Geophysical fluid mechanics

Stephen M. Griffies
Princeton University
Atmospheric and Oceanic Sciences Program
SMG@princeton.edu
Draft from May 31, 2025

Griffies, Stephen M., 1962-

Geophysical fluid mechanics

This book was typeset using LaTeX.

Contents

CONTENTS

PREFACE

Geophysical fluid mechanics (GFM) is a branch of theoretical physics concerned with natural fluid motion on a rotating and gravitating planet or star, making use of concepts and methods from classical continuum mechanics and thermodynamics. The primary inspiration for the subject comes from the motion of fluids in the earth's atmosphere and ocean, though the principles and methods are also applicable to extra-terrestrial planetary fluid flows. Geophysical fluids are in near rigid-body motion with the rotating planet, thus prompting a description from the rotating (non-inertial) planetary reference frame. Body forces from gravity plus planetary rotation (Coriolis and centrifugal) are fundamental features of the motion, as are contact forces from stresses (pressure and friction). We limit attention to the motion of a single phase of matter (gas or liquid), with the study of multiphase geophysical fluid mechanics, which is relevant to a moist atmosphere, outside our scope. Electromagnetic forces, important for the study of plasmas and astrophysical fluid motions, are also ignored.

Geophysical fluid flows manifest over a huge range of space and time scales, with linear and nonlinear interactions transferring information across these scales. Physical insights into such flows typically result from examining a hierarchy of conceptual models using a variety of methods and perspectives. Some models are formulated within the context of a perfect fluid comprising a single material constituent with fundamental processes limited to the reversible and mechanical. Some models consider constant density fluids, as commonly considered in classical hydrodynamics. Other models are posed using a real fluid that is comprised of multiple matter constituents exposed to irreversible process such as mixing of momentum through viscous friction, mixing of matter through matter diffusion, and/or the mixing of enthalpy through conduction. Some models ignore rotation, and thus tacitly apply to flows with length scales too short to feel the Coriolis acceleration, whereas others ignore buoyancy to focus on the dynamics of a homogeneous rotating fluid.

We develop geophysical fluid mechanics from a mathematical physics perspective, with a grounding in fundamentals offering a robust and versatile framework for exploring the gamut of special cases and approximations encountered in applications. Topics are approached by establishing general principles prior to the examination of case studies. Consistent with this approach, our treatment focuses on developing the mechanics of geophysical fluid motion, with that focus supporting theoretical explorations that often extend beyond that required for phenomenological purposes. Correspondingly, we embrace the opportunity to examine physics through multiple lenses that render a variety of complementary insights. In a nutshell, if a physical system can be formulated and analyzed in more than one way, then we do so if it enhances pedagogy and exposes layers of understanding. As a result, brevity is sacrificed to support exposition and exploration.

The presentation is based on the premise that skills in theoretical physics are optimally taught by nurturing physical reasoning, with physical reasoning supported by mathematical precision coupled to the elucidation of concepts using words and pictures. Correspondingly, the presentation is both deductive and descriptive. The deductive approach supports a precise understanding through the use of elementary physical notions that are expressed mathematically. The descriptive approach builds skills in reasoning along with the ability to articulate physical ideas using words

and pictures that complement the maths. Readers are supported by development of salient physical concepts and mathematical methods in the process of building understanding. With sufficient study, this book should be accessible to the advanced undergraduate student or entering graduate student in fields such as applied mathematics, astrophysics, atmospheric physics, engineering, geophysics, ocean physics, planetary physics, and theoretical physics.

We generally offer details to mathematical derivations. Doing so nurtures the mathematical skills required for the budding theorist, with the reader strongly encouraged to work through the various derivations to fully embrace each detail and concept. Exposing mathematical details also helps to unpack many of the physical concepts encapsulated by equations. It is notable that the concepts encountered in this book generally accord with common experience, thus affording a means to check on the validity of the maths. Furthermore, as we are studying physics, mathematical equations must satisfy dimensional consistency, with this constraint offering the physicist a powerful tool for exposing spurious mathematical statements.

We consider this book's intellectual journey as one taken together by the author and reader, thus motivating use of the first person plural pronouns *we* and *us*. We furthermore cultivate the deductive and descriptive approaches by embracing the synergism between physics and maths, whereby physics informs the maths and maths reveals the physics. This synergism is facilitated by a presentation style inspired by *Mermin* (1989), who identified the following characteristics for the clear articulation of mathematical physics.

- RULE 1: All displayed equations are given numbers to facilitate cross-referencing. Additionally, any equation supporting another equation or a discussion is itself afforded an equation number.

- RULE 2: Cross-referenced equations are referred to by their equation number as well as descriptive phrases or names (e.g., "the vector-invariant velocity equation (40.33)" rather than "equation (40.33)"). Coupling maths to words supports learning and reduces the need to flip pages to view the cited equation.

- RULE 3: Equations are part of the prose and are thus subject to punctuation.

Concerning the book's title

The study of rotating and stratified geophysical fluid motion largely started in the first half of the 20th century, and has evolved much over its history. During recent decades the study has seen particular evolution through deepening physical foundations, refining mathematical formulations, increasing the intellectual and predictive value of numerical simulations, extending applications across terrestrial and planetary systems, and expanding observational and laboratory measurements and techniques. What has emerged is a recognition that a fruitful study of rotating and stratified fluid flows makes use of ideas that go beyond the traditional notions of *geophysical fluid dynamics* (GFD). A contemporary practitioner develops insights by weaving together concepts and tools from mathematics, classical mechanics, fluid mechanics, thermodynamics, scalar mechanics, numerical simulations, laboratory experiments, field measurements, and data science. Acknowledging this broadening of the practice motivates the term *mechanics* in this book's title, rather than the more focused *dynamics*. It is a minor change in verbiage that reflects a broadening of the perspective pursued here.

Two pillars of theoretical geophysical fluid mechanics

We conceive of two pillars to theoretical geophysical fluid mechanics that are synergistic, thus offering lessons, guidance, and feedback to the other. The elements pillar of geophysical fluid

mechanics comprises the physical and mathematical formulation of conceptual models used to garner insight into rotating and stratified fluid motion. This pillar is concerned with setting the stage by deductively and descriptively exposing how physical concepts are mathematically expressed to describe geophysical fluid flows. We provide a thorough treatment of the element pillar in part since it is commonly offered only a terse treatment in other books. We emphasize that the elements pillar is far more than equation manipulation, although one certainly must become adept at that task. Instead, at its core, the elements pillar allows the physicist to reveal the fundamental physical concepts in a precise mathematical manner. Doing so supports understanding while building the foundations for applications encountered in the emergent phenomena pillar. The emergent phenomena pillar of geophysical fluid mechanics studies solutions to equations that describe phenomena, such as waves, instabilities, turbulence, and general circulation, all of which emerge from the fundamental equations based on first principles. These phenomena can emerge in manners that are far from simple to understand deductively, particularly when considering nonlinear behavior such as turbulence. Our treatment of the emergent pillar is limited to waves and instabilities, all of which are treated using the methods of linear mathematical physics.[1]

Some themes found in this book

This book covers a number of topics in theoretical geophysical fluid mechanics. Throughout, we encounter a number of themes that appear in various guises, with the following offering a brief survey.

Causation and budgets

A great deal of this book is concerned with deriving and understanding equations that describe the evolution of fluid properties, with such equations (differential or integral) derived from physical principles such as Newton's laws of motion, Hamilton's principle of stationary action, Noether's theorem, thermodynamic laws, mass conservation, and vorticity mechanics. These *budget equations* form the theoretical foundation of continuum mechanics. As part of this development we often seek information about what *causes* fluid motion, making use of a variety of kinematic and mathematical frameworks. The causality question is posed when studying the equation of motion, which says that acceleration (motion) arises from a net force (the cause of motion). Even though seemingly a clear decomposition of cause and effect, this fundamental statement of Newtonian mechanics offers little more than the definition of a force. We break the self-referential loop, and thus make physical progress, after specifying the nature of the force (e.g., gravitational, electromagnetic), as well as by offering properties of these forces as per Newton's third law (the action/reaction law).[2]

In geophysical fluid mechanics, we sometimes refer to time evolving budget equations as *evolution equations* or, more commonly, *prognostic equations*, with terms in the prognostic equation referred to as *time tendencies*. For prognostic equations, knowledge of the processes contributing to the net time tendency enables a prediction of flow properties. The question arises how to practically determine the tendencies acting in the fluid, particularly when tendencies are generally dependent on the flow itself. This question is not always simple to answer. Such is the complexity and beauty inherent in nonlinear field theories such as fluid mechanics, where cause and effect are intrinsically coupled.

[1] The further one moves along the axis of nonlinearity, the more Sisyphean the task of connecting fundamental processes to emergent phenomena. This perspective is lucidly discussed by *Anderson* (1972).

[2] For more on this perspective of Newton's laws, see Chapter 1 of *Symon* (1971) or Chapter 2 of *Marion and Thornton* (1988).

We can sometimes make progress by turning the problem around, whereby kinematic knowledge of the motion offers inferential knowledge of the processes contributing to the motion. This situation is exemplified by pressure forces acting within a non-divergent flow whereby pressure provides the force that acts, instantaneously and globally, to maintain the constraint that the velocity is non-divergent.[3] We may also make use of constraints that restrict the flow in manners that assist in prediction and understanding.

Constraints

Determining the forces, either directly or indirectly, provides physical insight into the cause of fluid flow and its changes. This approach is sometimes referred to a *momentum-based viewpoint* since it is based on working directly with the momentum equation (i.e., Newton's second law of motion). However, we are commonly unable to deduce the forces due to complexities inherent in nonlinear field theories. Furthermore, there are many occasions when we are simply uninterested in the forces. In these cases, we are motivated to use constraints that can allow us to sidestep forces but still garner insights into the motion.

One example of a constraint concerns the inability of fluid to flow through a solid static material boundary. To understand how this constraint impacts the macroscopic fluid motion, we do not need to understand details of the electromagnetic forces that underlie the resistance, at an atomic level, to this motion. Instead, we simply impose the kinematic boundary condition whereby the component of the velocity that is normal to the boundary vanishes at the boundary. The forces active within the fluid, no matter what flavor they may take, are constrained to respect the kinematic boundary condition. Another example concerns the study of vorticity developed in Part VII of this book. A variety of vorticity constraints offer the means to deduce flow properties without determining forces. Indeed, the *vorticity-based viewpoint* often provides a framework that is more versatile in practice than the momentum-based approach, thus prompting the importance of vortex mechanics in this book.

Associations and balances

Besides seeking causal relations pointing toward the future, many basic questions of fluid mechanics arise either instantaneously, as in the constraints maintaining non-divergent flows, or when the flow is steady, in which case properties at each point in space have no time dependence. In steady flows, the net acceleration, and hence the net force, vanish at each point within the fluid, although the fluid itself can still be moving (steady flows are not necessarily static). For steady flows we are unconcerned with causality since time changes have been removed. In this manner, the steady state equations are *diagnostic* rather than prognostic. Diagnostic relations thus provide mechanical statements about *associations* between physical processes that manifest as *balances*. The *geostrophic balance* is the canonical association in geophysical fluid mechanics, where the horizontal Coriolis force is balanced by the horizontal pressure gradient force. Another balance concerns the vertical pressure gradient and its near balance with the weight of fluid above a point in the fluid, with this *hydrostatic balance* approximately maintained at the large scale even for moving geophysical fluids. Further associations arise when studying steady vorticity balances, with the *Sverdrup balance* a key example that is commonly used in ocean circulation theory.

We summarize the above by saying that diagnostic equations are concerned with the way things are, whereas prognostic equations point to how things will be. So although a predictive theory requires prognostic equations that manifest causal relations, an understanding of how

[3] For non-divergent flow, pressure acts as the *Lagrange multiplier* enforcing flow non-divergence. See Section 48.2 for details.

fluid motion appears, and in particular how it is constrained, is revealed by studying diagnostic relations that expose associations through balances.

Mathematical transformations between kinematic perspectives

Geophysical fluid flows are complex. Hence, it proves useful to avail ourselves of a variety of methods and perspectives that support a mechanistic description of the motion. Many methods are associated with distinct kinematic lenses that reveal particular facets of the flow that might be less visible using alternative lenses. Examples include the Eulerian (spatial) and Lagrangian (material) kinematics used throughout fluid mechanics; the dual position space ($\boldsymbol{x}$-space) and wavevector space ($\boldsymbol{k}$-space) used for wave mechanics; the variety of vertical coordinates used for vertically stratified flows; and the analysis of motion in property spaces exemplified by watermass or thermodynamic analysis. We make use of these perspectives throughout this book, and offer the mathematical tools needed to transform between them.

Newtonian mechanics and Hamilton's principle

Throughout this book we pursue the maxim: *If there is more than one way to formulate a problem, then pursue them!* A canonical example concerns the complementary perspectives available from Newtonian mechanics and Hamilton's principle of stationary action. Each offers consistent results yet approaches mechanics from fundamentally distinct conceptual and operational perspectives. In a Newtonian approach to fluid mechanics, governing differential equations are formulated using a continuum version of Newton's law of motion, in which forces (causes) and accelerations (effects) are articulated as a means to understand and predict the flow. The alternative approach of Hamilton's principle of stationary action approaches mechanics via a variational formulation involving the *action*. Hamilton's principle says that the action functional is extremized by the physically realized system. The action is the space-time integral of the difference between kinetic and potential/internal energies, and by extremizing the action we reveal the governing Euler-Lagrange differential equations. The Euler-Lagrange equations are identical to Newton's equations for those cases where Newton's equations are available,[4] and yet the route to deriving these equations is very distinct. It is by pursuing these disinct paths that we uncover new insights and develop distinct tools for analysis.

Hamilton's principle is not typically covered in fluid mechanics books. This absence contrasts to its ubiquity of Hamilton's principle in other areas of theoretical physics. There are historical reasons for this disconnect, some of which are discussed in the introduction to Part IX of this book. We have chosen to include facets of Hamilton's principle in this book with the hope that doing so partially remedies the disconnect.[5] More specifically, we include Hamilton's principle since it provides novel perspectives on the fundamental equations of geophysical fluid mechanics, and renders insights and tools for the study of emergent phenomena such as waves and instabilities. The reader interested in a serious pursuit of theoretical mechanics should, at some point, make friends with Hamilton's principle. The effort is nontrivial as it requires brain muscles not exercised when studying Newtonian mechanics. But the conceptual and technical payoff is significant.

[4] Hamilton's principle yields the Maxwell's equations of electromagnetism. Indeed, it is used throughout modern physics in areas far beyond those of Newtonian mechanics.

[5] There certainly are examples where Hamilton's principle is discussed in fluid mechanics books, with *Salmon* (1998), *Olbers et al.* (2012), and *Badin and Crisciani* (2018) notable examples that have inspired this author. Even so, these books remain the exception rather than the norm. As a result, the broader geophysical fluid mechanics community, even those pursuing theoretical aspects, are largely unaware of the beauty and power of Hamilton's principle. This situation contrasts to nearly every other area of mechanics, in which Hamilton's principle is a central part of the theoretical development.

Non-dimensionalization and scale analysis

Mathematical symbols describing a physical system generally have physical dimensions. Examining the physical dimensions of an equation supports an understanding of the physical content of the equation, and provides a powerful means to identify errors in mathematical manipulations. It is for this reason that we prefer to expose physical dimensions throughout this book, rather than the alternative approach of working predominantly with non-dimensional equations. Even so, *scale analysis*, as realized through *non-dimensionalization*, offers an essential tool for deriving mathematical equations used to describe particular flow regimes.

There are two general types of dimensional scales that we use to non-dimensionalize a mathematical physics equation. The first is the *external scale*, with examples in this book being the gravitational acceleration, Coriolis parameter, and specified background or reference state. External scales are set by the geophysical parameter regime in which the flow occurs, and as such they are under direct control of the theorist. The second is the *emergent scale*, which emerges from the flow itself. Emergent scales, such as the length scale and velocity scale of the flow, are specified by the subjective interest of the physicist though they are not under their direct control. That is, we choose to focus on flows with a particular scale for purposes of examining the corresponding equations that describe that flow regime. A key example concerns our study of planetary geostrophy and quasi-geostrophy in Part VIII of this book, where we choose to focus on flows of a particular scale where the Coriolis acceleration is of leading order importance.

We thus consider the operational aspects of scale analysis to be largely subjective in nature. Namely, we approach the analysis with a subjective bias towards the flow regime of interest, which in turn affects choices for non-dimensional parameters that lead to the corresponding asymptotic equations that describe the regime. Hence, scale analysis is deductive while being strongly guided by our subjective interests.

Geophysical Fluid Mechanics and Climate Science

Fluid mechanics has a history of applications that span science and engineering, from blood flow to the stability of stars and the evolution of galaxies. A key 21st century application of geophysical fluid mechanics concerns the questions of earth system science associated with the uncontrolled greenhouse gas experiment pursued by industrialized civilization's carbon centered energy use. Leading order questions about climate warming have been sufficiently addressed to recognize that the planet has reached a crisis point threatening many features of the biosphere. Even so, mechanistic answers to a number of questions remain at the cutting edge of research. What will happen to the atmospheric jet stream and storm tracks in a world without summer Arctic sea ice? Will tropical storms be more powerful in a warmer world? What are the patterns for coastal sea level rise and their connections to large-scale ocean circulation? What are the key processes acting to bring relatively warm ocean waters to the base of high latitude ice shelves? How stable are the ocean and atmosphere's large-scale overturning circulations and their associated heat transport? Are there feasible and sustainable climate intervention options that equitably reduce the negative impacts of climate warming without introducing new problems? These questions, and countless others, constitute key intellectual challenges of climate science in particular and Earth system science more generally.

Numerical circulation models, observational field campaigns (both *in situ* and remote), and laboratory experiments, are core platforms for Earth system science. Many of these platforms have reached a level of maturity allowing them to vividly reveal details of the complex and multi-scaled nature of planetary fluid flow. Geophysical fluid mechanics is key to the design of observational field campaigns and novel laboratory and numerical experiments, and it provides the intellectual framework for developing mechanistic analyses and robust interpretations of measurements and simulations. In this way, geophysical fluid mechanics furthers predictive

capability for weather and climate forecast systems and it enhances confidence in projections for future climate. In a world of increasingly large volumes of simulated and measured data, we conjecture that the marriage of fundamental physical theory to data science tools will enable the significant science and engineering advances needed to address key questions of Earth system science.

About the cover

I took the cover photo of an iceberg, ocean, clouds, and sea bird (can you find the bird?) in the Orkney Passage region of the Southern Ocean during a research cruise from March-May 2017 aboard the British ship James Clark Ross. I am grateful to Alberto Naveira Garabato, the chief scientist on this cruise, for taking me to this amazing part of the planet. Although I largely pursue theoretical research, experiences with seagoing field research have greatly enhanced my scientific viewpoint and profoundly deepened a connection to the natural forces and phenomena that are in part described by geophysical fluid mechanics.

Gratitudes

This book greatly benefited from interactions with students in the Princeton University Atmospheric and Oceanic Sciences Program. In particular, parts of this book serve as the basis for the two-semester graduate course, AOS 571 and AOS 572, as well as for a variety of special topics classes (AOS/GEO 585) and lecture series. Further inspiration was offered by students, postdocs, and fellow researchers and scholars encountered on my path. I also thank those who provided specific suggestions, corrections, and comments on various drafts of this book, whose names are too many to list.

I am grateful for having been part of the unique research and learning environment cultivated at NOAA's Geophysical Fluid Dynamics Laboratory (GFDL), where I worked from 1993 until 2025, as well as Princeton University's Atmospheric and Oceanic Sciences (AOS) program, where I have taught and mentored since 2014. The focus of my research concerns ocean physics and the ocean's role in climate. The community at GFDL and Princeton AOS provide an ideal setting for those interested in broadening scientific perspectives while diving deep into particular research areas. As part of my research and mentoring in this community, I have encountered thinkers whose style, questions, and insights have taken root in my work. This work has also afforded me the opportunity to travel the world to interact with colleagues whose wisdom and love of the scientific endeavor are infectious and inspiring. Throughout these interactions, I have entered into trusting and non-judgmental spaces where deep learning and understanding arise. Partaking in these spaces, where heart and mind meld, has been among the most fulfilling experiences of my life.

Developing a book of this nature is a not a simple endeavor. It starts modestly, grows over time, and eventually becomes a passion and obsession. I was particularly drawn to writing during the COVID-19 pandemic that kept the world largely sequestered at home, and I am grateful that my life situation allowed for this work to safely flourish during these otherwise very difficult times. Writing this book has been an exercise in rational thought that exemplifies the maxim "to write is to learn", as articulated by *Zinnser* (1993). It was furthermore fed by spiritual food from meditation, yoga, family, and community. In particular, each step of this project was supported by my wife, Adi, and our son, Francisco. I am deeply grateful for their patience and trust as I satisfied the goal of writing this book through countless nights, weekends, and holidays. I treasure being part of this family and I dedicate this work to you two amazing human beings.

Caveats and limitations

This book remains a work in progress not yet ready for publication. There are many loose threads detailed at the start of many chapters. In addition, here are items targeted for completion prior to release of this book to a publisher.

- Mathematical topics
  - linear operator theory
  - Cartesian, cylindrical, and spherical harmonics
  - Lie derivative following Section F.3 of *Tromp* (2025a)
  - Frenet-Serret equations for three-dimensional flow as in Section 15.3.4 of *Dahlen and Tromp* (1998).
- Application of Hamilton's principle
  - Referential flow using Hamilton's principle
  - waves and mean flow interactions
  - shallow water and Hamilton's principle
  - semi-geostrophy and Hamilton's principle
  - quasi-geostrophy and Hamilton's principle
  - Ray theory using Hamilton's principle as in *Tracy et al.* (2014)
- Wave mechanics
  - equatorial shallow water waves
  - Rossby wave packets and motion in non-homogeneous background
  - Laplace's tidal equations and spherical harmonnics
- Flow stability
  - Charney problem of baroclinic instability
  - Arnold's stability theorem
  - Rayleigh-Benard convection
- Miscellaneous
  - More exercises
  - More figures
  - Continued refinement to notation
  - Continued scrutiny from readers
  - *Glossary for this chapter*, similar to that done by *Thorne and Blandford* (2017), placed at the end of each chapter. Besides defining the terms, point to the section where the term is defined and used more thoroughly. Have a bold index term for the glossary entries. Build a full book glossary from the chapter glossaries.

A GUIDE TO THIS BOOK

No book is an island, with this book generously making use of other books, review articles, research papers, and online tutorials. Many readers find value in studying a subject from a variety of perspectives and voices, thus justifying the proliferation of books with overlapping subject matter. Sometimes it is merely one or two sentences that allow for an idea or concept to click within the reader's brain, whereas other topics require the full gamut of detailed derivations and discussions coming from multiple voices. For these reasons we provide pointers to written and/or video presentations that offer supportive views on material in this book. Many further resources are available through a quick internet search.

There is no pretense that any reader will penetrate all topics in this book, nor read this book cover-to-cover. This recognition is particularly apparent in a world where research and educational agendas often spread rather than focus attention. Hence, an attempt has been made to facilitate picking up this book at a variety of starting points. For that purpose, each chapter is written in a reasonably self-contained manner and with a brief guide at the start of each chapter listing pre-requisite material. As such, some equations and derivations are reproduced in more than one place, thus obviating the need to back reference. Certainly each chapter cannot be fully self-contained since this is a book with material building from earlier chapters. We thus make generous use of cross-referencing to point out allied material treated elsewhere in the book.

Organization

This book is organized into parts according to their particular focus, with each chapter starting with a brief guide to the material and pointing to dependencies to other chapters. Some chapters focus on topics required for a basic understanding of the subject and offer exercises to test that understanding. Other chapters offer monograph style topics that further the foundations and exemplify applications largely taken from a selection of the author's research interests. Not all topics are treated equally, with some topics probed deeply whereas others are given little more than a superficial treatment. Indeed, there are even more topics that are omitted. Each of these shortcomings reflect on the author's limited energy and experience, rather than a judgement of importance for any given topic.

MATHEMATICAL METHODS AND CONCEPTS

In Part I of this book, we study a suite of mathematical topics that are of use for studying geophysical fluid mechanics. These chapters concern topics found in applied mathematics and/or mathematical physics texts. However, we approach the material with a distinctively geophysical fluid mechanics perspective. Many readers can skim these chapters without sacrificing too much from later chapters, assuming they have a working knowledge of Cartesian tensors (Chapter 1) as well as vector differential and integral calculus (Chapter 2). Where unfamiliar mathematics topics arise in later chapters, the reader is encouraged to return to this part of the book to help develop the necessary skills.

The chapters in this part of the book serve the needs of readers aiming for mathematical

acuity in a physical setting. Quite simply, mathematics is the best language for doing theoretical physics such as that developed in this book. So although we do not argue that all of the mathematical apparatus studied here are indispensible for "getting an answer", the physicist finds merit in developing a well honed mathematical brain by nurturing efficient, and often elegant, ways to think about physics. Those aiming to become a practitioner of geophysical fluid mechanics will benefit from a variety of mathematical methods such as those offered in this part of the book.

CLASSICAL MECHANICS

In Part II we survey topics in classical mechanics with a distinctively geophysical fluids perspective. Here we encounter the motion of particles moving around a rotating planet using methods from both Newtonian mechanics and Lagrangian mechanics, as well as notions from classical field theory that form the foundation for continuum mechanics and wave mechanics. Many students entering a course on geophysical fluid mechanics have just a cursory exposure to classical mechanics, so that material in Part II aims to partially remedy this limited exposure.

KINEMATICS OF FLUID FLOW

Mechanics is comprised of kinematics (the study of intrinsic properties of motion) and dynamics (the study of forces and energies causing motion). In Part III we initiate a study of fluid mechanics by focusing on the kinematics of fluid flow and matter transported by that flow. Our treatment exposes both the Eulerian and Lagrangian viewpoints and emphasizes the variety of kinematic notions and tools key to describing fluid motion. We also encounter facets of material transport as described by the tracer equation, thus laying the foundation for *tracer mechanics* pursued in Part XIII. Fluid flow, and the transport of matter within that flow, have many features fundamentally distinct from point particle and rigid body motion, and it takes practice to intellectually digest these differences.

Quite often a course in geophysical fluid mechanics skims over fluid kinematics, preferring instead to focus on dynamics. Indeed, some kinematic topics can seem esoteric on first encounter, particularly the study of Lagrangian kinematics. However, an incomplete understanding of fluid kinematics can lead to difficulties appreciating facets of fluid dynamics. The reader is thus encouraged to fully study the kinematics chapters, and to revisit the material as the needs arise in later chapters.

THERMODYNAMICS

We study equilibrium thermodynamics in Part IV of this book, assuming little to no prior exposure to the subject. We pay particular attention to the role of gravity in modifying the treatment of thermodynamic equilibrium states, with gravity an essential facet of geophysical fluids and yet a force commonly ignored in standard treatments. However, we ignore phase transitions, thus making this part of the book a mere introduction to the study of a moist atmosphere. A reader can skip this part of the book with minimal disruption to later chapters. Even so, thermodynamics is an incredibly rich subject that is central to how we think about geophysical flows, in particular how energy moves through fluid systems. We thus consider thermodynamics forms a central pillar in our treatment of geophysical fluid mechanics.

DYNAMICS OF GEOPHYSICAL FLUID FLOW

In Part V we encounter the foundational topics of geophysical fluid dynamics. Within these chapters we study how Newton's laws of mechanics and the principles of thermodynamics are used to describe fluid motion on a rotating and gravitating planet. We approach the subject by

focusing on how forces that act on fluid elements lead to accelerations and thus to motion. These forces act both throughout the volume of a fluid element (*body forces* from gravity, Coriolis, and centrifugal) as well as on the boundary of a fluid element (*contact forces* from pressure and friction). We also complement the Newtonian approach, which focuses on forces, with Hamilton's Principle, which focuses on energy.

SHALLOW WATER MECHANICS

In Part VI we study the mechanics of a shallow water fluid, with a shallow water fluid comprised of hydrostatically balanced homogeneous fluid layers. The layers are also typically assumed to be immiscible, so that interactions between layers occur only via mechanical forces from pressure acting at the layer interfaces. The shallow water fluid allows us to focus on rotation and stratification without the complexities of vertically continuous stratification and thermodynamics. Many physical insights garnered by studying shallow water fluids extend to more realistic fluids, thus making the shallow water model very popular among theorists and teachers. Indeed, *Zeitlin* (2018) provides an example of just how far one can go in understanding geophysical fluids with shallow water theory.

VORTICITY AND POTENTIAL VORTICITY

In Part VII we develop the concepts of vorticity and potential vorticity. Vorticity plays a role in the motion of all geophysical fluids since motion on a rotating planet provides a nonzero *planetary vorticity* even to fluids at rest on the planet. This feature of geophysical fluids contrasts to many other areas of fluid mechanics, where irrotational flows are commonly encountered. Potential vorticity is a strategically chosen component of the vorticity vector that melds mechanics (vorticity) to thermodynamics (stratification). Material conservation properties of potential vorticity are striking and render important constraints on fluid motion. Indeed, perhaps the most practical reason to study vorticity concerns the various constraints imposed on the flow moving on a rotating and gravitating planet. These constraints provide conceptual insights and predictive power.

NEARLY GEOSTROPHIC BALANCED FLOWS

Balanced models are introduced in Part VIII, with our attention limited to the shallow water and continuously stratified versions of quasi-geostrophy and planetary geostrophy. Balanced models generally remove the horizontally divergent motions associated with gravity waves, thus allowing a focus on the large-scale vortical motions. Balanced models have a rich history among theoretical geophysical fluid studies, providing insights into both laminar oceanic flows through planetary geostrophy, and wave-turbulent atmospheric and oceanic flows through quasi-geostrophy.

LINEAR WAVE MECHANICS

In Part X we study a variety of geophysical waves and associated mathematical methods used for their characterization. We include waves not commonly included in a book on geophysical fluids, such as sound and capillary waves, with these waves included due to their ubiquity in the natural environment as well as their pedagogical value. Most focus, however, is given to waves arising from the Coriolis acceleration (inertial waves, planetary Rossby waves, topographic Rossby waves) and gravitational acceleration (surface gravity waves, internal gravity waves). Furthermore, we study linear waves and their corresponding wave packets, first studying their behavior in a homogeneous background environment where Fourier methods are available. Thereafter, we introduce the methods needed to study linear waves on a gently varying background, including the methods of geometrical optics and wave action where Fourier methods are not suited.

FLOW INSTABILITIES

In Part XI we study instabilities that arise in geophysical fluid motions. We distinguish two classes of fluid instabilities: *local* or *parcel* instabilities versus *global* or *wave* instabilities. Local instabilities are afforded a local necessary and sufficient condition to determine whether the fluid base state is unstable to perturbations. In contrast, global instabilities arise from the constructive interference of waves and so involve the solution of an eigenvalue problem to determine properties of unstable waves. At most, a necessary condition can be derived to determine whether a global instability exists. Our study of fluid instabilities introduces a suite of case studies that foster analysis and conceptual methods to establish a foundation for further study. Geophysical fluid instability analysis remains an active area of research, with insights into the suite of primary and secondary instabilities providing compelling stories for how the ocean and atmosphere work.

GENERALIZED VERTICAL COORDINATES

In Part XII we provide a thorough and unified treatment of the generalized vertical coordinate description of geophysical fluid mechanics. The chapters dive into details of the maths, kinematics, dynamics, and applications. This material is central to many current research activities, including subgrid scale parameterizations and the design of numerical atmosphere and ocean models.

SCALAR FIELDS

For Part XIII of this book, we unpack the mechanics of scalar fields with a focus mostly on the ocean. Here we consider active tracers (temperature and salinity), passive tracers, and buoyancy. Much of this study forms the basis of *tracer mechanics*, which has proven very important for the ocean since it is generally very difficult to measure vector fields such as velocity and vorticity, whereas tracer distributions are far more readily measured. We also consider facets of sea level analysis in this part of the book.

Written and spoken communication

To thrive in research and teaching requires one to master elements of both written and spoken communication. Here we offer a few pointers.

CLEAR THINKING LEADS TO CLEAR COMMUNICATION

Clear communication is the sign of clear thinking. Some people communicate better in writing, where one has the opportunity to carefully organize thoughts and refine the writing style. Others are better at speaking, where spontaneous and interactive reflections and experience can bolster the clarity of a presentation.

As inspiration for both the clear and obscure, pick up one a textbook or lecture notes and analyze the presentation for clarity. Where is the presentation confusing? Where is the material crystal clear? Then pick up a journal article and perform the same analysis. What is appealing? What is unappealing? Then go to the internet and find a science or engineering lecture, old or new. What makes the speaker engaging and clear, or boring and obscure?

EMPATHY IS KEY

Empathy is a basic facet of effective communication and teaching, where the writer, speaker, or teacher places their mind inside that of an interested and smart reader or listener. Identify with their quest to understand new ideas and to comprehend the foundations and assumptions. Are

the assumptions justified based on the audience? How compelling is the scientific story? Are missing steps crucial to understanding or easily dispensed with for streamlining the presentation?

CLARITY HELPS, BUT SOME MATERIAL IS JUST TOUGH

Although poor communication hinders our ability to digest new ideas and concepts, it is also important to appreciate that some material is tough no matter how well it is communicated. We should aim to make a subject matter as simple as possible, but not simpler (paraphrasing Einstein). Furthermore, it sometimes takes a few generations of teaching before some scientific material can be sufficiently digested to allow for the core conceptual nuggets to be revealed. As an example, try reading Newton or Maxwell's original works as compared to a modern presentation of Classical Mechanics or Electromagnetism. So as we strive for clear communication, we cannot presume that clarity is sufficient to remove the struggles everyone experiences when learning.

Pointers on physics problem solving

Most people are not born with *a priori* physics problem solving skills. Rather, it takes extensive practice to develop the necessary brain muscle. Here are some general pointers to keep in mind when diving into a physics problem, whether it is for a class or the basis of a broader research question.

CHECK FOR DIMENSIONAL CONSISTENCY

The symbols we use in mathematical physics correspond to geometrical objects (e.g., points, vectors, tensors) describing a physical concept (e.g., position in space, velocity, temperature, angular momentum, stress). Hence, the symbols generally carry physical dimensions. The physical dimensions we are concerned with in this book are length (L), time (T), mass (M), and temperature. We do not consider electromagnetism. Physical dimensions of the equations must be self-consistent. For example, if one writes an equation $A = B$, where A and B have different physical dimensions, then the equation makes no sense physically. Something is wrong. Although not always sufficient to uncover errors, dimensional analysis is an incredibly powerful necessary step in debugging the maths.

CHECK FOR TENSORIAL CONSISTENCY

In the same way that mathematical equations in physics need to maintain dimensional consistency, they must also respect tensor rules. For example, the equation $A = B$ makes mathematical sense if A and B are both scalars. Likewise, $\mathbf{A} = \mathbf{B}$ makes sense if $\mathbf{A}$ and $\mathbf{B}$ are both vectors. However, if both $\mathbf{A}$ and $\mathbf{B}$ are vectors, then the equation $\mathbf{A} = \nabla \cdot \mathbf{B}$ does not make sense because the left hand side is a vector and the right hand side is a scalar. A more subtle example is when $\mathbf{A}$ is a vector yet $\mathbf{B}$ is an axial vector. In this case, $\mathbf{A}$ remains invariant under a change from right hand to left hand coordinates whereas $\mathbf{B}$ flips sign. Maintaining basic tensorial rules can be considered the next level of sophistication beyond dimensional analysis.

USE WORDS AND PICTURES

Words and pictures are important elements in explaining a physical concept and/or a problem in physics. Hence, it is good practice to liberally sprinkle sentences in between the key equations for the purpose of explaining what the maths means using clear English. Here are some practical payoffs to the student for this style of presentation.

- The process of explaining the maths using words and pictures requires one to dive deeper into the logic of a physics problem. Doing so often reveals weak points, incomplete or unmentioned assumptions, and errors. This process is a very important learning stage in preparing to stand in front of an audience to present results and to answer questions. It is a key facet of research and teaching.
- Physics teachers are often more forgiving of math errors if you convince the teacher that you have a sensible physical understanding of the problem. Plain English and pictures are very useful means for this purpose.

THERE IS OFTEN MORE THAN ONE PATH TO A SOLUTION

In physics, there is often more than one path to a solution to a problem or the formulation of a concept. Pursuing distinct paths offers novel physical and mathematical insights, exposes otherwise hidden assumptions, and simply allows one to double-check the veracity of a solution. Some of the most profound advances in physics came from pursuing distinct formulations. One example concerns the distinct formulation of mechanics offered by Newton (1642-1746), and then later by Lagrange (1736-1813) and then Hamilton (1805-1865). Had Lagrange or Hamilton rested on the merits of their predecessors, we may well have had a very different intellectual evolution of 19th and 20th century physics.

Princeton University AOS 571 and AOS 572

Princeton University's AOS 571 and AOS 572 are two courses that focus on geophysical fluid mechanics. The first semester, AOS 571, is concerned with developing conceptual and mathematical foundations of the subject by studying elemental features of planetary fluid motion, and by providing a mathematical physics basis for understanding these patterns. The second semester, AOS 572, makes use of the foundations from AOS 571 to study emergent phenomena arising from waves and instabilities.

DETAILS OF YOUR TEACHER AND THE COURSE

Dr. Stephen M. Griffies
`SMG@princeton.edu`
`https://stephengriffies.github.io/`
Worked homeworks to be uploaded onto Canvas before class on the due-day.
Class materials are enabled via Canvas.
Class communication is enabled via Ed Discussion.
AOS 571 class lectures were recorded during Covid shutdown (autumn 2020), and they are available on Canvas.

.1 Class structure and expectations

Our goal for this two-semester sequence of courses is develop an understanding of basic geophysical fluid mechanics, and in doing so to learn how to formulate and to solve problems. To help reach these goals, we study selected chapters from this book. Note that you will be expected to read far more material than covered in class.

As with any other topic in physics, garnering an understanding and appreciation of geophysical fluid mechanics can require effort and practice. To help that process, you are expected to read the assigned material, work through the derivations, and hand-in homework exercises. You will have many opportunities to develop the necessary brain muscle assuming you maintain the discipline to keep up with the material. Please ask questions, preferably in class, when you are unsure of anything.

CULTIVATING A SAFE SPACE FOR HEALTHY LEARNING

A fundamental feature of any class concerns the learning environment. My aim as class teacher is to foster an inclusive, friendly, generous, patient, and non-judgmental space for learning. Key principles that support this space include equity, diversity and inclusion, each of which are intrinsically valuable and an essential feature of ethical research and education. We also acknowledge and honor past generations whose efforts, some of which were garnered through force and oppression, have led to the rewarding environment in Princeton where we study and conduct research. It is our sincere hope that practicing the above principles will support present and future generations in a way that helps to heal past injustices. Cultivating this

safe and grateful space supports deep learning while genuinely appreciating contributions from individuals without regard to race, ethnicity, culture, religion, sexual orientation, gender identity and expression, physical ability, age, socioeconomic status or nationality. As a participant in this space, we each celebrate diversity and nurture an inclusive and friendly community that is optimized for shared learning and mutual understanding.

For many, this class will require a tremendous amount of effort. It will require much focus and energy to master the material even for those with an established background. Regardless your background, talents, or interests, I am here to help. So please reach out if you are struggling. I also encourage you to develop working relations with your classmates. Homework exercises can be done collaboratively, and working with others offers great opportunities for learning.

Even if you prefer to work alone, I ask that you develop some form of a relation with one or more of your classmates. Part of this recommendation is based on the need to informally monitor our mutual health, particularly given that graduate school can be stressful. Even so, it can be a time for building deep friendships and community as we share in the process of learning how to thrive as budding researchers and scholars.

CLASS LECTURES AND CLASS BOOK

The class lectures closely follow selected material from Griffies (2025). Prior to each class, you are expected to read through the assigned sections and view the assigned videos. During class we will discuss salient points from the readings and videos. To allow sufficient time for interactive discussion and questions, not all of the assigned reading material will be directly covered in class. Hence, you are expected to read and to understand more material than is covered on the chalkboard. Correspondingly, you are welcome to bring any questions related to the reading to the class, even if the material was not covered in class.

The pace of the lectures will be gauged by questions during the class and my sense for how well you are grokking the material. You are encouraged to follow lectures by having a copy of the class book on-hand, preferably electronically to conserve paper.

PLEASE DISCONNECT ELECTRONICS FROM INTERNET DURING CLASS

To support your learning and teaching experience, and those of your classmates, please ensure that you turn all electronic devices into airplane mode so that you are not tempted to divert attention to non-class issues. To get the most from the lectures and class time requires focused attention and active participation.

.2 Some pointers for the problem sets

Here we consider some context for the class problem sets, which are an important part of learning the material.

AIM FOR A BALANCE BETWEEN THOROUGH AND BRIEF

There is often a conflict between showing full mastery of a problem and keeping the solution write-up brief. In general, there is no need to re-derive equations already presented in the book. Proper referencing of the equation is all that you need; i.e., tell me something like "starting from equation (X.YY) from Griffies book draft dated DD.MM.YY." Additionally, when presenting a derivation, you may choose to show just the key steps rather than all intermediate steps. Determining what is a "key" step is largely up to you, but it should be something you learn to do in time. Nonetheless, you are encouraged to show more than one approach to a solution.

QUESTIONS FOR POINTS OF CLARIFICATION

Questions for points of clarification will be entertained if you feel the problem is ill-posed or if you are totally lost. Email through Ed Discussion is the most efficient means to communicate to me. Responses will generally be sent back through Ed Discussion so that all students can see the response, thus keeping everyone with the same information. Correspondingly, questions within 24 hours of the deadline are generally not entertained so to ensure that all students have time to see the response.

MISTAKES OFFER IMPORTANT OPPORTUNITIES FOR LEARNING

Everyone makes mistakes, some more than others. The toughest part is the self-imposed shame or embarrassment. Please try to keep a positive mind about your mistakes. As you will discover, mistakes offer significant opportunities for learning. I am a poster-child for this process!

So do not be overly anxious if you find many marks on your homeworks and exams. Rather, aim to use mistakes as learning opportunities. That is how life in academics (life in general!) works. Furthermore, be completely honest with yourself to candidly identify weaknesses. I will do my best to work personally with you if something remains uncertain or you feel there is a weakness in your skills that needs some extra help. Please seek help should you wish it. And finally, please do question my marks should you feel they are unfair or incorrect. I am prone to mistakes in my grading.

PRESENTATION OF THE SOLUTION: PLEASE USE LATEX

Please write clearly and legibly. I strongly encourage you to learn and to use LaTeX as this mark-up language is an indispensible tool for writing documents with or without mathematics. Indeed, LaTeX is required for all AOS 572 assignments, so it is wise to start using it for AOS 571. If you choose to hand-write your solutions, then please ensure that the equations and words are clearly written. In my experience, sloppy hand-writing generally leads to graders who are less forgiving of errors. You must convince the grader that you understand the solution and present the maths in a legible manner.

DEADLINES ARE STRICT IN ORDER TO BE FAIR TO EVERYONE

Please do your best to be on time with handing in homeworks and exams, with disasters, personal tragedy, and significant accidents the only excuses for late assignments. Fairness to those meeting the deadlines is the fundamental reason to insist on this rule. Additionally, I generally aim to grade the homework soon after everyone hands it in, and then to provide solutions for quick feedback. Doing so helps to identify issues and obstacles sooner rather than later. If someone is given extra time, then that delays the feedback time, thus eating into the learning experience for everyone else.

> In brief: a homework problem will receive zero credit if handed in late, with rare exceptions.

GENERAL RUBRIC FOR MARKING YOUR WORK

Problem sets are marked using the following general rules, with grading less forgiving as the class progresses through the year. The following mistakes are marked by an increasing amount moving through the list.

POINTS ABOUT GRADING YOUR WORK

1. SIGN ERRORS: Sign errors are a nuisance. We all must spend time to uncover them. One means of detecting errors is to try explaining the maths to yourself or someone else. Does the result make sense? If not, then perhaps there is a sign error. I am generally not too upset with sign errors if they have minimal physical relevance. But when they indicate a physical misconception then I will mark it more harshly.
2. MATH ERRORS: Math errors, such as those associated with basic calculus mistakes, are generally marked.
3. DIMENSIONAL AND TENSORIAL ERRORS: I am relatively unforgiving of dimensional mistakes and tensorial inconsistencies.
4. PHYSICALLY MISSING THE POINT: Evidence of physically missing the point will generally invoke the most negative marks depending on the depth of the misconception. The best way to convince me you grasp the basic physics is to use words and pictures. If the maths is missing or totally wrong, but you present some sensible words and pictures, then that will help earn some credit.

.3 Course material and strategies for thriving

The course material consists of a class book plus a selection of online videos. Ideally, the book material is to be read and the videos viewed **prior to each class**. Salient points related to the material will be presented during class on the chalkboard, along with further discussion and questions. We will *not* cover all the material in class that is expected to be learned as part of the reading assignments and problem sets. Since there is no laboratory portion of this class, it is very important to view the various videos linked to each lecture. More generally, you are strongly encouraged to peruse this library of classic videos that have stood the test of time for their pedagogy on various topics in fluid mechanics. Additionally, the Homsy Multi-media Fluid Mechanics lectures offer an incredibly valuable tool for basic fluid mechanics concepts. The full content of Homsy is available online through the Princeton University library.

STRATEGIES FOR THRIVING IN THIS COURSE

- ESSENTIALS FROM PROF. BAZETT FOR THE START OF THE SEMESTER
  - View this 12-minute lecture on study tips.
  - View this 12-minute lecture on how to learn effectively.
  - View this 19-minute lecture on how to write LaTeX documents using Overleaf.
- PRIOR TO EACH CLASS
  - Review material from previous lecture (5 to 10 minutes).
  - View assigned videos (5 to 45 minutes).
  - Read assigned class book sections (30-120 minutes).
- AFTER EACH CLASS
  - Reread class book material and review assigned videos.
  - Identify questions for class discussion or during Q & A session.
  - As needed, view recorded class lecture from 2020 to fill in gaps.
  - Work assigned exercises alone and then gather with classmates to discuss and complete.
- QUESTIONS: Address questions by reaching out during class, after class, during office hours, during group gatherings, or via Ed Discussion. There are no silly questions!

.4 Grades for AOS 571

AOS 571 CLASS GRADE = PROBLEM SETS (75%) + FINAL EXAM (25%)

Worked problem sets are due on Canvas prior to the start of class when they are due. Each problem set normally is allocated one week for completion, unless otherwise noted. Students can make use of any resources for solving problem sets, including other people. Clarification of questions can also be obtained via email to me. If you find a solution from a source other than your own head, then be sure that you fully understand both the essence and the detail of the solution. Although you are encouraged to discuss the problems with other students, you are cheating yourself if you merely parrot another person's answer without fully grokking it yourself.

There is no pretense that the exercises offered in class are clearly formulated. Indeed, a certain degree of ambiguity reflects the *status quo* in research, where formulating a novel and insightful question is generally the most difficult part of the research process. Additionally, the solutions may not be 100% correct or ideal from a pedagogical perspective. Rather, they represent a work in progress. If mistakes or ambiguities are found, then please share your questions and concerns.

There is a takehome final exam during exam period. You are asked to do the work as a solo student, with no help or consultation from another human. However, you can make use of books, notes, online resources, etc. The questions are generally taken from published papers with relevant references provided to the student.

.5 AOS 571 course outline

Here we offer specifics of the course material covered during AOS 571. There are 24 class lecture periods of 80-90 minutes each. Most of the following topics take a full class, though some are shorter and some are longer.

0. Lecture-0 consists of pre-class study of the course introduction and mathematics refresher. It is assumed that each student knows this material when starting the first lecture, so please be prepared. And yes, there is a lot of pre-class reading. But for many, this reading will be review from previous classes and so it should be relatively simple.
    - Watch this 9-minute video from Prof. Hall introducing some basic images from terrestrial fluid flows.
    - Watch this 16-minute video from 3Blue1Brown on the divergence and curl operations with examples taken from fluid mechanics.
    - Read the preface to this book.
    - Read Chapter 1 on Cartesian tensors.
    - Read Chapter 2 on vector calculus.
    - Read Chapter 11 on Newtonian particle mechanics.
    - Read Chapter 16 on the continuum approximation used for describing fluids as a continuous media.
1. Geophysical particle mechanics
    - Chapter 13: kinematics of a particle moving around a rotating sphere, including position, velocity, acceleration, Cartesian and spherical coordinates, rotating reference frame, Coriolis acceleration, planetary centrifugal acceleration
    - Chapter 13: dynamics of a particle moving around a rotating sphere using Newton's equation of motion, rotating reference frames, gravitational geopotential
    - Watch the first 5-minutes from this UCLA Spin Lab video on Coriolis effect.
    - Exercises 11.1, 13.3, 13.4, 13.7.
2. Symmetries, conservation laws, and constrained motion
    - Chapter 14: mechanical energy, potential momentum, inertial oscillations, axial angular momentum
    - Exercises 14.1 and 14.2.
3. Fluid kinematics
    - Chapter 17: Eulerian and Lagrangian fluid kinematics, Galilean invariance, material time derivative, flow lines
    - 4-minute video on Eulerian and Lagrangian descriptions from Prof. Hogg
    - 27-minute video on Eulerian and Lagrangian descriptions from Prof. Lumley.
    - Exercises 17.2, 17.4, and 17.7.
4. Mass conservation
    - Chapter 19: continuity equation, mass budget for fluid elements and finite regions, kinematic boundary conditions

- 5-minute video on mass conservation from Prof. Hogg.
- Exercises 19.1, 19.2, 19.3, and 19.4

5. Tracer conservation

   - Chapter 20: barycentric velocity, tracer equation, budgets for infinitesimal fluid elements, budgets for finite fluid regions, Leibniz-Reynolds transport theorem, boundary conditions

6. Kinematics of non-divergent flows

   - Chapter 21: scalar streamfunction, vector streamfunction, area and volume conservation, meridional-depth overturning circulation
   - 4-minute video on streamlines from Prof. Hogg.
   - Exercises 21.4, 21.5, 21.6, 21.8, 21.9

7. Momentum dynamics

   - Chapter 24: momentum dynamics, accelerations, contact forces, body forces, special forms of the momentum equation, axial angular momentum
   - 6-minute video on momentum from Prof. Hogg.
   - Exercises 24.2, 24.4 and 24.7

8. Stress in fluids

   - Chapter 25: stresses and the stress tensor, linear momentum budget, relating stress to strain, form stress, boundary conditions
   - 2.5-minute video on stress and strain from Prof. Hogg.
   - 8-minute video on stress from Prof. Hogg.
   - Exercise 25.1

9. Energy dynamics and filtered equations

   - Chapter 26: kinetic energy, gravitational potential energy
   - 8-minute video on hydrostatic pressure from Prof. Hogg.
   - Exercises 26.2, 26.3, and 26.6.

10. Pressure in fluids

    - Chapter 27: primitive equations, hydrostatic approximation, hydrostatic pressure
    - Chapter 28: pressure form stress
    - Exercises 27.1, 27.2

11. The Boussinesq ocean

    - Chapter 29: oceanic Boussinesq approximation, hydrostatic scaling, pressure and non-divergent velocity
    - Exercises 29.2, 29.4, 29.5

12. Buoyancy

    - Chapter 30: Archimedes' principle, buoyancy, stratification, gravitational stability, mass density for perfect and realistic fluids

- 49-minute video from Prof. Lewin for an overview of buoyancy as well as other features of fluid mechanics.
- Exercises 30.1, 30.4

13. Geostrophic mechanics

- Chapter 31: Rossby number, geostrophy, planetary geostrophic equations, Taylor-Proudman, thermal wind, isopycnal form stress
- 30-minute video from Prof. Fultz for an overview of rotating fluids.
- 4-minute video from the UCLA SpinLab for examples of Taylor columns.
- Exercises 31.1, 31.2

14. Natural coordinates and Ekman mechanics

- Chapter 32: natural coordinates for horizontal (tangent plane) flow; centripetal, centrifugal, and Coriolis accelerations; exact geostrophic flow; inertial motion of fluid particles; cyclostrophic balance; gradient wind balance
- Chapter 33 on Ekman mechanics: natural coordinates, spiral motion across isobars, non-dimensionalization and the Ekman number, net mass transport
- Start around the 23-minute mark of this video from Prof. Fultz for his discussion of Ekman layers.
- Exercises 33.1, 33.2

15. Formulation of shallow water models

- Chapter 35: thickness equation, momentum equation, reduced gravity model, stacked shallow water layers, shallow water layer in a rotating tank
- 30-minute video on shallow water model from Prof. Hall.
- Exercises 35.1, 35.5

16. Shallow water dynamics

- Chapter 36: geostrophy, thermal wind, form stress, mechanical energy including available potential energy
- Exercises 36.2, 36.7, 36.8

17. Vorticity and circulation

- Chapter 37: vorticity and circulation
- 23-minute video on vorticity from Prof. Shapiro (part 1 of 2)
- Exercises 37.2, 37.3, 37.4, 37.5, 37.6.

18. Two-dimensional non-divergent barotropic vorticity model

- Chapter 38: two-dimensional barotropic vorticity model; properties of this model.
- Exercises 38.5, 38.6

19. Shallow water vorticity and potential vorticity

- Chapter 39: shallow water vorticity and potential vorticity
- Exercises 39.3, 39.4

20. Vorticity mechanics

    - Chapter 40: vortex lines and tubes, Kelvin's circulation theorem, mechanics of baroclinicity, stretching and twisting of vortex lines, β-effect
    - 21-minute video on vorticity from Prof. Shapiro (part 2 of 2).
    - 5-minute video on vortex rings and Helmholtz's theorems from the Physics Girl.
    - Exercises 40.4, 40.5, 40.8, 40.11

21. Potential vorticity mechanics

    - Chapter 41: Ertel potential vorticity, PV evolution with friction and other irreversible processes.
    - Exercise 41.1

22. Balanced models I (single layer)

    - Chapter 43: Buckingham's Π theorem, asymptotic expansion in terms of small Rossby number, shallow water planetary geostrophy and quasi-geostrophy

23. Balanced models II (continuous stratification)

    - Chapter 44: asymptotic derivation of continuously stratified planetary geostrophy and properties of these equations.
    - Chapter 45: asymptotic derivation of continuously stratified quas-geostrophy and properties of these equations.

.6 Grades for AOS 572

AOS 572 CLASS GRADE = PROBLEM SETS (60%) + FINAL REPORT/PRESENTATION (40%)

The style of the problem sets is just as in AOS 571, but with one important addition:

> ALL PROBLEM SETS MUST BE PREPARED USING LaTeX.

This requirement supports your skills in preparing scientific documents using LaTeX, preferably making use of your Princeton Overleaf account. It will also prepare you for the written report.

Rather than a final exam, you will prepare a final project for AOS 572. The project consists of a written report on a non-original topic (i.e., it is not research) and a corresponding tutorial presentation emphasizing a portion of the written report. The topic of the final project is to be decided by the student and teacher and it concerns a topic directly related to waves and/or instabilities, with the topic chosen no later than mid-term. The topic either is one that is *not* covered in the class, or one that is pursued in much more depth than covered in class. Grades are based on mastery of the subject, skills at pedagogically communicating the subject using written and oral methods, and ability to answer fair questions from anyone in the audience.

Here are further details for the project.

- WRITTEN REPORT = 30% OF CLASS GRADE

    1. The report surveys the physics and maths of the chosen topic in a manner allowing it to be taught to AOS 572 students. There should be deductive/pedagogical math derivations along with physical principles and connections to topics in other AOS classes. Citations should be given for all sources.

2. The report is *not* original research. Rather, it represents an intelletually digested view of a topic from the literature that is pedagogically connected to material covered in the class.
3. The report is not purely descriptive. Instead, it must meld the three pieces of clear mathematical physics: words, equations, and schematics.
4. Figures can be original or taken from other books and papers.
5. The report must be typeset in LaTeX using Overleaf and using the provided LaTeX template.
6. The report should be no less than 20 pages (excluding references), and no more than 30 pages total.
7. A thorough report draft (via Overleaf) is due no later than one week prior to the oral presentation, thus allowing the teacher to offer feedback to be addressed in the final draft.
8. Start writing soon after the middle of the semester. Homework assignments will lighten then (though not vanish) to allow time for the report.
9. Feel free to discuss with others the content of the report. However, 100% of the writing and presentation must originate from each respective student. Do not use use any generative artificial intelligence for generating the report.
10. Refer to Mermin (1989) and Griffies et al (2013) for specific pointers on writing styles. Marks will be taken off when ignoring these styles.
11. Grading rubric
    (a) intro/background (20)
    (b) concepts/methods (60)
    (c) pedagogy/clarity/style (20)

- ORAL PRESENTATION = 10% OF CLASS GRADE

1. The presentation is to the full class (and any interested visitors) using a chalkboard with zero electronic media (i.e., no slides and no videos). Eliminating all electronic media focuses efforts on the intellectual content of the report and the presentation rather than tweaking presentation aesthetics. It also provides important experience for working on the chalkboard rather than "hiding" behind electronic slides.
2. The presentation should be designed to last 15 minutes without interruptions. It is not simple to stand in front of a class and convey information. So you are strongly encouraged to practice the presentation beforehand to optimize time and clarity.
3. The 15 minute presentation is not intended to cover the full written report. Rather, the purpose is to teach the class just one or two key concepts from the report. Teaching requires a tremendous amount of study and practice. Be humble with goals for the 15 minute lecture.
4. After the presentation, 15 minutes is then devoted to questions from students, visitors, and the teacher.
5. All students must be present for all presentations.

- GRADING RUBRIC

1. intro/background (20)
2. concepts/methods (20)

3. pedagogy/speaking skills (20)
4. understanding: presentation (20)
5. understanding: questions (20)

.7 AOS 572 course outline

Here we offer specifics of the course material covered during AOS 572, which is roughly organized as 2/3-waves and 1/3-instabilities.

1. Fourier analysis
    - Chapter 8: Fourier analysis
    - This video, also from 3Blue1Brown provides a visual introduction to Fourier transforms.
    - This video from 3Blue1Brown provides a visual introduction to Fourier series.
    - Exercises 8.1 and 8.2
2. Plane waves and wave packets
    - Chapter 49
    - Exercises 49.1, 49.3, 49.4.
3. Acoustic waves
    - Chapter 51
    - The second half of this video offers an introduction to acoustic waves.
    - Exercises 51.1, 51.2
4. Surface gravity and capillary waves (Part I)
    - Chapter 52
    - Exercises 52.2, 52.3
5. Surface gravity and capillary waves (Part II)
    - Chapter 52
    - Exercises 52.5, 52.7
6. Inertial waves
    - Chapter 53
7. Two-dimensional barotropic Rossby waves I
    - Chapter 54
    - Exercises 54.1 and 54.2
8. Two-dimensional barotropic Rossby waves II
    - Chapter 54
9. Shallow water waves I
    - Chapter 55

- The first half of this video offers an introduction to shallow water waves.
- Exercises 55.1 and 55.5

10. Shallow water waves II
    - Chapter 55
    - 14-minute video on gravity waves from Prof. N. Hall
    - Exercises 56.1 and 56.2
11. Internal gravity waves I
    - Chapter 57
    - Tank experiment from Prof. Peter Rhines' lab
    - Simulations from Prof. Dale Durran
12. Internal gravity waves II
    - Chapter 57
    - Exercise 57.1
13. Forced internal gravity waves
    - Chapter 58
    - Exercises 58.1 and 58.2
14. Centrifugal instability
    - Chapter 59
    - Sections 17.1 and 17.2 of *Cushman-Roisin and Beckers* (2011)
15. Inertial instability and symmetric instability
    - Chapter 59
    - Section 17.2 of *Cushman-Roisin and Beckers* (2011)
    - Exercises 59.1, 59.2 and 59.3
16. Rayleigh-Taylor instability
    - Chapter 60
    - Wikipedia for Rayleigh-Taylor
17. Kelvin-Helmholtz instability
    - Chapter 60
    - Sections 9.1 of *Vallis* (2017)
    - Wikipedia for Kelvin-Helmholtz
18. Horizontal shear instability I
    - Section 54.5
    - Chapter 61
    - Section 3.12 of *Smyth and Carpenter* (2019)
    - Sections 9.2-9.3 of *Vallis* (2017)

- Chapter 10 of *Cushman-Roisin and Beckers* (2011)

19. Horizontal shear instability II

    - Chapter 61
    - Section 3.12 of *Smyth and Carpenter* (2019)
    - Sections 9.2-9.3 of *Vallis* (2017)
    - Chapter 10 of *Cushman-Roisin and Beckers* (2011)
    - Exercise 61.2

20. Stratified shear instability

    - Chapter 61
    - Section 11.7 of *Kundu et al.* (2016)
    - Sections 14.1 and 14.3 of *Cushman-Roisin and Beckers* (2011)
    - Chapter 4 of *Smyth and Carpenter* (2019)

21. Quasi-geostrophic waves

    - Chapter 62
    - Chapter 8 of *Smyth and Carpenter* (2019)
    - Sections 9.4-9.8 of *Vallis* (2017)
    - Sections 17.3-17.6 of *Cushman-Roisin and Beckers* (2011)
    - Rotating tank experiment from Prof. Wing
    - Rotating tank experiment from MIT

22. Baroclinic instability II

    - Chapter 62
    - Chapter 8 of *Smyth and Carpenter* (2019)
    - Sections 9.4-9.8 of *Vallis* (2017)
    - Sections 17.3-17.6 of *Cushman-Roisin and Beckers* (2011)

23. Baroclinic instability III

    - Chapter 62
    - Chapter 8 of *Smyth and Carpenter* (2019)
    - Sections 9.4-9.8 of *Vallis* (2017)
    - Sections 17.3-17.6 of *Cushman-Roisin and Beckers* (2011)

24. A survey of turbulence

    - Chapters 11 and 12 of *Vallis* (2017)
    - Turbulence and the 5/3 spectrum from 3Blue1Brown
    - Rayleigh-Bernard convection generated turbulence as simulated using Dedelas
    - 3d turbulence video from Prof. Stewart
    - MicroHH simulations
    - Steve Brunton lecture

- Decaying two dimensional turbulence
- Forced two dimensional turbulence from Prof. Ed Zaron
- Two dimensional turbulence and cascade from Prof. Ryan Abernathey
- Shallow water turbulence from Prof. Ed Zaron
- Geostrophic turbulence from Prof. Bill Young
- CM2.6 surface temperature simulation
- Neverworld2 shallow water simulations

Part I

Mathematical methods

We assume that readers of this book have a wide range of prior exposure to and penchant for mathematical physics. For example, many graduate students in the atmospheric and oceanic sciences might have seen elements of vector calculus during their first and/or second year of undergraduate studies (or perhaps even in high school), but may have used these methods only sporadically in subsequent years. This situation is distinct from those having a degree in physics or engineering, whose mathematical training is nurtured throughout their undergraduate and graduate years. Those not having received a thorough mathematical physics/engineering undergraduate training must fill gaps to intellectually digest the physics in this book. This situation motivates writing the chapters in this part of the book, which offers an eclectic suite of mathematical concepts and tools to help in the study and practice of geophysical fluid mechanics.

Concerning the value and importance of mathematical physics

When considering the impressive skill of numerical simulations of geophysical flows now common in the 21st century, the analytical training received by a 20th century theoretical scientist and engineer may seem like an unnecessary relic. Why bother to become adept at the huge variety of methods and tricks for deriving and/or analytically solving equations of mathematical physics? One answer is simply that such knowledge and skills provide a wealth of fundamental physical understanding. Namely, mathematics remains the most precise and powerful language of physics. So anyone presuming to do physical science or engineering must have some level of skills in mathematics. Quite simply, to sidestep a training in mathematical methods risks missing a huge opportunity to grok the physics. Namely, conceptual insights arise from the use of mathematics to expose the physical and geometrical meaning of physics equations, even for those equations that cannot be analytically solved. From this perspective, we propose that there is a growing, not declining, need for practitioners to understand the physical principles and mathematical methods at the heart of the compelling pictures generated by ever-increasingly powerful computers, satellites, and *in situ* measures of geophysical fluid flows.

The depth to which one can pursue mathematical physics goes far beyond that presented in this book. For example, a modern mathematical treatment of continuum mechanics makes use of differential geometry and differential forms as presented in such books as *Schutz* (1980), *Frankel* (2004), and *Tromp* (2025a). However, to develop familiarity and trust with differential forms requires a nontrivial intellectual investment. At best, we offer glimpses of that approach through forays into tensor analysis, with pointers to such approaches in the literature to motivate the interested reader to dive deeper by accessing the literature.

Physics provides relations between geometric objects

Mathematical objects of use for the study of fluid mechanics include scalar fields (e.g., temperature, mass density, specific entropy), vector fields (e.g., velocity, vorticity), and second order tensor fields (e.g., diffusion tensor, stress tensor, moment of inertia tensor). These and other fields have a value at each point in the continuous space and time used in continuum mechanics. Furthermore, their existence is independent of the arbitrary coordinate choices used for the mathematical description. In the study of geophysical fluid mechanics, we use physical principles to develop differential equations relating geometric objects referred to here as *tensors*. Mathematical tools of analysis are then used to compute the numbers required to compare with experiments and field measurements, and to formulate discrete equations for numerical simulations.

Our perspective can be summarized by "physics as geometry", which forms a foundation to theoretical physics such as that detailed in *Thorne and Blandford* (2017) and *Tromp* (2025a). This perspective has both conceptual and practical use for our study throughout this book. In

this part of the book we develop certain mathematical tools of geometry and analysis that are later used to formulate theoretical geophysical fluid equations and conceptual models. Our aim is to develop mathematics to help both pack and unpack the physics encapsulated by equations, pictures, and words. This aim extends to those cases where closed form analytical solutions are unavailable, which is the norm for nonlinear field theories such as fluid mechanics or even in many cases when the equations are linearized. Such qualitative and conceptual tools are of great value for the analysis of numerical simulations and field measurements.

TENSOR ANALYSIS AND GEOPHYSICAL FLUID MECHANICS

There are many occasions where a geophysical fluid system is more physically transparent when using a particular coordinate description or reference frame. However, there is no *a priori* coordinate choice that fits all cases. Thus, being adept at transforming from one mathematical description to another eases the study and pays huge dividends to the practioner. Tensor analysis is the proven means for systematically performing such transformations, thus motivating its use in fluid mechanics and other areas of continuum mechanics. In its more abstract realization via differential (or exterior) forms (not pursued in this book), tensor analysis provides the means to mathematically express physical ideas without any display of coordinate artefacts, thus exposing the underlying physical and mathematical essence.

The following offers an incomplete list of geophysical fluid systems where various coordinate descriptions or reference frames are encountered, and thus where tensor analysis can be put to use. Granted, many of these physical systems can be studied without the formalism of tensor analysis. However, by doing so one often encounters clumsy manipulations that obfuscate the underlying physical concepts. Indeed, imagine the tedium required to write continuous field equations in multiple dimensions prior to vector analysis.[6] That situation is akin to the tedium and awkward nature required to work across multiple coordinate systems and reference frames absent the formalism of tensor analysis. Hence, an adept use of vector analysis and its generalization to tensor analysis reveals how maths can inform the physics and how physics can is embodied by the maths.

- RELATING EULERIAN AND LAGRANGIAN KINEMATICS: There is a duality in fluid kinematics between Eulerian and Lagrangian descriptions of fluid motion. To develop an understanding of this duality we make use of tensor analysis to facilitate the transformation between the two kinematic descriptions. Whereas Cartesian coordinates offer a complete description for Eulerian kinematics, Lagrangian kinematics requires general tensor analysis (Chapters 3 and 4) since fluid particles deform with the fluid motion and thus render a non-orthogonal coordinate description.

  For many purposes in continuum mechanics, one can pursue a description of motion without the choice of an origin, thus making use of some general results from differential geometry and tensor analysis. Our pursuit is less ambitious since we always have in mind a fluid system on a rotating planet or laboratory placed in a background Euclidean space with universal Newtonian time. Hence, for our puposes we acknowledge that there is a natural origin for a spatial description (e.g., planetary center or fixed location in the laboratory).

- APPROXIMATELY SPHERICAL PLANET: Geophysical fluids move on an approximately spherical planet, making spherical coordinates the preferred choice for studying planetary flows.[7] The surface of a sphere is non-Euclidean object that is embedded in a background

[6] The original treatment of electrodynamics by Maxwell was before the notations of vector analysis were invented by Gibbs, Heaviside, and others. Hence, reading Maxwell's original maths is, by today's standards, tedious and challenging.

[7] *Staniforth* (2022) provides compelling arguments for moving beyond spherical coordinates for realistic atmospheric and oceanic modeling.

Euclidean space. We make use of tensor methods to transform between planetary Cartesian coordinates (origin at the center of the planet) and spherical coordinates. Notably, spherical coordinates are locally orthogonal, so that one can, if desired, make use of spherical coordinates without the machinery of tensor analysis. Even so, having two ways to develop the spherical equations provides useful pedagogy when learning tensor analysis since results are readily checked with prior experience.

- ROTATING TANK: Rotating laboratory fluids move in a circular tank, with cylindrical polar coordinates respecting symmetry of the domain. We make use of tensor methods to transform between Cartesian and cylindrical polar coordinates when considering rotating tank systems. Cylindrical polar coordinates are locally orthogonal, so that the comments above about spherical coordinates also hold here.

- ROTATING REFERENCE FRAME: Geophysical fluids move around a rotating earth and the fluid maintains a nearly rigid-body motion. Terrestrial observers also move in near rigid-body motion with the planet. We are thus motivated to study geophysical fluids from a rotating reference frame. We use rudimentary tensor methods to transform between a fixed inertial frame and the non-inertial rotating reference frame, with this transformation revealing non-inertial accelerations (planetary Coriolis and planetary centrifugal) that impact on the observed fluid flow.

- GALILEAN TRANSFORMATIONS: Geophysical fluids move in a space-time defined by universal *Newtonian time* (all clocks measure same time) and Euclidean space, with the product of these two defining *Galilean space-time*. When studying fluid motion it can be convenient to move from one Galilean reference frame to another, with the movement referred to as a *Galilean transformation*. Tensor methods are quite useful to develop the mathematical relations between two Galilean reference frames.

- STRATIFIED FLUIDS AND GENERALIZED VERTICAL COORDINATES: Geophysical fluids move in a gravitational field that acts to stratify the fluid according to its local buoyancy (high buoyancy fluid sits above low buoyancy fluid). When there is a one-to-one invertible relation between the height and the buoyancy, then it can be useful to describe the vertical position of a fluid element according to its buoyancy rather than its height. This buoyancy or "isopycnal" vertical coordinate choice leads to a non-orthogonal coordinate description of the fluid motion. There are other vertical coordinates that can be of use for other situations, such as the terrain following coordinates commonly used for atmospheric simulations and coastal ocean models. Transforming between Cartesian coordinates and such *generalized vertical coordinates* is greatly facilitated by the use of general tensor analysis.

Our use of tensor analysis is minimized both to reduce the necessary mathematical overhead for the reader, and because much of the physics in this book is suitably displayed with Cartesian coordinates, in which case tensor analysis and vector calculus are nearly identical. Furthermore, even in those cases where tensor analysis has an obvious benefit, such as the generalized vertical coordinates of Part XII, we do not pursue the full power of tensor analysis since doing so requires more development of the mathematical formalism than warranted for this book.

SUMMARY OF THE MATH CHAPTERS

Some of the chapters in this part of the book are essential for nearly all subsequent chapters (e.g., Chapters 1 and 2), with the bulk of this book accessible to those with a strong undergraduate training in multivariate calculus and the rudiments of analytic geometry. Other chapters target those interested in penetrating various special topics presented in this book. Readers are encouraged to take a close look at each chapter if only to know where to find topics of use later in the book or later in one's career.

- CARTESIAN TENSOR ALGEBRA: Chapter 1 is a synopsis of Cartesian tensor analysis. This topic provides a systematization of ideas from Cartesian geometry and linear algebra. Material in this chapter is essential for nearly every topic in this book.

- CARTESIAN TENSOR CALCULUS: Chapter 2 extends the algebraic ideas from Chapter 1 to differential and integral calculus. This chapter provides a resume of multivariate or vector calculus of use for fluid mechanics. Material in this chapter is essential for nearly every topic in this book.

- GENERAL TENSOR INTRODUCTION: Chapter 3 provides an introduction to general tensor analysis and its applications to geophysical fluids. The discussion is accessible to anyone who has read Chapters 1 and 2, as it builds directly from that earlier discussion. Chapter 3 is highly recommended for all readers of this book, even for those who do not wish to study details of general tensors in Chapter 4.

- GENERAL TENSOR ANALYSIS: Chapter 4 extends the Cartesian tensor algebra and calculus from Chapters 1 and 2 to allow for arbitrary, or general, coordinates. This chapter is essential for the mathematics underlying non-Cartesian coordinates, such as spherical coordinates, generalized vertical coordinates (Part XII of this book), and Lagrangian/-material coordinates (e.g., Chapters 17 and 18). Note that we retain the assumption that all tensors are embedded within a background Euclidean space, which offers some simplification relative to that needed to study topics such as general relativity.

- PARTIAL DIFFERENTIAL EQUATIONS: Chapter 6 provides a summary of linear partial differential equations (PDEs) commonly encountered in mathematical physics. Even though the equations of fluid mechanics are nonlinear, their linear counterparts offer much insight into fluid behavior, with particular applications to the study of waves, instabilities, and tracer transport.

- DIRAC DELTA: Chapter 7 develops properties of the Dirac delta generalized function, which provides one of the most magical tools available for the theorist. The Dirac delta has particular use in the study of Fourier analysis and Green's functions.

- FOURIER ANALYSIS: Chapter 8 summarizes salient points from Fourier series and Fourier transforms. We make particular use of Fourier analysis in the study of wave mechanics in Part X of this book.

- GREEN'S FUNCTIONS: Chapter 9 surveys Green's function methods used to solve linear partial differential equations. Green's function methods build on the superposition principle possessed by linear systems, and they foster insights into both the mathematical and physical content of linear differential equations.

- VARIATIONAL CALCULUS: Chapter 10 offers an introduction to the calculus of variations, which proves of great use for our study of mechanics via Hamilton's Principle.

- GEOMETRY OF CURVES AND SURFACES: Chapter 5 introduces rudimentary differential geometry used to characterize curves (such as fluid particle trajectories) and surfaces (such as isopycnals) embedded in a background Euclidean space. Here we encounter such notions as normal and tangent directions as well as the curvature of a surface.

In closing this introduction, we quote from page 1 of the classical text on theoretical physics by *Morse and Feshbach* (1953). Their perspective and goals have inspired and guided the chapters in this part of the book.

Our task in this book is to discuss the mathematical techniques which are useful in the calculation and analysis of the various types of fields occurring in modern physical theory. Emphasis will be given primarily to the exposition of the interrelation between the equations and physical properties of the fields, and at times details of the mathematical rigor will be sacrified when it might interfere with the clarification of the physical background. Mathematical rigor is important and cannot be neglected, but the theoretical physicist must first gain a thorough understanding of the physical implications of the symbolic tools [they are] using before formal rigor can be of help. Other volumes are available which provide the rigor; this book will have fulfilled its purpose if it provides physical insight into the manifold field equations which occur in modern theory, together with a comprehension of the physical meaning behind the various mathematical techniques employed for their solution.

Chapter 1

TENSOR ALGEBRA

A mathematical study of geophysical fluid flow makes use of *Galilean relativity*, which is built from *Newtonian universal time* (all clocks in the universe measure the same time) and flat *Euclidean space* (the intrinsic curvature vanishes). This Galilean space-time structure induces the familiar Euclidean norm or *metric* when measuring the spatial distance between two points. That is, the Euclidean space measures distance using *Pythagorus' theorem*. This Pythagorean method to measure distance holds even when the points are restricted to non-Euclidean manifolds (e.g., point on a sphere or points on an arbitrary surface such as a constant buoyancy surface), so long as those manifolds are embedded within the Euclidean background space. We can thus make use of Cartesian coordinates as the starting point for a mathematical formulation of geophysical fluid mechanics, whether using Eulerian or Lagrangian kinematics (Chapters 17 and 18) or generalized vertical coordinates (Part XII).

Tensors are geometric objects that have no concern for coordinate system nor origin. As noted above, we are concerned with tensors living in three-dimensional Euclidean space as well as tensors living on a non-Euclidean manifold (e.g., a sphere or an isopycnal) that is embedded within Euclidean space. The study of *Cartesian tensors* restricts attention to tensors described by *Cartesian coordinates* in Euclidean space, or for tensors on flat surfaces embedded in Euclidean space. The isomorphism between three-dimensional Euclidean space and the space of three-dimensional real numbers allows one to associate each point of Euclidean space, $\mathbf{x} \in \mathbb{E}^3$, with unique *Cartesian coordinates*, $\boldsymbol{x} \in \mathbb{R}^3$, for that point. This isomorphism renders a connection between geometry and analysis, thus offering two perspectives on the equations of mathematical physics.

Transformations to alternative coordinates are made if they offer insight to symmetry of the flow and/or the geometry of the space on which the flow occurs. For Cartesian coordinate systems with the same origins and of equivalent handedness, such transformations are related by rotations, which are orthogonal transformations. More general transformations to non-Cartesian coordinates are the topic of general tensor analysis, with details provided in Chapters 3 and 4.

In this chapter we introduce tensor analysis with a focus on algebraic relations. Our treatment shares much with the mathematical physics literature, such as Chapter 2 of *Aris* (1962), Chapter 1 of *Segel* (1987), and Chapter 2 of *Lovelock and Rund* (1989) (whose use the term *affine tensors* rather than *Cartesian tensors*). Additionally, we provide a particular emphasis on the distinction between tensors as geometric objects versus their subjective representations using coordinates, with this emphasis of fundamental importance particularly when working with general tensors. We also introduce the notion of a one-form as a tensor that is dual to vectors, and in turn we distinguish *covariant* and *contravariant* tensor representations. The distinctions between one-forms and vectors are not central to this book, since the two representations are connected through the metric tensor, which we always assume is available for our use.

The extra bit of formalism associated with covariant and contravariant tensor representations is not needed for Cartesian tensors, so that most textbook treatments of Cartesian tensors ignore it. However, it serves our purpose to smooth the transition to the general tensors studied in

Chapters 3 and 4. Indeed, for that purpose we typically write $\mathcal{G}_{ab}$ as the representation of the metric tensor, which for Cartesian tensors reduces to the Kronecker symbol, $\mathcal{G}_{ab} = \delta_{ab}$.

CHAPTER GUIDE

This chapter is a prerequisite for nearly every chapter to follow. It should be accessible to those having a working knowledge of linear algebra.

We make use of *covariant* index notation for the representation of tensors (indices placed downstairs), as well as the *contravariant* index notation (indices placed upstairs).[a] For Cartesian coordinates in Euclidean space, there is no numerical distinction between covariant and contravariant index placements (see Section 1.4.5). Even so, we make use of the covariant/contravariant notation in anticipation of its use for general tensors in Chapters 3 and 4 (see in particular Section 3.5). This notation also facilitates the Einstein summation convention, in which repeated indices are summed over their range. So although this chapter focuses on Cartesian tensors, we keep our eye on their more general cousins, with a particular aim to reveal those assumptions suited to Cartesian tensor analysis yet that are unsuited to general tensor analysis.

[a] The mnemonic "co-low" helps remember the index placement.

1.1 Loose ends

- Move from δ_{ab} to $\mathfrak{g}_{ab}$ so to get used to the general coordinates. That will make life easier when move to chapters 3 and 4.

1.2 Points, positions, and notation

Consider a point, $\mathscr{P} \in \mathbb{E}^3$, living in three-dimensional Euclidean space. As a geometric object, a point has an existence that is independent of any coordinate representation. Now let $\mathbf{x}$ be the position for this point relative to an arbitrary origin. Once an origin is fixed, the position, $\mathbf{x}$, also has an existence that is independent of coordinates, and so we consider $\mathbf{x} \in \mathbb{E}^3$. Namely, the position for a point in Euclidean space is a line segment with an arrow pointing from the origin to the point. In this manner, the point, $\mathscr{P}$, and its position, $\mathbf{x}$, have no concern for coordinate systems. Even so, to make use of geometric objects for analysis requires specifying a set of coordinates, and in this chapter we focus on Cartesian coordinates.

1.2.1 Cartesian representation of the position

The isomorphism between Euclidean space and the real numbers allows us to associate a unique Cartesian *coordinate representation*, $\boldsymbol{x} \in \mathbb{R}^3$, for the position of every point in Euclidean space. We write this Cartesian coordinate representation as

$$\mathbf{x} = \hat{\boldsymbol{x}}\, x + \hat{\boldsymbol{y}}\, y + \hat{\boldsymbol{z}}\, z \quad \mathbf{x} \in \mathbb{E}^3 \tag{1.1a}$$

$$\boldsymbol{x} = (x, y, z) \qquad \boldsymbol{x} \in \mathbb{R}^3. \tag{1.1b}$$

These equations state that each position, $\mathbf{x} \in \mathbb{E}^3$, has a unique coordinate representation, $\boldsymbol{x} \in \mathbb{R}^3$, with the coordinate representation written here using three-dimensional Cartesian coordinates. A Cartesian coordinate representation is provided by an ordered triplet of real numbers, (x, y, z). Each element of the triplet measures the coordinate distance (with *physical dimensions* of length)

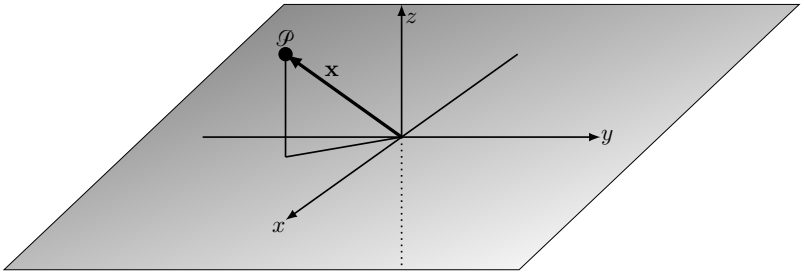

FIGURE 1.1: An arbitrary point in Euclidean space, $\mathscr{P} \in \mathbb{E}^3$, has an objective existence independent of a subjective choice of coordinate system used to describe its position. Its position, $\mathbf{x}$, relative to a chosen origin has an existence independent of the orientation of the coordinate system. The position is here represented by a right-handed Cartesian coordinate system according to $\mathbf{x} = \hat{\boldsymbol{x}}\, x + \hat{\boldsymbol{y}}\, y + \hat{\boldsymbol{z}}\, z$, with the coordinate representation, $\boldsymbol{x} = (x, y, z) \in \mathbb{R}^3$. The Cartesian basis vectors are given by the normalized triplet of unit vectors $(\hat{\boldsymbol{x}}, \hat{\boldsymbol{y}}, \hat{\boldsymbol{z}})$. There is a continuous infinity of possible Cartesian coordinate systems that are rotated with respect to the one shown here.

along the axes defined by their corresponding Cartesian unit vectors, $(\hat{\boldsymbol{x}}, \hat{\boldsymbol{y}}, \hat{\boldsymbol{z}})$, with these unit vectors pointing in directions of increasing coordinate values. The Cartesian unit vectors are a right-handed set of linearly independent vectors that form a basis for three dimensional Euclidean space.[1] As such, the position for any point in Euclidean space can be represented in terms of these three basis vectors.

1.2.2 A soft convention for upright versus slanted notation

We use an upright symbol for a geometric object living in Euclidean space. The position, $\mathbf{x} \in \mathbb{E}^3$, is an example (in LaTeX, the upright is written `\mathbf{x}`), as are the tensors introduced later. The corresponding slanted symbol is used for a coordinate representation of the position, $\boldsymbol{x}$, or of a tensor, with coordinate representations living in the space of real numbers (using LaTeX, the slanted boldface is written `{\bm x}`). Each coordinate representation is realized by specifying a subjectively chosen set of coordinates. For this chapter the coordinates are Cartesian with $\boldsymbol{x} \in \mathbb{R}^3$ and with each coordinate having a physical dimension of length. So in summary, the upright notation is used for the position and for tensors, and the slanted notation is used for their coordinate representations.

The distinction between an upright and slanted version of a symbol is fundamental conceptually, in that it distinguishes tensors as geometric objects from their coordinate specific representations. Even so, the distinction is not critical in practice since an equation can be generalized from a specific set of coordinates (e.g., Cartesian) to arbitrary coordinates, so long as the equation respects the tensor rules discussed in Section 3.1.2.

1.2.3 Indices and Einstein's summation convention

Coordinate representations of the position and of tensors require indices to distinguish the various objects that appear in tensor analysis. The practioner of tensor analysis becomes quite adept with the rules of *index gymnastics*, and we nurture the necessary brain-muscle in this chapter.[2] The choice for where to place indices follows a convention that originates from that used for the position. This convention then sets the stage for subsequent usage with tensors.

[1] The unit vectors are sometimes denoted $(\hat{\boldsymbol{i}}, \hat{\boldsymbol{j}}, \hat{\boldsymbol{k}})$ in the literature. We do not use that notation in this book.
[2] See Section 3.5 for a summary of the rules.

We choose to write the coordinate representation of the position as

$$\mathbf{x} = \hat{\boldsymbol{x}}\, x^1 + \hat{\boldsymbol{y}}\, x^2 + \hat{\boldsymbol{z}}\, x^3 = \sum_{a=1}^{3} \boldsymbol{e}_a\, x^a = \boldsymbol{e}_a\, x^a, \tag{1.2}$$

with the superscripts acting as tensor labels rather than as multiplicative powers. The final equality in equation (1.2) introduced the *Einstein summation convention*, in which we drop the summation symbol while repeated indices are summed over their range. Although seemingly trivial, the summation convention proves central to a variety of tensor manipulations, and so it is important to make friends with it. The second equality in equation (1.2) introduced a generic notation for the basis vectors

$$\boldsymbol{e}_1 = \hat{\boldsymbol{x}} \quad \text{and} \quad \boldsymbol{e}_2 = \hat{\boldsymbol{y}} \quad \text{and} \quad \boldsymbol{e}_3 = \hat{\boldsymbol{z}}, \tag{1.3}$$

with this notation allowing us to succinctly write the coordinate representation as $\mathbf{x} = \boldsymbol{e}_a\, x^a$.

We emphasize that the indices denote components of a specific coordinate representation, $x^a = (x^1, x^2, x^3)$, as well as members from the set of basis vectors, $\boldsymbol{e}_a = (\boldsymbol{e}_1, \boldsymbol{e}_2, \boldsymbol{e}_3)$. These labels are not multiplicative powers nor partial derivative operations.[3] Furthermore, placement of the downstairs tensor indices on the basis vectors pairs with the upstairs indices placed on the coordinate representations of the position. Such index placements establish a convention that is used for tensors.

1.2.4 Alternative Cartesian coordinates

We have thus far written $\boldsymbol{x}$ as the Cartesian coordinate representation of the position, $\mathbf{x}$. Now consider an alternative Cartesian coordinate system in which the position is represented by $\overline{\boldsymbol{x}}$. In Section 1.10 we work through the mathematics of the transformation between the two sets of Cartesian coordinates, $\boldsymbol{x}$ and $\overline{\boldsymbol{x}}$. For now we use the existence of this alternative coordinate system to exemplify the distinction between a geometric object (e.g., the position), versus its coordinate representation. Namely, the position for a particular point in space, $\mathbf{x}$, can be represented in either of the following equivalent manners

$$\mathbf{x} = \sum_{a=1}^{3} \boldsymbol{e}_a\, x^a \quad \text{with} \quad \boldsymbol{x} = (x^1, x^2, x^3) \tag{1.4a}$$

$$\mathbf{x} = \sum_{\overline{a}=1}^{3} \boldsymbol{e}_{\overline{a}}\, x^{\overline{a}} \quad \text{with} \quad \overline{\boldsymbol{x}} = (x^{\overline{1}}, x^{\overline{2}}, x^{\overline{3}}). \tag{1.4b}$$

That is, the position, $\mathbf{x}$, points from the origin to the point $\mathscr{P}$, and it can be represented using any number of Cartesian coordinates, with two such coordinates here written as $\boldsymbol{x}$ and $\overline{\boldsymbol{x}}$. Since both coordinate sets are Cartesian, their respective basis vectors, $\boldsymbol{e}_a$, and $\boldsymbol{e}_{\overline{a}}$, are orthonormal.

1.3 Tensors

We extend the study of points and their positions in Section 1.2 to now consider *tensors* as geometrical objects that live in $\mathbb{E}^3$ or a suitable submanifold. Just like the position for a point, each tensor has a coordinate representation that allows for its use in analysis. Importantly, a

[3] In this book we generally eschew the notation where partial derivatives are denoted by a subscript. One exception occurs in our discussion of the evolution of mass density in Sections 72.2 and 72.3.

tensor has no dependence on either the choice for coordinates nor the choice for origin.[4] In this section we introduce the *Kronecker tensor*, which is the *unit tensor*, as well as vectors and one-forms.

1.3.1 Kronecker (unit) tensor

The Cartesian basis vectors each have unit magnitude (normalized), meaning that their scalar products satisfy[5]

$$\hat{\boldsymbol{x}} \cdot \hat{\boldsymbol{x}} = \hat{\boldsymbol{y}} \cdot \hat{\boldsymbol{y}} = \hat{\boldsymbol{z}} \cdot \hat{\boldsymbol{z}} = 1, \tag{1.5}$$

which can be written more generally as

$$\boldsymbol{e}_a \cdot \boldsymbol{e}_b = \delta_{ab}, \tag{1.6}$$

with δ_{ab} the *Kronecker symbols*, which form the $(0,2)$ Cartesian representation of the *Kronecker tensor*, also known as the *unit tensor*, which is given by[6]

$$\boldsymbol{e}_a \cdot \boldsymbol{e}_b = \delta_{ab} = \begin{cases} 1 & \text{if } a = b \\ 0 & \text{if } a \neq b. \end{cases} \tag{1.7}$$

As seen in Section 1.4, the Kronecker tensor provides the Cartesian coordinate representation of the *metric tensor* for Euclidean space. In Section 4.1 we introduce alternative representations for the metric based on the use of general coordinates.

Use of a hat over a vector in equation (1.3) signifies that the vector is normalized to unity. For Cartesian coordinates we generally work with the normalized basis vectors (1.3), or their orthogonal transformations related by a rotation (Section 1.10). Indeed, a normalized vector can change only through rotation since by definition it remains of unit norm and so cannot change its magnitude (see Section 2.1.4). For general tensors, we sometimes find it more convenient to work with unnormalized basis vectors. Hence, the basis vectors, $\boldsymbol{e}_a$, are not assumed to be normalized and so are not adorned with a hat.

1.3.2 Vectors as tensors

The position, $\mathbf{x}$, identifies locations in space relative to a chosen origin, and it is commonly referred to as the *position vector*. However, we reserve the term "vector" for a particular example of geometric objects (i.e., *tensors*) that are independent of coordinates as well as origin. Geometrically, we define a vector as a line segment with an arrow that points in a particular direction. In this manner, a vector has no concern for any subjectively chosen origin. We encounter a number of vectors in physics, such as the velocity, acceleration, and force.

It is notable that the velocity is the time derivative of the position of a point particle that moves through space, and the acceleration is the second time derivative. Taking a time derivative of the position removes dependence on the origin. So although the position of a point particle is not a tensor, its time derivative is a first order tensor, as is the acceleration. This result hints at the nature of vectors as living in the tangent space to points on a manifold, which is a concept we return to in Section 4.2.3 when studying general tensors.[7]

[4]The position, $\mathbf{x}$, depends on the arbitrarily chosen origin. Consequently, the position is not a vector (a first order tensor). This distinction is easily forgotten since the position is often referred to as the "position vector". See Section 1.3.2 for more on this point.

[5]The Cartesian scalar (or dot or inner) product is discussed more formally in Section 1.4.

[6]The notation $(0,2)$ signifies the number of upstairs or contravariant indices, 0 here, and the number of downstairs or covariant indices, 2 here.

[7]The *flow map* or *motion field* introduced in Section 18.2 is the generalization of position and trajectory to continuum matter. Like the position, the flow map is not a tensor, though its time derivative, the velocity field, is a tensor.

Following the notation for the position and its coordinate representation, we use an upright bold symbol, $\mathbf{F}$, for a vector and write its coordinate representations with a slanted $\boldsymbol{F}$:

$$\mathbf{F} = F^a\,\boldsymbol{e}_a \in \mathbb{E}^3 \quad \text{and} \quad \boldsymbol{F} = (F^1, F^2, F^3) \in \mathbb{R}^3. \tag{1.8}$$

The coordinate components, (F^1, F^2, F^3) are dependent on the choice for coordinate basis vectors. As there is one index on the components of a vector, they are referred to as *first order tensors*. Furthermore, the contravariant representation of a first order tensor (i.e., as a vector) is referred to as its $(1, 0)$ representation.

1.3.3 One-forms as the dual to vectors

Equation (1.8) represents the first order tensor, $\mathbf{F}$, in terms of a suite of basis vectors, $\boldsymbol{e}_a$, and the contravariant coordinate representation, F^a. We define *one-forms* as the duals to vectors in a manner analogous to how row and column vectors are dual objects in linear algebra.[8] We do so by introducing a basis of one-forms, written as $\boldsymbol{e}^a$, with the upstairs index chosen to distinguish from the downstairs index used for the vector basis, $\boldsymbol{e}_a$. Following Figure 2.8 of *Misner et al.* (1973) and Figure C.6 of *Tromp* (2025a), we offer the following geometric interpretation of a basis of one-forms as a dual to a basis of vectors. Namely, a particular member of a vector basis corresponds geometrically to a unit length line segment with an arrow pointing in the direction of increasing coordinate value. A member of a one-form basis has the dual geometric interpretation as a surface or sheet whose outward normal direction is given by the corresponding basis vector.

Equation (1.8) offers a coordinate representation of a first order tensor in terms of a vector basis, $\boldsymbol{e}_a$. If we insist on a tensor as a geometric object, then we can also represent the same tensor in terms of a set of basis one-forms, in which case

$$\mathbf{F} = F_a\,\boldsymbol{e}^a \in \mathbb{E}^3. \tag{1.9}$$

We say that the first order tensor, $\mathbf{F}$, is here represented in terms of a one-form basis, $\boldsymbol{e}^a$, with the *covariant* expansion coefficients, F_a, providing the corresponding $(0, 1)$ coordinate representation of the tensor.

1.3.4 Scalar product and the duality condition

Using the language of *Misner et al.* (1973), we say that a one-form eats a vector to produce a scalar. Equivalently, a vector eats a one-form and also produces the same scalar. We realize this machine analogy by defining the *scalar product* as follows.[9] Namely, we define a scalar product between a first order tensor represented as a vector, $\mathbf{F} = F^a\,\boldsymbol{e}_a$, and a first order tensor represented as a one-form, $\mathbf{G} = G_a\,\boldsymbol{e}^a$, as

$$\mathbf{F} \cdot \mathbf{G} = (F^a\,\boldsymbol{e}_a) \cdot (G_b\,\boldsymbol{e}^b) = F^a\,G_b\,(\boldsymbol{e}_a \cdot \boldsymbol{e}^b). \tag{1.10}$$

To proceed, assume the vector basis and one-form basis satisfy the following *duality condition*

$$\boldsymbol{e}_a \cdot \boldsymbol{e}^b = \delta_a{}^b = \delta^b{}_a. \tag{1.11}$$

[8] The introduction of one-forms has little practical motivation for Cartesian tensors since there are no numerical distinctions between one-forms and vectors (as shown in Section 1.4.5). So why add this extra bit of formalism? It turns out that one-forms are needed when working with general tensors, with the associated formalism further detailed and motivated in Section 4.2. We introduce the extra baggage in the study of Cartesian tensors to anticipate the treatment with general tensors. It also offers a means to help keep track of the index notation. The added formalism is not onerous after a bit of head-scratching, and it is well worth the price in support of the transition to general tensors.

[9] Section 4.2 furthers this approach and offers a bit more clarity. Here we are a bit informal in order to avoid going too deep into the flowering weeds.

We here introduced $\delta_a{}^b = \delta^b{}_a$, which is the representation of the Kronecker delta where one index is downstairs and the other is upstairs. In Cartesian tensors, this representation of the Kronecker tensor is numerically identical to δ_{ab} introduced by equation (1.7)

$$\delta_{ab} = \delta_a{}^b = \delta^b{}_a = \begin{cases} 1 & a = b \\ 0 & a \neq b. \end{cases} \tag{1.12}$$

Furthermore, the identity $\delta_a{}^b = \delta^b{}_a$ means that the Kronecker tensor is symmetric; i.e., swapping which index comes first (i.e., rows and columns when expressed as a matrix) does not alter the tensor.[10] Making use of duality condition leads to the equivalent expressions of a scalar product between a vector and one-form

$$\mathbf{F} \cdot \mathbf{G} = (F^a \, \boldsymbol{e}_a) \cdot (G_b \, \boldsymbol{e}^b) = F^a \, G_b \, \boldsymbol{e}_a \cdot \boldsymbol{e}^b = F^a \, G_b \, \delta_a{}^b = F^a \, G_a. \tag{1.13}$$

The result is indeed a scalar since the indices are contracted. Returning to the geometric picture from Section 1.3.3, the duality condition (1.11) says that the scalar product of a vector basis element and one-form basis element equals to unity if the vector basis is the outward normal to the one-form basis, whereas the scalar product is zero otherwise.

1.4 Distance and metric

In defining the Cartesian unit vectors, $(\hat{\boldsymbol{x}}, \hat{\boldsymbol{y}}, \hat{\boldsymbol{z}})$, to have unit magnitudes, we presumed knowledge of how to measure the magnitude of a vector. We here make this notion precise.

1.4.1 Distance between points

Consider two points in Euclidean space, $\mathscr{P}$ and $\mathscr{P} + \mathrm{d}\mathscr{P}$, where the differential, d, symbolizes a small increment in space. These two points are specified by their respective positions, $\mathbf{x}$ and $\mathbf{x} + \mathrm{d}\mathbf{x}$. Representing these positions using a particular set of Cartesian coordinates renders

$$\mathbf{x} = \boldsymbol{x} = x^a \, \boldsymbol{e}_a \quad \text{and} \quad \mathbf{x} + \mathrm{d}\mathbf{x} = (x^a + \mathrm{d}x^a) \, \boldsymbol{e}_a. \tag{1.14}$$

Euclidean space is afforded a metric whereby the squared distance between two points is measured via *Pythagoras' theorem*

$$\begin{aligned}
[\text{distance}(\mathscr{P}, \mathscr{P} + \mathrm{d}\mathscr{P})]^2 &= (\mathbf{x} + \mathrm{d}\mathbf{x} - \mathbf{x}) \cdot (\mathbf{x} + \mathrm{d}\mathbf{x} - \mathbf{x}) && \text{definition of distance} && (1.15a) \\
&= \mathrm{d}x^a \, \mathrm{d}x^b \, (\boldsymbol{e}_a \cdot \boldsymbol{e}_b) && \text{coordinate representation} && (1.15b) \\
&= \mathrm{d}x^a \, \mathrm{d}x^b \, \delta_{ab} && \text{basis orthonormality (1.6)} && (1.15c) \\
&= (\mathrm{d}x^1)^2 + (\mathrm{d}x^2)^2 + (\mathrm{d}x^3)^2 && \text{expanding the sum} && (1.15d) \\
&= (\mathrm{d}x)^2 + (\mathrm{d}y)^2 + (\mathrm{d}z)^2 && \text{use familiar } x, y, z \text{ notation.} && (1.15e)
\end{aligned}$$

Evidently, the Kronecker or unit tensor, $\mathbf{I}$, which has Cartesian coordinate representation δ_{ab}, provides the means to compute distances in Euclidean space when using Cartesian coordinates. We thus say that the Kronecker delta provides the Cartesian representation of the Euclidean *metric tensor*.

[10] The duality condition (1.11) is analogous to the orthogonality between a row vector basis and column vector basis.

1.4.2 Use of more general notation for the metric tensor

The Kronecker symbols, δ_{ab}, are but one of the many representations available for the metric tensor applicable to Euclidean space. We encounter a number of other representations when using, for example, spherical coordinates, cylindrical polar coordinates, generalized vertical coordinates, and Lagrangian coordinates. For these other coordinates we need a more general expression for the metric. For this purpose we write the metric tensor representation as $\mathcal{g}_{ab}$, so that

$$\mathcal{g}_{ab} \overset{\text{Cartesian}}{=} \delta_{ab} \quad \text{for Euclidean space with Cartesian coordinates.} \tag{1.16}$$

Although we are mostly concerned in this chapter with Cartesian tensors, we introduce the more general expression for the metric tensor to readily expose those results that hold for general tensors.

1.4.3 Magnitude of a vector

By defining the distance between two points, we now have the means to define the squared magnitude of an arbitrary vector

$$|\mathbf{F}|^2 = \mathbf{F} \cdot \mathbf{F} = F^a \, F^b \, (\boldsymbol{e}_a \cdot \boldsymbol{e}_b) = F^a \, F^b \, \mathcal{g}_{ab} \overset{\text{Cartesian}}{=} \sum_{a=1}^{3} F^a \, F^a, \tag{1.17}$$

with the final equality holding for Cartesian tensors with $\mathcal{g}_{ab} = \delta_{ab}$. Correspondingly, we have the *scalar product* between two vectors

$$\mathbf{F} \cdot \mathbf{G} = F^a \, G^b \, (\boldsymbol{e}_a \cdot \boldsymbol{e}_b) = F^a \, G^b \, \mathcal{g}_{ab} \overset{\text{Cartesian}}{=} \sum_{a=1}^{3} F^a \, G^a, \tag{1.18}$$

which we already encountered in Section 1.3.4. Given our expression for the scalar product and the magnitude of vectors, we can introduce a geometrical interpretation by defining the angle between the vectors according to

$$\cos\vartheta \equiv \frac{\mathbf{F} \cdot \mathbf{G}}{|\mathbf{F}| \, |\mathbf{G}|} = \frac{F^a \, G^b \, \mathcal{g}_{ab}}{\sqrt{F^c \, F^d \, \mathcal{g}_{cd}} \, \sqrt{G^e \, G^f \, \mathcal{g}_{ef}}}. \tag{1.19}$$

Though a bit pedantic, the use of distinct indices within each of the terms emphasizes that each of the scalar products is self-contained. We illustrate this equation in Figure 1.2 for Cartesian coordinates. It is useful to verify that this definition is consistent with $-1 \leq \cos\vartheta \leq 1$. Furthermore, note that this definition of an angle between two vectors makes use of the metric tensor, thus emphasizing that angles on a manifold, just like distances, require a metric.[11]

1.4.4 Relating covariant and contravariant tensor representations

When a manifold has a metric tensor, then we can seamlessly transfer between the covariant and contravariant representation of a tensor. In this manner, the metric tensor links the one-forms

[11] This point about the need for a metric tensor might seem pedantic to those having only worked with Euclidean space with Cartesian coordinates, where the formalism of linear algebra and calculus tacitly builds in the Kronecker metric from the start. However, the study of calculus can be generalized to differential manifolds that have no metric. For example, the mathematics of thermodynamics is based on differential manifolds that have no metric, and thus no sense for distance or angles between two points in thermodynamic space (see *Schutz* (1980) and *Frankel* (2004) for discussions). *Nurser et al.* (2022) offer another example for studies of fluid motion in continuous property spaces rather than Euclidean space.

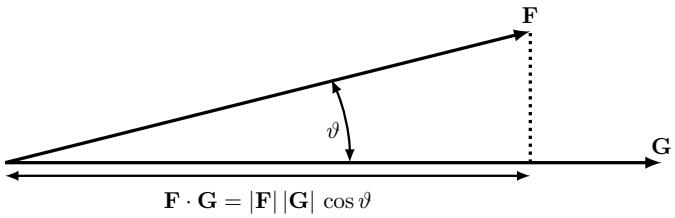

FIGURE 1.2: Illustrating the geometry of the scalar product (also known as the dot product or inner product) between two arbitrary vectors, $\boldsymbol{F} \cdot \boldsymbol{G} = |\boldsymbol{F}|\,|\boldsymbol{G}| \cos\vartheta$.

and vectors so to make their distinction important conceptually yet unimportant in practice. We here introduce the formalism for this conversion.[12]

The operational means to convert between the covariant to contravariant expressions of a tensor arises through *contraction* of a tensor with the metric tensor, where contraction refers to summation over a common index. For Cartesian coordinates on Euclidean space, we saw in Section 1.4 that the metric tensor is represented by the Kronecker tensor. To raise and lower indices on Cartesian tensors, one contracts with the metric tensor, so that, for example,

$$\begin{aligned}
\mathbf{F} &= F^a\,\boldsymbol{e}_a && \text{contravariant representation} && (1.20a)\\
&= (\mathcal{g}^{ab}\,F_b)\,(\mathcal{g}_{ac}\,\boldsymbol{e}^c) && \text{raise/lower indices with metric, } \mathcal{g}_{ab} \text{ and its inverse, } \mathcal{g}^{ab} && (1.20b)\\
&= \mathcal{g}^{ab}\,\mathcal{g}_{ac}\,F_b\,\boldsymbol{e}^c && \text{rearrange} && (1.20c)\\
&= F_a\,\boldsymbol{e}^a && \mathcal{g}^{ab}\,\mathcal{g}_{ac} = \delta^b{}_c. && (1.20d)
\end{aligned}$$

For the case of Cartesian tensors, with $\mathcal{g}_{ab} \overset{\text{Cartesian}}{=} \delta_{ab}$ and $\mathcal{g}^{ab} \overset{\text{Cartesian}}{=} \delta^{ab}$, these relations are no more than a repackaging of results already presented in earlier subsections. But what we have identified here is the role of the metric tensor in moving an index from downstairs to upstairs, and that is what we mean by converting between the covariant and contravariant representations. This operation holds for any representation of the metric, as indicated here by use of $\mathcal{g}_{ab}$ and its inverse, $\mathcal{g}^{ab}$. In particular, we can trivially move an index up if contracted with another index that moves down, so that the scalar product is given by the equivalent expressions

$$\mathbf{F} \cdot \mathbf{G} = F^a\,G_a = F_a\,G^a. \tag{1.21}$$

Again, all of these manipulations hold for general coordinates when using a general coordinate representation of the metric tensor.

1.4.5 Covariant and contravariant are identical for Cartesian tensors

As seen in Section 1.4.1, the Kronecker tensor is the metric tensor for Euclidean space using Cartesian coordinates. As a result, there is no distinction for Cartesian tensors between covariant, contravariant, one-form, etc. For example, consider the identity

$$F_a = \delta_{ab}\,F^b, \tag{1.22}$$

which is how we lower an index to obtain the covariant representation, F_a, from the contarcovariant representation, F^b. Since δ^{ab} vanishes unless $a = b$, where it equals unity, we have, for

[12] The conversion is superfluous for Cartesian tensors since there is no distinction between covariant and contravariant, which is exhibited in Section 1.4.5. Even so, let us agree to play the game in support of the general tensor case where the distinction is important.

each index a, the following identity

$$F_a = F^a. \tag{1.23}$$

This identity holds for all Cartesian tensors, such as the basis vectors and basis one-forms are identical

$$\boldsymbol{e}_1 = \boldsymbol{e}^1 = \hat{\boldsymbol{x}} \quad \text{and} \quad \boldsymbol{e}_2 = \boldsymbol{e}^2 = \hat{\boldsymbol{y}} \quad \text{and} \quad \boldsymbol{e}_3 = \boldsymbol{e}^3 = \hat{\boldsymbol{z}}. \tag{1.24}$$

Hence, there is no need to distinguish upstairs and downstairs indices when working with Cartesian tensors. Even so, we continue to play the game given the need for a distinction when considering general tensors.

1.5 Tensor fields

To make use of tensor analysis for studying continuum mechanics requires the use of *tensor fields*, with a tensor field providing a tensor at each point in space and time. Space and time relations between tensor fields arise from physical theories expressed by differential and integral equations.

1.5.1 Scalar fields

A physical *scalar field*, F, provides a number with physical dimensions at each point in space and time. Example physical scalar fields encountered in this book include temperature, mass density, buoyancy, salinity, humidity, and mechanical energy. Consider a point, $\mathscr{P} \in \mathbb{E}^3$, that has a position, $\mathbf{x}$. The scalar field, F, has a value written

$$\mathrm{F}(\mathbf{x}, t) = \text{scalar property, F, evaluated at position } \mathbf{x} \text{ and time instance } t. \tag{1.25}$$

Now choose a particular set of spatial coordinates, $\boldsymbol{x} \in \mathbb{R}^3$. The scalar field, F, as sampled at a point represented by coordinates $\boldsymbol{x}$ and at time t, is specified by evaluating a function

$$F(\boldsymbol{x}, t) = \text{property F measured using coordinates } \boldsymbol{x} \text{ and time } t. \tag{1.26}$$

As per the notational convention introduced in Section 1.2.2, we here use the upright, F, for the scalar field, whereas the slanted, F, symbolizes the scalar field represented by a scalar function that depends on the chosen Cartesian space coordinates.

Bringing equations (1.25) and (1.26) together, we say that with $\boldsymbol{x}$ as the Cartesian coordinate expression for the position, $\mathbf{x}$, then

$$F(\boldsymbol{x}, t) = \mathrm{F}(\mathbf{x}, t) \quad \text{with } \boldsymbol{x} \text{ the coordinate representation of } \mathbf{x}. \tag{1.27}$$

If we instead choose another set of coordinates, $\overline{\boldsymbol{x}}$, then the property F sampled at a spatial point represented by coordinates $\overline{\boldsymbol{x}}$ is specified by another function,

$$\overline{F}(\overline{\boldsymbol{x}}, t) = \text{property F representated by coordinates } \overline{\boldsymbol{x}} \text{ and time } t. \tag{1.28}$$

If the two sets of Cartesian coordinates represent the same position, $\mathbf{x}$, then

$$\mathrm{F}(\mathbf{x}, t) = F(\boldsymbol{x}, t) = \overline{F}(\overline{\boldsymbol{x}}, t). \tag{1.29}$$

The distinction between a scalar field, $\mathrm{F}(\mathbf{x}, t)$, and scalar function, $F(\boldsymbol{x}, t)$, is conceptually fundamental. Even so, in practice the distinction is somewhat pedantic, and so it will be ignored when it is safe to do so.

1.5.2 Vector fields

The vector field, $\mathbf{F}(\mathbf{x}, t)$, provides a vector at each point in space, indicated by the position, $\mathbf{x}$, and each instance in time, t. Example vector fields considered in this book include velocity, acceleration, and forces. Choosing a particular coordinate representation of a vector field leads to the representation

$$\mathbf{F}(\mathbf{x}, t) = \boldsymbol{F}(\boldsymbol{x}, t). \tag{1.30}$$

The right hand side provides a vector function, $\boldsymbol{F}$, that represents the vector field, $\mathbf{F}$, with the vector function specific to the chosen Cartesian coordinates, $\boldsymbol{x}$. Another set of Cartesian coordinates, $\overline{\boldsymbol{x}}$, generally requires a distinct vector function, $\overline{\boldsymbol{F}}$, that renders an alternative representation of the vector field $\mathbf{F}(\mathbf{x}, t)$,

$$\mathbf{F}(\mathbf{x}, t) = \overline{\boldsymbol{F}}(\overline{\boldsymbol{x}}, t). \tag{1.31}$$

Just as found for scalar fields in equation (1.29), we have the identity for vector fields and their vector function representations

$$\mathbf{F}(\mathbf{x}, t) = \boldsymbol{F}(\boldsymbol{x}, t) = \overline{\boldsymbol{F}}(\overline{\boldsymbol{x}}, t). \tag{1.32}$$

In Section 1.10 we detail the mechanics of how to transform coordinate components of the vector field written using two sets of Cartesian coordinates, and in Chapter 4 we do the same for general coordinates. Each component, F^a, of a vector field, when written in terms of a particular set of coordinates, is itself a function of those coordinates

$$\boldsymbol{F}(\boldsymbol{x}, t) = F^a(\boldsymbol{x}, t)\, \boldsymbol{e}_a. \tag{1.33}$$

However, each component function, $F^a(\boldsymbol{x}, t)$, cannot be considered a scalar field since the vector components transform according to the coordinate transformation rules detailed in Section 1.10, with these transformation rules distinct from those holding for a scalar field. This point is very basic to tensor analysis, and yet it can be readily overlooked upon first encounter.

1.6 Second order tensors and tensor products

The metric tensor, stress tensor (Chapter 24), moment of inertia tensor (Section 37.9.4) and diffusion tensor (Chapter 69) are examples of second order tensors encountered in this book. Second order tensors have a coordinate representation given by any of the equivalent expressions

$$\mathbf{T} = T^{ab}\, \boldsymbol{e}_a \otimes \boldsymbol{e}_b = T^a{}_b\, \boldsymbol{e}_a \otimes \boldsymbol{e}^b = T_a{}^b\, \boldsymbol{e}^a \otimes \boldsymbol{e}_b = T_{ab}\, \boldsymbol{e}^a \otimes \boldsymbol{e}^b, \tag{1.34}$$

with T^{ab}, $T^a{}_b$, $T_a{}^b$, and T_{ab} the variety of coordinate representations of the second order tensor, $\mathbf{T}$. This expression for a general second order tensor allows us to write the Kronecker or unit tensor in the form

$$\mathbf{I} = \delta^{ab}\, \boldsymbol{e}_a \otimes \boldsymbol{e}_b = \delta^a{}_b\, \boldsymbol{e}_a \otimes \boldsymbol{e}^b = \delta_a{}^b\, \boldsymbol{e}^a \otimes \boldsymbol{e}_b = \delta_{ab}\, \boldsymbol{e}^a \otimes \boldsymbol{e}^b, \tag{1.35}$$

as well as the metric tensor

$$\mathbb{g} = \mathbb{g}^{ab}\, \boldsymbol{e}_a \otimes \boldsymbol{e}_b = \mathbb{g}^a{}_b\, \boldsymbol{e}_a \otimes \boldsymbol{e}^b = \mathbb{g}_a{}^b\, \boldsymbol{e}^a \otimes \boldsymbol{e}_b = \mathbb{g}_{ab}\, \boldsymbol{e}^a \otimes \boldsymbol{e}^b, \tag{1.36}$$

where the metric and its inverse satisfy the identities

$$\mathbb{g}^{ac}\, \mathbb{g}_{cb} = \mathbb{g}^a{}_b = \delta^a{}_b \quad \text{and} \quad \mathbb{g}_{ac}\, \mathbb{g}^{cb} = \mathbb{g}_a{}^b = \delta_a{}^b. \tag{1.37}$$

Notably, there is not a scalar product between the basis vectors in equations (1.34) or (1.35). Rather, the $\otimes$ symbol represents the *tensor product* of the basis vectors and/or basis one-forms. The tensor product generalizes the *outer product* of linear algebra, with components given by

$$(\boldsymbol{e}_a \otimes \boldsymbol{e}_b)_{ij} = (\boldsymbol{e}_a)_i \, (\boldsymbol{e}_b)_j. \tag{1.38}$$

1.6.1 Three representations of a second order tensor

Equation (1.34) provides three distinct representations for the second order tensor. We define these representations as

$$\mathbf{T}^\natural = T^a{}_b \, \boldsymbol{e}_a \otimes \boldsymbol{e}^b = T_a{}^b \, \boldsymbol{e}^a \otimes \boldsymbol{e}_b \quad \text{natural or } (1,1) \text{ representation} \tag{1.39a}$$

$$\mathbf{T}^\sharp = T^{ab} \, \boldsymbol{e}_a \otimes \boldsymbol{e}_b \quad \text{sharp or } (2,0) \text{ representation} \tag{1.39b}$$

$$\mathbf{T}^\flat = T_{ab} \, \boldsymbol{e}^a \otimes \boldsymbol{e}^b \quad \text{flat or } (0,2) \text{ representation.} \tag{1.39c}$$

1.6.2 More on the tensor product

Consider two arbitrary vectors, $\mathbf{A}$ and $\mathbf{B}$, and form a second order tensor by taking their tensor product

$$\mathbf{A} \otimes \mathbf{B} = A^a \, B^b \, \boldsymbol{e}_a \otimes \boldsymbol{e}_b = A^a \, B_b \, \boldsymbol{e}_a \otimes \boldsymbol{e}^b = A_a \, B^b \, \boldsymbol{e}^a \otimes \boldsymbol{e}_b. \tag{1.40}$$

It can prove useful to organize elements of the tensor product for a particular coordinate representation according to the rules of matrix multiplication

$$\boldsymbol{A} \otimes \boldsymbol{B} = \begin{bmatrix} A^1 \\ A^2 \\ A^3 \end{bmatrix} \begin{bmatrix} B^1 & B^2 & B^3 \end{bmatrix} = \begin{bmatrix} A^1 \, B^1 & A^1 \, B^2 & A^1 \, B^3 \\ A^2 \, B^1 & A^2 \, B^2 & A^2 \, B^3 \\ A^3 \, B^1 & A^3 \, B^2 & A^3 \, B^3 \end{bmatrix}. \tag{1.41}$$

This example makes it clear that the tensor product between two tensors is not commutative,

$$\mathbf{A} \otimes \mathbf{B} \neq \mathbf{B} \otimes \mathbf{A}, \tag{1.42}$$

but instead it satisfies

$$(\mathbf{A} \otimes \mathbf{B})^{\mathrm{T}} = \mathbf{B} \otimes \mathbf{A}, \tag{1.43}$$

where the T superscript is the *transpose operation* (swapping index locations). Likewise, considering the horizontal basis vectors for Cartesian coordinates renders the following tensor products

$$\boldsymbol{e}_1 \otimes \boldsymbol{e}_1 = \hat{\boldsymbol{x}} \otimes \hat{\boldsymbol{x}} = \begin{bmatrix} 1 & 0 & 0 \\ 0 & 0 & 0 \\ 0 & 0 & 0 \end{bmatrix} \qquad \boldsymbol{e}_2 \otimes \boldsymbol{e}_2 = \hat{\boldsymbol{y}} \otimes \hat{\boldsymbol{y}} = \begin{bmatrix} 0 & 0 & 0 \\ 0 & 1 & 0 \\ 0 & 0 & 0 \end{bmatrix} \tag{1.44a}$$

$$\boldsymbol{e}_1 \otimes \boldsymbol{e}_2 = \hat{\boldsymbol{x}} \otimes \hat{\boldsymbol{y}} = \begin{bmatrix} 0 & 1 & 0 \\ 0 & 0 & 0 \\ 0 & 0 & 0 \end{bmatrix} \qquad \boldsymbol{e}_2 \otimes \boldsymbol{e}_1 = \hat{\boldsymbol{y}} \otimes \hat{\boldsymbol{x}} = \begin{bmatrix} 0 & 0 & 0 \\ 1 & 0 & 0 \\ 0 & 0 & 0 \end{bmatrix}, \tag{1.44b}$$

and similar results when including $\boldsymbol{e}_3 = \hat{\boldsymbol{z}}$.

1.7 Vector cross product

The *vector cross product* provides a means to measure area associated with two vectors and to specify the *orientation* of that area. Note that when the vectors have physical dimensions distinct from length, then their vector cross product is not the area as a squared length. Even

so, the geometric interpretation remains, only with the physical dimensions adjusted accordingly. We here introduce the vector cross product, focusing on the Cartesian expression. We require a bit more nuance for the case of general tensors, with details presented in Section 4.8. Even so, the algebraic relations derived here also hold for general tensors.

1.7.1 Orienting an area via the Levi-Civita tensor

Consider a flat plane defined by any two of the Cartesian basis vectors, $\boldsymbol{e}_a$ and $\boldsymbol{e}_b$ where $a \neq b$. We seek a means to specify what side of the plane is up and what side is down. Doing so allows us to orient objects within space.[13] Notably, there is no objective means for this specification, since "up" and "down" are subject to our chosen orientation. Therefore, we must choose a convention. For that purpose, we follow the *right hand rule*, in which the out-stretched thumb, index, and middle fingers of the right hand orient the three Cartesian basis vectors.

We algebraically specify the right hand rule for the basis vectors through the relation

$$\boldsymbol{e}_a \times \boldsymbol{e}_b = \epsilon_{abc}\, \boldsymbol{e}^c. \tag{1.45}$$

The left hand side introduces the *vector cross product* of two basis vectors, with the $\times$ symbol used for the product. The right hand side identifies the vector cross product as a one-form. That is, as seen in Section 1.7.4, the cross product of two $(1,0)$ tensors produces a $(0,1)$ tensor.

The cross product (1.45) introduced the *Levi-Civita tensor*, whose Cartesian components are given by the totally anti-symmetric *permutation symbol*

$$\epsilon_{123} = 1 \tag{1.46a}$$

$$\epsilon_{abc} = \begin{cases} 1, \text{ even permutation of } abc \ (123, 312, 231) \\ -1, \text{ odd permutation of } abc \ (321, 132, 213) \\ 0, \text{ all other } abc. \end{cases} \tag{1.46b}$$

Exchanging any two indices is an odd permutation and results in a sign swap

$$\epsilon_{abc} = -\epsilon_{bac} = -\epsilon_{acb} \implies \epsilon_{123} = -\epsilon_{213}. \tag{1.47}$$

In contrast, the cycling of indices is an even permutation and it preserves the sign

$$\epsilon_{abc} = \epsilon_{cab} = \epsilon_{bca} \implies \epsilon_{123} = \epsilon_{312} = \epsilon_{231}. \tag{1.48}$$

Correspondingly, the vector cross product changes sign when its elements are commuted

$$\boldsymbol{e}_a \times \boldsymbol{e}_b = \epsilon_{abc}\, \boldsymbol{e}^c = -\epsilon_{bac}\, \boldsymbol{e}^c = -\boldsymbol{e}_b \times \boldsymbol{e}_a. \tag{1.49}$$

1.7.2 Axial (or pseudo) vector

The vector cross product defines a one-form whose coordinate representation changes its sign upon changing from a right handed to left handed orientation of the coordinate system. One often sees the term *axial vectors* or *pseudo vectors* used for this one-form. The angular velocity is a prominent pseudo vector encountered in this book.

[13] There are surfaces, such as the Möbius strip and Klein bottle, that are not orientable. We only consider orientiable surfaces in this book.

1.7.3 Orthogonality relations between cross products

The permutation symbol ensures that $\boldsymbol{e}_a \times \boldsymbol{e}_b$ is orthogonal to both $\boldsymbol{e}_a$ and $\boldsymbol{e}_b$. To prove this property we write

$$\begin{aligned} \boldsymbol{e}_a \cdot (\boldsymbol{e}_a \times \boldsymbol{e}_b) &= \boldsymbol{e}_a \cdot \epsilon_{abc}\, \boldsymbol{e}^c && \text{equation (1.45)} && (1.50a)\\ &= \epsilon_{abc}\, \delta_a{}^c && \text{duality (1.11)} && (1.50b)\\ &= 0 && \epsilon_{abc}\, \delta_a{}^c = 0. && (1.50c) \end{aligned}$$

The final equality holds since $\epsilon_{abc} = -\epsilon_{cba}$ whereas $\delta_a{}^c = \delta^c{}_a$, with a vanishing double contraction of an anti-symmetric tensor and a symmetric tensor.[14] The same procedure shows that $\boldsymbol{e}_b \cdot (\boldsymbol{e}_a \times \boldsymbol{e}_b) = 0$. Hence, the one-form defined by the vector cross product of two vectors is orthogonal to both of the vectors. Evidently, the vector cross product is oriented orthogonal to the plane defined by the two vectors, with a direction determined by the right hand rule.

1.7.4 Vector product of two arbitrary vectors

The expression (1.45) for the vector product of two basis vectors renders the vector product of two arbitrary vectors

$$\begin{aligned} \mathbf{P} \times \mathbf{Q} &= P^a\, \boldsymbol{e}_a \times Q^b\, \boldsymbol{e}_b && (1.51a)\\ &= P^a\, Q^b\, \boldsymbol{e}_a \times \boldsymbol{e}_b && (1.51b)\\ &= P^a\, Q^b\, \epsilon_{abc}\, \boldsymbol{e}^c && (1.51c)\\ &= (P^2\, Q^3 - P^3\, Q^2)\, \boldsymbol{e}^1 + (P^3\, Q^1 - P^1\, Q^3)\, \boldsymbol{e}^2 + (P^1\, Q^2 - P^2\, Q^1)\, \boldsymbol{e}^3. && (1.51d) \end{aligned}$$

For a particular representation, we can write the vector product in the form of a determinant

$$\boldsymbol{P} \times \boldsymbol{Q} = \det \begin{bmatrix} \boldsymbol{e}^1 & \boldsymbol{e}^2 & \boldsymbol{e}^3 \\ P^1 & P^2 & P^3 \\ Q^1 & Q^2 & Q^3 \end{bmatrix}. \tag{1.52}$$

As with the basis vectors, the vector product is orthogonal to both of the individual vectors, such as

$$\begin{aligned} \mathbf{P} \cdot (\mathbf{P} \times \mathbf{Q}) &= (P^d\, \boldsymbol{e}_d) \cdot (P^a\, Q^b\, \epsilon_{abc}\, \boldsymbol{e}^c) && (1.53a)\\ &= P^a\, P^d\, Q^b\, \epsilon_{abc}\, \delta^c{}_d && (1.53b)\\ &= P^a\, P^c\, Q^b\, \epsilon_{abc} && (1.53c)\\ &= 0, && (1.53d) \end{aligned}$$

where the final equality follows since the product, $P^c\, P^a$, is symmetric on the labels ac ($P^c\, P^a = P^a\, P^c$), whereas ϵ_{abc} is anti-symmetric on these same labels.

1.7.5 Geometric interpretation of the vector cross product

The expression (1.51d) leads to the identity

$$\begin{aligned} |\mathbf{P} \times \mathbf{Q}|^2 &= |\mathbf{P}|^2\, |\mathbf{Q}|^2 - (\mathbf{P} \cdot \mathbf{Q})^2 && (1.54a)\\ &= |\mathbf{P}|^2\, |\mathbf{Q}|^2\, (1 - \cos^2 \vartheta) && (1.54b)\\ &= |\mathbf{P}|^2\, |\mathbf{Q}|^2 \sin^2 \vartheta, && (1.54c) \end{aligned}$$

[14] We further illustrate this property for matrices in Exercise 1.2.

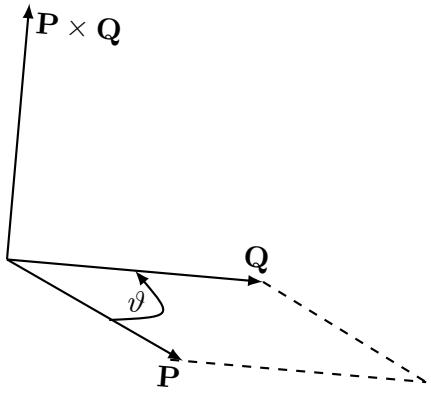

FIGURE 1.3: The magnitude of the vector product between two vectors is given by the product of their magnitudes and the sine of the angle between them, $|\mathbf{P}\times\mathbf{Q}| = |\mathbf{P}|\,|\mathbf{Q}|\sin\vartheta$. This magnitude equals to the area of the parallelogram formed by the two vectors. The vector cross product is a one-form that is directed perpendicular to the plane determined by the two vectors and oriented according to the right hand rule. The right hand rule is found by placing the fingers of the right hand along the first vector, $\mathbf{P}$. Closing the fingers in the direction of the second vector, $\mathbf{Q}$ (as here depicted by the arrow on the arc for the angle ϑ), then ensures that the thumb provides the orientation for the vector cross product, $\mathbf{P}\times\mathbf{Q}$.

where we used the scalar product expression (1.19) to introduce the angle subtended by the two vectors. Trigonometry indicates that the area of the parallelogram defined by the two vectors, $\mathbf{P}$ and $\mathbf{Q}$, is given by $|\mathbf{P}|\,|\mathbf{Q}|\sin\vartheta$. Hence, the vector cross product has a magnitude given by this area

$$\text{area}(\mathbf{P},\mathbf{Q}) = |\mathbf{P}|\,|\mathbf{Q}|\sin\vartheta = |\mathbf{P}\times\mathbf{Q}|. \tag{1.55}$$

Since $\mathbf{P}\times\mathbf{Q}$ is a one-form orthogonal to the plane defined by $\mathbf{P}$ and $\mathbf{Q}$, we can write the vector product in the purely geometric manner

$$\mathbf{P}\times\mathbf{Q} = \hat{\boldsymbol{n}}\,\text{area}(\mathbf{P},\mathbf{Q}) = \hat{\boldsymbol{n}}\,|\mathbf{P}|\,|\mathbf{Q}|\sin\vartheta, \tag{1.56}$$

where $\hat{\boldsymbol{n}}$ is a *unit normal one-form* (also known as the *normal direction*) that points normal to the area and in a direction given by the right hand rule. This formula is illustrated in Figure 1.3.

1.7.6 Decomposing the vector cross product

To further our geometric interpretation of the vector cross product using Cartesian coordinates, let $\mathbf{P}$ be the vertical unit vector, $\mathbf{P} = \hat{\boldsymbol{z}}$. The vector cross product then produces

$$\begin{aligned}
\mathbf{Q}^{\hat{\boldsymbol{z}}\perp} &= \hat{\boldsymbol{z}}\times\mathbf{Q} && \text{(1.57a)}\\
&= \hat{\boldsymbol{z}}\times[\mathbf{Q} - (\hat{\boldsymbol{z}}\cdot\mathbf{Q})\,\hat{\boldsymbol{z}}] && \text{(1.57b)}\\
&= (\hat{\boldsymbol{z}}\times\hat{\boldsymbol{x}})\,(\hat{\boldsymbol{x}}\cdot\mathbf{Q}) + (\hat{\boldsymbol{z}}\times\hat{\boldsymbol{y}})\,(\hat{\boldsymbol{y}}\cdot\mathbf{Q}) && \text{(1.57c)}\\
&= \hat{\boldsymbol{y}}\,(\hat{\boldsymbol{x}}\cdot\mathbf{Q}) - \hat{\boldsymbol{x}}\,(\hat{\boldsymbol{y}}\cdot\mathbf{Q}). && \text{(1.57d)}
\end{aligned}$$

By construction, $\mathbf{Q}^{\hat{\boldsymbol{z}}\perp}$ is in the horizontal plane and it is perpendicular to the horizontal projection of $\mathbf{Q}$

$$\mathbf{Q}^{\hat{\boldsymbol{z}}\perp}\cdot\hat{\boldsymbol{z}} = 0 \quad\text{and}\quad \mathbf{Q}^{\hat{\boldsymbol{z}}\perp}\cdot\mathbf{Q} = 0 \Longrightarrow \mathbf{Q}^{\hat{\boldsymbol{z}}\perp}\cdot[\mathbf{Q} - (\hat{\boldsymbol{z}}\cdot\mathbf{Q})\,\hat{\boldsymbol{z}}] = 0. \tag{1.58}$$

Hence, $\mathbf{Q}^{\hat{\boldsymbol{z}}\perp}$ is geometrically computed by rotating the horizontal component of $\mathbf{Q}$ by $\pi/2$ radians counter-clockwise about the $\hat{\boldsymbol{z}}$ axis. That interpretation holds for all coordinate directions:

$$\hat{\boldsymbol{x}}\times\mathbf{Q} = \hat{\boldsymbol{z}}\,(\hat{\boldsymbol{y}}\cdot\mathbf{Q}) - \hat{\boldsymbol{y}}\,(\hat{\boldsymbol{z}}\cdot\mathbf{Q}) = \text{project } \mathbf{Q} \text{ to y-z plane + rotate } \pi/2 \text{ CCW around } \hat{\boldsymbol{x}} \tag{1.59a}$$

$$\hat{\boldsymbol{y}} \times \mathbf{Q} = \hat{\boldsymbol{x}}\,(\hat{\boldsymbol{z}} \cdot \mathbf{Q}) - \hat{\boldsymbol{z}}\,(\hat{\boldsymbol{x}} \cdot \mathbf{Q}) = \text{project } \mathbf{Q} \text{ to z-x plane + rotate } \pi/2 \text{ CCW around } \hat{\boldsymbol{y}} \quad (1.59b)$$

$$\hat{\boldsymbol{z}} \times \mathbf{Q} = \hat{\boldsymbol{y}}\,(\hat{\boldsymbol{x}} \cdot \mathbf{Q}) - \hat{\boldsymbol{x}}\,(\hat{\boldsymbol{y}} \cdot \mathbf{Q}) = \text{project } \mathbf{Q} \text{ to x-y plane + rotate } \pi/2 \text{ CCW around } \hat{\boldsymbol{z}}. \quad (1.59c)$$

This geometric interpretation may appear a bit arcane. However, it serves to couple the analytical to the geometrical, and so supports our understanding. We also encounter it in various guises particularly when studying vorticity in Part VII of this book.

1.8 Measuring volume

The vector cross product offers a means to measure area defined by two vectors. We now see how it can be of use to measure the volume determined by three non-parallel vectors. This result has particular relevance to the volume element used for integration over space. As for the vector cross product in Section 1.7, we require a bit more nuance for the case of general tensors and present details in Section 4.5. So the material in the present section assumes Cartesian tensors.

1.8.1 Volume defined by three vectors

Consider the scalar product of an arbitrary vector, $\mathbf{R}$, with the vector product of two vectors, $(\mathbf{P} \times \mathbf{Q}) \cdot \mathbf{R}$. This scalar product projects that portion of the vector, $\mathbf{R}$, onto the direction parallel to the normal to the plane defined by $\mathbf{P} \times \mathbf{Q}$. Given that $|\mathbf{P} \times \mathbf{Q}|$ is the area of the parallelogram defined by $\mathbf{P}$ and $\mathbf{Q}$, we see that $(\mathbf{P} \times \mathbf{Q}) \cdot \mathbf{R}$ is the volume of the parallelepiped defined by the three vectors.

The sign of the volume depends on the orientation of the three vectors, $\mathbf{P}$, $\mathbf{Q}$ and $\mathbf{R}$. We assign a convention so that the volume is positive if the vectors are oriented in a right hand sense. Ignoring this convention, we can simply place an absolute value around the triple product to ensure a positive volume.

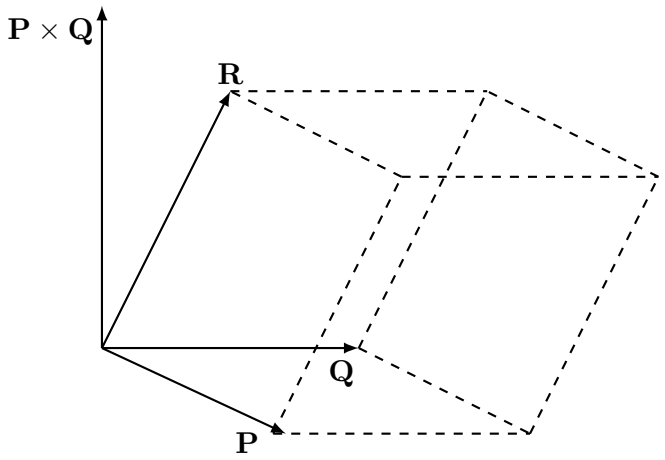

FIGURE 1.4: Three linearly independent vectors determine a volume given by $|(\mathbf{P} \times \mathbf{Q}) \cdot \mathbf{R}| = |(\mathbf{R} \times \mathbf{P}) \cdot \mathbf{Q}| = |(\mathbf{Q} \times \mathbf{R}) \cdot \mathbf{P}|$. We see this identity geometrically by noting that the area of the base is given by $|\mathbf{P} \times \mathbf{Q}|$, so that the volume of the parallelepiped is given by the base area times the height, $|(\mathbf{P} \times \mathbf{Q}) \cdot \mathbf{R}|$. Cyclic permutation then leads to the equality with the other two expressions.

We prove cyclic symmetry of $(\mathbf{P} \times \mathbf{Q}) \cdot \mathbf{R}$ through the following manipulations

$$(\mathbf{P} \times \mathbf{Q}) \cdot \mathbf{R} = (P^a\,\boldsymbol{e}_a \times Q^b\,\boldsymbol{e}_b) \cdot R^d\,\boldsymbol{e}_d \quad \text{expose coordinates and basis vectors} \quad (1.60a)$$

$$= P^a\,Q^b\,(\boldsymbol{e}_a \times \boldsymbol{e}_b) \cdot R^d\,\boldsymbol{e}_d \quad \text{rearrange} \quad (1.60b)$$

$$
\begin{aligned}
&= P^a\, Q^b\, (\epsilon_{abc}\, \boldsymbol{e}^c) \cdot \boldsymbol{e}_d\, R^d && \text{vector product as per equation (1.45)} && \text{(1.60c)}\\
&= P^a\, Q^b\, \epsilon_{abc}\, (\boldsymbol{e}^c \cdot \boldsymbol{e}_d)\, R^d && \text{rearrange} && \text{(1.60d)}\\
&= P^a\, Q^b\, \epsilon_{abc}\, \delta^c{}_d\, R^d && \text{duality: } \boldsymbol{e}^c \cdot \boldsymbol{e}_d = \delta^c{}_d = \delta_d{}^c && \text{(1.60e)}\\
&= P^a\, Q^b\, \epsilon_{abc}\, R^c && d \text{ index is contracted: } \delta^c{}_d\, R^d = R^c && \text{(1.60f)}\\
&= R^c\, P^a\, Q^b\, \epsilon_{abc} && \text{rearrange} && \text{(1.60g)}\\
&= R^a\, P^b\, Q^c\, \epsilon_{bca} && \text{relabel: } a \to b \text{ and } b \to c \text{ and } c \to a && \text{(1.60h)}\\
&= R^a\, P^b\, Q^c\, \epsilon_{abc} && \text{even permutation: } \epsilon_{bca} = \epsilon_{abc} && \text{(1.60i)}\\
&= (\mathbf{R} \times \mathbf{P}) \cdot \mathbf{Q} && \text{redintroduce boldface notation.} && \text{(1.60j)}
\end{aligned}
$$

This identity yields the geometric result illustrated in Figure 1.4

$$\text{volume}(\mathbf{P}, \mathbf{Q}, \mathbf{R}) = (\mathbf{P} \times \mathbf{Q}) \cdot \mathbf{R} = (\mathbf{R} \times \mathbf{P}) \cdot \mathbf{Q} = (\mathbf{Q} \times \mathbf{R}) \cdot \mathbf{P}. \tag{1.61}$$

1.8.2 Cartesian volume element for integration

We need the volume of an infinitesimal region when performing an integration over space. When making use of Cartesian coordinates we need the volume of a rectangular prism defined by infinitesimal distances along each of the Cartesian coordinate axes. We thus set

$$\mathbf{P} = \hat{\boldsymbol{x}}\, \mathrm{d}x \quad \text{and} \quad \mathbf{Q} = \hat{\boldsymbol{y}}\, \mathrm{d}y \quad \text{and} \quad \mathbf{R} = \hat{\boldsymbol{z}}\, \mathrm{d}z, \tag{1.62}$$

in which case the volume element is

$$\mathrm{d}V = (\mathbf{P} \times \mathbf{Q}) \cdot \mathbf{R} = \mathrm{d}x\, \mathrm{d}y\, \mathrm{d}z\, (\hat{\boldsymbol{x}} \times \hat{\boldsymbol{y}}) \cdot \hat{\boldsymbol{z}} = \mathrm{d}x\, \mathrm{d}y\, \mathrm{d}z. \tag{1.63}$$

This expression for the volume element could have been written down without the formalism of a vector triple product. However, in Chapter 3 we find the expression, $(\mathbf{P} \times \mathbf{Q}) \cdot \mathbf{R}$, provides a useful starting point to derive the volume element using arbitrary coordinates.

1.8.3 $n-$space volumes and the Levi-Civita tensor

Let us now combine the geometric specification (1.56) of the vector product as a means to measure area, with the algebraic specification (1.51d), and do so by writing

$$\text{2-volume} = \epsilon(\mathbf{P}, \mathbf{Q}) = \epsilon_{ab}\, P^a\, Q^b = \det \begin{bmatrix} P^1 & Q^1 \\ P^2 & Q^2 \end{bmatrix}. \tag{1.64}$$

In this equation, ϵ_{ab} is the totally anti-symmetric second order tensor, whose Cartesian component expression can be organized as a 2×2 matrix

$$\begin{bmatrix} \epsilon_{11} & \epsilon_{12} \\ \epsilon_{21} & \epsilon_{22} \end{bmatrix} = \begin{bmatrix} 0 & 1 \\ -1 & 0 \end{bmatrix}. \tag{1.65}$$

In words, the first equality in equation (1.64) states that the ϵ-tensor in two dimensions takes two vectors as its argument and produces a 2-volume (i.e., an area). The three dimensional generalization yields

$$\text{3-volume} = \epsilon(\mathbf{P}, \mathbf{Q}, \mathbf{R}) = \epsilon_{abc}\, P^a\, Q^b\, R^c = \det \begin{bmatrix} P^1 & Q^1 & R^1 \\ P^2 & Q^2 & R^2 \\ P^3 & Q^3 & R^3 \end{bmatrix}. \tag{1.66}$$

Suppressing the first vector argument in the 3-volume produces the surface area one-form defined by the other two vectors

$$\text{surface area one-form} = \epsilon(\ \ , \mathbf{Q}, \mathbf{R}). \tag{1.67}$$

By construction, the vectorial surface area is orthogonal to both $\mathbf{Q}$ and $\mathbf{R}$ since

$$\epsilon(\mathbf{Q}, \mathbf{Q}, \mathbf{R}) = \epsilon(\mathbf{R}, \mathbf{Q}, \mathbf{R}) = 0. \tag{1.68}$$

1.9 Practice with the Cartesian Levi-Civita tensor

The Levi-Civita tensor is a versatile tool for deriving identities in tensor algebra. We illustrated some of these features in the previous discussion and here illustrate some more, assuming Cartesian tensors. These examples, and others in this chapter, generally expose elements of the *index gymnastics* involved with tensor manipulations. A bit of practice readily allows one to skip many of the steps that are exposed in the following.

1.9.1 Contractions of the Levi-Civita tensor

Explicit substitution readily verifies that the identity

$$\delta^d{}_f\, \epsilon_{bcf}\, \epsilon_{aed} = \epsilon_{bc}{}^d\, \epsilon_{aed} = \delta_{ba}\, \delta_{ce} - \delta_{be}\, \delta_{ca}. \tag{1.69}$$

If $c = e$ then this identity reduces to

$$\epsilon_{be}{}^d\, \epsilon_{aed} = 2\, \delta_{ba}. \tag{1.70}$$

We make use of these, and related, identities throughout this book.

1.9.2 Double vector product

The triple cross product can be derived according to

$$\begin{aligned}
\mathbf{P} \times (\mathbf{Q} \times \mathbf{R}) &= P^a\, Q^b\, R^c\, \boldsymbol{e}_a \times (\boldsymbol{e}_b \times \boldsymbol{e}_c) && \text{(1.71a)}\\
&= P^a\, Q^b\, R^c\, \boldsymbol{e}_a \times (\epsilon_{bcd}\, \boldsymbol{e}^d) && \text{(1.71b)}\\
&= P^a\, Q^b\, R^c\, \epsilon_{bcd}\, \boldsymbol{e}_a \times \boldsymbol{e}_f\, \delta^{df} && \text{(1.71c)}\\
&= P^a\, Q^b\, R^c\, \epsilon_{bcd}\, \delta^{df}\, \epsilon_{afg}\, \boldsymbol{e}^g && \text{(1.71d)}\\
&= P^a\, Q^b\, R^c\, \epsilon_{bc}{}^f\, \epsilon_{fga}\, \boldsymbol{e}^g && \text{(1.71e)}\\
&= P^a\, Q^b\, R^c\, (\delta_{bg}\, \delta_{ca} - \delta_{ba}\, \delta_{cg})\, \boldsymbol{e}^g && \text{(1.71f)}\\
&= (\mathbf{P} \cdot \mathbf{R})\, \mathbf{Q} - (\mathbf{P} \cdot \mathbf{Q})\, \mathbf{R}, && \text{(1.71g)}
\end{aligned}$$

where we used

$$\epsilon_{bcd}\, \delta^{df}\, \epsilon_{afg} = \delta^{df}\, \epsilon_{dbc}\, \epsilon_{afg} = \epsilon^f{}_{bc}\, \epsilon_{afg} = \epsilon^f{}_{bc}\, \epsilon_{fga} = \delta_{bg}\, \delta_{ca} - \delta_{ba}\, \delta_{cg}, \tag{1.72}$$

which corresponds to the identity (1.69).

1.9.3 Scalar product of two vector products

We make further use of the Levi-Civita identity (1.69) to derive the following identity for the scalar product of two vector cross products

$$(\mathbf{P}\times\mathbf{Q})\cdot(\mathbf{R}\times\mathbf{S}) = (\epsilon_{abc}\,P^a\,Q^b)\,(\epsilon_{def}\,R^d\,S^e)\,\boldsymbol{e}^c\cdot\boldsymbol{e}^f \tag{1.73a}$$

$$= P^a\,Q^b\,R^d\,S^e\,\delta^{cf}\,\epsilon_{abc}\,\epsilon_{def} \tag{1.73b}$$

$$= (\mathbf{P}\cdot\mathbf{R})\,(\mathbf{Q}\cdot\mathbf{S}) - (\mathbf{P}\cdot\mathbf{S})\,(\mathbf{Q}\cdot\mathbf{R}). \tag{1.73c}$$

1.10 Transforming the representations of Cartesian tensors

The Cartesian basis vectors are mutually orthogonal, and once their orientation is chosen they are fixed in space. However, the choice of orientation is arbitrary.[15] We can consider an alternative specification to the Cartesian basis vectors by performing a linear transformation according to

$$\boldsymbol{e}_{\overline{a}} = \mathcal{R}^{a}{}_{\overline{a}}\,\boldsymbol{e}_a. \tag{1.74}$$

This expression introduced components to the *transformation matrix*, $\mathcal{R}^{a}{}_{\overline{a}}$, that moves tensors between the unbarred and the barred Cartesian coordinates. In Cartesian tensor analysis, the transformation is independent of space. The transformation matrix is a function of space and time for the general tensors. Even so, much of the formalism developed here has a straightforward generalization to the general tensors considered in Chapter 4.

Although the transformation in equation (1.74) carries two indices, it is not a tensor. Instead, it is a matrix operator used to transform from one set of basis vectors to another.[16] Indeed, the slightly rightward placement of the lower index for the transformation in equation (1.74) is a convention used to express the transformation as a matrix

$$\mathcal{R}^{a}{}_{\overline{a}} \longleftrightarrow \mathcal{R} = \begin{bmatrix} \mathcal{R}^{1}{}_{\overline{1}} & \mathcal{R}^{1}{}_{\overline{2}} & \mathcal{R}^{1}{}_{\overline{3}} \\ \mathcal{R}^{2}{}_{\overline{1}} & \mathcal{R}^{2}{}_{\overline{2}} & \mathcal{R}^{2}{}_{\overline{3}} \\ \mathcal{R}^{3}{}_{\overline{1}} & \mathcal{R}^{3}{}_{\overline{2}} & \mathcal{R}^{3}{}_{\overline{3}} \end{bmatrix}. \tag{1.75}$$

Note that typically we dispense with the double-headed arrow correspondence symbol, and simply think of $\mathcal{R}^{a}{}_{\overline{a}}$ as $\mathcal{R}$. In that way we have the transpose of the transformation written as

$$(\mathcal{R}^{\mathrm{T}})^{a}{}_{\overline{a}} = \mathcal{R}_{\overline{a}}{}^{a} = \begin{bmatrix} \mathcal{R}^{1}{}_{\overline{1}} & \mathcal{R}^{2}{}_{\overline{1}} & \mathcal{R}^{3}{}_{\overline{1}} \\ \mathcal{R}^{1}{}_{\overline{2}} & \mathcal{R}^{2}{}_{\overline{2}} & \mathcal{R}^{3}{}_{\overline{2}} \\ \mathcal{R}^{1}{}_{\overline{3}} & \mathcal{R}^{2}{}_{\overline{3}} & \mathcal{R}^{3}{}_{\overline{3}} \end{bmatrix}. \tag{1.76}$$

We have occasion to work with the transpose transformation matrix since, as we show in Section 1.10.2, transformations between Cartesian coordinates with orthonormal basis vectors are orthogonal transformations, which means that the inverse of the transformation matrix equals to the transpose.

1.10.1 Inverse transformation

Assuming the transformation is invertible leads to the inverse transformation

$$\boldsymbol{e}_a = (\mathcal{R}^{-1})^{\overline{a}}{}_{a}\,\boldsymbol{e}_{\overline{a}}. \tag{1.77}$$

[15] The choice for origin is also arbitrary. Here we assume the origins to be the same, so that it is only the orientation that differs between the two Cartesian coordinate systems.

[16] We have more to say about the distinction between a matrix and tensor in Section 1.10.7.

As a self-consistency check we combine this relation with equation (1.74) to render

$$\boldsymbol{e}_a = (\mathcal{R}^{-1})^{\overline{a}}{}_a \, \boldsymbol{e}_{\overline{a}} = (\mathcal{R}^{-1})^{\overline{a}}{}_a \, \mathcal{R}^{c}{}_{\overline{a}} \, \boldsymbol{e}_c. \tag{1.78}$$

This relation holds since

$$(\mathcal{R}^{-1})^{\overline{a}}{}_a \, \mathcal{R}^{c}{}_{\overline{a}} = \delta^{c}{}_{a}, \tag{1.79}$$

or as a matrix identity

$$\mathcal{R}^{-1} \, \mathcal{R} = I. \tag{1.80}$$

1.10.2 Orthogonal transformation

We now assume that the two sets of Cartesian basis vectors are orthonormal, which leads to the following constraint on the transformation matrix

$$\begin{aligned}
\delta_{\overline{a}\overline{b}} &= \boldsymbol{e}_{\overline{a}} \cdot \boldsymbol{e}_{\overline{b}} && && \text{(1.81a)}\\
&= \mathcal{R}^{a}{}_{\overline{a}} \, \boldsymbol{e}_a \cdot \mathcal{R}^{b}{}_{\overline{b}} \, \boldsymbol{e}_b && \text{relate barred to unbarred basis vectors} && \text{(1.81b)}\\
&= \mathcal{R}^{a}{}_{\overline{a}} \, \mathcal{R}^{b}{}_{\overline{b}} \, \boldsymbol{e}_a \cdot \boldsymbol{e}_b && \text{rearrange} && \text{(1.81c)}\\
&= \mathcal{R}^{a}{}_{\overline{a}} \, \mathcal{R}^{b}{}_{\overline{b}} \, \delta_{ab} && \text{orthonormality of basis vectors} && \text{(1.81d)}\\
&= (\mathcal{R}^{\mathrm{T}})_{\overline{a}}{}^{a} \, \delta_{ab} \, \mathcal{R}^{b}{}_{\overline{b}} && \text{rearrangement,} && \text{(1.81e)}
\end{aligned}$$

where $\mathcal{R}^{\mathrm{T}}$ is the transpose of the transformation matrix whose components are (note the positioning of the indices as per equation (1.76))

$$(\mathcal{R}^{\mathrm{T}})_{\overline{a}}{}^{a} = \mathcal{R}^{a}{}_{\overline{a}}. \tag{1.82}$$

Written as a matrix equation, the identity (1.81e) means that

$$\mathcal{R}^{\mathrm{T}} \, \mathcal{R} = I. \tag{1.83}$$

This identity defines an *orthogonal transformation*, whereby the inverse matrix equals to the matrix transpose

$$\mathcal{R}^{-1} = \mathcal{R}^{\mathrm{T}}. \tag{1.84}$$

Consequently, the Cartesian basis vectors transform under rotations according to

$$\boldsymbol{e}_{\overline{a}} = \mathcal{R}^{a}{}_{\overline{a}} \, \boldsymbol{e}_a \quad \text{and} \quad \boldsymbol{e}_a = (\mathcal{R}^{\mathrm{T}})^{\overline{a}}{}_a \, \boldsymbol{e}_{\overline{a}}. \tag{1.85}$$

These transformation rules have implications for how components to vectors and tensors transform.

1.10.3 Geometric interpretation of orthogonal transformations

Orthogonal transformations convert one set of Cartesian coordinates to another. Geometrically, an orthogonal transformation corresponds to a rotation so long as the determinant of the transformation is $+1$, with Figure 1.5 illustrating this axis rotation in two dimensions.[17] For this two dimensional example, the rotation matrix can be written in terms of the cosine of the

[17] If the determinant of the transformation is -1, then the transformation involves a reflection in addition to a rotation, with the reflection changing the handedness of the basis vectors. We only consider right handed basis vectors in this book, so that we only consider orthogonal transformations of Cartesian tensors.

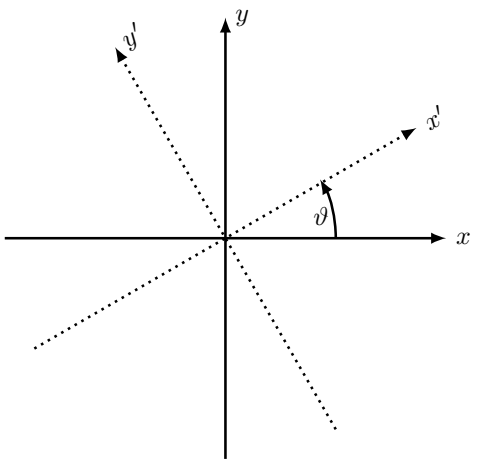

FIGURE 1.5: Counter-clockwise rotation through an angle ϑ of a right-handed horizontal Cartesian axes.

angles between the unit vectors; i.e., the *direction cosines*

$$\mathcal{R}^{a}{}_{\overline{a}} = \begin{bmatrix} \cos\vartheta & \sin\vartheta \\ -\sin\vartheta & \cos\vartheta \end{bmatrix} = \begin{bmatrix} \cos\vartheta & \cos(\pi/2-\vartheta) \\ \cos(\pi/2+\vartheta) & \cos\vartheta \end{bmatrix} = \begin{bmatrix} \boldsymbol{e}_1\cdot\boldsymbol{e}_{\overline{1}} & \boldsymbol{e}_1\cdot\boldsymbol{e}_{\overline{2}} \\ \boldsymbol{e}_2\cdot\boldsymbol{e}_{\overline{2}} & \boldsymbol{e}_2\cdot\boldsymbol{e}_{\overline{2}} \end{bmatrix}. \tag{1.86}$$

The final form of the rotation matrix reveals that it is built from the projection of the rotated basis vectors onto the original basis vectors. This result holds for rotations in three dimensions as well, thus leading to

$$\mathcal{R}^{a}{}_{\overline{a}} = \begin{bmatrix} \boldsymbol{e}_1\cdot\boldsymbol{e}_{\overline{1}} & \boldsymbol{e}_1\cdot\boldsymbol{e}_{\overline{2}} & \boldsymbol{e}_1\cdot\boldsymbol{e}_{\overline{3}} \\ \boldsymbol{e}_2\cdot\boldsymbol{e}_{\overline{1}} & \boldsymbol{e}_2\cdot\boldsymbol{e}_{\overline{2}} & \boldsymbol{e}_2\cdot\boldsymbol{e}_{\overline{3}} \\ \boldsymbol{e}_3\cdot\boldsymbol{e}_{\overline{1}} & \boldsymbol{e}_3\cdot\boldsymbol{e}_{\overline{2}} & \boldsymbol{e}_3\cdot\boldsymbol{e}_{\overline{3}} \end{bmatrix}. \tag{1.87}$$

With the basis vectors all normalized, elements of the rotation matrix are given by the cosine of the angle between the respective basis vectors. As such, one sometimes refers to this rotation matrix as the *direction cosines* matrix.

1.10.4 Transforming the coordinate representation of a vector

We introduced the transformation (1.77) according to how it acts on the basis vectors. Now consider how it acts on the coordinate representation of an arbitrary vector, as revealed by moving around brackets

$$\mathbf{P} = P^a\,\boldsymbol{e}_a = P^a\,(\mathcal{R}^{\mathrm{T}})^{\overline{a}}{}_a\,\boldsymbol{e}_{\overline{a}} \equiv P^{\overline{a}}\,\boldsymbol{e}_{\overline{a}}. \tag{1.88}$$

The second equality made use of equation (1.85) for the transformation of the basis vector under an orthogonal transformation. The final equality reveals the transformation of the vector components according to

$$P^{\overline{a}} = P^a\,(\mathcal{R}^{\mathrm{T}})^{\overline{a}}{}_a = P^a\,\mathcal{R}_a{}^{\overline{a}}. \tag{1.89}$$

1.10.5 Invariance of the scalar product

The above properties of an orthogonal transformation ensure that the scalar product takes on the same form regardless the choice of Cartesian coordinates

$$\mathbf{P}\cdot\mathbf{Q} = P^a\,Q^b\,\delta_{ab} \qquad \text{expose tensor indices \& Kronecker delta} \tag{1.90a}$$

$$= P^a\, Q^b\, \boldsymbol{e}_a \cdot \boldsymbol{e}_b \qquad \text{orthonormal basis vectors: } \boldsymbol{e}_a \cdot \boldsymbol{e}_b = \delta_{ab} \tag{1.90b}$$

$$= P^a\, Q^b\, (\mathcal{R}^{\mathrm{T}})^{\overline{a}}{}_a\, \boldsymbol{e}_{\overline{a}} \cdot (\mathcal{R}^{\mathrm{T}})^{\overline{b}}{}_b\, \boldsymbol{e}_{\overline{b}} \qquad \text{rotate basis vectors to barred frame} \tag{1.90c}$$

$$= P^a\, (\mathcal{R}^{\mathrm{T}})^{\overline{a}}{}_a\, Q^b\, (\mathcal{R}^{\mathrm{T}})^{\overline{b}}{}_b\, \boldsymbol{e}_{\overline{a}} \cdot \boldsymbol{e}_{\overline{b}} \qquad \text{rearrange} \tag{1.90d}$$

$$= P^{\overline{a}}\, Q^{\overline{b}}\, \boldsymbol{e}_{\overline{a}} \cdot \boldsymbol{e}_{\overline{b}} \qquad \text{transform vector components (1.88)} \tag{1.90e}$$

$$= P^{\overline{a}}\, Q^{\overline{b}}\, \delta_{\overline{a}\overline{b}} \qquad \text{orthonormal basis vectors: } \boldsymbol{e}_{\overline{a}} \cdot \boldsymbol{e}_{\overline{b}} = \delta_{\overline{a}\overline{b}}. \tag{1.90f}$$

1.10.6 Transforming the coordinate representation of a second order tensor

We determine how the Cartesian coordinate components of a second order tensor, T^{ab}, transform by following the now familiar procedure for transforming the basis vectors. The key new facet is that we now have two basis vectors to carry around rather than just one

$$\mathbf{T} = T^{ab}\, \boldsymbol{e}_a \otimes \boldsymbol{e}_b \qquad \text{expose indices and basis vectors} \tag{1.91a}$$

$$= T^{ab}\, (\mathcal{R}^{\mathrm{T}})^{\overline{a}}{}_a\, \boldsymbol{e}_{\overline{a}} \otimes (\mathcal{R}^{\mathrm{T}})^{\overline{b}}{}_b\, \boldsymbol{e}_{\overline{b}} \qquad \text{rotate basis vectors to barred frame} \tag{1.91b}$$

$$= T^{ab}\, (\mathcal{R}^{\mathrm{T}})^{\overline{a}}{}_a\, (\mathcal{R}^{\mathrm{T}})^{\overline{b}}{}_b\, \boldsymbol{e}_{\overline{a}} \otimes \boldsymbol{e}_{\overline{b}} \qquad \text{rearrange} \tag{1.91c}$$

$$\equiv T^{\overline{a}\overline{b}}\, \boldsymbol{e}_{\overline{a}} \otimes \boldsymbol{e}_{\overline{b}} \qquad \text{define transformed tensor components.} \tag{1.91d}$$

The final equality introduced the transformed components to the second order tensor

$$T^{\overline{a}\overline{b}} = T^{ab}\, (\mathcal{R}^{\mathrm{T}})^{\overline{a}}{}_a\, (\mathcal{R}^{\mathrm{T}})^{\overline{b}}{}_b. \tag{1.92}$$

Transformation of the $(1,1)$ representation of a second order tensor is given by

$$T^{\overline{a}}{}_{\overline{b}} = T^a{}_b\, (\mathcal{R}^{\mathrm{T}})^{\overline{a}}{}_a\, \mathcal{R}^b{}_{\overline{b}}, \tag{1.93}$$

which compares to equation (1.92) for the fully contravariant representation, $T^{\overline{a}\overline{b}}$. The transformation of the components to higher order tensors follows analogously by carrying around further basis vectors or basis one-forms.

1.10.7 Distinguishing between tensors and matrices

Matrices are useful for organizing the coordinate components to a tensor. For example, the coordinate components to a first-order tensor (a vector)

$$\boldsymbol{F} = F^1\, \boldsymbol{e}_1 + F^2\, \boldsymbol{e}_2 + F^3\, \boldsymbol{e}_3, \tag{1.94}$$

can be organized into a *row vector*

$$\boldsymbol{F} = (F^1, F^2, F^3). \tag{1.95}$$

We are justified in assigning the name "vector" in this context since we know that the array elements comprise the coordinate representation of the vector, $\mathbf{F}$. However, if we just see an array of numbers, say (Q^1, Q^2, Q^3), on its own, then we generally have no idea whether the elements of that array are related to each other, or if the list is just an ordering of numbers. If merely a list of numbers, then nothing necessarily changes when we alter coordinates. But if the array is the coordinate representation of a vector, then we know that the elements of the row vector are related, and we know how they change when the coordinates are rotated.

Consider two examples of objects that are not tensors. First, the rotation matrix, $\mathcal{R}^a{}_{\overline{a}}$, has elements built from the direction cosines according to equation (1.87). Although carrying two indices, this matrix is not the coordinate representation of a second order tensor. Rather, it is

simply the matrix used to transform the components of tensors from one coordinate system to another. The rotation matrix is not a geometric object like a vector or tensor, but it is an ordered array that contains information for how a coordinate transformation alters the representation of geometric objects.

Although jumping ahead somewhat, we mention one further example encountered when studying general tensors in Chapter 4. Namely, the *Christoffel symbols* in Section 4.11.1 are built from the spatial derivatives of the basis vectors. Although these derivatives are zero for Cartesian basis vectors, they are not necessarily zero when using general coordinates. The Christoffel symbols carry three indices, and yet they are not elements of a third order tensor since they do not transform as elements to a tensor. One way to understand this property is to note that a tensor that vanishes in one coordinate system is zero for all coordinate systems. It turns out that all of the Christoffel symbols vanish for Euclidean space using Cartesian coordinates, because the Cartesian basis vectors are spatially constant. However, there are some nonzero Christoffel symbols when representing Euclidean space with spherical coordinates or other general coordinates. By this example, we conclude that the Christoffel symbols cannot be components of a tensor.

The key point we re-emphasize is that a tensor is a geometric object that can be represented using any arbitrary set of coordinates. Since the tensor has an objective existence independent of coordinates, its coordinate components are constrained to transform in a precise manner when changing coordinates. These properties of tensors are generally not shared with arbitrary matrices, hence the importance of making the distinction between tensors and matrices.

1.11 Homogeneity and isotropy of second order tensors

We have many occasions to consider symmetry properties of tensor fields, with homogeneity and isotropy two such properties. When developing these properties for second order Cartesian tensors, we make use of the $(1,1)$ tensor representation

$$T^a{}_b = T^{ac}\,\mathbb{g}_{cb}, \tag{1.96}$$

which is the natural representation of a second order tensor (Section 1.6.1). We also follow this approach in Section 1.12 when decomposing a second order tensor into its irreducible parts.[18]

1.11.1 Transpose of a second order tensor

When represented as a matrix, the transpose of a second order tensor is obtained by swapping the rows and columns. In a similar manner we generate the transpose through the following

$$T_a{}^b = (T^b{}_a)^{\mathrm{T}} = \mathbb{g}_{ac}\,T^c{}_d\,\mathbb{g}^{db} = \mathbb{g}_{ac}\,T^{cb} \tag{1.97a}$$

$$T^b{}_a = (T_a{}^b)^{\mathrm{T}} = \mathbb{g}^{bc}\,T_c{}^d\,\mathbb{g}_{da} = T^{bd}\,\mathbb{g}_{da}. \tag{1.97b}$$

The transpose for the sharp and flat representations of the second order tensor follow a bit more simply

$$(T^{ab})^{\mathrm{T}} = T^{ba} \quad \text{and} \quad (T_{ab})^{\mathrm{T}} = T_{ba}. \tag{1.98}$$

[18] We certainly can perform such decompositions with other representations of a tensor. But we choose to focus on the $(1,1)$ representation here.

1.11.2 Trace of a tensor

The trace of a second order tensor is given by the contraction

$$\text{trace}(\mathbf{T}) = T^{ac}\,\mathcal{g}_{ca} = T^{a}{}_{a} = T^{1}{}_{1} + T^{2}{}_{2} + T^{3}{}_{3}, \tag{1.99}$$

which is the sum of the diagonal components of the natural representation.

1.11.3 Homogeneous tensors

A tensor field is *homogeneous* if it possesses the same value at each point in space. For example, a uniform temperature field is homogeneous, as is a uniform velocity field. As defined, a homogeneous tensor field has no spatial dependence and thus it does not provide any means to distinguish points in space. Likewise, a time independent tensor is said to be homogeneous in time.

1.11.4 Isotropic tensors

A tensor field is *isotropic* if its representation remains independent of coordinate basis. A scalar tensor is, by definition, isotropic since it has no information about spatial directions. A nonzero vector field cannot be isotropic since it points in a particular direction and so its representation is dependent on the orientation of the basis vectors.

A second order Cartesian tensor, $\mathbf{J}$, is isotropic if its components are unchanged when undergoing rotation, so that

$$J^{\overline{a}}{}_{\overline{b}} = J^{a}{}_{b}\,\mathcal{R}^{b}{}_{\overline{b}}\,(\mathcal{R}^{\mathrm{T}})^{\overline{a}}{}_{a} \equiv J^{a}{}_{b}, \tag{1.100}$$

where we used equation (1.93) for the component transformation. For nonzero tensors, equation (1.100) is satisfied only if we can write

$$J^{a}{}_{b} = \lambda\,\delta^{a}{}_{b}, \tag{1.101}$$

with λ an arbitrary scalar. We verify this property through noting that

$$\delta^{a}{}_{b}\,\mathcal{R}^{b}{}_{\overline{b}}\,(\mathcal{R}^{\mathrm{T}})^{\overline{a}}{}_{a} = \mathcal{R}^{a}{}_{\overline{b}}\,(\mathcal{R}^{\mathrm{T}})^{\overline{a}}{}_{a} = \delta^{\overline{a}}{}_{\overline{b}}, \tag{1.102}$$

where the final equality made use of orthogonality of the rotation matrix. Hence, the most general second order isotropic tensor is proportional to the Kronecker (identity) tensor.

1.11.5 Decomposition into isotropic and anisotropic tensors

We often find it useful to decompose an arbitrary second order tensor into its anisotropic and isotropic components according to

$$T^{a}{}_{b} = \underbrace{T^{a}{}_{b} - \frac{T^{p}{}_{p}\,\delta^{a}{}_{b}}{N}}_{\text{anisotropic}} + \underbrace{\frac{T^{p}{}_{p}\,\delta^{a}{}_{b}}{N}}_{\text{isotropic}} \tag{1.103}$$

where

$$N = \delta^{p}{}_{p} \tag{1.104}$$

is the number of space dimensions, which equals to the trace of the Kronecker tensor. By extracting the isotropic portion, we know that the remaining portion is anisotropic by construction.

1.12 Irreducible parts of a second order tensor

Second order tensors have nine degrees of freedom when working in $N = 3$ dimensional space. It can be useful to decompose these tensors into their *irreducible tensorial parts* as presented here, with these parts generally representing distinct kinematic properties that help to understand the physical nature of the tensor. The decomposition shares much with the decomposition into anisotropic and isotropic tensors in Section 1.11.5, and with the following results holding for general tensors.

Any second order tensor can be decomposed into its symmetric and anti-symmetric parts according to

$$\mathbf{T} = (\mathbf{T} + \mathbf{T}^{\mathrm{T}})/2 + (\mathbf{T} - \mathbf{T}^{\mathrm{T}})/2 = \mathbf{S} + \mathbf{A}. \tag{1.105}$$

Working with the components in the $(1,1)$ representation of the tensor leads to

$$T^a{}_b = \underbrace{(T^a{}_b + T_b{}^a)/2}_{\text{symmetric}} + \underbrace{(T^a{}_b - T_b{}^a)/2}_{\text{anti-symmetric}} \equiv S^a{}_b + A^a{}_b. \tag{1.106}$$

The *symmetric tensor*, $\mathbf{S}$, is so-named because it satisfies

$$\mathbf{S} = \mathbf{S}^{\mathrm{T}} \longleftrightarrow S^a{}_b = S_b{}^a. \tag{1.107}$$

That is, swapping rows and columns leaves elements of a symmetric tensor unchanged. In three space dimensions, a symmetric second order tensor has six (rather than nine) degrees of freedom. The *anti-symmetric tensor* (also called the *skew-symmetric tensor*) satisfies

$$\mathbf{A} = -\mathbf{A}^{\mathrm{T}} \longleftrightarrow A^a{}_b = -A_b{}^a, \tag{1.108}$$

which means it has three degrees of freedom (for $N = 3$ space dimensions) and has zero elements along its diagonal

$$A^1{}_1 = A^2{}_2 = A^3{}_3 = 0. \tag{1.109}$$

The final irreducible part of a tensor is the *trace*, which we introduced in Section 1.11.2 and it is given by the sum of the diagonal elements

$$T^a{}_a = T^1{}_1 + T^2{}_2 + T^3{}_3 = S^a{}_a, \tag{1.110}$$

with the second equality following since the skew symmetric tensor, $\mathbf{A}$, has zero for its diagonal elements. We are thus led to the irreducible decomposition of an arbitrary second order tensor

$$T^a{}_b = \underbrace{S^p{}_p\,\delta^a{}_b/N}_{\text{trace}} + \underbrace{(S^a{}_b - S^p{}_p\,\delta^a{}_b/N)}_{\text{deviator}} + \underbrace{A^a{}_b}_{\text{skew}}. \tag{1.111}$$

The combination,

$$(S^{\mathrm{dev}})^a{}_b = S^a{}_b - S^p{}_p\,\delta^a{}_b/N, \tag{1.112}$$

is known as the *deviatoric tensor* or *deviator*, which, by construction, has zero trace

$$(S^{\mathrm{dev}})^a{}_a = 0. \tag{1.113}$$

1.13 Dot and double-dot notation for contractions

As seen many times in this chapter, we often use a dot notation for the *contraction* of two first order tensors, such as for the scalar product, $\mathbf{F} \cdot \mathbf{G}$, encountered in equation (1.13). The are additional occasions to contract higher order tensors, yet in this case we must follow a convention

to know what indices participate in the contraction. Following *Tromp* (2025a) and others, we define the dot as a contraction between the last index of the first tensor and the first index of the second tensor. For example, let $\boldsymbol{T}$ be a second order tensor and $\boldsymbol{A}$ a first order tensor. Their dot product is thus equal to a first order tensor

$$\boldsymbol{T} \cdot \boldsymbol{A} = \boldsymbol{F}, \tag{1.114}$$

which can be written in components as

$$T^a{}_b \, A^b = T^{ab} \, A_b = F^a. \tag{1.115}$$

Alternatively, consider the dot product, $\boldsymbol{A} \cdot \boldsymbol{T} = \boldsymbol{G}$, which has components

$$A^b \, T_b{}^a = A^b \, (T^a{}_b)^{\mathrm{T}} = A_b \, (T^{ab})^{\mathrm{T}} = A_b \, T^{ba} = G^a. \tag{1.116}$$

Evidently, $\boldsymbol{F} = \boldsymbol{G}$, only if the second order tensor is symmetric, $\boldsymbol{T} = \boldsymbol{T}^{\mathrm{T}}$.

There are occasions in which it is of interest to contract both indices between two second order tensors, in which we make use of the colon with the following index convention

$$\boldsymbol{D} : \boldsymbol{T} = D^{ab} \, T_{ab} = D_{ab} \, T^{ab}. \tag{1.117}$$

This double contraction is most commonly performed between two symmetric tensors, in which case ordering of the indices does not matter.

1.14 Exercises

EXERCISE 1.1: PRODUCT OF SYMMETRIC MATRICES
Let $A = A^{\mathrm{T}}$ and $B = B^{\mathrm{T}}$ be two symmetric matrices. Under what condition is their product also symmetric: $A\,B = (A\,B)^{\mathrm{T}}$?

EXERCISE 1.2: PRODUCT OF SYMMETRIC AND ANTI-SYMMETRIC MATRICES AND TENSORS
Let $A = -A^{\mathrm{T}}$ be an anti-symmetric matrix, and $S = S^{\mathrm{T}}$ be a symmetric matrix. Show that the trace of their product vanishes: $\mathrm{trace}(A\,S) = 0$. Alternatively, in terms of tensors, show that the double contraction of an anti-symmetric tensor with a symmetric tensor vanishes: $\mathbb{A}^m{}_n \, \mathbb{S}^n{}_m = 0$.

EXERCISE 1.3: PROJECTION OPERATOR
Consider an arbitrary direction in space specified by the unit direction, $\hat{\boldsymbol{n}}$, with components, $\hat{n}_a$. Define the symmetric tensor

$$P_{ab} = \mathbb{g}_{ab} - \hat{n}_a \, \hat{n}_b, \tag{1.118}$$

so that

$$P_{ab} \, T^{bc} = T_a{}^c - T^{bc} \, \hat{n}_a \, \hat{n}_b. \tag{1.119}$$

Show that $P_{ab} \, T^{bc}$ is the projection of $\mathbf{T}$ onto the plane perpendicular to the direction $\hat{\boldsymbol{n}}$. Do so by showing that

$$P_{ab} \, T^{bc} \, (\mathbb{g}^{ad} \, \hat{n}_d) = 0 \quad \forall \, c. \tag{1.120}$$

This result motivates referring to P_{ab} as a *projection operator*.

Chapter 2

CARTESIAN VECTOR CALCULUS

This chapter presents elements of differential and integral calculus. We build from the tensor algebra of Chapter 1 to here develop elements of Cartesian tensor calculus, also known as *vector calculus*.

CHAPTER GUIDE

The material in this chapter can be found in various forms in nearly all books on calculus with analytic geometry. Particular treatments, with applications to physics, are given in the following. Recall from Chapter 1 that we are mindful of the distinction between a tensor and its coordinate representation. We retain that distinction in this chapter, though mostly focus on particular Cartesian coordinate representations since we are concerned with analytical/operational aspects of tensor fields.

- FEYNMAN LECTURES: Chapters 2 and 3 in Volume II of the Feynman Lectures offers insightful discussions of vector differential calculus. Although written for students of electrodynamics, many of Feynman's examples are drawn from fluid mechanics.
- DIV, GRAD, CURL AND ALL THAT (*Schey*, 2004): This text presents the methods and theorems of vector calculus in a manner that greatly assists the development of intuition.
- Chapter 2 in *Segel* (1987) provides a lucid review of vector calculus using Cartesian tensors.
- THEORY AND PROBLEMS OF VECTOR ANALYSIS (*Spiegel*, 1974A): This "Schaum's Outline Series" book has nearly 500 worked exercises and provides a useful resource to develop problem solving in vector calculus. Some of the exercises in Section 2.9 at the end of this chapter are drawn from *Spiegel* (1974a).
- This video from 3Blue1Brown provides some compelling graphics to support intuition for the divergence and curl operators.
- This Youtube channel from Steve Brunton offers some pedagogical lectures on vector calculus.

2.1 Gradient of a scalar field

Consider a real valued scalar field defined on Euclidean space that is a function of Cartesian coordinates, $\psi(\boldsymbol{x})$. We can estimate the value of the field at an adjacent point an infinitesimal distance away, $\boldsymbol{x} + \mathrm{d}\boldsymbol{x}$, through use of a truncated Taylor series

$$\psi(\boldsymbol{x} + \mathrm{d}\boldsymbol{x}) = \psi(\boldsymbol{x}) + \frac{\partial \psi}{\partial x^1}\,\mathrm{d}x^1 + \frac{\partial \psi}{\partial x^2}\,\mathrm{d}x^2 + \frac{\partial \psi}{\partial x^3}\,\mathrm{d}x^3 + \mathcal{O}\left(\mathrm{d}\boldsymbol{x} \cdot \mathrm{d}\boldsymbol{x}\right) \tag{2.1a}$$

$$\approx \left[1 + \mathrm{d}x^a\,\partial_a\right]\psi(\boldsymbol{x}), \tag{2.1b}$$

where we dropped higher order terms to reach the final approximate expression. We also introduced the shorthand notation for the partial derivative operator

$$\partial_a = \frac{\partial}{\partial x^a}, \tag{2.2}$$

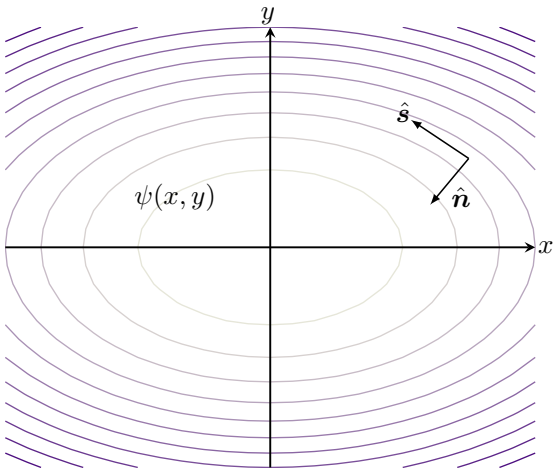

FIGURE 2.1: Contours of a scalar field $\psi(x, y) = -x^2/2 - y^2$. At any point in space, the gradient, $\nabla\psi = -(x\,\hat{\boldsymbol{x}} + 2\,y\,\hat{\boldsymbol{y}})$, points in the direction of steepest increase (ascent) and orients the unit normal, $\hat{\boldsymbol{n}} = |\nabla\psi|^{-1}\,\nabla\psi$. The unit tangent, $\hat{\boldsymbol{s}}$, points in a direction tangent to a ψ isosurface so that it is everywhere orthogonal to the direction of steepest ascent: $\hat{\boldsymbol{n}} \cdot \hat{\boldsymbol{s}} = 0$. We follow the convention in which the unit normal is oriented to the left of the unit tangent when facing in the tangent direction.

which is a notation used throughout this book. Notice how the index on the partial derivative naturally sits downstairs, in the covariant position. We can thus introduce the Cartesian gradient operator according to

$$\nabla = \hat{\boldsymbol{x}}\,\partial_x + \hat{\boldsymbol{y}}\,\partial_y + \hat{\boldsymbol{z}}\,\partial_z = \boldsymbol{e}^a\,\partial_a, \tag{2.3}$$

in which case

$$\psi(\boldsymbol{x} + \mathrm{d}\boldsymbol{x}) \approx (1 + \mathrm{d}\boldsymbol{x} \cdot \nabla)\,\psi(\boldsymbol{x}). \tag{2.4}$$

The second equality in equation (2.3) made use of the basis one-forms in Cartesian coordinates from Section 1.3.3. Evidently, the gradient operator naturally appears as a one-form.

2.1.1 Direction of steepest ascent

Using the approximate relation (2.4), and the geometric expression (1.19) for the scalar product, renders

$$\psi(\boldsymbol{x} + \mathrm{d}\boldsymbol{x}) - \psi(\boldsymbol{x}) \approx |\mathrm{d}\boldsymbol{x}|\,|\nabla\psi|\cos\vartheta, \tag{2.5}$$

where ϑ is the angle between the differential increment, $\mathrm{d}\boldsymbol{x}$, and the gradient, $\nabla\psi$. Orienting the increment $\mathrm{d}\boldsymbol{x}$ so that $\vartheta = 0$ ensures that $\psi(\boldsymbol{x} + \mathrm{d}\boldsymbol{x}) - \psi(\boldsymbol{x})$ is maximal. Consequently, $\nabla\psi$ points in the direction of *steepest ascent* across constant ψ isosurfaces (Figure 2.1). The opposite direction is that of *steepest descent*, where $\vartheta = \pi$.

2.1.2 Tangent to an isosurface

Consider a family of isosurfaces defined by points satisfying

$$\psi(\boldsymbol{x}) = \text{constant}. \tag{2.6}$$

Figure 2.1 shows a two dimensional example where the isosurfaces are lines where ψ is a constant. As another example, consider $\psi(\boldsymbol{x}) = \psi(r)$, where $r^2 = \boldsymbol{x} \cdot \boldsymbol{x}$ is the squared radius of a sphere. Isosurfaces for this spherically symmetric function are spherical surfaces of radius r.

In general, moving along an isosurface keeps the scalar field unchanged. Let $\hat{\boldsymbol{s}}$ have magnitude unity and point in the direction tangent to the isosurface at any point determined by the Cartesian

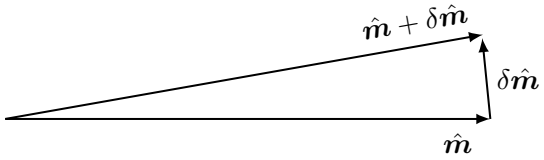

FIGURE 2.2: The infinitesimal change to a unit direction, $\delta\hat{\boldsymbol{m}}$, is orthogonal to itself: $\delta\hat{\boldsymbol{m}} \cdot \hat{\boldsymbol{m}} = 0$. The reason is that the unit direction is constrained to retain its unit length, so that the only way that it can change is to change its direction. In this image we have $|\hat{\boldsymbol{m}} + \delta\hat{\boldsymbol{m}}| = |\hat{\boldsymbol{m}}| = 1$, which requires $\delta\hat{\boldsymbol{m}} \cdot \hat{\boldsymbol{m}} = 0$. Evidently, $\delta\hat{\boldsymbol{m}}$ is orthogonal to $\hat{\boldsymbol{m}}$ in the limit that $\delta\hat{\boldsymbol{m}}$ gets tiny.

coordinate, $\boldsymbol{x}$. By construction[1]

$$\psi(\boldsymbol{x} + \hat{\boldsymbol{s}}\, \mathrm{d}s) - \psi(\boldsymbol{x}) = 0, \tag{2.7}$$

where $\mathrm{d}s$ is an infinitesimal arc length along the tangent direction. In words, this identity says that if we move an infinitesimal distance in the direction tangent to the isosurface, then the function ψ does not change its value. Now expanding this identity in a Taylor series leads to the vanishing of the tangential partial derivative

$$\hat{\boldsymbol{s}} \cdot \nabla\psi = \partial_s \psi = 0. \tag{2.8}$$

That is, isosurfaces of a function ψ are defined by directions along which the partial derivative of the function vanishes. For the spherically symmetric function, $\psi(\boldsymbol{x}) = \psi(r)$, the tangent vector points in either of the two angular directions along the spherical surface.

2.1.3 Unit normal to an isosurface

We may normalize the direction of maximal ascent, in which case we define the unit normal (a one-form)

$$\hat{\boldsymbol{n}} = |\nabla\psi|^{-1}\, \nabla\psi. \tag{2.9}$$

By construction, the gradient computed in the $\hat{\boldsymbol{n}}$ direction yields the maximum change for the function so that the *normal derivative* is given by

$$\hat{\boldsymbol{n}} \cdot \nabla\psi = |\nabla\psi|. \tag{2.10}$$

For the spherically symmetric example,

$$\hat{\boldsymbol{n}} = \frac{\boldsymbol{x}}{|\boldsymbol{x}|} = \hat{\boldsymbol{r}}, \tag{2.11}$$

where $\hat{\boldsymbol{r}}$ is the unit vector pointing radially outward from the origin. In this case the normal derivative is equal to the radial derivative

$$\hat{\boldsymbol{n}} \cdot \nabla\psi = \partial_r \psi \qquad \text{spherically symmetric } \psi. \tag{2.12}$$

2.1.4 Unit directions change only via rotation

Consider an arbitrary unit direction, $\hat{\boldsymbol{m}}$, that is generally a function of space. The unit direction has unit magnitude,

$$\hat{\boldsymbol{m}} \cdot \hat{\boldsymbol{m}} = 1, \tag{2.13}$$

[1] Sometimes in this book we write $\hat{\boldsymbol{t}}$ for the unit tangent.

with this property holding at each point in space. Unit directions can only be modified through changes in their orientation since their magnitude is everywhere fixed at unity. Hence, they differ in space only through rotations. An important consequence of this property is that the infinitesimal spatial change to a unit direction is perpendicular to unit direction itself (see Figure 2.2). We see this property through considering an arbitrary infinitesimal change, symbolized by δ, in which

$$0 = \delta(1) = \delta\left(\hat{\boldsymbol{m}} \cdot \hat{\boldsymbol{m}}\right) = 2\,\hat{\boldsymbol{m}} \cdot \delta\hat{\boldsymbol{m}}. \tag{2.14}$$

In Section 11.2, we formally show that the constraint

$$\delta\hat{\boldsymbol{m}} \cdot \hat{\boldsymbol{m}} = 0 \tag{2.15}$$

means that unit direction changes can only arise from rotations. Even so, the above assertion should make intuitive sense, with Figure 2.2 illustrating this property.

2.1.5 Showing that $\delta\hat{\boldsymbol{n}} \cdot \hat{\boldsymbol{n}} = 0$

As an illustration of the constraint (2.15), we verify that it holds for the special case of a unit normal defined according to equation (2.9) for surfaces of constant scalar field

$$\hat{\boldsymbol{n}} = |\nabla\psi|^{-1}\,\nabla\psi. \tag{2.16}$$

The proof follows first by writing

$$\delta\hat{\boldsymbol{n}} = |\nabla\psi|^{-1}\,\left[\delta(\nabla\psi) - \hat{\boldsymbol{n}}\,\delta|\nabla\psi|\right], \tag{2.17}$$

so that

$$|\nabla\psi|\,\hat{\boldsymbol{n}} \cdot \delta\hat{\boldsymbol{n}} = \hat{\boldsymbol{n}} \cdot \delta(\nabla\psi) - \delta(|\nabla\psi|) = \frac{\nabla\psi \cdot \delta(\nabla\psi)}{|\nabla\psi|} - \delta|\nabla\psi|. \tag{2.18}$$

We now make use of the identity

$$\delta(|\nabla\psi|) = \delta(\sqrt{\nabla\psi \cdot \nabla\psi}) = \frac{1}{2\sqrt{\nabla\psi \cdot \nabla\psi}}\delta(\nabla\psi \cdot \nabla\psi) = \frac{\nabla\psi \cdot \delta(\nabla\psi)}{|\nabla\psi|}, \tag{2.19}$$

in which case we have shown that $\delta\hat{\boldsymbol{n}} \cdot \hat{\boldsymbol{n}} = 0$.

2.1.6 Notation for the derivative operators

The discussion in this section made use of the Cartesian partial derivative operator, ∂_a, as well as the gradient operator, ∇. The Cartesian gradient operator becomes the covariant gradient operator when moving to general tensors, with the covariant gradient also written as ∇. When acting on first or higher order tensors, the covariant gradient picks up some extra terms beyond the familiar partial derivatives. To facilitate a translation of the equations in this chapter to those in general tensors, we commonly make use of the ∇_a symbol rather than ∂_a. Again, they are identical for Cartesian tensors.

2.2 Divergence of a vector field

The divergence of a vector field, $\mathbf{F}$, is the scalar product of the gradient operator with the vector

$$\text{div}(\mathbf{F}) = \nabla \cdot \mathbf{F} = \nabla_a F^a \begin{cases} > 0 \Rightarrow \text{diverging vector field} \\ < 0 \Rightarrow \text{converging vector field} \\ = 0 \Rightarrow \text{divergence-free (or non-divergent) vector field.} \end{cases} \tag{2.20}$$

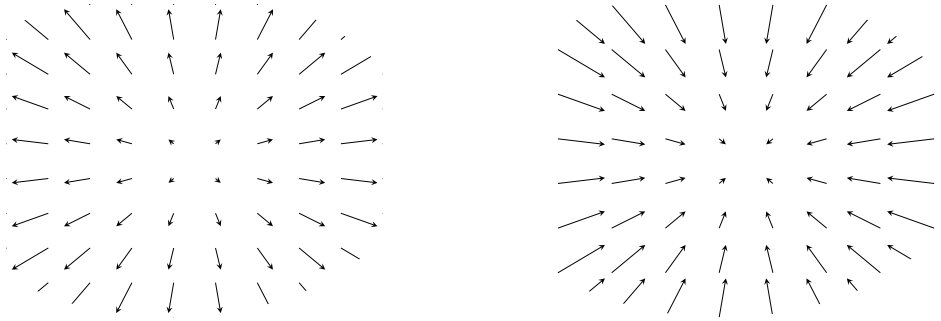

FIGURE 2.3: Two vector fields with a non-zero horizontal divergence. Left panel: The vector field $\mathbf{F} = x\,\hat{\boldsymbol{x}} + y\,\hat{\boldsymbol{y}}$ has a spatially constant positive divergence at each point with $\nabla \cdot \mathbf{F} = 2$. We thus say that the vector field is "diverging from each point." Right panel: with the opposite sign, the vector field $\mathbf{G} = -\mathbf{F} = -x\,\hat{\boldsymbol{x}} - y\,\hat{\boldsymbol{y}}$ has a spatially constant negative divergence at each point with $\nabla \cdot \mathbf{G} = -2$. We thus say that the vector field is "converging to each point." Note that these two vector fields have zero curl, $\nabla \times \mathbf{F} = \nabla \times \mathbf{G} = 0$.

If the vector field in the surrounding neighborhood of a point is directed away from that point, then the vector field is diverging as if there is a source at the point (Figure 2.3). In this case the divergence of the vector field is positive. The converse occurs for a vector field converging to a point as if there is a sink.

If the vector field under consideration is the velocity field of a moving fluid, then these considerations are directly related to the conservation of matter that we study in Chapter 19. That discussion motivates us to consider a positive divergence for a vector field as representing the creation of "stuff" at a point where there is a positive divergence. Again for the case of a fluid velocity, there is a net divergence if more fluid leaves a point than enters, and the converse holds if the velocity field is converging. We further discuss these ideas as part of our study of the divergence theorem in Section 2.7.

2.2.1 Divergence of a scalar field times a vector field

We have many opportunities to make use of properties of the divergence operator following from application of the chain rule. For example, use of the chain rule indicates that the divergence of a scalar field times a vector field is given by

$$\nabla \cdot (\phi\,\mathbf{F}) = \nabla_a(\phi\,F^a) \tag{2.21a}$$
$$= F^a\,\nabla_a\phi + \phi\,\nabla_a F^a \tag{2.21b}$$
$$= \mathbf{F} \cdot \nabla\phi + \phi\,\nabla \cdot \mathbf{F}. \tag{2.21c}$$

2.2.2 Laplacian of a scalar field

The Laplacian of a scalar field is the divergence of the gradient

$$\nabla^2\psi = \nabla \cdot \nabla\psi. \tag{2.22}$$

Scalar fields that have a vanishing Laplacian are said to be *harmonic*

$$\nabla^2\psi = 0 \qquad \text{harmonic function.} \tag{2.23}$$

The name *harmonic* originates from the relation of harmonic functions to characteristic vibrational modes of a taut string such as those found on musical instruments (when played with skill). Furthermore, harmonic functions play a central role in complex analysis.

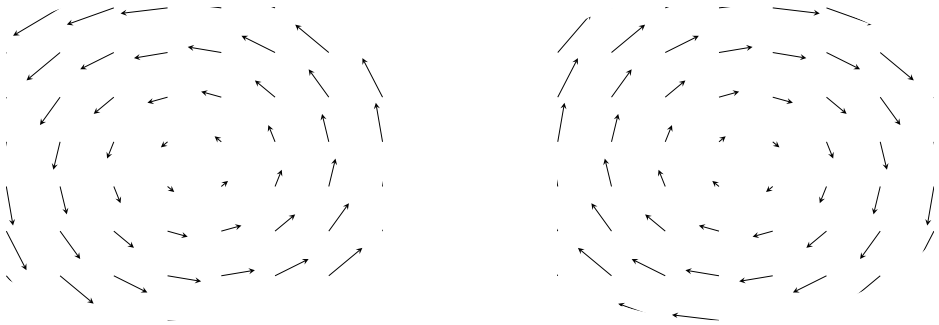

FIGURE 2.4: A horizontal vector field with a constant curl and zero divergence. Left panel: $\mathbf{F} = -y\,\hat{\boldsymbol{x}} + x\,\hat{\boldsymbol{y}}$, $\implies \nabla \times \mathbf{F} = 2\,\hat{\boldsymbol{z}}$ and $\nabla \cdot \mathbf{F} = 0$. Right panel: $\mathbf{G} = -\mathbf{F}$ so that $\nabla \times \mathbf{G} = -2\,\hat{\boldsymbol{z}}$.

2.3 Curl of a vector field

The curl characterizes how a vector field spins around each point in space. For example, in Part VII of this book we study the vorticity field, which is the curl of the velocity.

2.3.1 Computing the curl

We measure the curl of a vector by computing the cross product of the gradient operator with the vector field. Hence, just like the cross product from Section 1.7, the curl is specified by both a magnitude and a direction

$$
\begin{aligned}
\operatorname{curl}(\mathbf{F}) &= \nabla \times \mathbf{F} && && \text{(2.24a)}\\
&= \boldsymbol{e}^a\, \nabla_a \times \boldsymbol{e}_b\, F^b && \text{coordinate representation} && \text{(2.24b)}\\
&= \boldsymbol{e}^a\, \times \nabla_a\, (\boldsymbol{e}_b\, F^b) && \text{move derivative operator} && \text{(2.24c)}\\
&= (\boldsymbol{e}^a \times \boldsymbol{e}_b)\, \nabla_a F^b + F^b\, (\boldsymbol{e}^a \times \nabla_a \boldsymbol{e}_b) && \text{product rule} && \text{(2.24d)}\\
&= (\boldsymbol{e}^a \times \boldsymbol{e}_b)\, \nabla_a F^b && \nabla_a \boldsymbol{e}_b = 0 \text{ for Cartesian coordinates} && \text{(2.24e)}\\
&= \delta^{ad}\, (\boldsymbol{e}_d \times \boldsymbol{e}_b)\, \nabla_a F^b && \delta^{ad}\, \boldsymbol{e}_d = \boldsymbol{e}^a = 0 && \text{(2.24f)}\\
&= (\epsilon_{dbg}\, \nabla^d\, F^b)\, \boldsymbol{e}^g && \delta^{ad}\, \nabla_a = \nabla^d. && \text{(2.24g)}
\end{aligned}
$$

To reach this result we set $\nabla_a \boldsymbol{e}_b = 0$ since the Cartesian basis vectors are spatially constant.[2] We also made use of the relation (1.45) for the cross product of basis vectors. Expanding the final expression, using the Cartesian identity $\nabla^d = \nabla_d = \partial_d$, leads to

$$
\operatorname{curl}(\boldsymbol{F}) = \nabla \times \boldsymbol{F} = \left[\frac{\partial F^3}{\partial x^2} - \frac{\partial F^2}{\partial x^3}\right] \boldsymbol{e}^1 + \left[\frac{\partial F^1}{\partial x^3} - \frac{\partial F^3}{\partial x^1}\right] \boldsymbol{e}^2 + \left[\frac{\partial F^2}{\partial x^1} - \frac{\partial F^1}{\partial x^2}\right] \boldsymbol{e}^3, \tag{2.25}
$$

which can also be written as a determinant

$$
\nabla \times \boldsymbol{F} = \det \begin{bmatrix} \boldsymbol{e}^1 & \boldsymbol{e}^2 & \boldsymbol{e}^3 \\ \partial_1 & \partial_2 & \partial_3 \\ F^1 & F^2 & F^3 \end{bmatrix}. \tag{2.26}
$$

The horizontal vector field $\mathbf{F} = x\,\hat{\boldsymbol{x}} + y\,\hat{\boldsymbol{y}}$ shown in Figure 2.3 has zero curl yet non-zero divergence. Figure 2.4 shows another vector field, $\mathbf{F} = -y\,\hat{\boldsymbol{x}} + x\,\hat{\boldsymbol{y}}$, with zero divergence yet nonzero curl

[2] Basis vectors corresponding to non-Cartesian coordinates are spatially dependent (see Chapters 3 and 4). However, they do have a zero covariant gradient, so that the manipulations here quite closely resemble those for general tensors.

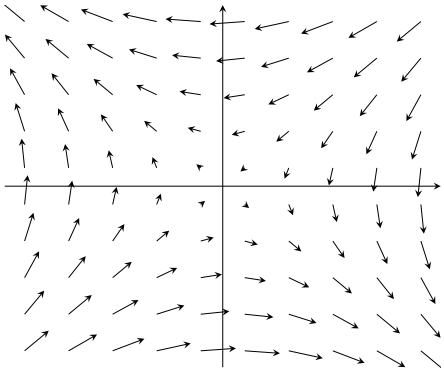

FIGURE 2.5: A horizontal vector field with a zero curl, where $\mathbf{F} = -\nabla\psi$ with the scalar potential given by $\psi = \sin(x/10)\,\sin(y/10)$.

$\nabla \times \mathbf{F} = 2\,\hat{\boldsymbol{z}}$. We encounter this vector again in Section 37.6, where we see that it corresponds to the velocity of fluid undergoing a rigid-body motion in a rotating reference frame, and with its curl measuring the vorticity induced by the rotation.

2.3.2 Curl-free vector fields

There are some cases of physically relevant vector fields that have a vanishing curl

$$\nabla \times \boldsymbol{F} = 0. \tag{2.27}$$

We sometimes refer to such curl-free vectors as *irrotational*. In fluid mechanics a curl-free velocity field has zero vorticity, which is a property maintained by linear gravity waves in the absence of rotation (Section 55.5). We illustrate a curl-free vector field in Figure 2.5.

The curl of a gradient vanishes, which follows from

$$\nabla \times \nabla\psi = \boldsymbol{e}^a\,\nabla_a \times \boldsymbol{e}^b\,\nabla_b\psi = (\boldsymbol{e}^a \times \boldsymbol{e}^b)\,\nabla_a\nabla_b\psi = 0, \tag{2.28}$$

where the final equality follows since $\boldsymbol{e}^a \times \boldsymbol{e}^b$ is anti-symmetric on the labels ab

$$\boldsymbol{e}^a \times \boldsymbol{e}^b = -\boldsymbol{e}^b \times \boldsymbol{e}^a, \tag{2.29}$$

whereas $\nabla_a\nabla_b$ is symmetric on these labels

$$\nabla_a\nabla_b = \nabla_b\nabla_a. \tag{2.30}$$

This property allows us to introduce a scalar field whose gradient equals to the curl-free vector field

$$\mathbf{F} = -\nabla\psi \qquad \text{scalar potential.} \tag{2.31}$$

The scalar ψ is known as the *scalar potential*. We may be familiar with the scalar potential for the gravitational force, in which ψ is called the gravitational potential (see Section 13.10 and Chapter 34).

2.3.3 Vector fields that are both curl-free and divergence-free

Consider a vector field that has zero curl *and* zero divergence. The curl-free property means that

$$\nabla \times \mathbf{F} = 0 \Longrightarrow \mathbf{F} = -\nabla\psi. \tag{2.32}$$

The divergence-free property means that ψ is a harmonic function (Section 2.2.2)

$$\nabla \cdot \nabla\psi = \nabla^2\psi = 0. \tag{2.33}$$

The velocity field arising from a linear non-rotating gravity wave (Section 55.5) in a Boussinesq fluid (Section 29.1) maintains zero vorticity and zero divergence. Furthermore, curl-free and divergence-free velocity fields are commonly encountered in engineering applications such as aerodynamics (e.g., see *Acheson* (1990) for many elementary examples).

2.3.4 Practice deriving identities involving the curl

We close this section by deriving a suite of identities involving the curl operator. These identities arise in various places within this book, particulely when developing dynamical equations for vorticity. Furthermore, by making use of the rules for general tensor analysis developed in Chapters 3 and 4, these identities take on the same form regardless the coordinate choice. The derivations are presented in detail to facilitate understanding of the various steps involving index gymnastics. After some practice, many of the steps can be readily skipped.

Vanishing divergence of the curl

Making use of equation (2.24g) for the curl leads to its zero divergence

$$\begin{aligned}
\nabla \cdot (\nabla \times \mathbf{F}) &= \boldsymbol{e}^a \nabla_a \cdot [\epsilon_{dbg} \nabla^d F^b) \boldsymbol{e}^g] && \text{equation (2.24g)} && (2.34a)\\
&= \boldsymbol{e}^a \cdot \boldsymbol{e}^g \epsilon_{dbg} \nabla_a \nabla^d F^b && \nabla_a \cdot (\epsilon_{dbg} \boldsymbol{e}^g) = 0 && (2.34b)\\
&= \delta^{ag} \epsilon_{dbg} \nabla_a \nabla^d F^b && \text{orthonormality, } \boldsymbol{e}^a \cdot \boldsymbol{e}^g = \delta^{ag} && (2.34c)\\
&= (\epsilon_{dbg} \nabla^g \nabla^d) F^b && \delta^{ag} \nabla_a = \nabla^g && (2.34d)\\
&= 0 && \epsilon_{dbg} \nabla^g \nabla^d = 0. && (2.34e)
\end{aligned}$$

The final equality holds since $\nabla^g \nabla^d$ is symmetric on the indices, gd, whereas ϵ_{dbg} is anti-symmetric on these same two indices.

Divergence of the cross product of two gradients vanishes

In a similar manner we find that the divergence acting on the cross product of two gradients vanishes:

$$\begin{aligned}
\nabla \cdot (\nabla\phi \times \nabla\psi) &= \boldsymbol{e}^a \nabla_a \cdot (\boldsymbol{e}^b \nabla_b\phi \times \boldsymbol{e}^c \nabla_c\psi) && \text{introduce basis one-forms and indices} && (2.35a)\\
&= \boldsymbol{e}^a \cdot (\boldsymbol{e}^b \times \boldsymbol{e}^c) \nabla_a (\nabla_b\phi \, \nabla_c\psi) && \nabla_a \boldsymbol{e}^b = 0 && (2.35b)\\
&= \epsilon^{abc} \nabla_a (\nabla_b\phi \, \nabla_c\psi) && \boldsymbol{e}^a \cdot (\boldsymbol{e}^b \times \boldsymbol{e}^c) = \boldsymbol{e}^a \cdot \epsilon^{bcd} \boldsymbol{e}_d = \epsilon^{bca} = \epsilon^{abc} && (2.35c)\\
&= 0, && && (2.35d)
\end{aligned}$$

where the result vanishes since $\nabla_a\nabla_b\phi$ and $\nabla_a\nabla_c\psi$ are both symmetric on their indices, whereas ϵ^{abc} is anti-symmetric on these indices. This derivation can be streamlined by dropping the basis vectors and basis one-forms:

$$\nabla \cdot (\nabla\phi \times \nabla\psi) = \nabla_a(\epsilon^{abc} \nabla_b\phi \, \nabla_c\psi) = \epsilon^{abc} (\nabla_{ab}\phi \, \nabla_c\psi + \nabla_b\phi \, \nabla_{ac}\psi) = 0. \tag{2.36}$$

Divergence of a cross product

The divergence of a cross product is determined through the following manipulations:

$$\begin{aligned}
\nabla \cdot (\mathbf{F} \times \mathbf{E}) &= \boldsymbol{e}^a \nabla_a \cdot (F^b \boldsymbol{e}_b \times E^c \boldsymbol{e}_c) && \text{expose indices and basis vectors} && (2.37a)\\
&= \boldsymbol{e}^a \cdot (\boldsymbol{e}_b \times \boldsymbol{e}_c) \nabla_a (F^b E^c) && \nabla_a \boldsymbol{e}_b = 0 && (2.37b)\\
&= \boldsymbol{e}^a \cdot (\epsilon_{bcd} \boldsymbol{e}^d) \nabla_a (F^b E^c) && \text{cross product equation (1.45)} && (2.37c)\\
&= \delta^{ad} \epsilon_{bcd} \nabla_a (F^b E^c) && \text{orthonormality, } \delta^{ad} = \boldsymbol{e}^a \cdot \boldsymbol{e}^d && (2.37d)\\
&= \epsilon_{bcd} \nabla^d (F^b E^c) && \text{raise index: } \delta^{ad} \nabla_a = \nabla^d && (2.37e)\\
&= \epsilon_{bcd} (F^b \nabla^d E^c + E^c \nabla^d F^b) && \text{product rule} && (2.37f)\\
&= -\mathbf{F} \cdot (\nabla \times \mathbf{E}) + \mathbf{E} \cdot (\nabla \times \mathbf{F}) && \text{equation (2.24g) for curl.} && (2.37g)
\end{aligned}$$

Curl of a scalar times a vector

The curl of a scalar times a vector, $\psi \mathbf{F}$, is determined by

$$\begin{aligned}
\nabla \times (\psi \mathbf{F}) &= \epsilon_{dbg} \nabla^d (\psi F^b) \boldsymbol{e}^g && \text{equation (2.24g) for curl} && (2.38a)\\
&= \boldsymbol{e}^g \epsilon_{dbg} [(\nabla^d \psi) F^b + \psi \nabla^d F^b] && \text{zero derivative for basis one-forms and } \epsilon && (2.38b)\\
&= \psi \nabla \times \mathbf{F} + \nabla \psi \times \mathbf{F} && \text{reintroduce boldface notation.} && (2.38c)
\end{aligned}$$

Curl of a cross product

The curl of a cross product of two vectors is given by

$$\begin{aligned}
\nabla \times (\mathbf{F} \times \mathbf{E}) &= \boldsymbol{e}^a \nabla_a \times (\boldsymbol{e}_b F^b \times \boldsymbol{e}_c E^c) && (2.39a)\\
&= \boldsymbol{e}^a \times (\boldsymbol{e}_b \times \boldsymbol{e}_c) \nabla_a (F^b E^c) && (2.39b)\\
&= \boldsymbol{e}^a \times (\epsilon_{bcd} \boldsymbol{e}^d) \nabla_a (F^b E^c) && (2.39c)\\
&= \epsilon^{ade} \epsilon_{bcd} \boldsymbol{e}_e \nabla_a (F^b E^c) && (2.39d)\\
&= -\epsilon^{aed} \epsilon_{bcd} \boldsymbol{e}_e \nabla_a (F^b E^c) && (2.39e)\\
&= -(\delta^a{}_b \delta^e{}_c - \delta^a{}_c \delta^e{}_b) \boldsymbol{e}_e \nabla_a (F^b E^c) && (2.39f)\\
&= (-\delta^a{}_b \boldsymbol{e}_c + \delta^a{}_c \boldsymbol{e}_b) \nabla_a (F^b E^c) && (2.39g)\\
&= \mathbf{F} (\nabla \cdot \mathbf{E}) + (\mathbf{E} \cdot \nabla) \mathbf{F} - \mathbf{E} (\nabla \cdot \mathbf{F}) - (\mathbf{F} \cdot \nabla) \mathbf{E}, && (2.39h)
\end{aligned}$$

where we made use of the identity (1.69) for the contraction of two Levi-Civita tensors.

Curl of a curl

The curl of a curl is given by

$$\nabla \times (\nabla \times \mathbf{F}) = \boldsymbol{e}^a \times (\boldsymbol{e}^b \times \boldsymbol{e}_c) \nabla_a \nabla_b F^c. \tag{2.40}$$

The double cross product is computed by

$$\begin{aligned}
\boldsymbol{e}^a \times (\boldsymbol{e}^b \times \boldsymbol{e}_c) &= \delta_{cd} \boldsymbol{e}^a \times (\boldsymbol{e}^b \times \boldsymbol{e}^d) && (2.41a)\\
&= \delta_{cd} \epsilon^{bde} \boldsymbol{e}^a \times \boldsymbol{e}_e && (2.41b)\\
&= \delta_{cd} \delta^{af} \epsilon^{bde} \epsilon_{feg} \boldsymbol{e}^g && (2.41c)\\
&= \delta_{cd} \delta^{af} (-\delta^b{}_f \delta^d{}_g + \delta^b{}_g \delta^d{}_f) \boldsymbol{e}^g && (2.41d)
\end{aligned}$$

$$= -\delta^{ab}\,\boldsymbol{e}_c + \delta^a{}_c\,\boldsymbol{e}^b, \tag{2.41e}$$

where we made use of the identity (1.69) for the contraction of two Levi-Civita tensors. We are then left with

$$\begin{aligned}\nabla\times(\nabla\times\mathbf{F}) &= (-\delta^{ab}\,\boldsymbol{e}_c + \delta^a{}_c\,\boldsymbol{e}^b)\,\nabla_a\nabla_b\,F^c && (2.42a)\\ &= -\nabla^b\,\nabla_b(\boldsymbol{e}_c\,F^c) + \nabla_c\,(\boldsymbol{e}^b\,\nabla_b F^c) && (2.42b)\\ &= -\nabla^2\mathbf{F} + \nabla(\nabla\cdot\mathbf{F}). && (2.42c)\end{aligned}$$

This identity is particularly useful for non-divergent vector fields, in which

$$\nabla\times(\nabla\times\mathbf{F}) = -\nabla^2\mathbf{F} \quad \text{if } \nabla\cdot\mathbf{F} = 0. \tag{2.43}$$

Relating advection, curl, and kinetic energy

We apply some of the previous results to derive a relation required to derive the vorticity equation (Section 40.3.1). In particular, we show that

$$(\mathbf{v}\cdot\nabla)\mathbf{v} = \omega\times\mathbf{v} + \nabla(\mathbf{v}\cdot\mathbf{v})/2, \tag{2.44}$$

where

$$\omega = \nabla\times\mathbf{v} \tag{2.45}$$

is the vorticity, $\mathbf{v}\cdot\mathbf{v}/2$ is the kinetic energy per mass, and $\mathbf{v}$ is the fluid velocity field. Revealing a large number of the steps leads to[3]

$$\begin{aligned}\omega\times\mathbf{v} &= (\nabla\times\boldsymbol{v})\times\boldsymbol{v} && \omega = \nabla\times\mathbf{v} && (2.46a)\\ &= (\boldsymbol{e}^a\,\nabla_a\times\boldsymbol{e}_b\,v^b)\times\boldsymbol{e}_c\,v^c && \text{expand } \mathbf{v} \text{ and } \nabla && (2.46b)\\ &= -\boldsymbol{e}_c\times(\boldsymbol{e}^a\times\boldsymbol{e}_b)\,(\nabla_a v^b)\,v^c && \text{rearrange} && (2.46c)\\ &= (-\delta_{cb}\,\boldsymbol{e}^a + \delta^a{}_c\,\boldsymbol{e}_b)\,(\nabla_a v^b)\,v^c && \text{identity (2.41e)} && (2.46d)\\ &= -v_b\,\nabla v^b + v^c\,\nabla_c\,(\boldsymbol{e}_b\,v^b) && \text{contract some indices} && (2.46e)\\ &= (\boldsymbol{v}\cdot\nabla)\,\boldsymbol{v} - \nabla(\boldsymbol{v}\cdot\boldsymbol{v}/2) && \text{contract remaining indices and rearrange.} && (2.46f)\end{aligned}$$

2.4 Path integral of a scalar function

Consider the integral of a scalar function, ψ, over an arbitrary one-dimensional path in space, $\mathcal{C}$

$$\mathcal{J} = \int_A^B \psi(\alpha)\,\mathrm{d}\alpha. \tag{2.47}$$

Since any path is a one-dimensional curve, a point along the path can be specified by a single parameter, denoted here by α with endpoints $\alpha = A$ and $\alpha = B$.[4] We now consider some explicit examples of how to parameterize a curve to thus enable an explicit evaluation of the integral.[5]

[3] See Section 4.4.4 of *Griffies* (2004) for an alternative derivation.

[4] We have more to say about the geometry of paths in Sections 5.1 and 5.2.

[5] In the more general language of differential forms, the evaluation of a path integral requires one to parameterize points along the path so to then write the path integral as a Riemann integral. This process is known as *pulling back* the path integral to a Riemann integral. *Shifrin* (2004) provies a treatment accessible to those having studied undergraduate calculus.

2.4.1 Cartesian coordinates

Lay down a Cartesian coordinate system with an arbitrary origin, in which case the Cartesian coordinate representation of a point along the path is written

$$\boldsymbol{x}(\alpha) = \hat{\boldsymbol{x}}\, x(\alpha) + \hat{\boldsymbol{y}}\, y(\alpha) + \hat{\boldsymbol{z}}\, z(\alpha), \tag{2.48}$$

along with the endpoints along the path

$$\boldsymbol{x}(A) = \boldsymbol{x}_A \quad \text{and} \quad \boldsymbol{x}(B) = \boldsymbol{x}_B. \tag{2.49}$$

In this way the path integral is written

$$\mathcal{J} = \int_A^B \psi(\alpha)\, \mathrm{d}\alpha = \int_A^B \psi[\boldsymbol{x}(\alpha)]\, \mathrm{d}\alpha. \tag{2.50}$$

To bring the integral (2.50) fully into a Cartesian parameterized form requires a coordinate transformation from α to $\boldsymbol{x}$ along the curve. For this purpose, consider two points on the path that are separated by an infinitesimal parameter difference, in which the difference in their Cartesian coordinates is given by

$$\mathrm{d}\boldsymbol{x} = \boldsymbol{x}(\alpha + \mathrm{d}\alpha) - \boldsymbol{x}(\alpha) = \frac{\mathrm{d}\boldsymbol{x}}{\mathrm{d}\alpha}\, \mathrm{d}\alpha. \tag{2.51}$$

We thus have

$$(\mathrm{d}\alpha)^2 = \frac{\mathrm{d}\boldsymbol{x} \cdot \mathrm{d}\boldsymbol{x}}{\mathrm{d}\boldsymbol{x}/\mathrm{d}\alpha \cdot \mathrm{d}\boldsymbol{x}/\mathrm{d}\alpha}. \tag{2.52}$$

Assuming $\mathrm{d}\alpha > 0$ then leads to the integral (2.50) taking on the rather clumsy, but nonetheless general, form

$$\mathcal{J} = \int_A^B \psi(\alpha)\, \mathrm{d}\alpha = \int_A^B \psi[\boldsymbol{x}(\alpha)]\, \mathrm{d}\alpha = \int_A^B \psi[\boldsymbol{x}(\alpha)] \sqrt{\frac{\mathrm{d}\boldsymbol{x} \cdot \mathrm{d}\boldsymbol{x}}{\mathrm{d}\boldsymbol{x}/\mathrm{d}\alpha \cdot \mathrm{d}\boldsymbol{x}/\mathrm{d}\alpha}}. \tag{2.53}$$

2.4.2 Arc length parameterization

Now consider a common special case for path parameterization where $\alpha = s$ is the arc length along the path[6]

$$\mathcal{J} = \int_A^B \psi(\alpha)\, \mathrm{d}\alpha = \int_{s_A}^{s_B} \psi[\boldsymbol{x}(s)]\, \mathrm{d}s. \tag{2.54}$$

For Euclidean space using Cartesian coordinates, the differential increment of arc length is given by

$$\mathrm{d}s = \sqrt{\mathrm{d}\boldsymbol{x} \cdot \mathrm{d}\boldsymbol{x}}. \tag{2.55}$$

Inserting $\boldsymbol{x}(s)$ into this expression renders

$$\mathrm{d}s = \sqrt{\mathrm{d}\boldsymbol{x} \cdot \mathrm{d}\boldsymbol{x}} = \mathrm{d}s \sqrt{\frac{\mathrm{d}\boldsymbol{x}}{\mathrm{d}s} \cdot \frac{\mathrm{d}\boldsymbol{x}}{\mathrm{d}s}}. \tag{2.56}$$

This expression is self-consistent if

$$\sqrt{\frac{\mathrm{d}\boldsymbol{x}}{\mathrm{d}s} \cdot \frac{\mathrm{d}\boldsymbol{x}}{\mathrm{d}s}} = 1, \tag{2.57}$$

[6]We offer a more focused discussion of curves and tangents in Section 5.2.1 (see in particular equation (5.9)).

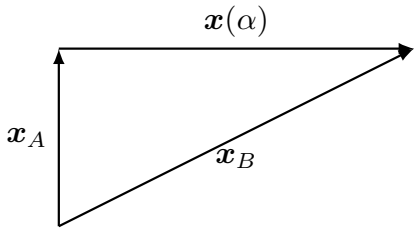

FIGURE 2.6: A linear path, $\boldsymbol{x}(\alpha)$ extending from $\boldsymbol{x}_A$ to $\boldsymbol{x}_B$ can be parameterized by a non-dimensional parameter $\alpha \in [0,1]$ via $\boldsymbol{x}(\alpha) = \boldsymbol{x}_A + (\boldsymbol{x}_B - \boldsymbol{x}_A)\,\alpha$. Alternatively, it can be parameterized by the arc-length along the path via $\boldsymbol{x}(s) = \boldsymbol{x}_A + \hat{\boldsymbol{s}}\,s$ with $s \in [0, L]$, $L = |\boldsymbol{x}_B - \boldsymbol{x}_A|$, and $\hat{\boldsymbol{s}}$ the unit tangent vector pointing from $\boldsymbol{x}_A$ to $\boldsymbol{x}_B$.

which is merely a rewrite of the defining expression (2.55). Note that the derivative of the curve with respect to the arc-length, $\mathrm{d}\boldsymbol{x}/\mathrm{d}s$, defines a unit tangent vector to the curve

$$\hat{\boldsymbol{s}} = \frac{\mathrm{d}\boldsymbol{x}}{\mathrm{d}s} \Longrightarrow \hat{\boldsymbol{s}} \cdot \hat{\boldsymbol{s}} = 1. \tag{2.58}$$

2.4.3 Linear path example

As a specific example, consider a straight line between two points, $\boldsymbol{x}_A$ and $\boldsymbol{x}_B$, as in Figure 2.6. We can parameterize the line using a dimensionless parameter α according to

$$\boldsymbol{x}(\alpha) = \boldsymbol{x}_A + (\boldsymbol{x}_B - \boldsymbol{x}_A)\,\alpha \qquad \alpha \in [0,1]. \tag{2.59}$$

Alternatively, we can parameterize using the arc length

$$\boldsymbol{x}(s) = \boldsymbol{x}_A + \hat{\boldsymbol{s}}\,s \qquad s \in [0, L], \tag{2.60}$$

where $L = \int_A^B \mathrm{d}s = |\boldsymbol{x}_B - \boldsymbol{x}_A|$ is the total arc length of the line, and where $\hat{\boldsymbol{s}}$ is the unit tangent vector pointing along the path from $\boldsymbol{x}_A$ to $\boldsymbol{x}_B$

$$\hat{\boldsymbol{s}} = \frac{\boldsymbol{x}'(s)}{|\boldsymbol{x}'(s)|} = \frac{\boldsymbol{x}_B - \boldsymbol{x}_A}{|\boldsymbol{x}_B - \boldsymbol{x}_A|}. \tag{2.61}$$

As defined we have $|\boldsymbol{x}'(s)| = |\hat{\boldsymbol{s}}| = 1$, so that the path integral is given by

$$\mathcal{I} = \int_{\mathcal{C}} \psi(\alpha)\,\mathrm{d}\alpha = \int_0^L \psi[\boldsymbol{x}(s)]\,\mathrm{d}s. \tag{2.62}$$

2.5 Path integral of a vector field

Generalizing to a vector field, $\mathbf{F}(\mathbf{x})$, we could conceivably integrate each component of the vector along the curve independently, making use of the approach for scalars functions in Section 2.4. In practice, however, that quantity rarely appears in physics.[7] Instead, we more commonly wish to integrate that component of $\mathbf{F}$ that projects onto a curve

$$\int_{\mathcal{C}} \mathbf{F} \cdot \mathrm{d}\boldsymbol{x} = \int_{\mathcal{C}} \mathbf{F} \cdot \frac{\mathrm{d}\boldsymbol{x}}{\mathrm{d}s}\,\mathrm{d}s = \int_{\mathcal{C}} \mathbf{F} \cdot \hat{\boldsymbol{s}}\,\mathrm{d}s, \tag{2.63}$$

[7] The mathematical reason it does not appear is that for a general manifold, the addition of vectors is only defined locally within a tangent space. This limitation prevents us from integrating general tensors over a volume.

where $\hat{\boldsymbol{s}} = \mathrm{d}\boldsymbol{x}/\mathrm{d}s$ is tangent to the curve given by equation (2.58). A common example for the path integral of a vector concerns the work performed by a force field applied to a physical system that is moving along a path (this example is studied in Section 11.1.4).

2.5.1 Circulation

For the case of a closed curve or a circuit (see Section 5.1), we refer to the path integral as the *circulation* and use the convention of putting an arrowed circle on the integral sign

$$\text{circulation of vector field} = \oint_{\mathcal{C}} \mathbf{F} \cdot \mathrm{d}\boldsymbol{x}. \tag{2.64}$$

The arrow indicates that we conventionally traverse the closed path in a counter-clockwise (right hand) manner when looking down on the path from above. Note that by choosing a viewpoint as "above", we necessarily allow for an unambiguous definition of "counter-clockwise", thus chosing an *orientation*.

2.5.2 Circulation example

Consider the vector field, $\mathbf{F}$, expressed using Cartesian coordinates by the following vector function

$$\boldsymbol{F}(\boldsymbol{x}) = -y\,\hat{\boldsymbol{x}} + x\,\hat{\boldsymbol{y}}, \tag{2.65}$$

as shown in Figure 2.4. What is the circulation computed around a circle of radius r whose center is the origin? To compute this circulation we make use of plane polar coordinates, in which $x = r\,\cos\alpha$ and $y = r\,\sin\alpha$, with $\alpha \in [0, 2\pi]$ the polar angle measured from the positive x-axis. The position of a point on the circle is thus written $\boldsymbol{x}(\alpha) = r\,(\hat{\boldsymbol{x}}\,\cos\alpha + \hat{\boldsymbol{y}}\,\sin\alpha)$, and the tangent to the circle is $\mathrm{d}\boldsymbol{x}(\alpha)/\mathrm{d}\alpha = r\,(-\hat{\boldsymbol{x}}\,\sin\alpha + \hat{\boldsymbol{y}}\,\cos\alpha)$. The integrand to the circulation (2.63) is given by

$$\boldsymbol{F} \cdot \frac{\mathrm{d}\boldsymbol{x}(\alpha)}{\mathrm{d}\alpha} = r\,(y\,\sin\alpha + x\cos\alpha) = r^2. \tag{2.66}$$

Hence, the circulation around the constant radius circle is twice the area of the circle

$$\oint_{\mathcal{C}} \boldsymbol{F} \cdot \mathrm{d}\boldsymbol{x} = 2\,\pi\,r^2. \tag{2.67}$$

We apply this result in Section 40.6.2 to geophysical fluids when computing the vorticity induced by the rotating planet.

2.5.3 Fundamental theorem of calculus

The special case of $\mathbf{F} = -\nabla\psi$ for a scalar field ψ recovers the fundamental theorem of calculus

$$\psi(\boldsymbol{x}_B) - \psi(\boldsymbol{x}_A) = \int_{\boldsymbol{x}_A}^{\boldsymbol{x}_B} \mathrm{d}\psi = \int_{\boldsymbol{x}_A}^{\boldsymbol{x}_B} \nabla\psi \cdot \mathrm{d}\boldsymbol{x}. \tag{2.68}$$

It follows that for any closed curve with $\boldsymbol{x}_A = \boldsymbol{x}_B$, the circulation of $\nabla\psi$ vanishes

$$\oint_{\mathcal{C}} \mathrm{d}\psi = \oint_{\mathcal{C}} \nabla\psi \cdot \mathrm{d}\boldsymbol{x} = 0. \tag{2.69}$$

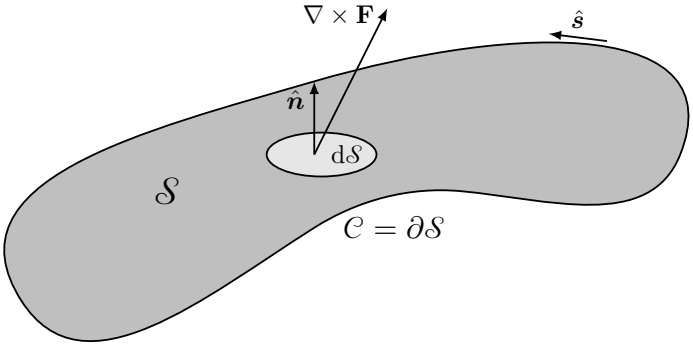

FIGURE 2.7: Illustrating the geometry of Stokes' theorem (2.70). The unit outward normal, $\hat{\boldsymbol{n}}$, points outward from the surface, $\mathcal{S}$, thus defining the positive or up direction. The integrand $(\nabla \times \boldsymbol{F}) \cdot \hat{\boldsymbol{n}}$ is the projection of the curl of a vector field onto the surface outward normal. The boundary of the area, $\mathcal{C} = \partial\mathcal{S}$, is traversed counterclockwise following the unit tangent vector, $\hat{\boldsymbol{s}}$, when computing the circulation. Counter-clockwise is oriented relative to the positive side of the surface as defined by the outward normal.

2.6 Stokes' curl theorem

Stokes' curl theorem relates the integral of a vector field, projected onto the tangent of a boundary around an orientable surface, to the integral of the unit normal projected onto the curl of the vector over the area of the surface.[8] The geometry of Stokes' theorem is illustrated in Figure 2.7. This theorem is used extensively in our study of circulation and vorticity in Part VII of this book.

2.6.1 Statement of Stokes' theorem

For an oriented[9] two-dimensional surface, $\mathcal{S}$, with a closed boundary, $\partial\mathcal{S}$, Stokes' theorem says that the circulation around the boundary equals to the area integrated curl projected onto the surface outward unit normal

$$\oint_{\partial\mathcal{S}} \mathbf{F} \cdot \mathrm{d}\boldsymbol{x} = \int_{\mathcal{S}} (\nabla \times \mathbf{F}) \cdot \hat{\boldsymbol{n}} \, \mathrm{d}\mathcal{S}. \tag{2.70}$$

In this equation,

$$\mathrm{d}\boldsymbol{x} = \frac{\mathrm{d}\boldsymbol{x}}{\mathrm{d}s} \, \mathrm{d}s = \hat{\boldsymbol{s}} \, \mathrm{d}s \tag{2.71}$$

is the vector line element along the closed path (circuit), $\hat{\boldsymbol{s}}$ is the unit tangent vector along the path, and s is the arc-distance along the path. For the surface integral we have the outward unit normal, $\hat{\boldsymbol{n}}$, and $\mathrm{d}\mathcal{S}$ is the infinitesimal surface area element. The orientation of the outward normal determines, through the right hand rule, the counter-clockwise direction for the path integral.

[8] As noted in a footnote on page 13 of *Truesdell* (1954), Lord Kelvin and later Hankel independently discovered what we here refer to as Stokes' theorem. Stokes' name became attached to the theorem since he included its derivation on an examination for students.

[9] For a surface to be orientable means that we can unambiguously describe its two sides, thus allowing us to determine a positive (top) side and negative (bottom) side. We are here only concerned with surfaces that are orientable, thus precluding non-orientable surfaces such as the Möbius strip.

2.6.2 Stokes' theorem for a rectangular region

To build experience with Stokes' theorem, consider the case of a rectangle in the x-y plane with dimensions L_x and L_y, and make use of Cartesian coordinates. In this case the outward normal is $\hat{\boldsymbol{n}} = \hat{\boldsymbol{z}}$, so that

$$(\nabla \times \boldsymbol{F}) \cdot \hat{\boldsymbol{z}} = \frac{\partial F^2}{\partial x} - \frac{\partial F^1}{\partial y}, \tag{2.72}$$

in which case the right hand side of Stokes' theorem reduces to

$$\int_{\mathcal{S}} (\nabla \times \boldsymbol{F}) \cdot \hat{\boldsymbol{n}} \, \mathrm{d}S = \int_0^{L_x} \int_0^{L_y} \left(\frac{\partial F^2}{\partial x} - \frac{\partial F^1}{\partial y} \right) \mathrm{d}x \, \mathrm{d}y. \tag{2.73}$$

Integration around the rectangle then leads to a direct verification of Stokes' theorem

$$\int_0^{L_x} \int_0^{L_y} \left(\frac{\partial F^2}{\partial x} - \frac{\partial F^1}{\partial y} \right) \mathrm{d}x \, \mathrm{d}y = \int_0^{L_y} F^2(x,y) \Big|_{x=0}^{x=L_x} \mathrm{d}y - \int_0^{L_x} F^1(x,y) \Big|_{y=0}^{y=L_y} \mathrm{d}x \tag{2.74a}$$

$$= \int_0^{L_x} F^1(x,0) \, \mathrm{d}x + \int_0^{L_y} F^2(L_x,y) \, \mathrm{d}y + \int_{L_x}^0 F^1(x,L_y) \, \mathrm{d}x + \int_{L_y}^0 F^2(0,y) \, \mathrm{d}y \tag{2.74b}$$

$$= \oint_{\partial \mathcal{S}} \boldsymbol{F} \cdot \mathrm{d}\boldsymbol{x}. \tag{2.74c}$$

We can generalize this result to verify Stokes' theorem for an arbitrary surface. We do so by breaking the surface into a lattice of tiny rectangles. Integrating around the tiny rectangles and summing their contributions leads to a cancellation of the line integrals over all interior boundaries. The cancellation occurs since an internal edge of a rectangle is integrated once in each direction thus cancelling its contribution. The only nonzero contribution comes from integration over the boundary, $\partial \mathcal{S}$.

2.6.3 Stokes' theorem for a second order tensor

We now prove an expression of Stokes' theorem that holds for second order tensors. For this purpose, write the vector, $\mathbf{F}$, as

$$\mathbf{F} = \mathbf{c} \cdot \mathbf{T}, \tag{2.75}$$

where $\mathbf{c}$ is a spatially constant vector and $\mathbf{T}$ is a second order tensor. We thus have the curl given by

$$\nabla \times \mathbf{F} = \nabla \times (\mathbf{c} \cdot \mathbf{T}) = (\nabla \times \mathbf{T}) \cdot \mathbf{c}, \tag{2.76}$$

so that Stokes' theorem (2.70) takes the form

$$\left[\int_{\mathcal{S}} (\nabla \times \mathbf{T}) \cdot \hat{\boldsymbol{n}} \, \mathrm{d}\mathcal{S} \right] \cdot \mathbf{c} = \left[\oint_{\partial \mathcal{S}} \mathbf{T} \cdot \mathrm{d}\boldsymbol{x} \right] \cdot \mathbf{c}. \tag{2.77}$$

Since $\mathbf{c}$ is an arbitrary constant vector, this equality holds in general

$$\int_{\mathcal{S}} (\nabla \times \mathbf{T}) \cdot \hat{\boldsymbol{n}} \, \mathrm{d}\mathcal{S} = \oint_{\partial \mathcal{S}} \mathbf{T} \cdot \mathrm{d}\boldsymbol{x}. \tag{2.78}$$

In Section 2.7 we make use of a similar trick with constant vectors to derive corollaries to the divergence theorem.

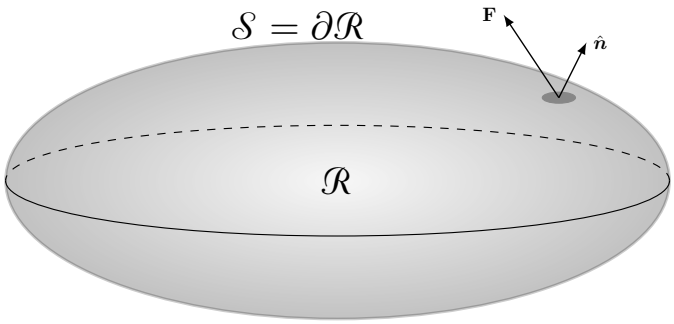

FIGURE 2.8: Illustrating the geometry of Gauss's divergence theorem for an ellipsoidal volume, $\mathcal{R}$, with closed boundary surface, $\mathcal{S} = \partial\mathcal{R}$. The outward unit normal along the boundary, $\hat{\boldsymbol{n}}$, is projected onto the vector field, $\mathbf{F}$, via the scalar product, $\mathbf{F} \cdot \hat{\boldsymbol{n}}$. Gauss's divergence theorem says that integrating $\mathbf{F} \cdot \hat{\boldsymbol{n}}$ over the closed boundary surface, $\mathcal{S}$, yields the same answer as computing the volume integral of the divergence, $\nabla \cdot \mathbf{F}$, over the closed region, $\mathcal{R}$, bounded by the closed surface $\mathcal{S}$.

2.7 Gauss's divergence theorem

For a continuously differentiable vector field $\mathbf{F}$, Gauss's divergence theorem states that

$$\int_{\mathcal{R}} \nabla \cdot \mathbf{F} \, \mathrm{d}V = \oint_{\partial\mathcal{R}} \mathbf{F} \cdot \hat{\boldsymbol{n}} \, \mathrm{d}\mathcal{S}, \tag{2.79}$$

where $\hat{\boldsymbol{n}}$ is the outward unit normal to the boundary surface, $\partial\mathcal{R}$, and $\mathrm{d}\mathcal{S}$ is the surface area element on the boundary. In words, the left hand side of Gauss's theorem is the volume integral of the divergence of a continuously differentiable vector field over a connected volume, $\mathcal{R}$. The right hand side is the unit normal projection of the vector field that is area integrated over the closed surface, $\partial\mathcal{R}$, bounding the volume. We follow the convention that $\oint_{\partial\mathcal{R}}$ refers to a surface integral over a closed surface that bounds a volume. This notation contrasts with the surface integral, $\int_{\mathcal{S}}$, that generally does not enclose a volume. Figure 2.8 illustrates the geometry of Gauss's divergence theorem. In physics jargon, we say that the divergence of a vector field, $\nabla \cdot \mathbf{F}$, integrated over a volume equals to the flux of that vector field, $\mathbf{F} \cdot \hat{\boldsymbol{n}}$, integrated over the area bounding the volume.

2.7.1 An example rectangular volume

To build intuition for Gauss's divergence theorem, consider a rectangular volume with dimensions L_x, L_y, and L_z and make use of Cartesian coordinates. The volume integral on the left hand side of equation (2.79) gives

$$\int_{\mathcal{R}} \left[\frac{\partial F^1}{\partial x} + \frac{\partial F^2}{\partial y} + \frac{\partial F^3}{\partial z} \right] \mathrm{d}x \, \mathrm{d}y \, \mathrm{d}z. \tag{2.80}$$

Focusing on just the leftmost term, integration in x gives

$$\int_{\mathcal{R}} \frac{\partial F^1}{\partial x} \, \mathrm{d}x \, \mathrm{d}y \, \mathrm{d}z = \int_{y=0}^{y=L_y} \int_{z=0}^{z=L_z} [F^1(L_x, y, z) - F^1(0, y, z)] \, \mathrm{d}y \, \mathrm{d}z \tag{2.81a}$$

$$= \int_{\mathcal{S}_1 + \mathcal{S}_2} \boldsymbol{F} \cdot \hat{\boldsymbol{n}} \, \mathrm{d}\mathcal{S}, \tag{2.81b}$$

where $\mathcal{S}_1$ is the rectangle's face with outward unit normal $\hat{\boldsymbol{n}} = \hat{\boldsymbol{x}}$ and $\mathcal{S}_2$ is the rectangle's face with unit normal $\hat{\boldsymbol{n}} = -\hat{\boldsymbol{x}}$. Repeating this procedure on the other terms in equation (2.80) gives the area integrated flux through the full boundary. To verify the theorem for a general volume

V, we take the approach used to prove Stokes' theorem. First, divide the volume into many rectangular sub-volumes. Then apply the above result to each sub-volume and sum up the result. The area integrated fluxes through internal rectangular faces cancel exactly. Therefore, the sum of all the area integrated fluxes equals to just the flux integrated over the external boundary, thus yielding the divergence theorem.

2.7.2 Gradient theorem for the volume integral of scalar fields

We consider various corollaries of the divergence theorem, the first of which arises from considering the special case of a vector field $\mathbf{F} = \phi\,\mathbf{c}$ with $\mathbf{c}$ an arbitrary *constant* vector. Substitution into the divergence theorem (2.79) yields

$$\oint_{\partial\mathcal{R}} \phi\,\mathbf{c}\cdot\hat{\boldsymbol{n}}\,\mathrm{d}\mathcal{S} = \int_{\mathcal{R}} \nabla\cdot(\phi\,\mathbf{c})\,\mathrm{d}V. \tag{2.82}$$

Pulling the constant vector out of the integrals and rearrangement leads to

$$\mathbf{c}\cdot\left[\oint_{\partial\mathcal{R}} \phi\,\hat{\boldsymbol{n}}\,\mathrm{d}\mathcal{S} - \int_{\mathcal{R}} \nabla\phi\,\mathrm{d}V\right] = 0. \tag{2.83}$$

Since $\mathbf{c}$ is an arbitrary constant vector, this equality is generally true if and only if

$$\oint_{\partial\mathcal{R}} \phi\,\hat{\boldsymbol{n}}\,\mathrm{d}\mathcal{S} = \int_{\mathcal{R}} \nabla\phi\,\mathrm{d}V. \tag{2.84}$$

In words, this result says that the integral of a scalar field over the boundary of a closed surface, when weighted by the outward unit normal to the surface, equals to the volume integral of the gradient of the scalar field integrated over the region bounded by the closed surface. We make use of this result in Section 24.2.3 when studying how stresses contribute to the motion of a fluid element, with particular application to the case of pressure.

2.7.3 Surface integral of the outward unit normal

A corollary of equation (2.84) can be found by setting the scalar field, ϕ, to a constant so that $\nabla\phi = 0$. We thus find that the area integral of the outward unit normal vanishes when integrated over the surface of a closed volume

$$\oint_{\partial\mathcal{R}} \hat{\boldsymbol{n}}\,\mathrm{d}\mathcal{S} = 0. \tag{2.85}$$

This identity also holds for two-dimensions, so that the outward normal has a zero line integral around a closed curve.

An example of the identity (2.85) can be seen by integrating over a closed rectangular volume, whereby the area integrals cancel component-wise. Another example is the sphere, where $\hat{\boldsymbol{n}} = \hat{\boldsymbol{r}}$ is the radial outward unit vector, so that integration of the radial unit vector over the spherical surface identically vanishes. For some purposes we can take equation (2.85) as the definition of a *simply closed volume* (or simply closed curve for the two dimensional case).

2.7.4 Integral of the curl of a vector field

Another identity follows from Gauss's theorem by setting

$$\mathbf{F} = \mathbf{c}\times\mathbf{v} \tag{2.86}$$

where $\mathbf{c}$ is a constant vector. As a result,

$$\nabla \cdot \mathbf{F} = -\mathbf{c} \cdot (\nabla \times \mathbf{v}), \tag{2.87}$$

which follows from the identity (2.37g). We are thus led to the following identities

$$\int_{\mathcal{R}} \nabla \cdot \mathbf{F} \, \mathrm{d}V = -\mathbf{c} \cdot \int_{\mathcal{R}} \nabla \times \mathbf{v} \, \mathrm{d}V \quad \text{equation (2.87)} \tag{2.88a}$$

$$= \oint_{\partial \mathcal{R}} (\mathbf{c} \times \mathbf{v}) \cdot \hat{\boldsymbol{n}} \, \mathrm{d}\mathcal{S} \quad \text{divergence theorem (2.79)} \tag{2.88b}$$

$$= \boldsymbol{c} \cdot \oint_{\partial \mathcal{R}} (\mathbf{v} \times \hat{\boldsymbol{n}}) \, \mathrm{d}\mathcal{S} \quad \text{since } \boldsymbol{c} \text{ is a constant.} \tag{2.88c}$$

Since these identities hold for arbitrary $\mathbf{c}$, we are led to

$$\int_{\mathcal{R}} (\nabla \times \mathbf{v}) \, \mathrm{d}V = \oint_{\partial \mathcal{R}} (\hat{\boldsymbol{n}} \times \mathbf{v}) \, \mathrm{d}\mathcal{S}. \tag{2.89}$$

2.7.5 First and second form of Green's identities

The further corollary to the divergence theorem arises from considering another special vector field

$$\mathbf{F} = \psi \, \nabla \phi, \tag{2.90}$$

with ψ and ϕ scalar fields. Substitution into the divergence theorem (2.79) leads to

$$\oint_{\partial \mathcal{R}} \psi \frac{\partial \phi}{\partial n} \, \mathrm{d}\mathcal{S} = \int_{\mathcal{R}} [\nabla \psi \cdot \nabla \phi + \psi \, \nabla^2 \phi] \, \mathrm{d}V \qquad \text{Green's first integral identity.} \tag{2.91}$$

We can make this result more symmetric by swapping ψ and ϕ and then subtracting, to render

$$\oint_{\partial \mathcal{R}} \left[\psi \frac{\partial \phi}{\partial n} - \phi \frac{\partial \psi}{\partial n} \right] \mathrm{d}\mathcal{S} = \int_{\mathcal{R}} [\psi \, \nabla^2 \phi - \phi \, \nabla^2 \psi] \, \mathrm{d}V \qquad \text{Green's second integral identity.} \tag{2.92}$$

Setting $\phi = 1$ yields

$$\oint_{\partial \mathcal{R}} \frac{\partial \psi}{\partial n} \, \mathrm{d}\mathcal{S} = \int_{\mathcal{R}} \nabla^2 \psi \, \mathrm{d}V \iff \oint_{\partial \mathcal{R}} \nabla \psi \cdot \hat{\boldsymbol{n}} \, \mathrm{d}\mathcal{S} = \int_{\mathcal{R}} \nabla \cdot \nabla \psi \, \mathrm{d}V. \tag{2.93}$$

We make use of these identities in Chapter 9 when studying the Green's function method for solving linear partial differential equations.

2.7.6 Integral of a curl over a closed surface

Application of Gauss's divergence theorem leads us to conclude that the following integral vanishes

$$\oint_{\partial \mathcal{R}} (\nabla \times \mathbf{F}) \cdot \hat{\boldsymbol{n}} \, \mathrm{d}\mathcal{S} = \int_{\mathcal{R}} \nabla \cdot (\nabla \times \mathbf{F}) \, \mathrm{d}V = 0, \tag{2.94}$$

where the final equality follows since the divergence of a curl vanishes. Hence, the integral of the unit normal projection of the curl of a vector field, as computed over an oriented closed surface, vanishes. We can understand this result geometrically by splitting the closed volume into two regions and then applying Stokes' theorem separately to the two regions (see Figure 2.9)

$$\oint_{\partial \mathcal{R}} (\nabla \times \mathbf{F}) \cdot \hat{\boldsymbol{n}} \, \mathrm{d}\mathcal{S} = \int_{\mathcal{S}_1} (\nabla \times \mathbf{F}) \cdot \hat{\boldsymbol{n}} \, \mathrm{d}\mathcal{S}_1 + \int_{\mathcal{S}_2} (\nabla \times \mathbf{F}) \cdot \hat{\boldsymbol{n}} \, \mathrm{d}\mathcal{S}_2 \tag{2.95a}$$

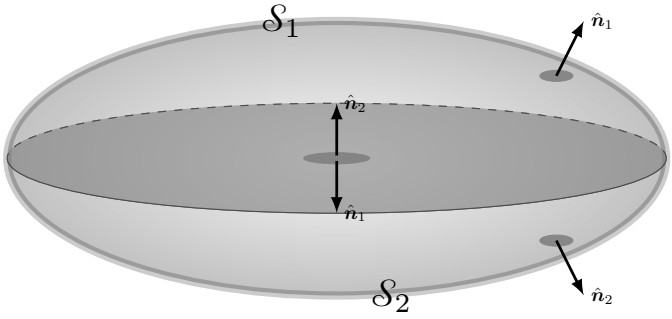

FIGURE 2.9: The integral of the unit normal component of the curl of a function vanishes when integrated over an oriented closed surface, $\partial\mathcal{R}$, which forms the boundary to a closed volume, $\mathcal{R}$. This result follows from both Gauss's divergence theorem as well as Stokes' curl theorem. For Gauss's theorem we find $\oint_{\partial\mathcal{R}}(\nabla\times\mathbf{F})\cdot\hat{\boldsymbol{n}}\,\mathrm{d}\mathcal{S} = \int_{\mathcal{R}}\nabla\cdot(\nabla\times\mathbf{F})\,\mathrm{d}V = 0$, which follows since the divergence of the curl vanishes. For Stokes' theorem we split the closed volume into two so that its boundary surface has also been split into two, $\partial\mathcal{R} = \mathcal{S}_1 + \mathcal{S}_2$. Separately applying Stokes' theorem to $\mathcal{S}_1$ and $\mathcal{S}_2$ leads to the calculation of the circulation around the common boundary along the equatorial plane. Since orientation of the outward unit normal along the equatorial plane is opposite for the two regions, the two circulations exactly cancel since they are computed in opposite directions.

$$= \oint_{\partial\mathcal{S}_1}\mathbf{F}\cdot\mathrm{d}\boldsymbol{x} - \oint_{\partial\mathcal{S}_2}\mathbf{F}\cdot\mathrm{d}\boldsymbol{x} \tag{2.95b}$$

$$= 0. \tag{2.95c}$$

The minus sign appearing in front of $\oint_{\partial\mathcal{S}_2}$ occurs since the orientation of the circulation integral is opposite that for $\oint_{\partial\mathcal{S}_1}$. We are thus left with a cancellation of the circulations. When applied to the vorticity of fluid flow (Chapter 37), we see that

$$\oint_{\partial\mathcal{R}}\omega\cdot\hat{\boldsymbol{n}}\,\mathrm{d}\mathcal{S} = \int_{\mathcal{R}}\nabla\cdot\omega\,\mathrm{d}V = 0, \tag{2.96}$$

where $\omega = \nabla\times\mathbf{v}$ is the vorticity and $\boldsymbol{v}$ is the fluid velocity.

2.7.7 The domain integral of a non-divergent Cartesian vector field

Consider a vector field that has zero divergence everywhere within a domain, $\mathcal{R}$. Consequently, $\int_{\mathcal{R}}\nabla\cdot\mathbf{F}\,\mathrm{d}V = \oint_{\partial\mathcal{R}}\mathbf{F}\cdot\hat{\boldsymbol{n}}\,\mathrm{d}\mathcal{S} = 0$. Now what can we say about $\int_{\mathcal{R}}\mathbf{F}\,\mathrm{d}V$? One might be tempted to say that it vanishes. But that is generally an incorrect statement as we now show.[10]

Making use of Cartesian coordinates, and the non-divergence property, know that

$$0 = \int_{\mathcal{R}} x^a\,\nabla\cdot\boldsymbol{F}\,\mathrm{d}V = \int_{\mathcal{R}}[\nabla\cdot(x^a\,\boldsymbol{F}) - F^a]\,\mathrm{d}V, \tag{2.97}$$

where we used $\partial_b x^a = \delta^a{}_b$. Use of the divergence theorem leads to

$$\int_{\mathcal{R}} F^a\,\mathrm{d}V = \int_{\mathcal{R}}\nabla\cdot(x^a\,\boldsymbol{F})\,\mathrm{d}V = \oint_{\partial\mathcal{R}} x^a\,(\hat{\boldsymbol{n}}\cdot\boldsymbol{F})\,\mathrm{d}\mathcal{S}. \tag{2.98}$$

The right hand side does not generally vanish since $\hat{\boldsymbol{n}}\cdot\boldsymbol{F}$ does not generally vanish at each point along $\partial\mathcal{R}$. Hence, we find that $\int_{\mathcal{R}}\boldsymbol{F}\,\mathrm{d}V = 0$ only for those domains where $\hat{\boldsymbol{n}}\cdot\boldsymbol{F} = 0$ at each point along $\partial\mathcal{R}$.

[10] As a technical note, we observe that the integral of a vector field is only well defined in Euclidean space and using Cartesian coordinates. A general manifold requires extra formalism for the purpose of comparing vectors at two different points.

2.7.8 Gradient tensor theorem for $\nabla \otimes \boldsymbol{F}$

Certain elements from Stokes' theorem in Section 2.6 and the divergence theorem from Section 2.7 can be summarized in the following *gradient tensor theorem* that originates from *Gibbs* (1884) (equation (2), page 65, §161), and has been further discussed by *Lilly et al.* (2024) for applications in fluid mechanics. For this purpose, recall the definition of the *tensor product* from Section 1.6. We are led to the tensor product of the gradient operator and a vector field, here using Cartesian coordinates

$$\nabla \otimes \boldsymbol{F} = \boldsymbol{e}^a \partial_a \otimes \boldsymbol{e}_b \, F^b = (\boldsymbol{e}^a \otimes \boldsymbol{e}_b) \, \partial_a F^b. \tag{2.99}$$

Integrating over a domain leads to

$$\begin{aligned}
\int_{\mathcal{R}} \nabla \otimes \boldsymbol{F} \, \mathrm{d}V &= \int_{\mathcal{R}} \boldsymbol{e}^a \partial_a \otimes \boldsymbol{e}_b \, F^b \, \mathrm{d}V && \text{expose tensor indices} && \text{(2.100a)} \\
&= \int_{\mathcal{R}} \partial_a (\boldsymbol{e}^a \otimes \boldsymbol{e}_b \, F^b) \, \mathrm{d}V && \text{Cartesian basis is constant} && \text{(2.100b)} \\
&= \left[\int_{\mathcal{R}} \partial_a (\boldsymbol{e}^a \, F^b) \, \mathrm{d}V \right] \otimes \boldsymbol{e}_b && \text{Cartesian basis is constant} && \text{(2.100c)} \\
&= \left[\oint_{\partial \mathcal{R}} \hat{n}_a \, \boldsymbol{e}^a \, F^b \, \mathrm{d}\mathcal{S} \right] \otimes \boldsymbol{e}_b && \text{divergence theorem} && \text{(2.100d)} \\
&= \oint_{\partial \mathcal{R}} \hat{n}_a \, \boldsymbol{e}^a \otimes \boldsymbol{e}_b \, F^b \, \mathrm{d}\mathcal{S} && \text{Cartesian basis is constant} && \text{(2.100e)} \\
&= \oint_{\partial \mathcal{R}} \hat{\boldsymbol{n}} \otimes \boldsymbol{F} \, \mathrm{d}\mathcal{S} && \text{boldface notation.} && \text{(2.100f)}
\end{aligned}$$

Use of the divergence theorem in equation (2.100d) is an application of the scalar gradient theorem (2.84) separately to each component of F^b, so that

$$\oint_{\partial \mathcal{R}} F^b \, \hat{\boldsymbol{n}} \, \mathrm{d}\mathcal{S} = \int_{\mathcal{R}} \nabla F^b \, \mathrm{d}V. \tag{2.101}$$

The assumption of Cartesian tensors is seemingly basic to the above derivation of the *gradient tensor theorem*

$$\int_{\mathcal{R}} \nabla \otimes \mathbf{F} \, \mathrm{d}V = \oint_{\partial \mathcal{R}} \hat{\boldsymbol{n}} \otimes \mathbf{F} \, \mathrm{d}\mathcal{S}. \tag{2.102}$$

In fact, when making use of the *covariant derivative* of a vector as defined in Section 4.11, as well as the *metricity condition* from Section 4.13, the derivation also follows for arbitrary coordinates. The only modification is to interpret the derivative operator, ∇, as a covariant derivative operator rather than a partial derivative operator. However, while offering a variety of uses of the gradient tensor theorem for fluids moving on flat surfaces and described by arbitrary coordinates, *Lilly et al.* (2024) also shows that the theorem cannot be generalized to arbitrary curved surfaces.

2.8 Exact and inexact differentials

Thus far in this chapter all differentials have been *exact*. However, the thermodynamics discussed in Part IV makes use of both exact and inexact differentials. We here introduce the mathematics of such differentials. Our focus concerns differentials taken between space points, though we note that in some applications it may be appropriate to consider space-time displacements.

2.8.1 Exact differentials

Consider an arbitrary scalar function of space, $F(\boldsymbol{x})$. A differential increment for that function, computed between two close points $\boldsymbol{x}$ and $\boldsymbol{x} + \mathrm{d}\boldsymbol{x}$, is given by

$$\mathrm{d}F(\boldsymbol{x}) = F(\boldsymbol{x} + \mathrm{d}\boldsymbol{x}) - F(\boldsymbol{x}) \tag{2.103a}$$
$$= \mathrm{d}\boldsymbol{x} \cdot \nabla F, \tag{2.103b}$$

where we dropped higher order terms due to the infinitesimal nature of the increments. It follows that we can determine the finite increment between two points through integration

$$F(\boldsymbol{x}_B) - F(\boldsymbol{x}_A) = \int_{\boldsymbol{x}_A}^{\boldsymbol{x}_B} \mathrm{d}F(\boldsymbol{x}) = \int_{\boldsymbol{x}_A}^{\boldsymbol{x}_B} \mathrm{d}\boldsymbol{x} \cdot \nabla F. \tag{2.104}$$

These results are familiar from elementary calculus, with the increment $\mathrm{d}F$ given by equation (2.103b) termed an *exact* differential. Importantly, the finite increment, $F(\boldsymbol{x}_B) - F(\boldsymbol{x}_A)$, depends only on the endpoint values of F. It does not depend on the path taken to go from $\boldsymbol{x}_A$ to $\boldsymbol{x}_B$. Correspondingly, the integral of an exact differential vanishes when computed around a closed loop

$$\oint \mathrm{d}F = 0. \tag{2.105}$$

2.8.2 Inexact differentials

Consider a differential expression written as

$$\boldsymbol{A} \cdot \mathrm{d}\boldsymbol{x} = A\,\mathrm{d}x + B\,\mathrm{d}y + C\,\mathrm{d}z, \tag{2.106}$$

where $\boldsymbol{A} = A\,\hat{\boldsymbol{x}} + B\,\hat{\boldsymbol{y}} + C\,\hat{\boldsymbol{z}}$ is an arbitrary vector here represented using Cartesian coordinates. If $\nabla \times \boldsymbol{A} = 0$, then $\boldsymbol{A}$ can be written as the gradient of a scalar

$$\nabla \times \boldsymbol{A} = 0 \Longrightarrow \boldsymbol{A} = \nabla F, \tag{2.107}$$

in which case we have an exact differential expression

$$\boldsymbol{A} \cdot \mathrm{d}\boldsymbol{x} = \nabla F \cdot \mathrm{d}\boldsymbol{x} = \mathrm{d}F. \tag{2.108}$$

That is, the differential $\mathrm{d}F = \boldsymbol{A} \cdot \mathrm{d}\boldsymbol{x}$ is exact if

$$\nabla \times \boldsymbol{A} = 0 \Longrightarrow \mathrm{d}F = \boldsymbol{A} \cdot \mathrm{d}\boldsymbol{x} \qquad \text{exact differential.} \tag{2.109}$$

If $\nabla \times \boldsymbol{A} \neq 0$, then $\boldsymbol{A} \cdot \mathrm{d}\boldsymbol{x}$ is termed an *inexact differential*. We make use of the following notation for inexact differentials,

$$đG = \boldsymbol{A} \cdot \mathrm{d}\boldsymbol{x}, \tag{2.110}$$

(note the symbol $đ$ for the inexact differential). Notably, the path integral of an inexact differential depends on the path taken between the endpoints. Correspondingly, the integral of an inexact differential around a closed loop does not generally vanish

$$\oint đG \neq 0. \tag{2.111}$$

2.8.3 Integrating factors

Consider again the inexact differential, $đG = \boldsymbol{A} \cdot \mathrm{d}\boldsymbol{x}$, and assume there exists a scalar function, ϕ, so that the product, $\phi^{-1}\, đG$, is exact. For ϕ to exist it must be such that

$$\nabla \times (\boldsymbol{A}\, \phi^{-1}) = 0. \tag{2.112}$$

Consequently, we can write

$$\boldsymbol{A} = \phi\, \nabla F, \tag{2.113}$$

so that

$$đG = \boldsymbol{A} \cdot \mathrm{d}\boldsymbol{x} = \phi\, \nabla F \cdot \mathrm{d}\boldsymbol{x} = \phi\, \mathrm{d}F. \tag{2.114}$$

The function, ϕ, is known as an *integrating factor*. As seen in our study of thermodynamics in Chapter 22 (see in particular Section 22.2.3), pressure is the integrating factor for mechanical work, temperature is the integrating factor for heating, and the chemical potential is the integrating factor for chemical work.

2.8.4 An example using the velocity field

Consider the scalar product, $\mathbf{v} \cdot \mathrm{d}\mathbf{x}$, where $\mathbf{v}$ is the velocity field for a fluid and $\mathrm{d}\mathbf{x}$ is a differential increment in space directed along a path. Furthermore, introduce the curl of the velocity, which defines the vorticity (Section 37.2) $\omega = \nabla \times \mathbf{v}$. For cases where the vorticity vanishes, $\omega = 0$, then $\mathrm{d}\Psi = \mathbf{v} \cdot \mathrm{d}\mathbf{x}$ is an exact differential. Consequently, Stokes' theorem means that the circulation vanishes for an irrotational velocity field computed around an arbitrary closed loop (Section 37.4)

$$\mathcal{C} \equiv \oint_{\partial S} \mathbf{v} \cdot \mathrm{d}\mathbf{x} = \int_S \boldsymbol{\omega} \cdot \hat{\boldsymbol{n}}\, \mathrm{d}S = 0. \tag{2.115}$$

Another way to see this result is to note that a vanishing curl means that the velocity field can be expressed as the gradient of a scalar, $\mathbf{v} = \nabla\psi$, so that $\mathrm{d}\Psi = \nabla\psi \cdot \mathrm{d}\mathbf{x}$, which is manifestly exact.

2.8.5 Heuristic physics of exact and inexact differential operations

Consider a hiker climbing a mountain. The mechanical work, which is force applied over a distance, is a function of the path taken. Some paths are smooth and well marked, whereas others are rough and poorly marked. Likewise, the frictional heating (of the hiker's feet, for example) depend on details of the path (and the shoes!). So although the start and finish points are fixed, the work exerted and heat generated in going between these points is a function of the path.

In contrast, the change in gravitational potential energy between the start and finish points is a function only of the elevation difference between the start and finish points. It does not depend on the path between the points. So the gravitational potential energy increment between the two points is an exact differential, with the potential energy for each point a function of the elevation at the point.

The First Law of thermodynamics, studied in Part IV, states that the sum of path-dependent processes (work and heat) used in going from one thermodynamic state to another equals to the difference in the internal energy between the two states. That is, the sum of the inexact differentials for heat and work equal to the exact differential for internal energy.

2.9 Exercises

Throughout these exercises we consider a point whose position vector, relative to an arbitrary origin, is represented using Cartesian coordinates according to

$$\boldsymbol{x} = x\,\hat{\boldsymbol{x}} + y\,\hat{\boldsymbol{y}} + z\,\hat{\boldsymbol{z}} \tag{2.116}$$

and whose squared distance from the origin is

$$r^2 = \boldsymbol{x}\cdot\boldsymbol{x} = x^2 + y^2 + z^2. \tag{2.117}$$

EXERCISE 2.1: PRACTICE WITH THE GRADIENT OPERATOR
Prove the following identities:

(a) $\nabla(|\boldsymbol{x}|) = \boldsymbol{x}\,|\boldsymbol{x}|^{-1} \equiv \hat{\boldsymbol{r}}$

(b) $\nabla \ln|\boldsymbol{x}| = \boldsymbol{x}\,|\boldsymbol{x}|^{-2} = \hat{\boldsymbol{r}}\,|\boldsymbol{x}|^{-1}$

(c) $\nabla|\boldsymbol{x}|^{-1} = -\boldsymbol{x}\,|\boldsymbol{x}|^{-3} = -\hat{\boldsymbol{r}}\,|\boldsymbol{x}|^{-2}$.

EXERCISE 2.2: PRACTICE WITH THE LAPLACIAN OPERATOR
Show that the Laplacian of the function

$$\psi = \frac{z\,x^2}{r^2} \tag{2.118}$$

is given by

$$\nabla^2\psi = \frac{2\,z\,(r^2 - 5\,x^2)}{r^4}. \tag{2.119}$$

Perform the proof using both Cartesian coordinates as well as spherical coordinates (see Figure 4.3), making use of the following expressions for Laplacian operator acting on a scalar field

$$\nabla^2\psi(x,y,z) = \frac{\partial^2\psi}{\partial x^2} + \frac{\partial^2\psi}{\partial y^2} + \frac{\partial^2\psi}{\partial z^2} \tag{2.120a}$$

$$\nabla^2\psi(\lambda,\phi,r) = \frac{1}{r^2\,\cos\phi}\left[\frac{1}{\cos\phi}\frac{\partial^2\psi}{\partial\lambda^2} + \frac{\partial}{\partial\phi}\left(\cos\phi\frac{\partial\psi}{\partial\phi}\right) + \cos\phi\,\frac{\partial}{\partial r}\left(r^2\,\frac{\partial\phi}{\partial r}\right)\right]. \tag{2.120b}$$

EXERCISE 2.3: MORE PRACTICE WITH OPERATORS
Prove the following identities with $r \neq 0$:

(a) $\nabla^2 r^{-1} = 0$

(b) $\nabla\cdot(\boldsymbol{x}/r^3) = 0$

(c) $\nabla\cdot(\boldsymbol{A}\times\boldsymbol{x}) = \boldsymbol{x}\cdot(\nabla\times\boldsymbol{A})$ for an arbitrary vector field $A(\boldsymbol{x})$.

(d) $\nabla\times[\boldsymbol{x}\,f(r)] = 0$ for an arbitrary function $f(r) = f(|\boldsymbol{x}|)$.

EXERCISE 2.4: RIGID-BODY ROTATION
Define a velocity field according to

$$\boldsymbol{v} = \boldsymbol{\Omega}\times\boldsymbol{x} \tag{2.121}$$

with $\boldsymbol{\Omega}$ a spatially constant angular rotation velocity (e.g., rotation of the earth). This velocity field describes rigid-body rotation as discussed in Section 37.6. Show that $2\,\boldsymbol{\Omega} = \nabla\times\boldsymbol{v}$. See also Exercise 37.2.

EXERCISE 2.5: DIVERGENCE-FREE AND IRROTATIONAL VECTOR
Let Φ be a harmonic function so that $\nabla^2\Phi = 0$. Show that $\boldsymbol{v} = -\nabla\Phi$ satisfies

(a) $\nabla \cdot \boldsymbol{v} = 0$

(b) $\nabla \times \boldsymbol{v} = 0$.

In this way we prove that all harmonic scalar fields correspond to a divergence-free and curl-free vector field.

EXERCISE 2.6: CONSERVATIVE VECTOR FIELD AND SCALAR POTENTIAL
Show that the curl, $\nabla \times \boldsymbol{F}$, of the following vector field vanishes

$$\boldsymbol{F} = 2\,x\,z\,\hat{\boldsymbol{x}} + 2\,y\,z^2\,\hat{\boldsymbol{y}} + (x^2 + 2\,y^2\,z - 1)\,\hat{\boldsymbol{z}}. \tag{2.122}$$

Hence, deduce that $\boldsymbol{F}$ is a *conservative vector field*, meaning that it can be written as the gradient of a scalar potential ψ according to $\boldsymbol{F} = -\nabla\psi$, where (to within an arbitrary constant)

$$\psi = -[x^2\,z + (y\,z)^2 - z]. \tag{2.123}$$

EXERCISE 2.7: PRODUCT RULE IDENTITIES
Prove the following identities with $\boldsymbol{F}$ a Cartesian vector in $\mathbb{R}^3$:

(a) $\boldsymbol{F} = \partial_n\,(F^n\,\boldsymbol{x}) - \boldsymbol{x}\,\nabla \cdot \boldsymbol{F}$

(b) $2\,F^m = [\boldsymbol{x} \times (\nabla \times \boldsymbol{F})]^m - \partial_m(\boldsymbol{x} \cdot \boldsymbol{F}) + \nabla \cdot (\boldsymbol{x}\,F^m)$.

Make use of Cartesian tensors and show all relevant steps, including use of the Levi-Civita tensor from Section 1.7.1 for the cross-product.

As discussed in Section 12.4.1 of *Bühler* (2014a), these product rule identities have use for the study of impulses imparted by a body force per volume, $\boldsymbol{F}$, to a fluid on an unbounded domain where the force has compact support (i.e., the force vanishes outside a finite domain). In that case the above product rule identities allow us to make use of the corresponding integral identities

$$\int \boldsymbol{F}\,\mathrm{d}V = -\int \boldsymbol{x}\,\nabla \cdot \boldsymbol{F}\,\mathrm{d}V = \frac{1}{2}\int \boldsymbol{x} \times (\nabla \times \boldsymbol{F})\,\mathrm{d}V. \tag{2.124}$$

EXERCISE 2.8: BELTRAMI FLOW
Beltrami flow is defined by velocity and vorticity fields satisfying

$$\nabla \cdot \boldsymbol{v} = 0 \tag{2.125a}$$

$$\boldsymbol{\omega} = \nabla \times \boldsymbol{v} = \lambda\boldsymbol{v} \tag{2.125b}$$

where λ is a constant with dimensions of inverse length. Show that the following velocity field is a Beltrami flow

$$\boldsymbol{v} = (A\,\sin z + C\,\cos y)\,\hat{\boldsymbol{x}} + (B\,\sin x + A\,\cos z)\,\hat{\boldsymbol{y}} + (C\,\sin y + B\,\cos x)\,\hat{\boldsymbol{z}}, \tag{2.126}$$

where A, B, C are constants with dimensions of length per time. Hint: the solution follows directly from computing

$$\lambda\,u = \partial_y w - \partial_z v \quad \text{and} \quad \lambda\,v = \partial_z u - \partial_x w \quad \text{and} \quad \lambda\,w = \partial_x v - \partial_y u. \tag{2.127}$$

EXERCISE 2.9: PRACTICE WITH PATH INTEGRALS
Consider the vector field written using Cartesian coordinates,

$$\boldsymbol{F} = x\,y^2\,\hat{\boldsymbol{x}} + 2\,\hat{\boldsymbol{y}} + x\,\hat{\boldsymbol{z}}. \tag{2.128}$$

Let $\mathcal{L}$ be a path parameterized by

$$x = c\,t \qquad y = c/t \qquad z = d \qquad t \in [1, 2], \tag{2.129}$$

where c and d are constants. Show that the following identities hold

$$\int_{\mathcal{L}} \boldsymbol{F}\,\mathrm{d}t = c^3 \ln 2\,\hat{\boldsymbol{x}} + 2\,\hat{\boldsymbol{y}} + \frac{3\,c}{2}\,\hat{\boldsymbol{z}} \tag{2.130a}$$

$$\int_{\mathcal{L}} \boldsymbol{F}\,\mathrm{d}y = -\frac{3\,c^4}{8}\,\hat{\boldsymbol{x}} - c\,\hat{\boldsymbol{y}} - c^2\,\ln 2\hat{\boldsymbol{z}} \tag{2.130b}$$

$$\int_{\mathcal{L}} \boldsymbol{F}\cdot\mathrm{d}\boldsymbol{x} = c^4 \ln 2 - c, \tag{2.130c}$$

where $\mathrm{d}\boldsymbol{x} = \hat{\boldsymbol{x}}\,\mathrm{d}x + \hat{\boldsymbol{y}}\,\mathrm{d}y + \hat{\boldsymbol{z}}\,\mathrm{d}z$. Although all three integrals are computed along the same path, they are not necessarily of the same type. In particular, the first two integrals are vector fields, whereas the third integral is a scalar.

EXERCISE 2.10: STOKES' THEOREM ON A PLANE

Show that

$$\mathcal{I} = \oint_{\partial\mathcal{S}} \left[y\,(4\,x^2 + y^2)\,\mathrm{d}x + x\,(2\,x^2 + 3\,y^2)\,\mathrm{d}y\right] = \frac{\pi}{2}\,b\,a^3 \tag{2.131}$$

when integrating around the boundary of an ellipse $\mathcal{S}$ defined by

$$\frac{x^2}{a^2} + \frac{y^2}{b^2} = 1, \tag{2.132}$$

where a, b are constants. Hint: make use of Stokes' theorem on a plane, otherwise known as Green's Theorem. Also make use of the substitution $x = a\cos\phi$ and the identity

$$\int_{\pi}^{0} \sin^2(2\,\phi)\,\mathrm{d}\phi = -\frac{\pi}{2}. \tag{2.133}$$

EXERCISE 2.11: PRACTICE WITH GAUSS'S DIVERGENCE THEOREM

We here demonstrate the validity of Gauss's divergence theorem for a particular vector field

$$\boldsymbol{F} = \frac{\alpha\,\boldsymbol{x}}{(r^2 + a^2)^{3/2}}, \tag{2.134}$$

where α and a are constants and $r^2 = \boldsymbol{x}\cdot\boldsymbol{x}$ is the squared radial distance to a point. Using fluid mechanics jargon, we think of $\boldsymbol{F}$ as a matter flux with physical dimensions of M L^{-2} T^{-1} (mass length^{-2} time^{-1}). Now compute the transport of $\boldsymbol{F}$ through a spherical surface, $\mathcal{S}$, of radius $|\boldsymbol{x}| = a\sqrt{3}$

$$\Phi = \oint_{|\boldsymbol{x}|=a\sqrt{3}} \boldsymbol{F}\cdot\hat{\boldsymbol{n}}\,\mathrm{d}\mathcal{S} = \frac{3\,\pi\,\alpha\,\sqrt{3}}{2}. \tag{2.135}$$

With $\boldsymbol{F}$ a matter flux then Φ has physical dimensions of M T^{-1}, so that it is the *mass transport* through the spherical surface. Next, show that this transport is equal to the integral of the divergence over the volume of the sphere

$$\Phi = \int_{|\boldsymbol{x}|=a\sqrt{3}} \nabla\cdot\boldsymbol{F}\,\mathrm{d}V. \tag{2.136}$$

We thus verify, for this particular vector field, the divergence theorem

$$\int_{\mathcal{R}} \nabla \cdot \boldsymbol{F} \, \mathrm{d}V = \oint_{\partial\mathcal{R}} \boldsymbol{F} \cdot \hat{\boldsymbol{n}} \, \mathrm{d}\mathcal{S}, \tag{2.137}$$

where $\hat{\boldsymbol{n}}$ is the outward unit normal on the bounding surface $\mathcal{S}$.

EXERCISE 2.12: MORE PRACTICE WITH GAUSS'S DIVERGENCE THEOREM
Prove the following identities, which are readily shown using Gauss's divergence theorem.

(a) $\oint_{\partial\mathcal{R}} \boldsymbol{x} \cdot \hat{\boldsymbol{n}} \, \mathrm{d}\mathcal{S} = 3 \int_{\mathcal{R}} \mathrm{d}V = 3\,V$, where $\mathcal{R}$ is a closed region bounded by $\partial\mathcal{R}$ and with volume $\int_{\mathcal{R}} \mathrm{d}V = V$.

(b) $\oint_{\partial\mathcal{R}} (\hat{\boldsymbol{n}} \times \boldsymbol{F}) \, \mathrm{d}\mathcal{S} = \int_{\mathcal{R}} \nabla \times \boldsymbol{F} \, \mathrm{d}V$, for an arbitrary vector field $\boldsymbol{F}$ and with $\hat{\boldsymbol{n}}$ the outward unit normal on the bounding surface $\partial\mathcal{R}$. Hint: in a manner similar to the result shown in Section 2.7.2, make use of Gauss's theorem with $\boldsymbol{A} = \boldsymbol{F} \times \boldsymbol{C}$ where $\boldsymbol{C}$ is a constant vector.

(c) Let $\partial\mathcal{R}$ be a closed surface bounding a volume $\mathcal{R}$, and let $\boldsymbol{x}$ denote the position vector of a point measured from an arbitrary origin. Prove the following

$$\oint_{\partial\mathcal{R}} \frac{\hat{\boldsymbol{n}} \cdot \boldsymbol{x}}{r^3} \, \mathrm{d}\mathcal{S} = \begin{cases} 0 & \text{if the origin lies outside of } \partial\mathcal{R} \\ 4\pi & \text{if the origin lies inside of } \partial\mathcal{R}. \end{cases} \tag{2.138}$$

Chapter 3

GENERAL TENSORS IN BRIEF

Vector calculus, as formalized by the Cartesian tensor analysis of Chapters 1 and 2, is sufficient for many areas of geophysical fluid mechanics. However, there are a number of applications where general tensors helps the physics to shine through the maths. We are thus motivated to move beyond Cartesian tensor analysis to here consider general tensors, thus enabling a more versatile and precise mathematical formalism. Besides enhancing our tools for geophysical fluid mechanics, general tensor analysis is found throughout physics so that understanding the formalism, if only its rudiments, can greatly help to understand the broader physics literature.

Geophysical fluid mechanics applications require only a modest level of new formalism in the transition from Cartesian tensors to general tensors. The following reasons support a somewhat minimalist use of general tensor analysis and differential geometry.

- Geophysical fluids are embedded within the same Euclidean space used for Newtonian particle mechanics (Chapter 11). Notably, Euclidean space has zero intrinsic curvature so we say that it is a *flat space*. So although we are concerned with fluid motion on curved static manifolds (e.g., spherical planets); motion on curved and fluctuating manifolds (e.g., Lagrangian coordinates, also isopycnal coordinates); and in describing motion using non-orthogonal coordinates (e.g., generalized vertical coordinates), the fluid remains embedded within a background Euclidean space. Through that embedding, the local geometry inherits features from the Euclidean space. In particular, we continue to measure distance between points in space via the Pythagorean theorem and the associated Kronecker metric, δ_{ij}.

- We make use of universal *Newtonian time*. Hence, time is measured the same by all observers and reference frames. So although the spatial coordinates used by geophysical fluid mechanics can be a function of time, the time coordinate is always independent of space.

- We assume that the position of a fluid particle is described by a vector extending from an origin, typically assumed to be the center of the planet. In so doing, we retain the notion of a position as a directed line segment starting from an origin, just as for Cartesian tensor analysis in Section 1.2. Alternative treatments dispense with the notion of an origin and corresponding position vector. Instead, these treatments generalize the concept of a vector to a directed partial derivative operator. We briefly motivate this generalization in Section 3.4.3.[1] Such treatments are essential in some areas of continuum mechanics, particularly when working with arbitrary manifolds where there is no special point that can serve as the origin. Even so, we retain the notion of an origin for our purposes since it is needed to discuss motion on a rotating planet. Namely, on a rotating planet the planet's center

[1] For a thorough discussion of this general approach to defining vectors and tensors, the reader can refer to one of the many books on mathematical physics, such as *Schutz* (1980) (see his Section 2.7) or *Frankel* (2004) (see his Section 1.3). Additionally, *Tromp* (2025b) as well as the appendices to *Tromp* (2025a) provide a treament focused on applications to continuum mechanics.

provides a natural coordinate origin and the rotational axis breaks the isotropy of space. It follows that to understand the planetary Coriolis acceleration and planetary centrifugal acceleration, which arise from a rotating terrestrial observer's description of planetary fluid motion, requires an acknowledgement of the rotational axis and planetary center.

Each of these features of the space and time used for geophysical fluid mechanics means that our mathematical needs are less than the general relativist who studies fluids moving in strong gravity fields and/or over galactic distances. Even so, we do need some of the tools, and that is the goal for this chapter as well as Chapter 4.

READER'S GUIDE TO THIS CHAPTER

This brief chapter offers an overview sufficient to appreciate why we need general tensors for certain subjects in this book. We do so by offering a conceptual platform for general tensor analysis, with details presented in Chapter 4. We focus on tensor analysis on spatial manifolds endowed with a metric, thus touching on the rudiments of *Riemannian differential geometry*. Furthermore, we restrict attention to manifolds embedded in Euclidean space, thus providing a natural extension of the Cartesian tensor analysis from Chapters 1 and 2.

3.1 Covariance as coordinate invariance

Physical relations are independent of subjective choices for their mathematical representations. This principle motivates us to seek mathematical expressions between objects whose meaning transcends a particular coordinate representation. At its most basic level, there is no *a priori* notion of the underlying geometry, with an insistence on such generalities leading to general relativity and the notion of *general covariance*. General covariance means that the physical equations take on the same form regardless the coordinates, even though when unpacked into coordinate components the terms in these equations generally are effected by coordinate choice.

We do not need general covariance in this book, given that we work on a background Euclidean space on which the fluid moves, and we make use of a universal Newtonian time measured by all observers. That is, we work with *Galilean space-time*. Nonetheless, within the restricted class of Galilean space-time, we do insist that the mathematical expression of a physical relation in an inertial reference frame be independent of the coordinate choice.

We refer to the above property of the physical equations as *Galilean covariance*, or more specifically *coordinate invariance*. This property is ensured when the equations of mathematical physics are relations between geometric objects such as points, vectors, and tensors. We thus focus in this chapter and in Chapter 4 with the operational goal of laying down the foundations for expressing the continuum equations of fluid mechanics in a form that exposes their underlying geometric foundation. Doing so allows us to avoid being distracted by coordinate dependent statements, while also offering a framework for the practice of using specific coordinates as well as non-inertial reference frames.

Although physics does not care about coordinates, physicists often do. Namely, it is convenient, and sometimes necessary, to work with specific coordinates suited to the symmetry of the physical system, particularly when comparing theory to experiment or when coding a numerical model. After deriving a physical law in one set of coordinates, it is often of interest to establish the form of the law in another set of coordinates. How does the physical law, typically represented as a differential equation, transform into other coordinates? So long as the equations are written in a proper tensorial form then the equations are form invariant. What constitutes "proper tensorial form" is a topic for this chapter and Chapter 4.

When the equations do not manifest form invariance (i.e., covariance), then that signals either a mistake or, more relevant to our study, a subjective view that arises when describing motion from a non-inertial reference frame. In Part II, we study the accelerations that result from viewing physical systems from a non-inertial reference frame, with such accelerations (planetary centrifugal and planetary Coriolis) fundamental to geophysical fluid mechanics. For this chapter and Chapter 4, we focus on coordinate invariance as a statement that the equations look the same regardless the choice of coordinates. Consequently, "physics as geometry" has a major practical implication. Namely, we can establish the validity of a physical relation in any convenient set of coordinates (including Cartesian), and then extend that relation to all coordinates so long as we respect the basic rules of tensor analysis.

3.1.1 Covariance versus covariant

The term *covariance* is here used as a noun, referring to the coordinate invariant form of equations. In traditional tensor analysis we also make use of *covariant* as an adjective, which refers to how a particular coordinate representation of a tensor transforms under coordinate changes (i.e., covariant labels are downstairs). The two uses are readily confused, particularly when encountering the *covariant derivative* in Chapter 4, which can have either a covariant or contra-variant tensor representation. It is referred to as the *covariant derivative* since it remains invariant under coordinate transformations.

It is unfortunate that we do not have two distinct names for these terms, though note that context and experience serve to clarify their uses. We also note that the older use of covariant (i.e.,for a downstairs tensor label) is becoming far less common in modern treatments. For this book, we retain the usage only where convenient.

3.1.2 Tensor operations

Extending a mathematical equation to all coordinates requires the equations to respect certain tensor rules. In brief, all tensor indices are properly matched and each derivative is covariant as specified in Section 4.10. In chapter 4, we provide the details needed to understand general

coordinate invariance. In this chapter we outline the procedure. The elegance and power rendered by coordinate invariance is the key reason that tensor analysis is ubiquitous in theoretical physics.

To ensure an equation respects coordinate invariance requires us to understand certain properties of tensors and operations with tensors that produce components of new tensors. We here summarize the specific properties characterizing coordinate invariance (taken after page 153 of *Schutz*, 1985):

1. Manipulations of tensor components are called *permissible tensor operations* if they produce components of new tensors. The following are permissible operations:
   (a) Multiplication of a tensor by a scalar produces a new tensor of the same type.
   (b) Addition of components of two tensors of the same type gives components of a new tensor of the same type. In particular, only tensors of the same type can be equal.
   (c) Multiplication of components of two tensors of arbitrary type gives components of a new tensor whose type is given by the sum of the types for the individual tensors. This operation is called the *outer product* or *tensor product* and is denoted by the operator $\otimes$. For example, $\mathbf{A} \otimes \mathbf{B}$ is a second order tensor built from the outer product of two vectors, $\mathbf{A}$ and $\mathbf{B}$. The discussion in Section 1.6 of tensor products largely holds for general tensors as well.
   (d) Covariant differentiation (Sections 4.10 and 4.11) increases by one the order of a tensor, with the covariant derivative operator denoted by ∇.
   (e) Contraction on a pair of indices of the components of a tensor reduces by one the order of a tensor.
   (f) A corollary of the multiplication rule is that if the inner product of two objects yields a tensor, and if one of these objects is itself a tensor then so too is the other. This result is known as the *quotient* rule.
2. If two tensors of the same type have equal components in a given coordinate system, then they have equal components in all coordinate systems. Hence, the tensors are identical. As a corollary, if a tensor is zero in one coordinate system, then it is zero in all coordinate systems. Conversely, if an object vanishes in one set of coordinates but is nonzero in another, then that object is *not* a tensor.
3. If a mathematical equation consists of tensors combined only by the permissible tensor operations, and if the equation is true in one coordinate system, then it is true in any coordinate system. If the equations involve covariant derivatives, then the equations remain form invariant under changes in coordinates. For the partial differential equations of geophysical fluid mechanics, covariant differentiation is the key to coordinate invariance.

3.1.3 Comments

The remainder of this chapter, as well as Chapter 4, we provide details needed for unpacking the notions of coordinate invariance and specifying particular tensor operations. Even without penetrating these details, the reader should be able to appreciate why coordinate invariance is so central to physics.

3.2 Points, trajectories, and coordinates

Consider a point in space, $\mathcal{P}$, at a particular time, τ. If this point represents the position of a point particle that moves, then as time increases the point traces out a curve in space-time. We call that curve the *trajectory* of the particle. In general, a trajectory through space-time could be

determined by a point particle satisfying Newton's laws, as discussed in Chapter 11. Or it could be that of a fluid particle within a continuum, whose motion defines the Lagrangian reference frame (Section 17.2). Or it could trace the path of something else such as a fish, balloon, boat, or airplane. As the trajectory is a one-dimensional curve, it is specified mathematically by a single parameter (see Section 5.2.1). We choose the time measured by an observer on the trajectory for this parameter. This time is referred to as *proper time* in special relativity. Yet since we are working with Newtonian time, there is no ambiguity concerning past, present, and future. In this manner, time is monotonically increasing and it has the same value at all points in space.

A point in the fluid as well as the trajectory in space-time are both geometric objects that exist independently of any coordinate representation. Even so, we find the need to represent points, trajectories, vectors, and other geometric objects using coordinates. For example, coordinates are needed to make quantitative statements about fluid flow in relation to observers. What is its speed and direction relative to a chosen reference frame? What is the distance from an origin or from another particle?

3.2.1 Time as a parameter and time as a coordinate

In special and general relativity, there is a mixing of space and time that warrants the use of four-dimensional space-time tensor analysis. In contrast, for classical mechanics forming the foundation of geophysical fluid mechanics, time is a monotonically increasing parameter that is numerically the same value throughout all of space. We thus make use of the same universal (or Newtonian) time since the fluid velocity and wave speeds are far smaller than the speed of light. Hence, for our studies we generally restrict attention to the space + time formalism of classical mechanics rather than the space-time formalism of relativity. Even so, we have some occasions for using the space-time formalism, such as mentioned in Section 3.5.4.

The time parameter, τ, specifies a point along a trajectory in space. When making use of Lagrangian methods for fluid mechanics, we refer to τ as T, the *Lagrangian time* coordinate. An alternative measure of time is given by t, which measures time at positions fixed throughout space. This time is the *Eulerian time* coordinate of fluid mechanics, which is the time measured by a fixed laboratory reference frame.

This distinction between the two times is pedantic given that $\tau = T = t$ (up to a constant offset) in the Galilean relativity considered in this book. Nonetheless, it is convenient to make the distinction when measuring how fluid properties change since these changes are subject to motion of the observer. For example, changes following a trajectory, found by computing the trajectory time derivative $\partial/\partial\tau = \partial/\partial T$, are generally distinct from changes found by computing the time derivative $\partial/\partial t$, in which the spatial coordinates are held fixed.

When the trajectory is defined by a fluid particle, we refer to $\partial/\partial T$ as the *material or Lagrangian time derivative*. This time derivative is the same as when working with Newtonian particle mechanics as in Chapter 11. In contrast, if the spatial coordinates are fixed in space, then $\partial/\partial t$ is an Eulerian time derivative. When alternative spatial coordinates are used, some of which can move (see Section 3.2.2), then $\partial/\partial t$ can be a mixture of Lagrangian and Eulerian or perhaps neither. We return to these time derivatives in Section 17.4 when discussing fluid kinematics.

3.2.2 The importance of index placement

In Chapters 1 and 2 we introduced the *covariant* (downstairs) and *contravariant* (upstairs) representation of Cartesian tensors. That distinction is unimportant for Cartesian tensors since the Cartesian representation of the metric tensor is given by the Kronecker symbol, δ_{ab}. In contrast, for general tensors the position of a tensor label has significance.

We are inspired by the choice for index placement by the placement of indices on coordinates. For that purpose we choose to express each of the coordinates in an ordered list according to

$$\xi^\alpha = (\xi^0, \xi^1, \xi^2, \xi^3), \tag{3.1}$$

with ξ^α representing a *generalized coordinate*. The α index is a coordinate label; it is not an exponent or power. We use a convention whereby Greek labels run from $\alpha = 0, 1, 2, 3$ with $\alpha = 0$ the time coordinate and $\alpha = a = 1, 2, 3$ the three labels for locating a point in space. The following shorthand notations are commonly used in this book

$$\xi^\alpha = (\xi^0, \xi^1, \xi^2, \xi^3) = (\xi^0, \xi^a) = (\xi^0, \boldsymbol{\xi}). \tag{3.2}$$

3.3 Example coordinate descriptions

We here offer coordinate examples used for describing geophysical fluid systems. As the time coordinate remains universal in our study, the following is only concerned with the spatial coordinates, $a = 1, 2, 3$.

3.3.1 Locally orthogonal coordinates

In Sections 4.21, 4.22, and 4.23 we detail three sets of commonly used locally orthogonal coordinates: Cartesian, cylindrical-polar, and spherical. In Cartesian coordinates, (x, y, z), the position vector for a point in space is written

$$\boldsymbol{x} = x\,\hat{\boldsymbol{x}} + y\,\hat{\boldsymbol{y}} + z\,\hat{\boldsymbol{z}} \qquad \text{Cartesian.} \tag{3.3}$$

For spherical coordinates, (λ, ϕ, r), the position vector is (see Figure 4.3)

$$\boldsymbol{x} = r\,\hat{\boldsymbol{r}} \qquad \text{spherical,} \tag{3.4}$$

and cylindrical-polar coordinates, (r, ϑ, z), (see Figure 4.2) we have

$$\boldsymbol{x} = r\,\hat{\boldsymbol{r}} + z\,\hat{\boldsymbol{z}} \qquad \text{cylindrical-polar.} \tag{3.5}$$

Note that in spherical coordinates, r is the distance from the origin to the point and $\hat{\boldsymbol{r}}$ points from the origin to the point. In contrast, for cylindrical-polar coordinates, r is the distance from the z-axis and $\hat{\boldsymbol{r}}$ is the horizontal vector pointing from the z-axis to the point. Each of these coordinate representations identify positions in space relative to a fixed coordinate origin.

As shown in Section 3.4, Cartesian coordinates have basis vectors that maintain a fixed direction throughout space. This feature lends simplicity to Cartesian coordinates and its corresponding Cartesian tensor analysis (Chapters 1 and 2). In contrast, the spherical basis vectors are spatially dependent. Likewise, the radial and angular basis vectors for polar cylindrical coordinates are spatially dependent, whereas the vertical direction is the same as the Cartesian vertical direction. Additionally, the spherical and cylindrical coordinates do not all have the same physical dimensions. Each of these features of spherical and cylindrical coordinates places them outside the purview of Cartesian tensor analysis.

3.3.2 Isopycnal coordinates

In geophysical fluids that are stably stratified in the vertical, it is common to measure the vertical position of a fluid element by specifying its entropy, buoyancy, or potential density depending

on the application. We generically write these *isentropic*, *buoyancy*, or *isopycnal* coordinates as

$$\xi^a = (x, y, b) \qquad \text{with} \qquad b = b(x, y, z, t) \qquad \text{isopycnal coordinates,} \tag{3.6}$$

where $b = b(x, y, z, t)$ is a generic symbol for entropy, buoyancy, or potential density. Entropy, buoyancy, and potential density are materially invariant for perfect fluid flow (flow absent irreversible processes such as mixing or heating). Hence, all fluid particle motion occurs on surfaces of constant b. Under such perfect fluid conditions, isopycnal coordinates are of great use for describing fluid mechanics of stably stratified geophysical flows.[2]

The isopycnal coordinates are generally not orthogonal since the direction normal to a buoyancy surface is not generally vertical. Hence, even if the horizontal coordinates are Cartesian, the use of b to measure the vertical precludes the use of Cartesian tensor analysis. Furthermore, we note the distinct physical dimensions of the three spatial coordinates (x, y, b), again necessitating the use of general tensor analysis. We develop the mathematical physics of such *generalized vertical coordinate* descriptions in Part XII of this book.

3.3.3 Lagrangian or material coordinates

We can conceive of a fluid as a continuum of fluid particles that are distinguished by continuum marker coordinates or labels. The initial position for a fluid particle offers a suitable (and common) choice for these *material coordinates*. The fluid dynamical equations of motion (i.e., Newton's Law of motion) can be formulated using material coordinates so long as the material coordinate maintains a 1-to-1 invertible relation to points in space. This kinematical framework is termed *Lagrangian* or *material*. The resulting dynamical equations share much in common with Newtonian particle mechanics, though with the added feature of contact forces acting between the fluid elements. We introduce Lagrangian coordinates in Section 17.1.2 and further develop their formalism in Chapter 18. Lagrangian descriptions are then used throughout this book. Transformations between material coordinates and spatial coordinates are facilitated by the methods of general tensor analysis.

3.3.4 Tracer coordinates

Consider a triplet of linearly independent tracer concentrations, $C^a = C^a(x, y, z, t)$, that spans $\mathbb{R}^3$. Hence, at any point in space there is a unique intersection of three tracer isosurfaces, so that we can uniquely determine a point in space by specifying the value for the three tracer concentrations. Correspondingly, we can use tracer concentrations as the spatial coordinates

$$\xi^a = (C^1, C^2, C^3). \tag{3.7}$$

In some cases there are only two linearly independent tracers, in which case the two may be used in combination with a third spatial coordinate such as depth or pressure. Furthermore, the case of one tracer coordinate formally reduces to the isopycnal coordinate system from Section 3.3.2.[3]

3.3.5 Coordinates are not tensors

When labels are placed on a coordinate, such as in equation (3.2), we do not refer to a as a *tensor index*. Rather, a is simply a label that delineates the spatial coordinates. We make this distinction in nomenclature since, as noted in Section 1.3.2, coordinates are not tensors. Rather,

[2] We can make use of the isopycnal coordinate system to determine the vertical position so long as there is a one-to-one invertible relation between z and b at each horizontal point and at each time instance.

[3] See *Nurser et al.* (2022) for a description of fluid flow in the space defined by arbitrary continuous properties such as tracers.

coordinates specify the location of points in space, whereas tensors are geometric objects that live in that space.

We can transform coordinates from one form to another, with those coordinate transformations inducing changes to the representation of tensors. Cartesian coordinate transformations are restricted to rigid rotations; i.e., all Cartesian coordinate transformations result in the same rotation of the Cartesian coordinates at each point in space. Hence, coordinate transformations between Cartesian coordinates are linear transformations. In contrast, coordinate transformations can generally be nonlinear, such as the transformation between Cartesian and spherical coordinates. Nonlinear coordinate transformations require the tools of general tensor analysis to transform the coordinate representation of tensors.

3.4 The velocity vector and basis vectors

Consider two points in space, $\mathscr{P}(\tau-\Delta\tau/2)$ and $\mathscr{P}(\tau+\Delta\tau/2)$ that sit along a particular trajectory separated by an infinitesimal time increment, $\mathrm{d}\tau$. Let $\mathbf{x}(\tau-\Delta\tau/2)$ and $\mathbf{x}(\tau+\Delta\tau/2)$ be the corresponding position, so that the velocity for this trajectory is defined by

$$\mathbf{v}(\tau) = \lim_{\Delta\tau\to 0} \frac{\mathbf{x}(\tau+\Delta\tau/2)-\mathbf{x}(\tau-\Delta\tau/2)}{\Delta\tau} = \frac{\mathrm{d}\mathbf{x}(\tau)}{\mathrm{d}\tau}. \tag{3.8}$$

The velocity points in the direction determined by the difference between two points on a trajectory, in the limit as the time separation between the points vanishes. Consequently, the velocity points in a direction tangent to the trajectory. Notably, the above definition for the velocity makes no use of coordinates and it is independent of any choice for origin used to define the position, $\mathbf{x}$. Hence, the velocity is determined by geometry of the trajectory and specification of the trajectory's time parameter. Evidently, velocity is fundamentally an arrow with a length and direction. That is, the velocity is a geometric object that we refer to as the *velocity vector*, and as such it is a tensor.

3.4.1 Coordinate representation

Assume a choice for an arbitrary set of spatial coordinates, ξ^a, to represent points in space. These coordinates are used to measure the spatial position of the trajectory according to

$$\mathscr{P}(\tau) = \mathbf{x}(\tau) = \mathbf{x}[\xi^a(\tau)], \tag{3.9}$$

where $\xi^a(\tau)$ is the spatial coordinate position on the trajectory at time τ. This coordinate representation for the trajectory induces a coordinate representation for the velocity through use of the chain rule

$$\mathbf{v}(\tau) = \frac{\mathrm{d}\mathbf{x}(\tau)}{\mathrm{d}\tau} = \frac{\mathrm{d}\xi^a}{\mathrm{d}\tau}\frac{\partial\mathbf{x}}{\partial\xi^a} \equiv v^a\,\boldsymbol{e}_a. \tag{3.10}$$

The expansion coefficients

$$v^a = \frac{\mathrm{d}\xi^a}{\mathrm{d}\tau} \tag{3.11}$$

provide a representation for the velocity vector, $\boldsymbol{v}(\tau)$, within the coordinate system, ξ^a.

3.4.2 Basis vectors

As seen by equation (3.10), for each number, v^a, there is a corresponding basis vector, $\boldsymbol{e}_a$, whose value at the point $\mathbf{x}=\mathscr{P}$ is given by

$$\boldsymbol{e}_a(\mathscr{P}) = \frac{\partial\mathbf{x}}{\partial\xi^a}. \tag{3.12}$$

The basis vectors are generally a function of space and time, with Cartesian coordinates a notable exception, whose basis vectors are space-time constants.

3.4.3 Vector fields living on a tangent space

The definition of velocity as a vector tangent to the trajectory is a general property of all vectors. Namely, a vector at a point on a manifold lives within the *tangent space* to the manifold, with a distinct tangent space defined at each point of the manifold.[4] So although we started by considering the position of two points relative to an origin, as afforded by Euclidean space, we do not need two points nor do we need an origin to define a vector. Instead, we simply consider a vector at a point on a manifold to be an object defined within the tangent space at the point. In this manner we can dispense with an origin when defining vectors, but in so doing we must be careful when comparing vectors living on a curved manifold. Namely, the comparison of two vectors (e.g., their sums or integrals) can only occur when they live in the same tangent space. So before comparing two vectors, they must be brought to the same tangent space so they can be compared. Herein lies the fundamental reason for extending the partial derivative operator to a covariant derivative when acting on vectors and higher order tensors.

3.4.4 Concerning basis vectors as differential operators

Throughout this section we used nomenclature consistent with Section 2.3 of *Misner et al.* (1973), *Tromp* (2025b), and appendix C.3 of *Tromp* (2025a). A slight modification of this nomenclature, commonly found in the mathematical physics literature (e.g., Sections 2.7 and 2.8 of *Schutz* (1980)), abstracts the identity (3.12) to identify the basis vector as the partial derivative

$$\boldsymbol{e}_a = \frac{\partial}{\partial \xi^a} \qquad \text{not used in this book.} \tag{3.13}$$

Identifying basis vectors as partial derivative operators emphasizes the ability to define a vector without the need to specify an origin. However, care should be exercised when using this identification for applications in physics. Namely, dropping $\mathscr{P}$ changes the physical dimensions of the basis vectors relative to the definition (3.12). For example, the Cartesian basis vectors, $\boldsymbol{e}_a(\mathscr{P}) = \partial_a \mathbf{x}$, are the dimensionless unit vectors $\hat{\boldsymbol{x}}, \hat{\boldsymbol{y}}, \hat{\boldsymbol{z}}$. In contrast, the alternative basis vectors, $\boldsymbol{e}_a = \partial_a$, have dimension of inverse length. For dimensional consistency with the treatment in Cartesian tensors, we consider the basis vectors to be the partial derivative operator acting on a point on the manifold as in equation (3.12), rather than the partial derivative operators as in equation (3.13).

3.5 Notational conventions

We here summarize notational conventions associated with tensor manipulations, sometimes referred to as *index gymnastics*. Many of these conventions are familiar from our study of Cartesian tensors in Chapters 1 and 2, so that the presentation here is relatively terse.

3.5.1 Covariant, contravariant, and Einstein summation

For general tensors, the Einstein summation convention assumes that tensor labels (also called tensor indices) are summed over their range when a lower *covariant* index matches an upper

[4] The *tangent bundle* is the collection of all tangent spaces for each point of a manifold. A vector field maps each point of a manifold to the tangent bundle.

contravariant index. In this way we have an arbitrary vector represented as

$$\mathbf{F} = \sum_{a=1}^{3} F^a \, \boldsymbol{e}_a = F^a \, \boldsymbol{e}_a. \tag{3.14}$$

By extension, the placement of tensor labels (covariant versus contravariant) has specific meaning in general tensor analysis. In particular, it is necessary to ensure *conservation of indices* across an equal sign, balancing across both upstairs (contravariant) indices and downstairs (covariant) indices.

The names *covariant* and *contravariant* originate from their relation to the labels placed on a coordinate basis vectors (Section 3.4.2), and thus how they change under coordinate transformations relative to how basis vectors change (Section 4.1). The covariant tensor label accords with the downstairs label placement for a coordinate basis, whereas the upstairs contravariant label is contrary to the coordinate basis (e.g., see Section 2.26 of *Schutz* (1980). A useful mneumonic is "co-low" to signal that the covariant label is downstairs ("low").

Although we make use of the names covariant and contravariant when useful, these terms are used infrequently in modern tensor analysis, which instead considers tensors as geometric objects and so it is not primarily concerned with the coordinate representations of tensors. Additionally, when allowing for a metric tensor (Section 4.1), then the metric can move tensor indices up and down, thus blurring the distinction between covariant and contravariant representations.

3.5.2 Upright and slanted notation

As detailed in Section 1.2.2 we use a bold upright symbol for a geometric object living in Euclidean space. The position, $\mathbf{x} \in \mathbb{E}^3$, is an example, as are tensors written as $\mathbf{F}$. In contrast, a slanted bold symbol is used for a coordinate representation of the position, $\boldsymbol{x}$, or of a tensor, $\boldsymbol{F}$, with coordinate representations living in the space of real numbers. Each coordinate representation is realized by specifying a subjectively chosen set of coordinates. The tensor does not change when changing coordinates, but rather its coordinate representation changes. Tensor analysis provides a systematic means to transform coordinate representations.

The upright versus slanted notation is fundamental conceptually, since it is important to appreciate that tensors are geometric objects that are not subject to the whims of a particular coordinate choice. Correspondingly, physically robust differential and integral equations are coordinate invariant. Even so, the upright-slanted notation can be softly adhered to without much cause for concern, so long as we are careful to write the coordinate equations using rules of tensor analysis. In that case, the coordinate equations are unaltered in form when changing coordinates; i.e., they are tensor equations. Developing a practical and conceptual understanding of what careful means in this context requires the tensor analysis material presented in Chapter 4.

3.5.3 Physical dimensions

When representing a tensor, such as a vector, in terms of a particular coordinate basis,

$$\mathbf{F} = F^a \, \boldsymbol{e}_a, \tag{3.15}$$

the physical dimensions of the basis vectors, $\boldsymbol{e}_a$, determine those of the coordinate representation, F^a. For Cartesian coordinates, the basis vectors are each non-dimensional, so that the physical dimensions of the coordinate representation, F^a, equal to those of the vector, $\mathbf{F}$. However, for other coordinate choices, the basis vectors can carry distinct physical dimensions, thus affecting the dimensions of the coordinate representation. This point is often ignored in the mathematics literature, where physical dimensions are of no concern. Hence, care should be exercised when

translating math equations to a physics application. In this book, we are concerned with physics, so that mathematical equations must have physically consistent dimensions. Indeed, checking for dimensional consistency is a very useful means to find bugs in mathematical manipulations.

3.5.4 Space-time notation

As introduced in Section 3.2.2, we make use of a Greek label when incorporating time to the tensor indices, with $\alpha = 0$ denoting the time coordinate. Time is universal in the Newtonian world of geophysical fluid mechanics, so that the time coordinate is independent of space. However, many spatial coordinates are functions of both space and time. Therefore, the time derivative of a tensor field computed in one set of spatial coordinates generally differs from another set of spatial coordinates.

Following equation (3.2) used for coordinates, we make use of the following index notation and ordered list for contravariant components of space-time 4-vectors

$$F^\alpha = (F^0, F^1, F^2, F^3) = (F^0, F^a) = (F^0, \boldsymbol{F}). \tag{3.16}$$

In Cartesian coordinates, the time component of the velocity 4-vector is unity

$$v^\alpha = (1, v^1, v^2, v^3) = (1, v^a) = (1, \boldsymbol{v}) \qquad \text{4-velocity in arbitrary coordinates.} \tag{3.17}$$

There are a variety of points in this book where the space-time formalism is paerticularly convenient. For example, we use the space-time formalism in Section 4.9 when performing the transformation of partial derivatives, and we use this formalism in Section 17.5 for Galilean transformation and Section 17.6 for the transformation of the material time operator. This notation is especially useful when studying field theory and Hamilton's principle in Part IX of this book.

We emphasize that throughout this book, the time coordinate is not a function of space, which is required since we use universal Newtonian time. For strictly Eulerian coordinates (coordinates fixed in space), the space coordinates are not functions of time. However, the we do sometimes allow for the space coordinates to be functions of time, such as when using generalized vertical coordinates in Part XII of this book.

Chapter 4

General tensors

In this chapter we generalize the tensor algebra of Chapter 1 and vector calculus of Chapter 2 to general tensors. Our focus concerns tensor analysis needed to describe the physics of particles and continua embedded in a background Euclidean space. This restricted generalization is sufficient for purposes in geophysical fluid mechanics (see the start of Chapter 3 for more on this point). Furthermore, since time remains universal, our main focus concerns space tensors. Even so, we do find occasion to make use of Galilean space-time tensors, such as when considering a space-time transformation of the partial time derivative operator (Section 4.9), where the time derivative cares about the motion of space coordinates even though the time itself is universal. We also make use of space-time tensors for much of our study of Hamilton's principle in Part IX of this book.

The tensor analysis from Chapters 1 2 was largely focused on *Cartesian tensors*. Cartesian tensor analysis provides a systematic formulation of vector analysis, with the Euclidean metric provided by the Kronecker delta (i.e., the unit tensor) forming the foundation for Cartesian tensors. Here, we extend the formalism by allowing for an arbitrary spatial metric (still embedded in a background Euclidean space), and in so doing penetrate a bit into the world of *Riemannian differential geometry*.

READER'S GUIDE TO THIS CHAPTER

This chapter is necessary for understanding the mathematics of Lagrangian fluid kinematics (Part III of this book), generalized vertical coordinates in Part XII of this book (Chapters 64, and 65), as well as general curvilinear coordinates such as cylindrical-polar and spherical (Sections 4.22 and 4.23). Otherwise, this chapter can be skimmed on first reading and returned to later when the need arises. Some material in this chapter is an updated version of Chapters 20 and 21 from *Griffies* (2004). Other resources include the treatment of tensors for fluid mechanics as given by *Aris* (1962), the physics treatment of *Thorne and Blandford* (2017) and the continuum mechanics treatment of *Tromp* (2025a) and *Tromp* (2025b).

Note that a mathematically deductive approach to tensor analysis first considers calculus on differential manifolds that are not endowed with a metric. That study constitutes the subject matter of *differential forms* through use of *exterior calculus*. This topic is beyond our scope, with the interested reader encouraged to study *Frankel* (2012).

4.1 The metric tensor and coordinate transformations

In the study of fluid mechanics we find the need to measure the distance between two points in space at a particular time instance. Since we assume all points live on a smooth and orientable manifold (e.g., a sphere, an isopycnal in a stably stratified fluid, the Lagrangian manifold defined by fluid particle labels), it is sufficient to consider the distance between two infinitesimally close points and use integration to measure finite distances. The measurement of distance requires a metric tensor, which is the subject of this section.

4.1.1 Cartesian coordinates in Euclidean space

Consider a Cartesian coordinate representation for the spatial position of two points, with point $\mathscr{P}$ having space coordinates $\xi^a = x^a$ and the other point $\mathscr{Q}$ an infinitesimal distance away at $x^a + \mathrm{d}x^a$. Furthermore, let

$$\mathrm{d}\boldsymbol{x} = \mathrm{d}x^a \, \boldsymbol{e}_a \tag{4.1}$$

be the infinitesimal space vector pointing from $\mathscr{P}$ to $\mathscr{Q}$. Since the space is Euclidean, the squared distance between the two points is based on the Euclidean norm; i.e., the familiar scalar or dot product (Section 1.4)

$$\mathrm{d}s^2 = \mathrm{d}\boldsymbol{x} \cdot \mathrm{d}\boldsymbol{x} = \boldsymbol{e}_a \cdot \boldsymbol{e}_b \, \mathrm{d}x^a \mathrm{d}x^b = \delta_{ab} \, \mathrm{d}x^a \mathrm{d}x^b. \tag{4.2}$$

In this expression,

$$(\mathrm{d}s)^2 \equiv \mathrm{d}s^2 \tag{4.3}$$

is the squared infinitesimal arc-length separating the two points. The Kronecker symbol, δ_{ab}, is symmetric

$$\delta_{ab} = \delta_{ba}, \tag{4.4}$$

and vanishes when $a \neq b$ and is unity when $a = b$

$$\delta_{ab} = \begin{cases} 0 & \text{if } a \neq b \\ 1 & \text{if } a = b. \end{cases} \tag{4.5}$$

The Kronecker symbol is a representation of the unit tensor.

4.1.2 The metric as a symmetric second order tensor

As defined by equation (4.2), δ_{ab} forms the Cartesian representation of the *metric tensor* for Euclidean space. The metric is a second order tensor, meaning that its coordinate representation carries two tensor labels. Contracting the metric tensor with two vectors leads to a number, namely the squared distance between the two points. Hence, the metric establishes the means to measure the distance between two points that live on a manifold.

We write this distance-measuring property of the metric tensor in a geometric manner through

$$\text{distance}(\mathbf{P}, \mathbf{Q}) = \sqrt{\mathbb{g}(\mathbf{P}, \mathbf{Q})}. \tag{4.6}$$

Here, $\mathbb{g}$ is the metric tensor with coordinate representation $\mathbb{g}_{ab}$ and $\mathbf{P}$, $\mathbf{Q}$ are infinitesimally close vectors with coordinate representations

$$\mathbf{P} = \xi^a \, \boldsymbol{e}_a \quad \text{and} \quad \mathbf{Q} = \mathbf{P} + \mathrm{d}\xi^a \, \boldsymbol{e}_a. \tag{4.7}$$

Equation (4.6) indicates that the metric tensor takes two vectors as argument and produces a scalar. Furthermore, since

$$\text{distance}(\mathbf{P}, \mathbf{Q}) = \text{distance}(\mathbf{Q}, \mathbf{P}) \geq 0, \tag{4.8}$$

the metric tensor is a symmetric and positive tensor that produces zero only when $\mathbf{P} = \mathbf{Q}$.

4.1.3 Coordinate representation of the metric tensor

Given the geometric expression (4.6) for the metric, we determine its representation in an arbitrary coordinate system by considering the squared distance between the coordinate basis vectors

$$\text{distance}(\boldsymbol{e}_a, \boldsymbol{e}_b) = \sqrt{\mathbb{g}(\boldsymbol{e}_a, \boldsymbol{e}_b)}. \tag{4.9}$$

This relation determines the coordinate components of the metric tensor

$$\mathbb{g}(\boldsymbol{e}_a, \boldsymbol{e}_b) \equiv \mathbb{g}_{ab}. \tag{4.10}$$

Furthermore, for a manifold embedded in Euclidean space (as considered in this book) this relation is written

$$\mathbb{g}_{ab} = \boldsymbol{e}_a \cdot \boldsymbol{e}_b = \sum_{i=1}^{3} (\boldsymbol{e}_a)_i \, (\boldsymbol{e}_b)_i. \tag{4.11}$$

In this manner, we see that the metric tensor components are determined by computing the Euclidean scalar product between the basis vectors. We also see that if the basis vectors are orthogonal, then the metric tensor coordinate representation has vanishing components for $a \neq b$.

4.1.4 Transforming the coordinate representation of the metric tensor

We find opportunities to represent the metric tensor in various coordinate systems. Here, we consider the transformation from Cartesian coordinates, $\xi^a = x^a$, to arbitrary coordinates, $\xi^{\overline{a}}$. Use of the chain rule along with index gymnastics leads to the equivalent expression for the squared infinitesimal distance between two points

$$\begin{aligned}
\mathrm{d}s^2 &= \delta_{ab} \, \mathrm{d}\xi^a \, \mathrm{d}\xi^b && \text{squared distance with Cartesian coordinates} && (4.12a)\\
&= \delta_{ab} \, \frac{\partial \xi^a}{\partial \xi^{\overline{a}}} \frac{\partial \xi^b}{\partial \xi^{\overline{b}}} \, \mathrm{d}\xi^{\overline{a}} \, \mathrm{d}\xi^{\overline{b}} && \text{chain rule to new coordinates} && (4.12b)\\
&\equiv \delta_{ab} \Lambda^a{}_{\overline{a}} \, \Lambda^b{}_{\overline{b}} \, \mathrm{d}\xi^{\overline{a}} \, \mathrm{d}\xi^{\overline{b}} && \text{define the transformation matrix, } \Lambda && (4.12c)
\end{aligned}$$

$$\equiv \mathcal{G}_{\overline{a}\overline{b}}\, \mathrm{d}\xi^{\overline{a}}\, \mathrm{d}\xi^{\overline{b}}, \qquad \text{define the new coordinate components, } \mathcal{G}_{\overline{a}\overline{b}}, \tag{4.12d}$$

where

$$\mathcal{G}_{\overline{a}\overline{b}} = \delta_{ab}\, \Lambda^{a}{}_{\overline{a}}\, \Lambda^{b}{}_{\overline{b}} \tag{4.13}$$

defines the components to the metric tensor as represented by the coordinates $\xi^{\overline{a}}$.

In equation (4.12c) we introduced elements to the *transformation matrix*

$$\Lambda^{a}{}_{\overline{a}} = \frac{\partial \xi^{a}}{\partial \xi^{\overline{a}}}. \tag{4.14}$$

This matrix of partial derivatives has a non-zero entry when a coordinate in one representation changes while moving along the direction of a coordinate in the other representation. As for any partial derivative, the complement coordinates are held fixed when performing the derivative. Although carrying indices, the numbers $\Lambda^{a}{}_{\overline{a}}$ are *not* components of a tensor. Instead, they are components of a matrix used to transform tensor representations from one coordinate system to another. Organized as a matrix, we follow a convention whereby the row is denoted by the label closest to Λ, here being a, whereas the column is denoted by the label furthest from Λ, here dnoted by $\overline{a}$, so that

$$\Lambda^{a}{}_{\overline{a}} = \begin{bmatrix} (\partial\xi^{1}/\partial\xi^{\overline{1}})_{\overline{2},\overline{3}} & (\partial\xi^{1}/\partial\xi^{\overline{2}})_{\overline{1},\overline{3}} & (\partial\xi^{1}/\partial\xi^{\overline{3}})_{\overline{1},\overline{2}} \\ (\partial\xi^{2}/\partial\xi^{\overline{1}})_{\overline{2},\overline{3}} & (\partial\xi^{2}/\partial\xi^{\overline{2}})_{\overline{1},\overline{3}} & (\partial\xi^{2}/\partial\xi^{\overline{3}})_{\overline{1},\overline{2}} \\ (\partial\xi^{3}/\partial\xi^{\overline{1}})_{\overline{2},\overline{3}} & (\partial\xi^{3}/\partial\xi^{\overline{2}})_{\overline{1},\overline{3}} & (\partial\xi^{3}/\partial\xi^{\overline{3}})_{\overline{1},\overline{2}} \end{bmatrix}. \tag{4.15}$$

Again, the lower index is displaced to the right to delineate which index refers to the column. The extra labels denote those coordinates held fixed when performing the partial derivatives. The transformation matrix is nonsingular for one-to-one invertible coordinate transformations, in which case its determinant, called the *Jacobian of the transformation*, is nonvanishing and single signed. Finally, we sometimes find it useful to write the un-barred coordinates as an ordered list in a column, $\boldsymbol{\xi} = (\xi^{1}, \xi^{2}, \xi^{3})^{T}$, in which case the transformation matrix takes on the abbreviated form

$$\Lambda^{a}{}_{\overline{a}} = \begin{bmatrix} (\partial\boldsymbol{\xi}/\partial\xi^{\overline{1}})_{\overline{2},\overline{3}} & (\partial\boldsymbol{\xi}/\partial\xi^{\overline{2}})_{\overline{1},\overline{3}} & (\partial\boldsymbol{\xi}/\partial\xi^{\overline{3}})_{\overline{1},\overline{2}} \end{bmatrix}. \tag{4.16}$$

Use of this expression for the transformation matrix leads to the arbitrary coordinate representation of the metric tensor

$$\mathcal{G}_{\overline{a}\overline{b}} = \boldsymbol{e}_{\overline{a}} \cdot \boldsymbol{e}_{\overline{b}} = \begin{bmatrix} \dfrac{\partial\boldsymbol{\xi}}{\partial\xi^{\overline{1}}} \cdot \dfrac{\partial\boldsymbol{\xi}}{\partial\xi^{\overline{1}}} & \dfrac{\partial\boldsymbol{\xi}}{\partial\xi^{\overline{1}}} \cdot \dfrac{\partial\boldsymbol{\xi}}{\partial\xi^{\overline{2}}} & \dfrac{\partial\boldsymbol{\xi}}{\partial\xi^{\overline{1}}} \cdot \dfrac{\partial\boldsymbol{\xi}}{\partial\xi^{\overline{3}}} \\ \dfrac{\partial\boldsymbol{\xi}}{\partial\xi^{\overline{2}}} \cdot \dfrac{\partial\boldsymbol{\xi}}{\partial\xi^{\overline{1}}} & \dfrac{\partial\boldsymbol{\xi}}{\partial\xi^{\overline{2}}} \cdot \dfrac{\partial\boldsymbol{\xi}}{\partial\xi^{\overline{2}}} & \dfrac{\partial\boldsymbol{\xi}}{\partial\xi^{\overline{2}}} \cdot \dfrac{\partial\boldsymbol{\xi}}{\partial\xi^{\overline{3}}} \\ \dfrac{\partial\boldsymbol{\xi}}{\partial\xi^{\overline{3}}} \cdot \dfrac{\partial\boldsymbol{\xi}}{\partial\xi^{\overline{1}}} & \dfrac{\partial\boldsymbol{\xi}}{\partial\xi^{\overline{3}}} \cdot \dfrac{\partial\boldsymbol{\xi}}{\partial\xi^{\overline{2}}} & \dfrac{\partial\boldsymbol{\xi}}{\partial\xi^{\overline{3}}} \cdot \dfrac{\partial\boldsymbol{\xi}}{\partial\xi^{\overline{3}}} \end{bmatrix}. \tag{4.17}$$

The dot appearing in this equation is the usual Cartesian scalar product, which we are afforded since the background space is Euclidean.

So in summary, the transformation matrix is the central tool needed for the practical use of tensor analysis. It is defined by the partial derivatives of one coordinate with respect to another. The transformation matrix is not a tensor and so it is not a geometric object. Rather, it is dependent on how the two coordinate systems are related, and it provides the means to transform coordinate representations of tensors between these coordinates. Given our assumption of motion in the background Euclidean space, we commonly assume one of the two coordinates to be Cartesian. Yet this assumption is certainly not necessary.

4.1.5 Basis vectors

We transform the basis vectors from Cartesian into arbitrary coordinates through the transformation

$$\boldsymbol{e}_{\overline{a}} = \Lambda^{a}{}_{\overline{a}}\, \boldsymbol{e}_{a}. \tag{4.18}$$

Use of the transformation matrix (4.16) renders the arbitrary coordinate basis vectors

$$\boldsymbol{e}_{\overline{1}} = \frac{\partial \boldsymbol{\xi}}{\partial \xi^{\overline{1}}} \qquad \text{and} \qquad \boldsymbol{e}_{\overline{2}} = \frac{\partial \boldsymbol{\xi}}{\partial \xi^{\overline{2}}} \qquad \text{and} \qquad \boldsymbol{e}_{\overline{3}} = \frac{\partial \boldsymbol{\xi}}{\partial \xi^{\overline{3}}}, \tag{4.19}$$

which corresponds to the metric tensor written as in equation (4.17).

4.1.6 Finite distance between points

Once the metric is determined, the distance along a curve between two finitely separated points is given by integration

$$L = \int \sqrt{\mathrm{d}s^2} = \int_{\varphi_1}^{\varphi_2} \left| \mathbb{g}_{ab} \frac{\mathrm{d}\xi^a}{\mathrm{d}\varphi} \frac{\mathrm{d}\xi^b}{\mathrm{d}\varphi} \right|^{1/2} \mathrm{d}\varphi, \tag{4.20}$$

where φ is a parameter specifying the curve (e.g., the arc length as in Section 2.4), with φ_1 and φ_2 specifying the endpoints of the curve.

4.2 One-forms

The metric tensor, $\mathbb{g}$, is a function of two vectors, so that when the metric eats the two vectors the result is the scalar distance between the vectors (equation (4.6))

$$\text{distance}(\mathbf{A}, \mathbf{B}) = \sqrt{\mathbb{g}(\mathbf{A}, \mathbf{B})}. \tag{4.21}$$

What if the metric only eats one vector? The resulting geometric object is known as a *one-form*

$$\widetilde{\mathbf{A}} \equiv \mathbb{g}(\mathbf{A}, \ ), \tag{4.22}$$

with the tilde used to distinguish a one-form from a vector.

4.2.1 Coordinate representation of a one-form

We can determine the coordinate representation of a one-form by eating a basis vector

$$\widetilde{\mathbf{A}}(\boldsymbol{e}_b) = \mathbb{g}(\mathbf{A}, \boldsymbol{e}_b) = \mathbb{g}(A^a\, \boldsymbol{e}_a, \boldsymbol{e}_b) = \mathbb{g}(\boldsymbol{e}_a, \boldsymbol{e}_b)\, A^a = \mathbb{g}_{ab} A^a. \tag{4.23}$$

To reach this result we pulled the coordinate representation A^a outside of the metric tensor since the tensor eats vectors rather than numbers. This equation defines the coordinate representation of the one-form, $\widetilde{\mathbf{A}}$, in terms of its *dual* vector, $\boldsymbol{A}$, and the metric tensor

$$A_b = \mathbb{g}_{ab} A^a. \tag{4.24}$$

Evidently, the metric tensor provides the means to lower an index on the representation of a vector, thus producing the representation of a one-form. It is this seamless transition between one-forms and vectors that motivates us to drop the tilde notation on the one-form.

4.2.2 Basis one-forms and the duality condition

Just as for vectors, we find use for a basis of one-forms to specify their coordinate representation. The basis of one-forms, $\boldsymbol{e}^a$, are defined through the *duality condition* (sometimes referred to as the *bi-orthogonality relation*)

$$\mathfrak{g}(\boldsymbol{e}^a, \boldsymbol{e}_b) = \boldsymbol{e}^a \cdot \boldsymbol{e}_b = \delta^a{}_b, \tag{4.25}$$

where

$$\delta^a{}_b = \mathfrak{g}^{ac}\,\mathfrak{g}_{cb} \tag{4.26}$$

are components to the Kronecker tensor, taking the value of unity when $a = b$ and zero otherwise

$$\delta^a{}_b = \begin{bmatrix} 1 & 0 & 0 \\ 0 & 1 & 0 \\ 0 & 0 & 1 \end{bmatrix}. \tag{4.27}$$

Note that it is only for Cartesian coordinates that we have

$$\delta^a{}_c = \mathfrak{g}^{ab}\,\delta_{bc} \qquad \text{Cartesian coordinates,} \tag{4.28}$$

which follows since $\mathfrak{g}^{ab} = \delta^{ab}$ in Cartesian coordinates (recall Section 1.3.4).

We can obtain an explicit expression for the basis one-forms in arbitrary coordinates by transforming from Cartesian coordinates through use of the inverse transformation

$$\boldsymbol{e}^{\overline{a}} = \Lambda^{\overline{a}}{}_a\,\boldsymbol{e}^a, \tag{4.29}$$

which renders

$$\boldsymbol{e}^{\overline{1}} = \hat{\boldsymbol{x}}\,\frac{\partial \xi^{\overline{1}}}{\partial x} + \hat{\boldsymbol{y}}\,\frac{\partial \xi^{\overline{1}}}{\partial y} + \hat{\boldsymbol{z}}\,\frac{\partial \xi^{\overline{1}}}{\partial z} = \nabla \xi^{\overline{1}} \tag{4.30a}$$

$$\boldsymbol{e}^{\overline{2}} = \hat{\boldsymbol{x}}\,\frac{\partial \xi^{\overline{2}}}{\partial x} + \hat{\boldsymbol{y}}\,\frac{\partial \xi^{\overline{2}}}{\partial y} + \hat{\boldsymbol{z}}\,\frac{\partial \xi^{\overline{2}}}{\partial z} = \nabla \xi^{\overline{2}} \tag{4.30b}$$

$$\boldsymbol{e}^{\overline{3}} = \hat{\boldsymbol{x}}\,\frac{\partial \xi^{\overline{3}}}{\partial x} + \hat{\boldsymbol{y}}\,\frac{\partial \xi^{\overline{3}}}{\partial y} + \hat{\boldsymbol{z}}\,\frac{\partial \xi^{\overline{3}}}{\partial z} = \nabla \xi^{\overline{3}}. \tag{4.30c}$$

In Section 4.9.3 we verify that the basis one-forms satisfy the duality condition (4.25) with the basis vectors

$$\boldsymbol{e}^{\overline{a}} \cdot \boldsymbol{e}_{\overline{b}} = \delta^{\overline{a}}{}_{\overline{b}}. \tag{4.31}$$

4.2.3 Metric as a mapping between vectors and one-forms

We can contract the expression (4.24) with components of the inverse metric tensor, $\mathfrak{g}^{ab}$, to render

$$\mathfrak{g}^{ab} A_b = \mathfrak{g}^{ab}\,\mathfrak{g}_{bc} A^c = \delta^a{}_c A^c = A^a. \tag{4.32}$$

This identity, as well as equation (4.24), show that the metric provides a map between coordinate representations of one-forms and vectors.

To every vector there is a corresponding one-form. We say that the one-forms and vectors are *dual*, with the mapping between one-forms and vectors rendered by the metric tensor. Abstractly, we say that a vector at a point on a manifold lives on the *tangent space* at that point, whereas its one-form dual lives on the *cotangent space*. The metric tensor provides a link between the tangent space and cotangent space. This link blurs the distinction between one-forms and vectors, and more generally between covariant and contra-variant representations of tensors. For Cartesian tensor analysis, the duality between one-forms and vectors is the duality between

row vectors and column vectors. Furthermore, as for Cartesian tensors, we construct an inner product by contracting one-forms and vectors to produce a scalar. Finally, the duality relation given by equation (4.24) offers us the means to raise and lower tensor indices in a manner akin to the transpose operation in linear algebra that produces a row vector from a column vector.

4.2.4 Transformation of the coordinate representation

The transformation matrix (4.14) provides the means to convert any arbitrary coordinate representation of a tensor from one coordinate system to another. For example, consider the coordinate representation of a vector, which is realized by letting the vector eat one of the basis one-forms

$$\mathbf{A}(\boldsymbol{e}^a) = A^a. \tag{4.33}$$

Now consider another coordinate system with basis one-forms $\boldsymbol{e}^{\overline{a}}$, so that the vector has a representation

$$\mathbf{A}(\boldsymbol{e}^{\overline{a}}) = A^{\overline{a}}. \tag{4.34}$$

Transforming the basis one-form using the transformation matrix leads to

$$A^{\overline{a}} = \mathbf{A}(\boldsymbol{e}^{\overline{a}}) = \mathbf{A}(\Lambda^{\overline{a}}{}_a\, \boldsymbol{e}^a) = \Lambda^{\overline{a}}{}_a\, \mathbf{A}(\boldsymbol{e}^a) = \Lambda^{\overline{a}}{}_a\, A^a. \tag{4.35}$$

The transformation of an arbitrary one-form representation takes place with the inverse transformation matrix

$$A_{\overline{a}} = \mathbf{A}(\boldsymbol{e}_{\overline{a}}) = \mathbf{A}(\Lambda^a{}_{\overline{a}}\, \boldsymbol{e}_a) = \Lambda^a{}_{\overline{a}}\, \mathbf{A}(\boldsymbol{e}_a) = \Lambda^a{}_{\overline{a}}\, A_a. \tag{4.36}$$

4.2.5 Arbitrary coordinate representation of inverse metric

The inverse metric tensor has an arbitrary coordinate representation given by

$$\mathcal{G}^{\overline{a}\overline{b}} = \boldsymbol{e}^{\overline{a}} \cdot \boldsymbol{e}^{\overline{b}} = \begin{bmatrix} \nabla\xi^{\overline{1}} \cdot \nabla\xi^{\overline{1}} & \nabla\xi^{\overline{1}} \cdot \nabla\xi^{\overline{2}} & \nabla\xi^{\overline{1}} \cdot \nabla\xi^{\overline{3}} \\ \nabla\xi^{\overline{2}} \cdot \nabla\xi^{\overline{1}} & \nabla\xi^{\overline{2}} \cdot \nabla\xi^{\overline{2}} & \nabla\xi^{\overline{2}} \cdot \nabla\xi^{\overline{3}} \\ \nabla\xi^{\overline{3}} \cdot \nabla\xi^{\overline{1}} & \nabla\xi^{\overline{3}} \cdot \nabla\xi^{\overline{2}} & \nabla\xi^{\overline{3}} \cdot \nabla\xi^{\overline{3}} \end{bmatrix}. \tag{4.37}$$

Proof that $\mathcal{G}^{\overline{a}\overline{b}}\, \mathcal{G}_{\overline{b}\overline{c}} = \delta^{\overline{a}}{}_{\overline{c}}$ requires use of the chain rule relations derived in Section 4.9.3.

4.3 Scalar product

In Section 1.4.3 we defined the scalar product between two Cartesian vectors. The natural generalization is given by

$$\mathbf{P} \cdot \mathbf{Q} = P^a\, Q^b\, \boldsymbol{e}_a \cdot \boldsymbol{e}_b = P^a\, Q^b\, \mathcal{G}_{ab} = P^a\, Q_a = P_b\, Q^b, \tag{4.38}$$

where the second equality made use of the metric tensor coordinate representation given by equation (4.11). We can conceive of the scalar product in a somewhat more general manner by recalling that a one-form, $\mathbf{P}$ operates on a vector, $\mathbf{Q}$, and conversely, a vector operates on a one-form. Exposing components leads to

$$\mathbf{P}(\mathbf{Q}) = \mathbf{P}(Q^a\, \boldsymbol{e}_a) = Q^a\, \mathbf{P}(\boldsymbol{e}_a) = Q^a\, P_a, \tag{4.39}$$

which equals to

$$\mathbf{Q}(\mathbf{P}) = \mathbf{Q}(P_a\, \boldsymbol{e}^a) = P_a\, \mathbf{Q}(\boldsymbol{e}^a) = P_a\, Q^a. \tag{4.40}$$

The scalar product is invariant to coordinate changes, as seen through

$$\mathbf{Q}(\mathbf{P}) = \mathbf{Q}(P_a\, \boldsymbol{e}^a) = P_a\, Q^a = \mathbf{Q}(P_{\overline{a}}\, \boldsymbol{e}^{\overline{a}}) = P_{\overline{a}}\, Q^{\overline{a}}. \tag{4.41}$$

The invariance is also revealed by working just with the coordinate representations and introducing the transformation matrix elements

$$P_a\, Q^a = (\Lambda^{\overline{a}}{}_a\, P_{\overline{a}})\, (\Lambda^a{}_{\overline{b}}\, Q^{\overline{b}}) = \Lambda^{\overline{a}}{}_a\, \Lambda^a{}_{\overline{b}}\, P_{\overline{a}}\, Q^{\overline{b}} = \delta^{\overline{a}}{}_{\overline{b}}\, P_{\overline{a}}\, Q^{\overline{b}} = P_{\overline{a}}\, Q^{\overline{a}}. \tag{4.42}$$

4.4 Worked example: oblique coordinates

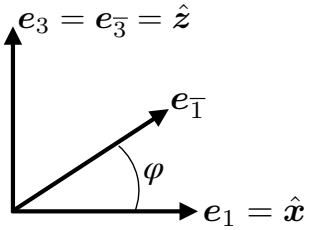

FIGURE 4.1: Oblique basis vectors for the x-z plane where $\boldsymbol{e}_{\overline{1}} = \boldsymbol{e}_1 \cos\varphi + \boldsymbol{e}_3 \sin\varphi$ and $\boldsymbol{e}_{\overline{3}} = \boldsymbol{e}_3$, with $\boldsymbol{e}_1 = \hat{\boldsymbol{x}}$ and $\boldsymbol{e}_3 = \hat{\boldsymbol{z}}$. These coordinate basis vectors are related to those used for generalized vertical coordinates shown in the left panel of Figure 63.2.

We pause in the development to exemplify some of the formalism for *oblique coordinates* for the x-z plane as specified by the basis vectors

$$\boldsymbol{e}_{\overline{1}} = \boldsymbol{e}_1 \cos\varphi + \boldsymbol{e}_3 \sin\varphi = \hat{\boldsymbol{x}} \cos\varphi + \hat{\boldsymbol{z}} \sin\varphi \qquad \text{and} \qquad \boldsymbol{e}_{\overline{3}} = \boldsymbol{e}_3 = \hat{\boldsymbol{z}}. \tag{4.43}$$

The oblique coordinate basis vectors, $\boldsymbol{e}_{\overline{a}}$, are orthogonal when the angle $\varphi = 0, \pi$; otherwise they are non-orthogonal. Also note that if $\varphi = \pi/2, 3\pi/2$ then $\boldsymbol{e}_{\overline{1}} = \pm \boldsymbol{e}_{\overline{3}}$, in which case the vectors no longer form a basis for the x-z plane. So in the following we assume $\varphi \in (-\pi/2, \pi/2)$. These coordinates are oriented so that they correspond to the generalized vertical coordinate basis vectors depicted in Figure 63.2. Finally, for the purposes of this section we ignore the 2 direction and just work within the x-z plane. Hence, tensor indices carry values 1 and 3 with 2 ignored.

4.4.1 Turning the crank

We here exhibit the results of turning the crank for the oblique coordinates.

Transformation matrix and its inverse

We can construct the transformation matrix through $\boldsymbol{e}_{\overline{a}} = \Lambda^a{}_{\overline{a}}\, \boldsymbol{e}_a$, and use of the coordinate basis definition (4.43)

$$\boldsymbol{e}_{\overline{1}} = \Lambda^1{}_{\overline{1}}\, \boldsymbol{e}_1 + \Lambda^3{}_{\overline{1}}\, \boldsymbol{e}_3 \Longrightarrow \Lambda^1{}_{\overline{1}} = \cos\varphi, \quad \Lambda^3{}_{\overline{1}} = \sin\varphi \tag{4.44a}$$

$$\boldsymbol{e}_{\overline{3}} = \Lambda^1{}_{\overline{3}}\, \boldsymbol{e}_1 + \Lambda^3{}_{\overline{3}}\, \boldsymbol{e}_3 \Longrightarrow \Lambda^1{}_{\overline{3}} = 0, \quad \Lambda^3{}_{\overline{3}} = 1, \tag{4.44b}$$

so that the transformation matrix is

$$\Lambda^a{}_{\overline{a}} = \begin{bmatrix} \Lambda^1{}_{\overline{1}} & \Lambda^1{}_{\overline{3}} \\ \Lambda^3{}_{\overline{1}} & \Lambda^3{}_{\overline{3}} \end{bmatrix} = \begin{bmatrix} \cos\varphi & 0 \\ \sin\varphi & 1 \end{bmatrix}, \tag{4.45}$$

and a matrix inversion yields the inverse transformation matrix

$$\Lambda^{\overline{a}}{}_{a} = \begin{bmatrix} \Lambda^{\overline{1}}{}_{1} & \Lambda^{\overline{1}}{}_{3} \\ \Lambda^{\overline{3}}{}_{1} & \Lambda^{\overline{3}}{}_{3} \end{bmatrix} = \frac{1}{\cos\varphi} \begin{bmatrix} 1 & 0 \\ -\sin\varphi & \cos\varphi \end{bmatrix}. \tag{4.46}$$

Basis one-forms

The basis one-forms using oblique coordinates are determined by

$$\boldsymbol{e}^{\overline{a}} = \Lambda^{\overline{a}}{}_{a}\, \boldsymbol{e}^{a} = \Lambda^{\overline{a}}{}_{1}\, \boldsymbol{e}^{1} + \Lambda^{\overline{a}}{}_{3}\, \boldsymbol{e}^{3} \tag{4.47}$$

with $\boldsymbol{e}^{1} = \hat{\boldsymbol{x}}$ and $\boldsymbol{e}^{3} = \hat{\boldsymbol{z}}$ for Cartesian coordinates. Making use of the inverse transformation matrix (4.46) leads to

$$\boldsymbol{e}^{\overline{1}} = \Lambda^{\overline{1}}{}_{1}\, \boldsymbol{e}^{1} + \Lambda^{\overline{1}}{}_{3}\, \boldsymbol{e}^{3} = \frac{\hat{\boldsymbol{x}}}{\cos\varphi} \tag{4.48a}$$

$$\boldsymbol{e}^{\overline{3}} = \Lambda^{\overline{3}}{}_{1}\, \boldsymbol{e}^{1} + \Lambda^{\overline{3}}{}_{3}\, \boldsymbol{e}^{3} = -\hat{\boldsymbol{x}} \tan\varphi + \hat{\boldsymbol{z}}. \tag{4.48b}$$

We can readily verify the bi-orthogonality relation (4.25) whereby

$$\boldsymbol{e}_{\overline{a}} \cdot \boldsymbol{e}^{\overline{b}} = \delta^{\overline{b}}{}_{\overline{a}}. \tag{4.49}$$

Representing a vector

The inverse transformation matrix (4.46) can be used to relate the Cartesian coordinate representation of an arbitrary vector, $\mathbf{P} = P^{a}\, \boldsymbol{e}_{a}$, to the oblique coordinate representation, $\mathbf{P} = P^{\overline{a}}\, \boldsymbol{e}_{\overline{a}}$. Doing so leads to the contravariant components written using oblique coordinates

$$P^{\overline{a}} = \Lambda^{\overline{a}}{}_{a}\, P^{a} = \Lambda^{\overline{a}}{}_{1}\, P^{1} + \Lambda^{\overline{a}}{}_{3}\, P^{3} \implies P^{\overline{1}} = \frac{1}{\cos\varphi}\, P^{1} \text{ and } P^{\overline{3}} = -\tan\varphi\, P^{1} + P^{3}. \tag{4.50}$$

Likewise, the covariant representation can be found by using the transformation matrix (4.45) to render

$$P_{\overline{a}} = \Lambda^{a}{}_{\overline{a}}\, P_{a} = \Lambda^{1}{}_{\overline{a}}\, P_{1} + \Lambda^{3}{}_{\overline{a}}\, P_{3} \implies P_{\overline{1}} = P_{1}\cos\varphi + P_{3}\sin\varphi \text{ and } P_{\overline{3}} = P_{3}, \tag{4.51}$$

where $P^{a} = P_{a}$ for the Cartesian coordinate representation.

Representing the metric tensor

The covariant representation of the metric tensor is given by

$$\mathcal{g}_{\overline{a}\,\overline{b}} = \delta_{ab}\, \Lambda^{a}{}_{\overline{a}}\, \Lambda^{b}{}_{\overline{b}} = \begin{bmatrix} \mathcal{g}_{\overline{1}\overline{1}} & \mathcal{g}_{\overline{1}\overline{3}} \\ \mathcal{g}_{\overline{3}\overline{1}} & \mathcal{g}_{\overline{3}\overline{3}} \end{bmatrix} = \begin{bmatrix} 1 & \sin\varphi \\ \sin\varphi & 1 \end{bmatrix}, \tag{4.52}$$

and its inverse is

$$\mathcal{g}^{\overline{a}\,\overline{b}} = \delta^{ab}\, \Lambda^{\overline{a}}{}_{a}\, \Lambda^{\overline{b}}{}_{b} = \begin{bmatrix} \mathcal{g}^{\overline{1}\overline{1}} & \mathcal{g}^{\overline{1}\overline{3}} \\ \mathcal{g}^{\overline{3}\overline{1}} & \mathcal{g}^{\overline{3}\overline{3}} \end{bmatrix} = \frac{1}{(\cos\varphi)^{2}} \begin{bmatrix} 1 & -\sin\varphi \\ -\sin\varphi & 1 \end{bmatrix}. \tag{4.53}$$

Squared magnitude

The squared magnitude of a vector is given by

$$\begin{aligned}
\mathbf{P} \cdot \mathbf{P} &= \mathcal{G}_{\overline{a}\overline{b}}\, P^{\overline{a}}\, P^{\overline{b}} && \text{(4.54a)}\\
&= P_{\overline{b}}\, P^{\overline{b}} && \text{(4.54b)}\\
&= (P_1 \cos\varphi + P_3 \sin\varphi)\, \frac{1}{\cos\varphi}\, P^1 + P_3\, (P^3 - \tan\varphi\, P^1) && \text{(4.54c)}\\
&= P_1\, P^1 + P_3\, P^3 && \text{(4.54d)}\\
&= \delta_{ab}\, P^a\, P^b. && \text{(4.54e)}
\end{aligned}$$

4.4.2 Comments

Oblique coordinate offer a pedagogical step towards the more complex case of generalized vertical coordinates studied in Chapter 63. Indeed, much of the tensor algebra needed for generalized vertical coordinates is concisely summarized in the above steps using oblique coordinates.

4.5 Volume element and the Jacobian of transformation

Recall from Section 1.8.2 that we derived an expression for the volume of an infinitesimal region of Euclidean space, $\mathbb{R}^3$, using Cartesian coordinates

$$\mathrm{d}V = \mathrm{d}x\, \mathrm{d}y\, \mathrm{d}z\, (\hat{\boldsymbol{x}} \times \hat{\boldsymbol{y}}) \cdot \hat{\boldsymbol{z}} = \mathrm{d}x\, \mathrm{d}y\, \mathrm{d}z. \tag{4.55}$$

This volume element is used for integrating over a region of $\mathbb{R}^3$ when using Cartesian coordinates. We now generalize this result to arbitrary coordinates.

4.5.1 Jacobian of transformation

From multi-variate calculus, the relation between $\mathrm{d}\xi^1\, \mathrm{d}\xi^2\, \mathrm{d}\xi^3$ and $\mathrm{d}\xi^{\overline{1}}\, \mathrm{d}\xi^{\overline{2}}\, \mathrm{d}\xi^{\overline{3}}$ for two sets of coordinates is given by

$$\begin{aligned}
\mathrm{d}\xi^1\, \mathrm{d}\xi^2\, \mathrm{d}\xi^3 &= \frac{\partial \boldsymbol{\xi}}{\partial \overline{\boldsymbol{\xi}}}\, \mathrm{d}\xi^{\overline{1}}\, \mathrm{d}\xi^{\overline{2}}\, \mathrm{d}\xi^{\overline{3}} && \text{(4.56a)}\\
&= \frac{\partial(\xi^1, \xi^2, \xi^3)}{\partial(\xi^{\overline{1}}, \xi^{\overline{2}}, \xi^{\overline{3}})}\, \mathrm{d}\xi^{\overline{1}}\, \mathrm{d}\xi^{\overline{2}}\, \mathrm{d}\xi^{\overline{3}} && \text{(4.56b)}\\
&= \left[\frac{\partial \boldsymbol{\xi}}{\partial \xi^{\overline{1}}} \times \frac{\partial \boldsymbol{\xi}}{\partial \xi^{\overline{2}}}\right] \cdot \frac{\partial \boldsymbol{\xi}}{\partial \xi^{\overline{3}}}\, \mathrm{d}\xi^{\overline{1}}\, \mathrm{d}\xi^{\overline{2}}\, \mathrm{d}\xi^{\overline{3}} && \text{(4.56c)}\\
&= \det(\Lambda^a{}_{\overline{a}})\, \mathrm{d}\xi^{\overline{1}}\, \mathrm{d}\xi^{\overline{2}}\, \mathrm{d}\xi^{\overline{3}}, && \text{(4.56d)}
\end{aligned}$$

where $\det(\Lambda^a{}_{\overline{a}})$ is the determinant of the transformation matrix, also known as the *Jacobian of transformation*. The transformation is well defined so long as the Jacobian does not vanish. We maintain labels on the transformation matrix inside the determinant symbol to help indicate the sense for the transformation. This notation also helps maintain proper conservation of tensor indices.

4.5.2 Jacobian related to the determinant of the metric

Recall the expression (4.12d) for the transformation of the metric

$$\mathcal{G}_{\overline{a}\overline{b}} = \Lambda^a{}_{\overline{a}} \Lambda^b{}_{\overline{b}}\, \mathcal{G}_{ab} = (\Lambda^{\mathrm{T}})_{\overline{a}}{}^a\, \mathcal{G}_{ab}\, \Lambda^b{}_{\overline{b}}. \tag{4.57}$$

Taking determinants of both sides yields[1]

$$\det(\mathfrak{g}_{\overline{a}\overline{b}}) = \det((\Lambda^{\mathrm{T}})_{\overline{a}}{}^{a})\,\det(\mathfrak{g}_{ab})\,\det(\Lambda^{b}{}_{\overline{b}}) = [\det(\Lambda)]^2\,\det(\mathfrak{g}_{ab}). \tag{4.58}$$

To reach this result we used the property of determinants that $\det(A\,B) = \det(A)\det(B)$ for any two matrices, and determinant of a matrix equals to the determinant of its transpose so that, $\det(\Lambda^{\mathrm{T}}) = \det(\Lambda)$. Consequently,

$$\det(\Lambda^{a}{}_{\overline{a}}) = \frac{\sqrt{\det(\mathfrak{g}_{\overline{a}\overline{b}})}}{\sqrt{\det(\mathfrak{g}_{ab})}}. \tag{4.59}$$

4.5.3 Invariant/covariant volume element

Equation (4.59) leads to the equivalent expressions for the volume element

$$\mathrm{d}V \equiv \sqrt{\det(\mathfrak{g}_{ab})}\,\mathrm{d}\xi^1\,\mathrm{d}\xi^2\,\mathrm{d}\xi^3 = \sqrt{\det(\mathfrak{g}_{\overline{a}\overline{b}})}\,\mathrm{d}\xi^{\overline{1}}\,\mathrm{d}\xi^{\overline{2}}\,\mathrm{d}\xi^{\overline{3}}. \tag{4.60}$$

This relation provides a general coordinate expression for the volume element, which we refer to as the *invariant volume element*, or equivalently the *covariant volume element*. For the special case when the unbarred coordinates are Cartesian, $\mathfrak{g}_{ab} = \delta_{ab}$, so that $\det(\mathfrak{g}_{ab}) = 1$ and

$$\det(\Lambda^{a}{}_{\overline{a}}) = \sqrt{\det(\mathfrak{g}_{\overline{a}\overline{b}})} \qquad \text{unbarred coordinates are Cartesian.} \tag{4.61}$$

This is a rather useful expression for our purposes, since we can always use Cartesian as the unbarred coordinates given that geophysical fluids move in a background Euclidean space.

We find that $\sqrt{\det(\mathfrak{g}_{ab})}$ appears throughout general tensor analysis, so that it is useful to introduce the shorthand

$$g = \sqrt{\det(\mathfrak{g}_{ab})}. \tag{4.62}$$

The indices are mere placeholders and play no role in the summation convention.

4.6 The permutation symbol and the determinant

As discussed in Section 1.7.1, the Cartesian components of the Levi-Civita tensor are given by the permutation symbol, ϵ_{abc}. To help determine the general coordinate representation of the Levi-Civita tensor, we here develop some identities satisfied by the determinant of the transformation matrix.

4.6.1 Connecting the permutation symbol to the determinant

Consider a two-dimensional space with a transformation matrix $\Lambda^{a}{}_{\overline{a}}$ between two sets of coordinates. The determinant of the transformation is given by

$$\det(\Lambda^{a}{}_{\overline{a}}) = \Lambda^{1}{}_{\overline{1}}\,\Lambda^{2}{}_{\overline{2}} - \Lambda^{1}{}_{\overline{2}}\,\Lambda^{2}{}_{\overline{1}}. \tag{4.63}$$

Introducing the permutation symbol ϵ_{ab} allows us to write this expression in a more tidy manner

$$\det(\Lambda^{a}{}_{\overline{a}}) = \epsilon_{ab}\,\Lambda^{a}{}_{\overline{1}}\,\Lambda^{b}{}_{\overline{2}} \tag{4.64}$$

[1] Note that we leave the indices exposed on the metric tensor when inside of the determinant operator. These indices are not subject to index conservation, with the determinant a number and so carrying no indices. Rather, the indices are kept around to remind us what coordinates are used to represent the metric tensor.

with

$$\epsilon_{12} = 1 \qquad \text{and} \qquad \epsilon_{21} = -1. \tag{4.65}$$

The permutation symbol is defined to have numerically the same values whether the labels are raised or lowered: $\epsilon^{ab} = \epsilon_{ab}$.

We can generalize the above to any number of dimensions, each of which adds one more label to the permutation symbol and one more number added to the permutation string. We already encountered the three dimensional version in Section 1.7.1 when discussing the vector cross product, in which case the permutation symbol is

$$\epsilon_{123} = 1 \tag{4.66a}$$

$$\epsilon_{abc} = \begin{cases} 0 & \text{if any two labels are the same,} \\ 1 & \text{if } a,b,c \text{ is an even permutation of } 1,2,3, \\ -1 & \text{if } a,b,c \text{ is an odd permutation of } 1,2,3. \end{cases} \tag{4.66b}$$

Likewise, the determinant of the transformation matrix takes the form

$$\det(\Lambda^{a}{}_{\overline{a}}) = \frac{\partial \boldsymbol{\xi}}{\partial \overline{\boldsymbol{\xi}}} = \frac{\partial(\xi^1,\xi^2,\xi^3)}{\partial(\xi^{\overline{1}},\xi^{\overline{2}},\xi^{\overline{3}})} = \epsilon_{abc}\,\Lambda^{a}{}_{\overline{1}}\,\Lambda^{b}{}_{\overline{2}}\,\Lambda^{c}{}_{\overline{3}}. \tag{4.67}$$

4.6.2 Further identities satisfied by the determinant

The following identity in two dimensions can be readily verified through enumeration

$$\epsilon_{ab}\,\Lambda^{a}{}_{\overline{a}}\,\Lambda^{b}{}_{\overline{b}} = \epsilon_{\overline{a}\overline{b}}\,\det(\Lambda^{a}{}_{\overline{a}}), \tag{4.68}$$

which follows directly from the definition of the determinant and can be explicity verified so long as we assume the permutation symbol, $\epsilon_{\overline{a}\overline{b}}$, is numerically identical to ϵ_{ab}. Now contract both sides of this relation with $\epsilon^{\overline{a}\overline{b}}$ to isolate the determinant

$$\frac{1}{2}\,\epsilon^{\overline{a}\overline{b}}\,\epsilon_{ab}\,\Lambda^{a}{}_{\overline{a}}\,\Lambda^{b}{}_{\overline{b}} = \det(\Lambda^{a}{}_{\overline{a}}), \tag{4.69}$$

where we used

$$\epsilon^{\overline{a}\overline{b}}\,\epsilon_{\overline{a}\overline{b}} = \epsilon^{\overline{12}}\,\epsilon_{\overline{12}} + \epsilon^{\overline{21}}\,\epsilon_{\overline{21}} = 2. \tag{4.70}$$

The three dimensional version takes the form

$$\epsilon_{abc}\,\Lambda^{a}{}_{\overline{a}}\,\Lambda^{b}{}_{\overline{b}}\,\Lambda^{c}{}_{\overline{c}} = \epsilon_{\overline{a}\overline{b}\overline{c}}\,\det(\Lambda^{a}{}_{\overline{a}}), \tag{4.71}$$

so that

$$\frac{1}{3!}\,\epsilon^{\overline{a}\overline{b}\overline{c}}\,\epsilon_{abc}\,\Lambda^{a}{}_{\overline{a}}\,\Lambda^{b}{}_{\overline{b}}\,\Lambda^{c}{}_{\overline{c}} = \det(\Lambda^{a}{}_{\overline{a}}). \tag{4.72}$$

The identity (4.72) is an elegant means to write the determinant and it serves many needs. Here is another relation that can be of use

$$\Lambda^{\overline{a}}{}_{a}\,\det(\Lambda^{a}{}_{\overline{a}}) = \frac{1}{2!}\,\epsilon^{\overline{a}\overline{b}\overline{c}}\,\epsilon_{abc}\,\Lambda^{b}{}_{\overline{b}}\,\Lambda^{c}{}_{\overline{c}}. \tag{4.73}$$

The right hand side is $(-1)^{\overline{a}+a}$ times the determinant of the 2×2 matrix built from excluding the $\overline{a}$ and a elements from $\Lambda^{a}{}_{\overline{a}}$, with this reduced determinant known as the *cofactor*. To prove equation (4.73) we contract both sides by $\Lambda^{a}{}_{\overline{a}}$ and use the identity $\Lambda^{a}{}_{\overline{a}}\,\Lambda^{\overline{a}}{}_{a} = 3$, in which case we recover the expression for the determinant in equation (4.72).

4.6.3 Derivative of the Jacobian with respect to a matrix element

In the study of Hamilton's principle for fluid mechanics in Chapter 47, we have the need to compute the derivative of the Jacobian determinant with respect to an element of the transformation matrix. For this purpose we make use of the identity

$$\frac{\partial \Lambda^{a}{}_{\overline{a}}}{\partial \Lambda^{d}{}_{\overline{d}}} = \delta^{a}{}_{d}\,\delta^{\overline{d}}{}_{\overline{a}}, \tag{4.74}$$

which then leads to

$$\frac{\partial \det(\Lambda^{a}{}_{\overline{a}})}{\partial \Lambda^{d}{}_{\overline{d}}} = \frac{1}{3!}\,\epsilon^{\overline{a}\overline{b}\overline{c}}\,\epsilon_{abc}\,\frac{\partial}{\partial \Lambda^{d}{}_{\overline{d}}}\left[\Lambda^{a}{}_{\overline{a}}\,\Lambda^{b}{}_{\overline{b}}\,\Lambda^{c}{}_{\overline{c}}\right] = \frac{1}{2}\,\epsilon^{\overline{d}\overline{b}\overline{c}}\,\epsilon_{dbc}\,\Lambda^{b}{}_{\overline{b}}\,\Lambda^{c}{}_{\overline{c}} = \Lambda^{\overline{d}}{}_{d}\,\det(\Lambda^{a}{}_{\overline{a}}), \tag{4.75}$$

where the final equality made use of equation (4.73). Evidently, the derivative of the determinant with respect to a matrix element equals to the determinant multiplied by the element of the inverse matrix.

4.6.4 Product of two Jacobians

Consider the case of two coordinate transformations that are each 1-to-1 and invertible. Summarize these transformations as

$$\xi^{a} \to \xi^{a'} \to \xi^{\overline{a}}, \tag{4.76}$$

with the corresponding transformation matrices written

$$\Lambda^{a'}{}_{a} = \frac{\partial \xi^{a'}}{\partial \xi^{a}} \quad \text{and} \quad \Lambda^{\overline{a}}{}_{a'} = \frac{\partial \xi^{\overline{a}}}{\partial \xi^{a'}} \quad \text{and} \quad \Lambda^{\overline{a}}{}_{a} = \frac{\partial \xi^{\overline{a}}}{\partial \xi^{a}}. \tag{4.77}$$

We now prove the very useful chain rule formula for determinants

$$\det(\Lambda^{a'}{}_{a})\det(\Lambda^{\overline{a}}{}_{a'}) = \det(\Lambda^{\overline{a}}{}_{a}). \tag{4.78}$$

To prove this identity, consider the two-dimensional case, where we have

$$\det(\Lambda^{a'}{}_{a})\det(\Lambda^{\overline{a}}{}_{a'}) = (1/4)\,(\Lambda^{1'}{}_{1}\,\Lambda^{2'}{}_{2} - \Lambda^{1'}{}_{2}\,\Lambda^{2'}{}_{1})(\Lambda^{\overline{1}}{}_{1'}\,\Lambda^{\overline{2}}{}_{2'} - \Lambda^{\overline{1}}{}_{2'}\,\Lambda^{\overline{2}}{}_{1'}) = (1/2)\,(\Lambda^{\overline{1}}{}_{1}\,\Lambda^{\overline{2}}{}_{2} - \Lambda^{\overline{1}}{}_{2}\,\Lambda^{\overline{2}}{}_{1}) = \det(\Lambda^{\overline{a}}{}_{a}), \tag{4.79}$$

where we made use of the chain rule identity

$$\frac{\partial x^{1'}}{\partial x^{1}}\,\frac{\partial x^{\overline{1}}}{\partial x^{1'}} = -\frac{\partial x^{\overline{1}}}{\partial x^{1}}, \tag{4.80}$$

and its analogs with the other indices. The proof extends to any number of dimensions, and we make particular use of it when working with particle relabeling symmetry in Section 47.7.

4.7 The Levi-Civita tensor and the volume element

The metric tensor introduced in Section 4.1 provides a means to measure distance between two points. The Levi-Civita tensor allows us to compute volumes (or areas for two dimensional manifolds). We make particular use of this tensor to compute the volume element used for integration. This section generalizes the Cartesian coordinate discussion provided in Section 1.8.3.

4.7.1 General coordinate representation of the Levi-Civita tensor

The relation (4.68) indicates that the permutation symbol, ϵ_{ab}, *does not* transform as the components to a second order covariant tensor, unless the determinant of the transformation is unity. The same can be said for the permutation symbol, ϵ_{abc}, with equation (4.71) indicating that it does not transform as the components to a third order covariant tensor, unless the determinant of the transformation is unity. Unit determinants occur for special transformations, such as rotations (i.e., Cartesian to Cartesian coordinate transformation as in Chapter 1) and the identity transformation. Indeed, we have already noted that the permutation symbol has the same representation regardless the coordinate choice. As we now show, the permutation symbol is the Cartesian coordinate representation of the Levi-Civita tensor.

The above relations for the determinant motivate us to introduce the general coordinate form of the *Levi-Civita tensor*

$$\varepsilon_{abc} \equiv \sqrt{\det(\mathbb{g}_{ab})}\,\epsilon_{abc}. \tag{4.81}$$

We highlight the distinct symbols in this definition, with ε the Levi-Civita tensor and ϵ the permutation symbol. By construction, the components to the Levi-Civita tensor transform as

$$\begin{aligned}
\Lambda^{a}{}_{\bar{a}}\,\Lambda^{b}{}_{\bar{b}}\,\Lambda^{c}{}_{\bar{c}}\,\varepsilon_{abc} &= \Lambda^{a}{}_{\bar{a}}\,\Lambda^{b}{}_{\bar{b}}\,\Lambda^{c}{}_{\bar{c}}\,\sqrt{\det(\mathbb{g}_{ab})}\,\epsilon_{abc} && \text{(4.82a)}\\
&= \sqrt{\det(\mathbb{g}_{ab})}\,\epsilon_{\bar{a}\bar{b}\bar{c}}\,\det(\Lambda^{a}{}_{\bar{a}}) && \text{(4.82b)}\\
&= \sqrt{\det(\mathbb{g}_{\bar{a}\bar{b}})}\,\epsilon_{\bar{a}\bar{b}\bar{c}} && \text{(4.82c)}\\
&= \varepsilon_{\bar{a}\bar{b}\bar{c}}, && \text{(4.82d)}
\end{aligned}$$

where equations (4.59) and (4.81) were used. Therefore, ε_{abc} transforms as components to a third order covariant tensor (a $(0,3)$ tensor). Likewise,

$$\varepsilon^{abc} = \frac{\epsilon^{abc}}{\sqrt{\det(\mathbb{g}_{ab})}} \tag{4.83}$$

transforms as the components to a third order contravariant tensor (a $(3,0)$ tensor). These transformation rules allow us to identify ε as a tensor rather than just a combination of numbers.

4.7.2 The volume element

As a third order tensor, the Levi-Civita tensor takes three vectors as its argument. In particular, for three infinitesimal vectors we have

$$\begin{aligned}
\varepsilon(\boldsymbol{e}_1\,\mathrm{d}\xi^1, \boldsymbol{e}_2\,\mathrm{d}\xi^2, \boldsymbol{e}_3\,\mathrm{d}\xi^3) &= \mathrm{d}\xi^1\,\mathrm{d}\xi^2\,\mathrm{d}\xi^3\,\varepsilon(\boldsymbol{e}_1, \boldsymbol{e}_2, \boldsymbol{e}_3) && \text{(4.84a)}\\
&= \mathrm{d}\xi^1\,\mathrm{d}\xi^2\,\mathrm{d}\xi^3\,\varepsilon_{123} && \text{(4.84b)}\\
&= \mathrm{d}\xi^1\,\mathrm{d}\xi^2\,\mathrm{d}\xi^3\,\sqrt{\det(\mathbb{g}_{ab})}\,\epsilon_{123} && \text{(4.84c)}\\
&= \mathrm{d}V, && \text{(4.84d)}
\end{aligned}$$

where we used equation (4.60) for the final step. This result means that geometrically, the Levi-Civita tensor measures the volume defined by three vectors

$$\varepsilon(\mathbf{A}, \mathbf{B}, \mathbf{C}) = \text{volume}(\mathbf{A}, \mathbf{B}, \mathbf{C}). \tag{4.85}$$

This interpretation accords with the Cartesian coordinate discussion of the Levi-Civita tensor in Section 1.8.3.

4.8 Vector cross product

The vector cross product of two Cartesian basis vectors yields the third, so that

$$\hat{\boldsymbol{x}} \times \hat{\boldsymbol{y}} = \hat{\boldsymbol{z}} \qquad \text{and cyclic permutations.} \tag{4.86}$$

The coordinate invariant generalization of this relation is given by

$$\boldsymbol{e}_a \times \boldsymbol{e}_b \equiv \varepsilon_{abc}\, \boldsymbol{e}^c. \tag{4.87}$$

As defined, the vector cross product of two vectors leads to a one-form. We are thus led to the general coordinate expression for the vector cross product of two arbitrary vectors

$$\mathbf{P} \times \mathbf{Q} = P^a\, Q^b\, \boldsymbol{e}_a \times \boldsymbol{e}_b \tag{4.88a}$$

$$= P^a\, Q^b\, \varepsilon_{abc}\, \boldsymbol{e}^c. \tag{4.88b}$$

4.9 Coordinate transformation of partial derivatives

Throughout this book, the background space is Euclidean and time is universal (i.e., we maintain the notion of absolute simultaneity). We are thus concerned with space tensors rather than the space-time tensors of special and general relativity. Nonetheless, our description of space generally makes use of curved generalized vertical coordinate surfaces that are time dependent. Curved surfaces motivate the use of general tensors. Time dependence of these surfaces motivates a space-time formulation (Section 3.5.4), in particular for the purpose of transforming the partial time derivative operator. In this section we establish some properties of the space-time transformation matrix and then make use of this matrix for transforming space and time partial time derivatives. We have further use of a space-time formulation in Sections 17.5 and 17.6, also for considering the transformation of partial derivatives.

4.9.1 The space-time transformation matrix

As discussed in Section 4.1.4, transformations between coordinate representations are enabled by the transformation matrix built from partial derivatives of the coordinate transformations. The transformation matrix with a universal Newtonian time plus spatial coordinates (that are functions of space and time) takes on the form

$$\Lambda^{\alpha}{}_{\overline{\alpha}} = \frac{\partial \xi^{\alpha}}{\partial \xi^{\overline{\alpha}}} = \begin{bmatrix} \frac{\partial \xi^0}{\partial \xi^{\overline{0}}} & \frac{\partial \xi^0}{\partial \xi^{\overline{1}}} & \frac{\partial \xi^0}{\partial \xi^{\overline{2}}} & \frac{\partial \xi^0}{\partial \xi^{\overline{3}}} \\ \frac{\partial \xi^1}{\partial \xi^{\overline{0}}} & \frac{\partial \xi^1}{\partial \xi^{\overline{1}}} & \frac{\partial \xi^1}{\partial \xi^{\overline{2}}} & \frac{\partial \xi^1}{\partial \xi^{\overline{3}}} \\ \frac{\partial \xi^2}{\partial \xi^{\overline{0}}} & \frac{\partial \xi^2}{\partial \xi^{\overline{1}}} & \frac{\partial \xi^2}{\partial \xi^{\overline{2}}} & \frac{\partial \xi^2}{\partial \xi^{\overline{3}}} \\ \frac{\partial \xi^3}{\partial \xi^{\overline{0}}} & \frac{\partial \xi^3}{\partial \xi^{\overline{1}}} & \frac{\partial \xi^3}{\partial \xi^{\overline{2}}} & \frac{\partial \xi^3}{\partial \xi^{\overline{3}}} \end{bmatrix} = \begin{bmatrix} 1 & 0 & 0 & 0 \\ \frac{\partial \xi^1}{\partial \xi^{\overline{0}}} & \frac{\partial \xi^1}{\partial \xi^{\overline{1}}} & \frac{\partial \xi^1}{\partial \xi^{\overline{2}}} & \frac{\partial \xi^1}{\partial \xi^{\overline{3}}} \\ \frac{\partial \xi^2}{\partial \xi^{\overline{0}}} & \frac{\partial \xi^2}{\partial \xi^{\overline{1}}} & \frac{\partial \xi^2}{\partial \xi^{\overline{2}}} & \frac{\partial \xi^2}{\partial \xi^{\overline{3}}} \\ \frac{\partial \xi^3}{\partial \xi^{\overline{0}}} & \frac{\partial \xi^3}{\partial \xi^{\overline{1}}} & \frac{\partial \xi^3}{\partial \xi^{\overline{2}}} & \frac{\partial \xi^3}{\partial \xi^{\overline{3}}} \end{bmatrix}. \tag{4.89}$$

The final equality made use of our assumption that $\xi^{\overline{0}} = \xi^0$ since the time coordinate remains universal. Hence, when computing $\partial \xi^0 / \partial \xi^{\overline{a}}$ we keep $\xi^{\overline{0}}$ fixed so that the derivative vanishes as in the specific case of

$$\left[\frac{\partial \xi^0}{\partial \xi^{\overline{1}}}\right]_{\xi^{\overline{0}}, \xi^{\overline{2}}, \xi^{\overline{3}}} = \left[\frac{\partial \xi^0}{\partial \xi^{\overline{1}}}\right]_{\xi^{0}, \xi^{\overline{2}}, \xi^{\overline{3}}} = 0. \tag{4.90}$$

Zero elements in the first row of the transformation matrix (4.89) reveals that time is not a function of space

$$\frac{\partial \xi^0}{\partial \xi^{\overline{a}}} = 0, \tag{4.91}$$

which is expected since we are assuming universal *Newtonian time* in which time is independent of space. In contrast, nonzero elements in the first column indicate that our description of space is generally a function of time

$$\frac{\partial \xi^a}{\partial \xi^{\overline{0}}} \neq 0. \tag{4.92}$$

We see the same overall structure in the inverse space-time transformation matrix

$$\Lambda^{\overline{\alpha}}{}_{\alpha} = \frac{\partial \xi^{\overline{\alpha}}}{\partial \xi^{\alpha}} = \begin{bmatrix} \frac{\partial \xi^{\overline{0}}}{\partial \xi^0} & \frac{\partial \xi^{\overline{0}}}{\partial \xi^1} & \frac{\partial \xi^{\overline{0}}}{\partial \xi^2} & \frac{\partial \xi^{\overline{0}}}{\partial \xi^3} \\ \frac{\partial \xi^{\overline{1}}}{\partial \xi^0} & \frac{\partial \xi^{\overline{1}}}{\partial \xi^1} & \frac{\partial \xi^{\overline{1}}}{\partial \xi^2} & \frac{\partial \xi^{\overline{1}}}{\partial \xi^3} \\ \frac{\partial \xi^{\overline{2}}}{\partial \xi^0} & \frac{\partial \xi^{\overline{2}}}{\partial \xi^1} & \frac{\partial \xi^{\overline{2}}}{\partial \xi^2} & \frac{\partial \xi^{\overline{2}}}{\partial \xi^3} \\ \frac{\partial \xi^{\overline{3}}}{\partial \xi^0} & \frac{\partial \xi^{\overline{3}}}{\partial \xi^1} & \frac{\partial \xi^{\overline{3}}}{\partial \xi^2} & \frac{\partial \xi^{\overline{3}}}{\partial \xi^3} \end{bmatrix} = \begin{bmatrix} 1 & 0 & 0 & 0 \\ \frac{\partial \xi^{\overline{1}}}{\partial \xi^0} & \frac{\partial \xi^{\overline{1}}}{\partial \xi^1} & \frac{\partial \xi^{\overline{1}}}{\partial \xi^2} & \frac{\partial \xi^{\overline{1}}}{\partial \xi^3} \\ \frac{\partial \xi^{\overline{2}}}{\partial \xi^0} & \frac{\partial \xi^{\overline{2}}}{\partial \xi^1} & \frac{\partial \xi^{\overline{2}}}{\partial \xi^2} & \frac{\partial \xi^{\overline{2}}}{\partial \xi^3} \\ \frac{\partial \xi^{\overline{3}}}{\partial \xi^0} & \frac{\partial \xi^{\overline{3}}}{\partial \xi^1} & \frac{\partial \xi^{\overline{3}}}{\partial \xi^2} & \frac{\partial \xi^{\overline{3}}}{\partial \xi^3} \end{bmatrix}. \tag{4.93}$$

4.9.2 Determinant of the transformation matrix

The determinant of the space-time transformation and its inverse remains identical to the determinant of their purely space portions

$$\det(\Lambda^{\alpha}{}_{\overline{\alpha}}) = \det(\Lambda^{a}{}_{\overline{a}}) \qquad \text{and} \qquad \det(\Lambda^{\overline{\alpha}}{}_{\alpha}) = \det(\Lambda^{\overline{a}}{}_{a}), \tag{4.94}$$

which follows since the first row in both transformations has only a single non-zero value, $\Lambda^{0}{}_{\overline{0}} = 1$ and $\Lambda^{\overline{0}}{}_{0} = 1$. Hence, the relations developed in Sections 4.5 and 4.6 for the volume element and Jacobian of transformation remain unchanged when adding the universal time coordinate.

4.9.3 Multiplying the transformation matrix and its inverse

We here verify that the transformation matrix (4.89) indeed has its inverse given by (4.93). For this purpose we must prove the space-time duality relations

$$\delta^{\alpha}{}_{\beta} = \Lambda^{\alpha}{}_{\overline{\beta}}\,\Lambda^{\overline{\beta}}{}_{\beta} \qquad \text{and} \qquad \delta^{\overline{\alpha}}{}_{\overline{\beta}} = \Lambda^{\overline{\alpha}}{}_{\beta}\,\Lambda^{\beta}{}_{\overline{\beta}}, \tag{4.95}$$

where $\delta^{\alpha}{}_{\beta}$ and $\delta^{\overline{\alpha}}{}_{\overline{\beta}}$ are components to the identity tensor. The proof relies on writing the space-time coordinate transformation as a composite function

$$\xi^{\overline{\alpha}} = \xi^{\overline{\alpha}}(\xi^{\alpha}) = \xi^{\overline{\alpha}}[\xi^{\alpha}(\xi^{\overline{\beta}})]. \tag{4.96}$$

Taking partial derivatives and using the chain rule renders

$$\delta^{\overline{\alpha}}{}_{\overline{\beta}} = \frac{\partial \xi^{\overline{\alpha}}}{\partial \xi^{\overline{\beta}}} = \frac{\partial \xi^{\overline{\alpha}}}{\partial \xi^{\alpha}}\,\frac{\partial \xi^{\alpha}}{\partial \xi^{\overline{\beta}}} = \Lambda^{\overline{\alpha}}{}_{\alpha}\,\Lambda^{\alpha}{}_{\overline{\beta}} \qquad \text{and} \qquad \delta^{\alpha}{}_{\beta} = \frac{\partial \xi^{\alpha}}{\partial \xi^{\beta}} = \frac{\partial \xi^{\alpha}}{\partial \xi^{\overline{\alpha}}}\,\frac{\partial \xi^{\overline{\alpha}}}{\partial \xi^{\beta}} = \Lambda^{\alpha}{}_{\overline{\alpha}}\,\Lambda^{\overline{\alpha}}{}_{\beta}. \tag{4.97}$$

Furthermore, the space subcomponents decouple from time, which can be seen by considering a few representative cases

$$1 = \delta^{0}{}_{0} = \Lambda^{0}{}_{\overline{\alpha}}\,\Lambda^{\overline{\alpha}}{}_{0} = \Lambda^{0}{}_{\overline{0}}\,\Lambda^{\overline{0}}{}_{0} \tag{4.98a}$$

$$1 = \delta^1{}_1 = \Lambda^1{}_{\overline{\alpha}}\,\Lambda^{\overline{\alpha}}{}_1 = \Lambda^1{}_{\overline{a}}\,\Lambda^{\overline{a}}{}_1 \tag{4.98b}$$

$$0 = \delta^0{}_1 = \Lambda^0{}_{\overline{\alpha}}\,\Lambda^{\overline{\alpha}}{}_1 = \Lambda^0{}_{\overline{0}}\,\Lambda^{\overline{0}}{}_1 \tag{4.98c}$$

$$0 = \delta^1{}_2 = \Lambda^1{}_{\overline{\alpha}}\,\Lambda^{\overline{\alpha}}{}_2 = \Lambda^1{}_{\overline{a}}\,\Lambda^{\overline{a}}{}_2. \tag{4.98d}$$

Consequently, the spatial components satisfy

$$\delta^a{}_b = \Lambda^a{}_{\overline{b}}\,\Lambda^{\overline{b}}{}_b \qquad \text{and} \qquad \delta^{\overline{a}}{}_{\overline{b}} = \Lambda^{\overline{a}}{}_b\,\Lambda^b{}_{\overline{b}}, \tag{4.99}$$

which allows for a splitting of the spatial components from the time component.

4.9.4 Transformation of space and time partial derivatives

Application of the chain rule leads to the transformation of the partial derivative operator

$$\partial_{\overline{\alpha}} = \frac{\partial}{\partial \xi^{\overline{\alpha}}} = \frac{\partial \xi^\alpha}{\partial \xi^{\overline{\alpha}}}\frac{\partial}{\partial \xi^\alpha} = \Lambda^\alpha{}_{\overline{\alpha}}\,\partial_\alpha. \tag{4.100}$$

Extracting the time and space components from the transformation matrix (4.89) yields

$$\partial_{\overline{0}} = \Lambda^\alpha{}_{\overline{0}}\,\partial_\alpha = \partial_0 + \Lambda^a{}_{\overline{0}}\,\partial_a \tag{4.101a}$$

$$\partial_{\overline{a}} = \Lambda^\alpha{}_{\overline{a}}\,\partial_\alpha = \Lambda^a{}_{\overline{a}}\,\partial_a. \tag{4.101b}$$

Notably, the time derivative operator in one coordinate system transforms into both space and time derivative operators in the new coordinate system. We expect this result since the time derivative in one coordinate system is computed with its spatial coordinates held fixed, but these coordinates are generally moving with respect to the other coordinate system. In contrast, the spatial components to the partial derivative operator transform among just the other spatial components; there is no mixing with the time derivative operator. This property of the spatial derivative operator follows from the use of universal Newtonian time. It allows us to focus on space tensors in the following sections.

4.10 Covariant derivative of a scalar

In this section and quite a few that follow it, we study the *covariant derivative operator*, which, as we will see, provides the means to take derivatives of tensors on a curved space. Operationally, we return to a focus on space tensor analysis by considering the contraction of spatial components to the partial derivative operator with the basis of one-forms. This contraction renders the geometric expression of the gradient operator acting on a scalar tensor

$$\text{grad}(\mathrm{F}) = \nabla \mathrm{F} = \boldsymbol{e}^a\,\partial_a F = \boldsymbol{e}^{\overline{a}}\,\partial_{\overline{a}} F. \tag{4.102}$$

This expression motivates us to define the *covariant derivative operator*

$$\nabla = \boldsymbol{e}^a\,\partial_a, \tag{4.103}$$

so that we refer to equation (4.102) as either the gradient acting on a scalar or the covariant derivative acting on a scalar.

4.11 Covariant derivative of a vector

The covariant derivative operator can act on a vector, in which case we consider $\nabla\mathbf{F}$. To perform calculations requires us to unpack the manifestly covariant expression $\nabla\mathbf{F}$ by introducing a

coordinate representation

$$\nabla \mathbf{F} = (\boldsymbol{e}^b\, \partial_b)\, (F^a\, \boldsymbol{e}_a). \tag{4.104}$$

4.11.1 Derivative of a vector and Christoffel symbols

The chain rule leads to the expression for the partial derivative operator acting on a vector field

$$\begin{aligned}
\partial_b \boldsymbol{F} &= \partial_b(\boldsymbol{e}_a\, F^a) && \text{coordinate representation of the vector } \boldsymbol{F} && (4.105a)\\
&= (\partial_b\, F^a)\, \boldsymbol{e}_a + F^a\, \partial_b\, \boldsymbol{e}_a && \text{chain rule} && (4.105b)\\
&= (\partial_b\, F^a)\, \boldsymbol{e}_a + F^a\, \Gamma^c_{ba}\, \boldsymbol{e}_c && \text{define Christoffel symbols} && (4.105c)\\
&= (\partial_b\, F^a + F^c\, \Gamma^a_{bc})\, \boldsymbol{e}_a && \text{reorganize} && (4.105d)\\
&\equiv (\nabla_b F^a)\, \boldsymbol{e}_a && \text{covariant derivative acting on vector component.} && (4.105e)
\end{aligned}$$

In the third equality we introduced the *Christoffel symbols*

$$\partial_b\, \boldsymbol{e}_a \equiv \Gamma^c_{ba}\, \boldsymbol{e}_c. \tag{4.106}$$

The Christoffel symbols carry information about the partial derivatives of the basis vectors. They vanish in Cartesian coordinates yet are generally nonzero. In the final equality we introduced components to the covariant derivative acting on the vector components

$$\nabla_b F^a \equiv \partial_b F^a + \Gamma^a_{bc}\, F^c. \tag{4.107}$$

Contracting $\partial_b \boldsymbol{F}$ with the basis one-form $\boldsymbol{e}^b$ leads to the coordinate invariant expression for the covariant derivative of a vector field

$$\nabla \mathbf{F} = \boldsymbol{e}^b\, (\partial_b\, \boldsymbol{F}) = (\boldsymbol{e}^b\, \nabla_b\, F^a)\, \boldsymbol{e}_a. \tag{4.108}$$

4.11.2 An alternative derivation

A heuristic explanation of these ideas follows by applying the elementary calculus notions to a vector field $\mathbf{F}$ as represented by arbitrary coordinates ξ^a, in which case

$$\partial_b \boldsymbol{F} = \lim_{\Delta \to 0} \frac{\boldsymbol{F}(\boldsymbol{x} + \Delta \boldsymbol{e}_b) - \boldsymbol{F}(\boldsymbol{x})}{\Delta}, \tag{4.109}$$

where $\boldsymbol{x} = \boldsymbol{e}_a\, \xi^a$ is the representation of the position for an arbitrary point and $\boldsymbol{e}_b$ specifies the direction for computing the partial derivative. The basis vectors, $\boldsymbol{e}_a$, are spatially independent for Cartesian coordinates, so that the derivative of a vector is computed merely by taking the derivative of each Cartesian component

$$\partial_b \boldsymbol{F} = (\partial_b F^a)\, \boldsymbol{e}_a \qquad \text{Cartesian coordinates.} \tag{4.110}$$

However, for general coordinates both the vector components and the basis vectors are spatially dependent, in which case

$$\begin{aligned}
\boldsymbol{F}(\boldsymbol{x} + \Delta \boldsymbol{e}_b) - \boldsymbol{F}(\boldsymbol{x}) &= [F^a + \Delta\, \partial_b F^a]\, [\boldsymbol{e}_a + \Delta\, \partial_b\, \boldsymbol{e}_a] - F^a\, \boldsymbol{e}_a && (4.111a)\\
&= \Delta\, \partial_b (F^a\, \boldsymbol{e}_a) + \mathcal{O}(\Delta^2). && (4.111b)
\end{aligned}$$

This is the same result as found in the first step of the chain rule used in equation (4.105a). Following through that derivation then leads to the same coordinate expression for the covariant derivative acting on a vector field.

4.11.3 Christoffel symbols as the metric connection

Recall from elementary calculus that the derivative of a function is computed by comparing the function at two points in space, dividing by the distance between those points, and taking the limit as the points get infinitesimally close. This operation is well defined for scalar fields on arbitrary manifolds. However, it is problematic for vectors since the vectors live on distinct tangent spaces and so cannot be directly compared (see Section 3.4 for more on tangent spaces). For example, how do we compare two vectors at distinct points on a sphere? To do so we must provide a method to move one vector to the position of the other before comparing. As seen through the above discussion of covariant derivative of a vector, the Christoffel symbols provide the means to move vectors. Namely, they connect the two vectors by carrying information about how the basis vectors change in space. It is for this reason that some refer to the Christoffel symbols as the *metric connection* or the *connection coefficients*.

The Christoffel symbols are coordinate dependent. For example, the Christoffel symbols all vanish in Euclidean space when using Cartesian coordinates, whereas they are nonzero with other coordinates. As discussed in Section 3.1, a tensor that vanishes in one coordinate system remains zero for all coordinate systems. We thus conclude that the Christoffel symbols are *not* components to a tensor. Rather, they carry information regarding the partial derivatives of the coordinate basis vectors and as such they are fundamentally tied to a chosen coordinate system.

4.11.4 Transformation of the Christoffel symbols

We noted above that the Christoffel symbols do not transform as components to a tensor. We here derive just how the Christoffel symbols transform under coordinate transformations. For that purpose, note that the covariant derivative of a vector defines a tensor, so that its components must transform according to

$$\nabla_{\bar{b}} F^{\bar{a}} = \Lambda^{b}{}_{\bar{b}} \Lambda^{\bar{a}}{}_{a} \, \nabla_b F^a. \tag{4.112}$$

We expand the left hand side according to

$$\begin{aligned}
\nabla_{\bar{b}} F^{\bar{a}} &= \partial_{\bar{b}} F^{\bar{a}} + \Gamma^{\bar{a}}_{\bar{b}\bar{c}} F^{\bar{c}} && \text{(4.113a)} \\
&= \partial_{\bar{b}} (\Lambda^{\bar{a}}{}_{a} F^a) + \Gamma^{\bar{a}}_{\bar{b}\bar{c}} \Lambda^{\bar{c}}{}_{a} F^a && \text{(4.113b)} \\
&= (\partial_{\bar{b}} \Lambda^{\bar{a}}{}_{a} + \Lambda^{\bar{a}}{}_{a} \partial_{\bar{b}} + \Gamma^{\bar{a}}_{\bar{b}\bar{c}} \Lambda^{\bar{c}}{}_{a}) F^a && \text{(4.113c)} \\
&= (\partial_{\bar{b}} \Lambda^{\bar{a}}{}_{a} + \Lambda^{\bar{a}}{}_{a} \Lambda^{b}{}_{\bar{b}} \partial_b + \Gamma^{\bar{a}}_{\bar{b}\bar{c}} \Lambda^{\bar{c}}{}_{a}) F^a && \text{(4.113d)}
\end{aligned}$$

The expanded right hand side of equation (4.112) is given by

$$\Lambda^{b}{}_{\bar{b}} \Lambda^{\bar{a}}{}_{a} \, \nabla_b F^a = \Lambda^{b}{}_{\bar{b}} \Lambda^{\bar{a}}{}_{a} \, (\partial_b F^a + \Gamma^{a}_{bc} F^c). \tag{4.114}$$

Notice how the $\Lambda^{b}{}_{\bar{b}} \Lambda^{\bar{a}}{}_{a} \, \partial_b F^a$ term cancels from equation (4.113d), thus rendering

$$\partial_{\bar{b}} \Lambda^{\bar{a}}{}_{a} \, F^a + \Gamma^{\bar{a}}_{\bar{b}\bar{c}} \Lambda^{\bar{c}}{}_{a} \, F^a = \Lambda^{b}{}_{\bar{b}} \Lambda^{\bar{a}}{}_{a} \, \Gamma^{a}_{bc} \, F^c \tag{4.115}$$

Relabeling the tensor indices on the right hand side term and rearranging leads to

$$(\partial_{\bar{b}} \Lambda^{\bar{a}}{}_{a} + \Gamma^{\bar{a}}_{\bar{b}\bar{c}} \Lambda^{\bar{c}}{}_{a} - \Lambda^{b}{}_{\bar{b}} \Lambda^{\bar{a}}{}_{d} \, \Gamma^{d}_{ba}) \, F^a = 0. \tag{4.116}$$

This equality holds for all vectors, so that we have the identity satisfied by the Christoffel symbols and the transformation matrix

$$\partial_{\bar{b}} \Lambda^{\bar{a}}{}_{a} + \Gamma^{\bar{a}}_{\bar{b}\bar{c}} \Lambda^{\bar{c}}{}_{a} = \Lambda^{b}{}_{\bar{b}} \, \Lambda^{\bar{a}}{}_{d} \, \Gamma^{d}_{ba}. \tag{4.117}$$

Finally, we can contract with $\Lambda^{a}{}_{\overline{d}}$ to render

$$\Gamma^{\overline{a}}_{\overline{bd}} = \Lambda^{a}{}_{\overline{d}}\,\Lambda^{b}{}_{\overline{b}}\,\Lambda^{\overline{a}}{}_{d}\,\Gamma^{d}_{ba} - \Lambda^{a}{}_{\overline{d}}\,\partial_{\overline{b}}\,\Lambda^{\overline{a}}{}_{a}. \tag{4.118}$$

The presence of a nonzero term, $\Lambda^{a}{}_{\overline{d}}\,\partial_{\overline{b}}\,\Lambda^{\overline{a}}{}_{a}$, means that $\Gamma^{\overline{a}}_{\overline{bd}}$ does not transform as components to a tensor.

4.12 Covariant derivative of a one-form

The product of a one-form and a vector is a scalar. As seen in Section 4.10, the covariant derivative of a scalar field is given by the gradient operator

$$\nabla(\mathbf{E}\cdot\mathbf{F}) = \boldsymbol{e}^{b}\,\partial_{b}\,(E_{a}\,F^{a}). \tag{4.119}$$

Expanding the partial derivative yields

$$\begin{aligned}
\partial_{b}(E_{a}\,F^{a}) &= F^{a}\,\partial_{b}E_{a} + E_{a}\,\partial_{b}F^{a} && \text{(4.120a)}\\
&= F^{a}\,\partial_{b}E_{a} + E_{a}\,(\nabla_{b}F^{a} - \Gamma^{a}_{bc}F^{c}) && \text{(4.120b)}\\
&= F^{a}(\partial_{b}E_{a} - \Gamma^{c}_{ba}E_{c}) + E_{a}\,\nabla_{b}F^{a} && \text{(4.120c)}\\
&\equiv F^{a}\,\nabla_{b}E_{a} + E_{a}\,\nabla_{b}F^{a}. && \text{(4.120d)}
\end{aligned}$$

The last equality defines the covariant derivative when acting on the components to a one form

$$\nabla_{b}E_{a} = \partial_{b}E_{a} - \Gamma^{c}_{ba}E_{c}, \tag{4.121}$$

which leads to the coordinate invariant expression for the covariant derivative of a one-form

$$\nabla\mathbf{E} = (\boldsymbol{e}^{b}\,\partial_{b})\,\mathbf{E} = (\boldsymbol{e}^{b}\,\nabla_{b}E_{a})\,\boldsymbol{e}^{a}. \tag{4.122}$$

4.13 Covariant derivative of the metric tensor

When written in Cartesian coordinates, the covariant derivative of components to the metric tensor for Euclidean space vanishes,

$$\nabla_{c}\mathfrak{g}_{ab} = \nabla_{c}\delta_{ab} = 0, \tag{4.123}$$

because the Cartesian representation of the metric is the unit tensor, δ_{ab}, in which case all Christoffel symbols vanish. Previous results establish the tensorial nature of the covariant derivative. Hence, $\nabla_{c}\mathfrak{g}_{ab} = 0$ is a valid result for *all* coordinates. This result is often called the *metricity* condition. It represents a self-consistency condition required for the manifolds considered in this book. Importantly, it holds only so long as the covariant derivative and the metric tensor are represented by the same coordinates. Namely, if we consider an alternative coordinate system to represent the covariant derivative, say $\nabla_{\overline{c}}$, then we generally have $\nabla_{\overline{c}}\mathfrak{g}_{ab} \neq 0$.

4.14 Christoffel symbols in terms of the metric tensor

We can develop an expression for the covariant derivative when acting on the components to a second order tensor. When applied to the metric tensor, its vanishing covariant derivative (equation (4.123)) then leads to the identity

$$0 = \nabla_{c}\mathfrak{g}_{ab} = \partial_{c}\mathfrak{g}_{ab} - \Gamma^{d}_{ca}\,\mathfrak{g}_{db} - \Gamma^{d}_{cb}\,\mathfrak{g}_{ad}. \tag{4.124}$$

We can solve this equation for the Christoffel symbols

$$\Gamma^c_{ab} = \frac{1}{2}\,\mathcal{G}^{cd}\,(\partial_b\,\mathcal{G}_{da} + \partial_a\,\mathcal{G}_{db} - \partial_d\,\mathcal{G}_{ab}). \tag{4.125}$$

This expression exhibits the symmetry property of the lower two indices on the Christoffel symbols

$$\Gamma^c_{ab} = \Gamma^c_{ba}. \tag{4.126}$$

This symmetry property holds for for spaces with zero *torsion*, such as the Euclidean space considered in this book.

As an aside, we remark on the notation used for the Christoffel symbols. For that purpose, introduce the *torsion tensor*,

$$\mathcal{T}_{ab}{}^c = \Gamma^c_{ab} - \Gamma^c_{ba}. \tag{4.127}$$

For Euclidean space the torsion tensor vanishes identically, and this property holds for manifolds embedded in Euclidean space that inherit the connection properties of Euclidean space. That is, no matter what coordinates we use, each element of the torsion tensor is zero, $\mathcal{T}_{ab}{}^c = 0$. Having $\mathcal{T}_{ab}{}^c = 0$ for all coordinates assures us that the torsion is indeed a tensor. As a tensor we make use of the tensor notation with the upstairs c on the torsion tensor displaced to the right, $\mathcal{T}_{ab}{}^c$. In contrast, the non-tensorial Christoffel symbols have the c vertically aligned and so not displaced. This purposeful usage of notation is indicative of tensor analysis.

4.15 Covariant divergence of a vector

The covariant divergence of the components to a vector results in a scalar

$$\nabla_a F^a = \partial_a F^a + \Gamma^a_{ab} F^b. \tag{4.128}$$

We now bring this expression into a form more convenient for practical calculations.

4.15.1 Contraction of the Christoffel symbols

Expression (4.125) for the Christoffel symbols yields the contraction

$$\Gamma^a_{ab} = \frac{1}{2}\,\mathcal{G}^{ad}(\partial_b\,\mathcal{G}_{da} + \partial_a\,\mathcal{G}_{db} - \partial_d\,\mathcal{G}_{ab}) = \frac{1}{2}\,\mathcal{G}^{ad}\,\partial_b\,\mathcal{G}_{ad} \tag{4.129}$$

where symmetry of both the metric tensor and its inverse was used.

4.15.2 Exponential of the determinant

For the matrix representation of a symmetric positive definite tensor, such as the metric tensor, we can write

$$\begin{aligned}
\det(A) &= e^{\ln\det(A)} && \text{identity} && \text{(4.130a)}\\
&= e^{\ln(\Pi_i \Lambda_i)} && \text{determinant related to product of eigenvalues} && \text{(4.130b)}\\
&= e^{\Sigma_i \ln \Lambda_i} && \text{identity} && \text{(4.130c)}\\
&= e^{\mathrm{Tr}(\ln A)} && \text{sum of eigenvalues related to trace of matrix.} && \text{(4.130d)}
\end{aligned}$$

Each of these identities is trivial to verify using a set of coordinates in which the matrix is diagonal. For any symmetric and positive definite matrix, such a set of coordinates always exists, in which case

$$\partial_c \ln\det(A) = \partial_c[\mathrm{Tr}(\ln A)] = \mathrm{Tr}(\partial_c \ln A) = \mathrm{Tr}(A^{-1}\partial_c A). \tag{4.131}$$

With A now set equal to the metric tensor, $\mathbb{g}_{ab}$, this result yields

$$\partial_c \ln \det(\mathbb{g}_{ab}) = \mathbb{g}^{ab}\, \partial_c\, \mathbb{g}_{ab} \tag{4.132}$$

which in turn yields for the contracted Christoffel symbol

$$\Gamma^a_{ac} = \partial_c \ln(\sqrt{\det(\mathbb{g}_{ab})}) = \partial_c \ln g. \tag{4.133}$$

This result brings the covariant divergence of a vector to the form

$$\nabla \cdot \mathbf{F} = \nabla_a\, F^a = \partial_a F^a + F^a\, \partial_a \ln g = g^{-1}\, \partial_a (g\, F^a). \tag{4.134}$$

This is a very convenient result. In particular, it only requires partial derivatives in the chosen coordinate system, with all the coordinate dependent properties summarized by $g = \sqrt{\det(\mathbb{g}_{ab})}$.

4.16 Covariant Laplacian of a scalar

Making use of equation (4.134) with

$$F^a = \mathbb{g}^{ab}\, \partial_b \psi \tag{4.135}$$

leads to the covariant Laplacian of a scalar field

$$\nabla_a\, (\mathbb{g}^{ab}\, \partial_b\, \psi) = \frac{1}{\sqrt{\det(\mathbb{g}_{ab})}}\, \partial_a\, [\sqrt{\det(\mathbb{g}_{ab})}\; \mathbb{g}^{ab}\, \partial_b \psi] = g^{-1}\, \partial_a\, (g\;\; \mathbb{g}^{ab}\, \partial_b \psi). \tag{4.136}$$

This expression is fundamental to the evolution of scalar fields under the impacts from diffusion (Chapter 69).

4.17 Covariant divergence of a second order tensor

We find many occasions to compute the covariant divergence a second order tensor, such as the stress tensor appearing in the momentum equation (Chapter 24) or the eddy transport tensor appearing in the tracer equation (Chapter 71). Following the methods used for derivating the covariant derivative of a vector in Section 4.11 (see also Section 21.6 of *Griffies* (2004)), we have the covariant divergence of the $(2, 0)$ (sharp) representation of a second order tensor

$$\nabla_a T^{ab} = \partial_a T^{ab} + \Gamma^b_{ad}\, T^{da} + \Gamma^a_{ad}\, T^{bd}. \tag{4.137}$$

It is convenient to split the tensor components into the symmetric and antisymmetric parts

$$S^{ab} = (T^{ab} + T^{ba})/2 \quad \text{and} \quad R^{ab} = (T^{ab} - T^{ba})/2. \tag{4.138}$$

The covariant divergence of the symmetric components is

$$\nabla_a S^{ab} = g^{-1} \partial_a (g\, S^{ab}) + \Gamma^b_{ad}\, S^{ad}, \tag{4.139}$$

where we used equation (4.133) for the contraction of the Christoffel symbol. For the anti-symmetric tensor, the $\Gamma^b_{ad}\, R^{ad}$ term drops out since Γ^b_{ad} is symmetric on the indices a, d, whereas R^{ad} is anti-symmetric. We are thus led to the covariant divergence of an anti-symmetric tensor

$$\nabla_a R^{ab} = g^{-1}\, \partial_a (g\, R^{ab}). \tag{4.140}$$

This relation is analogous to the covariant divergence of a vector given by equation (4.134). In particular, the vector components

$$F^b \equiv \nabla_a R^{ab} \tag{4.141}$$

are divergence-free since

$$\nabla_b F^b = g^{-1}\,\partial_b(g\,F^b) = g^{-1}\,\partial_b(g\,\nabla_a R^{ab}) = g^{-1}\,\partial_b\partial_a(g\,R^{ab}) = 0, \tag{4.142}$$

which follows from anti-symmetry of the components R^{ab} under interchange of a, b and symmetry of $\partial_b\partial_a$.

4.18 Covariant curl of a vector

The Levi-Civita tensor from Section 4.7

$$\varepsilon_{abc} = \sqrt{\det(\mathbb{g}_{ab})}\,\epsilon_{abc} = g\,\epsilon_{abc}, \tag{4.143}$$

as well as its inverse

$$\varepsilon^{abc} = (1/\sqrt{\det(\mathbb{g}_{ab})})\,\epsilon^{abc} = (1/g)\,\epsilon^{abc}, \tag{4.144}$$

are useful in generalizing the curl operation from Cartesian coordinates in Euclidean space to arbitrary coordinates on a curved manifold embedded in Euclidean space. For this purpose we define the covariant curl according to the coordinate invariant expression

$$\mathrm{curl}(\boldsymbol{F}) = \boldsymbol{e}_a\,\varepsilon^{abc}\,(\nabla_b F_c) = \boldsymbol{e}^a\,\varepsilon_{abc}\,(\nabla^b F^c). \tag{4.145}$$

This expression simplifies by making use of equation (4.121) for the covariant derivative, $\nabla_b\,F_c = \partial_b F_c - \Gamma^a_{cb}\,F_a$. Conveniently, the contraction $\varepsilon^{abc}\,\Gamma^a_{cb}$ vanishes identically since $\varepsilon^{abc} = -\varepsilon^{acb}$ whereas $\Gamma^a_{cb} = \Gamma^a_{bc}$. Hence, we are left with a general expression for the covariant curl that involves just the partial derivatives

$$\mathrm{curl}(\boldsymbol{F}) = \boldsymbol{e}_a\,\varepsilon^{abc}\,\partial_b F_c = \boldsymbol{e}_a\,\varepsilon^{abc}\,\partial_b(\mathbb{g}_{cd}F^d) = \boldsymbol{e}_a\,(1/g)\,\epsilon^{abc}\,\partial_b(\mathbb{g}_{cd}F^d), \tag{4.146}$$

where the second equality made use of the identity $F_c = \mathbb{g}_{cd}F^d$.

4.19 Gauss's divergence theorem

The integral theorems from Cartesian vector analysis transform in a straightforward manner to arbitrary coordinates in arbitrary smooth and oriented spaces. An easy way to prove the theorems is to invoke the ideas of general coordinate invariance from Section 3.1, in which the integral theorems are written in a tensorially proper manner with partial derivatives changed to covariant derivatives. The divergence theorem offers a particularly simple example. For this purpose, make use of the volume element (4.60)

$$\mathrm{d}V = \sqrt{\det(\mathbb{g}_{ab})}\,\mathrm{d}\xi^1\,\mathrm{d}\xi^2\,\mathrm{d}\xi^3, \tag{4.147}$$

multiplied by the covariant divergence (4.134). Hence, the volume integral of the divergence is given by

$$\int_{\mathcal{R}} (\nabla_a\,F^a)\,\mathrm{d}V = \int_{\mathcal{R}} \partial_a[\sqrt{\det(\mathbb{g}_{ab})}\,F^a]\,\mathrm{d}\xi^1\,\mathrm{d}\xi^2\,\mathrm{d}\xi^3 = \oint_{\partial\mathcal{R}} F^a\,\hat{n}_a\,\mathrm{d}\mathcal{S}. \tag{4.148}$$

In this equation, $\hat{\boldsymbol{n}}$ is the outward *normal one-form* for the boundary, $\partial\mathcal{R}$, with $\mathrm{d}\mathcal{S}$ the invariant area element on the boundary, and $\hat{n}_a$ the covariant components of the outward normal.

4.20 Stokes' curl theorem

The Cartesian form of Stokes' Theorem from Section 2.6 is generalized in a manner similar to the divergence theorem

$$\oint_{\partial\mathcal{S}} \boldsymbol{F}\cdot\mathrm{d}\boldsymbol{x} = \int_{\mathcal{S}} \mathrm{curl}(\boldsymbol{F})\cdot\hat{\boldsymbol{n}}\,\mathrm{d}\mathcal{S}, \tag{4.149}$$

where $\mathrm{d}\boldsymbol{x}$ is the vector line element along the path and $\partial\mathcal{S}$ is the closed path defining the boundary to a simply connected two-dimensional surface, $\mathcal{S}$. For the circulation on the left hand side we have

$$\boldsymbol{F}\cdot\mathrm{d}\boldsymbol{x} = F^a\,\boldsymbol{e}_a\cdot\boldsymbol{e}_b\,\mathrm{d}x^b = F_b\,\mathrm{d}x^b = F_{\bar{b}}\,\mathrm{d}\xi^{\bar{b}}. \tag{4.150}$$

For the curl on the right hand side we have

$$\mathrm{curl}(\boldsymbol{F})\cdot\hat{\boldsymbol{n}} = \varepsilon^{abc}\,(\partial_b F_c)\,\boldsymbol{e}_a\cdot\hat{\boldsymbol{n}} = \varepsilon^{abc}\,(\partial_b F_c)\,\hat{n}_a = \varepsilon^{\bar{a}\bar{b}\bar{c}}\,(\partial_{\bar{b}} F_{\bar{c}})\,\hat{n}_{\bar{a}}, \tag{4.151}$$

thus leading to the expression of Stokes' theorem in arbitrary coordinates

$$\oint_{\partial\mathcal{S}} F_{\bar{b}}\,\mathrm{d}\xi^{\bar{b}} = \int_{\mathcal{S}} \varepsilon^{\bar{a}\bar{b}\bar{c}}\,(\partial_{\bar{b}} F_{\bar{c}})\,\hat{n}_{\bar{a}}\,\mathrm{d}\mathcal{S}. \tag{4.152}$$

4.21 Summary of Cartesian coordinates

Whenever developing a general tensor relation it is useful to check its validity by considering Cartesian coordinates, in which case we can make use of familiar rules from vector calculus. We here summarize some results from our discussion of Cartesian tensors in Chapters 1 and 2.

4.21.1 The basics

We start by expressing the trajectory of a point through space in the following equivalent forms

$$\mathbf{x}(\tau) = \boldsymbol{e}_1\,x(\tau) + \boldsymbol{e}_2\,y(\tau) + \boldsymbol{e}_3\,z(\tau) = \hat{\boldsymbol{x}}\,x(\tau) + \hat{\boldsymbol{y}}\,y(\tau) + \hat{\boldsymbol{z}}\,z(\tau) \tag{4.153}$$

with the basis vectors written

$$\boldsymbol{e}_1 = \hat{\boldsymbol{x}} \qquad \text{and} \qquad \boldsymbol{e}_2 = \hat{\boldsymbol{y}} \qquad \text{and} \qquad \boldsymbol{e}_3 = \hat{\boldsymbol{z}}. \tag{4.154}$$

The orthogonal unit vectors for Cartesian coordinates are normalized so that

$$\boldsymbol{e}_1\cdot\boldsymbol{e}_1 = \boldsymbol{e}_2\cdot\boldsymbol{e}_2 = \boldsymbol{e}_3\cdot\boldsymbol{e}_3 = 1. \tag{4.155}$$

Furthermore, the basis vectors are identical to the basis one-forms

$$\boldsymbol{e}_1 = \boldsymbol{e}^1 = \hat{\boldsymbol{x}} \qquad \text{and} \qquad \boldsymbol{e}_2 = \boldsymbol{e}^2 = \hat{\boldsymbol{y}} \qquad \text{and} \qquad \boldsymbol{e}_3 = \boldsymbol{e}^3 = \hat{\boldsymbol{z}}, \tag{4.156}$$

in which we see there is no importance placed on whether a tensor index is up or down. Since the Cartesian basis vectors are independent of both space and time, we compute the coordinate representation of the velocity vector through taking the time derivative as

$$\boldsymbol{v}(\tau) = \frac{\mathrm{d}\boldsymbol{x}}{\mathrm{d}\tau}, \tag{4.157}$$

which takes on the expanded expressions

$$\boldsymbol{v}(\tau) = \boldsymbol{e}_1\,\frac{\mathrm{d}x(\tau)}{\mathrm{d}\tau} + \boldsymbol{e}_2\,\frac{\mathrm{d}y(\tau)}{\mathrm{d}\tau} + \boldsymbol{e}_3\,\frac{\mathrm{d}z(\tau)}{\mathrm{d}\tau} \tag{4.158a}$$

$$= \hat{\boldsymbol{x}}\, v^1(\tau) + \hat{\boldsymbol{y}}\, v^2(\tau) + \hat{\boldsymbol{z}}\, v^3(\tau). \tag{4.158b}$$

$$= \hat{\boldsymbol{x}}\, u(\tau) + \hat{\boldsymbol{y}}\, v(\tau) + \hat{\boldsymbol{z}}\, w(\tau), \tag{4.158c}$$

where (u, v, w) is the notation commonly used in this book for the three velocity components.

4.21.2 Concerning the horizontal gradient operator

Geophysical fluids are affected by gravity, and gravity breaks the spatial symmetry between the locally vertical (i.e., radial) and horizontal (i.e., local tangent plane) for fluid motion on a planet. We have thus many occasions where the horizontal is treated distinctly from the vertical. For that purpose we often find it useful to decompose the gradient operator into its horizontal and vertical components, writing the operator in one of the following manners

$$\nabla = \nabla_{\mathsf{h}} + \nabla_z = \nabla_{\mathsf{h}} + \hat{\boldsymbol{z}}\, \partial_z, \tag{4.159}$$

where the horizontal gradient operator, using Cartesian coordinates, is

$$\nabla_{\mathsf{h}} = \hat{\boldsymbol{x}}\, \nabla_x + \hat{\boldsymbol{y}}\, \nabla_y. \tag{4.160}$$

In earlier drafts of this book, as well as in many publications, we find the horizontal gradient operator written as ∇_z rather than ∇_{h}. In this alternative notation, the subscript z indicates that the derivative acts along surfaces of constant z. However, this notation is easily confused in this book. In particular, the ∇ operator has tensor labels that distinguish its components, in which case the vertical component to the Cartesian gradient operator is $\nabla_z = \hat{\boldsymbol{z}}\, \partial_z$. Herein lies the source of much confusion. To avoid that confusion we have chosen to use the ∇_{h} in this book for the horizontal gradient operator. To further reduce potential for confusion, we make use of the upright and sans serif h label. This label is not a tensor index but instead indicates that the operator is computed along a locally constant horizontal direction, and so is part of the operator's name. The h label is also placed quite close to the ∇ symbol, nearly attached, in order to further distinguish it from a tensor index.

4.21.3 Summary

In Cartesian coordinates, mathematical operators and integral theorems take their familiar form from vector calculus. We here list those encountered throughout this book.

$$\boldsymbol{x} = (x^1, x^2, x^3) = (x, y, z) \qquad \text{Cartesian coordinates} \tag{4.161}$$

$$\boldsymbol{F} = \hat{\boldsymbol{x}} F^1 + \hat{\boldsymbol{y}} F^2 + \hat{\boldsymbol{z}} F^3 = \hat{\boldsymbol{x}} F_1 + \hat{\boldsymbol{y}} F_2 + \hat{\boldsymbol{z}} F_3 \qquad \text{covariant = contravariant} \tag{4.162}$$

$$\frac{\partial}{\partial x^a} = \partial_a \;\text{ or }\; (\partial_x, \partial_y, \partial_z) \qquad \text{partial derivative operator} \tag{4.163}$$

$$\nabla = \hat{\boldsymbol{x}}\, \partial_x + \hat{\boldsymbol{y}}\, \partial_y + \hat{\boldsymbol{z}}\, \partial_z \qquad \text{gradient = covariant derivative} \tag{4.164}$$

$$\nabla_{\mathsf{h}} = \hat{\boldsymbol{x}}\, \partial_x + \hat{\boldsymbol{y}}\, \partial_y \qquad \text{horizontal gradient operator} \tag{4.165}$$

$$\nabla \cdot \boldsymbol{F} = \partial_x F^x + \partial_y F^y + \partial_z F^z \qquad \text{divergence of a vector} \tag{4.166}$$

$$\nabla_{\mathsf{h}} \cdot \boldsymbol{F} = \partial_x F^x + \partial_y F^y \qquad \text{horizontal divergence of a vector} \tag{4.167}$$

$$(\nabla \times \boldsymbol{F})_a = \epsilon_{abc}\, \partial^b F^c \qquad \text{components to the curl} \tag{4.168}$$

$$\nabla \cdot \nabla\psi = \nabla^2 \psi = (\partial_{xx} + \partial_{yy} + \partial_{zz})\, \psi \qquad \text{Laplacian of a scalar} \tag{4.169}$$

$$\int_{\mathcal{R}} \nabla \cdot \boldsymbol{F}\, \mathrm{d}V = \oint_{\partial\mathcal{R}} \boldsymbol{F} \cdot \hat{\boldsymbol{n}}\, \mathrm{d}\mathcal{S} \qquad \text{Gauss's divergence theorem} \tag{4.170}$$

$$\oint_{\partial\mathcal{S}} \boldsymbol{F} \cdot \mathrm{d}\boldsymbol{x} = \int_{\mathcal{S}} (\nabla \times \boldsymbol{F}) \cdot \hat{\boldsymbol{n}}\, \mathrm{d}\mathcal{S}. \qquad \text{Stokes' curl theorem.} \tag{4.171}$$

4.22 Summary of cylindrical-polar coordinates

Many physical systems exhibit circular symmetry in two-dimensions or cylindrical symmetry in three-dimensions. Motion of liquid in a rotating circular tank provides the primary physical example encountered in this book. In the following, we emulate the discussion presented for the spherical coordinates in Section 4.23, here focusing on the cylindrical-polar coordinates shown in Figure 4.2. Our task is somewhat simpler than for the spherical coordinates since the vertical/axial position, z, remains unchanged from its Cartesian value. In a slight corruption of notation, we use the symbol r for the radial distance from the vertical axis in cylindrical-polar coordinates (Figure 4.2), which is distinct from the radial distance, r, used to measure the distance from the origin in spherical coordinates (Figure 4.3).[2]

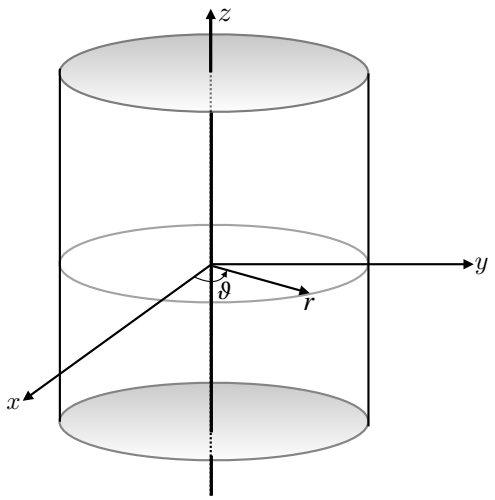

FIGURE 4.2: This schematic illustrates the geometry and notation for cylindrical-polar coordinates. The Cartesian triad of orthonormal basis vectors, $(\hat{\boldsymbol{x}}, \hat{\boldsymbol{y}}, \hat{\boldsymbol{z}})$ points along the orthogonal axes. The cylindrical-polar triad of orthonormal basis vectors, $(\hat{\boldsymbol{r}}, \hat{\boldsymbol{\vartheta}}, \hat{\boldsymbol{z}})$, makes use of the radial unit vector $\hat{\boldsymbol{r}}$, which points outward from the vertical axis, the angular unit vector $\hat{\boldsymbol{\vartheta}}$, which points in the counter-clockwise direction around the circle, and the vertical unit vector $\hat{\boldsymbol{z}}$. Note that the radial unit vector used for cylindrical-polar coordinates is distinct from that radial vector used in spherical coordinates shown in Figure 4.3.

The coordinate transformation between Cartesian coordinates and cylindrical-polar coordinates is given by

$$x = r\cos\vartheta \equiv \xi^{\overline{1}}\cos\xi^{\overline{2}} \tag{4.172a}$$

$$y = r\sin\vartheta \equiv \xi^{\overline{1}}\sin\xi^{\overline{2}} \tag{4.172b}$$

$$z = \xi^{\overline{3}}. \tag{4.172c}$$

The radial coordinate for cylindrical-polar coordinates

$$r = \sqrt{x^2 + y^2} \tag{4.173}$$

measures the distance from the vertical z-axis, and the angular coordinate $0 \leq \vartheta \leq 2\pi$ measures the angle counter-clockwise from the positive x-axis. We introduce the unbarred and barred labels for the Cartesian and cylindrical polar coordinates

$$(x, y, z) = (\xi^1, \xi^2, \xi^3) \equiv \xi^a \qquad \text{and} \qquad (r, \vartheta, z) = (\xi^{\overline{1}}, \xi^{\overline{2}}, \xi^{\overline{3}}) \equiv \xi^{\overline{a}}. \tag{4.174}$$

[2] Many mathematics texts use ρ for the cylindrical radial distance. We choose not to follow that convention, since ρ is reserved in this book for mass density.

Although the vertical coordinate, z, remains the same in both Cartesian and cylindrical-polar coordinates, and it is orthogonal to the other coordinates, we find it useful to introduce a distinct symbols, ξ^3 and $\xi^{\overline{3}}$, to specify what other coordinates are held fixed when performing partial derivative operations.

4.22.1 Cartesian and cylindrical-polar transformation

The coordinate transformation (4.172a)-(4.172c) leads to the transformation matrix

$$\Lambda^a{}_{\overline{a}} = \begin{bmatrix} \partial\xi^1/\partial\xi^{\overline{1}} & \partial\xi^1/\partial\xi^{\overline{2}} & \partial\xi^1/\partial\xi^{\overline{3}} \\ \partial\xi^2/\partial\xi^{\overline{1}} & \partial\xi^2/\partial\xi^{\overline{2}} & \partial\xi^2/\partial\xi^{\overline{3}} \\ \partial\xi^3/\partial\xi^{\overline{1}} & \partial\xi^3/\partial\xi^{\overline{2}} & \partial\xi^3/\partial\xi^{\overline{3}} \end{bmatrix} = \begin{bmatrix} \cos\vartheta & -r\sin\vartheta & 0 \\ \sin\vartheta & r\cos\vartheta & 0 \\ 0 & 0 & 1 \end{bmatrix} \tag{4.175}$$

and the inverse transformation is given by

$$\Lambda^{\overline{a}}{}_a = \frac{1}{r}\begin{bmatrix} r\cos\vartheta & r\sin\vartheta & 0 \\ -\sin\vartheta & \cos\vartheta & 0 \\ 0 & 0 & r \end{bmatrix}. \tag{4.176}$$

The determinant of the transformation (Jacobian) is given by

$$\det(\Lambda^a{}_{\overline{a}}) = r, \tag{4.177}$$

which vanishes along the vertical axis, which is where the transformation is singular. Otherwise, the coordinate transformation is one-to-one and invertible.

4.22.2 Basis vectors

The cylindrical-polar coordinate basis vectors, $\boldsymbol{e}_{\overline{a}}$, are related to the Cartesian coordinate basis vectors, $\boldsymbol{e}_a$, through the transformation $\boldsymbol{e}_{\overline{a}} = \Lambda^a{}_{\overline{a}}\,\boldsymbol{e}_a$. The transformation matrix (4.175) leads to

$$\boldsymbol{e}_r = \hat{\boldsymbol{x}}\cos\vartheta + \hat{\boldsymbol{y}}\sin\vartheta \tag{4.178a}$$
$$\boldsymbol{e}_\vartheta = r\,(-\hat{\boldsymbol{x}}\sin\vartheta + \hat{\boldsymbol{y}}\cos\vartheta) \tag{4.178b}$$
$$\boldsymbol{e}_{\overline{z}} = \hat{\boldsymbol{z}}. \tag{4.178c}$$

It is convenient to introduce the following orthonormal unit vectors $(\hat{\boldsymbol{r}}, \hat{\boldsymbol{\vartheta}}, \hat{\boldsymbol{z}})$, which point in directions of increasing r, ϑ, and z, and which are related to the basis vectors via

$$\boldsymbol{e}_r = \hat{\boldsymbol{r}} \qquad \text{and} \qquad \boldsymbol{e}_\vartheta = r\,\hat{\boldsymbol{\vartheta}} \qquad \text{and} \qquad \boldsymbol{e}_{\overline{z}} = \hat{\boldsymbol{z}}, \tag{4.179}$$

along with the inverse relations

$$\hat{\boldsymbol{x}} = \hat{\boldsymbol{r}}\cos\vartheta - \hat{\boldsymbol{\vartheta}}\sin\vartheta \tag{4.180a}$$
$$\hat{\boldsymbol{y}} = \hat{\boldsymbol{r}}\sin\vartheta + \hat{\boldsymbol{\vartheta}}\cos\vartheta \tag{4.180b}$$
$$\hat{\boldsymbol{z}} = \hat{\boldsymbol{z}}. \tag{4.180c}$$

4.22.3 Basis one-forms

Since cylindrical-polar coordinates are orthogonal, we can readily derive the one-form basis through inverting the vector basis

$$\boldsymbol{e}^r = \hat{\boldsymbol{r}} \qquad \text{and} \qquad \boldsymbol{e}^\vartheta = r^{-1}\hat{\boldsymbol{\vartheta}} \qquad \text{and} \qquad \boldsymbol{e}^{\overline{z}} = \hat{\boldsymbol{z}}, \tag{4.181}$$

which satisfy the duality condition (Section 4.2.2)

$$\boldsymbol{e}^{\bar{b}} \cdot \boldsymbol{e}_{\bar{a}} = \delta^{\bar{b}}{}_{\bar{a}}. \tag{4.182}$$

4.22.4 Position and velocity

In cylindrical-polar coordinates, the position of a point is specified by the radial position plus the vertical position

$$\boldsymbol{x}(\tau) = r\,\boldsymbol{e}_r + z\,\boldsymbol{e}_{\bar{z}}. \tag{4.183}$$

The velocity requires all three coordinates since the radial basis vector is a function of the angular positions, which are in turn functions of time. Use of the chain rule renders

$$\begin{aligned}
\boldsymbol{v}(\tau) &= \frac{\mathrm{d}\boldsymbol{x}}{\mathrm{d}\tau} && \text{(4.184a)}\\
&= \boldsymbol{e}_r \frac{\mathrm{d}r}{\mathrm{d}\tau} + r\frac{\mathrm{d}\boldsymbol{e}_r}{\mathrm{d}\tau} + \boldsymbol{e}_{\bar{z}}\frac{\mathrm{d}z}{\mathrm{d}\tau} && \text{(4.184b)}\\
&= \boldsymbol{e}_r \frac{\mathrm{d}r}{\mathrm{d}\tau} + r\frac{\partial \boldsymbol{e}_r}{\partial\vartheta}\frac{\mathrm{d}\vartheta}{\mathrm{d}\tau} + \boldsymbol{e}_{\bar{z}}\frac{\mathrm{d}z}{\mathrm{d}\tau} && \text{(4.184c)}\\
&= \boldsymbol{e}_r \frac{\mathrm{d}r}{\mathrm{d}\tau} + \boldsymbol{e}_{\vartheta}\frac{\mathrm{d}\vartheta}{\mathrm{d}\tau} + \boldsymbol{e}_{\bar{z}}\frac{\mathrm{d}z}{\mathrm{d}\tau} && \text{(4.184d)}\\
&= \boldsymbol{e}_r\, v^r + \boldsymbol{e}_{\vartheta}\, v^{\vartheta} + \boldsymbol{e}_{\bar{z}}\, v^{\bar{z}}. && \text{(4.184e)}
\end{aligned}$$

To reach this result we made use of the identity

$$\boldsymbol{e}_{\vartheta} = r\frac{\partial \boldsymbol{e}_r}{\partial\vartheta} = r\,\hat{\boldsymbol{\vartheta}}. \tag{4.185}$$

4.22.5 Metric tensor

Cylindrical-polar coordinates are orthogonal with the metric tensor and its inverse represented by the diagonal matrices

$$\mathfrak{g}_{\bar{a}\bar{b}} = \boldsymbol{e}_{\bar{a}} \cdot \boldsymbol{e}_{\bar{b}} = \begin{bmatrix} 1 & 0 & 0 \\ 0 & r^2 & 0 \\ 0 & 0 & 1 \end{bmatrix} \qquad \text{and} \qquad \mathfrak{g}^{\bar{a}\bar{b}} = \boldsymbol{e}^{\bar{a}} \cdot \boldsymbol{e}^{\bar{b}} = \begin{bmatrix} 1 & 0 & 0 \\ 0 & r^{-2} & 0 \\ 0 & 0 & 1 \end{bmatrix}. \tag{4.186}$$

4.22.6 Volume element and Levi-Civita tensor

The square root of the determinant of the metric tensor written in cylindrical-polar coordinates (from equation (4.186)) is given by

$$\sqrt{\det(\mathfrak{g}_{\bar{a}\bar{b}})} = r \tag{4.187}$$

so that the volume element is

$$\mathrm{d}V = r\,\mathrm{d}r\,\mathrm{d}\vartheta\,\mathrm{d}z. \tag{4.188}$$

The covariant Levi-Civita tensor has the cylindrical-polar representation

$$\varepsilon_{\bar{a}\bar{b}\bar{c}} = r\,\epsilon_{\bar{a}\bar{b}\bar{c}}. \tag{4.189}$$

4.22.7 Vector cross product of basis vectors

As a check on the formalism for vector cross products, let us verify the relation (4.87) for the cross product of two basis vectors using cylindrical-polar coordinates

$$\boldsymbol{e}_{\overline{a}} \times \boldsymbol{e}_{\overline{b}} = \varepsilon_{\overline{a}\overline{b}\overline{c}}\, \boldsymbol{e}^{\overline{c}} \Longrightarrow \boldsymbol{e}_{\overline{a}} \times \boldsymbol{e}_{\overline{b}} = r\, \epsilon_{\overline{a}\overline{b}\overline{c}}\, \boldsymbol{e}^{\overline{c}}. \tag{4.190}$$

Making use of the cylindrical-polar coordinate basis vectors and one-forms renders

$$\boldsymbol{e}_r \times \boldsymbol{e}_{\vartheta} = r\,(\hat{\boldsymbol{r}} \times \hat{\boldsymbol{\vartheta}}) = r\, \boldsymbol{e}^{\overline{z}} = \varepsilon_{r\vartheta\overline{z}}\, \boldsymbol{e}^{\overline{z}} \tag{4.191a}$$

$$\boldsymbol{e}_{\vartheta} \times \boldsymbol{e}_{\overline{z}} = r\,(\hat{\boldsymbol{\vartheta}} \times \hat{\boldsymbol{z}}) = r\, \hat{\boldsymbol{r}} = r\, \boldsymbol{e}^{r} = \varepsilon_{\vartheta\overline{z}r}\, \boldsymbol{e}^{r} \tag{4.191b}$$

$$\boldsymbol{e}_{\overline{z}} \times \boldsymbol{e}_{r} = \hat{\boldsymbol{z}} \times \hat{\boldsymbol{r}} = \hat{\boldsymbol{\vartheta}} = r\, \boldsymbol{e}^{\vartheta} = \varepsilon_{\overline{z}r\vartheta}\, \boldsymbol{e}^{\vartheta}. \tag{4.191c}$$

To reach these results we made use of the cross products for the unit vectors

$$\hat{\boldsymbol{r}} \times \hat{\boldsymbol{\vartheta}} = \hat{\boldsymbol{z}} \qquad \text{and} \qquad \hat{\boldsymbol{\vartheta}} \times \hat{\boldsymbol{z}} = \hat{\boldsymbol{r}} \qquad \text{and} \qquad \hat{\boldsymbol{z}} \times \hat{\boldsymbol{r}} = \hat{\boldsymbol{\vartheta}}. \tag{4.192}$$

4.22.8 Components of a vector field

A vector field, $\mathbf{F}$, has Cartesian components, F^a, related to its cylindrical-polar components, $F^{\overline{a}}$, via the transformation matrix, $F^{\overline{a}} = \Lambda^{\overline{a}}{}_{a}\, F^a$. This transformation leads to

$$F^{\overline{1}} = F^x \cos\vartheta + F^y \sin\vartheta \tag{4.193a}$$

$$F^{\overline{2}} = r^{-1}\,[-F^x \sin\vartheta + F^y \cos\vartheta] \tag{4.193b}$$

$$F^{\overline{3}} = F^z. \tag{4.193c}$$

Introducing the cylindrical-polar unit vectors (4.179) leads to the more tidy expressions

$$F^{\overline{1}} = \hat{\boldsymbol{r}} \cdot \boldsymbol{F} \tag{4.194a}$$

$$r\, F^{\overline{2}} = \hat{\boldsymbol{\vartheta}} \cdot \boldsymbol{F} \tag{4.194b}$$

$$F^{\overline{3}} = \hat{\boldsymbol{z}} \cdot \boldsymbol{F}, \tag{4.194c}$$

where $\boldsymbol{F}$ is the Cartesian representation of the vector.

4.22.9 Differential operators

In cylindrical-polar coordinates, the gradient operator $\nabla = \boldsymbol{e}^a \partial_a$ is given by

$$\nabla = \hat{\boldsymbol{r}}\, \frac{\partial}{\partial r} + \frac{\hat{\boldsymbol{\vartheta}}}{r}\, \frac{\partial}{\partial \vartheta} + \hat{\boldsymbol{z}}\, \frac{\partial}{\partial z} \tag{4.195}$$

and the covariant divergence of a vector field is

$$\nabla_{\overline{a}} F^{\overline{a}} = r^{-1}\, \partial_{\overline{a}}\,(r\, F^{\overline{a}}) \tag{4.196a}$$

$$= r^{-1} \left(\partial_r [r\, F^{\overline{1}}] + \partial_{\vartheta} [r\, F^{\overline{2}}] + \partial_{\overline{z}} [r\, F^{\overline{3}}] \right) \tag{4.196b}$$

$$= \frac{1}{r}\, \frac{\partial (r\, \hat{\boldsymbol{r}} \cdot \boldsymbol{F})}{\partial r} + \frac{1}{r}\, \frac{\partial\, (\hat{\boldsymbol{\vartheta}} \cdot \boldsymbol{F})}{\partial \vartheta} + \frac{\partial (\hat{\boldsymbol{z}} \cdot \boldsymbol{F})}{\partial z}, \tag{4.196c}$$

where $\boldsymbol{F}$ is the Cartesian coordinate representation. The covariant Laplacian of a scalar, $\nabla^2\psi = \nabla\cdot\nabla\psi$, is

$$\nabla^2\psi = \nabla\cdot\left[\hat{\boldsymbol{r}}\,\frac{\partial\psi}{\partial r} + \frac{\hat{\boldsymbol{\vartheta}}}{r}\,\frac{\partial\psi}{\partial\vartheta} + \hat{\boldsymbol{z}}\,\frac{\partial\psi}{\partial z}\right] \tag{4.197a}$$

$$= \frac{1}{r}\,\frac{\partial}{\partial r}\left[r\,\frac{\partial\psi}{\partial r}\right] + \frac{1}{r^2}\,\frac{\partial^2\psi}{\partial\vartheta^2} + \frac{\partial^2\psi}{\partial z^2}. \tag{4.197b}$$

The covariant curl (Section 4.18) is

$$(\operatorname{curl}\mathbf{F})^{\bar{1}} = r^{-1}\left[\partial_\vartheta\,F^{\bar{3}} - \partial_{\bar{z}}\,(r^2\,F^{\bar{2}})\right] \tag{4.198a}$$

$$(\operatorname{curl}\mathbf{F})^{\bar{2}} = r^{-1}\left[\partial_{\bar{z}}\,F^{\bar{1}} - \partial_r\,F^{\bar{3}}\right] \tag{4.198b}$$

$$(\operatorname{curl}\mathbf{F})^{\bar{3}} = r^{-1}\left[\partial_r\,(r^2\,F^{\bar{2}}) - \partial_\vartheta\,F^{\bar{1}}\right], \tag{4.198c}$$

which can be written more conventionally as

$$(\operatorname{curl}\mathbf{F})^{\bar{1}} = \frac{1}{r}\,\frac{\partial(\hat{\boldsymbol{z}}\cdot\boldsymbol{F})}{\partial\vartheta} - \frac{\partial(\hat{\boldsymbol{\vartheta}}\cdot\boldsymbol{F})}{\partial z} \tag{4.199a}$$

$$r\,(\operatorname{curl}\mathbf{F})^{\bar{2}} = \frac{\partial(\hat{\boldsymbol{r}}\cdot\boldsymbol{F})}{\partial z} - \frac{\partial(\hat{\boldsymbol{z}}\cdot\boldsymbol{F})}{\partial r} \tag{4.199b}$$

$$(\operatorname{curl}\mathbf{F})^{\bar{3}} = \frac{1}{r}\,\frac{\partial(r\,\hat{\boldsymbol{\vartheta}}\cdot\boldsymbol{F})}{\partial r} - \frac{1}{r}\,\frac{\partial(\hat{\boldsymbol{r}}\cdot\boldsymbol{F})}{\partial\vartheta}. \tag{4.199c}$$

4.22.10 Summary

We here summarize the cylindrical coordinate version of some common mathematical operators.

$$(r,\vartheta,z) = (x^{\bar{1}},x^{\bar{2}},x^{\bar{3}}) \tag{4.200}$$

$$F^{\bar{1}} = \hat{\boldsymbol{r}}\cdot\boldsymbol{F} \qquad r\,F^{\bar{2}} = \hat{\boldsymbol{\vartheta}}\cdot\boldsymbol{F} \qquad F^{\bar{3}} = \hat{\boldsymbol{z}}\cdot\boldsymbol{F} \tag{4.201}$$

$$\nabla = \hat{\boldsymbol{r}}\,\frac{\partial}{\partial r} + \frac{\hat{\boldsymbol{\vartheta}}}{r}\,\frac{\partial}{\partial\vartheta} + \hat{\boldsymbol{z}}\,\frac{\partial}{\partial z} \tag{4.202}$$

$$\nabla_{\bar{a}}F^{\bar{a}} = \frac{1}{r}\,\frac{\partial(r\,\hat{\boldsymbol{r}}\cdot\boldsymbol{F})}{\partial r} + \frac{1}{r}\frac{\partial\,(\hat{\boldsymbol{\vartheta}}\cdot\boldsymbol{F})}{\partial\vartheta} + \frac{\partial(\hat{\boldsymbol{z}}\cdot\boldsymbol{F})}{\partial z}. \tag{4.203}$$

$$\nabla^2\psi = \frac{1}{r}\,\frac{\partial}{\partial r}\left[r\,\frac{\partial\psi}{\partial r}\right] + \frac{1}{r^2}\,\frac{\partial^2\psi}{\partial\vartheta^2} + \frac{\partial^2\psi}{\partial z^2} \tag{4.204}$$

$$(\nabla\times\boldsymbol{F})_{\bar{a}} = \varepsilon_{\bar{a}\bar{b}\bar{c}}\partial_{\bar{b}}F^{\bar{c}} \qquad \text{see equations (4.198a) – (4.198c)} \tag{4.205}$$

4.23 Summary of spherical coordinates

We now consider spherical coordinates defined by Figure 4.3 and related to Cartesian coordinates through the coordinate transformation[3]

$$x = r\cos\phi\,\cos\lambda \tag{4.206a}$$

$$y = r\cos\phi\,\sin\lambda \tag{4.206b}$$

$$z = r\sin\phi. \tag{4.206c}$$

[3]Figure 4.3 depicts a rotating spherical planet. We here focus on the coordinate transformations when applied within the non-inertial rotating reference frame of a terrestrial observer. Connections to observers in an inertial non-rotating reference frame are studied in Chapter 13.

The radial coordinate

$$r = |\boldsymbol{x}| = \sqrt{\boldsymbol{x}\cdot\boldsymbol{x}} = \sqrt{x^2+y^2+z^2} \tag{4.207}$$

measures the distance from the center of the sphere to the position of the point. The spherical angle coordinates,

$$0 \le \lambda \le 2\pi \qquad \text{longitude} \tag{4.208}$$

$$-\pi/2 \le \phi \le \pi/2 \qquad \text{latitude,} \tag{4.209}$$

specify the longitude, measuring the radians of the position east of the prime meridian, and latitude, measuring the radians north ($\phi > 0$) or south ($\phi < 0$) from the equator. To streamline notation in the following, we introduce the unbarred and barred labels for the Cartesian and spherical coordinates, respectively

$$(x,y,z) = (\xi^1,\xi^2,\xi^3) \equiv \xi^a \qquad \text{and} \qquad (\lambda,\phi,r) = (\xi^{\overline{1}},\xi^{\overline{2}},\xi^{\overline{3}}) \equiv \xi^{\overline{a}}. \tag{4.210}$$

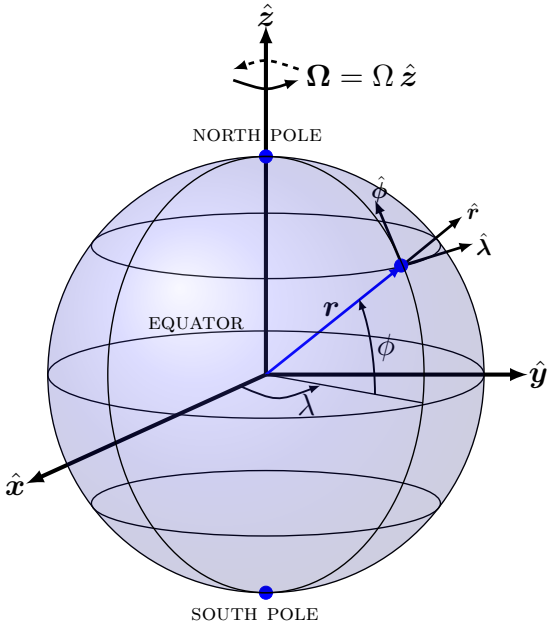

FIGURE 4.3: Geometry and notation for motion around a rotating sphere. For geophysical applications, the sphere rotates counter-clockwise when looking down from the north polar axis and it has an angular speed Ω. The planetary Cartesian triad of orthonormal basis vectors, $(\hat{\boldsymbol{x}},\hat{\boldsymbol{y}},\hat{\boldsymbol{z}})$ points along the orthogonal axes and rotates with the sphere. The planetary spherical triad (also rotating with the sphere) of orthonormal basis vectors, $(\hat{\boldsymbol{\lambda}},\hat{\boldsymbol{\phi}},\hat{\boldsymbol{r}})$, makes use of the longitudinal unit vector $\hat{\boldsymbol{\lambda}}$, which points in the longitudinal direction (positive eastward), the latitudinal unit vector $\hat{\boldsymbol{\phi}}$, which points in the latitudinal direction (positive northward) and the radial unit vector $\hat{\boldsymbol{r}}$, which point in the radial direction (positive away from the center).

4.23.1 Cartesian and spherical transformation

Following the general discussion in Section 4.1.4, we consider the infinitesimal distance along one of the Cartesian coordinate axes, $\mathrm{d}\xi^a$. The chain rule allows us to relate this distance to those along the axes of the spherical coordinate system

$$\mathrm{d}\xi^a = \frac{\partial \xi^a}{\partial \xi^{\overline{a}}}\,\mathrm{d}\xi^{\overline{a}} = \Lambda^a{}_{\overline{a}}\,\mathrm{d}\xi^{\overline{a}}. \tag{4.211}$$

The partial derivatives $\partial\xi^a/\partial\xi^{\overline{a}}$ form components to the transformation matrix that transforms between coordinate representations. For the coordinate transformation (4.206a)-(4.206c), the transformation matrix is given by

$$\Lambda^a{}_{\overline{a}} = \begin{bmatrix} \partial\xi^1/\partial\xi^{\overline{1}} & \partial\xi^1/\partial\xi^{\overline{2}} & \partial\xi^1/\partial\xi^{\overline{3}} \\ \partial\xi^2/\partial\xi^{\overline{1}} & \partial\xi^2/\partial\xi^{\overline{2}} & \partial\xi^2/\partial\xi^{\overline{3}} \\ \partial\xi^3/\partial\xi^{\overline{1}} & \partial\xi^3/\partial\xi^{\overline{2}} & \partial\xi^3/\partial\xi^{\overline{3}} \end{bmatrix} = \begin{bmatrix} -r\cos\phi\sin\lambda & -r\sin\phi\,\cos\lambda & \cos\phi\cos\lambda \\ r\cos\phi\cos\lambda & -r\sin\phi\,\sin\lambda & \cos\phi\sin\lambda \\ 0 & r\cos\phi & \sin\phi \end{bmatrix}. \tag{4.212}$$

The determinant of the transformation (Jacobian) is given by

$$\det(\Lambda^a{}_{\overline{a}}) = r^2\cos\phi. \tag{4.213}$$

The Jacobian vanishes at the north and south poles ($\phi = \pm\pi/2$), where the transformation is singular. Otherwise, the transformation is one-to-one and invertible. Methods familiar from linear algebra render the inverse transformation matrix

$$\Lambda^{\overline{a}}{}_a = \frac{1}{r^2\cos\phi}\begin{bmatrix} -r\sin\lambda & r\cos\lambda & 0 \\ -r\cos\phi\,\sin\phi\,\cos\lambda & -r\cos\phi\sin\phi\sin\lambda & r\cos^2\phi \\ r^2\cos^2\phi\cos\lambda & r^2\,\cos^2\phi\sin\lambda & r^2\cos\phi\sin\phi \end{bmatrix}, \tag{4.214}$$

so that

$$\Lambda^{\overline{a}}{}_a\,\Lambda^a{}_{\overline{b}} = \delta^{\overline{a}}{}_{\overline{b}} \quad \text{and} \quad \Lambda^a{}_{\overline{b}}\,\Lambda^{\overline{b}}{}_b = \delta^a{}_b. \tag{4.215}$$

4.23.2 Basis vectors

The spherical coordinate basis vectors, $\boldsymbol{e}_{\overline{a}}$, are related to the Cartesian coordinate basis vectors, $\boldsymbol{e}_a$, through the transformation

$$\boldsymbol{e}_{\overline{a}} = \Lambda^a{}_{\overline{a}}\,\boldsymbol{e}_a. \tag{4.216}$$

The transformation matrix (4.212) leads to

$$\boldsymbol{e}_\lambda = r\cos\phi\,(-\hat{\boldsymbol{x}}\sin\lambda + \hat{\boldsymbol{y}}\cos\lambda) \tag{4.217a}$$
$$\boldsymbol{e}_\phi = r(-\hat{\boldsymbol{x}}\sin\phi\,\cos\lambda - \hat{\boldsymbol{y}}\sin\phi\,\sin\lambda + \hat{\boldsymbol{z}}\cos\phi) \tag{4.217b}$$
$$\boldsymbol{e}_r = \hat{\boldsymbol{x}}\cos\phi\,\cos\lambda + \hat{\boldsymbol{y}}\cos\phi\,\sin\lambda + \hat{\boldsymbol{z}}\sin\phi. \tag{4.217c}$$

It is convenient to introduce the orthonormal unit vectors, $(\hat{\boldsymbol{\lambda}}, \hat{\boldsymbol{\phi}}, \hat{\boldsymbol{r}})$, which point in directions of increasing λ, ϕ, and r, so that the basis vectors are written

$$\boldsymbol{e}_\lambda = r\cos\phi\,\hat{\boldsymbol{\lambda}} \qquad \text{and} \qquad \boldsymbol{e}_\phi = r\,\hat{\boldsymbol{\phi}} \qquad \text{and} \qquad \boldsymbol{e}_r = \hat{\boldsymbol{r}}, \tag{4.218}$$

in which case we have the relations

$$\hat{\boldsymbol{\lambda}} = -\hat{\boldsymbol{x}}\sin\lambda + \hat{\boldsymbol{y}}\cos\lambda \tag{4.219a}$$
$$\hat{\boldsymbol{\phi}} = -\hat{\boldsymbol{x}}\cos\lambda\,\sin\phi - \hat{\boldsymbol{y}}\sin\lambda\,\sin\phi + \hat{\boldsymbol{z}}\cos\phi \tag{4.219b}$$
$$\hat{\boldsymbol{r}} = \hat{\boldsymbol{x}}\,\cos\lambda\,\cos\phi + \hat{\boldsymbol{y}}\sin\lambda\,\cos\phi + \hat{\boldsymbol{z}}\sin\phi \tag{4.219c}$$

along with their inverse

$$\hat{\boldsymbol{x}} = -\hat{\boldsymbol{\lambda}}\sin\lambda - \hat{\boldsymbol{\phi}}\cos\lambda\sin\phi + \hat{\boldsymbol{r}}\,\cos\lambda\,\cos\phi \tag{4.220a}$$
$$\hat{\boldsymbol{y}} = \hat{\boldsymbol{\lambda}}\cos\lambda - \hat{\boldsymbol{\phi}}\,\sin\lambda\,\sin\phi + \hat{\boldsymbol{r}}\sin\lambda\,\cos\phi \tag{4.220b}$$
$$\hat{\boldsymbol{z}} = \hat{\boldsymbol{\phi}}\,\cos\phi + \hat{\boldsymbol{r}}\,\sin\phi. \tag{4.220c}$$

4.23.3 Basis one-forms

Since spherical coordinates are locally orthogonal, we can readily derive the one-form basis through inverting the vector basis

$$\boldsymbol{e}^{\lambda} = (r\cos\phi)^{-1}\,\hat{\boldsymbol{\lambda}} \qquad \text{and} \qquad \boldsymbol{e}^{\phi} = r^{-1}\hat{\boldsymbol{\phi}} \qquad \text{and} \qquad \boldsymbol{e}^{r} = \hat{\boldsymbol{r}}, \tag{4.221}$$

which satisfy the duality condition (bi-orthogonality relation) with the basis vectors (Section 4.2.2)

$$\boldsymbol{e}^{\overline{b}} \cdot \boldsymbol{e}_{\overline{a}} = \delta^{\overline{b}}{}_{\overline{a}}. \tag{4.222}$$

4.23.4 Position and velocity

In spherical coordinates, the position of a point is fully specified by the radial position

$$\boldsymbol{x}(\tau) = r\,\boldsymbol{e}_r = r\,\hat{\boldsymbol{r}}. \tag{4.223}$$

However, the velocity requires all three spherical coordinates since the radial basis vector is a function of the angular positions, which are functions of time. Use of the chain rule renders

$$\begin{aligned}
\boldsymbol{v}(\tau) &= \frac{\mathrm{d}\boldsymbol{x}(\tau)}{\mathrm{d}\tau} && \text{(4.224a)}\\
&= \boldsymbol{e}_r\,\frac{\mathrm{d}r}{\mathrm{d}\tau} + r\,\frac{\mathrm{d}\boldsymbol{e}_r}{\mathrm{d}\tau} && \text{(4.224b)}\\
&= \boldsymbol{e}_r\,\frac{\mathrm{d}r}{\mathrm{d}\tau} + r\,\frac{\partial\boldsymbol{e}_r}{\partial\lambda}\,\frac{\mathrm{d}\lambda}{\mathrm{d}\tau} + r\,\frac{\partial\boldsymbol{e}_r}{\partial\phi}\,\frac{\mathrm{d}\phi}{\mathrm{d}\tau} && \text{(4.224c)}\\
&\equiv \boldsymbol{e}_r\,\frac{\mathrm{d}r}{\mathrm{d}\tau} + \boldsymbol{e}_\lambda\,\frac{\mathrm{d}\lambda}{\mathrm{d}\tau} + \boldsymbol{e}_\phi\,\frac{\mathrm{d}\phi}{\mathrm{d}\tau} && \text{(4.224d)}\\
&= \boldsymbol{e}_r\,v^r + \boldsymbol{e}_\lambda\,v^\lambda + \boldsymbol{e}_\phi\,v^\phi. && \text{(4.224e)}
\end{aligned}$$

To reach this result we made use of the identities satisfied by the spherical basis vectors

$$\boldsymbol{e}_\lambda = r\,\frac{\partial\boldsymbol{e}_r}{\partial\lambda} \qquad \text{and} \qquad \boldsymbol{e}_\phi = r\,\frac{\partial\boldsymbol{e}_r}{\partial\phi}, \tag{4.225}$$

which can be readily verified by equations (4.217a)-(4.217c).

4.23.5 Metric tensor

Since spherical coordinates are orthogonal, the metric tensor is diagonal and it is given by

$$\mathfrak{g}_{\overline{a}\overline{b}} = \boldsymbol{e}_{\overline{a}} \cdot \boldsymbol{e}_{\overline{b}} = \begin{bmatrix} (r\cos\phi)^2 & 0 & 0 \\ 0 & r^2 & 0 \\ 0 & 0 & 1 \end{bmatrix}, \tag{4.226}$$

along with the inverse metric tensor

$$\mathfrak{g}^{\overline{a}\overline{b}} = \boldsymbol{e}^{\overline{a}} \cdot \boldsymbol{e}^{\overline{b}} = \begin{bmatrix} (r\cos\phi)^{-2} & 0 & 0 \\ 0 & r^{-2} & 0 \\ 0 & 0 & 1 \end{bmatrix}. \tag{4.227}$$

Volume element and Levi-Civita tensor

The square root of the determinant of the metric tensor written in spherical coordinates (from equation (4.226)) is given by

$$\sqrt{\det(\mathfrak{g}_{\overline{a}\overline{b}})} = r^2 \cos\phi \tag{4.228}$$

so that the volume element is

$$\mathrm{d}V = r^2 \cos\phi \, \mathrm{d}r \, \mathrm{d}\lambda \, \mathrm{d}\phi. \tag{4.229}$$

The covariant Levi-Civita tensor has the spherical representation

$$\varepsilon_{\overline{a}\overline{b}\overline{c}} = (r^2 \cos\phi) \, \epsilon_{\overline{a}\overline{b}\overline{c}}, \tag{4.230}$$

where $\epsilon_{\overline{a}\overline{b}\overline{c}}$ are components to the permutation symbol (i.e., the Cartesian components to the Levi-Civita tensor) from Section 1.7.1.

Vector cross product of basis vectors

As a check on the formalism for cross products, let us verify the relation (4.87) for the vector cross product of two basis vectors using spherical coordinates

$$\boldsymbol{e}_{\overline{a}} \times \boldsymbol{e}_{\overline{b}} = \varepsilon_{\overline{a}\overline{b}\overline{c}} \, \boldsymbol{e}^{\overline{c}} \Longrightarrow \boldsymbol{e}_{\overline{a}} \times \boldsymbol{e}_{\overline{b}} = (r^2 \cos\phi) \epsilon_{\overline{a}\overline{b}\overline{c}} \, \boldsymbol{e}^{\overline{c}}. \tag{4.231}$$

Making use of the spherical coordinate basis vectors and one-forms renders

$$\boldsymbol{e}_r \times \boldsymbol{e}_\lambda = (r\cos\phi) \, (\hat{\boldsymbol{r}} \times \hat{\boldsymbol{\lambda}}) = (r\cos\phi) \, \hat{\boldsymbol{\phi}} = (r^2 \cos\phi) \, \boldsymbol{e}^\phi = \varepsilon_{r\lambda\phi} \, \boldsymbol{e}^\phi \tag{4.232a}$$

$$\boldsymbol{e}_\lambda \times \boldsymbol{e}_\phi = (r^2\cos\phi) \, (\hat{\boldsymbol{\lambda}} \times \hat{\boldsymbol{\phi}}) = (r^2 \cos\phi) \, \hat{\boldsymbol{r}} = (r^2 \cos\phi) \, \boldsymbol{e}^r = \varepsilon_{\lambda\phi r} \, \boldsymbol{e}^r \tag{4.232b}$$

$$\boldsymbol{e}_\phi \times \boldsymbol{e}_r = r \, (\hat{\boldsymbol{\phi}} \times \hat{\boldsymbol{r}}) = r \, \hat{\boldsymbol{\lambda}} = (r^2 \cos\phi) \, \boldsymbol{e}^\lambda = \varepsilon_{\phi r\lambda} \, \boldsymbol{e}^\lambda. \tag{4.232c}$$

To reach these results we made use of the cross products for the spherical coordinate unit vectors

$$\hat{\boldsymbol{r}} \times \hat{\boldsymbol{\lambda}} = \hat{\boldsymbol{\phi}} \qquad \text{and} \qquad \hat{\boldsymbol{\lambda}} \times \hat{\boldsymbol{\phi}} = \hat{\boldsymbol{r}} \qquad \text{and} \qquad \hat{\boldsymbol{\phi}} \times \hat{\boldsymbol{r}} = \hat{\boldsymbol{\lambda}}. \tag{4.233}$$

4.23.6 Components of a vector field

A vector field, $\mathbf{F}$, has Cartesian components, F^a, related to its spherical components, $F^{\overline{a}}$, via the transformation matrix, $F^{\overline{a}} = \Lambda^{\overline{a}}{}_a \, F^a$. This transformation leads to

$$F^{\overline{1}} = (r\cos\phi)^{-1} \, [-F^x \sin\lambda + F^y \cos\lambda] \tag{4.234a}$$

$$F^{\overline{2}} = r^{-1} \, [-F^x \sin\phi\cos\lambda - F^y \sin\phi \sin\lambda + F^z \cos\phi] \tag{4.234b}$$

$$F^{\overline{3}} = F^x \cos\phi\cos\lambda + F^y \cos\phi \sin\lambda + F^z \sin\phi. \tag{4.234c}$$

Making use of the spherical unit vector (4.219a)-(4.219c) leads to the more tidy relations

$$(r\cos\phi) \, F^{\overline{1}} = \hat{\boldsymbol{\lambda}} \cdot \boldsymbol{F} \tag{4.235a}$$

$$r \, F^{\overline{2}} = \hat{\boldsymbol{\phi}} \cdot \boldsymbol{F} \tag{4.235b}$$

$$F^{\overline{3}} = \hat{\boldsymbol{r}} \cdot \boldsymbol{F}, \tag{4.235c}$$

where $\boldsymbol{F} = F^a \, \boldsymbol{e}_a$ is the Cartesian representation.

4.23.7 Differential operators

In spherical coordinates the gradient operator $\nabla = \boldsymbol{e}^a \partial_a$ takes on the form

$$\nabla = \hat{\boldsymbol{\lambda}} \, (r \, \cos\phi)^{-1} \, \partial_\lambda + \hat{\boldsymbol{\phi}} \, r^{-1} \, \partial_\phi + \hat{\boldsymbol{r}} \, \partial_r, \tag{4.236}$$

and the covariant divergence of a vector field is given by

$$\begin{aligned}
\nabla_{\overline{a}} F^{\overline{a}} &= (r^2 \cos\phi)^{-1} \partial_{\overline{a}} [r^2 \cos\phi \, F^{\overline{a}}] && \text{(4.237a)} \\
&= (r^2 \cos\phi)^{-1} \left(\partial_\lambda [r^2 \cos\phi \, F^{\overline{1}}] + \partial_\phi [r^2 \cos\phi \, F^{\overline{2}}] + \partial_r [r^2 \cos\phi \, F^{\overline{3}}] \right) && \text{(4.237b)} \\
&= \frac{1}{r \cos\phi} \frac{\partial(\hat{\boldsymbol{\lambda}} \cdot \boldsymbol{F})}{\partial\lambda} + \frac{1}{r \cos\phi} \frac{\partial \, (\hat{\boldsymbol{\phi}} \cdot \boldsymbol{F} \, \cos\phi)}{\partial\phi} + \frac{1}{r^2} \frac{\partial \, (\hat{\boldsymbol{r}} \cdot \boldsymbol{F} \, r^2)}{\partial r}. && \text{(4.237c)}
\end{aligned}$$

The covariant Laplacian of a scalar, $\nabla^2 \psi = \nabla \cdot \nabla \psi$, is given by

$$\begin{aligned}
\nabla^2 \psi &= \nabla \cdot \left[\hat{\boldsymbol{\lambda}} \, (r \cos\phi)^{-1} \, \partial_\lambda \psi + \hat{\boldsymbol{\phi}} \, r^{-1} \, \partial_\phi \psi + \hat{\boldsymbol{r}} \, \partial_r \psi \right] && \text{(4.238a)} \\
&= \frac{1}{(r \cos\phi)^2} \frac{\partial^2 \psi}{\partial\lambda^2} + \frac{1}{r^2 \cos\phi} \frac{\partial}{\partial\phi} \left[\cos\phi \, \frac{\partial\psi}{\partial\phi} \right] + \frac{1}{r^2} \frac{\partial}{\partial r} \left[r^2 \, \frac{\partial\psi}{\partial r} \right]. && \text{(4.238b)}
\end{aligned}$$

The covariant curl (Section 4.18) takes the form

$$\begin{aligned}
(\text{curl} \, \boldsymbol{F})^{\overline{1}} &= (r^2 \cos\phi)^{-1} \left[\partial_\phi \, F^{\overline{3}} - \partial_r \, (r^2 \, F^{\overline{2}}) \right] && \text{(4.239a)} \\
(\text{curl} \, \boldsymbol{F})^{\overline{2}} &= (r^2 \cos\phi)^{-1} \left[\partial_r \, (r^2 \cos^2\phi \, F^{\overline{1}}) - \partial_\lambda \, F^{\overline{3}} \right] && \text{(4.239b)} \\
(\text{curl} \, \boldsymbol{F})^{\overline{3}} &= (r^2 \cos\phi)^{-1} \left[\partial_\lambda \, (r^2 \, F^{\overline{2}}) - \partial_\phi \, (r^2 \cos^2\phi \, F^{\overline{1}}) \right], && \text{(4.239c)}
\end{aligned}$$

which can be written in the more conventional form[4]

$$\begin{aligned}
r \cos\phi \, (\text{curl} \, \boldsymbol{F})^{\overline{1}} &= \frac{1}{r} \left[\frac{\partial(\hat{\boldsymbol{r}} \cdot \boldsymbol{F})}{\partial\phi} - \frac{\partial(r \, \hat{\boldsymbol{\phi}} \cdot \boldsymbol{F})}{\partial r} \right] && \text{(4.240a)} \\
r \, (\text{curl} \, \boldsymbol{F})^{\overline{2}} &= \frac{1}{r} \left[\frac{\partial(r \, \hat{\boldsymbol{\lambda}} \cdot \boldsymbol{F})}{\partial r} - \frac{1}{\cos\phi} \frac{\partial(\hat{\boldsymbol{r}} \cdot \boldsymbol{F})}{\partial\lambda} \right] && \text{(4.240b)} \\
(\text{curl} \, \boldsymbol{F})^{\overline{3}} &= \frac{1}{r \cos\phi} \left[\frac{\partial(\hat{\boldsymbol{\phi}} \cdot \boldsymbol{F})}{\partial\lambda} - \frac{\partial(\cos\phi \, \hat{\boldsymbol{\lambda}} \cdot \boldsymbol{F})}{\partial\phi} \right]. && \text{(4.240c)}
\end{aligned}$$

4.23.8 Summary

We here summarize the spherical coordinate version of some common mathematical operators:

$$\begin{aligned}
&(\lambda, \phi, r) = (x^{\overline{1}}, x^{\overline{2}}, x^{\overline{3}}) && \text{(4.241)} \\
&(r \cos\phi) \, F^{\overline{1}} = \hat{\boldsymbol{\lambda}} \cdot \boldsymbol{F} \qquad r \, F^{\overline{2}} = \hat{\boldsymbol{\phi}} \cdot \boldsymbol{F} \qquad F^{\overline{3}} = \hat{\boldsymbol{r}} \cdot \boldsymbol{F} && \text{(4.242)} \\
&\nabla = \hat{\boldsymbol{\lambda}} \, (r \, \cos\phi)^{-1} \, \partial_\lambda + \hat{\boldsymbol{\phi}} \, r^{-1} \, \partial_\phi + \hat{\boldsymbol{r}} \, \partial_r && \text{(4.243)} \\
&\nabla_{\!\text{h}} = \hat{\boldsymbol{\lambda}} \, (r \, \cos\phi)^{-1} \, \partial_\lambda + \hat{\boldsymbol{\phi}} \, r^{-1} \, \partial_\phi && \text{(4.244)} \\
&\nabla_{\overline{a}} F^{\overline{a}} = \frac{1}{r \cos\phi} \frac{\partial(\hat{\boldsymbol{\lambda}} \cdot \boldsymbol{F})}{\partial\lambda} + \frac{1}{r \cos\phi} \frac{\partial \, (\hat{\boldsymbol{\phi}} \cdot \boldsymbol{F} \, \cos\phi)}{\partial\phi} + \frac{1}{r^2} \frac{\partial \, (\hat{\boldsymbol{r}} \cdot \boldsymbol{F} \, r^2)}{\partial r} && \text{(4.245)} \\
&\nabla^2 \psi = \frac{1}{(r \cos\phi)^2} \frac{\partial^2 \psi}{\partial\lambda^2} + \frac{1}{r^2 \cos\phi} \frac{\partial}{\partial\phi} \left[\cos\phi \, \frac{\partial\psi}{\partial\phi} \right] + \frac{1}{r^2} \frac{\partial}{\partial r} \left[r^2 \, \frac{\partial\psi}{\partial r} \right] && \text{(4.246)}
\end{aligned}$$

[4] Equations (4.240a)-(4.240c) correspond to equation (2.33) of *Vallis* (2017).

$$(\nabla \times \boldsymbol{F})_{\overline{a}} = \varepsilon_{\overline{a}\overline{b}\overline{c}} \partial_{\overline{b}} F^{\overline{c}} \qquad \text{see equations (4.240a) – (4.240c).} \tag{4.247}$$

4.24 General orthogonal coordinates

We can generalize the spherical and cylindrical-polar coordinates by considering a nonsingular and orthogonal set of coordinates defined such that the metric tensor takes on the diagonal form

$$\mathfrak{g}_{\overline{a}\overline{b}} = \boldsymbol{e}_{\overline{a}} \cdot \boldsymbol{e}_{\overline{b}} = \begin{bmatrix} h_{\overline{1}} & 0 & 0 \\ 0 & h_{\overline{2}} & 0 \\ 0 & 0 & h_{\overline{3}} \end{bmatrix}, \tag{4.248}$$

where $h_{\overline{a}} > 0$ are "stretching" functions. The corresponding volume element is expressed as

$$\mathrm{d}V = h_{\overline{1}} h_{\overline{2}} h_{\overline{3}} \, \mathrm{d}\xi^{\overline{1}} \, \mathrm{d}\xi^{\overline{2}} \, \mathrm{d}\xi^{\overline{3}}. \tag{4.249}$$

These *generalized orthogonal curvilinear coordinates* have a corresponding orthogonal set of basis vectors

$$\boldsymbol{e}_{\overline{a}} = h_{\overline{a}} \, \hat{\mathbf{e}}_{(\overline{a})} \qquad \text{no implied sum.} \tag{4.250}$$

The objects $\hat{\mathbf{e}}_{(\overline{a})}$ are the dimensionless unit directions. The corresponding one-form basis is given by

$$\boldsymbol{e}^{\overline{a}} = (h_{\overline{a}})^{-1} \, \hat{\mathbf{e}}_{(\overline{a})}. \tag{4.251}$$

The index on the unit directions is enclosed in parentheses to advertise that it is not tensorial; i.e., the unit directions do not transform as tensors. Rather, the functions $h_{\overline{a}}$ carry the tensorial properties of the basis vectors $\boldsymbol{e}_{\overline{a}}$. Results for the trajectory and velocity are straightforward generalizations of the spherical results in Section 4.23 and cylindrical-polar results from Section 4.22. A detailed presentation of generalized orthogonal coordinates is found in Section 21.11 of *Griffies* (2004), with these coordinates commonly used for ocean and atmospheric models.

4.25 Comments on gradient operators

A feature common to non-Cartesian coordinates concerns the presence of spatially dependent factors in front of certain components of the gradient operators. Indeed, recall the gradient for the three coordinates discussed in this chapter:

$$\nabla = \hat{\boldsymbol{x}} \frac{\partial}{\partial x} + \hat{\boldsymbol{y}} \frac{\partial}{\partial y} + \hat{\boldsymbol{z}} \frac{\partial}{\partial z} \qquad \text{Cartesian} \tag{4.252a}$$

$$\nabla = \hat{\boldsymbol{r}} \frac{\partial}{\partial r} + \frac{\hat{\boldsymbol{\vartheta}}}{r} \frac{\partial}{\partial \vartheta} + \hat{\boldsymbol{z}} \frac{\partial}{\partial z} \qquad \text{cylindrical-polar} \tag{4.252b}$$

$$\nabla = \frac{\hat{\boldsymbol{\lambda}}}{r \cos\phi} \frac{\partial}{\partial \lambda} + \frac{\hat{\boldsymbol{\phi}}}{r} \frac{\partial}{\partial \phi} + \hat{\boldsymbol{r}} \frac{\partial}{\partial r} \qquad \text{spherical,} \tag{4.252c}$$

where we recall that r for the spherical coordinates measures the distance from the origin, whereas r for cylindrical-polar coordinates measures the distance from the vertical axis. Observe the r^{-1} dependence for the angular components of the gradient for both spherical and cylindrical-polar coordinates. This dependence arises since as r increases, the surfaces of constant r become flatter, a result of their larger radius of curvature.

To further help understand the meaning of the r^{-1} factor, consider two points with the same r but distinct angular coordinates. As r increases, so too does the distance between the two points, even though their angular positions remain unchanged. Speaking prosaically, this property is why the outer portion of a pizza pie is bigger than the inner portion. Correspondingly, when

measuring the derivative of a function in the angular direction, that derivative must be weighted by r^{-1} to account for the difference in the arc-distance (more precisely the geodesic distance) between the two points. The same idea explains the $\cos\phi$ factor on the longitudinal derivative in spherical coordinates. Each of these notions are encapsulated in the spatial dependence of the basis vectors for non-Cartesian coordinates.

A practical implication of the r and $r\cos\phi$ factors appearing in the gradient operators arises when performing a vertical integral of the fluid mechanical equations. Such integrals are often used to study reduced order versions of the full three-dimensional equations. But to be used in practice, such integrals must be done either with Cartesian coordinates or for those cases where it is acceptable to set the r^{-1} factor to a constant, such as occurs for the shallow fluid approximation discussed in Section 27.1.2. Indeed, the vertically integrated equations are of most practical use only when making a shallow fluid approximation. If this point seems obscure now, it will be clarified when studying the depth integrated mechanical energy in Section 27.1.6, the depth integrated momentum equation in Section 28.4, the depth integrated angular momentum equation in Section 28.5, and the depth integrated vorticity equations in Sections 44.3, 44.5, and 44.6.

Chapter 5

CURVES AND SURFACES

We encounter curves and surfaces throughout the study of geophysical fluid mechanics, with fluid particle pathlines through space-time and isopycnal/isentropic surfaces providing two examples. Indeed, curves and surfaces are encountered throughout physics. Hence, there is a well developed mathematical framework to describe the geometric properties of these objects. Our goal in this chapter is to introduce some of the basics of curves and surfaces embedded in Euclidean space.

Although the curves and surfaces of geophysical fluid mechanics are commonly moving as part of the fluid flow, we are concerned in this chapter with describing their instantaneous spatial properties. Hence, time does not appear in this chapter. Furthermore, although curves and surfaces can overturn and intersect themselves, we restrict attention to orientable curves and surfaces whose normal direction has a nonzero projection onto the vertical; i.e., they have no overhangs and no wrapping (Figure 5.1). This constraint is satisfied by the surfaces of constant generalized vertical coordinates (e.g., isopycnal surfaces) considered in Chapter 63 and in many other places in this book. It allows us to make use of coordinates known as the *Monge gauge* in condensed matter physics.

READER'S GUIDE TO THIS CHAPTER

This chapter requires an understanding of the Cartesian calculus of Chapter 2. The differential geometry presented here is mostly written at the level of undergraduate calculus, so that it can be readily skipped for those recalling the basic ideas and formula. The interested reader can find far more development by studying a variety of mathematical physics texts that discuss geometry. One point of direct connection is provided by the physics of fluctuating membranes as discussed in Section 10.4 of the condensed matter physics textbook from *Chaikin and Lubensky* (1995).

5.1 Definitions and notation

The basic notions of curves and surfaces embedded in Euclidean space are rather intuitive. Nonetheless, it is important to be precise in our usage. For this purpose we here offer some notation and definitions.

5.1.1 Definitions

We assume the notion of a curve and surface embedded in Euclidean space to be self-evident, offering analytical expressions for curves in Section 5.2 and surfaces in Section 5.3. Given such, we here define some related notions used in our study of fluid mechanics.

- ORIENTABLE: An *orientable curve* is a curve that allows for normal and tangent directions to specify directions and sides to the curve. Likewise, an *orientable surface* has two sides, allowing one to choose a positive side and a negative side. A Möbius strip is the canonical surface that is not orientable since it only has one side. Likewise, the boundary of a Möbius strip is a non-orientable curve. We only consider orientable objects in this book.

- PATH or CONTOUR: A path or contour is a continuous piecewise smooth oriented curve. A *simple path* or *simple contour* does not cross itself. We already encountered contours when considering path integrals in Chapter 2.

- CIRCUIT: A circuit is a path that closes, and a *simple circuit* is a circuit that does not cross itself. Finally, a *reducible circuit* is a circuit that can be continuously deformed to a point within the domain without leaving the domain. For example, a circuit within the ocean that encloses an island or continent cannot be deformed to a point since doing so requires the circuit to cross onto land and thus to leave the ocean.

5.1.2 Notation

In this chapter we write the Cartesian position of a point on a surface as

$$\boldsymbol{S} = x\,\hat{\boldsymbol{x}} + y\,\hat{\boldsymbol{y}} + \eta(x,y)\,\hat{\boldsymbol{z}} \qquad \text{position on surface,} \tag{5.1}$$

with the vertical position written as

$$z = \eta(x,y) \qquad \text{vertical position on surface.} \tag{5.2}$$

If we are instead referring to a point on a planar curve in the x-z-plane, then we drop the y-dependence to have

$$\boldsymbol{S} = x\,\hat{\boldsymbol{x}} + \eta(x)\,\hat{\boldsymbol{z}} \qquad \text{position on planar curve.} \tag{5.3}$$

Time dependence is dropped throughout this chapter since we focus on the spatial geometry of curves and surfaces at a particular time instance.

We assume the outward normal direction on the curve or the surface has a nonzero projection into the vertical as shown in Figure 5.1. Indeed, we are only able to write the vertical position as $z = \eta(x,y)$ so long as there are no overturns in the surface, in which case the outward unit normal direction is

$$\hat{\boldsymbol{n}} = \frac{\nabla(z-\eta)}{|\nabla(z-\eta)|} = \frac{\hat{\boldsymbol{z}} - \nabla\eta}{\sqrt{1+|\nabla\eta|^2}}. \tag{5.4}$$

Figure 5.2 provides an example surface along with the notation.

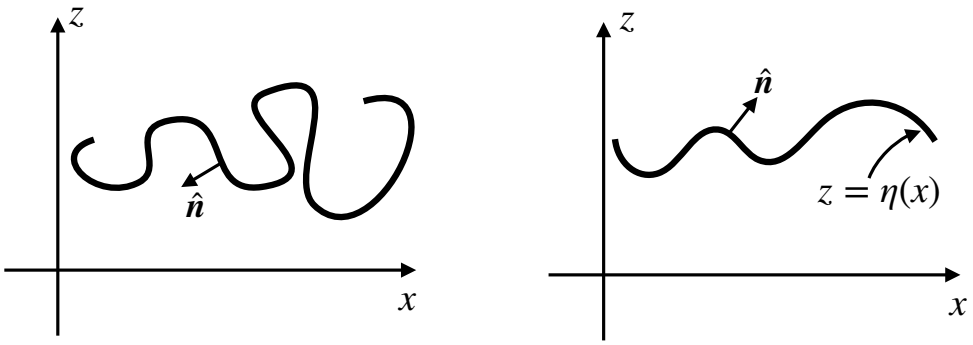

FIGURE 5.1: Two sample curves on the x-z plane. The left panel shows a curve whose outward unit normal, $\hat{\boldsymbol{n}}$, encounters points where $\hat{\boldsymbol{n}} \cdot \hat{\boldsymbol{z}} = 0$ and where $\hat{\boldsymbol{n}} \cdot \hat{\boldsymbol{z}}$ changes sign. This curve, and its generalization to a surface, are not treated in this chapter. The right panel shows a more gently undulating curve where $\hat{\boldsymbol{n}} \cdot \hat{\boldsymbol{z}} \neq 0$ everywhere, and thus where $\hat{\boldsymbol{n}} \cdot \hat{\boldsymbol{z}}$ is single signed. For curves such as the right panel, we can express the vertical position as a 1-to-1 function of the horizontal position, $z = \eta(x)$. Again, this curve has its natural generalization to a gently undulating surface whereby $z = \eta(x, y)$ provides a unique mapping between horizontal position and vertical. The assumption regarding no overhanging curves and surfaces is consistent with our study of surfaces defined by a constant generalized vertical coordinate (e.g., isopycnals or isentropes) in Chapter 63.

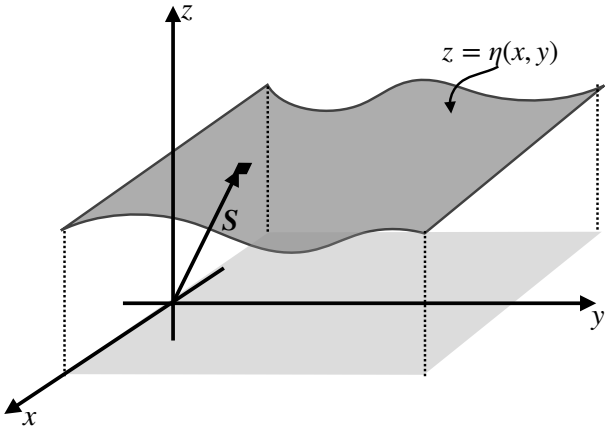

FIGURE 5.2: Example two-dimensional surface embedded in Euclidean space. The position of a point on the surface is given by the Cartesian position vector $\boldsymbol{S} = x\,\hat{\boldsymbol{x}} + y\,\hat{\boldsymbol{y}} + \eta(x, y)\,\hat{\boldsymbol{z}}$. The relation $z = \eta(x, y)$ provides a 1-to-1 mapping between the horizontal position and the vertical position of a point on the surface. Correspondingly, the surface is uniquely specified by finding the envelope of points where $z - \eta(x, y) = 0$. The lightly shaded region represents the projection of the curved surface onto the flat horizontal x-y plane below.

5.1.3 Surfaces with $x = \gamma(y, z)$ or $y = \psi(x, z)$

We generally find it most useful to specify a point on a surface according to equation (5.1), whereby we write $z = \eta(x, y)$ for the vertical position as a function of the horizontal position. This approach is typical for our applications since the surfaces we encounter most commonly in stratified geophysical flows have a normal direction that has a non-zero projection into the $\hat{\boldsymbol{z}}$ direction. However, there are occasions where it is more convenient to define a point on a surface according to

$$\boldsymbol{S} = \gamma(y, z)\,\hat{\boldsymbol{x}} + y\,\hat{\boldsymbol{y}} + z\,\hat{\boldsymbol{z}} \qquad \text{alternative specification.} \tag{5.5}$$

Here, we specify the x position on the surface as a function of y and z via the function $\gamma(y, z)$. The unit normal is thus specified by

$$\hat{\boldsymbol{n}} = \frac{\nabla(x - \gamma)}{|\nabla(x = \gamma)|} = \frac{\hat{\boldsymbol{x}} - \hat{\boldsymbol{y}}\,\partial_y\gamma - \hat{\boldsymbol{z}}\,\partial_z\gamma}{1 + \sqrt{(\partial_y\gamma)^2 + (\partial_z\gamma)^2}}. \tag{5.6}$$

Hence, this specification is useful for those surfaces with normal direction having a non-zero $\hat{\boldsymbol{x}}$ component everywhere on the surface, in which case we are afforded the ability to define $\gamma(y,z)$. Alternatively, if the surface instead has a normal direction with a non-zero $\hat{\boldsymbol{y}}$ component everywhere, then we would find it more suitable to define a point on the surface according to

$$\boldsymbol{S} = x\,\hat{\boldsymbol{x}} + \psi(x,z)\,\hat{\boldsymbol{y}} + z\,\hat{\boldsymbol{z}}, \tag{5.7}$$

where $y = \psi(x,z)$ provides the y position of a point on the surface as a function of x, z.

For the remainder of this chapter we return to the specification (5.1) whereby $z = \eta(x,y)$. However, there are occasions when we find it more suitable to define the surface using either equation (5.5) or (5.7). For example, we make use of the specification (5.5) in Section 21.7 when studying the meridional-depth overturning streamfunction.

5.2 Planar curves in 2D Euclidan space

We here describe the geometry of a curve on the x-z-plane (a *planar curve*) as depicted in Figure 5.3. These curves are one-dimensional objects living in a two-dimensional Euclidean space. Extensions to curves on non-Euclidean surfaces, such as the sphere or an isopycnal, are straightforward when those surfaces are embedded in the background Euclidean space assumed in this book.

5.2.1 Differential increments along the curve

As a one-dimensional geometric object, an arbitrary curve can be parameterized by a single coordinate, referred to here as φ. Let $\boldsymbol{S}(\varphi)$ specify the position of a point along the curve. Correspondingly, the differential increment between two infinitesimally close points on the curve is given by

$$\boldsymbol{S}(\varphi + \mathrm{d}\varphi) - \boldsymbol{S}(\varphi) = \mathrm{d}\boldsymbol{S} = \frac{\mathrm{d}\boldsymbol{S}}{\mathrm{d}\varphi}\,\mathrm{d}\varphi \equiv \boldsymbol{t}\,\mathrm{d}\varphi, \tag{5.8}$$

where

$$\boldsymbol{t} = \frac{\mathrm{d}\boldsymbol{S}}{\mathrm{d}\varphi} \tag{5.9}$$

is tangent to the curve. If $\varphi = s$ is the arc length along the curve, then $\boldsymbol{t} = \hat{\boldsymbol{t}}$ is a unt vector

$$\hat{\boldsymbol{t}} \cdot \hat{\boldsymbol{t}} = \frac{\mathrm{d}\boldsymbol{S}}{\mathrm{d}s} \cdot \frac{\mathrm{d}\boldsymbol{S}}{\mathrm{d}s} = 1. \tag{5.10}$$

In some treatments in this book we also write

$$\hat{\boldsymbol{s}} = \hat{\boldsymbol{t}} \tag{5.11}$$

to correspond to s for arc length. Recall we made use of the arc length along a curve in Section 2.4 when describing path integration.

5.2.2 Length along the curve

As in equation (5.3) we can represent the position of a point along the curve using Cartesian coordinates

$$\boldsymbol{S} = x\,\hat{\boldsymbol{x}} + \eta(x)\,\hat{\boldsymbol{z}}. \tag{5.12}$$

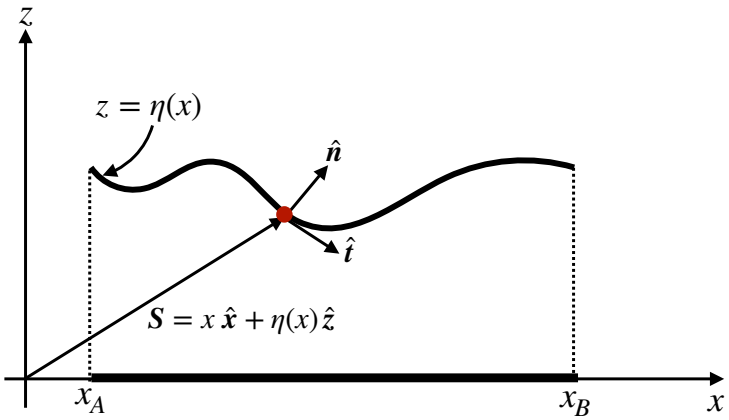

FIGURE 5.3: An orientable path in the x-z plane defined by a planar curve that does not intersect itself. The Cartesian position of a point on the curve is given by $\boldsymbol{S} = x\,\hat{\boldsymbol{x}} + \eta(x)\,\hat{\boldsymbol{z}}$, where $z = \eta(x)$ provides the vertical position of the point as a function of the horizontal position. The projection of the curve onto the horizontal x-axis occupies a range $x_A \leq x \leq x_B$. One way to define the curve is by finding the envelope of points where $z - \eta(x) = 0$, in which case we can readily find the unit normal direction pointing upward as $\hat{\boldsymbol{n}} = \nabla(z-\eta)/|\nabla(z-\eta)| = [\hat{\boldsymbol{z}} - (\mathrm{d}\eta/\mathrm{d}x)\,\hat{\boldsymbol{x}}]\,[1 + (\mathrm{d}\eta/\mathrm{d}x)^2\,]^{-1/2}$, and the unit tangent vector $\hat{\boldsymbol{t}} = [\hat{\boldsymbol{x}} + (\mathrm{d}\eta/\mathrm{d}x)\,\hat{\boldsymbol{z}}]\,[1 + (\mathrm{d}\eta/\mathrm{d}x)^2\,]^{-1/2}$.

Hence, letting $\varphi = x$ parameterize the curve leads to the representation of the tangent direction

$$\boldsymbol{t} = \frac{\mathrm{d}\boldsymbol{S}}{\mathrm{d}x} = \hat{\boldsymbol{x}} + \frac{\mathrm{d}\eta}{\mathrm{d}x}\,\hat{\boldsymbol{z}}, \tag{5.13}$$

which has the magnitude

$$\boldsymbol{t}\cdot\boldsymbol{t} = 1 + (\mathrm{d}\eta/\mathrm{d}x)^2, \tag{5.14}$$

so that the unit tangent vector is

$$\hat{\boldsymbol{t}} = \frac{\hat{\boldsymbol{x}} + (\mathrm{d}\eta/\mathrm{d}x)\,\hat{\boldsymbol{z}}}{\sqrt{1 + (\mathrm{d}\eta/\mathrm{d}x)^2}}. \tag{5.15}$$

Likewise, the curve's unit normal vector is given by

$$\hat{\boldsymbol{n}} = \frac{\nabla(z-\eta)}{|\nabla(z-\eta)|} = \frac{\hat{\boldsymbol{z}} - (\mathrm{d}\eta/\mathrm{d}x)\,\hat{\boldsymbol{x}}}{\sqrt{1 + (\mathrm{d}\eta/\mathrm{d}x)^2}}, \tag{5.16}$$

with orthogonality manifest

$$\hat{\boldsymbol{t}}\cdot\hat{\boldsymbol{n}} = 0. \tag{5.17}$$

The squared length of an infinitesimal segment along the curve is given by

$$(\mathrm{d}s)^2 = \mathrm{d}\boldsymbol{S}\cdot\mathrm{d}\boldsymbol{S} = \left[\frac{\mathrm{d}\boldsymbol{S}}{\mathrm{d}x}\cdot\frac{\mathrm{d}\boldsymbol{S}}{\mathrm{d}x}\right]\mathrm{d}x\,\mathrm{d}x, \tag{5.18}$$

so that the finite length of the curve is determined by the integral

$$L = \int_0^L \mathrm{d}s = \int_{x_A}^{x_B} |\mathrm{d}\boldsymbol{S}/\mathrm{d}x|\,\mathrm{d}x = \int_{x_A}^{x_B} \sqrt{1 + (\mathrm{d}\eta/\mathrm{d}x)^2}\,\mathrm{d}x, \tag{5.19}$$

where $x_A \leq x \leq x_B$ is the range over which x runs for the projection of the curve onto the x-axis (see Figure 5.3).

5.2.3 Curvature of a curve

Curvature measures the amount that the unit normal changes along the curve. For a planar curve, the curvature at a point equals to the inverse radius of a circle that shares the same tangent plane to the curve at the point (see Figure 5.4). We refer to the radius as the *radius of curvature* and the corresponding circle as the *curvature circle*. To formulate an analytic expression for the radius of curvature at a point on a curve, orient the Cartesian coordinate axes so that the point is at the origin and the tangent plane sits along the x-axis as in Figure 5.4. Consequently, the outward unit normal, $\hat{\boldsymbol{n}}$, is parallel to the $\hat{\boldsymbol{z}}$ direction.

A Taylor series expansion about the origin tells us that the vertical position of a point along the curve and near to the origin can be written

$$\eta(x) = \eta(0) + x\left[\frac{\mathrm{d}\eta}{\mathrm{d}x}\right]_{x=0} + \frac{x^2}{2}\left[\frac{\mathrm{d}^2\eta}{\mathrm{d}x^2}\right]_{x=0} + \mathcal{O}(x^3) \tag{5.20a}$$

$$= \frac{x^2}{2}\left[\frac{\mathrm{d}^2\eta}{\mathrm{d}x^2}\right]_{x=0} + \mathcal{O}(x^3). \tag{5.20b}$$

This result follows since we placed the origin so that $\eta(0) = 0$, and aligned the x-axis so that it is tangent at the origin, in which case $\mathrm{d}\eta/\mathrm{d}x = 0$ at $x = 0$. Hence, η has a quadratic behavior near the origin.

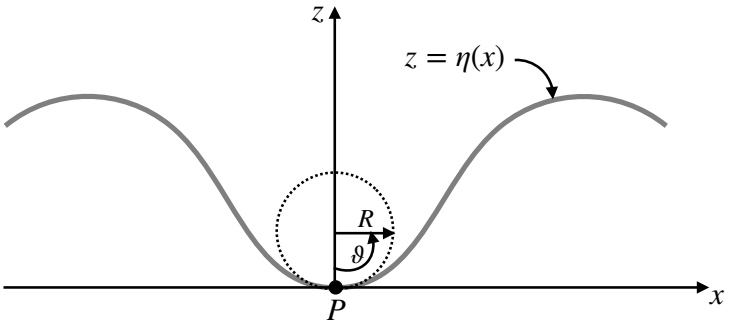

FIGURE 5.4: The radius of curvature at a point on a curve, P, equals to the radius of the curvature circle that shares the same tangent plane as the curve at the point P. When constructing the curvature circle we make use of the angle, ϑ, to measure the height of a point along the circle, $h(x) = R\,(1 - \cos\vartheta) \approx R\,\vartheta^2/2 \approx x^2/(2R)$. Setting $R^{-1} = \mathrm{d}^2\eta/\mathrm{d}x^2$ provides a second order accurate fit of the curvature circle to the curve at the point P.

Now place a circle with center along the z-axis so that it is tangent to the curve at the origin, as depicted in Figure 5.4. What is the radius, R, of the circle that best fits the curve at the origin? To answer this question note that the height of a point on the circle is given by $h(x) = R\,(1 - \cos\vartheta)$, where $\vartheta = 0$ for a point at the origin and $\vartheta = \pi$ at the diametrically opposite point. For small ϑ this height takes the form

$$h(x) \approx R\,[1 - 1 + \vartheta^2/2] = x^2/(2R), \tag{5.21}$$

where $\vartheta = x/R$ near the origin. For the height of a point on the curve (equation (5.20b)) to match the height along the circle, to second order accuracy, requires us to set the circle's radius to

$$\frac{1}{R} = \frac{\mathrm{d}^2\eta}{\mathrm{d}x^2}. \tag{5.22}$$

Equation (5.22) thus provides an expression for the radius of curvature, R, whose inverse is the curvature

$$\text{curvature} = \frac{1}{R}. \tag{5.23}$$

This result supports our expectation that the second derivative measures the curvature. As the

radius, R, gets larger, the curvature decreases, which means that local regions along the circle appear more flat. In the opposite limit the curvature grows as R decreases. Note that we could have chosen to orient the circle on the opposite side of the tangent (on the convex side), in which case the radius of curvature is negative. That is, $R > 0$ when the unit normal points towards the concave side (side where the curve rises towards $\hat{\boldsymbol{n}}$), whereas $R < 0$ when the unit normal points towards the convex side (side where the curve falls away from $\hat{\boldsymbol{n}}$).

In closing this section we note that

$$-\nabla \cdot \hat{\boldsymbol{n}} = \frac{\mathrm{d}^2\eta/\mathrm{d}x^2}{[1 + (\mathrm{d}\eta/\mathrm{d}x)^2\,]^{3/2}}. \tag{5.24}$$

When evaluated at the point of interest along the curve, we set $\mathrm{d}\eta/\mathrm{d}x = 0$ so that

$$-\nabla \cdot \hat{\boldsymbol{n}} = \frac{\mathrm{d}^2\eta}{\mathrm{d}x^2} = \frac{1}{R}. \tag{5.25}$$

This result supports our earlier statement that curvature measures the change in the normal direction along the curve. In fact, the identity

$$-\nabla \cdot \hat{\boldsymbol{n}} = \frac{1}{R} \tag{5.26}$$

holds for an arbitrary point along the curve since it is a coordinate invariant statement.

Equation (5.25) provides a useful means to check the sign of the radius of curvature. Namely, the point of interest in Figure 5.4 is a local minimum, so that $\mathrm{d}^2\eta/\mathrm{d}x^2 > 0$ and the radius of curvature is thus positive, $R > 0$. In contrast, the radius of curvature is negative at points where $\mathrm{d}^2\eta/\mathrm{d}x^2 < 0$.

5.3 Surfaces embedded in 3D Euclidean space

We now extend the previous discussion to a two-dimensional surface embedded in three-dimensional Euclidean space such as in Figure 5.2. In general, a 2D surface in 3D space can be parameterized by two variables, φ_1 and φ_2, so that infinitesimal increments along the surface satisfy

$$\mathrm{d}\boldsymbol{S} = \frac{\partial \boldsymbol{S}}{\partial \varphi_1}\,\mathrm{d}\varphi_1 + \frac{\partial \boldsymbol{S}}{\partial \varphi_2}\,\mathrm{d}\varphi_2 = \boldsymbol{t}_1\,\mathrm{d}\varphi_1 + \boldsymbol{t}_2\,\mathrm{d}\varphi_2. \tag{5.27}$$

The vectors $\boldsymbol{t}_1$ and $\boldsymbol{t}_2$ are tangent to the surface at the point (φ_1, φ_2), and yet they are not generally orthogonal to one another.

Making use of the Cartesian expression (5.1)

$$\boldsymbol{S} = x\,\hat{\boldsymbol{x}} + y\,\hat{\boldsymbol{y}} + \eta(x, y)\,\hat{\boldsymbol{z}} \tag{5.28}$$

brings the two tangent directions and the unit tangent directions into the form

$$\boldsymbol{t}_1 = \frac{\partial \boldsymbol{S}}{\partial x} = \hat{\boldsymbol{x}} + \frac{\partial \eta}{\partial x}\,\hat{\boldsymbol{z}} \quad \text{and} \quad \hat{\boldsymbol{t}}_1 = \frac{\hat{\boldsymbol{x}} + (\partial\eta/\partial x)\,\hat{\boldsymbol{z}}}{\sqrt{1 + (\partial\eta/\partial x)^2}} \tag{5.29a}$$

$$\boldsymbol{t}_2 = \frac{\partial \boldsymbol{S}}{\partial y} = \hat{\boldsymbol{y}} + \frac{\partial \eta}{\partial y}\,\hat{\boldsymbol{z}} \quad \text{and} \quad \hat{\boldsymbol{t}}_2 = \frac{\hat{\boldsymbol{y}} + (\partial\eta/\partial y)\,\hat{\boldsymbol{z}}}{\sqrt{1 + (\partial\eta/\partial y)^2}}. \tag{5.29b}$$

Likewise, the surface unit normal vector is given by

$$\hat{\boldsymbol{n}} = \frac{\nabla(z - \eta)}{|\nabla(z - \eta)|} = \frac{\hat{\boldsymbol{z}} - \nabla\eta}{|\hat{\boldsymbol{z}} - \nabla\eta|} = \frac{\hat{\boldsymbol{z}} - \nabla\eta}{\sqrt{1 + |\nabla\eta|^2}}, \tag{5.30}$$

and it is straightforward to show orthogonality with the two tangent vectors

$$\hat{\boldsymbol{t}}_1 \cdot \hat{\boldsymbol{n}} = \hat{\boldsymbol{t}}_2 \cdot \hat{\boldsymbol{n}} = 0. \tag{5.31}$$

5.3.1 Area on the surface

Recall from Section 1.7.5 that the magnitude of a vector product of two vectors equals to the area of the parallelogram subtended by the vectors. Hence, the area of an infinitesimal surface element with sides $\mathrm{d}\varphi_1$ and $\mathrm{d}\varphi_2$ is given by

$$\mathrm{d}\mathcal{S} = \left| \frac{\partial \boldsymbol{S}}{\partial \varphi_1} \times \frac{\partial \boldsymbol{S}}{\partial \varphi_2} \right| \mathrm{d}\varphi_1 \, \mathrm{d}\varphi_2. \tag{5.32}$$

Making use of Cartesian coordinates brings the area element to

$$\mathrm{d}\mathcal{S} = \sqrt{1 + |\nabla \eta|^2} \, \mathrm{d}x \, \mathrm{d}y = \sqrt{1 + |\nabla \eta|^2} \, \mathrm{d}A, \tag{5.33}$$

where

$$\mathrm{d}A = \mathrm{d}x \, \mathrm{d}y \tag{5.34}$$

is the area of the surface projected onto the horizontal plane. Hence, the area of a finite region is given by the integral

$$\mathcal{S} = \int \mathrm{d}\mathcal{S} = \int |\nabla(z - \eta)| \, \mathrm{d}A = \int \sqrt{1 + |\nabla \eta|^2} \, \mathrm{d}x \, \mathrm{d}y, \tag{5.35}$$

where the second and third integrals extend over the region defined by the projection of the surface onto the horizontal (see Figure 5.2).

5.3.2 Curvature of a surface

We now seek an expression for the curvature of a point on the surface. Since the surface has two dimensions, we expect the curvature to be measured by two numbers rather than the single curvature for the curve discussed in Section 5.2.3. The method for developing the curvature is analogous to that used for a curve, yet with a bit more mathematics needed to allow for the extra dimension. Figure 5.5 depicts the situation.

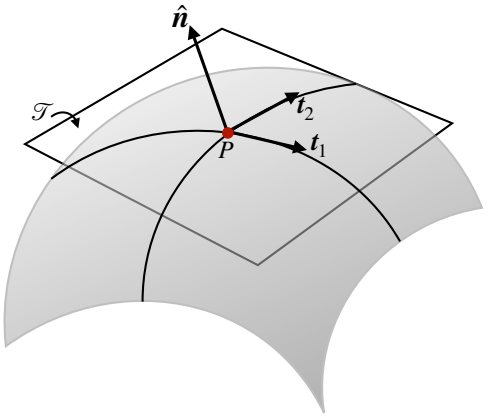

FIGURE 5.5: Depicting the elements needed to construct the curvature of a surface at an arbitrary point, P. The local unit normal direction is given by $\hat{\boldsymbol{n}}$, along with the two tangent vectors $\boldsymbol{t}_1$ and $\boldsymbol{t}_2$. The tangent vectors span the space of the tangent plane, $\mathcal{T}$, shown as a flat surface that is tangent at the chosen point on the surface. In this case the surface falls away from the normal direction, as per a convex surface, so that the two radii of curvature are negative. Other surfaces can be concave, whereby both radii of curvature are positive, or hyperbolic (saddle), whereby one is positive and another negative.

Let $\boldsymbol{x} = (x_1, x_2) = (x, y)$ be Cartesian coordinates on a tangent plane local to an arbitrary point on the surface, with the origin of the coordinate system taken at the point. Near to the point, we can estimate the vertical distance of a point on the surface from the tangent plane according to the quadratic form

$$\eta \approx \frac{1}{2}\, x_m\, \mathbb{C}^{mn}\, x_n, \tag{5.36}$$

where $\mathbb{C}$ is the matrix of second partial derivatives evaluated at the point

$$\mathbb{C} = \begin{bmatrix} \dfrac{\partial^2 \eta}{\partial x_1^2} & \dfrac{\partial^2 \eta}{\partial x_1 \partial x_2} \\ \dfrac{\partial^2 \eta}{\partial x_1 \partial x_2} & \dfrac{\partial^2 \eta}{\partial x_2^2} \end{bmatrix}. \tag{5.37}$$

As a symmetric matrix, $\mathbb{C}$ is diagonalizable and it has two eigenvalues, R_1^{-1} and R_2^{-1}, along with its associated eigenvectors, $\boldsymbol{c}_1$ and $\boldsymbol{c}_2$. The quadratic form (5.36) can thus be written as

$$\eta \approx \frac{1}{2}\, R_1^{-1}\, (\boldsymbol{x} \cdot \boldsymbol{c}_1)^2 + \frac{1}{2}\, R_2^{-1}\, (\boldsymbol{x} \cdot \boldsymbol{c}_2)^2. \tag{5.38}$$

R_1 and R_2 are the principle radii of curvature for the surface at the point P. They correspond, respectively, to the radii of the curvature circles in the $\hat{\boldsymbol{n}}$-$\boldsymbol{c}_1$ and $\hat{\boldsymbol{n}}$-$\boldsymbol{c}_2$ planes. If the radius of curvature, R_m, is positive, then the surface curves towards $\hat{\boldsymbol{n}}$ along the $\hat{\boldsymbol{n}}$-$\boldsymbol{c}_i$ plane, and conversely if R_m is negative. The surface takes the shape of a saddle when the two radii of curvature have opposite signs.

There are two scalar invariants of the matrix $\mathbb{C}$ that commonly arise in applications.

- $\mathrm{Tr}(\mathbb{C}) = R_1^{-1} + R_2^{-1}$, which is twice the mean curvature for the surface. With the unit normal vector given by equation (5.4), one can show that

$$-\nabla \cdot \hat{\boldsymbol{n}} = \frac{\nabla^2 \eta}{[1 + (\nabla \eta)^2\,]^{3/2}}. \tag{5.39}$$

  A bit of algebra leads us to conclude that

$$-\nabla \cdot \hat{\boldsymbol{n}} = \frac{\nabla^2 \eta}{[1 + (\nabla \eta)^2\,]^{3/2}} = \frac{1}{R_1} + \frac{1}{R_2}, \tag{5.40}$$

  for any point along the surface, thus generalizing the result (5.25) found for a curve. Furthermore, if $|\nabla \eta| \ll 1$ then we have

$$\nabla^2 \eta \approx \frac{1}{R_1} + \frac{1}{R_2}, \tag{5.41}$$

  with this result proving useful in the study of surface tension in Section 25.11.

- $\det(\mathbb{C}) = 1/(R_1\, R_2)$ is known as the *Gaussian curvature*, which is the product of the two curvatures.

5.3.3 Curves on the surface $z = \eta(x, y)$

We now consider a curve, as in Section 5.2, defined along a two dimensional surface, $z = \eta(x, y)$, with the curve defined by lines of constant $z = \eta(x, y)$. For example, if $\eta(x, y)$ is the solid earth topography, then lines of constant η are contours of constant topography. By definition, these contours have no projection into the vertical direction (i.e., they do not go uphill or downhill),

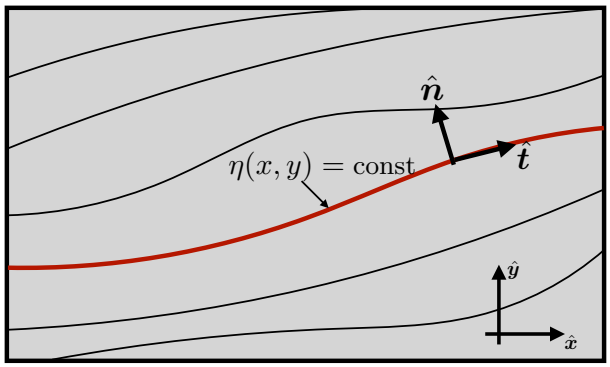

FIGURE 5.6: Geometry depicting a contour along a particular line of constant $z = \eta(x, y)$, such as for a constant elevation path along a mountain or valley. The along-contour unit tangent direction is $\hat{\boldsymbol{t}} = \mathrm{d}\boldsymbol{x}/\mathrm{d}s$, with s the arc length along the contour. The unit normal direction pointing to the left of the contour direction is $\hat{\boldsymbol{n}}$, with $\hat{\boldsymbol{n}} \cdot \hat{\boldsymbol{t}} = 0$ and $\hat{\boldsymbol{t}} \times \hat{\boldsymbol{n}} = \hat{\boldsymbol{z}}$. Both $\hat{\boldsymbol{n}}$ and $\hat{\boldsymbol{t}}$ are horizontal unit vectors.

and they are determined by

$$\mathrm{d}\eta = 0 = \nabla\eta \cdot \mathrm{d}\boldsymbol{x}, \tag{5.42}$$

where $\mathrm{d}\boldsymbol{x} = \hat{\boldsymbol{x}}\,\mathrm{d}x + \hat{\boldsymbol{y}}\,\mathrm{d}y$ is the horizontal space increment along the contour. Following the introduction of arc length in Section 5.2.1, we write

$$\mathrm{d}\eta = 0 = \nabla\eta \cdot \mathrm{d}\boldsymbol{x} = \nabla\eta \cdot \frac{\mathrm{d}\boldsymbol{x}}{\mathrm{d}s}\,\mathrm{d}s = \nabla\eta \cdot \hat{\boldsymbol{t}}\,\mathrm{d}s, \tag{5.43}$$

where $\hat{\boldsymbol{t}}$ is a unit vector pointing in the direction of the contour. To build an orthogonal triad of coordinates, we then define an orthogonal unit vector, $\hat{\boldsymbol{n}}$, that points to the left of the contour direction so that

$$\hat{\boldsymbol{n}} \cdot \hat{\boldsymbol{t}} = 0 \quad \text{and} \quad \hat{\boldsymbol{t}} \times \hat{\boldsymbol{n}} = \hat{\boldsymbol{z}}, \tag{5.44}$$

as depicted in Figure 5.6. We provide an example use of this formalism in Exercise 5.1.

5.4 Exercises

EXERCISE 5.1: JACOBIAN EVALUATED ALONG A CONTOUR
Consider the vector cross product of two functions, $\psi(x, y)$ and $Q(x, y)$

$$\hat{\boldsymbol{z}} \cdot (\nabla\psi \times \nabla Q) = \partial_x\psi\,\partial_y Q - \partial_y\psi\,\partial_x Q \equiv J(\psi, Q), \tag{5.45}$$

where the final equality defined the Jacobian operator. Show that when evaluated along a contour of constant Q, the Jacobian is given by

$$J(\psi, Q) = -(\hat{\boldsymbol{n}} \cdot \nabla Q)\,(\hat{\boldsymbol{t}} \cdot \nabla\psi) \tag{5.46}$$

where $\hat{\boldsymbol{t}}$ is the unit tangent along the contour and $\hat{\boldsymbol{n}}$ is a unit vector pointing to the left of the tangent (e.g., see Figure 5.6).

EXERCISE 5.2: CURVATURE OF A CIRCLE
Make use of equation (5.26), as well as the polar coordinates from Section 4.22, to show that for

a circle of radius r we have

$$-\nabla \cdot \hat{\boldsymbol{n}} = \frac{1}{r}, \tag{5.47}$$

where $\hat{\boldsymbol{n}} = -\hat{\boldsymbol{r}}$ points to the left when moving around the circle in a counterclockwise direction. Hence, the radius of curvature for the circle equals to the circle's radius.

Chapter 6

LINEAR PARTIAL DIFFERENTIAL EQUATIONS

Fluid mechanics is a classical field theory whose mathematical description involves partial differential equations (PDEs). Although most of these partial differential equations are nonlinear, some are linear. Regardless, an understanding of linear partial differential equations provides useful insights into the physics and maths of geophysical fluids. For this purpose, we here explore the rudiments of linear partial differential equations.

CHAPTER GUIDE

This chapter renders an appreciation for the mathematical structure and physical behavior of many equations encountered in geophysical fluid mechanics. Indeed, it is remarkable how useful it is, both mathematically and physically, to develop a basic understanding of linear partial differential equations. Furthermore, those aiming to develop solution methods, either analytical or numerical, should have a working knowledge of this chapter along with the Green's function method detailed in Chapter 9. Throughout this chapter we assume Cartesian coordinates.

There are many resources devoted to the theory and application of partial differential equations throughout physics, engineering, and applied mathematics. Chapter 8 of *Hildebrand* (1976) offers a pedagogical starting point whereas *Stakgold* (2000a,b) thoroughly develops the theory and methods available for boundary value problems encountered in physics. *Duchateau and Zachmann* (1986) concisely summarize partial differential equations and provide nearly 300 worked exercises, with much of the presentation in this chapter following their treatment.

6.1 Loose threads

- Exercises that illustrate the separation of variables method.
- Discuss the notion of spherical harmonics and cylindrical harmonics.

6.2 The advection equation

Consider a tracer concentration, C, which for present purposes is a scalar field that is a function of space and time. As derived in Section 69.3, the tracer concentration in the absence of diffusion satisfies the advection equation

$$(\partial_t + \boldsymbol{v} \cdot \nabla) C = 0. \tag{6.1}$$

The space and time derivatives acting on C are both first order, indicating that the advection equation is a first order partial differential equation. It is a nonlinear partial differential equation for those *active* tracers such as temperature, where active tracers affect the velocity, $\boldsymbol{v}$, through changes to density and hence to pressure. In contrast, the advection equation is linear for *passive* tracers (e.g., colored dye, dust), which are tracers whose effects on velocity are negligible (Section 20.1.5). We limit the present discussion to passive tracers so that the advection equation is linear.

6.2.1 Constant advection velocity

Consider one space dimension and let the advection velocity be constant in space and time,

$$(\partial_t + U \partial_x) C = 0, \tag{6.2}$$

where U is a constant velocity in the $\hat{\boldsymbol{x}}$ direction. An inspired guess reveals that

$$C(x,t) = \Gamma(\alpha) = \Gamma(x - Ut) \tag{6.3}$$

is a general solution to equation (6.2). Here, Γ is an arbitrary differentiable function that is determined by the initial conditions of the tracer field. Furthermore, there is only one argument to Γ, here written as $\alpha = x - Ut$. As discussed in Section 6.3, $\alpha = x - Ut$ is referred to as a *characteristic curve* for the constant speed one-dimensional advection equation.

Verification of the solution (6.3) is readily found by noting

$$\frac{\partial C}{\partial x} = \frac{\mathrm{d}\Gamma(\alpha)}{\mathrm{d}\alpha}\frac{\partial \alpha}{\partial x} = \Gamma'(\alpha)\frac{\partial (x - Ut)}{\partial x} = \Gamma' \tag{6.4a}$$

$$\frac{\partial C}{\partial t} = \frac{\mathrm{d}\Gamma(\alpha)}{\mathrm{d}\alpha}\frac{\partial \alpha}{\partial t} = \Gamma'(\alpha)\frac{\partial (x - Ut)}{\partial t} = -\Gamma' U. \tag{6.4b}$$

We have thus verified that

$$(\partial_t + \boldsymbol{v} \cdot \nabla) C = -\Gamma' U + U \Gamma' = 0. \tag{6.5}$$

The functional dependence,

$$C(x, t) = \Gamma(\alpha) = \Gamma(x - Ut), \tag{6.6}$$

reveals that as time progresses with $U > 0$, an observer that moves in the positive $\hat{\boldsymbol{x}}$ direction with a speed U maintains a constant value for the tracer concentration. This behavior means that the tracer concentration is transported by advection with a speed U without changing its structure. We illustrate this behavior in Figure 6.1.

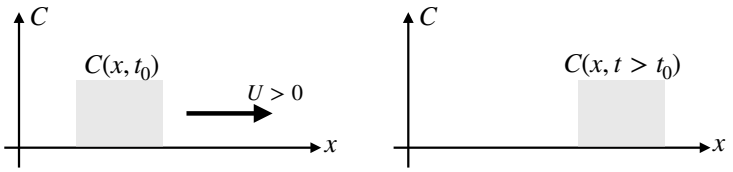

FIGURE 6.1: Illustrating the advection of a scalar field resulting from a constant advection velocity $\boldsymbol{v} = U\hat{\boldsymbol{x}}$ with $U > 0$. The initially square pulse of tracer concentration is translated, unchanged, by the constant advection velocity.

6.2.2 Arbitrary functions resulting from PDEs

As revealed from the above example, the solution to a partial differential equation is typically given in terms of an arbitrary function with a specified dependence on the independent variables. The function itself is unspecified without additional information from initial and/or boundary conditions. For example, consider an initial tracer concentration in the form of a sine-wave

$$C(x, t = 0) = C_0 \sin(k\, x), \tag{6.7}$$

with k a wavenumber (dimensions of inverse length), and allow the domain to be infinite in extent (no boundaries). When advected by a constant advection velocity, the solution to the advection equation is a tracer concentration in the form of a sine-wave moving in the positive $\hat{\boldsymbol{x}}$ direction with speed U

$$C(x, t) = C_0 \sin[k\,(x - Ut)]. \tag{6.8}$$

The arbitrary functional degree of freedom is a generalization of the case with ordinary differential equations, whose solutions are determined up to constants that are specified by initial and/or boundary conditions.

6.2.3 Further study

Advection plays a fundamental role in the transport of matter, energy, and momentum within fluids. As seen in our discussion of fluid kinematics in Chapter 17, advection appears in the fluid mechanical equations when viewing the fluid from the fixed laboratory or *Eulerian* reference

frame. We thus encounter advection throughout this book, with further development of the physics in Section 69.3 and mathematics in Section 69.4.

6.3 Characteristic curves for first order PDEs

The advection equation is the canonical first order partial differential equation commonly found in fluid mechanics. A more general form for a first order partial differential equation in one space dimension is given by[1]

$$P(x,t,\psi)\,\partial_x\psi + Q(x,t,\psi)\,\partial_t\psi = R(x,t,\psi), \tag{6.9}$$

where P, Q, and R are arbitrary smooth functions, x, t are the independent variables, and ψ is the unknown dependent function. This partial differential equation is linear if P, Q, and R are independent of ψ, and quasi-linear if P and Q are independent of ψ and R is at most a linear function of ψ. In this section we develop a formalism that determines the functional dependence of solutions to these partial differential equations. This *method of characteristics* is quite useful for exposing general properties of the solutions, even for those cases where the solution is not analytically available.

6.3.1 General formulation

In the first order partial differential equation given by equation (6.9), assume there is a functional relation

$$\Upsilon(x,t,\psi) = \text{constant} \tag{6.10}$$

that determines the dependent function, ψ, consistent with equation (6.9). We refer to Υ as an *integral surface* that specifies a solution to the partial differential equation. If Υ specifies an integral surface, it must satisfy

$$\mathrm{d}\Upsilon = 0 = \frac{\partial\Upsilon}{\partial x}\,\mathrm{d}x + \frac{\partial\Upsilon}{\partial t}\,\mathrm{d}t + \frac{\partial\Upsilon}{\partial\psi}\,\mathrm{d}\psi, \tag{6.11}$$

which holds since the differential of a constant vanishes. For the two dependent variables, x and t, the condition (6.11) leads to the differential constraints

$$\frac{\mathrm{d}\Upsilon}{\mathrm{d}t} = 0 = \frac{\partial\Upsilon}{\partial\psi}\frac{\partial\psi}{\partial t} + \frac{\partial\Upsilon}{\partial t} \tag{6.12a}$$

$$\frac{\mathrm{d}\Upsilon}{\mathrm{d}x} = 0 = \frac{\partial\Upsilon}{\partial\psi}\frac{\partial\psi}{\partial x} + \frac{\partial\Upsilon}{\partial x}. \tag{6.12b}$$

Assuming $\partial\Upsilon/\partial\psi \neq 0$ allows us to write

$$\frac{\partial\psi}{\partial t} = -\frac{\partial\Upsilon/\partial t}{\partial\Upsilon/\partial\psi} \quad \text{and} \quad \frac{\partial\psi}{\partial x} = -\frac{\partial\Upsilon/\partial x}{\partial\Upsilon/\partial\psi} \tag{6.13}$$

so that the first order partial differential equation (6.9) takes on the equivalent form

$$P\frac{\partial\Upsilon}{\partial x} + Q\frac{\partial\Upsilon}{\partial t} + R\frac{\partial\Upsilon}{\partial\psi} = 0. \tag{6.14}$$

[1] Much from this section is taken from Section 8.2 of *Hildebrand* (1976).

Through this construct we have symmetrized the appearance of the functions P, Q, R appearing in the partial differential equation (6.9). Consistency of equation (6.14) with

$$\mathrm{d}\Upsilon = \frac{\partial \Upsilon}{\partial x}\,\mathrm{d}x + \frac{\partial \Upsilon}{\partial t}\,\mathrm{d}t + \frac{\partial \Upsilon}{\partial \psi}\,\mathrm{d}\psi = 0, \tag{6.15}$$

requires

$$P = \rho\,\mathrm{d}x \quad \text{and} \quad Q = \rho\,\mathrm{d}t \quad \text{and} \quad R = \rho\,\mathrm{d}\psi, \tag{6.16}$$

for some non-dimensional function, $\rho(x, t, \psi)$. Eliminating the unknown function ρ renders the ordinary differential equations

$$\frac{\mathrm{d}x}{P} = \frac{\mathrm{d}t}{Q} = \frac{\mathrm{d}\psi}{R}. \tag{6.17}$$

Paths in (x, t, ψ) space that satisfy these differential equations are known as *characteristic curves*. Note that if any one of the functions P, Q, or R vanish, then we merely remove that term from these relations.

6.3.2 Examples

We now determine characteristic curves for some specific examples. First consider the linear homogeneous advection equation with constant advection speed

$$U\,\frac{\partial \psi}{\partial x} + \frac{\partial \psi}{\partial t} = 0, \tag{6.18}$$

in which we identify $P = U$, $Q = 1$, and $R = 0$. The single ordinary differential equation defining the characteristic curve is given by

$$\frac{\mathrm{d}x}{U} = \frac{\mathrm{d}t}{1}, \tag{6.19}$$

so that characteristics are given by the family of space-time lines

$$\mathrm{d}(x - U\,t) = 0 \Longrightarrow x - U\,t = \alpha, \tag{6.20}$$

with α an arbitrary constant. These lines determine the paths in space-time along which advective signals are transmitted.

Now add a constant source to the linear advection equation

$$U\,\frac{\partial \psi}{\partial x} + \frac{\partial \psi}{\partial t} = R. \tag{6.21}$$

The two ordinary differential equations defining the characteristic curve are

$$\frac{\mathrm{d}x}{U} = \frac{\mathrm{d}t}{1} = \frac{\mathrm{d}\psi}{R}. \tag{6.22}$$

In addition to the relation $x - U\,t = \alpha_1$ determined from the homogeneous case, we also have $\psi - R\,t = \alpha_2$ for α_2 an arbitrary constant. Hence, the characteristic equations render the general solution of the form

$$\Gamma[x - U\,t, \psi - R\,t] = \text{constant}, \tag{6.23}$$

for Γ an arbitrary function. One example solution is given by

$$\psi = f(x - U\,t) + R\,t, \tag{6.24}$$

for an arbitrary smooth function, f. This solution has the form of a traveling signal, $f(x - U\,t)$, plus a linear signal, $R\,t$.

For the final example, consider the linear advection equation with non-constant coefficients and non-constant source

$$x\,\frac{\partial \psi}{\partial x} + t\,\frac{\partial \psi}{\partial t} = \psi, \tag{6.25}$$

in which the ordinary differential equations determining the characteristics are given by

$$\frac{\mathrm{d}x}{x} = \frac{\mathrm{d}t}{t} = \frac{\mathrm{d}\psi}{\psi}. \tag{6.26}$$

The first equality leads to the identity

$$\mathrm{d}(\ln x) = \mathrm{d}(\ln t) \Longrightarrow t/x = \alpha_1. \tag{6.27}$$

Similarly, by equating the first and third terms in equation (6.26) we have

$$\psi/x = \alpha_2. \tag{6.28}$$

Hence, the general solution of the partial differential equation (6.25) is given by e

$$\Gamma(t/x, \psi/x) = 0 \Rightarrow \psi = x\,F(t/x) \tag{6.29}$$

for an arbitrary smooth function F.

6.4 Classifying second order partial differential equations

There are many second order partial differential equations appearing in fluid mechanics, a general form of which in one space dimension is given by

$$A\,\frac{\partial^2 \psi}{\partial x^2} + B\frac{\partial^2 \psi}{\partial x\,\partial t} + C\frac{\partial^2 \psi}{\partial t^2} = \Lambda. \tag{6.30}$$

For linear partial differential equations, A, B, C are arbitrary functions of space and time that are independent of ψ. Furthermore, Λ is a function of space and time and at most a linear function of ψ and its derivatives. The most general solution to a linear partial differential equation consists of the sum of any *particular solution* and a solution to the homogeneous problem (where $\Lambda = 0$).

The terms involving second derivatives in equation (6.30) determine the character of the solutions, with importance placed on the sign of the discriminant $B^2 - 4\,A\,C$. By analogy with conic sections we classify second order partial differential equations as follows:

$$\text{PDE form} = \begin{cases} \text{hyperbolic} & B^2 - 4\,A\,C > 0 \\ \text{elliptic} & B^2 - 4\,A\,C < 0 \\ \text{parabolic} & B^2 - 4\,A\,C = 0. \end{cases} \tag{6.31}$$

We can further motivate this terminology by considering the case of a homogeneous constant coefficient partial differential equation and an assumed solution of the form

$$\psi(x,t) = f(m\,x + t). \tag{6.32}$$

Plugging into the second order partial differential equation (6.30) with $\Lambda = 0$ leads to

$$A\,m^2 + B\,m + C = 0. \tag{6.33}$$

The two solutions, m_1 and m_2, are both real for the hyperbolic case, conjugate complex for the elliptic case, and a perfect square for the parabolic case.

6.5 Elliptic partial differential equations

The elliptic case from Section 6.4 has discriminant $B^2 - 4\,A\,C < 0$, in which case there are two imaginary characteristics. The canonical example elliptic equation is *Laplace's equation*

$$(\partial_{xx} + \partial_{yy})\,\psi = 0, \tag{6.34}$$

where we converted from the time coordinate, t, to the space coordinate y. Formally, this transition is realized by setting $t = \mathrm{i}\,y$, where $\mathrm{i} = \sqrt{-1}$. Laplace's equation is satisfied by time-independent (i.e., *steady state*) solutions to the heat/diffusion equation (Section 6.6). Another common elliptic equation is *Poisson's equation*, which results from adding a source to Laplace's equation

$$(\partial_{xx} + \partial_{yy})\,\psi = \Lambda. \tag{6.35}$$

As a frequent shorthand, we define the *Laplacian operator* (for three space-dimensions)

$$\nabla^2 = \partial_{xx} + \partial_{yy} + \partial_{zz}. \tag{6.36}$$

This expression generalizes to arbitrary coordinates (e.g., see Sections 4.22, and 4.23 for cylindrical and spherical coordinate examples).

As there is no time in the Laplace and Poisson equations, information is transmitted instantaneously so that the structure of the solution is determined by boundary conditions or boundary *data*. Strictly speaking, instantaneous information transfer is not physical since all physical signals have a finite propagation speed no greater than the speed of light. However, an infinite speed can be a useful mathematical construct motivated by the physics. For example, acoustic signals (Chapter 51) propagate in fluids much faster than other waves and fluid particle speeds. For many purposes of large-scale planetary fluid mechanics, it is suitable to assume acoustic speeds are infinite, and in so doing we *filter* or remove acoustic modes from of the dynamical equations.[2] In the process, the hyperbolic equation describing acoustic waves is converted into an elliptic equation.

6.5.1 Harmonic functions

Solutions to Laplace's equation, $\nabla^2\psi = 0$, are known as *harmonic functions*. The name "harmonic" originates from the study of fundamental modes of oscillation, such as arise from musical instruments or more generally the motion of linear oscillators. Such fundamental modes are solutions to the Laplace equation with boundary conditions depending on the instrument. On domains with certain symmetries, the solution to Laplace's equation can be written in terms of the sine and cosine trignometric functions. Notably, these functions are solutions to the one-dimensional Helmholtz equation (see Section 6.7.3), or equivalently to the *simple harmonic oscillator equation* (see Section 15.6). As a result, the sine and cosine functions, though not satisfying Laplace's equation, provide building blocks to the harmonic functions that do satisfy Laplace's equation.

Here are some example harmonic functions for two space dimensions:

$$\psi = x^3 - 3\,x\,y^2 \qquad \psi = \ln(x^2 + y^2) \qquad \psi = e^{\gamma\,x}\cos(\gamma\,y) \qquad \psi = a\,x + b\,y, \tag{6.37}$$

[2] A scuba diver feeling the beat of a ship underwater, or an audience member at a rock concert may question why we wish to filter out acoustic waves from the dynamics. Even so, in Chapter 51 we see that acoustic energy is in fact tiny relative to planetary waves and gravity waves, and utterly negligible for studies of large scale geophysical fluid motions.

with arbitrary constants a, b, γ. Furthermore, with

$$\nabla^2(\psi\,\phi) = \psi\,\nabla^2\phi + 2\,\nabla\phi\cdot\nabla\psi + \phi\,\nabla^2\psi, \tag{6.38}$$

we see that the product of two harmonic functions ($\nabla^2\psi = \nabla^2\phi = 0$) is itself harmonic if and only if their gradients are orthogonal, $\nabla\psi\cdot\nabla\phi = 0$. In the remainder of this section we present some properties of harmonic functions and develop self-consistency for the boundary data appearing in the Laplacian boundary value problem defined by equations (6.41a)-(6.41b) stated below.

6.5.2 Mean value property of harmonic functions

Harmonic functions possess a remarkable *mean value property*, which we prove in Section 9.3.10 using methods from Green's function theory. Here, we consider its implications.

The mean value property says that the value of a harmonic function, ψ, at a point $\boldsymbol{x}_0$ within an open region of $\mathcal{R}$ equals to the average of ψ taken over the surface of a sphere within $\mathcal{R}$ that is centered at $\boldsymbol{x}_0$. In equations this property states that

$$\psi(\boldsymbol{x}_0) = \frac{\oint_{\mathcal{S}_R}\psi(\boldsymbol{x})\,\mathrm{d}\mathcal{S}}{\oint_{\mathcal{S}_R}\mathrm{d}\mathcal{S}}, \tag{6.39}$$

where $\mathcal{S}_R$ is a sphere with radius R centered at $\boldsymbol{x}_0$ with "area" given by

$$\oint_{\mathcal{S}_R}\mathrm{d}\mathcal{S} = \begin{cases} 2\pi R & n = 2 \text{ space dimensions} \\ 4\pi R^2 & n = 3 \text{ space dimensions.} \end{cases} \tag{6.40}$$

We illustrate this property in Figure 6.2.

The mean-value property of harmonic functions holds anywhere within the domain where $\nabla^2\psi = 0$, so long as the sphere is fully contained within that domain. It implies that there can be no extrema of ψ within the domain, since if there was an extrema then it could not satisfy the mean-value property. Hence, all extrema of harmonic functions live on the domain boundary. This property lends mathematical support for considering harmonic functions to be solutions to continuous physical systems that are in equilibrium or a steady state. As a physical example, consider a temperature field, $T(\boldsymbol{x})$, in a region with zero heat sources and zero fluid flow. As shown in Section 68.3.4, the steady state temperature satisfies $\nabla^2 T = 0$, and as such it is harmonic and hence has no extrema within the domain.

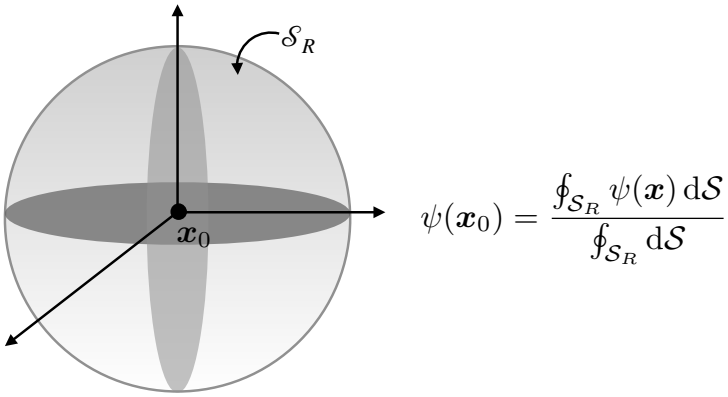

FIGURE 6.2: The value of a harmonic function at a point $\boldsymbol{x}_0$ equals to the area average of the function over a sphere of arbitrary radius (so long as $\nabla^2\psi = 0$ inside the sphere) centered at $\boldsymbol{x}_0$. We here illustrate this property for 3-dimensions, but it holds for arbitrary space dimensions.

6.5.3 Laplace's boundary value problem

Laplace's equation requires boundary conditions to fully specify the harmonic function. We here consider Laplace's *boundary value problem* in the form

$$\nabla^2 \psi = 0 \qquad \boldsymbol{x} \in \mathcal{R} \tag{6.41a}$$

$$\alpha\, \psi + \beta\, \hat{\boldsymbol{n}} \cdot \nabla \psi = \sigma \qquad \boldsymbol{x} \in \partial\mathcal{R}, \tag{6.41b}$$

where $\mathcal{R}$ is a smooth and simply connected volume, $\partial\mathcal{R}$ is the boundary surface enclosing $\mathcal{R}$ with outward unit normal, $\hat{\boldsymbol{n}}$, and with α, β, and σ given boundary data functions.

We can establish constraints on the boundary conditions that lead to a self-consistent Laplacian boundary value problem (6.41a)-(6.41b). We do so through the use of Gauss's divergence theorem (Section 2.7) in which integration over the full domain leads to

$$0 = \int_{\mathcal{R}} \nabla^2 \psi \, \mathrm{d}V = \oint_{\partial\mathcal{R}} \hat{\boldsymbol{n}} \cdot \nabla \psi \, \mathrm{d}\mathcal{S}. \tag{6.42}$$

In physical applications the boundary condition (6.41b) usually appears with either $\alpha = 0$ or $\beta = 0$, and these two cases are associated with distinct self-consistency constraints.

Dirichlet boundary condition

The case with $\beta = 0$ is referred to as a *Dirichlet boundary condition* whereby

$$\psi = \sigma \qquad \boldsymbol{x} \in \partial\mathcal{R}, \tag{6.43}$$

where we set $\alpha = 1$ without loss of generality. In this case all boundary data result in a self-consistent Laplacian boundary value problem so there is no constraint on σ. Thinking again about temperature, this boundary condition specifies the temperature on the domain boundary to equal $T = \sigma$, with all boundary functions σ consistent with a harmonic temperature distribution within the domain interior.

Neumann boundary condition

The case with $\alpha = 0$ results in a *Neumann boundary condition*. Without loss of generality we set $\beta = 1$ and reach the following self-consistency condition

$$\oint_{\partial\mathcal{R}} \sigma \, \mathrm{d}\mathcal{S} = 0. \tag{6.44}$$

A self-consistent boundary condition for Laplace's equation with the Neumann boundary condition must satisfy this surface integral constraint. For the temperature example, this boundary condition says that to realize a steady state harmonic temperature distribution within a region, we can at most apply a zero area averaged boundary heating. If the boundary constraint (6.44) is not satisfied, then the interior temperature field cannot be harmonic so that it will not be in a steady state.

6.5.4 Poisson's equation

The generic boundary value problem for Poisson's equation takes on the form

$$\nabla^2 \psi = \Lambda \qquad \boldsymbol{x} \in \mathcal{R} \tag{6.45a}$$

$$\alpha\, \psi + \beta\, \hat{\boldsymbol{n}} \cdot \nabla \psi = \sigma \qquad \boldsymbol{x} \in \partial\mathcal{R}, \tag{6.45b}$$

where $\Lambda(\boldsymbol{x})$ is a specified source function. We here present, without proof, some general properties of solutions to Poisson's equation and develop self-consistency conditions for the boundary data appearing in equation (6.45b).

6.5.5 Extended max-min principle for Poisson's equation

A *subharmonic function*, ψ, satisfies the Poisson equation with a non-negative source

$$\nabla^2\psi = \Lambda \geq 0 \qquad \boldsymbol{x} \in \mathcal{R}. \tag{6.46}$$

Here, the source function makes the curvature of a subharmonic function positive. Correspondingly, every point within $\mathcal{R}$ satisfies the minimum principle

$$\psi(\boldsymbol{x}_0) \leq \frac{\oint_{\mathcal{S}_R} \psi(\boldsymbol{x})\,\mathrm{d}\mathcal{S}}{\oint_{\mathcal{S}_R} \mathrm{d}\mathcal{S}}, \tag{6.47}$$

for spheres, $\mathcal{S}_R$, that are fully within $\mathcal{R}$ and where $\nabla^2\psi = \Lambda$. The signs switch for superharmonic functions whereby $\nabla^2\psi \leq 0$ for $\boldsymbol{x} \in \mathcal{R}$

Returning to the temperature example, consider a temperature field in a region with a positive heat source, $\Lambda > 0$. The steady state temperature in the presence of zero fluid flow satisfies Poisson's equation $\nabla^2 T = \Lambda \geq 0$ for regions with the heat source. The minimum principle (6.47) means that the temperature at any point within the heating region is less than the temperature averaged over a sphere centered on the point, so long as the sphere remains within the region of heating. It is only in the absence of a heat source or sink, where $\nabla^2 T = 0$, that we recover the mean-value property of harmonic functions given by equation (6.39).

6.5.6 Poisson's boundary value problem

We follow the method in Section 6.5.3 to develop constraints on the boundary conditions applied as part of the Poisson boundary value problem (6.45a)-(6.45b). Use of Gauss's divergence theorem leads to the constraint

$$\oint_{\partial\mathcal{R}} \hat{\boldsymbol{n}} \cdot \nabla\psi \,\mathrm{d}\mathcal{S} = \int_{\mathcal{R}} \Lambda \,\mathrm{d}V. \tag{6.48}$$

We separately consider Dirichlet and Neumann boundary conditions.

Dirichlet boundary condition

The Dirichlet condition with $\beta = 0$ leads to

$$\psi = \sigma \qquad \boldsymbol{x} \in \partial\mathcal{R}. \tag{6.49}$$

Just as for Laplace's boundary value problem, all boundary data result in a self-consistent Poisson boundary value problem, so there is no constraint on σ. Thinking again about temperature, this boundary condition specifies the temperature on the domain boundary to equal $T = \sigma$, with all boundary functions, σ, consistent with the interior heating, Λ, and a temperature field satisfying $\nabla^2 T = \Lambda$ within the interior.

Self-consistent Neumann boundary condition

The *Neumann* boundary condition leads to the following self-consistency condition

$$\oint_{\partial\mathcal{R}} \sigma \, \mathrm{d}\mathcal{S} = \int_{\mathcal{R}} \Lambda \, \mathrm{d}V. \tag{6.50}$$

A self-consistent boundary condition for Poisson's equation with a Neumann boundary condition must satisfy this surface integral constraint. For the temperature example, this boundary condition says that the area integrated boundary data must be consistent with the volume integrated source function in order for the temperature to satisfy Poisson's equation. Otherwise, the temperature field will evolve in time and thus not be in a steady state. Compatibility of the boundary conditions ensures the existence of a solution to the Poisson equation that is unique up to an arbitrary constant.

6.6 Parabolic partial differential equations

The parabolic case from Section 6.4, $B^2 - 4\,A\,C = 0$, contains a single real characteristic. The canonical example is the *heat equation*, which is also known as the *diffusion equation*

$$\frac{\partial \psi}{\partial t} = \kappa \, \frac{\partial^2 \psi}{\partial x^2}, \tag{6.51}$$

where $\kappa > 0$ is the kinematic diffusivity with dimensions of squared length per time.

6.6.1 Initial and initial-boundary value problems

The *Cauchy Problem* is the name given to the initial value problem for the heat equation over all space, here given by Euclidean space

$$\frac{\partial \psi}{\partial t} = \kappa \, \nabla^2 \psi \qquad \boldsymbol{x} \in \mathbb{R}^n, t > 0 \tag{6.52a}$$

$$\psi(\boldsymbol{x}, t = 0) = \sigma(\boldsymbol{x}) \qquad \boldsymbol{x} \in \mathbb{R}^n \tag{6.52b}$$

$$|\psi(\boldsymbol{x}, t)| < \infty \qquad \boldsymbol{x} \in \mathbb{R}^n, t > 0. \tag{6.52c}$$

The general initial-boundary value problem over a finite domain $\mathcal{R}$ takes the form

$$\frac{\partial \psi}{\partial t} = \kappa \, \nabla^2 \psi \qquad \boldsymbol{x} \in \mathcal{R}, t > 0 \tag{6.53a}$$

$$\psi(\boldsymbol{x}, t = 0) = \sigma(\boldsymbol{x}) \qquad \boldsymbol{x} \in \mathcal{R} \tag{6.53b}$$

$$\alpha(\boldsymbol{x}) \, \psi(\boldsymbol{x}, t) + \beta(\boldsymbol{x}) \, \hat{\boldsymbol{n}} \cdot \nabla \psi(\boldsymbol{x}, t) = g(\boldsymbol{x}, t) \qquad \boldsymbol{x} \in \partial\mathcal{R}, t > 0, \alpha\,\beta \geq 0. \tag{6.53c}$$

Following from the discussion of Laplace's and Poisson's boundary value problems, choices for the boundary functions α and β impact on the character of the boundary conditions. The Neumann condition is most commonly applied to set the flux of a tracer or temperature at the boundaries. The alternative use of the Dirichlet condition is commonly applied for idealized "diagnostic" tracers in geophysical fluid applications (see *Haine et al.* (2025) for a review of such idealized ocean tracers).

6.6.2 Smoothing property

The extended max-min principle from Section 6.5.5 holds also for the heat equation, which is consistent with solutions to the heat equation generally decaying their initial condition towards

zero by reducing the amplitude of all extrema. Hence, no extrema are introduced in the interior of the domain by the heat equation; extrema only arise via boundary and/or initial conditions. Furthermore, the steady state limit of the heat equation is a harmonic function, and so solves Laplace's equation whereby the mean-value property holds (Section 6.5.2).

Illustrating the smoothing property in a finite domain

We illustrate the smoothing property for the specific case of the one-dimensional initial-boundary value problem with homogeneous Dirichlet boundary conditions

$$\frac{\partial \psi}{\partial t} = \kappa \frac{\partial^2 \psi}{\partial x^2} \qquad 0 < x < L,\ t > 0 \tag{6.54a}$$

$$\psi(x,t) = I(x) \qquad 0 < x < L,\ t = 0 \tag{6.54b}$$

$$\psi(0,t) = \psi(L,t) = 0 \qquad t > 0. \tag{6.54c}$$

A variety of methods, such as separation of variables, can be used to derive the following Fourier series solution[3]

$$\psi(x,t) = \sum_{n=1}^{\infty} I_n \, e^{-\kappa t (n\pi/L)^2} \sin(n\pi x/L) \qquad \text{with} \qquad I_n = \frac{2}{L} \int_0^L I(x) \sin(n\pi x/L) \, \mathrm{d}x. \tag{6.55}$$

As per the smoothing property of diffusion, note how the amplitude of each Fourier mode decays exponentially in time.

Smoothing property for an initial value problem on the real line

Now consider the one-dimensional heat equation on the real line, with the only boundary conditions being regularity at infinity

$$\frac{\partial \psi}{\partial t} = \kappa \frac{\partial^2 \psi}{\partial x^2} \qquad -\infty < x < \infty,\ t > 0 \tag{6.56a}$$

$$\psi(x,t) = I(x) \qquad -\infty < x < \infty,\ t = 0. \tag{6.56b}$$

One can show by direct differentiation that the following Gaussian is a solution[4]

$$\psi(x,t) = \frac{1}{\sqrt{4\pi\kappa t}} \int_{-\infty}^{\infty} I(\xi) \, \exp\left[-\frac{(x-\xi)^2}{4\kappa t}\right] \mathrm{d}\xi. \tag{6.57}$$

Again, this function smooths/damps the initial condition function $I(x)$ as time increases.

6.6.3 Duhamel's superposition integral for the heat equation

Consider a scalar field that starts from zero initial conditions and evolves according to the heat equation in the presence of a source

$$\frac{\partial \Psi}{\partial t} = \kappa \nabla^2 \Psi + f(\boldsymbol{x}) \qquad \boldsymbol{x} \in \mathbb{R}^n,\ t > 0 \tag{6.58a}$$

$$\Psi(\boldsymbol{x},t) = 0 \qquad \boldsymbol{x} \in \mathbb{R}^n,\ t = 0. \tag{6.58b}$$

[3] We discuss Fourier series in Chapter 8.

[4] In Section 9.5 we develop Green's function methods to derive the integral solution (6.57).

Now consider the converse, in which another scalar field evolves without a source and yet is initialized according to the source

$$\frac{\partial \psi}{\partial t} = \kappa \nabla^2 \psi \qquad \boldsymbol{x} \in \mathbb{R}^n,\ t > 0 \tag{6.59a}$$

$$\psi(\boldsymbol{x}, t) = f(\boldsymbol{x}) \qquad \boldsymbol{x} \in \mathbb{R}^n,\ t = 0. \tag{6.59b}$$

Remarkably, these two scalar fields are related by *Duhamel's superposition integral*

$$\Psi(\boldsymbol{x}, t) = \int_0^t \psi(\boldsymbol{x}, t - \tau)\, \mathrm{d}\tau. \tag{6.60}$$

We verify the connection by direct differentiation

$$\frac{\partial \Psi(\boldsymbol{x}, t)}{\partial t} = \psi(\boldsymbol{x}, 0) + \int_0^t \frac{\partial \psi(\boldsymbol{x}, t - \tau)}{\partial t}\, \mathrm{d}\tau = f(\boldsymbol{x}) + \kappa \nabla^2 \Psi(\boldsymbol{x}, t). \tag{6.61}$$

Duhamel's superposition integral allows us to move the source between the partial differential operator and the initial conditions. It says that the forced solution, $\Psi(\boldsymbol{x}, t)$, is built by time integrating the "retarded" values of the unforced solution, ψ, from the initial time, $t = 0$, to the current time, t. A more general presentation allows for the source function to be a function of time, $f(\boldsymbol{x}, t)$, in which case we develop a family of solutions, $\psi_f(\boldsymbol{x}, t; \tau)$, generated by reinitializing $\psi_f(\boldsymbol{x}, t = \tau; \tau) = f(\boldsymbol{x}, \tau)$ and then superposing the members of this family to generate $\Psi(\boldsymbol{x}, t)$. This more general solution method is encompassed by the Green's functions of Section 9.5.

As an example, consider the initial value problem for the heat equation on a line as given by equations (6.56a)-(6.56b)

$$\frac{\partial \psi}{\partial t} = \kappa \frac{\partial^2 \psi}{\partial x^2} \qquad -\infty < x < \infty,\ t > 0 \tag{6.62a}$$

$$\psi(x, t) = f(x) \qquad -\infty < x < \infty,\ t = 0, \tag{6.62b}$$

whose solution is given by the Gaussian function in equation (6.57). Duhamel's superposition integral (6.60) says that

$$\Psi(x, t) = \int_0^t \psi(x, t - \tau)\, \mathrm{d}\tau = \int_0^t \frac{1}{\sqrt{4\,\pi\,\kappa\,(t - \tau)}} \int_{-\infty}^{\infty} f(\xi)\, \exp\left[-\frac{(x - \xi)^2}{4\,\kappa\,(t - \tau)} \right] \mathrm{d}\tau\, \mathrm{d}\xi \tag{6.63}$$

satisfies the forced (inhomogeneous) initial value problem with zero initial condition

$$\frac{\partial \Psi}{\partial t} = \kappa \frac{\partial^2 \Psi}{\partial x^2} + f(x) \qquad -\infty < x < \infty,\ t > 0 \tag{6.64a}$$

$$\Psi(x, t) = 0 \qquad -\infty < x < \infty,\ t = 0. \tag{6.64b}$$

We make use of this result in our discussion of Green's functions in Chapter 9.

6.6.4 Further study

We examine physical and mathematical properties of the heat/diffusion equation in Sections 68.3 and 68.4. Section 9.11 of *Hildebrand* (1976) offers a lucid discussion of Duhamel's superposition integral.

6.7 Hyperbolic partial differential equations

The hyperbolic case from Section 6.4 has $B^2 - 4\,A\,C > 0$ and thus contains two real characteristics. The the linear homogeneous wave equation is the canonical example of a hyperbolic partial differential equation

$$(\partial_{tt} - U^2\,\partial_{xx})\psi = 0. \tag{6.65}$$

Solutions have the form of a moving signal in both directions that move along the two characteristics

$$\psi(x,t) = \mathcal{F}(x - Ut) + \mathcal{G}(x + U\,t), \tag{6.66}$$

where $\mathcal{F}$ and $\mathcal{G}$ are differentiable functions whose form is determined by the initial conditions. Note that we can factor the differential operator into the form

$$(\partial_t - U\,\partial_x)\,(\partial_t + U\,\partial_x)\psi = 0. \tag{6.67}$$

Consequently, if either one of the linear first-order partial differential equations are satisfied

$$(\partial_t - U\,\partial_x)\psi = 0 \tag{6.68a}$$
$$(\partial_t + U\,\partial_x)\psi = 0 \tag{6.68b}$$

then ψ will satisfy the full wave equation. These first-order partial differential equations are the one-dimensional advection equations considered in Section 6.3 with opposite advection direction, and each of which has a single characteristic. In this manner, we can think of advection by constant velocity as the square root of the wave equation. Similarly, some disciplines refer to the linear advection equation (6.2), with constant advection speed, as the *one-way wave equation*. It represents the simplest of the hyperbolic partial differential equations.

6.7.1 Initial value problem for the infinite-domain wave equation

Since there are two time derivatives, specification of a solution requires initial conditions for the field and its first time derivative. To illustrate the structure of a solution to the wave equation, we develop a solution to the *Cauchy problem*, which is the initial value problem for the one-dimensional wave equation on the real line (infinite spatial domain so no boundary conditions)

$$\partial_{tt}\psi = c^2\,\partial_{xx}\psi \qquad -\infty < x < \infty,\ t > 0 \qquad \text{wave equation on a line} \tag{6.69a}$$
$$\psi = F(x) \qquad -\infty < x < \infty,\ t = 0 \qquad \text{initial condition} \tag{6.69b}$$
$$\partial_t\psi = G(x) \qquad -\infty < x < \infty,\ t = 0 \qquad \text{initial tendency,} \tag{6.69c}$$

where the initial condition data, F, G, are arbitrary functions of space and c is a constant wave speed. Following from the discussion of characteristics in Section 6.3, we are motivated to perform a linear transformation of the wave equation into wave characteristic coordinates

$$\xi = x + c\,t \qquad \text{and} \qquad \eta = x - c\,t \Longrightarrow (\xi + \eta)/2 = x \qquad \text{and} \qquad (\xi - \eta)/(2c) = t. \tag{6.70}$$

Wave signals propagate in directions defined by constant ξ and η, so that these coordinates isolate the signal transmission. Furthermore, as we will see, this coordinate transformation facilitates a direct integration of the wave equation.

Transformation to characteristic coordinates

To help organize the linear transformation to characteristic coordinates, write equation (6.70) as a matrix-vector equation

$$\begin{bmatrix} \xi \\ \eta \end{bmatrix} = \begin{bmatrix} c & 1 \\ -c & 1 \end{bmatrix} \begin{bmatrix} t \\ x \end{bmatrix} \Longleftrightarrow \begin{bmatrix} t \\ x \end{bmatrix} = \frac{1}{2} \begin{bmatrix} c^{-1} & -c^{-1} \\ 1 & 1 \end{bmatrix} \begin{bmatrix} \xi \\ \eta \end{bmatrix}. \tag{6.71}$$

Furthermore, introduce tensor indices (see Chapter 1)

$$\mu = (0, 1) \quad \text{and} \quad \overline{\mu} = (\overline{0}, \overline{1}), \tag{6.72}$$

where indices 0 and $\overline{0}$ represent time and indices 1 and $\overline{1}$ represent space, in which case the time and space coordinates are written

$$x^{\mu} = (x^0, x^1) = (t, x) \quad \text{and} \quad x^{\overline{\mu}} = (x^{\overline{0}}, x^{\overline{1}}) = (\xi, \eta). \tag{6.73}$$

Use of this index notation brings the linear transformation (6.71) into the tidy form

$$x^{\overline{\mu}} = \Lambda^{\overline{\mu}}{}_{\nu}\, x^{\nu} \Longleftrightarrow x^{\mu} = \Lambda^{\mu}{}_{\overline{\nu}}\, x^{\overline{\nu}}, \tag{6.74}$$

where the transformation matrices are given by the constant matrices[5]

$$\Lambda^{\overline{\mu}}{}_{\nu} = \begin{bmatrix} \partial x^{\overline{1}}/\partial x^1 & \partial x^{\overline{1}}/\partial x^2 \\ \partial x^{\overline{1}}/\partial x^2 & \partial x^{\overline{2}}/\partial x^2 \end{bmatrix} = \begin{bmatrix} c & 1 \\ -c & 1 \end{bmatrix} \tag{6.75}$$

and

$$\Lambda^{\mu}{}_{\overline{\nu}} = \begin{bmatrix} \partial x^1/\partial x^{\overline{1}} & \partial x^1/\partial x^{\overline{2}} \\ \partial x^2/\partial x^{\overline{1}} & \partial x^2/\partial x^{\overline{2}} \end{bmatrix} = \frac{1}{2} \begin{bmatrix} c^{-1} & -c^{-1} \\ 1 & 1 \end{bmatrix}. \tag{6.76}$$

Note the use of an upstairs position for the row index on the transformation matrix, which conforms to the use with general tensors from Chapter 3. The coordinate transformation (6.74) and the transformation matrices (6.75)-(6.76) then lead to the partial derivative relationship

$$\partial_{\overline{\nu}} = \Lambda^{\mu}{}_{\overline{\nu}}\, \partial_{\mu} \Longleftrightarrow \partial_{\nu} = \Lambda^{\overline{\mu}}{}_{\nu}\, x_{\overline{\mu}}, \tag{6.77}$$

so that

$$\frac{\partial^2}{\partial x^2} = \left[\frac{\partial}{\partial \xi} + \frac{\partial}{\partial \eta} \right]^2 = \frac{\partial^2}{\partial \xi^2} + 2\, \frac{\partial}{\partial \xi}\, \frac{\partial}{\partial \eta} + \frac{\partial^2}{\partial \eta^2} \tag{6.78a}$$

$$c^{-2}\, \frac{\partial^2}{\partial t^2} = \left[\frac{\partial}{\partial \xi} - \frac{\partial}{\partial \eta} \right]^2 = \frac{\partial^2}{\partial \xi^2} - 2\, \frac{\partial}{\partial \xi}\, \frac{\partial}{\partial \eta} + \frac{\partial^2}{\partial \eta^2}. \tag{6.78b}$$

General solution for the initial value problem

The operator transformations (6.78a) and (6.78b) bring the initial value problem (6.69a)-(6.69c) into the form

$$\frac{\partial^2 \psi}{\partial \xi \partial \eta} = 0 \qquad -\infty < \eta < \xi < \infty \tag{6.79a}$$

$$\psi(\xi, \eta) = F(\xi) \qquad -\infty < \xi < \infty,\ \xi = \eta \tag{6.79b}$$

[5] For linear coordinate transformations such as considered here, the space-time coordinates as well as tensors transform with the same transformation matrices.

$$\frac{\partial \psi}{\partial \xi} - \frac{\partial \psi}{\partial \eta} = c^{-1} G(\xi) \qquad -\infty < \xi < \infty, \; \xi = \eta. \tag{6.79c}$$

Integrating equation (6.79a) leads to $\partial_\xi \psi = \theta(\xi)$ so that

$$\psi(\xi, \eta) = \Phi(\eta) + \int^{\xi} \theta(s) \, \mathrm{d}s \equiv \Phi(\eta) + \Theta(\xi), \tag{6.80}$$

for two functions $\Phi(\eta)$ and $\Theta(\xi)$. The initial conditions (6.79b) and (6.79c) determine relations between $\Phi(\eta)$ and $\Theta(\xi)$ and the initial data

$$\Theta(\xi) = \frac{1}{2} \left[F(\xi) + \frac{1}{c} \int^{\xi} G(s) \, \mathrm{d}s \right] \tag{6.81a}$$

$$\Phi(\eta) = \frac{1}{2} \left[F(\eta) - \frac{1}{c} \int^{\eta} G(s) \, \mathrm{d}s \right], \tag{6.81b}$$

in which case the general solution to the initial value problem (6.69a)-(6.69c) takes the form

$$\psi(x,t) = \frac{1}{2} \left[F(x + c\,t) + F(x - c\,t) \right] + \frac{1}{2c} \int_{x-ct}^{x+ct} G(s) \, \mathrm{d}s, \tag{6.82}$$

where we reintroduced the variables (x, t). This solution is known as the *D'Alembert formula* for the wave equation. Note how the initial profile, $F(x)$, is propagated along the two characteristics, $\xi = x + c\,t$ and $\eta = x - c\,t$, without any change. In contrast, the initial tendency, $\partial_t \psi(x, t = 0) = G(x)$, is smoothed through the time integration. This behavior contrasts to the heat equation in Section 6.6, with its single time derivative resulting in a smoothing of the full solution.

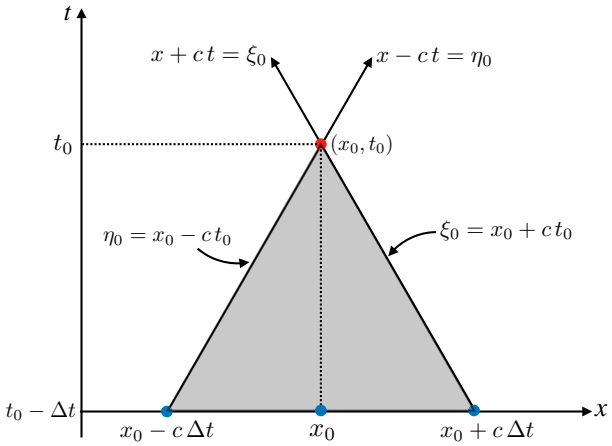

FIGURE 6.3: Equation (6.82) is the general solution to the wave equation initial value problem on a line, in which case an arbitrary space-time point, (x_0, t_0), is causally connected via wave signals to all space-time points within the shaded region in its past. This *domain of influence* is bounded by the two wave characteristics, $\xi_0 = x_0 + c\,t_0$ and $\eta_0 = x_0 - c\,t_0$, with these characteristics the pathway for propagating information about the initial wave profile, $\psi(x, t = 0) = F(x)$. Points in between the characteristics are causally connected via the initial time tendency, $\partial_t \psi(x, t = 0) = G(x)$, which is integrated over the region $x_0 - c\,t_0 \leq x \leq x_0 + c\,t_0$. Points outside the domain of influence are causally disconnected from the point (x_0, t_0).

6.7.2 Domain of influence for wave signals

The wave solution (6.82) at a point in space time, (x_0, t_0), depends on data to its past within a causality triangle, or *domain of influence*, as shown in Figure 6.3. The domain of influence is bounded by the two wave characteristics, $\xi_0 = x_0 + c\,t_0$ and $\eta_0 = x_0 - c\,t_0$. These characteristics

are the pathways for propagating information about the initial wave profile, $\psi(x, t = 0) = F(x)$. Points in between the characteristics are causally connected via the initial time tendency, $\partial_t \psi(x, t = 0) = G(x)$, which is integrated over the region $x_0 - c\,t_0 \leq x \leq x_0 + c\,t_0$. Points outside the domain of influence are causally disconnected from the point (x_0, t_0).

6.7.3 Helmholtz equation

Consider the wave equation with a constant wave speed

$$(\partial_{tt} - c^2 \nabla^2)\, \psi = 0. \tag{6.83}$$

Assuming a monochromatic periodic time dependence ansatz[6] of the form

$$\psi(\boldsymbol{x}, t) = e^{-\mathrm{i}\,\omega\, t}\, \Psi(\boldsymbol{x}) \tag{6.84}$$

results in the *Helmholtz equation* for the amplitude function

$$[\nabla^2 + (\omega/c)^2]\, \Psi = 0. \tag{6.85}$$

The Helmholtz equation thus plays a central role in wave theory. In particular, it is the relevant equation when we are uninterested in the initial value problem for waves, but instead are interested in the steady state where the wave field is fully established. In Exercise 51.1, we encounter this equation when deriving the standing acoustic modes in a rectangular cavity. We further encounter Helmholtz-like equations throughout our study of wave mechanics in Part X of this book.

6.7.4 Duhamel's superposition integral for the wave equation

We here present *Duhamel's superposition integral* for the wave equation, following from the similar discussion for the heat equation in Section 6.6.3. For this purpose, consider the forced wave equation with time independent forcing

$$\partial_{tt} \Psi = c^2\, \nabla^2 \Psi + G(\boldsymbol{x}) \qquad \boldsymbol{x} \in \mathbb{R}^n,\ t > 0 \tag{6.86a}$$

$$\Psi(\boldsymbol{x}, t) = 0 \qquad \boldsymbol{x} \in \mathbb{R}^n,\ t = 0, \tag{6.86b}$$

and the corresponding unforced wave equation with inhomogenous initial time tendency

$$\partial_{tt} \psi = c^2\, \nabla^2 \psi \qquad \boldsymbol{x} \in \mathbb{R}^n, t > 0 \tag{6.87a}$$

$$\psi(\boldsymbol{x}, t) = 0 \qquad \boldsymbol{x} \in \mathbb{R}^n,\ t = 0. \tag{6.87b}$$

$$\partial_t \psi(\boldsymbol{x}, t) = G(\boldsymbol{x}) \qquad \boldsymbol{x} \in \mathbb{R}^n,\ t = 0. \tag{6.87c}$$

The two scalar fields are related by Duhamel's superposition integral

$$\Psi(\boldsymbol{x}, t) = \int_0^t \psi(\boldsymbol{x}, t - \tau)\, \mathrm{d}\tau. \tag{6.88}$$

We can verify this formula through direct differentiation

$$\partial_t \Psi(\boldsymbol{x}, t) = \int_0^t \frac{\partial \psi(\boldsymbol{x}, t - \tau)}{\partial t}\, \mathrm{d}\tau \tag{6.89a}$$

[6] *Ansatz* is a German word meaning an educated guess for the form of the solution. Monochromatic refers to the time dependence where each portion of the wave oscillates with the same angular frequency, ω. We study wave kinematics in Chapter 49.

$$\partial_{tt}\Psi(\boldsymbol{x},t) = \partial_t\psi(\boldsymbol{x},0) + \int_0^t \partial_{tt}\psi(\boldsymbol{x},t-\tau)\,\mathrm{d}\tau = G(\boldsymbol{x}) + c^2\,\nabla^2\Psi(\boldsymbol{x},t). \tag{6.89b}$$

As an example, consider the initial value problem for wave equation on a line with time independent forcing

$$\partial_{tt}\Psi = c^2\,\partial_{xx}\Psi + G(x) \qquad -\infty < x < \infty,\ t > 0 \tag{6.90a}$$
$$\Psi(x,t) = 0 \qquad -\infty < x < \infty,\ t = 0 \tag{6.90b}$$
$$\partial_t\Psi(x,t) = 0 \qquad -\infty < x < \infty,\ t = 0. \tag{6.90c}$$

Duhamel's superposition integral says that Ψ is related to the solution of the unforced wave equation with initial time tendency given by the forcing

$$\partial_{tt}\psi = c^2\,\partial_{xx}\psi \qquad -\infty < x < \infty,\ t > 0 \tag{6.91a}$$
$$\psi(x,t) = 0 \qquad -\infty < x < \infty, t = \tau \tag{6.91b}$$
$$\partial_t\psi(x,t) = G(x) \qquad -\infty < x < \infty,\ t = \tau > 0. \tag{6.91c}$$

We know from Section 6.7.1 that the solution, ψ, is given by the D'Alembert formula in equation (6.82), only here with the initial condition function set to zero

$$\psi(x,t) = \frac{1}{2c}\int_{x-ct}^{x+ct} G(s)\,\mathrm{d}s. \tag{6.92}$$

Hence, D'Alembert's formula says that the solution to the forced wave equation (6.90a)-(6.90c) is given by the superposition integral

$$\Psi(x,t) = \frac{1}{2c}\int_0^t \int_{x-c\,(t-\tau)}^{x+c\,(t-\tau)} G(s)\,\mathrm{d}s. \tag{6.93}$$

Introducing the *antiderivative* function via

$$\mathcal{G}(s) = \int^s G(s')\,\mathrm{d}s' \iff \frac{\partial \mathcal{G}(s)}{\partial s} = G(s) \tag{6.94}$$

allows us to interpret the solution (6.93) as the superposition of two oppositely traveling waves

$$\Psi(x,t) = \frac{1}{2c}\int_0^t \Big[\mathcal{G}[x + c\,(t-\tau)] - \mathcal{G}[x - c\,(t-\tau)]\Big]\mathrm{d}\tau. \tag{6.95}$$

6.7.5 Further study

Stakgold (2000a,b) provides a thorough discussion of the wave equation and the related Helmholtz equation. We further our understanding of wave maths and physics in Part X of this book, where we refer to the hyperbolic waves of this section as *non-dispersive waves*. For non-dispersive waves, the linear superposition of many waves retains its integrity since each wave travels with the same speed. However, most waves of interest for geophysical fluid mechanics are *dispersive*, so that waves mix among themselves; i.e., they change wavelengths as they propagate. Dispersive waves are described by linear partial differential equations that are not necessarily hyperbolic. For example, surface gravity waves of Chapter 52 satisfy an elliptic equation, with time dependence arising from boundary conditions. The dispersion of surface gravity waves leads to the familiar spreading of waves on the surface of a pond whereby longer waves travel faster than shorter waves.

6.8 Euler's theorem for homogeneous functions

Consider a suite of Q independent variables, $X_1, X_2, ...X_Q$, and an arbitrary function of these variables, $F(X_1, X_2, ...X_Q)$. We say that this function is a *homogeneous function* of degree γ if the following property holds

$$F(\lambda X_1, \lambda X_2, ...\lambda X_Q) = \lambda^\gamma F(X_1, X_2, ...X_Q), \tag{6.96}$$

with λ an arbitrary scalar. The left hand side is the function evaluated with each of the independent variables scaled by the same number, λ. The right hand side is the function evaluated with the unscaled variables, but multiplied by the scale raised to the power γ.

A particularly remarkable and useful property of such functions can be found by taking $\partial/\partial\lambda$ on both sides of the identity (6.96). The left hand side has the following partial derivative, as found through the chain rule

$$\begin{aligned}\frac{\partial F(\lambda X_1, \lambda X_2, ...\lambda X_Q)}{\partial \lambda} &= \frac{\partial F(X_1, X_2, ...X_Q)}{\partial X_1}\frac{\partial(\lambda X_1)}{\partial \lambda} + ...\frac{\partial F(X_1, X_2, ...X_Q)}{\partial X_Q}\frac{\partial(\lambda X_Q)}{\partial \lambda} \\ &= \sum_{q=1}^{Q}\left[\frac{\partial F(X_1, X_2, ...X_Q)}{\partial X_q}\right]_{X_{r\neq q}} X_q \end{aligned} \tag{6.97}$$

The derivative of the right hand side of equation (6.96) is given by

$$\frac{\partial[\lambda^\gamma F(X_1, X_2, ...X_Q)]}{\partial \lambda} = \gamma\,\lambda^{\gamma-1} F(X_1, X_2, ...X_Q). \tag{6.98}$$

Bringing these results together leads to *Euler's theorem* for homogeneous functions, which is found by setting $\lambda = 1$

$$\sum_{q=1}^{Q} X_q \left[\frac{\partial F(X_1, X_2, ...X_Q)}{\partial X_q}\right]_{X_{r\neq q}} = \gamma\, F(X_1, X_2, ...X_Q). \tag{6.99}$$

Example homogeneous functions include the intensive thermodynamic properties from Part IV of this book, with such properties homogeneous functions of degree $\gamma = 0$, meaning they are scale invariant. For example, a bucket of homogeneous water has the same temperature whether or not we remove an arbitrary sample of the water. In contrast, as discussed below, extensive thermodynamic properties are homogeneous functions of degree $\gamma = 1$. Section 22.3 presents the thermodynamic implications of such mathematical properties. We also make use of these properties in proving the *Virial theorem* of classical mechanics in Section 12.7.

6.9 Evolution of time averages

In geophysical fluid mechanics, we generically refer to an equation with a time derivative, such as a parabolic or hyperbolic equation, as a *prognostic equation* or an *evolution equation*. In the analysis of such equations, for example when analyzing simulation output or time series data, it is common to take the time average in order to focus on lower frequency behavior. This section provides a technical discussion concerning this time averaging operation, with the material here following *Bladwell et al.* (2022).

For this purpose, ignore all space coordinates and write a generic prognostic equation in the form

$$\frac{\mathrm{d}A}{\mathrm{d}t} = \mathcal{B}. \tag{6.100}$$

For example, the quantity A might be the velocity or temperature at a point in space, and $\mathcal{B}$ might be the acceleration due to pressure or the heating due to temperature diffusion. We term $\mathrm{d}A/\mathrm{d}t$ the *time tendency* of the quantity A whereas $\mathcal{B}$ is the "forcing" that gives rise to the time tendency. In the analysis of fluid flows, we commonly wish to diagnose terms appearing in the evolution equations for the purpose of ascribing physical understanding to the flow regime; e.g., what forces are more active in certain regions. Although sitting a bit outside the scope of a chapter on partial differential equations, the material in this section exposes some common questions that arise when time averaging terms appearing in the prognostic equations of geophysical fluid mechanics.

Time integration of equation (6.100) leads to

$$A(t) = A(t_0) + \int_{t_0}^{t} \mathcal{B}(s)\,\mathrm{d}s, \tag{6.101}$$

thus providing an expression for the instantaneous value of A at an arbitrary time t, assuming knowledge of the initial value, $A(t_0)$, as well as the time integral of $\mathcal{B}$. In practice, particularly when working with numerical models, we typically have access to time averages over some time interval (e.g., days, months, years, decades) rather than instantaneous (snapshot) values of A. Furthermore, instantaneous snapshots can be prone to relatively large fluctuations that expose the diagnostic calculations to numerical precision errors (e.g., small differences between relatively large fluctuating values). We are thus interested in relating time averages of A to time averages of $\mathcal{B}$.

6.9.1 Time averages

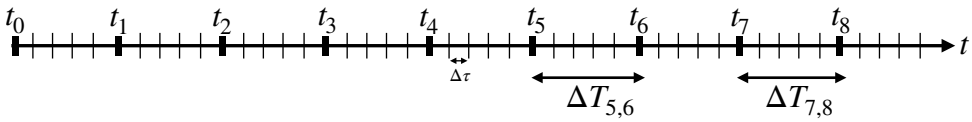

FIGURE 6.4: Example time axis for the discussion of time averaging. The labeled times, t_n, can represent, for example, days, months or years with the time interval, $\Delta T_{n,n+1} = t_{n+1} - t_n$, not necessarily the same (e.g., different number of days in a month or a leap year versus non-leap year). The smaller unlabeled time steps represent the time steps for the model's prognostic equations (e.g., days, hours, seconds, etc.), with fixed time step $\Delta\tau$.

Introduce a discrete partitioning of the time axis as in Figure 6.4 and define an unweighted time average over a chosen time interval $\Delta T_{n,n+1} = t_{n+1} - t_n > 0$

$$\overline{A}_{n,n+1} = \frac{1}{\Delta T_{n,n+1}} \int_{t_n}^{t_{n+1}} A(t)\,\mathrm{d}t \tag{6.102a}$$

$$\overline{\mathcal{B}}_{n,n+1} = \frac{1}{\Delta T_{n,n+1}} \int_{t_n}^{t_{n+1}} \mathcal{B}(t)\,\mathrm{d}t. \tag{6.102b}$$

These integrals are realized in practice as a discrete sum over the model time steps, with only the lower limit inclusive so as to not double-count endpoints; i.e., $[t_n, t_{n+1})$. We allow for non-constant time intervals, $\Delta T_{n,n+1}$, as arises in monthly and yearly (with leap-years) time averages.

Substituting expression (6.101) into the time mean (6.102a) renders

$$\overline{A}_{n,n+1} - A(t_0) = \frac{1}{\Delta T_{n,n+1}} \int_{t_n}^{t_{n+1}} \left[\int_{t_0}^{t} \mathcal{B}(s)\,\mathrm{d}s \right] \mathrm{d}t, \tag{6.103}$$

and a similar expression over a later time interval $[t_p, t_{p+1})$ with $p \geq n+1$ leads to the difference between time averages

$$\overline{A}_{p,p+1} - \overline{A}_{n,n+1} = \frac{1}{\Delta T_{p,p+1}} \int_{t_p}^{t_{p+1}} \left[\int_{t_0}^{t} \mathcal{B}(s)\, \mathrm{d}s \right] \mathrm{d}t - \frac{1}{\Delta T_{n,n+1}} \int_{t_n}^{t_{n+1}} \left[\int_{t_0}^{t} \mathcal{B}(s)\, \mathrm{d}s \right] \mathrm{d}t. \quad (6.104)$$

The formalism allows us to take differences between time averages over intervals that are separated, such as might be of interest in taking decadal means between the beginning and end of a century, for example. Importantly, the initial value, $A(t_0)$, is absent from the difference in time means so that there are only time integrated quantities appearing in equation (6.104).

6.9.2 Massaging the double time integrals

The double time integrals in equation (6.104) can be massaged into a simpler form. We start by making the following decomposition and noting that $t_n \leq t \leq t_{n+1}$

$$\int_{t_n}^{t_{n+1}} \left[\int_{t_0}^{t} \mathcal{B}(s)\, \mathrm{d}s \right] \mathrm{d}t = \int_{t_n}^{t_{n+1}} \left[\int_{t_0}^{t_n} \mathcal{B}(s)\, \mathrm{d}s + \int_{t_n}^{t} \mathcal{B}(s)\, \mathrm{d}s \right] \mathrm{d}t \quad (6.105a)$$

$$= \Delta T_{n,n+1} \int_{t_0}^{t_n} \mathcal{B}(s)\, \mathrm{d}s + \int_{t_n}^{t_{n+1}} \left[\int_{t_n}^{t} \mathcal{B}(s)\, \mathrm{d}s \right] \mathrm{d}t. \quad (6.105b)$$

We are thus led to the difference

$$\begin{aligned} \overline{A}_{p,p+1} - \overline{A}_{n,n+1} &= \left[\int_{t_0}^{t_p} \mathcal{B}(s)\, \mathrm{d}s - \int_{t_0}^{t_n} \mathcal{B}(s)\, \mathrm{d}s \right] \\ &+ \frac{1}{\Delta T_{p,p+1}} \int_{t_p}^{t_{p+1}} \left[\int_{t_p}^{t} \mathcal{B}(s)\, \mathrm{d}s \right] \mathrm{d}t - \frac{1}{\Delta T_{n,n+1}} \int_{t_n}^{t_{n+1}} \left[\int_{t_n}^{t} \mathcal{B}(s)\, \mathrm{d}s \right] \mathrm{d}t \\ &= \int_{t_n}^{t_p} \mathcal{B}(t)\, \mathrm{d}t + \frac{1}{\Delta T_{p,p+1}} \int_{t_p}^{t_{p+1}} \left[\int_{t_p}^{t} \mathcal{B}(s)\, \mathrm{d}s \right] \mathrm{d}t - \frac{1}{\Delta T_{n,n+1}} \int_{t_n}^{t_{n+1}} \left[\int_{t_n}^{t} \mathcal{B}(s)\, \mathrm{d}s \right] \mathrm{d}t. \end{aligned} \quad (6.106)$$

The double integrals in equation (6.106) take place over triangular time domains, such as shown in Figure 6.5.

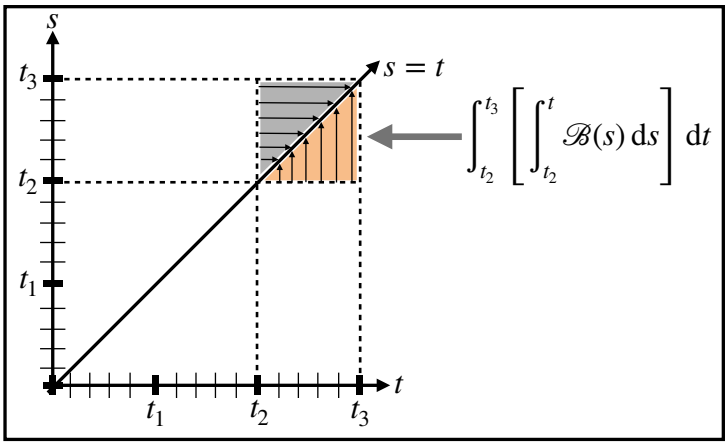

FIGURE 6.5: Gold region depicts the time integration domain used in one of the double integrals from equation (6.106) for the special case of $n = 2$. Note that the gray triangular region generally leads to a distinct integral.

6.9.3 Making use of a double integral identity

We here derive an identity (originally due to *Cauchy* (1823)) that reduces the double integral in equation (6.106) to a single integral to expose the underlying geometry of the time windowing. For this purpose we make use of the following identity

$$\int_{t_n}^{t_{n+1}} \left[\int_{t_n}^{t} \mathcal{B}(s)\,\mathrm{d}s \right] \mathrm{d}t = \int_{t_n}^{t_{n+1}} (t_{n+1} - t)\,\mathcal{B}(t)\,\mathrm{d}t. \tag{6.107}$$

To prove this identity we make the substitution $\mathcal{B}(s) = \mathrm{d}A/\mathrm{d}s$ from equation (6.100) and then show that both sides to equation (6.107) yield the same result. For the left hand side we have

$$\begin{aligned}
\int_{t_n}^{t_{n+1}} \left[\int_{t_n}^{t} \mathcal{B}(s)\,\mathrm{d}s \right] \mathrm{d}t &= \int_{t_n}^{t_{n+1}} \left[\int_{t_n}^{t} \frac{\mathrm{d}A(s)}{\mathrm{d}s}\,\mathrm{d}s \right] \mathrm{d}t && \text{(6.108a)} \\
&= \int_{t_n}^{t_{n+1}} \left[\int_{t_n}^{t} \mathrm{d}A(s) \right] \mathrm{d}t && \text{(6.108b)} \\
&= \int_{t_n}^{t_{n+1}} [A(t) - A(t_n)]\mathrm{d}t && \text{(6.108c)} \\
&= \int_{t_n}^{t_{n+1}} A(t)\,\mathrm{d}t - (t_{n+1} - t_n)\,A(t_n), && \text{(6.108d)}
\end{aligned}$$

whereas the right hand side is

$$\begin{aligned}
\int_{t_n}^{t_{n+1}} (t_{n+1} - t)\,\mathcal{B}(t)\,\mathrm{d}t &= \int_{t_n}^{t_{n+1}} (t_{n+1} - t)\,\frac{\mathrm{d}A(t)}{\mathrm{d}t})\,\mathrm{d}t && \text{(6.109a)} \\
&= \int_{t_n}^{t_{n+1}} (t_{n+1} - t)\,\mathrm{d}A(t) && \text{(6.109b)} \\
&= \int_{t_n}^{t_{n+1}} \mathrm{d}[A(t)\,(t_{n+1} - t)] + A(t)\,\mathrm{d}t && \text{(6.109c)} \\
&= -A(t_n)\,(t_{n+1} - t_n) + \int_{t_n}^{t_{n+1}} A(t)\,\mathrm{d}t, && \text{(6.109d)}
\end{aligned}$$

which is identical to the left hand side given by equation (6.108d). We have thus proven the double integral formula (6.107).

The right hand side of the double integral formula (6.107) can be written

$$\int_{t_n}^{t_{n+1}} (t_{n+1} - t)\,\mathcal{B}(t)\,\mathrm{d}t = t_{n+1}\,\Delta T_{n,n+1}\,\overline{\mathcal{B}}_{n,n+1} - \int_{t_n}^{t_{n+1}} t\,\mathcal{B}(t)\,\mathrm{d}t, \tag{6.110}$$

which might be useful in some contexts. However, it is awkward for our purposes since it exposes the absolute time, t_{n+1}, in the first term on the right hand side and the time, t, within the integral. Since we generally do not hold any initial time as special (i.e., the initial time, t_0, is arbitrary), it is preferable to retain the time differences throughout the formulation. Hence, when making use of the double integral identity (6.107) we bring equation (6.106) into the form

$$\begin{aligned}
\overline{A}_{p,p+1} - \overline{A}_{n,n+1} &= \int_{t_n}^{t_p} \mathcal{B}(t)\,\mathrm{d}t + \int_{t_p}^{t_{p+1}} \frac{(t_{p+1} - t)\,\mathcal{B}(t)}{t_{p+1} - t_p}\,\mathrm{d}t - \int_{t_n}^{t_{n+1}} \frac{(t_{n+1} - t)\,\mathcal{B}(t)}{t_{n+1} - t_n}\,\mathrm{d}t && \text{(6.111a)} \\
&= \int_{t_n}^{t_{n+1}} \frac{(t - t_n)\,\mathcal{B}(t)}{t_{n+1} - t_n}\,\mathrm{d}t + \int_{t_{n+1}}^{t_p} \mathcal{B}(t)\,\mathrm{d}t + \int_{t_p}^{t_{p+1}} \frac{(t_{p+1} - t)\,\mathcal{B}(t)}{t_{p+1} - t_p}\,\mathrm{d}t. && \text{(6.111b)}
\end{aligned}$$

The first right hand side term is a weighted integral with a linearly increasing weight from zero

to unity, whereas the final right hand side term has a linearly descreasing weight from unity to zero. The middle term has a unity weight throughout and it vanishes if $p = n + 1$, as when the averaging regions are adjacent. Figure 6.6. illustrates the time windowing used for equation (6.111b).

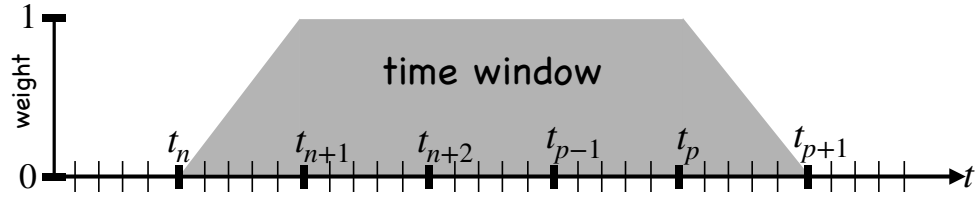

FIGURE 6.6: Illustrating the time window weighting used in computing the right hand side of equation (6.111b). Note that if $p = n + 1$, then the middle term in equation (6.111b) and there is no plateau region of unit weight, in which case the window region becomes two adjacent triangles.

As a final means to write equation (6.111b), extend the middle term to the end of the time period and then subtract the extra piece and recombine to render

$$\overline{A}_{p,p+1} - \overline{A}_{n,n+1} = \int_{t_{n+1}}^{t_{p+1}} \mathcal{B}(t)\,\mathrm{d}t + \int_{t_n}^{t_{n+1}} \frac{(t - t_n)\,\mathcal{B}(t)}{t_{n+1} - t_n}\,\mathrm{d}t - \int_{t_p}^{t_{p+1}} \frac{(t - t_p)\,\mathcal{B}(t)}{t_{p+1} - t_p}\,\mathrm{d}t. \tag{6.112}$$

The first term on the right hand side is an unweighted integral from the end of the first interval to the end of the final interval, whereas the other two terms both have increasing weights over their respective integration intervals. This form allows for some advantages diagnostically since we only need to save unweighted integrals plus linearly increasing weighted integrals; there is no need to save decreasing weighted integrals.

6.10 Exercises

EXERCISE 6.1: HELMHOLTZ DECOMPOSITION FOR CORIOLIS ACCELERATION
Consider a vector field

$$\boldsymbol{F} = 2\,\boldsymbol{\Omega} \times \boldsymbol{v}, \tag{6.113}$$

where $\boldsymbol{\Omega}$ is a spatial constant and $\nabla \cdot \boldsymbol{v} = 0$. As seen in Part V of this book, the vector $\boldsymbol{F}$ is minus the Coriolis acceleration. Since the velocity is non-divergent, there exists a vector potential so that

$$\boldsymbol{v} = \nabla \times \boldsymbol{B}. \tag{6.114}$$

Show that we can perform a Helmholtz decomposition of the Coriolis acceleration so that

$$\boldsymbol{F} = 2\,\boldsymbol{\Omega} \times \boldsymbol{v} = -\nabla\Psi + \nabla \times \boldsymbol{A}, \tag{6.115}$$

where

$$-\nabla^2\Psi = -2\,\boldsymbol{\Omega} \cdot (\nabla \times \boldsymbol{v}) \tag{6.116a}$$
$$\nabla \times \boldsymbol{A} = (\boldsymbol{\Omega} \cdot \nabla)\,\boldsymbol{B} + \nabla\lambda, \tag{6.116b}$$

with λ an arbitrary gauge function.

Chapter 7

The Dirac delta

The *Dirac delta* provides an idealization of a point source. In mathematics, the Dirac delta is known as a *generalized function* or a *distribution* (e.g., chapter 5 of *Stakgold* (2000b)). We use the nomenclature *Dirac delta*, rather than the commonly used "Dirac delta function", as a hint that this object is not a typical sort of function. Indeed, the Dirac delta has the very peculiar properties of vanishing everywhere except at a single point where it is infinite. Consequently, it has a nonzero integral, which is normalized to unity. Furthermore, when multiplied by an arbitrary smooth test function and then integrated over the point where the Dirac delta "fires", the result is the test function evaluated at the point. This behavior is referred to as the *sifting property*. When the test function is unity, then the sifting property reduces to the normalization, so that the sifting property serves as the defining property of the Dirac delta.

Our treatment of the Dirac delta is *physically formal* in that we offer a deductive formulation that is motivated from a physical perspective rather than serving the needs for a *mathematically rigorous* presentation.[1] The physically formal treatment presented here is supported by *heuristic* arguments taken from Newtonian gravity (see Section 13.10); electrostatics (e.g., *Jackson* (1975)); and the diffusion of temperature or matter within a continuous media.[2]

READER'S GUIDE TO THIS CHAPTER

Properties of the Dirac delta are derived in many treatments within the mathematical physics literature. In particular, the Dirac delta is ubiquitous in the study of quantum mechanics. We here made use of Appendix A of *Gasiorowicz* (1974) and Appendix C of *Pope* (2000).

[1] The term *physically formal* is often used in the mathematical physics and applied mathematics literature as a complement to *mathematically rigorous*. A mathematically rigorous treatment for the topics of this chapter require an array of mathematical apparatus, particularly in topics of functional analysis, that are outside our scope.

[2] A heuristic technique or argument employs a practical method not guaranteed to be fully rational or deductive from all perspectives, but is sufficient for establishing a self-consistent formalism. The study of the Dirac delta is an example where physical heuristics established a formalism whose mathematical rigor followed later.

7.1 Motivation from Newtonian gravity

In Newtonian gravity[3] we encounter the Poisson equation for the gravitational potential, Φ, arising from an arbitrary mass density, ρ

$$\nabla^2 \Phi = 4\,\pi\, G^{\text{grv}}\,\rho, \tag{7.1}$$

with G^{grv} Newton's gravitational constant. The gravitational potential for an arbitrary spherically symmetric mass, when sampled at a point outside the mass, equals to the potential of a point mass located at the origin. Making precise the notion of a "point mass" provides a physical venue for introducing the Dirac delta, which we interpret as the mass density for a point mass.

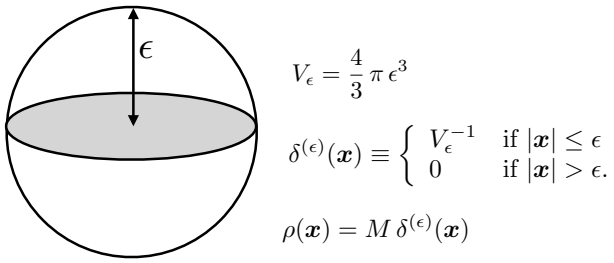

FIGURE 7.1: Depicting a spherical region of radius, $\epsilon > 0$, and with fixed mass, M, whose volume is given by $V_\epsilon = \frac{4}{3}\,\pi\,\epsilon^3$. The Dirac delta is given by the limit as the radius tends to zero, $\delta(\boldsymbol{x}) \equiv \lim_{\epsilon\to 0}\,\delta^{(\epsilon)}(\boldsymbol{x})$. That is, the Dirac delta is the mass density for a point mass.

For that purpose, consider a mass, M, distributed uniformly within a sphere of radius, $\epsilon > 0$, and volume,

$$V_\epsilon = \frac{4}{3}\,\pi\,\epsilon^3, \tag{7.2}$$

and let the sphere be centered at the origin of a coordinate system (see Figure 7.1). The mass distribution has a mass density,

$$\rho(\boldsymbol{x}) = M\,\delta^{(\epsilon)}(\boldsymbol{x}), \tag{7.3}$$

where we introduced the $\epsilon-$distribution

$$\delta^{(\epsilon)}(\boldsymbol{x}) \equiv \begin{cases} V_\epsilon^{-1} & \text{if } |\boldsymbol{x}| \le \epsilon \\ 0 & \text{if } |\boldsymbol{x}| > \epsilon. \end{cases} \tag{7.4}$$

By construction, an integral over a domain, $\mathcal{R}$, that fully encompasses the sphere yields the mass

$$\int_{\mathcal{R}} \rho\,\mathrm{d}V = M \int_{\mathcal{R}} \delta^{(\epsilon)}(\boldsymbol{x})\,\mathrm{d}V = M, \tag{7.5}$$

with this result holding even as the radius of the sphere becomes arbitrarily small, $\epsilon \to 0$. We

[3] We consider Newtonian gravity in a bit more detail in Section 13.10.1.

define the Dirac delta as the limiting ϵ-distribution

$$\delta(\boldsymbol{x}) \equiv \lim_{\epsilon \to 0} \delta^{(\epsilon)}(\boldsymbol{x}). \tag{7.6}$$

Evidently, the Dirac delta is the mass density for a mass source that is zero everywhere in space except at a single point. Hence, the Dirac delta distribution is infinite at the location of the point source. This dual property, namely an object defined only at a single point and yet having an infinite value at that point, allows the Dirac delta to have a nonzero integral, which is normalized according to

$$\int_{\mathcal{R}} \delta(\boldsymbol{x}) \, \mathrm{d}V = 1, \tag{7.7}$$

where the region, $\mathcal{R}$, includes the point $\boldsymbol{x} = 0$ where the Dirac delta "fires". Concerns with how to interpret the infinite value of $\delta(\boldsymbol{x})$ at $\boldsymbol{x} = 0$ are ameliorated by recognizing that $\delta(\boldsymbol{x})$ is evaluated only as part of an integral. Connecting to other physical analogs beyond the point mass source, we can consider the Dirac delta as the charge density (charge per volume) for a point charge in electrostatics, or the mass density for a point source of trace matter within a fluid.

7.2 Sifting property of the Dirac delta

Multiply an ϵ-distribution by an arbitrary smooth function, $\psi(\boldsymbol{x})$. Since the ϵ-distribution has support only within the ϵ-sphere surrounding the origin, an integral of $\delta^{(\epsilon)}(\boldsymbol{x})\,\psi(\boldsymbol{x})$ over the sphere, in the limit that $\epsilon \to 0$, leads to the *sifting property*

$$\lim_{\epsilon \to 0} \int_{\mathcal{R}} \delta^{(\epsilon)}(\boldsymbol{x})\,\psi(\boldsymbol{x}) \, \mathrm{d}V = \int_{\mathcal{R}} \delta(\boldsymbol{x})\,\psi(\boldsymbol{x}) \, \mathrm{d}V = \psi(\boldsymbol{x} = 0). \tag{7.8}$$

Evidently, the Dirac delta sifts out the smooth function as evaluated at the location of the Dirac delta source. The normalization property (7.7) and the sifting property (7.8) are the two defining features of the Dirac delta. To derive further properties implied by normalization and sifting, we find it useful to write

$$\psi(\boldsymbol{x}) = \int_{\mathcal{R}} \delta(\boldsymbol{x} - \boldsymbol{y})\,\psi(\boldsymbol{y}) \, \mathrm{d}V, \tag{7.9}$$

which reduces to the normalization property (7.7) when $\psi = 1$.

The sifting property (7.9) holds whether the Dirac delta has argument $\boldsymbol{x} - \boldsymbol{y}$ or $\boldsymbol{y} - \boldsymbol{x}$

$$\psi(\boldsymbol{x}) = \int_{\mathcal{R}} \delta(\boldsymbol{x} - \boldsymbol{y})\,\psi(\boldsymbol{y}) \, \mathrm{d}V = \int_{\mathcal{R}} \delta(\boldsymbol{y} - \boldsymbol{x})\,\psi(\boldsymbol{y}) \, \mathrm{d}V, \tag{7.10}$$

in which case we conclude that the Dirac delta is a symmetric or even distribution

$$\delta(\boldsymbol{x}) = \delta(-\boldsymbol{x}). \tag{7.11}$$

7.3 Dirac delta carries physical dimensions

As emphasized throughout this chapter, the Dirac delta carries physical dimensions given by the inverse dimension of its argument. For example, $\delta(x)$ has dimensions inverse length (here, x is a Cartesian space coordinate), $\delta(t)$ has dimensions inverse time (t is time), and $\delta(\phi)$ is non-dimensional (ϕ is latitude in radians). The dimensional properties of a Dirac delta are manifest from its corresponding sifting property. It is notable that many treatments, particularly

in the maths literature, ignore the physical dimensions of the Dirac delta. Hence, it is important to exercise care when transferring Dirac delta identities from a maths text to a physics context.

7.4 Example $\delta^{(\epsilon)}(x)$ distributions

In one-dimension, the construction of the Dirac delta following equation (7.6) is given by

$$\delta^{(\epsilon)}(x) = \epsilon^{-1} \quad \text{for } |x| < \epsilon/2 \text{ and } 0 \text{ for } |x| > \epsilon/2, \tag{7.12}$$

with this function depicted in Figure 7.2.

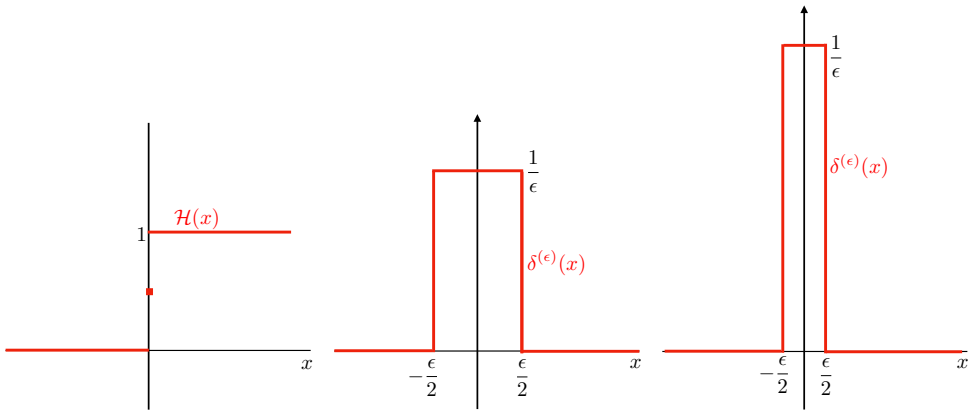

FIGURE 7.2: Left panel: Heaviside step function, $\mathcal{H}(x)$, as given by equation (7.19). Middle and right panels: the square pulse function, $\delta^{(\epsilon)}(x)$, given by equation (7.12), with the far right panel having a smaller value for $\epsilon > 0$ than the middle panel. We see that $\lim_{\epsilon\to 0}\delta^{(\epsilon)}(x) = \delta(x) = \mathrm{d}\mathcal{H}(x)/\mathrm{d}x$, with $\int_{\mathbb{R}}\delta^{(\epsilon)}(x)\,\mathrm{d}x = 1$ for each ϵ.

There are many other ϵ-distributions whose limiting behavior also result in a Dirac delta, as defined by the unit normalization and sifting properties

$$\lim_{\epsilon\to 0}\delta^{(\epsilon)}(x) = \delta(x). \tag{7.13}$$

Indeed, any even function that is normalized to unity and whose central peak's width is infinitesimal can be used to define a suitable $\delta^{(\epsilon)}(x)$, with the following examples (see Figure 7.3) appearing in applications ($\epsilon > 0$ for each example)

$$\delta^{(\epsilon)}(x) = \frac{\mathrm{e}^{-|x|/\epsilon}}{2\,\epsilon} \tag{7.14a}$$

$$\delta^{(\epsilon)}(x) = \frac{\mathrm{e}^{-x^2/\epsilon^2}}{\epsilon\sqrt{\pi}} \tag{7.14b}$$

$$\delta^{(\epsilon)}(x) = \frac{\epsilon}{\pi\,(x^2+\epsilon^2)} \tag{7.14c}$$

$$\delta^{(\epsilon)}(x) = \frac{\sin(x/\epsilon)}{\pi\,x} \tag{7.14d}$$

$$\delta^{(\epsilon)}(x) = \frac{\epsilon\sin^2(x/\epsilon)}{\pi\,x^2}. \tag{7.14e}$$

With x corresponding to a spatial position, note how each of these one-dimensional functions has physical dimensions of inverse length. The sifting property holds since each function is even and becomes infinitely peaked yet infinitesimally narrow as $\epsilon \to 0$. We verify the normalization

condition for equation (7.14a) through

$$\frac{1}{2\,\epsilon}\int_{-\infty}^{\infty} \mathrm{e}^{-|x|/\epsilon}\,\mathrm{d}x = \frac{1}{2\,\epsilon}\int_{-\infty}^{0} \mathrm{e}^{x/\epsilon}\,\mathrm{d}x + \frac{1}{2\,\epsilon}\int_{0}^{\infty} \mathrm{e}^{-x/\epsilon}\,\mathrm{d}x = \frac{1}{2} + \frac{1}{2} = 1. \tag{7.15}$$

The other expressions for $\delta^{(\epsilon)}(x)$ likewise have unit integrals over the real line and so satisfy the normalization property. The expression (7.14b) is related to the causal free space Green's function for the diffusion equation studied in Section 9.5.2. The expression (7.14d) is notable for its connection to Fourier analysis from Chapter 8. Namely, from the discussion in Section 8.5.1 we have the integral expression

$$\delta(x) = \frac{1}{2\,\pi}\lim_{\epsilon\to 0}\int_{-1/\epsilon}^{1/\epsilon} \mathrm{e}^{\mathrm{i}\,k\,x}\,\mathrm{d}k = \frac{1}{2\,\pi\,\mathrm{i}\,x}\lim_{\epsilon\to 0}(\mathrm{e}^{\mathrm{i}\,x/\epsilon} - \mathrm{e}^{-\mathrm{i}\,x/\epsilon}) = \lim_{\epsilon\to 0}\frac{\sin(x/\epsilon)}{\pi\,x}. \tag{7.16}$$

Equivalently, we have the identity

$$\delta(x) = \frac{1}{2\,\pi}\int_{-\infty}^{\infty} \mathrm{e}^{\mathrm{i}\,k\,x}\,\mathrm{d}k = \frac{1}{\pi}\int_{-\infty}^{\infty} \cos(k\,x)\,\mathrm{d}k, \tag{7.17}$$

which follows from the Euler identity (8.3) and anti-symmetry of the sin function

$$\int_{-\infty}^{\infty} \sin(k\,x)\,\mathrm{d}k = 0. \tag{7.18}$$

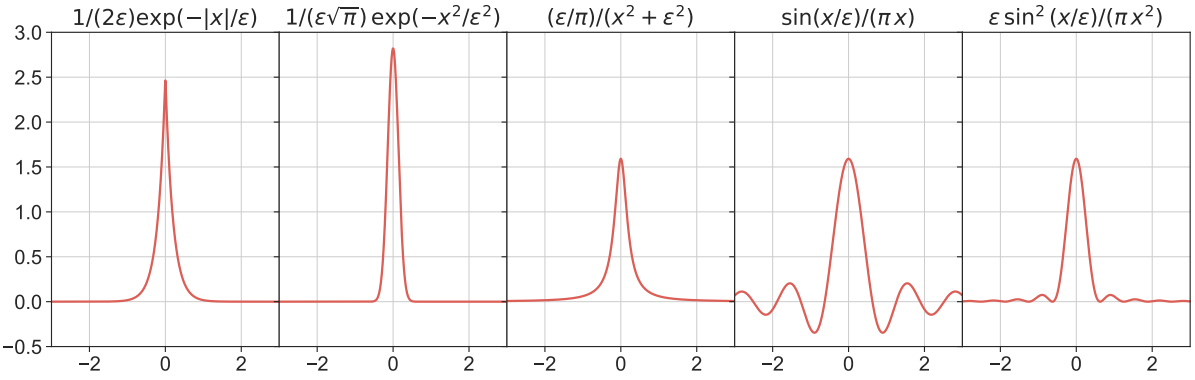

FIGURE 7.3: Plots of the functions $\delta^{(\epsilon)}(x)$ from equations (7.14a)-(7.14e) for $\epsilon = 0.2$, each of which converges to the Dirac delta as $\epsilon \to 0$.

7.5 Connection to the Heaviside step function

The Heaviside step function (Figure 7.2) is given by[4]

$$\mathcal{H}(x) = \begin{cases} 0 & \text{if } x < 0 \\ 1/2 & \text{if } x = 0 \\ 1 & \text{if } x > 0, \end{cases} \tag{7.19}$$

[4]In some treatments, $\mathcal{H}(x)$ is undefined at $x = 0$. For our purposes, the properties of the Heaviside step function remain unchanged whether it is defined at $x = 0$ or not. See footnote on page 20 of *Stakgold* (2000a) for more details.

and it is related to the sgn function

$$\operatorname{sgn}(x) = \begin{cases} -1 & \text{if } x < 0 \\ 0 & \text{if } x = 0 \\ 1 & \text{if } x > 0, \end{cases} \tag{7.20}$$

according to

$$\operatorname{sgn}(x) = 2\,\mathcal{H}(x) - 1. \tag{7.21}$$

Both the Heaviside and sgn functions are piecewise continuous and have infinite derivatives at $x = 0$. In particular, the derivative of the Heaviside step function equals to the Dirac delta

$$\frac{\mathrm{d}\mathcal{H}(x)}{\mathrm{d}x} = \delta(x). \tag{7.22}$$

This identity is most apparent by considering the square pulse approximation to the Dirac delta given by equation (7.12), in which we find

$$\delta(x) = \lim_{\epsilon \to 0} \delta^{(\epsilon)}(x) = \lim_{\epsilon \to 0} \frac{\mathcal{H}(x + \epsilon/2) - \mathcal{H}(x - \epsilon/2)}{\epsilon} = \frac{\mathrm{d}\mathcal{H}(x)}{\mathrm{d}x}. \tag{7.23}$$

To be convinced of the second equality, separately consider the cases with $x < -\epsilon/2$, $x > \epsilon/2$, and $|x| < \epsilon/2$. Equivalently, we see that the Heaviside step function is the cumulative distribution of the Dirac delta

$$\int_{-\infty}^{x} \delta(y)\,\mathrm{d}y = \int_{-\infty}^{x} \frac{\mathrm{d}\mathcal{H}(y)}{\mathrm{d}y}\,\mathrm{d}y = \mathcal{H}(x) - \mathcal{H}(-\infty) = \mathcal{H}(x). \tag{7.24}$$

Connecting to the language of probability theory, the Dirac delta corresponds to a probability density function peaked over an infinitesimal region, whereas the Heaviside step function is the corresponding probability distribution function.

As we see when studying Green's functions in Chapter 9, there are many other functions whose derivatives yield the Dirac delta. In particular, the Green's function is a continuous function whose first derivative has a jump and second derivative equals to a Dirac delta. Just as there is no unique function, $\delta^{(\epsilon)}(\boldsymbol{x})$, whose limit yields a Dirac delta, there is no unique function whose derivative (or 2nd derivative) equals to a Dirac delta. The key point is that any "function" that respects the sifting property (7.9) is a legitimate Dirac delta.

7.6 Scaling property of the Dirac delta

Write the sifting property (7.9) in the form

$$\psi(x) = \int_{-L}^{L} \delta(x - y)\,\psi(y)\,\mathrm{d}y \qquad \text{with } |x| < L, \tag{7.25}$$

where we introduced the constant, L, to keep track of the integration limits. Now scale the coordinates by a non-dimensional constant, $\alpha \neq 0$, so that $x = \alpha\,\xi$, $y = \alpha\,\eta$, and $\mathrm{d}y = \alpha\,\mathrm{d}\eta$, in which case the sifting property (7.25) becomes

$$\psi(\alpha\,\xi) = \int_{-L/\alpha}^{L/\alpha} \alpha\,\delta(\alpha\,\xi - \alpha\,\eta)\,\psi(\alpha\,\eta)\,\mathrm{d}\eta. \tag{7.26}$$

The sifting property (7.25) also implies

$$\psi(\alpha\,\xi) = \int_{-L/\alpha}^{L/\alpha} \delta(\xi - \eta)\,\psi(\alpha\,\eta)\,\mathrm{d}\eta, \tag{7.27}$$

so that equating the two expressions (7.26) and (7.27) suggests that $\delta(x) = \alpha\,\delta(\alpha\,x)$. However, this expression fails for $\alpha < 0$. Namely, from the symmetry property (7.11) we know that $\delta(x) = \delta(-x)$ so that $\delta(\alpha\,x) = \delta(-\alpha\,x)$. Hence, the scaling property holds for an arbitrary nonzero constant in the following form with the absolute value of the constant,

$$\delta(x) = |\alpha|\,\delta(\alpha\,x). \tag{7.28}$$

Stated more simply, the symmetry property (7.11), $\delta(x) = \delta(-x)$, is a special case of the scaling property with $\alpha = -1$. For this connection to hold requires application of the absolute value operation, $|-1| = 1$, thus leading to the expression (7.28).

7.7 Dirac delta with a function argument

Consider the integral

$$\int_{\mathcal{R}} \psi(x)\,\delta[f(x)]\,\mathrm{d}x, \tag{7.29}$$

for some smooth function, $f(x)$. The argument to the Dirac delta vanishes where the function vanishes, so this integral is nonzero only if $f(x)$ has at least one root somewhere. Assume there are N roots of $f(x)$, where $f(x_n) = 0$. Let us furthermore assume the roots are simple, so that $f(x)$ has a non-zero first derivative at each root, $f'(x_n) \neq 0$. Consequently, near any of the simple roots we can write the Taylor expansion

$$f(x) \approx f'(x_n)\,(x - x_n). \tag{7.30}$$

We are thus led to

$$\int_{\mathcal{R}} \psi(x)\,\delta[f(x)]\,\mathrm{d}x = \sum_{n=1}^{N} \int_{\mathcal{R}} \psi(x)\,\delta[f'(x_n)\,(x - x_n)]\,\mathrm{d}x \tag{7.31a}$$

$$= \sum_{n=1}^{N} \frac{1}{|f'(x_n)|} \int_{\mathcal{R}} \psi(x)\,\delta(x - x_n)\,\mathrm{d}x \tag{7.31b}$$

$$= \sum_{n=1}^{N} \frac{\psi(x_n)}{|f'(x_n)|}, \tag{7.31c}$$

where the second equality made use of the scaling property (7.28). Evidently, we we find the generalized scaling property for the Dirac delta

$$\delta[f(x)] = \sum_{n=1}^{N} \frac{\delta(x - x_n)}{|f'(x_n)|} \qquad \text{for } f(x) \text{ having } N \text{ simple roots with } f'(x_n) \neq 0. \tag{7.32}$$

As an example, consider the quadratic function, $f(x) = x^2 - \alpha^2$, which has two simple roots, $x_1 = \alpha$ and $x_2 = -\alpha$, and corresponding derivatives, $f'(x_1) = 2\alpha$ and $f'(x_2) = -2\alpha$. The generalized scaling property (7.32) leads to

$$\delta(x^2 - \alpha^2) = \frac{\delta(x - \alpha) + \delta(x + \alpha)}{2\,|\alpha|}, \tag{7.33}$$

and the corresponding sifting result

$$\int_{\mathcal{R}} \psi(x)\,\delta(x^2-\alpha^2)\,\mathrm{d}x = \frac{\psi(\alpha)+\psi(-\alpha)}{2\,|\alpha|}. \tag{7.34}$$

7.8 Equivalence classes of Dirac deltas

We commonly write a variety of equations satisfied by the Dirac that are outside of an integral sign, such as equations (7.32) and (7.33). Those equations are placeholders or shorthands for relations that hold inside of integrals and when multiplied by a smooth test function. For example, consider

$$\psi(a)\,A(a) = \int_{\mathcal{R}} \psi(x)\,A(x)\,\delta(x-a)\,\mathrm{d}x, \tag{7.35}$$

which is equivalent to

$$\psi(a)\,A(a) = \int_{\mathcal{R}} \psi(x)\,A(a)\,\delta(x-a)\,\mathrm{d}x. \tag{7.36}$$

We conclude that

$$A(x)\,\delta(x-a) = A(a)\,\delta(x-a). \tag{7.37}$$

As a corollary, let $A(a)=1$ so that

$$A(x)\,\delta(x-a) = \delta(x-a). \tag{7.38}$$

We can thus consider the Dirac delta as an equivalance class

$$[A(x)\,\delta(x)] \sim [\delta(x)]. \tag{7.39}$$

That is, if a Dirac delta within an integral is multiplied by a non-dimensional function, $A(x)$, satisfying $A(0)=1$, then we can disregard $A(x)$ since it does not modify how the Dirac delta acts within the integral. That is, $A(x)$ does not modify the sifting property of $\delta(x)$, and so it has no impact on how $\delta(x)$ affects test functions inside of integrals.

7.9 Taylor series decomposition of the Dirac delta

The first derivative of a Dirac delta represents an idealization of a dipole (e.g., see exercise 1.14 of *Stakgold* (2000a)). How does a Dirac dipole act on a test function? To answer this question, make use of the identity

$$\int_{-\epsilon}^{\epsilon} \frac{\mathrm{d}[\psi(x)\,\delta(x)]}{\mathrm{d}x}\,\mathrm{d}x = \psi(\epsilon)\,\delta(\epsilon) - \psi(-\epsilon)\,\delta(-\epsilon). \tag{7.40}$$

Each term on the right hand side vanishes when $\epsilon > 0$ since the Dirac delta never fires. Applying the product rule inside of the integral renders the identity

$$\int_{-\epsilon}^{\epsilon} \frac{\mathrm{d}[\psi(x)\,\delta(x)]}{\mathrm{d}x}\,\mathrm{d}x = \int_{-\epsilon}^{\epsilon} \left[\psi(x)\,\frac{\mathrm{d}\delta(x)}{\mathrm{d}x} + \delta(x)\,\frac{\mathrm{d}\psi(x)}{\mathrm{d}x}\right]\mathrm{d}x = 0, \tag{7.41}$$

so that

$$\int_{-\epsilon}^{\epsilon} \psi(x)\,\frac{\mathrm{d}\delta(x)}{\mathrm{d}x}\,\mathrm{d}x = -\left[\frac{\mathrm{d}\psi(x)}{\mathrm{d}x}\right]_{x=0}. \tag{7.42}$$

Consequently, the Dirac dipole acts to sift minus the first derivative of the test function. For example, let $\psi(x) = x$, in which case

$$\int_{-\epsilon}^{\epsilon} x \frac{\mathrm{d}\delta(x)}{\mathrm{d}x}\,\mathrm{d}x = -1 \Longrightarrow \int_{-\epsilon}^{\epsilon} \left[x \frac{\mathrm{d}\delta(x)}{\mathrm{d}x} + \delta(x)\right]\mathrm{d}x = 0, \tag{7.43}$$

which can be formally written

$$x\,(\mathrm{d}\delta(x)/\mathrm{d}x) = -\delta(x). \tag{7.44}$$

We follow the same procedure to derive the sifting property of the second derivative of the Dirac delta

$$\int_{\mathcal{R}} \psi \frac{\mathrm{d}^2\delta}{\mathrm{d}x^2}\,\mathrm{d}x = \int_{\mathcal{R}} \left[\frac{\mathrm{d}}{\mathrm{d}x}\left(\psi \frac{\mathrm{d}\delta}{\mathrm{d}x}\right) - \frac{\mathrm{d}\psi}{\mathrm{d}x}\frac{\mathrm{d}\delta}{\mathrm{d}x}\right]\mathrm{d}x. \tag{7.45}$$

The right hand side first term integrates to boundary contributions, each of which vanish if we assume the Dirac delta is in the interior of the domain, and we assume the test function is well behaved on the boundaries. Integration by parts one more time renders

$$\int_{\mathcal{R}} \psi \frac{\mathrm{d}^2\delta}{\mathrm{d}x^2}\,\mathrm{d}x = -\int_{\mathcal{R}} \frac{\mathrm{d}\psi}{\mathrm{d}x}\frac{\mathrm{d}\delta}{\mathrm{d}x}\,\mathrm{d}x = -\int_{\mathcal{R}} \frac{\mathrm{d}}{\mathrm{d}x}\left(\delta \frac{\mathrm{d}\psi}{\mathrm{d}x}\right)\mathrm{d}x + \int_{\mathcal{R}} \delta \frac{\mathrm{d}^2\psi}{\mathrm{d}x^2}\,\mathrm{d}x = \int_{\mathcal{R}} \delta \frac{\mathrm{d}^2\psi}{\mathrm{d}x^2}\,\mathrm{d}x, \tag{7.46}$$

where the boundary term vanishes from the penultimate equation. This procedure readily generalizes to the identity holding for any integer $n > 0$

$$\int_{\mathcal{R}} \psi(x) \frac{\mathrm{d}^n\delta(x)}{\mathrm{d}x^n}\,\mathrm{d}x = (-1)^n \int_{\mathcal{R}} \delta(x) \frac{\mathrm{d}^n\psi(x)}{\mathrm{d}x^n}\,\mathrm{d}x = (-1)^n \left[\frac{\mathrm{d}^n\psi(x)}{\mathrm{d}x^n}\right]_{x=0}. \tag{7.47}$$

Hence, the $n'th$ derivative of the Dirac delta acts to sift the $n'th$ derivative of a test function as multiplied by $(-1)^n$.

The sifting property in the form of equation (7.47) allows us to define the Taylor series of a Dirac delta as follows. Consider the expression for the test function at an arbitrary point $x = a$, written using both a Taylor series and the sifting property

$$\psi(a) = \psi(0) + \sum_{n=1}^{\infty} \frac{a^n}{n!}\,\psi^{(n)}(0) = \int_{\mathcal{R}} \psi(x)\,\delta(x-a)\,\mathrm{d}x, \tag{7.48}$$

where we introduced the shorthand

$$\psi^{(n)}(0) = \left[\frac{\mathrm{d}^n\psi(x)}{\mathrm{d}x^n}\right]_{x=0}. \tag{7.49}$$

Making use of the sifting property (7.47) also yields

$$\psi(0) + \sum_{n=1}^{\infty} \frac{a^n}{n!}\,\psi^{(n)}(0) = \int_{\mathcal{R}} \psi(x) \left[\delta(x) + \sum_{n=1}^{\infty} \frac{a^n}{n!}\,(-1)^n\,\delta^{(n)}(x)\right]\mathrm{d}x, \tag{7.50}$$

where we introduced the shorthand

$$\delta^{(n)}(x) = \frac{\mathrm{d}^n\delta(x)}{\mathrm{d}x^n}. \tag{7.51}$$

We are thus led to the identity

$$\psi(a) = \int_{\mathcal{R}} \psi(x)\,\delta(x-a)\,\mathrm{d}x = \int_{\mathcal{R}} \psi(x) \left[\delta(x) + \sum_{n=1}^{\infty} \frac{a^n}{n!}\,(-1)^n\,\delta^{(n)}(x)\right]\mathrm{d}x, \tag{7.52}$$

which renders the Taylor series

$$\delta(x-a) = \delta(x) + \sum_{n=1}^{\infty} \frac{a^n}{n!} (-1)^n \, \delta^{(n)}(x). \tag{7.53}$$

7.10 Spectral decomposition of the Dirac delta

Consider a discrete set of orthonormal polynomials, $P_n(x)$, that satisfy

$$\int_{\mathcal{R}} w(x) \, P_n(x) \, P_m(x) \, \mathrm{d}x = \delta_{mn}, \tag{7.54}$$

where m, n are integers, $w(x)$ is a weight function, and δ_{mn} is the Kronecker delta. We assume these polynomials form a complete basis for the domain, $\mathcal{R}$, with the Legendre polynomials, Hermite polynomials, and Laguerre polynomials examples that arise in physics.

Now consider an arbitrary smooth test function, $\psi(x)$, defined over the domain $\mathcal{R}$. Completeness of the polynomials means that we can represent $\psi(x)$ as the infinite series, which is sometimes referred to as a *spectral decomposition*

$$\psi(x) = \sum_n \Phi_n \, P_n(x) = \sum_n \left[\int_{\mathcal{R}} w(y) \, P_n(y) \, \psi(y) \, \mathrm{d}y \right] P_n(x), \tag{7.55}$$

where the expansion coefficients, Φ_n, are determined by projecting ψ onto the polynomials along with the weighting function. Rearranging the spectral decomposition (7.55) allows us to write

$$\psi(x) = \int_{\mathcal{R}} \left[\sum_m w(y) \, P_m(y) \, P_m(x) \right] \psi(y) \, \mathrm{d}y = \int_{\mathcal{R}} \delta(x-y) \, \psi(y) \, \mathrm{d}y, \tag{7.56}$$

where the second equality made use of the sifting property (7.9) of the Dirac delta. We thus identify the spectral decomposition of the Dirac delta

$$\delta(x-y) = \sum_m w(y) \, P_m(y) \, P_m(x). \tag{7.57}$$

7.11 The product of Dirac deltas

The product of two Dirac deltas is not defined if the deltas act on the same space dimension. For example, one possible definition of the product of two x-space Dirac deltas could be

$$\delta(x) \, \delta(x) \stackrel{?}{=} \lim_{\epsilon_1 \to 0} \delta^{(\epsilon_1)}(x) \lim_{\epsilon_2 \to 0} \delta^{(\epsilon_2)}(x). \tag{7.58}$$

If we take ϵ_1 to zero before ϵ_2 then

$$\delta(x) \, \delta(x) \stackrel{?}{=} \delta(x) \lim_{\epsilon_2 \to 0} \delta^{(\epsilon_2)}(x). \tag{7.59}$$

The problem is seen by taking the integral along the real line,

$$\int \delta(x) \, \delta(x) \, \mathrm{d}x \stackrel{?}{=} \int \delta(x) \lim_{\epsilon_2 \to 0} \delta^{(\epsilon_2)}(x) \, \mathrm{d}x = \lim_{\epsilon_2 \to 0} \delta^{(\epsilon_2)}(0) = \delta(0) = \infty. \tag{7.60}$$

Evidently, the product of two Dirac deltas, when acting on the same dimension, is not defined since the integral is not finite. However, when the two Diracs act over distinct coordinate

dimensions, such as the x and y Cartesian coordinates, then there is no problem since each dimension has a corresponding integration

$$\int_{\mathcal{R}} \delta(x)\,\delta(y)\,\mathrm{d}x\,\mathrm{d}y = \left[\int_{\mathcal{R}_x} \delta(x)\,\mathrm{d}x\right]\left[\int_{\mathcal{R}_y} \delta(y)\,\mathrm{d}y\right] = 1, \tag{7.61}$$

where the domains $\mathcal{R}_x$ and $\mathcal{R}_y$ contain the origin. We pursue this point in Section 7.12 when decomposing the Dirac delta for three space dimensions into its coordinate components.

7.12 Cartesian, spherical, and cylindrical-polar coordinates

We here display the form of the Dirac delta for three space dimensions using Cartesian, spherical, and cylindrical coordinates.

7.12.1 Cartesian coordinates

We can decompose the three-dimensional Dirac delta according to the Cartesian coordinates

$$\delta(\boldsymbol{x}) = \delta(x)\,\delta(y)\,\delta(z), \tag{7.62}$$

so that, with the domain $\mathcal{R}$ containing the origin, we have

$$\int_{\mathcal{R}} \delta(\boldsymbol{x})\mathrm{d}V = \int_{\mathcal{R}} \delta(x)\,\delta(y)\,\delta(z)\,\mathrm{d}x\,\mathrm{d}y\,\mathrm{d}z = 1. \tag{7.63}$$

Each of the Dirac deltas, $\delta(x)$, $\delta(y)$, and $\delta(z)$ has physical dimensions of inverse length, so that their product, $\delta(x)\,\delta(y)\,\delta(z)$, has the dimension inverse volume.

7.12.2 Spherical coordinates

We sometimes find it useful to make use of the spherical coordinates from Section 4.23, in which the Dirac delta takes the form

$$\delta(\boldsymbol{x}) = \frac{\delta(r)\,\delta(\phi)\,\delta(\lambda)}{r^2\cos\phi}, \tag{7.64}$$

so that

$$\int_{\mathcal{R}} \delta(\boldsymbol{x})\,\mathrm{d}x\,\mathrm{d}y\,\mathrm{d}z = \int_{\mathcal{R}} \delta(\boldsymbol{x})\,r^2\cos\phi\,\mathrm{d}r\,\mathrm{d}\phi\,\mathrm{d}\lambda = \int_{\mathcal{R}} \delta(r)\,\delta(\phi)\,\delta(\lambda)\,\mathrm{d}r\,\mathrm{d}\phi\,\mathrm{d}\lambda = 1. \tag{7.65}$$

Notice how the dimensions of a particular Dirac delta equals to the inverse dimensions of its argument, so that both $\delta(\phi)$ and $\delta(\lambda)$ are dimensionless whereas $\delta(r)$ has the dimension of inverse length.

7.12.3 Cylindrical-polar coordinates

When written using the cylindrical-polar coordinates from Section 4.22, we have

$$\delta(\boldsymbol{x}) = \frac{\delta(r)\,\delta(\vartheta)\,\delta(z)}{r}, \tag{7.66}$$

so that

$$\int_{\mathcal{R}} \delta(\boldsymbol{x})\,\mathrm{d}x\,\mathrm{d}y\,\mathrm{d}z = \int_{\mathcal{R}} \delta(\boldsymbol{x})\,r\,\mathrm{d}r\,\mathrm{d}\vartheta\,\mathrm{d}z = \int_{\mathcal{R}} \delta(r)\,\delta(\vartheta)\,\delta(z)\,\mathrm{d}r\,\mathrm{d}\vartheta\,\mathrm{d}z = 1. \tag{7.67}$$

Again, the dimensions of a particular Dirac delta equals to the inverse dimensions of its argument, so that $\delta(\vartheta)$ is dimensionless whereas $\delta(r)$ and $\delta(z)$ have dimensions of inverse length.

7.13 Temporal Dirac delta and impulses

Poisson's equation (7.1) for the gravitational potential is an elliptic partial differential equation (see Section 6.5), in which there is no time derivative. We now introduce the temporal Dirac delta to support the study of evolution equations, such as when developing a Green's function theory for the diffusion equation in Section 9.5, the wave equation in Section 9.6, and the advection-diffusion equation of Section 69.9. The temporal Dirac delta is a point source that is turned on just at one time instance and it is normalized according to

$$\int_{\mathcal{T}} \delta(t)\,\mathrm{d}t = 1, \tag{7.68}$$

where $\mathcal{T}$ is a time interval containing the source time, $t = 0$. This normalization means that $\delta(t)$ has dimensions of inverse time. The temporal Dirac delta also possesses the sifting property from Section 7.2, in which

$$\int_{\mathcal{T}} \delta(t)\,\psi(t)\,\mathrm{d}t = \psi(t=0). \tag{7.69}$$

In the study of transient behavior of dynamical systems, it is often of interest to examine the response of the system to an idealized force, $\mathcal{F}(t)$, where the force occurs over a small time increment. The time integral of this force is referred to as the *impulse*

$$I(\tau) = \int_{-\tau}^{\tau} \mathcal{F}(t)\,\mathrm{d}t. \tag{7.70}$$

If the force is further idealized to occur just at a single moment in time, and it is normalized to unity, then we have the *unit impulse*, which is the integral of the Dirac delta

$$I(\tau) = 1 = \int_{-\tau}^{\tau} \delta(t)\,\mathrm{d}t. \tag{7.71}$$

The corresponding response of the dynamical system is referred to as the *impulse response function*. If the dynamical system is linear, then the impulse response function equals to the Green's function for the initial value problem. We further discuss the response function in Section 9.7.

7.14 Shifting the space-time position of the source

We can arbitrarily place the Dirac source at $(\boldsymbol{x}_0, t_0)$, in which case the Dirac delta is written

$$\delta(\boldsymbol{x} - \boldsymbol{x}_0)\,\delta(t - t_0) = \delta(x - x_0)\,\delta(y - y_0)\,\delta(z - z_0)\,\delta(t - t_0). \tag{7.72}$$

Defining the region, $\mathcal{R}$, to now encompass the source point in space, $\boldsymbol{x} = \boldsymbol{x}_0$, and the time increment $\mathcal{T}$ to encompasses the source time, $t = t_0$, we have the normalization condition

$$\int_{\mathcal{R}} \int_{\mathcal{T}} \delta(\boldsymbol{x} - \boldsymbol{x}_0)\,\delta(t - t_0)\,\mathrm{d}V\,\mathrm{d}t = 1, \tag{7.73}$$

as well as the sifting property

$$\int_{\mathcal{R}} \int_{\mathcal{T}} \psi(\boldsymbol{x}, t)\, \delta(\boldsymbol{x} - \boldsymbol{x}_0)\, \delta(t - t_0)\, \mathrm{d}V\, \mathrm{d}t = \psi(\boldsymbol{x}_0, t_0). \tag{7.74}$$

Chapter 8

Fourier analysis

In this chapter we survey salient features of Fourier analysis, with particular application to the study of wave mechanics in Part X of this book. Fourier analysis is the canonical means to *spectrally decompose* a signal into orthogonal components, here given by trigonometric functions. Fourier analysis is particularly relevant to the study of wave mechanics considered in Part X of this book, thus motivating the use of wave mechanics terminology in this chapter. We assume Cartesian coordinates throughout this chapter, given that our treatment of Fourier analysis assumes flat Euclidean space.[1] Furthermore, we are only concerned in this book with physical systems, in which all physical quantities are real numbers. Hence, our use of complex numbers, common in Fourier analysis, is solely for convenience.

The following lists conventions for Fourier analysis followed in this book, with further context for these conventions given later in the chapter.

- P is the period for functions represented using a Fourier series. Some treatments instead write the period as $P = 2\,L$.
- A factor of $1/2\pi$ is placed on the inverse Fourier transform as per equation (8.68c), whereas there is unity for the Fourier transform. An alternative convention is commonly used in quantum mechanics whereby $1/\sqrt{2\pi}$ appears on both the Fourier transform and its inverse. We have more to say about this convention in Section 8.3.7. Note that the $1/2\pi$ factor for the inverse Fourier transform in one-dimension becomes $(1/2\pi)^n$ for n-dimensions. In this chapter we focus on $n = 1$ since generalizations to higher dimensions are straightforward.
- Fourier space is referred to as $\boldsymbol{k}$-space or *wavevector space*, which is a dual vector space (through the Fourier integral transform) to $\boldsymbol{x}$-space or *position space*. Some treatments refer to $\boldsymbol{x}$-space as "physical space". We avoid that language since for describing a physical system, $\boldsymbol{x}$-space is no more or less physical than $\boldsymbol{k}$-space. Instead, they emphasize complementary features and both offer physical insights.

CHAPTER GUIDE

The following references offer compatible treatments to that here, with many also providing far more details: Chapters 2 and 5 of *Spiegel* (1974b), Appendix A of *Gasiorowicz* (1974), Appendix I of *Cohen-Tannoudji et al.* (1977), Sections 5.10-5.15 of *Hildebrand* (1976), Section 5.6 of *Stakgold* (2000b), and Section 6.4.2 of *Thorne and Blandford* (2017). However, there are slight inconsistencies in conventions that warrant care if taking results from the literature, such as integral tables for Fourier transforms. This video from 3Blue1Brown provides an insightful introduction to Fourier series, and this video, also from 3Blue1Brown provides a corresponding introduction to Fourier transforms.

[1] Spherical harmonics offers a generalization of Cartesian Fourior analysis to the sphere.

8.1 Complex numbers

All physical fields are real in the physics considered in this book. Even so, we sometimes make use of complex numbers for convenience, particularly when studying linear waves since manipulating exponentials is simpler than the alternative sines and cosines. We here summarize a few salient points for working with complex numbers in physics.

8.1.1 Modulus and phase

A complex number, $\mathcal{A}$, is the sum of its real and imaginary parts, which we write as[2]

$$\mathcal{A} = \mathrm{Re}[\mathcal{A}] + \mathrm{i}\ \mathrm{Im}[\mathcal{A}], \tag{8.1}$$

and its complex conjugate is written

$$\mathcal{A}^* = \mathrm{Re}[\mathcal{A}] - \mathrm{i}\ \mathrm{Im}[\mathcal{A}]. \tag{8.2}$$

Making use of the *Euler identity*,[3]

$$\mathrm{e}^{\mathrm{i}\alpha} = \cos\alpha + \mathrm{i}\sin\alpha, \tag{8.3}$$

[2] In this book, we generally use the LaTeX *mathcal* notation for complex numbers.
[3] There are few equations in mathematics that are more elegant and powerful than Euler's identity.

allows us to write a complex number as

$$\mathcal{A} = \sqrt{\mathcal{A}\,\mathcal{A}^*}\,\mathrm{e}^{\mathrm{i}\,\alpha} = |\mathcal{A}|\,(\cos\alpha + \mathrm{i}\sin\alpha) \quad \text{with } \tan\alpha = \mathrm{Im}[\mathcal{A}]/\,\mathrm{Re}[\mathcal{A}]. \tag{8.4}$$

The term

$$|\mathcal{A}| = \sqrt{\mathcal{A}\,\mathcal{A}^*} = \sqrt{\mathrm{Re}[\mathcal{A}]^2 + \mathrm{Im}[\mathcal{A}]^2} \tag{8.5}$$

is the *modulus* of the complex number $\mathcal{A}$. The notation $|\mathcal{A}|$ is motivated since the modulus is a generalization of the absolute value used for real numbers. The angle, α, is called the *argument* in the maths literature, whereas we refer to it as the *phase* to correspond to its name in wave mechanics. We illustrate these formulae in Figure 8.1 within the complex plane.

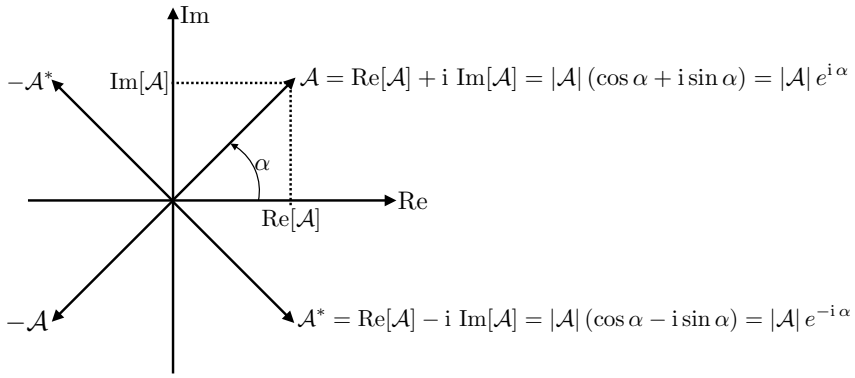

FIGURE 8.1: Illustrating the complex plane and its representation of a complex number, $\mathcal{A} = \mathrm{Re}[\mathcal{A}] + \mathrm{i}\ \mathrm{Im}[\mathcal{A}] = |\mathcal{A}|\,(\cos\alpha + \mathrm{i}\sin\alpha) = |\mathcal{A}|\,\mathrm{e}^{\mathrm{i}\,\alpha}$, along with its complex congugate, $\mathcal{A}^* = |\mathcal{A}|\,\mathrm{e}^{-\mathrm{i}\,\alpha}$, as well as $-\mathcal{A}^*$ and $-\mathcal{A}$.

The complex conjugate of the product of two complex numbers is the product of the conjugate, which can be shown by

$$\mathcal{A}\,\mathcal{B} = |\mathcal{A}|\,|\mathcal{B}|\,\mathrm{e}^{\mathrm{i}\,(\alpha+\beta)} \tag{8.6a}$$

$$\mathcal{A}^*\,\mathcal{B}^* = |\mathcal{A}|\,|\mathcal{B}|\,\mathrm{e}^{-\mathrm{i}\,(\alpha+\beta)} = (\mathcal{A}\,\mathcal{B})^*. \tag{8.6b}$$

When we write a complex number in this book, it is the real part that is of physical interest

$$\mathrm{Re}[\mathcal{A}] = \sqrt{\mathcal{A}\,\mathcal{A}^*}\cos\alpha = |\mathcal{A}|\cos\alpha. \tag{8.7}$$

Hence, for most purposes we evaluate the product, $\mathcal{A}\,\mathcal{A}$, as the product of the real parts

$$\mathrm{Re}[\mathcal{A}]\,\mathrm{Re}[\mathcal{A}] = |\mathcal{A}|^2\cos^2\alpha. \tag{8.8}$$

Likewise, with $\mathcal{B} = |\mathcal{B}|\,\mathrm{e}^{\mathrm{i}\,\beta}$, we interpret the product $\mathcal{A}\,\mathcal{B}$ as

$$\mathrm{Re}[\mathcal{A}]\,\mathrm{Re}[\mathcal{B}] = |\mathcal{A}|\,|\mathcal{B}|\cos\alpha\cos\beta. \tag{8.9}$$

These considerations are particularly important when computing energetics of wave fields. Namely, energetics involves the product of real fields rather than the product of complex fields. So if we work with the complex representation of a wave, then we must compute its real part prior to computing the product; i.e., the real part of the product of two complex fields is not equal to the product of the real parts

$$\mathrm{Re}[\mathcal{A}\,\mathcal{B}] \neq \mathrm{Re}[\mathcal{A}]\,\mathrm{Re}[\mathcal{B}]. \tag{8.10}$$

The following identities are particularly useful when computing energetics of wave fields as in

Section 61.4.6

$$\mathrm{Re}[\mathrm{i}\,\mathcal{A}] = \mathrm{Re}[\mathrm{i}\,\mathrm{Re}[\mathcal{A}] - \mathrm{Im}[\mathcal{A}]] = -\,\mathrm{Im}[\mathcal{A}] \tag{8.11a}$$
$$\mathrm{Re}[\mathcal{A}^*\,\mathcal{B}] = |\mathcal{A}|\,|\mathcal{B}|\cos(-\alpha+\beta) = \mathrm{Re}[\mathcal{A}\,\mathcal{B}^*] \tag{8.11b}$$
$$\mathrm{Im}[\mathcal{A}^*\,\mathcal{B}] = |\mathcal{A}|\,|\mathcal{B}|\sin(-\alpha+\beta) = -|\mathcal{A}|\,|\mathcal{B}|\sin(\alpha-\beta) = -\,\mathrm{Im}[\mathcal{A}\,\mathcal{B}^*]. \tag{8.11c}$$

8.1.2 Phase averaging

There are many occasions in the study of waves where it is useful to average over the extent of a wave, either in space or time. Doing so provides a measure for the "wave averaged" properties. To add precision to this notion, consider two real wave fields written in the form of a traveling plane wave

$$A = \mathrm{Re}[\mathcal{A}\,\mathrm{e}^{\mathrm{i}\,(\boldsymbol{k}\cdot\boldsymbol{x}-\omega\,t)}] = |\mathcal{A}|\cos(\boldsymbol{k}\cdot\boldsymbol{x}-\omega\,t+\alpha) \tag{8.12a}$$
$$B = \mathrm{Re}[\mathcal{B}\,\mathrm{e}^{\mathrm{i}\,(\boldsymbol{k}\cdot\boldsymbol{x}-\omega\,t)}] = |\mathcal{B}|\cos(\boldsymbol{k}\cdot\boldsymbol{x}-\omega\,t+\beta), \tag{8.12b}$$

where $\boldsymbol{k}\cdot\boldsymbol{x}-\omega\,t$ is the space-time dependence found for a traveling plane wave, with $\boldsymbol{k}$ the wavevector and ω the angular frequency (e.g., Section 49.5). We wrote the complex wave amplitudes as

$$\mathcal{A} = |\mathcal{A}|\,\mathrm{e}^{\mathrm{i}\,\alpha} \quad \text{and} \quad \mathcal{B} = |\mathcal{B}|\,\mathrm{e}^{\mathrm{i}\,\beta}, \tag{8.13}$$

where α and β are phase shifts relative to $\boldsymbol{k}\cdot\boldsymbol{x}-\omega\,t$. To introduce the notion of a *phase average*, introduce a constant phase shift, φ, according to

$$\alpha = \alpha' + \varphi \quad \text{and} \quad \beta = \beta' + \varphi, \tag{8.14}$$

in which case we define a *phase average* as

$$\langle\cdots\rangle \equiv \frac{1}{2\pi}\int_0^{2\pi}(\cdots)\,\mathrm{d}\varphi, \tag{8.15}$$

so that a phase average is computed by sampling over the extent of a single wavelength or single wave period. The phase average of a traveling plane wave is zero

$$\langle A\rangle = \frac{1}{2\pi}\int_0^{2\pi}|\mathcal{A}|\cos(\boldsymbol{k}\cdot\boldsymbol{x}-\omega\,t+\alpha'+\varphi)\,\mathrm{d}\varphi = 0, \tag{8.16}$$

whereas the phase average for the product of two real wave fields does not generally vanish

$$\langle A\,B\rangle = \frac{1}{2\pi}\int_0^{2\pi}|\mathcal{A}|\,|\mathcal{B}|\cos(\boldsymbol{k}\cdot\boldsymbol{x}-\omega\,t+\alpha'+\varphi)\cos(\boldsymbol{k}\cdot\boldsymbol{x}-\omega\,t+\beta'+\varphi)\,\mathrm{d}\varphi \tag{8.17a}$$
$$= \frac{1}{4\pi}\int_0^{2\pi}|\mathcal{A}|\,|\mathcal{B}|\,[\cos(\alpha'-\beta')+\cos(2\,\boldsymbol{k}\cdot\boldsymbol{x}-2\,\omega\,t+2\,\varphi+\alpha'-\beta')]\,\mathrm{d}\varphi \tag{8.17b}$$
$$= \frac{1}{2}\,|\mathcal{A}|\,|\mathcal{B}|\cos(\alpha'-\beta') \tag{8.17c}$$
$$= \frac{1}{2}\,\mathrm{Re}[\mathcal{A}^*\,\mathcal{B}] \tag{8.17d}$$
$$= \frac{1}{2}\,\mathrm{Re}[\mathcal{A}\,\mathcal{B}^*]. \tag{8.17e}$$

We see that the phase average of a product acts to remove information about the common phase, leaving only information about the modulus of the wave amplitudes and their phase difference.

For example,

$$\langle A^2 \rangle = |\mathcal{A}|^2/2, \tag{8.18}$$

so that the phase average for the square of a real wave field is one-half the squared modulus of the wave amplitude. Similarly, if $\mathcal{B} = \mathrm{i}\,\mathcal{A}$ then

$$\langle A\,B \rangle = \frac{1}{2\pi} \int_0^{2\pi} |\mathcal{A}|\,|\mathcal{B}|\,\cos(\pi/2)\,\mathrm{d}\varphi = 0, \tag{8.19}$$

in which we say that the real wave fields A and B are *out of phase*.

8.1.3 Euler's identity motivates the use of complex numbers

As noted earlier, there is no physical reason to introduce complex numbers in classical physics. However, there are many mathematical reasons. In particular, it is generally more convenient to use complex Fourier analysis than real Fourier analysis when establishing various theoretical results in wave mechanics.

The central reason to employ complex numbers is the shear elegance and power of Euler's identity (8.3). We encountered examples in Section 8.1.2 when discussing phase averaging. One more example concerns the sum of two waves, such as the sum of the two real wave fields (8.12a) and (8.12b)

$$C = A + B = |\mathcal{A}|\cos(\boldsymbol{k}\cdot\boldsymbol{x} - \omega\,t + \alpha) + |\mathcal{B}|\cos(\boldsymbol{k}\cdot\boldsymbol{x} - \omega\,t + \beta). \tag{8.20}$$

It is certainly possible to determine an expression for the combined wave, C, through the use of trigonometric identities. However, it is far less tedious to compute the sum via Euler's identity, in which case

$$\begin{aligned}
C &= |\mathcal{A}|\cos(\boldsymbol{k}\cdot\boldsymbol{x} - \omega\,t + \alpha) + |\mathcal{B}|\cos(\boldsymbol{k}\cdot\boldsymbol{x} - \omega\,t + \beta) && \text{(8.21a)}\\
&= \mathrm{Re}[|\mathcal{A}|\,\mathrm{e}^{\mathrm{i}\,(\boldsymbol{k}\cdot\boldsymbol{x} - \omega\,t + \alpha)} + |\mathcal{B}|\,\mathrm{e}^{\mathrm{i}\,(\boldsymbol{k}\cdot\boldsymbol{x} - \omega\,t + \beta)}] && \text{(8.21b)}\\
&= \mathrm{Re}[(|\mathcal{A}|\,\mathrm{e}^{\mathrm{i}\,\alpha} + |\mathcal{B}|\,\mathrm{e}^{\mathrm{i}\,\beta})\,\mathrm{e}^{\mathrm{i}\,(\boldsymbol{k}\cdot\boldsymbol{x} - \omega\,t)}] && \text{(8.21c)}\\
&\equiv \mathrm{Re}[|\mathcal{C}|\,\mathrm{e}^{\mathrm{i}\,(\boldsymbol{k}\cdot\boldsymbol{x} - \omega\,t + \gamma)}] && \text{(8.21d)}\\
&= |\mathcal{C}|\cos(\boldsymbol{k}\cdot\boldsymbol{x} - \omega\,t + \gamma), && \text{(8.21e)}
\end{aligned}$$

where we introduced the complex amplitude

$$|\mathcal{C}|\,\mathrm{e}^{\mathrm{i}\,\gamma} \equiv |\mathcal{A}|\,\mathrm{e}^{\mathrm{i}\,\alpha} + |\mathcal{B}|\,\mathrm{e}^{\mathrm{i}\,\beta}. \tag{8.22}$$

We can further use Euler's identity and some trigonometric identities to determine the real amplitude and phase shift for the combined wave

$$\begin{aligned}
|\mathcal{C}|^2 &= |\mathcal{A}|^2 + |\mathcal{B}|^2 + 2\,|\mathcal{A}|\,|\mathcal{B}|\cos(\alpha - \beta) && \text{(8.23a)}\\
\tan\gamma &= \frac{|\mathcal{A}|\sin\alpha + |\mathcal{B}|\sin\beta}{|\mathcal{A}|\cos\alpha + |\mathcal{B}|\cos\beta}. && \text{(8.23b)}
\end{aligned}$$

The curious reader is encouraged to use just real analysis to compute the expression (8.21e), along with the real amplitude (8.23a) and phase shift (8.23b).

8.2 Fourier series

Consider an arbitrary real function, $F(x)$, defined over the real line and that is piecewise continuous on every finite interval, as is its first derivative.[4] We also assume the function satisfies the periodicity condition[5]

$$F(x+P) = F(x), \tag{8.24}$$

where $P > 0$ is the period.[6] The periodicity condition (8.24) holds for every point on the real line so that

$$F(x+n\,P) = F(x) \quad \text{for arbitrary positive or negative integer } n. \tag{8.25}$$

How general are periodic functions defined over the full real line? To answer this question, consider a function defined only over a finite domain, $x \in [\alpha, \beta]$, and that is periodic over that domain

$$G(\alpha) = G(\beta). \tag{8.26}$$

Quite trivially, we can construct the extended function, $F(x)$, that equals to $G(x)$ for $x \in [\alpha, \beta]$ and that is periodic over the real line, $F(x) = F(x+P)$, with period $P = \beta - \alpha$. For this reason, it is sufficient to focus on periodic functions defined over the full real line, $x \in (-\infty, \infty)$.

8.2.1 Fourier series of sines and cosines

A *Fourier series* decomposes an arbitrary periodic function in terms of the function's mean value over a period, plus an infinite series of sines and cosines[7]

$$F(x) = a_0 + \sum_{n=1}^{\infty} [a_n \cos(k_n\,x) + b_n \sin(k_n\,x)], \tag{8.27}$$

where we introduced the discrete *wavenumber*

$$k_n = 2\,\pi\,n/P. \tag{8.28}$$

Clearly the Fourier series (8.27) satisfies the periodicity condition, $F(x) = F(x+n\,P)$. Mathematically, the Fourier series is enabled by completeness of the trigonometric functions as a basis for periodic functions over a finite interval. Furthermore, the real coefficients, a_n and b_n, are determined through use of orthonormality conditions satisfied by the sine and cosine functions

$$\frac{2}{P}\int_{x_0}^{x_0+P} \cos(k_n\,x)\sin(k_m\,x)\,\mathrm{d}x = 0 \tag{8.29a}$$

$$\frac{2}{P}\int_{x_0}^{x_0+P} \cos(k_n\,x)\cos(k_m\,x)\,\mathrm{d}x = \delta_{mn} \tag{8.29b}$$

$$\frac{2}{P}\int_{x_0}^{x_0+P} \sin(k_n\,x)\sin(k_m\,x)\,\mathrm{d}x = \delta_{mn}, \tag{8.29c}$$

[4] These properties for $F(x)$ are commonly satisfied for functions considered in this book.

[5] We use the notation x as for a spatial coordinate. Yet everything that follows holds if x is interpreted as time.

[6] Some treatments, such as Chapter 2 of *Spiegel* (1974b), assume the function has period $F(x) = F(x+2L)$, in which case $P = 2L$. In general, care is needed when making use of expressions from the literature to account for slight differences in conventions.

[7] There are certain mathematical conditions required of $F(x)$ that allow for the Fourier series to be an identity. These conditions are typically satisfied by functions encountered in physics. See Section 5.10 of *Hildebrand* (1976) for more details.

where δ_{mn} is the Kronecker delta, which is unity if $m = n$ and vanishes otherwise.[8] Furthermore, note that the constant, x_0, is arbitrary and with the equalities holding for any value. We can understand this arbitrariness by noting that the integral over a single period of a periodic function is unchanged when shifting the start point of the integration. All that matters is that we extend over a single period.[9]

The orthonormality conditions (8.29a)-(8.29c) directly lead to the following expressions for the Fourier series expansion coefficients

$$a_0 = \frac{1}{P}\int_{x_0}^{x_0+P} F(x)\,\mathrm{d}x \tag{8.30a}$$

$$a_{n>0} = \frac{2}{P}\int_{x_0}^{x_0+P} \cos(k_n\,x)\,F(x)\,\mathrm{d}x \tag{8.30b}$$

$$b_0 = 0 \tag{8.30c}$$

$$b_{n>0} = \frac{2}{P}\int_{x_0}^{x_0+P} \sin(k_n\,x)\,F(x)\,\mathrm{d}x. \tag{8.30d}$$

Evidently, a_0 is the mean value of $F(x)$ over a single period. As an exercise, we verify equation (8.30b) by multiplying the Fourier series (8.27) by $\cos(k_m\,x)$ for $m > 0$ and integrating over a period

$$\int_{x_0}^{x_0+P} \cos(k_m\,x)\,F(x)\,\mathrm{d}x = \int_{x_0}^{x_0+P} \cos(k_m\,x)\left[a_0 + \sum_{n=1}^{\infty}[a_n\cos(k_n\,x) + b_n\sin(k_n\,x)]\right]\mathrm{d}x \tag{8.31a}$$

$$= (P/2)\,a_n\,\delta_{mn}, \tag{8.31b}$$

where the second equality used the orthogonality conditions (8.29a)-(8.29c). We use analogous steps to verify equation (8.30d),

$$\int_{x_0}^{x_0+P} \sin(k_m\,x)\,F(x)\,\mathrm{d}x = \int_{x_0}^{x_0+P} \sin(k_m\,x)\left[a_0 + \sum_{n=1}^{\infty}[a_n\cos(k_n\,x) + b_n\sin(k_n\,x)]\right]\mathrm{d}x \tag{8.32a}$$

$$= (P/2)\,b_n\,\delta_{mn}. \tag{8.32b}$$

8.2.2 Functions with a particular parity

Any function, $F(x)$, can be written as the sum

$$F(x) = \frac{F(x)+F(-x)}{2} + \frac{F(x)-F(-x)}{2} = F^{\text{even}}(x) + F^{\text{odd}}(x). \tag{8.33}$$

The function $F^{\text{odd}}(x)$ is said to have *odd parity* since it swaps sign upon the transformation $x \to -x$

$$F^{\text{odd}}(-x) = -F^{\text{odd}}(x), \tag{8.34}$$

whereas F^{even} has *even parity* since it maintains the same value upon the transformation $x \to -x$

$$F^{\text{even}}(-x) = F^{\text{even}}(x). \tag{8.35}$$

[8] As seen in Section 1.4, the Kronecker delta is the representation of the Euclidean metric when represented by Cartesian coordinates. For equations (8.29b) and (8.29c), we use the Kronecker delta merely as a signal of orthonormality of the trigonometric functions.

[9] We make use of this arbitrariness in Section 8.3.1 where we choose a particularly useful value for developing the notion of a Fourier integral.

The cosine and sine functions used in the Fourier series have even and odd parities, respectively

$$\cos(k_n\,x) = \cos(-k_n\,x) \quad \Longrightarrow \text{cosine has even parity} \tag{8.36a}$$
$$\sin(k_n\,x) = -\sin(-k_n\,x) \Longrightarrow \text{sine has odd parity.} \tag{8.36b}$$

As we show next, the Fourier series expansion of F^{even} and F^{odd} involve only a portion of the full series (8.27).

8.2.3 Fourier series of periodic functions with parity

Consider an even parity periodic function

$$F^{\text{even}}(x) = F^{\text{even}}(x+P), \tag{8.37}$$

so that this function has a Fourier series representation (equation (8.27))

$$F^{\text{even}}(x) = a_0 + \sum_{n=1}^{\infty}[a_n\cos(k_n\,x) + b_n\sin(k_n\,x)]. \tag{8.38}$$

Making use of the even parity property, $F^{\text{even}}(-x) = F^{\text{even}}(x)$, on the left hand side, as well as the parity properties (8.36a) and (8.36b) of the cosine and sine functions on the right hand side, leads to

$$F^{\text{even}}(x) = a_0 + \sum_{n=1}^{\infty}[a_n\cos(k_n\,x) - b_n\sin(k_n\,x)]. \tag{8.39}$$

For the series expansions (8.38) and (8.39) to be consistent for arbitrary even functions requires $b_n = 0$ for all n. Evidently, an even periodic function only has a Fourier cosine series expansion

$$F^{\text{even}}(x) = a_0 + \sum_{n=1}^{\infty} a_n\cos(k_n\,x), \tag{8.40}$$

An analogous result holds for an odd parity periodic function, in which $a_n = 0$ so that F^{odd} only has sine functions for its Fourier expansion

$$F^{\text{odd}}(x) = \sum_{n=1}^{\infty} b_n\sin(k_n\,x). \tag{8.41}$$

As a self-consistency check on the cosine expansion (8.40), compute the b_n coefficients according to equation (8.30d) whereby (setting $x_0 = -P/2$ for convenience)

$$b_{n>0} = \frac{2}{P}\int_{-P/2}^{P/2}\sin(k_n\,x)\,F^{\text{even}}(x)\,\mathrm{d}x \qquad \text{equation (8.30d)} \tag{8.42a}$$
$$= \frac{2}{P}\int_{P/2}^{-P/2}\sin(-k_n\,y)\,F^{\text{even}}(-y)\,(-\mathrm{d}y) \qquad \text{let } x=-y \tag{8.42b}$$
$$= \frac{2}{P}\int_{P/2}^{-P/2}\sin(k_n\,y)\,F^{\text{even}}(-y)\,\mathrm{d}y \qquad \sin(-k_n y) = -\sin(k_n y) \tag{8.42c}$$
$$= -\frac{2}{P}\int_{-P/2}^{P/2}\sin(k_n\,y)\,F^{\text{even}}(-y)\,\mathrm{d}y. \qquad \text{swap integration limits} \tag{8.42d}$$
$$= -\frac{2}{P}\int_{-P/2}^{P/2}\sin(k_n\,y)\,F^{\text{even}}(y)\,\mathrm{d}y. \qquad F^{\text{even}}(y) = F^{\text{even}}(-y). \tag{8.42e}$$

The only way to satisfy this equation is for $b_n = 0$ for each n, thus verifying the expansion (8.40). The same sort of argument is used to prove that $a_n = 0$ when computing the Fourier series expansion of an odd function, thus verifying the Fourier sine expansion (8.41) (see Exercise).

8.2.4 Complex Fourier series of exponentials

Rather than a sum of sines and cosines, we can use the Euler identity (8.3) to decompose a periodic function into a series of exponentials by introducing the complex expansion coefficients

$$c_0 = a_0 \tag{8.43a}$$
$$c_{-n} = (a_n + \mathrm{i}\, b_n)/2 \quad \text{for } n > 0 \tag{8.43b}$$
$$c_n = (a_n - \mathrm{i}\, b_n)/2 \quad \text{for } n > 0. \tag{8.43c}$$

Making use of the expressions (8.30b) and (8.30d) yields

$$c_n = \frac{1}{P} \int_{x_0}^{x_0+P} \mathrm{e}^{-\mathrm{i}\, k_n\, x}\, F(x)\, \mathrm{d}x. \tag{8.44}$$

The reality condition, commonly referred to as *conjugate symmetry*,

$$c_{-n} = c_n^*, \tag{8.45}$$

holds since we are only considering real functions, $F(x)$. Inverting the relations (8.43a)-(8.43c)

$$a_0 = c_0 \tag{8.46a}$$
$$a_n = c_n + c_{-n} \qquad \text{for } n > 0 \tag{8.46b}$$
$$b_n = \mathrm{i}\,(c_n - c_{-n}) \quad \text{for } n > 0 \tag{8.46c}$$

then allows us to write the Fourier series (8.27) as

$$F(x) = a_0 + \sum_{n=1}^{\infty} [a_n \cos(k_n\, x) + b_n \sin(k_n\, x)] \tag{8.47a}$$
$$= c_0 + \sum_{n=1}^{\infty} [(c_n + c_{-n}) \cos(k_n\, x) + \mathrm{i}\,(c_n - c_{-n}) \sin(k_n\, x)] \tag{8.47b}$$
$$= c_0 + \sum_{n=1}^{\infty} c_n\, [\cos(k_n\, x) + \mathrm{i} \sin(k_n\, x)] + \sum_{n=1}^{\infty} c_{-n}\, [\cos(k_n\, x) - \mathrm{i} \sin(k_n\, x)] \tag{8.47c}$$
$$= c_0 + \sum_{n=1}^{\infty} c_n\, \mathrm{e}^{\mathrm{i}\, k_n\, x} + \sum_{n=1}^{\infty} c_{-n}\, \mathrm{e}^{-\mathrm{i}\, k_n\, x} \tag{8.47d}$$
$$= c_0 + \sum_{n=1}^{\infty} c_n\, \mathrm{e}^{\mathrm{i}\, k_n\, x} + \sum_{n=1}^{\infty} c_{-n}\, \mathrm{e}^{\mathrm{i}\, k_{-n}\, x} \tag{8.47e}$$
$$= \sum_{n=-\infty}^{\infty} c_n\, \mathrm{e}^{\mathrm{i}\, k_n\, x}, \tag{8.47f}$$

where the penultimate step made use of equation (8.28) for the wavenumber, whereby

$$k_n = 2\,\pi\, n/P = -k_{-n}. \tag{8.48}$$

The exponential expression in equation (8.47f) is commonly more convenient for manipulations, with the conjugate symmetry condition (8.45) of fundamental importance when working with

real functions. Importantly, note that the real coefficients, a_n and b_n, are defined for $n \geq 0$ (with $b_0 = 0$) , whereas the complex coefficients, c_n, are defined for all integers.

8.2.5 Bessel-Parseval relations

Making use of the conjugate symmetry condition (8.45) allows us to write the square of a real periodic function

$$F(x)\,F(x) = \left[\sum_{n=-\infty}^{\infty} c_n\,\mathrm{e}^{\mathrm{i}\,k_n\,x}\right]\left[\sum_{m=-\infty}^{\infty} c_m\,\mathrm{e}^{\mathrm{i}\,k_m\,x}\right] \qquad \text{equation (8.47f)} \tag{8.49a}$$

$$= \left[\sum_{n=-\infty}^{\infty} c_n\,\mathrm{e}^{\mathrm{i}\,k_n\,x}\right]\left[\sum_{m=-\infty}^{\infty} c_{-m}\,\mathrm{e}^{-\mathrm{i}\,k_m\,x}\right] \qquad \text{swap } m \text{ summation order} \tag{8.49b}$$

$$= \left[\sum_{n=-\infty}^{\infty} c_n\,\mathrm{e}^{\mathrm{i}\,k_n\,x}\right]\left[\sum_{m=-\infty}^{\infty} c^*_m\,\mathrm{e}^{-\mathrm{i}\,k_m\,x}\right] \qquad \text{conjugate symmetry (8.45)} \tag{8.49c}$$

$$= \sum_{n,m=-\infty}^{\infty} c_n\,c^*_m\,\mathrm{e}^{\mathrm{i}\,(k_n-k_m)\,x} \qquad \text{combine sums.} \tag{8.49d}$$

The *Bessel-Parseval relation* (sometimes just referred to as *Parseval's identity*) results from performing an average of equation (8.49d) over a single period

$$\frac{1}{P}\int_{x_0}^{x_0+P} F(x)\,F(x)\,\mathrm{d}x = \sum_{n=-\infty}^{\infty} c_n\,c^*_n = \sum_{n=-\infty}^{\infty} |c_n|^2 = \sum_{n=-\infty}^{\infty} c_n\,c_{-n}. \tag{8.50}$$

To reach this identity we used the orthonormality condition holding for the exponentials

$$\frac{1}{P}\int_{x_0}^{x_0+P} \mathrm{e}^{\mathrm{i}\,(k_n-k_m)x}\,\mathrm{d}x = \delta_{mn}, \tag{8.51}$$

and the final equality in equation (8.50) follows from conjugate symmetry (8.45) that holds since F is real. The analogous form of Parseval's identity holds when using the sine/cosine version of the Fourier series (8.27), whereby

$$F(x)\,F(x) = \left[a_0 + \sum_{n=1}^{\infty}[a_n\cos(k_n\,x) + b_n\sin(k_n\,x)]\right]\left[a_0 + \sum_{m=1}^{\infty}[a_m\cos(k_m\,x) + b_m\sin(k_m\,x)]\right], \tag{8.52}$$

with integration and the orthonormality relations (8.29a)-(8.29c) resulting in

$$\frac{1}{P}\int_{x_0}^{x_0+P} F(x)\,F(x)\,\mathrm{d}x = a_0^2 + \frac{1}{2}\sum_{n=1}^{\infty}(a_n^2 + b_n^2). \tag{8.53}$$

We find it useful to double-check this form of Parseval's identity while confirming we are consistently using both the real and complex forms of the Fourier series. For this purpose, substitute the expressions (8.43a)-(8.43c) for c_n into the final form of Parsevel's identity (8.50) to yield

$$\sum_{n=-\infty}^{\infty} c_n\,c_{-n} = c_0^2 + \sum_{n=-\infty}^{-1} c_n\,c_{-n} + \sum_{n=1}^{\infty} c_n\,c_{-n} = c_0^2 + 2\sum_{n=1}^{\infty} c_n\,c_{-n} = a_0^2 + \frac{1}{2}\sum_{n=1}^{\infty}(a_n^2 + b_n^2), \tag{8.54a}$$

which agrees with equation (8.53).

We can go one further step by introducing a second real and periodic function, $H(x) = H(x + m\,P)$, in which case

$$H(x) = \sum_{n=-\infty}^{\infty} d_n \, \mathrm{e}^{\mathrm{i}\, k_n \, x}. \tag{8.55}$$

The Bessel-Parseval relation (8.50) can thus be generalized to

$$\frac{1}{P} \int_{x_0}^{x_0+P} F(x)\, H(x)\, \mathrm{d}x = \sum_{n=-\infty}^{\infty} c_n \, d_n^* = \sum_{n=-\infty}^{\infty} c_n \, d_{-n}. \tag{8.56}$$

8.3 Fourier integrals

We develop *Fourier integrals* as the limit of a Fourier series and then derive some properties of these integrals. Our treatment is heuristic.[10]

8.3.1 Fourier's integral theorem

Consider a real periodic function, $F(x) = F(x + n\,P)$ with n an integer, and decompose it according to the Fourier series (8.27). Also, insert the expressions (8.30a)-(8.30d) for the expansion coefficients and specify the arbitrary constant $x_0 = -P/2$ in order to symmetrize the integral limits. The resulting Fourier series is given by

$$F(x) = \frac{2}{P} \int_{-P/2}^{P/2} F(u) \left[\frac{1}{2} + \sum_{n=1}^{\infty} [\cos(k_n\, u) \cos(k_n\, x) + \sin(k_n\, u) \sin(k_n\, x)] \right] \mathrm{d}u. \tag{8.57}$$

We now consider the limit as $P \to \infty$, in which case the period becomes infinite so that the function, $F(x)$, is no longer periodic over a finite interval. Precisely, we make the following assumptions and conversions.

- FINITE INTEGRAL: We assume the absolute value of the function has a finite integral for arbitrary P, which in turn means that its average tends to zero as P becomes infinite:

$$\int_{-P/2}^{P/2} |F(u)|\, \mathrm{d}u < \infty \Longrightarrow \lim_{P\to\infty} \frac{1}{P} \int_{-P/2}^{P/2} F(u)\, \mathrm{d}u = 0. \tag{8.58}$$

- INFINITESIMAL WAVENUMBER INCREMENT: We introduce the wavenumber increment

$$k_{n+1} - k_n = \Delta k = 2\pi/P, \tag{8.59}$$

  which becomes infinitesimal as P becomes large. As a result, the infinite sum over discrete wavenumbers transitions to an integral over continuous wavenumbers

$$\lim_{P\to\infty} \sum_{n=1}^{\infty} \frac{2}{P} = \frac{1}{\pi} \int_0^{\infty} \mathrm{d}k. \tag{8.60}$$

Making use of these results in equation (8.57) leads to

$$F(x) = \frac{1}{\pi} \int_0^{\infty} \left[\cos(k\, x) \int_{-\infty}^{\infty} F(u) \cos(k\, u)\, \mathrm{d}u + \sin(k\, x) \int_{-\infty}^{\infty} F(u) \sin(k\, u)\, \mathrm{d}u \right] \mathrm{d}k, \tag{8.61}$$

[10] The derivation of the Fourier transform equations in this section follows that given by Chapter 5 of *Spiegel* (1974b), particularly worked exercise 5.11, yet note that L in *Spiegel* (1974b) is given by $L = P/2$.

which is known as *Fourier's integral theorem*. We can bring Fourier's integral theorem a bit closer to the discrete Fourier sum (8.27) by introducing the real amplitude functions

$$A(k) \equiv \frac{1}{\pi}\int_{-\infty}^{\infty} F(u)\cos(k\,u)\,\mathrm{d}u \quad \text{and} \quad B(k) \equiv \frac{1}{\pi}\int_{-\infty}^{\infty} F(u)\sin(k\,u)\,\mathrm{d}u, \tag{8.62}$$

thus resulting in the tidy expression of the Fourier integral theorem (8.61)

$$F(x) = \int_{0}^{\infty} [A(k)\cos(k\,x) + B(k)\sin(k\,x)]\,\mathrm{d}k. \tag{8.63}$$

This version of Fourier's integral theorem forms the foundation for the remainder of this section, which largely consists of rewriting this identity in a variety of forms. Before doing so, we emphasize the following points.

All physical fields produce real numbers

As noted at the start of this chapter, all physical fields in this book are real. Hence, every term in equation (8.63) is real, including the amplitude functions, $A(k)$ and $B(k)$. So although many versions of Fourier analysis involve complex numbers, as we describe in Section 8.3.2, the introduction of complex numbers is based on mathematical convenience and so it is not physically motivated.

Concerning the functional degrees of freedom

For each function, $F(x)$, there are two amplitude functions, $A(k)$ and $B(k)$. However, there is no explosion of functional degrees of freedom since $F(x)$ is defined over the full real line, $-\infty < x < \infty$ whereas $A(k)$ and $B(k)$ are defined with $k \geq 0$. The equal functional degrees of freedom manifest when using the complex version of the Fourier integral theorem in Section 8.3.2.

Parity properties of the amplitude functions

The parity properties of the amplitude functions, $A(k)$ and $B(k)$, are directly inherited from the cosine and sine functions appearing in their definition (8.62), so that we find

$$A(k) = A(-k) \quad \text{and} \quad B(k) = -B(-k). \tag{8.64}$$

As shown in Section 8.3.5, these properties are reflected in the nature of the integral theorem when representing functions, $F(x)$, with a particular parity.

Allowing the wavenumber to range over the full real line

The integral over wavenumber, k, in equation (8.62) extends from $k = 0$ to $k = \infty$. When moving to a complex representation that involves the Fourier transform in Section 8.3.2, the integral is extended to $-\infty < k < \infty$. As discussed in Section 49.6.10, the extension to $k < 0$ can be interpreted as a plane wave moving in the direction opposite to the wave with $k > 0$.

8.3.2 Fourier transform

Introducing the *Fourier transform*, $\mathcal{F}(k)$, allows us to connect to the complex Fourier series from Section (8.2.4)

$$\mathcal{F}(k) \equiv \pi\,[A(k) - \mathrm{i}\,B(k)] = \int_{-\infty}^{\infty} F(u)\,\mathrm{e}^{-\mathrm{i}\,k\,u}\,\mathrm{d}u \quad \Longleftarrow \text{Fourier transform.} \tag{8.65}$$

We can write the Fourier integral theorem (8.63) in terms of $\mathcal{F}(k)$ according to

$$F(x) = \int_0^\infty [A(k)\cos(k\,x) + B(k)\sin(k\,x)]\,\mathrm{d}k \tag{8.66a}$$

$$= \frac{1}{2\pi}\int_0^\infty \left[\cos(k\,x)\left[\mathcal{F}(k) + \mathcal{F}^*(k)\right] + \mathrm{i}\,\sin(k\,x)\left[\mathcal{F}(k) - \mathcal{F}^*(k)\right]\right]\mathrm{d}k \tag{8.66b}$$

$$= \frac{1}{2\pi}\int_0^\infty \left[\mathcal{F}(k)\,\mathrm{e}^{\mathrm{i}\,k\,x} + \left[\mathcal{F}(k)\,\mathrm{e}^{\mathrm{i}\,k\,x}\right]^*\right]\mathrm{d}k. \tag{8.66c}$$

From its definition (8.65), we know that the complex conjugate of the Fourier transform satisfies the *conjugate symmetry* identity

$$\mathcal{F}^*(k) = \int_{-\infty}^\infty F(u)\,\mathrm{e}^{\mathrm{i}\,k\,u}\,\mathrm{d}u = \mathcal{F}(-k). \tag{8.67}$$

This identity is directly analogous to the discrete Fourier transform identity (8.45), both of which hold due to the reality of the function, $F(x)$. We are thus led to the complex version of the Fourier integral theorem (8.63)

$$F(x) = \frac{1}{2\pi}\int_0^\infty \mathcal{F}(k)\,\mathrm{e}^{\mathrm{i}\,k\,x}\,\mathrm{d}k + \frac{1}{2\pi}\int_0^\infty \mathcal{F}(-k)\,\mathrm{e}^{-\mathrm{i}\,k\,x}\,\mathrm{d}k \tag{8.68a}$$

$$= \frac{1}{2\pi}\int_0^\infty \mathcal{F}(k)\,\mathrm{e}^{\mathrm{i}\,k\,x}\,\mathrm{d}k - \frac{1}{2\pi}\int_0^{-\infty} \mathcal{F}(k)\,\mathrm{e}^{\mathrm{i}\,k\,x}\,\mathrm{d}k \tag{8.68b}$$

$$= \frac{1}{2\pi}\int_{-\infty}^\infty \mathcal{F}(k)\,\mathrm{e}^{\mathrm{i}\,k\,x}\,\mathrm{d}k. \tag{8.68c}$$

With $\mathcal{F}(k)$ referred to as the Fourier transform we sometimes refer to $F(x)$ as the *inverse Fourier transform*. Correspondingly, $\mathcal{F}(k)$ and $F(x)$ are *Fourier transform pairs*.

8.3.3 A comment on conjugate symmetry

As noted above, reality of the function, $F(x)$, is ensured by a Fourier transform that satisfies the conjugate symmetry property (8.67). We make use of this property in much of our analysis in this book, such as when studying wave packets in Chapter 49. However, there are reasons to sometimes dispense with conjugate symmetry. One example is provided in Sections 49.6.4 and 52.9.1 when providing information about a wave packet's initial tendency rather than its initial position. Evidently, the identity (8.66c) ensures that $F(x)$ is real, even if the Fourier amplitudes, $\mathcal{F}(k)$, do not satisfy conjugate symmetry. That is, conjugate symmetry is a sufficient condition to ensure $F(x)$ is real, but it is not a necessary condition.

8.3.4 Integrals over a symmetric interval

Consider the integral of a function, $F(x)$, defined over an arbitrary, but symmetric, interval $x \in [-L, L]$. Decomposing this function into its even an odd components leads to

$$\int_{-L}^{L} F(x)\,\mathrm{d}x = \frac{1}{2}\int_{-L}^{L}[F(x) + F(-x)]\,\mathrm{d}x + \frac{1}{2}\int_{-L}^{L}[F(x) - F(-x)]\,\mathrm{d}x \tag{8.69a}$$

$$\equiv \int_{-L}^{L} F^{\text{even}}(x)\mathrm{d}x + \int_{-L}^{L} F^{\text{odd}}(x)\,\mathrm{d}x. \tag{8.69b}$$

The integral of the even parity component can be written

$$\int_{-L}^{L} F^{\text{even}}(x)\,\mathrm{d}x = \int_{-L}^{0} F^{\text{even}}(x)\,\mathrm{d}x + \int_{0}^{L} F^{\text{even}}(x)\,\mathrm{d}x \tag{8.70a}$$

$$= -\int_{L}^{0} F^{\text{even}}(-x)\,\mathrm{d}x + \int_{0}^{L} F^{\text{even}}(x)\,\mathrm{d}x \tag{8.70b}$$

$$= 2\int_{0}^{L} F^{\text{even}}(x)\,\mathrm{d}x. \tag{8.70c}$$

Evidently, the integral of an even parity function over a symmetric interval equals to twice the integral over half the interval

$$\int_{-L}^{L} F^{\text{even}}(x)\,\mathrm{d}x = 2\int_{0}^{L} F^{\text{even}}(x)\,\mathrm{d}x. \tag{8.71}$$

In a similar manner we find that the integral of an odd parity function over a symmetric interval vanishes

$$\int_{-L}^{L} F^{\text{odd}}(x)\,\mathrm{d}x = \int_{-L}^{0} F^{\text{odd}}(x)\,\mathrm{d}x + \int_{0}^{L} F^{\text{odd}}(x)\,\mathrm{d}x \tag{8.72a}$$

$$= -\int_{L}^{0} F^{\text{odd}}(-x)\,\mathrm{d}x + \int_{0}^{L} F^{\text{odd}}(x)\,\mathrm{d}x \tag{8.72b}$$

$$= \int_{0}^{L} [F^{\text{odd}}(-x) + F^{\text{odd}}(x)]\,\mathrm{d}x \tag{8.72c}$$

$$= 0. \tag{8.72d}$$

We thus find that the integral of an arbitrary function over a symmetric interval is given by twice the integral of the even component over half the interval

$$\int_{-L}^{L} F(x)\,\mathrm{d}x = 2\int_{0}^{L} F_{\text{even}}(x)\,\mathrm{d}x = \int_{0}^{L} [F(x) + F(-x)]\,\mathrm{d}x. \tag{8.73}$$

We make use of these relations in developing parity conditions for Fourier transforms, in which case the integral limits are infinity, $L = \infty$.

8.3.5 Fourier cosine and sine transforms

The Fourier integral theorem simplifies when acting on functions of a particular parity. As any function can be decomposed into its even and odd parity components (see Section 8.3.4), it is common to make use of the simplification by introducing the cosine and sine transforms. These transforms allow one to work with all real valued functions when convenient, rather than the complex valued functions used with the standard Fourier transform of Section 8.3.2.

Fourier cosine transform for even functions: $F(x) = F(-x)$

Consider an even function, $F(x) = F(-x)$, and expand it in terms of the Fourier integral theorem (8.63)

$$F(x) = \int_{0}^{\infty} [A(k)\cos(k\,x) + B(k)\sin(k\,x)]\,\mathrm{d}k. \tag{8.74}$$

Since $F(x) = F(-x)$ it follows that

$$F(x) = F(-x) = \int_0^\infty [A(k)\cos(k\,x) - B(k)\sin(k\,x)]\,\mathrm{d}k, \tag{8.75}$$

which follows from the odd parity of the sine function. For this relation to hold requires $B(k) = 0$, which indeed follows from its definition

$$\begin{aligned}
\pi\,B(k) &= \int_{-\infty}^\infty F(u)\sin(k\,u)\,\mathrm{d}u && \text{(8.76a)}\\
&= \int_{-\infty}^0 F(u)\sin(k\,u)\,\mathrm{d}u + \int_0^\infty F(u)\sin(k\,u)\,\mathrm{d}u && \text{(8.76b)}\\
&= \int_0^\infty [-F(u) + F(u)]\sin(k\,u)\,\mathrm{d}u && \text{(8.76c)}\\
&= 0. && \text{(8.76d)}
\end{aligned}$$

These simplification of Fourier's integral theorem motivate us to define the *Fourier cosine transform* for functions with even parity

$$F_\mathrm{C}(k) \equiv (\pi/2)\,A(k) = \frac{1}{2}\int_{-\infty}^\infty F(u)\cos(k\,u)\,\mathrm{d}u = \int_0^\infty F(u)\cos(k\,u)\,\mathrm{d}u, \tag{8.77}$$

so that Fourier's integral theorem (8.75) for an even parity function is

$$F(x) = \int_0^\infty A(k)\cos(k\,x)\,\mathrm{d}k = \frac{2}{\pi}\int_0^\infty F_\mathrm{C}(k)\cos(k\,x)\,\mathrm{d}k. \tag{8.78}$$

Correspondingly, the Fourier cosine transform of an odd parity function vanishes.

Fourier sine transform for odd functions: $F(x) = -F(-x)$

We now consider the case of an odd function, $F(x) = -F(-x)$, and expand it in terms of the Fourier integral theorem (8.63)

$$F(x) = \int_0^\infty [A(k)\cos(k\,x) + B(k)\sin(k\,x)]\,\mathrm{d}k = \int_0^\infty [-A(k)\cos(k\,x) + B(k)\sin(k\,x)]\,\mathrm{d}k, \tag{8.79}$$

where the second equality follows since $F(x) = -F(-x)$ and the parity of the cosine and sine functions. This relation is consistent only if $A(k) = 0$ for odd functions, which indeed follows from its definition

$$\begin{aligned}
\pi\,A(k) &= \int_{-\infty}^\infty F(u)\cos(k\,u)\,\mathrm{d}u && \text{(8.80a)}\\
&= \int_{-\infty}^0 F(u)\cos(k\,u)\,\mathrm{d}u + \int_0^\infty F(u)\cos(k\,u)\,\mathrm{d}u && \text{(8.80b)}\\
&= \int_0^\infty [F(-u) + F(u)]\cos(k\,u)\,\mathrm{d}u && \text{(8.80c)}\\
&= 0. && \text{(8.80d)}
\end{aligned}$$

We are thus motivated to define the *Fourier sine transform* for functions with odd parity

$$F_\mathrm{S}(k) \equiv (\pi/2)\,B(k) = \frac{1}{2}\int_{-\infty}^\infty F(u)\sin(k\,u)\,\mathrm{d}u = \int_0^\infty F(u)\sin(k\,u)\,\mathrm{d}u, \tag{8.81}$$

so that Fourier's integral theorem (8.79) for an odd parity function takes the form

$$F(x) = \int_0^\infty B(k)\sin(k\,x)\,\mathrm{d}k = \frac{2}{\pi}\int_0^\infty F_{\mathrm{S}}(k)\sin(k\,x)\,\mathrm{d}k. \tag{8.82}$$

Correspondingly, the Fourier sine transform of an even parity function vanishes.

8.3.6 Parseval-Plancherel formulas

In Section 8.2.5 we showed that a Fourier series expansion of a periodic function satisfies the Parseval identities (8.50) and (8.56). Here we derive the analog for Fourier integral transforms. For this purpose, consider the integral of the product of two real functions

$$\int_{-\infty}^\infty G(x)\,F(x)\,\mathrm{d}x = \frac{1}{2\pi}\int_{-\infty}^\infty G(x)\left[\int_{-\infty}^\infty \mathcal{F}(k)\,\mathrm{e}^{\mathrm{i}\,k\,x}\,\mathrm{d}k\right]\mathrm{d}x, \tag{8.83}$$

where we expressed $F(x)$ in terms of its inverse Fourier transform (8.68c). Now swap the integration order and rearrange to render

$$\int_{-\infty}^\infty G(x)\,F(x)\,\mathrm{d}x = \frac{1}{2\pi}\int_{-\infty}^\infty \left[\int_{-\infty}^\infty G(x)\,\mathrm{e}^{-\mathrm{i}\,k\,x}\,\mathrm{d}x\right]^*\mathcal{F}(k)\,\mathrm{d}k, \tag{8.84}$$

where we noted that

$$\left[\mathrm{e}^{\mathrm{i}\,k\,x}\right]^* = \mathrm{e}^{-\mathrm{i}\,k\,x} \quad \text{and} \quad G^* = G. \tag{8.85}$$

We recognize the bracketed term in equation (8.84) as the complex conjugate Fourier transform of G, thus bringing us to the identity

$$\int_{-\infty}^\infty G(x)\,F(x)\,\mathrm{d}x = \frac{1}{2\pi}\int_{-\infty}^\infty [\mathcal{G}(k)]^*\,\mathcal{F}(k)\,\mathrm{d}k. \tag{8.86}$$

For the special case with $G = F$ we recover the *Parseval-Plancherel formula*, commonly referred to as *Parseval's identity*

$$\int_{-\infty}^\infty [F(x)]^2\,\mathrm{d}x = \frac{1}{2\pi}\int_{-\infty}^\infty |\mathcal{F}(k)|^2\,\mathrm{d}k. \tag{8.87}$$

If $[F(x)]^2$ is proportional to the energy, then Parseval's identity expresses the identity of energy when expressed in either $\boldsymbol{x}$-space or $\boldsymbol{k}$-space.[11]

8.3.7 Concerning the placement of $1/2\pi$

There is no universal convention for the pre-factors appearing in the Fourier transform pairs (8.65) and (8.68c). That is, the unity for the Fourier transform pre-factor in equation (8.65), versus the $1/2\pi$ pre-factor for the inverse Fourier transform (8.68c), could just as well be swapped, or alternatively they could both be equal to $1/\sqrt{2\pi}$. However these factors are chosen, their product must equal to $1/2\pi$.

Furthermore, the $1/2\pi$ factor in the inverse Fourier transform (8.68c) can be eliminated through use of the *reduced wavenumber*, $\bar{k}$, defined as

$$\bar{k} = k/2\pi, \tag{8.88}$$

[11]The $1/2\pi$ factor in the Parsevel identity (8.87) can be eliminated by distributing a $1/\sqrt{2\pi}$ equally between the Fourier transform and the inverse Fourier transform. That convention is generally followed in the quantum mechanics literature but not in the fluid mechanics literature. See Section 8.3.7 for more on the 2π factor.

in which case the inverse Fourier transform (8.68c) is given by

$$F(x) = \int_{-\infty}^{\infty} \mathcal{F}(\hbar)\, \mathrm{e}^{\mathrm{i}\, 2\,\pi\, \hbar x}\, \mathrm{d}\hbar \tag{8.89}$$

An analogous approach is used when working in the time-frequency domain and using the frequency, f, rather than the angular frequency, ω, where $f = \omega/2\pi$ (see Section 8.4). Even though $\hbar$ is somewhat more elegant, we generally work with the wavenumber, k, thus necessitating care to properly place the $1/2\pi$ factor.

8.3.8 Fourier transforms and derivatives

Here we examine some properties of the Fourier transform of derivatives. Note that for all of the results, we must assume that the function and its Fourier transform decay to zero at infinity at a rate sufficient to ensure that all integrals are all bounded.

Each derivative operation multiplies by $(\mathrm{i}\, k)^p$

Consider a function expressed as the inverse Fourier transform (8.68c)

$$F(x) = \frac{1}{2\pi} \int_{-\infty}^{\infty} \mathcal{F}(k)\, \mathrm{e}^{\mathrm{i}\, k\, x}\, \mathrm{d}k, \tag{8.90}$$

where $\mathcal{F}(k)$ is the Fourier transform of $F(x)$ as per equation (8.65). Now take the p'th derivative of $F(x)$ and note that the derivative operator commutes with the $\boldsymbol{k}$-space integral

$$\frac{\mathrm{d}^p F(x)}{\mathrm{d}x^p} = \frac{1}{2\pi} \int_{-\infty}^{\infty} \mathcal{F}(k)\, (\mathrm{i}\, k)^p\, \mathrm{e}^{\mathrm{i}\, k\, x}\, \mathrm{d}k, \tag{8.91}$$

where we set

$$\frac{\mathrm{d}^p\, (\mathrm{e}^{\mathrm{i}\, k\, x})}{\mathrm{d}x^p} = (\mathrm{i}\, k)^p\, \mathrm{e}^{\mathrm{i}\, k\, x}. \tag{8.92}$$

Equation (8.91) indicates that each derivative increases the power of $(\mathrm{i}\, k)$ inside the $\boldsymbol{k}$-space integral, in which case the relative contributions from higher wavenumbers are enhanced relative to lower wavenumbers.[12]

Furthering the above result

To further the above remarks, consider a function, $G(x)$, that is expressed as an inverse Fourier transform

$$G(x) = \frac{1}{2\pi} \int_{-\infty}^{\infty} \mathcal{G}(k)\, \mathrm{e}^{\mathrm{i}\, k\, x}\, \mathrm{d}k, \tag{8.93}$$

and define $G(x)$ as the p'th derivative of $F(x)$

$$G^{(p)}(x) = \frac{\mathrm{d}^p F(x)}{\mathrm{d}x^p}. \tag{8.94}$$

From equation (8.91) we make the identification

$$\mathcal{G}^{(p)}(k) = (\mathrm{i}\, k)^p\, \mathcal{F}(k). \tag{8.95}$$

[12] As noted at the start of this subsection, we must assume a finite wavenumber cutoff to ensure the integral (8.91) is bounded. That is, we must assume a length scale below which there is no structure in $F(x)$, which then means that $\mathcal{F}(k)$ vanishes (or is exponentially small) for wavenumbers above some finite wavenumber. This assumption is typically satisfied by physical fields.

Hence, the Fourier transform of the derivative of a function results in a power of $(\mathrm{i}\,k)$ for each derivative, so that, for example,

$$\mathcal{G}^{(1)}(k) = \mathrm{i}\,k\,\mathcal{F}(k) \tag{8.96a}$$

$$\mathcal{G}^{(2)}(k) = -k^2\,\mathcal{F}(k). \tag{8.96b}$$

For $p = 1$ we see that the Fourier transform of the derivative of a function has a $\pi/2$ phase shift relative to the function, whereas for $p = 2$ there is a π phase shift.

Directly computing the Fourier transform of the derivative of a function

There is yet another way to compute the Fourier transform of the derivative of a function, through use of integration by parts

$$\mathcal{G}^{(1)}(k) = \int_{-\infty}^{\infty} \frac{\mathrm{d}F}{\mathrm{d}x}\,\mathrm{e}^{-\mathrm{i}\,k\,x}\,\mathrm{d}x \tag{8.97a}$$

$$= \int_{-\infty}^{\infty} \left[\frac{\mathrm{d}(F\,\mathrm{e}^{-\mathrm{i}\,k\,x})}{\mathrm{d}x} - F\,\frac{\mathrm{d}(\mathrm{e}^{-\mathrm{i}\,k\,x})}{\mathrm{d}x}\right]\mathrm{d}x \tag{8.97b}$$

$$= \int_{-\infty}^{\infty} \left[\frac{\mathrm{d}(F\,\mathrm{e}^{-\mathrm{i}\,k\,x})}{\mathrm{d}x} + (\mathrm{i}\,k)\,F(x)\,\mathrm{e}^{-\mathrm{i}\,k\,x}\right]\mathrm{d}x. \tag{8.97c}$$

If we assume $F(x)$ decays to zero as $x \to \pm\infty$, then the total derivative vanishes, in which case we are left with

$$\mathcal{G}^{(1)}(k) = (\mathrm{i}\,k)\int_{-\infty}^{\infty} F(x)\,\mathrm{e}^{-\mathrm{i}\,k\,x}\,\mathrm{d}x = (\mathrm{i}\,k)\,\mathcal{F}(k). \tag{8.98}$$

This result agrees with equation (8.96a) derived earlier. Higher derivatives can be computed likewise.

A Fourier series example with two Fourier components

To further illustrate the role of derivatives and how they enhance the relative contribution of small scales versus large scales, consider a finite sized one-dimensional periodic domain. For a function, $F(x)$, that is periodic on this domain we can represent it according to its Fourier series (8.27), and assume there are just two non-zero wavenumbers contributing to the function

$$F(x) = a_1\cos(k_1\,x) + a_{10}\cos(k_{10}\,x), \tag{8.99}$$

with $a_1/a_{10} = 0.95/0.05 = 19$. As illustrated in Figure 8.2, the function $F(x)$ is the sum of a low wavenumber Fourier component, $a_1\cos(k_1\,x)$, plus a high wavenumber component, $a_{10}\cos(k_{10}\,x)$. The second derivative of this function is given by

$$\mathrm{d}^2F(x)/\mathrm{d}x^2 = -a_1\,k_1^2\cos(k_1\,x) - a_{10}\,k_{10}^2\cos(k_{10}\,x), \tag{8.100}$$

so that each wavenumber contribution is multiplied by its respective wavenumber squared. Evidently, the contribution from $n = 10$ is enhanced relative to the $n = 1$ contribution by the ratio $(k_{10}/k_1)^2 = (10/1)^2 = 100$. In general, any nonzero a_n coefficient in the expansion of a function is amplified by its respective wavenumber when taking a derivative, so that higher wavenumber features are enhanced relative to lower wavenumber features.

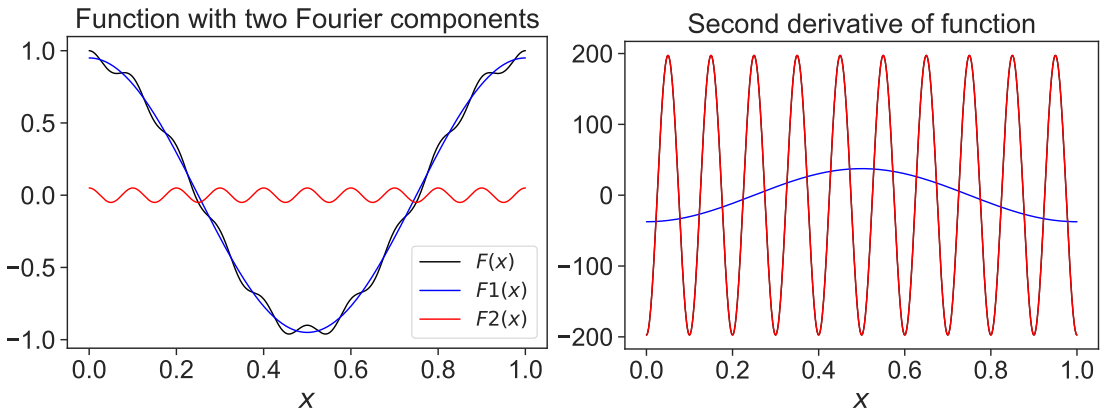

FIGURE 8.2: Left panel: a function comprised of two Fourier components, $F(x) = F_1(x) + F_2(x) = a_1 \cos(k_1\, x) + a_{10} \cos(k_{10}\, x)$, with a low wavenumber $k_1 = 2\,\pi/L$, and a high wavenumber, $k_{10} = 2\,\pi/(L/10)$, along with the amplitudes $a_1 = 0.95$ and $a_{10} = 0.05$. We choose $L = 1$ in arbitrary units. Given that $a_1/a_{10} = 19$, the low wavenumber component dominates $F(x)$. Right panel: the second derivative of the function, $\mathrm{d}^2F(x)/\mathrm{d}x^2 = -a_1\, k_1^2 \cos(k_1\, x) - a_{10}\, k_{10}^2 \cos(k_{10}\, x)$, which is dominated by the high wavenumber component, with the high wavenumber component having an amplitude that is roughly five times larger than the low wavenumber component, $a_{10}\, k_{10}^2/(a_1\, k_1^2) \approx 5$.

Streamfunction and vorticity example

An example from fluid mechanics occurs with a horizontally non-divergent barotropic fluid from Chapter 38. In this case the vorticity, ζ, is the Laplacian of the streamfunction, ψ, so that

$$\zeta = \nabla^2 \psi. \tag{8.101}$$

Taking the Fourier transform of this equation reveals that the Fourier transform of the vorticity equals to $-k^2$ times the Fourier transform of the streamfunction. Hence, if there is any structure in the streamfunction at scale k, then the vorticity at that same scale is amplified by k^2. Consequently, the vorticity field has higher wavenumber features (i.e., smaller spatial scales) than the streamfunction field.

8.4 Time-frequency Fourier transforms

Our notation has thus far been based on space, x, and wavenumber, k. However, all formula hold whatever interpretation one gives to these coordinates, with time and frequency commonly used as well as space and wavenumber. Even so, for the time/frequency Fourier analysis we follow the typical physics convention of swapping sign in the exponents. Doing so accords with conventions in wave mechanics as pursued in Chapter 49. With that motivation we define the time/frequency Fourier transform and its inverse according to

$$\mathcal{F}(\omega) = \int_{-\infty}^{\infty} F(t)\, \mathrm{e}^{\mathrm{i}\,\omega\, t}\, \mathrm{d}t \tag{8.102a}$$

$$F(t) = \frac{1}{2\pi} \int_{-\infty}^{\infty} \mathcal{F}(\omega)\, \mathrm{e}^{-\mathrm{i}\,\omega\, t}\, \mathrm{d}\omega, \tag{8.102b}$$

where ω is the angular frequency. The time integral extends from $-\infty$ to ∞, meaning that it extends arbitrarily far in the past and arbitrarily far into the future. The negative angular frequency arises from the same symmetrization of the integral limits made when moving to the complex Fourier transform in Section 8.3.2. As in our discussion of wave mechanics in Section 49.6.10, we here find it important to interpret the negative angular frequency, $\omega < 0$, which we

do next.

8.4.1 How to interpret negative frequency for waves

As noted at the start of this chapter, we generally make use of Fourier analysis for the study of waves in Part X of this book. When working in $\boldsymbol{x}$-space and $\boldsymbol{k}$-space, we can consider the components of a wavevector to be positive or negative given that the wavevector determines the direction of a wave. We consider this particular point in Section 49.6.10. Since information about the direction of the wave is fully carried by the wavevector, we consider the angular frequency of a wave to be a non-negative number, $\omega \geq 0$ (Section 49.4), which corresponds to a non-negative wave period, $2\pi/\omega$. Hence, when working with waves, we interpret the expression (8.102b) for the inverse Fourier transform, with its negative frequency integral limits, as a convenient mathematical means to bring the Fourier sine and cosine functions together into a single integral. Yet we do not give any physical meaning to $\omega < 0$.

To provide details to support the above comments, return to the Fourier integral theorem (8.63), only now interpreted for time and angular frequency

$$F(t) = \int_0^\infty [A(\omega)\cos(\omega\, t) + B(\omega)\sin(\omega\, t)]\mathrm{d}\omega. \tag{8.103}$$

Note that the frequency integral extends only over non-negative frequencies, consistent with ω as a frequency. In contrast, the amplitude functions are built from integrals over all time according to equation (8.62)

$$A(\omega) = \frac{1}{\pi}\int_{-\infty}^{\infty} F(t)\cos(\omega\, t)\,\mathrm{d}t \quad \text{and} \quad B(\omega) = \frac{1}{\pi}\int_{-\infty}^{\infty} F(t)\sin(\omega\, t)\,\mathrm{d}t, \tag{8.104}$$

so that[13]

$$\mathcal{F}(\omega) = \pi\,[A(\omega) + \mathrm{i}\,B(\omega)]. \tag{8.105}$$

We have no problem with negative time simply because the origin of time is arbitrary. In contrast, we ascribe no physical meaning to a negative frequency, but instead interpret a negative frequency as a mathematical expedient enabling us to write equation (8.102b) in a compact form. We emphasize this point by writing

$$\begin{aligned}
F(t) &= \frac{1}{2\pi}\int_{-\infty}^{\infty} \mathrm{e}^{-\mathrm{i}\,\omega\, t}\,\mathcal{F}(\omega)\,\mathrm{d}\omega && \text{Fourier eq. (8.102b)} && \text{(8.106a)}\\
&= \frac{1}{2}\int_{-\infty}^{\infty} [\cos(\omega\, t) - \mathrm{i}\sin(\omega\, t)]\,[A(\omega) + \mathrm{i}\,B(\omega)]\mathrm{d}\omega && \text{Euler + eq. (8.104)} && \text{(8.106b)}\\
&= \frac{1}{2}\int_{-\infty}^{\infty} [A(\omega)\cos(\omega\, t) + B(\omega)\sin(\omega\, t)]\mathrm{d}\omega && \text{parity properties} && \text{(8.106c)}\\
&= \int_0^{\infty} [A(\omega)\cos(\omega\, t) + B(\omega)\sin(\omega\, t)]\mathrm{d}\omega && \text{parity properties.} && \text{(8.106d)}
\end{aligned}$$

So again, we compute the inverse Fourier transform as in equation (8.102b) with a frequency interval including negative frequencies. Yet there is no physical meaning given to the negative frequencies. Instead, they simply offer the means to unify the Fourier cosine and sine amplitude functions according to the above identities.

[13] Compare equation (8.105) to equation (8.65). The sign difference arises from the sign convention: we use $\mathrm{e}^{-\mathrm{i}\,\omega\, t}$ for the time-domain inverse Fourier transform (8.102b), whereas $\mathrm{e}^{\mathrm{i}\,k\,x}$ for the space-domain inverse Fourier transform (8.68c).

8.4.2 Frequency versus angular frequency

As noted in Section 8.3.7, we can eliminate the $1/2\pi$ factor appearing in the inverse Fourier transform (8.102b) through using the frequency, f (cycles per time), rather than the angular frequency, ω (radians per time),

$$f = \omega/2\pi, \tag{8.107}$$

in which case the Fourier transform partners (8.102a) and (8.102b) take the form

$$\mathcal{F}(f) = \int_{-\infty}^{\infty} F(t)\, \mathrm{e}^{\mathrm{i}\, 2\pi\, f\, t}\, \mathrm{d}t \tag{8.108a}$$

$$F(t) = \int_{-\infty}^{\infty} \mathcal{F}(f)\, \mathrm{e}^{-\mathrm{i}\, 2\pi\, f\, t}\, \mathrm{d}f. \tag{8.108b}$$

Even though f is rather elegant from this perspective, we generally use the angular frequency, ω (along with the angular wavenumber, k), thus necessitating care with the placement of the $1/2\pi$ factor for the Fourier transform pair given by equations (8.102a) and (8.102b).

8.5 Example Fourier transform pairs

In this section we offer a few examples of Fourier transform pairs.

8.5.1 Dirac delta in x-space

Consider the Dirac delta from Chapter 7,

$$F(x) = \delta(x). \tag{8.109}$$

Following from its sifting property (7.8), we find that the Fourier transform (equation (8.65)) of the Dirac delta is given by

$$\mathcal{F}(k) = \int_{-\infty}^{\infty} \delta(x)\, \mathrm{e}^{-\mathrm{i}\, k\, x}\, \mathrm{d}x = 1. \tag{8.110}$$

This result provides an extreme example of the *complementarity* relation maintained between the Fourier transform and its inverse. Namely, if a function is concentrated in $\boldsymbol{x}$-space then its Fourier transform is widely distributed in $\boldsymbol{k}$-space. The Dirac delta, $\delta(x)$, is infinitely concentrated in $\boldsymbol{x}$-space at the origin, whereas it has a uniform and constant distribution in $\boldsymbol{k}$-space. That is, the $\boldsymbol{x}$-space distribution is infinitesimally narrow whereas the $\boldsymbol{k}$-space distribution is infinitely broad. As a consistency check, we note the physical dimensionality of the terms in equation (8.110). The Dirac delta, $\delta(x)$, has dimensions of inverse length (Section 7.12), so that $\delta(x)\, \mathrm{d}x$ is non-dimensional. We thus expect its Fourier transform, $\mathcal{F}(k)$, to be non-dimensional.

It follows that the inverse Fourier transform (equation (8.68c)) of the Dirac delta is given by

$$\delta(x - x_0) = \frac{1}{2\pi} \int_{-\infty}^{\infty} \mathrm{e}^{\mathrm{i}\, k\, (x - x_0)}\, \mathrm{d}k \tag{8.111}$$

where we introduced an arbitrary shift from the origin, x_0. Note that

$$\int_{-\infty}^{\infty} \sin[k\, (x - x_0)]\, \mathrm{d}k = 0, \tag{8.112}$$

which follows since the $\boldsymbol{k}$-space integral is over a symmetric domain yet the integrand has odd

$\boldsymbol{k}$-space parity. Consequently, we have

$$\delta(x - x_0) = \frac{1}{2\pi} \int_{-\infty}^{\infty} \cos[k\,(x - x_0)]\,\mathrm{d}k = \frac{2}{2\pi} \int_{0}^{\infty} \cos[k\,(x - x_0)]\,\mathrm{d}k. \tag{8.113}$$

This equation is a rather remarkable expression that can be heuristically explained by noting that for all values of $x - x_0 \neq 0$, the cosine function oscillates so that any positive values are exactly matched by negative values, thus yielding a zero integral. However, when $x - x_0 = 0$, the integral diverges to infinity.

8.5.2 Dirac delta in $\boldsymbol{k}$-space

We now assume exact information about the wave number by setting the Fourier transform to

$$\mathcal{F}(k) = \delta(k - k_0), \tag{8.114}$$

which has physical dimensions of length. The resulting inverse Fourier transform is given by the dimensionless function

$$F(x) = \frac{1}{2\pi} \int_{-\infty}^{\infty} \delta(k - k_0)\,\mathrm{e}^{\mathrm{i}\,k\,x}\,\mathrm{d}k = \frac{\mathrm{e}^{\mathrm{i}\,k_0\,x}}{2\pi}. \tag{8.115}$$

So as a complement to the case in Section 8.5.1, we here find that exact information about the $\boldsymbol{k}$-space location (i.e., the wavenumber is exactly k_0) results in zero information about the $\boldsymbol{x}$-space position.

8.5.3 Gaussian

Consider a normalized Gaussian function,

$$F(x) = (4\,\pi\,\sigma)^{-1/2}\,\mathrm{e}^{-x^2/4\sigma} \quad \text{with} \quad \int_{-\infty}^{\infty} F(x)\,\mathrm{d}x = 1, \tag{8.116}$$

and where the mean and variance are

$$\langle x \rangle = \int_{-\infty}^{\infty} x\,F(x)\,\mathrm{d}x = 0 \quad \text{and} \quad \langle x^2 \rangle = \int_{-\infty}^{\infty} x^2\,F(x)\,\mathrm{d}x = 2\,\sigma. \tag{8.117}$$

Its Fourier transform is given by

$$\mathcal{F}(k) = (4\,\pi\,\sigma)^{-1/2} \int_{-\infty}^{\infty} \mathrm{e}^{-x^2/4\sigma}\,\mathrm{e}^{-\mathrm{i}\,k\,x}\,\mathrm{d}x = \mathrm{e}^{-\sigma\,k^2}, \tag{8.118}$$

with evaluation of this integral following from the calculus of residues.[14] We expect the Fourier transform to be real since $F(x)$ has even parity so that its Fourier sine transform vanishes (see Section 8.3.5). What is remarkable, however, is that the Fourier transform is also a Gaussian. This property is unique to the Gaussian and it is illustrated in Figure 8.3.

To compute the variance of the Fourier transform (in $\boldsymbol{k}$-space) requires us to first normalize it according to

$$(\sigma/\pi)^{1/2} \int_{-\infty}^{\infty} \mathrm{e}^{-\sigma\,k^2}\,\mathrm{d}k = 1, \tag{8.119}$$

[14] In Section 49.7.5 we discuss a few of the necessary steps for evaluating the integral (8.118), as part of our study of Gaussian wave packets.

so that its variance is

$$\langle k^2 \rangle = (\sigma/\pi)^{1/2} \int_{-\infty}^{\infty} k^2 \, \mathrm{e}^{-\sigma\, k^2} \, \mathrm{d}k = (2\,\sigma)^{-1}. \tag{8.120}$$

We thus find that the product of the variances is unity

$$\langle x^2 \rangle \langle k^2 \rangle = 1. \tag{8.121}$$

Hence, if the Gaussian is narrow in $\boldsymbol{x}$-space, as per a small value of σ, then it is broad in $\boldsymbol{k}$-space, and vice versa. This behavior offers another example of the complementarity property of Fourier transform pairs.

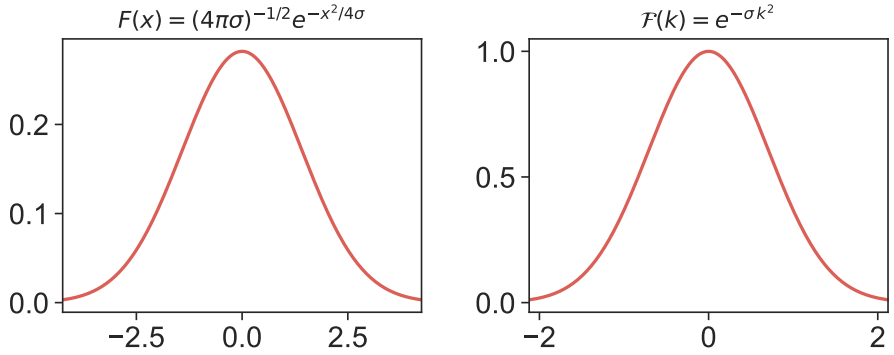

FIGURE 8.3: Left panel: the Gaussian function, $F(x) = (4\,\pi\,\sigma)^{-1/2}\,\mathrm{e}^{-x^2/4\sigma}$, which has a variance, $\langle x^2 \rangle = 2\,\sigma$, with the horizontal axes having a range $\pm 3\,\sqrt{\langle x^2 \rangle} = \pm 3\,(2\,\sigma)^{1/2}$. Right panel: the Fourier transform, $\mathcal{F}(k) = \mathrm{e}^{-\sigma\,k^2}$, which has a variance $\langle k^2 \rangle = (2\,\sigma)^{-1}$ and the horizontal axes range $\pm 3\,\sqrt{\langle k^2 \rangle} = \pm 3\,(2\,\sigma)^{-1/2}$. We set $\sigma = 1$ in arbitrary units.

8.6 Exercises

EXERCISE 8.1: BESSEL-PARSEVAL IDENTITY FOR TWO FUNCTIONS
Show all steps necessary to derive the generalized Bessel-Parseval identity (8.56)

EXERCISE 8.2: SOLVING AN ODE (PROBLEM 9.8 OF *Fetter and Walecka* (2003))
In this exercise we find a general expression for a forced ordinary differential equation using Fourier transform methods to determine the Green's function. We provide a detailed study of Green's functions in Chapter 9, though understanding of that material is not needed for this exercise.

(a) Use a Fourier transform to solve the one-dimensional ordinary differential equation

$$\frac{\mathrm{d}^2 H(x)}{\mathrm{d}x^2} - \lambda^2\, H(x) = -F(x), \tag{8.122}$$

for $\lambda > 0$ and assuming that $H(x)$ vanishes as $|x| \to \infty$. Express your answer in the form of a Green's function, $G(x, x')$, so that the solution can be written

$$H(x) = \int_{-\infty}^{\infty} G(x, x')\, F(x')\, \mathrm{d}x'. \tag{8.123}$$

(b) Find an explicit expression for the Green's function. Hint: you might wish to make use of an integral table.

(c) What are the physical dimensions of the Green's function, G? Relative to F, what are the dimensions of H?

(d) Discuss the limit $\lambda \to 0$.

Chapter 9

Green's functions

The mathematical problem of classical continuum mechanics concerns a field, $\psi(\boldsymbol{x}, t)$, that represents a physical property such as material tracer concentration, velocity streamfunction, temperature, Newtonian gravitational potential, or electrostatic potential. The space-time structure of the field is the result of a space-time distributed source (e.g., tracer source, potential vorticity distribution, mass distribution, or electric charge distribution) along with differential operators (e.g., time derivative, advection, Laplacian diffusion, wave operator) that connect the field across points in space-time, as well as initial and boundary conditions along selected space-time regions.[1]

For fluid mechanics, the differential equations describing the dynamical field, ψ, are generally nonlinear. However, in some notable cases it is possible to linearize the governing equations and learn much about the underlying mathematical and physical properties of the system. For example, the linear wave theory in Part X of this book renders great insights into the space-time structure of geophysical fluids. The advection-diffusion equation describing a passive tracer (Chapter 69) is also a linear partial differential equation, even when the dynamical flow field is determined by nonlinear field equations. Finally, the Poisson equation for pressure in a Boussinesq ocean (Section 29.3) is linear, under certain assumptions about the boundary conditions.

The conceptual foundation of the Green's function method is based on observing that if the field equations are linear, then ψ can be constructed by accumulating (i.e., convolving) contributions to the field induced by point-sized portions of the distributed source (including sources on the space-time boundaries). More precisely, we write $G(\boldsymbol{x}, t|\boldsymbol{x}_0, t)$ as the field at an observation space-time point, $(\boldsymbol{x}, t)$ (the *field point*), that is caused by a point source at $(\boldsymbol{x}_0, t_0)$ (the *source point*). We then observe that $\psi(\boldsymbol{x}, t)$ caused by a source that is distributed through space and time is the product of G multiplied by the source and integrated over the space-time domain. Similar superpositions are made for the initial and boundary conditions. The function, G, is referred to as the *Green's function* in honor of the 19th century mathematical physicist who introduced the method. As revealed in this chapter, even without an analytical expression for the Green's function (which are, in fact, only available under certain idealized cases), an appreciation of Green's function method deepens both physical and mathematical understanding of the various linear partial differential equations encountered in this book

The above arguments rely on the *superposition principle* that holds for linear systems. It does so by finding a particular solution (the Green's function) to a linear initial-boundary value problem with a singular point source (the *Dirac delta* from Chapter 7) and homogeneous boundary conditions. The solution to the original problem is found by integrating (convolving) the Green's function with the boundary conditions, initial conditions, and distributed sources. The Green's function is generally simpler to determine than the solution to the original initial-boundary value problem, thus providing the key practical reason to pursue the method. Furthermore,

[1] In some cases, sources are present only along spatial boundaries.

the Green's function provides a formal inverse to the linear partial differential operator in a manner reminiscent of matrix inversion used to solve a matrix-vector problem. Just as for the matrix-vector problem, once we have the Green's function we can write the solution to any of the associated initial-boundary value problems regardless the details of the distributed source, initial data, or boundary data. Herein lies the power of the Green's function method and why it has found much use across mathematical physics.

READER'S GUIDE TO THIS CHAPTER

We develop the *Green's function method* for a variety of linear initial-boundary value problems. Use of the common symbol, G, for the Green's function, and $\mathcal{G}$ for *free-space Green's function*, minimizes the adornments otherwise needed to distinguish Green's functions derived for each of the distinct equations. Confusion is avoided by noting that properties of any particular Green's function are specific to the section where the function is discussed. The modified Green's function, $\widetilde{G}$, is the one place we do provide extra adornment, with this function encountered in our study of the Poisson equation with Neumann boundary conditions. Furthermore, it is useful on certain occasions to write the gradient operator as either $\nabla_{\boldsymbol{x}}$ or $\nabla_{\boldsymbol{x}_0}$, depending on what argument of a Green's function is being differentiated (i.e., the field point or source point). This notation is particularly helpful in organizing manipulations in this chapter.

Much in this chapter is based on the treatments found in Chapter 7 of *Morse and Feshbach* (1953) as well as *Stakgold* (2000a,b). Both of these treatments are highly recommended for those wishing to pursue Green's function methods in more depth and to see further applications.

9.1 Loose threads

- Derive the 1d free space Green's function in Section 9.2.
- Include some applied math sorts of exercises that solve the diffusion equation and find the Green's function in idealized domains.
- Present the method of images for idealized domains

9.2 Free space Green's functions for elliptic operators

We study the Dirac delta in Chapter 7 by considering the Newtonian gravitational potential in the presence of a point mass source. This physical example also serves to introduce the notion of a Green's function, in this case a particularly simple Green's function known as a *free space Green's function* for Laplace's equation. The free space Green's function serves an important role in the analytical theory of Green's functions, and it offers a pedagogical introduction to

Green's functions satisfying boundary conditions. We here derive explicit expressions for the Laplace free space Green's function as well as that for the screened Poisson equation.

9.2.1 Gravitational potential from a point mass source

Consider the gravitational potential, Φ, in three space dimensions and in the presence of a point mass source at $\boldsymbol{x} = \boldsymbol{x}_0$ in the absence of boundaries (i.e., in *free space*), and with an assumed decay of the potential when moving away from the source. In the study of Green's functions this potential is referred to as the *fundamental solution* to Laplace's equation.[2] In other contexts it is referred to as the *free space Green's function*, which is the terminology we choose since it emphasizes the absence of any spatial boundaries. From our discussion of Newtonian gravity in Section 7.1, the free space Green's function for Newtonian gravity satisfies the Poisson equation with a singular mass source

$$\nabla^2_{\boldsymbol{x}} \Phi(\boldsymbol{x}|\boldsymbol{x}_0) = 4\pi G^{\text{grv}} M \delta(\boldsymbol{x} - \boldsymbol{x}_0), \tag{9.1}$$

where we wrote the singular mass density in terms of the Dirac delta

$$\rho(\boldsymbol{x}|\boldsymbol{x}_0) = M \delta(\boldsymbol{x} - \boldsymbol{x}_0). \tag{9.2}$$

We added the "grv" label to Newton's gravitational constant, G^{grv}, rather than use the more common nomenclature, G, in order to distinguish the gravitational constant from a Green's function.

The gravitational potential in equation (9.1) has two arguments, $\Phi(\boldsymbol{x}|\boldsymbol{x}_0)$. The first argument, $\boldsymbol{x}$, is the point where the field is sampled and is referred to as the *field point* or sometimes the *observation point*. The second argument, $\boldsymbol{x}_0$, is where the source is located and is thus referred to as the *source point*. Figure 9.1 summarizes the notation. The Laplacian operator acts on the field point, $\boldsymbol{x}$, so that it is useful to write it with an $\boldsymbol{x}$ subscript, $\nabla^2_{\boldsymbol{x}}$, for clarity. The dimensonal multiplier, $4\pi G^{\text{grv}} M$, acting on the Dirac delta in equation (9.1) is specific to the physical problem, here being for Newtonian gravity. In this case the Green's function has dimensions of $\text{L}^2\ \text{T}^{-2}$ since it is a gravitational potential. In other cases, the Green's function will have distinct dimensions, whereas the Dirac delta remains with the same dimensions.[3]

The gravitational potential for a point mass source, in the absence of any boundaries, is the free space Green's function for Newtonian gravity. Anticipating our study in Section 13.10.2, we write this free space Green's function in the form

$$\Phi(\boldsymbol{x}|\boldsymbol{x}_0) = -\frac{M G^{\text{grv}}}{|\boldsymbol{x} - \boldsymbol{x}_0|}. \tag{9.3}$$

This function is singular when sampling the field at the source location, $\boldsymbol{x} = \boldsymbol{x}_0$, and it decreases according to the inverse distance when moving away from the source.

9.2.2 Free space Green's function

Abstracting the previous discussion motivates us to define the free space Green's function, $\mathcal{G}(\boldsymbol{x}|\boldsymbol{x}_0)$, for the Laplace operator as the solution to the singular Poisson equation

$$-\nabla^2_{\boldsymbol{x}} \mathcal{G}(\boldsymbol{x}|\boldsymbol{x}_0) = \delta(\boldsymbol{x} - \boldsymbol{x}_0). \tag{9.4}$$

[2] For example, see Section 5.8 of *Stakgold* (2000b) where he provides a discussion of a variety of such free space or fundamental solutions.

[3] As emphasized throughout this book, checking for physical dimensional consistency offers a powerful means to ensure that a mathematical expression makes physical sense. If the equation is not dimensionally consistent, then something is wrong either with the maths or the physics.

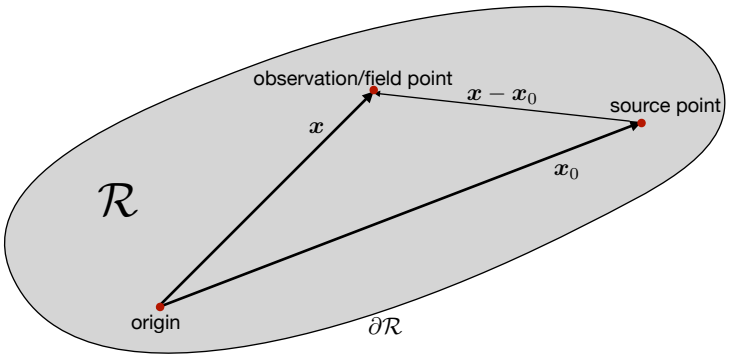

FIGURE 9.1: Depicting the geometry of a typical Green's function problem in space, shown here for a finite domain, $\mathcal{R}$, with boundary $\partial\mathcal{R}$. Note that the free-space Green's function has no prescribed boundary conditions, whereas other Green's functions typically do. The field observation point, $\boldsymbol{x}$, is where the Green's function is sampled, whereas the source point, $\boldsymbol{x}_0$, is where the Dirac delta source is located. The origin is at an arbitrary position within the domain. The Green's function, $G(\boldsymbol{x}|\boldsymbol{x}_0)$, is the response of the field as sampled at $\boldsymbol{x}$ arising from the Dirac delta placed at $\boldsymbol{x}_0$

It is conventional in many treatments to place a minus sign on the Laplacian operator to correspond to how it appears in the diffusion equation of Section 9.5. In one, two and three space dimensions the free space Green's function is given by

$$\mathcal{G}(x|x_0) = -|x - x_0|/2 \qquad \text{for } x, x_0 \in \mathbb{R}^1 \tag{9.5a}$$

$$\mathcal{G}(\boldsymbol{x}|\boldsymbol{x}_0) = -(2\,\pi)^{-1} \ln|\boldsymbol{x} - \boldsymbol{x}_0|, \quad \text{for } \boldsymbol{x}, \boldsymbol{x}_0 \in \mathbb{R}^2 \tag{9.5b}$$

$$\mathcal{G}(\boldsymbol{x}|\boldsymbol{x}_0) = (4\,\pi\,|\boldsymbol{x} - \boldsymbol{x}_0|)^{-1} \qquad \text{for } \boldsymbol{x}, \boldsymbol{x}_0 \in \mathbb{R}^3. \tag{9.5c}$$

When considering the Dirac delta as the mass density for a point mass, the corresponding gravitational acceleration is proportional to the gradient of the free space Green's function. From these expressions for the free space Green's functions, we see that for one space dimension, a point mass yields a gravity field that is a constant on either side of the mass point, with the acceleration pointing towards the mass. For two space dimensions, a point mass source produces a gravitational acceleration that points to the mass, and with a magnitude that falls off as the inverse distance from the source. Finally, for three space dimensions, the gravitational acceleration points towards the mass and falls off as the inverse squared distance.

We examine the three-dimensional Green's function in Section 9.2.3 and provide a derivation in Section 9.2.4. We then derive the two-dimensional Green's function (9.5b) in Section 9.2.5, and make use of it for studying flow around a point vortex in Section 38.2.8. Finally, we encounter the one-dimensional Green's function in Section 9.3.11 when studying the one-dimensional Poisson equation.

9.2.3 Properties of the three-dimensional Green's function

We here verify that the expression (9.5c) is indeed the free space Green's function for $\mathbb{R}^3$, with this discussion providing exposure to some of the formal manipulations encountered with Dirac deltas and Green's functions.

To simplify notation, place the Dirac delta at $\boldsymbol{x}_0 = 0$ so that

$$\mathcal{G}(\boldsymbol{x}|0) = \frac{1}{4\,\pi\,r}, \tag{9.6}$$

where $|\boldsymbol{x}| = r$ is the radial distance from the origin. Introduce the continuous and non-singular

function

$$G^{(\epsilon)}(\boldsymbol{x}) = \frac{1}{4\pi} \begin{cases} r^{-1} & \text{for } r > \epsilon \\ \epsilon^{-1} & \text{for } r \leq \epsilon, \end{cases} \tag{9.7}$$

with $\epsilon > 0$, in which case $G^{(\epsilon)}(\boldsymbol{x})$ has removed the singularity at $r = 0$. Now consider the integral

$$\mathcal{I}(\epsilon) = -\int_{r \leq \epsilon} \psi(\boldsymbol{x}) \, \nabla^2 G^{(\epsilon)}(\boldsymbol{x}) \, \mathrm{d}V, \tag{9.8}$$

for an arbitrary smooth function, ψ, and for a spherical region of radius $r = \epsilon$ centered on the origin. Since ψ is a smooth function, taking the limit as $\epsilon \to 0$ allows us to remove ψ from the integral and evaluate it at the origin

$$\lim_{\epsilon \to 0} \mathcal{I}(\epsilon) = -\psi(r = 0) \lim_{\epsilon \to 0} \left[\int_{r \leq \epsilon} \nabla^2 G^{(\epsilon)}(\boldsymbol{x}) \, \mathrm{d}V \right]. \tag{9.9}$$

Making use of the divergence theorem brings the volume integral to a surface integral over the ϵ-sphere

$$\lim_{\epsilon \to 0} \mathcal{I}(\epsilon) = -\psi(r = 0) \lim_{\epsilon \to 0} \left[\int_{r = \epsilon} \hat{\boldsymbol{r}} \cdot \nabla(1/r) \, r^2 \, \mathrm{d}r \right] = \psi(r = 0), \tag{9.10}$$

where we introduced spherical coordinates from Section 4.23. This result establishes both the sifting property and normalization property for $-\nabla^2 G^{(\epsilon)}(\boldsymbol{x})$. These two properties are the defining features of a Dirac delta, in which case we have established the identity

$$-\nabla^2 G^{(\epsilon)}(\boldsymbol{x}) = -\nabla^2 (4\,\pi\,|\boldsymbol{x}|)^{-1} = \delta(\boldsymbol{x}). \tag{9.11}$$

9.2.4 Deriving the three-dimensional Green's function

As a means to further understand the free space Green's function (9.5c), we here offer a derivation using Fourier transform methods. For that purpose, introduce the Fourier representation (8.113) of the Dirac delta so that[4]

$$-\nabla^2_{\boldsymbol{x}} \mathcal{G}(\boldsymbol{x}|\boldsymbol{x}_0) = \delta(\boldsymbol{x} - \boldsymbol{x}_0) = \frac{1}{(2\pi)^3} \int \mathrm{e}^{\mathrm{i}\,\boldsymbol{k}\cdot(\boldsymbol{x}-\boldsymbol{x}_0)} \, \mathrm{d}\boldsymbol{k}, \tag{9.12}$$

where $\mathrm{d}\boldsymbol{k}$ is the $\boldsymbol{k}$-space volume element. It is straightforward to verify that

$$\mathcal{G}(\boldsymbol{x}|\boldsymbol{x}_0) = \frac{1}{(2\pi)^3} \int \frac{\mathrm{e}^{\mathrm{i}\,\boldsymbol{k}\cdot(\boldsymbol{x}-\boldsymbol{x}_0)}}{|\boldsymbol{k}|^2} \, \mathrm{d}\boldsymbol{k} \tag{9.13}$$

solves the Green's function equation (9.12), thus providing a Fourier integral expression for the free space Green's function.

Now evaluate the integral (9.13) to derive a closed form expression by introducing spherical coordinates in $\boldsymbol{k}$-space, whereby[5]

$$k_x = |\boldsymbol{k}| \cos\phi \cos\lambda \quad \text{and} \quad k_y = |\boldsymbol{k}| \cos\phi \sin\lambda \quad \text{and} \quad k_z = |\boldsymbol{k}| \sin\phi. \tag{9.14}$$

We are free to orient the axes as suits the integration, with the following choice very convenient

$$\boldsymbol{k} \cdot (\boldsymbol{x} - \boldsymbol{x}_0) = |\boldsymbol{k}| \, |\boldsymbol{x} - \boldsymbol{x}_0| \sin\phi, \tag{9.15}$$

[4] This approach follows Section 28 of *Dennery and Krzywicki* (1967).
[5] See Section 4.23 for a discussion of spherical coordinates.

thus bringing the integral (9.13) to

$$\mathcal{G}(\boldsymbol{x}|\boldsymbol{x}_0) = \frac{1}{(2\pi)^3}\int_0^\infty \mathrm{d}|\boldsymbol{k}| \int_{-\pi/2}^{\pi/2} \cos\phi\,\mathrm{d}\phi \int_0^{2\pi} \mathrm{e}^{\mathrm{i}\,|\boldsymbol{k}|\,|\boldsymbol{x}-\boldsymbol{x}_0|\sin\phi}\,\mathrm{d}\lambda. \tag{9.16}$$

The λ integral trivially picks up a factor of 2π since the integrand is independent of λ. Performing the ϕ integral takes just a bit more work

$$\int_{-\pi/2}^{\pi/2} \mathrm{e}^{\mathrm{i}\,|\boldsymbol{k}|\,|\boldsymbol{x}-\boldsymbol{x}_0|\sin\phi}\,\cos\phi\,\mathrm{d}\phi = \int_{-\pi/2}^{\pi/2} \mathrm{e}^{\mathrm{i}\,|\boldsymbol{k}|\,|\boldsymbol{x}-\boldsymbol{x}_0|\sin\phi}\,\mathrm{d}(-\sin\phi) \tag{9.17a}$$

$$= -\int_{-1}^{1} \mathrm{e}^{\mathrm{i}\,|\boldsymbol{k}|\,|\boldsymbol{x}-\boldsymbol{x}_0|\alpha}\,\mathrm{d}\alpha \tag{9.17b}$$

$$= \frac{2\sin[|\boldsymbol{k}|\,|\boldsymbol{x}-\boldsymbol{x}_0|]}{|\boldsymbol{k}|\,|\boldsymbol{x}-\boldsymbol{x}_0|}, \tag{9.17c}$$

so that the Green's function is

$$\mathcal{G}(\boldsymbol{x}|\boldsymbol{x}_0) = \frac{4\pi}{(2\pi)^3}\int_0^\infty \frac{\sin[|\boldsymbol{k}|\,|\boldsymbol{x}-\boldsymbol{x}_0|]}{|\boldsymbol{k}|\,|\boldsymbol{x}-\boldsymbol{x}_0|}\,\mathrm{d}|\boldsymbol{k}| = \frac{4\pi}{(2\pi)^3\,|\boldsymbol{x}-\boldsymbol{x}_0|}\int_0^\infty \frac{\sin\alpha}{\alpha}\,\mathrm{d}\alpha. \tag{9.18}$$

The integral in equation (9.18) can be readily found in an integral table. Nonetheless, we use this integral as an opportunity to introduce a version of *Feynman's trick*, which for this integral proceeds by considering the *LaPlace transform*

$$F(s) = \int_0^\infty \mathrm{e}^{-s\,\alpha}\,\frac{\sin\alpha}{\alpha}\,\mathrm{d}\alpha, \tag{9.19}$$

where $s \geq 0$ is a parameter. The desired integral is $F(0)$, but we first determine $F(s)$ by taking its derivative

$$\frac{\mathrm{d}F(s)}{\mathrm{d}s} = -s\int_0^\infty \mathrm{e}^{-s\,\alpha}\,\sin\alpha\,\mathrm{d}\alpha. \tag{9.20}$$

Integrating by parts two times leads to

$$-\frac{\mathrm{d}F(s)}{\mathrm{d}s} = \frac{1}{1+s^2}, \tag{9.21}$$

which can be directly integrated to find

$$-F(s) = \tan^{-1}(s) + C. \tag{9.22}$$

To determine the constant of integration, C, take the limit $s \to \infty$, in which case $F(s)$ as given by equation (9.19) vanishes so that

$$C = -\lim_{s\to\infty} \tan^{-1}(s) = -\pi/2, \tag{9.23}$$

in which case

$$F(s) = -\tan^{-1}(s) + \pi/2 = \int_0^\infty \mathrm{e}^{-s\,\alpha}\,\frac{\sin\alpha}{\alpha}\,\mathrm{d}\alpha. \tag{9.24}$$

Setting $s = 0$ and noting that $\tan^{-1}(s=0) = 0$ leads to the desired integral

$$\int_0^\infty \mathrm{e}^{-s\,\alpha}\,\frac{\sin\alpha}{\alpha}\,\mathrm{d}\alpha = \pi/2, \tag{9.25}$$

and then to the free space Green's function (9.5c)

$$\mathcal{G}(\boldsymbol{x}|\boldsymbol{x}_0) = (4\,\pi\,|\boldsymbol{x} - \boldsymbol{x}_0|)^{-1}. \tag{9.26}$$

9.2.5 The two-dimensional Green's function

To simplify the derivation of the two-dimensional free space Green's function (9.5b), place the Dirac delta at the origin so that $\boldsymbol{x}_0 = 0$. Furthermore, the Dirac delta induces no angular asymmetry, so that it is convenient to use polar coordinates since the Green's function is independent of the polar angle. As detailed in Section 4.22, the two-dimensional Laplace operator acting on a circularly symmetric function leads to the Green's function equation

$$-\frac{1}{r}\frac{\mathrm{d}}{\mathrm{d}r}\left[r\,\frac{\mathrm{d}\mathcal{G}}{\mathrm{d}r}\right] = \frac{\delta(r)\,\delta(\vartheta)}{r}, \tag{9.27}$$

where we made use of equation (7.66) for the polar coordinate form of the Dirac delta. Integrating over the angle to remove $\delta(\vartheta)$ renders

$$-\frac{1}{r}\frac{\mathrm{d}}{\mathrm{d}r}\left[r\,\frac{\mathrm{d}\mathcal{G}}{\mathrm{d}r}\right] = -\frac{\delta(r)}{2\,\pi\,r}. \tag{9.28}$$

One radial integral that includes the origin yields

$$\frac{\mathrm{d}\mathcal{G}}{\mathrm{d}r} = -\frac{1}{2\,\pi\,r}, \tag{9.29}$$

with a second radial integral leading to

$$\mathcal{G}(r|0) - \mathcal{G}(r_0|0) = -(2\pi)^{-1}\ln(r/r_0), \tag{9.30}$$

where $r_0 \neq 0$ is an arbitrary reference radius. Without loss of generality we set $\mathcal{G}(r_0|0) = -(2\pi)^{-1}\ln r_0$ so that

$$\mathcal{G}(r|0) = -(2\pi)^{-1}\ln r, \tag{9.31}$$

whose more general expression is given by equation (9.5b).

9.2.6 Green's function for the screened Poisson equation

As a bit more practice with free space Green's functions, introduce an extension of the Coulomb potential of electrostatics by considering the following elliptic equation

$$(-\nabla^2 + \mu^2)\,\psi = \Lambda, \tag{9.32}$$

where $\mu^2 > 0$ is a constant with dimesion L^{-2}. As noted in Section 50 of *Fetter and Walecka* (2003), this equation occurs in the Yukawa theory of mesons and the Debye-Hückel screening of ionic solutions, hence the name *screened Poisson equation*. Although not of direct use for our studies of geophysical fluid mechanics, we see in Section 9.6.8 that there is a direct connection to the Helmholtz equation, which is important for geophysical wave theory.

Consider the screened Poisson equation (9.32) in the absence of boundaries, so that its corresponding free space Green's function satisfies

$$(\nabla^2 - \mu^2)\,\mathcal{G}(\boldsymbol{x}|\boldsymbol{x}_0) = -\delta(\boldsymbol{x} - \boldsymbol{x}_0). \tag{9.33}$$

Since there are no boundaries, we can make use of the Fourier transform method from Section

9.2.4 to derive the free space Green's function, which satisfies

$$(-\nabla^2 + \mu^2)\, \mathcal{G}(\boldsymbol{x}|\boldsymbol{x}_0) = \frac{1}{(2\pi)^3} \int \mathrm{e}^{\mathrm{i}\, \boldsymbol{k}\cdot(\boldsymbol{x}-\boldsymbol{x}_0)}\, \mathrm{d}\boldsymbol{k}, \tag{9.34}$$

and has the Fourier integral expression

$$\mathcal{G}(\boldsymbol{x}|\boldsymbol{x}_0) = \frac{1}{(2\pi)^3} \int \frac{\mathrm{e}^{\mathrm{i}\, \boldsymbol{k}\cdot(\boldsymbol{x}-\boldsymbol{x}_0)}\, \mathrm{d}\boldsymbol{k}}{|\boldsymbol{k}|^2 + \mu^2}. \tag{9.35}$$

Setting $\mu = 0$ recovers expression (9.13) for Laplace's free space Green's function. As for that case, we introduce spherical wavevector coordinates (9.14) and orient the axes according to $\boldsymbol{x} - \boldsymbol{x}_0$ so that equation (9.15) holds. We thus have integral

$$\mathcal{G}(\boldsymbol{x}|\boldsymbol{x}_0) = \frac{2\pi}{(2\pi)^3} \int_0^\infty \left[\int_{-\pi/2}^{\pi/2} \frac{\mathrm{e}^{\mathrm{i}\, |\boldsymbol{k}|\, |\boldsymbol{x}-\boldsymbol{x}_0| \sin\phi}}{|\boldsymbol{k}|^2 + \mu^2} \mathrm{d}(-\sin\phi) \right] \mathrm{d}|\boldsymbol{k}| \tag{9.36a}$$

$$= \frac{1}{2\pi^2\, |\boldsymbol{x} - \boldsymbol{x}_0|} \int_0^\infty \frac{|\boldsymbol{k}| \sin[|\boldsymbol{k}||\boldsymbol{x} - \boldsymbol{x}_0|]\, \mathrm{d}|\boldsymbol{k}|}{|\boldsymbol{k}|^2 + \mu^2} \tag{9.36b}$$

$$= \frac{\mathrm{e}^{-\mu\, |\boldsymbol{x}-\boldsymbol{x}_0|}}{4\pi\, |\boldsymbol{x} - \boldsymbol{x}_0|}, \tag{9.36c}$$

where the final equality made use of an integral table.[6] The Green's function (9.36c) for the screened Poisson equation earns its name since it exponentially decays when moving away from the origin at $\boldsymbol{x} = \boldsymbol{x}_0$, with this behavior contrasting to the much slower $1/|\boldsymbol{x} - \boldsymbol{x}_0|$ decay of the electrostatics Coulomb potential with $\mu = 0$.

9.3 Poisson equation with Dirichlet boundaries

In this section we develop the Green's function method for Poisson's equation with a *Dirichlet boundary condition*

$$-\nabla^2 \psi = \Lambda, \quad \text{for } \boldsymbol{x} \in \mathcal{R} \qquad \text{and} \qquad \psi = \sigma, \quad \text{for } \boldsymbol{x} \in \partial\mathcal{R}. \tag{9.37}$$

We focus on the three-dimensional case, though the results hold for one and two dimensions as well. The mathematical goal is to determine an integral expression for ψ in terms of the distributed source, $\Lambda(\boldsymbol{x})$, and boundary data, $\sigma(\boldsymbol{x})$.

9.3.1 Constraints on the source and boundary normal derivative

Assuming there exists a solution to the boundary value problem (9.37), we can derive a constraint on the normal derivative of ψ along the domain boundary.[7] This constraint is revealed by integrating the Poisson equation (9.37) over the spatial domain, with the left hand side yielding

$$-\int_{\mathcal{R}} \nabla^2 \psi \, \mathrm{d}V = -\oint_{\partial\mathcal{R}} \nabla\psi \cdot \hat{\boldsymbol{n}} \, \mathrm{d}\mathcal{S}, \tag{9.38}$$

where we made use of the divergence theorem and with $\partial\mathcal{R}$ the closed boundary of the domain, $\mathcal{R}$. Equating this result to the integral of the source, Λ, leads to the constraint

$$\oint_{\partial\mathcal{R}} \nabla\psi \cdot \hat{\boldsymbol{n}} \, \mathrm{d}\mathcal{S} = -\int_{\mathcal{R}} \Lambda \, \mathrm{d}V. \tag{9.39}$$

[6] See Section 50 of *Fetter and Walecka* (2003) for details of the calculation.

[7] To be self-contained, we here repeat discussion of the constraint (9.39) that is also provided in Section 6.5.6.

We can physically interpret the constraint (9.39) by invoking a steady state tracer diffusion interpretation of the Poisson equation, with $\nabla\psi \cdot \hat{\boldsymbol{n}}$ interpreted as a flux of ψ-stuff through the boundary. For a steady state solution to exist in the presence of specified boundary tracer concentration as well as with an interior source function, there must be a balance between the boundary integrated flux and the volume integrated source. In particular, this balance is required to maintain the specified Dirichlet boundary values in the presence an interior source. Absent this balance, there will be depletion or accumulation of ψ within the domain that leads to a transient adjustment, thus breaking the steady state assumption.[8] Notably, the constraint (9.39) can be realized for arbitrary Dirichlet boundary data, σ.

9.3.2 Uniqueness of the solution

To establish uniqueness of the solution to the boundary value problem (9.37), consider two functions, ψ_A and ψ_B, each satisfying the same boundary value problem (9.37). In turn, their difference, $\Psi = \psi_A - \psi_B$, is a harmonic function that satisfies a homogeneous Dirichlet boundary condition

$$-\nabla^2\Psi = 0, \quad \text{for } \boldsymbol{x} \in \mathcal{R} \qquad \text{and} \qquad \Psi = 0, \quad \text{for } \boldsymbol{x} \in \partial\mathcal{R}. \tag{9.40}$$

We offer a proof by contraction to establish that $\Psi = 0$ is the only solution to this boundary value problem. Namely, we assume $\Psi \neq 0$ and then show that to be an inconsistent assumption. First consider the case where Ψ is a constant. A constant is certainly a harmonic function, $\nabla^2\Psi = 0$. But only the zero constant, $\Psi = 0$, satisfies the homogeneous Dirichlet boundary condition. Next, assume Ψ has spatial dependence so that $\nabla\Psi \neq 0$ and examine the non-negative integral over the full domain

$$\mathcal{I} = \int_{\mathcal{R}} \nabla\Psi \cdot \nabla\Psi \, \mathrm{d}V. \tag{9.41}$$

Since $\nabla^2\Psi = 0$ we have $\nabla\Psi \cdot \nabla\Psi = \nabla \cdot (\Psi \, \nabla\Psi)$ so that

$$\mathcal{I} = \int_{\mathcal{R}} \nabla \cdot (\Psi \, \nabla\Psi) \, \mathrm{d}V = \oint_{\partial\mathcal{R}} \Psi \, \nabla\Psi \cdot \hat{\boldsymbol{n}} \, \mathrm{d}\mathcal{S}, \tag{9.42}$$

where we used the divergence theorem for the second equality. But since $\Psi = 0$ on $\partial\mathcal{R}$ we find that $\mathcal{I} = 0$. Since the integrand of $\mathcal{I}$ is non-negative, $\mathcal{I} = 0$ can only be realized by $\nabla\Psi = 0$ everywhere, which in turn means that Ψ is a constant. But we just saw that the only constant that satisfies the homogeneous Dirichlet boundary condition is $\Psi = 0$ everywhere. We thus conclude that $\Psi = 0$ is the only harmonic function with zero Dirichlet boundary conditions, in which case the solution, ψ, to the boundary value problem (9.37) is indeed unique.

9.3.3 The Green's function problem

The Green's function, $G(\boldsymbol{x}|\boldsymbol{x}_0)$, corresponding to the boundary value problem (9.37) is the solution to the Poisson equation with a Dirac delta source (rather than Λ) and a homogeneous Dirichlet boundary condition (rather than σ)

$$-\nabla^2_{\boldsymbol{x}} G(\boldsymbol{x}|\boldsymbol{x}_0) = \delta(\boldsymbol{x} - \boldsymbol{x}_0) \quad \text{for } \boldsymbol{x}, \boldsymbol{x}_0 \in \mathcal{R} \quad \text{and} \quad G(\boldsymbol{x}|\boldsymbol{x}_0) = 0 \quad \text{for } \boldsymbol{x} \in \partial\mathcal{R}. \tag{9.43}$$

In three space dimensions, the Dirac delta has dimensions of inverse volume (Section 7.3), so that the Green's function has dimensions of inverse length. By construction, the Green's function is harmonic everywhere except at the location of the Dirac delta source, $\boldsymbol{x} = \boldsymbol{x}_0$. Furthermore, the

[8] An analogous interpretation holds when ψ is the gravitational potential resulting from the mass source, Λ. For ψ to be a specified value along the domain boundary requires the volume integrated mass source to balance a gravitational acceleration integrated along the boundary.

Green's function satisfies a homogenous Dirichlet boundary condition whenever the field point, $\boldsymbol{x}$, is on the boundary and for any source position, $\boldsymbol{x}_0$.

Although the Green's function cares about the existence of spatial boundaries, it is independent of the boundary data, σ, and the distributed source, Λ, that appear in the boundary value problem (9.37) for ψ. In that manner, the Green's function is connected to the original boundary value problem only through the differential operator (here the Laplacian) and the type of boundary condition (here a Dirichlet condition).

9.3.4 Decomposing the Green's function

Linearity enables us to decompose the Green's function into the sum of the free space Green's function, $\mathcal{G}(\boldsymbol{x}|\boldsymbol{x}_0)$, plus a harmonic function

$$G(\boldsymbol{x}|\boldsymbol{x}_0) = \mathcal{G}(\boldsymbol{x}|\boldsymbol{x}_0) + H(\boldsymbol{x}|\boldsymbol{x}_0), \tag{9.44}$$

where the free space Green's function and harmonic function satisfy

$$-\nabla^2_{\boldsymbol{x}}\mathcal{G}(\boldsymbol{x}|\boldsymbol{x}_0) = \delta(\boldsymbol{x}-\boldsymbol{x}_0) \quad \text{for} \quad \boldsymbol{x},\boldsymbol{x}_0 \in \mathbb{R}^n \tag{9.45a}$$

$$-\nabla^2_{\boldsymbol{x}}H(\boldsymbol{x}|\boldsymbol{x}_0) = 0 \quad \text{for} \quad \boldsymbol{x},\boldsymbol{x}_0 \in \mathcal{R} \tag{9.45b}$$

$$-H(\boldsymbol{x}|\boldsymbol{x}_0) = \mathcal{G}(\boldsymbol{x}|\boldsymbol{x}_0) \quad \text{for} \quad \boldsymbol{x} \in \partial\mathcal{R}. \tag{9.45c}$$

Given the free space Green's function for the corresponding space dimension, n, from equations (9.5a), (9.5b), or (9.5c), then the mathematical problem of finding $G(\boldsymbol{x}|\boldsymbol{x}_0)$ reduces to finding the harmonic function, $H(\boldsymbol{x}|\boldsymbol{x}_0)$, satisfying the inhomogeneous Dirichlet boundary condition (9.45c). Hence, the decomposition (9.44) is quite useful in practice as it isolates the singular or non-smooth behavior from the Dirac delta within the known free space Green's function, whereas the harmonic function is smooth.

9.3.5 Jump condition induced by the Dirac source

Following the consistency condition established in Section 9.3.1, we integrate the Green's function partial differential equation (9.43) over a volume, $\mathcal{R}_0$, that encloses the Dirac delta source point at $\boldsymbol{x}_0 \in \mathcal{R}_0$. Doing so leads to

$$\int_{\mathcal{R}} \nabla_{\boldsymbol{x}} \cdot \nabla_{\boldsymbol{x}} G(\boldsymbol{x}|\boldsymbol{x}_0)\, \mathrm{d}V_0 = \oint_{\partial\mathcal{R}} \hat{\boldsymbol{n}} \cdot \nabla_{\boldsymbol{x}} G(\boldsymbol{x}|\boldsymbol{x}_0)\, \mathrm{d}\mathcal{S}_0 = -1, \tag{9.46}$$

where we used the divergence theorem for the first equality. This result means that for any domain enclosing the Dirac source point, the normal derivative of the Green's function must satisfy this integral jump condition across the region boundary. Decomposing the Green's function per equation (9.44) reveals that it is the free space Green's function that contributes to the jump

$$\int_{\mathcal{R}} \nabla_{\boldsymbol{x}} \cdot \nabla_{\boldsymbol{x}} \mathcal{G}(\boldsymbol{x}|\boldsymbol{x}_0)\, \mathrm{d}V_0 = \oint_{\partial\mathcal{R}} \hat{\boldsymbol{n}} \cdot \nabla_{\boldsymbol{x}} \mathcal{G}(\boldsymbol{x}|\boldsymbol{x}_0)\, \mathrm{d}\mathcal{S}_0 = -1, \tag{9.47}$$

whereas the harmonic contribution has no jump

$$\int_{\mathcal{R}} \nabla_{\boldsymbol{x}} \cdot \nabla_{\boldsymbol{x}} H(\boldsymbol{x}|\boldsymbol{x}_0)\, \mathrm{d}V_0 = \oint_{\partial\mathcal{R}} \hat{\boldsymbol{n}} \cdot \nabla_{\boldsymbol{x}} H(\boldsymbol{x}|\boldsymbol{x}_0)\, \mathrm{d}\mathcal{S}_0 = 0. \tag{9.48}$$

9.3.6 Reciprocity of the Green's function

The Green's function satisfies the following *reciprocity condition*

$$G(\boldsymbol{x}|\boldsymbol{x}_0) = G(\boldsymbol{x}_0|\boldsymbol{x}). \tag{9.49}$$

Reciprocity says that the Green's function at the field point, $\boldsymbol{x}$, arising from a Dirac delta source at the source point, $\boldsymbol{x}_0$ is identical to the Green's function at the field point, $\boldsymbol{x}_0$, arising from a Dirac delta source at point, $\boldsymbol{x}$. By inspection, the free space Green's functions (9.5a)-(9.5c) satisfy reciprocity. Hence, by implication the harmonic function, $H(\boldsymbol{x}|\boldsymbol{x}_0)$, also satisfies reciprocity. We here offer a direct derivation of reciprocity by using steps similar to those used for establishing the second form of Green's integral identity (2.92).

Proof of reciprocity

Consider two Green's functions, $G(\boldsymbol{x}|\boldsymbol{a})$ and $G(\boldsymbol{x}|\boldsymbol{b})$, arising from Dirac delta sources at points $\boldsymbol{a} \in \mathcal{R}$ and $\boldsymbol{b} \in \mathcal{R}$

$$-\nabla^2_{\boldsymbol{x}} G(\boldsymbol{x}|\boldsymbol{a}) = \delta(\boldsymbol{x}-\boldsymbol{a}) \quad \text{and} \quad -\nabla^2_{\boldsymbol{x}} G(\boldsymbol{x}|\boldsymbol{b}) = \delta(\boldsymbol{x}-\boldsymbol{b}). \tag{9.50}$$

Multiplying the first equation by $G(\boldsymbol{x},\boldsymbol{b})$ and the second by $G(\boldsymbol{x},\boldsymbol{a})$, then subtracting leads to

$$-G(\boldsymbol{x}|\boldsymbol{b})\,\nabla^2_{\boldsymbol{x}} G(\boldsymbol{x}|\boldsymbol{a}) + G(\boldsymbol{x}|\boldsymbol{a})\,\nabla^2_{\boldsymbol{x}} G(\boldsymbol{x}|\boldsymbol{b}) = G(\boldsymbol{x}|\boldsymbol{b})\,\delta(\boldsymbol{x}-\boldsymbol{a}) - G(\boldsymbol{x}|\boldsymbol{a})\,\delta(\boldsymbol{x}-\boldsymbol{b}). \tag{9.51}$$

Now integrate this equation over the region $\mathcal{R}$, with the right hand side rendering

$$\int_{\mathcal{R}} [G(\boldsymbol{x}|\boldsymbol{b})\,\delta(\boldsymbol{x}-\boldsymbol{a}) - G(\boldsymbol{x}|\boldsymbol{a})\,\delta(\boldsymbol{x}-\boldsymbol{b})]\,\mathrm{d}V = G(\boldsymbol{a},\boldsymbol{b}) - G(\boldsymbol{b},\boldsymbol{a}), \tag{9.52}$$

where we made use of the sifting property (7.8). Integrating the left hand side of equation (9.51) leads to

$$\int_{\mathcal{R}} [-G(\boldsymbol{x}|\boldsymbol{b})\,\nabla^2_{\boldsymbol{x}} G(\boldsymbol{x}|\boldsymbol{a}) + G(\boldsymbol{x}|\boldsymbol{a})\,\nabla^2_{\boldsymbol{x}} G(\boldsymbol{x}|\boldsymbol{b})]\,\mathrm{d}V \tag{9.53a}$$

$$= \int_{\mathcal{R}} [-\nabla_{\boldsymbol{x}} \cdot [G(\boldsymbol{x}|\boldsymbol{b})\,\nabla_{\boldsymbol{x}} G(\boldsymbol{x}|\boldsymbol{a})] + \nabla_{\boldsymbol{x}} \cdot [G(\boldsymbol{x}|\boldsymbol{a})\,\nabla_{\boldsymbol{x}} G(\boldsymbol{x}|\boldsymbol{b})]]\,\mathrm{d}V \tag{9.53b}$$

$$= \oint_{\partial\mathcal{R}} [-G(\boldsymbol{x}|\boldsymbol{b})\,\nabla_{\boldsymbol{x}} G(\boldsymbol{x}|\boldsymbol{a}) + G(\boldsymbol{x}|\boldsymbol{a})\,\nabla_{\boldsymbol{x}} G(\boldsymbol{x}|\boldsymbol{b})] \cdot \hat{\boldsymbol{n}}\,\mathrm{d}\mathcal{S}, \tag{9.53c}$$

where we made use of the divergence theorem for the second equality. The final result vanishes when making use of the homogeneous Dirichlet boundary condition (9.43). We are thus led to

$$G(\boldsymbol{a},\boldsymbol{b}) = G(\boldsymbol{b},\boldsymbol{a}), \tag{9.54}$$

which is the reciprocity condition (9.49).

Comments on self-adjoint operators

The reciprocity relation (9.49) for Green's functions holds for *self-adjoint* differential operators.[9] Self-adjointness reflects properties of both the differential operator and the boundary conditions, with the discussion in this section revealing that the Laplacian operator is self-adjoint with Dirichlet boundary conditions. Operators that are not self-adjoint, such as the diffusion operator

[9] See Theorem 8.10 of *Duchateau and Zachmann* (1986).

in Section 9.5, satisfy a slightly more general reciprocity relation that we consider in Section 9.5.7.

The absence of self-adjointness reflects some form of symmetry breaking either through the operator itself or through the boundary and/or initial conditions. The diffusion operator has a single time derivative, ∂_t, which breaks symmetry between past and future thus leading to the absence of self-adjointness. Furthermore, self-adjointness is a property that depends on the nature of the chosen inner product, with the inner product in the present discussion defined by integration over the domain $\mathcal{R}$. See *Stakgold* (2000a,b) for a thorough discussion accessible to physicists.

9.3.7 The integral solution

We have the elements in place to determine ψ as an integral expression involving $G(\boldsymbol{x}|\boldsymbol{x}_0)$ along with the prescribed source, Λ, and boundary data, σ. To do so we follow steps similar to those used to establish reciprocity. Recall the Poisson boundary value problem (9.37) for ψ and the associated Green's function problem (9.43),

$$-\nabla^2_{\boldsymbol{x}}\psi(\boldsymbol{x}) = \Lambda(\boldsymbol{x}) \tag{9.55a}$$

$$-\nabla^2_{\boldsymbol{x}}G(\boldsymbol{x}|\boldsymbol{x}_0) = \delta(\boldsymbol{x}-\boldsymbol{x}_0). \tag{9.55b}$$

Multiply the $\psi(\boldsymbol{x})$ equation by $G(\boldsymbol{x}|\boldsymbol{x}_0)$ and the $G(\boldsymbol{x}|\boldsymbol{x}_0)$ equation by $\psi(\boldsymbol{x})$ to find

$$-G(\boldsymbol{x}|\boldsymbol{x}_0)\,\nabla^2_{\boldsymbol{x}}\psi(\boldsymbol{x}) = G(\boldsymbol{x}|\boldsymbol{x}_0)\,\Lambda(\boldsymbol{x}) \tag{9.56a}$$

$$-\psi(\boldsymbol{x})\,\nabla^2_{\boldsymbol{x}}G(\boldsymbol{x}|\boldsymbol{x}_0) = \psi(\boldsymbol{x})\,\delta(\boldsymbol{x}-\boldsymbol{x}_0), \tag{9.56b}$$

and then subtract these two equations

$$-G(\boldsymbol{x}|\boldsymbol{x}_0)\,\nabla^2_{\boldsymbol{x}}\psi(\boldsymbol{x}) + \psi(\boldsymbol{x})\,\nabla^2_{\boldsymbol{x}}G(\boldsymbol{x}|\boldsymbol{x}_0) = G(\boldsymbol{x}|\boldsymbol{x}_0)\,\Lambda(\boldsymbol{x}) - \psi(\boldsymbol{x})\,\delta(\boldsymbol{x}-\boldsymbol{x}_0). \tag{9.57}$$

Now integrate over observational points, $\boldsymbol{x}$, sampled over the region $\mathcal{R}$, in which case the right hand side becomes

$$\int_{\mathcal{R}} [G(\boldsymbol{x}|\boldsymbol{x}_0)\,\Lambda(\boldsymbol{x}) - \psi(\boldsymbol{x})\,\delta(\boldsymbol{x}-\boldsymbol{x}_0)]\,\mathrm{d}V = -\psi(\boldsymbol{x}_0) + \int_{\mathcal{R}} G(\boldsymbol{x}|\boldsymbol{x}_0)\,\Lambda(\boldsymbol{x})\,\mathrm{d}V, \tag{9.58}$$

where we made use of the sifting property (7.8) to expose the function, ψ, at the location of the Dirac source, $\boldsymbol{x}_0$. Integrating the left hand side of equation (9.57) yields

$$\int_{\mathcal{R}} [-G(\boldsymbol{x}|\boldsymbol{x}_0)\,\nabla^2_{\boldsymbol{x}}\psi(\boldsymbol{x}) + \psi(\boldsymbol{x})\,\nabla^2_{\boldsymbol{x}}G(\boldsymbol{x}|\boldsymbol{x}_0)]\,\mathrm{d}V \tag{9.59a}$$

$$= \int_{\mathcal{R}} \nabla_{\boldsymbol{x}} \cdot [-G(\boldsymbol{x}|\boldsymbol{x}_0)\,\nabla_{\boldsymbol{x}}\psi(\boldsymbol{x}) + \psi(\boldsymbol{x})\,\nabla_{\boldsymbol{x}}G(\boldsymbol{x}|\boldsymbol{x}_0)]\,\mathrm{d}V \tag{9.59b}$$

$$= \oint_{\partial\mathcal{R}} [-G(\boldsymbol{x}|\boldsymbol{x}_0)\,\nabla_{\boldsymbol{x}}\psi(\boldsymbol{x}) + \psi(\boldsymbol{x})\,\nabla_{\boldsymbol{x}}G(\boldsymbol{x}|\boldsymbol{x}_0)] \cdot \hat{\boldsymbol{n}}_{\boldsymbol{x}}\,\mathrm{d}\mathcal{S}. \tag{9.59c}$$

Bringing the two sides to equation (9.57) together leads to

$$\psi(\boldsymbol{x}_0) = \int_{\mathcal{R}} \Lambda(\boldsymbol{x})\,G(\boldsymbol{x}|\boldsymbol{x}_0)\,\mathrm{d}V + \oint_{\partial\mathcal{R}} [G(\boldsymbol{x}|\boldsymbol{x}_0)\,\nabla_{\boldsymbol{x}}\psi(\boldsymbol{x}) - \psi(\boldsymbol{x})\,\nabla_{\boldsymbol{x}}G(\boldsymbol{x}|\boldsymbol{x}_0)] \cdot \hat{\boldsymbol{n}}_{\boldsymbol{x}}\,\mathrm{d}\mathcal{S}. \tag{9.60}$$

As a final step, we make use of the Dirichlet boundary conditions (homogeneous for the Green's function and prescribed function for ψ), relabel $\boldsymbol{x}_0 \leftrightarrow \boldsymbol{x}$, and make use of reciprocity,

$G(\boldsymbol{x}|\boldsymbol{x}_0) = G(\boldsymbol{x}_0|\boldsymbol{x})$, so that

$$\psi(\boldsymbol{x}) = \underbrace{\int_{\mathcal{R}} \Lambda(\boldsymbol{x}_0)\, G(\boldsymbol{x}|\boldsymbol{x}_0)\, \mathrm{d}V_0}_{\text{volume integral over } \mathcal{R}} - \underbrace{\oint_{\partial\mathcal{R}} [\sigma(\boldsymbol{x}_0)\, \nabla_{\boldsymbol{x}_0} G(\boldsymbol{x}|\boldsymbol{x}_0)] \cdot \hat{\boldsymbol{n}}_{\boldsymbol{x}_0}\, \mathrm{d}\mathcal{S}_0}_{\text{boundary area integral over } \partial\mathcal{R}}, \tag{9.61}$$

where we inserted the boundary data $\psi(\boldsymbol{x}) = \sigma(\boldsymbol{x})$ for $\boldsymbol{x} \in \partial\mathcal{R}$. We have thus established ψ as a volume integral of the Green's function with the source, Λ, plus a boundary integral of the Green's function with the boundary data. Note that the Green's function is independent of the source, Λ, and the boundary data, so that $G(\boldsymbol{x}|\boldsymbol{x}_0)$ can be used to express ψ for arbitrary source functions and boundary data.

9.3.8 Properties of the Dirichlet solution

We refer to the inward normal gradient of the Green's function as the *boundary Green's function*

$$G^{\mathrm{bd}}(\boldsymbol{x}|\boldsymbol{x}_0) \equiv -\hat{\boldsymbol{n}}_{\boldsymbol{x}_0} \cdot \nabla_{\boldsymbol{x}_0} G(\boldsymbol{x}|\boldsymbol{x}_0) = -\frac{\partial G(\boldsymbol{x}|\boldsymbol{x}_0)}{\partial \hat{n}_{\boldsymbol{x}_0}}, \tag{9.62}$$

in which case the Dirichlet solution (9.61) takes the form

$$\psi(\boldsymbol{x}) = \int_{\mathcal{R}} \Lambda(\boldsymbol{x}_0)\, G(\boldsymbol{x}|\boldsymbol{x}_0)\, \mathrm{d}V_0 + \oint_{\partial\mathcal{R}} \sigma(\boldsymbol{x}_0)\, G^{\mathrm{bd}}(\boldsymbol{x}|\boldsymbol{x}_0)\, \mathrm{d}\mathcal{S}_0. \tag{9.63}$$

This form for the solution, which is depicted in Figure 9.2, emphasizes the role of the Green's function in the region interior as the mediator between the distributed source, Λ, and all surrounding points $\boldsymbol{x} \in \mathcal{R}$, along with the boundary Green's function acting as mediator between information prescribed along the boundary, $\boldsymbol{x} \in \partial\mathcal{R}$, and interior points. In this subsection we summarize certain properties of the solution (9.61) and (9.63), and infer (through insisting on self-consistency) corresponding properties of the Green's function and boundary Green's function.

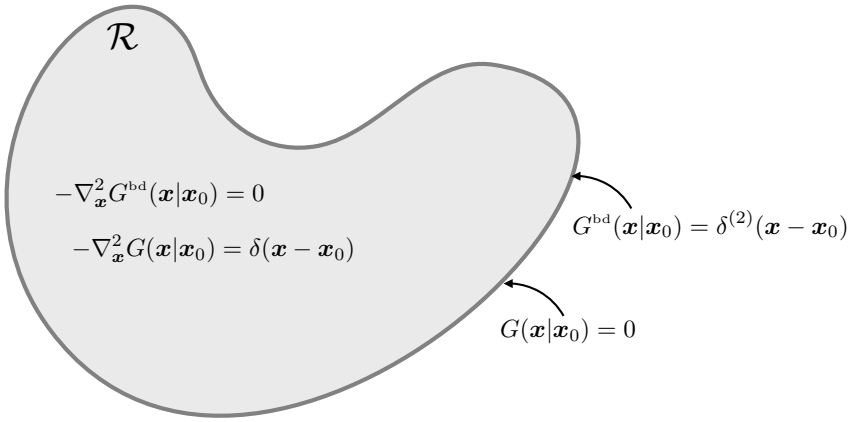

FIGURE 9.2: Decomposing the Green's function solution (9.61) for a Poisson boundary value problem with Dirichlet boundary conditions. The decomposition is written in terms of an interior Green's function, $G(\boldsymbol{x}|\boldsymbol{x}_0)$, that satisfies equation (9.43), and a boundary Green's function, $G^{\mathrm{bd}}(\boldsymbol{x}|\boldsymbol{x}_0)$, that satisfies equation (9.69). Note that we derive the properties for the boundary Green's function in Section 9.3.9.

Verifying the partial differential equation for $\boldsymbol{x} \in \mathcal{R}$

We derived the Dirichlet solution (9.61) with manipulations that are reversible; i.e., equal signs at every step. Hence, we know that the expression (9.61) indeed satisfies the Dirichlet boundary

value problem (9.37). Even so, the exercise of directly verifying the solution reveals insights into properties of the Green's function.

As a starting point, decompose the Green's function according to equation (9.44) to bring the solution (9.44) to the form

$$\psi(\boldsymbol{x}) = \int_{\mathcal{R}} \Lambda(\boldsymbol{x}_0)\,[\mathcal{G}(\boldsymbol{x}|\boldsymbol{x}_0) + H(\boldsymbol{x}|\boldsymbol{x}_0)]\,\mathrm{d}V_0 + \oint_{\partial\mathcal{R}} \sigma(\boldsymbol{x}_0)\,G^{\mathrm{bd}}(\boldsymbol{x}|\boldsymbol{x}_0)\,\mathrm{d}\mathcal{S}_0. \tag{9.64}$$

Now assume the field point, $\boldsymbol{x}$, is located at a point within the interior of the region, $\boldsymbol{x} \in \mathcal{R}$, and operate with $-\nabla^2_{\boldsymbol{x}}$ on equation (9.64) to find

$$-\nabla^2_{\boldsymbol{x}}\psi(\boldsymbol{x}) = -\int_{\mathcal{R}} \Lambda(\boldsymbol{x}_0)\,\nabla^2_{\boldsymbol{x}}[\mathcal{G}(\boldsymbol{x}|\boldsymbol{x}_0) + H(\boldsymbol{x}|\boldsymbol{x}_0]\,\mathrm{d}V_0 + \oint_{\partial\mathcal{R}} \sigma(\boldsymbol{x}_0)\,[-\nabla^2_{\boldsymbol{x}}G^{\mathrm{bd}}(\boldsymbol{x}|\boldsymbol{x}_0)]\,\mathrm{d}\mathcal{S}_0. \tag{9.65}$$

Note that we brought the Laplacian operator, $\nabla^2_{\boldsymbol{x}}$, inside the integral since the integral is over $\boldsymbol{x}_0$. For the first term on the right hand side of equation (9.45b), set $\nabla^2_{\boldsymbol{x}}H(\boldsymbol{x}|\boldsymbol{x}_0) = 0$ as per equation (9.45b), and use the free space Green's function identity $-\nabla^2_{\boldsymbol{x}}\mathcal{G}(\boldsymbol{x}|\boldsymbol{x}_0) = \delta(\boldsymbol{x} - \boldsymbol{x}_0)$. Then use the sifting property of the Dirac delta, $\int_{\mathcal{R}} \Lambda(\boldsymbol{x}_0)\,\delta(\boldsymbol{x} - \boldsymbol{x}_0)\,\mathrm{d}V_0 = \Lambda(\boldsymbol{x})$. To show that the boundary contribution vanishes, make use of the following

$$\begin{aligned}
\nabla^2_{\boldsymbol{x}}G^{\mathrm{bd}}(\boldsymbol{x}|\boldsymbol{x}_0) &= \nabla^2_{\boldsymbol{x}}[-\nabla_{\boldsymbol{x}_0}G(\boldsymbol{x}|\boldsymbol{x}_0)\cdot\hat{\boldsymbol{n}}_{\boldsymbol{x}_0}] && \text{(9.66a)}\\
&= \hat{\boldsymbol{n}}_{\boldsymbol{x}_0}\cdot\nabla_{\boldsymbol{x}_0}[-\nabla^2_{\boldsymbol{x}}G(\boldsymbol{x}|\boldsymbol{x}_0)] && \text{(9.66b)}\\
&= \hat{\boldsymbol{n}}_{\boldsymbol{x}_0}\cdot\nabla_{\boldsymbol{x}_0}\delta(\boldsymbol{x} - \boldsymbol{x}_0). && \text{(9.66c)}
\end{aligned}$$

With $\boldsymbol{x}_0 \in \partial\mathcal{R}$ yet $\boldsymbol{x} \notin \partial\mathcal{R}$, the Dirac delta never fires, thus eliminating the boundary contribution. We have thus verified that $-\nabla^2\psi = \Lambda$ for points $\boldsymbol{x} \in \mathcal{R}$.

Verifying the Dirichlet boundary condition for $\boldsymbol{x} \in \partial\mathcal{R}$

To verify that the boundary conditions are satisfied by the Dirichlet solution (9.61), bring the field point, $\boldsymbol{x}$, onto the boundary

$$\boldsymbol{x} \to \boldsymbol{x}_{\partial\mathcal{R}} \in \partial\mathcal{R}. \tag{9.67}$$

For such boundary points, the volume integral in the solution (9.61) vanishes since the Dirichlet Green's function vanishes on the boundary, $G(\boldsymbol{x}_{\partial\mathcal{R}}|\boldsymbol{x}_0) = 0$. Self-consistency with the Dirichlet boundary data, $\psi(\boldsymbol{x}_{\partial\mathcal{R}}) = \sigma(\boldsymbol{x}_{\partial\mathcal{R}})$, leads to the identity

$$\sigma(\boldsymbol{x}) = \oint_{\partial\mathcal{R}} \sigma(\boldsymbol{x}_0)\,G^{\mathrm{bd}}(\boldsymbol{x}|\boldsymbol{x}_0)\,\mathrm{d}\mathcal{S}_0 = -\oint_{\partial\mathcal{R}} \sigma(\boldsymbol{x}_0)\,\nabla_{\boldsymbol{x}_0}G(\boldsymbol{x}_{\partial\mathcal{R}}|\boldsymbol{x}_0)\cdot\hat{\boldsymbol{n}}_{\boldsymbol{x}_0}\,\mathrm{d}\mathcal{S}_0 \quad \text{for } \boldsymbol{x} \in \partial\mathcal{R}. \tag{9.68}$$

This integral equation is consistent so long as $G^{\mathrm{bd}}(\boldsymbol{x}|\boldsymbol{x}_0)$ satisfies the boundary condition

$$G^{\mathrm{bd}}(\boldsymbol{x}|\boldsymbol{x}_0) = -\hat{\boldsymbol{n}}_{\boldsymbol{x}_0}\cdot\nabla_{\boldsymbol{x}_0}G(\boldsymbol{x}|\boldsymbol{x}_0) = \delta^{(2)}(\boldsymbol{x} - \boldsymbol{x}_0) \quad \text{for } \boldsymbol{x}, \boldsymbol{x}_0 \in \partial\mathcal{R}, \tag{9.69}$$

where $\delta^{(2)}(\boldsymbol{x} - \boldsymbol{x}_0)$ is the surface Dirac delta with physical dimensions of inverse area. This property of the boundary Green's function is consistent with the jump condition (9.72) found for the one-dimensional Poisson equation. It furthermore leads to the corresponding integral identity

$$\oint_{\partial\mathcal{R}} G^{\mathrm{bd}}(\boldsymbol{x}|\boldsymbol{x}_0)\,\mathrm{d}\mathcal{S}_0 = \oint_{\partial\mathcal{R}} \delta^{(2)}(\boldsymbol{x} - \boldsymbol{x}_0)\,\mathrm{d}\mathcal{S}_0 = 1 \quad \text{for } \boldsymbol{x}, \boldsymbol{x}_0 \in \partial\mathcal{R}. \tag{9.70}$$

We emphasize[10] that the expressions (9.69) and (9.70) are found by first placing the source point, $\boldsymbol{x}_0$, on the boundary and thereafter moving the field point to the boundary, $\boldsymbol{x} \to \boldsymbol{x}_{\partial\mathcal{R}} \in \partial\mathcal{R}$.

[10] As per page 801 of *Morse and Feshbach* (1953).

We return to the normalization (9.70) in Section 9.3.9 when discussing the partial differential equation satisfied by the boundary Green's function.

Linear superposition

The Dirichlet solution (9.61) manifests the linear superposition principle by writing $\psi = \psi_1 + \psi_2$ as given by Table 9.1. By construction, ψ_1 satisfies Poisson's equation with homogeneous Dirichlet boundary conditions, whereas ψ_2 satisfies Laplace's equation with inhomogeneous Dirichlet boundary conditions.

PDE: $\boldsymbol{x} \in \mathcal{R}$	BC: $\boldsymbol{x} \in \partial\mathcal{R}$	SOLUTION $\psi = \psi_1 + \psi_2$
$-\nabla^2\psi_1 = \Lambda$	$\psi_1 = 0$	$\psi_1(\boldsymbol{x}) = \int_{\mathcal{R}} G(\boldsymbol{x}\vert\boldsymbol{x}_0)\,\Lambda(\boldsymbol{x}_0)\,\mathrm{d}V_0$
$-\nabla^2\psi_2 = 0$	$\psi_2 = \sigma$	$\psi_2(\boldsymbol{x}) = \oint_{\partial\mathcal{R}} G^{\mathrm{bd}}(\boldsymbol{x}\vert\boldsymbol{x}_0)\,\sigma(\boldsymbol{x}_0)\,\mathrm{d}\mathcal{S}_0$

TABLE 9.1: Decomposing the Dirichlet solution (9.61) into $\psi = \psi_1 + \psi_2$, with ψ_1 and ψ_2 satisfying the properties shown in this table. For the boundary contribution we made use of the boundary Green's function, $G^{\mathrm{bd}}(\boldsymbol{x}|\boldsymbol{x}_0) = -\nabla_{\boldsymbol{x}_0} G(\boldsymbol{x}|\boldsymbol{x}_0) \cdot \hat{\boldsymbol{n}}_{\boldsymbol{x}_0}$, as given by equation (9.62) and whose properties are further developed in Section 9.3.9.

9.3.9 Boundary Green's function

Boundary value problem for the boundary Green's function

As part of the development in Section 9.3.8, we revealed that the boundary Green's function satisfies the following boundary value problem

$$-\nabla^2_{\boldsymbol{x}} G^{\mathrm{bd}}(\boldsymbol{x}|\boldsymbol{x}_0) = 0 \quad \text{for } \boldsymbol{x} \in \mathcal{R} \quad \text{and} \quad G^{\mathrm{bd}}(\boldsymbol{x}|\boldsymbol{x}_0) = \delta^{(2)}(\boldsymbol{x} - \boldsymbol{x}_0) \quad \text{for} \quad \boldsymbol{x}, \boldsymbol{x}_0 \in \partial\mathcal{R}. \tag{9.71}$$

As seen by equation (9.43), the Dirichlet Green's function, $G(\boldsymbol{x}|\boldsymbol{x}_0)$, feels the Dirac source in the interior of the domain, $\boldsymbol{x} \in \mathcal{R}$, and satisfies homogeneous Dirichlet boundary conditions for $\boldsymbol{x} \in \partial\mathcal{R}$. As a complement, the boundary Green's function, $G^{\mathrm{bd}}(\boldsymbol{x}|\boldsymbol{x}_0)$, is harmonic everywhere in the domain interior and yet equals to the Dirac source along the boundary. By construction, the boundary Green's function incorporates boundary information into the region as part of the Dirichlet solution (9.63). We make further use of the boundary Green's function when studying the diffusion equation in Section 9.5 and the advection-diffusion equation in Section 69.9, in which case the boundary Green's function is referred to as the *boundary propagator*.

Normalization of the boundary Green's function

Consider the special case of constant boundary data, $\sigma = \sigma_{\mathrm{const}}$, in which case the harmonic function in Table 9.1 is itself a constant, $\psi_B(\boldsymbol{x}) = \sigma_{\mathrm{const}}$. Consequently, the boundary Green's function satisfies

$$-\oint_{\partial\mathcal{R}} \nabla_{\boldsymbol{x}_0} G(\boldsymbol{x}|\boldsymbol{x}_0) \cdot \hat{\boldsymbol{n}}_{\boldsymbol{x}_0}\,\mathrm{d}\mathcal{S}_0 = \oint_{\partial\mathcal{R}} G^{\mathrm{bd}}(\boldsymbol{x}|\boldsymbol{x}_0)\,\mathrm{d}\mathcal{S}_0 = 1. \tag{9.72}$$

This is the same normalization derived above in equation (9.70). It is built by placing Dirac delta sources along the boundary, $\boldsymbol{x}_0 \in \partial\mathcal{R}$, and then area integrating over the boundary area. It holds for any field point, $\boldsymbol{x} \in \mathcal{R}$. Although derived by considering the special case of constant boundary data, equation (9.72) holds in general since the Green's function is independent of the boundary data.

To help understand the identity (9.72), consider the Green's function to be the steady state temperature or tracer concentration resulting from a Dirac delta source placed within

the domain interior. The area integrated condition (9.72) acts to maintain the homogeneous Dirichlet boundary condition, $G(\boldsymbol{x}_{\partial\mathcal{R}}|\boldsymbol{x}_0) = 0$, for every point $\boldsymbol{x}_{\partial\mathcal{R}} \in \partial\mathcal{R}$. It does so by providing a boundary flux, via the normal gradient, whose area integral precisely cancels the unit positive source from the Dirac delta.

Equation (9.72) represents a normalization of the boundary Green's function at each point within the region interior, and it is consistent with the boundary condition given in equation (9.71). If we place Dirac delta sources along the boundary and integrate over the boundary, then every point within the domain feels a net unit source from these boundary sources, which is reflected by the normalization of the boundary Green's function. We return to this normalization when considering the boundary propagator for the diffusion equation in Section 9.5.13.

9.3.10 Mean value property for harmonic functions

Recall the discussion in Section 6.5.2 of the mean value property of harmonic functions. This property says that the value of a harmonic function, ψ, at a point $\boldsymbol{x}$ within an open region of $\mathcal{R}$ equals to the average of ψ taken over the surface of a sphere within $\mathcal{R}$ that is centered at $\boldsymbol{x}$. We here prove the mean value property through use of Green's function methods. For this purpose, specialize the Dirichlet solution (9.61) to the case of zero source, $\Lambda = 0$, so that the harmonic field is determined solely through the boundary Green's function and boundary data

$$\psi(\boldsymbol{x}) = -\oint_{\partial\mathcal{R}} \psi(\boldsymbol{x}_0)\, \nabla_{\boldsymbol{x}_0} G(\boldsymbol{x}|\boldsymbol{x}_0) \cdot \hat{\boldsymbol{n}}_{\boldsymbol{x}_0}\, \mathrm{d}\mathcal{S}_0. \tag{9.73}$$

Recall the discussion in Section (9.3.4) whereby the Green's function is decomposed into the sum of the free space Green's function plus a harmonic function that equals to minus the free space Green's function on the boundary. Furthermore, to simplify the algebra, without loss in generality, set the coordinate system so that the field point is at the origin, $\boldsymbol{x} = 0$, and let $\boldsymbol{y}$ be the source point, in which case

$$\psi(0) = -\oint_{\partial\mathcal{R}} \psi(\boldsymbol{y})\, \nabla_{\boldsymbol{y}} G(0|\boldsymbol{y}) \cdot \hat{\boldsymbol{n}}_{\boldsymbol{y}}\, \mathrm{d}\mathcal{S}_{\boldsymbol{y}}. \tag{9.74}$$

Two dimensions

Making use of the free space Green's function (9.5b) leads to the solution for two space dimensions

$$\psi(0) = \frac{1}{2\pi} \oint_{\partial\mathcal{R}} \psi(\boldsymbol{y})\, \nabla_{\boldsymbol{y}} \left[\ln|\boldsymbol{y}| - 2\,\pi\, H(0|\boldsymbol{y})\right] \cdot \hat{\boldsymbol{n}}_{\boldsymbol{y}}\, \mathrm{d}\ell \tag{9.75}$$

Now specialize the region, $\mathcal{R}$, to be a circle with center at $\boldsymbol{x} = 0$, radius R, and make use of polar coordinates so that $\mathrm{d}\ell = R\,\mathrm{d}\vartheta$ (Section 4.22). For this domain the free space Green's function is a constant on the circle's perimeter so that

$$\psi(0) = \frac{1}{2\,\pi} \int_0^{2\pi} \psi(R,\vartheta)\, \mathrm{d}\vartheta - \int_0^{2\pi} \partial_r H(0|R,\vartheta)\, \mathrm{d}\vartheta. \tag{9.76}$$

The harmonic function, H, satisfies

$$-\nabla_{\boldsymbol{y}}^2 H(0|\boldsymbol{y}) = 0 \quad \text{for } |\boldsymbol{y}| < R \quad \text{and} \quad H(0|\boldsymbol{y}) = (1/2\pi)\ln R \quad \text{for } |\boldsymbol{y}| = R. \tag{9.77}$$

The unique solution is given by the constant

$$H(0|\boldsymbol{y}) = (1/2\pi)\ln R, \tag{9.78}$$

which has a zero derivative so that equation (9.76) reduces to the mean value expression

$$\psi(0) = \frac{1}{2\,\pi} \int_0^{2\pi} \psi(R, \vartheta)\, \mathrm{d}\vartheta = \frac{\int_0^{2\pi} \psi(R, \vartheta)\, \mathrm{d}\vartheta}{\int_0^{2\pi} \mathrm{d}\vartheta}. \tag{9.79}$$

That is, the value of the harmonic function, ψ, at the center of a circle of arbitrary radius, R, equals to its average integrated over the circle's perimeter.

Three dimensions

The same arguments hold for three space dimensions, now making use of the free space Green's function (9.5c) and spherical coordinates (Section 4.23), in which case

$$\psi(0) = \frac{1}{4\,\pi} \int_0^{2\pi} \left[\int_{-\pi/2}^{\pi/2} \psi(R, \lambda, \phi)\, \mathrm{d}\lambda \right] \cos\phi\, \mathrm{d}\phi = \frac{\int_0^{2\pi} \left[\int_{-\pi/2}^{\pi/2} \psi(R, \lambda, \phi)\, \mathrm{d}\lambda \right] \cos\phi\, \mathrm{d}\phi}{\int_0^{2\pi} \left[\int_{-\pi/2}^{\pi/2} \mathrm{d}\lambda \right] \cos\phi\, \mathrm{d}\phi}. \tag{9.80}$$

9.3.11 1D Poisson equation with Dirichlet boundaries

To illustrate the Green's function method, we here work through the one-dimensional Poisson equation on a finite domain with Dirichlet boundary conditions

$$-\frac{\mathrm{d}^2\psi}{\mathrm{d}x^2} = \Lambda \qquad \text{for } -L < x < L \tag{9.81a}$$

$$\psi(x) = \sigma^{\pm} \qquad \text{for } x = \pm L, \tag{9.81b}$$

where $\Lambda(x)$ is an interior source and $\sigma^{\pm}$ is prescribed boundary data. The corresponding Green's function satisfies

$$-\frac{\mathrm{d}^2 G(x|x_0)}{\mathrm{d}x^2} = \delta(x - x_0) \qquad \text{for } -L < x < L \tag{9.82a}$$

$$G(x|x_0) = 0 \qquad \text{for } x = \pm L. \tag{9.82b}$$

Since the Dirac delta has dimensions of inverse length, equation (9.82a) implies that the Green's function has the dimensions of length. The Green's function solution (9.61) takes on the following form for one-dimension

$$\psi(x_0) = \int_{-L}^{L} G(x|x_0)\, \Lambda(x)\, \mathrm{d}x - \left[\psi(x)\, \frac{\mathrm{d}G(x|x_0)}{\mathrm{d}x} \right]_{x=L} + \left[\psi(x)\, \frac{\mathrm{d}G(x|x_0)}{\mathrm{d}x} \right]_{x=-L}. \tag{9.83}$$

Furthermore, by integrating the differential equation (9.81a) over the domain we are led to the identity

$$\left.\frac{\mathrm{d}\psi}{\mathrm{d}x}\right|_{x=L} - \left.\frac{\mathrm{d}\psi}{\mathrm{d}x}\right|_{x=-L} = -\int_{-L}^{L} \Lambda(x)\, \mathrm{d}x, \tag{9.84}$$

which is the one-dimensional version of the compatibility constraint (9.39). Likewise, the one-dimensional version of the Green's function jump condition (9.46) is given by

$$\lim_{\epsilon \to 0} \left[\frac{\mathrm{d}G(x|x_0)}{\mathrm{d}x} \right]_{x=x_0+\epsilon} - \lim_{\epsilon \to 0} \left[\frac{\mathrm{d}G(x|x_0)}{\mathrm{d}x} \right]_{x=x_0-\epsilon} = -1. \tag{9.85}$$

The solution to the Green's function equation (9.82a) is given by the linear function

$$G(x|x_0) = \begin{cases} (x - x_0)/2 + A\,x + B & \text{for } -L \le x \le x_0 \\ -(x - x_0)/2 + C\,x + D & \text{for } x_0 \le x \le L. \end{cases} \tag{9.86}$$

Note that we extracted the term $\mathcal{G}(x|x_0) = -|x - x_0|/2$, which is the free space Green's function (9.5a). Doing so is not necessary, yet it does help to reduce the algebra needed to determine the constants A, B, C, D, which are found by invoking the (i) jump condition for $\mathrm{d}G(x|x_0)/\mathrm{d}x$ at $x = x_0$, (ii) continuity of $G(x|x_0)$ at $x = x_0$, and (iii) homogeneous Dirichlet boundary conditions at $x = \pm L$.

The jump condition (9.85) leads to $A = C$ so that

$$G(x|x_0) = \begin{cases} (x - x_0)/2 + A\,x + B & \text{for } -L \le x \le x_0 \\ -(x - x_0)/2 + A\,x + D & \text{for } x_0 \le x \le L. \end{cases} \tag{9.87}$$

A finite jump in the Green's function derivative at $x = x_0$ means that the Green's function is continuous at $x = x_0$,

$$\lim_{\epsilon \to 0} G(x = x_0 + \epsilon|x_0) = \lim_{\epsilon \to 0} G(x = x_0 - \epsilon|x_0). \tag{9.88}$$

Making use of this condition in equation (9.87) yields $B = D$ so that

$$G(x|x_0) = \begin{cases} (x - x_0)/2 + A\,x + B & \text{for } -L \le x \le x_0 \\ -(x - x_0)/2 + A\,x + B & \text{for } x_0 \le x \le L. \end{cases} \tag{9.89}$$

The two remaining constants are determined by specifying the homogeneous Dirichlet boundary conditions, $G(x = \pm L|x_0) = 0$, in which we find $A = -x_0/(2\,L)$ and $B = L/2$, so that the Green's function is the linear kink function

$$G(x|x_0) = \frac{1}{2\,L} \begin{cases} (L - x_0)\,(L + x) & \text{for } -L \le x \le x_0 \\ (L + x_0)\,(L - x) & \text{for } x_0 \le x \le L, \end{cases} \tag{9.90}$$

which is depicted in Figure 9.3. Note the reciprocity condition is manifest in the expression (9.90). Also note that we can write the Green's function as the sum of the free space Green's function plus a harmonic function

$$G(x|x_0) = -|x - x_0|/2 + \frac{L^2 - x\,x_0}{2\,L} = \mathcal{G}(x|x_0) + H(x|x_0), \tag{9.91}$$

where

$$-\frac{\mathrm{d}^2 H(x|x_0)}{\mathrm{d}x^2} = 0 \quad \text{and} \quad H(x = \pm L|x_0) = -\mathcal{G}(x = \pm L|x_0). \tag{9.92}$$

9.4 Poisson equation with Neumann boundaries

Consider the Poisson equation with *Neumann boundary conditions*

$$-\nabla^2 \psi = \Lambda, \quad \text{for } \boldsymbol{x} \in \mathcal{R} \qquad \text{and} \qquad \hat{\boldsymbol{n}} \cdot \nabla \psi = \Sigma, \quad \text{for } \boldsymbol{x} \in \partial\mathcal{R}. \tag{9.93}$$

Rather than specifying the value of ψ along the boundary, the Neumann condition specifies the normal derivative. As we see, this slight change in the boundary conditions leads to some rather basic distinctions from the Dirichlet problem.

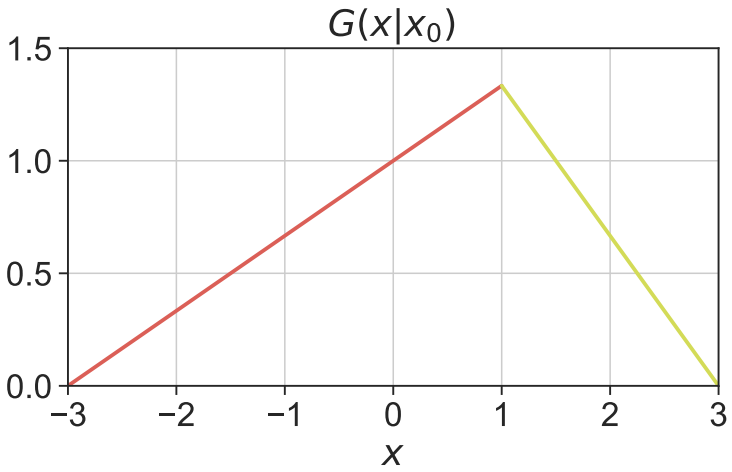

FIGURE 9.3: The Green's function (9.90) for the one-dimensional Poisson equation satisfying homogeneous Dirichlet boundary conditions at $x = \pm L$. The Dirac delta source is located at $x = x_0$, which is the point where the Green's function has its maximum displacement of $(L^2 - x_0^2)/(2\,L)$. The Green's function is continuous and yet its first derivative has a finite discontinuity at the location of the Dirac source. Its second derivative is minus the Dirac delta, as per the Green's function equation (9.82a). We here choose $x_0 = 1$ and $L = 3\,x_0$, with arbitrary units.

9.4.1 Constraints on the source and boundary data

As in our discussion of Dirichlet boundary conditions in Section 9.3.1, we can realize a solution to the boundary value problem (9.93) only so long as the constraint (9.39) is satisfied. For Neumann boundary conditions, we specify the normal derivative along the boundary so that the constraint (9.39) is now imposed on the volume source and boundary data[11]

$$\oint_{\partial\mathcal{R}} \Sigma \, \mathrm{d}\mathcal{S} = -\int_{\mathcal{R}} \Lambda \, \mathrm{d}V. \tag{9.94}$$

If the source and boundary data do not satisfy this constraint, then there is no solution to the Poisson problem (9.93). If the Poisson problem arises physically from steady state tracer diffusion, then the constraint (9.94) imposes a balance between the diffusive flux integrated around the boundary (left hand side) with the volume integrated tracer source (right hand side). In the absence of this balance, there is no solution to the Poisson problem thus indicating the presence of transients (e.g., time dependent diffusion). If the Poisson problem arises from Newtonian gravity, then the condition (9.94) means that the area integrated gravitational acceleration specified on the boundary must be consistent with the volume integrated mass source distributed within the domain.

9.4.2 Uniqueness of the solution up to a constant

As for the Dirichlet problem in Section 9.3.2, consider the uniqueness of the solution to the boundary value problem (9.93). We do so, again, by considering two functions, ψ_A and ψ_B, each satisfying the boundary value problem (9.93) and noting that their difference, $\Psi = \psi_A - \psi_B$, satisfies the homogeneous problem

$$-\nabla^2 \Psi = 0, \quad \text{for } \boldsymbol{x} \in \mathcal{R} \qquad \text{and} \qquad \hat{\boldsymbol{n}} \cdot \nabla \Psi = 0, \quad \text{for } \boldsymbol{x} \in \partial\mathcal{R}. \tag{9.95}$$

[11] To be self-contained, we here repeat the discussion of the constraint (9.94) that is also provided in Section 6.5.6.

The same arguments we used in Section 9.3.2 lead us to conclude that $\nabla\Psi = 0$, but for the Neumann problem this result is consistent with Ψ being an arbitrary spatial constant. We can understand this arbitrariness since the Neumann boundary condition involves a derivative, with the derivative of a constant vanishing. We thus conclude that the solution to the boundary value problem (9.93) is unique up to an arbitrary constant.

9.4.3 Modified Green's function problem

The standard Green's function corresponding to the Poisson boundary value problem (9.93) is the solution to the Poisson equation with a Dirac delta source and a homogeneous Neumann boundary condition

$$-\nabla^2_{\boldsymbol{x}} G(\boldsymbol{x}|\boldsymbol{x}_0) = \delta(\boldsymbol{x}-\boldsymbol{x}_0) \quad \text{for } \boldsymbol{x}, \boldsymbol{x}_0 \in \mathcal{R} \tag{9.96a}$$

$$\hat{\boldsymbol{n}} \cdot \nabla_{\boldsymbol{x}} G(\boldsymbol{x}|\boldsymbol{x}_0) = 0, \quad \text{for } \boldsymbol{x} \in \partial\mathcal{R}. \tag{9.96b}$$

However, there is no solution to the Green's function problem (9.96a)-(9.96b) since the self-consistency condition (9.94) is not satisfied. Namely, an integral over the Dirac delta source leads to unity, which is not consistent with use of the homogeneous Neumann boundary condition (9.96b).

We are led to consider the *modified Green's function* that satisfies[12]

$$-\nabla^2_{\boldsymbol{x}} \widetilde{G}(\boldsymbol{x}|\boldsymbol{x}_0) = \delta(\boldsymbol{x}-\boldsymbol{x}_0) - 1/\mathcal{V} \quad \text{for } \boldsymbol{x}, \boldsymbol{x}_0 \in \mathcal{R} \tag{9.97a}$$

$$\hat{\boldsymbol{n}} \cdot \nabla_{\boldsymbol{x}} \widetilde{G}(\boldsymbol{x}|\boldsymbol{x}_0) = 0, \quad \text{for } \boldsymbol{x} \in \partial\mathcal{R}. \tag{9.97b}$$

Introducing the region volume to the source in equation (9.97a)

$$\mathcal{V} = \int_{\mathcal{R}} \mathrm{d}V, \tag{9.98}$$

ensures that the self-consistency condition (9.94) is satisfied by $\widetilde{G}$

$$-\int_{\mathcal{R}} \nabla^2_{\boldsymbol{x}} \widetilde{G}(\boldsymbol{x}|\boldsymbol{x}_0)\,\mathrm{d}V_{\boldsymbol{x}} = -\oint_{\partial\mathcal{R}} \hat{\boldsymbol{n}}_{\boldsymbol{x}} \cdot \nabla_{\boldsymbol{x}} \widetilde{G}(\boldsymbol{x}|\boldsymbol{x}_0)\,\mathrm{d}V_{\boldsymbol{x}} = 0 \tag{9.99a}$$

$$\int_{\mathcal{R}} \delta(\boldsymbol{x}-\boldsymbol{x}_0)\,\mathrm{d}V - \frac{1}{\mathcal{V}}\int_{\mathcal{R}} \mathrm{d}V = 0. \tag{9.99b}$$

Making use of the method from Section 9.3.7, we readily derive an integral expression for the solution, ψ, in terms of the modified Green's function,

$$\psi(\boldsymbol{x}) - \langle\psi\rangle = \int_{\mathcal{R}} \Lambda(\boldsymbol{x}_0)\,\widetilde{G}(\boldsymbol{x}|\boldsymbol{x}_0)\,\mathrm{d}V_0 + \oint_{\partial\mathcal{R}} \Sigma(\boldsymbol{x}_0)\,\widetilde{G}(\boldsymbol{x}|\boldsymbol{x}_0)\,\mathrm{d}\mathcal{S}_0, \tag{9.100}$$

where $\Sigma = \hat{\boldsymbol{n}} \cdot \nabla\psi$ is the Neumann boundary data given in the problem statement (9.93), and we introduced the domain average

$$\langle\psi\rangle = \frac{1}{\mathcal{V}}\int_{\mathcal{R}} \psi\,\mathrm{d}V. \tag{9.101}$$

[12] See Exercise 6.46 of *Stakgold* (2000a) or exercise 8.10 of *Duchateau and Zachmann* (1986). *Hildebrand* (1976) in his Section 11.11 refers to the solution of equation (9.97a) (9.97b) as *Hilbert's function*. *Kellogg* (1953) on his page 246 refers to $G^{(1)}$ as the Green's function of the second kind. For simplicity in nomenclature we refer to $\widetilde{G}$ as the *modified Green's function*. Both *Hildebrand* (1976) and Section 1.10 of *Jackson* (1975) consider the complement modification of the Green's function, whereby the Neumann boundary condition is not homogeneous whereas the source remains a Dirac delta.

9.4.4 Reciprocity of the modified Green's function

The reciprocity condition (9.49) satisfied by the Dirichlet Green's function is a very useful property. What is required to respect this property for the modified Green's function? To answer that question, consider the Green's function problem (9.97a)-(9.97b) for two source points, $\boldsymbol{a} \in \mathcal{R}$ and $\boldsymbol{b} \in \mathcal{R}$

$$-\nabla^2_{\boldsymbol{x}} \widetilde{G}(\boldsymbol{x}|\boldsymbol{a}) = \delta(\boldsymbol{x}-\boldsymbol{a}) - 1/\mathcal{V} \quad \text{and} \quad \hat{\boldsymbol{n}} \cdot \nabla_{\boldsymbol{x}} \widetilde{G}(\boldsymbol{x}|\boldsymbol{a}) = 0 \tag{9.102a}$$

$$-\nabla^2_{\boldsymbol{x}} \widetilde{G}(\boldsymbol{x}|\boldsymbol{b}) = \delta(\boldsymbol{x}-\boldsymbol{b}) - 1/\mathcal{V} \quad \text{and} \quad \hat{\boldsymbol{n}} \cdot \nabla_{\boldsymbol{x}} \widetilde{G}(\boldsymbol{x}|\boldsymbol{b}) = 0. \tag{9.102b}$$

Multiplying equation (9.102a) by $\widetilde{G}(\boldsymbol{x}|\boldsymbol{b})$ and equation (9.102b) by $\widetilde{G}(\boldsymbol{x}|\boldsymbol{a})$, subtracting, then integrating over the domain, and using the homogeneous Neumann boundary conditions leads to

$$\widetilde{G}(\boldsymbol{x}|\boldsymbol{b}) - \widetilde{G}(\boldsymbol{x}|\boldsymbol{a}) = \frac{1}{\mathcal{V}} \int_{\mathcal{R}} [\widetilde{G}(\boldsymbol{x}|\boldsymbol{b}) - \widetilde{G}(\boldsymbol{x}|\boldsymbol{a})] \, \mathrm{d}V. \tag{9.103}$$

Reciprocity holds if the modified Green's function has a constant integral over the domain,

$$\int_{\mathcal{R}} \widetilde{G}(\boldsymbol{x}|\boldsymbol{x}_0) \, \mathrm{d}V = \text{constant}, \tag{9.104}$$

with zero a convenient constant that we use in the following. In words, we see that if the domain integral of the modified Green's function is the independent of where the Dirac delta is placed, then the modified Green's function satisfies the reciprocity condition

$$\int_{\mathcal{R}} \widetilde{G}(\boldsymbol{x}|\boldsymbol{x}_0) \, \mathrm{d}V = 0 \Longrightarrow \widetilde{G}(\boldsymbol{x}|\boldsymbol{x}_0) = \widetilde{G}(\boldsymbol{x}_0|\boldsymbol{x}). \tag{9.105}$$

9.4.5 Decomposing the modified Green's function

Motivated by the decomposition (9.44) for the Dirichlet Green's function, we linearly decompose the modified Green's function as the sum of the free space Green's function, $\mathcal{G}(\boldsymbol{x}|\boldsymbol{x}_0)$, plus another function

$$\widetilde{G}(\boldsymbol{x}|\boldsymbol{x}_0) = \mathcal{G}(\boldsymbol{x}|\boldsymbol{x}_0) + \widetilde{H}(\boldsymbol{x}|\boldsymbol{x}_0), \tag{9.106}$$

where

$$-\nabla^2_{\boldsymbol{x}} \widetilde{H}(\boldsymbol{x}|\boldsymbol{x}_0) = -1/\mathcal{V} \qquad \text{for} \quad \boldsymbol{x}, \boldsymbol{x}_0 \in \mathcal{R} \tag{9.107a}$$

$$-\hat{\boldsymbol{n}} \cdot \nabla_{\boldsymbol{x}} \widetilde{H}(\boldsymbol{x}|\boldsymbol{x}_0) = \hat{\boldsymbol{n}} \cdot \nabla_{\boldsymbol{x}} \mathcal{G}(\boldsymbol{x}|\boldsymbol{x}_0) \quad \text{for} \quad \boldsymbol{x} \in \partial\mathcal{R}. \tag{9.107b}$$

This decomposition is self-consistent since the free space Green's function satisfies the global boundary constraint

$$\oint_{\partial\mathcal{R}} \hat{\boldsymbol{n}} \cdot \nabla_{\boldsymbol{x}} \mathcal{G}(\boldsymbol{x}|\boldsymbol{x}_0) \, \mathrm{d}\mathcal{S}_{\boldsymbol{x}} = -1, \tag{9.108}$$

and likewise, equation (9.107a) means that

$$\oint_{\partial\mathcal{R}} \hat{\boldsymbol{n}} \cdot \nabla_{\boldsymbol{x}} \widetilde{H}(\boldsymbol{x}|\boldsymbol{x}_0) \, \mathrm{d}\mathcal{S}_{\boldsymbol{x}} = 1. \tag{9.109}$$

Hence, the local boundary condition (9.107b) is consistent with these two global boundary constraints.

9.4.6 Verifying the solution

It is a useful exercise to verify that the solution (9.100) indeed solves the Poisson boundary value problem with Neumann boundary conditions (equation (9.93)). First consider a point in the interior of the region, $\boldsymbol{x} \in \mathcal{R}$, and apply $-\nabla^2_{\boldsymbol{x}}$ on equation (9.100) to find

$$-\nabla^2_{\boldsymbol{x}}\psi(\boldsymbol{x}) = \int_{\mathcal{R}} \Lambda(\boldsymbol{x}_0)\,[-\nabla^2_{\boldsymbol{x}}\widetilde{G}(\boldsymbol{x}|\boldsymbol{x}_0)]\,\mathrm{d}V_0 + \oint_{\partial\mathcal{R}} \Sigma(\boldsymbol{x}_0)\,[-\nabla^2_{\boldsymbol{x}}\widetilde{G}(\boldsymbol{x}|\boldsymbol{x}_0)]\,\mathrm{d}\mathcal{S}_0 \tag{9.110a}$$

$$= \int_{\mathcal{R}} \Lambda(\boldsymbol{x}_0)\,[\delta(\boldsymbol{x}-\boldsymbol{x}_0) - 1/\mathcal{V}]\,\mathrm{d}V_0 + \oint_{\partial\mathcal{R}} \Sigma(\boldsymbol{x}_0)\,[\delta(\boldsymbol{x}-\boldsymbol{x}_0) - 1/\mathcal{V}]\,\mathrm{d}\mathcal{S}_0 \tag{9.110b}$$

$$= \Lambda(\boldsymbol{x}) - \frac{1}{\mathcal{V}}\left[\int_{\mathcal{R}} \Lambda(\boldsymbol{x}_0)\,\mathrm{d}V_0 + \oint_{\partial\mathcal{R}} \Sigma(\boldsymbol{x}_0)\,\mathrm{d}\mathcal{S}_0\right] + \oint_{\partial\mathcal{R}} \Sigma(\boldsymbol{x}_0)\,\delta(\boldsymbol{x}-\boldsymbol{x}_0)\,\mathrm{d}\mathcal{S}_0. \tag{9.110c}$$

For points in the interior, the boundary integral with the Dirac delta never fires since $\boldsymbol{x} \notin \partial\mathcal{R}$, so that $\oint_{\partial\mathcal{R}} \Sigma(\boldsymbol{x}_0)\,\delta(\boldsymbol{x}-\boldsymbol{x}_0)\,\mathrm{d}\mathcal{S}_0$ vanishes. Furthermore, the $1/\mathcal{V}$ term drops out due to the consistency condition (9.94). We have thus verified that $-\nabla^2\psi = \Lambda$ holds for points in the interior of the domain.

To verify that the boundary condition is met, act with the gradient, $\nabla_{\boldsymbol{x}}$, on the solution (9.100)

$$\nabla_{\boldsymbol{x}}\psi(\boldsymbol{x}) = \int_{\mathcal{R}} \Lambda(\boldsymbol{x}_0)\,[\nabla_{\boldsymbol{x}}\widetilde{G}(\boldsymbol{x}|\boldsymbol{x}_0)]\,\mathrm{d}V_0 + \oint_{\partial\mathcal{R}} \Sigma(\boldsymbol{x}_0)\,[\nabla_{\boldsymbol{x}}\widetilde{G}(\boldsymbol{x}|\boldsymbol{x}_0)]\,\mathrm{d}\mathcal{S}_0. \tag{9.111}$$

Now move the field point onto the boundary, $\boldsymbol{x} \to \boldsymbol{x}_{\boldsymbol{x}_{\partial\mathcal{R}}} \in \partial\mathcal{R}$, and project the gradient onto the unit normal direction, $\hat{\boldsymbol{n}}_{\boldsymbol{x}}$, at the point $\boldsymbol{x}_{\partial\mathcal{R}}$. This projection leads to $\hat{\boldsymbol{n}}_{\boldsymbol{x}} \cdot \nabla_{\boldsymbol{x}}\psi(\boldsymbol{x}_{\boldsymbol{x}_{\partial\mathcal{R}}}) = \Sigma(\boldsymbol{x}_{\boldsymbol{x}_{\partial\mathcal{R}}})$ on the left hand side, and it annihilates the volume term on the right hand side since $\hat{\boldsymbol{n}}_{\boldsymbol{x}} \cdot \nabla_{\boldsymbol{x}}\widetilde{G}(\boldsymbol{x}_{\boldsymbol{x}_{\partial\mathcal{R}}}|\boldsymbol{x}_0) = 0$. We are thus left with

$$\hat{\boldsymbol{n}}_{\boldsymbol{x}} \cdot \nabla_{\boldsymbol{x}}\psi(\boldsymbol{x}) = \Sigma(\boldsymbol{x}) = \oint_{\partial\mathcal{R}} \Sigma(\boldsymbol{x}_0)\,[\hat{\boldsymbol{n}}_{\boldsymbol{x}} \cdot \nabla_{\boldsymbol{x}}\widetilde{G}(\boldsymbol{x}|\boldsymbol{x}_0)]\,\mathrm{d}\mathcal{S}_0 \quad \text{for } \boldsymbol{x} \in \partial\mathcal{R}. \tag{9.112}$$

We emphasize that both arguments of the Green's function are on the boundary, $\boldsymbol{x}, \boldsymbol{x}_0 \in \partial\mathcal{R}$, with the Dirac source point, $\boldsymbol{x}_0$, integrated around the boundary whereas the field point, $\boldsymbol{x}$, is an arbitrary point on the boundary. Equation (9.68) is the analogous integral equation for the solution with Dirichlet boundary conditions. We are ensured a solution to the integral equation (9.112) if the Green's function satisfies the property

$$\hat{\boldsymbol{n}}_{\boldsymbol{x}} \cdot \nabla_{\boldsymbol{x}}\widetilde{G}(\boldsymbol{x}|\boldsymbol{x}_0) = \delta^{(2)}(\boldsymbol{x}-\boldsymbol{x}_0) \quad \text{for } \boldsymbol{x}, \boldsymbol{x}_0 \in \partial\mathcal{R}, \tag{9.113}$$

which takes on the integral expression

$$\oint_{\partial\mathcal{R}} \hat{\boldsymbol{n}}_{\boldsymbol{x}} \cdot \nabla_{\boldsymbol{x}}\widetilde{G}(\boldsymbol{x}|\boldsymbol{x}_0)\,\mathrm{d}\mathcal{S}_0 = \oint_{\partial\mathcal{R}} \delta^{(2)}(\boldsymbol{x}-\boldsymbol{x}_0)\,\mathrm{d}\mathcal{S}_0 \quad \text{for } \boldsymbol{x} \in \partial\mathcal{R}. \tag{9.114}$$

Table 9.2 compares the boundary properties of the Green's functions for the Dirichlet and Neumann problems.

9.4.7 Extracting a harmonic portion to the solution

The analysis in Section 9.4.6 reveals that we can write the Neumann solution (9.100) in the form

$$\psi(\boldsymbol{x}) - \langle\psi\rangle = \underbrace{\int_{\mathcal{R}} \Lambda(\boldsymbol{x}_0)\,\mathcal{G}(\boldsymbol{x}|\boldsymbol{x}_0)\,\mathrm{d}V_0}_{\psi^{\Lambda}} + \underbrace{\int_{\mathcal{R}} \Lambda(\boldsymbol{x}_0)\,\widetilde{H}(\boldsymbol{x}|\boldsymbol{x}_0)\,\mathrm{d}V_0 + \oint_{\partial\mathcal{R}} \Sigma(\boldsymbol{x}_0)\,\widetilde{G}(\boldsymbol{x}|\boldsymbol{x}_0)\,\mathrm{d}\mathcal{S}_0}_{\psi^{\text{harmonic}}}. \tag{9.115}$$

BOUNDARY CONDITION	GREEN'S FUNCTION PROPERTY	EQUATION
Dirichlet	$\hat{\boldsymbol{n}}_{\boldsymbol{x}_0} \cdot \nabla_{\boldsymbol{x}_0} G(\boldsymbol{x}\|\boldsymbol{x}_0) = -\delta^{(2)}(\boldsymbol{x} - \boldsymbol{x}_0)$	(9.69)
Neumann	$\hat{\boldsymbol{n}}_{\boldsymbol{x}} \cdot \nabla_{\boldsymbol{x}} G(\boldsymbol{x}\|\boldsymbol{x}_0) = \delta^{(2)}(\boldsymbol{x} - \boldsymbol{x}_0)$	(9.113)

TABLE 9.2: Comparing the boundary normal derivatives for the Poisson equation Green's function with Dirichlet and Neumann boundary conditions. Each point is on the boundary, $\boldsymbol{x}, \boldsymbol{x}_0 \in \partial\mathcal{R}$, and the Dirac delta is two-dimensional so it has dimensions of inverse area. The properties satisfied by these Green's functions are realized by first placing the source point, $\boldsymbol{x}_0$, on the boundary and then moving the field point to the boundary, $\boldsymbol{x} \to \boldsymbol{x}_{\partial\mathcal{R}} \in \partial\mathcal{R}$. For the Dirichlet condition, the normal derivative is computed at the source point, whereas the Neumann condition computes the normal derivative at the field point.

The function, ψ^Λ, is directly computable since both the source function, Λ, and free space Green's function, $\mathcal{G}(\boldsymbol{x}|\boldsymbol{x}_0)$, are known. The Neumann boundary value problem (9.93) has thus been reduced to finding the harmonic function, ψ^{harmonic}, which satisfies the Neumann boundary value problem

$$-\nabla^2 \psi^{\text{harmonic}}(\boldsymbol{x}) = 0 \qquad \text{for } \boldsymbol{x} \in \mathcal{R} \tag{9.116a}$$

$$\hat{\boldsymbol{n}} \cdot \nabla \psi^{\text{harmonic}}(\boldsymbol{x}) = \Sigma(\boldsymbol{x}) - \int_{\mathcal{R}} \Lambda(\boldsymbol{x}_0)\, \hat{\boldsymbol{n}}_{\boldsymbol{x}} \cdot \nabla_{\boldsymbol{x}} \mathcal{G}(\boldsymbol{x}|\boldsymbol{x}_0)\, \mathrm{d}V_0 \quad \text{for } \boldsymbol{x} \in \partial\mathcal{R}. \tag{9.116b}$$

We verify that the boundary value problem (9.116a)-(9.116b) is self-consistent by integrating the boundary condition (9.116b) around the domain boundary

$$\int_{\partial\mathcal{R}} \hat{\boldsymbol{n}} \cdot \nabla \psi^{\text{harmonic}}(\boldsymbol{x})\, \mathrm{d}\mathcal{S}_{\boldsymbol{x}} = \int_{\partial\mathcal{R}} \Sigma(\boldsymbol{x})\, \mathrm{d}\mathcal{S}_{\boldsymbol{x}} - \int_{\partial\mathcal{R}} \left[\int_{\mathcal{R}} \Lambda(\boldsymbol{x}_0)\, \hat{\boldsymbol{n}}_{\boldsymbol{x}} \cdot \nabla_{\boldsymbol{x}} \mathcal{G}(\boldsymbol{x}|\boldsymbol{x}_0)\, \mathrm{d}V_0 \right] \mathrm{d}\mathcal{S}_{\boldsymbol{x}}. \tag{9.117}$$

In the final term we can interchange the surface integral over $\boldsymbol{x}$ with the volume integral over $\boldsymbol{x}_0$ to have

$$\int_{\partial\mathcal{R}} \left[\int_{\mathcal{R}} \Lambda(\boldsymbol{x}_0)\, \hat{\boldsymbol{n}}_{\boldsymbol{x}} \cdot \nabla_{\boldsymbol{x}} \mathcal{G}(\boldsymbol{x}|\boldsymbol{x}_0)\, \mathrm{d}V_0 \right] \mathrm{d}\mathcal{S}_{\boldsymbol{x}} = \int_{\mathcal{R}} \Lambda(\boldsymbol{x}_0) \left[\int_{\partial\mathcal{R}} \hat{\boldsymbol{n}}_{\boldsymbol{x}} \cdot \nabla_{\boldsymbol{x}} \mathcal{G}(\boldsymbol{x}|\boldsymbol{x}_0)\, \mathrm{d}\mathcal{S}_{\boldsymbol{x}} \right] \mathrm{d}V_0 \tag{9.118a}$$

$$= -\int_{\mathcal{R}} \Lambda(\boldsymbol{x}_0)\, \mathrm{d}V_0, \tag{9.118b}$$

where the second equality made use of the identity (9.108) satisfied by the free space Green's function. Making use of the constraint (9.94) satisfied by the source and boundary data leads to

$$\int_{\partial\mathcal{R}} \hat{\boldsymbol{n}} \cdot \nabla \psi^{\text{harmonic}}(\boldsymbol{x})\, \mathrm{d}\mathcal{S}_{\boldsymbol{x}} = 0, \tag{9.119}$$

as required for a harmonic function.

9.4.8 The Dirac delta sheet and boundary data

The Dirichlet solution (9.61) has the Green's function in the volume integral but its normal gradient in the surface integral. In contrast, the Neumann solution (9.100) involves the Green's function, $\widetilde{G}$, within both the volume integral and the surface integral. For the Neumann problem we can thus consider a slightly modified formulation of how the boundary data is incorporated. To motivate this formulation, assume the only nontrivial Neumann boundary data appears along the flat plane surface, $z = z_{\text{b}}$, with all other boundaries maintaining the homogeneous boundary

condition, $\hat{\boldsymbol{n}} \cdot \nabla\psi = 0$. In this special case the Neumann solution (9.100) takes the form

$$\psi(\boldsymbol{x}) - \langle\psi\rangle = \int_{\mathcal{R}} \Lambda(\boldsymbol{x}_0)\, \widetilde{G}(\boldsymbol{x}|\boldsymbol{x}_0)\, \mathrm{d}V_0 + \int_{z=z_\mathrm{b}} \Sigma(x_0, y_0)\, \widetilde{G}(\boldsymbol{x}|\boldsymbol{x}_0)\, \mathrm{d}x_0\, \mathrm{d}y_0 \tag{9.120a}$$

$$= \int_{\mathcal{R}} [\Lambda(\boldsymbol{x}_0) + \Sigma(x_0, y_0)\, \delta(z_0 - z_\mathrm{b})]\, \widetilde{G}(\boldsymbol{x}|\boldsymbol{x}_0)\, \mathrm{d}V_0 \tag{9.120b}$$

$$\equiv \int_{\mathcal{R}} \Lambda^*(\boldsymbol{x}_0)\, \widetilde{G}(\boldsymbol{x}|\boldsymbol{x}_0)\, \mathrm{d}V_0. \tag{9.120c}$$

These manipulations have absorbed the non-homogeneous Neumann boundary condition into a modified source, $\Lambda^*(\boldsymbol{x})$. We are thus led to two equivalent formulations for the Poisson boundary value problem with Neumann conditions. The first is given by equation (9.93), whereby ψ is the solution to the Poisson equation with source, Λ, and with inhomogeneous Neumann boundary data, Σ. The second formulation considers ψ to be the solution to Poisson's equation with homogeneous Neumann boundary conditions yet with a modified source function

$$\Lambda^*(\boldsymbol{x}) = \Lambda(\boldsymbol{x}) + \Sigma(x, y)\, \delta(z - z_\mathrm{b}) = \Lambda(\boldsymbol{x}) + \partial_z\psi(\boldsymbol{x})\, \delta(z - z_\mathrm{b}). \tag{9.121}$$

As a check, note that the physical dimensionality of $\Lambda^*(\boldsymbol{x})$ is indeed correct since the Dirac delta, $\delta(z - z_\mathrm{b})$, has dimensions of inverse length. We interpret the term, $\Sigma(x, y)\, \delta(z - z_\mathrm{b})$, as a flux or *Dirac delta sheet* that sits just inside the boundary (at $z = z_\mathrm{b} - \epsilon$ with $\epsilon \to 0$), which allows this data to be incorporated into the volume source data rather than be part of the boundary data. The specific form (9.121) can be generalized to the expression

$$\Lambda^*(\boldsymbol{x}) = \Lambda(\boldsymbol{x}) + \Sigma(\boldsymbol{x})\, \delta[\hat{\boldsymbol{n}} \cdot (\boldsymbol{x} - \boldsymbol{x}_{\partial\mathcal{R}})] = \Lambda(\boldsymbol{x}) + \hat{\boldsymbol{n}} \cdot \nabla\psi(\boldsymbol{x})\, \delta[\hat{\boldsymbol{n}} \cdot (\boldsymbol{x} - \boldsymbol{x}_{\partial\mathcal{R}})], \tag{9.122}$$

where the argument to the Dirac delta picks out the coordinates in the direction of the outward unit normal. The transformed Neumann problem thus takes the generic form

$$-\nabla^2\psi = \Lambda^*, \quad \text{for } \boldsymbol{x} \in \mathcal{R} \qquad \text{and} \qquad \hat{\boldsymbol{n}} \cdot \nabla\psi = 0, \quad \text{for } \boldsymbol{x} \in \partial\mathcal{R}. \tag{9.123}$$

Again, the solution to the boundary value problem (9.123) is identical to the solution of the original problem (9.93).

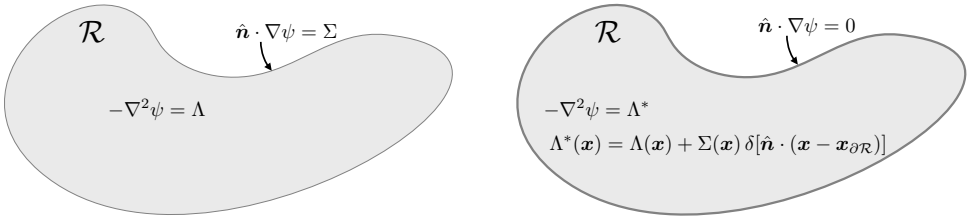

FIGURE 9.4: Use of Neumann boundary conditions for the Poisson boundary value problem allows for two equivalent formulations of the boundary condition. The first, shown in the left, considers the Poisson equation $-\nabla^2\psi = \Lambda$ in the interior, $\boldsymbol{x} \in \mathcal{R}$, along with boundary data along $\boldsymbol{x} \in \partial\mathcal{R}$, where $\hat{\boldsymbol{n}} \cdot \nabla\psi = \Sigma$. The second formulation, shown on the right, absorbs the boundary data into the interior source via a Dirac delta sheet that is placed infinitesimally close, on the inside, of the boundary. In this approach the Poisson equation has a modified source, $\Lambda^*(\boldsymbol{x}) = \Lambda(\boldsymbol{x}) + \Sigma(\boldsymbol{x})\, \delta[\hat{\boldsymbol{n}} \cdot (\boldsymbol{x} - \boldsymbol{x}_{\partial\mathcal{R}})]$, and the Neumann boundary condition becomes homogeneous, $\hat{\boldsymbol{n}} \cdot \nabla\psi = 0$. The delta sheet is here depicted by the slightly thicker line placed around the boundary.

Notably, the same data, Σ, is needed for both equations (9.123) and (9.93), so there is nothing fundamentally special or efficient about one formulation or the other. Rather, it is a matter of convenience. For example, the formulation using Λ^* has found some favor in the study of quasi-geostrophic potential vorticity (*Bretherton*, 1966), and we pursue this approach in Section 45.7. We also make use of a similar construct in Sections 72.6.3 and 73.4.3 for studies

of boundary buoyancy fluxes crossing the ocean surface.

9.4.9 One-dimensional Poisson equation with Neumann boundaries

To exemplify the results from this section, consider the one-dimensional Poisson equation with Neumann boundary conditions

$$-\frac{\mathrm{d}^2\psi}{\mathrm{d}x^2} = \Lambda \qquad \text{for } -L < x < L \tag{9.124a}$$

$$\frac{\mathrm{d}\psi}{\mathrm{d}x} = \Sigma^{\pm} \qquad \text{for } x = \pm L, \tag{9.124b}$$

with $\Sigma^{\pm}$ prescribed boundary data. The corresponding modified Green's function, $\widetilde{G}(x|x_0)$, satisfies the boundary value problem

$$-\frac{\mathrm{d}^2\widetilde{G}(x|x_0)}{\mathrm{d}x^2} = \delta(x-x_0) - \frac{1}{2\,L} \qquad \text{for } -L < x, x_0 < L, \tag{9.125a}$$

$$\frac{\mathrm{d}\widetilde{G}(x|x_0)}{\mathrm{d}x} = 0 \qquad \text{for } x = \pm L. \tag{9.125b}$$

Including the extra source term, $-1/(2L)$, in the differential equation (9.125a) compensates for the integral of the Dirac source, so that the integral of equation (9.125a)

$$-\left.\frac{\mathrm{d}\widetilde{G}}{\mathrm{d}x}\right|_{x=L} + \left.\frac{\mathrm{d}\widetilde{G}}{\mathrm{d}x}\right|_{x=-L} = 0, \tag{9.126}$$

is consistent with homogeneous Neumann boundary conditions satisfied by $\widetilde{G}$. The one-dimensional version of the solution (9.100) takes the form

$$\psi(x_0) - \langle\psi\rangle = \int_{-L}^{L} \widetilde{G}(x|x_0)\,\Lambda(x)\,\mathrm{d}x + \left[\widetilde{G}\,\frac{\mathrm{d}\psi}{\mathrm{d}x}\right]_{x=L} - \left[\widetilde{G}\,\frac{\mathrm{d}\psi}{\mathrm{d}x}\right]_{x=-L}, \tag{9.127}$$

where we introduced the domain average

$$\langle\psi\rangle = \frac{1}{2\,L}\int_{-L}^{L}\psi(x)\,\mathrm{d}x. \tag{9.128}$$

Exposing the free space Green's function, $-|x-x_0|/2$, as for the Dirichlet solution in Section 9.3.11, we have the quadratic expression for the Green's function

$$\widetilde{G}(x|x_0) = \begin{cases} (x-x_0)/2 + x^2/(4\,L) + A\,x + B & \text{for } -L \le x \le x_0 \\ -(x-x_0)/2 + x^2/(4\,L) + C\,x + D & \text{for } x_0 \le x \le L, \end{cases} \tag{9.129}$$

where A, B, C, D are constants. The quadratic term is the new piece relative to the Dirichlet expression in Section 9.3.11. Use of the homogeneous Neumann boundary conditions at $x = \pm L$ determines $A = 0$ and $C = 0$ so that the Green's function is

$$\widetilde{G}(x|x_0) = \begin{cases} (x-x_0)/2 + x^2/(4\,L) + B & \text{for } -L \le x \le x_0 \\ -(x-x_0)/2 + x^2/(4\,L) + D & \text{for } x_0 \le x \le L, \end{cases} \tag{9.130}$$

along with its first derivative

$$\frac{\mathrm{d}\widetilde{G}(x|x_0)}{\mathrm{d}x} = \begin{cases} 1/2 + x/(2\,L) & \text{for } -L \le x \le x_0 \\ -1/2 + x/(2\,L) & \text{for } x_0 \le x \le L. \end{cases} \tag{9.131}$$

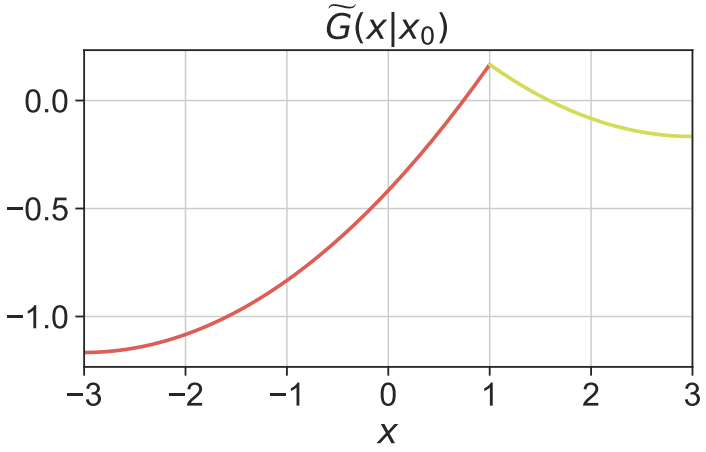

FIGURE 9.5: Depicting the Green's function, $\widetilde{G}(x|x_0)$, given by equation (9.134). This function has a kink at the source point, here chosen as $x = x_0 = 1$ and with $L = 3\,x_0$ (units are arbitrary). Notice that the Green's function has a zero derivative at $x = \pm L$, as required since it satisfies the homogeneous Neumann boundary conditions.

The jump condition at $x = x_0$ offers no new information, since the jump is already satisfied by exposing the free space Green's function. However, insisting that the Green's function be continuous at $x = x_0$ leads to $B = D$, thus yielding the Green's function

$$\widetilde{G}(x|x_0) = \begin{cases} (x - x_0)/2 + x^2/(4\,L) + B & \text{for } -L \leq x \leq x_0 \\ -(x - x_0)/2 + x^2/(4\,L) + B & \text{for } x_0 \leq x \leq L. \end{cases} \tag{9.132}$$

The final constant, B, can be specified by insisting on the reciprocity condition by constraining the global integral of $\widetilde{G}$ to be zero as per equation (9.105), which yields

$$B = (x_0^2/2 - L^2/3)/(2\,L), \tag{9.133}$$

and thus the Green's function

$$\widetilde{G}(x|x_0) = \frac{1}{4\,L} \begin{cases} x^2 + x_0^2 + 2\,L\,(x - x_0) & \text{for } -L \leq x \leq x_0 \\ x^2 + x_0^2 - 2\,L\,(x - x_0) & \text{for } x_0 \leq x \leq L, \end{cases} \tag{9.134}$$

with reciprocity manifest. We plot this Green's function in Figure 9.5, revealing a kink at the Dirac source location, $x = x_0$, and the quadratic behaviour when moving away from the source.

9.5 Green's functions for the diffusion equation

In this section we study the *diffusion equation*, also known as the *heat equation*. We first encountered the diffusion equation in Section 6.6, where it served as the canonical parabolic partial differential equation. It is more thoroughly explored in Chapter 69, with much of the current chapter a foundation for the Green's function treatment of the advection-diffusion tracer equation in Section 69.9. Correspondingly, we offer physical interpretations of the results in this section according to the tracer diffusion equation, where the tracer can be material (e.g., ocean salinity or atmospheric moisture) or thermodynamic (e.g., temperature or potential enthalpy). Time evolution presents a fundamentally new element to the diffusion equation relative to the Poisson equation encountered in Sections 9.2, 9.3, and 9.4.

9.5.1 Time independence of the spatial domain

Certain geophysical applications of interest in this book make use of spatial regions, $\mathcal{R}$, that have time dependent boundaries. The ocean free surface is the key example. Indeed, we consider time dependent boundaries when studying the tracer advection-diffusion equation in Section 69.9. However, the advent of a time dependent domain boundary adds some additional conceptual and technical details that are best confronted only after developing a Green's function brain muscle in the current chapter. For that reason, we assume $\mathcal{R}$ is static in this chapter.

9.5.2 Causal free space Green's function

Consider a Dirac delta source of tracer at the space-time point, $(\boldsymbol{x}_0, t_0)$, and assume a continuous media where there is no advection, such as found in a stagnant fluid or elastic solid. The simplest solution to the diffusion equation is known as the *causal free space Green's function*, $\mathcal{G}$, which is defined for $t \in (-\infty, \infty)$ and satisfies

$$(\partial_t - \kappa \nabla_{\boldsymbol{x}}^2)\, \mathcal{G}(\boldsymbol{x}, t|\boldsymbol{x}_0, t_0) = \delta(t - t_0)\, \delta(\boldsymbol{x} - \boldsymbol{x}_0) \qquad \boldsymbol{x} \in \mathbb{R}^n \tag{9.135a}$$

$$\mathcal{G}(\boldsymbol{x}, t|\boldsymbol{x}_0, t_0) \to 0 \qquad |\boldsymbol{x} - \boldsymbol{x}_0| \to \infty \tag{9.135b}$$

$$\mathcal{G}(\boldsymbol{x}, t|\boldsymbol{x}_0, t_0) = 0 \qquad t < t_0, \tag{9.135c}$$

where $\mathbb{R}^n$ is Euclidean space with $n = 1, 2, 3$ considered here, and where $\kappa > 0$ is a constant kinematic diffusivity (dimensions $\mathrm{L}^2\ \mathrm{T}^{-1}$). Equation (9.135b) ensures that the free space Green's function decays as the field point gets further away from the source point. The *causality condition* (9.135c) means that the Green's function vanishes throughout all of space for times prior to the time, t_0, at which the Dirac source occurs. Given the dimensions of the Dirac source, we see that the Green's function has dimensions of L^{-n}.

The causal free-space Green's function is given by[13]

$$\mathcal{G}(\boldsymbol{x}, t|\boldsymbol{x}_0, t_0) = \frac{\mathcal{H}(t - t_0)}{[4\,\pi\,\kappa\,(t - t_0)]^{n/2}} \mathrm{e}^{-(\boldsymbol{x} - \boldsymbol{x}_0)^2/[4\,\kappa\,(t - t_0)]}, \tag{9.136}$$

where the Heaviside step function, $\mathcal{H}$ (equation (7.19)), enforces causality. The amplitude of the Green's function exponentially decays when moving away from the source location, thus satisfying the condition (9.135b). Additionally, as time progresses beyond the source time, the Green's function decays according to the pre-factor, $(t - t_0)^{-n/2}$. As seen by equation (7.14b), as time approaches the Dirac delta time, $t \downarrow t_0$, the Green's function becomes a Dirac delta in space[14]

$$\lim_{t \downarrow t_0} \mathcal{G}(\boldsymbol{x}, t|\boldsymbol{x}_0, t_0) = \delta(\boldsymbol{x} - \boldsymbol{x}_0). \tag{9.137}$$

9.5.3 Causal Green's function

We next introduce the *causal Green's function* for the diffusion equation. This Green's function is defined for $t \in (-\infty, \infty)$ and satisfies the following equations when assuming Neumann boundary conditions

$$\frac{\partial[G(\boldsymbol{x}, t|\boldsymbol{x}_0, t_0)]}{\partial t} - \nabla_{\boldsymbol{x}} \cdot [\mathbb{K} \cdot \nabla_{\boldsymbol{x}} G(\boldsymbol{x}, t|\boldsymbol{x}_0, t_0)] = \delta(t - t_0)\, \delta(\boldsymbol{x} - \boldsymbol{x}_0) \qquad \boldsymbol{x} \in \mathcal{R} \tag{9.138a}$$

$$\hat{\boldsymbol{n}} \cdot \mathbb{K} \cdot \nabla_{\boldsymbol{x}} G(\boldsymbol{x}, t|\boldsymbol{x}_0, t_0) = 0 \qquad \boldsymbol{x} \in \partial\mathcal{R}, \boldsymbol{x}_0 \notin \partial\mathcal{R} \tag{9.138b}$$

$$G(\boldsymbol{x}, t|\boldsymbol{x}_0, t_0) = 0 \qquad t < t_0. \tag{9.138c}$$

[13] See Section 5.8 of *Stakgold* (2000b) for a derivation of the free space solution (9.136).
[14] See also exercise 5.3 in *Stakgold* (2000b) for the one-dimensional case.

The Neumann boundary condition is relevant when one knows the boundary flux of heat or tracer concentration. Note that the nicety regarding the placement of the field and source points for the boundary conditions. Namely, the homogeneous Neumann boundary condition (9.138b) holds when the field point, $\boldsymbol{x}$, is on the boundary and yet the source point, $\boldsymbol{x}_0$, is not on the boundary. We later extend the boundary condition (see equation (9.181)) to allow both $\boldsymbol{x}, \boldsymbol{x}_0 \in \partial\mathcal{R}$.

Dirichlet boundary conditions are used when knowing the boundary values for the field, in which case the corresponding causal Green's function satisfies

$$\frac{\partial[G(\boldsymbol{x}, t|\boldsymbol{x}_0, t_0)]}{\partial t} - \nabla_{\boldsymbol{x}} \cdot [\mathbb{K} \cdot \nabla_{\boldsymbol{x}} G(\boldsymbol{x}, t|\boldsymbol{x}_0, t_0)] = \delta(t - t_0)\, \delta(\boldsymbol{x} - \boldsymbol{x}_0) \qquad \boldsymbol{x} \in \mathcal{R} \tag{9.139a}$$

$$G(\boldsymbol{x}, t|\boldsymbol{x}_0, t_0) = 0 \qquad \boldsymbol{x} \in \partial\mathcal{R} \tag{9.139b}$$

$$G(\boldsymbol{x}, t|\boldsymbol{x}_0, t_0) = 0 \qquad t < t_0. \tag{9.139c}$$

The Dirichlet condition is particularly relevant for passive tracers in the atmosphere and ocean, such as those studied in Section 69.9. In both the Neumann and Dirichlet cases, we generalized the free space solution from Section 9.5.2 by introducing a space-time dependent diffusivity tensor, $\mathbb{K}(\boldsymbol{x}, t)$, which is a symmetric second order tensor with dimensions $\mathrm{L}^2\ \mathrm{T}^{-1}$ (we study diffusion tensors in Chapter 69 and 71). The Green's function has dimensions of inverse volume, L^{-3}, which is implied since the Dirac delta source has dimensions of inverse volume times inverse time, $\mathrm{L}^{-3}\ \mathrm{T}^{-1}$.

In the presence of boundaries, the spatial position of the Dirac delta source impacts the value of the causal Green's function. In contrast, the causality condition (9.138c) means that the Green's function is dependent only on the time since the introduction of the source, $t - t_0$. Hence, there is no added generality afforded by setting the source time, t_0, to be distinct from $t_0 = 0$. Even so, we retain t_0 to maintain symmetry with the spatial location $\boldsymbol{x}_0$. Doing so also helps to distinguish the Dirac source time, t_0, from the initial time, t_{init}, with the intitial time introduced in Section 9.5.9.

Finally, notice that the causality conditions (9.138c) and (9.139c) strictly hold for $t < t_0$. As seen in equation (9.178), when the source time is evaluated at $t_0 = t_{\text{init}}$, then the limit as the field time goes to the initial time, $t \downarrow t_{\text{init}}$, results in a spatial Dirac delta $\delta(\boldsymbol{x} - \boldsymbol{x}_0)$. That is, the Green's function is initialized by a Dirac delta source at $\boldsymbol{x} = \boldsymbol{x}_0$.

9.5.4 An integral consistency condition

It is notable that there is a Green's function for the diffusion equation in the presence of homogeneous Neumann conditions, whereas there is no Green's function for the Poisson equation with Neumann boundaries (Section 9.4.3). Time dependence in the diffusion equation is the key distinction.

To determine a self-consistency condition for the Green's function partial differential equation (9.138a), integrate it over the static spatial domain, $\mathcal{R}$, and make use of the divergence theorem to find

$$\frac{\mathrm{d}}{\mathrm{d}t} \int_{\mathcal{R}} G(\boldsymbol{x}, t|\boldsymbol{x}_0, t_0)\, \mathrm{d}V_{\boldsymbol{x}} = \delta(t - t_0) + \oint_{\partial\mathcal{R}} \hat{\boldsymbol{n}} \cdot \mathbb{K}(\boldsymbol{x}) \cdot \nabla_{\boldsymbol{x}} G(\boldsymbol{x}, t|\boldsymbol{x}_0, t_0)\, \mathrm{d}\mathcal{S}_{\boldsymbol{x}}. \tag{9.140}$$

The boundary integral term on the right hand side vanishes for the homogeneous Neumann boundary conditions (9.138b), in which the domain integrated Green's function evolves only as a result of the Dirac delta source firing at $t = t_0$. For the case of homogeneous Dirichlet boundary conditions (9.139b), the domain integrated Green's function evolves both from the Dirac source and from the generally nonzero fluxes crossing the domain boundaries.

Now integrate equation (9.140) over a time intervel, $t_0 - \epsilon \leq t \leq t_0 + \epsilon$, thus resulting in

$$\int_{\mathcal{R}} G(\boldsymbol{x}, t = t_0 + \epsilon | \boldsymbol{x}_0, t_0) \, \mathrm{d}V_{\boldsymbol{x}} = 1 + \int_{t_0-\epsilon}^{t_0+\epsilon} \oint_{\partial\mathcal{R}} \hat{\boldsymbol{n}} \cdot \mathbb{K}(\boldsymbol{x}) \cdot \nabla_{\boldsymbol{x}} G(\boldsymbol{x}, t | \boldsymbol{x}_0, t_0) \, \mathrm{d}\mathcal{S}_{\boldsymbol{x}} \, \mathrm{d}t, \tag{9.141}$$

where we used causality (9.138c) to set $G(\boldsymbol{x}, t = t_0 - \epsilon | \boldsymbol{x}_0, t_0) = 0$. The unit impulse on the right hand side results from the integrated Dirac delta source that fires at $t = t_0$. For homogeneous Neumann boundaries, the domain integrated Green's function is unity at all times $t > t_0$

$$\int_{\mathcal{R}} G(\boldsymbol{x}, t = t_0 + \epsilon | \boldsymbol{x}_0, t_0) \, \mathrm{d}V_{\boldsymbol{x}} = 1 \qquad \text{for Neumann boundaries.} \tag{9.142}$$

That is, the Green's function is normalized to unity when integrated over the full domain. This result follows from the conservation of domain integrated tracer, which holds in the absence of boundary fluxes (homogeneous Neumann conditions) and for all times.

9.5.5 A temporal consistency condition

We can develop another consistency condition by integrating the partial differential equation (9.138a) over a time interval that straddles the Dirac source time, $t \in [t_0 - \epsilon, t_0 + \epsilon]$, in which case

$$G(\boldsymbol{x}, t_0 + \epsilon | \boldsymbol{x}_0, t_0) = \delta(\boldsymbol{x} - \boldsymbol{x}_0) + \int_{t_0-\epsilon}^{t_0+\epsilon} \nabla_{\boldsymbol{x}} \cdot [\mathbb{K} \cdot \nabla_{\boldsymbol{x}} G(\boldsymbol{x}, t | \boldsymbol{x}_0, t_0)] \, \mathrm{d}t. \tag{9.143}$$

where we used causality (9.138c) to set $G(\boldsymbol{x}, t_0 - \epsilon | \boldsymbol{x}_0, t_0) = 0$. The divergence operator commutes with the time integral so that the right hand side term can be written

$$\int_{t_0-\epsilon}^{t_0+\epsilon} \nabla_{\boldsymbol{x}} \cdot [\mathbb{K} \cdot \nabla_{\boldsymbol{x}} G(\boldsymbol{x}, t | \boldsymbol{x}_0, t_0)] \, \mathrm{d}t = \nabla_{\boldsymbol{x}} \cdot \int_{t_0-\epsilon}^{t_0+\epsilon} \mathbb{K} \cdot \nabla_{\boldsymbol{x}} G(\boldsymbol{x}, t | \boldsymbol{x}_0, t_0) \, \mathrm{d}t. \tag{9.144}$$

Now take the limit as $\epsilon \to 0$, and assume the integrand is smooth in time so that the integral vanishes,[15] thus leaving the relation

$$\lim_{\epsilon \to 0} G(\boldsymbol{x}, t_0 + \epsilon | \boldsymbol{x}_0, t_0) = \delta(\boldsymbol{x} - \boldsymbol{x}_0). \tag{9.145}$$

Evidently, the Green's function, when evaluated at the source time $t = t_0$, equals to the spatial Dirac delta source. This property is shared with the causal free space Green's function in Section 9.5.2 (see equation (9.137)).

9.5.6 Adjoint causal Green's function

We make use of the *adjoint causal Green's function* for solving initial-boundary value problems for the diffusion equation. The adjoint causal Green's function is defined for $t \in (-\infty, \infty)$ and satisfies the following boundary value problem for the Neumann conditions, with these equations representing the adjoint to the Green's function equations (9.138a)-(9.138c)

$$-\frac{\partial [G^{\ddagger}(\boldsymbol{x}, t | \boldsymbol{x}_0, t_0)]}{\partial t} - \nabla_{\boldsymbol{x}} \cdot \Big[\mathbb{K} \cdot \nabla_{\boldsymbol{x}} G^{\ddagger}(\boldsymbol{x}, t | \boldsymbol{x}_0, t_0) \Big] = \delta(t - t_0) \, \delta(\boldsymbol{x} - \boldsymbol{x}_0) \quad \boldsymbol{x} \in \mathcal{R} \tag{9.146a}$$

$$\hat{\boldsymbol{n}} \cdot \mathbb{K} \cdot \nabla_{\boldsymbol{x}} G^{\ddagger}(\boldsymbol{x}, t | \boldsymbol{x}_0, t_0) = 0 \qquad \boldsymbol{x} \in \partial\mathcal{R}, \boldsymbol{x}_0 \notin \partial\mathcal{R} \tag{9.146b}$$

$$G^{\ddagger}(\boldsymbol{x}, t | \boldsymbol{x}_0, t_0) = 0 \qquad t > t_0. \tag{9.146c}$$

[15] This assumption is not fully satisfactory. Even so, we infer the property (9.145) derived when studying properties of the Green's function solution to the initial-boundary value problem for the diffusion equation.

Similarly, the adjoint Green's function satisfying Dirichlet boundary conditions is determined by

$$-\frac{\partial[G^\ddagger(\boldsymbol{x},t|\boldsymbol{x}_0,t_0)]}{\partial t} - \nabla_{\boldsymbol{x}}\cdot\left[\mathbb{K}\cdot\nabla_{\boldsymbol{x}}G^\ddagger(\boldsymbol{x},t|\boldsymbol{x}_0,t_0)\right] = \delta(t-t_0)\,\delta(\boldsymbol{x}-\boldsymbol{x}_0) \quad \boldsymbol{x}\in\mathcal{R} \tag{9.147a}$$

$$G^\ddagger(\boldsymbol{x},t|\boldsymbol{x}_0,t_0) = 0 \quad \boldsymbol{x}\in\partial\mathcal{R} \tag{9.147b}$$

$$G^\ddagger(\boldsymbol{x},t|\boldsymbol{x}_0,t_0) = 0 \quad t > t_0. \tag{9.147c}$$

Note the sign change on the time derivative in equations (9.146a) and (9.147a) relative to equations (9.138a) and (9.139a). This change results since the single partial time derivative is not a self-adjoint operator, reflecting the lack of time symmetry of the diffusion equation (i.e., the diffusion equation distinguishes between past and future). Also note the backward causal condition, equations (9.146c) and (9.147c). Physically we might wish to interpret the adjoint Green's function as a solution to the *concentration equation*, which is the diffusion equation run backwards in time.

9.5.7 Reciprocity of the Green's function and its adjoint

When studying Poisson's equation we made use of reciprocity (9.49) satisfied by the Poisson equation Green's function. We desire a corresponding reciprocity condition for the causal Green's function from the diffusion equation. Deriving reciprocity requires a bit more work for the diffusion equation due to the added time derivative term, which renders the adjoint diffusion operator distinct from the diffusion operator. That is, the diffusion operator is not *self-adjoint* due to sign change on the time derivative, whereas the Laplacian operator is self-adjoint.

Before starting this derivation, note that we did not derive the adjoint in Section 9.5.6, instead we merely wrote it down. However, introduction of the adjoint Green's function is largely motivated by the following derivation of the reciprocity relation. In this derivation we find that the Green's function for the diffusion equation satisfies a reciprocity relation with the adjoint Green's function (equation (9.156) below). Hence, as part of the following derivation we indirectly see how to construct the adjoint problem.

Setting up the derivation

To derive reciprocity, consider the partial differential equation (9.138a) with a Dirac delta source $\delta(t-t_1)\,\delta(\boldsymbol{x}-\boldsymbol{x}_1)$, and the adjoint partial differential equation (9.146a) with a distinct Dirac delta source $\delta(t-t_2)\,\delta(\boldsymbol{x}-\boldsymbol{x}_2)$. Multiply each of these equations by the complement Green's function and subtract

$$\begin{aligned}
&G^\ddagger(\boldsymbol{x},t|\boldsymbol{x}_2,t_2)(\partial_t G(\boldsymbol{x},t|\boldsymbol{x}_1,t_1) - \nabla_{\boldsymbol{x}}\cdot[\mathbb{K}\cdot\nabla_{\boldsymbol{x}}G(\boldsymbol{x},t|\boldsymbol{x}_1,t_1)])\\
-&G(\boldsymbol{x},t|\boldsymbol{x}_1,t_1)(-\partial_t G^\ddagger(\boldsymbol{x},t|\boldsymbol{x}_2,t_2) - \nabla_{\boldsymbol{x}}\cdot[\mathbb{K}\cdot\nabla_{\boldsymbol{x}}G^\ddagger(\boldsymbol{x},t|\boldsymbol{x}_2,t_2)])\\
&= G^\ddagger(\boldsymbol{x},t|\boldsymbol{x}_2,t_2)\,\delta(t-t_1)\,\delta(\boldsymbol{x}-\boldsymbol{x}_1) - G(\boldsymbol{x},t|\boldsymbol{x}_1,t_1)\,\delta(t-t_2)\,\delta(\boldsymbol{x}-\boldsymbol{x}_2).
\end{aligned} \tag{9.148}$$

The Dirac delta source locations, $\boldsymbol{x}_1\in\mathcal{R}$ and $\boldsymbol{x}_2\in\mathcal{R}$, are arbitrary points within the spatial domain $\mathcal{R}$. Likewise, the source times, t_1 and t_2, are arbitrary. In the following, we find it useful for organizational purposes to introduce an arbitrarily large time, T, so that

$$-T < t_1, t_2 < T, \tag{9.149}$$

with T later dropping out from the results through use of the causality conditions.

Integration and use of the sifting property

An integral of the right hand side of equation (9.148) over the spatial domain, $\boldsymbol{x} \in \mathcal{R}$, and over the time domain, $t \in [-T, T]$, for the observational space-time points $(\boldsymbol{x}, t)$, leads to

$$\int_{-T}^{T} \int_{\mathcal{R}} \Big[G^{\ddagger}(\boldsymbol{x}, t|\boldsymbol{x}_2, t_2)\, \delta(t - t_1)\, \delta(\boldsymbol{x} - \boldsymbol{x}_1) - G(\boldsymbol{x}, t|\boldsymbol{x}_1, t_1)\, \delta(t - t_2)\, \delta(\boldsymbol{x} - \boldsymbol{x}_2) \Big] \, \mathrm{d}V \, \mathrm{d}t$$
$$= G^{\ddagger}(\boldsymbol{x}_1, t_1|\boldsymbol{x}_2, t_2) - G(\boldsymbol{x}_2, t_2|\boldsymbol{x}_1, t_1). \quad (9.150)$$

As shown in the following, the same integral of the left hand side of equation (9.148) vanishes, which then establishes the reciprocity property between the Green's function and the adjoint Green's function.

Moving the time derivative from G to $G^{\ddagger}$ and picking up a minus sign

The left hand side of equation (9.148) requires us to massage just the first term since, as we will show, this term equals to the second so that the left hand side of equation (9.148) vanishes. To prove this assertion, start by examining the time derivative. Since the spatial domain, $\mathcal{R}$, is assumed to be static,[16] we can swap the time and space derivatives to find

$$\int_{-T}^{T} G^{\ddagger}(\boldsymbol{x}, t|\boldsymbol{x}_2, t_2)\, \partial_t\, G(\boldsymbol{x}, t|\boldsymbol{x}_1, t_1)\, \mathrm{d}t$$
$$= \int_{-T}^{T} \Big[\partial_t \Big(G^{\ddagger}(\boldsymbol{x}, t|\boldsymbol{x}_2, t_2)\, G(\boldsymbol{x}, t|\boldsymbol{x}_1, t_1) \Big) - \partial_t G^{\ddagger}(\boldsymbol{x}, t|\boldsymbol{x}_2, t_2)\, G(\boldsymbol{x}, t|\boldsymbol{x}_1, t_1) \Big] \, \mathrm{d}t. \quad (9.151)$$

We now set

$$G(\boldsymbol{x}, t = -T|\boldsymbol{x}_1, t_1) = 0 \quad \text{and} \quad G^{\ddagger}(\boldsymbol{x}, t = +T|\boldsymbol{x}_2, t_2) = 0, \quad (9.152)$$

which result from the causality conditions (9.138c) and (9.146c). Hence, in moving the time derivative from G to $G^{\ddagger}$ we pick up a minus sign, which, again, means that the time derivative is not self-adjoint

$$\int_{-T}^{T} G^{\ddagger}(\boldsymbol{x}, t|\boldsymbol{x}_2, t_2)\, \partial_t\, G(\boldsymbol{x}, t|\boldsymbol{x}_1, t_1)\, \mathrm{d}t = -\int_{-T}^{T} \partial_t G^{\ddagger}(\boldsymbol{x}, t|\boldsymbol{x}_2, t_2)\, G(\boldsymbol{x}, t|\boldsymbol{x}_1, t_1)\, \mathrm{d}t. \quad (9.153)$$

The Laplacian is self-adjoint with a symmetric diffusion tensor

Consider next the spatial derivative term on the left hand side of equation (9.148)

$$-\int_{\mathcal{R}} G^{\ddagger}(\boldsymbol{x}, t|\boldsymbol{x}_2, t_2)\, \nabla_{\boldsymbol{x}} \cdot [\mathbb{K} \cdot \nabla_{\boldsymbol{x}} G(\boldsymbol{x}, t|\boldsymbol{x}_1, t_1)] \, \mathrm{d}V =$$
$$\int_{\mathcal{R}} \Big[-\nabla_{\boldsymbol{x}} \cdot \Big(G^{\ddagger}(\boldsymbol{x}, t|\boldsymbol{x}_2, t_2)\, \mathbb{K} \cdot \nabla_{\boldsymbol{x}} G(\boldsymbol{x}, t|\boldsymbol{x}_1, t_1) \Big) + \nabla_{\boldsymbol{x}} G^{\ddagger}(\boldsymbol{x}, t|\boldsymbol{x}_2, t_2) \cdot \mathbb{K} \cdot \nabla_{\boldsymbol{x}} G(\boldsymbol{x}, t|\boldsymbol{x}_1, t_1) \Big] \, \mathrm{d}V. \quad (9.154)$$

Use of the divergence theorem and either the homogeneous Neumann boundary condition (9.138b) or homogeneous Dirichlet condition (9.139b) allow us to drop the total derivative term. The same manipulation, with either the Neumann condition (9.146b) or Dirichlet condition (9.147b) satisfied by the adjoint Green's function $G^{\ddagger}(\boldsymbol{x}, t|\boldsymbol{x}_2, t_2)$, allows us to seamlessly move

[16] As noted in Section 9.5.1, in Section 69.9 we dispense with the assumption of a time independent spatial domain. Doing so requires extra care, both physically and mathematically, thus motivating us to postpone that discussion until we have more experience.

the Laplacian operator from $G(\boldsymbol{x}, t|\boldsymbol{x}_1, t_1)$ onto $G^\ddagger(\boldsymbol{x}, t|\boldsymbol{x}_2, t_2)$, thus manifesting the self-adjoint nature of the Laplacian operator even in the presence of a symmetric diffusion tensor

$$\int_{\mathcal{R}} G^\ddagger(\boldsymbol{x}, t|\boldsymbol{x}_2, t_2)\, \nabla_{\boldsymbol{x}} \cdot [\mathbb{K} \cdot \nabla_{\boldsymbol{x}} G(\boldsymbol{x}, t|\boldsymbol{x}_1, t_1)]\, \mathrm{d}V = \int_{\mathcal{R}} \nabla_{\boldsymbol{x}} \cdot \left[\mathbb{K} \cdot \nabla_{\boldsymbol{x}} G^\ddagger(\boldsymbol{x}, t|\boldsymbol{x}_2, t_2)\right] G(\boldsymbol{x}, t|\boldsymbol{x}_1, t_1)\, \mathrm{d}V. \quad (9.155)$$

Reciprocity of the Green's function and the adjoint Green's function

The above manipulations show that the space-time integral for the left hand side of equation (9.148) vanishes. Consequently, we are left with the reciprocity relation satisfied by the Green's function and adjoint Green's function for the diffusion equation

$$G^\ddagger(\boldsymbol{x}, t|\boldsymbol{x}_0, t_0) = G(\boldsymbol{x}_0, t_0|\boldsymbol{x}, t). \quad (9.156)$$

The Green's function, $G(\boldsymbol{x}_0, t_0|\boldsymbol{x}, t)$, results from placing a Dirac delta source at $(\boldsymbol{x}, t)$ and using the forward diffusion equation to determine the response at $(\boldsymbol{x}_0, t_0)$ with $t < t_0$. The adjoint Green's function, $G^\ddagger(\boldsymbol{x}, t|\boldsymbol{x}_0, t_0)$, results from placing a Dirac delta source at $(\boldsymbol{x}_0, t_0)$ and using the adjoint diffusion equation to determine the response at $(\boldsymbol{x}, t)$, again with $t < t_0$. The reciprocity relation (9.156) shows that the two responses are identical. We emphasize that reciprocity is a property that emerges from properties of the differential operator, the boundary conditions, and the causality condition.

Reciprocity in the form of equation (9.156) means we have no need to bother solving the adjoint Green's function equation for $G^\ddagger(\boldsymbol{x}, t|\boldsymbol{x}_0, t_0)$ since the adjoint Green's function equals to the Green's function after swapping the space-time points for the field and source. Hence, it is sufficient to determine the Green's function, $G(\boldsymbol{x}, t|\boldsymbol{x}_0, t_0)$, and then use reciprocity to determine $G^\ddagger(\boldsymbol{x}, t|\boldsymbol{x}_0, t_0)$. The simplicity of the reciprocity relation (9.156) is central to the practical use of the Green's function method for the diffusion equation.

9.5.8 Composition property of the Green's function

Following from the reciprocity relation derived in Section 9.5.7, we here derive the *composition property* satisfied by the Green's functions for the diffusion equation. This property connects the Green's function to Markov processes, in which the composition property is known as the *Chapman-Kolmogorov relation* (*Gardiner*, 1985). The derivation closely follows that given in Section 9.5.7 for reciprocity, though it is a bit simpler. *Larson* (1999) and *Holzer* (2009) discuss the composition property in the context of the advection-diffusion equation, to which we return to in Section 69.9.6. *Holzer* (2009) also provides further connections to probability theory, thus promoting the interpretation of the Green's function as a transition probability.

Setting up the derivation

Consider again the Green's function partial differential equation (9.138a) with a Dirac delta source at $(t_1, \boldsymbol{x}_1)$,

$$\partial_t G(\boldsymbol{x}, t|\boldsymbol{x}_1, t_1) - \nabla_{\boldsymbol{x}} \cdot [\mathbb{K} \cdot \nabla_{\boldsymbol{x}} G(\boldsymbol{x}, t|\boldsymbol{x}_1, t_1)] = \delta(t - t_1)\, \delta(\boldsymbol{x} - \boldsymbol{x}_1), \quad (9.157)$$

and the adjoint Green's function partial differential equation (9.146a) with a distinct Dirac delta source at $(t_2, \boldsymbol{x}_2)$

$$\partial_t G^\ddagger(\boldsymbol{x}, t|\boldsymbol{x}_2, t_2) + \nabla_{\boldsymbol{x}} \cdot [\mathbb{K} \cdot \nabla_{\boldsymbol{x}} G^\ddagger(\boldsymbol{x}, t|\boldsymbol{x}_2, t_2)] = -\delta(t - t_2)\, \delta(\boldsymbol{x} - \boldsymbol{x}_2). \quad (9.158)$$

Multiply each of these equations by the complement Green's function and add the two equations.[17] Adding the time derivatives leads to

$$G^{\ddagger}(\boldsymbol{x},t|\boldsymbol{x}_2,t_2)\,\partial_t G(\boldsymbol{x},t|\boldsymbol{x}_1,t_1) + G(\boldsymbol{x},t|\boldsymbol{x}_1,t_1)\,\partial_t G^{\ddagger}(\boldsymbol{x},t|\boldsymbol{x}_2,t_2) = \partial_t\left[G^{\ddagger}(\boldsymbol{x},t|\boldsymbol{x}_2,t_2)\,G(\boldsymbol{x},t|\boldsymbol{x}_1,t_1)\right], \quad (9.159)$$

and adding the space derivatives leads to

$$\begin{aligned} &- G^{\ddagger}(\boldsymbol{x},t|\boldsymbol{x}_2,t_2)\,\nabla_{\boldsymbol{x}}\cdot[\mathbb{K}\cdot\nabla_{\boldsymbol{x}}G(\boldsymbol{x},t|\boldsymbol{x}_1,t_1)] + G(\boldsymbol{x},t|\boldsymbol{x}_1,t_1)\,\nabla_{\boldsymbol{x}}\cdot[\mathbb{K}\cdot\nabla_{\boldsymbol{x}}G^{\ddagger}(\boldsymbol{x},t|\boldsymbol{x}_2,t_2)] \\ &\quad = \nabla_{\boldsymbol{x}}\cdot[-G^{\ddagger}(\boldsymbol{x},t|\boldsymbol{x}_2,t_2)\,\mathbb{K}\cdot\nabla_{\boldsymbol{x}}G(\boldsymbol{x},t|\boldsymbol{x}_1,t_1) + G(\boldsymbol{x},t|\boldsymbol{x}_1,t_1)\,\mathbb{K}\cdot\nabla_{\boldsymbol{x}}G^{\ddagger}(\boldsymbol{x},t|\boldsymbol{x}_2,t_2)]. \end{aligned} \quad (9.160)$$

Integrating over the full spatial domain and using the homogeneous Neumann or Dirichlet boundary conditions removes the space derivative terms, thus leaving

$$\frac{\mathrm{d}}{\mathrm{d}t}\int_{\mathcal{R}}[G^{\ddagger}(\boldsymbol{x},t|\boldsymbol{x}_2,t_2)\,G(\boldsymbol{x},t|\boldsymbol{x}_1,t_1)]\,\mathrm{d}V = G^{\ddagger}(\boldsymbol{x}_1,t|\boldsymbol{x}_2,t_2)\,\delta(t-t_1) - G(\boldsymbol{x}_2,t|\boldsymbol{x}_1,t_1)\,\delta(t-t_2), \quad (9.161)$$

where we pulled the time derivative outside of the space integration since $\mathcal{R}$ is a static domain (Section 9.5.1).

Time integration and use of causality

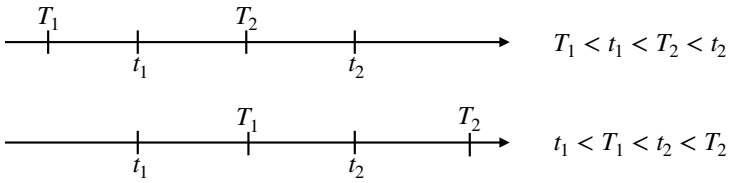

FIGURE 9.6: Two possible placements of the time steps used to derive the Green's function composition property.

Integrate equation (9.161) over time, in which case

$$\int_{\mathcal{R}}[G^{\ddagger}(\boldsymbol{x},T_2|\boldsymbol{x}_2,t_2)\,G(\boldsymbol{x},T_2|\boldsymbol{x}_1,t_1) - G^{\ddagger}(\boldsymbol{x},T_1|\boldsymbol{x}_2,t_2)\,G(\boldsymbol{x},T_1|\boldsymbol{x}_1,t_1)]\,\mathrm{d}V = \int_{T_1}^{T_2}[G^{\ddagger}(\boldsymbol{x}_1,t|\boldsymbol{x}_2,t_2)\,\delta(t-t_1) - G(\boldsymbol{x}_2,t|\boldsymbol{x}_1,t_1)\,\delta(t-t_2)]\,\mathrm{d}t, \quad (9.162)$$

where $T_1 < T_2$ are time endpoints for the time integration. The causality conditions (9.138c) and (9.146c) lead to the following identities, depending on the placements of T_1, T_2 relative to t_1, t_2 as shown in Figure 9.6

$$G^{\ddagger}(\boldsymbol{x}_1,t_1|\boldsymbol{x}_2,t_2) = \int_{\mathcal{R}} G^{\ddagger}(\boldsymbol{x},T_2|\boldsymbol{x}_2,t_2)\,G(\boldsymbol{x},T_2|\boldsymbol{x}_1,t_1)\,\mathrm{d}V \quad \text{if } T_1 < t_1 < T_2 < t_2 \quad (9.163a)$$

$$G(\boldsymbol{x}_2,t_2|\boldsymbol{x}_1,t_1) = \int_{\mathcal{R}} G^{\ddagger}(\boldsymbol{x},T_1|\boldsymbol{x}_2,t_2)\,G(\boldsymbol{x},T_1|\boldsymbol{x}_1,t_1)\,\mathrm{d}V \quad \text{if } t_1 < T_1 < t_2 < T_2. \quad (9.163b)$$

[17] Recall that in Section 9.5.7 we subtracted the two equations to derive the reciprocity relation.

Use of the reciprocity relation (9.156) then leads to the composition relations

$$G(\boldsymbol{x}_2, t_2|\boldsymbol{x}_1, t_1) = \int_{\mathcal{R}} G(\boldsymbol{x}_2, t_2|\boldsymbol{x}, T_2)\, G(\boldsymbol{x}, T_2|\boldsymbol{x}_1, t_1)\, \mathrm{d}V \quad \text{if } T_1 < t_1 < T_2 < t_2 \tag{9.164a}$$

$$G(\boldsymbol{x}_2, t_2|\boldsymbol{x}_1, t_1) = \int_{\mathcal{R}} G(\boldsymbol{x}_2, t_2|\boldsymbol{x}, T_1)\, G(\boldsymbol{x}, T_1|\boldsymbol{x}_1, t_1)\, \mathrm{d}V \quad \text{if } t_1 < T_1 < t_2 < T_2. \tag{9.164b}$$

These equations are identical since both include an arbitrary intermediate time that is bounded by $t_1 < t_2$, thus allowing us to write the general composition property of the Green's function

$$G(\boldsymbol{x}_2, t_2|\boldsymbol{x}_1, t_1) = \int_{\mathcal{R}} G(\boldsymbol{x}_2, t_2|\boldsymbol{x}, \tau)\, G(\boldsymbol{x}, \tau|\boldsymbol{x}_1, t_1)\, \mathrm{d}V \quad \text{if } t_1 < \tau < t_2. \tag{9.165}$$

Interpreting the Green's function composition property

The Green's function, $G(\boldsymbol{x}_2, t_2|\boldsymbol{x}_1, t_1)$, on the left hand side of the composition property (9.165) is the response from a Dirac delta source diffused from $(\boldsymbol{x}_1, t_1)$ and measured at the field space-time point $(\boldsymbol{x}_2, t_2)$. The right hand side says that this response, $G(\boldsymbol{x}_2, t_2|\boldsymbol{x}_1, t_1)$, is identical to the composition of a Green's function feeling the source at $(\boldsymbol{x}_1, t_1)$ but now sampled at an intermediate space-time position, $(\boldsymbol{x}, \tau)$, and then further diffused to $(\boldsymbol{x}_2, t_2)$, with integration over all possible intermediate positions $\boldsymbol{x}$. Furthermore, note that the intermediate sampling can occur at an arbitrary intermediate time, τ, so long as $t_1 < \tau < t_2$. The composition property allows us to conceive of a long-time interval Green's function as the composition of an arbitrary number of shorter time interval Green's functions.

9.5.9 The integral solution

Having established reciprocity (9.156), we are ready to derive an integral expression for the field, $\psi(\boldsymbol{x}, t)$, satisfying the diffusion equation initial-boundary value problem with either the Neumann boundary conditions

$$\partial_t \psi(\boldsymbol{x}, t) - \nabla \cdot [\mathbb{K} \cdot \nabla_{\boldsymbol{x}} \psi(\boldsymbol{x}, t)] = \Lambda(\boldsymbol{x}, t) \quad \boldsymbol{x} \in \mathcal{R} \tag{9.166a}$$

$$\hat{\boldsymbol{n}} \cdot \mathbb{K} \cdot \nabla_{\boldsymbol{x}} \psi(\boldsymbol{x}, t) = \Sigma(\boldsymbol{x}, t) \quad \boldsymbol{x} \in \partial\mathcal{R} \tag{9.166b}$$

$$\psi(\boldsymbol{x}, t = t_{\text{init}}) = I(\boldsymbol{x}) \qquad \boldsymbol{x} \in \mathcal{R}, \tag{9.166c}$$

or Dirichlet boundary conditions

$$\partial_t \psi(\boldsymbol{x}, t) - \nabla \cdot [\mathbb{K} \cdot \nabla_{\boldsymbol{x}} \psi(\boldsymbol{x}, t)] = \Lambda(\boldsymbol{x}, t) \quad \boldsymbol{x} \in \mathcal{R} \tag{9.167a}$$

$$\psi(\boldsymbol{x}, t) = \sigma(\boldsymbol{x}, t) \quad \boldsymbol{x} \in \partial\mathcal{R} \tag{9.167b}$$

$$\psi(\boldsymbol{x}, t = t_{\text{init}}) = I(\boldsymbol{x}) \qquad \boldsymbol{x} \in \mathcal{R}. \tag{9.167c}$$

In these equations we introduced the initial time, $t = t_{\text{init}}$, which is distinct from the Dirac delta source time, $t = t_0$. We are interested in the evolution of ψ after specification of the initial data, $\psi(\boldsymbol{x}, t = t_{\text{init}}) = I(\boldsymbol{x})$. Correspondingly, t_{init} defines the lower limit on time integrals in the following. Use of the $\nabla_{\boldsymbol{x}}$ notation is not needed for these equations, since there is no source point, $\boldsymbol{x}_0$, in any of the expressions. However, writing $\nabla_{\boldsymbol{x}}$ helps us remain organized during the following manipulations. Finally, note that the diffusion tensor appearing in these equations means that the source function, $\Lambda(\boldsymbol{x}, t)$, in equations (9.166a) and (9.167a), as well as the boundary data, $\Sigma(\boldsymbol{x}, t)$, in equation (9.166b), have different physical dimensions from their counterparts found in the Poisson boundary value problems (9.37) and (9.93).

The following derivation emulates that for the Poisson equation in Section 9.3.7, yet with distinct features arising from time evolution and the corresponding need to use the adjoint causal

Green's function, $G^\ddagger$. We expose many details as doing so reveals general notions and tricks arising with Green's function methods for initial-boundary value problems.

Setting up the derivation

To start the derivation, multiply the diffusion equation (9.166a) by the adjoint Green's function, $G^\ddagger(\boldsymbol{x},t|\boldsymbol{x}_0,t_0)$, and the adjoint Green's function equation (9.146a) by $\psi(\boldsymbol{x},t)$. Subtracting and rearranging leads to

$$\partial_t(G^\ddagger\,\psi)+\nabla\cdot[\psi\,\mathbb{K}\cdot\nabla_{\boldsymbol{x}}G^\ddagger-G^\ddagger\,\mathbb{K}\cdot\nabla\psi] = G^\ddagger(\boldsymbol{x},t|\boldsymbol{x}_0,t_0)\,\Lambda(\boldsymbol{x},t)-\psi(\boldsymbol{x},t)\,\delta(\boldsymbol{x}-\boldsymbol{x}_0)\,\delta(t-t_0), \quad (9.168)$$

where we temporarily suppressed arguments on the left hand side for brevity. Since the spatial domain is assumed to be static, we can integrate this equation over space and time without concern for the order of integration.

Time integration

A time integral of the first left hand side term in equation (9.168) leads to[18]

$$\int_{t_{\text{init}}}^{T}\partial_t[G^\ddagger(\boldsymbol{x},t|\boldsymbol{x}_0,t_0)\,\psi(\boldsymbol{x},t)]\,\mathrm{d}t = G^\ddagger(\boldsymbol{x},T|\boldsymbol{x}_0,t_0)\,\psi(\boldsymbol{x},T) - G^\ddagger(\boldsymbol{x},t_{\text{init}}|\boldsymbol{x}_0,t_0)\,\psi(\boldsymbol{x},t_{\text{init}}) \quad (9.169a)$$

$$= -G^\ddagger(\boldsymbol{x},t_{\text{init}}|\boldsymbol{x}_0,t_0)\,I(\boldsymbol{x}), \quad (9.169b)$$

where we made use of the backward causal condition (9.146c) satisfied by the adjoint Green's function to set $G^\ddagger(\boldsymbol{x},t=T|\boldsymbol{x}_0,t_0)=0$, and used the initial condition (9.166c) to introduce the initial value data, $\psi(\boldsymbol{x},t_{\text{init}})=I(\boldsymbol{x})$.

Space integration

A space integral over all observation points, and use of the divergence theorem, brings the divergence term on the left side of equation (9.168) into

$$\int_{\mathcal{R}}\nabla\cdot[\psi(\boldsymbol{x},t)\,\mathbb{K}\cdot\nabla_{\boldsymbol{x}}G^\ddagger(\boldsymbol{x},t|\boldsymbol{x}_0,t_0) - G^\ddagger(\boldsymbol{x},t|\boldsymbol{x}_0,t_0)\,\mathbb{K}\cdot\nabla_{\boldsymbol{x}}\psi(\boldsymbol{x},t)]\,\mathrm{d}V$$

$$= \oint_{\partial\mathcal{R}}\Big[\psi(\boldsymbol{x},t)\,\mathbb{K}\cdot\nabla_{\boldsymbol{x}}G^\ddagger(\boldsymbol{x},t|\boldsymbol{x}_0,t_0) - G^\ddagger(\boldsymbol{x},t|\boldsymbol{x}_0,t_0)\,\mathbb{K}\cdot\nabla_{\boldsymbol{x}}\psi(\boldsymbol{x},t)\Big]\cdot\hat{\boldsymbol{n}}\,\mathrm{d}\mathcal{S}. \quad (9.170)$$

We keep both boundary terms pending specification of whether the fields satisfy Dirichlet or Neumann boundary conditions. This boundary integral has the same appearance as found for the Poisson equation in Section 9.3.7, with the added feature here of the diffusion tensor. Also, recall that the diffusion tensor is generally a function of space and time, $\mathbb{K}(\boldsymbol{x},t)$, with the dependence supressed for brevity.

[18] Recall that T is an arbitrarily large but finite time. It drops out from the final answer, but proves useful for organizational purposes in intermediate steps.

Integrating the right hand side of equation (9.168)

A space and time integral for the right hand side of equation (9.168), along with the sifting properties of the Dirac delta, render

$$\int_{t_{\text{init}}}^{T}\left[\int_{\mathcal{R}}[G^{\ddagger}(\boldsymbol{x},t|\boldsymbol{x}_0,t_0)\,\Lambda(\boldsymbol{x},t)-\psi(\boldsymbol{x},t)\,\delta(\boldsymbol{x}-\boldsymbol{x}_0)\,\delta(t-t_0)]\,\mathrm{d}V\right]\mathrm{d}t$$
$$=-\psi(\boldsymbol{x}_0,t_0)+\int_{t_{\text{init}}}^{T}\left[\int_{\mathcal{R}}G^{\ddagger}(\boldsymbol{x},t|\boldsymbol{x}_0,t_0)\,\Lambda(\boldsymbol{x},t)\mathrm{d}V\right]\mathrm{d}t. \quad (9.171)$$

Notice how this integration over the observation space-time points, $(\boldsymbol{x},t)$, serves to pick out the field, ψ, evaluated at the space-time point, $(\boldsymbol{x}_0,t_0)$, where the Dirac delta source is located.

Rearrangement and use of reciprocity

Bringing the above results together leads to the expression

$$\psi(\boldsymbol{x}_0,t_0)=\int_{\mathcal{R}}G^{\ddagger}(\boldsymbol{x},t_{\text{init}}|\boldsymbol{x}_0,t_0)\,I(\boldsymbol{x})\,\mathrm{d}V+\int_{t_{\text{init}}}^{t_0}\left[\int_{\mathcal{R}}G^{\ddagger}(\boldsymbol{x},t|\boldsymbol{x}_0,t_0)\,\Lambda(\boldsymbol{x},t)\,\mathrm{d}V\right]\mathrm{d}t$$
$$+\int_{t_{\text{init}}}^{t_0}\left[\oint_{\partial\mathcal{R}}\left[G^{\ddagger}(\boldsymbol{x},t|\boldsymbol{x}_0,t_0)\,\mathbb{K}\cdot\nabla_{\boldsymbol{x}}\psi(\boldsymbol{x},t)-\psi(\boldsymbol{x},t)\,\mathbb{K}\cdot\nabla_{\boldsymbol{x}}G^{\ddagger}(\boldsymbol{x},t|\boldsymbol{x}_0,t_0)\right]\cdot\hat{\boldsymbol{n}}\,\mathrm{d}\mathcal{S}\right]\mathrm{d}t. \quad (9.172)$$

The time integrals are restricted to the range $t\in[t_{\text{init}},t_0]$ through use of the causality condition (9.146c) for the adjoint Green's function. Hence, the arbitrary time, T, drops out from the solution and there is no dependence on fields at times later than t_0 nor before t_{init}.

Use of reciprocity (9.156) allows us to replace the adjoint Green's function with the Green's function to thus bring equation (9.172) to

$$\psi(\boldsymbol{x}_0,t_0)=\int_{\mathcal{R}}G(\boldsymbol{x}_0,t_0|\boldsymbol{x},t_{\text{init}})\,I(\boldsymbol{x})\,\mathrm{d}V+\int_{t_{\text{init}}}^{t_0}\left[\int_{\mathcal{R}}G(\boldsymbol{x}_0,t_0|\boldsymbol{x},t)\,\Lambda(\boldsymbol{x},t)\,\mathrm{d}V\right]\mathrm{d}t$$
$$+\int_{t_{\text{init}}}^{t_0}\left[\oint_{\partial\mathcal{R}}[G(\boldsymbol{x}_0,t_0|\boldsymbol{x},t)\,\mathbb{K}\cdot\nabla_{\boldsymbol{x}}\psi(\boldsymbol{x},t)-\psi(\boldsymbol{x},t)\,\mathbb{K}\cdot\nabla_{\boldsymbol{x}}G(\boldsymbol{x}_0,t_0|\boldsymbol{x},t)]\cdot\hat{\boldsymbol{n}}\,\mathrm{d}\mathcal{S}\right]\mathrm{d}t. \quad (9.173)$$

Finally, it is convenient to relabel $(\boldsymbol{x}_0,t_0)\leftrightarrow(\boldsymbol{x},t)$ to write

$$\psi(\boldsymbol{x},t)=\underbrace{\int_{\mathcal{R}}G(\boldsymbol{x},t|\boldsymbol{x}_0,t_{\text{init}})\,I(\boldsymbol{x}_0)\,\mathrm{d}V_0}_{\text{space integral of } G \text{ times } I \text{ on } \mathcal{R}}+\underbrace{\int_{t_{\text{init}}}^{t}\left[\int_{\mathcal{R}}G(\boldsymbol{x},t|\boldsymbol{x}_0,t_0)\,\Lambda(\boldsymbol{x}_0,t_0)\,\mathrm{d}V_0\right]\mathrm{d}t_0}_{\text{space-time integral of } G \text{ times } \Lambda \text{ over } \mathcal{R}}$$
$$+\underbrace{\int_{t_{\text{init}}}^{t}\left[\oint_{\partial\mathcal{R}}[G(\boldsymbol{x},t|\boldsymbol{x}_0,t_0)\,\mathbb{K}\cdot\nabla_{\boldsymbol{x}_0}\psi(\boldsymbol{x}_0,t_0)-\psi(\boldsymbol{x}_0,t_0)\,\mathbb{K}\cdot\nabla_{\boldsymbol{x}_0}G(\boldsymbol{x},t|\boldsymbol{x}_0,t_0)]\cdot\hat{\boldsymbol{n}}_{\boldsymbol{x}_0}\,\mathrm{d}\mathcal{S}_0\right]\mathrm{d}t_0}_{\text{space-time integral of boundary terms over } \partial\mathcal{R}}. \quad (9.174)$$

Specializing to Neumann boundary conditions leads to

$$\psi^{\text{Neumann}}(\boldsymbol{x},t)=\int_{\mathcal{R}}G(\boldsymbol{x},t|\boldsymbol{x}_0,t_{\text{init}})\,I(\boldsymbol{x}_0)\,\mathrm{d}V_0+\int_{t_{\text{init}}}^{t}\left[\int_{\mathcal{R}}G(\boldsymbol{x},t|\boldsymbol{x}_0,t_0)\,\Lambda(\boldsymbol{x}_0,t_0)\,\mathrm{d}V_0\right]\mathrm{d}t_0$$
$$+\int_{t_{\text{init}}}^{t}\left[\oint_{\partial\mathcal{R}}G(\boldsymbol{x},t|\boldsymbol{x}_0,t_0)\,\Sigma(\boldsymbol{x}_0,t_0)\,\mathrm{d}\mathcal{S}_0\right]\mathrm{d}t_0, \quad (9.175)$$

whereas the solution with Dirichlet boundary conditions is

$$\psi^{\text{Dirichlet}}(\boldsymbol{x},t) = \int_{\mathcal{R}} G(\boldsymbol{x},t|\boldsymbol{x}_0,t_{\text{init}})\, I(\boldsymbol{x}_0)\,\mathrm{d}V_0 + \int_{t_{\text{init}}}^{t}\left[\int_{\mathcal{R}} G(\boldsymbol{x},t|\boldsymbol{x}_0,t_0)\,\Lambda(\boldsymbol{x}_0,t_0)\,\mathrm{d}V_0\right]\mathrm{d}t_0$$
$$- \int_{t_{\text{init}}}^{t}\left[\oint_{\partial\mathcal{R}} \sigma(\boldsymbol{x}_0,t_0)\,\mathbb{K}(\boldsymbol{x}_0,t_0)\cdot\nabla_{\boldsymbol{x}_0} G(\boldsymbol{x},t|\boldsymbol{x}_0,t_0)\cdot\hat{\boldsymbol{n}}_{\boldsymbol{x}_0}\,\mathrm{d}\mathcal{S}_0\right]\mathrm{d}t_0. \quad (9.176)$$

9.5.10 Properties of the solution: initial conditions

Many properties of the solution (9.174) are also reflected in the Poisson equation solutions from Sections 9.3.8 and 9.4.7. In particular, the solution manifests the linear superposition principle, with the solution given by the sum of three terms arising from the initial conditions, distributed volume source, and spatial boundary conditions. We expect to have this connection given that the steady state diffusion equation satisfies a generalized Poisson equation (generalized by the presence of a diffusion tensor). Uniqueness of the solution (9.174) also follows as in the discussion of the Poisson equation in Sections 9.3.2 and 9.4.2. Namely, consider two solutions to the diffusion equation and take their difference, $\Psi = \psi_A - \psi_B$. We readily see that Ψ satisfies the homogeneous diffusion equation with homogeneous boundary conditions along with a zero initial condition. Ψ thus remains zero for both the Dirichlet and Neumann cases, thus proving that the solution to both problems is unique.

A fundamentally new piece of physics and maths arises from time dependence. By sampling the solution (9.174) as time decreases towards the initial time, $t \downarrow t_{\text{init}}$, and noting the initial condition $\psi(\boldsymbol{x},t_{\text{init}}) = I(\boldsymbol{x})$, we are led to[19]

$$\lim_{t\downarrow t_{\text{init}}} \psi(\boldsymbol{x},t) = I(\boldsymbol{x}) = \lim_{t\downarrow t_{\text{init}}} \int_{\mathcal{R}} G(\boldsymbol{x},t|\boldsymbol{x}_0,t_{\text{init}})\, I(\boldsymbol{x}_0)\,\mathrm{d}V_0. \quad (9.177)$$

This temporal sampling of the field time is distinguished from the source time, which here is fixed at the initial time, t_{init}. Self-consistency in equation (9.177) implies that the Green's function for both Neumann and Dirichlet boundary conditions satisfies the initial condition

$$\lim_{t\downarrow t_{\text{init}}} G(\boldsymbol{x},t|\boldsymbol{x}_0,t_{\text{init}}) = \delta(\boldsymbol{x}-\boldsymbol{x}_0) \quad \text{with } \boldsymbol{x},\boldsymbol{x}_0 \in \mathcal{R}. \quad (9.178)$$

That is, the Green's function is initialized by a Dirac delta pulse at the source point, $\boldsymbol{x}_0$, which is a result already derived in Section 9.5.5 (equation (9.145)) through use of causality. This result then leads to the identity

$$\lim_{t\downarrow t_{\text{init}}} \int_{\mathcal{R}} G(\boldsymbol{x},t|\boldsymbol{x}_0,t_{\text{init}})\, I(\boldsymbol{x}_0)\,\mathrm{d}V_0 = \int_{\mathcal{R}} \delta(\boldsymbol{x}-\boldsymbol{x}_0)\, I(\boldsymbol{x}_0)\,\mathrm{d}V_0 = I(\boldsymbol{x}). \quad (9.179)$$

9.5.11 Properties of the solution with Neumann boundary conditions

Acting with $\mathbb{K}(\boldsymbol{x},t)\cdot\nabla_{\boldsymbol{x}}$ on the Neumann solution (9.175); evaluating the expression on the boundary $\boldsymbol{x} = \boldsymbol{x}_{\partial\mathcal{R}} \in \partial\mathcal{R}$; and then projecting onto the outward unit normal, $\hat{\boldsymbol{n}}_{\boldsymbol{x}}$, serves to annihilate the volume integrals as per the homogeneous Neumann condition satisfied by the Green's function (9.138b). We are thus left with

$$\hat{\boldsymbol{n}}_{\boldsymbol{x}}\cdot\mathbb{K}(\boldsymbol{x},t)\cdot\nabla_{\boldsymbol{x}}\psi(\boldsymbol{x},t) = \Sigma(\boldsymbol{x},t) \quad (9.180a)$$
$$= \int_{t_{\text{init}}}^{t}\left[\oint_{\partial\mathcal{R}} \hat{\boldsymbol{n}}_{\boldsymbol{x}}\cdot\mathbb{K}(\boldsymbol{x},t)\cdot\nabla_{\boldsymbol{x}} G(\boldsymbol{x},t|\boldsymbol{x}_0,t_0)\,\Sigma(\boldsymbol{x}_0,t_0)\,\mathrm{d}\mathcal{S}_0\right]\mathrm{d}t_0. \quad (9.180b)$$

[19] Since t_{init} is the initial time, the limit $t \downarrow t_{\text{init}}$ means that $t = t_{\text{init}} + \epsilon$ with $\epsilon \to 0$.

Self-consistency implies that the Green's function for the Neumann problem, when evaluated on the spatial boundary, satisfies

$$\hat{\boldsymbol{n}}_{\boldsymbol{x}} \cdot \mathbb{K}(\boldsymbol{x}, t) \cdot \nabla_{\boldsymbol{x}} G(\boldsymbol{x}, t | \boldsymbol{x}_0, t_0) = \delta(t - t_0)\, \delta^{(2)}(\boldsymbol{x} - \boldsymbol{x}_0) \quad \text{with } \boldsymbol{x}, \boldsymbol{x}_0 \in \partial\mathcal{R}, \tag{9.181}$$

where $\delta^{(2)}(\boldsymbol{x} - \boldsymbol{x}_0)$ is a surface Dirac delta with physical dimensions inverse area. The boundary condition (9.181) generalizes the property (9.113) holding for the Poisson equation Green's function. Furthermore, it extends the homogeneous Neumann condition (9.138b) holding when $\boldsymbol{x} \in \partial\mathcal{R}$ and $\boldsymbol{x}_0 \notin \partial\mathcal{R}$ to now allow $\boldsymbol{x} \in \partial\mathcal{R}$ and $\boldsymbol{x}_0 \in \partial\mathcal{R}$.

When studying the Poisson boundary value problem in Section 9.4.8, we saw how to transform the Neumann boundary condition into the interior by modifying the source function. The diffusion equation Neumann solution (9.175) allows for the same transformation by writing

$$\psi^{\text{Neumann}}(\boldsymbol{x}, t) = \int_{\mathcal{R}} G(\boldsymbol{x}, t | \boldsymbol{x}_0, t_{\text{init}})\, I(\boldsymbol{x}_0)\, \mathrm{d}V_0 + \int_{t_{\text{init}}}^{t} \left[\int_{\mathcal{R}} G(\boldsymbol{x}, t | \boldsymbol{x}_0, t_0)\, \Lambda^*(\boldsymbol{x}_0, t_0)\, \mathrm{d}V_0 \right] \mathrm{d}t_0, \tag{9.182}$$

where the modified source function follows from that used for the Poisson equation (9.122)

$$\Lambda^*(\boldsymbol{x}_0, t_0) = \Lambda(\boldsymbol{x}_0, t_0) + \Sigma(\boldsymbol{x}_0, t_0)\, \delta[\hat{\boldsymbol{n}} \cdot (\boldsymbol{x}_0 - \boldsymbol{x}_{\partial\mathcal{R}})]. \tag{9.183}$$

9.5.12 Properties of the solution with Dirichlet boundary conditions

Evaluating the Dirichlet solution (9.176) on a spatial boundary, $\boldsymbol{x} = \boldsymbol{x}_{\partial\mathcal{R}} \in \partial\mathcal{R}$, eliminates both of the volume integrals so that we are left with

$$\psi^{\text{dirichlet}}(\boldsymbol{x}_{\partial\mathcal{R}}, t) = \sigma(\boldsymbol{x}_{\partial\mathcal{R}}, t) = -\int_{t_{\text{init}}}^{t} \left[\oint_{\partial\mathcal{R}} \sigma(\boldsymbol{x}_0, t_0)\, \mathbb{K} \cdot \nabla_{\boldsymbol{x}_0} G(\boldsymbol{x}, t | \boldsymbol{x}_0, t_0) \cdot \hat{\boldsymbol{n}}_{\boldsymbol{x}_0}\, \mathrm{d}\mathcal{S}_0 \right] \mathrm{d}t_0. \tag{9.184}$$

Self-consistency implies that the Green's function for the Dirichlet problem, when evaluated on the spatial boundary, satisfies

$$\hat{\boldsymbol{n}}_{\boldsymbol{x}_0} \cdot \mathbb{K}(\boldsymbol{x}_0, t_0) \cdot \nabla_{\boldsymbol{x}_0} G(\boldsymbol{x}, t | \boldsymbol{x}_0, t_0) = -\delta(t - t_0)\, \delta^{(2)}(\boldsymbol{x} - \boldsymbol{x}_0) \quad \text{with } \boldsymbol{x}, \boldsymbol{x}_0 \in \partial\mathcal{R}, \tag{9.185}$$

which is a generalization of the property (9.69) holding for the Poisson equation Green's function. It is notable that this boundary condition appears with the opposite sign to the analog (9.181) holding for the Neumann conditions.

9.5.13 The boundary propagator for the Dirichlet problem

In Sections 9.3.8 and 9.3.9 we studied the boundary Green's function for the Poisson equation. Here we extend those ideas to the *boundary propagator* for the diffusion equation, with the boundary propagator mediating the transfer of Dirichlet boundary information into the interior. Boundary propagators for diffusion and advection-diffusion (Section 69.9) have extensive use in geophysical fluids given that many tracers have no interior sources.

Defining the boundary propagator

To focus on the role of the boundary propagator, consider a tracer in which the initial conditions and interior source both vanish: $I(\boldsymbol{x}) = 0$ and $\Lambda(\boldsymbol{x}, t) = 0$. Assuming Dirichlet boundary

conditions, the initial-boundary value problem (9.166a)-(9.166c) simplifies to

$$\partial_t \psi(\boldsymbol{x},t) - \nabla_{\boldsymbol{x}} \cdot [\mathbb{K} \cdot \nabla_{\boldsymbol{x}} \psi(\boldsymbol{x},t)] = 0 \qquad \boldsymbol{x} \in \mathcal{R} \tag{9.186a}$$

$$\psi(\boldsymbol{x},t) = \sigma(\boldsymbol{x},t) \quad \boldsymbol{x} \in \partial\mathcal{R} \tag{9.186b}$$

$$\psi(\boldsymbol{x}, t = t_{\text{init}}) = 0 \qquad \boldsymbol{x} \in \mathcal{R}, \tag{9.186c}$$

with the corresponding Dirichlet Green's function solution (9.176) taking the form

$$\psi(\boldsymbol{x},t) = -\int_{t_{\text{init}}}^{t} \left[\oint_{\partial\mathcal{R}} \sigma(\boldsymbol{x}_0,t_0)\, \mathbb{K}(\boldsymbol{x}_0,t_0) \cdot \nabla_{\boldsymbol{x}_0} G(\boldsymbol{x},t|\boldsymbol{x}_0,t_0) \cdot \hat{\boldsymbol{n}}_{\boldsymbol{x}_0}\, \mathrm{d}\mathcal{S}_0 \right] \mathrm{d}t_0. \tag{9.187}$$

We define the *boundary propagator* as the kernel in this equation

$$G^{\text{bp}}(\boldsymbol{x},t|\boldsymbol{x}_0,t_0) \equiv -\mathbb{K}(\boldsymbol{x}_0,t_0) \cdot \nabla_{\boldsymbol{x}_0} G(\boldsymbol{x},t|\boldsymbol{x}_0,t_0) \cdot \hat{\boldsymbol{n}}_{\boldsymbol{x}_0} \quad \text{with } \boldsymbol{x}_0 \in \partial\mathcal{R}, \tag{9.188}$$

with this definition giving G^{bp} the dimensions of $\mathrm{L}^{-2}\ \mathrm{T}^{-1}$. Use of the boundary propagator brings the Dirichlet solution (9.187) into the succinct form

$$\psi(\boldsymbol{x},t) = \int_{t_{\text{init}}}^{t} \left[\oint_{\partial\mathcal{R}} \sigma(\boldsymbol{x}_0,t_0)\, G^{\text{bp}}(\boldsymbol{x},t|\boldsymbol{x}_0,t_0)\, \mathrm{d}\mathcal{S}_0 \right] \mathrm{d}t_0. \tag{9.189}$$

Boundary value problem satisfied by the boundary propagator

If we know the Green's function, $G(\boldsymbol{x},t|\boldsymbol{x}_0,t_0)$, then we can compute the boundary propagator through the definition (9.188). Alternatively, we can directly determine the boundary propagator by solving its boundary value problem. Following from the definition (9.188) and the boundary condition (9.185), we know that

$$G^{\text{bp}}(\boldsymbol{x},t|\boldsymbol{x}_0,t_0) = \delta(t-t_0)\, \delta^{(2)}(\boldsymbol{x}-\boldsymbol{x}_0) \quad \text{with } \boldsymbol{x},\boldsymbol{x}_0 \in \partial\mathcal{R}. \tag{9.190}$$

Hence, the boundary propagator, when evaluated along the boundary, is a Dirac delta source that fires at time $t = t_0$ at the location $\boldsymbol{x} = \boldsymbol{x}_0 \in \partial\mathcal{R}$. To determine the partial differential equation satisfied by the boundary propagator, make use of the solution (9.189) and compute its time derivative

$$\partial_t \psi(\boldsymbol{x},t) = \oint_{\partial\mathcal{R}} \sigma(\boldsymbol{x}_0,t)\, G^{\text{bp}}(\boldsymbol{x},t|\boldsymbol{x}_0,t)\, \mathrm{d}\mathcal{S}_0 + \int_{t_{\text{init}}}^{t} \left[\oint_{\partial\mathcal{R}} \sigma(\boldsymbol{x}_0,t_0)\, \frac{\partial G^{\text{bp}}(\boldsymbol{x},t|\boldsymbol{x}_0,t_0)}{\partial t}\, \mathrm{d}\mathcal{S}_0 \right] \mathrm{d}t_0. \tag{9.191}$$

The first right hand side term vanishes since the boundary propagator satisfies causality just like the Green's function when sampled at interior points

$$G^{\text{bp}}(\boldsymbol{x},t|\boldsymbol{x}_0,t_0) = 0 \quad \text{if } t_{\text{init}} < t \leq t_0 \text{ and } \boldsymbol{x} \notin \partial\mathcal{R}. \tag{9.192}$$

Similarly, equation (9.189) ensures that

$$\nabla_{\boldsymbol{x}} \cdot [\mathbb{K}(\boldsymbol{x},t) \cdot \nabla_{\boldsymbol{x}} \psi(\boldsymbol{x},t)] = \int_{t_{\text{init}}}^{t} \left[\oint_{\partial\mathcal{R}} \sigma(\boldsymbol{x}_0,t_0)\, \nabla_{\boldsymbol{x}} \cdot [\mathbb{K}(\boldsymbol{x},t) \cdot \nabla_{\boldsymbol{x}} G^{\text{bp}}(\boldsymbol{x},t|\boldsymbol{x}_0,t_0)] \right] \mathrm{d}\mathcal{S}_0\, \mathrm{d}t_0. \tag{9.193}$$

We are thus led to

$$\partial_t \psi(\boldsymbol{x},t) - \nabla_{\boldsymbol{x}} \cdot [\mathbb{K}(\boldsymbol{x},t) \cdot \nabla_{\boldsymbol{x}} \psi(\boldsymbol{x},t)]$$

$$= \int_{t_{\text{init}}}^{t} \left[\oint_{\partial\mathcal{R}} \sigma(\boldsymbol{x}_0, t_0) \left[\frac{\partial G^{\text{bp}}(\boldsymbol{x}, t|\boldsymbol{x}_0, t_0)}{\partial t} - \nabla_{\boldsymbol{x}} \cdot [\mathbb{K}(\boldsymbol{x}, t) \cdot \nabla_{\boldsymbol{x}} G^{\text{bp}}(\boldsymbol{x}, t|\boldsymbol{x}_0, t_0)] \right] \mathrm{d}\mathcal{S}_0 \right] \mathrm{d}t_0. \quad (9.194)$$

Since the left hand side vanishes via the partial differential equation (9.186a), and since the boundary data, σ, is arbitrary, we are led to the causal boundary value problem for the boundary propagator

$$\partial_t G^{\text{bp}}(\boldsymbol{x}, t|\boldsymbol{x}_0, t_0) - \nabla_{\boldsymbol{x}} \cdot [\mathbb{K} \cdot \nabla_{\boldsymbol{x}} G^{\text{bp}}(\boldsymbol{x}, t|\boldsymbol{x}_0, t_0)] = 0 \qquad \boldsymbol{x} \in \mathcal{R} \quad (9.195a)$$

$$G^{\text{bp}}(\boldsymbol{x}, t|\boldsymbol{x}_0, t_0) = 0 \qquad t < t_0 \quad (9.195b)$$

$$G^{\text{bp}}(\boldsymbol{x}, t|\boldsymbol{x}_0, t_0) = \delta(t - t_0)\, \delta^{(2)}(\boldsymbol{x} - \boldsymbol{x}_0) \qquad \boldsymbol{x}, \boldsymbol{x}_0 \in \partial\mathcal{R}. \quad (9.195c)$$

In words, we see that upon firing the Dirac delta source on the boundary at time $t = t_0$ and point $\boldsymbol{x} = \boldsymbol{x}_0 \in \partial\mathcal{R}$, the boundary propagator diffuses the Dirac source into the region interior. Whereas the Dirichlet Green's function, $G(\boldsymbol{x}, t|\boldsymbol{x}_0, t_0)$, is zero along the boundary and yet feels the Dirac delta source within the interior, the boundary propagator, $G^{\text{bp}}(\boldsymbol{x}, t|\boldsymbol{x}_0, t_0)$, places the Dirac delta source on the boundary and feels no source within the interior. Just as the causality condition means that the Green's function is a function of $t - t_0$, so too is the boundary propagator. Furthermore, a focus on the boundary propagator rather than the Green's function allows us to dispense with the need to compute the normal gradient of the Green's function at the boundary, with that calculation rather awkward in practice.

Normalization of the boundary propagator

Consider the special case of a uniform constant Dirichlet boundary data, $\sigma = \sigma_{\text{constant}}$, in the solution (9.189). Diffusion acts on this constant boundary data to spread it throughout the region. After sufficient time the solution will reach a steady state whereby $\psi = \sigma_{\text{constant}}$ at every point withing the domain. This result means that the boundary Green's function satisfies the normalization condition

$$\lim_{t_{\text{init}} \to -\infty} \int_{t_{\text{init}}}^{t} \left[\oint_{\partial\mathcal{R}} G^{\text{bp}}(\boldsymbol{x}, t|\boldsymbol{x}_0, t_0)\, \mathrm{d}\mathcal{S}_0 \right] \mathrm{d}t_0 = 1, \quad (9.196)$$

where the lower time limit is meant to indicate some arbitrary time sufficiently far in the past so that a steady state has been reached. This normalization condition holds for every point within the domain and for any time, t. It corresponds to the normalization condition (9.72) satisfied by the boundary Green's function for the Poisson equation.

9.6 Green's functions for the wave equation

The linear wave equation from Section 6.7 describes the motion of non-dispersive waves such as the acoustic waves of Chapter 51 and shallow water gravity waves of Section 55.5. These are a small subset of the waves encountered in geophysical fluid mechanics, most of which are dispersive. Even so, it is useful to here introduce the Green's function formalism for non-dispersive waves both because of its intrinsic interest, and because it offers a step towards the dispersive waves. Much of the development in this section emulates that for the diffusion equation in Section 9.5, in particular the details of causality that are shared between the diffusion equation and wave equation.

9.6.1 Initial-boundary value problem for the wave equation

Consider the following initial-boundary value problem for a wave function satisfying the linear non-dispersive wave equation

$$(\partial_{tt} - c^2\nabla^2)\,\psi(\boldsymbol{x},t) = \Lambda(\boldsymbol{x},t) \qquad \boldsymbol{x}\in\mathcal{R},\quad t > t_{\text{init}} \tag{9.197a}$$

$$\psi(\boldsymbol{x},t) = I(\boldsymbol{x}) \qquad \boldsymbol{x}\in\mathcal{R},\quad t = t_{\text{init}} \tag{9.197b}$$

$$\partial_t\psi(\boldsymbol{x},t) = J(\boldsymbol{x}) \qquad \boldsymbol{x}\in\mathcal{R},\quad t = t_{\text{init}} \tag{9.197c}$$

$$\psi(\boldsymbol{x},t) = \sigma(\boldsymbol{x},t) \qquad \boldsymbol{x}\in\partial\mathcal{R}, \tag{9.197d}$$

where $\mathcal{R}$ is a spatial region, and with Λ, I, J, and σ known functions. We choose to focus on the Dirichlet boundary problem here, though note that the Neumann boundary condition is handled similarly.[20] Compatiability between the boundary conditions and initial conditions is ensured if

$$\sigma(\boldsymbol{x},t) = I(\boldsymbol{x}) \qquad \boldsymbol{x}\in\partial\mathcal{R},\quad t = t_{\text{init}}. \tag{9.198}$$

As for the diffusion equation in Section 9.5.9, we introduced the initial time, $t = t_{\text{init}}$, which is distinct from the Dirac delta source time, $t = t_0$, appearing in the Green's function equations. Correspondingly, the Dirac delta source is fired *after* the initial time,

$$t_{\text{init}} < t_0, \tag{9.199}$$

which follows since we are interested in evolution of ψ after specification of the initial data. Correspondingly, t_{init} defines the lower limit on time integrals in the following. For the upper limit we introduce an arbitrary time $T > t_0$, with T dropping out due to causality in a manner just like it did for the diffusion equation in Section 9.5.9.

9.6.2 Uniqueness of the solution

We here consider the question of uniqueness to the solution of the wave equation. If there are two distinct solutions, ψ_1 and ψ_2, that each solve the initial-boundary value problem (9.197a)–(9.197d), then their difference, $\Psi = \psi_1 - \psi_2$, must solve the following homogeneous system

$$(\partial_{tt} - c^2\nabla^2)\,\Psi(\boldsymbol{x},t) = 0 \qquad \boldsymbol{x}\in\mathcal{R},\quad t > t_{\text{init}} \tag{9.200a}$$

$$\Psi(\boldsymbol{x},t) = 0 \qquad \boldsymbol{x}\in\mathcal{R},\quad t = t_{\text{init}} \tag{9.200b}$$

$$\partial_t\Psi(\boldsymbol{x},t) = 0 \qquad \boldsymbol{x}\in\mathcal{R},\quad t = t_{\text{init}} \tag{9.200c}$$

$$\Psi(\boldsymbol{x},t) = 0 \qquad \boldsymbol{x}\in\partial\mathcal{R}. \tag{9.200d}$$

Now multiply the homogeneous wave equation (9.200a) by $\partial_t\Psi$ and integrate over the domain, with integration by parts leading to an energy equation

$$\frac{\mathrm{d}}{\mathrm{d}t}\int_{\mathcal{R}} [(\partial_t\Psi)^2 + c^2\,\nabla\Psi\cdot\nabla\Psi]\,\mathrm{d}V = 2\,c^2\int_{\partial\mathcal{R}} (\partial_t\Psi)\,\nabla\Psi\cdot\hat{\boldsymbol{n}}\,\mathrm{d}\mathcal{S}. \tag{9.201}$$

Since $\Psi = 0$ on the boundary (equation (9.200d)), we know that $\partial_t\Psi = 0$ also holds on the boundary, so that the right hand side vanishes, meaning that the energy integral is a constant

$$\int_{\mathcal{R}} [(\partial_t\Psi)^2 + c^2\,\nabla\Psi\cdot\nabla\Psi]\,\mathrm{d}V = C. \tag{9.202}$$

[20] See Section 8.5 of *Duchateau and Zachmann* (1986) for the general Robin boundary value problem.

At the initial time, both $\Psi = 0$ and $\partial_t \Psi = 0$, in which case $\nabla \Psi = 0$ as well, which means that $C = 0$. Since the integrand is non-negative, we can only satisfy this constraint if Ψ is a space-time constant. With $\Psi = 0$ as the initial condition, then $\Psi = 0$ holds for all time, which then proves our assertion that the wave equation solution is unique.

9.6.3 Relating modified initial condition solutions

Consider the following initial-boundary value problem

$$
\begin{aligned}
(\partial_{tt} - c^2 \nabla^2)\, u(\boldsymbol{x}, t) &= 0 && \boldsymbol{x} \in \mathcal{R}, \quad t > t_{\text{init}} && \text{(9.203a)} \\
u(\boldsymbol{x}, t) &= 0 && \boldsymbol{x} \in \mathcal{R}, \quad t = t_{\text{init}} && \text{(9.203b)} \\
\partial_t u(\boldsymbol{x}, t) &= F(\boldsymbol{x}) && \boldsymbol{x} \in \mathcal{R}, \quad t = t_{\text{init}} && \text{(9.203c)} \\
u(\boldsymbol{x}, t) &= 0 && \boldsymbol{x} \in \partial\mathcal{R}, \quad t \geq 0, && \text{(9.203d)}
\end{aligned}
$$

as well as the slightly modified problem

$$
\begin{aligned}
(\partial_{tt} - c^2 \nabla^2)\, v(\boldsymbol{x}, t) &= 0 && \boldsymbol{x} \in \mathcal{R}, \quad t > t_{\text{init}} && \text{(9.204a)} \\
v(\boldsymbol{x}, t) &= F(\boldsymbol{x}) && \boldsymbol{x} \in \mathcal{R}, \quad t = t_{\text{init}} && \text{(9.204b)} \\
\partial_t v(\boldsymbol{x}, t) &= 0 && \boldsymbol{x} \in \mathcal{R}, \quad t = t_{\text{init}} && \text{(9.204c)} \\
v(\boldsymbol{x}, t) &= 0 && \boldsymbol{x} \in \partial\mathcal{R}, , \quad t \geq 0 && \text{(9.204d)}
\end{aligned}
$$

where the only difference appears in the initial conditions. Compatibility between the initial condition and boundary condition requires that $F(\boldsymbol{x}) = 0$ on $\partial\mathcal{R}$. In the following we show that

$$
v = \partial_t u, \tag{9.205}
$$

so that finding u is sufficient for finding v. Furthermore, by superposition we can handle any arbitrary initial displacement and time derivative.

For the proof, introduce the function

$$
\beta = \partial_t u, \tag{9.206}
$$

with our goal to show that β satisfies the same equations as v and then, from the uniqueness theorem in Section 9.6.2, we conclude that $\beta = v$. First observe that

$$
(\partial_{tt} - c^2\, \nabla^2)\beta = (\partial_{tt} - c^2\, \nabla^2)\partial_t u = \partial_t(\partial_{tt} - c^2\, \nabla^2)u = 0, \tag{9.207}
$$

so that β satisfies the homogeneous wave equation. Since u vanishes on $\partial\mathcal{R}$ for all time, $t \geq 0$, then it has a vanishing time derivative there as well, which means that $\beta = 0$ on $\partial\mathcal{R}$. For the initial condition, observe that

$$
\beta(\boldsymbol{x}, 0) = \partial_t u(\boldsymbol{x}, 0) = F(\boldsymbol{x}). \tag{9.208}
$$

Finally, we have

$$
\partial_t \beta(\boldsymbol{x}, t) = \partial_{tt} u(\boldsymbol{x}, t) = c^2 \nabla^2 u(\boldsymbol{x}, t). \tag{9.209}
$$

Since $u(\boldsymbol{x}, t = 0) = 0$, we know that $\nabla^2 u(\boldsymbol{x}, t = 0) = 0$, which means that

$$
\partial_t \beta(\boldsymbol{x}, 0) = 0. \tag{9.210}
$$

We have thus established that β satisfies the same initial-boundary value problem as v, which means that $\beta = v$.

9.6.4 Causal free space Green's function

The causal free space Green's function for the wave equation satisfies

$$(\partial_{tt} - c^2\nabla^2_{\boldsymbol{x}})\,\mathcal{G}(\boldsymbol{x},t|\boldsymbol{x}_0,t_0) = \delta(t-t_0)\,\delta(\boldsymbol{x}-\boldsymbol{x}_0) \qquad \boldsymbol{x},\boldsymbol{x}_0 \in \mathbb{R}^n \tag{9.211a}$$

$$\mathcal{G}(\boldsymbol{x},t|\boldsymbol{x}_0,t_0) = 0 \qquad \boldsymbol{x},\boldsymbol{x}_0 \in \mathbb{R}^n,\ \ t \le t_0 \tag{9.211b}$$

$$\partial_t\mathcal{G}(\boldsymbol{x},t|\boldsymbol{x}_0,t_0) = \delta(\boldsymbol{x}-\boldsymbol{x}_0) \qquad \boldsymbol{x},\boldsymbol{x}_0 \in \mathbb{R}^n,\ \ t = t_0, \tag{9.211c}$$

where $c > 0$ is a constant wave speed (dimensions L T^{-1}). An initial condition (9.211c) on the time derivative is needed since the wave equation has two time derivatives, and it is chosen as a Dirac source. Note that we do not impose a regularity condition at infinity, in contrast to equation (9.135b) for the diffusion equation free space Green's function. The reason is that we can conceive, at least in principle, of waves reaching out to infinity at time infinity. Finally, given the dimensions of the Dirac source, we see that the Green's function has dimensions of $\mathrm{T\,L}^{-n}$.

Consider the slightly simpler Green's function problem by focusing on times $t > t_0$ and setting $t_0 = 0$ and $\boldsymbol{x}_0 = 0$, in which case we have

$$(\partial_{tt} - c^2\nabla^2)\,g(\boldsymbol{x},t) = 0 \qquad \boldsymbol{x} \in \mathbb{R}^n,\ \ t > 0 \tag{9.212a}$$

$$g(\boldsymbol{x},t) = 0 \qquad \boldsymbol{x} \in \mathbb{R}^n,\ \ t = 0+ \tag{9.212b}$$

$$\partial_t g(\boldsymbol{x},t) = \delta(\boldsymbol{x}) \qquad \boldsymbol{x} \in \mathbb{R}^n,\ \ t = 0+, \tag{9.212c}$$

where $t = 0+$ refers to a time that is arbitrarily close to, but greater than, $t = 0$. We now show that

$$\mathcal{G}(\boldsymbol{x},t|\boldsymbol{x}_0 = 0, t_0 = 0) = \mathcal{H}(t)\,g(\boldsymbol{x},t), \tag{9.213}$$

or more generally

$$\mathcal{G}(\boldsymbol{x},t|\boldsymbol{x}_0,t_0) = \mathcal{H}(t-t_0)\,g(\boldsymbol{x},t|\boldsymbol{x}_0,t_0). \tag{9.214}$$

This result is not too surprising since, by causality, $\mathcal{G}(\boldsymbol{x},t|\boldsymbol{x}_0,t_0)$ vanishes for times prior to when the Dirac delta is fired, so we suspect it should be proportional to a Heaviside step function just like for the diffusion equation in Section 9.5.2.

A proof of equation (9.214) requires the time derivatives (dropping the $\boldsymbol{x}$ label for brevity)

$$\partial_t\mathcal{G}(t) = \delta(t)\,g(t) + \mathcal{H}(t)\,\partial_t g(t) \tag{9.215a}$$

$$\partial_{tt}\mathcal{G}(t) = (\mathrm{d}\delta(t)/\mathrm{d}t)\,g(t) + 2\,\delta(t)\,\partial_t g(t) + \mathcal{H}(t)\,\partial_{tt}g(t). \tag{9.215b}$$

To massage the $\partial_{tt}\mathcal{G}$ term, introduce a prime symbol for time derivative so that[21]

$$\delta'(t)\,g(t) + \delta(t)\,\partial_t g(t) = \delta'(t)\,g(t) - t\,\delta'(t)\,\partial_t g(t) \qquad \text{dipole identity (7.44)} \tag{9.216a}$$

$$= \delta'(t)\,[g(t) - t\,\partial_t g(t)] \qquad \text{reorganize} \tag{9.216b}$$

$$= \delta'(t)\,g(0) + t\,\delta'(t)\,[\partial_t g(0) - \partial_t g(t)] \qquad \text{Taylor series around } t = 0 \tag{9.216c}$$

$$= \delta'(t)\,g(0) - \delta(t)\,[\partial_t g(0) - \partial_t g(t)] \qquad \text{dipole identity (7.44).} \tag{9.216d}$$

Causality, along with the initial condition (9.212b), means that $g(t = 0) = 0$, so that the first term vanishes. When multiplying a function and the Dirac delta, it is sufficient to evaluate that function at the place where the Dirac fires. For the second term, the Dirac delta fires at $t = 0$, which is where $\partial_t g(0) - \partial_t g(t) = 0$, so that second term vanishes. We are thus led to

$$\partial_{tt}\mathcal{G}(t) = \delta(t)\,\partial_t g(t) + \mathcal{H}(t)\,\partial_{tt}g(t). \tag{9.217}$$

[21] These manipulations are motivated from page 61 of *Stakgold* (2000b), including his footnote.

Likewise, we find

$$\delta(t)\,\partial_t g(\boldsymbol{x},t) = \delta(t)\,\partial_t g(\boldsymbol{x},0) = \delta(t)\,\delta(\boldsymbol{x}), \tag{9.218}$$

where the final equality made use of the initial condition (9.212c). Bringing all the pieces together leads to

$$(\partial_{tt} - c^2\,\nabla^2)\mathcal{G} = \mathcal{H}(t)\,(\partial_{tt} - c^2\,\nabla^2)g + \delta(t)\,\delta(\boldsymbol{x}) = \delta(t)\,\delta(\boldsymbol{x}), \tag{9.219}$$

with the final equality holding since $(\partial_{tt} - c^2\,\nabla^2)g = 0$ as per equation (9.212a). We have thus shown that the causal free-space Green's function for the wave equation can be decomposed as in equation (9.214), in which case it is sufficient to solve equations (9.212a)-(9.212c).

9.6.5 Expressions for the free space Green's functions

Following the methods from Section 28.4 of *Dennery and Krzywicki* (1967), Section 8.5 of *Duchateau and Zachmann* (1986), and Section 5.8 of *Stakgold* (2000b), the causal free-space Green's function for the wave equation is given by[22]

$$\mathcal{G}(x,t|x_0,t_0) = \frac{\mathcal{H}[c\,(t-t_0) - |x-x_0|]}{2c} \qquad \text{for } \mathbb{R}^1 \tag{9.220a}$$

$$\mathcal{G}(\boldsymbol{x},t|\boldsymbol{x}_0,t_0) = \frac{\mathcal{H}[c\,(t-t_0) - |\boldsymbol{x}-\boldsymbol{x}_0|]}{2\,\pi\,c\,\sqrt{[c\,(t-t_0)]^2 - |\boldsymbol{x}-\boldsymbol{x}_0|^2}} \qquad \text{for } \mathbb{R}^2 \tag{9.220b}$$

$$\mathcal{G}(\boldsymbol{x},t|\boldsymbol{x}_0,t_0) = \frac{\delta[c\,(t-t_0) - |\boldsymbol{x}-\boldsymbol{x}_0|]}{4\,\pi\,c\,|\boldsymbol{x}-\boldsymbol{x}_0|} \qquad \text{for } \mathbb{R}^3. \tag{9.220c}$$

These wave solutions manifest causality since they vanish for regions in space-time that are unconnected to the source, as accords with the domain of influence shown by Figure 6.3.

There is an essential distinction between the three-dimensional Green's function (9.220c) relative to the one and two dimensional Green's functions (9.220a) and (9.220b). Namely, in three dimensions the Green's function is a spherical front that is infinitely sharp (i.e., a Dirac front) that propagates outward at speed c from the source point at $\boldsymbol{x} = \boldsymbol{x}_0$. The one and two dimensional Green's function fronts also move with speed c, yet these fronts are trailed by a wake as realized by the Heaviside step function. Furthermore, observe that the two dimensional wake decays according to the inverse distance from the front.

9.6.6 Causal Green's function for the wave equation

The causal Green's function corresponding to the initial-boundary value problem (9.197a)-(9.197d) is given by

$$(\partial_{tt} - c^2\nabla^2)\,G(\boldsymbol{x},t|\boldsymbol{x}_0,t_0) = \delta(\boldsymbol{x}-\boldsymbol{x}_0)\,\delta(t-t_0) \qquad \boldsymbol{x},\boldsymbol{x}_0 \in \mathcal{R} \tag{9.221a}$$

$$G(\boldsymbol{x},t|\boldsymbol{x}_0,t_0) = 0 \qquad \boldsymbol{x} \in \mathcal{R},\ \ t < t_0 \tag{9.221b}$$

$$G(\boldsymbol{x},t|\boldsymbol{x}_0,t_0) = 0 \qquad \boldsymbol{x} \in \partial\mathcal{R}. \tag{9.221c}$$

The following properties are of use for subsequent development.

- The time dependence only appears as the difference, $t - t_0$, so that there is no need to retain both time variables. Correspondingly,

$$\partial_t G(\boldsymbol{x},t|\boldsymbol{x}_0,t_0) = -\partial_{t_0} G(\boldsymbol{x},t|\boldsymbol{x}_0,t_0). \tag{9.222}$$

[22] Recall from Section 7.5 that the Heaviside step function is a non-dimensional function, whereas the Dirac delta has dimensions given by the inverse dimensions of its argument. These properties are key to checking that the given Green's functions in equations (9.220a)-(9.220c) have dimensions T L^{-n}, where n is the space dimenson.

- The wave operator is self-adjoint. Even so, swapping t and t_0 results in a swapped causality relation so that if $G(\boldsymbol{x}, t|\boldsymbol{x}_0, t_0)$ is the causal Green's function that satisfies equations (9.221a)-(9.221c), then $G(\boldsymbol{x}_0, t_0|\boldsymbol{x}, t)$ represents an *anti-causal* Green's function in that it satisfies

$$(\partial_{tt} - c^2\nabla^2)\, G(\boldsymbol{x}_0, t_0|\boldsymbol{x}, t) = \delta(\boldsymbol{x} - \boldsymbol{x}_0)\, \delta(t - t_0) \qquad \boldsymbol{x}, \boldsymbol{x}_0 \in \mathcal{R} \tag{9.223a}$$

$$G(\boldsymbol{x}_0, t_0|\boldsymbol{x}, t) = 0 \qquad \boldsymbol{x} \in \mathcal{R}, \quad t > t_0 \tag{9.223b}$$

$$G(\boldsymbol{x}_0, t_0|\boldsymbol{x}, t) = 0 \qquad \boldsymbol{x} \in \partial\mathcal{R}. \tag{9.223c}$$

- By the same arguments used in Section 9.6.4, we can determine the causal Green's function by solving the following initial-boundary value problem

$$(\partial_{tt} - c^2\nabla^2)\, g(\boldsymbol{x}, t|\boldsymbol{x}_0, t_0) = 0 \qquad \boldsymbol{x}, \boldsymbol{x}_0 \in \mathcal{R} \quad t > t_0 \tag{9.224a}$$

$$g(\boldsymbol{x}, t|\boldsymbol{x}_0, t_0) = 0 \qquad \boldsymbol{x} \in \mathcal{R}, \quad t = t_0 \tag{9.224b}$$

$$\partial_t g(\boldsymbol{x}, t|\boldsymbol{x}_0, t_0) = \delta(\boldsymbol{x} - \boldsymbol{x}_0) \qquad \boldsymbol{x} \in \mathcal{R}, \quad t = t_0 \tag{9.224c}$$

$$g(\boldsymbol{x}, t|\boldsymbol{x}_0, t_0) = 0 \qquad \boldsymbol{x} \in \partial\mathcal{R}. \tag{9.224d}$$

As in equation (9.214) for the free space Green's function, we have

$$G(\boldsymbol{x}, t|\boldsymbol{x}_0, t_0) = \mathcal{H}(t - t_0)\, g(\boldsymbol{x}, t|\boldsymbol{x}_0, t_0). \tag{9.225}$$

9.6.7 Green's function solution to the wave equation

The self-adjoint nature of the wave operator simplifies the derivation of the Green's function solution relative to that needed for the diffusion equation in Section 9.5. To proceed, multiply the swapped Green's function equation (9.223a) by the wave function and integrate over the space-time domain

$$\psi(\boldsymbol{x}_0, t_0) = \int_{\mathcal{R}} \int_{t_{\text{init}}}^{T} \psi(\boldsymbol{x}, t)\, (\partial_{tt} - c^2\nabla^2)\, G(\boldsymbol{x}_0, t_0|\boldsymbol{x}, t)\, \mathrm{d}t\, \mathrm{d}V_{\boldsymbol{x}}. \tag{9.226}$$

Dropping arguments for brevity, we move the wave operator from the Green's function to the wave function, thus leading to

$$\psi\, (\partial_{tt} - c^2\nabla^2)\, G = G\, (\partial_{tt} - c^2\, \nabla^2)\psi + \partial_t(\psi\, \partial_t G - G\, \partial_t\psi) - c^2\, \nabla \cdot (\psi\, \nabla G - G\, \nabla\psi). \tag{9.227}$$

Making use of the partial differential equation (9.197a) satisfied by the wave equation brings the first right hand side term to

$$G(\boldsymbol{x}_0, t_0|\boldsymbol{x}, t)\, (\partial_{tt} - c^2\, \nabla^2)\psi(\boldsymbol{x}, t) = G(\boldsymbol{x}_0, t_0|\boldsymbol{x}, t)\, \Lambda(\boldsymbol{x}, t). \tag{9.228}$$

The space integral of the space derivative term in equation (9.227) is given by

$$\int_{\mathcal{R}} \nabla_{\boldsymbol{x}} \cdot (\psi\, \nabla_{\boldsymbol{x}} G - G\, \nabla_{\boldsymbol{x}}\psi)\, \mathrm{d}V_{\boldsymbol{x}} = \int_{\partial\mathcal{R}} \sigma(\boldsymbol{x}, t)\, \nabla_{\boldsymbol{x}} G(\boldsymbol{x}_0, t_0|\boldsymbol{x}, t) \cdot \hat{\boldsymbol{n}}\, \mathrm{d}\mathcal{S}_{\boldsymbol{x}}, \tag{9.229}$$

where we used the Dirichlet boundary condition (9.197d) satisfied by ψ and the homogeneous Dirichlet condition (9.223c) satisfied by the Green's function.

We need to do a bit more work for the time integral of the time derivative term in equation

(9.227), which is given by

$$\int_{t_{\text{init}}}^{T} \partial_t(\psi\,\partial_t G - G\,\partial_t\psi)\,\mathrm{d}t = [\psi(\boldsymbol{x},t)\,\partial_t G(\boldsymbol{x}_0,t_0|\boldsymbol{x},t) - G(\boldsymbol{x}_0,t_0|\boldsymbol{x},t)\,\partial_t\psi(\boldsymbol{x},t)]\Big|_{t_{\text{init}}}^{T}. \tag{9.230}$$

The initial conditions (9.197b) and (9.197c), along with the anti-causality condition (9.223b), render

$$\int_{t_{\text{init}}}^{T} \partial_t(\psi\,\partial_t G - G\,\partial_t\psi)\,\mathrm{d}t = -I(\boldsymbol{x})\,\partial_t G(\boldsymbol{x}_0,t_0|\boldsymbol{x},t_{\text{init}}) + J(\boldsymbol{x})\,G(\boldsymbol{x}_0,t_0|\boldsymbol{x},t_{\text{init}}) \tag{9.231a}$$

$$= I(\boldsymbol{x})\,\partial_{t_0} G(\boldsymbol{x}_0,t_0|\boldsymbol{x},t_{\text{init}}) + J(\boldsymbol{x})\,G(\boldsymbol{x}_0,t_0|\boldsymbol{x},t_{\text{init}}), \tag{9.231b}$$

where the second equality used the property (9.222) of the time derivatives acting on the Green's function. Notice that the upper time limit, T, drops out due to the anti-causality condition.

Bringing terms together leads to the Green's function solution to the wave equation

$$\begin{aligned}\psi(\boldsymbol{x}_0,t_0) = &\int_{\mathcal{R}}\int_{t_{\text{init}}}^{t_0} \Lambda(\boldsymbol{x},t)\,G(\boldsymbol{x}_0,t_0|\boldsymbol{x},t)\,\mathrm{d}t\,\mathrm{d}V_{\boldsymbol{x}}\\ &- c^2\int_{\partial\mathcal{R}}\int_{t_{\text{init}}}^{t_0} \sigma(\boldsymbol{x},t)\nabla_{\boldsymbol{x}}G(\boldsymbol{x}_0,t_0|\boldsymbol{x},t)\cdot\boldsymbol{n}\,\mathrm{d}\mathcal{S}_{\boldsymbol{x}}\\ &+ \int_{\mathcal{R}} [I(\boldsymbol{x})\,\partial_{t_0} G(\boldsymbol{x}_0,t_0|\boldsymbol{x},t_{\text{init}}) + J(\boldsymbol{x})\,G(\boldsymbol{x}_0,t_0|\boldsymbol{x},t_{\text{init}})]\,\mathrm{d}V_{\boldsymbol{x}}.\end{aligned} \tag{9.232}$$

Again notice that the upper time limit, T, drops out due to the anti-causality condition. Hence, the Green's function solution (9.232) only depends on processes happening between the initial time, t_{init}, and current time, t_0, thus manifesting causality. This solution shares much with the diffusion equation in Section 9.5, but here with the addition of a second initial condition due to the second order time derivative appearing in the wave equation, whereas there is only a single time derivative in the diffusion equation.

9.6.8 The Helmholtz equation

Consider the wave equation (9.197a) in unbounded space

$$(\partial_{tt} - c^2\,\nabla^2)\,\psi = \lambda. \tag{9.233}$$

Now introduce the time-frequency Fourier transforms, $\Psi(\boldsymbol{x},\omega)$ and $\Lambda(\boldsymbol{x},\omega)$ (see equations (8.102a) and (8.102b)) whereby

$$\psi(\boldsymbol{x},t) = \frac{1}{2\pi}\int_{-\infty}^{\infty} \Psi(\boldsymbol{x},\omega)\,\mathrm{e}^{-\mathrm{i}\,\omega\,t}\,\mathrm{d}\omega \quad\text{and}\quad \lambda(\boldsymbol{x},t) = \frac{1}{2\pi}\int_{-\infty}^{\infty} \Lambda(\boldsymbol{x},\omega)\,\mathrm{e}^{-\mathrm{i}\,\omega\,t}\,\mathrm{d}\omega, \tag{9.234}$$

thus yielding the frequency domain version of the wave equation

$$[\nabla^2 + (\omega/c)^2]\,\Psi = -\Lambda/c^2. \tag{9.235}$$

This is the *Helmholtz equation* first introduced in Section 6.7.3, and its corresponding free space Green's function satisfies the singular elliptic problem

$$[\nabla^2 + (\omega/c)^2]\,\mathcal{G}(\boldsymbol{x}|\boldsymbol{x}_0;\omega) = -\delta(\boldsymbol{x}-\boldsymbol{x}_0). \tag{9.236}$$

Observe that the Helmholtz operator, $\nabla^2 + (\omega/c)^2$, differs from the screened Poisson operator, $\nabla^2 - \mu^2$ (equation (9.32)), due to the differing signs on the constant. One may relate the two by

setting

$$\mu = -\mathrm{i}\,\omega/c. \tag{9.237}$$

This connection proves rather important for both the physics and the maths, yet with details involving aspects of causality and complex analysis that are beyond our scope.[23] It is satisfying that the details do confirm that the Helmholtz free space Green's function is related to the screened Poisson Green's function (9.36c) simply by setting $\mu = -\mathrm{i}\,\omega/c$, so that

$$\mathcal{G}(\boldsymbol{x}|\boldsymbol{x}_0;\omega) = \frac{\mathrm{e}^{\mathrm{i}\,|\boldsymbol{x}-\boldsymbol{x}_0|\,\omega/c}}{4\,\pi\,|\boldsymbol{x}-\boldsymbol{x}_0|}. \tag{9.238}$$

9.7 Initial value problems and response functions

In this section we focus on initial value problems and study the response functions that help to characterize a dynamical system. For this purpose, consider the first order ordinary differential equation

$$[\mathrm{d}/\mathrm{d}t + \lambda(t)]\,\psi(t) = F(t) \quad \text{with } \psi(t \le t_{\text{init}}) = 0, \tag{9.239}$$

where ψ is some geophysical field, such as the anomalous sea surface temperature, λ is a feedback parameter that is positive for a damped system, and F is a forcing function such as that introduced by atmospheric variability on the surface ocean. We are only concerned with temporal behavior so that all spatial information is ignored. This equation has found widespread use in the climate dynamics community, largely following the work of *Hasselmann* (1976).

The material in this section could well have been presented near the start of this chapter since we are only concerned with ordinary differential equations. However, placing it at the end helps to tie together material sprinkled throughout this chapter, and to connect to applications of Green's functions for studies of climate dynamics.

9.7.1 Impulse response function

Consider the system (9.239) with $\lambda > 0$ a time-independent feedback parameter damping the system back to zero, and with the forcing given by a weighted Dirac delta

$$[\mathrm{d}/\mathrm{d}t + \lambda]\,G(t|t_0) = \alpha\,\delta(t - t_0) \quad \text{with } G(t|t_0) = 0 \text{ for } t < t_0, \tag{9.240}$$

where $\alpha > 0$ is a constant dimensionless scaling coefficient. We refer to the resulting causal Green's function, $G(t|t_0)$, as the *impulse response function* since it represents the response of the dynamical system to an impulse provided by the Dirac delta.[24]

Initial condition for the impulse response function

To determine the initial condition for the Green's function, integrate equation (9.240) over an interval containing the source time, t_0, to render

$$\lim_{\epsilon \to 0} \left[G(t_0 + \epsilon|t_0) - G(t_0 - \epsilon|t_0) + \int_{t_0-\epsilon}^{t_0+\epsilon} \lambda\,G(t|t_0)\,\mathrm{d}t \right] = \alpha. \tag{9.241}$$

[23] *Fetter and Walecka* (2003) present a lucid discussion of the role of causality in their Section 50. See also Section 5.8 and 7.12 of *Stakgold* (2000b) for a detailed presentation of the mathematical derivations.

[24] Recall our discussion of impulse in Section 7.13.

Causality means that $G(t_0 - \epsilon|t_0) = 0$ so that

$$\lim_{\epsilon\to 0} G(t_0 + \epsilon|t_0) + \lim_{\epsilon\to 0}\int_{t_0}^{t_0+\epsilon} \lambda\, G(t|t_0)\,\mathrm{d}t = \alpha. \tag{9.242}$$

We assume that the integral vanishes in the limit of $\epsilon \to 0$, which is a sensible assumption since the only means to have a nonzero integral is if the Green's function had a singularity similar to a Dirac delta. We are thus led to the initial condition for the Green's function

$$G(t = t_0|t_0) = \alpha. \tag{9.243}$$

Solution for the impulse response function

The causality condition $G(t < t_0|t_0) = 0$ can be satisfied by introducing the Heaviside step function from Section 7.5

$$G(t|t_0) = \mathcal{H}(t - t_0)\, g(t) \quad \text{with} \quad [\mathrm{d}/\mathrm{d}t + \lambda]\, g = 0 \quad \text{and} \quad g(t = t_0) = \alpha, \tag{9.244}$$

with the solution readily determined to be the damped exponential

$$G(t|t_0) = \mathcal{H}(t - t_0)\, \alpha\, \mathrm{e}^{-\lambda\,(t-t_0)}. \tag{9.245}$$

We verify this function satisfies the initial value problem (9.240) by noting that

$$\mathrm{d}G(t|t_0)/\mathrm{d}t = \alpha\,\delta(t - t_0)\,\mathrm{e}^{-\lambda\,(t-t_0)} - \lambda\, G(t|t_0) = \alpha\,\delta(t - t_0) - \lambda\, G(t|t_0). \tag{9.246}$$

To reach the second equality, we noted that the $\mathrm{e}^{-\lambda\,(t-t_0)}$ term multiplying the Dirac delta is unity at $t = t_0$, and so it does not alter the sifting property of the Dirac delta. Hence, following the discussion leading to equation (7.39), we can drop $\mathrm{e}^{-\lambda\,(t-t_0)}$ from the Dirac. As illustrated in Figure 9.7, the impulse response function (9.245) has a particularly simple interpretation as the damped exponential response of the dynamical system to a Dirac impulse fired at $t = t_0$.

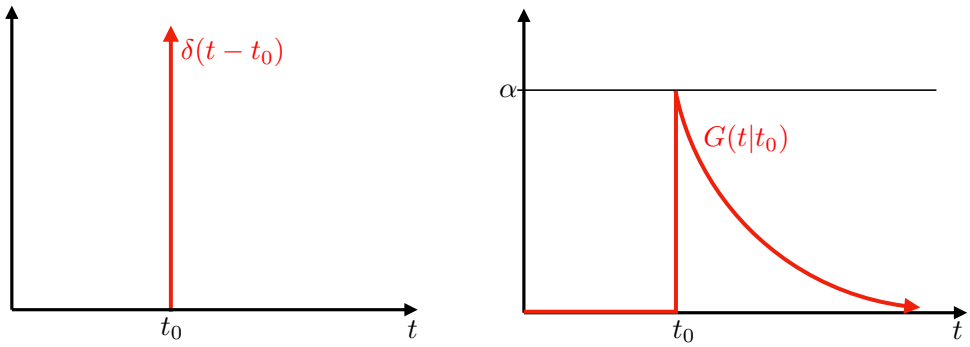

FIGURE 9.7: Left panel: Dirac delta that is fired at time $t = t_0$. Right panel: The impulse response function (9.245) resulting from the Dirac delta impulse as realized for the damped linear system (9.240).

9.7.2 Step response function

Rather than hit the system at a particular moment in time with a Dirac delta, we may choose to impose a force that turns on and remains on after some initial time, as per a Heaviside step function. The *step response function*, $S(t|t_0)$, measures the response of the dynamical system to this step forcing and it satisfies the differential equation

$$[\mathrm{d}/\mathrm{d}t + \lambda]\, S(t|t_0) = \alpha\,\mathcal{H}(t - t_0) \quad \text{with } S(t|t_0) = 0 \text{ for } t < t_0. \tag{9.247}$$

Note that in the steady state at $t \to \infty$, the step response function asymptotes to the constant

$$\lim_{t\to\infty} S(t|t_0) = \alpha/\lambda. \tag{9.248}$$

Connection to the impulse response function

Taking the time derivative, $\mathrm{d}/\mathrm{d}t_0$, on the step response function equation (9.247) leads to

$$[\mathrm{d}/\mathrm{d}t + \lambda]\, \mathrm{d}S(t|t_0)/\mathrm{d}t_0 = \alpha\, \mathrm{d}\mathcal{H}(t-t_0)/\mathrm{d}t_0. \tag{9.249}$$

The derivative of the Heaviside step function equals to the Dirac delta as per equation (7.22), in which

$$\mathrm{d}\mathcal{H}(t-t_0)/\mathrm{d}t_0 = -\mathrm{d}\mathcal{H}(t-t_0)/\mathrm{d}t = -\delta(t-t_0). \tag{9.250}$$

Use of this result in equation (9.249), and comparison to the impulse response function equation (9.240), yields the identity

$$\frac{\mathrm{d}S(t|t_0)}{\mathrm{d}t_0} = -G(t|t_0). \tag{9.251}$$

This identity holds even when the feedback parameter is a function of time, $\lambda = \lambda(t)$, since the time derivative operator, $\mathrm{d}/\mathrm{d}t_0$, has no affect on $\lambda(t)$.

Initial condition for the step response function

To determine the initial condition for the step response function, integrate equation (9.247) over an interval bounding t_0 and take the limit as that interval vanishes

$$\lim_{\epsilon\to 0}\left[S(t_0+\epsilon|t_0) - S(t_0-\epsilon|t_0) + \int_{t_0-\epsilon}^{t_0+\epsilon} \lambda\, S(t|t_0)\,\mathrm{d}t = \int_{t_0-\epsilon}^{t_0+\epsilon} \mathcal{H}(t-t_0)\,\mathrm{d}t\right]. \tag{9.252}$$

Causality means that $S(t_0-\epsilon|t_0) = 0$. Furthermore, the integral of the Heaviside is given by

$$\lim_{\epsilon\to 0}\int_{t_0-\epsilon}^{t_0+\epsilon} \mathcal{H}(t-t_0)\,\mathrm{d}t = \lim_{\epsilon\to 0}\int_{t_0}^{t_0+\epsilon} \mathcal{H}(t-t_0)\,\mathrm{d}t = \lim_{\epsilon\to 0}\epsilon = 0, \tag{9.253}$$

so that

$$\lim_{\epsilon\to 0} S(t_0+\epsilon|t_0) = \epsilon\,\lambda \Longrightarrow S(t=t_0|t_0) = 0. \tag{9.254}$$

That is, the step response function starts at zero and then grows in time in response to the Heaviside step function forcing.

Solution for the step response function

It is straightforward to show that the causal step response function is given by the saturating exponential

$$S(t|t_0) = \frac{\alpha}{\lambda}\left[1 - \mathrm{e}^{-\lambda\,(t-t_0)}\right]\mathcal{H}(t-t_0). \tag{9.255}$$

Figure 9.8 depicts this function along with the Heaviside step forcing. Furthermore, we verify the connection between $S(t|t_0)$ and $G(t|t_0)$ by computing

$$\mathrm{d}S(t|t_0)/\mathrm{d}t_0 = -\alpha\,\mathcal{H}(t-t_0)\,\mathrm{e}^{-\lambda\,(t-t_0)} - \frac{\alpha}{\lambda}\left[1-\mathrm{e}^{-\lambda\,(t-t_0)}\right]\delta(t-t_0) \tag{9.256a}$$

$$= -G(t|t_0) - \frac{\alpha}{\lambda}\left[1-\mathrm{e}^{-\lambda\,(t-t_0)}\right]\delta(t-t_0). \tag{9.256b}$$

The second term on the right hand side vanishes since

$$\int_{t_0-\epsilon}^{t_0+\epsilon} \left[1 - \mathrm{e}^{-\lambda\,(t-t_0)}\right] \delta(t-t_0)\,\mathrm{d}t = 0, \tag{9.257}$$

in which case we have

$$\mathrm{d}S(t|t_0)/\mathrm{d}t_0 = -G(t|t_0). \tag{9.258}$$

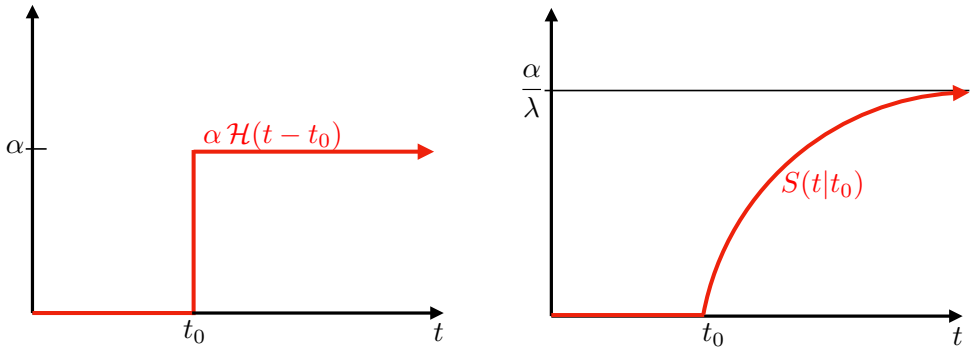

FIGURE 9.8: Left panel: Heaviside step function is fired at time $t = t_0$ and stays on afterward. Right panel: The step response function (9.255) resulting from the Heaviside step forcing impulse as realized for the damped linear system (9.240).

9.7.3 Reciprocity relation

The initial value problem (9.239) is not self-adjoint. Hence, we need to develop a reciprocity condition for the impulse response function and its adjoint, following the procedure used for the diffusion equation in Section 9.5.7. Again, the impulse response function satisfies

$$[\mathrm{d}/\mathrm{d}t + \lambda]\, G(t|t_1) = \alpha\,\delta(t-t_1) \quad \text{with } G(t|t_1) = 0 \text{ for } t < t_1 \text{ and } G(t_1|t_1) = \alpha, \tag{9.259}$$

and the adjoint impulse response function satisfies

$$[-\mathrm{d}/\mathrm{d}t + \lambda]\, G^{\ddagger}(t|t_2) = \alpha\,\delta(t-t_2) \quad \text{with } G^{\ddagger}(t|t_2) = 0 \text{ for } t > t_2 \text{ and } G^{\ddagger}(t_2|t_2) = \alpha. \tag{9.260}$$

We here introduced two Dirac delta source times, t_1, t_2, which both occur after the initial time and before the end time

$$t_{\text{init}} < t_1, t_2 < T. \tag{9.261}$$

As we will see, causality eliminates the final time, T, from the solution for ψ. We retain it merely for bookeeping.

Determining the reciprocity relation between $G^{\ddagger}$ and G follows by multiplying equation (9.259) by $G^{\ddagger}(t|t_2)$ and multiplying equation (9.260) by $G(t|t_1)$ and then subtracting

$$\frac{\mathrm{d}}{\mathrm{d}t}\left[G(t|t_1)\,G^{\ddagger}(t|t_2)\right] = \alpha\,[G^{\ddagger}(t|t_2)\,\delta(t-t_1) - G(t|t_1)\,\delta(t-t_2)]. \tag{9.262}$$

Now integrate this equation over the time range $t_{\text{init}} \le t \le T$. For the right hand side we assume α to be a constant, which then leads to the difference $G^{\ddagger}(t_1|t_2) - G(t_2|t_1)$. For the left hand side, use of the causality conditions in equations (9.259) and (9.260) render

$$\int_{t_{\text{init}}}^{T} \frac{\mathrm{d}}{\mathrm{d}t}\left[G(t|t_1)\,G^{\ddagger}(t|t_2)\right]\mathrm{d}t = 0, \tag{9.263}$$

thus yielding the reciprocity relation

$$G^{\ddagger}(t|t_0) = G(t_0|t). \tag{9.264}$$

The feedback parameter, λ, dropped out from the derivation, with the reciprocity relation holding even if λ is time dependent. However, we again needed to assume the coefficient α to be constant.

9.7.4 Response function for general forcing

We now return to the initial value problem (9.239) and determine the response, ψ, to a general forcing function, $F(t)$, that turns on at some initial time $t = t_0 > t_{\text{init}}$. As for our earlier discussions of Green's functions, we express the general response function as an integral over impulse responses. For this purpose, multiply equation (9.239) by $G^{\ddagger}(t|t_0)$ and the adjoint equation (9.260) by $\psi(t)$, subtract, and then integrate to find

$$\alpha\,\psi(t_0) = \int_{t_{\text{init}}}^{T} G^{\ddagger}(t|t_0)\,F(t)\,\mathrm{d}t - \int_{t_{\text{init}}}^{T} \frac{\mathrm{d}}{\mathrm{d}t}\Big[G^{\ddagger}(t|t_0)\,\psi(t)\Big]\,\mathrm{d}t. \tag{9.265}$$

Making use of the causality condition $G^{\ddagger}(t|t_0) = 0$ for $t > t_0$ leads to

$$\alpha\,\psi(t_0) = G^{\ddagger}(t_{\text{init}}|t_0)\,\psi(t_{\text{init}}) + \int_{t_{\text{init}}}^{t_0} G^{\ddagger}(t|t_0)\,F(t)\,\mathrm{d}t, \tag{9.266}$$

where we retained the possibility of $\psi(t_{\text{init}}) \neq 0$ for a bit of generality. The reciprocity condition (9.264) brings this equation to the form

$$\alpha\,\psi(t_0) = G(t_0|t_{\text{init}})\,\psi(t_{\text{init}}) + \int_{t_{\text{init}}}^{t_0} G(t_0|t)\,F(t)\,\mathrm{d}t, \tag{9.267}$$

and swapping symbols, $t \leftrightarrow t_0$, yields

$$\alpha\,\psi(t) = G(t|t_{\text{init}})\,\psi(t_{\text{init}}) + \int_{t_{\text{init}}}^{t} G(t|t_0)\,F(t_0)\,\mathrm{d}t_0. \tag{9.268}$$

As anticipated, the general response is written as an initial response plus the integral of the general forcing with the impulse response function. Causality ensures that ψ is dependent only on forcing that is active between the initial time, t_{init}, and current time, t. To garner further insights into the general expression (9.268), consider the special case of constant feedback parameter, λ, in which the impulse response function is (9.245) so that

$$\psi(t) = \mathrm{e}^{-\lambda\,(t-t_{\text{init}})}\,\psi(t_{\text{init}}) + \int_{t_{\text{init}}}^{t} \mathrm{e}^{-\lambda\,(t-t_0)}\,F(t_0)\,\mathrm{d}t_0. \tag{9.269}$$

9.7.5 Connection to the boundary propagator

Recall our discussion in Section 9.5.13 of the boundary propagator, $G^{\text{bp}}(\boldsymbol{x}, t|\boldsymbol{x}_0, t_0)$, for the diffusion equation, which solves the causal boundary value problem (9.195a)-(9.195c). Again, the boundary propogator measures the response of the system at $(\boldsymbol{x}, t)$ to a Dirac delta space-time source imposed along the surface boundary. The details of the diffusion process are encoded into the boundary propagator so that the propagator is able to build up the response, ψ, to a general boundary forcing function, σ, as per equation (9.189). The discussion in the present section thus prompts us to consider the boundary propagator as an impulse response function for spatially

distributed sources whose influence through space and time is mediated by diffusion.

9.7.6 Comments and further study

Many applications of Green's function methods in geophysical fluid mechanics and climate dynamics do not make use of analytical methods to solve for the Green's function. Instead, they make use of numerical estimates based on time stepping passive tracers in ocean and atmosphere models, with source functions approximating Dirac delta sources. Many applications have focused on boundary propagators, which as shown in this section are equivalant to impulse response functions for boundary sources. We return to this point when discussing the passive tracer equation in Section 69.9.

Hasselmann et al. (1993) introduced the impulse response function and step response function to the study of climate model drift. *Marshall et al.* (2014) and *Zanna et al.* (2019) presented further studies using this framework. Some of the mathematical formulation of impulse response and step response functions as presented here follow that offered in Exercise 1.52 of *Stakgold* (2000a).

9.8 Helmholtz decomposition

In characterizing the kinematic properties of vector fields, such as the velocity vector for a moving fluid, *Helmholtz* (1867) introduced a method to decompose any vector into two distinct components whose properties are readily analyzed: one component vector has a zero divergence and the second vector has a zero curl. This *Helmholtz decomposition* has extensive applications throughout fluid mechanics. See also *Bhatia et al.* (2013) for a review, as well as an earlier treatment in Section 26 of *Serrin* (1959). We make particular use of the Helmholtz decomposition when introducing a scalar or vector potential for studying the kinematics of non-divergent fluid flows (Chapter 21). In this section we provide further insights into features of the Helmholtz decomposition, with much of the discussion following *Denaro* (2003) and *Bhatia et al.* (2013). Note that our treatment makes use of Cartesian vector analysis, with more general treatments, such as Chapter 14 of *Frankel* (2012), outside our scope.

To introduce the Helmholtz decomposition, consider a vector field, $\boldsymbol{F}$, written using Cartesian coordinates and in free space (i.e., no boundaries), and assume the field decays to zero outside of a finite domain. In this case we can decompose $\boldsymbol{F}$ into

$$\boldsymbol{F} = -\nabla D + \nabla \times \boldsymbol{R}, \tag{9.270}$$

where

$$D(\boldsymbol{x}) = \frac{1}{4\pi} \int_{\mathcal{R}} \frac{\nabla \cdot \boldsymbol{F}(\boldsymbol{x}')}{|\boldsymbol{x} - \boldsymbol{x}'|} \, \mathrm{d}V' \tag{9.271a}$$

$$\boldsymbol{R}(\boldsymbol{x}) = \frac{1}{4\pi} \int_{\mathcal{R}} \frac{\nabla \times \boldsymbol{F}(\boldsymbol{x}')}{|\boldsymbol{x} - \boldsymbol{x}'|} \, \mathrm{d}V'. \tag{9.271b}$$

The scalar potential, D, and vector potential, $\boldsymbol{R}$, are here given by the Green's function solutions derived in Section 9.3.7.

The Helmholtz decomposition (9.271a) and (9.271b) is both elegant and straightforward. It offers motivation to seek a similar decomposition for domains of relevance to geophysical fluids, where boundaries play a fundamental role. However, there are many mathematical nuances associated with Helmholtz decompositions in more general situations, each depending on the domain topology and nature of the prescribed boundary conditions. Our goal in this section is to explore the mathematics for a few common boundary conditions for a fluid on simply connected

manifolds.[25] We offer rather brief comments for the more general non-simply connected case as the mathematics is beyond our scope.[26]

9.8.1 Summarizing the Helmholtz decomposition

The Helmholtz decomposition on a simply connected manifold, $\mathcal{R}$, states that a vector field, $\boldsymbol{F}$, is fully determined by specifying its divergence, $\nabla \cdot \boldsymbol{F}$, and curl, $\nabla \times \boldsymbol{F}$, for points $\boldsymbol{x} \in \mathcal{R}$, along with the normal component, $\hat{\boldsymbol{n}} \cdot \boldsymbol{F}$, or the tangential component[27], $\hat{\boldsymbol{n}} \times \boldsymbol{F}$, along the domain boundary, $\partial\mathcal{R}$. Here, $\hat{\boldsymbol{n}}$ is the outward normal along the boundary. Expressed with equations, the Helmholtz decomposition is given by

$$\boldsymbol{F} = -\nabla D + \nabla \times \boldsymbol{R} = \text{gradient term (curl-free)} + \text{rotation term (divergence-free)}. \tag{9.272}$$

The scalar potential, D, is arbitrary up to a constant, and the vector potential, $\boldsymbol{R}$, is arbitrary up to the gradient of a scalar field. This ambiguity in specifying D and $\boldsymbol{R}$ is referred to as *gauge invariance* or *gauge freedom*, and we encounter it in other contexts within this book. For present purposes, gauge freedom allows us to choose the *Coulomb gauge* that is commonly used in electromagnetics (*Jackson*, 1975), whereby $\boldsymbol{R}$ is prescribed to be divergence-free

$$\nabla \cdot \boldsymbol{R} = 0. \tag{9.273}$$

As seen next, this constraint simplifies the boundary value problem satisfied by $\boldsymbol{R}$.

Taking the divergence of (9.272) reveals that the scalar potential satisfies the Poisson equation

$$-\nabla^2 D = \nabla \cdot \boldsymbol{F} \quad \text{for } \boldsymbol{x} \in \mathcal{R}. \tag{9.274}$$

Taking the curl of the decomposition (9.272), and using the curl identity (2.42c) along with the Coulomb gauge (9.273)

$$\nabla \times (\nabla \times \boldsymbol{R}) = \nabla(\nabla \cdot \boldsymbol{R}) - \nabla^2 \boldsymbol{R} = -\nabla^2 \boldsymbol{R}, \tag{9.275}$$

leads to the vector Poisson equation

$$-\nabla^2 \boldsymbol{R} = \nabla \times \boldsymbol{F} \quad \text{for } \boldsymbol{x} \in \mathcal{R}. \tag{9.276}$$

The two elliptic equations, (9.274) and (9.276), are supplemented by boundary conditions for points $\boldsymbol{x} \in \partial\mathcal{R}$. The choice of boundary conditions depend on information available about the vector $\boldsymbol{F}$ along the boundary. We here consider the following three sets of boundary conditions, with $\hat{\boldsymbol{n}}$ the outward unit normal along $\partial\mathcal{R}$:

$$\text{normal component} \qquad -\hat{\boldsymbol{n}} \cdot \nabla D = \hat{\boldsymbol{n}} \cdot \boldsymbol{F} \quad \text{and} \quad \hat{\boldsymbol{n}} \cdot (\nabla \times \boldsymbol{R}) = 0 \tag{9.277a}$$

$$\text{tangential component} \qquad \hat{\boldsymbol{n}} \times \nabla D = 0 \quad \text{and} \quad \hat{\boldsymbol{n}} \times (\nabla \times \boldsymbol{R}) = \hat{\boldsymbol{n}} \times \boldsymbol{F} \tag{9.277b}$$

$$\text{vanishing boundary} \qquad \hat{\boldsymbol{n}} \cdot \nabla D = 0 \quad \text{and} \quad \hat{\boldsymbol{n}} \times (\nabla \times \boldsymbol{R}) = 0 \Longrightarrow \boldsymbol{F} = 0. \tag{9.277c}$$

The homogeneous Neumann boundary condition $\hat{\boldsymbol{n}} \cdot (\nabla \times \boldsymbol{R}) = 0$ in equation (9.277a) means

[25] A manifold is simply connected if a closed curve can be continuously shrunk to a point while remaining on the manifold. For example, the domain of the global ocean on a water covered planet is a simply connected manifold. Adding land masses in the form of islands or continents makes the ocean domain non-simply connected.

[26] Section 5.2 of *Bhatia et al.* (2013) provides a few comments on the non-simply connected case, whereas chapter 14 of *Frankel* (2012) provides details for the mathematically experienced reader.

[27] *Helmholtz* (1867) only considered vector fields with a specified normal component along boundaries. This situation is most common in fluid mechanical applications. *Denaro* (2003) showed how specification of the tangential component along the boundary also allows for a Helmholtz decomposition. We explore both boundary conditions in this section.

that $(\nabla \times \boldsymbol{R})$ is parallel to the boundary. Likewise, $\hat{\boldsymbol{n}} \times \nabla D = 0$ in equation (9.277b) means that ∇D is parallel to the boundary. If $\boldsymbol{F} = \boldsymbol{v}$ is the fluid velocity field, then $\boldsymbol{v} \cdot \hat{\boldsymbol{n}} = 0$ is the no-normal flow kinematic condition that holds for static solid boundaries (Section 19.6.1). Furthermore, the vanishing boundary condition (9.277c) holds for the velocity with the dynamic no-slip boundary condition discussed in Section 25.10.3.

9.8.2 Concerning a harmonic contribution

Consider a vector $\boldsymbol{H}$ that is both divergent-free and curl-free

$$\nabla \cdot \boldsymbol{H} = 0 \quad \text{and} \quad \nabla \times \boldsymbol{H} = 0. \tag{9.278}$$

$\boldsymbol{H}$ is a harmonic vector function (Section 6.5.1), which is seen by noting that with $\nabla \cdot \boldsymbol{H} = 0$ then (see equation (2.42c)) $\boldsymbol{H}$ satisfies the vector Laplace equation

$$\nabla \times (\nabla \times \boldsymbol{H}) = -\nabla^2 \boldsymbol{H} = 0, \tag{9.279}$$

so that each component of $\boldsymbol{H}$ is a harmonic function.

An arbitrary vector, $\boldsymbol{F}$, generally contains a portion that is harmonic, in which case we consider the three-component decomposition

$$\boldsymbol{F} = -\nabla E + \nabla \times \boldsymbol{S} + \boldsymbol{H} = \text{gradient term} + \text{rotation term} + \text{harmonic term}. \tag{9.280}$$

However, as we show in this section, there are many physically interesting cases in which the original two-component Helmholtz decomposition (9.272) is sufficient. That is, for many cases the two-component Helmholtz decomposition is able to include contributions from the harmonic portion of $\boldsymbol{F}$ as part of either ∇D or $\nabla \times \boldsymbol{R}$.

Normal component boundary condition

The constraint $\nabla \times \boldsymbol{H} = 0$ can be satisfied by writing $\boldsymbol{H} = -\nabla\phi$, which then brings the decomposition (9.280) into the form

$$\boldsymbol{F} = -(\nabla E + \nabla\phi) + \nabla \times \boldsymbol{S}. \tag{9.281}$$

We connect this decomposition to the orginal form of the Helmholtz decomposition in equation (9.272) by identifying

$$\nabla E + \nabla\phi \equiv \nabla D \quad \text{and} \quad \nabla \times \boldsymbol{S} \equiv \nabla \times \boldsymbol{R}. \tag{9.282}$$

In so doing, the harmonic term, here captured by $\nabla\phi$, is absorbed into the scalar potential, D. This method for absorbing the harmonic term is suited to the normal component boundary condition (9.277a), in which

$$-\hat{\boldsymbol{n}} \cdot \boldsymbol{F} = \hat{\boldsymbol{n}} \cdot (\nabla E + \nabla\phi) = \hat{\boldsymbol{n}} \cdot \nabla D \implies \hat{\boldsymbol{n}} \cdot \nabla E = -\hat{\boldsymbol{n}} \cdot (\boldsymbol{F} + \nabla\phi). \tag{9.283}$$

In practice, we determine D and $\boldsymbol{R}$ as per the two-component decomposition (9.272), with the harmonic contribution to $\boldsymbol{F}$ contained as part of the scalar potential, D.

Tangential component boundary condition

The constraint $\nabla \cdot \boldsymbol{H} = 0$ is satisfied by writing $\boldsymbol{H} = \nabla \times \boldsymbol{A}$, so that the decomposition (9.280) takes on the form

$$\boldsymbol{F} = -\nabla E + \nabla \times (\boldsymbol{S} + \boldsymbol{A}). \tag{9.284}$$

We connect this decomposition to the orginal form of the Helmholtz decomposition of equation (9.272) by identifying

$$\nabla E \equiv \nabla D \quad \text{and} \quad \nabla \times (\boldsymbol{S} + \boldsymbol{A}) \equiv \nabla \times \boldsymbol{R}. \tag{9.285}$$

In so doing, the harmonic term, here captured by $\nabla \times \boldsymbol{A}$, is included in the vector potential, $\boldsymbol{R}$. This method for absorbing the harmonic term is suited for the tangential component boundary condition (9.277b), in which case

$$\hat{\boldsymbol{n}} \times \boldsymbol{F} = \hat{\boldsymbol{n}} \times (\boldsymbol{S} + \boldsymbol{A}) = \hat{\boldsymbol{n}} \times \boldsymbol{R} \Longrightarrow \hat{\boldsymbol{n}} \times \boldsymbol{S} = \hat{\boldsymbol{n}} \times (\boldsymbol{F} - \boldsymbol{A}). \tag{9.286}$$

Non-divergent velocity vector with no-normal flow boundary condition

As discussed in Chapters 21 and 29, many geophysical fluid flows maintain a non-divergent velocity field. Such velocity fields also maintain the no-normal flow boundary condition at static material boundaries (Section 19.6.1). For this vector field the scalar potential is harmonic and satisfies the vanishing Neumann boundary condition

$$-\nabla^2 D = 0 \quad \text{for} \quad \boldsymbol{x} \in \mathcal{R} \tag{9.287a}$$

$$\hat{\boldsymbol{n}} \cdot \nabla D = 0 \quad \text{for} \quad \boldsymbol{x} \in \partial\mathcal{R}. \tag{9.287b}$$

The solution to this boundary value problem is a spatially constant D, so that the velocity field is fully specified by a vector potential

$$\boldsymbol{F} = \nabla \times \boldsymbol{R}. \tag{9.288}$$

In the presence of a time dependent boundary condition, such as a fluctuating free surface, the scalar potential is not generally a spatial constant. We encounter an example when studying surface gravity waves in Section 52.3.

Vanishing boundary condition

The case with $\boldsymbol{F} = 0$ on the boundary means that

$$\boldsymbol{F} \cdot \hat{\boldsymbol{n}} = 0 \quad \text{and} \quad \hat{\boldsymbol{n}} \times \boldsymbol{F} = 0 \quad \text{for } \boldsymbol{x} \in \partial\mathcal{R}. \tag{9.289}$$

We proceed with both of the previous boundary condition constraints whereby

$$\nabla E + \nabla \phi = \nabla D \quad \text{and} \quad \nabla \times \boldsymbol{S} = \nabla \times \boldsymbol{R} \tag{9.290a}$$

$$\nabla E = \nabla D \quad \text{and} \quad \nabla \times (\boldsymbol{A} + \boldsymbol{S}) = \nabla \times \boldsymbol{R}. \tag{9.290b}$$

These two sets of constraints are mutually satisfied only when

$$\nabla \phi = 0 \quad \text{and} \quad \nabla \times \boldsymbol{A} = 0, \tag{9.291}$$

so that the harmonic term vanishes identically for the case of $\boldsymbol{F} = 0$ along the boundary.

Summary comments

We have shown that for a simply connected domain, it is possible to absorb an arbitrary harmonic portion of $\boldsymbol{F}$ into either the scalar potential D (for the normal component boundary conditions (9.277a)) or vector potential, $\boldsymbol{R}$ (for tangential component boundary conditions (9.277b)). Furthermore, the harmonic term vanishes altogether for the vanishing boundary condition (e.g., no-slip velocity boundary condition).

We infer from this discussion that if both the normal and tangential components of $\boldsymbol{F}$ are specified nonzero values on the boundary, then the harmonic term cannot be fully absorbed into one of the potentials D or $\boldsymbol{R}$. Rather, the harmonic term must be explictly computed, in which case the three-component decomposition (9.280) is referred to as the *Helmholtz-Hodge decomposition*.

These considerations are analogous to the Cauchy-Stokes decomposition summarized by Figure 18.6. That is, Cauchy-Stokes decomposes the motion of a fluid element into three processes: a deformation plus a rigid rotation plus a uniform translation. The deformation corresponds to the curl-free vector in the Helmholtz decomposition ($-\nabla D$), the rotation corresponds to the divergent free vector ($\nabla \times \boldsymbol{R}$), and the uniform translation corresponds to the harmonic vector.

9.8.3 Self-consistency conditions

We here establish existence conditions for the scalar potential, D, and vector potential, $\boldsymbol{R}$, that satisfy the decomposition (9.272). We separately do so for the two sets of boundary conditions (9.277a) and (9.277b). The proof consists of showing that the source term on the right hand side of the Poisson equation is self-consistent with the boundary condition.

Normal component boundary condition

Consider the scalar Poisson equation with Neumann boundary conditions

$$-\nabla^2 \chi = \Lambda \quad \text{for } \boldsymbol{x} \in \mathcal{R} \tag{9.292a}$$

$$-\hat{\boldsymbol{n}} \cdot \nabla \chi = \sigma \quad \text{for } \boldsymbol{x} \in \partial\mathcal{R}. \tag{9.292b}$$

As discussed in Section 6.5.6, this elliptic boundary value problem has a solution so long as the source, Λ, and boundary condition, σ, satisfy a self-consistency condition given by equation (6.50)

$$\int_{\mathcal{R}} \Lambda \, \mathrm{d}V = \oint_{\partial\mathcal{R}} \sigma \, \mathrm{d}\mathcal{S}. \tag{9.293}$$

Now specialize to the Helmholtz decomposition (9.272) whereby $\chi = D$ is the scalar potential with source $\Lambda = \nabla \cdot \boldsymbol{F}$ and boundary condition $\sigma = \hat{\boldsymbol{n}} \cdot \boldsymbol{F}$. Gauss's divergence theorem (2.79) readily verifies self-consistency

$$\int_{\mathcal{R}} \Lambda \, \mathrm{d}V = \int_{\mathcal{R}} \nabla \cdot \boldsymbol{F} \, \mathrm{d}V = \oint_{\partial\mathcal{R}} \boldsymbol{F} \cdot \hat{\boldsymbol{n}} \, \mathrm{d}\mathcal{S} = \oint_{\partial\mathcal{R}} \sigma \, \mathrm{d}\mathcal{S}. \tag{9.294}$$

As noted in Section 6.5.6, self-consistency ensures the existence of a solution to the Neumann problem that is unique up to an arbitrary constant. Hence, ∇D is unique so that

$$\nabla \times \boldsymbol{R} = \boldsymbol{F} + \nabla D \tag{9.295}$$

is also unique (we further discuss uniqueness in Section 9.8.5). Finally, the inhomogeneous Neumann boundary condition satisfied by the scalar potential, $-\hat{\boldsymbol{n}} \cdot \nabla D = \hat{\boldsymbol{n}} \cdot \boldsymbol{F}$, means that the curl satisfies the homogeneous Neumann boundary condition

$$\hat{\boldsymbol{n}} \cdot (\nabla \times \boldsymbol{R}) = \hat{\boldsymbol{n}} \cdot (\boldsymbol{F} + \nabla D) = 0, \tag{9.296}$$

so that $(\nabla \times \boldsymbol{R})$ is parallel to the boundary.

Tangential component boundary condition

Consider the vector Poisson equation

$$-\nabla^2 \boldsymbol{\Psi} = \boldsymbol{\Lambda} \qquad \text{for } \boldsymbol{x} \in \mathcal{R} \tag{9.297a}$$

$$\hat{\boldsymbol{n}} \times (\nabla \times \boldsymbol{\Psi}) = \hat{\boldsymbol{n}} \times \boldsymbol{\Sigma} \quad \text{for } \boldsymbol{x} \in \partial\mathcal{R}, \tag{9.297b}$$

with an assumed non-divergence condition (Coulomb gauge) placed on $\boldsymbol{\Psi}$

$$\nabla \cdot \boldsymbol{\Psi} = 0. \tag{9.298}$$

The region $\mathcal{R}$ is assumed to be a bounded three-dimensional volume with a closed boundary surface, $\partial\mathcal{R}$. Now let $\mathcal{S}$ be an arbitrary simply connected portion of $\partial\mathcal{R}$, and write $\partial\mathcal{S}$ for the closed contour that bounds $\mathcal{S}$. Integrate the normal projection of the vector Poisson equation over $\mathcal{S}$ and make use of Stokes' theorem (Section 2.6) to render

$$\int \boldsymbol{\Lambda} \cdot \hat{\boldsymbol{n}} \, \mathrm{d}\mathcal{S} = -\int \nabla^2 \boldsymbol{\Psi} \cdot \hat{\boldsymbol{n}} \, \mathrm{d}\mathcal{S} = \int \nabla \times (\nabla \times \boldsymbol{\Psi}) \cdot \hat{\boldsymbol{n}} \, \mathrm{d}\mathcal{S} = \oint_{\partial\mathcal{S}} (\nabla \times \boldsymbol{\Psi}) \cdot \hat{\boldsymbol{t}} \, \mathrm{d}s, \tag{9.299}$$

with $\hat{\boldsymbol{t}}$ the unit tangent vector pointing counter-clockwise along the closed contour, and $\mathrm{d}s$ the increment of arc-length along the contour (see Section 2.4). The assumed boundary condition (9.297b) means that for $\boldsymbol{x} \in \partial\mathcal{R}$ we can write

$$\nabla \times \boldsymbol{\Psi} = \boldsymbol{\Sigma} + \boldsymbol{m}, \tag{9.300}$$

where $\boldsymbol{m}$ is parallel to $\hat{\boldsymbol{n}}$ so that $\hat{\boldsymbol{n}} \times \boldsymbol{m} = 0$. In turn, with $\boldsymbol{m}$ parallel to $\hat{\boldsymbol{n}}$ then it is also perpendicular to the unit tangent vector, $\hat{\boldsymbol{t}} \cdot \boldsymbol{m} = 0$, so that

$$\oint_{\partial\mathcal{S}} (\nabla \times \boldsymbol{\Psi}) \cdot \hat{\boldsymbol{t}} \, \mathrm{d}s = \oint_{\partial\mathcal{S}} \boldsymbol{\Sigma} \cdot \hat{\boldsymbol{t}} \, \mathrm{d}s. \tag{9.301}$$

We are thus led to the self-consistency condition between the source, $\boldsymbol{\Lambda}$, and boundary condition, $\boldsymbol{\Sigma}$

$$\int \boldsymbol{\Lambda} \cdot \hat{\boldsymbol{n}} \, \mathrm{d}\mathcal{S} = \oint_{\partial\mathcal{S}} \boldsymbol{\Sigma} \cdot \hat{\boldsymbol{t}} \, \mathrm{d}s, \tag{9.302}$$

with this condition holding for any arbitrary simply connected region, $\mathcal{S}$, that lives on the boundary, $\partial\mathcal{R}$.

Now apply the self-consistency condition (9.302) to the Helmholtz decomposition (9.272), in which case $\boldsymbol{\Psi} = \boldsymbol{R}$, $\boldsymbol{\Lambda} = \nabla \times \boldsymbol{F}$, and $\boldsymbol{\Sigma} = \boldsymbol{F}$. Making use of Stokes' theorem readily verifies self-consistency

$$\int \boldsymbol{\Lambda} \cdot \hat{\boldsymbol{n}} \, \mathrm{d}\mathcal{S} = \int (\nabla \times \boldsymbol{F}) \cdot \hat{\boldsymbol{n}} \, \mathrm{d}\mathcal{S} = \oint_{\partial\mathcal{S}} \boldsymbol{F} \cdot \hat{\boldsymbol{t}} \, \mathrm{d}s = \oint_{\partial\mathcal{S}} \boldsymbol{\Sigma} \cdot \hat{\boldsymbol{t}} \, \mathrm{d}s. \tag{9.303}$$

We appeal to the scalar Poisson equation to conclude that self-consistency between the source and boundary conditions ensures the existence of a vector potential, $\boldsymbol{R}$, that is unique up to the gradient of a scalar. Hence, the gradient of the scalar potential is itself unique. Finally, we note that the assumed boundary condition (9.277b) for the vector potential, $\hat{\boldsymbol{n}} \times (\nabla \times \boldsymbol{R}) = \hat{\boldsymbol{n}} \times \boldsymbol{F}$, means that the scalar potential satisfies the homogeneous boundary condition

$$\hat{\boldsymbol{n}} \times \boldsymbol{F} = \hat{\boldsymbol{n}} \times (\nabla \times \boldsymbol{R}) = \hat{\boldsymbol{n}} \times (\boldsymbol{F} - \nabla D) \Longrightarrow \hat{\boldsymbol{n}} \times \nabla D = 0. \tag{9.304}$$

We thus see that ∇D is aligned parallel to $\hat{\boldsymbol{n}}$ along the boundary.

9.8.4 Orthogonality with the L^2 inner product

Consider an L^2 inner product for vector functions defined according to the volume integral of their scalar product

$$\langle \boldsymbol{A}, \boldsymbol{B} \rangle \equiv \int_{\mathcal{R}} \boldsymbol{A} \cdot \boldsymbol{B} \, \mathrm{d}V. \tag{9.305}$$

We here show that $\langle \nabla D, (\nabla \times \boldsymbol{R}) \rangle = 0$. That is, the Helmholtz decomposition (9.272) serves to decompose a vector into two orthogonal component vectors, where orthogonality is defined over the L^2 inner product (9.305). This orthogonality property is of great importance for the practical use of the Helmholtz decomposition.

Orthogonality with the normal component boundary condition

Assuming the normal component boundary conditions (9.277a), we readily find that the two vectors ∇D and $\nabla \times \boldsymbol{R}$ have a vanishing inner product

$$\langle \nabla D, \nabla \times \boldsymbol{R} \rangle = \int_{\mathcal{R}} \nabla D \cdot (\nabla \times \boldsymbol{R}) \, \mathrm{d}V = \int_{\mathcal{R}} \nabla \cdot (D \, \nabla \times \boldsymbol{R}) \, \mathrm{d}V = \int_{\partial\mathcal{R}} D \, (\nabla \times \boldsymbol{R}) \cdot \hat{\boldsymbol{n}} \, \mathrm{d}\mathcal{S} = 0, \tag{9.306}$$

where the final equality made use of the homogeneous boundary condition $(\nabla \times \boldsymbol{R}) \cdot \hat{\boldsymbol{n}} = 0$.

Orthogonality with the tangential boundary condition

Now assume the tangential component boundary conditions (9.277b). For this case we make use of the following identities holding for Cartesian tensors

$$\begin{aligned}
\nabla D \cdot (\nabla \times \boldsymbol{R}) &= \partial_i D \, (\nabla \times \boldsymbol{R})_i && \text{expose Cartesian tensor indices} && (9.307a)\\
&= \partial_i D \, \epsilon^{ijk} \, \partial_j R_k && \text{vector product as per equation (1.51d)} && (9.307b)\\
&= \partial_j (\epsilon^{ijk} \, \partial_i D \, R_k) && \text{since } \epsilon^{ijk} \partial_i \partial_j D = 0 \text{ and } \partial_j \epsilon^{ijk} = 0 && (9.307c)\\
&= -\partial_j (\epsilon^{jik} \, \partial_i D \, R_k) && \epsilon^{ijk} = -\epsilon^{jik} && (9.307d)\\
&= -\nabla \cdot (\nabla D \times \boldsymbol{R}) && \text{reintroduce Cartesian vector notation.} && (9.307e)
\end{aligned}$$

As a result we have orthogonality

$$\langle \nabla D, \nabla \times \boldsymbol{R} \rangle = \int_{\mathcal{R}} \nabla \cdot (\boldsymbol{R} \times \nabla D) \, \mathrm{d}V = \int_{\mathcal{R}} (\boldsymbol{R} \times \nabla D) \cdot \hat{\boldsymbol{n}} \, \mathrm{d}\mathcal{S} = \int_{\partial\mathcal{R}} (\nabla D \times \hat{\boldsymbol{n}}) \cdot \boldsymbol{R} \, \mathrm{d}\mathcal{S} = 0, \tag{9.308}$$

where the final equality made use of the homogeneous boundary condition $(\nabla D \times \hat{\boldsymbol{n}}) = 0$.

Comments

We have shown that the set of boundary conditions (9.277a) and (9.277b) are sufficient to produce an L^2-orthogonal Helmholtz decomposition on a simply connected domain. However, we have *not* shown that these boundary conditions are necessary for orthogonality, with other boundary conditions generally available. Since orthogonality is central to the practical use of the Helmholtz decomposition, it is important to verify whether orthogonality property holds when using alternative boundary conditions.

9.8.5 Uniqueness of the decomposition

We already commented on the uniqueness of the scalar and vector potentials in Section 9.8.3. We here further that discussion by offering a uniqueness proof following a "proof by contradiction"

method. For this approach we write the Helmholtz decomposition as

$$\boldsymbol{F} = -\nabla D_1 + \nabla \times \boldsymbol{R}_1 = -\nabla D_2 + \nabla \times \boldsymbol{R}_2, \tag{9.309}$$

and show that the only consistent solution has $D_1 = D_2$ and $\boldsymbol{R}_1 = \boldsymbol{R}_2$. Note that uniqueness is a function of the boundary conditions. That is, the normal component boundary conditions (9.277a) generally lead to a decomposition that is distinct from the tangential component boundary conditions (9.277b).

Uniqueness with the normal component boundary condition

From the assumed relation (9.309) we have

$$0 = -\nabla(D_1 - D_2) + \nabla \times (\boldsymbol{R}_1 - \boldsymbol{R}_2). \tag{9.310}$$

Taking the scalar product of this equality with $\nabla \times (\boldsymbol{R}_1 - \boldsymbol{R}_2)$ and then integrating over the domain leads to

$$0 = -\int_{\mathcal{R}} [\nabla(D_1 - D_2) \cdot \nabla \times (\boldsymbol{R}_1 - \boldsymbol{R}_2)] \, \mathrm{d}V + \int_{\mathcal{R}} [\nabla \times (\boldsymbol{R}_1 - \boldsymbol{R}_2)]^2 \, \mathrm{d}V. \tag{9.311}$$

The first integral vanishes, as seen by

$$\begin{aligned} -\int_{\mathcal{R}} [\nabla(D_1 - D_2) \cdot \nabla \times (\boldsymbol{R}_1 - \boldsymbol{R}_2)] \, \mathrm{d}V &= \int_{\mathcal{R}} [\nabla D_1 \cdot (\nabla \times \boldsymbol{R}_2) + \nabla D_2 \cdot (\nabla \times \boldsymbol{R}_1)] \, \mathrm{d}V && \text{(9.312a)} \\ &= \int_{\mathcal{R}} \nabla \cdot [D_1 (\nabla \times \boldsymbol{R}_2) + D_2 (\nabla \times \boldsymbol{R}_1)] \, \mathrm{d}V && \text{(9.312b)} \\ &= \int_{\partial\mathcal{R}} [D_1 (\nabla \times \boldsymbol{R}_2) + D_2 (\nabla \times \boldsymbol{R}_1)] \cdot \hat{\boldsymbol{n}} \, \mathrm{d}\mathcal{S} && \text{(9.312c)} \\ &= 0, && \text{(9.312d)} \end{aligned}$$

where the first equality follows from orthogonality as per equation (9.306); the second equality holds since the divergence of the curl vanishes (Section 2.3.4); the third equality follows from Gauss's divergence theorem (Section 2.7); and the fourth equality follows from the homogeneous boundary conditions, $\hat{\boldsymbol{n}} \cdot (\nabla \times \boldsymbol{R}_1) = \hat{\boldsymbol{n}} \cdot (\nabla \times \boldsymbol{R}_2) = 0$, satisfied with the normal component boundary conditions (9.277a). We are thus left with the equality

$$\int_{\mathcal{R}} [\nabla \times (\boldsymbol{R}_1 - \boldsymbol{R}_2)]^2 \, \mathrm{d}V = 0, \tag{9.313}$$

which is generally satisfied only when $\nabla \times \boldsymbol{R}_1 = \nabla \times \boldsymbol{R}_2$ so that $\nabla D_1 = \nabla D_2$. We have thus shown that the Helmholtz decomposition $\boldsymbol{F} = -\nabla D + \nabla \times \boldsymbol{R}$ is unique with the normal component boundary conditions (9.277a).

Uniqueness with the tangential component boundary condition

Now consider the tangential component boundary conditions (9.277b). The proof proceeds much like above, only now we take the scalar product of equation (9.310) with $\nabla(D_1 - D_2)$ and integrate over the domain. In doing so we encounter the term

$$\begin{aligned} -\int_{\mathcal{R}} [\nabla(D_1 - D_2) \cdot \nabla \times (\boldsymbol{R}_1 - \boldsymbol{R}_2)] \, \mathrm{d}V &= \int_{\mathcal{R}} [\nabla D_1 \cdot (\nabla \times \boldsymbol{R}_2) + \nabla D_2 \cdot (\nabla \times \boldsymbol{R}_1)] \, \mathrm{d}V && \text{(9.314a)} \\ &= \int_{\mathcal{R}} \nabla \cdot [\nabla D_1 \times \boldsymbol{R}_2 + \nabla D_2 \times \boldsymbol{R}_1] \, \mathrm{d}V && \text{(9.314b)} \end{aligned}$$

$$= \int_{\partial\mathcal{R}} [\boldsymbol{R}_2 \cdot (\hat{\boldsymbol{n}} \times \nabla D_1) + \boldsymbol{R}_1 \cdot (\hat{\boldsymbol{n}} \times \nabla D_2)] \tag{9.314c}$$

$$= 0, \tag{9.314d}$$

where the second equality made use of the identity (9.307e) derived when examining orthogonality, the third equality made of the divergence theorem, and the fourth equality holds according to the homogenous boundary conditions $\hat{\boldsymbol{n}} \times \nabla D = 0$ following from equation (9.277b). We are thus led to

$$\int_{\mathcal{R}} [\nabla(D_1 - D_2)]^2 \, \mathrm{d}V = 0, \tag{9.315}$$

which generally holds only if $\nabla D_1 = \nabla D_2$ and hence $\nabla \times \boldsymbol{R}_1 = \nabla \times \boldsymbol{R}_2$. We have thus shown that the Helmholtz decomposition is unique with the tangential component boundary conditions (9.277b).

Chapter 10

Calculus of variations

The *calculus of variations* (or *variational calculus*) provides a mathematical framework to determine a function that extremizes a given integral. The integral is a *functional*, which is a function of functions. As discussed by *Yourgrau and Mandelstam* (1968), the intellectual origins of variational methods date from extremum questions posed by the ancient Greeks, which then found their modern realization in the work of Fermat in optics (e.g., see Chapter 1 in *Tracy et al.* (2014)), and in the mechanics of Newton, the Bernoulli brothers, Euler, Legendre, Lagrange, and Hamilton. Variational methods are central to much of 20th century physics, including classical and quantum field theory. The calculus of variations is also central to optimization methods, information theory, and data assimilation.

Discussions of the calculus of variations are given in classical mechanics texts, with the present chapter building from Chapter 2 of *Goldstein* (1980), Chapter 5 of *Marion and Thornton* (1988), Chapter 2 of *Basdevant* (2007), and Appendix B of *Tracy et al.* (2014). Our treatment is relatively brief, working first through the derivation of the *Euler equation* and then providing a few analytical examples. Variational methods can handle constraints that affect the solution to the extremum problem, though we do not consider constraints in this chapter. Rather, we leave the treatment of constraints for the analytical mechanics studied in Chapter 12 and fluid mechanics in Chapter 47.

READER'S GUIDE TO THIS CHAPTER

The calculus of variations is fundamental to various parts of this book through the use of *Hamilton's Principle*, with applications to analytical mechanics in Chapter 12, classical field theory in Chapter 46, fluid mechanics in Chapter 47, and wave mechanics in Chapter 50 (and other waves chapters in Part X). In these mechanical examples, the functional is known as the *Lagrangian* and the integral is called the *action*.

When making use of variational methods in other chapters of this book, we typically provide background to the calculus of variations sufficient to deal with the problem at hand. Consequently, the present chapter can be readily skipped. Even so, this chapter serves those wanting a more complete understanding of the method's foundations, as well a sampling of the numerous analytical examples enabled by variational methods.

10.1 Mathematical formulation

The fundamental goal of the calculus of variations concerns the determination of a function that extremizes a given integral. For example, what is the shortest path between two points on a plane? Experience indicates that the shortest path is a straight line, and with the formalism of the calculus of variations supporting this experience (Section 10.2). The question is non-local in that it seeks information about the distance between two distinct points in space. The answer, as we will see, is the solution to a differential equation that determines a specific function.

Let (x, y) be the Cartesian coordinates for a point in $\mathbb{E}^2$ (i.e., the plane), and assume that $y = y(x)$ specifies y as a differentiable function of x. In this chapter we focus on functions of one variable, with extensions to higher dimensions straightforward and presented where needed later in this book. Now consider an integral of the form

$$\mathcal{J} = \int_{x_1}^{x_2} L[y(x), y'(x), x]\, \mathrm{d}x, \tag{10.1}$$

where L is a functional and

$$y'(x) = \frac{\mathrm{d}y}{\mathrm{d}x} \tag{10.2}$$

is the first derivative of $y(x)$. Functionals dependent on higher derivatives of y can be considered. However, in mechanics (i.e., Hamilton's principle) we do not encounter higher than the first derivative, so that a functional of the form (10.1) is sufficient for our needs. We seek a function, y, that extremizes the integral, $\mathcal{J}$, for a given functional, L, and with specified end points, x_1 and x_2. The calculus of variations provides a systematic method to determine this extremal function. Note that we write x, which typically means space point in this book. However, it can also mean time, t, which is typicallly the case in mechanics.

In formulating the solution to the extremum problem, it is important to recognize that the functional, L, depends implicitly on x as realized through its dependence on $y(x)$ and $y'(x)$. It also depends explicitly on x, as indicated by the final argument in equation (10.1). This tandem implicit and explicit dependence is perhaps the most technically confusing point about the calculus of variations, making it essential to clearly state how derivatives of L are taken. This point is further explained in Section 10.1.4.

10.1.1 Variation of a function

Assume that $y(x)$ is the function that extremizes $\mathcal{J}$, and assume this function is unique. As a result, any function distinct from $y(x)$ is not an extremum of $\mathcal{J}$. One means to consider such non-extremal functions is by introducing a non-dimensional parameter, α, that defines

$$Y(x, \alpha) = y(x) + \alpha\, \eta(x), \tag{10.3}$$

where $\eta(x)$ is an arbitrary smooth function that vanishes at the endpoints

$$\eta(x_1) = \eta(x_2) = 0. \tag{10.4}$$

Specifying these endpoint conditions means that $Y(x, \alpha)$ equals to the extremum function at the endpoints

$$Y(x_1, \alpha) = y(x_1) \quad \text{and} \quad Y(x_2, \alpha) = y(x_2). \tag{10.5}$$

Furthermore, by definition,

$$Y(x, 0) = y(x) \tag{10.6}$$

is the extremum function for all x. We say that $Y(x, \alpha)$ is a function of the spatial point, x, and the parameter, α. It follows that varying α allows $Y(x, \alpha)$ to sample the space of functions that are close, but not identical, to the extreme function, $y(x)$.

10.1.2 The δ variation operator acting on a function

As a notational shorthand, it is very useful to make use of the non-dimensional *variation operator*, δ, defined so that

$$Y(x, \alpha) = y(x) + \alpha\, \eta(x) = y(x) + \delta y(x) = (1 + \delta)\, y(x), \tag{10.7}$$

where $\delta y(x)$ defines the variation of the function. Notably, δ acts only on the function and not the space point, so that x remains unchanged upon acting with δ. Correspondingly, δ commutes with the derivative operator

$$\delta[y'(x)] = \delta[\mathrm{d}y(x)/\mathrm{d}x] = \mathrm{d}[\delta y(x)]/\mathrm{d}x. \tag{10.8}$$

As a final shorthand, we often write

$$y(x) \to y(x) + \delta y(x), \tag{10.9}$$

to indicate that a function, $y(x)$, is to be replaced by $(1 + \delta)\, y(x)$ each place it is found. In Figure 10.1 we illustrate $y(x) + \delta y(x)$, where $y(x)$ is a straight line whereas $\delta y(x)$ are arbitrary curved paths for which $\delta y(x_1) = \delta y(x_2) = 0$.

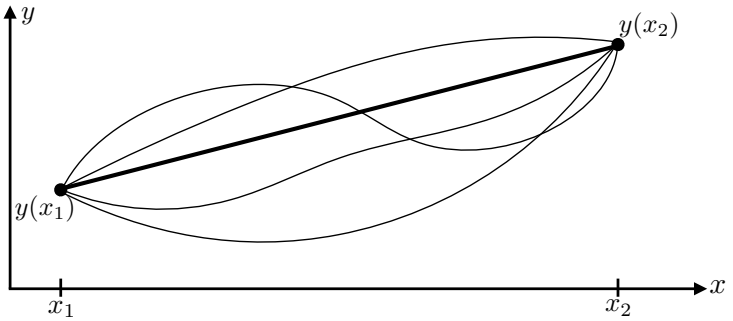

FIGURE 10.1: Illustrating some variations to the function, $y(x)$, here depicted as a straight line whereas $y(x)+\delta y(x)$ are curved paths. Note that each variation satisfies $\delta y(x_1) = \delta y(x_2) = 0$.

10.1.3 Derivative of the integral

Introducing the function, $Y(x, \alpha)$, into the integral (10.1) yields

$$\mathcal{J}(\alpha) = \int_{x_1}^{x_2} L[Y(x, \alpha), Y'(x, \alpha), x]\, \mathrm{d}x, \tag{10.10}$$

where we exposed the α dependence of the integral by writing $\mathcal{J}(\alpha)$, and where

$$Y'(x,\alpha) = \frac{\partial Y(x,\alpha)}{\partial x} = y'(x) + \alpha\,\eta'(x). \tag{10.11}$$

By construction, the integral, $\mathcal{J}(\alpha)$, is an extremum at $\alpha = 0$, which means that its derivative vanishes there

$$\left.\frac{\mathrm{d}\mathcal{J}}{\mathrm{d}\alpha}\right|_{\alpha=0} = 0. \tag{10.12}$$

The integration limits in equation (10.10) are independent of α, so that the chain rule renders

$$\frac{\mathrm{d}\mathcal{J}(\alpha)}{\mathrm{d}\alpha} = \int_{x_1}^{x_2} \left[\frac{\partial L}{\partial Y}\frac{\partial Y}{\partial \alpha} + \frac{\partial L}{\partial Y'}\frac{\partial Y'}{\partial \alpha}\right] \mathrm{d}x. \tag{10.13}$$

Making use of the identities

$$\frac{\partial Y}{\partial \alpha} = \eta \quad \text{and} \quad \frac{\partial Y'}{\partial \alpha} = \eta' \tag{10.14}$$

leads to

$$\frac{\mathrm{d}\mathcal{J}(\alpha)}{\mathrm{d}\alpha} = \int_{x_1}^{x_2} \left[\frac{\partial L}{\partial Y}\,\eta + \frac{\partial L}{\partial Y'}\,\eta'\right] \mathrm{d}x \tag{10.15a}$$

$$= \int_{x_1}^{x_2} \left[\frac{\partial L}{\partial Y} - \frac{\mathrm{d}}{\mathrm{d}x}\left(\frac{\partial L}{\partial Y'}\right)\right] \eta\,\mathrm{d}x + \int_{x_1}^{x_2} \frac{\mathrm{d}}{\mathrm{d}x}\left[\frac{\partial L}{\partial Y'}\,\eta\right] \mathrm{d}x, \tag{10.15b}$$

where the second equality follows from integration by parts. Since $\eta(x_1) = \eta(x_2) = 0$, the total derivative term vanishes from equation (10.15b), thus leaving

$$\frac{\mathrm{d}\mathcal{J}(\alpha)}{\mathrm{d}\alpha} = \int_{x_1}^{x_2} \left[\frac{\partial L}{\partial Y} - \frac{\mathrm{d}}{\mathrm{d}x}\left(\frac{\partial L}{\partial Y'}\right)\right] \eta\,\mathrm{d}x. \tag{10.16}$$

We emphasize the importance of distinguishing the derivative operators as they appear in equation (10.16), whereby

$$\frac{\partial L}{\partial Y'} = \left(\frac{\partial L}{\partial Y'}\right)_{Y,x} \tag{10.17a}$$

$$\frac{\mathrm{d}}{\mathrm{d}x}\left[\frac{\partial L}{\partial Y'}\right] = \left[\frac{\partial Y}{\partial x}\frac{\partial}{\partial Y}\Big)_{Y',x} + \frac{\partial Y'}{\partial x}\frac{\partial}{\partial Y'}\Big)_{Y,x} + \frac{\partial}{\partial x}\Big)_{Y,Y'}\right] \frac{\partial L}{\partial Y'}. \tag{10.17b}$$

The ∂_Y and $\partial_{Y'}$ terms in equation (10.17b) arise from the implicit x dependence through Y and Y', with the explicit x dependence leading to the ∂_x term. Being mindful of these operations greatly reduces confusion when manipulating the equations of variational calculus. In the following, we typically drop the subscripts to reduce notational clutter. Yet where confusion arises it is useful to return to the above two equations for clarification.

10.1.4 Variation of the integral and the Fréchet derivative

Rather than computing the derivative of the integral as in Section 10.1.3, it is common in the physics literature to compute the variation of the integral through use of the δ operator, which in turn motivates defining the *functional derivative*, or sometimes called the *Fréchet derivative*. In this approach we write

$$\delta\mathcal{J} = \delta \int_{x_1}^{x_2} L[y(x), y'(x), x]\,\mathrm{d}x = \int_{x_1}^{x_2} \delta L[y(x), y'(x), x]\,\mathrm{d}x, \tag{10.18}$$

where the variation operator commutes with the spatial integral since, as noted in Section 10.1.2, δ does not touch the space coordinate. To compute the variation of the functional, L, we make use of the chain rule and by noting that $\delta x = 0$, so that

$$\delta\mathcal{J} = \int_{x_1}^{x_2} \left[\frac{\partial L}{\partial y}\,\delta y + \frac{\partial L}{\partial y'}\delta y'\right] \mathrm{d}x \tag{10.19a}$$

$$= \int_{x_1}^{x_2} \left[\frac{\partial L}{\partial y} - \frac{\mathrm{d}}{\mathrm{d}x}\left(\frac{\partial L}{\partial y'}\right)\right] \delta y\,\mathrm{d}x + \int_{x_1}^{x_2} \frac{\mathrm{d}}{\mathrm{d}x}\left(\frac{\partial L}{\partial y'}\,\delta y\right) \mathrm{d}x \tag{10.19b}$$

$$= \int_{x_1}^{x_2} \left[\frac{\partial L}{\partial y} - \frac{\mathrm{d}}{\mathrm{d}x}\left(\frac{\partial L}{\partial y'}\right)\right] \delta y\,\mathrm{d}x \tag{10.19c}$$

$$= \alpha \left[\frac{\mathrm{d}\mathcal{J}(\alpha)}{\mathrm{d}\alpha}\right]_{\alpha=0}, \tag{10.19d}$$

where the penultimate equality holds since $\delta y(x_1) = \delta y(x_2) = 0$, and the final equality set $\delta y = \alpha\,\eta$ and used equation (10.16) for $\mathrm{d}\mathcal{J}(\alpha)/\mathrm{d}\alpha$. Evidently, equation (10.19d) provides a direct connection between the variation of the integral to the derivative of the integral via

$$\delta\mathcal{J} = \alpha \left[\frac{\mathrm{d}\mathcal{J}(\alpha)}{\mathrm{d}\alpha}\right]_{\alpha=0}. \tag{10.20}$$

The variation operator formalism in equation (10.19c) suggests we define the functional derivative, also known as the Fréchet derivative, via

$$\frac{\delta\mathcal{J}}{\delta y(x^*)} = \int_{x_1}^{x_2} \left[\frac{\partial L}{\partial y} - \frac{\mathrm{d}}{\mathrm{d}x}\left(\frac{\partial L}{\partial y'}\right)\right] \frac{\delta y(x)}{\delta y(x^*)}\,\mathrm{d}x = \left[\frac{\partial L}{\partial y(x^*)} - \frac{\mathrm{d}}{\mathrm{d}x^*}\left(\frac{\partial L}{\partial y'(x^*)}\right)\right] \mathrm{d}x^*, \tag{10.21}$$

where

$$\frac{\delta y(x)}{\delta y(x^*)} = \delta(x - x^*)\,\mathrm{d}x^*, \tag{10.22}$$

with $\delta(x - x^*)$ the Dirac delta studied in Chapter 7, and with x^* an arbitrary space point.[1] It is notable that the $\mathrm{d}x^*$ factor appearing in equation (10.22) is typically ignored in most treatments, since it plays no role in the Euler equations that follow from setting $\delta\mathcal{J}/\delta y(x^*) = 0$ (Section 10.1.5). However, this factor is necessary for dimensional consistency since the Dirac delta has dimensions of inverse length. So in summary, the Fréchet derivative of the integral is given by

$$\frac{\delta\mathcal{J}}{\delta y} = \left[\frac{\partial L}{\partial y} - \frac{\mathrm{d}}{\mathrm{d}x}\left(\frac{\partial L}{\partial y'}\right)\right] \mathrm{d}x. \tag{10.23}$$

The Fréchet derivative provides the functional analog to the gradient operator, with this derivative vanishing at an extremum of $\mathcal{J}$.

10.1.5 The Euler equation

The derivative (10.16) vanishes when $\alpha = 0$, by construction, in which case

$$0 = \left.\frac{\mathrm{d}\mathcal{J}(\alpha)}{\mathrm{d}\alpha}\right|_{\alpha=0} = \int_{x_1}^{x_2} \left[\frac{\partial L}{\partial y} - \frac{\mathrm{d}}{\mathrm{d}x}\left(\frac{\partial L}{\partial y'}\right)\right] \eta\,\mathrm{d}x, \tag{10.24}$$

where the derivatives inside the integral are now taken with respect to y since $Y(0, x) = y(x)$. Since $\eta(x)$ is an arbitrary function, this equation is satisfied only if the integrand vanishes, which

[1] Use of the δ symbol for both the variational operator as well as the Dirac delta is unfortunate but universal.

leads to *Euler's equation*

$$\frac{\partial L}{\partial y} - \frac{\mathrm{d}}{\mathrm{d}x}\left(\frac{\partial L}{\partial y'}\right) \Longleftrightarrow y(x) \text{ extremizes } \mathcal{J}[y(x), y'(x), x]. \tag{10.25}$$

Euler's equation is equivalently found by setting the Fréchet derivative (10.23) to zero

$$\frac{\delta \mathcal{J}}{\delta y} = 0 \Longrightarrow \left[\frac{\partial L}{\partial y} - \frac{\mathrm{d}}{\mathrm{d}x}\left(\frac{\partial L}{\partial y'}\right)\right] = 0. \tag{10.26}$$

Note that in our study of mechanics in Chapter 12, we refer to the Euler equation as the *Euler-Lagrange equation*, given work done by Lagrange to extend variational methods to mechanics.

10.1.6 The second form of Euler's equation

The total derivative of the functional is given, through the chain rule, by

$$\frac{\mathrm{d}L}{\mathrm{d}x} = \left[\frac{\partial L}{\partial x}\right]_{y,y'} + \frac{\mathrm{d}y}{\mathrm{d}x}\left[\frac{\partial L}{\partial y}\right]_{y',x} + \frac{\mathrm{d}^2 y}{\mathrm{d}x^2}\left[\frac{\partial L}{\partial y'}\right]_{y,x} \tag{10.27a}$$

$$= \frac{\partial L}{\partial x} + y'\frac{\partial L}{\partial y} + y''\frac{\partial L}{\partial y'}, \tag{10.27b}$$

where the second equality dropped the subscript notation to reduce clutter. In turn, we have

$$\frac{\mathrm{d}}{\mathrm{d}x}\left[y'\frac{\partial L}{\partial y'}\right] = y''\frac{\partial L}{\partial y'} + y'\frac{\mathrm{d}}{\mathrm{d}x}\left[\frac{\partial L}{\partial y'}\right], \tag{10.28}$$

with substitution from equation (10.27b) rendering

$$\frac{\mathrm{d}}{\mathrm{d}x}\left[L - y'\frac{\partial L}{\partial y'}\right] = \frac{\partial L}{\partial x} + y'\left[\frac{\partial L}{\partial y} - \frac{\mathrm{d}}{\mathrm{d}x}\left(\frac{\partial L}{\partial y'}\right)\right]. \tag{10.29}$$

The final term on the right hand side vanishes due to Euler's equation (10.25), thus leading to the *second form of Euler's equation*

$$\frac{\mathrm{d}}{\mathrm{d}x}\left[L - y'\frac{\partial L}{\partial y'}\right] = \frac{\partial L}{\partial x}. \tag{10.30}$$

This equation is particularly useful when the functional, L, has no explicit dependence on x, in which case the right hand side vanishes. Furthermore, when applied to mechanics, the term $y'\,\partial L/\partial y' - L$ is the Hamiltonian (e.g., see Section 12.9.4).

10.1.7 Nature of the extremum

The Euler equation (10.25) has a solution, $y(x)$, that is an extremum to the integral $\mathcal{J}[y(x), y'(x), x]$. In this manner, we connect a question about the extremum of an integral to the solution of a differential equation. However, is the extremum a minimum, maximum, or inflection? To answer that question requires taking the second derivative of the integral,

$$\delta^2 \mathcal{J} = \alpha^2 \left[\frac{\mathrm{d}^2 \mathcal{J}(\alpha)}{\mathrm{d}\alpha^2}\right]_{\alpha=0}. \tag{10.31}$$

In practice this is a rather difficult calculation to perform. Furthermore, in many cases the nature of the extremum is apparent by inspection. For example, in Section 10.2 we determine the

path between any two points on a plane, with a straight line an extremum that is the minimum path since one is free to consider an alternative path this is arbitrarily longer.

10.2 Shortest path between two points on a plane

Let $(x, y) \in \mathbb{R}^2$ be the Cartesian coordinates for a point in $\mathbb{E}^2$ (i.e., a flat plane), where $y = y(x)$ specifies y as a differentiable function of x. We seek an expresion for the function, $y(x)$, that represents the shortest path between two arbitrary points in $\mathbb{E}^2$. The answer is a straight line

$$y = y_1 + \frac{x - x_1}{x_2 - x_1}(y_2 - y_1) = \frac{y_1(x_2 - x) + y_2(x - x_1)}{x_2 - x_1}, \quad \text{with } y_1 = y(x_1) \text{ and } y_2 = y(x_2), \tag{10.32}$$

with the calculus of variations unnecessary to determine this function. Even so, we find it useful to consider this question using the calculus of variations in order to garner experience and confidence with the formalism.

In $\mathbb{E}^2$, the distance between two infinitesimally close points is given by Pythagoras' theorem

$$\mathrm{d}s = [(\mathrm{d}x)^2 + (\mathrm{d}y)^2]^{1/2} = \sqrt{1 + (y')^2}\,\mathrm{d}x, \tag{10.33}$$

so that the finite distance between two points is given by the integral

$$\mathcal{J} = \int_{x_1}^{x_2} \mathrm{d}s = \int_{x_1}^{x_2} \sqrt{1 + (y')^2}\,\mathrm{d}x = \int_{x_1}^{x_2} L\,\mathrm{d}x, \tag{10.34}$$

where the functional is

$$L = \sqrt{1 + (y')^2}. \tag{10.35}$$

Terms in the Euler equation (10.25) are thus given by

$$\frac{\partial L}{\partial y} = 0 \quad \text{and} \quad \frac{\partial L}{\partial y'} = \frac{y'}{\sqrt{1 + (y')^2}}, \tag{10.36}$$

so that the Euler equation is

$$\frac{\mathrm{d}}{\mathrm{d}x}\left[\frac{y'}{\sqrt{1 + (y')^2}}\right] = 0, \tag{10.37}$$

whose solution is indeed the straight line given by equation (10.32).

10.3 Shortest time falling between two points

The *brachistochrone* is a smooth curve upon which a frictionless bead moves under the effects from gravity and travels in the shortest time between two points, A and B, where these two points are not underneath one another.[2] We illustrate the physical system in Figure 10.2. The integral expression for time of the excursion is given by

$$T = \int_A^B \mathrm{d}t = \int_{s_A}^{s_B} \frac{\mathrm{d}s}{v(s)}, \tag{10.38}$$

where s is the arc length and $v(s)$ is the speed of the bead as a function of the arc length. The minimal time is achieved by the particle moving in a single plane, which we set as the x-z plane

[2] If the two points A and B are vertically oriented, then the brachistochrone is the straight vertical line connecting these two points.

without loss of generality. In this case the differential arc length is given by

$$\mathrm{d}s = \sqrt{(\mathrm{d}x)^2 + (\mathrm{d}z)^2} = \sqrt{1 + (z')^2}\,\mathrm{d}x, \tag{10.39}$$

where we assumed that the vertical position, z, is a monotonic function of the horizontal position, x, thus enabling a functional expression $z = z(x)$ for the curve.[3]

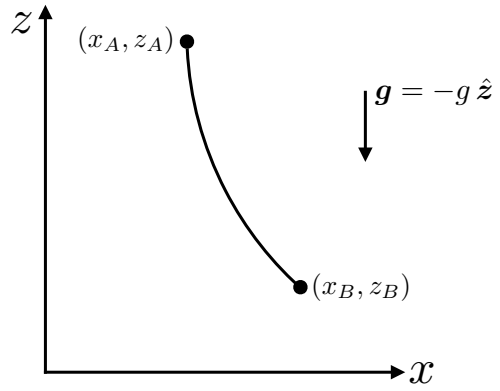

FIGURE 10.2: A bead falls along a frictionless wire from point A to point B. It traverses this path in the least amount of time if the wire is in the shape of a *cycloid*. This brachistochrone problem is readily solved using variational methods.

Mechanical energy of the bead is constant since the bead is frictionless.[4] If the bead starts from rest at point A, then the mechanical energy at this point is just given by the gravittional potential energy, $g\,m\,z_A$, where m is the mass of the bead, z_A is its vertical position, and we choose the zero for potential energy at $z = 0$. We thus find that the speed at any point along the path is given by

$$v^2/2 + g\,z = g\,z_A \Longrightarrow v = \sqrt{2\,g\,(z_A - z)}, \tag{10.40}$$

in which the time integral (10.38) becomes

$$T = \int_{s_A}^{s_B} \frac{\mathrm{d}s}{v(s)} = \int_{x_A}^{x_B} \frac{\sqrt{1 + (z')^2}}{\sqrt{2\,g\,(z_A - z)}}\,\mathrm{d}x. \tag{10.41}$$

The functional appearing in the time integral (10.41) is given by

$$L = L[z(x), z'(x)] = \frac{\sqrt{1 + (z')^2}}{\sqrt{2\,g\,(z_A - z)}}. \tag{10.42}$$

With no explicit dependence on x, the second form of Euler's equation, given by equation (10.30), leads to the identity

$$L - z'\,\frac{\partial L}{\partial z'} = \frac{1}{\sqrt{2\,g\,(z_A - z)\,(1 + (z')^2)}} = c^{-1}, \tag{10.43}$$

where c is a constant with dimensions of speed (L T^{-1}). We can write the solution to this equation by introducing the angle parameter θ, so that

$$x = [c^2/(4g)]\,(\sin\theta - \theta) \quad \text{and} \quad z_A - z = [c^2/(4g)]\,(1 - \cos\theta) \tag{10.44a}$$

$$\mathrm{d}x/\mathrm{d}\theta = [c^2/(4g)]\,(\cos\theta - 1) \quad \text{and} \quad \mathrm{d}(z_A - z)/\mathrm{d}\theta = [c^2/(4g)]\sin\theta. \tag{10.44b}$$

[3]Some treatments, such as Example 5.2 of *Marion and Thornton* (1988), solve for $x = x(z)$, which is possible since the is a one-to-one relation between x and z.

[4]In Section 11.1.5 we prove this property of conservative classical discrete systems.

This is the equation for a *cycloid*, which is the curve shown in Figure 10.3 that is traced by a point on a circle that is rolling (without slipping) along a straight line on a plane.[5]

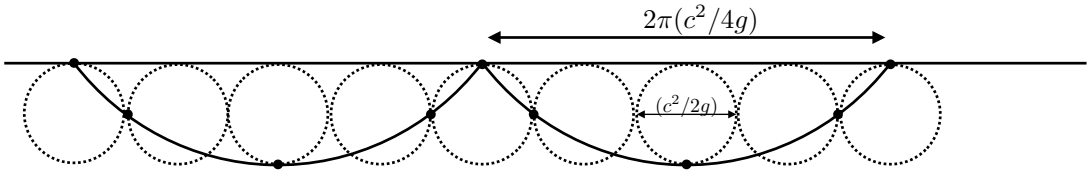

FIGURE 10.3: A cycloid is the curve traced by a point on a circle that is rolling (without slipping) along a straight line on a plane. As per equation (10.44a), the radius of the circle is $c^2/(4g)$ so that its circumference is $2\,\pi\,c^2/(4g)$. We depict the circle each quarter rotation as it moves along the line, with the black dot fixed relative to the circle and tracing out the cycloid.

10.4 Shape of a hanging massive string

Consider a string or cable with uniform mass per length, σ, which is suspended from each end as depicted in Figure 10.4. What is the shape of the string when in mechanical equilibrium? To answer this question one can make use of mechanics through studying the tensile forces acting within the string and the gravitational forces acting on the string, with equilibrium realized when the net forces and torques sum to zero. Alternatively, we can assume the shape minimizes the gravitational potential energy of the string, in which case there is no need to determine any of the forces. Instead we make use of variational calculus to determine the minimum potential energy state.

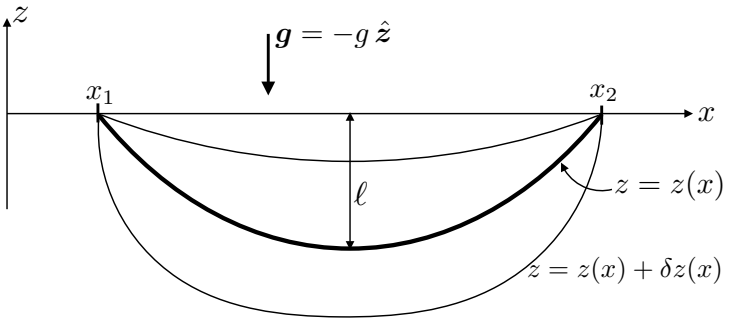

FIGURE 10.4: A massive string or cable is supported at its two ends at a vertical position $z_1 = z(x_1) = z_2 = z(x_2)$. The string is placed in a vertically directed gravitational field with acceleration, $\boldsymbol{g} = -g\,\hat{\boldsymbol{z}}$, where g is the constant gravitational acceleration. Variational methods determine the shape of the string as given by the hyperbolic cosine in equation (10.50), which is known as a *catenary*. This is the ideal shape taken by stationary power lines, spider webs, clothes lines, and chains, for example.

The variational problem arises from writing the gravitational potential energy as

$$P = g\,\sigma \int_{s(x_1)}^{s(x_2)} z(x)\,\mathrm{d}s, \tag{10.45}$$

where s is the arc distance along the curve and g is the constant gravitational acceleration. Along the curve, the arc-length differential is

$$\mathrm{d}s = \sqrt{(\mathrm{d}x)^2 + (\mathrm{d}z)^2} = \sqrt{1 + (z')^2}\,\mathrm{d}x, \tag{10.46}$$

[5] See Example 5-2 of *Marion and Thornton* (1988) for more details of the cycloid.

where $z'(x) = \mathrm{d}z/\mathrm{d}x$ is the derivative. Hence, the potential energy is

$$P = g\,\sigma \int_{x_1}^{x_2} z(x)\,\sqrt{1+(z')^2}\,\mathrm{d}x = g\,\sigma \int_{x_1}^{x_2} L[z(x), z'(x)]\,\mathrm{d}x, \tag{10.47}$$

where we introduced the functional

$$L[z(x), z'(x)] = z(x)\,\sqrt{1+(z')^2}. \tag{10.48}$$

This functional is reminiscent of that found for the shortest path problem as given by equation (10.35), yet here there is an extra $z(x)$ factor multiplying the square root term.

Since the functional (10.48) has no explicit x dependence, we make use of the second form of the Euler equation, in which

$$L - y'\,\frac{\partial L}{\partial y'} = z\,\sqrt{1+(z')^2}\left[1 - \frac{(z')^2}{1+(z')^2}\right] = \ell \Longrightarrow z/\ell = 1+(z')^2, \tag{10.49}$$

where ℓ is a constant of integration with dimensions of length. The solution to this differential equation that satisfies the two endpoint conditions $z(x_1) = z(x_2)$ is given by

$$z = \ell\cosh[(2\,x - x_1 - x_2)/(2\ell)], \tag{10.50}$$

which is referred to as a *catenary* and is depicted in Figure 10.4. The constant, ℓ, is the vertical position of the midpoint of the curve, which is also the lowest point

$$z = \ell \quad \text{at } x = (x_1 + x_2)/2. \tag{10.51}$$

10.5 Minimal surface of revolution

Figure 10.5 shows an axially symmetric surface that is bounded by two circles with distinct radii and that are aligned along the $\hat{\boldsymbol{z}}$ axis. This surface is formed by connecting two points in the x-z plane, (x_1, z_1) and (x_2, z_2), and then revolving the curve around the z-axis. What is the shape of the surface that results in the minimum surface area? One guess is that the surface is a cone built from straight lines extending from the lower circle to the upper circle. In fact, it turns out to be built from catenaries; i.e., the same shape as found in Section 10.4 for the hanging massive string, with the resulting surface known as a *catenoid*.

Given the rotational symmetry assumed for the surface, it is sufficient to fix attention to the x-z plane. Furthermore, we assume there is a monotonic relation between z and x, so that we can write $z = z(x)$ for any point on the surface in the x-z plane. In this case the surface area is given by

$$A = 2\,\pi \int_{x_1}^{x_2} x\,\sqrt{1+(z')^2}\,\mathrm{d}x, \tag{10.52}$$

where the 2π factor arises from the angular integral and circular symmetry. The x factor is the radius of the circle and

$$\mathrm{d}s = \sqrt{1+(z')^2}\,\mathrm{d}x \tag{10.53}$$

is the thickness of a tiny strip along the surface and in the x-z plane (see Figure 10.5). The integrand to the surface area in equation (10.52) is identical to the integrand in equation (10.47) for the potential energy of a hanging string. Hence, the minimal surface is constructed from catenaries. That is, in any particular plane passing through the center of the circles (e.g., the x-z plane), use a catenary to connect a point on the upper surface to a point on the lower surface, and then spin this catenary around the vertical axis. The resulting surface of revolution has the minimal surface area and it is known as a catenoid.

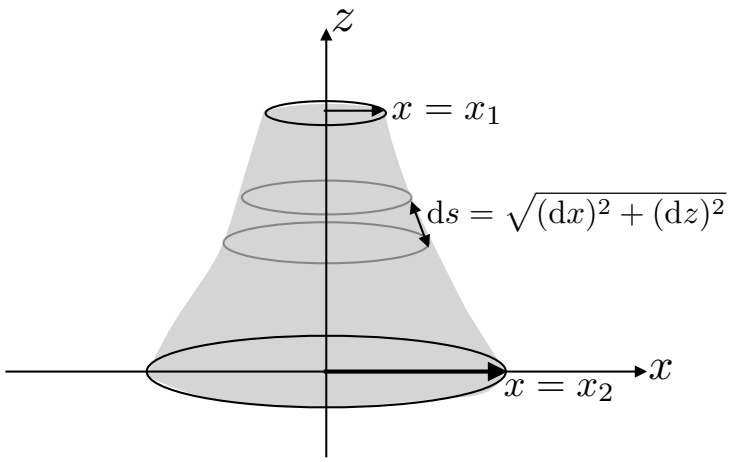

FIGURE 10.5: This figure shows an axially symmetric surface that connects two circles aligned along the $\hat{\boldsymbol{z}}$ axis. The thickness of a strip along the surface and within the x-z plane is given by $\mathrm{d}s = \sqrt{(\mathrm{d}x)^2 + (\mathrm{d}z)^2} = \sqrt{1 + (z')^2}\,\mathrm{d}x$. The shape of the minimal surface that connects the two circles is known as a *catenoid*. The catenoid is built from connecting the two circles with a catenary and then rotating the catenary around the vertical axis.

As noted in Section 2-2 of *Goldstein* (1980), a more thorough treatment of this problem identifies those configurations in which there is no catenary that can connect the circles, or when the minimal surface is discontinuous rather than continuous. Such cases might represent inflection points rather than minimal surfaces. Also note that circles with similar or identical radii, then the function $z(x)$ is not monotonic, in which case the problem can be split into two regions over which $z(x)$ is monotonic.

Part II

Classical mechanics

Planetary rotation and gravitation are two defining features of geophysical fluid mechanics. Furthermore, geophysical fluids exhibit motions whose speed is small relative to that of the rotating planet. We thus say that geophysical fluids are in near rigid-body motion, making it convenient to use a rotating (non-inertial) terrestrial reference frame to describe the fluid motion. Rotating and gravitating motion around a planet introduce new physical ideas beyond more familiar non-rotating physical systems. Rather than introduce rotating physics within the context of fluid mechanics, we first focus on the point particle system to establish a foundation for rotating physics. In the process, we also review facets of classical particle mechanics that are useful in the continuum mechanics of a moving fluid. Additionally, we examine systems of particles and then take their continuum limit, thus introducing notions relevant to the continuum mechanics of fluids.

Classical mechanics considers space to be Euclidean and time to be universal. Euclidean space has no curvature, so that Cartesian coordinates are commonly sufficient (though not always the most convenient) for developing the equations of motion. Universal time (sometimes referred to as *Newtonian time*) means that an event occuring at one point in space at time, t, also occurs at the same time everywhere else in space. That is, classical mechanics is based on *absolute simultaneity* holding throughout all of Euclidean space. The marriage of Euclidean space and Newtonian time is referred to as *Galilean relativity*.

There is a payoff for studying these chapters on classical mechanics even for the experienced physicist. Namely, topics familiar from previous studies are presented from the viewpoint of what later proves central to the study of geophysical fluid mechanics. In particular, we encounter Newtonian mechanics, Lagrangian mechanics, Hamilton's principle, trajectories, linear momentum, angular momentum, body forces, accelerations due to the rotating reference frame (planetary Coriolis and planetary centrifugal), space-time symmetries and conservation laws, center of mass coordinates, harmonic oscillators, pendula, planetary Cartesian coordinates, and planetary spherical coordinates.

We start by reviewing foundational elements of Newtonian particle mechanics in Chapter 11, considering a single point particle, a system of particles, and particles coupled by linear oscillators. We here also introduce some kinematic properties of non-inertial reference frames. Thereafter, in Chapters 13 and 14 we focus on the geophysically relevant case of a classical point particle moving around a rotating and gravitating sphere as described from the rotating terrestrial reference frame. In Chapter 12 we study Lagrangian mechanics, which formulates classical mechanics in a manner that complements Newtonian mechanics. We then follow in Chapter 15 with a suite of case studies that exemplify the power of Lagrangian mechanics. It is notable that Lagrangian mechanics focuses on energy rather than forces, and its Euler-Lagrange differential equations (derived from Hamilton's stationary action principle) are equivalent to Newton's equations of motion. Although leading to the same end point, the energy approach of Lagrange, coupled to the variational approach of Hamilton's principle, provide a powerful means to formulate otherwise intractable problems in classical physics. It also offers the natural mathematical foundation for connecting symmetries to conservation laws via Noether's theorem. Finally, it forms the starting point for a field theoretic perspective on continuum mechanics as introduced in Chapter 46.

Chapter 11

NEWTONIAN MECHANICS

Classical physics is concerned with describing the motion of matter, with Newtonian classical mechanics based on using Newton's laws to deduce the cause of motion. Classical matter is organized into three categories: (i) massive point particles; (ii) extended and continuous rigid media (rigid bodies); (iii) extended and continuous non-rigid media (e.g., elastic solids, fluids). A point particle has zero dimensions and so it occupies a single point in space. Rigid bodies occupy a finite region of space and are comprised of a continuum of matter particles that maintain fixed relative positions, thus constraining the media to maintain constant mass and volume. Particles in an extended non-rigid continuous media can move relative to one another, so that the media maintains constant mass though with a generally changing volume.[1] In this chapter we focus on mechanics of point particles as a venue to introduce rudimentary features of classical mechanics.

A mechanical description of motion is decomposed into *kinematics* and *dynamics*, with kinematics concerned with the nature of motion and dynamics concerned with the causes of motion. More specifically, kinematics is concerned with the position, velocity, and acceleration, whereas dynamics, through Newton's laws, provide the means to determine how motion is altered in the presence of forces. The mechanics of Newton are summarized by three laws of motion:

- FIRST LAW: In an inertial reference frame, every massive body remains at rest or in uniform motion unless acted on by a net force. This law is sometimes referred to as the *law of inertia*.
- SECOND LAW: In an inertial reference frame, application of a net force to a body alters its linear momentum.
- THIRD LAW: To each action there is an equal and oppositely directed reaction.

The first and second laws offer definitions for an inertial reference frame and for a force. The third law provides a statement about how forces act, thus providing physical substance to the first and second laws.[2] The third law holds for central forces, such as arise in Newtonian gravity and electrostatics. However, it does not hold for all forces, such as the Lorentz force acting on a moving charged particle.

The decomposition of matter into point particles, rigid bodies, and continuous media, directly corresponds to the kinematic decomposition of motion into translations, rotations, and dilations.[3] Namely, point particles move by translations through space, with this space-time motion referred to as a *trajectory*. The motion of a rigid body consists of its center of mass translations plus rotations of the body relative to the center of mass. Finally, the motion of a continuous media

[1] We typically abbreviate "extended non-rigid continuous media" as "continuous media". There is little room for confusion with rigid bodies since in this book we provide only tangential attention to the dynamics of rigid bodies.

[2] For more on this perspective of Newton's laws, see Chapter 1 of *Symon* (1971) or Chapter 2 of *Marion and Thornton* (1988).

[3] This decomposition is referred to as the *Cauchy-Stokes decomposition* and is studied in Section 18.8.6.

consists of the translations and rotations of a rigid body, plus changes in the relative positions of the particles that can lead to changes in the volume of the media, with such motions referred to as *dilatations*.

CHAPTER GUIDE

In this chapter we study the rudiments of Newtonian particle mechanics for a single massive point particle and for a system of such particles. Along the way, we expose core concepts such as space, time, mass, force, and rotation. Notably, within the bounds of classical physics, we must remain satisfied with common experience definitions for many of the foundational concepts that are not deduced from more fundamental principles.

Every classical mechanics textbook has some form of the material presented in this chapter. The books from *Goldstein* (1980) and *Fetter and Walecka* (2003) are targeted at the entering physics graduate student, whereas *French* (1971), *Symon* (1971), *Marion and Thornton* (1988), and *Taylor* (2005) are targeted at second or third year undergraduates. This chapter is required for understanding the mechanics of a particle moving around a rotating sphere in Chapters 13 and 14. It also serves as a baseline for the complementary approach taken by the *Lagrangian mechanics* studied in Chapters 12 and 15. We make use of Cartesian tensors for ease of presentation.

11.1 Newtonian mechanics of a point particle

In this section we study the Newtonian mechanics of a single point particle of constant mass, with the point particle occupying a single point in space and so having zero extent.

11.1.1 Position, velocity, and acceleration

The Cartesian position, $\boldsymbol{x}$, of a point particle at a Newtonian time instance, t, is written

$$\boldsymbol{x} = \boldsymbol{X}(t) = X^1(t)\,\hat{\boldsymbol{x}} + X^2(t)\,\hat{\boldsymbol{y}} + X^3(t)\,\hat{\boldsymbol{z}} = x(t)\,\hat{\boldsymbol{x}} + y(t)\,\hat{\boldsymbol{y}} + z(t)\,\hat{\boldsymbol{z}}. \tag{11.1}$$

The spatial position is measured relative to an arbitrary origin, with the vector, $\boldsymbol{X}$, pointing from the origin to the position of the particle. Universal *Newtonian time*, t, is a monotonically increasing parameter that allows for the unambiguous distinction between past, present, and future. That is, time parameterizes the particle's position in Euclidean space, with $\boldsymbol{X}(t)$ providing the mathematical representation for the *trajectory* in space as determined over a finite span of time.

The time derivative of the position defines the *velocity*, and the time derivative of the velocity is the *acceleration*

$$\boldsymbol{V}(t) = \frac{\mathrm{d}\boldsymbol{X}(t)}{\mathrm{d}t} = \dot{\boldsymbol{X}}(t) \quad \text{and} \quad \boldsymbol{A}(t) = \frac{\mathrm{d}\boldsymbol{V}(t)}{\mathrm{d}t} = \dot{\boldsymbol{V}}(t) = \ddot{\boldsymbol{X}}(t), \tag{11.2}$$

where we introduced the commonly used dot notation for the time derivative. By definition, the velocity is instantaneously tangent to the trajectory, and the acceleration is instantaneously tangent to the velocity. Newton's law connects the acceleration to the net force, in which case we have no concern for higher time derivatives than the second.

11.1.2 Linear momentum and Newton's second law

The *linear momentum* of the particle equals to the mass of the particle, m, times its velocity

$$\boldsymbol{P} = m\,\dot{\boldsymbol{X}} = m\,\boldsymbol{V}. \tag{11.3}$$

The linear momentum changes when it experiences a net force. The vector sum of all forces is written $\boldsymbol{F}$, and Newton's second law of motion states that there exists *inertial reference frames* where motion of the particle is described by the differential equation

$$\frac{\mathrm{d}\boldsymbol{P}}{\mathrm{d}t} = \boldsymbol{F}. \tag{11.4}$$

If the particle mass is fixed, then this equation becomes a second order differential equation for the particle position as a function of time

$$\boldsymbol{A} = \frac{\mathrm{d}\boldsymbol{V}}{\mathrm{d}t} = \frac{\mathrm{d}^2\boldsymbol{X}}{\mathrm{d}t^2} = \boldsymbol{F}/m. \tag{11.5}$$

Many conclusions in mechanics are expressed in terms of conservation laws (Chapter 14), which provide relations or conditions whereby mechanical properties of a physical system remain time invariant (i.e., time independent). Newton's second law provides our first conservation law since, in the absence of a net force, the linear momentum remains unchanged: $\mathrm{d}\boldsymbol{P}/\mathrm{d}t = 0$. Depending on the nature of the forces, this conservation law might hold for one, two, or all three of the vector components to the linear momentum. Note that for a constant mass particle, a time independent linear momentum means that the velocity remains constant, which is a statement of Newton's first law (the law of inertia).

11.1.3 Galilean relativity and inertial reference frames

If the forces acting on the particle are not directly dependent on the particle velocity, then the inertial frame equation of motion (11.5) is unchanged if shifting the velocity by a constant. Such velocity-independent forces (such as Newton's gravitational force) are commonly found in the conservative (non-dissipative) motion of charge-free particles. This arbitrariness in the velocity reflects a *symmetry* respected by the equation of motion, where symmetry refers to an operation that can be performed on the system without changing any physics. This particular symmetry is known in various contexts as *Galilean invariance*, *Galilean relativity*, or *Newtonian relativity*.

Galilean relativity holds for all inertial reference frames in non-relativistic mechanics. It is thus notable that there is no *absolute reference frame*, since we cannot mechanically distinguish any of the inertial reference frames that differ by an arbitrary constant velocity. That is, there is no classical experiment that can distinguish between two arbitrary inertial reference frames, so long as the experiments are described by Newton's equation of motion (11.5) and the force is independent of the velocity. The operational reason we cannot make a distinction is that the equation of motion is indistinguishable in the two inertial frames. As a corollary, two inertial reference frames can at most be moving relative to one another by a constant velocity. Otherwise, at least one of the reference frames is accelerating, which in turn means that this accelerating reference frame is not an inertial frame.

This discussion offers an example of the mathematical transformation theory introduced in Part I of this book. Mathematically, the Galilean transformation is written

$$\bar{t} = t \qquad \text{and} \qquad \overline{\boldsymbol{X}} = \boldsymbol{X} + \boldsymbol{U}t, \tag{11.6}$$

where the barred position vector is measured in the moving reference frame. Time remains unchanged since we make use of Newtonian universal time. In contrast, the coordinate position for the particle in the new frame equals to that in the original reference frame plus a contribution from the constant velocity, $\boldsymbol{U}$. We may sometimes refer to the barred reference frame as a *Galilean boosted* frame. The particle velocity in the moving (boosted) reference frame is given by

$$\overline{\boldsymbol{V}} = \frac{\mathrm{d}\overline{\boldsymbol{X}}}{\mathrm{d}\bar{t}} = \frac{\mathrm{d}\boldsymbol{X}}{\mathrm{d}t} + \frac{\mathrm{d}\left(\boldsymbol{U}t\right)}{\mathrm{d}t} = \boldsymbol{V} + \boldsymbol{U}, \tag{11.7}$$

where we set $\mathrm{d}\boldsymbol{U}/\mathrm{d}t = 0$ since $\boldsymbol{U}$ has a fixed magnitude and direction (as per our assumption that it is a constant vector). As expected, the velocity is shifted by the constant reference frame velocity $\boldsymbol{U}$, whereas the acceleration in the two reference frames is identical

$$\overline{\boldsymbol{A}} = \frac{\mathrm{d}^2\overline{\boldsymbol{X}}}{\mathrm{d}\bar{t}^2} = \frac{\mathrm{d}\boldsymbol{V}}{\mathrm{d}t} = \boldsymbol{A}. \tag{11.8}$$

11.1.4 Mechanical work and kinetic energy

When a force is applied to a particle as it moves along its trajectory, the force does *mechanical work* on the particle. This force affects the motion, with the work performed by the force computed by the line integral along the trajectory

$$W = \int_{\boldsymbol{x}_1}^{\boldsymbol{x}_2} \boldsymbol{F} \cdot \mathrm{d}\boldsymbol{x}, \tag{11.9}$$

where

$$\boldsymbol{x}_1 = \boldsymbol{X}(t = t_1) \quad \text{and} \quad \boldsymbol{x}_2 = \boldsymbol{X}(t = t_2) \tag{11.10}$$

are the spatial coordinates of the endpoints for the trajectory at times t_1 and t_2, and $\mathrm{d}\boldsymbol{x}$ is the differential vector increment along the trajectory. Since the particle is moving along its

dynamical trajectory, we can write

$$\mathrm{d}\boldsymbol{x} = \boldsymbol{V}\,\mathrm{d}t \tag{11.11}$$

and make use of Newton's equation of motion (11.5) to reach

$$W = \int_{\boldsymbol{x}_1}^{\boldsymbol{x}_2} \boldsymbol{F}\cdot\mathrm{d}\boldsymbol{x} = \int_{t_1}^{t_2} m\,\frac{\mathrm{d}\boldsymbol{V}}{\mathrm{d}t}\cdot\boldsymbol{V}\,\mathrm{d}t = \frac{m}{2}\int_{t_1}^{t_2}\frac{\mathrm{d}(\boldsymbol{V}\cdot\boldsymbol{V})}{\mathrm{d}t}\,\mathrm{d}t = K(t_2) - K(t_1), \tag{11.12}$$

where we defined the kinetic energy of the particle

$$K = \frac{m}{2}\,\boldsymbol{V}\cdot\boldsymbol{V}. \tag{11.13}$$

We conclude that the work done on the particle over a time interval is equal to its change in kinetic energy. The result (11.12) is called the *work-energy theorem*.

11.1.5 Mechanical energy conservation

Consider the work done on a particle as it moves between two points in space. Now compute the work done on the particle as it moves along another path between the same initial and final positions. If the work done on the particle is independent of the path taken between the points, then the force is said to be *conservative*.

Conservation of mechanical energy

Recalling our discussion of exact differentials in Section 2.8, we know that a conservative force can be written as the gradient of a *force potential*

$$\boldsymbol{F}^{\text{cons}} = -\nabla P, \tag{11.14}$$

where P is called the *potential* or the *potential energy*. Inserting the potential into the work equation (11.12) leads to an expression of *mechanical energy* conservation

$$W = \int_{\boldsymbol{x}_1}^{\boldsymbol{x}_2} \boldsymbol{F}^{\text{cons}}\cdot\mathrm{d}\boldsymbol{x} = \Delta K = -\Delta P \Longrightarrow K(t_2) + P(t_2) = K(t_1) + P(t_1). \tag{11.15}$$

That is, the sum of the kinetic energy plus potential energy remains constant for a particle moving in a conservative force field. The conservation of kinetic plus potential energy within a conservative force field offers our third conservation law: the conservation of *mechanical energy*.

As a result of mechanical energy conservation (11.15), we see that if a particle takes a closed trajectory within a conservative force field, then there is zero integrated work applied to the particle

$$W = \oint_{\mathcal{C}} \boldsymbol{F}^{\text{cons}}\cdot\mathrm{d}\boldsymbol{x} = 0, \tag{11.16}$$

where $\mathcal{C}$ is an arbitrary closed trajectory. Another way to see that $W = 0$ for a closed trajectory is to write

$$W = \oint_{\mathcal{C}} \boldsymbol{F}^{\text{cons}}\cdot\mathrm{d}\boldsymbol{x} = \oint_{\mathcal{C}} m\,\frac{\mathrm{d}\boldsymbol{V}}{\mathrm{d}t}\cdot\boldsymbol{V}\,\mathrm{d}t = \frac{m}{2}\oint_{\mathcal{C}}\mathrm{d}(\boldsymbol{V}\cdot\boldsymbol{V}) = 0, \tag{11.17}$$

with the zero resulting since $\mathrm{d}(\boldsymbol{V}\cdot\boldsymbol{V})$ is an exact differential (see Section 2.8 for exact differentials).

Conservative force from the effective gravity field

The earth's gravitational field as well as the planetary centrifugal acceleration (due to motion on a rotating planet) both give rise to conservative forces. We discuss these ideas in Section

13.10.4, where we see that the combined gravitational and planetary centrifugal accelerations are encapsulated by the gradient of the geopotential, Φ. In this case, the effective gravitational force acting on a point particle of mass, m, is given by

$$\boldsymbol{F}^{\text{geo}} = -m\,\nabla\Phi. \tag{11.18}$$

Consequently, the work done on the particle by the effective gravitational field is

$$W = \int_{\boldsymbol{x}_1}^{\boldsymbol{x}_2} \boldsymbol{F}^{\text{geo}} \cdot \mathrm{d}\boldsymbol{x} = -m \int_{\boldsymbol{x}_1}^{\boldsymbol{x}_2} \nabla\Phi \cdot \mathrm{d}\boldsymbol{x} = -m\,[\Phi(\boldsymbol{x}_2) - \Phi(\boldsymbol{x}_1)]. \tag{11.19}$$

The effective gravitational force field does positive work on the particle if $\Phi(\boldsymbol{x}_1) > \Phi(\boldsymbol{x}_2)$. That is, work is applied to the particle as it moves from a high geopotential at $\boldsymbol{x}_1$ to a lower geopotential at $\boldsymbol{x}_2$, in which case the work-energy theorem (11.12) means that the kinetic energy increases. Conversely, if $\Phi(\boldsymbol{x}_1) < \Phi(\boldsymbol{x}_2)$, then gravity does negative work on the particle. In this case the potential energy of the particle increases as it moves to a higher geopotential, while, through the work-energy theorem, the kinetic energy of the particle decreases.

11.1.6 Friction as a non-conservative force

Friction is the canonical non-conservative force that typically depends on the velocity field. For example, a common form of the frictional force is given by *Rayleigh drag*

$$\boldsymbol{F}^{\text{Rayleigh}} = -\gamma\, m\, \boldsymbol{V}, \tag{11.20}$$

where $\gamma > 0$ is a constant with dimensions of inverse time. Newton's equation of motion with Rayleigh drag (and no other forces) takes the form

$$\frac{\mathrm{d}\boldsymbol{V}}{\mathrm{d}t} = -\gamma\, \boldsymbol{V}. \tag{11.21}$$

Notably, Rayleigh drag is not Galilean invariant since it is dependent on the velocity. We can understand this lack of Galilean invariance by noting that the friction force identifies the state of rest ($\boldsymbol{V} = 0$) as a special reference frame.

The solution to the first order ordinary differential equation (11.21) is the exponential decay

$$\boldsymbol{V}(t) = \boldsymbol{V}(0)\, e^{-\gamma\, t}, \tag{11.22}$$

with $\boldsymbol{V}(0)$ the velocity at time $t = 0$. We thus see that Rayleigh drag exponentially drives the velocity towards zero. Correspondingly, Rayleigh drag dissipates the kinetic energy according to twice the exponential decay

$$\frac{\mathrm{d}K}{\mathrm{d}t} = m\,\boldsymbol{V} \cdot \frac{\mathrm{d}\boldsymbol{V}}{\mathrm{d}t} = -2\,\gamma\, K \Longrightarrow K(t) = K(0)\, e^{-2\,\gamma\, t}, \tag{11.23}$$

where $K(0) = \boldsymbol{V}(0) \cdot \boldsymbol{V}(0)/2$.

11.2 Kinematics of rigid-body rotations

The motion of a point particle is described by its trajectory, $\boldsymbol{X}(t)$, which provides the particle location in Euclidean space as time progresses. At each time instance the trajectory's velocity, $\mathrm{d}\boldsymbol{X}/\mathrm{d}t$, can be decomposed into radial motion towards or away from an arbitrary fixed origin, plus rotation about an instantaneously defined axis through the origin. In this section we focus on the rotational motion, so that the particle moves on a trajectory that is a fixed distance from

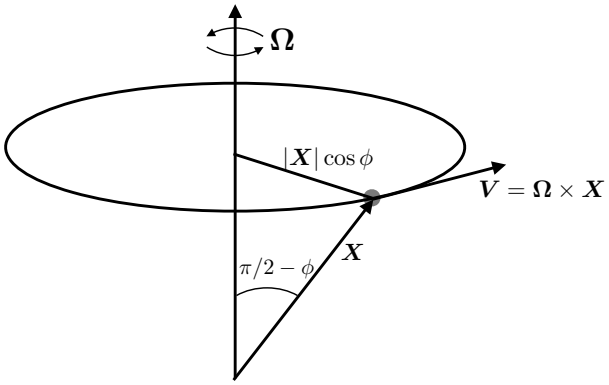

FIGURE 11.1: Kinematics of the rotational motion of a particle moving a fixed distance from an origin, whereby the motion at each instance can be represented as a rotation around an instanteneously determined axis that passes through the origin. Rotational motion is characterized by the angular velocity, $\boldsymbol{\Omega}$, that is oriented according to the right hand rule, so that rotation is counter-clockwise relative to $\hat{\boldsymbol{\Omega}}$. The velocity corresponding to this rotational motion is $\boldsymbol{V} = \boldsymbol{\Omega} \times \boldsymbol{X}$, which is perpendicular to both the particle position, $\boldsymbol{X}$, and the angular velocity, $\boldsymbol{\Omega}$. The angle, ϕ, is the angle relative to plane perpendicular to the rotation axis that passes through the origin. This choice for angle is motivated from the geophysical latitude as per Figure 4.3. In contrast, it is conventional in the mechanics literature to use the co-latitude, $\pi/2 - \phi$, which is the angle relative to the rotational axis. This figure anticipates our study of motion viewed from the rotating terrestrial reference frame in Chapter 13 (see also Figure 4.3 for the geometry of a rotating sphere).

the origin, $\mathrm{d}|\boldsymbol{X}|/\mathrm{d}t = 0$. We make use of results encountered when studying rigid body motion, with those results available here since $|\boldsymbol{X}|$ is fixed. We thus refer to the motion as *rigid-body rotational* motion. Besides offering insights into the nature of motion, the rigid-body rotations have direct application to the rigid-body rotating reference frame used by terrestrial observers. We pick up on that application in Section 11.4.

11.2.1 Angular velocity vector

A particle that moves on a trajectory, $\boldsymbol{X}(t)$, that is a fixed distance from an origin (as per points in a rigid body), can only exhibit rotational motion around an axis that extends through the origin. In general, the rotational axis has an evolving orientation in space. Yet at any time instance, the particle motion is specified by the axis around which rotation occurs, as well as the angular rate of rotation. Bringing the rotation rate and the axis orientation together leads to the notion of the *angular velocity* vector (dimensions of radians per time)

$$\boldsymbol{\Omega} = |\boldsymbol{\Omega}| \, \hat{\boldsymbol{\Omega}}, \tag{11.24}$$

where $\hat{\boldsymbol{\Omega}}$ is the unit vector specifying the direction of the rotational axis, and $|\boldsymbol{\Omega}|$ is the angular speed of the rotation. We choose the direction of the rotational axis according to the right hand rule. Although an arbitrary choice (i.e., we could just as well work with the left hand rule), the right hand rule establishes a convention from which we pursue the mechanical description. Figure 11.1 provides an example of rotational motion of a particle around an axis passing through a fixed origin.

11.2.2 Velocity of rigid-body rotation

Since the particle moves along a trajectory that has a fixed distance from the origin, its velocity is given by

$$\frac{\mathrm{d}\boldsymbol{X}}{\mathrm{d}t} = |\boldsymbol{X}| \, \frac{\mathrm{d}\hat{\boldsymbol{X}}}{\mathrm{d}t}, \tag{11.25}$$

where $\mathrm{d}\hat{\boldsymbol{X}}/\mathrm{d}t$ is the time derivative of the unit vector that points from the origin to the particle. Following from Figure 11.1, we see that the unit vector evolves under rotations according to

$$\frac{\mathrm{d}\hat{\boldsymbol{X}}}{\mathrm{d}t} = \boldsymbol{\Omega} \times \hat{\boldsymbol{X}}, \tag{11.26}$$

with this time derivative perpendicular to both $\boldsymbol{\Omega}$ and $\hat{\boldsymbol{X}}$. Multiplying by the constant $|\boldsymbol{X}|$ renders the rigid-body velocity vector

$$\frac{\mathrm{d}\boldsymbol{X}}{\mathrm{d}t} = \boldsymbol{V} = \boldsymbol{\Omega} \times \boldsymbol{X}, \tag{11.27}$$

with this velocity perpendicular to both the position vector and the rotational axis

$$\boldsymbol{V} \cdot \boldsymbol{\Omega} = 0 \quad \text{and} \quad \boldsymbol{V} \cdot \boldsymbol{X} = 0, \tag{11.28}$$

with this orientation reflected in Figure 11.1. We are also led to the corresponding linear momentum

$$\boldsymbol{P} = m\,\boldsymbol{V} = m\,\boldsymbol{\Omega} \times \boldsymbol{X}. \tag{11.29}$$

Evidently, motion that is further away from the rotational axis has a larger velocity magnitude (speed) for a given angular velocity, and thus a larger linear momentum. This property accords with our experience on a merry-go-round, in which there is a higher speed at the outer rim of the merry-go-round relative to points near the center.

11.2.3 Rigid-body rotation of an arbitrary vector

The results from Section 11.2.2, in particular the key result in equation (11.27), hold for any vector undergoing rigid-body rotation with a fixed origin. This result appears many times in this book, thus motivating us to here discuss it a bit further from slightly complementary perspectives. Indeed, we offer yet another derivation in Section 11.4.2 when studying rotating reference frames. Note that although we consider the position vector, $\boldsymbol{X}(t)$, derivations in this subsection are general, so that the results hold for an arbitrary vector of fixed magnitude that rotates about a fixed origin.

Proof that $\boldsymbol{X} \cdot \mathrm{d}\boldsymbol{X}/\mathrm{d}t = 0$ for rigid-body rotations

The rigid-body rotation of a vector does not change the vector's magnitude, so that

$$|\boldsymbol{X}(t)| = |\boldsymbol{X}(t + \delta t)|, \tag{11.30}$$

where δt is a small time increment during which the vector experiences a rigid-body rotation. The condition (11.30) can be written in the equivalent form

$$\frac{\mathrm{d}(\boldsymbol{X} \cdot \boldsymbol{X})}{\mathrm{d}t} = 0, \tag{11.31}$$

which then leads to the constraint

$$\boldsymbol{X} \cdot \frac{\mathrm{d}\boldsymbol{X}}{\mathrm{d}t} = 0. \tag{11.32}$$

Evidently, the time derivative of a vector undergoing a rigid-body rotation about a fixed origin is itself perpendicular to the vector.

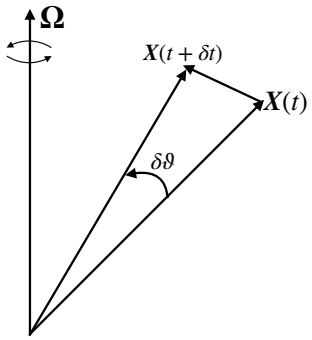

FIGURE 11.2: The change in a vector under a pure rotation leaves its origin fixed and the vector magnitude unchanged, $|\boldsymbol{X}(t)| = |\boldsymbol{X}(t+\delta t)|$. Only the vector direction changes by the angle $\delta\vartheta = \Omega\,\delta t$. Infinitesimal changes generated by the angular velocity $\boldsymbol{\Omega}$ lead to the vector differences $\boldsymbol{X}(t+\delta t) - \boldsymbol{X}(t) = \delta t\,\boldsymbol{\Omega} \times \boldsymbol{X}(t)$. Evidently, $\boldsymbol{\Omega}$ generates the rotation of vectors around its axis.

Geometric derivation of $\mathrm{d}\boldsymbol{X}/\mathrm{d}t = \boldsymbol{\Omega} \times \boldsymbol{X}$ *for rigid-body rotations*

In Figure 11.2 we consider the vector at two time instances, $\boldsymbol{X}(t+\delta t)$ and $\boldsymbol{X}(t)$, with the change in the vector generated by an infinitesimal rotation around the axis defined by the angular velocity vector, $\boldsymbol{\Omega}$. Evidently, Figure 11.2 reveals that the infinitesimal difference, $\boldsymbol{X}(t+\delta t) - \boldsymbol{X}(t)$, equals to the vector cross product of the angular velocity with the vector

$$\boldsymbol{X}(t+\delta t) - \boldsymbol{X}(t) = \delta t\,\boldsymbol{\Omega} \times \boldsymbol{X}(t). \tag{11.33}$$

Dividing by δt leads to

$$\frac{\mathrm{d}\boldsymbol{X}}{\mathrm{d}t} = \boldsymbol{\Omega} \times \boldsymbol{X}. \tag{11.34}$$

This time derivative satisfies the constraint (11.32) since $\boldsymbol{X} \cdot (\boldsymbol{\Omega} \times \boldsymbol{X}) = 0$, meaning that the magnitude of the vector indeed remains fixed. It is via equation (11.34) that we say $\boldsymbol{\Omega}$ generates rotations of $\boldsymbol{X}$.

Analytical derivation of $\mathrm{d}\boldsymbol{X}/\mathrm{d}t = \boldsymbol{\Omega} \times \boldsymbol{X}$ *for rigid-body rotations*

Let the direction of the angular velocity, $\boldsymbol{\Omega}$, be vertical, and let $\boldsymbol{X}$ be confined to the horizontal plane. In a time increment, δt, the vector is rotated by an angle

$$\delta\vartheta = |\boldsymbol{\Omega}|\,\delta t. \tag{11.35}$$

In the limit of small $\delta\vartheta$, the difference vector, $\boldsymbol{X}(t+\delta t) - \boldsymbol{X}(t)$, is perpendicular to $\boldsymbol{X}(t)$ and is of magnitude equal to the arc length

$$\delta s = |\boldsymbol{X}(t)|\,\delta\vartheta = |\boldsymbol{X}(t)|\,|\boldsymbol{\Omega}|\,\delta t. \tag{11.36}$$

Observe that the vector, $\boldsymbol{\Omega} \times \boldsymbol{X}(t)$, points in the same direction as the vector, $\boldsymbol{X}(t+\delta t) - \boldsymbol{X}(t)$, and is of length $|\boldsymbol{X}(t)|\,|\boldsymbol{\Omega}|$. We conclude that

$$\boldsymbol{X}(t+\delta t) - \boldsymbol{X}(t) = \boldsymbol{\Omega} \times \boldsymbol{X}(t)\,\delta t. \tag{11.37}$$

Dividing through by δt and taking the limit $\delta t \to 0$ gives

$$\frac{\mathrm{d}\boldsymbol{X}}{\mathrm{d}t} = \boldsymbol{\Omega} \times \boldsymbol{X}. \tag{11.38}$$

The proof for the case in which $\boldsymbol{\Omega}$ has a component along $\boldsymbol{X}$ is a straightforward generalization. The rotation of the trajectory is still confined to a plane, but only the component of $\boldsymbol{\Omega}$ normal to $\boldsymbol{X}$ generates rotation.

11.2.4 Angular momentum of rigid-body rotations

The *angular momentum* is the moment of the linear momentum

$$\boldsymbol{L} = \boldsymbol{X} \times \boldsymbol{P}. \tag{11.39}$$

Newton's second law (11.4) leads to the time derivative

$$\frac{\mathrm{d}\boldsymbol{L}}{\mathrm{d}t} = \boldsymbol{X} \times \boldsymbol{F}, \tag{11.40}$$

where $\dot{\boldsymbol{X}} \times \boldsymbol{P} = \dot{\boldsymbol{X}} \times m\,\dot{\boldsymbol{X}} = 0$. The cross product, $\boldsymbol{X} \times \boldsymbol{F}$, is the *torque* acting on the system relative to the chosen origin, with torques having dimensions of a force times a length. Equation (11.40) leads to our second conservation law: a particle has a constant angular momentum when experiencing zero torques, with this statement dependent on the choice of origin for the angular momentum and the corresponding torques.[4]

Inserting the rigid-body velocity (11.27) into the angular momentum (11.39) renders

$$\boldsymbol{L} = \boldsymbol{X} \times \boldsymbol{P} = m\,\boldsymbol{X} \times (\boldsymbol{\Omega} \times \boldsymbol{X}) = m\,[\boldsymbol{\Omega}\,|\boldsymbol{X}|^2 - \boldsymbol{X}\,(\boldsymbol{\Omega} \cdot \boldsymbol{X})] \equiv \boldsymbol{M} \cdot \boldsymbol{\Omega}. \tag{11.41a}$$

In the final equality we introduced the moment of inertia (a symmetric rank two tensor) for a point particle, with components given by

$$M^{pq} = m\,(\boldsymbol{X} \cdot \boldsymbol{X}\,\delta^{pq} - X^p\,X^q). \tag{11.42}$$

The moment of inertia tensor measures the inertia appropriate for determining angular momentum relative to a rotational axis. We encounter the moment of inertia tensor for a continuous fluid in Section 37.9.4 when studying the angular momentum of a region of fluid (see equation (37.76)).

The utility and relevance of angular momentum stems from its conservation for systems exhibiting rotational symmetry about special points or special directions. For example, motion on a smooth sphere exhibits rotational symmetry with respect to the center of the sphere. Consequently, all components of angular momentum for a particle are constant in the absence of externally applied torques. For motion around a smooth rotating sphere, the rotational axis breaks the three dimensional isotropy so that we only have a single angular momentum conservation; namely, the *axial angular momentum*. We study the connection between symmetry and conservation laws in Chapter 14, with particular focus on axial angular momentum in Section 14.5.

11.2.5 Kinetic energy of rigid-body rotations

If the particle is undergoing rigid-body rotational motion so that $\boldsymbol{V} = \boldsymbol{\Omega} \times \boldsymbol{X}$ (equation (11.27)), then the squared velocity for the particle is given by

$$\begin{aligned}
\delta_{mn}\,V^m\,V^n &= \delta_{mn}\,(\epsilon^{mpq}\,\Omega_p\,X_q)\,(\epsilon^{nst}\,\Omega_s\,X_t) && \text{(11.43a)}\\
&= \delta_{mn}\,\epsilon^{mpq}\,\epsilon^{nst}\,\Omega_p\,X_q\,\Omega_s\,X_t && \text{(11.43b)}\\
&= (\delta^{ps}\,\delta^{qt} - \delta^{pt}\,\delta^{qs})\,\Omega_p\,X_q\,\Omega_s\,X_t && \text{(11.43c)}
\end{aligned}$$

[4] We emphasize that angular momentum, torque, and angular velocity, are each defined relative to a chosen origin and chosen axis. For geophysical motion, the natural origin is the center of the planet, with angular momentum and torques computed relative to the polar rotation axis. We return to these ideas in Section 14.5.

$$= (\boldsymbol{X} \cdot \boldsymbol{X})\,(\boldsymbol{\Omega} \cdot \boldsymbol{\Omega}) - (\boldsymbol{X} \cdot \boldsymbol{\Omega})^2, \tag{11.43d}$$

where we made use of the Cartesian identity (1.69) holding for the permutation symbol. Introducing the moment of inertia tensor (11.42) renders the kinetic energy for the rotating particle

$$K = \tfrac{1}{2}\,\boldsymbol{\Omega} \cdot \boldsymbol{M} \cdot \boldsymbol{\Omega} = \tfrac{1}{2}\,\Omega_m\, M^{mn}\,\Omega_n. \tag{11.44}$$

11.2.6 Further study

The kinematics of rotational motion have their origin in the work of Euler. A more thorough discussion of rotational kinematics can be found in Section 4-6 of *Goldstein* (1980).

11.3 Accelerated and non-rotating reference frames

Inertial reference frames have a special status in Newtonian mechanics since it is in these reference frames that Newton's second law holds as per equations (11.4) or (11.5). Inertial reference frames are not accelerating, and as such they are related by the Galilean transformations considered in Section 11.1.3. Inertial reference frames are an idealization only approximately met in practice. For motion taking place within many terrestrial laboratories, the earth or *laboratory reference frame* provides a good approximation to an inertial reference frame. However, when the size of the physical system increases, and/or the length scale of the motion increases, then we must account for the earth's rotation. This is the situation holding for most of the geophysical fluid motions of concern in this book.

In this section we initiate our study of non-inertial reference frames by working in a frame that is accelerating along a straight line without turning (i.e. no rotation), such as when observing motion from a train accelerating on a straight track. We follow this study in Section 11.4 by examining motion from a rotating reference frame that has a fixed origin, thus allowing us to make use of the rigid-body rotating mechanics from Section 11.2. Although the rigid rotating frame in Section 11.4 is more directly connected to the description of geophysical motion from a rotating terrestrial reference frame, it is useful to warm up to the study of non-inertial reference frames by first studying the non-rotating case in the present section.

11.3.1 Reference frame induced accelerations and forces

Let $\mathcal{R}$ be an inertial reference frame so that Newton's law of motion takes on the familiar form (11.5)

$$m\,\dot{\boldsymbol{V}} = \boldsymbol{F}, \tag{11.45}$$

where $\boldsymbol{F}$ is the net force vector, with such forces arising from force fields (e.g., gravity or electromagnetic) or from contact forces that arise from interactions between bodies. Now consider another reference frame, $\mathcal{R}^*$, that moves with velocity $\boldsymbol{V}^{\text{frame}}$ relative to $\mathcal{R}$, and let $\boldsymbol{V}^*$ be the velocity of a particle measured relative to the $\mathcal{R}^*$. Accordingly, the velocity of a particle is decomposed into two terms

$$\boldsymbol{V} = \boldsymbol{V}^{\text{frame}} + \boldsymbol{V}^*. \tag{11.46}$$

Making use of this relation in Newton's law (11.45), and rearranging, leads to

$$m\,\dot{\boldsymbol{V}}^* = m\,(\dot{\boldsymbol{V}} - \dot{\boldsymbol{V}}^{\text{frame}}) = \boldsymbol{F} - m\,\dot{\boldsymbol{V}}^{\text{frame}}. \tag{11.47}$$

If $\dot{\boldsymbol{V}}^{\text{frame}}$ vanishes, then Newton's law (11.47) remains form invariant and we refer to $\mathcal{R}^*$ as another inertial reference frame that is realized via a Galilean transformation from the original (see Section 11.1.3 for Galilean transformations between two inertial reference frames). For the

more general case with a non-vanishing $\dot{\boldsymbol{V}}^{\text{frame}}$, we encounter an extra force in equation (11.47) when working in a non-inertial reference frame

$$\boldsymbol{F}^{\text{frame}} = -m\,\boldsymbol{A}^{\text{frame}} \equiv -m\,\dot{\boldsymbol{V}}^{\text{frame}}. \tag{11.48}$$

That is, by choosing to write equation (11.47) in the form of Newton's law, but from the perspective of the non-inertial reference frame, we must include a force that arises solely due to acceleration of the reference frame

$$m\,\dot{\boldsymbol{V}}^{*} = \boldsymbol{F} + \boldsymbol{F}^{\text{frame}}. \tag{11.49}$$

To appreciate the minus sign in equation (11.48), consider the backward force felt on the driver when accelerating forward in a car.

Equation (11.48) is somewhat overloaded. Namely, when the non-inertial reference frame is rotating, then the coordinate basis vectors are time dependent, and that time dependence must be considered when transforming vectors. As a result, we only make direct use of equation (11.48) when studying linear accelerating frames in Section 11.3.3, since in this case the basis vectors in the two reference frames are the same. The case of rotating reference frames in Section 11.4 requires a bit more work.

11.3.2 A comment on terminology

The reference frame induced force, $\boldsymbol{F}^{\text{frame}}$, from equation (11.48) is sometimes called a "fictitious force" or a "pseudo-force". We eschew that terminology since reference frame induced forces can play a dominant role in describing motion viewed from the non-inertial reference frame. So from the non-inertial reference frame perspective, there is nothing fictional about them $\boldsymbol{F}^{\text{frame}}$.

Chapter 12 of *French* (1971) refers to $\boldsymbol{F}^{\text{frame}}$ as an *inertial force* along with the corresponding *inertial acceleration*. As noted on pages 493-494 of *French* (1971), such forces that are experienced by an object due to the acceleration of a reference frame are "forces of inertia" that allow one to return Newton's law back to its familiar form found in inertial reference frames. Though ubiquitous in the literature, this terminology is prone to confusion since these so-called inertial forces arise due to non-inertial motion of the reference frame, and as such would more clearly be referred to as "non-inertial terms" or "non-inertial forces" (see Section 9.3 of *Marion and Thornton* (1988)). We aim to avoid confusion by being somewhat pedantic when discussing forces induced by a non-inertial reference frame.

11.3.3 Simple pendulum in an accelerating train

Consider a non-inertial reference frame that accelerates along a line without turning (i.e., no rotation). For example, we feel a backwards acceleration while the vehicle accelerates forward, and the converse while the vehicle slows to a stop. The opposite sense of the acceleration is accounted for by the minus sign in the expression (11.48).

As a specific example, consider a pendulum with constant mass, m, on a massless string of length L. Hang the pendulum from the top of a train car in a gravity field and assume the train has an acceleration, $\dot{\boldsymbol{V}}^{\text{frame}}$, along a straight track. When viewed from the inertial reference frame, the pendulum satisfies Newton's law in the familiar form

$$m\,\dot{\boldsymbol{V}} = \boldsymbol{F}. \tag{11.50}$$

The force, $\boldsymbol{F}$, arises from the pendulum's weight, $m\,\boldsymbol{g}$, as well as the string tension, $\boldsymbol{T}$, so that

$$m\,\dot{\boldsymbol{V}} = \boldsymbol{T} + m\,\boldsymbol{g}. \tag{11.51}$$

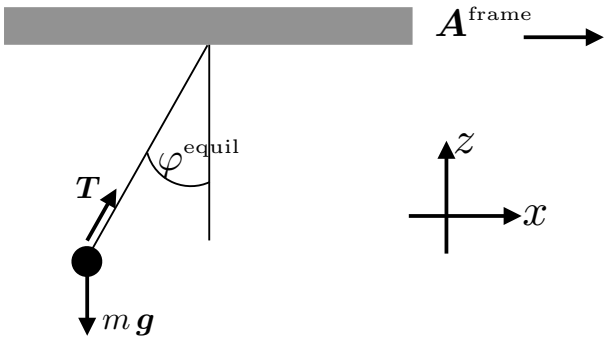

FIGURE 11.3: A pendulum oscillating from the ceiling of a train car, with the train moving with velocity $\boldsymbol{V}^{\text{frame}} = \hat{\boldsymbol{x}}\,|\boldsymbol{V}^{\text{frame}}|$. Forces acting on the pendulum arise from the string tension, $\boldsymbol{T}$, and the weight, $\boldsymbol{g}\,m = -\hat{\boldsymbol{z}}\,g\,m$. In the accelerating (non-inertial) reference frame, the additional force appears, $-\hat{\boldsymbol{x}}\,m\,|\boldsymbol{V}^{\text{frame}}|$. When viewed in the accelerating reference frame, the pendulum reaches its equilibrium ($\dot{\boldsymbol{V}}^{*} = 0$) at an angle satisfying $\tan\varphi^{\text{equil}} = |\dot{\boldsymbol{V}}^{\text{frame}}|/g$.

When viewed in the accelerating reference frame the equation of motion takes the form

$$m\,\dot{\boldsymbol{V}}^{*} = \boldsymbol{T} + m\,\boldsymbol{g} - m\,\dot{\boldsymbol{V}}^{\text{frame}} = \boldsymbol{T} + m\,(\boldsymbol{g} - \dot{\boldsymbol{V}}^{\text{frame}}). \tag{11.52}$$

Since the same mass, m, multipled both the gravitational force and the force due to the accelerating reference frame, we can define an effective gravity by writing

$$m\,\dot{\boldsymbol{V}}^{*} = \boldsymbol{T} + m\,\boldsymbol{g}^{\text{eff}} \quad \text{with} \quad \boldsymbol{g}^{\text{eff}} = \boldsymbol{g} - \dot{\boldsymbol{V}}^{\text{frame}}. \tag{11.53}$$

The effective gravity is not vertical when the reference frame accelerates. For example, if the reference frame accelerates in the $+\hat{\boldsymbol{x}}$ direction, then

$$\boldsymbol{g}^{\text{eff}} = -g\,\hat{\boldsymbol{z}} - \dot{V}^{\text{frame}}\,\hat{\boldsymbol{x}} = -g\,(\hat{\boldsymbol{z}} + \hat{\boldsymbol{x}}\,\dot{V}^{\text{frame}}/g). \tag{11.54}$$

We depict this situation in Figure 11.3.

What happens when the acceleration of the pendulum vanishes in the inertial reference frame? In this case the string tension exactly balances the weight so that from equation (11.51) we find

$$\boldsymbol{T} = -m\,\boldsymbol{g} \quad \Longleftarrow \quad \text{no acceleration in inertial frame, } \mathcal{R}. \tag{11.55}$$

Evidently, the pendulum comes to rest in the inertial frame with a string tension that exactly balances the vertical gravitational force acting on the pendulum mass. Hence, the pendulum hangs vertically.

The same question posed from the non-inertial reference frame leads to the distinct string tension

$$\boldsymbol{T} = -m\,\boldsymbol{g}^{\text{eff}} \quad \Longleftarrow \quad \text{no acceleration in non-inertial frame, } \mathcal{R}^{*}. \tag{11.56}$$

That is, the string tension now balances the effective gravity, so that the resting pendulum is not vertical but instead it is aligned with the effective gravity. We can readily find the angle of the resting pendulum, relative to the vertical, through the expression (11.54) for the effective gravity, so that

$$\tan\varphi^{\text{equil}} = |\dot{\boldsymbol{V}}^{\text{frame}}|/g. \tag{11.57}$$

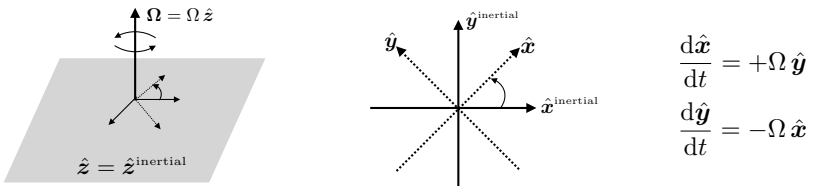

FIGURE 11.4: Depicting the coordinate axes in an inertial reference frame, $(\hat{\boldsymbol{x}}^{\text{inertial}}, \hat{\boldsymbol{y}}^{\text{inertial}}, \hat{\boldsymbol{z}}^{\text{inertial}})$, and a corresponding rigid-body rotating reference frame, $(\hat{\boldsymbol{x}}, \hat{\boldsymbol{y}}, \hat{\boldsymbol{z}})$. The origin for the two reference frames is the same, and the rotation is around the vertical axis so that $\hat{\boldsymbol{z}} = \hat{\boldsymbol{z}}^{\text{inertial}}$ and $\boldsymbol{\Omega} = \Omega\,\hat{\boldsymbol{z}}$. Left panel: perspective view of the inertial and rotating reference frames. Middle panel: horizontal (plan view) and rotation of the horizontal basis vectors in the rotating reference frame. Right panel: expressing the time derivatives of the horizontal basis vectors according to the rigid-body rotation equation (11.60).

11.4 Rigid-body rotating reference frames

We now consider a rotating reference frame. For simplicity, as well as to connect to the terrestrial case, assume rotation is around a fixed axis that passes through a fixed origin, such as that depicted in Figure 11.4. In this manner, the reference frame rotates as a rigid-body, thus enabling use of the kinematics from Section 11.2.[5]

In this chapter we make use of Cartesian coordinates for both the inertial reference frame, $\mathcal{R}$, and the rigid-body rotating reference frame, $\mathcal{R}^*$, with orientation chosen so that the basis vectors of the rotating frame rotate counter-clockwise around the vertical axis, $\hat{\boldsymbol{z}}$. As we see in this section, a proper accounting for the basis vector rotation is critical for computing non-inertial accelerations.

11.4.1 Incorrect calculation of Coriolis acceleration

Directly plugging into the expression (11.48) leads to the force in the non-inertial reference frame

$$\begin{aligned}
\boldsymbol{F}^{\text{frame}} &= -m\,\dot{\boldsymbol{V}}^{\text{rigid}} && \text{(11.58a)}\\
&= -m\,\frac{\mathrm{d}(\boldsymbol{\Omega}\times\boldsymbol{X})}{\mathrm{d}t} && \text{(11.58b)}\\
&= -m\,\boldsymbol{\Omega}\times\boldsymbol{V} && \text{(11.58c)}\\
&= -m\,\boldsymbol{\Omega}\times(\boldsymbol{V}^{\text{rigid}} + \boldsymbol{V}^*). && \text{(11.58d)}
\end{aligned}$$

The first term is the correct expression for the centrifugal acceleration (see Figure 11.5), yet the second term is missing a factor of two for the Coriolis acceleration. As hinted at following equation (11.48), the error arises since the coordinate basis vectors change as the reference frame rotates, and this time dependence must be considered when computing the acceleration seen in a non-inertial reference frame.

[5]Rigid-body rotating reference frame is what one generally means when studying rotating physics. However, there are more general forms of rotation, whereby angular rotation is a function of space and time. We do not consider time dependent rotating frames in this book. However, the rigid-body frame of the earth's rotation is experienced as a latitudinally dependent rotation rate due to sphericity of the planet. Spatial dependence of the rotating terrestrial frame is the origin for the planetary Rossby waves studied in Part X of this book.

11.4.2 Rigid-body rotation of an arbitrary vector

We here offer yet another means to derive the key result from Section 11.2.3 concerning the time derivative of a vector undergoing rigid-body rotation around a fixed origin. For this purpose, consider a vector that is measured in the rotating reference frame and represented using Cartesian coordinates

$$\boldsymbol{Q} = \sum_{i*=1}^{3} Q^{i*}\,\hat{\boldsymbol{e}}_{i*} = Q^{i*}\,\hat{\boldsymbol{e}}_{i*}, \tag{11.59}$$

where the second equality made use of Einstein summation convention. Also, we introduced the rotating reference frame Cartesian basis vectors, $\hat{\boldsymbol{e}}_{1*} = \hat{\boldsymbol{x}}$, $\hat{\boldsymbol{e}}_{2*} = \hat{\boldsymbol{y}}$, and $\hat{\boldsymbol{e}}_{3*} = \hat{\boldsymbol{z}}$, which are rigidly rotating with the reference frame. Following the discussion in Section 11.2.2, rigid-body rotation of the basis vectors leads to a time derivative according to equation (11.26), so that

$$\frac{\mathrm{d}\hat{\boldsymbol{e}}_{i*}}{\mathrm{d}t} = \boldsymbol{\Omega} \times \hat{\boldsymbol{e}}_{i*}. \tag{11.60}$$

Hence, the time derivative of $\boldsymbol{Q}$, when represented in the rotating reference frame, is given by two terms,

$$\frac{\mathrm{d}\boldsymbol{Q}}{\mathrm{d}t} = \frac{\mathrm{d}Q^{i*}}{\mathrm{d}t}\,\hat{\boldsymbol{e}}_{i*} + Q^{i*}\,(\boldsymbol{\Omega} \times \hat{\boldsymbol{e}}_{i*}) = \frac{\mathrm{d}Q^{i*}}{\mathrm{d}t}\,\hat{\boldsymbol{e}}_{i*} + \boldsymbol{\Omega} \times \boldsymbol{Q}. \tag{11.61}$$

The first expression on the right hand side is the time derivative of the vector's components as measured in the rotating reference frame, which we write as

$$\dot{\boldsymbol{Q}}^{*} \equiv \frac{\mathrm{d}Q^{i*}}{\mathrm{d}t}\,\hat{\boldsymbol{e}}_{i*}. \tag{11.62}$$

The second term in equation (11.61) arises from rigid-body rotation of the rotating reference frame's coordinate basis.

11.4.3 Coriolis and centrifugal accelerations

We can make use of equation (11.61) for an arbitrary vector, including the particle's position vector. In this case the velocity of the particle is decompsed into

$$\frac{\mathrm{d}\boldsymbol{X}}{\mathrm{d}t} = \frac{\mathrm{d}X^{i*}}{\mathrm{d}t}\,\hat{\boldsymbol{e}}_{i*} + \boldsymbol{\Omega} \times \boldsymbol{X} = \boldsymbol{V}^{*} + \boldsymbol{U}_{\mathrm{rigid}}. \tag{11.63}$$

Evidently, the velocity as measured in the inertial frame equals to the velocity measured in the non-inertial reference frame, $\boldsymbol{V}^{*}$, plus the rigid-body rotating velocity,

$$\boldsymbol{U}_{\mathrm{rigid}} = \boldsymbol{\Omega} \times \boldsymbol{X}. \tag{11.64}$$

Taking the second derivative of the position vector leads to the decomposition of the acceleration measured in the inertial reference frame

$$\begin{aligned}
\frac{\mathrm{d}^2\boldsymbol{X}}{\mathrm{d}t^2} &= \frac{\mathrm{d}^2X^{i*}}{\mathrm{d}t^2}\,\hat{\boldsymbol{e}}_{i*} + \frac{\mathrm{d}X^{i*}}{\mathrm{d}t}\,(\boldsymbol{\Omega} \times \hat{\boldsymbol{e}}_{i*}) + \boldsymbol{\Omega} \times \frac{\mathrm{d}\boldsymbol{X}}{\mathrm{d}t} && \text{(11.65a)}\\
&= \boldsymbol{A}^{*} + \boldsymbol{\Omega} \times \boldsymbol{V}^{*} + \boldsymbol{\Omega} \times (\boldsymbol{V}^{*} + \boldsymbol{V}^{\mathrm{rigid}}) && \text{(11.65b)}\\
&= \boldsymbol{A}^{*} + 2\,\boldsymbol{\Omega} \times \boldsymbol{V}^{*} + \boldsymbol{\Omega} \times \boldsymbol{V}^{\mathrm{rigid}}. && \text{(11.65c)}
\end{aligned}$$

Hence, the acceleration as measured in the rigid-body rotating reference frame is given by

$$\boldsymbol{A}^{*} = \boldsymbol{A} \underbrace{-2\,\boldsymbol{\Omega} \times \boldsymbol{V}^{*}}_{\text{Coriolis}} \underbrace{-\boldsymbol{\Omega} \times \boldsymbol{V}^{\mathrm{rigid}}}_{\text{centrifugal}}. \tag{11.66}$$

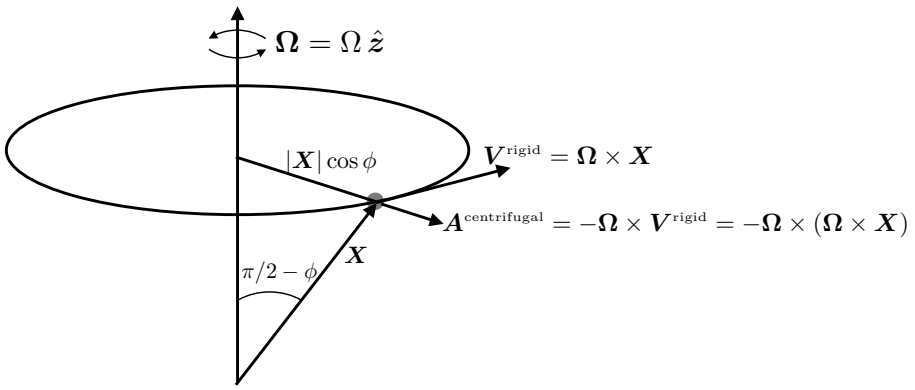

FIGURE 11.5: Depicting the kinematics of a rigid-body rotating reference frame, with rotation around a fixed vertical axis that passes through a fixed origin. The orientation is geophysically motivated as per Figure 4.3. In addition to the angular velocity, $\boldsymbol{\Omega}$, and rigid-body velocity, $\boldsymbol{V}^{\rm rigid} = \boldsymbol{\Omega} \times \boldsymbol{X}$, both depicted in Figure 11.1, we also show the centrifugal acceleration, $\boldsymbol{A}^{\rm cent} = -\boldsymbol{\Omega} \times \boldsymbol{V}^{\rm rigid} = -\boldsymbol{\Omega} \times (\boldsymbol{\Omega} \times \boldsymbol{X})$, that points outward away from the rotational axis.

We here identified the Coriolis and centrifugal accelerations

$$\boldsymbol{A}^{\rm Coriolis} = -2\,\boldsymbol{\Omega} \times \boldsymbol{V}^* \quad \text{and} \quad \boldsymbol{A}^{\rm centrifugal} = -\boldsymbol{\Omega} \times \boldsymbol{V}^{\rm rigid} = -\boldsymbol{\Omega} \times (\boldsymbol{\Omega} \times \boldsymbol{X}), \tag{11.67}$$

with both of these accelerations arising from the rigid-body rotation of the non-inertial reference frame. We have much to say in this book about these accelerations, particularly as realized by the rotating earth.

11.5 Newtonian mechanics for a system of particles

We here extend the single particle mechanics from Section 11.1 to the case of N particles with mass, $m_{(i)}$, position, $\boldsymbol{X}_{(i)}(t)$, and velocity, $\boldsymbol{V}_{(i)}(t) = \mathrm{d}\boldsymbol{X}_{(i)}/\mathrm{d}t$, where i is an integer labeling the particles,[6] and we assume the particle mass remains fixed in time. In the following, we find it useful to introduce the total mass of the system as well as the vector center of mass according to

$$M = \sum_{i=1}^{N} m_{(i)} \quad \text{and} \quad \boldsymbol{X} = \frac{1}{M} \sum_{i=1}^{N} m_{(i)}\,\boldsymbol{X}_{(i)}. \tag{11.68}$$

11.5.1 Forces on the particles

We conceive of two contributions to the forces acting on each particle. The first arises from *external force* fields that are independent of the N particles, $\boldsymbol{F}^{(\rm ext)}_{(i)}$. For example, we may consider a system of particles moving in the gravitational field of the planet, with the planet's gravitational field assumed to be independent of the particles. The second force arises from the interactions between the particles, which we refer to as an *internal force*. We write the internal force vector as $\boldsymbol{F}_{(ji)}$, which is taken to be the force on particle i due to interactions with particle j. We furthermore assume that there are no self-forces so that

$$\boldsymbol{F}_{(ii)} = 0. \tag{11.69}$$

[6] We place the particle index within parentheses to emphasize that it is not a tensor index. Correspondingly, particle indices do not follow the summation convention of tensor indices.

The net force acting on particle i is thus written

$$\boldsymbol{F}_{(i)} = \boldsymbol{F}^{(\text{ext})}_{(i)} + \sum_{j=1}^{N} \boldsymbol{F}_{(ji)}, \tag{11.70}$$

and the net force acting on the full system of particles is

$$\sum_{i=1}^{N} \boldsymbol{F}_{(i)} = \sum_{i=1}^{N} \boldsymbol{F}^{(\text{ext})}_{(i)} + \sum_{i=1}^{N}\sum_{j=1}^{N} \boldsymbol{F}_{(ji)}. \tag{11.71}$$

The final sum can be written

$$\sum_{i=1}^{N}\sum_{j=1}^{N} \boldsymbol{F}_{(ji)} = \frac{1}{2}\sum_{i=1}^{N}\sum_{j=1}^{N} (\boldsymbol{F}_{(ji)} + \boldsymbol{F}_{(ij)}), \tag{11.72}$$

where, again, $\boldsymbol{F}_{(ji)}$ is the force on particle i due to interactions with particle j, and $\boldsymbol{F}_{(ij)}$ is the force on particle j due to interactions with particle i. This identity follows since the sums are finite so that limits on double sums can be swapped. In the next subsection we see why it is useful to write the internal forces in this manner.

11.5.2 Weak and strong form of Newton's third law

Newton's third law states that the force acting on particle i due to particle j is equal to, yet oppositely directed, the force acting on particle j due to particle i:

$$\boldsymbol{F}_{(ij)} = -\boldsymbol{F}_{(ji)}. \tag{11.73}$$

For those forces satisfying Newton's third law, the total force acting on the N particle system arises from just the external force, since the internal forces cancel pairwise

$$\sum_{i=1}^{N}\sum_{j=1}^{N} \boldsymbol{F}_{(ij)} = \sum_{i=1}^{N} \boldsymbol{F}^{(\text{ext})}_{(i)} = \boldsymbol{F}^{(\text{ext})}. \tag{11.74}$$

As discussed in Section 13.10.2, the gravitational force acting between two point masses offers an example force that satisfies Newton's third law, in which case the force is given by the inverse square expression

$$\boldsymbol{F}_{(ji)} = -\frac{G\, m_{(i)}\, m_{(j)}\, (\boldsymbol{X}_{(i)} - \boldsymbol{X}_{(j)})}{|\boldsymbol{X}_{(i)} - \boldsymbol{X}_{(j)}|^3} = -\boldsymbol{F}_{(ji)}, \tag{11.75}$$

where G is Newton's gravitational constant discussed in Section 13.10.1. Notice how the gravitational force acts along the line connecting the two particles, so that

$$(\boldsymbol{X}_{(i)} - \boldsymbol{X}_{(j)}) \times \boldsymbol{F}_{(ji)} = 0. \tag{11.76}$$

The electrostatic force acting on charged particles in an electric field is given by Coulombs law, which is also an inverse squared force and that acts along the line between the two particles.

Newton's gravity force and the Coulomb electrostatic force are known as *central forces*. Central forces are said to satisfy the *strong form* of Newton's third law, in that both $\boldsymbol{F}_{(ij)} = -\boldsymbol{F}_{(ji)}$ and $(\boldsymbol{X}_{(i)} - \boldsymbol{X}_{(j)}) \times \boldsymbol{F}_{(ji)} = 0$. Slightly more general forces arise that satisfy $\boldsymbol{F}_{(ji)} = -\boldsymbol{F}_{(ij)}$ and yet

$(\boldsymbol{X}_{(i)} - \boldsymbol{X}_{(j)}) \times \boldsymbol{F}_{(ji)} \neq 0$, with such forces said to satisfy the *weak form* of Newton's third law:

$$\boldsymbol{F}_{(ij)} = -\boldsymbol{F}_{(ji)} \quad \text{and} \quad (\boldsymbol{X}_{(i)} - \boldsymbol{X}_{(j)}) \times \boldsymbol{F}_{(ji)} = 0 \Longrightarrow \text{central force; strong 3rd law} \tag{11.77a}$$

$$\boldsymbol{F}_{(ij)} = -\boldsymbol{F}_{(ji)} \quad \text{and} \quad (\boldsymbol{X}_{(i)} - \boldsymbol{X}_{(j)}) \times \boldsymbol{F}_{(ji)} \neq 0 \Longrightarrow \text{non-central force; weak 3rd law.} \tag{11.77b}$$

Any force that depends on the velocity of the particle is not a central force.[7] The distinction between the weak and strong form of Newton's third law becomes important when studying particle angular momentum in Section 11.5.4. When studying stresses in fluids in Chapter 25, we assume the strong form of Newton's third law.

11.5.3 Newton's second law of motion

The linear momentum of a particle is its mass times the velocity

$$\boldsymbol{P}_{(i)} = m_{(i)}\, \boldsymbol{V}_{(i)} \quad \text{no implied summation.} \tag{11.78}$$

Assuming the mass of the particle is constant, the corresponding equation of motion is given by Newton's second law

$$\dot{\boldsymbol{P}}_{(i)} = m_{(i)}\, \dot{\boldsymbol{V}}_{(i)} = \boldsymbol{F}^{(\text{ext})}_{(i)} + \sum_{j=1}^{N} \boldsymbol{F}_{(ji)}. \tag{11.79}$$

Assuming the internal forces satisfy either the weak or strong form of Newton's third law as in equations (11.77a)-(11.77b), we find that the total momentum for the N particle system evolves according to just the total external force

$$\dot{\boldsymbol{P}} = \sum_{i=1}^{N} \dot{\boldsymbol{P}}_{(i)} = \frac{\mathrm{d}^2}{\mathrm{d}t^2} \sum_{i=1}^{N} m_{(i)}\, \boldsymbol{X}_{(i)} = M\, \ddot{\boldsymbol{X}} = \boldsymbol{F}^{(\text{ext})}. \tag{11.80}$$

That is, the time change in the total linear momentum is given by the total mass times the acceleration of the center of mass, which equals, through Newton's second and third laws, to the total external force acting on the system. We thus find that the center of mass maintains a fixed velocity if there is no net external force acting on the many particle system. This result accords with common experience whereby we cannot lift ourselves up by our own bootstraps.

11.5.4 Angular momentum

The total angular momentum for the many particle system is given by

$$\boldsymbol{L} = \sum_{i=1}^{N} \boldsymbol{L}_{(i)} = \sum_{i=1}^{N} \boldsymbol{X}_{(i)} \times \boldsymbol{P}_{(i)} = \sum_{i=1}^{N} m_{(i)}\, \boldsymbol{X}_{(i)} \times \boldsymbol{V}_{(i)}, \tag{11.81}$$

and its time derivative is given by

$$\dot{\boldsymbol{L}} = \sum_{i=1}^{N} m_{(i)}\, \boldsymbol{X}_{(i)} \times \dot{\boldsymbol{V}}_{(i)} = \sum_{i=1}^{N} \boldsymbol{X}_{(i)} \times \boldsymbol{F}^{(\text{ext})}_{(i)} + \sum_{i=1}^{N} \sum_{j=1}^{N} \boldsymbol{X}_{(i)} \times \boldsymbol{F}_{(ji)}, \tag{11.82}$$

[7] The force acting on a classical charged particle moving in an electromagnetic field is known as the Lorentz force. The Lorentz force depends on the velocity of the charged particle and so it is not a central force, with the Lorentz force only satisfying the weak form of Newton's third law. See page 45 of *Marion and Thornton* (1988) for more discussion.

where we set $\dot{\boldsymbol{X}}_{(i)} \times \boldsymbol{V}_{(i)} = \dot{\boldsymbol{X}}_{(i)} \times \dot{\boldsymbol{X}}_{(i)} = 0$, and made use of the particle equation of motion (11.79). We identify the term

$$\boldsymbol{\Gamma}^{(\text{ext})} \equiv \sum_{i=1}^{N} \boldsymbol{X}_{(i)} \times \boldsymbol{F}_{(i)}^{(\text{ext})} \tag{11.83}$$

as the total torque acting on the N particle system arising from the external force acting on each particle. The internal torque contribution can be written

$$\sum_{i=1}^{N}\sum_{j=1}^{N} \boldsymbol{X}_{(i)} \times \boldsymbol{F}_{(ji)} = \frac{1}{2}\sum_{i=1}^{N}\sum_{j=1}^{N}(\boldsymbol{X}_{(i)} \times \boldsymbol{F}_{(ji)} + \boldsymbol{X}_{(j)} \times \boldsymbol{F}_{(ij)}) = \frac{1}{2}\sum_{i=1}^{N}\sum_{j=1}^{N}(\boldsymbol{X}_{(i)} - \boldsymbol{X}_{(j)}) \times \boldsymbol{F}_{(ji)}, \tag{11.84}$$

where the first equality follows from interchanging particle indices, and the second equality follows from the weak form of Newton's third law given by equation (11.77b). If we furthermore assume the force satisfies the strong form of Newton's third law (11.77a), as for a central force, then the total angular momentum evolves according to just the total external torque

$$\dot{\boldsymbol{L}} = \boldsymbol{\Gamma}^{(\text{ext})}. \tag{11.85}$$

That is, we require the strong form of Newton's third law to ensure that the total angular momentum is only affected by the torques created by external forces. If the forces only satisfy the weak form of Newton's third law, then evolution of the total angular momentum is generally affected by internal torques. Such torques arise in the presence of nonmechanical forces, such as a magnetic force between charged particles when the electromagnetic field contains intrinsic angular momentum. We have no occasion to study internal torques in this book, so that all physical systems are assumed to satisfy the strong form of Newton's third law.

11.5.5 Center of mass coordinates

It is sometimes preferable to move to an internal set of coordinates that dispenses with the arbitrary fixed origin. In this case we place the coordinate origin at the moving center of mass,

$$\boldsymbol{X}_{(i)} = \boldsymbol{X} + \boldsymbol{X}'_{(i)}, \tag{11.86}$$

with a corresponding velocity expression

$$\boldsymbol{V}_{(i)} = \boldsymbol{V} + \boldsymbol{V}'_{(i)}. \tag{11.87}$$

Making use of the definition of the center of mass coordinate (11.68), we readily find that the relative position and relative velocity each have a vanishing mass weighted sum over all the particles

$$\sum_{i=1}^{N} m_{(i)}\, \boldsymbol{X}'_{(i)} = 0 \quad \text{and} \quad \sum_{i=1}^{N} m_{(i)}\, \boldsymbol{V}'_{(i)} = 0. \tag{11.88}$$

11.5.6 Angular momentum in center of mass coordinates

The total angular momentum of the N particle system, expressed in the center of mass coordinates, is given by

$$\boldsymbol{L} = \sum_{i=1}^{N} m_{(i)}\, \boldsymbol{X}_{(i)} \times \boldsymbol{V}_{(i)} \tag{11.89a}$$

$$= \sum_{i=1}^{N} m_{(i)} \left(\boldsymbol{X} + \boldsymbol{X}'_{(i)} \right) \times \left(\boldsymbol{V} + \boldsymbol{V}'_{(i)} \right) \tag{11.89b}$$

$$= M \, \boldsymbol{X} \times \boldsymbol{V} + \sum_{i=1}^{N} m_{(i)} \, \boldsymbol{X}'_{(i)} \times \boldsymbol{V}'_{(i)} \tag{11.89c}$$

$$= \boldsymbol{L}^{(\mathrm{cm})} + \boldsymbol{L}', \tag{11.89d}$$

where we used equation (11.88) to reach the third equality. The first term is the angular momentum of the center of mass relative to the fixed origin

$$\boldsymbol{L}^{(\mathrm{cm})} = M \, \boldsymbol{X} \times \boldsymbol{V}, \tag{11.90}$$

whereas the second term is the internal angular momentum measured relative to the center of mass

$$\boldsymbol{L}' = \sum_{i=1}^{N} m_{(i)} \, \boldsymbol{X}'_{(i)} \times \boldsymbol{V}'_{(i)}. \tag{11.91}$$

Evolution of the center of mass angular momentum takes on the form

$$\dot{\boldsymbol{L}}^{(\mathrm{cm})} = M \, \boldsymbol{X} \times \dot{\boldsymbol{V}} = \boldsymbol{X} \times \boldsymbol{F}^{(\mathrm{ext})}, \tag{11.92}$$

with the right hand side the torque from the net external force computed relative to the center of mass position. Correspondingly, evolution of the total angular momentum is

$$\dot{\boldsymbol{L}} = \sum_{i=1}^{N} m_{(i)} \, \boldsymbol{X}_{(i)} \times \dot{\boldsymbol{V}}_{(i)} \tag{11.93a}$$

$$= \sum_{i=1}^{N} (\boldsymbol{X} + \boldsymbol{X}'_{(i)}) \times \boldsymbol{F}^{\mathrm{ext}}_{(i)} \tag{11.93b}$$

$$= \boldsymbol{X} \times \boldsymbol{F}^{\mathrm{ext}} + \sum_{i=1}^{N} \boldsymbol{X}'_{(i)} \times \boldsymbol{F}^{\mathrm{ext}}_{(i)} \tag{11.93c}$$

$$= \dot{\boldsymbol{L}}^{(\mathrm{cm})} + \dot{\boldsymbol{L}}'. \tag{11.93d}$$

We thus see that the rate of change for the angular momentum computed relative to the center of mass is given by the torques from the external forces applied to each particle, computed relative to the center of mass

$$\dot{\boldsymbol{L}}' = \sum_{i=1}^{N} \boldsymbol{X}'_{(i)} \times \boldsymbol{F}^{\mathrm{ext}}_{(i)}. \tag{11.94}$$

11.5.7 Energy in center of mass coordinates

Making use of the identity (11.88), we find that the total kinetic energy is given by

$$K = \frac{1}{2} \sum_{i=1}^{N} m_{(i)} \, \boldsymbol{V}_{(i)} \cdot \boldsymbol{V}_{(i)} = \frac{M}{2} \boldsymbol{V} \cdot \boldsymbol{V} + \frac{1}{2} \sum_{i=1}^{N} m_{(i)} \, \boldsymbol{V}'_{(i)} \cdot \boldsymbol{V}'_{(i)} = K^{(\mathrm{cm})} + K', \tag{11.95}$$

which is the sum of the center of mass kinetic energy, $K^{(\mathrm{cm})}$, plus the kinetic energy of the internal motions relative to the center of mass, K'.

Consider two configurations of the N particle system, configuration A at time t_A and configuration B at time t_B. Let $\boldsymbol{X}_{(iA)}$ be the position of particle i in configuration A, and $\boldsymbol{X}_{(iB)}$

the position of this particle in configuration B, and assume the two configurations are connected by trajectories determined by the equation of motion for each particle. Extending our discussion of work in Section 11.1.4, we see that the work done by forces acting on the N particle system as it moves between these two configurations is given by

$$W_{AB} = \sum_{i=1}^{N} \int_{\boldsymbol{X}_{(iA)}}^{\boldsymbol{X}_{(iB)}} \boldsymbol{F}_{(i)} \cdot \mathrm{d}\boldsymbol{x}_{(i)} \tag{11.96a}$$

$$= \sum_{i=1}^{N} \int_{t_A}^{t_B} \boldsymbol{F}_{(i)} \cdot \boldsymbol{V}_{(i)} \, \mathrm{d}t \tag{11.96b}$$

$$= \sum_{i=1}^{N} \int_{t_A}^{t_B} m_{(i)} \, \dot{\boldsymbol{V}}_{(i)} \cdot \boldsymbol{V}_{(i)} \, \mathrm{d}t \tag{11.96c}$$

$$= \frac{1}{2} \sum_{i=1}^{N} \int_{t_A}^{t_B} m_{(i)} \, \frac{\mathrm{d}}{\mathrm{d}t} (\boldsymbol{V}_{(i)} \cdot \boldsymbol{V}_{(i)}) \, \mathrm{d}t \tag{11.96d}$$

$$= K_A - K_B, \tag{11.96e}$$

where K_A and K_B are the kinetic energies in the two configurations.

Rather than making use of Newton's law of motion to introduce the kinetic energy, we can decompose the force vector in the expression for work, thus giving

$$W_{AB} = \sum_{i=1}^{N} \int_{\boldsymbol{X}_{(iA)}}^{\boldsymbol{X}_{(iB)}} \boldsymbol{F}_{(i)} \cdot \mathrm{d}\boldsymbol{x}_{(i)} \tag{11.97a}$$

$$= \sum_{i=1}^{N} \int_{\boldsymbol{X}_{(iA)}}^{\boldsymbol{X}_{(iB)}} \boldsymbol{F}_{(i)}^{(\mathrm{ext})} \cdot \mathrm{d}\boldsymbol{x}_{(i)} + \frac{1}{2} \sum_{i=1}^{N} \sum_{j=1}^{N} \int_{\boldsymbol{X}_{(iA)}}^{\boldsymbol{X}_{(iB)}} \boldsymbol{F}_{(ji)} \cdot (\mathrm{d}\boldsymbol{x}_{(i)} - \mathrm{d}\boldsymbol{x}_{(j)}), \tag{11.97b}$$

where the minus sign on the final term arises from Newton's third law satisfied by the internal forces. Now assume that both the internal and external forces are conservative, so that they can separately be written as the gradient of respective potential energies. For the external potential energy acting on particle i, we assume it is a function just of the position of that particle

$$\boldsymbol{F}_{(i)}^{\mathrm{ext}} = -\nabla_i P^{\mathrm{ext}}(\boldsymbol{X}_{(i)}), \tag{11.98}$$

where ∇_i is the gradient operator acting on the position in space, $\boldsymbol{x}_{(i)}$, of the trajectory at a particular time, $\boldsymbol{x}_{(i)} = \boldsymbol{X}_{(i)}(t)$. Furthermore, assume the interparticle potential energy between particles i and j is a function just of the distance between the two particles, which is a property of central forces. In this case we have

$$\boldsymbol{F}_{(ji)} = -\nabla_{ij} P(|\boldsymbol{X}_{(i)} - \boldsymbol{X}_{(j)}|), \tag{11.99}$$

where ∇_{ij} is the gradient operator acting on the relative position, $\boldsymbol{x}_{(i)} - \boldsymbol{x}_{(j)}$, of the two particles at a particular time instance. These assumptions then bring the work into the form

$$W_{AB} = -\sum_{i=1}^{N} \int_{\boldsymbol{X}_{(iA)}}^{\boldsymbol{X}_{(iB)}} \nabla_i P^{(\mathrm{ext})} \cdot \mathrm{d}\boldsymbol{x}_{(i)} - \frac{1}{2} \sum_{i=1}^{N} \sum_{j=1}^{N} \int_{\boldsymbol{X}_{(iA)}}^{\boldsymbol{X}_{(iB)}} \nabla_{ij} P \cdot (\mathrm{d}\boldsymbol{x}_{(i)} - \mathrm{d}\boldsymbol{x}_{(j)}) \tag{11.100a}$$

$$= -\sum_{i=1}^{N} \int_{\boldsymbol{X}_{(iA)}}^{\boldsymbol{X}_{(iB)}} \mathrm{d}P_{(i)}^{(\mathrm{ext})} - \frac{1}{2} \sum_{i=1}^{N} \sum_{j=1}^{N} \int_{\boldsymbol{X}_{(iA)}}^{\boldsymbol{X}_{(iB)}} \mathrm{d}P(|\boldsymbol{X}_{(i)} - \boldsymbol{X}_{(j)}|) \tag{11.100b}$$

$$\equiv -[P^{(\mathrm{tot})}(A) - P^{(\mathrm{tot})}(B)], \tag{11.100c}$$

where the total potential energy is

$$P^{(\text{tot})} = \sum_{i=1}^{N} P_{(i)}^{(\text{ext})} + \frac{1}{2} \sum_{i=1}^{N} \sum_{j=1}^{N} P(|\boldsymbol{X}_{(i)} - \boldsymbol{X}_{(j)}|). \tag{11.101}$$

Combining this result and the expression of work in terms of kinetic energy leads to the conservation of mechanical energy for the conservative N particle system

$$K + P^{(\text{tot})} = \text{constant}. \tag{11.102}$$

11.5.8 Comments and further reading

This section largely follows Section 2 of *Fetter and Walecka* (2003). Note that when considering a continuous fluid in Part V, the interparticle forces manifest as pressure and friction, whereas the external force is given by gravitation, planetary centrifugal, and planetary Corioliis. Furthermore, we always assume the fluids in this book satisfy the strong form of Newton's third law.

11.6 Exercises

EXERCISE 11.1: ACCELERATION WITH $\mathrm{d}\boldsymbol{\Omega}/\mathrm{d}t \neq 0$
Geophysical applications warrant taking the planetary rotation to be a constant vector, $\mathrm{d}\boldsymbol{\Omega}/\mathrm{d}t = 0$, and that assumption is made throughout this book. However, for some applications, such as for rotating machines, we cannot make that assumption. What extra term appears in the acceleration vector (11.48) when $\mathrm{d}\boldsymbol{\Omega}/\mathrm{d}t \neq 0$? Hint: rework the derivation of equation (11.65c) retaining $\mathrm{d}\boldsymbol{\Omega}/\mathrm{d}t \neq 0$.

Chapter 12

Analytical mechanics

In this chapter we formulate the equations describing classical particle motion according to *Lagrangian mechanics* as well as *Hamiltonian mechanics*. We also make use of *Hamilton's principle of stationary action*, which offers a basis for classical mechanics that is distinct from, though consistent with, Newton's laws of motion. That is, within classical mechanics, neither Newton's laws of motion nor Hamilton's principle are derived from more fundamental physical principles. As we see in this chapter, as well as Chapter 15 and Part IX, the lens afforded by Lagrangian and Hamiltonian mechanics, as well as Hamilton's principle, render insights into the nature of motion and dynamics, while also providing powerful tools for its quantitative and qualitative description.

We refer to this formulation of mechanics as *analytical mechanics*. The name is motivated since a great deal of general analysis is placed up front as part of formulating the equations of motion. As seen through the examples discussed in Chapter 15, analytical mechanics allow us to sidestep many difficulties inherent in Newtonian mechanics arising from the need to determine forces, with forces often difficult if not impossible to determine *a priori*. Remarkably, analytical mechanics, through the method of Lagrange multipliers, allows one to determine even the most complex of forces *a posteriori*.

CHAPTER GUIDE

We here assume an understanding of Newton's law of motion from Chapter 11. We also use a modest level of tensor notation for some of the manipulations. Book supplements to this chapter include intermediate and advanced treatments of classical mechanics, such as *Landau and Lifshitz* (1976), *Goldstein* (1980), *Marion and Thornton* (1988), *Fetter and Walecka* (2003), *José and Saletan* (1998), and *Taylor* (2005).

12.1 Loose threads

- Liouville's theorem and motion in phase space in Section 12.10.7.
- Adiabatic invariants: prove the general theorem as in *José and Saletan* (1998) or *Landau and Lifshitz* (1976).
- Hamilton-Jacobi theory in brief.

12.2 Motivation for studying analytical mechanics

As encountered in this chapter, the formulation of *Lagrangian mechanics* requires a nontrivial effort in general formalism. Most of this effort is required to account for constraints and to

remove the need to know anything about forces, including forces of constraint. *Hamiltonian mechanics* is another approach that parallels Lagrangian mechanics in that it also accounts for constraints and has no concern for forces, yet it focuses more on the geometry of *phase space* rather than the *configuration space* of Lagrangian mechanics (these terms are defined later in this chapter). We refer to *analytical mechanics* as the study of constrained motion using the methods of either Lagrange or Hamilton. Analytical mechanics, particularly Hamiltonian mechanics, proved foundational to the invention of quantum mechanics.

As payoff for the extra formalism needed beyond that of Newtonian mechanics, analytical mechanics provides an extremely straightforward means to derive the Euler-Lagrange equation of motion for physical systems. The key reason for the simplification is that with analytical mechanics we only need energies to derive the equation of motion. Energy is a scalar and thus is invariant under coordinate transformations, so that the Euler-Lagrange equations of motion take on the same form regardless the coordinates. In contrast, Newton's laws are simple to state in principle. However, they are vector equations since they require information about forces, and as such they can be very difficult to formulate for mechanical systems beyond the simplest.

Philosophically, we observe that the Newtonian approach is concerned with motion of a system arising from an outside agency, namely a net force that brings about a change in the linear momentum, or a net torque that changes the angular momentum. In contrast, the Lagrangian approach is concerned with properties of the physical system, namely its potential and kinetic energies. We propose that a complete understanding of a classical physical system comes from pursuing both the energy approaches of analytical mechanics (of Lagrange and Hamilton) and the force approach of Newtonian mechanics.

Before diving into the details of analytical mechanics, we offer the following list of characteristics as motivation for the study.

Generalized coordinates

As seen in Chapter 11, Newtonian mechanics is naturally expressed using Cartesian coordinates, whereas it takes some work (using tensor methods) to develop the equations using non-Cartesian coordinates (such as the spherical coordinates used in Chapter 13). In contrast, the equation of motion arising in Lagrangian mechanics, referred to as the *Euler-Lagrange equation*, has the same form using any coordinate system. Lagrangian mechanics is thus suited to the use of *generalized coordinates*, with such coordinates tailored to the particulars of each physical system. Hamiltonian mechanics goes one further step to render insights into the geometry of classical motion.

Dynamical constraints

Noether's theorem connects space-time symmetries of a physical system to the dynamical conservation laws maintained by motion of the system. These conservation laws provide *dynamical constraints* on the motion. The deduction of these constraints is naturally arrived at using Lagrangian mechanics coupled to *Hamilton's principle of stationary action.*

Forces of constraint

In addition to dynamical constraints, there are any number of further constraints that arise from details of the particular motion, such as the imposition of spatial boundaries, rods or springs connecting particles, or other geometric conditions. From the perspective of classical mechanics, such constraints might be considered purely kinematical. For example, the motion of a frictionless bead threaded by a wire is constrained to move along a trajectory defined by the shape of the wire. Such constraints reduce the spatial degrees of freedom of the particle motion. However, it is rarely simple, and often impossible in practice, to provide an *a priori*

determination of the *forces of constraint* (also called *reactive forces*) that maintain the constraints. Since Newtonian mechanics requires all forces for determining the motion, it offers an impractical basis for studying systems where the forces of constraint are unknown *a priori*. In contrast, the equations of motion from Lagrangian mechanics do not require forces, neither those from external fields nor the forces of constraint. As such, Lagrangian mechanics provides the basis for the formulation of a huge range of phenomena. Indeed, it is for this reason that it forms the core of engineering mechanics.

Diagnosing forces

Although Lagrangian mechanices does not need forces, it does provide the means to determine forces if so desired, including forces of constraint. It does so through the method of *Lagrange multipliers*.

Continuum mechanics

Each of the above motivations, developed in this chapter for particle mechanics, has its generalizations to continuum mechanics. That is, Lagrangian mechanics and Hamilton's principle are suited to continuum field theories such as geophysical fluid mechanics. We touch upon some of this use in the chapters forming Part IX to this book, which formulates the equations of geophysical fluid mechanics using Hamilton's principle. Further motivation is provided when we study waves in Part X of this book and instabilities in Part XI.

12.3 Constraints

A particle that moves in three dimensional Euclidean space has at most three independent *degrees of freedom*, meaning that three numbers are needed to specify the particle's spatial position at a particular time. If the particle moves without any forces then it is said to be a *free particle*, and we describe free particle motion in Section 12.9.1. Even without forces on the particle, the motion of a free particle is constrained by *dynamical constraints* that arise from symmetries of the space and time through which the particle moves; e.g., linear momentum, angular momentum, and mechanical energy are conserved (Section 12.9). In addition, there are further constraints that arise from *forces of constraint*, as we now discuss.

12.3.1 Holonomic constraints

When constraints are placed on the spatial position of the particles, then they are referred to as *holonomic constraints*. For example, consider the motion of a particle restricted to a frictionless two dimensional surface. As a result, its three Cartesian coordinates are related by a function of the form

$$\Psi[x(t), y(t), z(t)] = \mathcal{C}, \tag{12.1}$$

where $\mathcal{C}$ is a constant. If, for example, the particle is confined to move on the surface of a sphere of radius, R, then the constraint takes the form

$$\Psi[x(t), y(t), z(t)] = x(t)^2 + y(t)^2 + z(t)^2 = R^2. \tag{12.2}$$

By this restriction the particle has two independent spatial degrees of freedom rather than the three available without the constraint.

Holonomic constraints are enforced by *forces of constraint*, which are also known as *reactive forces*. Forces of constraint reduce the degrees of freedom possessed by the motion. According to *d'Alembert's principle*, forces of constraint instantaneously perform no work on the physical

system, which is the property that we use to define forces of constraint.[1] For the particle moving on a surface, we readily see that the forces of constraint that keep the particle on the surface perform no work since the forces act, at each time instance, in a direction that is perpendicular to the surface and hence perpendicular to the trajectory. Furthermore, note that the forces of constraint can be conservative (written as the gradient of a scalar potential energy function) or non-conservative (such as friction). Indeed, within the confines of classical mechanics, we generally have little fundamental knowledge of the forces of constraints. Rather, we only see their impact on the motion.

An equivalent expression for the algebraic constraint (12.1) is given by differential expressions

$$\mathrm{d}\Psi = 0 \quad \text{or} \quad \frac{\mathrm{d}\Psi}{\mathrm{d}t} = \frac{\partial \Psi}{\partial x^a}\,\dot{x}^a + \frac{\partial \Psi}{\partial t} = 0, \tag{12.3}$$

where we wrote $(x, y, z) = (x^1, x^2, x^3)$ and made use of the summation convention from tensor alegebra. We refer to holonomic constraints as *integrable* since the differential constraint (12.3) can be integrated to yield the algebraic constraint (12.1).

12.3.2 Non-holonomic constraints

There are physical systems where the constraints take on a more general *non-holonomic* form. The canonical non-holonomic constraint involves both the position and velocity and so it is written

$$\Psi(\boldsymbol{X}, \dot{\boldsymbol{X}}, t) = C. \tag{12.4}$$

The exact differential of this constraint includes the position, velocity, and time, so that

$$\mathrm{d}\Psi = \frac{\partial \Psi}{\partial x^a}\,\dot{x}^a + \frac{\partial \Psi}{\partial \dot{x}^a}\,\ddot{x}^a + \frac{\partial \Psi}{\partial t} = 0. \tag{12.5}$$

We note that some non-holonomic constraints are, in effect, holonomic in that they can be integrated. For example, consider the contraint

$$H_a\,\dot{x}^a + I = 0, \tag{12.6}$$

where H_a and I are functions of time that can be written as

$$H_a = \frac{\partial \Psi}{\partial x^a} \quad \text{and} \quad I = \frac{\partial \Psi}{\partial t}. \tag{12.7}$$

For this special case, the constraint (12.6) takes the form of the differential holonomic constraint (12.3), in which we say that the constraint (12.6) is *semi-holonomic*. But more generally non-holonomic constraints are non-integrable and require methods that are not fully covered by the generalized coordinates or Lagrange multipliers considered in this chapter.

12.3.3 Dynamical constraints

At the start of this section we noted the possibility of a dynamical constraint. Such constraints typically involve both the position and velocity of the particle, and so might at first be considered non-holonomic. However, they do not arise from an external force of constraint. Rather, they arise from space and time symmetries. For example, in Section 12.9.4 we detail conditions under

[1] Recall from Section 11.1.4 that mechanical work arises when a force acts in a direction aligned with the motion of a physical system. If the force is perpendicular to the motion, then that force performs no work and so does not alter the kinetic energy of the system. Hence, d'Alembert's principle says that forces of constraint act perpendicular to the motion. See Section 14 of *Fetter and Walecka* (2003) for more on d'Alembert's principle.

which the mechanical energy is a constant of the motion, whereby the sum of the kinetic and potential energies are constant. For a particle, this dynamical constraint takes the form

$$m\,\dot{\boldsymbol{X}}\cdot\dot{\boldsymbol{X}}/2 + V(\boldsymbol{X}) = K(\boldsymbol{X},\dot{\boldsymbol{X}}). \tag{12.8}$$

Evidently, this constraint involves the position of the particle, through the potential energy $V(\boldsymbol{X})$, and the velocity, through the kinetic energy, $m\,\dot{\boldsymbol{X}}\cdot\dot{\boldsymbol{X}}/2$. It holds everywhere along the particle's trajectory as determined by the equation of motion

$$m\,\ddot{\boldsymbol{X}} = -\nabla V. \tag{12.9}$$

12.3.4 Comments

In this chapter we only consider dynamical constraints and holonomic constraints. The study of non-holonomic constraints can be rather subtle, and it is outside our scope.

12.4 Coordinate description of motion

We here review the Cartesian coordinate formalism needed to describe the motion of a system of N particles, and then transform to generalized coordinates that are optimized to describing constrained motion.

12.4.1 Cartesian coordinates for N particles

Following the notation from Section 11.5, we specify the position of each discrete particle by its Cartesian position vector,

$$\boldsymbol{X}_{(i)} = \hat{\boldsymbol{x}}\,x^1_{(i)} + \hat{\boldsymbol{y}}\,x^2_{(i)} + \hat{\boldsymbol{z}}\,x^3_{(i)} = \boldsymbol{e}_a\,x^a_{(i)}, \tag{12.10}$$

where $i = 1,..N$ is the particle index, $x^a_{(i)}$ is the a'th Cartesian coordinate for particle i, and $\boldsymbol{e}_a$ is the a'th Cartesian basis vector where $a = 1,2,3$. We place the particle index inside a parentheses to distinguish it from the coordinate indices, and we make use of the Einstein summation convention for the Cartesian index in the final equality. Each of the Cartesian coordinates for the particle position are functions of time, though we sometimes suppress time dependence for brevity.

The notation in equation (12.10) is somewhat cluttered on many occasions. To help de-clutter the notation we sometimes find it convenient to meld each of the Cartesian position vectors together into an ordered list of length $3N$

$$\boldsymbol{X} = (x^1, x^2, x^3, x^4, x^5, ..., x^{3N-2}, x^{3N-1}, x^{3N}). \tag{12.11}$$

This list is organized so that the first triplet, $n = 1,2,3$, contains the coordinates for the first particle, the second triplet, $n = 4,5,6$, is for the second particle, and so on up to the final triplet where $n = 3N-2, 3N-1, 3N$ is for particle N. In so ordering the indices we are able to drop the particle label since there is a clear mapping between particle number and position within the list.

12.4.2 An introduction to generalized coordinates

Cartesian coordinates are sufficient for describing motion through Euclidean space, and they offer a suitable description particularly when there are no constraints on the motion. However, when constraints reduce the degrees of freedom, we are motivated to choose each coordinate to directly correspond to an independent degree of freedom. We refer to such coordinates as

generalized coordinates. Generalized coordinates can be any coordinate that specifies the spatial position of the matter comprising the physical system. For example, latitude and longitude provide generalized coordinates for a particle moving on the surface of a sphere, whereas the polar angle serves as a generalized coordinate for motion around the circumference of a planar circle. In these two examples, we see that generalized coordinates are typically not Cartesian coordinates.

A further example of the value of generalized coordinates arises in the description of *rigid body* motion. A rigid body is comprised of a huge number of particles that are each constrained by inter-particle forces that keep the particles rigidly fixed relative to one another.[2] Internal forces of constraint that maintain the rigid spacing provide no net force nor net torqe on the body as a whole, so that only externally applied forces and torques lead to time changes in the body's translation and/or rotation. Correspondingly, the internal forces of constraint perform no net work on the body, which reflects d'Alembert's principle. Given that the particles are rigidly fixed relative to one another, the spatial configuration of the rigid body is specified by the position of the center of mass (three coordinates) and the orientation of the rigid body in space (three angles). The spatial configuration of a rigid body is thus fully described by just six degrees of freedom.[3]

12.4.3 Cartesian and generalized coordinates for N particles

Assume there are C holonomic constraints placed on the spatial coordinates of the system that are written in the form

$$\Psi_c(x^1, ..., x^{3N}, t) = \mathcal{C}_c, \quad \text{for} \quad c = 1, ..., C, \tag{12.12}$$

where $\mathcal{C}_c$ are constants. As a result, there are

$$D = 3N - C \tag{12.13}$$

spatial degrees of freedom. We can thus choose D generalized coordinates, $\xi^\sigma, \sigma = 1, 2, ..., D$, that are linearly independent and so fully describe the spatial position of the constrained system. For example, if a particle is constrained to move on a spherical shell of radius R, then the two spherical angular coordinates are suitable generalized coordinates corresponding to the single constraint equation, $r = R$.

With the spatial configuration of the physical system fully described by the generalized coordinates, we can determine the Cartesian position, $\boldsymbol{X}$, for the particles according to the functional relation

$$\boldsymbol{X} = \boldsymbol{X}(\xi^1, \xi^2, ..., \xi^D, t), \tag{12.14}$$

where the explicit time dependence in this relation offers generality that can be useful (e.g., motion on a spherical shell whose radius is time dependent). In turn, the exact differential of the Cartesian position is related to that of the generalized coordinates according to the chain rule

$$\mathrm{d}\boldsymbol{X} = \sum_{\sigma=1}^{D} \frac{\partial \boldsymbol{X}}{\partial \xi^\sigma} \, \mathrm{d}\xi^\sigma + \frac{\partial \boldsymbol{X}}{\partial t} \, \mathrm{d}t. \tag{12.15}$$

[2] In any real solid, the atoms are not rigidly fixed. But when concerned only with the macroscopic (classical) motion of a solid body, we can readily approximate its matter constituents as rigidly fixed relative to each other.

[3] See any of the references at the start of this chapter for detailed analysis of rigid body motion.

12.4.4 Virtual displacements

When discussing forces of constraint in Section (12.3), we included the qualifier "instantaneous" or "time instance" when referring to the inability of a force of constraint to do work on the physical system. This qualifier is needed when the constraints are explicit functions of time, such as for motion on a spherical shell whose radius changes in time. We formalize this qualifier by introducing the concept of a *virtual displacement*. A virtual displacement is a tiny spatial displacement of a physical system that occurs at a fixed time instance. Furthermore, virtual displacements respect the forces of constraint, which means they are *kinematically admissable* displacements.

Conceptually, we imagine freezing the physical system at a specific time instance, and then probing alternative realizations of the physical system by considering tiny kinematically admissable displacements; i.e., displacements that are consistent with the forces of constraints. By choosing a particular time instance, virtual displacements are not concerned with the dynamics since dynamics requires information about time changes. For a particle moving on a spherical shell, spherical angle displacements at a fixed time respect the constraint that the particle remains on the shell, so that tiny displacements of the spherical angles provide suitable virtual displacements.

Any perturbation of generalized coordinates represents a possible virtual displacement. In turn, a virtual displacement written in terms of Cartesian coordinates follows from the exact differential (12.15) with $\mathrm{d}t = 0$

$$\delta \boldsymbol{X} = \sum_{\sigma=1}^{D} \frac{\partial \boldsymbol{X}}{\partial \xi^\sigma} \, \delta\xi^\sigma. \tag{12.16}$$

In this expression we introduced the δ symbol for a virtual displacement as distinct from an exact differential. Virtual displacements hold a prominent role in Lagrangian mechanics as well as Hamilton's principle. In the context of Hamilton's principle, virtual displacements are generalized to the *variations* considered when probing alternative trajectories of a physical system.

Note that the δ symbol is commonly used in this book for tiny displacements or perturbations of a physical system that allow one to probe dynamical stability and examine alternative realizations of the motion. Not all cases where we use the δ symbol are virtual displacements. For example, in Section 14.6.2 we examined the constraints imposed by axial angular momentum conservation, with the use of δ in that context distinctly not virtual since the perturbations generally occur over a time interval.

12.4.5 Particle moving on a spherical shell

As an example of the ideas presented in this section, consider a particle constrained to move a constant radial distance from a fixed center. This motion on a spherical shell is enabled through the imposition of forces of constaint that keep the particle from either moving radially outward or radially inward. The forces of constraint can perform no work on the particle since they act in the radial direction, whereas the motion is in the spherical angular directions. For a particular realization, consider particle motion on the surface of a solid massive and frictionless spherical shell. The gravitational force from the shell provides a radially inward force that keeps the particle from moving outward, whereas the solid surface of the shell provides the radially outward force that keeps the particle from moving inward.[4] It is as if the particle was confined to a narrow gap between two spherical surfaces that only allow motion in the angular directions.

[4]The constraint against moving inward arises from inter-atomic forces that keep the particle from penetrating into the solid shell. From the perspective of the classical particle motion, we are unconcerned with such inter-atomic forces, but instead only concerned with their effects on the classical motion of the particle.

Neither of the constraining forces performs work on the particle since they act perpendicular to the particle's motion.

The coordinates used to specify the particle position are constrained to the spherical shell with fixed radius, R. Hence, the particle spatial position is fully specified by the latitude, ϕ, and longitude, λ, which are related to Cartesian coordinates via equations (4.206a)–(4.206c) (see also Figure 4.3)

$$x = R\cos\phi\,\cos\lambda \quad \text{and} \quad y = R\cos\phi\,\sin\lambda \quad \text{and} \quad z = R\sin\phi, \tag{12.17}$$

which manifests the constraint placed on the three Cartesian coordinates

$$\boldsymbol{X}(t)\cdot\boldsymbol{X}(t) = x(t)^2 + y(t)^2 + z(t)^2 = R^2. \tag{12.18}$$

Note that the corresponding exact differentials

$$\mathrm{d}x = R\,(-\mathrm{d}\phi\sin\phi\cos\lambda - \mathrm{d}\lambda\cos\phi\sin\lambda) \tag{12.19a}$$
$$\mathrm{d}y = R\,(-\mathrm{d}\phi\sin\phi\sin\lambda + \mathrm{d}\lambda\cos\phi\cos\lambda) \tag{12.19b}$$
$$\mathrm{d}z = R\,\mathrm{d}\phi\cos\phi, \tag{12.19c}$$

are within the spherical shell since they are orthogonal to the radial unit vector

$$\hat{\boldsymbol{r}}\cdot(\hat{\boldsymbol{x}}\,\mathrm{d}x + \hat{\boldsymbol{y}}\,\mathrm{d}y + \hat{\boldsymbol{z}}\,\mathrm{d}z) = 0, \tag{12.20}$$

where the radial unit vector is given by equation (4.219c)

$$\hat{\boldsymbol{r}} = \hat{\boldsymbol{x}}\,\cos\lambda\,\cos\phi + \hat{\boldsymbol{y}}\sin\lambda\,\cos\phi + \hat{\boldsymbol{z}}\sin\phi. \tag{12.21}$$

12.5 Lagrange's equations of motion

In this section we step through the derivation of *Lagrange's equation of motion*. This equation is equivalent to Newton's equation of motion, and yet it eliminates the forces of constraint and is written fully in terms of generalized coordinates. A key facet of the derivation concerns the need to articulate the functional dependency of the Cartesian position and velocity, $\boldsymbol{X}$ and $\dot{\boldsymbol{X}}$, on the generalized coordinates, generalized velocities, and time, $(\xi^\sigma, \dot{\xi}^\sigma, t)$.

12.5.1 Eliminating the forces of constraint

The inability of forces of constraint to perform work under virtual displacements (d'Alembert's principle) provides the key insight needed to eliminate the forces of constraint from the equations of motion. For this purpose, start by writing Newton's equation of motion using Cartesian coordinates

$$\dot{P}^n = F^n + F^n_{\text{constraint}} \quad \text{for } n = 1, ..., 3N, \tag{12.22}$$

where F^n is the n'th component of the net applied force (e.g., gravity, electromagnetism) and $F^n_{\text{constraint}}$ is the n'th component of the force of constraint. It is convenient to make use of the $3N$ ordered list notation of equation (12.11), in which we organize the linear momentum time derivatives and applied forces

$$\dot{\boldsymbol{P}} = (\dot{P}^1, \dot{P}^2, \dot{P}^3, \dot{P}^4, \dot{P}^5, ..., \dot{P}^{3N-2}, \dot{P}^{3N-1}, \dot{P}^{3N}) \tag{12.23a}$$
$$\boldsymbol{F} = (F^1, F^2, F^3, F^4, F^5, ..., F^{3N-2}, F^{3N-1}, F^{3N}), \tag{12.23b}$$

so that Newton's equation (12.22) for the N particle system becomes

$$\dot{\boldsymbol{P}} = \boldsymbol{F} + \boldsymbol{F}_{\text{constraint}}. \tag{12.24}$$

Through d'Alembert's principle we eliminate the forces of constraint by multiplying Newton's equation (12.24) by the vector of Cartesian virtual displacements, $\delta\boldsymbol{X}$, and summing over all $3N$ Cartesian coordinates

$$(\dot{\boldsymbol{P}} - \boldsymbol{F}) \cdot \delta\boldsymbol{X} = 0. \tag{12.25}$$

To reach this equation we set

$$\boldsymbol{F}_{\text{constraint}} \cdot \delta\boldsymbol{X} = 0, \tag{12.26}$$

due to d'Alembert's principle. To help appreciate d'Alembert's principle written as equation (12.26), again refer to the case of a particle moving on a spherical shell from Section 12.4.5, whereby the force of constraint is directed radially whereas a virtual displacement is directed along an angle within the shell.

Equation (12.25) is a statement of d'Alembert's principle using Cartesian coordinates. It succeeds in eliminating the forces of constraint, which is one of our goals. However, we cannot set each of the $3N$ terms individually to zero since each Cartesian component of the virtual displacement, $\delta\boldsymbol{X}$, is not generally independent of the other. To provide a more useful expression requires us to transform the Cartesian virtual displacements into generalized coordinate virtual displacements. This part of the derivation requires a few steps, and we do so by separately considering $\boldsymbol{F} \cdot \delta\boldsymbol{X}$ and $\dot{\boldsymbol{P}} \cdot \delta\boldsymbol{X}$.

12.5.2 Work by the applied forces acting on virtual displacements

Although the forces of constraint perform no work on the virtual displacements, the applied forces generally do perform work, as given by

$$\delta W = \boldsymbol{F} \cdot \delta\boldsymbol{X} = \boldsymbol{F} \cdot \sum_{\sigma=1}^{D} \frac{\partial \boldsymbol{X}}{\partial \xi^\sigma}\, \delta\xi^\sigma = \sum_{\sigma=1}^{D} Q_\sigma\, \delta\xi^\sigma. \tag{12.27}$$

The second equality made use of equation (12.16) to write the Cartesian virtual displacement in terms of the generalized coordinate displacements. The third equality defined the *generalized force*, which is the representation of the applied force using generalized coordinates

$$Q_\sigma = \boldsymbol{F} \cdot \frac{\partial \boldsymbol{X}}{\partial \xi^\sigma}. \tag{12.28}$$

We thus identify the product, $Q_\sigma\, \delta\xi^\sigma$ (no implied sum), as the work done by the generalized force, Q_σ, on the generaliized virtual displacement, $\delta\xi^\sigma$. Correspondingly, the total work done by all generalized forces is given by the sum in equation (12.27). Observe that the generalized force can be computed from the defining expression (12.28), given knowledge of the force vector, $\boldsymbol{F}$, and coordinate transformation matrix, $\partial\boldsymbol{X}/\partial\xi^\sigma$. Alternatively, and often more conveniently, recall that the virtual displacements of the generalized coordinates are linearly independent so that we can compute the generalized force by computing the virtual work arising from a single virtual displacement, with all other displacements set to zero.

12.5.3 Massaging $\dot{\boldsymbol{P}} \cdot \delta \boldsymbol{X}$

As for equation (12.27), we transform the Cartesian virtual displacements into generalized coordinate virtual displacements according to

$$\dot{\boldsymbol{P}} \cdot \delta \boldsymbol{X} = \dot{\boldsymbol{P}} \cdot \sum_{\sigma=1}^{D} \frac{\partial \boldsymbol{X}}{\partial \xi^\sigma} \delta \xi^\sigma = \sum_{n=1}^{3N} \sum_{\sigma=1}^{D} \dot{p}^n \frac{\partial x^n}{\partial \xi^\sigma} \delta \xi^\sigma, \tag{12.29}$$

which takes on the following form if each particle has the same constant mass, m,

$$\dot{\boldsymbol{P}} \cdot \delta \boldsymbol{X} = m \sum_{n=1}^{3N} \sum_{\sigma=1}^{D} \ddot{x}^n \frac{\partial x^n}{\partial \xi^\sigma} \delta \xi^\sigma \tag{12.30a}$$

$$= m \sum_{n=1}^{3N} \sum_{\sigma=1}^{D} \left[\frac{\mathrm{d}}{\mathrm{d}t} \left(\dot{x}^n \frac{\partial x^n}{\partial \xi^\sigma} \right) - \dot{x}^n \frac{\mathrm{d}}{\mathrm{d}t} \left(\frac{\partial x^n}{\partial \xi^\sigma} \right) \right] \delta \xi^\sigma. \tag{12.30b}$$

To massage this expression further requires us to be careful about the functional dependencies for the terms inside the square bracket.

Alternative expression for the transformation matrix elements

For the first right hand side term in equation (12.30b), recall that the functional dependence for the Cartesian expression of the particle velocity is found by making use of the exact differential (12.15), where division by $\mathrm{d}t$ leads to

$$\dot{\boldsymbol{X}} = \sum_{\sigma=1}^{D} \frac{\partial \boldsymbol{X}}{\partial \xi^\sigma} \dot{\xi}^\sigma + \frac{\partial \boldsymbol{X}}{\partial t}. \tag{12.31}$$

The Cartesian position, $\boldsymbol{X}$, is a function of the generalized coordinates and time as per equation (12.14), which then means that the partial derivatives, $\partial \boldsymbol{X}/\partial \xi^\sigma$ and $\partial \boldsymbol{X}/\partial t$, each have the same functional dependence. We thus conclude that the Cartesian velocity is a function of the generalized coordinates, the generalized velocities, and time

$$\dot{\boldsymbol{X}} = \dot{\boldsymbol{X}}(\xi^1, ..., \xi^D, \dot{\xi}^1, ..., \dot{\xi}^D, t). \tag{12.32}$$

Furthermore, equation (12.31) says that each element of $\dot{\boldsymbol{X}}$ is a linear function of the generalized velocities, $\dot{\xi}^\sigma$, from which it follows that

$$\frac{\partial \dot{x}^n}{\partial \dot{\xi}^\sigma} = \frac{\partial x^n}{\partial \xi^\sigma}. \tag{12.33}$$

This rather remarkable identity says that component-wise, the partial derivative of the Cartesian velocity, with respect to the generalized coordinate velocity, equals to the partial derivative of the Cartesian coordinate with respect to the generalized coordinate.

Making use of the identity (12.33) for the first right hand side term in equation (12.30b) leads to

$$m \sum_{n=1}^{3N} \sum_{\sigma=1}^{D} \frac{\mathrm{d}}{\mathrm{d}t} \left[\dot{x}^n \frac{\partial x^n}{\partial \xi^\sigma} \right] = m \sum_{n=1}^{3N} \sum_{\sigma=1}^{D} \frac{\mathrm{d}}{\mathrm{d}t} \left[\dot{x}^n \frac{\partial \dot{x}^n}{\partial \dot{\xi}^\sigma} \right] \tag{12.34a}$$

$$= \frac{m}{2} \sum_{n=1}^{3N} \sum_{\sigma=1}^{D} \frac{\mathrm{d}}{\mathrm{d}t} \left[\frac{\partial (\dot{x}^n \, \dot{x}^n)}{\partial \dot{\xi}^\sigma} \right] \tag{12.34b}$$

$$= \sum_{\sigma=1}^{D} \frac{\mathrm{d}}{\mathrm{d}t} \left[\frac{\partial K}{\partial \dot{\xi}^\sigma} \right], \tag{12.34c}$$

where we introduced the kinetic energy of the N particle system

$$K = \frac{m}{2} \sum_{n=1}^{3N} \dot{x}^n \, \dot{x}^n = \frac{m}{2} \sum_{i=1}^{N} \dot{\boldsymbol{X}}_{(i)} \cdot \dot{\boldsymbol{X}}_{(i)} = \frac{m}{2} \sum_{i=1}^{N} \dot{x}^a_{(i)} \, \delta_{ab} \, \dot{x}^b_{(i)}, \tag{12.35}$$

with the final equality introducing the Kronecker metric, δ_{ab}, for Euclidean space. Note that the functional dependence (12.32) for the Cartesian velocities is transferred to the kinetic energy so that

$$K = K(\xi^1, ..., \xi^D, \dot{\xi}^1, ..., \dot{\xi}^D, t). \tag{12.36}$$

Proving that $\mathrm{d}/\mathrm{d}t(\partial x^n/\partial \xi^\sigma) = \partial \dot{x}^n/\partial \xi^\sigma$

For the next step we prove the identity

$$\frac{\mathrm{d}}{\mathrm{d}t} \frac{\partial x^n}{\partial \xi^\sigma} = \frac{\partial}{\partial \xi^\sigma} \frac{\mathrm{d}x^n}{\mathrm{d}t} \tag{12.37}$$

by evaluating both sides and showing they are equal. For the left hand side, recall from the derivation of equation (12.33) that the transformation matrix element, $\partial x^n/\partial \xi^\sigma$, is a function of the generalized coordinates and time, so that its total time derivative is

$$\frac{\mathrm{d}}{\mathrm{d}t} \frac{\partial x^n}{\partial \xi^\sigma} = \left[\frac{\partial}{\partial t} + \sum_{\mu=1}^{D} \dot{\xi}^\mu \frac{\partial}{\partial \xi^\mu} \right] \frac{\partial x^n}{\partial \xi^\sigma}. \tag{12.38}$$

Next, evaluate the right hand side of equation (12.37) directly by expanding the total time derivative. Importantly, recall the functional dependence of the Cartesian velocity in equation (12.32), and note that the partial derivative, $\partial/\partial \xi^\sigma$, is computed while holding fixed the explicit time dependence and the dependence on the generalized velocity, $\dot{\xi}^\sigma$. We thus find

$$\frac{\partial}{\partial \xi^\sigma} \frac{\mathrm{d}x^n}{\mathrm{d}t} = \frac{\partial}{\partial \xi^\sigma} \left[\frac{\partial}{\partial t} + \sum_{\mu=1}^{D} \dot{\xi}^\mu \frac{\partial}{\partial \xi^\mu} \right] x^n = \left[\frac{\partial}{\partial t} + \sum_{\mu=1}^{D} \dot{\xi}^\mu \frac{\partial}{\partial \xi^\mu} \right] \frac{\partial x^n}{\partial \xi^\sigma}, \tag{12.39}$$

which follows since (i) partial derivative operators commute, and (ii) the partial derivative, $\partial/\partial \xi^\sigma$, is computed while holding the generalized velocity, $\dot{\xi}^\mu$, fixed. Since equations (12.38) and (12.39) are identical, we have proven the identity (12.37).

Making use of equation (12.37) for the second right hand side term in equation (12.30b) leads to

$$\sum_{n=1}^{3N} \sum_{d=1}^{D} m^n \dot{x}^n \frac{\mathrm{d}}{\mathrm{d}t} \left(\frac{\partial x^n}{\partial \xi^\sigma} \right) \delta \xi^\sigma = m \sum_{n=1}^{3N} \sum_{\sigma=1}^{D} \dot{x}^n \frac{\partial}{\partial \xi^\sigma} \frac{\mathrm{d}x^n}{\mathrm{d}t} \, \delta \xi^\sigma = \sum_{d=1}^{D} \frac{\partial K}{\partial \xi^\sigma} \, \delta \xi^\sigma, \tag{12.40}$$

where we again introduced the kinetic energy (12.35) of the N particle system.

12.5.4 Lagrange's equation of motion

We now combine the expression (12.27) for the work done by the generalized force against the virtual displacements, along with the identities (12.34c) and (12.40), to find

$$\sum_{d=1}^{D}\left[\frac{\mathrm{d}}{\mathrm{d}t}\left[\frac{\partial K}{\partial \dot{\xi}^{\sigma}}\right]-\frac{\partial K}{\partial \xi^{\sigma}}-Q_{\sigma}\right]\delta\xi^{\sigma}=0. \tag{12.41}$$

We have thus succeeded in eliminating the forces of constraint *and* expressing the equations in terms of just the generalized coordinates. Since each of the virtual displacements of the generalized coordinates, $\delta\xi^{\sigma}, \sigma = 1, ...D$, are linearly independent, satisfying equation (12.41) for arbitrary virtual displacements requires *Lagrange's equations of motion*

$$\frac{\mathrm{d}}{\mathrm{d}t}\left[\frac{\partial K}{\partial \dot{\xi}^{\sigma}}\right]-\frac{\partial K}{\partial \xi^{\sigma}}=Q_{\sigma} \quad \text{for } \sigma = 1, ..., D. \tag{12.42}$$

Lagrange's equation is a partial differential equation for the kinetic energy that is driven by generalized forces. This equation holds separately for each of the D generalized coordinates.

12.5.5 Conservative forces and the Lagrangian function

Conservative forces are those that can be derived as minus the spatial gradient of a potential energy scalar, P. We commonly assume conservative forces when working with Lagrangian mechanics as discussed in Section 12.5.5. When written using Cartesian coordinates, the potential energy for a conservative system is time independent. However, when transforming to generalized coordinates as per equation (12.14), the potential energy can pick up an explicit time dependence along with the expected dependence on generalized coordinates. We thus write the potential energy as

$$\text{potential energy} = P^{\text{cartesian}}(\boldsymbol{X}) = P^{\text{generalized}}(\xi^1, ..., \xi^D, t), \tag{12.43}$$

where $P^{\text{cartesian}}$ and $P^{\text{generalized}}$ are distinct scalar functions that both measure the potential energy. Notably, the potential energy is not a function of the Cartesian velocity nor the generalized velocity, so that

$$\frac{\partial P^{\text{cartesian}}}{\partial \dot{x}^n}=0 \quad \text{and} \quad \frac{\partial P^{\text{generalized}}}{\partial \dot{\xi}^{\sigma}}=0. \tag{12.44}$$

As per our discussion of scalar functions in Section 1.5.1, we drop the extra superscript notation on the potential energy in equation (12.43), with the understanding that the functional dependency determines which particularl function is meant. In this manner, the generalized force takes the form

$$Q_{\sigma}=\sum_{n=1}^{3N}F^{n}\frac{\partial x^{n}}{\partial \xi^{\sigma}}=-\sum_{n=1}^{3N}\frac{\partial P(\boldsymbol{X})}{\partial x^{n}}\frac{\partial x^{n}}{\partial \xi^{\sigma}}=-\frac{\partial P(\xi^1, ..., \xi^D, t)}{\partial \xi^{\sigma}}, \tag{12.45}$$

where the second equality follows from the chain rule. Consequently, we can rewrite Lagrange's equation (12.42) as

$$\frac{\mathrm{d}}{\mathrm{d}t}\left[\frac{\partial (K-P)}{\partial \dot{\xi}^{\sigma}}\right]-\frac{\partial (K-P)}{\partial \xi^{\sigma}}=0 \quad \text{for } \sigma = 1, ..., D. \tag{12.46}$$

The difference between the kinetic energy and potential energy is referred to as the *Lagrangian*

$$L = K - P, \tag{12.47}$$

so that Lagrange's equation of motion (12.46) takes on the more commonly written form

$$\frac{\mathrm{d}}{\mathrm{d}t}\left[\frac{\partial L}{\partial \dot{\xi}^\sigma}\right] - \frac{\partial L}{\partial \xi^\sigma} = 0 \quad \text{for } \sigma = 1, ..., D. \tag{12.48}$$

The Lagrangian inherits the functional dependence of the kinetic energy as given by equation (12.36)

$$L = L(\xi^1, ..., \xi^D, \dot{\xi}^1, ..., \dot{\xi}^D, t). \tag{12.49}$$

Furthermore, we refer to the space defined by the $\xi^\sigma, \dot{\xi}^\sigma, \sigma = 1, ..., D$ as *configuration space*. As such, Lagrange's equation (12.48) is a partial differential equation for motion in configuration space.

In Lagrange's equation (12.48), when computing the partial derivatives, $\partial/\partial\xi^\sigma$ and $\partial/\partial\dot{\xi}^\sigma$, all other variables are held fixed. When computing the total time derivative, $\mathrm{d}/\mathrm{d}t$, we must be sure to account for the functional dependence of L according to equation (12.49), so that

$$\frac{\mathrm{d}}{\mathrm{d}t}\left[\frac{\partial L}{\partial \dot{\xi}^\mu}\right] = \left[\frac{\partial}{\partial t} + \dot{\xi}^\sigma \frac{\partial}{\partial \xi^\sigma} + \ddot{\xi}^\sigma \frac{\partial}{\partial \dot{\xi}^\sigma}\right] \frac{\partial L}{\partial \dot{\xi}^\mu}. \tag{12.50}$$

12.5.6 Connection to Newton's equation of motion

As a partial differential equation for the scalar Lagrangian function, Lagrange's equation (12.48) is quite distinct from Newton's equation of motion, which is a vector ordinary differential equation for the acceleration determined by the forces. However, these two equations are directly connected since we used Newton's equation to derive Lagrange's equation.

To further reveal the equivalance, consider the unconstrained case for a single particle, in which the Lagrangian as written in Cartesian coordinates as

$$L = (m/2)\,(\dot{x}^2 + \dot{y}^2 + \dot{z}^2) - P(x, y, z), \tag{12.51}$$

which leads to

$$\frac{\mathrm{d}}{\mathrm{d}t}\left[\frac{\partial L}{\partial \dot{x}}\right] = m\,\ddot{x} \quad \text{and} \quad \frac{\mathrm{d}}{\mathrm{d}t}\left[\frac{\partial L}{\partial \dot{y}}\right] = m\,\ddot{y} \quad \text{and} \quad \frac{\mathrm{d}}{\mathrm{d}t}\left[\frac{\partial L}{\partial \dot{z}}\right] = m\,\ddot{z}. \tag{12.52}$$

Lagrange's equation thus becomes Newton's equation of motion

$$\boldsymbol{F} = m\,\ddot{\boldsymbol{X}} \quad \text{with} \quad \boldsymbol{F} = -\nabla_{\boldsymbol{x}} P. \tag{12.53}$$

12.5.7 Kinetic energy in terms of generalized velocities

We wrote the kinetic energy in equation (12.35) in terms of the Cartesian velocities. Here we make use of the coordinate transformation (12.31) to expose the generalized velocities according to

$$K = \frac{m}{2}\sum_{i=1}^{N} \dot{x}^a_{(i)}\,\delta_{ab}\,\dot{x}^b_{(i)} \tag{12.54a}$$

$$= \frac{m}{2}\sum_{i=1}^{N}\left[\frac{\partial x^a_{(i)}}{\partial t} + \sum_{\sigma=1}^{D}\dot{\xi}^\sigma \frac{\partial x^a_{(i)}}{\partial \xi^\sigma}\right]\delta_{ab}\left[\frac{\partial x^b_{(i)}}{\partial t} + \sum_{\mu=1}^{D}\dot{\xi}^\mu \frac{\partial x^b_{(i)}}{\partial \xi^\mu}\right], \tag{12.54b}$$

where we made use of the notation in equation (12.10) with the implied summation over $a, b = 1, 2, 3$. Expanding this product leads to three terms, two of which arise from the time dependent coordinate transformation, whereby $\partial_t \boldsymbol{X}_{(i)} \neq 0$. The third term is given by the

quadratic form

$$\frac{m}{2}\sum_{i=1}^{N}\sum_{\sigma=1}^{D}\sum_{\mu=1}^{D}\frac{\partial x^a_{(i)}}{\partial \xi^\sigma}\,\delta_{ab}\,\frac{\partial x^b_{(i)}}{\partial \xi^\mu}\,\dot{\xi}^\sigma\,\dot{\xi}^\mu = \frac{m}{2}\sum_{\sigma=1}^{D}\sum_{\mu=1}^{D}G_{\sigma\mu}(\boldsymbol{\xi})\,\dot{\xi}^\sigma\,\dot{\xi}^\mu. \tag{12.55}$$

We here introduced the symmetric tensor

$$G_{\sigma\mu} = \sum_{i=1}^{N}\frac{\partial x^a_{(i)}}{\partial \xi^\sigma}\,\delta_{ab}\,\frac{\partial x^b_{(i)}}{\partial \xi^\mu}, \tag{12.56}$$

which is the metric tensor for the space of generalized coordinates. For the special (and common) case of a time independent coordinate transformation, the metric is a function just of the generalized coordinates

$$G_{\sigma\mu} = G_{\sigma\mu}(\boldsymbol{\xi}), \tag{12.57}$$

and the kinetic energy reduces to the quadratic form

$$K = \frac{m}{2}\sum_{\sigma=1}^{D}\sum_{\mu=1}^{D}G_{\sigma\mu}(\boldsymbol{\xi})\,\dot{\xi}^\sigma\,\dot{\xi}^\mu \quad \text{if } \partial_t \boldsymbol{X}_{(i)} = 0. \tag{12.58}$$

12.5.8 Comments

The derivation in this section closely follows sections 13, 14, and 15 of *Fetter and Walecka* (2003). In summary, the approach started from Newton's equation of motion and then introduced virtual displacements, d'Alembert's principle, generalized coordinates, and then pursues a series of manipulations that carefully account for the functional dependencies of various quantities. In the next section we take an alternative approach that starts from *Hamilton's stationary action principle*, which is a more streamlined approach that renders Lagrange's equation and is thus consistent with Newton's equation of motion. The more tedious approach of the current section serves to expose certain details about are both useful for understanding the foundation of the theory, and find use in different contexts within this book.

12.6 Hamilton's principle of stationary action

In this section we show that Lagrange's equations of motion (12.48) for a conservative physical system can be derived from a variational principle, known as *Hamilton's principle of stationary action*. Hamilton's principle states that the *action*, which is the time integral of the Lagrangian, is stationary if and only if Lagrange's equation of motion are satisfied. Hamilton's principle is logically on the same level as Newton's laws of motion in that neither are derived from more fundamental principles. Rather, they each offer the starting point for two distinct, but consistent, formulations of mechanics.

12.6.1 Notation

As for our derivation of Lagrange's equations in Section 12.5, it is useful to work with generalized coordinates in order to seamlessly account for constraints. To reduce notation clutter we use the boldface notation introduced in equation (12.11) for Cartesian coordinates. Here, the generalized coordinates and generalized velocities for a system with D degrees of freedom are organized into a list of length D according to

$$\boldsymbol{\xi} = (\xi^1, ..., \xi^D) \quad \text{and} \quad \dot{\boldsymbol{\xi}} = (\dot{\xi}^1, ..., \dot{\xi}^D). \tag{12.59}$$

In this manner, the kinetic energy, potential energy, and Lagrangian are written with the functional dependence

$$K = K(\boldsymbol{\xi}, \dot{\boldsymbol{\xi}}, t) \quad \text{and} \quad P = P(\boldsymbol{\xi}, t) \quad \text{and} \quad L = L(\boldsymbol{\xi}, \dot{\boldsymbol{\xi}}, t). \tag{12.60}$$

We also assume the following shorthand for partial derivatives

$$\frac{\partial K}{\partial \boldsymbol{\xi}} = (\partial K/\partial \xi^1, \partial K/\partial \xi^2, ..., \partial K/\partial \xi^D) \quad \text{and} \quad \frac{\partial K}{\partial \dot{\boldsymbol{\xi}}} = (\partial K/\partial \dot{\xi}^1, \partial K/\partial \dot{\xi}^2, ..., \partial K/\partial \dot{\xi}^D). \tag{12.61}$$

With this notation, Lagrange's equations of motion (12.48) take the form

$$\frac{\mathrm{d}}{\mathrm{d}t}\left[\frac{\partial L}{\partial \dot{\boldsymbol{\xi}}}\right] - \frac{\partial L}{\partial \boldsymbol{\xi}} = 0. \tag{12.62}$$

12.6.2 The action

Consider the trajectory of an N particle system with $D \leq 3N$ degrees of freedom, and assume knowledge of the trajectory at two points in time, $t_A < t_B$. The action is the time integral of the Lagrangian[5]

$$\mathcal{S} = \int_{t_A}^{t_B} L(\boldsymbol{\xi}, \dot{\boldsymbol{\xi}}, t)\, \mathrm{d}t, \tag{12.63}$$

where we exposed the functional dependence (12.49) for the Lagrangian function. As defined, the action has physical dimensions of energy times time, which is the same as angular momentum

$$\mathcal{S} \ [\equiv] \ \mathrm{M}\ (\mathrm{L}/\mathrm{T})^2\ \mathrm{T} = \mathrm{M}\ \mathrm{L}^2\ \mathrm{T}^{-1}. \tag{12.64}$$

Hamilton's principle states that the physically realized trajectory is an extremum of the action. The action integral (12.63) must have an extremum arising from the physically realized trajectory, regardless the time interval. However, the extremum is not necessarily a minimum.[6] Indeed, it is typically nontrivial to deduce the nature of the extremum given that one must compute the second variation of the action. Even so, we only rely on there being an extremum of the action in order to derive the equations of motion. It is for this reason that we prefer the name *Hamilton's principle of stationary action* rather than the commonly used *Hamilton's principle of least action*.

12.6.3 Variation of the action

To prove that the action is stationary for the physical trajectory, $\boldsymbol{\xi}(t)$, consider a perturbed trajectory via

$$\boldsymbol{\xi}'(t) = \boldsymbol{\xi}(t) + \epsilon\, \boldsymbol{\chi}(t). \tag{12.65}$$

As so defined, we have the perturbation written

$$\delta\boldsymbol{\xi}(t) = \boldsymbol{\xi}'(t) - \boldsymbol{\xi}(t) = \epsilon\, \boldsymbol{\chi}(t), \tag{12.66}$$

and the corresponding perturbation to the generalized velocity

$$\delta\dot{\boldsymbol{\xi}}(t) = \dot{\boldsymbol{\xi}}'(t) - \dot{\boldsymbol{\xi}}(t) = \epsilon\, \dot{\boldsymbol{\chi}}(t) = (\mathrm{d}/\mathrm{d}t)\, \delta\boldsymbol{\xi}. \tag{12.67}$$

[5] In some chapters of this book (e.g., Chapters 22, 22, and 26), $\mathcal{S}$ is the entropy per mass. The distinct meanings for the same symbol will be clear from the context.

[6] This point is emphasized in a footnote in Section 2 of *Landau and Lifshitz* (1976).

In these equations, ϵ is a small non-dimensional constant that scales the perturbation function, $\boldsymbol{\chi}(t)$. Furthermore, the perturbation function vanishes at the initial time and final time

$$\boldsymbol{\chi}(t_A) = \boldsymbol{\chi}(t_B) = 0, \tag{12.68}$$

and $\boldsymbol{\chi}(t)$ is consistent with the constraints applied to the system. For example, if the motion is constrained to the surface of a spherical shell, then so too is $\boldsymbol{\chi}$. Furthermore, note that equation (12.67) reveals that variations in the generalized velocities are not independent of variations of the generalized coordinates.

We refer to $\delta\boldsymbol{\xi}(t)$ as the *variation* of the trajectory, with Figure 12.1 providing an example. Variations provide a method to probe physically unrealized paths for the purpose of characterizing and understanding what is special about the physically realized path. This approach builds from the virtual displacements considered in Section 12.4.4. Indeed, the path variations are virtual displacements from the physical path. Like a virtual displacement, path variations are made during a single time instance so that $\mathrm{d}t = 0$.

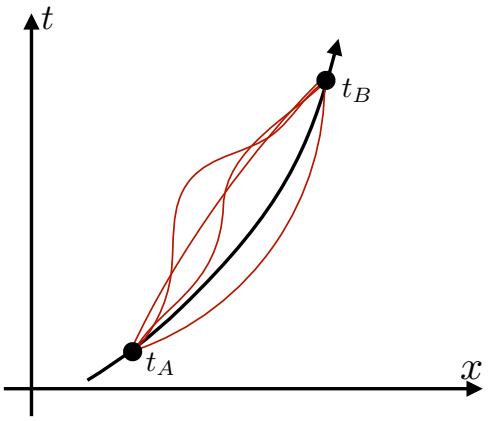

FIGURE 12.1: The physically realized trajectory, $\boldsymbol{\xi}(t)$, is depicted by the black line, with a sampling of the infinite number of possible variations, $\boldsymbol{\xi}'(t) = \boldsymbol{\xi}(t) + \delta\boldsymbol{\xi}(t)$, depicted in red. We assume knowledge of the trajectory at the start time, t_A, and end time, t_B. Hence, the physical trajectory and its variations are coincident at times t_A and t_B. Variations provide a means to probe physically unrealized paths for the purpose of characterizing and understanding what is special about the physically realized path.

The Lagrangian function takes on the following form when evaluated with the modified trajectory (12.65)

$$L(\boldsymbol{\xi}', \dot{\boldsymbol{\xi}}', t) = L(\boldsymbol{\xi} + \epsilon\,\boldsymbol{\chi}, \dot{\boldsymbol{\xi}} + \epsilon\,\dot{\boldsymbol{\chi}}, t) \approx L(\boldsymbol{\xi}, \dot{\boldsymbol{\xi}}, t) + \epsilon \left[\boldsymbol{\chi} \cdot \frac{\partial L(\boldsymbol{\xi}, \dot{\boldsymbol{\xi}}, t)}{\partial \boldsymbol{\xi}} + \dot{\boldsymbol{\chi}} \cdot \frac{\partial L(\boldsymbol{\xi}, \dot{\boldsymbol{\xi}}, t)}{\partial \dot{\boldsymbol{\xi}}} \right]. \tag{12.69}$$

We only expand the Taylor series to leading order since ϵ is tiny so that all higher order terms are negligible. The notation in equation (12.69) is a shorthand for the more complete sums over the degrees of freedom

$$\boldsymbol{\chi} \cdot \frac{\partial L(\boldsymbol{\xi}, \dot{\boldsymbol{\xi}}, t)}{\partial \boldsymbol{\xi}} = \sum_{\sigma=1}^{D} \chi^\sigma \frac{\partial L(\boldsymbol{\xi}, \dot{\boldsymbol{\xi}}, t)}{\partial \xi^\sigma} \quad \text{and} \quad \dot{\boldsymbol{\chi}} \cdot \frac{\partial L(\boldsymbol{\xi}, \dot{\boldsymbol{\xi}}, t)}{\partial \dot{\boldsymbol{\xi}}} = \sum_{\sigma=1}^{D} \dot{\chi}^\sigma \frac{\partial L(\boldsymbol{\xi}, \dot{\boldsymbol{\xi}}, t)}{\partial \dot{\xi}^\sigma}. \tag{12.70}$$

From equation (12.69) we deduce the variation of the Lagrangian that arises from variation of the trajectories

$$\delta L(\boldsymbol{\xi}, \dot{\boldsymbol{\xi}}, t) = L(\boldsymbol{\xi}', \dot{\boldsymbol{\xi}}', t) - L(\boldsymbol{\xi}, \dot{\boldsymbol{\xi}}, t) \approx \epsilon \left[\boldsymbol{\chi} \cdot \frac{\partial L(\boldsymbol{\xi}, \dot{\boldsymbol{\xi}}, t)}{\partial \boldsymbol{\xi}} + \dot{\boldsymbol{\chi}} \cdot \frac{\partial L(\boldsymbol{\xi}, \dot{\boldsymbol{\xi}}, t)}{\partial \dot{\boldsymbol{\xi}}} \right], \tag{12.71}$$

along with the corresponding variation of the action

$$\delta \mathcal{S} = \int_{t_A}^{t_B} \delta L(\boldsymbol{\xi}, \dot{\boldsymbol{\xi}}, t)\, \mathrm{d}t. \tag{12.72}$$

Integrating by parts on the final term in equation (12.71) leads to the equivalent expression for variation of the Lagrangian

$$\delta L = \epsilon \boldsymbol{\chi} \cdot \left[\frac{\partial L}{\partial \boldsymbol{\xi}} - \frac{\mathrm{d}}{\mathrm{d}t} \left(\frac{\partial L}{\partial \dot{\boldsymbol{\xi}}} \right) \right] + \frac{\mathrm{d}}{\mathrm{d}t} \left[\epsilon \boldsymbol{\chi} \cdot \frac{\partial L(\boldsymbol{\xi}, \dot{\boldsymbol{\xi}}, t)}{\partial \dot{\boldsymbol{\xi}}} \right]. \tag{12.73}$$

Since the perturbation function, $\boldsymbol{\chi}$, vanishes at t_A and t_B according to equation (12.68), the total time derivative plays no role in the action variation, in which case

$$\delta \mathcal{S} = \epsilon \int_{t_A}^{t_B} \boldsymbol{\chi} \cdot \left[\frac{\partial L}{\partial \boldsymbol{\xi}} - \frac{\mathrm{d}}{\mathrm{d}t} \left(\frac{\partial L}{\partial \dot{\boldsymbol{\xi}}} \right) \right] \mathrm{d}t. \tag{12.74}$$

12.6.4 Stationary action and the Euler-Lagrange equations

Equation (12.74) says that variation of the action vanishes (i.e., the action is stationary) for all values of $\boldsymbol{\chi}$ if and only if the integrand is zero for each of the generalized coordinates. We are thus led to the condition

$$\delta \mathcal{S} = 0 \Longleftrightarrow \frac{\mathrm{d}}{\mathrm{d}t} \left[\frac{\partial L}{\partial \dot{\xi}^\sigma} \right] - \frac{\partial L}{\partial \xi^\sigma} = 0 \quad \text{for } \sigma = 1, ..., D, \tag{12.75}$$

which is Lagrange's equation of motion (12.48) derived in Section 12.5 starting from Newton's equation of motion. In the context of Hamilton's principle, Lagrange's equations (12.75) are referred to as the *Euler-Lagrange* equations, given the work by Euler on variational principles.

12.6.5 Derivative of the action with respect to ϵ

The discussion in Section 12.6.3 illustrates the how to vary the action, and its usage becomes second nature once doing it a few times. We here present a slightly alternative approach that, in the end, is totally equivalant to the variation approach but which offers a few more insights.

Consider the action evaluated on the perturbed trajectory

$$\mathcal{S}' = \int_{t_A}^{t_B} L(\boldsymbol{\xi}', \dot{\boldsymbol{\xi}}', t)\, \mathrm{d}t = \int_{t_A}^{t_B} L(\boldsymbol{\xi} + \epsilon \boldsymbol{\chi}, \dot{\boldsymbol{\xi}} + \epsilon \dot{\boldsymbol{\chi}}', t)\, \mathrm{d}t. \tag{12.76}$$

Now take the derivative of the perturbed action with respect to ϵ

$$\frac{\mathrm{d}\mathcal{S}'}{\mathrm{d}\epsilon} = \int_{t_A}^{t_B} \left[\frac{\partial L(\boldsymbol{\xi}', \dot{\boldsymbol{\xi}}', t)}{\partial \boldsymbol{\xi}'} \cdot \frac{\partial \boldsymbol{\xi}'}{\partial \epsilon} + \frac{\partial L(\boldsymbol{\xi}', \dot{\boldsymbol{\xi}}', t)}{\partial \dot{\boldsymbol{\xi}}'} \cdot \frac{\partial \dot{\boldsymbol{\xi}}'}{\partial \epsilon} \right] \mathrm{d}t. \tag{12.77}$$

Now evaluate the derivatives of the trajectory and the velocity to find

$$\frac{\mathrm{d}\mathcal{S}'}{\mathrm{d}\epsilon} = \int_{t_A}^{t_B} \left[\frac{\partial L(\boldsymbol{\xi}', \dot{\boldsymbol{\xi}}', t)}{\partial \boldsymbol{\xi}'} \cdot \boldsymbol{\chi} + \frac{\partial L(\boldsymbol{\xi}', \dot{\boldsymbol{\xi}}', t)}{\partial \dot{\boldsymbol{\xi}}'} \cdot \dot{\boldsymbol{\chi}} \right] \mathrm{d}t, \tag{12.78}$$

with integration by parts and use of the initial and final conditions yielding

$$\frac{\mathrm{d}\mathcal{S}'}{\mathrm{d}\epsilon} = \int_{t_A}^{t_B} \boldsymbol{\chi} \cdot \left[\frac{\partial L(\boldsymbol{\xi}', \dot{\boldsymbol{\xi}}', t)}{\partial \boldsymbol{\xi}'} - \frac{\mathrm{d}}{\mathrm{d}t} \left(\frac{\partial L(\boldsymbol{\xi}', \dot{\boldsymbol{\xi}}', t)}{\partial \dot{\boldsymbol{\xi}}'} \right) \right] \mathrm{d}t. \tag{12.79}$$

This expression has the same look as the variation in equation (12.74), and yet here the action is evaluated on the perturbed trajectory rather than the physically realized trajectory. Hamilton's principle says that the action is extremal for the physically realized trajectory, which means that

$$\left[\frac{\mathrm{d}\mathcal{S}'}{\mathrm{d}\epsilon} \right]_{\epsilon=0} = 0. \tag{12.80}$$

That is, Hamilton's principle says that the physically realized trajectory extremizes the action, which means that the action has a zero derivative at $\epsilon = 0$. As expected, this statement leads to the same Euler-Lagrange equations (12.75) as derived using the variational approach.

Considering the small parameter to be continuous, we can formally connect this discussion to the δ variation operator by writing

$$\left[\frac{\mathrm{d}\mathcal{S}'}{\mathrm{d}\epsilon} \right] \mathrm{d}\epsilon = \delta\mathcal{S}' \quad \text{and} \quad \frac{\mathrm{d}\boldsymbol{\xi}'}{\mathrm{d}\epsilon} \mathrm{d}\epsilon = \delta\boldsymbol{\xi}'. \tag{12.81}$$

12.6.6 Mechanical equivalence of Lagrangians

The Euler-Lagrange equation (12.75) remains unchanged if we multiply the Lagrangian by a constant. This property, though seemingly trivial, has important implications for scaling properties of the energy of physical systems. We deduce such properties in Section 12.7. Additionally, the Euler-Lagrange equation is unchanged by adding the total time derivative of an arbitrary function of the generalized coordinates and time

$$L^{\text{new}} = L^{\text{old}} + \frac{\mathrm{d}\Gamma(\boldsymbol{\xi}, t)}{\mathrm{d}t}. \tag{12.82}$$

To show the equivalance, note that the action transforms into

$$\mathcal{S}^{\text{new}} = \mathcal{S}^{\text{old}} + \Gamma[\boldsymbol{\xi}(t_B), t_B] - \Gamma[\boldsymbol{\xi}(t_A), t_A]. \tag{12.83}$$

The added terms are evaluated at t_A and t_B, where the trajectories are held fixed. Hence, these terms have zero variation so that

$$\delta\mathcal{S}^{\text{new}} = \delta\mathcal{S}^{\text{old}}, \tag{12.84}$$

which then means that the associated Euler-Lagrange equation is unchanged.

12.6.7 Summary of the method

As a recap, we here defined the action (12.63) as the time integral of the Lagrangian between a start time and end time, $t_A < t_B$. The trajectory is assumed to be known at t_A and t_B. Besides knowing all details of the physical system at $t = t_A$ and at $t = t_B$, there is nothing special about these two times. For example, we do *not* imagine the physical system starts from some rest state at t_A. Instead, we only imagine that information about a physical system is somehow known at at t_A and t_B. The physical question concerns the trajectory in between these two time instances. To determine this trajectory, we consider how the action is modified by considering an arbitrary variation of the trajectory for times between the end times, again with the trajectory fixed at the start and end times. We found that the Euler-Lagrange equations (12.75) are satisfied if and only if the action is stationary with respect to trajectory variations. That is, the physically

realized trajectory is that trajectory that makes the action stationary; i.e., it is an extremum of the action. This result constitutes Hamilton's principle of stationary action.

Since the physically realized trajectory is the one that satisfies the Euler-Lagrange equations, all other trajectories are unphysical and as such they are not constrained by dynamical principles. Instead, these virtual trajectories are only constrained by the geometry of the system and by the need to respect the prescribed initial and final conditions. As such, Hamilton's principle tests all kinematically possible trajectories and selects the dynamically unique trajectory through insisting on stationarity of the action. Uniqueness of the dynamical trajectory constitutes a tacit assumption of Hamilton's principle. Proof of uniqueness follows from uniqueness of solutions to the Euler-Lagrange differential equations.

12.6.8 Some philosophical points

As already noted, Hamilton's principle provides an alternative to Newton's laws for the formulation of mechanics. Indeed, it is remarkable how complementary these two approaches are. Namely, Newton's laws are concerned with forces and accelerations acting at a point in space and time. Stating Newton's law of motion is relatively straightforward and, with the benefit of centuries of hindsight and experience, rather self-evident.[7] In contrast, Hamilton's principle says that the difference between the kinetic and potential energies, as integrated on a trajectory over a time interval, is extremized by the physically realized trajectory. Understanding the mathematical and physical statement of Hamilton's principle, and making use of it operationally, requires nontrivial formulational effort via the methods of analytical mechanics. Even so, upon mastering its formulation, the application of Hamilton's principle via the Euler-Lagrange equations can prove of great practical value for solving physical problems that are outside the reach of Newtonian methods.

The Newtonian description offers the canonical cause and effect perspective, whereby a force (the cause) creates an effect (the acceleration). In contrast, Hamilton's principle states that the physically realize motion takes place so that the action (an integral over time) is an extrema. From this view, Hamilton's principle can be viewed as offering a purpose for the motion, namely to extremize the action.[8] We do not pursue this discussion further as it goes beyond our goals, though the interested reader might find Chapter 14 of *Yourgrau and Mandelstam* (1968) of interest for its philosophical insights.

12.7 Mechanical similarity and the virial theorem

As noted in Section 12.6.6, the Euler-Lagrange equation (12.75) remains unchanged if we multiply the Lagrangian by a constant. In this section we uncover a suite of rather general scaling properties that can be inferred as a result of this seemingly trivial symmetry. Remarkably, these properties are found without solving the equations of motion.

12.7.1 Potential energy as a homogeneous function

To derive the advertised results, we must assume that the potential energy is a homogeneous function, which means that it scales according to

$$P(\lambda x^1, \lambda x^2, \lambda x^3) = \lambda^\gamma P(x^1, x^2, x^3), \tag{12.85}$$

[7] Being self-evident in retrospect is often a characteristic of a foundational physical concept.

[8] A *teleological* explanation considers phenomena in terms of the purpose it serves rather than of the cause by which it arises.

where λ is a non-dimensional scale factor and γ is an integer that sets the degree of homogeneity. The left hand side of equation (12.85) is the potential energy evaluated with each of its Cartesian coordinates scaled by the same number, λ. That is, the left hand side has length scales modified by λ. The right hand side is the potential energy evaluated with the unscaled coordinates (unscaled length), but it is multiplied by the scale, λ, raised to the power γ.

Note that we represented the potential energy in equation (12.85) in terms of the Cartesian coordinates, since doing so readily ensures that scaling is consistently applied to each of the distinct coordinates by the same number. We also only considered the potential energy for a single particle. Extending to an arbitrary number of particles simply means adding more coordinates to the potential energy, with the scale, λ, also applied to these additional coordinates.

We prove Euler's theorem for homogeneous functions in Section 6.8, which for potential energy constitutes the identity

$$\gamma\, P(\boldsymbol{X}) = x^a\, \partial P(\boldsymbol{X})/\partial x^a. \tag{12.86}$$

This equation says that the potential energy, as multiplied by the degree of homogeneity, γ, has an equivalent expression in terms of the coordinates multiplied by the corresponding partial derivative of the potential energy. Introducing the conservative force associated with the potential energy

$$\boldsymbol{F} = -\nabla P, \tag{12.87}$$

we see that Euler's theorem for potential energy means that

$$\gamma\, P = -\boldsymbol{X} \cdot \boldsymbol{F} \tag{12.88}$$

We emphasize that the rather simple expression (12.88) for the potential energy holds only for potential energies that are homogeneous functions. Though restrictive, there are a number of physically interesting systems with homogeneous potential energies, including the following.

- $\gamma = -1$: the potential energy of particles in a gravity field or electrostatic field is inversely related to the distance between the particles, so that $\gamma = -1$.

- $\gamma = 1$: for a particle moving in a uniform field, such as a uniform gravity field, the potential energy has $\gamma = 1$.

- $\gamma = 2$: Small amplitude oscillations, such as those exhibited by a pendulum (Section 15.1) or simple harmonic oscillator (Section 15.6), have $\gamma = 2$.

Note that the trivial case of $\gamma = 0$ corresponds to a potential energy that is a constant, and thus leads to a zero force.

12.7.2 Mechanical similarity

Consider a physical system in which we scale the length by λ, just as considered for the potential energy in equation (12.85). This scaling alters the Lagrangian in a manner that alters the Euler-Lagrange equations. However, if we couple scaling of the length with a corresponding scaling of the time, then it is conceivable that we can find a combination of these two scalings that results in an overall factor multiplying the Lagrangian, in which case the Euler-Lagrange equation are unaltered. We refer to this confluence of scaling as *mechanical similarity*.

We are thus led to examine symmetry of the Lagrangian under the space-time scaling transformation

$$x^a \to \lambda\, x^a \iff x^{a'}/x^a = \lambda \quad \text{and} \quad t \to \beta\, t \iff t'/t = \beta, \tag{12.89}$$

where λ and β are two non-dimensional scales. This space-time scaling leads to a scaling of the velocity components

$$\dot{x}^a \to (\lambda/\beta)\, \dot{x}^a. \tag{12.90}$$

Since the kinetic energy is proportional to the square of the velocity, the scaling of space and time given by equation (12.89) renders the Lagrangian scaling

$$L = K - P \to \lambda^\gamma\, P - (\lambda/\beta)^2\, K. \tag{12.91}$$

In order for this scaling to not alter the Euler-Lagrange equations requires

$$\beta = \lambda^{1-\gamma/2} \Longrightarrow (t'/t) = \beta = \lambda^{1-\gamma/2} = (x'/x)^{1-\gamma/2}. \tag{12.92}$$

which we refer to as *mechanical similarity*. This equation means that if we scale time by β, so that $(t'/t) = \beta$, then we do not change the equations of motion if length is scaled according to $(l/l')^{1-\gamma/2}$. We can now infer the following results according to the scaling of the potential energy presented in Section 12.7.1.

- $\gamma = -1$ leads to $(t'/t) = (x'/x)^{3/2}$, or $(t'/t)^2 = (x'/x)^3$. This equality accords with *Kepler's third law*, which states that the square of the orbit period scales as the cube of the orbit size.
- $\gamma = 1$ leads to $(t'/t) = (x'/x)^{1/2}$, or $(t'/t)^2 = (x'/x)$. This equality accords with the quadratic time dependence for a particle freely falling through a uniform gravity field.
- $\gamma = 2$ leads to $(t'/t) = 1$, which accords with the amplitude independence for the period of small oscillations exhibited by a pendulum.

12.7.3 Virial theorem and time averaged energy

To derive the *virial theorem*, we assume that the physical system maintains motion within a bounded region of space and with bounded velocity. This assumption is maintained by geophysical motion. The virial theorem provides a relation between the time averaged kinetic energy and time averaged potential energy for such bounded motion.

The kinetic energy is a quadratic function of velocity. Hence, as a function of velocity, the kinetic energy is a homogeneous function of degree two. Euler's theorem for homogeneous functions thus means that

$$2\, K = m\, \delta_{ab}\, \dot{x}^a\, \dot{x}^b/2 = \dot{x}^a\, (\partial K/\partial \dot{x}^a) = \dot{x}^a\, \mathcal{P}_a, \tag{12.93}$$

where we introduced the Cartesian momentum,

$$\mathcal{P}_a \equiv \frac{\partial L}{\partial \dot{x}^a} = \frac{\partial K}{\partial \dot{x}^a}, \tag{12.94}$$

which is generalized in Section 12.10 for generalized coordinates. Here it merely represents a useful shorthand, allowing us to write

$$\begin{aligned} 2\, K &= \dot{x}^a\, \mathcal{P}_a && \text{(12.95a)}\\ &= \frac{\mathrm{d}(x^a\, \mathcal{P}_a)}{\mathrm{d}t} - x^a\, \dot{\mathcal{P}}_a && \text{(12.95b)}\\ &= \frac{\mathrm{d}(x^a\, \mathcal{P}_a)}{\mathrm{d}t} + x^a\, \partial P/\partial x^a && \text{(12.95c)}\\ &= \frac{\mathrm{d}(x^a\, \mathcal{P}_a)}{\mathrm{d}t} + \gamma\, P. && \text{(12.95d)} \end{aligned}$$

In the penultimate step (12.95c) we set

$$\dot{\mathcal{P}}_a = -\partial P/\partial x^a \tag{12.96}$$

according to Newton's law of motion, and in the final step (12.95d) we made use of Euler's theorem (12.86) for the potential energy. Taking the time average of equation (12.95d), and assuming the time average of the time derivative vanishes, then leads to the relation between the time averaged kinetic energy and time averaged potential energy

$$2\,\overline{K} = \gamma\,\overline{P}. \tag{12.97}$$

Note that the time average of the derivative vanishes if the time average is computed over a long enough time, given that the motion is assumed to be bounded. Additionally, if the motion is periodic then we can exactly remove the time derivative by taking the time average over the period of the motion.

The virial theorem (12.97) relates the time averaged kinetic energy and the time averaged potential energy in physical systems with a potential energy that is a homogeneous function of degree γ. In this book we find particular use for the case of $\gamma = 2$, which corresponds to motion of a simple harmonic oscillator, in which the virial theorem says that the potential and kinetic energies have equal time averages. This result is referred to as the *equipartition of energy*. In addition to harmonic oscillators and small amplitude pendula, we find in Part X of this book that the equipartition of energy holds for linear wave motion, with the potential energy of linear waves generally a homogeneous function of degree two.

12.7.4 Further reading

This section shares much with Section 10 of *Landau and Lifshitz* (1976) as well as Section 6.13 of *Marion and Thornton* (1988).

12.8 Lagrange multipliers and forces of constraint

Derivation of Lagrange's equation of motion in Section 12.5 succeeded in eliminating the forces of constraint from the formulation. Likewise in the discussion of Hamilton's principle in Section 12.6, we assumed the $D = 3N - C$ generalized coordinates directly correspond to the D degrees of freedom available to the constrained physical system. In this section we present a method to infer the C forces of constraint through the method of *Lagrange multipliers*, with this inference of use when aiming to study force balances.

12.8.1 Holonomic constraints and their variation

Following equation (12.12), consider $3N$ coordinates, $\xi^\sigma, \sigma = 1, ..., 3N$, and assume they are constrained by C holonomic constraints of the form

$$\Psi_c(\xi^1, ..., \xi^{3N}, t) = C_c, \quad \text{for} \quad c = 1, ..., C, \tag{12.98}$$

where C_c are constants. This equation is nearly the same as equation (12.12), only now we allow the coordinates to be non-Cartesian if that is suits to the problem.[9] Varying the trajectory then

[9] Strictly, the $3N$ coordinates, ξ^σ, are not "generalized coordinates" since that term refers to coordinates that directly correspond to the $D = 3N - C$ degrees of freedom. Even so, that distinction is not important for what follows.

leads to a variation of the constraint equations (12.98) that takes the form

$$\delta\Psi_c = \sum_{\sigma=1}^{3N} \frac{\partial \Psi_c}{\partial \xi^\sigma}\,\delta\xi^\sigma = 0, \quad \text{for} \quad c = 1, ..., C. \tag{12.99}$$

This equation provides C constraints that must be satisfied by the $3N$ variations, $\delta\xi^\sigma$. Recall that a variation is a virtual process (Section 12.4.4) and so it occurs at a time instance, which explains why there is no $\mathrm{d}t$ term in equation (12.99). Also note that variation of a constant vanishes, so that $\delta\, C_c = 0$, thus rendering a zero on the right hand side of equation (12.99).

12.8.2 Lagrange multipliers and the modified Euler-Lagrange equations

Recall the variation of the action given by equation (12.74), only now write this variation assuming there are $3N$ coordinates

$$\delta\mathcal{S} = \int_{t_A}^{t_B} \sum_{\sigma=1}^{3N} \delta\xi^\sigma \left[\frac{\partial L}{\partial \xi^\sigma} - \frac{\mathrm{d}}{\mathrm{d}t}\left(\frac{\partial L}{\partial \dot{\xi}^\sigma}\right)\right] \mathrm{d}t = 0. \tag{12.100}$$

Contrary to what we did in Section 12.6.4, we cannot separately set $\delta\xi^\sigma$ to zero to then render the Euler-Lagrange equations (12.75). The reason is that the $3N$ variations, $\delta\xi^\sigma$, are constrained according to equation (12.101), thus making the variations dependent on one another. The method of Lagrange multipliers allows for us to incorporate the constraints while keeping all $3N$ coordinates.

To do so, introduce C Lagrange multipliers, $\Lambda^c(t)$, which are functions of time and whose form is to be specified below. Multiply each of the C constraint equations (12.99) by Λ^c and sum over all of the constraints

$$\sum_{c=1}^{C} \Lambda^c\,\delta\Psi_c = \sum_{c=1}^{C}\sum_{\sigma=1}^{3N} \Lambda^c \frac{\partial \Psi_c}{\partial \xi^\sigma}\,\delta\xi^\sigma = 0. \tag{12.101}$$

Now the action variation in equation (12.100) is unchanged by adding zero to the right hand side, and if we add zero in the form of equation (12.101) then that brings the constraints into the action variation via

$$\delta\mathcal{S} = \int_{t_A}^{t_B} \sum_{\sigma=1}^{3N} \delta\xi^\sigma \left[\frac{\partial L}{\partial \xi^\sigma} - \frac{\mathrm{d}}{\mathrm{d}t}\left(\frac{\partial L}{\partial \dot{\xi}^\sigma}\right) + \sum_{c=1}^{C} \Lambda^c \frac{\partial \Psi_c}{\partial \xi^\sigma}\right] \mathrm{d}t = 0. \tag{12.102}$$

This equation has $D = 3N - C$ independent variations and C constrained variations. Let us organize the coordinates, ξ^σ, so that the $\sigma = 1, ...D$ coordinates have independent variations, whereas the remaining are constrained. Hence, coefficients of the independent variations in equation (12.102) must vanish in order to satisfy Hamilton's stationary action principle, using the same logic as for Section 12.6.4. For the remaining $\sigma = D+1, ..., D+C$ constrained variations, we can *choose* the C Lagrange multipliers so that the coefficients of these dependent variations also vanish. In this manner the coefficients multiplying *all* of the $3N$ variations, $\delta\xi^\sigma$, vanish, which then leads to the modified Euler-Lagrange equations along with the C holonomic constraints

$$\frac{\mathrm{d}}{\mathrm{d}t}\left[\frac{\partial L}{\partial \dot{\xi}^\sigma}\right] - \frac{\partial L}{\partial \xi^\sigma} = \sum_{c=1}^{C} \Lambda^c \frac{\partial \Psi_c}{\partial \xi^\sigma} \quad \text{for } \sigma = 1, ..., 3N \tag{12.103a}$$

$$\Psi_c(\xi^1, ..., \xi^{3N}, t) = C_c, \quad \text{for} \quad c = 1, ..., C. \tag{12.103b}$$

12.8.3 The extended Lagrangian with multipliers

The modified Euler-Lagrange equation (12.103a) and corresponding holonomic constraints (12.103b) can be summarized by defining the extended Lagrangian as

$$L^* = L + \sum_{c=1}^{C} \Lambda^c \, \Psi_c. \tag{12.104}$$

As defined, the extended Lagrangian has the functional depedence

$$L^* = L(\xi^1, ...\xi^{3N}, \dot{\xi}^1, ...\dot{\xi}^{3N}, t, \Lambda^1, ...\Lambda^C), \tag{12.105}$$

so that it is a function of the coordinates, ξ^σ, velocities, $\dot{\xi}^\sigma$, and time, t, as well as the Lagrange multipliers, $\Lambda^1, ..., \Lambda^C$. We thus find the partial derivatives

$$\frac{\partial L^*}{\partial \dot{\xi}^\sigma} = \frac{\partial L}{\partial \dot{\xi}^\sigma} \tag{12.106a}$$

$$\frac{\partial L^*}{\partial \xi^\sigma} = \frac{\partial L}{\partial \xi^\sigma} + \sum_{c=1}^{C} \Lambda^c \frac{\partial \Psi_c}{\partial \xi^\sigma} \tag{12.106b}$$

$$\frac{\partial L^*}{\partial \Lambda^c} = \Psi_c. \tag{12.106c}$$

In this manner we can write the Euler-Lagrange equation (12.103a) and corresponding holonomic constraints (12.103b) as

$$\frac{\mathrm{d}}{\mathrm{d}t}\left[\frac{\partial L^*}{\partial \dot{\xi}^\sigma}\right] = \frac{\partial L^*}{\partial \xi^\sigma} \tag{12.107a}$$

$$\frac{\partial L^*}{\partial \Lambda^c} = \Psi_c. \tag{12.107b}$$

12.8.4 Determining the forces of constraint

There are $3N$ equations in the modified Euler-Lagrange equation (12.103a), and C constraints in equation (12.103b). By adding to the burden of what is to be determined, we now have the means to infer the forces of constraint. For that purpose, re-introduce the kinetic energy and potential energy to write equation (12.103a) as

$$\frac{\mathrm{d}}{\mathrm{d}t}\left[\frac{\partial K}{\partial \dot{\xi}^\sigma}\right] - \frac{\partial K}{\partial \xi^\sigma} = -\frac{\partial P}{\partial \xi^\sigma} + \sum_{c=1}^{C} \Lambda^c \frac{\partial \Psi_c}{\partial \xi^\sigma} \quad \text{for } \sigma = 1, ..., 3N, \tag{12.108}$$

where the potential energy is independent of the coordinate velocities, $\partial P/\partial \dot{\xi}^\sigma = 0$, as follows from equation (12.44). Recalling the Lagrange's equation in the form (12.42), we identify the right hand side of equation (12.108) as the generalized force

$$Q_\sigma = -\frac{\partial P}{\partial \xi^\sigma} + \sum_{c=1}^{C} \Lambda^c \frac{\partial \Psi_c}{\partial \xi^\sigma} \quad \text{for } \sigma = 1, ..., 3N. \tag{12.109}$$

Now $-\partial P/\partial \xi^\sigma$ is the applied conservative force, so we identify the remaining term is the force of constraint

$$Q_\sigma^{\text{constraint}} = \sum_{c=1}^{C} \Lambda^c \frac{\partial \Psi_c}{\partial \xi^\sigma} \quad \text{for } \sigma = 1, ..., 3N. \tag{12.110}$$

12.9 Symmetries and conservation laws

Part of the allure of Hamilton's principle and the corresponding Euler-Lagrange equations concerns the ability to deduce quantities that are conserved by the physically realized dynamical system. These dynamical conservation laws are associated with symmetries, with this connection between symmetries (kinematics) and conservation laws (dynamics) first made by *Noether* (1918) (see *Noether and Tavel* (2018) for an English translation). In this section we focus on space and time symmetries. In particular, we connect the conservation of linear momentum to *space homogeneity*; conservation of angular momentum to *space isotropy*; and conservation of mechanical energy to *time homogeneity*. The present section focuses on deriving the mathematical expressions of the conservation law. In so doing, we further our understanding of Hamilton's principle and the associated manipulations needed for its practical use. We study implications of these conservation laws in Chapter 14 for particles moving viewed in a rotating reference frame, such as appropriate for a terrestrial observer on a rotating planet.

To connect a symmetry to a conservation law, it is sufficient to focus on the Lagrangian since it encapsulates the mechanics. That is, we examine how the Lagrangian is affected by the chosen symmetry operation. Furthermore, since we are concerned with conservation laws realized by the physical system, the Lagrangian satisfies the Euler-Lagrange equations of motion. Additionally, we here only consider continuous space and time symmetries. Therefore, to determine implications of a symmetry it is sufficient to examine how the Lagrangian varies under an infinitesimal symmetry transformation. This treatment is convenient since infinitesimal transformations are simpler mathematically than finite transformations. In effect, we only need to go to leading order in a Taylor expansion to deduce the conservation laws. Additionally, we remove all forces of constraint, so that it is sufficient to work with Cartesian coordinates.

So in brief, we observe that if the mechanical system is to respect a particular symmetry, then its action must remain invariant under the symmetry transformation; i.e., its variation must vanish. Variation of the action vanishes if variation of the Lagrangian vanishes, with a zero variation of the Lagrangian directly leading to the differential conservation law associated with the symmetry.[10]

12.9.1 Free particle motion

Before we work through the conservation laws arising from space-time symmetries, we here study what is perhaps the simplest physical system, the *free particle*. Doing so provides a warm-up to the more general systems considered next. Free particle motion occurs when a particle experiences no forces at all (neither applied nor constraining) in an inertial reference frame. We infer from this statement that the particle can only move in an empty space that is homogeneous and isotropic, since otherwises it would necessarily experience a force that altered its path.[11]

For the particle to experience space as homogeneous (the particle does not care about the point in space) and time as homogeneous (the particle does not care about the origin of time),

[10] In Section 12.6.6 we found that the action is unaffected the total time derivative of a function that depends only on the generalized coordinates and time. Even so, to derive the conservation laws in this section, we set the Lagrangian variation to zero.

[11] This statement carries importance nuances when moving to general relativity, which is outside of our scope. So for this book, we consider space to be Euclidean, so that free particle motion is along a straight line in this space. Furthermore, it is notable that free particle motion appears to be forced motion when viewed from a non-inertial reference frame (Sections 11.3 and 11.4). As such, the symmetries of a non-inertial reference frame are generally distinct from an inertial reference frame. We here focus on inertial reference frames since it is here that free particle motion in empty space experiences no force, and velocity remains constant.

then the Lagrangian for the particle cannot contain any explicit dependence on space or time,

$$\frac{\partial L}{\partial t} = 0 \quad \text{and} \quad \frac{\partial L}{\partial x} = \frac{\partial L}{\partial y} = \frac{\partial L}{\partial z} = 0, \tag{12.111}$$

where it is convenient to use Cartesian coordinates since there are no constraints. For mechanics to be the same for all space directions (isotropic space), then the Lagrangian must be independent of the velocity direction. We are led to a Lagrangian that is a function just of the velocity magnitude, or more conveniently the velocity squared. That is, the free particle Lagrangian is given by the kinetic energy

$$L = m\,(\dot{x}^2 + \dot{y}^2 + \dot{z}^2)/2, \tag{12.112}$$

where we chose Cartesian coordinates since the motion is unconstrained. We already knew this result must hold since the potential energy is zero in the absence of forces. Even so, this discussion serves to illustrate the power of arguments based on symmetry, with such arguments fundamental to how we make practical use of Hamilton's principle.

With the Lagrangian given by just the kinetic energy for unconstrained motion, then the Euler-Lagrange equation leads to constancy of the velocity

$$\frac{\mathrm{d}}{\mathrm{d}t}\frac{\partial L}{\partial \dot{x}} = \frac{\mathrm{d}}{\mathrm{d}t}\frac{\partial L}{\partial \dot{y}} = \frac{\mathrm{d}}{\mathrm{d}t}\frac{\partial L}{\partial \dot{z}} = 0 \Longrightarrow \dot{\boldsymbol{X}} = \text{constant}. \tag{12.113}$$

This result is *Newton's first law* discussed in Chapter 11, and sometimes referred to as the *law of inertia*.

12.9.2 Space homogeneity and linear momentum conservation

We here examine the implications of an N particle system moving through a space that is homogeneous in an inertial reference frame. Moving beyond the free particle case of Section 12.9.1, we allow for conservative forces of interaction between the particles as measured by the potential energy function, $P(\boldsymbol{X})$. To respect spatial homogeneity requires mechanical properties of the system to be unchanged if we shift the coordinate position for each particle by an arbitrary amount. For ease in deriving the associated conservation law we examine how the Lagrangian changes when considering an infinitesimal shift in all of the particle positions

$$\boldsymbol{X}_{(i)} \to \boldsymbol{X}_{(i)} + \boldsymbol{\epsilon} \Longrightarrow \delta \boldsymbol{X}_{(i)} = \boldsymbol{\epsilon}, \tag{12.114}$$

where $\boldsymbol{\epsilon}$ is a constant displacement vector that is the same for all particles. A constant shift in particle positions does nothing to the particle velocities. Hence, upon shifting all particle positions by a constant, the Lagrangian becomes, to first order in $\boldsymbol{\epsilon}$,

$$L(\boldsymbol{X}', \dot{\boldsymbol{X}}', t) = L(\boldsymbol{X} + \boldsymbol{\epsilon}, \dot{\boldsymbol{X}}, t) \approx L(\boldsymbol{X}, \dot{\boldsymbol{X}}, t) + \epsilon^a \sum_{i=1}^{N} \frac{\partial L}{\partial x^a_{(i)}}, \tag{12.115}$$

so that variation of the Lagrangian is

$$\delta L = \epsilon^a \sum_{i=1}^{N} \frac{\partial L}{\partial x^a_{(i)}}. \tag{12.116}$$

A zero variation of the Lagrangian ensures that the physical system is unaffected by shifts in the particle positions. Since the perturbation vector, $\boldsymbol{\epsilon}$, is arbitrary, the Lagrangian has zero

variation only if

$$\delta L = 0 \Longrightarrow \sum_{i=1}^{N} \frac{\partial L}{\partial x^a_{(i)}} = 0 \quad \text{for } a = 1, 2, 3. \tag{12.117}$$

Using this result in the Euler-Lagrange equation (12.75) leads to a conservation law for each of the three spatial directions

$$\frac{\mathrm{d}}{\mathrm{d}t} \sum_{i=1}^{N} \frac{\partial L}{\partial \dot{x}_{(i)}} = \frac{\mathrm{d}}{\mathrm{d}t} \sum_{i=1}^{N} \frac{\partial L}{\partial \dot{y}_{(i)}} = \frac{\mathrm{d}}{\mathrm{d}t} \sum_{i=1}^{N} \frac{\partial L}{\partial \dot{z}_{(i)}} = 0. \tag{12.118}$$

Evidently, when space is homogeneous and an N particle system respects this symmetry, then the linear momentum of the system is a constant of the motion

$$\sum_{i=1}^{N} \frac{\partial L}{\partial \dot{x}^a_{(i)}} = m \sum_{i=1}^{N} \dot{x}^a_{(i)} = \text{constant}. \tag{12.119}$$

This result is the law of inertia for the N particle system. Note that if there is spatial symmetry in only a select number of directions, then only the corresponding momenta are conserved.

Another implication for the homogeneity condition (12.117) is that the sum of the forces acting on the N particle system vanishes

$$\sum_{i=1}^{N} \frac{\partial L}{\partial x^a_{(i)}} = -\sum_{i=1}^{N} \frac{\partial P}{\partial x^a_{(i)}} = \sum_{i=1}^{N} F^a_{(i)} = 0. \tag{12.120}$$

For the case of $N = 1$ we recover the free particle discussed in Section 12.9.1, whereby the particle experiences no forces if it moves through a space that is homogeneous. However, an N particle system respects spatial homogeneity if the sum of all the inter-particle forces vanishes. Equation (12.120) is a statement of *Newton's third law* as studied in Section 11.5.2, where we also noted that a central force between particles provides a prominent example of a force that respects the third law.

12.9.3 Space isotropy and angular momentum conservation

We now consider the conservation law associated with the isotropy of space. Spatial isotropy means that the mechanical system is invariant under the same rotation of both the positions and velocities for the N particles. Let $\delta\boldsymbol{\phi}$ be an infinitesimal rotation vector and consider the following variation of the Cartesian representations of the particle positions and velocities

$$\delta \boldsymbol{X}_{(i)} = \delta\boldsymbol{\phi} \times \boldsymbol{X}_{(i)} \quad \text{and} \quad \delta \dot{\boldsymbol{X}}_{(i)} = \delta\boldsymbol{\phi} \times \dot{\boldsymbol{X}}_{(i)}, \tag{12.121}$$

which made use of Section 11.2 for how infinitesimal rigid rotations affect changes to vectors. The corresponding variation of the Lagrangian is given by

$$\delta L = \sum_{i=1}^{N} \left[\frac{\partial L}{\partial x^a_{(i)}} \delta x^a_{(i)} + \frac{\partial L}{\partial \dot{x}^a_{(i)}} \delta \dot{x}^a_{(i)} \right] = \sum_{i=1}^{N} \frac{\mathrm{d}}{\mathrm{d}t} \left[\frac{\partial L}{\partial \dot{x}^a_{(i)}} \delta x^a_{(i)} \right], \tag{12.122}$$

where we used the Euler-Lagrange equation (12.75) to reach the second equality. With the kinetic energy in terms of Cartesian coordinates given by equation (12.35), we can introduce the Cartesian component of linear momentum

$$P^a_{(i)} = \frac{\partial L}{\partial \dot{x}^a_{(i)}}, \tag{12.123}$$

in which case the Lagrangian has zero variation under infinitesimal rotations if

$$\sum_{i=1}^{N} \frac{\mathrm{d}}{\mathrm{d}t}\left[P^a_{(i)}\,\delta\dot{x}^a_{(i)}\right] = \delta\boldsymbol{\phi}\cdot\sum_{i=1}^{N}\frac{\mathrm{d}}{\mathrm{d}t}(\boldsymbol{X}_{(i)}\times\boldsymbol{P}_{(i)}) = 0. \tag{12.124}$$

With $\delta\boldsymbol{\phi}$ arbitrary, we are left with conservation of angular momentum for the N particle system

$$\sum_{i=1}^{N}\frac{\mathrm{d}}{\mathrm{d}t}(\boldsymbol{X}_{(i)}\times\boldsymbol{P}_{(i)}) = 0. \tag{12.125}$$

For a space that possesses partial isotropy, that component of angular momentum associated with the isotropy is conserved. This case is particularly relevant for planetary physics, whereby planetary rotation reduces spatial isotropy to just that of the rotational axis (see Section 14.5.1).

12.9.4 Time homogeneity and Hamiltonian evolution

Time homogeneity

We now consider how a mechanical system behaves under a shift in time, $t \to t+\epsilon$, while keeping the generalized positions and generalized velocities unchanged. In this case the Lagrangian becomes

$$L(\boldsymbol{\xi},\dot{\boldsymbol{\xi}},t+\epsilon) \approx L(\boldsymbol{\xi},\dot{\boldsymbol{\xi}},t) + \epsilon\,\partial_t L \implies \delta L = \epsilon\,\partial_t L. \tag{12.126}$$

Hence, for a mechanical system to manifest time homogeneity the Lagrangian must have no explicit time dependence,

$$\left[\frac{\partial L}{\partial t}\right]_{\xi^\sigma,\dot{\xi}^\sigma} = 0 \iff \text{time symmetry.} \tag{12.127}$$

Derivation of the Hamiltonian evolution

The total time derivative of the Lagrangian (following equation (12.50)) takes on the form

$$\frac{\mathrm{d}L}{\mathrm{d}t} - \left[\frac{\partial L}{\partial t}\right]_{\xi^\sigma,\dot{\xi}^\sigma} = \sum_{\sigma=1}^{D}\left[\dot{\xi}^\sigma\,\frac{\partial L}{\partial \xi^\sigma} + \ddot{\xi}^\sigma\,\frac{\partial L}{\partial\dot{\xi}^\sigma}\right] \tag{12.128a}$$

$$= \sum_{\sigma=1}^{D}\left[\dot{\xi}^\sigma\,\frac{\mathrm{d}}{\mathrm{d}t}\frac{\partial L}{\partial\dot{\xi}^\sigma} + \ddot{\xi}^\sigma\,\frac{\partial L}{\partial\dot{\xi}^\sigma}\right] \tag{12.128b}$$

$$= \sum_{\sigma=1}^{D}\frac{\mathrm{d}}{\mathrm{d}t}\left[\dot{\xi}^\sigma\,\frac{\partial L}{\partial\dot{\xi}^\sigma}\right], \tag{12.128c}$$

where the second equality used the Euler-Lagrange equation (12.75). We are thus led to

$$\frac{\mathrm{d}H}{\mathrm{d}t} = -\left[\frac{\partial L}{\partial t}\right]_{\xi^\sigma,\dot{\xi}^\sigma} \quad\text{with}\quad H = \left[\sum_{\sigma=1}^{D}\dot{\xi}^\sigma\,\frac{\partial L}{\partial\dot{\xi}^\sigma} - L\right], \tag{12.129}$$

where H is known as the *Hamiltonian*. Evidently, if there is no explicit time dependence in the Lagrangian then the Hamiltonian is a constant of the motion

$$\left[\frac{\partial L}{\partial t}\right]_{\xi^\sigma,\dot{\xi}^\sigma} = 0 \implies \frac{\mathrm{d}H}{\mathrm{d}t} = 0. \tag{12.130}$$

Connecting the Hamiltonian to the mechanical energy

From Section 12.5.7 we wrote the kinetic energy in terms of generalized coordinates. In the special case of a time independent transformation between Cartesian and generalized coordinates, the kinetic energy is given by equation (12.55)

$$K = \frac{m}{2} \sum_{\sigma=1}^{D} \sum_{\mu=1}^{D} G_{\sigma\mu}(\boldsymbol{\xi}) \, \dot{\xi}^{\sigma} \, \dot{\xi}^{\mu}. \tag{12.131}$$

We thus find

$$\frac{\partial L}{\partial \dot{\xi}^{\nu}} = \frac{\partial K}{\partial \dot{\xi}^{\nu}} = \frac{m}{2} \sum_{\sigma=1}^{D} \sum_{\mu=1}^{D} G_{\sigma\mu} \left(\delta^{\sigma}_{\nu} \, \dot{\xi}^{\mu} + \delta^{\mu}_{\nu} \, \dot{\xi}^{\sigma} \right) = m \sum_{\sigma=1}^{D} G_{\sigma\nu} \, \dot{\xi}^{\sigma}, \tag{12.132}$$

where we used $G_{\sigma\mu} = G_{\mu\sigma}$ for the final equality. In this case, the Hamiltonian equals to the total mechanical energy

$$H = \sum_{\nu=1}^{D} \dot{\xi}^{\nu} \frac{\partial L}{\partial \dot{\xi}^{\nu}} - L = m \sum_{\nu=1}^{D} \sum_{\sigma=1}^{D} G_{\sigma\nu} \, \dot{\xi}^{\nu} \, \dot{\xi}^{\sigma} - \frac{m}{2} \sum_{\nu=1}^{D} \sum_{\sigma=1}^{D} G_{\sigma\nu} \, \dot{\xi}^{\nu} \, \dot{\xi}^{\sigma} + P = K + P, \tag{12.133}$$

which is the familiar form of mechanical energy found in our study of energetics in Newtonian mechanics from Section 11.1.5.

Further distinguishing the Hamiltonian and the mechanical energy

We emphasize that the Hamiltonian is a constant of the motion if the Lagrangian has no explicit time dependence; e.g., equation (12.130). However, the Hamiltonian equals to the mechanical energy only if there is a time independent coordinate transformation between Cartesian and generalized coordinates. Typically $\partial_t L = 0$ means that $\partial_t \boldsymbol{X}_{(i)} = 0$. However, such is not always that case (e.g., see page 82 of *Fetter and Walecka* (2003)). So when $\partial_t L = 0$ but $\partial_t \boldsymbol{X}_{(i)} \neq 0$, the Hamiltonian remains a constant of the motion, but the mechanical energy is time dependent. Hence, we must qualify our earlier statement that time homogeneity leads to a constant mechanical energy. The more precise statement is that the Hamiltonian is a constant of the motion when time does not explicitly appear in the Lagrangian; however, the Hamiltonian is equal to the mechanical energy only if there is a time independent relation between Cartesian coordinates and generalized coordinates.

12.9.5 Further study

Conservation laws and symmetries in classical mechanics are lucidly discussed in Chapters 1 and 2 of *Landau and Lifshitz* (1976). Pedagogical presentations on these topics can be found in this online lecture from the Space Time series and this online lecture from Physics with Elliot. This essay about Emmy Noether provides insights into this mathematician whose work, conducted under some very unfortunate circumstances, forever connected symmetry and conservation laws, with this connection providing the basis for nearly all modern theories of physics.

12.10 Hamiltonian mechanics

In this section we develop the rudiments of *Hamiltonian mechanics*, which is related to Lagrangian mechanics through a Legendre transformation.[12]

[12] We also encounter Legendre transformations in our study of thermodynamics in Part IV of this book.

12.10.1 Generalized momenta

Define the *generalized momenta*, also known as the *canonical momenta*, according to

$$\mathcal{P}_\sigma \equiv \frac{\partial L}{\partial \dot{\xi}^\sigma} = \mathcal{P}_\sigma(\boldsymbol{\xi}, \dot{\boldsymbol{\xi}}, t), \tag{12.134}$$

where the functional dependence is inherited from the Lagrangian. Also note the care in placing the σ index downstairs in the covariant position, which is quite useful in the following. With the generalized momenta, the Euler-Lagrange equations (12.75) take the form

$$\dot{\mathcal{P}}_\sigma = \frac{\partial L}{\partial \xi^\sigma}. \tag{12.135}$$

Evidently, if the Lagrangian has no explicit dependence on a particular generalized coordinate, then the corresponding generalized momenta is a constant of the motion. Such generalized coordinates are termed *cyclic*, and we more to say about cyclic coordinates in Section 12.10.5.

12.10.2 Legendre transformation

In terms of the generalized momenta, the Hamiltonian function (12.130) is written

$$H = -L + \sum_{\sigma=1}^{D} \dot{\xi}^\sigma \, \mathcal{P}_\sigma. \tag{12.136}$$

This definition of the Hamiltonian represents a *Legendre transformation* from the Lagrangian to the Hamiltonian, whereby we swap around some of the functional dependence. Namely, we already know that the Lagrangian has functional dependence on generalized coordinates, generalized velocities, and time. In this subsection we show that the Hamiltonian is a functional of the generalized coordinates, generalized momenta, and time. We say that the Legendre transformation (12.136) moves from the configuration space of Lagrangian mechanics to the *phase space* of *Hamiltonian mechanics*.

Exact differential of the Hamiltonian

The Lagrangian functional dependence (12.49)

$$L = L(\boldsymbol{\xi}, \dot{\boldsymbol{\xi}}, t), \tag{12.137}$$

leads to the exact differential of the Hamiltonian (12.136)

$$\mathrm{d}H = -\frac{\partial L}{\partial t}\,\mathrm{d}t + \sum_{\sigma=1}^{D}\left[-\frac{\partial L}{\partial \xi^\sigma}\,\mathrm{d}\xi^\sigma - \frac{\partial L}{\partial \dot{\xi}^\sigma}\,\mathrm{d}\dot{\xi}^\sigma + \mathcal{P}_\sigma\,\mathrm{d}\dot{\xi}^\sigma + \dot{\xi}^\sigma\,\mathrm{d}\mathcal{P}_\sigma\right]. \tag{12.138}$$

With the generalized momenta given by equation (12.134), the exact differential reduces to

$$\mathrm{d}H = -\frac{\partial L}{\partial t}\,\mathrm{d}t + \sum_{\sigma=1}^{D}\left[-\frac{\partial L}{\partial \xi^\sigma}\,\mathrm{d}\xi^\sigma + \dot{\xi}^\sigma\,\mathrm{d}\mathcal{P}_\sigma\right]. \tag{12.139}$$

This relation means that the Hamiltonian has the following functional dependence

$$H = H(\xi^1, ..., \xi^D, \mathcal{P}_1, ..., \mathcal{P}_D, t). \tag{12.140}$$

Namely, the Hamiltonian is a functional of the generalized coordinates, generalized momenta, and a (possibly) explicit function of time. Furthermore, as for the Lagrangian function, the Hamiltonian is an implicit function of time as realized through time dependence to the generalized coordinates and generalized momenta.

Relations between partial derivatives

The functional dependence (12.140) means that the exact differential of the Hamiltonian is given by

$$\mathrm{d}H = \left[\frac{\partial H}{\partial t}\right]_{\xi^\sigma,\mathrm{P}_\sigma} \mathrm{d}t + \sum_{\sigma=1}^{D} \left(\left[\frac{\partial H}{\partial \xi^\sigma}\right]_{\mathcal{P}_\sigma,t} \mathrm{d}\xi^\sigma + \left[\frac{\partial H}{\partial \mathcal{P}_\sigma}\right]_{\xi^\sigma,t} \mathrm{d}\mathcal{P}_\sigma \right), \tag{12.141}$$

which is equal also to equation (12.139), here rewritten as

$$\mathrm{d}H = -\left[\frac{\partial L}{\partial t}\right]_{\xi^\sigma,\dot{\xi}^\sigma} \mathrm{d}t + \sum_{\sigma=1}^{D} \left(-\left[\frac{\partial L}{\partial \xi^\sigma}\right]_{\dot{\xi}^\sigma,t} \mathrm{d}\xi^\sigma + \dot{\xi}^\sigma \,\mathrm{d}\mathcal{P}_\sigma \right). \tag{12.142}$$

In both equations (12.141) and (12.142) we exposed subscripts on the partial derivatives to be clear on what coordinates are held fixed when computing the derivatives. Equating terms between equations (12.141) and (12.142) leads to

$$\left[\frac{\partial H}{\partial t}\right]_{\xi^\sigma,\mathrm{P}_\sigma} = -\left[\frac{\partial L}{\partial t}\right]_{\xi^\sigma,\dot{\xi}^\sigma} \tag{12.143a}$$

$$\left[\frac{\partial H}{\partial \xi^\sigma}\right]_{\mathcal{P}_\sigma,t} = -\left[\frac{\partial L}{\partial \xi^\sigma}\right]_{\dot{\xi}^\sigma,t} \tag{12.143b}$$

$$\left[\frac{\partial H}{\partial \mathcal{P}_\sigma}\right]_{\xi^\sigma,t} = \frac{\mathrm{d}\xi^\sigma}{\mathrm{d}t}. \tag{12.143c}$$

12.10.3 Hamilton's equations of motion

The manipulations in Section 12.10.2 are mathematical identities that arise from the functional dependencies of the Lagrangian and Hamiltonian, and the Legendre transformation (12.136). We return to physics by assuming the Lagrangian satisfies the Euler-Lagrange equations as written in the form (12.135)

$$\dot{\mathcal{P}}_\sigma = \left[\frac{\partial L}{\partial \xi^\sigma}\right]_{\dot{\xi}^\sigma,t}, \tag{12.144}$$

which brings the exact differential (12.142) to

$$\mathrm{d}H = \left[\frac{\partial H}{\partial t}\right]_{\xi^\sigma,\mathrm{P}_\sigma} \mathrm{d}t + \sum_{\sigma=1}^{D} \left(-\dot{\mathcal{P}}_\sigma \,\mathrm{d}\xi^\sigma + \dot{\xi}^\sigma \,\mathrm{d}\mathcal{P}_\sigma \right). \tag{12.145}$$

We are thus led to *Hamilton's equations of motion*

$$\dot{\mathcal{P}}_\sigma = \frac{\mathrm{d}\mathcal{P}_\sigma}{\mathrm{d}t} = -\left[\frac{\partial H}{\partial \xi^\sigma}\right]_{\mathcal{P}_\sigma,t} \tag{12.146a}$$

$$\dot{\xi}^\sigma = \frac{\mathrm{d}\xi^\sigma}{\mathrm{d}t} = \left[\frac{\partial H}{\partial \mathcal{P}_\sigma}\right]_{\xi^\sigma,t}, \tag{12.146b}$$

which are $2\,D$ first order differential equations for the time derivatives of the generalized coordinates and generalized momenta. These equations are to be compared to the Euler-

Lagrange equations (12.75), which are D second order differential equations for the generalized coordinates.

As a result of Hamilton's equations (12.146a) and (12.146b), we can readily compute the time derivative of the Hamiltonian

$$\frac{\mathrm{d}H}{\mathrm{d}t} = \left[\frac{\partial H}{\partial t}\right]_{\xi^\sigma,\mathrm{P}_\sigma} + \sum_{\sigma=1}^{D}\left(\left[\frac{\partial H}{\partial \xi^\sigma}\right]_{\mathcal{P}_\sigma,t}\dot{\xi}^\sigma + \left[\frac{\partial H}{\partial \mathcal{P}_\sigma}\right]_{\xi^\sigma,t}\dot{\mathcal{P}}_\sigma\right) \tag{12.147a}$$

$$= \left[\frac{\partial H}{\partial t}\right]_{\xi^\sigma,\mathrm{P}_\sigma} + \sum_{\sigma=1}^{D}\left(-\dot{\mathcal{P}}_\sigma\,\dot{\xi}^\sigma + \dot{\mathcal{P}}_\sigma\,\dot{\xi}^\sigma\right) \tag{12.147b}$$

$$= \left[\frac{\partial H}{\partial t}\right]_{\xi^\sigma,\mathrm{P}_\sigma} \tag{12.147c}$$

$$= -\left[\frac{\partial L}{\partial t}\right]_{\xi^\sigma,\dot{\xi}^\sigma}, \tag{12.147d}$$

where the final equality follows from equation (12.129). Evidently, the Hamiltonian is a constant of the motion if it has no explicit time dependence. This result corresponds to Noether's theorem as discussed in Section 12.9.4.

12.10.4 Operational steps

When deriving Hamilton's equations of motion for a particular physical problem, we typically start by writing down the Lagrangian and then using the Legendre transformation (12.136) to derive the Hamiltonian. Before performing the partial derivatives in Hamilton's equations (12.147c)-(12.146b), it is essential to express the Hamiltonian as a function of the generalized coordinates and generalized momenta. Doing so requires removing all appearances of the generalized velocity in favor of the generalized momenta.

In much of this section, we exposed subscripts on the partial derivatives to identify what variables are held fixed when taking the derivatives. Such care is important for developing a proper understanding of the equations and their manipulation. We also found such care important for developing Lagrangian mechanics earlier in this chapter. For both formulations, some exposure to the methodology readily allows one to dispense with the extra clutter of the subscripts. Even so, it can be quite valuable to expose the subscripts when debugging any particular formulation.

12.10.5 Cyclic versus ignorable coordinates

We commented in Section 12.10.1 that if the Lagrangian is independent of a coordinate, referred to as a *cyclic coordinate*, then its corresponding generalized momenta is a constant of the motion. Even so, the corresponding generalized velocity is not necessarily zero and so it cannot be ignored. However, in the Hamiltonian formulation we can ignore a cyclic coordinate since the generalized momenta now a time-independent parameter of the Hamiltonian. As such, there is no corresponding equation of motion. We thus find the Hamiltonian dynamical system has two less degrees of freedom, one for the cyclic coordinate and one for the corresponding constant generalized momenta, thus motivating the name *ignorable coordinate* when a cyclic coordinate is encountered in the Hamiltonian formulation.

12.10.6 Modified Hamilton's principle

Hamilton's variational principle in the form of equation (12.75) leads to the Euler-Lagrange equations. We can derive a related variational principle that leads to Hamilton's equations. To

do so, insert the definition of the Hamiltonian from equation (12.136) into the action to render

$$\mathcal{S} = \int_{t_A}^{t_B} L(\xi^\sigma, \dot{\xi}^\sigma, t)\,\mathrm{d}t = \int_{t_A}^{t_B} \left[-H(\xi^\sigma, \mathcal{P}_\sigma, t) + \sum_{\sigma=1}^{D} \dot{\xi}^\sigma\, \mathcal{P}_\sigma \right] \mathrm{d}t. \tag{12.148}$$

We now consider a variation of the generalized coordinates and generalized momenta, in which the action is varied according to

$$\delta\mathcal{S} = \sum_{\sigma=1}^{D} \int_{t_A}^{t_B} \left[-\frac{\partial H}{\partial \xi^\sigma}\,\delta\xi^\sigma - \frac{\partial H}{\partial \mathcal{P}_\sigma}\,\delta\mathcal{P}_\sigma + \delta\dot{\xi}^\sigma\,\mathcal{P}_\sigma + \dot{\xi}^\sigma\,\delta\mathcal{P}_\sigma \right] \mathrm{d}t. \tag{12.149}$$

Variations of the generalized momenta and generalized coordinates are independent. However, variation of the generalized coordinates and generalized velocities are connected just like when deriving the Euler-Lagrange equations in Section 12.6.3. Hence, an integration by parts leads to

$$\int_{t_A}^{t_B} \delta\dot{\xi}^\sigma\,\mathcal{P}_\sigma\,\mathrm{d}t = \int_{t_A}^{t_B} \frac{\mathrm{d}(\delta\xi^\sigma)}{\mathrm{d}t}\,\mathcal{P}_\sigma\,\mathrm{d}t = \int_{t_A}^{t_B} \left[\frac{\mathrm{d}(\delta\xi^\sigma\,\mathcal{P}_\sigma)}{\mathrm{d}t} - \delta\xi^\sigma\,\dot{\mathcal{P}}_\sigma \right] \mathrm{d}t. \tag{12.150}$$

The total time derivative in the final expression vanishes since the coordinate variation vanishes at the initial and final times. We are thus left with the action variation

$$\delta\mathcal{S} = \sum_{\sigma=1}^{D} \int_{t_A}^{t_B} \left[-\left(\dot{\mathcal{P}}_\sigma + \frac{\partial H}{\partial \xi^\sigma} \right) \delta\xi^\sigma + \left(\dot{\xi}^\sigma - \frac{\partial H}{\partial \mathcal{P}_\sigma} \right) \delta\mathcal{P}_\sigma \right] \mathrm{d}t. \tag{12.151}$$

Since $\delta\xi^\sigma$ and $\delta\mathcal{P}_\sigma$ are independent, we realize a stationary action if and only if Hamilton's equations are satisfied

$$\dot{\xi}^\sigma = \frac{\partial H}{\partial \mathcal{P}_\sigma} \quad \text{and} \quad \dot{\mathcal{P}}_\sigma = -\frac{\partial H}{\partial \xi^\sigma}. \tag{12.152}$$

12.10.7 Incompressible motion in phase space

Chapter 13

PARTICLE MECHANICS AROUND A ROTATING PLANET

In this chapter we study the mechanics of a point particle of fixed mass that moves around a rotating and massive planet, making use of the Newtonian mechanics from Chapter 11. The motion of a point particle provides a model for objects such as satellites moving around rotating planets. For this analysis, the motion of the planet is prescribed with a fixed kinetic energy and fixed angular momentum around a fixed axis of rotation. Hence, we are concerned just with mechanics of the moving particle.

Our description of the particle is examined from the rigid-body rotating (non-inertial) reference frame (Section 11.4), which is the natural frame for an observer fixed on the planet surface. We generally ignore friction and other non-gravitational forces, so that the only force appearing in an inertial reference frame is that from the gravitational field produced by the massive spherical planet. As discussed in Section 11.4, there are two extra accelerations (planetary centrifugal and planetary Coriolis) that appear when viewing motion from the rigid-body rotating terrestrial reference frame.

CHAPTER GUIDE

This chapter builds from the Newtonian mechanics of Chapter 11, here specializing to the geophysically relevant case of a particle moving around a rotating planet. Introducing the spherical coordinate equations of motion represent a key technical element of this chapter, thus going beyond the Cartesian coordinates used in Chapter 11. The use of spherical coordinates prompts the introduction of basic Cartesian and general tensor algebra as presented in Chapters 1, 3, 4, and Section 4.23. We offer the salient features of tensor technology in this chapter where needed, thus providing a reasonably self-contained presentation.

13.1 The rotating earth

The earth's *angular velocity* is comprised of two main contributions: the spin of the earth about its axis and the orbit of the earth about the sun (see Figure 13.1). Other astronomical motions can be neglected for geophysical fluid mechanics. Therefore, in the course of a single period of 24 hours, or $24 \times 3600 = 86400$ seconds, the earth experiences an angular rotation of $(2\pi + 2\pi/365.24)$ radians. As such, the angular rotation rate is given by

$$\Omega = \frac{2\pi + 2\pi/365.24}{86400\text{s}} = \left[\frac{\pi}{43082}\right] \text{s}^{-1} = 7.2921 \times 10^{-5}\ \text{s}^{-1}. \tag{13.1}$$

The earth's angular velocity, both its direction through the polar axis and its magnitude, is assumed constant in time for purposes of geophysical fluid mechanics

$$\frac{d\boldsymbol{\Omega}}{dt} = 0. \tag{13.2}$$

The angular velocity (13.1) seems quite small. However, a terrestrial reference frame on the earth surface undergoes *rigid-body rotation* with speed

$$U_{\text{rigid-body}}(\phi) = \Omega\, R_e \cos\phi \approx 465\ \text{m s}^{-1} \cos\phi = 1672\ \text{km hr}^{-1} \cos\phi, \tag{13.3}$$

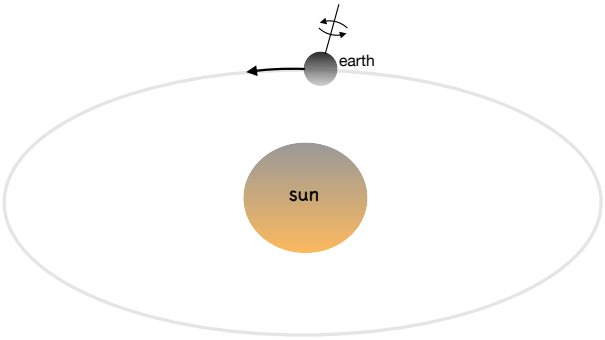

FIGURE 13.1: The angular velocity of the earth arises from the spin about the polar axis plus the orbit of the planet around the sun. This angular velocity determines the strength of the Coriolis acceleration and the planetary centrifugal acceleration. The polar axis has an angle of roughly 23.4° relative to the orbital/ecliptic plane with respect to the sun. This angle is referred to as the *obliquity*, and the obliquity is the reason for the seasonal cycle (e.g., the summer season occurrs in the hemisphere receiving more solar radiation). For an interesting perspective on planetary rotation, see this video from Veritasium.

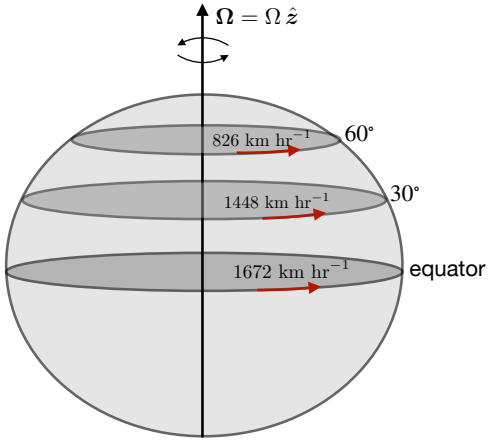

FIGURE 13.2: For an observer at rest on the earth's surface, the rigid-body speed is $\Omega\, R_e \cos\phi = 7.2921 \times 10^{-5}$ s^{-1} $\times\, 6.371 \times 10^6$ m $\cos\phi \approx 465$ m s^{-1} $\cos\phi = 1672$ km hr^{-1} $\cos\phi$. We here display rigid-body speeds for motion at the equator, 30° latitude, and 60° latitude. These speeds are much larger than motion of the ocean and atmosphere relative to the earth, thus motivating a description of geophysical fluid motion from the rotating terrestrial frame moving with the rigid-body.

where we set the earth's radius to

$$R_e = 6.371 \times 10^6 \text{ m}. \tag{13.4}$$

This speed is quite large relative to a fixed frame outside the planet (see Figure 13.2)

$$U_{\text{rigid-body}}(0^\circ) = 1672 \text{ km hr}^{-1} \tag{13.5a}$$
$$U_{\text{rigid-body}}(30^\circ) = 1448 \text{ km hr}^{-1} \tag{13.5b}$$
$$U_{\text{rigid-body}}(60^\circ) = 826 \text{ km hr}^{-1}. \tag{13.5c}$$

Motion of the atmosphere and ocean are generally close to rigid-body motion, so that their speeds relative to the planet are much smaller than the speed of the rotating planet itself. So in addition to being directly relevant to terrestrial observers, we find it most interesting to study geophysical motion in the rotating planetary frame (a non-inertial frame) rather than a frame fixed relative to the stars (an approximate inertial frame).

13.2 Changes to basis vectors under rigid-body rotation

In Section 11.2, we studied the kinematics of a vector with fixed length that is rotating about a fixed origin. The key kinematic result (11.34) exposes how rotation generates a time change to the rigid-body rotation of a vector

$$\frac{\mathrm{d}\boldsymbol{Q}}{\mathrm{d}t} = \boldsymbol{\Omega} \times \boldsymbol{Q}, \tag{13.6}$$

where $\boldsymbol{Q}$ is an arbitrary vector. We here make use of this relation to determine how the basis vectors for Cartesian coordinates, cylindrical-polar coordinates, and spherical coordinates change under rotation.

13.2.1 Changes to Cartesian basis vectors under rotation

With $\boldsymbol{\Omega} = \Omega\,\hat{\boldsymbol{z}}$ as for a rotating spherical earth, equation (13.6) says that the change in planetary Cartesian unit vectors under rigid-body rotation is given by

$$\frac{\mathrm{d}\hat{\boldsymbol{x}}}{\mathrm{d}t} = \boldsymbol{\Omega} \times \hat{\boldsymbol{x}} = \Omega\,\hat{\boldsymbol{y}} \qquad \text{and} \qquad \frac{\mathrm{d}\hat{\boldsymbol{y}}}{\mathrm{d}t} = \boldsymbol{\Omega} \times \hat{\boldsymbol{y}} = -\Omega\,\hat{\boldsymbol{x}} \qquad \text{and} \qquad \frac{\mathrm{d}\hat{\boldsymbol{z}}}{\mathrm{d}t} = \boldsymbol{\Omega} \times \hat{\boldsymbol{z}} = 0. \tag{13.7}$$

13.2.2 Changes to cylindrical-polar coordinate unit vectors under rotation

Now consider the polar coordinates from Section 4.22 with rotation continuing to be oriented about the vertical axis, $\boldsymbol{\Omega} = \Omega\,\hat{\boldsymbol{z}}$. In the horizontal plane we have the radial and angular unit vectors

$$\hat{\boldsymbol{r}} = \hat{\boldsymbol{x}} \cos\vartheta + \hat{\boldsymbol{y}} \sin\vartheta \tag{13.8a}$$

$$\hat{\boldsymbol{\vartheta}} = -\hat{\boldsymbol{x}} \sin\vartheta + \hat{\boldsymbol{y}} \cos\vartheta. \tag{13.8b}$$

We can directly verify that the time derivative of these unit vectors is given by

$$\frac{\mathrm{d}\hat{\boldsymbol{r}}}{\mathrm{d}t} = (\Omega + \dot{\vartheta})\,\hat{\boldsymbol{\vartheta}} = (\Omega + \dot{\vartheta})\,(\hat{\boldsymbol{z}} \times \hat{\boldsymbol{r}}) \tag{13.9a}$$

$$\frac{\mathrm{d}\hat{\boldsymbol{\vartheta}}}{\mathrm{d}t} = -(\Omega + \dot{\vartheta})\,\hat{\boldsymbol{r}} = (\Omega + \dot{\vartheta})\,(\hat{\boldsymbol{z}} \times \hat{\boldsymbol{\vartheta}}). \tag{13.9b}$$

Notice how these unit vectors change both due to the rotation of the reference frame, Ω, plus the change in the angular position relative to the reference frame, $\dot{\vartheta}$. We thus see that unit vectors, such as those for spherical coordinates and cylindrical-polar coordinates, change due to the rigid-body rotation, just like the Cartesian unit vectors. Additionally, non-Cartesian unit vectors change when their orientation is modified relative to the Cartesian coordinate axes at a rate distinct from the rigid-body. This situation occurs when a trajectory moves relative to the rigid-body, with further discussion for spherical coordinates in Sections 13.7.2 and 13.9.

13.2.3 Changes to spherical coordinate unit vectors under rotation

As a third example, consider the rotation of spherical coordinate unit vectors, whose form was derived in Section 4.23.2

$$\hat{\boldsymbol{\lambda}} = -\hat{\boldsymbol{x}} \sin\lambda + \hat{\boldsymbol{y}} \cos\lambda \tag{13.10a}$$

$$\hat{\boldsymbol{\phi}} = -\hat{\boldsymbol{x}} \cos\lambda\, \sin\phi - \hat{\boldsymbol{y}} \sin\lambda\, \sin\phi + \hat{\boldsymbol{z}} \cos\phi \tag{13.10b}$$

$$\hat{\boldsymbol{r}} = \hat{\boldsymbol{x}}\, \cos\lambda\, \cos\phi + \hat{\boldsymbol{y}} \sin\lambda\, \cos\phi + \hat{\boldsymbol{z}} \sin\phi. \tag{13.10c}$$

Again, each of the spherical basis vectors, $(\hat{\boldsymbol{\lambda}}, \hat{\boldsymbol{\phi}}, \hat{\boldsymbol{r}})$, are normalized, so that their evolution arises just from rotations.

Start with deriving the time derivative of the radial unit vector, $\hat{\boldsymbol{r}}$. We know that it can rotate either through rigid-body motion of the rotating reference frame, or through changes in the spherical angles, (λ, ϕ), relative to the rotating reference frame. We see these two forms of time changes by taking the time derivative

$$\frac{\mathrm{d}\hat{\boldsymbol{r}}}{\mathrm{d}t} = \frac{\mathrm{d}}{\mathrm{d}t}(\hat{\boldsymbol{x}}\, \cos\lambda\, \cos\phi + \hat{\boldsymbol{y}} \sin\lambda\, \cos\phi + \hat{\boldsymbol{z}} \sin\phi). \tag{13.11}$$

Expanding the right hand side leads to

$$\frac{\mathrm{d}}{\mathrm{d}t}(\hat{\boldsymbol{x}}\, \cos\lambda\, \cos\phi) = \frac{\mathrm{d}\hat{\boldsymbol{x}}}{\mathrm{d}t} \cos\lambda \cos\phi - \hat{\boldsymbol{x}}\, \dot{\lambda} \sin\lambda \cos\phi - \hat{\boldsymbol{x}}\, \dot{\phi} \cos\lambda \sin\phi \tag{13.12a}$$

$$\frac{\mathrm{d}}{\mathrm{d}t}(\hat{\boldsymbol{y}} \sin\lambda\, \cos\phi) = \frac{\mathrm{d}\hat{\boldsymbol{y}}}{\mathrm{d}t} \sin\lambda \cos\phi + \hat{\boldsymbol{y}}\, \dot{\lambda} \cos\lambda \cos\phi - \hat{\boldsymbol{y}}\, \dot{\phi} \sin\lambda \sin\phi \tag{13.12b}$$

$$\frac{\mathrm{d}}{\mathrm{d}t}(\hat{\boldsymbol{z}} \sin\phi) = \hat{\boldsymbol{z}}\, \dot{\phi} \cos\phi. \tag{13.12c}$$

Making use of equation (13.7) for the change in planetary Cartesian unit vectors due to rotation, and substituting the expressions (4.219a)-(4.219c) for the spherical unit vectors, leads to

$$\frac{\mathrm{d}\hat{\boldsymbol{r}}}{\mathrm{d}t} = \hat{\boldsymbol{\lambda}}\, (\dot{\lambda} + \Omega) \cos\phi + \hat{\boldsymbol{\phi}}\, \dot{\phi}. \tag{13.13}$$

We thus confirm that changes to $\hat{\boldsymbol{r}}$ arise just from changes to its angular orientation. To help understand this expression, take the case of rigid-body motion, in which $\dot{\lambda} = \dot{\phi} = 0$, so that $\hat{\boldsymbol{r}}$ changes only through motion of the rotating reference frame. Any additional longitudinal motion arising from $\dot{\lambda} \neq 0$ renders further changes in the $\hat{\boldsymbol{\lambda}}$ direction. Finally, meridional motion through $\dot{\phi} \neq 0$ modifies the unit vector in the $\hat{\boldsymbol{\phi}}$ direction. Similar manipulations and considerations lead to the time derivatives for the angular unit vectors

$$\frac{\mathrm{d}\hat{\boldsymbol{\phi}}}{\mathrm{d}t} = -\hat{\boldsymbol{\lambda}}\, (\Omega + \dot{\lambda}) \sin\phi - \hat{\boldsymbol{r}}\, \dot{\phi} \tag{13.14a}$$

$$\frac{\mathrm{d}\hat{\boldsymbol{\lambda}}}{\mathrm{d}t} = (\Omega + \dot{\lambda})\, (\hat{\boldsymbol{\phi}} \sin\phi - \hat{\boldsymbol{r}} \cos\phi). \tag{13.14b}$$

Further details for deriving equations (13.13), (13.14a), and (13.14b) are given in the solution to Exercise 13.2.

13.3 A synopsis of tensor algebra

In Part I of this book, we detailed the use of tensor analysis for geophysical motions. We here summarize some of the salient points that are of use in this chapter for manipulating spherical coordinates.

13.3.1 Why we need general tensors

Cartesian tensors are sufficient for many purposes of fluid mechanics, such as when using Cartesian coordinates for a tangent plane approximation to study geophysical fluid motion (e.g., Section 24.5). However, we make routine use of spherical coordinates when describing geophysical motion, and cylindrical-polar coordinates for studies of rotating tank experiments (see Section 36.8). Finally, we use generalized vertical coordinates in the description of stratified flows (Part XII). The basis vectors for curvilinear coordinates and generalized vertical coordinates change

direction when moving through space. In contrast, Cartesian basis vectors always point in the same direction. This distinction between the basis vectors is the key reason curvilinear coordinates and generalized vertical coordinates require a more general formalism than required by Cartesian tensors.

Even though general tensors are of use in this book, we can keep much of the heavy technology at a modest distance, with exposure only in selected places. The key crutch we rely on is that the planet is assumed to be embedded in a background three-dimensional Euclidean space. That is, we are not considering the curved space-time of general relativity nor the marriage of space and time afforded by special relativity. Rather, we restrict our concern to *Galilean relatively*, which is based on three-dimensional Euclidean space plus universal Newtonian time. These assumptions greatly simplify our use of general tensors.

13.3.2 The coordinate representation of a vector

The coordinate representation of a vector follows from decomposing the vector into components aligned according to a set of basis vectors, in which case we write

$$\vec{Q} = \sum_{a=1}^{3} Q^a \, \vec{e}_a = Q^a \, \vec{e}_a, \tag{13.15}$$

where the Einstein summation convention is defined by the final equality. In this equation,

$$\vec{e}_a = (\vec{e}_1, \vec{e}_2, \vec{e}_3) \tag{13.16}$$

is a set of linearly independent basis vectors, and Q^a are the corresponding coordinate representations of the vector $\vec{Q}$. The basis vectors may be normalized to unit magnitude, as in the case of Cartesian coordinates, or may be unnormalized as for spherical coordinates (see Section 4.23.2). Note that we commonly make use of the boldface notation for a vector rather than the arrowed symbol (Section 3.5)

$$\boldsymbol{Q} = \vec{Q} = Q^a \, \vec{e}_a. \tag{13.17}$$

The basis vectors in equation (13.15) have a lower index while the coordinate representation of a vector has an upper index. Why? For arbitrary coordinates (e.g., spherical), we make a distinction between a coordinate representation with an index upstairs (*contravariant*) versus the downstairs (*covariant*) representation. Moving between the covariant and contravariant representations requires a metric tensor.

When working with general coordinates, it is necessary to distinguish between a basis vector, $\vec{e}_a$, and its dual partner known as a *one-form*, $\widetilde{e}^a$. Duality is here defined by the familiar (Euclidean) inner product that leads to the bi-orthogonality relation

$$\vec{e}_a \cdot \widetilde{e}^b = \delta^b_{\ a}, \tag{13.18}$$

with $\delta^b_{\ a}$ the Kronecker delta tensor

$$\delta^b_{\ a} = \begin{cases} 1 & \text{if } b = a \\ 0 & \text{if } b \neq a. \end{cases} \tag{13.19}$$

In linear algebra, a row vector is dual to its column vector, with that analog appropriate for the present context. Cartesian basis vectors equal to the basis one-forms, in which case there is no distinction between contravariant and covariant. However, the distinction is important for more general coordinates used in geophysical fluids.

13.3.3 Generalized coordinates

We find it convenient to write ξ^a as the a'th component of a *generalized coordinate* used to describe space. In this chapter we choose the unbarred generalized coordinates as planetary Cartesian coordinates, so that

$$(\xi^1, \xi^2, \xi^3) = (x, y, z), \tag{13.20}$$

whereas the barred generalized coordinates are the planetary spherical coordinates[1]

$$(\xi^{\overline{1}}, \xi^{\overline{2}}, \xi^{\overline{3}}) = (\lambda, \phi, r). \tag{13.21}$$

These two sets of coordinates are related by the coordinate transformation provided in Section 4.23 (see in particular Figure 4.3)

$$x = r\cos\phi\,\cos\lambda \qquad \text{and} \qquad y = r\cos\phi\,\sin\lambda \qquad \text{and} \qquad z = r\sin\phi. \tag{13.22}$$

The equation set (13.22) provides the coordinate transformation between a particular point in three-dimensional Euclidean space that is represented by Cartesian coordinates and spherical coordinates.

13.3.4 Transformation between coordinate representations

The coordinate representation of a tensor is a subjective analytical description of an objective geometric object. That is, the subjectively chosen coordinate representation of a vector, such as that given by equation (13.15), does not affect the vector as a geometric object. Hence, we can represent the vector using any arbitrary set of coordinates

$$\vec{Q} = Q^a\,\vec{e}_a = Q^{\overline{a}}\,\vec{e}_{\overline{a}}. \tag{13.23}$$

In this equation, $Q^{\overline{a}}$ is the representation of the vector $\vec{Q}$ in a coordinate system defined by the basis vector $\vec{e}_{\overline{a}}$, whereas Q^a is the representation in the unbarred coordinate system with basis vectors $\vec{e}_a$.

The coordinate representation of a vector transforms when changing coordinates. The transformation is mediated by the *transformation matrix*, which is the matrix composed of the partial derivatives of one coordinate set with respect to the other. For example, the relation between the coordinate representation of the velocity vector and acceleration vector, as well as the coordinate basis vectors, are given by

$$V^{\overline{a}} = \Lambda^{\overline{a}}_{\ a}\,V^a \qquad \text{and} \qquad A^{\overline{a}} = \Lambda^{\overline{a}}_{\ a}\,A^a \qquad \text{and} \qquad \vec{e}_{\overline{a}} = \Lambda^{a}_{\ \overline{a}}\,\vec{e}_a. \tag{13.24}$$

The general expression for the transformation matrix is given by the matrix of partial derivatives

$$\Lambda^{a}_{\ \overline{a}} = \begin{bmatrix} \partial\xi^1/\partial\xi^{\overline{1}} & \partial\xi^1/\partial\xi^{\overline{2}} & \partial\xi^1/\partial\xi^{\overline{3}} \\ \partial\xi^2/\partial\xi^{\overline{1}} & \partial\xi^2/\partial\xi^{\overline{2}} & \partial\xi^2/\partial\xi^{\overline{3}} \\ \partial\xi^3/\partial\xi^{\overline{1}} & \partial\xi^3/\partial\xi^{\overline{2}} & \partial\xi^3/\partial\xi^{\overline{3}} \end{bmatrix}. \tag{13.25}$$

For the particular case where the unbarred coordinates are Cartesian and the barred are spherical, we have from Section 4.23.1 the transformation matrix along with its inverse

$$\Lambda^{a}_{\ \overline{a}} = \begin{bmatrix} -r\cos\phi\sin\lambda & -r\sin\phi\,\cos\lambda & \cos\phi\cos\lambda \\ r\cos\phi\cos\lambda & -r\sin\phi\,\sin\lambda & \cos\phi\sin\lambda \\ 0 & r\cos\phi & \sin\phi \end{bmatrix} \tag{13.26}$$

[1] We will have occasion to use other generalized coordinates in this book, with particular attention given to generalized vertical coordinates in Part XII.

$$\Lambda^{\overline{a}}_{\ a} = \frac{1}{r^2 \cos\phi} \begin{bmatrix} -r\sin\lambda & r\cos\lambda & 0 \\ -r\cos\phi\,\sin\phi\,\cos\lambda & -r\cos\phi\sin\phi\sin\lambda & r\cos^2\phi \\ r^2\cos^2\phi\cos\lambda & r^2\,\cos^2\phi\sin\lambda & r^2\cos\phi\sin\phi \end{bmatrix}. \tag{13.27}$$

It is straightforward to verify the orthonormality relations satisfied by these matrices

$$\Lambda^{\overline{a}}_{\ a}\,\Lambda^{a}_{\ \overline{b}} = \delta^{\overline{a}}_{\ \overline{b}} \qquad \text{and} \qquad \Lambda^{a}_{\ \overline{a}}\,\Lambda^{\overline{a}}_{\ b} = \delta^{a}_{\ b}. \tag{13.28}$$

Hence, if we have the Cartesian representation of a vector, such as the velocity or acceleration, then we can use these transformation rules to derive the spherical representation through matrix multiplication, as per equation (13.24).

13.3.5 Two meanings for the same symbol

We highlight the need to hold two meanings in mind for (x, y, z) and (r, λ, ϕ), or for any set of generalized coordinates (ξ^1, ξ^2, ξ^3). One meaning specifies a point in Euclidean space. The other meaning refers to the position in space for a moving material particle, in which case the coordinate position is a function of time. We commonly write the second meaning using the capital, $\boldsymbol{X}(t)$, to denote the particle trajectory. To accord with common usage for the Cartesian and spherical coordinates, we write the components to $\boldsymbol{X}(t)$ using the smaller case, so that the Cartesian position of the particle is

$$\boldsymbol{X}(t) = \hat{\boldsymbol{x}}\, x(t) + \hat{\boldsymbol{y}}\, y(t) + \hat{\boldsymbol{z}}\, z(t), \tag{13.29}$$

whereas the spherical position is

$$\boldsymbol{X}(t) = \hat{\boldsymbol{r}}(t)\, r(t). \tag{13.30}$$

Time dependence of the unit vectors depends on the reference frame. For an inertial reference frame, the Cartesian unit vectors are fixed in space, whereas for the rigid-body rotating frame, the Cartesian basis vectors rotate around the vertical axis. Likewise, the spherical unit vector rotates with the rotating reference frame. Yet even in an inertial reference frame, $\hat{\boldsymbol{r}}$ is a function of time since it points from the origin towards the moving particle.

13.4 The velocity vector

The velocity is the time derivative of the position vector

$$\boldsymbol{V} = \frac{\mathrm{d}\boldsymbol{X}}{\mathrm{d}t}. \tag{13.31}$$

This equation is manifestly geometric in that the velocity at a space-time point is the tangent vector to the trajectory at that point. When expressing this relation using a coordinate representation we note that time dependence lives with both the coordinate representation of the position vector as well as the basis vectors

$$\boldsymbol{V} = \frac{\mathrm{d}\boldsymbol{X}}{\mathrm{d}t} = \frac{\mathrm{d}\,(\xi^a\,\vec{e}_a)}{\mathrm{d}t} = \frac{\mathrm{d}\xi^a}{\mathrm{d}t}\,\vec{e}_a + \xi^a\,\frac{\mathrm{d}\vec{e}_a}{\mathrm{d}t}. \tag{13.32}$$

13.4.1 Coordinate velocity

The first term on the right hand side of equation (13.32) is the velocity as measured within the chosen reference frame using the chosen coordinates

$$\boldsymbol{V}_{\text{coord}} \equiv \frac{\mathrm{d}\xi^a}{\mathrm{d}t}\,\vec{e}_a. \tag{13.33}$$

This is the contribution to velocity as measured in the reference frame that moves with the basis vectors. In the context of geophysical motions, this is the velocity measured in the rotating terrestrial reference frame using Cartesian, spherical, or other chosen coordinates.

13.4.2 Temporal changes to the basis vectors

The second term on the right hand side of equation (13.32) arises from changes to the basis vectors. There are three means for a basis vector to change, and we encounter them when considering coordinate representations later in this chapter. Two changes arise from rotations, each of which change the basis vector's direction without changing its magnitude. The third change leads to a modification of the basis vector's magnitude.

- RIGID-BODY ROTATION: For a rigid-body rotation of the reference frame, the rigid-body velocity is given by (see Section 11.2.2)

$$\boldsymbol{U}_{\text{rigid}} = \boldsymbol{\Omega} \times \boldsymbol{X}. \tag{13.34}$$

- ROTATION RELATIVE TO RIGID-BODY: A vector can also rotate at a rate that differs from the rigid-body.

- CHANGE IN MAGNITUDE: Finally, if the basis vectors are not normalized to have unit magnitude, then they can change their magnitude during motion.

13.5 Decomposition of the inertial frame acceleration

The acceleration measured in an inertial reference frame is given by the time derivative of the velocity measured in this frame, so that the acceleration is the second derivative of the position vector

$$\boldsymbol{A} = \frac{\mathrm{d}\boldsymbol{V}}{\mathrm{d}t} = \frac{\mathrm{d}^2\boldsymbol{X}}{\mathrm{d}t^2}. \tag{13.35}$$

This equation is independent of any coordinate representation so that the physical and geometrical content are manifest. When introducing a coordinate representation, the resulting expression becomes subject to details of the chosen coordinates and those details possibly obscure the underlying geometric meaning. Hence, it is important to keep the geometric expression in mind when offering an interpretation for coordinate dependent terms.

Introducing a coordinate representation $\boldsymbol{X} = \xi^a \, \vec{e}_a$ into the acceleration (13.35), and making use of the chain rule, leads to

$$\begin{aligned}
\boldsymbol{A} &= \frac{\mathrm{d}}{\mathrm{d}t} \frac{\mathrm{d}\boldsymbol{X}}{\mathrm{d}t} && \text{(13.36a)} \\
&= \frac{\mathrm{d}}{\mathrm{d}t} \frac{\mathrm{d}\,(\xi^a \, \vec{e}_a)}{\mathrm{d}t} && \text{(13.36b)} \\
&= \frac{\mathrm{d}}{\mathrm{d}t} \left[\frac{\mathrm{d}\,\xi^a}{\mathrm{d}t} \, \vec{e}_a + \xi^a \, \frac{\mathrm{d}\,\vec{e}_a}{\mathrm{d}t} \right] && \text{(13.36c)} \\
&= \frac{\mathrm{d}^2\xi^a}{\mathrm{d}t^2} \, \vec{e}_a + 2 \, \frac{\mathrm{d}\xi^a}{\mathrm{d}t} \, \frac{\mathrm{d}\vec{e}_a}{\mathrm{d}t} + \xi^a \, \frac{\mathrm{d}^2\vec{e}_a}{\mathrm{d}t^2}. && \text{(13.36d)}
\end{aligned}$$

The first term on the right hand side is the acceleration of the coordinate representation as measured in the rotating reference frame

$$\boldsymbol{A}_{\text{coord}} \equiv \frac{\mathrm{d}^2\xi^a}{\mathrm{d}t^2} \, \vec{e}_a. \tag{13.37}$$

It is the acceleration measured by an observer in the rotating frame using coordinates ξ^a. The remaining two terms arise from changes to the basis vectors, and they give rise to the Coriolis and planetary centrifugal accelerations associated with the rotating reference frame. In non-Cartesian coordinates, they also give rise to a *metric acceleration* arising from the change in directions of the unit vectors associated with motion of the particle relative to the rotating reference frame (Section 13.4.2). Note that the factor of two on the middle term (the Coriolis term) in equation (13.36d) results from the two time derivatives that act on the basis vectors that arise when computing the acceleration. We already encountered this factor of two when deriving the Cartesian expression of the Coriolis acceleration in Section 11.4.3.

13.6 Representing the position vector

We make use of some results from Section 4.23 relating Cartesian and spherical coordinates and as defined by Figure 4.3. In particular, we use the *planetary* Cartesian basis vectors, $(\hat{\boldsymbol{x}}, \hat{\boldsymbol{y}}, \hat{\boldsymbol{z}})$, and corresponding spherical basis vectors, $(\hat{\boldsymbol{\lambda}}, \hat{\boldsymbol{\phi}}, \hat{\boldsymbol{r}})$, thus leading to the coordinate representations of the position vector relative to the center of a rotating sphere

$$\begin{aligned}
\boldsymbol{X} &= x\,\hat{\boldsymbol{x}} + y\,\hat{\boldsymbol{y}} + z\,\hat{\boldsymbol{z}} && \text{(13.38a)}\\
&= (r\cos\phi\,\cos\lambda)\,\hat{\boldsymbol{x}} + (r\cos\phi\,\sin\lambda)\,\hat{\boldsymbol{y}} + (r\sin\phi)\,\hat{\boldsymbol{z}} && \text{(13.38b)}\\
&= r\,\hat{\boldsymbol{r}} && \text{(13.38c)}\\
&= |\boldsymbol{X}|\,\hat{\boldsymbol{r}}. && \text{(13.38d)}
\end{aligned}$$

The expression for the position vector is quite simple when written in spherical coordinates, as it is merely the distance from the origin with a direction that points radially from the origin to the particle.

13.7 Representing the velocity vector

As seen in Section 13.4, the inertial frame velocity vector has a coordinate representation written as

$$\boldsymbol{V} = \frac{\mathrm{d}\boldsymbol{X}}{\mathrm{d}t} = \frac{\mathrm{d}(\xi^a\,\vec{e}_a)}{\mathrm{d}t} = \frac{\mathrm{d}\xi^a}{\mathrm{d}t}\,\vec{e}_a + \xi^a\,\frac{\mathrm{d}\vec{e}_a}{\mathrm{d}t}. \tag{13.39}$$

Contributions arise from both the time changes in the coordinates, ξ^a, and time changes to the basis vectors, $\vec{e}_a$. We now consider the Cartesian and spherical forms for these changes.

13.7.1 Planetary Cartesian coordinate representation

The basis vectors for the Cartesian coordinates, $(\vec{e}_1, \vec{e}_2, \vec{e}_3) = (\hat{\boldsymbol{x}}, \hat{\boldsymbol{y}}, \hat{\boldsymbol{z}})$, are normalized, so they do not change their magnitude. Furthermore, they move only through rigid-body motion of the rotating reference frame. We refer to these coordinates as *planetary Cartesian coordinates* since they are oriented according to the rotating planet with origin at the planet's center. In Section 24.5 we introduce the distinct *tangent plane Cartesian coordinates*. Tangent plane Cartesian coordinates are also moving with the rotating planet. Yet they are defined according to a tangent plane at a point on the surface of the planet. It is important to distinguish these two uses for Cartesian coordinates in geophysical fluid mechanics.

The angular velocity is oriented around the polar axis

$$\boldsymbol{\Omega} = \Omega\,\hat{\boldsymbol{z}}, \tag{13.40}$$

so that the rigid-body velocity of the rotating reference frame only has components in the $\hat{\boldsymbol{x}}$ and

$\hat{\boldsymbol{y}}$ directions

$$\boldsymbol{U}_{\text{rigid}} = \boldsymbol{\Omega} \times \boldsymbol{X} = \Omega\,(-\hat{\boldsymbol{x}}\,y + \hat{\boldsymbol{y}}\,x). \tag{13.41}$$

The inertial frame velocity thus has the following representation in terms of planetary Cartesian coordinates

$$\begin{aligned}
\boldsymbol{V} &= \frac{\mathrm{d}}{\mathrm{d}t}\left[\hat{\boldsymbol{x}}\,x + \hat{\boldsymbol{y}}\,y + \hat{\boldsymbol{z}}\,z\right] && \text{(13.42a)}\\
&= \left[\hat{\boldsymbol{x}}\,\frac{\mathrm{d}x}{\mathrm{d}t} + \hat{\boldsymbol{y}}\,\frac{\mathrm{d}y}{\mathrm{d}t} + \hat{\boldsymbol{z}}\,\frac{\mathrm{d}z}{\mathrm{d}t}\right] + x\,\frac{\mathrm{d}\hat{\boldsymbol{x}}}{\mathrm{d}t} + y\,\frac{\mathrm{d}\hat{\boldsymbol{y}}}{\mathrm{d}t} + z\,\frac{\mathrm{d}\hat{\boldsymbol{z}}}{\mathrm{d}t} && \text{(13.42b)}\\
&= \left[-y\,\Omega + \frac{\mathrm{d}x}{\mathrm{d}t}\right]\hat{\boldsymbol{x}} + \left[x\,\Omega + \frac{\mathrm{d}y}{\mathrm{d}t}\right]\hat{\boldsymbol{y}} + \frac{\mathrm{d}z}{\mathrm{d}t}\,\hat{\boldsymbol{z}} && \text{(13.42c)}\\
&= \boldsymbol{V}_{\text{Cartesian}} + \boldsymbol{\Omega} \times \boldsymbol{X} && \text{(13.42d)}\\
&= \boldsymbol{V}_{\text{Cartesian}} + \boldsymbol{U}_{\text{rigid}}, && \text{(13.42e)}
\end{aligned}$$

where we defined the Cartesian velocity vector

$$\boldsymbol{V}_{\text{Cartesian}} \equiv \frac{\mathrm{d}x}{\mathrm{d}t}\,\hat{\boldsymbol{x}} + \frac{\mathrm{d}y}{\mathrm{d}t}\,\hat{\boldsymbol{y}} + \frac{\mathrm{d}z}{\mathrm{d}t}\,\hat{\boldsymbol{z}}, \tag{13.43}$$

which is the velocity as measured in the rotating reference frame when using planetary Cartesian coordinates. We also made use of equation (13.7) to express the time rate of change for the planetary Cartesian unit vectors, with this change arising solely from the planetary rotation. Note that the results here are valid for $\boldsymbol{\Omega}$ varying in time.

13.7.2 Planetary spherical coordinate representation

The position vector in the planetary spherical coordinate representation is given by

$$\boldsymbol{X} = r\,\hat{\boldsymbol{r}}. \tag{13.44}$$

The basis vector $\hat{\boldsymbol{r}}$ is normalized, so that its evolution arises just from rotations, and we determined that time evolution in equation (13.13)

$$\frac{\mathrm{d}\hat{\boldsymbol{r}}}{\mathrm{d}t} = \hat{\boldsymbol{\lambda}}\,(\dot{\lambda} + \Omega)\cos\phi + \hat{\boldsymbol{\phi}}\,\dot{\phi}. \tag{13.45}$$

Consequently, the velocity as viewed in the inertial frame has the following spherical coordinate representation

$$\begin{aligned}
\boldsymbol{V} &= \frac{\mathrm{d}\boldsymbol{X}}{\mathrm{d}t} && \text{(13.46a)}\\
&= \frac{\mathrm{d}(r\,\hat{\boldsymbol{r}})}{\mathrm{d}t} && \text{(13.46b)}\\
&= r\,\frac{\mathrm{d}\hat{\boldsymbol{r}}}{\mathrm{d}t} + \frac{\mathrm{d}r}{\mathrm{d}t}\,\hat{\boldsymbol{r}} && \text{(13.46c)}\\
&= r_\perp\,(\dot{\lambda} + \Omega)\,\hat{\boldsymbol{\lambda}} + r\,\dot{\phi}\,\hat{\boldsymbol{\phi}} + \dot{r}\,\hat{\boldsymbol{r}} && \text{(13.46d)}\\
&= (u + r_\perp\,\Omega)\,\hat{\boldsymbol{\lambda}} + v\,\hat{\boldsymbol{\phi}} + w\,\hat{\boldsymbol{r}} && \text{(13.46e)}\\
&= \boldsymbol{V}_{\text{spherical}} + \boldsymbol{U}_{\text{rigid}}. && \text{(13.46f)}
\end{aligned}$$

In this equation we introduced the spherical coordinate velocity vector

$$\boldsymbol{V}_{\text{spherical}} = r_\perp\,\dot{\lambda}\,\hat{\boldsymbol{\lambda}} + r\,\dot{\phi}\,\hat{\boldsymbol{\phi}} + \dot{r}\,\hat{\boldsymbol{r}} \equiv u\,\hat{\boldsymbol{\lambda}} + v\,\hat{\boldsymbol{\phi}} + w\,\hat{\boldsymbol{r}}, \tag{13.47}$$

where we defined the components to the spherical velocity vector

$$u \equiv r_\perp \frac{\mathrm{d}\lambda}{\mathrm{d}t} \qquad \text{and} \qquad v \equiv r \frac{\mathrm{d}\phi}{\mathrm{d}t} \qquad \text{and} \qquad w \equiv \frac{\mathrm{d}r}{\mathrm{d}t}, \tag{13.48}$$

and with

$$r_\perp = |\boldsymbol{X}| \cos\phi = r \cos\phi \tag{13.49}$$

the distance to the polar axis. The spherical velocity, $\boldsymbol{V}_{\text{spherical}}$, is the velocity measured in the rotating reference frame when using planetary spherical coordinates. We also noted that the rigid-body velocity has the spherical coordinate representation

$$\boldsymbol{U}_{\text{rigid}} = \boldsymbol{\Omega} \times \boldsymbol{X} = r_\perp \, \Omega \, \hat{\boldsymbol{\lambda}}. \tag{13.50}$$

That is, the rigid-body velocity is purely zonal.

13.7.3 Transforming from Cartesian to spherical

We make use of the tensor analysis from Section 13.3 to transform from the Cartesian representation of the velocity vector to the spherical representation. This approach leads to an equivalent result to that pursued thus far in this section, but it is somewhat more systematic and it offers useful experience with the formalities of coordinate transformations. In particular, we make use of the transformation rule (13.24) along with the transformation matrix (13.26) and its inverse (13.27) to have

$$V^{\overline{1}} = V^r = \Lambda^{\overline{1}}_{\ 1} \, V^1 + \Lambda^{\overline{1}}_{\ 2} \, V^2 + \Lambda^{\overline{1}}_{\ 3} \, V^3 \tag{13.51a}$$

$$V^{\overline{2}} = V^\lambda = \Lambda^{\overline{2}}_{\ 1} \, V^1 + \Lambda^{\overline{2}}_{\ 2} \, V^2 + \Lambda^{\overline{2}}_{\ 3} \, V^3 \tag{13.51b}$$

$$V^{\overline{3}} = V^\phi = \Lambda^{\overline{3}}_{\ 1} \, V^1 + \Lambda^{\overline{3}}_{\ 2} \, V^2 + \Lambda^{\overline{3}}_{\ 3} \, V^3, \tag{13.51c}$$

where the Cartesian components are

$$V^1 = \dot{x} - \Omega \, y = \dot{r} \cos\phi \cos\lambda - r \, \dot{\phi} \sin\phi \cos\lambda - r \, (\dot{\lambda} + \Omega) \cos\phi \sin\lambda \tag{13.52a}$$

$$V^2 = \dot{y} + \Omega \, x = \dot{r} \cos\phi \sin\lambda - r \, \dot{\phi} \sin\phi \sin\lambda + r \, (\dot{\lambda} + \Omega) \cos\phi \cos\lambda \tag{13.52b}$$

$$V^3 = \dot{z} = \dot{r} \sin\phi + r \, \dot{\phi} \cos\phi. \tag{13.52c}$$

Making use of the inverse transformation matrix components $\Lambda^{\overline{a}}_{\ b}$ given by equation (13.27), as well as the relation (13.24) between the coordinate basis vectors, leads to

$$\vec{V} = \boldsymbol{V} = V^{\overline{a}} \, \vec{e}_{\overline{a}} = r_\perp \, (\dot{\lambda} + \Omega) \, \hat{\boldsymbol{\lambda}} + r \, \dot{\phi} \, \hat{\boldsymbol{\phi}} + \dot{r} \, \hat{\boldsymbol{r}}, \tag{13.53}$$

which is the same as equation (13.46f) determined without the formalism of tensor algebra.

13.7.4 Axial angular momentum

As seen in Section 14.5, the zonal component of the inertial frame velocity, times the *moment arm* (distance from the rotation axis), equals to the axial angular momentum per unit mass

$$L^z = m \, r_\perp \, \hat{\boldsymbol{\lambda}} \cdot \boldsymbol{V} = m \, r_\perp \, (u + r_\perp \, \Omega). \tag{13.54}$$

The distance to the rotational axis is given by $r_\perp$, and this is the moment arm for the axial angular momentum. For cases with rotational symmetry around polar axis, as for motion of a particle around a smooth sphere, the axial angular momentum is a constant of the motion. As

discussed in Section 14.5, this conservation law provides a constraint on the particle trajectory and it plays a role in the motion of geophysical fluids (Section 24.7).

13.8 Planetary Cartesian representation of acceleration

The acceleration measured in an inertial reference frame is given by the second time derivative of the position vector

$$\boldsymbol{A} = \frac{\mathrm{d}\boldsymbol{V}}{\mathrm{d}t} = \frac{\mathrm{d}^2\boldsymbol{X}}{\mathrm{d}t^2}. \tag{13.55}$$

We here consider its representation using planetary Cartesian coordinates (x, y, z) and the Cartesian basis $(\vec{e}_1, \vec{e}_2, \vec{e}_3) = (\hat{\boldsymbol{x}}, \hat{\boldsymbol{y}}, \hat{\boldsymbol{z}})$. The results here were anticipated by the discussion in Section 11.4.3. We find it useful to go through the derivation again, here with more focus on the geophysical applications of this book.

13.8.1 Planetary Cartesian representation

For the study of geophysical fluid motion, we assume the planetary angular velocity, $\boldsymbol{\Omega}$, is a constant in time

$$\frac{\mathrm{d}\boldsymbol{\Omega}}{\mathrm{d}t} = 0. \tag{13.56}$$

Making use of the results from Section 13.2.1 leads to

$$\frac{\mathrm{d}\vec{e}_a}{\mathrm{d}t} = \boldsymbol{\Omega} \times \vec{e}_a \tag{13.57}$$

and

$$\frac{\mathrm{d}^2\vec{e}_a}{\mathrm{d}t^2} = \frac{\mathrm{d}}{\mathrm{d}t}\left(\boldsymbol{\Omega} \times \vec{e}_a\right) = \boldsymbol{\Omega} \times \frac{\mathrm{d}\vec{e}_a}{\mathrm{d}t} = \boldsymbol{\Omega} \times \left(\boldsymbol{\Omega} \times \vec{e}_a\right), \tag{13.58}$$

which yields the acceleration

$$\begin{aligned}
\boldsymbol{A} &= \frac{\mathrm{d}}{\mathrm{d}t}\frac{\mathrm{d}\boldsymbol{X}}{\mathrm{d}t} && \text{(13.59a)}\\
&= \frac{\mathrm{d}^2\xi^a}{\mathrm{d}t^2}\,\vec{e}_a + 2\,\frac{\mathrm{d}\xi^a}{\mathrm{d}t}\left(\boldsymbol{\Omega} \times \vec{e}_a\right) + \xi^a\,\boldsymbol{\Omega} \times \left(\boldsymbol{\Omega} \times \vec{e}_a\right) && \text{(13.59b)}\\
&= \hat{\boldsymbol{x}}\left[\ddot{x} - 2\,\Omega\,\dot{y} - \Omega^2 x\right] + \hat{\boldsymbol{y}}\left[\ddot{y} + 2\,\Omega\,\dot{x} - \Omega^2 y\right] + \hat{\boldsymbol{z}}\,\ddot{z} && \text{(13.59c)}\\
&= \ddot{x}\,\hat{\boldsymbol{x}} + \ddot{y}\,\hat{\boldsymbol{y}} + \ddot{z}\,\hat{\boldsymbol{z}} + 2\,\Omega\left(-\dot{y}\,\hat{\boldsymbol{x}} + \dot{x}\,\hat{\boldsymbol{y}}\right) - \Omega^2\left(x\,\hat{\boldsymbol{x}} + y\,\hat{\boldsymbol{y}}\right) && \text{(13.59d)}\\
&= \boldsymbol{A}_{\text{Cartesian}} + 2\,\boldsymbol{\Omega} \times \boldsymbol{V}_{\text{Cartesian}} + \boldsymbol{\Omega} \times \left(\boldsymbol{\Omega} \times \boldsymbol{X}\right) && \text{(13.59e)}\\
&= \boldsymbol{A}_{\text{Cartesian}} - \boldsymbol{A}_{\text{Coriolis}} - \boldsymbol{A}_{\text{centrifugal}}. && \text{(13.59f)}
\end{aligned}$$

The acceleration is thus decomposed into three terms that we now discuss.

Coordinate acceleration in the rotating reference frame

The first acceleration on the right hand side of equation (13.59f) is

$$\boldsymbol{A}_{\text{Cartesian}} = \frac{\mathrm{d}^2x}{\mathrm{d}t^2}\,\hat{\boldsymbol{x}} + \frac{\mathrm{d}^2y}{\mathrm{d}t^2}\,\hat{\boldsymbol{y}} + \frac{\mathrm{d}^2z}{\mathrm{d}t^2}\,\hat{\boldsymbol{z}} = \ddot{x}\,\hat{\boldsymbol{x}} + \ddot{y}\,\hat{\boldsymbol{y}} + \ddot{z}\,\hat{\boldsymbol{z}}, \tag{13.60}$$

which is the coordinate acceleration measured in the rotating frame using planetary Cartesian coordinates.

Planetary Coriolis acceleration

The second term on the right hand side of equation (13.59f) is the planetary Coriolis acceleration

$$\boldsymbol{A}_{\text{Coriolis}} = -2\,\boldsymbol{\Omega} \times \boldsymbol{V}_{\text{Cartesian}}. \tag{13.61}$$

One key feature of the Coriolis acceleration is that it vanishes when there is no motion relative to the rotating reference frame. The Coriolis acceleration plays a fundamental role in geophysical fluid mechanics and is central to our studies in this book.

Planetary centrifugal/centripetal acceleration

The third contribution to acceleration in equation (13.59f) is the planetary *centrifugal acceleration*, which is also minus the planetary *centripetal acceleration*

$$\boldsymbol{A}_{\text{centrifugal}} = -\boldsymbol{A}_{\text{centripetal}} = -\boldsymbol{\Omega} \times (\boldsymbol{\Omega} \times \boldsymbol{X}). \tag{13.62}$$

The planetary centrifugal acceleration points outward from (perpendicular to) the polar axis of rotation whereas the planetary centripetal acceleration points inward; they are action/reaction pairs. They can be written as the gradient of a scalar potential

$$\boldsymbol{A}_{\text{centrifugal}} = -\nabla \Phi_{\text{centrifugal}} \tag{13.63}$$

with

$$-\Phi_{\text{centrifugal}} \equiv \frac{(\boldsymbol{\Omega} \times \boldsymbol{x}) \cdot (\boldsymbol{\Omega} \times \boldsymbol{x})}{2} = \frac{\Omega^2\, r_\perp^2}{2} = \frac{(\Omega\, r \cos\phi)^2}{2} = \frac{\Omega^2\,(x^2+y^2)}{2}, \tag{13.64}$$

so that

$$\boldsymbol{A}_{\text{centrifugal}} = -\nabla \Phi_{\text{centrifugal}} = \Omega^2\, \nabla(x^2+y^2)/2. \tag{13.65}$$

The planetary centripetal acceleration (pointing towards the rotational axis) keeps the rotating particle from flying outward away from the rotational axis. On a massive rotating sphere, the planetary centripetal acceleration acting on the moving particle is provided by that component of the gravitational acceleration (Section 13.10) that is directed towards the rotation axis. The planetary centripetal acceleration's opposing partner, the planetary centrifugal acceleration, arises from the rotating planet and it accounts for the slight equatorial bulge of the earth. For a human scale example, note that the centrifugal acceleration pulls a person outward from the center of a rotating merry-go-round, whereas the person's arms provide the opposing centripetal acceleration to keep from from flying outward. In summary, the centrifugal acceleration arises from rotation of the non-inertial reference frame, and as such is a non-inertial acceleration, whereas the centripetal acceleration arises from a "real" force that balances the centrifugal acceleration.

13.8.2 Summary

For the purpose of formulating the equation of motion in the rotating terrestrial frame, we write the rigid-body rotating frame acceleration as

$$\boldsymbol{A}_{\text{Cartesian}} = \boldsymbol{A} + \boldsymbol{A}_{\text{Coriolis}} + \boldsymbol{A}_{\text{centrifugal}} \tag{13.66a}$$

$$= \boldsymbol{A} - 2\,\boldsymbol{\Omega} \times \boldsymbol{V}_{\text{Cartesian}} - \nabla \Phi_{\text{centrifugal}} \tag{13.66b}$$

and summarize the following accelerations (force per unit mass).

- INERTIAL: Newton's law of motion is formulated within an inertial reference frame making use of the acceleration, $\boldsymbol{A}$, that is directly affected by forces such as gravitation.

- PLANETARY CORIOLIS: The planetary Coriolis acceleration,

$$\boldsymbol{A}_{\text{Coriolis}} = -2\,\boldsymbol{\Omega} \times \boldsymbol{V}_{\text{Cartesian}} = -2\,\Omega\,\hat{\boldsymbol{z}} \times \boldsymbol{V}_{\text{Cartesian}} = -2\,\Omega \left[-\frac{\mathrm{d}y}{\mathrm{d}t}\,\hat{\boldsymbol{x}} + \frac{\mathrm{d}x}{\mathrm{d}t}\,\hat{\boldsymbol{y}} \right], \tag{13.67}$$

  arises from the choice to describe motion within the rotating terrestrial reference frame. The Coriolis acceleration gives rise to a rich suite of fundamentally new phenomena relative to non-rotating motion, with much of this book focused in describing such phenomena. It has components only in the horizontal planetary Cartesian plane spanned by the unit vectors $(\hat{\boldsymbol{x}}, \hat{\boldsymbol{y}})$. That is, the Coriolis acceleration occurs in a plane parallel to the equatorial plane. We expect this orientation of the Coriolis acceleration since it arises from rotation about the $\hat{\boldsymbol{z}}$ axis, so that there can be no component of the Coriolis acceleration aligned with $\hat{\boldsymbol{z}}$.

- PLANETARY CENTRIFUGAL: The planetary centrifugal acceleration,

$$\boldsymbol{A}_{\text{centrifugal}} = -\nabla\Phi_{\text{centrifugal}} = \Omega^2\,\boldsymbol{r}_\perp = \Omega^2\,(x\,\hat{\boldsymbol{x}} + y\,\hat{\boldsymbol{y}}), \tag{13.68}$$

  is the second term arising from the rotating reference frame. As for the Coriolis acceleration, the planetary centrifugal acceleration has components only in the horizontal planetary Cartesian plane spanned by the unit vectors $(\hat{\boldsymbol{x}}, \hat{\boldsymbol{y}})$; i.e., the planetary centrifugal acceleration occurs in a plane parallel to the equatorial plane, which is again expected since the planetary centrifugal acceleration arises from rotation of the planet about the polar axis. The planetary centrifugal acceleration is directed outward from (perpendicular to) to the polar axis of rotation. We see this orientation in Figure 13.4 to be discussed later. Furthermore, the planetary centrifugal acceleration is nonzero even when the particle is fixed relative to the rotating planet, whereas the Coriolis acceleration is zero when the particle has zero motion relative to the planet.

  The planetary centrifugal acceleration can be written as the gradient of a scalar potential, $\boldsymbol{A}_{\text{centrifugal}} = -\nabla\Phi_{\text{centrifugal}}$ where $\Phi_{\text{centrifugal}} = -\Omega^2\,(x^2 + y^2)/2$ (equation (13.64)). Hence, the planetary centrifugal acceleration can be combined with the gravitational acceleration in the equation of motion (see Section 13.10). The resulting "effective gravity" leads to a conservative force field that is modified relative to the central gravitational field of the non-rotating spherical planet. We detail these points in Section 13.10.4.

13.8.3 Further study

We build up our understanding of the Coriolis acceleration as the book develops, such as in Section 14.6 where we offer a thorough examination of its facets. Further related study can be found in Section 3.5 of *Apel* (1987). Visualizations from rotating tank experiments are useful to garner an experiential understanding of the Coriolis acceleration. The first few minutes of this video from Prof. Fultz of the University of Chicago is particularly insightful.

13.9 Spherical representation of acceleration

The spherical representation of the velocity viewed in an inertial reference frame is given by equation (13.46f)

$$\boldsymbol{V} = \frac{\mathrm{d}\boldsymbol{X}}{\mathrm{d}t} = (u + r_\perp\,\Omega)\,\hat{\boldsymbol{\lambda}} + v\,\hat{\boldsymbol{\phi}} + w\,\hat{\boldsymbol{r}} = \boldsymbol{V}_{\text{sphere}} + r_\perp\,\Omega\,\hat{\boldsymbol{\lambda}}, \tag{13.69}$$

where we introduced the spherical velocity from equation (13.48)

$$\boldsymbol{V}_{\text{sphere}} \equiv u\,\hat{\boldsymbol{\lambda}} + v\,\hat{\boldsymbol{\phi}} + w\,\hat{\boldsymbol{r}}. \tag{13.70}$$

We also make use of the notation for the zonal component of the velocity as measured in the inertial reference frame,

$$u_{\text{I}} = u + r_{\perp}\,\Omega. \tag{13.71}$$

Just as for computing the velocity vector, the corresponding acceleration measured in the inertial reference frame must take into account changes in both the spherical coordinates and spherical basis vectors

$$\boldsymbol{A} = \frac{\mathrm{d}}{\mathrm{d}t}\left(u_{\text{I}}\,\hat{\boldsymbol{\lambda}} + v\,\hat{\boldsymbol{\phi}} + w\,\hat{\boldsymbol{r}}\right) \tag{13.72a}$$

$$= \frac{\mathrm{d}u_{\text{I}}}{\mathrm{d}t}\,\hat{\boldsymbol{\lambda}} + \frac{\mathrm{d}v}{\mathrm{d}t}\,\hat{\boldsymbol{\phi}} + \frac{\mathrm{d}w}{\mathrm{d}t}\,\hat{\boldsymbol{r}} + u_{\text{I}}\,\frac{\mathrm{d}\hat{\boldsymbol{\lambda}}}{\mathrm{d}t} + v\,\frac{\mathrm{d}\hat{\boldsymbol{\phi}}}{\mathrm{d}t} + w\,\frac{\mathrm{d}\hat{\boldsymbol{r}}}{\mathrm{d}t}. \tag{13.72b}$$

The spherical unit vectors change due to both the rigid-body rotation of the rotating reference frame, plus motion of the particle relative to the rotating frame. Making use of equations (13.13), (13.14a), and (13.14b) for the changes to the spherical coordinate unit vectors leads to the decomposition of the acceleration viewed from the inertial frame

$$\boldsymbol{A}\cdot\hat{\boldsymbol{\lambda}} = \frac{\mathrm{d}u_{\text{I}}}{\mathrm{d}t} + \left[\frac{\mathrm{d}\lambda}{\mathrm{d}t} + \Omega\right](w\cos\phi - v\sin\phi) \tag{13.73a}$$

$$\boldsymbol{A}\cdot\hat{\boldsymbol{\phi}} = \frac{\mathrm{d}v}{\mathrm{d}t} + \left[\frac{\mathrm{d}\lambda}{\mathrm{d}t} + \Omega\right] u_{\text{I}}\,\sin\phi + w\,\frac{\mathrm{d}\phi}{\mathrm{d}t} \tag{13.73b}$$

$$\boldsymbol{A}\cdot\hat{\boldsymbol{r}} = \frac{\mathrm{d}w}{\mathrm{d}t} - \left[\frac{\mathrm{d}\lambda}{\mathrm{d}t} + \Omega\right] u_{\text{I}}\,\cos\phi - v\,\frac{\mathrm{d}\phi}{\mathrm{d}t}. \tag{13.73c}$$

Use of the identities

$$u = r_{\perp}\,\frac{\mathrm{d}\lambda}{\mathrm{d}t} \qquad \text{and} \qquad u_{\text{I}} = u + r_{\perp}\,\Omega \qquad \text{and} \qquad \frac{\mathrm{d}u_{\text{I}}}{\mathrm{d}t} = \frac{\mathrm{d}u}{\mathrm{d}t} + \Omega\,(w\cos\phi - v\sin\phi), \tag{13.74}$$

along with some reorganization, then renders the spherical coordinate representation of the inertial frame acceleration

$$\begin{aligned}
\boldsymbol{A} = \hat{\boldsymbol{\lambda}}&\left[\frac{\mathrm{d}u}{\mathrm{d}t} + \frac{u\,(w - v\tan\phi)}{r} + 2\,\Omega\,(w\cos\phi - v\sin\phi)\right] \\
+\,\hat{\boldsymbol{\phi}}&\left[\frac{\mathrm{d}v}{\mathrm{d}t} + \frac{v\,w + u^2\tan\phi}{r} + 2\,\Omega\,u\sin\phi + r_{\perp}\,\Omega^2\sin\phi\right] \\
+\,\hat{\boldsymbol{r}}&\left[\frac{\mathrm{d}w}{\mathrm{d}t} - \frac{u^2 + v^2}{r} - 2\,\Omega\,u\cos\phi - r_{\perp}\,\Omega^2\cos\phi\right].
\end{aligned} \tag{13.75}$$

13.9.1 Transforming from Cartesian to spherical

As in Section 13.7.3, we can make use of the tensor algebra from Section 13.3 to transform from the Cartesian representation of the acceleration vector to the spherical representation. Following the same steps as for the velocity leads to

$$A^{\overline{a}} = \Lambda^{\overline{a}}_{\ a}\,A^{a} \tag{13.76}$$

where the Cartesian components to the acceleration are

$$A^1 = \ddot{x} - 2\,\Omega\,\dot{y} - \Omega^2\,x \tag{13.77a}$$

$$A^2 = \ddot{y} + 2\,\Omega\,\dot{x} - \Omega^2\,y \tag{13.77b}$$

$$A^3 = \ddot{z}. \tag{13.77c}$$

Making use of the coordinate transformation (13.22) allows us to express these Cartesian components of the acceleration in terms of spherical coordinates. Then we make use of the inverse transformation matrix components $\Lambda^{\overline{a}}_{b}$ given by equation (13.27), as well as the relation (13.24) between the coordinate basis vectors, which leads to

$$\vec{A} = \boldsymbol{A} = A^a\,\vec{e}_a = A^{\overline{a}}\,\vec{e}_{\overline{a}} \tag{13.78}$$

with the spherical coordinate representation given by equation (13.75) as derived without the formalism of tensor algebra. Both approaches require algebraic manipulations, so that it is useful to have two approaches to double-check results.

13.9.2 Decomposing the acceleration

We decompose the inertial frame acceleration (13.75) into the following terms

$$\boldsymbol{A} = \boldsymbol{A}_{\text{sphere}} + \boldsymbol{A}_{\text{metric}} - \boldsymbol{A}_{\text{Coriolis}} - \boldsymbol{A}_{\text{centrifugal}}, \tag{13.79}$$

with signs chosen so that in the rigid-body rotating frame the acceleration is written

$$\underbrace{\boldsymbol{A}_{\text{sphere}} + \boldsymbol{A}_{\text{metric}}}_{\text{net spherical acceleration}} = \boldsymbol{A} + \boldsymbol{A}_{\text{Coriolis}} + \boldsymbol{A}_{\text{centrifugal}}. \tag{13.80}$$

We identify the net spherical acceleration as the sum of the coordinate acceleration and metric acceleration. In the absence of reference frame rotation, this sum provides an expression for the acceleration as represented by spherical coordinates. For example, if we are describing the motion of a satellite from an inertial reference frame using spherical coordinates, then we would use $\boldsymbol{A}_{\text{sphere}} + \boldsymbol{A}_{\text{metric}}$. The Coriolis and planetary centrifugal terms arise from the rigid-body rotation of the planet.

13.9.3 Spherical coordinate acceleration

The spherical coordinate acceleration is given by the time change in the spherical velocity components

$$\boldsymbol{A}_{\text{sphere}} = \frac{\mathrm{d}u}{\mathrm{d}t}\,\hat{\boldsymbol{\lambda}} + \frac{\mathrm{d}v}{\mathrm{d}t}\,\hat{\boldsymbol{\phi}} + \frac{\mathrm{d}w}{\mathrm{d}t}\,\hat{\boldsymbol{r}}. \tag{13.81}$$

This term has no contribution from changes to the spherical unit vectors.

13.9.4 Metric acceleration

We define the *metric acceleration* as that contribution to the acceleration arising from time dependence of the spherical unit vectors that appears when taking the time derivative of the velocity vector. For spherical coordinates we have

$$\boldsymbol{A}_{\text{metric}} = \hat{\boldsymbol{\lambda}}\left[\frac{u\,(w - v\tan\phi)}{r}\right] + \hat{\boldsymbol{\phi}}\left[\frac{v\,w + u^2\tan\phi}{r}\right] - \hat{\boldsymbol{r}}\left[\frac{u^2 + v^2}{r}\right] \tag{13.82a}$$

$$= \hat{\boldsymbol{\lambda}}\left[\frac{u\,(w\cos\phi - v\sin\phi)}{r\cos\phi}\right] + \hat{\boldsymbol{\phi}}\left[\frac{v\,w\cos\phi + u^2\sin\phi}{r\cos\phi}\right] - \hat{\boldsymbol{r}}\left[\frac{u^2 + v^2}{r}\right] \tag{13.82b}$$

$$= \frac{1}{r}\left[u \tan\phi\,(\hat{\boldsymbol{r}} \times \boldsymbol{V}_{\text{sphere}}) + w\,\boldsymbol{U}_{\text{sphere}} - \hat{\boldsymbol{r}}\,\boldsymbol{U}_{\text{sphere}} \cdot \boldsymbol{U}_{\text{sphere}}\right], \tag{13.82c}$$

where we wrote the horizontal (angular) and vertical (radial) components of the spherical velocity according to

$$\boldsymbol{V}_{\text{sphere}} = \boldsymbol{U}_{\text{sphere}} + \hat{\boldsymbol{r}}\,w = \hat{\boldsymbol{\lambda}}\,u + \hat{\boldsymbol{\phi}}\,v + \hat{\boldsymbol{r}}\,w. \tag{13.83}$$

Note that

$$\boldsymbol{V}_{\text{sphere}} \cdot \boldsymbol{A}_{\text{metric}} = 0, \tag{13.84}$$

so that the metric acceleration is orthogonal to the spherical velocity, in which case with (see equation (13.46f)) $\boldsymbol{V} = \boldsymbol{V}_{\text{sphere}} + r_\perp\,\Omega\,\hat{\boldsymbol{\lambda}}$ we have

$$\boldsymbol{V} \cdot \boldsymbol{A}_{\text{metric}} = \Omega\,u\,(-v\sin\phi + w\cos\phi). \tag{13.85}$$

Furthermore, the metric acceleration vanishes when the curvature of the sphere vanishes (i.e., $r \to \infty$), as per a flat plane.

13.9.5 Planetary centrifugal acceleration

The spherical coordinate representation of the planetary centrifugal acceleration is given by

$$\boldsymbol{A}_{\text{centrifugal}} = -\nabla\Phi_{\text{centrifugal}} = \Omega^2\,(x\,\hat{\boldsymbol{x}} + y\,\hat{\boldsymbol{y}}) = r_\perp\,\Omega^2\,(-\hat{\boldsymbol{\phi}}\sin\phi + \hat{\boldsymbol{r}}\cos\phi). \tag{13.86}$$

The planetary centrifugal acceleration points outward from the axis of rotation (see Figure 13.4 to be discussed later), so that it has no component in the longitudinal direction. Furthermore, note that

$$\boldsymbol{V} \cdot \boldsymbol{A}_{\text{centrifugal}} = \boldsymbol{V}_{\text{sphere}} \cdot \boldsymbol{A}_{\text{centrifugal}} = r_\perp\,\Omega^2\,(-v\sin\phi + w\cos\phi). \tag{13.87}$$

13.9.6 Planetary Coriolis acceleration

The spherical coordinate representation of the Coriolis acceleration makes use of the spherical representation of the earth's angular velocity

$$\boldsymbol{\Omega} = \Omega\,\hat{\boldsymbol{z}} = \Omega\,(\hat{\boldsymbol{\phi}}\,\cos\phi + \hat{\boldsymbol{r}}\,\sin\phi). \tag{13.88}$$

Although $\boldsymbol{\Omega} = \Omega\,\hat{\boldsymbol{z}}$ is fixed in absolute space, its representation using spherical coordinates is a function of latitudinal position on the sphere, with components in the local radial and local meridional directions. This spatial dependence gives rise to much of the characteristic features of geophysical flows associated with the *beta*-effect studied in Section 40.6.2.

We use the representation (13.88) to write the spherical coordinate representation of the Coriolis acceleration

$$\boldsymbol{A}_{\text{Coriolis}} = -2\,\boldsymbol{\Omega} \times \boldsymbol{V}_{\text{sphere}} \tag{13.89a}$$

$$= -2\,\Omega\,(\hat{\boldsymbol{\phi}}\,\cos\phi + \hat{\boldsymbol{r}}\,\sin\phi) \times (u\,\hat{\boldsymbol{\lambda}} + v\,\hat{\boldsymbol{\phi}} + w\,\hat{\boldsymbol{r}}) \tag{13.89b}$$

$$= -2\,\Omega\left[\hat{\boldsymbol{\lambda}}\,(w\cos\phi - v\sin\phi) + \hat{\boldsymbol{\phi}}\,u\sin\phi - \hat{\boldsymbol{r}}\,u\cos\phi\right]. \tag{13.89c}$$

As a check on this result, note that

$$\boldsymbol{A}_{\text{Coriolis}} \cdot \hat{\boldsymbol{z}} = 0, \tag{13.90}$$

as it must since there is no component of the Coriolis acceleration that is parallel to the rotation axis. Furthermore, as for the metric acceleration, we see that the Coriolis acceleration is

orthogonal to the spherical velocity

$$\boldsymbol{V}_{\text{sphere}} \cdot \boldsymbol{A}_{\text{Coriolis}} = 0, \tag{13.91}$$

so that

$$\boldsymbol{V} \cdot \boldsymbol{A}_{\text{Coriolis}} = 2\, r_\perp\, \Omega^2\, (v \sin\phi - w \cos\phi). \tag{13.92}$$

We commonly find it convenient to introduce a shorthand notation

$$\boldsymbol{f} = (2\,\Omega\, \sin\phi)\, \hat{\boldsymbol{r}} \qquad \text{and} \qquad \boldsymbol{f}^* = (2\,\Omega\, \cos\phi)\, \hat{\boldsymbol{\phi}}, \tag{13.93}$$

so that the Coriolis acceleration is decomposed into two terms

$$\boldsymbol{A}_{\text{Coriolis}} = -(\boldsymbol{f} + \boldsymbol{f}^*) \times \boldsymbol{V}_{\text{sphere}}. \tag{13.94}$$

These two terms take on the form

$$\boldsymbol{A}^{\boldsymbol{f}}_{\text{Coriolis}} = -(2\,\Omega\, \sin\phi)\, \hat{\boldsymbol{r}} \times (u\, \hat{\boldsymbol{\lambda}} + v\, \hat{\boldsymbol{\phi}} + w\, \hat{\boldsymbol{r}}) = 2\,\Omega \sin\phi\, (v\, \hat{\boldsymbol{\lambda}} - u\, \hat{\boldsymbol{\phi}}), \tag{13.95}$$

which is purely in the spherical angular directions, and

$$\boldsymbol{A}^{\boldsymbol{f}^*}_{\text{Coriolis}} = -(2\,\Omega\, \cos\phi)\, \hat{\boldsymbol{\phi}} \times (u\, \hat{\boldsymbol{\lambda}} + v\, \hat{\boldsymbol{\phi}} + w\, \hat{\boldsymbol{r}}) = 2\,\Omega \cos\phi\, (u\, \hat{\boldsymbol{r}} - w\, \hat{\boldsymbol{\lambda}}), \tag{13.96}$$

which has a zonal and radial component.

13.9.7 Centrifugal acceleration from particle plus planetary motion

The radial component to the inertial frame acceleration (13.75) can be written in the form

$$\boldsymbol{A} \cdot \hat{\boldsymbol{r}} = \frac{\mathrm{d}w}{\mathrm{d}t} - (u_{\text{I}}^2 + v^2)/r. \tag{13.97}$$

Evidently, the contribution from $(u_{\text{I}}^2 + v^2)/r$ term leads to a vertical (radially outward) acceleration in the radial equation of motion (13.134) discussed in Section 13.11.2. We identify it as the radial acceleration arising from the particle's centrifugal acceleration due to angular motion of the particle around the sphere, combined with the local vertical contribution from the planetary centrifugal acceleration of Section 13.9.5.

13.9.8 Coriolis acceleration for large-scale motions

Let us again write the Coriolis acceleration in equation (13.89c), now underlining two terms

$$\boldsymbol{A}_{\text{Coriolis}} = -2\,\Omega \left[\hat{\boldsymbol{\lambda}}\, (\underline{w \cos\phi} - v \sin\phi) + \hat{\boldsymbol{\phi}}\, u \sin\phi - \hat{\boldsymbol{r}}\, \underline{u \cos\phi}\right]. \tag{13.98}$$

For many applications in geophysical fluid mechanics, the term $\hat{\boldsymbol{r}}\, (2\,\Omega\, u \cos\phi)$ is much smaller than the competing gravitational acceleration that also contributes to the radial acceleration, thus prompting $\hat{\boldsymbol{r}}\, (2\,\Omega\, u \cos\phi)$ to be dropped from the $\hat{\boldsymbol{r}}$ equation of motion.[2] Furthermore, the vertical velocity term is often much smaller than the horizontal velocity term appearing in the $\hat{\boldsymbol{\lambda}}$ component. Dropping these two terms results in the Coriolis acceleration used for large-scale dynamics, such as when considering the hydrostatic primitive equations for geophysical fluids (Section 27.1)

$$\boldsymbol{A}^{\text{large-scale}}_{\text{Coriolis}} \equiv -2\,\Omega \sin\phi\, (-\hat{\boldsymbol{\lambda}}\, v + \hat{\boldsymbol{\phi}}\, u) \equiv -f\, \hat{\boldsymbol{r}} \times \boldsymbol{V}_{\text{sphere}}. \tag{13.99}$$

[2]The term $\hat{\boldsymbol{r}}\, (2\,\Omega\, u \cos\phi)$ is called the Eötvös correction in the study of marine gravity.

For the last equality we introduced the Coriolis parameter

$$f \equiv 2\,\Omega \sin\phi. \tag{13.100}$$

As illustrated in Figure 13.3, we see that it is the radial (i.e., the local vertical) component of the earth's angular rotation that plays the most important role in large-scale geophysical fluid mechanics

$$\boldsymbol{\Omega} \cdot \hat{\boldsymbol{r}} = \Omega\, \hat{\boldsymbol{z}} \cdot \hat{\boldsymbol{r}} = \Omega\, (\hat{\boldsymbol{\phi}}\, \cos\phi + \hat{\boldsymbol{r}}\, \sin\phi) \cdot \hat{\boldsymbol{r}} = \Omega \sin\phi = f/2. \tag{13.101}$$

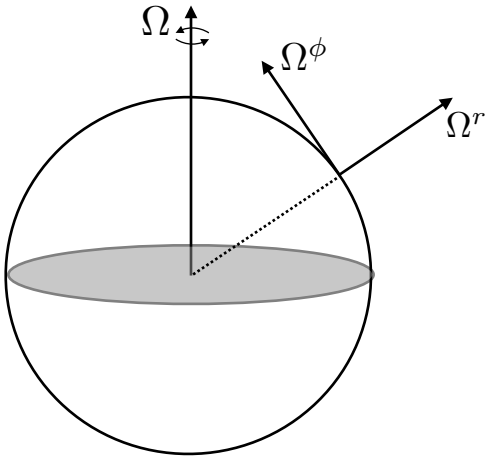

FIGURE 13.3: This figure illustrates the two components of the earth's rigid-body rotational velocity, $\boldsymbol{\Omega} = \Omega\, \hat{\boldsymbol{z}} = \Omega\, (\hat{\boldsymbol{\phi}} \cos\phi + \hat{\boldsymbol{r}} \sin\phi)$. The radial component (also known as the local vertical component), $\Omega^r = \Omega \sin\phi$, is generally more important for large scale geophysical fluid motions than the meridional component, $\Omega^\phi = \Omega \cos\phi$.

13.10 Newtonian gravity

Thus far we have focused on the kinematics of a particle moving around a rotating planet, with this motion viewed from the rotating planetary reference frame. We now acknowledge that the particle is moving in the prescribed gravitational field of the massive planet. The gravitational force acting on the particle is the only force felt by the point particle when viewed in an inertial reference frame. Since the point particle contains no internal structure and it has no surface area, the total energy for the particle equals to the mechanical energy (Chapter 14). We here discuss the gravitational potential energy and the associated gravitational force, all within the context of Newtonian mechanics.

13.10.1 Newtonian gravity from Poisson's equation

The Newtonian gravitational potential, $\Phi_{\rm N}$, in the presence of a mass distribution with density, ρ, satisfies Poisson's equation (see Section 6.5)

$$\nabla^2 \Phi_{\rm N} = 4\,\pi\, G\, \rho, \tag{13.102}$$

where

$$G = 6.674 \times 10^{-11}\ \text{N m}^2\ \text{kg}^{-2} = 6.674 \times 10^{-11}\ \text{m}^3\ \text{kg}^{-1}\ \text{s}^{-2} \tag{13.103}$$

is Newton's gravitational constant. Gravity is a conservative force, so that the gradient of the gravitational potential gives the gravitational acceleration

$$\boldsymbol{g} = -\nabla \Phi_{\rm N}. \tag{13.104}$$

The gravitational potential has dimensions of $\mathrm{L}^2\ \mathrm{T}^{-2}$ so that its gradient indeed has the dimensions of acceleration, $\mathrm{L}\ \mathrm{T}^{-2}$. Note that the gravitational potential responds instantaneously to any changes in the mass distribution. It took a few centuries, and the genius of Einstein, to provide a local connection between mass and gravity as rendered by space-time curvature and gravitational waves.[3]

A volume integral of Poisson's equation (13.102), computed over a region in space, leads to

$$\int_{\mathcal{R}} \nabla^2 \Phi_{\mathrm{N}} \, \mathrm{d}V = 4\,\pi\,G \int_{\mathcal{R}} \rho \, \mathrm{d}V. \tag{13.105}$$

The integral on the right hand side is the mass contained in the region,

$$M = \int_{\mathcal{R}} \rho \, \mathrm{d}V, \tag{13.106}$$

whereas the divergence theorem (Section 2.7) allows us to write the left hand side as a surface integral

$$\int_{\partial\mathcal{R}} \nabla \Phi_{\mathrm{N}} \cdot \hat{\boldsymbol{n}} \, \mathrm{d}\mathcal{S} = 4\,\pi\,G\,M. \tag{13.107}$$

With a continuous mass density, ρ, the Newtonian gravitational potential, Φ_{N}, can be written in terms of the Green's function solution in equation (9.61), along with the free space Green's function in equation (9.5c), so that

$$\Phi_{\mathrm{N}}(\boldsymbol{x}) = -G \int_{\mathcal{R}} \frac{\rho(\boldsymbol{x}_0)}{|\boldsymbol{x} - \boldsymbol{x}_0|} \, \mathrm{d}V_0 \quad \text{and} \quad \boldsymbol{g}(\boldsymbol{x}) = -\nabla \Phi_{\mathrm{N}} = -G \int_{\mathcal{R}} \frac{\rho(\boldsymbol{x}_0)\,(\boldsymbol{x} - \boldsymbol{x}_0)}{|\boldsymbol{x} - \boldsymbol{x}_0|^3} \, \mathrm{d}V_0. \tag{13.108}$$

The potential is built from the convolution of the free space Green's function with the mass distribution. The gravitational acceleration manifests the inverse squared gravitational force arising from Newtonian gravity.

13.10.2 Gravitational field outside a spherical earth

In this book we assume the mass density of the planet to be spherically symmetric, in which case the gravitational potential is a function only of the radial distance from the center of the mass distribution, $\Phi_{\mathrm{e}} = \Phi_{\mathrm{e}}(r)$. Letting the integration region, $\mathcal{R}$, be a sphere of radius $r > R_{\mathrm{e}}$, where R_{e} is the radius of the planet, and making use of spherical coordinates from Section 4.23.8, brings equation (13.107) to

$$4\,\pi\,r^2 \, \frac{\partial \Phi_{\mathrm{e}}}{\partial r} = 4\,\pi\,G\,M. \tag{13.109}$$

Integration leads to the gravitational potential for an arbitrary point outside the spherically symmetric mass distribution[4]

$$\Phi_{\mathrm{e}} = -\frac{G\,M}{r}, \tag{13.110}$$

where we set the integration constant to zero. Evidently, when sampling the gravity field at a radius equal to or larger than the spherical planet radius, the gravitational potential is identical to that of a point mass at the origin. The gradient of the gravitational potential (13.110) yields the inverse-squared dependence of the gravitational acceleration

$$\boldsymbol{g}_{\mathrm{e}} = -\nabla \Phi_{\mathrm{e}} = -\frac{G\,M}{r^2}\,\hat{\boldsymbol{r}} = -\frac{G\,M}{r^3}\,\boldsymbol{r}, \tag{13.111}$$

[3] See *Thorne and Blandford* (2017) for a study of general relativity and gravitational waves.
[4] In Exercise 13.10 we derive the gravitational potential inside of a spherical body.

along with the gravitational force acting on a point particle of mass m

$$\boldsymbol{F}_{\text{gravity}} = m\,\boldsymbol{g}_{\text{e}} = -m\,\nabla\Phi_{\text{e}}. \tag{13.112}$$

Furthermore, the gravitational potential energy of the particle (dimensions M L^2 T^{-2}) is

$$P = m\,\Phi_{\text{e}}. \tag{13.113}$$

13.10.3 Approximate gravitational acceleration

For most applications of atmospheric and oceanic fluid dynamics, it is sufficient to assume the gravitational acceleration is constant and equal to its value at the earth's surface. This assumption holds so long as the radial position of the particle is a distance from the earth surface that is small relative to the earth radius. We generally make this assumption throughout this book.[5] In this case we can assume the earth's gravitational acceleration, g_{e}, is a constant so that

$$\boldsymbol{g}_{\text{e}} = -g_{\text{e}}\,\hat{\boldsymbol{r}}, \tag{13.114}$$

where

$$g_{\text{e}} = \frac{G\,M_{\text{e}}}{R_{\text{e}}^2} \approx 9.8 \text{ m s}^{-2}. \tag{13.115}$$

To reach this value, we assumed a sphere of mass equal to the earth mass

$$M_{\text{e}} = 5.977 \times 10^{24} \text{ kg}, \tag{13.116}$$

and radius

$$R_{\text{e}} = 6.371 \times 10^{6} \text{ m} \tag{13.117}$$

determined so that the sphere has the same volume as the earth.

The corresponding gravitational potential for the particle is given by

$$\Phi_{\text{e}} = g_{\text{e}}\,r, \tag{13.118}$$

with the gravitational acceleration

$$\boldsymbol{g}_{\text{e}} = -\nabla\Phi_{\text{e}} = -g_{\text{e}}\,\hat{\boldsymbol{r}}, \tag{13.119}$$

and the gravitational potential energy

$$m\,\Phi_{\text{e}} = m\,g_{\text{e}}\,r. \tag{13.120}$$

We emphasize that the expression for the gravitational potential, (13.118), and potential energy, (13.120), are accurate only so long as the radial position of the particle is a distance from the earth surface that is small relative to the earth radius. Furthermore, note that the approximate gravitational potential (13.118) is positive whereas the unapproximated potential (13.110) is negative. However, the absolute zero of the potential has no physical significance. Instead, what is important is the change between two points in space, with both expressions for the gravitational potential increasing when moving away from the earth center.

[5] In the study of tides in Chapter 34, we no longer make the assumption of constant gravitational field.

13.10.4 Effective gravitational force from the geopotential

Combining the potential for the planetary centrifugal acceleration as given by equation (13.64) with the gravitational potential (13.110), leads to the *geopotential*

$$\Phi = r\,[g_e - \boldsymbol{U}^2_{\text{rigid}}/(2r)] \quad \text{with} \quad \boldsymbol{U}_{\text{rigid}} = r\cos\phi\,\Omega\,\hat{\boldsymbol{\lambda}}, \tag{13.121}$$

where $\boldsymbol{U}_{\text{rigid}}$ is the rigid body velocity of the planet, as per equation (13.50). The expression (13.121) for the geopotential is relevant for motion that is close enough to the earth surface that we can assume the earth's gravitational acceleration, g_e, is constant (see discussion in Section 13.10.3). In Exercise 13.7 we derive the geopotential for the more general case when this assumption is not made.

The contribution from the planetary centrifugal term in the geopotential (13.121) can be estimated by making use of terrestrial values, in which $R = R_e = 6.371 \times 10^6$ m (equation (13.117)), and $\Omega_e = 7.292 \times 10^{-5}$ s^{-1} (Section 13.1). The planetary centrifugal term is its largest at the equator, $\phi = 0$, where

$$\frac{\boldsymbol{U}^2_{\text{rigid}}}{2\,R_e} \approx 0.017 \text{ m s}^{-2}, \tag{13.122}$$

so that the ratio of the gravitational to planetary centrifugal accelerations is (at most)

$$\frac{g_e}{\boldsymbol{U}^2_{\text{rigid}}/(2R_e)} = \frac{M_e\,G/R_e^2}{\Omega_e^2\,R_e/2} \approx 576. \tag{13.123}$$

The geopotential is thus dominated by the earth's gravitational potential. Even so, the planetary centrifugal acceleration leads to a slight equatorial bulge on the earth. To account for this slight non-sphericity, geophysical fluid models generally interpret the radial direction, $\hat{\boldsymbol{r}}$, as pointing parallel to $\nabla\Phi$ rather than parallel to $\nabla\Phi_e$. We have more to say on this topic of geopotential coordinates in Section 13.11.3.

13.10.5 Further study

Newton's gravitational law is standard material from freshman physics. Some commonly used physical properties of the earth are summarized in Appendix Two of *Gill* (1982).

13.11 Newton's law of motion

As seen in Section 11.1, Newton's law of motion says that in an inertial reference frame, the time derivative of the linear momentum arises only from externally applied forces. In our study, we are only concerned with the gravitational force that the constant mass particle feels in an inertial frame. In this case, Newton's equation of motion says that

$$m\,\boldsymbol{A} = -m\,\nabla\Phi_e. \tag{13.124}$$

This is a relatively simple equation of motion. Its representation is somewhat complex, yet useful for practical purposes, when moving to the rigid-body rotating reference frame of terrestrial observers and when represented using spherical coordinates.[6]

[6]As emphasized by *Early* (2012), the acceleration from gravity, from the perspective of general relativity, cannot be distinguished from accelerations encountered when describing motion in a non-inertial reference frame. *Early* (2012) provides an accounting of such motion while clarifying what is meant by "inertial oscillations" for particles constrained to move around the earth along a constant geopotential (we also consider inertial oscillations in Section 15.5). Even so, we here consider gravity as distinct from Coriolis and centrifugal since, in Newtonian mechanics, gravity appears when the particle is viewed from an inertial reference frame.

13.11.1 Cartesian coordinate representation

The inertial frame acceleration using planetary Cartesian coordinates is decomposed according to equation (13.66b)

$$\boldsymbol{A} = \boldsymbol{A}_{\text{Cartesian}} - \boldsymbol{A}_{\text{Coriolis}} - \boldsymbol{A}_{\text{centrifugal}} \tag{13.125a}$$
$$= \boldsymbol{A}_{\text{Cartesian}} + 2\,\boldsymbol{\Omega} \times \boldsymbol{V}_{\text{Cartesian}} + \nabla\Phi_{\text{centrifugal}}. \tag{13.125b}$$

We thus have the equation of motion as viewed within the rigid-body rotating frame and using Cartesian coordinates

$$\boldsymbol{A}_{\text{Cartesian}} = \boldsymbol{A} - 2\,\boldsymbol{\Omega} \times \boldsymbol{V}_{\text{Cartesian}} - \nabla\Phi_{\text{centrifugal}} \tag{13.126a}$$
$$= -\nabla\Phi_{\text{e}} - 2\,\boldsymbol{\Omega} \times \boldsymbol{V}_{\text{Cartesian}} - \nabla\Phi_{\text{centrifugal}} \tag{13.126b}$$
$$= -2\,\boldsymbol{\Omega} \times \boldsymbol{V}_{\text{Cartesian}} - \nabla\Phi, \tag{13.126c}$$

where the geopotential is the sum of the gravitational and planetary centrifugal potentials (equation (13.121))

$$\Phi = \Phi_{\text{e}} + \Phi_{\text{centrifugal}}. \tag{13.127}$$

We can write the equation of motion in the vector form within the rotating reference frame

$$\frac{\mathrm{d}^2\boldsymbol{X}}{\mathrm{d}t^2} + 2\,\boldsymbol{\Omega} \times \dot{\boldsymbol{X}} = -\nabla\Phi. \tag{13.128}$$

Note for this equation, the basis vectors are not time differentiated again since their rigid-body rotation has already been taken care of when exposing the Coriolis and planetary centrifugal accelerations. That is, the time derivatives are all computed within the rigid-body rotating reference frame. This equation of motion is the standard form that occurs also for a fluid, though with the addition of contact forces from pressure and friction as studied in Chapter 24.

Since the rotation of the reference frame is assumed to be constant in time, the equation of motion (13.128) can be written

$$\frac{\mathrm{d}\boldsymbol{M}}{\mathrm{d}t} = \frac{\mathrm{d}}{\mathrm{d}t}(\boldsymbol{V}_{\text{Cartesian}} + 2\,\boldsymbol{\Omega} \times \boldsymbol{X}) = -\nabla\Phi, \tag{13.129}$$

where we introduced the *potential momentum* per mass

$$\boldsymbol{M} = \boldsymbol{V}_{\text{Cartesian}} + 2\,\boldsymbol{\Omega} \times \boldsymbol{X}. \tag{13.130}$$

Evidently, the potential momentum is a constant of the motion for particles moving along directions parallel to the geopotential (so long as the geopotential is a constant). We emphasize that the potential momentum per mass is distinct from the inertial frame velocity (13.42e). Namely, the factor of 2 in the potential momentum arises from the Coriolis acceleration, whereas the inertial frame velocity has $\boldsymbol{\Omega} \times \boldsymbol{X}$ arising from the rigid-body rotation of the planet. We further discuss potential momentum in Section 14.3.

13.11.2 Spherical coordinate representation

We now follow the spherical coordinate discussion in Section 13.9 by writing the inertial frame acceleration using planetary spherical coordinates and decomposing this acceleration into terms that arise in a rigid-body rotating non-inertial frame

$$\boldsymbol{A}_{\text{sphere}} + \boldsymbol{A}_{\text{metric}} = \boldsymbol{A}_{\text{Coriolis}} + \boldsymbol{A} + \boldsymbol{A}_{\text{centrifugal}} = -2\,\boldsymbol{\Omega} \times \boldsymbol{V}_{\text{sphere}} - \nabla\Phi. \tag{13.131}$$

The effective gravitational force is not a central force due to the contribution from the planetary centrifugal acceleration. We see this fact more explicitly by using the equations in Section 13.9 to write the spherical equations of motion

$$\dot{u} + \frac{u\,(w - v\tan\phi)}{r} + 2\,\Omega\,(w\cos\phi - v\sin\phi) = 0 \tag{13.132}$$

$$\dot{v} + \frac{v\,w + u^2\tan\phi}{r} + 2\,\Omega\,u\sin\phi = -r_\perp\,\Omega^2\sin\phi \tag{13.133}$$

$$\dot{w} - \frac{u^2 + v^2}{r} - 2\,\Omega\,u\cos\phi = r_\perp\,\Omega^2\cos\phi - g_{\mathrm{e}}, \tag{13.134}$$

where, again, $r_\perp = r\cos\phi$.

The Ω^2 term in both the meridional equation (13.133), and the radial equation (13.134), are the two components of the planetary centrifugal acceleration, $\boldsymbol{A}_{\text{centrifugal}} = r_\perp\,\Omega^2\,(-\hat{\boldsymbol{\phi}}\sin\phi + \hat{\boldsymbol{r}}\cos\phi)$. The planetary centrifugal acceleration is directed outward from the planetary axis of rotation, and it is balanced by an inward directed planetary centripetal acceleration provided by that portion of the gravitational acceleration directed oppositely to the planetary centrifugal. Notably, a particle initially at rest on a smooth spherical planet accelerates meridionally toward the equator due to the meridional component of the planetary centrifugal acceleration. The initial meridional acceleration for this particle is derived from equation (13.133), whereby $\dot{v} = -r_\perp\,\Omega^2\sin\phi$.

Imagine setting the planetary centripetal acceleration to zero, in which case the particle would still feel the central force from gravity but its trajectory would differ. As seen in Section 13.10.4, the earth's gravitational acceleration is much larger than the planetary centrifugal acceleration, so that in the absence of the planetary centrifugal acceleration the particle would still be bound to the planet. But in more extreme conditions where the rotational rate is much higher (e.g., a rotating neutron star), removing the centripetal acceleration causes a huge modification to the particle trajectory.

13.11.3 Geopotential coordinate representation

As we saw in Section 13.10.2, the radius of a sphere that best fits the volume of the earth is given by $R_{\mathrm{e}} = 6.371 \times 10^6$ m. The non-central nature of the effective gravitational force (arising from central gravity plus planetary centrifugal) leads to an oblate spheroidal shape for planets such as the earth. The result is a distinction between the earth's equatorial and polar radii (Appendix Two of *Gill* (1982))

$$R_{\text{equator}} = 6.378 \times 10^6\,\mathrm{m} \qquad \text{and} \qquad R_{\text{pole}} = 6.357 \times 10^6\,\mathrm{m}, \tag{13.135}$$

with a corresponding ratio

$$1 - \frac{R_{\text{pole}}}{R_{\text{equator}}} \approx 3 \times 10^{-3}. \tag{13.136}$$

An oblate spheroid shape does a better job fitting the actual earth shape than a sphere, thus motivating the use of oblate spheroid coordinates for describing planetary scale mechanics. In this case, the radial coordinate is constant on the oblate spheroid shaped geopotential, and the effective gravitational acceleration is precisely aligned with the geopotential direction. If we consider an ocean covered rotating spherical planet, then at static equilibrium the sea surface corresponds to an oblate spheroidal geopotential.

Even though oblate spheroidal coordinates are better than spherical for describing geopotentials, it is possible, to a high degree of accuracy, to describe the earth's geometry as spherical (*Veronis*, 1973). Doing so simplifies the mathematics since oblate spheroidal coordinates are less convenient and less familiar than standard spherical coordinates. We are thus led to assume

that the radial coordinate measures distances perpendicular to the geopotential, yet to use geometric/metric functions based on spherical coordinates. The error in this approach is small for the earth, and well worth the price since there is no component to the effective gravitational force that is within the geopotential surface.

We illustrate the change in coordinates in Figure 13.4, with the figure caption also explaining how the force balances are reorganized. Absorbing the planetary centrifugal term into an effective gravitational potential then leads to the effective gravitational acceleration vector

$$-\nabla\Phi = -g\,\hat{\boldsymbol{r}}, \tag{13.137}$$

with g the effective gravitational acceleration. Using this convention, the particle equations of motion take the following form

$$\dot{u} + \frac{u\,(w - v\tan\phi)}{r} + 2\,\Omega\,(w\cos\phi - v\sin\phi) = 0 \tag{13.138a}$$

$$\dot{v} + \frac{v\,w + u^2\tan\phi}{r} + 2\,\Omega\,u\sin\phi = 0 \tag{13.138b}$$

$$\dot{w} - \frac{u^2 + v^2}{r} - 2\,\Omega\,u\cos\phi = -g. \tag{13.138c}$$

Notably, in geopotential coordinates the effective gravitational acceleration only impacts the radial equation of motion. There is no longer a component of the effective gravity pointing meridionally.

13.11.4 Comments

Figure 13.4, including its rather long caption, offers a view on the transition from spherical coordinates to geopotential coordinates. The use of geopotential coordinates is rather accurate and extremely convenient for most purposes of geophysical fluid mechanics, with a notable exception being the study of tides and sea level, in which detailed models of the earth's mass distribution and gravity field are used (see *Gregory et al.* (2019) for a review).

Although precise, the transition to geopotential coordinates is somewhat subtle in principle since we are reorganizing how the planetary centrifugal acceleration appears. It is through this reorganization that we can largely ignore the planetary centrifugal acceleration in our studies of geophysical motions since it is absorbed by the geopotential. The single exception for our studies concerns the rotating laboratory tank experiments in Section 27.5, where we find it more convenient to expose the centrifugal acceleration.

13.11.5 Further study

Section 4.12 of *Gill* (1982) and section 2.2.1 of *Vallis* (2017) present the terrestrial scaling needed to justify spherical coordinates with a radial effective gravitational potential. *Morse and Feshbach* (1953) and *Veronis* (1973) present details of oblate spheroidal coordinates. See also the textbook from *Staniforth* (2022) for a careful presentation of the equations for earth's gravity.

The transition from spherical to geopotential coordinates for geophysical fluid mechanics has been the topic of some confusion, as evidenced by the papers from *Stewart and McWilliams* (2022), *Chang and Wolfe* (2022), *Chang et al.* (2023), and *McWilliams* (2024). For the purposes of this book, the key point is that gravity is directed vertically and thus provides no acceleration in the local horizontal directions.

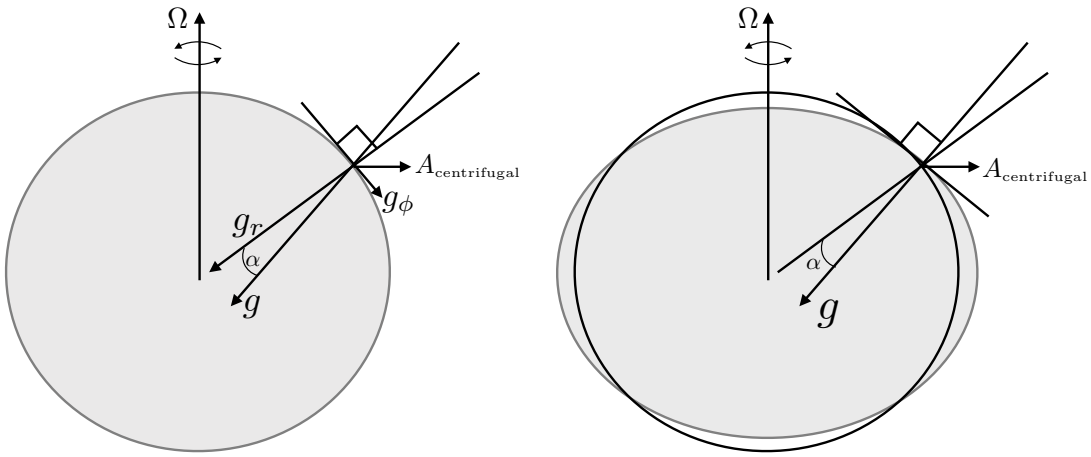

FIGURE 13.4: This figure illustrates the spherical (left panel) versus geopotential (right panel) coordinate systems used to study geophysical motions. The left panel shows the non-central nature of the effective gravitational acceleration, $\boldsymbol{g}$, on a rotating spherical planet, with the effective gravity given by the sum of the gravitational acceleration, $-g_e\,\hat{\boldsymbol{r}}$, plus planetary centrifugal acceleration (equation (13.86)), $\boldsymbol{A}_{\text{centrifugal}} = r_\perp\,\Omega^2\,(-\hat{\boldsymbol{\phi}}\sin\phi + \hat{\boldsymbol{r}}\cos\phi)$. The gravitational acceleration points radially to the center of the earth whereas the planetary centrifugal acceleration points outward away from the polar axis of rotation, thus leading to an effective gravitational acceleration $\boldsymbol{g} = \hat{\boldsymbol{r}}\,(-g_e + r_\perp\,\Omega^2\cos\phi) - \hat{\boldsymbol{\phi}}\,r_\perp\,\Omega^2\sin\phi = \hat{\boldsymbol{r}}\,g^r + \hat{\boldsymbol{\phi}}\,g^\phi$. The angle between the radial gravity and the effective gravity, α, is determined by a *plumb line* and is a function of the rotation rate, earth radius, gravitational acceleration, and latitude. The expression for α is determined in Exercise 13.5. A particle initially at rest on a smooth spherical planet accelerates meridionally toward the equator due to the meridional component of the planetary centrifugal acceleration (from equation (13.133) we have $\dot{v} = -r_\perp\,\Omega^2\sin\phi$). The right panel shows a *geopotential vertical coordinate*, $r = R + z$, that measures the distance perpendicular to the oblate spheroid shaped geopotential surface. The geopotential vertical coordinate precisely aligns the effective gravitational force with the vertical coordinate, so that there is no component of the effective gravity along the surface directions ($g_\phi = 0$). Equivalently, the central gravitational acceleration now has a meridional component on the oblate spheroid that exactly balances the meridional component to the planetary centrifugal acceleration, leaving an effective gravity that is only vertical. Hence, a frictionless oblate spheroidal planet allows for a particle at rest on the planet's surface to remain at rest (see equation (13.138b)). Note that this figure is not drawn to scale, with the oblate nature highly exaggerated compared to the real earth system (see equation (13.136)), and the planetary centrifugal acceleration much smaller than the gravitational (see equation (13.123)). This figure is taken after Figure 2.2 of *Vallis* (2017) and Figure 2.8 of *Olbers et al.* (2012).

13.12 Exercises

EXERCISE 13.1: WORKING THROUGH THE SPHERICAL ACCELERATION

Convince yourself that the spherical form of the acceleration given by equation (13.75) is indeed correct.

EXERCISE 13.2: DERIVING THE SPHERICAL UNIT VECTOR TIME DERIVATIVES

In this exercise we work through details for deriving the time derivative of the spherical coordinate unit vector from Section 13.2.3.

(A) Fill in the details for deriving equation (13.13)

(B) Fill in the details for deriving equation (13.14a)

(C) Fill in the details for deriving equation (13.14b)

EXERCISE 13.3: VELOCITY AND ACCELERATION IN CYLINDRICAL-POLAR COORDINATES

In Section 4.22 we worked through the transformation from Cartesian coordinates to cylindrical-polar coordinates for describing motion in a rotating reference frame. We also made use of polar coordinates in Section 13.2.2 to illustrate how polar unit vectors change under rotations. The cylindrical-polar coordinates are useful when describing physical systems such as rotating

fluid columns (e.g., fluids in a rotating circular tank as in Section 36.8) or when studying cyclostrophically balanced flow (Section 32.5). Here we work through the details using a cylindrical-polar coordinate system in the rigid-body rotating reference frame.

In particular, we here derive the cylindrical-polar coordinate representation of the velocity and acceleration vectors for a particle moving in a reference frame rigid-body rotating with a constant rate about the vertical axis ($\boldsymbol{\Omega} = \Omega\,\hat{\boldsymbol{z}}$). The derivation is directly analogous to the spherical coordinate representation presented in the chapter. Specifically, in Section 13.7.2 we determined a spherical coordinate representation of the velocity vector, and then in Section 13.9 we found the spherical coordinate representation of the acceleration vector.

(A) Determine the representation of the inertial frame velocity vector, $\boldsymbol{V} = \mathrm{d}\boldsymbol{X}/\mathrm{d}t$, in terms of cylindrical-polar coordinates. Hint: remember to include the solid body motion of the rotating reference frame, which was discussed in Section 13.2.2.

(B) Determine the representation of the inertial frame acceleration vector, $\boldsymbol{A} = \mathrm{d}\boldsymbol{V}/\mathrm{d}t$, in terms of cylindrical-polar coordinates.

(C) Writing the inertial frame acceleration in the form

$$\boldsymbol{A} = \boldsymbol{A}_{\text{cylindrical-polar}} + \boldsymbol{A}_{\text{metric}} - \boldsymbol{A}_{\text{centrifugal}} - \boldsymbol{A}_{\text{Coriolis}}, \tag{13.139}$$

give the mathematical expressions for these terms:

- $\boldsymbol{A}_{\text{cylindrical-polar}}$ = acceleration in the rotating reference frame using cylindrical-polar coordinates;
- $\boldsymbol{A}_{\text{metric}}$ = acceleration due to motion of the cylindrical-polar unit vectors relative to the rotating reference frame;
- $\boldsymbol{A}_{\text{centrifugal}}$ = centrifugal acceleration;
- $\boldsymbol{A}_{\text{Coriolis}}$ = Coriolis acceleration.

EXERCISE 13.4: VELOCITY PROJECTED ONTO ACCELERATION

The kinetic energy per mass of a particle is given by

$$\mathcal{K} = \boldsymbol{V} \cdot \boldsymbol{V}/2, \tag{13.140}$$

where $\boldsymbol{V}$ is the velocity of the particle viewed in the inertial reference frame. Hence, in an inertial reference frame it is trivial to show that

$$\frac{\mathrm{d}\mathcal{K}}{\mathrm{d}t} = \boldsymbol{V} \cdot \boldsymbol{A} \tag{13.141}$$

through use of the chain rule, where $\boldsymbol{A} = \mathrm{d}\boldsymbol{V}/\mathrm{d}t$ is the inertial frame acceleration. Verify that this identity also holds when viewing the motion in the rigid-body rotating reference frame. For simplicity make use of planetary Cartesian coordinates.

EXERCISE 13.5: ANGLE OF A PLUMB LINE

A *plumb line* defines the local vertical direction, which is parallel to the effective gravity. As illustrated in Figure 13.4, the planetary centrifugal acceleration causes the plumb line to not extend through the earth center.

(A) What is the angle that the plumb line makes with a line that extends through the earth center? Hint: read the caption to Figure 13.4, and orient your thinking according to the left panel of this figure. Make use of the spherical coordinate version of the equations of motion (13.132)–(13.134).

(B) Explain why the plumb line angle, α, vanishes at both the equator and the poles.

EXERCISE 13.6: GEOMETRY OF CONSTANT GEOPOTENTIAL SURFACES

Here we examine some properties of the geopotential given by equation (13.121), where the squared rigid-body speed is $\boldsymbol{U}^2_{\text{rigid}} = (\Omega\, r \cos\phi)^2$. We only consider geopotentials that are close to the radius of the planet, so that we can assume the gravitational acceleration, g_{e}, is constant and takes on its value at R_{e} as in Sections 13.10.2 and 13.10.4.

(A) Sketch surfaces of constant geopotential according to equation (13.121).

(B) By equating the geopotential going around the pole to that going around the equator, show that the polar radius is less than the equatorial radius when $\Omega > 0$.

(C) Taking the terrestrial values of g_{e}, R_{equator}, and Ω, what is the polar radius R_{pole}? Compare to the measured value of the polar radius given by equation (13.135).

EXERCISE 13.7: GENERAL FORM OF THE GEOPOTENTIAL

In Exercise 13.6, as in Sections 13.10.3 and 13.10.4, we only considered geopotentials that are close to the radius of the planet. Show that geopotentials have larger radius at the equator than at the poles even when not making this assumption. Hint: maintain the general form of the gravitational potential as given by equation (13.110), then add the potential for the planetary centrifugal acceleration (13.64). Evaluate the geopotential at the pole and then show that this same geopotential surface has a larger radial position anywhere equatorward of the pole.

EXERCISE 13.8: SCALING TO JUSTIFY USE OF GEOPOTENTIAL COORDINATES

Summarize the argument that justifies the use of geopotential coordinates while retaining the spherical geometry. Make use of your favorite textbook discussion such that given in Chapter 2 of *Vallis* (2017).

EXERCISE 13.9: ACCELERATIONS ACTING ON A RESTING PARTICLE

In this exercise we consider the accelerations acting on a particle at rest (in the rotating frame) on a smooth/frictionless rotating spherical planet and a rotating oblate spheroidal planet. We also consider similar questions in Section 14.8.

(A) Motion of a particle on a rotating spherical planet is described using the spherical coordinates from Section 13.11.2 with the corresponding equations of motion (13.132)-(13.134). Suppose that we drop a particle on a rotating sphere and that we describe its motion using the spherical coordinates. Discuss the initial acceleration of the particle that is released from rest.

(B) Motion of a particle on a rotating oblate spheroid planet is described using the geopotential coordinates from Section 13.11.3 with the corresponding equations of motion (13.138a)-(13.138c). Suppose that we drop a particle on a rotating oblate spheroid and that we describe its motion using the geopotential coordinates. Discuss the initial acceleration of the particle that is released from rest. Note that we return to this freely falling particle in Section 14.8.3.

EXERCISE 13.10: GRAVITATIONAL POTENTIAL INSIDE A SPHERE

In Section 13.10.2 we found the gravitational, Φ_{e}, for a point outside of the spherical earth. Here we find the gravitational potential inside of the earth. That is, solve the Poisson equation

$$\nabla^2 \Phi_{\text{e}} = 4\,\pi\, G\, \rho, \tag{13.142}$$

for a radial position $r < R_{\text{e}}$. Hint: follow the approach in Section 13.10.1 and then match the potential at $r = R_{\text{e}}$. Hint: the solution can be found in many undergraduate physics texts.

Chapter 14

SYMMETRIES AND CONSERVATION LAWS

Symmetries are discrete or continuous operations that leave a physical system unchanged. For example, let $\boldsymbol{X}$ be a trajectory satisfying Newton's equation of motion and $\mathcal{A}$ be an operation. If $\mathcal{A}[\boldsymbol{X}]$ also satisfies Newton's equation of motion then $\mathcal{A}$ is a symmetry of the physical system. As studied in Section 12.9, *Noether's theorem* provides a connection between symmetries and *conservation laws*, with conservation laws providing *dynamical constraints* on the motion. In this chapter we study a variety of dynamical constraints respected by particle motion. We then use these dynamical constraints as a means to study the nature of the motion and, in turn, to further our understanding. We are particularly interested in studying motion as observed from a rigid-body rotating reference frame, as per a terrestrial observer on the rotating earth.

One of the key reasons to make use of conserved quantities concerns their additive nature. Namely, a conserved quantity for a system composed of several weakly interacting parts is given by the sum of the conserved quantity for the individual parts. As a result, symmetries and conservation laws are fundamental to how we garner a qualitative and quantitative understanding of motion in which, for many purposes, it is more useful to know the dynamically conserved properties of any realized motion than details of any particular trajectory.

CHAPTER GUIDE

This chapter relies on our study of particle mechanics in Chapter 13. In Section 12.9 we provide the mathematical basis for Noether's theorem through the study of Lagrangian mechanics and Hamilton's principle. However, full reading of that material is not necessary for the present chapter.

14.1 Trajectories and dynamical constraints

Time integration (twice) of the equation of motion provides an expression for the trajectory of a particle. To assist in this integration we find it very useful to make use of *dynamical constraints* respected by the motion. Dynamical constraints manifest as conservation laws and can be essential for any practical determination of the trajectory. Dynamical constraints also provide predictive statements of value when studying the stability of motion and for developing numerical methods for simulations.

Knowledge of the trajectory is important if we are interested in details of a particular realization of the motion. For example, the particle might be an idealization of a satellite orbiting the planet, with an accurate trajectory needed to predict its location at a future time. However, for other purposes we might wish to know that all particles, no matter what trajectory, conserve *angular momentum* and mechanical energy. This information about the dynamical constraints satisfied by the motion offers the ability to understand basic properties of the motion and to predict its response to perturbations, even without determining trajectories. Dynamical constraints imposed by conservation laws are especially relevant for fluids since it is rare to determine the analytical expression for the motion of fluid particles, making the knowledge of constraints incredibly valuable.

14.1.1 Connecting symmetries to conservation laws

The discovery of conservation laws often comes from inspired manipulations of the equations of motion. However, there is a more robust and fundamental means to deduce conservation laws through their connection to symmetries, with a symmetry manifesting as an operation that leaves the physical system unchanged. For example, does the physical system remain unchanged when shifting the origin of time? If so, then mechanical energy is a constant of the motion.

Likewise, if there is rotational symmetry around an axis, then the associated angular momentum is a constant of the motion.

The connection between symmetries (kinematics) and conservation laws (dynamics) was made by *Noether* (1918) (see *Noether and Tavel* (2018) for an English translation). We provide the mathematical expression of Noether's theorem in Section 12.9 as part of our study of Hamilton's principle. It is sufficient for this chapter to make use of this theorem as a conceptual framework for understanding conservation laws and their connections to symmetries. Quite simply, if there is a symmetry then there is a corresponding conservation law, and vice versa.

It is very useful to identify conserved quantities as a means to understand and to dynamically constrain the motion. This perspective holds even when the symmetries giving rise to conserved quantities are broken through the introduction of non-conservative forces such as friction. For example, as seen in Section 11.1.6, friction breaks time translation symmetry and so leads to the dissipation of mechanical energy. Nonetheless, understanding the conservative motion, and the associated energy conservation law, offers insights for the case with friction. In this chapter, we offer two examples to support this point: mechanical energy conservation and axial angular momentum conservation. These conservation laws also hold in a modified form for the continuum fluid (e.g., Chapter 24). Additional conservation properties also arise that are unique to the continuum, with conservation of potential vorticity the most notable one for geophysical fluids (Chapter 41).

14.1.2 Further study

Conservation laws and symmetries in classical mechanics are lucidly discussed in Chapters 1 and 2 of *Landau and Lifshitz* (1976). Pedagogical presentations on these topics can be found in this online lecture from the Space Time series and this online lecture from Physics with Elliot. This essay about Emmy Noether provides insights into this mathematician whose work, conducted under some very unfortunate circumstances, forever connected symmetries to conservation laws, with this connection providing the basis for nearly all modern theories of physics.

14.2 Time reversal symmetry

As a warm-up to the ideas of symmetry, consider the question about time reversibility. A deterministic process is time-reversible if the time-reversed process satisfies the same dynamical equations as the forward-time process. That is, the dynamical equations are symmetric under a change in the sign of time so that the time-reversed evolution of one state is equivalent to the forward-time evolution of a corresponding state. We here discuss time reversal symmetry in the context of the point particle with trajectory, $\boldsymbol{X}(t)$, and velocity, $\boldsymbol{V}(t) = \mathrm{d}\boldsymbol{X}(t)/\mathrm{d}t$.

If $\boldsymbol{X}(t)$ is a solution to the equations of motion, then what is needed for

$$\boldsymbol{X}^*(t^*) = \boldsymbol{X}(-t) \quad \text{and} \quad \boldsymbol{V}^*(t^*) = \mathrm{d}\boldsymbol{X}^*(t^*)/\mathrm{d}t^* = -\mathrm{d}\boldsymbol{X}(-t)/\mathrm{d}t \tag{14.1}$$

to define the same trajectory traversed backwards in time, where $t^* = -t$? We answer this question by recalling from Section 13.11.1 that with planetary rotation a constant in time then the Cartesian coordinate equation of motion is given by

$$\frac{\mathrm{d}}{\mathrm{d}t}\left[\frac{\mathrm{d}\boldsymbol{X}(t)}{\mathrm{d}t} + 2\,\boldsymbol{\Omega} \times \boldsymbol{X}(t)\right] = -\nabla\Phi(t). \tag{14.2}$$

We are interested in the constraints that ensure the following equation is satisfied

$$\frac{\mathrm{d}}{\mathrm{d}t^*}\left[\frac{\mathrm{d}\boldsymbol{X}^*(t^*)}{\mathrm{d}t^*} + 2\,\boldsymbol{\Omega}^* \times \boldsymbol{X}^*(t^*)\right] = -\nabla\Phi(t^*). \tag{14.3}$$

The effective gravitational acceleration remains time reversible if

$$\Phi^*(t^*) = \Phi(t), \tag{14.4}$$

which is trivially satisfied for $\Phi = g\,z$. The Coriolis acceleration is velocity dependent so that it generally breaks time reversal symmetry. However, we can recover time symmetry by assuming that the rotation direction switches when time reverses so that

$$\boldsymbol{\Omega}^* = -\boldsymbol{\Omega}. \tag{14.5}$$

With this transformation, a trajectory, $\boldsymbol{X}(t)$, that solves the forward equation (14.2) yields a trajectory $\boldsymbol{X}(-t)$ that solves the same equation but with time (and $\boldsymbol{\Omega}$) reversed. We return in Section 25.8.12 to the question of time reversal symmetry for the Euler equations of perfect fluid mechanics.

14.3 Potential momentum

In Section 13.11.1 we introduced the *potential momentum*, and we here further study its conservation properties. Recall that it is a constant of the motion when a particle moves on a time independent geopotential in a direction where the geopotential does not change. That is, the conservation of potential momentum arises from a spatial symmetry of the geopotential.

14.3.1 Basics

Start with the planetary Cartesian coordinate equation of motion

$$\frac{\mathrm{d}}{\mathrm{d}t}\left[\dot{\boldsymbol{X}} + 2\,\boldsymbol{\Omega} \times \boldsymbol{X}\right] = -\nabla\Phi. \tag{14.6}$$

Now introduce the *potential momentum* per mass

$$\boldsymbol{M} \equiv \dot{\boldsymbol{X}} + 2\,\boldsymbol{\Omega} \times \boldsymbol{X} = \hat{\boldsymbol{x}}\,(u - 2\,\Omega\,y) + \hat{\boldsymbol{y}}\,(v + 2\,\Omega\,x) + \hat{\boldsymbol{z}}\,w, \tag{14.7}$$

in which case the equation of motion takes the form

$$\dot{\boldsymbol{M}} = -\nabla\Phi. \tag{14.8}$$

Now let $\hat{\boldsymbol{s}}$ be a unit vector tangent to the geopotential surface so that $\hat{\boldsymbol{s}} \cdot \nabla\Phi = 0$. Assuming the geopotential surface is time independent so that $\hat{\boldsymbol{s}}$ is also time independent, then the equation of motion (14.8) leads to

$$\frac{\mathrm{d}(\hat{\boldsymbol{s}} \cdot \boldsymbol{M})}{\mathrm{d}t} = 0. \tag{14.9}$$

That is, the projection of the potential momentum onto a static geopotential surface is a constant of motion. This dynamical constraint arises since we cannot distinguish one point on the geopotential from another; i.e., there is a symmetry associated with motion along the static geopotential. Noether's theorem (Section 14.1.1) then says that this geometric symmetry leads to a constant of the motion, here given by that component of potential momentum within the geopotential surface. We illustrate this situation in Figure 14.1 with a horizontal geopotential surface.

Consider a particle with potential momentum, $\boldsymbol{M}$, and move it from an arbitrary point to a reference position with $\boldsymbol{X} = 0$. Upon reaching the reference position, the horizontal velocity of the particle must equal to $\boldsymbol{M}$ in order to maintain the same potential momentum. This example

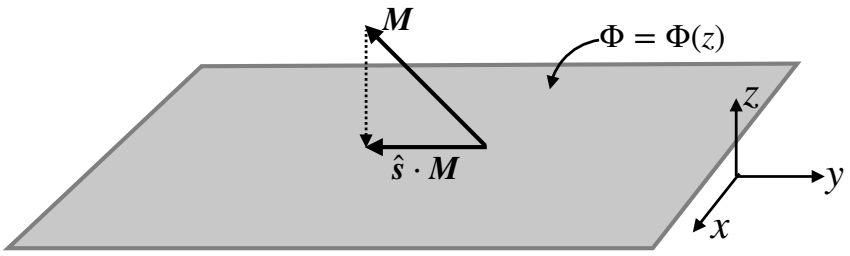

FIGURE 14.1: The projection of the potential momentum onto the geopotential surface is a constant of the motion, $\mathrm{d}(\hat{\boldsymbol{s}} \cdot \boldsymbol{M})/\mathrm{d}t = 0$. Here the geopotential surface is the x-y-plane so that $\hat{\boldsymbol{x}} \cdot \boldsymbol{M} = u - 2\,\Omega\, y$ and $\hat{\boldsymbol{y}} \cdot \boldsymbol{M} = v + 2\,\Omega\, x$ are the two conserved components of potential momentum.

motivates the name "potential momentum", since $\boldsymbol{M}$ measures the potential for relative motion contained in the particle as it moves along a geopotential.

14.3.2 Comment about terminology

As noted on page 51 of *Markowski and Richardson* (2010), one might see potential momentum referred to as *pseudo angular momentum*, with some dropping the "pseudo" portion to the name. In either case, it is important to note that potential momentum is distinct from angular momentum. In particular, there is no moment-arm as part of the potential momentum, nor is there any axial symmetry corresponding to the conservation law.

Many authors use the term *absolute momentum* rather than potential momentum, perhaps in reference to the momentum measured in the absolute or inertial reference frame. However, that connection is incorrect since the inertial frame velocity is (Section 13.7.1)

$$\boldsymbol{V} = \boldsymbol{V}_{\text{Cartesian}} + \boldsymbol{U}_{\text{rigid-body}} = \boldsymbol{V}_{\text{Cartesian}} + \boldsymbol{\Omega} \times \boldsymbol{X}. \tag{14.10}$$

The factor of two multiplying the rotation rate in the potential momentum arises from the Coriolis acceleration. In contrast, the rigid-body rotation velocity contributes to the inertial frame velocity and it has a factor of unity multiplying the rotation rate.

14.4 Free particle motion on the f-plane

In Section 24.5 we introduce the tangent plane approximation for motion on a rotating sphere. In this approximation, motion occurs on a geopotential surface with the surface approximated as a horizontal flat plane. Furthermore, we use local tangent plane Cartesian coordinates (which are distinct from the planetary Cartesian coordinates used in Chapter 13 and illustrated in Figure 4.3). The f-plane approximation furthermore sets the Coriolis parameter to a constant,

$$f = 2\,\Omega \sin \phi_0, \tag{14.11}$$

where ϕ_0 is a chosen latitude. Consequently, a *free particle* constrained to move on a constant geopotential under the f-plane approximation maintains a constant horizontal potential momentum

$$\frac{\mathrm{d}M_x}{\mathrm{d}t} = \frac{\mathrm{d}(u - f\,y)}{\mathrm{d}t} = 0 \tag{14.12a}$$

$$\frac{\mathrm{d}M_y}{\mathrm{d}t} = \frac{\mathrm{d}(v + f\,x)}{\mathrm{d}t} = 0, \tag{14.12b}$$

where we introduced the horizontal velocity components $(u, v) = (\dot{x}, \dot{y})$. These two conservation laws provide dynamical constraints on the free particle motion on a constant geopotential

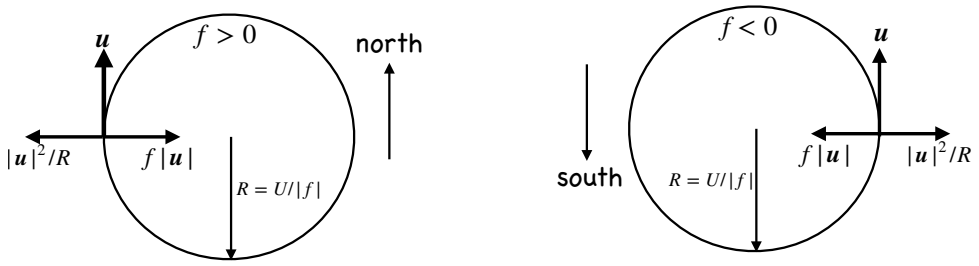

FIGURE 14.2: Free particle motion on a horizontal f-plane occurs when the particle's centrifugal acceleration balances its planetary Coriolis acceleration. Left panel: $f > 0$ for the northern hemisphere, revealing that the motion is an anti-cyclonic (clockwise) circular motion with radius $|R| = U/|f|$. The Coriolis acceleration is to the right, pointing into the center of the inertial circle, whereas the centrifugal acceleration points away from the center. Right panel: Counterclockwise motion in the southern hemisphere with the same balance between Coriolis and centrifugal accelerations.

surface.[1]

14.4.1 Oscillator equation

Taking the time derivative of the zonal equation (14.12a) and using the meridional equation (14.12b) leads to

$$\ddot{u} - f\,\dot{v} = \ddot{u} + f^2 u = 0. \tag{14.13}$$

Similar manipulations for the meridional velocity equation render the free oscillator equation for each component of the horizontal velocity

$$\frac{\mathrm{d}^2 u}{\mathrm{d}t^2} + f^2 u = 0 \qquad \text{and} \qquad \frac{\mathrm{d}^2 v}{\mathrm{d}t^2} + f^2 v = 0. \tag{14.14}$$

Motions that satisfy this equation are termed *inertial oscillations*.

14.4.2 Particle trajectory and velocity

Time integrating the equation of motion (14.14) renders the particle trajectory and its velocity

$$\boldsymbol{X}(t) = (U/f)\,[\hat{\boldsymbol{x}}\sin(ft) + \hat{\boldsymbol{y}}\cos(ft)] \tag{14.15a}$$
$$\boldsymbol{U}(t) = U\,[\hat{\boldsymbol{x}}\cos(ft) - \hat{\boldsymbol{y}}\sin(ft)], \tag{14.15b}$$

where $U > 0$ is the particle speed, which is a constant, and we assumed the initial conditions

$$\boldsymbol{X}(0) = (U/f)\,\hat{\boldsymbol{y}} \qquad \text{and} \qquad \boldsymbol{U}(0) = U\,\hat{\boldsymbol{x}}. \tag{14.16}$$

From the particle trajectory equation (14.15a), we see that the free particle motion is circular with a radius

$$R = U/|f|. \tag{14.17}$$

As depicted in Figure 14.2, northern hemisphere ($f > 0$) free particle motion occurs in the clockwise direction whereas southern hemisphere motion is counter-clockwise. This motion arises from the rightward deflection by the Coriolis in the northern hemisphere and leftward in the southern. Consequently, particle motion occurs in an anti-cyclonic sense (opposite to the sense of the rotating reference frame). As studied in Section 32.4, this motion arises from a balance

[1] It is important to recall from Section 13.10.4 that motion on a geopotential incorporates the acceleration from both the central gravitational field and the planetary centrifugal acceleration. Hence, there is no planetary centrifugal term when studying free particle motion on the f-plane.

between the Coriolis acceleration of the rotating frame and the centrifugal acceleration arising from the particle's circular motion. The only way to realize this balance is for the particle to move anti-cyclonically, with the Coriolis acceleration pointing towards the inside of the circle and the centrifugal acceleration pointing outside. Finally, note that the potential momentum vanishes since

$$\boldsymbol{M}(t) = \boldsymbol{U}(t) + f\,\hat{\boldsymbol{z}} \times \boldsymbol{X}(t) = 0. \tag{14.18}$$

Adding an arbitrary constant to the initial position makes the potential momentum equal to a nonzero constant.

14.4.3 Period of the circular motion

The circular motion of the free particle possesses a constant speed and moves around a circle with a period

$$T_{\text{inertial}} = \frac{2\,\pi}{f} = \frac{11.97}{|\sin\phi_0|}\,\text{hour}, \tag{14.19}$$

where we set $\Omega = 7.292 \times 10^{-5}\text{s}^{-1}$ (equation (13.1)). This period is the time it takes to go around the circle. It is smallest at the poles, where the latitude $\phi_0 = \pm\pi/2$ and $T_{\text{smallest}} \approx 12\,\text{hour}$. At the equator, $\phi_0 = 0$, so that the radius of the inertial circle is infinite and inertial oscillations are unavailable. Furthermore, T_{inertial} is the time for a Foucault pendulum (Section 15.3) to turn through π radians, so that T_{inertial} is sometimes referred to as one-half a pendulum day.

14.4.4 Inertial oscillations

The circular free particle motion studied in this section is sometimes referred to as an *inertial oscillation*. Again, this circular motion occurs on a constant geopotential and on the f-plane when there is a balance between the Coriolis acceleration from planetary rotation and centrifugal acceleration arising from the curved motion of a particle on a constant geopotential. Importantly, the centrifugal acceleration here is not the planetary centrifugal acceleration (Section 13.10.4), with the planetary centrifugal acceleration absorbed into the effective gravity that is a fixed constant along a geopotential.

Furthermore, the name "inertial" does not refer to motion as observed in an inertial reference frame. Instead, it is used as a synonym for free particle motion, with the free motion here in the directions along a constant geopotential.[2] More generally, there has been some confusion in the literature concerning the forces acting in inertial oscillations, particularly when not making a tangent plane approximation. *Early* (2012) clarifies the fundamental physics. We return to these matters in Section 15.4, there making use of Lagrangian mechanics to examine the energetics and forces acting on the free particle.

14.4.5 Comments and further study

Inertial oscillations of fluid elements are described by the above constant potential momentum equation of motion. Such oscillations are commonly measured by ocean current meters, especially in higher latitude regions where diurnal (day-night) variations in wind forcing have a strong projection onto the inertial period. This resonant forcing puts energy into inertial or near-inertial motions. It is quite amazing that such oscillations are indeed found in the ocean, given that we have ignored pressure and friction, which are two forces that impact on fluid motion (whereas pressure and friction do not affect point particles). A key reason we can observe such motion is that upper ocean currents are often generated by winds even in the absence of horizontal

[2] See Section 11.3.2 for comments on the somewhat confusing terminology used to refer to the Coriolis acceleration and centrifugal acceleration as "inertial" accelerations.

pressure gradients. Hence, there are occasions when the motion is not strongly affected by pressure gradients or friction, thus allowing for the inertial oscillations to manifest.

We study inertial waves in Chapter 53 as part of our study of rapidly rotating fluid motion. We also encounter inertial motions in Section 32.4 as part of our characterization of horizontal fluid motion according to the balance between forces. A rotating fluid in a tank offers a useful controlled setting to observe inertial waves in a fluid, such as shown near the 18 minute mark in this video from Prof. Fultz.

14.5 Angular momentum

We introduced the concept of angular momentum in Section 11.2.4, with angular momentum the moment of linear momentum and given by the following expression for the point particle

$$\boldsymbol{L} = m\, \boldsymbol{X} \times \boldsymbol{V}. \tag{14.20}$$

In this section we study the angular momentum computed relative to the center of a spherical planet; i.e., where $\boldsymbol{X}$ is the position of the particle with respect to the sphere's center. For a non-rotating sphere, there is spherical symmetry, meaning that rotations around any axis extending out from the sphere's center represent symmetry operations. Noether's theorem then says that the angular momentum projected onto any of these axes is a constant of the motion for a particle moving around the non-rotating sphere. For a rotating spherical planet, the polar rotational axis is distinguished from all other axes, so that the spherical symmetry of the non-rotating planet is broken down to symmetry around just the rotational axis. Indeed, for oblate spheroidal planets, the rotation axis is the only symmetry axis. Noether's theorem then says that it is only the axial component of angular momentum that is conserved for the rotating planet.

To be more specific, we ask whether a point particle knows anything about the longitudinal angle, λ, on the rotating planet (Figure 14.3)? Assuming the planet is smooth (i.e., no mountains), and the planet rotates around the polar axis (along the planetary $\hat{\boldsymbol{z}}$ direction), then there is an arbitrariness in the value of the longitude. That is, the physical system remains unchanged if we shift the longitudinal angle by a constant. Noether's theorem then says that this symmetry leads to a corresponding conservation of angular momentum around the polar axis.

We here display the manipulations that show axial angular momentum, $L^z = \hat{\boldsymbol{z}} \cdot \boldsymbol{L}$, is a constant of the motion for motion around the rotating sphere, and furthermore show that the other components to angular momentum, $L^x = \hat{\boldsymbol{x}} \cdot \boldsymbol{L}$ and $L^y = \hat{\boldsymbol{y}} \cdot \boldsymbol{L}$, are not constant. Many of the same concepts and mathematical manipulations occur when considering angular momentum conservation for a fluid in Section 24.7.

14.5.1 Axial angular momentum

The axial angular momentum is the component of the angular momentum through the polar axis, and it can be written in the following equivalent manners

$$L^z = \boldsymbol{L} \cdot \hat{\boldsymbol{z}} = m\, (\boldsymbol{X} \times \boldsymbol{V}) \cdot \hat{\boldsymbol{z}} = m\, (\hat{\boldsymbol{z}} \times \boldsymbol{X}) \cdot \boldsymbol{V} = m\, r \cos\phi\, (\hat{\boldsymbol{\lambda}} \cdot \boldsymbol{V}) = m\, r_\perp\, (\hat{\boldsymbol{\lambda}} \cdot \boldsymbol{V}). \tag{14.21}$$

Evidently, the component of angular momentum along the polar axis equals to the component of the linear momentum in the longitudinal direction, multiplied by the distance to the polar rotational axis (the moment-arm)

$$r_\perp = r \cos\phi. \tag{14.22}$$

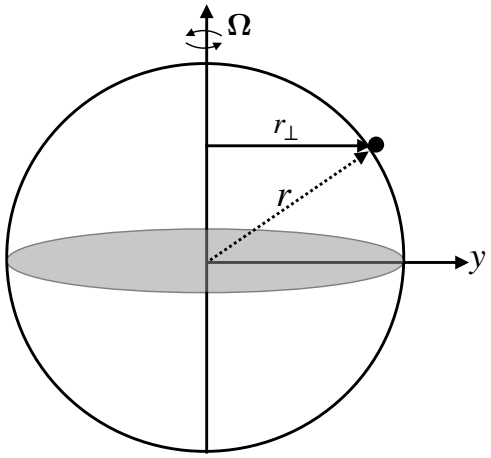

FIGURE 14.3: Axial angular momentum is the component of the angular momentum through the polar axis, $L^z = \hat{\boldsymbol{z}} \cdot \boldsymbol{L}$. It is the moment of the zonal momentum around the polar axis, with the moment-arm, $r_\perp = r\,\cos\phi = \sqrt{x^2 + y^2}$, the distance to the axis of rotation, whereas $r^2 = \sqrt{x^2 + y^2 + z^2}$ is the radial distance to the center of the planet. It can be written in the equivalent manners $L^z = m\,r_\perp\,(\hat{\boldsymbol{\lambda}} \cdot \boldsymbol{V}) = m\,r_\perp^2\,(\dot{\lambda} + \Omega) = m\,r_\perp\,(u + r_\perp\,\Omega)$. The axial angular momentum is a constant of the motion for the particle moving on a smooth rotating planet in the absence of friction.

In deriving equation (14.21), we made use of the identity (see equation (4.233))

$$\hat{\boldsymbol{z}} \times \boldsymbol{X} = r\,\hat{\boldsymbol{z}} \times \hat{\boldsymbol{r}} = r_\perp\,\hat{\boldsymbol{\lambda}}, \tag{14.23}$$

which we use below for proving that axial angular momentum is a constant of the motion.

We can write the axial angular momentum from equation (14.21) in terms of the rotating frame quantities. To do so, decompose the inertial frame velocity written using spherical coordinates according to equation (13.46f), which yields

$$L^z = m\,r_\perp\,(\hat{\boldsymbol{\lambda}} \cdot \boldsymbol{V}) = m\,r_\perp^2\,(\dot{\lambda} + \Omega) = m\,r_\perp\,(u + r_\perp\,\Omega). \tag{14.24}$$

Evidently, when measured from the rotating terrestrial frame, the axial angular momentum consists of two terms: one from the zonal velocity of the particle relative to the rotating planet and another from the rigid-body motion of the planet.

14.5.2 Axial angular momentum is a constant of the motion

The time derivative of the axial angular momentum is given by

$$\begin{aligned}
m^{-1}\,\mathrm{d}L^z/\mathrm{d}t &= \mathrm{d}/\mathrm{d}t\,[(\boldsymbol{X} \times \boldsymbol{V}) \cdot \hat{\boldsymbol{z}}] && \text{definition of axial angular momentum} && (14.25a)\\
&= \mathrm{d}/\mathrm{d}t\,[(\hat{\boldsymbol{z}} \times \boldsymbol{X}) \cdot \boldsymbol{V}] && \text{cyclic permutation from equation (1.60j)} && (14.25b)\\
&= (\hat{\boldsymbol{z}} \times \boldsymbol{V}) \cdot \boldsymbol{V} + (\hat{\boldsymbol{z}} \times \boldsymbol{X}) \cdot \boldsymbol{A} && \mathrm{d}\boldsymbol{X}/\mathrm{d}t = \boldsymbol{V},\ \mathrm{d}\boldsymbol{V}/\mathrm{d}t = \boldsymbol{A},\ \text{and } \mathrm{d}\hat{\boldsymbol{z}}/\mathrm{d}t = 0 && (14.25c)\\
&= (\hat{\boldsymbol{z}} \times \boldsymbol{X}) \cdot \boldsymbol{A} && (\hat{\boldsymbol{z}} \times \boldsymbol{V}) \cdot \boldsymbol{V} = 0 && (14.25d)\\
&= r_\perp\,\hat{\boldsymbol{\lambda}} \cdot \boldsymbol{A}. && \hat{\boldsymbol{z}} \times \boldsymbol{X} = r_\perp\,\hat{\boldsymbol{\lambda}} \text{ from equation (14.23).} && (14.25e)
\end{aligned}$$

The inertial frame acceleration arises just from the central-force gravitational field (equation (13.124))

$$\boldsymbol{A} = -\nabla\Phi_\mathrm{e} = -g_\mathrm{e}\,\hat{\boldsymbol{r}}. \tag{14.26}$$

Evidently, the central gravity force has no affect on the axial angular momentum since $\hat{\boldsymbol{\lambda}} \cdot \hat{\boldsymbol{r}} = 0$. We are thus led to axial angular momentum conservation

$$\frac{\mathrm{d}L^z}{\mathrm{d}t} = 0. \tag{14.27}$$

Conservation of axial angular momentum plays an important role in constraining the particle motion, and we explore those constraints in Section 14.6.

14.5.3 L^x and L^y are not constants of the motion

To display the symmetry breaking nature of rotation around the polar axis, we here show that the angular momentum components, $\hat{\boldsymbol{x}} \cdot \boldsymbol{L}$ and $\hat{\boldsymbol{y}} \cdot \boldsymbol{L}$, are not constants of the motion. For $L^x = \hat{\boldsymbol{x}} \cdot \boldsymbol{L}$ we write

$$m^{-1}\, L^x = (\hat{\boldsymbol{x}} \times \hat{\boldsymbol{X}}) \cdot \boldsymbol{V} = r\, (\hat{\boldsymbol{x}} \times \hat{\boldsymbol{r}}) \cdot \boldsymbol{V}, \tag{14.28}$$

so that its time derivative is

$$m^{-1}\, \mathrm{d}L^x/\mathrm{d}t = (\mathrm{d}\hat{\boldsymbol{x}}/\mathrm{d}t \times \boldsymbol{X}) \cdot \boldsymbol{V} + (\hat{\boldsymbol{x}} \times \dot{\boldsymbol{X}}) \cdot \boldsymbol{V} + r\, (\hat{\boldsymbol{x}} \times \hat{\boldsymbol{r}}) \cdot \boldsymbol{A} \tag{14.29a}$$

$$= r\, \Omega\, (\hat{\boldsymbol{y}} \times \hat{\boldsymbol{r}}) \cdot \boldsymbol{V}, \tag{14.29b}$$

where we used equation (13.7) to write $\mathrm{d}\hat{\boldsymbol{x}}/\mathrm{d}t = \Omega\, \hat{\boldsymbol{y}}$. Similarly, we have

$$m^{-1}\, L^y = (\hat{\boldsymbol{y}} \times \hat{\boldsymbol{X}}) \cdot \boldsymbol{V} = r\, (\hat{\boldsymbol{y}} \times \hat{\boldsymbol{r}}) \cdot \boldsymbol{V}, \tag{14.30}$$

so that its time derivative is

$$m^{-1}\, \mathrm{d}L^y/\mathrm{d}t = (\mathrm{d}\hat{\boldsymbol{y}}/\mathrm{d}t \times \boldsymbol{X}) \cdot \boldsymbol{V} = -r\, \Omega\, (\hat{\boldsymbol{x}} \times \hat{\boldsymbol{r}}) \cdot \boldsymbol{V}, \tag{14.31}$$

where $\mathrm{d}\hat{\boldsymbol{y}}/\mathrm{d}t = -\Omega\, \hat{\boldsymbol{x}}$ from equation (13.7). Evidently, both $\mathrm{d}L^x/\mathrm{d}t$ and $\mathrm{d}L^y/\mathrm{d}t$ vanish when $\Omega = 0$. Otherwise, when $\Omega \neq 0$ then both L^x and L^y are not constant, leaving just L^z as a constant of the motion.

14.6 Facets of the Coriolis acceleration

The Coriolis acceleration is a primary feature of motion in the ocean and atmosphere, and for any motion that spans large distances over the planet (e.g., projectiles, satellites). There are a variety of methods available to lend understanding to facets of Coriolis, though few can replace time pondering its implications. In this section we offer a few thought experiments to help build understanding. As part of those thought experiments, we show that acceleration induced by axial angular momentum conserving motion connects to the Coriolis acceleration appearing in the zonal momentum equation. This connection offers a clear example of how conservation principles, which lead to constraints, directly affect motion.

14.6.1 Two pictures to help frame the discussion

Before working through the mathematical analysis needed to quantitatively understand the Coriolis acceleration, we consider two depictions of the Coriolis acceleration as it acts on a moving particle whose motion is viewed in a rotating reference frame. These pictures capture essential features of the Coriolis acceleration for studies of geophysical fluid motion.

Figure 14.4 shows the motion of a particle on a rotating and frictionless table. We can choose to observe this motion from the comfort of the laboratory frame, which we assume approximates an inertial frame, or we can view the motion from the rotating table (preferably viewed by a

camera on the table so as to avoid becoming too dizzy). The figure caption details the motion from the two reference frames. Evidently, the rotating reference frame observer sees the particle motion deflected to the right, regardless the direction that the particle moves on the table. In contrast, the inertial reference frame observer views the table moving to the left according to the counter-clockwise motion of the table, whereas the particle moves along a straight line. We emphasize that the motion is objectively the same; it is the same particle moving through space along the same single trajectory. However, the perspectives of observers in the two reference frames clearly differ.

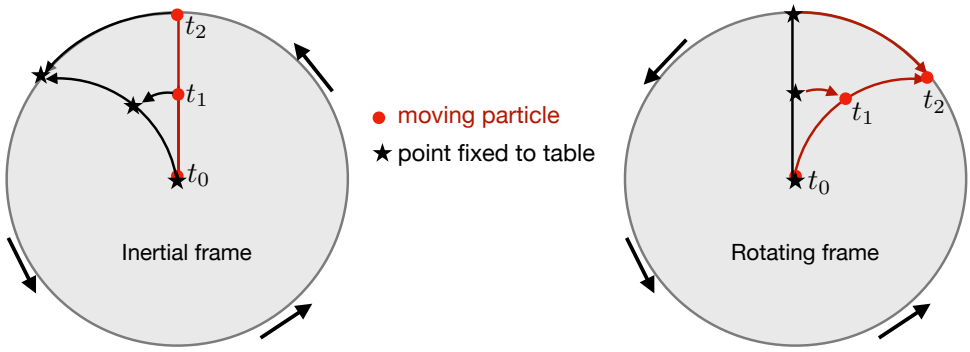

FIGURE 14.4: Illustrating the motion of a particle on a frictionless table (e.g., a perfectly slick ice rink), with the table rotating in the counter-clockwise sense around its center (corresponding to the planetary rotation as viewed from the northern hemisphere). The particle (red dot) moves outward from the center of the table at time t_0 to the edge at time t_2, with an intermediate position at time t_1. The left panel shows the motion viewed from an inertial (non-rotating) reference frame, whereby the particle moves along a straight line from the center to the edge. During this transit, the table moves underneath the particle. Stars designate points painted on the table, with the stars moving to the left as the table rotates. The right panel depicts the motion viewed within the frame at rest with the rotating table (rigid-body rotating non-inertial reference frame). Here, the positions on the table remain fixed (the stars do not move), whereas the particle moves along a rightward curved trajectory as it reaches the edge. The rotating frame observer interprets the rightward deflection as due to the Coriolis acceleration.

The rotating table example in Figure 14.4 captures the essence of how the Coriolis acceleration deflects particles moving along horizontal trajectories around the rotating planet. Namely, each point on the planet is akin to a rotating table. Importantly, the rotation rate (and sign) is a function of latitude since the imprint of the planetary rotation depends on the latitude. So although the planet rotates at a constant angular velocity, the imprint of that rotation has a latitudinal dependence due to the spherical geometry of the planet. This added feature of planetary Coriolis acceleration is referred to as the *beta effect*, and it is is a fundamental distinction from the rotating flat table of Figure 14.4 where each point on the table feels the same angular rotation vector. Facets of the beta effect are revealed through the course of this book.

Figure 14.5 summarizes features of the Coriolis acceleration seen for motion on a rotating planet. Here, the particle trajectories are deflected to the right in the northern hemisphere, where the planetary rotation is counter-clockwise just as in the rotating table example. However, for the southern hemisphere the planetary rotation is clockwise, so that the Coriolis deflection is to the left. To help understand the sign switch, imagine viewing the planet from above the north pole, whereby the rotation of the planet is counter-clockwise. Now view the planet from below the south pole, in which case the earth is seen to rotate clockwise.[3] This sign swap reflects the *axial vector* nature of the angular velocity vector, with axial vectors discussed in Section 1.7.2.

[3]Those who do not trust their mind's eye are encouraged to perform the thought experiment with a globe.

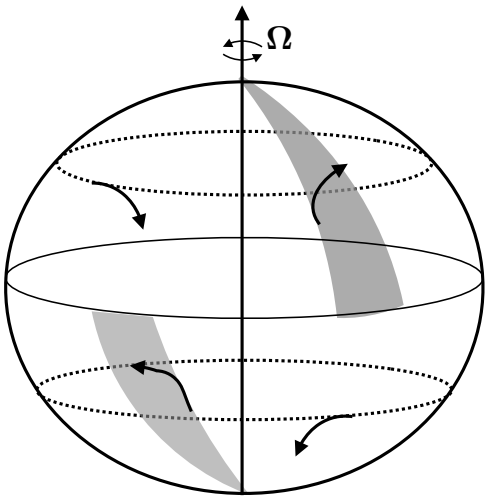

FIGURE 14.5: For a particle moving at constant radial distance from the planet center, the Coriolis acceleration deflects to the right in the northern hemisphere and to the left in the southern hemisphere. This figure summarizes key features of the Coriolis acceleration for large-scale geophysical motions. The one exception is the missing vertical acceleration induced by the Coriolis acceleration, with this vertical deflection discussed in Section 14.6.8. It is notable that this vertical acceleration is tiny compared to that from gravity, and so it is commonly ignored.

14.6.2 Constraints from axial angular momentum conservation

There are various ways to express the constraints resulting from conservation of axial angular momentum, most notably whether we describe the motion from the inertial frame or rotating frame. Here we explore the constraints viewed by the rotating terrestrial observer. Since the mass, m, of the particle is constant, we find it a bit more convenient to work with the axial angular momentum per mass, which from Section 14.5.1 takes on the form

$$l^z = L^z/m = r_\perp \, \hat{\boldsymbol{\lambda}} \cdot \boldsymbol{V} = r_\perp^2 \, (\dot\lambda + \Omega) = r_\perp \, (u + r_\perp \, \Omega), \tag{14.32}$$

where the zonal velocity component is given by equation (13.48)

$$u = r_\perp \, \dot\lambda = r \cos\phi \, \dot\lambda. \tag{14.33}$$

Note that for most geophysical applications, $l^z > 0$ since rigid-body motion dominates over the relative zonal velocity:

$$r_\perp \, \Omega > |u| \qquad \text{for most terrestrial motions,} \tag{14.34}$$

with $r_\perp \, \Omega = 465$ m s^{-1} at the equator (see Figure 13.2). In Exercise 14.1 we consider the interesting, but geophysically uncommon, case where $l^z \leq 0$.

Constraints on δu and $\delta\dot\lambda$ in terms of $\delta r_\perp$

To determine the constraints, we set $\delta l^z = 0$, where δ refers to any small change brought about by some perturbation whose origins are not of concern. When writing $l^z = r_\perp^2 \, (\dot\lambda + \Omega)$ we have

$$\delta l^z = 2 \, r_\perp \, \delta r_\perp \, (\dot\lambda + \Omega) + r_\perp^2 \, \delta\dot\lambda = 2 \, l^z \, \frac{\delta r_\perp}{r_\perp} + r_\perp^2 \, \delta\dot\lambda, \tag{14.35}$$

where we set $\delta\Omega = 0$ since the earth's rotation rate is assumed to be fixed. Furthermore, we find it useful to express the perturbations in terms of l^z since it is a constant of the motion. Likewise,

when writing $l^z = r_\perp\,(u + r_\perp\,\Omega)$ we have

$$\delta l^z = \delta r_\perp\,(u + r_\perp\,\Omega) + r_\perp\,(\delta u + \Omega\,\delta r_\perp) = \Omega\,r_\perp\,\delta r_\perp\,\left[1 + \frac{l^z}{\Omega\,r_\perp^2}\right] + r_\perp\,\delta u. \tag{14.36}$$

Setting $\delta l^z = 0$ then leads to the expressions for the constraints

$$\delta\dot{\lambda} = -\frac{2\,l^z}{r_\perp^2}\,\frac{\delta r_\perp}{r_\perp} \Longleftrightarrow \delta u = -\Omega\,\delta r_\perp\left[1 + \frac{l^z}{\Omega\,r_\perp^2}\right]. \tag{14.37}$$

As noted above, $l^z > 0$ is generally the case for geophysical fluid motion. Consequently, axial angular momentum conserving motion that brings the particle closer to the rotation axis ($\delta r_\perp < 0$) leads to an eastward velocity change (angular velocity $\delta\dot{\lambda} > 0$ and zonal velocity $\delta u > 0$). The opposite occurs for motion with $\delta r_\perp > 0$. These results hold in both the northern and southern hemispheres.

Unpacking $\delta r_\perp$ in terms of δr and $\delta\phi$

Since $r_\perp = r\cos\phi$, the distance to the rotational axis can be perturbed through changing either the radial position or the meridional position

$$\delta r_\perp = (\cos\phi)\,\delta r - (r\sin\phi)\,\delta\phi. \tag{14.38}$$

Assuming these perturbations occur over a small time increment, δt, allows us to write

$$\delta r_\perp/\delta t = w\cos\phi - v\sin\phi, \tag{14.39}$$

where we made use of equation (13.48) to introduce the meridional and vertical velocity components

$$v = r\,\delta\phi/\delta t = r\,\dot{\phi} \quad \text{and} \quad w = \delta r/\delta t = \dot{r}. \tag{14.40}$$

For motion in the earth's atmosphere and ocean, perturbations to vertical distance, δr, are far smaller than the distance to the earth's center, $\delta r \ll r$, since the thickness of the ocean and atmosphere are very small compared to the earth's radius. In this case, when $\phi \neq 0$, then $\delta r_\perp$ is affected much more by meridional motion at constant radial position (second term on right hand side of equation (14.39)) than by vertical motion at constant latitude (first term on right hand side of equation (14.39)). We return to this observation in Section 14.6.9 when discussing the shallow fluid approximation used to develop the primitive equations for the atmosphere and ocean (Section 27.1.2).

14.6.3 Axial angular momentum conservation and Coriolis acceleration

Consider a particle at rest in the rotating frame so that its axial angular momentum equals to that arising from the rigid-body motion of the planet, $l^z = r_\perp^2\,\Omega$. If we perturb this initial state while conserving axial angular momentum, equation (14.37) says there must be an associated change in the zonal velocity given by

$$\delta\dot{\lambda} = -2\,\Omega\,\frac{\delta r_\perp}{r_\perp} \quad \text{and} \quad \delta u = -2\,\Omega\,\delta r_\perp. \tag{14.41}$$

If the perturbation occurs over a time increment, δt, then we have

$$\delta\dot{\lambda}/\delta t = \ddot{\lambda} = -2\,\Omega\,\frac{\delta r_\perp/\delta t}{r_\perp} = -2\,\Omega\,(w\cos\phi - v\sin\phi)/r_\perp \tag{14.42a}$$

$$\delta u/\delta t = \dot{u} = -2\,\Omega\,(\delta r_\perp/\delta t) = -2\,\Omega\,(w\cos\phi - v\sin\phi), \tag{14.42b}$$

where we used equation (14.39) for $\delta r_\perp/\delta t$. The expression for $\dot{u}$ is precisely the same as the Coriolis acceleration appearing in the zonal momentum equation (13.138a)

$$\dot{u} + \frac{u\,(w - v\tan\phi)}{r} = \underbrace{-2\,\Omega\,(w\cos\phi - v\sin\phi).}_{\text{Coriolis acceleration}} \tag{14.43}$$

We thus find that the Coriolis acceleration appearing in the zonal momentum equation is identical to the zonal acceleration induced by constraining the motion to conserve axial angular momentum. That is, by unpacking the constraint of axial angular momentum conservation to reveal the zonal momentum equation, the Coriolis acceleration is revealed to be part of the package. Furthermore, we see that both vertical and meridional motion lead to zonal accelerations through the Coriolis acceleration or, equivalently, through axial angular momentum conservation.

14.6.4 Deriving $\dot{u}$ from $\mathrm{d}L^z/\mathrm{d}t = 0$

The discussion in Section 14.6.3 can be formalized by analyzing how the conservation of axial angular momentum leads to an expression for the zonal acceleration, $\dot{u}$. For this purpose, compute the time derivative of the first form of the axial angular momentum in equation (14.32), in which case

$$\frac{\mathrm{d}l^z}{\mathrm{d}t} = \frac{\mathrm{d}[(r\cos\phi)^2\,(\dot{\lambda} + \Omega)]}{\mathrm{d}t} \tag{14.44a}$$

$$= 2\,(\dot{r}\cos\phi - r\,\dot{\phi}\sin\phi)\,(\dot{\lambda}\,r\cos\phi + r\,\Omega\cos\phi) + (r\cos\phi)^2\,\ddot{\lambda} \tag{14.44b}$$

$$= 2\,(w\cos\phi - v\sin\phi)\,(u + r\,\Omega\cos\phi) + (r\cos\phi)^2\,\ddot{\lambda}, \tag{14.44c}$$

where we introduced the (u, v, w) velocity components according to equation (13.48). With the zonal velocity $u = \dot{\lambda}\,r_\perp = \dot{\lambda}\,r\cos\phi$, we have

$$r\cos\phi\,\ddot{\lambda} = \dot{u} + \frac{u}{r\cos\phi}\,(v\sin\phi - w\cos\phi)\,, \tag{14.45}$$

so that equation (14.44c) takes the form

$$\frac{\mathrm{d}l^z}{\mathrm{d}t} = 2\,(w\cos\phi - v\sin\phi)\,(u + r\,\Omega\cos\phi) + (r\cos\phi)^2\,\ddot{\lambda} \tag{14.46a}$$

$$= (w\cos\phi - v\sin\phi)\,(u + 2\,r\,\Omega\cos\phi) + \dot{u}\,r\cos\phi. \tag{14.46b}$$

Setting $\mathrm{d}l^z/\mathrm{d}t = 0$ and rearranging then leads to a prognostic equation for the zonal velocity

$$\frac{\mathrm{d}u}{\mathrm{d}t} = \left[\frac{u}{r\cos\phi} + 2\,\Omega\right](v\sin\phi - w\cos\phi). \tag{14.47}$$

The first term in the bracket arises from curvature of the sphere (the "metric acceleration") whereas the second term is the Coriolis acceleration.

The same result can be obtained by performing the time derivative on the second form of the axial angular momentum in equation (14.32), in which case

$$\frac{\mathrm{d}l^z}{\mathrm{d}t} = \frac{\mathrm{d}\,[u\,r\,\cos\phi + \Omega\,(r\,\cos\phi)^2]}{\mathrm{d}t} \tag{14.48a}$$

$$= \dot{u}\,r\,\cos\phi + u\,\dot{r}\,\cos\phi - u\,r\,\dot{\phi}\,\sin\phi + 2\,\Omega\,r\,\cos\phi\,(\dot{r}\,\cos\phi - r\,\dot{\phi}\,\sin\phi). \tag{14.48b}$$

Again, setting $\mathrm{d}l^z/\mathrm{d}t = 0$ and rearranging leads to the zonal acceleration (14.47).

14.6.5 Zonal acceleration induced by meridional motion

We now consider a few thought experiments to help understand how axial angular momentum conservation gives rise to the Coriolis acceleration appearing in the zonal momentum equation. Start by considering a particle moving meridionally ($\delta\phi \neq 0$) while maintaining a constant radial position ($\delta r = 0$). The axial angular momentum constraint (14.42b) induces a zonal acceleration

$$\dot{u} = 2\,\Omega\, v \sin\phi, \tag{14.49}$$

which, as seen by equation (14.43), is the Coriolis acceleration appearing in the zonal momentum equation arising from the meridional motion. For poleward motion in either hemisphere, the product $v \sin\phi$ is always positive.[4] Hence, axial angular momentum conserving motion towards either pole induces an eastward acceleration, whereas a westward acceleration is induced for equatorward motion. For the northern hemisphere, the induced acceleration deflects the particle to the right when looking downstream whereas in the southern hemisphere the induced acceleration deflects the particle to the left. These deflections are illustrated in Figure 14.5.

A rudimentary means to understand the deflections arising from meridional motion is to view a particle trajectory from an inertial reference frame off the planet. For a meridional trajectory, the spinning earth causes the trajectory to pick up zonal motion relative to the earth surface, zonally to the right in the northern hemisphere and zonally to the left in the southern hemisphere. Equivalently, consider a projectile starting from rest on the planet and shot poleward. Since the projectile started closer to the equator, it has a zonal velocity component that is larger than the more poleward ground underneath it as it flies away from the equator. Hence, as it moves poleward it also picks up an eastward velocity component, which is to the right of the poleward motion in the northern hemisphere and to the left in the southern.

14.6.6 Zonal acceleration induced by radial (vertical) motion

Now consider a particle moving radially while holding the latitude fixed ($\delta r \neq 0$ and $\delta\phi = 0$). The axial angular momentum constraint (14.42b) induces a zonal acceleration

$$\dot{u} = -2\,\Omega\, w \cos\phi, \tag{14.50}$$

which, as seen by equation (14.43), is the Coriolis acceleration appearing in the zonal momentum equation arising from the vertical motion. Hence, for vertically downward motion ($w < 0$), axial angular momentum conservation induces a positive zonal acceleration, $\dot{u} > 0$, which we expect from axial angular momentum conservation since the particle is moving closer to the rotation axis.

14.6.7 Meridional acceleration from Coriolis

We showed in Section 14.6.4 that the zonal equation of motion determining $\dot{u}$ is another way of writing the conservation of axial angular momentum. The same, however, cannot be said for the meridional equation of motion, which is given by equation (13.138b)

$$\dot{v} + \frac{v\,w + u^2 \tan\phi}{r} = -2\,\Omega\, u \sin\phi. \tag{14.51}$$

[4] Recall from Figure 4.3 that $\sin\phi \leq 0$ in the Southern Hemisphere, where $-\pi/2 \leq \phi \leq 0$. In contrast, $\sin\phi \geq 0$ in the Northern Hemisphere, where $0 \leq \phi \leq \pi/2$.

The Coriolis acceleration is on the right hand side. In the northern hemisphere ($\sin\phi > 0$), the Coriolis acceleration gives rise to a rightward (equatorward) acceleration, $-2\,\Omega\,u\sin\phi < 0$, when the particle is moving eastward, $u > 0$, thus inducing a negative meridional acceleration, $\dot{v} < 0$. Conversely, if the particle is moving to the west so that $u < 0$, then the Coriolis acceleration is again to the right, only this time it provides a poleward acceleration, $\dot{v} > 0$. The analogous considerations hold in the southern hemisphere where the particle is deflected to the left by the Coriolis acceleration. These motions are reflected in Figure 14.5. Once the particle picks up a meridional component to the motion, then we return to the axial angular momentum constraint (14.42b) to see how zonal flow is affected.

14.6.8 Vertical acceleration from Coriolis

As for the meridional Coriolis acceleration in Section 14.6.7 there is no angular momentum constraint that connects to the Coriolis acceleration appearing in the vertical velocity equation (13.138c)

$$\dot{w} - \frac{u^2 + v^2}{r} = 2\,\Omega\,u\cos\phi - g. \tag{14.52}$$

In both hemispheres the cosine factor is positive, $\cos\phi > 0$. Hence, the Coriolis acceleration is positive (upward) for eastward motion and negative (downward) for westward motion. Note that for typical geophysical motion, the Coriolis acceleration is tiny compared to that arising from gravity.

14.6.9 When lateral motions dominate vertical motions

We here consider two approximations relevant to large scale geophysical fluid motions.

1. The particle kinetic energy is dominated by lateral motions on the sphere (i.e., motion at constant radial position).

2. Vertical (radial) excursions are much smaller than the earth radius.

When applied to a fluid, the first assumption leads to the hydrostatic approximation (Section 27.2), and the second assumption leads to the shallow fluid approximation (Section 27.1.2). Self-consistency of the equations of motion means that these two assumptions must be applied together.

Dropping the vertical velocity component to the kinetic energy leads to

$$K \approx \frac{m}{2}\,[(u + r_\perp\,\Omega)^2 + v^2]. \tag{14.53}$$

The second assumption means that the axial angular momentum takes the approximate form

$$L^z \approx m\,R_\perp\,(u + \Omega\,R_\perp) = m\,R_\perp^2\,(\dot{\lambda} + \Omega), \tag{14.54}$$

where

$$r = R + z \approx R \qquad \text{and} \qquad R_\perp = R\cos\phi. \tag{14.55}$$

The approximate angular momentum (14.54) ignores contributions from vertical motion in changing the moment-arm. Indeed, as noted in Section 14.6.2, vertical movements within the atmosphere and ocean (relatively thin fluid layers over the earth's surface) lead to a relatively small modification to the moment-arm, so the assumption that $r_\perp \approx R\cos\phi$ is reasonable. With $r \approx R$, the zonal acceleration (14.47) is modified to the form

$$\frac{\mathrm{d}u}{\mathrm{d}t} = v\left[\frac{u\tan\phi}{R} + f\right] \qquad \text{where} \qquad f = 2\,\Omega\,\sin\phi. \tag{14.56}$$

That is, we dropped the vertical velocity component, w, from the general form of the acceleration (14.47). Correspondingly, the meridional momentum equation takes the form

$$\frac{\mathrm{d}v}{\mathrm{d}t} = -u\left[\frac{u\tan\phi}{R} + f\right]. \tag{14.57}$$

These approximate forms for the zonal and meridional accelerations appear in the primitive equations developed in Section 27.1.

14.6.10 Comments

A concise summary of many features of rotating physics is provided by this video from SciencePrimer.

14.7 Mechanical energy conservation

Does the particle know anything about the origin of time? Since the angular velocity of the planet and the gravitational acceleration are both assumed constant in time, then shifting the time by an arbitrary constant will leave the physical system unaltered. That is, the physical system remains unchanged if we shift all clocks by a constant amount. Through Noether's theorem, this symmetry in time leads to mechanical energy conservation, which means that the particle's mechanical energy is a fixed constant. We here prove that mechanical energy is constant in time by manipulating the equations of motion. Many of the manipulations also occur when considering the mechanical energy conservation laws for a continuum fluid discussed in Chapter 24.

14.7.1 Some properties of kinetic energy

In this subsection we establish some basic properties of kinetic energy for a particle. As we saw in Section 11.1.4, changes in the kinetic energy of a particle equal to the *mechanical work* done on the particle as it moves along its trajectory

$$K(t_2) - K(t_1) = \int_{\boldsymbol{x}_1}^{\boldsymbol{x}_2} \boldsymbol{F}\cdot\mathrm{d}\boldsymbol{x} = \int_{t_1}^{t_2} \boldsymbol{F}\cdot\boldsymbol{V}\,\mathrm{d}t, \tag{14.58}$$

where $\boldsymbol{V}\,\mathrm{d}t = \mathrm{d}\boldsymbol{x}$ defines the vector increment along the trajectory, and $\boldsymbol{x}_{1,2}$ are the endpoints of the trajectory at times $t_{1,2}$. The integrand, $\boldsymbol{F}\cdot\boldsymbol{V}$, is known as the *power*. Hence, equation (14.58) says that the time integral of the power equals to the difference in kinetic energy between the final and initial times.

The kinetic energy is *not* Galilean invariant since movement to another inertial reference frame leads to the kinetic energy change

$$\overline{\boldsymbol{V}} = \boldsymbol{V} + \boldsymbol{U} \Longrightarrow \overline{K} = K + \frac{m}{2}(2\,\boldsymbol{V}\cdot\boldsymbol{U} + \boldsymbol{U}\cdot\boldsymbol{U}), \tag{14.59}$$

where $\boldsymbol{U}$ is a constant boost velocity so that $\mathrm{d}\boldsymbol{U}/\mathrm{d}t = 0$. We do not expect kinetic energy to be Galilean invariant since kinetic energy measures energy of motion relative to a chosen reference frame. Even so, the time change of the kinetic energy in a different inertial frame is given by the power in the new frame

$$\frac{\mathrm{d}\overline{K}}{\mathrm{d}t} = \frac{\mathrm{d}K}{\mathrm{d}t} + m\,\boldsymbol{A}\cdot\boldsymbol{U} = \boldsymbol{F}\cdot\boldsymbol{V} + \boldsymbol{F}\cdot\boldsymbol{U} = \boldsymbol{F}\cdot\overline{\boldsymbol{V}}. \tag{14.60}$$

Hence, we can directly connect kinetic energy changes to forces within an arbitrary inertial reference frame.

Cartesian expression for kinetic energy

Consider the expression for kinetic energy when introducing the velocity of the rotating reference frame. Writing the inertial frame velocity in the planetary Cartesian form

$$\boldsymbol{V} = \boldsymbol{V}_{\text{Cartesian}} + \boldsymbol{U}_{\text{rigid}}, \tag{14.61}$$

leads to

$$K = \frac{m}{2}\left[\boldsymbol{V}_{\text{Cartesian}} \cdot \boldsymbol{U}_{\text{Cartesian}} + 2\,\boldsymbol{V}_{\text{Cartesian}} \cdot \boldsymbol{U}_{\text{rigid}} + \boldsymbol{U}_{\text{rigid}} \cdot \boldsymbol{U}_{\text{rigid}}\right] \tag{14.62}$$

The first term arises from motion of the particle relative to the rotating sphere; the second arises from coupling between relative velocity and rigid-body velocity; and the third arises from rigid-body motion of the sphere.

Spherical expression for kinetic energy: Part I

To expose spherical symmetry of the physical system, we express the kinetic energy in terms of the planetary spherical coordinates defined in Figure 4.3. Doing so for the rigid-body velocity leads to equation (13.50)

$$\boldsymbol{U}_{\text{rigid}} = \Omega\, r \cos\phi\, \left(-\sin\lambda\, \hat{\boldsymbol{x}} + \cos\lambda\, \hat{\boldsymbol{y}}\right). \tag{14.63}$$

Likewise, the velocity components measured in the rotating frame are given by

$$\dot{X} = \frac{\mathrm{d}\left(r\cos\phi\cos\lambda\right)}{\mathrm{d}t} = \dot{r}\,\cos\phi\,\cos\lambda - r\dot{\phi}\,\sin\phi\,\cos\lambda - r\dot{\lambda}\,\cos\phi\,\sin\lambda \tag{14.64a}$$

$$\dot{Y} = \frac{\mathrm{d}\left(r\cos\phi\sin\lambda\right)}{\mathrm{d}t} = \dot{r}\,\cos\phi\,\sin\lambda - r\dot{\phi}\,\sin\phi\,\sin\lambda + r\dot{\lambda}\,\cos\phi\,\cos\lambda \tag{14.64b}$$

$$\dot{Z} = \frac{\mathrm{d}\left(r\sin\phi\right)}{\mathrm{d}t} = \dot{r}\,\sin\phi + r\dot{\phi}\,\cos\phi. \tag{14.64c}$$

Bringing terms together then leads to the kinetic energy in terms of spherical coordinates

$$K = \frac{m}{2}\left[(\dot{r}^2 + r^2\dot{\phi}^2 + \dot{\lambda}^2\, r^2\cos^2\phi) + (2\,\Omega\, r^2\dot{\lambda}\,\cos^2\phi) + (\Omega\, r\,\cos\phi)^2\right]. \tag{14.65}$$

Spherical expression for kinetic energy: Part II

An alternative means for deriving the kinetic energy in equation (14.65) makes use of the spherical coordinate form of the inertial frame velocity given by equation (13.46f), in which case

$$\boldsymbol{V} = (u + r_\perp\,\Omega)\,\hat{\boldsymbol{\lambda}} + v\,\hat{\boldsymbol{\phi}} + w\,\hat{\boldsymbol{r}}, \tag{14.66}$$

so that

$$K = \frac{m}{2}\left[(u + r_\perp\,\Omega)^2 + v^2 + w^2\right], \tag{14.67}$$

where $r_\perp = r\cos\phi$. Additionally, as discussed in Section 14.5, the axial angular momentum is given by

$$L^z = m\, r_\perp\,(u + r_\perp\,\Omega) \equiv m\, l^z, \tag{14.68}$$

and this property is a constant of the motion when there is azimuthal (zonal) symmetry. It is thus convenient to write the kinetic energy as

$$K = \frac{m}{2}\left[(l^z/r_\perp)^2 + v^2 + w^2\right]. \tag{14.69}$$

Geopotential expression for mechanical energy

As seen in Section 14.7.4 below, the mechanical energy using geopotential coordinates takes on the form

$$M_{\text{geop}} = \frac{m}{2}\left[u^2 + v^2 + w^2 + 2\,g\,r\right], \tag{14.70}$$

where each of these symbols takes on their geopotential interpretation.

14.7.2 Planetary Cartesian mechanical energy

The time derivative of the kinetic energy is given by

$$\frac{\mathrm{d}K}{\mathrm{d}t} = m\,\boldsymbol{V}\cdot\frac{\mathrm{d}\boldsymbol{V}}{\mathrm{d}t} = m\,\boldsymbol{V}\cdot\boldsymbol{A} = -m\,\boldsymbol{V}\cdot\nabla\Phi_{\text{e}}. \tag{14.71}$$

For the final equality we introduced the gravitational potential given that the particle only feels an external force from gravity as per equation (13.124). The gravitational potential is given by (see equation (13.118))

$$\Phi_{\text{e}} = g_{\text{e}}\,r, \tag{14.72}$$

so that

$$\frac{\mathrm{d}K}{\mathrm{d}t} = -m\,\boldsymbol{V}\cdot\nabla\Phi_{\text{e}} = -m\,g_{\text{e}}\,\dot{r}. \tag{14.73}$$

This result means that kinetic energy is reduced when moving the particle away from the earth center ($\dot{r} > 0$). Moving away from the earth requires work to overcome the gravitational acceleration pointing towards the earth. This work to overcome the gravitational attraction is taken away from the kinetic energy of the particle. Furthermore, the work is added to the gravitational potential energy, whose evolution is given by (see equation (13.120))

$$\frac{\mathrm{d}P_{\text{e}}}{\mathrm{d}t} = m\,g_{\text{e}}\,\dot{r}, \tag{14.74}$$

where we assumed a constant gravitational acceleration, g_{e}. Consequently, as the particle moves away from the earth center, its reduction in kinetic energy is exactly compensated by an increase in potential energy. Hence, the mechanical energy for the particle remains constant throughout the motion

$$\frac{\mathrm{d}(K + P_{\text{e}})}{\mathrm{d}t} = 0, \tag{14.75}$$

where the mechanical energy is the sum of the inertial frame kinetic energy plus the gravitational potential energy

$$\begin{aligned} M &= K + P_{\text{e}} && \text{(14.76a)}\\ &= \frac{m}{2}\,\boldsymbol{V}\cdot\boldsymbol{V} + m\,\Phi_{\text{e}} && \text{(14.76b)}\\ &= \frac{m}{2}\left[(u + r_\perp\,\Omega)^2 + v^2 + w^2\right] + m\,g_{\text{e}}\,r && \text{(14.76c)}\\ &= \frac{m}{2}\left[(l^z/r_\perp)^2 + v^2 + w^2\right] + m\,g_{\text{e}}\,r. && \text{(14.76d)} \end{aligned}$$

14.7.3 Planetary spherical mechanical energy

It is physically revealing to expose the exchange of mechanical energy between kinetic and gravitational potential energies. Furthermore, knowledge of the total mechanical energy at any time affords knowledge for all time since the mechanical energy (in the absence of dissipation) remains constant. Following from the discussion in Section 14.6, where we examined the constraints on particle motion due to conservation of axial angular momentum, we here ask similar questions about mechanical energy conservation. We make use of the spherical form of the equations of motion, equations (13.132)-(13.134), which expose the planetary centrifugal and Coriolis accelerations, and pursue the calculation for geopotential coordinates in Section 14.7.4.

We find it convenient to write the momentum equations (13.132)-(13.134) in terms of the distance to the polar axis, $r_\perp = r\cos\phi$, and its time derivative, $\dot r_\perp = w\cos\phi - v\sin\phi$

$$\frac{\mathrm{d}}{\mathrm{d}t}\left[r_\perp\, u + \Omega\, r_\perp^2\right] = 0 \tag{14.77a}$$

$$\dot v = -\frac{v\,w}{r} - \frac{u\tan\phi}{r}\,(u + 2\,\Omega\, r_\perp) - r_\perp\,\Omega^2\sin\phi \tag{14.77b}$$

$$\dot w = \frac{u^2+v^2}{r} + 2\,\Omega\, u\,\cos\phi + r_\perp\,\Omega^2\cos\phi - g_\mathrm{e}. \tag{14.77c}$$

Equation (14.77a) expresses the conservation of axial angular momentum, $\dot l^z = 0$, where the axial angular momentum per mass is $l^z = r_\perp\,(u + r_\perp\,\Omega)$ (Section 14.5). For the mechanical energy, we have

$$\dot M = 0 \qquad \text{with} \qquad M = \frac{m}{2}\left[(l^z/r_\perp)^2 + v^2 + w^2\right] + m\,g_\mathrm{e}\,r, \tag{14.78}$$

where $l^z/r_\perp = u + r_\perp\,\Omega$ is the zonal component to the inertial frame velocity (equation (13.46f)). We now show that $\dot M = 0$ arises from the momentum equations. Performing the time derivative, and setting $\mathrm{d}l^z/\mathrm{d}t = 0$, leads to

$$\frac{1}{m}\,\dot M = \frac{1}{2}\,\frac{\mathrm{d}}{\mathrm{d}t}\left[(l^z/r_\perp)^2 + v^2 + w^2 + 2\,g_\mathrm{e}\,r\right] = -\frac{(l^z)^2\,\dot r_\perp}{(r_\perp)^3} + v\,\dot v + w\,(\dot w + g_\mathrm{e}). \tag{14.79}$$

Use of the meridional momentum equation (14.77b) renders

$$v\,\dot v = -v\left[\frac{v\,w}{r} + \frac{u\tan\phi}{r}\,(u + 2\,\Omega\, r_\perp) + r_\perp\,\Omega^2\sin\phi\right] \tag{14.80a}$$

$$= -\frac{v^2\,w}{r} - \frac{v\tan\phi}{r}\,(u + r_\perp\,\Omega)^2. \tag{14.80b}$$

Likewise, the vertical momentum equation (14.77c) renders

$$w\,(\dot w + g_\mathrm{e}) = \frac{v^2\,w}{r} + \frac{w}{r}\left[u^2 + 2\,\Omega\, u\, r_\perp + (r_\perp\,\Omega)^2\right] \tag{14.81a}$$

$$= \frac{v^2\,w}{r} + \frac{w}{r}\,(u + r_\perp\,\Omega)^2, \tag{14.81b}$$

so that

$$v\,\dot v + w\,(\dot w + g_\mathrm{e}) = r^{-1}\,(-v\tan\phi + w)\,(u + r_\perp\,\Omega)^2 = \frac{(l^z)^2\,\dot r_\perp}{(r_\perp)^3}. \tag{14.82}$$

Combining this result with equation (14.79) leads to the expected $\dot M = 0$. Hence, angular momentum conservation combined with the meridional and vertical momentum equations is equivalent to mechanical energy conservation.

14.7.4 Geopotential mechanical energy

Now consider the mechanical energy conservation when using geopotential coordinates with the equations of motion (13.138a)-(13.138c)

$$\dot{u} + \frac{u\,(w - v\tan\phi)}{r} + 2\,\Omega\,(w\cos\phi - v\sin\phi) = 0 \tag{14.83a}$$

$$\dot{v} + \frac{v\,w + u^2\tan\phi}{r} + 2\,\Omega\,u\sin\phi = 0 \tag{14.83b}$$

$$\dot{w} - \frac{u^2 + v^2}{r} - 2\,\Omega\,u\cos\phi = -g. \tag{14.83c}$$

Multiplying each equation by its respective velocity component and summing yields

$$\frac{1}{m}\,\dot{M}_{\text{geop}} = \frac{1}{2}\,\frac{\mathrm{d}}{\mathrm{d}t}\left[u^2 + v^2 + w^2 + 2\,g\,r\right] = 0. \tag{14.84}$$

The conserved mechanical energy for the particle written in geopotential coordinates

$$M_{\text{geop}} = m\,(u^2 + v^2 + w^2)/2 + m\,g\,r. \tag{14.85}$$

This expression should be compared to that written using spherical coordinates in equation (14.78). Since the coordinates are different (spherical versus geopotential), the velocity components (u, v, w) are slightly different in the two coordinate systems, as is the radial position. So care is needed when comparing the two expressions.

14.8 Sample particle trajectories

Here we examine some trajectories to illustrate how the dynamical properties discussed in this chapter, particularly angular momentum conservation, help to determine trajectories. The discussion complements that considered in Exercise 13.9.

14.8.1 Free fall starting from rest in the inertial reference frame

Consider a particle freely falling to the center of the sphere starting with zero axial angular momentum. Although the trajectory from an inertial reference frame is rather trivial, we need to do a bit more work in the non-inertial rotating frame, where we make use of the spherical coordinate equations to write

$$\dot{\lambda} = -\Omega \quad \text{and} \quad u = -r_\perp\,\Omega \quad \text{and} \quad v = 0 \quad \text{and} \quad \dot{w} = -g_{\text{e}}. \tag{14.86}$$

Evidently, the longitude, latitude, and vertical position are given by

$$(\lambda - \lambda_0) = -\Omega\,t \quad \text{and} \quad \phi = \phi_0 \quad \text{and} \quad (w - w_0) = -g_{\text{e}}\,t, \tag{14.87}$$

where λ_0 is the initial longitude, ϕ_0 is the initial latitude, and w_0 the initial vertical velocity. So the position with respect to the earth's longitude adjusts westward according to $(\lambda - \lambda_0) = -\Omega\,t$, which is needed to maintain a fixed absolute longitude. Likewise, the vertical free fall with $(w - w_0) = -g_{\text{e}}\,t$ accords with the free fall seen in the inertial reference frame. Integrating the vertical equation leads to the radial position

$$r - r_0 = w_0\,t - g_{\text{e}}\,t^2/2. \tag{14.88}$$

If we drop the particle from rest, so that $w_0 = 0$, then the particle falls a distance H within a time

$$T = (2\,H/g_e)^{1/2}. \tag{14.89}$$

During this time the particle deflects its longitude to the west by an amount

$$\lambda - \lambda_0 = -\Omega\,T = -\Omega\,(2\,H/g_e)^{1/2}. \tag{14.90}$$

It is useful to check self-consistency by verifying that the rotating reference frame description measures a zero axial angular momentum throughout the free fall. We first do so by noting that $l^z = r_\perp^2\,(\dot\lambda + \Omega) = 0$ since $\dot\lambda = -\Omega$. Taking the time derivative leads to

$$\dot l^z = r\,r_\perp\,\dot r_\perp\,(\Omega + \dot\lambda) + r_\perp^2\,\ddot\lambda = 0, \tag{14.91}$$

since $\dot\lambda = -\Omega$ and so $\ddot\lambda = 0$. Furthermore, we can write $l^z = r_\perp\,(u + r_\perp\,\Omega) = 0$, which also means that

$$\dot l^z = \dot r_\perp\,(u + r_\perp\,\Omega) + r_\perp\,(\dot u + \dot r_\perp\,\Omega) = 0, \tag{14.92}$$

where we noted that $u = -r_\perp\,\Omega$ means that $\dot u = -\dot r_\perp\,\Omega$.

14.8.2 Falling with $\dot u = 0$

Now consider a trajectory that maintains a constant zonal velocity, $\dot u = 0$, which, with $u = r_\perp\,\dot\lambda$, means that

$$\dot u = \dot r_\perp\,\dot\lambda + r_\perp\,\ddot\lambda = 0. \tag{14.93}$$

To maintain a constant axial angular momentum means

$$\dot l^z = 2\,r_\perp\,\dot r_\perp\,(\dot\lambda + \Omega) + r_\perp^2\,\ddot\lambda = r_\perp\,\dot r_\perp\,(\dot\lambda + 2\,\Omega), \tag{14.94}$$

where the second step made use of the assumed $\dot u = 0$ condition from equation (14.93). Equation (14.94) can be satisfied by either $\dot r_\perp = 0$ or $\dot\lambda = -2\,\Omega$. Yet setting one of these conditions means that the other must also hold in order to maintain $\dot u = 0$ from equation (14.93). We are thus led to

$$\dot u = 0 \quad \text{and} \quad \dot l^z = 0 \Longleftrightarrow \dot\lambda = -2\,\Omega \quad \text{and} \quad \dot r_\perp = 0 \quad \text{and} \quad l^z = -\Omega\,r_\perp^2. \tag{14.95}$$

Evidently, a particle moving westward with $\dot\lambda = -2\,\Omega$, and maintaining a fixed distance from the polar rotation axis, maintains both constant axial angular momentum and a constant zonal velocity

$$u = -2\,\Omega\,r_\perp. \tag{14.96}$$

Furthermore, observe that a constant distance from the rotation axis, $\dot r_\perp = 0$, means that

$$\dot r_\perp = 0 \Longrightarrow w\cos\phi = v\sin\phi. \tag{14.97}$$

This relation couples vertical and meridional motion in the rotating reference frame in a manner that keeps the distance to the rotational axis fixed. For example, the vertical velocity vanishes at the equator. Additionally, if the particle is falling so that $w\cos\phi < 0$, then there is an equatorward meridional velocity to keep the distance from the rotational axis fixed. In this manner, the particle is falling not towards the earth center but instead towards the equatorial plane, all while maintaining a fixed zonal velocity with $\dot u = 0$.

To garner further insight into the trajectory, we examine the meridional and vertical accelerations. For this purpose, recall the meridional equation of motion (13.133), written as

$$r\,\dot v + v\,w + u^2\tan\phi + \Omega\,r\sin\phi\,(2\,u + r_\perp\,\Omega) = 0. \tag{14.98}$$

Now multiply by $\cos\phi$ and set $w\cos\phi = v\sin\phi$ to reach

$$r_\perp\,\dot{v} + (u^2 + v^2)\sin\phi + \Omega\, r_\perp \sin\phi\,(2\,u + r_\perp\,\Omega) = 0. \tag{14.99}$$

Next set $u = -2\,r_\perp\,\Omega$ to have

$$r_\perp\,\dot{v} + [(\Omega\, r_\perp)^2 + v^2]\sin\phi = 0, \tag{14.100}$$

which, when setting $l^z/r_\perp = -\Omega\, r_\perp$, leads to the meridional acceleration

$$r_\perp\,\dot{v} = -[(l^z/r_\perp)^2 + v^2]\sin\phi. \tag{14.101}$$

Evidently, the meridional acceleration is negative in the northern hemisphere (where $\sin\phi > 0$) and positive in the southern, so that the particle always accelerates toward the equator. Similarly, use of the vertical acceleration from equation (13.134) leads to

$$r\,(\dot{w} + g_e) = u^2 + v^2 + r_\perp\,\Omega\,u + (r_\perp\,\Omega)^2 = v^2 + (r_\perp\,\Omega)^2 = v^2 + (l^z/r_\perp)^2 > 0. \tag{14.102}$$

Hence, the vertical acceleration ($\dot{w} < 0$) is always smaller in magnitude than the earth's gravitational acceleration. Finally, combining the conditions (14.101) and (14.102) means that the meridional and vertical accelerations are related by

$$\dot{v}\cos\phi + (\dot{w} + g_e)\sin\phi = 0. \tag{14.103}$$

So when the particle reaches the equator at $\phi = 0$, we know from equation (14.97) that the vertical velocity vanishes, and from equation (14.103) we see that the merdional acceleration also vanishes. In contrast, at the poles where $\phi = \pm\pi/2$, the vertical acceleration is $\dot{w} = -g_e$ whereas equation (14.97) says that the meridional velocity vanishes.

14.8.3 Free fall from rest in the rotating frame

We here consider the case of a particle initially at rest in the rotating reference frame that is allowed to freely fall. As in Exercise 13.9b, we make use of geopotential coordinates since the particle will initially fall parallel to the effective gravity direction; i.e., the *plumb line*. We consider the trajectory just in the zonal and vertical plane, assuming $v = 0$ throughout the free fall. Setting $v = \dot{v} = 0$ in the geopotential coordinate equations of motion (13.138a) and (13.138c) yields

$$\dot{u} + \frac{u\,w}{r} + 2\,\Omega\,w\cos\phi = 0 \tag{14.104a}$$

$$\dot{w} - \frac{u^2}{r} - 2\,\Omega\,u\cos\phi = -g. \tag{14.104b}$$

We now linearize by dropping the uw/r and u^2/r terms to render

$$\dot{u} = -2\,\Omega\,w\cos\phi \quad \text{and} \quad \dot{w} = 2\,\Omega\,u\cos\phi - g. \tag{14.105}$$

Now write $w = w_0 + w_1$, where

$$\dot{w}_0 = -g \quad \text{and} \quad \dot{w}_1 = 2\,\Omega\,u\cos\phi, \tag{14.106}$$

so that $w_0 = -g\,t$. To first order in Ω, the zonal velocity satisfies

$$\dot{u} = 2\,\Omega\,g\,t\,\cos\phi \Longrightarrow u = \Omega\,g\,t^2\cos\phi. \tag{14.107}$$

We are thus left with the free fall particle velocity that is valid to first order in Ω

$$\boldsymbol{V} = (\Omega\, g\, t^2 \cos\phi)\, \hat{\boldsymbol{\lambda}} - g\, t\, \hat{\boldsymbol{r}}. \tag{14.108}$$

The eastward velocity component arises from the need for the particle to conserve axial angular momentum as it falls closer to the polar axis.

Time integrating the velocity equation (14.108) leads to the particle trajectory

$$\boldsymbol{X} = (1/3)\, (\Omega\, g\, t^3 \cos\phi)\, \hat{\boldsymbol{\lambda}} - (g\, t^2/2)\, \hat{\boldsymbol{r}} + \boldsymbol{X}_0, \tag{14.109}$$

where $\boldsymbol{X}_0$ is an arbitrary initial position. The time it takes for the particle to fall a vertical distance H is given by

$$T = (2\, H/g)^{1/2}, \tag{14.110}$$

and within this time interval the particle is deflected eastward by a distance

$$D = (1/3)\, (\Omega\, g\, \cos\phi)\, (2\, H/g)^{3/2}. \tag{14.111}$$

14.9 Dynamical constraints from spatial symmetries

We close this chapter by summarizing the conservation laws that arise from spatial symmetries. These conservation laws complement the discussion in Section 14.7 for mechanical energy conservation arising from time symmetry.

14.9.1 Linear momentum conservation

As seen in Section 11.1.2, linear momentum remains constant for a particle moving without any forces acting on it; i.e., a *free particle*. This type of motion is not common for geophysical particles or fluids since they feel gravity and so are not free. Even so, we consider this limiting case as a point of comparison for the other conservation laws.

The conservation of linear momentum is simply viewed within the particle's inertial reference frame, where a vanishing inertial frame acceleration leads to a constant inertial frame velocity

$$\boldsymbol{A} = \mathrm{d}\boldsymbol{V}/\mathrm{d}t = 0. \tag{14.112}$$

In a Euclidean space, a vanishing acceleration means the particle is moving in a straight line with constant velocity.[5] When viewed from a rotating frame using Cartesian coordinates, a vanishing inertial frame acceleration means that the Cartesian acceleration balances Coriolis and centrifugal accelerations

$$\ddot{\boldsymbol{X}} = -2\, \boldsymbol{\Omega} \times \dot{\boldsymbol{X}} - \nabla \Phi_{\text{centrifugal}}. \tag{14.113}$$

This equation is clearly not a very useful means to describe unaccelerated free particle motion. We can provide a bit more compactness to this equation by introducing the potential momentum (14.7) so that

$$\mathrm{d}\boldsymbol{M}/\mathrm{d}t = -\nabla \Phi_{\text{centrifugal}}. \tag{14.114}$$

While the inertial frame acceleration vanishes ($\boldsymbol{A} = \mathrm{d}\boldsymbol{V}/\mathrm{d}t = 0$), time changes to the potential momentum are balanced by the gradient of the centrifugal potential.

[5] Recall that a zero acceleration as in equation (14.112) is an expression of Newton's first law (law of inertia), which was stated in the start of Chapter 11.

14.9.2 Potential momentum conservation

Conservation of potential momentum arises from symmetry of particle motion on a constant geopotential surface. The conservation law is most readily viewed within the rotating frame, whereby equation (14.9) is given by

$$\frac{\mathrm{d}(\hat{\boldsymbol{s}} \cdot \boldsymbol{M})}{\mathrm{d}t} = 0. \tag{14.115}$$

A geopotential is a two-dimensional surface so that this conservation law corresponds to two dynamical constraints such as shown in Figure 14.1.

14.9.3 Angular momentum conservation

As detailed in Section 14.5, the angular momentum computed with respect to the axis of rotation is a constant of the motion (Figure 14.3). This conservation law arises from symmetry of the system about the rotational axis. Axial (z-axis) angular momentum conservation takes the form

$$\mathrm{d}L^z/\mathrm{d}t = 0, \tag{14.116}$$

where the axial angular momentum is

$$L^z = m\, r_\perp^2\, (\dot{\lambda} + \Omega) \qquad \text{with} \qquad r_\perp = \sqrt{x^2 + y^2} = r \cos\phi. \tag{14.117}$$

The distance from the rotation axis, $r_\perp$, is the *moment arm* for the axial angular momentum. The longitude, λ, measures the angle in the counter-clockwise direction from the positive x-axis, and $\dot{\lambda}$ is the time change of the longitude.

14.10 Exercises

EXERCISE 14.1: NEGATIVE AXIAL ANGULAR MOMENTUM

In Section 14.6 we assume the axial angular momentum is positive, which is geophysically the common situation since axial angular momentum from the rigid-body motion is so large relative to motion of geophysical fluids. But let us consider the uncommon case where the particle moves zonally westward at a speed greater than the planetary rotation speed so that

$$\dot{\lambda} + \Omega < 0 \Longleftrightarrow u + \Omega\, r_\perp < 0, \tag{14.118}$$

which means the axial angular momentum per mass of the particle is negative

$$l^z = r_\perp\, (u + r_\perp\, \Omega) = -|l^z| < 0. \tag{14.119}$$

Throughout this exercise we seek answers based on conservation of axial angular momentum. When checking to see whether an answer agrees with common sense, be careful since motion of this sort is not commonly experienced by terrestrial observers. Correspondingly, it is useful to check answers by viewing the motion from the perspective of an inertial reference frame rather than the rotating terrestrial reference frame. For example, the particular case where $\dot{\lambda} = -\Omega$, in which case the particle has zero angular momentum, corresponds to a particle that is stationary in the inertial reference frame while the planet rotates underneath.

(A) Discuss what happens to $\delta\dot{\lambda}$ for the particle that is deflected poleward with constant radius while conserving axial angular momentum. Hint: consider the first form of equation (14.37).

(B) Discuss what happens to δu for the particle as it is deflected poleward with constant radius while conserving axial angular momentum. Separately discuss the three cases where

(i) $|l^z| = 0$
(ii) $|l^z| < \Omega\, r_\perp^2$.
(iii) $|l^z| > \Omega\, r_\perp^2$

Hint: consider the second form of equation (14.37).

(C) Is fluid particle motion with $u + \Omega\, r_\perp < 0$ relevant for the terrestrial atmosphere and ocean? Why? To help answer this question, what is $\Omega\, r_\perp$ for $\phi = \pi/4$ and $r = R_e$? Note, we already provided the result for the equator just after equation (14.34). Compare these speeds to that of a category 5 tropical cyclone.

EXERCISE 14.2: SPHERICAL COMPONENTS TO ANGULAR MOMENTUM

In Section 14.5 we studied angular momentum relative to the center of the sphere, $\boldsymbol{L} = m\, \boldsymbol{X} \times \boldsymbol{V}$. In particular, we considered the evolution equations for the planetary Cartesian compoents $\hat{\boldsymbol{x}} \cdot \boldsymbol{L}$, $\hat{\boldsymbol{y}} \cdot \boldsymbol{L}$, and $\hat{\boldsymbol{z}} \cdot \boldsymbol{L}$. Here we consider the projection of the angular momentum onto the planetary spherical directions $\hat{\boldsymbol{\lambda}}, \hat{\boldsymbol{\phi}}$ and $\hat{\boldsymbol{r}}$. For a space that is spherically symmetric around the center of the sphere, we do not expect $\hat{\boldsymbol{\lambda}} \cdot \boldsymbol{L}$ or $\hat{\boldsymbol{\phi}} \cdot \boldsymbol{L}$ to be constants of the motion. The reason is that neither $\hat{\boldsymbol{\lambda}}$ nor $\hat{\boldsymbol{\phi}}$ extend outward from the center of the sphere, so that rotations around either of these axes do not manifest a symmetry operation. Nevertheless, it is interesting to explore properties of $\hat{\boldsymbol{\lambda}} \cdot \boldsymbol{L}$ and $\hat{\boldsymbol{\phi}} \cdot \boldsymbol{L}$ as an exercise in the angular momentum formalism, and to display how their evolution relates to that of the linear momentum on the sphere.

(A) Write an expression for the zonal component to the angular momentum, $\hat{\boldsymbol{\lambda}} \cdot \boldsymbol{L}$, in terms of $\dot{\phi}$ and r. Hint: check that the physical dimensions are correct, and that the sign accords with the right hand rule.

(B) Derive an expression for the time derivative, $\mathrm{d}(\hat{\boldsymbol{\lambda}} \cdot \boldsymbol{L})/\mathrm{d}t$, in terms of $\dot{\phi}$ and $\dot{r}$.

(C) Write an alternative expression for the time derivative, $\mathrm{d}(\hat{\boldsymbol{\lambda}} \cdot \boldsymbol{L})/\mathrm{d}t$, in terms $u = r_\perp\, \dot{\lambda}$ and Ω. Hint: recall the spherical coordinate version of the meridional momentum equation (13.133).

(D) Derive an expression for the meridional component to the angular momentum, $\hat{\boldsymbol{\phi}} \cdot \boldsymbol{L}$, and write it in terms of r, Ω, $\dot{\lambda}$, and ϕ.

(E) Derive an expression for the time derivative, $\mathrm{d}(\hat{\boldsymbol{\phi}} \cdot \boldsymbol{L})/\mathrm{d}t$.

(F) Derive an expression for $\hat{\boldsymbol{r}} \cdot \boldsymbol{L}$.

Chapter 15

CASE STUDIES IN ANALYTICAL MECHANICS

The discussion in Chapter 12 certainly does support the name *analytical mechanics*, given that there is a nontrival degree of analysis needed to reformulate the laws of mechanics beyond their Newton's law expression. In this chapter, we work through some case studies for the purpose of illustrating the use of analytical mechanics for practical problems. These studies further exemplify and clarify the foundations of the theory while exploring geophysically interesting dynamical systems. It is through such examples that the power and elegance of analytical mechanics shines.

CHAPTER GUIDE

This chapter relies on the formulation of analytical mechanics from Chapter 12. We also make use of material from our study of particle mechanics around a rotating planet from Chapter 13.

15.1 Planar simple pendulum

Consider a planar simple pendulum as illustrated in Figure 15.1, where motion is restricted to the x-z plane. This pendulum consists of a point mass, m, attached to a massless string of fixed length, ℓ, oscillating around a fixed point within a constant gravity field with acceleration $-g\,\hat{\boldsymbol{z}}$. We derive the equations of motion for this system using both Newtonian mechanics and Lagrangian mechanics.

Before diving into the specifics of the simple pendulum, we note that it exemplifies the two key properties of any oscillatory system, including linear waves studied in Part X of this book. The first property is a restoring force that kicks in when the system is displaced a small distance from its equilibrium. For the simple pendulum the restoring force is provided by the gravitational acceleration. The second property is inertia as that then allows the system to overshoot its equilibrium position, with mass providing the pendulum's inertia. The exchange between the restoring force and inertia lead to oscillations, and the natural oscillation frequencies are a function of the inertia and the restoring force.

15.1.1 Free particle motion using polar coordinates

Before addressing the simple pendulum, we find it useful to consider the equations for a free particle moving in the x-z plane without gravity and without any string. Cartesian coordinates provide the natural set of coordinates for describing this motion, in which the $\hat{\boldsymbol{x}}$ and $\hat{\boldsymbol{z}}$ components to the Cartesian velocity velocity remain constant in space and time. We also consider polar coordinates, with the polar angle defined by φ as depicted in Figure 15.1, anticipating the motion of a simple pendulum using these coordinates. The coordinate transformation between Cartesian and polar is given by

$$x = r \sin\varphi \tag{15.1a}$$
$$z = -r \cos\varphi \tag{15.1b}$$
$$\hat{\boldsymbol{r}} = \hat{\boldsymbol{x}} \sin\varphi - \hat{\boldsymbol{z}} \cos\varphi \tag{15.1c}$$
$$\hat{\boldsymbol{\varphi}} = \hat{\boldsymbol{x}} \cos\varphi + \hat{\boldsymbol{z}} \sin\varphi. \tag{15.1d}$$

The Cartesian unit vectors are fixed in space, but the time derivatives of the polar unit vectors are

$$\dot{\hat{\boldsymbol{r}}} = \dot{\varphi}\,\hat{\boldsymbol{\varphi}} \quad \text{and} \quad \dot{\hat{\boldsymbol{\varphi}}} = -\dot{\varphi}\,\hat{\boldsymbol{r}}. \tag{15.2}$$

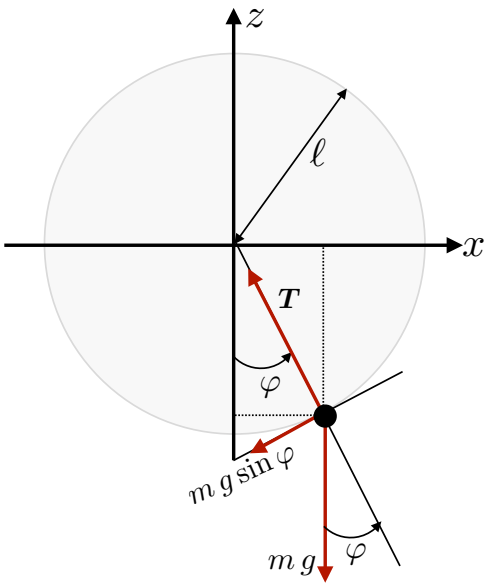

FIGURE 15.1: A simple pendulum is comprised of a point mass, m, attached to a massless string of fixed length, ℓ, with the string attached to a fixed point taken as the origin of a Cartesian coordinate system. The string makes an angle, φ, with respect to the vertical, and gravity points down with a constant acceleration, $-g\,\hat{\boldsymbol{z}}$. The force provided by the string on the particle, $\boldsymbol{T}$, points radially inward and balances the projection of the weight along the string plus the centrifugal acceleration due to motion of the particle. The point mass moves along the circumference of the circle. The string force is directed orthogonal to the motion so that it does no work on the point mass, and as such the string provides a force of constraint. The component of the weight directed along the circumference forces motion of the oscillator, with this force having magnitude $m\,g|\sin\varphi|$.

These results render the particle position, its velocity, and its acceleration

$$\boldsymbol{X} = r\,(\hat{\boldsymbol{x}}\,\sin\varphi - \hat{\boldsymbol{z}}\cos\varphi) = r\,\hat{\boldsymbol{r}} \tag{15.3a}$$

$$\dot{\boldsymbol{X}} = \dot{r}\,\hat{\boldsymbol{r}} + r\,\dot{\varphi}\,\hat{\boldsymbol{\varphi}} \tag{15.3b}$$

$$\ddot{\boldsymbol{X}} = (\ddot{r} - r\,\dot{\varphi}^2)\,\hat{\boldsymbol{r}} + (2\,\dot{r}\,\dot{\varphi} + r\,\ddot{\varphi})\,\hat{\boldsymbol{\varphi}}. \tag{15.3c}$$

Free particle motion has zero acceleration,

$$\ddot{x} = 0 \quad \text{and} \quad \ddot{z} = 0, \tag{15.4}$$

which means each Cartesian velocity component is a space and time constant. This trivial result has some nuance when written in polar coordinates

$$\ddot{r} - r\,\dot{\varphi}^2 = 0 \quad \text{and} \quad 2\,\dot{r}\,\dot{\varphi} + r\,\ddot{\varphi} = 0. \tag{15.5}$$

Of relevance to the pendulum, observe that forces are needed for both equations to maintain a fixed r.

Pursuing a Lagrangian mechanics approach, we compute the Euler-Lagrange equation (12.75) using (r, φ) as the two generalized coordinates. For the free particle, the Lagrangian equals to the kinetic energy

$$L = m\,(\dot{r}^2 + r^2\,\dot{\varphi}^2)/2, \tag{15.6}$$

so that the two Euler-Lagrange equations are

$$\frac{\mathrm{d}}{\mathrm{d}t}\frac{\partial L}{\partial \dot{r}} = \frac{\partial L}{\partial r} \Longrightarrow \ddot{r} = r\,\dot{\varphi}^2 \tag{15.7a}$$

$$\frac{\mathrm{d}}{\mathrm{d}t}\frac{\partial L}{\partial \dot{\varphi}} = \frac{\partial L}{\partial \varphi} \Longrightarrow \frac{\mathrm{d}\,(r^2\,\dot{\varphi})}{\mathrm{d}t} = 0. \tag{15.7b}$$

The radial equation says that the radial acceleration balances the centrifugal acceleration. The angular equation reflects the property of a Lagrangian that is independent of the generarlized coordinate, φ, so that its corresponding generalized momentum, the angular momentum computed relative to the origin, is a constant of the motion.

15.1.2 Newtonian mechanics of the simple pendulum

Now allow the particle to feel the constant gravitational field and the force by the string. Notably, the string force keeps the particle at a fixed distance, $r = \ell$, from the origin so that the particle motion only has a single degree of freedom. The position, velocity, and acceleration for the particle are thus given by

$$\boldsymbol{X} = \ell\,(\hat{\boldsymbol{x}}\sin\varphi - \hat{\boldsymbol{z}}\cos\varphi) = \ell\,\hat{\boldsymbol{r}} \tag{15.8a}$$

$$\dot{\boldsymbol{X}} = \ell\,\dot{\varphi}\,(\hat{\boldsymbol{x}}\cos\varphi + \hat{\boldsymbol{z}}\sin\varphi) = \ell\,\dot{\varphi}\,\hat{\boldsymbol{\varphi}} \tag{15.8b}$$

$$\ddot{\boldsymbol{X}} = \ell\,\ddot{\varphi}\,\hat{\boldsymbol{\varphi}} - \ell\,\dot{\varphi}^2\,\hat{\boldsymbol{r}}, \tag{15.8c}$$

with polar coordinates now ideally suited to the physical system. The force provided by the string points radially inward and it must be sufficient to exactly balance the projection of the particle weight along the string direction, plus the centrifugal acceleration of the particle as it oscillates along the circumference of the circle

$$\boldsymbol{T} = -m\,(g\cos\varphi + \ell\,\dot{\varphi}^2)\,\hat{\boldsymbol{r}}. \tag{15.9}$$

This string force constrains the particle to remain a fixed distance, $r = \ell$, from the center of the circle. Since the particle motion is directed along the circumference and the string force is radially directed, then the string force does no work on the particle. Evidently, the force provided by the string is a force of constraint. We reconsider this force of constraint from the Lagrangian perspective in Section 15.1.6.

Newton's equation of motion takes the form

$$m\,\ddot{\boldsymbol{X}} = -m\,g\,\hat{\boldsymbol{z}} + \boldsymbol{T}. \tag{15.10}$$

Projecting into the angular direction, $\hat{\boldsymbol{\varphi}}$, eliminates the string force and leads to the nonlinear oscillator equation

$$\ddot{\varphi} + (g/\ell)\sin\varphi = 0, \tag{15.11}$$

where we used

$$\hat{\boldsymbol{z}}\cdot\hat{\boldsymbol{\varphi}} = \sin\varphi. \tag{15.12}$$

When the angle is small we can approximate $\sin\varphi \approx \varphi$, in which case we have a linear oscillator equation

$$\ddot{\varphi} + (g/\ell)\,\varphi = 0, \tag{15.13}$$

with natural angular frequency, $\omega_0 = \sqrt{g/\ell}$ and period $2\,\pi/\omega_0 = 2\,\pi\,\sqrt{\ell/g}$.

15.1.3 Euler-Lagrange equation for the simple pendulum

With a single degree of freedom for the simple pendulum, we choose the angle, φ, as the generalized coordinate. The kinetic energy, potential energy (referenced to $z = 0$), and Lagrangian are thus

given by

$$K = (m/2)\,(\dot{x}^2 + \dot{z}^2) = (m/2)\,\ell^2\,\dot{\varphi}^2 \tag{15.14a}$$

$$P = -m\,g\,\ell\cos\varphi \tag{15.14b}$$

$$L = m\,(\ell^2\,\dot{\varphi}^2/2 + g\,\ell\cos\varphi), \tag{15.14c}$$

with the corresponding Euler-Lagrange equation (12.75)

$$\frac{\mathrm{d}}{\mathrm{d}t}\left[\frac{\partial L}{\partial\dot{\varphi}}\right] = \frac{\partial L}{\partial\varphi} \Longrightarrow \ddot{\varphi} + (g/\ell)\sin\varphi = 0. \tag{15.15}$$

As expected, we derived the same oscillator equation (15.11) as when using Newtonian mechanics. However, the path to this equation is somewhat more streamlined since we had no need to consider forces.

15.1.4 The Hamiltonian is a constant of the motion

The coordinate transformation between the Cartesian coordinates and generalized coordinate does not depend explicitly on time, nor does the Lagrangian. Hence, from Section 12.9.4 we know that the Hamiltonian equals to the mechanical energy, and it is a constant of the motion

$$H = -L + \dot{\varphi}\,\frac{\partial L}{\partial\dot{\varphi}} = K + P. \tag{15.16}$$

We readily confirm that $\dot{H} = 0$ by computing

$$\dot{K} + \dot{P} = m\,\ell^2\,\dot{\varphi}\,[\ddot{\varphi} + (g/\ell)\sin\varphi] = 0, \tag{15.17}$$

where the second equality follows from the Euler-Lagrange equation of motion (15.15).

15.1.5 Hamilton's equations of motion

When proving that the Hamiltonian is a constant of the motion in Section 15.1.4, we did not first write the Hamiltonian in terms of the generalized coordinates and momenta. Instead, we directly computed the time derivative and used the Euler-Lagrange equation to show that $\dot{H} = 0$. However, as mentioned in Section 12.10.4, to derive Hamilton's equations of motion we must first write the Hamiltonian in terms of the generalized coordinates and generalized momenta. The generalized momenta for the pendulum is given by

$$\mathcal{P}_\varphi = \frac{\partial L}{\partial\dot{\varphi}} = m\,\ell^2\,\dot{\varphi}, \tag{15.18}$$

so that the Hamiltonian is

$$H(\varphi, \mathcal{P}_\varphi) = \frac{\mathcal{P}_\varphi^2}{2\,m\,\ell^2} - m\,g\,\ell\cos\varphi. \tag{15.19}$$

Hamilton's equations of motion (12.146a) and (12.146b) take on the general form

$$\dot{\mathcal{P}}_\sigma = -\frac{\partial H}{\partial\xi^\sigma} \quad \text{and} \quad \dot{\xi}^\sigma = \frac{\partial H}{\partial\mathcal{P}_\sigma}, \tag{15.20}$$

which for the pendulum are

$$\dot{\mathcal{P}}_\varphi = -m\,g\,\ell\sin\varphi \quad \text{and} \quad \dot{\varphi} = \frac{\mathcal{P}_\varphi}{m\,\ell^2}. \tag{15.21}$$

Reorganization of the $\dot{\mathcal{P}}_\varphi$ equation renders the Euler-Lagrange equation (15.15). In contrast, the $\dot{\varphi}$ equation is identical to the definition of the generalized momenta given by equation (15.18), so that this equation offers no new information.

15.1.6 Force of constraint provided by the string

Following the Lagrange multiplier method from Section 12.8, we here derive the force of constraint acting on the particle. As already noted, the force of constraint is provided by the string, and this force is always orthogonal to the particle motion. Indeed, we wrote this force by inspection in equation (15.9). Here we compute this force via the Lagrange multiplier. In particular, we follow the approach in Section 12.8 and identify the single constraint equation as

$$\Psi(r) = r = \ell, \tag{15.22}$$

so that $\partial\Psi/\partial r = 1$ and equation (12.110) then says that the Lagrange multiplier is the force of constraint corresponding to the radial coordinate

$$\Lambda = Q_r. \tag{15.23}$$

Following the procedure detailed in Section 12.8.3, we consider the extended Lagrangian (12.104) for the pendulum

$$L = m\,(\dot{r}^2 + r^2\,\dot{\varphi}^2)/2 + m\,g\,r\cos\varphi + \Lambda\,(r - \ell). \tag{15.24}$$

The corresponding Euler-Lagrange equations are

$$m\,\ddot{r} = m\,r\,\dot{\varphi}^2 + m\,g\cos\varphi + \Lambda \tag{15.25a}$$

$$m\,\frac{\mathrm{d}(r^2\,\dot{\varphi})}{\mathrm{d}t} = -m\,g\,r\sin\varphi \tag{15.25b}$$

$$r = \ell. \tag{15.25c}$$

The angular equation of motion (15.25a) remains unaffected by the Lagrange multiplier since there are no constraints on motion in the angular direction. So the set of three equations for the three unknowns, (r, φ, Λ), is given by

$$2\,\dot{r}\,\dot{\varphi} + r\,\ddot{\varphi} + g\sin\varphi = 0 \quad \text{and} \quad \Lambda = m\,(\ddot{r} - r\,\dot{\varphi}^2 - g\cos\varphi) \quad \text{and} \quad r = \ell. \tag{15.26}$$

Satisfying the constraint, $r = \ell$, means that $\dot{r} = 0$ and $\ddot{r} = 0$ so that the force of constraint is

$$Q_r = \Lambda = -m\,(\ell\,\dot{\varphi}^2 + g\cos\varphi) < 0, \tag{15.27}$$

where the inequality follows since $\ell\,\dot{\varphi}^2 + g\cos\varphi > 0$. This result agrees with equation (15.9) for the force provided by the string, $\boldsymbol{T}$, so that we identify

$$\boldsymbol{T} = Q_r\,\hat{\boldsymbol{r}} = -m\,(\ell\,\dot{\varphi}^2 + g\cos\varphi)\,\hat{\boldsymbol{r}}. \tag{15.28}$$

15.1.7 Comments

As anticipated, the Euler-Lagrange equation of motion is both equal to Newton's equation of motion and simple to derive. It is simpler to derive largely due to the scalar nature of the Lagrangian versus the vector nature of Newton's equation of motion. Namely, it is easier to derive the kinetic energy and potential energy than the acceleration and forces. Even though we do not need forces for analytical mechanics, the calculation of forces offers great physical

insights into the nature of the physical system. Conservative forces are deduced as per Newtonian mechanics via the gradient of the force potential, and forces of constraint are inferred through the method of Lagrange multipliers.

15.2 Variable length pendulum

What if we let the length of the pendulum's string be a prescribed function of time? That is, we let the string length be a time dependent parameter of the physical system. In this case the Hamiltonian is an explicit function of time, through the string length, and so mechanical energy is not a constant of the motion. Correspondingly, the force of constraint acting along the string does work as the string changes, with this work the cause of the nonzero time derivative of the Hamiltonian. We are familiar with forces of constraint providing no work on a physical system, with this property enshrined in *d'Alembert's principle* studied in Section 12.3.1. Indeed, at any particular instance, the forces of constraint perform no work on a virtual displacement. However, when allowing time to evolve then the force of constraint acting along the string does work and that work results in an energy change.

Along with a time change in the pendulum's energy, there is a time change to the pendulum's angular frequency. Quite remarkably, the ratio of the energy to the angular frequency remains nearly constant for small amplitude oscillations, so long as changes to the string length are slow. The ratio of the energy to frequency is known as an *adiabatic invariant*. This adiabatic invariant arises when studying linear waves moving through a time dependent media. Additionally, adiabatic invariants played an important role in the development of quantum mechanics.

15.2.1 Work done by the force of constraint

Recall from Section 15.1.6 that we introduced the extended Lagrangian with a Lagrange multiplier, Λ, representing the force of constraint,

$$L = m\,(\dot{r}^2 + r^2\,\dot{\varphi}^2)/2 + m\,g\,r\cos\varphi + \Lambda\,(r-\ell), \tag{15.29}$$

where (r, φ, Λ) are three generalized coordinates, and the corresponding Hamiltonian is

$$H = -L + \dot{\varphi}\,\frac{\partial L}{\partial \dot{\varphi}} + \dot{r}\,\frac{\partial L}{\partial \dot{r}} = m\,(\dot{r}^2 + r^2\,\dot{\varphi}^2)/2 - m\,g\,r\cos\varphi - \Lambda\,(r-\ell). \tag{15.30}$$

The corresponding Euler-Lagrange equations (15.26) are here repeated for completeness

$$2\,\dot{r}\,\dot{\varphi} + r\,\ddot{\varphi} + g\sin\varphi = 0 \quad \text{and} \quad \Lambda = m\,(\ddot{r} - r\,\dot{\varphi}^2 - g\cos\varphi) \quad \text{and} \quad r(t) = \ell(t). \tag{15.31}$$

Evidently, the force of constraint, Λ, picks up a new contribution from the second time derivative, $\ddot{r}$, whereas this contribution vanished in Section 15.1.6 where we assumed ℓ has a fixed length.

Both the Lagrangian (15.29) and Hamiltonian (15.30) are explicit functions of time via the time dependent string length, $\ell(t)$. Hence, the Hamiltonian has a time derivative, which can be evaluated in either of the following manners

$$\frac{\mathrm{d}H}{\mathrm{d}t} = \left[\frac{\partial H}{\partial t}\right]_{r,\varphi,\mathcal{P}_r,\mathcal{P}_\varphi} = \frac{\partial H}{\partial \ell}\,\frac{\mathrm{d}\ell}{\mathrm{d}t} = -\left[\frac{\partial L}{\partial t}\right]_{r,\varphi,r,\dot{r},\dot{\varphi}} = \dot{\ell}\,\Lambda, \tag{15.32}$$

so that the energy of the pendulum changes due to work done by the force of constraint acting in the presence of a changing string length. We can double-check the result (15.32) by making

use of the equations of motion (15.31), which now requires us to set $r = \ell$ so that

$$\frac{\mathrm{d}H}{\mathrm{d}t} = \dot{H} = m\,\dot{l}\,(\ddot{l} + \ell\,\dot{\varphi}^2 - g\cos\varphi) + m\,\ell\,\dot{\varphi}\,(\ell\,\ddot{\varphi} + g\sin\varphi) = m\,\dot{\ell}\,(\ddot{\ell} - \ell\,\dot{\varphi}^2 - g\cos\varphi) = \dot{\ell}\,\Lambda. \tag{15.33}$$

15.2.2 Small amplitude oscillations

Assuming the angular displacements of the pendulum are small leads to the Lagrangian and Hamiltonian for a linear variable length pendulum

$$L = m\,\ell^2\,(\dot{\varphi}^2 - (g/\ell)\,\varphi^2)/2 + m\,g\,\ell + m\,\dot{\ell}^2/2, \tag{15.34a}$$

$$H = m\,\ell^2\,(\dot{\varphi}^2 + (g/\ell)\,\varphi^2)/2 - m\,g\,\ell - m\,\dot{\ell}^2/2, \tag{15.34b}$$

along with the corresponding Euler-Lagrange equation of motion

$$\frac{\mathrm{d}(\ell^2\,\dot{\varphi})}{\mathrm{d}t} + g\,\ell\,\varphi = 0. \tag{15.35}$$

Note that the term $m\,\ell^2\,(\dot{\varphi}^2 - (g/\ell)\,\varphi^2)/2$ appearing in the Lagrangian (15.34a) is the kinetic energy minus the potential energy for a simple harmonic oscillator, as studied in Section 15.6. We thus identify the angular frequency of the oscillator as

$$\omega^2(t) = g/\ell(t), \tag{15.36}$$

with $2\pi/\omega$ equal to the period of the oscillations.

15.2.3 Two time scales for the pendulum

For the linear pendulum with a fixed length, the angular displacement is given by $\varphi = A\cos(\omega\,t)$, where A is a constant amplitude and we set the initial conditions so that $\varphi(t=0) = A$. If the string length changes very slowly, then we expect the oscillations to continue yet with a time dependent frequency and amplitude. We are thus motivated to consider the ansatz

$$\varphi(t) = A(t)\cos\theta(t), \tag{15.37}$$

where the amplitude, $A(t)$, has a time dependence, as does the phase, $\theta(t)$. Furthermore, we note that the time scale for the phase derivative accords with the angular frequency

$$\dot{\theta} \approx \omega. \tag{15.38}$$

In Section 15.2.4 we find equality holds to leading order.

A string whose length slowly changes is one whose inverse time scale for changes, T^{-1}, is much smaller than the angular frequency for the pendulum, so that

$$\dot{\ell}/\ell = T^{-1} \ll \omega \approx \dot{\theta} \Longrightarrow \dot{\ell}^2 \ll \ell\,g \tag{15.39}$$

where the second inequality follows since $\omega^2 = g/\ell$. The inequality $T^{-1} \ll \dot{\theta}$ means that the phase of the oscillation varies rapidly relative to the string length. Another corresponding assumption concerns the amplitude of the oscillation, which we assume also slowly changes

$$\dot{A}/A = T^{-1} \ll \omega. \tag{15.40}$$

Finally, the relation $\omega^2 = g/\ell$, along with the inequality (15.39), shows that relative changes to

the angular frequency are also small

$$2\,\dot{\omega}/\omega = -\dot{\ell}/\ell \Longrightarrow |\dot{\omega}| \ll \omega^2 = g/\ell. \tag{15.41}$$

These scaling relations can be summarized by stating that the phase of the oscillation changes rapidly whereas all other quantities change slowly.

In the Lagrangian (15.34a) and Hamiltonian (15.34b), we encounter the sum, $m\,g\,\ell + m\,\dot{\ell}^2/2$. The first term, $-m\,g\,\ell$, is the gravitational potential energy of a pendulum at zero angular displacement, $\varphi = 0$. Over the time scale of an oscillation, this term is roughly a constant and it can be ignored by merely readjusting the zero of the potential energy. Likewise, the term $m\,\dot{\ell}^2/2$ is the kinetic energy associated with changes to the string length. This term changes slowly and it is much smaller than the kinetic energy from angular motion, $m\,\ell^2\,\dot{\varphi}^2/2$. We thus ignore this term as well in the following analysis.

15.2.4 Adiabatic invariant

Making use of the ansatz (15.37) yields time changes to the pendulum's angle

$$\dot{\varphi} = \dot{A}\cos\theta - A\,\dot{\theta}\sin\theta \approx -A\,\dot{\theta}\sin\theta, \tag{15.42}$$

where we made use of the assumed scales in Section 15.2.3 to reach the approximation. We are thus led to the approximate form of the Lagrangian (15.34a) (recall we are ignoring the terms $m\,g\,\ell + m\,\dot{\ell}^2/2$)

$$L \approx m\,\ell^2\,A^2\,(\dot{\theta}^2\sin^2\theta - \omega^2\cos^2\theta)/2. \tag{15.43}$$

As part of the time scale separation in Section 15.2.3, we assume the phase of the oscillation changes rapidly relative to changes in the angular frequency as well as changes to $\dot{\theta}$ and ℓ. Hence, we are motivated to perform a phase average,[1] in which case $\sin^2\theta$ and $\cos^2\theta$ are replaced by $1/2$

$$\langle L\rangle = m\,\ell^2\,A^2\,(\dot{\theta}^2 - \omega^2)/4. \tag{15.44}$$

We treat the amplitude and phase as generalized coordinates that are connected to the angular displacement via the oscillator ansatz (15.37). Their respective phase averaged Euler-Lagrange equations are

$$\frac{\mathrm{d}}{\mathrm{d}t}\frac{\partial L}{\partial \dot{A}} = \frac{\partial L}{\partial A} \Longrightarrow \dot{\theta}^2 = \omega^2 \tag{15.45a}$$

$$\frac{\mathrm{d}}{\mathrm{d}t}\frac{\partial L}{\partial \dot{\varphi}} = \frac{\partial L}{\partial \varphi} \Longrightarrow \frac{\mathrm{d}(\ell^2\,A^2\,\dot{\theta})}{\mathrm{d}t} = 0. \tag{15.45b}$$

Equation (15.45a) says that the phase has a time derivative equal to the instantaneous frequency. It also results in a zero phase averaged Lagrangian

$$\langle L\rangle = 0. \tag{15.46}$$

To interpret equation (15.45b) note that the phase averaged Hamiltonian (15.34b) is (recall we are ignoring the terms $m\,g\,\ell + m\,\dot{\ell}^2/2$)

$$\langle H\rangle = m\,\ell^2\,A^2\,(\dot{\theta}^2 + \omega^2)/4 = m\,\ell^2\,A^2\,\omega^2/2, \tag{15.47}$$

[1] We introduced phase averaging in Section 8.1.2 when studying Fourier analysis.

so that the Euler-Lagrange equation (15.45b) can be written

$$\frac{\mathrm{d}(H/\omega)}{\mathrm{d}t} = 0. \tag{15.48}$$

Evidently, although energy and angular frequency change due to the variable string length, their ratio is constant when the oscillations are small and the changes to the string length are slow. The ratio, H/ω, is known as the *phase averaged action*, and equation (15.48) says that it is an adiabatic invariant. Conservation of the phase averaged action results from symmetry of the phase in the phase averaged Lagrangian (15.44). That is, we can shift the phase by a constant and not alter the Lagrangian. This result exemplifies the importance of identifying any (sometimes quite innocent looking) symmetries of a dynamical system, as they inevitably lead to a conservation law.

15.2.5 Further study

A general discussion of adiabatic invariants is given in Section 49 of *Landau and Lifshitz* (1976), Section 11.7 of *Goldstein* (1980), and Section 6.4 of *José and Saletan* (1998). See also Section 7.1 of *Salmon* (1998) for a discussion of the adiabatic invariant for the harmonic oscillator. Furthermore, we encounter adiabatic invariants in Section 50.5 when studying waves in a media that changes in space and time, with the *wave action* the corresponding invariant.

Adiabatic invariants formed an important part in the foundations of quantum mechanics. For example, the energy of a photon is given by

$$E = \hbar\omega, \tag{15.49}$$

where $\hbar = h/2\pi$ is the reduced Planck's constant, thus revealing that E/ω is a constant.

15.3 The Foucault pendulum

In this section we use Lagrangian mechanics to study motion of the *Foucault pendulum*, which is a frictionless spherical pendulum in a gravity field on a rotating planet. To illustrate the rotation of the planet, we setup the pendulum to oscillate in a fixed plane as viewed in an inertial reference frame, and as such it precesses when viewed from the planetary rotating reference frame. In this manner, the Foucault pendulum provides a remarkable illustration of the planetary Coriolis acceleration, and hence of the planetary rotation.

15.3.1 Assumptions about the Coriolis acceleration

We illustrate the Foucault pendulum in Figure 15.2, which is a spherical pendulum that feels the effects of the earth's rotation. For any point on the earth, the planetary rotation has a projection in the local vertical and local meridional directions (see Figure 13.3). However, for our study of the Foucault pendulum we only consider the local vertical component to the planetary rotation. This approximate approach accords with our study of large-scale fluid flows in this book. Even though the Foucault pendulum is tiny compared to the planetary fluid flows, the motion of the particle respects the same assumptions relevant for large-scale fluid motions. We detail these assumptions in the next paragraph.

As studied in Section 13.9.8, the meridional component to the planetary rotation leads to a Coriolis acceleration that has both a radial component and longitudinal component. The radial Coriolis acceleration is far smaller than the effective gravitational acceleration so that this contribution to the Coriolis acceleration can be ignored. The longitudinal Coriolis acceleration is determined by the vertical velocity of the particle. For the Foucault pendulum we assume the

vertical motion is much smaller than the horizontal velocity. Hence, this piece of the longitudinal Coriolis acceleration is negligible compared to the other portion that arises from horizontal motion. For these two reasons, the most significant portion of the Coriolis acceleration acting on the pendulum arises just from the local vertical component to the planetary rotation. As such, the Coriolis acceleration acts just in the local horizontal tangent plane.

Furthermore, since the horizontal length scales of the pendulum are tiny relative to the earth's radius, we assume the Coriolis parameter (equation (13.100))

$$f = 2\,\Omega \sin\phi, \tag{15.50}$$

to be constant and evaluated at the fixed point of the pendulum, which we refer to as the *f-plane approximation* in Section 24.5. In equation (15.50), Ω is the angular frequency of the planetary rotation (Section 13.1), and ϕ is the planetary latitude (Figure 4.3).

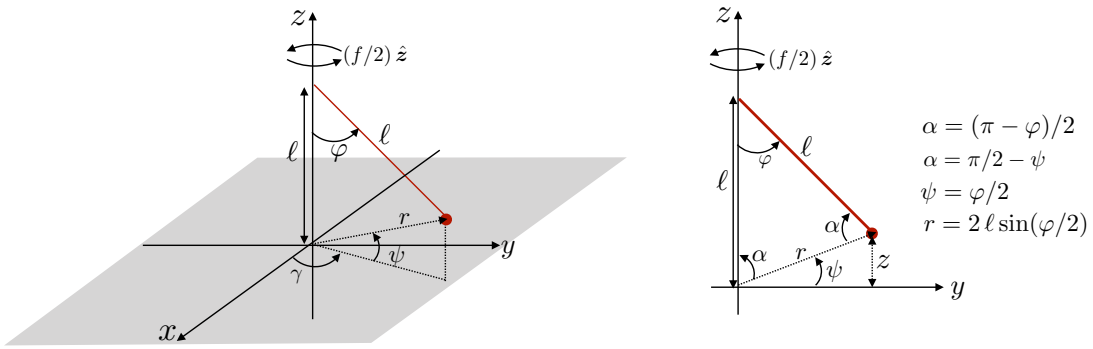

FIGURE 15.2: A Foucault pendulum is a frictionless spherical pendulum on a rotating planet. Taking the f-plane approximation, we assume rotation of the reference frame occurs around the local vertical axis with angular frequency $(f/2)\,\hat{\boldsymbol{z}}$, with $f = 2\,\Omega \sin\phi$ the Coriolis parameter and ϕ the latitude of the fixed point of the pendulum. To avoid confusion with the planetary spherical angles (where we use ϕ for latitude and λ for longitude as in Figure 4.3), we here use the local spherical coordinates with $\psi \geq 0$ the angle the pendulum makes with the horizontal x-y plane, and $0 \leq \gamma \leq 2\pi$ the angle it makes with the x-axis in a counter-clockwise sense. The angle made by the string relative to the vertical axis is $\varphi \geq 0$, just as for the simple pendulum in Figure 15.1. The right panel shows a projection onto the y-z plane ($\gamma = \pi/2$), which clearly illustrates the relation $\psi = \varphi/2$. Furthermore, the law of cosines expresses the radial position as a function of the angle, φ, and the string length, $r^2 = 2\,\ell^2\,(1 - \cos\varphi) = 4\,\ell^2 \sin^2(\varphi/2)$.

15.3.2 Position vector for the point mass

To avoid confusion with the planetary spherical coordinates of Figure 4.3, we write the pendulum's spherical angles as ψ (angle relative to the horizontal plane with $\psi \geq 0$ for the pendulum) and γ (angle relative to $\hat{\boldsymbol{x}}$, with $0 \leq \gamma \leq 2\pi$). In this manner, the coordinates for the point mass at the end of the string are given by

$$x = r\cos\psi\cos\gamma = 2\,\ell\sin(\varphi/2)\cos(\varphi/2)\cos\gamma = \ell\sin\varphi\cos\gamma \tag{15.51a}$$

$$y = r\cos\psi\sin\gamma = 2\,\ell\sin(\varphi/2)\cos(\varphi/2)\sin\gamma = \ell\sin\varphi\sin\gamma \tag{15.51b}$$

$$z = r\sin\psi = 2\,\ell\sin^2(\varphi/2) = \ell\,(1 - \cos\varphi). \tag{15.51c}$$

For these equations we made use of the law of cosines to write the radial distance from the origin, r, in terms of the string length, ℓ, and the angle of the string from the vertical, φ,

$$r = \ell\sqrt{2\,(1 - \cos\varphi)} = 2\,\ell\sin(\varphi/2). \tag{15.52}$$

Equations (15.51a)–(15.51c) provide an expression for the particle position

$$\boldsymbol{X}(t) = \ell\,[\hat{\boldsymbol{x}}\sin\varphi\cos\gamma + \hat{\boldsymbol{y}}\sin\varphi\sin\gamma + \hat{\boldsymbol{z}}\,(1-\cos\varphi)], \tag{15.53}$$

which is written in terms of just the two angles, φ and γ, which serve as our generalized coordinates.

15.3.3 Lagrangian for the Foucault pendulum

We are describing the motion of the particle within a rotating reference frame, with the horizontal axes rotating around the vertical as viewed in a local tangent plane on the planet. Hence, from the rigid-body rotation study in Section 11.2.2, we have (see equation (11.34)) the time change of the local horizontal Cartesian unit vectors

$$\dot{\hat{\boldsymbol{x}}} = (f/2)\,\hat{\boldsymbol{z}}\times\hat{\boldsymbol{x}} = (f/2)\,\hat{\boldsymbol{y}} \quad \text{and} \quad \dot{\hat{\boldsymbol{y}}} = (f/2)\,\hat{\boldsymbol{z}}\times\hat{\boldsymbol{y}} = -(f/2)\,\hat{\boldsymbol{x}}. \tag{15.54}$$

The corresponding velocity vector for the particle is

$$\begin{aligned}\dot{\boldsymbol{X}} = {}& \ell\,\dot\varphi\cos\varphi\,(\hat{\boldsymbol{x}}\cos\gamma + \hat{\boldsymbol{y}}\sin\gamma) + \ell\,\dot\gamma\sin\varphi\,(-\hat{\boldsymbol{x}}\sin\gamma + \hat{\boldsymbol{y}}\cos\gamma)\\ &+ \ell\,\hat{\boldsymbol{z}}\,\dot\varphi\sin\varphi + (f/2)\,\hat{\boldsymbol{z}}\times\boldsymbol{X},\end{aligned} \tag{15.55}$$

with rearrangement leading to

$$\begin{aligned}\dot{\boldsymbol{X}} = {}& \ell\,\hat{\boldsymbol{x}}\,(\dot\varphi\cos\varphi\cos\gamma - (\dot\gamma + f/2)\sin\varphi\sin\gamma)\\ &+ \ell\,\hat{\boldsymbol{y}}\,(\dot\varphi\cos\varphi\sin\gamma + (\dot\gamma + f/2)\sin\varphi\cos\gamma) + \ell\,\hat{\boldsymbol{z}}\,\dot\varphi\sin\varphi.\end{aligned} \tag{15.56}$$

Notice the appearance of $\dot\gamma + f/2$, which is the net angular frequency for motion around the vertical axis.

Computing the squared velocity and rearranging then leads to the particle's kinetic energy

$$K = (m\,\ell^2/2)\,(\dot\varphi^2 + (\dot\gamma + f/2)^2\sin^2\varphi), \tag{15.57}$$

which arises from motion in the two angular directions plus the rigid-body motion of the rotating reference frame. The gravitational potential energy, referenced to the coordinate system origin, is given by

$$P = m\,g\,\ell\,(1-\cos\varphi), \tag{15.58}$$

so that the Lagrangian is

$$L = K - P = (m\,\ell^2/2)\,(\dot\varphi^2 + (\dot\gamma + f/2)^2\sin^2\varphi) + m\,g\,\ell\,(\cos\varphi - 1). \tag{15.59}$$

15.3.4 Euler-Lagrange equations of motion

The absence of an explicit appearance of γ in the Lagrangian (15.59) means that the γ component of the generalized momentum, $\mathscr{P}_\gamma$, is a constant of the motion

$$\frac{\mathrm{d}\mathscr{P}_\gamma}{\mathrm{d}t} = 0 \quad \text{with} \quad \mathscr{P}_\gamma = \frac{\partial L}{\partial\dot\gamma} = m\,\ell^2\,(\dot\gamma + f/2)\sin^2\varphi. \tag{15.60}$$

We interpret $\mathscr{P}_\gamma$ as the axial angular momentum for the unconstrained rotational motion around the local vertical axis, with $\ell\sin\varphi$ the distance of the particle from the vertical axis and $\dot\gamma + f/2$

the net angular frequency for motion around the axis.[2] The φ equation is derived from

$$\frac{\partial L}{\partial \dot{\varphi}} = m\,\ell^2\,\dot{\varphi} \quad \text{and} \quad \frac{\partial L}{\partial \varphi} = m\,\ell^2\,(\dot{\gamma} + f/2)^2 \sin\varphi\cos\varphi - m\,g\,\ell\sin\varphi, \tag{15.61}$$

which leads to

$$\ddot{\varphi} + (g/\ell)\sin\varphi = (\dot{\gamma} + f/2)^2 \sin\varphi\cos\varphi. \tag{15.62}$$

This equation reduces to the planar pendulum equation (15.15) for the special case of motion within a vertical plane so that $\dot{\gamma} = 0$, and in the absence of planetary rotation so that $f = 0$. It also reduces to the planar pendulum for the case where $\dot{\gamma} = -f/2$, in which the pendulum contains zero axial angular momentum. We return to the case of zero axial angular momentum in Section 15.3.6.

15.3.5 Mechanical energy conservation

Since the Cartesian expression (15.53) for the position vector has no explicit time dependence, and neither does the Lagrangian (15.53), we know that the Hamiltonian equals to the mechanical energy and it is a constant of the motion

$$H = K + P = (m\,\ell^2/2)\,(\dot{\varphi}^2 + (\dot{\gamma} + f/2)^2 \sin^2\varphi) + m\,g\,\ell\,(1 - \cos\varphi). \tag{15.63}$$

Using the Euler-Lagrange equations of motion (15.60) and (15.62), it is straightforward to show that (see Exercise 15.1)

$$\frac{\mathrm{d}H}{\mathrm{d}t} = 0. \tag{15.64}$$

15.3.6 The case of zero axial angular momentum

Let us view the Foucault pendulum from a non-rotating inertial frame off the planet. Upon release from a position of rest, the inertial observer sees a pendulum that oscillates in a plane that is fixed with respect to the non-rotating inertial frame. In contrast, the rotating reference frame sees the pendulum's oscillation plane rotate oppositvely to the planet. The situation is directly analogous to the frictionless motion of a particle on a rotating table as illustrated in Figure 14.4. For the Foucault pendulum, the particle is constrained to oscillate on the end of a string. However, its motion couples to the rotation and so the rotating reference frame experiences a Coriolis acceleration. In picturing the motion, it is important to remember the assumption of zero friction, so that the apparatus holding the pendulum can rotate with the planet and yet not impart any frictional force to cause the pendulum to also rotate with the planet. In this manner, the pendulum maintains a fixed planar motion as viewed in the inertial reference frame.

Our thought experiment focuses on the special case of zero axial angular momentum (where, again, the axis here refers to the local vertical axis of the pendulum). In this case, the Euler-Lagrange equations of motion reduce to the relatively simple set

$$(\dot{\gamma} + f/2)\sin^2\varphi = 0 \quad \text{and} \quad \ddot{\varphi} + (g/\ell)\sin\varphi = 0. \tag{15.65}$$

The first equation is generally satisfied with $\dot{\gamma} = -f/2$, whereas the second equation is that for the planar pendulum from Section 15.1. The zero axial angular momentum motion decouples the evolution equations for γ and φ.

[2] Compare this result to our study in Section 14.5 of axial angular momentum for planetary motion. In that discussion we considered motion around the planetary rotational axis. Here, the rotational axis for the Foucault pendulum is approximated by the local vertical, as per our assumptions discussed in Section 15.3.1.

Evidently, with $\dot{\gamma} = -f/2$ then γ evolves as $\gamma = -(f/2)\,t$. We refer to this motion as a *precession* of the pendulum motion around the vertical rotational axis. The precession of γ means that the Foucault pendulum is seen by a rotating frame observer to have its oscillation plane rotate opposite to the planetary rotation (anti-cyclonically). In the northern hemisphere the pendulum's rotational plane precesses clockwise, whereas it precesses counter-clockwise in the southern hemisphere. Again, as per the motion of a frictionless ball on a rotating table seen in Figure 14.4, the precession can be interpreted as the persistent effects of the rightward deflection by the Coriolis acceleration in the northern hemisphere and leftward deflction in the southern (see Section 14.6). The period of the precession is

$$T^{\text{precession}} = \frac{2\,\pi}{|f|/2} = \frac{2\,\pi}{\Omega|\sin\phi|}. \tag{15.66}$$

Hence, a Foucault pendulum positioned at either poles (where the latitude, $\phi = \pm\pi/2$) exhibits a complete precession once per day, whereas at the equator ($\phi = 0$) there is no precession (formally an infinite period). Observe that the precession period is twice the period of inertial oscillations studied in Section 14.4.

15.3.7 Comments

Our treatment of Foucault's pendulum is distinguished from certain standard treatments, such as Section 12 of *Fetter and Walecka* (2003) and Example 9-5 of *Marion and Thornton* (1988). First, we made use of Lagrangian mechanics whereas both of these alternative treatments used Newtonian mechanics. Consequently, we had no occasion to consider the forces acting within the string, as these forces of constraint are removed when using the angles φ and γ as generalized coordinates. Second, we made use of an approximate Coriolis acceleration as described in Section 15.3.1, where we only considered the local vertical component of the earth's rotation. The standard treatments reduce to this same approximate Coriolis acceleration, though they generally wait until later in the analysis to introduce the assumption. We found it useful to introduce the approximation earlier since it corresponds closely to how we treat the Coriolis acceleration for motion of the large-scale circulation in the ocean and atmosphere. It also simplifies the analysis. Third, we focused on the zero axial angular momentum case, which trivially yields the precession rate $\dot{\gamma} = -f/2$. Since the axial angular momentum is a constant of the motion, we can set it to a zero value initially and it will remain so throughout the experiment (ignoring friction). It is this situation that is realized by a careful initial release of the Foucault pendulum so as to not introduce any lateral bias to the motion. In this manner, the spherical pendulum oscillates in a fixed plane when viewed by an inertial observer, while the planetary rotation occurs underneath the oscillating pendulum so that the planetary observer sees a precession.

15.4 Motion on constant potential energy surfaces

In this section we study motion constrained to move on surfaces of constant potential energy. Since the potential energy is a function of the coordinates (and not the velocity), the constraint is holonomic thus enabling use of generalized coordinates and Lagrange multipliers.

15.4.1 Anticipating the results

Much can be anticipated before doing any analysis, and it is useful to do so. For each case gravity provides the external conservative force and we ignore friction as well as any other external forces. The first case considers motion in the presence of a horizontally symmetric gravitational potential, which leads to a vertically directed gravitational acceleration. Motion in the horizontal directions is free (again, we ignore friction and any other forces). Hence, linear momentum

in the horizontal directions is a constant of the motion, as is angular momentum around the vertical axis centered anywhere in the field. Also, since the potential and the Lagrangian have no explicit time dependence, the Hamiltonian (mechanical energy) is a constant. Horizontal motion is maintained by a force of constraint, such as provided by a frictionless flat table, with this force exactly balancing the weight of the particle.

Next we study motion in the force field of a spherically symmetric gravitational potential such as generated by a spherical mass source. In this case the generalized coordinates are the two spherical angles (latitude and longitude), with the angular momentum around any axis a constant of the motion, as is the Hamiltonian. The force of constraint must counteract the gravitational force (pointing into the center) as well as the centrifugal force arising from the angular velocity (pointing away from the center). Indeed, particles with enough kinetic energy can have sufficient centrifugal acceleration to overcome the gravitational acceleration, in which case the force of constraint must keep the particle from flying outward.

15.4.2 Lagrangian using Cartesian coordinates

The unconstrained Lagrangian in Cartesian coordinates is given by

$$L = (m/2)\,(\dot{x}^2 + \dot{y}^2 + \dot{z}^2) - P(x, y, z), \tag{15.67}$$

where we assume the potential energy has no explicit time dependence, in which case the Hamiltonian is a constant of the motion (see Section 12.9.4)

$$\dot{H} = 0 \quad \text{with} \quad H = (m/2)\,(\dot{x}^2 + \dot{y}^2 + \dot{z}^2) + P. \tag{15.68}$$

Now introduce a Lagrange multiplier, Λ, to constrain the particle motion to a surface of constant potential energy, $P = \mathcal{C}$, so that the modified Lagrangian is

$$L^* = L + \Lambda\,(P - \mathcal{C}) = K - P\,(1 - \Lambda) - \Lambda\,\mathcal{C}. \tag{15.69}$$

The corresponding Euler-Lagrange equations of motion (12.107a) and (12.107b) are

$$m\,\ddot{\boldsymbol{X}} = -(1 - \Lambda)\,\nabla P \quad \text{and} \quad P = \mathcal{C}. \tag{15.70}$$

For particle motion along the $P = \mathcal{C}$ surface we know that the exact differential of the potential energy vanishes, which means that

$$\mathrm{d}P = \nabla P \cdot \mathrm{d}\boldsymbol{X} = 0 \Longrightarrow \nabla P \cdot \dot{\boldsymbol{X}} = 0. \tag{15.71}$$

This condition means that the velocity is parallel to constant potential energy surfaces, which it must be to maintain constant potential energy. Furthermore, taking the dot product of $\dot{\boldsymbol{X}}$ with the equation of motion (15.70), and using the constraint $\nabla P \cdot \dot{\boldsymbol{X}} = 0$, reveals that the kinetic energy is a constant of the motion

$$\dot{\boldsymbol{X}} \cdot \ddot{\boldsymbol{X}} = 0 \Longrightarrow \dot{K} = 0. \tag{15.72}$$

We can readily anticipate this result since with a constant potential energy and a constant Hamiltonian, then the kinetic energy is also a constant of the motion.

The Lagrange multiplier scales the force of constraint that counteracts the conservative force arising from the gradient of the potential energy. Making use of the general expression (12.110) yields the force of constraint

$$Q_\sigma^{\text{constraint}} = \Lambda\,\frac{\partial P}{\partial x^\sigma} = -\Lambda\,F_\sigma, \tag{15.73}$$

where F_σ is the conservative force arising from the potential energy. Setting $\Lambda = 1$ ensures that the force of constraint acts to exactly oppose the conservative force, thus rendering a zero acceleration along the σ direction. The case of $\Lambda = 1$ is encountered for the particle moving along a horizontal geopotential. However, when the particle experiences any acceleration due to curved motion (e.g., motion around the sphere), then $\Lambda \neq 1$. The reason is that in addition to the conservative force from gravity, the particle encounters the centrifugal acceleration due to its angular motion around the sphere. If the sphere is itself rotating, as considered in Section 15.5, then there are additional accelerations (planetary centrifugal and planetary Coriolis) that must be accounted for when determining the force of constraint. These points will become clearer as we work through the various examples.

15.4.3 Plane symmetric potential energy

If the potential energy arises from a gravitational force field in the $-\hat{\boldsymbol{z}}$ direction, then gravitational potential energy is given by

$$P = m\, g\, z, \tag{15.74}$$

and the corresponding force of constraint is

$$Q_z^{\text{constraint}} = m\, g. \tag{15.75}$$

Evidently, the force of constraint acts vertically upward to exactly balance the downward weight of the particle so that the particle remains on a fixed z surface. A particle moving on a flat frictionless table provides the canonical example of this situation, where the table provides the force of constraint that balances the particle weight.

With $\Lambda = 1$ the horizontal motion has no acceleration

$$\ddot{x} = \ddot{y} = 0. \tag{15.76}$$

It is notable that all three coordinate directions have zero acceleration. However, motion in the horizontal directions is unconstrained and so the horizontal motion is free, whereas motion in the vertical direction is constrained due to the force of constraint balancing the weight.

15.4.4 Spherically symmetric potential energy

Now consider motion in the presence of a spherically symmetric potential, such as for a particle moving around a non-rotating spherical earth. We make use of spherical coordinates, with the transformation between planetary Cartesian coordinates and planetary spherical coordinates given by equations (4.206a)-(4.206c)

$$x = r\cos\phi\,\cos\lambda \quad \text{and} \quad y = r\cos\phi\,\sin\lambda \quad \text{and} \quad z = r\sin\phi, \tag{15.77}$$

where $0 \leq \lambda \leq 2\pi$ is the longitude, and $-\pi/2 \leq \phi \leq \pi/2$ is the latitude (see Figure 4.3). The velocity components are given by

$$\dot{x} = \dot{r}\cos\phi\cos\lambda - r\,\dot{\phi}\sin\phi\cos\lambda - r\,\dot{\lambda}\cos\phi\sin\lambda \tag{15.78a}$$

$$\dot{y} = \dot{r}\cos\phi\sin\lambda - r\,\dot{\phi}\sin\phi\sin\lambda + r\,\dot{\lambda}\cos\phi\cos\lambda \tag{15.78b}$$

$$\dot{z} = \dot{r}\sin\phi + r\,\dot{\phi}\cos\phi, \tag{15.78c}$$

which then leads (after a bit of algebra) to the kinetic energy

$$K = (m/2)\,(\dot{x}^2 + \dot{y}^2 + \dot{z}^2) = (m/2)\,(\dot{r}^2 + r^2\,\dot{\phi}^2 + r^2\,\dot{\lambda}^2\cos^2\phi). \tag{15.79}$$

We could have written this expression down by inspection if using the spherical coordinate expression (13.46d). However, the approach shown here is useful in general. Namely, we first write the kinetic energy in Cartesian coordinates, and then transform to coordinates that respect the symmetry of the system and thus provide suitable generalized coordinates.

Assuming the particle motion moves at a radius close to that of the mean earth radius allows us to approximate the gravitational potential energy according to equation (13.120)

$$P = m\,\Phi_{\text{e}} = m\,g_{\text{e}}\,r, \tag{15.80}$$

where $g_{\text{e}} \approx 9.8$ m s^{-2} (Section 13.10.3). We are thus led to the Lagrangian

$$L = (m/2)\,(\dot{r}^2 + r^2\,\dot{\phi}^2 + r^2\,\dot{\lambda}^2\cos^2\phi) - m\,g_{\text{e}}\,r. \tag{15.81}$$

Since the Lagrangian and the potential energy are not explicit functions of time, then the Hamiltonian is a constant of the motion

$$\dot{H} = 0 \quad \text{with} \quad H = (m/2)\,(\dot{r}^2 + r^2\,\dot{\phi}^2 + r^2\,\dot{\lambda}^2\cos^2\phi) + m\,g_{\text{e}}\,r. \tag{15.82}$$

We next modify the Lagrangian by adding a Lagrange multiplier to constrain the motion to remain on a constant potential energy surface, $P = P(R)$, in which case

$$L^* = L + \Lambda\,[P - P(R)] = (m/2)\,(\dot{r}^2 + r^2\,\dot{\phi}^2 + r^2\,\dot{\lambda}^2\cos^2\phi) - P\,(1-\Lambda) - \Lambda\,P(R). \tag{15.83}$$

The corresponding Euler-Lagrange equations are

$$\ddot{r} = r\,(\dot{\phi}^2 + \dot{\lambda}^2\cos^2\phi) - (1-\Lambda)\,g_{\text{e}} \tag{15.84a}$$

$$\frac{\mathrm{d}(r^2\,\dot{\phi})}{\mathrm{d}t} = -r^2\,\dot{\lambda}^2\cos\phi\sin\phi \tag{15.84b}$$

$$\frac{\mathrm{d}(r^2\,\dot{\lambda}\cos^2\phi)}{\mathrm{d}t} = 0 \tag{15.84c}$$

$$r = R. \tag{15.84d}$$

The third equation corresponds to angular momentum conservation arising from the spherical symmetry. Satisfying the constraint, $r = R$, means that there is no radial acceleration, $\ddot{r} = 0$, and that the potential energy is fixed at the constant

$$P = m\,g_{\text{e}}\,R. \tag{15.85}$$

Equation (15.84a) thus leads to

$$m\,R^2\,(\dot{\phi}^2 + \dot{\lambda}^2\cos^2\phi) = (1-\Lambda)\,P, \tag{15.86}$$

and the Hamiltonian (which is a constant of the motion) takes the form

$$H = m\,R^2\,(\dot{\phi}^2 + \dot{\lambda}^2\cos^2\phi)/2 + P. \tag{15.87}$$

Making use of this constant Hamiltonian in equation (15.86) gives us

$$\Lambda = 3 - 2\,H/P = 1 - 2\,K/P, \tag{15.88}$$

with the kinetic energy a constant of the motion since both H and P are also constants.[3] The

[3] Again, $H = K + P$ is a constant due to time symmetry whereas P is a constant due to the force of constraint that keeps the particle at a fixed radius.

radial force of constraint is thus given by

$$Q_r = \Lambda \frac{\partial P}{\partial r} = (1 - 2\,K/P)\, m\, g_{\mathrm{e}}. \tag{15.89}$$

To help interpret the force of constraint (15.89), write the kinetic energy in the form

$$2\,K = m\,R^2\,(\dot{\phi}^2 + \dot{\lambda}^2 \cos^2\phi) = m\,(v^2 + u^2) = m\,R\,A^{\text{centrifugal}}, \tag{15.90}$$

where we introduced the spherical velocity components according to equation (13.48), and defined the centrifugal acceleration arising from the angular motion of the particle around the sphere,

$$A^{\text{centrifugal}} = R\,(\dot{\phi}^2 + \dot{\lambda}^2 \cos^2\phi) = (u^2 + v^2)/R, \tag{15.91}$$

which is positive and points outward away from the axis of rotation. We can now write the force of constraint in the physically transparent manner

$$Q_r = m\,g_{\mathrm{e}}\,(1 - A^{\text{centrifugal}}/g_{\mathrm{e}}). \tag{15.92}$$

Evidently, if the gravitational acceleration is greater than the centrifugal acceleration, then the force of constraint is directed radially outward with a magnitude less than the weight of the particle. In contrast, if the centrifugal acceleration is greater than the gravitational acceleration, then the force of constraint must point radially inward to keep the particle on a constant radius. If the centrifugal acceleration equals to the gravitational acceleration, then the particle remains at a fixed radius with a zero force of constraint.

15.5 Motion on geopotential surfaces

We extend the results from Section 15.4 to now consider motion on geopotential surfaces that arise from central gravity plus planetary centrifugal. For the rotating spherical planet, the geopotentials are oblate spheroidal shaped surfaces (Section 13.10.4), whereas they are parabolic for the case of a rotating plane (Section 15.5.3). The force of constraint accounts for the gravitational acceleration, the centrifugal acceleration from the particle motion, the centrifugal acceleration of the rotating reference frame, and a portion of the Coriolis acceleration. We greatly simplify the analysis by moving from spherical coordinates to geopotential coordinates as motivated by our earlier work in Section 13.11.3.

15.5.1 Oblate spheroidally symmetric potential energy

Building from the analysis in Sections 15.4.3 and 15.4.4, consider a rotating spherical planet with constant angular rotation rate, $\boldsymbol{\Omega} = \Omega\,\hat{\boldsymbol{z}}$, directed through the vertical planetary Cartesian axis. We describe motion from the rotating reference frame, in which the planetary spherical coordinates and planetary Cartesian coordinates are fixed with respect to the rotating planet. This is the same convention taken in Chapter 13 and used throughout this book. As we show, the particle motion maintains a constant axial angular momentum (due to zonal symmetry), a constant Hamiltonian (due to time symmetry), and constant geopotential (due to the imposed constraint). Notably, however, the kinetic energy is not a constant of the motion.

The Lagrangian and the oblate spheroidal geopotential

The spherical coordinate expression for the particle's kinetic energy is

$$K = (m/2)\,(\dot{r}^2 + r^2\,\dot{\phi}^2 + r^2\,(\dot{\lambda} + \Omega)^2 \cos^2\phi). \tag{15.93}$$

The only change relative to equation (15.79) is the presence of Ω, which arises from the rigid-body rotation of the planet around the polar axis. The gravitational potential energy is just like for the non-rotating case, thus leading to the Lagrangian

$$\begin{aligned} L &= K - P && \text{(15.94a)} \\ &= (m/2)\,(\dot{r}^2 + r^2\,\dot{\phi}^2 + r^2\,(\dot{\lambda} + \Omega)^2\cos^2\phi) - m\,g_{\mathsf{e}}\,r && \text{(15.94b)} \\ &= (m/2)\,[\dot{r}^2 + r^2\,\dot{\phi}^2 + r^2\,\dot{\lambda}\,(\dot{\lambda} + 2\,\Omega)\cos^2\phi] - m\,(g_{\mathsf{e}}\,r - (1/2)\,\Omega^2\,r^2\cos^2\phi) && \text{(15.94c)} \\ &= K^{\text{truncate}} - m\,\Phi. && \text{(15.94d)} \end{aligned}$$

The third equality introduced the truncated kinetic energy

$$K^{\text{truncate}} = K - (m/2)\,\Omega^2\,r^2\cos^2\phi = (m/2)\,[\dot{r}^2 + r^2\,\dot{\phi}^2 + r^2\,\dot{\lambda}\,(\dot{\lambda} + 2\,\Omega)\cos^2\phi], \tag{15.95}$$

which is the kinetic energy absent the contribution from the centrifugal acceleration from the rigid-body planetary rotation. It is notable that K^{truncate} is not guaranteed to be non-negative. In equation (15.94d) we also introduced the geopotential for a rotating spherical planet

$$\Phi(r,\phi) = g_{\mathsf{e}}\,r - (1/2)\,\Omega^2\,r^2\cos^2\phi, \tag{15.96}$$

which we discussed in Section (13.10.4). In particular, surfaces of constant geopotential have larger radius at the equator than at the pole, which characterizes the earth's oblate spheroidal shape.

The Lagrange multiplier and Euler-Lagrange equations

Introducing a Lagrange multiplier to enforce the constraint of motion on a constant geopotential leads to the modified Lagrangian

$$L^* = L + \Lambda\,m\,(\Phi - \Phi^{\text{const}}) = K^{\text{truncate}} - m\,\Phi\,(1 - \Lambda) - \Lambda\,m\,\Phi^{\text{const}}, \tag{15.97}$$

where Φ^{const} is a constant. The corresponding Euler-Lagrange equations of motion are

$$\begin{aligned} \ddot{r} &= r\,\dot{\phi}^2 + r\,\dot{\lambda}\,(\dot{\lambda} + 2\,\Omega)\cos^2\phi - (1 - \Lambda)\,\partial\Phi/\partial r && \text{(15.98a)} \\ \frac{\mathrm{d}(r^2\,\dot{\phi})}{\mathrm{d}t} &= -r^2\,\dot{\lambda}\,(\dot{\lambda} + 2\,\Omega)\cos\phi\sin\phi - (1 - \Lambda)\,\partial\Phi/\partial\phi && \text{(15.98b)} \\ \frac{\mathrm{d}(r^2\,(\dot{\lambda} + \Omega)\cos^2\phi)}{\mathrm{d}t} &= 0 && \text{(15.98c)} \\ \Phi &= \Phi^{\text{const}}. && \text{(15.98d)} \end{aligned}$$

In the absence of planetary rotation, with $\Omega = 0$, equations (15.98a)–(15.98d) reduce to the Euler-Lagrange equations (15.84a)–(15.84d) for motion around the non-rotating sphere. Furthermore, with some work, and in the absence of the geopotential constraint (i.e., $\Lambda = 0$), we can massage these equations to agree with the spherical coordinate equations (13.132)–(13.134) describing motion around a rotating sphere and derived using Newtonian methods.

Energy constants of the motion

Because the Lagrangian and the gravitational potential energy both have no explicit time dependence, the Hamiltonian, H, is a constant of the motion (see Section 12.9.4), where

$$H = K + m\,g_{\mathsf{e}}\,r = K^{\text{truncate}} + (m/2)\,\Omega^2\,r^2\cos^2\phi + m\,g_{\mathsf{e}}\,r = K^{\text{truncate}} + m\,\Phi + m\,\Omega^2\,r^2\cos^2\phi. \tag{15.99}$$

With the motion constrained to maintain a constant geopotential, $\dot{\Phi} = 0$ and $\dot{H} = 0$, then

$$\frac{\mathrm{d}(K + m\, g_{\mathrm{e}}\, r)}{\mathrm{d}t} = 0 \quad \text{and} \quad \frac{\mathrm{d}(K^{\text{truncate}} + m\, \Omega^2\, r^2 \cos^2\phi)}{\mathrm{d}t} = 0. \tag{15.100}$$

In contrast to the case of motion around a non-rotating sphere studied in Section 15.4.4, the kinetic energy is here not a constant of the motion since the particle is not constrained to a constant spherical radius, $\dot{r} \neq 0$. Rather, the particle is constrained to a constant geopotential, which has an oblate spheroidal shape. This facet of the motion adds complexity to the description, which we alleviate in Section 15.5.2 by moving to geopotential coordinates. Until then, it is useful to offer some more details of the spherical coordinate formulation.

Velocity on the geopotential

Motion along the geopotential means that

$$\dot{\boldsymbol{X}} \cdot \nabla\Phi = 0, \tag{15.101}$$

so that the particle velocity is directed parallel to the geopotential surface. Writing the velocity in spherical coordinates according to equation (13.46d)

$$\dot{\boldsymbol{X}} = r\cos\phi\,(\dot{\lambda} + \Omega)\,\hat{\boldsymbol{\lambda}} + r\,\dot{\phi}\,\hat{\boldsymbol{\phi}} + \dot{r}\,\hat{\boldsymbol{r}}, \tag{15.102}$$

and using the spherical coordinate gradient operator (4.243)

$$\nabla = \hat{\boldsymbol{\lambda}}\,(r\,\cos\phi)^{-1}\,\partial_\lambda + \hat{\boldsymbol{\phi}}\,r^{-1}\,\partial_\phi + \hat{\boldsymbol{r}}\,\partial_r, \tag{15.103}$$

renders

$$\dot{\boldsymbol{X}} \cdot \nabla\Phi = \dot{\phi}\,\partial\Phi/\partial\phi + \dot{r}\,\partial\Phi/\partial r = 0, \tag{15.104}$$

which means that

$$r\,\Omega^2\cos\phi\,(r\,\dot{\phi}\sin\phi - \dot{r}\cos\phi) + \dot{r}\,g_{\mathrm{e}} = 0. \tag{15.105}$$

Evidently, any radial motion must be accompanied by meridional motion in order to remain on the geopotential. Furthermore, if there is no radial motion then there is no meridional motion, in which case the particle moves along a constant latitude circle.

15.5.2 Oblate spheroidally symmetric earth[4]

The analysis in Section 15.5.1 can be greatly simplified by acknowledging that the earth has evolved to approximate the oblate spheroidal shape of the geopotential (15.96). Following *Veronis* (1973) and *Gill* (1982), and as detailed in Section 13.11.3 (see in particular Figure 13.4), we interpret the radial direction as aligned with the effective gravitational acceleration (central gravity plus planetary centrifugal), so that the geopotential takes on the much simpler form

$$\Phi = g\,r, \tag{15.106}$$

where g is the effective gravitational acceleration and geopotential surfaces are now surfaces of constant r. In this manner the constrained Lagrangian is

$$L = (m/2)\,(\dot{r}^2 + r^2\,\dot{\phi}^2 + r^2\,\dot{\lambda}\,(\dot{\lambda} + 2\,\Omega)\cos^2\phi) - m\,g\,r + m\,\Lambda\,(\Phi - \Phi^{\text{const}}). \tag{15.107}$$

This Lagrangian is nearly the same as for the non-rotating sphere given by equation (15.83), with the exception of the $2\,\Omega$ term. The force of constraint is required to keep the particle

[4]The analysis in this section is inspired by *Early* (2012).

moving on a constant geopotential, which here means the particle maintains a fixed $r = R$.

To examine the force of constraint, we generate the Euler-Lagrange equations

$$\ddot{r} = r\,\dot{\phi}^2 + r\,\dot{\lambda}\,(\dot{\lambda} + 2\,\Omega)\cos^2\phi - (1 - \Lambda)\,g \tag{15.108a}$$

$$\frac{\mathrm{d}(r^2\,\dot{\phi})}{\mathrm{d}t} = -r^2\,\dot{\lambda}\,(\dot{\lambda} + 2\,\Omega)\cos\phi\sin\phi \tag{15.108b}$$

$$\frac{\mathrm{d}(r^2\,(\dot{\lambda} + \Omega)\cos^2\phi)}{\mathrm{d}t} = 0 \tag{15.108c}$$

$$\Phi = \Phi^{\text{const}} = g\,R. \tag{15.108d}$$

With $r = R$ for the constrained motion, the radial equation (15.108a) allows us to solve for the Lagrange multiplier

$$\Lambda = 1 - (R/g)\,(\dot{\phi}^2 + \dot{\lambda}^2\cos^2\phi + 2\,\Omega\,\dot{\lambda}\cos^2\phi) = 1 - g^{-1}\,(A^{\text{centrifugal}} + A^{\text{coriolis}}), \tag{15.109}$$

where we introduced the centrifugal acceleration arising from the angular particle motion (as for the non-rotating sphere in equation (15.91))

$$A^{\text{centrifugal}} = R\,(\dot{\phi}^2 + \dot{\lambda}^2\cos^2\phi), \tag{15.110}$$

as well as the Coriolis acceleration

$$A^{\text{coriolis}} = 2\,\Omega\,R\,\dot{\lambda}\cos^2\phi, \tag{15.111}$$

which is positive for eastward motion and negative if westward. The force of constraint is thus given by

$$Q_r = \Lambda\,\frac{\partial P}{\partial r} = m\,g\,[1 - (A^{\text{centrifugal}} + A^{\text{coriolis}})/g]. \tag{15.112}$$

Compared to the non-rotating case in equation (15.92), we here see the inclusion of the Coriolis acceleration contribution as well as the minor difference between g_{e} and g.

15.5.3 An f-plane geopotential surface

We now return to planar symmetry as in Section 15.4.3, here examining motion of a particle as viewed in a rotating reference frame with constant angular rotation rate, $(f/2)\,\hat{\boldsymbol{z}}$. Furthermore, we assume the motion is on an f-plane (Section 24.5), which means that surfaces of constant geopotential from Section 15.5.2 are now approximated as horizontal, and it is only the vertical component of planetary rotation that is considered.

This particle has a kinetic energy

$$K = (m/2)\,(\dot{x}_{\text{I}}^2 + \dot{y}_{\text{I}}^2 + \dot{z}_{\text{I}}^2) = (m/2)\,[(\dot{x} - f\,y/2)^2 + (\dot{y} + f\,x/2)^2 + \dot{z}^2], \tag{15.113}$$

where

$$\dot{X}_{\text{I}} = \dot{\boldsymbol{X}} + (f/2)\,\hat{\boldsymbol{z}} \times \boldsymbol{X} \tag{15.114}$$

relates the velocity measured in the inertial reference frame, $\dot{\boldsymbol{X}}_{\text{I}}$, to the velocity, $\dot{\boldsymbol{X}}$, measured in the rotating reference frame. Expanding the kinetic energy leads to

$$K = (m/2)\,[\dot{x}\,(\dot{x} - f\,y) + \dot{y}\,(\dot{y} + f\,x) + \dot{z}^2] + (m/2)\,(f/2)^2\,(x^2 + y^2). \tag{15.115}$$

We are thus led to the Lagrangian

$$L^{\text{cartesian}} = (m/2)\,[\dot{x}\,(\dot{x} - f\,y) + \dot{y}\,(\dot{y} + f\,x) + \dot{z}^2] - m\,\Phi^{\text{parabolic}}, \tag{15.116}$$

where we introduced the geopotential

$$\Phi^{\text{parabolic}} = g_e\, z - (1/2)\,(f/2)^2\,(x^2 + y^2), \tag{15.117}$$

whose isosurfaces are parabolic.

Following the geopotential coordinate approach from Section 15.5.2, we reinterpret the local vertical direction as perpendicular to surfaces of constant $\Phi^{\text{parabolic}}$, in which case the Lagrangian (15.116) simplifies to

$$L = (m/2)\,[\dot{x}\,(\dot{x} - f\,y) + \dot{y}\,(\dot{y} + f\,x) + \dot{z}^2] - m\,\Phi, \tag{15.118}$$

with the geopotential

$$\Phi = g\,z. \tag{15.119}$$

To constrain the particle motion to remain on a constant geopotential, $\Phi = \Phi^{\text{const}}$, we introduce a Lagrange multiplier to produce the modified Lagrangian

$$L^* = (m/2)\,[\dot{x}\,(\dot{x} - f\,y) + \dot{y}\,(\dot{y} + f\,x) + \dot{z}^2] - m\,\Phi + \Lambda\,(\Phi - \Phi^{\text{const}}), \tag{15.120}$$

which generates the Euler-Lagrange equations

$$\frac{\mathrm{d}(\dot{x} - f\,y)}{\mathrm{d}t} = 0 \tag{15.121a}$$

$$\frac{\mathrm{d}(\dot{y} + f\,x)}{\mathrm{d}t} = 0 \tag{15.121b}$$

$$\frac{\mathrm{d}\dot{z}}{\mathrm{d}t} = -(1 - \Lambda)\,g \tag{15.121c}$$

$$\Phi = \Phi^{\text{const}}. \tag{15.121d}$$

To maintain zero vertical acceleration requires a unit Lagrange multiplier

$$\Lambda = 1, \tag{15.122}$$

which was also found in Section 15.4.3 for motion on a flat non-rotating plane. As for that case, we here find that the force of constraint must exactly balance the weight of the particle. Contrary to the full earth case in Section 15.5.2, there is no contribution to the force of constraint from the Coriolis acceleration. The reason is that we here only consider the local vertical component of the earth's rotation, whereas in Section 15.5.2 we made no such approximation.

The horizontal equations of motion (15.121a) and (15.121b) describe the f-plane inertial oscillations studied in Section 14.4. This horizontal motion is that of a free particle on an f-plane and as observed in the rotating reference frame. Consistent with the motion being free in the horizontal, it maintains a constant kinetic energy

$$K = m\,(\dot{x}^2 + \dot{y}^2)/2 \quad \text{and} \quad \dot{K} = m\,(\dot{x}\,\ddot{x} + \dot{y}\,\ddot{y}) = m\,f\,(\dot{x}\,\dot{y} - \dot{y}\,\dot{x}) = 0. \tag{15.123}$$

15.6 Simple harmonic oscillator

We here study the mechanics of *simple harmonic oscillators*. We start with the case of a single harmonic oscillator and then consider a line of coupled oscillators. We take the continuum limit of the coupled oscillators, thus providing a platform for introducing longitudinal waves, such as the acoustic waves studied in Chapter 51, as well as the use of Lagrangian mechanics for continuous media.

15.6.1 Physical picture

Consider a tiny piece of matter (idealized as a point) with constant mass, m. Assume this mass is constrained to move along one direction on a frictionless table. Equivalently, assume the mass moves in one direction a vacuum without any gravity field. Let the coordinate position, x, of the mass be measured by the trajectory, $x = X(t)$, and apply a horizontal force to the mass that is a function just of the position, $F(x)$. Newton's equation of motion for the point mass is given by

$$m\,\ddot{X} = F(x), \tag{15.124}$$

where $F(x)$ is evaluated at the horizontal position of the mass, $x = X(t)$. Now assume the point mass only moves a small distance from its equilibrium position, $x = \Delta$, which is defined by the position where the force vanishes, $F(\Delta) = 0$. We thus approximate the horizontal force by its leading order Taylor expansion

$$F(x) \approx F(\Delta) + (x - \Delta)\left[\frac{\mathrm{d}F(x)}{\mathrm{d}x}\right]_{x=\Delta} = (x - \Delta)\left[\frac{\mathrm{d}F(x)}{\mathrm{d}x}\right]_{x=\Delta}, \tag{15.125}$$

where higher order terms are dropped, and we set $F(\Delta) = 0$.

15.6.2 Oscillations from a Hooke's law restoring force

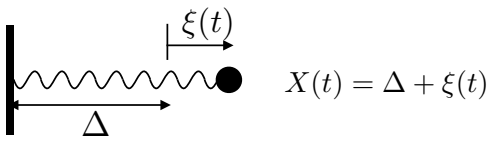

FIGURE 15.3: A simple harmonic oscillator as realized by an object of fixed mass m (approximated as a point mass) attached to a massless spring with motion in just one direction. The only force acting on the mass arises from the spring, whose spring constant, Γ, is constant. The trajectory of the point mass, $X(t) = \Delta + \xi(t)$, measures the position relative to the wall on the left, with Δ the equilibrium position (where the spring force vanishes), and $\xi(t)$ the displacement from the equilibrium position. We here depict the system where the spring is extended to the right so that $\xi(t) > 0$. In this case, the restoring force from the spring accelerates the mass to the left.

Now specialize the force to be restorative so that

$$F(x) = -\Gamma\,(x - \Delta) \quad \text{with} \quad \Gamma = \left[\frac{\mathrm{d}F(x)}{\mathrm{d}x}\right]_{x=\Delta} > 0. \tag{15.126}$$

This linear force provides the canonical *Hooke's law* force, such as realized by an idealized massless spring as depicted in Figure 15.3.[5] Introducing the displacement relative to an equilibrium position (see Figure 15.3)

$$\xi(t) = X(t) - \Delta, \tag{15.127}$$

along with the Hooke's law restoring force (15.126), we find Newton's law for the particle trajectory takes the form of the linear *oscillator equation*

$$m\,\ddot{X} + \Gamma\,(X - \Delta) = m\,\ddot{\xi} + \Gamma\,\xi = 0 \Longrightarrow \ddot{\xi} + \omega_0^2\,\xi = 0 \quad \text{with} \quad \omega_0^2 = \Gamma/m. \tag{15.128}$$

[5] We encounter a more complex example of Hooke's law in Section 25.8 when studying the relation between stress and strain rate for viscous fluids.

A solution to the oscillator equation can be written

$$X(t) - \Delta = \xi(t) = A\cos(\omega_0 t + \alpha), \tag{15.129}$$

where A is the oscillation amplitude and α a phase shift, with both A and α time independent and specified by initial conditions. We thus find that the Hooke's law restoring force leads to an oscillatory trajectory (15.129) centered on the equilibrium position, $x = \Delta$. The angular frequency, ω_0, determines the period of oscillation according to

$$T^{\text{per}} = 2\pi/\omega_0 = 2\pi\,(m/\Gamma)^{1/2}. \tag{15.130}$$

The period increases with the square root of the mass (longer period for larger mass) and decreases with the square root of the Hooke's law restoring constant (shorter period for larger Hooke's law constant).

15.6.3 Hamiltonian as a constant of the motion

The Hooke's law force has no explicit dependence on time, $\partial F/\partial t = 0$, so that the oscillating point mass has no concern for the time origin. From our discussion of time symmetry in Section 12.9.4, we know that the simple harmonic oscillator maintains a constant Hamiltonian, which is here also equal to the mechanical energy. A constancy of the Hamiltonian via Noether's theorem then means that the oscillator exchanges mechanical energy between its kinetic energy and potential energy while holding their sum constant.

Potential energy and kinetic energy of the oscillator

During its motion, the point mass experiences work done by the spring and this work is given by

$$W = -\int_{\Delta}^{\Delta+\xi} F\,\mathrm{d}x = \Gamma\int_{\Delta}^{\Delta+\xi}(x-\Delta)\,\mathrm{d}x = \Gamma\,\xi^2/2. \tag{15.131}$$

This work to displace the mass renders a potential energy for the point mass relative to the zero potential energy it possesses when located at its equilibrium position with $\xi = 0$. Through the work-energy theorem from Section 11.1.4, we find that temporal changes in the potential energy are associated with temporal changes in kinetic energy

$$W = -m\int_{\Delta}^{\Delta+\xi}\ddot{X}\,\mathrm{d}x = -m\int_{t_0}^{t}\ddot{X}\,\dot{X}\,\mathrm{d}t = -\frac{m}{2}\int_{t_0}^{t}\frac{\mathrm{d}\dot{X}^2}{\mathrm{d}t}\,\mathrm{d}t = -K(t) + K(t_0), \tag{15.132}$$

where

$$K = m\,\dot{X}^2/2 = m\,\dot{\xi}^2/2 \tag{15.133}$$

is the kinetic energy for the oscillating particle. Hence, as the point mass oscillates, changes to its potential energy are exactly compensated by equal and opposite changes to its kinetic energy, thus reflecting the constant mechanical energy for the harmonic oscillator. Another way to see that the mechanical energy remains constant is to note that the sum of the potential plus kinetic energies has a zero time derivative

$$(\mathrm{d}/\mathrm{d}t)\,[m\,\dot{\xi}^2 + \Gamma\,\xi^2]/2 = \dot{\xi}\,[m\,\ddot{\xi} + \Gamma\,\xi] = 0, \tag{15.134}$$

where the final equality made use of the equation of motion (15.128). Indeed, making use of the trajectory (15.129) we readily see that the mechanical energy is given by the constant

$$[m\,\dot{\xi}^2 + \Gamma\,\xi^2]/2 = (A^2/2)\,[m\,\omega_0^2\sin^2(\omega_0 t + \alpha) + \Gamma\cos^2(\omega_0 t + \alpha)] = \Gamma\,A^2/2, \tag{15.135}$$

where we set $\omega_0^2 = \Gamma/m$ as per equation (15.128). The total energy is thus proportional to the square of the amplitude and linearly proportional to the Hooke's law constant.

15.6.4 Equipartition of time averaged energies

When time averaged over a single oscillation period of length $2\pi/\omega_0$, the averaged kinetic energy and potential energy are identical

$$\frac{\omega_0}{2\pi}\int_0^{2\pi/\omega_0} (m\,\dot{\xi}^2/2)\,\mathrm{d}t = \Gamma\,A^2/4 \tag{15.136a}$$

$$\frac{\omega_0}{2\pi}\int_0^{2\pi/\omega_0} (\Gamma\,\xi^2/2)\,\mathrm{d}t = \Gamma\,A^2/4. \tag{15.136b}$$

Energy equipartition means that within a single oscillation period, there is an exact exchange between kinetic energy and potential energy, so that their time averages are identical.

Energy equipartition is a rather generic property of linear oscillating systems, and we encounter it again for linear waves, such as the acoustic waves in Section 51.6.2. It follows as a general result of the *virial theorem* proved in Section 12.7.3. In particular, it holds for systems in which the potential energy is a homogeneous function of degree two (see Section 12.7.1).

15.6.5 Lagrangian formulation

Having established the potential energy (15.131) for the oscillator, we can write the Lagrangian as

$$L = m\,\dot{\xi}^2/2 - \Gamma\,\xi^2, \tag{15.137}$$

with ξ a suitable generalized coordinate that captures the single degree of freedom for the oscillator. The Euler-Lagrange equation is

$$\frac{\mathrm{d}}{\mathrm{d}t}\frac{\partial L}{\partial \dot{\xi}} = \frac{\partial L}{\partial \xi} \implies \ddot{\xi} + \omega_0^2\,\xi = 0, \tag{15.138}$$

which is the same as equation (15.128) derived from Newtonian methods.

15.6.6 Further study

The study of harmonic oscillators can be found in most classical mechanics texts, with our treatment following Sections 3.1 and 3.2 of *Marion and Thornton* (1988).

15.7 Coupled harmonic oscillators

We here extend the study of a single harmonic oscillator in Section 15.6 to the case of N identical frictionless point mass particles connected by massless linear Hooke's law springs with identical spring constant, Γ. Let

$$X_{\mathfrak{n}}(t) = {}_{\mathfrak{n}}\Delta + \xi_{\mathfrak{n}}(t) \tag{15.139}$$

be the position of particle $\mathfrak{n}$ relative to the left-most rigid wall, with $x = {}_{\mathfrak{n}}\Delta$ the equilibrium position for particle $\mathfrak{n}$ and $\xi_{\mathfrak{n}}(t)$ the displacement of the particle at time t from its equilibrium. The $\xi_{\mathfrak{n}}$ displacements serve as generalized coordinates for this system with N degrees of freedom.[6]

[6] In Section 12.4.1 that we wrote $X_{(i)}$ for the Cartesian position of particle i. This notation is important to distinguish the particle label from a tensor index. In this section, we instead use the upright $\mathfrak{n}$ to write $X_{\mathfrak{n}}$ to distinguish the particle label, $\mathfrak{n}$, from a tensor index, n. Additionally, in this section we are only concerned with motion along a single direction, so that any label is a particle label.

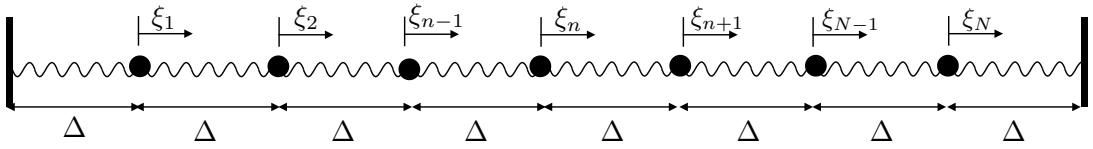

FIGURE 15.4: A line of $N = 7$ coupled simple harmonic oscillators as realized by identical point objects with fixed mass, m, each attached to two massless springs and moving in one direction. The only horizontal force acting on the masses arises from the springs, each with identical spring constants, Γ, and equilibrium length, Δ. The trajectory of any particular mass, $X_{\text{n}}(t)$, measures the position relative to the equilibrium at $X_{\text{n}}(t) = 0$, where the force from the springs vanishes. The system is here shown in its equilibrium where the distance between each mass is Δ, and the displacments all vanish, $\xi_{\text{n}} = 0$. Each point mass is attached to two springs, with the end springs attached to a rigid wall.

To develop the equation of motion, observe that the force acting on a particle is comprised of two terms associated with the two springs, one on the left and one on the right. Consider first the end particles where one of its springs is attached to a rigid wall. For convenience, we label a point at the left wall as $_{\text{n}} = 0$ and $_{\text{n}} = N + 1$ for a point on the right wall. For the $_{\text{n}} = 1$ mass we have the force from the left spring given by

$$F_{\text{n}=0\to\text{n}=1} = -\Gamma\,\xi_1, \tag{15.140}$$

just as for a single harmonic oscillator considered in Section 15.6.2. The force on particle 1 from the right spring is given by

$$F_{\text{n}=2\to\text{n}=1} = -\Gamma\,(\xi_1 - \xi_2). \tag{15.141}$$

We understand the nature of this force by noting that if $\xi_1 > 0$ then the spring is compressed to the right, so that the restoring force is to the left as the spring expands. Conversely, if $\xi_2 > 0$ then the spring is expanded to the right, in which case the particle is itself accelerated to the right. Hence, the equation of motion for this mass is given by

$$m\,\ddot{\xi}_1 = -\Gamma\,\xi_1 - \Gamma\,(\xi_1 - \xi_2). \tag{15.142}$$

Anticipating the force balance that acts on the interior masses, we introduce two dummy deviations, each with fixed value of zero,

$$\xi_0 \equiv 0 \quad \text{and} \quad \xi_{N+1} \equiv 0. \tag{15.143}$$

We thus have the equation of motion for the $_{\text{n}} = 1$ point mass given by

$$M\,\ddot{\xi}_1 = -\Gamma\,(\xi_1 - \xi_0) - \Gamma\,(\xi_1 - \xi_2), \tag{15.144}$$

and analogous considerations hold for the $_{\text{n}} = N$ point mass

$$m\,\ddot{\xi}_N = -\Gamma\,(\xi_N - \xi_{N-1}) - \Gamma\,(\xi_N - \xi_{N+1}). \tag{15.145}$$

The interior masses have analogous equations so that the generic equation of motion for particles $_{\text{n}} = 1, N$ is given by

$$m\,\ddot{\xi}_{\text{n}} = -\Gamma\,(\xi_{\text{n}} - \xi_{\text{n}-1}) - \Gamma\,(\xi_{\text{n}} - \xi_{\text{n}+1}) \Longrightarrow \ddot{\xi}_{\text{n}} = \omega_0^2\,(\xi_{\text{n}+1} - 2\,\xi_{\text{n}} + \xi_{\text{n}-1}). \tag{15.146}$$

It is useful to write the case for $N = 2$ oscillators for reference

$$\ddot{\xi}_1 = \omega_0^2\,(-2\,\xi_1 + \xi_2) \tag{15.147a}$$

$$\ddot{\xi}_2 = \omega_0^2\,(-2\,\xi_2 + \xi_1), \tag{15.147b}$$

as well as for $N = 3$ oscillators

$$\ddot{\xi}_1 = \omega_0^2 \left(-2\,\xi_1 + \xi_2\right) \tag{15.148a}$$

$$\ddot{\xi}_2 = \omega_0^2 \left(\xi_3 - 2\,\xi_2 + \xi_1\right) \tag{15.148b}$$

$$\ddot{\xi}_3 = \omega_0^2 \left(-2\,\xi_3 + \xi_2\right). \tag{15.148c}$$

15.7.1 Mechanical energy for coupled oscillators

Following our discussion of mechanical energy for a single oscillator in Section 15.6.3, we multiply the equation of motion (15.146) by $\dot{\xi}_n$ and sum over the $n = 1, N$ oscillators. The acceleration term leads to the time change for the total kinetic energy of the full coupled oscillator system

$$m \sum_{n=1}^{N} \dot{\xi}_n \ddot{\xi}_n = \frac{m}{2} \sum_{n=1}^{N} \frac{\mathrm{d}\dot{\xi}_n^2}{\mathrm{d}t}. \tag{15.149}$$

Summation over the left portion of the force in equation (15.146) can be written

$$\sum_{n=1}^{N} \dot{\xi}_n \left(\xi_n - \xi_{n-1}\right) = \sum_{n=1}^{N+1} \dot{\xi}_n \left(\xi_n - \xi_{n-1}\right), \tag{15.150}$$

which follows since $\xi_{N+1} \equiv 0$ so that the extra term in the summation vanishes. The summation over the right portion of the force in equation (15.146) can be written

$$\sum_{n=1}^{N} \dot{\xi}_n \left(\xi_n - \xi_{n+1}\right) = \sum_{n=2}^{N+1} \dot{\xi}_{n-1} \left(\xi_{n-1} - \xi_n\right) = \sum_{n=1}^{N+1} \dot{\xi}_{n-1} \left(\xi_{n-1} - \xi_n\right). \tag{15.151}$$

To reach the first equality we changed indices on the terms in the summation, and modified the summation limits accordingly. For the second equality we expanded the summation range by noting that $\xi_0 \equiv 0$, thus allowing us to bring the lower summation limit from $n = 2$ to $n = 1$. Combining equations (15.150) and (15.151) leads to

$$\Gamma \sum_{n=1}^{N} \dot{\xi}_n \left(\xi_n - \xi_{n-1}\right) + \Gamma \sum_{n=1}^{N} \dot{\xi}_n \left(\xi_n - \xi_{n+1}\right) = \frac{\Gamma}{2} \frac{\mathrm{d}}{\mathrm{d}t} \sum_{n=1}^{N+1} \left(\xi_n - \xi_{n-1}\right)^2, \tag{15.152}$$

which is the time derivative of the potential energy, P, arising from the expansion and contraction of the Hooke's law springs, where

$$P = \frac{\Gamma}{2} \sum_{n=1}^{N+1} \left(\xi_n - \xi_{n-1}\right)^2 = \frac{\Gamma}{2} \left[\xi_1^2 + \sum_{n=2}^{N} \left(\xi_n - \xi_{n-1}\right)^2 + \xi_N^2\right], \tag{15.153}$$

where we set $\xi_0 = 0$ and $\xi_{N+1} = 0$.

Bringing the kinetic energy and potential energy together leads to the conservation of mechanical energy for the coupled oscillator system

$$\frac{\mathrm{d}}{\mathrm{d}t} \sum_{n=1}^{N+1} \left[\frac{m}{2} \dot{\xi}_n^2 + \frac{\Gamma}{2} \left(\xi_n - \xi_{n-1}\right)^2\right] = 0. \tag{15.154}$$

Just as for the single oscillator, we see that the coupled oscillator system maintains a fixed mechanical energy in which energy is exchanged between kinetic and potential energy reservoirs.

15.7.2 Lagrangian formulation

The Lagrangian for the coupled oscillator system is given by

$$L = \sum_{n=1}^{N+1} \left[\frac{m}{2} (\dot{\xi}_n)^2 - \frac{\Gamma}{2} (\xi_n - \xi_{n-1})^2 \right]. \tag{15.155}$$

To derive the Euler-Lagrange equations we require the following derivatives

$$\frac{\partial L}{\partial \dot{\xi}_p} = m \sum_{n=1}^{N+1} \dot{\xi}_n \, \delta_{n,p} = m \, \dot{\xi}_p, \tag{15.156a}$$

$$\frac{\partial L}{\partial \xi_p} = \Gamma \sum_{n=1}^{N+1} (\xi_n - \xi_{n-1}) \, (\delta_{n,p} - \delta_{n-1,p}) = -\Gamma \, (\xi_{p+1} - 2\,\xi_p + \xi_{p-1}), \tag{15.156b}$$

which lead to the Euler-Lagrange equation

$$\ddot{\xi}_p = \omega_0^2 \, (\xi_{p+1} - 2\,\xi_p + \xi_{p-1}). \tag{15.157}$$

As expected, the Euler-Lagrange equation of motion agrees with Newton's equation (15.146) derived using Newtonian methods.

15.7.3 Further study

Our presentation of coupled harmonic oscillators was inspired by Section 24 of *Fetter and Walecka* (2003), though we made use of a kinematic treatment anticipating the generalized Lagrangian mean approach used in fluid mechanics and introduced in Section 70.2.

15.8 Exercises

EXERCISE 15.1: CONSERVATION OF ENERGY FOR THE FOUCAULT PENDULUM
Using the Euler-Lagrange equations of motion (15.60) and (15.62), show that $\dot{H} = 0$ for the Foucault pendulum, where the Hamiltonian is given by equation (15.63).

Chapter 16

CONTINUUM APPROXIMATION

Ordinary gases and liquids are canonical examples of fluids, with gases filling any container with its molecules widely separated, whereas molecules in liquids are much closer together so that liquids are far less compressible than gases. Viewed macroscopically, a fluid is mechanically characterized by deforming continuously when applying a tangential or shearing stress, so that a fluid has no preferred shape.[1] Consequently, a fluid responds to a shearing stress by flowing. Even so, fluids can maintain their shape when experiencing a bulk compression, otherwise known as a *normal stress*, with liquids and gases generally distinguished by their very different compressibilities.

For geophysical fluid mechanics, we are concerned with the atmosphere (mostly a gas) and the ocean (mostly a liquid). We are furthermore interested in macroscopic properties of fluid motion, with no interest in describing molecular degrees of freedom. Nor do we consider rarefied gas dynamics, which is a subject appropriate for the upper bounds of the atmosphere where pressures are extremely low and the molecular mean free path relatively large. For these reasons we pursue a phenomenological approach that makes use of conservation laws describing the motion of a continuous fluid media. This treatment is based on the *continuum approximation*, which assumes that mathematical limits for fluid volumes tending to zero are reached on length and time scales very large compared to molecular space and time scales. The temporal realization of the continuum approximation is based on recognizing that macroscopic motion associated with fluid flows (e.g., advection, waves, and mixing) evolves with time scales far longer than the time scales of molecular motions. Hence, from a macroscopic perspective, we assume that all fluid motions are continuous in both space and time.

The huge space and time scale separation that supports the continuum approximation allows us to make use of differential calculus for describing the mechanics of fluid motion. That is, the continuum approximation makes fluid mechanics a continuous field theory, thus sitting within the broader discipline of *continuum mechanics*. Correspondingly, the differential laws describing fluid motion are partial differential equations. Even so, it must be admitted that the equations of continuum mechanics are motivated by the continuum approximation rather than deductively resulting from it. That is, a deductive derivation of continuum field theory, starting from molecular dynamics, is nontrivial even for an ideal gas, and largely non-existent for liquids. For our purpose, we remain satisfied to postulate that a continuum description is suited for the fluid mechanics of atmosphere and ocean flows, and to examine the postulate *a posteriori* via experimental measurements. Centuries of experiments with fluid motions in the environment and laboratory lend credence to the continuum description. We consider these tests to offer sufficient motivation to use continuum mechanics as the foundation for our study of geophysical fluid mechanics.

[1] A stress is a force per area, and we study stresses in Chapter 25. A shearing or tangential stress gives rise to fluid acceleration that causes fluid elements to deform.

READER'S GUIDE TO THIS CHAPTER

This chapter presents salient points supporting the use of a space and time continuous description of fluid mechanics. Section 16.2 summarizes the key results and Section 16.3 provides a bit more detail by quoting from kinetic theory. Our overall goal here is to unpack the dictum *macroscopically small yet microscopically large*, which summarizes the regime assumed when formulating the equations of continuum mechanics. For this purpose, we borrow from the kinetic theory of gases as treated in statistical physics books such as *Reif* (1965) and *Huang* (1987). Chapter 1 of *Salmon* (1998) also provides a compelling discussion with application to geophysical fluid mechanics. No prior exposure to these treatments is necessary, nor do we dive into the many details.

We return to elements of this chapter in Section 26.5 when describing *local thermodynamic equilibrium*. Together, the continuum approximation and the hypothesis of local thermodynamic equilibrium form two key pillars of continuum mechanics.

16.1 Loose ends

- Add a figure for Section 16.2.4.
- Can one be more precise about the scale in Figure 16.2 where measurements become fuzzy?

16.2 A variety of length scales

Matter is comprised of molecules. However, fluid mechanics is not concerned with the motion of individual molecular degrees of freedom. Rather, fluid mechanics is concerned with phenomenological conservation laws describing the flow of a continuous fluid material. In this section we outline certain properties of matter that motivate the continuum approximation and the corresponding study of continuum mechanics. More details are offered in Section 16.3, although a full discussion is outside the purview of fluid mechanics, with interested readers encouraged to penetrate the literature in statistical physics and kinetic theory.

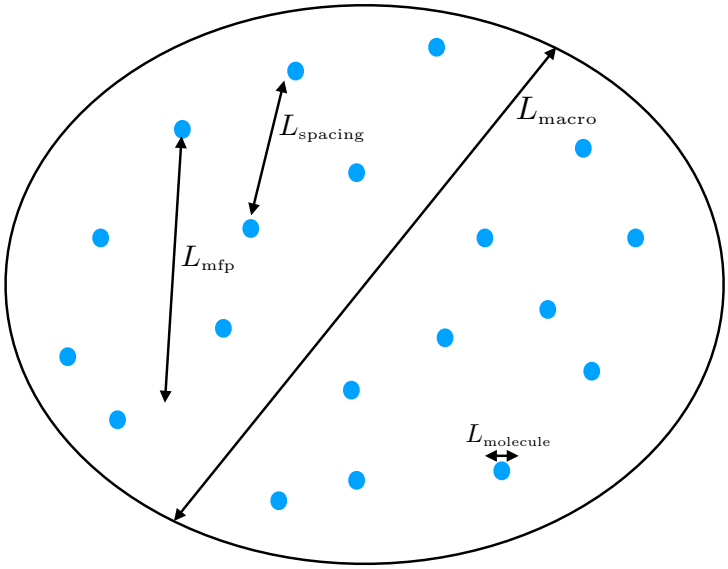

FIGURE 16.1: Schematic to illustrate the length scales considered when making the continuum approximation. The blue circles represent molecules with diameter L_{molecule}. On average, molecules are separated by a spacing, L_{spacing}, that is much larger than the size of the molecule. The mean free path, L_{mfp}, is the average distance a molecule travels between collisions with other molecules, with L_{mfp} generally larger than L_{molecule} since the mean free path takes into account the trajectory of a molecule between collisions, rather than just its immediate neighbors. The smallest macroscopic length scale for fluid flow is denoted L_{macro}. There is no objective value for L_{macro}, though for our purposes we assume it is on the order of $L_{\text{macro}} \sim 10^{-4}$ m, which corresponds roughly to the precision of a flow measurement. In this case, $L_{\text{macro}} \approx 10^3\, L_{\text{mfp}}$ for an ideal gas at standard conditions. A region of air with volume L^3_{macro} contains roughly 10^{13} air molecules, whereas that same volume contains roughly 10^{16} water molecules. For either case, the Law of Large Numbers greatly helps in taking the continuum limit. Note that this schematic is not drawn to scale!

16.2.1 Macroscopic and microscopic length scales

In fluid mechanics, as in other areas of continuum mechanics, we are concerned with the motion of matter over geometric scales that have a lower bound that is macroscopically small (e.g., $L_{\text{macro}} \sim 10^{-4}$ m) yet microscopically large (e.g., $L_{\text{macro}} \gg L_{\text{mfp}} \sim 10^{-7}$ m, where L_{mfp} is the molecular mean free path). For example, a region of air with volume L^3_{macro} contains roughly 10^{13} air molecules at standard temperature ($T_{\text{stand}} = 0°\text{C} = 273.15$ K) and standard atmospheric pressure ($p_{\text{stand}} = 101.325 \times 10^3$ Pa), whereas that same volume contains roughly 10^{16} water molecules. These numbers illustrate the notions of macroscopically small yet microscopically large. That is, a macroscopically small region, which provides a lower bound for the precision of flow measurements, generally contains an enormous number of microscopic molecules. It is only when reaching length scales on the order of the molecular mean free path that we need to be concerned with the discrete nature of matter. Figure 16.1 offers a schematic to illustrate these distinct length scales.

16.2.2 Fields at each space point

When measured on length scales of the mean free path, material properties exhibit very large fluctuations on time scales of order $L_{\text{mfp}}/v_{\text{rms}}$, where v_{rms} is the root-mean-square speed of a fluid molecule (see Section 16.3.4). However, on macroscopic scales encompassing many molecular degrees of freedom, fluid matter appears continuous in both space and time. The incredibly large number of molecules within a macroscopically tiny region motivates our assumption that physical properties are homogeneous over regions of size L_{macro}. For our purposes, this *continuum approximation* works with macroscopically small but finite sized fluid elements whose mean dynamical properties (e.g., velocity, vorticity) and thermodynamical properties (e.g., mass

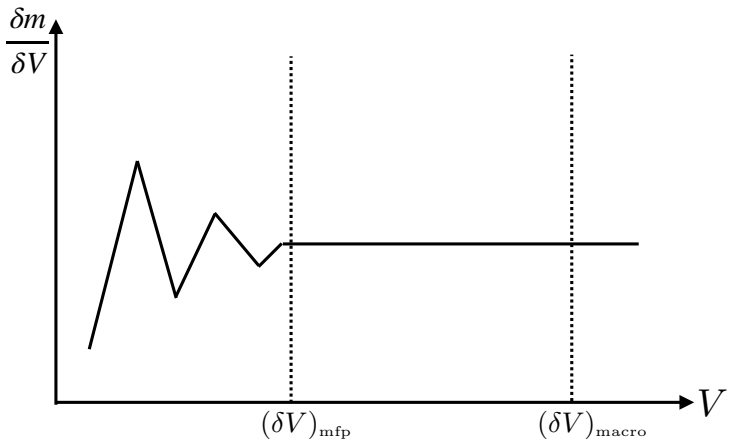

FIGURE 16.2: The measurement of mass density of a fluid becomes erratic for volumes on the order of that determined by the molecular mean free path, $(\delta V)_{\text{mfp}} \sim L^3_{\text{mfp}}$. For the fluid mechanical study of fluid motion, we are concerned with length scales much larger than the mean free path, $L_{\text{macro}} \gg L_{\text{mfp}}$, in which case the mass density is a smooth function of space and time. This figure is adapted from Figure 1.2.1 of *Batchelor* (1967).

density, matter concentration, temperature, pressure, specific entropy) are defined at each point within the continuous fluid media and at each time instance. As a result, we assume that any differential space increment, $\mathrm{d}\boldsymbol{x}$, has magnitude on the order of L_{macro}, even though we make use of differential calculus and its associated infinitesimals.

Let us be a bit more precise by considering the measurement of mass density for a prescribed region of fluid, δV. To compute the mass density we take the ratio of the mass of fluid in the region, δm, to the region volume. When the region volume is macroscopic, and thus contains many molecules, we can maintain a relatively fixed mass for this region since molecular fluctuations have a relatively tiny effect on δm. Correspondingly, we can maintain a precise measurement of the mass density, $\delta m/\delta V$. However, when the volume of the region become microscopic, whereby it has a volume on the order of $\delta V \sim L^3_{\text{mfp}}$, then molecular fluctuations generally lead to a relatively large fluctuation in the region's mass. We thus lose the notion of a smooth and continuous mass density when the volume approaches that set by the molecular mean free path. This situation is depicted in Figure 16.2.

The ratio of the molecular mean free path to the macroscopic length scale is known as the *Knudsen number*

$$\text{Kn} = \frac{L_{\text{mfp}}}{L_{\text{macro}}}. \tag{16.1}$$

For this book, we are concerned with fluid conditions where the mean free path is microscopic so that the Knudsen number is tiny

$$\text{Kn} \ll 1. \tag{16.2}$$

For tiny Knudsen numbers, we are led to make use of the continuum approximation. The continuum approximation allows us to employ fluid properties that take values at each point within a space and time continuum, $(\boldsymbol{x}, t)$. For example, we make use of the mass density, $\rho(\boldsymbol{x}, t)$, fluid velocity, $\boldsymbol{v}(\boldsymbol{x}, t)$, pressure $p(\boldsymbol{x}, t)$, temperature $T(\boldsymbol{x}, t)$, tracer concentration, $C(\boldsymbol{x}, t)$, and other fields.

We contrast the above to the study of a rarefied gas, such as in the outer reaches of the earth's atmosphere. With a relatively small number density of molecules, rarefied gases have macroscopic mean free paths so that there are relatively few molecular collisions in a given time increment. Correspondingly, a rarefied gas is far from thermodynamic equilibrium and the continuum approximation is not well suited to its description.

16.2.3 Reynolds number and the macroscopic length scale

The continuum field equations of fluid mechanics are formally established for fluid motions with length scales on the order of L_{macro} and larger. We stated earlier that L_{macro} is on the order of 10^{-4} m, with that length loosely based on noting that most macroscopic measurements in a fluid cannot distinguish flow features smaller than a millimetre. We here describe another means to determine L_{macro}.

Namely, we set L_{macro} to the length scale at which the Reynolds number is order unity

$$\text{Re}_{\text{macro}} = \frac{U\, L_{\text{macro}}}{\nu} \sim 1. \tag{16.3}$$

In this equation, $\nu > 0$ is the kinematic viscosity (dimensions squared length per time), which is a property of the fluid. The velocity scale, U, is set by the scale for a macroscopic fluid velocity fluctuation. The Reynolds number measures the ratio of inertial accelerations (accelerations felt by fluid elements) to frictional accelerations from viscous forces (forces due to the rubbing of fluid elements against one another in the presence of viscosity). We provide more details concerning the Reynolds number when studying fluid stresses in Chapter 25. For present purposes, we note that when the Reynolds number is on the order of unity, viscous forces play a leading role in the acceleration of the fluid. Furthermore, at this scale the viscous accelerations serve to dissipate kinetic energy of the macroscopic motion, with this dissipation a particularly important process in fluid turbulence. We are thus motivated to define L_{macro} as the length scale where viscosity is of leading order importance.

The kinematic viscosity is the ratio of the *dynamic viscosity* and the mass density. For air, the kinematic viscosity is (page 75 of *Gill* (1982))

$$\nu_{\text{air}} = \frac{1.7 \times 10^{-5} \text{ kg m}^{-1} \text{ s}^{-1}}{1.3 \text{ kg m}^{-3}} = 1.3 \times 10^{-5} \text{ m}^2 \text{ s}^{-1}, \tag{16.4}$$

and a typical fluid velocity fluctuation has a scale 10^{-1} m s^{-1}, so that

$$L_{\text{macro}} \approx 10^{-4} \text{ m} = 0.1 \text{ mm}. \tag{16.5}$$

Water has a kinematic viscosity (page 75 of *Gill* (1982))

$$\nu_{\text{water}} = \frac{10^{-3} \text{ kg m}^{-1} \text{ s}^{-1}}{1000 \text{ kg m}^{-3}} \approx 10^{-6} \text{ m}^2 \text{ s}^{-1}, \tag{16.6}$$

and a fluid velocity fluctuation about 10 times smaller than air. Hence, the macroscopic length scale for water is on the order of that for air, both of which are roughly 10^{-4} m. We are thus further compelled to consider the macroscopic length scale to be on the order 10^{-4} m and larger.

16.2.4 Resolution of measurements and simulations

When we measure fluid motions in the laboratory or field, we generally do not measure the motions at scales on the order of L_{macro}. That is, our measurement devices generally have a spatial resolution coarser than L_{macro}, so that $L_{\text{measure}} \gg L_{\text{macro}}$. Likewise, numerical simulations are generally designed using discrete grids with length scales $L_{\text{numerical}} \gg L_{\text{macro}}$. The equations describing motions at the measurement/simulation length scales involve effects from fluctuations occurring at the smaller (unmeasured) scales. The reason for this coupling is that the fluid equations are nonlinear so that scales interact. These fluctuations, generally associated with turbulent or chaotic motions, have statistical correlations that can play a role, sometimes a dominant role, in the evolution of flow features at the measured/simulated scales. The parameterization of these correlations in terms of measured/simulated motions constitutes the

turbulence closure problem. We do not study turbulence closure in this book though we do identify the role of turbulence at certain points.

It is important to acknowledge the limited ability of macroscopic measurements to accurately characterize fine scale motions. For this purpose define a gradient length scale

$$L_{\text{gradient}} = \frac{|\boldsymbol{v}|}{|\nabla \boldsymbol{v}|}, \tag{16.7}$$

where $\boldsymbol{v}$ is the velocity of a fluid element relative to some mean velocity, and $|\nabla \boldsymbol{v}|$ is the magnitude of velocity gradients. Decomposing fluctuations into Fourier modes allows us to see that an accurate measurement of velocity fluctuations with length scales L_{gradient} requires a measurement length scale that satisfies

$$2\,\pi\, L_{\text{measure}} \leq L_{\text{gradient}}. \tag{16.8}$$

This constraint means that to measure velocity fluctuations on a scale L_{gradient} requires a finer measurement sampling with $L_{\text{measure}} = L_{\text{gradient}}/(2\,\pi)$. Note that this discussion of length scales transfers seamlessly over to time scales through dividing the length scale by the velocity scale. Correspondingly, fluctuations with time scales shorter than $2\,\pi\, T_{\text{measure}}$ cannot be accurately measured.

16.2.5 Fields at each time instance

The continuum approximation means that fields are defined at every point in the space continuum and at each time in the time continuum. As motivation for the time continuum, we note that there are a huge number of molecular collisions per second, with molecules moving at incredibly high speeds (see Section 16.3 for some numbers). There are added features of the continuous time assumption that are best studied as part of the hypothesis of local thermodynamic equilibrium in Section 26.5.

16.2.6 The Deborah number

Although the focus of this book concerns the atmosphere and ocean, which are clearly fluids, it is useful to mention that not all materials clearly fit into the category of solid or fluid. For example, in geophysics we encounter frozen materials within the cryosphere and rocky material as part of the crust and deeper earth interior. Both materials appear quite hard and solid from human perspectives, and yet they flow over longer time scales and as such they are not rigid solids.

We are led to recognize that the characterization of whether a material is a solid or fluid depends on the time scale of the macroscopic observation, t_{observe}, versus the time scale for the internal relaxations within the material, t_{relax}. The ratio of these two time scales is referred to as the *Deborah number*[2]

$$\text{Db} = \frac{t_{\text{relax}}}{t_{\text{observe}}}. \tag{16.9}$$

For the fluid mechanics considered in this book, we are concerned with tiny Deborah numbers, in which the relaxation time scales are determined by the relatively rapid molecular collisions that take place on time scales of order 10^{-10} s (see Section 16.3.5), whereas the observation time scales are determined by macroscropic deformations that are $\approx 10^{0}$ s, so that

$$\text{Db} \ll 1 \Longrightarrow \text{viscous fluid}. \tag{16.10}$$

[2]See *Reiner* (1964) for the Biblical origins of the Deborah number.

In contrast, for many geophysical materials, as well as polymers encountered in material science, the relaxation time scales are relatively large, in which case the Deborah number can be order unity or even larger

$$\mathrm{Db} = \begin{bmatrix} \mathcal{O}(1) & \Longrightarrow \text{viscoelastic material} \\ \gg 1 & \Longrightarrow \text{elastic solid.} \end{bmatrix} \tag{16.11}$$

16.3 Results from kinetic theory

If the reader is content to accept the continuum approximation on face value, then the material in this section can be readily skipped. For others, this section outlines results from the kinetic theory of ideal gases in support of the continuum approximation. Deductive treatments that transition from molecular mechanics to macroscopic fluid mechanics is a topic of the kinetic theory of gases and liquids, which is outside our scope. In Section 16.3.7, we provide literature pointers for those wishing more rigor.

16.3.1 A mole and Avogadro's number

There are a tremendous number of molecules in the tiniest drop of water or puff of air. Just how many? To answer this question, we introduce the notion of a mole of matter. A mole is defined as the mass of a material substance that contains Avogadro's number of that substance, where

$$A^{\mathrm{v}} = 6.022 \times 10^{23} \text{ mole}^{-1}. \tag{16.12}$$

Avogadro's number, A^{v}, is the proportionality constant converting from one molar mass of a substance to the mass of a substance. Avogadro's number is conventionally specified so that one mole of the carbon isotope, ^{12}C, contains exactly 12 grams. Hence, 12 grams of ^{12}C contains 6.022×10^{23} atoms of ^{12}C. Avogadro's number provides a connection between scales active in the microscopic world of molecules to the macroscopic world of everyday experience.

Dry air (air with no water vapor) is comprised of oxygen molecules O_2, at roughly 22% by molecular mass, and nitrogen molecules N_2, at roughly 78% molecular mass.[3] The molar mass of dry air is thus

$$M^{\mathrm{air}} = 0.22 * 32 \text{ g mole}^{-1} + 0.78 * 28 \text{ g mole}^{-1} \approx 28.8 \text{ g mole}^{-1}. \tag{16.13}$$

Pure (fresh) water is comprised of two hydrogen atoms and one oxygen atom. The molar mass of pure water is thus given by

$$M^{\mathrm{water}} = 2 * 1 \text{ g mole}^{-1} + 16 \text{ g mole}^{-1} = 18 \text{ g mole}^{-1}. \tag{16.14}$$

16.3.2 Ideal gas law

The ideal gas law is given by

$$p\,V = n\,R^{\mathrm{g}}\,T, \tag{16.15}$$

where p is the pressure, V is the volume, n is the number of moles, R^{g} is the universal gas constant,[4] and T is the absolute or thermodynamic temperature (temperature relative to absolute zero). Measuring the temperature in Kelvin leads to the universal gas constant

$$R^{\mathrm{g}} = 8.314 \text{ J mole}^{-1} \text{ K}^{-1} = 8.314 \text{ kg m}^2 \text{ s}^{-2} \text{ mole}^{-1} \text{ K}^{-1}, \tag{16.16}$$

[3] We here ignore the presence of other trace gases, such as CO_2 and H_2O, although these gases are critical for understanding atmospheric radiation and hence the earth's energy budget.

[4] We write R^{g} rather than the more conventional R to distinguish from R commonly used in this book for the radius of a sphere.

where the second equality replaced the energy unit, Joule, by its MKS equivalent,

$$\mathrm{J} = \mathrm{kg\ m^2\ s^{-2}}. \tag{16.17}$$

Use of the ideal gas law (16.15) says that one mole of ideal gas at standard temperature ($T_{\text{stand}} = 0°\mathrm{C} = 273.15$ K) and standard atmospheric pressure ($p_{\text{stand}} = 101.325 \times 10^3$ Pa) occupies the following volume

$$V = \frac{n\, R^{\mathsf{g}}\, T_{\text{stand}}}{p_{\text{stand}}} \tag{16.18a}$$

$$= \frac{(1\ \text{mole})\,(8.314\ \mathrm{kg\ m^2\ s^{-2}\ mole^{-1}\ K^{-1}})\,(273.15\ \mathrm{K})}{101.325 \times 10^3\ \mathrm{kg\ m^{-1}\ s^{-2}}} \tag{16.18b}$$

$$\approx 2.25 \times 10^{-2}\ \mathrm{m^3}, \tag{16.18c}$$

where we introduced the MKS units for pressure (force per unit area)

$$\mathrm{Pa} = \mathrm{N\ m^{-2}} = \mathrm{kg\ m^{-1}\ s^{-2}}. \tag{16.19}$$

Hence, the number density (number of molecules per volume) for a mole of ideal gas is given by

$$n^{\mathsf{gas}} = \frac{\text{number per mole}}{\text{volume per mole}} \tag{16.20a}$$

$$= \frac{A^{\mathsf{v}}}{V} \tag{16.20b}$$

$$= \frac{6.022 \times 10^{23}}{2.25 \times 10^{-2}\ \mathrm{m^3}} \tag{16.20c}$$

$$= 2.68 \times 10^{25}\ \mathrm{m^{-3}}. \tag{16.20d}$$

Specializing to air, we compute the mass density of air at standard temperature and pressure as

$$\rho^{\mathsf{air}} = \frac{M^{\mathsf{air}}}{V} = \frac{28.8 \times 10^{-3}\ \mathrm{kg}}{2.25 \times 10^{-2}\ \mathrm{m^3}} = 1.28\ \mathrm{kg\ m^{-3}}, \tag{16.21}$$

where we set $M^{\mathsf{air}} = 28.8 \times 10^{-3}$ kg according to equation (16.13). This ideal gas density is close to the 1.225 kg m^{-3} density measured for air at standard conditions, thus supporting use of the ideal gas law for dry air. Differences arise from trace constituents in air as well as inter-molecular forces (an ideal gas has no inter-molecular forces).

16.3.3 Molecular mean free path

We are in search of length scales relevant for molecular motion. One length scale is that of the molecule itself. Another is set by the average distance between molecules. Finally, we may consider the distance between molecular collisions, with the molecular mean free path the mean distance that a molecule travels before colliding with another molecule. The mean free path is generally larger than the average molecular distance since for molecules to collide requires their trajectories to intersect, and that generally happens over a distance larger than the averaged molecular distance.

Arguments from kinetic theory of gases, applied to an ideal gas, lead to the expression

$$L_{\text{mfp}} = \frac{1}{\pi \sqrt{2}\, n^{\mathsf{gas}}\, d^2} \tag{16.22}$$

where d is the diameter of the molecule. The mean diameter of air molecules is roughly

$$d_{\text{molecule air}} \approx 2 \times 10^{-10} \text{ m}. \tag{16.23}$$

Hence, the mean free path for air molecules at standard temperature and pressure is

$$L_{\text{mfp}} = \frac{1}{\pi \sqrt{2}\, n^{\text{gas}}\, d^2_{\text{molecule air}}} \tag{16.24a}$$

$$= \frac{1}{\pi \sqrt{2}\, (2.68 \times 10^{25} \text{ m}^{-3})\, (2 \times 10^{-10} \text{ m})^2} \tag{16.24b}$$

$$= 2 \times 10^{-7} \text{ m}. \tag{16.24c}$$

The mean free path for an air molecule is roughly 1000 times larger than the molecular diameter (e.g., Figure 16.1).

16.3.4 Root mean square molecular speed

What is the mean speed for molecules moving through a gas? Again, kinetic theory for ideal gases offers an explicit expression, here written in terms of the pressure and density of the gas

$$v_{\text{rms}} = \sqrt{\frac{3\, p}{\rho}} = \sqrt{\frac{3\, R^{\text{g}}\, T}{M}}. \tag{16.25}$$

Note the direct relation between pressure, temperature, and speed. That is, molecules move faster at higher temperature, and thus impart larger pressure on their surrounding environment. At standard pressure and temperature, the root-mean-square speed for an air molecule is given by

$$v_{\text{rms}} = \sqrt{\frac{3\, p_{\text{stand}}}{\rho^{\text{air}}}} \tag{16.26a}$$

$$= \sqrt{\frac{3\, (101.325 \times 10^3 \text{ kg m}^{-1} \text{ s}^{-2})}{1.28 \text{ kg m}^{-3}}} \tag{16.26b}$$

$$= 487 \text{ m s}^{-1}. \tag{16.26c}$$

To get a sense for the relative scale of this speed, note that the speed of sound in air at standard temperature and pressure is 331 m s^{-1}. So these molecules are moving faster than sound! These speeds are correspondingly much higher than the speeds typical for fluid elements in the atmosphere and ocean.

16.3.5 Time scales for molecular collisions

Assuming one collision occurs within a mean free path, and the molecules are moving at the root-mean-square speed, we can estimate the time between collision according to

$$t_{\text{collision}} = \frac{L_{\text{mfp}}}{v_{\text{rms}}} \tag{16.27}$$

The corresponding time for air is given by

$$t_{\text{air}} = \frac{2 \times 10^{-7} \text{ m}}{487 \text{ m s}^{-1}} = 4.1 \times 10^{-10} \text{ s}. \tag{16.28}$$

Inverting this number, we see that there are roughly $t_{\text{air}}^{-1} = 2.5 \times 10^9 \text{ s}^{-1}$ collisions per second. The huge number of molecular collisions per second means that for all macroscopic processes, including highly turbulent geophysical fluid flow, the dynamical time scales for the macroscopic motion are many orders of magnitude longer than the time scales for molecular motions.

16.3.6 Macroscopically small and microscopically large

For environmental measurements of the atmosphere and ocean, or for conventional measurements in laboratories, we can detect differences in fluid properties (e.g., mass density, velocity, tracer concentration, thermodynamic state properties) for length scales no smaller than

$$L_{\text{macro}} = 10^{-4} \text{ m}. \tag{16.29}$$

For macroscopic purposes, fluid properties are homogeneous over regions with length scales on the order of L_{macro}. Although macroscopically rather tiny, a fluid region of volume L_{macro}^3 is huge microscopically. We can see so by computing the number of molecules in this region.

At standard conditions, a volume of air of size L_{macro}^3 contains

$$N_{\text{air molecules}} = V\, n^{\text{gas}} = (10^{-4} \text{ m})^3\, (2.68 \times 10^{25} \text{ m}^{-3}) \approx 3 \times 10^{13} \text{ air molecules}. \tag{16.30}$$

To compute the number of water molecules in this same volume, we first use the water mass density of

$$\rho^{\text{water}} \approx 10^3 \text{ kg m}^{-3} \tag{16.31}$$

to determine the water mass in this region

$$M^{\text{water}} = \rho^{\text{water}}\, V = (1000 \text{ kg m}^{-3})\, (10^{-12} \text{ m}^3) = 10^{-9} \text{ kg}. \tag{16.32}$$

Water has a molar mass of 0.018 kg mole^{-1}, so a volume of $(10^{-4} \text{ m})^3$ contains

$$N_{\text{water molecules}} = \left(\frac{10^{-9} \text{ kg}}{0.018 \text{ kg mole}^{-1}} \right) \times 6.022 \times 10^{23} \text{ molecules mole}^{-1} = 3 \times 10^{16} \text{ water molecules}. \tag{16.33}$$

Water thus has roughly 10^3 more molecules in this volume than air at standard pressure, which reflects the roughly 10^3 times larger mass density for water. Evidently, both water and air contain a huge number of molecules in this macroscopically tiny region.

16.3.7 Further study

Pedagogical treatments of the ideal gas law and kinetic theory can be found in most books on introductory physics or chemistry. *Vallis* (2017) provides extensions of the ideal gas law for an atmosphere with moisture.

For discussions of the continuum approximation reflecting that given here, see the discussion on page 1 of *Olbers et al.* (2012), or the more thorough treatments in Section 1.2 of *Batchelor* (1967), Section 2.1 of *Pope* (2000), or Section 1.4 of *Kundu et al.* (2016). Chapter 1 of *Salmon* (1998) touches on elements from kinetic theory and details for how to coarse grain average over molecular degrees of freedom (see his pages 3 and 4 and Sections 9, 10, and 11). An analogous treatment is given by exercise 2.1 of *Pope* (2000). A rigorous account of kinetic theory is offered in many treatments of statistical mechanics. That given by *Reif* (1965) and *Huang* (1987) are accessible to those with a physics undergraduate training. When reading the statistical mechanics literature, look for discussions of the "hydrodynamical limit," which concerns the transition from discrete particle mechanics to continuum mechanics.

Part III

Kinematics of fluid flows

In this part of the book we focus on the kinematics of a classical and non-relativistic continuous fluid flows. We take inspiration from treatments given in the continuum mechanics literature (e.g., chapter 4 of *Malvern* (1969) and Part I of *Tromp* (2025a)), though with a bias towards elements particularly useful in fluid mechanics (e.g., chapter 2 of *Truesdell* (1954)). There are a variety of rather subtle points connected with fluid flow kinematics, and such subtleties can lead to confusion (it certainly has for this author!). The present treatment aims for a reasonably deductive level of rigor while appealing to the physicist. The interested student is encouraged to read a variety of treatments to survey the presentations, as each author stresses unique nuances that can be important both for understanding and for applications.

Kinematic properties of fluid flows in an inertial reference frame also hold for flow on steady rotating planets such as considered in this book. The reason is that steady rigid-body rotation does not directly impart strain to the flow, where strain refers to the relative motion between fluid particles (Chapter 17). Rotation does impart a planetary component to the vorticity of geophysical fluids, with important implications for the study of vorticity in Part VII. However, for the purpose of fluid kinematics studied in this part of the book, we can safely ignore planetary rotation.

Eulerian and Lagrangian reference frames

The *Eulerian and Lagrangian reference frames* provide dual kinematic descriptions of fluid flows. The Eulerian frame describes fluid motion relative to a frame fixed in the laboratory, whereas the Lagrangian frame follows a moving material fluid particle. The Eulerian frame is inertial (when the laboratory is not accelerating), whereas the Lagrangian frame is non-inertial since fluid particles generally accelerate. Having two descriptions of the same motion provides a synergy that is extensively used in fluid mechanics. Fully realizing this synergy requires skills to move between the Eulerian and Lagrangian descriptions, with tools from mathematical transformation theory of Part I used for this purpose. Whereas Cartesian coordinates offer a complete description for Eulerian kinematics, Lagrangian kinematics requires general tensor analysis (Chapters 3 and 4) since fluid particles deform with the fluid motion and thus render a non-orthogonal coordinate description. Elements of Eulerian and Lagrangian kinematics are the focus of Chapter 17, and Chapter 18 further develops the formal theory of fluid kinematics, with applications to the study of material lines, areas, and volumes.

We acknowledge that for most flows encountered in geophysical fluid mechanics, a Lagrangian description has practical limitations. These limitations arise from the chaotic and turbulent nature of the flow that render a description based on fluid particle trajectories of little use after even a brief time. This is perhaps the key reason that Eulerian approaches are far more common in fluid mechanics, whereas Lagrangian approaches are more common in solid mechanics where materials maintain their shape far longer. Nevertheless, Lagrangian formulations of continuum mechanics offer insights to the fundamental theorems of fluid flows, thus motivating the Lagrangian approach in tandem with the Eulerian.

A historical note is appropriate here. As emphasized by *Truesdell* (1953), as well as Section 14 of *Truesdell* (1954), it was Euler who first introduced the material coordinates used with the Lagrangian reference frame. In recognition of this historical error, we sometimes use "material" in place of "Lagrangian". Even so, we do make use of "Lagrangian" in most places, thus according with its common usage in geophysical fluid mechanics. Relatedly, again according to *Truesdell* (1953), it was d'Alembert who introduced the spatial coordinates used for the Eulerian description.

Mass and matter conservation are part of fluid kinematics

The conservation of mass plays a central role in physics. For fluids, mass conservation constrains the flow regardless what forces act on the fluid. Hence, we include mass conservation

as a part of fluid kinematics rather than fluid dynamics. Mass conservation, and its expression as volume conservation for non-divergent flows, are the topics of Chapters 19 and 21. Chapter 20 develops the allied study of matter conservation and matter flow, with this study forming the foundations for *tracer mechanics* that we return to in earnest within Part XIII of this book.

FLUID KINEMATICS + FLUID DYNAMICS = FLUID MECHANICS

Kinematics is concerned with the intrinsic properties of motion, including properties of the space and time in which motion occurs. It is the complement to dynamics, which is concerned with the causes of motion that arise through the action of forces. In one sense, kinematics deduces the acceleration whereas dynamics deduces the forces, with Newton's second law linking the two via the equation of motion: $\boldsymbol{F} = m\,\boldsymbol{a}$. In fluid mechanics, kinematics studies the flow of a fluid and its matter constituents, whereas dynamics studies the forces causing the motion. Furthermore, as discussed in Chapter 14, symmetries of a mechanical system lead, through Noether's Theorem, to dynamical conservation laws. That is, symmetries, which embody kinematic properties, lead to dynamical invariants maintained by the motion, with these invariants constraining the motion. The intellectual avenues pursued in developing a mechanical description of fluid motion are many and varied, with fluid kinematics and fluid dynamics intimately woven into the fabric of that description.

A KINEMATICAL RESULT IS VALID FOREVER

As motivation for studying this part of the book, we offer the following quote from page 2 of *Truesdell* (1954), with Clifford Truesdell one the giants of 20th century continuum mechanics who was clearly fond of kinematics.

> All dynamical statements I have relegated to parenthetical sections, appendices, or footnotes, not in a foolish attempt to diminish their physical importance, but rather to let the argument course freely, uninterrupted by merely interpretative remarks, and to leave the propositions free for application to such special dynamical situations as may be of interest either now or in the future–for I cannot too strongly urge that a kinematical result is a result valid forever, no matter how time and fashion may change the "laws" of physics.

Chapter 17

FUNDAMENTALS OF FLUID KINEMATICS

In describing fluid motion, we use the dual lenses offered by the *Eulerian* and the *Lagrangian* reference frames. The Eulerian reference frame ($\boldsymbol{x}$-space) uses a spatial description with coordinates that are fixed in Euclidean space, whereas the Lagrangian reference frame ($\boldsymbol{a}$-space) uses a material description with coordinates that are fixed on fluid particles. These dual descriptions (spatial versus material) form the foundation for fluid kinematics. We give attention to the needs of both Eulerian and Lagrangian kinematics in this chapter and elsewhere in this book, and how to transform between the two.[1]

The Eulerian description is more commonly used in fluid mechanics since the kinematic property of central focus is the fluid velocity as a field, $\boldsymbol{v}(\boldsymbol{x}, t)$, whereas trajectories for fluid particles are not needed for most purposes. In contrast, the Lagrangian approach is more commonly used in solid mechanics, in which one is concerned with motion of material particles relative to a reference or base configuration (typically the initial state). The two descriptions are mathematically related by a one-to-one invertible mapping. To transform from the Lagrangian to Eulerian description requires taking the time derivative of the trajectory to produce the velocity, whereas to transform from the Eulerian to Lagrangian description requires solving a set of ordinary differential equations to compute a trajectory from the time integral of the velocity. The Eulerian description requires less information than the Lagrangian since it does not determine trajectories. However, there is a price to pay for reducing the information, in which case the mechanical foundations can be somewhat obscured using the Eulerian approach, with this comment manifest in our study of Hamilton's principle in Chapter 47.

READER'S GUIDE TO THIS CHAPTER

This chapter introduces concepts and tools used in nearly every subsequent chapter of this book that concerns a description of fluid motion.

[1] As noted by *Truesdell* (1953), as well as the long footnote on pages 30-31 of *Truesdell* (1954), the Lagrangian reference frame originates from the work of Leonard Euler (1707-1783), so that the term "Lagrangian reference frame" is a historical error. Even so, we continue this error given the near ubiquitous terminology used in the geophysical fluid mechanics literature, thus referring to the material frame as the Lagrangian frame.

17.1 Introduction to fluid kinematics

We here introduce some basic concepts that form the foundation for the discussions in this chapter.

17.1.1 Strong and weak formulations

The continuum approximation (Chapter 16) allows us to consider fluid flow from a field theoretic perspective, whereby physical properties are described by fields that take on values at each point of a space and time continuum. Consequently, we make use of a differential equation formulation of the governing continuum equations as well as an integral formulation. The differential formulation is sometimes referred to as the *strong* formulation. This name is motivated by the need to make assumptions about the smoothness of the continuum fields. Absent such smoothness assumptions, the differential equations lack predictive skill. Some phenomena (e.g., shocks in fluids and faults in solids) do not satisfy the necessary smoothness assumptions, thus making the strong formulation unsuitable. In those cases it can be useful to employ an integral formulation, with the integral formulation known as the *weak* formulation since it requires fewer assumptions about smoothness.

In this book, we are not concerned with shocks or other discontinuities in the fluid flow. Consequently, we make use of both the strong and weak formulations. We are afforded a connection between the weak and strong formulations through the *Leibniz-Reynolds transport*

theorem derived in Section 20.2.4. Each formulation is suited for particular needs. For example, the strong formulation provides a concise view of the fluid equations and allows for manipulations and transformations based on the rules of differential calculus and differential gemoetry studied in Part I. In contrast, the weak formulation is needed to develop budgets over finite fluid regions. Correspondingly, the weak formulation provides a starting point for the derivation of finite volume budgets that serve as the basis for analysis methods and numerical methods (e.g., *Griffies et al.* (2020)).

17.1.2 Lagrangian and Eulerian descriptions

There are two reference frames commonly used as the basis for describing motion of a continuum. For the continuous fluid motions considered in this book, these two reference frames retain a 1-to-1 and invertible relation that allows for the mathematical and conceptual transformation between the frames.

- LAGRANGIAN OR MATERIAL DESCRIPTION: This description makes use of a reference frame that is defined by motion of material fluid particles (Section 17.2.1). That is, the Lagrangian reference frame is comoving with the continuum of fluid particles. The mechanical description aims to determine the continuum of trajectories, with each trajectory delineated by a continuous material coordinate that labels each fluid particle. The Lagrangian reference frame is non-inertial since fluid particles generally experience accelerations via changes to their speed and/or direction.

- EULERIAN OR LABORATORY DESCRIPTION: This description makes use of a reference frame that observes fluid motion relative to fixed spatial positions, $\boldsymbol{x}$, within a "laboratory". This *Eulerian* description measures fluid properties as the fluid streams by a fixed observer. It is not concerned with determining trajectories. Instead, Eulerian kinematics focuses on fluid properties as continuous fields that are functions of spatial position, $\boldsymbol{x}$, and time, t.

The Eulerian and Lagrangian descriptions complement one another. The Lagrangian description renders insights partly due to its direct analog to point particle mechanics of Part II in this book. Alternatively, the Eulerian description is commonly more straightforward when developing numerical methods for simulations, or when making laboratory or field measurements. Throughout this book, we make use of both Eulerian and Lagrangian kinematic descriptions. A goal of this chapter is to provide the foundation for these two descriptions and to develop tools for transforming between them.

In non-geophysical treatments of fluid mechanics, it is typical to assume that the laboratory reference frame of the Eulerian observer is fixed in space, and thus is an inertial reference frame. However, for geophysical fluid mechanics we generally consider an Eulerian reference frame fixed with respect to the rotating planet (a rotating laboratory frame), and the earth laboratory frame is not inertial. However, the discussion in this chapter is not concerned with the non-inertial features that give rise to planetary centrifugal and Coriolis accelerations (see Chapter 13). Instead, we note that the constant rotation of the planet does not impart any strain to the fluid.[2] Consequently, non-rotating fluid kinematics is sufficient for most purposes of geophysical fluid kinematics.

17.2 Conceptually partitioning the continuum

As part of a continuum description of fluid motion, we make use of conceptual physical systems to frame the mechanics and describe the motion. We start by describing the material fluid

[2]This point is made more formally when studying the kinematics of fluid strain in Section 18.6.

particle in Section 17.2.1, which is a zero-dimensional point moving with the fluid flow, and then expand to infinitesimal fluid regions (fluid parcels and fluid elements) that are bounded by imagined partitions. The boundaries of fluid regions can be either open or closed to matter and energy exchange depending on the character of the fluid. Importantly, there is no pretense that the partitions used to define fluid parcels and fluid elements can be experimentally determined. Rather, partitions are drawn within the continuum fluid by the theorist for purposes of formulation and conceptualization. We are afforded the ability to draw these partitions through the continuum description of fluid mechanics.[3]

17.2.1 Fluid particles

A point in Euclidean space is specified by a spatial coordinate, $\boldsymbol{x}$, and an instant in *Newtonian time* is specified by the time, t. Euclidean space plus Newtonian time is referred to as a *Galilean space-time*. Each point within a matter continuum undergoes motion according to the laws of continuum mechanics. We define a *fluid particle* as a zero dimensional mathematical point that follows motion of the continuous material fluid, with that motion specified by the velocity field (left panel in Figure 17.1). Since it has zero spatial extent, a fluid particle has no impact on the flow. Notably, a fluid particle is not a molecule or atom since even molecules and atoms have nonzero spatial extent and so impact their surroundings. Even so, a fluid particle does represesent a point in the material fluid continuum rather than just a point in space.

The position of a fluid particle in space and time is uniquely specified by its material coordinate plus time (we discuss material coordinates in Section 17.3.1). The trajectory or pathline of a fluid particle is an *integral curve* of the velocity field, where each point along a trajectory has a tangent that defines the velocity vector (Section 17.7).[4] The accumulation of a continuum of fluid particle trajectories define the pathlines that prescribe the Lagrangian or material reference frame (Section 17.1.2).

Fluid particles are directly analogous to *test mass particles* in Newtonian gravitation that are used to map gravitational field lines, and *test electric charges* in electromagnetism used for mapping the electromagnetic field. However, fluid particles have zero mass and are fully defined kinematically through specifying the velocity field. Fluid particles can be used to study perfect fluids, which necessarily have a single matter constitutent, as well as real fluids with multiple matter constituents. For the perfect fluid, fluid particles trace out *integral curves* of the velocity field, whereas for a real fluid the fluid particles provide integral curves for the *barycentric velocity* studied in Section 20.1.

Some books define fluid particles as finite sized fluid regions, much like the fluid parcel described in Section 17.2.2 or the fluid element in Section 17.2.4. Some treatments also suggest that a fluid particle is akin to a fluid molecule. We instead find it conceptually simpler and far less problematic to define a fluid particle as a mathematical point with zero spatial extent and zero mass, thus serving solely as a conceptual probe for the fluid flow and as a means to specify the Lagrangian reference frame.[5]

17.2.2 Material fluid parcels in perfect fluids

For many purposes we find it useful to study fluid mechanics in the absence of irreversible processes such as friction, heat exchange, and diffusive mixing. In this case the fluid is referred

[3]This conceptual formulation of fluid mechanics, namely as a continuous collection of infinitesimally small fluid elements, originates from the work of Leonard Euler (1707-1783). For an insightful and authoritative discussion on this topic, see *Truesdell* (1953) as well as the long footnote on pages 30-31 of *Truesdell* (1954).

[4]When orienting time along the vertical axis, then the tangent to the trajectory is actually the inverse velocity: slope $= \mathrm{d}t/\mathrm{d}x = 1/u$. We follow the convention used in special relativity, where the trajectory is known as the *world line*, and world lines live within the cone bounded by the world line of photons.

[5]Our definition of fluid particle agrees with Section 2.2 of *Pope* (2000).

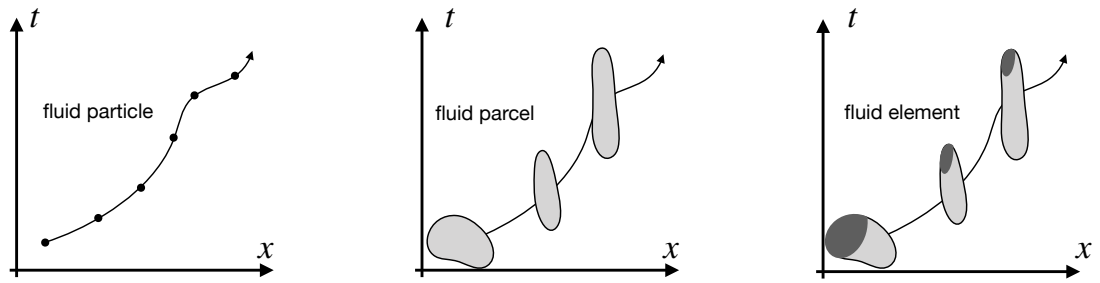

FIGURE 17.1: Schematic of the motion in space-time for the conceptual systems used in our considerations of fluid kinematics. Left panel: a fluid particle has zero spatial extent and has zero impact on the flow. Its motion in space-time defines a path/trajectory as determined by integral curves of the velocity field, $\boldsymbol{v}(\boldsymbol{x}, t)$. Note that slope of the curve on this space-time diagram is the inverse of the velocity: slope $= \mathrm{d}t/\mathrm{d}x = 1/u$. The trajectories of fluid particles define the Lagrangian reference frame. Middle panel: a material fluid parcel is comprised of a fixed material content (and thus a fixed mass) and fixed thermodynamic properties. Fluid parcels are infinitesimal deformable regions of a perfect fluid whose motion within a straining velocity field changes the parcel's shape. The center of mass for the fluid parcel follows a path that is approximated by that of a fluid particle at the center of mass. Right panel: a fluid element is comprised of a fixed mass but with matter and thermodynamic properties exchanged across its boundary, here depicted by the loss of dark gray matter and increase of light gray matter through exchanges with the surrounding fluid. The fluid element moves with the barycentric velocity (see Section 20.1), which is the center of mass velocity for the constituents contained in the fluid element. Both fluid parcels and fluid elements change their shape in the presence of fluid strain. Over time, a fluid parcel and a fluid element change their shape, with most realistic flows resulting in flows that require a reinitialization of the parcel/element boundaries in order to maintain coherency as identifiable fluid regions.

to as an *ideal fluid* or equivalently a *perfect fluid*. We prefer the term *perfect fluid* to avoid confusions with an ideal gas often found useful in studying the atmosphere. Namely, ideal gases can posses irreversible processes so that they need not be perfect fluids.

Perfect fluid mechanics is concerned with motion of a homogeneous fluid (e.g., pure water or pure air) with zero viscosity (no friction), and in the absence of any heat exchange (adiabatic).[6] In describing perfect fluids we commonly make use of *material fluid parcels*, which are infinitesimal deformable fluid regions (middle panel in Figure 17.1). A material fluid parcel maintains a fixed matter content so that it has a fixed mass. Furthermore, it does not experience irreversible exchanges of momentum arising from friction since the perfect fluid has zero viscosity. Hence, its only interaction with the surrounding fluid environment is through reversible mechanical exchanges from pressure. The material fluid parcel is thus a closed thermodynamic system that is open to reversible mechanical interactions.

A material parcel is not a point. Rather, it has an infinitesimal volume that deforms with the flow. Conceptually we can imagine the material fluid parcel as a tiny region of fluid surrounded by a perfectly slippery bag that is also perfectly insulating. This bag is closed to matter exchange so that its enclosed fluid particles are not exchanced with surrounding environment. Even so, the fluid parcel deforms in response to mechanical interactions mediated by pressure. Additionally, the bag expands or contracts according to the density of the fluid within the bag. This conceptual picture is qualified by noting that we never have occasion or need to precisely specify the boundary of a material fluid parcel. Rather, we make use of the conceptual framework provided by fluid parcels as a means to formulate the differential equations of perfect fluid mechanics.

[6] We study frictional stresses arising from viscosity in Chapter 25, with viscosity the means for the irreversible transfer of momentum within a non-perfect fluid. We study enthalpy in the Chapter 22, with a perfect fluid maintaining constant enthalpy since it is entirely adiabatic.

17.2.3 Finite sized material objects in perfect fluids

Any extended region in a perfect fluid, either infinitesimal or finite, remains exactly coherent (fixed matter content) as the region moves through the fluid. The reason for such coherency is that a perfect fluid supports no mixing or other irreversible processes that would otherwise act to diffuse the matter content. A closed material region in a perfect fluid is a finite volume generalization of a material fluid parcel. Conversely, a material fluid parcel is the infinitesimal limit of a closed material fluid region. Likewise, we can define finite sized material regions of any shape, each of which retains a fixed mass and fixed matter content as it moves through a perfect fluid. We study the kinematics of perfect fluid material lines, surfaces, and volumes in Chapter 18.

17.2.4 Fluid elements in real fluids

A fluid element is an infinitesimal and deformable fluid region of fixed mass yet non-fixed matter and non-fixed thermodynamic properties (right panel in Figure 17.1). For a homogeneous fluid comprised of a single matter constituent and no irreversible processes, then a fluid element reduces to a material fluid parcel. However, there is a distinction for real fluids such as the ocean and atmosphere, both of which have multiple constituents and support irreversible processes.

The exchange of matter across the boundary of a fluid element arises from the irreversible mixing of matter constituents within the fluid (Sections 20.1 and 68.3). As detailed in Section 20.1, diffusive matter exchange leaves the mass of the fluid element unchanged since the fluid element velocity is determined by its center of mass (*barycentric velocity*). Just as for a material fluid parcel, we have no need to experimentally specify the boundary of a fluid element. Instead, fluid elements are conceptual systems used to formulate the differential equations of a real fluid. Much of the kinematics in the current chapter holds for both material fluid parcels and fluid elements. However, in Chapter 19 and elsewhere, we make the distinction when studying the kinematics of multi-constituent fluids.

Many authors do not distinguish between material fluid parcels and fluid elements, choosing instead to retain a single overloaded term for both a perfect fluid and real fluid. However, this overloaded terminology can lead to confusion. We are thus motivated to maintain a distinction between fluid parcel (single component perfect fluid with no mixing) and fluid element (multi-component real fluid with mixing). The distinction offers an added signal for when the fluid under study is perfect (fluid parcel) or real (fluid element).

17.2.5 Test fluid element in real fluids

A *test fluid element* is a fluid element that has no effect on the surrounding fluid environment and is used as a conceptual probe of the fluid much like the fluid particle in Section 17.2.1. Unlike the fluid particle, the test fluid element has nonzero spatial extent and it can exchange matter and energy with its surrounding environment. The test fluid element is of particular use when studying buoyancy in Chapter 30. In that context, we further refine our treatment of the test fluid element, where we assume that it feels the same contact forces as the fluid, but distinct body forces.[7]

17.2.6 Finite sized fluid region in real fluids

A finite sized region within a real fluid is the most general subsystem we consider, with the region having boundaries that are open to the exchange of matter, mechanical forces, and thermodynamic properties with the surrounding environment. Here, we are often concerned with details of the region boundary and study the transport of properties across that boundary.

[7] We study contact and body forces in Sections 24.2 and 25.2.

17.2.7 Comments

Throughout the study of fluid kinematics, it is important to maintain an appreciation for the continuum approximation. In particular, the continuum approximation affords information about the continuous velocity field at each point of space and each instance of time. The velocity field allows us to determine fluid particle trajectories (via time integration), as well as the motion of fluid parcels in perfect fluids and fluid elements in real fluids. As part of a diagnostic framework for laboratory or field experiments, it can be useful to seed the fluid flow with a large number of tiny objects that approximate fluid particles whose motion approximates fluid particle trajectories. Similarly, in numerical experiments we may seed the flow with numerical fluid particles and compute their trajectories (*van Sebille et al.*, 2018). If we initially seed these particles in a tiny region, then deformation of the region provides the means to study deformation of fluid parcels and fluid elements as they move through the fluid. Likewise, seeding particles over larger regions allows one to study how finite sized regions are deformed.

When thinking about fluids parcels and elements, we should acknowledge that they are convenient concepts, and yet we do not delineate their boundaries either conceptually or in practice. This situation contrasts the study of other areas of continuum mechanics, where discrete regions of the media are identifiable. For a fluid, the notion of identifying a fluid element, such as by wrapping a tiny region of fluid with an imaginary permeable sack, is a fiction that works for some thought experiments, but it is not taken literally. The perspective leads us to discount (i.e., consider incorrect) a description of continuum mechanics that depends on fluid elements as distinct and identifiable objects. Rather, we aim for a theoretical description independent of details for the fluid element boundaries. In this case, we are afforded the ability to describe a fluid as continuum matter with properties that are unambiguously defined at every point in the fluid.

17.3 Material and spatial coordinates

A material description is afforded by the Lagrangian reference frame, whereby each fluid particle is labeled with a continuous material coordinate, $\boldsymbol{a}$, along with a material time coordinate, T, thus leading to the $\boldsymbol{a}$-space or material space description.[8] This description complements the Eulerian or $\boldsymbol{x}$-space description, whereby each point in Euclidean space, $\boldsymbol{x}$, is labeled by its position relative to a fixed origin and with time, t. The $\boldsymbol{a}$-space description determines the history of each material fluid particle's trajectory, whereas the $\boldsymbol{x}$-space description determines the fluid velocity as viewed at each spatial point $\boldsymbol{x}$. Note that $t = T$ since we are working with universal Newtonian time. However, it is very useful to distinguish the two times, since when taking time derivatives it is important to know whether the time derivative is computed holding $\boldsymbol{x}$ fixed or $\boldsymbol{a}$ fixed.

17.3.1 Fluid particle trajectories

In describing the motion of a classical point particle (Chapter 13), we specify its spatial position according to a time dependent position vector, $\boldsymbol{X}(T)$. At a given time, T, the position vector points to the spatial point $\boldsymbol{x}$, in which case we write

$$\boldsymbol{x} = \boldsymbol{X}(T) \qquad \text{point particle.} \tag{17.1}$$

[8]The continuum mechanics literature often writes $\boldsymbol{X}$ rather than $\boldsymbol{a}$ for the material particle label. That nomenclature is motivated since $\boldsymbol{X}$ is commonly chosen as the initial Cartesian position at a referential time. We instead write the material coordinate as $\boldsymbol{a}$. The reason for our notation is that, as noted in Section 17.3.2, there are examples where one, two, or three of the $\boldsymbol{a}$ coordinates are not positions in Euclidean space, but instead are determined by, for example, the buoyancy or tracer concentration.

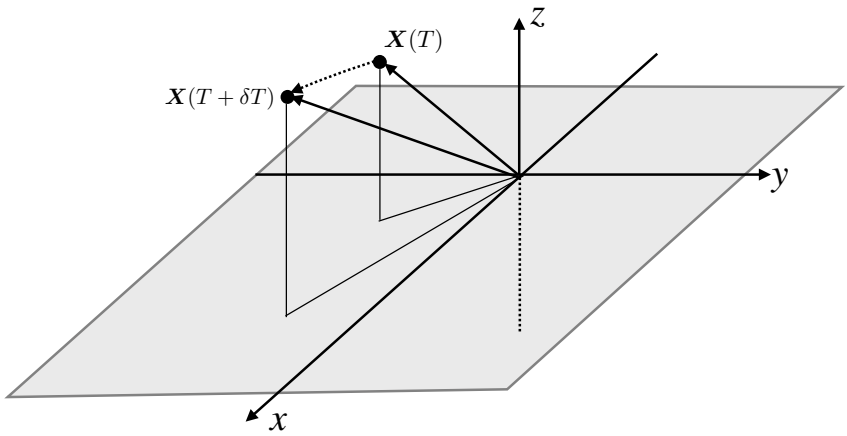

FIGURE 17.2: A short segment of a fluid particle trajectory in Euclidean space. The trajectory passes through the point $\boldsymbol{x} = \boldsymbol{X}(T)$ at time T and $\boldsymbol{x} + \delta\boldsymbol{x} = \boldsymbol{X}(T + \delta T)$ at time $T + \delta T$. Eulerian kinematics describes the fluid flow from the perspective of an observer fixed with respect to the laboratory frame. Lagrangian kinematics describes the fluid flow from the perspective of an observer comoving with fluid particles. Note that we have here chosen an origin for use in defining the fluid particle trajectory. If we only cared about the velocity, which is the difference of the trajectory between two infinitesimally close time instants, then there is no need to prescribe a particular origin. The reason is that in the process of computing the time difference, we remove dependence on the origin.

A sample trajectory is shown in Figure 17.2. We emphasize the notation convention used here, which may seem pedantic but in later discussions proves essential. Namely, the time dependent spatial position of a particle is denoted with, $\boldsymbol{X}(T)$, whose instantaneous space position is denoted by the lowercase, $\boldsymbol{x}$. This convention aims to distinguish time dependent functions, such as $\boldsymbol{X}(T)$, from the value of these functions, $\boldsymbol{x}$, evaluated at a time instance. In Section 18.2 we introduce the fluid *motion*, which serves as a slighly more formal, and general, means to distinguish points on a particle trajectory from points in space.

When there are N discrete particles, we distinguish the various particle trajectories by introducing a discrete label for each of the trajectories (e.g., see Section 11.5). The spatial position of particle i at time T is thus written

$$\boldsymbol{x} = \boldsymbol{X}_{(i)}(T). \tag{17.2}$$

When the matter is a continuum, then the discrete label becomes a continuous vector, $\boldsymbol{a}$, which is referred to as the *material* coordinate along with material time, T. At time T, the spatial position of a fluid particle labelled by the material coordinate, $\boldsymbol{a}$, is written

$$\boldsymbol{x} = \boldsymbol{X}(\boldsymbol{a}, T) \qquad \text{continuum of matter.} \tag{17.3}$$

The continuous vector, $\boldsymbol{a}$, labels a point of matter within the continuum fluid. Correspondingly, by allowing time to progress, the function $\boldsymbol{X}(\boldsymbol{a}, T)$ provides the trajectory for the fluid particle labelled by the material coordinate, $\boldsymbol{a}$.

In this book we ignore special relativistic effects, so that both the material reference frame and the laboratory reference frame measure the same universal Newtonian time, $t = T$. In contrast, the spatial coordinates are distinct for the Eulerian and Lagrangian references frames. Again, the spatial coordinates for the Eulerian frame are given by the position in Euclidean space relative to a fixed laboratory frame, with this specification making use of any convenient set of coordinates, such as Cartesian, spherical, polar, etc. (see Sections 4.21, 4.22, and 4.23). The three components of a material Lagrangian coordinate, $\boldsymbol{a}$, remain fixed according to the value assigned to each fluid particle. Additionally, the three coordinates for both the Eulerian and Lagrangian description must be linearly independent to allow for a unique specification of the fluid particle.

17.3.2 Example material coordinates

One common choice for material coordinate is the spatial position of each fluid particle at the referential time,

$$\boldsymbol{a} = (a, b, c) = (\mathring{x}, \mathring{y}, \mathring{z}) = \text{Cartesian position at } T = t_0 \text{ for particle labelled by } \boldsymbol{a}. \tag{17.4}$$

Even if not making this choice, initial position coordinates are quite useful conceptually as a grounding in the maths of material coordinates.

Now consider a perfect fluid (single material component with no irreversible processes). For this fluid, the specific entropy of each fluid parcel remains fixed at its initial value. When the fluid is placed in a gravitational field, layers of constant specific entropy are generally found to be monotonically stacked, or *stratified*, in the vertical direction (Chapter 30). As a result, we can uniquely specify a fluid parcel by giving its horizontal coordinate position, (x, y), as well as the specific entropy. The material coordinates for a parcel can thus be written as

$$\boldsymbol{a} = (a, b, c) = (\mathring{x}, \mathring{y}, \theta) = \text{Cartesian horizontal and } \theta \text{ at } T = t_0, \tag{17.5}$$

where θ is a measure of the specific entropy (or potential temperature as discussed in Section 23.3). In this example, the physical dimensions of the individual material coordinates can generally differ. It is this generality that necessitates the use of general tensor methods when developing the mechanical equations using arbitrary Lagrangian coordinates. The case of a single Lagrangian coordinate combined with two horizontal Eulerian coordinates is commonly used for geophysical fluid mechanics, with the mathematical physics of these *generalized vertical coordinates* detailed in Part XII of this book.

In combination with using specific entropy as a generalized vertical coordinate, we might further choose to specify a horizontal position according to the value of tracer concentration. So long as there is a one-to-one mapping between tracer space and geographic space, then we can consider a tracer concentration as a viable Lagrangian coordinate. This approach is less common than the generalized vertical coordinate approach, since tracers are rarely monotonically organized in any particular horizontal direction. Even so, the formalism can be extended to this case.

17.4 Lagrangian and Eulerian time derivatives

As noted in Section 17.3.2, we assume non-relativistic motion so that the Lagrangian reference frame and the Eulerian reference frame both measure the same universal Newtonian time, t. However, when computing time derivatives, the Eulerian frame does so by fixing the space coordinate, $\boldsymbol{x}$, whereas the Lagrangian frame does so by fixing the material coordinate, $\boldsymbol{a}$. These two time derivatives generally measure distinct changes in the fluid since one is computed in the laboratory frame and the other in the material frame. Relating their changes constitutes a key result of fluid kinematics. We derive an expression for the relation by first focusing on time derivatives acting on scalar fields, such as the temperature, and then derive the relation for vector fields, such as the velocity.

17.4.1 Infinitesimal space-time increment of a function

Consider a fluid property as represented by a space-time dependent scalar field, Π. For example, Π could be the temperature, kinetic energy per mass, or the mass density. When measured at a point in space this fluid property is written mathematically as

$$\Pi = \Pi(\boldsymbol{x}, t). \tag{17.6}$$

The difference between $\Pi(\boldsymbol{x}, t)$ and $\Pi(\boldsymbol{x} + \mathrm{d}\boldsymbol{x}, t + \mathrm{d}t)$ delivers the differential space and time increment, computed to leading order via a Taylor series expansion

$$\mathrm{d}\Pi = \Pi(\boldsymbol{x} + \mathrm{d}\boldsymbol{x}, t + \mathrm{d}t) - \Pi(\boldsymbol{x}, t) \tag{17.7a}$$
$$= \mathrm{d}t\, \partial_t \Pi + \mathrm{d}\boldsymbol{x} \cdot \nabla \Pi. \tag{17.7b}$$

In this equation, $\mathrm{d}t$ is the infinitesimal time increment, and $\mathrm{d}\boldsymbol{x}$ is the vector of infinitesimal space increments. For example, making use of Cartesian coordinates leads to the increment

$$\mathrm{d}\boldsymbol{x} = \hat{\boldsymbol{x}}\, \mathrm{d}x + \hat{\boldsymbol{y}}\, \mathrm{d}y + \hat{\boldsymbol{z}}\, \mathrm{d}z. \tag{17.8}$$

We ignore higher order terms in equation (17.7b) since the space and time increments are infinitesimal.[9]

17.4.2 Total time derivative of a function

In fluid mechanics, it is often useful to sample properties of the fluid from moving reference frames. In this case, the sampling position is a function of time. Determining how a field evolves when sampled in this moving reference frame requires us to allow the sampling position to itself be a function of time. Operationally, we have the total time derivative of Π determined by dividing both sides of equation (17.7b) by the infinitesimal time increment

$$\frac{\mathrm{d}\Pi}{\mathrm{d}t} = \frac{\partial \Pi}{\partial t} + \frac{\mathrm{d}\boldsymbol{x}}{\mathrm{d}t} \cdot \nabla \Pi. \tag{17.9}$$

The first term measures the time derivative of Π at the specific space point, $\boldsymbol{x}$, and as such it measures the Eulerian time derivative. The second term accounts for changes in Π arising from movement of the reference frame relative to a point, $\boldsymbol{x}$, according to the velocity, $\mathrm{d}\boldsymbol{x}/\mathrm{d}t$. Equation (17.9) holds regardless the velocity of the moving frame. Even so, we find it useful to specialize to the two common reference frames used in fluid mechanics.

17.4.3 Eulerian: evolution measured in the spatial frame

The Eulerian time derivative considers the evolution of a fluid property when sampled at a fixed space point

$$\text{Eulerian time derivative} = \frac{\partial \Pi(\boldsymbol{x}, t)}{\partial t}. \tag{17.10}$$

This result follows from specializing the total time derivative in equation (17.9) to the case of fixed spatial points, so that $\mathrm{d}\boldsymbol{x}/\mathrm{d}t = 0$. In the geophysical fluids literature, the Eulerian time derivative is often termed the *time tendency* and flows with a nonzero time tendency are said to be *developing flows* or *evolving flows*. When the Eulerian time derivative vanishes everywhere the flow is said to be in a *steady state* or in a *steady flow* condition, with all points in the laboratory frame measuring a zero time change for fluid properties. Note that steady flows are not generally static; rather, they are simply unchanging locally.

17.4.4 Lagrangian: evolution measured in the material frame

The Lagrangian or material time derivative measures the evolution of a fluid property sampled along the trajectory of a moving fluid particle. The Lagrangian time derivative for a field is

$$\text{Lagrangian time derivative} = \frac{\mathrm{D}\Pi}{\mathrm{D}t} = \frac{\partial \Pi}{\partial t} + \boldsymbol{v} \cdot \nabla \Pi. \tag{17.11}$$

[9] Mathematically, equation (17.7b) defines the *exterior derivative* of a scalar field.

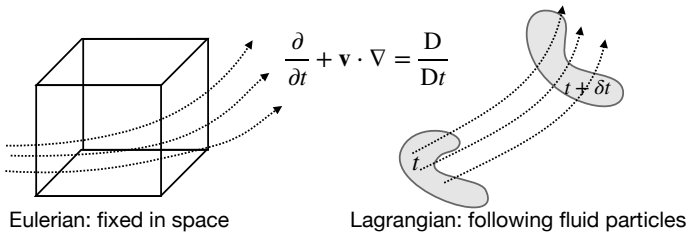

FIGURE 17.3: Illustrating the distinctions between the Eulerian (laboratory) and Lagrangian (material) reference frames for describing fluid motion. For the Eulerian description we consider a fixed control volume in the laboratory frame and measure properties as the fluid moves through the volume. For the Lagrangian description we tag fluid particles and measure fluid properties as sampled along the particle trajectories. The Eulerian representation of the material time derivative has two terms, one due to time changes local to the fixed laboratory point, and one due to the advection of properties that are swept by the local position.

The second equality follows by setting $\mathrm{d}\boldsymbol{x}/\mathrm{d}t = \boldsymbol{v}$ in equation (17.9) since we are sampling points along the fluid particle trajectory $\boldsymbol{x} = \boldsymbol{X}(\boldsymbol{a}, t)$. The operator $\partial/\partial t$ is the Eulerian time derivative from equation (17.10), whereas $\boldsymbol{v} \cdot \nabla$ is referred to as the *advection* operator. Use of the capital D for the material time operator

$$\frac{\mathrm{D}}{\mathrm{D}t} = \frac{\partial}{\partial t} + \boldsymbol{v} \cdot \nabla \tag{17.12}$$

signals that the time derivative is computed along a fluid particle trajectory. This notation distinguishes the material time derivative from the more generic total time derivative of equation (17.9). In some texts the material time derivative is referred to as the *convective time derivative*, since the term "convection" is often used rather than "advection".[10] It is also sometimes referred to as the *substantial time derivative* since it refers to the time changes following a material substance.

Equation (17.12) provides an Eulerian expression (right hand side) to the material time derivative, $\mathrm{D}/\mathrm{D}t$. There are two Eulerian contributions: the local (fixed space point) time tendency $\partial/\partial t$ and advection, $\boldsymbol{v} \cdot \nabla$. Advection arises in the Eulerian reference frame due to the fluid passing by the fixed laboratory observer, whereas it is absent from the material reference frame since the material frame moves with the fluid particles. Figure 17.3 illustrates the differences between the Eulerian and Lagrangian perspectives.

A *steady flow* is one with zero Eulerian time derivatives so that a steady flow does not imply a vanishing Lagrangian time derivative. Rather, a steady flow is a statement that the flow is time independent when viewed from the Eulerian (laboratory) reference frame. Hence, a steady flow generally has changing properties when sampled along a fluid particle trajectory. That is, there can be a nonzero Lagrangian evolution (via advection) even when the Eulerian time tendency vanishes.

17.4.5 Example material time derivative operations

The material time derivative operator is perhaps the most important operator in fluid mechanics, and its relation to the Eulerian time derivative plus advection is a key result of fluid kinematics. Therefore, it is critical to develop experience with this operator and its generalizations. The examples here offer a starting point.

[10] In the geophysical fluids literature, "convection" generally refers to vertical motion induced by gravitational instability, such as when heavy fluid is above light fluid. In contrast, the engineering literature often refers to "convection" in the same manner as we use the term "advection."

Material invariant/constant

Consider a scalar function, $\Pi(\boldsymbol{x}, t)$, that remains constant on a material trajectory so that its material time derivative vanishes

$$\frac{\mathrm{D}\Pi}{\mathrm{D}t} = 0. \tag{17.13}$$

Material constancy is generally referred to as *material invariance*. We may also say that the property, Π, is *materially constant*. At a fixed point in space, a materially invariant property has its Eulerian time derivative arising only via advection

$$\frac{\partial \Pi}{\partial t} = -\boldsymbol{v} \cdot \nabla \Pi. \tag{17.14}$$

For geometric insight into relation (17.14), introduce the unit normal vector to the surface of constant Π

$$\hat{\boldsymbol{n}} = \frac{\nabla \Pi}{|\nabla \Pi|}. \tag{17.15}$$

Material invariance of Π thus means that the normalized Eulerian time tendency equals to the negative of the projection of the fluid velocity into the direction normal to constant Π surfaces

$$\frac{\partial \Pi / \partial t}{|\nabla \Pi|} = -\boldsymbol{v} \cdot \hat{\boldsymbol{n}}. \tag{17.16}$$

That is, the normal projection of the fluid velocity, $\boldsymbol{v}$, is matched precisely to the moving surface of constant Π. No fluid particles cross the surface. We return to this result in Section 19.6.2 when studying the kinematic boundary conditions at a variety of surfaces.

Time derivative measured in an arbitrary moving frame

Now consider a reference frame moving at an arbitrary velocity, $\boldsymbol{v}^{(\mathrm{s})}$. Examples include the quasi-Lagrangian reference frames of a float in the ocean or balloon in the atmosphere. Due to their finite size and associated drag effects, these objects only approximate material particle motion, so that $\boldsymbol{v}^{(\mathrm{s})} \neq \boldsymbol{v}$. Returning to the general expression (17.9) for the total time derivative, we have the time derivative operator as measured in this non-material moving reference frame

$$\frac{\boldsymbol{v}^{(\mathrm{s})}}{\mathrm{D}t} = \frac{\partial}{\partial t} + \boldsymbol{v}^{(\mathrm{s})} \cdot \nabla. \tag{17.17}$$

A function that remains constant within this general moving frame thus satisfies

$$\frac{\boldsymbol{v}^{(\mathrm{s})}\Pi}{\mathrm{D}t} = 0 \Longrightarrow \frac{\partial \Pi}{\partial t} = -\boldsymbol{v}^{(\mathrm{s})} \cdot \nabla \Pi. \tag{17.18}$$

Introducing the normal direction $\hat{\boldsymbol{n}} = |\nabla \Pi|^{-1} \nabla \Pi$ leads to

$$\frac{\partial \Pi / \partial t}{|\nabla \Pi|} = -\boldsymbol{v}^{(\mathrm{s})} \cdot \hat{\boldsymbol{n}}, \tag{17.19}$$

which is an analog to the material invariance condition (17.16).

17.4.6 Worked example: velocity and acceleration from a trajectory

Following example 3.2 from *Kundu et al.* (2016), consider a one-dimensional fluid motion whereby the trajectory of a fluid particle is given by

$$\boldsymbol{X}(t) = \hat{\boldsymbol{x}}\, X(t) = \hat{\boldsymbol{x}} \left[K\,(t - t_0) + x_0^3 \right]^{1/3}, \tag{17.20}$$

where K is a constant with dimensions volume per time and x_0 is the particle position at time $t = t_0$. The particle velocity and particle acceleration are determined through time differentiation

$$\frac{\mathrm{d}\boldsymbol{X}}{\mathrm{d}t} = \hat{\boldsymbol{x}}\, \frac{K}{3\,X^2} \qquad \text{and} \qquad \frac{\mathrm{d}^2\boldsymbol{X}}{\mathrm{d}t^2} = -\hat{\boldsymbol{x}}\, \frac{2K^2}{9\,X^5}. \tag{17.21}$$

The Eulerian velocity field is then determined by

$$\boldsymbol{v}(\boldsymbol{x}, t) \equiv \left[\frac{\mathrm{d}\boldsymbol{X}}{\mathrm{d}t} \right]_{\boldsymbol{x} = \boldsymbol{X}(t)} = \hat{\boldsymbol{x}}\, \frac{K}{3\,x^2}, \tag{17.22}$$

which reveals that the flow is steady since there is no time dependence to the Eulerian velocity field. The Eulerian acceleration is given by the material time derivative of the Eulerian velocity, which is equal to the second time derivative of the trajectory evaluated at the field point

$$\frac{\mathrm{D}u}{\mathrm{D}t} = \frac{\partial u}{\partial t} + \boldsymbol{v} \cdot \nabla u = 0 + u\,\partial_x u = -[K/(3\,x^2)]\,[(2K)/(3\,x^3)] = -\frac{2\,K^2}{9\,x^5} = \left[\frac{\mathrm{d}^2 X(t)}{\mathrm{d}t^2} \right]_{\boldsymbol{x} = \boldsymbol{X}(t)}. \tag{17.23}$$

17.4.7 Material time derivative of a vector field

We now develop the material time derivative of a vector field, such as the velocity. We expect there to be a bit more baggage to carry around since a vector field representation requires basis vectors, with such vectors generally a function of space and time. Indeed, as we see, the application to a vector field requires the covariant derivative operator from Section 4.11.

To start, consider Cartesian coordinates in Euclidean space. There is no special treatment needed in this case, in which each component of a vector field, $\boldsymbol{G} = \hat{\boldsymbol{x}}\, G^1 + \hat{\boldsymbol{y}}\, G^2 + \hat{\boldsymbol{z}}\, G^3$, has a material time derivative

$$\mathrm{D}G^m/\mathrm{D}t = (\partial_t + \boldsymbol{v} \cdot \nabla)\, G^m = (\partial_t + v^n\, \partial_n)\, G^m. \tag{17.24}$$

That is, for Cartesian coordinates in Euclidean space, each component of a vector field has a material time derivative with the same form as that for a scalar field. Extending to arbitrary coordinates requires us to take into account the space-time dependence of the basis vectors used to represent a vector. The same ideas arose in Chapter 13 when deriving expressions for the velocity and acceleration of a particle using spherical coordinates.

So let us write the vector field according to

$$\boldsymbol{G} = G^m\, \boldsymbol{e}_m, \tag{17.25}$$

where $\boldsymbol{e}_m$ are basis vectors for the chosen coordinate system. In order for the material time derivative of a vector field to itself be a tensor, we need to use the covariant derivative as part of the advection operator, so that we have

$$\frac{\mathrm{D}}{\mathrm{D}t} = \partial_t + v^n\, \nabla_n, \tag{17.26}$$

so that

$$\frac{\mathrm{D}\boldsymbol{G}}{\mathrm{D}t} = (\partial_t + v^n \nabla_n)(G^m \boldsymbol{e}_m). \tag{17.27}$$

For Cartesian coordinates, the basis vectors, $\boldsymbol{e}_m$, are space-time constants, in which case we recover equation (17.24). For more general Eulerian coordinates, the basis vectors are time independent so that

$$\frac{\mathrm{D}\boldsymbol{G}}{\mathrm{D}t} = \boldsymbol{e}_m (\partial_t + v^n \nabla_n) G^m \quad \text{Eulerian coordinates.} \tag{17.28}$$

This result noted that the covariant derivative of the basis vectors vanishes, $\nabla_n \boldsymbol{e}_m = 0$, which follows since the metric tensor also has a zero covariant derivative (Section 4.13). Also in equation (17.28) we introduced the covariant derivative acting on a vector component

$$\nabla_n G^m = \partial_n G^m + \Gamma^m_{np} G^p, \tag{17.29}$$

and with $\Gamma^m_{np} = \Gamma^m_{pn}$ the Christoffel symbols (Section 4.11) that measure the spatial dependence of the basis vectors

$$\partial_n \boldsymbol{e}_m = \Gamma^p_{nm} \boldsymbol{e}_p. \tag{17.30}$$

In spherical coordinates the basis vectors are time independent, in which case $\partial_t \boldsymbol{e}_m = 0$. However, this time derivative term is present in some other coordinates, such as the generalized vertical coordinates studied in Part XII of this book. So for the case of generalized vertical coordinates, the basis vectors are time dependent so that the material time derivative of a vector is

$$\frac{\mathrm{D}\boldsymbol{G}}{\mathrm{D}t} = G^m \partial_t \boldsymbol{e}_m + \boldsymbol{e}_m (\partial_t + v^n \nabla_n) G^m. \tag{17.31}$$

17.4.8 Summarizing some terminology

We here summarize some terminology used to refer to the variety of equations in geophysical fluid mechanics. Some of this terminology was introduced in this chapter, whereas others will be encountered later.

- PROGNOSTIC: This is an equation that determines the time tendency (Eulerian evolution) of a quantity such as the temperature or velocity.
- DIAGNOSTIC: This is an equation that determines the value of a field at a particular time instance. An example is the non-divergence condition satisfied by velocity in an incompressible flow (Chapter 21) as well in a Boussinesq ocean (Chapter 29). There are generally no time derivatives appearing in diagnostic equations, though this property is generally a function of the chosen coordinate system.
- STEADY STATE: All Eulerian time derivatives vanish, so that all fluid properties are time independent when measured in the laboratory frame.
- MATERIAL INVARIANCE: The Lagrangian time derivative vanishes for a property that is a material invariant.

17.5 Galilean transformation

Recall from Section 11.1.3 that Galilean invariance means that the laws of motion are the same in all inertial reference frames. Furthermore, two inertial reference frames can only be moving with a constant velocity relative to one another. As for the particle, Galilean invariance for a fluid means that the material acceleration of a fluid particle remains the same when viewed in

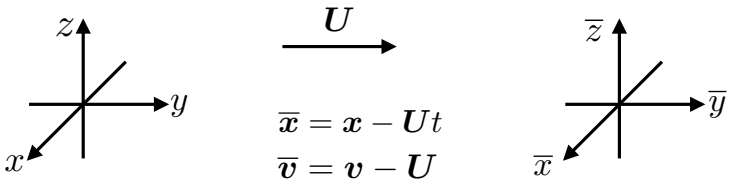

FIGURE 17.4: Illustrating the Galilean transformation between two inertial reference frames. The time coordinate is unchanged, $\bar{t} = t$, whereas space coordinates are related by $\overline{\boldsymbol{x}} = \boldsymbol{x} - \boldsymbol{U}t$ with $\boldsymbol{U}$ a constant boost velocity. We refer to the barred frame as the boosted reference frame and the unbarred frame as the rest frame, though since both frames are inertial there is no unique rest frame.

an arbitrary inertial reference frame. Some care is required when translating this invariance into a mathematical statement when decomposing the material acceleration into its Eulerian components. Our considerations here provide a useful warmup to the more general discussion in Section 17.6, where we transform space and time derivative operators between an inertial frame and a rotating frame.

Operationally, we determine whether an equation is Galilean invariant by examining the differential operators appearing in the equation. Hence, in the following we examine how differential operators transform when moving to a Galilean boosted reference frame. We then examine how the material time operator transforms, since this operator appears in the calculation of velocity and acceleration.

17.5.1 Specifying the Galilean transformation

A Galilean transformation is illustrated in Figure 17.4 and it is given mathematically by the linear space-time transformation

$$\bar{t} = t \qquad \text{and} \qquad \overline{\boldsymbol{x}} = \boldsymbol{x} - \boldsymbol{U}t \qquad \text{and} \qquad \overline{\boldsymbol{v}} = \boldsymbol{v} - \boldsymbol{U}. \tag{17.32}$$

We say that the barred coordinates measure space and time in the moving (boosted) reference frame and the unbarred coordinates measure space and time in the rest (unboosted) frame. As time increases, fixing a position, $\overline{\boldsymbol{x}}$, in the boosted frame, so that $\overline{\boldsymbol{v}} = 0$, is equivalent to moving with velocity $\boldsymbol{v} = \boldsymbol{U}$ in the unboosted frame. Conversely, fixing a position, $\boldsymbol{x}$, in the rest frame, so that $\boldsymbol{v} = 0$, is equivalent to movement with velocity $\overline{\boldsymbol{v}} = -\boldsymbol{U}$ in the boosted frame.

Since both reference frames are inertial, there is no experiment on a Galilean invariant physical system that can determine which frame is at rest or which is moving. Instead, what is relevant is that the two inertial frames are moving relative to one another. Furthermore, note that time remains unchanged (universal Newtonian time), whereas the position of a point in the new frame equals to that in the original reference frame plus a contribution from the constant velocity, $\boldsymbol{U}$. The inverse transformation is trivially given by

$$t = \bar{t} \qquad \text{and} \qquad \boldsymbol{x} = \overline{\boldsymbol{x}} + \boldsymbol{U}\bar{t} \qquad \text{and} \qquad \boldsymbol{v} = \overline{\boldsymbol{v}} + \boldsymbol{U}. \tag{17.33}$$

17.5.2 Transformation matrix

We make use of the transformation matrix formalism to derive relations between the partial differential operators, with details of the transformation matrix presented in Section 4.9. The reader having skipped that section should still be able to understand the gist of the following. For simplicity we work in the 1+1 dimensional case with time along with one space dimension.

Writing the space and time coordinates as

$$(t, x) = (x^0, x^1) \quad \text{and} \quad (\bar{t}, \overline{x}) = (x^{\bar{0}}, x^{\bar{1}}) \tag{17.34}$$

renders the transformation of partial derivatives (following the chain rule)

$$\frac{\partial}{\partial x^{\overline{\alpha}}} = \frac{\partial x^{\alpha}}{\partial x^{\overline{\alpha}}} \frac{\partial}{\partial x^{\alpha}}, \tag{17.35}$$

where $\alpha = 0, 1$ is a tensor index that has $\alpha = 0$ for the time coordinate. The transformation matrix for the Galilean transformation is thus given by the 2×2 matrix

$$\frac{\partial x^{\overline{\alpha}}}{\partial x^{\alpha}} = \begin{bmatrix} \partial x^{\overline{0}}/\partial x^{0} & \partial x^{\overline{0}}/\partial x^{1} \\ \partial x^{\overline{1}}/\partial x^{0} & \partial x^{\overline{1}}/\partial x^{1} \end{bmatrix} = \begin{bmatrix} 1 & 0 \\ -U & 1 \end{bmatrix}, \tag{17.36}$$

and the inverse is

$$\frac{\partial x^{\alpha}}{\partial x^{\overline{\alpha}}} = \begin{bmatrix} 1 & 0 \\ U & 1 \end{bmatrix}. \tag{17.37}$$

The Jacobian determinant of the transformation matrix is unity, so that the Galilean transformation always has an inverse.

17.5.3 Transforming the differential operators

Given the transformation matrix, we can compute the Eulerian time derivative as measured in the moving frame by using the chain rule

$$\frac{\partial}{\partial x^{\overline{0}}} = \frac{\partial x^{0}}{\partial x^{\overline{0}}} \frac{\partial}{\partial x^{0}} + \frac{\partial x^{1}}{\partial x^{\overline{0}}} \frac{\partial}{\partial x^{1}} = \frac{\partial}{\partial x^{0}} + U \frac{\partial}{\partial x^{1}} = \frac{\partial}{\partial t} + U \frac{\partial}{\partial x}. \tag{17.38}$$

In words, this identity says that the time derivative computed between two inertial reference frames differs due to an advective term (with the constant Galilean boost velocity) arising from the relative motion of the two inertial observers. A time derivative measured in the boosted reference frame keeps the position, $\overline{x}$, fixed, so that even if ∂_t is zero, we can still have a nonzero $\partial_{\overline{t}}$ due to advection, $U\,\partial_{\overline{x}}$.

In the same manner we find that the space derivatives are related by

$$\frac{\partial}{\partial x^{\overline{1}}} = \frac{\partial x^{0}}{\partial x^{\overline{1}}} \frac{\partial}{\partial x^{0}} + \frac{\partial x^{1}}{\partial x^{\overline{1}}} \frac{\partial}{\partial x^{1}} = \frac{\partial}{\partial x^{1}}. \tag{17.39}$$

Evidently, the space derivative operator remains form invariant under a Galilean transformation. This result holds also for the other two space dimensions.

Bringing pieces together we find that the material time derivative operator is form invariant under a Galilean transformation

$$\begin{aligned} \frac{\mathrm{D}}{\mathrm{D}t} &= \frac{\partial}{\partial t} + \boldsymbol{v} \cdot \nabla && \text{(17.40a)} \\ &= \frac{\partial}{\partial \overline{t}} - \boldsymbol{U} \cdot \overline{\nabla} + (\overline{\boldsymbol{v}} + \boldsymbol{U}) \cdot \overline{\nabla} && \text{(17.40b)} \\ &= \frac{\partial}{\partial \overline{t}} + \overline{\boldsymbol{v}} \cdot \overline{\nabla} && \text{(17.40c)} \\ &= \frac{\overline{\mathrm{D}}}{\mathrm{D}\overline{t}}\,, && \text{(17.40d)} \end{aligned}$$

where we used the shorthand

$$\overline{\boldsymbol{v}} \cdot \overline{\nabla} = \overline{u} \frac{\partial}{\partial x^{\overline{1}}} + \overline{v} \frac{\partial}{\partial x^{\overline{2}}} + \overline{w} \frac{\partial}{\partial x^{\overline{3}}}. \tag{17.41}$$

So although the individual pieces to the material time operator are modified by a Galilean

transformation, the material time derivative operator is form invariant. Hence, if a scalar function has a material time derivative in one inertial reference frame, it has the same material time operator in any other inertial reference frame. To be more precise, let F represent some scalar property. When measured at a space-time point $(\mathscr{P}, t)$ using the coordinate system, $x^\alpha = (\boldsymbol{x}, t)$, we write[11]

$$\mathrm{F}(\mathscr{P}, t) = F(\boldsymbol{x}, t), \tag{17.42}$$

and its material time derivative is

$$\frac{\mathrm{D}F(\boldsymbol{x}, t)}{\mathrm{D}t} = (\partial_t + v^m \, \partial_m) \, F. \tag{17.43}$$

Likewise, when evaluated at the same point but using the boosted coordinates, $x^{\overline{\alpha}} = (\overline{\boldsymbol{x}}, \overline{t})$, then

$$\mathrm{F}(\mathscr{P}) = \overline{F}(\overline{x}, \overline{t}), \tag{17.44}$$

with its material time derivative

$$\frac{\mathrm{D}\Pi(\mathscr{P})}{\mathrm{D}\overline{t}} = (\partial_{\overline{t}} + v^{\overline{m}} \, \partial_{\overline{m}}) \, \overline{F}. \tag{17.45}$$

We provide an explicit example in Exercise 17.6.

17.5.4 Comments

There are many features of geophysical fluid flows that break Galilean invariance. For example, a solid boundary breaks Galilean invariance since it establishes a special reference frame and thus breaks the symmetry of unbounded space. Additionally, a rotating planet distinguishes between longitude and latitude even if the planet is perfectly smooth. Nonetheless, as a starting point in our study of the equations of fluid mechanics it is useful to establish their properties under a Galilean transformation. In general, if space is Galilean invariant and yet the equations of motion are not, then we question the physical relevance of the equations. Exercise 38.11 provides an example of this reasoning.

There are further symmetries of the equations of fluid mechanics, especially when there is no dissipation (inviscid). Section 2.2 of *Frisch* (1995), Section 2.9 of *Pope* (2000), and Section 1.4 of *Badin and Crisciani* (2018) provide a discussion of these further symmetries.

17.6 Transforming the material time derivative

In the discussion of Galilean invariance in Section 17.5, we showed that the material time derivative operator remains form invariant under changes to the inertial reference frame. Here, we consider an arbitrary transformation, with a focus on its action on a scalar field. The development offers a case study for how to transform from one reference frame to another.

17.6.1 Definition of the material time derivative

We first determine the transformation by focusing on the conceptual definition of the material time derivative. Namely, the material time derivative measures time changes of a fluid property in the reference frame comoving with a fluid particle. The Lagrangian reference frame follows fluid particles, so it is the natural reference frame for measuring material time changes. In contrast, the Eulerian reference frame is fixed in a laboratory. The material time derivative

[11] Recall the notational convention from Section 1.5.1.

acting on a scalar when computed from the laboratory reference frame consists of an Eulerian time tendency plus an advection operator

$$\frac{\mathrm{D}}{\mathrm{D}t} = \frac{\partial}{\partial t} + \boldsymbol{v} \cdot \nabla. \tag{17.46}$$

Importantly, this expression holds regardless the choice of laboratory reference frame, either inertial or non-inertial. The particle reference frame is unconcerned with the subjective choice made by the observer in the laboratory reference frame. Our choice of laboratory frame only impacts on the form of the Eulerian time derivative and on the advection operator. The sum of the two terms returns the same material time derivative operator, no matter what laboratory frame is chosen.

17.6.2 Example: a rotating reference frame

Consider two reference frames. The first is at rest and so serves as an inertial frame, whereas the second is rotating (and thus non-inertial) with rotational axis aligned with the vertical direction as in Figure 4.3. Introduce Cartesian coordinates for the inertial frame, with corresponding basis vectors $(\hat{\overline{\boldsymbol{x}}}, \hat{\overline{\boldsymbol{y}}}, \hat{\overline{\boldsymbol{z}}})$. Let these inertial frame unit vectors be related to rotating frame unit vectors according to

$$\hat{\overline{\boldsymbol{x}}} = \hat{\boldsymbol{x}} \cos\vartheta - \hat{\boldsymbol{y}} \sin\vartheta \tag{17.47a}$$

$$\hat{\overline{\boldsymbol{y}}} = \hat{\boldsymbol{x}} \sin\vartheta + \hat{\boldsymbol{y}} \cos\vartheta \tag{17.47b}$$

$$\hat{\overline{\boldsymbol{z}}} = \hat{\boldsymbol{z}}, \tag{17.47c}$$

and let time be the same in the two reference frames. The angle ϑ measures the counter-clockwise angle between the inertial frame direction $\hat{\overline{\boldsymbol{x}}}$ and the moving frame direction $\hat{\boldsymbol{x}}$, with this angle a linear function of time

$$\vartheta = \Omega\, t. \tag{17.48}$$

The above relations between the two sets of basis vectors translates into the same relations between the corresponding coordinate representations for an arbitrary vector. Including time, we have the relation between inertial coordinates (the barred frame) and rotating coordinates (unbarred frame)

$$\overline{t} = t \tag{17.49a}$$

$$\overline{x} = x \cos\vartheta - y \sin\vartheta \tag{17.49b}$$

$$\overline{y} = x \sin\vartheta + y \cos\vartheta \tag{17.49c}$$

$$\overline{z} = z. \tag{17.49d}$$

The inverse transformation can be easily found

$$t = \overline{t} \tag{17.50a}$$

$$x = \overline{x} \cos\vartheta + \overline{y} \sin\vartheta \tag{17.50b}$$

$$y = -\overline{x} \sin\vartheta + \overline{y} \cos\vartheta \tag{17.50c}$$

$$z = \overline{z}. \tag{17.50d}$$

We are now prepared to make use of the transformation formalism developed in Section 4.9, and applied for the Galilean transformation in Section 17.5. We include time as part of the formalism by introducing the Greek label $\alpha = 0, 1, 2, 3$ so that the transformation matrix

between the inertial frame and rotating frame is given by

$$\frac{\partial x^{\overline{\alpha}}}{\partial x^{\alpha}} = \begin{bmatrix} \partial x^{\overline{0}}/\partial x^{0} & \partial x^{\overline{0}}/\partial x^{1} & \partial x^{\overline{0}}/\partial x^{2} & \partial x^{\overline{0}}/\partial x^{3} \\ \partial x^{\overline{1}}/\partial x^{0} & \partial x^{\overline{1}}/\partial x^{1} & \partial x^{\overline{1}}/\partial x^{2} & \partial x^{\overline{1}}/\partial x^{3} \\ \partial x^{\overline{2}}/\partial x^{0} & \partial x^{\overline{2}}/\partial x^{1} & \partial x^{\overline{2}}/\partial x^{2} & \partial x^{\overline{2}}/\partial x^{3} \\ \partial x^{\overline{3}}/\partial x^{0} & \partial x^{\overline{3}}/\partial x^{1} & \partial x^{\overline{3}}/\partial x^{2} & \partial x^{\overline{3}}/\partial x^{3} \end{bmatrix} = \begin{bmatrix} 1 & 0 & 0 & 0 \\ -\Omega\,\overline{y} & \cos\vartheta & -\sin\vartheta & 0 \\ \Omega\,\overline{x} & \sin\vartheta & \cos\vartheta & 0 \\ 0 & 0 & 0 & 1 \end{bmatrix}. \tag{17.51}$$

Similarly, the inverse transformation is given by

$$\frac{\partial x^{\alpha}}{\partial x^{\overline{\alpha}}} = \begin{bmatrix} \partial x^{0}/\partial x^{\overline{0}} & \partial x^{0}/\partial x^{\overline{1}} & \partial x^{0}/\partial x^{\overline{2}} & \partial x^{0}/\partial x^{\overline{3}} \\ \partial x^{1}/\partial x^{\overline{0}} & \partial x^{1}/\partial x^{\overline{1}} & \partial x^{1}/\partial x^{\overline{2}} & \partial x^{1}/\partial x^{\overline{3}} \\ \partial x^{2}/\partial x^{\overline{0}} & \partial x^{2}/\partial x^{\overline{1}} & \partial x^{2}/\partial x^{\overline{2}} & \partial x^{2}/\partial x^{\overline{3}} \\ \partial x^{3}/\partial x^{\overline{0}} & \partial x^{3}/\partial x^{\overline{1}} & \partial x^{3}/\partial x^{\overline{2}} & \partial x^{3}/\partial x^{\overline{3}} \end{bmatrix} = \begin{bmatrix} 1 & 0 & 0 & 0 \\ \Omega\,y & \cos\vartheta & \sin\vartheta & 0 \\ -\Omega\,x & -\sin\vartheta & \cos\vartheta & 0 \\ 0 & 0 & 0 & 1 \end{bmatrix}. \tag{17.52}$$

The derivative operators transform according to

$$\frac{\partial}{\partial x^{\alpha}} = \frac{\partial x^{\overline{\alpha}}}{\partial x^{\alpha}}\,\frac{\partial}{\partial x^{\overline{\alpha}}}, \tag{17.53}$$

in which case

$$\frac{\partial}{\partial t} = \frac{\partial}{\partial \overline{t}} + (\boldsymbol{\Omega} \times \overline{\boldsymbol{x}}) \cdot \overline{\nabla} \tag{17.54a}$$

$$\frac{\partial}{\partial x} = \cos\vartheta\,\frac{\partial}{\partial \overline{x}} + \sin\vartheta\,\frac{\partial}{\partial \overline{y}} \tag{17.54b}$$

$$\frac{\partial}{\partial y} = -\sin\vartheta\,\frac{\partial}{\partial \overline{x}} + \cos\vartheta\,\frac{\partial}{\partial \overline{y}} \tag{17.54c}$$

$$\frac{\partial}{\partial z} = \frac{\partial}{\partial \overline{z}}. \tag{17.54d}$$

The velocity vector components transform according to

$$v^{\alpha} = \frac{\partial x^{\alpha}}{\partial x^{\overline{\alpha}}}\,v^{\overline{\alpha}}, \tag{17.55}$$

so that

$$v^{0} = v^{\overline{0}} \tag{17.56a}$$

$$u = \Omega\,y + \overline{u}\cos\vartheta + \overline{v}\sin\vartheta \tag{17.56b}$$

$$v = -\Omega\,x - \overline{u}\sin\vartheta + \overline{v}\cos\vartheta \tag{17.56c}$$

$$w = \overline{w}, \tag{17.56d}$$

where

$$v^{0} = v^{\overline{0}} = 1. \tag{17.57}$$

Bringing these result together leads to the transformation of the horizontal advection operator

$$u\,\frac{\partial}{\partial x} + v\,\frac{\partial}{\partial y} = (\overline{\boldsymbol{u}} - \boldsymbol{\Omega} \times \overline{\boldsymbol{x}}) \cdot \overline{\nabla}. \tag{17.58}$$

Combining this result with the transformed Eulerian time derivative leads to the material time derivative

$$\frac{\mathrm{D}}{\mathrm{D}t} = \frac{\partial}{\partial t} + \boldsymbol{v} \cdot \nabla \tag{17.59a}$$

$$= \frac{\partial}{\partial t} + u\,\frac{\partial}{\partial x} + v\,\frac{\partial}{\partial y} + w\,\frac{\partial}{\partial z} \tag{17.59b}$$

$$= \frac{\partial}{\partial \overline{t}} + (\boldsymbol{\Omega}\times\overline{\boldsymbol{x}})\cdot\overline{\nabla} + (\overline{\boldsymbol{u}} - \boldsymbol{\Omega}\times\overline{\boldsymbol{x}})\cdot\overline{\nabla} + \overline{w}\,\frac{\partial}{\partial \overline{z}} \tag{17.59c}$$

$$= \frac{\partial}{\partial \overline{t}} + \overline{\boldsymbol{v}}\cdot\overline{\nabla}. \tag{17.59d}$$

As advertised, the operator is form invariant under time dependent transformations to a non-inertial reference frame.

17.6.3 Invariance using space-time tensors

We can generalize the previous result by writing the material time derivative operator using space-time tensor notation from Section 3.5.4, in which case

$$\frac{\mathrm{D}}{\mathrm{D}t} = \frac{\partial}{\partial t} + \boldsymbol{v}\cdot\nabla = \frac{\partial}{\partial x^0} + v^m\,\frac{\partial}{\partial x^m} = v^\alpha\,\frac{\partial}{\partial x^\alpha}, \tag{17.60}$$

where we introduced the velocity 4-vector

$$(v^0, v^1, v^2, v^3) = (1, v^1, v^2, v^3). \tag{17.61}$$

All space-time indices are contracted in equation (17.60), which means the material time derivative is a space-time scalar. Consequently, we can change coordinates or change reference frames without changing the material time operator.

We verify the above conclusion via the following manipulations using the chain rule

$$\frac{\mathrm{D}}{\mathrm{D}t} = \partial_0 + v^m\,\partial_m \tag{17.62a}$$

$$= \Lambda^{\overline{\alpha}}_{\ 0}\,\partial_{\overline{\alpha}} + \Lambda^{a}_{\ \overline{\alpha}}\,v^{\overline{\alpha}}\,\Lambda^{\overline{\beta}}_{\ a}\,\partial_{\overline{\beta}} \tag{17.62b}$$

$$= \Lambda^{\overline{\alpha}}_{\ 0}\,\partial_{\overline{\alpha}} + \Lambda^{a}_{\ \overline{\alpha}}\,\Lambda^{\overline{\beta}}_{\ a}\,v^{\overline{\alpha}}\,\partial_{\overline{\beta}}, \tag{17.62c}$$

where we wrote the transformation matrix and its inverse in the form (see Section 4.1.4 for more details)

$$\Lambda^{\alpha}_{\ \overline{\alpha}} \equiv \frac{\partial x^\alpha}{\partial x^{\overline{\alpha}}} \quad \text{and} \quad \Lambda^{\overline{\alpha}}_{\ \alpha} \equiv \frac{\partial x^{\overline{\alpha}}}{\partial x^\alpha}. \tag{17.63}$$

Next make use of the identity

$$\Lambda^{a}_{\ \overline{\alpha}}\,\Lambda^{\overline{\beta}}_{\ a} = \Lambda^{\alpha}_{\ \overline{\alpha}}\,\Lambda^{\overline{\beta}}_{\ \alpha} - \Lambda^{0}_{\ \overline{\alpha}}\,\Lambda^{\overline{\beta}}_{\ 0} \qquad a = 1,2,3 \text{ and } \alpha = 0,1,2,3 \tag{17.64a}$$

$$= \delta^{\overline{\beta}}_{\ \overline{\alpha}} - \Lambda^{0}_{\ \overline{\alpha}}\,\Lambda^{\overline{\beta}}_{\ 0} \qquad \Lambda^{\alpha}_{\ \overline{\alpha}}\,\Lambda^{\overline{\beta}}_{\ \alpha} = \delta^{\overline{\beta}}_{\ \overline{\alpha}} \text{ by chain rule} \tag{17.64b}$$

$$= \delta^{\overline{\beta}}_{\ \overline{\alpha}} - \delta^{0}_{\ \overline{\alpha}}\,\Lambda^{\overline{\beta}}_{\ 0} \qquad \Lambda^{0}_{\ \overline{\alpha}} = \delta^{0}_{\ \overline{\alpha}} \text{ for Newtonian time.} \tag{17.64c}$$

Use of this identity in equation (17.62c) renders

$$\frac{\mathrm{D}}{\mathrm{D}t} = \Lambda^{\overline{\alpha}}_{\ 0}\,\partial_{\overline{\alpha}} + \left[\delta^{\overline{\beta}}_{\ \overline{\alpha}} - \delta^{0}_{\ \overline{\alpha}}\,\Lambda^{\overline{\beta}}_{\ 0}\right] v^{\overline{\alpha}}\,\partial_{\overline{\beta}} \tag{17.65a}$$

$$= \Lambda^{\overline{\alpha}}_{\ 0}\,\partial_{\overline{\alpha}} + v^{\overline{\alpha}}\,\partial_{\overline{\alpha}} - v^{\overline{0}}\,\Lambda^{\overline{\beta}}_{\ 0}\,\partial_{\overline{\beta}} \tag{17.65b}$$

$$= v^{\overline{\alpha}}\,\partial_{\overline{\alpha}} \tag{17.65c}$$

$$= \partial_{\overline{t}} + v^{\overline{a}}\,\partial_{\overline{a}}, \tag{17.65d}$$

where we used $v^{\overline{0}} = 1$. This proof means that the material time derivative remains form invariant

no matter what coordinate choice is made for the laboratory reference frame.

17.6.4 Comments

As argued at the start of this section, there is no reason for a time derivative computed in a material frame to be concerned with the coordinates chosen for the laboratory frame. Hence, we expect there to be form invariance across all chosen laboratory coordinates. It is satisfying to see the tools of coordinate transformations put to use verifying this result.

17.7 Fluid flow lines

There are three types of flow lines commonly used to visualize fluid motion: *pathlines*, *streamlines*, and *streaklines*. These flow lines are identical for time independent (steady) flow, where steady flow means that all fields are constant in time when observed in the Eulerian reference frame. However, these flow lines differ for unsteady flow. They each offer complementary information about the flow field, and have uses in both theoretical and experimental contexts. We have use for pathlines and streamlines in this book, yet also introduce streaklines for completeness.

17.7.1 Material pathlines from fluid particle trajectories

As introduced in Section 17.3.1, a fluid particle traces out a *trajectory* as it moves through space and time (Figure 17.2). We use the term material *pathline* for a fluid particle trajectory, with a collection of pathlines providing a means to visualize fluid particle motion throughout the flow. In this book we are only concerned with *smooth velocity fields*, which allow for an unambiguous specification of the particle trajectory at each point of the fluid.

As introduced in Section 18.3.2, a fluid particle trajectory is a curve in space, $\boldsymbol{\varphi}(\boldsymbol{a}, T)$, that is traced by fixing the material coordinate, $\boldsymbol{a}$, and letting time, T, advance.[12] Trajectories are computed by time integrating the ordinary differential equation

$$\frac{\partial \boldsymbol{\varphi}(\boldsymbol{a}, T)}{\partial T} = \boldsymbol{v}[\boldsymbol{\varphi}(\boldsymbol{a}, T), T] \tag{17.66a}$$

$$\boldsymbol{\varphi}(\boldsymbol{a}, T = t_0) = \boldsymbol{a}, \tag{17.66b}$$

where the Lagrangian velocity of the fluid particle is written as the Eulerian velocity when evaluated on a trajectory[13]

$$\boldsymbol{v}^{\text{L}}(\boldsymbol{a}, T) = \boldsymbol{v}[\boldsymbol{x} = \boldsymbol{\varphi}(\boldsymbol{a}, T), t = T], \tag{17.67}$$

and we have assumed the material coordinates are known at some arbitrary initial time, $T = t_0$. Again, the partial time derivative is computed with the material coordinate held fixed, so that the material coordinate distinguishes between particle trajectories.

Since the trajectory is determined by integrating the ordinary differential equation (17.66a), the fluid particle trajectory provides an *integral curve* for the velocity vector. Furthermore, by construction, trajectories are tangent to the velocity field at each point, and there is a trajectory that passes through each point of space at each time instance.

In the laboratory, we can insert tiny particles into the fluid to offer a means for visualizing the flow, with a time exposed photograph providing an estimate of fluid particle pathlines. Experimental particles provide an accurate estimate of fluid particle pathlines if the particles do

[12] As studied in Chapter 18, trajectories are the Euclidean space manifestation of the *flow map*, which acts to smoothly deform the matter continuum through space as the fluid moves. For this reason, we sometimes write $\boldsymbol{\varphi}(\boldsymbol{a}, T) = \boldsymbol{X}(\boldsymbol{a}, T)$ to correspond to the particle mechanics studied in Part II of this book.

[13] We have more to say about equation (17.67) in Chapter 18.

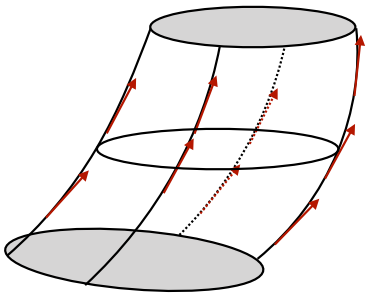

FIGURE 17.5: This image shows an example streamtube. The side boundaries of a streamtube consist of streamlines. At each point of a streamline, the local tangent vector equals to the velocity field (see equation (17.69)). Streamlines are identical to pathlines only for steady flow; they differ for unsteady flows. Hence, for unsteady flows, particle trajectories generally cross through the streamtube boundary.

not disperse through diffusion (see Chapter 69). As another example, consider cars moving at night with a time exposed photograph revealing pathlines formed by car head and tail lights. Like cars, the material pathlines in a fluid can intersect, cross, and become quite complex, particularly when the flow is turbulent.

17.7.2 Fluid streamlines and streamtubes

Streamlines are curves whose tangent is parallel to the instantaneous fluid velocity field. Streamlines can intersect only at a stagnation point; i.e., a point where the fluid is not moving. Let

$$\mathrm{d}\boldsymbol{x} = \hat{\boldsymbol{x}}\,\mathrm{d}x + \hat{\boldsymbol{y}}\,\mathrm{d}y + \hat{\boldsymbol{z}}\,\mathrm{d}z \tag{17.68}$$

be an infinitesimal increment along a streamline written using Cartesian coordinates. The family of streamlines at a given time, t, satisfy the tangent constraint

$$\boldsymbol{v} \times \mathrm{d}\boldsymbol{x} = 0, \tag{17.69}$$

which is equivalent to

$$\frac{\mathrm{d}x}{u(\boldsymbol{x},t)} = \frac{\mathrm{d}y}{v(\boldsymbol{x},t)} = \frac{\mathrm{d}z}{w(\boldsymbol{x},t)}. \tag{17.70}$$

Alternatively, we can introduce a pseudo-time parameter, s, that determines a position along a streamline. Streamlines are the curves $\boldsymbol{x} = \boldsymbol{\varphi}(s;\boldsymbol{a},t)$ computed with $(\boldsymbol{a},t)$ held fixed, but with the pseudo-time varied

$$\frac{\partial\boldsymbol{\varphi}(s;\boldsymbol{a},T)}{\partial s} = \boldsymbol{v}[\boldsymbol{\varphi}(s;\boldsymbol{a},T),T] \tag{17.71a}$$

$$\boldsymbol{\varphi}(s=0;\boldsymbol{a},T) = \boldsymbol{a}. \tag{17.71b}$$

Again, both the material coordinate $\boldsymbol{a}$ and time T are held fixed when determining streamlines, so that $(\boldsymbol{a},T)$ act as parameters to distinguish streamlines. Streamlines thus do not know about the time evolution of unsteady flow. Instead, streamlines only sample a snapshot of the velocity field; they are freshly computed at each time instance.

A *streamtube* is a bundle of streamlines crossing through an arbitrary closed curve (see Figure 17.5). Hence, at each time instance, streamtube sides are parallel to the velocity vector. Furthermore, when the flow is steady then streamlines are identical to material particle pathlines. Hence, a streamtube is a material tube for steady flow, in which case no fluid particles cross the streamtube boundary.

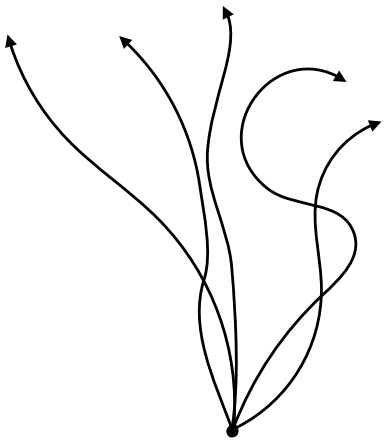

FIGURE 17.6: A suite of trajectories emanating from a single point. Common approximate realizations include the paths of fluid particles that leave a chimney, or the smoke from a source like a burning stick or torch. A streakline is defined as the accumulation of positions at time T of particles that passed through the common point at some earlier time $s < T$.

17.7.3 Distinguishing streamlines and pathlines

The tangent to a streamline gives the velocity at a single point in time, whereas the tangent to a material pathline (i.e., a trajectory) gives the velocity at subsequent times. These tangents are identical when the flow is steady. However, if the flow is time dependent (unsteady), then streamlines differ from material pathlines. Furthermore, for unsteady flow, the pseudo-time parameter, s, determining the streamlines in equation (17.71a) is not equal to the time, t, used to compute fluid particle trajectories in equation (17.66a). Consequently, the condition $\boldsymbol{v} \cdot \hat{\boldsymbol{n}} = 0$ satisfied at each time instance by a streamline still allows fluid particles to cross streamlines. The reason is that a material pathline moves with the fluid in such a way that

$$(\boldsymbol{v} - \boldsymbol{v}^{\text{line}}) \cdot \hat{\boldsymbol{n}} = 0 \Longrightarrow \boldsymbol{v} \cdot \hat{\boldsymbol{n}} = \boldsymbol{v}^{\text{line}} \cdot \hat{\boldsymbol{n}} \qquad \text{material lines,} \tag{17.72}$$

where $\boldsymbol{v}^{\text{line}}$ is the velocity of a point on the material pathline. The material pathline thus moves so that no fluid particles cross it. Only when the flow is steady, so that $\boldsymbol{v}^{\text{line}} \cdot \hat{\boldsymbol{n}} = 0$, will material pathlines and streamlines be equal. That is, the streamline constraint $\boldsymbol{v} \cdot \hat{\boldsymbol{n}} = 0$ is not a material constraint when $\boldsymbol{v}^{\text{line}} \cdot \hat{\boldsymbol{n}} \neq 0$. The key point is that streamlines do not probe the time behavior of the flow, so they do not know whether the velocity is steady or unsteady.

17.7.4 Fluid streaklines

A *streakline* is a curve obtained by connecting the positions for all fluid particles that emanate from a fixed point in space (see Figure 17.6). Streaklines are simple to define conceptually and to realize experimentally. However, they are a bit convoluted to specify mathematically. We present two formulations.

At any time T, the streakline passing through a fixed point $\boldsymbol{y}$ is a curve going from $\boldsymbol{y}$ to $\boldsymbol{\varphi}(\boldsymbol{y}, T)$, the position reached by the particle initialized at $T = 0$ at the point $\boldsymbol{y}$. A particle is on the streakline if it passed the fixed point $\boldsymbol{y}$ at some time between 0 and T. If this time was s, then the material coordinate of the particle would be given by $\boldsymbol{a}(\boldsymbol{y}, s)$ relating the material coordinate to its corresponding laboratory position). Furthermore, at time T, this particle is at $\boldsymbol{x}$, so that the equation of the streakline at time T is

$$\boldsymbol{x} = \boldsymbol{\varphi}[\boldsymbol{a}(\boldsymbol{y}, s), T] \qquad 0 \leq s \leq T. \tag{17.73}$$

We can connect the streakline specification to that given for a pathline and streamline

through the following. A streakline at some time instance $\tilde{T}$ is a curve defined by fixing $\tilde{T}$ and varying s over $s \leq \tilde{T}$ in the function $\boldsymbol{\varphi}(s; \boldsymbol{a}, \tilde{T})$. We determine the curves $\boldsymbol{x} = \boldsymbol{\varphi}(s; \boldsymbol{a}, \tilde{T})$ by solving the following set of initial value problems for trajectories with initial conditions imposed at $T = s$ rather than $T = 0$

$$\frac{\partial \boldsymbol{\varphi}(s; \boldsymbol{a}, T)}{\partial T} = \boldsymbol{v}[\boldsymbol{\varphi}(s; \boldsymbol{a}, T), T] \tag{17.74a}$$

$$\boldsymbol{\varphi}(T = s; \boldsymbol{a}, T) = \boldsymbol{a}. \tag{17.74b}$$

Note that $\boldsymbol{a}$ remains fixed, as we start all trajectories determining a streakline from the same initial point (e.g., the chimney does not move). A streakline can thus be generated by emitting a dye from a point over a time interval equal to the range of s, with the dye following fluid particle trajectories.

17.7.5 An analytic example of flow lines

Consider the following two-dimensional example as taken from Section 4.13 of *Aris* (1962). Let the Eulerian velocity field be given by

$$u = \frac{x}{\tau + t} \quad \text{and} \quad v = \frac{y}{\tau} \quad \text{and} \quad w = 0, \tag{17.75}$$

where $\tau > 0$ is a constant with the dimensions of time. Also write $\boldsymbol{X}(\boldsymbol{a}, T) = \boldsymbol{\varphi}(\boldsymbol{x}, T)$ for the trajectories, with $t = T$ the time coordinate.

Pathlines

Pathlines are determined by solving the trajectory equations

$$\frac{\mathrm{d}X(T)}{\mathrm{d}T} = \frac{X(T)}{\tau + T} \quad \text{and} \quad \frac{\mathrm{d}Y(T)}{\mathrm{d}T} = \frac{Y(T)}{\tau} \quad \text{and} \quad \frac{\mathrm{d}Z(T)}{\mathrm{d}T} = 0, \tag{17.76}$$

which are found to be

$$X(T) = X_0\,(1 + T/\tau) \tag{17.77a}$$

$$Y(T) = Y_0\, e^{T/\tau} \tag{17.77b}$$

$$Z(T) = Z_0, \tag{17.77c}$$

where $\boldsymbol{X}(T = 0) = \boldsymbol{X}_0$. Sample trajectories are shown in Figure 17.7 over time $T \in [0, 2]$. We can eliminate time to yield a curve in the horizontal (x, y) plane

$$y = Y_0\, e^{(x - X_0)/X_0}. \tag{17.78}$$

Streamlines

Streamlines are determined by solving the differential equations

$$\frac{\mathrm{d}X(s;T)}{\mathrm{d}s} = \frac{X(s;T)}{\tau + T} \quad \text{and} \quad \frac{\mathrm{d}Y(s;T)}{\mathrm{d}s} = \frac{Y(s;T)}{\tau} \quad \text{and} \quad \frac{\mathrm{d}Z(s;T)}{\mathrm{d}s} = 0, \tag{17.79}$$

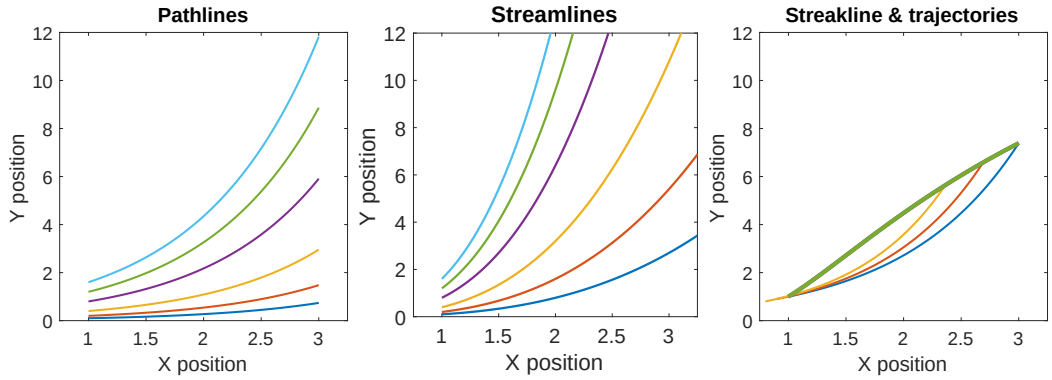

FIGURE 17.7: Left panel: sample pathlines $X(T) = X_0\,(1 + T/\tau)$ and $Y(T) = Y_0\,e^{T/\tau}$ (see equations (17.77a) and (17.77b)) during times $T \in [0, 2\tau]$. The trajectories drawn here all start at $X_0 = 1$ and set the parameter $\tau = 1$. Note that those pathlines with $X_0 = 0$ remain on the y-axis, and those with $Y_0 = 0$ remain on the x-axis. Middle panel: Sample streamlines $X(s;T) = X_0\,e^{s/(\tau+T)}$ and $Y(s;T) = Y_0\,e^{s/\tau}$ (see equations (17.80a) and (17.80b). We set $T = 2$ and let the pseudo-time run from $s \in [0, 4]$. All streamlines shown here start at $X_0 = 1$. Note that those that start with $X_0 = 0$ remain on the y-axis, and those that start with $Y_0 = 0$ remain on the x-axis. Right panel: sample analytic streakline (dark bold line) at $T = 2$ according to equations (17.83a) and (17.83b). This streakline is determined by the position of particles at $T = 2$ that pass through $(X, Y) = (1, 1)$ during times $t \in (-\infty, 2)$. We show three sample trajectories that fall onto the streakline. The longest trajectory starts at $(X, Y) = (1, 1)$ at $T = 0$, whereas the two shorter trajectories pass through $(X, Y) = (1, 1)$ at some time $0 < T < 2$. Notice the distinction between all three flow lines, which is to be expected since the flow field is unsteady.

where time, T, is a fixed parameter whereas the pseudo-time, s, is varied. Integration renders the streamlines

$$X(s;T) = X_0\,e^{s/(\tau+T)} \tag{17.80a}$$

$$Y(s;T) = Y_0\,e^{s/\tau} \tag{17.80b}$$

$$Z(s;T) = Z_0. \tag{17.80c}$$

Sample streamlines are shown in Figure 17.7. Note that we can eliminate the pseudo-time s to render a curve in the horizontal (x, y) plane

$$y = Y_0 \left[\frac{x}{X_0}\right]^{(\tau+T)/\tau} \tag{17.81a}$$

$$z = Z_0. \tag{17.81b}$$

Streaklines

For streaklines, invert the trajectory expressions (17.77a)-(17.77b) to find the material coordinates $\boldsymbol{a}(\boldsymbol{y}, s)$ in the form

$$a_1 = \frac{y_1}{1 + s/\tau} \quad \text{and} \quad a_2 = y_2\,e^{-s/\tau} \quad \text{and} \quad a_3 = y_3. \tag{17.82}$$

We next evaluate the trajectory expressions (17.77a)-(17.77b) with $\boldsymbol{a}$ as the initial positions to find the streaklines

$$X(s;\boldsymbol{a},T) = \frac{y_1\,(1 + T/\tau)}{1 + s/\tau} \tag{17.83a}$$

$$Y(s;\boldsymbol{a},T) = y_2\,e^{(T-s)/\tau} \tag{17.83b}$$

$$Z(s;\boldsymbol{a},T) = y_3. \tag{17.83c}$$

Figure 17.7 illustrates the streakline for a particular point $(X, Y) = (1, 1)$.

17.7.6 Further study

A discussion of flow lines can be found in most books on fluid mechanics. The presentation here borrows from Sections 4.11-4.13 of *Aris* (1962), Section 3.3 of *Kundu et al.* (2016), and online lecture notes on fluid kinematics from Professor McIntyre of Cambridge University.

17.8 Exercises

EXERCISE 17.1: FLUID VELOCITY AND ACCELERATION DERIVED FROM A TRAJECTORY
This exercise is based on Q1.6 of *Johnson* (1997). As described in this chapter, Eulerian kinematics focuses on the velocity field, $\boldsymbol{v}(\boldsymbol{x}, t)$, which provides the fluid velocity as a function of the space and time. The complementary Lagrangian kinematics is based on describing fluid motion from the perspective of a moving fluid particle labeled by a material coordinate, $\boldsymbol{a}$. For definiteness, let the material coordinate be the position of a fluid particle at some arbitrary initial time, $\boldsymbol{a} = \boldsymbol{X}_0$.

Consider the following expression for the position of a fluid particle

$$\boldsymbol{X}(T) = X(T)\,\hat{\boldsymbol{x}} + Y(T)\,\hat{\boldsymbol{y}} + Z(T)\,\hat{\boldsymbol{z}} = X_0\,\mathrm{e}^{2\,(T/\tau)^2}\,\hat{\boldsymbol{x}} + Y_0\,\mathrm{e}^{-(T/\tau)^2}\,\hat{\boldsymbol{y}} + Z_0\,\mathrm{e}^{-(T/\tau)^2}\,\hat{\boldsymbol{z}}, \quad (17.84)$$

where τ is a constant with dimensions of time.

(a) Derive an expression for the Lagrangian velocity (i.e., velocity of the fluid particle), $\boldsymbol{V} = \dot{\boldsymbol{X}} = \mathrm{d}\boldsymbol{X}/\mathrm{d}T$.

(b) Derive an expression for the Eulerian velocity field, $\boldsymbol{v}(\boldsymbol{x}, t)$.

(c) Derive an expression for the Lagrangian acceleration, $\boldsymbol{A} = \dot{\boldsymbol{V}} = \mathrm{d}\boldsymbol{V}/\mathrm{d}T$. To simplify the expression, write $\boldsymbol{A}$ in terms of $\boldsymbol{V}$, $\dot{X}$, $\dot{Y}$, and $\dot{Z}$.

(d) Derive an expression for the Eulerian acceleration, which is given by the material time derivative of the Eulerian velocity field,

$$\frac{\mathrm{D}\boldsymbol{v}}{\mathrm{D}t} = (\partial_t + \boldsymbol{v}\cdot\nabla)\,\boldsymbol{v}. \quad (17.85)$$

(e) Show that the Lagrangian acceleration and Eulerian acceleration are the same when evaluated at the same point in space and time,

$$\frac{\mathrm{D}\boldsymbol{v}}{\mathrm{D}t} = \boldsymbol{A} \quad \text{if } t = T \text{ and } \boldsymbol{x} = \boldsymbol{X}(T). \quad (17.86)$$

EXERCISE 17.2: FLUID VELOCITY AND ACCELERATION DERIVED FROM A TRAJECTORY
This exercise is just like Exercise 17.1, only with a different expression for the trajectory, and here considering only a single space dimension. Following the example in Section 17.4.6, consider the one-dimensional fluid particle trajectory

$$\boldsymbol{X}(T) = \hat{\boldsymbol{x}}\,X(T) = \hat{\boldsymbol{x}}\left[k\,(T - t_0)^2 + x_0^3\right]^{1/3}, \quad (17.87)$$

where k is a constant with dimensions $\mathrm{L}^3\ \mathrm{T}^{-2}$, x_0 is the particle position at time t_0, and $\hat{\boldsymbol{x}}$ is the fixed Cartesian unit vector.

(a) Determine the velocity of the fluid particle.

(b) Determine the acceleration of the fluid particle.

(c) Determine the Eulerian velocity field.

(d) Determine the Eulerian acceleration field and show that it equals to the particle acceleration when evaluated at the spatial point, $\boldsymbol{x} = \boldsymbol{X}(T)$.

EXERCISE 17.3: STREAMLINES AND PATHLINES
Consider the spatially constant oscillating horizontal velocity field

$$\boldsymbol{u} = U\,[\hat{\boldsymbol{x}}\cos(\omega\,t) + \hat{\boldsymbol{y}}\sin(\omega\,t)], \tag{17.88}$$

where U is the constant flow speed and ω is the angular frequency of the oscillating flow. In this example we determine the streamlines and pathlines, which serves to clearly illustrate their distinction for this spatially constant time dependent flow.

(a) Derive the equation $y = y(x)$ for the streamline that passes through the origin at time $t = 0$.

(b) Derive the equation for the pathline that passes through the origin at time $t = 0$. Write the equation in a form that eliminates time, so to reveal the geometric shape of the pathlines.

EXERCISE 17.4: MATERIAL EVOLUTION OF THE PARTIAL DERIVATIVE OF A FUNCTION
In this exercise we establish some properties of the material time derivative operator when acting on spatial derivatives of a scalar field.

(a) If a scalar field Π is materially constant, prove that the material evolution of its spatial derivative is given by

$$\frac{\mathrm{D}(\partial_i\Pi)}{\mathrm{D}t} = -\partial_i\boldsymbol{v}\cdot\nabla\Pi. \tag{17.89}$$

For example, if $\mathrm{D}\Pi/\mathrm{D}t = 0$, then the zonal partial derivative $\partial_x\Pi$ has a material time derivative given by

$$\frac{\mathrm{D}(\partial\Pi/\partial x)}{\mathrm{D}t} = -\frac{\partial\boldsymbol{v}}{\partial x}\cdot\nabla\Pi. \tag{17.90}$$

(b) What is the material time derivative of $\nabla\Pi$ for the case that Π is not materially constant? Write your answer in a manner that clearly shows that the partial space derivative does not commute with the material time derivative. That is,

$$\frac{\mathrm{D}(\partial_i\Pi)}{\mathrm{D}t} \neq \partial_i\frac{\mathrm{D}\Pi}{\mathrm{D}t}. \tag{17.91}$$

Show what term appears on the right hand side to produce an equality.

Hint: Some might find it more suitable to first solve the general case. Also, use Cartesian tensors for convenience.

EXERCISE 17.5: SURFACE MOVING WITH THE FLUID
This exercise is based on Q1.5 of *Johnson* (1997). Consider a non-dimensional velocity field (all symbols are non-dimensional in this exercise)

$$\boldsymbol{v}(x,y,z,t) = t\,(2\,x\,\hat{\boldsymbol{x}} - y\,\hat{\boldsymbol{y}} - z\,\hat{\boldsymbol{z}}) \tag{17.92}$$

and a surface defined by the function

$$F(x,y,z,t) = x^2\,\mathrm{e}^{-2\,t^2} + (y^2 + 2\,z^2)\,\mathrm{e}^{t^2} = \text{constant}. \tag{17.93}$$

Show that

$$\frac{\mathrm{D}F}{\mathrm{D}t} = (\partial_t + \boldsymbol{v}\cdot\nabla)F = 0, \tag{17.94}$$

which means that the surface follows fluid particles.

EXERCISE 17.6: TRACER CONCENTRATION AND A GALILEAN TRANSFORMATION
Consider a tracer concentration written using (x,t) coordinates[14]

$$\Pi(x,t) = \Pi_0\,\mathrm{e}^{-x^2/(4\,\kappa\,t)}, \tag{17.95}$$

where Π_0 is a constant and where κ is a constant diffusivity with dimensions of $\mathrm{L}^2\ \mathrm{T}^{-1}$.

(a) Compute the material time derivative, $\mathrm{D}\Pi/\mathrm{D}t$, with an assumed zero fluid flow.

(b) Perform a Galilean boost to a reference frame moving with constant velocity, $U\,\hat{\boldsymbol{x}}$. In this frame the fluid velocity is no longer static, but is now seen to be moving. Compute the material time derivative of $\overline{\Pi}(\overline{x},\bar{t})$ in this reference frame. Hint: you should find that

$$\frac{\mathrm{D}\overline{\Pi}(\overline{x},\bar{t})}{\mathrm{D}\bar{t}} = \frac{\mathrm{D}\Pi(x,t)}{\mathrm{D}t}, \tag{17.96}$$

where (x,t) are space-time coordinates in the rest frame, $(\overline{x},\bar{t})$ are coordinates in the boosted frame, and $\overline{\Pi}(\overline{\boldsymbol{x}},\bar{t})$ is the functional representation of the tracer concentration in the boosted frame.

Hint: make use of ideas detailed in Section 17.5

EXERCISE 17.7: UNSTATED ASSUMPTION IN LUMLEY'S VIDEO
This 27-minute video on Eulerian and Lagrangian descriptions from Prof. Lumley offers a pedagogical discussion of these two perspectives on fluid motion. However, there is one unstated assumption in this video that limits the applicability of his expressions for the material time derivative. What is that assumption? Hint: read Section 17.4.7.

[14] We study tracers in Chapter 20. No prior knowledge of tracers is needed for this exercise.

Chapter 18

Flow and deformation

Motion of the matter continuum provides a *flow map* that continuously and smoothly reshapes the continuum as time evolves. In this chapter we develop an understanding of how this motion of the continuum, assumed to occur in Euclidean space, modifies geometric objects and shapes placed in the flow. The kinematics of this modification is directly connected to flow *deformation*, and we consider two methods to characterize deformation. One is based on the *motion field* that produces a *flow map* of the continuum. This method makes use of the *deformation matrix* (computed from derivatives of the flow map) that deforms material objects. The second method (which is dual to the first) is based on the *velocity gradient tensor*, which is conveniently decomposed into its symmetric component, the *strain rate tensor* (also called the *deformation rate tensor*), and its anti-symmetric component known as the *rotation* tensor.

The kinematic ideas in this chapter make extensive use of material fluid particles as introduced in Section 17.2.1. Fluid particles are mathematical points that move with the fluid flow, and there is a continuum of such particles comprising any continuous region of fluid. We do not ask questions about the number of such particles on a material object, nor do we question whether particles are created or destroyed as a material object changes its length, area, or volume. Instead, we make use of fluid particles as a conceptual construct to describe motion of the continuum, and we use their trajectories to define the Lagrangian reference frame. Point fluid particles are not approximations to molecules. Instead, they are mathematical constructs that offer a lens to view motion of the matter continuum.

As part of a study of flow kinematics, we commonly consider thought experiments by drawing an imaginary geometric object within a fluid and following the object as the fluid flows. A particularly relevant object is one whose material points follow a fluid particle trajectory. We study the kinematics of such material fluid objects by using rudimentary Lagrangian and Eulerian methods. Extra attention is given to the kinematics of two-dimensional flow due to the relative mathematical ease and the associated intuition that proves useful for more general three dimensional flows.

READER'S GUIDE FOR THIS CHAPTER

This chapter builds from the kinematics of Chapter 17, and makes extensive use of both the Eulerian and Lagrangian references frames. We assign the Latin labels i, j, k for the spatial (Eulerian) description in $\boldsymbol{x}$-space, whereas material (Lagrangian) labels use the capital letters, I, J, K for $\boldsymbol{a}$-space. Coordinates in both $\boldsymbol{x}$-space and $\boldsymbol{a}$-space sometimes assumed to be arbitrary, so that we make use of notions from general tensor analysis as per Chapters 3 and 4, with distinctions made between covariant and contravariant labels enabling the Einstein summation convention. We require tensor analysis to systematically transform between the Eulerian and Lagrangian descriptions, and we review the salient formalism in this chapter as applied to $\boldsymbol{x}$-space and $\boldsymbol{a}$-space.

Even so, at certain points we make use of Cartesian coordinates for the Eulerian space

since doing so allows for the use of familiar notions from Cartesian tensor analysis (Chapter 2) when studying how points in the flow move relative to one another. Extending certain of these kinematic concepts to general coordinates requires more mathematical apparatus than considered in this book (e.g., Lie derivatives).

References for this chapter include the text by *Salmon* (1998), who provides an accessible treatment of Eulerian and Lagrangian fluid mechanics. Chapter 4 of *Aris* (1962) treats fluid kinematics in the context of tensor analysis. Chapter 4 of *Malvern* (1969), Chapters 1 and 2 of *Tromp* (2025a), and *Tromp* (2025b) provide insightful summaries of continuum kinematics, with Eulerian (spatial) and Lagrangian (material) two of the four descriptions that have found use in continuum mechanics. The other two descriptions are the *referential description* and the *relative description*. We make some use of the referential description in Section 18.2, which is commonly used in solid mechanics.

18.1 Loose threads

- Convert Figure 18.6 into Keynote and gray shade the color.

18.2 Motion generates the flow map

The discussion in Section 17.3 is directly motivated by particle mechanics, and it serves as a useful introduction to fluid kinematics. It also serves to emphasize the primary role of particle trajectories for use in describing fluid motion through Euclidean space. In this section we provide a more formal treatment building from particle trajectories. In particular, we present a rudimentary mathematical structure framing the motion of continuum matter.

18.2.1 Defining the motion field and its flow map

The matter continuum moves through Euclidean space as Newtonain time progresses. We define the *motion field*, $\boldsymbol{\varphi}$, as the mathematical object that generates a nonlinear time dependent and invertible *flow map*, with the map between the continuous matter distribution in a reference or base state and the continuous matter distribution in a future state. That is, the motion field is the reason there is a flow map, so that the nomenclature "motion field" and "flow map" are used interchangeably in this book since they both refer to movement of the continuum.

We write the motion field or flow map as

$$\boldsymbol{x} = \boldsymbol{\varphi}(\boldsymbol{a}, T) \quad \text{and} \quad x^i = \varphi^i(\boldsymbol{a}, T) \quad \text{for} \quad i = 1, 2, 3. \tag{18.1}$$

The function, $\boldsymbol{\varphi}$, has a nonlinear dependence on the material coordinate, a^I, which labels a material point in the continuum, as well as the material time, T. The uppercase index, $I = 1, 2, 3$, is used for material coordinates. Equation (18.1) says that the spatial point, $\boldsymbol{x}$, for a fluid particle in the spatial manifold, $\mathcal{S}$, is determined once we specify the material coordinate, $\boldsymbol{a}$, and the time, $T = t$. We thus conceive of the motion of the material continuum through Euclidean space as providing the map that continuously and smoothly reshapes the material configuration. We are only concerned in this book with evolution that renders no holes or rips in the matter continuum; i.e., no discontinuities such as shocks in fluids or faults in solids.[1] Hence, the flow

[1] *Tromp* (2025a) and *Tromp* (2025b) further generalizes the motion by working fully within the context of manifolds and differential geometry, thus removing the need to conceive of the motion of particles in Euclidean space. Besides allowing for the power of differential geometry, that level of abstraction allows *Tromp* (2025a) and *Tromp* (2025b) to consider rips in matter continuum, thus opening up the formalism to treating faults and earthquakes. For the present book, we do not employ that level of abstraction since the geophysical fluid motion

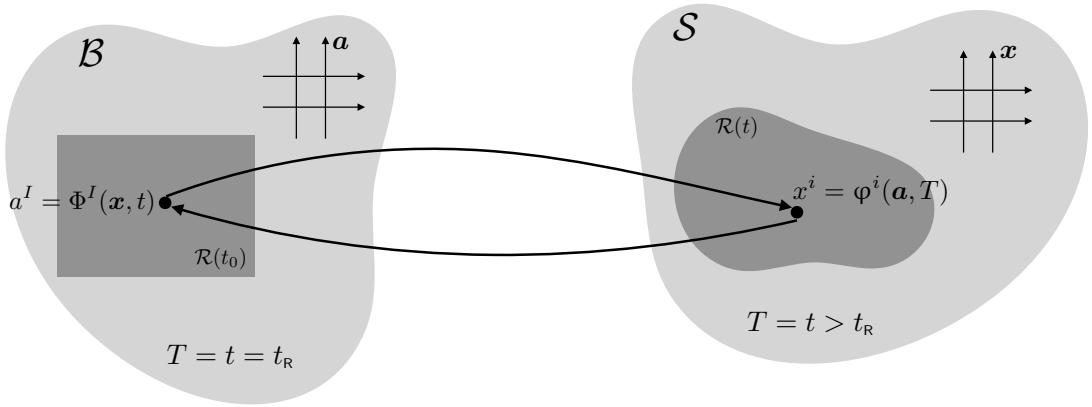

FIGURE 18.1: In the left panel, the matter continuum at reference time, $T = t_{\mathsf{R}}$, defines a reference or base manifold, $\mathcal{B}$. Each point in $\mathcal{B}$ is specified by its material (Lagrangian) coordinate, $\boldsymbol{a}$, thus defining the $\boldsymbol{a}$-space descriptions. Within the base manifold we also depict a subregion, $\mathcal{R}(t_{\mathsf{R}})$. The motion field, $\boldsymbol{\varphi}(\boldsymbol{a}, T)$, acts as a one-to-one invertible flow map that smoothly evolves the matter continuum from the base manifold, $\mathcal{B}$, to the deformed or spatial manifold, $\mathcal{S}$, at $t = T > t_{\mathsf{R}}$. The motion field also maps the subregion $\mathcal{R}(t_{\mathsf{R}})$ of $\mathcal{B}$ to the subregion $\mathcal{R}(t)$ of $\mathcal{S}$. The inverse motion or inverse flow map, $\boldsymbol{\Phi}$, defines the one-to-one inverse flow map going from $\mathcal{S}$ to $\mathcal{B}$. A point on the spatial manifold is specified by its point in space, $\boldsymbol{x}$, thus providing the Eulerian $\boldsymbol{x}$-space description. We here depict the $\boldsymbol{a}$-space and $\boldsymbol{x}$-space coordinates as orthogonal Cartesian coordinates, yet they can be arbitrary coordinates by making use of the general tensor formalism in Chapters 3 and 4. Indeed, it is common for the Lagrangian coordinates to have arbitrary physical dimensions (i.e., not length), as discussed in Section 17.3.2.

map (18.1) is smooth, one-to-one, and invertible.[2]

We encountered the idea of motion creating a flow map when studying flow lines in Section 17.7. Namely, by fixing a particular material coordinate, $\boldsymbol{a}$, and letting time progress, the flow map, $\boldsymbol{\varphi}(\boldsymbol{a}, T)$, defines a fluid particle trajectory moving through Euclidean space

$$\boldsymbol{\varphi}(\boldsymbol{a}, T) = \boldsymbol{X}(\boldsymbol{a}, T). \tag{18.2}$$

Given this identity, we could have maintained the notation for trajectories introduced in Section 17.3, rather than introduce the new symbol, $\boldsymbol{\varphi}$. Indeed, in many cases in this book it is convenient to use the notation $\boldsymbol{X}(\boldsymbol{a}, T)$ to connect to trajectories of point particles moving through Euclidean space, as studied in Part II of this book. However, the $\boldsymbol{\varphi}$ notation is more general, allowing for the consideration of motion without presuming it is embedded within Euclidean space. Even though such generalities are not essential for this book, it is of use for more general treatments of continuum mechanics (e.g., *Tromp* (2025a) and *Tromp* (2025b)). Furthermore, it is effective nomenclature for our use when interpreting the flow map as a coordinate transformations between $\boldsymbol{a}$-space and $\boldsymbol{x}$-space, as we do in Section 18.3.2.

As depicted in Figure 18.1, the $\boldsymbol{a}$-space coordinates can be specified by the Cartesian positions of the fluid particles at a specified reference time, $T = t_{\mathsf{R}}$. Indeed, this choice is common in the continuum mechanics literature. The continuum matter deforms as it evolves according to the motion field, $\boldsymbol{\varphi}(\boldsymbol{a}, T)$, with this deformation typically leading to rather complex coordinate lines. Hence, a coordinate description of fluid motion using Lagrangian kinematics necessarily involves features of the general tensor analysis from Chapters 3 and 4.

of concern this book concerns the smooth motion of fluid particles through Euclidean space.

[2]Invertibility of the flow map holds even in the presence of irreversible mixing. The reason is that mixing retains the notion of distinct fluid particles, even though the mixing of fluid particles generates entropy.

18.2.2 Depicting the motion and its inverse

In Figure 18.1 we depict the motion field and the corresponding flow map of the matter continuum. The base or reference state of the continuum is referred to as $\mathcal{B}$, and it defines a smooth *reference manifold* or *base manifold* on which we can perform differential calculus (i.e., there are no rips or discontinuities in the fluid continuum). Each point of $\mathcal{B}$ is specified by a value for the material (also Lagrangian) coordinate, $\boldsymbol{a}$. As time progresses, the motion field smoothly and invertibly maps each point of $\mathcal{B}$ to a deformed state of the matter continuum. A point in the deformed fluid state is described by a point in the manifold, $\mathcal{S}$. We measure a position on $\mathcal{S}$ using the spatial (or Eulerian) coordinates, x^i, according to the flow map (18.1), thus motivating the name *spatial manifold* for $\mathcal{S}$.

Since the flow map provided by the motion is invertible, there is an inverse flow map, $\boldsymbol{\Phi}$. The inverse flow map takes each point occupied by fluid in the spatial manifold, $\mathcal{S}$, to a unique point on the reference manifold, $\mathcal{B}$. That is, given the Eulerian position of a fluid particle, $\boldsymbol{x}$, we have a unique material coordinate $\boldsymbol{a}$, which is specified by the inverse flow map

$$\boldsymbol{a} = \boldsymbol{\Phi}(\boldsymbol{x}, t) \quad \text{and} \quad a^I = \Phi^I(\boldsymbol{x}, t). \tag{18.3}$$

The invertible nature of the flow map means that a fluid particle trajectory does not split, nor do two trajectories occupy the same point at the same time. We acknowledge that fluid particle trajectories generally become increasingly complex in turbulent flow (indeed, even for some laminar flows). Consequently, the Lagrangian description is less convenient after a certain time has elapsed, thus motivating the reinitialization of fluid particle trajectories for practical calculations. Even so, as long as trajectories do not split or merge, the trajectories are well defined in principle, and so is the corresponding Lagrangian formulation.

18.2.3 Comments

We mostly interpret the flow map as a coordinate transformation, as discussed in Section 18.3.2. Even so, it is useful to appreciate the complementary view in terms of motion as a flow map between distinct manifolds, as presented in this section. This kinematic persepective is commonly taken in solid mechanics.

18.3 Material and spatial representations

According to the presentation in Section 18.2, we specify a point of matter on the reference (or base) manifold, $\mathcal{B}$, by providing its material coordinate, $\boldsymbol{a}$. Similarly, a point on the spatial manifold, $\mathcal{S}$, is specified by the Eulerian point in space, $\boldsymbol{x}$. The motion field generates a one-to-one and invertible flow map, $\boldsymbol{\varphi}(\boldsymbol{a}, T)$, which affords the ability to move seamlessly between the base manifold and the spatial manifold. For example, by specifying the material point, $\boldsymbol{a}$, on $\mathcal{B}$, then that information uniquely specifies the fluid particle's spatial location, $(\boldsymbol{x}, t)$, on $\mathcal{S}$, according to

$$\boldsymbol{x} = \boldsymbol{\varphi}(\boldsymbol{a}, T) \quad \text{and} \quad t = T. \tag{18.4}$$

Alternatively, by specifying the spatial point of a fluid particle, $(\boldsymbol{x}, t)$, on $\mathcal{S}$, then we uniquely specify the material point $(\boldsymbol{a}, T)$ on $\mathcal{B}$, via the inverse motion

$$\boldsymbol{a} = \boldsymbol{\Phi}(\boldsymbol{x}, t) \quad \text{and} \quad T = t. \tag{18.5}$$

18.3.1 Notation

We write $\mathrm{d}\boldsymbol{x}$ for the differential increment between two Eulerian positions in $\boldsymbol{x}$-space. Likewise, $\mathrm{d}\boldsymbol{a}$ is the differential increment between two positions in $\boldsymbol{a}$-space. Finally, we write $\delta\boldsymbol{x}$ for the

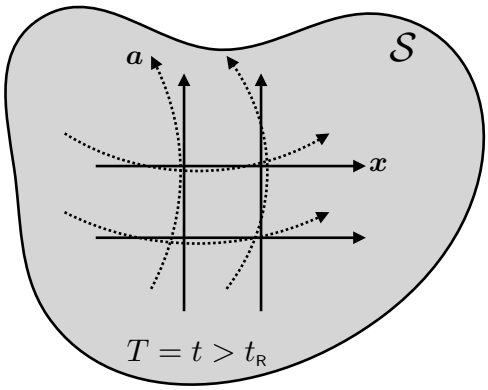

FIGURE 18.2: Two coordinate systems used to represent the spatial manifold, $\mathcal{S}$. The first is the spatial (Eulerian) representation, $\boldsymbol{x}$, which is fixed in space. The second is the material (Lagrangian) representation, $\boldsymbol{a}$, which is fixed on material particles. When projected onto the spatial manifold, the lines of constant $\boldsymbol{a}$ are deformed as the fluid evolves, although they are typically assumed orthogonal on the base manifold as in Figure 18.1. The transformation between these two sets of coordinates is facilitated by the motion field, $\boldsymbol{\varphi}$, as given by equation (18.1). The coordinate transformation perspective complements the mapping perspective from Figure 18.1.

differential distance in $\boldsymbol{x}$-space between two material fluid particles specified by $\boldsymbol{a}$ and $\mathrm{d}\boldsymbol{a}$.

18.3.2 The flow map as a coordinate transformation

Equation (18.4) has the appearance of an invertible coordinate transformation between spatial and material coordinates. However, the coordinate transformations studied in Chapter 4 concern two alternative coordinate representations for points on a single manifold, and yet, as illustrated by Figure 18.1, equation (18.4) provides a flow map between two points on two manifolds, with one point on the reference manifold and one on the spatial manifold. Even so, the motion field provides a smooth, one-to-one and invertible mapping between these points. Consequently, we are afforded an alternative interpretation of the motion field, namely as a coordinate transformation via equation (18.4). That is, the flow map defines a *point transformation* between a spatial representation of a fluid particle (fixed laboratory frame; Eulerian) and a material representation of the same fluid particle (moving reference frame co-moving with fluid particles; Lagrangian).[3] We make use of the general tensor analysis from Chapter 4 to formalize the mathematical transformation between the two coordinates and their respective representations of fluid properties, and depict this point transformation in Figure 18.2.

The velocity of a fluid particle is given by the time derivative of the flow map

$$\boldsymbol{v}^{\text{L}}(\boldsymbol{a}, T) = \partial_T \boldsymbol{\varphi}(\boldsymbol{a}, T) \iff (v^{\text{L}})^i = \partial_T \varphi^i, \tag{18.6}$$

where the L superscript indicates that the velocity is written as a function of the material coordinates and time.[4] This expression for the fluid particle velocity equals to the Eulerian velocity field as sampled along the fluid particle trajectory

$$\boldsymbol{v}^{\text{L}}(\boldsymbol{a}, T) = \boldsymbol{v}[\boldsymbol{x} = \boldsymbol{\varphi}(\boldsymbol{a}, T), t = T]. \tag{18.7}$$

Equivalently, we can produce the Eulerian expression for the velocity by inverting the expression for the flow map, $\boldsymbol{\varphi}(\boldsymbol{a}, T)$, as per equation (18.5) to obtain the material coordinate, $\boldsymbol{a}(\boldsymbol{x}, t)$, thus rendering

$$\boldsymbol{v}^{\text{L}}(\boldsymbol{a}, T) = \boldsymbol{v}^{\text{L}}[\boldsymbol{a}(\boldsymbol{x}, t), T]. \tag{18.8}$$

[3] The point transformation perspective follows from Section 4.11 of *Aris* (1962) and is commonly considered in fluid mechanics.

[4] The L superscript is *not* a tensor index.

The right hand expression is defined at all spatial points, $\boldsymbol{x}$, so that we can define the Eulerian velocity field according to

$$\boldsymbol{v}(\boldsymbol{x},t) = \boldsymbol{v}^{\mathsf{L}}[\boldsymbol{a}(\boldsymbol{x},t), T=t]. \tag{18.9}$$

In the converse situation we have the Eulerian velocity field, $\boldsymbol{v}(\boldsymbol{x},t)$ at all points in space. The flow map, and hence the Lagrangian description, can be determined by integrating the first order ordinary differential equation

$$\partial_T \boldsymbol{\varphi}(\boldsymbol{a},T) = \boldsymbol{v}[\boldsymbol{x}=\boldsymbol{\varphi}(\boldsymbol{a},T),t]. \tag{18.10}$$

This is a nonlinear differential equation since the flow map appears on the left hand side as its time derivative, as well as within the argument to the velocity on the right hand side.

18.3.3 Material time derivative of a scalar field

To further help understand the role of the motion field, as well as the time derivative following a fluid particle trajectory, consider a scalar fluid property, Π, and measure it along the fluid particle trajectory

$$\Pi^{\mathsf{L}}(\boldsymbol{a},T) = \text{property } \Pi \text{ following the trajectory } \boldsymbol{\varphi}(\boldsymbol{a},T). \tag{18.11}$$

As a complement, measuring the property at a spatial point renders the Eulerian representation[5]

$$\Pi^{\mathsf{E}}(\boldsymbol{x},t) = \text{property } \Pi \text{ at a spatial point } \boldsymbol{x} \text{ at time } t. \tag{18.12}$$

Since the arguments differ, the functions Π^{L} and Π^{E} are generally distinct. The Eulerian and Lagrangian values for the fluid property agree when they are evaluated at the same point in space and time, hence

$$\Pi^{\mathsf{L}}(\boldsymbol{a},T) = \Pi^{\mathsf{E}}[\boldsymbol{x}=\boldsymbol{\varphi}(\boldsymbol{a},T), t=T]. \tag{18.13}$$

The time derivative of $\Pi^{\mathsf{L}}(\boldsymbol{a},T)$ following the fluid particle motion is given by the partial derivative

$$\frac{\partial \Pi^{\mathsf{L}}(\boldsymbol{a},T)}{\partial T} = \quad \text{time derivative following fluid particle motion,} \tag{18.14}$$

which is computed while holding the material coordinates fixed. The chain rule renders the Eulerian expression for the same time derivative

$$\frac{\partial \Pi^{\mathsf{L}}(\boldsymbol{a},T)}{\partial T} = \frac{\partial \Pi^{\mathsf{E}}[\boldsymbol{x}=\boldsymbol{\varphi}(\boldsymbol{a},T), t=T]}{\partial T} \tag{18.15a}$$

$$= \frac{\partial \Pi^{\mathsf{E}}(\boldsymbol{x},t)}{\partial t} + \frac{\partial \boldsymbol{\varphi}(\boldsymbol{a},T)}{\partial T} \cdot \nabla \Pi^{\mathsf{E}}(\boldsymbol{x},t) \tag{18.15b}$$

$$= (\partial_t + \boldsymbol{v}^{\mathsf{L}}(\boldsymbol{a},T)\cdot\nabla)\Pi^{\mathsf{E}}(\boldsymbol{x},t), \tag{18.15c}$$

$$= (\partial_t + \boldsymbol{v}^{\mathsf{E}}(\boldsymbol{x},t)\cdot\nabla)\Pi^{\mathsf{E}}(\boldsymbol{x},t). \tag{18.15d}$$

In equation (18.15c) we introduced the Lagrangian expression for the fluid particle velocity from Section 18.3.2

$$\boldsymbol{v}^{\mathsf{L}}(\boldsymbol{a},T) \equiv \boldsymbol{v}[\boldsymbol{x}=\boldsymbol{\varphi}(\boldsymbol{a},T), t=T] = \partial_T \boldsymbol{\varphi}(\boldsymbol{a},T), \tag{18.16}$$

where, again, the time derivative of the motion field is computed while holding the material coordinate, $\boldsymbol{a}$, fixed. For equation (18.15d) we equated the Lagrangian and Eulerian expressions for the particle velocity when they are evaluated at the same point in space and time, as given

[5] In most occasions throughout this book, we do not expose the E superscript to denote an Eulerian expression for a fluid property. But for the present purposes it is useful to be somewhat pedantic in order to clearly distinguish the two functional representations of the scalar property, Π.

by equation (17.67). Equation (18.15d) accords with equation (17.11) derived using distinct methods.

18.3.4 The flow map is a function, not a tensor

The flow map is a function that assigns the position in space for fluid particles at a particular time instance. As such, the flow map generalizes to the continuum the notion of position for a continuum of point fluid particles. In Section 1.3.2 we emphasized that the point particle position is not a tensor, motivating us to eschew the term "position vector." Likewise, the flow map is not a tensor (even though it is written with the boldface notation), which is why we eschew the term "flow map vector" or "motion vector field." Even so, as for the position, the time derivative of the flow map defines a tensor, namely the velocity of the flow.

18.4 The deformation matrix as a transformation matrix

In an analysis of fluid flow, we make routine use of the spatial coordinates ($\boldsymbol{x}$-space) of an Eulerian description and material coordinates ($\boldsymbol{a}$-space) of a Lagrangian description. Following the interpretation in Section 18.3.2 of the flow map as a coordinate transformation, we here introduce the *transformation matrix* that facilitates the coordinate transformation of physical objects between Eulerian and Lagrangian descriptions. Since the flow map is invertible, so too is the transformation matrix, which means that its determinant, the *Jacobian*, remains nonzero and hence is single signed. We refer to the transformation matrix as the *deformation matrix*, for reasons motivated below.

18.4.1 The deformation (transformation) matrix $F^i{}_I$

We introduced the transformation matrix in Section 4.1.4 for coordinate transformations. We here write the transformation matrix as the matrix of partial derivatives of the flow map and organize the elements to this matrix according to the following convention

$$F^i{}_I = \frac{\partial \varphi^i}{\partial a^I} \equiv \begin{bmatrix} \partial\varphi^1/\partial a^1 & \partial\varphi^1/\partial a^2 & \partial\varphi^1/\partial a^3 \\ \partial\varphi^2/\partial a^1 & \partial\varphi^2/\partial a^2 & \partial\varphi^2/\partial a^3 \\ \partial\varphi^3/\partial a^1 & \partial\varphi^3/\partial a^2 & \partial\varphi^3/\partial a^3 \end{bmatrix}. \tag{18.17}$$

The upper Eulerian label, i, denotes the row and the lower material label, I, is the column. The transformation matrix, $F^i{}_I$, provides a means to measure how trajectories are deformed by the flow. Namely, each element of $F^i{}_I$ measures how much the i-component of a fluid particle trajectory is modified when altering the I-component of the material coordinate. *Malvern* (1969) refers to $F^i{}_I$ as a two-point tensor, given that it connects points in $\boldsymbol{x}$-space to points in $\boldsymbol{a}$-space as per Figure 18.1. However, as discussed in Section 4.1.4, the transformation matrix is *not* a tensor, so we do not refer to $F^i{}_I$ as a tensor.[6] Rather, we refer to the transformation matrix, $F^i{}_I$, as the *deformation matrix* in deference to its role as the transformation matrix between spatial and material coordinates as per Figure 18.2, and given its measure of how trajectories are deformed by the flow of matter.

In Section 18.6 we study how the deformation matrix leads to the evolution of the vector connecting two material points in the fluid. As a preface to that discussion, consider the special case where the material coordinate is the reference spatial position. In this case, the partial derivatives measure how particle trajectories are modified when altering the reference position of the particles. If the fluid has no deformation, then particle trajectories remain unaffected if

[6] In Section 1.10.7, we discuss the distinction between a second order tensor and a matrix.

changing the material coordinate (i.e., the reference position), in which case the deformation matrix is the identity tensor

$$F^i{}_I = \delta^i{}_I \quad \text{if there is no flow deformation.} \tag{18.18}$$

Generally each component of the deformation matrix is nonzero so that trajectories are deformed by the flow and as such they are dependent on the reference position.

18.4.2 The inverse deformation matrix $F^I{}_i \equiv (F^{-1})^I{}_i$

Since the transformation between $\boldsymbol{a}$-space and $\boldsymbol{x}$-space is invertible, we sometimes have occasion to consider the inverse transformation matrix, which we write as

$$F^I{}_i \equiv (F^{-1})^I{}_i = \frac{\partial \Phi^I}{\partial x^i} \equiv \begin{bmatrix} \partial\Phi^1/\partial x^1 & \partial\Phi^1/\partial x^2 & \partial\Phi^1/\partial x^3 \\ \partial\Phi^2/\partial x^1 & \partial\Phi^2/\partial x^2 & \partial\Phi^2/\partial x^3 \\ \partial\Phi^3/\partial x^1 & \partial\Phi^3/\partial x^2 & \partial\Phi^3/\partial x^3 \end{bmatrix}, \tag{18.19}$$

where $a^I = \Phi^I(\boldsymbol{x}, t)$ defines the mapping from $\boldsymbol{x}$-space to $\boldsymbol{a}$-space according to equation (18.3). As the inverse matrix, we are afforded the identities

$$F^I{}_i \, F^i{}_J = \delta^I{}_J \quad \text{and} \quad F^I{}_i \, F^j{}_I = \delta^j{}_i. \tag{18.20}$$

18.4.3 A terse notation for the deformation matrix and its inverse

The deformation appears throughout our study of fluid mechanics given its role as the transformation matrix between material and position coordinates. Here we summarize the notation

$$F^i{}_I = \frac{\partial \varphi^i(\boldsymbol{a}, T)}{\partial a^I} = \frac{\partial x^i}{\partial a^I} \qquad \text{deformation matrix} \tag{18.21a}$$

$$F^I{}_i = (F^{-1})^I{}_i = \frac{\partial \Phi^I(\boldsymbol{x}, t)}{\partial x^i} = \frac{\partial a^I}{\partial x^i} \quad \text{inverse deformation matrix.} \tag{18.21b}$$

The final equality in each line introduces a shorthand whose definition is given by the preceeding equality. This shorthand is suited to manipulations with the deformation matrix and its determinant. Furthermore, recall that use of the symbol x^i does not imply that the Eulerian coordinates are Cartesian.

18.4.4 Jacobian determinant of the deformation matrix $F^i{}_I$

The Jacobian determinant of the deformation matrix can be written in either of the following ways

$$\det(F^i{}_I) = \frac{\partial \boldsymbol{x}}{\partial \boldsymbol{a}} = \frac{\partial \boldsymbol{\varphi}}{\partial \boldsymbol{a}} = \det \begin{bmatrix} \partial\varphi^1/\partial a^1 & \partial\varphi^1/\partial a^2 & \partial\varphi^1/\partial a^3 \\ \partial\varphi^2/\partial a^1 & \partial\varphi^2/\partial a^2 & \partial\varphi^2/\partial a^3 \\ \partial\varphi^3/\partial a^1 & \partial\varphi^3/\partial a^2 & \partial\varphi^3/\partial a^3 \end{bmatrix}. \tag{18.22}$$

The notation $\partial\boldsymbol{\varphi}/\partial\boldsymbol{a} = \partial\boldsymbol{x}/\partial\boldsymbol{a}$ offers a useful means to distinguish between the determinant of the deformation (18.17), versus the determinant of the inverse deformation matrix, written as

$$\det(F^I{}_i) = \frac{\partial \boldsymbol{a}}{\partial \boldsymbol{x}} = \frac{\partial \boldsymbol{\Phi}}{\partial \boldsymbol{x}} = \det \begin{bmatrix} \partial\Phi^1/\partial x^1 & \partial\Phi^1/\partial x^2 & \partial\Phi^1/\partial x^3 \\ \partial\Phi^2/\partial x^1 & \partial\Phi^2/\partial x^2 & \partial\Phi^2/\partial x^3 \\ \partial\Phi^3/\partial x^1 & \partial\Phi^3/\partial x^2 & \partial\Phi^3/\partial x^3 \end{bmatrix}. \tag{18.23}$$

The Jacobian is single-signed since the mapping between $\boldsymbol{a}$-space and $\boldsymbol{x}$-space is one-to-one invertible.

18.4.5 A discrete algorithm for the deformation matrix

To help further understanding of the deformation matrix (18.17), we here sketch an algorithm for its discrete approximation. For this purpose, consider two-dimensional flow and write the trajectory of a particular fluid particle using Cartesian coordinates

$$\boldsymbol{X}(T) = X^1(T)\,\hat{\boldsymbol{x}} + X^2(T)\,\hat{\boldsymbol{y}}, \tag{18.24}$$

and use a Cartesian representation for the corresponding material coordinate

$$\boldsymbol{a} = a^1\,\hat{\boldsymbol{x}} + a^2\,\hat{\boldsymbol{y}}. \tag{18.25}$$

Now lay down a two-dimensional lattice with discrete indices (e, f) for each of the nodal points (grid points) on the lattice, and with corresponding spatial coordinates

$$\boldsymbol{x}(e, f) = x(e, f)\,\hat{\boldsymbol{x}} + y(e, f)\,\hat{\boldsymbol{y}}. \tag{18.26}$$

This lattice discretizes the two-dimensional space and so provides a discrete approximation to the Eulerian reference frame. Initialize fluid particles at each of the lattice grid points,

$$\boldsymbol{X}(e, f; T = 0) = \boldsymbol{x}(e, f) = \boldsymbol{a}(e, f), \tag{18.27}$$

with the discrete material coordinates defined by the initial positions. Then time step the trajectories using the velocity field to compute the particle pathlines, $\boldsymbol{X}[\boldsymbol{a}(e, f); T]$, as illustrated in Figure 18.3. At any particular time, the Eulerian position of a fluid particle is found by interpolating from the lattice grid points. Setting the material coordinates equal to the initial position then leads to the finite difference approximation to the deformation matrix

$$F^i{}_I = \begin{bmatrix} F^1{}_1 & F^1{}_2 \\ F^2{}_1 & F^2{}_2 \end{bmatrix} \approx \begin{bmatrix} \frac{X^1(e+1,f;T)-X^1(e-1,f;T)}{X^1(e+1,f;0)-X^1(e-1,f;0)} & \frac{X^1(e,f+1;T)-X^1(e,f-1;T)}{X^2(e,f+1;0)-X^2(e,f-1;0)} \\ \frac{X^2(e+1,f;T)-X^2(e-1,f;T)}{X^1(e+1,f;0)-X^1(e-1,f;0)} & \frac{X^2(e,f+1;T)-X^2(e,f-1;T)}{X^2(e,f+1;0)-X^2(e,f-1;0)} \end{bmatrix}. \tag{18.28}$$

If the grid is regular in both directions, then the initial positions have a separation, Δ, given by the grid spacing so that

$$F^i{}_I \approx \frac{1}{2\Delta} \begin{bmatrix} X^1(e+1, f; T) - X^1(e-1, f; T) & X^1(e, f+1; T) - X^1(e, f-1; T) \\ X^2(e+1, f; T) - X^2(e-1, f; T) & X^2(e, f+1; T) - X^2(e, f-1; T) \end{bmatrix}. \tag{18.29}$$

This expression illustrates how the deformation matrix provides a measure of trajectory spreading as fluid particles move away from their initial positions. As a check on the formulation, consider the case without any deformation. In this case $X^1(e, f; T) = X^1(e; T)$ and $X^2(e, f; T) = X^2(f; T)$ so that the transformation matrix is diagonal, and furthermore, $X^1(e+1; T) - X^1(e-1; T) = 2\,\Delta$ and $X^2(f + 1; T) - X^2(f - 1; T) = 2\,\Delta$, so that the transformation matrix is the identity.

18.4.6 Comments and further study

When transforming between Eulerian and Lagrangian coordinates, it is the deformation matrix,

$$F^i{}_I = \partial\varphi^i/\partial a^I, \tag{18.30}$$

and its Jacobian determinant,

$$\det(F^i{}_I) = \partial\boldsymbol{x}/\partial\boldsymbol{a} = \partial\boldsymbol{\varphi}/\partial\boldsymbol{a}, \tag{18.31}$$

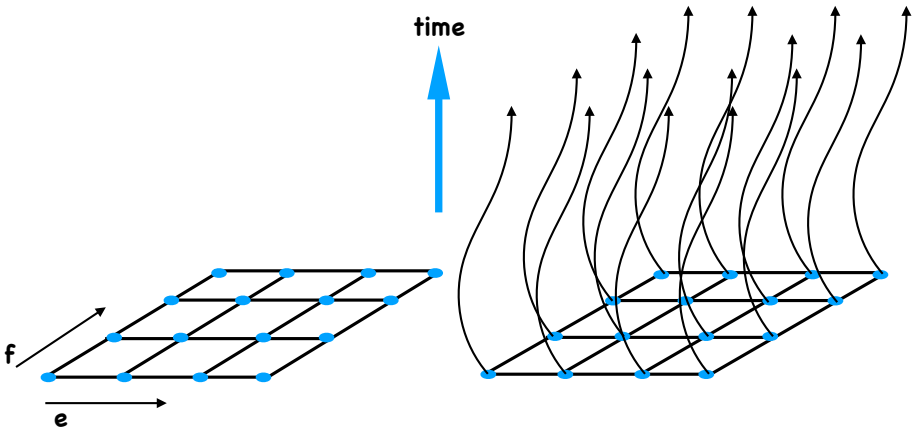

FIGURE 18.3: Illustrating the discrete algorithm of Section 18.4.5 to approximate the deformation matrix, $F^i{}_I$. The left panel shows the two-dimensional grid with nodal points defining the initial positions for fluid particles. Each position on the grid is labeled by a unique integer pair, (e, f). The initial position of each particle is taken as the material coordinate, with the discrete label (e, f) maintained by the particles as they evolve. The right panel shows the pathlines for the fluid particles after time $T > 0$. When working on a discrete grid, the position of the fluid particles is not generally at a nodal point. Hence, the position must be found by interpolating betwen the node points.

that encapsulates information about the transformation between Eulerian ($\boldsymbol{x}$-space) coordinates and Lagrangian ($\boldsymbol{a}$-space) coordinates. In particular, it is the deformation matrix (and its inverse) that transforms the representation of tensors between Eulerian coordinates and Lagrangian coordinates. The rules of coordinate transformation between Eulerian and Lagrangian representations are identical to those between any other set of coordinates (e.g., Chapters 1-4). However, for continuum mechanics the transformation between Eulerian and Lagrangian coordinates is given special treatment due to the central roles played by Eulerian and Lagrangian kinematics.

This video from the *National Committee for Fluid Mechanics Films* offers insightful visualizations to help understand Eulerian and Lagrangian fluid descriptions. This lecture from Prof. Brunton discusses fluid kinematics related to finite time Lyapunov exponents, whose calculation requires estimating the transformation matrix in Section 18.4.5 along with its eigenvalues and eigenvectors.

18.5 The metric tensor

Throughout this book we are concerned with the motion of continuum matter through Euclidean space. Euclidean space is endowed with the Kronecker metric as a means to measure the distance between points in space. When using Cartesian coordinates to describe Euclidean space, we can make use of Cartesian tensor analysis as detailed in Chapters 1 and 2. However, for fluid mechanics we are interested in a variety of coordinates, both for Eulerian and Lagrangian descriptions. In particular, material coordinates used for the Lagrangian description follow fluid particles. As such, these coordinates deform with the flow and so cannot remain Cartesian even if initialized as Cartesian. Consequently, we require general tensor analysis as detailed in Chapters 3 and 4. Having introduced the deformation matrix as the transformation matrix between $\boldsymbol{x}$-space and $\boldsymbol{a}$-space, we here introduce the metric tensor, $\mathbb{g}$, and its representations using Eulerian and Lagrangian coordinates. The discussion here specializes the more general presentation provided in Section 4.1.

18.5.1 Representing the metric tensor with $\boldsymbol{x}$-coordinates

Consider two very close points in Euclidean space as represented by arbitrary Eulerian coordinates,[7] x^a and $x^a + \mathrm{d}x^a$. The squared arc-distance between these points is given by

$$\mathrm{d}s^2 = \mathfrak{g}_{ij}\,\mathrm{d}x^i\,\mathrm{d}x^j, \tag{18.32}$$

with $\mathfrak{g}_{ij}$ the components to the metric tensor. Invertible transformations between two sets of arbitrary Eulerian coordinates,

$$\overline{\boldsymbol{x}} = \overline{\boldsymbol{x}}(\boldsymbol{x}) \quad \text{or component-wise} \quad x^{\overline{i}} = x^{\overline{i}}(x^i), \tag{18.33}$$

are facilitated by the transformation matrix built from the partial derivatives of the coordinate transformation. For example, the metric tensor transforms as a second order covariant tensor

$$\mathfrak{g}_{\overline{ij}} = \mathfrak{g}_{ij}\,\frac{\partial x^i}{\partial x^{\overline{i}}}\,\frac{\partial x^j}{\partial x^{\overline{j}}}, \tag{18.34}$$

which has an inverse transformation

$$\mathfrak{g}_{ij} = \mathfrak{g}_{\overline{ij}}\,\frac{\partial x^{\overline{i}}}{\partial x^i}\,\frac{\partial x^{\overline{j}}}{\partial x^j}. \tag{18.35}$$

The Eulerian coordinates are independent of time, t. Consequently, the metric tensor represented using Eulerian coordinates is time independent

$$\partial_t \mathfrak{g}_{ij} = 0 \Longrightarrow \mathfrak{g}_{ij} = \mathfrak{g}_{ij}(\boldsymbol{x}). \tag{18.36}$$

Note that if the coordinates, x^i, are Cartesian, then the Euclidean space metric tensor is represented by the Kronecker or unit tensor

$$\mathfrak{g}_{ij} = \delta_{ij} \quad \text{Euclidean space with Cartesian coordinates.} \tag{18.37}$$

18.5.2 Representing the metric tensor with $\boldsymbol{a}$-coordinates

In a directly analogous fashion to the transformation (18.34) between two Eulerian coordinates, we use the deformation matrix from Section 18.4.1 to transform the metric tensor from general Eulerian coordinates to general Lagrangian coordinates via

$$\mathfrak{g}_{IJ} = \mathfrak{g}_{ij}\,\frac{\partial x^i}{\partial a^I}\,\frac{\partial x^j}{\partial a^J} = \mathfrak{g}_{ij}\,F^i{}_I\,F^j{}_J. \tag{18.38}$$

This representation of the metric tensor is useful when measuring the length of material line elements[8]

$$\delta s^2 = \mathfrak{g}_{ij}\,\mathrm{d}\varphi^i\,\mathrm{d}\varphi^j = \mathfrak{g}_{ij}\,\frac{\partial \varphi^i}{\partial a^I}\,\frac{\partial \varphi^j}{\partial a^J}\,\mathrm{d}a^I\,\mathrm{d}a^J = \mathfrak{g}_{ij}\,F^i{}_I\,F^j{}_J\,\mathrm{d}a^I\,\mathrm{d}a^J = \mathfrak{g}_{IJ}\,\mathrm{d}a^I\,\mathrm{d}a^J. \tag{18.39}$$

This expression is directly analogous to the squared differential length (18.32) found in $\boldsymbol{x}$-space. Although the Eulerian representation of the metric tensor is time independent as per equation (18.36), the Lagrangian representation is time dependent due to the time dependence of the deformation matrix, so that

$$\mathfrak{g}_{IJ} = \mathfrak{g}_{IJ}(\boldsymbol{a}, T). \tag{18.40}$$

[7] We here use x^a as any arbitrary Eulerian coordinates, either Cartesian or more general.

[8] To help understand equation (18.39), it can be useful to be reminded of the notation conventions summarized in Sections 18.3.1, 18.4.3, and 18.4.4.

When the Eulerian coordinates are Cartesian, so that $g_{ij} = \delta_{ij}$, then the Lagrangian form of the metric tensor is known as *Cauchy-Green strain rate* tensor

$$\mathcal{g}_{IJ} = F^i{}_I \, F^j{}_J \, \delta_{ij} \quad \text{Cauchy-Green strain tensor.} \tag{18.41}$$

Note that in Section 1.6 of *Tromp* (2025a), $\mathcal{g}_{IJ}$ in equation (18.41) is referred to as the *right Cauchy-Green deformation rate tensor*, which is the term also used in *Malvern* (1969). We prefer the term "strain" rather than "deformation" to help reduce confusion with the deformation matrix, $F^i{}_I$.

18.5.3 Exposing the functional dependencies

In equation (18.40) we noted that the metric tensor represented using Lagrangian coordinates is seen as a function of $(\boldsymbol{a}, T)$. Likewise, the metric tensor represented using Eulerian coordinates is written in terms of the Eulerian coordinates, $g_{ij}(\boldsymbol{x})$. Written in terms of their transformations we have

$$g_{ij}(\boldsymbol{x}) = F^I{}_i(\boldsymbol{x}, t) \, F^J{}_j(\boldsymbol{x}, t) \, g_{IJ}(\boldsymbol{a} = \Phi(\boldsymbol{x}, t), T = t) \tag{18.42a}$$

$$g_{IJ}(\boldsymbol{a}, T) = F^i{}_I(\boldsymbol{a}, T) \, F^j{}_J(\boldsymbol{a}, T) \, g_{ij}(\boldsymbol{x} = \varphi(\boldsymbol{a}, T)). \tag{18.42b}$$

In these equations we inserted the motion field, $\varphi(\boldsymbol{a}, T)$, and its inverse, $\Phi(\boldsymbol{x}, t)$, when written on the right hand sides to these equations.

As noted in Section 18.5.1, the Eulerian representation of the metric tensor has no dependence on the Eulerian time, t. In contrast, the Lagrangian representation is generally a function of Lagrangian time, T. This distinction becomes less clear, however, when using coordinates commonly used in geophysical fluid mechanics, in which the set of coordinates are neither fully Eulerian nor fully Lagrangian, with the primary example being the generalized vertical coordinates studied in Part XII of this book. In that case, we generally have a metric tensor that is time dependent, even though some of the coordinates are Eulerian.

18.5.4 Determinant of the metric tensor and deformation matrix

The determinant of the metric tensor appears in the covariant volume element derived in Section 4.5.3 and extended to Eulerian and Lagrangian coordinates in Section 18.7. Furthermore, the metric tensor is a positive-definite tensor, so that we know its determinant is positive. As a shorthand, we find it useful to introduce the following notation for the square root of the determinant as represented using Eulerian and Lagrangian coordinates

$$g^{\mathsf{E}} = \sqrt{\det[\mathcal{g}(\boldsymbol{x})]} \quad \text{and} \quad g^{\mathsf{L}} = \sqrt{\det[\mathcal{g}(\boldsymbol{a}, T)]}. \tag{18.43}$$

With this notation, we take the determinant of equation (18.38) to render

$$(g^{\mathsf{L}})^2 = \det(F^i{}_I) \, \det(F^j{}_J) \, (g^{\mathsf{E}})^2 = \left[\frac{\partial \boldsymbol{x}}{\partial \boldsymbol{a}}\right]^2 (g^{\mathsf{E}})^2. \tag{18.44}$$

Rearrangement leads to

$$\frac{\partial \boldsymbol{x}}{\partial \boldsymbol{a}} = \frac{\partial \boldsymbol{\varphi}}{\partial \boldsymbol{a}} = \frac{g^{\mathsf{L}}}{g^{\mathsf{E}}}, \tag{18.45}$$

where we assumed the Jacobian determinant is positive. Note that if the Eulerian coordinates are Cartesian, then $g^{\mathsf{E}} = 1$ so that

$$\frac{\partial \boldsymbol{x}}{\partial \boldsymbol{a}} = \frac{\partial \boldsymbol{\varphi}}{\partial \boldsymbol{a}} = g^{\mathsf{L}} \quad \text{Cartesian Eulerian coordinates.} \tag{18.46}$$

18.6 Kinematic description of relative motion

Material curves are one-dimensional geometric objects that follow fluid particles. We initialize a material curve by drawing a line in the fluid and then following the curve as it deforms according to the trajectories of the fluid particles. The material curve is stretched and folded by the fluid flow as illustrated in Figure 18.4. We here develop the rudimentary kinematics of such motion by considering evolution of the relative vector connecting two fluid particles in Euclidean space. We specialize to Eulerian Cartesian coordinates to simplify comparison of the particle position vectors. That is, we assume the flow map generated by the motion, $\boldsymbol{\varphi}(\boldsymbol{a}, T)$, is represented by the Cartesian position of the fluid particles. As we will see, evolution of these two points is determined by the deformation matrix introduced in Section 18.4.

18.6.1 Differential increment for $\boldsymbol{a}$-space and $\boldsymbol{x}$-space

We start by developing expressions for the differential increment of a function in $\boldsymbol{x}$-space and in material $\boldsymbol{a}$-space.[9] These relations are useful when manipulating relations in either $\boldsymbol{x}$-space or $\boldsymbol{a}$-space.

Spatial increments

Consider a scalar fluid property, Π, and represent it with the spatial coordinates of an Eulerian description, $\Pi(\boldsymbol{x}, t)$. In Section 17.4.1, we considered the space and time increment of a scalar function. Here we consider just the space increment, as defined by the differential increment of a function evaluated at the same time but at two infinitesimally close points in space. Writing this increment for a scalar renders

$$\mathrm{d}\Pi(\boldsymbol{x}, t) = \Pi(\boldsymbol{x} + \mathrm{d}\boldsymbol{x}, t) - \Pi(\boldsymbol{x}, t) = (\mathrm{d}x^i \, \partial_i)\Pi(\boldsymbol{x}, t). \tag{18.47}$$

Material increments

Consider the same fluid property, Π, now evaluated on a material fluid particle trajectory, and write this Lagrangian function as in Section 18.3.3

$$\Pi^{\mathrm{L}}(\boldsymbol{a}, T) \equiv \Pi[\boldsymbol{x} = \boldsymbol{\varphi}(\boldsymbol{a}, T), t = T]. \tag{18.48}$$

Now consider an infinitesimal increment of $\Pi^{\mathrm{L}}(\boldsymbol{a}, T)$ within material coordinate space. This increment measures the difference of the fluid property, Π, when evaluated on two fluid particles, one labelled by $\boldsymbol{a}$ and the other by $\boldsymbol{a} + \mathrm{d}\boldsymbol{a}$. Just like when working in $\boldsymbol{x}$-space, we take a Taylor series and truncate to leading order, so that

$$\begin{aligned} \mathrm{d}\Pi^{\mathrm{L}}(\boldsymbol{a}, T) &= \Pi[\boldsymbol{\varphi}(\boldsymbol{a} + \mathrm{d}\boldsymbol{a}, T), T] - \Pi[\boldsymbol{\varphi}(\boldsymbol{a}, T), T] && \text{(18.49a)} \\ &= \Pi^{\mathrm{L}}(\boldsymbol{a} + \mathrm{d}\boldsymbol{a}, T) - \Pi^{\mathrm{L}}(\boldsymbol{a}, T) && \text{(18.49b)} \\ &= (\mathrm{d}a^I \, \partial_I)\Pi^{\mathrm{L}}(\boldsymbol{a}, T). && \text{(18.49c)} \end{aligned}$$

Duality between Eulerian and Lagrangian perspectives

It is self-evident that the value of a fluid property at a spatial point $\boldsymbol{x}$ (Eulerian perspective) equals to the property evaluated on a moving fluid particle (Lagrangian perspective) at the

[9] From a mathematical perspective, we develop the exterior derivatives for a selection of scalar functions, and detail their expressions using both Eulerian and Lagrangian coordinates.

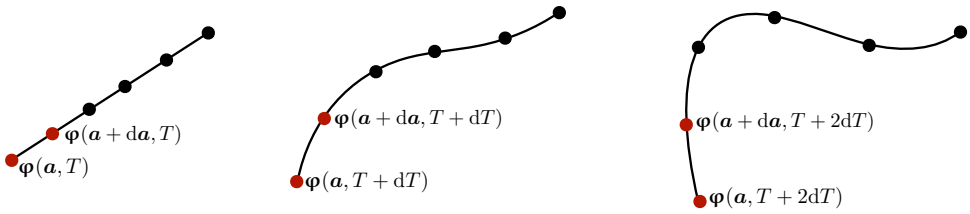

FIGURE 18.4: Three time instances of a material curve, highlighting two fluid particles whose trajectories are $\boldsymbol{\varphi}(\boldsymbol{a},T)$ and $\boldsymbol{\varphi}(\boldsymbol{a}+\mathrm{d}\boldsymbol{a},T)$. All points along the curve move through the fluid by following the trajectories of the fluid particles. Kinematics of the relative vector separating two fluid particles is determined by properties of the deformation matrix in Section 18.6, or the deformation rate in Section 18.8.

instance the particle passes through $\boldsymbol{x}$. Mathematically, this identity takes the form

$$\Pi^{\text{L}}(\boldsymbol{a},T)=\Pi[\boldsymbol{x}=\boldsymbol{\varphi}(\boldsymbol{a},T),t=T]=\Pi(\boldsymbol{x},t)\quad\text{if }\boldsymbol{\varphi}(\boldsymbol{a},T)=\boldsymbol{x}. \tag{18.50}$$

Likewise, if the infinitesimal increment in space, $\delta\boldsymbol{x}$, equals to the vector increment of the two fluid particles,

$$\mathrm{d}\boldsymbol{\varphi}(\boldsymbol{a},T)=\boldsymbol{\varphi}(\boldsymbol{a}+\mathrm{d}\boldsymbol{a},T)-\boldsymbol{\varphi}(\boldsymbol{a},T), \tag{18.51}$$

then the functional increments are identical

$$\mathrm{d}\Pi^{\text{L}}(\boldsymbol{a},T)=\delta\Pi(\boldsymbol{x},t)\quad\text{if }\mathrm{d}\boldsymbol{\varphi}(\boldsymbol{a},T)=\delta\boldsymbol{x}, \tag{18.52}$$

where

$$\delta\Pi(\boldsymbol{x},t)=\Pi(\boldsymbol{x}+\delta\boldsymbol{x},t)-\Pi(\boldsymbol{x},t)=(\delta x^i\,\partial_i)\,\Pi(\boldsymbol{x},t) \tag{18.53a}$$

$$\mathrm{d}\Pi^{\text{L}}(\boldsymbol{a},T)=\Pi^{\text{L}}(\boldsymbol{a}+\mathrm{d}\boldsymbol{x},T)-\Pi^{\text{L}}(\boldsymbol{a},T)=(\mathrm{d}a^I\,\partial_I)\,\Pi^{\text{L}}(\boldsymbol{a},T). \tag{18.53b}$$

These identities allow us to develop relations using either a Lagrangian or an Eulerian description, and then to interpret the resulting equations in their dual perspective available from an Eulerian or a Lagrangian description.

18.6.2 A role for the deformation matrix

Consider two fluid particles with material coordinates, $\boldsymbol{a}$ and $\boldsymbol{a}+\mathrm{d}\boldsymbol{a}$, along with their corresponding trajectories $\boldsymbol{\varphi}(\boldsymbol{a},T)$ and $\boldsymbol{\varphi}(\boldsymbol{a}+\mathrm{d}\boldsymbol{a},T)$ (see Figure 18.4). Assuming the trajectories are represented using Cartesian coordinates, we can write the vector connecting these two particles (the relative vector) as

$$\mathrm{d}\boldsymbol{\varphi}(\boldsymbol{a},T)=\boldsymbol{\varphi}(\boldsymbol{a}+\mathrm{d}\boldsymbol{a},T)-\boldsymbol{\varphi}(\boldsymbol{a},T). \tag{18.54}$$

Expanding to leading order yields an expression of *Cauchy's solution* (further explored in Section 18.6.4)

$$\mathrm{d}\boldsymbol{\varphi}(\boldsymbol{a},T)=\boldsymbol{\varphi}(\boldsymbol{a}+\mathrm{d}\boldsymbol{a},T)-\boldsymbol{\varphi}(\boldsymbol{a},T)\approx(\mathrm{d}a^I\,\partial_I)\,\boldsymbol{\varphi}(\boldsymbol{a},T). \tag{18.55}$$

Making use of the assumed Cartesian coordinates for the flow map allows us to write the material increment in terms of the deformation matrix[10]

$$\mathrm{d}\varphi^i=\mathrm{d}a^I\,\partial_I\varphi^i=\mathrm{d}a^I\,F^i{}_I, \tag{18.56}$$

where we introduced the deformation matrix from Section 18.4.1, $F^i{}_I\equiv\partial_I\varphi^i$.

[10]The connection between differential increment and deformation gradient does not hold when using general coordinates for the flow map. The reason is that we cannot naively compare vectors on a general manifold. More work is needed, with details provided in Chapter 1 of *Tromp* (2025a) as well as in *Tromp* (2025b).

18.6.3 Kinematic evolution equation

Now consider the material time derivative of the material increment

$$\frac{\partial[\mathrm{d}\boldsymbol{\varphi}(\boldsymbol{a},T)]}{\partial T} = \frac{\partial\boldsymbol{\varphi}(\boldsymbol{a}+\delta\boldsymbol{a},T)}{\partial T} - \frac{\partial\boldsymbol{\varphi}(\boldsymbol{a},T)}{\partial T} \tag{18.57a}$$

$$= \boldsymbol{v}^{\text{L}}(\boldsymbol{a}+\mathrm{d}\boldsymbol{a},T) - \boldsymbol{v}^{\text{L}}(\boldsymbol{a},T) \tag{18.57b}$$

$$= \mathrm{d}\boldsymbol{v}^{\text{L}}(\boldsymbol{a},T). \tag{18.57c}$$

In these equations, we introduced the Lagrangian velocity,

$$\boldsymbol{v}^{\text{L}}(\boldsymbol{a},T) = \boldsymbol{v}[\boldsymbol{x}=\boldsymbol{\varphi}(\boldsymbol{a},T), t=T], \tag{18.58}$$

as per equation (18.16). As for the manipulations in Section 18.6.2, we can massage the expression (18.57c) by performing a Taylor series expansion and truncating to leading order

$$\frac{\partial[\mathrm{d}\boldsymbol{\varphi}(\boldsymbol{a},T)]}{\partial T} = \mathrm{d}\boldsymbol{v}^{\text{L}}(\boldsymbol{a},T) = (\mathrm{d}a^I\,\partial_I)\boldsymbol{v}^{\text{L}}(\boldsymbol{a},T). \tag{18.59}$$

Alternatively, we can choose to evaluate this expression using an Eulerian perspective (see Section 18.6.1), in which case

$$\frac{\mathrm{D}(\delta\boldsymbol{x})}{\mathrm{D}t} = \delta\boldsymbol{v}(\boldsymbol{x},t) = (\delta x^i\,\partial_i)\boldsymbol{v}(\boldsymbol{x},t). \tag{18.60}$$

In Section 18.6.4 we examine this equation according to Cauchy, thus furthering our understanding of how the relative displacement vector evolves.

18.6.4 Cauchy's solution for evolution of the relative vector

We can determine a general solution to the kinematic evolution equation (18.60) following the method used by Cauchy[11] to solve the perfect fluid barotropic vorticity equation discussed in Section 40.5. Indeed, we already encountered the Cauchy solution in Section 18.6.2. We rederive it here as an exercise in the formalism that can be of general use when working with Lagrangian coordinates.

Derivation using the motion field and deformation matrix

For this derivation we make use of the motion field, $\varphi^i(\boldsymbol{a},T)$, and the deformation matrix, $\partial_I\varphi^i = F^i{}_I$, in which we start from equation (18.60) yet written using Lagrangian coordinates

$$\partial_T(\delta x^i) = \delta x^j\,\partial_j(\partial_T\varphi^i) = \delta x^j\,F^J{}_j\,\partial_J(\partial_T\varphi^i), \tag{18.61}$$

where the second equality used the deformation matrix to convert from an Eulerian derivative to a Lagrangian derivative: $\partial_j = F^J{}_j\,\partial_J$. Noting that $\partial_J\,\partial_T = \partial_T\,\partial_J$, and introducing the deformation matrix, $\partial_J\varphi^i = F^i{}_J$, we find

$$\partial_T(\delta x^i) = \delta x^j\,F^J{}_j\,\partial_T F^i{}_J = -\delta x^j\,(\partial_T F^J{}_j)\,F^i{}_J. \tag{18.62}$$

The second equality follows since $F^J{}_j\,F^i{}_J = \delta^i{}_j$ is time independent. Now contract both sides of this equation with $F^K{}_i$ and note that $F^K{}_i\,F^i{}_J = \delta^J{}_K$, so that

$$F^K{}_i\,\partial_T(\delta x^i) = -\delta x^j\,\partial_T F^K{}_j \Longrightarrow \partial_T(F^K{}_i\,\delta x^i) = 0. \tag{18.63}$$

[11] See *Frisch and Villone* (2014) for an insightful discussion of the enduring impact of Cauchy's solution.

Choosing the material coordinates equal to the reference positions

If we choose the material coordinates as the reference positions of fluid particles,

$$\boldsymbol{a} = \boldsymbol{x}(t = t_{\mathsf{R}}) = \mathring{\boldsymbol{x}}, \tag{18.64}$$

then the inverse transformation matrix element at the reference time is given by the unit tensor

$$F^K{}_j = \delta^K{}_j \quad \text{at } t = t_{\mathsf{R}}, \tag{18.65}$$

so that the material invariance in equation (18.63) leads to

$$\delta x^j \, F^K{}_j = \delta \mathring{x}^K. \tag{18.66}$$

Inverting this equation by contracting with $F^i{}_K$ and using $F^i{}_K \, F^K{}_j = \delta^i{}_j$ leads to *Cauchy's solution*

$$\delta x^i = \delta \mathring{x}^K \, F^i{}_K = \delta \mathring{x}^K \, \partial_K \varphi^i(\boldsymbol{a}, T). \tag{18.67}$$

Discussion of Cauchy's solution (18.67)

The Cauchy solution (18.67) says that the increment along a line segment defined by fluid particles, $\delta\boldsymbol{x} = \delta\boldsymbol{\varphi}$, expands or contracts according to the time and space dependent deformation matrix, $F^i{}_K$. This result follows from our assumption that the increment is defined by fixed $\boldsymbol{a}$-space coordinates, which then constrains the increment's $\boldsymbol{x}$-space evolution. It is also an expression that we wrote down, rather trivially, in Section 18.6.2 when performing a truncated Taylor series expansion of the spatial increment between two material fluid particles that follow the flow. Both approaches offer distinct insights as well as confidence in the validity of the result.[12] The ability to derive kinematic results using either simple (indeed trivial) methods versus more long-winded methods is somewhat exemplary of fluid kinematics.

Extension to vorticity

As seen in Section 40.3, the relative vorticity, $\boldsymbol{\omega} = \nabla \times \boldsymbol{v}$, for a homogeneous inviscid, barotropic fluid satisfies the same kinematic equation (18.60) as for a material line increment

$$\frac{\mathrm{D}\boldsymbol{\omega}}{\mathrm{D}t} = (\boldsymbol{\omega} \cdot \nabla) \, \boldsymbol{v}(\boldsymbol{x}, t). \tag{18.68}$$

We can thus invoke the Cauchy solution to write the vorticity

$$\omega^i(t) = \omega^K(t = 0) \, F^i{}_K, \tag{18.69}$$

which is one form of Kelvin's circulation theorem studied in Section 40.2.

18.7 The volume element

Consider the volume, $\mathrm{d}V$, of an infinitesimal region of $\boldsymbol{x}$-space as depicted in Figure 18.5. The volume has a zero Eulerian time derivative,

$$\partial_t[\mathrm{d}V] = 0, \tag{18.70}$$

which trivially follows since the region is Eulerian. The volume has dimensions of L^3, and it can be represented using either Cartesian coordinates, $\boldsymbol{x}^{\mathsf{cart}}$, or arbitrary coordinates, $\boldsymbol{x}$. We first

[12] If there is more than one way to solve a problem, then do so, even if one of those ways is much more tedious!

consider the general case and then specialize to Cartesian.

18.7.1 Arbitrary Eulerian and Lagrangian coordinates

Using the expression (4.60) for the invariant volume element we have

$$\mathrm{d}V = g^{\mathsf{E}}\,\mathrm{d}^3x, \tag{18.71}$$

where $g^{\mathsf{E}} = \sqrt{\det(\mathbb{g}_{ij}(\boldsymbol{x}))}$ from Section 18.5.4, which is the square root of the metric as written using the arbitrary Eulerian coordinates, $\boldsymbol{x}$. Following the interpretation from Section 18.3.2 whereby $\boldsymbol{a}$-space is a coordinate transformation of $\boldsymbol{x}$-space, we can write that Eulerian volume element using arbitrary material coordinates, $\boldsymbol{a}$, just like we did for two sets of Eulerian coordinates in equation (18.71). Namely,

$$\mathrm{d}V = g^{\mathsf{E}}(\boldsymbol{x})\,\mathrm{d}^3x = g^{\mathsf{L}}(\boldsymbol{a},T)\,\mathrm{d}^3a, \tag{18.72}$$

where $g^{\mathsf{L}} = \sqrt{\det(\mathbb{g}_{IJ})}$ is the square root of the Euclidean metric using the material coordinates (equation (18.43)), and g^{L} is a function of material space and time.

18.7.2 Cartesian Eulerian coordinates

To help solidify the general results developed in this section, consider the specific case of Eulerian Cartesian coordinates (still written as $\boldsymbol{x}$) and material coordinates set by the Cartesian reference positions of fluid particles,

$$\boldsymbol{a} = \boldsymbol{\varphi}(\boldsymbol{a}, T = t_{\mathsf{R}}) = \mathring{\boldsymbol{x}}. \tag{18.73}$$

We are led to the coordinate transformed expression for the volume element

$$\mathrm{d}V = \mathrm{d}^3x = (\partial\boldsymbol{x}/\partial\mathring{\boldsymbol{x}})\,\mathrm{d}^3\mathring{x}, \tag{18.74}$$

where $\partial\boldsymbol{x}/\partial\mathring{\boldsymbol{x}}$ is the Jacobian of transformation between the present Cartesian positions of fluid particles moving with the flow,

$$\boldsymbol{x} = \boldsymbol{\varphi}(\mathring{\boldsymbol{x}}, T), \tag{18.75}$$

and their reference Cartesian positions

$$\mathring{\boldsymbol{x}} = \boldsymbol{\varphi}(\mathring{\boldsymbol{x}}, T = t_{\mathsf{R}}). \tag{18.76}$$

The material coordinate volume element, $\mathrm{d}^3\mathring{x} = \mathrm{d}\mathring{x}\,\mathrm{d}\mathring{y}\,\mathrm{d}\mathring{z}$, is the Cartesian expression for the volume of fluid in the reference flow state that fits into the Eulerian volume, $\mathrm{d}^3x = \mathrm{d}V$, at time $t > t_{\mathsf{R}}$. The Jacobian is a function of time for a moving fluid and so is the volume $\mathrm{d}^3\mathring{x}$, but their product is time independent by construction. Furthermore, it is notable that the Jacobian is the ratio of the volume elements

$$\frac{\partial\boldsymbol{x}}{\partial\mathring{\boldsymbol{x}}} = \frac{\mathrm{d}^3x}{\mathrm{d}^3\mathring{x}}. \tag{18.77}$$

When material coordinates are given by the reference fluid particle positions, $\boldsymbol{a} = \mathring{\boldsymbol{x}} = \boldsymbol{\varphi}(\boldsymbol{a}, T = t_{\mathsf{R}})$, then the Jacobian is unity at the reference time, $T = t_{\mathsf{R}}$. This choice for material coordinate is commonly made in the solid mechanics literature (e.g., Chapter 1 of *Tromp* (2025a)), and it is suggested by the referential manifold perspective of Figure 18.12. However, for geophysical fluid mechanics we do not build this assumption into the formalism. The reason is that we often find it useful to set $\boldsymbol{a}$ to a non-spatial coordinate, such as discussed in Section 17.3.2, in which case the Jacobian is not unity at the reference time.

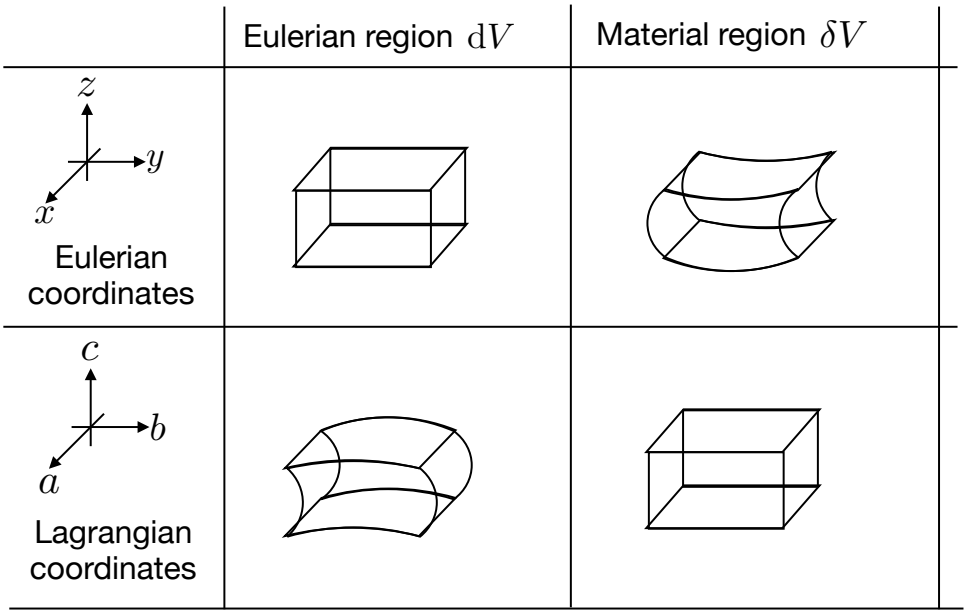

FIGURE 18.5: Depicting the volume of tiny regions of the fluid using Eulerian ($\boldsymbol{x}$-space) coordinates (top row) and Lagrangian ($\boldsymbol{a}$-space) coordinates (bottom row). The left column considers an Eulerian region with volume, $\mathrm{d}V = g^{\mathsf{E}}\,\mathrm{d}^3x = g^{\mathsf{L}}\,\mathrm{d}^3a$, with this volume independent of Eulerian time, t. The right column depicts the complement material region, in which the material coordinate volume, δV, is assumed to have zero material time derivative, so that it is a function just of $\boldsymbol{a}$.

18.7.3 The volume of a fixed region of $\boldsymbol{a}$-space

Now consider a tiny material region that moves through the fluid and whose volume is written δV, as in Figure 18.5, and with the volume independent of material time. The volume has dimensions of L^3, and it can be represented using either the reference Cartesian positions, $\boldsymbol{a} = \mathring{\boldsymbol{x}}$, or arbitrary material coordinates, $\boldsymbol{a}$, which leads to

$$\delta V = g^{\mathsf{E}}\,\delta^3x = g^{\mathsf{L}}\,\mathrm{d}^3a, \tag{18.78}$$

which are the same expressions we derived in Section 18.7.1 for the Eulerian volume element. However, in the present case the material volume increment, d^3a, is materially constant whereas the Eulerian increment, δ^3x, is a function of time.

18.8 The velocity gradient tensor and relative velocity

In this section we return to the expression (18.55) of the Cauchy solution for the relative position vector between two fluid particles[13]

$$\mathrm{d}\boldsymbol{\varphi}(\boldsymbol{a},T) = \boldsymbol{\varphi}(\boldsymbol{a}+\mathrm{d}\boldsymbol{a},T) - \boldsymbol{\varphi}(\boldsymbol{a},T) = (\mathrm{d}a^I\,\partial_I)\,\boldsymbol{\varphi}(\boldsymbol{a},T). \tag{18.79}$$

Rather then developing the solution into the form (18.67), which exposes the deformation matrix, we here take a material time derivative, in which case the deformation matrix is seen to determine evolution of the relative velocity.

[13]We continue to assume Cartesian coordinates for the Eulerian description, whereas the material description can be arbitrary.

18.8.1 Evolution of the relative velocity

Taking the material time derivative of the left hand side to equation (18.79) leads to the relative velocity vector

$$\partial_T(\mathrm{d}\boldsymbol{\varphi}) = \mathrm{d}(\partial_T\boldsymbol{\varphi}) = \mathrm{d}\boldsymbol{v}^{\mathrm{L}}, \tag{18.80}$$

where we introduced the velocity vector as evaluated on a fluid particle

$$\boldsymbol{v}^{\mathrm{L}}(\boldsymbol{a}, T) = \partial_T\boldsymbol{\varphi}(\boldsymbol{a}, T). \tag{18.81}$$

Combining equation (18.80) with the material time derivative acting on the right hand side of equation (18.79) renders

$$\mathrm{d}\boldsymbol{v}^{\mathrm{L}} = (\mathrm{d}a^I\,\partial_I)\,\partial_T\boldsymbol{\varphi} = (\mathrm{d}a^I\,\partial_I)\,\boldsymbol{v}^{\mathrm{L}}, \tag{18.82}$$

where the material time derivative operator commutes with the material increment operator $\mathrm{d}a^I\,\partial_I$, and with equation (18.82) agreeing with the earlier identity (18.53b). Making use of the deformation matrix renders the component form of equation (18.82)

$$(\mathrm{d}v^{\mathrm{L}})^i = (\mathrm{d}a^I\,\partial_I)\,\partial_T\varphi^i = \mathrm{d}a^I\,\partial_T\,\partial_I\,\varphi^i = \mathrm{d}a^I\,\partial_T F^i{}_I. \tag{18.83}$$

Hence, the relative velocity of two fluid particles is directly determined by the material time derivative of the deformation matrix.

18.8.2 Velocity gradient tensor

We make use of the duality developed in Section 18.6.1 to write the Lagrangian expression (18.82) in terms of Eulerian position coordinates

$$\delta\boldsymbol{v}(\boldsymbol{x}, t) = (\delta x^j\,\partial_j)\,\boldsymbol{v}(\boldsymbol{x}, t) \Longleftrightarrow \delta v^i = (\delta x^j\,\partial_j)\,v^i. \tag{18.84}$$

Alternatively, we can return to the identity (18.80), and again make use of the duality to write the material time derivative of the position increment

$$\frac{\mathrm{D}(\delta x^i)}{\mathrm{D}t} = \delta v^i = (\delta x^j\,\partial_j)\,v^i. \tag{18.85}$$

This equation says that the material evolution of δx^i is determined by the velocity derivatives, $\partial_j v^i$. These derivatives form elements to the Cartesian Eulerian form of the second order *velocity gradient tensor*

$$G^i{}_j = \partial_j v^i, \tag{18.86}$$

so that equation (18.85) can be written

$$\frac{\mathrm{D}(\delta x^i)}{\mathrm{D}t} = G^i{}_j\,\delta x^j. \tag{18.87}$$

To help understand how the velocity gradient tensor affects the evolution of $\delta\boldsymbol{x}$, it is useful to decompose the tensor into its symmetric and anti-symmetric components. For this purpose we need the transpose of the tensor, which is written[14]

$$(G^{\mathrm{T}})^i{}_j = G_j{}^i. \tag{18.88}$$

We can thus write the velocity gradient tensor as

$$\mathbf{G} = (\mathbf{G} + \mathbf{G}^{\mathrm{T}})/2 + (\mathbf{G} - \mathbf{G}^{\mathrm{T}})/2 \equiv \mathbf{S} + \mathbf{R}, \tag{18.89}$$

[14] Recall we discussed the transpose of a second order tensor in Section 1.11.1.

where

$$\mathbf{S} = (\mathbf{G} + \mathbf{G}^{\mathrm{T}})/2 \qquad \text{strain (deformation) rate tensor (symmetric)} \tag{18.90a}$$

$$\mathbf{R} = (\mathbf{G} - \mathbf{G}^{\mathrm{T}})/2 \qquad \text{rotation tensor (anti-symmetric).} \tag{18.90b}$$

As seen in the following, the strain rate and rotation tensors affect the motion of a material fluid object in distinct manners. Note that the strain rate tensor is commonly referred to as the *deformation rate* tensor in the literature. We choose the strain rate nomenclature to help reduce confusion with the deformation matrix, $F^i{}_I$ from Section 18.4.1.

18.8.3 Stretching and tilting of material lines

Consider a material line element initially aligned with the vertical axis

$$\delta\boldsymbol{x}_{t=0} = \hat{\boldsymbol{z}}\,\delta Z_0. \tag{18.91}$$

The evolution equation (18.87) means that the initial evolution of this material line element takes on the form

$$\frac{\mathrm{D}(\delta x)}{\mathrm{D}t} = \underbrace{\delta Z_0 \left[\frac{\partial u}{\partial z}\right]}_{\text{tilting}} \qquad \text{and} \qquad \frac{\mathrm{D}(\delta y)}{\mathrm{D}t} = \underbrace{\delta Z_0 \left[\frac{\partial v}{\partial z}\right]}_{\text{tilting}} \qquad \text{and} \qquad \frac{\mathrm{D}(\delta z)}{\mathrm{D}t} = \underbrace{\delta Z_0 \left[\frac{\partial w}{\partial z}\right]}_{\text{stretching}}. \tag{18.92}$$

In the presence of a vertical derivative in the horizontal velocity field (vertical shear), the first and second terms create a non-zero projection of the material line element onto the horizontal plane. That is, these terms *tilt* the material line element. Additionally, in the presence of a vertical derivative of the vertical velocity, the material line element is expanded or compressed along its initial axis. This term is called *stretching*. We return to the tilting and stretching mechanisms when discussing the dynamics of vorticity in Chapter 40. There, we see that vortex lines in a perfect fluid flow are material lines. Consequently, vortex lines are also affected by tilting and stretching just like a material line.

18.8.4 Evolution of line element length from the strain rate

Recall the expression (18.39) for the squared length of a material line element

$$\mathrm{d}\boldsymbol{\varphi} \cdot \mathrm{d}\boldsymbol{\varphi} = \mathrm{d}\varphi^i\,\delta_{ij}\,\mathrm{d}\varphi^j = (\mathrm{d}a^I\partial_I)\varphi^i\,\delta_{ij}\,(\mathrm{d}a^J\partial_J)\varphi^j, \tag{18.93}$$

whose material time derivative is given by

$$\partial_T(\mathrm{d}\boldsymbol{\varphi} \cdot \mathrm{d}\boldsymbol{\varphi}) = 2\,(\mathrm{d}a^I\partial_I)\boldsymbol{v}^\llcorner \cdot (\mathrm{d}a^J\partial_J)\boldsymbol{\varphi}. \tag{18.94}$$

We can express this result using Eulerian $\boldsymbol{x}$-space coordinates through the duality in Section 18.6.1, which leads to

$$(\delta a^I\,\partial_I)\boldsymbol{v}^\llcorner = (\delta x^i\,\partial_i)\boldsymbol{v} \quad \text{and} \quad (\delta a^I\,\partial_I)\boldsymbol{\varphi} = \delta\boldsymbol{x}, \tag{18.95}$$

so that

$$\frac{\mathrm{D}(\delta\boldsymbol{x} \cdot \delta\boldsymbol{x})}{\mathrm{D}t} = 2\,\delta x^i\,\delta x^k\,\delta_{jk}\,\partial_i v^j = 2\,\delta x^i\,\delta x^k\,\delta_{jk}\,G^j{}_i. \tag{18.96}$$

Since the product $\delta x^i\,\delta x^k$ is symmetric on the indices i,k, it projects out the symmetric portion of the velocity gradient tensor, which is the strain rate tensor, thus yielding

$$\frac{1}{2}\frac{\mathrm{D}(\delta\boldsymbol{x}\cdot\delta\boldsymbol{x})}{\mathrm{D}t} = 2\,\delta x^i\,\delta x^k\,\delta_{jk}\,S^j{}_i. \tag{18.97}$$

Consequently, the strain rate tensor, $\mathbf{S}$, determines the rate at which a material curve changes its length.

To further understand the result (18.97), consider two fluid particles initialized very close together. Equation (18.97) says that the distance between the two particles is modified so long as there are nonzero strain rates in the fluid flow. In the special case of a zero strain rate tensor, then the separation between the two fluid particles is fixed. Evidently, in the absence of a strain rate, the two fluid particles move in a locally and instantaneously rigid manner.

Since the strain rate tensor is symmetric, it has six degrees of freedom. Furthermore, it can be diagonalized, with the diagonal elements equal to the eigenvalues (e.g., see section 2.2 of *Segel* (1987)). Each eigenvalue measures the rate that material lines oriented according to the principle axes (eigenvectors) expand/contract under the impacts of straining motion in the fluid. According to equation (18.97), the expansion/contraction is exponential when aligned along the principle axes, with the exponential rate determined by the eigenvalues of $\mathbf{S}$. Furthermore, as shown in Section 18.10, the sum of these eigenvalues (given by the trace of the strain rate tensor) measures the rate that a material volume changes through the divergence of the velocity

$$S^i{}_i = \partial_i v^i = \nabla\cdot\boldsymbol{v}. \tag{18.98}$$

18.8.5 Rigid rotation of the line element

As defined by equation (18.90b), the rotation tensor is given by

$$\mathbf{R} = (\mathbf{G}-\mathbf{G}^{\mathrm{T}})/2. \tag{18.99}$$

Notably, the rotation tensor is anti-symmetric so that

$$\mathbf{R} = -\mathbf{R}^{\mathrm{T}}, \tag{18.100}$$

and as such it has three degrees of freedom. At this point we return to the full gamut of Cartesian tensor notation by bringing all indices downstairs.[15] We also introduce the vorticity vector,

$$\boldsymbol{\omega} = \nabla\times\boldsymbol{v}, \tag{18.101}$$

which is related to the rotation tensor via

$$2\,R^i{}_j = -\epsilon^i{}_{jk}\,\omega^k \Longleftrightarrow \mathbf{R} = \frac{1}{2}\begin{bmatrix} 0 & -\omega^3 & \omega^2 \\ \omega^3 & 0 & -\omega^1 \\ -\omega^2 & \omega^1 & 0 \end{bmatrix} \Longleftrightarrow \omega^k = -\epsilon^{kij}\,R_{ij}, \tag{18.102}$$

where the final expression made use of the identity (1.69) in the form

$$\epsilon^{ijl}\,\epsilon_{ijm} = 2\,\delta^l{}_m. \tag{18.103}$$

It is furthermore straightforward to show that the doubly contracted rotation tensor equals to half the squared vorticity

$$R^i{}_j\,R^j{}_i = |\boldsymbol{\omega}|^2/2. \tag{18.104}$$

[15] To work with general tensors at this stage requires more tools than warranted for this discussion.

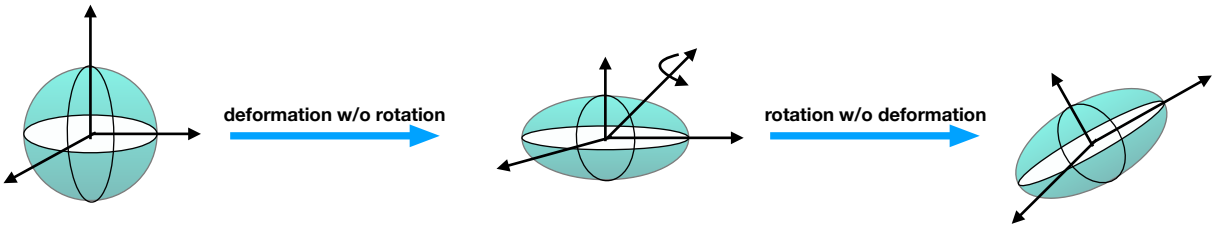

FIGURE 18.6: Schematic illustrating the Cauchy-Stokes decomposition of how fluid flow can modify a spherical material region according to equation (18.106). First the sphere can be deformed without rotation, with this process encompassed by the strain rate tensor, $\mathbf{S}$. Next it can be rigidly rotated without changing its shape, as encompassed by the rotation tensor, $\mathbf{R}$. The axes shown represent the principle axes so that deformation corresponds to expansion or contraction along the principle axes directions.

The contribution of the rotation matrix to evolution of the material line element is given by

$$\left[\frac{\mathrm{D}(\delta x^i)}{\mathrm{D}t}\right]_{\text{rot}} = R^i{}_j\,\delta x^j = -(\epsilon^i{}_{jk}\,\omega^k/2)\,\delta x^j \implies \left[\frac{\mathrm{D}(\delta \boldsymbol{x})}{\mathrm{D}t}\right]_{\text{rot}} = \frac{1}{2}\,(\boldsymbol{\omega}\times\delta\boldsymbol{x})\,. \tag{18.105}$$

This relation is in the form of a pure rotation of the material line element, $\delta\boldsymbol{x}$, as generated by the vector, $\boldsymbol{\omega}/2$ (recall the discussion of rigid-body rotations in Section 11.2). We thus conclude that the anti-symmetric rotation tensor, $\mathbf{R}$, provides a rigid rotation to a material line element about the axis defined by the vorticity vector. It rotates the objects without altering the size (length, area, volume).

18.8.6 Cauchy-Stokes decomposition

The above discussion of how fluid motion impacts on a material curve falls under the more general insights from the *Cauchy-Stokes decomposition theorem*. This theorem says that the arbitrary motion of a region in a continuous media can be decomposed into a uniform translation, dilation along three perpendicular axes, plus a rigid body rotation. Mathematically, this decomposition can be written by expanding equation (18.87) to read

$$v^i(\boldsymbol{x},t) = v^i(\boldsymbol{x}_0,t) + G^i{}_j\,\delta x^j = v^i(\boldsymbol{x}_0,t) + S^i{}_j\,\delta x^j + R^i{}_j\,\delta x^j. \tag{18.106}$$

Figure 18.6 illustrates the deformation and rotation portion of this decomposition. A more thorough discussion of this theorem can be found in Chapter 4 of *Aris* (1962) and Section 3.1 of *Segel* (1987).

18.8.7 Evolution of the deformation matrix

In equation (18.83) we found that the relative velocity of two fluid particles is directly determined by the material time derivative of the deformation matrix. As an exercise in the formalism, we here determine how the deformation matrix evolves materially, in which we compute

$$\begin{aligned}
\partial_T F^i{}_I &= \partial_T\,\partial_I \varphi^i && \text{definition (18.17) of deformation matrix} && (18.107a)\\
&= \partial_I\,\partial_T \varphi^i && \text{Lagrangian space and time derivatives commute} && (18.107b)\\
&= \partial_I (v^{\text{L}})^i && \text{flow velocity (18.16)} && (18.107c)\\
&= \partial_I v^i && \text{dual representation of flow velocity} && (18.107d)\\
&= (\partial\varphi^j/\partial a^I)\,\partial_j v^i && \text{chain rule} && (18.107e)\\
&= F^j{}_I\,G^i{}_j. && \text{definitions (18.17) and (18.86)} && (18.107f)
\end{aligned}$$

Evidently, material evolution of the deformation matrix is given by

$$\partial_T F^i{}_I = G^i{}_j \, F^j{}_I, \tag{18.108}$$

so that the deformation matrix experiences larger changes in regions with stronger gradients in the flow, as measured by the velocity gradient tensor, $G^i{}_j$. Making use of equation (18.108) in equation (18.83) thus leads to the expression for the relative velocity increment

$$(\mathrm{d}v^{\text{L}})^i = \partial_T F^i{}_I \, \mathrm{d}a^I = G^i{}_j \, F^j{}_I \, \mathrm{d}a^I. \tag{18.109}$$

18.8.8 Evolution of the Cauchy-Green strain tensor

As noted in Section 18.5.1, the Eulerian representation of the metric tensor is independent of Eulerian time, so that $\partial_t \mathcal{G}_{ij} = 0$. Following from the discussion in Section 18.8.7 for evolution of the deformation matrix, we here consider the material time evolution of the $\boldsymbol{a}$-space representation of the metric tensor

$$\partial_T \mathcal{G}_{IJ} = \partial_T \left[\mathcal{G}_{ij} \, F^i{}_I \, F^j{}_J \right] = \partial_T \mathcal{G}_{ij} \left[F^i{}_I \, F^j{}_J \right] + \mathcal{G}_{ij} \, \partial_T [\partial_I \varphi^i \, \partial_J \varphi^j]. \tag{18.110}$$

The first equality made use of equation (18.38) for the metric tensor written in terms of Lagrangian coordinates, and the second equality made use of equation (18.17) for the deformation matrix, $F^i{}_I$. Now use equation (18.16) for velocity of the fluid flow to arrive at

$$\partial_T [\partial_I \varphi^i \, \partial_J \varphi^j] = \partial_I (\partial_T \varphi^i) \, \partial_J \varphi^j + \partial_J (\partial_T \varphi^j) \, \partial_I \varphi^i \tag{18.111a}$$

$$= \partial_I (v^{\text{L}})^i \, \partial_J \varphi^j + \partial_J (v^{\text{L}})^j \, \partial_I \varphi^i. \tag{18.111b}$$

Examine one of these terms, with the Eulerian metric contracted, to find

$$\mathcal{G}_{ij} \, \partial_I (v^{\text{L}})^i \, \partial_J \varphi^j = \mathcal{G}_{ij} \, F^k{}_I \, \partial_k (v^{\text{L}})^i \, F^j{}_J \quad \text{chain rule and deformation matrix (18.17)} \tag{18.112a}$$

$$= \mathcal{G}_{ij} \, F^k{}_I \, G^i{}_k \, F^j{}_J \quad \text{introduce gradient tensor (18.86)} \tag{18.112b}$$

$$= \mathcal{G}_{ij} \, G^i{}_I \, F^j{}_J \quad \text{transformation of } \boldsymbol{x}\text{-space to } \boldsymbol{a}\text{-space} \tag{18.112c}$$

$$= G_{jI} \, F^j{}_J \quad \text{metric tensor to lower } i\text{-index} \tag{18.112d}$$

$$= G_{JI} \quad \text{transformation of } \boldsymbol{x}\text{-space to } \boldsymbol{a}\text{-space.} \tag{18.112e}$$

Bringing terms together leads to

$$\partial_T \mathcal{G}_{IJ} = \partial_T \mathcal{G}_{ij} \left[F^i{}_I \, F^j{}_J \right] + G_{JI} + G_{IJ} = \partial_T \mathcal{G}_{ij} \left[F^i{}_I \, F^j{}_J \right] + 2 \, S_{IJ}, \tag{18.113}$$

where the second equality introduced the Lagrangian representation of the strain rate tensor (18.90a). If we choose Cartesian coordinates for the Eulerian $\boldsymbol{x}$-space description so that $\mathcal{G}_{ij} = \delta_{ij}$, then $\mathcal{G}_{IJ}$ is the Cauchy-Green strain tensor from equation (18.41), with equation (18.113) leading to

$$\partial_T \mathcal{G}_{IJ} = 2 \, S_{IJ} \quad \text{material evolution of Cauchy-Green strain tensor.} \tag{18.114}$$

Evidently, the Cauchy-Green strain tensor has a material evolution directly determined by the Lagrangian expression for the strain rate tensor.

18.9 Evolution of material surfaces

We here extend the discussion of the material line element in Sections 18.6 and 18.8 to the case of a material surface such as that shown in Figure 18.7. Considerations are given to both three-dimensional and two-dimensional flows. Furthermore, we employ Cartesian tensors

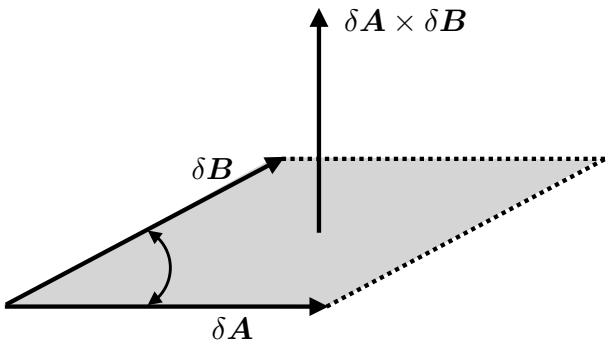

FIGURE 18.7: A material surface as defined by the cross product of two material line elements, $\delta\boldsymbol{\mathcal{S}} = \delta\boldsymbol{A}\times\delta\boldsymbol{B}$. In the special case of $\delta\boldsymbol{A} = \hat{\boldsymbol{x}}\,\delta x$ and $\delta\boldsymbol{B} = \hat{\boldsymbol{y}}\,\delta y$, then $\delta\boldsymbol{\mathcal{S}} = \delta x\,\delta y\,\hat{\boldsymbol{z}}$.

throughout this section. Even so, we use covariant and contra-variant index placement to facilitate use of the Einstein summation convention.

18.9.1 Surfaces in three-dimensional flow

Following from the geometric interpretation of the vector product in Section 1.7.5, we here define a material surface by (see Figure 18.7)

$$\delta\boldsymbol{\mathcal{S}} = \delta\boldsymbol{A}\times\delta\boldsymbol{B} \quad \text{and in components} \quad \delta\mathcal{S}_i = \epsilon_{ijk}\,\delta A^j\,\delta B^k \tag{18.115}$$

where $\delta\boldsymbol{A}$ and $\delta\boldsymbol{B}$ are non-parallel infinitesimal material lines. The surface projected onto the unit normal direction, $\hat{\boldsymbol{n}}$, is given by

$$\hat{\boldsymbol{n}}\cdot\delta\boldsymbol{\mathcal{S}} = \hat{\boldsymbol{n}}\cdot(\delta\boldsymbol{A}\times\delta\boldsymbol{B}). \tag{18.116}$$

The evolution of the material surface is given by

$$\frac{\mathrm{D}(\delta\boldsymbol{\mathcal{S}})}{\mathrm{D}t} = \frac{\mathrm{D}(\delta\boldsymbol{A})}{\mathrm{D}t}\times\delta\boldsymbol{B} + \delta\boldsymbol{A}\times\frac{\mathrm{D}(\delta\boldsymbol{B})}{\mathrm{D}t} \tag{18.117a}$$

$$= [(\delta\boldsymbol{A}\cdot\nabla)\,\boldsymbol{v}]\times\delta\boldsymbol{B} + \delta\boldsymbol{A}\times[(\delta\boldsymbol{B}\cdot\nabla)\,\boldsymbol{v}], \tag{18.117b}$$

where the second equality made use of the material line evolution equation (18.60). To proceed we expose indices and make use of some tensor identities

$$\frac{\mathrm{D}(\delta\mathcal{S}_i)}{\mathrm{D}t} = \epsilon_{ijk}\,[(\delta A^q\,\partial_q)\,v^j]\,\delta B^k + \epsilon_{ijk}\,\delta A^j\,[(\delta B^q\,\partial_q)\,v^k] \tag{18.118a}$$

$$= \epsilon_{ijk}\,[\delta A^q\,\delta B^k\,\partial_q v^j + \delta A^j\,\delta B^q\,\partial_q v^k] \tag{18.118b}$$

$$= \epsilon_{ijk}\,\partial_q v^j\,[\delta A^q\,\delta B^k - \delta A^k\,\delta B^q] \tag{18.118c}$$

$$= \epsilon_{ijk}\,\partial_q v^j\,\epsilon^{rqk}\,\delta\mathcal{S}_r \tag{18.118d}$$

$$= (\delta^r{}_i\,\delta^q{}_j - \delta^r{}_j\,\delta^q{}_i)\,\partial_q v^j\,\delta\mathcal{S}_r \tag{18.118e}$$

$$= (\nabla\cdot\boldsymbol{v})\,\delta\mathcal{S}_i - (\partial_i\boldsymbol{v})\cdot\delta\boldsymbol{\mathcal{S}}. \tag{18.118f}$$

To reach this result we made use of the following identities available for the permutation symbol from Chapter 1

$$\delta A^q\,\delta B^k - \delta A^k\,\delta B^q = \epsilon^{rqk}\,\delta\mathcal{S}_r \tag{18.119a}$$

$$\delta^r{}_i\,\delta^q{}_j - \delta^r{}_j\,\delta^q{}_i = \epsilon_{ijk}\,\epsilon^{rqk}. \tag{18.119b}$$

18.9.2 Evolution of the material surface area

Now orient the material surface area according to its outward unit normal vector

$$\delta \boldsymbol{\mathcal{S}} = \hat{\boldsymbol{n}}\, \delta \mathcal{S} \quad \text{and in components} \quad \delta \mathcal{S}_i = \hat{n}_i\, \delta \mathcal{S}, \tag{18.120}$$

where the magnitude of the area element is written

$$\delta \mathcal{S} = |\delta \boldsymbol{\mathcal{S}}|. \tag{18.121}$$

Doing so brings equation (18.118f) to the form

$$\frac{1}{\delta \mathcal{S}} \frac{\mathrm{D}(\hat{n}_i\, \delta \mathcal{S})}{\mathrm{D}t} = (\nabla \cdot \boldsymbol{v})\, \hat{n}_i - (\partial_i \boldsymbol{v}) \cdot \hat{\boldsymbol{n}}. \tag{18.122}$$

Evidently, we can develop evolution equations for the surface area, $\delta \mathcal{S}$, and the unit normal vector, $\hat{\boldsymbol{n}}$.

For the surface area evolution we take the inner product of equation (18.122) with $\hat{n}_i$ to yield

$$\frac{1}{\delta \mathcal{S}} \frac{\mathrm{D}\delta \mathcal{S}}{\mathrm{D}t} = \nabla \cdot \boldsymbol{v} - [(\hat{\boldsymbol{n}} \cdot \nabla)\boldsymbol{v}] \cdot \hat{\boldsymbol{n}} \tag{18.123}$$

where we set $\hat{\boldsymbol{n}} \cdot \hat{\boldsymbol{n}} = 1$ and followed the discussion in Section 2.1.5 to find that

$$\hat{\boldsymbol{n}} \cdot \hat{\boldsymbol{n}} = 1 \Longrightarrow \hat{\boldsymbol{n}} \cdot \frac{\mathrm{D}\hat{\boldsymbol{n}}}{\mathrm{D}t} = 0, \tag{18.124}$$

so that the normal vector is always perpendicular to its material time derivative. Rearrangement of equation (18.123) then leads to the kinematic evolution equation for the area

$$\frac{1}{\delta S} \frac{\mathrm{D}\delta \mathcal{S}}{\mathrm{D}t} = [\partial_i - \hat{n}_i\, (\hat{\boldsymbol{n}} \cdot \nabla)]\, v_i. \tag{18.125}$$

We next provide some interpretation of this result.

Surface derivative operator

The derivative operator on the right hand side of equation (18.125),

$$\partial_i^{\mathsf{surf}} \equiv \partial_i - \hat{n}_i\, (\hat{\boldsymbol{n}} \cdot \nabla), \tag{18.126}$$

is a *surface derivative operator* since it subtracts from the gradient operator the projection onto the local normal, thus leaving a gradient operator just in the tangent plane of the surface. The area evolution equation (18.125) can thus be written in the tidy form

$$\frac{1}{\delta S} \frac{\mathrm{D}\delta \mathcal{S}}{\mathrm{D}t} = \nabla^{\mathsf{surf}} \cdot \boldsymbol{v}, \tag{18.127}$$

so that the relative area of the material surface changes according to the surface divergence of the velocity field.

Special case of a horizontal surface

To help understand the kinematic equation (18.127), consider the special case of a horizontal surface with a vertical unit normal vector, $\hat{\boldsymbol{n}} = \hat{\boldsymbol{z}}$, so that

$$\frac{1}{\delta S} \frac{\mathrm{D}(\delta \mathcal{S})}{\mathrm{D}t} = \nabla \cdot \boldsymbol{v} - \hat{\boldsymbol{z}} \cdot \partial_z \boldsymbol{v} = \nabla_{\mathsf{h}} \cdot \boldsymbol{u}. \tag{18.128}$$

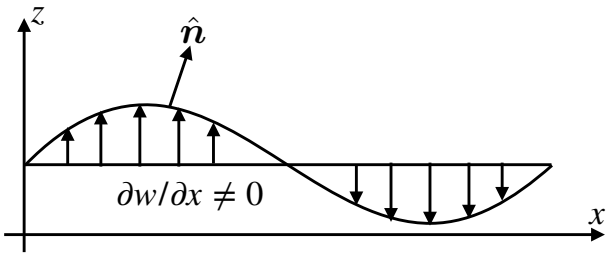

FIGURE 18.8: Horizontal shear in the vertical velocity, $\nabla_h w$, creates undulations in an initially horizontal material surface that leads to a horizontal component in the normal vector. We here show the case where $\partial w/\partial x \neq 0$, thus leading to a zonal component to the normal vector according to $\mathrm{D}\hat{n}_x/\mathrm{D}t = -\partial_x w$.

.

In this case we see that the area of a horizontal surface increases when the horizontal velocity diverges, and the area decreases when the horizontal velocity converges. We expect this behavior since the surface is material and is thus moving with the flow. We encounter this result again in Section 18.9.4 for two-dimensional flow, in which the area is always horizontal.

As another special case, consider a three dimensional flow that is non-divergent, $\nabla \cdot \boldsymbol{v} = 0$ (see Chapter 21). In this case the area changes are only due to the projection of the normal gradient onto the normal direction. So again considering a horizontal area with $\hat{\boldsymbol{n}} = \hat{\boldsymbol{z}}$, the area evolution in a non-divergent flow is given by

$$\frac{1}{\delta S}\frac{\mathrm{D}(\delta S)}{\mathrm{D}t} = -\hat{\boldsymbol{z}} \cdot (\hat{\boldsymbol{z}} \cdot \nabla)\, \boldsymbol{v} = -\partial_z w, \tag{18.129}$$

which follows from equation (18.128) with $\partial_x u + \partial_y v + \partial_z w = \nabla_h \cdot \boldsymbol{u} + \partial_z w = 0$.

18.9.3 Evolution of the normal vector

We make use of the area evolution equation (18.127) within equation (18.122) to derive an evolution equation for the normal vector

$$\begin{aligned}
\frac{\mathrm{D}\hat{n}_i}{\mathrm{D}t} &= -\hat{n}_i \frac{1}{\delta S}\frac{\mathrm{D}(\delta S)}{\mathrm{D}t} + (\partial_j v^j)\,\hat{n}_i - (\partial_i v^j)\,\hat{n}_j && \text{(18.130a)}\\
&= -\hat{n}_i\,[\partial_j v^j - \hat{n}_j\,(\hat{\boldsymbol{n}} \cdot \nabla)\, v^j] + (\partial_j v^j)\,\hat{n}_i - (\partial_i v^j)\,\hat{n}_j && \text{(18.130b)}\\
&= -\hat{n}_j\,[\partial_i - \hat{n}_i\,\hat{\boldsymbol{n}} \cdot \nabla]\, v^j && \text{(18.130c)}\\
&= -\hat{n}_j\,\partial^{\mathsf{surf}}\, v^j && \text{(18.130d)}\\
&= -\hat{\boldsymbol{n}} \cdot \partial^{\mathsf{surf}}\, \boldsymbol{v}. && \text{(18.130e)}
\end{aligned}$$

Equation (18.130c) provides a simple means to verify that the kinematic constraint (18.124) is satisfied, in which $\hat{\boldsymbol{n}} \cdot \mathrm{D}\hat{\boldsymbol{n}}/\mathrm{D}t = 0$.

To help understand the evolution equation (18.130e), consider again a horizontal area with its normal vector initially in the vertical. The evolution of this normal vector is thus given by

$$\frac{\mathrm{D}\hat{n}_i}{\mathrm{D}t} = -(\partial_i - \hat{z}_i\,\partial_z)\, w, \tag{18.131}$$

with each component evolving according to

$$\frac{\mathrm{D}\hat{n}_1}{\mathrm{D}t} = -\partial_x w \quad \text{and} \quad \frac{\mathrm{D}\hat{n}_2}{\mathrm{D}t} = -\partial_y w \quad \text{and} \quad \frac{\mathrm{D}\hat{n}_3}{\mathrm{D}t} = 0. \tag{18.132}$$

Hence, an initially vertical normal vector tilts into the horizontal direction according to minus the horizontal shear in the vertical velocity. As illustrated in Figure 18.8, we understand this

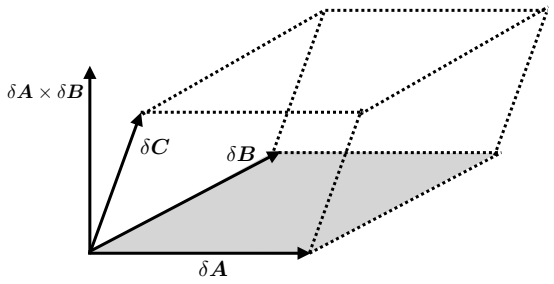

FIGURE 18.9: A parallelepiped defined by three material lines with volume (to within a sign) given by $\delta V = (\delta\boldsymbol{A}\times\delta\boldsymbol{B})\cdot\delta\boldsymbol{C}$. See also the discussion surrounding Figure 1.4.

result by noting that such a shear creates undulations in the initially horizontal surface that render a horizontal component to the normal vector.

18.9.4 Material area in two-dimensional flow

Now consider a material area for two-dimensional fluid flow with velocity, $\boldsymbol{v} = (u, v, 0)$, and $\delta\boldsymbol{A} = \hat{\boldsymbol{x}}\,\delta x$, $\delta\boldsymbol{B} = \hat{\boldsymbol{y}}\,\delta y$, with zero dependence on z. In this case, the area of an infinitesimal material region is

$$\delta\mathcal{S} = (\delta\boldsymbol{A}\times\delta\boldsymbol{B})\cdot\hat{\boldsymbol{z}} = \delta x\,\delta y, \tag{18.133}$$

and its evolution is given by

$$\frac{\mathrm{D}(\delta\mathcal{S})}{\mathrm{D}t} = (\delta\boldsymbol{B}\times\hat{\boldsymbol{z}})\cdot(\delta\boldsymbol{A}\cdot\nabla)\,\boldsymbol{u} + (\hat{\boldsymbol{z}}\times\delta\boldsymbol{A})\cdot(\delta\boldsymbol{B}\cdot\nabla)\,\boldsymbol{u} \tag{18.134a}$$

$$= \delta x\,\delta y\,\nabla\cdot\boldsymbol{u}, \tag{18.134b}$$

so that

$$\frac{1}{\delta\mathcal{S}}\frac{\mathrm{D}(\delta\mathcal{S})}{\mathrm{D}t} = \nabla\cdot\boldsymbol{u}. \tag{18.135}$$

Hence, the area of the material region evolves according to the divergence of the horizontal velocity. Correspondingly, the area remains constant in a horizontally non-divergent flow. This result follows from specializing the three-dimensional result (18.118f) to the case of two-dimensional flow by assuming no dependence on the vertical direction.

18.10 Volume, thickness, and the Jacobian

As studied in Chapter 19, the mass of a material parcel is constant. However, its volume is not generally constant since the fluid density is not generally uniform. We here derive the expression for how volume evolves for a material parcel. We also derive the material evolution equation for the Jacobian of transformation between position space and material space. We find that the relative change for both the parcel volume and the Jacobian are determined by divergence of the velocity field. We retain Cartesian tensor notation throughout this section. Note that some of these results were anticipated in Sections 18.5 and 18.7.

18.10.1 Material parcel volume

Consider a material region with a volume δV spanned by the infinitesimal material lines $\delta\boldsymbol{A}$, $\delta\boldsymbol{B}$, and $\delta\boldsymbol{C}$ (see Figure 18.9). To within a sign the volume is given by

$$\delta V = (\delta\boldsymbol{A}\times\delta\boldsymbol{B})\cdot\delta\boldsymbol{C}. \tag{18.136}$$

Making use of the material line evolution equation (18.60) renders

$$\frac{\mathrm{D}(\delta V)}{\mathrm{D}t} = (\delta \boldsymbol{B} \times \delta \boldsymbol{C}) \cdot (\delta \boldsymbol{A} \cdot \nabla)\boldsymbol{v} + (\delta \boldsymbol{C} \times \delta \boldsymbol{A}) \cdot (\delta \boldsymbol{B} \cdot \nabla)\boldsymbol{v} + (\delta \boldsymbol{A} \times \delta \boldsymbol{B}) \cdot (\delta \boldsymbol{C} \cdot \nabla)\boldsymbol{v}. \quad (18.137)$$

Now specialize to the case where the parcel is a parallepiped oriented according to the coordinate axes

$$\delta \boldsymbol{A} = \hat{\boldsymbol{x}}\, \delta x \quad \text{and} \quad \delta \boldsymbol{B} = \hat{\boldsymbol{y}}\, \delta y \quad \text{and} \quad \delta \boldsymbol{C} = \hat{\boldsymbol{z}}\, \delta z, \quad (18.138)$$

so that

$$\delta V = \delta x\, \delta y\, \delta z. \quad (18.139)$$

Plugging into equation (18.137) leads to

$$\frac{1}{\delta V}\frac{\mathrm{D}(\delta V)}{\mathrm{D}t} = \nabla \cdot \boldsymbol{v}. \quad (18.140)$$

This result is a three-dimensional generalization of the material area equation (18.135).

We offer an alternative derivation of equation (18.140) in Section 19.2, where no assumptions are made concerning the shape of the material region. That derivation leads us to conclude that the relative volume of a material parcel increases when the parcel moves through a region where the velocity diverges ($\nabla \cdot \boldsymbol{v} > 0$). We think of a diverging velocity field as "spreading out" the material parcel boundary, thus increasing its volume. In contrast, the volume of a material parcel decreases where the fluid velocity converges ($\nabla \cdot \boldsymbol{v} < 0$)

$$\nabla \cdot \boldsymbol{v} > 0 \Longrightarrow \text{material volume increases in diverging flow} \Longrightarrow \text{parcel expands} \quad (18.141a)$$
$$\nabla \cdot \boldsymbol{v} < 0 \Longrightarrow \text{material volume decreases in converging flow} \Longrightarrow \text{parcel contracts.} \quad (18.141b)$$

Some authors refer to $\nabla \cdot \boldsymbol{v}$ as the *dilatation* (e.g., page 15 of *Pope* (2000)), since the velocity divergence measures the rate that the volume of a fluid element is expanded (dilates) or contracts.

18.10.2 Evolution of the column thickness

A material volume, δV, evolves according to the divergence of the velocity (equation (18.140)), whereas the material area, $\delta \mathcal{S}$, evolves according to the surface divergence of the velocity (equation (18.127)). Now consider a material volume whose cross-sectional area is $\delta \mathcal{S}$ and whose thickness is δh, with δh measuring the thickness in a direction defined by the unit normal, $\hat{\boldsymbol{n}}$. That is, the material volume is cylindrical. We can deduce the evolution of the thickness since we know the evolution of the volume and area

$$\frac{1}{\delta V}\frac{\mathrm{D}(\delta V)}{\mathrm{D}t} = \frac{1}{\delta h\, \delta \mathcal{S}}\frac{\mathrm{D}(\delta h\, \delta \mathcal{S})}{\mathrm{D}t} = \frac{1}{\delta h}\frac{\mathrm{D}(\delta h)}{\mathrm{D}t} + \frac{1}{\delta \mathcal{S}}\frac{\mathrm{D}(\delta \mathcal{S})}{\mathrm{D}t}. \quad (18.142)$$

Use of equations (18.140) and (18.127) render

$$\frac{1}{\delta h}\frac{\mathrm{D}(\delta h)}{\mathrm{D}t} = \nabla \cdot \boldsymbol{v} - \nabla^{\mathsf{surf}} \cdot \boldsymbol{v} = \hat{n}_i\, (\hat{\boldsymbol{n}} \cdot \nabla)\, v_i. \quad (18.143)$$

For example, consider the special case with $\hat{\boldsymbol{n}} = \hat{\boldsymbol{z}}$, in which

$$\frac{1}{\delta h}\frac{\mathrm{D}(\delta h)}{\mathrm{D}t} = \frac{\partial w}{\partial z}, \quad (18.144)$$

so that the column thickness evolves according to the vertical derivative of the vertical velocity. This result accords with our discussion of stretching in Section 18.8.3.

18.10.3 Evolution of the Jacobian of transformation

Recall the discussion in Sections 18.7.3 and 18.7.1, where we showed how the Jacobian satisfies

$$\mathrm{d}^3x = \frac{\partial \boldsymbol{\varphi}(\boldsymbol{a},T)}{\partial \boldsymbol{a}}\,\mathrm{d}^3a \Longrightarrow \frac{\partial \boldsymbol{\varphi}(\boldsymbol{a},T)}{\partial \boldsymbol{a}} = \frac{\mathrm{d}^3x}{\mathrm{d}^3a}, \tag{18.145}$$

where

$$\mathrm{d}^3a = \mathrm{d}a^1\,\mathrm{d}a^2\,\mathrm{d}a^3 \tag{18.146}$$

is the material coordinate volume for the parcel, and d^3x is the Eulerian coordinate volume. The material coordinate volume is a constant following a particle trajectory, whereas the Eulerian coordinate volume is not a constant, so that

$$\frac{\mathrm{D}}{\mathrm{D}t}\frac{\partial \boldsymbol{\varphi}}{\partial \boldsymbol{a}} = \frac{1}{\mathrm{d}^3a}\frac{\mathrm{D}(\mathrm{d}^3x)}{\mathrm{D}t} \tag{18.147a}$$

$$= \frac{\mathrm{d}^3x}{\mathrm{d}^3a}\,\nabla\cdot\boldsymbol{v} \tag{18.147b}$$

$$= \frac{\partial \boldsymbol{\varphi}}{\partial \boldsymbol{a}}\,\nabla\cdot\boldsymbol{v}. \tag{18.147c}$$

The second equality made use of the equation (18.140), which expresses the material time change for the volume of a material fluid parcel, as measured in position space, in terms of the velocity divergence. We thus see that the relative change of the Jacobian is determined by the divergence of the velocity

$$\left[\frac{\partial \boldsymbol{\varphi}}{\partial \boldsymbol{a}}\right]^{-1}\frac{\mathrm{D}}{\mathrm{D}t}\left[\frac{\partial \boldsymbol{\varphi}}{\partial \boldsymbol{a}}\right] = \nabla\cdot\boldsymbol{v}. \tag{18.148}$$

This equation is identical to the parcel volume equation (18.140), which is expected given the relation between the Jacobian and the parcel volume. In Exercise 18.5, we derive this result using the explicit expression for the Jacobian in terms of the permutation symbol, ϵ.

18.11 Kinematics of two-dimensional flow

In this section we consider the rudiments of two-dimensional flow as a venue to illustrate topics presented earlier in this chapter such as dilation, rotation, and strains. In so doing we expose kinematic properties commonly used to characterize two-dimensional flow, with generalizations to three-dimensions available with a bit more maths. We retain Cartesian tensors throughout this section.

The starting point is Figure 18.10, which shows a square region of fluid exposed to a variety of flow regimes. We can kinematically describe these changes by making use of the velocity gradient tensor introduced in Section 18.8, here written for the two-dimensional flow with horizontal velocity components, (u,v)

$$[\partial_j v^i] = \begin{bmatrix} \partial u/\partial x & \partial u/\partial y \\ \partial v/\partial x & \partial v/\partial y \end{bmatrix} \tag{18.149a}$$

$$= \begin{bmatrix} \partial u/\partial x & (1/2)\,(\partial u/\partial y + \partial v/\partial x) \\ (1/2)\,(\partial u/\partial y + \partial v/\partial x) & \partial v/\partial y \end{bmatrix} + \frac{\zeta}{2}\begin{bmatrix} 0 & -1 \\ 1 & 0 \end{bmatrix} \tag{18.149b}$$

$$= \mathbf{S} + \mathbf{R}, \tag{18.149c}$$

where

$$\zeta = \hat{\boldsymbol{z}}\cdot\nabla\times\boldsymbol{v} = \partial v/\partial x - \partial u/\partial y \tag{18.150}$$

is the vertical component to the vorticity.

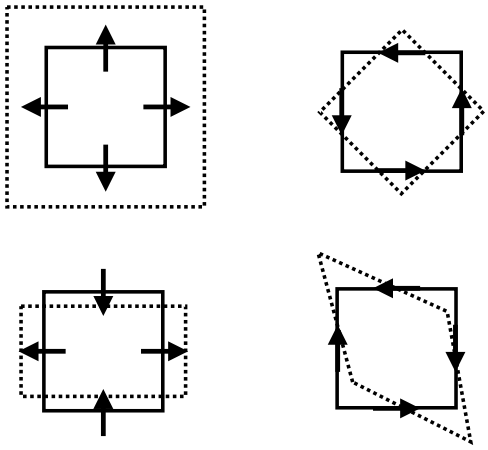

FIGURE 18.10: Illustrating the varieties of changes for an initially square material fluid region in two-dimensional flow. Upper left: purely divergent flow, whereby $\nabla \cdot \boldsymbol{u} > 0$ yet with zero vorticity, thus leading to an increase in the area. An example flow generating this motion is realized by $\boldsymbol{u} = \gamma\,(x\,\hat{\boldsymbol{x}} + y\,\hat{\boldsymbol{y}}) = \gamma\,\boldsymbol{x}$ (with $\gamma > 0$ a constant of dimensions inverse time) so that the divergence is $\nabla \cdot \boldsymbol{u} = 2\,\gamma$. Upper right: rotational flow with nonzero vertical vorticity component, $\zeta = \hat{\boldsymbol{z}} \cdot (\nabla \times \boldsymbol{u})$, yet zero divergence, thus leading to a pure rotation of the square patch. An example flow generating this motion is realized by $\boldsymbol{u} = \hat{\boldsymbol{z}} \times \nabla\psi = \gamma\,(-y\,\hat{\boldsymbol{x}} + x\,\hat{\boldsymbol{y}}) = -\gamma\,\hat{\boldsymbol{z}} \times \boldsymbol{x}$ with streamfunction $\psi = (\gamma/2)\,(x^2 + y^2)$ and vorticity $\zeta = \nabla^2\psi = 2\,\gamma$. Lower left: result of a pure tension/compression straining flow (also called a deformation flow) with zero divergence and zero vorticity, leading to compression in one direction and dilation in the orthogonal direction. An example flow is given by $\boldsymbol{u} = \hat{\boldsymbol{z}} \times \nabla\psi = \gamma\,(x\,\hat{\boldsymbol{x}} - y\,\hat{\boldsymbol{y}})$ with streamfunction $\psi = -\gamma\,x\,y$. The deformation of the region is measured by the tension strain, $\partial_x u - \partial_y v = 2\,\gamma$. Lower right: pure shearing strain flow with zero divergence and zero vorticity. An example flow is given by $\boldsymbol{u} = -\gamma\,(y\,\hat{\boldsymbol{x}} + x\,\hat{\boldsymbol{y}})$ with streamfunction $\psi = -(\gamma/2)\,(x^2 - y^2)$. The deformation of the region is measured by the shearing strain, $\partial_y u + \partial_x v = -2\,\gamma$. This figure is adapted from Figure 2.4 of *Hoskins and James* (2014).

18.11.1 Diverging flow

Recall from Section 18.9.4 that a material surface in two-dimensional flow changes its area according to the divergence. The upper left panel of Figure 18.10 thus illustrates equation (18.135)

$$\frac{1}{\delta\mathcal{S}}\,\frac{\mathrm{D}(\delta\mathcal{S})}{\mathrm{D}t} = \nabla \cdot \boldsymbol{u} = S^i{}_i = S^1{}_1 + S^2{}_2, \tag{18.151}$$

where $\delta\mathcal{S}$ is the area and $S^i{}_i$ is the trace of the strain rate tensor. That is, a diverging flow as depicted by this figure, with $\nabla \cdot \boldsymbol{u} > 0$, leads to an expansion of the area. The opposite occurs for a converging flow, where the area compresses.

18.11.2 Flow with nonzero deformation

The lower left panel of Figure 18.10 shows the square within a deformational flow whereby it contracts along the y-axis and dilates along the x-axis. This flow is non-divergent, $\nabla \cdot \boldsymbol{u} = 0$, and has zero vorticity, $\zeta = 0$, so that the area remains constant and the orientation is fixed. However, it has shear that acts to deform the area. This particular non-divergent deformational flow is determined by

$$\boldsymbol{u} = \hat{\boldsymbol{z}} \times \nabla\psi, \tag{18.152}$$

with the streamfunction, $\psi = -\gamma\,x\,y$ where γ is a constant inverse time scale and hence the strength of the strain. The resulting velocity components are $u = -\partial\psi/\partial y = \gamma\,x$ and $v = \partial\psi/\partial x = -\gamma\,y$.

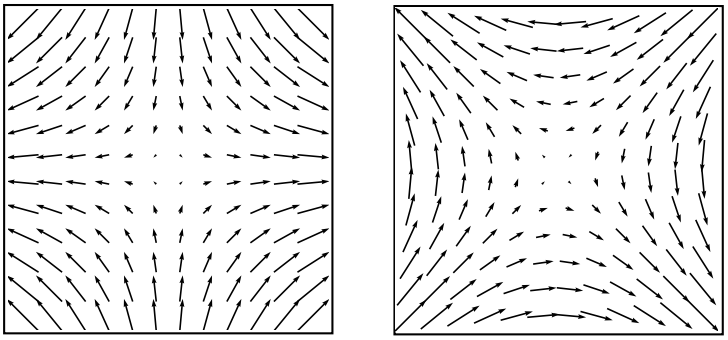

FIGURE 18.11: Two-dimensional horizontally non-divergent and irrotational flow with nonzero deformation/strain. Left panel: pure tension strain as determined by the streamfunction, $\psi = -\gamma\, x\, y$, so that the velocity $\boldsymbol{u} = \hat{\boldsymbol{z}} \times \boldsymbol{\nabla}\psi = \gamma\,(x\,\hat{\boldsymbol{x}} - y\,\hat{\boldsymbol{y}})$. The y-axis orients the direction along which flow contracts (compression) whereas the x-axis is the dilation axis (tension). Right panel: pure shearing flow as determined by the streamfunction $\psi = -(\gamma/2)\,(x^2 - y^2)$ so that the velocity is $\boldsymbol{u} = \hat{\boldsymbol{z}} \times \boldsymbol{\nabla}\psi = \gamma\,(-y\,\hat{\boldsymbol{x}} - x\,\hat{\boldsymbol{y}})$. We set $\gamma = 1$ for both examples.

18.11.3 Rotational flow with nonzero vorticity

The upper right panel of Figure 18.10 illustrates the effects from flow with a non-zero vorticity, $\zeta = \partial v/\partial x - \partial u/\partial y$. We provide extensive discussion of vorticity in Part VII of this book, with vorticity measuring the spin of a fluid particle within the flow. The nonzero spin imparts a rotation to an area element, with the flow in the upper right panel of Figure 18.10 bringing about a counter-clockwise rotation. All components of the strain tensor vanish for a purely rotational flow, so that there is no deformation of the square as it rotates.

There are two combinations of the strain rate tensor elements that are useful in describing deformational flows:

$$\text{tension strain} = S_{\text{T}} = S^1{}_1 - S^2{}_2 = \partial u/\partial x - \partial v/\partial y \tag{18.153a}$$

$$\text{shearing strain} = S_{\text{S}} = 2\,S^1{}_2 = \partial u/\partial y + \partial v/\partial x. \tag{18.153b}$$

The tension strain and shearing strain are also known as tension and shearing *deformation rates*. Note that negative tension is known as *compression*. For the deformation flow with streamfunction $\psi = -\gamma\, x\, y$, we have

$$S_{\text{T}} = 2\,\gamma \qquad \text{and} \qquad S_{\text{S}} = 0, \tag{18.154}$$

so that this velocity leads to a purely tension straining flow. In contrast, the following non-divergent irrotational flow is a purely shearing strain flow

$$\psi = -(\gamma/2)\,(x^2 - y^2) \qquad u = -\gamma\, y \qquad v = -\gamma\, x \qquad S_{\text{T}} = 0 \qquad S_{\text{S}} = -2\,\gamma, \tag{18.155}$$

as depicted by the right panel of Figure 18.11. This pure shearing flow leads to the deformation of the fluid square shown in the lower right panel of Figure 18.10.

18.11.4 Further study

Elements of this section can be found in Section 2.3 of *Hoskins and James* (2014). More detailed examinations of two-dimensional flow kinematics are offered by *Weiss* (1991) and *Lilly* (2018). Furthermore, we here introduced the streamfunction, ψ, for non-divergent two-dimensional flow, yet provide a more thorough discussion in Section 21.4.

18.12 Exercises

EXERCISE 18.1: MATERIAL EVOLUTION OF THE ACCELERATION DIVERGENCE
This exercise is based on problem 10(a) from Section 3.1 of *Segel* (1987). Here, we derive the relation

$$\nabla \cdot \frac{\mathrm{D}\boldsymbol{v}}{\mathrm{D}t} = \frac{\mathrm{D}(\nabla \cdot \boldsymbol{v})}{\mathrm{D}t} + S^i{}_j \, S^j{}_i - R^i{}_j \, R^j{}_i, \tag{18.156}$$

where $S^i{}_j \, S^j{}_i$ and $R^i{}_j \, R^j{}_i$ are the doubly contracted strain rate tensor and squared rotation tensor (Sections 18.8.4 and 18.8.5). Make use of Cartesian tensors for your solution.

EXERCISE 18.2: VELOCITY FIELD WITH ZERO STRAIN (*Aris* (1962) EXERCISE 4.41.1)
If the strain rate tensor vanishes, show that the velocity field can be written

$$\boldsymbol{v} = \boldsymbol{U} + \boldsymbol{\Omega} \times \boldsymbol{x}, \tag{18.157}$$

where $\boldsymbol{\Omega}$ is a constant angular rotation rate and $\boldsymbol{U}$ is a constant velocity. That is, a fluid velocity equal to a constant rotation plus translation renders zero strain. Hint: if $\mathbf{S} = 0$, what does that imply about the velocity field? You may also wish to make use of the general decomposition (18.106).

EXERCISE 18.3: STRAIN RATE TENSOR AND ROTATION TENSOR (*Aris* (1962) EXERCISE 4.43.3)
Consider a two-dimensional flow with horizontal velocity

$$\boldsymbol{u} = (F/r)\,(\hat{\boldsymbol{x}}\, y - \hat{\boldsymbol{y}}\, x), \tag{18.158}$$

where $F = F(r)$ is an arbitrary function of the radial distance $r = \sqrt{x^2 + y^2}$ and with dimensions of L T^{-1}. Throughout this exercise, be sure your solution is dimensionally consistent.

(a) Show that the velocity field is non-divergent.

(b) Determine an analytic expression for the streamlines and draw a picture.

(c) Determine the elements to the strain rate tensor, $\mathbf{S}$, given by equation (18.149c). Write the expression using polar coordinates $x = r\cos\varphi$ and $y = r\sin\varphi$ (see Section 4.22) and the structure function

$$G(r) = r\,\frac{\mathrm{d}(F/r)}{\mathrm{d}r} = (F' - F/r)/2 \quad \text{with } F' = \mathrm{d}F/\mathrm{d}r. \tag{18.159}$$

(d) Determine elements to the rotation tensor, $\mathbf{R}$, given by equation (18.149c), also written in polar coordinates.

EXERCISE 18.4: STRAIN RATE TENSOR AND ROTATION TENSOR FOR PARALLEL SHEAR FLOW
Consider a two-dimensional parallel shear flow with horizontal velocity

$$\boldsymbol{u} = a\, x\, \hat{\boldsymbol{y}}, \tag{18.160}$$

where a is a constant with dimension inverse time.

(a) Compute the strain rate tensor, $\mathbf{S}$ (equation (18.149c)) for this velocity field.

(b) Compute the rotation tensor, $\mathbf{R}$ (equation (18.149c)) for this velocity field.

(c) Decompose the velocity field according to equation (18.106), and show that each of the velocity components is non-divergent. That is, write

$$\boldsymbol{u} = \boldsymbol{u}^0 + \boldsymbol{u}^{(\mathrm{S})} + \boldsymbol{u}^{(\mathrm{A})} \qquad \text{with} \qquad \nabla \cdot \boldsymbol{u}^{(\mathrm{S})} = \nabla \cdot \boldsymbol{u}^{(\mathrm{A})} = 0, \tag{18.161}$$

with u_i^0 the velocity at the point where $\delta x_i = x_i - x_i^0 = 0$. The velocity $\boldsymbol{u}^{(\mathrm{S})}$ has a constant strain but no vorticity whereas $\boldsymbol{u}^{(\mathrm{A})}$ has a constant vorticity but no strain. Hint: both $\boldsymbol{u}^{(\mathrm{S})}$ and $\boldsymbol{u}^{(\mathrm{A})}$ have nonzero $\hat{\boldsymbol{x}}$ and $\hat{\boldsymbol{y}}$ components.

(d) Determine the streamfunctions for $\boldsymbol{u}^{(\mathrm{S})}$ and $\boldsymbol{u}^{(\mathrm{A})}$.

(e) Sketch the velocity vectors $\boldsymbol{u}^{(\mathrm{S})}$ and $\boldsymbol{u}^{(\mathrm{A})}$.

EXERCISE 18.5: EVOLUTION OF THE JACOBIAN USING ϵ-TENSOR GYMNASTICS

There is another way to derive the identity (18.148) for the evolution of the Jacobian. This other method is somewhat more tedious. However, it exercises some useful methods of index gymnastics involving the ϵ-tensor. It also has a natural generalization to curved spaces. This exercise is only for aficionados of tensor analysis.

An explicit expression for the Jacobian of transformation is given by

$$\frac{\partial \boldsymbol{\varphi}}{\partial \boldsymbol{a}} = \frac{1}{3!}\,\epsilon_{mnp}\,\epsilon^{IJK}\,\frac{\partial \varphi^m}{\partial a^I}\,\frac{\partial \varphi^n}{\partial a^J}\,\frac{\partial \varphi^p}{\partial a^K}. \tag{18.162}$$

Take the material derivative of this expression and show that we get the same expression as equation (18.148). Hint: make use of the identity

$$\frac{\mathrm{D}}{\mathrm{D}t}\,\frac{\partial \varphi^m}{\partial a^I} = \frac{\partial v^m}{\partial a^I}, \tag{18.163}$$

which holds since the material time derivative is taken with the material coordinates, $\boldsymbol{a}$, held fixed. Also make use of the identity (4.75) for the derivative of the Jacobian with respect to one of the matrix elements. Finally, note that similar manipulations are encountered in Section 47.5.4.

Chapter 19

MASS CONSERVATION

Throughout this book, we assume that matter is neither created nor destroyed anywhere within the fluid continuum, and furthermore that the fluid remains in a single phase.[1] These assumptions constrain the fluid motion and as such they form an important facet of fluid kinematics. In this chapter, we derive a variety of mathematical expressions for mass conservation in a single component fluid (materially homogeneous fluid), along with associated kinematic constraints placed on fluid motion. These constraints are examined both in the fluid interior and at boundaries, and from both Eulerian and Lagrangian viewpoints.

READER'S GUIDE TO THIS CHAPTER

We are here concerned with single-component fluids, with generalizations to multiple-component fluids given in Chapter 20. We build on the understanding of the Eulerian and Lagrangian kinematic descriptions developed in Chapters 17 and 18. For some discussions we require the tools from general tensor analysis as summarized in Chapter 18 for Eulerian ($\boldsymbol{x}$-space) and Lagrangian ($\boldsymbol{a}$-space).

[1] Chemical reactions transform matter from one form to the another. Nuclear reactions convert between matter and nuclear energy. Phase changes convert matter from one phase to another. These processes are all outside the scope of this book.

19.1 Eulerian fluid regions

We here develop expressions for the mass budget within an Eulerian region, both infinitesimal and finite. Recall that Eulerian regions are fixed in space and thus have constant volumes.

19.1.1 Finite volume expression

Consider a finite sized cubic region that is fixed in space as shown in Figure 19.1. The mass contained within the cube is given by

$$\Delta M = \rho \, \Delta V = \rho \, \Delta x \, \Delta y \, \Delta z, \tag{19.1}$$

where the cube volume,

$$\Delta V = \Delta x \, \Delta y \, \Delta z, \tag{19.2}$$

is constant in time as per an Eulerian region. Since we will be taking the limit as the size of the cube becomes infinitesimal, it is sufficient to approximate the mass density as that at the cube center, $\rho = \rho(x, y, z, t)$. In the absence of mass sources within the fluid, the mass within the cube changes only through the accumulation or depletion of mass transported across the six cube faces.

Focusing on the mass transport in the meridional direction as illustrated in Figure 19.1, the accumulation of mass within the cube through this transport is determined by the difference in mass transport crossing the two adjacent cell faces

$$\text{mass change from meridional transport} = (\Delta x \, \Delta z) \, [(v \, \rho)_{y - \Delta y/2} - (v \, \rho)_{y + \Delta y/2}]. \tag{19.3}$$

Expanding the difference into a Taylor series and truncating after leading order yields

$$\text{mass change from meridional transport} \approx -(\Delta x \, \Delta y \, \Delta z) \, \frac{\partial (v \, \rho)}{\partial y}. \tag{19.4}$$

The same analysis for the zonal and vertical directions leads to the mass budget for the cube

$$\frac{\partial (\rho \, \Delta V)}{\partial t} = -\Delta V \left[\frac{\partial (u \, \rho)}{\partial x} + \frac{\partial (v \, \rho)}{\partial y} + \frac{\partial (w \, \rho)}{\partial z} \right]. \tag{19.5}$$

Hence, the cube mass changes according to convergence of mass across the cube boundaries. Cancelling the constant volume ΔV (again, the volume is assumed fixed as per an Eulerian region) renders the *flux-form* Eulerian mass continuity equation

$$\frac{\partial \rho}{\partial t} + \nabla \cdot (\rho \, \boldsymbol{v}) = 0. \tag{19.6}$$

The mass continuity equation (19.6) is in the form of a *flux-form conservation law*, in which the local time tendency of a field is determined by the convergence of a flux

$$\frac{\partial \rho}{\partial t} = -\nabla \cdot (\rho \, \boldsymbol{v}). \tag{19.7}$$

The *mass flux*, $\rho \, \boldsymbol{v}$, with dimensions $M \, L^{-2} \, T^{-1}$, measures the mass per time of matter crossing

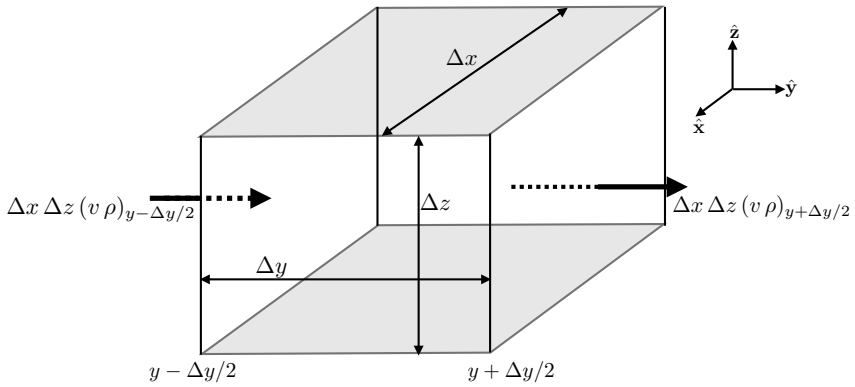

FIGURE 19.1: A finite sized cube or cell region with fixed dimensions and position (an Eulerian region) used to formulate the Eulerian form of mass conservation. We highlight two cell faces with area $\Delta x\,\Delta z$ and with meridional mass transport crossing the faces given by $\Delta x\,\Delta z\,(v\,\rho)_{y-\Delta y/2}$ and $\Delta x\,\Delta z\,(v\,\rho)_{y+\Delta y/2}$. To establish signs we assume the meridional velocity is positive, $v > 0$, so that mass enters the face at $y - \Delta y/2$ and leaves the face at $y + \Delta y/2$. Differences between these two transports leads to an accumulation of mass within the cell. The resulting mass budget holds regardless the direction of the flow velocity.

a unit area oriented with an outward normal in each of the three Cartesian directions. If more mass is transported into a region than leaves (i.e., mass converges), then the mass density increases, and vice versa for a mass flux that diverges from a region. It is notable that the mass flux also serves as a measure of the *momentum flux*, which we discuss in Chapter 24.

19.1.2 Arbitrary Eulerian region

The discussion for the infinitesimal cube can be generalized by making use of Gauss's divergence theorem from Section 2.7. For that purpose, consider an arbitrary static and simply closed region within the fluid such as in Figure 19.2. Integrating the continuity equation (19.6) over that region leads to

$$\int_{\mathcal{R}} \frac{\partial \rho}{\partial t}\,\mathrm{d}V = -\int_{\mathcal{R}} \nabla \cdot (\rho\,\boldsymbol{v})\,\mathrm{d}V. \tag{19.8}$$

Since the region is static we can move the partial time derivative outside on the left hand side. Furthermore, the divergence theorem can be applied to the right hand side to convert the volume integral to a surface integral over the boundaries of the static domain. The resulting mass budget is given by

$$\frac{\mathrm{d}}{\mathrm{d}t}\int_{\mathcal{R}} \rho\,\mathrm{d}V = -\oint_{\partial\mathcal{R}} \rho\,\boldsymbol{v}\cdot\hat{\boldsymbol{n}}\,\mathrm{d}\mathcal{S}, \tag{19.9}$$

where $\hat{\boldsymbol{n}}$ is the outward unit normal vector along the closed boundary of the region, and $\mathrm{d}\mathcal{S}$ is the surface area element along that boundary. This equation says that the mass within a fixed region of the fluid changes in time (left hand side) according to the accumulation of mass crossing the region boundary (right hand side). The minus sign means that the mass decreases in the region if there is a net mass transport leaving the domain in the direction of the outward normal.

19.2 Material fluid parcels

We here derive the differential expressions for mass conservation of a constant mass fluid parcel within a Lagrangian reference frame. The differential expressions for volume and density arise as a corollary. This discussion complements the Eulerian discussion from Section 19.1. To motivate

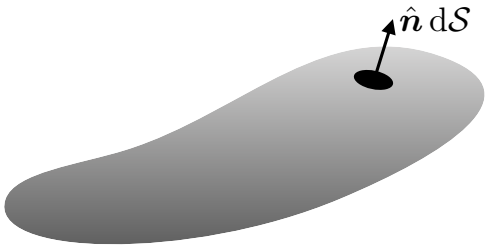

FIGURE 19.2: An arbitrarily shaped simply closed region, $\mathcal{R}$, within the fluid. If the region is fixed in space, then it represents a general Eulerian region for considering mass budgets. A surface area element, $\mathrm{d}\mathcal{S}$, is oriented according to the outward normal, $\hat{\boldsymbol{n}}$.

the derivations we expand the flux-form mass continuity equation (19.6) to have

$$\frac{1}{\rho}\frac{\mathrm{D}\rho}{\mathrm{D}t} = -\nabla\cdot\boldsymbol{v}, \tag{19.10}$$

where $\mathrm{D}/\mathrm{D}t = \partial_t + \boldsymbol{v}\cdot\nabla$ is the material time derivative operator from Section 17.4.4. We now derive this form of the mass continuity using Lagrangian methods.

19.2.1 Lagrangian expression for mass conservation

The mass of an infinitesimal fluid parcel that moves with the fluid flow is written[2]

$$\delta M = \rho\,\delta V, \tag{19.11}$$

where δV is the volume and

$$\rho = \delta M/\delta V \tag{19.12}$$

is the mass density of the moving parcel. Mass conservation means that the fluid parcel has a constant mass as it moves with the flow, so that its material time derivative vanishes

$$\frac{\mathrm{D}(\delta M)}{\mathrm{D}t} = 0. \tag{19.13}$$

Equation (19.13) is the most basic form of mass conservation for a fluid parcel. However, one often has need to express this result in terms of parcel density and parcel volume

$$\frac{\mathrm{D}(\delta M)}{\mathrm{D}t} = \frac{\mathrm{D}\,(\rho\,\delta V)}{\mathrm{D}t} = \delta M\left[\frac{1}{\rho}\frac{\mathrm{D}\rho}{\mathrm{D}t} + \frac{1}{\delta V}\frac{\mathrm{D}(\delta V)}{\mathrm{D}t}\right]. \tag{19.14}$$

Comparing to the mass continuity equation (19.10) leads to[3]

$$\frac{1}{\delta M}\frac{\mathrm{D}(\delta M)}{\mathrm{D}t} = \frac{1}{\rho}\frac{\mathrm{D}\rho}{\mathrm{D}t} + \nabla\cdot\boldsymbol{v}. \tag{19.15}$$

Setting $\mathrm{D}(\delta M)/\mathrm{D}t = 0$ renders the continuity equation (19.10) derived from the Eulerian expression

$$\frac{1}{\rho}\frac{\mathrm{D}\rho}{\mathrm{D}t} = -\nabla\cdot\boldsymbol{v}. \tag{19.16}$$

The parcel volume contracts in regions where the velocity converges (we prove that property in Sections 18.10.1 and 19.3.1). The continuity equation (19.16) then says that regions of volume

[2]Recall that we use the δ symbol to signal a property measured in the Lagrangian reference frame.

[3]In Section 18.10.1 we derived the material evolution of volume, and will again see this result in equation (19.25).

contraction are where the parcel density increases whereas the opposite occurs for regions where the velocity diverges.

19.2.2 Summary of material kinematic equations

Let us now summarize the variety of differential evolution equations for mass, volume, and density as viewed from a material reference frame

$$\frac{\mathrm{D}(\delta M)}{\mathrm{D}t} = 0 \qquad \text{parcel mass is constant} \tag{19.17}$$

$$\frac{1}{\delta V}\frac{\mathrm{D}(\delta V)}{\mathrm{D}t} = \nabla \cdot \boldsymbol{v} \qquad \text{parcel volume increases in divergent flow} \tag{19.18}$$

$$\frac{1}{\rho}\frac{\mathrm{D}\rho}{\mathrm{D}t} = -\nabla \cdot \boldsymbol{v} \qquad \text{parcel density increases in convergent flow.} \tag{19.19}$$

To help remember the signs on the right hand side, recall that as the fluid diverges from a point ($\nabla \cdot \boldsymbol{v} > 0$), it expands the boundaries of the material parcel and so increases the parcel volume as per equation (19.18). Since the parcel has a fixed mass, the diverging velocity field causes the material parcel density to decrease ($-\nabla \cdot \boldsymbol{v} < 0$) as per equation (19.19).

19.3 Material fluid regions

We now extend the kinematics of material fluid parcels in Section 19.2 to finite sized material fluid regions. Just as for material fluid parcels, the finite sized material fluid region retains the same matter content, and thus maintains a constant mass.[4] We contrast the discussion here with that for Eulerian regions (fixed in space) considered in Section 19.1. One key operational distinction between the Eulerian and Lagrangian domains is that partial time derivative, ∂_t, commutes with integration over a fixed Eulerian domain, whereas material time derivative, ∂_T, commutes with integration over a Lagrangian domain as per Reynolds transport theorem derived in Section 19.5.

19.3.1 Evolution of volume

Consider a finite material region, $\mathcal{R}(\boldsymbol{v})$, whose volume is given by the integral

$$V = \int_{\mathcal{R}(\boldsymbol{v})} \mathrm{d}V, \tag{19.20}$$

with $\mathrm{d}V$ the volume element. The region changes its shape according to motion of the fluid particles fixed to the boundary of the material region. We designate this region as

$$\mathcal{R}(\boldsymbol{v}) = \text{region following flow}, \tag{19.21}$$

with the $\boldsymbol{v}$ argument emphasizing that the region moves with the flow velocity. The material region expands when the flow moves outward and contracts when the flow moves inward. These statements take on the following mathematical expression

$$\frac{\mathrm{d}}{\mathrm{d}t}\int_{\mathcal{R}(\boldsymbol{v})} \mathrm{d}V = \oint_{\partial\mathcal{R}(\boldsymbol{v})} \boldsymbol{v} \cdot \hat{\boldsymbol{n}}\, \mathrm{d}\mathcal{S}, \tag{19.22}$$

[4] Recall that throughout this chapter we are focused on single-component fluids, so there is no diffusion of matter considered here. We relax this restriction in Chapter 20.

where $\hat{\boldsymbol{n}}$ is the outward normal on the region's closed boundary, $\mathrm{d}\mathcal{S}$ is the area element on the boundary, and

$$\boldsymbol{v} \cdot \hat{\boldsymbol{n}}\, \mathrm{d}\mathcal{S} = \text{volume transport (volume per time) at the boundary } \partial\mathcal{R}. \tag{19.23}$$

Use of the divergence theorem then leads to the equivalent expression

$$\frac{\mathrm{d}}{\mathrm{d}t} \int_{\mathcal{R}(\boldsymbol{v})} \mathrm{d}V = \int_{\mathcal{R}(\boldsymbol{v})} \nabla \cdot \boldsymbol{v}\, \mathrm{d}V. \tag{19.24}$$

We now take the limit as the material region becomes a material parcel, in which case we recover the differential expression

$$\frac{1}{\delta V} \frac{\mathrm{D}(\delta V)}{\mathrm{D}t} = \nabla \cdot \boldsymbol{v}, \tag{19.25}$$

where we make use of $\mathrm{D}/\mathrm{D}t$ since the infinitesimal volume is moving with the fluid. This equation is also derived in Section 18.10.1 using different methods.

19.3.2 Mass conservation

The mass of fluid contained in a finite material region is given by

$$M = \int_{\mathcal{R}(\boldsymbol{v})} \rho\, \mathrm{d}V. \tag{19.26}$$

As a material fluid region, it maintains a constant mass as it moves through the fluid so that

$$\frac{\mathrm{d}}{\mathrm{d}t} \int_{\mathcal{R}(\boldsymbol{v})} \rho\, \mathrm{d}V = 0. \tag{19.27}$$

Just as for the volume in Section 19.3.1, taking the limit as the material region becomes infinitesimally small, the region mass conservation statement (19.27) becomes the parcel mass conservation statement (19.13)

$$\frac{\mathrm{D}(\delta M)}{\mathrm{D}t} = \frac{\mathrm{D}(\rho\, \delta V)}{\mathrm{D}t} = 0. \tag{19.28}$$

19.4 Mass conservation and the motion field

In Sections 18.2 and 18.3 we described motion of the matter continuum in terms of the *motion field*, $\boldsymbol{\varphi}(\boldsymbol{a}, T)$. The motion field smoothly and continuously maps the reference or *base manifold*, $\mathcal{B}$, to the *spatial manifold*, $\mathcal{S}$, as time evolves. In that manner, the motion field provides a *flow map*. Here we frame mass conservation in this rather formal language of Lagrangian fluid mechanics, with Figure 19.3 providing a summary of the ideas.

19.4.1 Mass for a fluid parcel

Following the discussion of material volume elements in Section 18.7.3, write the mass of a fluid parcel on the referential or base manifold, $\mathcal{B}$, as (see equation (18.78))

$$\delta M = \rho^{\mathsf{L}}(\boldsymbol{a}, T = t_{\mathsf{R}}) \sqrt{\det[\mathbb{g}^{\mathsf{L}}(\boldsymbol{a}, T = t_{\mathsf{R}})]}\, \mathrm{d}^3 a = \mathring{\rho}^{\mathsf{L}}(\boldsymbol{a})\, \mathring{g}^{\mathsf{L}}(\boldsymbol{a})\, \mathrm{d}^3 a \tag{19.29}$$

In this equation, $\mathrm{d}^3 a$ is the region of material space that is occupied by the parcel, with this region specified on the base manifold so that it does not change as the parcel evolves via the

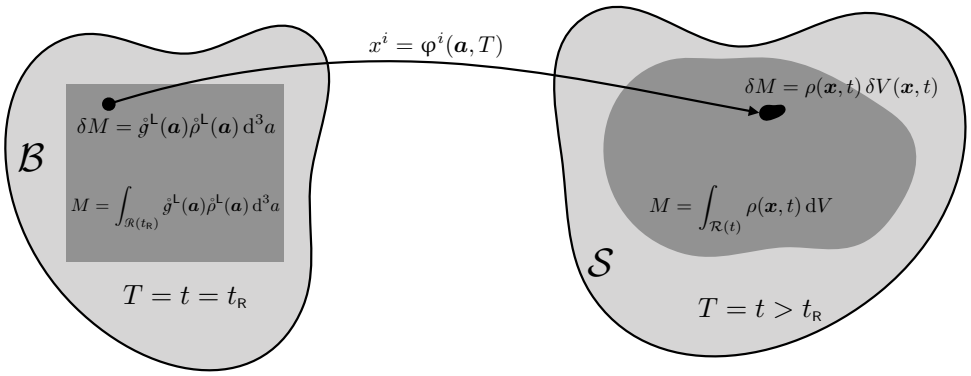

FIGURE 19.3: Following from Figure 18.1, we here depict conservation of mass in terms of the mapping between the referential or base manifold, $\mathcal{B}$, at time $T = t = t_{\mathsf{R}}$, and the spatial manifold, $\mathcal{S}$, at some future time. The mapping is affected by the motion field, $\boldsymbol{\varphi}(\boldsymbol{a}, T)$, which provides a flow map for the matter continuum. Mass conservation means that each infinitesimal fluid parcel within the matter continuum has a constant mass as it evolves from the base manifold to the spatial manifold. When represented using material coordinates on the base manifold, the parcel (small black circular region) has a mass given by $\delta M = \mathring{\rho}(\boldsymbol{a})\,\mathrm{d}^3a$, and mass within a finite subregion, $\mathcal{R}(t_{\mathsf{R}})$ of the base manifold (dark gray region) is given by the integral, $M = \int_{\mathcal{R}(t_{\mathsf{R}})} \mathring{\rho}(\boldsymbol{a})\,\mathrm{d}^3a$. When represented using Eulerian coordinates on the spatial manifold, the parcel has a mass, $\delta M = \rho(\boldsymbol{x}, t)\,\delta V(\boldsymbol{x}, t)$, and the mass within the finite subregion, $\mathcal{R}(t)$, that moves with the motion field, is given by the integral, $M = \int_{\mathcal{R}(t)} \rho(\boldsymbol{x}, t)\,\mathrm{d}V$. Mass conservation for parcels, according to equation (19.40), means that the mass densities are related by $\mathring{\rho}(\boldsymbol{a}) = \rho^{\mathsf{L}}(\boldsymbol{a}, T)\,g^{\mathsf{L}}(\boldsymbol{a}, T)$, or when using Cartesian Eulerian coordinates we have $\mathring{\rho}(\boldsymbol{a}) = \rho^{\mathsf{L}}(\boldsymbol{a}, T)\,\partial\boldsymbol{\varphi}(\boldsymbol{a}, T)/\partial\boldsymbol{a}$. In either case, $\mathring{\rho}(\boldsymbol{a})$ is independent of the material time, T

motion field. We use the shorthand

$$\mathring{g}^{\mathsf{L}}(\boldsymbol{a}) = g^{\mathsf{L}}(\boldsymbol{a}, T = t_{\mathsf{R}}) = \sqrt{\det[\mathbb{g}^{\mathsf{L}}(\boldsymbol{a}, T = t_{\mathsf{R}})]} \tag{19.30}$$

for the square root of the Euclidean metric using the Lagrangian coordinates, computed at the reference time $T = t_{\mathsf{R}}$ and written as per equation (18.43). The mass density, $\rho^{\mathsf{L}}(\boldsymbol{a}, T = t_{\mathsf{R}})$, is the density of the fluid parcel computed at the base time, $T = t_{\mathsf{R}}$.

As the fluid evolves, the motion field maps the base manifold, $\mathcal{B}$, to the spatial manifold, $\mathcal{S}$, as depicted in Figure 19.3. Mass conservation means that mass of the fluid parcel, δM, remains unchanged as its center of mass moves along a fluid particle trajectory, so that

$$\delta M = \rho^{\mathsf{L}}(\boldsymbol{a}, T)\,g^{\mathsf{L}}(\boldsymbol{a}, T)\,\mathrm{d}^3a = \mathring{\rho}^{\mathsf{L}}(\boldsymbol{a})\,\mathring{g}^{\mathsf{L}}(\boldsymbol{a})\,\mathrm{d}^3a. \tag{19.31}$$

When measured using Eulerian coordinates on the spatial manifold, the parcel mass is written

$$\delta M = \rho(\boldsymbol{x}, t)\,\delta V(\boldsymbol{x}, t). \tag{19.32}$$

In this equation, $\delta V(\boldsymbol{x}, t)$ is the parcel volume measured using $\boldsymbol{x}$ coordinates, with this volume having dimensions L^3, and being a function of space and time. The mass density, $\rho(\boldsymbol{x}, t)$, is the mass of the parcel per unit volume, $\delta V(\boldsymbol{x}, t)$. Writing the parcel mass using arbitrary Eulerian coordinates renders

$$\delta M = \rho(\boldsymbol{x}, t)\,\delta V = \rho(\boldsymbol{x}, t)\,g^{\mathsf{E}}(\boldsymbol{x})\,\mathrm{d}^3x, \tag{19.33}$$

where $g^{\mathsf{E}}(\boldsymbol{x}) = \sqrt{\det[\mathbb{g}^{\mathsf{E}}(\boldsymbol{x})]}$ is the square root of the metric determinant when using arbitrary Eulerian coordinates.[5] Equating the Lagrangian expression (19.31) to the Eulerian expression (19.33) yields the identity

$$\rho^{\mathsf{L}}(\boldsymbol{a}, T)\,g^{\mathsf{L}}(\boldsymbol{a}, T)\,\mathrm{d}^3a = \rho(\boldsymbol{x}, t)\,g^{\mathsf{E}}(\boldsymbol{x})\,\mathrm{d}^3x. \tag{19.34}$$

[5] Recall from Section 18.5.1 that the Eulerian representation of the metric tensor is independent of the Eulerian time coordinate, t.

If the Eulerian coordinates are taken to be Cartesian, then equation (18.46) means that the Jacobian of the transformation between $\boldsymbol{x}$-space and $\boldsymbol{a}$-space can be written in terms of the Lagrangian metric tensor determinant,

$$\frac{\partial \boldsymbol{\varphi}}{\partial \boldsymbol{a}} = g^{\text{L}}(\boldsymbol{a}, T) \quad \text{Cartesian Eulerian coordinates.} \tag{19.35}$$

With this choice, the parcel mass can be written as

$$\delta M = \rho^{\text{L}}(\boldsymbol{a}, T)\, (\partial \boldsymbol{\varphi}/\partial \boldsymbol{a})\, \mathrm{d}^3 a \quad \text{Cartesian Eulerian coordinates.} \tag{19.36}$$

19.4.2 Parcel mass conservation and the Jacobian

The coordinate volume in material space is a material constant, so that

$$\partial_T(\mathrm{d}^3 a) = 0. \tag{19.37}$$

Consequently, setting $\partial_T(\delta M) = \partial_T(\rho\, \delta V) = 0$ in equation (19.31) leads to the expression of mass conservation

$$\frac{\partial}{\partial T}\left[\rho^{\text{L}}(\boldsymbol{a}, T)\, g^{\text{L}}(\boldsymbol{a}, T)\right] = 0. \tag{19.38}$$

Evidently, the product of the mass density times the square root of the metric determinant remains constant when following the trajectory of a fluid particle. Specializing to the case of Cartesian Eulerian coordinates allows us to replace the metric determinant with the Jacobian as per equation (18.46), so that

$$\frac{\partial}{\partial T}\left[\rho^{\text{L}}(\boldsymbol{a}, T)\, \frac{\partial \boldsymbol{\varphi}(\boldsymbol{a}, T)}{\partial \boldsymbol{a}}\right] = 0 \quad \text{Cartesian Eulerian coordinates.} \tag{19.39}$$

Equation (19.29) for mass conservation leads to

$$\mathring{\rho}^{\text{L}}(\boldsymbol{a})\, \mathring{g}^{\text{L}}(\boldsymbol{a}) = \rho^{\text{L}}(\boldsymbol{a}, T)\, g^{\text{L}}(\boldsymbol{a}, T) \overset{\text{Cartesian Eulerian}}{=} \rho^{\text{L}}(\boldsymbol{a}, T)\, \frac{\partial \boldsymbol{\varphi}(\boldsymbol{a}, T)}{\partial \boldsymbol{a}}. \tag{19.40}$$

Defining material coordinates as the base manifold particle positions is commonly made in the solid mechanics literature (e.g., Chapter 1 of *Tromp* (2025a)). However, for geophysical fluid mechanics we do not build this assumption into the formalism. The reason is that we often find it useful to set $\boldsymbol{a}$ to non-spatial coordinates, such as discussed in Section 17.3.2.

19.4.3 Another derivation of mass conservation

Yet another derivation of mass conservation follows from the identity (18.148), in which

$$\frac{\mathrm{D}}{\mathrm{D}t}\left[\rho(\boldsymbol{x}, t)\, \delta V(\boldsymbol{x}, t)\right] = \frac{\mathrm{D}}{\mathrm{D}t}\left[\rho\, \frac{\partial \boldsymbol{\varphi}}{\partial \boldsymbol{a}}\, \mathrm{d}^3 a\right] \tag{19.41a}$$

$$= \left[\frac{\mathrm{D}\rho}{\mathrm{D}t} + \rho\, \nabla \cdot \boldsymbol{v}\right]\left[\frac{\partial \boldsymbol{\varphi}}{\partial \boldsymbol{a}}\right] \mathrm{d}^3 a \tag{19.41b}$$

$$= \left[\frac{\mathrm{D}\rho}{\mathrm{D}t} + \rho\, \nabla \cdot \boldsymbol{v}\right] \delta V(\boldsymbol{x}, t). \tag{19.41c}$$

The Eulerian form of mass conservation given by equation (19.16) is recovered when noting that the mass of a material parcel is constant, so that $\mathrm{D}\rho/\mathrm{D}t = -\rho\, \nabla \cdot \boldsymbol{v}$.

19.4.4 Mass conservation for material fluid regions

Now consider a finite region of the base manifold, $\mathcal{R}(t_{\mathsf{R}})$, as depicted in Figure 19.3. The mass of matter in this region is given by the integral

$$M = \int_{\mathcal{R}(t_{\mathsf{R}})} \mathring{\rho}^{\mathsf{L}}(\boldsymbol{a})\, \mathring{g}^{\mathsf{L}}(\boldsymbol{a})\, \mathrm{d}^3 a. \tag{19.42}$$

If the region follows the fluid flow so that $\mathcal{R}(t > t_{\mathsf{R}})$ is comprised of the same fluid particles, then the domain in $\boldsymbol{a}$-space remains unchanged, in which case we write it as $\mathcal{R}(\boldsymbol{a})$. Furthermore, a region that moves with fluid particles has a mass given by

$$M = \int_{\mathcal{R}(\boldsymbol{a})} \rho^{\mathsf{L}}(\boldsymbol{a}, T)\, g^{\mathsf{L}}(\boldsymbol{a}, T)\, \mathrm{d}^3 a \overset{\text{Cartesian Eulerian}}{=} \int_{\mathcal{R}(\boldsymbol{a})} \rho^{\mathsf{L}}(\boldsymbol{a}, T)\, \frac{\partial \boldsymbol{\varphi}(\boldsymbol{a}, T)}{\partial \boldsymbol{a}}\, \mathrm{d}^3 a. \tag{19.43}$$

When measured on the spatial manifold using Eulerian coordinates, the mass is given by

$$M = \int_{\mathcal{R}(t)} \rho(\boldsymbol{x}, t)\, \mathrm{d}V \overset{\text{Cartesian Eulerian}}{=} \int_{\mathcal{R}(t)} \rho(\boldsymbol{x}, t)\, \mathrm{d}^3 x, \tag{19.44}$$

with the Eulerian domain, $\mathcal{R}(t)$, a function of time.

A one-dimensional example

To help understand the equality between equations (19.42)–(19.44), consider a one-dimensional example, in which the mass on a material line is given by

$$\int_{x_1(t)}^{x_2(t)} \rho(x, t)\, \mathrm{d}x = \int_{a[x_1(t)]}^{a[x_2(t)]} \rho^{\mathsf{L}}(a, T)\, \frac{\partial \varphi(a, T)}{\partial a}\, \mathrm{d}a = \int_{a_1}^{a_2} \rho^{\mathsf{L}}(a, T)\, \frac{\partial \varphi(a, T)}{\partial a}\, \mathrm{d}a = \int_{a_1}^{a_2} \mathring{\rho}^{\mathsf{L}}(a)\, \mathring{g}^{\mathsf{L}}(a)\, \mathrm{d}a. \tag{19.45}$$

The first equality introduced the Jacobian, $\partial\varphi/\partial a$, for the one-dimensional coordinate transformation from $\boldsymbol{x}$-space to $\boldsymbol{a}$-space, with corresponding changes to the integration limits. We can make this coordinate transformation since there is a 1-to-1 relation between the $\boldsymbol{a}$-space and $\boldsymbol{x}$-space representation of a material fluid parcel. We also introduced the Lagrangian expression for the mass density following a fluid particle

$$\rho^{\mathsf{L}}(a, T) = \rho[x = \varphi(a, T), t = T]. \tag{19.46}$$

The second equality in equation (19.45) wrote the integral bounds in terms of the material coordinate. Since we are considering a material region that follows fluid particles, the integral bounds have fixed material coordinate values, $a[x_1(t)] = a_1$ and $a[x_2(t)] = a_2$. The final equality in equation (19.45) introduced base manifold density and metric determinant,

$$\mathring{\rho}^{\mathsf{L}}(a)\, \mathring{g}^{\mathsf{L}}(a) = \rho^{\mathsf{L}}(a, T)\, \frac{\partial \varphi(a, T)}{\partial a}, \tag{19.47}$$

which is independent of time, as required for mass conservation for a material fluid parcel as given by equation (19.39).

An exercise in the formalism

As an exercise using the Lagrangian formalism, consider the time derivative of the mass within a material fluid region and assume Cartesian $\boldsymbol{x}$-space so that

$$\frac{\mathrm{d}}{\mathrm{d}t}\left[\int_{\mathcal{R}[\boldsymbol{v}(\boldsymbol{x},t)]} \rho \,\mathrm{d}V\right] = \frac{\mathrm{d}}{\mathrm{d}t}\left[\int_{\mathcal{R}[\boldsymbol{v}(\boldsymbol{x},t)]} \rho \,\mathrm{d}^3x\right] \qquad \mathrm{d}V = \mathrm{d}^3x \text{ for Cartesian } \boldsymbol{x}\text{-space} \tag{19.48a}$$

$$= \frac{\partial}{\partial T}\left[\int_{\mathcal{R}(\boldsymbol{a})} \rho^{\text{L}} \frac{\partial \boldsymbol{\varphi}}{\partial \boldsymbol{a}} \,\mathrm{d}^3a\right] \qquad \text{transform } \boldsymbol{x} \text{ to } \boldsymbol{a} \tag{19.48b}$$

$$= \int_{\mathcal{R}(\boldsymbol{a})} \frac{\partial}{\partial T}\left[\rho^{\text{L}} \frac{\partial \boldsymbol{\varphi}}{\partial \boldsymbol{a}} \mathrm{d}^3a\right] \qquad \partial_T \text{ commutes w/ integral} \tag{19.48c}$$

$$= \int_{\mathcal{R}[\boldsymbol{v}(\boldsymbol{x},t)]} \frac{\mathrm{D}}{\mathrm{D}t}\left[\rho \,\mathrm{d}^3x\right] \qquad \text{transform } \boldsymbol{a} \text{ to } \boldsymbol{x} \tag{19.48d}$$

$$= \int_{\mathcal{R}[\boldsymbol{v}(\boldsymbol{x},t)]} \left[\frac{\mathrm{D}\rho}{\mathrm{D}t} + \rho \nabla \cdot \boldsymbol{v}\right] \mathrm{d}V \qquad \text{chain rule + eq. (18.140)} \tag{19.48e}$$

$$= \int_{\mathcal{R}[\boldsymbol{v}(\boldsymbol{x},t)]} \left[\frac{1}{\rho}\frac{\mathrm{D}\rho}{\mathrm{D}t} + \nabla \cdot \boldsymbol{v}\right] \rho \,\mathrm{d}V \qquad \text{rearrange.} \tag{19.48f}$$

When expressing the integral bounds using $\boldsymbol{a}$-space coordinates, the integral bounds have no material T-dependence since they are fixed on fluid particles. We can thus move the ∂_T derivative inside of the integral sign to reach the third equality. The fourther equality made use of equation (19.41c) and converted back to $\boldsymbol{x}$-space. In this manner, upon entering the integral and using Eulerian coordinates, the time derivative is written as a material time derivative, $\mathrm{D}/\mathrm{D}t$, since it is a time derivative computed by following the fluid particles that define the material region. As the material region, $\mathcal{R}$, has a materially constant mass, we recover the mass continuity equation (19.16) by setting the integrand in equation (19.48f) to zero.

19.5 Reynolds transport theorem

On first encounter, the method from Section 19.4.4 that involves moving between Eulerian ($\boldsymbol{x}$-space) and Lagrangian ($\boldsymbol{a}$-space) representations is clumsy at best and a black box at worse. However, with some practice it becomes an elegant means to study the time evolution of fluid properties integrated over a material region. The method is formalized by the *Reynolds transport theorem*.

19.5.1 Derivation of the theorem

Manipulations leading to the mass conservation statement (19.48f) can be generalized by considering the material time derivative of a mass-weighted field ψ (e.g., a tracer concentration as in Section 20.1)

$$\frac{\mathrm{D}(\psi\,\rho\,\delta V)}{\mathrm{D}t} = \frac{\mathrm{D}\psi}{\mathrm{D}t}\,\rho\,\delta V + \psi\,\frac{\mathrm{D}(\rho\,\delta V)}{\mathrm{D}t} \tag{19.49a}$$

$$= \rho\,\delta V\left[\frac{\mathrm{D}\psi}{\mathrm{D}t} + \frac{\psi}{\rho}\frac{\mathrm{D}\rho}{\mathrm{D}t} + \psi\,\nabla\cdot\boldsymbol{v}\right] \tag{19.49b}$$

$$= \delta V\left[\frac{\partial(\rho\,\psi)}{\partial t} + \nabla\cdot(\rho\,\psi\,\boldsymbol{v})\right]. \tag{19.49c}$$

The first equality used the product rule, which holds for material time derivatives. Mass conservation means that the material derivative $\mathrm{D}(\rho\,\delta V)/\mathrm{D}t = 0$. However, we choose to write mass conservation in the form of equation (19.41c), which allows us to introduce the flux-form Eulerian expression after replacing the material time derivative with its Eulerian form from equation (17.11). Another means to derive this result is to write

$$\rho\,\frac{\mathrm{D}\psi}{\mathrm{D}t} = \rho\left[\frac{\partial\psi}{\partial t} + \boldsymbol{v}\cdot\nabla\psi\right] \tag{19.50a}$$

$$= \rho\left[\frac{\partial\psi}{\partial t} + \boldsymbol{v}\cdot\nabla\psi\right] + \psi\left[\frac{\partial\rho}{\partial t} + \nabla\cdot(\boldsymbol{v}\,\rho)\right] \tag{19.50b}$$

$$= \frac{\partial(\rho\,\psi)}{\partial t} + \nabla\cdot(\rho\,\boldsymbol{v}\,\psi). \tag{19.50c}$$

Following the discussion in Section 19.4.4, we can extend the material parcel result (19.49c) to a finite size material region. Again, each point in the material region is following a fluid particle. The result is known as the *Reynolds transport theorem*, which can be written in the following equivalent manners

$$\frac{\mathrm{d}}{\mathrm{d}t}\int_{\mathcal{R}(\boldsymbol{v})}\psi\,\rho\,\mathrm{d}V = \int_{\mathcal{R}(\boldsymbol{v})}\frac{\mathrm{D}\psi}{\mathrm{D}t}\rho\,\mathrm{d}V \qquad \text{material region} \tag{19.51a}$$

$$= \int_{\mathcal{R}(\boldsymbol{v})}\left[\frac{\partial(\rho\,\psi)}{\partial t} + \nabla\cdot(\rho\,\psi\,\boldsymbol{v})\right]\mathrm{d}V \qquad \text{identity (19.50c)} \tag{19.51b}$$

$$= \int_{\mathcal{R}(\boldsymbol{v})}\frac{\partial(\rho\,\psi)}{\partial t}\,\mathrm{d}V + \oint_{\partial\mathcal{R}(\boldsymbol{v})}\rho\,\psi\,\boldsymbol{v}\cdot\hat{\boldsymbol{n}}\,\mathrm{d}\mathcal{S} \qquad \text{divergence theorem (2.79).} \tag{19.51c}$$

Note that we returned to the notation $\mathcal{R}(\boldsymbol{v})$ for material region as introduced in Section 19.3.1. This notation is sufficient to designate that the region is following fluid particles whose velocity is the fluid velocity, $\boldsymbol{v}$. The surface integral term, $\boldsymbol{v}\cdot\hat{\boldsymbol{n}}$, generally does not vanish. Rather, it is given by $\boldsymbol{v}\cdot\hat{\boldsymbol{n}} = \boldsymbol{v}^{(\mathrm{s})}\cdot\hat{\boldsymbol{n}}$, where $\boldsymbol{v}^{(\mathrm{s})}$ is the velocity of a point on the boundary of the material region. Only when the material boundary is static can we set $\boldsymbol{v}\cdot\hat{\boldsymbol{n}} = 0$. We further consider this issue in Section 19.6 when studying kinematic boundary conditions.

19.5.2 Comments on notation for the time derivative

In this book we write $\mathrm{d}/\mathrm{d}t$ for the time derivative operator acting on an integral. Furthermore, when the domain is specialized to follow fluid particles, we identify the special nature of such domains by introducing the fluid velocity argument to the domain name, $\mathcal{R}(\boldsymbol{v})$. This notation designates that all points in the domain, $\mathcal{R}$, move with the fluid velocity, $\boldsymbol{v}$, since all points have fluid particles attached. However, many authors choose an alternative notation by using the material time derivative, $\mathrm{D}/\mathrm{D}t$, when acting on an integral over a material region. We thus have the following equality across the two notational conventions

$$\frac{\mathrm{D}}{\mathrm{D}t}\int_{\mathcal{R}}\psi\,\rho\,\mathrm{d}V = \frac{\mathrm{d}}{\mathrm{d}t}\int_{\mathcal{R}(\boldsymbol{v})}\psi\,\rho\,\mathrm{d}V. \tag{19.52}$$

The use of one convention versus the other is a matter of taste. We follow Section 2.1 of *Batchelor* (1967) by restricting the $\mathrm{D}/\mathrm{D}t$ operator to act only on space-time fields, such as $\psi(\boldsymbol{x}, t)$. Hence,

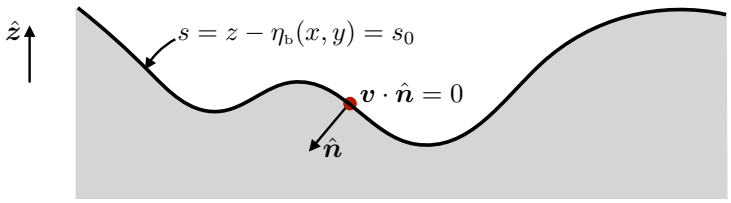

FIGURE 19.4: Illustrating the no-normal flow boundary condition maintained for a solid material boundary, on which $\boldsymbol{v} \cdot \hat{\boldsymbol{n}} = 0$ (equation (19.53)). When the solid boundary denotes the solid-earth (ground or ocean bottom), and when the boundary does not overturn (i.e., $\hat{\boldsymbol{n}} \cdot \hat{\boldsymbol{z}}$ is single-signed), then the position of the interface can be written $s(x,y,z) = z - \eta_{\rm b}(x,y) = s_0$, with s_0 a constant (equation (19.54)). Correspondingly, the outward unit normal is given by $\hat{\boldsymbol{n}} = -\nabla s/|\nabla s| = -(\hat{\boldsymbol{z}} - \nabla \eta_{\rm b})/\sqrt{1 + |\nabla \eta_{\rm b}|^2}$ as given by equation (19.55).

the $\mathrm{D}/\mathrm{D}t$ operator is not used when acting on integrals over spatial regions. Following this convention leads us to write $\mathscr{R}(\boldsymbol{v})$ for a region that moves with the fluid flow and to retain $\mathrm{d}/\mathrm{d}t$ when acting on the integral over that region.

The $\mathscr{R}(\boldsymbol{v})$ notation is not generally used in the literature, with many authors dropping the $\boldsymbol{v}$ and thus letting words designate whether a region follows the flow or otherwise. As we have occasion in this book to consider a variety of fluid regions, we find it essential to introduce the somewhat more explicit notation, $\mathscr{R}(\boldsymbol{v})$, to denote a region moving with the flow velocity, $\boldsymbol{v}$. This usage aims to help the reader freely swim along with the mathematical flow rather than struggling to stay afloat in an ocean of confused or non-specific notation.

19.6 Kinematic boundary conditions

When a fluid encounters a boundary, either at the edge of the fluid region or an imaginary boundary within the fluid itself, the flow must accommodate the boundary. Conversely, the boundary must accommodate the flow. Some boundaries are impermeable, so that they do not allow matter to cross. For material boundaries, any fluid originally in contact with the boundary stays in contact; at most the fluid can move tangential to the boundary without leaving it. We can understand this rather remarkable constraint placed on material boundaries by noting that no two fluid particles can occupy the same point along the material boundary, nor can there be a cavity next to the boundary as the boundary moves through the fluid. Other boundaries are permeable, thus allowing matter to cross. In this section we develop kinematic boundary conditions appropriate for the variety of cases encountered in fluid mechanics.

19.6.1 Static material surface

Consider a moving fluid that encounters a static material surface, such as the solid-earth. At the boundary, we can decompose the fluid velocity into a component that moves in the plane locally tangent to the boundary and another component that is normal to the boundary. To ensure that no fluid crosses the static boundary, the normal component must vanish at the boundary surface. Hence, the kinematic boundary condition for a moving fluid that encounters a static material boundary is (see Figure 19.4)

$$\boldsymbol{v} \cdot \hat{\boldsymbol{n}} = 0 \qquad \text{no-normal flow condition on static material boundary.} \tag{19.53}$$

Recall our discussion of streamlines in Section 17.7.2, where $\boldsymbol{v} \cdot \hat{\boldsymbol{n}} = 0$ along a streamline. Evidently, the static material boundary is a flow streamline so that fluid that is in contact with the boundary remains in contact. This result holds even in the case of a time dependent flow.[6]

[6] Specification of the tangential velocity along a material boundary requires dynamical information, such as the no-slip boundary from Section 25.8.7, that is unavailable from purely kinematic considerations.

For many cases in practice, the material surface is monotonic in the vertical, meaning there are no overturns. In this case, it is useful to introduce some differential geometry (at the level of introductory calculus) to unpack the boundary condition (19.53). Doing so helps to develop a geometric formalism especially useful for the more complicated moving boundary conditions in Sections 19.6.2 and 19.6.3. For this purpose, introduce a coordinate expression for the boundary according to

$$s(x, y, z) = z - \eta_{\mathrm{b}}(x, y) = s_0 \qquad \text{static material boundary,} \tag{19.54}$$

with $z = \eta_{\mathrm{b}}(x, y)$ the vertical position of the boundary and s_0 a constant. The outward unit normal vector at the boundary is thus given by

$$\hat{\boldsymbol{n}} = -\frac{\nabla s}{|\nabla s|} = -\frac{\nabla(z - \eta_{\mathrm{b}})}{|\nabla(z - \eta_{\mathrm{b}})|} = -\frac{\hat{\boldsymbol{z}} - \nabla\eta_{\mathrm{b}}}{\sqrt{1 + |\nabla\eta_{\mathrm{b}}|^2}}. \tag{19.55}$$

Consequently, the no-flux boundary condition (19.53) takes the form

$$\nabla(z - \eta_{\mathrm{b}}) \cdot \boldsymbol{v} = w - \boldsymbol{u} \cdot \nabla\eta_{\mathrm{b}} = 0 \qquad \text{at } z = \eta_{\mathrm{b}}(x, y), \tag{19.56}$$

where the velocity is decomposed into its horizontal and vertical components, $\boldsymbol{v} = (\boldsymbol{u}, w)$. Hence, to maintain the no-flux boundary condition requires the vertical velocity component to precisely balance the projection of the horizontal velocity onto the slope of the material surface. If the material surface is flat, so that $\nabla\eta_{\mathrm{b}} = 0$, then the kinematic boundary condition reduces to $w = 0$. Alternatively, if the flow is purely horizontal and thus moves along a constant η_{b} isoline, then $\boldsymbol{u} \cdot \nabla\eta_{\mathrm{b}} = 0$ so that $w = 0$.

19.6.2 Moving (free) material surface

We next consider the kinematic constraints imposed by a moving surface that does not allow matter to cross the surface.[7]

General expression of the kinematic boundary condition

To ensure that no matter crosses the surface, the normal component of the velocity for a point on the surface must match the normal component of the fluid at the surface. We are thus led to the kinematic boundary condition for a moving material surface

$$(\boldsymbol{v} - \boldsymbol{v}^{(\mathrm{s})}) \cdot \hat{\boldsymbol{n}} = 0 \qquad \text{moving material boundary condition.} \tag{19.57}$$

We illustrate this boundary condition in Figure 19.5, where $\boldsymbol{v}^{(\mathrm{s})}$ is the velocity of a point fixed on the moving material surface and $\boldsymbol{v}$ is the velocity of the fluid particles.

As for the static material boundary, there is no constraint on the tangential component of the velocities, since it is only the normal component that measures the flow of matter across the boundary. Hence, the boundary condition (19.57) does not mean $\boldsymbol{v}$ and $\boldsymbol{v}^{(\mathrm{s})}$ are identical. It only says that their normal components are the same when evaluated on the material surface. As a Corollary, we see that $\boldsymbol{v} \cdot \hat{\boldsymbol{n}}$ is not generally zero so that a moving material boundary does *not* coincide with a flow streamline (see discussion in Sections 17.7.2 and 17.7.3).

[7] As we discuss in Chapter 20, with multiple matter components a surface that follows the barycentric velocity and so allows for zero net mass to cross it can still allow for the exchange of component matter in the presence of matter diffusion. In the current chapter, we are only considering a single matter constituent, so that zero mass crossing a surface also means there are no fluid particles crossing the surface.

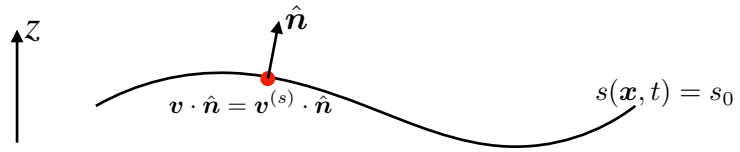

FIGURE 19.5: Illustrating the boundary condition for a moving material surface, on which $\hat{\boldsymbol{n}} \cdot (\boldsymbol{v} - \boldsymbol{v}^{(s)}) = 0$ (equation (19.57)), so that no fluid particles cross the surface. The boundary condition means that the velocity of the surface, $\boldsymbol{v}^{(s)}$, has the same normal component as the velocity of a fluid particle, $\boldsymbol{v}$. The material nature of the surface is not compromised if $\boldsymbol{v} \neq \boldsymbol{v}^{(s)}$, so long as their normal components are identical, $\hat{\boldsymbol{n}} \cdot \boldsymbol{v} = \hat{\boldsymbol{n}} \cdot \boldsymbol{v}^{(s)}$. For many cases, we can specify the surface by the value of a function that is a constant on the surface: $s(\boldsymbol{x}, t) = s_0$ for some constant s_0 (equation (19.58)), in which case the unit normal direction is given by $\hat{\boldsymbol{n}} = |\nabla s|^{-1} \nabla s$ (equation (19.59)). For example, s could represent a surface of constant temperature, or a constant Archimedean buoyancy (Chapter 30) in a buoyancy stratified fluid.

Specialized expression of the boundary condition

Now specialize the kinematic condition (19.57) to the case of a material surface, $\mathcal{S}$, as specified by a scalar function whose value remains a fixed constant when it is evaluated on the surface

$$s(\boldsymbol{x}, t) = s_0 \quad \text{when } \boldsymbol{x} \in \mathcal{S}. \tag{19.58}$$

An example of such a function is the Archimedean buoyancy (Chapter 30) or the Conservative Temperature (Section 26.11). Correspondingly, the surface unit normal vector is given by

$$\hat{\boldsymbol{n}} = |\nabla s|^{-1} \nabla s. \tag{19.59}$$

From Section 17.4.5, we know that a point fixed on an arbitrary surface has a velocity that satisfies (see equation (17.19))

$$\frac{\partial s}{\partial t} + \boldsymbol{v}^{(s)} \cdot \nabla s = 0 \qquad \text{on an iso-surface } s(\boldsymbol{x}, t) = s_0. \tag{19.60}$$

Note that we offer another derivation of this equation later in this subsection. Use of the identity

$$\frac{\partial s}{\partial t} = \frac{\mathrm{D}s}{\mathrm{D}t} - \boldsymbol{v} \cdot \nabla s \tag{19.61}$$

renders

$$\frac{\mathrm{D}s}{\mathrm{D}t} - \boldsymbol{v} \cdot \nabla s + \boldsymbol{v}^{(s)} \cdot \nabla s = \frac{\mathrm{D}s}{\mathrm{D}t} + (\boldsymbol{v}^{(s)} - \boldsymbol{v}) \cdot \nabla s = 0. \tag{19.62a}$$

Since $(\boldsymbol{v}^{(s)} - \boldsymbol{v}) \cdot \nabla s = 0$ from the boundary condition (19.57), we are left with the material constancy condition

$$\frac{\mathrm{D}s}{\mathrm{D}t} = \frac{\partial s}{\partial t} + \boldsymbol{v} \cdot \nabla s = 0 \qquad \text{on material surface } s(\boldsymbol{x}, t) = s_0. \tag{19.63}$$

Consequently, matter does not cross a surface of constant s as long as s is materially constant. This is an important kinematic property that reappears in many forms throughout fluid mechanics.[8]

Boundary condition for a material interface

Consider the interface between two immiscible fluids. Assume this interface has an outward normal that has a nonzero vertical component, so that there are no breaking waves, for example.

[8] As noted on page 137 of *Serrin* (1959), the kinematic condition (19.63) originates from Kelvin in 1848 and Lagrange in 1781.

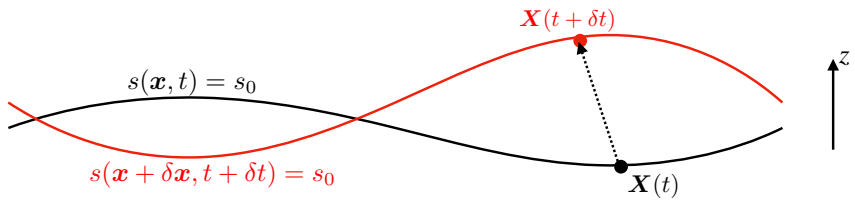

FIGURE 19.6: A surface within a fluid at two time instants, along with the position of a fluid particle on the surface at $\boldsymbol{X}(t)$ and $\boldsymbol{X}(t+\delta t)$. The velocity of a point on the surface is given by $\boldsymbol{v}^{(s)}=[\boldsymbol{X}(t+\delta t)-\boldsymbol{X}(t)]/\delta t=\delta\boldsymbol{X}/\delta t$. The equation $s(\boldsymbol{x},t)=z-\eta(x,y,t)=s_0$ specifies the vertical position for points on the surface as a function of horizontal position and time. At both time instances the vertical position is determined by $s(\boldsymbol{x},t)=s(\boldsymbol{x}+\delta\boldsymbol{x},t+\delta t)=s_0$.

In this case we can express the vertical position of a point on the interface as

$$s(x,y,z,t)=z-\eta(x,y,t)=s_0. \tag{19.64}$$

The function $\eta(x,y,t)$ is the vertical deviation of the interface relative to the horizontal. The kinematic boundary condition (19.63) thus takes the form

$$\frac{\mathrm{D}s}{\mathrm{D}t}=\frac{\mathrm{D}(z-\eta)}{\mathrm{D}t}=0. \tag{19.65}$$

Hence, the vertical velocity component at the interface equals to the material time derivative of the interface displacement

$$\frac{\mathrm{D}z}{\mathrm{D}t}=\frac{\mathrm{D}\eta}{\mathrm{D}t}\Longrightarrow w=\frac{\partial\eta}{\partial t}+\boldsymbol{u}\cdot\nabla\eta \qquad \text{material b.c. at interface } z=\eta(x,y,t). \tag{19.66}$$

This boundary condition can be equivalently written in the form

$$\boldsymbol{v}\cdot\hat{\boldsymbol{n}}=\frac{\partial\eta/\partial t}{\sqrt{1+|\nabla\eta|^2}}, \tag{19.67}$$

where

$$\hat{\boldsymbol{n}}=\frac{\nabla\,(z-\eta)}{|\nabla\,(z-\eta)|}=\frac{-\nabla\eta+\hat{\boldsymbol{z}}}{\sqrt{1+|\nabla\eta|^2}} \tag{19.68}$$

is the outward unit normal at the material surface. These equations provide kinematic relation for the motion of an surface within a perfect fluid. It also provides the kinematic relation for the interface separating two immiscible fluid layers. A particular example concerns the boundary condition placed on the ocean free surface in the special case of no water penetrating the surface (i.e., no rain or evaporation).

A geometric derivation of the material boundary condition

The material invariance condition $\mathrm{D}s/\mathrm{D}t=0$ is a key kinematic result. We thus offer an alternative derivation to help solidify its meaning. As before, define the surface according to

$$s(\boldsymbol{x},t)=z-\eta(x,y,t)=s_0, \tag{19.69}$$

which specifies the vertical position of a point on the surface at time t. Now consider the position of the surface after a small time interval, $t+\delta t$ (see Figure 19.6). The vertical position of the surface at the new time is determined by the same condition

$$s(\boldsymbol{x}+\delta\boldsymbol{x},t+\delta t)=s_0, \tag{19.70}$$

where $\boldsymbol{\varphi}(t+\delta t) = \boldsymbol{x} + \delta\boldsymbol{x}$ is the displaced position of a point on the surface that started at $\boldsymbol{\varphi}(t) = \boldsymbol{x}$, and

$$\boldsymbol{v}^{(\mathrm{s})} = [\boldsymbol{\varphi}(t+\delta t) - \boldsymbol{\varphi}(t)]/\delta t = \delta\boldsymbol{x}/\delta t \tag{19.71}$$

is the velocity of a point stuck to the surface. Expanding equation (19.70) in a Taylor series to leading order yields

$$s(\boldsymbol{x}, t) + \delta\boldsymbol{x} \cdot \nabla s + \delta t\, \partial_t s = s_0. \tag{19.72}$$

Since $s(\boldsymbol{x}, t) = s_0$ from equation (19.69) we thus have

$$\frac{\partial s}{\partial t} + \frac{\delta\boldsymbol{x}}{\delta t} \cdot \nabla s = \frac{\partial s}{\partial t} + \frac{\delta\boldsymbol{x}}{\delta t} \cdot \hat{\boldsymbol{n}}\, |\nabla s| = 0, \tag{19.73}$$

where $\hat{\boldsymbol{n}} = |\nabla s|^{-1}\, \nabla s$ is the surface unit normal direction. This result means that when positioned at a fixed point in space, it is the normal component of the displacement that corresponds to a temporal modification of $s(\boldsymbol{x}, t)$

$$\frac{\partial s}{\partial t} = -\boldsymbol{v}^{(\mathrm{s})} \cdot \hat{\boldsymbol{n}}\, |\nabla s|. \tag{19.74}$$

In contrast, any tangential displacement along an s-isosurface leaves $s(\boldsymbol{x}, t)$ unchanged. Hence, when following motion of points on the surface, we are only concerned with motion along the direction set by the normal component of the velocity of that point, $\hat{\boldsymbol{n}}\, (\boldsymbol{v}^{(\mathrm{s})} \cdot \hat{\boldsymbol{n}})$. It is this velocity component that corresponds to movement of the surface normal to itself, thus leading to nonzero motion through space.

Writing equation (19.74) in a more conventional form leads to the differential equation satisfied by a point fixed on the moving surface

$$\frac{\partial s}{\partial t} + \boldsymbol{v}^{(\mathrm{s})} \cdot \nabla s = 0. \tag{19.75}$$

Again, assuming the surface is material means that

$$\boldsymbol{v}^{(\mathrm{s})} \cdot \hat{\boldsymbol{n}} = \boldsymbol{v} \cdot \hat{\boldsymbol{n}}, \tag{19.76}$$

so that motion of the surface normal to itself is identical to that of the fluid in the same direction. Use of the boundary condition (19.76) in equation (19.75) renders the material invariance condition

$$\frac{\mathrm{D}s}{\mathrm{D}t} = \frac{\partial s}{\partial t} + \boldsymbol{v} \cdot \nabla s = 0. \tag{19.77}$$

19.6.3 Dynamic and permeable surface

We now consider the kinematic boundary condition for a moving permeable surface that separates two fluid media (e.g., ocean and atmosphere) or two regions within a single media (e.g., surface of constant buoyancy within the ocean or within the atmosphere). As before, the kinematic boundary condition is a statement about the mass transport through the boundary. Whereas the previous conditions enforced a zero mass transport through the boundary at each point of the boundary, here we allow for a generally non-zero transport (mass per time). We write this transport condition as

$$\rho\, (\boldsymbol{v} - \boldsymbol{v}^{(\mathrm{s})}) \cdot \hat{\boldsymbol{n}}\, \mathrm{d}\mathcal{S} = -\mathcal{Q}_{\mathrm{m}}\, \mathrm{d}\mathcal{S} \qquad \text{moving non-material boundary condition.} \tag{19.78}$$

In this equation, $\mathrm{d}\mathcal{S}$ is an infinitesimal area element on the surface, and $\mathcal{Q}_{\mathrm{m}}$ measures the mass per time per surface area (mass flux) crossing the boundary. The minus sign is a convention to be motivated in the following. We now massage this kinematic boundary condition into alternative forms.

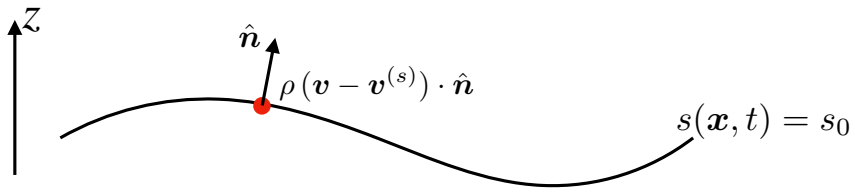

FIGURE 19.7: Illustrating the boundary condition for a moving permeable surface, such as the interface between two miscible fluid layers. On this surface, the boundary condition states that $\rho\,(\boldsymbol{v}-\boldsymbol{v}^{(s)})\cdot\hat{\boldsymbol{n}}\,\mathrm{d}\mathcal{S}=-\mathcal{Q}_\mathrm{m}\,\mathrm{d}\mathcal{S}$ (as per equation (19.78)). In the special case of an ocean free surface with no overturns, this boundary condition reduces to the surface kinematic boundary condition (19.94).

Coordinate representation of the permeable surface

The expression (19.60) for $\boldsymbol{v}^{(\mathrm{s})}\cdot\hat{\boldsymbol{n}}$ holds for a point on an arbitrary surface, even if that surface is permeable, so that

$$\boldsymbol{v}^{(\mathrm{s})}\cdot\hat{\boldsymbol{n}}=-\frac{\partial s/\partial t}{|\nabla s|}. \tag{19.79}$$

Furthermore, the projection of the fluid velocity onto the normal direction can be written

$$\frac{\mathrm{D}s}{\mathrm{D}t}=\frac{\partial s}{\partial t}+\boldsymbol{v}\cdot\nabla s\Longrightarrow\boldsymbol{v}\cdot\hat{\boldsymbol{n}}=\frac{1}{|\nabla s|}\left[\frac{\mathrm{D}s}{\mathrm{D}t}-\frac{\partial s}{\partial t}\right]. \tag{19.80}$$

Bringing these results together leads to

$$\rho\,(\boldsymbol{v}-\boldsymbol{v}^{(\mathrm{s})})\cdot\hat{\boldsymbol{n}}\,\mathrm{d}\mathcal{S}=\frac{\rho\,\mathrm{d}\mathcal{S}}{|\nabla s|}\frac{\mathrm{D}s}{\mathrm{D}t}\Longrightarrow\mathcal{Q}_\mathrm{m}=-\frac{\rho}{|\nabla s|}\frac{\mathrm{D}s}{\mathrm{D}t}. \tag{19.81}$$

This equation says that the mass transport crossing the surface is proportional to the material time derivative of the surface coordinate. The material time derivative vanishes when there is no mass transport across the surface, which is a result already seen in Section 19.6.2.

In terms of the horizontal projection of the surface area

Assume that the surface is not vertical, so that its normal direction has a nonzero component in the vertical (e.g., waves that do not overturn). This assumption means that

$$\frac{\partial s}{\partial z}\neq 0, \tag{19.82}$$

so that we can further massage the boundary condition (19.81) by writing the area factor in the form

$$\frac{\mathrm{d}\mathcal{S}}{|\nabla s|}=\frac{\mathrm{d}\mathcal{S}}{\sqrt{(\partial s/\partial x)^2+(\partial s/\partial y)^2+(\partial s/\partial z)^2}} \tag{19.83a}$$

$$=\frac{\mathrm{d}\mathcal{S}}{|\partial s/\partial z|\sqrt{[(\partial s/\partial x)/(\partial s/\partial z)]^2+[(\partial s/\partial y)/(\partial s/\partial z)]^2+1}} \tag{19.83b}$$

$$=\frac{\mathrm{d}\mathcal{S}}{|\partial s/\partial z|\sqrt{1+\tan^2\vartheta}} \tag{19.83c}$$

$$=\left|\frac{\partial z}{\partial s}\right||\cos\vartheta|\,\mathrm{d}\mathcal{S} \tag{19.83d}$$

$$=\left|\frac{\partial z}{\partial s}\right|\mathrm{d}A. \tag{19.83e}$$

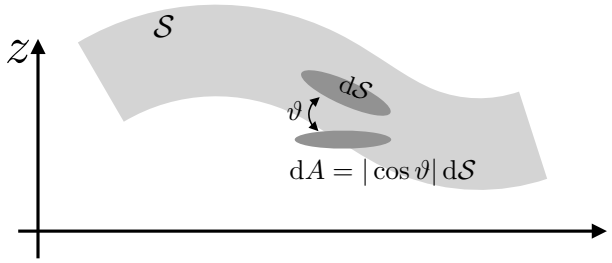

FIGURE 19.8: Illustrating the relation between an infinitesimal area element on a surface, $\mathrm{d}\mathcal{S}$, to its horizontal projection, $\mathrm{d}A = |\cos\vartheta|\,\mathrm{d}\mathcal{S}$, according to equation (19.87). The angle, ϑ, must be bounded away from $\pm\pi/2$, thus enabling a nonzero horizontal area projection. For the specific case of a surface defined by $s = z - \eta(x, y, t)$, then $\partial s/\partial z = 1$ and $\mathrm{d}\mathcal{S} = \sqrt{1 + (\nabla\eta)^2}\,\mathrm{d}A$ (equation (19.91)).

The equality (19.83c) introduced the angle, ϑ, between the boundary surface and the horizontal plane. The squared slope of this surface is given by

$$\tan^2\vartheta = \frac{\nabla_{\mathsf{h}} s \cdot \nabla_{\mathsf{h}} s}{(\partial s/\partial z)^2} = \nabla_{\mathsf{hs}} z \cdot \nabla_{\mathsf{hs}} z \tag{19.84}$$

with

$$\nabla_{\mathsf{h}} = \hat{\boldsymbol{x}} \left[\frac{\partial}{\partial x}\right]_{y,z} + \hat{\boldsymbol{y}} \left[\frac{\partial}{\partial y}\right]_{x,z} \tag{19.85}$$

the horizontal gradient operator on constant z surfaces, and

$$\nabla_{\mathsf{hs}} = \hat{\boldsymbol{x}} \left[\frac{\partial}{\partial x}\right]_{y,s} + \hat{\boldsymbol{y}} \left[\frac{\partial}{\partial y}\right]_{x,s} \tag{19.86}$$

the horizontal gradient operator on constant s surfaces, along with $z(x, y, s, t)$ for the vertical position of the constant s surface.[9] The equality (19.83d) made use of a trigonometric identity, and the equality (19.83e) introduced the horizontal projection of the area,

$$\mathrm{d}A = |\cos\vartheta|\,\mathrm{d}\mathcal{S}. \tag{19.87}$$

See Figure 19.8 for an illustration.

These results bring the kinematic boundary condition (19.81) into the form

$$\begin{aligned} \rho\,(\boldsymbol{v} - \boldsymbol{v}^{(\mathsf{s})}) \cdot \hat{\boldsymbol{n}}\,\mathrm{d}\mathcal{S} &= -\mathcal{Q}_{\mathrm{m}}\,\mathrm{d}\mathcal{S} && \text{(19.88a)} \\ &= \rho\,\frac{\mathrm{D}s}{\mathrm{D}t}\left|\frac{\partial z}{\partial s}\right|\mathrm{d}A && \text{(19.88b)} \\ &\equiv -Q_{\mathsf{m}}\,\mathrm{d}A. && \text{(19.88c)} \end{aligned}$$

As defined, the flux Q_{m} is the net mass per time per horizontal area crossing the boundary surface

$$Q_{\mathsf{m}} = -\rho\,(\boldsymbol{v} - \boldsymbol{v}^{(\mathsf{s})}) \cdot \hat{\boldsymbol{n}}\,\frac{\mathrm{d}\mathcal{S}}{\mathrm{d}A} = -\rho\,\frac{\mathrm{D}s}{\mathrm{D}t}\left|\frac{\partial z}{\partial s}\right|. \tag{19.89}$$

We motivate the minus sign through the ocean free surface case in the following.

[9] We study such operators in Chapter 63 as part of the mathematical development of generalized vertical coordinates.

Kinematic boundary condition at the ocean free surface

Consider the ocean free surface located at

$$s(x,y,z,t) = z - \eta(x,y,t) = 0 \qquad \text{ocean free surface.} \tag{19.90}$$

For this boundary, $\partial s/\partial z = 1$ so that the area elements are related by

$$\mathrm{d}\mathcal{S} = |\nabla(z-\eta)|\,\mathrm{d}A = \sqrt{1+|\nabla\eta|^2}\,\mathrm{d}A. \tag{19.91}$$

The normal projection for the velocity of a point fixed on the free surface is given by

$$\boldsymbol{v}^{(\eta)} \cdot \hat{\boldsymbol{n}} = -\frac{\partial s/\partial t}{|\nabla s|} = \frac{\partial \eta/\partial t}{|\nabla(z-\eta)|} = \frac{\partial \eta/\partial t}{\sqrt{1+|\nabla\eta|^2}} \Longrightarrow \boldsymbol{v}^{(\eta)} \cdot \hat{\boldsymbol{n}}\,\mathrm{d}\mathcal{S} = \partial_t \eta\,\mathrm{d}A, \tag{19.92}$$

so that the mass flux crossing the free surface is

$$-\mathcal{Q}_{\mathrm{m}} = \rho\,(\boldsymbol{v} - \boldsymbol{v}^{(\eta)}) \cdot \hat{\boldsymbol{n}}. \tag{19.93}$$

The boundary condition (19.89) thus takes the form

$$\rho\,(\boldsymbol{v} - \boldsymbol{v}^{(\eta)}) \cdot \hat{\boldsymbol{n}}\,\frac{\mathrm{d}\mathcal{S}}{\mathrm{d}A} = \rho\left[\frac{\mathrm{D}(z-\eta)}{\mathrm{D}t}\right] = -Q_{\mathsf{m}} \Longrightarrow w + \rho^{-1}\,Q_{\mathsf{m}} = \frac{\partial \eta}{\partial t} + \boldsymbol{u}\cdot\nabla\eta. \tag{19.94}$$

We now motivate the sign convention chosen for equation (19.88c) by considering the special case of a flat free surface and a resting fluid with $\boldsymbol{v} = 0$. Adding mass to the ocean raises the free surface, so that $\partial\eta/\partial t > 0$. Hence, the chosen sign convention means that $Q_{\mathsf{m}} > 0$ corresponds to mass added to the ocean.

Kinematic boundary condition on a buoyancy surface

Now consider the interface to be a surface of constant potential density in the ocean (or analogously a surface of constant specific entropy in the atmosphere). These buoyancy isosurfaces are also known as isopycnals, and we use the symbol[10]

$$s = \sigma(x,y,z,t) \tag{19.95}$$

for a particular isopycnal, σ. The mass transport crossing the isopycnal is written

$$Q_{\mathsf{m}} = \rho\,\frac{\mathrm{D}\sigma}{\mathrm{D}t}\left|\frac{\partial z}{\partial \sigma}\right| \equiv \rho\, w^{(\dot\sigma)}, \tag{19.96}$$

where we introduced the *diapycnal transport velocity*

$$w^{(\dot\sigma)} \equiv \frac{\mathrm{D}\sigma}{\mathrm{D}t}\left|\frac{\partial z}{\partial \sigma}\right|. \tag{19.97}$$

A key aspect of physical oceanography concerns the development of theories for processes that cause a non-zero diapycnal transport. Examples include breaking waves, which act to mix matter across density surfaces; i.e., to *entrain* water from one density class to another.

[10] In this book, we use σ as an arbitrary generalized vertical coordinate, here chosen to be an isopycnal.

19.7 Volume and mass budgets for a bounded fluid column

We close this chapter by deriving the budget for the volume per horizontal area in a column of a bounded fluid, as well as the budget for the mass per horizontal area in this as shown in Figure 19.9. Such fluid columns are relevant to the study of mass budgets over the full depth of the ocean. Since the upper boundary of the domain is the free surface, and since the free surface is a function of time, the region is not strictly Eulerian even though the sides are fixed in space. Furthermore, the free surface is permeable, as are the sides, so that the region is not material. The derivation offers experience working with the kinematic boundary conditions, as well as some exposure to the use of Leibniz's rule from calculus.

19.7.1 Kinematic free surface equation

We here derive an equation for the free surface evolution, with this equation providing a budget for the volume per horizontal area in the column. The derivation proceeds by vertically integrating the mass continuity equation (19.16) over the depth of an ocean column, from $z = \eta_b(x, y)$ at the bottom to $z = \eta(x, y, t)$ at the free surface. Use of the bottom and surface kinematic boundary conditions renders a kinematic expression for the free surface time tendency.

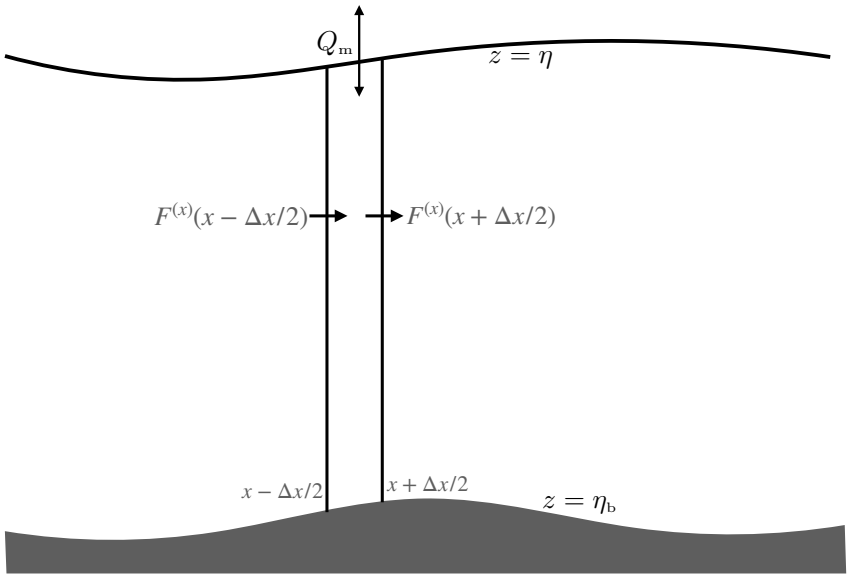

FIGURE 19.9: A longitudinal-vertical slice of ocean fluid from the surface at $z = \eta(x, y, t)$ to bottom at $z = \eta_b(x, y)$. The horizontal boundaries of the column at $x - \Delta x/2$ and $x + \Delta x/2$ are static and are penetrated by zonal mass transport, $F^{(x)}$. The zonal mass transport is computed by integrating the zonal mass flux, ρu over the area of the column sides. A similar transport acts in the meridional direction as well. The ocean bottom at the solid-earth boundary, $z = \eta_b(x, y)$, is static with no mass crossing this interface. The ocean surface at $z = \eta(x, y, t)$ is time dependent with mass flux, Q_m, crossing this interface.

Vertically integrating the continuity equation (19.16) for a compressible fluid renders

$$-\int_{\eta_b}^{\eta} \frac{1}{\rho} \frac{D\rho}{Dt} \, dz = \int_{\eta_b}^{\eta} \nabla \cdot \boldsymbol{v} \, dz \tag{19.98a}$$

$$= w(\eta) - w(\eta_b) + \int_{\eta_b}^{\eta} \nabla_h \cdot \boldsymbol{u} \, dz \tag{19.98b}$$

$$= w(\eta) - w(\eta_b) + \nabla_h \cdot \left[\int_{\eta_b}^{\eta} \boldsymbol{u} \, dz \right] - \boldsymbol{u}(\eta) \cdot \nabla_h \eta + \boldsymbol{u}(\eta_b) \cdot \nabla_h \eta_b \tag{19.98c}$$

$$= [w(\eta) - \boldsymbol{u}(\eta) \cdot \nabla_h \eta] - [w(\eta_b) - \boldsymbol{u}(\eta_b) \cdot \nabla_h \eta_b] + \nabla_h \cdot \left[\int_{\eta_b}^{\eta} \boldsymbol{u} \, dz \right], \tag{19.98d}$$

where we made use of *Leibniz's rule* from calculus in order to move the horizontal divergence outside of the integral. Also note that $\nabla \cdot \boldsymbol{u} = \nabla_h \cdot \boldsymbol{u}$ since $\boldsymbol{u}$ is the horizontal velocity, and likewise for $\nabla \eta_b$ and $\nabla \eta$ since η_b and η are both functions of horizontal space and time, and so have no z dependence.

Use of the surface kinematic boundary condition (19.94) and no-normal flow bottom boundary condition yield

$$\frac{\partial \eta}{\partial t} = \frac{Q_m}{\rho(\eta)} - \nabla \cdot \boldsymbol{U} - \int_{\eta_b}^{\eta} \frac{1}{\rho} \frac{\mathrm{D}\rho}{\mathrm{D}t} \, \mathrm{d}z \tag{19.99}$$

where

$$\boldsymbol{U} = \int_{\eta_b}^{\eta} \boldsymbol{u} \, \mathrm{d}z \tag{19.100}$$

is the depth integrated horizontal transport. Hence, as deduced from the mass continuity equation, the ocean free surface time tendency is affected by the passage of mass across the surface boundary (as normalized by the surface density), the convergence of depth integrated flow, and the depth integral of the material changes in density. The density term contributes to a positive sea surface height tendency when density decreases, and vice versa when density increases. *Griffies and Greatbatch* (2012) provide a more complete analysis of the sea surface height budget (19.99) by unpacking the physical processes leading to the material evolution of density, which they refer to as the *non-Boussinesq steric effect*.

19.7.2 Budget for mass per horizontal area

The mass per horizontal area in the fluid column is given by $\int_{\eta_b}^{\eta} \rho \, \mathrm{d}z$. Use of Leibniz's rule, the bottom kinematic boundary condition, (19.56), surface kinematic boundary condition (19.94), and the mass continuity equation (19.6), leads to

$$\begin{aligned}
\frac{\mathrm{d}}{\mathrm{d}t}\left[\int_{\eta_b}^{\eta} \rho \, \mathrm{d}z\right] &= \rho(\eta) \frac{\partial \eta}{\partial t} + \int_{\eta_b}^{\eta} \frac{\partial \rho}{\partial t} \, \mathrm{d}z && \text{(19.101a)} \\
&= \rho(\eta) \frac{\partial \eta}{\partial t} - \int_{\eta_b}^{\eta} \nabla \cdot (\rho \boldsymbol{v}) \, \mathrm{d}z && \text{(19.101b)} \\
&= \rho(\eta) \left[\frac{\partial \eta}{\partial t} - w(\eta)\right] + \rho(\eta_b) \, w(\eta_b) - \int_{\eta_b}^{\eta} \nabla_h \cdot (\rho \boldsymbol{u}) \, \mathrm{d}z && \text{(19.101c)} \\
&= \rho(\eta) \left[\frac{\partial \eta}{\partial t} + \boldsymbol{u} \cdot \nabla \eta - w(\eta)\right] + \rho(\eta_b) \left[w(\eta_b) - \boldsymbol{u}(\eta_b) \cdot \nabla \eta_b\right] - \nabla_h \cdot \boldsymbol{U}^{\rho} && \text{(19.101d)} \\
&= Q_m - \nabla_h \cdot \boldsymbol{U}^{\rho}, && \text{(19.101e)}
\end{aligned}$$

where

$$\boldsymbol{U}^{\rho} = \int_{\eta_b}^{\eta} \rho \, \boldsymbol{u} \, \mathrm{d}z. \tag{19.102}$$

Hence, the mass per horizontal area within a column evolves according to

$$\frac{\mathrm{d}}{\mathrm{d}t}\left[\int_{\eta_b}^{\eta} \rho \, \mathrm{d}z\right] = Q_m - \nabla \cdot \boldsymbol{U}^{\rho}, \tag{19.103}$$

with terms on the right hand side representing the convergence of mass onto the column either through the sides or upper surface. We consider an alternative derivation of this budget in Exercise 19.3.

19.8 Exercises

EXERCISE 19.1: VELOCITY THAT DOES NOT PENETRATE A CURVE
Consider a static curve defined by

$$s(x, y) = x\, y = \text{constant}. \tag{19.104}$$

Provide an example velocity, $\boldsymbol{v} = u\,\hat{\boldsymbol{x}} + v\,\hat{\boldsymbol{y}} + w\,\hat{\boldsymbol{z}}$, that has nonzero horizontal components and that satisfies $\boldsymbol{v} \cdot \hat{\boldsymbol{n}} = 0$, where $\hat{\boldsymbol{n}}$ is the unit normal to the curve. Be sure that your answer has the proper dimensions for a velocity. Hint: see Section 38.4.5.

EXERCISE 19.2: CENTER OF MASS MOTION
Consider a material fluid region, $\mathcal{R}(\boldsymbol{v})$, with constant mass written as

$$M = \int_{\mathcal{R}(\boldsymbol{v})} \rho \, \mathrm{d}V. \tag{19.105}$$

Assume Cartesian coordinates throughout this exercise.[11]

(a) Show mathematically that the center of mass for the region moves with the region's total linear momentum

$$\frac{\mathrm{d}}{\mathrm{d}t}\left[\frac{1}{M}\int_{\mathcal{R}(\boldsymbol{v})} \boldsymbol{x}\,\rho\,\mathrm{d}V\right] = \frac{1}{M}\int_{\mathcal{R}(\boldsymbol{v})} \frac{\mathrm{D}\boldsymbol{x}}{\mathrm{D}t}\,\rho\,\mathrm{d}V = \frac{1}{M}\int_{\mathcal{R}(\boldsymbol{v})} \boldsymbol{v}\,\rho\,\mathrm{d}V. \tag{19.106}$$

Precisely describe the reasoning behind each step. Note: a brief solution is sufficient, so long as the reasoning is sound.

(b) Show mathematically (or precisely describe why) that the time change in the linear momentum for the region is given by

$$\frac{\mathrm{d}}{\mathrm{d}t}\left[\int_{\mathcal{R}(\boldsymbol{v})} \rho\,\boldsymbol{v}\,\mathrm{d}V\right] = \int_{\mathcal{R}(\boldsymbol{v})} \frac{\mathrm{D}\boldsymbol{v}}{\mathrm{D}t}\,\rho\,\mathrm{d}V. \tag{19.107}$$

Precisely describe the reasoning behind each step. Note: a brief solution is sufficient, so long as the reasoning is sound.

EXERCISE 19.3: MASS BUDGET FOR A FLUID COLUMN
We here provide an alternative derivation of equation (19.103), the budget for the mass per horizontal area over a column of fluid.

The mass within an arbitrary fluid region is given by

$$M = \int_{\mathcal{R}} \rho \, \mathrm{d}V. \tag{19.108}$$

Consider the fluid mass within the column shown in Figure 19.9. In this column, the vertical side-walls are fixed in time, the bottom surface, $z = \eta_{\mathsf{b}}(x, y)$, is at the solid-earth boundary, and the top, $z = \eta(x, y, t)$, is the fluctuating ocean free surface. Convince yourself that the mass for this column can be written

$$M = \iint \left[\int_{\eta_{\mathsf{b}}(x,y)}^{\eta(x,y,t)} \rho\,\mathrm{d}z\right] \mathrm{d}x\,\mathrm{d}y, \tag{19.109}$$

[11] Note the for a general manifold, the addition of vectors is only defined locally within a tangent space. This limitation prevents us from integrating general tensors over a volume. However, for Cartesian tensors we can perform integration in a naive manner just as for scalars.

where the horizontal (x, y) integrals extend over the horizontal extent of the column. Mass conservation for this column means that the change in mass arises just through boundary fluxes, so that

$$\frac{\mathrm{d}M}{\mathrm{d}t} = -\int \rho\, \Delta \boldsymbol{v} \cdot \hat{\boldsymbol{n}}\, \mathrm{d}\mathcal{S}, \tag{19.110}$$

where $\hat{\boldsymbol{n}}$ is the outward normal to the surface of the fluid region, $\mathrm{d}\mathcal{S}$ is the area of an infinitesimal element on the surface, and the minus sign means that fluid leaving the region contributes to a reduction in mass within the region. The term

$$\Delta \boldsymbol{v} = \boldsymbol{v} - \boldsymbol{v}^{(\mathsf{s})} \tag{19.111}$$

is the velocity of the fluid relative to the velocity of the boundary; e.g., see the kinematic boundary condition discussion in Section 19.6.3. We also derive a general form of this relation in equation (20.50), though this exercise can be solved without knowing the details of that derivation.

(a) Mass transported in the zonal direction ($\hat{\boldsymbol{x}}$) that crosses the column's vertical boundary at x is given by

$$F^{(x)}(x, y, t) = \int_{y-\Delta y/2}^{y+\Delta y/2} \left[\int_{\eta_{\mathsf{b}}(x,y')}^{\eta(x,y',t)} u(x, y', z', t)\, \rho(x, y', z', t)\, \mathrm{d}z' \right] \mathrm{d}y' \tag{19.112a}$$

$$\equiv \int_{y-\Delta y/2}^{y+\Delta y/2} U^{\rho}(x, y', t)\, \mathrm{d}y', \tag{19.112b}$$

and similarly for mass transport in the meridional direction

$$F^{(y)}(x, y, t) = \int_{x-\Delta x/2}^{x+\Delta x/2} \left[\int_{\eta_{\mathsf{b}}(x',y)}^{\eta(x',y,t)} v(x', y, z', t)\, \rho(x', y, z', t)\, \mathrm{d}z' \right] \mathrm{d}x' \tag{19.113a}$$

$$\equiv \int_{x-\Delta x/2}^{x+\Delta x/2} V^{\rho}(x', y, t)\, \mathrm{d}x', \tag{19.113b}$$

where

$$\boldsymbol{U}^{\rho}(x, y, t) = \int_{\eta_{\mathsf{b}}(x,y)}^{\eta(x,y,t)} \boldsymbol{u}(x, y, z', t)\, \rho(x, y, z', t)\, \mathrm{d}z' = \hat{\boldsymbol{x}}\, U^{\rho} + \hat{\boldsymbol{y}}\, V^{\rho}. \tag{19.114}$$

What are the physical dimensions [in terms of length (L), mass (M), and time (T)] for the mass transports, $F^{(x)}$ and $F^{(y)}$?

(b) Using these expressions for the mass crossing the vertical side boundaries of a fluid column, take the limit as the horizontal cross-sectional area of the column becomes infinitesimally small to show that the evolution equation for the mass per unit area of the column is given by

$$\frac{\mathrm{d}}{\mathrm{d}t} \left[\int_{\eta_{\mathsf{b}}}^{\eta} \rho\, \mathrm{d}z \right] = -\nabla \cdot \boldsymbol{U}^{\rho} + Q_{\mathsf{m}}, \tag{19.115}$$

where Q_{m} is the mass transport entering the ocean through the surface, per horizontal area, as defined by equation (19.88c), so that

$$\int Q_{\mathsf{m}}\, \mathrm{d}A = -\int \rho\, \Delta \boldsymbol{v} \cdot \hat{\boldsymbol{n}}\, \mathrm{d}\mathcal{S} \qquad \text{at } z = \eta. \tag{19.116}$$

The derivation of equation (19.115) is part of this exercise, using methods distinct from

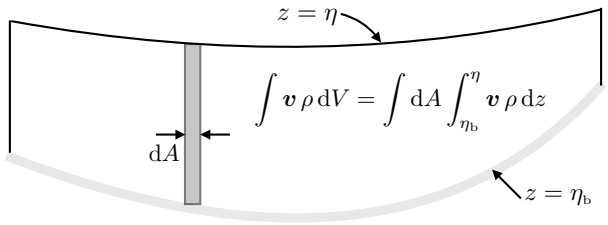

FIGURE 19.10: Cross-section of the integration region for Exercise 19.4, with the region extending from the ocean bottom at $z = \eta_b(x, y)$ and the free surface at $z = \eta(x, y, t)$. The sides are assumed to be vertical and rigid. An infinitesimal column is shown with cross-sectional area $\mathrm{d}A$, extending from the bottom to the surface. The cross-sectional area for the column is time independent, so that a time derivative passes across the area integral to act only on the upper limit $z = \eta$ and the integrand in equation (19.119).

those used in Section 19.7.2.

(c) In words, the mass budget in equation (19.115) says that mass changes in a column of fluid if there is a convergence of mass into the column across its vertical boundaries (first term on right hand side), and a mass flux entering the column across the ocean surface (second term on right hand side). What are the physical dimensions of all terms in equation (19.115)?

EXERCISE 19.4: CHANGE IN LINEAR MOMENTUM OF A FLUID REGION

Consider a closed ocean basin with zero boundary fluxes of matter; i.e., zero precipitation/evaporation and zero mass fluxes through the solid-earth bottom. Consequently, this region is bounded by material surfaces and so it maintains constant matter content with fixed mass

$$M = \int_{\mathcal{R}} \rho \, \mathrm{d}V. \tag{19.117}$$

Show that the time change in the linear momentum for this ocean basin is given by

$$\frac{\mathrm{d}}{\mathrm{d}t} \left[\int_{\mathcal{R}} \rho \, \boldsymbol{v} \, \mathrm{d}V \right] = \int_{\mathcal{R}} \frac{\mathrm{D}\boldsymbol{v}}{\mathrm{D}t} \, \rho \, \mathrm{d}V. \tag{19.118}$$

This result is identical to that derived in Exercise 19.2. Rather than just repeating the solution method used there, make use of Leibniz's rule, the kinematic boundary condition detailed in Section 19.6.2, and mass conservation.

As noted in the footnote for Exercise 19.2, addition of vectors is only defined locally within a tangent space when working on a general manifold. This limitation prevents us from integrating vectors over an arbitrary manifold. However, for Cartesian tensors in Euclidean space, we can perform integration in a naive manner just as for scalars, thus enabling us to perform the integration in equation (19.118). Hence, throughout this exercise we use Cartesian tensors in Euclidean space.

Hint: Refer to Figure 19.10 for a schematic of the integration where we have expanded the volume integral into the form

$$\frac{\mathrm{d}}{\mathrm{d}t} \left[\int_{\mathcal{R}} \rho \, \boldsymbol{v} \, \mathrm{d}V \right] = \frac{\mathrm{d}}{\mathrm{d}t} \left[\int \left(\int_{\eta_b}^{\eta} \rho \, \boldsymbol{v} \, \mathrm{d}z \right) \mathrm{d}A \right], \tag{19.119}$$

where the horizontal integral extends over the rigid and fixed horizontal area of the basin, $\mathrm{d}A = \mathrm{d}x \, \mathrm{d}y$ is the time independent horizontal area element, $z = \eta_b(x, y)$ is the solid-earth bottom and $z = \eta(x, y, t)$ is the ocean free surface. Time dependence appears in the upper boundary at $z = \eta$ and within the integrand. Perform the time derivative operation and make use of mass continuity and the kinematic boundary condition. Also make use of the trigonometry

presented in Section 19.6.3 (in particular equation (19.87)). Unlike the formulation in Exercise 19.2, there is no use of a material time derivative in this approach. Rather, it is a straightforward (albeit tedious) use of integration over a domain with fixed horizontal/bottom boundaries and a time dependent free surface boundary.

Chapter 20

CONSERVATION EQUATIONS FOR MATERIAL TRACERS

As seen in Chapter 19, the assumption of *mass conservation* has many implications for the motion of single-component fluids. In this chapter we extend that discussion to the case of a fluid comprised of multiple matter constituents referred to as *material tracers* (e.g., seawater comprised of fresh water, salt, nitrogen, oxygen, carbon, nutrients, biogeochemicals). In so doing we develop differential and integral budget equations for extensive properties, such as mass or tracer content, along with *continuity equations* for intensive properties, such as mass density and tracer concentration. The Leibniz-Reynolds transport theorem provides the link between the differential and integral formulations.

The *barycentric velocity* is a key element in the formulation of mass budgets with multiple matter constituents, with the barycentric velocity equal to the center of mass velocity for a fluid element. As we see in this chapter, the barycentric velocity plays the same role for multi-component fluids as the fluid parcel velocity does for single-component fluids. Differences between the barycentric velocity and the velocity of a specific fluid constituent can lead to the exchange of matter constituents across the boundary of the fluid element, with that exchange typically represented as diffusion.

The continuity equation describing material tracer concentration is referred to as the *tracer equation*. As we see in Section 26.11.3, it is also the equation satisfied (to a high degree of accuracy) by Conservative Temperature, which is the scalar field used to describe the relative enthalpy of a fluid element. We thus have many opportunities in this book to encounter the tracer equation.

READER'S GUIDE TO THIS CHAPTER

The formulation pursued in this chapter is inspired by similar treatments in the chemical physics literature (e.g., Chapter 11 of *Aris* (1962), Chapter II of *DeGroot and Mazur* (1984), or Section 2.1 of *Kreuzer* (1981)), who develop a theory for transport processes in multi-component fluids. For this chapter, we assume an understanding of the Eulerian and Lagrangian kinematic descriptions detailed in Chapter 17 and the mass conservation analysis in Chapter 19. Much of the material from this chapter is used for the study of scalar fields such as potential enthalpy (i.e., Conservative Temperature) and material tracers. Furthermore, the Leibniz-Reynolds transport theorem of Section 20.2.4 is a kinematic result central to all finite volume budgets in fluid mechanics.

20.1 The tracer equation

As defined in Section 17.2, a fluid element is an infinitesimal region of constant mass that lives within the moving fluid continuum. Although possessing a constant mass, it generally has a non-constant material composition. That is, a fluid element is a non-material fluid parcel. Fluid element boundaries are open to the exchange of matter (i.e., tracers) with adjacent fluid elements. They are also open to the exchange of thermodynamic properties such as temperature and specific entropy.

The kinematics of fluid elements share certain features with material fluid parcels. For example, we can uniquely specify the position of a fluid element's center of mass by providing a material coordinate and time. Correspondingly, we can generalize the Reynolds transport theorem for integration over a constant mass fluid region (Section 20.2.4). We make use of fluid elements to develop the mass budgets for multi-component fluids such as the ocean and atmosphere. The constituent mass budgets are commonly referred to as *tracer equations*.

20.1.1 Mass conservation for each constituent

In this subsection we formulate the mass conservation equation for each constituent within the fluid. The mass equation is formulated by taking an integral (weak formulation) over a fixed (Eulerian) region.

Density and velocity for each matter constituent

Consider a fluid with $\mathsf{n} = 1, N$ matter constituents. For example, seawater has $N = 2$ when concerned just with its freshwater and salt content, whereas $N > 2$ when also concerned with other material constituents such as CO_2 and biogeochemical species. Now focus on a fixed (Eulerian) region of the fluid with volume, V, and total mass, M. Inside of the region, assume we can somehow count the number of molecules of each constituent and determine their corresponding velocities. This information can be used to construct the molecular center of mass

velocity for each constituent, $\boldsymbol{v}^{(\mathsf{n})}$, as well as the mass density,

$$\rho^{(\mathsf{n})} = V^{-1}\, M^{(\mathsf{n})}. \tag{20.1}$$

In the continuum limit, the volume and mass in the region get tiny ($V \to \mathrm{d}V$ and $M \to \mathrm{d}M$), yet the mass density remains smooth and finite (see Figure 16.2 and corresponding discussion). Hence, the constituent velocity and mass density are continuous fields whose values are available at each point within the continuum fluid.

Integral formulation of the constituent mass budget

Consider an arbitrary region, $\mathscr{R}$, assumed to be fixed in space (an Eulerian region). The mass of component n within $\mathscr{R}$ is given by the integral

$$M^{(\mathsf{n})} = \int_{\mathscr{R}} \rho^{(\mathsf{n})}\, \mathrm{d}V, \tag{20.2}$$

and it changes in time according to the finite volume budget equation (there is no implied summation on the right hand side)

$$\frac{\mathrm{d}}{\mathrm{d}t} \int_{\mathscr{R}} \rho^{(\mathsf{n})}\, \mathrm{d}V = -\oint_{\partial\mathscr{R}} \rho^{(\mathsf{n})}\, \boldsymbol{v}^{(\mathsf{n})} \cdot \hat{\boldsymbol{n}}\, \mathrm{d}\mathcal{S}. \tag{20.3}$$

This equation is a constituent form of the finite volume mass budget given for a single-component fluid by equation (19.9). Since the region, $\mathscr{R}$, is assumed to be fixed in space, we can move the time derivative across the integral to reveal

$$\int_{\mathscr{R}} \left[\frac{\partial \rho^{(\mathsf{n})}}{\partial t} + \nabla \cdot (\rho^{(\mathsf{n})}\, \boldsymbol{v}^{(\mathsf{n})}) \right] \mathrm{d}V = 0, \tag{20.4}$$

where we also used the divergence theorem to convert the surface integral to a volume integral. Arbitrariness of the region means that this integral expression must be satisfied at each point of the continuum, thus leading to the Eulerian form of the constituent mass continuity equation

$$\partial_t \rho^{(\mathsf{n})} + \nabla \cdot (\rho^{(\mathsf{n})}\, \boldsymbol{v}^{(\mathsf{n})}) = 0. \tag{20.5}$$

This equation can also be written using a material time derivative

$$\frac{\mathrm{D}^{(\mathsf{n})} \rho^{(\mathsf{n})}}{\mathrm{D}t} = -\rho^{(\mathsf{n})}\, \nabla \cdot \boldsymbol{v}^{(\mathsf{n})} \qquad \text{for each of the } \mathsf{n} = 1, N \text{ constituents}, \tag{20.6}$$

where the constituent material time derivative is given by

$$\frac{\mathrm{D}^{(\mathsf{n})}}{\mathrm{D}t} = \frac{\partial}{\partial t} + \boldsymbol{v}^{(\mathsf{n})} \cdot \nabla. \tag{20.7}$$

We thus have N statements of mass conservation corresponding to each constituent material fluid parcel moving according to the velocity, $\boldsymbol{v}^{(\mathsf{n})}$.

20.1.2 Total mass conservation

Summing the Eulerian mass continuity equation (20.5) over all constituents leads to the continuity equation for the total mass

$$\partial_t \rho + \nabla \cdot (\rho\, \boldsymbol{v}) = 0, \tag{20.8}$$

where the total mass density and *barycentric velocity* are given by

$$\rho = \sum_{\mathsf{n}=1}^{N} \rho^{(\mathsf{n})} \quad \text{and} \quad \boldsymbol{v} = \rho^{-1} \sum_{\mathsf{n}=1}^{N} \rho^{(\mathsf{n})}\, \boldsymbol{v}^{(\mathsf{n})}. \tag{20.9}$$

Introducing the material time derivative following the barycentric velocity, $\mathrm{D}/\mathrm{D}t = \partial/\partial t + \boldsymbol{v}\cdot\nabla$, leads to the equivalent material form for the mass conservation equation

$$\frac{\mathrm{D}\rho}{\mathrm{D}t} = -\rho\,\nabla\cdot\boldsymbol{v}. \tag{20.10}$$

The *barycenter* of a distribution of matter is the center of inertia for that matter. We choose the term barycentric velocity for $\boldsymbol{v}$ to distinguish it from the molecular *center of mass velocity*, $\boldsymbol{v}^{(\mathsf{n})}$, of each material constituent. The barycentric velocity plays a key role in conservation laws for multi-component fluids, largely since equations (20.8) and (20.10) are identical to the mass conservation equations that hold for the homogeneous fluid derived in Section 19.2.

20.1.3 The tracer equation

Rather than keep track of each constituent velocity, $\boldsymbol{v}^{(\mathsf{n})}$, and the corresponding material parcels, it is generally more convenient to focus on the fluid element that moves with the barycentric velocity. For this purpose, consider again the constituent mass continuity equation (20.5)

$$(\partial_t + \boldsymbol{v}^{(\mathsf{n})}\cdot\nabla)\rho^{(\mathsf{n})} = -\rho^{(\mathsf{n})}\nabla\cdot\boldsymbol{v}^{(\mathsf{n})}, \tag{20.11}$$

and insert the barycentric velocity to both sides by adding $0 = \boldsymbol{v} - \boldsymbol{v}$

$$[\partial_t + (\boldsymbol{v} - \boldsymbol{v} + \boldsymbol{v}^{(\mathsf{n})})\cdot\nabla]\rho^{(\mathsf{n})} = -\rho^{(\mathsf{n})}\nabla\cdot[\boldsymbol{v} - \boldsymbol{v} + \boldsymbol{v}^{(\mathsf{n})}]. \tag{20.12}$$

Rearrangment leads to

$$(\partial_t + \boldsymbol{v}\cdot\nabla)\rho^{(\mathsf{n})} = -\rho^{(\mathsf{n})}\nabla\cdot\boldsymbol{v} - \nabla\cdot[\rho^{(\mathsf{n})}\,(\boldsymbol{v}^{(\mathsf{n})} - \boldsymbol{v})], \tag{20.13}$$

which can be written

$$\frac{\mathrm{D}\rho^{(\mathsf{n})}}{\mathrm{D}t} = -\rho^{(\mathsf{n})}\,\nabla\cdot\boldsymbol{v} - \nabla\cdot\boldsymbol{J}^{(\mathsf{n})}, \tag{20.14}$$

where we defined the constituent *tracer mass flux*

$$\boldsymbol{J}^{(\mathsf{n})} = \rho^{(\mathsf{n})}\,(\boldsymbol{v}^{(\mathsf{n})} - \boldsymbol{v}), \tag{20.15}$$

which arises from the difference between the constituent velocity and the barycentric velocity. The dimensions of $\boldsymbol{J}^{(\mathsf{n})}$ are mass of constituent, n, per time per area.

The material mass conservation equation (20.14) takes on the Eulerian form

$$\partial_t\rho^{(\mathsf{n})} + \nabla\cdot(\boldsymbol{v}\,\rho^{(\mathsf{n})}) = -\nabla\cdot\boldsymbol{J}^{(\mathsf{n})}. \tag{20.16}$$

Introducing the tracer concentration $C^{(\mathsf{n})}$ according to

$$C^{(\mathsf{n})} = \frac{\rho^{(\mathsf{n})}}{\rho} = \frac{\delta M^{(\mathsf{n})}}{\delta M} = \frac{\text{mass of constituent } n \text{ in fluid element}}{\text{mass of fluid element}}, \tag{20.17}$$

leads to the tracer flux

$$\boldsymbol{J}^{(\mathsf{n})} = \rho\, C^{(\mathsf{n})}\,(\boldsymbol{v}^{(\mathsf{n})} - \boldsymbol{v}), \tag{20.18}$$

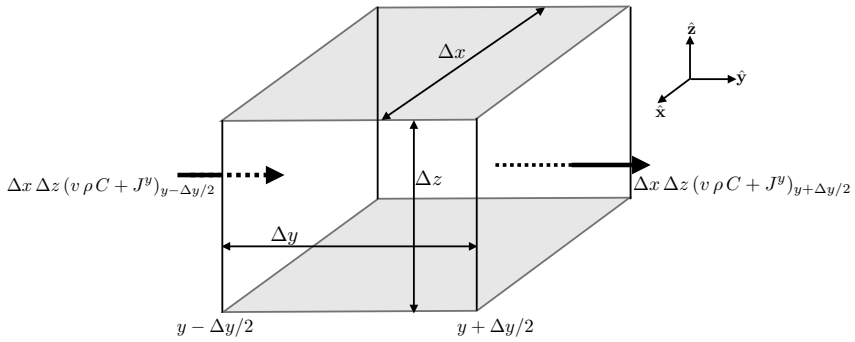

FIGURE 20.1: A finite sized cube as in Figure 19.1, here used to illustrate the budget of tracer mass over an Eulerian region. In addition to the advective flux of tracer moving with the barycentric velocity, $\boldsymbol{v}$, there is a flux, $\boldsymbol{J}$, that arises from differences between the barycentric velocity and the constituent velocity. We here only show fluxes in the $\hat{\boldsymbol{y}}$ direction, with corresponding fluxes in the $\hat{\boldsymbol{x}}$ and $\hat{\boldsymbol{z}}$ directions also contributing to the tracer budget.

and the flux-form tracer budget

$$\partial_t(\rho\, C^{(\mathsf{n})}) + \nabla \cdot (\boldsymbol{v}\, \rho\, C^{(\mathsf{n})} + \boldsymbol{J}^{(\mathsf{n})}) = 0. \tag{20.19}$$

In Figure 20.1 we illustrate the contributions to the tracer evolution according to equation (20.19).

Eulerian and Lagrangian forms of the tracer equation

The flux-form equation (20.19) has a corresponding material time derivative form derived by expanding the derivatives

$$\begin{aligned} C^{(\mathsf{n})}\, \partial_t \rho + \rho\, \partial_t C^{(\mathsf{n})} + \rho\, \boldsymbol{v} \cdot \nabla C^{(\mathsf{n})} + C^{(\mathsf{n})}\, \nabla \cdot (\rho\, \boldsymbol{v}) & \\ = C^{(\mathsf{n})}\, (\partial_t \rho + \nabla \cdot (\rho\, \boldsymbol{v})) + \rho\, (\partial_t + \boldsymbol{v} \cdot \nabla) C^{(\mathsf{n})}. & \end{aligned} \tag{20.20}$$

The first term on the right hand side vanishes through mass continuity in the form of equation (20.8). The second term on the right hand side is the material time derivative of the tracer concentration. We are thus led to the equivalent forms for the tracer equation

$$\partial_t(\rho\, C^{(\mathsf{n})}) + \nabla \cdot [\boldsymbol{v}\, \rho\, C^{(\mathsf{n})}] = \rho\, \frac{\mathrm{D} C^{(\mathsf{n})}}{\mathrm{D}t} = -\nabla \cdot \boldsymbol{J}^{(\mathsf{n})}. \tag{20.21}$$

The same result was also derived in equation (19.50c) when discussing Reynolds transport theorem for a single-component fluid.

Advective plus non-advective (diffusive) tracer fluxes

The above definitions allow us to decompose the advective tracer flux, defined according to the tracer velocity, into an advective flux based on the barycentric velocity plus a *non-advective flux*

$$\rho\, C^{(\mathsf{n})}\, \boldsymbol{v}^{(\mathsf{n})} = \rho\, C^{(\mathsf{n})}\, (\boldsymbol{v}^{(\mathsf{n})} - \boldsymbol{v} + \boldsymbol{v}) = \boldsymbol{J}^{(\mathsf{n})} + \rho\, C^{(\mathsf{n})}\, \boldsymbol{v}. \tag{20.22}$$

The non-advective flux, $\boldsymbol{J}^{(\mathsf{n})} = \rho\, C^{(\mathsf{n})}\, (\boldsymbol{v}^{(\mathsf{n})} - \boldsymbol{v})$ (equation (20.18)), vanishes when the tracer velocity equals to the barycentric velocity, $\boldsymbol{v}^{(\mathsf{n})} = \boldsymbol{v}$. Correspondingly, the non-advective flux also vanishes for a single-component fluid, since in that case there is only one matter component and so the constituent velocity equals to the barycentric velocity. We sometimes refer to the non-advective flux as a *diffusive flux* since it is common in practice to parameterize this term as a

downgradient diffusive flux. However, as seen in Section 26.10.2, not all non-advective processes are downgradient. We also offer further discussion of diffusion due to turbulent processes in Chapters 68 and 71.

20.1.4 Compatibility between total mass and tracer mass

By construction, the flux-form of the tracer equation (20.19) is compatible with the flux-form continuity equation

$$\partial_t(\rho\, C^{(\mathsf{n})}) + \nabla \cdot [\rho\, \boldsymbol{v}\, C^{(\mathsf{n})} + \boldsymbol{J}^{(\mathsf{n})}] = 0 \iff \partial_t \rho + \nabla \cdot (\rho\, \boldsymbol{v}) = 0. \tag{20.23}$$

Compatibility is manifest by summing the tracer equation over all constituents and using the identities

$$\sum_{\mathsf{n}=1}^{N} C^{(\mathsf{n})} = 1 \qquad \text{and} \qquad \sum_{\mathsf{n}=1}^{N} \boldsymbol{J}^{(\mathsf{n})} = 0. \tag{20.24}$$

Furthermore, through use of the barycentric velocity (20.9), we are ensured that the continuity equation (20.8) for the total density of a fluid element contains just the barycentric velocity. There is no contribution from $\boldsymbol{J}^{(\mathsf{n})}$ since $\sum_{\mathsf{n}=1}^{N} \boldsymbol{J}^{(\mathsf{n})} = 0$.

20.1.5 Passive tracers

As defined in equation (20.17), the concentration of a material tracer is the mass of the trace constituent per mass of a fluid element. Such material tracers modify the barycentric velocity (20.9) since they carry mass and thus affect the mass density. We here define the idealized or theoretical construct known as a *passive tracer*. A passive tracer satisfies the advection-diffusion equation, but it has zero impact on the velocity and is thus dynamically passive. The passive tracer is thus analogous to the massless fluid particle of Section 17.2 whose trajectories define the Lagrangian reference frame. However, the passive tracer is transported both via advection and diffusion. Hence, we make use of passive tracers to probe the advective and diffusive features of the flow without modifying the flow. For example, a passive tracer can be used to define tracer pathways and time scales for transport between fluid regions. Passive tracers enable use of Green's function methods for describing their evolution, with some discussion given in Section 69.9, and a more thorough review provided by *Haine et al.* (2025) for ocean applications.

In Chapter 18 and Section 19.6.2, we discussed the notion of a material fluid object, which is an object comprised of fluid particles that follow the velocity, $\boldsymbol{v}$. In a single-component fluid, such material objects are impenetrable to matter, by construction. For a multi-component fluid, we can also consider objects that move with the barycentric velocity. However, trace matter generally crosses the material object through diffusion since $\boldsymbol{v}^{(\mathsf{n})} \neq \boldsymbol{v}$. Hence, there is no perfectly impenetrable fluid object in a fluid with any form of diffusion, including molecular diffusion. Even so, we can consider a passive tracer that follows the barycentric velocity, and selectively decide whether that passive tracer is affected by diffusion or not. Such theoretical options are afforded the passive tracer given that it is a conceptual idealization used to probe the fluid flow properties. Hence, the passive tracer is not subject to the same physical constraints as a material tracer.

20.1.6 Summary of some conceptual points

What is a fluid element? How does it maintain constant mass but not constant matter? Here we aim to review some of the conceptual points that answer these questions, building from our initial specification of fluid elements and fluid parcels in Section 17.2.

Revisiting a fluid element

The mass continuity equation (20.10) motivates us to define a fluid element as an infinitesimal fluid parcel that moves with barycentric velocity, $\boldsymbol{v}$, and maintains a constant total mass

$$\delta M = \sum_{\mathsf{n}=1}^{N} \delta M^{(\mathsf{n})}. \tag{20.25}$$

The fluid element does not maintain a constant mass for each constituent, since the fluid element moves at the barycentric velocity, $\boldsymbol{v}$, which generally differs from the constituent velocities, $\boldsymbol{v}^{(\mathsf{n})}$. Consequently, a fluid element boundary is permeable to matter transport that leaves its mass constant but allows for exchanges of matter constituents with adjacent fluid elements. Hence, if some matter leaves the fluid element, then an equal amount must enter the element in order to maintain a constant mass.

The exchange of matter across a fluid element's boundary can arise from the direct motion of matter crossing the boundary, or from the motion of the fluid element boundary relative to the matter. This point is central to resolving conundrums associated with the notion of constituent matter exchange constrained to retain constant mass.

Conceptual summary of the formulation

The formulation pursued in this section is based on considering the multi-component fluid to be a continuum with distinct matter constituents (e.g., salt and freshwater for the ocean or water vapor and dry air for the atmosphere). Furthermore, the mass concentration for each constituent is represented by a scalar field whose value at any point in space-time gives the mass of tracer per mass of fluid. We then formulate mass conservation equations (i.e., continuity equations) for each matter constituent following methods used for the single-component fluid in Chapter 19. By choosing to use the *barycentric* (center of mass) velocity for describing fluid flow, the mass continuity equation for the total mass in a fluid element takes on the same form as for a single-component fluid. The resulting constituent mass budgets (i.e., tracer equations) have non-advective (diffusive) fluxes since the velocity of each matter constituent is generally distinct from the barycentric velocity.

To expose a bit of the details, we saw in this section that the tracer equation expresses the balance of mass for each trace constituent in the fluid. Furthermore, a nonzero tracer flux, $\boldsymbol{J}^{(\mathsf{n})} = \rho C^{(\mathsf{n})} (\boldsymbol{v}^{(\mathsf{n})} - \boldsymbol{v})$, arises when the barycentric velocity, $\boldsymbol{v}$, differs from the constituent velocity, $\boldsymbol{v}^{(\mathsf{n})}$. In that case, matter and thermodynamic properties are exchanged between fluid elements, with the exchange made without altering the mass of a fluid element. In the presence of random motion within a turbulent fluid, or in the presence of random interactions with molecular degrees of freedom, tracer exchange is akin to a random walk. Such exchange is commonly parameterized by a diffusion process (see Chapter 68). Correspondingly, the mass of tracers in a fluid element is altered in the presence of differences in tracer concentration between fluid elements (i.e., tracer concentration gradients). However, the total mass of the element remains fixed.

How to maintain constant mass

As defined, a fluid element provides a generalization to multi-component fluids of the notion of a constant mass material fluid parcel that we used in describing a single-component fluid (see Section 17.2). Later in this chapter we encounter a finite volume extension of the fluid element, which we refer to as a *Lagrangian region*. A Lagrangian region has boundaries that follow the barycentric velocity, $\boldsymbol{v}$, so that the region maintains constant mass as per our discussion of Reynolds transport theorem in Section 20.2.6.

To maintain constant mass, any matter that leaves the fluid element by crossing its boundary is compensated by an equal mass that enters the boundary. Kinematically, there are two means for matter to cross a boundary. First, the matter itself can move across the boundary, with the limiting case being a stationary boundary with matter moving across. Second, the boundary can move relative to the matter, with the limiting case being stationary matter with the boundary moving. In either case, by choosing to follow the barycentric velocity, a fluid element's boundary (or a corresponding Lagrangian region's boundary) adjusts so that mass remains constant.

The strategic choice to formulate the kinematics of multi-component fluids using the barycentric velocity is directly analogous to the choice in Newtonian mechanics to describe motion relative to the center of mass for a system of many moving objects such as planets or point particles (see Section 11.5). In particular, by describing the motion of a multi-component fluid using the barycentric velocity, we simplify the kinematics by linking to the kinematics of single-component fluids while also supporting a generalization in the form of constituent tracer equations. As seen in Part V of this book, a dynamical description of fluid motion is also facilitated by working with constant mass fluid elements/regions.

The importance of compatibility

In Section 20.1.4, we introduced the notion of compatibility between the tracer equation and mass continuity equation. On first encounter, one might consider it a rather trivial consequence of the formulation. Indeed, mathematically it is rather trivial, as it directly follows from our choice to describe motion according to the barycentric velocity. However, it is a notion that can sometimes be overlooked when in the midst of a formulation that decomposes the flow into mean components and deviations, as occurs with studies of turbulent flows. The key point to remember is that whatever form the mean-field mass continuity equation takes, one must retain a clear formulation of mass conservation. Doing so may require modification of the effective barycentric velocity in the presence of turbulent fluctuations.

As an example, let $\overline{\rho}$ and $\overline{\boldsymbol{v}}$ be the mean density and mean velocity, where "mean" can represent any number of averaging operators, and let primes denote deviations from the means. The mass continuity equation for the mean density thus takes the form

$$\partial_t \overline{\rho} + \nabla \cdot (\overline{\rho}\, \overline{\boldsymbol{v}}) = 0. \tag{20.26}$$

Introducing the density-weighted velocity

$$\boldsymbol{v}^{\mathrm{H}} \equiv \overline{\rho\, \boldsymbol{v}}/\overline{\rho} = \overline{\boldsymbol{v}} + \overline{\rho'\, \boldsymbol{v}'}/\overline{\rho} \tag{20.27}$$

renders the mean continuity equation

$$\partial_t \overline{\rho} + \nabla \cdot (\overline{\rho}\, \boldsymbol{v}^{\mathrm{H}}) = 0. \tag{20.28}$$

The density-weighted velocity, $\boldsymbol{v}^{\mathrm{H}}$, is motivated by the work of *Hesselberg* (1926) and *Favre* (1965), with further details for its use in the full suite of dynamical equations summarized in Chapter 8 of *Griffies* (2004). Rather than pursue details here, we use it simply to illustrate how one may choose to work with averaged equations in a manner that retains a clear sense for mass conservation. Namely, by introducing $\boldsymbol{v}^{\mathrm{H}}$, which can be considered a modified barycentric velocity, the mean mass conservation equation (20.28) takes on the same form as the un-averaged mass equation (20.8). In this manner we see that $\boldsymbol{v}^{\mathrm{H}}$, rather than $\overline{\boldsymbol{v}}$, advects the mean fluid mass density.

20.1.7 Further study

We used many words in this section to develop the mass budget for fluid elements in a multi-component fluid. The reason for such verbosity is that the formulation can be confusing on first encounter. Even so, it is important to keep in mind that the basic notions are quite simple. Further extension of these ideas incorporates chemical reactions that transfer mass from one matter constituent to others, while retaining fixed net mass. This extension is relevant for studies of atmospheric chemistry and ocean bioegeochemistry. Development of these extensions, using nomenclature similar to that used here, is provided in Chapter 11 of *Aris* (1962), Chapter II of *DeGroot and Mazur* (1984), and Section 2.1 of *Kreuzer* (1981).

The tracer fluxes introduced when formulating the tracer equation are typically parameterized by downgradient diffusion. However, as discussed in our study of the ocean entropy budget in Section 26.10, the transport of a scalar field can arise both from spatial gradients in that field as well as gradients in other fluid properties. These fluxes arise as a result of fundamental constraints from the second law of thermodynamics, and as such they are part of the suite of processes contributing to the transport of scalar properties in a multi-component fluid.

20.2 Budgets for arbitrary fluid regions

Thus far in this chapter we have considered the evolution of mass within a variety of fluid regions, including infinitesimal and finite domains either moving with the fluid or fixed in space. We have also considered similar domains in Chapter 19 where the fluid domains were typically material regions. In this section we synthesize these presentations by considering mass budgets over an arbitrary finite sized domain within multi-component fluids. The resulting mass equations form the basis for matter budgets used in geophysical fluid mechanics.

20.2.1 Extensive and intensive fluid properties

Consider a bucket of seawater that has homogeneous temperature and salinity. Removing a cup of water from this bucket does not alter the temperature or salinity, but it does alter the enthalpy, salt mass, and freshwater mass. We are thus motivated to characterize physical properties as *extensive* or *intensive*. For the bucket of seawater, temperature and salinity are intensive quantities, whose value does not change when removing seawater from the bucket. Further intensive properties include number density (number of particles per volume), mass density (mass of substance per volume), tracer concentration (mass of tracer per mass of fluid), temperature, velocity (linear momentum per mass), kinetic energy per mass, entropy per mass, and enthalpy per mass. An extensive property changes when the size of the sample changes, with examples including particle number, mass, length, volume, kinetic energy, entropy, enthalpy, and linear momentum.[1]

We are concerned in this section with how scalar extensive properties change as a function of time.[2] Determining the evolution of such properties constitutes a budget analysis for the scalar property. What are the processes responsible for these changes? Where are the changes coming from? Those are basic questions asked when performing a budget analysis. In addition to physical and biogeochemical processes active within the fluid, details of the region over which one performs a budget have an important impact on the budget. Is the region open to matter and energy transport, or is it closed? Is the region static (Eulerian) or do boundaries move? If the boundaries move, do they move with the barycentric velocity (Lagrangian) or are they moving in some other manner?

[1] We again encounter intensive and extensive properties when studying thermodynamics in Chapter 22.
[2] We consider budget equations for vector linear momentum in Chapter 24.

In the following, let Π represent an intensive scalar property of a fluid element so that $\Pi\,\rho\,\delta V$ is the corresponding extensive property

$$\Pi = \text{intensive fluid property such as tracer concentration} \tag{20.29a}$$

$$\Pi\,\rho\,\delta V = \text{extensive fluid property such as tracer mass.} \tag{20.29b}$$

For example, if Π is the tracer concentration in a fluid element (i.e., mass of tracer per mass of fluid), then the corresponding extensive property, $\Pi\,\rho\,\delta V$, is the mass of tracer in the fluid element. Anticipating our discussion in Section 26.11, then if Π is the Conservative Temperature, Θ, of a fluid element, then the corresponding extensive property, $\Theta\,c_{\mathrm{p}}\,\rho\,\delta V$, is the potential enthalpy with c_{p} the specific heat capacity.

We furthermore assume that Π satisfies the scalar conservation equation, written here in both its material (or advective) form and flux-form

$$\rho\,\frac{\mathrm{D}\Pi}{\mathrm{D}t} = -\nabla\cdot\boldsymbol{J} \qquad \Longleftrightarrow \qquad \frac{\partial(\rho\,\Pi)}{\partial t} + \nabla\cdot(\rho\,\Pi\,\boldsymbol{v} + \boldsymbol{J}) = 0, \tag{20.30}$$

where $\boldsymbol{J}$ is a flux such as that associated with the tracer equation derived in Section 20.1.3. Depending on the context, the budget equation (20.30) is sometimes referred to as a *conservation law* for Π. Notably, satisfaction of a conservation law does not mean that Π is constant either at a point in space nor following a fluid particle. Instead, there are two cases of "constancy" that naturally arise. First, with $-\nabla\cdot\boldsymbol{J} = 0$, the scalar field is constant following a material fluid particle

$$-\nabla\cdot\boldsymbol{J} = 0 \Longrightarrow \frac{\mathrm{D}\Pi}{\mathrm{D}t} = 0. \tag{20.31}$$

In this case we say that Π is a *material invariant* or a *material constant*. Second, if the Eulerian time derivative vanishes, $\partial_t\Pi = 0$, then Π remains constant at a fixed spatial point in the fluid and we say that Π is in a *steady state*. Furthermore, recall that the Eulerian reference frame is stationary with respect to a laboratory frame, with the laboratory frame inertial when connected by a Galilean transformation to the universal Newtonian reference frame (Section 17.1.2). Hence, if the flow in one laboratory frame is steady, then flow in all laboratory frames is steady so long as the laboratory frames are connected by a Galilean transformation (see Section 17.5).

20.2.2 General form of the finite domain integral

We are concerned here with the evolution of extensive fluid properties integrated over an arbitrary region. Let us make use of the following notation for such integrals

$$\mathcal{I}[\mathcal{R}(t), t] = \int_{\mathcal{R}(t)} \Pi\,\rho\,\mathrm{d}V \equiv \int_{\mathcal{R}(t)} \varphi\,\mathrm{d}V, \tag{20.32}$$

where we introduced the shorthand

$$\varphi = \rho\,\Pi. \tag{20.33}$$

The integrand in equation (20.32) is a function of space and time, $\varphi = \varphi(\boldsymbol{x}, t)$, and the integration region is generally a function of time, $\mathcal{R}(t)$. In previous sections, $\mathcal{R}$ was a material region of fixed matter content (Section 19.3) or a constant mass fluid region open to the exchange of matter with the surroundings (Section 20.1). In both of these cases the region was denoted by $\mathcal{R}(\boldsymbol{v})$ since it moved with the fluid flow. Here we make no *a priori* assumption about the region.

The total time derivative of $\mathcal{I}$ can be written as

$$\frac{\mathrm{d}\mathcal{I}}{\mathrm{d}t} = \left[\frac{\partial\mathcal{I}}{\partial t}\right]_{\mathcal{R}} + \frac{\mathrm{d}\mathcal{R}}{\mathrm{d}t}\left[\frac{\partial\mathcal{I}}{\partial\mathcal{R}}\right]_{t}. \tag{20.34}$$

The first term on the right hand side is the time derivative of the integral when holding the region fixed in space as per an Eulerian time derivative. The second term accounts for changes due to evolution of the region as weighted by dependence of the integral on the region itself. How the integral changes in time depends on both the evolution of the fluid property relative to the chosen region and evolution of the fluid region itself. Equation (20.34) is directly analogous to the total time derivative of a field in a moving fluid as given by equation (17.9).

20.2.3 Eulerian (static) domain

We first consider an Eulerian domain, which is fixed in space and thus static so that

$$\frac{\mathrm{d}\mathcal{I}}{\mathrm{d}t} = \left[\frac{\partial \mathcal{I}}{\partial t}\right]_{\mathcal{R}} = \frac{\partial}{\partial t}\left[\int_{\mathcal{R}} \Pi\, \rho \,\mathrm{d}V\right] = \int_{\mathcal{R}} \left[\frac{\partial(\rho\,\Pi)}{\partial t}\right] \mathrm{d}V. \tag{20.35}$$

Movement of the time derivative across the integral sign is available since the domain boundaries are static; i.e., the second term on the right hand side of equation (20.34) vanishes. Furthermore, since the domain is static, the volume element, $\mathrm{d}V$, provides a static partition of the total domain volume so that $\mathrm{d}V$ does not appear inside the time derivative. This case corresponds to the Eulerian budgets depicted in Figures 19.1, 19.2, and 20.1.

20.2.4 Deriving the Leibniz-Reynolds transport theorem

We now allow the domain boundaries to be time dependent so that both terms in the total time derivative (20.34) contribute. The resulting *Leibniz-Reynolds transport theorem* is a general expression of conservation over an arbitrary region. We derive this theorem here using two methods, one naive and another a bit more rigorous. Interpretation and application of this theorem are then presented in Section 20.2.5.

A rectangular region

Consider a one-dimensional domain with time dependent endpoints. Integrals of this type commonly arise when integrating over the depth of the atmosphere or ocean, in which case the boundary terms are replaced by the kinematic boundary conditions studied in Section 19.6. The chain rule for differentiating integrals is known as *Leibniz's rule*. It results in the time derivative acting on the upper integral limit, the lower limit, and the integrand

$$\frac{\mathrm{d}}{\mathrm{d}t}\left[\int_{x_1(t)}^{x_2(t)} \varphi(x,t)\,\mathrm{d}x\right] = \int_{x_1(t)}^{x_2(t)} \frac{\partial \varphi}{\partial t}\,\mathrm{d}x + \frac{\mathrm{d}}{\mathrm{d}t}\left[\int_{x_1(t)}^{x_2(t)}\right] \varphi(x,t)\,\mathrm{d}x \tag{20.36a}$$

$$= \int_{x_1(t)}^{x_2(t)} \frac{\partial \varphi}{\partial t}\,\mathrm{d}x + \frac{\mathrm{d}x_2(t)}{\mathrm{d}t}\varphi(x_2,t) - \frac{\mathrm{d}x_1(t)}{\mathrm{d}t}\varphi(x_1,t), \tag{20.36b}$$

with the terms $\mathrm{d}x_{1,2}/\mathrm{d}t$ the velocities of the endpoints.

We can generalize the one-dimensional result (20.36b) to three dimensions by assuming the three dimensional domain is expressible by Cartesian coordinates whose extents are mutually independent. That is, we assume the domain, $\mathcal{R}(t)$, is rectangular. In this case we can immediately generalize equation (20.36b) to

$$\frac{\mathrm{d}}{\mathrm{d}t}\left[\int_{\mathcal{R}} \varphi\,\mathrm{d}V\right] = \int_{\mathcal{R}} \frac{\partial \varphi}{\partial t}\,\mathrm{d}V + \oint_{\partial\mathcal{R}} \varphi\, \boldsymbol{v}^{(\mathrm{b})} \cdot \hat{\boldsymbol{n}}\,\mathrm{d}\mathcal{S}, \tag{20.37}$$

where we introduced the shorthand for the velocity of a point on the region boundary

$$\boldsymbol{v}^{(\mathrm{b})} = \frac{\mathrm{d}\boldsymbol{x}}{\mathrm{d}t}. \tag{20.38}$$

The identity (20.37) is the *Leibniz-Reynolds transport theorem.*

An arbitrary simply connected region

We now present the derivation for an arbitrary simply connected domain, $\mathcal{R}(t)$, thus generalizing the domain geometry while offering further insight into the transport theorem. For this purpose, again let the region boundary, $\partial\mathcal{R}$, have an outward unit normal, $\hat{\boldsymbol{n}}$, and let points on the boundary move with the velocity, $\boldsymbol{v}^{(\mathrm{b})}$. In Figure 20.2 we depict the region geometry as it evolves over a time step of size, Δt. In particular, this figure illustrates the identity[3]

$$\mathcal{R}(t+\Delta t/2) = \mathcal{R}(t-\Delta t/2) + [\mathcal{R}(t+\Delta t/2) - \mathcal{R}(t-\Delta t/2)], \tag{20.39}$$

with the corresponding equation for the region volume given by

$$\int_{\mathcal{R}(t+\Delta t/2)} \mathrm{d}V = \int_{\mathcal{R}(t-\Delta t/2)} \mathrm{d}V + \int_{\mathcal{R}(t+\Delta t/2)-\mathcal{R}(t-\Delta t/2)} \mathrm{d}V. \tag{20.40}$$

From Figure 20.2 we see that the volume of the time incremented region, $\mathcal{R}(t+\Delta t/2)-\mathcal{R}(t-\Delta t/2)$, in the limit $\Delta t \to 0$, is given by

$$\lim_{\Delta t\to 0} \frac{1}{\Delta t} \int_{\mathcal{R}(t+\Delta t/2)-\mathcal{R}(t-\Delta t/2)} \mathrm{d}V = \lim_{\Delta t\to 0} \frac{1}{\Delta t} \left[\int_{\mathcal{R}(t+\Delta t/2)} \mathrm{d}V - \int_{\mathcal{R}(t-\Delta t/2)} \mathrm{d}V \right] \tag{20.41a}$$

$$= \frac{\mathrm{d}}{\mathrm{d}t} \left[\int_{\mathcal{R}(t)} \mathrm{d}V \right] \tag{20.41b}$$

$$= \oint_{\partial\mathcal{R}(t)} \boldsymbol{v}^{(\mathrm{b})} \cdot \hat{\boldsymbol{n}} \, \mathrm{d}\mathcal{S}. \tag{20.41c}$$

The final equality follows since $\boldsymbol{v}^{(\mathrm{b})} \cdot \hat{\boldsymbol{n}}$ measures the rate that the boundary is moving normal to itself, so that its area integral over $\partial\mathcal{R}(t)$ measures the rate that the volume of $\mathcal{R}(t)$ changes. It is the analog to the Lagrangian result (19.22) measuring the change in volume of a material region following the fluid flow.

The above ideas used to derive the volume budget equation (20.41c) are now applied when $\varphi(\boldsymbol{x}, t)$ is included within the integral, in which case we consider

$$\frac{\mathrm{d}}{\mathrm{d}t} \left[\int_{\mathcal{R}(t)} \varphi(t) \, \mathrm{d}V \right] = \lim_{\Delta t\to 0} \frac{1}{\Delta t} \left[\int_{\mathcal{R}(t+\Delta t/2)} \varphi(t+\Delta t/2) \, \mathrm{d}V - \int_{\mathcal{R}(t-\Delta t/2)} \varphi(t-\Delta t/2) \, \mathrm{d}V \right]. \tag{20.42}$$

Note that for brevity we suppressed the $\boldsymbol{x}$ functional dependence of $\varphi(\boldsymbol{x}, t)$. Expanding the first integral on the right hand side around the central time leads to the expression, which is accurate to $\mathcal{O}(\Delta t)^2$,

$$\int_{\mathcal{R}(t+\Delta t/2)} \varphi(t+\Delta t/2) \, \mathrm{d}V$$

[3]For those familiar with numerical methods, note that we make use of centered finite time differences in this discussion. Doing so offers a second order accurate expression of the finite difference approximations to the time derivative, whereas forward or backward differences are only first order accurate. Central differences also provides an intuitive centering of the time differences around the central time, t.

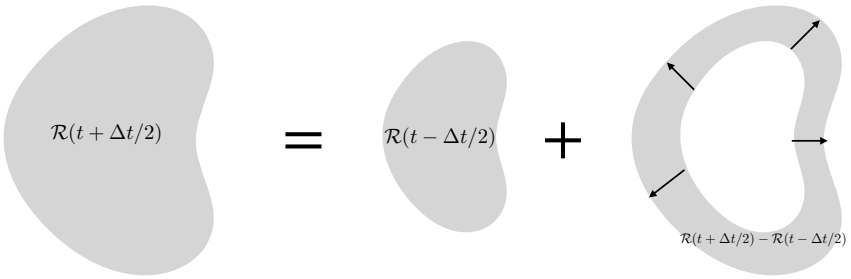

FIGURE 20.2: Illustrating the geometry of the Leibniz-Reynolds transport theorem. The region at time $t + \Delta t/2$, is written as $\mathcal{R}(t + \Delta t/2)$, which results from changing $\mathcal{R}(t - \Delta t/2)$ by the increment $\mathcal{R}(t + \Delta t/2) - \mathcal{R}(t - \Delta t/2)$. We here depict the case with an expanding boundary that renders a larger volume at $t + \Delta t/2$. At each point along the boundary the velocity of the boundary, $\boldsymbol{v}^{(\mathrm{b})}$, has an outward normal projection, $\boldsymbol{v}^{(\mathrm{b})} \cdot \hat{\boldsymbol{n}}$. The product $\boldsymbol{v}^{(\mathrm{b})} \cdot \hat{\boldsymbol{n}}\, \Delta t$ measures the distance that the boundary moves over the time increment, Δt. Hence, area integrating $\boldsymbol{v}^{(\mathrm{b})} \cdot \hat{\boldsymbol{n}}$ over the boundary yields the rate that the region volume changes.

$$= \int_{\mathcal{R}(t)} \left[\varphi(t) + \frac{\Delta t}{2} \frac{\partial \varphi(t)}{\partial t} \right] \mathrm{d}V + \int_{\mathcal{R}(t+\Delta t/2) - \mathcal{R}(t)} \left[\varphi(t) + \frac{\Delta t}{2} \frac{\partial \varphi(t)}{\partial t} \right] \mathrm{d}V. \quad (20.43)$$

We have a similar expansion for the second integral in equation (20.42)

$$\int_{\mathcal{R}(t-\Delta t/2)} \varphi(t - \Delta t/2)\, \mathrm{d}V$$
$$= \int_{\mathcal{R}(t)} \left[\varphi(t) - \frac{\Delta t}{2} \frac{\partial \varphi(t)}{\partial t} \right] \mathrm{d}V + \int_{\mathcal{R}(t-\Delta t/2) - \mathcal{R}(t)} \left[\varphi(t) - \frac{\Delta t}{2} \frac{\partial \varphi(t)}{\partial t} \right] \mathrm{d}V, \quad (20.44)$$

thus leading to the finite difference

$$\int_{\mathcal{R}(t+\Delta t/2)} \varphi(t + \Delta t/2)\, \mathrm{d}V - \int_{\mathcal{R}(t-\Delta t/2)} \varphi(t - \Delta t/2)\, \mathrm{d}V$$
$$= \Delta t \int_{\mathcal{R}(t)} \frac{\partial \varphi(t)}{\partial t}\, \mathrm{d}V + \int_{\mathcal{R}(t+\Delta t/2) - \mathcal{R}(t-\Delta t/2)} \varphi(t)\, \mathrm{d}V, \quad (20.45)$$

which is again accurate to $\mathcal{O}(\Delta t)^2$. Following our derivation of equation (20.41c) leads us to

$$\int_{\mathcal{R}(t+\Delta t/2) - \mathcal{R}(t-\Delta t/2)} \varphi(t)\, \mathrm{d}V = \Delta t \oint_{\partial \mathcal{R}(t)} \varphi\, \boldsymbol{v}^{(\mathrm{b})} \cdot \hat{\boldsymbol{n}}\, \mathrm{d}\mathcal{S}, \quad (20.46)$$

where all terms on the right hand side surface integral are evaluated at the central time, t. Bringing the pieces together, and taking the limit as $\Delta t \to 0$, leads to the Leibniz-Reynolds transport theorem

$$\frac{\mathrm{d}}{\mathrm{d}t} \left[\int_{\mathcal{R}(t)} \varphi(t)\, \mathrm{d}V \right] = \int_{\mathcal{R}(t)} \frac{\partial \varphi}{\partial t}\, \mathrm{d}V + \oint_{\partial \mathcal{R}(t)} \varphi\, \boldsymbol{v}^{(\mathrm{b})} \cdot \hat{\boldsymbol{n}}\, \mathrm{d}\mathcal{S}, \quad (20.47)$$

which agrees with the earlier result given by equation (20.37).

20.2.5 Interpreting the Leibniz-Reynolds transport theorem

The Leibniz-Reynolds transport theorem (20.37) is a central kinematic result in fluid mechanics. In particular, it forms the starting point for all finite volume budgets. Although we made use of Cartesian coordinates for both derivations, the result is a coordinate invariant measure of how an extensive fluid property evolves within a region. Hence, by the rules of tensor analysis from

Chapter 4, the result holds for arbitrary coordinates. Furthermore, we can extend it to multiply connected domains for which one sums over the distinct sub-domains to render the complete budget. These results confirm our notions regarding extensive properties, such as fluid mass, tracer mass, and enthalpy, and how they are budgeted throughout the fluid. Namely, these quantities are simply counted over the various regions of the fluid.

Comments on the boundary velocity

The appearance of the boundary velocity, $\boldsymbol{v}^{(\mathrm{b})}$, warrants some comment. As defined by equation (20.38), it measures the velocity of a point on the domain boundary. Notably, the resulting budget only requires information about the normal component to that velocity, $\boldsymbol{v}^{(\mathrm{b})} \cdot \hat{\boldsymbol{n}}$. For example, the domain boundary could be exhibiting arbitrary motion in the direction tangent to the bounding surface. Yet such tangential motion is of no concern for a budget developed over the domain since we are only concerned with transport across the boundary. Indeed, information concerning the tangential component is not available without making dynamical assumptions that go beyond the kinematics considered here. We encountered the same ideas when studying the kinematic boundary conditions in Section 19.6.

Transport theorem for region volume

As part of the general derivation, we derived the expression (20.41c) for the volume changes of the region, which is recovered by setting $\varphi = 1$ in the transport theorem (20.37)

$$\frac{\mathrm{d}}{\mathrm{d}t}\left[\int_{\mathscr{R}} \mathrm{d}V\right] = \oint_{\partial\mathscr{R}} \boldsymbol{v}^{(\mathrm{b})} \cdot \hat{\boldsymbol{n}}\, \mathrm{d}\mathcal{S}. \tag{20.48}$$

This result says that the volume for an arbitrary region changes in time so long as there is motion of the region boundary normal to itself. As noted above, we can compare this expression to that for a material region given by equation (19.22), with the expressions identical when $\boldsymbol{v}^{(\mathrm{b})} \cdot \hat{\boldsymbol{n}} = \boldsymbol{v} \cdot \hat{\boldsymbol{n}}$ for a material region. Note that the general volume budget (20.48) holds for both divergent and non-divergent flows, with further specialization to the non-divergent (incompressible) case considered in Section 21.6.2.

Transport theorem for a scalar field

We can derive a corollary to the transport theorem (20.37) that proves useful for budget analyses over moving regions. For this purpose, make use of the flux-form of the scalar conservation equation (20.30) so that the transport theorem is written

$$\frac{\mathrm{d}}{\mathrm{d}t}\left[\int_{\mathscr{R}} \rho\, \Pi\, \mathrm{d}V\right] = -\oint_{\partial\mathscr{R}} \left[\rho\, \Pi\, (\boldsymbol{v} - \boldsymbol{v}^{(\mathrm{b})}) + \boldsymbol{J}\right] \cdot \hat{\boldsymbol{n}}\, \mathrm{d}\mathcal{S}. \tag{20.49}$$

Setting $\Pi = 1$ gives an expression for the change in mass for the region

$$\frac{\mathrm{d}}{\mathrm{d}t}\left[\int_{\mathscr{R}} \rho\, \mathrm{d}V\right] = -\oint_{\partial\mathscr{R}} \rho\, (\boldsymbol{v} - \boldsymbol{v}^{(\mathrm{b})}) \cdot \hat{\boldsymbol{n}}\, \mathrm{d}\mathcal{S}. \tag{20.50}$$

The transport theorem (20.49) has a straightforward interpretation. Namely, the left hand side is the time tendency for the total Π-stuff within the moving region. The right hand side is the surface area integral of the flux of Π-stuff through the boundary of the region. The first right hand side term arises from the difference between the barycentric fluid velocity and the velocity of the boundary, and the second term arises from the non-advective (e.g., diffusive) flux. Both fluxes are projected onto the outward normal at the boundary and then integrated over the

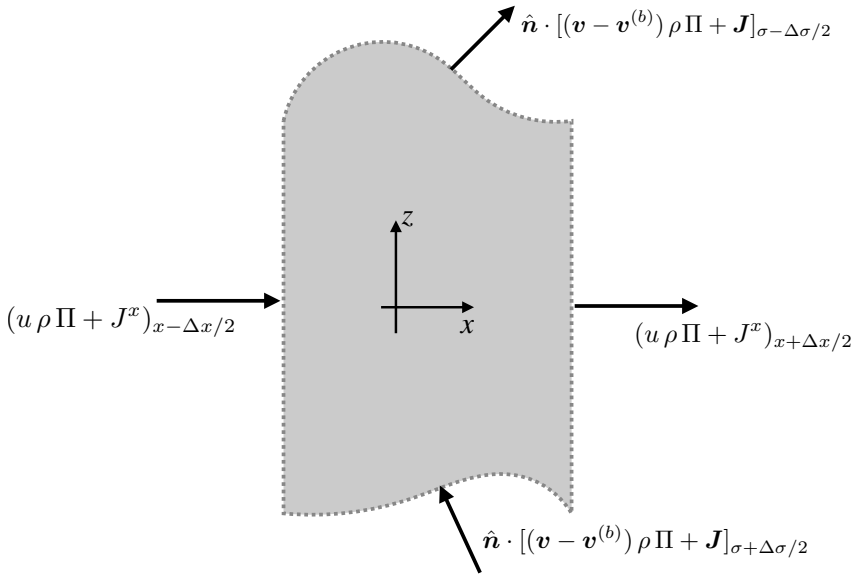

FIGURE 20.3: This figure depicts the contributions to the Leibniz-Reynolds transport theorem (20.49). The theorem is applied to a domain corresponding to a numerical model grid cell with the top and bottom interfaces defined by generalized vertical coordinates of Chapters 63, 64, and 65. In particular, the vertical cell faces are assumed to have fixed positions, so that $(\boldsymbol{v} - \boldsymbol{v}^{(b)}) \cdot \hat{\boldsymbol{n}} = \boldsymbol{v} \cdot \hat{\boldsymbol{n}}$ for these cell faces. Hence, the fluxes crossing these faces are due to advection by the barycentric velocity plus and contributions from non-advective (e.g., diffusive) fluxes. However, the top and bottom faces of the cell are allowed to move according to the generalized vertical coordinate surfaces. Hence, transport through these faces must take into account the nonzero velocity of the boundaries. Note that numerical models generally assume the top and bottom interfaces have a nonzero projection in the vertical direction so that they never overturn (e.g., *Griffies et al.* (2020)).

surface area. Hence, the budget is not affected by fluxes tangential to the boundary. Finally, for the mass budget (20.50), the non-advective flux vanishes since the mass of a fluid element moves according to the barycentric velocity of Section (20.1.2).

In Figure 20.3 we illustrate the transport theorem (20.49) for the special case of a discrete numerical model grid cell. This cell has fixed positions for the vertical sides whereas the top and bottom interfaces are time dependent. This application of the transport theorem provides the framework for finite volume methods in numerical models (e.g., *Griffies et al.* (2020)). We offer further discussion of the kinematics of such *general vertical coordinate* models in Chapter 64 and their dynamics in Chapter 65.

20.2.6 Revisiting Reynolds transport theorem

Consider the special case of a region that is moving with the fluid flow, in which case we provide a more general derivation of the *Reynolds transport theorem* than originally given for material regions in Section 19.5. The following results are special cases of the general expression (20.49).

Reynolds Transport Theorem

Let us apply the result (20.37) to a region that follows the fluid flow as defined by the barycentric velocity, $\boldsymbol{v}$. For this moving region, the time derivative of the region boundaries in equation (20.37) is given by the fluid velocity thus leading to

$$\frac{\mathrm{d}}{\mathrm{d}t}\left[\int_{\mathcal{R}(\boldsymbol{v})} \varphi \, \mathrm{d}V\right] = \int_{\mathcal{R}(\boldsymbol{v})} \left[\frac{\partial \varphi}{\partial t} + \nabla \cdot (\boldsymbol{v}\, \varphi)\right] \mathrm{d}V = \int_{\mathcal{R}(\boldsymbol{v})} \left[\frac{\mathrm{D}\varphi}{\mathrm{D}t} + \varphi\, \nabla \cdot \boldsymbol{v}\right] \mathrm{d}V. \tag{20.51}$$

This result is the Reynolds transport theorem. The derivation given here is more general than that in Section 19.5, with that derivation assuming the region to be material (i.e., no matter crosses the region boundary). For the present derivation we only assumed that the region boundaries move so that $(\boldsymbol{v} - \boldsymbol{v}^{(\mathrm{b})}) \cdot \hat{\boldsymbol{n}} = 0$, where again $\boldsymbol{v}$ is the barycentric velocity. We did not assume the region boundaries are material. We can thus make use of Reynolds transport theorem (20.51) for constant mass regions of a multi-component fluid so long as $(\boldsymbol{v} - \boldsymbol{v}^{(\mathrm{b})}) \cdot \hat{\boldsymbol{n}} = 0$. Furthermore, the region boundary is generally permeable via the non-advective (diffusive) tracer fluxes.

Alternative form of Reynolds Transport Theorem

We can put the Reynolds Transport Theorem (20.51) into another useful form by reintroducing $\varphi = \rho \, \Pi$ and making use of mass continuity

$$\frac{1}{\rho} \frac{\mathrm{D}\rho}{\mathrm{D}t} = -\nabla \cdot \boldsymbol{v}. \tag{20.52}$$

Doing so yields the rather tidy result

$$\begin{aligned}
\frac{\mathrm{d}}{\mathrm{d}t} \left[\int_{\mathcal{R}(\boldsymbol{v})} \Pi \, \rho \, \mathrm{d}V \right] &= \int_{\mathcal{R}(\boldsymbol{v})} \left[\frac{\mathrm{D}\varphi}{\mathrm{D}t} + \varphi \, \nabla \cdot \boldsymbol{v} \right] \mathrm{d}V && \text{Reynolds (20.51)} && (20.53a) \\
&= \int_{\mathcal{R}(\boldsymbol{v})} \left[\frac{\mathrm{D}(\rho \, \Pi)}{\mathrm{D}t} + \rho \, \Pi \, \nabla \cdot \boldsymbol{v} \right] \mathrm{d}V && \varphi = \rho \, \Pi && (20.53b) \\
&= \int_{\mathcal{R}(\boldsymbol{v})} \left[\Pi \left(\frac{\mathrm{D}\rho}{\mathrm{D}t} + \rho \, \nabla \cdot \boldsymbol{v} \right) + \rho \, \frac{\mathrm{D}\Pi}{\mathrm{D}t} \right] \mathrm{d}V && \text{product rule} && (20.53c) \\
&= \int_{\mathcal{R}(\boldsymbol{v})} \frac{\mathrm{D}\Pi}{\mathrm{D}t} \, \rho \, \mathrm{d}V. && \text{mass continuity (20.10)} && \\
& && && (20.53d)
\end{aligned}$$

Heuristically, this result follows since $\rho \, \mathrm{d}V$ is a constant when following the flow, so that passage of the time derivative across the material integral only picks up the material derivative of Π.

We can take the result (20.53d) one more step by inserting the material form of the scalar conservation equation (20.30) so that

$$\frac{\mathrm{d}}{\mathrm{d}t} \left[\int_{\mathcal{R}(\boldsymbol{v})} \Pi \, \rho \, \mathrm{d}V \right] = - \oint_{\partial \mathcal{R}(\boldsymbol{v})} \boldsymbol{J} \cdot \hat{\boldsymbol{n}} \, \mathrm{d}\mathcal{S}, \tag{20.54}$$

which is a special case of the general transport theorem (20.49) found by setting $(\boldsymbol{v} - \boldsymbol{v}^{(\mathrm{b})}) \cdot \hat{\boldsymbol{n}} = 0$ along the region boundary. This result says that the change in Π-stuff within a region moving with the barycentric velocity arises only from the area integrated non-advective flux crossing normal to the boundary. It is a finite volume generalization of the mass conservation statement for a fluid element as discussed in Section 20.1.3. We can set $\Pi = 1$ to render a statement of mass conservation for a Lagrangian region

$$\frac{\mathrm{d}}{\mathrm{d}t} \left[\int_{\mathcal{R}(\boldsymbol{v})} \rho \, \mathrm{d}V \right] = 0, \tag{20.55}$$

where the non-advective flux, $\boldsymbol{J}$, vanishes for the mass.

20.2.7 Summary of the time derivatives acting on integrals

We here summarize the variety of time derivatives acting on integrals of scalar fields

$$\frac{\mathrm{d}}{\mathrm{d}t}\int_{\mathcal{R}} \rho\,\Pi\,\mathrm{d}V = \begin{cases} \int_{\mathcal{R}} \frac{\partial(\rho\,\Pi)}{\partial t}\,\mathrm{d}V = -\oint_{\partial\mathcal{R}} (\rho\,\boldsymbol{v}\,\Pi + \boldsymbol{J})\cdot\hat{\boldsymbol{n}}\,\mathrm{d}\mathcal{S} & \text{Eulerian } \mathcal{R} \\ \int_{\mathcal{R}(\boldsymbol{v})} \rho\,\frac{\mathrm{D}\Pi}{\mathrm{D}t}\,\mathrm{d}V = -\oint_{\partial\mathcal{R}(\boldsymbol{v})} \boldsymbol{J}\cdot\hat{\boldsymbol{n}}\,\mathrm{d}\mathcal{S} & \text{Lagrangian } \mathcal{R}(\boldsymbol{v}) \\ -\oint_{\partial\mathcal{R}} [\rho\,\Pi\,(\boldsymbol{v}-\boldsymbol{v}^{(\mathrm{b})}) + \boldsymbol{J}]\cdot\hat{\boldsymbol{n}}\,\mathrm{d}\mathcal{S} & \text{arbitrary } \mathcal{R}, \end{cases} \tag{20.56}$$

with the scalar fields assumed to satisfy the flux-form conservation equation

$$\rho\,\frac{\mathrm{D}\Pi}{\mathrm{D}t} = -\nabla\cdot\boldsymbol{J} \Longleftrightarrow \partial_t(\rho\,\Pi) + \nabla\cdot(\rho\,\boldsymbol{v}\,\Pi + \boldsymbol{J}) = 0. \tag{20.57}$$

As discussed in Section 17.1.1, the partial differential equation (20.57) is referred to as the *strong formulation* of the scalar budget, whereas the integral expressions in equation (20.56) provide a variety of *weak formulations*. We thus see how the Leibniz-Reynolds transport theorem provides the mathematical framework to move between the strong form and weak form of the scalar bugets.

20.3 Brute force illustration of Leibniz-Reynolds

The Leibniz-Reynolds transport theorem

$$\frac{\mathrm{d}}{\mathrm{d}t}\left[\int_{\mathcal{R}} \rho\,\Pi\,\mathrm{d}V\right] = -\int_{\partial\mathcal{R}} \left[\rho\,\Pi\,(\boldsymbol{v}-\boldsymbol{v}^{(\mathrm{b})}) + \boldsymbol{J}\right]\cdot\hat{\boldsymbol{n}}\,\mathrm{d}\mathcal{S}, \tag{20.58}$$

is an incredibly useful and elegant expression of the scalar budget over an arbitrary domain. Correspondingly, we make great use of it throughout this book. To further our understanding, we here consider the scalar budget for an ocean domain such as in Figure 20.4. Rather than make direct use of Leibniz-Reynolds, we use a brute force approach by expanding the volume integral according to

$$\frac{\mathrm{d}}{\mathrm{d}t}\left[\int_{\mathcal{R}} \rho\,\Pi\,\mathrm{d}V\right] = \frac{\mathrm{d}}{\mathrm{d}t}\left[\int_{A(t)} \mathrm{d}A \int_{\eta_{\mathrm{b}}}^{\eta} \rho\,\Pi\,\mathrm{d}z\right]. \tag{20.59}$$

In this equation, $\int_{A(t)} \mathrm{d}A$ is an integral over the horizontal area of the domain, with the lateral boundaries of the domain generally a function of time. This exercise requires the use of various kinematic boundary conditions and provides further practice with the Leibniz rule.

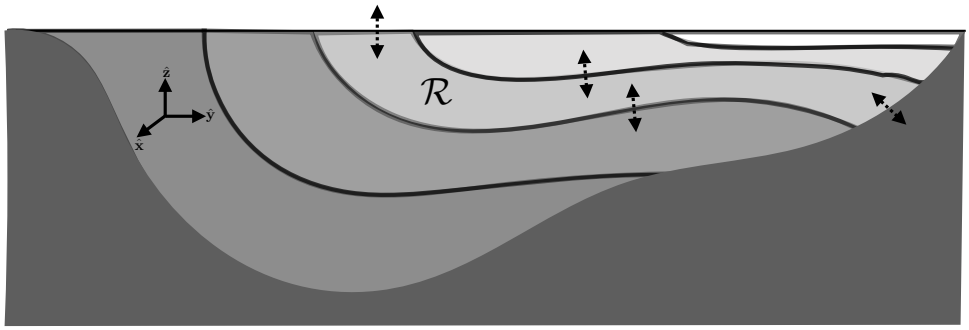

FIGURE 20.4: A depiction of fluid layers in which we formulate the budget for the total mass of scalar (e.g., tracer or potential enthalpy). The scalar mass within the layer, such as that one denoted by $\mathcal{R}$, is modified by dia-surface transport across interior layer interfaces, as well as transport across the surface and bottom boundaries. Note that an arbitrary layer might never intersect the bottom or surface boundaries. However, the layers depicted here each intersect boundaries, with such layers requiring extra care in formulating their budgets.

20.3.1 Leibniz's rule plus kinematic boundary conditions

Performing the time derivative in equation (20.59) and using Leibniz's rule yields

$$\frac{\mathrm{d}}{\mathrm{d}t}\left[\int_{\mathscr{R}} \rho\,\Pi\,\mathrm{d}V\right] = \int_{A(t)} [\partial_t \eta\,(\rho\,\Pi)_{z=\eta}]\,\mathrm{d}A + \frac{\mathrm{d}A}{\mathrm{d}t}\left[\int_{\eta_\mathsf{b}}^{\eta} \rho\,\Pi\,\mathrm{d}z\right]_{\text{bounds}} + \int_{A(t)} \mathrm{d}A \int_{\eta_\mathsf{b}}^{\eta} \frac{\partial(\rho\,\Pi)}{\partial t}\,\mathrm{d}z. \tag{20.60}$$

The first term on the right hand side arises from time dependence to the free surface. This term is present even if the horizontal boundaries are rigid. The second term on the right hand side is evaluated along the lateral boundaries of the domain. If the boundaries are fixed in time, as in a rectangular box of seawater or a periodic channel, then $\mathrm{d}A/\mathrm{d}t = 0$. The more general case has a lateral boundary that is time dependent such as along a beach where fluid moves up and down the sloping shoreline. However, in that case the thickness of fluid vanishes at the lateral boundary, $\eta - \eta_\mathsf{b} = 0$, thus again revealing that the second term on the right hand side drops from the budget to render

$$\frac{\mathrm{d}}{\mathrm{d}t}\left[\int_{\mathscr{R}} \rho\,\Pi\,\mathrm{d}V\right] = \int_{A(t)} [\partial_t \eta\,(\rho\,\Pi)_{z=\eta}]\,\mathrm{d}A + \int_{A(t)} \mathrm{d}A \int_{\eta_\mathsf{b}}^{\eta} \frac{\partial(\rho\,\Pi)}{\partial t}\,\mathrm{d}z. \tag{20.61}$$

For the second term on the right hand side of equation (20.61) we make use of the scalar equation (20.57) and Leibniz's rule to write

$$\int_{\eta_\mathsf{b}}^{\eta} \frac{\partial(\rho\,\Pi)}{\partial t}\,\mathrm{d}z = -\int_{\eta_\mathsf{b}}^{\eta} \nabla_\mathsf{h} \cdot (\rho\,\Pi\,\boldsymbol{u} + \boldsymbol{J}_h)\,\mathrm{d}z - \int_{\eta_\mathsf{b}}^{\eta} \frac{\partial(\rho\,\Pi\,w + J^z)}{\partial z}\,\mathrm{d}z \tag{20.62a}$$

$$= -\nabla_\mathsf{h} \cdot \int_{\eta_\mathsf{b}}^{\eta} (\rho\,\Pi\,\boldsymbol{u} + \boldsymbol{J}_h)\,\mathrm{d}z + \nabla(\eta - z) \cdot (\rho\,\Pi\,\boldsymbol{v} + \boldsymbol{J})_{z=\eta} + \nabla(z - \eta_\mathsf{b}) \cdot (\rho\,\Pi\,\boldsymbol{v} + \boldsymbol{J})_{z=\eta_\mathsf{b}} \tag{20.62b}$$

where we wrote $\boldsymbol{J} = \boldsymbol{J}_h + \hat{\boldsymbol{z}}\,J^z$. The surface terms ($z = \eta$) combine with the $\partial_t \eta$ term appearing in equation (20.61) to yield

$$\rho\,\Pi\left[\frac{\partial \eta}{\partial t} + \boldsymbol{u} \cdot \nabla\eta - w\right] = \Pi\,Q_\mathsf{m}, \tag{20.63}$$

where we used the surface kinematic boundary condition (19.94) to introduce the surface boundary mass flux Q_m. The bottom kinematic boundary condition eliminates the advective contribution at the bottom, $z = \eta_\mathsf{b}$, via the no normal flow condition (19.56)

$$\nabla(z - \eta_\mathsf{b}) \cdot \boldsymbol{v} = w - \boldsymbol{u} \cdot \nabla\eta_\mathsf{b} = 0 \qquad \text{at } z = \eta_\mathsf{b}(x, y). \tag{20.64}$$

Finally, when integrated over the horizontal extent of the domain, the horizontal convergence term from equation (20.62b) vanishes. The reason it vanishes is because either the thickness of fluid vanishes at the horizontal boundaries (as along a beach); there is a no flux boundary condition if the boundary is a vertical wall; or the domain is periodic.

20.3.2 Summarizing the result

Bringing the results together yields the budget equation

$$\frac{\mathrm{d}}{\mathrm{d}t}\left[\int_{\mathscr{R}} \rho\,\Pi\,\mathrm{d}V\right] = \int_{z=\eta} (\Pi\,Q_\mathsf{m} + \nabla(\eta - z) \cdot \boldsymbol{J})\,\mathrm{d}A + \int_{z=\eta_\mathsf{b}} \nabla(z - \eta_\mathsf{b}) \cdot \boldsymbol{J}\,\mathrm{d}A. \tag{20.65}$$

We now use the identity (19.83e) between horizontal area element, $\mathrm{d}A = \mathrm{d}x\,\mathrm{d}y$, and area element on the surface

$$\hat{\boldsymbol{n}}\,\mathrm{d}\mathcal{S} = -\nabla(\eta - z)\,\mathrm{d}A \qquad \text{at } z = \eta \tag{20.66a}$$

$$\hat{\boldsymbol{n}}\,\mathrm{d}\mathcal{S} = -\nabla(z - \eta_{\mathsf{b}})\,\mathrm{d}A \qquad \text{at } z = \eta_{\mathsf{b}}, \tag{20.66b}$$

to write

$$\frac{\mathrm{d}}{\mathrm{d}t}\left[\int_{\mathscr{R}} \rho\,\Pi\,\mathrm{d}V\right] = -\int_{z=\eta} (-\Pi\,\mathcal{Q}_{\mathsf{m}} + \hat{\boldsymbol{n}}\cdot\boldsymbol{J})\mathrm{d}\mathcal{S} - \int_{z=\eta_{\mathsf{b}}} \hat{\boldsymbol{n}}\cdot\boldsymbol{J}\,\mathrm{d}\mathcal{S}, \tag{20.67}$$

where

$$Q_{\mathsf{m}}\,\mathrm{d}A = \mathcal{Q}_{\mathsf{m}}\,\mathrm{d}\mathcal{S} = -\rho\,(\boldsymbol{v} - \boldsymbol{v}^{(\eta)})\cdot\hat{\boldsymbol{n}}\,\mathrm{d}\mathcal{S} \tag{20.68}$$

according to equation (19.88c). The budget for fluid mass is realized by setting Π to a constant and thus dropping the non-advective flux

$$\frac{\mathrm{d}}{\mathrm{d}t}\left[\int_{\mathscr{R}} \rho\,\mathrm{d}V\right] = \int_{z=\eta} \mathcal{Q}_{\mathsf{m}}\,\mathrm{d}\mathcal{S} = -\int_{z=\eta} \rho\,(\boldsymbol{v} - \boldsymbol{v}^{(\eta)})\cdot\hat{\boldsymbol{n}}\,\mathrm{d}\mathcal{S}. \tag{20.69}$$

The manipulations in this section have succeeded in bringing the scalar and mass budgets into the form of the Leibniz-Reynolds transport theorem (20.58). The process of doing so required far more tedium as compared to the elegance of merely starting from equation (20.58). Even so, our efforts provide a useful means to ground the formalism by unpacking the many steps summarized by Leibniz-Reynolds. Furthermore, many of these steps are encountered in practical calculations of finite volume budgets.

20.4 Boundary conditions

We here study the boundary conditions relevant at the variety of boundaries encountered by a fluid. To be specific, consider Π to be a tracer concentration,

$$\Pi = C, \tag{20.70}$$

though note that the formalism holds for an arbitrary scalar satisfying the budget equation

$$\partial_t(\rho\,C) + \nabla\cdot(\rho\,C\,\boldsymbol{v} + \boldsymbol{J}) = 0. \tag{20.71}$$

We continue to focus on a fluid layer such as shown in Figure 20.4, paying particular interest to fluid layers that intersect surface (as for the ocean) and/or bottom boundaries (as for the ocean or atmosphere). We commonly think of this layer as defined by isosurfaces of generalized vertical coordinates whose layers are monotonically stacked in the vertical according to the discussion from Sections 63.9.1 and 64.2. However, the treatment given here allows for the layers to be non-monotonic in the vertical (e.g., overturns are allowed), so that these results can be used for the water mass transformation analysis discussed in Chapter 73. For example, the layers can be defined by surfaces of constant Conservative Temperature or salinity within the ocean, with these fields generally exhibiting regions of non-monotonic vertical stratification.

The Leibniz-Reynolds transport theorem (20.49) provides the starting point

$$\frac{\mathrm{d}}{\mathrm{d}t}\left[\int_{\mathscr{R}} \rho\,C\,\mathrm{d}V\right] = -\int_{\partial\mathscr{R}} \left[\rho\,C\,(\boldsymbol{v} - \boldsymbol{v}^{(\mathsf{b})}) + \boldsymbol{J}\right]\cdot\hat{\boldsymbol{n}}\,\mathrm{d}\mathcal{S}, \tag{20.72}$$

The left hand side of equation (20.72) is the time tendency for the mass of tracer within the region, such as the region $\mathscr{R}$ shown in Figure 20.4. This tendency is affected by transport across

the layer boundaries, with three boundaries considered here. We ignore interior sources, though note that the formalism can be readily extended in their presence.

20.4.1 Interior layer boundary conditions

The boundary transport across interior layer interfaces,

$$\text{interior boundary transport} = [\rho C\,(\boldsymbol{v} - \boldsymbol{v}^{(\mathrm{b})}) + \boldsymbol{J}] \cdot \hat{\boldsymbol{n}}\, \mathrm{d}\mathcal{S}, \tag{20.73}$$

measures the tracer mass transport due to advective fluxes across the moving layer boundaries (first term) and sugbrid scale fluxes (second term). The advective flux is sometimes known as the *dia-surface transport*, with the kinematics of this transport discussed in Section 64.3.

20.4.2 Solid-earth boundary conditions

At the static material bottom boundary, the no-normal flow condition means that

$$\boldsymbol{v} \cdot \hat{\boldsymbol{n}} = 0. \tag{20.74}$$

Consider the velocity of a point attached to the layer interface, $\boldsymbol{v}^{(\mathrm{b})}$, and focus on where the interface intersects the bottom boundary. At this point, $\boldsymbol{v}^{(\mathrm{b})}$ tracks the position of the interface as it intersects the bottom boundary. By construction, the movement of this intersection point is tangential to the bottom boundary so that it too is orthogonal to the boundary outward normal direction

$$\boldsymbol{v}^{(\mathrm{b})} \cdot \hat{\boldsymbol{n}} = 0. \tag{20.75}$$

Hence, the only contribution to the tracer budget at the bottom boundary comes through the non-advective flux, $\boldsymbol{J}$

$$\text{bottom boundary transport} = -\boldsymbol{J} \cdot \hat{\boldsymbol{n}}\, \mathrm{d}\mathcal{S}. \tag{20.76}$$

This equation says that if there is any transport through the bottom boundary (left hand side), then it induces a non-advective transport within the ocean whose normal component at the boundary equals to the bottom transport (right hand side).

Geothermal heating is the canonical solid-earth transport in the ocean. Assuming a known geothermal heat flux, $\mathcal{Q}_{\text{geo-heat}}$, it leads to a non-advective ocean boundary flux

$$\mathcal{Q}_{\text{geo-heat}} = -c_{\mathrm{p}}\, \boldsymbol{J}(\Theta) \cdot \hat{\boldsymbol{n}}, \tag{20.77}$$

where c_{p} is the ocean heat capacity and Θ is the Conservative Temperature (discussed in Section 26.11 and Chapter 72). Furthermore, if we assume the non-advective flux is parameterized as the downgradient diffusive flux (as in equation (72.54)), then the geothermal boundary condition (20.77) takes the form

$$\mathcal{Q}_{\text{geo-heat}} = c_p\, \rho\, (\boldsymbol{K} \cdot \nabla\Theta) \cdot \hat{\boldsymbol{n}}, \tag{20.78}$$

where $\boldsymbol{K}$ is the diffusion tensor (Chapters 68 and 71).

For those cases where the geothermal heating vanishes, or more generally for tracers that have zero bottom boundary flux, then the tracer must satisfy the following no-normal flux (Neumann) boundary condition

$$\text{no flux bottom boundary} = (\boldsymbol{K} \cdot \nabla\Theta) \cdot \hat{\boldsymbol{n}} = 0. \tag{20.79}$$

In the case where diffusion next to the boundary is isotropic, as per molecular diffusion, then we reach the simpler result

$$\text{no flux bottom boundary} = \nabla C \cdot \hat{\boldsymbol{n}} = 0. \tag{20.80}$$

Namely, in this case, tracer isosurfaces are oriented normal to the boundary as depicted in Figure 20.5. Notably, this kinematic boundary condition holds at each point in time. For the dynamical tracers like temperature and salinity, this boundary condition affects flow near the boundary by modifying the density field and thus the pressure.

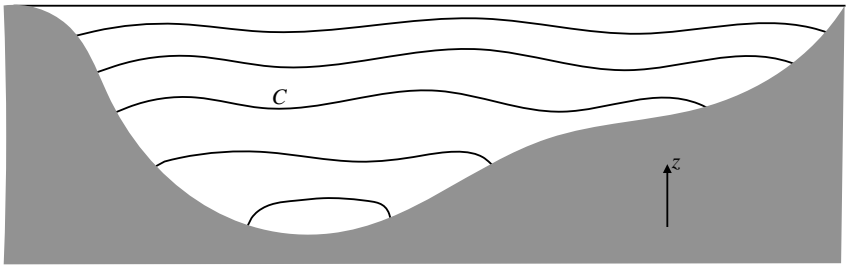

FIGURE 20.5: In the absence of a bottom boundary tracer flux (e.g., geothermal heating), and in the presence of isotropic downgradient diffusion, the isosurfaces of tracer, C, intersect solid boundaries normal to the boundary as per equation (20.80): $\nabla C \cdot \hat{\boldsymbol{n}} = 0$, where $\hat{\boldsymbol{n}}$ is the outward normal direction. This constraint holds at each time instance.

20.4.3 Upper ocean surface boundary conditions

Let us write the upper ocean surface boundary tracer transport as

$$\mathcal{Q}_\mathsf{C} \, \mathrm{d}\mathcal{S} = \text{net tracer mass per time crossing ocean surface.} \tag{20.81}$$

The surface boundary transport is generally comprised of two terms: a non-advective term just like at the solid-earth in Section 20.4.2, plus an advective term afforded since the ocean surface is permeable. If we assume that the tracer transported via the advected matter is either a dissolved tracer, such as salinity, or a thermodynamic tracer, such as Conservative Temperature, then we can write the net tracer flux as

$$\mathcal{Q}_\mathsf{C} = C_\mathrm{m} \, \mathcal{Q}_\mathsf{m} + \mathcal{Q}_\mathsf{C}^{\text{non-adv}}, \tag{20.82}$$

where $\mathcal{Q}_\mathsf{C}^{\text{non-adv}}$ is the non-advective tracer flux, C_m is the tracer concentration within the mass transported across the surface, and $\mathcal{Q}_\mathsf{m}$ the mass per time per surface area of matter that crosses the boundary, as defined according to the kinematic boundary condition (19.78)

$$\mathcal{Q}_\mathsf{m} = -\rho \, \hat{\boldsymbol{n}} \cdot (\boldsymbol{v} - \boldsymbol{v}^{(\eta)}) \qquad \text{surface ocean boundary.} \tag{20.83}$$

As for the solid-earth boundary condition, specification of $\mathcal{Q}_\mathsf{C}$ requires information concerning the flux of tracer mass into or out of the ocean, and this flux equals to the net flux on the ocean side of the surface

$$\mathcal{Q}_\mathsf{C} = C_\mathrm{m} \, \mathcal{Q}_\mathsf{m} + \mathcal{Q}_\mathsf{C}^{\text{non-adv}} \equiv -[\rho \, C \, (\boldsymbol{v} - \boldsymbol{v}^{(\mathrm{b})}) + \boldsymbol{J}] \cdot \hat{\boldsymbol{n}} = C \, \mathcal{Q}_\mathsf{m} - \boldsymbol{J} \cdot \hat{\boldsymbol{n}}, \tag{20.84}$$

We thus see that the surface transport of tracer mass induces the following non-advective flux within the ocean at $z = \eta$

$$-\boldsymbol{J} \cdot \hat{\boldsymbol{n}} = \mathcal{Q}_\mathsf{C} - C \, \mathcal{Q}_\mathsf{m} = \mathcal{Q}_\mathsf{C}^{\text{non-adv}} + (C_\mathrm{m} - C) \, \mathcal{Q}_\mathsf{m}. \tag{20.85}$$

Figure 20.6 offers a schematic to summarize these results. We make use of these results when discussing the surface ocean boundary conditions in Sections 72.5 and 73.8.3.

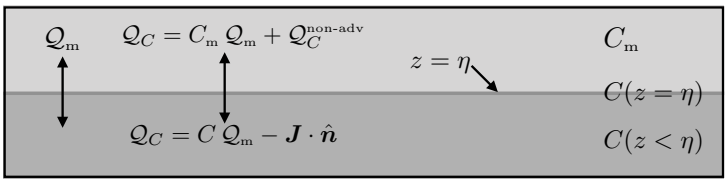

FIGURE 20.6: A schematic of an infinitesimal region of the ocean surface boundary at $z = \eta(x, y, t)$, with $z < \eta$ the ocean region. $\mathcal{Q}_{\rm m}\, d\mathcal{S}$ is the mass transport (mass per time) that crosses the interface and carries a tracer concentration, $C_{\rm m}$. $\mathcal{Q}_{\rm c}\, d\mathcal{S}$ is the tracer mass transport that crosses the ocean surface. Continuity across the $z = \eta$ boundary means that the tracer mass transport at $z = \eta - \epsilon$ (ocean side) equals to that at $z = \eta + \epsilon$ (atmospheric side), with $\epsilon > 0$ a tiny number. The tracer concentration at the interface, $C(z = \eta)$, is not determined by kinematics. Many analyses and numerical model applications approximate $C(z = \eta)$ as the bulk tracer concentration within the upper few meters of the ocean, depending on details of the upper ocean turbulence. However, as vertical grid spacing is refined to be finer than roughly a meter, this assumption must be reconsidered.

20.5 Evolution of region mean tracer

We here consider an application of the formalism developed in this chapter by deriving evolution equations for the averaged tracer concentration as defined by

$$\langle C \rangle = \frac{1}{M} \int_{\mathcal{R}} \rho\, C\, dV \quad \text{with} \quad M = \int_{\mathcal{R}} \rho\, dV, \tag{20.86}$$

where the region domain, $\mathcal{R}$, is arbitrary.

20.5.1 Formulation

Use of the product rule leads to

$$\frac{d[\langle C \rangle\, M]}{dt} = M\, \frac{d\langle C \rangle}{dt} + \langle C \rangle\, \frac{dM}{dt} = M\, \frac{d\langle C \rangle}{dt} - \langle C \rangle \oint_{\partial \mathcal{R}} \rho\, (\boldsymbol{v} - \boldsymbol{v}^{(b)}) \cdot \hat{\boldsymbol{n}}\, d\mathcal{S}, \tag{20.87}$$

where the second equality made use of the mass budget (20.50). Inserting the transport theorem (20.49) for the left hand side yields

$$M\, \frac{d\langle C \rangle}{dt} = - \oint_{\partial \mathcal{R}} \left[\rho\, (C - \langle C \rangle)\, (\boldsymbol{v} - \boldsymbol{v}^{(b)}) + \boldsymbol{J} \right] \cdot \hat{\boldsymbol{n}}\, d\mathcal{S}. \tag{20.88}$$

The first term on the right hand side vanishes if the averaged tracer concentration equals to the boundary concentration. That is, the region averaged tracer concentration is unchanged if the boundary fluxes of mass have a tracer concentration that matches the region average.

20.5.2 Application to a numerical ocean model grid cell

If the region is an ocean model grid cell that is adjacent to the ocean surface (see Figure 20.3 or 20.6), then use of the surface boundary condition (20.84) leads to

$$M\, \frac{d\langle C \rangle}{dt} = \int_{z=\eta} (C - \langle C \rangle)\, \mathcal{Q}_{\rm m}\, dA - \int_{\partial \mathcal{R}_{\rm int}} \rho\, (C - \langle C \rangle)\, (\boldsymbol{v} - \boldsymbol{v}^{(b)}) \cdot \hat{\boldsymbol{n}}\, d\mathcal{S} - \oint_{\partial \mathcal{R}} \boldsymbol{J} \cdot \hat{\boldsymbol{n}}\, d\mathcal{S}, \tag{20.89}$$

where $\partial \mathcal{R}_{\rm int}$ is the interior boundary to the grid cell. As noted above, the first term on the right hand side vanishes if $C(z = \eta) = \langle C \rangle$. This situation is commonly assumed for temperature in the surface grid cell of an ocean model. That is, the temperature of evaporation, precipitation, and river runoff is commonly taken as the temperature in the surface model grid cell. In contrast, $C(z = \eta) = 0$ is commonly the case for material tracers such as salt, whose concentration is

commonly close to zero within boundary water fluxes.

20.6 Exercises

EXERCISE 20.1: EQUATION FOR TRACER MASS PER FLUID VOLUME
In some treatments it can be suitable to define a volumetric tracer concentration as the mass of tracer per volume of fluid

$$\phi = \frac{\text{mass of constituent } n \text{ in fluid element}}{\text{volume of fluid element}} = C\,\rho, \tag{20.90}$$

where C is the mass concentration defined by equation (20.17) and satisfying the tracer equation (20.21). Derive the corresponding equation satisfied by ϕ.

EXERCISE 20.2: EVOLUTION OF THE INTEGRATED DENSITY WEIGHTED POSITION
In Exercise 19.2 we developed an evolution equation for the center of mass motion for a region with fixed mass. Here we derive a slightly more general result holding for an arbitrary region, $\mathscr{R}$, within the fluid. Namely, for Cartesian coordinates, use the Leibniz-Reynolds transport theorem (20.37) as well as the mass continuity equation (19.6) to derive the identity

$$\frac{\mathrm{d}}{\mathrm{d}t}\int_{\mathscr{R}} \rho\,\boldsymbol{x}\,\mathrm{d}V = \int_{\mathscr{R}} \rho\,\boldsymbol{v}\,\mathrm{d}V + \oint_{\partial\mathscr{R}} \rho\,\boldsymbol{x}\,[(\boldsymbol{v}-\boldsymbol{v}^{(\mathrm{b})})\cdot\hat{\boldsymbol{n}}]\,\mathrm{d}\mathcal{S}, \tag{20.91}$$

where $\boldsymbol{x}$ is the position vector for a point within the fluid. Notice that for a mass conserving Lagrangian region (i.e., a region that moves with the fluid flow), the boundary term vanishes since in this case $(\boldsymbol{v}-\boldsymbol{v}^{(\mathrm{b})})\cdot\hat{\boldsymbol{n}} = 0$, which then reduces equation (20.91) to equation (19.106) derived in Exercise 19.2.

Chapter 21

NON-DIVERGENT FLOWS

In this chapter, we study the kinematics of a non-divergent flow velocity field, $\nabla \cdot \boldsymbol{v} = 0$. In many areas of fluid mechanics, a non-divergent velocity[1] is said to describe an *incompressible flow*, with this term motivated by the case of flow within a constant density or incompressible fluid. In other areas of fluid mechanics, non-divergent flows are referred to as *solenoidal*, in analog to the non-divergent or solenoidal magnetic field occurring in classical electrodynamics. As seen when studying the Boussinesq ocean in Chapter 29, a fluid with a non-divergent flow can still experience compressibility effects and the associated density variations. That is, the study of a Boussinesq ocean concerns the incompressible flow of a compressible fluid, thus exemplifying the important distinction between a *fluid property* versus a *flow property*.

READER'S GUIDE TO THIS CHAPTER

We presume an understanding of the kinematics of mass conservation from Chapter 19 as well as many of the results from Cartesian tensor analysis in Chapter 2. This chapter introduces many concepts and tools of use in the remainder of the book.

[1] A somewhat trivial example of a non-divergent fluid flow is given by $\boldsymbol{v}(x,y,z) = u(y,z)\,\hat{\boldsymbol{x}} + v(x,z)\,\hat{\boldsymbol{y}} + w(x,y)\,\hat{\boldsymbol{z}}$. There are many further flows that are non-divergent, such as realized by the Boussinesq ocean studied in Chapter 29.

21.1 Loose threads

- Need more work for the general Ψ in Section 21.7.4 to prove that it is a streamfunction.

21.2 Introduction to non-divergent flow

For many purposes in fluid mechanics, we can make the simplifying assumption regarding the fluid kinematics whereby the volume of a fluid element is approximated as a constant. In particular, this situation holds for the Boussinesq ocean discussed in Chapter 29. Recalling the expression

$$\frac{1}{\delta V}\frac{\mathrm{D}(\delta V)}{\mathrm{D}t} = \nabla \cdot \boldsymbol{v} \tag{21.1}$$

from Section 18.10.1, we see that a constant volume for a fluid element constrains the velocity field to be non-divergent

$$\frac{1}{\delta V}\frac{\mathrm{D}(\delta V)}{\mathrm{D}t} = 0 \implies \nabla \cdot \boldsymbol{v} = 0. \tag{21.2}$$

Flow satisfying $\nabla \cdot \boldsymbol{v} = 0$ is said to be *incompressible* since the volume of a fluid element is materially invariant. We illustrate this situation in Figure 21.1.

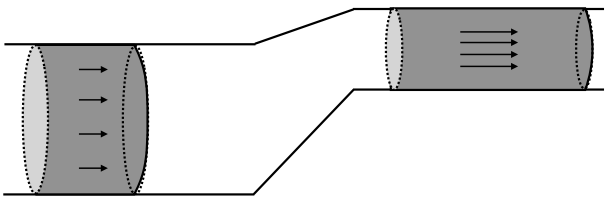

FIGURE 21.1: Illustrating volume continuity for a non-divergent velocity flow in a pipe. On the left the pipe has a relatively large diameter whereas on the right the pipe is narrower. A plug of water on the left moves through the pipe and becomes longer when it moves into the narrower region so that the volume of the plug remains the same. Correspondingly, the speed of the flow increases when moving into the narrower portion of the pipe.

A slightly less onerous constraint arises from the *anelastic approximation*, whereby

$$\nabla \cdot (\rho \boldsymbol{v}) = 0. \tag{21.3}$$

The anelastic approximation is sometimes motivated for the atmosphere. However, it is less commonly used for atmospheric dynamics than the Boussinesq ocean is used for the ocean. We thus focus on the Boussinesq case here, whereby $\nabla \cdot \boldsymbol{v} = 0$.

The non-divergence constraint (21.2) reduces by one the number of functional degrees of freedom possessed by the velocity field. What that means in practice is that we need one fewer velocity component to determine the flow since one component can be diagnosed from the other two components. This property manifests by our ability to introduce a streamfunction to specify the velocity, as further developed in this chapter.

21.3 Kinematic boundary conditions

For non-divergent flow, there are slight modifications to the boundary conditions detailed in Section 19.6. Whereas the material conditions remain identical, the non-material conditions are applied with a constant reference density, ρ_o, rather than the local *in situ* density, ρ. The reason is that we switch from specifying a mass transport condition as per equation (19.78) to a volume transport condition

$$\rho_o \, (\boldsymbol{v} - \boldsymbol{v}^{(s)}) \cdot \hat{\boldsymbol{n}} \, d\mathcal{S} = -\mathcal{Q}_m \, d\mathcal{S} = -Q_m \, dA \qquad \text{moving non-material boundary condition,} \tag{21.4}$$

where the second equality introduced the mass flux per unit horizontal area, Q_m, according to equation (19.88c). Correspondingly, the kinematic boundary condition (19.94) applied at the ocean free surface takes on the form

$$\rho_o \frac{D(z-\eta)}{Dt} = -Q_m \implies w + \frac{Q_m}{\rho_o} = \frac{\partial \eta}{\partial t} + \boldsymbol{u} \cdot \nabla \eta. \tag{21.5}$$

Making use of the non-divergence condition on the velocity allows us to write this equation in the equivalent forms[2]

$$\partial_t \eta - Q_m/\rho_o = (\hat{\boldsymbol{z}} - \nabla \eta) \cdot \boldsymbol{v} = \nabla(z-\eta) \cdot \boldsymbol{v} = \nabla \cdot [(z-\eta)\, \boldsymbol{v}]. \tag{21.6}$$

In Section 21.8 we derive the kinematic free surface equation (21.81), which also shows that $\partial_t \eta - Q_m/\rho_o$ is a total divergence.

21.4 Streamfunction for two-dimensional flow

Vertical stratification of buoyancy plus the effects from planetary rotation inhibit vertical motion in geophysical flows. Therefore, as an idealization it is sometimes useful to assume the geophysical fluid flow is horizontal (two-dimensional) as well as non-divergent. The non-divergent constraint for two-dimensional flow can be satisfied by writing the horizontal velocity in the form

$$\boldsymbol{u} = \nabla \times (z \, \nabla \psi) = \hat{\boldsymbol{z}} \times \nabla \psi = \hat{\boldsymbol{z}} \times \nabla_h \psi = -\hat{\boldsymbol{x}} \frac{\partial \psi}{\partial y} + \hat{\boldsymbol{y}} \frac{\partial \psi}{\partial x}, \tag{21.7}$$

where

$$\nabla_h = \hat{\boldsymbol{x}} \, \partial_x + \hat{\boldsymbol{y}} \, \partial_y \tag{21.8}$$

is the horizontal gradient operator. The constraint $\nabla_h \cdot \boldsymbol{u} = 0$ is satisfied since the partial derivative operators commute

$$\frac{\partial^2 \psi}{\partial x \partial y} = \frac{\partial^2 \psi}{\partial y \partial x}. \tag{21.9}$$

We refer to ψ as the *streamfunction*, with this name motivated by the following considerations.[3]

[2] In equation (21.6), we set $z = \eta$ after applying the gradient operator in the penultimate expression and the divergence in the final expression.

[3] In this section we could choose to relax notation by dispensing with the z subscript on the horizontal gradient operator, ∇_h, since we are here concerned only with two-dimensional horizontal flow. Even so, we find it useful to be pedantic as doing so clearly distinguishes the two-dimensional formulations in this section from the analogous three-dimensional case considered in Section 21.5.

21.4.1 Streamfunction isolines are streamlines

At any fixed time instance, the exact differential of the streamfunction is

$$\mathrm{d}\psi = \frac{\partial \psi}{\partial x}\,\mathrm{d}x + \frac{\partial \psi}{\partial y}\,\mathrm{d}y = v\,\mathrm{d}x - u\,\mathrm{d}y, \tag{21.10}$$

where the second equality follows from equation (21.7). Instantaneous lines along which ψ is a constant satisfy

$$\mathrm{d}\psi = 0 \implies \frac{\mathrm{d}x}{u} = \frac{\mathrm{d}y}{v}. \tag{21.11}$$

Furthermore, the normal direction to constant ψ lines

$$\hat{\boldsymbol{n}} = \frac{\nabla_{\!\mathrm{h}}\psi}{|\nabla_{\!\mathrm{h}}\psi|} = \frac{v\,\hat{\boldsymbol{x}} - u\,\hat{\boldsymbol{y}}}{|\boldsymbol{u}|} \tag{21.12}$$

is normal to the velocity

$$\boldsymbol{u}\cdot\nabla_{\!\mathrm{h}}\psi = u\,v - v\,u = 0. \tag{21.13}$$

Consequently, at each time instance, lines of constant ψ are streamlines, which means (following Section 17.7.2) that curves of constant ψ define integral curves for the instantaneous velocity field. This property motivates the name *streamfunction*. Furthermore, through each point of a two-dimensional non-divergent flow and at any particular time instance, there is one and only one streamline passing through that point.

21.4.2 Streamfunction is constant on material boundaries

As a corollary to the results from Section 21.4.1, we know that the streamfunction is a spatial constant when evaluated along static material boundaries where $\boldsymbol{u}\cdot\hat{\boldsymbol{n}} = 0$. This property follows from equation (21.13). We can also see it from

$$0 = \boldsymbol{u}\cdot\hat{\boldsymbol{n}} = (\hat{\boldsymbol{z}}\times\nabla_{\!\mathrm{h}}\psi)\cdot\hat{\boldsymbol{n}} = (\hat{\boldsymbol{n}}\times\hat{\boldsymbol{z}})\cdot\nabla_{\!\mathrm{h}}\psi = \hat{\boldsymbol{t}}\cdot\nabla_{\!\mathrm{h}}\psi, \tag{21.14}$$

where $\hat{\boldsymbol{t}}$ a unit vector pointing tangent to the boundary. The operator $\hat{\boldsymbol{t}}\cdot\nabla_{\!\mathrm{h}}\psi$ is the derivative of ψ computed along the boundary tangent at any given boundary point. Hence, $\hat{\boldsymbol{t}}\cdot\nabla_{\!\mathrm{h}}\psi = 0$ means that ψ is a spatial constant along the boundary. Even though spatially constant, ψ along the boundary is generally a function of time.

We emphasize that a constant streamfunction along a boundary, $\hat{\boldsymbol{t}}\cdot\nabla_{\!\mathrm{h}}\psi = 0$, is distinct from a vanishing normal derivative at the boundary. Indeed, the streamfunction for a two-dimensional non-divergent flow generally has a nonzero normal derivative at boundaries, $\hat{\boldsymbol{n}}\cdot\nabla_{\!\mathrm{h}}\psi \neq 0$.

21.4.3 The streamfunction and fluid transport

Consider an arbitrary curve in the fluid with endpoints $\boldsymbol{x}_1$ and $\boldsymbol{x}_2$ as depicted in Figure 21.2. At any particular time instance, the difference in streamfunction between these two points is given by

$$\psi(\boldsymbol{x}_2) - \psi(\boldsymbol{x}_1) = \int_{\boldsymbol{x}_1}^{\boldsymbol{x}_2} \mathrm{d}\psi = \int_{\boldsymbol{x}_1}^{\boldsymbol{x}_2} \left[\mathrm{d}x\,\frac{\partial\psi}{\partial x} + \mathrm{d}y\,\frac{\partial\psi}{\partial y}\right] = \int_{\boldsymbol{x}_1}^{\boldsymbol{x}_2} \nabla_{\!\mathrm{h}}\psi\cdot\mathrm{d}\boldsymbol{x} = \int_{\boldsymbol{x}_1}^{\boldsymbol{x}_2} \nabla_{\!\mathrm{h}}\psi\cdot\hat{\boldsymbol{t}}\,\mathrm{d}s. \tag{21.15}$$

For the final equality we wrote

$$\mathrm{d}\boldsymbol{x} = \hat{\boldsymbol{t}}\,\mathrm{d}s, \tag{21.16}$$

where

$$\mathrm{d}s = |\mathrm{d}\boldsymbol{x}| \tag{21.17}$$

is the element of arc length along the curve, and $\hat{\boldsymbol{t}}$ is the unit tangent vector that points in the direction along the curve from $\boldsymbol{x}_1$ to $\boldsymbol{x}_2$. Now introduce the unit normal vector along the curve according to

$$\hat{\boldsymbol{t}} = \hat{\boldsymbol{n}} \times \hat{\boldsymbol{z}}, \tag{21.18}$$

where $\hat{\boldsymbol{n}}$ points to the left when facing in the $\hat{\boldsymbol{t}}$ direction. We thus have

$$\psi(\boldsymbol{x}_2) - \psi(\boldsymbol{x}_1) = \int_{\boldsymbol{x}_1}^{\boldsymbol{x}_2} \nabla_h \psi \cdot (\hat{\boldsymbol{n}} \times \hat{\boldsymbol{z}}) \, \mathrm{d}s = \int_{\boldsymbol{x}_1}^{\boldsymbol{x}_2} (\hat{\boldsymbol{z}} \times \nabla_h \psi) \cdot \hat{\boldsymbol{n}} \, \mathrm{d}s = \int_{\boldsymbol{x}_1}^{\boldsymbol{x}_2} \boldsymbol{u} \cdot \hat{\boldsymbol{n}} \, \mathrm{d}s, \tag{21.19}$$

with the final equality an expression for the net area transport of fluid normal to the curve (dimensions of area per time). As the chosen curve connecting the points is arbitrary, we conclude that the difference in streamfunction values between two points measures the transport across any curve connecting the points. Correspondingly, the stronger the gradient in the streamfunction, the larger the transport since

$$|\boldsymbol{u}| = |\nabla_h \psi|. \tag{21.20}$$

Given the connection between the transport between two points and the value of the streamfunction at those two points, we are motivated to name ψ the *transport streamfunction*.

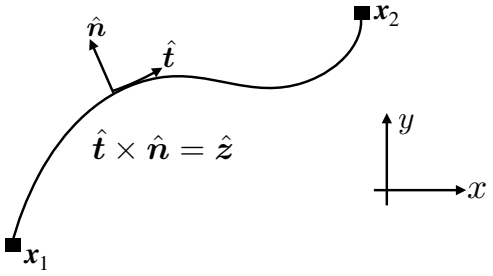

FIGURE 21.2: Depicting the transport between two points in a two-dimensional fluid. The transport is the line integral, $\int_{\boldsymbol{x}_1}^{\boldsymbol{x}_2} \boldsymbol{u} \cdot \hat{\boldsymbol{n}} \, \mathrm{d}s$, from point $\boldsymbol{x}_1$ to $\boldsymbol{x}_2$, with the unit normal, $\hat{\boldsymbol{n}}$, pointing to the left when facing in the direction of the local unit tangent vector, $\hat{\boldsymbol{t}}$. By construction, $\hat{\boldsymbol{t}} \times \hat{\boldsymbol{n}} = \hat{\boldsymbol{z}}$, where $\hat{\boldsymbol{z}}$ points vertically out of the page. For a two-dimensionally non-divergent flow, $\nabla_h \cdot \boldsymbol{u} = 0$, the transport between any two points is the streamfunction difference at these two points, $\int_{\boldsymbol{x}_1}^{\boldsymbol{x}_2} \boldsymbol{u} \cdot \hat{\boldsymbol{n}} \, \mathrm{d}s = \psi(\boldsymbol{x}_1) - \psi(\boldsymbol{x}_2)$. This result holds regardless the path taken between these two points, so long as the path remains simple; i.e., it does not intersect itself.

21.4.4 Gauge symmetry

For a two-dimensional non-divergent flow, the constraint $\nabla_h \cdot \boldsymbol{u} = 0$ reduces the functional degrees of freedom from two (the two velocity components (u, v)) to one (the streamfunction). However, the streamfunction is arbitrary up to a constant, k, since

$$\psi' = \psi + k \Rightarrow \boldsymbol{u}' = \boldsymbol{u}. \tag{21.21}$$

So the value of the streamfunction at a particular point has no unambiguous physical meaning. Rather, only the difference in streamfunction between two points is physically relevant. The ability to add a constant to the streamfunction is termed a *gauge symmetry*.

21.4.5 Exact differential formulation

We here connect our discussion of velocity streamfunction to the discussion of exact differentials in Section 2.8. For that purpose introduce the differential

$$\boldsymbol{A} \cdot \mathrm{d}\boldsymbol{x} \equiv (\boldsymbol{u} \times \hat{\boldsymbol{z}}) \cdot \mathrm{d}\boldsymbol{x} = v \, \mathrm{d}x - u \, \mathrm{d}y. \tag{21.22}$$

By construction

$$\hat{\boldsymbol{z}} \cdot (\nabla_{\mathrm{h}} \times \boldsymbol{A}) = 0 \qquad \text{since} \qquad \nabla_{\mathrm{h}} \cdot \boldsymbol{u} = 0, \tag{21.23}$$

which means that $\boldsymbol{A} \cdot \mathrm{d}\boldsymbol{x}$ is an exact differential (Section 2.8.1). Consequently, we can write

$$\boldsymbol{A} \cdot \mathrm{d}\boldsymbol{x} = (\boldsymbol{u} \times \hat{\boldsymbol{z}}) \cdot \mathrm{d}\boldsymbol{x} = \nabla_{\mathrm{h}}\psi \cdot \mathrm{d}\boldsymbol{x} = \mathrm{d}\psi, \tag{21.24}$$

which then leads to the results derived earlier in this section where ψ is the transport streamfunction.

21.4.6 Concerning the Helmholtz decomposition

We close the discussion in this section by tidying up some mathematical niceties concerning the Helmholtz decomposition studied in Section 9.8. For two-dimensional flows the decomposition takes the form

$$\boldsymbol{u} = \hat{\boldsymbol{z}} \times \nabla_{\mathrm{h}}\Gamma + \nabla_{\mathrm{h}}\Phi, \tag{21.25}$$

for some functions Γ and Φ. For non-divergent flows, Φ is constrained to be harmonic[4]

$$\nabla \cdot \boldsymbol{u} = 0 \Longrightarrow \nabla_{\mathrm{h}}^2\Phi = \nabla_{\mathrm{h}} \cdot \nabla_{\mathrm{h}}\Phi = 0. \tag{21.26}$$

As summarized in Table 21.1, it is sufficient to make use of just a streamfunction, ψ, for vortical flow and just a *velocity potential*, ϕ, for irrotational flow.[5] In the following we verify why it is sufficient to make use of this truncated version of the Helmholtz decomposition for non-divergent two-dimensional flows.

NON-DIVERGENT VORTICAL FLOW	NON-DIVERGENT IRROTATIONAL FLOW
$\nabla_{\mathrm{h}} \cdot \boldsymbol{u} = 0$	$\nabla_{\mathrm{h}} \cdot \boldsymbol{u} = 0$
$\nabla_{\mathrm{h}} \times \boldsymbol{u} \neq 0$	$\nabla_{\mathrm{h}} \times \boldsymbol{u} = 0$
$\boldsymbol{u} = \hat{\boldsymbol{z}} \times \nabla_{\mathrm{h}}\psi$	$\boldsymbol{u} = \nabla_{\mathrm{h}}\phi$
$\hat{\boldsymbol{z}} \cdot (\nabla_{\mathrm{h}} \times \boldsymbol{u}) = \nabla_{\mathrm{h}}^2\psi$	$\nabla_{\mathrm{h}}^2\phi = 0.$

TABLE 21.1: Summarizing some mathematical properties of non-divergent two-dimensional velocity fields, $\nabla \cdot \boldsymbol{u} = 0$. The streamfunction is ψ whereas the harmonic velocity potential is ϕ.

Non-divergent vortical flow

Return to the exact differential formulation from Section 21.4.5. In that formulation we noted that $\nabla_{\mathrm{h}} \cdot \boldsymbol{u} = 0$ means that the differential $\boldsymbol{A} \cdot \mathrm{d}\boldsymbol{x} = (\boldsymbol{u} \times \hat{\boldsymbol{z}}) \cdot \mathrm{d}\boldsymbol{x}$ is exact. Making use of the Helmholtz decomposition (21.25) renders

$$\begin{aligned} \boldsymbol{A} \cdot \mathrm{d}\boldsymbol{x} &= (\boldsymbol{u} \times \hat{\boldsymbol{z}}) \cdot \mathrm{d}\boldsymbol{x} && \text{(21.27a)} \\ &= [(\hat{\boldsymbol{z}} \times \nabla_{\mathrm{h}}\Gamma) \times \hat{\boldsymbol{z}} + \nabla_{\mathrm{h}}\Phi \times \hat{\boldsymbol{z}}] \cdot \mathrm{d}\boldsymbol{x} && \text{(21.27b)} \\ &= [\nabla_{\mathrm{h}}\Gamma + \nabla_{\mathrm{h}}\Phi \times \hat{\boldsymbol{z}}] \cdot \mathrm{d}\boldsymbol{x}. && \text{(21.27c)} \end{aligned}$$

To reveal the exactness of the right hand side requires the harmonic property of Φ so that we can write

$$\hat{\boldsymbol{z}} \cdot [\nabla_{\mathrm{h}} \times (\nabla_{\mathrm{h}}\Phi \times \hat{\boldsymbol{z}})] = -\nabla_{\mathrm{h}}^2\Phi = 0 \Longrightarrow \nabla_{\mathrm{h}}\Phi \times \hat{\boldsymbol{z}} \equiv \nabla_{\mathrm{h}}\Upsilon, \tag{21.28}$$

in which case

$$\boldsymbol{A} \cdot \mathrm{d}\boldsymbol{x} \equiv v\,\mathrm{d}x - u\,\mathrm{d}y = \mathrm{d}(\Gamma + \Upsilon) \equiv \mathrm{d}\psi. \tag{21.29}$$

[4] Recall our discussion of harmonic functions in Sections 2.2.2 and 6.5.1.

[5] The vorticity, $\nabla_{\mathrm{h}} \times \boldsymbol{u}$, is a measure of the spin in the fluid and is the focus of Part VII of this book.

We conclude that for non-divergent vortical flow, we lose no generality by working just with the streamfunction, ψ, of Section 21.4.3. There is no need to also include a harmonic function.

Non-divergent irrotational flow

Consider now non-divergent and irrotational flow. The irrotational condition holds so long as Γ is harmonic

$$\hat{\boldsymbol{z}} \cdot [\nabla_h \times (\hat{\boldsymbol{z}} \times \nabla_h \Gamma)] = \nabla_h^2 \Gamma = 0. \tag{21.30}$$

Consequently, we can write

$$\hat{\boldsymbol{z}} \times \nabla_h \Gamma = \nabla_h \gamma, \tag{21.31}$$

in which case

$$\boldsymbol{u} = \hat{\boldsymbol{z}} \times \nabla_h \Gamma + \nabla_h \Phi = \nabla_h (\gamma + \Phi) \equiv \nabla_h \phi. \tag{21.32}$$

Hence, for non-divergent irrotational flow, it is sufficient to work just with the harmonic velocity potential, ϕ.

21.4.7 A caveat: transport with curl-free + divergent flow

Consider a horizontal velocity that has a non-zero divergence, $\nabla \cdot \boldsymbol{u} \neq 0$, and yet it has a zero curl, $\nabla \times \boldsymbol{u} = 0$. The zero curl allows us to write $\boldsymbol{u} = \nabla_h \phi$, with ϕ the velocity potential. Hence, $\mathrm{d}\Phi = \nabla_h \phi \cdot \mathrm{d}\boldsymbol{x}$ is an exact differential and so its closed loop integral vanishes: $\oint \mathrm{d}\Phi = 0$. However, there is no connection between velocity potential and transport. That is, we cannot conclude anything about the net transport across a closed curve based on properties of ϕ.

21.5 Vector streamfunction for three-dimensional flow

A three-dimensional non-divergent velocity, $\nabla \cdot \boldsymbol{v} = 0$, can be specified by a vector streamfunction

$$\boldsymbol{v} = \nabla \times \boldsymbol{\Psi}. \tag{21.33}$$

The constraint $\nabla \cdot \boldsymbol{v} = 0$ is trivially satisfied since the divergence of the curl vanishes

$$\nabla \cdot (\nabla \times \boldsymbol{\Psi}) = 0. \tag{21.34}$$

21.5.1 Gauge symmetry

For three-dimensional non-divergent flow, the constraint $\nabla \cdot \boldsymbol{v} = 0$ reduces the three functional degrees of freedom down to two, meaning that one of the velocity components can be diagnosed from the other two. Gauge symmetry manifests through the ability to add the gradient of an arbitrary function to the streamfunction, $\boldsymbol{\Psi}$, without altering $\boldsymbol{v}$:

$$\boldsymbol{\Psi}' = \boldsymbol{\Psi} + \nabla\lambda \Rightarrow \boldsymbol{v}' = \boldsymbol{v}, \tag{21.35}$$

which follows since $\nabla \times \nabla\lambda = 0$. Hence, the vector streamfunction has no absolute physical meaning since it can be modified by adding an arbitrary gauge function.

21.5.2 The streamfunction and transport through a surface

The volume transport (volume per time) of fluid crossing a surface is defined by the area integral

$$\mathcal{T}(\mathcal{S}) = \int_{\mathcal{S}} \boldsymbol{v} \cdot \hat{\boldsymbol{n}} \, \mathrm{d}\mathcal{S}, \tag{21.36}$$

where $\hat{\boldsymbol{n}}$ is the outward unit normal vector on the surface. Introducing the vector streamfunction and making use of Stokes' Theorem (Section 2.6) then leads to

$$\mathcal{T}(\mathcal{S}) = \int_{\mathcal{S}} \boldsymbol{v} \cdot \hat{\boldsymbol{n}} \, \mathrm{d}\mathcal{S} = \int_{\mathcal{S}} (\nabla \times \boldsymbol{\Psi}) \cdot \hat{\boldsymbol{n}} \, \mathrm{d}\mathcal{S} = \oint_{\partial \mathcal{S}} \boldsymbol{\Psi} \cdot \hat{\boldsymbol{t}} \, \mathrm{d}s, \tag{21.37}$$

where $\hat{\boldsymbol{t}}\,\mathrm{d}s$ is the oriented arc distance increment along the boundary of $\mathcal{S}$, and $\oint_{\partial \mathcal{S}}$ is the oriented line integral around the boundary $\partial\mathcal{S}$. Hence, the volume transport of fluid through the surface depends only on the vector streamfunction on the perimeter of the surface. Furthermore, if the transport through the surface vanishes (e.g., no-flux material surface such as a solid earth boundary), then on the surface the vector streamfunction can be written as the gradient of an arbitrary scalar field, $\boldsymbol{\Psi} = \nabla\chi$, since

$$\oint_{\partial \mathcal{S}} \boldsymbol{\Psi} \cdot \hat{\boldsymbol{t}} \, \mathrm{d}s = \oint_{\partial \mathcal{S}} \nabla\chi \cdot \hat{\boldsymbol{t}} \, \mathrm{d}s = \oint_{\partial \mathcal{S}} \nabla\chi \cdot \mathrm{d}\boldsymbol{x} = \oint_{\partial \mathcal{S}} \mathrm{d}\chi = 0. \tag{21.38}$$

Because $\boldsymbol{\Psi}$ has a connection to fluid transport, we sometimes refer to it as the *transport streamfunction*, just as for the streamfunction ψ in two-dimensional non-divergent flows (Section 21.4.3).

21.5.3 Scalar streamfunctions and transport

We can expose the two degrees of freedom of the vector streamfunction by writing it as the product of a scalar field and the gradient of another scalar field

$$\boldsymbol{\Psi} = \gamma \nabla\psi \tag{21.39}$$

so that the velocity is given by[6]

$$\boldsymbol{v} = \nabla \times \boldsymbol{\Psi} = \nabla\gamma \times \nabla\psi. \tag{21.40}$$

By construction the velocity satisfies

$$\boldsymbol{v} \cdot \nabla\gamma = \boldsymbol{v} \cdot \nabla\psi = 0, \tag{21.41}$$

so that the velocity is parallel to surfaces of constant γ and ψ. Correspondingly, the velocity streamlines are intersections of the γ and ψ isosurfaces, as depicted in Figure 21.3. We thus refer to γ and ψ as the two *scalar streamfunctions* for the three dimensional non-divergent flow. However, note that γ and ψ have different dimensions. By convention, we choose γ to have dimensions of length, so that it is not a traditional streamfunction, whereas ψ has the traditional streamfunction dimensions of length squared per time.

As a check that the formalism is sensible, consider the special case of two-dimensional flow so that all streamlines are in the horizontal x-y plane. Taking $\gamma = z$ then renders

$$\boldsymbol{\Psi} = z \nabla\psi \quad \text{and} \quad \boldsymbol{v} = \nabla \times \boldsymbol{\Psi} = \hat{\boldsymbol{z}} \times \nabla\psi, \tag{21.42}$$

which agrees with the scalar streamfunction in equation (21.7) for two dimensional non-divergent flow.

The volume transport through a surface defined by the two streamfunction isosurfaces takes

[6] Equation (21.40) is sometimes referred to as *Euler's form*, for, as noted on page 21 of *Truesdell* (1954), it was Euler who originally proved its validity.

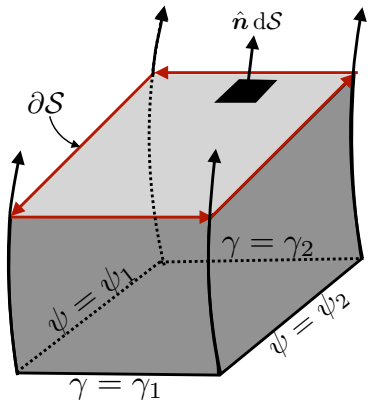

FIGURE 21.3: Isosurfaces of constant scalar streamfunctions, γ and ψ, for a three dimensional non-divergent flow. Streamlines are defined by the intersections of the γ and ψ isosurfaces, as shown by four streamlines along the corners of this particular volume. The volume transport of fluid through the surface, $\mathcal{S}$, is determined by the line integral, $\oint_{\partial\mathcal{S}} \gamma\,\mathrm{d}\psi = -\oint_{\partial\mathcal{S}} \psi\,\mathrm{d}\gamma = (\gamma_1 - \gamma_2)\,(\psi_2 - \psi_1)$, around the boundary circuit.

the form

$$\mathcal{T}(\mathcal{S}) = \int_{\mathcal{S}} \boldsymbol{v}\cdot\hat{\boldsymbol{n}}\,\mathrm{d}\mathcal{S} = \oint_{\partial\mathcal{S}} \boldsymbol{\Psi}\cdot\hat{\boldsymbol{t}}\,\mathrm{d}s = \oint_{\partial\mathcal{S}} \gamma\,\nabla\psi\cdot\hat{\boldsymbol{t}}\,\mathrm{d}s = \oint_{\partial\mathcal{S}} \gamma\,\mathrm{d}\psi = -\oint_{\partial\mathcal{S}} \psi\,\mathrm{d}\gamma. \tag{21.43}$$

To reach the penultimate step we set

$$\mathrm{d}\psi = \nabla\psi\cdot\mathrm{d}\boldsymbol{x} = \nabla\psi\cdot\hat{\boldsymbol{t}}\,\mathrm{d}s, \tag{21.44}$$

and for the final step we used the identity

$$\oint_{\partial\mathcal{S}} \gamma\,\mathrm{d}\psi = \oint_{\partial\mathcal{S}} \mathrm{d}(\gamma\,\psi) - \oint_{\partial\mathcal{S}} \psi\,\mathrm{d}\gamma = -\oint_{\partial\mathcal{S}} \psi\,\mathrm{d}\gamma. \tag{21.45}$$

This identity follows from

$$\oint_{\partial\mathcal{S}} \mathrm{d}(\gamma\,\psi) = 0, \tag{21.46}$$

which holds since $\mathrm{d}(\gamma\,\psi)$ is an exact differential and its line integral vanishes when computed around a closed path.[7] The volume transport for the particular surface shown in Figure 21.3 is given by

$$\mathcal{T}(\mathcal{S}) = \oint_{\partial\mathcal{S}} \gamma\,\mathrm{d}\psi = \gamma_1\,(\psi_2 - \psi_1) + \gamma_2\,(\psi_1 - \psi_2) = (\gamma_1 - \gamma_2)\,(\psi_2 - \psi_1). \tag{21.47}$$

Hence, the volume transport through a streamtube defined by isosurfaces of γ and ψ is given by the product of the difference between the isosurfaces.

21.5.4 Concerning a harmonic velocity potential

As for the two-dimensional case discussed in Section 21.4.6, we consider the relevance of an arbitrary harmonic velocity potential, χ, so that the velocity takes the form

$$\boldsymbol{v} = \nabla\times\boldsymbol{\Gamma} + \nabla\chi \qquad \text{with} \qquad \nabla^2\chi = 0. \tag{21.48}$$

[7] The identity (21.46) follows from the fundamental theorem of calculus, whereby the closed loop integral of an exact differential vanishes.

Since $\nabla \cdot \nabla\chi = 0$ we can write $\nabla\chi$ as the curl of another vector

$$\nabla \cdot \nabla\chi = 0 \implies \nabla\chi = \nabla \times \mathbf{\Lambda}, \tag{21.49}$$

in which case the velocity takes the form

$$\boldsymbol{v} = \nabla \times \mathbf{\Gamma} + \nabla\chi = \nabla \times (\mathbf{\Gamma} + \mathbf{\Lambda}) \equiv \nabla \times \mathbf{\Psi}. \tag{21.50}$$

Consequently, just as for the two-dimensional case, we are at liberty to work with the transport streamfunction $\mathbf{\Psi}$ if that suits our needs. Otherwise, we can work with the harmonic potential, χ, which is commonly used when the velocity is both non-divergent and irrotational, such as for our studies of surface gravity waves in Chapter 52.

21.5.5 The vertical gauge streamfunction

To explicitly reveal the two functional degrees of freedom possessed by the non-divergent velocity field, we establish that the velocity field can be constructed from the following *vertical gauge* streamfunction[8]

$$\mathbf{\Psi}^{\text{vg}} = \hat{\boldsymbol{x}}\, \Psi_1^{\text{vg}} + \hat{\boldsymbol{y}}\, \Psi_2^{\text{vg}}, \tag{21.51}$$

which has a zero vertical component, $\Psi_3^{\text{vg}} = 0$. In addition to proving that $\boldsymbol{v} = \nabla \times \mathbf{\Psi}^{\text{vg}}$, we show that $\mathbf{\Psi}^{\text{vg}}$ provides a measure of the horizontal volume transport of fluid beneath a chosen depth. It is this property of $\mathbf{\Psi}^{\text{vg}}$ that makes it commonly used for studies of ocean mesoscale eddy parameterizations, such as in Section 69.5.1.

Proof that $\boldsymbol{v} = \nabla \times \mathbf{\Psi}^{vg}$

In terms of the vertical gauge streamfunction, the velocity components are given by

$$u = -\frac{\partial \Psi_2^{\text{vg}}}{\partial z} \qquad \text{and} \qquad v = \frac{\partial \Psi_1^{\text{vg}}}{\partial z} \qquad \text{and} \qquad w = \frac{\partial \Psi_2^{\text{vg}}}{\partial x} - \frac{\partial \Psi_1^{\text{vg}}}{\partial y}. \tag{21.52}$$

Vertically integrating the u, v equations from the bottom at $z = \eta_{\text{b}}(x, y)$ up to an arbitrary geopotential leads to[9]

$$\mathbf{\Psi}^{\text{vg}}(x, y, z, t) = \int_{\eta_{\text{b}}(x,y)}^{z} \boldsymbol{u}(x, y, z', t)\, \mathrm{d}z' \times \hat{\boldsymbol{z}} \equiv \boldsymbol{U}(x, y, z, t) \times \hat{\boldsymbol{z}}, \tag{21.53}$$

where

$$\boldsymbol{U}(x, y, z, t) = \int_{\eta_{\text{b}}(x,y)}^{z} \boldsymbol{u}(x, y, z', t)\, \mathrm{d}z' \tag{21.54}$$

is the horizontal transport of fluid from the bottom up to a chosen vertical position above the bottom. We trivially see that $u = -\partial\Psi_2^{\text{vg}}/\partial z$ and $v = \partial\Psi_1^{\text{vg}}/\partial z$. It takes a bit more work to verify that this streamfunction also renders w through noting that

$$\frac{\partial \Psi_2^{\text{vg}}}{\partial x} = u(\eta_{\text{b}})\, \partial_x \eta_{\text{b}} - \int_{\eta_{\text{b}}}^{z} \partial_x u\, \mathrm{d}z' \qquad \text{and} \qquad \frac{\partial \Psi_1^{\text{vg}}}{\partial y} = \int_{\eta_{\text{b}}}^{z} \partial_y v\, \mathrm{d}z' - v(\eta_{\text{b}})\, \partial_y \eta_{\text{b}}, \tag{21.55}$$

[8] There are occasions in which it is suitable to use either $\mathbf{\Psi} = \hat{\boldsymbol{x}}\, \Psi_1 + \hat{\boldsymbol{z}}\, \Psi_3$ or $\mathbf{\Psi} = \hat{\boldsymbol{y}}\, \Psi_2 + \hat{\boldsymbol{z}}\, \Psi_3$. In this section we focus on the vertical gauge (21.51) since that is more commonly used in applications.

[9] We expose the functional dependencies in equations (21.53) and (21.54), as it can be useful when first encountering these equations. Otherwise, we typically use a more terse notation.

so that

$$\frac{\partial \Psi_2^{\text{vg}}}{\partial x} - \frac{\partial \Psi_1^{\text{vg}}}{\partial y} = \boldsymbol{u}(\eta_{\text{b}}) \cdot \nabla \eta_{\text{b}} - \int_{\eta_{\text{b}}}^{z} \left[\frac{\partial u}{\partial x} + \frac{\partial v}{\partial y} \right] \mathrm{d}z' = w(\eta_{\text{b}}) + \int_{\eta_{\text{b}}}^{z} \frac{\partial w}{\partial z'} \, \mathrm{d}z' = w(z), \tag{21.56}$$

where we used the bottom kinematic boundary condition (19.56) to write $\boldsymbol{u}(\eta_{\text{b}}) \cdot \nabla \eta_{\text{b}} = w(\eta_{\text{b}})$. We conclude that knowledge of the vector streamfunction (21.53), which just has two functional degrees of freedom, contains all the information of the three velocity components.

We close by noting that the transport through the solid-earth bottom, $z = \eta_{\text{b}}(x, y)$, vanishes according to equation (21.37) discussed below. We can trivially verify this result for the vertical gauge since

$$\boldsymbol{\Psi}^{\text{vg}}(z = \eta_{\text{b}}) = 0, \tag{21.57}$$

so that $\oint_{\partial \mathcal{S}} \boldsymbol{\Psi}^{\text{vg}} \cdot \hat{\boldsymbol{t}} \, \mathrm{d}s = 0$ on the bottom.

Comments on the vertical gauge streamfunction

Consider a streamfunction with nonzero components in all three directions

$$\overline{\boldsymbol{\Psi}} = \hat{\boldsymbol{x}} \, \overline{\Psi}_1 + \hat{\boldsymbol{y}} \, \overline{\Psi}_2 + \hat{\boldsymbol{z}} \, \overline{\Psi}_3. \tag{21.58}$$

Following Section 21.5.1, introduce a gauge transformation so that

$$\boldsymbol{\Psi} = \overline{\boldsymbol{\Psi}} + \nabla \lambda. \tag{21.59}$$

Is it possible to remove one of the components of $\overline{\boldsymbol{\Psi}}$? For example, can we find a λ so that $\boldsymbol{\Psi}$ is a horizontal vector and is thus a vertical gauge streamfunction? For that to occur we need, at each time instance, to satisfy

$$\nabla \lambda(x, y, z) = -\hat{\boldsymbol{z}} \, \overline{\Psi}_3(x, y, z). \tag{21.60}$$

This equation is not generally solvable since the gradient of a function, $\lambda(x, y, z)$, has vector components in all three directions rather than just in the vertical. We conclude that the vertical gauge streamfunction is not the result of a gauge transformation from a streamfunction of the form (21.58). Even so, it is a legitimate streamfunction, as noted by the above proof that $\boldsymbol{v} = \nabla \times \boldsymbol{\Psi}^{\text{vg}}$.

21.6 Evolution of volume and area

In this section we develop kinematic equations for the evolution of volume and area within a non-divergent flow, starting with a material region and then considering an arbitrary region.

21.6.1 Material volumes and areas

As shown by equation (21.2), the volume of a fluid element remains constant in a non-divergent flow. Correspondingly, a fluid region moving with the velocity field maintains a constant volume

$$\frac{\mathrm{d}}{\mathrm{d}t} \int_{\mathcal{R}(\boldsymbol{v})} \mathrm{d}V = \int_{\mathcal{R}(\boldsymbol{v})} \frac{\mathrm{D}(\delta V)}{\mathrm{D}t} = \int_{\mathcal{R}(\boldsymbol{v})} (\nabla \cdot \boldsymbol{v}) \, \mathrm{d}V = \oint_{\partial \mathcal{R}(\boldsymbol{v})} \boldsymbol{v} \cdot \hat{\boldsymbol{n}} \, \mathrm{d}\mathcal{S} = 0. \tag{21.61}$$

The appearance of a material time derivative on the inside of the integral arises since the integral is computed following fluid particles whose trajectories define integral curves of the flow (see Section 20.2.7). Likewise, following from the area element equation (18.135), the area of a region

moving with a two-dimensional non-divergent flow remains materially constant

$$\frac{\mathrm{d}}{\mathrm{d}t}\int_{\mathcal{S}(\boldsymbol{v})} \mathrm{d}\mathcal{S} = \int_{\mathcal{S}(\boldsymbol{v})} \frac{\mathrm{D}(\delta\mathcal{S})}{\mathrm{D}t} = \int_{\mathcal{S}(\boldsymbol{v})} (\nabla\cdot\boldsymbol{u})\,\mathrm{d}\mathcal{S} = \oint_{\partial\mathcal{S}(\boldsymbol{v})} \boldsymbol{u}\cdot\hat{\boldsymbol{n}}\,\mathrm{d}s = 0. \tag{21.62}$$

This area preservation property is illustrated in Figure 21.4, in which a two-dimensional non-divergent flow is seen to deform an initially square patch of fluid while retaining a constant area for the patch.

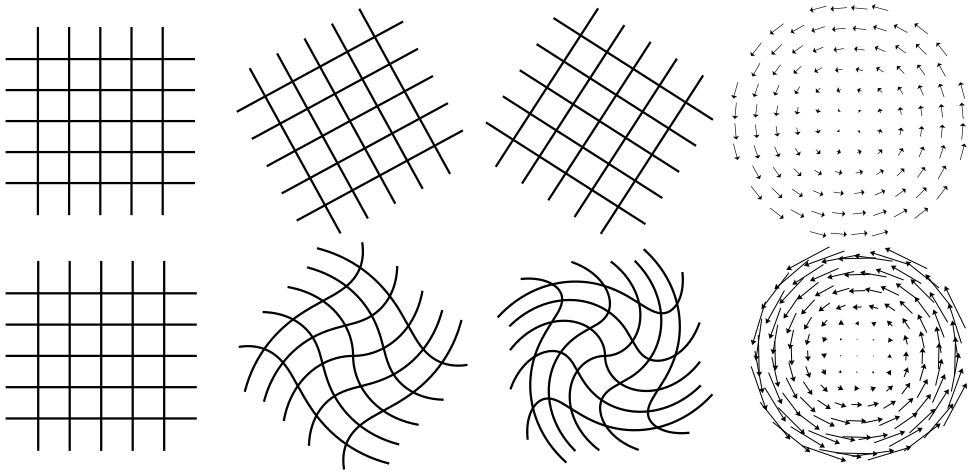

FIGURE 21.4: Illustrating the rotation and straining of fluid patches in a two-dimensional circular and non-divergent flow with non-dimensional velocity, $\boldsymbol{v} = f(|\boldsymbol{x}|)\,\hat{\boldsymbol{z}}\times\boldsymbol{x} = f(|\boldsymbol{x}|)\,(x\,\hat{\boldsymbol{y}} - y\,\hat{\boldsymbol{x}}) = f(|\boldsymbol{x}|)\,\hat{\boldsymbol{\vartheta}}$, where $\boldsymbol{x} = x\,\hat{\boldsymbol{x}} + y\,\hat{\boldsymbol{y}}$ is the position vector for a fluid particle relative to the origin (at center of the panels), and $\hat{\boldsymbol{\vartheta}}$ is the angular unit vector pointed counter-clockwise relative to the positive x-axis (see Section 4.22). As discussed in Section 21.6, the area of each fluid patch remains fixed as it moves with the non-divergent flow. The top row shows a rigid rotational flow (pure rotation with zero strain) with $f(|\boldsymbol{x}|) = 1$, with time increasing to the right and with the right-most column showing the rigid rotating fluid flow. The bottom row shows the result from a rotating and straining flow with $f(|\boldsymbol{x}|) = \sqrt{x^2+y^2}$. Thanks to Kentaro Hanson for providing the Python notebook to generate the grid advection panels.

21.6.2 Arbitrary volume and area

We make use of the Leibniz-Reynolds transport theorem from Section 20.2.4 to develop the evolution equation for the volume of an arbitrary region. In particular, equation (20.48) gives

$$\frac{\mathrm{d}}{\mathrm{d}t}\left[\int_{\mathcal{R}} \mathrm{d}V\right] = \oint_{\partial\mathcal{R}} \boldsymbol{v}^{(b)}\cdot\hat{\boldsymbol{n}}\,\mathrm{d}\mathcal{S}. \tag{21.63}$$

This result holds for both divergent and non-divergent flows. But for non-divergent flows we can go one step further by noting that

$$0 = \int_{\mathcal{R}} \nabla\cdot\boldsymbol{v}\,\mathrm{d}V = \oint_{\partial\mathcal{R}} \boldsymbol{v}\cdot\hat{\boldsymbol{n}}\,\mathrm{d}\mathcal{S}. \tag{21.64}$$

Importantly, this result holds only when integrating around the boundary of the closed volume, $\partial\mathcal{R}$. It does not necessarily mean that $\boldsymbol{v}\cdot\hat{\boldsymbol{n}} = 0$ holds at every point along the boundary. Indeed, when the boundary is time dependent, then $\boldsymbol{v}\cdot\hat{\boldsymbol{n}} \neq 0$ generally holds along the boundary.

Making use of equation (21.64) allows us to write

$$\frac{\mathrm{d}}{\mathrm{d}t}\left[\int_{\mathcal{R}} \mathrm{d}V\right] = \oint_{\partial\mathcal{R}} \boldsymbol{v}^{(b)}\cdot\hat{\boldsymbol{n}}\,\mathrm{d}\mathcal{S} = -\oint_{\partial\mathcal{R}} (\boldsymbol{v}-\boldsymbol{v}^{(b)})\cdot\hat{\boldsymbol{n}}\,\mathrm{d}\mathcal{S}. \tag{21.65}$$

This result is identical to the mass budget equation (20.50) for the special case of a constant reference density appropriate for a Boussinesq ocean. The dia-surface transport, $(\boldsymbol{v} - \boldsymbol{v}^{(b)}) \cdot \hat{\boldsymbol{n}} \, \mathrm{d}\mathcal{S}$, measures the volume per time crossing the boundary of the region, whether that region has a static or moving boundary. For example, if the boundary is the ocean free surface, then we can make use of the surface kinematic boundary condition (21.4).

21.7 Meridional-depth circulation

Geophysical fluid flow is generally three-dimensional. However, it is sometimes useful to summarize aspects of that flow by integrating the mass transport over one of the directions. A common approach is to integrate over the zonal direction either between two solid-wall boundaries (as in an ocean basin) or over a periodic domain (as in the atmosphere or within the Southern Ocean). Doing so leaves a two-dimensional transport in the meridional-depth plane

$$V^\rho = \int_{x_1}^{x_2} \rho \, v \, \mathrm{d}x \qquad \text{and} \qquad W^\rho = \int_{x_1}^{x_2} \rho \, w \, \mathrm{d}x, \tag{21.66}$$

where

$$x_1 = x_1(y, z) \quad \text{and} \quad x_2 = x_2(y, z) \tag{21.67}$$

are expressions for the zonal boundaries as a function of (y, z), with Figure 21.5 offering a schematic. In some cases the zonal direction is periodic, as in the case of the global zonally integrated circulation in the atmosphere or for the Drake Passage latitudes in the Southern Ocean. In such cases we can dispense with x_1 and x_2 as the integration extends around the periodic domain. In other cases the basin has zonal boundaries, as in the Atlantic and Indian-Pacific oceans, and as depicted in Figure 21.5.

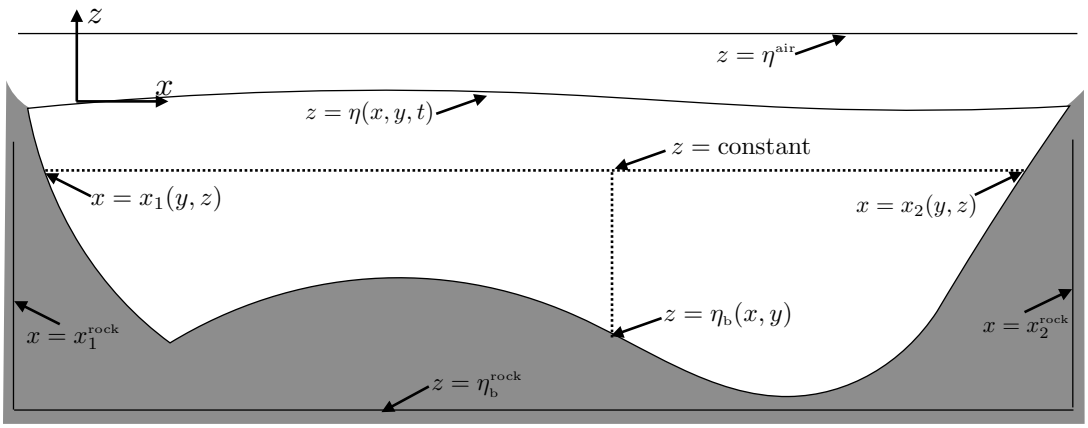

FIGURE 21.5: Geometry needed to compute the meridional-depth streamfunction. The zonal boundaries are written $x = x_1(y, z)$ and $x = x_2(y, z)$, which are generally functions of latitude and vertical position. The bottom is written as $z = \eta_{\text{b}}(x, y)$ and the vertical position of an arbitrary constant depth surface is written $z = \text{constant}$. We also display the constant zonal positions, $x_{1,2}^{\text{rock}}$, which are fully within the rock, as well as the bottom position, $\eta_{\text{b}}^{\text{rock}}$, which is also within the rock. These rock coordinates allow us to dispense with much of the kinematic formalities needed to compute the streamfunction, with fluid flow taken as zero inside the rock.

In this section we derive a streamfunction for the zonally integrated flow, with a streamfunction available when the zonally integrated flow is non-divergent. We focus on the meridional-depth streamfunction, with extention in Section 64.11 to the case of a circulation partitioned according to generalized vertical coordinates.

21.7.1 The zonally integrated transport is non-divergent

In Section 5.1.3 we introduced the geometry of surfaces specified by the zonal position as in equation (21.67). There, we noted that by writing the functions $x_1(y,z)$ and $x_2(y,z)$, we must assume that the normal direction along the boundary everywhere has a nonzero and single-signed projection in the $\hat{\boldsymbol{x}}$ direction. If that is indeed the case (we dispense with this assumption below), then we can write the normal direction as

$$\hat{\boldsymbol{n}}_i = \frac{\nabla(x - x_i)}{|\nabla(x - x_i)|} = \frac{\hat{\boldsymbol{x}} - \hat{\boldsymbol{y}}\,\partial_y x_i - \hat{\boldsymbol{z}}\,\partial_z x_i}{|\sqrt{1 + (\partial_y x_i)^2 + (\partial_z x_i)^2}|}, \tag{21.68}$$

for boundaries $i = 1, 2$. Furthermore, the no-normal flow boundary condition at the bottom (Section 19.6.1) takes on the form

$$\boldsymbol{v} \cdot \hat{\boldsymbol{n}}_i = 0 \implies u = v\,\partial_y x_i + w\,\partial_z x_i \quad \text{at } x = x_i(y,z). \tag{21.69}$$

We make use of this boundary condition in this section to prove that the zonally integrated flow is non-divergent.

To see how to create a streamfunction, consider the zonal integrated area transport for a non-divergent flow[10]

$$V(y,z,t) = \int_{x_1(y,z)}^{x_2(y,z)} v(x',y,z,t)\,\mathrm{d}x' \qquad \text{and} \qquad W(y,z,t) = \int_{x_1(y,z)}^{x_2(y,z)} w(x',y,z,t)\,\mathrm{d}x'. \tag{21.70}$$

Taking the meridional derivative of the meridional transport, and making use of Leibniz's rule and the non-divergence condition, leads to

$$\frac{\partial V}{\partial y} = \frac{\partial}{\partial y}\left[\int_{x_1}^{x_2} v(x',y,z)\,\mathrm{d}x\right] \tag{21.71a}$$

$$= v(x_2)\,\partial_y x_2 - v(x_1)\,\partial_y x_1 + \int_{x_1}^{x_2} \frac{\partial v}{\partial y}\,\mathrm{d}x \tag{21.71b}$$

$$= v(x_2)\,\partial_y x_2 - v(x_1)\,\partial_y x_1 - \int_{x_1}^{x_2} \left[\frac{\partial u}{\partial x} + \frac{\partial w}{\partial z}\right]\mathrm{d}x \tag{21.71c}$$

$$= -[u - v\,\partial_y x - w\,\partial_z x]_{x=x_2} + [u - v\,\partial_y x - w\,\partial_z x]_{x=x_1} - \frac{\partial}{\partial z}\int_{x_1}^{x_2} w(x',y,z)\,\mathrm{d}x \tag{21.71d}$$

$$= -\frac{\partial W}{\partial z}. \tag{21.71e}$$

To reach the final equality we made use of the no-normal flow boundary condition in the form of equation (21.69), so that the boundary terms vanish identically. We thus conclude that the zonally integrated transport is non-divergent

$$\frac{\partial V}{\partial y} + \frac{\partial W}{\partial z} = 0. \tag{21.72}$$

[10]The case for a steady compressible flow follows analogously since in that case $\nabla \cdot (\rho\,\boldsymbol{v}) = 0$, in which case we would consider $(\rho\,v, \rho\,w)$ rather than (v, w).

21.7.2 Meridional-depth streamfunction

As a consequence of the non-divergence condition (21.72), we can introduce a meridional-depth streamfunction

$$\Psi(y,z,t) = -\int_{\eta_b^{\text{rock}}}^{z} V(y,z',t)\,\mathrm{d}z' = -\int_{\eta_b^{\text{rock}}}^{z} \left[\int_{x_1(y,z')}^{x_2(y,z')} v(x',y,z',t)\,\mathrm{d}x'\right]\mathrm{d}z', \tag{21.73}$$

whose derivatives specify the zonally integrated flow. An idealized version of the meridional-depth circulation is shown in Figure 21.6, with this circulation in the form of an overturning cell. Note that the z dependence for the streamfunction (21.73) arises just from the upper limit of the vertical integral. Furthermore, the lower limit of $z = \eta_b^{\text{rock}}$ is a spatial constant that is chosen so that the lower limit on the integral is beneath the fluid anywhere in the full domain, with the convention that there is zero transport for any region below the fluid bottom (i.e., no fluid transport in rock). This specification for the lower integration limit ensures that the streamfunction has its spatial dependence just on (y,z). We further discuss this extension into the rock in Section 21.7.4.

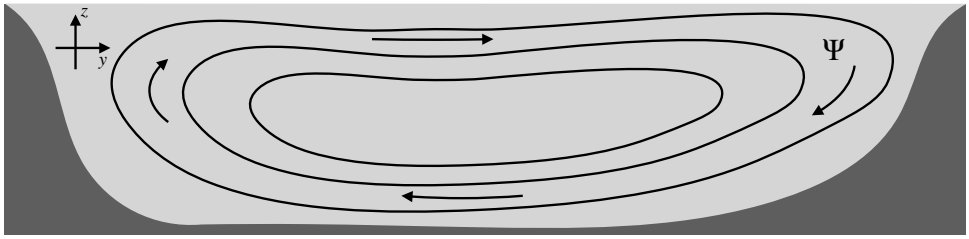

FIGURE 21.6: An idealized depiction of a steady meridional-depth overturning circulation for the zonally integrated flow. Shown here are streamlines (isolines of constant Ψ) for the zonally integrated flow between two solid boundaries or over a zonally periodic domain. The flow is assumed to be non-divergent, as per equation (21.72). In the upper reaches of the fluid, flow moves northward (positive y), with downward motion as it reaches the northern boundary, then southward motion at depth and eventual return towards the surface near the southern boundary.

21.7.3 Verifying that Ψ is a streamfunction

It is a useful exercise to verify that Ψ as defined by equation (21.73) is indeed a streamfunction for the zonally integrated flow. Suppressing the time dependence for notational brevity, we first show that

$$\frac{\partial \Psi}{\partial z} = -\frac{\partial}{\partial z}\left[\int_{\eta_b^{\text{rock}}}^{z} V(y,z')\,\mathrm{d}z'\right] = -V(y,z), \tag{21.74}$$

where we used Leibniz's rule and noted that only the upper integration limit is a function of z. For the meridional derivative we have

$$\frac{\partial \Psi}{\partial y} = -\int_{\eta_b^{\text{rock}}}^{z} \frac{\partial V(y,z')}{\partial y}\,\mathrm{d}z' = \int_{\eta_b^{\text{rock}}}^{z} \frac{\partial W(y,z')}{\partial z'}\,\mathrm{d}z' = W(y,z), \tag{21.75}$$

where we used the non-divergent condition (21.72), and we also set

$$W(z = \eta_b^{\text{rock}}) = 0, \tag{21.76}$$

which follows from our convention that η_b^{rock} is below the deepest fluid region. Also, we are able to move the $\partial/\partial y$ derivative across the lower limit of the integral since η_b^{rock} is a constant. We have thus shown that Ψ is a streamfunction since its derivatives equal to the zonally integrated

flow.

To evaluate the streamfuction (21.73) at the ocean surface, $z = \eta(x, y, t)$, we follow a method similar to how we deal with the bottom. Namely, introduce a constant η^{air} that is larger than any value of $\eta(x, y, t)$ and with the convention that the transport is zero in regions above the ocean surface. In this case the streamfunction computed across the full depth of the domain is given by minus the net meridional transport across the chosen latitude

$$\Psi(y, z = \eta^{\text{air}}) = -\int_{\eta_b^{\text{rock}}}^{\eta^{\text{air}}} V \, dz' = -\int_{\eta_b^{\text{rock}}}^{\eta^{\text{air}}} \left[\int_{x_1}^{x_2} v \, dx \right] dz'. \tag{21.77}$$

Volume conservation means that this transport vanishes in the steady state but it is generally nonzero in the presence of transients or boundary volume fluxes.

21.7.4 Generalizing to arbitrary domains

The method of extending the integration into the rock, and thus transforming a spatially dependent integration limit to a constant, serves to capture the flow while simplifying the practical calculation of the streamfunction. Indeed, it is a necessary method for computing the streamfunction in realistic domains such as those where the zonal boundaries are not monotonic functions of latitude or depth. A further generalization is found by introducing zonal rock coordinate values, $x_{1,2}^{\text{rock}}$, which are fully outside of the ocean fluid domain as depicted in Figure 21.5. Making use of these values allows us to write the streamfunction (21.73) in the equivalent form

$$\Psi(y, z, t) = -\int_{x_1^{\text{rock}}}^{x_2^{\text{rock}}} \left[\int_{\eta_b(x', y)}^{z} v(x', y, z', t) \, dz' \right] dx'. \tag{21.78}$$

Relative to equation (21.73), we moved the zonal integral to the outside and vertical integral to the inside. Reference to Figure 21.5 offers a pictural explanation for why this integral is identical to equation (21.73). The streamfunction expression (21.78) offers a more suitable framework for studying circulation partitioned according to surfaces of constant generalized vertical coordinate rather than constant depth. That formulation requires kinematics arising from generalized vertical coordinates, and so its discussion is postponed until Section 64.11.

21.7.5 $\Psi(y, z)$ does not generally delineate particle pathlines

In Section 17.7 we showed that a fluid particle pathline equals to a streamline when the flow is steady, and then in Section 21.4.1 we showed that streamfunction isolines are streamlines. One might then be led to infer that for a steady flow, the meridional-depth streamfunction delineates fluid particle pathlines in the y-z plane. That inference, however, is generally wrong. The reason is that that zonal integration removes spatial degrees of freedom that can hide crucial flow properties.

Two examples are the Ferrel Cell in the atmosphere (*Andrews et al.*, 1987) and overturning circulation in the Southern Ocean (*Döös and Webb*, 1994) (see *Karoly et al.* (1997) for a unified discussion of their streamfunctions). For both of these circulations, fluid particles in the fluid interior are mostly confined to constant potential density or specific entropy surfaces. Since these surfaces are not flat, and generally have slopes in the zonal direction, then closed north-south motion on such surfaces can appear as closed isolines when projected into the meridional-depth plane. The accumulation of such motions on vertically stacked potential density surfaces creates a single closed meridional-depth streamfunction contour. This closed streamfunction contour suggests that fluid particle motion extends from near the top of the fluid column to near the bottom of the fluid column. In fact, no such motion occurs for a single fluid particle since the potential density surfaces generally do not extend from the top to bottom of the column.

This example motivates the study of overturning circulation as projected onto potential density coordinates (for the ocean) or isentropic coordinates (for the atmosphere). The associated circulation streamfunctions expose flow properties that are complementary to the meridional-depth streamfunction. We postpone the development of such streamfunctions until Section 64.11, after developing the kinematics of generalized vertical coordinates.

21.8 Kinematic free surface equation

We here derive the volume budget over a column of fluid. This budget provides a kinematic expression for the free surface evolution in a non-divergent flow.

21.8.1 Derivation

Vertically integrate the constraint, $\nabla \cdot \boldsymbol{v} = 0$, over the depth of an ocean column, from $z = \eta_\mathsf{b}(x, y)$ at the bottom to $z = \eta(x, y, t)$ at the free surface and use the bottom and surface kinematic boundary conditions. This calculation yields

$$0 = \int_{\eta_\mathsf{b}}^{\eta} \nabla \cdot \boldsymbol{v} \, \mathrm{d}z \tag{21.79a}$$

$$= w(\eta) - w(\eta_\mathsf{b}) + \int_{\eta_\mathsf{b}}^{\eta} \nabla \cdot \boldsymbol{u} \, \mathrm{d}z \tag{21.79b}$$

$$= w(\eta) - w(\eta_\mathsf{b}) + \nabla \cdot \left[\int_{\eta_\mathsf{b}}^{\eta} \boldsymbol{u} \, \mathrm{d}z \right] - \boldsymbol{u}(\eta) \cdot \nabla \eta + \boldsymbol{u}(\eta_\mathsf{b}) \cdot \nabla \eta_\mathsf{b} \tag{21.79c}$$

$$= [w(\eta) - \boldsymbol{u}(\eta) \cdot \nabla \eta] - [w(\eta_\mathsf{b}) - \boldsymbol{u}(\eta_\mathsf{b}) \cdot \nabla \eta_\mathsf{b}] + \nabla \cdot \left[\int_{\eta_\mathsf{b}}^{\eta} \boldsymbol{u} \, \mathrm{d}z \right], \tag{21.79d}$$

where we made use of Leibniz's Rule to move the horizontal divergence outside of the integral. We now make use of the surface kinematic boundary condition (21.5) and the bottom no-flow condition

$$w(\eta) - \boldsymbol{u} \cdot \nabla \eta = -Q_\mathsf{m}/\rho_\circ + \partial_t \eta \qquad z = \eta \tag{21.80a}$$

$$w = \boldsymbol{u} \cdot \nabla \eta_\mathsf{b} \qquad z = \eta_\mathsf{b} \tag{21.80b}$$

to render the free surface equation for a fluid with a non-divergent flow

$$\partial_t \eta = Q_\mathsf{m}/\rho_\circ - \nabla \cdot \boldsymbol{U}, \tag{21.81}$$

where

$$\boldsymbol{U} = \int_{\eta_\mathsf{b}}^{\eta} \boldsymbol{u} \, \mathrm{d}z \tag{21.82}$$

is the depth integrated horizontal transport. For the special case of a steady state with zero boundary mass flux, the depth integrated flow is non-divergent

$$\nabla \cdot \boldsymbol{U} = 0 \qquad \text{if } Q_\mathrm{m} = 0 \text{ and } \partial \eta / \partial t = 0. \tag{21.83}$$

21.8.2 Comments

Comparing to the surface kinematic boundary condition

Recall that we can write the surface kinematic boundary condition for a non-divergent flow in the special form of equation (21.6). Comparing to the free surface equation (21.81) renders the

identity

$$\partial_t \eta - Q_{\rm m}/\rho_{\circ} = -\nabla \cdot \boldsymbol{U} = \nabla \cdot [(z-\eta)\, \boldsymbol{v}], \tag{21.84}$$

where the final expression is evaluated at $z = \eta$ after evaluating the divergence.

Concerning the evolution of sea level

Comparing the free surface equation (21.81) holding for a non-divergent flow to the free surface equation (19.99) holding for a divergent flow indicates that the non-divergent case is missing a contribution from the material changes in density

$$\frac{\partial \eta}{\partial t} = \frac{Q_{\rm m}}{\rho_{\circ}} - \nabla \cdot \boldsymbol{U} \qquad \text{Boussinesq ocean } (\nabla \cdot \boldsymbol{v} = 0) \tag{21.85a}$$

$$\frac{\partial \eta}{\partial t} = \frac{Q_{\rm m}}{\rho(\eta)} - \nabla \cdot \boldsymbol{U} - \int_{\eta_{\rm b}}^{\eta} \frac{1}{\rho} \frac{\mathrm{D}\rho}{\mathrm{D}t}\, \mathrm{d}z \qquad \text{non-Boussinesq ocean } (\nabla \cdot \boldsymbol{v} \neq 0). \tag{21.85b}$$

The material time changes to density arise from mixing and boundary fluxes of buoyancy. The particular absence of an impact from surface buoyancy fluxes means that the free surface in a Boussinesq ocean is not impacted by global thermal expansion, such as that arising from ocean warming. *Greatbatch* (1994) and *Griffies and Greatbatch* (2012) provide a recipe for diagnostically addressing this formulational limitation, thus enabling a study of global mean sea level with Boussinesq ocean models.

21.9 Exercises

EXERCISE 21.1: NON-DIVERGENT AND IRROTATIONAL FLOW IN POLAR COORDINATES
Consider the following two-dimensional velocity field written using polar coordinates (Section 4.22)

$$\boldsymbol{u}(r, \vartheta) = \hat{\boldsymbol{r}}\, U\, (1 - a^2/r^2) \cos\vartheta - \hat{\boldsymbol{\vartheta}}\, U\, (1 + a^2/r^2) \sin\vartheta, \tag{21.86}$$

with U and a constants.

(a) Show that the flow is non-divergent, $\nabla \cdot \boldsymbol{u} = 0$.

(b) Show that the flow is irrotational, $\nabla \times \boldsymbol{u} = 0$.

EXERCISE 21.2: NON-DIVERGENT FLOW AND TRAJECTORIES
This exercise is based on Q1.8 of *Johnson* (1997). Consider a fluid particle trajectory given by

$$\boldsymbol{X}(T) = X_0\, \mathrm{e}^{\alpha T}\, \hat{\boldsymbol{x}} + Y_0\, \mathrm{e}^{\beta T}\, \hat{\boldsymbol{y}} + Z_0\, \mathrm{e}^{\gamma T}\, \hat{\boldsymbol{z}} = X(T)\, \hat{\boldsymbol{x}} + Y(T)\, \hat{\boldsymbol{y}} + Z(T)\, \hat{\boldsymbol{z}}, \tag{21.87}$$

where $\boldsymbol{X}_0$ is the initial particle position, and α, β, γ are constants with dimensions of inverse time.

(a) Show that the Eulerian velocity field, $\boldsymbol{v}$, is steady so that it is independent of time, $\boldsymbol{v}(\boldsymbol{x})$.

(b) What condition ensures that the flow is non-divergent, $\nabla \cdot \boldsymbol{v} = 0$?

EXERCISE 21.3: STREAMLINES FOR CELLULAR FLOW
Sketch the velocity field for this streamfunction

$$\psi(x, y) = A\, \sin(k\, x)\, \sin(l\, y), \tag{21.88}$$

where (k, l) are the zonal and meridional components to the wavevector, respectively. Hint: assume any convenient value for k,l and the amplitude, A, but indicate what values were chosen. Furthermore, show vectors so that the sense of the flow is clear.

EXERCISE 21.4: ZERO NET AREA TRANSPORT THROUGH STATIC CLOSED CURVE
For a two-dimensional non-divergent flow, show that there is zero net area transport of fluid crossing an arbitrary static and simply connected closed curve. Consequently, the area remains unchanged for any closed region moving with the fluid flow. Note that in two space dimensions, the area transport of fluid across a line has dimensions $\mathrm{L}^2\ \mathrm{T}^{-1}$, thus representing an area transport.

EXERCISE 21.5: ZERO NET VOLUME TRANSPORT THROUGH STATIC CLOSED SURFACE
For a three-dimensional non-divergent flow, show that there is zero net volume transport of fluid crossing an arbitrary static and simply connected closed surface within the fluid interior. Note that in three space dimensions, the transport of fluid across a surface has dimensions $\mathrm{L}^3\ \mathrm{T}^{-1}$, thus representing a volume transport.

EXERCISE 21.6: NET FLUID TRANSPORT ACROSS AN ARBITRARY SURFACE
Consider flow in a container with static sides/bottom. Draw an arbitrary static surface, $\mathcal{S}$, within the fluid from one side of the container to the other as in Figure 21.7. Integrate the fluid volume transport over the surface, $\int_{\mathcal{S}} \boldsymbol{v} \cdot \hat{\boldsymbol{n}}\, \mathrm{d}\mathcal{S}$.

(a) For a non-divergent flow, show that the volume transport, $\int_{\mathcal{S}} \boldsymbol{v} \cdot \hat{\boldsymbol{n}}\, \mathrm{d}\mathcal{S}$, vanishes. That is, the net volume transport across the surface is zero.

(b) Specialize the above result to a horizontal surface so that we see there is zero integrated vertical volume transport across the surface, $\int_{\mathcal{S}} w\, \mathrm{d}x\, \mathrm{d}y = 0$. Discuss these results. Note: see Section 64.3.8 for the more general case of a non-static surface.

(c) Rework part (a) for the case of a compressible fluid so that fluid elements conserve their mass rather than their volume, in which case mass continuity is given by equation (19.10)

$$\frac{1}{\rho} \frac{\mathrm{D}\rho}{\mathrm{D}t} = -\nabla \cdot \boldsymbol{v}. \tag{21.89}$$

Again, we are to compute the volume transport across a surface, but now for the case of a compressible flow rather than non-divergent flow.

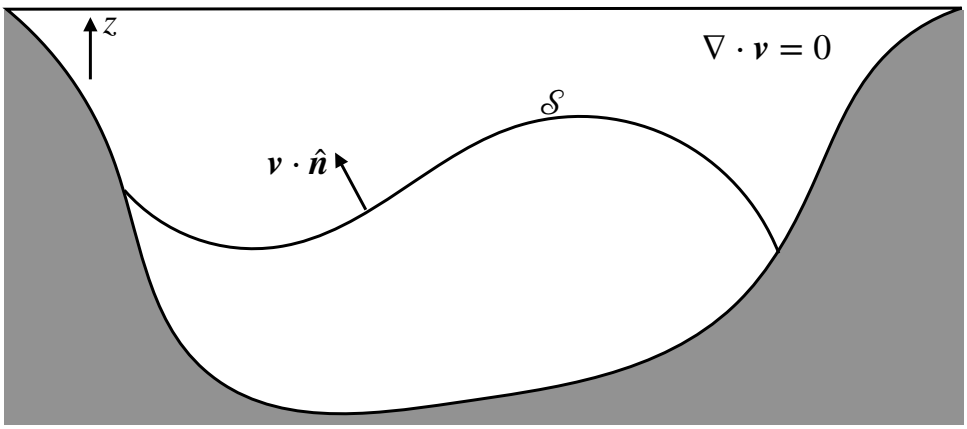

FIGURE 21.7: Schematic for exercise 21.6, whereby we show that the net flow vanishes across a static surface, $\mathcal{S}$, that extends from one boundary to the other within a non-divergent flow.

EXERCISE 21.7: RIGID-BODY ROTATION
Consider a velocity field corresponding to a time-independent rigid-body rotation on a plane

$$\boldsymbol{u} = \Omega\, \hat{\boldsymbol{z}} \times \boldsymbol{x} = \Omega\, (-y\, \hat{\boldsymbol{x}} + x\, \hat{\boldsymbol{y}}), \tag{21.90}$$

where $\Omega > 0$ is a constant rotation rate.

(a) Compute the relative vorticity, $\boldsymbol{\omega} = \nabla \times \boldsymbol{u}$.

(b) Compute the streamfunction $\boldsymbol{u} = \hat{\boldsymbol{z}} \times \nabla\psi$. Draw streamfunction contours; i.e., lines of constant streamfunction. Put arrows to orient the flow along the streamlines.

(c) Describe the geometry of material lines. Hint: since the velocity field is time-independent, material parcel trajectories are coincident with streamlines.

EXERCISE 21.8: ALTERNATIVE FORM OF MERIDIONAL-DEPTH STREAMFUNCTION
In equation (21.73), we introduced the meridional-depth overturning streamfunction

$$\Psi(y, z, t) = -\int_{\eta_{\mathrm{b}}^{\min}}^{z} V(y, z', t)\, \mathrm{d}z'. \tag{21.91}$$

Show that an alternative streamfunction is given by

$$\Gamma(y, z, t) = \int_{y_s}^{y} W(y', z, t)\, \mathrm{d}y', \tag{21.92}$$

where y_s is a constant latitude southward of the southern-most latitude where fluid exists. That is, show that

$$\frac{\partial \Gamma}{\partial y} = W \quad \text{and} \quad \frac{\partial \Gamma}{\partial z} = -V. \tag{21.93}$$

EXERCISE 21.9: VOLUME TRANSPORT THROUGH STREAMTUBE ENDS
Recall our discussion of streamtubes in Section 17.7.2 (see in particular Figure 17.5). Show that for a non-divergent flow field, the volume transport (volume per time) through the two streamtube ends balances

$$\int_{\mathcal{S}_1} \boldsymbol{v} \cdot \hat{\boldsymbol{n}}_1\, \mathrm{d}\mathcal{S} + \int_{\mathcal{S}_2} \boldsymbol{v} \cdot \hat{\boldsymbol{n}}_2\, \mathrm{d}\mathcal{S} = 0, \tag{21.94}$$

where $\hat{\boldsymbol{n}}_1$ and $\hat{\boldsymbol{n}}_2$ are the outward normals at the two end caps $\mathcal{S}_1$ and $\mathcal{S}_2$. Since the end caps have oppositely directed outward normals, equation (21.94) says that the volume transport entering one streamtube end equals to that leaving the other end. Furthermore, the area of the streamtube is inversely proportional to the local normal velocity, so that flow speeds up when moving through a narrower region of the tube.

The identity (21.94) holds whether the flow is steady or not. Yet for an unsteady flow, streamlines and pathlines are not generally equivalent. So although the volume transport through the two ends is the same, the material contained in that transport is not necessarily the same. That is, the pathlines of fluid particles are not necessarily parallel to streamlines, so that fluid particles can generally cross the streamtube boundaries.

EXERCISE 21.10: AREA AVERAGE OF FREE SURFACE TIME TENDENCY
Consider a non-divergent ocean flow bounded by a free upper surface and a solid bottom. Let $z = \eta_{\mathrm{b}}(x, y)$ be the vertical position of the static bottom, and $z = \eta(x, y, t)$ be the position of the transient free surface, so that the thickness of the layer is $h = -\eta_{\mathrm{b}} + \eta$ (see Figure 21.8). The horizontal extent of the layer is a function of time, and is defined by a vanishing thickness $h = -\eta_{\mathrm{b}} + \eta = 0$ (e.g., ocean water reaching the shoreline). Assume no material crosses either

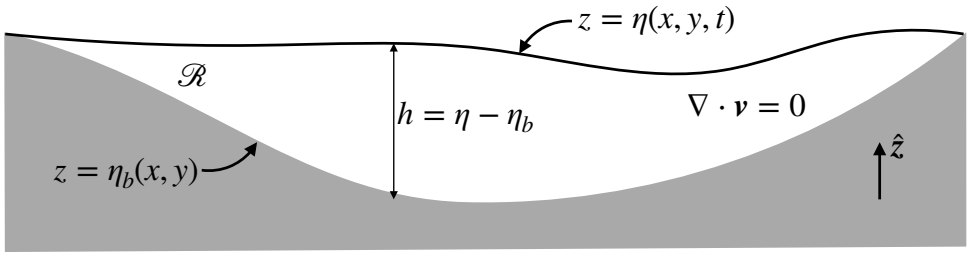

FIGURE 21.8: Schematic for exercise 21.10 with $z = \eta(x, y, t)$ the free surface at the top of the fluid. This exercise shows that the area integrated time tendency for the free surface vanishes in the absence of mass transport across the free surface.

the surface or bottom boundaries, so that both boundaries are material surfaces. Show that the free surface has a time derivative, $\partial\eta/\partial t$, whose area average vanishes. Discuss this result.

EXERCISE 21.11: VOLUME INTEGRAL OF THE NON-DIVERGENT CARTESIAN VELOCITY FIELD
Consider a non-divergent ocean flow in Cartesian coordinates bounded by a free upper surface and a solid bottom over a domain $\mathscr{R}$. Let $z = \eta_b(x, y)$ be the vertical position of the static bottom, and $z = \eta(x, y, t)$ be the position of the transient free surface as in Figure 21.8. Prove that the domain integral of the velocity is given by

$$\int_{\mathscr{R}} \boldsymbol{v} \, \mathrm{d}V = \int_{z=\eta} \boldsymbol{x} \, (\boldsymbol{v} \cdot \hat{\boldsymbol{n}}) \, \mathrm{d}\mathcal{S} = \int_{z=\eta} \boldsymbol{x} \, (\partial_t \eta - Q_m/\rho_o) \, \mathrm{d}x \, \mathrm{d}y. \tag{21.95}$$

Hint: make use of the results from Section 2.7.7 and then use the kinematic boundary conditions from Section 21.3. Note that to enable this exercise we assume Cartesian coordinates, which is required when integrating a vector.

EXERCISE 21.12: VERIFYING THAT Ψ IS A STREAMFUNCTION
In Section 21.7.3 we verified that the meridional-depth streamfunction, Ψ, is indeed a streamfunction when it is written in the form of equation (21.73). Provide an analogous derivation to show that the alternative expression in equation (21.78) is indeed also a streamfunction. Hint: the derivation closely follows that in Section 21.7.3.

Part IV

Equilibrium thermodynamics

Thermodynamics is a phenomenological discipline focused on relations between macroscopic properties of physical systems, in particular how those properties change as the system transitions from one state to another. Thermodynamics is a necessary ingredient for understanding the stability, evolution, and transformation of macroscopic systems, with such topics at the heart of geophysical fluid mechanics. In this part of the book we develop elements of equilibrium thermodynamics relevant to a multi-component fluid. We limit concern to a single phase of matter (liquid or gas), noting that a more complete treatment relevant to geophysical fluids must consider multiple phases and their transitions.

We focus on classical thermodynamics, which means we are generally concerned with macroscopic states of a fluid system; i.e., a *macrostate* that is specified by a few macroscopic properties such as temperature, pressure, and matter concentration. For our purposes, a macrostate is synonymous with *thermodynamic state*. This nomenclature must be modified when discussing statistical mechanics and quantum mechanics, whereby the complementary notion of a microstate takes on a far more central role than considered in this book.

The name "thermodynamics" suggests that the discipline concerns how heat moves through a system. Indeed, that topic formed the focus of the subject in the 19th century, as exemplified by *Maxwell* (1872). However, treatments following the formulation from Gibbs generally focus on energy and entropy, from which temperature is derived. Energy and entropy are logically distinct concepts that together form the basis for thermodynamics. Energy is a concept borrowed from mechanics. *Internal energy* refers to the energy of microscopic degress of freedom, with this energy the concern of Chapter 22, where we focus on transitions between thermodynamic equilibrium states in the absence of gravity. In Chapter 23 we extend the equilibrium theory to include a geopotential, with this study directly relevant to geophysical fluid mechanics.

Our study of thermodynamics is incompletely addressed in this part of the book. Further treatment concerns the melding of thermodynamics with the mechanics describing macroscropic fluid motion. After introducing the basics of momentum and mechanical energy for macroscopic motion in Chapter 24, we return to thermodynamics in Chapter 26 as applied to a moving fluid. That study necessarily moves beyond the restrictions of equilibrium thermodynamics considered in Chapters 22 and 23, but only slightly. The key assumption we make in Chapter 26 is that each fluid element is locally within thermodynamic equilibrium. The assumption of local thermodynamic equilibrium allows us to bring forward the key facets of equilibrium thermodynamics to the nonequilibrium thermodynamics required for moving fluids.

Thermodynamics is a deep subject whose subtleties rarely cease to puzzle and amaze both the novice and expert. For some perspective, consider the following reflections from two giants of physics on the enduring and profound nature of thermodynamics.

> Thermodynamics is a funny subject. The first time you go through it, you do not understand it at all. The second time you go through it, you think you understand it, except for one or two points. The third time you go through it, you know you do not understand it, but by that time you are so used to the subject it does not bother you anymore. *Attributed to Arnold Sommerfeld, unknown source*

> A theory is the more impressive the greater the simplicity of its premises, the more different kinds of things it relates, and the more extended is its area of applicability. Therefore the deep impression which classical thermodynamics made upon me. It is the only physical theory of universal content concerning which I am convinced that, within the framework of the applicability of its basic concepts, it will never be overthrown. *Einstein* (1949)

Chapter 22

EQUILIBRIUM THERMODYNAMICS

We here study equilibrium thermodynamics following classical treatments, with emphasis on the needs for atmosphere and ocean fluid mechanics. Thermodynamics is conceptually subtle but technically straightforward, thus making this chapter relatively long on words yet short on equations.

CHAPTER GUIDE

Our treatment follows *Callen* (1985), *Reif* (1965), chapter 2 of *Landau and Lifshitz* (1980), and chapter 2 of *Ebeling and Feistel* (2011). Mathematical tools required for thermodynamics include the basics of partial differential calculus from Chapter 2.

22.1 Conceptual foundations

In our study of equilibrium thermodynamics, we are concerned with macroscopic fluid systems whose evolution tends toward states in which its properties are determined by intrinsic factors rather than depending on memory of previous external influences. These particular *macrostates* are known as *thermodynamic equilibria.* One aim for thermodynamics is the determination of a new thermodynamic equilibrium after the removal of a constraint. When a constraint is removed, the system moves through a sequence of macrostates as it evolves towards its new equilibrium, with the time evolution through such macrostates referred to as a *process.* Any macrostate is comprised of a huge number of microscopic degrees of freedom; i.e., *microstates.* The allure of thermodynamics is that we can describe macroscopic systems, and the process of moving from one thermodynamic equilibria to another, using just a handful of macroscopically measurable properties.

22.1.1 Thermodynamic equilibrium

Equilibrium thermodynamics is the study of physical systems in *thermodynamic equilibrium* and how these systems transit from one thermodynamic equilibrium state to another through quasi-static processes. We explore the defining characteristics of thermodynamic equilibrium within this chapter. At a basic level, a system in thermodynamic equilibrium could remain in that state for all time, with details of the equilibrium dependent on the constraints imposed on the system. When such constraints are removed, then a system generally transitions to another equilibrium state. Note that "for all time" is a loaded term. More precisely, we mean "for a time extremely long compared to any time scale relevant to the physical system under consideration".

A system in thermodynamic equilibrium experiences no time changes to the system's macroscopic properties. However, all mechanical steady states are not necessarily in thermodynamic equilibrium. For example, consider a region of fluid with nonzero heat fluxes yet with no heat flux convergence so the temperature of the region does not change. As we see in this chapter, a temporally constant temperature is a signature of a macroscopic steady state, whereas the flow of heat is the sign of thermodynamic disequilibrium. The distinction is sometimes subtle and always important.

To provide motivation for the study of thermodynamic equilibrium, consider an isolated system, defined as a physical system that does not exchange heat, matter, or mechanical forces

with its surroundings, though possibly experiencing body forces such as from gravity.[1] Given sufficient time, all isolated systems will reach their thermodynamic equilibrium consistent with the constraints on that system. Geophysical fluids are routinely exposed to mechanical and thermal interactions with their surrounding environment, and as such as they are not isolated. Even so, it is useful to understand the basic properties of isolated systems and their corresponding thermodynamic equilibrium, as doing so provides the starting point for understanding how systems deviate from thermodynamic equilibrium. Furthermore, a fundamental assumption of thermodynamics applied to moving fluids (Chapter 26) is that each fluid element is in a local thermodynamic equilibrium, even while the macroscopic fluid does not reach a global thermodynamic equilibrium. Hence, we are motivated to study equilibrium thermodynamics since it forms the foundations for a study of moving fluids, even when those moving fluids are globally far from thermodynamic equilibrium.

22.1.2 Exchanges between thermodynamic systems

In the study of thermodynamics it is important to characterize how a physical system interacts with its surrounding environment through mechanical, thermal, and material interactions and exchanges. Infinitesimal fluid elements, and their accumulation into finite fluid regions, constitute the physical systems we are concerned with in this book.[2] We are concerned with systems that routinely interact mechanically with their surroundings so that the systems are mechanically open; i.e., they feel pressure from the surrounding environment. Hence, we here focus on characterizing how a physical system interacts thermally and materially with its surroundings.

- THERMALLY OPEN (DIABATIC) AND MATERIALLY OPEN: An open physical system exchanges matter, thermodynamic properties, and mechanical forces with its surrounding environment. All naturally occuring fluid systems are open in this manner.

- THERMALLY OPEN (DIABATIC) AND MATERIALLY CLOSED: We have occasion to consider a thermodynamic system that is mechanically and thermally open yet materially closed. Such systems maintain a fixed matter content yet exchange thermal and mechanical energy with their surrounding environment.

- THERMALLY CLOSED (ADIABATIC) AND MATERIALLY CLOSED: We sometimes consider a thermodynamic system that is both materially and thermally closed and yet mechanically open. In fluid mechanics, such systems constitute *material fluid parcels* (Section 17.2), defined as infinitesimal regions that maintain fixed matter and thermal properties yet move according to the mechanical forces acting on the parcel. A *perfect fluid* is a continuum of infinitesimal material fluid parcels.

Again, each of the above interactions is mechanically open, so that the system is exposed to mechanical forces, either contact forces such as pressure and friction or body forces such as gravity and Coriolis. For pedagogical purposes we first study thermodynamics of fluid elements that are thermally open yet materially closed and then extend to fluid elements that are both thermally and materially open. As a somewhat overloaded terminology, "adiabatic" in fluid mechanics is often used for a fluid element that is *both* thermally closed *and* materially closed. However, we maintain the distinction in our treatment to maintain consistency with the physics literature.

[1] We define body and contact forces in Section 24.2 when studying Newton's second law.
[2] See Section 17.2.4 for a reminder of how we define fluid elements.

22.1.3 Extensive and intensive properties

We characterize thermodynamic properties according to whether they are *extensive* or *intensive*. Extensive properties scale with the size of the system, with examples including mass, internal energy and entropy. Mathematically, we say that extensive properties scale with a power 1 with the size of the system (we return to this point in Section 6.8).

A *homogeneous fluid* is one in which all *intensive properties* are identical, with temperature, pressure, and chemical potential the canonical examples. This characteristic of intensive properties contrasts to extensive properties. Hence, intensive properties do not scale with the size of a system. That is, intensive properties are scale invariant and thus scale with power 0 as the size of the system changes. Intensive properties describe possible gradients within a thermodynamic system. In the absence of an externally imposed force field such as gravity, intensive properties are uniform for systems in thermodynamic equilibrium (we show this property in Sections 22.2.8 and 23.1.2). However, as discussed in Section 23.1, hydrostatic balance is realized in thermodynamic equilibrium for a fluid in an externally imposed gravity field, in which case pressure is not uniform.

Extensive and intensive properties come as conjugate pairs in thermodynamics, whereby intensive properties always multiply their conjugate extensive property (e.g., pressure-volume and temperature-entropy) when appearing in the various forms of the first law of thermodynamics. In this chapter, extensive properties are labeled with a superscript e (except for the mass and volume), with this label *not* a tensor index. In Section 22.5 we introduce the internal energy per mass and entropy per mass, as doing so is most convenient when studying thermodynamic systems of fixed mass. In this manner we can convert the extensive properties to their specific (per mass) form in which case we drop the e superscript. It is the specific form of extensive properties that provides a straightforward transfer to the study of constant mass fluid elements.

22.1.4 Thermodynamic configuration space

The configuration space of a thermodynamic system is not specified by coordinates in geographical space. Rather, it is specified by a suite of continuous thermodynamic properties and then studying how those properties change for processes arising from the removal of constraints. In this manner, we conceive of thermodynamic properties as defining coordinates for a point within *thermodynamic configuration space*.[3] Each point in thermodynamic configuration space is a thermodynamic equilibrium state, whereas non-equilibrium thermodynamic states.

We observe that one commonly encounters thermodynamic configuration space diagrams with orthogonal axes specifying values of thermodynamic properties. However, there is no notion of distance or angle between points in thermodynamic configuration space since there is no metric structure.[4] Mathematically, we say that thermodynamic configuration space comprises a *differentiable manifold*.[5]

22.1.5 Reversible processes and quasi-static processes

In our study of classical point particle mechanics in Section 14.2, we noted that the particle motion time reversal symmetric in the absence of dissipation.[6] That is, for mechanically

[3] We follow Section 4.2 of *Callen* (1985) in this presentation of thermodynamic configuration space.

[4] See Section 4.1 for a discussion of the metric tensor used in geographic space.

[5] A summary of the mathematical structure of equilibrium thermodynamics can be found in this online tutorial from Salamon et al. Note that there are some formulations of thermodynamics that do introduce a metric through properties of the entropy. In so doing, these formulations transform the differentiable manifold to a Riemannian manifold. There are tradeoffs when doing so, with *Andresen et al.* (1988) offering a survey of the tradeoffs. Here, we follow the approach of Gibbs as articulated in the books by *Reif* (1965) and *Callen* (1985).

[6] We extend the point particle discussion to a perfect fluid in Section 25.8.12.

reversible processes, there is no physical means to distinguish the time direction. Consequently, an animation of the motion looks sensible when viewed either forward or backward in time.

We here extend the notion of mechanical reversibility to thermodynamic processes. Namely, a thermodynamically *reversible process* can traverse a path through thermodynamic configuraton space in either direction. It follows that a reversible process continuously moves between thermodynamic equilibria, which in turn means that a reversible process traces out a continuous path through thermodynamic configuration space. As seen in Section 22.2.7, the net entropy of a physical system plus its surrounding environment remains unchanged by reversible processes, whereas irreversible processes are characterized by an increase in the net entropy.

Like a reversible process, a *quasi-static process* moves continuosly between thermodynamic equilibrium states, so it traces out a path in thermodynamic configuration space. However, a quasi-static process can be either reversible or irreversible. If a quasi-static process is irreversible, then its path in thermodynamic configuration space is in a direction that increases the net entropy of the system plus environment, whereas if it is reversible then the path leaves the net entropy unchanged. In this manner, all reversible processes are quasi-static, and yet some quasi-static processes are irreversible.[7]

A quasi-static process is fully defined by its continuous path through thermodynamic configuration space. Hence, it does not involve time or rates of change. Evidently, a quasi-static process is not a real physical process. However, we can use a real physical process to approximate a quasi-static process, so long as the quasi-static process has a monotonically nondecreasing entropy. For example, consider a quasi-static path that moves from point A to point B in thermodynamic configuration space. Approximating this path with a real physical process involves intermediate states that are not in necessarily thermodynamic equilibrium, so that the intermediate states are not representable by points in a thermodynamic configuration space. The accuracy of the approximation is a function of the rate to which thermodynamic equilibrium is approached, which itself is a function of the degree to which constraints are modified as the real physical system moves from A to B.

We are afforded the means to unambiguously measure thermodynamic properties (e.g., temperature, pressure, chemical potential) only when a physical system is in thermodynamic equilibrium. Hence, when a system traverses a quasi-static path through thermodynamic configuration space, its properties are well defined, whereas when a system is out of equilibrium the properties are fuzzy. This importance placed on thermodynamic equilibrium is of clear concern when applying thermodynamics to a moving geophysical fluid, in which case the fluid is generally far from equiliibrium. We return to this important point in Chapter 26 where we introduce the hypothesis of *local thermodynamic equilibrium*, which is the foundation upon which equilibrium thermodynamics is extended to continuous media such as a fluid.

22.1.6 Internal energy and total energy

As discussed in Chapter 16, there are a huge number of microscopic (molecular) degrees of freedom that are averaged over when describing a fluid as a continuous media. *Internal energy* embodies the energy of microscopic degrees of freedom not explicitly considered in a macroscopic continuum treatment. Internal energy is not readily accessed or harnessed, which contrasts to the mechanical energy of the macroscopic motion.

For a simple ideal gas (Section 23.4), internal energy arises from the translational kinetic energy of molecular motion, as well as degrees of freedom associated with rotation and vibration. Kinetic theory studies of a simple ideal gas suggests that we conceive of internal energy as *thermal energy*. That is, we idealize molecules as point masses whose kinetic energy is directly related to

[7] Some authors do not make a distinction between a quasi-static process and a reversible process. Our treatment follows *Callen* (1985) (see his sections 4.2 and 4.3) and *Reif* (1965) (see his sections 2.9 and 2.10), whereby reversible processes are subsets of quasi-static processes.

temperature, and with the internal energy of an ideal gas directly proportional to temperature. However, for a general fluid, particularly for liquids, the internal energy is far more than a measure of the kinetic energy of molecules, as real molecules exhibit intermolecular potential energy arising from molecular interactions. In general, the concept of internal energy is rather slippery. We are thus motivated to sidestep internal when getting serious about quantitative notions, such as when studying energetics of fluid flow in Chapter 26. We do so by appealing to the conservation of *total energy* as postulated in Section 22.1.7. Even so, to lay the foundations we largely focus on internal energy in this chapter.

22.1.7 Postulates of thermodynamics

Thermodynamics is not a first principles theory, though it does have its roots in statistical mechanics. We follow *Callen* (1985) by building thermodynamics from a set of postulates from which deductive results are derived. The following postulates render a logical basis for the subject, with the bulk of this chapter exemplifying these postulates and developing implications.

- ⋆ THERMODYNAMIC EQUILIBRIUM: There exists states of thermodynamic equilibrium that are completely characterized macroscopically by a few extensive properties, including internal energy, volume, and mass (or mole number). For each thermodynamic equilibrium there exists a scalar intensive property, called the *thermodynamic temperature*, or more brielfly the temperature, that is uniquely defined. Furthermore, the termpature has the same value for two systems in thermodynamic equilibrium with one another.

- ⋆ ZEROTH LAW OF THERMODYNAMICS: When two systems, A and B, are each separately in thermodynamic equilibrium with a third system, C, then the systems A and B are also in thermodynamic equilibrium with one another.

- ⋆ MAXIMUM ENTROPY: *Entropy* is an extensive property of a macrostate. The values assumed by the other extensive properties are those that maximize the entropy over the manifold of constrained thermodynamic equilibrium states. This postulate is fundamental to how we determine properties of thermodynamic equilibria.

- ⋆ ENTROPY INCREASES: The entropy of a composite macroscopic system is additive over the constituent subsystems. Furthermore, entropy is a continuous and differential function that is a monotonically increasing function of the internal energy. This postulate is fundamental to how we use thermodynamics for composite systems such as a fluid.

- ⋆ TOTAL ENERGY IS CONSERVED: The total energy of a thermodynamic system is locally (in space and time) conserved while undergoing a thermodynamic process. This property constitutes the *first law of thermodynamics*. For a macroscopic fluid, total energy is the sum of the internal energy arising from microscopic degrees of freedom plus the mechanical energy of macroscopic degrees of freedom. In this chapter, as well as Chapter 23, we are mostly concerned with internal energy, whereas Chapters 24 and 26 extend the discussion to include mechanical energy. Space and time locality of total energy conservation means that physical processes are not allowed in which total energy disappears from one point in space or time only to reappear at a distant point. As a corollary, we are afforded a local budget equation for total energy, whereby energy is transferred from one form to another and with particular forms of this budget equation a topic of Chapter 26. Note that energy is well defined for both microstates and macrostates, whereas entropy is only defined for macrostates.

- ⋆ THIRD LAW OF THERMODYNAMICS: Internal energy and entropy are extensive scalar quantities that are finite for finite systems and bounded from below. In the limit of

zero thermodynamic temperature for single-phase systems (single state of matter), the derivatives of entropy with respect to extensive variables disappear asymptotically. Many take the zero temperature limit to have zero entropy, though statistical fluctuations break this assumption (see page 51 of *Ebeling and Feistel* (2011) for discussion). We have little direct use for the third law, though it takes on an important role when considering quantum statistical mechanics.

The two postulates concerning entropy (entropy maximum and entropy increasing) constitute the *second law of thermodynamics*. Statistical mechanics reveals the statistical nature of entropy and the second law. In Sections 22.2.8 and 23.1.2, we see how it provides the basis for determining properties at thermodynamic equilibrium, and for how systems approach equilibrium. We make further use of the second law in Chapter 26 to constrain certain processes acting in a multicomponent fluid.

22.2 Materially closed systems

We here apply the foundational concepts from Section 22.1 to develop the thermodynamics of a physical system that is materially closed.

22.2.1 First law of thermodynamics

The first law of thermodynamics for a materially closed system establishes a relationship between infinitesimal changes of internal energy of a physical system, the work done to or by the system, and the thermal energy transferred between the system and its surrounding environment. The first law takes on the mathematical form

$$\mathrm{d}\mathcal{I}^{\mathrm{e}} = đ\mathcal{W} + đ\mathcal{Q} \qquad \Longleftarrow \text{materially closed.} \tag{22.1}$$

In this equation, $\mathrm{d}\mathcal{I}^{\mathrm{e}}$ is the exact differential of the internal energy; $đ\mathcal{W}$ is the change in internal energy due to work applied to the system (*working*); and $đ\mathcal{Q}$ is the internal energy change due to thermal energy transferred to the system (*heating*). We only have occasion to study mechanical work in this book, though note that there are other forms such as those arising from electromagnetic forces.

The first law of thermodynamics is a statement of energy conservation for a physical system, where energy changes arise from working and heating applied to the system or by the system. We are only interested in changes to the energy, with the absolute value of the energy of no concern. We focus on the internal energy by ignoring the mechanical energy associated with moving fluids. This assumption is relaxed in Chapter 26, where we include mechanical energy of macroscopic motion (Section 26.4) along with internal energy, thus forming the total energy of a moving fluid.

22.2.2 The nature of working and heating

Working and heating are both path-dependent thermodynamic processes that transform a system from one thermodynamic state to another. That is, working and heating represent *path functions* whose value depends on their history. They are mathematically represented by inexact differentials as denoted by the đ symbol. It is remarkable that the first law in equation (22.4) shows that the sum of two inexact differentials equals to an exact differential which, in the absence of macroscopic motion, is the exact differential of the internal energy.

The internal energy is a *state function* that is a property of the thermodynamic state of a system and not a function of the path history taken to reach that state. The term *thermodynamic potential* is synonymous with state function. It follows that if the internal energy change occurs

in the absence of heating then the working process must occur as a path independent process. The converse holds if internal energy changes without any working. Furthermore, the first law (22.4) allows us to decompose changes to internal energy according to mechanical and thermal contributions. However, it is not possible to perform that decomposition for the internal energy itself.

Working and heating denote actions applied to a system (verbs) rather than properties of a system (nouns). They are energy *in transition* that arise at the boundary of a thermodynamic system. We raise this somewhat pedantic yet subtle point since the terms "work" and "heat" are often used instead of "working" and "heating". Indeed, we will often make use of that language in this book. However, such usage should be used with care as it can spuriously lead one to seek information concerning the "work content" or "heat content" of a physical system; i.e., to incorrectly consider work and heat as state properties (i.e., nouns). Rather, in thermodynamics we only consider the work imparted to change a system's energy (working), or likewise the thermal energy used to change a system (heating).

These conceptual points are particularly relevant when asking questions about the heat transported by a fluid (with dimensions energy per time and SI units of Watt = Joule per second). One is then led to analyze a heat budget, in which it is tempting to define the "heat content" of a fluid element or fluid region according to its temperature, mass, and heat capacity. But the notion of heat content spuriously conflates a thermodynamic process whereby a system moves from one state to another (heating) with a thermodynamic state property (e.g., enthalpy, which is a property of the state; see Section 22.6.4). Furthermore, any definition of heat content is ambiguous due to the arbitrariness of the temperature scale; i.e., heat content based on the Celsius scale is distinct from that based on the Kelvin scale. Therefore, when working with heat transport, care should be exercised if also including the notion of heat content. One way to detect an error is to ask whether a particular conclusion is modified by changing the temperature scale. If so, then one should revisit assumptions of the analysis since the results might be unphysical.

22.2.3 Mechanical work from pressure

As forces do work on a physical system they change its internal energy and mechanical energy. We are here concerned only with the effects on internal energy, though note that mechanical changes that alter internal energy are generally balanced by compensating changes to mechanical energy (see Section 26.7). One way to perform mechanical work is via changes to the volume of a fluid element through the action of pressure (a contact force per area) on the boundary of the fluid element. For example, if a fluid element increases its volume, it must do work against the surrounding environment to overcome the compressive force from pressure.

When volume changes occur quasi-statically, then we can write the *pressure work* in the mathematical form

$$đ\mathcal{W} = -p \, dV, \tag{22.2}$$

where p is the pressure that acts on the boundaries of the fluid element. The assumption that the mechanical process is quasi-static allows us to unambiguously define pressure acting on the system, and thus to write equation (22.2) for the work. The negative sign arises since the compression of a fluid element into a smaller volume, $dV < 0$, requires positive mechanical work be applied to the fluid element, $đ\mathcal{W} > 0$. The mathematical form of pressure work derives from the general form of mechanical work given by

$$\text{work} = \text{force} \times \text{distance} = \text{force/area} \times \text{distance} \times \text{area} = \text{force/area} \times \text{volume}. \tag{22.3}$$

Stated alternatively, we note that pressure is a force per unit area acting on a surface, and the product of the surface area and its normal displacement is the volume swept out during a time increment.

We offer the following points in regards to this form of mechanical work.

- Pressure is an intensive property that measures the *intensity* of a force (per area) that is conjugate to the extensive property, V. In general, work applied to a thermodynamic system, thus leading to a change in the internal energy, takes on the form of an intensive property multiplying the change of an extensive property.
- From a mathematical perspective, pressure is the *integrating factor* that connects the inexact (path dependent) differential đ$\mathcal{W}$ to the exact differential dV. We studied the mathematics of inexact differentials in Section 2.8.
- For a quasi-static process, pressure changes the internal energy of a fluid through the pressure work according to equation (22.2). As seen in Section 26.3, pressure also changes the kinetic energy of a moving fluid by changing the fluid speed. When combining the internal energy and mechanical energy budgets in Section 26.7, we see how pressure affects the total energy of a fluid element.
- Surface tension acting on fluid interfaces can give rise to mechanical work. However, we generally ignore surface tension in this book since it is negligible for scales larger than a few centimeters (see Section 25.11).

22.2.4 Entropy and the quasi-static transfer of internal degrees of freedom

The internal energy of a thermodynamic system can change when the molecular degrees of freedom are energized. For a materially closed system whose internal energy changes in a quasi-static manner, we consider the thermal energy change as relates to entropy changes via

$$đ\mathcal{Q} = T \, d\mathcal{S}^e \qquad \text{materially closed system.} \tag{22.4}$$

T is the thermodynamic temperature (measured relative to absolute zero) and it is an intensive variable whereas $\mathcal{S}^e$ is the extensive form of entropy. Entropy is an extensive state function so that T provides the integrating factor connecting the inexact differential đ$\mathcal{Q}$ to the exact differential d$\mathcal{S}^e$. A nonzero đ$\mathcal{Q}$ in a geophysical fluid can arise from radiative fluxes external to the fluid element; internal sources from viscous friction; and the exchange of thermal energy through the mixing of fluid properties. Since heating has dimensions of energy, the entropy has dimensions of energy per temperature.

22.2.5 Gibbs' fundamental thermodyanamic relation

We summarize the discussion of this section by writing the first law for quasi-static materially closed processes

$$d\mathcal{J}^e = -p \, dV + T \, d\mathcal{S}^e \quad \Longleftarrow \quad \text{quasi-static materially closed processes.} \tag{22.5}$$

This equation is known as the *Gibbs relation* or more commonly the *fundamental thermodyanamic relation* for quasi-static materially closed processes moving from one thermodynamic equilibrium state to another. This relation suggests that we interpret minus the pressure as the amount of internal energy required to add one unit of volume to the system while holding entropy fixed. Likewise, temperature is the internal energy required to add one unit of entropy to the system while holding volume fixed.

The fundamental thermodynamic relation (22.5) is an integrable differential equation, with a solution found by performing a path integral within thermodynamic configuration space. The solution provides one of the extensive properties, such as internal energy or entropy, as a function of the other extensive properties. However, we generally do not require this solution since it is

the differentials, as determined by the Gibbs relation, that are sufficient for determining practical thermodyanamic properties such as temperature, pressure, and chemical potential.

All differentials within the fundamental thermodynamic relation (22.5) are exact differentials of state functions. This property is a result of assuming the thermodynamic processes are quasi-static, in which case we can determine the integrating factors pressure and temperature to thus replace the inexact differentials đ$\mathcal{W}$ and đ$\mathcal{Q}$ with exact differentials. Even with the quasi-static restriction, equation (22.5) offers great utility (with its extension to materially open systems given in Section 22.5). Since we are only concerned with quasi-static changes to fluid elements in this book, the fundamental thermodynamic relation (22.5) provides the central expression of the first law of thermodynamics for our purposes.

It follows from the first law expression in equation (22.5) that the internal energy is a natural function of volume and entropy

$$\mathrm{d}\mathcal{I}^{\mathrm{e}} = -p\,\mathrm{d}V + T\,\mathrm{d}\mathcal{S}^{\mathrm{e}} \Longrightarrow \mathcal{I}^{\mathrm{e}} = \mathcal{I}^{\mathrm{e}}(V, \mathcal{S}^{\mathrm{e}}). \tag{22.6}$$

Conversely, the entropy for a materially closed system is naturally a function of volume and internal energy

$$T\,\mathrm{d}\mathcal{S}^{\mathrm{e}} = \mathrm{d}\mathcal{I}^{\mathrm{e}} + p\,\mathrm{d}V \Longrightarrow \mathcal{S}^{\mathrm{e}} = \mathcal{S}^{\mathrm{e}}(V, \mathcal{I}^{\mathrm{e}}). \tag{22.7}$$

We see that both of the extensive state functions, $\mathcal{I}^{\mathrm{e}}$ and $\mathcal{S}^{\mathrm{e}}$, are functions of extensive properties, with such dependence having implications for the scaling discussed in Section 22.3.1. Furthermore, we note that both $\mathcal{I}^{\mathrm{e}}$ and $\mathcal{S}^{\mathrm{e}}$ are functions of the volume of a system, but not of the shape. This behavior is strictly only appropriate for fluids, and it ignores effects from interfaces. Both of these assumptions are suitable for our study of geophysical fluids.

22.2.6 Partial derivatives

The fundamental thermodynamic relation (22.6) appears in terms of internal energy, which is written as a natural function of the extensive properties volume and entropy. We arrive at two partial derivative identities by expanding the exact derivative of internal energy

$$\mathrm{d}\mathcal{I}^{\mathrm{e}} = \left[\frac{\partial \mathcal{I}^{\mathrm{e}}}{\partial V}\right]_{\mathcal{S}^{\mathrm{e}},M} \mathrm{d}V + \left[\frac{\partial \mathcal{I}^{\mathrm{e}}}{\partial \mathcal{S}^{\mathrm{e}}}\right]_{V,M} \mathrm{d}\mathcal{S}^{\mathrm{e}} \tag{22.8}$$

and then identifying this expression with the fundamental thermodynamic relation (22.6) to reveal

$$\left[\frac{\partial \mathcal{I}^{\mathrm{e}}}{\partial \mathcal{S}^{\mathrm{e}}}\right]_{V,M} = T \tag{22.9}$$

$$\left[\frac{\partial \mathcal{I}^{\mathrm{e}}}{\partial V}\right]_{\mathcal{S}^{\mathrm{e}},M} = -p. \tag{22.10}$$

Each equation relates an intensive property (right hand side) to the partial derivative of internal energy with respect to an extensive property. Furthermore, since each of the extensive properties is a homogeneous function of degree one, then it follows that the intensive properties are homogeneous functions of degree zero. That is, the intensive properties, T and p, do not scale with the size of the system. Rather, intensive properties are scale invariant. We arrive at analogous partial derivative identities for entropy, $\mathcal{S}^{\mathrm{e}}(V, \mathcal{I}^{\mathrm{e}})$, by expanding its exact differential and then comparing to equation (22.7)

$$\left[\frac{\partial \mathcal{S}^{\mathrm{e}}}{\partial \mathcal{I}^{\mathrm{e}}}\right]_{V,M} = \frac{1}{T} \tag{22.11}$$

$$\left[\frac{\partial \mathcal{S}^{\mathrm{e}}}{\partial V}\right]_{\mathcal{J}^{\mathrm{e}},M} = \frac{p}{T}. \tag{22.12}$$

Recall that partial derivatives are defined with the complement variables held fixed during the differentiation. Hence, so long as we are clear about functional dependence, extra subscripts such as those exposed in equations (22.9)-(22.10) are not needed for the partial derivatives. Nonetheless, traditional thermodynamic notation exposes all of the subscripts in order to remain explicit about the dependent and independent variables. Such notation, though clumsy, can be essential when in the midst of manipulations with thermodynamic potentials and their derivatives.

22.2.7 Entropy and thermodynamic processes

A *reversible process* can, at each stage, go either forward or backward in time so that there is symmetry in time. In the absence of non-conservative forces (e.g., dissipation such as friction), Newton's dynamical laws are reversible. For example, one observes nothing unphysical about the motion of an ideal pendulum with time moving backward rather than forward.[8]

From a thermodynamic perspective, a reversible process does not alter the net entropy of a physical system plus its surrounding environment. Reversible thermodynamic processes are quasi-static and yet not all quasi-static processes are reversible. For example, a process that involves friction can evolve quasi-statically and yet frictional processes, as with any dissipative process, increases entropy. When the net entropy changes, we say the process occurs *irreversibly*, with the second law of thermodynamics stating that the net entropy change is positive. Quasi-static is a property of how a system changes, whereas reversibility is a statement about how both the system and its surrounding environment change. Any natural process is irreversible, with irreversibility providing an arrow for the evolution of physical systems; i.e., it breaks the symmetry between past and future.

The entropy differential for a quasi-static process in a materially closed system is given by $\mathrm{d}\mathcal{S}^{\mathrm{e}} = đ\mathcal{Q}/T$, with $T > 0$ (recall T is the Kelvin thermodynamic temperature) so that the entropy differential has the same sign as the heating differential, and entropy for a materially closed system remains unchanged in the absence of heating. The idealization of a heat bath allows us to perform reversible heating; i.e., heating without change in net entropy for a thermodynamic system plus the heat bath. Heat baths are held at a fixed temperature, which is the idealization of the case when the surrounding environment is arbitrarily larger than the thermodynamic system under consideration. Now imagine exchanging heat between a thermodynamic system and a series of heat baths to progressively alter the system's temperature by differential, $\mathrm{d}T$. In each exchange of heat, the entropy of the system plus heat bath is constructed to remain unchanged since we are exchanging an equal magnitude of entropy between them

$$\mathrm{d}\mathcal{S}^{\mathrm{e}}_{\mathrm{net}} = \mathrm{d}\mathcal{S}^{\mathrm{e}}_{\mathrm{system}} + \mathrm{d}\mathcal{S}^{\mathrm{e}}_{\mathrm{bath}} = đ\mathcal{Q}/T - đ\mathcal{Q}/T = 0. \tag{22.13}$$

To reverse the process, we merely reverse the heat exchanges between the thermodynamic system and the heat baths.

As noted above, when any thermodynamic process occurs irreversibly there is a net increase in entropy of the universe, which is a statement of the second law of thermodynamics. In statistical mechanics, entropy is computed by counting the number of microstates accessible to any given macrostate. Reversible processes do not modify the number of accessible microstates so there is zero change in the entropy. In contrast, irreversible processes increase entropy by increasing the number of accessible microstates.

[8] We briefly discussed time-reversal symmetry in Section 14.2. We also consider time symmetry for the perfect fluid equations (Euler equations) in Section 25.8.12.

22.2.8 Properties of thermodynamic equilibrium

Consider two systems labelled[9] by α and β that are separately in thermodynamic equilibrium with internal energies, $\mathcal{I}^{\mathrm{e}}_\alpha$, $\mathcal{I}^{\mathrm{e}}_\beta$, and volumes, V_α, V_β. Allow these two systems to interact mechanically and thermally, but do not allow for any exchange of matter. Furthermore, assume that the interactions conserve the total internal energy and volume of the combined system so that the system maintains the following constraints during the interaction process

$$\mathrm{d}(\mathcal{I}^{\mathrm{e}}_\alpha + \mathcal{I}^{\mathrm{e}}_\beta) = 0 \quad \text{and} \quad \mathrm{d}(V_\alpha + V_\beta) = 0. \tag{22.14}$$

When the composite system reaches thermodynamic equilibrium, the entropy maximum postulate forming the second law of thermodynamics (Section 22.1.7) means that

$$\mathrm{d}\mathcal{S}^{\mathrm{e}} = \mathrm{d}(\mathcal{S}^{\mathrm{e}}_\alpha + \mathcal{S}^{\mathrm{e}}_\beta) = 0 \tag{22.15}$$

for the combined composite system. Importantly, this condition holds only at equilibrium, whereas the constraints (22.14) hold throughout the process of reaching equilibrium. From equation (22.7) we know that entropy is naturally a function of volume and internal energy so that

$$\mathrm{d}\mathcal{S}^{\mathrm{e}} = \left[\frac{\partial \mathcal{S}^{\mathrm{e}}_\alpha}{\partial \mathcal{I}^{\mathrm{e}}_\alpha}\right]_{V_\alpha, M_\alpha} \mathrm{d}\mathcal{I}^{\mathrm{e}}_\alpha + \left[\frac{\partial \mathcal{S}^{\mathrm{e}}_\alpha}{\partial V_\alpha}\right]_{\mathcal{I}^{\mathrm{e}}_\alpha, M_\alpha} \mathrm{d}V_\alpha + \left[\frac{\partial \mathcal{S}^{\mathrm{e}}_\beta}{\partial \mathcal{I}^{\mathrm{e}}_\beta}\right]_{V_\beta, M_\beta} \mathrm{d}\mathcal{I}^{\mathrm{e}}_\beta + \left[\frac{\partial \mathcal{S}^{\mathrm{e}}_\beta}{\partial V_\beta}\right]_{\mathcal{I}^{\mathrm{e}}_\beta, M_\beta} \mathrm{d}V_\beta \tag{22.16a}$$

$$= \frac{1}{T_\alpha}\,\mathrm{d}\mathcal{I}^{\mathrm{e}}_\alpha + \frac{p_\alpha}{T_\alpha}\,\mathrm{d}V_\alpha + \frac{1}{T_\beta}\,\mathrm{d}\mathcal{I}^{\mathrm{e}}_\beta + \frac{p_\beta}{T_\beta}\,\mathrm{d}V_\beta \tag{22.16b}$$

$$= \left[\frac{1}{T_\alpha} - \frac{1}{T_\beta}\right]\mathrm{d}\mathcal{I}^{\mathrm{e}}_\alpha + \left[\frac{p_\alpha}{T_\alpha} - \frac{p_\beta}{T_\beta}\right]\mathrm{d}V_\alpha, \tag{22.16c}$$

where we used the partial derivative identities (22.11) and (22.12) for the second equality, and the constraints (22.14) for the final equality. Again, $\mathrm{d}\mathcal{S}^{\mathrm{e}} = 0$ at thermodynamic equilibrium, and this condition holds for arbitrary and independent $\mathrm{d}\mathcal{I}^{\mathrm{e}}_\alpha$ and $\mathrm{d}V_\alpha$. We are thus led to the thermal and mechanical equilibrium conditions

$$T_\alpha = T_\beta \quad \text{and} \quad p_\alpha = p_\beta \quad \text{at thermodynamic equilibrium.} \tag{22.17}$$

That is, the temperature and pressure are uniform when the composite system reaches thermodynamic equilibrium.[10]

To understand how the two systems thermally approach thermodynamic equilibrium, assume the volumes of the two systems are fixed so that there is no mechanical work from pressure. Furthermore, assume the two systems are initially separated by an adiabatic wall with initial temperatures $T^{\mathrm{init}}_\alpha > T^{\mathrm{init}}_\beta$. Now allow for the flow of heat by switching from an adiabatic wall to a diathermal wall. Since the temperature differs for the two systems, they are mutually out of equilibrium. Heat flows in a manner to bring the two systems into equilibrium, during which time entropy of the composite system increases. At the new equilibrium, temperature is uniform and entropy has reached its maximum within the constraints imposed on the composite system. At a time instant after the wall changes from adiabatic to diathermal, the infinitesimal entropy change takes the form

$$\mathrm{d}\mathcal{S}^{\mathrm{e}} = \left[\frac{1}{T^{\mathrm{init}}_\alpha} - \frac{1}{T^{\mathrm{init}}_\beta}\right]\mathrm{d}\mathcal{I}^{\mathrm{e}}_\alpha > 0, \tag{22.18}$$

[9] The labels α and β are not tensor labels. Instead, they merely label the system under consideration.

[10] As seen in Chapter 23, pressure at thermodynamic equilibrium is not a uniform constant for a system within a gravity field.

where the inequality follows from the second law of thermodynamics (Section 22.1.7). If $T_\alpha^{\text{init}} > T_\beta^{\text{init}}$, then an increase in entropy requires $\mathrm{d}\mathcal{J}_\alpha^{\text{e}} < 0$, which means that heat leaves the system α and flows to the system β. Hence, as the composite system approaches thermodynamic equilibrium, heat flows from the region with higher temperature to the region with lower temperature. This result, deduced from the second law of thermodynamics, accords with common experience.

Further to the time scale for equilibration, we note that mechanical equilibrium (pressure equality) generally arises much sooner than thermal equilibrium (temperature equality). The reason is that mechanical equilibrium is facilitated by force imbalances that lead to macroscopic motion (e.g., acoustic waves), whereas thermal equilibrium arises from microscopic motion (e.g., molecular diffusion). This time scale separation means that real fluid systems are far closer to mechanical equilibrium than thermal equilibrium.

22.3 Characterizing materially open systems

A thermodynamic system is generally open to the transfer of matter across its boundaries. We here summarize methods used to characterize systems and processes that allow for the movement of matter, with extensive use of Euler's theorem for homogeneous functions as presented in Section 6.8.

22.3.1 Homogeneous functions

Following Section 6.8, consider a suite of Q independent variables, $X_1, X_2, ...X_Q$, and an arbitrary function of these variables, $F(X_1, X_2, ...X_Q)$. We say that this function is a *homogeneous function* of degree γ if the following property holds

$$F(\lambda X_1, \lambda X_2, ...\lambda X_Q) = \lambda^\gamma F(X_1, X_2, ...X_Q), \tag{22.19}$$

with λ an arbitrary scalar. The left hand side is the function evaluated with each of the independent variables scaled by the same number, λ. The right hand side is the function evaluated with the unscaled variables, but multiplied by the scale raised to the power γ. As proved in Section 6.8, *Euler's theorem* for homogeneous functions states that

$$\sum_{q=1}^{Q} X_q \left[\frac{\partial F(X_1, X_2, ...X_Q)}{\partial X_q}\right]_{X_{r\neq q}} = \gamma\, \lambda^{\gamma-1} F(X_1, X_2, ...X_Q). \tag{22.20}$$

The simplest homogeneous function are those of degree $\gamma = 0$, with examples including intensive thermodynamic propertie, meaning these properties are scale invariant. For example, a bucket of homogeneous water has the same temperature whether or not we remove an arbitrary sample of the water. In contrast, as discussed below, extensive thermodynamic properties are homogeneous functions of degree $\gamma = 1$.

Both the internal energy, $\mathcal{I}^{\text{e}}$, and entropy, $\mathcal{S}^{\text{e}}$, are extensive properties of a fluid system. Consequently, the transfer of matter across the system boundaries leads to an additive change in $\mathcal{I}^{\text{e}}$ and $\mathcal{S}^{\text{e}}$. The internal energy and entropy thus have their natural functional dependencies (22.6) and (22.7) extended to include the matter content

$$\mathcal{I}^{\text{e}} = \mathcal{I}^{\text{e}}(V, \mathcal{S}^{\text{e}}, M_n) \qquad \text{and} \qquad \mathcal{S}^{\text{e}} = \mathcal{S}^{\text{e}}(V, \mathcal{I}^{\text{e}}, M_n), \tag{22.21}$$

where the M_n argument is shorthand for $M_1, M_2...M_N$ for the N matter constituents.[11]

[11] Note that in this subsection the subscript refers to the matter constituents, $n = 1, ...N$, whereas in Section 22.3.1 we used $q = 1., , , Q$ to label the number of independent variables.

What happens when we scale the system by an arbitrary parameter λ? Under this scale operation, the extensive variables, $\mathcal{I}^{\mathrm{e}}$, $\mathcal{S}^{\mathrm{e}}$, as well as the volume, V, and masses, M_n, scale by the same scale factor. The relation (22.21) thus leads to the scaling

$$\lambda\,\mathcal{I}^{\mathrm{e}}(V,\mathcal{S}^{\mathrm{e}},M_n)=\mathcal{I}^{\mathrm{e}}(\lambda\,V,\lambda\,\mathcal{S}^{\mathrm{e}},\lambda\,M_n)\qquad\text{and}\qquad\lambda\,\mathcal{S}^{\mathrm{e}}(V,\mathcal{I}^{\mathrm{e}},M_n)=\mathcal{S}^{\mathrm{e}}(\lambda\,V,\lambda\,\mathcal{I}^{\mathrm{e}},\lambda\,M_n),\quad(22.22)$$

thus revealing that $\mathcal{I}^{\mathrm{e}}(V,\mathcal{S}^{\mathrm{e}},M_n)$ and $\mathcal{S}^{\mathrm{e}}(\lambda\,V,\lambda\,\mathcal{I}^{\mathrm{e}},\lambda\,M_n)$ are homogeneous functions of degree one. Making use of Euler's theorem (22.20) with $\gamma=1$ leads to

$$\mathcal{I}^{\mathrm{e}}(V,\mathcal{S}^{\mathrm{e}},M_n)=V\left[\frac{\partial\mathcal{I}^{\mathrm{e}}}{\partial V}\right]_{\mathcal{S}^{\mathrm{e}},M_n}+\mathcal{S}^{\mathrm{e}}\left[\frac{\partial\mathcal{I}^{\mathrm{e}}}{\partial\mathcal{S}^{\mathrm{e}}}\right]_{V,M_n}+\sum_{n=1}^{N}M_n\left[\frac{\partial\mathcal{I}^{\mathrm{e}}}{\partial M_n}\right]_{V,\mathcal{S}^{\mathrm{e}},M_{m\neq n}}\quad(22.23a)$$

$$\mathcal{S}^{\mathrm{e}}(V,\mathcal{I}^{\mathrm{e}},M_n)=V\left[\frac{\partial\mathcal{S}^{\mathrm{e}}}{\partial V}\right]_{\mathcal{I}^{\mathrm{e}},M_n}+\mathcal{I}^{\mathrm{e}}\left[\frac{\partial\mathcal{S}^{\mathrm{e}}}{\partial\mathcal{I}^{\mathrm{e}}}\right]_{V,M_n}+\sum_{n=1}^{N}M_n\left[\frac{\partial\mathcal{S}^{\mathrm{e}}}{\partial M_n}\right]_{V,\mathcal{I}^{\mathrm{e}},M_{m\neq n}}.\quad(22.23b)$$

These are very special expressions for the internal energy and entropy that are of great use throughout thermodynamics.

22.3.2 Chemical potential and the Euler form

We can further massage the results (22.23a) and (22.23b) by making use of the partial derivative identities from Section 22.2.6 to render

$$\mathcal{I}^{\mathrm{e}}=-p\,V+T\,\mathcal{S}^{\mathrm{e}}+\sum_{n=1}^{N}M_n\left[\frac{\partial\mathcal{I}^{\mathrm{e}}}{\partial M_n}\right]_{V,\mathcal{S}^{\mathrm{e}},M_{m\neq n}}\quad(22.24)$$

$$T\,\mathcal{S}^{\mathrm{e}}=p\,V+\mathcal{I}^{\mathrm{e}}+\sum_{n=1}^{N}T\,M_n\left[\frac{\partial\mathcal{S}^{\mathrm{e}}}{\partial M_n}\right]_{V,\mathcal{I}^{\mathrm{e}},M_{m\neq n}}.\quad(22.25)$$

Self-consistency requires

$$\left[\frac{\partial\mathcal{I}^{\mathrm{e}}}{\partial M_n}\right]_{V,\mathcal{S}^{\mathrm{e}}}=-T\left[\frac{\partial\mathcal{S}^{\mathrm{e}}}{\partial M_n}\right]_{V,\mathcal{I}^{\mathrm{e}},M_{m\neq n}},\quad(22.26)$$

which motivates defining the *chemical potential*

$$\mu_n\equiv\left[\frac{\partial\mathcal{I}^{\mathrm{e}}}{\partial M_n}\right]_{V,\mathcal{S}^{\mathrm{e}},M_{m\neq n}}=-T\left[\frac{\partial\mathcal{S}^{\mathrm{e}}}{\partial M_n}\right]_{V,\mathcal{I}^{\mathrm{e}},M_{m\neq n}}\quad(22.27)$$

thus leading to

$$\mathcal{I}^{\mathrm{e}}=T\,\mathcal{S}^{\mathrm{e}}-p\,V+\sum_{n=1}^{N}\mu_n\,M_n\Longleftrightarrow T\,\mathcal{S}^{\mathrm{e}}=\mathcal{I}^{\mathrm{e}}+p\,V-\sum_{n=1}^{N}\mu_n\,M_n.\quad(22.28)$$

These are the *Euler forms* for the internal energy and entropy.

By definition, the chemical potential, μ_n, is an intensive property that measures the change in the internal energy, $\mathcal{I}^{\mathrm{e}}$, when altering the mass, M_n, of the constituent n, while fixing the entropy, volume, and mass of the other components. Equivalently, it is minus the temperature weighted change in the entropy, $\mathcal{S}^{\mathrm{e}}$, when altering the mass, M_n while fixing the volume, internal energy, and mass of the other components. We can define a chemical potential for a single component system, in which it is the change arising from altering the mass of the system. Despite its name, the chemical potential does not necessarily refer to the existence of chemical reactions, though we note that it does appear prominently in the thermodynamics of chemical reactions (*Atkins and de Paula*, 2006).

22.3.3 Molar mass and molar chemical potential

It is sometimes convenient to write the mass of a constituent as the product of the number of moles, N_n, and the mass per mole, $\mathfrak{M}_n$ (the *molar mass*), so that

$$M_n = N_n \, \mathfrak{M}_n \quad \text{no implied sum.} \tag{22.29}$$

In this way, an infinitesimal mass change is given by

$$\mathrm{d}M = \sum_{n=1}^{N} \mathrm{d}M_n = \sum_{n=1}^{N} \mathrm{d}(N_n \, \mathfrak{M}_n) = \sum_{n=1}^{N} \mathfrak{M}_n \, \mathrm{d}N_n, \tag{22.30}$$

so that mass changes are signalled by changes in the number of moles. We furthermore note the identity (no implied sum)

$$M_n \, \mu_n = M_n \left[\frac{\partial \mathcal{J}^{\mathrm{e}}}{\partial M_n} \right]_{V, \mathcal{S}^{\mathrm{e}}, M_{m \neq n}} = N_n \, \mathfrak{M}_n \left[\frac{\partial \mathcal{J}^{\mathrm{e}}}{\partial (N_n \, \mathfrak{M}_n)} \right]_{V, \mathcal{S}^{\mathrm{e}}, N_{m \neq n}} = N_n \, \tilde{\mu}_n, \tag{22.31}$$

where we defined the molar chemical potential determined according to mole number

$$\tilde{\mu}_n = \left[\frac{\partial \mathcal{J}^{\mathrm{e}}}{\partial N_n} \right]_{V, \mathcal{S}^{\mathrm{e}}, N_{m \neq n}} = \mathfrak{M}_n \, \mu_n. \tag{22.32}$$

We are similarly led to the identities (no implied sum)

$$M_n \, \mathrm{d}\mu_n = N_n \, \mathrm{d}\tilde{\mu}_n \quad \text{and} \quad \mu_n \, \mathrm{d}M_n = \tilde{\mu}_n \, \mathrm{d}N_n. \tag{22.33}$$

22.3.4 Chemical work and the Gibbs-Duhem relation

Changes to the matter composition of a system changes the internal energy through *chemical work*, written as $đ\mathcal{C}$. If the changes to the matter composition occur quasi-statically then the chemical work is written

$$đ\mathcal{C} = \sum_{n=1}^{N} \mu_n \, \mathrm{d}M_n = \sum_{n=1}^{N} \tilde{\mu}_n \, \mathrm{d}N_n \tag{22.34}$$

so that the chemical potential is the integrating factor connecting the inexact differential measuring the chemical work to the exact differential change in matter content. The chemical potential is the energy absorbed or released due to an infinitesimal change in the matter content. As shown in Section 23.1.2, matter in a mixture tends to move from regions of high chemical potential to lower chemical potential, thus motivating the name "potential" in analog to the gravitational potential.

The inclusion of chemical work brings the first law of thermodynamics to the form

$$\mathrm{d}\mathcal{J}^{\mathrm{e}} = đ\mathcal{W} + đ\mathcal{Q} + đ\mathcal{C} \qquad \text{materially open} \tag{22.35a}$$

$$\mathrm{d}\mathcal{J}^{\mathrm{e}} = -p \, \mathrm{d}V + T \, \mathrm{d}\mathcal{S}^{\mathrm{e}} + \sum_{n=1}^{N} \mu_n \, \mathrm{d}M_n \qquad \text{quasi-static and materially open.} \tag{22.35b}$$

Use of the quasi-static form of the first law (22.35b) along with the differential of the result

(22.28) leads to the *Gibbs-Duhem* relation[12]

$$\mathcal{S}^{\mathrm{e}}\,\mathrm{d}T - V\,\mathrm{d}p + \sum_{n=1}^{N} M_n\,\mathrm{d}\mu_n = 0. \tag{22.36}$$

As a corollary we see that for processes occuring at constant temperature and pressure that

$$\sum_{n=1}^{N} M_n\,\mathrm{d}\mu_n = \sum_{n=1}^{N} N_n\,\mathrm{d}\tilde{\mu}_n = 0 \quad \text{constant } T, p. \tag{22.37}$$

22.3.5 Gibbs potential

We offer a formal study of thermodynamic potentials in Section 22.6. Among those, we find Gibbs potential of particular use for geophysical fluid mechanics and thus introduce it here

$$\mathcal{G}^{\mathrm{e}} = \mathcal{I}^{\mathrm{e}} - T\,\mathcal{S}^{\mathrm{e}} + p\,V = \sum_{n=1}^{N} \mu_n\,M_n. \tag{22.38}$$

The reason that the Gibbs potential is so useful is that it is a natural function of temperature, pressure, and matter content,

$$\mathcal{G}^{\mathrm{e}} = \mathcal{G}^{\mathrm{e}}(T, p, M_n), \tag{22.39}$$

with T, p, M_n readily measured fluid properties. This convenient functional dependence is confirmed by taking the differential, $\mathrm{d}\mathcal{G}^{\mathrm{e}}$, and using the fundamental thermodynamic relation (22.35b) to find

$$\mathrm{d}\mathcal{G}^{\mathrm{e}} = -\mathcal{S}^{\mathrm{e}}\,\mathrm{d}T + V\,\mathrm{d}p + \sum_{n=1}^{N} \mu_n\,\mathrm{d}M_n. \tag{22.40}$$

In turn, we can derive the following partial derivatives,

$$\left[\frac{\partial \mathcal{G}^{\mathrm{e}}}{\partial T}\right]_{p,M_n} = -\mathcal{S}^{\mathrm{e}} \quad \text{and} \quad \left[\frac{\partial \mathcal{G}^{\mathrm{e}}}{\partial p}\right]_{T,M_n} = V \quad \text{and} \quad \left[\frac{\partial \mathcal{G}^{\mathrm{e}}}{\partial M_n}\right]_{p,T,M_{m\neq n}} = \mu_n \tag{22.41}$$

along with the second derivative identities

$$\left[\frac{\partial \mu_n}{\partial p}\right]_{T,M_n} = \frac{\partial}{\partial p}\Big]_{T,M_n}\left[\frac{\partial \mathcal{G}^{\mathrm{e}}}{\partial M_n}\right]_{p,T,M_{m\neq n}} = \frac{\partial}{\partial M_n}\Big]_{p,T,M_{m\neq n}}\left[\frac{\partial \mathcal{G}^{\mathrm{e}}}{\partial p}\right]_{T,M_n} = \left[\frac{\partial V}{\partial M_n}\right]_{p,T,M_{m\neq n}} \tag{22.42a}$$

$$\left[\frac{\partial \mu_n}{\partial T}\right]_{p,M_n} = \frac{\partial}{\partial T}\Big]_{p,M_n}\left[\frac{\partial \mathcal{G}^{\mathrm{e}}}{\partial M_n}\right]_{p,T,M_{m\neq n}} = \frac{\partial}{\partial M_n}\Big]_{p,T,M_{m\neq n}}\left[\frac{\partial \mathcal{G}^{\mathrm{e}}}{\partial T}\right]_{p,M_n} = -\left[\frac{\partial \mathcal{S}^{\mathrm{e}}}{\partial M_n}\right]_{p,T,M_{m\neq n}}. \tag{22.42b}$$

The second derivative identities are particular examples of *Maxwell relations*, wtih Maxwell relations the result from commutativity of the partial derivative operation.

22.3.6 Extensive functions of (T, p, M_n)

Just as for the internal energy and entropy, the Gibbs function, $\mathcal{G}^{\mathrm{e}}(T, p, M_n)$, is an extensive function. Since the temperature and pressure are both intensive properties, we follow the scale

[12] In Exercise 22.1 we work through the derivation of Gibbs-Duhem (22.36) in a bit more detail.

analysis from Section 22.3.1 to arrive at the Euler form of the Gibbs function

$$\mathcal{G}^{\mathrm{e}}(T,p,M_n) = \sum_{n=1}^{N} M_n \left[\frac{\partial \mathcal{G}^{\mathrm{e}}}{\partial M_n}\right]_{p,T,M_{m\neq n}} = \sum_{n=1}^{N} \mu_n\, M_n, \tag{22.43}$$

which is consistent with the definition (22.38). Indeed, any extensive property written as a function of (T,p,M_n) can be written in the same fashion. For example, the internal energy, entropy, and volume take the form

$$\mathcal{I}^{\mathrm{e}}(T,p,M_n) = \sum_{n=1}^{N} M_n \left[\frac{\partial \mathcal{I}^{\mathrm{e}}}{\partial M_n}\right]_{p,T,M_{m\neq n}} = \sum_{n=1}^{N} N_n \left[\frac{\partial \mathcal{I}^{\mathrm{e}}}{\partial N_n}\right]_{p,T,N_{m\neq n}} \tag{22.44a}$$

$$\mathcal{S}^{\mathrm{e}}(T,p,M_n) = \sum_{n=1}^{N} M_n \left[\frac{\partial \mathcal{S}^{\mathrm{e}}}{\partial M_n}\right]_{p,T,M_{m\neq n}} = \sum_{n=1}^{N} N_n \left[\frac{\partial \mathcal{S}^{\mathrm{e}}}{\partial N_n}\right]_{p,T,N_{m\neq n}} \tag{22.44b}$$

$$V(T,p,M_n) = \sum_{n=1}^{N} M_n \left[\frac{\partial V}{\partial M_n}\right]_{p,T,M_{m\neq n}} = \sum_{n=1}^{N} N_n \left[\frac{\partial V}{\partial N_n}\right]_{p,T,N_{m\neq n}}. \tag{22.44c}$$

The partial derivatives, $[\partial(\mathcal{G}^{\mathrm{e}},\mathcal{I}^{\mathrm{e}},\mathcal{S}^{\mathrm{e}},V)/\partial N_n]_{p,T,N_{m\neq n}}$, are intensive properties known as the *partial Gibbs potential*, *partial internal energy*, *partial entropy*, and *partial volume*. These relations mean that we can regard each of the extensive quantites as the sum of contributions from each of the material components as determined by their partial properties. For the particular case of a single matter component we have

$$\mathcal{G}^{\mathrm{e}}(T,p,M) = M\left[\frac{\partial \mathcal{G}^{\mathrm{e}}}{\partial M}\right]_{p,T} = \mu\, M \tag{22.45a}$$

$$\mathcal{I}^{\mathrm{e}}(T,p,M) = M\left[\frac{\partial \mathcal{I}^{\mathrm{e}}}{\partial M}\right]_{p,T} = N\left[\frac{\partial \mathcal{I}^{\mathrm{e}}}{\partial N}\right]_{p,T} \tag{22.45b}$$

$$\mathcal{S}^{\mathrm{e}}(T,p,M) = M\left[\frac{\partial \mathcal{S}^{\mathrm{e}}}{\partial M}\right]_{p,T} = N\left[\frac{\partial \mathcal{S}^{\mathrm{e}}}{\partial N}\right]_{p,T} \tag{22.45c}$$

$$V(T,p,M) = M\left[\frac{\partial V}{\partial M}\right]_{p,T} = N\left[\frac{\partial V}{\partial N}\right]_{p,T}. \tag{22.45d}$$

22.4 Thermodynamic equilibrium with matter flow

Consider a single-component fluid ($N=1$) that consists of two regions or systems, labelled by α and β, with each of these two systems separately in thermodynamic equilibrium. Assume the composite system is enclosed in a container with fixed volume, $V_\alpha + V_\beta = V$. Allow the two systems to interact thermally, mechanically, and materially. What are the properties of thermodynamic equilibrium for the composite system, $\alpha \oplus \beta$?

To answer this question, we follow the procedure in Section 22.2.8, here here considering the case where matter flows between the systems in addition to thermal transfer and mechanical interactions. Such processes occur as the composite system approaches thermodynamic equilibrium. Initially, the α and β systems are separately in thermodynamic equilibrium with internal energies, $(\mathcal{I}^{\mathrm{e}}_\alpha, \mathcal{I}^{\mathrm{e}}_\beta)$, volumes, (V_α, V_β), and masses, (M_α, M_β). During the process of reaching thermodynamic equilibrium, the internal energy, volume, and mass of the composite system

remains constant so that[13]

$$\mathrm{d}(\mathcal{I}^{\mathrm{e}}_\alpha + \mathcal{I}^{\mathrm{e}}_\beta) = 0 \quad \text{and} \quad \mathrm{d}(V_\alpha + V_\beta) = 0 \quad \text{and} \quad \mathrm{d}(M_\alpha + M_\beta) = 0. \tag{22.46}$$

From equation (22.21) we know that entropy is a natural function of volume, internal energy, and mass of each matter constituent. With only a single matter constituent we have

$$\mathrm{d}\mathcal{S}^{\mathrm{e}} = \frac{1}{T_\alpha}\,\mathrm{d}\mathcal{I}^{\mathrm{e}}_\alpha + \frac{p_\alpha}{T_\alpha}\,\mathrm{d}V_\alpha - \frac{\mu_\alpha}{T_\alpha}\,\mathrm{d}M_\alpha + \frac{1}{T_\beta}\,\mathrm{d}\mathcal{I}^{\mathrm{e}}_\beta + \frac{p_\beta}{T_\beta}\,\mathrm{d}V_\beta - \frac{\mu_\beta}{T_\beta}\,\mathrm{d}M_\beta \tag{22.47a}$$

$$= \left[\frac{1}{T_\alpha} - \frac{1}{T_\beta}\right]\mathrm{d}\mathcal{I}^{\mathrm{e}}_\alpha + \left[\frac{p_\alpha}{T_\alpha} - \frac{p_\beta}{T_\beta}\right]\mathrm{d}V_\alpha - \left[\frac{\mu_\alpha}{T_\alpha} - \frac{\mu_\beta}{T_\beta}\right]\mathrm{d}M_\alpha, \tag{22.47b}$$

where we used the partial derivative identities (22.11), (22.12), and (22.27). As before, $\mathrm{d}\mathcal{S}^{\mathrm{e}} = 0$ at thermodynamic equilibrium, and this condition holds for arbitrary and independent $\mathrm{d}\mathcal{I}^{\mathrm{e}}_\alpha$, $\mathrm{d}V_\alpha$, and $\mathrm{d}M_\alpha$. We are thus led to the thermal, mechanical, and material conditions for thermodynamic equilibrium

$$T_\alpha = T_\beta \quad \text{and} \quad p_\alpha = p_\beta \quad \text{and} \quad \mu_\alpha = \mu_\beta. \tag{22.48}$$

That is, the temperature, pressure, and chemical potential are uniform when the composite system reaches thermodynamic equilibrium. Note that this thermodynamic equilibrium condition means that each term in the Gibbs-Duhem relation (22.36) separately vanishes. Furthermore, since the Gibbs potential equals to the mass times the chemical potential for a single component system (equation (22.43)), equality of the chemical potentials at equilibrium means that

$$\mu_\alpha = \mu_\beta \implies \frac{\mathcal{G}^{\mathrm{e}}_\alpha}{M_\alpha} = \frac{\mathcal{G}^{\mathrm{e}}_\beta}{M_\beta}. \tag{22.49}$$

As for the direction of heat flow discussed in Section 22.2.8, we can determine the direction for matter flow as $\alpha \oplus \beta$ approaches thermodynamic equilibrium. For this purpose, assume the temperature and volumes are already uniform, but the matter content initially differs. At the instance the two systems start interacting, the entropy differential is given by

$$T\,\mathrm{d}\mathcal{S}^{\mathrm{e}} = -(\mu_\alpha - \mu_\beta)\,\mathrm{d}M_\alpha > 0, \tag{22.50}$$

where T is the equilibrium temperature of the two systems, and where the inequality holds according to the second law of thermodynamics (Section 22.1.7). If $\mu_\alpha > \mu_\beta$, then this inequality requires $\mathrm{d}M_\alpha < 0$. Hence, in the process of approaching thermodynamic equilibrium, matter flows from regions of high chemical potential to regions of low chemical potential. This behavior allows us to consider the chemical potential in a manner directly akin to temperature. That is, temperature differences measure the potential for heat to be fluxed, and likewise chemical potential differences measure the potential for matter to be fluxed. The chemical potential is central to the study of changes in matter states (e.g., solid to liquid, liquid to gas), as well as for chemical reactions (e.g., *Guggenheim*, 1967; *Atkins and de Paula*, 2006).

22.5 Materially open systems with fixed total mass

In our study of geophysical fluids, we make use of a continuum of fluid elements. Each fluid element is open mechanically, thermally, and materially while maintaining constant mass as it quasi-statically evolves through local thermodynamic equilibrium states. Hence, when

[13] We here assume there is no macroscopic mechanical energy, so that the total energy is the internal energy. In Section 26.8 we relax this assumption by considering macroscopic motion.

formulating the equations of linear irreversible thermodynamics in Chapter 26, we make use of thermodynamic equations written in their "per unit mass" form. Here we present these equations, as well as extend our understanding of the formalism.

22.5.1 Matter concentrations

We generally make use of matter or tracer concentration as written

$$C_n = M_n/M \Longrightarrow \sum_{n=1}^{N} C_n = 1, \tag{22.51}$$

with the constant mass constraint $\sum_{n=1}^{N} C_n = 1$ meaning that only $N-1$ of the concentrations are linearly independent. Recall that we previously made use of tracer concentrations in Section 20.1 when developing the tracer equation.

22.5.2 Fundamental thermodynamic relation per unit mass

We scale away the mass of the system by setting the scale factor $\lambda = M^{-1}$ in our discussion in Section 22.3.1 of how extensive properties scale. The result is the *specific* (per mass) versions of the extensive properties

$$\mathcal{J}^{\mathrm{e}} = M\,\mathcal{J} \tag{22.52a}$$
$$\mathcal{S}^{\mathrm{e}} = M\,\mathcal{S} \tag{22.52b}$$
$$V = M/\rho = M\,\nu_{\mathrm{s}} \tag{22.52c}$$
$$M_n = M\,C_n, \tag{22.52d}$$

where

$$\nu_{\mathrm{s}} = 1/\rho \tag{22.53}$$

is the *specific volume* and the total mass, M, is held fixed. In the equality (22.52d), C_n is the mass fraction or concentration of species n in the fluid (Section 22.5.1). Substituting the specific quantities (22.52a)-(22.52d) into the fundamental thermodynamic relation (22.35b) leads to the fundamental thermodynamic relation in terms of specific thermodynamic quantities

$$\mathrm{d}\mathcal{J} = T\,\mathrm{d}\mathcal{S} - p\,\mathrm{d}\rho^{-1} + \sum_{n} \mu_n\,\mathrm{d}C_n. \tag{22.54}$$

This is the form of the fundamental thermodynamic relation most commonly used in this book. Again, this relation holds for quasi-static processes where the total mass of the system is fixed, thus making it relevant for our study of constant mass fluid elements in Chapter 26.

22.5.3 Seawater as a binary fluid

The atmosphere is a multi-component and multi-phase fluid that is well approximated as a mixture of water vapor and dry air. However, we do not consider moist atmospheric processes in this book nor do we consider phases changes. In contrast, there are many occasions in this book that require us to consider seawater as a binary fluid system of salt dissolved in fresh water so

that their concentrations satisfy the constraint[14]

$$C_{\text{salt}} + C_{\text{water}} = 1 \implies \mathrm{d}C_{\text{water}} = -\mathrm{d}C_{\text{salt}}. \tag{22.55}$$

We are thus able to write the Gibbs fundamental thermodynamic relation (22.54) in the form

$$\mathrm{d}\mathcal{J} = T\,\mathrm{d}\mathcal{S} - p\,\mathrm{d}\rho^{-1} + \mu_{\text{water}}\,\mathrm{d}C_{\text{water}} + \mu_{\text{salt}}\,\mathrm{d}C_{\text{salt}} \tag{22.56a}$$

$$= T\,\mathrm{d}\mathcal{S} - p\,\mathrm{d}\rho^{-1} + \mu\,\mathrm{d}C, \tag{22.56b}$$

where

$$C = C_{\text{salt}} \tag{22.57}$$

is the concentration of salt (mass of salt per mass of seawater), and

$$\mu = \mu_{\text{salt}} - \mu_{\text{water}} \tag{22.58}$$

is the *relative chemical potential*, often referred to as the *seawater chemical potential*. We return in Section 22.58 to discuss how the chemical potentials are computed according to partial derivatives of the Gibbs potential, which is the preferred method for the ocean and atmosphere.

The *absolute salinity* S, with units parts per thousand (gram per kilogram), is related to C_{salt} via

$$S = 1000\, C_{\text{salt}}. \tag{22.59}$$

The range of absolute salinity in the ocean (roughly $0 \leq S \leq 40$) is more convenient than the range of C_{salt}, making salinity more commonly used in oceanography.

22.5.4 Further study

Chapters 1 and 2 of *Olbers et al.* (2012) provide a more complete suite of thermodynamic relations for seawater.

22.6 Thermodynamic potentials

Internal energy and entropy are referred to as state functions (functions only of the current state) as well as *thermodynamic potentials*, and they are related by equation (22.28), here written in its specific form as appropriate for constant mass fluid elements

$$\mathcal{I} = T\,\mathcal{S} - p\,\nu_{\text{s}} + \sum_{n=1}^{N} \mu_n\, C_n \iff T\,\mathcal{S} = \mathcal{I} + p\,\nu_{\text{s}} - \sum_{n=1}^{N} \mu_n\, C_n. \tag{22.60}$$

Each thermodynamic potential is a natural function of certain other thermodynamic properties, as determined by the fundamental thermodynamic relation.

It is useful to have access to a suite of thermodynamic potentials (internal energy, entropy, enthalpy, Gibbs potential, Helmbolz free energy) that have different natural functional dependencies, which in turn yield distinct expressions for the fundamental equation of state. Thermodynamic potentials are related mathematically through a *Legendre transformation*. Motivation for their introduction comes from the distinct laboratory and environmental conditions whereby the

[14] Salt in the ocean is largely comprised of chloride ions, sodium ions, sulphate ions, magnesium ions, calcium ions, potassium ions, and hydro-carbonate ions. The composition of the principal ions in seawater is roughly a constant, thus allowing us to be concerned only with the "salt" content and concentration rather than that for the individual components. In turn, we can accurately consider seawater as a two-component fluid comprised of fresh water and salt. See Section 1.4 of *Kamenkovich* (1977), Section 3.1 of *Gill* (1982), Section 1.2 of *Olbers et al.* (2012), or Section 1.4 of *Vallis* (2017) for more details.

controlling parameters may differ. In this section we introduce the variety of thermodynamic potentials commonly used for fluid mechanics, and exhibit their natural functional dependencies.

In this section, we specialize to the case of a binary fluid, which is most commonly the case for the ocean and atmosphere. If there are more than two matter constituents, then the term $\mu \, \mathrm{d}C$ appearing in these formula become $\sum_{n=1}^{N} \mu_n \, \mathrm{d}C_n$. Partial derivatives are also modified accordingly. We choose the binary case since it is typically sufficient for the earth's atmosphere and ocean.

As a point of practice, it is important to commit to a single choice for the thermodynamic potential when manipulating thermodynamic equations. The reason is that functional dependencies change when switching to a different thermodynamic potential, thus exposing oneself to mistakes when swapping formulations midstream.

22.6.1 Equations of state

Equations (22.9), (22.10), and (22.27) provide expressions for intensive properties, T, p, and μ_n, in terms of the partial derivatives of the internal energy in terms of extensive functions $\mathcal{S}^{\mathrm{e}}$, V, and M_n. Hence, we can write T, p, and μ_n in the functional form

$$T = T(\mathcal{S}^{\mathrm{e}}, V, M_m) \qquad \text{and} \qquad p = p(\mathcal{S}^{\mathrm{e}}, V, M_m) \qquad \text{and} \qquad \mu_n = \mu_n(\mathcal{S}^{\mathrm{e}}, V, M_m). \tag{22.61}$$

These equations are known as *equations of state*. Knowledge of all the equations of state is equivalent to knowledge of the fundamental thermodynamic relation (22.35b). In the following, we develop similar equations of state based on other thermodynamic potentials.

22.6.2 Internal energy

Recall the fundamental thermodynamic relation (22.56b) written for a binary fluid

$$\mathrm{d}\mathcal{I} = T \, \mathrm{d}\mathcal{S} - p \, \mathrm{d}\nu_{\mathrm{s}} + \mu \, \mathrm{d}C. \tag{22.62}$$

Equation (22.62) identifies the specific internal energy, $\mathcal{I}$, as a natural function of specific entropy, $\mathcal{S}$, specific volume, ν_{s}, and matter concentration, C

$$\mathcal{I} = \mathcal{I}(\mathcal{S}, \nu_{\mathrm{s}}, C). \tag{22.63}$$

Knowledge of the fundamental thermodynamic relation (22.62) allows us to derive a variety of thermodynamic relations via partial differentiation. For example, we can identify

$$\left[\frac{\partial \mathcal{I}}{\partial \mathcal{S}}\right]_{\nu_{\mathrm{s}}, C} = T \qquad \text{and} \qquad \left[\frac{\partial \mathcal{I}}{\partial \nu_{\mathrm{s}}}\right]_{\mathcal{S}, C} = -p \qquad \text{and} \qquad \left[\frac{\partial \mathcal{I}}{\partial C}\right]_{\mathcal{S}, \nu_{\mathrm{s}}} = \mu, \tag{22.64}$$

which are the specific (per mass) forms of equations (22.9), (22.10), and (22.27).

We see that equations (22.64) provide a relation between T, p, μ as derivatives of a function, the internal energy, which is itself a function $\mathcal{I}(\mathcal{S}, \nu_{\mathrm{s}}, C)$. Hence, we may consider T, p, μ each as a function of $(\mathcal{S}, \nu_{\mathrm{s}}, C)$, and thus write the equations of state

$$T = T(\mathcal{S}, \nu_{\mathrm{s}}, C) \qquad \text{and} \qquad p = p(\mathcal{S}, \nu_{\mathrm{s}}, C) \qquad \text{and} \qquad \mu = \mu(\mathcal{S}, \nu_{\mathrm{s}}, C), \tag{22.65}$$

which are the equations of state (22.61) written in terms of specific (per mass) quantities. In turn, the exact differentials of the intensive properties are

$$T = T(\mathcal{S}, \nu_{\mathrm{s}}, C) \Longrightarrow \mathrm{d}T = \left[\frac{\partial T}{\partial \mathcal{S}}\right]_{\nu_{\mathrm{s}}, C} \mathrm{d}\mathcal{S} + \left[\frac{\partial T}{\partial \nu_{\mathrm{s}}}\right]_{C, \mathcal{S}} \mathrm{d}\nu_{\mathrm{s}} + \left[\frac{\partial T}{\partial C}\right]_{\mathcal{S}, \nu_{\mathrm{s}}} \mathrm{d}C \tag{22.66}$$

$$p = p(\mathcal{S}, \nu_s, C) \Longrightarrow dp = \left[\frac{\partial p}{\partial \mathcal{S}}\right]_{\nu_s, C} d\mathcal{S} + \left[\frac{\partial p}{\partial \nu_s}\right]_{C, \mathcal{S}} d\nu_s + \left[\frac{\partial p}{\partial C}\right]_{\mathcal{S}, \nu_s} dC \tag{22.67}$$

$$\mu = \mu(\mathcal{S}, \nu_s, C) \Longrightarrow d\mu = \left[\frac{\partial \mu}{\partial \mathcal{S}}\right]_{\nu_s, C} d\mathcal{S} + \left[\frac{\partial \mu}{\partial \nu_s}\right]_{C, \mathcal{S}} d\nu_s + \left[\frac{\partial \mu}{\partial C}\right]_{\mathcal{S}, \nu_s} dC. \tag{22.68}$$

22.6.3 Entropy

Rearrangement of the fundamental thermodynamic relation (22.62) leads to the exact differential for specific entropy

$$d\mathcal{S} = \frac{1}{T} d\mathcal{I} + \frac{p}{T} d\nu_s - \frac{\mu}{T} dC. \tag{22.69}$$

In this form, specific entropy has the functional dependence

$$\mathcal{S} = \mathcal{S}(\mathcal{I}, \nu_s, C), \tag{22.70}$$

whose knowledge provides yet another form of the fundamental equation of state. This functional dependence, along with equation (22.69), lead to the following identities

$$\left[\frac{\partial \mathcal{S}}{\partial \mathcal{I}}\right]_{\nu_s, C} = \frac{1}{T} \quad \text{and} \quad \left[\frac{\partial \mathcal{S}}{\partial \nu_s}\right]_{\mathcal{I}, C} = \frac{p}{T} \quad \text{and} \quad \left[\frac{\partial \mathcal{S}}{\partial C}\right]_{\mathcal{I}, \nu_s} = -\frac{\mu}{T}. \tag{22.71}$$

As for internal energy in Section 22.6.2, equation (22.71) provides a relation between T, p, μ as derivatives of a function, the entropy, which is itself a function $\mathcal{S}(\mathcal{I}, \nu_s, C)$. Hence, we may consider T, p, μ as each a function of $(\mathcal{I}, \nu_s, C)$ to thus write the equations of state

$$T = T(\mathcal{I}, \nu_s, C) \quad \text{and} \quad p = p(\mathcal{I}, \nu_s, C) \quad \text{and} \quad \mu = \mu(\mathcal{I}, \nu_s, C). \tag{22.72}$$

22.6.4 Enthalpy

Thus far we have worked only with the fundamental thermodynamic relation (22.62). We now introduce the specific enthalpy

$$\mathcal{H} = \mathcal{I} + p\,\nu_s = T\,\mathcal{S} + \sum_{n=1}^{N} \mu_n\, C_n, \tag{22.73}$$

where the second equality made use of equation (22.60). Specializing to the case of a binary fluid, such as the ocean or atmosphere, and use of the fundamental thermodynamic relation (22.62), leads to the exact differential for enthalpy

$$d\mathcal{H} = d\mathcal{I} + d(p\,\nu_s) \tag{22.74a}$$

$$= T\,d\mathcal{S} - p\,d\nu_s + \mu\,dC + p\,d\nu_s + \nu_s\,dp \tag{22.74b}$$

$$= T\,d\mathcal{S} + \nu_s\,dp + \mu\,dC. \tag{22.74c}$$

Recalling that for quasi-static processes, $T\,d\mathcal{S}$ equals to the thermal energy added to a fluid element. Hence, for processes occuring at constant pressure and constant matter content, changes in enthalpy are determined by the thermal energy added to the system. This connection motivates the name *heat function* sometimes applied to enthalpy (e.g., page 4 of *Landau and Lifshitz* (1987)).

Equation (22.74c) provides the fundamental thermodynamic relation with enthalpy rather than internal energy. Consequently, the *Legendre transformation* (22.73) renders a functional dependence for enthalpy

$$\mathcal{H} = \mathcal{H}(\mathcal{S}, p, C), \tag{22.75}$$

which in turn leads to the following partial derivative identities

$$\left[\frac{\partial \mathcal{H}}{\partial \mathcal{S}}\right]_{p,C} = T \qquad \text{and} \qquad \left[\frac{\partial \mathcal{H}}{\partial p}\right]_{\mathcal{S},C} = \nu_{\mathrm{s}} \qquad \text{and} \qquad \left[\frac{\partial \mathcal{H}}{\partial C}\right]_{\mathcal{S},p} = \mu. \tag{22.76}$$

As for internal energy in Section 22.6.2, equations (22.76) provide a relation between T, ν_{s}, μ as derivatives of a function, the enthalpy, which is itself a function $\mathcal{H}(\mathcal{S}, p, C)$. Hence, we may consider T, ν_{s}, μ as each a function of $(\mathcal{S}, p, C)$ to thus render the following equations of state

$$T = T(\mathcal{S}, p, C) \qquad \text{and} \qquad \nu_{\mathrm{s}} = \nu_{\mathrm{s}}(\mathcal{S}, p, C) \qquad \text{and} \qquad \mu = \mu(\mathcal{S}, p, C). \tag{22.77}$$

Enthalpy's functional dependence (22.75) is more convenient for studies of geophysical fluids than that for internal energy, $\mathcal{I}(\mathcal{S}, \nu_{\mathrm{s}}, C)$, or for entropy $\mathcal{S}(\mathcal{I}, \nu_{\mathrm{s}}, C)$.

- In the laboratory or field, we generally have direct mechanical means for measuring pressure in a fluid, whereas specific volume requires indirect methods involving the equation of state for density discussed in Section 30.3.

- Correspondingly, the interaction between fluid elements typically occurs at near constant pressure. Hence, fluid elements exchange both their entropy and enthalpy when the exchange occurs as constant pressure.

- Specific entropy remains constant on a fluid element in the absence of mixing or other irreversible effects. Correspondingly, enthalpy remains constant for constant pressure motion without mixing. Conversely, in the presence of mixing at constant pressure, fluid elements mix their specific enthalpy, specific entropy, and tracer concentration.

22.6.5 Helmholtz free energy

The Helmholtz free energy is defined by the Legendre transformation

$$\mathcal{F} = \mathcal{I} - T\,\mathcal{S} = -p\,\nu_{\mathrm{s}} + \sum_{n=1}^{N} \mu_n\, C_n, \tag{22.78}$$

where the second equality made use of equation (22.60). The exact differential of the Helmholtz free energy is given by

$$\begin{aligned} \mathrm{d}\mathcal{F} &= \mathrm{d}\mathcal{I} - \mathrm{d}(T\,\mathcal{S}) && \text{(22.79a)} \\ &= \mathrm{d}\mathcal{I} - T\,\mathrm{d}\mathcal{S} - \mathcal{S}\,\mathrm{d}T && \text{(22.79b)} \\ &= -\mathcal{S}\,\mathrm{d}T - p\,\mathrm{d}\nu_{\mathrm{s}} + \mu\,\mathrm{d}C, && \text{(22.79c)} \end{aligned}$$

where we used the fundamental thermodynamic relation (22.56b) for the final equality. Isothermal and constant concentration processes render the changes to the free energy equal to the pressure work applied to the system.

The Helmholtz free energy has the functional dependence

$$\mathcal{F} = \mathcal{F}(T, \nu_{\mathrm{s}}, C), \tag{22.80}$$

which then leads to the partial derivatives identities

$$\left[\frac{\partial \mathcal{F}}{\partial T}\right]_{\nu_{\mathrm{s}},C} = -\mathcal{S} \qquad \text{and} \qquad \left[\frac{\partial \mathcal{F}}{\partial \nu_{\mathrm{s}}}\right]_{T,C} = -p \qquad \text{and} \qquad \left[\frac{\partial \mathcal{F}}{\partial C}\right]_{T,\nu_{\mathrm{s}}} = \mu. \tag{22.81}$$

As for internal energy in Section 22.6.2, equations (22.81) provide a relation between $\mathcal{S}, p, \mu$ as derivatives of a function, the Helmholtz free energy, which is itself a function $\mathcal{F}(T, \nu_s, C)$. Hence, we may consider $\mathcal{S}, p, \mu$ each as a function of (T, ν_s, C) to render the equations of state

$$\mathcal{S} = \mathcal{S}(T, \nu_s, C) \qquad \text{and} \qquad p = p(T, \nu_s, C) \qquad \text{and} \qquad \mu = \mu(T, \nu_s, C). \tag{22.82}$$

22.6.6 Gibbs potential

The Gibbs potential is defined by the Legendre transformation

$$\mathcal{G} = \mathcal{I} + p\,\nu_s - T\,\mathcal{S} = \mathcal{H} - T\,\mathcal{S} = \sum_{n=1}^{N} \mu_n\, C_n, \tag{22.83}$$

where the final equality made use of equation (22.60). The exact differential of the Gibbs potential is given by

$$\begin{aligned} \mathrm{d}\mathcal{G} &= \mathrm{d}\mathcal{H} - \mathrm{d}(T\,\mathcal{S}) && \text{(22.84a)} \\ &= T\,\mathrm{d}\mathcal{S} + \nu_s\,\mathrm{d}p + \mu\,\mathrm{d}C - T\,\mathrm{d}\mathcal{S} - \mathcal{S}\,\mathrm{d}T && \text{(22.84b)} \\ &= -\mathcal{S}\,\mathrm{d}T + \nu_s\,\mathrm{d}p + \mu\,\mathrm{d}C, && \text{(22.84c)} \end{aligned}$$

where we made use of the fundamental thermodynamic relation (22.74c) written in terms of enthalpy. The Gibbs potential has the functional dependence

$$\mathcal{G} = \mathcal{G}(T, p, C), \tag{22.85}$$

which leads to the partial derivatives identities

$$\left[\frac{\partial \mathcal{G}}{\partial T}\right]_{p,C} = -\mathcal{S} \qquad \text{and} \qquad \left[\frac{\partial \mathcal{G}}{\partial p}\right]_{T,C} = \nu_s \qquad \text{and} \qquad \left[\frac{\partial \mathcal{G}}{\partial C}\right]_{T,p} = \mu. \tag{22.86}$$

As for internal energy in Section 22.6.2, equations (22.86) provide a relation between $\mathcal{S}, \nu_s, \mu$ as derivatives of a function, the Gibbs potential, which is itself a function $\mathcal{G}(T, p, C)$. Hence, we may consider $\mathcal{S}, \nu_s, \mu$ each as a function of (T, p, C) to render the following functional relations

$$\mathcal{S} = \mathcal{S}(T, p, C) \qquad \text{and} \qquad \nu_s = \nu_s(T, p, C) \qquad \text{and} \qquad \mu = \mu(T, p, C). \tag{22.87}$$

The form of the fundamental dependencies (22.85), and the associated equations of state (22.87), are often used in fluid mechanics and physical chemistry. The reason is that temperature, pressure, and concentration are readily measured in the laboratory and the environment. We can thus readily measure the partial derivatives of $\mathcal{G}$, and the functional dependence (22.87) provides a convenient means to express $\mathcal{S}$, ν_s, and μ (e.g., see the adiabatic lapse rate discussion in Section 23.2).

Given its convenient functional dependence, the Gibbs potential plays a central role in developing the thermodynamics of seawater as formulated by *Feistel* (1993) and codifed by *IOC et al.* (2010). We thus endeavor to exhibit how quantities (e.g., response functions as in Section 22.7) can be computed based on knowledge of the Gibbs potential and its partial derivatives. For example, use of equation (22.86) renders the expression for the enthalpy

$$\mathcal{H} = \mathcal{G} + T\,\mathcal{S} = \mathcal{G} - T\left[\frac{\partial \mathcal{G}}{\partial T}\right]_{p,C}. \tag{22.88}$$

22.6.7 Chemical potential and the Gibbs potential

Throughout this section we have displayed equations for the chemical potential of a binary fluid in terms of the partial derivatives of the thermodynamic potentials, such as equation (22.86) using the Gibbs potential. Here we consider some details that lead to further understanding of the partial derivatives. We start by writing the chemical potential of fresh water and salt as contained within seawater in terms of the partial derivatives of the extensive Gibbs potential

$$\mu_{\text{water}} = \left[\frac{\partial \mathcal{G}^{\text{e}}}{\partial M_{\text{water}}}\right]_{T,p,M_{\text{salt}}} \quad \text{and} \quad \mu_{\text{salt}} = \left[\frac{\partial \mathcal{G}^{\text{e}}}{\partial M_{\text{salt}}}\right]_{T,p,M_{\text{water}}}. \tag{22.89}$$

The total mass of a sample of seawater is given by $M = M_{\text{water}} + M_{\text{salt}}$. Consequently, to compute these partial derivatives requires us to alter the mass of the sample as we hold the mass of one component fixed while varying the mass of the other component. This sort of partial derivative is less convenient for our purposes since we prefer to work with constant mass samples, such as we encounter with constant mass fluid elements. For that purpose we introduce the specific Gibbs potential, in which case the chemical potential of fresh water is

$$\mu_{\text{water}} = \left[\frac{\partial \mathcal{G}^{\text{e}}}{\partial M_{\text{water}}}\right]_{T,p,M_{\text{salt}}} = \left[\frac{\partial (M\,\mathcal{G})}{\partial M_{\text{water}}}\right]_{T,p,M_{\text{salt}}} = \mathcal{G} + M\left[\frac{\partial \mathcal{G}}{\partial M_{\text{water}}}\right]_{T,p,M_{\text{salt}}}. \tag{22.90}$$

The specific Gibbs potential is a natural function of T, p, C_n, and since $C_{\text{water}} + C_{\text{salt}} = 1$ we can write the Gibbs potential in terms of just one of the concentrations, typically chosen as C_{salt}. We are thus led to

$$\mu_{\text{water}} = \mathcal{G} + M\left[\frac{\partial \mathcal{G}}{\partial M_{\text{water}}}\right]_{T,p,M_{\text{salt}}} \tag{22.91a}$$

$$= \mathcal{G} + M\left[\frac{\partial \mathcal{G}}{\partial C_{\text{water}}}\right]_{T,p}\left[\frac{\partial C_{\text{water}}}{\partial M_{\text{water}}}\right]_{M_{\text{salt}}} \tag{22.91b}$$

where the concentration partial derivative is given by

$$\left[\frac{\partial C_{\text{water}}}{\partial M_{\text{water}}}\right]_{M_{\text{salt}}} = \left[\frac{\partial}{\partial M_{\text{water}}}\right]_{M_{\text{salt}}}\left[\frac{M_{\text{water}}}{M_{\text{water}} + M_{\text{salt}}}\right] = \frac{C_{\text{salt}}}{M}, \tag{22.92}$$

thus leading to the chemical potential of fresh water within seawater

$$\mu_{\text{water}} = \mathcal{G} + C_{\text{salt}}\left[\frac{\partial \mathcal{G}}{\partial C_{\text{water}}}\right]_{T,p} = \mathcal{G} - C_{\text{salt}}\left[\frac{\partial \mathcal{G}}{\partial C_{\text{salt}}}\right]_{T,p}. \tag{22.93}$$

We are thus able to work with the specific Gibbs function for a constant mass fluid element and compute its concentration partial derivative. Similar manipulations lead to the chemical potential for salt within seawater

$$\mu_{\text{salt}} = \mathcal{G} + C_{\text{water}}\left[\frac{\partial \mathcal{G}}{\partial C_{\text{salt}}}\right]_{T,p} = \mathcal{G} + (1 - C_{\text{salt}})\left[\frac{\partial \mathcal{G}}{\partial C_{\text{salt}}}\right]_{T,p}. \tag{22.94}$$

We are thus led to the seawater chemical potential

$$\mu = \mu_{\text{salt}} - \mu_{\text{water}} = \left[\frac{\partial \mathcal{G}}{\partial C_{\text{salt}}}\right]_{T,p}, \tag{22.95}$$

which agrees with equation (22.86).

22.7 Response functions

Response functions measure the change in a thermodynamic property as the system is forced in some manner. We here introduce the heat capacity, thermal expansion coefficient, and haline contraction coefficient, which are three response functions commonly encountered in ocean and atmospheric fluid mechanics.

22.7.1 Specific heat capacities

The heat capacity measures the change in heat associated with a change in temperature at constant matter composition. There are two distinct heat capacities generally considered in fluid mechanics: one with specific volume held fixed and the other with pressure held fixed

$$c_{\mathsf{v}} \equiv \frac{1}{M}\left[\frac{đ\mathcal{Q}}{\partial T}\right]_{\nu_{\mathsf{s}},C} \qquad \text{SI units } \mathrm{m}^2\ \mathrm{s}^{-2}\ \mathrm{K}^{-1}. \tag{22.96}$$

$$c_{\mathsf{p}} \equiv \frac{1}{M}\left[\frac{đ\mathcal{Q}}{\partial T}\right]_{p,C} \qquad \text{SI units } \mathrm{m}^2\ \mathrm{s}^{-2}\ \mathrm{K}^{-1}. \tag{22.97}$$

Each of these quantities are specific heat capacities since we have divided by the mass. If heating occurs quasi-statically, we can make use of the equation (22.4) that relates heating and entropy, applied here in its specific (per mass) form $M^{-1}\, đ\mathcal{Q} = T\, d\mathcal{S}$. The result is a state function form of the specific heat capacities

$$c_{\mathsf{v}} = T\left[\frac{\partial \mathcal{S}}{\partial T}\right]_{\nu_{\mathsf{s}},C} = -T\left[\frac{\partial}{\partial T}\right]_{\nu_{\mathsf{s}},C}\left[\frac{\partial \mathcal{G}}{\partial T}\right]_{p,C} \tag{22.98}$$

$$c_{\mathsf{p}} = T\left[\frac{\partial \mathcal{S}}{\partial T}\right]_{p,C} = -T\left[\frac{\partial}{\partial T}\right]_{p,C}\left[\frac{\partial \mathcal{G}}{\partial T}\right]_{p,C} \tag{22.99}$$

where the second equalities in both of the above equations introduced the Gibbs potential according to equation (22.86). Furthermore, we can make use of the fundamental thermodynamic relation (22.54) with specific volume and matter concentration held fixed to yield

$$c_{\mathsf{v}} = T\left[\frac{\partial \mathcal{S}}{\partial T}\right]_{\nu_{\mathsf{s}},C} = \left[\frac{\partial \mathcal{I}}{\partial T}\right]_{\nu_{\mathsf{s}},C}. \tag{22.100}$$

The second form of c_{v} motivates the name *internal energy capacity* rather than heat capacity at fixed volume. Equation (22.100) implies that internal energy, for a process occuring at constant specific volume and constant tracer concentration, can be written in terms of a *caloric equation of state*

$$\mathcal{I} = \mathcal{I}(T) \quad \text{constant } \nu_{\mathsf{s}} \text{ and } C. \tag{22.101}$$

Making use of the fundamental thermodynamic relation (22.74c) written in terms of enthalpy leads to the constant pressure heat capacity

$$c_{\mathsf{p}} = T\left[\frac{\partial \mathcal{S}}{\partial T}\right]_{p,C} = \left[\frac{\partial \mathcal{I}}{\partial T}\right]_{p,C} + p\left[\frac{\partial \nu_{\mathsf{s}}}{\partial T}\right]_{p,C} = \left[\frac{\partial \mathcal{H}}{\partial T}\right]_{p,C}. \tag{22.102}$$

The constant pressure heat capacity is equivalently referred to as the *enthalpy capacity*.

22.7.2 Thermal expansion coefficient

The thermal expansion coefficient measures relative changes in density as temperature changes at constant pressure and concentration

$$\alpha_{\rm T} = -\frac{1}{\rho}\left[\frac{\partial \rho}{\partial T}\right]_{p,C} = \frac{1}{\nu_{\rm s}}\left[\frac{\partial \nu_{\rm s}}{\partial T}\right]_{p,C} = \frac{1}{(\partial \mathcal{G}/\partial p)_{T,C}}\left[\frac{\partial}{\partial T}\right]_{p,C}\left[\frac{\partial \mathcal{G}}{\partial p}\right]_{T,C} \tag{22.103}$$

where the final equality introduced the Gibbs function according to equation (22.86). The minus sign in the definition is introduced since density typically reduces when temperature increases, so that for most substances $\alpha_{\rm T} > 0$. Freshwater near its freezing point is an important counter-example, with $\alpha_{\rm T} < 0$ allowing for solid ice to float on liquid water.

22.7.3 Haline contraction coefficient

A similar response function measures changes to density arising from changes in the salt concentration (salinity) in seawater

$$\beta_{\rm S} = \frac{1}{\rho}\left[\frac{\partial \rho}{\partial S}\right]_{p,T} = -\frac{1}{\nu_{\rm s}}\left[\frac{\partial \nu_{\rm s}}{\partial S}\right]_{p,T} = -\frac{1}{(\partial \mathcal{G}/\partial p)_{T,S}}\left[\frac{\partial}{\partial S}\right]_{T,p}\left[\frac{\partial \mathcal{G}}{\partial p}\right]_{T,S} \tag{22.104}$$

where $S = 1000\, C$ is the salinity (22.59). Seawater density typically increases (fluid element volume contracts) when salinity increases, so that $\beta_{\rm S} > 0$.

22.7.4 Speed of sound (acoustic) waves

Changes in density with respect to pressure at a fixed entropy define the inverse squared sound speed[15]

$$\frac{1}{c_{\rm s}^2} = \left[\frac{\partial \rho}{\partial p}\right]_{\mathcal{S}} = -\frac{1}{(\nu_{\rm s})^2}\left[\frac{\partial \nu_{\rm s}}{\partial p}\right]_{\mathcal{S}} = -\frac{1}{[(\partial \mathcal{G}/\partial p)_{T,S}]^2}\left[\frac{\partial}{\partial p}\right]_{\mathcal{S}}\left[\frac{\partial \mathcal{G}}{\partial p}\right]_{T,S}. \tag{22.105}$$

The sound speed is a strong function of pressure, generally increasing with higher pressure, as well as temperature, generally decreasing with lower temperature. For the ocean, these two effects compete when moving into the ocean interior. In the upper 500 m to 1000 m, decreasing temperatures cause the sound speed to reduce whereas at deeper regions the higher pressures overcome the temperature effect thus increasing the sound speed. The result is a sound speed minimum between 500 m and 1000 m. The sound speed minimum and the associated acoustic waveguide play an important role in ocean acoustics, in particular for how certain whales are able to communicate across ocean basins. We consider the sound speed for an ideal gas in Section 23.4.8.

22.8 Maxwell relations for single component fluids

Thermodynamics makes use of basic properties of exact differentials for the purpose of developing identities between partial derivatives. Maxwell relations refer to a suite of partial derivative identities that follow from the equality of mixed second partial derivatives of thermodynamic potentials. We already made use of some Maxwell relations in Section 22.3.5 when discussing the Gibbs potential, and we use another in Section 23.2 for expressing the adiabatic lapse rate in terms of readily measurable thermo-mechanical properties. In this section we develop the Maxwell relations encountered with single component fluids, with similar relations readily derived for multi-component fluids.

[15] We study sound waves in Chapter 51.

22.8.1 Maxwell relation from internal energy

As seen from Section 22.6.2, the natural functional dependence for internal energy in a single-component fluid is given by its fundamental thermodynamic relation (22.62)

$$\mathrm{d}\mathcal{I} = \left[\frac{\partial \mathcal{I}}{\partial \mathcal{S}}\right]_{\nu_s} \mathrm{d}\mathcal{S} + \left[\frac{\partial \mathcal{I}}{\partial \nu_s}\right]_{\mathcal{S}} \mathrm{d}\nu_s = T\,\mathrm{d}\mathcal{S} - p\,\mathrm{d}\nu_s \Longrightarrow \mathcal{I} = \mathcal{I}(\mathcal{S}, \nu_s). \tag{22.106}$$

The mixed second partial derivatives are equal

$$\frac{\partial}{\partial \nu_s}\Big]_{\mathcal{S},C} \frac{\partial}{\partial \mathcal{S}}\Big]_{\nu_s,C} \mathcal{I} = \frac{\partial}{\partial \mathcal{S}}\Big]_{\nu_s,C} \frac{\partial}{\partial \nu_s}\Big]_{\mathcal{S},C} \mathcal{I}, \tag{22.107}$$

so that, via the fundamental thermodynamic relation (22.106), we have the Maxwell relation

$$\left[\frac{\partial T}{\partial \nu_s}\right]_{\mathcal{S}} = -\left[\frac{\partial p}{\partial \mathcal{S}}\right]_{\nu_s}. \tag{22.108}$$

22.8.2 Summary of the Maxwell relations

The other thermodynamic potentials, and their associated fundamental thermodynamical relations, lead to further Maxwell relations as summarized here

$$\mathrm{d}\mathcal{I} = T\,\mathrm{d}\mathcal{S} - p\,\mathrm{d}\nu_s \Longrightarrow \left[\frac{\partial T}{\partial \nu_s}\right]_{\mathcal{S}} = -\left[\frac{\partial p}{\partial \mathcal{S}}\right]_{\nu_s} \tag{22.109}$$

$$\mathrm{d}\mathcal{H} = T\,\mathrm{d}\mathcal{S} + \nu_s\,\mathrm{d}p \Longrightarrow \left[\frac{\partial T}{\partial p}\right]_{\mathcal{S}} = \left[\frac{\partial \nu_s}{\partial \mathcal{S}}\right]_{p} \tag{22.110}$$

$$\mathrm{d}\mathcal{G} = -\mathcal{S}\,\mathrm{d}T + \nu_s\,\mathrm{d}p \Longrightarrow \left[\frac{\partial \mathcal{S}}{\partial p}\right]_{T} = -\left[\frac{\partial \nu_s}{\partial T}\right]_{p}. \tag{22.111}$$

$$\mathrm{d}\mathcal{F} = -\mathcal{S}\,\mathrm{d}T - p\mathrm{d}\nu_s \Longrightarrow \left[\frac{\partial \mathcal{S}}{\partial \nu_s}\right]_{T} = \left[\frac{\partial p}{\partial T}\right]_{\nu_s}. \tag{22.112}$$

These four Maxwell relations for single-component fluids involve permutations on cross derivatives of $(T, \mathcal{S})$ and (p, ν_s). In statistical mechanics, $(T, \mathcal{S})$ determine the density of accessible microscopic states forming the thermodynamic system, whereas (p, ν_s) involves an external control parameter and its corresponding generalized force.

22.9 Exercises

EXERCISE 22.1: DERIVATION OF THE GIBBS-DUHEM RELATION
Show all of the steps leading to the Gibbs-Duhem relation (22.36).

EXERCISE 22.2: CHEMICAL POTENTIAL IDENTITY
As seen in Section 26.6.6, we have need to consider the partial derivative

$$\left[\frac{\partial \mathcal{H}}{\partial C}\right]_{T,p} \tag{22.113}$$

when determining the chemical work done by mixing within a fluid. Prove the identity

$$\left[\frac{\partial \mathcal{H}}{\partial C}\right]_{T,p} = \left[\frac{\partial \mathcal{H}}{\partial C}\right]_{\mathcal{S},p} - T\left[\frac{\partial \mu}{\partial T}\right]_{C,p} = \mu - T\left[\frac{\partial \mu}{\partial T}\right]_{C,p}. \tag{22.114}$$

Hint: as seen in Section 22.6.4, the natural functional dependence for enthalpy is $\mathcal{H}(\mathcal{S}, p, C)$, whereas in Section 22.6.6 we found the natural function dependence of the Gibbs potential to be $\mathcal{G}(T, p, C)$. Equate the exact differential expressions for enthalpy using the two functional dependencies $\mathcal{H}(\mathcal{S}, p, C)$ and $\mathcal{H}(T, p, C)$, and then derive a Maxwell relation based on the fundamental thermodynamic relation written in terms of the Gibbs potential.

EXERCISE 22.3: CONSTANT OF MOTION FOR ADIABATIC PROCESSES

Show that for a simple ideal gas, isentropic processes (i.e., both adiabatic and of constant matter concentration) maintain

$$p\,\nu_{\mathsf{s}}^{c_{\mathsf{p}}/c_{\mathsf{v}}} = \text{constant}, \tag{22.115}$$

where $\nu_{\mathsf{s}} = \rho^{-1}$ is the specific volume.

Chapter 23

THERMODYNAMICS WITH A GEOPOTENTIAL

We here extend the equilibrium thermodynamics from Chapter 22 to allow for gravitational effects as embodied by the geopotential (which also includes the planetary centrifugal acceleration). Thermodynamic equilibrium of a fluid in a constant gravitational field is consistent with mechanical equilibrium; i.e., the fluid is in hydrostatic balance. We develop certain properties of hydrostatic fluids, such as the adiabatic lapse rate, potential temperature, and a variety of identities holding for an ideal gas (which offers a useful approximation to the atmosphere).

CHAPTER GUIDE

This chapter develops the rudiments of equilibrium thermodynamics in the presence of gravity, building on the foundations established in Chapter 22. Surprisingly, there are relatively few presentations of gravity within standard thermodynamic texts, even though its presence is ubiquitous for terrestrial experiments. Chapter 9 of *Guggenheim* (1967) and §25 of *Landau and Lifshitz* (1980) are notable exceptions that include external fields, such as gravity, along with Section 1.8 of the oceanography text from *Kamenkovich* (1977).

23.1 Thermodynamic equilibrium with a geopotential

What does thermodynamic equilibrium look like in the presence of a gravity field? To answer this question, we here consider a single-component system in the presence of a static gravity field. To further connect to geophysical fluids, we let the geopotential, Φ, represent the effects from central gravity plus the planetary centrifugal acceleration (Section 13.10.4). Throughout this analysis, we assume the acceleration from the geopotential is prescribed and is thus not affected by the mass of the thermodynamic system that feels the geopotential. Furthermore, we assume the force from the geopotential is terrestrial, so that it is weak enough to ignore general relativistic effects.[1]

23.1.1 The first law

As seen in Section 22.2.3, a thermodynamic system subjected to a pressure field undergoes pressure work as its volume changes. Analogously, when the mass of a thermodynamic system changes within a geopotential field, then it is subjected to geopotential work, which takes the form

$$đ\mathcal{W}^{\text{geopotential}} = \Phi \, \mathrm{d}M. \tag{23.1}$$

We thus see that the geopotential is an intensive property with mass its corresponding extensive property. Consequently, the first law for a quasi-static process is modified from equation (22.35b) to now read

$$\mathrm{d}\mathcal{J}^{\mathrm{e}} = -p \, \mathrm{d}V + T \, \mathrm{d}\mathcal{S}^{\mathrm{e}} + (\mu + \Phi) \, \mathrm{d}M \iff \mathrm{d}\mathcal{S}^{\mathrm{e}} = T^{-1} \left[p \, \mathrm{d}V + \mathrm{d}\mathcal{J}^{\mathrm{e}} - (\mu + \Phi) \, \mathrm{d}M \right], \tag{23.2}$$

where μ is the chemical potential in the absence of a geopotential

$$\left[\frac{\partial \mathcal{J}^{\mathrm{e}}}{\partial M} \right]_{V, \mathcal{S}^{\mathrm{e}}} = \mu + \Phi \quad \text{and} \quad \left[\frac{\partial \mathcal{J}^{\mathrm{e}}}{\partial M} \right]_{V, \mathcal{S}^{\mathrm{e}}, \Phi = 0} = \mu. \tag{23.3}$$

The corresponding Gibbs-Duhem relation (22.36) now takes on the form

$$-V \, \mathrm{d}p + \mathcal{S}^{\mathrm{e}} \, \mathrm{d}T + M \, \mathrm{d}(\mu + \Phi) = 0. \tag{23.4}$$

23.1.2 Thermodynamic equilibrium with varying volume

Following our discussion in Section 22.4, we consider two adjoining fluid regions that are allowed to adjust toward thermodynamic equilibrium in the presence of a geopotential field. The entropy

[1] The relevant non-dimensional ratio is given by Φ/c^2, with c the speed of light. See *Santiago and Visser* (2018) for a concise review of how gravity leads to a spatially dependent temperature in thermal equilibrium through Tolman's temperature gradient. These considerations are important when Φ/c^2 is order unity. For terrestrial purposes, $\Phi/c^2 \ll 1$, so that relativistic gravitational effects are entirely negligible.

differential in equation (22.47b) now takes on the form

$$\mathrm{d}\mathcal{S}^{\mathrm{e}} = \left[\frac{1}{T_\alpha} - \frac{1}{T_\beta}\right] \mathrm{d}\mathcal{J}^{\mathrm{e}}_\alpha + \left[\frac{p_\alpha}{T_\alpha} - \frac{p_\beta}{T_\beta}\right] \mathrm{d}V_\alpha - \left[\frac{\mu_\alpha + \Phi_\alpha}{T_\alpha} - \frac{\mu_\beta + \Phi_\beta}{T_\beta}\right] \mathrm{d}M_\alpha, \tag{23.5}$$

which follows from the constraints (22.46) that assume fixed internal energy, mass, and volume for the composite system $\alpha \oplus \beta$. Equilibrium is characterized by $\mathrm{d}\mathcal{S}^{\mathrm{e}} = 0$, which leads to a uniform temperature, as for the case with uniform Φ. A further extension of Section 22.4 suggests that $\mathrm{d}p = 0$ and $\mathrm{d}(\mu + \Phi) = 0$ at equilibrium. However, our understanding of fluid statics leads us to expect pressure to vary according to the hydrostatic balance discussed in Section 24.6. That is, a uniform pressure does not arise for equilibrium with a nonuniform geopotential. For that purpose we consider different constraints as seen below.

23.1.3 Thermodynamic equilibrium with fixed volume

To recover hydrostatic balance at thermodynamic equilibrium, consider the case with each volume remaining fixed. In this manner we have

$$\mathrm{d}(\mathcal{J}^{\mathrm{e}}_\alpha + \mathcal{J}^{\mathrm{e}}_\beta) = 0 \quad \text{and} \quad \mathrm{d}V_\alpha = \mathrm{d}V_\beta = 0 \quad \text{and} \quad \mathrm{d}(M_\alpha + M_\beta) = 0. \tag{23.6}$$

An example consists of two vertically positioned fluid boxes, with $\nabla\Phi$ defining the local vertical direction and with adjustment towards equilibrium consisting of mass moving from one box to the other. By fixing each of the region volumes, pressure does no work so that internal energy changes only through entropy and mass changes

$$\mathrm{d}\mathcal{J}^{\mathrm{e}} = T\,\mathrm{d}\mathcal{S}^{\mathrm{e}} + (\mu + \Phi)\,\mathrm{d}M \iff \mathrm{d}\mathcal{S}^{\mathrm{e}} = T^{-1}\left[\mathrm{d}\mathcal{J}^{\mathrm{e}} - (\mu + \Phi)\,\mathrm{d}M\right]. \tag{23.7}$$

Correspondingly, we find that thermodynamic equilibrium results when

$$\mathrm{d}T = 0 \quad \text{and} \quad \mathrm{d}(\mu + \Phi) = 0. \tag{23.8}$$

To interpret the equilibrium condition, $\mathrm{d}(\mu + \Phi) = 0$, take the derivative with respect to geopotential, holding temperature and mass fixed, to render

$$\left[\frac{\partial \mu}{\partial \Phi}\right]_{T,M} = -1. \tag{23.9}$$

Anticipating the hydrostatic balance, we assume that pressure at thermodynamic equilibrium is a monotonic function of Φ, so that

$$\left[\frac{\partial \mu}{\partial \Phi}\right]_{T,M} = \left[\frac{\partial \mu}{\partial p}\right]_{T,M} \left[\frac{\mathrm{d}p}{\mathrm{d}\Phi}\right]_{T,M} = -1. \tag{23.10}$$

Making use of the Maxwell relation (22.42a) and the identity (22.45d) leads to

$$\left[\frac{\mathrm{d}p}{\mathrm{d}\Phi}\right]_{T,M} = -M/V = -\rho, \tag{23.11}$$

where $\rho = M/V$ is the mass density. We thus recover the exact hydrostatic balance[2]

$$\mathrm{d}p = -\rho\,\mathrm{d}\Phi. \tag{23.12}$$

[2]We discuss the exact hydrostatic balance in Section 24.6, and discuss the approximate hydrostatic balance in Chapter 27.

That is, thermodynamic equilibrium in a gravity field consists of a uniform temperature with pressure satisfying the exact hydrostatic balance.

23.1.4 Vertical salinity gradient at thermodynamic equilibrium

Consider the case of seawater as approximated as a two-component fluid, so that the entropy exact differential is given by

$$\mathrm{d}\mathcal{S}^{\mathrm{e}} = T^{-1} \left[p \, \mathrm{d}V + \mathrm{d}\mathcal{J}^{\mathrm{e}} - (\mu_{\mathrm{salt}} + \Phi) \, \mathrm{d}M_{\mathrm{salt}} - (\mu_{\mathrm{water}} + \Phi) \, \mathrm{d}M_{\mathrm{water}} \right]. \tag{23.13}$$

Separately holding the salt and freshwater masses fixed,[3] we apply the same formalism as pursued in Section 23.1.3 for a single component fluid, thus leading to

$$\mathrm{d}T = 0 \quad \text{and} \quad \mathrm{d}(\mu_{\mathrm{salt}} + \Phi) = 0 \quad \text{and} \quad \mathrm{d}(\mu_{\mathrm{sater}} + \Phi) = 0. \tag{23.14}$$

Subtracting the second and third equilibrium condition leads to the equilibrium condition for the seawater chemical potential,

$$\mathrm{d}(\mu_{\mathrm{salt}} - \mu_{\mathrm{water}}) = \mathrm{d}\mu = 0. \tag{23.15}$$

Now recall the seawater chemical potential is given by equation (22.95) in terms of the salinity derivative of the specific Gibbs potential

$$\mu = \mu_{\mathrm{salt}} - \mu_{\mathrm{water}} = \left[\frac{\partial \mathcal{G}}{\partial S} \right]_{T,p}, \tag{23.16}$$

where $S = C_{\mathrm{salt}}$ is the salt concentration. Hence, we may consider the seawater chemical potential to be a function of the temperature, pressure, and salt concentration

$$\mu = \mu(T, p, S). \tag{23.17}$$

The equilibrium conditions $\mathrm{d}T = 0$ and $\mathrm{d}\mu = 0$ lead to

$$\frac{\partial \mu}{\partial S} \, \mathrm{d}S + \frac{\partial \mu}{\partial p} \, \mathrm{d}p = 0. \tag{23.18}$$

The hydrostatic relation $\mathrm{d}p = -\rho \, \mathrm{d}\Phi$ leads to

$$\frac{\partial \mu}{\partial S} \frac{\mathrm{d}S}{\mathrm{d}\Phi} = \rho \frac{\partial \mu}{\partial p}. \tag{23.19}$$

Of when the geopotential takes on the simple form, $\Phi = g \, z$, then

$$\frac{\partial \mu}{\partial S} \frac{\mathrm{d}S}{\mathrm{d}z} = g \, \rho \frac{\partial \mu}{\partial p}. \tag{23.20}$$

We thus conclude that at thermodynamic equilibrium, the salinity maintains a nonzero geopotential gradient whereas the *in situ* temperature is uniform.

23.1.5 Comments and further study

A depth independent *in situ* temperature is not observed in the ocean or atmosphere. Likewise, as noted on page 28 of *Kamenkovich* (1977), the vertical salinity gradient implied by the

[3] This constraint is appropriate since we are looking for the entropy extrema for an isolated system with no boundary fluxes of either salt or freshwater.

equilibrium relation (23.19) is not observed in the ocean. Both results point to the absence of thermodynamic equilibrium for the macroscale atmosphere and ocean. The absence of global thermodynamic equilibrium is expected since both the atmosphere and ocean are not isolated systems. Furthermore, the fluids are both turbulently mixed rather than mixed solely by molecular processes, with turbulent mixing not leading to thermodynamic equilibrium.[4]

Although we do not generally observe temperature close to thermodynamic equilibrium, we do find a horizontally local hydrostatic balance to be well maintained by the large-scale atmosphere and ocean. In addition to being a thermodynamic equilibrium state, hydrostatic balance is a mechanical equilibrium state (Section 24.6). We thus conclude that for a moving and turbulent geophysical fluid, the mechanical equilibrium state of hydrostatic balance is far more robust than full thermodynamic equilibrium of *in situ* temperature and material tracers. The reason is that mechanical equilibrium is enabled by macroscopic motion (e.g., acoustic waves), whereas thermodynamic equilibrium required for uniform *in situ* temperature is enabled by the far slower molecular diffusion.

The presentation in this section largely follows §25 of *Landau and Lifshitz* (1980) and Section 1.8 of *Kamenkovich* (1977).

23.2 Adiabatic lapse rate

The temperature of a fluid can change without the transfer of heat. This *adiabatic* temperature change arises when the fluid pressure changes. We here introduce the *adiabatic lapse rate*, which measures the vertical variations in temperature for a static fluid placed in a gravity field. There are two lapse rates commonly considered: one related to height and one related to pressure. We introduce some manipulations commonly performed with thermodynamic state functions and their partial derivatives, with the goal of expressing the lapse rate in terms of commonly measured response functions.

23.2.1 Isentropic rearrangement

Consider a finite region of a static fluid in a gravitational field. Assume the fluid is initially in a horizontal layer in thermodynamic equilibrium so that it has a uniform *in situ* temperature. Now rearrange the fluid into a vertical column, and do so without changing the entropy; i.e., without the transfer of heat across the fluid boundary (adiabatically) and without mixing any of its matter constituents. Performing this rearrangement raises the center of mass of the fluid and thus increases the gravitational potential energy. This process requires mechanical work against the gravitational field.

Gravity makes pressure at the bottom of the vertical fluid column greater than at the top. This pressure difference modifies the temperature in the column, thus putting the fluid out of global thermodynamic equilibrium. We seek a general expression for how changes in pressure affects changes in temperature for a static fluid, with the pressure changes imparted reversibly and adiabatically so that entropy does not change. Mathematically, we seek an expression for the partial derivative

$$\hat{\Gamma} \equiv \left[\frac{\partial T}{\partial p}\right]_{C,\mathcal{S}}, \tag{23.21}$$

which is known as the *adiabatic lapse rate*. The adiabatic lapse rate can be measured directly, with empirical expressions fit to laboratory measurements. Additionally, it is convenient to

[4] As emphasized in Section 22.1 and in Chapter 26, the macroscale atmosphere and ocean are not in thermodynamic equilibrium, and yet these fluids maintain local thermodynamic equilibrium at the scale of fluid elements.

express it in terms of other thermodynamic response functions in order to garner further physical insight. The necessary manipulations form the bulk of this section.

23.2.2 Thermodynamic formulation

When the matter concentration is held fixed, the equation of state (22.87) allows us to consider entropy as a function of temperature and pressure so that

$$\mathrm{d}\mathcal{S} = \left[\frac{\partial \mathcal{S}}{\partial T}\right]_p \mathrm{d}T + \left[\frac{\partial \mathcal{S}}{\partial p}\right]_T \mathrm{d}p. \tag{23.22}$$

Substituting the definition of heat capacity from equation (22.99) leads to

$$T\,\mathrm{d}\mathcal{S} = c_{\mathrm{p}}\,\mathrm{d}T + T\left[\frac{\partial \mathcal{S}}{\partial p}\right]_T \mathrm{d}p. \tag{23.23}$$

It is useful to eliminate $(\partial \mathcal{S}/\partial p)_T$ in favor of a more easily measurable quantity. For that purpose we make use of the Maxwell relation (22.111) to write

$$\left[\frac{\partial \mathcal{S}}{\partial p}\right]_T = -\left[\frac{\partial \nu_{\mathrm{s}}}{\partial T}\right]_p. \tag{23.24}$$

Introducing the thermal expansion coefficient (22.103) yields an expression for changes in entropy in terms of changes in temperature and pressure

$$T\,\mathrm{d}\mathcal{S} = c_{\mathrm{p}}\,\mathrm{d}T - T\left[\frac{\partial \nu_{\mathrm{s}}}{\partial T}\right]_p \mathrm{d}p = c_{\mathrm{p}}\,\mathrm{d}T - \left[\frac{T\,\alpha_{\mathrm{T}}}{\rho}\right]\mathrm{d}p. \tag{23.25}$$

Since c_{p} and α_{T} are readily measurable response functions, the expression (23.25) is a useful means to compute infinitesimal entropy changes when matter concentration is held constant.

23.2.3 Adiabatic lapse rate for pressure changes

Equation (23.25) means that the change in temperature associated with changes in pressure, with $\mathrm{d}\mathcal{S} = 0$ and $\mathrm{d}C = 0$, can be written

$$\hat{\Gamma} = \left[\frac{\partial T}{\partial p}\right]_{C,\mathcal{S}} = \frac{T\,\alpha_{\mathrm{T}}}{\rho\, c_{\mathrm{p}}}. \tag{23.26}$$

This relation holds for any form of pressure changes, such as those due to hydrostatic pressure changes or pressure fluctuations in an acoustic wave (see Section 51.4.4). Temperature indeed changes when pressure changes, even though there has been no heat exchanged with the environment. With $\hat{\Gamma}$ so defined, we can write the entropy change in equation (23.25) as

$$T\,\mathrm{d}\mathcal{S} = c_{\mathrm{p}}\,(\mathrm{d}T - \hat{\Gamma}\,\mathrm{d}p). \tag{23.27}$$

The term $\mathrm{d}T - \hat{\Gamma}\,\mathrm{d}p$ subtracts from the *in situ* temperature differential the pressure induced changes in temperature. In Section 23.3 we introduce the *potential temperature*, which is defined just for the purpose of removing changes due to pressure.

23.2.4 Adiabatic lapse rate for height changes

A static fluid in a gravity field is in exact hydrostatic balance, whereby the pressure at a point equals to the weight per area above that point (Section 24.6). Hydrostatic balance in a constant

gravity field maintains the following relation between the pressure differential and the vertical differential

$$\mathrm{d}p = -g\,\rho\,\mathrm{d}z. \tag{23.28}$$

Use of the chain rule within the lapse rate expression (23.26) leads to

$$\Gamma = \left[\frac{\partial T}{\partial z}\right]_{C,\mathbb{S}} = \left[\frac{\partial T}{\partial p}\right]_{C,\mathbb{S}} \left[\frac{\partial p}{\partial z}\right] = -\rho\, g \left[\frac{T\,\alpha_{\mathrm{T}}}{\rho\, c_{\mathrm{p}}}\right] = -\frac{g\,T\,\alpha_{\mathrm{T}}}{c_{\mathrm{p}}}. \tag{23.29}$$

This form for the lapse rates measures the change in temperature (the *lapse*) within a constant composition fluid element as it is isentropically moved vertically through a hydrostatic pressure field.

23.2.5 Further study

In Section 23.4.9 we consider the adiabatic lapse rate for the special case of a simple ideal gas. For this gas, the internal energy of a fluid element is represented entirely by its temperature, and pressure is caused solely by molecular thermal motion. For water, however, molecular interaction energies are important, and pressure arises not only from thermal motion but also from interaction forces of the densely packed molecules. It is these differences between the behavior of water and a perfect gas that were examined by *McDougall and Feistel* (2003) in terms of molecular dynamics. In particular, they note that the lapse rate, being proportional to the thermal expansion coefficient, can be negative when the thermal expansion is negative. A negative thermal expansion coefficient occurs in cool fresh water, such as the Baltic Sea, whereby its temperature decreases as work is done on the fluid element as pressure increases.

The addition of water to the atmosphere modifies the lapse rate, as the air is then no longer well approximated by an ideal gas. Chapter 18 of *Vallis* (2017) offers a pedagogical discussion of the thermodynamics of a moist tropical atmosphere.

23.3 Potential temperature

As discussed in Section 23.1, thermodynamic equilibrium of a fluid in a geopotential field sees the hydrostatic pressure balancing the weight of fluid. Thermodynamic equilibrium is also characterized by a uniform *in situ* temperature, T, which requires removal of the temperature gradient associated with the adiabatic lapse rate discussed in Section 23.2. The molecular diffusive processes (see Section 26.11) that homogenize *in situ* temperature are very slow, so that geophysical fluids are rarely in thermodynamic equilibrium. We here introduce the notion of *potential temperature*, which offers a measure of temperature that removes the adiabatic lapse rate. With some qualifiers discussed below, turbulent mixing processes active in geophysical fluids lead to a nearly homogenous potential temperature. As such, potential temperature is a more practical thermodynamic tracer than *in situ* temperature.

23.3.1 Motivating the definition of potential properties

We observe that the processes of heating and cooling of the ocean occur predominantly near the ocean surface. In contrast, transport in the ocean interior is nearly adiabatic and isohaline (i.e., nearly isentropic). The physical picture is suggested whereby the surface ocean boundary layer experiences irreversible processes that set characteristics of water masses that move quasi-reversibly within the ocean interior. As a means to characterize and thus to label these *water masses*, oceanographers prefer to use properties that maintain constant values when moving within the quasi-isentropic ocean interior. Salinity is a good label for this purpose since it is only altered by mixing between waters of varying concentrations, and in turn it is materially

constant in the absence of mixing.[5] This behavior constitutes a basic property of material tracers (tracers that measure the mass per mass of a constituent as discussed in Section 20.1). However, it is *not* a property of the *in situ* temperature, T, which changes even in the absence of mixing due to pressure effects. We are thus motivated to seek a thermodynamic property that evolves analogously to material tracers, so that it can be used as a second material label for fluid elements. A similar motivation stems from the analysis of atmospheric motions.

A thermodynamic property that remains constant when a fluid element is moved from one pressure to another, without the transfer of heat or matter and without any kinetic energy dissipation, is said to be a *potential property*. The *potential temperature* is the example that concerns us in this section. As we will see, in some special cases the potential temperature is directly proportional to the specific entropy. More practically, it offers a means to estimate the heat transport within a geophysical fluid.

Conservative Temperature, Θ, is another potential property discussed in Section 26.11, with Conservative Temperature defined as the potential enthalpy divided by a constant heat capacity. As detailed in *McDougall* (2003), Conservative Temperature provides a more convenient and accurate measure of heat transport in a geophysical fluid than potential temperature. As such, Θ is now more commonly used in applications than potential temperature, θ, (*McDougall et al.*, 2021).

23.3.2 Temperature changes from pressure changes

Motion of a fluid element, without exchange of heat (adiabatic) or matter (constant concentration), generally changes the pressure of the fluid element. In turn, this motion causes the *in situ* temperature to have a differential that is in proportion to the adiabatic lapse rate given by (Section 23.2)

$$\mathrm{d}T = \hat{\Gamma}\, \mathrm{d}p. \tag{23.30}$$

Consequently, and as already noted, the *in situ* temperature is not a useful thermodynamic variable to label fluid elements since it changes even in the absence of irreversible mixing processes. Instead, it is more useful to remove the adiabatic pressure effects. This is the key reason for introducing potential temperature.

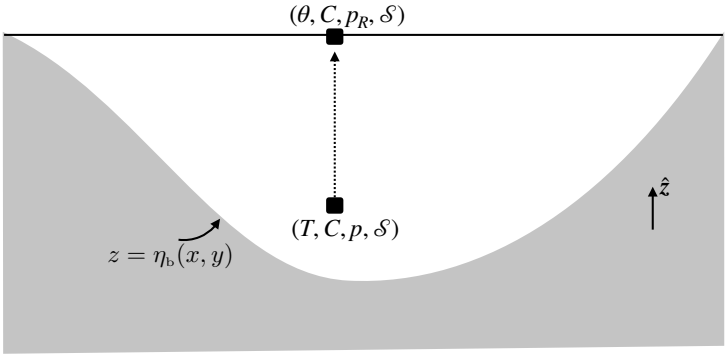

FIGURE 23.1: Potential temperature is the *in situ* temperature that a fluid element of fixed material composition would have if isentropically displaced from its *in situ* pressure to a reference pressure, p_R. The schematic here depicts that displacement for a seawater fluid element with *in situ* temperature, T, salinity, $S = 1000\, C$, pressure, p, and specific entropy, $\mathcal{S}$. The element is moved to the ocean surface with the standard sea level atmospheric pressure providing the reference pressure.

[5] There are nuances concerning what we mean by "salinity", with details given by *IOC et al.* (2010) (in particular, see Sections A.8 and A.9). We are not directly concerned with these nuances in this book, though note that they are important for ocean measurements and the interpretation of salinity as used in numerical ocean models (*McDougall et al.*, 2021).

23.3.3 Defining the potential temperature

Operationally, the potential temperature is based on removing adiabatic pressure effects from *in situ* temperature. That is, potential temperature is defined as the *in situ* temperature that a fluid element of fixed material composition would have if it were isentropically transported from its *in situ* pressure to a reference pressure $p_{\rm R}$, with the reference pressure typically taken at the ocean/land surface (see Figure 23.1). Mathematically, the potential temperature, θ, is the reference temperature obtained via integration of $\mathrm{d}T = \hat{\Gamma}\,\mathrm{d}p$ for an isentropic *in situ* temperature change with respect to pressure

$$\int_{\theta}^{T} \mathrm{d}T' = \int_{p_{\rm R}}^{p} \hat{\Gamma}(T, p', C)\,\mathrm{d}p' \Longrightarrow T = \theta(T, p_{\rm R}, C) + \int_{p_{\rm R}}^{p} \hat{\Gamma}(T, p', C)\,\mathrm{d}p', \tag{23.31}$$

with $\hat{\Gamma}$ the lapse rate defined in terms of pressure changes (equation (23.26)). By definition, the *in situ* temperature, T, equals the potential temperature, θ, at the reference pressure, $p = p_{\rm R}$. Elsewhere, they differ by an amount determined by the adiabatic lapse rate. Furthermore, we see that

$$\left[\frac{\partial T}{\partial p}\right]_{C,\mathcal{S}} = \left[\frac{\partial \theta}{\partial p}\right]_{C,\mathcal{S}} + \hat{\Gamma}. \tag{23.32}$$

However, by definition

$$\left[\frac{\partial T}{\partial p}\right]_{C,\mathcal{S}} = \hat{\Gamma} \tag{23.33}$$

so that

$$\left[\frac{\partial \theta}{\partial p}\right]_{C,\mathcal{S}} = 0. \tag{23.34}$$

That is, by construction, the potential temperature depends explicity on the concentration, C, and *in situ* temperature, T, and has a parametric dependence on the reference pressure. It has no explicit dependence on the *in situ* pressure when holding tracer concentration and entropy fixed. Finally, we emphasize that the potential temperature is a function of tracer concentration, C. Hence, the potential temperature generally changes if the tracer concentration changes. For example, potential temperature in the ocean changes if the salinity changes.

23.3.4 Potential temperature and specific entropy

An alternative definition of the potential temperature follows by noting that the entropy of a fluid element remains unchanged as it is reversibly moved to the reference pressure. Consequently, writing entropy as a function of the *in situ* temperature, pressure, and matter concentration as in equation (22.87)

$$\mathcal{S} = \mathcal{S}(T, p, C) \tag{23.35}$$

leads to the defining identity for potential temperature

$$\mathcal{S} = \mathcal{S}(T, p, C) = \mathcal{S}(\theta, p_{\rm R}, C). \tag{23.36}$$

This relation directly connects changes in entropy to changes in potential temperature

$$\mathrm{d}\mathcal{S} = \left[\frac{\partial \mathcal{S}(\theta, p_{\rm R}, C)}{\partial \theta}\right]_{C} \mathrm{d}\theta. \tag{23.37}$$

Consequently, the reversible transport of a fluid element with constant matter concentration ($\mathrm{d}C = 0$) occurs with both a constant specific entropy and constant potential temperature.

We can go even further than the relation (23.37) by recalling that equation (23.27) relates

the differential of specific entropy to temperature and pressure

$$T\,\mathrm{d}\mathcal{S} = c_{\mathrm{p}}\,(\mathrm{d}T - \hat{\Gamma}\,\mathrm{d}p), \tag{23.38}$$

where $\hat{\Gamma}$ is the adiabatic lapse rate defined in terms of pressure changes (equation (23.26)), and we set $\mathrm{d}C = 0$. To relate $\mathrm{d}T - \hat{\Gamma}\,\mathrm{d}p$ to $\mathrm{d}\theta$ we write the potential temperature equation (23.31) in the form

$$\theta(T, p_{\mathrm{R}}, C) = T - \int_{p_{\mathrm{R}}}^{p} \hat{\Gamma}(T, p', C)\,\mathrm{d}p' = T - \Psi(T, p, C, p_{\mathrm{R}}), \tag{23.39}$$

so that the differentials are related by

$$\mathrm{d}\theta = \mathrm{d}T - \mathrm{d}\Psi. \tag{23.40}$$

We evaluate $\mathrm{d}\Psi$ using the chain rule and then specialize to the case of constant composition and with a fixed reference pressure

$$\mathrm{d}\Psi = \frac{\partial\Psi}{\partial T}\,\mathrm{d}T + \frac{\partial\Psi}{\partial p}\,\mathrm{d}p + \frac{\partial\Psi}{\partial C}\,\mathrm{d}C + \frac{\partial\Psi}{\partial p_{\mathrm{R}}}\,\mathrm{d}p_{\mathrm{R}} \tag{23.41a}$$

$$= \frac{\partial\Psi}{\partial T}\,\mathrm{d}T + \frac{\partial\Psi}{\partial p}\,\mathrm{d}p \tag{23.41b}$$

$$\equiv \int_{p_{\mathrm{R}}}^{p} \frac{\partial\hat{\Gamma}(T, p', C)}{\partial T}\,\mathrm{d}p' + \hat{\Gamma}(T, p, C)\,\mathrm{d}p. \tag{23.41c}$$

Evaluating this differentials at the reference pressure removes the integral so that

$$\mathrm{d}\Psi = \hat{\Gamma}(T, p_{\mathrm{R}}, C)\,\mathrm{d}p, \tag{23.42}$$

in which case the potential temperature differential is

$$\mathrm{d}\theta = \mathrm{d}T - \hat{\Gamma}(T, p_{\mathrm{R}}, C)\,\mathrm{d}p. \tag{23.43}$$

Making use of this relation in equation (23.38) renders an expression for the entropy differential in terms of the potential temperature differential

$$\mathrm{d}\mathcal{S} = c_{\mathrm{p}}\,\theta^{-1}\,\mathrm{d}\theta \qquad p = p_{\mathrm{R}} \text{ and } \mathrm{d}C = 0. \tag{23.44}$$

Although evaluated at the reference pressure, as part of exercise 26.4 we see that this relation holds for an ideal gas at all pressures. Furthermore, as part of exercise 26.5 we see that this relation also holds for all pressures in certain liquids.

23.4 Thermodynamic relations for a simple ideal gas

In an ideal gas, we ignore the potential energy of intermolecular interaction forces between molecules. Also, the molecules in an ideal gas are assumed to occupy zero volume (i.e., they are point particles), although they do collide elastically. As a result, the internal energy of an ideal gas is just due to translation, rotation, and vibration of molecules. We refer to a *simple ideal gas* as an ideal gas where the internal energy is a linear function of temperature. In this section we develop a variety of thermodynamic relations for a simple ideal gas atmosphere in exact hydrostatic balance. Although the real atmosphere is moving, and thus not in exact hydrostatic balance, and the real atmosphere is not a simple ideal gas (i.e., it has moisture and that alters the thermodynamic relations), it turns out that many of the relations established here are rather accurate approximations to the real atmosphere. Furthermore, by exposing these

relations for the ideal gas, we further our understanding of the more general thermodynamic relations established earlier in this chapter.

23.4.1 Equation of state

An ideal gas satisfies the following equation of state (see Section 16.3.2)

$$P\,V = n\,R^{\mathsf{g}}\,T, \tag{23.45}$$

where p is the pressure, V is the volume, n is the number of moles,

$$R^{\mathsf{g}} = 8.314 \text{ J mole}^{-1} \text{ K}^{-1} = 8.314 \text{ kg m}^2 \text{ s}^{-2} \text{ mole}^{-1} \text{ K}^{-1} \tag{23.46}$$

is the *universal gas constant*, and T is the absolute temperature in Kelvin (see Section 16.3.2). The number of moles equals to the mass, M, of the gas divided by the mass per mole, M_{mole}

$$n = M/M_{\text{mole}}. \tag{23.47}$$

The mass density, $\rho = M/V$, is thus given by

$$\rho = \frac{p\,M_{\text{mole}}}{T\,R^{\mathsf{g}}} \equiv \frac{p}{T\,R^{\mathsf{M}}}, \tag{23.48}$$

where

$$R^{\mathsf{M}} = R^{\mathsf{g}}/M_{\text{mole}} \tag{23.49}$$

is the *specific gas constant* as defined by the universal gas constant normalized by the molar mass for the constituent. For air we have (Section 16.3.2)

$$M^{\mathsf{air}} = 28.8 \times 10^{-3} \text{ kg mole}^{-1} \tag{23.50}$$

so that air's specific gas constant is

$$R^{\mathsf{air}} = \frac{R^{\mathsf{g}}}{M^{\mathsf{air}}} = \frac{8.314 \text{ kg m}^2 \text{ s}^{-2} \text{ mole}^{-1} \text{ K}^{-1}}{28.8 \times 10^{-3} \text{ kg mole}^{-1}} = 2.938 \times 10^2 \text{ m}^2 \text{ s}^{-2} \text{ K}^{-1}. \tag{23.51}$$

The relation (23.48) is known as a *thermal equation of state*, or more succinctly just an equation of state (see Section 30.3 for more discussion). It shows that the mass density of an ideal gas is directly proportional to the pressure: increasing pressure increases density. In contrast, mass density is inversely proportional to the temperature: increases in temperature lead to lower mass density. This behavior for the ideal gas density is reflected in certain real gases and liquids.[6]

23.4.2 Internal energy

An ideal gas is comprised of molecules that interact only through elastic collisions. There are no inter-molecular forces. Furthermore, the volume of the individual molecules is ignored in comparison to the volume of empty space between the molecules, so they are approximated as point masses. Consequently, the internal energy for an ideal gas is independent of density and of the matter concentration. It is hence a function only of the temperature, which measures the kinetic energy of the elastic point molecules

$$\mathcal{I} = \mathcal{I}(T) \qquad \text{ideal gas.} \tag{23.52}$$

[6] A notable counter-example is water near its freezing point, which becomes more dense as temperature rises. This anomalous behavior is why a body of water freezes from the top down rather than from the bottom up.

Consequently, the exact differential of internal energy for an ideal gas is

$$\mathrm{d}\mathcal{J} = c_{\mathrm{v}}\,\mathrm{d}T. \tag{23.53}$$

The appearance of c_{v}, the constant volume specific heat capacity discussed in Section 22.7.1, arises in order for the ideal gas internal energy to satisfy the general equation (22.100). The heat capacity for an ideal gas is generally a function of temperature. However, for many applications it is sufficient to consider a simple ideal gas, in which c_{v} is a constant so that

$$\mathcal{J} = c_{\mathrm{v}}\,T + \text{constant} \qquad \text{simple ideal gas.} \tag{23.54}$$

The arbitrary constant of integration is generally set to zero so that the internal energy vanishes at absolute zero.

23.4.3 Heat capacity

The heat capacity is a constant for a simple ideal gas (equation 23.54). Results from statistical mechanics show that the thermal/internal energy per molecule equals to $k_{\mathrm{B}}\,T/2$ per excited molecular degree of freedom, where

$$k_{\mathrm{B}} = 1.3806 \times 10^{-23}\ \mathrm{m^2\ kg\ s^{-2}\ K^{-1}} \tag{23.55}$$

is the *Boltzmann constant*. Dry air is mostly comprised of the diatomic molecules N_2 and O_2. Diatomic molecules at temperatures of the lower atmosphere have two rotational and three translational degrees of freedom,[7] so that $\mathcal{J}_{\text{molecule}} = 5\,k_{\mathrm{B}}\,T/2$.

We convert this energy per molecule to an energy per mole of diatomic molecules by multiplying by Avogadro's number (equation (16.12))

$$\mathcal{J}_{\text{mole diatomic}} = 5\,A^{\mathrm{v}}\,k_{\mathrm{B}}\,T/2 = 5\,R^{\mathrm{g}}\,T/2, \tag{23.56}$$

where the gas constant is given by

$$\begin{aligned} R^{\mathrm{g}} &= A^{\mathrm{v}}\,k_{\mathrm{B}} && \text{(23.57a)}\\ &= \left(6.022 \times 10^{23}\ \mathrm{mole^{-1}}\right)\left(1.3806 \times 10^{-23}\ \mathrm{m^2\ kg\ s^{-2}\ K^{-1}}\right) && \text{(23.57b)}\\ &= 8.314\ \mathrm{kg\ m^2\ s^{-2}\ mole^{-1}\ K^{-1}}. && \text{(23.57c)} \end{aligned}$$

Finally, dividing by the molar mass for dry air (equation (16.13))

$$M^{\mathrm{air}} = 0.028\ \mathrm{kg\ mole^{-1}} \tag{23.58}$$

leads to the simple ideal gas approximation to the dry air heat capacity

$$c_{\mathrm{v}} = \frac{5\,R^{\mathrm{g}}}{2\,M^{\mathrm{air}}} = 742\ \mathrm{m^2\ s^{-2}\ K^{-1}}. \tag{23.59}$$

The measured heat capacity for dry air at standard temperature (300 K) is 718 $\mathrm{m^2\ s^{-2}\ K^{-1}}$, so the simple ideal gas estimate is only $(742 - 718)/718 = 3.3\%$ too large.

[7] At high temperatures, two vibrational degrees of freedom are also excited so that $\mathcal{J}_{\text{molecule}} = 7\,k_{\mathrm{B}}\,T/2$ at high temperatures.

23.4.4 Enthalpy

The enthalpy is generally given by equation (22.73), which for a simple ideal gas takes the form

$$\mathcal{H} = \mathcal{I} + p/\rho = c_{\mathsf{v}}\, T + \frac{T\, R^{\mathsf{g}}}{M_{\text{mole}}} = T\,(c_{\mathsf{v}} + R^{\mathsf{M}}) \tag{23.60}$$

where $R^{\mathsf{M}} = R^{\mathsf{g}}/M_{\text{mole}}$ (equation (23.49)) is the specific gas constant for the gas. Recall that the constant pressure heat capacity is given by equation (22.102)

$$c_{\mathsf{p}} = T\left[\frac{\partial \mathcal{S}}{\partial T}\right]_{p,C} = \left[\frac{\partial \mathcal{H}}{\partial T}\right]_{p,C}. \tag{23.61}$$

Consequently, for a simple ideal gas we have

$$c_{\mathsf{p}} = c_{\mathsf{v}} + R^{\mathsf{M}} \qquad \text{and} \qquad \mathcal{H} = c_{\mathsf{p}}\, T. \tag{23.62}$$

23.4.5 Thermal expansion coefficient

The thermal expansion coefficient for an ideal gas is given by

$$\alpha_{\mathrm{T}} = -\frac{1}{\rho}\frac{\partial \rho}{\partial T} = \frac{1}{T}, \tag{23.63}$$

so that as temperature increases the thermal expansion decreases.

23.4.6 Fundamental thermodynamic relations

The fundamental thermodynamic relation, written in terms of internal energy (equation (22.56b)) and enthalpy (equation (22.73)), are given by

$$\mathrm{d}\mathcal{I} = T\,\mathrm{d}\mathcal{S} - p\,\mathrm{d}\nu_{\mathrm{s}} + \mu\,\mathrm{d}C \tag{23.64}$$

$$\mathrm{d}\mathcal{H} = T\,\mathrm{d}\mathcal{S} + \nu_{\mathrm{s}}\,\mathrm{d}p + \mu\,\mathrm{d}C. \tag{23.65}$$

For a simple ideal gas these relations take the form

$$c_{\mathsf{v}}\,\mathrm{d}T = T\,\mathrm{d}\mathcal{S} - p\,\mathrm{d}\nu_{\mathrm{s}} + \mu\,\mathrm{d}C \tag{23.66}$$

$$c_{\mathsf{p}}\,\mathrm{d}T = T\,\mathrm{d}\mathcal{S} + \nu_{\mathrm{s}}\,\mathrm{d}p + \mu\,\mathrm{d}C. \tag{23.67}$$

23.4.7 Isothermal compressibility

The isothermal compressibility measures the change in volume when holding the temperature and matter concentration fixed and it is determined by the partial derivatives

$$-\frac{1}{V}\left[\frac{\partial V}{\partial p}\right]_{T,C} = \frac{1}{\rho}\left[\frac{\partial \rho}{\partial p}\right]_{T,C}. \tag{23.68}$$

For an ideal gas the compressibility is given by

$$-\frac{1}{V}\left[\frac{\partial V}{\partial p}\right]_{T,C} = \frac{1}{p}, \tag{23.69}$$

so that the compressibility decreases when pressure increases.

23.4.8 Sound speed

As studied in Chapter 51, sound travels through a fluid through compression and expansion of the fluid media. So we expect the sound speed to be related to the compressibility. But rather than the isothermal compressibility considered above, sound waves are largely adiabatic waves so that the entropy is constant. We are thus in need of the isentropic compressibility to compute the sound speed. That is, as defined by equation (22.105), the sound speed is the pressure derivative of density computed with entropy and matter concentration held fixed. We make use of the fundamental relations (23.66) and (23.67), with $\mathrm{d}\mathcal{S} = 0$ and $\mathrm{d}C = 0$ to have

$$\frac{c_v}{c_p} = \frac{p}{\rho}\left[\frac{\partial \rho}{\partial p}\right]_{\mathcal{S},C} = (p/\rho)\, c_s^{-2} \implies c_s^2 = (p/\rho)(c_p/c_v) = T\, R^{\mathsf{M}}\, (c_p/c_v). \tag{23.70}$$

For an ideal diatomic gas, such as nitrogen and oxygen, the ratio $c_p/c_v = 7/5$. Taking $R^{\mathsf{M}} = 2.938 \times 10^2$ m^2 s^{-2} K^{-1} for air from equation (23.51) then leads to

$$c_s \approx 350 \text{ m s}^{-1} \quad \text{for } T = 300 \text{ K}. \tag{23.71}$$

23.4.9 Adiabatic lapse rate

For an ideal gas, the thermal expansion coefficient is given by (equation (23.63)) $\alpha_{\mathrm{T}} = T^{-1}$ so that the lapse rates are

$$\hat{\Gamma} = \frac{1}{\rho\, c_p} \qquad \text{and} \qquad \Gamma = -\frac{g}{c_p}. \tag{23.72}$$

The measured specific heat capacity for a dry atmosphere at standard temperature (300 K) is

$$c_p = 1005 \text{ m}^2 \text{ s}^{-2} \text{ K}^{-1} \tag{23.73}$$

so that the adiabatic lapse rate for a dry atmosphere is roughly

$$\Gamma_{\mathrm{d}} = -9.8 \text{ K}/(1000 \text{ m}). \tag{23.74}$$

Hence, temperature decreases by nearly 10 K when rising 1000 m in a dry and ideal gas atmosphere.

23.4.10 Geopotential thickness

We now establish basic relations for a static atmosphere satisfying the hydrostatic balance. These relations also hold to a very good approximation for the large-scale atmosphere given the dominance of approximate hydrostatic balance for these scales (see Section 27.2).

From the hydrostatic equation (24.56) we know that the pressure on a geopotential, Φ_1, equals to

$$p(\Phi_1) = \int_{\Phi_1}^{\infty} \rho(\Phi)\, \mathrm{d}\Phi \tag{23.75}$$

where we assumed that $p(\Phi_2 = \infty) = 0$. Equation (24.55) allows us to write the integrand as

$$\mathrm{d}\Phi = -\rho^{-1}\, \mathrm{d}p = -\frac{T\, R^{\mathsf{air}}\, \mathrm{d}p}{p}, \tag{23.76}$$

where the second equality assumed an ideal gas atmosphere. Vertical integration of equation (23.76) leads to the *hypsometric equation*, which provides the geopotential thickness between

two pressure isosurfaces

$$\Phi(z_2) - \Phi(z_1) = -R^{\text{air}} \int_{p_1}^{p_2} T \, \mathrm{d}(\ln p). \tag{23.77}$$

Recall that $\mathrm{d}p < 0$ if $\mathrm{d}z > 0$ since the hydrostatic pressure decreases when moving up in the atmosphere. We define the *geopotential height* according to

$$Z = \Phi / g, \tag{23.78}$$

where g is the gravitational acceleration at sea level. The geopotential height is close to the geometric height in the troposphere and lower stratosphere. The hypsometric equation (23.77) says that the geopotential thickness between two isobars is

$$Z_2 - Z_1 = \frac{R^{\text{air}}}{g} \int_{p_2}^{p_1} T \, \mathrm{d}(\ln p). \tag{23.79}$$

Defining the layer mean temperature

$$\langle T \rangle = \frac{\int_{p_2}^{p_1} T \, \mathrm{d}(\ln p)}{\int_{p_2}^{p_1} \mathrm{d}(\ln p)} \tag{23.80}$$

and the layer mean *scale height*

$$H = \frac{R^{\text{air}} \langle T \rangle}{g} \tag{23.81}$$

leads to the geopotential thickness

$$Z_2 - Z_1 = -H \ln(p_2 / p_1) \tag{23.82}$$

The geopotential thickness is thus directly proportional to the mean temperature within the pressure layer, with thicker layers, for example, with higher mean temperatures.

We can invert the geopotential thickness relation (23.82) for the pressures to render

$$p_1 = p_2 \, e^{-(Z_1 - Z_2)/H}. \tag{23.83}$$

This relation, or more commonly its simplified version (23.87) discussed below, is sometimes referred to as the *law of atmospheres* or the *barometric law*. The scale height is a function of pressure through its dependence on the layer averaged temperature in equation (23.81). For the special case of an atmosphere with a constant temperature, T, then the scale height is a constant[8]

$$H_{\text{const}} = \frac{R^{\text{air}} \, T_{\text{const}}}{g}. \tag{23.84}$$

Setting $T_{\text{const}} = 300$ K and using the specific gas constant for air from equation (23.51) leads to the scale height

$$H_{\text{const}} = \frac{2.938 \times 10^2 \text{ m}^2 \text{ s}^{-2} \text{ K}^{-1} \times 300 \text{ K}}{9.8 \text{ m s}^{-2}} \approx 9 \times 10^3 \text{ m}. \tag{23.85}$$

It is furthermore convenient to set $Z_2 = 0$ with $p_2 = p_{\text{slp}}$ the sea level pressure, whose global average is

$$\langle p_{\text{slp}} \rangle = 101.325 \times 10^3 \text{ N m}^{-2}. \tag{23.86}$$

[8] As we saw earlier in this chapter, a fluid has uniform temperature at thermodynamic equilibrium. However, the effects from turbulent motions, even very modest turbulent motions, readily break thermodynamic equilibrium. This topic was discussed on page 299 of *Maxwell* (1872), where he also credits input from Lord Kelvin.

The pressure in an isothermal atmosphere thus decreases exponentially with geopotential height according to the scale height

$$p(Z) = \langle p_{\text{slp}} \rangle \exp(-Z/H_{\text{const}}). \tag{23.87}$$

23.4.11 Potential temperature

The fundamental thermodynamic relation for a simple ideal gas (23.67) takes on the following form for an isentropic change

$$c_{\text{p}}\, \mathrm{d}T = \nu_{\text{s}}\, \mathrm{d}p. \tag{23.88}$$

Dividing both sides by temperature and using the ideal gas relation

$$\frac{\nu_{\text{s}}}{T} = \frac{R^{\text{M}}}{p} \tag{23.89}$$

leads to

$$c_{\text{p}}\, \mathrm{d}(\ln T) = R^{\text{M}}\, \mathrm{d}(\ln p). \tag{23.90}$$

Since c_{p} and R^{M} are constants, we can integrate this relation from the reference pressure to an arbitrary pressure

$$c_{\text{p}} \int_{\theta}^{T} \mathrm{d}(\ln T) = R^{\text{M}} \int_{p_{\text{R}}}^{p} \mathrm{d}(\ln p), \tag{23.91}$$

which renders the explicit expression for the potential temperature of a simple ideal gas

$$\theta = T \left[\frac{p_{\text{R}}}{p} \right]^{R^{\text{M}}/c_{\text{p}}} \qquad \text{where} \qquad c_{\text{p}} = \frac{7\, R^{\text{M}}}{2}, \tag{23.92}$$

with c_{p} the constant pressure heat capacity of a simple ideal gas of diatomic molecules (Section 23.4.3). In some treatments (e.g., Exercise 23.3) it is useful to introduce the *Exner function*

$$\Pi = \frac{c_{\text{p}}\, T}{\theta} = c_{\text{p}} \left[\frac{p}{p_{\text{R}}} \right]^{R^{\text{M}}/c_{\text{p}}}. \tag{23.93}$$

In Exercise 23.2 we show that $\partial\theta/\partial p = 0$ for the ideal gas, thus exemplifying the removal of explicit pressure effects from the potential temperature. Furthermore, it follows from equation (23.92) that the potential temperature differential is related to temperature and pressure differentials via

$$\frac{\delta\theta}{\theta} = \frac{\delta T}{T} - \frac{\delta p}{p}. \tag{23.94}$$

In particular, if the differential is computed between points in space within a fluid at a particular time instance, then we are led to the relationship between spatial gradients

$$\frac{\nabla\theta}{\theta} = \frac{\nabla T}{T} - \frac{\nabla p}{p}. \tag{23.95}$$

23.4.12 Further study

Atmospheric sciences and dynamic meteorology books have thorough discussions of ideal gas thermodynamics. Some of the material in section 2.7 of *Holton and Hakim* (2013) was used in the present section.

23.5 Exercises

EXERCISE 23.1: GEOPOTENTIAL HEIGHT
The *geopotential height* is the height above the earth of a chosen pressure surface.

(a) Show that an ideal gas atmosphere in exact hydrostatic balance with a uniform lapse rate

$$\frac{\mathrm{d}T}{\mathrm{d}z} = -|\Gamma| = \text{constant} \tag{23.96}$$

has a geopotential height at a pressure p given by

$$z = \frac{T_0}{|\Gamma|}\left[1 - \left[\frac{p_0}{p}\right]^{-R^{\mathsf{M}}\,|\Gamma|/g}\right], \tag{23.97}$$

where T_0 is the temperature at $z = 0$.

(b) For an isothermal atmosphere, obtain an expression for the geopotential height as a function of pressure, and show that this result is consistent with the expression (23.97) in the appropriate limit.

EXERCISE 23.2: POTENTIAL TEMPERATURE FOR AN IDEAL GAS
Show that $\partial\theta/\partial p = 0$ for the potential temperature of an ideal gas given by equation (23.92)

$$\theta = T\left[\frac{p_{\mathrm{R}}}{p}\right]^{R^{\mathsf{M}}/c_{\mathsf{p}}}. \tag{23.98}$$

Hint: remember that $\partial T/\partial p \neq 0$ since the partial derivative is computed with other variables fixed.

EXERCISE 23.3: THERMODYNAMIC RELATIONS FOR AN ATMOSPHERE
In this exercise, we establish some relations for an ideal gas atmosphere, and one relation holding for an arbitrary equation of state. We assume that the gravitational acceleration is constant throughout the full depth of the atmosphere. This assumption becomes questionable when integrating to the top of the atmosphere. We furthermore ignore differences in the horizontal cross-sectional area of a fluid column at the bottom and top of the atmosphere arising from the spherical nature of the planet. These two assumption are sufficient for our purposes.

(a) PRESSURE-HEIGHT IDENTITY: Prove the following identity and state your assumptions

$$\int_0^{p_{\mathrm{s}}} z\,\mathrm{d}p = \int_{z=0}^{z_{\mathrm{top}}} p\,\mathrm{d}z. \tag{23.99}$$

This identity will be of use for some of the following questions.

(b) IDEAL GAS $\mathcal{I}+\Phi$ INTEGRATED OVER DEPTH OF A HYDROSTATIC ATMOSPHERE: For an ideal gas atmosphere in exact hydrostatic balance, show that the integral of the gravitational potential energy plus internal energy from the surface to the top of the atmosphere is equal to the integral of the enthalpy of the atmosphere

$$\int_0^{z_{\mathrm{top}}} (\Phi + \mathcal{I})\,\rho\,\mathrm{d}z = \int_0^{z_{\mathrm{top}}} \mathcal{H}\,\rho\,\mathrm{d}z, \tag{23.100}$$

where

$$\mathcal{H} = p\,\alpha + \mathcal{I} \tag{23.101}$$

is the enthalpy per mass,

$$\Phi = g\,z \tag{23.102}$$

is the simple form of the geopotential, which is also the gravitational potential energy per mass (Section 13.10.4), and $\mathcal{I}$ is the internal energy per mass. The height integral extends from the surface where $z = 0$, to the top of the atmosphere where $z = z_{\text{top}}$.

(c) Vertical derivative of dry static energy: For an ideal gas atmosphere in hydrostatic balance, show that

$$\frac{\mathrm{d}\sigma}{\mathrm{d}z} = \Pi\,\frac{\mathrm{d}\theta}{\mathrm{d}z}, \tag{23.103}$$

where

$$\sigma = \mathcal{H} + \Phi \tag{23.104}$$

is the dry static energy and

$$\Pi = c_{\mathsf{p}}\,(T/\theta) \tag{23.105}$$

is the *Exner function* introduced in equation (23.93).

(d) First identity for horizontal pressure gradient: For an ideal gas atmosphere (either hydrostatic or non-hydrostatic), derive the following expression for the pressure gradient acceleration

$$-\frac{1}{\rho}\,\nabla p = -\theta\,\nabla\Pi. \tag{23.106}$$

It then follows that for any instant in time, we have the relation between differentials

$$\rho^{-1}\,\mathrm{d}p = \theta\,\mathrm{d}\Pi. \tag{23.107}$$

(e) Second identity for horizontal pressure gradient: For an ideal gas atmosphere (either hydrostatic or non-hydrostatic), derive the following expression for the pressure gradient acceleration

$$-\frac{1}{\rho}\,\nabla p = -\frac{c_s^2}{\rho\,\theta}\,\nabla(\rho\,\theta), \tag{23.108}$$

where c_s is the sound speed.

(f) $\mathcal{I} + \Phi$ integrated over depth of a hydrostatic atmosphere: Show that for a hydrostatic atmosphere with an arbitrary equation of state

$$\int_0^{p_{\text{s}}} (\Phi + \mathcal{I})\,\mathrm{d}p = \int_0^{p_{\text{s}}} \mathcal{H}\,\mathrm{d}p. \tag{23.109}$$

That is, show that the relation in the first part of this problem holds even without making the ideal gas assumption.

exercise 23.4: Unit Knudsen number

Recall from Section 16.2.2 that the Knudsen number is the ratio $\text{Kn} = L_{\text{mfp}}/L_{\text{macro}}$, where $L_{\text{macro}} \approx 10^{-4}$ m is the macroscopic length scale used in the discussion of the continuum approximation, and L_{mfp} is the molecular mean free path (Section 16.3.3). Throughout this exercise make use of $p_{\text{stand}} = 101.325 \times 10^3$ Pa for standard atmospheric pressure.

(a) Consider a mole of an isothermal and ideal gas atmosphere of $T = 300\text{K}$ with a constant gravitational acceleration. At what pressure is the Knudsen number unity? Write your answer as a fraction of standard sea atmospheric pressure, p_{stand}.

(b) Compute the altitude corresponding to the above pressure, assuming the sea level pressure is p_{slp} and the geopotential is $\Phi = g\,z$. Hint: make use of results from Section 23.4.10.

(c) Assuming $p = p_{\text{stand}}$, at what temperature is $\text{Kn} = 1$? Hint: assume the ideal gas law holds regardless the temperature.

(d) Comment on what is the least atmospherically relevant assumption made during this exercise.

Part V

Dynamics of fluid flows

Dynamics is the area of mechanics that examines the causes of motion. For a classical mechanical system, such as a geophysical fluid, understanding the cause of motion requires understanding forces and energies. The force approach follows the methods of Newtonian mechanics whereas the energy approach follows the methods of Hamilton's principle. The bulk of this part of the book takes the Newtonian approach by studying the variety of forces acting on a geophysical fluid. Even so, in Chapter 47 we establish elements of Hamilton's principle as applied to perfect geophysical fluids. Throughout this part of the book we encounter a suite of theoretical concepts that form the foundations of geophysical fluid mechanics. Our presentation typically moves from the general to the specific, with each chapter written in a manner that allows it to be picked up without relying too much on other chapters. The *general to specific* presentation allows us to establish general principles based on fundamental concepts and to then see how those concept manifest in specific contexts.

Forces of concern in geophysical fluid mechanics include the body force acting on a fluid element from the earth's gravity field along with the contact forces from pressure and friction that act between adjacent fluid elements. Additionally, by choosing to work in a non-inertial rotating terrestrial reference frame, we encounter body forces from the Coriolis and planetary centrifugal accelerations, just as encountered for geophysical particle mechanics in Part II of this book. Each of these forces play important roles in determining the diversity of geophysical fluid motion, and their analysis leads to dynamical insights into the nature and causes of fluid motion. We observe that forces in fluids are commonly inferred from kinematic properties of the motion, thus making use of the fluid kinematics from Part III.

SUMMARY OF THE DYNAMICS CHAPTERS

We start the development of dynamics by formulating the equations of motion (linear momentum and angular momentum) in Chapter 24 using Newtonian methods. In subsequent chapters we study the forces appearing in these equations, including friction (Chapter 25), pressure (Chapter 28), and buoyancy (Chapter 30). Buoyancy is the vertical pressure force, arising from density inhomogeneities, that are not balanced by gravity. As such, our study of buoyancy focuses on vertical forces, which contrasts to our study of pressure form stresses in Chapter 28, which focus on horizontal forces.

When studying buoyancy in Chapter 30, we make use of an equation of state that provides the mass density of a fluid element as a function of thermodynamical properties such as temperature, pressure, and matter concentration. In Chapter 26 we study the flow of energy through the fluid, including both mechanical energy of the macroscopic fluid and the internal energy of the molecular degrees of freedom. We thus study how mechanical energy is exchanged with internal energy in the presence of work done by pressure and heat generated by friction.

Chapters 27 and 29 introduce a variety of approximate equations that allow us to focus on selected dynamical regimes by filtering away selected phenomena. It is here that we encounter the hydrostatic approximation and the Boussinesq ocean approximation, both of which are commonly used for large-scale models of the ocean and atmosphere. Approximate balances are further examined in Chapter 31, where we study the mechanics of a rapidly rotating fluid. We here encounter the geostrophic balance, which is a diagnostic balance appropriate for describing large-scale geophysical flows in which the horizontal pressure acceleration is balanced by the Coriolis acceleration. Geostrophic balance is one of the variety of balances considered in Chapter 32, which introduces balanced flow regimes pertaining to horizontal motions. Chapter 33 examines the physics of an Ekman boundary layer in which the Coriolis acceleration balances vertical friction. Throughout this book, we generally assume a constant effective gravitational acceleration. However, observations of the ocean typically encouter motions arising from spatial-temporal variations of the gravity field that give rise to tides. Given this observation, we take a brief look in Chapter 34 at how to formulate the equations of geophysical fluid mechanics in the

presence of a space and time dependent gravitational acceleration. We close this part of the book in Chapter 47 by developing Hamilton's variational principle for perfect geophysical fluids.

Chapter 24

Momentum dynamics

We here formulate the fluid mechanical equations for linear momentum and axial angular momentum for geophysical fluid motions. We derive these equations of geophysical fluid dynamics (GFD) using Newton's laws of motion applied to a gravitationally stratified fluid continuum moving on a rotating planet where the rotation rate is constant in time. Relative to the point particle, the new dynamical feature afforded to the continuum concerns contact forces between fluid elements, which lead to pressure and frictional forces from mechanical interactions.

READER'S GUIDE TO THIS CHAPTER

We make liberal use of results from point particle mechanics studied in Part II as well as fluid kinematics from Part III. There are various places in this chapter where we consider integrals of vectors over finite regions, such as when forming the finite volume (weak form) momentum budget as well as the angular momentum budget. As written, such discussions hold for Cartesian tensors, such as for the planetary Cartesian coordinates from Chapter 13 or the tangent plane Cartesian coordinates from Section 24.5. More care than given here is needed for general tensors on general manifolds.

24.1 Loose threads

- Figures needed

24.2 Linear momentum equation

We here summarize elements of classical continuum mechanics and in turn apply Newton's second law to derive the linear momentum budget for a fluid continuum. We present the momentum budget over both a finite volume region of the fluid (weak formulation) and for an infinitesimal fluid element (strong formulation).

24.2.1 Body forces

Forces acting on an arbitrary region, $\mathcal{R}$, of a continuous matter distribution are of two general types. The first involves forces that originate from outside of the matter and act throughout the body, thus motivating the names *external* forces, *body* forces, or *long range forces*. Examples include gravitational forces (including the planetary gravitational force as well as astronomical tidal forces); planetary Coriolis force and planetary centrifugal force (due to the rotating planetary reference frame); and electromagnetic forces (due to motion of charged matter moving through an electromagnetic field, with such forces ignored in this book). The net body force acting on a finite volume of continuum matter is the volume integral of the body force per unit mass, $\boldsymbol{f}_{\text{body}}$, multiplied by the mass of the matter

$$\boldsymbol{F}_{\text{body}} = \int_{\mathcal{R}} \boldsymbol{f}_{\text{body}} \, \rho \, \mathrm{d}V. \tag{24.1}$$

For example, the effective gravitational force (combination of central gravity plus planetary centrifugal) acting on a volume of fluid is given by

$$\boldsymbol{F}_{\text{effective gravity}} = \int_{\mathcal{R}} \boldsymbol{g} \, \rho \, \mathrm{d}V, \tag{24.2}$$

where $\boldsymbol{g} = -\nabla\Phi$ is the effective acceleration of gravity with Φ the geopotential (Section 13.10.4). Likewise, the Coriolis force acting on the volume is given by

$$\boldsymbol{F}_{\text{Coriolis}} = -2 \int_{\mathcal{R}} (\boldsymbol{\Omega} \times \boldsymbol{v}) \, \rho \, \mathrm{d}V. \tag{24.3}$$

These body forces have the same appearance as for the point particle in Chapter 13, with the only difference being the material is now a continuous media rather than a point mass, thus requiring us to integrate over the region.

24.2.2 Contact forces

The second kind of forces are *internal* or *contact* forces, such as pressure forces and frictional forces. Contact forces are molecular in origin, though we are unconcerned with details of the molecular dynamics leading to these forces. In some areas of continuum mechanics, contact forces are referred to as *tractions*. These forces act on a region of a continuous media through the area integrated stresses acting on the boundary enclosing the region. Mathematically, we

compute the contact force exerted on the region by area integrating the *stress tensor* projected onto the normal direction along the region boundary

$$\boldsymbol{F}_{\text{contact}} = \oint_{\partial\mathcal{R}} \mathbb{T} \cdot \hat{\boldsymbol{n}} \, \mathrm{d}\mathcal{S}, \tag{24.4}$$

where $\hat{\boldsymbol{n}}$ is the outward normal direction orienting the domain boundary with $\mathrm{d}\mathcal{S}$ the associated area element, and $\mathbb{T}$ is the second order stress tensor. We have more to say about the stress tensor in the following as well as in Chapter 25. For now, we must be satisfied regarding equation 24.4 as the definition of a contact force.

Contact forces affect continuous media and they do so through the nonzero spatial extent of elements within the media, with this spatial extent allowing for interactions between adjacent fluid elements. Point particles (Part II) do not experience contact forces since point particles have no spatial extent. Hence, contact forces represent a fundamentally new feature, conceptually and operationally, to the fluid dynamical equations relative to the equations of point particles.

Stresses from friction and pressure

As detailed in Chapter 25, there are two types of stress that concern us: diagonal stresses associated with reversible momentum exchange through pressure, and stresses associated with the irreversible exchange of momentum through friction. Hence, it is convenient to decompose the stress tensor components according to

$$\mathbb{T}^{ab} = \mathbb{\tau}^{ab} - p \, g^{ab}. \tag{24.5}$$

In this equation, p is the pressure, which is a force per unit area acting in a compressive manner on the area of a surface. The second order tensor, g^{ab}, is a chosen coordinate representation of the inverse metric tensor and it equals to the Kronecker or unit tensor when choosing Cartesian coordinates in Euclidean space (Section 4.1). The frictional stress tensor is written $\mathbb{\tau}^{ab}$. It is also known as the *deviatoric* stress tensor as it represents deviations from the static case when stress is due solely to pressure. The friction stress tensor generally has zero trace, with pressure comprising the trace portion of the full stress tensor.

Substitution of the stress tensor (24.5) into the contact force expression (24.4) leads to

$$\boldsymbol{F}_{\text{contact}} = \oint_{\partial\mathcal{R}} (\mathbb{\tau} \cdot \hat{\boldsymbol{n}} - p \, \hat{\boldsymbol{n}}) \, \mathrm{d}\mathcal{S}, \tag{24.6}$$

where the integral is taken over the bounding surface of the domain whose outward normal is $\hat{\boldsymbol{n}}$. Given this expression for contact forces acting on the boundary of a fluid domain, it is seen that positive pressure ($p > 0$) acts in the direction opposite to the surface's outward normal so that pressure always acts in a compressive manner. Deviatoric stresses create more general forces on the bounding surface, which can have compressive, expansive, shearing, and/or rotational characteristics.

Exchange of momentum between fluid elements

We mathematically represent the exchange of momentum between fluid elements via a symmetric stress tensor, with symmetry implied by statements about angular momentum conservation (detailed in Section 25.4). The divergence of the stress tensor then leads to a force acting on the fluid element. The forces arising from molecular viscosity provide an irreversible exchange of momentum that reduce the kinetic energy of fluid elements (Section 26.3.3). This process is dissipative and thus referred to as friction. Furthermore, when averaging over turbulent realizations of a fluid, the impacts on the mean flow are generally far larger than those associated

with molecular viscosity, with these exchanges commonly parameterized via a symmetric stress tensor.

A gauge symmetry of pressure force

The contribution from pressure in the contact force (24.6) remains invariant if pressure is shifted by an arbitrary function of time

$$p(\boldsymbol{x}, t) \to p(\boldsymbol{x}, t) + F(t). \tag{24.7}$$

We see this invariance by noting that

$$\oint_{\partial \mathcal{R}} F(t)\, \hat{\boldsymbol{n}}\, \mathrm{d}\mathcal{S} = F(t) \oint_{\partial \mathcal{R}} \hat{\boldsymbol{n}}\, \mathrm{d}\mathcal{S} = 0, \tag{24.8}$$

where the final equality follows from a corollary of the divergence theorem as discussed in Section 2.7.3. Briefly, through the divergence theorem in Section 2.7.2 we know that

$$\oint_{\partial \mathcal{R}} p\, \hat{\boldsymbol{n}}\, \mathrm{d}\mathcal{S} = \int_{\mathcal{R}} \nabla p\, \mathrm{d}V, \tag{24.9}$$

so that if pressure is shifted by a spatial constant then the pressure gradient body force remains unchanged, as will the integrated pressure contact force.

We refer to this invariance of the pressure force as a *gauge symmetry*. It means that motion of the fluid remains unchanged if pressure is modified by a spatial constant that can generally be a function of time.

24.2.3 Equation of motion

The linear momentum of a fluid region is given by

$$\boldsymbol{P} = \int_{\mathcal{R}} \boldsymbol{v}\, \rho\, \mathrm{d}V. \tag{24.10}$$

Applying Newton's law of motion to the continuum leads to the finite volume equation of motion

$$\frac{\mathrm{d}}{\mathrm{d}t} \int_{\mathcal{R}} \boldsymbol{v}\, \rho\, \mathrm{d}V = \int_{\mathcal{R}} \rho\, \boldsymbol{f}_{\text{body}}\, \mathrm{d}V + \oint_{\partial \mathcal{R}} \mathbb{T} \cdot \hat{\boldsymbol{n}}\, \mathrm{d}\mathcal{S}. \tag{24.11}$$

The time derivative can be material, as for a constant mass fluid region moving with the barycentric velocity. Or it could be Eulerian, as for a fixed region in space (see Section 20.2), or it could be a time derivative following an arbitrary fluid region. Applying the divergence theorem (Section 2.7.2) to the area integral yields

$$\frac{\mathrm{d}}{\mathrm{d}t} \int_{\mathcal{R}} \rho\, \boldsymbol{v}\, \mathrm{d}V = \int_{\mathcal{R}} (\rho\, \boldsymbol{f}_{\text{body}} + \nabla \cdot \mathbb{T})\, \mathrm{d}V, \tag{24.12}$$

where we brought the contact forces into the volume integral through exposing the divergence of the stress tensor.

General form of the equation of motion for a fluid element

Since the volume under consideration is arbitrary, the integral relation (24.12) is satisfied for an arbitrary region. We apply the result to an infinitesimal fluid element moving with the flow

$$\frac{\mathrm{D}(\rho\,\boldsymbol{v}\,\delta V)}{\mathrm{D}t} = \delta V\,(\rho\,\boldsymbol{f}_{\text{body}} + \nabla\cdot\mathbb{T}). \tag{24.13}$$

Assuming the mass for the fluid element is constant then reveals the strong form of the equation of motion

$$\rho\,\frac{\mathrm{D}\boldsymbol{v}}{\mathrm{D}t} = \rho\,\boldsymbol{f}_{\text{body}} + \nabla\cdot\mathbb{T} \iff \rho\,\frac{\mathrm{D}v_a}{\mathrm{D}t} = \rho\,f_a + \partial_b\mathbb{T}_{ba}. \tag{24.14}$$

This equation is a continuum expression of Newton's equation of motion, and it is sometimes referred to as *Cauchy's equation of motion*. The right expression exposes the Cartesian tensor labels, with the "body" label dropped for brevity.

Momentum equation for a rotating fluid in a gravitational field

We now specialize the momentum equation (24.14) to suit the needs of geophysical fluid mechanics. We first write the stress tensor in terms of the deviatoric component from friction and a diagonal component from pressure (equation (24.6))

$$\rho\,\frac{\mathrm{D}\boldsymbol{v}}{\mathrm{D}t} = \rho\,\boldsymbol{f}_{\text{body}} - \nabla p + \nabla\cdot\mathbb{\tau}. \tag{24.15}$$

Next, move to a rotating terrestrial reference frame and thus expose the Coriolis acceleration and the effective gravitational force (Section 13.11)

$$\rho\,\frac{\mathrm{D}\boldsymbol{v}}{\mathrm{D}t} + 2\,\rho\,\boldsymbol{\Omega}\times\boldsymbol{v} = -\rho\,\nabla\Phi - \nabla p + \nabla\cdot\mathbb{\tau}. \tag{24.16}$$

This form of the equation of motion arises from extracting the rigid-body motion of the basis vectors to define the Coriolis acceleration (see Section 13.9). Any remaining changes to the basis vectors arise from motion of the fluid relative to the rigid-body rotating reference frame, and thus appear when expanding the material time derivative. The form (24.16) for the equation of motion offers a suitable starting point for studies of geophysical fluid dynamics. It sometimes goes by the name of *Navier-Stokes* equation. However, that name is more commonly applied to the non-rotating case with a specific form for the friction operator (see Section 25.8.7). We thus refer to equation (24.16) as Newton's law of motion for a rotating fluid.[1]

24.2.4 Euler equation for perfect fluid motion

The inviscid form of the momentum equation (24.15) is known as the *Euler equation* of perfect fluid mechanics

$$\rho\,\frac{\mathrm{D}\boldsymbol{v}}{\mathrm{D}t} = \rho\,\boldsymbol{f}_{\text{body}} - \nabla p, \tag{24.17}$$

where the body force is conservative. That is, the Euler equation is concerned just with fluid motion in the absence of dissipative processes. The inviscid form of the momentum equation (24.16) leads to the Euler equation in the presence of rotation and gravitation

$$\rho\,\frac{\mathrm{D}\boldsymbol{v}}{\mathrm{D}t} + 2\,\rho\,\boldsymbol{\Omega}\times\boldsymbol{v} = -\rho\,\nabla\Phi - \nabla p. \tag{24.18}$$

[1]The Navier-Stokes equations were first derived by Claude-Louis Navier in 1822 and later independently derived by George Stokes in 1845.

We have many occasions in this book to ignore dissipation, in which case we work with a particular form of the Euler equation. We further comment on the Euler equation in Section 25.8.7.

24.2.5 Further study

Chapter 5 of *Aris* (1962) offers an insightful discussion of continuum mechanics as applied to a fluid. Section 2.2 *Vallis* (2017) provides a thorough derivation of the dynamical equations of motion for the atmosphere and ocean. We offer further discussion of the mathematics and physics of stress in fluids in Chapters 25 and 28.

24.3 Spherical/geopotential coordinates

Geophysical fluids move on a rotating planet with the planet commonly assumed to have an oblate spherical geometry, though with the equations approximated by their spherical form using the geopotential vertical coordinate. To display the equations of motion, we make use of the acceleration as derived in Section 13.11.3 for the point particle, using the geopotential coordinate to measure radial distances from the center of the sphere, as well as the longitude and latitude angular coordinates defined by Figure 4.3. The point particle time derivative, which is computed following the particle, translates into a material time derivative for fluid elements. We are thus led to the spherical equations of motion in their full glory

$$\frac{\mathrm{D}u}{\mathrm{D}t} + \frac{u\,(w - v\tan\phi)}{r} + 2\,\Omega\,(w\cos\phi - v\sin\phi) = -\frac{1}{\rho\, r\cos\phi}\frac{\partial p}{\partial\lambda} + F^{\lambda} \tag{24.19}$$

$$\frac{\mathrm{D}v}{\mathrm{D}t} + \frac{v\,w + u^2\tan\phi}{r} + 2\,\Omega\,u\sin\phi = -\frac{1}{\rho\, r}\frac{\partial p}{\partial\phi} + F^{\phi} \tag{24.20}$$

$$\frac{\mathrm{D}w}{\mathrm{D}t} - \frac{u^2 + v^2}{r} - 2\,\Omega\,u\cos\phi = -g - \frac{1}{\rho}\frac{\partial p}{\partial r} + F^{r}, \tag{24.21}$$

where we introduced the spherical components to the friction acceleration

$$\boldsymbol{F} = F^{\lambda}\,\hat{\boldsymbol{\lambda}} + F^{\phi}\,\hat{\boldsymbol{\phi}} + F^{r}\,\hat{\mathbf{r}}, \tag{24.22}$$

which is determined by the divergence of the frictional stress tensor. We also note the spherical coordinate form for the gradient operator (Section 4.23.8)

$$\nabla = \frac{\hat{\boldsymbol{\lambda}}}{r\cos\phi}\frac{\partial}{\partial\lambda} + \frac{\hat{\boldsymbol{\phi}}}{r}\frac{\partial}{\partial\phi} + \hat{\mathbf{r}}\frac{\partial}{\partial r}, \tag{24.23}$$

as well as the material time derivative operator

$$\frac{\mathrm{D}}{\mathrm{D}t} = \frac{\partial}{\partial t} + \boldsymbol{v}\cdot\nabla = \frac{\partial}{\partial t} + \frac{u}{r\cos\phi}\frac{\partial}{\partial\lambda} + \frac{v}{r}\frac{\partial}{\partial\phi} + w\frac{\partial}{\partial r}. \tag{24.24}$$

We can write the spherical momentum equations in a bit more compact form by introducing the spherical coordinate velocity field (see equation (13.47))

$$\boldsymbol{v} = \boldsymbol{u} + \hat{\mathbf{r}}\,w = u\,\hat{\boldsymbol{\lambda}} + v\,\hat{\boldsymbol{\phi}} + w\,\hat{\mathbf{r}} \tag{24.25}$$

and the corresponding spherical coordinate acceleration

$$\boldsymbol{A}_{\text{sphere}} = \frac{\mathrm{D}u}{\mathrm{D}t}\,\hat{\boldsymbol{\lambda}} + \frac{\mathrm{D}v}{\mathrm{D}t}\,\hat{\boldsymbol{\phi}} + \frac{\mathrm{D}w}{\mathrm{D}t}\,\hat{\mathbf{r}}. \tag{24.26}$$

We also introduce the expression (13.82c) for the metric acceleration to render

$$\rho \frac{\mathrm{D}\boldsymbol{v}}{\mathrm{D}t} + 2\,\rho\,\boldsymbol{\Omega} \times \boldsymbol{v} = -\rho\,\nabla\Phi - \nabla p + \rho\,\boldsymbol{F}, \tag{24.27}$$

where we have the acceleration relative to the rotating frame

$$\frac{\mathrm{D}\boldsymbol{v}}{\mathrm{D}t} = \boldsymbol{A}_{\text{sphere}} + \frac{1}{r}\left[u \tan\phi\,(\hat{\boldsymbol{r}} \times \boldsymbol{v}) + w\,\boldsymbol{u} - \hat{\boldsymbol{r}}\,\boldsymbol{u}\cdot\boldsymbol{u}\right]. \tag{24.28}$$

For some purposes it is convenient to combine one piece of the metric acceleration to the Coriolis acceleration to yield

$$\boldsymbol{A}_{\text{sphere}} + \frac{1}{r}\left[w\,\boldsymbol{u} - \hat{\boldsymbol{r}}\,\boldsymbol{u}\cdot\boldsymbol{u}\right] + \left[2\,\boldsymbol{\Omega} + \frac{u\tan\phi\,\hat{\boldsymbol{r}}}{r}\right] \times \boldsymbol{v} = -\nabla\Phi - \rho^{-1}\,\nabla p + \boldsymbol{F}. \tag{24.29}$$

24.4 Vector-invariant velocity equation

The metric terms appearing in the momentum equation (24.29) are those terms proportional to r^{-1} that arise from spatial dependence of the spherical unit vectors.[2] An alternative formulation removes these terms in favor of the vorticity and kinetic energy. For that purpose we make use of the identity for the nonlinear self-advection term (equation (2.44))

$$(\boldsymbol{v}\cdot\nabla)\,\boldsymbol{v} = \boldsymbol{\omega} \times \boldsymbol{v} + \nabla(\boldsymbol{v}\cdot\boldsymbol{v})/2, \tag{24.30}$$

where $\boldsymbol{\omega} = \nabla \times \boldsymbol{v}$ is the vorticity that is studied in Part VII of this book. We derive the corresponding *vector-invariant* form of the velocity equation using Cartesian coordinates and then invoke general coordinate invariance (Section 3.1) to extend the result to arbitrary coordinates.[3] Making use of equation (24.30) thus leads to the material acceleration

$$\frac{\mathrm{D}\boldsymbol{v}}{\mathrm{D}t} = \frac{\partial \boldsymbol{v}}{\partial t} + \boldsymbol{\omega} \times \boldsymbol{v} + \nabla(\boldsymbol{v}\cdot\boldsymbol{v})/2 \tag{24.31}$$

so that the momentum equation (24.16) becomes the vector-invariant velocity equation

$$\frac{\partial \boldsymbol{v}}{\partial t} + (2\,\boldsymbol{\Omega} + \boldsymbol{\omega}) \times \boldsymbol{v} = -\nabla(\Phi + \boldsymbol{v}\cdot\boldsymbol{v}/2) + (1/\rho)\,(-\nabla p + \nabla\cdot\mathbb{T}). \tag{24.32}$$

The name *vector-invariant* is motivated since the form of this equation remains unchanged when using Cartesian or spherical coordinates. However, this name seems rather unnecessary since when formulated using the tensor formalism from Chapters 3 and 4, any mathematical physics equation remains form invariant.

24.4.1 Dynamic pressure

The *velocity equation* (24.32) is mathematically equivalent to the momentum equation (24.16). Even so, it provides a more convenient means to derive Bernoulli's theorem in Section 26.9.3 and the vorticity equation in Chapter 40. Furthermore, it highlights certain physical processes affecting accelerations that are not obviously seen from the momentum equation. One such process is the *dynamic pressure*, which arises from the kinetic energy per mass appearing in the velocity equation (24.32). Gradients in the kinetic energy per mass contribute a *dynamical*

[2] The metric terms are referred to as *Christoffel symbols* in Section 4.11, which is the section where we derive the covariant derivative of a vector.

[3] See Section 4.4.4 of *Griffies* (2004) for a detailed derivation using general coordinates.

pressure gradient that accelerates the fluid down the kinetic energy gradient, from regions of high kinetic energy per mass to regions of low kinetic energy per mass. To help understand this process, consider a Boussinesq fluid (Chapter 29), in which case the density factor is a constant, $\rho = \rho_o$, so that we can write the accelerations from pressure and kinetic energy as

$$-(1/\rho_o)\,\nabla p - \nabla(\boldsymbol{v}\cdot\boldsymbol{v}/2) = -\rho_o^{-1}\,\nabla(p + \rho_o\,\boldsymbol{v}\cdot\boldsymbol{v}/2) \equiv -\rho_o^{-1}\,\nabla p_{\text{stagnation}}. \tag{24.33}$$

In this equation we defined the *stagnation pressure* (page 149 of *Kundu et al.* (2016)), also called the *total head* (Section 3.1 of *Saffman* (1992))

$$p_{\text{stagnation}} \equiv p + \rho_o\,\boldsymbol{v}\cdot\boldsymbol{v}/2, \tag{24.34}$$

which is the sum of the mechanical pressure, p, plus the dynamic pressure, $\rho_o\,\boldsymbol{v}\cdot\boldsymbol{v}/2$.

The stagnation pressure is the mechanical pressure required to keep the local acceleration unchanged *if* the dynamic pressure is set to zero as per a stagnant fluid. This situation arises in practice in a device known as a *Pitot tube* used to measure the speed of flow in a pipe, with the Pitot tube making use of the Bernoulli theorem formulated in Section 26.9. Stagnation points also arise at special points along solid objects within a moving fluid, such as wings. The dynamic pressure, $\rho_o\,\boldsymbol{v}\cdot\boldsymbol{v}/2$, provides an isotropic force per area in addition to mechanical pressure, p. Hence, the stagnation pressure is the total isotropic contact force per area, thus motivating some treatments to refer the stagnation pressure as the *total pressure*.[4]

24.4.2 Magnus acceleration

The acceleration, $-\boldsymbol{\omega}\times\boldsymbol{v}$, appearing in the velocity equation (24.32) couples vorticity and velocity. This acceleration is known as the *Magnus effect* or *Magnus acceleration*. Since it acts only when there is both motion and vorticity, it is sometimes referred to as a *vortex force*.[5] As discussed in Chapter 37, vorticity is a measure of the spin of a fluid element. Evidently, the Magnus acceleration deflects a spinning fluid element in a direction perpendicular to its trajectory in a manner analogous to the Coriolis acceleration.[6]

24.4.3 Nonlinear accelerations for some example flows

We here consider some example two-dimensional velocities to help garner insights into the nonlinear accelerations. First note that there are certain flows where the self-advection term vanishes identically so that

$$(\boldsymbol{v}\cdot\nabla)\,\boldsymbol{v} = 0 \implies \boldsymbol{\omega}\times\boldsymbol{v} + \nabla(\boldsymbol{v}\cdot\boldsymbol{v})/2 = 0. \tag{24.35}$$

One example is a zonal flow with a meridional shear

$$\boldsymbol{v} = u(y)\,\hat{\boldsymbol{x}}, \tag{24.36}$$

in which case

$$(\boldsymbol{v}\cdot\nabla)\,\boldsymbol{v} = 0 \quad \text{and} \quad \boldsymbol{\omega} = -\partial_y u\,\hat{\boldsymbol{z}} \quad \text{and} \quad \boldsymbol{\omega}\times\boldsymbol{v} = -u\,\partial_y u\,\hat{\boldsymbol{y}} \quad \text{and} \quad \nabla(\boldsymbol{v}\cdot\boldsymbol{v}/2) = u\,\partial_y u\,\hat{\boldsymbol{y}}. \tag{24.37}$$

[4] In many applications, the mechanical pressure, p, is referred to as the *static pressure* so that the total/stagnation pressure is the sum of the static plus dynamic pressures. See section 4.9 of *Kundu et al.* (2016) for more discussion.

[5] Chapter 3 of *Saffman* (1992) pursues this interpretation in studying the forces acting on and by vortices.

[6] Besides causing a moving and spinning fluid element to deflect, the Magnus acceleration provides the mechanism whereby a solid spinning body immersed in a moving fluid is deflected, such as commonly experienced by spinning balls used for baseball, tennis, and cricket.

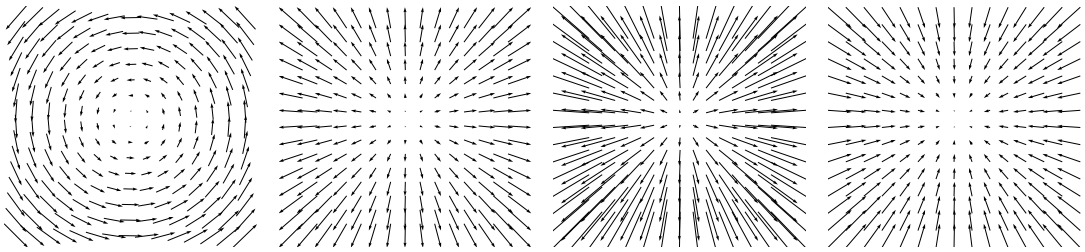

FIGURE 24.1: Illustrating the various nonlinear accelerations contributing to the velocity time tendency as per the vector-invariant velocity equation (24.32). Far left panel: the two-dimensional non-divergent velocity, $\boldsymbol{u} = \gamma\,(-y\,\hat{\boldsymbol{x}} + x\,\hat{\boldsymbol{y}})$. Middle left panel: self-advection acceleration $-(\boldsymbol{u}\cdot\nabla)\boldsymbol{u} = \gamma^2\boldsymbol{x}$. Middle right panel: Magnus acceleration $-\boldsymbol{\omega}\times\boldsymbol{u} = 2\,\gamma^2\,\boldsymbol{x}$. Far right panel: dynamic pressure gradient acceleration, $-\nabla(\boldsymbol{u}^2/2) = -\gamma^2\,\boldsymbol{x}$. Notice that the Magnus acceleration acts to the right of the flow, whereas the acceleration from the dynamic pressure gradient partially opposes the Magnus acceleration. The sum of the Magnus acceleration and dynamic pressure gradient acceleration equals to the acceleration from self-advection. In each panel we set $\gamma = 1$ and used arbitrary units.

An example flow with a nonzero self-advection is given by the two-dimensional flow of an ideal vortex

$$\boldsymbol{u} = \hat{\boldsymbol{z}}\times\nabla\psi = \gamma\,(-y\,\hat{\boldsymbol{x}} + x\,\hat{\boldsymbol{y}}), \tag{24.38}$$

where $\gamma > 0$ is a constant with dimensions of inverse time.[7] This flow has zero horizontal divergence, $\nabla\cdot\boldsymbol{u} = 0$, and constant vorticity

$$\hat{\boldsymbol{z}}\cdot\boldsymbol{\omega} = \zeta = 2\,\gamma. \tag{24.39}$$

The accelerations from self-advection, Magnus, and dynamic pressure are given by

$$-(\boldsymbol{u}\cdot\nabla)\,\boldsymbol{u} = \gamma^2\,\boldsymbol{x} \quad\text{and}\quad -\boldsymbol{\omega}\times\boldsymbol{v} = 2\,\gamma^2\,\boldsymbol{x} \quad\text{and}\quad -\nabla(\boldsymbol{u}\cdot\boldsymbol{u}/2) = -\gamma^2\,\boldsymbol{x}. \tag{24.40}$$

We depict these three accelerations, along with the velocity field, in Figure 24.1. Notice how the Magnus acceleration acts to the right of the flow, whereas the acceleration from the dynamic pressure gradient partially opposes the Magnus acceleration.

24.5 The tangent plane approximation

Spherical coordinates are suited for the study of planetary fluid dynamics for cases where the fluid samples the earth's curvature. However, spherical coordinates remain more complicated to work with than Cartesian coordinates. We are thus led to consider the utility of an idealized tangent plane configuration as part of a hierarchy of theoretical models to help understand geophysical fluid motion. This motivation leads to the f-plane and β-plane approximations, which are the two cases of the tangent plane approximation. We here expose these equations, with further use encountered later in the book. As formulated here, it is important to note that the tangent plane approximation is not based on assuming a locally flat sphere. Rather, the tangent plane approximation as based on assuming a locally flat geopotential. We further comment on this subtle distinction in Sections 24.5.2 and 24.5.5.

[7] We made use of this velocity in Section 18.11 in our study of kinematics in two-dimensional flow.

24.5.1 Basics of the tangent plane approximation

Consider a position at latitude $\phi = \phi_0$ and introduce a local Cartesian set of coordinates according to

$$(x, y, z) = (R_e\, \lambda \cos\phi_0, R_e\, (\phi - \phi_0), z) \tag{24.41}$$

$$(\hat{\boldsymbol{x}}, \hat{\boldsymbol{y}}, \hat{\boldsymbol{z}}) = (\hat{\boldsymbol{\lambda}}, \hat{\boldsymbol{\phi}}, \hat{\boldsymbol{r}}). \tag{24.42}$$

Use of these Cartesian coordinates leads to the following inviscid (i.e., no friction) equations of motion local to $\phi = \phi_0$

$$\frac{\mathrm{D}u}{\mathrm{D}t} + 2\,(\Omega^y\, w - \Omega^z\, v) = -\frac{1}{\rho}\frac{\partial p}{\partial x} \tag{24.43a}$$

$$\frac{\mathrm{D}v}{\mathrm{D}t} + 2\,(\Omega^z\, u - \Omega^x\, w) = -\frac{1}{\rho}\frac{\partial p}{\partial y} \tag{24.43b}$$

$$\frac{\mathrm{D}w}{\mathrm{D}t} + 2\,(\Omega^x\, v - \Omega^y\, u) = -\frac{1}{\rho}\frac{\partial p}{\partial z} - g, \tag{24.43c}$$

with rotational vector components

$$\boldsymbol{\Omega} = \Omega\,(\cos\phi_0\, \hat{\boldsymbol{y}} + \sin\phi_0\, \hat{\boldsymbol{z}}). \tag{24.44}$$

Note the absence of metric terms due to the use of Cartesian coordinates on a flat geometry.

24.5.2 Tangent plane is a geopotential approximation

As formulated above, the tangent plane approximation originates from the geopotential vertical coordinate system rather than the spherical coordinates (Section 13.11.3). In geopotential coordinates, the effective gravitational acceleration (central gravity plus planetary centrifugal) is aligned with the local vertical direction. Correspondingly, the resulting tangent plane equations have the effective gravitational force aligned in the $\hat{\boldsymbol{z}}$ direction. This very convenient property of the geopotential coordinate system was discussed in Section 13.10.4, with particular attention given by Figure 13.4.

In contrast, when studying motion in a rotating tank, such as in Section 27.5, it is convenient to separately account for the gravitational acceleration and rotating reference frame's centrifugal acceleration, so that both accelerations appear explicitly in the fluid equation of motion. It is thus important to distinguish the tangent plane equations (which absorb the rotating reference frame's centrifugal acceleration into the effective gravity acceleration) from the equations used for a rotating fluid in a laboratory tank (which separately account for gravity and centrifugal).[8]

24.5.3 Traditional approximation and the f-plane

The *traditional approximation* is discussed in Section 27.1.3, where we justify retaining only the local vertical component of the rotation vector for the study of large-scale planetary flows, thus resulting in

$$\mathrm{D}\boldsymbol{u}/\mathrm{D}t + f\, \hat{\boldsymbol{z}} \times \boldsymbol{u} = -\rho^{-1}\, \nabla_h p \quad \text{and} \quad \mathrm{D}w/\mathrm{D}t = -\rho^{-1}\, \partial_z p - g. \tag{24.45}$$

The f-plane makes further use of a constant Coriolis parameter

$$f = 2\,\Omega \sin\phi_0 \equiv f_\circ. \tag{24.46}$$

[8] As noted by *Durran* (1993), confusion can arise when forgetting this distinction.

The f-plane approximation is the simplest model for a rotating fluid on a locally flat geopotential, and as such it provides an end member in the hierarchy of theoretical models for rotating geophysical fluid flows.

24.5.4 β-plane approximation

As seen in Section 54.3, *Rossby waves* are planetary scale waves that sample the earth's curvature. The essential ingredient for their existence is the latitudinal dependence of the Coriolis parameter. To capture Rossby waves on a tangent plane requires the meridional gradient of the Coriolis parameter, with a linear dependence sufficient

$$f = f_\circ + R_e^{-1} (2\,\Omega\,\cos\phi_0)\,(y - y_0). \tag{24.47}$$

The β-plane approximation only depends on the meridional gradient of the Coriolis parameter, in which case we more succintly write

$$f = f_\circ + \beta\, y \tag{24.48}$$
$$\beta = \partial f / \partial y = (2\,\Omega / R_e) \cos\phi_0, \tag{24.49}$$

thus ignoring the constant $-(2\,\Omega\,\cos\phi_0)\,y_0/R_e$. The β-plane approximation is formally valid so long as the horizontal scale of motion, L, is not too large, in which case we require

$$\beta\, L \ll |f_\circ|. \tag{24.50}$$

24.5.5 Comments and caveats

We emphasized that the tangent plane assumes a locally flat geopotential, so that the gravitational acceleration remains locally vertical. Additionally, for the traditional approximation we retain only the local vertical component of the planetary rotation vector, which leads to a simpler expression for the Coriolis acceleration. It is tempting to extrapolate the traditional tangent plane to an infinite plane. However, doing so certainly breaks the assumption built into the truncated Taylor series used to mathematically justify the tangent plane. Furthermore, it leads to the unphysical situation of an infinite flat rotating plane without a centrifugal acceleration to distinguish a center of rotation. Additionally, an infinite β-plane leads to an unbounded rotation rate.

24.6 Exact hydrostatic balance

We are mostly interested in moving fluids within this book. Even so, it is useful to expose the signature of a static fluid supporting the trivial solution, $\boldsymbol{v} = 0$. The equation of motion (24.16) has an exact static solution so long as the pressure gradient force balances the effective gravitational force

$$\nabla p = -\rho\,\nabla\Phi, \tag{24.51}$$

and where the frictional stress tensor has zero divergence. Equation (24.51) constitutes the *exact hydrostatic balance*. As justified in Section 27.2, the hydrostatic balance is a very good approximation for the vertical momentum equation in large-scale geophysical fluids even when those fluids are moving. We will thus commonly make the *hydrostatic approximation* for moving fluids. For the current considerations, we are interested in a static fluid, in which case the hydrostatic balance (24.51) is an exact solution to the equation of motion.

24.6.1 Properties of exact hydrostatic balance

We make the following observations of the exact hydrostatic balance.

- Since ∇p is directly proportional to $\nabla\Phi$, surfaces of constant pressure (*isobars*) in a static fluid correspond to surfaces of constant geopotential.

- Since the curl of the pressure gradient vanishes, a static fluid maintains its density gradients parallel to geopotential gradients

$$\nabla\rho \times \nabla\Phi = 0, \tag{24.52}$$

  which in turn means that density surfaces are parallel to geopotentials so that

$$\rho = \rho(\Phi) \qquad \text{static fluid.} \tag{24.53}$$

  For the geopotential $\Phi = g\,z$, a static fluid is realized if the density depends only on the vertical position

$$\rho = \rho(z) \qquad \text{static fluid with } \Phi = g\,z. \tag{24.54}$$

  If the density gradient has any component perpendicular to $\nabla\Phi$, then pressure forces will affect fluid flow thus implying that the fluid is not in an exact hydrostatic balance.

- Projecting both sides of equation (24.51) onto an infinitesimal space increment, $\mathrm{d}\boldsymbol{x}$, renders

$$\mathrm{d}\boldsymbol{x}\cdot\nabla p = -\rho\,\mathrm{d}\boldsymbol{x}\cdot\nabla\Phi \Longrightarrow \frac{\mathrm{d}p}{\mathrm{d}\Phi} = -\rho. \tag{24.55}$$

  Hence, the difference in hydrostatic pressure between any two geopotentials is given by the integral

$$p(\Phi_2) - p(\Phi_1) = -\int_{\Phi_1}^{\Phi_2} \rho(\Phi)\,\mathrm{d}\Phi. \tag{24.56}$$

  If $\Phi = g\,z$ then we recover

$$p(z_2) - p(z_1) = -g\int_{z_1}^{z_2} \rho(z)\,\mathrm{d}z, \tag{24.57}$$

  so that the difference in hydrostatic pressure between two geopotentials is given by the weight per horizontal area of fluid between the two geopotentials. This relation is illustrated for an infinitesimally thin layer in Figure 24.2.

24.6.2 Comparison to approximate hydrostatic balance

A static fluid in a gravitational field exhibits hydrostatic balance whereby pressure at a point is a function solely of the geopotential, in which case $p = p(z)$ when $\Phi = g\,z$. Correspondingly, $\mathrm{d}p/\mathrm{d}z = -\rho\,g$, which means that we determine hydrostatic pressure at a point by computing the weight per horizontal area of fluid above that point. Likewise, density is just a function of geopotential since $\nabla\rho\times\nabla\Phi = 0$.

For an approximate hydrostatic fluid, pressure is a function of space and time, $p = p(\boldsymbol{x}, t)$, as is density, $\rho = \rho(\boldsymbol{x}, t)$. Hence, we are no longer ensured that pressure and density isolines are parallel. However, the approximate hydrostatic fluid retains a vertical pressure gradient given by

$$\frac{\partial p}{\partial z} = -\rho\,g \quad \text{approximate hydrostatic.} \tag{24.58}$$

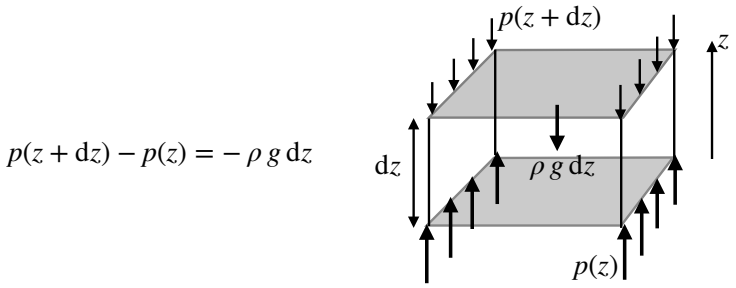

FIGURE 24.2: Illustrating the forces acting in a hydrostatically balanced fluid layer placed in a geopotential field $\Phi = g\,z$ with g constant. The layer has an infinitesimal thickness $\mathrm{d}z > 0$, density ρ, and horizontal cross-sectional area $\mathrm{d}A$. The pressure force acting on the top and bottom of the layer are compressive. Hence, the pressure force at the top of the layer acts downward, $\boldsymbol{F}^{\mathrm{press}}(z+\mathrm{d}z) = -\hat{\boldsymbol{z}}\, p(z+\mathrm{d}z)\, \mathrm{d}A$, whereas the pressure force at the bottom of the layer acts upward, $\boldsymbol{F}^{\mathrm{press}}(z) = +\hat{\boldsymbol{z}}\, p(z)\, \mathrm{d}A$. In a hydrostatically balanced fluid, the difference in pressure across the layer is exactly balanced by the weight per area of fluid within the layer. Consequently, $p(z+\mathrm{d}z) - p(z) = -g\,\rho(z)\,\mathrm{d}z$, so that pressure at the top of the layer is less than that at the bottom.

Hence, column by column, the pressure at a point in an approximate hydrostatic fluid is determined by the weight per horizontal area of fluid above that point. This key property is thus shared between fluids in exact and approximate hydrostatic balance. In Chapter 27 we have much more to say about fluid flows maintaining approximate hydrostatic balance.

24.7 Axial angular momentum

Following our discussion of a point particle in Section 14.5, the axial angular momentum of a fluid element is given by

$$L^z = (\rho\,\delta V)\, r_\perp\, (u + r_\perp\, \Omega) \equiv (\rho\,\delta V)\, l^z \tag{24.59}$$

where

$$l^z = r_\perp\, (u + r_\perp\, \Omega) \tag{24.60}$$

is the axial angular momentum per unit mass, and the distance to the polar rotation axis,

$$r_\perp = r\cos\phi \tag{24.61}$$

is the moment-arm for determining the torques acting on a fluid element. Making use of the zonal momentum equation (24.19), as well as the material time derivative of the moment arm

$$\frac{\mathrm{D}r_\perp}{\mathrm{D}t} = \frac{\mathrm{D}r}{\mathrm{D}t}\cos\phi - r\,\frac{\mathrm{D}\phi}{\mathrm{D}t}\sin\phi = w\cos\phi - v\sin\phi, \tag{24.62}$$

we find the material time change

$$\frac{\mathrm{D}l^z}{\mathrm{D}t} = (u + 2\,\Omega\, r_\perp)\,\frac{\mathrm{D}r_\perp}{\mathrm{D}t} + r_\perp\,\frac{\mathrm{D}u}{\mathrm{D}t} \tag{24.63a}$$

$$= (u + 2\,\Omega\, r_\perp)\,\frac{\mathrm{D}r_\perp}{\mathrm{D}t} + (u + 2\,\Omega\, r_\perp)\,(v\sin\phi - w\cos\phi) - \frac{1}{\rho}\,\frac{\partial p}{\partial\lambda} \tag{24.63b}$$

$$= (u + 2\,\Omega\, r_\perp)\left[\frac{\mathrm{D}r_\perp}{\mathrm{D}t} + v\sin\phi - w\cos\phi\right] - \frac{1}{\rho}\,\frac{\partial p}{\partial\lambda} \tag{24.63c}$$

$$= -\frac{1}{\rho}\,\frac{\partial p}{\partial\lambda}, \tag{24.63d}$$

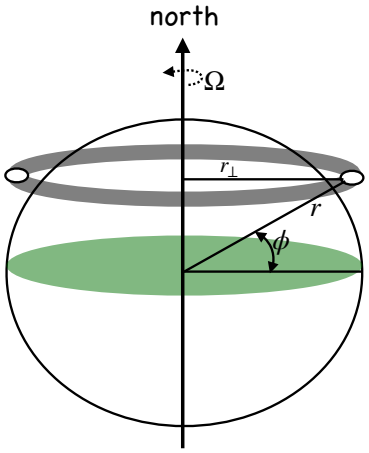

FIGURE 24.3: A ring of inviscid air circulating around a constant latitude circle over a smooth planet. This ring conserves is axial angular momentum. Consequently, axial angular momentum conserving motion of the ring induces a zonal acceleration if the ring alters its distance from the rotation axis, $r_\perp$, by moving meridionally or vertically.

so that

$$\rho \frac{\mathrm{D}l^z}{\mathrm{D}t} = -\frac{\partial p}{\partial \lambda} \implies \frac{\partial(\rho\, l^z)}{\partial t} + \nabla \cdot (\rho\, l^z\, \boldsymbol{v}) = -\frac{\partial p}{\partial \lambda}. \tag{24.64}$$

In the absence of a zonal pressure gradient, the axial angular momentum for a fluid element is materially invariant just like for the point particle discussed in Section 14.5. The physical constraints for motion of the point particle, as described in Section 14.6, also hold for the fluid element. In particular, we can equate the zonal Coriolis acceleration to the zonal acceleration induced by axial angular momentum conservation. For example, a fluid element initially at rest in a fluid with zero zonal pressure gradient will zonally accelerate when moved meridionally (e.g., as from a meridional pressure gradient) according to the needs of axial angular momentum conservation.

24.7.1 Axial angular momentum conserving motion of a ring of air

Atmospheric and oceanic flows rarely experience a zero zonal pressure gradient. However, on a smooth spherical planet without meridional boundaries there is a zero zonally integrated zonal pressure gradient

$$\oint_{\text{ring}} \frac{\partial p}{\partial \lambda}\, \mathrm{d}\lambda = 0. \tag{24.65}$$

Hence, a constant mass material ring of fluid circling the smooth planet (Figure 24.3) will preserve its axial angular momentum in the absence of friction

$$\frac{\mathrm{d}}{\mathrm{d}t} \oint_{\text{ring}} \rho\, l^z\, \mathrm{d}V = \oint_{\text{ring}} \rho \frac{\mathrm{D}l^z}{\mathrm{D}t}\, \mathrm{d}V = -\oint_{\text{ring}} \frac{\partial p}{\partial \lambda}\, \mathrm{d}V = 0. \tag{24.66}$$

We now consider some thought experiments to illustrate the zonal fluid motion induced by axial angular momentum conservation. Each example has an analog in the point particle thought experiments considered in Section 14.6.

Consider a latitudinal ring of constant mass inviscid fluid circling the earth at latitude ϕ_{A} and radial position r_{A}. If the ring is at rest in the rotating terrestrial reference frame, the angular momentum per mass for this ring is due to just the rigid-body motion of the planet,

$$l^z = \Omega\, (r_{\mathrm{A}} \cos \phi_{\mathrm{A}})^2. \tag{24.67}$$

Altering either the latitude (to ϕ_B) or radial position (to r_B) induces a corresponding zonal velocity, $u_B \neq 0$, that maintains fixed axial angular momentum

$$l^z = \Omega\,(r_A \cos\phi_A)^2 = r_B \cos\phi_B\,(u_B + \Omega\, r_B \cos\phi_B), \tag{24.68}$$

which means that

$$u_B = \Omega\,\frac{(r_A \cos\phi_A)^2 - (r_B \cos\phi_B)^2}{r_B \cos\phi_B}. \tag{24.69}$$

For example, moving the ring vertically to a radial distance, $r_B \neq r_A$, while maintaining a constant latitude, $\phi_B = \phi_A$, induces a zonal velocity

$$u_B = \Omega \cos\phi_A\,\frac{r_A^2 - r_B^2}{r_B}. \tag{24.70}$$

If the new radial position is less than the original, so that $r_A^2 > r_B^2$, then axial angular momentum conservation induces an eastward zonal velocity ($u_B > 0$); i.e., westerly winds. The opposite happens for an increase in the radial position. If we instead change the latitudinal position of the ring ($\phi_A \neq \phi_B$) while keeping the radial position fixed ($r_A = r_B$), then axial angular momentum conservation induces the zonal velocity

$$u_B = r_A\,\Omega\,\frac{\cos^2\phi_A - \cos^2\phi_B}{\cos\phi_B}. \tag{24.71}$$

Since $-\pi/2 \leq \phi \leq \pi/2$, we know that $\cos\phi \geq 0$ on the sphere, and $\cos\phi$ decreases moving poleward in either hemisphere. Hence, poleward latitudinal motion that preserves axial angular momentum induces eastward flow ($u_B > 0$), whereas eqatorward latitudinal motion induces westward flow ($u_B > 0$).

24.7.2 Realistic atmospheric axial angular momentum cycle

How realistic is it to have coherent rings of inviscid air circulating around the planet at all latitudes? To answer this question we insert some numbers for a ring of radius R_e that starts with zero relative velocity at the equator, $\phi_A = 0$, in which case equation (24.71) reduces to

$$u_B = r_A\,\Omega\,\frac{\sin^2\phi_B}{\cos\phi_B}. \tag{24.72}$$

The westerly winds induced by axial angular momentum conserving motion have the following speeds at a selection of latitudes

$$u(10^\circ) = 14 \text{ m s}^{-1} \qquad u(20^\circ) = 58 \text{ m s}^{-1} \qquad u(30^\circ) = 134 \text{ m s}^{-1}. \tag{24.73}$$

The values at higher latitudes grow unbounded since $\cos\phi \to 0$ as the poles are approached. So there is a problem with an idealized theory of atmospheric circulation based on axial angular momentum conserving rings of air.

Further investigation reveals that inviscid axial angular momentum conserving ideas extend only so far as the *Hadley circulation*, which extends only to the middle latitudes. There are two missing ingredients needed for a more realistic theory: (i) frictional dissipation between the atmosphere and land, which occurs within the planetary boundary layer; (ii) baroclinic eddies that contribute to poleward and vertical transport of angular momentum. It is outside of our scope to detail these physical processes and the corresponding atmospheric circulation. A pedagogical summary can be found in Section 10.3 of *Holton and Hakim* (2013) and Section 8.2 of *Marshall and Plumb* (2008).

24.7.3 Further study

In Section 28.5 we consider the zonally integrated axial angular momentum budget for the ocean with sloping solid-earth bottom boundary as well as the upper surface (ocean) boundary. In particular, we see how boundary form stresses (Section 28.1) affect the angular momentum in addition to boundary frictional stresses. That ocean analysis is analogous to that for the atmosphere given in Section 10.3 of *Holton and Hakim* (2013).

24.8 Exercises

EXERCISE 24.1: PRESSURE SOLUTION TO EULER'S EQUATION
This exercise is based on Q1.10 of *Johnson* (1997). Consider the Euler equation (24.18) in a non-rotating reference frame (zero Coriolis) and with constant density

$$\rho \frac{\mathrm{D}\boldsymbol{v}}{\mathrm{D}t} = -\nabla p - \rho\, g\, \hat{\boldsymbol{z}}. \tag{24.74}$$

Assume the Cartesian velocity field is given by

$$\boldsymbol{v}(\boldsymbol{x}, t) = \tau^{-2}\, (\hat{\boldsymbol{x}}\, x\, t + \hat{\boldsymbol{y}}\, y\, t - 2\, \hat{\boldsymbol{z}}\, z\, t), \tag{24.75}$$

where τ is a constant with dimensions of time.

(a) Show that the velocity field is non-divergent, $\nabla \cdot \boldsymbol{v} = 0$.

(b) Find the pressure field, $p(\boldsymbol{x}, t)$, satisfying $p(\boldsymbol{x} = 0, t) = P_0(t)$.

EXERCISE 24.2: CONDITIONS FOR UNIFORM FLOW WITHOUT GRAVITY AND ROTATION
Consider the Euler equation (24.18) in the absence of rotation (zero Coriolis) and gravitation (free space fluid)

$$\rho \frac{\mathrm{D}\boldsymbol{v}}{\mathrm{D}t} = -\nabla p. \tag{24.76}$$

Ignore all boundaries throughout this exercise, and assume density is a uniform constant.

(a) What equation does the pressure need to satisfy to ensure $\boldsymbol{v} \equiv \boldsymbol{v}_0$, where $\boldsymbol{v}_0$ is a constant in space and time?

(b) What equation does the pressure need to satisfy to ensure $\partial_t(\nabla \cdot \boldsymbol{v}) = 0$?

EXERCISE 24.3: DIAGNOSING THE PRESSURE FOR A GIVEN FLOW
Consider a two-dimensional perfect fluid with constant density, ρ, that satisfies the Euler equation in the absence of planetary rotation

$$\rho \frac{\mathrm{D}\boldsymbol{u}}{\mathrm{D}t} = -\nabla_{\mathrm{h}} p. \tag{24.77}$$

Provide a suitable pressure (to within a constant) that corresponds to the following steady (i.e., time independent) velocity fields, with $\gamma > 0$ a constant having dimensions inverse time, and $\boldsymbol{x} = \hat{\boldsymbol{x}}\, x + \hat{\boldsymbol{y}}\, y$ the horizontal position vector. Consider the following hints: (i) check your physical dimensions, (ii) check that $\nabla \times [(\boldsymbol{u} \cdot \nabla)\boldsymbol{u}] = 0$, (iii) check that $\nabla \cdot \boldsymbol{u} = 0$, which is required since ρ is a constant.

(a) $\boldsymbol{u} = \gamma\, \boldsymbol{x}$

(b) $\boldsymbol{u} = -\gamma\, \hat{\boldsymbol{z}} \times \boldsymbol{x}$

(c) $\boldsymbol{u} = \gamma\, (x\, \hat{\boldsymbol{x}} - y\, \hat{\boldsymbol{y}})$.

EXERCISE 24.4: THEOREM OF STRESS MEANS (*Aris* (1962) EXERCISE 5.12.2)
Make use of Cauchy's equation of motion (24.14) and the divergence theorem to prove the *theorem of stress means*

$$\oint_{\partial\mathcal{R}} \Psi\, \mathbb{T}_{pq}\, \hat{n}_q\, \mathrm{d}\mathcal{S} = \int_{\mathcal{R}} \left[\mathbb{T}_{pq}\, \partial_q \Psi + \rho\, \Psi \left(\frac{\mathrm{D} v_p}{\mathrm{D} t} - f_p \right) \right] \mathrm{d}V, \tag{24.78}$$

where Ψ is an arbitrary differentiable function, and $\hat{n}_q$ is the q'th component of the outward normal vector on $\partial\mathcal{R}$. This theorem finds use in certain formulations of continuum mechanics. Assume Cartesian tensors.

EXERCISE 24.5: AREA OF A STEADY 1D LAMINAR JET EMANATING FROM A DOWNWARD NOZZLE
Consider a steady state laminar jet of constant density and inviscid water emanating from a downward facing nozzle with a constant prescribed volume flow rate, Q (dimensions volume per time). Ignore surface tension and assume the air pressure acting on the surface of the jet is constant all along the jet. You can solve this exercise by making use of the steady vertical momentum equation and the steady mass continuity equation.

(a) Explain why we can set $\mathrm{d}p/\mathrm{d}z = 0$ within the jet once it leaves the nozzle.

(b) Determine an expression for the area of the jet, $A(z)$, as a function of distance, z, from the nozzle, with the nozzle placed at $z = 0$ and $z < 0$ a position beneath the nozzle. In addition to z, your expression will contain Q, g, and $A(0)$.

(c) Is the area of the jet getting smaller or larger as the water moves downward away from the nozzle? Does this answer agree with your experience?

(d) If the downward speed of water at the nozzle is $w(0) = 0.5$ m s^{-1}, then at what vertical position, z, is the area of the jet four times different than at $z = 0$?

EXERCISE 24.6: ROSSBY EFFECT
Consider a horizontal region of fluid whose velocity is rotationally symmetric and depth independent

$$\boldsymbol{u} = \boldsymbol{\Gamma} \times \boldsymbol{r}, \tag{24.79}$$

where

$$\boldsymbol{\Gamma} = \Gamma(r)\, \hat{\boldsymbol{z}} \tag{24.80}$$

is an angular velocity, $\hat{\boldsymbol{z}}$ is the vertical direction, and r is the radial distance to the origin. Furthermore, let $\Gamma(r)$ vanish for radial distances $r \geq R$ for some radius R. Let the fluid be moving on a β-plane with Coriolis parameter $f = f_\circ + \beta\, y = f_\circ + \beta\, r\, \sin\vartheta$, where ϑ is the polar angle relative to the x-axis (see Section 4.22 for definition of polar coordinates). Derive an integral expression for the Coriolis acceleration integrated over this fluid region. Discuss the direction of the acceleration.

You may find the following hints of use.

- The resulting integrated Coriolis acceleration is solely in the $\hat{\boldsymbol{y}}$ direction, and it vanishes when $\beta = 0$.
- The answer is given in *Rossby* (1948), and is sometimes known as the *Rossby effect*.

- We further consider such interactions between rotating fluid motion and the Coriolis parameter in Section 38.5.4 when studying the *beta drift* of axially symmetric vortices. There, we find that the beta drift leads to a northwestward drift rather than the northward drift from the Rossby effect. The reason for the discrepency is that *Rossby* (1948) ignored pressure effects that set up a secondary flow that induces westward drift, in addition to Rossby's northward drift. For this exercise, we ignore these pressure effects.

EXERCISE 24.7: CENTER OF MASS TRANSPORT THEOREM
Consider a field, ψ, that satisfies the standard conservation law

$$\rho \frac{\mathrm{D}\psi}{\mathrm{D}t} = -\nabla \cdot \boldsymbol{J}, \tag{24.81}$$

within a region, $\mathcal{R}(\boldsymbol{v})$, that moves with the fluid flow. We here derive some results that hold for Cartesian coordinates in Euclidean space.

(a) Prove the transport theorem valid for Cartesian tensors

$$\frac{\mathrm{d}}{\mathrm{d}t} \int_{\mathcal{R}(\boldsymbol{v})} \psi \, \boldsymbol{x} \, \rho \, \mathrm{d}V = \int_{\mathcal{R}(\boldsymbol{v})} (\boldsymbol{J} + \rho \, \psi \, \boldsymbol{v}) \, \mathrm{d}V - \oint_{\partial\mathcal{R}(\boldsymbol{v})} \boldsymbol{x} \, (\hat{\boldsymbol{n}} \cdot \boldsymbol{J}) \, \mathrm{d}\mathcal{S}. \tag{24.82}$$

Hint: multiply both sides of equation (24.81) by x_m.

(b) Offer an interpretation of equation (24.82). Hint: first consider the special case that the total ψ-stuff, defined by $\Psi \equiv \int_{\mathcal{R}(\boldsymbol{v})} \psi \, \rho \, \mathrm{d}V$, is constant when following the flow. Further hint: consider the more specialized case of $\psi = 1$ and $\boldsymbol{J} = 0$, and then make use of Exercise 19.2.

Chapter 25

Stress in fluids

As a continuous region of matter, a fluid element experiences two kinds of forces. The first concerns *external* or *body* forces and the second concerns *internal* or *contact* forces. Body forces act throughout the fluid element such as from a force field whose source is external to the matter acted upon. The accumulated effects from body forces within a fluid region result from volume integrating the body forces over the region. In geophysical fluid mechanics, we are concerned with body forces from the effective gravitational acceleration (central gravity plus planetary centrifugal) plus the body force from the Coriolis acceleration. Body forces are also experienced by the point particles studied in Part II in this book.

Internal or contact forces are the focus of this chapter, with such forces arising from intermolecular forces within the fluid media. Macroscopically, they give rise to the local exchange of dynamical properties between fluid elements, and they represent a fundamental distinction between forces acting on a fluid element and those acting on a point particle (Part II in this book). Dividing the contact force by the area upon which it acts leads to the *Cauchy stress vector*. As a force per unit area, stresses are associated with two directions: the direction of the force and the direction normal to the area acted upon by the force. Correspondingly, stresses acting on a fluid element are naturally organized into a second order *stress tensor*.[1] Details of the stress tensor govern the dynamic response of a continuous media to kinematic and thermodynamic properties of the media. Consequently, the equations of continuum mechanics posed by Cauchy find their specialization when prescribing the stress tensor, with this specification known as a *constitutive relation*.

We distinguish two types of mechanical stresses acting within a fluid: a *normal stress* and a *tangential stress*, which is commonly called a *shearing stress* in the fluid mechanical literature. Pressure is the canonical normal stress that acts normal to any surface within a fluid, and with pressure acting in a compressive manner. The ability of a fluid to resist compression is a function of the fluid's compressibility. Fluids flow in the presence of tangential or shearing stresses, with viscous friction acting to resist such motion.

Contact forces, which are given by the Cauchy stress times an area element, satisfy Newton's third law, also known as the action/reaction law (e.g., see beginning of Chapter 11). Hence, the net contact force acting on a finite region arises just from the contact forces acting at the region boundary. This property of contact forces means that a mechanically isolated region of a continuous media (i.e., a region unaffected by external forces or boundary contact forces) does not spontaneously translate its center of mass. Similarly, symmetry of the stress tensor means that an isolated region does not spontaneously alter its angular momentum.

Surface tension is a stress that acts on the boundaries of a fluid media, such as the boundary between oil and water or, more relevant to our study of geophysical flows, the boundary between air and water. Surface tension is unique in this chapter in that it does *not* satisfy Newton's third

[1] In the language of continuum mechanics, we here work exclusively with the *Cauchy stress tensor*. See Section 1.22 of *Tromp* (2025a) for more details.

law. As shown in Section 25.11, surface tension is generally negligible for length scales larger than a few centimeters. Even so, the effects of surface tension are important if studying physical processes associated with air-sea interactions, such as tracer, heat, and momentum exchange through bubbles, droplets, and capillary waves (we study capillary waves in Section 52.10).

CHAPTER GUIDE

We introduced contact forces in Chapter 24 when deriving the fluid equations of motion. In the present chapter we dive deeper into the study of contact forces and their corresponding stresses. We also discuss conditions placed on stress and velocity at boundaries. We organize fluid stresses into a second order Cauchy stress tensor and further decompose this stress into isoptropic (pressure) stresses and tangential (viscous) stresses. Understanding the mathematical and physical aspects of stress is important for the suite of fluid models studied in this book. Because the subject involves vectors and tensors, it can require more patience than analogous chapters that discuss scalar fields. To make the formalism less mathematically intense, we employ Cartesian tensors as discussed in Chapters 1 and 2, with all tensor indices downstairs. Results can be generalized to arbitrary coordinates through the general tensor analysis detailed in Chapter 4.

There are various places in this chapter where we consider integrals of vectors over finite regions, such as when forming the finite volume (weak form) momentum budget or angular momentum budget. Such discussions hold only for Cartesian tensors, with integration of general tensors requiring more care.

25.1 Loose threads

- Schematic of viscous transfer as in Figure 12.6 of *Kundu et al.* (2016)
- More on existence and uniqueness of Navier-Stokes as per *Doering and Gibbon* (1995).

25.2 Cauchy's stress principle and Newton's laws

We here develop some general properties of contact forces and the associated stresses. For that purpose, consider an arbitrary smooth closed region, $\mathcal{R}$, of fluid with volume $V = \int_{\mathcal{R}} \mathrm{d}V$ and mass $M = \int_{\mathcal{R}} \rho \, \mathrm{d}V$ (Figure 25.1). Furthermore, let $\partial\mathcal{R}$ be the bounding surface for the region, and let $\hat{\boldsymbol{n}}$ be the outward normal at a point on the boundary.

25.2.1 Cauchy's stress principle

The bounding surface of a fluid region experiences mechanical interactions with the surrounding fluid continuum (due to molecular forces) and these interactions lead to contact forces acting on the boundary. Let $\boldsymbol{\tau}$ be the stress vector (force per unit area) acting at a point on $\partial\mathcal{R}$. Cauchy's stress principle asserts that the stress vector is a function of the position, time, and boundary normal

$$\boldsymbol{\tau} = \boldsymbol{\tau}(\boldsymbol{x}, t, \hat{\boldsymbol{n}}). \tag{25.1}$$

The dependence on the boundary normal in equation (25.1) means that the stress acting on a surface is generally a function of the orientation of that surface. This form of the stress trivially holds for an exactly hydrostatic fluid where the stress vector is proportional to the pressure (Section 24.6). Furthermore, the stress from pressure is oriented along the inward normal, thus

reflecting the purely compressive nature of pressure

$$\boldsymbol{\tau} = -p(\boldsymbol{x}, t)\, \hat{\boldsymbol{n}} \qquad \text{static fluid in hydrostatic balance.} \tag{25.2}$$

Cauchy's stress principle is sensible for points within the fluid media, and its relevance has been supported by experimental studies over the time since Cauchy made this assertion in the 1820s. Furthermore, it holds for pressure and viscous stresses at the interface between fluid media or at solid-earth boundaries. However, Cauchy's stress principle does not hold for surface tension, which is proportional to the curvature of the surface separating two fluid media (e.g., atmosphere and ocean), where curvature involves spatial gradients of the normal vector. As discussed in Section 25.11, surface tension is important for length scales on the order of centimeters, and as such play a minor role in this book. Hence, with the single exception of surface tension, we rely on Cauchy's stress principle to formulate the fluid dynamical equations.

25.2.2 Newton's third law and local equilibrium of stresses

Newton's second law says that in an inertial reference frame, unbalanced forces acting on a physical system affect a time change to the linear momentum. Consider a region, $\mathcal{R}(\boldsymbol{v})$, whose fluid elements follow the barycentric velocity. Newton's second law then states that the material time evolution of the region's linear momentum is given by

$$\frac{\mathrm{d}}{\mathrm{d}t} \int_{\mathcal{R}(\boldsymbol{v})} \boldsymbol{v}\, \rho \, \mathrm{d}V = \int_{\mathcal{R}(\boldsymbol{v})} \boldsymbol{f}\, \rho \, \mathrm{d}V + \oint_{\partial \mathcal{R}(\boldsymbol{v})} \boldsymbol{\tau} \, \mathrm{d}\mathcal{S}, \tag{25.3}$$

where $\int_{\mathcal{R}(\boldsymbol{v})} \boldsymbol{f}\, \rho \, \mathrm{d}V$ is the domain integrated body force (from central gravity, planetary centrifugal, and Coriolis). To develop a general property for the contact forces, consider this balance for a region whose size gets infinitesimally small. Assuming the integrands for the two volume integrals are well behaved (i.e., smooth and bounded) as the region size goes to zero, we see that the volume integrals are proportional to L^3, where L is a length scale measuring the size of the region (e.g., side for a cubical region or diameter for a spherical region). In the same manner, we assume the stresses are well behaved in the case of an infinitesimal region. However, the integral of the contact forces goes to zero at the slower rate that is proportional to L^2. Self-consistency for the balance (25.3) over a region of infinitesimal size thus requires the contact forces to satisfy the limiting behavior

$$\lim_{L \to 0} \frac{1}{L^2} \oint_{\partial \mathcal{R}(\boldsymbol{v})} \boldsymbol{\tau} \, \mathrm{d}\mathcal{S} = 0. \tag{25.4}$$

This behavior means that contact forces at a point in the fluid must be in local equilibrium. Equation (25.4) is sometimes referred to as *Cauchy's fundamental lemma*.

A direct implication of the local equilibrium statement is that stress vectors that respect Cauchy's principle (25.1) satisfy

$$\boldsymbol{\tau}(\boldsymbol{x}, t, \hat{\boldsymbol{n}}) = -\boldsymbol{\tau}(\boldsymbol{x}, t, -\hat{\boldsymbol{n}}). \tag{25.5}$$

For example, the stress vector on one side of a surface is equal and oppositely directed to the stress vector acting on the other side. This equation is an expression of Newton's third law of mechanics (the action/reaction law; see Section 11.5), here written in terms of the stresses acting in a continuous media. It is of fundamental importance throughout our study of contact forces and their associated stresses acting within the fluid and at boundaries. We thus see how an application of Newton's second law, the linear momentum principle (25.3) for a continuous media, leads to a statement of Newton's third law in the form of equation (25.5) holding for contact forces.

As an example of the above ideas, the simplest stress we consider in this chapter is that from

pressure, with pressure acting solely in a compressive manner so that the stress vector takes the form

$$\boldsymbol{\tau}^{\text{press}}(\boldsymbol{x}, t, \hat{\boldsymbol{n}}) = -p(\boldsymbol{x}, t)\, \hat{\boldsymbol{n}}. \tag{25.6}$$

This stress trivially satisfies the Newton's third law relation (25.5) since

$$\boldsymbol{\tau}^{\text{press}}(\boldsymbol{x}, t, \hat{\boldsymbol{n}}) = -\boldsymbol{\tau}^{\text{press}}(\boldsymbol{x}, t, -\hat{\boldsymbol{n}}). \tag{25.7}$$

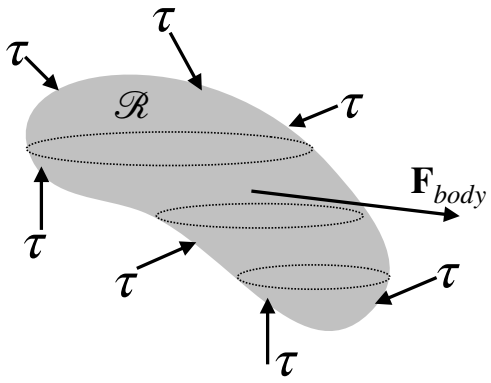

FIGURE 25.1: Schematic of the net body force, $\boldsymbol{F}_{\text{body}}$, acting on a finite region of fluid, plus the accumulation of stress vectors, $\boldsymbol{\tau}$, acting on the region boundaries. The net body force is determined by a volume integral of the body force (gravity, centrifugal, and Coriolis) at each point within the volume. In contrast, since the stresses are in local equilibrium, the volume integral of the stress divergence reduces to an area integral of the stress over the region boundary. Stress arises from pressure (compressive and normal) and strains (which then lead to viscous stresses when there is viscosity). The area integrated contribution from pressure to horizontal accelerations is referred to as *form stress*. The form stress coming from the bottom boundary is called the *topographic form stress*. The form stress appearing at the air-sea boundary is the *atmospheric form stress* if considering ocean dynamics and *oceanic form stress* if considering atmospheric dynamics. We study form stress in Chapter 28.

25.2.3 Comments on the local equilibrium relation

The local equilibrium relation (25.4), and the corresponding expression of Newton's third law, (25.5), might suggest that stresses cannot lead to motion. However, that suggestion is incorrect since stresses integrated over a finite region can lead to a net force that causes motion. Since contact forces within the domain interior cancel pointwise, the local equilibrium relation (25.4) says that the net contact force acting on the region arises only from the area integrated stresses acting on the region boundary. Local or pointwise mechanical equilibrium does not imply mechanical equilibrium for finite regions.

To further emphasize the above point, consider an ocean region bounded at its bottom by the solid earth and its upper surface by a massive atmosphere. Variations (divergences) in stresses over finite regions within the ocean fluid lead to accelerations; e.g., ocean circulation. However, when integrated over the full ocean domain, all stresses cancel from the interior of the fluid. Consequently, the net contact force acting on the full ocean domain reduces to the contact force acting just on the ocean boundaries. The boundary contact forces arise from mechanical interactions with the solid-earth and the overlying atmosphere. The center of mass for the ocean basin remains static if the accumulation of forces sum to zero, which includes the contact forces acting over its boundaries plus the volume integrated body forces from effective gravity (central gravity plus planetary centrifugal) and Coriolis.

In Figure 25.2 we illustrate the net pressure force acting on an arbitrary fluid domain. Pressure acts solely in a compressive manner as directed along the inward normal to the domain.

Area integration over a domain boundary renders the net pressure force acting on the domain

$$\boldsymbol{F}^{\text{pressure}} = -\oint_{\partial\mathscr{R}} p\,\hat{\boldsymbol{n}}\,\mathrm{d}\mathcal{S} = -\int_{\mathscr{R}} \nabla p\,\mathrm{d}V, \tag{25.8}$$

where the second equality follows from application of Gauss's divergence theorem for a scalar field (Section 2.7.2). When decomposed according to coordinate axes, the pressure force acting on the boundary has a component in both the vertical and horizontal directions, thus contributing to both vertical and horizontal accelerations. The vertical accelerations are closely balanced by the weight of fluid, with exact balance in the case of a hydrostatic fluid. The horizontal stresses from pressure are known as *form stress*. This name arises since the stress depends on the form, or shape, of the surface on which pressure acts.

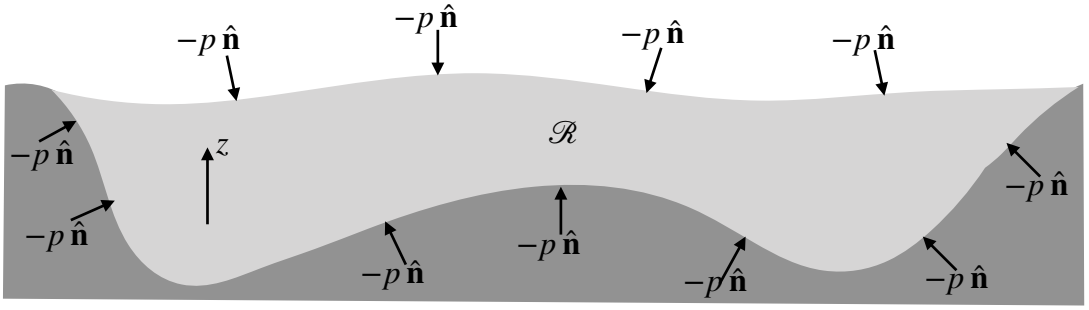

FIGURE 25.2: Schematic of contact forces from pressure acting on the boundaries to an ocean domain. Pressure forces are directed according to minus the local normal since pressure is a compressive force aligned with the inward normal direction. As with all contact forces, the pressure forces acting in the interior of the ocean are locally in mechanical equilibrium. Hence, when integrated over the global domain the net pressure forces only arise at the domain boundaries. That is, the net pressure force acting on the full ocean domain arises only at the interface between the solid-earth and the ocean, plus the interface between the atmosphere and the ocean. Note that the pressure force has a component in both the vertical and horizontal directions as per the orientation of the local normal vector. Further boundary stresses arise from viscous exchange, which generally have components perpendicular to the boundary normal; i.e., tangential to the boundary. Such stresses also satisfy Newton's third law.

25.2.4 Historical comments

We find it useful to quote from *Truesdell* (1952), who provides the following description of Cauchy's stress principle as given by equation (25.1).

> Upon any imagined closed surface, $\mathcal{S}$, there exists a distribution of stress vectors, $\boldsymbol{\tau}$, whose resultant and moment are equivalent to those of the actual forces of material continuity exerted by the material outside $\mathcal{S}$ upon that inside.

Worded in this manner, we can understand the relation between Newton's third law and Cauchy's stress principle. The profound nature of Cauchy's stress principle is further articulated, again from *Truesdell* (1952).

> [Cauchy's stress principle] has the simplicity of genius. Its profound originality can be grasped only when one realizes that a whole century of brilliant geometers had treated very special elastic problems in very complicated and sometimes incorrect ways without ever hitting upon this basic idea, which immediately became the foundation of the mechanics of distributed media.

25.3 The stress tensor

Cauchy's stress principle reduces the mathematical complexity of describing stress vectors. A further implication of this principle leads to *Cauchy's theorem*, which states that the stress vector, which is a function of space, time, and normal direction, can be expressed in terms of a stress tensor (a function of space and time) projected into the direction of the normal. The purpose of this section is to provide arguments supporting this theorem, with these arguments largely following the original from Cauchy in 1827.

25.3.1 The stress tetrahedron

For this purpose, consider the tetrahedron fluid region shown in Figure 25.3, where three of the four sides are aligned according to the Cartesian coordinate axes and the fourth side has an outward normal, $\hat{\boldsymbol{n}} = (\hat{n}_1, \hat{n}_2, \hat{n}_3)$, projecting into all three directions. The results developed for this rather contrived region using Cartesian coordinates also hold for an arbitrary region using arbitrary coordinates. The reason for this generality is that once we derive a tensorially correct result using one choice of coordinates, such as Cartesian used here, we can make use of general tensor analysis (Chapters 3 and 4) to move from specific coordinates to arbitrary coordinates.

In the limit that the tetrahedron size goes to zero, local equilibrium of the contact forces means that

$$-\sum_{m=1}^{3} \boldsymbol{\tau}_{(m)}\, \mathrm{d}A_m + \boldsymbol{\tau}_{\hat{\boldsymbol{n}}}\, \mathrm{d}A = 0, \tag{25.9}$$

where we use the shorthand expression for the outward normal directed stress vector

$$\boldsymbol{\tau}(\boldsymbol{x}, t, \hat{\boldsymbol{n}}) = \boldsymbol{\tau}_{\hat{\boldsymbol{n}}}. \tag{25.10}$$

In equation (25.9), $\boldsymbol{\tau}_{(m)}\, \mathrm{d}A_m$ (no implied summation) is the contact force vector acting on the face with outward normal parallel to the corresponding coordinate axis and $\boldsymbol{\tau}_{\hat{\boldsymbol{n}}}\, \mathrm{d}A$ is the contact force acting on the slanted face with outward normal $\hat{\boldsymbol{n}}$. The minus sign arises for the summation term since the outward normals for these three faces point in the negative coordinate directions, and our convention is for $\boldsymbol{\tau}_{(m)}$ to align with the positive coordinate directions. The areas for each face are related to the slanted face area through

$$\mathrm{d}A_m = \hat{n}_m\, \mathrm{d}A, \tag{25.11}$$

so that the local equilibrium relation (25.9) becomes

$$\boldsymbol{\tau}_{\hat{\boldsymbol{n}}} = \sum_{m=1}^{3} \hat{n}_m\, \boldsymbol{\tau}_{(m)}. \tag{25.12}$$

25.3.2 The stress tensor and stress vector

Equation (25.12) can be organized into a matrix-vector equation

$$\begin{bmatrix} (\tau_{\hat{n}})_1 & (\tau_{\hat{n}})_2 & (\tau_{\hat{n}})_3 \end{bmatrix} = \begin{bmatrix} \hat{n}_1 & \hat{n}_2 & \hat{n}_3 \end{bmatrix} \begin{bmatrix} \tau_{(1)1} & \tau_{(1)2} & \tau_{(1)3} \\ \tau_{(2)1} & \tau_{(2)2} & \tau_{(2)3} \\ \tau_{(3)1} & \tau_{(3)2} & \tau_{(3)3} \end{bmatrix}, \tag{25.13}$$

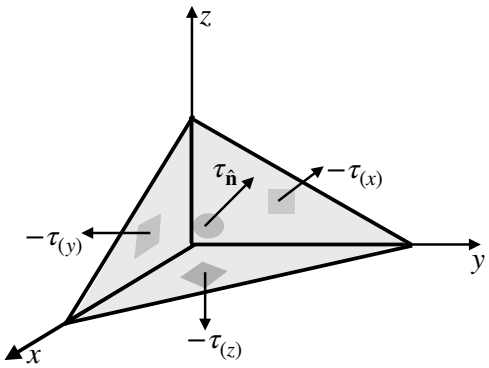

FIGURE 25.3: Cauchy's tetrahedron region of fluid with stresses acting on the four faces. Note that the stresses are not necessarily directed normal to the faces. Local equilibrium of stresses means that the accumulation of these four stresses around the region adds to zero as the region volume goes to zero.

where each matrix element is the n-component of the m-stress $\boldsymbol{\tau}_{(m)}$. We introduce a less cumbersome notation by writing

$$\begin{bmatrix} (\tau_{\hat{n}})_1 & (\tau_{\hat{n}})_2 & (\tau_{\hat{n}})_3 \end{bmatrix} = \begin{bmatrix} \hat{n}_1 & \hat{n}_2 & \hat{n}_3 \end{bmatrix} \begin{bmatrix} T_{11} & T_{12} & T_{13} \\ T_{21} & T_{22} & T_{23} \\ T_{31} & T_{32} & T_{33} \end{bmatrix}, \tag{25.14}$$

so that T_{mn} measures the force per area in the n-direction along a surface whose outward normal points in the m-direction, as depicted in Figure 25.4. Making use of T_{mn} in the expression (25.12) leads to

$$(\boldsymbol{\tau}_{\hat{\boldsymbol{n}}})_n = \sum_{m=1}^{3} \hat{n}_m \, T_{mn}, \tag{25.15}$$

which can be written more succinctly as

$$\boldsymbol{\tau}_{\hat{\boldsymbol{n}}} = \hat{\boldsymbol{n}} \cdot \boldsymbol{T}. \tag{25.16}$$

We thus see that the stress vector that acts on a surface that is oriented according to a normal vector, $\hat{\boldsymbol{n}}$, equals to the projection of the *stress tensor*, $\boldsymbol{T}$, onto the normal vector. Evidently, $\boldsymbol{\tau}_{\hat{\boldsymbol{n}}}$ is a vector with components within the tangent plane of the surface, as well as normal to the surface. Exposing functional dependence to equation (25.16) reveals

$$\boldsymbol{\tau}_{\hat{\boldsymbol{n}}}(\boldsymbol{x}, t, \hat{\boldsymbol{n}}) = \hat{\boldsymbol{n}} \cdot \boldsymbol{T}(\boldsymbol{x}, t), \tag{25.17}$$

which manifests Cauchy's theorem. Namely, the stress vector $\boldsymbol{\tau}_{\hat{\boldsymbol{n}}}$, which is a function of $(\boldsymbol{x}, t, \hat{\boldsymbol{n}})$, has been decomposed into a stress tensor, $\boldsymbol{T}$, which is a function of $(\boldsymbol{x}, t)$, as well as the projection of the stress tensor into a direction $\hat{\boldsymbol{n}}$. Finally, note a common example concerns the case of a vertical normal direction, $\hat{\boldsymbol{n}} = \hat{\boldsymbol{z}}$, as for the stress acting on a nearly horizontal sea surface. In this case the stress vector is

$$\boldsymbol{\tau}_{\hat{\boldsymbol{z}}} = \hat{\boldsymbol{x}} \, T_{31} + \hat{\boldsymbol{y}} \, T_{32} + \hat{\boldsymbol{z}} \, T_{33}. \tag{25.18}$$

The horizontal components are key to the transfer of horizontal stress between the atmosphere and ocean, thus providing a mechanical forcing to the ocean circulation. The vertical stress is less important particularly for hydrostatic fluids whose vertical momentum equation is dominated by hydrostatic balance.

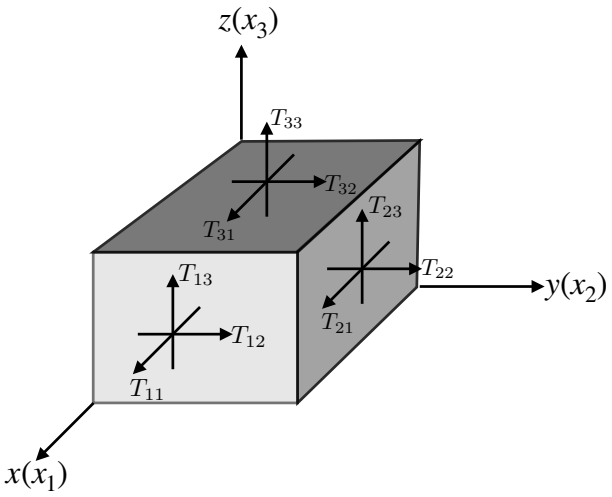

FIGURE 25.4: Illustrating the components to the stress tensor, T_{mn} and how they are organized according to the coordinate axes. The component T_{mn} is the stress that points in the n-direction along the face with outward normal in the m-direction.

25.3.3 Stress is a tensor

How do we know that T_{mn} form the components to a tensor rather than just being elements of a 3×3 matrix? To answer this question we note that each component of $\boldsymbol{T}$ is a force per area, with force a vector and area orientable by its outward normal. As it is built from vectors, which are first order tensors, we suspect that $\boldsymbol{T}$ should be a proper second order tensor. This suspicion is supported by the quotient rule from tensor analysis (Section 3.1.2). Namely, the quotient rule means that equation (25.15) indeed yields T_{mn} that are components to a second order tensor. As components to a second order tensor, the tensor components, T_{mn}, transform under a coordinate transformation according to the rules developed in Chapter 1 for Cartesian tensors and in Chapter 4 for general tensors. Through the power of tensor analysis, we thus see that our considerations, based on the rather contrived tetrahedron region in Figure 25.3, hold for an arbitrary region described by an arbitrary coordinate system.

25.4 Angular momentum and the stress tensor

The linear momentum principle afforded by Newton's law of motion allowed us to deduce the local equilibrium property (25.4) of the stress. We here derive a constraint placed on the stress tensor that is imposed by studying angular momentum. Phenomenologically, we observe that geophysical fluids, as with most common fluids, experience torques only as the moments of body forces acting throughout the volume of a fluid region, or as moments of contact forces acting on the surface bounding the fluid region. We now make use of this observation to deduce symmetry of the stress tensor.[2]

[2]Page 11 of *Batchelor* (1967) and Section 5.13 of *Aris* (1962) offer brief discussions of fluids in which internal force couplets lead to torques distinct from those considered here, and in which the stress tensor has an anti-symmetric component. *Dahler and Scriven* (1961) provide a more thorough account of such *polar materials*. Internal sources of angular momentum are studied in solid mechanics, with Section 5.3 of *Malvern* (1969) offering a discussion.

25.4.1 Basic formulation

Consider a constant mass fluid element that has a Cartesian position $\boldsymbol{x}$ relative to an arbitrary origin. The angular momentum of the fluid element with respect to the origin is

$$\boldsymbol{L} = \rho\, \delta V\, (\boldsymbol{x} \times \boldsymbol{v}), \tag{25.19}$$

and its material time evolution is

$$\frac{\mathrm{D}\boldsymbol{L}}{\mathrm{D}t} = \rho\, \delta V\, \boldsymbol{x} \times \frac{\mathrm{D}\boldsymbol{v}}{\mathrm{D}t}, \tag{25.20}$$

which follows since $\mathrm{D}(\rho\, \delta V)/\mathrm{D}t = 0$, $\mathrm{D}\boldsymbol{x}/\mathrm{D}t = \boldsymbol{v}$, and $\boldsymbol{v} \times \boldsymbol{v} = 0$. Making use of Cauchy's form for the equation of motion (24.14)

$$\rho \frac{\mathrm{D}\boldsymbol{v}}{\mathrm{D}t} = \rho\, \boldsymbol{f} + \nabla \cdot \boldsymbol{T} \tag{25.21}$$

allows us to write the angular momentum evolution as

$$\frac{\mathrm{D}\boldsymbol{L}}{\mathrm{D}t} = \delta V\, \boldsymbol{x}\, \times\, (\rho \boldsymbol{f} + \nabla \cdot \boldsymbol{T}). \tag{25.22}$$

The first term arises from body forces (e.g., central gravity, planetary centrifugal, and Coriolis) and the second term arises from the divergence of stresses. Expanding the stress divergence term renders

$$\begin{aligned}
\left[\frac{\mathrm{D}L_m}{\mathrm{D}t}\right]_{\text{stress}} &= \delta V\, \epsilon_{mnp}\, x_n\, (\nabla \cdot \boldsymbol{T})_p && \text{(25.23a)}\\
&= \delta V\, \epsilon_{mnp}\, x_n\, \partial_q T_{pq} && \text{(25.23b)}\\
&= \delta V\, \epsilon_{mnp}\, [\partial_q (x_n\, T_{pq}) - (\partial_q x_n)\, T_{pq}] && \text{(25.23c)}\\
&= \delta V\, \epsilon_{mnp}\, [\partial_q (x_n\, T_{pq}) - T_{pn}], && \text{(25.23d)}
\end{aligned}$$

where the final equality follows since $\partial_q x_n = \delta_{qn}$. Bringing this result back into the full expression (25.22) leads to

$$\frac{\mathrm{D}L_m}{\mathrm{D}t} = \delta V\, \epsilon_{mnp}\, [\rho\, x_n\, f_p + \partial_q (x_n\, T_{pq}) - T_{pn}]. \tag{25.24}$$

25.4.2 Physical interpretation

To facilitate a physical interpretation of the terms appearing in equation (25.24), integrate over an arbitrary Lagrangian region (region moving with the barycentric velocity, $\boldsymbol{v}$) so that

$$\frac{\mathrm{d}}{\mathrm{d}t} \int_{\mathcal{R}(\boldsymbol{v})} L_m = \int_{\mathcal{R}(\boldsymbol{v})} \epsilon_{mnp}\, [\rho\, x_n\, f_p + \partial_q (x_n\, T_{pq}) - T_{pn}]\, \mathrm{d}V. \tag{25.25}$$

As noted earlier, the first term on the right hand side arises from torques due to body forces acting over the region

$$\int_{\mathcal{R}(\boldsymbol{v})} \epsilon_{mnp}\, (\rho\, x_n\, f_p)\, \mathrm{d}V = \int_{\mathcal{R}(\boldsymbol{v})} (\boldsymbol{x} \times \boldsymbol{f})_m\, \rho\, \mathrm{d}V. \tag{25.26}$$

The second term on the right hand side of equation (25.25) can be transferred into a surface integral using the divergence theorem

$$\int_{\mathcal{R}(\boldsymbol{v})} \epsilon_{mnp}\, \partial_q (x_n\, T_{pq})\, \mathrm{d}V = \int_{\partial\mathcal{R}(\boldsymbol{v})} \epsilon_{mnp}\, x_n\, T_{pq}\, \hat{n}_q\, \mathrm{d}\mathcal{S} = \int_{\partial\mathcal{R}(\boldsymbol{v})} (\boldsymbol{x}\times\boldsymbol{\tau})_m\, \mathrm{d}\mathcal{S}, \tag{25.27}$$

where $\hat{n}_q$ is the $q'th$ component of the normal vector on the region boundary, $\partial\mathcal{R}(\boldsymbol{v})$, and

$$\tau_p = T_{pq}\, \hat{n}_q \tag{25.28}$$

is the $p'th$ component to the stress vector that is normal to $\hat{\boldsymbol{n}}$ (see equation (25.16)). Hence, the second term is the contribution to angular momentum evolution due to torques arising from the moment of contact forces acting on the region boundary.

25.4.3 Symmetry of the stress tensor

As noted at the start of this section, geophysical fluids have their angular momentum affected by torques arising from the moment of body forces acting throughout the fluid region, plus the moment of contact forces acting on the region boundary. There is a third term in equation (25.24) that does not fit into either category, and it is given by the volume integral

$$-\int_{\mathcal{R}(\boldsymbol{v})} \epsilon_{mnp}\, T_{pn}\, \mathrm{d}V = \int_{\mathcal{R}(\boldsymbol{v})} \epsilon_{mpn}\, T_{pn}\, \mathrm{d}V \equiv \int_{\mathcal{R}(\boldsymbol{v})} T^{\times}_m\, \mathrm{d}V, \tag{25.29}$$

where we defined

$$T^{\times}_m = \epsilon_{mpn}\, T_{pn}. \tag{25.30}$$

This term contributes a volume source to angular momentum and yet it is *not* associated with body forces. We might refer to it as a *torque density* (torque source per volume). As already noted, such torque sources are *not* relevant for geophysical fluids, in which case we conclude that geophysical fluids are affected only by symmetric stress tensors

$$T_{mn} = T_{nm} \Longrightarrow \epsilon_{mnp}\, T_{np} = 0. \tag{25.31}$$

Symmetry of the stress tensor is a central property of the stresses acting on most fluids, including geophysical fluids. We thus only consider symmetric stress tensors throughout this book.

To further support the above conclusion concerning a symmetric stress tensor, consider a particular component of the torque density, such as the vertical

$$T^{\times}_3 = \epsilon_{3pn}\, T_{pn} = T_{12} - T_{21}, \tag{25.32}$$

with the corresponding torque applied to a fluid element given by

$$T^{\times}_3\, \delta V = (T_{12} - T_{21})\, \delta x\, \delta y\, \delta z. \tag{25.33}$$

What sort of angular acceleration is induced by this torque when computed relative to the fluid element center? To answer this question, assume the fluid element is moving as a rigid body so that we can compute its angular acceleration by dividing the torque by the moment of inertia for the fluid element. The moment of inertia depends on the shape of the element, which is unspecified. Even so, we can estimate the moment of inertia computed relative to a vertical axis through the center of the element

$$I_3 = \alpha\, [(\delta x)^2 + (\delta y)^2]\, \rho\, \delta x\, \delta y\, \delta z, \tag{25.34}$$

where α is a dimensionless geometric factor. Dividing the torque (25.33) by the moment of inertia thus leads to an estimate of the angular acceleration

$$\text{angular acceleration} \approx \frac{T_3^\times}{I_3} \approx \frac{T_{12} - T_{21}}{[(\delta x)^2 + (\delta y)^2]\,\rho\,\alpha}. \tag{25.35}$$

Now consider the continuum limit, found as δx and δy are reduced to zero. In the absence of an unspecified counteracting torque, a finite angular acceleration in the continuum limit (where $(\delta x)^2 + (\delta y)^2 \to 0$) is ensured only if the stress tensor is symmetric so that the numerator vanishes.

25.5 Forces and torques in an exact hydrostatic fluid

In this section we return to the study of a static fluid in a gravitational field originally considered in Section 24.6. The exact solution is known as *exact hydrostatic balance*, which distinguishes it from the approximate hydrostatic balance appropriate for moving geophysical fluids under certain scaling regimes (Section 27.2). For a static fluid, all forces and all torques sum to zero at any point. Similarly, the integrated forces and integrated torques acting on any finite fluid region also vanish. The static fluid, although trivial dynamically, offers useful practice in applying the formalism of continuum mechanics to a system where we know the answer. Furthermore, there are interesting and important applications of these ideas, such as in the building of dams and underwater structures, both of which we certainly hope will remain static!

25.5.1 Force balance

The force balance in an exact hydrostatic fluid was addressed in Section 24.6 where we deduced the following relation between the pressure gradient and geopotential gradient

$$\nabla p = -\rho\,\nabla\Phi. \tag{25.36}$$

This equality holds at every point within the fluid, and as such it is a strong form of the hydrostatic balance.[3] Integrating over a finite fluid region, $\mathcal{R}$, and using the divergence theorem for scalar fields, (2.84), renders the finite volume or weak form of hydrostatic balance

$$\int_{\mathcal{R}} \rho\,\nabla\Phi\,\mathrm{d}V = -\int_{\mathcal{R}} \nabla p\,\mathrm{d}V = -\oint_{\partial\mathcal{R}} p\,\hat{\boldsymbol{n}}\,\mathrm{d}\mathcal{S}. \tag{25.37}$$

Expanding the above relations for the special case of $\Phi = g\,z$ leads to the differential statements

$$0 = \hat{\boldsymbol{x}}\cdot\nabla p = \hat{\boldsymbol{y}}\cdot\nabla p \qquad \text{and} \qquad \rho\,g = -\hat{\boldsymbol{z}}\cdot\nabla p, \tag{25.38}$$

with the first two equations implying that the exact hydrostatic pressure is only a function of z. The corresponding weak form of hydrostatic balance reads

$$g\,M = -\int_{\mathcal{R}} \nabla p\cdot\hat{\boldsymbol{z}}\,\mathrm{d}V = -\oint_{\partial\mathcal{R}} p\,(\hat{\boldsymbol{n}}\cdot\hat{\boldsymbol{z}})\,\mathrm{d}\mathcal{S}, \tag{25.39}$$

where $M = \int_{\mathcal{R}} \rho\,\mathrm{d}V$ is the mass in the fluid region, and the weak form of horizontal balances are

$$0 = \int_{\mathcal{R}} \nabla p\cdot\hat{\boldsymbol{x}}\,\mathrm{d}V = \oint_{\partial\mathcal{R}} p\,(\hat{\boldsymbol{n}}\cdot\hat{\boldsymbol{x}})\,\mathrm{d}\mathcal{S} \tag{25.40a}$$

[3] Recall the discussion of weak and strong formulation in Section 17.1.1. In brief, the weak formulation provides integral relations whereas the strong formulation provides differential relations.

$$0 = \int_{\mathcal{R}} \nabla p \cdot \hat{\boldsymbol{y}} \, dV = \oint_{\partial \mathcal{R}} p \, (\hat{\boldsymbol{n}} \cdot \hat{\boldsymbol{y}}) \, d\mathcal{S}. \tag{25.40b}$$

We emphasize that these finite volume balances hold for any arbitrarily shaped region within a static fluid.

25.5.2 Pressure force balance for a homogeneous fluid

To further our understanding of the pressure force balances in a static fluid, consider a constant density static ocean sitting under a massless atmosphere, in which case the hydrostatic pressure is

$$p = -\rho \, g \, z, \tag{25.41}$$

where $z < 0$ for the ocean. Now examine the pressure forces acting on the three sides of the triangle in Figure 25.5. This geometry is simple enough to explicitly compute the pressure forces, thus confirming the general properties in equations (25.39), (25.40a), and (25.40b).

The outward normal vectors along the three triangle faces are given by

$$\hat{\boldsymbol{n}}_{\rm A} = +\hat{\boldsymbol{y}} \qquad \text{and} \qquad \hat{\boldsymbol{n}}_{\rm B} = -\hat{\boldsymbol{z}} \qquad \text{and} \qquad \hat{\boldsymbol{n}}_{\rm C} = \hat{\boldsymbol{z}} \cos\varphi - \hat{\boldsymbol{y}} \sin\varphi, \tag{25.42}$$

where

$$\tan\varphi = \frac{z_2 - z_1}{y_2 - y_1} = \frac{\Delta z}{\Delta y} \tag{25.43}$$

is the slope of the hypotenuse relative to the horizontal. The integrated pressure force along the vertical face is thus given by

$$\boldsymbol{F}_{\rm A}^{\rm press} = -\int p \, \hat{\boldsymbol{n}}_{\rm A} \, d\mathcal{S} = \hat{\boldsymbol{y}} \, \Delta x \int_{z_1}^{z_2} \rho \, g \, z \, dz = \hat{\boldsymbol{y}} \, (\rho \, g/2) \, (z_2 + z_1) \, \Delta z \, \Delta x, \tag{25.44}$$

where Δx is the thickness of the triangle in the $\hat{\boldsymbol{x}}$ direction into the page. Note that $\boldsymbol{F}_{\rm A}^{\rm press}$ points in the $-\hat{\boldsymbol{y}}$ direction since $z_2 + z_1 < 0$. Likewise, the integrated pressure force along the horizontal face is given by

$$\boldsymbol{F}_{\rm B}^{\rm press} = -\int p \, \hat{\boldsymbol{n}}_{\rm B} \, d\mathcal{S} = -\hat{\boldsymbol{z}} \, \Delta x \int_{y_1}^{y_2} \rho \, g \, z_1 \, dy = -\hat{\boldsymbol{z}} \, \rho \, g \, z_1 \, \Delta y \, \Delta x, \tag{25.45}$$

which points upward since $z_1 < 0$.

The integrated pressure force along the sloped hypotenuse face, C, requires a bit of trigonometry. For this purpose we make use of the formalism from Section 19.6.3, in which the vertical position along the hypotenuse is written

$$z = \eta(y) = z_2 - (y_2 - y) \tan\varphi, \tag{25.46}$$

so that the horizontal projection of the surface area is given by equation (28.4)

$$d\mathcal{S} = |\nabla(z - \eta)| \, dx \, dy = \frac{dx \, dy}{|\cos\varphi|}. \tag{25.47}$$

Hence, the integrated pressure force on the hypotenuse is given by

$$\boldsymbol{F}_{\rm C}^{\rm press} = -\int p \, \hat{\boldsymbol{n}}_{\rm C} \, d\mathcal{S} \tag{25.48a}$$

$$= \frac{\hat{\boldsymbol{n}}_{\rm C}}{\cos\varphi} \, \Delta x \int_{y_1}^{y_2} \rho \, g \, \eta(y) \, dy \tag{25.48b}$$

$$= (\hat{\boldsymbol{z}} - \hat{\boldsymbol{y}} \tan\varphi)\, \rho\, g\, \Delta x\, [z_2\, \Delta y - y_2\, \Delta z - (1/2)\, (y_1 + y_2)\, \Delta y\, \tan\varphi] \tag{25.48c}$$

$$= (\hat{\boldsymbol{z}} - \hat{\boldsymbol{y}} \tan\varphi)\, \rho\, g\, \Delta x\, [z_2\, \Delta y - y_2\, \Delta z + (y_1 + y_2)\, \Delta z/2] \tag{25.48d}$$

$$= (\hat{\boldsymbol{z}} - \hat{\boldsymbol{y}} \tan\varphi)\, \rho\, g\, \Delta x\, \Delta y\, (z_1 + z_2)/2. \tag{25.48e}$$

Bringing these results together renders the net pressure forces in the two directions

$$\hat{\boldsymbol{y}} \cdot (\boldsymbol{F}_{\mathrm{A}}^{\mathrm{press}} + \boldsymbol{F}_{\mathrm{B}}^{\mathrm{press}} + \boldsymbol{F}_{\mathrm{C}}^{\mathrm{press}}) = (\rho\, g\, \Delta x/2)\, [(z_1 + z_2)\, \Delta z - \tan\varphi\, (z_1 + z_2)\, \Delta y] = 0 \tag{25.49a}$$

$$\hat{\boldsymbol{z}} \cdot (\boldsymbol{F}_{\mathrm{A}}^{\mathrm{press}} + \boldsymbol{F}_{\mathrm{B}}^{\mathrm{press}} + \boldsymbol{F}_{\mathrm{C}}^{\mathrm{press}}) = \rho\, g\, \Delta x\, \Delta y\, \Delta z/2 = M\, g, \tag{25.49b}$$

where the mass of the triangle is given by

$$M = \rho\, \Delta x\, \Delta y\, \Delta z/2. \tag{25.50}$$

We thus see that the area integrated horizontal pressure forces vanish, whereas the area integrated vertical pressure force balances the weight of the fluid. Again, these results are expected given the general expressions (25.39), (25.40a), and (25.40b) of force balance. Even so, being able to explictly compute the pressure forces acting around a region, and to confirm the general force balances, is a useful means to become familiar with hydrostatic pressure.

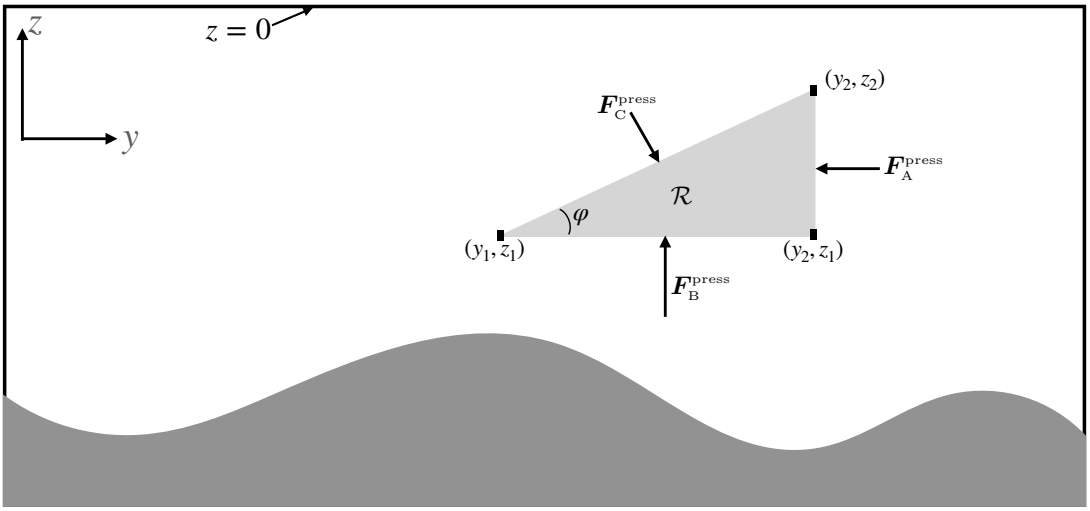

FIGURE 25.5: A right triangle region of fluid in a static ocean where $z < 0$. The positions for the three corners are shown as (y_1, z_1), (y_2, z_1), and (y_2, z_2), along with the pressure forces acting on the three sides. In exact hydrostatic balance, the area integrated pressure force acting over the triangle boundary vanishes, $-\oint_{\partial\mathcal{R}} p\, \hat{\boldsymbol{n}}\, \mathrm{d}\mathcal{S} = 0$. If the density of the fluid is assumed constant, then we can analytically compute the force balance as detailed in Section 25.5.2.

25.5.3 Torque balance

Torques arise in the presence of force *couplets*, which in turn lead to time changes in the angular momentum. In our discussion of the stress tensor in Section 25.4, we saw that a symmetric stress tensor removes volume sources of torque; i.e., there are no internal sources of force couplets. So the only means to impart a nonzero torque is for force couplets to arise from body forces (forces originating outside of the fluid region) and from contact forces that act between fluid elements within the region. In this section, we show that for a static fluid then the net torque vanishes both at an arbitrary point in the fluid as well as when integrated over an arbitrary region.

Strong form: zero torques acting on a fluid element

The torque is the moment of a force computed about a chosen origin. For a static geophysical fluid, the torque acting on a fluid element is given by the moment of the pressure force plus the moment of the effective gravity force (central gravity plus planetary centrifugal)

$$\boldsymbol{x} \times \boldsymbol{f}\, \rho\, \delta V = \boldsymbol{x} \times (-\rho^{-1}\, \nabla p - \nabla \Phi)\, \rho\, \delta V. \tag{25.51}$$

As seen in Section 25.5.1, the pressure and effective gravitational forces exactly balance at each point with a static fluid so that $\nabla p = -\rho\, \nabla \Phi$. Hence, there can be no torques at each point since there are no net forces at each point.

Weak form: zero torques acting on a finite fluid region

To show that the torque vanishes for a finite fluid region, we can merely integrate the fluid element result (25.51) over the finite region. Since the integral of zero is still zero, there are no torques on the region. An alternative approach makes use of the weak formulation by following the discussion in Section 25.4.2. In this approach, we start by writing the time change in angular momentum acting on a static fluid region

$$\frac{\mathrm{d}}{\mathrm{d}t} \int_{\mathcal{R}} \boldsymbol{L} = \int_{\mathcal{R}} [\boldsymbol{x} \times (-\rho\, \nabla \Phi)]\, \mathrm{d}V + \oint_{\partial \mathcal{R}} [\boldsymbol{x} \times (-\hat{\boldsymbol{n}}\, p)]\, \mathrm{d}\mathcal{S}. \tag{25.52}$$

Note that although the discusssion in Section 25.4.2 focused on a Lagrangian region, $\mathcal{R}(\boldsymbol{v})$, there is no distinction here between Lagrangian and Eulerian since the fluid is static.

The pressure contribution in equation (25.52) is written in its contact force form, which is appropriate for a weak formulation. However, to compare its contribution to the torque with that from effective gravity requires us to convert the area integral to a volume integral. For that purpose we use Cartesian tensor notation and expose full details

$$\oint_{\partial \mathcal{R}} (\hat{\boldsymbol{n}} \times \boldsymbol{x})_a\, p\, \mathrm{d}\mathcal{S} = \epsilon_{abc} \oint_{\partial \mathcal{R}} \hat{n}_b\, x_c\, p\, \mathrm{d}\mathcal{S} \qquad \text{permutation symbol (Section 1.7.1)} \tag{25.53a}$$

$$= \epsilon_{abc} \int_{\mathcal{R}} \partial_b (x_c\, p)\, \mathrm{d}V \qquad \text{divergence theorem} \tag{25.53b}$$

$$= \epsilon_{abc} \int_{\mathcal{R}} (\delta_{bc}\, p + x_c\, \partial_b p)\, \mathrm{d}V \qquad \text{product rule} \tag{25.53c}$$

$$= \epsilon_{abc} \int_{\mathcal{R}} x_c\, \partial_b p\, \mathrm{d}V \qquad \epsilon_{abc}\, \delta_{bc} = 0 \tag{25.53d}$$

$$= -\epsilon_{acb} \int_{\mathcal{R}} x_c\, \partial_b p\, \mathrm{d}V \qquad \epsilon_{abc} = -\epsilon_{acb} \tag{25.53e}$$

$$= -\int_{\mathcal{R}} (\boldsymbol{x} \times \nabla p)_a\, \mathrm{d}V \qquad \text{vector cross product notation.} \tag{25.53f}$$

This result then brings the angular momentum equation (25.52) to the form

$$\frac{\mathrm{d}}{\mathrm{d}t}\int_{\mathcal{R}} \boldsymbol{L} = \int_{\mathcal{R}} [\boldsymbol{x} \times (-\rho\,\nabla\Phi - \nabla p)]\,\mathrm{d}V. \tag{25.54}$$

At this point we can invoke the strong form force balance in equation (25.36), thus revealing that the integrand on the right hand side vanishes at each point in the fluid. However, this approach is no different than starting from the strong formulation of the torques in equation (25.51) and integrating over a finite region. An alternative approach, remaining fully within the weak formulation, states that if the region's angular momentum remains constant, then that defines a region experiencing zero net torque. This approach is the same as taken for the force balance, whereby we say that a fluid region experiencing no acceleration is one that has zero net forces acting on it. Hence, for a region with time invariant angular momentum we are led to the finite volume (weak form) torque balance

$$\int_{\mathcal{R}} [\boldsymbol{x} \times (\rho\,\nabla\Phi + \nabla p)]\,\mathrm{d}V = 0 \Longrightarrow \int_{\mathcal{R}} (\boldsymbol{x} \times \rho\,\nabla\Phi)\,\mathrm{d}V = -\int_{\partial\mathcal{R}} (\boldsymbol{x} \times \hat{\boldsymbol{n}}\,p)\,\mathrm{d}\mathcal{S}, \tag{25.55}$$

with this balance the direct analog for torques of the weak form of the force balances given by equations (25.39), (25.40a), and (25.40b).

25.6 Flux-form Eulerian momentum equation

We often find it useful to consider Cauchy's form of the momentum equation (25.21) in its flux-form Eulerian expression. Making use of Cartesian tensors, we expand the material time derivative acting on the velocity and introduce the mass conservation equation (19.6) so that

$$\begin{aligned}
\rho\,\frac{\mathrm{D}\boldsymbol{v}}{\mathrm{D}t} &= \rho\,[\partial_t \boldsymbol{v} + (\boldsymbol{v}\cdot\nabla)\,\boldsymbol{v}] && \text{(25.56a)}\\
&= \rho\,[\partial_t \boldsymbol{v} + (\boldsymbol{v}\cdot\nabla)\,\boldsymbol{v}] + \boldsymbol{v}\,(\partial_t\rho + \nabla\cdot(\rho\,\boldsymbol{v})] && \text{(25.56b)}\\
&= \partial_t(\rho\,\boldsymbol{v}) + \nabla\cdot[\rho\,\boldsymbol{v}\otimes\boldsymbol{v}], && \text{(25.56c)}
\end{aligned}$$

where $\boldsymbol{v}\otimes\boldsymbol{v}$ is the outer product of the velocity vector and it has Cartesian tensor components written as

$$(\boldsymbol{v}\otimes\boldsymbol{v})_{mn} = v_m\,v_n. \tag{25.57}$$

Consequently, the momentum equation (25.21) takes on the flux-form Eulerian expression

$$\partial_t(\rho\,\boldsymbol{v}) + \nabla\cdot[\rho\,\boldsymbol{v}\otimes\boldsymbol{v}] = \rho\,\boldsymbol{f} + \nabla\cdot\mathbb{T}. \tag{25.58}$$

Alternatively, we can move the advection of momentum term onto the right hand side so that

$$\partial_t(\rho\,\boldsymbol{v}) = \rho\,\boldsymbol{f} + \nabla\cdot[\boldsymbol{T} - \rho\,\boldsymbol{v}\otimes\boldsymbol{v}], \tag{25.59}$$

which takes on the component form

$$\partial_t(\rho\,v_m) = \rho\,f_m + \partial_n[T_{mn} - \rho\,v_m\,v_n]. \tag{25.60}$$

In this form we see that momentum advection can be interpreted as a stress that modifies the linear momentum per volume at a point in space. We refer to the stress,

$$T^{\text{kinetic}}_{mn} = -\rho\,(\boldsymbol{v}\otimes\boldsymbol{v})_{mn} = -\rho\,v_m\,v_n, \tag{25.61}$$

as the *mechanical stress* or *kinetic stress*, which arises from the mechanical interactions between moving fluid elements. The turbulent contribution to the mechanical stress is known as the *Reynolds stress*.

For a rotating fluid in a gravity field we set the body force to

$$\rho \boldsymbol{f} = -2\,\rho\,\boldsymbol{\Omega} \times \boldsymbol{v} - \rho \nabla \Phi, \tag{25.62}$$

and the divergence of the stress tensor is

$$\nabla \cdot \boldsymbol{T} = -\nabla p + \rho\,\boldsymbol{F}, \tag{25.63}$$

with $\boldsymbol{F}$ the frictional acceleration (see Section 25.8). In this case, Cauchy's equation (25.58) takes on the form

$$\frac{\partial(\rho\,\boldsymbol{v})}{\partial t} + \nabla \cdot (\rho\,\boldsymbol{v} \otimes \boldsymbol{v}) + 2\,\rho\,\boldsymbol{\Omega} \times \boldsymbol{v} = -\nabla p - \rho\,\nabla\Phi + \rho\,\boldsymbol{F}. \tag{25.64}$$

25.7 Linear momentum for arbitrary regions

Consider the budget of linear momentum for an arbitrary region, $\mathcal{R}$, moving in an arbitrary manner within the fluid. For this purpose we make use of the Leibniz-Reynolds Transport Theorem (20.37)

$$\frac{\mathrm{d}}{\mathrm{d}t}\left[\int_{\mathcal{R}} \varphi \,\mathrm{d}V\right] = \int_{\mathcal{R}} \frac{\partial \varphi}{\partial t}\,\mathrm{d}V + \oint_{\partial\mathcal{R}} \varphi\,\boldsymbol{v}^{(b)} \cdot \hat{\boldsymbol{n}}\,\mathrm{d}\mathcal{S}, \tag{25.65}$$

where $\boldsymbol{v}^{(b)}$ is the velocity of the region boundary, $\partial\mathcal{R}$, with $\hat{\boldsymbol{n}}$ the outward normal along the boundary. Applying this result to a component of the linear momentum per volume, $\varphi = \rho\,v_m$ (again, assuming Cartesian tensors), and making use of the flux-form Eulerian momentum equation (25.60) leads to

$$\begin{aligned}
\frac{\mathrm{d}}{\mathrm{d}t}\left[\int_{\mathcal{R}} \rho\,v_m \,\mathrm{d}V\right] &= \int_{\mathcal{R}} \partial_t(\rho\,v_m)\,\mathrm{d}V + \oint_{\partial\mathcal{R}} (\rho\,v_m)\,\boldsymbol{v}^{(b)} \cdot \hat{\boldsymbol{n}}\,\mathrm{d}\mathcal{S} && \text{(25.66a)}\\
&= \int_{\mathcal{R}} [\rho\,f_m + \partial_n(T_{mn} - \rho\,v_m\,v_n)]\,\mathrm{d}V + \oint_{\partial\mathcal{R}} (\rho\,v_m)\,\boldsymbol{v}^{(b)} \cdot \hat{\boldsymbol{n}}\,\mathrm{d}\mathcal{S} && \text{(25.66b)}\\
&= \int_{\mathcal{R}} \rho\,f_m\,\mathrm{d}V + \oint_{\partial\mathcal{R}} (T_{mn} - \rho\,v_m\,v_n)\,\hat{n}_n\,\mathrm{d}\mathcal{S} + \oint_{\partial\mathcal{R}} (\rho\,v_m)\,\boldsymbol{v}^{(b)} \cdot \hat{\boldsymbol{n}}\,\mathrm{d}\mathcal{S} && \text{(25.66c)}\\
&= \int_{\mathcal{R}} \rho\,f_m\,\mathrm{d}V + \oint_{\partial\mathcal{R}} [T_{mn} + \rho\,v_m\,(v_n^{(b)} - v_n)]\,\hat{n}_n\,\mathrm{d}\mathcal{S}. && \text{(25.66d)}
\end{aligned}$$

We can write this relation as

$$\frac{\mathrm{d}}{\mathrm{d}t}\left[\int_{\mathcal{R}} \rho\,\boldsymbol{v}\,\mathrm{d}V\right] = \int_{\mathcal{R}} \rho\,\boldsymbol{f}\,\mathrm{d}V + \oint_{\partial\mathcal{R}} [\boldsymbol{T} + \rho\,\boldsymbol{v} \otimes (\boldsymbol{v}^{(b)} - \boldsymbol{v})] \cdot \hat{\boldsymbol{n}}\,\mathrm{d}\mathcal{S}. \tag{25.67}$$

We conclude that the evolution of linear momentum over an arbitrary region is affected by the volume integrated body force acting over the region, plus the impacts from stresses acting on the region boundary. Notably, the stresses have a contribution from the advection of linear momentum across the region boundary, with advection computed relative to motion of the boundary. In Section 25.10 we specialize the budget (25.67) to an infinitesimally thin interface. That analysis is then used to develop stress conditions for a surface within a single fluid media, and the stress condition at the boundary between two fluids.

We refer to a *Lagrangian region* as one that moves so that the surface velocity and barycentric velocity satisfy $\boldsymbol{v}^{(b)} \cdot \hat{\boldsymbol{n}} = \boldsymbol{v} \cdot \hat{\boldsymbol{n}}$, in which case the mechanical stress is eliminated from the finite

volume momentum budget (25.67). Recall from our discussion of Lagrangian regions in Section 19.3.1, we denote a Lagrangian region by writing $\mathcal{R}(\boldsymbol{v})$ to emphasize that the region moves with the barycentric fluid velocity, $\boldsymbol{v}$. For this case the linear momentum is only affected by body forces as well as stresses contained in the stress tensor

$$(\boldsymbol{v} - \boldsymbol{v}^{(b)}) \cdot \hat{\boldsymbol{n}} = 0 \implies \frac{\mathrm{d}}{\mathrm{d}t} \left[\int_{\mathcal{R}(\boldsymbol{v})} \rho \, \boldsymbol{v} \, \mathrm{d}V \right] = \int_{\mathcal{R}(\boldsymbol{v})} \rho \, \boldsymbol{f} \, \mathrm{d}V + \oint_{\partial \mathcal{R}(\boldsymbol{v})} \boldsymbol{T} \cdot \hat{\boldsymbol{n}} \, \mathrm{d}\mathcal{S}. \tag{25.68}$$

This relation is Reynold's transport theorem (Section 20.2.6) as applied to linear momentum.

25.8 Constitutive relation between stress and strain rate

Thus far we have offered a rather general treatment of stress, developing its properties according to the conservation of linear momentum and angular momentum. We now develop *constitutive relations*, which relate stress to properties of the fluid as well as properties of the fluid flow.

25.8.1 Thermodynamic pressure and mechanical pressure

Consider a fluid in which the stress on an area element is always normal to the area element and is independent of the orientation. This fluid is in hydrostatic balance and the corresponding stress tensor and stress vector are written

$$T_{mn} = -p \, \delta_{mn} \iff \boldsymbol{T} \cdot \hat{\boldsymbol{n}} = -p \, \hat{\boldsymbol{n}}, \tag{25.69}$$

where p is the hydrostatic pressure field. Since the pressure introduced here arises from purely mechanical considerations, we refer to it as the *mechanical pressure*. For a compressible fluid at rest, we can identify the mechanical pressure with the *thermodynamic pressure* encountered in our study of equilibrium thermodynamics (Chapter 22). Furthermore, if we assume that local thermodynamic equilibrium is maintained for fluid elements within a moving fluid, then we are motivated to continue making this identification between mechanical pressure and thermodynamical pressure (see Section 4.5 of *Kundu et al.* (2016) or Section 1.10 of *Salmon* (1998)). However, we note that there is no fully deductive theory supporting this equality of pressures. The reader in search of a deductive theory will need to start by studying nonequilibrium statistical mechanics, which is outside our scope.

When the fluid flow is non-divergent (Chapter 21), we lose the equality between mechanical pressure and thermodynamical pressure, even when the fluid is at rest. The reason is that a non-divergent fluid flow is unable to do pressure work on a fluid element since the flow cannot change the fluid element's volume. Hence, for non-divergent flow there is no connection between pressure and changes to internal energy as per the first law of thermodynamics (Section 22.2). A non-divergent flow only has access to the mechanical pressure as revealed through the measurement of stresses. Furthermore, the mechanical pressure instantaneously conforms to the needs of non-divergence throughout the fluid (see Section 29.3 and Section 38.4). Correspondingly, energetic consistency requires us to make use of the geopotential in the equation of state for *in situ* density in an oceanic Boussinesq fluid (in which the velocity is non-divergent), rather than the thermodynamic pressure. We explore this point in Section 29.8.

25.8.2 Couette flow and the frictional stress tensor

Couette flow arises when fluid is placed between two long and straight concentric cylinders that can rotate. Relative motion between the two cylinders leads to fluid motion. For example, if the inner surface rotates, then fluid next to the cylinder wall will move with the cylinder. Any normal stresses on the fluid imparted by the cylinders are directed toward the cylinder axis and

so cannot render any tangential motion. This elegant experiment proves that fluid motion can be induced by purely tangential stresses. Furthermore, the tangential stress imparted by the inner cylinder transfers through the fluid to the outer cylinder. Indeed, if the inner cylinder rotates at a constant rate, then eventually the whole fluid-cylinder system rotates as a solid body. Couette flow thus exhibits how real fluids can support tangential stresses in response to tangential strains, thus providing a clear distinction from a perfect fluid where only normal stresses (i.e., pressure) are supported.

As evidenced by the Couette flow, a moving fluid has a more complex stress relation than a static fluid. In particular, the presence of tangential stresses in the fluid provides evidence for an additional piece to the stress tensor that we write as

$$T_{mn} = -p\,\delta_{mn} + \mathbb{T}_{mn} \iff \boldsymbol{T} = -p\,\mathbb{I} + \mathbb{T}. \tag{25.70}$$

The pressure term remains isotropic as for a fluid at rest, thus imparting normal stresses. The additional tensor, $\mathbb{T}$, is referred to as the *frictional stress tensor* or sometimes the *viscous stress tensor*.[4] The friction tensor captures the irreversible exchanges of momentum between moving (relative to one another) fluid elements, such as in Couette flow, with the irreversible momentum exchange supported by fluid viscosity. Viscosity is assumed to be identically zero in a perfect fluid, so that a perfect fluid can only support normal stresses from pressure even when the perfect fluid has relative motion.

As noted above, we assume the frictional stress tensor vanishes when there is zero relative motion within the fluid.[5] The physical idea is that fluid strains are needed to generate friction between fluid elements to support the transfer of momentum through the presence of viscosity. The determination of frictional stresses from kinematic properties (such as strain) requires a constitutive relation. The constitutive relation commonly used for geophysical fluids follows that for a *Newtonian fluid*, which is a particular type of *Stokesian fluid* whose frictional stresses are assumed to be linearly proportional to the strain rate.

The diagonal stresses, T_{11}, T_{22}, and T_{33}, are known as the *direct stresses* or *normal stresses*, whereas the off-diagonal stresses are *shear stresses*. The sum of the direct stresses forms the trace of the stress tensor and is given by

$$T_{qq} = T_{11} + T_{22} + T_{33} = -3\,p + \mathbb{T}_{qq}. \tag{25.71}$$

If $\mathbb{T}_{qq} = 0$ then it is known as the *deviatoric friction tensor*. As argued in Section 25.8.6, a deviatoric friction tensor is consistent with the assumption of equal mechanical and thermodynamical pressures.

25.8.3 D'Alembert's theorem for perfect fluids

Consider a finite impermeable solid body placed in a steady fluid flow, with the flow assumed to be uniform upstream and downstream. A particular realization is an arbitrarily long pipe flow with a solid object in the middle of the pipe. *D'Alembert's theorem* says that the force exerted by a perfect fluid on the solid body has no component along the direction of the pipe's central axis. A proof of this theorem, as provided in Section 13 of *Meyer* (1971), makes use of basic insights into momentum balances.

D'Alembert's theorem suggests a behavior that is contrary to common experience, whereby an object placed in a real fluid flow experiences a net force in the direction of the flow, so that there is a transfer of momentum between the fluid and the solid body. Consequently, D'Alembert's theorem became known as *D'Alembert's paradox*, thus motivating research during

[4] The viscous tensor is distinct from the viscosity tensor, which is a fourth order tensor not considered in this book. Section 4.5 of *Kundu et al.* (2016) and Chapter 17 in *Griffies* (2004) for a discussion of the viscosity tensor.

[5] This assumption follows those for a Stokes fluid as discussed in Section 5.21 of *Aris* (1962).

the 19th and early 20th centuries to understand stresses acting between a fluid and solid. It further put into question the ability to consider a fluid with arbitrarily small, but nonzero, viscosity as approximately a perfect fluid, where the viscosity identically vanishes.

The nonzero viscosity present in real fluid supports tangential stresses, in addition to normal (pressure) stresses present in perfect fluids. It is the tangential stresses, no matter how small in magnitude (but nonzero), that lead to a net force on the solid body. These ideas highlight the subtle nature of taking the limit of vanishing viscosity. Namely, a real fluid, no matter how small its viscosity (so long as it is nonzero), displays fundamentally distinct behavior relative to the perfect fluid. We return to this point in Section 25.8.7 when discussing the relation between the Navier-Stokes equation and the Euler equation.

25.8.4 Guidance from Galilean invariance

Consider a fluid in uniform motion in free space. Boosting the reference frame allows us to move to a reference frame where the fluid is static. Through Galilean invariance (Section 17.5) we expect the dynamics to remain unchanged. Since we assume friction vanishes when the fluid is static (as per a Stokesian fluid), Galilean invariance implies that the frictional stresses vanish when the fluid undergoes uniform motion in any direction.

Uniform motion of fluid elements is reflected in zero velocity gradients, which offers a key insight into how friction depends on strains. Namely, these considerations suggest that the friction tensor is a function of gradients in the velocity field, $\partial_m v_n$. Furthemore, as the stress tensor must be symmetric (Section 25.4), the simplest expression for the friction tensor is one that is linearly proportional to the strain rate tensor introduced in Section 18.8. Symmetry thus removes any dependence on the rotation (spin) tensor (Section 18.8.5).[6] Fluids that satisfy a linear constitutive relation between stress and the strain rate are known as *Newtonian fluids*. Furtheremore, this constitutive relation takes the same mathematical form as *Hooke's Law* used in the study of elastic materials or simple harmonic oscillators (see Section 15.6).[7]

25.8.5 A comment on Rayleigh drag

Rayleigh drag is a particular form of friction that makes use of the acceleration

$$\boldsymbol{F}_{\text{Rayleigh}} = -\gamma \boldsymbol{v}, \tag{25.72}$$

where $\gamma > 0$ is an inverse time scale. Rayleigh drag is *not* Galilean invariant since it decelerates all flows, even uniformly moving flows, towards rest where rest is defined by the laboratory frame. Furthermore, Rayleigh drag is not equal to the divergence of a frictional stress tensor, and so it does not arise from a contact stress. Even so, it has found some use for rudimentary purposes, particularly when aiming to derive analytic expressions for how friction acts on flows in a bulk sense. We provide an example in the study of Ekman dynamics in Section 33.2.3.

25.8.6 Constitutive relation for Newtonian fluids

There are many details involved with deriving the Newtonian fluid constitutive relation, with discussions provided in Section G of *Serrin* (1959), Chapter 5 of *Aris* (1962), Section 3.1 of *Segel* (1987), and Section 4.5 of *Kundu et al.* (2016) for general fluids, and Chapter 17 and 18 of *Griffies* (2004) for stratified fluids with particular focus on the ocean. We here offer a taste of

[6]The absence of a dependence on the rotation tensor is to be expected, since this tensor renders a rigid rotation on fluid elements, thus inducing no change in the distance between fluid particles. See Section 18.8.4.

[7]In fact, Hooke's Law provides a linear relationship between stress and strain, whereas for Newtonian fluids we consider a linear relationship between stress and strain rate.

these considerations by starting with the constitutive relation

$$\mathbb{T}_{mn} = \rho\,(2\,\nu\,\mathbb{S}_{mn} + \lambda\,\nabla\cdot\boldsymbol{v}\,\delta_{mn}), \tag{25.73}$$

with $\mathbb{S}_{mn}$ the components to the strain rate tensor introduced in Section 18.8.4 and whose trace equals to the velocity divergence

$$\mathbb{S}_{qq} = \nabla\cdot\boldsymbol{v}. \tag{25.74}$$

The first contribution to the frictional stress (25.73) includes the strain tensor multiplied by the *first kinematic viscosity*, $\nu > 0$ (dimensions of squared length per time). The second contribution arises just from flow divergence as scaled by a *second kinematic viscosity*, λ. The sum

$$\nu_{\text{bulk}} = \rho\,(\lambda + 2\,\nu/3) \tag{25.75}$$

is known as the *bulk viscosity*, which, as discussed in the following, will be set to zero. Finally, one sometimes finds it more convenient to work with the *dynamic viscosity*

$$\mu_{\text{vsc}} = \rho\,\nu. \tag{25.76}$$

Note that we set ρ to the constant Boussinesq reference density, ρ_o (Chapter 29), when working with a Boussinesq fluid.

Deviatoric friction tensor

As noted in Section 25.8.1, the pressure appearing in the stress tensor is a mechanical pressure that equals to minus one-third the trace of the stress tensor when the fluid is at rest

$$T^{\text{static}}_{qq} = -3\,p. \tag{25.77}$$

We assume that the frictional stress tensor does *not* alter this trace, so that the frictional stress tensor has zero trace and is known as a *deviatoric friction tensor*[8]

$$\mathbb{T}_{qq} = 0 = 3\,\nu_{\text{bulk}}\,\nabla\cdot\boldsymbol{v} \Longrightarrow \lambda = -2\,\nu/3, \tag{25.78}$$

so that the total stress tensor is given by

$$T_{mn} = -\delta_{mn}\,p + 2\,\mu_{\text{vsc}}\,\mathbb{S}^{\text{dev}}_{mn} \quad \text{with} \quad \mathbb{S}^{\text{dev}}_{mn} = \mathbb{S}_{mn} - \delta_{mn}\,\mathbb{S}_{qq}/3, \tag{25.79}$$

where $\mathbb{S}^{\text{dev}}$ is the *deviatoric strain rate tensor*. We next offer arguments for why the friction tensor used for geophysical flows should have zero trace.

Equality of the mechanical and thermodynamic pressures

The frictional stress tensor (25.73) is not the precise form typically used in geophysical fluid modeling. Instead, the velocity divergence term is generally dropped even for compressible flows, and the viscosity is anisotropic and more generally takes the form of a fourth order *viscosity tensor* (see Chapter 17 and 18 of *Griffies* (2004) for the ocean). Furthermore, what is generally respected in most geophysical applictions is the deviatoric nature of the friction tensor. That property is maintained since it is consistent with our assumption in Section 25.8.1 that the mechanical pressure equals to the thermodynamic pressure.

To see this equality between the pressures, introduce the mechanical pressure, p^{mech}, according

[8] A second order tensor in 3-dimensions, $\mathbb{D}$, has a *deviator* with components given by $\mathbb{D}^{\text{dev}}_{mn} = \mathbb{D}_{mn} - (1/3)\,\delta_{mn}\,\mathbb{D}_{qq}$. By construction, the trace of the deviator vanishes: $\mathbb{D}^{\text{dev}}_{qq} = 0$.

to the trace of the stress tensor

$$T_{qq} = -3\, p^{\text{mech}}. \tag{25.80}$$

That is, mechanical pressure is minus one-third the trace of the stress tensor whether the fluid is at rest or in motion. We can, in principle, measure this pressure by measuring the stresses. If we now return to the general form of the stress tensor

$$T_{mn} = -\delta_{mn}\, p + \rho\,(\lambda\, \nabla \cdot \boldsymbol{v}\, \delta_{mn} + 2\,\nu\, \mathbb{S}_{mn}), \tag{25.81}$$

with p here given by the thermodynamic pressure, then the trace is

$$T_{qq} = -3\, p + \rho\,(3\,\lambda + 2\,\nu)\, \nabla \cdot \boldsymbol{v}. \tag{25.82}$$

Setting the two traces (25.80) and (25.82) equal then leads to

$$p^{\text{mech}} - p = -\nu_{\text{bulk}}\, \nabla \cdot \boldsymbol{v}. \tag{25.83}$$

Hence, in regions where the flow converges, the mechanical pressure is greater than the thermodynamical pressure, $p^{\text{mech}} > p$, whereas where flow diverges then $p^{\text{mech}} < p$.

Stokes assumed $p = p^{\text{mech}}$ by taking a zero bulk viscosity, and he used arguments from kinetic theory of gases to support that choice.[9] This choice is generally taken for geophysical fluid applications, largely based on the assumption of local thermodynamic equilibrium mentioned in Section 25.8.1, and by noting that the flows are predominantly close to divergence-free.

Local thermodynamical equilibrium is not a good assumption in supersonic flows (e.g., shock waves), in which case $p \neq p^{\text{mech}}$ and the bulk viscosity is nonzero. Correspondingly, the divergence term and the second kinematic viscosity, $\lambda \neq -2\,\nu/3$, are important. Additionally, the second viscosity is important when concerned with the damping of acoustic waves (e.g., sounds absorption). Neither topics are considered in this book so that we have no further concern for the second viscosity.

Frictional force per volume

Taking the mechanical and thermodynamic pressures equal, so that the second kinematical viscosity satisfies equation (25.78), renders the frictional force per volume as given by the divergence of the frictional stress tensor

$$\rho\, F_n = \partial_m \mathbb{T}_{mn} = 2\, \partial_m(\mu_{\text{vsc}}\, \mathbb{S}^{\text{dev}}_{mn}). \tag{25.84}$$

The special case of a Boussinesq ocean with $\nabla \cdot \boldsymbol{v} = 0$

For a Boussinesq ocean (Chapter 29), the viscous friction (25.84) simplifies to

$$\rho_o\, F_n = 2\, \rho_o\, \partial_m(\nu\, \mathbb{S}_{mn}). \tag{25.85}$$

To reach this equality we set the dynamic viscosity to $\mu_{\text{vsc}} = \rho_o\, \nu$, with ρ_o the constant Boussinesq reference density. Furthermore, as studied in Chapter 29, the Boussinesq ocean has a non-divergent flow field so that $\nabla \cdot \boldsymbol{v} = \partial_m v_m = 0$, in which case

$$\mathbb{S}^{\text{dev}}_{mn} = \mathbb{S}_{mn} \quad \text{if } \nabla \cdot \boldsymbol{v} = 0. \tag{25.86}$$

Finally, for the case of a constant kinematic viscosity, we have the Boussinesq result reducing

[9] As noted in Section 62 of *Serrin* (1959), Stokes later admitted to having little confidence in this assumption.

to the Laplacian form, which is seen by

$$\begin{aligned}
\nu^{-1} F_n &= 2\,\partial_m \mathbb{S}_{mn} && \text{(25.87a)}\\
&= \partial_m(\partial_n v_m + \partial_m v_n) && \text{(25.87b)}\\
&= \partial_m(\partial_n v_m) + \partial_m(\partial_m v_n) && \text{(25.87c)}\\
&= \partial_n(\partial_m v_m) + \nabla^2 v_n && \text{(25.87d)}\\
&= \nabla^2 v_n, && \text{(25.87e)}
\end{aligned}$$

so that

$$\boldsymbol{F} = \nu\,\nabla^2 \boldsymbol{v}. \tag{25.88}$$

The relatively simple form of the Laplacian friction operator is commonly used for scale analysis, such as when introducing the Reynolds number in Section 25.9.

25.8.7 Navier-Stokes and Euler equations

The *Navier-Stokes* equation is a special form of the momentum equation found by assuming a Newtonian fluid constitutive relation. In this case the Navier-Stokes momentum equation (24.16), in the presence of rotation and gravity, takes on the form

$$\rho\,\frac{\mathrm{D}\boldsymbol{v}}{\mathrm{D}t} + 2\,\rho\,\boldsymbol{\Omega}\times\boldsymbol{v} = -\rho\,\nabla\Phi - \nabla p + \nabla\cdot(2\,\mu_{\text{vsc}}\,\mathbb{S}^{\text{dev}}), \tag{25.89}$$

where we set the friction tensor equal to $\mathbb{T} = 2\,\mu_{\text{vsc}}\,\mathbb{S}^{\text{dev}}$. Quite often when examining the mathematical properties of the Navier-Stokes equation, one assumes the flow to be non-divergent, in which case $\mathbb{S}^{\text{dev}} = \mathbb{S}$ since $\mathbb{S}_{qq} = \nabla\cdot\boldsymbol{v} = 0$. A further simplification occurs by assuming a constant density, ρ, and constant kinematic viscosity, ν, in which case the friction tensor reduces to the Laplacian form (25.88) so that the Navier-Stokes equation becomes

$$\frac{\mathrm{D}\boldsymbol{v}}{\mathrm{D}t} + 2\,\boldsymbol{\Omega}\times\boldsymbol{v} = -\nabla\Phi - \rho^{-1}\,\nabla p + \nu\,\nabla^2\boldsymbol{v}. \tag{25.90}$$

This form, or even simpler when ignoring rotation and gravity, is commonly studied by mathematicians concerned with existence and uniqueness properties of fluid flow solutions (e.g., see *Doering and Gibbon* (1995)). When assuming the fluid to be perfect, so that there are no viscous forces, the momentum equation is referred to as the *Euler equation*[10]

$$\frac{\mathrm{D}\boldsymbol{v}}{\mathrm{D}t} + 2\,\boldsymbol{\Omega}\times\boldsymbol{v} = -\nabla\Phi - \rho^{-1}\,\nabla p. \tag{25.91}$$

It is tempting to consider the Euler equations to be a continuous limit of the Navier-Stokes equation as the viscosity goes to zero. However, there is a key distinction between the two equations. Namely, the Navier-Stokes equations admit solutions that display statistically equilibriated turbulent motions, whereby energy cascades to the small scales through vortex stretching in three dimensional flows. This energy is ultimately dissipated by viscosity at the small spatial scales, and this mechanism holds no matter how small the viscosity, so long as it is nonzero. In contrast, for the Euler equations, with identically zero viscosity, energy cannot be dissipated at the small scales so that an equilibrium turbulent cascade is unavailable.

[10] Note that some authors refer to the Euler equations only in the case of a perfect fluid that has no body force, so that both rotation and gravitation vanish.

25.8.8 No-slip boundary conditions on solid boundaries

Another fundamental distinction between the Euler equation and Navier-Stokes equation concerns the boundary conditions. For the Navier-Stokes equation, the presence of a second order operator (the Laplacian), weighted by the viscosity, signals a distinct behavior of the flow next to boundaries. The Euler equation can only maintain a no-normal flow kinematic boundary condition at a boundary, with the kinematics detailed in Section 19.6. Yet the viscous fluid described by the Navier-Stokes equation must satisfy an additional boundary condition.

Evidence based on research in the 19th and 20th centuries suggests that fluids, such as air and water, adhere to solid boundaries and thus satisfy the *no-slip* boundary condition. Writing $\hat{\boldsymbol{n}}$ as the outward normal along the solid boundary, a no-slip boundary condition at a stationary solid boundary means that the flow has a zero component in the direction tangent to the boundary

$$\boldsymbol{v} - \hat{\boldsymbol{n}}\,(\hat{\boldsymbol{n}} \cdot \boldsymbol{v}) = 0 \quad \text{for } \boldsymbol{x} \text{ on solid boundary.} \tag{25.92}$$

When combined with the kinematic boundary condition, $\hat{\boldsymbol{n}} \cdot \boldsymbol{v} = 0$, we find that a no-slip boundary condition requires the fluid velocity to vanish at the solid boundary.[11] This boundary condition has basic implications for how stress acts between fluids and solids. We have more to say concerning this boundary condition in Section 25.10.[12]

25.8.9 Laplacian friction in terms of vorticity and divergence

The Laplacian friction operator with a constant viscosity is afforded the following decomposition

$$\begin{aligned}
\nu^{-1}\, F_n &= \partial_m(\partial_m v_n) && \text{(25.93a)}\\
&= \partial_m(\partial_m v_n - \partial_n v_m + \partial_n v_m) && \text{(25.93b)}\\
&= \partial_m(\partial_m v_n - \partial_n v_m) + \partial_n(\partial_m v_m) && \text{(25.93c)}\\
&= -2\,\partial_m \mathbb{R}_{mn} + \partial_n \nabla \cdot \boldsymbol{v} && \text{(25.93d)}\\
&= \partial_m(\epsilon_{mnp}\,\omega_p) + \partial_n \nabla \cdot \boldsymbol{v} && \text{(25.93e)}\\
&= -\epsilon_{nmp}\,\partial_m \omega_p + \partial_n \nabla \cdot \boldsymbol{v} && \text{(25.93f)}\\
&= -(\nabla \times \boldsymbol{\omega})_n + \partial_n \nabla \cdot \boldsymbol{v}. && \text{(25.93g)}
\end{aligned}$$

In the fourth equality we introduced the rotation tensor (18.99)

$$\mathbb{R}_{mn} = (1/2)\,(\partial_n v_m - \partial_m v_n), \tag{25.94}$$

which is related to the vorticity, $\boldsymbol{\omega} = \nabla \times \boldsymbol{v}$, via equation (18.102)

$$\mathbb{R}_{mn} = -\epsilon_{mnp}\,\omega_p/2. \tag{25.95}$$

These manipulations have served to decompose the Laplacian viscous acceleration, with a constant viscosity, into the two terms

$$\boldsymbol{F} = \nu\,[-\nabla \times \boldsymbol{\omega} + \nabla(\nabla \cdot \boldsymbol{v})]\,. \tag{25.96}$$

The Laplacian friction acceleration is thus due to the curl of the vorticity plus gradients in the velocity divergence. Many geophysical flows are dominated by vorticity, with the divergence relatively small. Indeed, the Boussinesq ocean discussed in Chapter 29 has $\nabla \cdot \boldsymbol{v} = 0$, in which

[11] More generally, if the solid boundary is moving, then the no-slip condition means that there is zero relative flow between the fluid and solid.

[12] See also the comments and footnote on page 86 of *Segel* (1987) as well as pages 83-84 of *Meyer* (1971).

case frictional acceleration arises only when the vorticity has a nonzero curl. Correspondingly, irrotational flows (where $\boldsymbol{\omega} = 0$) that are also non-divergent have zero Laplacian frictional acceleration.

25.8.10 Frictional stresses in a sheared flow

As a means to connect the above ideas in this section to the Couette flow discussed in Section 25.8.2, consider a non-divergent velocity that only has a zonal component with a vertical shear (Figure 25.6)

$$\boldsymbol{v} = u(z)\,\hat{\boldsymbol{x}}. \tag{25.97}$$

In this case the only nonzero components to the strain rate tensor are due to the vertical shear, $\mathbb{S}_{13} = \mathbb{S}_{31} = \partial_z u/2$. Now consider a horizontal area whose outward normal is parallel to the $\hat{\boldsymbol{z}}$ direction. The frictional force acting on that area is given by the area integral of the frictional stress

$$\boldsymbol{F}_{\text{area}} = \int \mathbb{T} \cdot \hat{\boldsymbol{n}}\,\mathrm{d}\mathcal{S} = \int \mathbb{T} \cdot \hat{\boldsymbol{z}}\,\mathrm{d}x\,\mathrm{d}y = \rho_{\circ}\,\frac{\hat{\boldsymbol{x}}}{2}\,\nu\,A\,\frac{\partial u}{\partial z}, \tag{25.98}$$

where $A = \int \mathrm{d}x\,\mathrm{d}y$ is the horizontal area, and where we used the constant reference density, $\rho_{\circ}$, for a Boussinesq fluid. Hence, the zonal stress arises from the nonzero vertical shear.

Momentum is deposited in regions where there is a divergence in the stress, in which case momentum is transferred from regions of high vertical shear to low vertical shear. At a point, the momentum is affected by the divergence of the friction stress at that point. For $\boldsymbol{v} = u(z)\,\hat{\boldsymbol{x}}$ we have

$$\left[\frac{\partial(\rho\,v_m)}{\partial t}\right]_{\text{viscous}} = \partial_n \mathbb{T}_{nm} \Longrightarrow \left[\frac{\partial(\rho\,u)}{\partial t}\right]_{\text{viscous}} = \partial_z\,(\mu_{\text{vsc}}\,\partial_z u), \tag{25.99}$$

so that zonal momentum is preferentially deposited to or removed from regions with high vertical curvature in the zonal velocity. Spatial variations in the dynamic viscosity, $\mu_{\text{vsc}} = \rho_{\circ}\,\nu$, also contribute to friction.

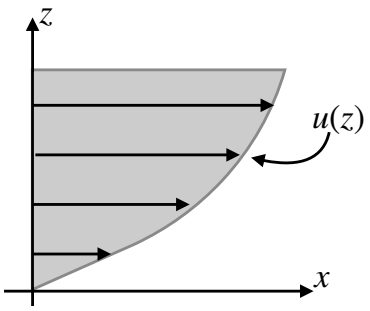

FIGURE 25.6: Sample profile of zonal velocity possessing a vertical shear: $\boldsymbol{v} = u(z)\,\hat{\boldsymbol{x}}$ and with a no-slip boundary condition at $z = 0$. The resulting zonal frictional stress arises from the nonzero vertical shear in the presence of viscosity.

25.8.11 The net stress tensor

Combining the frictional stress tensor with pressure and kinetic stress yields the flux-form momentum equation (25.64)

$$\frac{\partial(\rho\,\boldsymbol{v})}{\partial t} + 2\,\rho\,\boldsymbol{\Omega} \times \boldsymbol{v} + \rho\,\nabla\Phi = \nabla \cdot \boldsymbol{T}^{\text{net}}, \tag{25.100}$$

where we introduced the net stress tensor

$$\boldsymbol{T}^{\text{net}} = -p\,\mathbb{I} - \rho\,\boldsymbol{v}\otimes\boldsymbol{v} + \mathbb{T} = \begin{bmatrix} -p - \rho\,u^2 + \mathbb{T}_{11} & -\rho\,u\,v + \mathbb{T}_{12} & -\rho\,u\,w + \mathbb{T}_{13} \\ -\rho\,u\,v + \mathbb{T}_{12} & -p - \rho\,v^2 + \mathbb{T}_{22} & -\rho\,v\,w + \mathbb{T}_{23} \\ -\rho\,u\,w + \mathbb{T}_{13} & -\rho\,v\,w + \mathbb{T}_{23} & -p - \rho\,w^2 + \mathbb{T}_{33} \end{bmatrix}. \tag{25.101}$$

The left hand side of the momentum equation (25.100) includes the local time tendency plus the body forces from Coriolis and effective gravity. The right hand side is the divergence of the net stress tensor, with this tensor combining the pressure stress, kinetic stress, and frictional stress. Varieties of the net stress tensor appear in subsequent chapters of this book, with details dependent on the chosen approximations.

25.8.12 Properties under time reversal[13]

Make an animation of a dynamical system over a period of time, and then play the animation backwards in time. Is there anything about the time reversed animation to indicate it is not physically realizable? If not, then the dynamical system possesses symmetry under the reversal of time. We considered this question in Section 14.2 for the motion of a point particle. Here we ask the same question for the perfect fluid satisfying the Euler equation (25.91) in a rotating reference frame, in which we show there is time symmetry. We then show that time reversal symmetry is broken by viscous friction in the Navier-Stokes equation (25.90).

Perfect fluid satisfying the rotating Euler equation

Consider a particular solution, $\boldsymbol{v}(\boldsymbol{x},t)$, to the Euler equation in a rotating reference frame in either free space (i.e., no boundaries) or with static material boundaries where the flow satisfies the no normal flow boundary condition, $\boldsymbol{v}\cdot\hat{\boldsymbol{n}} = 0$. What transformation properties for the pressure, $p(\boldsymbol{x},t)$, density, $\rho(\boldsymbol{x},t)$, geopotential, $\Phi(\boldsymbol{x},t)$, and rotation, $\boldsymbol{\Omega}$, are sufficient for $\boldsymbol{v}^*(\boldsymbol{x},t^*) = -\boldsymbol{v}(\boldsymbol{x},-t)$ to be a solution? That is, by running time backwards, and changing the sign of the velocity, does this flow also satisfy the Euler equations?

In the following, we retain the space position unchanged. Hence, for brevity, we suppress the $\boldsymbol{x}$ dependence just focus on time, in which case we have the Euler equation (25.91) is written as

$$\rho(t)\,\frac{\mathrm{D}\boldsymbol{v}(t)}{\mathrm{D}t} + 2\,\rho(t)\,\boldsymbol{\Omega}\times\boldsymbol{v}(t) = -\rho(t)\,\nabla\Phi(t) - \nabla p(t). \tag{25.102}$$

We can ensure time reversal symmetry by assuming the following properties

$$\begin{aligned}
\boldsymbol{v}^*(\boldsymbol{x},t) &= -\boldsymbol{v}(\boldsymbol{x},-t) && \text{velocity reverses direction} && (25.103a)\\
p^*(\boldsymbol{x},t^*) &= p(\boldsymbol{x},-t) && \text{pressure retains same sign} && (25.103b)\\
\rho^*(\boldsymbol{x},t^*) &= \rho(\boldsymbol{x},-t) && \text{density retains same sign} && (25.103c)\\
\Phi^*(\boldsymbol{x},t^*) &= \Phi(\boldsymbol{x},-t) && \text{geopotential retains same sign} && (25.103d)\\
\boldsymbol{\Omega}^* &= -\boldsymbol{\Omega}. && \text{rotation reverses direction.} && (25.103e)
\end{aligned}$$

That is, if the rotating Euler equation is satisfied by $\boldsymbol{v}(\boldsymbol{x},t)$, $p(\boldsymbol{x},t)$, $\rho(\boldsymbol{x},t)$, $\Phi(\boldsymbol{x},t)$, and $\boldsymbol{\Omega}$, then the rotating Euler equation is also satisfied by $-\boldsymbol{v}(\boldsymbol{x},-t)$, $p(\boldsymbol{x},-t)$, $\rho(\boldsymbol{x},-t)$, $\Phi(\boldsymbol{x},-t)$, and $-\boldsymbol{\Omega}$. More explicitly, we verify time reversal symmetry by writing out the terms in the Euler equation

[13] This subsection was inspired by the discussion on page 77 of *Meyer* (1971), with the added feature here of the Coriolis acceleration.

$$\frac{\mathrm{D}\boldsymbol{v}^*(t^*)}{\mathrm{D}t^*} = \frac{\mathrm{D}\boldsymbol{v}(-t)}{\mathrm{D}t} \tag{25.104a}$$

$$\rho^*(t^*)\,\boldsymbol{\Omega}^* \times \boldsymbol{v}^*(t^*) = \rho(-t)\,\boldsymbol{\Omega} \times \boldsymbol{v}(-t) \tag{25.104b}$$

$$\rho^*(t^*)\,\Phi^*(t^*) = \rho(-t)\,\Phi(-t) \tag{25.104c}$$

$$\nabla p^*(t^*) = \nabla p(-t), \tag{25.104d}$$

so that satisfying the Euler equation (25.102) implies that also

$$\rho(-t)\,\frac{\mathrm{D}\boldsymbol{v}(-t)}{\mathrm{D}(-t)} + 2\,\rho(-t)\,\boldsymbol{\Omega} \times \boldsymbol{v}(-t) = -\rho(-t)\,\nabla\Phi(-t) - \nabla p(-t). \tag{25.105}$$

Note that a special case for the density condition (25.103c) is realized by a barotropic fluid[14], in which

$$\rho(\boldsymbol{x}, t) = \rho[p(\boldsymbol{x}, t)]. \tag{25.106}$$

The geopotential condition (25.103c) generally holds for static geopotentials, $\Phi = g\,z$, so that the gravity field does not care about the time direction. This property of gravity is characteristic of conservative forces. As noted in Section 14.2, the condition on rotation arises since the Coriolis acceleration is a function of the velocity.

Real fluid satisfying the rotating Navier-Stokes equation

Real fluids are not time reversible. For example, water leaving a tea pot does turn around and reenter the pot. Also, if air were a perfect fluid then one could only survive through breathing in a cross-wind since otherwise we would breath in the same air we just breathed out. Even though perfect fluids suffer from unrealistic features, it is of interest to expose symmetries of the Euler equations and to then study how these symmetries are broken. To see how dissipation breaks time reversal symmetry, consider the Laplacian viscous friction acceleration appearing in the Navier-Stokes equation (25.90)

$$\boldsymbol{F} = \nu\,\nabla^2\boldsymbol{v}, \tag{25.107}$$

where $\nu > 0$ is the kinematic viscosity. So long as the viscosity stays positive, we see that frictional acceleration changes sign under the transformation $\boldsymbol{v}^*(t^*) = -\boldsymbol{v}(-t)$, so that the friction operator becomes an anti-dissipation operator when time is reversed. As such, time reversed motion in the presence of viscous friction (again, with $\nu > 0$) is distinct from time forward motion. That is, friction breaks time reversal symmetry so that the Navier-Stokes equations are not time symmetric, meaning that we can distinguish between motion that is forward in time versus motion that is backward in time.

25.8.13 Comments and further study

There are more elaborate constitutive relations between the frictional stress tensor and strain rate tensor than those considered in this section. The most general form for a Newtonian fluid introduces a fourth-order viscosity tensor as in Section 4.5 of *Kundu et al.* (2016) and Chapter 17 in *Griffies* (2004). We also recommend the presention of stress in Chapter 5 of *Aris* (1962).

Geophysical fluids such as air and water are generally well treated using Newtonian constitutive relations. However, there are some geophysical turbulence theories that propose a non-Newtonian constitutive relation for part of their closures, whereby the constitutive relation makes use of products of the strain rate tensor for computing stress. *Anstey and Zanna*

[14] Barotropic fluids have a functional relation $\rho = \rho(p)$, and are discussed in Section 40.2.3.

(2017) offer a compelling approach with a subgrid scale stress tensor that is non-Newtonian and furthermore contains a non-zero trace, thus resulting in a modification to the mechanical pressure. Additional nonlinear relations can arise when the viscous tensor is a function of the flow, such as with the Smagorinsky scheme commonly used for Large Eddy Simulations (LES) (see *Smagorinsky* (1993) or Chapter 18 of *Griffies* (2004)).

25.9 Reynolds number and flow regimes

How important is friction relative to other terms in the momentum equation? In particular, how does it compare to the material acceleration? We consider that question in the context of the non-rotating and constant density Navier-Stokes equations with a constant viscosity, ρ,

$$\frac{\partial \boldsymbol{v}}{\partial t} + (\boldsymbol{v} \cdot \nabla)\, \boldsymbol{v} = -\rho^{-1}\, \nabla p + \nu\, \nabla^2 \boldsymbol{v}. \tag{25.108}$$

25.9.1 Non-dimensional Navier-Stokes

We non-dimensionalize the Navier-Stokes equation (25.108) to garner an understanding of relative magnitudes of the various terms. For that purpose, introduce the dimensional scales and corresponding non-dimensional fields

$$L = \text{length scale} \qquad U = \text{velocity scale} \qquad P = \text{pressure scale} \qquad T = \text{time scale}, \tag{25.109}$$

so that equation (25.108) takes the form

$$\frac{\partial \widehat{\boldsymbol{v}}}{\partial \widehat{t}} + \frac{U\,T}{L}\, (\widehat{\boldsymbol{v}} \cdot \widehat{\nabla})\, \widehat{\boldsymbol{v}} = -\frac{T\,P}{\rho\, U\, L}\, \widehat{\nabla} \widehat{p} + \frac{T\,\nu}{L^2}\, \widehat{\nabla}^2 \widehat{\boldsymbol{v}}, \tag{25.110}$$

where the hat fields are non-dimensional and defined according to

$$\nabla = L^{-1}\, \widehat{\nabla} \qquad \partial_t = T^{-1}\, \partial_{\widehat{t}} \qquad \boldsymbol{v} = U\, \widehat{\boldsymbol{v}} \qquad p = P\, \widehat{p}. \tag{25.111}$$

25.9.2 Ratio of inertial to frictional accelerations

We are concerned with three dimensional flows with only a single length and velocity scale, L and U. For the time scale we assume that it is determined by the fluid particle time scale, which is the *advective time*

$$T = L/U. \tag{25.112}$$

Furthermore, we assume that the scale of mechanical pressure is comparable to the dynamical stress induced by the flow itself, thus leading to the *dynamical pressure scaling*[15]

$$P = \rho\, U^2. \tag{25.113}$$

These assumed scales for time and pressure bring the non-dimensionl Navier-Stokes equation (25.110) into the rather tidy form

$$\frac{\partial \widehat{\boldsymbol{v}}}{\partial \widehat{t}} + (\widehat{\boldsymbol{v}} \cdot \widehat{\nabla})\, \widehat{\boldsymbol{v}} = -\widehat{\nabla} \widehat{p} + \frac{1}{\mathrm{Re}}\, \widehat{\nabla}^2 \widehat{\boldsymbol{v}}. \tag{25.114}$$

[15] When considering flows close to geostrophic balance in Sections 33.3.2 and 43.7.4, we find that pressure scales as $\rho\, f\, U\, L$, where f is the Coriolis parameter, which is distinct from the ρU^2 scaling found for flows not feeling the Coriolis acceleration.

Flow regimes of the non-dimensional Navier-Stokes equation are specified by the non-dimensional number, $\mathrm{Re} = L\,U/\nu$, which is the *Reynolds number*. By definition, the Reynolds number is the ratio of scales for material (inertial) acceleration to frictional acceleration

$$\mathrm{Re} = \frac{\text{inertial accelerations}}{\text{frictional accelerations}} = \frac{U/T}{\nu\,U/L^2} = \frac{L^2/T}{\nu} = \frac{L\,U}{\nu}. \tag{25.115}$$

25.9.3 Reynolds numbers for some example flows

Laboratory experiments with flow around and within various objects indicates the following regimes of flow as a function of the Reynolds number:

$$\mathrm{Re} \sim \begin{cases} \leq 10^2 & \text{laminar} \\ 10^2 - 10^3 & \text{quasi-periodic flow} \\ 10^3 - 10^4 & \text{transition to turbulence} \\ \geq 10^4 & \text{fully turbulent.} \end{cases} \tag{25.116}$$

These numbers are fuzzy given dependence on the geometry of the objects placed in the flow and their characteristic length scale. What is more general concerns the behavior of the flow, with a transition from laminar to turbulent typically occuring as the flow moves from relatively low to high Reynolds number.

For a given molecular kinematic viscosity, the Reynolds number is dependent on the velocity and length scales. Let us consider some examples. First, place a finger into a flowing stream of water, such as in a gentle mountain creek. Let the length scale for the finger be 10^{-2} m and the stream flow at a speed of $U \approx 0.1 - 1$ m s^{-1}. With the kinematic viscosity of water given by (page 75 of *Gill* (1982))

$$\nu_{\text{water}} = 10^{-6}\ \text{m}^2\ \text{s}^{-1}, \tag{25.117}$$

our finger poking into the mountain stream is associated with a flow Reynolds number on the order of

$$\mathrm{Re}_{\text{finger in stream}} = 10^3 - 10^4. \tag{25.118}$$

Evidently, mountain stream flow around a finger is at the lower end of the turbulent regime. We thus expect to see slightly turbulent whirls and eddies downstream from the finger.

Now consider an oceanographic length scale given by a Gulf Stream ring (see Figure 31.1) in which $L \approx 10^5$ m. Assuming the flow speed is on the same order as the mountain stream (good assumption) leads to a huge Reynolds number for Gulf Stream flow

$$\mathrm{Re}_{\text{Gulf Stream}} = 10^{10} - 10^{11}. \tag{25.119}$$

For the atmosphere, we take $L = 10^6$ m for a typical atmospheric weather system, $U = 10$ m s^{-1} for the speed, and

$$\nu_{\text{air}} = 1.4 \times 10^{-5}\ \text{m}^2\ \text{s}^{-1}, \tag{25.120}$$

for the kinematic viscosity of air at standard pressure (page 75 of *Gill* (1982)). Given the larger length and velocity scales, the Reynolds number for large-scale atmospheric circulation features is

$$\mathrm{Re}_{\text{weather system}} = 10^{12}. \tag{25.121}$$

Note that these large Reynolds numbers are associated with horizontal scales of geophysical flows. Vertical motions have much smaller L and U, so that the Reynolds number for vertical motions are significantly smaller than horizontal scales.

The above values for the Reynolds number from horizontal geophysical motions are huge relative to typical values found in engineering flows, with the large values arising from the large

length scales of the flows. Large Reynolds numbers signal the minor role that molecular friction plays in large-scale geophysical fluid flows. Even so, molecular friction is the process leading to mechanical energy dissipation at the small scales. A fundamental feature of large Reynolds number flow is the presence of turbulent motions. Turbulent flows are highly nonlinear and affect a transfer of mechanical energy across length and time scales. This cascade leads to the dissipation of mechanical energy at the small scales. It is at the small scales that flow curvature can be large enough for the relatively tiny values of molecular viscosity to dissipate the energy, thus preventing an *ultraviolet catastrophe*; i.e., preventing the unbounded pile up of mechanical energy at the smallest scales.[16]

The ocean and atmosphere exhibit a huge variety of turbulent regimes, from the macro-turbulence of quasi-geostrophic eddies to the microturbulence of boundary layers. Turbulence is not directly considered in this book. However, certain of its implications are identified in various places given that it is so basic to the ocean and atmosphere flows. *Vallis* (2017) offers a pedagogical entry point for the physics and maths of geophysical turbulence.

25.10 Stress on an interface

In this section we study the stress acting on an interface. This analysis applies to an arbitrary surface within a single media as well as for the boundary interface separating a liquid and a gas (air-sea boundary) or between a fluid and a rigid boundary (air-land or ocean-land). We ignore the effects from surface tension discussed in Section 25.11 since we are interested in length scales on the order of meters or larger (see in particular Section 25.11.5).

25.10.1 General formulation

Formulation of the stress boundary conditions follows from applying the finite volume momentum equation (25.67) to a cylindrical region straddling a moving interface such as that shown in Figure 25.7. The sides of the cylinder have thickness h and the top and bottom have area $\delta\mathcal{S}$. In the limit that the cylinder thickness goes to zero, the volume integrals in equation (25.67) vanish under the assumption of a smooth velocity field on both sides of the interface as well as smooth body forces. We are thus left with the constraint that the area integrated contact forces must vanish when integrated around the cylinder boundary

$$\oint_{\partial\text{cylinder}} [\boldsymbol{T} + \rho\,\boldsymbol{v} \otimes (\boldsymbol{v}^{(b)} - \boldsymbol{v})] \cdot \hat{\boldsymbol{n}}\, \mathrm{d}\mathcal{S} = \oint_{\partial\text{cylinder}} [-p\,\mathbb{I} + \mathbb{T} + \rho\,\boldsymbol{v} \otimes (\boldsymbol{v}^{(b)} - \boldsymbol{v})] \cdot \hat{\boldsymbol{n}}\, \mathrm{d}\mathcal{S} = 0. \quad (25.122)$$

The end-caps on the cylinder vanish as $h \to 0$, in which case we have no constraint based on the stresses acting on the end-caps. Instead, the $h \to 0$ limit leads us to conclude that the contact force on one side of the interface is equal and opposite to that on the other side. This condition is a direct statement of the Newton's third law as manifest via the local equilibrium of stresses discussed in Section 25.2.2. For the stresses acting on the interface in Figure 25.7 we have

$$[-p_{\mathrm{A}}\,\mathbb{I} + \mathbb{T}_{\mathrm{A}} + \rho_{\mathrm{A}}\,\boldsymbol{v}_{\mathrm{A}} \otimes (\boldsymbol{v}^{(b)} - \boldsymbol{v}_{\mathrm{A}})] \cdot \hat{\boldsymbol{n}}_{\mathrm{A}} + [-p_{\mathrm{B}}\,\mathbb{I} + \mathbb{T}_{\mathrm{B}} + \rho_{\mathrm{B}}\,\boldsymbol{v}_{\mathrm{B}} \otimes (\boldsymbol{v}^{(b)} - \boldsymbol{v}_{\mathrm{B}})] \cdot \hat{\boldsymbol{n}}_{\mathrm{B}} = 0. \quad (25.123)$$

Setting $\hat{\boldsymbol{n}} = \hat{\boldsymbol{n}}_{\mathrm{B}} = -\hat{\boldsymbol{n}}_{\mathrm{A}}$ leads to

$$[-p_{\mathrm{A}}\,\mathbb{I} + \mathbb{T}_{\mathrm{A}} + \rho_{\mathrm{A}}\,\boldsymbol{v}_{\mathrm{A}} \otimes (\boldsymbol{v}^{(b)} - \boldsymbol{v}_{\mathrm{A}})] \cdot \hat{\boldsymbol{n}} = [-p_{\mathrm{B}}\,\mathbb{I} + \mathbb{T}_{\mathrm{B}} + \rho_{\mathrm{B}}\,\boldsymbol{v}_{\mathrm{B}} \otimes (\boldsymbol{v}^{(b)} - \boldsymbol{v}_{\mathrm{B}})] \cdot \hat{\boldsymbol{n}}, \quad (25.124)$$

[16] Ultraviolet refers to the high wavenumber end of the flow spectrum. The name refers to the violet part of the visible electromagnetic spectrum, which has a higher wavenumber than the infrared part of the spectrum.

which is an expanded expression of Newton's third law given by equation (25.5). Recall that we are ignoring surface tension, which means there is no pressure jump across the interface (see Section 25.11). Hence, setting $p_{\rm A} = p_{\rm B}$ allows us to cancel pressure thus leaving an interface stress condition involving just the frictional stress and kinetic stress

$$[\mathbb{T}_{\rm A} + \rho_{\rm A}\, \boldsymbol{v}_{\rm A} \otimes (\boldsymbol{v}^{(b)} - \boldsymbol{v}_{\rm A})] \cdot \hat{\boldsymbol{n}} = [\mathbb{T}_{\rm B} + \rho_{\rm B}\, \boldsymbol{v}_{\rm B} \otimes (\boldsymbol{v}^{(b)} - \boldsymbol{v}_{\rm B})] \cdot \hat{\boldsymbol{n}}, \tag{25.125}$$

which is sometimes more suitably written as

$$(\mathbb{T}_{\rm A} - \mathbb{T}_{\rm B}) \cdot \hat{\boldsymbol{n}} = \boldsymbol{v}_{\rm B}\, [\rho_{\rm B}\, (\boldsymbol{v}^{(b)} - \boldsymbol{v}_{\rm B}) \cdot \hat{\boldsymbol{n}}] - \boldsymbol{v}_{\rm A}\, [\rho_{\rm A}\, (\boldsymbol{v}^{(b)} - \boldsymbol{v}_{\rm A}) \cdot \hat{\boldsymbol{n}}]. \tag{25.126}$$

Recall from Section 25.3 that $\mathbb{T}_{\rm A} \cdot \hat{\boldsymbol{n}}$ and $\mathbb{T}_{\rm B} \cdot \hat{\boldsymbol{n}}$ pick out that portion of the frictional stress tensor that acts on a surface whose outward normal is $\hat{\boldsymbol{n}}$. We now consider some examples to unpack the boundary condition (25.126).

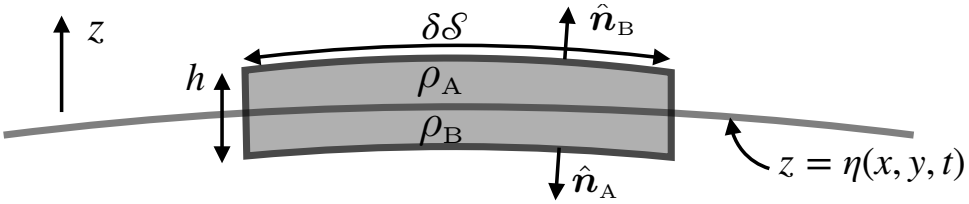

FIGURE 25.7: An infinitesimal cylindrical region used in formulating the stress boundary condition at an interface. The interface can be one that separates two fluid regions with densities $\rho_{\rm A}$ and $\rho_{\rm B}$. It can also represent the boundary between a fluid (region A) and solid (region B). The interface generally moves with velocity $\boldsymbol{v}^{(b)}$. We orient the interface through the outward normals according to (recall h is infinitesimal) $\hat{\boldsymbol{n}} = \hat{\boldsymbol{n}}_{\rm B} = -\hat{\boldsymbol{n}}_{\rm A}$, so that the outward normal for region A points into region B whereas the outward normal for region B points into region A. For this particular interface, the normal direction has a nonzero projection in the vertical, $\hat{\boldsymbol{n}} \cdot \hat{\boldsymbol{z}} \neq 0$, thus allowing us to define the interface vertical position according to $z = \eta(x, y, t)$. This interface represents an idealized geometry useful to formulate the stress condition at the boundary between fluid media, such as the air-sea interface, fluid-land interface, or interior fluid interface (e.g., buoyancy surface). The single geometric assumption is that there are no overturning motions so that $\hat{\boldsymbol{n}} \cdot \hat{\boldsymbol{z}} \neq 0$, with this assumption based on convenience. The stress condition is general and so does not require this assumption.

25.10.2 Solid material boundary

Consider a solid material boundary through which no matter crosses. Let region B be the solid side of the interface and region A the fluid side (region A is either the ocean or atmosphere). The material nature of the boundary means that no matter crosses it, in which case (see Section 19.6.2)

$$(\boldsymbol{v}^{(b)} - \boldsymbol{v}_{\rm A}) \cdot \hat{\boldsymbol{n}} = (\boldsymbol{v}^{(b)} - \boldsymbol{v}_{\rm B}) \cdot \hat{\boldsymbol{n}} = 0. \tag{25.127}$$

A nonzero $\boldsymbol{v}^{(b)}$ corresponds here to a moving solid boundary, such as the region next to the grounding line of an ice-shelf. More commonly, in geophysical fluid applications we have $\boldsymbol{v}^{(b)} = 0$ for solid boundaries. In either case, there is no contribution from the kinetic stress so that the stress condition (25.125) reduces to

$$\mathbb{T}_{\rm A} \cdot \hat{\boldsymbol{n}} = \mathbb{T}_{\rm B} \cdot \hat{\boldsymbol{n}} \Longleftrightarrow \mathbb{T}_{\rm A} \cdot \hat{\boldsymbol{n}}_{\rm A} = -\mathbb{T}_{\rm B} \cdot \hat{\boldsymbol{n}}_{\rm B}. \tag{25.128}$$

This identity is consistent with

$$\mathbb{T}_{\rm A} \cdot \hat{\boldsymbol{n}} = \boldsymbol{\tau}^{\text{friction A}}(\boldsymbol{x}, t, \hat{\boldsymbol{n}}) = -\boldsymbol{\tau}^{\text{friction A}}(\boldsymbol{x}, t, -\hat{\boldsymbol{n}}) = \mathbb{T}_{\rm B} \cdot \hat{\boldsymbol{n}} = \boldsymbol{\tau}^{\text{friction B}}(\boldsymbol{x}, t, \hat{\boldsymbol{n}}), \tag{25.129}$$

which expresses Newton's third law in the form of Cauchy's principle in equation (25.5). Hence, the frictional force imparted by the land on the fluid is equal and opposite to that imparted by

the fluid on the land.

25.10.3 No-slip condition at a static boundary

At solid boundaries, the kinematic boundary condition from Section 19.6.1 sets the normal component of the velocity to zero[17]

$$\boldsymbol{v} \cdot \hat{\boldsymbol{n}} = 0 \qquad \text{kinematic no-flux condition on static material boundary.} \tag{25.130}$$

However, kinematic is unable to specify the tangential component of the velocity along a solid boundary. What is it?

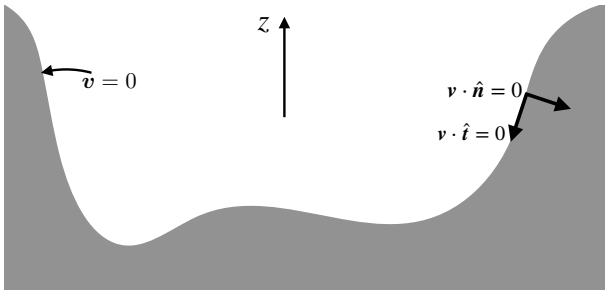

FIGURE 25.8: The no-slip boundary condition means that fluid has a zero tangential velocity component at the solid-fluid boundary, $\boldsymbol{v} \cdot \hat{\boldsymbol{t}} = 0$. Together, the kinematic no-normal flow boundary condition, $\boldsymbol{v} \cdot \hat{\boldsymbol{n}} = 0$, plus the dynamic no-slip boundary condition, $\boldsymbol{v} \cdot \hat{\boldsymbol{t}} = 0$, mean that the fluid sticks to the solid boundary. That is, the fluid particle velocity vanishes at a solid boundary when the no-slip condition holds.

Laboratory experiments over the 19th and 20th centuries indicate that there is no relative motion of molecules at solid-fluid interfaces.[18] That is, a fluid at the solid-fluid interface has a velocity matching that of the solid so that the fluid sticks to the solid boundary as depicted in Figure 25.8. The no-slip boundary condition means that both the normal and tangential components of the fluid velocity vanish next to static solid boundaries

$$\boldsymbol{v} \cdot \hat{\boldsymbol{n}} = \boldsymbol{v} \cdot \hat{\boldsymbol{t}} = 0 \qquad \text{no-slip condition on static solid boundaries.} \tag{25.131}$$

The no-slip boundary condition gives rise to an exchange of momentum between the solid and fluid, with this exchange mediated by viscosity. This boundary condition is the origin of the tangential stresses found in the Couette flow discussed in Section 25.8.2. In the absence of viscous friction, as per an inviscid perfect fluid, the no-slip boundary condition cannot be imposed since doing so would mathematically over-specify the flow. Consequently, for inviscid fluids the tangential component of the velocity remains unspecified at solid boundaries.

25.10.4 Lagrangian interface

Consider a Lagrangian interface within the fluid, with this interface defined so that

$$(\boldsymbol{v}^{(b)} - \boldsymbol{v}_{\mathrm{A}}) \cdot \hat{\boldsymbol{n}} = (\boldsymbol{v}^{(b)} - \boldsymbol{v}_{\mathrm{B}}) \cdot \hat{\boldsymbol{n}} = 0. \tag{25.132}$$

This condition is identical to the solid material boundary condition (25.127), so that the kinetic stress contribution to equation (25.125) vanishes. We thus have the frictional stress condition

[17] For convenience we here assume the solid boundary is static. Generalizations to moving solid boundaries are straightforward, requiring one to merely replace $\boldsymbol{v}$ with $\boldsymbol{v} - \boldsymbol{v}^{(b)}$ in the results of this subsection.

[18] As discussed in the historical essay by *Anderson* (2005), it was the work of Prandtl in 1905 that first exposed the fundamental nature of the no-slip boundary condition, and its role in establishing boundary layers around solid bodies immersed in a fluid flow.

(25.128) and a Newton's third law interpretation (25.129), yet now the frictional transfer takes place between two regions of the same fluid.

25.10.5 Permeable interface

Now allow for the interface to be permeable to matter, with matter conservation meaning that

$$\rho_{\mathrm{A}} \, (\boldsymbol{v}_{\mathrm{A}} - \boldsymbol{v}^{(b)}) \cdot \hat{\boldsymbol{n}} = \rho_{\mathrm{B}} \, (\boldsymbol{v}_{\mathrm{B}} - \boldsymbol{v}^{(b)}) \cdot \hat{\boldsymbol{n}}. \tag{25.133}$$

The kinetic stress thus adds to the frictional contribution in the stress boundary condition (25.125), with the kinetic stress providing a transfer of momentum across the interface through the transfer of matter that carries a nonzero linear momentum. Rearrangement of the stress boundary condition (25.125) with use of mass conservation (25.133) leads to

$$(\mathbb{T}_{\mathrm{A}} - \mathbb{T}_{\mathrm{B}}) \cdot \hat{\boldsymbol{n}} = (\boldsymbol{v}_{\mathrm{A}} - \boldsymbol{v}_{\mathrm{B}}) \, [\rho_{\mathrm{A}} \, (\boldsymbol{v}_{\mathrm{A}} - \boldsymbol{v}^{(b)}) \cdot \hat{\boldsymbol{n}}]. \tag{25.134}$$

We unpack this boundary condition by considering two cases.

Single continuous fluid media

If the interface is within a single continuous fluid media, then $\boldsymbol{v}_{\mathrm{A}} = \boldsymbol{v}_{\mathrm{B}}$ so that the frictional stress tensor boundary condition (25.128) again holds: $(\mathbb{T}_{\mathrm{A}} - \mathbb{T}_{\mathrm{B}}) \cdot \hat{\boldsymbol{n}} = 0$.

Air-sea boundary interface

Consider now the air-sea boundary where region B is the ocean and region A the atmosphere. Introduce the dia-surface mass flux according to equation (19.78)

$$\rho_{\mathrm{A}} \, (\boldsymbol{v}_{\mathrm{A}} - \boldsymbol{v}^{(b)}) \cdot \hat{\boldsymbol{n}} = \rho_{\mathrm{B}} \, (\boldsymbol{v}_{\mathrm{B}} - \boldsymbol{v}^{(b)}) \cdot \hat{\boldsymbol{n}} = -\mathcal{Q}_{\mathrm{m}}, \tag{25.135}$$

where $\mathcal{Q}_{\mathrm{m}}$ is the mass per time per surface area crossing the boundary. The minus sign is implied by the convention that $\mathcal{Q}_{\mathrm{m}} > 0$ means that mass enters the ocean side of the interface and leaves the atmosphere side. The stress boundary condition (25.134) takes the form

$$(\mathbb{T}_{\mathrm{atm}} - \mathbb{T}_{\mathrm{ocn}}) \cdot \hat{\boldsymbol{n}} = -(\boldsymbol{v}_{\mathrm{atm}} - \boldsymbol{v}_{\mathrm{ocn}}) \, \mathcal{Q}_{\mathrm{m}} \tag{25.136}$$

We might consider the velocity of the atmosphere to be unequal to that of the ocean, in which case the surface normal projection of the frictional stress tensor satisfies a jump condition in the presence of mass transport across the air-sea interface. However, following Section 1.9 of *Batchelor* (1967), available evidence suggests that when approaching the boundary interface, the velocity of the two media match, both their normal and tangential components. In this case we again return to the friction boundary condition (25.128), in which the normal projection of the frictional stress tensors match, even in the presence of mass transport across the boundary.

25.10.6 Summary comments

There are three terms in the general expression for the stress boundary condition (25.124), with contributions from pressure, friction, and kinetic stress. In the absence of surface tension (Section 25.11), pressure is continuous at the interface; i.e., its value is the same on both sides of the interface. In the absence of mass transport across the interface, then we find a continuous kinetic stress at the interface that then leads to a continuous frictional stress. However, mass transport crossing the interface leads to a jump in the friction for those cases where velocity has a jump across the interface. Even so, empirical evidence suggests that the velocity has no jump across the interface, in which case there is no jump in the normal stress.

The subject of boundary conditions for momentum are not simple, particularly in the presence of mass transport across the boundary. We have only briefly touched on the topic, with similar discussions provided by Section 1.9 of *Batchelor* (1967) and Section 4.10 of *Kundu et al.* (2016). Specialized treatments are needed when pursuing these topics in more detail.

25.10.7 Comments on boundary layers

A fundamental advance in the relevance of fluid mechanics for describing observed flows came from the 20th century work of Prandtl and others who noted the central role of viscosity, even the tiny molecular values, in forming boundary layers when fluids flow next to rigid bodies.[19] Prandtl's work focused on flows around airplane wings, thus supporting the development of aerodynamics as a scientific and engineering discipline. The key ideas transfer to geophysical flows where boundary layers form in the atmosphere and ocean as these fluids interact with the solid earth. Boundary layers also form where the atmosphere and ocean interact with one another.

A key facet of geophysical boundary layers concerns the dominance of turbulence in producing an eddy viscosity that is many orders larger than molecular viscosity. Indeed, molecular viscosity plays a role only in a very small region (the *laminar subregion*) immediately adjacent to the boundary. In contrast, the bulk of the boundary layer is dominated by turbulent flows. In Chapter 33 we study geophysical boundary layers that are affected by pressure, Coriolis, and turbulence induced friction. The role of rotation distinguishes geophysical boundary layers from engineering applications. The associated *Ekman boundary layers* are crucial for understanding circulation and transport in both the atmosphere and ocean.

25.11 Surface tension

Surface tension arises from the anisotropic forces acting on molecules that are within a mean free path distance from the surface between two immiscible liquids, between a liquid and gas, or between a fluid and a solid. Energetically, it arises since molecules have a preferance for locations within the bulk of the fluid (surrounded by identical neighbors) rather than at the boundary (where it encounters fewer identical neighbors). Surface tension acts to resist forces that act to increase the surface area, and it has many physical consequences that are part of our common experience. For example, it allows certain insects to walk on water even though their body density is greater than water. It also accounts for the predominantly spherical shape of rain drops and gas bubbles in liquids. As we study in Section 52.10, surface tension gives rise to capillary waves when there is a very slight breeze on the ocean surface, or when a tiny stone is thrown into a still pond (gravity waves dominate for larger stones). In the present section we focus on the mechanics of surface tension. Note that a first principles understanding of surface tension involves tools from physical chemistry that are outside of the scope of this book. Here, we develop the subject phenomenologically.

25.11.1 Capillary tube

Atmospheric pressure at the earth's surface is roughly $p_{\text{atm}} = 10^5$ N m^{-2}. As we saw in Section 25.8, pressure acts normal to a surface regardless the surface orientation. So fill a container of water whose weight per horizontal area is less than the atmospheric pressure, $\rho\, g\, h < p_{\text{atm}}$ and turn the container upside-down as in Figure 25.9. Does the water spill from the container? Common

[19] For a historical treatement of boundary layer theory see *Anderson* (2005), or for a pedagogical study see *Tennekes and Lumley* (1972). The associated mathematical methods of singular perturbation theory and matched asymptotic expansions (e.g., *Dyke* (1975)) offer an example of how the study of physical systems can spawn the development of new mathematical methods.

experience with drinking glasses indicate that water will spill. But what about containers with a very small cross-sectional area such as the pipettes used in chemistry laboratories? Pipettes, or more generally capillary tubes, hold the liquid regardless the orientation. They do so since their cross-sectional area is small enough to allow forces from surface tension to overcome gravitational instabilities acting at the liquid-gas interface. We return to this point in Section 60.2.3 when studying the *Rayleigh-Taylor* instability in the presence of surface tension. In the remainder of this section we discuss elements of surface tension with the goal to develop intuition as well as to determine the length scales where it becomes important.

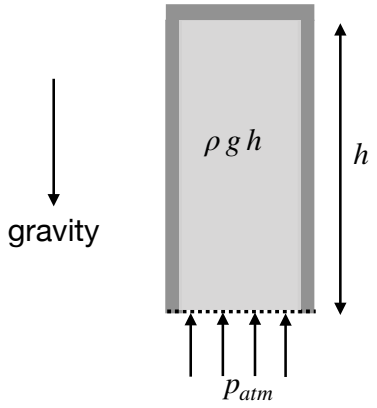

FIGURE 25.9: A container of water with density ρ and height h is placed upside-down. Atmospheric pressure, $p_{\rm atm}$, will support water with thickness $h < p_{\rm atm}/(\rho\, g) \approx 10$ m if the cross-sectional area of the container is small enough to allow for surface tension to overcome the gravitationally unstable waves that otherwise allow water to spill from the container. The liquid-gas interface supports both gravity waves (Section 52.3) and capillary waves (Section 52.10). If the wavelength is small enough then surface tension suppresses the growth of unstable gravity waves so that the liquid remains within the *capillary tube*. However, for longer waves allowed by increasing the cross-sectional area, then fluctuations allow the gravitational instability to overcome surface tension, thus breaking the interface and releasing water.

25.11.2 Force balance on an air-water interface

Consider two fluids with distinct densities. Air and water provide one example of special importance to understanding physics at the ocean-atmosphere boundary. Another example concerns two immiscible layers of water within the ocean or two layers of air within the atmosphere. For molecules well within either of the fluid regions, the intermolecular forces are statistically isotropic. In contrast, intermolecular forces are not isotropic for molecules within a mean free path distance from the interface.[20] Attractive (cohesive) intermolecular (van der Waals) forces dominate within a liquid whereas gas molecules generally feel more repulsive forces. Hence, a liquid molecule within the liquid-gas interface preferentially experiences an attractive force towards the liquid side of the interface, as depicted in Figure 25.10. Surface tension arises from the cohesive force per area acting between molecules in a direction that parallels the interface, with surface tension acting to resist perturbations to the interface shape.

Anisotropic attractive intermolecular forces cause the interface between the two fluids to behave as a stretched membrane that experiences a tensile force resisting any stretching of the interface. The magnitude of the tensile force per unit length (or energy per unit area) is the *surface tension*, γ (SI units N m^{-1} = kg s^{-2}), which measures the force needed to change the interface a unit length. Equivalently, the surface tension is the energy per area needed to change the surface area. The surface tension is a property of the two fluids, including their temperature,

[20] As discussed in Section 16.2, the mean free path is a statistical measure of the distance a molecule moves before hitting another molecule.

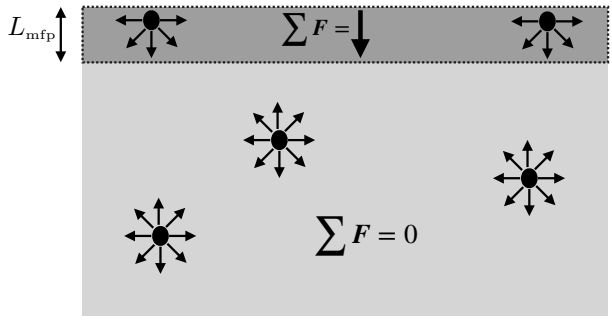

FIGURE 25.10: Surface tension at a liquid-gas interface arises from the anisotropic cohesive forces acting on liquid molecules within a mean-free-path distance, L_{mfp}, from the interface, which contrasts to the isotropic cohesive forces acting away from the interface. The net intermolecular force vanishes for interior molecules, whereas the net force acts inward on molecules at the interface. Surface tension refers to the cohesive force per area acting between molecules in a direction that is parallel to the interface.

as well as any impurities that might be included on the interface; e.g., oil on the surface of water effects properties of the capillary waves found on the air-sea interface (see Section 52.10). In the following we focus on the liquid-gas example to be specific and to expose issues that arise in studies of the air-sea interface. For a liquid-gas interface surrounding a liquid drop, the tensile force acts to curve the interface towards the liquid into a spherical shape.

The tensile force along a line segment is directed normal to the line and tangent to the interface

$$\boldsymbol{f}_{\text{interface}} = -\gamma\, \hat{\boldsymbol{n}} \times \delta \boldsymbol{x}, \tag{25.137}$$

where $\hat{\boldsymbol{n}}$ is a normal vector pointing towards the center of the curved interface, and $\delta \boldsymbol{x}$ is a line element oriented so that the normal $\hat{\boldsymbol{n}}$ points to the left facing in the direction of the line increment. Figure 25.11 depicts the surface tensile forces acting on the surface of a spherical bubble of water. Note that it is sometimes useful to consider the product $\gamma\, \mathrm{d}\mathcal{S}$ as the work (units of N m^{-1} = Joule) required to create an area, $\mathrm{d}\mathcal{S}$, on the interface. We make use of this energetic perspective in Section 25.11.3.

To develop an expression for the pressure jump across the liquid-gas interface, consider a spherical droplet of radius R shown in Figure 25.11 and focus on the circular cross-section cut through the center of the sphere. The net tensile force acting on the circumference of the circle is

$$\boldsymbol{F}_{\text{circle}} = \oint_{\text{circle}} \boldsymbol{f}_{\text{interface}} = -\oint_{\text{circle}} \gamma\, \hat{\boldsymbol{n}} \times \delta \boldsymbol{x} = -2\pi R\, \gamma\, \hat{\boldsymbol{z}}. \tag{25.138}$$

Equilibrium of the spherical droplet is realized by a pressure jump across the circular cross-sectional area

$$\pi R^2 \left(p_{\text{in}} - p_{\text{out}}\right) = 2\pi R\, \gamma \Longrightarrow \left(p_{\text{in}} - p_{\text{out}}\right) = 2\gamma / R. \tag{25.139}$$

Hence, the pressure jump is determined by the surface tension (a property of the two fluids) and the curvature of the sphere, R, which is also the radius of curvature for the sphere. Pressure is higher inside of the sphere (i.e., on the concave side of the interface), with this pressure required to balance the pressure outside the sphere plus the surface tension. Notably, equilibrium for smaller bubbles (with $R \to 0$) requires a larger pressure difference than for larger bubbles.

The pressure jump is known as the *capillary pressure*. It arises from surface tension and curvature of the interface. The relation (25.139) is a special case of the *Young-Laplace formula*, specialized here to a sphere.

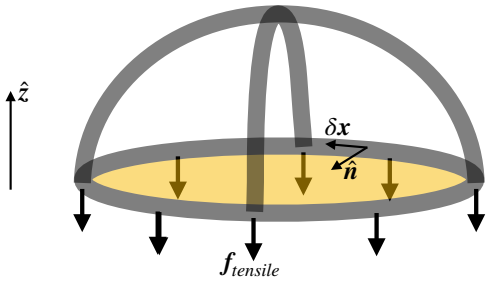

FIGURE 25.11: Surface tension on a spherical water droplet, with water on the inside of the sphere and air on the outside. The tensile forces act parallel to the spherical interface between the water and air. When cutting a circular cross-section as shown here, the surface tensile force acts downward. In equilibrium, the net tensile forces acting downward along the circumference of the hemisphere ($2\pi R\,\gamma$) are balanced by a pressure jump across the droplet, with the interior pressure larger than the exterior pressure. Focusing on the circular cross-section, this area remains static so long as $2\pi R\,\gamma = \pi R^2\,(p_{\text{in}} - p_{\text{out}})$, leading to a pressure jump across the droplet interface $p_{\text{in}} - p_{\text{out}} = 2\,\gamma/R$. This result is general: namely, according to the Young-Laplace formula (25.149), pressure is greater on the concave side of the interface than on the convex side.

25.11.3 Young-Laplace formula

We garner added insight into the physics of surface tension by considering the energetics required to enable a virtual displacement of a surface through a pressure field along with the work required to change the area of the surface. The resulting equation for the pressure jump across the surface is referred to as the *Young-Laplace formula*, which expresses the pressure jump in terms of the surface tension and the principle radii of curvature for the surface.

Consider a horizontal surface depicted in Figure 25.12 that represents the interface seperating fluid-A from fluid-B, with $\hat{\boldsymbol{n}}$ a unit normal vector oriented from fluid-A to fluid-B. Now consider a virtual displacement of each point along the interface by an infinitesimal distance, $\delta h = \eta(x, y, t)$, with $\hat{\boldsymbol{n}}\,\delta h$ connecting points on the initial position of the interface to the displaced position, where $\delta h > 0$ if the displacement is directed towards fluid-B and $\delta h < 0$ if directed towards fluid-A. The (signed) volume swept out by an infinitesimal area $\mathrm{d}A$ is given by $\delta h\,\mathrm{d}A$. There are two forms of work required to move the surface: pressure work required to change the fluid volume and area work required to change the surface area. The pressure work is given by

$$W_{\text{volume}} = -p_{\text{A}}\,\delta V_{\text{A}} - p_{\text{B}}\,\delta V_{\text{B}} = (p_{\text{B}} - p_{\text{A}})\,\delta V_{\text{A}} = (p_{\text{B}} - p_{\text{A}})\,\delta h\,\mathrm{d}A, \tag{25.140}$$

where we set $\delta V_{\text{A}} = -\delta V_{\text{B}} = \delta h\,\mathrm{d}A$. For example, if $p_{\text{B}} > p_{\text{A}}$ and the displacement is into fluid-B ($\delta h > 0$), then $W_{\text{volume}} > 0$. We thus find that $W_{\text{volume}} > 0$ to displace the surface into the fluid region with higher pressure, whereas $W_{\text{volume}} < 0$ if displacing the interface into a region with lower pressure.

In the presence of surface tension, work is needed to change to the interface area

$$W_{\text{area}} = \gamma\,\delta A, \tag{25.141}$$

where δA is the change in area of an infinitesimal element on the interface

$$\delta A = \mathrm{d}\mathcal{S} - \mathrm{d}A \tag{25.142a}$$

$$= \mathrm{d}A\,\left[\sqrt{1 + (\nabla\delta h)^2} - 1\right] \tag{25.142b}$$

$$\approx \mathrm{d}A\,(\nabla\delta h)^2/2. \tag{25.142c}$$

To reach this result we made use of equation (5.33) that relates the area of an infinitesimal element on a curved surface to the area of its horizontal projection (see Section 5.3.1). We next

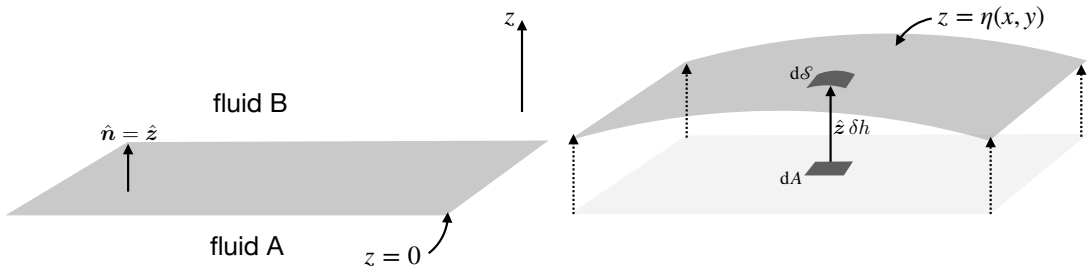

FIGURE 25.12: Left panel: initial position of a material interface separating two fluid regions, fluid-A and fluid-B. Right panel: infinitesimal displacement of the interface sweeps out a volume in space, here depicted with the interface moving upward. To determine the volume, extend a unit normal vector, $\hat{\boldsymbol{n}}$, from the initial interface position and pointing towards fluid-B. For this example, $\hat{\boldsymbol{n}} = \hat{\boldsymbol{z}}$. Let $\delta h = \eta$ be the distance along that normal to the new position, with $\delta h > 0$ if the displacement moves towards fluid-B and $\delta h < 0$ for displacements pointing to fluid-A. We assume that displacements at each interface point can move independently of adjacent points, so that the interface area generally changes. The Young-Laplace formula (25.149) says that the pressure jumps when crossing an interface that is subject to surface tension, with pressure higher on the concave side. In this example, Young-Laplace says pressure is higher on the Fluid-A side since that it is the concave side.

make use of the surface curvature detailed in Section 5.3.2, where equation (5.38) shows that the vertical displacement is given, for small displacements, by

$$-\delta h \approx \frac{1}{2}\, R_1^{-1}\, (\boldsymbol{x} \cdot \boldsymbol{e}_1)^2 + \frac{1}{2}\, R_2^{-1}\, (\boldsymbol{x} \cdot \boldsymbol{e}_2)^2. \tag{25.143}$$

R_1^{-1}, R_2^{-1} are the eigenvalues and $\boldsymbol{e}_1, \boldsymbol{e}_2$ are the corresponding eigenvectors of the matrix of second partial derivatives of $\delta h(x, y)$, whereas the inverse eigenvalues, R_1, R_2, are the radii of curvature of the displaced surface. To get signs correct, it is important to note that the radius of curvature is positive if the surface curves towards the outward normal direction, and negative otherwise (see Figure 5.5). For the example depicted in the right panel of Figure 25.12, and both radii of curvature are negative since the surface curves away from the outward normal (pointing from A to B). This convention explans the minus sign on the left side of equation (25.143).

Orienting the Cartesian axes along the eigenvector directions renders

$$(\nabla \delta h)^2 \approx (x/R_1)^2 + (y/R_2)^2 = (-\delta h)\, \left[\frac{1}{R_1} + \frac{1}{R_2}\right], \tag{25.144}$$

where we set

$$(-\delta h)/R_1 = (x/R_1)^2 \qquad \text{and} \qquad (-\delta h)/R_2 = (y/R_2)^2. \tag{25.145}$$

We are thus led to the area difference

$$\delta A \approx \mathrm{d}A\, (-\delta h)\, \left[\frac{1}{R_1} + \frac{1}{R_2}\right]. \tag{25.146}$$

Note that $\delta A > 0$ whether displacing the surface into a concave or convex direction, since the sign of δh accounts for the sign of the radii of curvature. For small displacements of the surface from its horizontal position, equation (5.41) allows us to connect the radii of curvature for a surface with the Laplacian of the displacement of the surface, in which case equation (25.146) takes on the form

$$\delta A \approx -\mathrm{d}A\, \delta h\, \nabla^2(\delta h). \tag{25.147}$$

Total work for the interface displacement is given by the sum of the area work and volume

work

$$W_{\text{area}} + W_{\text{volume}} = \mathrm{d}A\,\delta h\,\left[-\gamma\,(R_1^{-1} + R_2^{-1}) + p_{\text{B}} - p_{\text{A}}\right] = \mathrm{d}A\,\delta h\,\left[-\gamma\,\nabla^2\eta + p_{\text{B}} - p_{\text{A}}\right], \quad (25.148)$$

and equilibrium results if the net work vanishes, in which case

$$p_{\text{B}} - p_{\text{A}} = \gamma\,(R_1^{-1} + R_2^{-1}) = \gamma\nabla^2\eta, \quad (25.149)$$

where we set $\delta h = \eta$ as per Figure 25.12. This equation is the *Young-Laplace* formula, which reduces to equation (25.139) if $R_1 = R_2$ as for a sphere. It says that there is a pressure jump, known as the *capillary pressure*, across an interface as given by the surface tension times the sum of the inverse principle radii of curvature, or equivalently the surface tension times the Laplacian of the displacement. To help remember signs, note that the Young-Laplace formula (25.149) says that the pressure on the concave side of an interface is higher than on the convex side. Hence, pressure is higher on the inside of a bubble/droplet. For the example depicted in Figure 25.12, $\nabla^2\eta < 0$ since the surface is a local maximum, in which case $p_{\text{A}} > p_{\text{B}}$ since fluid A is on the concave side of the interface.

25.11.4 Soluble gas bubbles inside water

The previous considerations hold whether there is liquid or gas inside a spherical bubble or drop. As an example, consider a spherical gas bubble of radius $R = 10^{-6}$ m inside water and make use of the air-water surface tension $\gamma = 0.072$ N m^{-1} $= 0.072$ kg s^{-2}. We thus find the pressure jump is

$$p_{\text{in}} - p_{\text{out}} = 2\,\gamma/R \approx 144 \times 10^3 \text{ N m}^{-2} = 1.42\,p_{\text{atm}}, \quad (25.150)$$

where $p_{\text{atm}} = 1.01 \times 10^5$ N m^{-2} is standard atmospheric pressure. If the gas inside the bubble is water soluble, then the enhanced pressure inside the bubble will induce more gas to dissolve in the water, which in turn will cause the bubble to shrink and thus increase the pressure inside the bubble. Small bubbles of soluble gases can thus be squeezed towards zero radius by the effects of surface tension induced pressure.

25.11.5 When we can ignore surface tension

The sizable pressure jump (25.150) arises from the tiny radius of curvature of the bubble, with the pressure jump decreasing as the bubble radius increases. Rather than a bubble, consider an ocean surface capillary-gravity wave, such as those observed from a boat (e.g., Sections 52.3 and 52.10). Such waves may have wavelength on the order of 10^{-2} m or longer. If we set the radius of curvature to $R \sim 10^{-2}$ m, then equation (25.150) finds an entirely negligible pressure jump of $\Delta p \approx 10^{-4}\ p_{\text{a}}$.

Most geophysical fluid motion of concern in this book is associted with material interfaces having a radius of curvature on the order of meters or larger. It is for this reason that surface tension is generally ignored when studying geophysical fluid motion. That is, we can safely assume there is no pressure jump when approaching an interface between two fluid media, or between a fluid and a solid boundary. This discussion then justifies the approach considered in Section 25.10 when studying stresses at interfaces, in which we made use of Newton's third law at the interface.

Even so, the role of surface tension is central to the fundamental mechanisms of how matter, momentum, and energy are transferred across the air-sea interface. Relatedly, as we show in Section 52.10, capillary waves arise from surface tension, with capillary waves the initial response of the ocean free surface upon the imposition of a wind stress.

25.11.6 Further study

This 30-minute video from Prof. Trefethen provides a pedagogical summary of surface tension. The upside-down container of water in Figure 25.9 is based on a discussion of capillary-gravity waves in Section 3.1.3 of *Falkovich* (2011). We study capillary-gravity waves in Section 52.10. Section 1.9 of *Batchelor* (1967) discusses how surface tension acts between two fluid media, with that discussion extended into his Section 3.3 to develop boundary conditions for velocity and stress. The bubble example in Section 25.11.4 is taken from Section 1.3 of *Kundu et al.* (2016). Section 4.10 of *Kundu et al.* (2016) provides a detailed accounting of the force balance at an interface, offering more details than found in *Batchelor* (1967). The energetic arguments used to derive the Young-Laplace formula follows Section 61 of *Landau and Lifshitz* (1987). Section 46 of *Fetter and Walecka* (2003) discuss the dynamics of membranes under tension.

25.12 Exercises

EXERCISE 25.1: FORCE BALANCE FOR A NON-ACCELERATING TANGENT PLANE OCEAN
Consider an ocean basin, $\mathcal{R}$, on the rotating tangent plane as in Figure 25.2, with bottom interface separating the ocean fluid from the solid-earth, and upper interface separating the ocean fluid from the atmosphere, and where the atmosphere has a nonzero mass.[21] Assume no matter crosses the ocean boundaries; i.e., no evaporation, precipitation, nor river runoff. Hence, the ocean domain maintains a fixed mass

$$M = \int_{\mathcal{R}} \rho \, \mathrm{d}V \tag{25.151}$$

as well as fixed matter. In this case, the ocean domain is materially closed and so its center of mass position

$$\boldsymbol{X}^{\mathrm{com}} = M^{-1} \int_{\mathcal{R}} \boldsymbol{x} \, \rho \, \mathrm{d}V \tag{25.152}$$

has a velocity given by

$$\frac{\mathrm{d}\boldsymbol{X}^{\mathrm{com}}}{\mathrm{d}t} = M^{-1} \int_{\mathcal{R}} \boldsymbol{v} \, \rho \, \mathrm{d}V, \tag{25.153}$$

and corresponding acceleration

$$\frac{\mathrm{d}^2\boldsymbol{X}^{\mathrm{com}}}{\mathrm{d}t^2} = M^{-1} \int_{\mathcal{R}} \frac{\mathrm{D}\boldsymbol{v}}{\mathrm{D}t} \, \rho \, \mathrm{d}V. \tag{25.154}$$

Apply a horizontal stress over the ocean surface with a stress vector $\boldsymbol{\tau}^{\mathrm{surf}}$. This stress leads to motion of the ocean fluid. Allow for the ocean bottom to exchange momentum with the static solid-earth through a horizontal bottom turbulent stress, $\boldsymbol{\tau}^{\mathrm{bott}}$. Assume there are no vertical components to $\boldsymbol{\tau}^{\mathrm{surf}}$ and $\boldsymbol{\tau}^{\mathrm{bott}}$. Also use Cartesian coordinates so that Cartesian vector/tensor analysis is sufficient for this tangent plane analysis.

(a) What is the force balance for the full ocean domain if the center of mass experiences no acceleration. Express the corresponding force balance in words and in equations. Expose the contact forces arising from pressure and from turbulent stresses, as well as the body forces from Coriolis and gravity. The answer should be generally stated, with no need

[21] In some applications it is suitable to assume a zero mass atmosphere. For this exercise, however, we do not make that assumption.

for specific details. Hint: consider Figure 25.2 and include the missing forces to this diagram. Mathematically express the force balance as an integral expression as per the weak formulation of fluid mechanics (see Section 17.1.1).

(b) Express the vertical component of the force balance assuming the fluid is in an approximate hydrostatic balance, meaning that the pressure and gravitational forces are balanced.[22]

(c) Consider an ocean without any turbulent contact stresses at the boundaries, $\boldsymbol{\tau}^{\text{surf}} = \boldsymbol{\tau}^{\text{bott}} = 0$ and assume there is no motion anywhere in the fluid. What integral constraints are satisfied by the horizontal components of the pressure contact force? Hint: recall equations equations (25.40a) and (25.40b). Also note assume that the free surface is flat, which is consistent with the absence of motion.

(d) Assume the ocean is on an f-plane (Section 24.5) so that $\boldsymbol{\Omega} = \hat{\boldsymbol{z}}\,\Omega = \hat{\boldsymbol{z}}\,(f/2)$ is a constant vector. Also assume that the center of mass velocity vanishes, $\int_{\mathscr{R}} \rho\,\boldsymbol{v}\,\mathrm{d}V = 0$. Discuss the resulting zonal and meridional force balance. Hint: one of the forces appearing in part (a) now vanishes.

[22] In Section 27.2 we provide a discussion of when this approximation is appropriate for moving fluids. That discussion is not needed for the current exercise. Instead, we merely assume the vertical momentum balance is hydrostatic.

Chapter 26

Energy and entropy in a moving fluid

In this chapter we study the energetics of fluid flow. In particular, we are concerned with how energy is partitioned between the mechanical energy of macroscopic motion and the internal energy associated with internal degrees of freedom. To fully specify energy in fluid flows requires us to study the flow of entropy and the associated constraints arising from the second law of thermodynamics. For this purpose we extend the equilibrium thermodynamics of Chapters 22 and 23 to include time dependent moving fluid phenomena. Making this transition requires the hypothesis of *local thermodynamic equilibrium*.

READER'S GUIDE FOR THIS CHAPTER

This chapter builds from the momentum dynamics of Chapter 24 and the thermodynamics of Chapters 22 and 23. In addition to developing the budgets for mechanical energy and total energy (mechanical plus internal), we derive budgets for entropy and potential enthalpy. A particularly important practical outcome of this chapter concerns the derivation of the equation for potential enthalpy or Conservative Temperature, with this equation completing the suite of fundamental equations describing the evolution of a geophysical fluid. Finally, we also present a derivation of the momentum equation using Hamilton's variational principle, which makes use of Hamilton's principle for continuous fields in Chapter 46, and the methods of analytical mechanics in Chapter 12. To make the formalism less mathematically intense, we employ Cartesian tensors as discussed in Chapters 1 and 2, with all tensor indices downstairs.

26.1 Loose threads

- Figures needed
- Potential energy as per Section 108 of *Landau and Lifshitz* (1980)

26.2 Gravitational potential energy

Geophysical fluids move within a gravitational field created by the mass of the planet, including the mass of the fluid itself. We typically focus on a rather simple form for the effective gravitational acceleration exemplified by the geopotential $\Phi = g\,z$, where g is the gravitational acceleration that includes effects from both central gravity plus planetary centrifugal (Section 13.10.4). However, we offer some discussion of astronomical tide producing forces in Chapter 34, whereby the geopotential is a more complicated function of space and time, $\Phi(\boldsymbol{x}, t)$. In this section we study the potential energy of a fluid element due to its presence in a gravitational field, with the geopotential providing the effective gravitational potential energy per mass of fluid elements.[1]

26.2.1 Material evolution

The gravitational potential energy per mass of a fluid element is given by the geopotential, Φ, so that the gravitational potential energy is $\Phi\,\rho\,\delta V$. Hence, the evolution of potential energy for a constant mass fluid element is given by

$$\frac{\mathrm{D}(\Phi\,\rho\,\delta V)}{\mathrm{D}t} = \rho\,\delta V\,\frac{\mathrm{D}\Phi}{\mathrm{D}t}, \tag{26.1}$$

where $\mathrm{D}(\rho\,\delta V)/\mathrm{D}t = 0$ since the fluid element has a constant mass. The material time derivative for the geopotential

$$\frac{\mathrm{D}\Phi}{\mathrm{D}t} = \frac{\partial\Phi}{\partial t} + \boldsymbol{v}\cdot\nabla\Phi, \tag{26.2}$$

contains a local time dependence that arises from astronomical tide forcing or movement of mass on the planet (Chapter 34). As further explored in Section 26.4, the advective term represents an exchange of mechanical energy between the kinetic energy contained in fluid motion and the gravitational potential energy due to the fluid being within a gravitational field. This energy exchange arises from fluid motion across constant geopotential surfaces. For example, motion up the geopotential gradient, $\boldsymbol{v}\cdot\nabla\Phi > 0$, increases gravitational potential energy and motion down the geopotential gradient decreases potential energy. With the geopotential $\Phi = g\,z$, we have

$$\boldsymbol{v}\cdot\nabla\Phi = g\,w, \tag{26.3}$$

so that vertically upward motion ($w > 0$) increases potential energy.

26.2.2 Flux-form potential energy equation

Another way to reveal the same ideas is to make use of the kinematic identity (19.50c), so that the density weighted material time derivative of the geopotential is given by

$$\rho\,\frac{\mathrm{D}\Phi}{\mathrm{D}t} = \partial_t(\rho\,\Phi) + \nabla\cdot(\rho\,\boldsymbol{v}\,\Phi). \tag{26.4}$$

For the simple geopotential, $\Phi = g\,z$, we thus find

$$\rho\,\frac{\mathrm{D}\Phi}{\mathrm{D}t} = \rho\,g\,w \iff \partial_t(\rho\,\Phi) + \nabla\cdot(\rho\,\boldsymbol{v}\,\Phi) = \rho\,g\,w. \tag{26.5}$$

[1] In this chapter we generally refer to the more concise "gravitational potential energy" or even briefer "potential energy" rather than "potential energy from the effective gravitational field."

26.2.3 Reference geopotential

There is no change to the energetics if we modify the gravitational reference state by modifying the geopotential

$$\Phi \to \Phi + \Phi_{\rm r} \tag{26.6}$$

with $\Phi_{\rm r}$ an arbitrary constant. In particular, this offset has no effect on the evolution of gravitational potential energy of the constant mass fluid element since

$$\frac{\mathrm{D}(\Phi_{\rm r}\, \rho\, \delta V)}{\mathrm{D}t} = \Phi_{\rm r}\, \frac{\mathrm{D}(\rho\, \delta V)}{\mathrm{D}t} = 0. \tag{26.7}$$

Hence, as is well known from classical mechanics, it is not the value of the gravitational potential energy that is important, but instead it is the space and time changes that affect energetics.

26.2.4 Regionally integrated gravitational potential energy

Now consider the evolution of the gravitational potential energy integrated over a finite region $\mathcal{R}$. If the fluid region is closed to mass transport, as per a material boundary, then we can make use of the Leibniz-Reynolds transport theorem in the form of equation (20.53d) to write

$$\frac{\mathrm{d}}{\mathrm{d}t} \int_{\mathcal{R}} \Phi\, \rho\, \mathrm{d}V = \int_{\mathcal{R}} \frac{\mathrm{D}\Phi}{\mathrm{D}t}\, \rho\, \mathrm{d}V, \tag{26.8}$$

which is an extension of the material evolution equation (26.1). If the region is open to material mass transport, we make use Leibniz-Reynolds transport theorem in the form of equation (20.37) to find

$$\frac{\mathrm{d}}{\mathrm{d}t} \int_{\mathcal{R}} \rho\, \Phi\, \mathrm{d}V = \int_{\mathcal{R}} \frac{\partial(\rho\, \Phi)}{\partial t}\, \mathrm{d}V + \oint_{\partial \mathcal{R}} \rho\, \Phi\, \boldsymbol{v}^{(b)} \cdot \hat{\boldsymbol{n}} \mathrm{d}\mathcal{S} \tag{26.9a}$$

$$= \int_{\mathcal{R}} \left[\rho\, \frac{\mathrm{D}\Phi}{\mathrm{D}t} - \nabla \cdot (\rho\, \Phi\, \boldsymbol{v}) \right] \mathrm{d}V + \oint_{\partial \mathcal{R}} \rho\, \Phi\, \boldsymbol{v}^{(b)} \cdot \hat{\boldsymbol{n}} \mathrm{d}\mathcal{S} \tag{26.9b}$$

$$= \int_{\mathcal{R}} \rho\, \frac{\mathrm{D}\Phi}{\mathrm{D}t}\, \mathrm{d}V + \oint_{\partial \mathcal{R}} \rho\, \Phi\, (\boldsymbol{v}^{(b)} - \boldsymbol{v}) \cdot \hat{\boldsymbol{n}} \mathrm{d}\mathcal{S}, \tag{26.9c}$$

where $\boldsymbol{v}^{(b)}$ is the velocity of a point on the boundary of the domain. The evolution thus consists of the mass integrated material time evolution of the geopotential, plus a surface term that contributes to the transport of the geopotential across the regional boundaries.

If the region is a vertical column of ocean fluid with fixed horizontal cross-section, extending from the ocean surface to the ocean bottom, then there is horizontal transport across the vertical column bounds, plus vertical transport of mass across the ocean free surface. For the free surface we make use of the surface kinematic boundary condition (19.88c) to write

$$\int_{z=\eta} \rho\, \Phi\, (\boldsymbol{v}^{(b)} - \boldsymbol{v}) \cdot \hat{\boldsymbol{n}}\, \mathrm{d}\mathcal{S} = \int_{z=\eta} Q_{\mathsf{m}}\, \Phi\, \mathrm{d}A. \tag{26.10}$$

In this equation, Q_{m} is the mass per time per horizontal area of matter crossing the ocean free surface at $z = \eta$ where $Q_{\mathsf{m}} > 0$ for matter entering the ocean domain, and $\mathrm{d}\mathcal{S}$ is the area element on the free surface with $\mathrm{d}A$ its horizontal projection. As noted in Section 26.2.3, we can add a constant to the geopotential without affecting the energetics, which is here seen by noting that mass conservation means that

$$\frac{\mathrm{d}}{\mathrm{d}t} \int \rho\, \mathrm{d}V = - \int_{\mathcal{R}} \nabla \cdot [\rho\, (\boldsymbol{v} - \boldsymbol{v}^{(b)})] \mathrm{d}V, \tag{26.11}$$

which results from setting $\Phi = 1$ in equation (26.9c). In general, we expect the transfer of mass across the surface boundary to affect the gravitational potential energy both because it adds or removes mass to the ocean domain, and because it affects the geopotential. To help interpret the sign from the boundary term, it is useful to define the reference state geopotential so that $\Phi > 0$ at the ocean surface, no matter what the value of η. We can do so by defining the reference geopotential at or below the ocean bottom. In this case, adding mass increases the gravitational potential energy and removing mass reduces it.

Consider the special case of a geopotential $\Phi = g\,z$, so returning to a $z = 0$ reference state, in which case the global ocean potential energy equation is written

$$\frac{\mathrm{d}}{\mathrm{d}t} \int \rho\, z \,\mathrm{d}V = \int \rho\, w \,\mathrm{d}V + \int Q_{\mathsf{m}}\, \eta \,\mathrm{d}A, \tag{26.12}$$

where we cancelled the constant gravitational acceleration. Now decompose Q_{m} and η into their global area means and deviations

$$Q_{\mathsf{m}} = \overline{Q_{\mathsf{m}}} + Q'_{\mathsf{m}} \quad \text{and} \quad \eta = \overline{\eta} + \eta', \tag{26.13}$$

so that

$$g \int Q_{\mathsf{m}}\, \eta \,\mathrm{d}A = g\, \overline{Q_{\mathsf{m}}}\, \overline{\eta}\, A + g \int Q'_{\mathsf{m}}\, \eta' \,\mathrm{d}A. \tag{26.14}$$

As before, the $\overline{Q_{\mathsf{m}}}\, \overline{\eta}$ term alters potential energy relative to the arbitrary reference state, here taken as $z = 0$. The area correlation term increases potential energy in regions where $Q'_{\mathsf{m}}\, \eta' > 0$, which acts to increase the relative deviation of the free surface from its mean value. That is, $Q'_{\mathsf{m}}\, \eta' > 0$ in regions where $Q'_{\mathsf{m}} > 0$ and $\eta' > 0$ as well as in regions where $Q'_{\mathsf{m}} < 0$ and $\eta' < 0$. Conversely, the correlation term reduces potential energy where Q'_{m} and η' are anti-correlated, which acts to decrease the relative deviation of the free surface height.

26.2.5 Potential energy and vertical stratification

Consider the potential energy of a region of horizontally homogeneous fluid centered at a vertical position, $z = z_{\mathrm{c}}$, and with constant horizontal cross-sectional area, A. Assuming we do not move vertically far away from the central position, we can write the density in the linear form

$$\rho(z) = \rho(z_{\mathrm{c}}) + \frac{\mathrm{d}\rho(z_{\mathrm{c}})}{\mathrm{d}z}\,(z - z_{\mathrm{c}}) \equiv \rho_{\mathrm{c}} - K\,(z - z_{\mathrm{c}}), \tag{26.15}$$

where $K = -\mathrm{d}\rho(z_{\mathrm{c}})/\mathrm{d}z > 0$ is a shorthand for the vertical density gradient at the central point. The potential energy per volume ($\Delta V = A\,\Delta z$) for fluid in the vertical region $z \in [z_{\mathrm{c}} - \Delta z/2, z_{\mathrm{c}} + \Delta z/2]$ is given by

$$(g/\Delta z) \int z\,\rho \,\mathrm{d}z = (g/\Delta z) \int_{z_{\mathrm{c}} - \Delta z/2}^{z_{\mathrm{c}} + \Delta z/2} [\rho_{\mathrm{c}} - K\,(z - z_{\mathrm{c}})]\, z \,\mathrm{d}z \tag{26.16a}$$

$$= g\,\rho_{\mathrm{c}}\, z_{\mathrm{c}} - g\,K\,(\Delta z)^2/12. \tag{26.16b}$$

We thus see that the gravitational potential energy decreases as the vertical stratification, $K > 0$, increases, with the maximum potential energy when the stratification vanishes, $K = 0$. As seen in Section 26.2.6, potential energy is maximized when $K = 0$ since the center of mass moves vertically upward as the stratification reduces to zero.

26.2.6 Gravitational potential energy and mixing

Consider a fluid in exact hydrostatic balance (Section 24.6) with a gravitationally stable vertical stratification where light fluid is above heavy fluid.[2] Now introduce a physical process, such as vertical mixing associated with a kinetic energy source, that reduces the vertical stratification. Reducing vertical stratification requires mixing to move heavy fluid up and light fluid down. In so doing, the kinetic energy supporting the mixing is converted into gravitational potential energy since the center of mass for the fluid column rises.

We can formulate this thought experiment by considering a column of seawater that is vertically stratified in salinity, S, and Conservative Temperature, Θ, and another column that is vertically unstratified with constant values $S_{\rm m}$ and $\Theta_{\rm m}$.[3] We assume the mass of the two columns is the same so that the bottom pressure, $p_{\rm b}$, and surface pressure, $p_{\rm a}$, are the same for the two columns. However, the volumes will generally differ since the density differs, so that the two free surfaces, η and $\eta_{\rm m}$, differ. Assuming a geopotential for the homogenized column, $\Phi = g\, z_{\rm m}$, leads to the integrated potential energy

$$g \int_{\eta_{\rm b}}^{\eta_{\rm m}} \rho(S_{\rm m}, \Theta_{\rm m}, p)\, z_{\rm m}\, {\rm d}z_{\rm m} = -\int_{p_{\rm b}}^{p_{\rm a}} z_{\rm m}\, {\rm d}p, \tag{26.17}$$

where we used the hydrostatic balance to write

$${\rm d}p = -g\, \rho(S_{\rm m}, \Theta_{\rm m}, p)\, {\rm d}z_{\rm m}. \tag{26.18}$$

Likewise, the stratified column has an integrated potential energy

$$g \int_{\eta_{\rm b}}^{\eta} \rho(S, \Theta, p)\, z\, {\rm d}z = -\int_{p_{\rm b}}^{p_{\rm a}} z\, {\rm d}p, \tag{26.19}$$

so that the difference between the gravitational potential energies per horizontal area in the two columns is given by

$$g \int_{\eta_{\rm b}}^{\eta_{\rm m}} \rho(S_{\rm m}, \Theta_{\rm m}, p)\, z\, {\rm d}z - g \int_{\eta_{\rm b}}^{\eta} \rho(S, \Theta, p)\, z\, {\rm d}z = \int_{p_{\rm a}}^{p_{\rm b}} (z_{\rm m} - z)\, {\rm d}p = (p_{\rm b} - p_{\rm a})\, (\overline{z_{\rm m}} - \overline{z}). \tag{26.20}$$

In this equation we introduced the center of mass positions for the vertically homogeneous column, $\overline{z_{\rm m}}$, and the stratified column, $\overline{z}$, defined by

$$\overline{z_{\rm m}} = \frac{1}{p_{\rm b} - p_{\rm a}} \int_{p_{\rm a}}^{p_{\rm b}} z_{\rm m}\, {\rm d}p \quad \text{and} \quad \overline{z} = \frac{1}{p_{\rm b} - p_{\rm a}} \int_{p_{\rm a}}^{p_{\rm b}} z\, {\rm d}p. \tag{26.21}$$

There are two contributions to the potential energy difference in equation (26.20). The first is the mass per horizontal area, as measured by the difference in bottom pressure and applied surface pressure, $(p_{\rm b} - p_{\rm a})/g > 0$. The second is the difference between the center of mass for the two columns, $\overline{z_{\rm m}} - \overline{z}$, which is a positive number since homogenizing a fluid column moves heavier water up and lighter water down so that $\overline{z_{\rm m}} > \overline{z}$. Hence, the potential energy of the homogenized column is larger than the stratified column. We develop more experience with the energetics of mixing in Exercise 26.1.

[2] See Section 30.5 for a more precise discussion of gravitational stability.

[3] See Section 30.3 for discussion of the seawater equation of state. For present purposes it is sufficient to know that seawater density is a function of the material tracer S, the thermodynamic tracer, Θ, and pressure, p. When a column is vertically homogenized that means S and Θ are constant throughout the column. However, pressure remains hydrostatic and thus is not vertically constant. Since density is a function of pressure, it too retains a vertical gradient.

26.3 Kinetic energy of macroscopic motion

Mechanical energy is a dynamical property formed by adding the energy due to motion of fluid elements (kinetic energy) to the energy arising from the position of a fluid element within the gravitational field (gravitational potential energy). We studied the gravitational potential energy budget in Section 26.2. Here, we develop the budget for kinetic energy and then the full mechanical energy (kinetic plus gravitational potential) in Section 26.4. In Section 26.7 we then add the mechanical energy from macroscopic motion to the internal energy to develop the budget for total energy.

26.3.1 Kinetic energy budget from Cauchy's equation

We start the analysis by considering general features of the kinetic energy budget as seen from Cauchy's equation of motion (24.14)

$$\rho \frac{\mathrm{D}\boldsymbol{v}}{\mathrm{D}t} = \rho \boldsymbol{f}_{\text{body}} + \nabla \cdot (-p \mathbb{I} + \mathbb{\tau}), \tag{26.22}$$

with a body force per mass, $\boldsymbol{f}_{\text{body}}$, and contact stress from pressure, p, and the symmetric frictional stress tensor, $\mathbb{\tau}$. Taking the scalar product with $\boldsymbol{v}$ leads to

$$\rho \frac{\mathrm{D}\mathcal{K}}{\mathrm{D}t} = \rho \boldsymbol{v} \cdot \boldsymbol{f}_{\text{body}} + v_n \partial_m (-p \delta_{mn} + \tau_{mn}), \tag{26.23}$$

where

$$\mathcal{K} = \boldsymbol{v} \cdot \boldsymbol{v}/2 \tag{26.24}$$

is the kinetic energy per mass. We thus see that the kinetic energy of a fluid element is affected by work done by the body forces, $\rho \boldsymbol{v} \cdot \boldsymbol{f}_{\text{body}}$, along with work done by stresses through both pressure and friction.

Rearranging the stress term in equation (26.23) leads to

$$\rho \frac{\mathrm{D}\mathcal{K}}{\mathrm{D}t} = \rho \boldsymbol{v} \cdot \boldsymbol{f}_{\text{body}} + \nabla \cdot (-p \boldsymbol{v} + \boldsymbol{v} \cdot \mathbb{\tau}) + p \nabla \cdot \boldsymbol{v} - (\partial_m v_n) \tau_{mn}. \tag{26.25}$$

The $\nabla \cdot (-p \boldsymbol{v} + \boldsymbol{v} \cdot \mathbb{\tau})$ contribution represents the divergence of a flux arising from pressure and viscous stress, whereas the term $p \nabla \cdot \boldsymbol{v}$ arises from pressure work done on a fluid element as it changes volume. For the final term in equation (26.25), as note that the frictional stress tensor is symmetric so that

$$(\partial_m v_n) \tau_{mn} = \mathbb{S}_{mn} \tau_{mn}, \tag{26.26}$$

where we introduced the strain rate tensor from equation (18.90a)

$$2 \mathbb{S}_{mn} = \partial_n v_m + \partial_m v_n. \tag{26.27}$$

As shown in Section 26.3.3, the frictional stress tensors resulting from the constitutive relations in Section (25.8) mean that $\mathbb{S}_{mn} \tau_{mn}$ is non-negative, in which case viscous stresses dissipate kinetic energy.

26.3.2 Kinetic energy budget for a geophysical fluid

We now develop the kinetic energy budget for a fluid in a rotating reference frame, in which case the body force is provided by the effective gravity and Coriolis. For this purpose we make

use of the momentum equation (24.16), repeated here for convenience

$$\rho \frac{\mathrm{D}\boldsymbol{v}}{\mathrm{D}t} + 2\,\rho\,\boldsymbol{\Omega} \times \boldsymbol{v} = -\rho\,\nabla\Phi + \nabla\cdot(-p\,\mathbb{I} + \mathbb{T}) \tag{26.28a}$$

$$= -\rho\,\nabla\Phi - \nabla p + \rho\,\boldsymbol{F}, \tag{26.28b}$$

where we wrote

$$\boldsymbol{F} = \rho^{-1}\,\nabla\cdot\mathbb{T} \tag{26.29}$$

for acceleration due to viscous friction that arises from the divergence of the frictional stress tensor. Taking the scalar product the momentum equation in the form of equations (26.28a) and (26.28b) renders

$$\rho \frac{\mathrm{D}\mathcal{K}}{\mathrm{D}t} = -\rho\,\boldsymbol{v}\cdot\nabla\Phi - \boldsymbol{v}\cdot\nabla p + \rho\,\boldsymbol{v}\cdot\boldsymbol{F}. \tag{26.30}$$

We thus see that the kinetic energy of a fluid element is affected by work done by the geopotential, $-\rho\,\boldsymbol{v}\cdot\nabla\Phi$, along with work done by stresses through both pressure and friction. We detail these processes in the following.

Contribution from the geopotential

Kinetic energy increases for motion directed down the geopotential gradient

$$\boldsymbol{v}\cdot\nabla\Phi < 0 \implies \text{increases kinetic energy.} \tag{26.31}$$

For example, with a simple geopotential, $\Phi = g\,z$, kinetic energy increases where the vertical velocity is downward,

$$w < 0 \implies -w\,g\,\rho > 0 \longleftrightarrow \text{downward motion increases } \mathcal{K} \text{ of a fluid element.} \tag{26.32}$$

As seen in Section 26.2.1, this increase in kinetic energy due to motion down the geopotential gradient is exactly balanced by a decrease in gravitational potential energy. That is, an increase in kinetic energy through motion down the geopotential comes at the cost of a decrease in the gravitational potential energy. This exact conversion between kinetic energy and potential energy is also seen in Section 14.7 for motion of the point particle.

Contribution from the pressure gradient body force

Kinetic energy increases in regions where the velocity projects down the pressure gradient,

$$\boldsymbol{v}\cdot\nabla p < 0 \implies \text{increase kinetic energy,} \tag{26.33}$$

thus resulting in an increase in fluid speed imparted by the pressure gradient force. Conversely, kinetic energy is reduced in regions where the flow is directed up the pressure gradient. It is notable that geostrophic flows, studied in Section 31.4, have a velocity given by

$$\boldsymbol{v}_{\mathrm{g}} = (g\,\rho)^{-1}\,\hat{\boldsymbol{z}} \times \nabla p. \tag{26.34}$$

Consequently, geostrophic flows have $\boldsymbol{v}_{\mathrm{g}}\cdot\nabla p = 0$, so that the pressure gradient force has no impact on the horizontal kinetic energy of a geostrophic fluid.

Contribution from friction

Kinetic energy is reduced in regions where the velocity has a negative projection onto the direction of the friction vector, $\rho\,\boldsymbol{v}\cdot\boldsymbol{F} < 0$. As detailed in Section 26.3.3, the friction arising

from a viscous stress tensor appropriate for a Newtonian fluid gives rise to two contributions to kinetic energy: the divergence of a viscous flux plus a sign-definite sink.

26.3.3 Frictional dissipation of kinetic energy

We here detail the role of friction on kinetic energy

$$\text{friction power per volume} = \rho\, \boldsymbol{v} \cdot \boldsymbol{F} = \boldsymbol{v} \cdot (\nabla \cdot \mathbb{T}), \tag{26.35}$$

which is the frictional power per volume (energy per time per volume) that modifies the kinetic energy per volume of a fluid element, and with the frictional stress tensor, $\mathbb{T}$, determined by the constitutive equation (25.79). We anticipated this contribution in the general discussion of Section 26.3.1, and here provide details.

To proceed, we expose Cartesian tensor labels to have

$$\begin{aligned}
\rho\, \boldsymbol{v} \cdot \boldsymbol{F} &= v_m\, \rho\, F_m && \text{(26.36a)}\\
&= v_m\, \partial_n \mathbb{T}_{nm} && \text{(26.36b)}\\
&= 2\, v_m\, \partial_n (\rho\, \nu\, \mathbb{S}^{\text{dev}}_{mn}) && \text{(26.36c)}\\
&= 2\, \partial_n (\rho\, \nu\, v_m\, \mathbb{S}^{\text{dev}}_{mn}) - 2\, \rho\, \nu\, \partial_n v_m\, \mathbb{S}^{\text{dev}}_{mn} && \text{(26.36d)}\\
&= 2\, \nabla \cdot (\rho\, \nu\, \boldsymbol{v} \cdot \mathbb{S}^{\text{dev}}) - 2\, \rho\, \nu\, \mathbb{S}_{mn}\, \mathbb{S}^{\text{dev}}_{mn}, && \text{(26.36e)}
\end{aligned}$$

where we recall from Section 25.8.6 that the *deviatoric strain rate tensor* has elements given by

$$\mathbb{S}^{\text{dev}}_{mn} = \mathbb{S}_{mn} - \delta_{mn}\, \mathbb{S}_{qq}/3 \quad \text{with} \quad \mathbb{S}_{qq} = \nabla \cdot \boldsymbol{v}. \tag{26.37}$$

To reach equation (26.36e) required the identity

$$2\, \partial_n v_m\, \mathbb{S}^{\text{dev}}_{mn} = (\partial_n v_m + \partial_m v_n)\, \mathbb{S}^{\text{dev}}_{mn} + (\partial_n v_m - \partial_m v_n)\, \mathbb{S}^{\text{dev}}_{mn} = 2\, \mathbb{S}_{mn}\, \mathbb{S}^{\text{dev}}_{mn}, \tag{26.38}$$

where

$$(\partial_n v_m - \partial_m v_n)\, \mathbb{S}^{\text{dev}}_{mn} = 2\, \mathbb{R}_{mn}\, \mathbb{S}^{\text{dev}}_{mn} = 0 \tag{26.39}$$

due to symmetry of the deviatoric strain rate tensor, $\mathbb{S}^{\text{dev}}_{mn} = \mathbb{S}^{\text{dev}}_{nm}$, and anti-symmetry of the rotation tensor, $\mathbb{R}_{mn}$ (see Section 18.8 as well as Exercise 1.2). We can show that the second term in equation (26.36e) is sign-definite by noting that

$$\begin{aligned}
\mathbb{S}^{\text{dev}}_{mn}\, \mathbb{S}^{\text{dev}}_{mn} &= (\mathbb{S}_{mn} - \delta_{mn}\, \mathbb{S}_{qq}/3)^2 && \text{(26.40a)}\\
&= \mathbb{S}_{mn}\, \mathbb{S}_{mn} + \delta_{mn}\, \delta_{mn}\, \mathbb{S}_{qq}\, \mathbb{S}_{qq}/9 - 2\, \mathbb{S}_{mn}\, \delta_{mn}\, \mathbb{S}_{qq}/3 && \text{(26.40b)}\\
&= \mathbb{S}_{mn}\, \mathbb{S}_{mn} + (\mathbb{S}_{qq})^2/3 - 2\, (\mathbb{S}_{qq})^2/3 && \text{(26.40c)}\\
&= \mathbb{S}_{mn}\, (\mathbb{S}_{mn} - \delta_{mn}\, \mathbb{S}_{qq}/3) && \text{(26.40d)}\\
&= \mathbb{S}_{mn}\, \mathbb{S}^{\text{dev}}_{mn}. && \text{(26.40e)}
\end{aligned}$$

We are thus left

$$\rho\, \boldsymbol{v} \cdot \boldsymbol{F} = 2\, \nabla \cdot (\rho\, \nu\, \boldsymbol{v} \cdot \mathbb{S}^{\text{dev}}) - 2\, \rho\, \nu\, \mathbb{S}^{\text{dev}}_{mn}\, \mathbb{S}^{\text{dev}}_{mn}. \tag{26.41}$$

We interpret the two contributions to the frictional power in equation (26.41) as

$$\rho\, \boldsymbol{v} \cdot \boldsymbol{F} = \text{divergence of viscous flux} - \text{viscous dissipation}. \tag{26.42}$$

The divergence theorem means that when integrated over the full domain, the divergence of the viscous flux becomes a contribution from boundary stresses, and boundary stresses can either increase or decrease kinetic energy according to details of the boundary processes. In contrast,

the sign-definite dissipation term provides a sink to the kinetic energy at each point in the fluid interior. This frictional dissipation is commonly written

$$\epsilon \equiv [\boldsymbol{v} \cdot \boldsymbol{F}]_{\text{dissipate}} = 2\,\nu\,\mathbb{S}^{\text{dev}}_{mn}\,\mathbb{S}^{\text{dev}}_{mn} \geq 0. \tag{26.43}$$

The dimensions of ϵ are $\mathrm{L}^2\ \mathrm{T}^{-3}$, which in SI units are $\mathrm{m}^2\ \mathrm{s}^{-3} = \mathrm{W\ kg}^{-1}$. We thus refer to ϵ as the kinetic energy dissipation per mass arising from viscous effects. It is also sometimes referred to as the viscous power per mass. Note that we know that $\epsilon > 0$ since $\mathbb{S}^{\text{dev}}_{mn}\,\mathbb{S}^{\text{dev}}_{mn}$ is the sum of nine perfect squares, which is seen by expanding the Einstein summation convention

$$\mathbb{S}^{\text{dev}}_{mn}\,\mathbb{S}^{\text{dev}}_{mn} = \mathbb{S}^{\text{dev}}_{1n}\,\mathbb{S}^{\text{dev}}_{1n} + \mathbb{S}^{\text{dev}}_{2n}\,\mathbb{S}^{\text{dev}}_{2n} + \mathbb{S}^{\text{dev}}_{3n}\,\mathbb{S}^{\text{dev}}_{2n}, \tag{26.44}$$

where

$$\mathbb{S}^{\text{dev}}_{1n}\,\mathbb{S}^{\text{dev}}_{1n} = \mathbb{S}^{\text{dev}}_{11}\,\mathbb{S}^{\text{dev}}_{11} + \mathbb{S}^{\text{dev}}_{12}\,\mathbb{S}^{\text{dev}}_{12} + \mathbb{S}^{\text{dev}}_{13}\,\mathbb{S}^{\text{dev}}_{13}, \tag{26.45}$$

and likewise for $\mathbb{S}^{\text{dev}}_{2n}\,\mathbb{S}^{\text{dev}}_{2n}$ and $\mathbb{S}^{\text{dev}}_{3n}\,\mathbb{S}^{\text{dev}}_{3n}$.

26.3.4 Further study

The study of physical processes contributing to kinetic energy dissipation is central to the study of ocean mixing. The review by *MacKinnon et al.* (2013) provides a pedagogical starting point for this active area of physical oceanography.

As shown in Section 17.8 of *Griffies* (2004), we can relate the global integral of the kinetic energy dissipation to the friction vector by taking the functional derivative of the dissipation with respect to the velocity field. This connection follows from the self-adjoint nature of the friction operator and it can be a useful mathematical framework for developing numerical discretizations of the viscous friction operator (e.g., *Griffies and Hallberg* (2000)). In Section 68.5 we consider a similar connection between the tracer diffusion operator and tracer variance.

26.4 Mechanical energy budget

Mechanical energy of the macroscopic motion is the sum of the kinetic energy plus gravitational potential energy. We here develop the budget, both differential and integral, for mechanical energy.

26.4.1 Differential mechanical energy budget

Adding the material time evolution equations for kinetic energy per mass (equation (26.30)) and gravitational potential energy per mass (equation (26.5)) leads to the material form of the mechanical energy per mass

$$\rho \frac{\mathrm{D}\mathcal{M}}{\mathrm{D}t} = -\boldsymbol{v} \cdot \nabla p + 2\,\nabla \cdot (\rho\,\nu\,\boldsymbol{v} \cdot \mathbb{S}^{\text{dev}}) + \rho\,(-\epsilon + \partial_t \Phi) \tag{26.46a}$$

$$= -\nabla \cdot (p\,\boldsymbol{v} - 2\,\rho\,\nu\,\boldsymbol{v} \cdot \mathbb{S}^{\text{dev}}) + p\,\nabla \cdot \boldsymbol{v} + \rho\,(-\epsilon + \partial_t \Phi) \tag{26.46b}$$

$$= -\nabla \cdot \boldsymbol{J}_{\text{mech}} + p\,\nabla \cdot \boldsymbol{v} + \rho\,(-\epsilon + \partial_t \Phi), \tag{26.46c}$$

where

$$\mathcal{M} = \mathcal{K} + \Phi \tag{26.47}$$

is the mechanical energy per mass of a fluid element. Equation (26.46c) introduced the *mechanical energy flux*

$$\boldsymbol{J}_{\text{mech}} = p\,\boldsymbol{v} - 2\,\rho\,\nu\,\boldsymbol{v} \cdot \mathbb{S}^{\text{dev}} = -\boldsymbol{v} \cdot (-p\,\mathbb{I} + \mathbb{\tau}) = -\boldsymbol{v} \cdot \mathbb{T}, \tag{26.48}$$

where $\mathbb{T}$ is the stress tensor for a Newtonian fluid given by equation (25.79) . We can write the material time evolution equation (26.49) as a flux-form conservation equation

$$\partial_t(\rho\,\mathcal{M}) + \nabla\cdot(\rho\,\mathcal{M}\,\boldsymbol{v} + \boldsymbol{J}_{\text{mech}}) = p\,\nabla\cdot\boldsymbol{v} + \rho\,(-\epsilon + \partial_t\Phi). \tag{26.49}$$

Equation (26.46c) says that the material evolution of mechanical energy per mass arises from the convergence of the mechanical energy flux, $\boldsymbol{J}_{\text{mech}}$, plus the work done by pressure in a fluid with non-zero flow divergence, along with frictional dissipation (more discussed in Section 26.7.3), and time changes to the geopotential. Furthermore, as shown when studying total energy in Section 26.7, mechanical energy is exchanged with internal energy through pressure work and frictional dissipation. This exchange provides the fundamental link between the mechanical energy of macroscopic motion and the internal energy of microscropic degrees of freedom. As already anticipated, there is a cancellation of the mechanical energy exchanged between kinetic and potential energy due to motion through the gravitational field. However, the time-dependent geopotential provides a source of mechanical energy arising from processes external to the fluid, such as astronomical effects that drive tidal motions.

26.4.2 Gravitational potential energy budget for a finite volume

We here develop the gravitational potential energy budget for a finite volume, $\mathcal{R}$. Using the Leibniz-Reynolds transport theorem in the form of equation (20.47) yields

$$\frac{\mathrm{d}}{\mathrm{d}t}\left[\int_{\mathcal{R}} \rho\,\Phi\,\mathrm{d}V\right] = \int_{\mathcal{R}} \partial_t(\rho\,\Phi)\,\mathrm{d}V + \oint_{\partial\mathrm{R}} \rho\,\Phi\,\boldsymbol{v}^{(b)}\cdot\hat{\boldsymbol{n}}\,\mathrm{d}\mathcal{S}, \tag{26.50}$$

where $\boldsymbol{v}^{(b)}$ is the velocity of a point on the region boundary, $\partial\mathcal{R}$, and $\hat{\boldsymbol{n}}$ is the boundary outward normal. Next we replace the partial time derivative with

$$\partial_t(\rho\,\Phi) = \rho\,\frac{\mathrm{D}\Phi}{\mathrm{D}t} - \nabla\cdot(\rho\,\boldsymbol{v}\,\Phi), \tag{26.51}$$

in which case

$$\frac{\mathrm{d}}{\mathrm{d}t}\left[\int_{\mathcal{R}} \rho\,\Phi\,\mathrm{d}V\right] = \int_{\mathcal{R}} \rho\,\frac{\mathrm{D}\Phi}{\mathrm{D}t}\,\mathrm{d}V - \oint_{\partial\mathrm{R}} \rho\,\Phi\,(\boldsymbol{v}-\boldsymbol{v}^{(b)})\cdot\hat{\boldsymbol{n}}\,\mathrm{d}\mathcal{S}. \tag{26.52}$$

For the case of the full ocean domain we use the surface kinematic boundary condition (19.88a), and no-flux boundary condition on the bottom, to yield

$$\frac{\mathrm{d}}{\mathrm{d}t}\left[\int_{\mathcal{R}} \rho\,\Phi\,\mathrm{d}V\right] = \int_{\mathcal{R}} \rho\,\frac{\mathrm{D}\Phi}{\mathrm{D}t}\,\mathrm{d}V + \oint_{\partial\mathcal{R}} \Phi\,Q_{\mathsf{m}}\,\mathrm{d}A, \tag{26.53}$$

with Q_{m} the mass flux crossing the upper boundary at $z=\eta$, and $\mathrm{d}A$ the horizontal area element. For the simple geopotential, $\Phi = g\,z$, this equation takes the form

$$\frac{\mathrm{d}}{\mathrm{d}t}\left[\int_{\mathcal{R}} \rho\,\Phi\,\mathrm{d}V\right] = \int_{\mathcal{R}} \rho\,g\,w\,\mathrm{d}V + \oint_{\partial\mathcal{R}} \Phi\,Q_{\mathsf{m}}\,\mathrm{d}A. \tag{26.54}$$

This budget says that the gravitational potential energy for the global ocean domain changes due to the domain integrated vertical motion, plus contributions from the transfer of mass across the free surface boundary.

26.4.3 Mechanical energy budget for a finite volume

We here consider the mechanical energy budget for a finite volume region of fluid, first deriving the budget for a real fluid and then specializing to the perfect fluid without flow divergence.

Budget for a real fluid

To derive the finite volume budget we make use of the Leibniz-Reynolds transport theorem in the form of equation (20.49), as well as the flux-form mechanical energy budget (26.49), thus leading to

$$\frac{\mathrm{d}}{\mathrm{d}t}\left[\int_{\mathscr{R}} \rho \mathcal{M}\, \mathrm{d}V\right] = -\oint_{\partial\mathscr{R}} \rho \mathcal{M}\, (\boldsymbol{v} - \boldsymbol{v}^{(b)}) \cdot \hat{\boldsymbol{n}}\, \mathrm{d}\mathcal{S} - \oint_{\partial\mathscr{R}} \boldsymbol{J}_{\text{mech}} \cdot \hat{\boldsymbol{n}}\, \mathrm{d}\mathcal{S} + \int_{\mathscr{R}} [p\, \nabla \cdot \boldsymbol{v} + \rho\, (-\epsilon + \partial_t \Phi)]\, \mathrm{d}V. \quad (26.55)$$

The first term on the right hand side arises from the advective transport of mechanical energy across the moving boundary. The second term arises from the boundary work done by pressure and viscous stresses, with equation (26.48) yielding the equivalent expression in terms of the stress tensor

$$-\oint_{\partial\mathscr{R}} \boldsymbol{J}_{\text{mech}} \cdot \hat{\boldsymbol{n}}\, \mathrm{d}\mathcal{S} = \oint_{\partial\mathscr{R}} \boldsymbol{v} \cdot \mathbb{T} \cdot \hat{\boldsymbol{n}}\, \mathrm{d}\mathcal{S}. \quad (26.56)$$

The third term in equation (26.55) is a volume source arising from pressure work applied to each fluid parcel, viscous dissipation, and time tendencies in the geopotential.

Budget for a perfect fluid with zero flow divergence

Consider the particular case of a non-divergent flow ($\nabla \cdot \boldsymbol{v} = 0$), as in the Boussinesq ocean studied in Chapter 29. In this case, pressure does no work on fluid elements since each element maintains a constant volume.[4] Furthermore, assume the fluid is perfect and so do not have any viscous stresses. Finally, assume the geopotential is constant in time ($\partial_t \Phi = 0$). These assumptions bring the finite volume mechanical energy equation (26.55) to the form

$$\frac{\mathrm{d}}{\mathrm{d}t}\left[\int_{\mathscr{R}} \rho \mathcal{M}\, \mathrm{d}V\right] = -\oint_{\partial\mathscr{R}} \rho \mathcal{M}\, (\boldsymbol{v} - \boldsymbol{v}^{(b)}) \cdot \hat{\boldsymbol{n}}\, \mathrm{d}\mathcal{S} - \oint_{\partial\mathscr{R}} p\, \boldsymbol{v} \cdot \hat{\boldsymbol{n}}\, \mathrm{d}\mathcal{S}. \quad (26.57)$$

For this fluid, mechanical energy over a finite region changes via the advective transport of $\mathcal{M}$ across the region boundary, taking into account the distinctions between the fluid velocity and the velocity of the region boundary. Mechanical energy is also modified by pressure work acting on the region boundary. It is notable that even though the flow is non-divergent at each point, so that pressure cannot do work on fluid elements, pressure can still do work on the finite region through boundary effects. Indeed, if the region is material, then $(\boldsymbol{v} - \boldsymbol{v}^{(b)}) \cdot \hat{\boldsymbol{n}} = 0$, in which case mechanical energy is modified only through pressure work integrated over the region boundary. It follows that a steady state mechanical energy is realized for material regions only with a vanishing steady state boundary integrated pressure work.

26.5 Hypothesis of local thermodynamic equilibrium

We make use of the hypothesis of *local thermodynamic equilibrium* in Section 26.6 to couple the equilibrium thermodynamics in Chapters 22 and 23 to fluids in macroscopic motion. This hypothesis presumes that macroscopic fluid motion is comprised of a continuum of moving fluid elements[5] that are, individually, in local thermodynamic equilibrium. For a perfect fluid, macroscopic motion does not alter the entropy for a fluid element. That is, in the absence of mixing of fluid elements, advective transport is a reversible process. In contrast, mixing of properties between real fluid elements is irreversible and thus increases entropy.

[4] In Section 21.2 we show that $\nabla \cdot \boldsymbol{v} = 0$ means that fluid elements maintain a materially constant volume.
[5] See Section 17.2.4 for a reminder of fluid elements.

26.5.1 Elements of the local thermodynamic equilibrium hypothesis

For a real fluid, any finite sized region is generally out of thermodynamic equilibrium, as evidenced, say, by a non-uniform temperature over macroscopic length scales. Even so, the local thermodynamic equilibrium hypothesis assumes that infinitesimal fluid elements are in local thermodynamic equilibrium, thus affording the means to determine intensive thermodynamic properties (e.g., temperature, pressure, chemical potential) at each point within the fluid continuum. Furthermore, the hypothesis means that the functional dependence of state functions (e.g., internal energy, entropy, enthalpy) remains the same for the moving fluid as in thermodynamic equilibrium. This particular implication of the hypothesis provides the key operational means for extending to a moving real fluid the differential relations developed for equilibrium thermodynamics in Part IV of this book.

Theoretical foundations for the hypothesis of local thermodynamic equilibrium are rather difficult and somewhat unresolved. Indeed, many presentations postulate that the equations of equilibrium thermodynamics can be extended to moving continuous media, with justification provided *a posteriori* based on the resulting implications (e.g., Section III.2 of *DeGroot and Mazur* (1984)). We follow this approach here.[6] Fortunately, the hypothesis has proven successful for the atmosphere and ocean motions studied in this book, so that we accept it for our studies.[7] Further discussion of the hypothesis of local thermodynamic equilibrium can be found in Section 49 of *Landau and Lifshitz* (1987), chapter 5 of *Huang* (1987), and Section 19.2 of *Woods* (1975).[8]

26.5.2 Processes facilitating local equilibration

How does local thermodynamic equilibration come about, and how well should we expect it to be satisfied? If we assume a fluid element has length scale $L_{\text{macro}} = 10^{-4}$ m, as motivated in Section 16.2, then the question reduces to determining the time scale for a fluid element to be in have its mechanical and thermodynamical properties homogenized. We consider mechanical equilibrium to be related to the time scales for pressure to equilibrate, whereas thermodynamic equilibrium requires the additional considerations of material and thermal diffusion.

Pressure signals are transmitted by acoustic waves with speeds c_{s} (Chapter 51), so that we assume pressure equilibration times are proportional to $L_{\text{macro}}/c_{\text{s}}$. The sound speed for air at room temperature is roughly 350 m s^{-1}, so that pressure fluctuations are transmitted across an air element within roughly 3×10^{-7} s. The sound speed is about five times higher in water, thus leading to roughly 6×10^{-8} s for the pressure signal to cross an element of water. Both of these time scales are extremely tiny from a macroscopic perspective, thus supporting the assumption that pressure is rapidly equilibrated over the length scales of a fluid element.

The time scale for homogenization of temperature and matter concentrations are given by $L^2_{\text{macro}}/\kappa$, where κ is the respective molecular kinematic diffusivity for temperature or matter, which is on the order of 10^{-6}–10^{-5} m^2 s^{-1}. Hence, the time scale for a fluid element to homogenize its temperature and tracer concentration, through molecular diffusion, is 10^{-3} – 10^{-2} s. This time scale is far larger than the pressure time scale, yet it is still small relative to typical macroscopic processes associated with fluid particle motion.

[6] The hypothesis of local thermodynamic equilibrium can be motivated by noting that the microscopic motions of molecules have a much shorter equilibration time scale relative to the longer time scale of macroscopic processes of interest for fluid flow (Section 16.3.5). Even so, pursuit of that motivation has some nuances that go beyond our goals. Hence, our perspective is pragmatic, in which we assume local thermodynamic equilibrium and see what it implies.

[7] The hypothesis of local thermodynamic equilibrium is questionable for rarefied gas dynamics of the upper atmosphere, which is a subject outside the scope of this book.

[8] The extension of equilibrium thermodynamics to a moving fluid falls under the discipline of *quasi-equilibrium thermodynamics* or *linear irreversible thermodynamics*. The term "linear" in the name refers to an assumption that the system is close to thermodynamic equilibrium throughout its motion so that thermodynamic fluxes are linear functions of the gradients of the thermodynamic state variables.

26.6 Thermodynamics of a moving fluid

We here extend the formalism of equilibrium thermodynamics from Chapters 22 and 23 to the case of a moving fluid. One practical outcome of this development is a framework to understand how the internal energy of microscopic degrees of freedom is exchanged with the mechanical energy of macroscopic fluid motion. For that purpose, recall the fundamental thermodynamic relation (22.56b) for a two-component fluid such as seawater or the atmosphere

$$\mathrm{d}\mathcal{J} = T\,\mathrm{d}\mathcal{S} - p\,\mathrm{d}(1/\rho) + \mu\,\mathrm{d}C. \tag{26.58}$$

This equation expresses the first law of thermodynamics for a quasi-static process (Section 22.1.5), thus relating the exact differential of specific internal energy, $\mathcal{J}$, to the specific entropy, $\mathcal{S}$, specific volume, $1/\rho$, and matter concentration, C, along with the thermodynamic temperature, T, the pressure, p, and the relative chemical potential, μ.

Now consider a finite region of fluid comprised of a continuum of fluid elements. The fluid region is generally exposed to mechanical and thermal processes that support macroscopic fluid motion. However, as discussed in Section 26.5, we assume that each fluid element is in local thermodynamic equilibrium and separately satisfies the fundamental thermodynamic relation (26.58). We furthermore assume that the thermodynamic potentials have the same functional relation across all of the fluid elements. This assumption is basic to our ability to maintain a field theoretic description of the continuum. Namely, there is no objective definition of a fluid element. Instead, they are infinitesimal regions of a continuum. So we must make use of the same functional expression for thermodynamic potentials across all of the fluid elements. This assumption allows us to take space and time derivatives of thermodynamic potentials as considered next.

26.6.1 Concerning the transition to a continuous fluid

For a continuum fluid, each of the thermodynamic properties in the fundamental thermodynamic relation (26.58) are continuous functions of space and time. Furthermore, equation (26.58) provides a relation between exact differentials as detailed in Section 2.8. As exact differentials of continuous fields, we can make use of the space and time differentials detailed in Section 17.4.1 to write

$$\mathrm{d}\Psi = \Psi(\boldsymbol{x} + \mathrm{d}\boldsymbol{x}, t + \mathrm{d}t) - \Psi(\boldsymbol{x}, t) = \mathrm{d}t\,\partial_t\Psi + \mathrm{d}\boldsymbol{x}\cdot\nabla\Psi, \tag{26.59}$$

where Ψ is one of the thermodynamic properties, $\mathrm{d}t$ is the time differential, and $\mathrm{d}\boldsymbol{x}$ is the vector of space differentials. Following the discussion in Section 17.4.2, we are led to the total time derivative for a property following an arbitrary trajectory $\boldsymbol{x} = \boldsymbol{X}(t)$

$$\frac{\mathrm{d}\Psi}{\mathrm{d}t} = \frac{\partial\Psi}{\partial t} + \frac{\mathrm{d}\boldsymbol{X}}{\mathrm{d}t}\cdot\nabla\Psi. \tag{26.60}$$

Restricting the trajectory to that defined by a fluid particle, so that $\boldsymbol{v} = \mathrm{d}\boldsymbol{X}/\mathrm{d}t$, renders the material time derivative as in Section 17.4.4

$$\frac{\mathrm{D}\Psi}{\mathrm{D}t} = \frac{\partial\Psi}{\partial t} + \boldsymbol{v}\cdot\nabla\Psi. \tag{26.61}$$

We make use of this result in Section 26.6.4 to transition the quasi-static relation (26.58) to a moving fluid.

26.6.2 Space-time derivatives and thermodynamic partial derivatives

We need one more piece of formalism prior to transitioning the quasi-static relation (26.58) to a moving fluid. For this purpose, consider the particular case of specific enthalpy, in which case

$$\mathcal{H} = \mathcal{H}(\boldsymbol{x}, t) = \mathcal{H}[\mathcal{S}(\boldsymbol{x}, t), p(\boldsymbol{x}, t), C(\boldsymbol{x}, t)], \tag{26.62}$$

where the second equality exposed the natural functional dependence based on the fundamental thermodynamic relation (22.74c)

$$\mathrm{d}\mathcal{H} = T\,\mathrm{d}\mathcal{S} + (1/\rho)\,\mathrm{d}p + \mu\,\mathrm{d}C, \tag{26.63}$$

which holds for transitions between equilibrium states (Section 22.6.4). Again, this same functional dependence is assumed to hold for the case of an evolving fluid, so long as the evolution time scales are much slower than the time scales for reaching local thermodynamic equilibrium. We next make use of the chain-rule to render the spatial gradient

$$\nabla\mathcal{H} = \left[\frac{\partial\mathcal{H}}{\partial\mathcal{S}}\right]_{p,C}\nabla\mathcal{S} + \left[\frac{\partial\mathcal{H}}{\partial p}\right]_{\mathcal{S},C}\nabla p + \left[\frac{\partial\mathcal{H}}{\partial C}\right]_{\mathcal{S},p}\nabla C. \tag{26.64}$$

This spatial gradient probes properties of the field, $\mathcal{H}(\boldsymbol{x}, t)$, which is a function of three other fields, $\mathcal{S}(\boldsymbol{x}, t), p(\boldsymbol{x}, t), C(\boldsymbol{x}, t)$. From this field theory perspective, the thermodynamic partial derivatives are computed by holding the value of the complement thermodynamic properties fixed at a point in space and time. For example, exposing space and time positions renders the awkward, yet unambiguous, expression

$$\left[\frac{\partial\mathcal{H}}{\partial\mathcal{S}}\right]_{p,C} = \left[\frac{\partial\mathcal{H}[\mathcal{S}(\boldsymbol{x}, t), p(\boldsymbol{x}, t), C(\boldsymbol{x}, t)]}{\partial\mathcal{S}(\boldsymbol{x}, t)}\right]_{p(\boldsymbol{x},t),C(\boldsymbol{x},t)}. \tag{26.65}$$

We next apply the thermodynamic partial derivative identities (22.76) to write

$$\left[\frac{\partial\mathcal{H}}{\partial\mathcal{S}}\right]_{p,C} = \left[\frac{\partial\mathcal{H}[\mathcal{S}(\boldsymbol{x}, t), p(\boldsymbol{x}, t), C(\boldsymbol{x}, t)]}{\partial\mathcal{S}(\boldsymbol{x}, t)}\right]_{p(\boldsymbol{x},t),C(\boldsymbol{x},t)} = T(\boldsymbol{x}, t) \tag{26.66a}$$

$$\left[\frac{\partial\mathcal{H}}{\partial p}\right]_{\mathcal{S},C} = \left[\frac{\partial\mathcal{H}[\mathcal{S}(\boldsymbol{x}, t), p(\boldsymbol{x}, t), C(\boldsymbol{x}, t)]}{\partial p(\boldsymbol{x}, t)}\right]_{\mathcal{S}(\boldsymbol{x},t),C(\boldsymbol{x},t)} = 1/\rho(\boldsymbol{x}, t) \tag{26.66b}$$

$$\left[\frac{\partial\mathcal{H}}{\partial C}\right]_{\mathcal{S},p} = \left[\frac{\partial\mathcal{H}[\mathcal{S}(\boldsymbol{x}, t), p(\boldsymbol{x}, t), C(\boldsymbol{x}, t)]}{\partial C(\boldsymbol{x}, t)}\right]_{\mathcal{S}(\boldsymbol{x},t),p(\boldsymbol{x},t)} = \mu(\boldsymbol{x}, t), \tag{26.66c}$$

thus leading to[9]

$$\nabla\mathcal{H} = T\,\nabla\mathcal{S} + \rho^{-1}\,\nabla p + \mu\,\nabla C. \tag{26.67}$$

An analogous relation also holds for time derivatives, in which case

$$\partial_t\mathcal{H} = T\,\partial_t\mathcal{S} + \rho^{-1}\,\partial_t p + \mu\,\partial_t C. \tag{26.68}$$

We thus find a direct connection between exact differentials satisfied by the fundamental thermodynamic relations in equilibrium thermodynamics (Chapters 22 and 23), and partial

[9] Equation (26.67) is used on page 193 of *Landau and Lifshitz* (1987) as part of their derivation of the entropy budget for a moving fluid in the presence of heat conduction. It is also used on their page 229 to derive energetics for a fluid with both heat conduction and matter diffusion. See also their page 4 for more general discussion of how equilibrium thermodynamic relations imply relations between the space and time structure of thermodynamic functions in a moving fluid. Other treatments in the literature typically gloss over the transition of the fundamental thermodynamic relation of equilibrium thermodynamics to the quasi-equilibrium thermodynamics needed for moving fluids.

derivatives in both space and time. Such connections prove particularly useful in connecting between the mechanical force from pressure and gradients in thermodynamic properties. That is, the identity (26.67) offers an alternative means to express the pressure gradient acceleration appearing in the momentum equation (e.g., equation (24.15))[10]

$$-\rho^{-1} \nabla p = -\nabla \mathcal{H} + T \nabla \mathcal{S} + \mu \nabla C. \tag{26.69}$$

26.6.3 A caution for thermodynamic partial derivatives

One common confusion arises when not being clear on whether a mathematical expression refers to an equilibrium thermodynamic relation between thermodynamic variables, as in the fundamental thermodynamic relation (26.58), or whether it expresses a relation involving space-time field representations of thermodynamic properties. The distinction is particularly important when considering derivatives and integrals since it is necessary to know what variables are held fixed in the process of performing the operations.

For example, consider the middle relation in equation (22.86), which says that the partial derivative of the Gibbs potential with respect to pressure, holding temperature and tracer concentration fixed, equals to the specific volume

$$\left[\frac{\partial \mathcal{G}}{\partial p}\right]_{T,C} = \nu_s = \rho^{-1}. \tag{26.70}$$

However, if we encounter the Gibbs potential as a space-time function, and we use pressure as a generalized vertical coordinate, then we might find need to compute the distinct partial derivative

$$\left[\frac{\partial \mathcal{G}}{\partial p}\right]_{x,y,t} \neq \left[\frac{\partial \mathcal{G}}{\partial p}\right]_{T,C}. \tag{26.71}$$

When appropriate, we offer reminders to help avoid a cascade of misunderstandings. One point where this reminder is particularly useful is when discussing energetics for a Boussinesq fluid in Section 29.6.

26.6.4 First law for a moving fluid element

Sections 26.6.1 and 26.6.2 provide the key operational means for developing the equations of quasi-equilibrium thermodynamics, in which we apply the equilibrium thermodynamic relations to moving and evolving fluid elements. Consequently, the fundamental thermodynamic relation (26.58), which is the first law for a quasi-static process transitioning between thermodynamic equilibria, becomes for a moving fluid element

$$\frac{\mathrm{D}\mathcal{I}}{\mathrm{D}t} = T \frac{\mathrm{D}\mathcal{S}}{\mathrm{D}t} + \frac{p}{\rho^2} \frac{\mathrm{D}\rho}{\mathrm{D}t} + \mu \frac{\mathrm{D}C}{\mathrm{D}t}. \tag{26.72}$$

Making use of the space and time derivative results from Section 26.6.2 leads to the gradient and Eulerian time derivative identities

$$\nabla \mathcal{I} = T \nabla \mathcal{S} + p \rho^{-2} \nabla \rho + \mu \nabla C \tag{26.73a}$$

$$\partial_t \mathcal{I} = T \partial_t \mathcal{S} + p \rho^{-2} \partial_t \rho + \mu \partial_t C. \tag{26.73b}$$

We can further massage the first law (26.72) by recalling that mass conservation as discussed in Section 19.2 means that changes in the volume of a fluid element are related to density changes

[10] We make use of the identity (26.69) for studies of circulation in Section 40.2.5 and for potential vorticity in Section 41.6.

via

$$\frac{1}{\delta V}\frac{\mathrm{D}(\delta V)}{\mathrm{D}t} = \frac{1}{\nu_s}\frac{\mathrm{D}\nu_s}{\mathrm{D}t} = -\frac{1}{\rho}\frac{\mathrm{D}\rho}{\mathrm{D}t}. \tag{26.74}$$

Hence, equation (26.72) can be written

$$\delta M \frac{\mathrm{D}\mathcal{I}}{\mathrm{D}t} = T\,\delta M \frac{\mathrm{D}\mathcal{S}}{\mathrm{D}t} - p\frac{\mathrm{D}(\delta V)}{\mathrm{D}t} + \mu\,\delta M \frac{\mathrm{D}C}{\mathrm{D}t}, \tag{26.75}$$

where $\delta M = \rho\,\delta V$ is the mass of the fluid element. Since the mass of the fluid element is constant, equation (26.75) is the fluid element extension of the first law given by equation (26.58). Alternatively, we can use the further result from mass conservation (equation (19.25))

$$\frac{1}{\delta V}\frac{\mathrm{D}(\delta V)}{\mathrm{D}t} = \nabla\cdot\boldsymbol{v} \tag{26.76}$$

to write

$$\frac{\mathrm{D}\mathcal{I}}{\mathrm{D}t} = T\frac{\mathrm{D}\mathcal{S}}{\mathrm{D}t} - (p/\rho)\,\nabla\cdot\boldsymbol{v} + \mu\frac{\mathrm{D}C}{\mathrm{D}t}. \tag{26.77}$$

Processes affecting internal energy that appear on the right hand side are (i) entropy production, whose form is developed in Sections 26.10 and 26.7, (ii) mechanical work from pressure modifying the volume of the fluid element, and (iii) mixing (chemical work) through the exchange of matter constituents between fluid elements. We provide further details for the first law in Section 26.7 when considering the budget for the total energy of a fluid element.

26.6.5 Enthalpy budget

It is often more convenient to consider the specific enthalpy (Section 22.6.4),

$$\mathcal{H} = \mathcal{I} + p/\rho = \mathcal{I} + p\,\nu_s. \tag{26.78}$$

The mass continuity equation (19.19) and the internal energy equation (26.77) yield

$$\frac{\mathrm{D}\mathcal{H}}{\mathrm{D}t} = \frac{\mathrm{D}\mathcal{I}}{\mathrm{D}t} + \frac{1}{\rho}\frac{\mathrm{D}p}{\mathrm{D}t} - \frac{p}{\rho^2}\frac{\mathrm{D}\rho}{\mathrm{D}t} \Longrightarrow \frac{\mathrm{D}\mathcal{H}}{\mathrm{D}t} = T\frac{\mathrm{D}\mathcal{S}}{\mathrm{D}t} + \frac{1}{\rho}\frac{\mathrm{D}p}{\mathrm{D}t} + \mu\frac{\mathrm{D}C}{\mathrm{D}t}, \tag{26.79}$$

with the second expression consistent with equations (26.67) and (26.68) for the gradient and local time tendency of the specific enthalpy.

The specific enthalpy equation (26.79) says that for constant pressure processes, changes to specific enthalpy of a moving fluid element arise just from those processes that give rise to changes in specific entropy and changes in matter concentration

$$\frac{\mathrm{D}p}{\mathrm{D}t} = 0 \Longrightarrow \frac{\mathrm{D}\mathcal{H}}{\mathrm{D}t} = T\frac{\mathrm{D}\mathcal{S}}{\mathrm{D}t} + \mu\frac{\mathrm{D}C}{\mathrm{D}t}. \tag{26.80}$$

Since many boundary processes occur approximately at near constant pressure (e.g., air-sea fluxes), this result motivates formulating boundary fluxes of matter and thermal energy in terms of enthalpy fluxes rather than internal energy fluxes. Also, the mixing of fluid elements occurs locally in space so that pressure of fluid elements is the same when they mix, again making enthalpy a useful thermodynamic potential for the study of mixing.

26.6.6 Thermal and chemical processes and fluxes

The internal energy of a fluid element is modified by the diabatic transfer of thermal energy. We are generally concerned with two thermal fluxes, one due to conduction and one due to radiation

$$\boldsymbol{J}_{\text{therm}} = \boldsymbol{J}_{\text{cond}} + \boldsymbol{J}_{\text{rad}}. \tag{26.81}$$

Details of the radiant flux require topics outside our scope so we leave it unspecified. However, we consider forms for heat conduction in Section 26.10, with the simplest form being *Fourier's law* whereby $\boldsymbol{J}_{\text{cond}}$ is directed down the temperature gradient.

The internal energy of a fluid element also changes through changes in the matter concentration. This change occurs when fluid elements mix at constant pressure. As mentioned in Section 26.6.5, enthalpy is the proper thermodynamic potential to consider for examining the mixing of matter concentrations. We thus assume that the transfer of chemical energy associated with a matter flux, $\boldsymbol{J}_C$, leads to a corresponding chemical energy flux given by

$$\boldsymbol{J}_{\text{chem}} = \left[\frac{\partial \mathcal{H}}{\partial C}\right]_{T,p} \boldsymbol{J}_C. \tag{26.82}$$

The enthalpy partial derivative is computed at constant pressure and temperature so to isolate the energy change associated just with mixing of matter. It is important to distinguish this partial derivative with the distinct derivative that leads to the chemical potential as in equation (22.76)

$$\left[\frac{\partial \mathcal{H}}{\partial C}\right]_{\mathcal{S},p} = \mu. \tag{26.83}$$

As shown by Exercise 22.2, the two partial derivatives are related by

$$\left[\frac{\partial \mathcal{H}}{\partial C}\right]_{T,p} = \mu - T \left[\frac{\partial \mu}{\partial T}\right]_{p,C}, \tag{26.84}$$

so that

$$\boldsymbol{J}_{\text{chem}} = \left[\mu - T \left[\frac{\partial \mu}{\partial T}\right]_{p,C}\right] \boldsymbol{J}_C. \tag{26.85}$$

We make use of this relation when studying the entropy budget in Section 26.10.

Details of the thermal and chemical fluxes are undetermined at this point. We garner further insights through studying the entropy budget and second law of thermodynamics in Section 26.10 and the budget for total energy in Section 26.7. It is remarkable how far the laws of thermodynamics can be used to constrain the molecular flux laws. Even so, we note that the conductive and chemical fluxes are those that arise from molecular motions rather than turbulent motions, with turbulent fluxes determined by properties of the flow whereas $\boldsymbol{J}_{\text{cond}}$ and $\boldsymbol{J}_{\text{chem}}$ are determined by properties of the fluid.

26.6.7 First law in terms of potential temperature

Equation (23.44) says that the change in entropy for a fluid element moving with constant matter concentration and at the reference pressure is given in terms of the potential temperature

$$\frac{\mathrm{D}\mathcal{S}}{\mathrm{D}t} = \frac{c_p}{\theta} \frac{\mathrm{D}\theta}{\mathrm{D}t} \tag{26.86}$$

For a single-component fluid, the potential temperature equals to the *in situ* temperature when $p = p_{\mathrm{R}}$, in which case

$$c_p \frac{\mathrm{D}\theta}{\mathrm{D}t} = \theta \frac{\mathrm{D}\mathcal{S}}{\mathrm{D}t} \qquad \text{at } p = p_{\mathrm{R}} \text{ and } \mathrm{d}C = 0. \tag{26.87}$$

In general, this relation has little practical value since a fluid element generally does not maintain pressure at the reference pressure. Even so, in Exercise 26.4 we see that the relations hold for all pressures for the special case of an ideal gas, and in Exercise 26.5 we see they also hold for some liquids at all pressures.

26.6.8 Materially constant specific entropy for a perfect fluid

Each material fluid parcel within a perfect fluid maintains a constant specific entropy given that it experiences no dissipation (friction is absent), maintains a constant composition (mixing is absent), and encounters no heating (adiabatic). Consequently, specific entropy for each fluid parcel is reversibly stirred through advection

$$\frac{\mathrm{D}\mathcal{S}}{\mathrm{D}t} = \frac{\partial \mathcal{S}}{\partial t} + \boldsymbol{v} \cdot \nabla \mathcal{S} = 0. \tag{26.88}$$

A perfect fluid generally admits nonzero gradients of specific entropy, even as each fluid parcel moves without altering its specific entropy. The *homentropic fluid* is a special case where the entropy is a space-time constant throughout the fluid domain.

26.6.9 Further study

DeGroot and Mazur (1984) provide an authoritative accounting of quasi-equilibrium thermodynamics as applied to continuum matter such as a fluid. *Gregg* (1984) and *Davis* (1994) apply these methods to small-scale mixing in the ocean. Slightly different formulations can be found in *Landau and Lifshitz* (1987) and *Batchelor* (1967).

26.7 Budget for total energy

Recall from Section 14.7 that a point particle conserves its mechanical energy in the absence of friction. In contrast, the mechanical energy for a fluid element is not materially constant even when only conservative forces act on the element. The reason is that for the continuum fluid, there is (i) a conversion between mechanical energy and internal energy as pressure does work to alter the volume of fluid elements, and (ii) frictional dissipation of kinetic energy irreversibly converts some kinetic energy to internal energy through Joule heating (Section 26.7.3). In this section we combine the mechanical energy budget from Section 26.4 to the internal energy budget from Section 26.6, thus rendering the budget for total energy of a fluid element. We furthermore postulate that the domain integrated total energy changes only due to boundary effects, as well as possible changes in the geopotential such as via astronomical effects. This assumption then leads to further specifications of the processes contributing to the internal energy and enthalpy budgets.

26.7.1 Postulating the budget for total energy

In their specific (per mass) forms, the total energy of a fluid element is the sum of the internal energy, $\mathcal{I}$, of internal degress of freedom, plus the mechanical energy, $\mathcal{M}$, from macroscopic motion, with the mechanical energy the sum of the kinetic energy plus potential energy

$$\mathcal{E} = \mathcal{I} + \mathcal{M} = \mathcal{I} + \mathcal{K} + \Phi. \tag{26.89}$$

We postulate that this total energy per mass satisfies a conservation law whereby it is affected only by the convergence of a total energy flux, plus a source due to temporal changes in the geopotential

$$\rho \frac{\mathrm{D}\mathcal{E}}{\mathrm{D}t} = -\nabla \cdot \boldsymbol{J}_{\mathcal{E}} + \rho \, \partial_t \Phi. \tag{26.90}$$

Correspondingly, the flux-form equation for total energy is

$$\frac{\partial(\rho \, \mathcal{E})}{\partial t} + \nabla \cdot (\rho \, \boldsymbol{v} \, \mathcal{E} + \boldsymbol{J}_{\mathcal{E}}) = \rho \, \partial_t \Phi. \tag{26.91}$$

The flux of total energy is given by

$$\begin{aligned} \rho \, \boldsymbol{v} \, \mathcal{E} + \boldsymbol{J}_{\mathcal{E}} &= \rho \, \boldsymbol{v} \, \mathcal{E} + \boldsymbol{J}_{\text{therm}} + \boldsymbol{J}_{\text{chem}} + \boldsymbol{J}_{\text{mech}} && \text{(26.92a)} \\ &= \rho \, \boldsymbol{v} \, \mathcal{E} + \boldsymbol{J}_{\text{therm}} + \boldsymbol{J}_{\text{chem}} - \boldsymbol{v} \cdot (-p \, \mathbb{I} + \mathbb{T}) && \text{(26.92b)} \\ &= \rho \, \boldsymbol{v} \, (\mathcal{E} + p/\rho) + \boldsymbol{J}_{\text{therm}} + \boldsymbol{J}_{\text{chem}} - \boldsymbol{v} \cdot \mathbb{T}, && \text{(26.92c)} \end{aligned}$$

where $\boldsymbol{J}_{\text{therm}}$ and $\boldsymbol{J}_{\text{chem}}$ were discussed in Section 26.6.6, and $\boldsymbol{J}_{\text{mech}}$ was derived in Section 26.4. We have more to say concerning the flux of total energy in Section 26.9 when studying the Bernoulli potential.

We are led to postulate the total energy equation (26.90) through assuming that $\int_{\mathcal{R}} \rho \, \mathcal{E} \, \mathrm{d}V$ remains constant in time for a region, $\mathcal{R}$, that is closed to thermal, material, and mechanical interactions, and one where the geopotential is constant in time. This assumption is based on our understanding of molecular and atomic mechanics.

26.7.2 First law of thermodynamics for a moving fluid

We now have the total energy budget as postulated in the form of equation (26.90), along with the mechanical energy budget derived in equation (26.49). Subtracting the two yields the internal energy budget

$$\rho \frac{\mathrm{D}(\mathcal{E} - \mathcal{M})}{\mathrm{D}t} = \rho \frac{\mathrm{D}\mathcal{I}}{\mathrm{D}t} = -\nabla \cdot (\boldsymbol{J}_{\text{therm}} + \boldsymbol{J}_{\text{chem}}) - p \, \nabla \cdot \boldsymbol{v} + \rho \, \epsilon. \tag{26.93}$$

This equation provides yet another expression for the first law of thermodynmics for a moving fluid element. It says that the internal energy of a fluid element is modified through the convergence of thermal and chemical fluxes, pressure work that alters the volume of a fluid element, and frictional dissipation through viscosity. Both the pressure work and frictional dissipation are exchanged with mechanical energy, and so they appear with opposite signs in the budget for mechanical energy. We specify the thermal and chemical fluxes in Section 26.10 when studying the entropy budget.

We can make use of the enthalpy equation (26.79) to render the enthalpy budget

$$\rho \frac{\mathrm{D}\mathcal{H}}{\mathrm{D}t} - \frac{\mathrm{D}p}{\mathrm{D}t} = -\nabla \cdot (\boldsymbol{J}_{\text{therm}} + \boldsymbol{J}_{\text{chem}}) + \rho \, \epsilon. \tag{26.94}$$

This equation is used in Section 26.11 when studying the evolution of temperature.

26.7.3 Joule heating from friction

Frictional dissipation, $\epsilon > 0$, measures the conversion of kinetic energy into heat, and it is thus a conversion from mechanical energy to internal energy

$$\dot{Q}_{\text{Joule}} \equiv \epsilon. \tag{26.95}$$

This term is referred to as *Joule heating* in analog to the process that occurs in electrical circuits. The Joule heating of a fluid by molecular viscosity is larger in regions where the fluid strains are larger, signalling a more efficient transfer of power to the microscales where molecular viscosity can act on the flow.

In the ocean interior, measurements indicate that $\epsilon \approx 10^{-9}$ W kg^{-1}. Dividing by $c_p = 3900$ J kg^{-1} K^{-1} leads to a heating rate of less than 10^{-3} K century^{-1}, which is a very small rate of ocean heating. Consequently, ocean Joule heating has a negligible role in the ocean heat budget and as such is generally ignored. Atmospheric flows are roughly two orders faster so that the kinetic energy per mass is four orders larger. The larger flow speeds lead to larger shears thus creating larger viscous dissipation that reaches roughly $\epsilon \approx 2$ W m^{-2} globally averaged. Hence, Joule heating is an important part of the global atmosphere enthalpy budget (*Becker*, 2003).

26.7.4 Comments on gauge symmetry

Consider again the flux-form equation for total energy (26.91). It is notable that the time tendency for the total energy remains unchanged if we shift the flux of total energy by a curl,

$$\rho \mathcal{E} \boldsymbol{v} + \boldsymbol{J}_{\mathcal{E}} \to \rho \mathcal{E} \boldsymbol{v} + \boldsymbol{J}_{\mathcal{E}} + \nabla \times \boldsymbol{G}, \tag{26.96}$$

with $\boldsymbol{G}$ referred to as a *gauge function*. This arbitrariness in the definition of total energy flux is ubiquitous in physics; e.g., see the discussion of the electromagnetic field energy flux in Section 27-4 in Volume II of *Feynman et al.* (1963).[11] We conclude that the energy flux has no unique local physical meaning. Instead, it is only the convergence of the energy flux that has an unambiguous meaning given by its role in affecting a time change to the energy at a point in space.

We also encounter such *gauge symmetry* in the potential vorticity flux discussed in Chapter 42, as well as the vector streamfunction for an incompressible fluid in Section 21.5.1. In some cases we can exploit the symmetry to our subjective desires, such as discussed in Section 42.5.6 for potential vorticity. However, we know of no strategic use of gauge symmetry for the study of energy budgets.

26.7.5 Further study

The postulate of globally integrated total energy conservation in Section 26.7.1, and the associated discussion of energy budgets, follow that from Section 33 of *Serrin* (1959), Section II.4 of *DeGroot and Mazur* (1984), Chapter 14 of *Callen* (1985), Sections 49 and 58 of *Landau and Lifshitz* (1987), Chapters 3 and 4 of *Müller* (2006), Appendix B of *IOC et al.* (2010), Section 2.4 of *Olbers et al.* (2012), Chapter 1 of *Vallis* (2017), and Section 13.5.5 of *Thorne and Blandford* (2017).

26.8 Thermodynamic equilibrium with macroscopic motion

We derived the properties of thermodynamic equilibria in Section 22.2.8 for a single component fluid, and in Section 23.1 for a binary fluid in the presence of a geopotential. We here extend those discussions to the case of a finite region of a fluid undergoing macroscopic motion in the absence of gravity. We assume no external forces or torques, so that the total linear momentum and total angular momentum remain constant. As in our earlier discussions, we derive the properties of thermodynamic equilibrium by assuming entropy is an extremum at equilibrium. Furthermore, the extremum must be consistent with the variety of conserved quantities, thus

[11] The Feynman lectures are available online through the California Institute of Technology.

motivating the use of Lagrange multipliers as part of the formalism needed to determine the extremum.

26.8.1 Deriving the equilibrium conditions

To focus on the allowed macroscopic motion, we ignore external fields such as from gravity, in which case the total energy is the sum of the internal energy plus kinetic energy

$$\mathcal{E}^{\mathrm{e}} = \mathcal{I}^{\mathrm{e}} + P^2/(2\,M), \tag{26.97}$$

where $\boldsymbol{P} = M\,\boldsymbol{v}$ is the linear momentum of the system with velocity $\boldsymbol{v}$ and mass M, and $P^2 = \boldsymbol{P}\cdot\boldsymbol{P}$ is the squared momentum. If the macroscopic system is materially and mechanically closed then total energy remains constant, as does the linear momentum and angular momentum. Thermodynamic equilibrium is realized by maximizing the function

$$\Psi = \mathcal{S}^{\mathrm{e}} + \boldsymbol{A}\cdot\boldsymbol{P} + \boldsymbol{B}\cdot(\boldsymbol{x}\times\boldsymbol{P}), \tag{26.98}$$

where $\boldsymbol{x}$ is the position of the macroscopic system, and the vectors $\boldsymbol{A}$ and $\boldsymbol{B}$ are constant Lagrange multipliers. Note that for convenience we assume the system to be macroscopically small but microscopically large (e.g., a fluid element) so that we can assign a single position vector to the system.

Should entropy be a function of the total energy (which is a constant of the motion) or remain a function of just the internal energy? To answer this question we appeal to the statistical interpretation of entropy whereby the number of microstates corresponding to a particular macrostate is Galilean invariant.[12] The local rest state, where total energy equals to internal energy, is thus sufficient for defining the functional dependence[13]

$$\mathcal{S}^{\mathrm{e}} = \mathcal{S}^{\mathrm{e}}(V,\mathcal{I}^{\mathrm{e}}) = \mathcal{S}^{\mathrm{e}}[V,\mathcal{E}^{\mathrm{e}} - P^2/(2M)]. \tag{26.99}$$

Hence, maximizing Ψ with respect to the linear momentum component, P_m, requires the derivative

$$\left[\frac{\partial \mathcal{S}^{\mathrm{e}}}{\partial P_m}\right]_V = \left[\frac{\partial \mathcal{S}^{\mathrm{e}}}{\partial \mathcal{I}^{\mathrm{e}}}\right]_V \frac{\partial \mathcal{I}^{\mathrm{e}}}{\partial P_m} = -\frac{1}{T}\,\frac{P_m}{M} = -\frac{v_m}{T}, \tag{26.100}$$

so that the macroscopic velocity at equilibrium is

$$\frac{\partial \Psi}{\partial P_m} = 0 \Longrightarrow \boldsymbol{v} = T\,(\boldsymbol{A} + \boldsymbol{B}\times\boldsymbol{x}). \tag{26.101}$$

With temperature uniform throughout the macroscopic system at thermodynamic equilibrium, we find a velocity decomposed into a uniform translation plus a rigid-body rotation. That is, a closed macroscopic system in thermodynamic equilibrium can, at most, exhibit uniform translation plus rigid-body rotation. More general macroscopic motion is not possible when the system is in thermodynamic equilibrium. Furthermore, note that each component of the strain rate tensor vanishes for uniform translation plus a rigid-body rotation (see Exercise 18.2). For the Newtonian fluids considered in this book, a zero strain rate tensor means there are no frictional stresses (Section 25.8.6), thus ensuring no frictionally generated entropy.

The Cauchy-Stokes decomposition from Section 18.8.6 shows that at each time instance, motion of a fluid element can be kinematically decomposed into translation, rotation, and dilation. Dilation occurs through mechanical work. In its absence, and without heating or mixing, the fluid element moves through sequences of translations and rotations that maintain

[12] Recall our discussion of Galilean invariance in Section 17.5.

[13] See footnote on page 36 of *Landau and Lifshitz* (1980) for more discussion.

thermodynamic equilibrium. With dilation, heating, and/or matter mixing, we conceive of a moving fluid as a continuum of fluid elements that, on a time scale that is tiny relative to macroscopic processes, adjusts to thermodynamic equilibrium in response to interactions with the surrounding fluid environment.

26.8.2 Further study

We here followed the dicussion of §10 in *Landau and Lifshitz* (1980). See also a complementary discussion in Section 1.8 of *Kamenkovich* (1977), who considers a two-component fluid in the presence of gravity. *Kamenkovich* (1977) finds that although *in situ* temperature is a uniform constant in thermodynamic equilibrium, the salinity is not constant.

26.9 Bernoulli's theorem

The total energy equation (26.90) reveals that the material time change for the total energy of a fluid element is affected by the convergence of pressure times velocity. Hence, even in the absence of irreversible processes (i.e., a perfect fluid) and with a time-independent geopotential, the total energy of a fluid element is not materially invariant. The pressure flux, $p\,\boldsymbol{v}$, is a fundamental contribution to energy within the continuum. As shown in this section, it is the pressure work required for the fluid element to mechanically exist within the continuum. We thus refer to $p\,\boldsymbol{v}$ as the mechanical *injection work*. This conceptualization of $p\,\boldsymbol{v}$ arises in the context of exploring the remarkably versatile Bernoulli theorem, which is particularly useful in diagnosing energetic properties of steady flows.

26.9.1 Bernoulli potential

Consider the flux-form equation for the total energy, (26.91), written here as

$$\frac{\partial(\rho\,\mathcal{E})}{\partial t} + \nabla\cdot[\rho\,\boldsymbol{v}\,(\mathcal{E}+p/\rho) + \boldsymbol{J}_{\text{therm}} + \boldsymbol{J}_{\text{chem}} - \boldsymbol{v}\cdot\mathbb{T}] = \rho\,\partial_t\Phi. \tag{26.102}$$

The left hand side indicates that total energy of a fluid element is locally modified by the advective transport of the quantity

$$\mathcal{E} + p/\rho = (\mathcal{K}+\Phi) + (\mathcal{I} + p/\rho) = \mathcal{M} + \mathcal{H} \equiv \mathcal{B}, \tag{26.103}$$

where we introduced the *Bernoulli potential*, which is the sum of the mechanical energy per mass plus the enthalpy per mass

$$\mathcal{B} = \mathcal{M} + \mathcal{H} = \mathcal{K} + \Phi + \mathcal{I} + p/\rho. \tag{26.104}$$

For a perfect fluid there is no irreversible transfer of heat, matter, or momentum so that

$$\text{perfect fluid} \implies \boldsymbol{J}_{\text{therm}} = 0 \quad \text{and} \quad \boldsymbol{J}_{\text{chem}} = 0 \quad \text{and} \quad \mathbb{T} = 0. \tag{26.105}$$

Hence, we see that integration over a region with zero boundary transfer of $\boldsymbol{v}\,\mathcal{B}$ leads to the conservation of total energy for a perfect fluid with a time independent geopotential. Note that for some purposes it can be useful to write the total energy equation (26.102) as an equation for the Bernoulli function, which takes the form

$$\frac{\partial(\rho\,\mathcal{B})}{\partial t} + \nabla\cdot[\rho\,\boldsymbol{v}\,\mathcal{B} + \boldsymbol{J}_{\text{therm}} + \boldsymbol{J}_{\text{chem}} - \boldsymbol{v}\cdot\mathbb{T}] = \partial_t p + \rho\,\partial_t\Phi. \tag{26.106}$$

26.9.2 Mechanical injection work

Why is $\rho\,\mathcal{E}$ affected by the convergence of $\rho\,\boldsymbol{v}\,\mathcal{B}$ rather than the convergence of $\rho\,\boldsymbol{v}\,\mathcal{E}$? To answer this question,[14] again note that the Bernoulli potential is the sum of the total energy per mass of a fluid element, $\mathcal{E}$, plus the term p/ρ. So what is p/ρ? Imagine carving out a tiny region from within a continuous fluid with pressure p and specific volume $1/\rho$, leaving behind a "hole". The mechanical work required to carve out this hole is precisely equal to p/ρ. Correspondingly, we interpret p/ρ as the mechanical work required to inject a unit mass of fluid with specific volume $1/\rho$ into a region with pressure p. We thus refer to p/ρ as the *injection work*, and we in turn see that specific enthalpy, $\mathcal{H} = \mathcal{I} + p/\rho$ (equation (26.78)), measures the internal energy plus the mechanial work required for a fluid element to exist within a continuum.

We can support the above interpretation by considering the flux, $\rho\,\boldsymbol{v}\,\mathcal{B}$, in a perfect fluid that penetrates a static closed fluid region

$$\oint_{\partial\mathcal{R}} \rho\,\boldsymbol{v}\,\mathcal{B}\cdot\hat{\boldsymbol{n}}\,\mathrm{d}\mathcal{S} = \oint_{\partial\mathcal{R}} \rho\,\boldsymbol{v}\,\mathcal{E}\cdot\hat{\boldsymbol{n}}\,\mathrm{d}\mathcal{S} + \oint_{\partial\mathcal{R}} p\,\boldsymbol{v}\cdot\hat{\boldsymbol{n}}\,\mathrm{d}\mathcal{S}. \tag{26.107}$$

The first term on the right hand side is the flux of total energy (mechanical plus internal) that penetrates the region boundary, $\partial\mathcal{R}$. The second term is the mechanical work done by pressure acting on the boundary. The example in Section 26.9.5 further supports this perspective, whereby we develop the energetics of a control volume of fluid moving through a pipe.

26.9.3 Bernoulli's theorem for a steady perfect fluid

Consider a perfect fluid flow in steady state (vanishing Eulerian time derivatives). Steady state mass conservation means that

$$\frac{\partial\rho}{\partial t} = -\nabla\cdot(\rho\,\boldsymbol{v}) = 0. \tag{26.108}$$

This relation, along with a steady state energy in equation (26.102) (absent friction, heating, mixing, and with a time-independent geopotential), means that the steady state velocity field is locally tangent to isosurfaces of the Bernoulli potential

$$\boldsymbol{v}\cdot\nabla\mathcal{B} = 0. \tag{26.109}$$

We thus see that for the perfect fluid to be in a steady state, the Bernoulli potential is constant along streamlines, which is a result known as *Bernoulli's theorem*. Hence, as the fluid moves along a streamline, there is an exchange between the total energy per mass, $\mathcal{E}$, and the injection work, p/ρ, such that their sum remains constant.

A constant Bernoulli potential for steady flow is used frequently in engineering fluid dynamics to interpret flow around objects, such as for flow around a wing, in which case the sum $p+\rho\,\boldsymbol{v}^2/2$ is sometimes referred to as the *total pressure* or *stagnation pressure*. It leads to a realization of *Bernoulli's principle*, whereby in regions of low pressure the energy per mass is relatively large, whereas the converse holds in regions of high pressure. The change in energy is largely due to a change in the kinetic energy, so that flow is fast in regions of low pressure (e.g., top of the wing, flow around a train moving through a tunnel) and slow in regions of high pressure (e.g., bottom of the wing).[15] That is, the Bernoulli principle provides an energetic expression for why a fluid slows down when moving into a region of relatively high pressure, and speeds up when moving to a region of low pressure.

[14] This argument follows Section 13.5.4 of *Thorne and Blandford* (2017) as well as Section 6 of *Landau and Lifshitz* (1987).

[15] See this discussion and video for why it is incorrect to use Bernoulli's theorem for explaining the lift on an airplane wing.

26.9.4 Traditional derivation of Bernoulli's theorem

For completeness we offer a second derivation of Bernoulli's theorem that follows a more traditional route and reveals some useful manipulations. For this purpose, convert the advective-form momentum equation (24.16) into its vector-invariant form by making use of the vector identity (see Section 2.3.4)

$$\boldsymbol{\omega} \times \boldsymbol{v} = -\mathcal{K} + (\boldsymbol{v} \cdot \nabla)\, \boldsymbol{v}. \tag{26.110}$$

This identity allows us to eliminate velocity self-advection in favor of the vorticity and kinetic energy per mass

$$\frac{\partial \boldsymbol{v}}{\partial t} + \boldsymbol{\omega}_{\mathrm{a}} \times \boldsymbol{v} = -\frac{1}{\rho} \nabla p - \nabla \mathcal{M}, \tag{26.111}$$

where

$$\boldsymbol{\omega}_{\mathrm{a}} = \boldsymbol{\omega} + 2\, \boldsymbol{\Omega} \tag{26.112}$$

is the absolute vorticity (see Chapter 40) and we set the irreversible terms to zero since we are assuming a perfect fluid. The Eulerian time evolution for the kinetic energy per mass is therefore given by

$$\frac{\partial \mathcal{K}}{\partial t} = -\frac{1}{\rho}\, \boldsymbol{v} \cdot \nabla p - \boldsymbol{v} \cdot \nabla \mathcal{M}, \tag{26.113}$$

where we set $\boldsymbol{v} \cdot (\boldsymbol{\omega}_{\mathrm{a}} \times \boldsymbol{v}) = 0$.

For Bernoulli's theorem we are interested in the steady state, with a steady kinetic energy per mass realized by the balance

$$\rho^{-1}\, \boldsymbol{v} \cdot \nabla p = -\boldsymbol{v} \cdot \nabla \mathcal{M}. \tag{26.114}$$

We can connect this steady state balance to the Bernoulli potential by noting that for a steady perfect and single-component fluid, equation (26.69) allows us to write

$$\rho^{-1}\, \boldsymbol{v} \cdot \nabla p = \boldsymbol{v} \cdot (\nabla \mathcal{H} - T\, \nabla \mathcal{S}). \tag{26.115}$$

Combining with equation (26.114) renders

$$\boldsymbol{v} \cdot (\nabla \mathcal{H} + \nabla \mathcal{M} - T\, \nabla \mathcal{S}) = \boldsymbol{v} \cdot (\nabla \mathcal{B} - T\, \nabla \mathcal{S}) = 0. \tag{26.116}$$

A perfect fluid maintains materially constant specific entropy (Section 26.6.8), which in a steady state means that

$$\boldsymbol{v} \cdot \nabla \mathcal{S} = 0 \qquad \text{and} \qquad \boldsymbol{v} \cdot \nabla \mathcal{B} = 0 \qquad \Longleftarrow \text{steady state perfect fluid.} \tag{26.117}$$

That is, for a steady perfect fluid the velocity is aligned with isosurfaces of specific entropy and Bernoulli potential.

26.9.5 Steady flow in a pipe

To help further understand Bernoulli's theorem and the contribution from the mechanical work provided by pressure forces, consider the steady flow of a constant density perfect fluid in a frictionless pipe as depicted in Figure 26.1. For this system, Bernoulli's theorem says that the following simplified form of the Bernoulli potential is constant for flow along a streamline

$$\mathcal{B} = \boldsymbol{v}^2/2 + p/\rho + g\, z = \text{constant}. \tag{26.118}$$

Note that internal energy dropped out since for a constant density fluid the internal energy is a constant and so plays no role in the energetics. Equation (26.118) means that there is a precise

balance between the kinetic energy per mass, injection work, and geopotential for a steady and constant density fluid. For example, for flow following a constant geopotential, pressure is relatively low in regions of large kinetic energy whereas pressure is relatively high in regions of small kinetic energy. We further pursue this understanding by showing that the statement (26.118) of Bernoulli's theorem can be derived through traditional energetic arguments, whereby the mechanical work done on the fluid system equals to the system's change in kinetic energy (see Section 11.1.4 for the particle mechanics version of this *work-energy theorem*).

For this purpose, let the system under examination be a control volume of fluid as described in the caption to Figure 26.1, and examine the work done on the control volume over an arbitrary time increment, Δt. During this time, a mass of fluid given by

$$M = \rho\, A_1\, u_1\, \Delta t = \rho\, A_2\, u_2\, \Delta t \tag{26.119}$$

moves through the pipe, with $A_1\, u_1 = A_2\, u_2$ following from volume conservation, and we assumed that the $u_{1,2} = \Delta x_{1,2}/\Delta t$ measures the average velocity across the pipe cross-section. Mechanical work is applied to the fluid in the control volume by pressure acting on the end caps (contact force) and by gravity acting throughout the fluid (body force).

- PRESSURE WORK: At the left end cap, pressure from fluid to the left of the control volume does work on the control volume by the amount $p_1\, A_1\, \Delta x_1 = p_1\, M/\rho$. On the right end, the control volume does work on the fluid to its right, which means that a negative work is applied to the control volume in the amount $-p_2\, A_2\, \Delta x_2 = -p_2\, M/\rho$.

- GRAVITATIONAL WORK: Fluid downstream at the right end is higher than fluid upstream on the left end. The control volume must do work against gravity to achieve this altitude increase and this work is given by $-g\, M\, (z_2 - z_1)$.

As the fluid moves from left to right, the control volume changes its kinetic energy by the amount $(M/2)\,(u_2^2 - u_1^2)$. Equating this kinetic energy change to the work applied to the control volume renders

$$(1/2)\,(u_2^2 - u_1^2) = (1/\rho)\,(p_1 - p_2) - g\,(z_2 - z_1), \tag{26.120}$$

where the mass, M, dropped out. Rearrangement then leads to

$$u^2/2 + p/\rho + g\, z = \text{constant}, \tag{26.121}$$

which is a statement of Bernoulli's theorem (26.118).

Making use of volume conservation allows us to rearrange equation (26.120) to determine the pressure difference between the left and right end of the pipe

$$p_1 - p_2 = \rho\, g\,(z_2 - z_1) - (\rho/2)\, u_1^2\, [1 - (A_1/A_2)^2]. \tag{26.122}$$

To help understand this result, consider two special cases starting with $A_1 = A_2$. We see that for equal cross-sectional areas, the pressure drop equals to the increase in gravitational potential energy,

$$p_1 - p_2 = \rho\, g\,(z_2 - z_1) > 0 \quad \text{with } A_2 = A_1, \tag{26.123}$$

so that the pressure work equals to the gravitational work required to lift the fluid. Next consider $z_2 = z_1$ so that there is no change in gravitational potential energy but there is a change in cross-sectional area, in which case

$$p_1 - p_2 = -(\rho/2)\, u_1^2\, [1 - (A_1/A_2)^2] < 0 \quad \text{with } z_2 = z_1. \tag{26.124}$$

In this case there is a pressure increase as the fluid moves into a region with larger cross-sectional area ($A_2 > A_1$). This pressure increase slows the fluid speed, which accords with volume

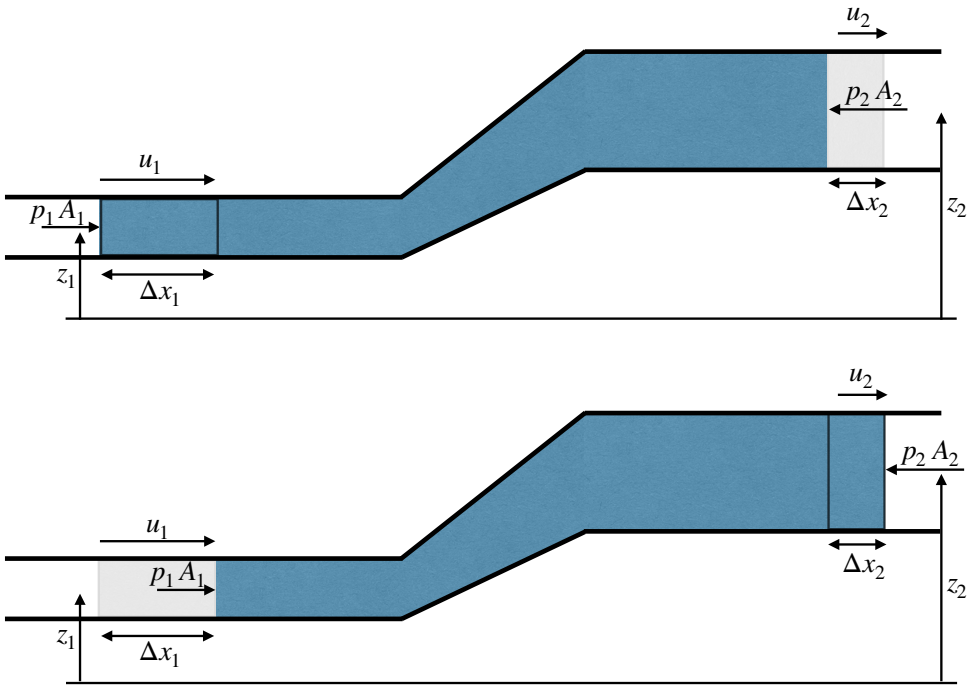

FIGURE 26.1: An example to illustrate the basic physics of Bernoulli's theorem and pressure work, whereby we depict the flow of a perfect and constant density fluid from left to right in a pipe of variable cross-section and variable height. We study the energetics of a control volume (dark blue region) moving with the fluid. The top panel shows the control volume at one time and the lower panel shows the control volume at a time Δt later, after which a mass of fluid, M, has moved through the system. Volume conservation means that $(u_1\,\Delta t)\,A_1 = (u_2\,\Delta t)\,A_2$, where $\Delta x_{1,2}$ is the horizontal displacement of the fluid plug over time Δt, $u_{1,2}$ is the cross-sectional area average velocity, $A_{1,2}$ is the pipe cross-sectional area, and $M = \rho\,\Delta x_1\,A_1 = \rho\,\Delta x_2\,A_2$ is the mass of fluid moving over the Δt time increment. Pressure forces, $p_{1,2}$, at the end caps point inward (compressive), with pressure on the left larger than that on the right to support the fluid moving to the right. As the fluid moves upward it increases its gravitational potential energy and in so doing the fluid does work against gravity.

conservation.

These examples support our understanding of how pressure provides mechanical work on fluid control volume boundaries, with that work required to maintain conservation of mechanical energy (seen in the above case with $A_2 = A_1$) and conservation of volume (see in the above case with $z_2 = z_1$). Indeed, taking the control volume to be a tiny fluid element furthers our understanding of the p/ρ injection work contribution to the Bernoulli potential (26.103).

26.9.6 Steady flow over a topographic bump

We build from the discussion of steady pipe flow in Section 26.9.5 by describing a more geophysically relevant case of steady single-component perfect fluid flowing over a topographic bump. In Figure 26.2 we illustrate this flow in the absence of rotation. As the fluid moves over the bump, it speeds up in order to maintain volume continuity. In regions of faster flow, Bernoulli's theorem (26.118) says that the pressure is lower, which is realized here by a lowering of the sea surface height over the bump. For a small bump, we can imagine that the flow remains symmetric with respect to the bump, so that the flow downstream of the bump is a reflection of the upstream flow. To maintain steady flow in the presence of a larger bump requires a larger pressure drop, which will eventually break the symmetry between downstream and upstream. For an even larger topographic bump, we find there is no way to satisfy Bernoulli's theorem, in which case the flow transitions into a time dependent *hydraulic jump*.

As for the pipe flow, the steady flow maintains two flow constants: the volume flow rate and

the simplified form of the Bernoulli potential in equation (26.118)

$$\mathcal{T} = v\,h\,\Delta \quad \text{and} \quad \mathcal{B} = \boldsymbol{v}^2/2 + p/\rho + g\,z, \tag{26.125}$$

where h is the thickness of the layer and Δ the width in the direction perpendicular to the flow. Also, recall that the Bernoulli potential is a constant along a particular streamline. However, for a constant density layer the Bernoulli potential is independent of depth, as we illustrate below. For simplicity we assume the flow is only a function of the along-stream coordinate, y, and furthermore assume the pressure on the upper interface is a uniform constant p_a. We also assume the top and botton interfaces of the layer are material, which then means they are each streamlines.

It is more convenient to work with the flow rate, $\mathcal{T} = v\,h\,\Delta$, than the velocity, v, in which case the Bernouilli potential is given by

$$\mathcal{B} = \mathcal{T}^2/(2\,h^2\,\Delta^2) + p/\rho + g\,z. \tag{26.126}$$

Far upstream of the bump the layer thickness takes on its unperturbed value, H, so that the Bernoulli potential along the surface streamline at $z = H$ is given by

$$\mathcal{B} = \mathcal{T}^2/(2\,H^2\,\Delta^2) + p_a/\rho + g\,H. \tag{26.127}$$

Notice how every term on the right hand side is positive, so that $\mathcal{B} > 0$. Also notice that the Bernoulli potential along the bottom streamline takes the same value

$$\mathcal{B} = \mathcal{T}^2/(2\,H^2\,\Delta^2) + p_b/\rho = \mathcal{T}^2/(2\,H^2\,\Delta^2) + (p_a + \rho\,h\,H)/\rho, \tag{26.128}$$

which results since the layer has constant density. Now express the Bernoulli potential in a region affected by the bump, in which case

$$\mathcal{B} = \mathcal{T}^2/(2\,h^2\,\Delta^2) + p_a/\rho + g\,\eta = \mathcal{T}^2/(2\,h^2\,\Delta^2) + p_a/\rho + g\,(h + \eta_b). \tag{26.129}$$

We observe that

$$\mathcal{B} - g\,\eta_b = T^2/(2\,h^2\,\Delta^2) + p_a/\rho + g\,h \geq 0, \tag{26.130}$$

with this quantity referred to as the *Bernoulli head*. The condition $\mathcal{B} - g\,\eta_b \geq 0$ holds so long as the flow maintains the assumptions of Bernouili's theorem. However, if the topography is too tall, then $\mathcal{B} - g\,\eta_b \leq 0$, in which case the flow can no longer satisfy the Bernoulli theorem. This result leads us to define a critical topography height

$$\eta_b^{\text{crit}} = \mathcal{B}/g = \mathcal{T}^2/(2\,H^2\,\Delta^2\,g) + p_a/(\rho\,g) + H. \tag{26.131}$$

When topography is larger than this height, the flow cannot reach a steady state and/or the flow develops a dependence on the direction perpendicular to the page. In either case, the assumptions of Bernoulli's theorem breakdown.

26.9.7 Further study

For an examination of Bernoulli's theorem for flows in a non-rotating reference frame, such as flow in laminar boundary layers, see this video from Prof. Shapiro. Chapter 3 of *Acheson* (1990) and the text from *Pratt and Whitehead* (2008) make use of Bernoulli's theorem for understanding flows over obstacles with and without the Coriolis acceleration. Their Section 1.4 forms the basis for the discussion in Section 26.9.6. See also Exercise 8.6 of *Klinger and Haine* (2019).

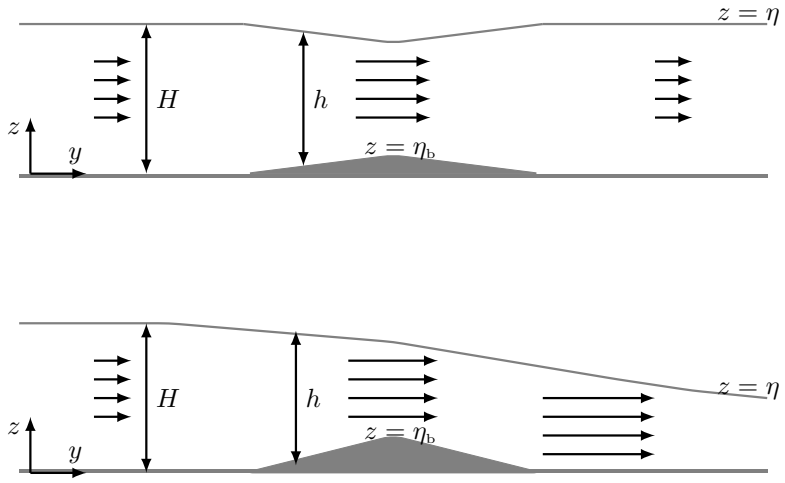

FIGURE 26.2: Depicting steady flow of a single-component fluid with constant density, ρ, flowing over a topographic bump and viewed from a non-rotating reference frame so there is no Coriolis acceleration. We assume all properties are a function only of the along-stream position, y, and $z = 0$ is taken at the position of a flat topography. For steady flow of a constant density fluid, the volume transport, $\mathcal{T}$, is constant and given by $\mathcal{T} = v\, h\, \Delta$, where Δ is the width of the flow in the direction perpendicular to the page, and $h = \eta - \eta_b$ is the layer thickness. The simplified form of the Bernouilli potential given by equation (26.118) is also constant along any streamline, $\mathcal{B} = \boldsymbol{v}^2/2 + p/\rho + g\, z =$ constant. The top panel shows the flow for a very small topographic bump, so that the flow is symmetric around the bump. The lower panel show flow for a larger bump that requires more fluid upstream of the bump to support enough pressure drop for steady flow to make it over the bump.

26.10 Entropy budget for the ocean

In this section we consider the entropy budget for the ocean and make use of the second law of thermodynamics to infer specific forms for the thermal and chemical fluxes introduced in Section 26.6.6. The discussion also holds for the atmosphere in the absence of phase transitions, though we focus on the ocean application to be specific. Hence, the matter concentration in this section is the salt concentration for seawater.

The entropy budget follows by rearranging the enthalpy equation (26.79)

$$T\,\rho\,\frac{\mathrm{D}\mathcal{S}}{\mathrm{D}t} = \rho\,\frac{\mathrm{D}\mathcal{H}}{\mathrm{D}t} - \frac{\mathrm{D}p}{\mathrm{D}t} - \mu\,\rho\,\frac{\mathrm{D}C}{\mathrm{D}t}, \tag{26.132}$$

with the enthalpy budget in the form (26.94) yielding

$$T\,\rho\,\frac{\mathrm{D}\mathcal{S}}{\mathrm{D}t} = -\nabla\cdot(\boldsymbol{J}_{\mathrm{therm}} + \boldsymbol{J}_{\mathrm{chem}}) + \rho\,\epsilon + \mu\,\nabla\cdot\boldsymbol{J}_C, \tag{26.133}$$

where we wrote the tracer equation as

$$\rho\,\frac{\mathrm{D}C}{\mathrm{D}t} = -\nabla\cdot\boldsymbol{J}_{\mathrm{C}}, \tag{26.134}$$

following Section 20.1.3. Through manipulations pursued in Section 26.10.1, we identify a non-advective entropy flux and a corresponding entropy source. This form of the entropy budget is useful since we can then invoke the second law to insist that the entropy source is non-negative, and that statement renders some constraints on the thermal and chemical fluxes.

26.10.1 Non-advective entropy flux and entropy source

To start the manipulations, divide equation (26.133) by T and rewrite in terms of a flux convergence plus a source

$$\rho \frac{\mathrm{D}\mathcal{S}}{\mathrm{D}t} = -\nabla \cdot \left[\frac{\boldsymbol{J}_{\text{therm}} + \boldsymbol{J}_{\text{chem}} - \mu \boldsymbol{J}_C}{T} \right] + \nabla(1/T) \cdot (\boldsymbol{J}_{\text{therm}} + \boldsymbol{J}_{\text{chem}} - \mu \boldsymbol{J}_C) - (\boldsymbol{J}_C/T) \cdot \nabla\mu + \frac{\rho\,\epsilon}{T}. \tag{26.135}$$

Recall from the identity (26.84) that we can write the chemical energy flux as

$$\boldsymbol{J}_{\text{chem}} = \left[\frac{\partial \mathcal{H}}{\partial C}\right]_{T,p} \boldsymbol{J}_C = \left[\mu - T \left[\frac{\partial \mu}{\partial T}\right]_{C,p}\right] \boldsymbol{J}_C = (\mu - T\,\mu_T)\,\boldsymbol{J}_C, \tag{26.136}$$

where we introduced a shorthand for the third equality. This identity then leads to

$$\boldsymbol{J}_{\text{chem}} - \mu\,\boldsymbol{J}_C = -T\,\mu_T\,\boldsymbol{J}_C, \tag{26.137}$$

in which case the entropy equation (26.135) becomes

$$\rho \frac{\mathrm{D}\mathcal{S}}{\mathrm{D}t} = -\nabla \cdot \left[\frac{\boldsymbol{J}_{\text{therm}} - T\,\mu_T\,\boldsymbol{J}_C}{T} \right] + \nabla(1/T) \cdot (\boldsymbol{J}_{\text{therm}} - T\,\mu_T\,\boldsymbol{J}_C) - (\boldsymbol{J}_C/T) \cdot \nabla\mu + \frac{\rho\,\epsilon}{T}. \tag{26.138}$$

We thus identify the non-advective entropy flux

$$\boldsymbol{J}_{\mathcal{S}} = \frac{\boldsymbol{J}_{\text{therm}}}{T} - \left[\frac{\partial \mu}{\partial T}\right]_{p,C} \boldsymbol{J}_C = \frac{\boldsymbol{J}_{\text{therm}}}{T} + \left[\frac{\partial \mathcal{S}}{\partial C}\right]_{T,p} \boldsymbol{J}_C, \tag{26.139}$$

where the second equality made use of the Maxwell relation

$$-\left[\frac{\partial \mathcal{S}}{\partial C}\right]_{T,p} = \left[\frac{\partial \mu}{\partial T}\right]_{p,C}, \tag{26.140}$$

which is derived as part of the solution to Exercise 22.2. The additional terms comprise the entropy source

$$\begin{aligned}
\Sigma_{\mathcal{S}} &= \frac{\rho\,\epsilon}{T} + \nabla(1/T) \cdot (\boldsymbol{J}_{\text{therm}} - T\,\mu_T\,\boldsymbol{J}_C) - (\boldsymbol{J}_C \cdot \nabla\mu)/T && \text{(26.141a)} \\
&= \frac{\rho\,\epsilon}{T} + \frac{\nabla T}{T^2} \cdot (T\,\mu_T\,\boldsymbol{J}_C - \boldsymbol{J}_{\text{therm}}) - (\boldsymbol{J}_C \cdot \nabla\mu)/T && \text{(26.141b)} \\
&= \frac{\rho\,\epsilon}{T} - \frac{\nabla T \cdot \boldsymbol{J}_{\text{therm}}}{T^2} + \frac{\boldsymbol{J}_C \cdot (\mu_T \nabla T - \nabla\mu)}{T} && \text{(26.141c)} \\
&= \frac{\rho\,\epsilon}{T} - \frac{\nabla T \cdot \boldsymbol{J}_{\text{therm}}}{T^2} - \frac{\boldsymbol{J}_C \cdot (\mu_C \nabla C + \mu_p \nabla p)}{T} && \text{(26.141d)} \\
&= \frac{\rho\,\epsilon}{T} - \frac{\nabla T \cdot \boldsymbol{J}_{\text{therm}}}{T^2} - \frac{\boldsymbol{J}_C}{T} \cdot \left[\left[\frac{\partial \mu}{\partial C}\right]_{T,p} \nabla C + \left[\frac{\partial \mu}{\partial p}\right]_{T,C} \nabla p \right], && \text{(26.141e)}
\end{aligned}$$

where we wrote the gradient of the chemical potential, $\mu(T, p, C)$, as

$$\nabla\mu = \left[\frac{\partial \mu}{\partial T}\right]_{p,C} \nabla T + \left[\frac{\partial \mu}{\partial p}\right]_{T,C} \nabla p + \left[\frac{\partial \mu}{\partial C}\right]_{T,p} \nabla C = \mu_T\,\nabla T + \mu_p\,\nabla p + \mu_C\,\nabla C. \tag{26.142}$$

The non-advective entropy flux (26.139) arises from the thermal and chemical fluxes, and the entropy source (26.141e) includes contributions from those fluxes as well as the frictional dissipation of mechanical energy.

26.10.2 Constraints from the second law of thermodynamics

The second law of thermodynamics states that the entropy source is non-negative

$$\Sigma_{\mathcal{S}} \geq 0 \Longleftarrow \text{second law of thermodynamics.} \tag{26.143}$$

This condition imposes constraints on the frictional dissipation, thermal flux, and tracer flux. Since frictional dissipation in Newtonian fluids (equation (26.43)) is non-negative, $\epsilon \geq 0$, we make use of the second law to constrain just the thermal flux and tracer flux. Furthermore, recall from equation (26.81) that the thernal flux is comprised of a radiant flux and conductive flux. We assume that radiant flux is determined by processes external to the fluid. We thus use the second law to constrain just the conductive portion of the thermal flux along with the tracer flux. That is, from the entropy source (26.141e) we have the second law constraint

$$-\nabla T \cdot \boldsymbol{J}_{\text{cond}} - T\, \mu_C\, \boldsymbol{J}_C \cdot \left[\nabla C + \frac{\mu_p}{\mu_C}\, \nabla p\right] \geq 0. \tag{26.144}$$

This constraint can be satisfied by assuming the conductive and tracer fluxes are of the form

$$\rho^{-1}\, \boldsymbol{J}_{\text{cond}} = -c_{\mathrm{p}}\, \kappa_T\, \nabla T - \kappa_{TC} \left[\nabla C + \frac{\mu_p}{\mu_C}\, \nabla p\right] \tag{26.145a}$$

$$\rho^{-1}\, \boldsymbol{J}_C = -\kappa_C \left[\nabla C + \frac{\mu_p}{\mu_C}\, \nabla p\right] - \kappa_{CT}\, \nabla T. \tag{26.145b}$$

The variety of molecular fluxes

The first term in the conductive thermal flux (26.145a) is known as *Fourier's law of conduction*

$$\boldsymbol{J}^{\text{Fourier}}_{\text{cond}} = -\rho\, c_{\mathrm{p}}\, \kappa_T\, \nabla T, \tag{26.146}$$

in which case the conductive thermal flux is directed down the gradient of the *in situ* temperature. The second term leads to a conductive thermal flux in the presence of matter concentration gradients and pressure gradients, and this process is known as the *Dufour effect*

$$\boldsymbol{J}^{\text{Dufour}}_{\text{cond}} = -\rho\, \kappa_{TC} \left[\nabla C + \frac{\mu_p}{\mu_C}\, \nabla p\right]. \tag{26.147}$$

The first term in the matter flux (26.145b) is known as *Fick's law of diffusion*

$$\boldsymbol{J}^{\text{Fick}}_C = -\rho\, \kappa_C\, \nabla C. \tag{26.148}$$

The second term in in the matter flux (26.145b) is known as *barodiffusion*

$$\boldsymbol{J}^{\text{barodiff}}_C = -(\rho\, \kappa_{CT}\, \mu_p / \mu_C)\, \nabla p, \tag{26.149}$$

which is a matter flux arising from a pressure gradient. Finally, the matter flux arising from temperature gradients is known as the *Soret effect*

$$\boldsymbol{J}^{\text{Soret}}_C = -\rho\, \kappa_{CT}\, \nabla T. \tag{26.150}$$

Thermodynamic equilibrium and the vertical gradient of salinity

In Section 23.1, we learned that thermodynamic equilibrium for a fluid in a gravity field leads to a uniform temperature, T, and a pressure in exact hydrostatic balance. The salt flux must vanish in thermodynamic equilibrium, but in the presence of a pressure gradient we have a

nonzero vertical salinity gradient from equation (26.145b) given by

$$\frac{\mathrm{d}C}{\mathrm{d}z} = -\frac{\mu_p}{\mu_C}\frac{\mathrm{d}p}{\mathrm{d}z} = \frac{\mu_p\,\rho\,g}{\mu_C}. \tag{26.151}$$

This relation is identical to equation (23.20) resulting from our study of conditions for thermodynamic equilibrium of a binary fluid in a gravity field. It is satisfying to see the same thermodynamic equilibrium condition arise from the rather different path taken here.

Invoking Onsager reciprocity condition

The Onsager reciprocity conditions[16] are now invoked to relate the two off-diagonal coefficients according to

$$T\,\mu_C\,\kappa_{CT} = \kappa_{TC}, \tag{26.152}$$

which brings the entropy condition to the form

$$c_{\mathrm{p}}\,\kappa_T\,|\nabla T|^2 + \kappa_C\,\mu_C\,T\left|\nabla C + \frac{\mu_p}{\mu_C}\nabla p\right|^2 + 2\,\kappa_{TC}\,\nabla T\cdot\left[\nabla C + \frac{\mu_p}{\mu_C}\nabla p\right] \geq 0. \tag{26.153}$$

This condition then constrains the phenomenological constants κ_C, κ_T and κ_{TC} so that

$$|\kappa_{TC}|^2 \leq \kappa_T\,\kappa_C\,c_{\mathrm{p}}\,T\,\mu_S. \tag{26.154}$$

Comments on measurements

The cross-diffusion coefficients, κ_{TC} and κ_{CT}, are both measured to be very small for seawater, so that the Dufour effect and Soret effect are commonly ignored. Furthermore, in an ocean in thermodynamic equilibrium, the vertical salinity gradient implied by equation (26.151) is roughly 3 g kg^{-1} per 1000 m. This vertical salinity gradient is far larger than measured in the ocean, thus providing evidence that turbulent fluxes, even in the ocean interior, dominate over molecular fluxes. That is, the observed ocean has sufficient turbulence to keep it well away from thermodynamic equilibrium.

26.10.3 A summary presentation

We here summarize the previous material by skipping details for the entropy flux, thermal flux, and matter flux. For this purpose, write the budget for the total energy in the form

$$\rho\,\frac{\mathrm{D}\mathcal{E}}{\mathrm{D}t} = -\nabla\cdot(p\,\boldsymbol{v} - \boldsymbol{v}\cdot\mathbb{T}) + \rho\left[-\epsilon + T\,\frac{\mathrm{D}\mathcal{S}}{\mathrm{D}t} + \mu\,\frac{\mathrm{D}C}{\mathrm{D}t}\right] + \rho\,\partial_t\Phi. \tag{26.155}$$

Now assume that the specific entropy and matter concentration satisfy the evolution equations

$$\rho\,\frac{\mathrm{D}\mathcal{S}}{\mathrm{D}t} = -\nabla\cdot\boldsymbol{J}_{\mathcal{S}} + \Sigma_{\mathcal{S}} \quad \text{and} \quad \rho\,\frac{\mathrm{D}C}{\mathrm{D}t} = -\nabla\cdot\boldsymbol{J}_C, \tag{26.156}$$

thus rendering

$$\rho\left[T\,\frac{\mathrm{D}\mathcal{S}}{\mathrm{D}t} + \mu\,\frac{\mathrm{D}C}{\mathrm{D}t}\right] = -T\,\nabla\cdot\boldsymbol{J}_{\mathcal{S}} + T\,\Sigma_{\mathcal{S}} - \mu\,\nabla\cdot\boldsymbol{J}_{\mathrm{C}} \tag{26.157a}$$

$$= -\nabla\cdot(T\,\boldsymbol{J}_{\mathcal{S}} + \mu\,\boldsymbol{J}_{\mathrm{C}}) + \nabla T\cdot\boldsymbol{J}_{\mathcal{S}} + \nabla\mu\cdot\boldsymbol{J}_{\mathrm{C}} + T\,\Sigma_{\mathcal{S}}, \tag{26.157b}$$

[16] See Chapter 14 of *Callen* (1985) for these conditions and their underlying dynamical connections.

which then brings the total energy equation (26.155) into the form

$$\rho \frac{\mathrm{D}\mathcal{E}}{\mathrm{D}t} = -\nabla \cdot (p\,\boldsymbol{v} - \boldsymbol{v} \cdot \mathbb{T} + T\,\boldsymbol{J}_{\mathcal{S}} + \mu\,\boldsymbol{J}_{\mathrm{C}}) + [-\rho\,\epsilon + \nabla T \cdot \boldsymbol{J}_{\mathcal{S}} + \nabla\mu \cdot \boldsymbol{J}_{\mathrm{C}} + T\,\Sigma_{\mathcal{S}}] + \rho\,\partial_t \Phi. \tag{26.158}$$

We now postulate that the globally integrated total energy is constant in the absence of boundary processes and with a time independent geopotential. In the presence of mechanical dissipation and matter constituent mixing, a necessary condition for such global energy conservation is for the specific entropy source to take the form

$$T\,\Sigma_{\mathcal{S}} = \rho\,\epsilon - \nabla T \cdot \boldsymbol{J}_{\mathcal{S}} - \nabla\mu \cdot \boldsymbol{J}_{\mathrm{C}}. \tag{26.159}$$

That is, the entropy source arises from frictional dissipation, entropy mixing, and matter mixing. With this form for the entropy source, the total energy budget (26.158) is given by the material form and the equivalent flux-form expressions

$$\rho \frac{\mathrm{D}\mathcal{E}}{\mathrm{D}t} = -\nabla \cdot (p\,\boldsymbol{v} - \boldsymbol{v} \cdot \mathbb{T} + T\,\boldsymbol{J}_{\mathcal{S}} + \mu\,\boldsymbol{J}_{\mathrm{C}}) + \rho\,\partial_t \Phi \tag{26.160a}$$

$$\frac{\partial(\rho\,\mathcal{E})}{\partial t} = -\nabla \cdot (\mathcal{E}\,\boldsymbol{v} + p\,\boldsymbol{v} - \boldsymbol{v} \cdot \mathbb{T} + T\,\boldsymbol{J}_{\mathcal{S}} + \mu\,\boldsymbol{J}_{\mathrm{C}}) + \rho\,\partial_t \Phi. \tag{26.160b}$$

The modified form of the internal energy budget (26.77) is found by subtracting the mechanical energy budget (26.49) from the total energy budget (26.160a)

$$\rho \frac{\mathrm{D}\mathcal{I}}{\mathrm{D}t} = \rho \frac{\mathrm{D}(\mathcal{E} - \mathcal{M})}{\mathrm{D}t} = -p\,\nabla \cdot \boldsymbol{v} - \nabla \cdot (T\,\boldsymbol{J}_{\mathcal{S}} + \mu\,\boldsymbol{J}_{\mathrm{C}}) + \rho\,\epsilon. \tag{26.161}$$

The corresponding enthalpy budget (26.79) is given by

$$\rho \frac{\mathrm{D}\mathcal{H}}{\mathrm{D}t} - \frac{\mathrm{D}p}{\mathrm{D}t} = -\nabla \cdot (T\,\boldsymbol{J}_{\mathcal{S}} + \mu\,\boldsymbol{J}_{\mathrm{C}}) + \rho\,\epsilon = -\nabla \cdot \boldsymbol{J}_{\mathcal{H}} + \rho\,\epsilon. \tag{26.162}$$

In the second equatlity we defined the enthalpy flux

$$\boldsymbol{J}_{\mathcal{H}} = T\,\boldsymbol{J}_{\mathcal{S}} + \mu\,\boldsymbol{J}_{\mathrm{C}} \tag{26.163a}$$

$$= \boldsymbol{J}_{\mathrm{therm}} - T \left[\frac{\partial\mu}{\partial T}\right]_{p,C} \boldsymbol{J}_C + \mu\,\boldsymbol{J}_C \tag{26.163b}$$

$$= \boldsymbol{J}_{\mathrm{therm}} + \left[\frac{\partial\mathcal{H}}{\partial C}\right]_{T,p} \boldsymbol{J}_C \tag{26.163c}$$

$$= \boldsymbol{J}_{\mathrm{therm}} + \boldsymbol{J}_{\mathrm{chem}}, \tag{26.163d}$$

where we used equation (26.139) for the entropy flux, $\boldsymbol{J}_{\mathcal{S}}$, equation (26.136) for the chemical flux, $\boldsymbol{J}_{\mathrm{chem}}$, and the thermodynamic identity (26.84) for the third equality. Furthermore, recall that the thermal flux, $\boldsymbol{J}_{\mathrm{therm}}$, is the sum of a conductive plus radiative contribution as per equation (26.81).

26.10.4 Comments

It is remarkable how the second law of thermodynamics is able to predict new physical processes through considering the various forms that the thermal and matter fluxes can take to ensure a positive entropy source. *Caldwell* (1973) and *Caldwell and Eide* (1981) estimate the Soret effect for seawater, where they propose some relevance of this effect in quiescent ocean regions with strong gradients. In contrast, for liquids the Dufour effect is about 1000 times smaller than Fickian heat conduction and so it is safely ignored throughout the ocean. *McDougall and*

Turner (1982) and *McDougall* (1983) studied double-diffusive convection in the presence of cross-diffusion, extending the oceanographic applications to arbitrary solutions with a pair of solutes. None of these studies consider the role of pressure gradients in generating fluxes.

For most purposes of oceanography, the fluxes considered in this section are far smaller than those induced by turbulent flow processes. In this case, the flux relations reduce to the Fickian and Fourier expressions yet with turbulent exchange coefficients rather than their molecular values. Turbulence thus makes molecular diffusive processes generally negligible for the ocean. Indeed, we already made this conclusion when noting that thermodynamic equilibrium implies a sizable vertical salinity gradient as given by equation (26.151). Whereas turbulence acts to produce a homogenous salinity (as well as potential temperature and potential enthalpy), molecular diffusion leads to a rather large vertical salinity gradient. Since the vertical salinity gradient implied by thermodynamic equilibrium is much larger than that measured in the ocean, we conclude that the ocean is far from a thermodynamic equilibrium state.

26.10.5 Further study

Much of our presentation in this section followed that from Sections 2.4 and 2.5 from *Olbers et al.* (2012) and Appendix B of *IOC et al.* (2010). *Graham and McDougall* (2013) extend these ideas to a turbulent ocean. The physical ideas underlying the Onsager reciprocity conditions are lucidly discussed in Chapter 14 of *Callen* (1985).

26.11 Temperature evolution

In specifying the state of a fluid element it is sensible to make use of the temperature, pressure, and tracer concentration given that these state properties are readily measured in the laboratory and environment. Furthermore, these properties are the natural variables for the Gibbs potential (Section 22.6.6). Hence, given values for (T, p, C) we can determine the Gibbs potential and then determine all other thermodynamic properties by taking partial derivatives.

How do we specify the evolution of (T, p, C) for a fluid element? Evolution of the matter concentration follows from the tracer equation (an advection-diffusion equation) as developed in Section 20.1. Pressure measures the compressive stress acting on each fluid element (Section 25.8), with its specification depending on the dominant dynamical balances (see Section 26.13). Temperature reflects the energy of the internal microscopic degrees of freedom within a fluid element, with its evolution the subject of this section. We show how Conservative Temperature, Θ, rather than *in situ* temperature, T, or potential temperature, θ, offers the simplest prognostic equation of the three temperature variables. The key reason is that Θ evolves almost precisely like a material tracer, driven by the convergence of fluxes, whereas the equations for T and θ contain extra source terms in additon to flux convergences.

26.11.1 Evolution of *in situ* temperature

In developing the temperature equation it is useful to start from the prognostic equation for enthalpy as developed in Sections 26.6.5. For that purpose we write the enthalpy equation (26.162) as

$$\rho \frac{\mathrm{D}\mathcal{H}}{\mathrm{D}t} = \frac{\mathrm{D}p}{\mathrm{D}t} - \nabla \cdot \boldsymbol{J}_{\mathcal{H}} + \rho\, \epsilon, \tag{26.164}$$

with the enthalpy flux, $\boldsymbol{J}_{\mathcal{H}}$, written in terms of the entropy and tracer fluxes as per equation (26.163d).

To reveal a prognostic equation for temperature, we write enthalpy as a function of (T, p, C)

so that

$$\frac{\mathrm{D}\mathcal{H}}{\mathrm{D}t} = \left[\frac{\partial\mathcal{H}}{\partial T}\right]_{p,C} \frac{\mathrm{D}T}{\mathrm{D}t} + \left[\frac{\partial\mathcal{H}}{\partial p}\right]_{T,C} \frac{\mathrm{D}p}{\mathrm{D}t} + \left[\frac{\partial\mathcal{H}}{\partial C}\right]_{T,p} \frac{\mathrm{D}C}{\mathrm{D}t}. \tag{26.165}$$

The partial derivatives can be related to response functions via the following. First, the specific heat capacity at constant pressure is given by equation (22.102)

$$\left[\frac{\partial\mathcal{H}}{\partial T}\right]_{p,C} = c_{\mathrm{p}}. \tag{26.166}$$

Next, we make use of the Gibbs potential identities in Section 22.6.6 to write

$$\left[\frac{\partial\mathcal{H}}{\partial p}\right]_{T,C} = \left[\frac{\partial\mathcal{G}}{\partial p}\right]_{T,C} - T\left[\frac{\partial}{\partial p}\right]_{T,C}\left[\frac{\partial\mathcal{G}}{\partial T}\right]_{p,C} \tag{26.167a}$$

$$= \nu_{\mathrm{s}} - T\left[\frac{\partial}{\partial T}\right]_{p,C}\left[\frac{\partial\mathcal{G}}{\partial p}\right]_{T,C} \tag{26.167b}$$

$$= \nu_{\mathrm{s}} - T\left[\frac{\partial\nu_{\mathrm{s}}}{\partial T}\right]_{p,C} \tag{26.167c}$$

$$= \nu_{\mathrm{s}}\,(1 - T\,\alpha_{\mathrm{T}}), \tag{26.167d}$$

where α_{T} is the thermal expansion coefficient given by equation (22.103). Use of these identities in the enthalpy equation (26.165) and rearrangement leads to the *in situ* temperature equation

$$c_{\mathrm{p}}\,\rho\,\frac{\mathrm{D}T}{\mathrm{D}t} = -\nabla\cdot\boldsymbol{J}_{\mathcal{H}} + \left[\frac{\partial\mathcal{H}}{\partial C}\right]_{T,p}\nabla\cdot\boldsymbol{J}_{\mathrm{C}} + \alpha_{\mathrm{T}}\,T\,\frac{\mathrm{D}p}{\mathrm{D}t} + \rho\,\epsilon. \tag{26.168}$$

The *in situ* temperature of a fluid element thus evolves according to convergence of the enthalpy fluxes, divergence of matter concentration fluxes, material time changes to pressure, and frictional dissipation. We can massage this expression a bit more by introducing the enthalpy flux (26.163c) so that

$$c_{\mathrm{p}}\,\rho\,\frac{\mathrm{D}T}{\mathrm{D}t} = -\nabla\cdot\boldsymbol{J}_{\mathrm{therm}} - \boldsymbol{J}_{C}\cdot\nabla\left[\frac{\partial\mathcal{H}}{\partial C}\right]_{T,p} + \alpha_{\mathrm{T}}\,T\,\frac{\mathrm{D}p}{\mathrm{D}t} + \rho\,\epsilon, \tag{26.169}$$

where constraints on the conductive portion of the thermal flux were discussed in Section 26.10.2.

26.11.2 Evolution of potential temperature

We can convert the *in situ* temperature equation (26.168) into a version of the potential temperature equation by recalling the expression (23.26) for the lapse rate

$$\hat{\Gamma} = \left[\frac{\partial T}{\partial p}\right]_{C,\mathcal{S}} = \frac{T\,\alpha_{\mathrm{T}}}{\rho\,c_{\mathrm{p}}} \tag{26.170}$$

so that equation (26.168) takes the form

$$c_{\mathrm{p}}\,\rho\left[\frac{\mathrm{D}T}{\mathrm{D}t} - \hat{\Gamma}\,\frac{\mathrm{D}p}{\mathrm{D}t}\right] = -\nabla\cdot\boldsymbol{J}_{\mathcal{H}} + \left[\frac{\partial\mathcal{H}}{\partial C}\right]_{T,p}\nabla\cdot\boldsymbol{J}_{\mathrm{C}} + \rho\,\epsilon. \tag{26.171}$$

Making use of the definition (23.31) for potential temperature renders

$$c_{\mathrm{p}}\,\rho\,\frac{\mathrm{D}\theta}{\mathrm{D}t} = -\nabla\cdot\boldsymbol{J}_{\mathcal{H}} + \left[\frac{\partial\mathcal{H}}{\partial C}\right]_{T,p}\nabla\cdot\boldsymbol{J}_{\mathrm{C}} + \rho\,\epsilon. \tag{26.172}$$

As expected, pressure changes are removed from the evolution equation for potential temperature.

26.11.3 Conservative Temperature for the ocean

Rather than expressing enthalpy as a function $\mathcal{H}(T, p, C)$, we make use of its natural coordinate dependence $\mathcal{H}(\mathcal{S}, p, C)$ from Section 22.6.4, which leads to the enthalpy equation in the form (26.162)

$$\rho \frac{\mathrm{D}\mathcal{H}}{\mathrm{D}t} = \frac{\mathrm{D}p}{\mathrm{D}t} - \nabla \cdot \boldsymbol{J}_{\mathcal{H}} + \rho\, \epsilon. \tag{26.173}$$

The pressure term arises just like for *in situ* temperature. Its presence suggests we introduce the *potential enthalpy*.

Potential enthalpy and Conservative Temperature

The potential enthalpy is defined to be the enthalpy of a fluid element moved to a reference pressure, p_{R}, while maintaining fixed specific entropy and fixed tracer concentration

$$\mathcal{H}^{\mathrm{pot}}(\mathcal{S}, C) = \mathcal{H}(\mathcal{S}, p_{\mathrm{R}}, C). \tag{26.174}$$

As for potential temperature (Section 23.3.3), it is most convenient to take p_{R} as the standard atmospheric pressure, thus corresponding to the standard pressure at the air-sea interface. This definition parallels that for potential temperature given by equation (23.36). It is also motivated by the exchange of enthalpy (heat) across the air-sea boundary, thus providing a natural means to study coupled air-sea processes.

By construction, the material time derivative of potential enthalpy is given by

$$\rho \frac{\mathrm{D}\mathcal{H}^{\mathrm{pot}}}{\mathrm{D}t} = \rho \left[\frac{\partial \mathcal{H}^{\mathrm{pot}}}{\partial \mathcal{S}}\right]_C \frac{\mathrm{D}\mathcal{S}}{\mathrm{D}t} + \rho \left[\frac{\partial \mathcal{H}^{\mathrm{pot}}}{\partial C}\right]_{\mathcal{S}} \frac{\mathrm{D}C}{\mathrm{D}t} \tag{26.175a}$$

$$= \theta \left(-\nabla \cdot \boldsymbol{J}_{\mathcal{S}} + \Sigma_{\mathcal{S}}\right) - \mu_{\mathrm{R}}\, \nabla \cdot \boldsymbol{J}_{\mathrm{C}} \tag{26.175b}$$

$$= (\theta/T)\left[\rho\, \epsilon - \nabla \cdot \boldsymbol{J}_{\mathrm{H}}\right] - \left[\mu_{\mathrm{R}} - (\theta/T)\, \mu\right] \nabla \cdot \boldsymbol{J}_{\mathrm{C}}, \tag{26.175c}$$

where we set

$$\theta = \left[\frac{\partial \mathcal{H}^{\mathrm{pot}}}{\partial \mathcal{S}}\right]_C \qquad \text{and} \qquad \mu_{\mathrm{R}} = \left[\frac{\partial \mathcal{H}^{\mathrm{pot}}}{\partial C}\right]_{\mathcal{S}} \tag{26.176}$$

and used equation (26.159) for the entropy source, $\Sigma_{\mathcal{S}}$. Now define the Conservative Temperature, Θ, via

$$c_{\mathrm{p}}^{\mathrm{ref}}\, \Theta \equiv \mathcal{H}^{\mathrm{pot}}(\mathcal{S}, C) = \mathcal{H}(\mathcal{S}, p_{\mathrm{R}}, C), \tag{26.177}$$

where $c_{\mathrm{p}}^{\mathrm{ref}}$ is an arbitrary reference specific heat capacity. For the ocean, *McDougall* (2003) suggested that $c_{\mathrm{p}}^{\mathrm{ref}}$ be chosen so that $\Theta = \theta$ at a salinity of 35 parts per thousand. *McDougall* (2003) furthermore argued that the terms appearing in the potential enthalpy equation (26.175c) are well approximated for the ocean by just the convergence of the enthalpy flux. Hence, the Conservative Temperature satisfies, to a very good approximation, the source-free tracer equation

$$\rho\, c_{\mathrm{p}}^{\mathrm{ref}} \frac{\mathrm{D}\Theta}{\mathrm{D}t} = -\nabla \cdot \boldsymbol{J}_{\mathrm{H}}. \tag{26.178}$$

Key points regarding the Conservative Temperature equation

The Conservative Temperature equation (26.178) is mathematically identical to the material tracer equation, and as such it offers an elegant means to prognose thermodynamic properties of the fluid and to perform budget analyses. We further emphasize two points in regards to this equation relative to the potential temperature equation (26.172).

- The source terms (those not associated with flux convergences) on the right hand side of the potential temperature equation are much larger than those in the Conservative

Temperature equation. In particular, *McDougall* (2003) and *Graham and McDougall* (2013) showed that the potential temperature sources are roughly 100 times larger in certain regions of the ocean than the Conservative Temperature sources.

- The heat capacity appearing in the Conservative Temperature equation is a fixed constant, by construction. This feature contrasts to the space-time variable heat capacity, $c_{\rm p}$, appearing in both the *in situ* temperature equation (26.168) and potential temperature equation (26.172). The space-time variations of $c_{\rm p}$ are not negligible (e.g., order 5% for the global ocean), thus making the non-constant heat capacity required for the T and θ equations very inconvenient for purposes of budget analyses (see *McDougall et al.* (2021) for more on this point).

We close by noting that the enthalpy flux, $\boldsymbol{J}_{\rm H}$, is related to the entropy flux and concentration flux as per equation (26.163d). As discussed in Section 2.6 of *Olbers et al.* (2012), the dominant terms appearing in this flux arise from entropy, which itself is largely due to fluxes of temperature. Consequently, the flux $\boldsymbol{J}_{\rm H}$ is well approximated as a flux just of Θ.

26.11.4 Alternative functional dependencies for specific enthalpy

Thus far in this section, we have considered specific enthalpy to be a function of (T, p, C) as well as its natural functional dependence, $(\mathcal{S}, p, C)$. The introduction of potential temperature and Conservative Temperature allow us to consider two more functional depenencies

$$\mathcal{H} = \mathcal{H}^{\rm natural}(\mathcal{S}, p, C) = \mathcal{H}^{\rm T}(T, p, C) = \mathcal{H}^{\theta}(\theta, p, C) = \mathcal{H}^{\Theta}(\Theta, p, C). \tag{26.179}$$

We use distinct notations for the functions since they each return specific enthalpy yet when fed distinct input. Given the more common use of either potential temperature or Conservative Temperature in atmosphere and ocean sciences, the final two functional dependencies are most commonly used in practice. Note that for brevity, we often drop the extra notation adorning the specific enthalpy symbol, except where confusion may arise. As an example of the above functional dependence, consider the exact differential of specific enthalpy when written using the (Θ, p, C) dependence, in which

$$\mathrm{d}\mathcal{H} = \left[\frac{\partial \mathcal{H}^{\Theta}}{\partial \Theta}\right]_{p,C} \mathrm{d}\Theta + \left[\frac{\partial \mathcal{H}^{\Theta}}{\partial p}\right]_{\Theta,C} \mathrm{d}p + \left[\frac{\partial \mathcal{H}^{\Theta}}{\partial C}\right]_{\Theta,p} \mathrm{d}C \tag{26.180a}$$

$$= \left[\frac{\partial \mathcal{H}^{\Theta}}{\partial \Theta}\right]_{p,C} \mathrm{d}\Theta + \rho^{-1}\, \mathrm{d}p + \left[\frac{\partial \mathcal{H}^{\Theta}}{\partial C}\right]_{\Theta,p} \mathrm{d}C, \tag{26.180b}$$

where we set

$$\rho^{-1} = \left[\frac{\partial \mathcal{H}^{\Theta}}{\partial p}\right]_{\Theta,C}, \tag{26.181}$$

which is a generalization of the partial derivative (22.76) holding for the natural functional dependence. Further discussion of the other partial derivatives are provided in *Graham and McDougall* (2013) as well as Appendices A.10 and A.11 of *IOC et al.* (2010).

26.11.5 Further study

The discussion in this section largely followed the more complete ocean discussion given in Section 2.6 of *Olbers et al.* (2012), which is itself based on *McDougall* (2003) and *Graham and McDougall* (2013).

Considerations for a realistic atmosphere involve phase changes (liquid-vapor and liquid-solid), with the associated latent heat exchanges are leading order contributions to the enthalpy budget

(see *Lauritzen et al.* (2022) for a comprehensive review). Additionally, the role of frictional dissipation is not negligible in the atmosphere whereas it is negligible in the ocean (see Section 26.7.3).

26.12 Conservation laws and potential properties

A central facet of theoretical physics concerns the development of concepts and tools to expose conservation laws and their underlying symmetries.[17] We routinely make use of such laws in geophysical fluid mechanics to provide constraints on the fluid motion and to study budgets of corresponding properties to help understand fundamental processes. As such, conservation laws offer great physical insight and predictive utility. We close this chapter by summarizing some conceptual points concerning conservation laws. In particular, we identify the need to distinguish laws that involve just the convergence of a flux from those that also include non-conservative "source" terms. We also distinguish between material and non-material conservation laws, in which properties satisfying material conservation laws are materially invariant in the absence of local mixing processes.

26.12.1 Flux-form conservation laws

Certain scalar properties studied in fluid mechanics satisfy conservation laws that are written as

$$\rho \frac{\mathrm{D}\psi}{\mathrm{D}t} = -\nabla \cdot \boldsymbol{J} \iff \frac{\partial(\rho\,\psi)}{\partial t} = -\nabla \cdot (\rho\, \boldsymbol{v}\, \psi + \boldsymbol{J}). \tag{26.182}$$

The right hand side of the flux-form expression (second equation) involves a flux that is comprised of an advective term, $\rho\, \boldsymbol{v}\, \psi$, plus a non-advective term, $\boldsymbol{J}$. Examples of conservation laws of this type include the material tracer concentration, $\psi = C$, as in equation (26.188); the Conservative Temperature, $\psi = \Theta$, as in equation (26.189); the total energy, $\psi = \mathcal{E}$, in the absence of astronomical forces, as in equation (26.160b); and the potential vorticity, $\psi = Q$, as in equation (41.49). In Chapter 20, we saw how this differential equation leads to finite volume conservation properties for the integral of ψ-stuff within a region, $\int_{\mathcal{R}} \psi\, \rho\, \mathrm{d}V$, with the evolution of this integral only affected by area integrated fluxes, $\rho\, \boldsymbol{v}\, \psi + \boldsymbol{J}$, penetrating the region boundary (mathematically seen by applying the divergence theorem).

Conservation laws of the form (26.182) are a direct consequence of the *local* conservation of ψ-stuff within the fluid. That is, the amount of ψ-stuff changes at a point only through the local convergence of fluxes onto that point, and likewise for a finite region. Such conservation laws are consistent with basic notions of causality and locality that appear throughout physics, with a discussion of such conservation laws offered in Section 27-1 of *Feynman et al.* (1963).

26.12.2 Conservation laws that are not flux-form

The presence of source/sinks are relevant for chemical or biogeochemical reactions, whereby matter is converted from one form to another. Such processes are not mathematically represented as the convergence of a flux. As such, they are not contained in the conservation law (26.182) and they are correspondingly referred to as *non-conservative processes*. Even without chemical reactions, not all fluid properties satisfy flux-form conservation laws of the form (26.182). For example, linear momentum of a fluid element is affected by pressure, Coriolis, and effective gravity, and these processes are not represented as the convergence of a flux.

As discussed in Chapter 14, conservation laws are associated with symmetries of the physical system. Correspondingly, non-conservative terms appearing in an evolution equation often reflect

[17] See Chapter 14 for the connection between conservation laws and symmetries, as embodied by Noether's theorem.

the breaking of a symmetry. For example, motion around a sphere does not conserve linear momentum even in the absence of forces, whereas linear momentum is conserved for free motion in a planar geometry.

26.12.3 Non-material or wave-like transport of properties

Pressure is of particular note since pressure perturbations travel through a compressible fluid via acoustic waves (Chapter 51), or, in the case of an incompressible flow, a pressure perturbation is felt globally and instantaneously as reflected in the elliptic Poisson equation satisfied by pressure (Section 29.3). More generally, the wave mediated transfer of forces, or other fluid properties such as momentum or mechanical energy, is an example of a non-material transfer; i.e., a transfer of information not arising from the transfer of matter. Non-material wave mediated transfer often occurs much faster than material transfer, with matter transport only mediated through advection and diffusion. Correspondingly, material substances (and potential enthalpy) are not directly affected by wave transport. Rather, waves affect material substances only so far as they affect advection and diffusion.

26.12.4 Material and non-material conservation laws

Mass invariance for a fluid element reflects matter conservation in classical physics, which in turn motivates the kinematic perspective pursued throughout this book that follows fluid elements whose mass remains constant. Relatedly, in the absence of irreversible mixing, the matter content of the fluid element remains invariant so that its tracer concentration is materially constant

$$\rho \frac{\mathrm{D}C}{\mathrm{D}t} = 0. \tag{26.183}$$

For example, in the absence of mixing, the salt content of seawater and the water content of moist air are materially invariant, so that the salt concentration and water concentration in a fluid element remains invariant. Correspondingly, in the presence of mixing between two fluid elements, the net material tracer in the combined fluid element equals to the sum of the tracer content in the contributing elements. We refer to fluid properties satisfying such conservation laws as *materially conservative properties*.

What about fluid properties that satisfy a local flux-form conservation law of the form (26.182), and yet do not remain materially invariant in the absence of mixing? For example, consider the total energy, $\mathcal{E}$, from Section 26.7. Even in the absence of entropy sources (i.e., no mixing) and astronomical forces (i.e., constant gravity), mechanical work from pressure modifies the internal energy of the fluid element via the energy equation (26.160a)

$$\rho \frac{\mathrm{D}\mathcal{E}}{\mathrm{D}t} = -\nabla \cdot (p \boldsymbol{v}). \tag{26.184}$$

Pressure work means that when two fluid elements are combined, the total energy of the combined fluid, $\mathcal{E}_{12}$, is not generally equal to the sum of their separate total energies,

$$\mathcal{E}_{12} \neq \mathcal{E}_1 + \mathcal{E}_2. \tag{26.185}$$

So although total energy is locally conserved in the sense that it is affected by a local flux convergence, it does not satisfy a material-like conservation law. We say that total energy is a *non-materially conservative* fluid property. Notably, when integrated globally over a domain closed to energy fluxes, including mechanical energy fluxes (meaning there is no pressure work applied to the domain boundaries), and when there are no time dependent astronomical forces, then the domain integrated total energy, $\int \rho \mathcal{E} \, \mathrm{d}V$, remains constant. This *global* conservation

law means that the total energy is conserved globally. Conservation laws for non-materially conserved properties, such as total energy, offer a less powerful constraint on fluid motion than the material conservation laws. Even so, global conservation can be of great use when studying energy transformations within a closed domain.

We summarize the above discussion by noting that for a fluid property to be locally conservative, it is necessary that the density weighted material derivative of that property be given by the convergence of a flux as in equation (26.182). To be materially conservative, a property must have its flux convergence vanish in the absence of mixing processes that are local in space and time. A diffusive flux satisfies this property (see Chapter 69 for more on diffusion). In contrast, the pressure flux convergence acting to modify total energy, $-\nabla \cdot (p\,\boldsymbol{v})$, can be nonzero even in regions where there is no mixing of matter since pressure is transported by waves (Section 26.12.3). So although total energy is locally conserved, its flux is dependent on non-local processes as mediated by waves, so that total energy satisfies a non-material conservation law.

26.12.5 Concerning potential properties

As introduced in Sections 23.3 and 26.11.3, to study fluid mixing it is useful to work with scalar fields that are not affected by adiabatic and isentropic pressure work. For this reason, rather than *in situ* temperature, we prefer to work with potential temperature, θ, or Conservative Temperature, Θ, both of which are potential properties as discussed in Section 23.3.1. Some potential properties are also endowed with the local conservation property discussed above, which makes local budgets available just like for a material tracer. For example, Conservative Temperature is very well approximated as a conservative property, with its non-flux form sources far smaller than potential temperature (Section 26.11.3). In contrast, neither *in situ* temperature nor total energy are potential properties since an adiabatic and isentropic change in pressure alters the *in situ* temperature and total energy of a fluid element.

26.12.6 Further study

Much from this section is motivated by the more extensive discussion in Sections A.8 and A.9 of *IOC et al.* (2010).

26.13 Equations for rotating and stratified fluids

We close this chapter by summarizing the physical content of the suite of partial differential equations describing rotating and stratified fluids.

$$\rho \frac{\mathrm{D}\boldsymbol{v}}{\mathrm{D}t} + 2\,\rho\,\boldsymbol{\Omega} \times \boldsymbol{v} = -\rho\,\nabla\Phi - \nabla p + \nabla \cdot \mathtt{T} \qquad \text{momentum} \tag{26.186}$$

$$\frac{\mathrm{D}\rho}{\mathrm{D}t} = -\rho\,\nabla \cdot \boldsymbol{v} \qquad \text{mass continuity} \tag{26.187}$$

$$\rho \frac{\mathrm{D}C}{\mathrm{D}t} = -\nabla \cdot \boldsymbol{J}(C) \qquad \text{matter conservation} \tag{26.188}$$

$$\rho \frac{\mathrm{D}\Theta}{\mathrm{D}t} = -\nabla \cdot \boldsymbol{J}(\Theta) \qquad \text{potential enthalpy conservation} \tag{26.189}$$

$$\rho = \rho(C, \Theta, p) \qquad \text{equation of state.} \tag{26.190}$$

It is a testament to the success of classical continuum mechanics that these equations are of use for describing fluid phenomena from the millimetre scale to the astrophysical scale. We summarize the following terms in these equations.

- LINEAR MOMENTUM AND VELOCITY: Newton's second law of motion, as developed for a fluid in Chapter 24, provides the prognostic equation for the velocity field, $\boldsymbol{v}$. Each of the three velocity components evolves according to its respective dynamical equation (26.186). As noted at the end of Section 24.2.3, we write the momentum equation in the form (26.186) by separating the time dependence of the basis vectors into a term arising from rigid-body rotation (which leads to planetary Coriolis and planetary centrifugal accelerations) and a term arising from the motion of the fluid relative to the rotating sphere (which leads to the metric acceleration when using non-Cartesian coordinates).

- MASS CONSERVATION: Kinematics provides a constraint on the velocity field according to the needs of mass conservation for a fluid element (Section 19.2). This constraint leads to the continuity equation (26.187).

- MATERIAL TRACER CONSERVATION: Kinematic constraints from the conservation of matter (Section 20.1) leads to the material tracer equation (26.188). Evolution is determined by the convergence of tracer fluxes, $\boldsymbol{J}$, with this flux specified by molecular diffusion as discussed in Section 68.3, or through other parameterized processes when sampling flow on scales larger than millimetres (see Chapter 71).

- THERMODYNAMIC TRACER: The Conservative Temperature, Θ, (Section 26.11.3), evolves according to the convergence of fluxes, just like a material tracer.

- DENSITY: The *in situ* density can be updated in time via mass continuity (equation (26.187)) or via knowledge of (C, Θ, p). We discussed the many forms of density for the ocean and atmosphere in Section 30.3.

- PRESSURE: There is no prognostic equation for pressure. Rather, pressure is diagnosed based on knowledge of other fields. Here are sketches of how that diagnostic calculation is performed.

  - For an ideal gas, pressure is diagnosed from the ideal gas relation (23.48) using the density and temperature.
  - For fluid flow maintaining an approximate hydrostatic balance (Section 27.2), pressure is diagnosed at a point through knowledge of the weight per area above the point.
  - For a non-divergent fluid flow as per the oceanic Boussinesq fluid (Chapter 29), pressure is no longer connected thermodynamically to partial derivatives of the thermodynamic potentials (Section 22.6). Instead, pressure is determined kinematically by the non-divergence constraint. In particular, for a non-hydrostatic Boussinesq fluid, pressure is diagnosed by solving a Poisson equation derived from taking the divergence of the momentum equation (see Section 29.3).

- GEOPOTENTIAL: The geopotential, Φ, is a function of the mass distribution of the planet and any relevant astronomical bodies. The simple geopotential is generally used in this book, with the single exception of Chapter 34 where we develop the equations for astronomical tides. The simple geopotential is specified by both the radial position (to give the height above an arbitrary reference level) plus the latitude (to give the centrifugal potential) (see Section 13.10.4). For geophysical fluid studies, the reference level is generally taken at the level of a resting sea surface. We thus often write the radial coordinate as

$$r = R_{\mathrm{e}} + z \tag{26.191}$$

  where $R_{\mathrm{e}} = 6.371 \times 10^6$ m is the radius of a sphere whose volume approximates that of the earth (equation (13.117)), and z is the geopotential coordinate measuring the height above sea level.

- EARTH'S SPIN: The earth's angular velocity, $\boldsymbol{\Omega}$, is time constant for geophysical fluid studies of concern here. Its value is discussed in Section 13.1.

- FRICTION: The friction vector,
$$\rho \boldsymbol{F} = \nabla \cdot \mathbb{T}, \tag{26.192}$$
is the divergence of a symmetric and trace-free deviatoric stress tensor, $\mathbb{T}$ (Section 25.8). The stress tensor is determined through a constitutive relation as a function of the strain and viscous properties.

- KINEMATIC AND DYNAMIC BOUNDARY CONDITIONS: Kinematic and dynamic boundary conditions consist of the exchange of matter, momentum, and enthalpy with the surrounding media, such as the solid earth or another fluid component (e.g., atmosphere-ocean exchange). We discuss the boundary conditions for matter in a homogeneous fluid in Section 19.6; matter in a multi-constituent fluid in Section 20.4; for momentum in Section 25.10; and for ocean buoyancy in Section 72.6.

26.14 Exercises

EXERCISE 26.1: ENERGETICS OF OCEAN MIXING

In this exercise we develop some basics for the energetics of mixing, thus providing more experience with the ideas developed in Section 26.2.6. We do so by examining a vertical column of seawater with uniform horizontal cross-sectional area, A. Let the initial conditions consist of two homogeneous regions stacked vertically, with thickness h_n, mass M_n, density ρ_n, Conservative Temperature Θ_n, and salinity S_n, where $n = 1$ is the lower region and $n = 2$ the upper region. Assume this column to be stably stratified so that $\Delta\rho = \rho_1 - \rho_2 > 0$. We then completely mix the two regions to produce a homogeneous column of fluid of mass M, salinity S, and Conservative Temperature Θ. We ignore pressure effects on density, so that the density is uniform in the two regions prior to mixing, and uniform in the full column after mixing. The conservation of mass, conservation of salt, and conservation of potential enthalpy (heat), mean that these scalar properties remain the same before and after the mixing, thus allowing us to compute the properties of the homogenized column

$$M = M_1 + M_2 \quad \text{and} \quad M\,\Theta = M_1\,\Theta_1 + M_2\,\Theta_2 \quad \text{and} \quad M\,S = M_1\,S_1 + M_2\,S_2. \tag{26.193}$$

(a) Compute the gravitational potential energy of the initial seawater column, taking the bottom of the column as the zero reference level.

(b) Compute the gravitational potential energy of the fluid column after homogenization. Verify that the gravitational potential energy of the homogenized column is greater than the initial column. For this question, assume the final thickness of the column equals to the sum of the initial thicknesses. This assumption is not exact but is very accurate for our purposes. For an exact calculation see equation (72.112) in our study of sea level in Section 72.7.7.

(c) If the same amount of energy used to increase in gravitational potential energy was instead used to increase kinetic energy of the homogenized fluid, what is the expression for the change in squared velocity? Write your expression in terms of the thicknesses, h_n, and densities, ρ_n.

(d) If the change in gravitational potential energy were converted to potential enthalpy of the homogenized fluid, what is the expression for the increase in Conservative Temperature, Θ? Again, write your expression in terms of the thicknesses, h_n, and densities, ρ_n.

(e) Compute the change in speed and change in Conservative Temperature for the previous parts of this exercise using the following values for a region of seawater: $c_{\text{p}} = 3992.1$ J kg^{-1} K^{-1}, $\rho_1 = 1020$ kg m^{-3}, $\Delta\rho = 1$ kg m^{-3}, $h_1 = 1$ m, and $h_2 = 1$ m.

EXERCISE 26.2: A MODIFIED FRICTIONAL STRESS TENSOR

Following the methods from Section 26.3.3, assume viscous friction in the momentum equation takes the form

$$\rho \boldsymbol{F} = \partial_n(\rho \nu \partial_n \boldsymbol{v}), \tag{26.194}$$

with $\nu > 0$ a scalar kinematic viscosity (generally non-constant). This friction operator corressponds to the frictional stress tensor

$$\text{ŧ}_{nm} = \rho \nu \partial_n v_m. \tag{26.195}$$

(a) Show that when integrated over the full domain

$$\int \boldsymbol{F} \cdot \boldsymbol{v} \, \rho \, \mathrm{d}V < 0, \tag{26.196}$$

where boundary terms are ignored. Hence, the global integrated kinetic energy is dissipated (reduced) through the impacts of viscosity in the interior of the domain. Note that for this exercise, it is sufficient to assume Cartesian tensors so that

$$\rho \boldsymbol{F} \cdot \boldsymbol{v} = \rho F_m v_m = \partial_n(\rho \nu \partial_n v_m) v_m. \tag{26.197}$$

(b) What property does the assumed ŧ_{nm} in equation (26.195) *not* satisfy, thus making it unsuitable as a frictional stress tensor? Discuss according to what we studied in Section 25.4.

EXERCISE 26.3: INTEGRATED FRICTIONAL DISSIPATION FOR AN INCOMPRESSIBLE FLUID

Consider an incompressible fluid ($\nabla \cdot \boldsymbol{v} = 0$ along with ρ is constant). Assume the fluid is contained in a region, $\mathcal{R}$, whose boundary, $\partial\mathcal{R}$, is static. Also assume the velocity satisfies the no-slip condition on $\partial\mathcal{R}$, as relevant for a viscous fluid. Show that the frictional dissipation of kinetic energy (Section 26.3.3) has a global integral

$$\int_{\mathcal{R}} \boldsymbol{v} \cdot \boldsymbol{F} \, \rho \, \mathrm{d}V = -\rho \nu \int_{\mathcal{R}} |\boldsymbol{\omega}|^2 \, \mathrm{d}V, \tag{26.198}$$

where $\boldsymbol{\omega} = \nabla \times \boldsymbol{v}$ is the vorticity. Hint: derive equation (18.156) from exercise 18.1, and specialize that equation to the case of an incompressible fluid.

EXERCISE 26.4: THERMODYNAMIC MANIPULATIONS FOR IDEAL GASES

This question develops some manipulations with the potential temperature.

(a) Beginning with the expression (23.92) for potential temperature of an ideal gas, show that

$$\mathrm{d}\theta = \frac{\theta}{T}\left[\mathrm{d}T - \frac{\nu_{\text{s}}}{c_{\text{p}}}\mathrm{d}p\right]. \tag{26.199}$$

(b) Given the result (26.199), show that an ideal gas satisfies the following relation

$$T \, \mathrm{d}\mathcal{S} = \frac{c_p T}{\theta} \, \mathrm{d}\theta. \tag{26.200}$$

Whereas the relation (23.44) holds for a general fluid only at the reference pressure, this exercise shows that it holds for an ideal gas at all pressures. As a result, a moving fluid of ideal gas satisfies the material time relation

$$T \frac{\mathrm{D}\mathcal{S}}{\mathrm{D}t} = \frac{c_p\, T}{\theta} \frac{\mathrm{D}\theta}{\mathrm{D}t} \Rightarrow \frac{c_p\, T}{\theta} \frac{\mathrm{D}\theta}{\mathrm{D}t} = \dot{Q}. \tag{26.201}$$

EXERCISE 26.5: THERMODYNAMIC MANIPULATIONS FOR A LIQUID
Consider seawater with specific entropy given by (see Section 1.7.2 of *Vallis* (2017))

$$\mathcal{S}(S,T,p) = \mathcal{S}_0 + c_{\mathrm{p0}} \ln(T/T_o)\,[1 + \beta^*_{\mathrm{S}}\,(S - S_o)] - \alpha_o\, p \left[\beta_{\mathrm{T}} + \beta_{\mathrm{T}}\, \gamma^* \frac{p}{2} + \beta^*_{\mathrm{T}}\,(T - T_o)\right], \tag{26.202}$$

and corresponding specific heat capacity at constant pressure

$$c_{\mathrm{p}}(S,T,p) = c_{\mathrm{p0}}\,[1 + \beta^*_{\mathrm{S}}\,(S - S_o)] - \alpha_o\, p\, \beta^*_{\mathrm{T}}\, T. \tag{26.203}$$

In these equations, T is the *in situ* temperature, S is the salinity, and p is the *in situ* pressure. All other terms on the right hand side to these expressions are empirical constants. Verify that the specific entropy differential for a fluid element with constant composition is given by

$$\theta\, \mathrm{d}\mathcal{S} = c_{\mathrm{p}}(S, \theta, p_{\mathrm{R}})\, \mathrm{d}\theta, \tag{26.204}$$

where θ is the potential temperature and p_{R} is the corresponding reference pressure. Consequently, we can write for a moving fluid element

$$\dot{Q} = \frac{c_{\mathrm{p}}\, T}{\theta} \frac{\mathrm{D}\theta}{\mathrm{D}t}, \tag{26.205}$$

where we evaluate the non-constant heat capacity at $c_{\mathrm{p}}(S, \theta, p_{\mathrm{R}})$. We see that certain liquids have an expression for heating that is analogous to that for an ideal gas, with the ideal gas case discussed in Exercise 26.4. Hint: Make use of the identity (23.36).

EXERCISE 26.6: BERNOULLI THEOREM AND TWO SHEETS OF PAPER (EXERCISE 1.22 OF *Sutherland* (2010))
Hold two sheets of paper from their top edge so they are two fingers-widths apart. Blow between the two sheets. Do they separate or come together. Explain what happens in terms of the physics discussed in this chapter. Hint: make use of the simplest form of Bernoulli's theorm from Section 26.9.

EXERCISE 26.7: DYNAMICALLY INCONSISTENT VELOCITY
Consider the two dimensional non-divergent vector field

$$\boldsymbol{u} = \Gamma\,(y^2\, \hat{\boldsymbol{x}} + x^2\, \hat{\boldsymbol{y}}), \tag{26.206}$$

with Γ a constant of dimensions $\mathrm{L}^{-1}\,\mathrm{T}^{-1}$. In this exercise we will show that it *cannot* be a physically realizable velocity field.

(a) Assuming $\boldsymbol{u}$ is a velocity field for fluid flow, then determine the pressure field giving rise to this velocity. Assume a constant density, non-rotating reference frame, zero friction, and no boundary effects. Do so by making use of the Bernoulli theorem in equation (26.118) for horizontal (constant z) flow, and thus provide the expression for pressure, and express that pressure along a streamline. Hint: compute the streamfunction corresponding to the velocity, and choose a convenient streamline upon which to evaluate the pressure.

(b) Now make use of the momentum equation to find the pressure gradient. Attempt to

integrate this equation to then find the pressure field. You should reach an inconsistency. Given this inconsistency, what can you conclude about the physical realizability of the given $\boldsymbol{u}$ as a velocity vector? Discuss. Hint: recall the discussion of exact differentials in Section 2.8.

EXERCISE 26.8: CROCCO'S THEOREM

Prove that the spatial gradient of the Bernoulli potential for a single-component steady state perfect fluid can be written

$$\mathcal{B} = T\,\nabla\mathcal{S} + \boldsymbol{v} \times \boldsymbol{\omega}_{\mathrm{a}}. \tag{26.207}$$

This result is known as Crocco's Theorem (*Crocco*, 1937). We derive two conclusions from this theorem. First, in a steady state, there is a nonzero vorticity non-parallel to the velocity whenever $\mathcal{B} - T\,\nabla\mathcal{S}$; i.e.,

$$\boldsymbol{v} \times \boldsymbol{\omega}_{\mathrm{a}} = \mathcal{B} - T\,\nabla\mathcal{S}. \tag{26.208}$$

Second, it means that the velocity for a single-component perfect fluid in steady state is aligned parallel to isosurfaces of both the Bernoulli potential and the specific entropy

$$\boldsymbol{v} \cdot \nabla\mathcal{B} = T\,\boldsymbol{v} \cdot \nabla\mathcal{S}. \tag{26.209}$$

We encounter another form of this theorem for the steady state shallow water equations in Exercise 39.7.

Hint: to help formulate the proof, study the discussion in Section 26.9.3 where we showed that the Bernoulli potential is constant along a steady flow streamline in a perfect fluid. Also recall equation (26.115), which is valid for a steady state and applied here to a single-component fluid.

Chapter 27

APPROXIMATE HYDROSTATIC FLOW

For a moving fluid with scales of motion that maintain a small vertical to horizontal aspect ratio, we show in this chapter that the vertical pressure gradient and gravitational acceleration individually remain far larger than other accelerations acting on a fluid element. In this case, the vertical momentum equation, even for the moving fluid, remains approximately in hydrostatic balance column-by-column. We thus have a flow whereby each vertical column is in hydrostatic balance, and yet there are horizontal pressure gradients that drive horizontal motion. Correspondingly, there is also vertical motion. In this chapter, we study the many facets of this *approximately hydrostatic flow*.

More generally, we observe that the ocean and atmosphere thermo-hydrodynamical equations (26.186)-(26.190) explain a huge range of phenomena. Yet by encapsulating so many physical scales of motion and associated dynamical processes, the equations are difficult to manage when studying a focused dynamical regime. Therefore, it is common to approximate or filter the equations to remove scales that are not of direct interest to the problem at hand, thus enabling a more telescopic view of the dynamics. The *hydrostatic primitive equations* provide an important example of this approach.

READER'S GUIDE TO THIS CHAPTER

The column-by-column hydrostatic balance found in the approximate hydrostatic flow is ubiquitous in large-scale fluid flows in the atmosphere and ocean. We thus make extensive use in this book of the corresponding expressions for the pressure gradients holding for such flows. Relatedly, the hydrostatic primitive equations have been very useful in the study of ocean and atmosphere circulation since their introduction in the 1950s, and we make use of them in various forms throughout the remainder of this book.

27.1 The hydrostatic primitive equations

The hydrostatic *primitive equations* provide a set of approximate equations for use in studying large-scale atmospheric and oceanic phenomena. Indeed, nearly all numerical models of the large-scale atmospheric and oceanic circulation are based on the primitive equations. They make use of the following three approximations.

27.1.1 Hydrostatic approximation

As discussed in Section 24.6, a static fluid in a gravity field maintains an exact hydrostatic balance, whereby the pressure at a point equals to the weight per area of fluid above that point. As shown in Section 27.2, the hydrostatic balance is very closely maintained column-by-column for the large scales in a moving geophysical fluid. Hence, it is appropriate for many purposes to take the *hydrostatic approximation* for the vertical momentum equation, with this approximation central to the study of large-scale geophysical fluid dynamics.

The hydrostatic approximation results in a balance within the vertical momentum equation (24.21) between the vertical pressure gradient and the effective gravitational force

$$\frac{\partial p}{\partial r} = -\rho\, g, \tag{27.1}$$

with this balance holding separately for each vertical column. Notably, there are no viscous or turbulent terms appearing in the hydrostatic balance.

Vertical integration of this equation, while assuming g is constant, renders a diagnostic expression for the hydrostatic pressure at a point as a function of the weight per horizontal area above the point

$$p(r, \lambda, \phi, t) = p(r_0, \lambda, \phi, t) + g \int_r^{r_0} \rho(r', \lambda, \phi, t)\, \mathrm{d}r'. \tag{27.2}$$

Note that we exposed the horizontal space dependence along with the time dependence for the density and hence the hydrostatic pressure. That is, an approximate hydrostatic fluid flow has horizontal pressure gradients as well as time dependence.

We emphasize that in making the hydrostatic approximation, we are *not* assuming that vertical motion vanishes. In fact, there is vertical motion. But with the hydrostatic approximation, the vertical motion is not prognosed by the vertical momentum equation. Instead, it must be diagnosed via the constraints imposed on the motion. We have more comment on this point in Section 27.2.7. Furthermore, there are no other terms appearing in the vertical momentum

equation, so that we retain just the vertical pressure gradient and the gravity term. Friction or boundary turbulent stresses do not appear in the hydrostatic balance, whereas they generally do appear in the non-hydrostatic vertical momentum equation.

27.1.2 Shallow fluid approximation

The ocean and atmosphere each form a fluid shell that envelopes the outer portion of the planet. The thickness of the these fluids is small relative to the earth's radius. The shallow fluid approximation[1] builds this scale separation into the equations of motion by setting the radial coordinate equal to the earth's radius

$$r = R_e + z \approx R_e. \tag{27.3}$$

This approximation is made where r appears as a multiplier, but not as a derivative operator. For example, the spherical coordinate gradient operator (24.23) takes the approximate form

$$\nabla = \frac{\hat{\boldsymbol{\lambda}}}{r \cos\phi} \frac{\partial}{\partial \lambda} + \frac{\hat{\boldsymbol{\phi}}}{r} \frac{\partial}{\partial \phi} + \hat{\boldsymbol{r}} \frac{\partial}{\partial r} \approx \frac{\hat{\boldsymbol{\lambda}}}{R_e \cos\phi} \frac{\partial}{\partial \lambda} + \frac{\hat{\boldsymbol{\phi}}}{R_e} \frac{\partial}{\partial \phi} + \hat{\boldsymbol{r}} \frac{\partial}{\partial r}. \tag{27.4}$$

This approximation proves useful when computing the depth integrated fluid mechanical equations for studies where we wish to remove the vertical degress of freedom. Examples include the depth integrated mechanical energy in Section 27.1.6, the depth integrated momentum equation in Section 28.4, the depth integrated angular momentum equation in Section 28.5, and the depth integrated vorticity equations in Sections 44.3, 44.5, and 44.6.

27.1.3 Traditional approximation

The *traditional approximation* comprises three approximations that come as a package in order to maintain physical consistency.

Coriolis acceleration

The traditional approximation sets to zero the Coriolis terms in the horizontal momentum equations involving the vertical velocity. We are thus concerned only with the local vertical component of the earth's angular rotation vector (see discussion in Section 13.9.8)

$$\boldsymbol{\Omega} = \Omega \hat{\boldsymbol{Z}} = \Omega \left(\hat{\boldsymbol{\phi}} \cos\phi + \hat{\boldsymbol{r}} \sin\phi \right) \to \Omega \sin\phi \, \hat{\boldsymbol{r}} = \boldsymbol{f}/2, \tag{27.5}$$

where

$$\boldsymbol{f} = (2\,\Omega \sin\phi)\, \hat{\boldsymbol{r}} \tag{27.6}$$

is the Coriolis parameter and $\hat{\boldsymbol{Z}}$ is the spherical earth unit vector pointing out of the north pole (Figure 4.3).[2]

Metric terms

The traditional approximation also drops the metric terms, uw/r and vw/r, associated with the vertical velocity as they appear in the horizontal momentum equations (24.19) and (24.20). These terms are generally smaller than the other terms since w is much smaller than the horizontal velocity for large-scale geophysical fluid flow.

[1] The shallow fluid approximation is distinct from the *shallow water approximation* treated in Part VI of this book.

[2] We use the capital $\hat{\boldsymbol{Z}}$ to distinguish this north pole unit vector from the local $\hat{\boldsymbol{z}} = \hat{\boldsymbol{r}}$ unit vector pointing vertical relative to a tangent plane discussed in Section 24.5.

Physical consistency

The shallow fluid approximation and both parts of the traditional approximation must be taken together in order to maintain a consistent energy and angular momentum conservation principle for the resulting equations. As shown in Exercise 27.1, taking one but not the other leads to a physically inconsistent set of equations

27.1.4 Summary of the hydrostatic primitive equations

The above approximations lead to the primitive equations written in spherical coordinates

$$\frac{\mathrm{D}u}{\mathrm{D}t} - \frac{u\,v\tan\phi}{R_e} - f\,v = -\frac{1}{\rho\,R_e\cos\phi}\,\frac{\partial p}{\partial\lambda} + F^\lambda \tag{27.7}$$

$$\frac{\mathrm{D}v}{\mathrm{D}t} + \frac{u^2\tan\phi}{R_e} + f\,u = -\frac{1}{\rho\,R_e}\,\frac{\partial p}{\partial\phi} + F^\phi \tag{27.8}$$

$$\frac{\partial p}{\partial z} = -g\,\rho, \tag{27.9}$$

where the gradient operator is given by equation (27.4). We can write these equations in the vector form

$$\rho\,\frac{\mathrm{D}\boldsymbol{u}}{\mathrm{D}t} + (f + u\tan\phi/R_e)\,\hat{\boldsymbol{z}}\times\rho\,\boldsymbol{u} = -\rho\,\nabla\Phi - \nabla p + \rho\,\boldsymbol{F}, \tag{27.10}$$

where

$$\boldsymbol{F} = \hat{\boldsymbol{\lambda}}\,F^\lambda + \hat{\boldsymbol{\phi}}\,F^\phi \tag{27.11}$$

is the horizontal friction acceleration, and the vertical component of equation (27.10) is the hydrostatic balance. Furthermore, the material time derivative in this equation signifies the relative acceleration

$$\frac{\mathrm{D}\boldsymbol{u}}{\mathrm{D}t} = \hat{\boldsymbol{\lambda}}\,\frac{\mathrm{D}u}{\mathrm{D}t} + \hat{\boldsymbol{\phi}}\,\frac{\mathrm{D}v}{\mathrm{D}t}. \tag{27.12}$$

27.1.5 Flux-form mechanical energy budget

For fluid flow maintaining the approximate hydrostatic approximation, the kinetic energy is dominated by the horizontal motions. Indeed, as we now show, the proper form of the kinetic energy is precisely that contained just in the horizontal motions. We do so by taking the scalar product of the horizontal velocity with the momentum equation (27.10) to render

$$\rho\,\frac{\mathrm{D}\mathcal{K}^{\mathrm{hyd}}}{\mathrm{D}t} = -\rho\,\boldsymbol{u}\cdot\nabla\Phi - \boldsymbol{u}\cdot\nabla p + \rho\,\boldsymbol{u}\cdot\boldsymbol{F}, \tag{27.13}$$

where we introduced the hydrostatic kinetic energy per mass

$$\mathcal{K}^{\mathrm{hyd}} = \boldsymbol{u}\cdot\boldsymbol{u}/2. \tag{27.14}$$

Making use of the hydrostatic balance in the presence of a simple geopotential, $\Phi = g\,z$ (so that $\boldsymbol{u}\cdot\nabla\Phi = 0$), leads to

$$\rho\,\frac{\mathrm{D}\mathcal{K}^{\mathrm{hyd}}}{\mathrm{D}t} = -(\boldsymbol{v}\cdot\nabla p - w\,\partial_z p) + \rho\,\boldsymbol{u}\cdot\boldsymbol{F} \tag{27.15a}$$

$$= -\nabla\cdot(\boldsymbol{v}\,p) + p\,\nabla\cdot\boldsymbol{v} - w\,g\,\rho + \rho\,\boldsymbol{u}\cdot\boldsymbol{F}, \tag{27.15b}$$

which leads to the flux-form conservation equation for kinetic energy

$$\partial_t(\rho\,\mathcal{K}^{\mathrm{hyd}}) + \nabla\cdot[\boldsymbol{v}\,(\rho\mathcal{K}^{\mathrm{hyd}} + p)] = p\,\nabla\cdot\boldsymbol{v} - \rho\,g\,w + \rho\,\boldsymbol{u}\cdot\boldsymbol{F}. \tag{27.16}$$

Furthermore, $\Phi = g\,z$ means that

$$\rho\,\mathrm{D}\Phi/\mathrm{D}t = \partial_t(\rho\,\Phi) + \nabla\cdot(\rho\,\boldsymbol{v}\,\Phi) = \rho\,g\,w, \tag{27.17}$$

in which case the flux-form equation for the mechanical energy per mass, $\mathcal{M}^{\mathrm{hyd}}$, is given by

$$\partial_t(\rho\,\mathcal{M}^{\mathrm{hyd}}) + \nabla\cdot[\rho\,\boldsymbol{v}\,(\mathcal{M}^{\mathrm{hyd}} + p/\rho)] = p\,\nabla\cdot\boldsymbol{v} + \rho\,\boldsymbol{u}\cdot\boldsymbol{F}, \tag{27.18}$$

where

$$\mathcal{M}^{\mathrm{hyd}} = \mathcal{K}^{\mathrm{hyd}} + \Phi = \boldsymbol{u}\cdot\boldsymbol{u}/2 + g\,z. \tag{27.19}$$

Equation (27.18) compares to the non-hydrostatic mechanical energy equation (26.49). The key difference is that the kinetic energy per mass is here just given by the horizontal flow (27.14). Additionally, the friction vector for the hydrostatic flow is horizontal. Otherwise, the physical interpretation of the mechanical energy budget accords with that for the non-hydrostatic flow given in Section 26.4.

27.1.6 Depth integrated mechanical energy budget

We here extend the analysis from Section 27.1.5 to derive the depth integrated mechanical energy budget for the hydrostatic primitive equations. The kinetic energy per area contained in the horizontal flow as integrated over a column is given by

$$\int_{\eta_{\mathsf{b}}}^{\eta}\rho\,\mathcal{K}^{\mathrm{hyd}}\,\mathrm{d}z = \frac{1}{2}\int_{\eta_{\mathsf{b}}}^{\eta}\rho\,\boldsymbol{u}\cdot\boldsymbol{u}\,\mathrm{d}z. \tag{27.20}$$

Leibniz's rule leads to the time tendency

$$\frac{\mathrm{d}}{\mathrm{d}t}\int_{\eta_{\mathsf{b}}}^{\eta}\rho\,\mathcal{K}^{\mathrm{hyd}}\,\mathrm{d}z = \partial_t\eta\,[\rho\,\mathcal{K}^{\mathrm{hyd}}]_{z=\eta} + \int_{\eta_{\mathsf{b}}}^{\eta}\partial_t(\rho\,\mathcal{K}^{\mathrm{hyd}})\,\mathrm{d}z. \tag{27.21}$$

Making use of the kinetic energy equation (27.16) as well as Leibniz's rule gives the budget

$$\begin{aligned}\frac{\mathrm{d}}{\mathrm{d}t}\int_{\eta_{\mathsf{b}}}^{\eta}\rho\,\mathcal{K}^{\mathrm{hyd}}\,\mathrm{d}z = {}& [\rho\,\mathcal{K}^{\mathrm{hyd}} + p_{\mathsf{a}}]_{z=\eta}\,(\partial_t\eta - w + \boldsymbol{u}\cdot\nabla\eta)_{z=\eta} + [\rho\,\mathcal{K}^{\mathrm{hyd}} + p_{\mathsf{b}}]_{z=\eta_{\mathsf{b}}}\,(w - \boldsymbol{u}\cdot\nabla\eta_{\mathsf{b}})_{z=\eta_{\mathsf{b}}} \\ & - \nabla_{\mathsf{h}}\cdot\int_{\eta_{\mathsf{b}}}^{\eta}(\rho\,\boldsymbol{u}\,\mathcal{K}^{\mathrm{hyd}} + \boldsymbol{u}\,p)\,\mathrm{d}z + \int_{\eta_{\mathsf{b}}}^{\eta}(p\,\nabla\cdot\boldsymbol{v} - \rho\,g\,w + \rho\,\boldsymbol{u}\cdot\boldsymbol{F})\,\mathrm{d}z.\end{aligned} \tag{27.22}$$

Note that when bringing ∇_{h} outside the vertical integral, besides making use of Leibniz's rule, we also assumed ∇_{h} is itself independent of z, which is trivially the case with Cartesian coordinates. However, for spherical coordinates the assumption requires the shallow fluid approximation so that the r^{-1} appearing in the gradient operator is replaced by R_{e}^{-1} as per equation (27.4). It is here that we see that the depth integrated equations are most usefully posed when working with the hydrostatic primitive equations.

The bottom kinematic boundary condition (19.56) and surface boundary condition (19.94) then give the depth-integrated kinetic energy budget

$$\begin{aligned}&\frac{\mathrm{d}}{\mathrm{d}t}\int_{\eta_{\mathsf{b}}}^{\eta}\rho\,\mathcal{K}^{\mathrm{hyd}}\,\mathrm{d}z = \\ &Q_{\mathsf{m}}\,[\mathcal{K}^{\mathrm{hyd}} + p_{\mathsf{a}}/\rho]_{z=\eta} - \nabla_{\mathsf{h}}\cdot\int_{\eta_{\mathsf{b}}}^{\eta}(\rho\,\boldsymbol{u}\,\mathcal{K}^{\mathrm{hyd}} + \boldsymbol{u}\,p)\,\mathrm{d}z + \int_{\eta_{\mathsf{b}}}^{\eta}(p\,\nabla\cdot\boldsymbol{v} - \rho\,g\,w + \rho\,\boldsymbol{u}\cdot\boldsymbol{F})\,\mathrm{d}z.\end{aligned} \tag{27.23}$$

The first term on the right hand side arises from the mass transport across the ocean surface,

along with the applied surface pressure. The second term is the convergence of the depth integrated flux of kinetic energy plus pressure. The final term is the depth integral of the buoyancy conversion term plus frictional work. Similar manipulations starting from the flux-form mechanical energy budget (27.18) lead to the depth integrated budget

$$\frac{\mathrm{d}}{\mathrm{d}t} \int_{\eta_b}^{\eta} \rho \mathcal{M}^{\mathrm{hyd}} \, \mathrm{d}z = Q_m \left[\mathcal{M}^{\mathrm{hyd}} + p_a/\rho \right]_{z=\eta} - \nabla_h \cdot \int_{\eta_b}^{\eta} (\rho \boldsymbol{u} \mathcal{M}^{\mathrm{hyd}} + \boldsymbol{u} p) \, \mathrm{d}z + \int_{\eta_b}^{\eta} (p \nabla \cdot \boldsymbol{v} + \rho \boldsymbol{u} \cdot \boldsymbol{F}) \, \mathrm{d}z. \quad (27.24)$$

27.1.7 Comments and further study

The primitive equations make use of the momentum equations, which contrasts to *non-primitive* equation methods that develop evolution equations for the vorticity and divergence. *Smagorinsky* (1963) was an early proponent of the hydrostatic primitive equations for use in studying the large-scale ocean and atmospheric circulation. These equations form the basis for many general circulation models of the atmosphere and ocean. However, it is notable that finer resolution simulations, that admit strong vertical motions, must make use of the non-hydrostatic equations. Non-hydrostatic simulations are particularly relevant when studying clouds in the atmosphere and fine-scale mixing in the ocean, with both of these processes involving nontrivial vertical accelerations that break the hydrostatic approximation. These models sometimes also time step the momentum equations, and as such are referred to as *non-hydrostatic primitive equation* models.

27.2 Elements of approximate hydrostatic pressure

For a static fluid with identically zero net acceleration, the vertical pressure gradient precisely balances the weight of fluid to thus realize exact hydrostatic balance. We discussed this static solution to the equations of motion in Sections 24.6 and 25.5. For a moving fluid with scales of motion that maintain a small vertical to horizontal aspect ratio, the presentation in this section reveals that the vertical pressure gradient and gravitational acceleration individually remain far larger than other accelerations acting on a fluid element. In this case, the vertical momentum equation, even for the moving fluid, remains approximately in hydrostatic balance column-by-column. We thus have a fluid flow whereby each vertical fluid column is in hydrostatic balance, and yet there are horizontal pressure gradients that drive motion. In this section we study aspects of such approximately hydrostatic fluid flows.

For simplicity in this section we make use of Cartesian coordinates rather than the spherical coordinates used in Section 27.1.

27.2.1 Expressions for the hydrostatic pressure

Making the hydrostatic approximation in the vertical momentum equation leads to the local balance

$$\frac{\partial p}{\partial z} = -\rho g. \quad (27.25)$$

Vertically integrating upward from a point within the ocean to the ocean surface leads to the hydrostatic pressure

$$p(x, y, z, t) = p_a(x, y, t) + g \int_z^{\eta} \rho(x, y, z', t) \, \mathrm{d}z'. \quad (27.26)$$

In this equation we wrote $p(\eta) = p_a$ for the pressure at the ocean free surface, $z = \eta(x, y, t)$, arising from the weight of the overlying atmosphere or sea ice; i.e., this is the applied pressure acting on the top of the ocean fluid. A similar integration applies to the atmosphere

$$p(x, y, z, t) = g \int_z^{z_{\text{top}}} \rho(x, y, z', t) \, \mathrm{d}z', \tag{27.27}$$

where $z = z_{\text{top}}$ is the top of the atmosphere, sometimes approximated by $z_{\text{top}} = \infty$. For both the ocean and the atmosphere, we assume g remains a constant over the vertical extent of the fluid, which is a sensible approximation even for the top of the atmosphere.

In both the ocean and atmosphere, the hydrostatic pressure at a vertical position, z, equals to the weight per horizontal area of matter above that position, with equations (27.26) and (27.27) providing explicit expressions in terms of *in situ* density and boundary contributions. These expressions offer a huge simplification for how we determine pressure, with the remainder of this section providing example implications.

27.2.2 Evolution of hydrostatic pressure

We expect that hydrostatic pressure evolves according to the convergence of mass onto the column of fluid above that point. The ocean hydrostatic pressure also changes due to time changes in the applied upper boundary pressure. Here we derive mathematical expressions that support these expectations, with Figure 27.1 providing a schematic.

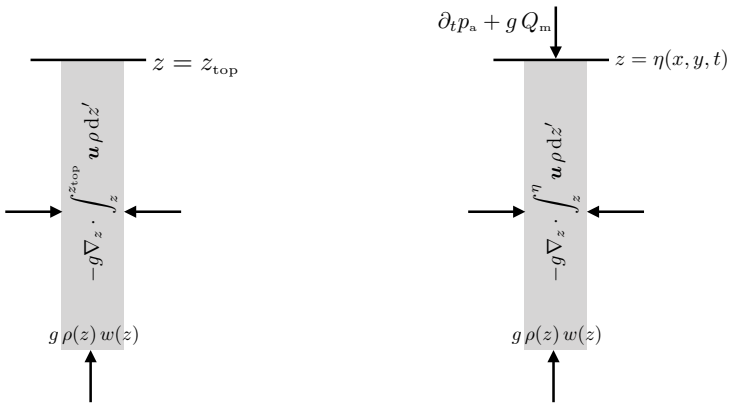

FIGURE 27.1: Evolution of hydrostatic pressure for a vertical position in the atmosphere (left panel) and ocean (right panel) according to equations (27.30) and (27.33a). Hydrostatic pressure at a vertical position, z, which here is the bottom of the fluid column, arises from the convergence of mass onto the column over the region above z. The ocean column also has a contribution from the time tendency of applied surface pressure plus the mass of coming across the top boundary. For the atmosphere as assume the top boundary is at $z_{\text{top}} = \infty$ and so there is no mass coming across that boundary.

Hydrostatic pressure in the atmosphere

A time derivative of the atmospheric hydrostatic pressure (27.27) renders

$$\partial_t p = g \int_z^{z_{\text{top}}} \partial_t \rho(x, y, z', t) \, \mathrm{d}z'. \tag{27.28}$$

Note the absence of a time derivative on z_{top}. We ensure this time derivative is not relevant by setting z_{top} to a constant value well above anything of physical relevance; e.g., $z_{\text{top}} \approx \infty$. Now

insert the mass continuity equation (19.6) and make further use of Leibniz's rule to write

$$\partial_t p = -g \int_z^{z_{\rm top}} \nabla \cdot (\boldsymbol{v}\, \rho)\, \mathrm{d}z' \tag{27.29a}$$

$$= g\, \rho(z)\, w(z) - g \int_z^{z_{\rm top}} \nabla_{\rm h} \cdot (\boldsymbol{u}\, \rho)\, \mathrm{d}z', \tag{27.29b}$$

where we set $w(z_{\rm top})\, \rho(z_{\rm top}) = 0$. The first term on the right hand side arises from the vertical mass flux into the fluid column from below. The second term arises from the horizontal convergence of mass as integrated over the column above the position, z. If the vertical position of the bottom limit on the integral is independent of horizontal position, then we can pull the horizontal divergence operator outside of the integral to render

$$\partial_t p = g\, \rho(z)\, w(z) - g\, \nabla_{\rm h} \cdot \int_z^{z_{\rm top}} \boldsymbol{u}\, \rho\, \mathrm{d}z'. \tag{27.30}$$

In Exercise 27.3 we derive an expression for the bottom pressure, $p(x, y, z = \eta_{\rm b}(x, y), t)$, where we must use Leibnitz's rule to pull the horizontal derivative outside of the integral.

Hydrostatic pressure in the ocean

The derivation for the ocean requires some more work since the ocean free surface is a permeable space and time dependent function. A time derivative of the ocean pressure expression (27.26) renders

$$\partial_t p = \partial_t p_{\rm a} + g\, \rho(\eta)\, \partial_t \eta + g \int_z^{\eta} \partial_t \rho(x, y, z', t)\, \mathrm{d}z', \tag{27.31}$$

where we made use of Leibniz's rule to take the time derivative of the upper limit at $z = \eta(x, y, t)$, and with the shorthand $\rho(\eta) = \rho(x, y, z = \eta, t)$. Now insert the mass continuity equation (19.6) and make further use of Leibniz's rule to write

$$\partial_t (p - p_{\rm a}) - g\, \rho(\eta)\, \partial_t \eta = g \int_z^{\eta} \partial_t \rho(x, y, z', t)\, \mathrm{d}z' \tag{27.32a}$$

$$= -g \int_z^{\eta} \nabla \cdot (\boldsymbol{v}\, \rho)\, \mathrm{d}z' \tag{27.32b}$$

$$= -g\, [\rho(\eta)\, w(\eta) - \rho(z)\, w(z)] - g \int_z^{\eta} \nabla_{\rm h} \cdot (\boldsymbol{u}\, \rho)\, \mathrm{d}z' \tag{27.32c}$$

$$= g\, \rho(z)\, w(z) + g\, [(-w + \boldsymbol{u} \cdot \nabla \eta)\, \rho]_{z=\eta} - g \nabla_{\rm h} \cdot \int_z^{\eta} \boldsymbol{u}\, \rho\, \mathrm{d}z' \tag{27.32d}$$

$$= g\, \rho(z)\, w(z) + g\, (Q_{\rm m} - \rho(\eta)\, \partial_t \eta) - g \nabla_{\rm h} \cdot \int_z^{\eta} \boldsymbol{u}\, \rho\, \mathrm{d}z', \tag{27.32e}$$

where the last step made use of the kinematic boundary condition (19.94) for the ocean free surface, with $Q_{\rm m}$ the mass flux entering the ocean across the free surface. Rearrangement, and cancellation of the $\rho(\eta)\, \partial_t \eta$ term appearing on both sides, leads to

$$\partial_t p = \partial_t p_{\rm a} + g\, \rho(z)\, w(z) + g\, Q_{\rm m} - g \nabla_{\rm h} \cdot \int_z^{\eta} \boldsymbol{u}\, \rho\, \mathrm{d}z'. \tag{27.33a}$$

The first term on the right hand side arises from time fluctuations of the applied pressure at $z = \eta$. The second and third terms measure the vertical convergence of mass onto the column of fluid sitting above the vertical position, with $\rho(z)\, w(z)$ the mass flux entering the column from below and $Q_{\rm m}$ the mass flux entering from across the free surface. The final term arises from the vertically integrated horizontal mass transport converging onto the column above the position of

interest.

27.2.3 Heuristic scaling

We here present a scale analysis to justify the hydrostatic approximation. This analysis serves to introduce a common method used in fluid mechanics to identify those processes that may be dominant for a particular flow regime. In particular, the flow regime of interest here occurs with a small vertical to horizontal aspect ratio

$$\alpha_{\text{aspect}} \equiv \frac{H}{L} \ll 1, \tag{27.34}$$

with H a typical length scale for vertical motion and L the horizontal length scale. This regime is fundamental to the large-scale circulation of the ocean and atmosphere. As the hydrostatic approximation is concered with the force balances in a fluid column, it is sufficient to ignore rotation when performing a scale analysis.

Consider the vertical momentum equation (24.43c) from the tangent plane and traditional approximations (Section 24.5), along with the associated scales for the various terms

$$\frac{\mathrm{D}w}{\mathrm{D}t} = -\frac{1}{\rho}\frac{\partial p}{\partial z} - g \tag{27.35a}$$

$$\frac{W}{T} + \frac{U\,W}{L} + \frac{W\,W}{H} = -\frac{1}{\rho}\frac{\partial p}{\partial z} - g. \tag{27.35b}$$

In the second equation we introduced the following scales for the terms appearing on the left hand side of the first equation.

- L is the horizontal scale of the motion.
- H is the vertical scale of the motion.
- W is the vertical velocity scale.
- U is the horizontal velocity scale. For this analysis we do not distinguish between the zonal and meridional velocity scales, writing U for both. This assumption is not always valid, such as when scaling for jet stream or equatorial flows, both of which have larger zonal speeds than meridional.
- T is the time scale of the motion. We assume that the time scale is determined by horizontal advection[3] so that $T \sim L/U$.

To get a sense for the numbers, consider large-scale atmospheric flows with $W = 10^{-2}$ m s^{-1}, $L = 10^5$ m, $H = 10^3$ m, $U = 10$ m s^{-1}. These numbers lead to $T = L/U = 10^4$ s and to the values for the vertical momentum equation

$$10^{-6}\ \text{m s}^{-2} \sim -\frac{1}{\rho}\frac{\partial p}{\partial z} - g. \tag{27.36}$$

With $g \sim 10$ m s^{-2}, the only term that can balance the gravitational acceleration is the vertical pressure gradient. A similar analysis holds for large-scale ocean flows where we set $W = 10^{-3}$ m s^{-1}, $L = 10^3$ m, $H = 10^1$ m, $U = 10^{-1}$ m s^{-1}. These numbers lead to $T = L/U = 10^4$ s and to

$$10^{-7}\ \text{m s}^{-2} \sim -\frac{1}{\rho}\frac{\partial p}{\partial z} - g. \tag{27.37}$$

[3]This assumption for time scale is not always appropriate, such as for studies of waves where we may instead consider time scales according to a wave speed and wave length.

In either case, large scale motion maintains an approximate hydrostatic balance whereby $\partial p/\partial z = -\rho\, g$.

We offer a more formal scale analysis in Section 29.2, making use of the oceanic Boussinesq equations derived in Chapter 29. For the remainder of this section we explore certain properties of a fluid flow maintaining an approximate hydrostatic balance.

27.2.4 Removal of a dynamically irrelevant background state

The previous analysis pointed to the dominance of the hydrostatic balance in the vertical momentum equation for large scale motions. However, is that analysis sufficient to understand what causes motion? To help answer that question, consider a density field that is decomposed into a constant, ρ_o, plus a deviation

$$\rho(\boldsymbol{x}, t) = \rho_o + \rho'(\boldsymbol{x}, t), \tag{27.38}$$

with a corresponding decomposition of the pressure field

$$p(\boldsymbol{x}, t) = p_0(z) + p'(\boldsymbol{x}, t) \qquad \text{with} \qquad \frac{\mathrm{d}p_0}{\mathrm{d}z} = -\rho_o\, g. \tag{27.39}$$

That is, the pressure is decomposed into a background *static pressure* field that is just a function of z, plus a deviation from the background pressure. In this case, the non-rotating vertical momentum equation takes the form

$$\rho\, \frac{\mathrm{D}w}{\mathrm{D}t} = -\frac{\partial p'}{\partial z} - \left[\frac{\mathrm{d}p_0}{\mathrm{d}z} + \rho_o\, g\right] = -\frac{\partial p'}{\partial z}. \tag{27.40}$$

We thus see that the exact hydrostatically balanced background pressure, $p_0(z)$, has no dynamical implications. Correspondingly, to garner a more relevant scaling for the hydrostatic balance it is appropriate to ask whether the dynamically active pressure, p', is approximately hydrostatic.

For flows with small aspect ratios, the vertical momentum equation remains approximately hydrostatic even when removing the dynamically inactive background pressure field. So our intuition about hydrostatic dominance holds unchanged even for the dynamical pressure. The formal justification of this approximation is nicely framed within the Boussinesq equations of Chapter 29 since the pressure force in these equations exposes just the dynamically active pressure. We thus postpone further discussion of hydrostatic scaling until Section 29.2.

27.2.5 Ocean dynamic topography

There are occasions in oceanography where it is useful to study the thickness of a layer bounded by isobars, here defined the thickness of fluid extending from the ocean free surface to a chosen pressure level in the ocean interior (see Figure 27.2)

$$D(p) = \eta - z(p). \tag{27.41}$$

Assuming a hydrostatic balance for each fluid column allows us to relate this expression to the vertical integral between two pressure surfaces of the specific volume, ρ^{-1}

$$D(p) = \int_{z(p)}^{\eta} \mathrm{d}z = g^{-1} \int_{p_a}^{p} \frac{\mathrm{d}p'}{\rho}, \tag{27.42}$$

where the second step used the hydrostatic balance and absorbed a minus sign by swapping integral limits. We refer to the thickness $D(p)$ as the *dynamic topography* with respect to a reference pressure, p. Note that $D(p)$ is sometimes also called the *steric sea level*.

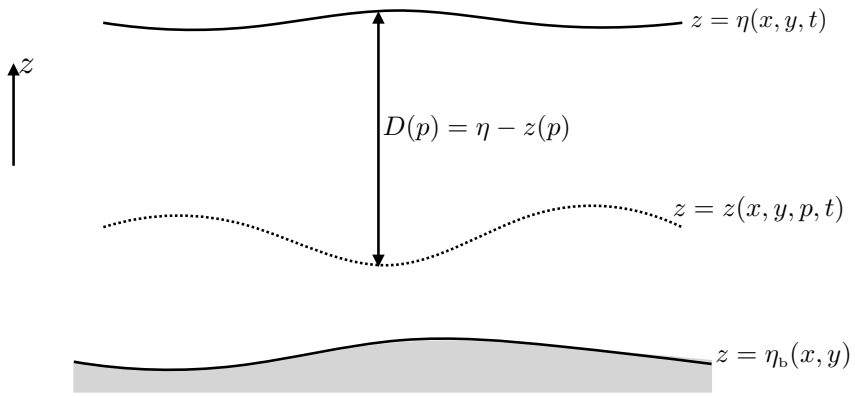

FIGURE 27.2: The ocean dynamic topography, $D(p) = \eta - z(p)$, is the thickness of a layer from the sea surface at $z = \eta(x, y, t)$ to the vertical position of a constant pressure surface, $z = z(x, y, p, t)$.

Evolution of the dynamic topography arises from changes in the pressure applied to the free surface as well as changes in the specific volume

$$g \frac{\partial D(p)}{\partial t} = -\frac{1}{\rho(\eta)} \frac{\partial p_a}{\partial t} + \int_{p_a}^{p} \frac{\partial \rho^{-1}}{\partial t} \, \mathrm{d}p. \tag{27.43}$$

Importantly, the time derivative here acts on the specific volume when computed on surfaces of constant pressure. If the depth, $z(p)$, of the constant pressure surface is static, then the evolution of layer thickness, $D(p)$, is identical to the sea surface, η. In general, there is no such static pressure level, thus making the time tendencies differ, though certain situations warrant this approximation.

27.2.6 Surfaces of atmospheric geopotential height and pressure

In Section 23.4.10 we computed the geopotential height within an exact hydrostatic and ideal gas atmosphere. We here apply those results to the case of approximate hydrostatic and ideal gas columns, making use of equation (23.82) for the difference in geopotential height between two constant pressure surfaces (isobars)

$$Z_2 - Z_1 = -(R^{\text{atm}} \langle T \rangle / g) \ln(p_2/p_1). \tag{27.44}$$

In this equation, $\langle T \rangle$ is the mean temperature within the column as computed according equation (23.80), and R^{atm} is the specific gas constant for air given by equation (23.51). The geopotential thickness is positive when the isobars have $p_2 < p_1$. This situation holds when level-2 sits at a higher altitude in the atmosphere than level-1, whereby the hydrostatic pressure decreases moving upward. Furthermore, the geopotential thickness is directly proportional to the column mean temperature so that a warmer column is thicker. This result is expected since for a given mass of air, a warmer column is less dense and so isobars are higher over warmer hydrostatic air columns than cooler columns. Correspondingly, when moving horizontally along a constant geopotential surface, we encounter higher pressure when moving into a region of warmer air. This situation is entirely analogous to that in Figure 27.4 when studying the horizontal pressure difference between two hydrostatic and equal mass columns of seawater.

27.2.7 Concerning vertical motion

Unbalanced vertical accelerations still exist in an approximate hydrostatic flow. Yet these vertical accelerations are not seen in the prognostic equations, since the vertical momentum

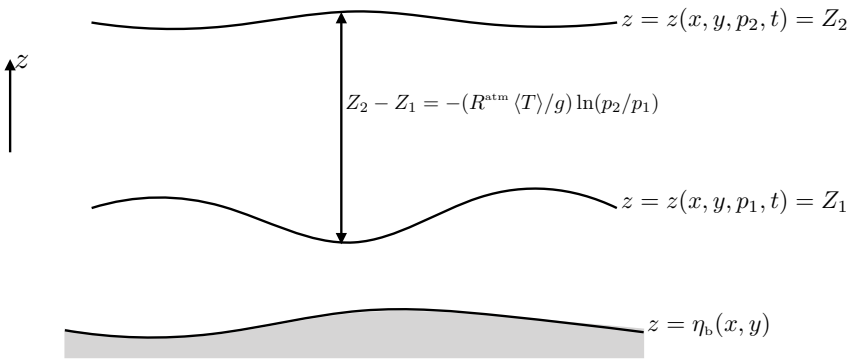

FIGURE 27.3: Thickness of the layer of an ideal gas atmosphere located between two constant pressure surfaces as given by equation (27.44): $Z_2 - Z_1 = -(R^{\text{atm}} \langle T \rangle / g) \ln(p_2/p_1)$. Evidently, when the flow is approximately hydrostatic, then $p_2 < p_1$ so that the thickness of the layer is positive. Also notice that the layer thickness increases when the column averaged temperature, $\langle T \rangle$, increases. Correspondingly, when moving horizontally along a constant geopotential surface (fixed z), we encounter higher pressure when moving into a region of warmer air and lower pressure when moving into a region of colder air.

equation reduces to a local hydrostatic balance. Hence, rather than compute vertical motion prognostically, vertical motion in an approximate hydrostatic flow must be diagnosed through constraints on the motion.

For example, an important constraint on the large-scale ocean circulation arises from vorticity and potential vorticity conservation, which are topics considered in Part VII of this book. Mass continuity discussed in Section 29.1.4 provides another constraint. In particular, horizontal velocity divergence in a non-divergent flow is balanced by vertical velocity convergence as per equation (29.17). The vertical pressure forces required to produce the vertical motion are those precisely needed to maintain volume continuity. In a hydrostatic flow, we do not directly compute these forces for the purpose of prognosing vertical accelerations. Rather, the vertical acceleration is inferred through kinematic constraints. The associated forces can be diagnosed given the velocity and the accelerations.

27.2.8 Further study

Section 2.7.4 in *Vallis* (2017) provides examples of scales over which the hydrostatic relation remains a useful approximation in geophysical fluid flows. Further discussions of dynamic topography are given in Appendix B.4 of *Griffies et al.* (2014) as well as in *Tomczak and Godfrey* (1994). This 8-minute video from Prof. Hogg offers an introduction to hydrostatic pressure.

27.3 Horizontal pressure gradients

In contrast to an exact hydrostatic fluid, where there is no motion, there are generally horizontal pressure gradients in an approximate hydrostatic fluid flow, and these horizontal gradients drive horizontal motion. Such horizontal pressure gradients can arise from horizontal differences in the mass density. We refer to such pressure gradients as *internal pressure gradients* since they arise from density gradients internal to the fluid, which are sometimes referred to as *baroclinic pressure gradients*. Horizontal pressure gradients can also arise from horizontal gradients in the total mass of a fluid column, with such pressure gradients referred to as *external pressure gradients*, which are sometimes referred to as *barotropic* pressure gradients.

In developing an understanding of the horizontal pressure accelerations in an approximate hydrostatic flow, it is useful to examine the variety of expressions for the pressure gradient,

which is the purpose of this section. We make use of these expressions studying case studies in Section 27.4.

27.3.1 Top down horizontal pressure gradient

In this section we examine the horizontal pressure gradient in an approximate hydrostatic flow, and do so by integrating from the top down. This approach complements that in Section 27.3.2, which starts from the bottom and integrates up.

External and internal contributions to the horizontal pressure gradient

Recall equation (27.26), which expresses the hydrostatic pressure at a point within the ocean

$$p(x,y,z,t) = p_{\text{a}}(x,y,t) + g \int_z^{\eta} \rho(x,y,z',t)\, \mathrm{d}z'. \tag{27.45}$$

In this equation, $p_{\text{a}} = p[x,y,z=\eta(x,y,t),t]$ is the pressure applied to the ocean free surface at $z=\eta(x,y,t)$ from any mass above the ocean, such as the atmosphere or cryosphere. In many idealized cases we assume the media above the ocean is massless, in which case $p_{\text{a}}=0$. Now introduce the globally referenced Archimedean buoyancy (see Chapter 30) as defined by

$$b = -g\,(\rho - \rho_{\circ})/\rho_{\circ}, \tag{27.46}$$

in which case the hydrostatic pressure is

$$p = -g\,\rho_{\circ}\, z + g\,\rho_{\circ}\,[\eta + p_{\text{a}}/(g\,\rho_{\circ})] - \rho_{\circ} \int_z^{\eta} b\, \mathrm{d}z'. \tag{27.47}$$

The first term is a background pressure that increases moving downward. However, this background pressure has no horizontal dependence and so it does not contribute to the horizontal pressure gradient. In contrast, the second and third terms have horizontal gradients and are thus sometimes referred to as the *dynamical pressure*. The second term arises from the free surface height plus the applied surface pressure. This term is uniformly felt throughtout the fluid column since it has no vertical dependence. The free surface term is the product of the large number, $g\,\rho_{\circ}$, times a small free surface undulation, η. The third term arises from buoyancy within the fluid computed relative to the constant background density, $\rho_{\circ}$, and this term is a function of vertical position. Furthermore, it is the vertical integral over a generally large depth range of the buoyancy. In this manner, the second and third terms can be of comparable magnitude.

The horizontal gradient of the hydrostatic pressure (27.47) is given by

$$\nabla_{\text{h}} p = \underbrace{\nabla_{\text{h}} p_{\text{a}} + g\,\rho(\eta)\,\nabla_{\text{h}}\eta}_{\text{external contribution}} - \underbrace{\rho_{\circ} \int_z^{\eta} \nabla_{\text{h}} b\, \mathrm{d}z'}_{\text{internal contribution}} = \underbrace{\nabla_{\text{h}} p_{\text{a}} + g\,\rho(\eta)\,\nabla_{\text{h}}\eta}_{\text{external contribution}} + \underbrace{g \int_z^{\eta} \nabla_{\text{h}}\rho\, \mathrm{d}z'}_{\text{internal contribution}}. \tag{27.48}$$

The internal contribution to the pressure gradient arises from horizontal gradients in Archimedean buoyancy that are integrated vertically over the region above the point of interest. The external contribution acts throughout the vertical fluid column since it is only a function of horizontal position and time. Every point within the fluid column instantly feels this term whenever there is a gradient in the applied surface pressure, the surface height, or the surface buoyancy, with $\rho_{\circ}[g - b(\eta)] = g\,\rho(\eta)$.

Mathematical comments regarding the external contribution

Observe that the external contributions to the horizontal pressure gradient in equation (27.48) are all functions of horizontal position and time, so there is no z dependence to hold fixed when computing $\nabla_{\!\mathsf{h}}$ on these terms. Even so, we sometimes retain the $\nabla_{\!\mathsf{h}}$ notation to align with that required to denote a horizontal gradient operator acting on three dimensional fields, such as buoyancy, $b(x, y, z, t)$, and density, $\rho(x, y, z, t)$).

To exemplify this comment, observe that the external contribution can be written as the horizontal pressure gradient evaluated at the ocean surface[4]

$$(\nabla_{\!\mathsf{h}} p)_{z=\eta} = \nabla_{\!\mathsf{h}} p_{\mathsf{a}} + g\, \rho(\eta)\, \nabla_{\!\mathsf{h}} \eta. \tag{27.49}$$

Hence, the pressure gradient in equation (27.48) can be written in the succinct form

$$\nabla_{\!\mathsf{h}} p = (\nabla_{\!\mathsf{h}} p)_{z=\eta} - \rho_{\mathsf{o}} \int_z^\eta \nabla_{\!\mathsf{h}} b \, \mathrm{d}z' = (\nabla_{\!\mathsf{h}} p)_{z=\eta} + g \int_z^\eta \nabla_{\!\mathsf{h}} \rho \, \mathrm{d}z'. \tag{27.50}$$

Observe that the component of the horizontal pressure gradient in a direction tangent to the free surface arises just from the $\nabla_{\!\mathsf{h}} p_{\mathsf{a}}$ term.

Mathematically, equation (27.49) decomposes the horizontal pressure gradient into the horizontal gradient of pressure along the curved free surface (the $\nabla_{\!\mathsf{h}} p_{\mathsf{a}}$ term), plus a term that accounts for curvature of the free surface (the $g\, \rho(\eta)\, \nabla_{\!\mathsf{h}} \eta$ term). As seen in Section 65.2, this decompostion of the horizontal pressure gradient, made throughout the fluid column, is a key step needed to formulate the equations of motion using generalized vertical coordinates.

27.3.2 Bottom up horizontal pressure gradient

It is sometimes useful to work with the bottom pressure and bottom topography, rather than the free surface height. For this purpose we invert the formulation from Section 27.3.1 by introducing the bottom pressure

$$p_{\mathsf{b}} = p_{\mathsf{a}} + g \int_{\eta_{\mathsf{b}}}^\eta \rho \, \mathrm{d}z, \tag{27.51}$$

in which case

$$\begin{aligned} p &= p_{\mathsf{a}} + g \int_z^\eta \rho \, \mathrm{d}z && \text{(27.52a)} \\ &= p_{\mathsf{a}} + g \int_{\eta_{\mathsf{b}}}^\eta \rho \, \mathrm{d}z - g \int_{\eta_{\mathsf{b}}}^z \rho \, \mathrm{d}z && \text{(27.52b)} \\ &= p_{\mathsf{b}} - g \int_{\eta_{\mathsf{b}}}^z (\rho - \rho_{\mathsf{o}} + \rho_{\mathsf{o}}) \, \mathrm{d}z && \text{(27.52c)} \\ &= p_{\mathsf{b}} - g\, \rho_{\mathsf{o}}\, (z - \eta_{\mathsf{b}}) + \rho_{\mathsf{o}} \int_{\eta_{\mathsf{b}}}^z b \, \mathrm{d}z', && \text{(27.52d)} \end{aligned}$$

so that the corresponding expression for the horizontal hydrostatic pressure gradient is

$$\nabla_{\!\mathsf{h}} p = \underbrace{\nabla_{\!\mathsf{h}} p_{\mathsf{b}} + g\, \rho(\eta_{\mathsf{b}})\, \nabla_{\!\mathsf{h}} \eta_{\mathsf{b}}}_{\text{external contribution}} + \underbrace{\rho_{\mathsf{o}} \int_{\eta_{\mathsf{b}}}^z \nabla_{\!\mathsf{h}} b \, \mathrm{d}z'}_{\text{internal contribution}} = \underbrace{\nabla_{\!\mathsf{h}} p_{\mathsf{b}} + g\, \rho(\eta_{\mathsf{b}})\, \nabla_{\!\mathsf{h}} \eta_{\mathsf{b}}}_{\text{external contribution}} - \underbrace{g \int_{\eta_{\mathsf{b}}}^z \nabla_{\!\mathsf{h}} \rho \, \mathrm{d}z'}_{\text{internal contribution}}. \tag{27.53}$$

[4]Namely, all terms in equation (27.49) are a function just of the horizontal position computed along the $z = \eta(x, y, t)$ ocean surface, so that we could write ∇ rather than $\nabla_{\!\mathsf{h}}$. Yet on the left hand side it is important to write $\nabla_{\!\mathsf{h}}$, since we are evaluating the horizontal pressure gradient at the surface.

The horizontal pressure gradient at the bottom

Just as for the pressure gradient expression (27.48), observe that equation (27.53) decomposes the horizontal pressure gradient into an external and internal contribution. The internal contribution arises from gradients in the buoyancy as integrated below the depth of interest. The external contributions arise from gradients in the bottom pressure, which measures the mass per area of fluid within the column, plus gradients in the bottom topography as weighted by the bottom buoyancy (27.59). The external contribution can be written as the horizontal pressure gradient evaluated at the ocean bottom

$$(\nabla_{\mathsf{h}} p)_{z=\eta_{\mathsf{b}}} = \nabla_{\mathsf{h}} p_{\mathsf{b}} + g\,\rho(\eta_{\mathsf{b}})\,\nabla_{\mathsf{h}}\eta_{\mathsf{b}}, \tag{27.54}$$

which accords with equation (27.49) for the horizontal pressure gradient evaluated at the ocean surface. Evidently, the horizontal pressure gradient at the ocean bottom equals to the gradient of the bottom pressure, plus a term that accounts for the bottom slope. Furthermore, the component of the horizontal pressure gradient in a direction tangent to the ocean bottom arises just from the $\nabla_{\mathsf{h}} p_{\mathsf{b}}$ term. Finally, we make use of expression (27.54) to produce a more succinct form of the horizontal pressure gradient (27.53)

$$\nabla_{\mathsf{h}} p = (\nabla_{\mathsf{h}} p)_{z=\eta_{\mathsf{b}}} + \rho_{\circ} \int_{\eta_{\mathsf{b}}}^{z} \nabla_{\mathsf{h}} b \, \mathrm{d}z' = (\nabla_{\mathsf{h}} p)_{z=\eta_{\mathsf{b}}} - g \int_{\eta_{\mathsf{b}}}^{z} \nabla_{\mathsf{h}} \rho \, \mathrm{d}z'. \tag{27.55}$$

Further decomposing the bottom pressure contribution

The bottom pressure contribution to equations (27.53) and (27.55) is generally dominated by gradients in the bottom topography. These gradients are static and so it can be useful to isolate the bottom topography by taking the horizontal gradient of equation (27.51) to find

$$\nabla_{\mathsf{h}} p_{\mathsf{b}} = \nabla p_{\mathsf{a}} + g\,\rho(\eta)\,\nabla\eta - g\,\rho(\eta_{\mathsf{b}})\,\nabla\eta_{\mathsf{b}} + g \int_{\eta_{\mathsf{b}}}^{\eta} \nabla_{\mathsf{h}}\rho \, \mathrm{d}z \tag{27.56a}$$

$$= \left[\nabla p_{\mathsf{a}} + g\,\rho(\eta)\,\nabla\eta - b(\eta_{\mathsf{b}})\,\nabla\eta_{\mathsf{b}} + g \int_{\eta_{\mathsf{b}}}^{\eta} \nabla_{\mathsf{h}}\rho \, \mathrm{d}z\right] - g\,\rho_{\circ}\,\nabla\eta_{\mathsf{b}}, \tag{27.56b}$$

in which case we write the bottom pressure gradient as

$$\nabla_{\mathsf{h}} p_{\mathsf{b}} = \nabla_{\mathsf{h}} p'_{\mathsf{b}} - g\,\rho_{\circ}\,\nabla_{\mathsf{h}}\eta_{\mathsf{b}}, \tag{27.57}$$

so that the horizontal pressure gradient takes the form

$$\nabla_{\mathsf{h}} p = \underbrace{\nabla_{\mathsf{h}} p'_{\mathsf{b}} - \rho_{\circ}\, b(\eta_{\mathsf{b}})\,\nabla_{\mathsf{h}}\eta_{\mathsf{b}}}_{\text{external contribution}} + \underbrace{\rho_{\circ} \int_{\eta_{\mathsf{b}}}^{z} \nabla_{\mathsf{h}} b \, \mathrm{d}z'}_{\text{internal contribution}}, \tag{27.58}$$

where we introduced the bottom buoyancy via

$$\rho_{\circ}\,[g - b(\eta_{\mathsf{b}})]\,\nabla\eta_{\mathsf{b}} = g\,\rho(\eta_{\mathsf{b}})\,\nabla\eta_{\mathsf{b}}. \tag{27.59}$$

27.4 Balancing internal and external pressure gradients

In this section we work through a set of case studies by considering a given density configuration that sets up an internal pressure gradient, and then seek a sea level configuration that establishes an external pressure gradient to balance the internal pressure gradient, thus leading to a net zero horizontal pressure gradient. We do not seek reasons for why the internal and external pressure

gradients balance, which require more than the hydrostatics used in this chapter. Rather, we consider the balanced state as a useful means to further an understanding of hydrostatic pressure. We are also motivated by noting that many ocean flows maintain a partial balance between internal and external pressure gradients along certain surfaces, which motivates the notion of a *level of no motion*, thus making the balanced state a useful starting point for examining the more complete dynamics of a particular flow.

As the starting point for these considerations, recall the expressions for the horizontal pressure gradient along the ocean surface (equation (27.49)) and ocean bottom (equation (27.54)). Here we list these equalities again, along with two more expressions that follow from evaluating equation (27.50) at the ocean bottom and equation (27.55) at the ocean surface

$$(\nabla_h p)_{z=\eta} = \nabla_h p_a + g\,\rho(\eta)\,\nabla_h \eta = (\nabla_h p)_{z=\eta_b} - g \int_{\eta_b}^{\eta} \nabla_h \rho \, dz \tag{27.60a}$$

$$(\nabla_h p)_{z=\eta_b} = \nabla_h p_b + g\,\rho(\eta_b)\,\nabla_h \eta_b = (\nabla_h p)_{z=\eta} + g \int_{\eta_b}^{\eta} \nabla_h \rho \, dz. \tag{27.60b}$$

27.4.1 Horizontal hydrostatic pressure gradient in a mass conserving fluid

As a warm-up to the continuous cases to follow, we work through an example emblematic of how one determines the sign for horizontal pressure gradients in an approximate hydrostatic balance. The example is posed for equal mass columns of mass conserving fluid in a bounded fluid layer, such as the ocean, but these considerations hold for the atmosphere where the upper boundary is the top of the atmosphere (i.e., effectively unbounded). We assume the flat bottom of the layer has a constant pressure so that the horizontal pressure gradient vanishes along the bottom, thus offering a particular example of the level of no motion.

Two columns with equal mass yet different densities

Consider two adjacent columns of seawater with equal mass but with distinct density; assume the density in each column is constant throughout the respective columns; and assume the atmospheric pressure is equal above the two water columns. Figure 27.4 offers a schematic, where we make the additional assumption that the two columns sit on a flat bottom. We can imagine setting up this configuration by starting with uniform density water, then warming the water in column B more than column A while maintaining constant mass in the two columns. This process sets up a horizontal density gradient with an associated horizontal gradient in the hydrostatic pressure. Furthermore, the less dense water in column B occupies more volume so that its free surface sits higher

$$\rho_B < \rho_A \Longrightarrow \eta_B > \eta_A. \tag{27.61}$$

What is the sign of the horizontal hydrostatic pressure gradient? As we show in the following, column B (the low density column) has larger hydrostatic pressure than column A (the high density column) for every point in the column, except at the bottom where the two bottom pressures are identical since the two columns have equal mass. The bottom thus represents a level of no motion.

Computing pressure starting from the equal bottom pressures

Since the two columns have equal mass and equal cross-sectional area, the hydrostatic pressures (weight per unit area) at the bottom of the two columns are equal and given by

$$p_{bot} = g\,\rho_A\,(\eta_A - \eta_b) = g\,\rho_B\,(\eta_B - \eta_b), \tag{27.62}$$

where $z = \eta_b(x, y)$ is the vertical position at the bottom, $z = \eta_A(x, y, t)$ is the top of column A, and $z = \eta_B(x, y, t)$ is the top of column B. Since the bottom pressures are identical, there is no horizontal pressure gradient at the bottom so that all pressure gradients exist above the bottom.

The hydrostatic pressure at an arbitrary position within column A is given by

$$p_A(z) = g\,\rho_A\,(\eta_A - z) = p_{bot} - g\,\rho_A\,(-\eta_b + z), \tag{27.63}$$

where we only expose here the z dependence to reduce clutter. The second equality arose by substituting the bottom pressure from equation (27.62) to eliminate the surface height η_A. Doing so is useful since we know that $\eta_A \neq \eta_B$, and yet the bottom pressure is the same for the two columns. The same approach for pressure in column B yields

$$p_B(z) = g\,\rho_B\,(\eta_B - z) = p_{bot} - g\,\rho_B\,(-\eta_b + z). \tag{27.64}$$

We can now take the difference between the two hydrostatic pressures to find

$$p_B(z) - p_A(z) = g\,(-\eta_b + z)\,(\rho_A - \rho_B) > 0. \tag{27.65}$$

Since $\rho_A > \rho_B$ and $z \geq \eta_b$ we see that at any point above the bottom, the hydrostatic pressure in column B (the lighter column) is greater than that in column A (the denser column). This horizontal difference in the hydrostatic pressure renders a force pointing from column B to column A. Vertically integrating this pressure difference over the thickness of column A leads to the net force per horizontal length

$$F_{\text{pressure B to A}} = \int_{\eta_b}^{\eta_A} [p_B(z) - p_A(z)]\,dz = (g/2)\,(\rho_A - \rho_B)\,(\eta_A - \eta_b)^2 > 0. \tag{27.66}$$

Inferring pressure gradients starting from the top

Another way to understand why the pressure force points from column B to column A is to note that at the top of both columns the pressures are the same (and equal to the uniform atmospheric pressure). However, since column B sits higher than column A, as we move down from $z = \eta_B$ the pressure increases in column B immediately, whereas the pressure in column A remains at the atmospheric pressure until entering the water column at $z = \eta_A < \eta_B$. So it is clear that the pressure in column B is greater than A starting from the surface and moving down. Since the two bottom pressures are equal, then we infer the pressure isolines as drawn in Figure 27.4.

27.4.2 Inverse barometer sea level

A zero horizontal pressure gradient at the ocean surface, in the presence of an applied surface pressure, is known as an *inverse barometer sea level*, whereby from equation (27.60a) we have

$$(\nabla_h p)_{z=\eta} = \nabla_h p_a + g\,\rho(\eta)\,\nabla_h \eta = 0, \tag{27.67}$$

which leads to

$$\nabla_h \cdot [g\,\rho(\eta)\,\nabla_h \eta] = -\nabla_h^2 p_a. \tag{27.68}$$

Assuming $\rho(\eta)$ is roughly constant, then the inverse barometer sea level is depressed under an atmospheric high pressure (where $\nabla_h^2 p_a < 0$) and it rises under an atmospheric low (where $\nabla_h^2 p_a > 0$), with Figure 27.5 providing a schematic. We again encounter the inverse barometer when studying shallow water theory in Section 35.2.2.

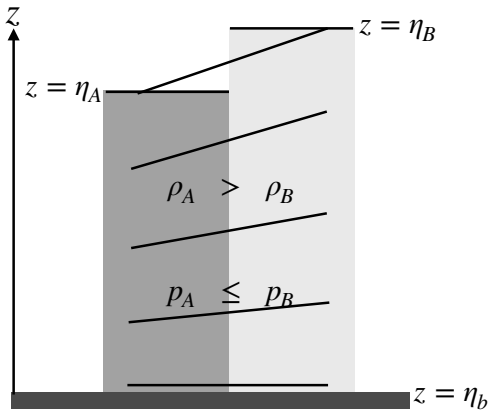

FIGURE 27.4: Two seawater columns on a flat bottom with equal mass but different densities with $\rho_A > \rho_B$. We assume the atmosphere above the columns has the same pressure over both columns, thus offering zero horizontal pressure force. Furthermore, the horizontal cross-sectional area of the two columns are the same so that the less dense water in column B has more volume and thus a greater thickness: $\eta_B > \eta_A$. Since the column masses are the same, the hydrostatic pressures (weight per horizontal area) at the bottom of the two columns are equal: $p_A(z = \eta_b) = p_B(z = \eta_b) = p_{bot}$. In oceanographic parlance, the bottom offers a "level of no motion" from which to reference the pressure field. At any position z above the bottom, equation (27.65) shows that the hydrostatic pressure in column B is greater than A: $p_B(z) - p_A(z) = g\,(-\eta_b + z)\,(\rho_A - \rho_B) > 0$. The horizontal gradient in hydrostatic pressure thus points from column B towards column A. The red lines show lines of constant pressure (isobars), which are horizontal next to the bottom but which slope upward to the right moving towards the surface. This configuration provides salient points about hydrostatic pressure relevant for the slightly more complex reduced gravity example in Figure 35.5. Also, it is useful to compare this schematic to Figure 31.4, which discusses the depth dependence of the horizontal gradient in hydrostatic pressure as per $\partial(\nabla_h p)/\partial z = -g\,\nabla_h \rho$.

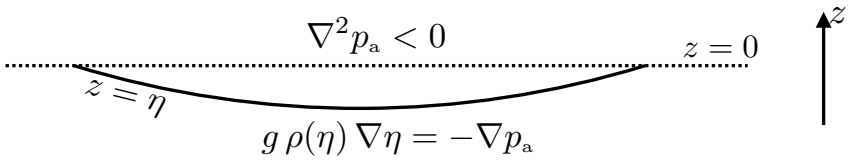

FIGURE 27.5: Illustrating the inverse barometer response of sea level under an atmospheric high pressure where $\nabla^2 p_a < 0$. The inverse barometer sea level is depressed according to equation (27.68).

27.4.3 Balanced pressure gradients above a level of no motion

Consider the case in which there is zero horizontal pressure gradient along a constant geopotential surface

$$z = \eta_{nm}. \tag{27.69}$$

We might find this configuration to be a relevant approximation of the sluggish flows in the deep ocean where flow can be much weaker than the upper ocean. Along this level there is zero horizontal geostrophic flow.[5] What is required from the hydrostatic pressure field to realize this level of no motion? Based on the expressions (27.50) and (27.55), the pressure field must satisfy

$$0 = (\nabla_h p)_{z=\eta_{nm}} = (\nabla_h p)_{z=\eta} + g \int_{\eta_{nm}}^{\eta} \nabla_h \rho \, dz = (\nabla_h p)_{z=\eta_b} - g \int_{\eta_b}^{\eta_{nm}} \nabla_h \rho \, dz. \tag{27.70}$$

[5] As studied in Chapter 31, geostrophic flow arises from a balance between the Coriolis acceleration and the horizontal pressure gradient acceleration. Hence, if there is a depth along which there is zero horizontal pressure gradient, then there is a corresponding zero horizontal geostrophic flow.

Each of these equations expresses a compensation or balance between external and internal contributions to the pressure gradient so that

$$(\nabla_h p)_{z=\eta} = -g \int_{\eta_{nm}}^{\eta} \nabla_h \rho \, dz \tag{27.71a}$$

$$(\nabla_h p)_{z=\eta_b} = g \int_{\eta_b}^{\eta_{nm}} \nabla_h \rho \, dz. \tag{27.71b}$$

In Figure 27.6 we illustrate the compensation (27.71a) that results if an external pressure gradient from a sloping sea level exactly balances the internal pressure gradient from horizontal density gradients so that

$$\rho(\eta) \, \nabla_h \eta = - \int_{\eta_{nm}}^{\eta} \nabla_h \rho \, dz. \tag{27.72}$$

This equation allows us to estimate the scale for the free surface slope by writing

$$\rho_o \, |\nabla_h \eta| \sim H \, |\nabla_h \rho| = (H \, \rho_o / g) \, |S \, N^2|, \tag{27.73}$$

where S is the slope of the density surfaces relative to the horizontal, $H = \eta - \eta_{nm}$ is the depth of the fluid, and N^2 is the squared buoyancy frequency. Assuming $|S| \approx 10^{-3}$, $H \approx 3 \times 10^3$ m, and $N^2 \approx 10^{-6}$ s^{-2} leads to the free surface slope

$$|\nabla_h \eta| \approx 10^{-7}. \tag{27.74}$$

Evidently, the free surface slope is much smaller (roughly 10^{-3} times smaller) than that of the interior density surfaces. We see this relative slopes again when studying the reduced gravity model in Section 35.3.

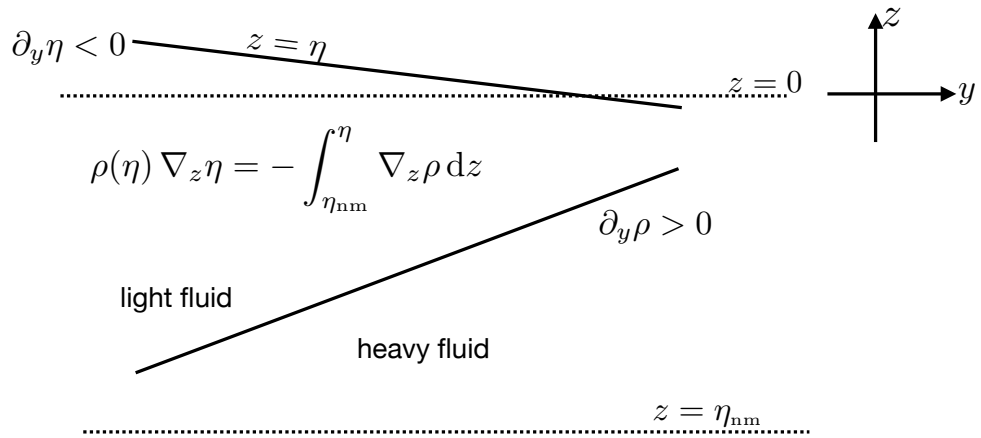

FIGURE 27.6: Illustrating the balance of internal and external horizontal pressure gradients that is needed to realize a level of zero horizontal pressure gradient at $z = \eta_{nm}$ (i.e., a *level of no motion*), and thus a level with zero geostrophic flow. The balance shown here is taken from equation (27.71a) with a zero applied pressure gradient, $\nabla p_a = 0$. Hence, compensation is between an external pressure gradient from the sea level that exactly balances the internal pressure gradient from horizontal density gradients. The relative slope of the free surface is exagerated here, with actual slopes scaling as in equation (27.74), which are generally much smaller (roughly 10^{-3} smaller) than the slope of density surfaces.

27.4.4 Balanced pressure gradients above a sloping side boundary

We now extend the example from Section 27.4.3 to study the case of compensated internal and external pressure gradients in the presence of a sloping coastal side boundary. Just like over a

flat bottom, realizing this compensation requires a sea level gradient to produce the external pressure gradient to balance the internal pressure gradient caused by the density field. As we find here, typical coastal density gradients, with lighter waters near the coast, leads to sea level rise near the coast and with this rise referred to as *steric setup*. The analysis is motivated by the studies of *Helland-Hansen* (1934), *Csanady* (1979) and *Bingham and Hughes* (2012). Note that to pursue an analytical calculation requires a number of common approximations. These approximations are often not realized in realistic flows. However, they lead to expressions whose relevance can be readily tested. Furthermore, they offer a useful starting point for more detailed analyses.

Idealized coastal density and topography

To enable an analytical calculation, consider a static density given by

$$\rho(y,z) = \rho_o + \rho'(y,z) \quad \text{with } |\rho'| \ll \rho_o, \tag{27.75}$$

and a bottom topography that is a monotonic function of the off-shore distance,

$$z = \eta_b(y) \quad \text{with } \partial_y \eta_b < 0. \tag{27.76}$$

An example coastal density configuration is depicted in Figure 27.7, whereby the topography deepens off-shore, $\partial_y \eta_b < 0$, and with lighter water next to the coast as might occur from freshening and warming in the shallow coastal waters. Along-shore gradients (in the $\hat{\boldsymbol{x}}$-direction) are typically far weaker than across shore gradients (in the $\hat{\boldsymbol{y}}$-direction). This observation then motivates assuming all fields to have zero ∂_x.

Depth of no motion intersecting a bottom of no motion

Assume a depth of no-motion at $z = \eta_{nm}$ that intersects the sloping coastal bottom at $z = \eta_b(y_{nm})$ as in Figure 27.7. Furthermore, assume there is no horizontal pressure gradient all along the bottom, from $y = y_{nm}$ to the coastline at $y = 0$, so that the bottom becomes a sloped surface of no geostrophic motion. Although there are many cases where geostrophic currents are nonzero next to sloping bottoms, it is useful to consider the no motion case as a baseline. Doing so facilitates diagnostic calculations reflective of the approach used for the open ocean away from coasts and thus forms a baseline dynamical balance. Equation (27.60b) then says that at each position along the bottom, from $y = y_{nm}$ to $y = 0$, the horizontal pressure at the sea surface balances the depth integrated horizontal density gradient

$$(\partial_y p)_{z=\eta} = -g \int_{\eta_b}^{\eta} \partial_y \rho \, dz. \tag{27.77}$$

Integrating to find the steric setup along a coast

To derive an approximation for the sea level at the coast relative to the interior, assume the surface density is a constant ($\rho(\eta) \approx \rho_o$), and the atmospheric pressure is constant ($\nabla p_a = 0$), which, with equation (27.60a), then renders

$$\partial_y \eta = -\frac{1}{\rho_o} \int_{\eta_b}^{\eta} \partial_y \rho \, dz. \tag{27.78}$$

This equation says that if density increases away from the coast, then sea level rises toward the coast, which, as already noted, we refer to as a *steric setup* of coastal sea level.

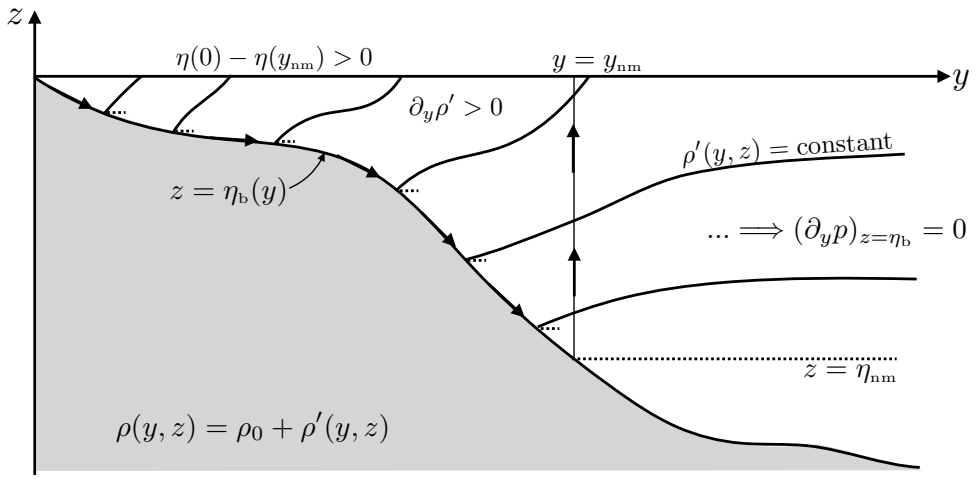

FIGURE 27.7: Density field in a region next to a coastal shelf and slope, illustrating the typical case with lighter water next to the coast, such as from freshening and warming in the shallow coastal waters. Along-shore density gradients (in the $\hat{\boldsymbol{x}}$-direction) are typically far weaker than across-shore gradients (in the $\hat{\boldsymbol{y}}$-direction), and they are here ignored. If there are no geostrophic currents at the bottom, so that $(\nabla_{\rm h} p)_{z=\eta_{\rm b}} = 0$ (indicated by the short horizontal dotted lines next to the bottom), then there is an exact compensation of external and internal pressure gradients as given in Section 27.4.3 and as illustrated by Figure 27.6. This pressure compensation is arrived at by sea level rising next to the coast. The arrows along the bottom and the vertical line at $y = y_{\rm nm}$ refer to the integration sense for the steric calculations of $\eta(y = 0)$ (equation (27.83)) and $\eta(y = y_{\rm nm})$ (equation (27.82)). Although many continental slope regions have nonzero flow at the bottom, the calculation of coastal steric setup assuming $(\nabla_{\rm h} p)_{z=\eta_{\rm b}} = 0$ offers a useful starting point for interpreting coastal sea level patterns.

With one further approximation, equation (27.78) can be integrated to provide an explicit expression for the steric sea level at the coast, relative to sea level away from the coast. For that purpose, set the upper limit on the right hand side integral to 0, thus yielding

$$\partial_y \eta = -\frac{1}{\rho_o} \int_{\eta_{\rm b}}^{0} \partial_y \rho \, \mathrm{d}z. \tag{27.79}$$

Now integrate this equation from the coast at $y = 0$ to the off-shore position at $y = y_{\rm nm}$, so that

$$\eta(0) - \eta(y_{\rm nm}) = \frac{1}{\rho_o} \int_0^{y_{\rm nm}} \left[\int_{\eta_{\rm b}(y)}^{0} \partial_y \rho(y,z) \, \mathrm{d}z \right] \mathrm{d}y. \tag{27.80}$$

Pulling the ∂_y derivative across the vertical integral, and using Leibniz's rule (Section 20.2.4), leads to

$$\eta(0) - \eta(y_{\rm nm}) = \frac{1}{\rho_o} \int_0^{y_{\rm nm}} \left[\frac{\partial}{\partial y} \int_{\eta_{\rm b}(y)}^{0} \rho(y,z) \, \mathrm{d}z + \rho(y, z = \eta_{\rm b}) \, \partial_y \eta_{\rm b} \right] \mathrm{d}y. \tag{27.81}$$

Since $\eta_{\rm b}(y = 0) = 0$ (sea level vanishes at the shoreline), the first integral on the right hand side is given by

$$\frac{1}{\rho_o} \int_0^{y_{\rm nm}} \left[\frac{\partial}{\partial y} \int_{\eta_{\rm b}(y)}^{0} \rho(y,z) \, \mathrm{d}z \right] \mathrm{d}y = \frac{1}{\rho_o} \int_{\eta_{\rm b}(y_{\rm nm})}^{0} \rho(y_{\rm nm}, z) \, \mathrm{d}z, \tag{27.82}$$

which is an integral that extends from the bottom at $\eta(y = y_{\rm nm})$ up to $z = 0$, as depicted in Figure 27.7.

The second integral in equation (27.81) is given by

$$\frac{1}{\rho_o} \int_0^{y_{\rm nm}} \rho[y, z = \eta_{\rm b}(y)] \, \partial_y \eta_{\rm b} \, \mathrm{d}y = -\frac{1}{\rho_o} \int_0^{\eta_{\rm b}(y_{\rm nm})} \rho_{\rm b} \, \mathrm{d}\eta_{\rm b}, \tag{27.83}$$

where we set

$$\mathrm{d}\eta_{\mathrm{b}} = -(\partial_y \eta_{\mathrm{b}})\, \mathrm{d}y, \tag{27.84}$$

which follows since η_{b} is a monotonic function of y, and with the minus sign accounting for $\partial_y \eta_{\mathrm{b}} < 0$ as assumed for Figure 27.7. The left hand integral in equation (27.83) is a y-integral of the bottom density times the topographic slope, integrated from the coastal position at $y = 0$ to the off-shore position at $y = y_{\mathrm{nm}}$. The right hand side is the bottom density, $\rho_{\mathrm{b}} = \rho[y, z = \eta_{\mathrm{b}}(y)]$, integrated along the bottom from $\eta_{\mathrm{b}}(0) = 0$ to $\eta_{\mathrm{b}}(y = y_{\mathrm{nm}})$, as depicted by the arrows along the bottom in Figure 27.7.[6]

Bringing terms together allows us to write equation (27.81) as

$$\eta(0) - \eta(y_{\mathrm{nm}}) = -\frac{1}{\rho_{\mathrm{o}}} \int_{\eta_{\mathrm{b}}(y_{\mathrm{nm}})}^{0} \rho_{\mathrm{b}}\, \mathrm{d}\eta_{\mathrm{b}} + \frac{1}{\rho_{\mathrm{o}}} \int_{\eta_{\mathrm{b}}(y_{\mathrm{nm}})}^{0} \rho(y_{\mathrm{nm}}, z)\, \mathrm{d}z. \tag{27.85}$$

As noted earlier, if the density is lighter near to the coast then $\eta(0) - \eta(y_{\mathrm{nm}}) > 0$. The various assumptions needed to derive equation (27.85) render this expression an approximation for more realistic sea levels near coasts. Even so, it offers a relatively simple expression that only requires density information, and as such it is a useful starting point for interpreting sea level patterns next to coasts and on continental shelves. In particular, the direct contributions to sea level from winds are missing from this calculation, so that deviations from steric setup typically signal contributions from winds.

27.5 Homogeneous fluid in a rotating tank

As an application of the ideas developed in this chapter and in earlier chapters, we develop the equations for a homogeneous fluid in a rotating tank such as occurs in laboratory studies of rotating fluids. One point of departure from planetary applications concerns the choice of vertical coordinate. Recall we introduced geopotential surfaces in Section 13.10.4, on which the effective gravitational force (sum of central gravity plus planetary centrifugal) is constant. Correspondingly, we introduced geopotential coordinates in Section 13.11.3 to simplify the equations for planetary fluid dynamics. In contrast, for the rotating tank we do not make use of geopotential coordinates. Instead, we expose the centrifugal acceleration (due to rotation of the tank), which allows for a clear display of the parabolic shape for the free surface when the fluid is in rigid-body motion.

27.5.1 What about the planet's rotation?

Do we need to worry about the planet's rotation? To answer this question, consider a typical record player with an angular speed of 45 revolutions per minute

$$\Omega_{\mathrm{record}} = 0.75 \text{ s}^{-1}. \tag{27.86}$$

This angular speed is roughly 10^4 times faster than the earth's angular speed of 7.29×10^{-5} s^{-1} (equation (13.1)). For a tank rotating at a rate on the same order as a record player, we are justified ignoring the rotating earth in comparison to the rotating tank. That is, we can safely ignore planetary Coriolis and planetary centrifugal accelerations, allowing us to instead focus on the non-inertial accelerations arising just from the tank rotating on a laboratory turntable.

[6] Note that *Csanady* (1979) and *Bingham and Hughes* (2012) refer to the integral (27.83) as a line integral computed along the bottom. However, it is not the sort of line integral considered in Section 2.4. The reason is that the integrand, ρ_{b}, is weighted by the bottom increment, $\mathrm{d}\eta_{\mathrm{b}} = -(\partial_y \eta_{\mathrm{b}})\, \mathrm{d}y$, rather than the arc-length along the bottom, $\mathrm{d}s = \mathrm{d}y \sqrt{1 + (\partial_y \eta_{\mathrm{b}})^2}$.

27.5.2 Formulating the equations of motion

In an inertial reference frame, a fluid element feels the gravitational force, pressure force, and friction, thus leading to the Cartesian coordinate equations of motion

$$\frac{\mathrm{D}u_{\mathrm{I}}}{\mathrm{D}t} = -\frac{1}{\rho}\frac{\partial p}{\partial x} + F^x \tag{27.87}$$

$$\frac{\mathrm{D}v_{\mathrm{I}}}{\mathrm{D}t} = -\frac{1}{\rho}\frac{\partial p}{\partial y} + F^y \tag{27.88}$$

$$\frac{\mathrm{D}w_{\mathrm{I}}}{\mathrm{D}t} = -\frac{1}{\rho}\frac{\partial p}{\partial z} - g + F^z, \tag{27.89}$$

where $\boldsymbol{v}_{\mathrm{I}}$ is the inertial velocity, ρ is the constant density, and we orient the coordinates so that the z-axis extends vertically upward from the center of the tank and parallel to the gravity acceleration. Correspondingly, the rotation vector for the tank is

$$\boldsymbol{\Omega} = \Omega\,\hat{\boldsymbol{z}} = (f/2)\,\hat{\boldsymbol{z}}. \tag{27.90}$$

To derive the rotating frame equations, return to some of the kinematics from Chapter 13, in which we write the position of a fluid particle as

$$\boldsymbol{X}(t) = X\,\hat{\boldsymbol{x}} + Y\,\hat{\boldsymbol{y}} + Z\,\hat{\boldsymbol{z}}. \tag{27.91}$$

We assume that the Cartesian unit vectors are fixed in the rotating frame and thus move as a rigid-body with the rotating tank. The inertial velocity is thus given by

$$\frac{\mathrm{d}\boldsymbol{X}}{\mathrm{d}t} = \left[\frac{\mathrm{d}X}{\mathrm{d}t}\right]\hat{\boldsymbol{x}} + \left[\frac{\mathrm{d}Y}{\mathrm{d}t}\right]\hat{\boldsymbol{y}} + \left[\frac{\mathrm{d}Z}{\mathrm{d}t}\right]\hat{\boldsymbol{z}} + \boldsymbol{\Omega}\times\boldsymbol{X}. \tag{27.92}$$

Correspondingly, the acceleration is given by

$$\frac{\mathrm{d}^2\boldsymbol{X}}{\mathrm{d}t^2} = \left[\frac{\mathrm{d}^2X}{\mathrm{d}t^2}\right]\hat{\boldsymbol{x}} + \left[\frac{\mathrm{d}^2Y}{\mathrm{d}t^2}\right]\hat{\boldsymbol{y}} + \left[\frac{\mathrm{d}^2Z}{\mathrm{d}t^2}\right]\hat{\boldsymbol{z}} + 2\,\boldsymbol{\Omega}\times\boldsymbol{v} + \boldsymbol{\Omega}\times(\boldsymbol{\Omega}\times\boldsymbol{X}), \tag{27.93}$$

where we defined the rotating frame Cartesian velocity as

$$\boldsymbol{v} = \left[\frac{\mathrm{d}X}{\mathrm{d}t}\right]\hat{\boldsymbol{x}} + \left[\frac{\mathrm{d}Y}{\mathrm{d}t}\right]\hat{\boldsymbol{y}} + \left[\frac{\mathrm{d}Z}{\mathrm{d}t}\right]\hat{\boldsymbol{z}}. \tag{27.94}$$

Setting the inertial acceleration equal to the inertial force per mass leads to the equations of motion in the rotating frame

$$\frac{\mathrm{D}u}{\mathrm{D}t} - 2\,\Omega\,v = -\frac{1}{\rho}\frac{\partial p}{\partial x} + \Omega^2\,x + F^x \tag{27.95}$$

$$\frac{\mathrm{D}v}{\mathrm{D}t} + 2\,\Omega\,u = -\frac{1}{\rho}\frac{\partial p}{\partial y} + \Omega^2\,y + F^y \tag{27.96}$$

$$\frac{\mathrm{D}w}{\mathrm{D}t} = -\frac{1}{\rho}\frac{\partial p}{\partial z} - g + F^z, \tag{27.97}$$

which take on the vector form

$$\frac{\mathrm{D}\boldsymbol{v}}{\mathrm{D}t} + f\,\hat{\boldsymbol{z}}\times\boldsymbol{v} = -\nabla\left[p/\rho + g\,z - \Omega^2\,(x^2+y^2)/2\right] + \boldsymbol{F}. \tag{27.98}$$

As expected, we encounter both a Coriolis and centrifugal acceleration due to the rotation of

the tank.

27.5.3 Rigid-body rotation and parabolic free surface shape

Consider a fluid at rest in a non-rotating tank, and then start the tank rotating. As in our discussion of Couette flow in Section 25.8.2, viscous effects transfer motion from the outside tank wall (where a no-slip boundary condition makes the fluid move with the wall) into the interior of the fluid. Given sufficient time and a constant rotation rate, the fluid reaches a steady state in rigid-body motion. Recall that rigid-body motion means that the velocity vanishes in the rotating reference frame.

As an application of the above equations of motion, we here determine the shape of the upper free surface for this steady rigid-body motion, offering two related derivations. Note that when the fluid reaches rigid-body motion, all strains vanish within the fluid so that frictional stresses vanish (see Section 25.8). Hence, the steady force balance is fully inviscid although the steady state required viscosity to reach it. The ability to ignore friction in the steady state greatly simplifies the analysis.

Component equations of motion

The velocity and acceleration in the rotating frame are zero when the fluid is in rigid-body rotation. The vertical momentum equation (27.97) thus reduces to the approximate hydrostatic balance

$$\frac{\partial p}{\partial z} = -\rho\, g. \tag{27.99}$$

In general we do not have hydrostatic balance for motion in a tank that deviates from rigid-body. However, when that motion is close to a rigid-body rotation, then the fluid is in an approximate hydrostatic balance. As seen in Section 27.2, this situation corresponds to the large-scale ocean and atmosphere.

Hydrostatic balance with a constant density means that the pressure is a linear function of depth

$$p(x, y, z) = \rho\, g\, (\eta - z), \tag{27.100}$$

where $z = \eta(x, y)$ is the vertical position of the free surface. The horizontal momentum equations (27.95)-(27.96) reduce to a balance between the pressure gradient and centrifugal accelerations

$$\frac{\partial p}{\partial x} = \rho\, x\, \Omega^2 \qquad \text{and} \qquad \frac{\partial p}{\partial y} = \rho\, y\, \Omega^2. \tag{27.101}$$

Pressure thus increases when moving radially away from the center. Substituting in the pressure as given by the hydrostatic relation (27.100) leads to relations satisfied by the rigid-body free surface

$$g\, \frac{\partial \eta}{\partial x} = x\, \Omega^2 \qquad \text{and} \qquad g\, \frac{\partial \eta}{\partial y} = y\, \Omega^2. \tag{27.102}$$

Integration leads to the quadratic expression for the free surface

$$\eta = \eta(0) + \frac{\Omega^2\, (x^2 + y^2)}{2\, g}, \tag{27.103}$$

where $\eta(0)$ is the free surface at the center of the tank where $x = y = 0$. The rigid-body rotating fluid thus has a quadratic free surface with the height of the surface increasing away from the center, as depicted in Figure 27.8. Notice how the fluid density dropped out from the problem, so that this parabolic shape holds for any homogeneous fluid in rigid-body motion.

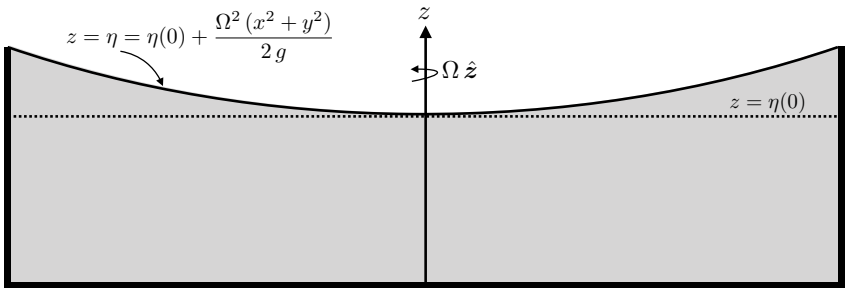

FIGURE 27.8: Rotating tank of homogeneous fluid that has reached a steady state with a parabolic free surface.

Vector force balance

A more telescopic means to determine the free surface shape is to set the forces to zero on the right hand side of the vector equation of motion (27.98) so that

$$p/\rho + g\, z - \Omega^2\, (x^2 + y^2)/2 = p_0/\rho, \tag{27.104}$$

where p_0 is a constant pressure to be specified below. Furthermore, we set friction to zero since the fluid is in rigid-body motion. Everywhere along the free surface, with $z = \eta$, the pressure equals to that applied to the free surface by the overlying media, $p = p_{\mathsf{a}}$ (e.g., atmospheric pressure). Hence, setting $z = \eta$ in equation (27.104) and solving for η yields

$$\eta = \frac{p_0 - p_{\mathsf{a}}}{\rho\, g} + \frac{\Omega^2\, (x^2 + y^2)}{2\, g}. \tag{27.105}$$

For simplicity, assume the applied pressure is spatially constant. Hence, setting p_0 according to the free surface at $x = y = 0$ brings the free surface to the parabolic form in equation (27.103)

$$\frac{p_0 - p_{\mathsf{a}}}{\rho\, g} = \eta(0) \Longrightarrow \eta = \eta(0) + \frac{\Omega^2\, (x^2 + y^2)}{2\, g}. \tag{27.106}$$

27.5.4 Further study

We study the angular momentum for the shallow water version of this system in Section 36.8. See section 6.6.4 of *Marshall and Plumb* (2008) for more discussion of laboratory rotating tank experiments.

27.6 Exercises

EXERCISE 27.1: PRIMITIVE EQUATIONS AND AXIAL ANGULAR MOMENTUM
The axial angular momentum of a fluid element satisfying the primitive equations is given by

$$L^z = (\rho\, \delta V)\, R_\perp\, (u + R_\perp\, \Omega) \equiv (\rho\, \delta V)\, l^z \tag{27.107}$$

where

$$R_\perp = R_{\mathsf{e}} \cos\phi \tag{27.108}$$

is the distance from the polar rotation axis to a point on the sphere with radius R_e, and

$$l^z = R_\perp \, (u + R_\perp \, \Omega) \tag{27.109}$$

is the angular momentum per unit mass. For this exercise, we develop some results for the axial angular momentum in the primitive equations. For this purpose, it can be useful to recall the discussion of axial angular momentum in Section 24.7, in which we did not assume primitive equations.

(a) Consider a constant mass fluid element in the absence of friction. Show that the primitive equation zonal momentum equation (27.7) implies that the material evolution of axial angular momentum per mass is given by

$$\frac{\mathrm{D}l^z}{\mathrm{D}t} = -\frac{1}{\rho}\frac{\partial p}{\partial \lambda}. \tag{27.110}$$

(b) Assume the zonal pressure gradient vanishes. Move the fluid element vertically while maintaining a fixed latitude. What happens to the zonal momentum of this primitive equation fluid element? Hint: be sure to remain within the "world" of the primitive equations.

(c) Give a very brief symmetry argument for why the axial angular momentum is materially conserved when $\partial p/\partial \lambda = 0$. Hint: recall the discussion of Noether's Theorem in Section 14.1.1.

(d) Consider the material evolution of primitive equation axial angular momentum per mass in the case where the zonal momentum equation retains the unapproximated form of the Coriolis acceleration. Discuss the resulting material evolution equation. Does this equation make sense based on the symmetry argument given in the previous part of this exercise?

EXERCISE 27.2: MASS BALANCE FOR A HYDROSTATIC OCEAN COLUMN

Equation (19.103) provides a kinematic expression for the column mass budget. Show that for a hydrostatic fluid flow, the mass balance for a fluid column (equation (19.115)) takes the form

$$\partial_t(p_\mathrm{b} - p_\mathrm{a}) = -g \, \nabla \cdot \boldsymbol{U}^\rho + g \, Q_\mathrm{m}, \tag{27.111}$$

where

$$\boldsymbol{U}^\rho = \int_{\eta_\mathrm{b}}^{\eta} \mathbf{u} \, \rho \, \mathrm{d}z \tag{27.112}$$

is the depth integrated horizontal mass transport,

$$p_\mathrm{b} = p_\mathrm{a} + g \int_{\eta_\mathrm{b}}^{\eta} \rho \, \mathrm{d}z \tag{27.113}$$

is the hydrostatic pressure at the ocean bottom, and $p_\mathrm{a}(x, y, t)$ is the pressure applied to the ocean surface from the overlying atmosphere or sea ice.

EXERCISE 27.3: EVOLUTION OF ATMOSPHERIC BOTTOM HYDROSTATIC PRESSURE

In deriving equation (27.30) we assumed the lower limit on the integral to be a horizontal constant. However, when integrating over the full atmospheric column, the lower limit varies horizontally given that the earth boundary is not flat. Return to equation (27.29b) and derive the evolution equation for the bottom pressure

$$\partial_t p_\mathrm{bot} = -g \, \nabla_\mathrm{h} \cdot \boldsymbol{U}^\rho, \tag{27.114}$$

where

$$p_{\text{bot}}(x, y, t) = p[x, y, z = \eta_{\text{b}}(x, y), t] \tag{27.115}$$

is the atmospheric pressure at the solid earth at $z = \eta_{\text{b}}(x, y)$,

$$\boldsymbol{U}^{\rho} = \int_{\eta_{\text{b}}}^{z_{\text{top}}} \boldsymbol{u}\, \rho \, \mathrm{d}z' \tag{27.116}$$

is the depth integrated horizontal mass transport, and z_{top} is the vertical position of the atmospheric top that is assumed to be independent of horizontal position.

Chapter 28

Pressure form stress

As introduced in our discussion of Cauchy's stress principle in Section 25.2, pressure form stress is the horizontal stress arising from pressure that acts on a sloped surface or interface. As a contact force per area, Newton's third law describes how form stress renders a transfer of pressure forces across interfaces, with pressure form stress affecting a vertical transfer of horizontal pressure forces. Hence, it provides an inviscid/reversible mechanism for the vertical transfer of horizontal momentum, thus complementing the vertical transfer associated with viscosity in the presence of tangential shear stresses (Section 25.8.2).

In this chapter we study pressure form stresses on a variety of interfaces encountered in geophysical fluids. We then develop two case studies to expose the role of pressure form stress in the force balances affecting motion of an ocean fluid column. The first case study is concerned with the evolution of vertically integrated horizontal linear momentum per mass. The second case study focuses on the axial angular momentum budget as a framework to study the dominant force balances in ocean channel flow and ocean gyre flow.

CHAPTER GUIDE

In this chapter we build from the study of stresses in Chapter 25, with an understanding of pressure form stress greatly enhancing our understanding of horizontal forces acting in geophysical fluids. The focus on horizontal forces in this chapter complements our studies in Chapter 30, whereby the net vertical acceleration from pressure and gravitational forces is repackaged into the buoyancy force.

28.1 Pressure form stresses at an interface

As depicted in Figure 28.1, there are three surfaces or interfaces across which we commonly study form stresses in geophysical fluids.

- ATMOSPHERE-OCEAN FORM STRESS: A form stress occurs at the air-sea interface. From the perspective of the ocean, the nonzero atmospheric pressure applied to the sea surface (the *sea level pressure*) provides a pressure acting on the sloped upper ocean free surface, thus rendering an *atmospheric form stress* acting on the ocean. Through *Newton's third law* (see Section 11.5.2), this form stress is met by the equal in magnitude but oppositely directed *ocean form stress* acting on the atmosphere.

- INTERIOR FLUID INTERFACIAL FORM STRESS: A form stress occurs on an internal interface within the fluid, and we study such *interfacial form stresses* in Section 28.3. Although the interface is arbitrary, it is dynamically very interesting to study form stresses acting on buoyancy isosurfaces. The reason is that buoyancy interfaces are directly connected to the geostrophic motion studied in Chapter 31. In particular, in Section 31.7 we study form stresses associated with buoyancy interfaces found in geostrophic flows.

- FLUID-TOPOGRAPHY FORM STRESS: A form stress exists at a solid/fluid boundary, at which the ocean or atmosphere impart a pressure force on the solid earth. Through Newton's third law, the pressure force imparted by the fluid on the solid earth is met equally in magnitude but oppositely in direction by a force provided by the solid earth onto the fluid. The horizontal projection of this force per area acting from the earth on the fluid is the *topographic form stress* and it is considered in Section 28.2.

28.1.1 Concerning the sign of a form stress

As a vector, pressure form stress has a direction and a magnitude, with three examples depicted in Figure 28.1. Even so, keeping track of the direction can be confusing if it is unclear who is the giver of the form stress and who is the receiver. To help in understanding the sign, imagine pushing against a heavy rock or boulder: you exert a force on the rock in one direction whereas, through Newton's third law, the rock exerts an equal and opposite force on you. Clarity is realized by specifying the origin of the force in order to determine its sign. For example, as illustrated in Figure 28.2, is one concerned with the force applied by the ocean bottom pressure

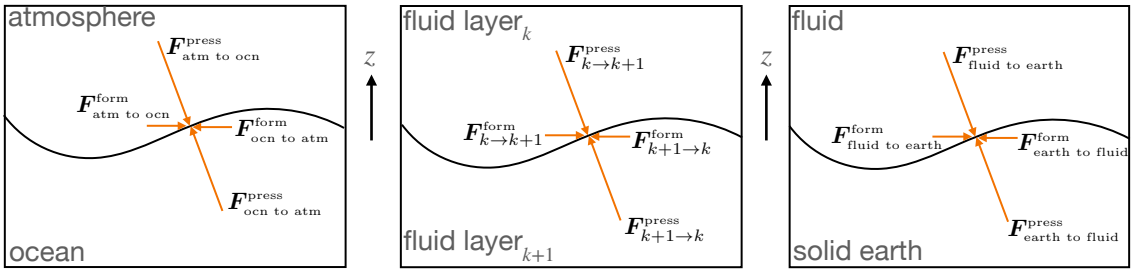

FIGURE 28.1: Illustrating the three interfaces of concern in geophysical fluid mechancs for the discussion of form stresses. Continuity of pressure at the interface, through Newtons' third law, means that the form stress on one side of the interface is equal and opposite to that acting on the other side. Left panel: a curved atmosphere-ocean interface leads to an atmospheric form stress acting on the ocean, $\boldsymbol{F}^{\text{form}}_{\text{atm to ocn}}$, and its equal and opposite oceanic form stress acting on the atmosphere, $\boldsymbol{F}^{\text{form}}_{\text{ocn to atm}} = -\boldsymbol{F}^{\text{form}}_{\text{atm to ocn}}$. Middle panel: a curved interior ocean interface (e.g., a buoyancy surface) leads to an interfacial form stress acting on the lower layer, $\boldsymbol{F}^{\text{form}}_{k\to k+1}$, and its equal and opposite interfacial form stress acting on the upper layer, $\boldsymbol{F}^{\text{form}}_{k+1\to k} = -\boldsymbol{F}^{\text{form}}_{k\to k+1}$. Right panel: a curved fluid-solid earth interface leads to a fluid form stress acting on the solid earth, $\boldsymbol{F}^{\text{form}}_{\text{fluid to earth}}$, and its equal and opposite oceanic form stress acting on the fluid, $\boldsymbol{F}^{\text{form}}_{\text{earth to fluid}} = -\boldsymbol{F}^{\text{form}}_{\text{fluid to earth}}$. The magnitude of the form stresses is a function of the pressure acting at the interface as well as the slope of the interface (steeper slopes lead to larger magnitude).

onto the earth (liquid ocean is giver and solid earth is receiver), or instead with the force from the earth applied onto the ocean fluid (earth is giver and ocean is receiver)? These forces have equal magnitude but opposite direction. Knowing the direction requires knowing the force giver and/or the force receiver.

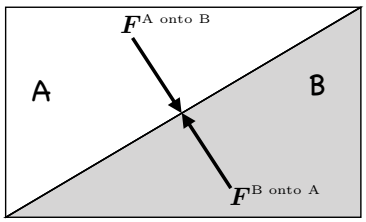

FIGURE 28.2: Contact forces, such as pressure, satisfy Newton's third law. Hence, the contact force at a point imparted by region A onto region B, $\boldsymbol{F}^{\text{A onto B}}$, is equal and opposite to the force imparted by region B onto region A so that $\boldsymbol{F}^{\text{A onto B}} = -\boldsymbol{F}^{\text{B onto A}}$. In the case where A=fluid (ocean or atmosphere) and B=solid earth, we generally to refer to the horizontal portion of $\boldsymbol{F}^{\text{earth onto fluid}}$, per horizontal area, as the *topographic form stress*.

28.1.2 Mathematical expression for form stress

To expose the mathematics of form stress, consider a surface, $\mathcal{S}$, such as that shown in Figure 28.3. To kinematically decompose the pressure force, assume the surface has no vertical section, with this assumption commonly satisfied by surfaces of interest for geophysical flows.

Assuming the surface has no vertical sections allows us to write the vertical position of a point on the surface as[1]

$$z = \eta(x, y, t). \tag{28.1}$$

[1]See the geometry discussion in Chapter 5 for more on the maths of such surfaces. Also see the discussion of generalized vertical coordinates in Chapters 63 and 64.

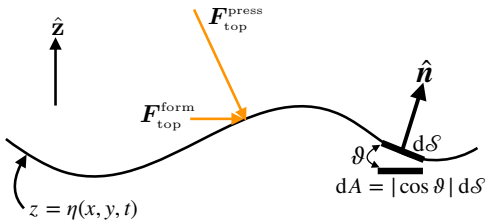

FIGURE 28.3: The pressure force acting on an arbitrary surface is given by $\boldsymbol{F}^{\text{press}} = -p\,\hat{\boldsymbol{n}}\,\mathrm{d}\mathcal{S}$, where $\mathrm{d}\mathcal{S}$ is the surface area element. We here depict the pressure acting on the top side of a surface, $\boldsymbol{F}^{\text{press}}_{\text{top}}$. Through Newton's third law, the pressure force vector acting on the top side of the interface is equal and opposite to the pressure force acting on the bottom side: $\boldsymbol{F}^{\text{press}}_{\text{top}} = -\boldsymbol{F}^{\text{press}}_{\text{b}}$. The horizontal component of this force vector arises from the slope; i.e., the geometric *form* of the surface. We thus refer to the horizontal pressure force per area as the *form stress*, $\boldsymbol{F}^{\text{form}}_{\text{top}} = -\boldsymbol{F}^{\text{form}}_{\text{b}}$. The area element on the surface, $\mathrm{d}\mathcal{S}$, has a horizontal projection given by $\mathrm{d}A = \mathrm{d}x\,\mathrm{d}y = \cos\vartheta\,\mathrm{d}\mathcal{S}$, with the angle assumed to be within the range $-\pi/2 < \vartheta < \pi/2$ so that the surface is nowhere vertical.

The outward normal pointing away from the top side of the surface is given by

$$\hat{\boldsymbol{n}}_{\text{top}} = \frac{\nabla(z-\eta)}{|\nabla(z-\eta)|} = \frac{\hat{\boldsymbol{z}} - \nabla\eta}{\sqrt{1+|\nabla\eta|^2}}. \tag{28.2}$$

Multiplying the pressure times the horizontal area element on the surface, $\mathrm{d}\mathcal{S}$, leads to the net pressure force acting at a point on the top side of the surface

$$\boldsymbol{F}^{\text{press}} = -p\,\hat{\boldsymbol{n}}_{\text{top}}\,\mathrm{d}\mathcal{S} = -p\,(\hat{\boldsymbol{z}} - \nabla\eta)\,\mathrm{d}A = -p\,(-\partial_x\eta\,\hat{\boldsymbol{x}} - \partial_y\eta\,\hat{\boldsymbol{y}} + \hat{\boldsymbol{z}})\,\mathrm{d}A. \tag{28.3}$$

In this equation we used the identity[2]

$$\mathrm{d}\mathcal{S} = |\nabla(z-\eta)|\,\mathrm{d}A = \sqrt{1+|\nabla\eta|^2}\,\mathrm{d}A, \tag{28.4}$$

with

$$\mathrm{d}A = \mathrm{d}x\,\mathrm{d}y \tag{28.5}$$

the horizontal projection of the surface area element (see Figure 28.3). We identify the form stress acting on the top side of this interface as

$$\text{pressure form stress acting on top side of interface} \equiv p\,\nabla\eta. \tag{28.6}$$

The name follows since the stress is determined by the "form" of the surface as measured by its slope, $\nabla\eta$. We can thus write the pressure force acting on the top side of the surface as the sum of a vertical pressure force plus a horizontal pressure form stress

$$\boldsymbol{F}^{\text{press}}_{\text{top}} = \hat{\boldsymbol{z}}\,[\hat{\boldsymbol{z}}\cdot\boldsymbol{F}^{\text{press}}_{\text{top}}] + \boldsymbol{F}^{\text{form}}_{\text{top}} = p\,(-\hat{\boldsymbol{z}} + \nabla\eta)\,\mathrm{d}A \qquad \text{pressure force on top of interface.} \tag{28.7}$$

Newton's third law, as manifested by Cauchy's Stress principle (Section 25.2) says that there is a local mechanical equilibrium of pressure contact forces within a fluid. Additionally, as seen in our discussion of stress on an interface in Section 25.10, this local equilibrium holds for pressure forces acting on interfaces separating two fluids, such as the atmosphere and ocean, as well as a fluid and the solid earth. Thus, the contact pressure force acting on the bottom side of the interface is equal in magnitude but oppositely directed to the contact force acting on the top

[2]The identity (28.4) follows from trigonometry summarized in Figure 28.3. See further details in the kinematic boundary conditions of Section 19.6 and the analogous dia-surface transport in Section 64.3.

side (see Section 25.8.2)

$$\boldsymbol{F}^{\text{press}}_{\text{bot}} = \hat{\boldsymbol{z}}\,[\hat{\boldsymbol{z}}\cdot\boldsymbol{F}^{\text{press}}_{\text{bot}}] + \boldsymbol{F}^{\text{form}}_{\text{bot}} = p\,(+\hat{\boldsymbol{z}} - \nabla\eta)\,\mathrm{d}A \qquad \text{pressure force on bottom of interface.} \tag{28.8}$$

28.1.3 Comments

We here offer three comments in regards to pressure form stress.

- NOT A MYSTERIOUS NOTION: The form stress, particularly interfacial form stress, can appear mysterious in some presentations. Part of the reason is that it sometimes appears seemingly without prior motivation as part of mathematical manipulations of the momentum equation. We illustrate these manipulations in Sections 28.2, 28.3, and 28.5, yet aim to offer sufficient physical motivation to help guide the maths. Another reason for the mystery is that the signs ascribed to form stress are often not clearly specified, with such ambiguities motivating the somewhat pedantic discussion in Section 28.1.1.

- UNBALANCED FORM STRESSES AND MOTION: Consider a container filled with water at rest. The horizontal pressure forces acting on the container sides are pressure form stresses between the water and the container. As discussed in Section 25.5, without motion we know that the form stresses balance over the whole of the fluid-container boundary, whereas horizontal motion occurs if the form stresses are out of balance. Quite generally, when concerned with fluid motion, we are interested in processes that lead to unbalanced form stresses. For example, when studying bottom topographic form stresses in the ocean, the bulk of the form stress acts to support the ocean water within the ocean basin. The dynamically active portion of the topographic form stress, associated with the fluid motion, is a small residual of the total form stress. Careful analysis is required to diagnose dynamically relevant patterns, with *Molemaker et al.* (2015) and *Gula et al.* (2015) presenting one method, and we explore their method as part of Exercise 40.14.

- DUAL FORM STRESS OFTEN CONFUSED WITH FORM STRESS: It is notable that much of the literature refers to $-\eta\nabla p$ as a form stress. However, as emphasized in Section 28.4.4, $-\eta\nabla p$ is not a form stress but is a *dual form stress*. Even though both have dimensions of a pressure, the dual form stress is not a pressure force in the sense that it does not act to accelerate a fluid element.

  The confusion between form stress and dual form stress perhaps originates from the common application of zonal averages. In this case we may wish to study the dynamics of the zonally averaged flow, particularly domains that are zonally periodic, in which we have the identity

  $$\oint p\,\partial_x\eta\,\mathrm{d}x = -\int \eta\,\partial_x p\,\mathrm{d}x. \tag{28.9}$$

  Hence, the zonally integrated form stress (left hand side) equals to the zonally integrated dual form stress (right hand side). However, care must be exercised in applying this identity in non-zonally periodic domains (we further pursue this point in Section 28.4). Even more fundamentally, $p\,\nabla\eta \neq -\eta\,\nabla p$. Consequently, it is generally necessary to distinguish the pressure form stress, which is a horizontal force per area that acts to accelerate fluid elements through Newton's law of motion, from the dual form stress, which does not appear in the equation of motion.

28.2 Form stresses on solid-fluid boundaries

In this section we focus on form stress arising from the shape of the solid earth interface with the atmosphere and ocean; i.e., the *fluid-topographic form stress*. As we are normally interested in the

form stress applied to the fluid, we focus on the *topographic form stress*. We also encounter the form stress associated with undulations in the ocean free surface and the atmospheric pressure at that interface, with the *atmospheric form stress* the stress imparted to the ocean from the atmosphere.

28.2.1 Zonally symmetric ridge

In Figure 28.4 we depict an idealized ridge with an example oceanic pressure field to illustrate the nature of topographic form stress acting on the ocean. Rather than assuming exact hydrostatic equilibrium as in Figure 25.5, with zero horizontal pressure gradients, we here consider pressure to be higher to the west of the ridge than to the east. Since the ridge is assumed to be symmetric in the zonal direction, we conclude that the topographic form stress, which acts just at the fluid-solid interface, is higher on the west side of the ridge than on the east. In turn, the net topographic form stress acting on the fluid is to the west, whereas the net oceanic form stress acting on the solid earth is to the east. We encounter this situation in Section 28.5.10 when studying the force balances for steady circulation in a zonally periodic channel.

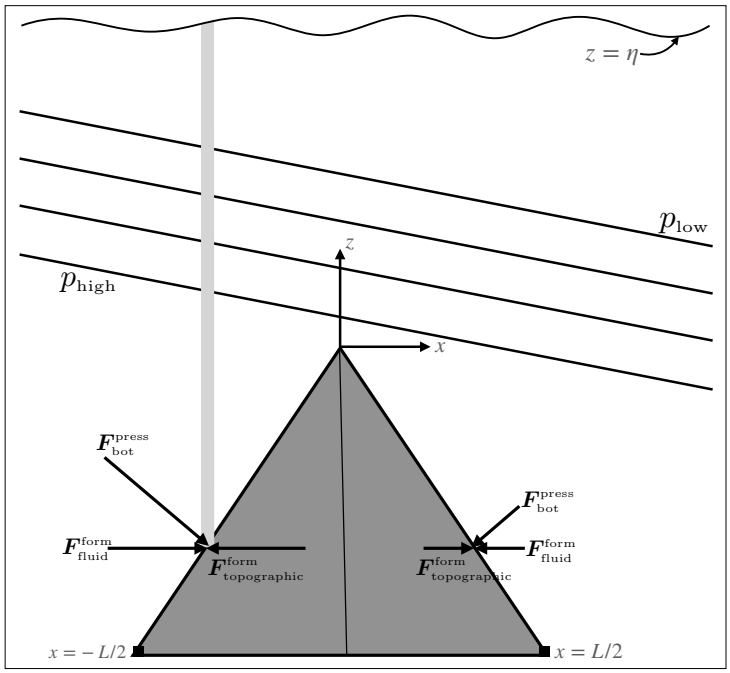

FIGURE 28.4: Depicting contact forces acting at a fluid-solid interface. The topographic form stress acts on the fluid and the equal in magnitude but oppositely directed fluid form stress acts on the solid earth. In this illustration the topography is assumed to be a ridge in the shape of an equilateral triangle. We also assume there is higher pressure to the west of the ridge than to the east as per the zonal balance discussed in Figure 28.8 for a Southern Ocean ridge. Hence, the topographic form stress has a larger magnitude on the western side of the ridge than on the eastern side. When integrated over the full ridge, there will be a net westward topographic form stress acting on the fluid and a net eastward fluid form stress acting on the solid earth. If the ridge was free to move, it would move to the east. The thin gray column extends from the solid earth bottom to the ocean free surface. As this column sits on the western side of the ridge, topographic form stress provides a westward acceleration at the column bottom. The net acceleration of the column is determined by integrating the contact forces around the column boundary and body forces throughout the column interior. We study the axial angular momentum budget for a fluid column in Section 28.5, with form stresses appearing in that budget.

28.2.2 Form stress transfer between the fluid and its boundaries

We now illustrate how topographic form stress appears mathematically in the study of momentum balances acting on a fluid. For definiteness, consider a column of ocean fluid extending from the bottom at $z = \eta_b(x, y)$ to the free surface at $z = \eta(x, y, t)$, and focus on the zonal force balance such as depicted in Figure 28.4. In computing the acceleration acting on this column at a particular horizontal position, we need to determine the depth integrated zonal pressure gradient

$$\text{depth integrated zonal pressure gradient} = -\int_{\eta_b}^{\eta} \frac{\partial p}{\partial x}\, dz. \tag{28.10}$$

We expose the contact force version of the pressure force by making use of Leibniz's Rule (Section 19.7) to write

$$-\int_{\eta_b}^{\eta} \frac{\partial p}{\partial x}\, dz = \underbrace{-\frac{\partial}{\partial x}\int_{\eta_b}^{\eta} p\, dz}_{\text{zonal deriv depth integrated pressure}} + \underbrace{\frac{\partial \eta}{\partial x}\, p_a}_{\text{atmospheric form stress}} - \underbrace{\frac{\partial \eta_b}{\partial x}\, p_b}_{\text{topographic form stress}}, \tag{28.11}$$

where p_a is the pressure applied to the ocean at its surface, $z = \eta$, and p_b is the pressure at the ocean bottom, $z = \eta_b$. The decomposition identifies the following three pressure contributions to the pressure force acting on the fluid column.

- ZONAL DERIVATIVE OF THE COLUMN INTEGRATED PRESSURE: The first term in equation (28.11) arises from the zonal derivative of pressure across the vertical sides of the column

$$\text{zonal derivative of layer integrated pressure} = -\frac{\partial}{\partial x}\int_{\eta_b}^{\eta} p\, dz. \tag{28.12}$$

  This term leads to a net eastward acceleration if the depth integrated pressure is higher to the west than the east.

- ATMOSPHERIC FORM STRESS AT THE FREE SURFACE: In the presence of a sloping free surface interface, equation (28.11) reveals that $\partial\eta/\partial x \neq 0$, the atmospheric pressure, p_a, imparts an atmospheric form stress onto the ocean

$$\text{zonal atmospheric form stress acting on ocean} = \frac{\partial \eta}{\partial x}\, p_a. \tag{28.13}$$

  For example, if the free surface slopes up to the east, $\partial\eta/\partial x > 0$, then the atmosphere provides a positive (eastward) zonal form stress onto the ocean. In turn, through Newton's third law, the ocean provides a westward zonal form stress to the atmosphere.

- TOPOGRAPHIC FORM STRESS ON OCEAN: Equation (28.11) also reveals that the bottom pressure, p_b, present at $z = \eta_b$ imparts a form stress to the solid earth

$$\text{zonal oceanic form stress acting on solid earth} = \frac{\partial \eta_b}{\partial x}\, p_b. \tag{28.14}$$

  In turn, through Newton's third law, the topographic form stress acting on the ocean is equal in magnitude but oppositely directed

$$\text{zonal topographic form stress acting on ocean} = -\frac{\partial \eta_b}{\partial x}\, p_b. \tag{28.15}$$

  For example, if the bottom rises to the east, so that $\partial\eta_b/\partial x > 0$, then the oceanic form stress acting on the solid earth is eastward whereas the topographic form stress acting

on the ocean is westward. As a check, we verify that the signs of these form stresses are consistent with those in Figure 28.4.

28.2.3 Decomposing topographic form stress

We follow the approach used in Section 27.3.2 to decompose here the contributions to the bottom pressure. Assuming the fluid maintains an approximate hydrostatic balance, and focusing on the oceanic case, allows us to decompose the bottom pressure according to

$$p_b = p_a + g \int_{\eta_b}^{\eta} \rho \, dz \tag{28.16a}$$

$$= \underbrace{g \, \rho_o \, [\eta + p_a/(g \, \rho_o)]}_{\text{external}} \; \underbrace{-g \, \rho_o \, \eta_b}_{\text{topog}} \; + \; \underbrace{g \int_{\eta_b}^{\eta} (\rho - \rho_o) \, dz}_{\text{internal}} \tag{28.16b}$$

$$\equiv p_{ext} + p_{topog} + p_{int}. \tag{28.16c}$$

We refer to the contribution from applied surface pressure plus surface height undulations as *external*, whereas those arising from density deviations relative to a constant reference density are termed *internal*. There is a further contribution from bottom topography itself.

Multiplying the decomposed pressure (28.16c) by the slope of the bottom topography renders an expression for the various contributions to topographic form stress

$$-p_b \nabla \eta_b = -p_{ext} \nabla \eta_b - p_{topog} \nabla \eta_b - p_{int} \nabla \eta_b. \tag{28.17}$$

The topographic term is static whereas the other two terms are time dependent. External contributions arise from undulations in the free surface as well as the applied pressure. This contribution fluctuates due to motions occuring on the relatively rapid time scales associated with external gravity waves or atmospheric pressure fluctuations such as through synoptic weather patterns. Internal contributions arise from the relatively slow internal movements of density surfaces, such as from internal gravity waves or even slower motions due to advection and diffusion. The study from *McCabe et al.* (2006) pursues this decomposition of the topographic form stress as part of their analysis of flow around a headland.

28.3 Interfacial form stress

In this section we focus on the form stress acting at an interface within the fluid itself, which is known as the *interfacial form stress*. As part of this discussion we expose some of the common manipulations found when considering finite volume integrated momentum budgets, whereby we decompose the horizontal pressure gradient acceleration acting on an infinitesimal column of fluid within the layer, as depicted in Figure 28.5. These manipulations are analogous to those considered in Section 28.2 for the topographic and atmospheric form stresses.

28.3.1 Interfacial form stresses transferred between layers

When studying the momentum of a column of fluid within a chosen layer, we need to compute the depth integrated zonal pressure gradient over a layer at a particular horizontal point

$$\text{layer integrated zonal pressure gradient} = -\int_{\eta_{k+1/2}}^{\eta_{k-1/2}} \frac{\partial p}{\partial x} \, dz, \tag{28.18}$$

where $z = \eta_{k-1/2}(x, y, t)$ is the vertical position for the interface at the top of the fluid layer and $z = \eta_{k+1/2}(x, y, t)$ is the vertical position for the bottom interface. If the layer integrated

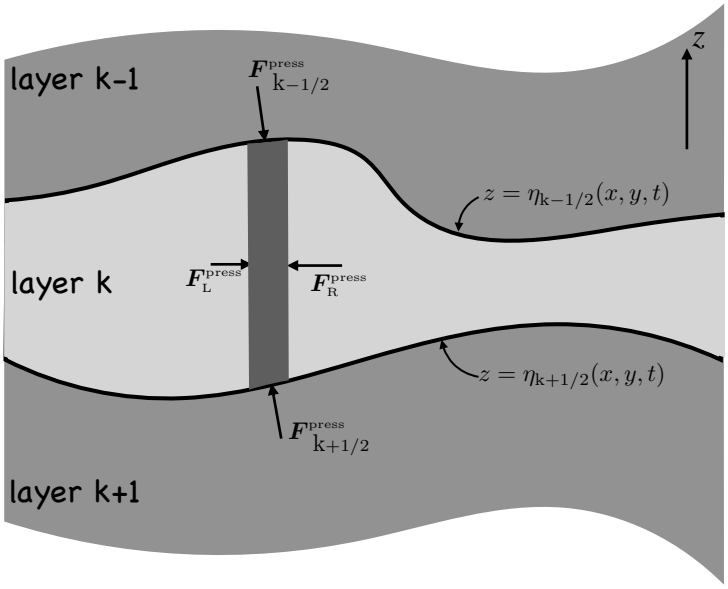

FIGURE 28.5: A schematic of the contact pressure force per area acting on the boundaries of a vertical column region within a fluid layer. The horizontal cross-sectional area of the column is depth independent. The interface at the lower boundary is at the vertical position $z = \eta_{\text{k}+1/2}(x, y, t)$, and the upper interface is at $z = \eta_{\text{k}-1/2}(x, y, t)$. In accordance with Newton's third law, pressures are continuous across each of the $\eta_{\text{k}\pm1/2}$ layer interfaces so that the pressure forces are equal in magnitude yet oppositely directed on the opposite sides to the interfaces. The boundaries of the dark gray columnar region feel a contact pressure force acting inward, as per the compressive nature of pressure. The left side of the column experiences a pressure, p_L; the right side experiences, p_R; the upper interface has a pressure, $p_{\text{k}-1/2}$, acting between the layer $\text{k}-1$ and layer k, and the lower interface has a pressure, $p_{\text{k}+1/2}$, acting between the layer $\text{k}+1$ and layer k. The interfacial form stress (IFS) is the name given to the horizontal pressure stress acting on the upper and lower layer interfaces. Through Newton's third law, the IFS imparted to layer k at the $z = \eta_{\text{k}-1/2}$ interface is equal and opposite to the IFS imparted to layer $\text{k}-1$ at this same interface. The same holds for the IFS at the $\text{k}+1/2$ interface. It is common to define the layers according to buoyancy (see Section 31.7) given its direct connection to pressure and dynamics. Even so, the ideas of pressure contact forces are generic and thus hold for arbitrarily defined layers. This figure is adapted from Figure A1 in *Loose et al.* (2023).

pressure gradient is downgradient to the east, then pressure accelerates the column to the east, and conversely when the layer integrated pressure gradient is downgradient to the west.

Although the depth integrated pressure gradient expression (28.18) is straightforward to understand, we also find it useful to consider the complementary perspective by studying the contact force version of the pressure acceleration. Proceeding as in Section 28.2 for topographic and atmospheric form stresses, we make use of Leibniz's Rule for a fluid layer

$$-\int_{\eta_{\text{k}+1/2}}^{\eta_{\text{k}-1/2}} \frac{\partial p}{\partial x}\,\mathrm{d}z = \underbrace{-\frac{\partial}{\partial x}\int_{\eta_{\text{k}+1/2}}^{\eta_{\text{k}-1/2}} p\,\mathrm{d}z}_{\text{zonal deriv layer integrated pressure}} + \underbrace{\frac{\partial \eta_{\text{k}-1/2}}{\partial x}\,p_{\text{k}-1/2}}_{\text{IFS at k-1/2 interface}} - \underbrace{\frac{\partial \eta_{\text{k}+1/2}}{\partial x}\,p_{\text{k}+1/2}}_{\text{IFS at k+1/2 interface}}, \tag{28.19}$$

where we introduced the pressures acting at a point on the interfaces

$$p_{\text{k}-1/2} = p(x, y, z = \eta_{\text{k}-1/2}, t) \qquad \text{and} \qquad p_{\text{k}+1/2} = p(x, y, z = \eta_{\text{k}+1/2}, t). \tag{28.20}$$

The decomposition identifies the following three pressure contributions, analogous to the decomposition in Section 28.2 for the topographic and atmospheric form stresses.

- ZONAL DERIVATIVE OF THE COLUMN INTEGRATED PRESSURE: The first term arises from

the zonal derivative of pressure across the vertical sides of the column within the layer

$$\text{zonal derivative of layer integrated pressure} = -\frac{\partial}{\partial x}\int_{\eta_{k+1/2}}^{\eta_{k-1/2}} p\,dz. \tag{28.21}$$

- INTERFACIAL FORM STRESS AT UPPER INTERFACE: The pressure at the $z = \eta_{k-1/2}$ interface is given by $p_{k-1/2}$. In the presence of a sloping interface, $\partial\eta_{k-1/2}/\partial x \neq 0$, this pressure imparts the following interfacial form stress (IFS) to layer-k:

$$\text{IFS on layer-k from the } \eta_{k-1/2} \text{ interface} = \frac{\partial\eta_{k-1/2}}{\partial x}\, p_{k-1/2}. \tag{28.22}$$

  For example, if the upper layer interface slopes up to the east, $\partial\eta_{k-1/2}/\partial x > 0$, then the interfacial form stress provides a positive (eastward) zonal force to layer-k. In turn, through Newton's third law, the layer above, labelled $k-1$, feels an interfacial form stress directed to the west.

- INTERFACIAL FORM STRESS AT LOWER INTERFACE: The pressure, $p_{k+1/2}$, present at the $z = \eta_{k+1/2}$ interface imparts an interfacial form stress to layer-k given by

$$\text{IFS on layer-}k \text{ from } \eta_{k+1/2} \text{ interface} = -\frac{\partial\eta_{k+1/2}}{\partial x}\, p_{k+1/2}. \tag{28.23}$$

  For example, if the layer slopes down to the east, $\partial\eta_{k+1/2}/\partial x < 0$, then the interfacial form stress accelerates layer-k to the east. In turn, through Newton's third law, the interfacial form stress acts to accelerate the layer below, labelled $k+1$, to the west.

Now apply the above to a column of ocean fluid, and extend the integration to include the full ocean column from the free upper surface to the rigid solid earth bottom. Evidently, all the intermediate interfacial form stresses vanish in the depth integral, with this cancellation a result of Newton's third law. Hence, accumulation of the interfacial form stresses throughout the ocean column leaves only the interfacial form stress at the top ($z = \eta$) and at the bottom ($z = \eta_b$). The corresponding boundary form stresses arise from mechanical interactions with the atmosphere ($z = \eta$) and solid earth ($z = \eta_b$), as discussed in Section 28.2. This result was already encountered in a more general context of contact forces in Section 25.2. It will also be found in our analysis of the depth integrated axial angular momentum budget in Section 28.5.

28.3.2 Zonally integrated interfacial form stress

Besides studying the force acting on a column at a particular horizontal position, it is interesting to study the net zonal force acting on the layer. For pressure, we thus need to consider the zonal integral of the layer integrated zonal pressure gradient

$$-\int\left[\int_{\eta_{k+1/2}}^{\eta_{k-1/2}} \frac{\partial p}{\partial x}\,dz\right]dx = \int\left[-\frac{\partial}{\partial x}\int_{\eta_{k+1/2}}^{\eta_{k-1/2}} p\,dz + \frac{\partial\eta_{k-1/2}}{\partial x}\,p_{k-1/2} - \frac{\partial\eta_{k+1/2}}{\partial x}\,p_{k+1/2}\right]dx. \tag{28.24}$$

If the domain is zonally periodic or is bounded by sloping shorelines (see Figure 28.6 discussed in Section 28.4.6), then the first term vanishes so that the zonally integrated pressure acting on the layer arises just from the interfacial form stresses

$$-\int\left[\int_{\eta_{k+1/2}}^{\eta_{k-1/2}} \frac{\partial p}{\partial x}\,dz\right]dx = \int\left[\frac{\partial\eta_{k-1/2}}{\partial x}\,p_{k-1/2} - \frac{\partial\eta_{k+1/2}}{\partial x}\,p_{k+1/2}\right]dx. \tag{28.25}$$

This zonal integral is only affected by zonal anomalies for the layer vertical positions and pressures

$$-\int \left[\int_{\eta_{k+1/2}}^{\eta_{k-1/2}} \frac{\partial p}{\partial x} \, dz \right] dx = \int \left[\frac{\partial \eta'_{k-1/2}}{\partial x} \, p'_{k-1/2} - \frac{\partial \eta'_{k+1/2}}{\partial x} \, p'_{k+1/2} \right] dx \tag{28.26a}$$

$$= \int \left[-\eta'_{k-1/2} \, \frac{\partial p'_{k-1/2}}{\partial x} + \eta'_{k+1/2} \, \frac{\partial p'_{k+1/2}}{\partial x} \right] dx, \tag{28.26b}$$

where primes denote deviations from the zonal mean. In Section 28.5.9 we offer details to prove that it is only the zonal anomalies that contribute to the zontal integral in a zonally periodic channel, or for domains with sloping shorelines. Furthermore, note that for the second equality we introduced the alternative expressions for the form stresses afforded by zonal periodicity or zonal sloped shorelines. We offer cautionary remarks on this replacement in Section 28.5.8 regarding this second equality.

28.3.3 Comments

Interfacial form stress acts on any arbitrary surface drawn in a fluid. Interfaces defined by buoyancy surfaces make the connection between the general concepts presented here to geostrophic mechanics, and they do so given the connection between buoyancy slopes and thermal wind (Section 31.4.3). Most studies of interfacial form stress are thus concerned with isopycnal interfacial form stress, with a discussion given in Section 31.7.

28.4 Depth integrated momentum for the primitive equations

In this section we develop the evolution equation for the depth integrated horizontal momentum per volume in a column of ocean fluid

$$\boldsymbol{U}^{\rho} = \int_{\eta_b}^{\eta} \rho \, \boldsymbol{u} \, dz, \tag{28.27}$$

extending from the ocean bottom at $z = \eta_b(x, y)$ to the ocean surface at $z = \eta(x, y, t)$. As we will see, the evolution equation clearly exposes how form stresses acting at the ocean surface and ocean bottom contribute to the column force balance. A study of the depth integrated momentum equation is commonly considered when the ocean fluid maintains an approximate hydrostatic balance (see Sections 27.2 and 29.2), and the shallow fluid approximation (Section 27.1.2). These two approximations constitute the hydrostatitc primitive equations (Section 27.1), which we assume holds in this section.

An important technical feature of the primitive equations is that the horizontal gradient operator, ∇_h, is depth independent, which is a property we use to develop the budget equations in this section. In particular, we need this assumption for equation (28.30c) below. We also made use of this property of ∇_h in Section 27.1.6 to derive the depth integrated kinetic energy budget for the primitive equations.

28.4.1 Flux-form horizontal momentum equation

Our starting point is the flux-form horizontal momentum equation (25.64) as specialized to a simple geopotential, $\Phi = g \, z$,

$$\frac{\partial (\rho \, \boldsymbol{u})}{\partial t} + \nabla \cdot [\rho \, \boldsymbol{v} \otimes \boldsymbol{u}] + f \, \hat{\boldsymbol{z}} \times (\rho \, \boldsymbol{u}) = -\nabla_h p + \rho \, \boldsymbol{F}. \tag{28.28}$$

In this equation, $\rho \boldsymbol{F}$ is the horizontal friction vector, and the outer product provides components to the kinetic stress (Section 25.6)

$$\rho \, [\boldsymbol{v} \otimes \boldsymbol{u}]_{mi} = \rho \, v_m \, u_i = -\mathbb{T}^{\text{kinetic}}_{mi}, \tag{28.29}$$

with $m = 1, 2, 3$ (for the full velocity vector, $\boldsymbol{v}$) extending over the full range whereas $i = 1, 2$ (for the horizontal velocity vector, $\boldsymbol{u}$) extending just over the horizontal range.

28.4.2 Leibniz's rule for the inertial and Coriolis accelerations

Leibniz's rule (Section 20.2.4) renders the following expressions for the depth integrated inertial acceleration and Coriolis acceleration

$$\int_{\eta_b}^{\eta} \frac{\partial(\rho \, \boldsymbol{u})}{\partial t} \, \mathrm{d}z = \partial_t \boldsymbol{U}^{\rho} - [\rho \, \boldsymbol{u} \, \partial_t \eta]_{z=\eta} \tag{28.30a}$$

$$\int_{\eta_b}^{\eta} \frac{\partial(w \, \rho \, \boldsymbol{u})}{\partial z} \, \mathrm{d}z = [w \, \rho \, \boldsymbol{u}]_{z=\eta} - [w \, \rho \, \boldsymbol{u}]_{z=\eta_b} \tag{28.30b}$$

$$\int_{\eta_b}^{\eta} \nabla_h \cdot [\rho \, \boldsymbol{u} \otimes \boldsymbol{u}] \, \mathrm{d}z = \nabla_h \cdot \left[\int_{\eta_b}^{\eta} \rho \, \boldsymbol{u} \otimes \boldsymbol{u} \, \mathrm{d}z \right] - [\boldsymbol{u} \cdot \nabla \eta \, (\rho \, \boldsymbol{u})]_{z=\eta} + [\boldsymbol{u} \cdot \nabla \eta_b \, (\rho \, \boldsymbol{u})]_{z=\eta_b} \tag{28.30c}$$

$$\int_{\eta_b}^{\eta} f \, \hat{\boldsymbol{z}} \times (\rho \, \boldsymbol{u}) \, \mathrm{d}z = f \, \hat{\boldsymbol{z}} \times \boldsymbol{U}^{\rho}. \tag{28.30d}$$

Use of the surface and bottom kinematic boundary conditions from Section 19.6

$$\partial_t \eta + \boldsymbol{u} \cdot \nabla \eta = w + \rho^{-1} \, Q_m \quad \text{for } z = \eta \tag{28.31a}$$

$$\boldsymbol{u} \cdot \nabla \eta_b = w \quad \text{for } z = \eta_b \tag{28.31b}$$

leads to the depth integrated inertial and Coriolis accelerations

$$\int_{\eta_b}^{\eta} [\partial_t(\rho \, \boldsymbol{u}) + \nabla \cdot [\boldsymbol{v} \otimes (\rho \, \boldsymbol{u})] + f \, \hat{\boldsymbol{z}} \times \rho \, \boldsymbol{u}] \, \mathrm{d}z$$

$$= (\partial_t + f \, \hat{\boldsymbol{z}} \times) \, \boldsymbol{U}^{\rho} - \boldsymbol{u}(\eta) \, Q_m - \nabla_h \cdot \int_{\eta_b}^{\eta} \mathbb{T}^{\text{kinetic}}_{\text{hor}} \, \mathrm{d}z, \tag{28.32}$$

where we introduced the horizontal kinetic stress tensor

$$\mathbb{T}^{\text{kinetic}}_{\text{hor}} = -\rho \, \boldsymbol{u} \otimes \boldsymbol{u}. \tag{28.33}$$

28.4.3 External and internal decomposition of the kinetic stress

For some applications it can be useful to introduce the density weighted depth averaged horizontal velocity

$$\overline{\boldsymbol{u}} = \frac{\int_{\eta_b}^{\eta} \rho \, \boldsymbol{u} \, \mathrm{d}z}{\int_{\eta_b}^{\eta} \rho \, \mathrm{d}z} = \frac{\boldsymbol{U}^{\rho}}{(p_b - p_a)/g}, \tag{28.34}$$

where p_b is the hydrostatic pressure at the ocean bottom, and p_a is the pressure applied to the ocean surface. The depth averaged velocity is referred to as the *external velocity*, whereas the deviation from the depth average

$$\boldsymbol{u}' = \boldsymbol{u} - \overline{\boldsymbol{u}}, \tag{28.35}$$

is referred to it as the *internal velocity*.[3] It follows by definition that the internal velocity has a zero density weighted vertical integral

$$\int_{\eta_\mathsf{b}}^{\eta} \rho\, \boldsymbol{u}'\, \mathrm{d}z = \int_{\eta_\mathsf{b}}^{\eta} \rho\, (\boldsymbol{u} - \overline{\boldsymbol{u}})\, \mathrm{d}z = 0. \tag{28.36}$$

Consequently, by making use of $\boldsymbol{u} = \overline{\boldsymbol{u}} + \boldsymbol{u}'$ we find the depth integrated kinetic stress

$$\int_{\eta_\mathsf{b}}^{\eta} \mathbb{T}^{\text{kinetic}}_{\text{hor}}\, \mathrm{d}z = -g^{-1}\, (p_\mathsf{b} - p_\mathsf{a})\, [\overline{\boldsymbol{u}} \otimes \overline{\boldsymbol{u}} + \overline{\boldsymbol{u}' \otimes \boldsymbol{u}'}]. \tag{28.37}$$

Note that absence of cross-terms (i.e., no internal-external correlation terms) appearing in the depth integrated stress (28.37). In this manner we have separated the contributions from kinetic stresses due to depth averaged horizontal velocities from those arising from depth-dependent horizontal velocities.

28.4.4 Decomposing the depth integrated horizontal pressure gradient

We here consider the depth integrated pressure and the corresponding depth integrated horizontal pressure gradient

$$P = \int_{\eta_\mathsf{b}}^{\eta} p\, \mathrm{d}z \quad \text{and} \quad \int_{\eta_\mathsf{b}}^{\eta} \nabla_\mathsf{h} p\, \mathrm{d}z. \tag{28.38}$$

Assuming each fluid column maintains an approximate hydrostatic balance allows us to decompose these integrals into elemental constituents. Doing so offers insights into the way pressure accelerates the fluid.

Depth integrated pressure and its connection to the potential energy

Write the depth integrated pressure as

$$P = \int_{\eta_\mathsf{b}}^{\eta} p\, \mathrm{d}z = \int_{\eta_\mathsf{b}}^{\eta} [\mathrm{d}(p\, z) - z\, \mathrm{d}p] = p_\mathsf{a}\, \eta - p_\mathsf{b}\, \eta_\mathsf{b} + \mathscr{P}, \tag{28.39}$$

where we used the hydrostatic balance for a vertical fluid column to write[4] $\mathrm{d}p = -g\, \rho\, \mathrm{d}z$, and we introduced the potential energy per horizontal area of a fluid column

$$\mathscr{P} = \int_{\eta_\mathsf{b}}^{\eta} g\, \rho\, z\, \mathrm{d}z. \tag{28.40}$$

Evidently, equation (28.39) decomposes the depth integrated pressure into a contribution from the applied surface pressure acting at the free surface, the bottom pressure acting at the ocean bottom (recall that $\eta_\mathsf{b} < 0$), and the potential energy per horizontal area of a fluid column.

[3] It is also common in the oceanography literature to refer to $\boldsymbol{u}'$ as the *baroclinic velocity* and $\overline{\boldsymbol{u}}$ as the *barotropic velocity*. We avoid that nomenclature since we prefer to use baroclinic and barotropic in reference to vorticity mechanics in Section 40.4.

[4] More generally, the differential of pressure is given by $\mathrm{d}p = \nabla p \cdot \mathrm{d}\boldsymbol{x}$ when probing three-dimensional spatial increments, $\mathrm{d}\boldsymbol{x}$. However, the integral in equation (28.39) is vertical, in which case $\mathrm{d}p = (\partial p/\partial z)\, \mathrm{d}z$. For the approximate hydrostatic fluid we thus have the transformation $\mathrm{d}p = -g\, \rho\, \mathrm{d}z$.

Depth integrated horizontal pressure gradient

For the depth integrated horizontal pressure gradient, we start by using Leibniz's rule to render

$$\nabla_{\mathrm{h}} P = \nabla_{\mathrm{h}} \int_{\eta_{\mathrm{b}}}^{\eta} p \, \mathrm{d}z = p_{\mathrm{a}} \, \nabla_{\mathrm{h}} \eta - p_{\mathrm{b}} \, \nabla_{\mathrm{h}} \eta_{\mathrm{b}} + \int_{\eta_{\mathrm{b}}}^{\eta} \nabla_{\mathrm{h}} p \, \mathrm{d}z. \tag{28.41}$$

Making use of the decomposition (28.39) leads to

$$\begin{aligned} -\int_{\eta_{\mathrm{b}}}^{\eta} \nabla_{\mathrm{h}} p \, \mathrm{d}z &= -\nabla_{\mathrm{h}} P + p_{\mathrm{a}} \nabla_{\mathrm{h}} \eta - p_{\mathrm{b}} \nabla_{\mathrm{h}} \eta_{\mathrm{b}} && \text{(28.42a)} \\ &= -\nabla_{\mathrm{h}} \left[p_{\mathrm{a}} \, \eta - p_{\mathrm{b}} \, \eta_{\mathrm{b}} + \mathscr{P} \right] + p_{\mathrm{a}} \nabla_{\mathrm{h}} \eta - p_{\mathrm{b}} \nabla_{\mathrm{h}} \eta_{\mathrm{b}} && \text{(28.42b)} \\ &= -\nabla_{\mathrm{h}} \mathscr{P} - \eta \nabla_{\mathrm{h}} p_{\mathrm{a}} + \eta_{\mathrm{b}} \nabla_{\mathrm{h}} p_{\mathrm{b}}. && \text{(28.42c)} \end{aligned}$$

These are very important results and so worth writing in a single identity

$$-\int_{\eta_{\mathrm{b}}}^{\eta} \nabla_{\mathrm{h}} p \, \mathrm{d}z = -\nabla_{\mathrm{h}} P + p_{\mathrm{a}} \nabla_{\mathrm{h}} \eta - p_{\mathrm{b}} \nabla_{\mathrm{h}} \eta_{\mathrm{b}} = -\nabla_{\mathrm{h}} \mathscr{P} - \eta \nabla_{\mathrm{h}} p_{\mathrm{a}} + \eta_{\mathrm{b}} \nabla_{\mathrm{h}} p_{\mathrm{b}}. \tag{28.43}$$

Equation (28.42a) exposes contributions from minus the horizontal gradient of the depth integrated pressure plus surface and bottom form stresses

$$\text{minus gradient of } \textstyle\int_{\eta_{\mathrm{b}}}^{\eta} p \, \mathrm{d}z + \text{boundary form stresses} = -\nabla_{\mathrm{h}} P + p_{\mathrm{a}} \nabla_{\mathrm{h}} \eta - p_{\mathrm{b}} \nabla_{\mathrm{h}} \eta_{\mathrm{b}}. \tag{28.44}$$

As a complement, equation (28.42c) exposes contributions from the gradient of the potential energy plus those from the *dual form stresses*,

$$\text{minus gradient of } \textstyle\int_{\eta_{\mathrm{b}}}^{\eta} g \, \rho \, z \, \mathrm{d}z + \text{boundary dual form stresses} = -\nabla_{\mathrm{h}} \mathscr{P} - \eta \nabla_{\mathrm{h}} p_{\mathrm{a}} + \eta_{\mathrm{b}} \nabla_{\mathrm{h}} p_{\mathrm{b}}. \tag{28.45}$$

It is notable that the literature commonly confuses form stresses with dual form stresses, along with contributions from depth integrated pressure and the potential energy. The role of these pressures is further studied for the axial angular momentum budget in Section 28.5, and furthermore within the column vorticity balance in Section 40.9.

Pressure balances for motionless flow that is exactly hydrostatic

As discussed in Section 24.6, the horizontal pressure gradient everywhere vanishes for a fluid in exact hydrostatic balance, $\nabla_{\mathrm{h}} p = 0$. Correspondingly, the free surface and surface applied pressure are spatially constant in order to maintain zero pressure gradients throughout the fluid. For the depth integral pressure gradient, the decompositions (28.42a) and (28.42c) lead to the exact hydrostatic fluid identities maintained at each vertical fluid column

$$\begin{aligned} \nabla_{\mathrm{h}} P &= -p_{\mathrm{b}} \, \nabla_{\mathrm{h}} \eta_{\mathrm{b}} && \text{(28.46a)} \\ \nabla_{\mathrm{h}} \mathscr{P} &= \eta_{\mathrm{b}} \, \nabla_{\mathrm{h}} p_{\mathrm{b}}. && \text{(28.46b)} \end{aligned}$$

The first identity says that the horizontal gradient of the depth integrated hydrostatic pressure exactly balances the topographic form stress. The second identity says that the horizontal gradient of the potential energy per area balances the dual topographic form stress.

Since the curl of the left hand side vanishes for both of equation (28.46a) and (28.46a), we find that the bottom pressure must be aligned with the bottom topography in order to maintain zero flow

$$\hat{\boldsymbol{z}} \cdot (\nabla \eta_{\mathrm{b}} \times \nabla p_{\mathrm{b}}) = 0. \tag{28.47}$$

In the language of vorticity, we say that there is no bottom pressure torque when the flow is

exactly hydrostatic (see Section 40.8.3). Conversely, nonzero flow is signaled by a misalignment of the contours of constant bottom pressure and bottom topography. We can also arrive at the identity (28.47) by taking the horizontal derivative of the bottom pressure. Since the fluid is static we have a spatially constant free surface and applied pressure, and a density that is horizontally uniform. Consequently,

$$\nabla_{\mathsf{h}} p_{\mathsf{b}} = g\, \nabla_{\mathsf{h}} \int_{\eta_{\mathsf{b}}}^{\eta} \rho \, \mathrm{d}z = -g\, \rho(z=\eta_{\mathsf{b}})\, \nabla_{\mathsf{h}} \eta_{\mathsf{b}}, \tag{28.48}$$

thus revealing that bottom pressure contours are indeed parallel to bottom topography contours when the fluid is in exact hydrostatic balance.

28.4.5 Depth integrated momentum equation

Bringing the pieces together leads to the depth integrated horizontal momentum equation for an approximate hydrostatic fluid

$$(\partial_t + f\, \hat{\boldsymbol{z}}\times)\, \boldsymbol{U}^{\rho} = \boldsymbol{u}(\eta)\, Q_{\mathsf{m}} + p_{\mathsf{a}} \nabla_{\mathsf{h}} \eta - p_{\mathsf{b}} \nabla_{\mathsf{h}} \eta_{\mathsf{b}} - \nabla_{\mathsf{h}} P + \nabla_{\mathsf{h}} \cdot \left[\int_{\eta_{\mathsf{b}}}^{\eta} \mathbb{T}^{\text{kinetic}}_{\text{hor}} \, \mathrm{d}z \right] + \int_{\eta_{\mathsf{b}}}^{\eta} \rho\, \boldsymbol{F} \, \mathrm{d}z. \tag{28.49}$$

In this equation we exposed minus the gradient of the depth integrated pressure along with the boundary form stresses, as per equation (28.42a). We could just as well have chosen to expose minus the gradient of the potential energy along with the boundary dual form stresses, as per equation (28.42c), in which case

$$(\partial_t + f\, \hat{\boldsymbol{z}}\times)\, \boldsymbol{U}^{\rho} = \boldsymbol{u}(\eta)\, Q_{\mathsf{m}} - \eta \nabla_{\mathsf{h}} p_{\mathsf{a}} + \eta_{\mathsf{b}} \nabla_{\mathsf{h}} p_{\mathsf{b}} - \nabla_{\mathsf{h}} \mathscr{P} + \nabla_{\mathsf{h}} \cdot \left[\int_{\eta_{\mathsf{b}}}^{\eta} \mathbb{T}^{\text{kinetic}}_{\text{hor}} \, \mathrm{d}z \right] + \int_{\eta_{\mathsf{b}}}^{\eta} \rho\, \boldsymbol{F} \, \mathrm{d}z. \tag{28.50}$$

For many applications we focus on the vertical divergence of horizontal frictional stress plus a term arising from horizontal strains, in which case

$$\int_{\eta_{\mathsf{b}}}^{\eta} \rho\, \boldsymbol{F} \, \mathrm{d}z = \int_{\eta_{\mathsf{b}}}^{\eta} (\rho\, \boldsymbol{F}^{\text{horz}} + \partial_z \boldsymbol{\tau}) \, \mathrm{d}z = \boldsymbol{D} + \boldsymbol{\tau}^{\eta} - \boldsymbol{\tau}^{\eta_{\mathsf{b}}} \equiv \boldsymbol{D} + \Delta\boldsymbol{\tau}, \tag{28.51}$$

where $\boldsymbol{\tau}^{\eta}$ is the horizontal stress vector at the surface (e.g., wind stress on the ocean surface), $\boldsymbol{\tau}^{\eta_{\mathsf{b}}}$ is the horizontal stress vector at the bottom (e.g., turbulent drag at the fluid-solid earth boundary), and

$$\boldsymbol{D} = \int_{\eta_{\mathsf{b}}}^{\eta} \rho\, \boldsymbol{F}^{\text{horz}} \, \mathrm{d}z \tag{28.52}$$

is the depth integrated friction arising from horizontal stresses within the fluid interior (e.g., viscous stresses as in Section 25.8). In this case the horizontal momentum equation (28.50) takes on the equivalent forms

$$(\partial_t + f\, \hat{\boldsymbol{z}}\times)\, \boldsymbol{U}^{\rho} = \boldsymbol{u}(\eta)\, Q_{\mathsf{m}} + p_{\mathsf{a}} \nabla_{\mathsf{h}} \eta - p_{\mathsf{b}} \nabla_{\mathsf{h}} \eta_{\mathsf{b}} - \nabla_{\mathsf{h}} P + \boldsymbol{A} + \boldsymbol{D} + \Delta\boldsymbol{\tau} \tag{28.53a}$$

$$(\partial_t + f\, \hat{\boldsymbol{z}}\times)\, \boldsymbol{U}^{\rho} = \boldsymbol{u}(\eta)\, Q_{\mathsf{m}} - \eta \nabla_{\mathsf{h}} p_{\mathsf{a}} + \eta_{\mathsf{b}} \nabla_{\mathsf{h}} p_{\mathsf{b}} - \nabla_{\mathsf{h}} \mathscr{P} + \boldsymbol{A} + \boldsymbol{D} + \Delta\boldsymbol{\tau}, \tag{28.53b}$$

where we introduced the shorthand for the nonlinear kinetic stress term

$$\boldsymbol{A} \equiv \nabla_{\mathsf{h}} \cdot \left[\int_{\eta_{\mathsf{b}}}^{\eta} \mathbb{T}^{\text{kinetic}}_{\text{hor}} \, \mathrm{d}z \right] = -\nabla_{\mathsf{h}} \cdot \left[\int_{\eta_{\mathsf{b}}}^{\eta} \rho\, \boldsymbol{u} \otimes \boldsymbol{u} \, \mathrm{d}z \right]. \tag{28.54}$$

28.4.6 Zonally integrated zonal momentum balance

Zonal integration and zonal averaging offer a common means to summarize elements of the flow, particularly in the atmosphere where zonal motions are much stronger than meridional due to the earth's rotation and the differential solar heating of the planet. Additionally, zonal averaging is of particular interest in the Southern Ocean, where the Drake Passage latitudes offer a zonally unbounded domain for ocean circulation. Even for zonally bounded ocean domains where gyre circulations occur, it is of interest to zonally integrate across the domain to study balances leading to meridional motion across the chosen latitude. We are thus motivated to integrate zonally across the full extent of the domain, with the resulting boundary contributions dependent on the geometry and topology of the domain.

Three canonical domains

We illustrate three canonical domains in Figure 28.6. For the zonally periodic domain, the zonal integral of any zonal derivative vanishes so that, for example,

$$\oint \partial_x P \, \mathrm{d}x = 0, \tag{28.55}$$

where we write $\oint \mathrm{d}x$ for integration over a zonally periodic domain. Additionally, zonal derivatives vanish for a zonally bounded domain with sloping shorelines

$$\int \partial_x P \, \mathrm{d}x = \Delta P = 0. \tag{28.56}$$

The reason this integral vanishes is that any depth integrated quantity, such as P, vanishes at the shoreline edge merely since the layer thickness vanishes at the shoreline edge. The same result holds for any other depth integrated quantity, including depth integrated axial angular momentum, mass transport, and potential energy.

It is only for the zonally bounded domain with vertical sidewalls (third panel in Figure 28.6) that we are unable to drop the zonal integral of the zonal pressure gradient. We observe that vertical sidewalls are common for numerical models and many theories of the ocean circulation. However, vertical sidewalls are the exception in Nature. For this reason, in the following we focus on the more geophysically relevant periodic configuration and the sloping shoreline configuration.

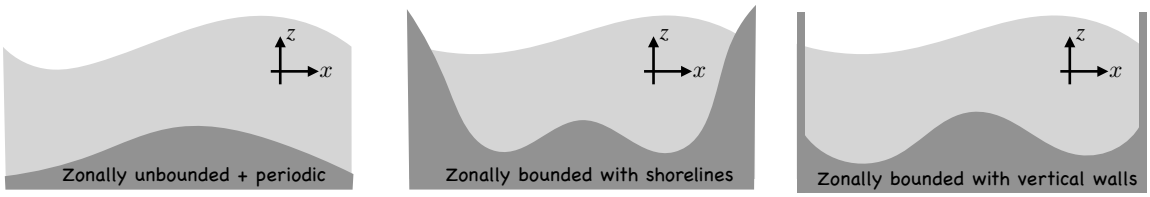

FIGURE 28.6: Three canonical zonal topologies/geometries considered in the study of fluid flow, particularly ocean flows. The light portion of each panel represents the fluid whereas the darker portion is the solid earth bottom topography. Left panel: zonally unbounded and periodic channel. Here, the topography, surface boundary forcing, and flow are zonally periodic. Middle panel: zonally bounded region where the zonal bounds occur along sloping shorelines at which the fluid thickness vanishes. The horizontal position of the vanishing thickness is time dependent since the fluid can move up and down the shoreline. Right panel: zonally bounded region where the fluid encounters a vertical sidewall so that the horizontal position of the fluid boundary is fixed, and so there is no horizontal position where the fluid thickness vanishes. Fixed vertical sidewall boundaries are commonly found in numerical model simulations and tacitly assumed in many theoretical treatments. Even so, vertical sidewall boundaries are uncommon in Nature.

Zonally integrated meridional mass transport

A zonal integral, either over a periodic domain or a domain with vanishing layer thickness along the shoreline, renders an expression for the meridional transport across the zonal-depth section

$$f \int V^\rho \, \mathrm{d}x = \int [p_\mathsf{a} \, \partial_x \eta - p_\mathsf{b} \, \partial_x \eta_\mathsf{b} - \partial_t U^\rho - u(\eta) \, Q_\mathsf{m} + (\boldsymbol{A} + \boldsymbol{D} + \Delta \boldsymbol{\tau}) \cdot \hat{\boldsymbol{x}}] \, \mathrm{d}x, \tag{28.57}$$

where we set $\int \partial_x P \, \mathrm{d}x = \int \partial_x \mathscr{P} \, \mathrm{d}x = 0$. Note that the Coriolis parameter was pulled outside the zonal integral since it is constant along a constant latitude line. As discussed in Section 28.5, this equation, or its analog for the axial angular momentum, provides a useful framework for studies of momentum balances in both the Southern Ocean and in ocean gyres. For the special case of a steady state in the absence of surface mass fluxes, so that $\partial_t U^\rho = 0$ and $Q_\mathsf{m} = 0$, and for a domain closed in the north and south, so that mass conservation renders $\int V^\rho \, \mathrm{d}x = 0$, then the balance (28.57) simplifies to

$$\int [p_\mathsf{a} \, \partial_x \eta - p_\mathsf{b} \, \partial_x \eta_\mathsf{b} + (\boldsymbol{A} + \boldsymbol{D} + \Delta \boldsymbol{\tau}) \cdot \hat{\boldsymbol{x}}] \, \mathrm{d}x = 0. \tag{28.58}$$

For those cases where nonlinear terms and interior friction are small, we find a balance between pressure form stresses at the boundaries plus boundary turbulent stresses. We defer to Section 28.5 any further remarks on this case.

28.4.7 Balances when $\nabla \cdot \boldsymbol{U}^\rho = 0$

There are many occasions in which the depth integrated flow is close to non-divergent, $\nabla \cdot \boldsymbol{U}^\rho = 0$. Such occurs particularly at the large scale and for cases where we neglect the mass transport accross the ocean surface, $Q_\mathsf{m} = 0$. Following the kinematics from Section 21.4, we introduce a *transport streamfunction* so that

$$\boldsymbol{U}^\rho = \hat{\boldsymbol{z}} \times \nabla \Psi, \tag{28.59}$$

with Ψ having dimensions of mass per time. Use of the transport streamfunction brings the Coriolis contribution to the form

$$f \, \hat{\boldsymbol{z}} \times \boldsymbol{U}^\rho = f \, \hat{\boldsymbol{z}} \times (\hat{\boldsymbol{z}} \times \nabla \Psi) = -f \, \nabla \Psi, \tag{28.60}$$

so that the momentum equations (28.53a) (28.53b) become

$$\partial_t \boldsymbol{U}^\rho = f \, \nabla_\mathsf{h} \Psi + p_\mathsf{a} \nabla_\mathsf{h} \eta - p_\mathsf{b} \nabla_\mathsf{h} \eta_\mathsf{b} - \nabla_\mathsf{h} P + \boldsymbol{A} + \boldsymbol{D} + \Delta \boldsymbol{\tau}. \tag{28.61a}$$

$$\partial_t \boldsymbol{U}^\rho = f \, \nabla_\mathsf{h} \Psi - \eta \nabla_\mathsf{h} p_\mathsf{a} + \eta_\mathsf{b} \nabla_\mathsf{h} p_\mathsf{b} - \nabla_\mathsf{h} \mathscr{P} + \boldsymbol{A} + \boldsymbol{D} + \Delta \boldsymbol{\tau} \tag{28.61b}$$

To reach a steady flow requires the following balances

$$-f \, \nabla_\mathsf{h} \Psi = p_\mathsf{a} \nabla_\mathsf{h} \eta - p_\mathsf{b} \nabla_\mathsf{h} \eta_\mathsf{b} - \nabla_\mathsf{h} P + \boldsymbol{A} + \boldsymbol{D} + \Delta \boldsymbol{\tau}. \tag{28.62a}$$

$$-f \, \nabla_\mathsf{h} \Psi = -\eta \nabla_\mathsf{h} p_\mathsf{a} + \eta_\mathsf{b} \nabla_\mathsf{h} p_\mathsf{b} - \nabla_\mathsf{h} \mathscr{P} + \boldsymbol{A} + \boldsymbol{D} + \Delta \boldsymbol{\tau} \tag{28.62b}$$

For some analysis it can be useful to project equation (28.62a) into the horizontal direction tangent to the bottom topography, denoted by the unit vector $\hat{\boldsymbol{t}}$. Doing so eliminates the $p_\mathsf{b} \nabla_\mathsf{h} \eta_\mathsf{b}$ term to have the steady along-topography flow balance

$$-f \, \hat{\boldsymbol{t}} \cdot \nabla_\mathsf{h} \Psi = \hat{\boldsymbol{t}} \cdot (p_\mathsf{a} \nabla_\mathsf{h} \eta - \nabla_\mathsf{h} P + \boldsymbol{A} + \boldsymbol{D} + \Delta \boldsymbol{\tau}). \tag{28.63}$$

28.5 Axial angular momentum budget for an ocean domain

We here develop the column integrated budget for axial angular momentum in an ocean region, such as shown in Figure 28.7. We then further specialize the budget by zonally integrating. The analysis shares features with the depth integrated linear momentum balance developed in Section 28.4. As in that discussion, we here assume the primitive equations (Section 27.1) so that the horizontal gradient operator is independent of depth (as for Sections 27.1.6 and 28.4, we need this assumption for equation (28.68b) below).

There is a close relation between the zonal momentum and axial angular momentum, with details provided in our study of geophysical particle dynamics in Sections 14.5 and 14.6. We choose to here study axial angular momentum since it has a slightly simpler budget (equation (28.64) discussed below) than the corresponding budget equation (28.53a) for zonal linear momentum. The simpler budget follows since axial angular momentum is directly connected to the axial symmetry of the rotating spherical planet (Sections 14.5 and 24.7).

To add a bit more generality to the analysis, we make use of spherical coordinates, though doing so offers only a modest degree of extra details beyond Cartesian coordinates. Although here focused on the ocean, many of the concepts and methods are directly relevant to a study of atmospheric axial angular momentum as introduced in Section 24.7 and discussed in Section 10.3 of *Holton and Hakim* (2013).

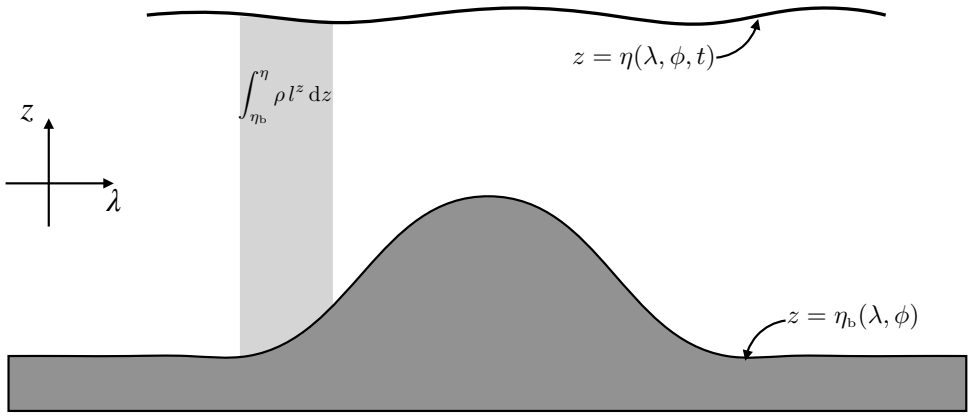

FIGURE 28.7: Schematic of the axial angular momentum for a fluid column, here depicted moving in an ocean with a topographic bump. In Section 28.5 we develop the budget for the depth and zonal integrated axial angular momentum in the ocean, where we see that the axial angular momentum is affected by a variety of boundary processes as well as interior transports and pressures.

28.5.1 Anticipating the budget

Before diving into the mathematical formulation, let us use some of the understanding gleaned from earlier sections of this chapter to anticipate the basic results. Doing so offers a framework to guide the maths, and to double check that the maths indeed renders a physically sensible budget.

For this purpose, consider a column of fluid such as shown in Figure 28.7. The forces acting on that column arise from contact forces (pressure stress, kinetic stress, and frictional stress) acting on the boundary (sides, top, and bottom), and body forces acting throughout the column (from effective gravity and Coriolis). There are further avenues for momentum to be transported across the ocean surface as part of the mass transported by rain, evaporation, and rivers. Each of these forces contribute a torque to the fluid column computed relative to the earth's rotational axis, thus modifying the axial angular momentum of the fluid column. In

the following development, we mathematically express the variety of forces and corresponding torques, thus building up the axial angular mometum budget.

28.5.2 Axial angular momentum

The axial angular momentum budget for a fluid element follows that developed in Section 24.7, here written with the addition of zonal friction

$$\rho \frac{\mathrm{D}l^z}{\mathrm{D}t} = -\frac{\partial p}{\partial \lambda} + r_\perp \rho F^\lambda, \tag{28.64}$$

where

$$l^z = r_\perp (u + r_\perp \Omega) \tag{28.65}$$

is the axial angular momentum per unit mass, and

$$r_\perp = r \cos\phi \tag{28.66}$$

is the distance to the polar rotation axis (the moment arm). For the primitive equations we set the radial position, r, to the earth radius, R_e, in the following.[5] Use of the Eulerian form of mass conservation (equation (19.6)) leads to the Eulerian flux-form budget

$$\frac{\partial(\rho l^z)}{\partial t} + \nabla \cdot (\rho \boldsymbol{v} l^z) = -\frac{\partial p}{\partial \lambda} + r_\perp \rho F^\lambda, \tag{28.67}$$

with $l^z \rho \, \mathrm{d}z$ the angular momentum per unit horizontal area. We use this form for the budget to develop the depth integrated axial angular momentum budget.

28.5.3 Depth integrated budget

Vertically integrating equation (28.67) over a column of ocean fluid renders a budget for the column-integrated axial angular momentum. As in Section 28.4.2, we here make use of Leibniz's Rule to reach the following identities that expose boundary contributions

$$\int_{\eta_b}^{\eta} \frac{\partial(\rho l^z)}{\partial t} \, \mathrm{d}z = \frac{\partial}{\partial t} \left[\int_{\eta_b}^{\eta} \rho l^z \, \mathrm{d}z \right] - \left[\rho l^z \frac{\partial \eta}{\partial t} \right]_{z=\eta} \tag{28.68a}$$

$$\int_{\eta_b}^{\eta} \nabla_h \cdot (\rho \boldsymbol{u} l^z) \mathrm{d}z = \nabla_h \cdot \left[\int_{\eta_b}^{\eta} \rho \boldsymbol{u} l^z \, \mathrm{d}z \right] - [\rho l^z \boldsymbol{u} \cdot \nabla \eta]_{z=\eta} + [\rho l^z \boldsymbol{u} \cdot \nabla \eta_b]_{z=\eta_b} \tag{28.68b}$$

$$\int_{\eta_b}^{\eta} \frac{\partial(\rho w l^z)}{\partial z} \, \mathrm{d}z = [w \rho l^z]_{z=\eta} - [w \rho l^z]_{z=\eta_b} . \tag{28.68c}$$

Equation (28.68c) made use of the primitive equations whereby the horizontal divergence operator is depth independent. The surface kinematic boundary condition (19.94) and bottom kinematic boundary condition (19.56) allow us to reach a reasonably tidy expression

$$\frac{\partial}{\partial t} \left[\int_{\eta_b}^{\eta} l^z \rho \, \mathrm{d}z \right] = [l^z Q_m]_{z=\eta} - \nabla_h \cdot \left[\int_{\eta_b}^{\eta} l^z \boldsymbol{u} \rho \, \mathrm{d}z \right] + \int_{\eta_b}^{\eta} \left[-\frac{\partial p}{\partial \lambda} + r_\perp \rho F^\lambda \right] \mathrm{d}z. \tag{28.69}$$

The budget (28.69) says that the depth integrated axial angular momentum per horizontal area in a horizontally fixed fluid column has a time tendency (left hand side) arising from the convergence of horizontal advection of axial angular momentum plus torques due to surface boundary mass fluxes, depth integrated zonal pressure gradients, and depth integrated irreversible stresses. This

[5] See also Exercise 27.1.

mathematical expression of the budget meets our expectations based on our understanding of the physical principles discussed in Section 28.5.1.

28.5.4 Atmospheric and topographic form stresses

We can further unpack the contribution from pressure in the budget (28.69) by making use of Leibniz's rule to write

$$-\int_{\eta_b}^{\eta} \frac{\partial p}{\partial \lambda}\, dz = -\frac{\partial P}{\partial \lambda} + p_a \frac{\partial \eta}{\partial \lambda} - p_b \frac{\partial \eta_b}{\partial \lambda}, \tag{28.70a}$$

where P is the depth-integrated pressure given by equation (28.38). We studied this decomposition of the pressure force in Section 28.2 and encountered it in Section 28.4.4. Again, we see that the depth integrated zonal pressure gradient has been decomposed into three terms: (i) zonal pressure differences integrated across the depth of the column, (ii) form stress imparted to the ocean from the atmospheric pressure, (iii) form stress imparted by the solid earth bottom topography onto the ocean.

28.5.5 Turbulent stresses at the surface and bottom

For turbulent stresses, we focus on the vertical transfer of zonal momentum arising from the vertical shear of horizontal stresses

$$\rho F^{\lambda} = \frac{\partial \tau^{\lambda}}{\partial z}, \tag{28.71}$$

where τ^{λ} is the zonal component to the stress vector.[6] When integrated vertically over an ocean column, $\int_{\eta_b}^{\eta} \rho F^{\lambda}\, dz$, this friction arises from stresses acting in the ocean surface and bottom boundary/Ekman layers (Chapter 33), where the stress arises from turbulent motions that transfer momentum vertically through these layers.

For the friction contribution, we make use of the primitive equations so that the axial moment-arm is approximated by its value at the ocean surface

$$r_{\perp} = r \cos\phi = (z + R) \cos\phi \approx R \cos\phi = R_{\perp}, \tag{28.72}$$

as per the shallow fluid approximation built into the hydrostatic primitive equations discussed in Section 27.1. This assumption allows us to write the frictional contribution to the angular momentum budget (28.69) in the form

$$\int_{\eta_b}^{\eta} r_{\perp}\, \rho F^{\lambda}\, dz \approx R_{\perp} \int_{\eta_b}^{\eta} \rho F^{\lambda}\, dz = R_{\perp}\, (\tau_a^{\lambda} - \tau_b^{\lambda}). \tag{28.73}$$

The final expression introduced τ_a^{λ}, which is the zonal component to the stress acting on the ocean surface imparted through interactions between the ocean and the overlying atmosphere and/or ice. The signs are such that $\tau_a^{\lambda} > 0$ transfers an eastward momentum to the ocean such as via a westerly wind stress. Likewise, the stress τ_b^{λ} is the zonal stress at the ocean bottom imparted through interactions between the ocean and the solid-earth. The signs are such that $\tau_b^{\lambda} > 0$ reflects the transfer of eastward momentum from the ocean to the solid-earth, or conversely the transfer of westward momentum from the earth to the ocean. The net contribution from vertical friction is thus given by the moment arm, $R_{\perp}$, multiplied by the difference in boundary stresses.

[6] As seen in equation (28.52), there are other turbulent terms associated with interior Reynolds stresses arising from horizontal shears. We omit these terms for the present analysis since they are generally smaller than stresses arising from vertical strains, and smaller than the turbulent stresses associated with surface and bottom boundary processes.

28.5.6 Summary budget for column integrated axial angular momentum

Bringing all the pieces together leads to the depth integrated axial angular momentum budget

$$\frac{\partial}{\partial t}\left[\int_{\eta_b}^{\eta} l^z \rho \, dz\right] = -\nabla_h \cdot \left[\int_{\eta_b}^{\eta} l^z \boldsymbol{u} \, \rho \, dz\right] - \frac{\partial P}{\partial \lambda} + [l^z Q_m]_{z=\eta} + p_a \frac{\partial \eta}{\partial \lambda} - p_b \frac{\partial \eta_b}{\partial \lambda} + R_\perp (\tau_a^\lambda - \tau_b^\lambda). \quad (28.74)$$

Other than assuming a specific form of the frictional stress given by equation (28.71), this result is the exact budget for the axial angular momentum in a column of ocean fluid satisfying the primitive equations.

Removing zonal means

We further isolate the processes contributing to the budget (28.74) by introducing the zonal mean operator

$$\overline{A} \equiv \frac{1}{L(\phi)} \int A \, d\lambda, \quad (28.75)$$

where

$$L(\phi) = (R_e \cos\phi) \, \Delta\lambda = R_\perp \, \Delta\lambda \quad (28.76)$$

is the zonal length of the domain as a function of latitude, ϕ, and $\Delta\lambda$ is the zonal extent of the domain in radians. For a domain that circles the planet, then $\Delta\lambda = 2\pi$. Other domains are possible, such as those in Figure 28.6. The corresponding zonal anomalies to the depth integrated pressure, sea surface height, and bottom topography are thus given by

$$P' = P - \overline{P} \qquad \text{and} \qquad \eta' = \eta - \overline{\eta} \qquad \text{and} \qquad \eta_b' = \eta_b - \overline{\eta_b}, \quad (28.77)$$

in which case equation (28.74) takes the form

$$\frac{\partial}{\partial t}\left[\int_{\eta_b}^{\eta} l^z \rho \, dz\right] = -\nabla_h \cdot \left[\int_{\eta_b}^{\eta} l^z \boldsymbol{u} \, \rho \, dz\right] - \frac{\partial P'}{\partial \lambda} + [l^z Q_m]_{z=\eta} + p_a \frac{\partial \eta'}{\partial \lambda} - p_b \frac{\partial \eta_b'}{\partial \lambda} + R_\perp (\tau_a^\lambda - \tau_b^\lambda). \quad (28.78)$$

Steady state balance

Steady state balances are of particular interest when studying the large-scale low frequency circulation. A steady state holds for the angular momentum budget (28.78) so long as the following balance is maintained

$$\nabla_h \cdot \left[\int_{\eta_b}^{\eta} l^z \boldsymbol{u} \, \rho \, dz\right] = -\frac{\partial P'}{\partial \lambda} + [l^z Q_m]_{z=\eta} + p_a \frac{\partial \eta'}{\partial \lambda} - p_b \frac{\partial \eta_b'}{\partial \lambda} + R_\perp (\tau_a^\lambda - \tau_b^\lambda). \quad (28.79)$$

Consequently, a steady state is realized if the horizontal divergence of depth integrated axial angular momentum advection (left hand side) is balanced by torques created by the variety of physical processes on the right hand side. We further examine these physical processes by studying the zonally integrated budget.

28.5.7 Steady domain integrated balance

Consider the area integral of the steady state balance (28.79) over the full ocean domain that is either periodic and/or has sloping side boundaries. In this case the divergence of the angular momentum transport integrates to zero, so that we are left with the balance

$$\int_{\phi_s}^{\phi_n} \left(\int_{\lambda_w(\phi)}^{\lambda_e(\phi)} \left[[l^z Q_m]_{z=\eta} + p_a' \frac{\partial \eta'}{\partial \lambda} - p_b' \frac{\partial \eta_b'}{\partial \lambda} + R_\perp (\tau_a^\lambda - \tau_b^\lambda) \right] d\lambda \right) R_e^2 \cos\phi \, d\phi = 0. \quad (28.80)$$

In computing the area integral, we chose to first integrate over the longitudinal domain, $\lambda_w(\phi) \leq \lambda \leq \lambda_e(\phi)$, which is a function of latitude, and then to integrate over the full latitudinal domain, $\phi_s \leq \phi \leq \phi_n$. In most applications the surface mass term, $[l^z Q_{\rm m}]_{z=\eta}$, is smaller than the other terms, in which case the balance is between the boundary form stresses and the boundary turbulent stresses.

In the angular momentum balance (28.80), we introduced the zonal anomalies for the applied surface pressure and the bottom pressure

$$p'_{\rm a}(\lambda,\phi) = p_{\rm a}(\lambda,\phi) - \overline{p_{\rm a}}(\phi) \qquad \text{and} \qquad p'_{\rm b}(\lambda,\phi) = p_{\rm b}(\lambda,\phi) - \overline{p_{\rm b}}(\phi). \tag{28.81}$$

We can introduce these anomalous fields since their zonal averages do not contribute to the budgets in either the periodic or sloping shoreline domains. To verify this property, note that

$$\int \overline{p_{\rm a}}\, \frac{\partial \eta'}{\partial \lambda}\, {\rm d}\lambda = \int \frac{\partial(\overline{p_{\rm a}}\, \eta')}{\partial \lambda}\, {\rm d}\lambda = 0. \tag{28.82}$$

For a periodic domain this term vanishes by inspection. For a zonally bounded domain with a sloping shoreline, it also vanishes since $\eta' = 0$ at the edge of the shoreline. Likewise, the bottom pressure term satisfies

$$\int \overline{p_{\rm b}}\, \frac{\partial \eta'_{\rm b}}{\partial \lambda}\, {\rm d}\lambda = \int \frac{\partial(\overline{p_{\rm b}}\, \eta'_{\rm b})}{\partial \lambda}\, {\rm d}\lambda = 0, \tag{28.83}$$

which follows either by periodicity or since $\eta'_{\rm b} = 0$ along the edge of a sloping shoreline. In conclusion, we see that it is only the zonal anomalies of the atmospheric and bottom pressures, and free surface and bottom topography, that impact the zonal mean zonal momenum balance (28.85) for the periodic and sloping shoreline domains.

28.5.8 Form stress versus dual form stress

We can further exploit symmetry of the periodic domain and sloping shoreline domain by writing the form stresses in equation (28.85) in an alternative manner that makes use of the dual form stress

$$\int \left[p'_{\rm a}\, \frac{\partial \eta'}{\partial \lambda} - p'_{\rm b}\, \frac{\partial \eta'_{\rm b}}{\partial \lambda} \right] {\rm d}\lambda = \int \left[-\frac{\partial p'_{\rm a}}{\partial \lambda}\, \eta' + \frac{\partial p'_{\rm b}}{\partial \lambda}\, \eta'_{\rm b} \right] {\rm d}\lambda. \tag{28.84}$$

Diagnostics of zonally integrated form stress can be more convenient using one form or the other, depending on dataset or numerical model framework. We have a choice since the zonal integral is the same, and that freedom is afforded since the spatial integral removes local information that appears as a total zonal derivative. However, we offer two caveats in this regard.

- The identity (28.84) does not hold for the bounded domain with vertical sidewalls (third panel of Figure 28.6). If working in such a domain and if one chooses to study patterns based on the right hand side dual form stress, then its zonal integral will not agree with that of the form stress on the left hand side. Correspondingly, physical interpretations based on the dual form stress are questionable.

- Although the zonal integrals in equation (28.84) agree for the periodic domain and sloping shoreline domain, there is no local identity between terms on the left hand side and right hand side. So if one wishes to make a statement about patterns of local form stresses acting on the depth integrated axial angular momentum, then it is necessary to return to the form stress appearing on the left hand side of equation (28.84).

28.5.9 Steady zonal and depth integrated budget

Now consider just a zonal integral of the steady angular momentum budget (28.79), again over a domain that is either periodic or has sloping shorelines (Figure 28.6). In both of these cases, we are left with the zonal and depth integrated steady angular momentum budget

$$\frac{1}{R\cos\phi}\int \frac{\partial}{\partial\phi}\left[\int_{\eta_b}^{\eta} l^z\, v\, \rho\, dz\right] d\lambda = \int \left[[l^z Q_m]_{z=\eta} + p'_a \frac{\partial\eta'}{\partial\lambda} - p'_b \frac{\partial\eta'_b}{\partial\lambda} + R_\perp\,(\tau^\lambda_a - \tau^\lambda_b)\right] d\lambda. \quad (28.85)$$

The meridional divergence of the advective transport of angular momentum is balanced, in the steady state, by the boundary terms on the right hand side.

28.5.10 Southern Ocean balances

Under certain cases the primary balance in equation (28.85) is between the form stress and boundary turbulent stress, whereby

$$\oint \left[p'_a \frac{\partial\eta'}{\partial\lambda} + R_\perp\,\tau^\lambda_a\right] d\lambda \approx \oint \left[p'_b \frac{\partial\eta'_b}{\partial\lambda} + R_\perp\,\tau^\lambda_b\right] d\lambda. \quad (28.86)$$

For much of the large-scale Southern Ocean circulation, the primary balance is even simpler: it is a balance between surface wind stress and topographic form stress

$$\oint \tau^\lambda_a\, d\lambda \approx \oint p'_b \frac{1}{R_\perp}\frac{\partial\eta'_b}{\partial\lambda}\, d\lambda = -\oint \eta'_b \frac{1}{R_\perp}\frac{\partial p'_b}{\partial\lambda}\, d\lambda, \quad (28.87)$$

with this balance exemplified in Figure 28.8. We now state in words what this balance means in the presence of a net eastward wind stress, $\oint \tau^\lambda_a\, d\lambda > 0$. The equivalent expressions on the right hand side allow complementary perspectives.

- For the first equality in equation (28.87) we see that a balance is realized if on the upwind side of a topographic bump there is an anomalously high bottom pressure, with the opposite on the downwind side. Correspondingly, there is a net westward topographic form stress imparted by the solid earth onto the ocean that balances the eastward surface wind stress imparted by the atmosphere onto the ocean.

- The second equality in equation (28.87) reveals that for $\eta'_b > 0$ (topographic ridge), a steady angular momentum balance is maintained so long as the bottom pressure decreases across the ridge from west to east, just as depicted in Figure 28.8.

28.5.11 Topographic form stress and ocean gyres

Hughes (2000) and *Hughes and de Cueves* (2001) are notable for having emphasized the importance of bottom topographic form stress, and the associated bottom pressure torque appearing in the vorticity equation (detailed in see Section 40.9). The key role for topographic form stress is well appreciated for channel flows since the work of *Munk and Palmén* (1951) who studied the Southern Ocean steady force balances (see also *Webb and de Cueves* (2007) for studies of the transient case). However, *Hughes* (2000) and *Hughes and de Cueves* (2001) showed that it is central even for steady ocean gyre circulations when allowing for sloping sides rather than vertical sides. Hence, sloping sides for the gyre domain allow for a steady momentum balance to occur between bottom form stress and wind stress, and a steady vorticity balance to occur between bottom pressure torque and wind stress curl. As a result, topographic form stress and bottom pressure torques allow for a mostly inviscid balance in ocean gyres much like for the

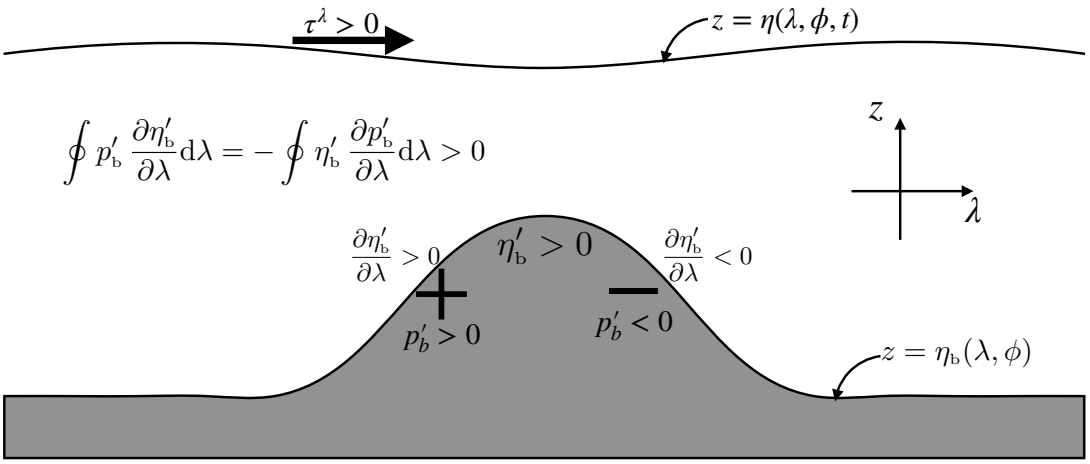

FIGURE 28.8: Depicting the balance between zonal wind stress and topographic form stress for a southern hemisphere zonally periodic ocean channel. For an eastward wind stress, the flow reaches a steady state if the upwind side of a topographic bump sees an anomalously high bottom pressure whereas on the downwind side it is anomalously low. The form stress imparted by the ocean onto the solid earth is eastward since the bottom pressure is higher in the west and lower in the east. Conversely, Newton's third law tells us that the topographic form stress imparted by the solid earth onto the ocean is westward. In this manner, the eastward force imparted by the atmosphere onto the ocean through wind stress is balanced by a westward topographic form stress imparted by the solid earth onto the ocean. Furthermore, the eastward bottom pressure gradient leads to a northward depth integrated geostrophic transport above the southern hemisphere ridge. Signs are swapped when flow moves over a depression, in which a westward bottom pressure gradient leads to southward geostrophic transport over the depression. We revisit these dynamical processes for the shallow water fluid in Figure 36.8.

zonally re-entrant Southern Ocean. We return to these points in Section 39.7, in particular in Section 39.7.6, when studying gyre circulations in a shallow water fluid.

28.5.12 Further study

Elements of this section are based on *Hughes* (2000) and *Hughes and de Cueves* (2001), as well as the analogous discussion of the global atmospheric axial angular momentum budget developed in Section 10.3 of *Holton and Hakim* (2013). *Straub* (1993) provides an analogous analysis with a focus on the Southern Ocean. The physical processes establishing the balances noted for the Southern Ocean remain under investigation, with further resources to the literature including Section 21.7 of *Vallis* (2017), and the reviews by *Rintoul et al.* (2001), *Rintoul and Naveira Garabato* (2013), and *Rintoul* (2018). We further revisit this balance in Section 36.7 for the shallow water system.

Chapter 29

The Boussinesq ocean

In some areas of fluid mechanics the speed of fluid particles can approach the speed of sound. In that case, the *Mach number*, which is the ratio of the fluid particle speed to the speed of sound waves, reaches unity or larger.[1] In such flows it is important to consider the influence of compressibility since the large flow speeds can lead to nontrivial local density changes through the convergence of advective mass fluxes.

Many of the geophysical flows studied in this book, particularly ocean flows, have Mach numbers well below unity. Hence, their local density changes are generally much smaller than the mean density.[2] Yet even with a small Mach number, pressure can play a nontrivial role in affecting density changes for those cases where motions extend over vertical distances comparable to the *scale height*. For the atmosphere, the scale height (Section 23.4.10) is roughly 10 km, whereas the ocean's scale height is generally deeper than the ocean. For this reason, compressibility effects are generally important for atmospheric motions, whereas they can be neglected for many purposes in ocean fluid mechanics.

Because compressibility effects are relatively weak in the ocean, the ocean velocity field is well approximated as non-divergent, thus allowing for the volume conserving kinematics from Chapter 21. Even with this approximation, it is crucial to note that the ocean is not an incompressible fluid since density is not uniform, and so we need something more than incompressible fluid mechanics.[3] It is for this purpose that we here develop the *Boussinesq ocean* equations, which sit somewhere between the fully compressible fluids (i.e., *non-Boussinesq* fluids) and incompressible flows.

In brief, the Boussinesq ocean velocity is non-divergent, thus representing an incompressible flow, and yet the Boussinesq ocean fluid admits density variations, as for a compressible fluid. That is, the study of a Boussinesq ocean concerns the incompressible flow of a compressible fluid, thus exemplifying the important distinction between a *fluid property* versus a *flow property*. Since the flow is non-divergent, the pressure in the Boussinesq ocean is not the thermodynamic pressure found in the compressible non-Boussinesq fluid studied in Part IV of this book. Rather, Boussinesq pressure serves a purely mechanical role by acting as the Lagrange multipler to constrain the Boussinesq flow to be non-divergent.[4]

[1] When a jet airplane or rocket moves at a speed greater than Mach one, such super-sonic motion generates a spectacularly loud and powerful sonic boom. In Section 51.5.2 we provide a more precise measure of the Mach number in terms of fluctuations of the density. For purposes of the present chapter, density fluctuations are very small and thus correspond to a tiny Mach number.

[2] In Section 51.5.2 in our study of acoustics, we see precisely how a density fluctuation is related to the Mach number.

[3] The fluid mechanics of constant density fluids is sometimes referred to as *hydrodynamics*. Certain idealized models of geophysical fluid mechanics follow the approaches of hydrodynamics; e.g., the single layer of constant density shallow water fluid studied in Part VI of this book. However, density variations are crucial for many atmosphere and ocean flows.

[4] We see this role for pressure as a Lagrange multiplier when studying Hamilton's principle for a Boussinesq ocean in Section 48.2. See also Section 59A of *Serrin* (1959) for more on pressure in a non-divergent flow.

READER'S GUIDE TO THIS CHAPTER

We here derive the Boussinesq ocean equations and explore their physical properties, including energetics. The Boussinesq ocean has broader application than just to the ocean, with many characteristics also holding for atmospheric flow satisfying the anelastic approximation (see Section 2.5 of *Vallis* (2017)). Furthermore, the Boussinesq ocean provides the starting point for many of the geophysical fluid models found later in this book. This is a relatively long chapter due to the broad use of the Boussinesq ocean in this book, which in turn motivates us to explore many of its facets.

29.1 The Boussinesq ocean approximation

For the ocean, density deviates no more than a few percent relative to the volume mean density. Although small, ocean density deviations act over large distances and are crucial for driving large-scale circulations. Such *thermohaline circulations* derive their driving force from variations in temperature and salinity that affect density and, in turn, modify the pressure. A key reason that small density changes can be so pivotal is that the density variations are multiplied by the relatively large gravitational acceleration when computing pressure. The oceanic Boussinesq approximation provides a systematic means to ignore small density deviations where it is safe to do so dynamically, while retaining density variations where they are critical such as when multiplied by gravity. In brief, the oceanic Boussinesq approximation makes use of (a slightly modified) compressibile thermodynamics plus an incompressible kinematics. The use of compressible thermodynamics allows for thermohaline processes to modify density and thus pressure, while the incompressible kinematics removes sound waves and renders the volume of a fluid element materially invariant.

29.1.1 Isolating the dynamically active pressure field

Pressure in a vertically stratified fluid can be decomposed into a static background hydrostatic pressure plus a deviation from the background pressure. We made use of this decomposition in Section 27.2.4 when developing the scaling for the hydrostatic approximation. The decomposition holds even when the fluid is non-hydrostatic. We consider the background pressure to be a function just of depth and as such it is determined by a static and horizontally homogeneous background density field. We are motivated to introduce this decomposition given that the background hydrostatic pressure field (again, it is just a function of depth) is dynamically inactive (as shown below). This decomposition is exact and motivated by the desire to isolate the dynamically active part of the equations of motion.

To achieve the pressure decomposition, start by decomposing density according to

$$\rho(\boldsymbol{x}, t) = \rho_{\circ}(z) + \rho'(\boldsymbol{x}, t) \tag{29.1}$$

where the deviation density is much smaller than the reference density

$$\rho' \ll \rho_\circ. \tag{29.2}$$

The following formulation for the momentum equation holds for the general case of $\rho_\circ(z)$. However, we note in Section 29.1.2 that setting $\rho_\circ(z) = \rho_\circ$ is motivated for studies of potential vorticity in the Boussinesq ocean. Indeed, a space and time constant reference density is generally synonymous with the oceanic Boussinesq approximation.[5]

The corresponding decomposition of pressure is given by the sum of a static and depth dependent background pressure, $p_\circ(z)$, and a deviation pressure, $p'(\boldsymbol{x}, t)$,

$$p(\boldsymbol{x}, t) = p_\circ(z) + p'(\boldsymbol{x}, t). \tag{29.3}$$

The background pressure is assumed to be in hydrostatic balance with the reference density

$$\frac{\mathrm{d}p_\circ}{\mathrm{d}z} = -\rho_\circ\, g, \tag{29.4}$$

with $p_\circ$ and $\rho_\circ$ both static. We offer the following points to clarify the decomposition of pressure in equation (29.3).

- Assuming the background pressure, $p_\circ(z)$, to be hydrostatic does *not* imply that the full pressure, $p(\boldsymbol{x}, t)$, is also hydrostatic. Rather, the decomposition merely serves to remove that portion of the pressure field that plays no role in establishing motion (we see this property below). So this decomposition holds whether the full pressure is approximately hydrostatic or fully non-hydrostatic.
- Furthermore, if $p(\boldsymbol{x}, t)$ is in an approximate hydrostatic balance (Section 27.2), the decomposition (29.3) does *not* remove all of the hydrostatic pressure from $p(\boldsymbol{x}, t)$. Rather, $p'(\boldsymbol{x}, t)$ is generally nonzero whether $p(\boldsymbol{x}, t)$ is in an approximate hydrostatic balance or fully non-hydrostatic.

With the above density and pressure decompositions, the momentum equation

$$\rho \left[\frac{\mathrm{D}\boldsymbol{v}}{\mathrm{D}t} + 2\, \boldsymbol{\Omega} \times \boldsymbol{v} \right] = -\nabla p - \hat{\boldsymbol{z}}\, g\, \rho \tag{29.5}$$

takes the equivalent form

$$(\rho_\circ + \rho') \left[\frac{\mathrm{D}\boldsymbol{v}}{\mathrm{D}t} + 2\, \boldsymbol{\Omega} \times \boldsymbol{v} \right] = -\nabla p' - g\, \rho'\, \hat{\boldsymbol{z}} - \left[\frac{\mathrm{d}p_\circ}{\mathrm{d}z} + \rho_\circ\, g \right] \hat{\boldsymbol{z}} \tag{29.6a}$$

$$= -\nabla p' - g\, \rho'\, \hat{\boldsymbol{z}}, \tag{29.6b}$$

where we used the hydrostatic balance (29.4) for the second equality. We thus see that the background hydrostatic pressure, $p_\circ(z)$, leads to no motion since it drops out from the momentum equation. The gradient pressure force is thus determined solely by the gradient of p'.

29.1.2 Boussinesq momentum equation

To develop the Boussinesq momentum equation, divide the momentum equation (29.6b) by the density, $\rho = \rho_\circ + \rho'$, and write the pressure and gravity terms as

$$\frac{\nabla p' + g\, \rho'\, \hat{\boldsymbol{z}}}{\rho_\circ + \rho'} = \frac{\nabla p' + g\, \rho'\, \hat{\boldsymbol{z}}}{\rho_\circ + \rho'} \left[\frac{\rho_\circ - \rho'}{\rho_\circ - \rho'} \right] = \frac{\nabla p' + g\, \rho'\, \hat{\boldsymbol{z}}}{\rho_\circ^2 - (\rho')^2} (\rho_\circ - \rho') \approx \frac{\nabla p' + g\, \rho'\, \hat{\boldsymbol{z}}}{\rho_\circ}, \tag{29.7}$$

[5] Exercise 29.3 offers a modest means to generalize this assumption.

where the final approximation results from dropping all terms that are second order in deviation quantities. This approximation then leads to the Boussinesq momentum equation

$$\frac{\mathrm{D}\boldsymbol{v}}{\mathrm{D}t} + 2\,\boldsymbol{\Omega} \times \boldsymbol{v} = -\frac{1}{\rho_\circ}\,\nabla p' + b\,\hat{\boldsymbol{z}}, \tag{29.8}$$

where we introduced the globally referenced *Archimedean buoyancy* (Chapter 30) as defined relative to the constant background density

$$b = -\frac{g\,\rho'}{\rho_\circ} = -\frac{g\,(\rho - \rho_\circ)}{\rho_\circ}. \tag{29.9}$$

Hence, the globally referenced Archimedean buoyancy is positive when the *in situ* density is less than the reference density so that $\rho' = \rho - \rho_\circ < 0$. That is, $b > 0$ when the fluid element is lighter (more buoyant) than the background reference density. Buoyancy is the product of the gravitational acceleration, which is a relatively large term, and the small number $\rho'/\rho_\circ$. Their product is generally not small so that it generally cannot be neglected from the momentum equation. This is a key point in producing a Boussinesq ocean equation set that contains dynamical processes arising from horizontal buoyancy gradients.

In the special case of a space and time constant reference density, $\rho_\circ(z) = \rho_\circ$, it is convenient to introduce the shorthand for the deviation pressure normalized by the reference density

$$\varphi = \frac{p'}{\rho_\circ} = \frac{p - p_\circ(z)}{\rho_\circ}. \tag{29.10}$$

In this case the Boussinesq momentum equation takes the form

$$\frac{\mathrm{D}\boldsymbol{v}}{\mathrm{D}t} + 2\,\boldsymbol{\Omega} \times \boldsymbol{v} = -\nabla\varphi + b\,\hat{\boldsymbol{z}}. \tag{29.11}$$

29.1.3 A vorticity motivation to set $\rho_\circ$ constant

We now anticipate a later discussion of vorticity and potential vorticity to motivate setting $\rho_\circ(z)$ to a constant. This paragraph is not critical for the remainder of this chapter, but worth returning to after studying baroclinicity for the Boussinesq fluid in Section 40.7.2. For that purpose, we note that the form of the pressure gradient acceleration found in equation (29.11) is particularly useful given that the curl of the right hand side eliminates pressure from the vorticity equation (Section 40.7.1). In contrast, for the more general form with $\rho_\circ(z)$ in equation (29.8), the Boussinesq baroclinicity vector (equation (40.152)) has a contribution from both pressure and buoyancy (we derive equation (29.12) in Exercise 40.7)

$$\boldsymbol{B} = \nabla\left[b - \frac{p'}{\rho_\circ^2}\frac{\mathrm{d}\rho_\circ}{\mathrm{d}z}\right] \times \hat{\boldsymbol{z}}. \tag{29.12}$$

The additional pressure contribution complicates the development of potential vorticity whereby we wish to have $\boldsymbol{B} \cdot \nabla b = 0$ (see Section 41.5.1). We are thus movitated to use a space and time constant reference density so that $\mathrm{d}\rho_\circ/\mathrm{d}z = 0$. Following this motivation, we generally assume $\rho_\circ$ is a constant in this book. Even so, in Exercise 29.3 we discuss a middle ground by defining a slightly more general buoyancy field while retaining a constant $\rho_\circ$.

29.1.4 Mass continuity

When decomposing density according to equation (29.1), the mass continuity equation (Section 19.2)

$$\frac{\mathrm{D}\rho}{\mathrm{D}t} = -\rho\,\nabla\cdot\boldsymbol{v}, \tag{29.13}$$

takes the form

$$\frac{\mathrm{D}\rho'}{\mathrm{D}t} = -(\rho_\circ + \rho')\,(\nabla_\mathrm{h}\cdot\boldsymbol{u} + \partial_z w). \tag{29.14}$$

For many geophysical flows, the material time derivative on the left hand side is much smaller than either of the two terms appearing on the right hand side. To help formalize this observation it is useful to introduce a time scale for the various terms in this equation

$$\left|\frac{1}{\rho}\frac{\mathrm{D}\rho'}{\mathrm{D}t}\right| \sim \frac{1}{T_\rho} \qquad |\partial_x u| \sim T_u^{-1} \qquad |\partial_y v| \sim T_v^{-1} \qquad |\partial_z w| \sim T_w^{-1}. \tag{29.15}$$

Quite often we find flows in which the time scales associated with the spatial deformations of the flow, in the direction of the flow, are much smaller than time scales for the material changes in density, whereby

$$T_u^{-1}, T_v^{-1}, T_w^{-1} \gg T_\rho^{-1}. \tag{29.16}$$

In this case the only way for the mass balance equation (29.14) to hold is for the three terms contributing to the divergence to balance one another

$$\partial_x u + \partial_y v + \partial_z w \approx 0. \tag{29.17}$$

Taking this balance to the limit motivates setting the velocity field for the Boussinesq ocean to be non-divergent

$$\nabla\cdot\boldsymbol{v} = 0. \tag{29.18}$$

Note that for density stratified flows we generally find the horizontal divergence of the horizontal velocity balancing the vertical convergence of the vertical velocity. For a Boussinesq ocean this balance is exact

$$\nabla_\mathrm{h}\cdot\boldsymbol{u} = -\partial_z w. \tag{29.19}$$

29.1.5 Dependence on reference density

How does the solution compare when considering two distinct reference densities, say $\rho_\circ \neq \rho_1$? To answer this question, write the inviscid Boussinesq velocity equation in the form

$$(\partial_t + \boldsymbol{v}_0\cdot\nabla)\,\boldsymbol{v}_0 + 2\,\boldsymbol{\Omega}\times\boldsymbol{v}_0 = -\nabla\varphi_0 + b_0\,\hat{\boldsymbol{z}} \tag{29.20a}$$

$$(\partial_t + \boldsymbol{v}_1\cdot\nabla)\,\boldsymbol{v}_1 + 2\,\boldsymbol{\Omega}\times\boldsymbol{v}_1 = -\nabla\varphi_1 + b_1\,\hat{\boldsymbol{z}}. \tag{29.20b}$$

Consider an initial condition in which

$$\rho_\circ\,\boldsymbol{v}_0 = \rho_1\,\boldsymbol{v}_1, \tag{29.21}$$

and with pressure and buoyancy initialized so that

$$\rho_\circ\,(-\nabla\varphi_0 + b_0\,\hat{\boldsymbol{z}}) = \rho_1\,(-\nabla\varphi_1 + b_1\,\hat{\boldsymbol{z}}) = -\nabla p - g\,\rho\,\hat{\boldsymbol{z}}. \tag{29.22}$$

Hence, the difference between equations (29.20a) and (29.20b) takes the form

$$\partial_t(\rho_\circ\,\boldsymbol{v}_0 - \rho_1\,\boldsymbol{v}_1) = -(\rho_\circ\,\boldsymbol{v}_0\cdot\nabla)\,\boldsymbol{v}_0 + (\rho_1\,\boldsymbol{v}_1\cdot\nabla)\,\boldsymbol{v}_1 \tag{29.23a}$$

$$= -[(\rho_1 - \rho_\circ)/\rho_\circ]\,(\boldsymbol{v}_1 \cdot \nabla)\,\boldsymbol{v}_1. \tag{29.23b}$$

The difference in reference densities allows for the nonlinear self-advection to evolve the difference $\rho_\circ\,\boldsymbol{v}_0 - \rho_1\,\boldsymbol{v}_1$. This property of the oceanic Boussinesq equations must be kept in mind if comparing numerical solutions using distinct reference densities. Namely, a Boussinesq ocean is dependent on the reference density through the nonlinear advection term.

29.1.6 Version I of the Boussinesq ocean equations

The first form of the oceanic Boussinesq equations emphasizes the role of buoyancy computed relative to a reference state of constant density, $\rho = \rho_\circ$. This form facilitates a focus on that portion of the pressure field giving rise to internal or baroclinic pressure gradients; i.e., those pressure gradients that generate motion independent of free surface undulations. The oceanic Boussinesq equations thus take the form

$$\frac{\mathrm{D}\boldsymbol{v}}{\mathrm{D}t} + 2\,\boldsymbol{\Omega} \times \boldsymbol{v} = -\nabla\varphi + b\,\hat{\boldsymbol{z}} + \boldsymbol{F} \qquad \text{velocity equation} \tag{29.24a}$$

$$\nabla \cdot \boldsymbol{v} = 0 \qquad \text{continuity equation} \tag{29.24b}$$

$$\frac{\mathrm{D}b}{\mathrm{D}t} = \dot{b} \qquad \text{buoyancy equation} \tag{29.24c}$$

$$b = -\frac{g\,\rho'}{\rho_\circ} = -\frac{g\,(\rho - \rho_\circ)}{\rho_\circ} \qquad \text{buoyancy defined} \tag{29.24d}$$

$$\varphi = \frac{p'}{\rho_\circ} = \frac{p - p_\circ(z)}{\rho_\circ} \qquad \text{dynamic pressure defined} \tag{29.24e}$$

$$\rho = \rho_\circ\,(1 - \alpha\,\Theta + \beta\,S) \qquad \text{linear equation of state} \tag{29.24f}$$

$$\frac{\mathrm{d}p_\circ}{\mathrm{d}z} = -\rho_\circ\,g \qquad \text{background hydrostatic pressure.} \tag{29.24g}$$

We offer the following comments on these equations.

- MATERIAL EVOLUTION OF BUOYANCY: The term $\dot{b}$ on the right hand side of the buoyancy equation (29.24c) is a placeholder for any process leading to a material change in buoyancy. We discuss some explicit examples of $\dot{b} \neq 0$ in Section 29.7.1.

- EQUATION OF STATE: The equation of state, (29.24f), is written as a linear function of salinity and Conservative Temperature, with the thermal expansion coefficient, α, and haline contraction coefficient, β, assumed constant.[6] This form for the equation of state eliminates processes such as cabbeling and thermobaricity, which are discussed in Section 72.3. These processes are important for certain features of the ocean, thus prompting the more general equation set written in Section 29.1.7. However, the linear equation of state is sufficient for many of our studies in this book, as is the further simplified form with zero haline contraction, $\beta = 0$.

- APPROXIMATED HYDROSTATIC BALANCE: Most numerical models of the large-scale ocean circulation are in approximate hydrostatic balance. Assuming this balance holds in the velocity equation (29.24a) leads to the split into a horizontal velocity equation plus a

[6] It is unfortunate that β is used for two prominent but very distinct properties of geophysical fluids. First, it is the meridional derivative of the Coriolis parameter: $\beta = \partial_y f$. Second, it is the haline contraction coefficient: $\beta = \rho^{-1}\partial\rho/\partial S$. These distinct uses will be clearly defined so to avoid confusion.

vertical hydrostatic balance

$$\frac{\mathrm{D}\boldsymbol{u}}{\mathrm{D}t} + 2\,\boldsymbol{\Omega} \times \boldsymbol{v} = -\nabla_{\mathrm{h}}\varphi + \boldsymbol{F}^{h} \qquad \text{horizontal velocity equation} \tag{29.25a}$$

$$\frac{\partial \varphi}{\partial z} = b \qquad \text{approximate hydrostatic balance,} \tag{29.25b}$$

where ∇_{h} is the horizontal gradient operator and $\boldsymbol{F}^{h}$ is the horizontal frictional acceleration. As emphasized in Section 27.1 when deriving the hydrostatic primitive equations, that approximate hydrostatic approximation leads to a vertical velocity equation with no friction nor Coriolis contribution. Rather, when making the hydrostatic approximation we just retain a balance between the vertical pressure gradient and gravity/buoyancy.

29.1.7 Version II of the Boussinesq ocean equations

The non-hydrostatic Boussinesq equations (29.24a)-(29.24g) are suited for many purposes in this book. However, the following form is better suited to studying or simulating realistic Boussinesq ocean flows, with such flows involving separate prognostic equations for salinity and Conservative Temperature rather than a single prognostic equation for buoyancy. We are thus movitated to consider the Boussinesq ocean equations in the form

$$\frac{\mathrm{D}\boldsymbol{v}}{\mathrm{D}t} + 2\,\boldsymbol{\Omega} \times \boldsymbol{v} = -(1/\rho_{\circ})\,(\nabla p + \rho\,\nabla\Phi) + \boldsymbol{F} \qquad \text{velocity equation} \tag{29.26a}$$

$$\nabla \cdot \boldsymbol{v} = 0 \qquad \text{continuity equation} \tag{29.26b}$$

$$\frac{\mathrm{D}S}{\mathrm{D}t} = \dot{S} \qquad \text{salinity equation} \tag{29.26c}$$

$$\frac{\mathrm{D}\Theta}{\mathrm{D}t} = \dot{\Theta} \qquad \text{Conservative Temperature equation} \tag{29.26d}$$

$$\rho = \rho(S, \Theta, \Phi) \qquad \text{equation of state.} \tag{29.26e}$$

We make the following comments concerning these equations.

- GEOPOTENTIAL: The geopotential is here considered to be a function of space and time, as relevant when studying the role of astronomical tidal forcing or changes to the mass distribution of the planet (see Chapter 34)

$$\Phi = \Phi(\boldsymbol{x}, t). \tag{29.27}$$

- EQUATION OF STATE: The equation of state is a function of salinity, Conservative Temperature, and geopotential, thus allowing for processes such as cabelling and thermobaricity (see Section 72.3). Furthermore, the pressure dependence in the equation of state is computed as per a homogeneous and resting hydrostatic fluid

$$\rho(S, \Theta, \Phi) = \rho(S, \Theta, p = -\rho_{\circ}\,\Phi). \tag{29.28}$$

  In Section 29.8 we provide an energetic argument for why it is appropriate to take this functional form rather than the more general form discussed in Section 30.3, in which density is a function of the full *in situ* pressure: $\rho = \rho(S, \Theta, p)$.

- HYDROSTATIC APPROXIMATION: As for version I of the Boussinesq ocean equations, we here list the equations when making the hydrostatic approximation in the vertical momentum equation, in which case the velocity equation (29.26a) splits into a horizontal velocity

equation and hydrostatic balance

$$\frac{\mathrm{D}\boldsymbol{u}}{\mathrm{D}t} + 2\,\boldsymbol{\Omega} \times \boldsymbol{v} = -(1/\rho_o)\,(\boldsymbol{\nabla}_h p + \rho\,\boldsymbol{\nabla}_h \Phi) + \boldsymbol{F}^h \qquad \text{horizontal velocity equation} \tag{29.29a}$$

$$\frac{\partial p}{\partial z} = -g\,\rho \qquad \text{hydrostatic balance.} \tag{29.29b}$$

29.1.8 Boussinesq inertial mass is not the gravitational mass

The *inertial mass* is the mass multiplying acceleration on the right hand side Newton's law of motion, $\boldsymbol{F} = m\,\boldsymbol{a}$, and it is correspondingly used to measure kinetic energy. The *gravitational mass* is the mass used to compute the gravitational force, and so it is the mass used when computing weight, buoyancy, and gravitational potential energy. The *principle of equivalence*, originating from the work of Galileo and forming a key element to Einstein's relativity theory, states that the gravitational mass and the inertial mass are the same. The principle of equivalance is embedded into the use of Newtonian mechanics, so much so that we routinely assume that inertial mass and gravitational mass are identical.

A Boussinesq ocean fluid element materially conserves its volume since the velocity is non-divergent (recall the kinematics of non-divergent flows studied in Chapter 21). In turn, the inertial mass of a Boussinesq fluid element is measured by multiplying its volume by the constant reference density, ρ_o. In contrast, whenever there is a gravitational acceleration multiplying density, the Boussinesq fluid element retains the full *in situ* density to measure the weight of the fluid element. Use of *in situ* density for the gravitational mass ensures an accurate representation of the gravitational force, hydrostatic pressure (Section 29.2.7), buoyancy (Chapter 30) and the gravitational potential energy (Sections 29.6 and 29.8). Evidently, the Boussinesq ocean *does not* respect the principle of equivalance since it distinguishes between the inertial mass and the gravitational mass.

The following offers a summary of various properties of a Boussinesq fluid element related to its distinct inertial mass and gravitational mass:

$$\text{inertial mass density} = \rho_o \tag{29.30a}$$

$$\text{inertial mass} = \rho_o\,\delta V \tag{29.30b}$$

$$\text{linear momentum} = \boldsymbol{v}\,\rho_o\,\delta V \tag{29.30c}$$

$$\text{kinetic energy} = \rho_o\,\delta V\,\boldsymbol{v}\cdot\boldsymbol{v}/2 \tag{29.30d}$$

$$\text{tracer mass} = C\,\rho_o\,\delta V \tag{29.30e}$$

$$\text{enthalpy content} = c_p\,\Theta\,\rho_o\,\delta V \tag{29.30f}$$

$$\text{gravitational mass density} = \rho \tag{29.30g}$$

$$\text{gravitational mass} = \rho\,\delta V \tag{29.30h}$$

$$\text{gravitational force (weight)} = -\rho\,\delta V\,\nabla\Phi \tag{29.30i}$$

$$\text{gravitational force (weight) with simple geopotential} = -g\,\rho\,\delta V\,\hat{\boldsymbol{z}} \tag{29.30j}$$

$$\text{gravitational potential energy} = \Phi\,\rho\,\delta V \tag{29.30k}$$

$$\text{gravitational potential energy with simple geopotential} = g\,z\,\rho\,\delta V. \tag{29.30l}$$

29.1.9 Summary points

We close this section by summarizing a number of conceptual points characterizing the Boussinesq ocean. It is useful to return to this list to help avoid common conceptual confusions.

Divergent and non-divergent velocity components

The velocity that results from the Boussinesq momentum equation (i.e., the prognostic Boussinesq velocity) is non-divergent. This is the velocity used for transport as per the material time derivative operator. Additionally, there is a divergent velocity field, $\boldsymbol{v}^{\mathrm{d}}$, that balances the material evolution of density

$$\frac{1}{\rho'} \frac{\mathrm{D}\rho'}{\mathrm{D}t} = -\nabla \cdot \boldsymbol{v}^{\mathrm{d}} \neq 0. \tag{29.31}$$

The divergent velocity is not used for any of the Boussinesq dynamical equations. Nonetheless, $\boldsymbol{v}^{\mathrm{d}} \neq 0$, as its divergence balances the material evolution of density according to equation (29.31). Consequently, there are acoustic waves (Chapter 51) supported by $\boldsymbol{v}^{\mathrm{d}}$ in a Boussinesq ocean.

Concerning density evolution and thermohaline circulation

The use of a non-divergent velocity for the Boussinesq ocean equations does not mean that the material time evolution of ρ vanishes. Instead, the scaling in Section 29.1.4 focuses just on the mass continuity equation. We must additionally acknowledge that as temperature and salinity evolve, so too does *in situ* density as determined through the equation of state. Indeed, equation (29.31) provides one expression for this evolution. Changes to density translate into changes in pressure, which in turn drive the large-scale *thermohaline circulation*.

The thermodynamic equation for Conservative Temperature or potential temperature is needed to determine density. There are various forms for the relation between temperature and density that depend on thermodynamic assumptions. We discuss the flavors for density in Section 30.3. For purposes of realistic ocean modeling, an accurate expression for density is critical, whereas for idealized modeling it is common to assume density equals to a constant times the temperature.

Buoyancy

We note the rather trivial point that there is identically zero buoyancy (Chapter 30), $b = -g\,(\rho - \rho_{\circ})/\rho_{\circ}$, in a fully homogeneous fluid where density is constant, $\rho = \rho_{\circ}$, everywhere. Hence, for an exactly incompressible fluid, where density is a fixed and uniform constant, there are no buoyancy forces. Such fluids serve many purposes, as exemplified by studies of a single layer of shallow water fluid in Part VI of this book. However, buoyancy forces are of primary importance for many other purposes in geophysical fluid mechanics. The Boussinesq ocean accounts for buoyancy forces, and the changes arising from processes such as heating and freshening, while making use of the more convenient kinematics of a non-divergent flow. We have far more to say concerning buoyancy in Chapter 30.

Distinguishing the Boussinesq ocean from the traditional Boussinesq approximation

The Boussinesq ocean equations are more general than the traditional Boussinesq approximation considered in other areas of fluid mechanics (e.g., *Chandrasekhar*, 1961). In particular, the traditional Boussinesq approximation assumes a linear equation of state. However, as we saw in Section 29.1.7, the Boussinesq ocean generally has a nonlinear equation of state, which is essential for realistic ocean circulation studies.

Connection to anelastic atmosphere

The atmosphere is far more compressible than the ocean, so that density variations cannot be neglected and the divergent nature of the velocity is important. However, there are some cases in which an atmospheric analog to the oceanic Boussinesq approximation can be useful.

The analog is known as the *anelastic approximation* and it is mathematically isomorphic to the oceanic Boussinesq approximation, in which case $\nabla \cdot (\rho \boldsymbol{v}) = 0$ is assumed. Section 2.5 of *Vallis* (2017) offers more details for the atmospheric anelastic approximation.

29.1.10 Further study

Section 2.4 of *Vallis* (2017) offers more details to show that density variations are small within the ocean. Further discussion of the oceanic Boussinesq approximation also can be found in Section 9.3 of *Griffies and Adcroft* (2008). This video from SciencePrimer provides a concise summary of ocean circulation arising from differences in density created by both thermal and haline (salinity) processes.

29.2 Scaling for the hydrostatic approximation

In Section 27.2 we considered a rudimentary scale analysis justifying the hydrostatic approximation for large-scale ocean and atmospheric flow. However, in that discussion we noted the need to remove a dynamically inactive hydrostatic pressure before addressing the question of whether the dynamically active pressure field is indeed approximately hydrostatic. That decomposition of pressure was performed in Section 29.1.1 as part of deriving the Boussinesq ocean equations. Hence, it is convenient to now return to the question of hydrostatic scaling within the context of the perfect non-rotating Boussinesq ocean equations.

29.2.1 Stratified non-rotating Boussinesq ocean equations

The stratified perfect Boussinesq equations in a non-rotating reference frame are

$$\frac{\mathrm{D}\boldsymbol{u}}{\mathrm{D}t} = -\nabla_{\mathrm{h}}\varphi \quad \text{and} \quad \frac{\mathrm{D}w}{\mathrm{D}t} = -\frac{\partial\varphi}{\partial z} + b \quad \text{and} \quad \nabla \cdot \boldsymbol{v} = 0 \quad \text{and} \quad \frac{\mathrm{D}b}{\mathrm{D}t} = 0. \tag{29.32}$$

To help isolate the dynamically important portion of pressure, we proceed much like in Section 29.1.1 whereby buoyancy is written

$$b = b'(x, y, z, t) + \tilde{b}(z). \tag{29.33}$$

The static buoyancy, $\tilde{b}(z)$, encompasses a background stratification that is in hydrostatic balance with its corresponding portion of the pressure field

$$\frac{\mathrm{d}\tilde{\varphi}}{\mathrm{d}z} = \tilde{b}(z). \tag{29.34}$$

The Boussinesq equations thus take the form

$$\frac{\mathrm{D}\boldsymbol{u}}{\mathrm{D}t} = -\nabla_{\mathrm{h}}\varphi' \quad \text{and} \quad \frac{\mathrm{D}w}{\mathrm{D}t} = -\frac{\partial\varphi'}{\partial z} + b' \quad \text{and} \quad \nabla \cdot \boldsymbol{v} = 0 \quad \text{and} \quad \frac{\mathrm{D}b'}{\mathrm{D}t} = -w\, N^2, \tag{29.35}$$

where

$$N^2 = \frac{\mathrm{d}\tilde{b}}{\mathrm{d}z} \tag{29.36}$$

is the squared buoyancy frequency from the background vertical stratification.[7] The decomposition into a background stratification helps to isolate the dynamical portion of the horizontal pressure gradient by removing a static depth dependent background. It also allows us to consider

[7] We discuss buoyancy frequency in Section 30.6. For present purposes, we merely note that it provides a measure of the vertical stratification of density, with $N^2 > 0$ signally a gravitationally stable density stratification.

the dynamically interesting, but simpler, case in which the background stratification dominates those perturbations around it.

29.2.2 Non-dimensionalization

Now introduce the dimensional scales (in uppercase) and corresponding non-dimensional quantities (with hats)

$$(x, y) = L\,(\widehat{x}, \widehat{y}) \qquad z = H\,\widehat{z} \qquad \boldsymbol{u} = U\,\widehat{\boldsymbol{u}} \qquad w = W\,\widehat{w} \tag{29.37}$$

$$t = T\,\widehat{t} \qquad \varphi' = \Phi\,\widehat{\varphi}' \qquad b' = B\,\widehat{b}' \qquad N^2 = \overline{N}^2\,\widehat{N}^2, \tag{29.38}$$

which yields the equations of motion

$$\frac{U}{T}\frac{\partial \widehat{u}}{\partial \widehat{t}} + \frac{U^2}{L}\widehat{u}\frac{\partial \widehat{u}}{\partial \widehat{x}} + \frac{U^2}{L}\widehat{v}\frac{\partial \widehat{u}}{\partial \widehat{y}} + \frac{UW}{H}\widehat{w}\frac{\partial \widehat{u}}{\partial \widehat{z}} = -\frac{\Phi}{L}\frac{\partial \widehat{\varphi}'}{\partial \widehat{x}} \tag{29.39a}$$

$$\frac{U}{T}\frac{\partial \widehat{v}}{\partial \widehat{t}} + \frac{U^2}{L}\widehat{u}\frac{\partial \widehat{v}}{\partial \widehat{x}} + \frac{U^2}{L}\widehat{v}\frac{\partial \widehat{v}}{\partial \widehat{y}} + \frac{UW}{H}\widehat{w}\frac{\partial \widehat{v}}{\partial \widehat{z}} = -\frac{\Phi}{L}\frac{\partial \widehat{\varphi}'}{\partial \widehat{y}} \tag{29.39b}$$

$$\frac{W}{T}\frac{\partial \widehat{w}}{\partial \widehat{t}} + \frac{UW}{L}\widehat{u}\frac{\partial \widehat{w}}{\partial \widehat{x}} + \frac{UW}{L}\widehat{v}\frac{\partial \widehat{w}}{\partial \widehat{y}} + \frac{WW}{H}\widehat{w}\frac{\partial \widehat{w}}{\partial \widehat{z}} = -\frac{\Phi}{H}\frac{\partial \widehat{\varphi}'}{\partial \widehat{z}} + B\,\widehat{b}' \tag{29.39c}$$

$$\frac{B}{T}\frac{\partial \widehat{b}'}{\partial \widehat{t}} + \frac{UB}{L}\widehat{u}\frac{\partial \widehat{b}'}{\partial \widehat{x}} + \frac{UB}{L}\widehat{v}\frac{\partial \widehat{b}'}{\partial \widehat{y}} + \frac{WB}{H}\widehat{w}\frac{\partial \widehat{b}'}{\partial \widehat{z}} = -W\,\overline{N}^2\,\widehat{w}\,\widehat{N}^2 \tag{29.39d}$$

$$\frac{U}{L}\frac{\partial \widehat{u}}{\partial \widehat{x}} + \frac{U}{L}\frac{\partial \widehat{v}}{\partial \widehat{y}} + \frac{W}{H}\frac{\partial \widehat{w}}{\partial \widehat{z}} = 0. \tag{29.39e}$$

29.2.3 Specifying the scales

We impose the following choices for scales based on the flow regimes of interest.

- TIME SCALE: Asssume that the time scale is determined by the horizontal velocity and the horizontal length scale

$$T = L/U. \tag{29.40}$$

- VERTICAL VELOCITY: It is common to assume the vertical velocity scales according to the continuity equation

$$\nabla_{\!\mathrm{h}} \cdot \boldsymbol{u} + \frac{\partial w}{\partial z} = 0 \Longrightarrow W = U\,\frac{H}{L} \equiv U\alpha_{\text{aspect}}, \tag{29.41}$$

  where the final equality introduced the vertical to horizontal aspect ratio, α_{aspect}. However, vertical density stratification acts to suppress vertical motion so that we introduce a non-dimensional number, ϵ

$$w = W\,\widehat{w} = \epsilon\left[\frac{HU}{L}\right]\widehat{w}. \tag{29.42}$$

  In Section 29.2.5 we motivate choosing ϵ as the squared *Froude number*.

- PRESSURE: Scale the pressure according to the non-rotating balance of the material time change in horizontal velocity and the horizontal pressure gradient

$$\frac{U}{T} + \frac{UU}{L} = \frac{\Phi}{L} \Longrightarrow \Phi = U^2. \tag{29.43}$$

  We made use of this *dynamical pressure scaling* in Section 25.9.2 when non-dimensionalizing the Navier-Stokes equation in a non-rotating reference frame. For flows in a rotating

reference frame that are in near geostrophic balance, we find that pressure instead scales with the Coriolis acceleration (Sections 33.3.2 and 43.7.4).

- BUOYANCY: We choose to scale buoyancy according to the hydrostatic balance

$$B = \frac{\Phi}{H} = \frac{U^2}{H}, \tag{29.44}$$

which is motivated by the importance of hydrostatic pressure in geophysical flows.

29.2.4 Non-dimensional Boussinesq equations of motion

With these choices, the equations of motion (29.39a)-(29.39e) take on form

$$\frac{\mathrm{D}\widehat{\boldsymbol{u}}}{\mathrm{D}\widehat{t}} = -\widehat{\nabla}\widehat{\varphi}' \tag{29.45}$$

$$\epsilon\, \alpha^2_{\text{aspect}} \frac{\mathrm{D}\widehat{w}}{\mathrm{D}\widehat{t}} = -\frac{\partial \widehat{\varphi}'}{\partial \widehat{z}} + \widehat{b}' \tag{29.46}$$

$$\left[\frac{U^2}{\overline{N}^2 H^2}\right] \frac{\widehat{\mathrm{D}}\widehat{b}'}{\mathrm{D}\widehat{t}} + \epsilon\, \widehat{N}^2\, \widehat{w} = 0 \tag{29.47}$$

$$\widehat{\nabla} \cdot \widehat{\boldsymbol{u}} + \epsilon \frac{\partial \widehat{w}}{\partial \widehat{z}} = 0 \tag{29.48}$$

where we introduced the non-dimensional material time derivative

$$\frac{\mathrm{D}}{\mathrm{D}\widehat{t}} = \frac{\partial}{\partial \widehat{t}} + \widehat{\boldsymbol{u}} \cdot \widehat{\nabla}_z + \epsilon\, \widehat{w}\, \frac{\partial}{\partial \widehat{z}}. \tag{29.49}$$

29.2.5 The role of the Froude number

At this point we make a choice for the parameter, ϵ, noting that there are many choices that one could consider. For our interests it is suitable to set ϵ equal to the squared *Froude number*

$$\epsilon = \mathrm{Fr}^2 = \frac{U^2}{\overline{N}^2 H^2}. \tag{29.50}$$

The Froude number measures the relative strength of vertical shears (i.e., vertical derivatives) of the horizontal velocity, U/H, versus the buoyancy stratification, N. Alternatively, it measures the ratio of the horizontal speed for a fluid particle, U, to an internal gravity wave speed, $N\,H$ (we study internal gravity waves in Chapter 57). Large Froude numbers indicate large fluid particle speeds relative to wave speeds, with $\mathrm{Fr} > 1$ a common indicator of hydraulic instability (see Section 55.5.4 for a shallow water example). In contrast, a relatively strong stratification (N^2 large) corresponds to a small Froude number and to flow that is stabilized by vertical stratification. Note that the squared Froude number is the inverse of the *Richardson number*

$$\mathrm{Ri} = \mathrm{Fr}^{-2} = \frac{\overline{N}^2 H^2}{U^2}. \tag{29.51}$$

It is a matter of taste whether one works with Fr or Ri.

The choice (29.50) leads to the vertical velocity scale

$$W = \mathrm{Fr}^2 \left[\frac{HU}{L}\right]. \tag{29.52}$$

For $\mathrm{Fr} < 1$, which is the case for stably stratified fluids, this result means that stratification

reduces the scale for the vertical velocity. The corresponding non-dimensional Boussinesq equations take the form

$$\frac{\mathrm{D}\widehat{u}}{\mathrm{D}\widehat{t}} = -\widehat{\nabla}_z \widehat{\varphi'} \tag{29.53}$$

$$\mathrm{Fr}^2\, \alpha^2_{\text{aspect}}\, \frac{\mathrm{D}\widehat{w}}{\mathrm{D}\widehat{t}} = -\frac{\partial \widehat{\varphi'}}{\partial \widehat{z}} + \widehat{b'} \tag{29.54}$$

$$\frac{\widehat{\mathrm{D}}\widehat{b'}}{\mathrm{D}\widehat{t}} + \widehat{N}^2\, \widehat{w} = 0 \tag{29.55}$$

$$\widehat{\nabla} \cdot \widehat{\boldsymbol{u}} + \mathrm{Fr}^2\, \frac{\partial \widehat{w}}{\partial \widehat{z}} = 0. \tag{29.56}$$

The condition for hydrostatic balance in a stratified fluid thus takes the form

$$\mathrm{Fr}^2\, \alpha^2_{\text{aspect}} \ll 1. \tag{29.57}$$

This result supports our initial suspicion that stratification suppresses vertical motion, thus reducing the vertical acceleration terms that break hydrostatic balance. That is, hydrostatic balance is more readily achieved for a stratified flow than for an unstratified flow. Note also that the horizontal divergence of the horizontal flow is reduced by the presence of stratification, which thus leads to a nearly horizontally non-divergent flow

$$\left| \widehat{\nabla} \cdot \widehat{\boldsymbol{u}} \right| = \left| \mathrm{Fr}^2\, \frac{\partial \widehat{w}}{\partial \widehat{z}} \right| \ll \left| \frac{\partial \widehat{w}}{\partial \widehat{z}} \right|. \tag{29.58}$$

Finally, this scaling reveals how the hydrostatic approximation becomes less accurate when $\mathrm{Fr}^2\, \alpha^2_{\text{aspect}} \sim 1$, which occurs when stratification is weak and/or the aspect ratio order unity.

29.2.6 Horizontal hydrostatic pressure gradient

In Section 29.2.6 we studied the horizontal pressure gradient between two columns of constant density for a hydrostatic fluid. In that example, the two columns were assumed to have equal mass, so the fluid is non-Boussinesq. Here, we reconsider that example for a Boussinesq ocean where volume is conserved rather than mass.

The expression for the hydrostatic pressure at a point within the fluid takes on the same form as that for a non-Boussinesq fluid (Section 27.2.1)

$$p_{\mathrm{h}}(x, y, z, t) = p_{\mathrm{a}}(x, y, t) + g \int_z^{\eta} \rho(x, y, z', t)\, \mathrm{d}z', \tag{29.59}$$

and the horizontal pressure gradient is thus given by

$$\nabla_{\mathrm{h}} p_{\mathrm{h}} = \nabla_{\mathrm{h}} p_{\mathrm{a}} + g\, \rho(\eta)\, \nabla_{\mathrm{h}} \eta + g \int_z^{\eta} \nabla_{\mathrm{h}} \rho\, \mathrm{d}z'. \tag{29.60}$$

For many studies with Boussinesq ocean, we are interested in the horizontal pressure gradients in the presence of a rigid lid ocean surface whereby $\eta = 0$. In this case we compute the *internal pressure gradient*

$$\nabla_{\mathrm{h}} p_{\mathrm{h}} = g \int_z^{0} \nabla_{\mathrm{h}} \rho\, \mathrm{d}z' \quad \text{rigid lid ocean.} \tag{29.61}$$

Hence, the internal horizontal pressure gradient at a vertical position z equals to the horizontal density gradient vertically integrated above that point. For example, if density increases poleward, then so too does the internal hydrostatic pressure.

29.2.7 Evolution of hydrostatic pressure

In Section 27.2.2 we developed the Eulerian evolution equation for hydrostatic pressure in a mass conserving non-Boussinesq fluid. Here we discuss the evolution in a Boussinesq ocean of the hydrostatic pressure at a point. To do so we take the Eulerian time tendency of the hydrostatic pressure (29.59), in which case

$$\partial_t p = \partial_t p_{\text{a}} + g\,\rho(\eta)\,\partial_t \eta + \int_z^\eta \partial_t \rho(x, y, z', t)\,\mathrm{d}z'. \tag{29.62}$$

This equation holds for both the Boussinesq and non-Boussinesq ocean. However, it is only for the mass conserving non-Boussinesq ocean that we can use mass continuity (19.6) to set $\partial_t \rho = -\nabla \cdot (\boldsymbol{v}\,\rho)$. Use of Leibniz's rule then reveals that the hydrostatic pressure evolves due to the convergence of mass onto the fluid column above that point (see Section 27.2.2 for the derivation). This result is expected since the hydrostatic pressure at a point is the weight per area of fluid above that point.

For a Boussinesq ocean, the volume conserving kinematics means that we cannot replace $\partial_t \rho$ with $-\nabla \cdot (\boldsymbol{v}\,\rho)$. Correspondingly, the weight of a fluid column can change merely through *in situ* density changes, so that the weight can change even if the matter content remains fixed; e.g., through heating. We expose details by noting that energetic consistency from Section 29.8 meana that the *in situ* density in a Boussinesq ocean has the functional dependence, $\rho(S, \Theta, \Phi)$, with Φ the geopotential. Hence, the Eulerian time derivative of density is given by

$$\partial_t \rho = (\partial \rho / \partial S)\,\partial_t S + (\partial \rho / \partial \Theta)\,\partial_t \Theta + (\partial \rho / \partial \Phi)\,\partial_t \Phi. \tag{29.63}$$

With a simple geopotential, $\Phi = g\,z$, we have $\partial_t \Phi = 0$ since the Eulerian time derivative is computed at fixed (x, y, z). This result leads to the time changes in the hydrostatic pressure for a Boussinesq ocean

$$\partial_t p = \partial_t p_{\text{a}} + g\,\rho(\eta)\,\partial_t \eta + \int_z^\eta [(\partial \rho / \partial S)\,\partial_t S + (\partial \rho / \partial \Theta)\,\partial_t \Theta]\,\mathrm{d}z'. \tag{29.64}$$

This equation reveals the direct dependence of the hydrostatic pressure on changes in S and Θ. Hence, heating and freshening, which alter the *in situ* density, directly alter the hydrostatic pressure in a Boussinesq ocean by altering the fluid's weight per area. This result contrasts to the mass conserving non-Boussinesq fluid, whose weight per area changes only through changes to its mass per area.

29.3 How pressure enforces non-divergent flow

We return now to the case of a non-hydrostatic fluid and consider the Boussinesq momentum equation (29.26a) written in the tangent plane form

$$\rho_{\text{o}}\,(\partial_t + \boldsymbol{v} \cdot \nabla)\,\boldsymbol{v} + f\,\boldsymbol{z} \times \rho_{\text{o}}\,\boldsymbol{v} = -\nabla p - \rho\,g\,\hat{\boldsymbol{z}} + \rho_{\text{o}}\,\boldsymbol{F}. \tag{29.65}$$

The non-divergence constraint on the velocity, $\nabla \cdot \boldsymbol{v} = 0$, must be maintained at each point in the fluid and at each time instance. How is that constraint maintained? As we show in this section, pressure provides the force that maintains non-divergence. Furthermore, pressure is determined through solving an elliptic boundary value problem. As we discussed in Section 6.5, elliptic partial differential equations transfer information instantaneously. Physically, this situation corresponds to the transition from a compressible non-Boussinesq fluid, in which pressure signals propagate via acoustic waves (Chapter 51), to the incompressible flow of a Boussinesq ocean, in which pressure adjusts instantaneously just as if the acoustic waves traveled

at infinite speed. The Boussinesq ocean sits between the compressible fluid and incompressible flow. That is, the Boussinesq prognostic velocity is non-divergent, and so it does not support acoustic waves, whereas the full velocity is divergent (Section 29.1.9), and this divergent portion supports acoustic waves, although such waves are never felt by the Boussinesq dynamical fields.

29.3.1 Poisson equation for pressure

To derive the pressure equation, we find it convenient to expose Cartesian tensor labels on the momentum equation (29.65)

$$\partial_t v_m + v_n \partial_n v_m + f\, \epsilon_{mnp}\, \delta_{3n}\, v_p = -\partial_m p/\rho_o - \delta_{3m}\, g\, \rho/\rho_o + F_m. \tag{29.66}$$

The time derivative is eliminated by taking the divergence through contracting with the operator ∂_m,

$$\partial_m \partial_t v_m = \partial_t \partial_m v_m = 0, \tag{29.67}$$

thus leading to

$$-\nabla^2 p/\rho_o = \partial_m (v_n \partial_n v_m + f\, \epsilon_{m3p}\, v_p + \delta_{3m}\, g\, \rho/\rho_o - F_m), \tag{29.68}$$

where the Laplacian operator is

$$\nabla^2 = \partial_m \partial_m. \tag{29.69}$$

Equation (29.68) can be written as the Poisson equation

$$-\nabla^2 p = \rho_o \nabla \cdot \boldsymbol{D}, \tag{29.70}$$

with the vector $\boldsymbol{D}$ given by the accelerations sans that from pressure

$$D_m = v_n \partial_n v_m + f\, \epsilon_{m3p}\, v_p + \delta_{3m}\, g\, \rho/\rho_o - F_m \tag{29.71a}$$

$$\boldsymbol{D} = (\boldsymbol{v} \cdot \nabla)\, \boldsymbol{v} + f\, \hat{\boldsymbol{z}} \times \boldsymbol{v} + g\, (\rho/\rho_o)\, \hat{\boldsymbol{z}} - \boldsymbol{F}. \tag{29.71b}$$

As when studying Green's functions in Chapter 9 (see also Section 29.3.3), it is useful to maintain the minus sign on the left hand side of equation (29.70) so that a positive divergence ($\nabla \cdot \boldsymbol{D} > 0$) represents a positive source for p. Equivalently, for a wavelike pressure perturbation we have

$$-\nabla^2 p \propto p, \tag{29.72}$$

so that a positive source, $-\nabla^2 p = \rho_o \nabla \cdot \boldsymbol{D} > 0$, leads to a local positive pressure anomaly, and conversely for a negative source.

29.3.2 Boundary conditions

To derive the boundary conditions for the Poisson equation (29.70), we find it useful to write the velocity equation as

$$\partial_t \boldsymbol{v} = -\nabla p/\rho_o - \boldsymbol{D}. \tag{29.73}$$

We consider a variety of boundaries in the following.

Static material surface

For a static material boundary we can make use of the no normal flow kinematic boundary condition (Section 19.6.1), in which case

$$\hat{\boldsymbol{n}} \cdot \partial_t \boldsymbol{v} = \partial_t\, (\hat{\boldsymbol{n}} \cdot \boldsymbol{v}) = 0 \Longrightarrow (\nabla p + \rho_o\, \boldsymbol{D}) \cdot \hat{\boldsymbol{n}} = 0 \qquad \text{for static material boundaries.} \tag{29.74}$$

This boundary condition takes the form

$$\hat{\boldsymbol{n}} \cdot \nabla p = -\rho_\circ \boldsymbol{D} \cdot \hat{\boldsymbol{n}} \qquad \text{for static material boundaries.} \tag{29.75}$$

Hence, maintenance of the no normal flow condition along a static material boundary requires a corresponding *Neumann boundary condition* for pressure.

Consider the case of $\hat{\boldsymbol{n}} = -\hat{\boldsymbol{z}}$ along a flat solid boundary at $z = \eta_\mathsf{b}$. In this case

$$-\rho_\circ \boldsymbol{D} \cdot \hat{\boldsymbol{n}} = g\,\rho - \hat{\boldsymbol{z}} \cdot \boldsymbol{F}, \tag{29.76}$$

so that along the boundary we have

$$-\rho_\circ \boldsymbol{D} \cdot \hat{\boldsymbol{n}} = \rho_\circ \hat{\boldsymbol{z}} \cdot [(\boldsymbol{v} \cdot \nabla)\,\boldsymbol{v} + g\,(\rho/\rho_\circ)\,\hat{\boldsymbol{z}} - \boldsymbol{F}] = g\,\rho - \hat{\boldsymbol{z}} \cdot \boldsymbol{F}, \tag{29.77}$$

where

$$\hat{\boldsymbol{z}} \cdot [(\boldsymbol{v} \cdot \nabla)\,\boldsymbol{v}] = (\boldsymbol{v} \cdot \nabla)\,w = 0, \tag{29.78}$$

since $w = 0$ on the flat solid boundary at $z = \eta_\mathsf{b}$. We are thus led to the pressure boundary condition (29.75)

$$-\partial_z p = \rho\,g\, - \hat{\boldsymbol{z}} \cdot \boldsymbol{F} \qquad \text{at } z = \eta_\mathsf{b}. \tag{29.79}$$

Rigid lid ocean surface

For many purposes it is sufficient to assume the upper ocean surface is rigid and flat ($z = \eta = 0$), in which case we follow the approach taken for the flat bottom boundary condition (29.79) to find the boundary condition

$$\partial_z p = -\rho\,g + \rho_\circ\,\hat{\boldsymbol{z}} \cdot \boldsymbol{F} \qquad \text{at } z = 0. \tag{29.80}$$

Free upper ocean surface

The ocean free surface is generally dynamic and permeable, so that the velocity does not satisfy a no normal flow condition along this surface (see Section 19.6). To develop the pressure boundary condition at the free surface, we invoke a dynamical principle rather than a kinematic principle. Namely, we invoke continuity of pressure across an interface, which follows from Newton's third law (recall our discussion of stress along an interface in Section 25.10). Hence, the pressure condition at the ocean free surface is the *Dirichlet boundary condition*

$$p = p_{\text{applied}} \quad \text{at } z = \eta(x, y, t), \tag{29.81}$$

where p_{applied} is the pressure applied to the ocean surface from the overlying atmosphere or cryosphere.

29.3.3 Green's function expression for pressure

Consider the pressure equation for the special case of a rigid lid upper ocean boundary

$$-\nabla^2 p = \rho_\circ \nabla \cdot \boldsymbol{D} \qquad \boldsymbol{x} \in \mathcal{R} \tag{29.82a}$$

$$\hat{\boldsymbol{n}} \cdot \nabla p = -\rho_\circ\,\hat{\boldsymbol{n}} \cdot \boldsymbol{D} \quad \boldsymbol{x} \in \partial\mathcal{R}. \tag{29.82b}$$

If we know the vector $\boldsymbol{D}$, then the pressure boundary value problem is linear, thus enabling use of Green's function methods from Chapter 9 to determine an expression for pressure. In fact, the pressure is only determined up to a constant. Likewise, the discussion in Section 9.4 for the Poisson equation with Neumann boundary conditions shows that there is no Green's function

for this boundary value problem. However, we can instead make use of the modified Green's function, $\widetilde{G}$, that satisfies equations (9.97a)-(9.97b)

$$-\nabla^2 \widetilde{G}(\boldsymbol{x}|\boldsymbol{y}) = \delta(\boldsymbol{x}-\boldsymbol{y}) - 1/\mathcal{V} \quad \boldsymbol{x} \in \mathcal{R} \tag{29.83a}$$

$$\hat{\boldsymbol{n}} \cdot \nabla_x \widetilde{G}(\boldsymbol{x}|\boldsymbol{y}) = 0 \qquad\qquad \boldsymbol{x} \in \partial\mathcal{R}, \tag{29.83b}$$

where $\mathcal{V} = \int_{\mathcal{R}} \mathrm{d}V$ is the domain volume. Making use of the solution (9.100) leads to the pressure

$$p(\boldsymbol{x}) - \langle p \rangle = \rho_\circ \int_{\mathcal{R}} (\nabla \cdot \boldsymbol{D})\, \widetilde{G}(\boldsymbol{x}|\boldsymbol{y})\, \mathrm{d}V_{\boldsymbol{y}} - \rho_\circ \oint_{\partial\mathcal{R}} (\hat{\boldsymbol{n}} \cdot \boldsymbol{D})\, \widetilde{G}(\boldsymbol{x}|\boldsymbol{y})\, \mathrm{d}\mathcal{S}_{\boldsymbol{y}}, \tag{29.84}$$

where the $\boldsymbol{y}$ subscripts indicate that the integrals are over $\boldsymbol{y}$, and $\langle p \rangle$ is the volume averaged pressure. The volume averaged pressure remains undetermined unless provided with further information. Since the volume average has a zero gradient, it plays no role in the pressure gradient.

As discussed in Section 9.4.5, we can extract the free space Green's function from the modified Green's function according to equation (9.106)

$$\widetilde{G}(\boldsymbol{x}|\boldsymbol{y}) = \mathcal{G}(\boldsymbol{x}|\boldsymbol{y}) + \widetilde{H}(\boldsymbol{x}|\boldsymbol{y}), \tag{29.85}$$

where $\widetilde{H}$ satisfies the boundary value problem

$$-\nabla^2_{\boldsymbol{x}} \widetilde{H}(\boldsymbol{x}|\boldsymbol{y}) = -1/\mathcal{V} \qquad \text{for} \quad \boldsymbol{x}, \boldsymbol{y} \in \mathcal{R} \tag{29.86a}$$

$$-\hat{\boldsymbol{n}} \cdot \nabla_{\boldsymbol{x}} \widetilde{H}(\boldsymbol{x}|\boldsymbol{y}) = \hat{\boldsymbol{n}} \cdot \nabla_{\boldsymbol{x}} \mathcal{G}(\boldsymbol{x}|\boldsymbol{y}) \quad \text{for} \quad \boldsymbol{x} \in \partial\mathcal{R}, \tag{29.86b}$$

and the free space Green's function is given by equation (9.5c)

$$-\nabla^2_{\boldsymbol{x}} \mathcal{G}(\boldsymbol{x}|\boldsymbol{y}) = \delta(\boldsymbol{x}-\boldsymbol{y}) \Longrightarrow \mathcal{G}(\boldsymbol{x}|\boldsymbol{y}) = (4\,\pi\,|\boldsymbol{x}-\boldsymbol{y}|)^{-1}. \tag{29.87}$$

Making use of the decomposition (29.85) and the expression (9.115) leads to the corresponding decomposition of the pressure

$$\begin{aligned} p(\boldsymbol{x}) - \langle p \rangle = \rho_\circ \int_{\mathcal{R}} (\nabla \cdot \boldsymbol{D})\, \mathcal{G}(\boldsymbol{x}|\boldsymbol{y})\, \mathrm{d}V_{\boldsymbol{y}} \\ + \underbrace{\rho_\circ \int_{\mathcal{R}} (\nabla \cdot \boldsymbol{D})\, \widetilde{H}(\boldsymbol{x}|\boldsymbol{y})\, \mathrm{d}V_{\boldsymbol{y}} + \rho_\circ \oint_{\partial\mathcal{R}} (\hat{\boldsymbol{n}} \cdot \boldsymbol{D})\, \widetilde{G}(\boldsymbol{x}|\boldsymbol{y})\, \mathrm{d}\mathcal{S}_{\boldsymbol{y}}}_{p^{\text{harmonic}}} \end{aligned} \tag{29.88}$$

where the under-braced term is harmonic, $\nabla^2 p^{\text{harmonic}} = 0$.

29.3.4 Characterizing the pressure sources

The right hand side of the Poisson equation (29.70) contains four sources for the pressure field. Linearity of the Poisson equation allows us to separately study the pressure resulting from these sources, with the net pressure the sum. We here summarize their basic features, borrowing from the treatment given in Section 38.4 for the kinematically simpler non-divergent barotropic model. As we find, three of the pressure sources contribute to non-hydrostatic pressures and one to hydrostatic pressure. Note that these pressure sources are *associated* with the pressure perturbations rather than *causing* the perturbations. Such is part of the nuance of pressure in a non-divergent flow.

Divergence of self-advection

The first source is given by the divergence of self-advection, which can be written

$$\nabla \cdot \boldsymbol{D}_{\text{self-advect}} = \partial_n(v_m\, \partial_m v_n) = (\partial_n v_m)\,(\partial_m v_n) + v_m\,(\partial_n \partial_m v_n) = (\partial_n v_m)\,(\partial_m v_n), \tag{29.89}$$

where we set

$$v_m\, \partial_n \partial_m v_n = v_m\, \partial_m \partial_n v_n = 0 \tag{29.90}$$

since $\partial_n v_n = 0$ follows from the non-divergent nature of the flow. Furthermore, introducing the strain rate tensor ($\mathbb{S}$ from equation (18.90a)) and rotation tensor ($\mathbb{R}$ equation (18.90b)), renders

$$2\,\mathbb{S}_{mn}\,\mathbb{S}_{mn} = (\partial_m v_n)\,(\partial_m v_n) + (\partial_m v_n)\,(\partial_n v_m) \tag{29.91}$$

$$2\,\mathbb{R}_{mn}\,\mathbb{R}_{mn} = (\partial_m v_n)\,(\partial_m v_n) - (\partial_m v_n)\,(\partial_n v_m), \tag{29.92}$$

so that

$$\nabla \cdot \boldsymbol{D}_{\text{self-advect}} = (\partial_n v_m)\,(\partial_m v_n) = \underbrace{\mathbb{S}_{mn}\,\mathbb{S}_{mn}}_{\text{splat}} - \underbrace{\mathbb{R}_{mn}\,\mathbb{R}_{mn}}_{\text{spin}}. \tag{29.93}$$

The vorticity or spin source provides a negative source to $-\nabla^2 p$. In contrast, the contribution from strain, sometimes referred to as *splat*, provides a positive source.[8] As detailed for horizontally non-divergent barotropic flow in Section 38.4, we understand why there is a negative pressure source from vortical (spinning) motion since, to retain a non-divergent flow, pressure must counteract the centrifugal acceleration arising from curved fluid motion. Likewise, a positive pressure source associated with straining motion is needed to counteract the convergent accelerations induced by strains.

Divergence of the Coriolis acceleration

The divergence of the Coriolis acceleration introduces a pressure source given by

$$-\nabla \cdot \nabla p_{\text{coriolis}} = \nabla \cdot \boldsymbol{D}_{\text{coriolis}} = \nabla \cdot (f\, \hat{\boldsymbol{z}} \times \boldsymbol{v}) = \beta\, u - f\, \zeta, \tag{29.94}$$

where $\zeta = \partial_x v - \partial_y u$ is the vertical component to the relative vorticity, and $\beta = \partial_y f$ is the planetary vorticity gradient. To help understand the $f\,\zeta$ term, consider two-dimensional flow with a cyclonic relative vorticity so that $f\,\zeta > 0$. Cyclonic flow feels an associated centrifugal acceleration directed "outward". To maintain a non-divergent two-dimensional flow requires an oppositely directed "inward" pressure gradient force. Hence, such rotating flow induces a low pressure source as a means to counteract the centrifugal acceleration

$$-\nabla \cdot \nabla p_{\text{coriolis}} < 0. \tag{29.95}$$

See section 38.4.6 for more discussion of this source as found in the non-divergent barotropic fluid.

Divergence of the gravitational force per volume

The divergence of the gravitational force per volume is given by

$$-\nabla \cdot \nabla p_{\text{gravity}} = \rho_o \nabla \cdot \boldsymbol{D}_{\text{gravity}} = \nabla \cdot (g\, \rho\, \hat{\boldsymbol{z}}) = g\, \partial_z \rho, \tag{29.96}$$

[8] The whimsically named *splat* source is so-named since it is large when a fluid element is squashed in a manner increasing fluid strains, akin to how strains appear when a fluid impacts or "splats" against a solid obstacle. Imagine a water balloon thrown against a wall.

with this pressure source absent in the depth-independent barotropic fluid of Section 38.4. The associated pressure gradient is that arising from the local hydrostatic component of the pressure field in which

$$\nabla \cdot (-\nabla p_{\text{gravity}} + g\,\rho\,\hat{\boldsymbol{z}}) = 0. \tag{29.97}$$

In regions where density decreases upward, $\partial_z \rho < 0$, a compressible fluid element that conserves its mass will expand when moving upward into less dense fluid. For a non-divergent flow that conserves the volume of fluid elements, there must be a counteracting force from pressure to halt the expansion of a fluid element. This counteracting force arises from the hydrostatic component to the pressure field that acts inward to squeeze the fluid element, with this pressure force originating from the negative pressure source, $-\nabla^2 p_{\text{gravity}} = g\,\partial_z \rho < 0$.

Divergence of the friction vector

The third source arises from the divergence of friction,

$$-\nabla \cdot \nabla p_{\text{friction}} = \rho_o \nabla \cdot \boldsymbol{D}_{\text{friction}} = -\rho_o \nabla \cdot \boldsymbol{F}. \tag{29.98}$$

With interior fluid friction arising from a nonzero strain rate (Section 25.8), we expect this pressure source to be most important in regions of large strains. Indeed, for an incompressible flow feeling only molecular viscosity, the friction operator is given by (see Section 25.8.7)

$$\boldsymbol{F} = \nu \nabla^2 \boldsymbol{v}, \tag{29.99}$$

where $\nu > 0$ is a constant molecular viscosity. In this case $\nabla \cdot \boldsymbol{F} = 0$, so that viscous friction does not contribute a pressure source. More general cases are considered in applications where the molecular viscosity is replaced by a flow dependent eddy viscosity so that $\nabla \cdot \boldsymbol{F} \neq 0$. For the case of a converging frictional acceleration, $\nabla \cdot \boldsymbol{F} < 0$, friction then leads to a positive pressure source to counteract the friction to thus maintain a non-divergent flow.

29.3.5 Comments and further study

The gravitational source contributes a local hydrostatic component to the pressure field, whereas the other three sources contribute non-hydrostatic pressure sources. In many applications, such as general circulation modeling of the ocean and atmosphere, the fluid is assumed to be approximately hydrostatic (Chapter 27). In this case vertical motion is diagnosed rather than prognosed, and the non-hydrostatic component of pressure is never needed to evolve the fluid motion. Even so, vertical derivatives in the non-hydrostatic pressure provide the vertical force needed for vertical accelerations. We have more to say on vertical motion in Section 30.11.

Markowski and Richardson (2010) provide lucid discussions of pressure forces acting in geophysical fluids. In particular their Section 2.5 inspired much of the current section.

29.4 Helmholtz decomposing the velocity equation

In this section we introduce some mathematical properties of the velocity equation for a Boussinesq ocean in a simply connected ocean domain, $\mathcal{R}$, with boundary, $\partial\mathcal{R}$. For this purpose, we again assume a tangent plane and so write the velocity equation (29.65) in the form

$$\partial_t \boldsymbol{v} = -\nabla p/\rho_o - \boldsymbol{D}, \tag{29.100}$$

where $\boldsymbol{D}$, as given by equation (29.71b), contains the various accelerations sans the pressure gradient

$$\boldsymbol{D} = (\boldsymbol{v} \cdot \nabla)\,\boldsymbol{v} + f\,\hat{\boldsymbol{z}} \times \boldsymbol{v} + g\,(\rho/\rho_o)\,\hat{\boldsymbol{z}} - \boldsymbol{F}. \tag{29.101}$$

29.4.1 Helmholtz decomposition

The Helmholtz decomposition from Section 9.8 says that on a simply connected domain, an arbitrary vector, such as the acceleration $\boldsymbol{D}$, can be decomposed as

$$\boldsymbol{D} = \boldsymbol{D}^{\text{rot}} + \boldsymbol{D}^{\text{div}} \tag{29.102}$$

where the two vectors on the right hand side satisfy

$$\nabla \cdot \boldsymbol{D}^{\text{rot}} = 0 \quad \text{and} \quad \nabla \times \boldsymbol{D}^{\text{rot}} \neq 0 \qquad \boldsymbol{D}^{\text{rot}} \text{ is divergent-free} \tag{29.103a}$$

$$\nabla \times \boldsymbol{D}^{\text{div}} = 0 \quad \text{and} \quad \nabla \cdot \boldsymbol{D}^{\text{div}} \neq 0 \qquad \boldsymbol{D}^{\text{div}} \text{ is curl-free.} \tag{29.103b}$$

We make use of the Helmholtz decomposition for a Boussinesq ocean by noting that the non-divergent velocity only has a rotational contribution

$$\boldsymbol{v} = \boldsymbol{v}^{\text{rot}}, \tag{29.104}$$

whereas the pressure gradient only has a divergent component

$$\nabla p = (\nabla p)^{\text{div}}. \tag{29.105}$$

In contrast, the acceleration, $\boldsymbol{D}$, generally has a rotational, a divergent, and a harmonic component as written in equation (29.102).

29.4.2 The pressure equation

Making use of the Helmholtz decomposition (29.102) brings the velocity equation (29.100) into the form

$$\partial_t \boldsymbol{v} = -\nabla p/\rho_o - \boldsymbol{D}^{\text{rot}} - \boldsymbol{D}^{\text{div}}. \tag{29.106}$$

The accelerations, $\partial_t \boldsymbol{v}$, and $\boldsymbol{D}^{\text{rot}}$, are each divergent-free. In contrast, the accelerations, $-\nabla p/\rho_o$ and $\boldsymbol{D}^{\text{div}}$, each have nonzero divergence. Self-consistency is maintained if the sum, $\nabla p/\rho_o + \boldsymbol{D}^{\text{div}}$, has zero divergence so that

$$\nabla \cdot (\nabla p/\rho_o + \boldsymbol{D}^{\text{div}}) = 0 \implies -\nabla^2 p = \rho_o \nabla \cdot \boldsymbol{D}^{\text{div}} = \rho_o \nabla \cdot \boldsymbol{D}. \tag{29.107}$$

This is the Poisson equation for the pressure field already derived in Section 29.3.1. We go one further step by observing that $\nabla p/\rho_o + \boldsymbol{D}^{\text{div}}$ is both curl-free and divergent-free, which we write as

$$\nabla p/\rho_o + \boldsymbol{D}^{\text{div}} = \boldsymbol{H} \quad \text{with} \quad \nabla \cdot \boldsymbol{H} = \nabla \times \boldsymbol{H} = 0. \tag{29.108}$$

29.4.3 The vorticity equation

As for the pressure equation in Section 29.4.2, we note that the accelerations $\nabla p/\rho_o$, and $\boldsymbol{D}^{\text{div}}$, are each curl-free. In contrast, the accelerations, $\partial_t \boldsymbol{v}$ and $\boldsymbol{D}^{\text{rot}}$, each have nonzero curl. Self-consistency thus requires $\partial_t \boldsymbol{v} + \boldsymbol{D}^{\text{rot}}$ to be curl-free

$$\nabla \times (\partial_t \boldsymbol{v} + \boldsymbol{D}^{\text{rot}}) = 0 \implies \partial_t (\nabla \times \boldsymbol{v}) = -\nabla \times \boldsymbol{D}^{\text{rot}}, \tag{29.109}$$

which is the relative vorticity equation that we further study in Chapter 40. Going one step further we note that the vector $\partial_t \boldsymbol{v} + \boldsymbol{D}^{\text{rot}}$ is both curl-free and divergent-free, which we write as

$$\partial_t \boldsymbol{v} + \boldsymbol{D}^{\text{rot}} = \boldsymbol{I} \quad \text{with} \quad \nabla \cdot \boldsymbol{I} = \nabla \times \boldsymbol{I} = 0. \tag{29.110}$$

29.4.4 The velocity equation

The above considerations have led us to the pressure gradient equation (29.108) and the velocity tendency equation (29.110)

$$\nabla p/\rho_o + \boldsymbol{D}^{\text{div}} = \boldsymbol{H} \tag{29.111}$$

$$\partial_t \boldsymbol{v} + \boldsymbol{D}^{\text{rot}} = \boldsymbol{I}, \tag{29.112}$$

where both $\boldsymbol{H}$ and $\boldsymbol{I}$ are divergent-free and curl-free. Adding these two equations leads to

$$\partial_t \boldsymbol{v} = -\nabla p/\rho_o - \boldsymbol{D}^{\text{rot}} - \boldsymbol{D}^{\text{div}} + \boldsymbol{H} + \boldsymbol{I}, \tag{29.113}$$

with this form of the velocity equation equivalent to the original Helmholtz decomposed equation (29.106) if we set

$$\boldsymbol{H} + \boldsymbol{I} = 0. \tag{29.114}$$

29.4.5 Comments

This section was inspired by *Marshall and Pillar* (2011), who applied a Helmholtz decomposition to study the variety of accelerations appearing in the Boussinesq velocity equation. A particularly revealing result of this decomposition, when setting $\boldsymbol{H} = \boldsymbol{I} = 0$, is the ability to make a 1-to-1 connection between terms in the Helmholtz decomposed velocity equation with terms in the relative vorticity equation. This correspondence can support dynamical understanding.

29.5 Tracer budgets in Eulerian regions

We are commonly interested in the tracer budget for a fluid region, and we examined a variety of regions in Section 20.2 for a compressible fluid. Here, we expose issues that arise for tracer budgets in a Boussinesq ocean, whereby the flow is non-divergent. We specialize to the study of an Eulerian region, $\mathcal{R}$, and emphasize how the non-divergent flow constrains the advective tracer transport and affects changes to the volume integrated tracer content.

29.5.1 Formulating the budget equation

Consider a tracer concentration, C, and compute its net content over an Eulerian region, $\mathcal{R}$

$$\rho_o \int_{\mathcal{R}} C \, \mathrm{d}V = \rho_o \, V \, \langle C \rangle, \tag{29.115}$$

where C satisfies the tracer equation

$$\partial_t(\rho_o \, C) + \nabla \cdot (\rho_o \, C \, \boldsymbol{v} + \boldsymbol{J}) = 0, \tag{29.116}$$

and

$$\langle C \rangle = \frac{\int_{\mathcal{R}} C \, \mathrm{d}V}{\int_{\mathcal{R}} \mathrm{d}V} = \frac{1}{V} \int_{\mathcal{R}} C \, \mathrm{d}V \tag{29.117}$$

is the volume averaged tracer concentration within the Eulerian region with fixed volume, $V = \int_{\mathcal{R}} \mathrm{d}V$. Following from the discussion of tracer budgets in Section 20.2, we have

$$\rho_o \frac{\mathrm{d}(V \, \langle C \rangle)}{\mathrm{d}t} = \rho_o \, V \, \frac{\mathrm{d}\langle C \rangle}{\mathrm{d}t} \tag{29.118a}$$

$$= \rho_o \frac{\mathrm{d}}{\mathrm{d}t} \int_{\mathcal{R}} C \, \mathrm{d}V \tag{29.118b}$$

$$= \int_{\mathcal{R}} \frac{\partial(\rho_o C)}{\partial t} \, dV \tag{29.118c}$$

$$= - \int_{\mathcal{R}} \nabla \cdot (\rho_o C \, \boldsymbol{v} + \boldsymbol{J}) \, dV \tag{29.118d}$$

$$= - \oint_{\partial \mathcal{R}} (\rho_o C \, \boldsymbol{v} + \boldsymbol{J}) \cdot \hat{\boldsymbol{n}} \, d\mathcal{S}, \tag{29.118e}$$

where we used the divergence theorem on the final equality with $\partial\mathcal{R}$ the boundary of $\mathcal{R}$ and the outward normal $\hat{\boldsymbol{n}}$. Changes in the total tracer contained within the region arise from the convergence of boundary fluxes due to the non-advective flux, $\boldsymbol{J}$, plus convergence of the advective tracer flux, $\rho_o C \, \boldsymbol{v}$. Since the region volume is constant in time, changes in the total tracer content directly affect the volume averaged tracer concentration, $\langle C \rangle$.

At any point along the boundary, the tracer content is modified if there is a non-advective flux, $\boldsymbol{J}$, directed across the boundary. There is no *a priori* constraint on $\boldsymbol{J}$, with local properties determining its sign and magnitude. In contrast, contributions from the boundary advective flux are constrained due to the non-divergent nature of the Boussinesq velocity, which we discuss next.

29.5.2 Interpreting advective tracer contributions

As seen by equation (29.118e), any advective flux, $\rho_o \, \boldsymbol{v} \, C$, that is directed into the region adds tracer to the region, whereas a flux directed outward reduces the region's tracer content. However, because the velocity is non-divergent, the tracer contained within the region is unaffected if we modify the advective tracer flux along the boundary by adding a number that is constant over the region $\mathcal{R}$. We see this property for any closed Eulerian region by writing[9]

$$0 = \int_{\mathcal{R}} \nabla \cdot \boldsymbol{v} \, dV = \oint_{\partial \mathcal{R}} \boldsymbol{v} \cdot \boldsymbol{n} \, d\mathcal{S}. \tag{29.119}$$

Hence, the velocity is, at each time instance, constrained so that the non-divergent flow cannot lead to the accumulation of fluid within any closed and static region. Correspondingly, the amount of fluid entering $\mathcal{R}$ exactly and instantaneously balances the amount of fluid leaving $\mathcal{R}$. We can thus add any spatial constant, k, to the advective flux without affecting the net tracer content change

$$\oint_{\partial \mathcal{R}} (C + k) \, \boldsymbol{v} \cdot \hat{\boldsymbol{n}} \, d\mathcal{S} = \oint_{\partial \mathcal{R}} C \, \boldsymbol{v} \cdot \hat{\boldsymbol{n}} \, d\mathcal{S} + k \oint_{\partial \mathcal{R}} \boldsymbol{v} \cdot \hat{\boldsymbol{n}} \, d\mathcal{S} = \oint_{\partial \mathcal{R}} C \, \boldsymbol{v} \cdot \hat{\boldsymbol{n}} \, d\mathcal{S}. \tag{29.120}$$

Boundary advection occuring with $C = k$ has no affect on the net tracer within a region since an equal amount of fluid enters as leaves.

To help interpret the role of advective fluxes on integrated tracer content, we find it useful to set the arbitrary spatial constant to $k = -\langle C \rangle$. In this manner, the advective contribution to the tracer budget takes the form

$$V \left[\frac{d\langle C \rangle}{dt} \right]_{\text{advective}} = - \oint_{\partial \mathcal{R}} C \, \boldsymbol{v} \cdot \hat{\boldsymbol{n}} \, d\mathcal{S} = - \oint_{\partial \mathcal{R}} (C - \langle C \rangle) \, \boldsymbol{v} \cdot \hat{\boldsymbol{n}} \, d\mathcal{S}. \tag{29.121}$$

Hence, advective transport through the region boundary changes the region integrated C, and thus the volume mean $\langle C \rangle$, only if the boundary transport occurs with C values that differ from the region average, $\langle C \rangle$.

[9] We considered property (29.119) in Exercise 21.5.

29.5.3 A rectangular region example

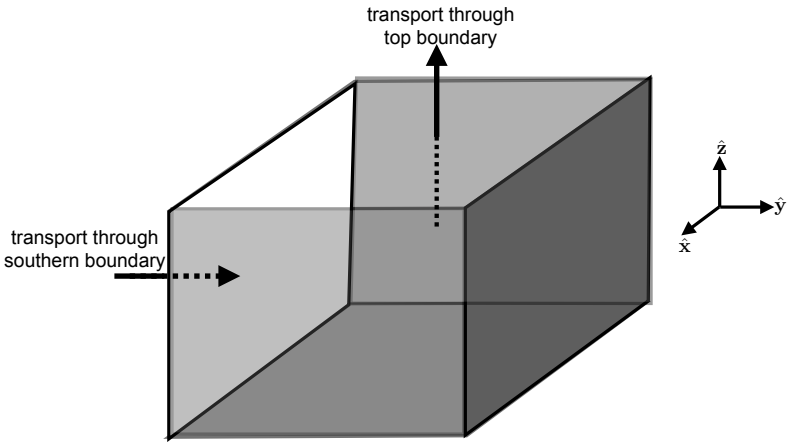

FIGURE 29.1: A rectangular ocean region for considering the tracer budget in a Boussinesq ocean. We assume the only open boundaries of the region are along the southern boundary and top boundary, with the remaining boundaries closed. Note that the top boundary can generally be within the ocean interior, and so does not need to be the top of the ocean. The non-divergent nature of the flow means that any fluid entering through the southern boundary must leave through the top boundary, and conversely. This constraint on the flow impacts on how the advective tracer transport affects changes to the volume integrated tracer within the region.

Consider the rectangular region of Figure 29.1 that is closed along its bottom, northern, eastern, and western boundaries, yet that is open along its top boundary and southern boundary. Specify flow along the southern boundary to be northward and let it bring fluid into the region with $C_{\text{south}} > \langle C \rangle$, thus acting to increase $\langle C \rangle$. Due to the non-divergent nature of the velocity, the northward transport of fluid through the southern boundary is exactly balanced by a vertically upward transport of fluid out of the top boundary. What does that vertical transport of fluid imply about changes to $\langle C \rangle$? The answer depends on the tracer concentration on the top boundary.

- If $C_{\text{top}} > \langle C \rangle$, then the relatively high values of tracer that leave through the top boundary act to decrease the net C within the region, thus counteracting the contribution of $C_{\text{south}} > \langle C \rangle$ that enters through the southern boundary. For the special case of equal C transports through the two boundaries, then there is no accumulation of C within the region so that $\langle C \rangle$ remains unchanged.

- If $C_{\text{top}} = \langle C \rangle$, then $\langle C \rangle$ increases due to the transport of C through the southern boundary, with no net transport across the top boundary.

- If $C_{\text{top}} < \langle C \rangle$, then the vertical transport of $C_{\text{top}} < \langle C \rangle$ increases $\langle C \rangle$ acting just like the $C_{\text{south}} > \langle C \rangle$ fluid that enters through the southern boundary. That is, we can increase $\langle C \rangle$ in the region by bringing fluid into the domain with C greater than $\langle C \rangle$, or by exporting fluid with C less than $\langle C \rangle$.

29.5.4 Comments

Constraints introduced by the non-divergent nature of the Boussinesq ocean render subtleties to the physical interpretation of how tracer fluxes affect the budget of tracer within a region. These constraints are absent from the compressible fluid, whose flow is generally divergent. The discussion in this section was motivated by Appendix B of *Gregory* (2000), who studied heat (enthalpy) budgets within a numerical Boussinesq ocean circulation model.

29.6 Mechanical energy analysis: Part I

The volume of a fluid element in a non-divergent flow remains materially invariant even as pressure acts on the element. Hence, pressure cannot perform mechanical work on the fluid. Consequently, a non-divergent flow supports no pressure work conversion between internal energy and kinetic energy, which contrasts to the case in a non-Boussinesq fluid (see Section 26.4). In this section we formulate a mechanical energy budget for the Boussinesq ocean, and find that this budget is closed for a perfect fluid so long as the geopotential is time-independent and there are no boundary effects. Many of the steps are directly analogous to those in a non-Boussinesq fluid detailed in Chapter 26, though with some important distinctions that are emphasized in this section as well as Section 29.8.

29.6.1 Governing equations

We develop the mechanical energy budget for an unforced non-hydrostatic Boussinesq ocean with density a function only of salinity and Conservative Temperature,

$$\rho = \rho(S, \Theta). \tag{29.122}$$

The more general pressure-dependent equation of state is considered in Section 29.8. Furthermore, we work with the velocity, density, and continuity equations in the form

$$\rho_o \left[\frac{\mathrm{D}\boldsymbol{v}}{\mathrm{D}t} + 2\,\boldsymbol{\Omega} \times \boldsymbol{v} \right] = -\nabla p - \rho\, \nabla \Phi \tag{29.123a}$$

$$\frac{\mathrm{D}\rho}{\mathrm{D}t} = \frac{\partial \rho}{\partial S}\frac{\mathrm{D}S}{\mathrm{D}t} + \frac{\partial \rho}{\partial \Theta}\frac{\mathrm{D}\Theta}{\mathrm{D}t} = \dot{\rho} \tag{29.123b}$$

$$\nabla \cdot \boldsymbol{v} = 0. \tag{29.123c}$$

Note that the geopotential, Φ, is generally a function of space and time, $\Phi = \Phi(\boldsymbol{x}, t)$, with thiisi dependence appropriate when studying astronomical tides or mass inhomogeneities creating spatial variations in the gravity field (see Chapter 34).

29.6.2 Kinetic energy

To obtain a kinetic energy equation, start by taking the dot product of the velocity, $\boldsymbol{v}$, and the momentum equation (29.123a) and note that the Coriolis acceleration drops out since it is orthogonal to the velocity

$$\boldsymbol{v} \cdot (2\,\boldsymbol{\Omega} \times \boldsymbol{v}) = 0. \tag{29.124}$$

The material time derivative takes the form

$$v_i \left[\frac{\partial v_i}{\partial t} + v_j \partial_j v_i \right] = \frac{\partial \mathcal{K}}{\partial t} + \boldsymbol{v} \cdot \nabla \mathcal{K} = \frac{\mathrm{D}\mathcal{K}}{\mathrm{D}t}, \tag{29.125}$$

where we introduced the kinetic energy per mass

$$\mathcal{K} = \boldsymbol{v} \cdot \boldsymbol{v}/2. \tag{29.126}$$

The equation for the Boussinesq kinetic energy per volume thus takes the form

$$\rho_o \frac{\mathrm{D}\mathcal{K}}{\mathrm{D}t} = -\boldsymbol{v} \cdot \nabla p - \rho\, \boldsymbol{v} \cdot \nabla \Phi. \tag{29.127}$$

Alternatively, we can write this equation in the flux-form

$$\frac{\partial(\rho_o \mathcal{K})}{\partial t} + \nabla \cdot [\boldsymbol{v}\,(\rho_o \mathcal{K} + p)] = -\rho\, \boldsymbol{v} \cdot \nabla\Phi, \tag{29.128}$$

where we used $\nabla \cdot \boldsymbol{v} = 0$ to write $\boldsymbol{v} \cdot \nabla p = \nabla \cdot (\boldsymbol{v}\, p)$. Note that in Exercise 29.4 we show that the kinetic energy evolution derived here for the non-hydrostatic fluid holds also for the hydrostatic fluid, yet with the kinetic energy in the hydrostatic fluid determined solely by the horizontal velocity.

The term $-\rho\, \boldsymbol{v} \cdot \nabla\Phi$ in the kinetic energy equation (29.128) is a source/sink that arises from fluid motion crossing surfaces of constant geopotential. Moving a fluid element down the geopotential gradient ($\boldsymbol{v} \cdot \nabla\Phi < 0$) increases the kinetic energy, and conversely when the fluid moves up the geopotential gradient. We sometimes refer to this process as *buoyancy work*, particularly when considered in the context of a vertically stratified fluid. We can further exemplify this term by taking the simplified form of the geopotential, $\Phi = g\, z$, in which $\boldsymbol{v} \cdot \nabla\Phi = g\, w$.

29.6.3 Gravitational potential and mechanical energies

We here develop the gravitational energy budget and then add to the kinetic energy to derive the mechanical energy budget.

Gravitational potential energy

A fluid element has a gravitational potential energy per mass given by the geopotential, Φ, which has a material time derivative

$$\frac{\mathrm{D}\Phi}{\mathrm{D}t} = \partial_t \Phi + \boldsymbol{v} \cdot \nabla\Phi. \tag{29.129}$$

The time-dependent geopotential provides an external source of potential energy to the system. Additionally, motion moving up the gradient of the geopotential ($\boldsymbol{v} \cdot \nabla\Phi > 0$) increases the potential energy per mass, and conversely for motion down the geopotential gradient.

Mechanical energy budget

Adding the gravitational potential energy equation (29.129) to the kinetic energy equation (29.127) renders the material evolution

$$\rho_o \frac{\mathrm{D}\mathcal{K}}{\mathrm{D}t} + \rho \frac{\mathrm{D}\Phi}{\mathrm{D}t} = -\nabla \cdot (\boldsymbol{v}\, p) + \rho\, \partial_t \Phi. \tag{29.130}$$

Note how the buoyancy work source, $\rho\, \boldsymbol{v} \cdot \nabla\Phi$, dropped out from this budget. Consequently, this term provides a reversible transfer of mechanical energy between gravitational potential energy per volume and the kinetic energy per volume. We saw the same transfer in Section 26.4 when studying the mechanical energy budget for a compressible non-Boussinesq fluid.

Equation (29.130) has nearly the same form as that for the non-Boussinesq fluid given by equation (26.49). However, for the Boussinesq ocean it does not lead to a flux-form conservation law for mechanical energy, even for the perfect fluid. Operationally, the derivations diverge at this point since for the non-Boussinesq fluid we make use of the mass continuity equation (19.6) to write the material evolution of density. In contrast, material density evolution in a Boussinesq ocean is determined by material changes in temperature, salinity, and pressure.

To develop a closed Boussinesq mechanical energy budget, add $\Phi\, \mathrm{D}\rho/\mathrm{D}t = \Phi\, \dot{\rho}$ to both sides

of equation (29.130) to render the material evolution for the mechanical energy *per volume*

$$\frac{\mathrm{D}}{\mathrm{D}t}\left[\rho_{\circ}\,\mathcal{K}+\rho\,\Phi\right]=-\nabla\cdot(\boldsymbol{v}\,p)+\rho\,\partial_t\Phi+\dot{\rho}\,\Phi, \tag{29.131}$$

which has the flux-form expression

$$\partial_t\left(\rho_{\circ}\,\mathcal{M}\right)+\nabla\cdot\left[\boldsymbol{v}\left(\rho_{\circ}\,\mathcal{M}+p\right)\right]=\rho\,\partial_t\Phi+\dot{\rho}\,\Phi, \tag{29.132}$$

where we defined the Boussinesq mechanical energy per volume as

$$\rho_{\circ}\,\mathcal{M}=\rho_{\circ}\,\mathcal{K}+\rho\,\Phi. \tag{29.133}$$

Note the $\rho_{\circ}$ determining the kinetic energy per volume, whereas ρ determines the gravitational potential energy. These distinct density factors result from the distinction made in the Boussinesq ocean between inertial mass and gravitational mass. We discussed this point in the opening to this chapter.

29.6.4 Finite volume mechanical energy bugdet

Recall that a scalar tracer concentration, C, satisfies a flux-form equation of the form (29.116)

$$\partial_t(\rho_{\circ}\,C)+\nabla\cdot(\rho_{\circ}\,C\,\boldsymbol{v}+\boldsymbol{J})=0, \tag{29.134}$$

where $\boldsymbol{J}$ is a subgrid tracer flux. Comparing to the mechanical energy equation (29.132), we see that mechanical energy has a non-zero source on the right hand side that cannot be written as the divergence of a flux. Additionally, the tracer vector, $\boldsymbol{J}$, corresponds in the energy equation to the pressure flux, $p\,\boldsymbol{v}$. With these correspondences between the tracer equation and mechanical energy equation, we can make direct use of the Leibniz-Reynolds transport theorem in the form of equation (20.49) to render the finite volume mechanical energy budget

$$\frac{\mathrm{d}}{\mathrm{d}t}\left[\int_{\mathcal{R}}\rho_{\circ}\,\mathcal{M}\,\mathrm{d}V\right]=-\oint_{\partial\mathcal{R}}\rho_{\circ}\,\mathcal{M}\,(\boldsymbol{v}-\boldsymbol{v}^{(\mathrm{b})})\cdot\hat{\boldsymbol{n}}\,\mathrm{d}\mathcal{S}-\oint_{\partial\mathcal{R}}p\,\boldsymbol{v}\cdot\hat{\boldsymbol{n}}\,\mathrm{d}\mathcal{S}+\int_{\mathcal{R}}\left[\rho\,\partial_t\Phi+\dot{\rho}\,\Phi\right]\mathrm{d}V, \tag{29.135}$$

where $\mathcal{R}$ is the finite volume region, $\partial\mathcal{R}$ is its boundary, $\boldsymbol{v}^{(\mathrm{b})}$ is the velocity of a point on the boundary, and $\hat{\boldsymbol{n}}$ is the outward normal on the boundary. The first term on the right hand side arises from the advective transport of mechanical energy across the moving region boundary, taking into account the difference between the fluid velocity and boundary velocity. The second term arises from the work done by pressure on the boundary, and the final term arises from time dependence to the geopotential plus material changes in density. It is notable that the flow is non-divergent at each point, so that pressure cannot do work in the interior of the region. Even so, pressure can do work on the boundary of the region where $\boldsymbol{v}\cdot\hat{\boldsymbol{n}}\neq 0$. Observe that the budget (29.135) for a Boussinesq fluid corresponds to the budget (26.55) for a non-Boussinesq fluid.

A material region is characterized by $(\boldsymbol{v}-\boldsymbol{v}^{(\mathrm{b})})\cdot\hat{\boldsymbol{n}}=0$ on the boundaries, in which case there is no transport of mechanical energy across the boundary. We are thus left with the mechanical energy budget (29.135)

$$\frac{\mathrm{d}}{\mathrm{d}t}\left[\int_{\mathcal{R}}\rho_{\circ}\,\mathcal{M}\,\mathrm{d}V\right]=-\oint_{\partial\mathcal{R}}p\,\boldsymbol{v}\cdot\hat{\boldsymbol{n}}\,\mathrm{d}\mathcal{S}+\int_{\mathcal{R}}\left(\rho\,\partial_t\Phi+\dot{\rho}\,\Phi\right)\mathrm{d}V. \tag{29.136}$$

Recall we are assuming $\rho=\rho(S,\Theta)$ in this section, so that

$$\dot{\rho}=(\partial\rho/\partial S)\,\dot{S}+(\partial\rho/\partial\Theta)\,\dot{\Theta}. \tag{29.137}$$

Hence, for a time-independent geopotential ($\partial_t \Phi = 0$) and in the absence of processes that contribute to a material evolution of S and Θ (i.e., $\dot{S} = 0$ and $\dot{\Theta} = 0$), then the finite volume Boussinesq mechanical energy for a material fluid region is affected only by pressure work on the boundaries.[10]

29.7 Boussinesq energetics with molecular dissipation

The ocean is a forced-dissipative system, with mechanical and buoyant forcing predominantly at the surface and bottom boundaries and mechanical dissipation via molecular viscosity. In this section we extend the discussion from Section 29.6 to here develop the mechanical energy budget in a Boussinesq ocean affected by forcing and dissipation. Much of this discussion represents a specialization of the more general presentation of energetics in Chapter 26, here focusing on the ocean interior and considering the addition of buouyancy sources.

In particular, we examine energetics for the Boussinesq ocean equations written in their form with Archimedean buoyancy

$$\mathrm{D}\boldsymbol{v}/\mathrm{D}t + 2\,\boldsymbol{\Omega} \times \boldsymbol{v} = -\nabla\varphi + \hat{\boldsymbol{z}}\, b + \nabla \cdot \mathbb{T}/\rho_o \tag{29.138a}$$

$$\mathrm{D}b/\mathrm{D}t = -\nabla \cdot \boldsymbol{F}^{\mathsf{b}} + Q_{\mathsf{b}} \tag{29.138b}$$

$$\nabla \cdot \boldsymbol{v} = 0. \tag{29.138c}$$

The term $\nabla \cdot \mathbb{T}/\rho_o$ is the divergence of a friction stress tensor, $-\nabla \cdot \boldsymbol{F}^{\mathsf{b}}$ is the convergence of a buoyancy flux vector, and Q_{b} is a buoyancy source either at the boundaries or the interior. The new element in this discussion, relative to Chapter 26, concerns the role of the buoyancy flux. One operational point to note is that for all subgrid scale and boundary conditions in a Boussinesq ocean, appearances of the *in situ* density present in a non-Boussinesq fluids are here converted to the Boussinesq reference density, ρ_o.

29.7.1 Forms for the buoyancy flux

Buoyancy flux for large-scale flows

For large-scale flows a particularly common form for the buoyancy flux is taken as

$$\boldsymbol{F}^{\mathsf{b}} = -\kappa\, \partial_z b\, \hat{\boldsymbol{z}} + \boldsymbol{v}^* b. \tag{29.139}$$

The first term is a downgradient vertical diffusive flux with the vertical *eddy diffusivity*, $\kappa > 0$, a function of the flow state so that

$$\kappa = \kappa(\boldsymbol{x}, t). \tag{29.140}$$

The second term is an advective flux, where the advective velocity, $\boldsymbol{v}^* = (\boldsymbol{u}^*, w^*)$, is assumed to be non-divergent

$$\nabla \cdot \boldsymbol{v}^* = \nabla_{\mathsf{h}} \cdot \boldsymbol{u}^* + \partial_z w^* = 0. \tag{29.141}$$

The velocity, $\boldsymbol{v}^*$, is commonly termed the *eddy-induced* velocity, with a particular choice for its parameterization discussed in Exercise 29.9 and further examined in Section 71.1.

[10] We find that $\dot{S}$ and $\dot{\Theta}$ are nonzero in the presence of boundary processes (e.g., heat fluxes, fresh water fluxes) and in the presence of mixing (e.g., as parameterized by diffusion). We study diffusion in Chapter 69 and then in Chapter 73 we provide a detailed look at the suite of processes contributing to nonzero $\dot{S}$ and $\dot{\Theta}$.

Boundary conditions

The normal component of the buouyancy flux vanishes at boundaries

$$\hat{\boldsymbol{n}} \cdot \boldsymbol{F}^{\mathsf{b}} = 0, \tag{29.142}$$

so that boundary buoyancy fluxes are assumed to sit within the source term, Q_{b}, via

$$Q_{\mathsf{b}} = Q^{\mathsf{surf}} \qquad \text{at } z = \eta(x, y, t) \tag{29.143a}$$
$$Q_{\mathsf{b}} = Q^{\mathsf{bot}} \qquad \text{at } z = \eta_{\mathsf{b}}(x, y) \tag{29.143b}$$
$$\boldsymbol{v}^* \cdot \hat{\boldsymbol{n}} = 0 \qquad \text{all boundaries,} \tag{29.143c}$$

where Q^{surf} is the surface buoyancy flux, Q^{bot} is the bottom buoyancy flux (e.g., geothermal heating), and $\hat{\boldsymbol{n}}$ is the outward normal at the boundaries. Both Q^{surf} and Q^{bot} are positive when directed upward. In Section 72.6 we detail the plethora of processes leading to boundary fluxes of buoyancy.

Molecular buoyancy flux assumed in this section

In the remainder of this section, we are most interested in the energetic role of molecular diffusion of buoyancy rather than turbulent mixing. In this case the buoyancy flux takes on the downgradient diffusive form

$$\boldsymbol{F}^{\mathsf{b}} = -\kappa \nabla b. \tag{29.144}$$

29.7.2 Mechanical forcing and dissipation

Following our discussion of frictional stresses in Section 25.8, we here write the frictional acceleration, $\boldsymbol{F}$, in the Boussinesq ocean as the divergence of the frictional stress tensor, $\mathbb{T}$,

$$\rho_{\circ} \boldsymbol{F} = \nabla \cdot \mathbb{T}. \tag{29.145}$$

Friction in large scale flows

For many large scale flows, the dominant contribution to frictional stresses arises from the vertical divergence of horizontal subgrid stresses, in which case the horizontal frictional acceleration vector takes the form

$$\rho_{\circ} \boldsymbol{F}^h = \partial_z \boldsymbol{\tau} = \rho_{\circ} \frac{\partial}{\partial z} \left[\nu^{\text{eddy}} \frac{\partial \boldsymbol{u}}{\partial z} \right], \tag{29.146}$$

where

$$\boldsymbol{\tau} = \rho_{\circ} \nu^{\text{eddy}} \partial_z \boldsymbol{u} \tag{29.147}$$

is the horizontal turbulent stress vector whose vertical derivative contributes to the vertical transfer of horizontal momentum. Whereas the molecular viscosity, ν, is a function of the fluid composition (Section 25.8), the *eddy viscosity*, ν^{eddy}, is a function of the flow so that

$$\nu^{\text{eddy}} = \nu^{\text{eddy}}(\boldsymbol{x}, t) \geq 0. \tag{29.148}$$

The eddy viscosity is typically many orders of magnitude larger than the molecular viscosity in regions of strong turbulent mixing.

Boundary stresses

Boundary stresses are written as

$$\hat{\boldsymbol{n}} \cdot \mathbb{T} = \boldsymbol{\tau}^{\text{surf}} \qquad \text{at } z = \eta(x, y, t) \tag{29.149a}$$

$$(-\hat{\boldsymbol{n}}) \cdot \mathbb{T} = \boldsymbol{\tau}^{\text{bott}} \qquad \text{at } z = \eta_{\text{b}}(x, y). \tag{29.149b}$$

The surface boundary stress vector, $\boldsymbol{\tau}^{\text{surf}}$, arises from the transfer of momentum between the ocean and atmosphere (or the ocean and ice). In numerical modeling practice, this stress is computed by a boundary layer parameterization that ingests the momentum from the atmosphere or ice and computes a stress that is transferred to the ocean through these boundary conditions. As per Newton's third law (the action/reaction law; see Section 25.10), the stress imparted to the ocean is equal and opposite the stress imparted to the atmosphere at its lower boundary.

The bottom stress vector, $\boldsymbol{\tau}^{\text{bott}}$, is often parameterized via a quadratic bottom drag

$$\boldsymbol{\tau}^{\text{bott}} = -C_{\text{D}} \, \rho_{\circ} \, \boldsymbol{v} \, |\boldsymbol{v}|, \tag{29.150}$$

where $C_{\text{D}} > 0$ is a dimensionless *drag coefficient* that is sometimes assumed to be a function of the bottom topographic roughness. This bottom stress acts to drag the ocean bottom velocity towards a state of rest. It is equal and opposite to the frictional stress transferred to the solid earth from the ocean. Note that this bottom drag acts similarly to the linear Rayleigh drag in equation (25.72). However, the bottom drag in equation (29.150) is nonlinear, whereas the Rayleigh drag is linear

$$\boldsymbol{F}_{\text{Rayleigh}} = -\gamma \, \boldsymbol{v}. \tag{29.151}$$

Molecular Laplacian friction assumed in this section

In the following, we are most interested in the energetic role of molecular viscosity rather than turbulent viscosity. In this case the frictional acceleration takes on the form

$$\boldsymbol{F} = \nu \, \nabla^2 \boldsymbol{v}. \tag{29.152}$$

Additionally, we ignore all boundary contributions in order to focus on the contributions from molecular viscosity.

29.7.3 Governing equations with molecular friction and diffusion

Assuming frictional acceleration given by molecular viscosity (29.152), and a buoyancy flux given by downgradient molecular diffusion (29.144), leads to the simplified form of the governing equations (29.138a)-(29.138c)

$$\mathrm{D}\boldsymbol{v}/\mathrm{D}t + 2 \, \boldsymbol{\Omega} \times \boldsymbol{v} = -\nabla \varphi + \hat{\boldsymbol{z}} \, b + \nu \, \nabla^2 \boldsymbol{v} \tag{29.153a}$$

$$\mathrm{D}b/\mathrm{D}t = \kappa \, \nabla^2 b + Q_{\text{b}} \tag{29.153b}$$

$$\nabla \cdot \boldsymbol{v} = 0. \tag{29.153c}$$

These are the equations to which we now examine energetics.

29.7.4 Kinetic energy evolution

To obtain a kinetic energy evolution equation, start by taking the dot product of the velocity, $\boldsymbol{v}$, with the momentum equation (29.153a). Since the Coriolis term drops out

$$\boldsymbol{v} \cdot (2 \, \boldsymbol{\Omega} \times \boldsymbol{v}) = 0, \tag{29.154}$$

the material time derivative takes the form (assuming Cartesian tensors for simplicity)

$$v_i \left[\partial_t v_i + v_j \partial_j v_i\right] = \partial_t \mathcal{K} + \boldsymbol{v} \cdot \nabla \mathcal{K} = \mathrm{D}\mathcal{K}/\mathrm{D}t, \tag{29.155}$$

where we introduced the kinetic energy per mass

$$\mathcal{K} = \boldsymbol{v} \cdot \boldsymbol{v}/2. \tag{29.156}$$

Hence, the kinetic energy equation takes the form

$$\mathrm{D}\mathcal{K}/\mathrm{D}t = -\nabla \cdot (\boldsymbol{v}\, \varphi) + w\, b + \nu\, \boldsymbol{v} \cdot \nabla^2 \boldsymbol{v}, \tag{29.157}$$

where we used $\nabla \cdot \boldsymbol{v} = 0$ to write $\boldsymbol{v} \cdot \nabla \varphi = \nabla \cdot (\boldsymbol{v}\, \varphi)$. Equation (29.157) says that the kinetic energy per mass of a Boussinesq fluid element is modified due to the advection of pressure, vertical motion in a buoyancy stratified fluid, and the projection of the velocity onto the frictional acceleration.

29.7.5 Frictional dissipation

Use of Cartesian coordinates allows us to write the Laplacian acting on a vector as (see Section 25.8.9)

$$\nabla^2 \boldsymbol{v} = -\nabla \times \boldsymbol{\omega}, \tag{29.158}$$

which then brings the Laplacian friction to the form

$$\begin{aligned}
-\boldsymbol{v} \cdot \nabla^2 \boldsymbol{v} &= \boldsymbol{v} \cdot \nabla \times \boldsymbol{\omega} && \text{(29.159a)}\\
&= v_m\, \epsilon_{mnp}\, \partial_n \omega_p && \text{(29.159b)}\\
&= \partial_n (\epsilon_{mnp}\, v_m\, \omega_p) - \epsilon_{mnp}\, \omega_p\, \partial_n v_m && \text{(29.159c)}\\
&= -\partial_n (\epsilon_{nmp}\, v_m\, \omega_p) + \epsilon_{nmp}\, (\partial_n v_m)\, \omega_p && \text{(29.159d)}\\
&= -\partial_n (\boldsymbol{v} \times \boldsymbol{\omega})_n + \omega_p\, \omega_p && \text{(29.159e)}\\
&= -\nabla \cdot (\boldsymbol{v} \times \boldsymbol{\omega}) + \boldsymbol{\omega} \cdot \boldsymbol{\omega}. && \text{(29.159f)}
\end{aligned}$$

The kinetic energy equation (29.157) can thus be written

$$\begin{aligned}
\mathrm{D}\mathcal{K}/\mathrm{D}t &= -\nabla \cdot (\boldsymbol{v}\, \varphi) + w\, b - \nu\, \boldsymbol{v} \cdot (\nabla \times \boldsymbol{\omega}) && \text{(29.160a)}\\
&= -\nabla \cdot [\boldsymbol{v}\, \varphi + \nu\, (\boldsymbol{v} \times \boldsymbol{\omega})] + w\, b - \nu\, \boldsymbol{\omega} \cdot \boldsymbol{\omega}. && \text{(29.160b)}
\end{aligned}$$

The physical dimensions for all terms in these equations are $\mathrm{L}^2\ \mathrm{T}^{-3}$: squared length per cubed time, which is the dimensions of energy per mass per time.

29.7.6 Domain integrated kinetic energy

Consider a region of fluid with no boundary contributions. Performing a volume average over that region leads to

$$\frac{\mathrm{d}}{\mathrm{d}t} \langle \mathcal{K} \rangle = \langle w\, b \rangle - \epsilon, \tag{29.161}$$

where the angle-brackets denote volume averaging

$$\langle A \rangle = \frac{\int A\, \mathrm{d}V}{\int \mathrm{d}V}. \tag{29.162}$$

To reach equation (29.161), we dropped all boundary terms, including the term $\hat{\boldsymbol{n}} \cdot (\boldsymbol{v} \times \boldsymbol{\omega})$, and introduced

$$\epsilon = \frac{\nu \int \boldsymbol{\omega} \cdot \boldsymbol{\omega} \, \mathrm{d}V}{\int \mathrm{d}V} = \nu \, \langle \boldsymbol{\omega} \cdot \boldsymbol{\omega} \rangle \geq 0, \tag{29.163}$$

which is the volume averaged kinetic energy dissipation rate arising from viscous effects (dimensions of $\mathrm{L}^2 \ \mathrm{T}^{-3}$). We thus see that there is more kinetic energy dissipation for a Boussinesq flow with larger domain averaged $\boldsymbol{\omega} \cdot \boldsymbol{\omega}$, and zero dissipation for flow with zero mean square vorticity.

Equation (29.161) says that the domain averaged kinetic energy per mass is reduced by viscous dissipation acting within the fluid domain. Furthermore, the averaged kinetic energy is increased in regions where buoyancy and vertical motion are positively correlated, $\langle w \, b \rangle > 0$, in which case light water preferentially moves vertically up and heavy water down. Conversely, the averaged kinetic energy is decreased when buoyancy and vertical motion are negatively correlated (light water preferentially moves down and heavy water up).

29.7.7 Potential energy evolution

Assuming the simple form of the geopotential

$$\Phi = g \, z \tag{29.164}$$

leads to

$$\mathrm{D}\Phi/\mathrm{D}t = g \, w = \boldsymbol{v} \cdot \nabla \Phi = \nabla \cdot (\boldsymbol{v} \, \Phi), \tag{29.165}$$

where the second equality follows from the definition of the material derivative, and since $\partial \Phi / \partial t = 0$. Multiplying the buoyancy equation (29.138b) by Φ, and the Φ equation (29.165) by b, then adding, leads to

$$\begin{aligned} \mathrm{D}(\Phi \, b)/\mathrm{D}t &= g \, b \, w + \Phi \, (Q_{\mathrm{b}} + \kappa \, \nabla^2 b) && \text{(29.166a)} \\ &= g \, b \, w + \Phi \, Q_{\mathrm{b}} + \nabla \cdot (\kappa \, \Phi \, \nabla b) - \kappa \, \nabla \Phi \cdot \nabla b && \text{(29.166b)} \\ &= g \, b \, w + \Phi \, Q_{\mathrm{b}} + \nabla \cdot (\Phi \, \kappa \, \nabla b) - g \, \kappa \, \partial_z b, && \text{(29.166c)} \end{aligned}$$

so that

$$\mathrm{D}P^{\mathrm{b}}/\mathrm{D}t = -b \, w - g^{-1} \, \Phi \, Q_{\mathrm{b}} - \nabla \cdot (g^{-1} \, \Phi \, \kappa \, \nabla b) + \kappa \, \partial_z b. \tag{29.167}$$

The product

$$P^{\mathrm{b}} = -g^{-1} \, \Phi \, b = z \, g \, \delta\rho / \rho_{\circ} \tag{29.168}$$

is the gravitational potential energy per mass associated with the deviation of density from the Boussinesq reference density, $\rho_{\circ}$. Equation (29.167) says that the gravitational potential energy per mass of a fluid element changes depending on the vertical motion of buoyancy (the $-b \, w$ term); from diabatic sources (the $\Phi \, Q_{\mathrm{b}}$ term); from a total divergence associated with buoyancy diffusion; and from the vertical diffusive flux of buoyancy. The diabatic source and diffusion are both irreversible terms, whereas the vertical motion term is reversible.

Writing the material evolution (29.167) in its flux-form leads to the Eulerian balance equation for the potential energy per mass

$$\partial_t P^{\mathrm{b}} + \nabla \cdot [\boldsymbol{v} \, P^{\mathrm{b}} + g^{-1} \, \Phi \, \kappa \, \nabla b] = -b \, w - g^{-1} \, \Phi \, Q_{\mathrm{b}} + \kappa \, \partial_z b. \tag{29.169}$$

Integrating over a region of constant volume and with zero boundary fluxes (other than fluxes associated with Q_{b}), leads to

$$\frac{\mathrm{d}}{\mathrm{d}t} \langle P^{\mathrm{b}} \rangle = -\langle b \, w \rangle - g^{-1} \langle \Phi \, Q_{\mathrm{b}} \rangle + \kappa \left\langle \frac{\partial b}{\partial z} \right\rangle. \tag{29.170}$$

The domain averaged potential energy per mass evolves according to the correlation between vertical motion and buoyancy; the correlation between heating and depth; and the domain averaged vertical diffusive flux of buoyancy. We now comment on the right hand side terms.

Downgradient diffusion in the vertical

In a stably stratified ocean, buoyancy is larger in the upper ocean than deeper ocean, in which case

$$\partial b/\partial z > 0 \qquad \text{stably stratified.} \tag{29.171}$$

A downgradient vertical diffusive flux acts to homogenize in the vertical. Consequently, when acting on a stably stratified fluid, diffusion moves buoyancy down from the upper ocean (where buoyancy is large) into the interior ocean (where buoyancy is less). Conversely, it moves low buoyancy upward. Consequently, diffusion makes the upper ocean less buoyant (heavier) and the deeper ocean more buoyant (lighter). We thus see that diffusion raises the ocean center of mass and as such it increases the domain averaged gravitational potential energy via equation (29.170).

As a further comment, recall that diffusion in a compressible fluid does not move mass (Section 20.1), but it generally does move volume. Conversely, for a Boussinesq ocean (which has a non-divergent flow, $\nabla \cdot \boldsymbol{v} = 0$), diffusion does not move volume but it generally does move mass. So since the flow is non-divergent, vertical diffusion can raise the center of mass through buoyancy diffusion even while it does not create any volume transport.

Diabatic heating

The diabatic heating term in equation (29.170), $-g^{-1}\langle \Phi\, Q_{\mathsf{b}} \rangle$, increases potential energy if there is a positive correlation between vertical position, $-g^{-1}\,\Phi = -z$, and heating

$$-g^{-1}\langle \Phi\, Q_{\mathsf{b}} \rangle = -\langle z\, Q_{\mathsf{b}} \rangle > 0. \tag{29.172}$$

That is, domain averaged potential energy increases if heating, $Q_{\mathsf{b}} > 0$, preferentially occurs in regions deeper than cooling. This situation is not typical in the ocean, where heating is generally shallower than cooling. Geothermal heating at the ocean bottom is perhaps the only example where heating is deeper than cooling.

Vertical motion

The vertical motion term appearing in equation (29.170),

$$b\, w = -g\, w\, \delta\rho/\rho_o \tag{29.173}$$

has a positive sign in the kinetic energy equation (29.157), wherea is has a negative sign in the potential energy equation (29.167). To help understand this term, consider the specific case of a negatively buoyant fluid element

$$b = -g\, \delta\rho/\rho_o < 0. \tag{29.174}$$

If this fluid element moves vertically upward, $w > 0$, the fluid acquires positive gravitational potential energy since relatively heavy water is moving upwards. This increase in potential energy is reflected in the term $-w\, b > 0$ appearing in the potential energy equation (29.167). This increase in gravitational potential energy is associated with a decrease in kinetic energy through the $w\, b < 0$ term appearing in equation (29.157). The conversion between potential and kinetic energy associated with the $w\, b$ term is a key process arising from vertical motion.

29.7.8 Mechanical energy

Adding the equation for kinetic energy per mass (29.157) to the potential energy equation (29.167) leads to the material evolution for the mechanical energy per mass

$$\frac{\mathrm{D}(\mathcal{K} + P^{\mathrm{b}})}{\mathrm{D}t} = -\nabla \cdot [\boldsymbol{v}\, \varphi + \nu\, \boldsymbol{v} \times \boldsymbol{\omega} + g^{-1}\, \kappa\, \Phi\, \nabla b] - \nu\, \boldsymbol{\omega} \cdot \boldsymbol{\omega} - g^{-1}\, \Phi\, Q_{\mathrm{b}} + \kappa\, \partial_z b. \tag{29.175}$$

Notice how the term $w\, b$ cancelled as it provides for a reversible transfer of mechanical energy between gravitational potential and kinetic. This reversible transfer has no effect on the mechanical energy. As emphasized by *Gent* (1993), frictional dissipation appears only in the equation for kinetic energy per mass (29.157), whereas buoyancy diffusion and sources only appear in the potential energy equation (29.167). When forming the mechanical energy equation, these terms appear together.

Writing the budget (29.175) in flux-form leads to

$$\frac{\partial(\mathcal{K} + P^{\mathrm{b}})}{\partial t} = -\nabla \cdot [\boldsymbol{v}\, (\mathcal{K} + P^{\mathrm{b}} + \varphi) + \nu\, \boldsymbol{v} \times \boldsymbol{\omega} + g^{-1}\, \kappa\, \Phi\, \nabla b] - \nu\, \boldsymbol{\omega} \cdot \boldsymbol{\omega} - g^{-1}\, \Phi\, Q_{\mathrm{b}} + \kappa\, \partial_z b. \tag{29.176}$$

The sum $\mathcal{K} + P^{\mathrm{b}} + \varphi$ appearing on the right hand side is the *Bernoulli function* for a Boussinesq fluid (see Section 26.7 for the non-Boussinesq form of the Bernoulli function). Integrating the local mechanical energy budget (29.176) over a region with constant volume, and dropping surface terms, leads to the domain averaged mechanical energy budget

$$\frac{\mathrm{d}}{\mathrm{d}t} \langle \mathcal{K} + P^{\mathrm{b}} \rangle = -\epsilon - \langle z\, Q_{\mathrm{b}} \rangle + \kappa \left\langle \frac{\partial b}{\partial z} \right\rangle . \tag{29.177}$$

29.7.9 Conditions for steady state mechanical energy

A steady state mechanical energy balance for the full ocean domain is realized when there is a balance between changes in domain averaged kinetic energy and changes in domain averaged potential energy

$$\frac{\mathrm{d}\langle \mathcal{K} \rangle}{\mathrm{d}t} = -\frac{\mathrm{d}\langle P^{\mathrm{b}} \rangle}{\mathrm{d}t}. \tag{29.178}$$

Setting the domain integrated mechanical energy time tendency to zero in equation (29.177) leads to the balance

$$\epsilon = -\langle z\, Q_{\mathrm{b}} \rangle + \kappa \left\langle \frac{\partial b}{\partial z} \right\rangle . \tag{29.179}$$

Recall from equation (29.163) that frictional dissipation is sign-definite

$$\epsilon \geq 0. \tag{29.180}$$

Consequently, a steady state mechanical energy for the ocean domain requires the right hand side of equation (29.179) to be positive. Such occurs when heating is preferentially below cooling (equation (29.172)), and when the diffusive flux moves buoyancy downward. We already discussed the diffusive flux in relation to equation (29.171) above. For the heat source term Q, we observe that locating a cooling source above the warming source will engender an overturning circulation, thus providing a kinetic energy source to balance the sink from viscous dissipation.

29.7.10 Further reading

Elements of this material originate from *Paparella and Young* (2002), and with Chapter 21 of *Vallis* (2017) offering a pedagogical discussion.

29.8 Mechanical energy analysis: Part II

In this section we build on the analysis from Section 29.6, here allowing density to be a function of salinity, Conservative Temperature, and pressure so that

$$\frac{\mathrm{D}\rho}{\mathrm{D}t} = \frac{\partial\rho}{\partial S}\frac{\mathrm{D}S}{\mathrm{D}t} + \frac{\partial\rho}{\partial\Theta}\frac{\mathrm{D}\Theta}{\mathrm{D}t} + \frac{\partial\rho}{\partial p}\frac{\mathrm{D}p}{\mathrm{D}t}. \tag{29.181}$$

Density thus materially evolves even in the absence of mixing or diabatic processes since $\mathrm{D}p/\mathrm{D}t$ is nonzero whenever flow crosses isobars. Hence, the flux-form mechanical energy equation (29.132) now takes on the form

$$\partial_t\left(\rho_\circ\,\mathcal{K} + \rho\,\Phi\right) + \nabla\cdot\left[\boldsymbol{v}\left(\rho_\circ\,\mathcal{K} + \rho\,\Phi + p\right)\right] = \rho\,\partial_t\Phi + \Phi\left[\frac{\partial\rho}{\partial S}\,\dot{S} + \frac{\partial\rho}{\partial\Theta}\,\dot{\Theta} + \frac{\partial\rho}{\partial p}\,\dot{p}\right]. \tag{29.182}$$

The right hand side terms provide sources that contribute to the evolution of mechanical energy. In the absence of mixing, diabatic processes, and with a time independent geopotential, the sources reduce to a term arising from motion across pressure surfaces. Such motion can occur for either reversible or irreversible processes. This pressure source term is rather awkward since it means the mechanical energy budget is not closed even when the flow is reversible (i.e., perfect fluid) and with time independent astronomical forces. We now follow the approach of *Young* (2010) to recover a closed Boussinesq mechanical energy budget by making use of a modified form of the gravitational potential energy.

29.8.1 Boussinesq dynamic enthalpy

In this section we introduce a new thermodynamic function that, in effect, provides us with an integrating factor to render a closed Boussinesq mechanical energy budget. This function is referred to as the *Boussinesq dynamic enthalpy*. Before considering that function we do a brief warm-up to refamiliarize ourself with the necessary thermodynamic formalism from Chapter 22.

Material time changes to a pressure integral of density

Consider a thermodynamic potential, $\widetilde{\Pi}(S,\Theta,p\,|\,p_{\mathrm{r}})$, defined according to the pressure integral of the *in situ* density

$$\widetilde{\Pi}(S,\Theta,p\,|\,p_{\mathrm{r}}) \equiv \int_{p_{\mathrm{r}}}^{p}\rho(S,\Theta,p')\,\mathrm{d}p' \Longrightarrow \left[\frac{\partial\widetilde{\Pi}}{\partial p}\right]_{S,\Theta} = \rho(S,\Theta,p), \tag{29.183}$$

where p_{r} is an arbitrary constant reference pressure. The notation $\widetilde{\Pi}(S,\Theta,p\,|\,p_{\mathrm{r}})$ emphasizes that p_{r} is a specified parameter whereas S,Θ,p are coordinates in thermodynamic configuration space (see Section 22.1.4). The integration in equation (29.183) is taken over pressure in a thermodynamic configuration space rather than an integral over a region in $\boldsymbol{x}$-space.[11] Accordingly, the infinitesimal increment of $\widetilde{\Pi}$ is given by

$$\delta\widetilde{\Pi} = \delta S\left[\frac{\partial\widetilde{\Pi}}{\partial S}\right]_{\Theta,p} + \delta\Theta\left[\frac{\partial\widetilde{\Pi}}{\partial\Theta}\right]_{S,p} + \delta p\left[\frac{\partial\widetilde{\Pi}}{\partial p}\right]_{S,\Theta} \tag{29.184a}$$

$$= \delta S\left[\frac{\partial\widetilde{\Pi}}{\partial S}\right]_{\Theta,p} + \delta\Theta\left[\frac{\partial\widetilde{\Pi}}{\partial\Theta}\right]_{S,p} + \rho(S,\Theta,p)\,\delta p. \tag{29.184b}$$

[11] This is an example where the discussion in Section 26.6.3 is key, whereby we must distinguish between fields in a thermodynamic configuration space versus fields in geographical space and time.

If the increment is computed following a moving fluid element then we are led to the material time derivative

$$\frac{\mathrm{D}\widetilde{\Pi}}{\mathrm{D}t} = \frac{\mathrm{D}S}{\mathrm{D}t}\left[\frac{\partial\widetilde{\Pi}}{\partial S}\right]_{\Theta,p} + \frac{\mathrm{D}\Theta}{\mathrm{D}t}\left[\frac{\partial\widetilde{\Pi}}{\partial\Theta}\right]_{S,p} + \rho(S,\Theta,p)\,\frac{\mathrm{D}p}{\mathrm{D}t}. \tag{29.185}$$

Material time changes to a geopotential integral of density

Using the same formalism as above, now consider a thermodynamic potential that is a function of salinity, Conservative Temperature, and geopotential

$$\Pi(S,\Theta,\Phi|\Phi_{\mathrm{r}}) \equiv \int_{\Phi_{\mathrm{r}}}^{\Phi} \rho(S,\Theta,\Phi')\,\mathrm{d}\Phi' \Longrightarrow \left[\frac{\partial\Pi}{\partial\Phi}\right]_{S,\Theta} = \rho(S,\Theta,\Phi), \tag{29.186}$$

where Φ_{r} is an arbitrary constant reference geopotential. We offer the following three comments concerning Π.

- For density that is independent of the geopotential, then $\Pi\,\mathrm{d}V = (\Phi - \Phi_{\mathrm{r}})\,\rho\,\mathrm{d}V$, which is the gravitational potential energy relative to a reference state. We thus interpret $\Pi(S,\Theta,\Phi)$ as a generalized gravitational potential energy per volume.
- One might consider Π to be the difference in hydrostatic pressure between Φ and Φ_{r} as per equation (24.56). However, the integral in equation (24.56) occurs in $\boldsymbol{x}$-space between two geopotentials and holding the (x,y) coordinates fixed during the integration, so that this integration generally crosses surfaces of constant S and Θ. In contrast, integration in equation (29.186) is taken from Φ_{r} to Φ within thermodynamic configuration space so that S and Θ are fixed while performing the geopotential integral. In this manner, the geopotential, rather than pressure, provides a coordinate within a Boussinesq thermodynamic configuration space along with S and Θ.
- *Young* (2010) provides motivation for calling Π the *Boussinesq dynamic enthalpy*.

Following the same formalism used to derive $\mathrm{D}\widetilde{\Pi}/\mathrm{D}t$ in equation (29.185), we here compute the material time derivative of the Boussinesq dynamic enthalpy

$$\frac{\mathrm{D}\Pi}{\mathrm{D}t} = \frac{\mathrm{D}S}{\mathrm{D}t}\left[\frac{\partial\Pi}{\partial S}\right]_{\Theta,\Phi} + \frac{\mathrm{D}\Theta}{\mathrm{D}t}\left[\frac{\partial\Pi}{\partial\Theta}\right]_{S,\Phi} + \rho(S,\Theta,\Phi)\,\frac{\mathrm{D}\Phi}{\mathrm{D}t}. \tag{29.187}$$

We now create a mechanical energy budget in the form

$$\frac{\mathrm{D}}{\mathrm{D}t}\left[\rho_{\circ}\,\mathcal{K} + \Pi\right] = -[\boldsymbol{v}\cdot\nabla p + \rho\,\boldsymbol{v}\cdot\nabla\Phi] + \dot{S}\left[\frac{\partial\Pi}{\partial S}\right]_{\Theta,\Phi} + \dot{\Theta}\left[\frac{\partial\Pi}{\partial\Theta}\right]_{S,\Phi} + \rho\,\frac{\mathrm{D}\Phi}{\mathrm{D}t} \tag{29.188a}$$

$$= -[\boldsymbol{v}\cdot\nabla p + \rho\,\boldsymbol{v}\cdot\nabla\Phi] + \dot{S}\left[\frac{\partial\Pi}{\partial S}\right]_{\Theta,\Phi} + \dot{\Theta}\left[\frac{\partial\Pi}{\partial\Theta}\right]_{S,\Phi} + \rho\,(\partial_t\Phi + \boldsymbol{v}\cdot\nabla\Phi) \tag{29.188b}$$

$$= -\boldsymbol{v}\cdot\nabla p + \rho\,\partial_t\Phi + \dot{S}\left[\frac{\partial\Pi}{\partial S}\right]_{\Theta,\Phi} + \dot{\Theta}\left[\frac{\partial\Pi}{\partial\Theta}\right]_{S,\Phi}, \tag{29.188c}$$

whose flux-form expression is given by

$$\partial_t\left(\rho_{\circ}\,\mathcal{K} + \Pi\right) + \nabla\cdot[\boldsymbol{v}\cdot(\rho_{\circ}\,\mathcal{K} + \Pi + p)] = \rho\,\partial_t\Phi + \dot{S}\left[\frac{\partial\Pi}{\partial S}\right]_{\Theta,\Phi} + \dot{\Theta}\left[\frac{\partial\Pi}{\partial\Theta}\right]_{S,\Phi}. \tag{29.189}$$

We thus see that in the absence of irreversible effects, and with a time independent geopotential, we have succeeded in deriving a closed (i.e., flux-form) mechanical energy budget for a Boussinesq

ocean, with

$$\rho_{\circ}\,\mathcal{M} = \rho_{\circ}\,\mathcal{K} + \Pi \xrightarrow{\rho=\rho(S,\Theta)} \rho_{\circ}\,\mathcal{K} + \rho\,(\Phi - \Phi_{\mathrm{r}}) \tag{29.190}$$

the appropriate Boussinesq expression for the mechanical energy per volume.

29.8.2 Regionally integrated Boussinesq dynamic enthalpy

Following the treatment for a compressible non-Boussinesq fluid in Section 26.2.4, we here study evolution of the gravitational potential energy integrated over a finite region, $\mathcal{R}$, that is open to material mass transport. Rather than working with the geopotential as done for the non-Boussinesq fluid, we here follow the discussion in Section 29.8.1 by making use of the Boussinesq dynamic enthalpy, thus ensuring a closed mechanical energy budget.

Budget with the equation of state: $\rho = \rho(S, \Theta, \Phi)$

For this purpose we make use the Leibniz-Reynolds transport theorem in the form of equation (20.37) to find

$$\frac{\mathrm{d}}{\mathrm{d}t}\int_{\mathcal{R}} \Pi\,\mathrm{d}V = \int_{\mathcal{R}} \partial_t \Pi\,\mathrm{d}V + \oint_{\partial\mathcal{R}} \Pi\,\boldsymbol{v}^{(b)}\cdot\hat{\boldsymbol{n}}\,\mathrm{d}\mathcal{S} = \int_{\mathcal{R}} \frac{\mathrm{D}\Pi}{\mathrm{D}t}\,\mathrm{d}V + \oint_{\partial\mathcal{R}} \Pi\,(\boldsymbol{v}^{(b)} - \boldsymbol{v})\cdot\hat{\boldsymbol{n}}\,\mathrm{d}\mathcal{S}, \tag{29.191}$$

where $\boldsymbol{v}^{(b)}$ is the velocity of a point on the boundary of the domain, $\partial\mathcal{R}$. We expose contributions from irreversible processes leading to material time changes to S and Θ by making use of the identity (29.187)

$$\frac{\mathrm{d}}{\mathrm{d}t}\int_{\mathcal{R}} \Pi\,\mathrm{d}V = \int_{\mathcal{R}} \left[\frac{\mathrm{D}S}{\mathrm{D}t}\left[\frac{\partial\Pi}{\partial S}\right]_{\Theta,\Phi} + \frac{\mathrm{D}\Theta}{\mathrm{D}t}\left[\frac{\partial\Pi}{\partial\Theta}\right]_{S,\Phi} + \rho\,\frac{\mathrm{D}\Phi}{\mathrm{D}t}\right]\mathrm{d}V + \oint_{\partial\mathcal{R}} \Pi\,(\boldsymbol{v}^{(b)} - \boldsymbol{v})\cdot\hat{\boldsymbol{n}}\,\mathrm{d}\mathcal{S}. \tag{29.192}$$

A constant can be added to the dynamic enthalpy without altering the energetics, which is seen by noting that volume conservation means that (equation (21.65))

$$\frac{\mathrm{d}}{\mathrm{d}t}\int \mathrm{d}V = -\int_{\partial\mathcal{R}} (\boldsymbol{v} - \boldsymbol{v}^{(b)})\cdot\hat{\boldsymbol{n}}\,\mathrm{d}\mathcal{S}. \tag{29.193}$$

If the region is a vertical column of fluid with fixed horizontal cross-section, extending from the ocean surface to the ocean bottom, then there is horizontal transport across the vertical boundaries, plus vertical transport of mass across the ocean free surface. For the free surface we make use of the surface kinematic boundary condition (19.88c) to write

$$\int_{z=\eta} (\Pi/\rho)\,\rho\,(\boldsymbol{v}^{(\eta)} - \boldsymbol{v})\cdot\hat{\boldsymbol{n}}\,\mathrm{d}\mathcal{S} = \int_{z=\eta} (\Pi/\rho)\,Q_{\mathsf{m}}\,\mathrm{d}A. \tag{29.194}$$

In this equation, Q_{m} is the mass per time per horizontal area of matter crossing the ocean free surface at $z = \eta$ where $Q_{\mathsf{m}} > 0$ for matter entering the ocean domain, and $\mathrm{d}\mathcal{S}$ is the area element on the free surface with $\mathrm{d}A$ its horizontal projection.

Budget with the equation of state: $\rho = \rho(S, \Theta)$

For the special case of an equation of state independent of pressure, $\rho = \rho(S, \Theta)$ (Section 29.6), we have $\Pi = \rho\,(\Phi - \Phi_{\mathrm{r}})$ so that equation (29.192) reduces to

$$\frac{\mathrm{d}}{\mathrm{d}t}\int_{\mathcal{R}} \rho\,(\Phi - \Phi_{\mathrm{r}})\,\mathrm{d}V = \int_{\mathcal{R}} \left[(\Phi - \Phi_{\mathrm{r}})\,\frac{\mathrm{D}\rho}{\mathrm{D}t} + \rho\,\frac{\mathrm{D}\Phi}{\mathrm{D}t}\right]\mathrm{d}V + \oint_{\partial\mathcal{R}} [\rho\,(\Phi - \Phi_{\mathrm{r}})\,(\boldsymbol{v}^{(b)} - \boldsymbol{v})]\cdot\hat{\boldsymbol{n}}\,\mathrm{d}\mathcal{S}. \tag{29.195}$$

Note that the reference geopotential, $\Phi_{\rm r}$, drops out since the Boussinesq form of the Leibniz-Reynolds transport theorem (i.e., equation (29.191) with ρ replacing Π) leads to the identity

$$\frac{\mathrm{d}}{\mathrm{d}t}\int_{\mathscr{R}} \rho \,\mathrm{d}V = \int_{\mathscr{R}} \frac{\mathrm{D}\rho}{\mathrm{D}t}\,\mathrm{d}V + \oint_{\partial\mathscr{R}} \rho\,(\boldsymbol{v}^{(b)} - \boldsymbol{v})\cdot\hat{\boldsymbol{n}}\,\mathrm{d}\mathcal{S}. \tag{29.196}$$

This equation means that the gravitational mass for a region of Boussinesq ocean (left hand side) changes through boundary terms, as for a non-Boussinesq fluid, plus processes that lead to material time changes in S and Θ

$$\rho = \rho(S,\Theta) \Longrightarrow \frac{\mathrm{D}\rho}{\mathrm{D}t} = \frac{\partial\rho}{\partial S}\frac{\mathrm{D}S}{\mathrm{D}t} + \frac{\partial\rho}{\partial\Theta}\frac{\mathrm{D}\Theta}{\mathrm{D}t}. \tag{29.197}$$

We understand the presence of the $\dot{S}$ and $\dot{\Theta}$ terms by noting that irreversible processes, such as mixing, do not alter volume in a Boussinesq ocean. Hence, if irreversible processes change density of a fluid element, then there must be a corresponding change in the gravitational mass of the element.

29.8.3 Density derivatives

When computing the derivatives of density, it is important to note whether the derivative is computed holding (Θ, S) fixed or holding (x, y) fixed. As seen here, this distinction can be confused for the Boussinesq ocean, especially when the geopotential takes the simple form $\Phi = g\,z$.

Vertical derivative of in situ density for a non-Boussinesq fluid

To motivate the discussion, recall the *in situ* density for a non-Boussinesq fluid is a function of the salinity, S, Conservative Temperature, Θ, and *in situ* pressure, p,

$$\rho = \rho(S,\Theta,p), \tag{29.198}$$

so that its spatial gradient is

$$\nabla\rho = \left[\frac{\partial\rho}{\partial S}\right]_{\Theta,p}\nabla S + \left[\frac{\partial\rho}{\partial\Theta}\right]_{S,p}\nabla\Theta + \left[\frac{\partial\rho}{\partial p}\right]_{S,\Theta}\nabla p = \left[\frac{\partial\rho}{\partial S}\right]_{\Theta,p}\nabla S + \left[\frac{\partial\rho}{\partial\Theta}\right]_{S,p}\nabla\Theta + \frac{1}{c_{\rm s}^2}\nabla p. \tag{29.199}$$

In the final step we introduced the inverse squared sound speed

$$\frac{1}{c_{\rm s}^2} = \left[\frac{\partial\rho}{\partial p}\right]_{S,\Theta}, \tag{29.200}$$

which is the partial derivative of density holding S and Θ fixed. Equation (29.199) says that the spatial gradient of density on the left hand side is determined by the sum of three terms that arise from spatial gradients of (S,Θ,p), each multiplied by their respective functional derivative of the equation of state for density. The vertical component of this equation arises when measuring vertical stratification, in which case

$$\left[\frac{\partial\rho}{\partial z}\right]_{x,y} = \left[\frac{\partial\rho}{\partial S}\right]_{\Theta,p}\left[\frac{\partial S}{\partial z}\right]_{x,y} + \left[\frac{\partial\rho}{\partial\Theta}\right]_{S,p}\left[\frac{\partial\Theta}{\partial z}\right]_{x,y} + \frac{1}{c_{\rm s}^2}\left[\frac{\partial p}{\partial z}\right]_{x,y}, \tag{29.201}$$

with $\partial p/\partial z = -\rho\,g$ for a hydrostatic fluid. Note that we exposed the (x, y) labels on the left hand side partial derivative. As seen next, these extra labels are especially important for the case of the Boussinesq ocean.

Vertical derivative of in situ density for a Boussinesq ocean

As seen earlier in this section, the *in situ* density for an energetically consistent Boussinesq ocean has the functional dependence

$$\rho = \rho(S, \Theta, \Phi). \tag{29.202}$$

That is, the geopotential, Φ, replaces pressure in the functional dependence, with the equation of state evaluated with a pressure $p_{\text{eos}} = -\rho_{\circ}\,\Phi$. Hence, the spatial gradient of *in situ* density for a Boussinesq ocean is

$$\nabla\rho = \left[\frac{\partial\rho}{\partial S}\right]_{\Theta,\Phi} \nabla S + \left[\frac{\partial\rho}{\partial\Theta}\right]_{S,\Phi} \nabla\Theta + \left[\frac{\partial\rho}{\partial\Phi}\right]_{S,\Theta} \nabla\Phi, \tag{29.203}$$

so that the vertical stratification is measured by

$$\left[\frac{\partial\rho}{\partial z}\right]_{x,y} = \left[\frac{\partial\rho}{\partial S}\right]_{\Theta,\Phi} \left[\frac{\partial S}{\partial z}\right]_{x,y} + \left[\frac{\partial\rho}{\partial\Theta}\right]_{S,\Phi} \left[\frac{\partial\Theta}{\partial z}\right]_{x,y} + \left[\frac{\partial\rho}{\partial\Phi}\right]_{S,\Theta} \left[\frac{\partial\Phi}{\partial z}\right]_{x,y}. \tag{29.204a}$$

This relation is analogous to the non-Boussinesq expression (29.201). In particular, the inverse squared sound speed for a Boussinesq ocean is given by

$$\left[\frac{\partial\rho}{\partial\Phi}\right]_{S,\Theta} = -\frac{\rho_{\circ}}{c_{\text{s}}^2}. \tag{29.205}$$

Although the prognostic flow is non-divergent for the Boussinesq ocean, the full velocity field is divergent (Section 29.1.9), thus supporting acoustic waves.

Now consider the special (and common) case of a simple geopotential, $\Phi = g\,z$, whereby the Boussinesq sound speed is given by

$$\left[\frac{\partial\rho}{\partial z}\right]_{S,\Theta} = -\frac{\rho_{\circ}\,g}{c_{\text{s}}^2}, \tag{29.206}$$

and the vertical stratification derivative is given by

$$\left[\frac{\partial\rho}{\partial z}\right]_{x,y} = \left[\frac{\partial\rho}{\partial S}\right]_{\Theta,z} \left[\frac{\partial S}{\partial z}\right]_{x,y} + \left[\frac{\partial\rho}{\partial\Theta}\right]_{S,z} \left[\frac{\partial\Theta}{\partial z}\right]_{x,y} + \left[\frac{\partial\rho}{\partial z}\right]_{S,\Theta}. \tag{29.207}$$

We here see why attachment of subscripts to the partial derivatives is essential to avoid confusion, since

$$\left[\frac{\partial\rho}{\partial z}\right]_{x,y} \neq \left[\frac{\partial\rho}{\partial z}\right]_{S,\Theta}. \tag{29.208}$$

The left hand side vertical derivative is computed holding the horizontal position fixed, as appropriate for computing the vertical stratification, whereas the right hand side vertical derivative is computed with (S, Θ) fixed, as appropriate for computing the sound speed. These two derivatives are conceptually distinct, with equation (29.207) exposing the mathematical distinction.

Horizontal derivative of in situ density for a Boussinesq ocean

The horizontal portion of the gradient (29.203), computed along surfaces of constant geopotential, is given by

$$\nabla_{\Phi}\rho = \left[\frac{\partial\rho}{\partial S}\right]_{\Theta,\Phi} \nabla_{\Phi} S + \left[\frac{\partial\rho}{\partial\Theta}\right]_{S,\Phi} \nabla_{\Phi}\Theta. \tag{29.209}$$

Hence, when the geopotential takes the simple form, $\Phi = g\,z$, then we have

$$\nabla_{\rm h}\rho = \left[\frac{\partial\rho}{\partial S}\right]_{\Theta,\Phi} \nabla_{\rm h} S + \left[\frac{\partial\rho}{\partial\Theta}\right]_{S,\Phi} \nabla_{\rm h}\Theta. \tag{29.210}$$

In either case, we see that the horizontal density gradient in a Boussinesq ocean is determined by the horizontal gradients of the Conservative Temperature and salinity.

29.8.4 Comments

Decoupling mechanical energy from internal energy

There are further nuances required to unravel energetics of the Boussinesq ocean, with details provided by *Young* (2010). When encountering these details for the first time one may wonder why bother since the non-Boussinesq energetics discussed in Sections 26.4 and 26.7 are, by comparison, very straightforward. However, the difficulty with non-Boussinesq energetics arises from the internal energy. Namely, since many geophysical flows, particularly those in the ocean, have speeds that are tiny compared to molecular speeds (see Section 16.3), the mechanical energy associated with geophysical flow is tiny relative to the internal energy arising from molecular motions. So when studying the total energy budget for a non-Boussinesq fluid, that energy is dominated by the internal energy. As detailed in *Young* (2010), the oceanic Boussinesq approximation allows us to focus on the Boussinesq mechanical energy arising just from the fluid flow, and it does so by decoupling mechanical energy from internal energy.

General form of the geopotential

The treatments in *Young* (2010) and Section 2.4.3 of *Vallis* (2017) focus on the simple form of the geopotential, $\Phi = g\,z$, in which case it appears that density in an energetically consistent Boussinesq ocean can at most have the space and time dependence

$$\rho = \rho[S(\boldsymbol{x},t), \Theta(\boldsymbol{x},t), p = -\rho_{\rm o}\, g\, z]. \tag{29.211}$$

However, the formalism developed by *Young* (2010) allows for a general geopotential, including those that arise from astronomical tidal forcing and from mass redistributions such as near ice shelves. In these cases we retain a consistent Boussinesq energetics with density of the more general form

$$\rho = \rho[S(\boldsymbol{x},t), \Theta(\boldsymbol{x},t), p = -\rho_{\rm o}\, \Phi(\boldsymbol{x},t)]. \tag{29.212}$$

Distinct manifestations of irreversible processes

It is notable that the irreversible terms from $\dot{S}$ and $\dot{\Theta}$ that appear in the mechanical energy equations (29.132), (29.188c) and (29.189) are absent from the non-Boussinesq budget in equation (26.49). Instead, for the non-Boussinesq fluid, the irreversible mixing processes manifest through their effects on flow convergence via the mass continuity equation

$$-\nabla\cdot\boldsymbol{v} = \frac{1}{\rho}\,\frac{\mathrm{D}\rho}{\mathrm{D}t}. \tag{29.213}$$

Since the Boussinesq ocean has a zero flow divergence, the role of mixing on the potential energy budget appears elsewhere within the mechanical energy budget.

29.9 Available potential energy

The gravitational potential energy per mass of a fluid element, as measured relative to the $z = 0$ geopotential, is given by $g \rho z$ (when assuming a simple geopotential). But how much of that potential energy can be transferred to generate kinetic energy? Not all of it since a state of zero potential energy means all of the fluid sits at $z = 0$, which is not generally possible. In Section 29.6 we noted that $-g^{-1} b \Phi$ is the potential energy per mass relative to the constant density background state. Pursuing this idea one more step, consider a background buoyancy, $b_{\text{ref}}(z)$, that has a non-zero depth dependence but with no horizontal dependence. Without any horizontal buoyancy gradients there are zero horizontal internal pressure gradients so that an initially static fluid will remain static.[12] Such fluids are said to have zero *baroclinicity*, with a proper treatment of baroclinicity in the context of vorticity given in Section 40.7. As seen in this vorticity discussion, a Boussinesq fluid with zero baroclinicity does not generate vorticity since its pressure gradients are perpendicular to buoyancy gradients, which are vertical for a reference state with $b = b_{\text{ref}}(z)$ (see Section 29.1.2 for the Boussinesq baroclinicity vector). These concepts from vorticity motivate us to compute the potential energy relative to a depth-dependent background buoyancy profile.

Lorenz (1955) suggested that a particularly relevant background buoyancy state is the one obtained by a reversible rearrangement or sorting of the original buoyancy to a state that has zero baroclinicity. A reversible rearrangement means there is no mixing when moving between the original state and the background state. The difference in gravitational potential energy between these two states is termed the *available potential energy* (APE), with the APE measuring the potential energy accessible for generating reversible motion.[13] Figure 29.2 illustrates the basic concept. In the remainder of this section we provide details to support a quantitative understanding of available potential energy. We restrict attention to the perfect Boussinesq ocean with a linear equation of state, and ignore the role of mixing and the rather difficult nuances related with the nonlinear equation of state. We also assume a simple connected domain.

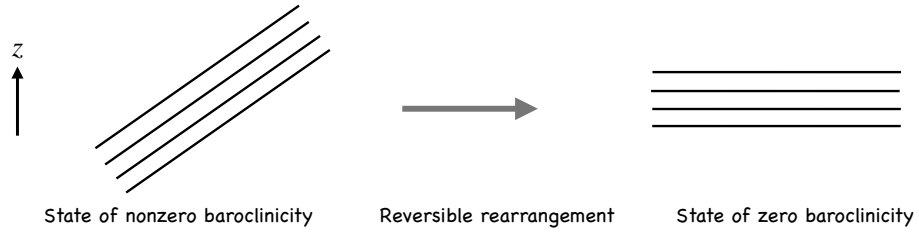

FIGURE 29.2: Isolines of constant buoyancy to illustrate the concept of available potential energy (APE) in a stably stratified Boussinesq ocean. The initial state (left panel) with non-zero baroclinicity is reversibly rearranged to have zero baroclinicity (right panel). The difference in gravitational potential energy between these two states defines the APE in the initial state. As shown in Section 29.9.3, the APE is a non-negative measure of the amount of gravitational potential energy that can, in principle, be reversibly converted to kinetic energy. Due to volume conservation and the absence of irreversible processes, the depth of a buoyancy surface in the background state shown in the right panel equals to the area average depth of the same buoyancy surface in the left panel (see Section 29.9.2).

[12] External pressure gradients, such as from sea level gradients or applied pressure gradients, are also assumed zero.

[13] Strictly, this is the potential energy available for producing motion *if* the fluid is allowed to relax to a state with zero baroclinicity. Yet as seen in Chapter 31, rotating stratified fluids generally reach a steady state (geostrophic balance) with nonzero baroclinicity (thermal wind). Even so, we ignore this concern by here following the standard treatment of available potential energy.

29.9.1 Analytic continuation of buoyancy surfaces

We use the term *outcrop* to refer to the vanishing of a buoyancy surface at the upper boundary, and *incrop* when it vanishes at the lower boundary. Figure 29.3 illustrates such surfaces. When considering a fluid in a domain with geometric boundaries, and when describing properties of the fluid according to thermodynamic coordinates such as buoyancy, we must decide how to describe these surfaces in regions where they do not exist; i.e., where they are outcropped or incropped. We follow the *Lorenz convention* described in *Lorenz* (1955), *Andrews* (1983), Section 4 of *Young* (2012), and Appendix A of *Ringler et al.* (2017).

This goal might appear to be pointless; i.e, if the surface does not exist in a region, then why do we need to specify any of its properties. However, the "analytic continuation" of buoyancy surfaces is very useful when developing their kinematics, with particular use for available potential energy in Section 29.9.3. Such concerns have further applications for studies of water mass transformation arising from boundary buoyancy fluxes (e.g., *Nurser et al.* (1999) as well as Chapter 73). Additionally, the buoyancy frequency along these surfaces is formally infinite since the extended buoyancy surfaces are squeezed into a zero thickness layer. Evidently, analytic continuation of buouyancy layers creates an infinite potential vorticity, which corresponds to the potential vorticity *delta sheets* as discussed by *Bretherton* (1966) and *Schneider et al.* (2003). In the following we limit our attention to domains with flat bottoms and vertical side-walls to minimize the niceties that arise with more general domains.

Buoyancy-area mean height of a buoyancy surface

Let $z = \eta(x, y, \mathcal{B}, t)$ be the vertical position ("height" for brief) of a surface with buoyancy $\mathcal{B}$. We make use of the area mean height when formulating available potential energy. One way to define the area mean is to integrate $\eta(x, y, \mathcal{B}, t)$ over the area of the buoyancy surface and then divide by the area of the buoyancy surface

$$\overline{\eta(\mathcal{B}, t)}^{\text{buoyancy}} = \frac{\int_{\mathcal{B}} \eta(x, y, \mathcal{B}, t) \, \mathrm{d}\mathcal{S}}{\int_{\mathcal{B}} \mathrm{d}\mathcal{S}}, \tag{29.214}$$

where $\int_{\mathcal{B}} \mathrm{d}\mathcal{S}$ is the area integral over the $\mathcal{B}$ buoyancy surface. Yet there are two problems with this area calculation. First, the area of a buoyancy surface is rather complicated to compute in practice, given that it can undulate, incrop, and outcrop. Second, the buoyancy surface area is time dependent thus making the area mean also time dependent.

Domain-area mean height of a buoyancy surface

An alternative method to compute the area mean height is to integrate over the area of the fluid domain

$$\overline{\eta(\mathcal{B})} = \frac{\int \eta(x, y, \mathcal{B}, t) \, \mathrm{d}A}{\int \mathrm{d}A}, \tag{29.215}$$

where

$$A = \int \mathrm{d}A = \int_{\text{fluid domain}} \mathrm{d}x \, \mathrm{d}y \tag{29.216}$$

is the time-independent horizontal area of the fluid domain. Time-independence of the area is a plus. In choosing the full domain area, we must specify the height of a buoyancy surface in those horizontal regions where the surface does not exist; i.e., where the surface outcrops or incrops. By doing so, we prove in Section 29.9.2 that the area mean height is time-independent for all buoyancy surfaces. This is another advantage of this approach. Finally, this area mean height

satisfies the monotonicity property

$$\overline{\eta(\mathcal{B}_1)} > \overline{\eta(\mathcal{B}_2)} \qquad \text{if} \qquad \mathcal{B}_1 > \mathcal{B}_2. \tag{29.217}$$

We make use of both the time-independence of the mean height and the monotonicity property when formulating the available potential energy in Section 29.9.3.

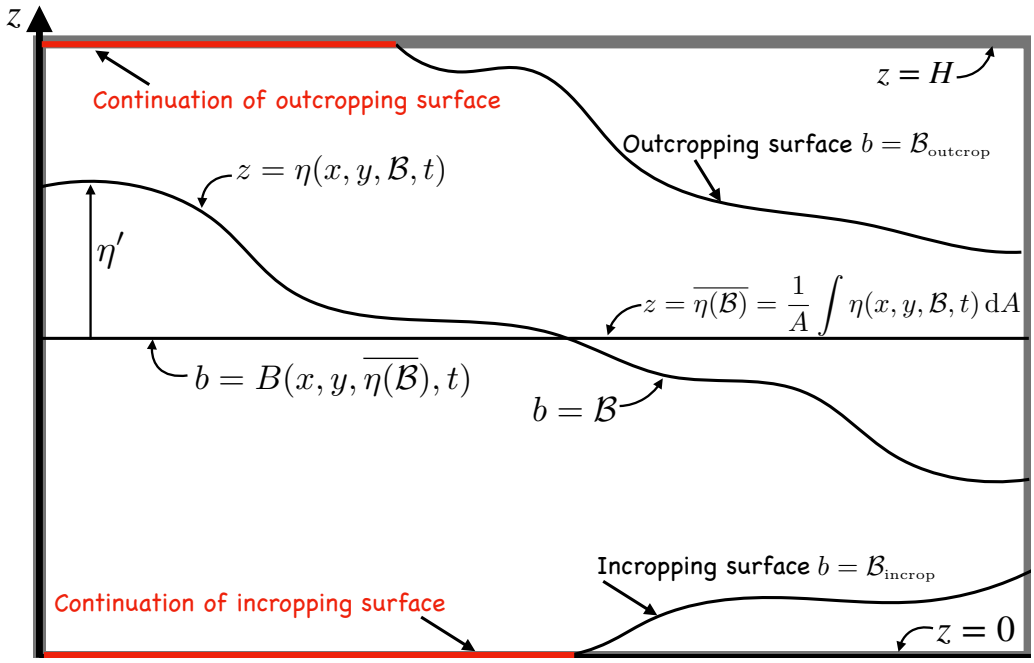

FIGURE 29.3: Geometry of buoyancy surfaces in a flat bottom box of perfect Boussinesq ocean with height H and horizontal area $\int \mathrm{d}A = A$. Three representative buoyancy surfaces are shown: one that spans the full domain with $b = \mathcal{B}$, one that incrops at the bottom with $b = \mathcal{B}_{\text{incrop}}$, and one that outcrops at the surface with $b = \mathcal{B}_{\text{outcrop}}$. The vertical height of a buoyancy surface is $z = \eta(x, y, \mathcal{B}, t)$; its area average (which is time independent; see Section 29.9.2) is $\overline{\eta(\mathcal{B})} = A^{-1} \int \eta(x, y, \mathcal{B}, t)\, \mathrm{d}A$; and its corresponding anomalous height is $\eta'(x, y, \mathcal{B}, t) = \eta(x, y, \mathcal{B}, t) - \overline{\eta(\mathcal{B})}$. As a complement, a particular point on the $z = \overline{\eta(\mathcal{B})}$ height surface has buoyancy $b = B(x, y, \overline{\eta(\mathcal{B})}, t)$, which then leads to an anomalous buoyancy $b'(x, y, \overline{\eta(\mathcal{B})}, t) = B(x, y, \overline{\eta(\mathcal{B})}, t) - \mathcal{B}$, where $\overline{B(x, y, \overline{\eta(\mathcal{B})}, t)} = \mathcal{B}$ (see equation (29.221)). To allow the formalism to be transparent across all buoyancy surfaces, we set $\eta(x, y, \mathcal{B}_{\text{outcrop}}, t) = H$ in regions where the surface has outcropped, and $\eta(x, y, \mathcal{B}_{\text{incrop}}, t) = 0$ where the surface has incropped (denoted by the red lines). As a complement, we set $\partial z / \partial b = 1/N^2 = 0$ for regions where the surface has either incropped or outcropped, thus formally imposing an infinitely stratified extension of the incropped and outcropped surfaces across the top and bottom domain boundaries. Through this analytic continuation of the buoyancy surfaces, we are ensured that the area mean height of all buoyancy surfaces forms a monotonic sequence from 0 to H, with $\overline{\eta(\mathcal{B}_1)} > \overline{\eta(\mathcal{B}_2)}$ if $\mathcal{B}_1 > \mathcal{B}_2$. When focused on a single buoyancy surface, we can reduce notational clutter by writing, for example, $\overline{\eta}$ rather than $\overline{\eta(\mathcal{B})}$, as well as $b'(\overline{\eta}) = B(\overline{\eta}) - \mathcal{B}$, and $\eta' = \eta - \overline{\eta}$.

Analytic continuation of surface height at outcrops and incrops

So how do we specify the height in outcrop regions? Let us motivate a specification by considering a buoyancy surface that sits near the top of the domain; i.e., its buoyancy is near the domain maximum, b_{max}. Assume this surface is not horizontal, with the surface $b = \mathcal{B}_{\text{outcrop}}$ in Figure 29.3 an example. Furthermore, let it cover less horizontal area than the full domain area. If we horizontally integrate just over regions where the surface does not outcrop, but still normalize by the total horizontal area of the domain, then the area mean height will be less than certain other buoyancy surfaces whose buoyancy is less and yet whose horizontal area is more. As a result we will not satisfy the monotonicity property (29.217). A way to recover monotonicity is

to analytically continue the buoyancy surface along the upper boundary so that its height in the outcropped region is set to $\eta(x_{\text{outcrop}}, y_{\text{outcrop}}, \mathcal{B}_{\text{outcrop}}, t) = H$. Doing so then ensures that the domain-area mean height for buoyancy surfaces will approach H as their buoyancy approaches the maximum buoyancy. We provide an analogous continuation of the surface within the bottom boundary so that

$$\eta(x, y, \mathcal{B}, t) = \begin{cases} H & \text{if } (x, y) \in \text{outcrop region} \\ 0 & \text{if } (x, y) \in \text{incrop region} \\ \eta(x, y, \mathcal{B}, t) & \text{otherwise.} \end{cases} \tag{29.218}$$

These two continuations of the buoyancy surfaces ensures that the domain-area mean height of all buoyancy surfaces forms a monotonic sequence and that the sequency extends from $0 \leq \overline{\eta(\mathcal{B})} \leq H$.

Analytic continuation of buoyancy stratification at outcrops and incrops

What does the analytic continuation (29.218) imply for buoyancy? As described, we allow all outcropped buoyancy surfaces to continue along the surface at $\eta = H$. All outcropped surfaces are thus squeezed into the infinitesimal upper fluid layer with buoyancy in that layer bounded above by the domain maximum buoyancy, b_{max}. Likewise, for the bottom of the domain we squeeze all incropped buoyancy surfaces into an infinitesimal layer bounded below by b_{min}, the minimum buoyancy in the domain. Consequently, the upper and lower boundaries are formally capped by infinitely stratified shells in which the inverse squared buoyancy frequency vanishes.

29.9.2 The dual relation between height and buoyancy

In deriving an expression for the APE in Section 29.9.3, we will find it useful to have relations between the unsorted and sorted buoyancy fields. We will also make use of the dual relation between the height of a constant buoyancy surface and the buoyancy of a constant height surface. For this purpose we examine certain kinematic properties of buoyancy surfaces in a stably stratified box of a perfect Boussinesq ocean as in Figure 29.3.

Volume beneath a buoyancy surface using height coordinates

Making use of notation from Figure 29.3, the volume of fluid contained beneath an arbitrary buoyancy surface is

$$V(\mathcal{B}) = \int \mathrm{d}A \int_0^{\eta(x,y,\mathcal{B},t)} \mathrm{d}z = \int \eta(x, y, \mathcal{B}, t)\, \mathrm{d}A = A\, \overline{\eta(\mathcal{B})}, \tag{29.219}$$

The following properties result from volume conservation in a perfect non-divergent flow in the absence of boundary fluxes (see Chapter 21).

- The volume of fluid beneath an arbitrary buoyancy surface is time-independent, as is the area mean height of this surface. This property allowed us to drop the time argument from $V(\mathcal{B})$ and $\overline{\eta(\mathcal{B})}$ in equation (29.219).
- The area mean height of a buoyancy surface is identical to the height of the surface when it is reversibly rearranged to be horizontal.

To verify these properties, recall that buoyancy surfaces are material in a perfect fluid so that no fluid crosses them even as they fluctuate. It follows that the volume of fluid beneath an arbitrary buoyancy surface is time-independent. Since the horizontal area of the domain is time-independent, equation (29.219) also means that the area averaged height of the buoyancy

surface is time-independent. Furthermore, any motion of a buoyancy surface in a perfect fluid is reversible, including motion that flattens the surface. Since its area mean height remains fixed, the area mean equals to the height of the surface when it is flat.

Area mean buoyancy on a constant depth surface

As a further realization of the dual relation between height and buoyancy, note that the area average buoyancy, $b = B(x, y, z, t)$ along a constant height surface is also constant in time

$$\overline{B(z)} = A^{-1} \int B(x, y, z, t) \, \mathrm{d}A = \text{time independent.} \tag{29.220}$$

This property follows since both buoyancy and volume are material constants following a fluid parcel in a perfect Boussinesq ocean. Hence, a fluid parcel carries both its buoyancy and volume unchanged so that the volume integrated buoyancy within any fluid region remains constant. Correspondingly, the area integrated buoyancy along any fixed height surface remains constant. It also follows that the area mean buoyancy at $z = \overline{\eta(\mathcal{B})}$ is $\mathcal{B}$

$$\overline{B[\overline{\eta(\mathcal{B})}]} = A^{-1} \int B(x, y, z = \overline{\eta(\mathcal{B})}, t) \, \mathrm{d}A = \mathcal{B}. \tag{29.221}$$

Volume beneath a buoyancy surface using buoyancy coordinates

Let us return to the volume beneath a buoyancy surface, only now use buoyancy coordinates to write

$$V(\mathcal{B}) = \int \mathrm{d}A \int_0^{\eta(x,y,\mathcal{B},t)} \mathrm{d}z = \int \mathrm{d}A \int_{b(x,y,0,t)}^{\mathcal{B}} \frac{\partial z}{\partial b} \, \mathrm{d}b = \int \mathrm{d}A \int_{b(x,y,0,t)}^{\mathcal{B}} \frac{\mathrm{d}b}{N^2} \tag{29.222}$$

where $b(x, y, 0, t)$ is the buoyancy at the bottom of the domain and

$$N^2 = \frac{\partial b}{\partial z} \tag{29.223}$$

is the squared buoyancy frequency. As noted in Section 29.9.1 and illustrated in Figure 29.3, we analytically continue the buoyancy surfaces into the surface and bottom boundaries so that

$$N^{-2}(x, y, \mathcal{B}) = \begin{cases} = 0 & \text{if } \mathcal{B} > b(x, y, H) \text{ (surface outcrop region)} \\ = 0 & \text{if } \mathcal{B} < b(x, y, 0) \text{ (bottom incrop region)} \\ = N^{-2}(x, y, \mathcal{B}) & \text{if } b(x, y, 0) \leq \mathcal{B} \leq b(x, y, H). \end{cases} \tag{29.224}$$

In this manner we can replace the lower limit in equation (29.222) with a constant buoyancy well below any buoyancy found in the domain, which we write as $b_{\min}$, so that

$$V(\mathcal{B}) = \int \mathrm{d}A \int_{b_{\min}}^{\mathcal{B}} \frac{\mathrm{d}b}{N^2} = \int_{b_{\min}}^{\mathcal{B}} \mathrm{d}b \int \frac{\mathrm{d}A}{N^2}. \tag{29.225}$$

Being able to commute the area and buoyancy integrals proves useful in the following.

29.9.3 Exact expression for APE

In this subsection we develop an expression for the APE of the perfect stably stratified Boussinesq ocean in a box. To start, consider the volume integrated gravitational potential energy per mass

of the fluid in Figure 29.3, relative to a constant density background state with $\rho = \rho_o$

$$\mathscr{P} = -\int \mathrm{d}A \int_0^H b\, z\, \mathrm{d}z = -\frac{1}{2}\int \mathrm{d}A \int_0^H b\, \mathrm{d}(z^2). \tag{29.226}$$

Integration by parts leads to the equivalent expression

$$\mathscr{P} = -\frac{1}{2}\int \mathrm{d}A \int_0^H \mathrm{d}(b\, z^2) + \frac{1}{2}\int \mathrm{d}A \int_{b(x,y,0)}^{b(x,y,H)} \eta^2(x,y,b)\, \mathrm{d}b \tag{29.227}$$

$$= -\frac{A\, H^2}{2}\, \overline{b(H)} + \frac{1}{2}\int \mathrm{d}A \int_{b(x,y,0)}^{b(x,y,H)} \eta^2(x,y,b)\, \mathrm{d}b, \tag{29.228}$$

where $\overline{b(H)}$ is the area averaged buoyancy at the top of the fluid domain, $z = H$. As discussed in Section 29.9.1, integration over the finite domain using a buoyancy coordinate leads us to set $\overline{b(H)} = b_{\max}$, the domain maximum buoyancy. Likewise, the second expression in equation (29.228) has its buoyancy integral range extended to $b_{\min}$ and $b_{\max}$. By doing so we can swap the area and buoyancy integrals to render

$$\mathscr{P} = \frac{A}{2}\left[-H^2\, b_{\max} + \int_{b_{\min}}^{b_{\max}} \overline{\eta^2(b)}\, \mathrm{d}b\right], \tag{29.229}$$

where $\overline{\eta^2(b)}$ is the area mean of the squared height of a buoyancy surface. The same calculation for the reference buoyancy, $b_{\mathrm{ref}}(z)$, leads to

$$\mathscr{P}_{\mathrm{ref}} = \frac{A}{2}\left[-H^2\, b_{\max} + \int_{b_{\min}}^{b_{\max}} \overline{\eta(b)}^2\, \mathrm{d}b\right], \tag{29.230}$$

where we noted that the height of a reference buoyancy surface equals to the area mean of the corresponding buoyancy surface

$$\eta(b_{\mathrm{ref}}) = \overline{\eta}(b = b_{\mathrm{ref}}), \tag{29.231}$$

and the reference buoyancy at the surface boundary equals to the maximum buoyancy, $b_{\mathrm{ref}}(H) = b_{\max}$.

Subtracting the gravitational potential energy of the reference/background state from the potential energy of the full state renders an expression for the available potential energy

$$\mathscr{P}_{\mathrm{APE}} = \mathscr{P} - \mathscr{P}_{\mathrm{ref}} = \frac{A}{2}\left[\int_{b_{\min}}^{b_{\max}} [\overline{\eta^2(b)} - \overline{\eta(b)}^2]\, \mathrm{d}b\right] = \int_{b_{\min}}^{b_{\max}} \overline{(\eta')^2}\, \mathrm{d}b \geq 0, \tag{29.232}$$

where (see Figure 29.3)

$$\eta(x,y,b,t) = \overline{\eta(b)} + \eta'(x,y,b,t). \tag{29.233}$$

The positive definite nature of the APE arises since either a positive or negative buoyancy surface undulation gives rise to motion.

Equation (29.232) is an exact expression for the APE of a perfect Boussinesq ocean in a flat bottom and simply connected domain. We encounter the same expression when studying the APE in a shallow water fluid in Section 36.5.6. It is the natural expression when working in buoyancy coordinates, whereby the APE is determined by height variations of constant buoyancy surfaces.

29.9.4 Approximate expression for APE

When working with geopotential coordinates it is useful to obtain an approximate expression for the APE in terms of buoyancy variations on constant height surfaces. That is the subject of this subsection.

Approximate version of APE in terms of buoyancy fluctuations

To develop an approximate expression for the APE we write the height of a buoyancy surface, $\eta(\mathcal{B})$, in the form (see caption to Figure 29.3 if confused by signs)

$$\eta(\mathcal{B}) \approx \overline{\eta(\mathcal{B})} + \left[\frac{\partial z}{\partial b}\right]_{z=\overline{\eta}} [\mathcal{B} - B(\overline{\eta})] = \overline{\eta} - \frac{b'}{N^2} \approx \overline{\eta} - \frac{b'}{N^2_{\text{ref}}}, \tag{29.234}$$

where the final step set $N^2(x, y, \overline{\eta}) \approx N^2_{\text{ref}}(\overline{\eta})$, which is valid to the same order as the approximation. We are thus led to the approximate expression

$$\eta' = \eta - \overline{\eta} \approx -\frac{b'}{N^2_{\text{ref}}} \tag{29.235}$$

so that the APE is given approximately by

$$\mathscr{P}_{\text{APE}} \approx A \left[\int_0^H \frac{\overline{(b')^2}}{2\, N^2_{\text{ref}}}\, \mathrm{d}z\right]. \tag{29.236}$$

This approximate expression is commonly used in practical calculations of APE, particularly when making use of field measurements (e.g., *Bishop et al.* (2020)).

Practical issues related to the sorted buoyancy profile

Figure 29.4 illustrates how to obtain the sorted buoyancy profile from a discretized version of a stably stratified fluid. The buoyancy of each cell is compared to that of all other cells and vertically stacked according to the relative buoyancy. The vertical position of the sorted grid cell is determined by accumulating the volume per horizontal area of the cell, starting from the bottom and moving up.

It is notable that cells with identical buoyancy lead to regions of zero vertical stratification in the sorted buoyancy profile. Such zero stratification regions commonly arise when sorting stratified fluid layers, where the buoyancy is constant within the layers. One is thus led to perform a vertical smoothing of the sorted profile to remove such unstratified regions, particularly if using the profile to define a background buoyancy frequency as required for the approximate APE calculation given by equation (29.236).

Budget for approximatae APE

To develop a budget for the approximate form of APE, start by considering the budget for buoyancy decomposed as

$$b(x, y, z, t) = b_{\text{ref}}(z) + b'(x, y, z, t), \tag{29.237}$$

so that the perfect fluid buoyancy equation takes on the form

$$\frac{\mathrm{D}b}{\mathrm{D}t} = 0 \Longrightarrow \frac{\mathrm{D}b'}{\mathrm{D}t} = -w\, N^2_{\text{ref}}. \tag{29.238}$$

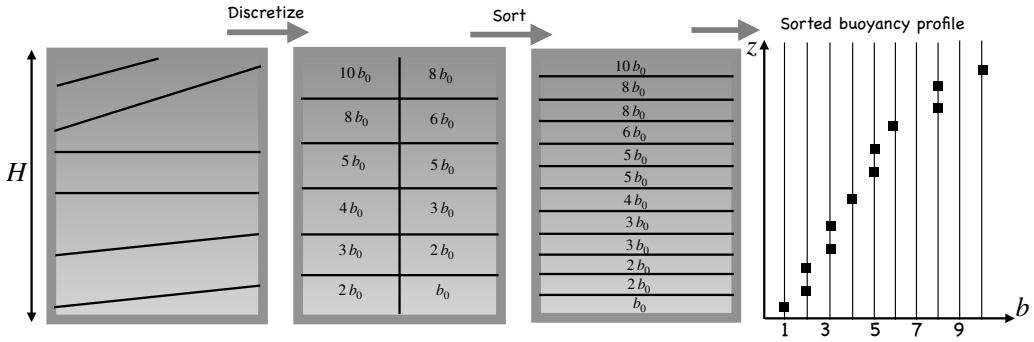

FIGURE 29.4: Illustrating how to sort buoyancy to determine the background or reference profile for computing APE. The first panel on the left shows a sample buoyancy field with black lines representing buoyancy isolines. The second panel shows a discretized version of the field, with b_0 a unit of buoyancy and each cell's buoyancy an integer multiple of b_0. For simplicity we assume the horizontal area of the domain is depth independent and that each of the discrete grid cells has the same volume and horizontal area. The third panel shows the result of sorting the discrete buoyancy field, with the most buoyant fluid above the less buoyant fluid. During the sort, the cell's volume remains constant (Boussinesq ocean) and the accumulated volume per horizontal area determines the vertical position of the sorted cell. The final panel shows the sorted profile $b_{\rm ref}(z)$. Note that regions of zero lateral buoyancy gradient in the unsorted buoyancy field lead to vertically unstratified regions in the sorted buoyancy.

Multiplying by b' leads to

$$\frac{\mathrm{D}[(b')^2/2]}{\mathrm{D}t} = -w\, b'\, N^2_{\rm ref}, \tag{29.239}$$

and then dividing by $N^2_{\rm ref}$ renders

$$\frac{\partial P_{\rm APE}}{\partial t} + \boldsymbol{v}\cdot\nabla P_{\rm APE} = -w\, b' \left[1 - \frac{b'}{2}\,\frac{\partial(1/N^2_{\rm ref})}{\partial z}\right], \tag{29.240}$$

where we defined the approximate APE per unit volume

$$P_{\rm APE} = (1/2)\,[b'/N_{\rm ref}]^2. \tag{29.241}$$

In the case of a depth-independent reference buoyancy frequency, we see that the APE per unit volume materially evolves with a source $-w\,b'$, which is analogous to the potential energy evolution where the source is $-w\,b$. Now adding equation (29.240) to the kinetic energy equation (29.128) with $\Phi = g\,z$ leads to

$$\frac{\partial(\mathcal{K} + P_{\rm APE})}{\partial t} + \boldsymbol{v}\cdot\nabla(\mathcal{K} + P_{\rm APE} + p/\rho_o) = -w\left[g - b_{\rm ref} - \frac{(b')^2}{2}\,\frac{\partial(1/N^2_{\rm ref})}{\partial z}\right]. \tag{29.242}$$

Note that a global area average on any surface eliminates the $w\,(g - b_{\rm ref})$ term since

$$\overline{w} = A^{-1}\int w\,\mathrm{d}A = 0, \tag{29.243}$$

which follows from $\nabla\cdot\boldsymbol{v} = 0$ (see Exercise 21.6). Further simplifications arise with depth-independent $N_{\rm ref}$, with the corresponding space and time spectra studied by *Bühler et al.* (2014).

29.9.5 Comments

Elements of this section follow from Section 3.11.1 of *Vallis* (2017). Available potential energy remains a compelling notion for many aspects of geophysical fluid studies. Unfortunately, for

the ocean proves difficult to extend the formalism beyond the perfect fluid Boussinesq system considered here. Particular difficulties arise from the nonlinear equation of state for seawater and the nontrivial ocean geometry with distinct basins and enclosed seas. Further difficulties arise when considering the non-simply connected nature of the ocean domain.

29.10 Exercises

EXERCISE 29.1: SYMMETRY UNDER A TIME-DEPENDENT TRANSLATION
In this exercise we consider the Euler equation in free space (no boundaries) where we focus only on the acceleration and the pressure gradient force. That is, we ignore any body forces from gravity and planetary rotation so that the Euler equation takes on the form

$$\rho_\circ \frac{\mathrm{D}\boldsymbol{v}}{\mathrm{D}t} = -\nabla p, \tag{29.244}$$

where we assume a Boussinesq ocean so that $\nabla \cdot \boldsymbol{v} = 0$.

Consider a shift in the reference frame used to describe the flow so that a coordinate position shifts according to

$$\boldsymbol{x} \to \boldsymbol{x} + \boldsymbol{c}(t), \tag{29.245}$$

where the vector $\boldsymbol{c}$ is time dependent but has the same value for all points in space.

(a) Is the shift (29.245) a Galilean transformation? Hint: recall the discussion of Galilean transformation in Section 17.5.

(b) What happens to pressure in the new reference frame? Hint: consider the elliptic problem for pressure as discussed in Section 29.3.1.

(c) Write the equation of motion (29.244) in this new reference frame.

EXERCISE 29.2: STEADY PARALLEL SHEARED FLOW ON A TANGENT PLANE
Consider the non-divergent parallel sheared flow

$$\boldsymbol{v} = \hat{\boldsymbol{x}}\, u(y), \tag{29.246}$$

so that the flow is steady, zonal, and has a meridional dependence. Assume the flow is on a tangent plane as discussed in Section 24.5.

(a) Show that this flow is an exact solution to the β-plane inviscid Boussinesq velocity equation.

(b) Express the corresponding pressure gradient in terms of u and other terms.

(c) Show that for an f-plane the stationary velocity can have an arbitrary orientation. Hint: it is sufficient to show that $\boldsymbol{v} = \hat{\boldsymbol{y}}\, v(x)$ is a stationary solution on the f-plane but not on the β-plane.

EXERCISE 29.3: A GENERALIZED BOUSSINESQ APPROXIMATION
In this exercise we derive a mild generalization to the Boussinesq approximation. This generalization facilitates a more accurate decomposition of pressure by introducing a new reference density, $\overline{\rho}(z)$, that is a static function of depth. The new decomposition also leads to a slightly modified buoyancy field.

The derivation starts with the usual decomposition of density using $\rho_\circ$ as a space and time constant

$$\rho(\boldsymbol{x}, t) = \rho_\circ + \rho'(\boldsymbol{x}, t), \tag{29.247}$$

thus leading to the Boussinesq momentum equation

$$\frac{\mathrm{D}\boldsymbol{v}}{\mathrm{D}t} + 2\,\boldsymbol{\Omega} \times \boldsymbol{v} = -\rho_\circ^{-1}\,(\nabla p + \hat{\boldsymbol{z}}\, g\, \rho). \tag{29.248}$$

But rather than take the traditional decomposition of the pressure and gravitational terms, we now write

$$\nabla p + \hat{\boldsymbol{z}}\, g\, \rho = \nabla[p - \overline{p}(z) + \overline{p}(z)] + \hat{\boldsymbol{z}}\, g\, [\rho - \overline{\rho}(z) + \overline{\rho}(z)] \tag{29.249a}$$

$$= \nabla[p - \overline{p}(z)] + \hat{\boldsymbol{z}}\, g\, [\rho - \overline{\rho}(z)]. \tag{29.249b}$$

This step introduced the density, $\overline{\rho}(z)$, and the corresponding hydrostatically balanced pressure

$$\frac{\mathrm{d}\overline{p}(z)}{\mathrm{d}z} = -g\,\overline{\rho}(z). \tag{29.250}$$

(a) Show that the pressure is decomposed as

$$p(\boldsymbol{x}, t) = [p(\boldsymbol{x}, t) - \overline{p}(z)] + \overline{p}(z) = \rho_\circ\, \tilde{\varphi} + \overline{p}(z). \tag{29.251}$$

What is $\tilde{\varphi}$?

(b) Introduce a buoyancy

$$\tilde{b} = -\frac{g\,(\rho - \overline{\rho})}{\rho_\circ}, \tag{29.252}$$

defined relative to the depth-dependent background density, $\overline{\rho}(z)$, rather than the globally constant density $\rho_\circ$. Show that the momentum equation is given by

$$\frac{\mathrm{D}\boldsymbol{v}}{\mathrm{D}t} + 2\,\boldsymbol{\Omega} \times \boldsymbol{v} = -\nabla\tilde{\varphi} + \hat{\boldsymbol{z}}\,\tilde{b}. \tag{29.253}$$

(c) Show that the baroclinicity vector appearing in the Boussinesq vorticity equation takes the form

$$\tilde{\boldsymbol{B}} = \nabla\tilde{b} \times \hat{\boldsymbol{z}}, \tag{29.254}$$

which is mathematically the same as with the traditional Boussinesq approximation from Section 29.1.2. We have thus succeeded in generalizing the pressure decomposition and buoyancy field, yet without corrupting the familiar Boussinesq vorticity dynamics.

EXERCISE 29.4: KINETIC ENERGY FOR A PERFECT HYDROSTATIC BOUSSINESQ FLUID

Consider a perfect *hydrostatic* Boussinesq ocean. Show that the kinetic energy per mass contained in the horizontal velocity,

$$\mathcal{K}_{\text{horz}} = \frac{\boldsymbol{u} \cdot \boldsymbol{u}}{2}, \tag{29.255}$$

satisfies the exact same equation as $\boldsymbol{v} \cdot \boldsymbol{v}/2$ does for a non-hydrostatic fluid, as given by equation (29.127). Assume the simple form for the geopotential, $\Phi = g\,z$.

EXERCISE 29.5: ENERGETICS FOR A PERFECT BOUSSINESQ OCEAN

In Section 29.6 we developed the energetic balances for a perfect Boussinesq ocean in a closed domain (domain where all boundary fluxes vanish). We here rederive the same energetics but

using the momentum, buoyancy, and continuity equations in the form that exposes buoyancy

$$\frac{\mathrm{D}\boldsymbol{v}}{\mathrm{D}t} + 2\,\boldsymbol{\Omega} \times \boldsymbol{v} = -\nabla\varphi + \hat{\boldsymbol{z}}\, b \tag{29.256a}$$

$$\frac{\mathrm{D}b}{\mathrm{D}t} = 0 \tag{29.256b}$$

$$\nabla \cdot \boldsymbol{v} = 0 \tag{29.256c}$$

$$b = b(S, \Theta). \tag{29.256d}$$

Assume the simple form for the geopotential, $\Phi = g\,z$, and assume a closed and static domain (i.e., an Eulerian domain with no boundary contributions). To help physically interpret terms, remember to isolate the total divergence terms and the remainder. Hint: this exercise is a simplification of the material presented in Section 29.7.

(a) Derive the material time evolution equation for the kinetic energy.

(b) Derive the material time evolution equation for $P^{\flat} = -g^{-1}\,\Phi\,b = -b\,z$, with $\Phi = g\,z$. Interpret $P^{\flat}$ and the processes that affect its material time evolution.

(c) Derive the mechanical energy equation written in its flux-form, where we define the mechanical energy per volume as $\rho_o\,(\mathcal{K} + P^{\flat})$. Note the presence of ρ_o multiplying both $\mathcal{K}$ and $P^{\flat}$. We thus derive an expression for $\rho_o\,\mathrm{D}(\mathcal{K} + P^{\flat})/\mathrm{D}t$, and show that it is not affected by $w\,b$. Discuss.

(d) Integrate the equation for the mechanical energy per mass to derive a global domain budget for mechanical energy. Discuss.

EXERCISE 29.6: KINETIC ENERGY AND THE HYDROSTATIC BOUSSINESQ EQUATIONS

In this exercise we develop some properties of the kinetic energy for the hydrostatic Boussinesq equations listed in Section 29.1.6. We here assume the horizontal frictional acceleration is determined by vertical viscous friction in equation (29.146), and the stress boundary conditions are given by equations (29.149a) and (29.150).

(a) Derive the flux-form expression for the kinetic energy budget.

(b) Why does the kinetic energy only have contributions from the horizontal velocity components?

(c) Discuss the role of vertical viscosity in transporting kinetic energy in the vertical.

(d) Discuss the role of vertical viscosity in dissipating kinetic energy.

(e) Discuss how wind stress and bottom drag impact the globally integrated kinetic energy. Assume bottom drag in the form of equation (29.150).

EXERCISE 29.7: POTENTIAL ENERGY AND THE HYDROSTATIC BOUSSINESQ EQUATIONS

In this exercise we develop some properties of the gravitational potential energy for the hydrostatic Boussinesq equations stated in Section 29.1.6.

(a) Derive the flux-form budget for gravitational potential energy written as $P^{\flat} = -g^{-1}\,\Phi\,b$ with $\Phi = g\,z$. Interpret $P^{\flat}$.

(b) Discuss the role of the subgrid scale eddy-induced advection in this budget as given by equation (29.139). In particular, discuss its impact on the center of mass of the fluid.

(c) Discuss the role of vertical diffusion in this budget as given by equation (29.139). In particular, discuss its impact on the center of mass of the fluid.

(d) Integrate the gravitational potential energy budget over the global ocean. Discuss how the surface boundary buoyancy flux, Q_{b}, impacts on the global potential energy budget through impacts on the center of mass of the fluid. Ignore any bottom geothermal heating.

EXERCISE 29.8: SQUARED BUOYANCY AND THE OCEAN MODEL EQUATIONS

In this exercise we develop some properties of the squared buoyancy for the hydrostatic Boussinesq equations stated in Section 29.1.6 using the subgrid scale buoyancy flux in equation (29.139).

(a) Write the flux-form budget describing the evolution of b^2, the squared buoyancy. Write the budget using the residual mean velocity defined by the sum

$$\boldsymbol{v}^{\dagger} = \boldsymbol{v} + \boldsymbol{v}^{*}. \tag{29.257}$$

Hint: start from the buoyancy equation written in the form

$$\mathrm{D}b/\mathrm{D}t = -\nabla \cdot \boldsymbol{F}^{\mathrm{b}}, \tag{29.258}$$

with $\boldsymbol{F}^{\mathrm{b}}$ discussed in Section 29.7.1.

(b) Discuss the impacts from vertical diffusion on the b^2 budget.

EXERCISE 29.9: PARAMETERIZED EDDY VELOCITY AND THE OCEAN MODEL EQUATIONS

In this exercise we develop some implications of assuming a specific form for the parameterized eddy velocity for the hydrostatic Boussinesq equations stated in Section 29.1.6. Namely, we consider the specific form for the parameterized eddy-induced velocity proposed by *Gent et al.* (1995)

$$\boldsymbol{u}^{*} = -\partial_z (B\, \boldsymbol{S}) \tag{29.259a}$$
$$w^{*} = \nabla_{\mathrm{h}} \cdot (B\, \boldsymbol{S}) \tag{29.259b}$$
$$\boldsymbol{S} = -\frac{\nabla_{\mathrm{h}} b}{N^2} \tag{29.259c}$$
$$\boldsymbol{v}^{*} \cdot \hat{\boldsymbol{n}} = 0 \qquad \text{at all ocean boundaries.} \tag{29.259d}$$

In this expression, $B > 0$ is an eddy diffusivity. To ensure $\boldsymbol{v}^{*} \cdot \hat{\boldsymbol{n}} = 0$ at all domain boundaries requires that $B = 0$ along these boundaries. The horizontal vector $\boldsymbol{S} = (S^{(x)}, S^{(y)}, 0)$ measures the slope of the buoyancy surfaces relative to the horizontal. We assume the ocean is stably stratified in the vertical, so that $\partial b/\partial z = N^2 > 0$.

(a) Determine the vector streamfunction $\boldsymbol{\Psi}^{*}$ such that

$$\boldsymbol{v}^{*} = \nabla \times \boldsymbol{\Psi}^{*}. \tag{29.260}$$

Choose the gauge with $\hat{\boldsymbol{z}} \cdot \boldsymbol{\Psi}^{*} = 0$.

(b) Show that

$$\int_{-H}^{\eta} \boldsymbol{u}^{*}\, \mathrm{d}z = 0. \tag{29.261}$$

That is, the parameterized horizontal flow has a zero depth integral.

(c) At any chosen meridional position y, the meridional buoyancy transport from advection (resolved plus parameterized) is computed by

$$\mathcal{B}^{(y)}(y,t) = \int_{x_1}^{x_2} \mathrm{d}x \int_{-H}^{\eta} b\,(v + v^*)\,\mathrm{d}z. \tag{29.262}$$

The zonal and vertical integrals are over the full zonal and vertical extent of the ocean domain. Show that the effects from v^* are to reduce the meridional gradients of buoyancy. That is, if buoyancy decreases poleward, then v^* will flux buoyancy poleward to reduce the gradient.

(d) How does the introduction of $\boldsymbol{v}^*$ to the buoyancy equation (29.24c) affect the global integrated *gravitational potential energy*? Discuss.

(e) How does the introduction of $\boldsymbol{v}^*$ to the buoyancy equation (29.24c) affect the global integrated *available potential energy*? Discuss.

Chapter 30

Buoyant acceleration of fluids

A large portion of the vertical pressure force acting on a geophysical fluid element is balanced by the gravitational force, with a precise balance holding for an exact hydrostatic fluid. If there are unbalanced density-induced pressure forces, then a fluid element experiences a *buoyant* acceleration that acts in the vertical. That is, buoyancy is the unbalanced vertical acceleration from pressure that acts on a fluid element placed within a fluid with density inhomogeneities in the presence of a gravity field. Correspondingly, buoyancy vanishes in a fluid with a homogeneous density, even though each fluid element still feels a gravitational force.[1] Buoyancy is a conceptually useful means to organize vertical forces from gravity in a fluid with varying density. Namely, if the vertical pressure forces acting on a fluid element are balanced by gravity, then the fluid element is *neutrally buoyant*; i.e., it floats. If these forces are unbalanced, then the fluid element has a nonzero vertical buoyant acceleration.

Our study of buoyancy starts by examining a *test fluid element*, with a test fluid element probing properties of the fluid environment without altering the environment.[2] We refer to the buoyancy of a test fluid element as the *Archimedean buoyancy*, with Archimedean buoyancy providing a generalization of the familiar buoyancy acting to keep extended bodies, like a ship, floating in a fluid.[3] Examining the buoyancy of test fluid elements leads to the notions of gravitational stability, neutral directions, and neutral trajectories.

References to buoyancy in the literature typically refer to the Archimedean buoyancy. Even so, Archimedean buoyancy is an incomplete rendering of the forces associated with density inhomogeneities and that act on a fluid element of any finite size. A more complete description recognizes that a fluid element affects its surrounding fluid environment. This recognition leads to the concept of *effective buoyancy*, with effective buoyancy accounting for the *static forces* that create vertical accelerations of a fluid element. More precisely, effective buoyancy is the vertical acceleration acting on a fluid element that remains when setting all velocity dependent accelerations to zero (hence the term "static forces"). The effective buoyancy has a contribution from Archimedean buoyancy, plus the vertical derivative of a pressure perturbation that depends only on the density field. This extra pressure perturbation force is the *back-reaction* on a fluid element due to the surrounding fluid environment.

[1] Even though buoyancy vanishes in a constant density fluid, there can still be vertical accelerations due to nonzero flow convergences or divergences. For example, we encounter such accelerations when studying shallow water flow in Chapter 35 (in particular see Section 35.2.8). Vertical acceleration of fluid elements also occurs in a constant density fluid in the presence of surface gravity waves or capillary waves, as studied in Chapter 52.

[2] As defined in Section 17.2.5, a test fluid element is directly analogous to a point test mass particle that probes a gravitational field and a point test electrical charge that probes an electromagnetic field. Neither the test fluid element, test mass particle, nor test charge alter the force fields that they probe.

[3] The Archimedean buoyancy of a test fluid element makes use of perhaps the most ancient of physical concepts in fluid mechanics. Archimedes was a mathematician, inventor, engineer, physicist, and astronomer who lived in Syracuse, Sicily from roughly 287 B.C.E to 212 B.C.E.

CHAPTER GUIDE

This chapter builds from the study of pressure in Chapters 24, 25, and 28. We also make use of the equations for a Boussinesq fluid derived in Chapter 29, in particular the Poisson equation satisfied by pressure in a non-divergent flow. An understanding of this chapter supports an understanding of how pressure and gravity work within a fluid with density inhomogeneities, thus creating vertical accelerations of fluid elements.

30.1 Loose threads

- Provide some examples of b_{eff} fields in Section 30.11 as taken from *Tarshish et al.* (2018).
- Solution needed for Exercise 30.5.

30.2 Archimedes' Principle for a fluid region

The Archimedean buoyancy acting on a massive body immersed in a static fluid is the vertical acceleration due to the gravitational acceleration of the body *relative* to the gravitational acceleration of the fluid displaced by the body. A body's Archimedean buoyancy is proportional to its density relative to the density of the displaced fluid. Hence, there is no Archimedean buoyancy without gravity nor is there an Archimedean buoyant acceleration without density differences. As shown in this section, these statements of *Archimedes' Principle* are a direct consequence of hydrostatics.

Archimedean buoyancy has wide applications for the study of bodies immersed within fluids; e.g. mechanics of marine organisms, ships, submarines, hot air balloons. Our interests concern the buoyancy of the fluid within itself, with this buoyancy fundamentally related to the density field. To extend the notions of Archimedean buoyancy to a fluid, we make use of a *test fluid element* originally defined in Section 17.2.5. A test fluid element is an imaginary probe that does not alter the fluid environment into which it is placed. It serves to map the Archimedean buoyancy of the fluid environment without modifying the fluid environment.

FIGURE 30.1: An arbitrary region of fluid, $\mathcal{R}$, within a density stratified fluid experiences a gravitational force acting down and a buoyant force acting up. The dark gray features represent the solid earth topography; i.e., mountains.

30.2.1 Hydrostatic pressure force

Consider an arbitrary finite region, $\mathcal{R}$, contained within an exactly hydrostatic fluid such as shown in Figure 30.1. Rather than an immersed body, such as a ship or balloon, we are interested in an arbitrary region of the fluid itself, such as an infinitesimal fluid element or a finite fluid volume. The mass of the fluid region is given by the integral of the fluid density over the region

$$M_{\text{fluid}} = \int_{\mathcal{R}} \rho \, \mathrm{d}V. \tag{30.1}$$

We seek an understanding of the forces acting on this region.

As discussed in Chapters 25 and 28, any surface, even an imaginary surface, within a fluid experiences a contact stress due to interactions between the fluid and the surface. For a fluid at rest in a gravitational field, the only contact stress arises from pressure. There are no tangential stresses from friction since there is, by assumption, no fluid motion. Pressure is a compressive normal stress, acting in the direction determined by minus the outward normal along the surface. Integrating the pressure over the closed boundary, $\partial\mathcal{R}$, leads to the pressure force acting on the region

$$\boldsymbol{F}_{\text{pressure}} = - \oint_{\partial\mathcal{R}} p \, \hat{\boldsymbol{n}} \, \mathrm{d}\mathcal{S}, \tag{30.2}$$

where p is the pressure, $\hat{\boldsymbol{n}}$ is the outward normal on the boundary, and $\mathrm{d}\mathcal{S}$ is the area element.

Since the region, $\mathcal{R}$, is part of the fluid itself, then we can use Gauss's divergence theorem in the form of equation (2.84) to render the equivalent expression for $\boldsymbol{F}_{\text{pressure}}$ in terms of the volume integral of the pressure gradient

$$\boldsymbol{F}_{\text{pressure}} = - \int_{\mathcal{R}} \nabla p \, \mathrm{d}V. \tag{30.3}$$

Furthermore, since the fluid is at rest, it maintains an exact hydrostatic balance so that its pressure only has a dependence on the vertical position within the fluid, $p = p(z)$. The hydrostatic pressure equals to the weight per horizontal area of fluid sitting above any point in the fluid so that its vertical derivative given by

$$\frac{\mathrm{d}p}{\mathrm{d}z} = -\rho \, g. \tag{30.4}$$

Hence, the force acting on the region is

$$\boldsymbol{F}_{\text{pressure}} = - \int_{\mathcal{R}} \nabla p \, \mathrm{d}V = - \int_{\mathcal{R}} \hat{\boldsymbol{z}} \, (\mathrm{d}p/\mathrm{d}z) \, \mathrm{d}V = \hat{\boldsymbol{z}} \, g \int_{\mathcal{R}} \rho \, \mathrm{d}V = \hat{\boldsymbol{z}} \, g \, M_{\text{fluid}}, \tag{30.5}$$

where we assumed a constant gravitational acceleration over $\mathcal{R}$. The hydrostatic pressure acting on the region imparts a vertical upward force equal to the weight of the fluid within the region. This result is a mathematical expression of *Archimedes' Principle* as applied to a fluid region.

Note that the net horizontal force acting over the region vanishes. The reason is that there are no horizontal pressure gradients within the fluid since, by assumption, the fluid is at rest and thus experiences no horizontal acceleration. So although the region $\mathcal{R}$ experiences horizontal compressive pressure forces acting along its boundary, $\partial\mathcal{R}$, these forces balance when integrated over the body, thus leaving a zero net horizontal acceleration. We studied such static force balances in Section 25.5.

30.2.2 Archimedean buoyancy force

Imagine replacing the fluid in the region $\mathcal{R}$ with another material whose density, ρ_{body}, generally differs from that of the displaced fluid, so that its mass is given by

$$M_{\text{body}} = \int_{\mathcal{R}} \rho_{\text{body}} \, \mathrm{d}V. \tag{30.6}$$

If the material has a density less than the displaced fluid, $\rho_{\text{body}} < \rho_{\text{fluid}}$, then we say that $\mathcal{R}$ has a net positive *buoyancy* force relative to the displaced fluid, in which case $\mathcal{R}$ experiences an upward acceleration. The converse holds if $\mathcal{R}$ is filled with matter that is more dense than the displaced fluid, in which case $\mathcal{R}$ sinks downward.

Mathematically we write this buoyancy force as

$$\boldsymbol{F}_{\text{buoy}} = \hat{\boldsymbol{z}}\, g \int_{\mathcal{R}} (\rho_{\text{fluid}} - \rho_{\text{body}}) \, \mathrm{d}V = \hat{\boldsymbol{z}}\, g \, (M_{\text{fluid}} - M_{\text{body}}). \tag{30.7}$$

In this manner, we define the Archimedean buoyancy as a *relative force*. The vertical buoyancy force is negative if the weight of the body is larger than that of the fluid it displaces, and conversely if the body has less weight. If the densities are equal, then the body is *neutrally buoyant* and thus experiences no net vertical force; i.e., it floats.

As we observed earlier, a nonzero buoyancy force that leads to vertical acceleration arises from an imbalance between the gravitational body force acting over the region, $\mathcal{R}$, with the pressure contact force acting on the region boundary, $\partial\mathcal{R}$. Furthermore, if $\mathcal{R}$ is a region of fluid itself, then the buoyancy forces arise from non-hydrostatic pressure forces since any vertical acceleration breaks the hydrostatic balance. We further examine these non-hydrostatic pressure forces in Section 30.11.

30.3 Mass density and its flavors

The density of a fluid element is central to determining its buoyancy. The *thermal equation of state*, or *equation of state* to be more brief (Section 23.4.1), provides an expression for the mass density as a function of pressure, temperature, and material tracer concentration (salinity in the ocean and humidity in the atmosphere). In this section we discuss the equation of state as well as the related flavors of mass density used to study stratified fluids.

30.3.1 Equation of state for the atmosphere and ocean

The atmosphere and ocean are commonly approximated as two-component fluids (air and water vapor for the atmosphere; freshwater and salt for ocean). We thus write the *in situ* density as a function

$$\rho = \rho(S, T, p). \tag{30.8}$$

This *equation of state* is a function of the *in situ* temperature, T, the *in situ* pressure, p, and the *in situ* salinity (ocean) or humidity (atmosphere), S.[4] The term *in situ* refers to a property measured locally at a point in the fluid. Such *in situ* properties contrast to *potential* properties, which are based on referencing to a chosen pressure (e.g., potential temperature described in Section 23.3).

Liquids such as seawater have rather complex equations of states obtained from empirical fits to measurements. Part of the complexity arises from the multi-component nature of seawater

[4]For our purposes when discussing the ocean, we set $S = 1000\, C$ with C the salt concentration, with this specification referred to as the *absolute salinity* by *IOC et al.* (2010). C generally has values around 0.035 so that S has values around 35.

(salt plus freshwater) as well as the nontrivial inter-molecular forces commonly found in liquids. In contrast, the dry atmosphere can, for many purposes, be well approximated as an ideal gas, which has a rather simple equation of state (see Section 23.4.1). Furthermore, even a moist atmosphere has an equation of state that can be massaged to look like that of an ideal gas (e.g., see Section 18.1 of *Vallis* (2017)). Hence, much of our discussion in this section is biased toward the ocean, where niceties of the equation of state are most important.

30.3.2 Modified temperature variables

As discussed in Section 23.3, the *in situ* temperature of a fluid element changes even if there is no heating applied to the element nor any changes to its material composition. Pressure changes provide a mechanical means for *in situ* temperature to change even in the presence of physical processes that are adiabatic and constant composition (e.g., laminar flow). Is it possible to remove such pressure effects and still have a field that describes the "temperature" of a fluid element? That is, can we define a temperature-like field that is only modified by irreversible processes such as heating and mixing? This question is answered by defining *potential temperature*, θ, as well as potential enthalpy or *Conservative Temperature*, Θ. Details are provided for potential temperature in Section 23.3 and Conservative Temperature in Section 26.11. For now it is sufficient to note that the mass density can be written as a function salinity, potential temperature, and pressure

$$\rho = \rho(S, \theta, p), \tag{30.9}$$

or as a function of salinity, Conservative Temperature, and pressure

$$\rho = \rho(S, \Theta, p). \tag{30.10}$$

For most purposes throughout this book, it is not important to distinguish between potential temperature and Conservative Temperature.[5] We choose to write Θ in most cases since Conservative Temperature offers the most general and self-consistent theoretical foundations for ocean thermodynamics, as per *McDougall* (2003) and *IOC et al.* (2010).

One comment on mathematical notation is key here. Namely, the functions $\rho(S, T, p)$, $\rho(S, \theta, p)$, and $\rho(S, \Theta, p)$ have distinct arguments and yet they all measure the same density. A more mathematically honest nomenclature distinguishes the functions by writing, say,

$$\rho = \mathcal{F}(S, T, p) = \mathcal{G}(S, \theta, p) = \mathcal{H}(S, \Theta, p). \tag{30.11}$$

However, we choose brevity in notation by allowing the functional dependence to signal the distinction. This overloaded notation is standard in the oceanography literature, with care needed to ensure clarity in understanding.[6]

30.3.3 Differential and material time changes

Recall from Section 30.2.2 that to compute the buoyancy acting on a fluid element, we compare the *in situ* density of the fluid element to that of its local surrounding fluid environment. To support that comparison, we must consider how *in situ* density in the fluid differs between two infinitesimally close points in the fluid. That is, we must compute the differential of *in situ* density.[7] Given the functional dependence for the equation of state written in terms of S, Θ, p

[5] One case where the distinction is important concerns an ideal gas atmosphere as discussed in Section 30.6.2.

[6] We made note of this point when introducing scalar fields in Section 1.5.1.

[7] Recall we introduced differentials in Section 2.8. For the mathematically inclined reader, we say that equation (30.12) provides the *exterior derivative* of density.

(equation (30.9)), the differential of *in situ* density is given by

$$\mathrm{d}\rho = \left[\frac{\partial\rho}{\partial S}\right]\mathrm{d}S + \left[\frac{\partial\rho}{\partial\Theta}\right]\mathrm{d}\Theta + \left[\frac{\partial\rho}{\partial p}\right]\mathrm{d}p \equiv \rho\,\beta\,\mathrm{d}S - \rho\,\alpha\,\mathrm{d}\Theta + c_{\mathrm{s}}^{-2}\,\mathrm{d}p. \tag{30.12}$$

The second equality introduced the following thermodynamic properties of the fluid[8]

$$\beta = \frac{1}{\rho}\left[\frac{\partial\rho}{\partial S}\right]_{\Theta,p} \qquad \text{haline contraction coefficient} \tag{30.13}$$

$$\alpha = -\frac{1}{\rho}\left[\frac{\partial\rho}{\partial\Theta}\right]_{S,p} \qquad \text{thermal expansion coefficient} \tag{30.14}$$

$$c_{\mathrm{s}}^2 = \left[\frac{\partial p}{\partial\rho}\right]_{S,\Theta} \qquad \text{squared sound speed.} \tag{30.15}$$

The haline contraction coefficient, β, is considered for the ocean, where *haline* refers to salinity.[9]

The density differential (30.12) leads to the expression for the material change in the *in situ* density moving along a fluid particle trajectory

$$\frac{1}{\rho}\frac{\mathrm{D}\rho}{\mathrm{D}t} = \beta\,\frac{\mathrm{D}S}{\mathrm{D}t} - \alpha\,\frac{\mathrm{D}\Theta}{\mathrm{D}t} + \frac{1}{\rho\,c_{\mathrm{s}}^2}\,\frac{\mathrm{D}p}{\mathrm{D}t}. \tag{30.16}$$

In the absence of mixing, the Conservative Temperature and salinity are materially constant.[10] In this case, the material time evolution of the *in situ* density is affected only through adiabatic processes that lead to material time changes to the pressure

$$\frac{\mathrm{D}\rho}{\mathrm{D}t} = \frac{1}{c_{\mathrm{s}}^2}\,\frac{\mathrm{D}p}{\mathrm{D}t} \quad \Longleftarrow \quad \text{adiabatic and isohaline changes.} \tag{30.17}$$

30.3.4 Potential density

As discussed in Section 30.3.2, the reversible motion of a perfect fluid element generally occurs with materially constant Conservative Temperature and materially constant tracer concentration. We thus find it convenient to combine the evolution of salinity and Conservative Temperature into the evolution of a single variable. *Potential density* is one such combination, which is defined as the density a fluid element would have if reversibly moved to a chosen reference pressure

$$\varrho = \varrho(S,\Theta|p_{\mathrm{ref}}) \equiv \rho(S,\Theta,p=p_{\mathrm{ref}}). \tag{30.18}$$

Hence, potential density is found by evaluating the equation of state for *in situ* density with the local value for S and Θ, yet with the pressure set to the fixed reference pressure, $p = p_{\mathrm{ref}}$. Potential density is thus parametrically a function of the reference pressure. As for the Conservative Temperature, the reference pressure is often taken at sea level. However, as noted in a few paragraphs below, that choice is neither necessary nor universal.

[8] A property of the fluid is not a function of the fluid flow but instead is a function of the fluid state.

[9] Note that in many chapters of this book, $\beta = \partial f/\partial y$ is the meridional derivative of the Coriolis parameter. We keep the two usages for β distinct so to avoid confusion.

[10] This statement has nuances that are discussed in Section 26.11 and in more detail in *IOC et al.* (2010). They can be ignored for present purposes.

Material evolution of potential density

With the definition (30.18), the material evolution of potential density is given by

$$\frac{1}{\varrho}\frac{\mathrm{D}\varrho}{\mathrm{D}t} = \beta(S,\Theta,p=p_{\rm ref})\,\frac{\mathrm{D}S}{\mathrm{D}t} - \alpha(S,\Theta,p=p_{\rm ref})\,\frac{\mathrm{D}\Theta}{\mathrm{D}t}, \tag{30.19}$$

where

$$\beta(S,\Theta,p=p_{\rm ref}) = \frac{1}{\varrho(S,\Theta,p=p_{\rm ref})}\left[\frac{\partial\rho(S,\Theta,p_{\rm ref})}{\partial S}\right]_{\Theta} \qquad \text{haline contraction at } p=p_{\rm ref} \tag{30.20}$$

$$\alpha(S,\Theta,p=p_{\rm ref}) = -\frac{1}{\varrho(S,\Theta,p=p_{\rm ref})}\left[\frac{\partial\rho(S,\Theta,p_{\rm ref})}{\partial \Theta}\right]_{S} \qquad \text{thermal expansion at } p=p_{\rm ref} \tag{30.21}$$

are the haline contraction and thermal expansion coefficients evaluated at the reference pressure, $p = p_{\rm ref}$. Since pressure is fixed at the reference value, there is no pressure derivative on the right hand side of equation (30.19). Conservative Temperature and salinity are materially constant for reversible processes; i.e., adiabatic motion that also maintains constant matter content (e.g., isohaline) for fluid elements. By construction, potential density is also materially constant for reversible processes since both terms on the right hand side of equation (30.19) vanish. This behavior is in contrast to *in situ* density, whose evolution is affected by pressure changes as revealed by equations (30.16) and (30.17).

Reference pressures for ϱ and Θ

The reference pressure for the potential density is commonly assumed to be the same as for the Conservative Temperature (and potential temperature). This assumption is particularly the norm for the atmosphere, where the reference pressure is generally taken at the sea level. Likewise for the ocean, the potential temperature and Conservative Temperature are generally computed using a standard sea level reference pressure. However, there are many occasions in the ocean to consider potential density with larger reference pressures, such as when considering physical processes (e.g., mixing) within the ocean interior. Doing so is motivated by the rather strong nonlinear effects associated with the seawater equation of state. In this case, pressure effects prompt one to choose a reference pressure closer to the *in situ* pressure near to the region of analysis. Even though it is common to choose a potential density reference pressure distinct from the surface pressure, the Conservative Temperature reference pressure generally remains at the surface. There is no fundamental problem with the use of distinct reference pressures for ϱ and Θ. In particular, all of the above properties of potential density remain unchanged.

30.3.5 Linear equation of state for the ocean

For certain purposes, it is useful to approximate the equation of state used to study ocean fluid mechanics. One common idealization is to compute density as a linear function of Conservative Temperature and salinity

$$\rho = \rho_o\,[1 - \alpha\,(\Theta - \Theta_0) + \beta\,(S - S_0)], \tag{30.22}$$

where α, β, ρ_o, Θ_0, and S_0 are constants. An even further simplification is to set salinity to a space-time constant, so that density is just a linear function of Conservative Temperature. Alternatively, we may choose $\beta = 0$, in which case salinity is a passive tracer that has no impact on density.

30.3.6 Comments on density in a hydrostatic ocean

In an approximate hydrostatic fluid (Section 27.2), we only have access to the hydrostatic pressure. As such, density can only be computed as a function of hydrostatic pressure. Furthermore, density is generally a function of pressure whereas hydrostatic pressure is directly determined by the vertical integral of density. This self-referential situation is resolved for the Boussinesq ocean in which energetic consistency requires the seawater equation of state to use the geopotential defined pressure, $p_{\text{eos}} = -\rho_{\circ}\,\Phi$, as the argument for density (Section 29.8), which takes on the static form, $p_{\text{eos}} = -\rho_{\circ}\,g\,z$, for a simple geopotential. For the non-Boussinesq hydrostatic ocean, we can make use of pressure as the vertical coordinate, thus allowing for density to be evaluated at a pressure prescribed by the value of the vertical coordinate.

30.3.7 Further study

Chapter 1 of *Vallis* (2017) provides a pedagogical discussion of the equation of state for an ideal gas atmosphere and for seawater, as well as a discussion of the various flavors of density. See also Section 18.1 of *Vallis* (2017) for the equation of state for an ideal gas with water vapor. The seawater equation of state is detailed by *IOC et al.* (2010), with an overview provided by *McDougall et al.* (2013).

30.4 Archimedean buoyancy of a test fluid element

We now return to the notions of Archimedean buoyancy (in brief, the "buoyancy") of a test fluid element. Again, buoyancy is the gravitational acceleration that acts on a massive body due to the difference between the density of the body and the density of the local surrounding fluid environment. For this section, we consider the massive body to be a test fluid element whose presence does not alter the density field.

30.4.1 Locally referenced Archimedean buoyancy

Consider a local definition of fluid buoyancy according to

$$b_{\text{loc}} = -g\,(\rho_{\text{test}} - \rho_{\text{env}})/\rho_{\text{env}} = g\,(1 - \rho_{\text{test}}/\rho_{\text{env}}), \tag{30.23}$$

where ρ_{env} is the local density of the fluid environment, and ρ_{test} is the density of the test fluid element within that environment. If the fluid element has a density greater than the environment, then it has a negative locally referenced buoyancy, and vice versa.

In probing the buoyancy of the fluid environment, we imagine moving the test fluid element from one point to another. In that movement, the test fluid element might retain all of its original properties, or those properties might be modified during the movement. That is, in determining the buoyancy we determine ρ_{test} by specifying its point of origin and how it is moved (e.g., with or without mixing?). Conventional approaches are specified later in this section. A key notion is that buoyancy as defined by equation (30.23) is a function of the path that the test fluid element takes to reach the environment point. This subjectivity lends ambiguity to the definition of local Archimedean buoyancy. We remove this ambiguity by asking specific questions. One central question we ask is if the test fluid element moves an infinitesimal distance while mixing its temperature and salinity with the environment, then what direction maintains a neutrally buoyant state for the test fluid element? This question forms the basis for defining *neutral directions*, which are studied in Section 30.5.

Working with locally referenced Archimedean buoyancy requires a redefinition of a reference state when moving from point to point within a fluid. The continuum of reference states allows for a local accounting of the gravitational stability and neutral directions. However, the

re-referencing cannot be seamlessly incorporated into the equations of motion since at each point one needs to redefine the reference state. As an alternative means to garner local information about forces associated with density gradients, we examine the nature of the pressure force in our discussion of *effective buoyancy* in Section 30.11.

30.4.2 Globally referenced Archimedean buoyancy

The definition (30.23) accepts that buoyancy is a relative field. Hence, at each fluid point we redefine the environment to compare the density of the test fluid element. However, there are cases in which it is sufficient to define a globally constant environment with a constant reference density, ρ_{ref}. In this case we consider the global buoyancy as

$$b_{\text{glb}} = g\,(1 - \rho/\rho_{\text{ref}}), \tag{30.24}$$

where we compute ρ according to the local environmental density. This definition is particularly useful for idealized cases where the *in situ* density is not a function of pressure. In this case buoyancy is a function only of Conservative Temperature and salinity so that we can make use of potential density to measure buoyancy (as explained below).

Although the numerical value of b_{glb} is a function of the reference density, what is more relevant is the buoyancy of one fluid element relative to another

$$\Delta b_{\text{glb}} = -g\,(\Delta\rho/\rho_{\text{ref}}). \tag{30.25}$$

The sign of this relative buoyancy does not depend on the reference density, with the sign all that we need to conclude whether one fluid element is more buoyant than another. Furthermore, with a globally constant environmental density, the buoyancy becomes a local function of space. That is, we no longer compare the fluid element density to a changing local density. Instead, we compute the local density and compare it to the reference density. We can thus determine b_{glb} at a point through information available just at that point. That is, b_{glb} is a space-time local field. Correspondingly, we can map b_{glb} and determine the relative buoyancy of fluid elements anywhere in the fluid.

30.5 Buoyancy stratification and neutral directions

What are the Archimedean buoyant forces that act on a fluid element? We answer this question by using a test fluid element to probe the local fluid environment without disturbing the environment. We do not consider time changes in this section. Rather, we here examine a snapshot of the fluid environment and use test fluid elements to probe the buoyant properties of that environment. In Section 30.8 we extend the notions of the present section to include time changes.

In probing the buoyant properties of a fluid, we are led to introduce *neutral directions*, which are directions that a test fluid element can move without any buoyancy force acting on that element. The concept of a neutral direction was pioneered by *McDougall* (1987a,b) with applications to the ocean. The thought experiments that build an understanding of neutral directions are applicable to any continuously stratified fluid, thus serving to teach fundamental aspects of buoyancy in both the ocean and atmosphere.

30.5.1 General considerations

As a fluid element moves through its surrounding fluid environment, it is exposed to a suite of physical processes that can modify its thermal, material, and mechanical properties; i.e., its Θ, S, and p. Modification of its pressure occurs through contact stresses with other fluid

elements (Chapters 25 and 28). Modification of its thermal and material properties occurs through the mixing-induced exchange of heat and matter such as via diffusion (Chapter 69). The exchange of thermal and material properties occurs in the presence of irreversible processes whereas mechanical exchanges occur either reversibly (pressure exchange) or irreversibly (viscous exchange; Section 25.3).

The *in situ* density of a fluid element generally changes when it moves through the fluid environment, with the density change determined by how the element interacts with the surrounding fluid. We conceive of two complementary interactions for the purpose of examining the local Archimedean buoyancy of the test fluid element.

- UNMIXED TEST FLUID ELEMENT: Displace the test fluid element without changing Θ and S yet allowing p to equilibrate with the local environment. We imagine this adiabatic and isohaline (i.e., isentropic) displacement to occur by surrounding the test element with a thermally and materially impermeable elastic sack. In this case there is no mixing of the test element with the environment. Furthermore, assume the test fluid element mechanically equilibrates its pressure with the surrounding fluid, so that the surrounding fluid does reversible pressure-work (Section 22.2) on the test fluid element. The test fluid element's *in situ* density changes through the changing pressure of the local environment.

- MIXED TEST FLUID ELEMENT: The complement thought experimence considers the displacement of a test fluid element with its Θ, S, and p equilibrating with the local environment. Such equilibration requires a complete mixing of the test fluid element's Θ and S with the local environment, as well as the mechanical equilibration of its pressure. Notably, the mixed test fluid element represents a proxy for the local enviromental properties, since its properties are identical to the local environment.

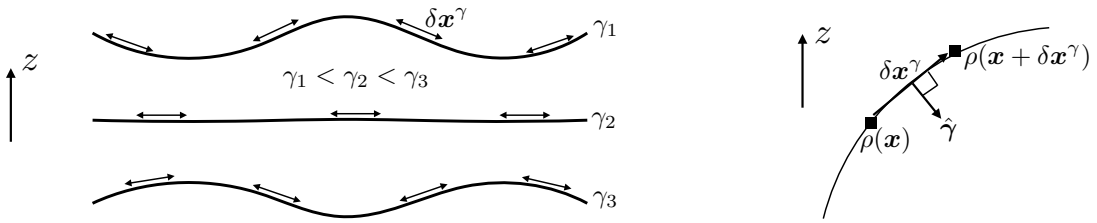

FIGURE 30.2: Depicting the notion of a neutral direction within a stably stratified fluid. The left panel shows surfaces of constant γ, which represents a surface of constant buoyancy. For example, with a density field that is a function just of Θ, then γ surfaces are parallel to surfaces of constant Θ (see comment at end of Section 30.5.3). Reversible displacements of test fluid elements along a constant γ surface incur no local buoyancy acceleration; i.e., the test fluid element floats along neutral directions. At each point along a γ surface, a neutral direction is defined by directions within the local tangent to the surface. Note that for a fluid with a nonzero neutral helicity (Section 30.7), it is not possible to define such neutral surfaces globally. So this figure holds only for a vanishing neutral helicity. Even so, we can define a neutral direction locally, as per the right panel, which shows a zoomed view of a small region on a γ surface. Infinitesimal neutral displacements, $\delta \boldsymbol{x}^\gamma$, are displacements that satisfy $\delta \boldsymbol{x}^\gamma \cdot \hat{\boldsymbol{\gamma}} = 0$, with this constraint leading to the neutrality condition (30.33). The dianeutral unit vector, $\hat{\boldsymbol{\gamma}}$, is the direction orthogonal to the local neutral direction, with $\hat{\boldsymbol{\gamma}}$ given by equation (30.30). Again, the neutrality condition holds locally at each point in the fluid, so neutral directions are defined even for a fluid with a nonzero neutral helicity.

If we displace the unmixed test fluid element to a region where its *in situ* density differs from the local environment, then the fluid element feels a local Archimedean buoyant acceleration. However, as we show in this section, there are directions that the test fluid element can move that leave its local Archimedean buoyancy zero; i.e., where the test fluid element retains the same *in situ* density as the local environment and so remains neutrally buoyant. These directions are referred to as *neutral directions*. In effect, the test fluid element floats along a neutral direction and illustrate this notion in Figure 30.2.

A complementary means to conceive of neutral directions is found by considering the mixed test fluid element that is displaced and equilibrates its Θ and S (through mixing), and p (through mechanical interactions) with the local environment. An arbitrary displacement leads to a change in the fluid element's *in situ* density due to changes in Θ, S, and p. However, if the mixed test element is displaced along the neutral direction, the mixing-induced changes from Θ and S exactly balance (as per the neutrality condition (30.33) derived below). In this manner, the only change to the *in situ* density arises from changes to the pressure felt by the test fluid element, with these changes identical to those felt by the unmixed test fluid element when moving along a neutral direction. We conclude that the buoyant acceleration vanishes along a neutral direction for both an umixed test fluid element as well as for a test fluid element that is mixed with the local environment.

30.5.2 Comparing *in situ* densities

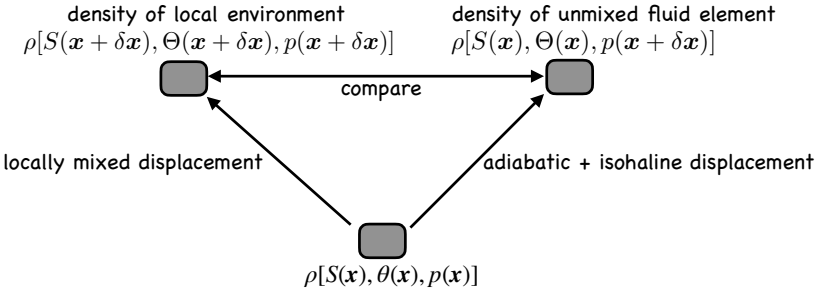

$$\rho[S(\boldsymbol{x}+\delta\boldsymbol{x}^\gamma), \Theta(\boldsymbol{x}+\delta\boldsymbol{x}^\gamma), p(\boldsymbol{x}+\delta\boldsymbol{x}^\gamma)] = \rho[S(\boldsymbol{x}), \Theta(\boldsymbol{x}), p(\boldsymbol{x}+\delta\boldsymbol{x}^\gamma)] \Longrightarrow \text{neutral direction}$$

FIGURE 30.3: Schematic of the two complementary thought experiments discussed in Section 30.5.2 used to determine neutral directions. The right path concerns a test fluid element that is thermally and materially closed but is mechanically open. Hence, as this test fluid element is displaced from its original location, $\boldsymbol{x}$, to a new position, $\boldsymbol{x}+\delta\boldsymbol{x}$, it equilibrates to the local pressure but retains the Θ and S of the origin. If the *in situ* density of the test fluid element is displaced along a direction where it maintains the same density as the local environment, then the locally defined Archimedean buoyancy vanishes and this displacement is aligned along a neutral direction. In this case, the displacement satisfies $\delta\boldsymbol{x}^\gamma \cdot \hat{\boldsymbol{\gamma}} = 0$, as per the neutrality condition (30.33). The complement perspective is shown by the left path as defined by a test fluid element that locally mixes with its environment. If the mixing-induced changes in Θ precisely compensate the mixing-induced changes in S, according to the neutrality condition (30.33), then the *in situ* density change for this test fluid element arise only from changes in pressure. But that change is just like for the ummixed test element on the right path. In this manner, both the mixed and unmixed test fluid elements at $\boldsymbol{x}+\delta\boldsymbol{x}$ define the same neutral direction.

To make the above ideas mathematically precise, refer to Figure 30.3 as we consider an infinitesimal displacement, $\delta\boldsymbol{x}$, of a test fluid element and examine how its *in situ* density changes. First consider the fluid element that equilibrates Θ, S, and p with the local environment along its displacement, so that its *in situ* density at the new location equals to that of the local environment, $\rho(\boldsymbol{x}+\delta\boldsymbol{x})$. To leading order, the difference in density between the original position and at the displaced position is computed according to the difference

$$\begin{aligned}
\delta\rho &= \rho(\boldsymbol{x}+\delta\boldsymbol{x}) - \rho(\boldsymbol{x}) && \text{(30.26a)}\\
&= \rho[S(\boldsymbol{x}+\delta\boldsymbol{x}), \Theta(\boldsymbol{x}+\delta\boldsymbol{x}), p(\boldsymbol{x}+\delta\boldsymbol{x})] - \rho[S(\boldsymbol{x}), \Theta(\boldsymbol{x}), p(\boldsymbol{x})] && \text{(30.26b)}\\
&\approx \delta\boldsymbol{x} \cdot \left[\frac{\partial\rho}{\partial\Theta} \nabla\Theta + \frac{\partial\rho}{\partial S} \nabla S + \frac{\partial\rho}{\partial p} \nabla p \right] && \text{(30.26c)}\\
&= \rho\, \delta\boldsymbol{x} \cdot \left[-\alpha \nabla\Theta + \beta \nabla S + \frac{1}{\rho\, c_s^2} \nabla p \right] . && \text{(30.26d)}
\end{aligned}$$

For the unmixed test fluid element there is no exchange (no mixing) of Θ and S with its surrounding fluid environment. Hence, changes to density of the test fluid element arise just from pressure changes

$$(\delta\rho)_{(\text{no mix})} = \rho(\boldsymbol{x}+\delta\boldsymbol{x})_{(\text{no mix})} - \rho(\boldsymbol{x}) \tag{30.27a}$$
$$= \rho[S(\boldsymbol{x}),\Theta(\boldsymbol{x}),p(\boldsymbol{x}+\delta\boldsymbol{x})] - \rho[S(\boldsymbol{x}),\Theta(\boldsymbol{x}),p(\boldsymbol{x})] \tag{30.27b}$$
$$\approx \rho\,\delta\boldsymbol{x}\cdot\left[\frac{1}{\rho\,c_{\rm s}^2}\,\nabla p\right]. \tag{30.27c}$$

Comparing the densities of the two displaced test fluid elements renders

$$\rho(\boldsymbol{x}+\delta\boldsymbol{x}) - \rho(\boldsymbol{x}+\delta\boldsymbol{x})_{(\text{no mix})} = \delta\rho - (\delta\rho)_{(\text{no mix})} \tag{30.28a}$$
$$= [\rho(\boldsymbol{x}+\delta\boldsymbol{x}) - \rho(\boldsymbol{x})] - [\rho(\boldsymbol{x}+\delta\boldsymbol{x})_{(\text{no mix})} - \rho(\boldsymbol{x})] \tag{30.28b}$$
$$= \rho[S(\boldsymbol{x}+\delta\boldsymbol{x}),\Theta(\boldsymbol{x}+\delta\boldsymbol{x}),p(\boldsymbol{x}+\delta\boldsymbol{x})] - \rho[S(\boldsymbol{x}),\Theta(\boldsymbol{x}),p(\boldsymbol{x}+\delta\boldsymbol{x})] \tag{30.28c}$$
$$\approx \rho\,\delta\boldsymbol{x}\cdot[-\alpha\,\nabla\Theta + \beta\,\nabla S]\,. \tag{30.28d}$$

We discuss this result in the following.

30.5.3 Neutral directions and the neutrality condition

Following the thought experiments illustrated in Figure 30.3, we find that if the density of the displaced and unmixed test fluid element is the same as the local environment, then the particular displacement defines a neutral direction. From equation (30.28d) we define a displacement along a neutral direction as a displacement that satisfies

$$\delta\boldsymbol{x}^{\gamma}\cdot[-\alpha\,\nabla\Theta+\beta\,\nabla S] = \delta\boldsymbol{x}^{\gamma}\cdot\hat{\boldsymbol{\gamma}}\,|-\alpha\,\nabla\Theta+\beta\,\nabla S| = 0, \tag{30.29}$$

where we introduced the *dianeutral direction* given by the unit vector

$$\hat{\boldsymbol{\gamma}} = \frac{-\alpha\,\nabla\Theta+\beta\,\nabla S}{|-\alpha\,\nabla\Theta+\beta\,\nabla S|}, \tag{30.30}$$

which points in the direction of increasing density.[11] Infinitesimal displacements, $\delta\boldsymbol{x}^{\gamma}$, that are orthogonal to the dianeutral direction, $\hat{\boldsymbol{\gamma}}$, occur along a neutral direction

$$\delta\boldsymbol{x}^{\gamma}\cdot\hat{\boldsymbol{\gamma}} = 0 \Longrightarrow \text{displacement along a neutral direction.} \tag{30.31}$$

These displacements of the unmixed test fluid element lead to no difference in the *in situ* density of the local environment and the fluid element. Hence, neutral displacements retain a vanishing local Archimedean buoyancy for the unmixed test fluid element. In contrast, displacements in the dianeutral direction alter the local buoyancy.

Let us write the neutral displacement in the form

$$\delta\boldsymbol{x}^{\gamma} = \hat{\boldsymbol{t}}^{\gamma}\,\delta s, \tag{30.32}$$

where δs is the arc-length along the displacement and $\hat{\boldsymbol{t}}^{\gamma}$ is the unit vector pointing along the neutral displacement. We can thus write equation (30.29) as

$$\alpha\,\hat{\boldsymbol{t}}^{\gamma}\cdot\nabla\Theta = \beta\,\hat{\boldsymbol{t}}^{\gamma}\cdot\nabla S, \tag{30.33}$$

[11] Equation (4) in *McDougall et al.* (2014) makes use of the opposite sign convention so that their dianeutral direction points towards decreasing density. We instead follow the water mass transformation convention as in equation (73.38), so that $\hat{\boldsymbol{\gamma}}$ points in the direction of increasing density.

which we refer to as the *neutrality condition*. The neutrality condition means that the α and β weighted gradients of Θ and S are exactly balanced when aligned along a neutral direction. So when considering neutral directions from the perspective of the mixed test fluid element, the mixing-induced changes in Θ precisely compensate mixing-induced changes in S as per the neutrality condition (30.33). As a result, the *in situ* density of the mixed test fluid element changes only via changes to the pressure (since Θ and S changes are compensated), which is precisely how the unmixed test fluid element changes its *in situ* density.

As a corollary, for those cases in which $\nabla S = 0$, so that S is a spatial constant, then neutral directions are aligned parallel to surfaces of constant Θ. In such fluids, Θ measures buoyancy so that fluid motion along surfaces of constant Θ feel no buoyant acceleration. We mentioned this case in Figure 30.2.

30.5.4 Comments and further study

Neutral directions were introduced to oceanography by *McDougall* (1987a,b), and they are the basis for how oceanographers think about buoyancy stratification. Our discussion of neutral directions was inspired by the concise presentation in Section 2.7.2 of *Olbers et al.* (2012). Our study of vertical gravitational stability follows Section 3.6 of *Gill* (1982) as well as Section 2.10 of *Vallis* (2017). In an actual fluid, the movement of any fluid, even a tiny fluid element, modifies the surrounding fluid so that a perfect test fluid element is a fiction. We return to this point in Section 30.11 when studying effective buoyancy.

It is notable that we did not present a dynamical argument for why physical processes favor neutral displacements. Rather, we appealed to intuition that suggests physical processes are more "free" to act in directions that feel no buoyant forces. More thorough arguments require dynamical principles, such as the equations of motion and associated energetic constraints. Even so, there is presently no dynamical argument for why the ocean prefers neutral displacements over arbitrary non-neutral displacements. However, empirical measurements of ocean mixing support the relevance of neutral directions for orienting tracer mixing within the ocean interior. More discussion of these points is given by *McDougall et al.* (2014), with mathematical implications presented in Chapter 71.

30.6 Buoyancy frequency and gravitational stability

In Section 30.5 we considered a general spatial displacement, $\delta\boldsymbol{x}$, of a test fluid element, and determined conditions for this displacement to keep the locally defined Archimedean buoyancy at zero. In this section we ask a slightly different question, focusing on a vertical displacement of the test fluid element without mixing (Figure 30.4), where the difference between the environmental density and the unmixed test element's density is

$$\rho(z+\delta z) - \rho(z+\delta z)_{(\text{no mix})} = \rho\,\delta z\,(-\alpha\,\partial_z\Theta + \beta\,\partial_z S). \tag{30.34}$$

We seek an understanding of whether the vertical fluid column is gravitationally stable to such displacements. Since we assume there is no motion of the fluid, the stability calculation determines whether the column is *statically stable* or *statically unstable*.[12]

Consider an upward displacement in equation (30.34) so that $\delta z > 0$. If the surrounding fluid environment has a lower density than the adiabatic and isohaline displaced test fluid element, $\rho(z+\delta z) < \rho(z+\delta z)_{(\text{no mix})}$, then the test element feels a buoyant force returning it to the

[12]We study fluid instabilities in Part XI of this book, with most attention given to instabilities associated with fluid flows. The *static instability* considered in this section occurs in the absence of fluid flow. Here, the instability arises simply because the density profile has heavier fluid above lighter fluid, with gravity acting to overturn this fluid column to produce a stable vertical stratification.

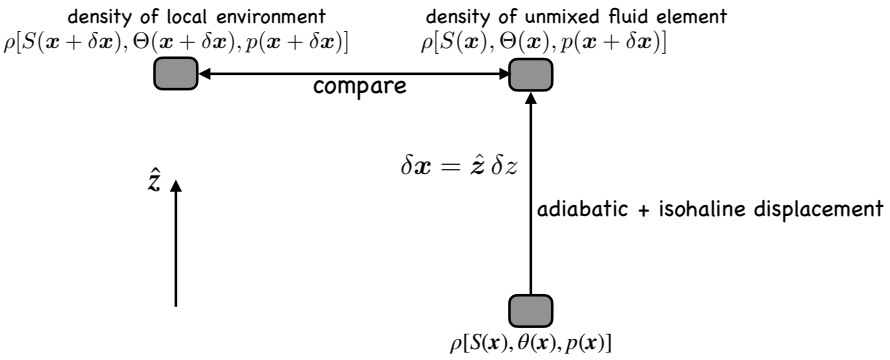

$$\rho[S(\boldsymbol{x}+\delta\boldsymbol{x}),\Theta(\boldsymbol{x}+\delta\boldsymbol{x}),p(\boldsymbol{x}+\delta\boldsymbol{x})] < \rho[S(\boldsymbol{x}),\Theta(\boldsymbol{x}),p(\boldsymbol{x}+\delta\boldsymbol{x})] \Longrightarrow \text{gravitationally stable}$$
$$\rho[S(\boldsymbol{x}+\delta\boldsymbol{x}),\Theta(\boldsymbol{x}+\delta\boldsymbol{x}),p(\boldsymbol{x}+\delta\boldsymbol{x})] > \rho[S(\boldsymbol{x}),\Theta(\boldsymbol{x}),p(\boldsymbol{x}+\delta\boldsymbol{x})] \Longrightarrow \text{gravitationally unstable}$$
$$\rho[S(\boldsymbol{x}+\delta\boldsymbol{x}),\Theta(\boldsymbol{x}+\delta\boldsymbol{x}),p(\boldsymbol{x}+\delta\boldsymbol{x})] = \rho[S(\boldsymbol{x}),\Theta(\boldsymbol{x}),p(\boldsymbol{x}+\delta\boldsymbol{x})] \Longrightarrow \text{gravitationally neutral}$$

FIGURE 30.4: Schematic of the calculation used to examine whether a fluid column is gravitationally stable under vertical displacement of a test fluid element, here realized by specializing the general displacement in Figure 30.3. An unmixed test fluid element (i.e., adiabatic and isohaline displacement) is displaced from its original location at a position $\boldsymbol{x}$ to a position $\boldsymbol{x}+\delta\boldsymbol{x}$, with $\delta\boldsymbol{x} = \hat{\boldsymbol{z}}\,\delta z$ and $\delta z > 0$ in this figure. We compare the density of the displaced unmixed test fluid element with the local environment to determine whether the density stratification of the fluid environment is gravitationally stable ($N^2 > 0$), unstable ($N^2 < 0$), or neutrally stable ($N^2 = 0$). Note that displacements with $N^2 > 0$ are associated with internal gravity waves studied in Chapter 57.

original vertical position. The restorative buoyant force per volume is written

$$g\,[\rho(z+\delta z) - \rho(z+\delta z)_{(\text{no mix})}] = g\,\rho\,\delta z\,(-\alpha\,\partial_z\Theta + \beta\,\partial_z S) \equiv -N^2\,\rho\,\delta z, \tag{30.35}$$

where we defined the squared *buoyancy frequency*

$$N^2 = g\,(\alpha\,\partial_z\Theta - \beta\,\partial_z S). \tag{30.36}$$

Gravitationally stable vertical motion results from a background density profile with $N^2 > 0$. In this case, the vertical displacement of an unmixed test fluid element moves the element into a region where buoyancy acts to return it to the original vertical position. This buoyant restoring force leads to buoyancy oscillations that can propagate in space-time in patterns referred to as *internal gravity waves*, which we study in Chapter 57.

A gravitationally unstable profile, in which the fluid has higher density over lower, is signalled by $N^2 < 0$. In this case the displacement of an unmixed test fluid element results in an exponential growth associated with *gravitational instability*. That is, when the fluid column is vertically stratified with $N^2 < 0$, a tiny vertical displacement of a test element leads to an even larger displacement, thus causing the perturbation to grow. The resulting gravitational instability causes the fluid to overturn so that it returns the fluid column to a gravitational stable state.

30.6.1 Locally referenced potential density

Equation (30.36) defines the squared buoyancy frequency in terms of the vertical temperature and salinity gradients. This expression is identical to the vertical gradient of the potential density (30.18), when the reference pressure for density is taken local to the point where the buoyancy frequency is computed. That is, the vertical gradient of the *locally referenced potential*

density provides a measure of the vertical stratification

$$N^2 = -g \left[\frac{1}{\varrho} \frac{\partial \varrho}{\partial z} \right]_{p_{\text{ref}}=p} = g \left[\alpha \, \frac{\partial \Theta}{\partial z} - \beta \, \frac{\partial S}{\partial z} \right]. \tag{30.37}$$

At a point in the fluid, the locally referenced potential density equals to the *in situ* density. However, when probing nearby points by displacing test fluid elements, and thus taking spatial variations into account, the two densities have distinct gradients. Namely, the gradient of the *in situ* density is affected by pressure gradients, whereas spatial gradients of the locally referenced potential density do not feel pressure effects.

30.6.2 Gravitational stability of an ideal gas atmosphere

We introduced the adiabatic lapse rate in Section 23.2 as a measure of how temperature varies as a function of pressure or depth. For an ideal gas atmosphere (Section 23.4), the temperature decreases when moving into a region of less pressure, and increases in regions of greater pressure. The squared buoyancy frequency for an ideal gas can be written (Exercise 30.2)

$$N^2 = \frac{g}{\theta} \frac{\partial \theta}{\partial z}. \tag{30.38}$$

The potential temperature for an ideal gas is given by equation (23.92)

$$\theta = T \left[\frac{p_{\text{ref}}}{p} \right]^{\varphi} \tag{30.39}$$

where

$$\varphi = R^{\text{M}} / c_{\text{p}} \tag{30.40}$$

is the dimensionless ratio of the gas constant to the heat capacity, both of which are constants for a simple ideal gas. Consequently, the squared buoyancy frequency takes the form

$$g^{-1} \, N^2 = \frac{\partial \ln \theta}{\partial z} = \frac{\partial \ln T}{\partial z} - \varphi \, \frac{\partial \ln p}{\partial z}. \tag{30.41}$$

Evidently, an *in situ* temperature that increases with height stabilizes the atmosphere, and a pressure that decreases with height also stabilizes. The more common situation is for an *in situ* temperature that decreases with height (e.g., it is typically colder on a mountain top than at sea level), with pressure also decreasing with height. Depending on the rate of their decrease, the atmosphere can be gravitationally stable (if temperature decreases gradually relative to pressure) or unstable.

For a hydrostatic fluid with a constant gravitational acceleration, the vertical derivative of pressure is given by (Section 27.2)

$$\frac{\partial p}{\partial z} = -\rho \, g, \tag{30.42}$$

so that pressure at a point in the fluid equals to the weight per area above that point (Section 24.6). Using this result leads to the squared buoyancy frequency for a hydrostatic ideal gas atmosphere

$$g^{-1} \, N^2 = \frac{\partial \ln T}{\partial z} + \frac{\varphi \, g \, \rho}{p} = \frac{1}{T} \left[\frac{\partial T}{\partial z} + \frac{g}{c_{\text{p}}} \right], \tag{30.43}$$

where we used the ideal gas relation $p = \rho T R^{\text{M}}$ for the final step. Equation (30.43) shows that the squared buoyancy frequency is positive (atmosphere is gravitationally stable) if the decrease

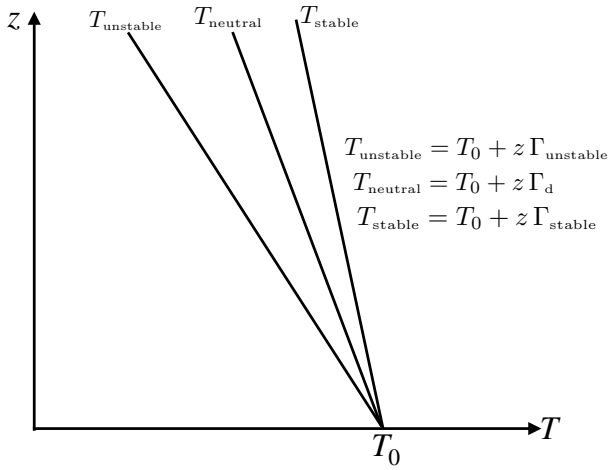

FIGURE 30.5: Three linear vertical profiles of *in situ* temperature in a dry ideal gas atmosphere. The neutrally stable profile has $T_{\text{neutral}} = T_0 + z\,\Gamma_{\text{d}}$, where $\Gamma_{\text{d}} = -g/c_{\text{p}} \approx -9.8$ K/(1000 m). A vertically unstable profile (heavy over light) has $T_{\text{unstable}} = T_0 + z\,\Gamma_{\text{unstable}}$ where $\Gamma_{\text{unstable}} < \Gamma_{\text{d}} = -g/c_{\text{p}}$. In contrast, the gravitationally stable atmosphere has $T_{\text{stable}} = T_0 + z\,\Gamma_{\text{stable}}$ where $\Gamma_{\text{stable}} > \Gamma_{\text{d}} = -g/c_{\text{p}}$.

with height of the *in situ* temperature is more gradual than the *adiabatic lapse rate*

$$N^2 = 0 \Longleftrightarrow \partial_z T = \Gamma_{\text{d}}, \tag{30.44}$$

where for a dry ideal gas atmosphere (i.e., an atmosphere with no moisture and thus no phase changes),[13] we find (see equation(23.74))

$$\Gamma_{\text{d}} = -g/c_{\text{p}} \approx -9.8 \text{ K/(1000 m)}. \tag{30.45}$$

Conversely, if the *in situ* temperature decreases upon ascent more quickly than the dry adiabatic lapse rate, then the vertical column is gravitationally unstable. In effect, the column becomes top heavy and subject to overturning. We summarize this gravitational stability criteria as follows:

$$\text{gravitationally stable} \qquad N^2 > 0 \Longleftrightarrow -\partial_z T < g/c_{\text{p}} \tag{30.46}$$

$$\text{gravitationally neutral} \qquad N^2 = 0 \Longleftrightarrow -\partial_z T = g/c_{\text{p}} \tag{30.47}$$

$$\text{gravitationally unstable} \qquad N^2 < 0 \Longleftrightarrow -\partial_z T > g/c_{\text{p}}, \tag{30.48}$$

with Figure 30.5 providing an illustration for three linear profiles of the *in situ* temperature.

30.6.3 Constant buoyancy frequency in idealized studies

In many idealized studies, pressure effects are ignored in the density, so that the squared buoyancy frequency is computed as the vertical derivative

$$N^2 = -\frac{g}{\rho}\frac{\partial \rho}{\partial z} \tag{30.49}$$

We thus see that if the density has the exponential structure

$$\rho(z) = \rho_{\text{o}}\, \text{e}^{-z/H}, \tag{30.50}$$

[13] A moist atmosphere has a lapse rate that has a smaller magnitude.

then the squared buoyancy frequency is

$$N^2 = g/H. \tag{30.51}$$

For a Boussinesq ocean (Chapter 29), one typically computes the squared buoyancy frequency as

$$N^2_{\text{Bous}} = -\frac{g}{\rho_o}\frac{\partial \rho}{\partial z} \tag{30.52}$$

so that the constant buoyancy frequency (30.51) arises from the linear density profile

$$\rho = \rho_o\,(1 - z/H). \tag{30.53}$$

Evidently, the Boussinesq density profile (30.53) is an approximation to the non-Boussinesq profile (30.50) in the case of very large H. When studying thermodynamics we derived the atmospheric scale height in equation (23.85), in which $H \approx 10$ km, which is within the troposphere. In contrast, the ocean scale depth is about an order of magnitude larger given the nearly incompressible nature of the ocean fluid, so that the scale depth for the ocean is well beneath the ocean bottom. This is yet another reason that the Boussinesq ocean is a useful approximation for many purposes of ocean mechanics.

30.7 Neutral helicity[14]

In our study of neutral directions in Section 30.5 we introduced the notion of a neutral displacement. We here consider a remarkable property of neutral displacements and the dianeutral direction, with this property first identified by *McDougall and Jackett* (1988).

30.7.1 Mathematical preliminaries

Consider a continuous and nonzero vector field, $\boldsymbol{N}(\boldsymbol{x})$, and write its normalized version as

$$\hat{\boldsymbol{n}} = \boldsymbol{N}/|\boldsymbol{N}|. \tag{30.54}$$

Let this vector field define a smooth two-dimensional surface, $\mathcal{S}$, so that wherever $\boldsymbol{N}$ is evaluated on $\mathcal{S}$ then it is perpendicular to $\mathcal{S}$ (see Figure 30.6 for an example). In general there is a continuum of such surfaces, yet we are here only interested in one of them. To be specific, assuming $\hat{\boldsymbol{n}} \cdot \hat{\boldsymbol{z}}$ is single-signed, let $\mathcal{S}$ be defined by the accumulation of points $\boldsymbol{x}_{\mathcal{S}} = x\,\hat{\boldsymbol{x}} + y\,\hat{\boldsymbol{y}} + \psi(x,y)\,\hat{\boldsymbol{z}}$, where $\psi(x,y)$ provides the vertical position of the surface as a continuous function of horizontal position.[15] In this case, $\boldsymbol{N} = \hat{\boldsymbol{z}} - \hat{\boldsymbol{x}}\,\partial_x\psi - \hat{\boldsymbol{y}}\,\partial_y\psi$ when evaluated on $\mathcal{S}$, so that $\boldsymbol{N} = \hat{\boldsymbol{x}}$ when the surface is flat. In the following, we say that these sorts of surfaces are *well-defined* since they are both smooth and everywhere have an outward normal vector.

Consider an arbitrary closed region, Ω, that lives on the surface, $\Omega \in \mathcal{S}$. Let $\hat{\boldsymbol{t}}$ be a unit tangent vector to the boundary of Ω and that is oriented counterclockwise around the boundary, $\partial\Omega$, as defined relative to $\boldsymbol{N}$ (see Figure 30.6). Since $\boldsymbol{N} \cdot \hat{\boldsymbol{t}} = 0$ by construction, we can integrate this identity around $\partial\Omega$ to have

$$\oint_{\partial\Omega} \boldsymbol{N} \cdot \hat{\boldsymbol{t}}\,\mathrm{d}s = 0 \Longrightarrow \int_{\Omega} (\nabla \times \boldsymbol{N}) \cdot \hat{\boldsymbol{n}}\,\mathrm{d}\mathcal{S} = 0, \tag{30.55}$$

where Stokes' theorem renders the second identity. Since the region, Ω, is arbitrary, the area

[14] This section greatly benefited from input by Geoffrey Stanley.

[15] We considered such surfaces in Section 19.6.2 when studying kinematic boundary conditions for flow encountering a material surface.

integral in equation (30.55) vanishes only if the integrand is identically zero for each point on $\mathcal{S}$. We thus conclude:

$$\text{well-defined surface } \mathcal{S} \implies \mathscr{H} \equiv \boldsymbol{N} \cdot (\nabla \times \boldsymbol{N}) = 0. \tag{30.56}$$

The contrapositive also holds so that[16]

$$\mathscr{H} \neq 0 \implies \text{ill-defined surface } \mathcal{S}. \tag{30.57}$$

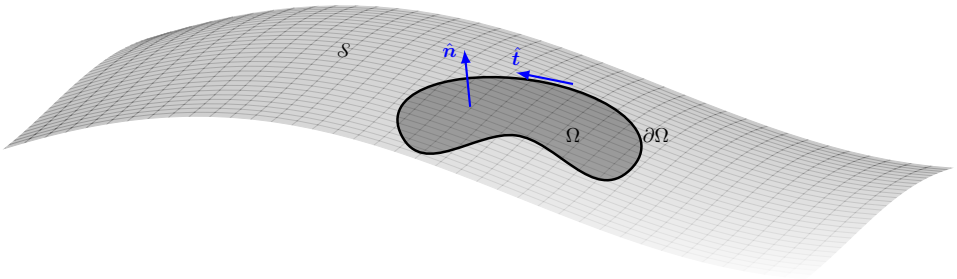

FIGURE 30.6: A smooth and orientable two-dimensional surface, $\mathcal{S}$, which we refer to as a "well-defined surface". At each point on $\mathcal{S}$ we can unambiguously define an outward normal, $+\hat{\boldsymbol{n}}$, and an inward normal, $-\hat{\boldsymbol{n}}$. Furthermore, we can consider an arbitrary simply connected closed region, Ω, with boundary $\partial\Omega$. The boundary is oriented by a unit tangent vector, $\hat{\boldsymbol{t}}$, that is perpendicular to the unit normal, $\hat{\boldsymbol{n}} \cdot \hat{\boldsymbol{t}} = 0$, and is oriented counterclockwise around $\partial\Omega$ according to $\hat{\boldsymbol{n}}$.

30.7.2 Neutral helicity is the reason neutral surfaces are ill-defined

Now apply the above general results to the question of whether we can define a surface with its outward normal parallel to the dianeutral direction, $\hat{\boldsymbol{\gamma}}$,

$$\boldsymbol{N} = -\alpha\,\nabla\Theta + \beta\,\nabla S = \hat{\boldsymbol{\gamma}}|\,-\alpha\,\nabla\Theta + \beta\,\nabla S|. \tag{30.58}$$

If such a surface exists, we refer to it as a surface *neutral surface*, since at each point on the surface its local normal direction is $\hat{\boldsymbol{\gamma}}$. From the discussion in Section 30.7.1 we know that neutral surfaces are well defined only if the *neutral helicity* vanishes, where the neutral helicity is

$$\mathscr{H}^{\gamma} = \boldsymbol{N} \cdot (\nabla \times \boldsymbol{N}) = (-\alpha\,\nabla\Theta + \beta\,\nabla S) \cdot [\nabla \times (-\alpha\,\nabla\Theta + \beta\,\nabla S)], \tag{30.59}$$

which can be written

$$\begin{aligned}
\mathscr{H}^{\gamma} &= (-\alpha\,\nabla\Theta + \beta\,\nabla S) \cdot [\nabla \times (-\alpha\,\nabla\Theta + \beta\,\nabla S)] && \text{(30.60a)}\\
&= -\alpha\,\nabla\Theta \cdot (\nabla \times \beta\,\nabla S) - \beta\,\nabla S \cdot (\nabla \times \alpha\,\nabla\Theta) && \text{(30.60b)}\\
&= -\alpha\,\nabla\Theta \cdot (\nabla\beta \times \nabla S) - \beta\,\nabla S \cdot (\nabla\alpha \times \nabla\Theta). && \text{(30.60c)}
\end{aligned}$$

[16] A contrapositive is a proposition or theorem formed by contradicting both the subject and predicate or both the hypothesis and conclusion of a given proposition or theorem. More succintly, the proposition "if A then B" has the contrapositive "if not-B then not-A". Likewise, the proposition has the converse "if B then A", and it has the inverse "if not-A then not-B".

Further expanding the spatial gradients of α and β

$$\nabla\alpha = (\partial\alpha/\partial\Theta)\,\nabla\Theta + (\partial\alpha/\partial S)\,\nabla S + (\partial\alpha/\partial p)\,\nabla p \tag{30.61a}$$
$$\nabla\beta = (\partial\beta/\partial\Theta)\,\nabla\Theta + (\partial\beta/\partial S)\,\nabla S + (\partial\beta/\partial p)\,\nabla p, \tag{30.61b}$$

then leads to

$$-\alpha\,\nabla\Theta\cdot(\nabla\beta\times\nabla S) = -\alpha\,\nabla\Theta\cdot(\partial_p\beta\,\nabla p\times\nabla S) = -\alpha\,\partial_p\beta\,\nabla p\cdot(\nabla S\times\nabla\Theta) \tag{30.62a}$$
$$-\beta\,\nabla S\cdot(\nabla\alpha\times\nabla\Theta) = -\beta\,\nabla S\cdot(\partial_p\alpha\,\nabla p\times\nabla\Theta) = \beta\,\partial_p\alpha\,\nabla p\cdot(\nabla S\times\nabla\Theta) \tag{30.62b}$$

which brings neutral helicity to the form

$$\mathscr{H}^\gamma = \nabla p\cdot(\nabla S\times\nabla\Theta)\,(\beta\,\partial_p\alpha - \alpha\,\partial_p\beta). \tag{30.63}$$

Introducing the thermobaricity parameter[17]

$$\mathscr{T} = \beta\,\partial_p(\alpha/\beta) = \beta^{-1}\,(\beta\,\partial_p\alpha - \alpha\,\partial_p\beta) \tag{30.64}$$

renders the tidy result

$$\mathscr{H}^\gamma = \beta\,\mathscr{T}\,\nabla p\cdot(\nabla S\times\nabla\Theta). \tag{30.65}$$

A nonzero neutral helicity (30.65) is fundamentally related to a nonzero thermobaricity parameter $\mathscr{T}$. It is also associated with the non-zero volume for a parallelopiped in (Θ, S, p) space[18]

$$\nabla p\cdot(\nabla S\times\nabla\Theta) = \nabla\Theta\cdot(\nabla p\times\nabla S) = \nabla S\cdot(\nabla\Theta\times\nabla p), \tag{30.66}$$

with this volume a function of the (S, Θ, p) arrangement.

Returning to the question of whether a neutral surface is well-defined, we see that with $\mathscr{H}^\gamma \neq 0$ then neutral surfaces are ill-defined. What does this result mean in practice? Consider a stably stratified ocean where $\hat{\boldsymbol{\gamma}}\cdot\hat{\boldsymbol{z}} \neq 0$ everywhere. Even for this ocean we are unable to find any finite smooth surface, $\mathcal{S}^\gamma$, whose outward normal equals to $\hat{\boldsymbol{\gamma}}$ everywhere on that surface. That is, we cannot find a single function, $\psi(x, y)$, where $\boldsymbol{N} = \hat{\boldsymbol{z}} - \hat{\boldsymbol{x}}\,\partial_x\psi - \hat{\boldsymbol{y}}\,\partial_y\psi$ everywhere on $\mathcal{S}^\gamma$.

30.7.3 Comments and further study

Figure 30.6 provides an example smooth surface; i.e., a canonical well-defined surface. What does an ill-defined surface look like? *McDougall and Jackett* (1988) answered by noting that neutral paths possess a helical structure, with each closed loop in (S, Θ) space displaced vertically in pressure. Besides being rather novel mathematically, this helical structure provides a source for irreversible (dianeutral) transformation of seawater. *Klocker and McDougall* (2010a,b) estimated the effects of this transformation on large-scale ocean overturning circulation. They found the effects from neutral helicity to be comparable to those from mixing, especially in the Southern Ocean.

Bennett (2019) discussed the geometry of neutral paths and made a connection to a theorem of Carathéodory developed in the context of thermodynamics. Additionally, *Stanley* (2019) showed that S and Θ (or ρ and p) on a neutral surface are functionally related but in a way that varies geographically. Stanley's topological analysis determined how different single-valued S-Θ relations in different geographic regions mesh together to form a globally continuous S-Θ relation. *Stanley et al.* (2021) then provided a corresponding method for determining approximate neutral surfaces. Such approximate neutral surfaces are globally well-defined, and with a local normal direction that is closely aligned with the dianeutral direction, $\hat{\boldsymbol{\gamma}}$.

[17] We further discuss the thermobaricity parameter in Section 72.3.

[18] See Section 1.8 for how three vectors define a volume in the space of the vectors.

30.8 Neutral trajectories

We here extend the notion of neutral directions and neutral displacements considered in Section 30.5 to here allow for time dependence. We thus consider *neutral trajectories*, which are infinitesimal paths in a transient fluid where a test fluid element moves without feeling any net local buoyant force.

30.8.1 Specifying the neutral trajectory

We define a neutral trajectory according to the following algorithm, which generalizes the neutral direction algorithm from Section 30.5.3.

> Consider two equal mass test fluid elements at points, $\boldsymbol{x}$ and $\boldsymbol{x}+\delta\boldsymbol{x}$. Exchange these elements over a time increment, δt, without mixing (i.e., adiabatic and isohaline). If the exchange leaves the local *in situ* density and pressure unchanged at the two points, then the exchange occurs along a *neutral trajectory*. The resulting infinitesimal displacement, $\delta\boldsymbol{x}^\gamma$, defines the neutral trajectory.[19] The rate of change along the neutral trajectory, $\boldsymbol{v}^\gamma = \delta\boldsymbol{x}^\gamma/\delta t$, defines the *neutral velocity*, $\boldsymbol{v}^\gamma$. As defined, neutral trajectories only have infinitesimal extents.

Stated differently, we examine infinitesimal displacements of a test fluid element, $\delta\boldsymbol{x}$, that occur without any mixing of S or Θ, and with the displacement realized over an infinitesimal time increment, $\delta t > 0$. If the displacement occurs along a neutral trajectory, written as $\delta\boldsymbol{x}^\gamma$, then at the new position the *in situ* density of the environment, $\rho(\boldsymbol{x}+\delta\boldsymbol{x}^\gamma, t+\mathrm{d}t)$, is equal to that of the element, $\rho[S(\boldsymbol{x},t), \Theta(\boldsymbol{x},t), p(\boldsymbol{x}+\mathrm{d}\boldsymbol{x}^\gamma, t+\delta t)]$. We are thus led to the following condition that serves to implicitly define a neutral displacement

$$\underbrace{\rho[S(\boldsymbol{x},t), \Theta(\boldsymbol{x},t), p(\boldsymbol{x}+\delta\boldsymbol{x}^\gamma, t+\delta t)]}_{\textit{in situ}\text{ density of displaced element at incremented time}} = \underbrace{\rho[S(\boldsymbol{x}+\delta\boldsymbol{x}^\gamma, t+\delta t), \Theta(\boldsymbol{x}+\delta\boldsymbol{x}^\gamma, t+\delta t), p(\boldsymbol{x}+\delta\boldsymbol{x}^\gamma, t+\delta t)]}_{\textit{in situ}\text{ density of environmental at displaced location and incremented time}}. \tag{30.67}$$

This condition for a neutral displacement says that the *in situ* density of the environment at $(\boldsymbol{x}+\delta\boldsymbol{x}^\gamma, t+\delta t)$ (right hand side) equals to the *in situ* density of a test fluid element that is transported to $(\boldsymbol{x}+\delta\boldsymbol{x}^\gamma, t+\delta t)$, while holding S and Θ at the original $(\boldsymbol{x}, t)$ values (left hand side).

30.8.2 Velocity of the neutral trajectory

The neutral trajectory condition (30.67) can be expressed as a differential relation by taking a leading order Taylor expansion of its left hand side

$$\rho[S(\boldsymbol{x},t), \Theta(\boldsymbol{x},t), p(\boldsymbol{x}+\delta\boldsymbol{x}^\gamma, t+\delta t)] = \rho(\boldsymbol{x},t) + \frac{\partial\rho}{\partial p}\left[\delta\boldsymbol{x}^\gamma\cdot\nabla p + \frac{\partial p}{\partial t}\,\delta t\right], \tag{30.68}$$

as well as its right hand side

$$\begin{aligned}\rho[S(\boldsymbol{x}+\delta\boldsymbol{x}^\gamma, t+\delta t), \Theta(\boldsymbol{x}+\delta\boldsymbol{x}^\gamma, t+\delta t), p(\boldsymbol{x}+\delta\boldsymbol{x}^\gamma, t+\delta t)] &= \rho(\boldsymbol{x},t) \\ &+ \frac{\partial\rho}{\partial p}\left[\delta\boldsymbol{x}^\gamma\cdot\nabla p + \frac{\partial p}{\partial t}\,\delta t\right] + \frac{\partial\rho}{\partial S}\left[\delta\boldsymbol{x}^\gamma\cdot\nabla S + \frac{\partial S}{\partial t}\,\delta t\right] + \frac{\partial\rho}{\partial\Theta}\left[\delta\boldsymbol{x}^\gamma\cdot\nabla\Theta + \frac{\partial\Theta}{\partial t}\,\delta t\right],\end{aligned} \tag{30.69}$$

[19] We use the same notation, $\delta\boldsymbol{x}^\gamma$, as used for neutral displacements in Section 30.5. The two displacements are equal when ignoring time dependence.

and then inserting into the density condition (30.67) to render

$$\delta \boldsymbol{x}^\gamma \cdot (-\alpha \, \nabla \Theta + \beta \, \nabla S) + (-\alpha \, \partial_t \Theta + \beta \, \partial_t S) \, \delta t = 0. \tag{30.70}$$

Dividing by the time increment leads to the equivalent condition

$$\boldsymbol{v}^\gamma \cdot (-\alpha \, \nabla \Theta + \beta \, \nabla S) + (-\alpha \, \partial_t \Theta + \beta \, \partial_t S) = -\alpha \, \frac{\mathrm{D}^\gamma \Theta}{\mathrm{D}t} + \beta \, \frac{\mathrm{D}^\gamma S}{\mathrm{D}t} = 0, \tag{30.71}$$

where

$$\boldsymbol{v}^\gamma = \frac{\delta \boldsymbol{x}^\gamma}{\delta t} \tag{30.72}$$

defines the three-dimensional velocity vector along a neutral trajectory, and we introduced the corresponding time derivative following a neutral trajectory

$$\frac{\mathrm{D}^\gamma}{\mathrm{D}t} = \frac{\partial}{\partial t} + \boldsymbol{v}^\gamma \cdot \nabla. \tag{30.73}$$

Notably, the neutral trajectory constraint (30.71) can be written as a relation between the pressure and density time derivatives along the neutral trajectory

$$\frac{\partial \rho}{\partial p} \, \frac{\mathrm{D}^\gamma p}{\mathrm{D}t} = \frac{\mathrm{D}^\gamma \rho}{\mathrm{D}t}. \tag{30.74}$$

We choose to focus on the form (30.71) in the following, since it exposes the tracesr S and Θ.

Equation (30.71) provides a time-dependent generalization of the neutrality condition (30.33) derived for a static ocean. This generalization says that for a neutral space-time trajectory, environmental changes in Θ encountered along the neutral trajectory are exactly compensated by environmental changes in S. Equation (30.71) also provides an explicit expression for the dianeutral component of the neutral velocity

$$\boldsymbol{v}^\gamma \cdot \hat{\boldsymbol{\gamma}} = \frac{\alpha \, \partial_t \Theta - \beta \, \partial_t S}{|-\alpha \, \nabla \Theta + \beta \, \nabla S|}, \tag{30.75}$$

where we introduced the dianeutral unit vector from equation (30.58)

$$\hat{\boldsymbol{\gamma}} = \frac{-\alpha \, \nabla \Theta + \beta \, \nabla S}{|-\alpha \, \nabla \Theta + \beta \, \nabla S|} = \frac{\boldsymbol{N}}{|\boldsymbol{N}|}. \tag{30.76}$$

30.8.3 Geometric expressions

Making use of the identity

$$\boldsymbol{v} \cdot \boldsymbol{N} = \boldsymbol{v} \cdot (-\alpha \, \nabla \Theta + \beta \, \nabla S), \tag{30.77}$$

along with equation (30.71) renders

$$\boldsymbol{N} \cdot (\boldsymbol{v} - \boldsymbol{v}^\gamma) = -\alpha \, \frac{\mathrm{D}\Theta}{\mathrm{D}t} + \beta \, \frac{\mathrm{D}S}{\mathrm{D}t}, \tag{30.78}$$

and further dividing by $|\boldsymbol{N}| = |-\alpha \, \nabla \Theta + \beta \, \nabla S|$ gives

$$(\boldsymbol{v} - \boldsymbol{v}^\gamma) \cdot \hat{\boldsymbol{\gamma}} = \frac{-\alpha \, \dot{\Theta} + \beta \, \dot{S}}{|-\alpha \, \nabla \Theta + \beta \, \nabla S|}, \tag{30.79}$$

which compares to equation (30.75) for $\boldsymbol{v}^\gamma \cdot \hat{\boldsymbol{\gamma}}$. The left hand side of equation (30.79) is familiar from our study of kinematics of surfaces in Section 19.6.2. Here, we do not have a globally

defined surface (due to helicity from Section 30.7). Yet we can consider an infinitesimal area element, $\delta\mathcal{S}$, that is oriented perpendicular to the dianeutral unit vector, $\hat{\boldsymbol{\gamma}}\,\delta\mathcal{S}$. The volume per time of fluid crossing that tiny area element is given by

$$\text{volume per time of fluid crossing } \delta\mathcal{S} = (\boldsymbol{v} - \boldsymbol{v}^\gamma) \cdot \hat{\boldsymbol{\gamma}}\,\delta\mathcal{S} = \frac{(-\alpha\,\dot{\Theta} + \beta\,\dot{S})\,\delta\mathcal{S}}{|-\alpha\,\nabla\Theta + \beta\,\nabla S|}. \tag{30.80}$$

The right hand side is nonzero for cases where S and Θ experience material changes, and when those material changes are not compensated so that $\alpha\,\dot{\Theta} \neq \beta\,\dot{S}$. In such cases, equation (30.80) says that a fluid particle velocity, $\boldsymbol{v}$, and a neutral trajectory velocity, $\boldsymbol{v}^\gamma$, have distinct projections onto the dianeutral direction, $\hat{\boldsymbol{\gamma}}$.

As illustrated in Figure 30.7, there are two general ways for the right hand side of equation (30.80) to vanish. First, in the absence of any irreversible processes, so that $\dot{\Theta} = 0$ and $\dot{S} = 0$, then both Θ and S are materially invariant fluid properties and $\delta\mathcal{S}$ is a material area element. The second way is to have compensated irreversible processes so that $\alpha\,\dot{\Theta} = \beta\,\dot{S}$. This compensation is reminscent of the compensation in equation (30.71) that is used to define the neutral velocity, $\boldsymbol{v}^\gamma$, via the motion of Θ and S surfaces as per equation (30.75). However, the condition $\alpha\,\dot{\Theta} = \beta\,\dot{S}$ concerns the irreversible processes acting on Θ and S, whereas equation (30.71) concerns a reversible thought experiment used to define neutral trajectories.

Neutral diffusion studied in Section 71.4 is a physical process where the $\alpha\,\dot{\Theta} = \beta\,\dot{S}$ compensation occurs, so long as the fluid has a linear equation of state (i.e., thermal expansion, α, and haline contraction, β, are constants). Yet compensation is broken when neutral diffusion occurs in the presence of a realistic (nonlinear) seawater equation of state, which introduces the processes of cabbeling and thermobaricity as discussed in Section 72.3.

30.8.4 Summarizing the neutral relations

We here summarize the various relations for a neutral direction (time snapshot of the fluid) and a neutral trajectory (motion through a transient fluid) by offering the geometrical perspective depicted in Figure 30.7.

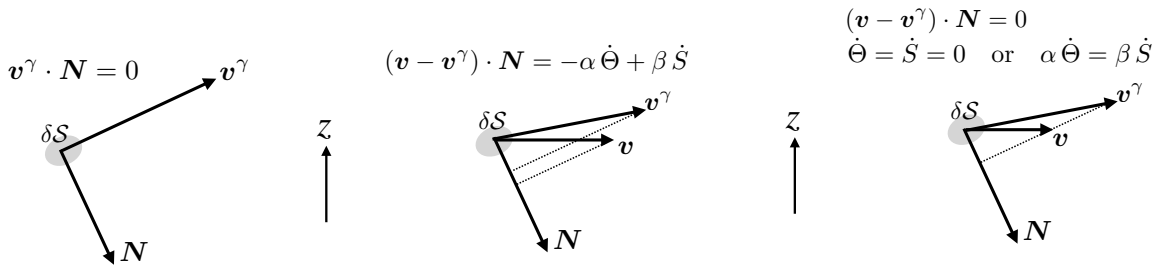

FIGURE 30.7: Depicting neutral directions and neutral trajectories. Left panel: for a time snapshot, as summarized by equation (30.81), then $\boldsymbol{v}^\gamma \cdot \hat{\boldsymbol{\gamma}} = \boldsymbol{v}^\gamma \cdot \boldsymbol{N}/|\boldsymbol{N}| = 0$, thus defining the neutral trajectory as perpendicular to the dianeutral direction, with $\boldsymbol{N} = -\alpha\,\dot{\Theta} + \beta\,\dot{S}$. Middle panel: time dependent fluid with $(\boldsymbol{v} - \boldsymbol{v}^\gamma) \cdot \boldsymbol{N} = -\alpha\,\dot{\Theta} + \beta\,\dot{S}$ as per equation (30.82d). Right panel: time dependent fluid yet with either $\dot{\Theta} = \dot{S} = 0$, as when there are no irreversible mixing processes, or if those processes are compensated so that $\alpha\,\dot{\Theta} = \beta\,\dot{S} = 0$, both of which render $(\boldsymbol{v}^\gamma - \boldsymbol{v}) \cdot \boldsymbol{N} = 0$.

Neutral direction

A neutral direction equals to a neutral trajectory in the special case of a static fluid, in which case Eulerian time derivatives vanish. In this case the constraint (30.70) reduces to the orthogonality condition

$$\delta\boldsymbol{x}^\gamma \cdot \hat{\boldsymbol{\gamma}} = \delta t\, \boldsymbol{v}^\gamma \cdot \hat{\boldsymbol{\gamma}} = 0. \tag{30.81}$$

Hence, for a static fluid, the neutral displacement, $\delta \boldsymbol{x}^\gamma = \delta t \, \boldsymbol{v}^\gamma$, and the corresponding neutral velocity, $\boldsymbol{v}^\gamma$, are everywhere orthogonal to the dianeutral vector, $\hat{\boldsymbol{\gamma}}$. This condition is illustrated in the left panel of Figure 30.7.

Neutral trajectory

The conditions given in Sections 30.8.2 and 30.8.3 can be written in the following equivalent manners

$$\frac{\mathrm{D}^\gamma \rho}{\mathrm{D}t} - \frac{\partial \rho}{\partial p} \frac{\mathrm{D}^\gamma p}{\mathrm{D}t} = 0 \tag{30.82a}$$

$$-\alpha \, \frac{\mathrm{D}^\gamma \Theta}{\mathrm{D}t} + \beta \, \frac{\mathrm{D}^\gamma S}{\mathrm{D}t} = 0 \tag{30.82b}$$

$$-\alpha \, \partial_t \Theta + \beta \, \partial_t S + \boldsymbol{v}^\gamma \cdot (-\alpha \, \nabla \Theta + \beta \, \nabla S) = 0 \tag{30.82c}$$

$$(\boldsymbol{v} - \boldsymbol{v}^\gamma) \cdot \boldsymbol{N} = -\alpha \, \dot{\Theta} + \beta \, \dot{S}, \tag{30.82d}$$

with equation (30.82d) depicted by the right two panels of Figure 30.7. These equations reflect the need for a neutral trajectory, whose velocity is $\boldsymbol{v}^\gamma$, to weave its path within the time dependent fluid environment. The special case with either $\dot{\Theta} = \dot{S} = 0$ (no irreversible processes) or $\alpha \, \dot{\Theta} = \beta \, \dot{S}$ (compensated irreversible processes) means that the neutral trajectory satisfies $(\boldsymbol{v} - \boldsymbol{v}^\gamma) \cdot \boldsymbol{N} = 0$, as depicted in the right panel of Figure 30.7.

30.8.5 Comments

By introducing time dependence we have enabled a step towards understanding how buoyancy works within an evolving fluid, thus moving beyond the time snapshot built into the neutral direction from Sections 30.5 and 30.7. Even so, the presentation in this section is limited in that it only considers infinitesimal excursions along a neutral trajectory. Indeed, this limitation is fundamental to the methods of neutral directions and neutral trajectories since they are designed to probe local buoyant forces; that is, the buoyancy of a test fluid element relative to its local environment. Moving beyond the infinitesimal trajectory leads to the concept of a test fluid element that remains coherent over a finite path while maintaining local mechanical equilibrium (i.e., pressure is equilibrated with the environment) and yet with fixed Θ and S. The finite trajectories for such fluid elements start along a neutral trajectory, but deviate upon moving further. *McDougall* (1987c) developed the mechanics of such fluid elements, with his study motivated by ocean coherent vortex structures such as reviewed by *McWilliams* (1985).

30.9 Pressure forces and vertical motion

As introduced in Section 27.2 and further detailed in Section 29.2, an approximate hydrostatic fluid is one in which the vertical pressure gradient locally balances the gravitational acceleration, with the horizontal gradient of hydrostatic pressure contributing to horizontal accelerations. Although vertical motion can occur in the approximately hydrostatic fluid, that motion is diagnosed rather than prognosed since the vertical momentum equation is reduced to local hydrostatic balance. For example, a diagnostic evaluation of the vertical velocity in a Boussinesq ocean is performed through vertically integrating the continuity equation, $\partial_z w = -\nabla_{\mathrm{h}} \cdot \boldsymbol{u}$, along with the specification of w at one point within the vertical column.

As we see in equation (30.92c) derived below, the vertical derivative of the non-hydrostatic pressure is the only inviscid force contributing to a vertical acceleration. So even if the fluid satisfies the assumptions of approximate hydrostatic balance, it is the non-hydrostatic pressure force that enables vertical accelerations. That is, for the approximately hydrostatic fluid, the

local hydrostatic balance holds, $\partial p/\partial z = -\rho\, g$, and yet there can still be a nonzero vertical acceleration, $\mathrm{D}w/\mathrm{D}t \neq 0$. This situation is directly analogous to the Boussinesq ocean as derived in Section 29.1. For the Boussinesq ocean, we have a non-divergent flow field, $\nabla \cdot \boldsymbol{v} = 0$, and yet the fluid itself is compressible so that density has space and time variations, $\mathrm{D}\rho/\mathrm{D}t \neq 0$.

We are concerned in this section with how pressure and gravity contribute to motion, and offer two methods to organize their accelerations starting from the momentum equation with the geopotential, $\Phi = g\, z$,

$$\rho\, \mathrm{D}\boldsymbol{v}/\mathrm{D}t + 2\, \boldsymbol{\Omega} \times \rho\, \boldsymbol{v} = -\nabla p - g\, \rho\, \hat{\boldsymbol{z}} + \rho\, \boldsymbol{F}. \tag{30.83}$$

Analysis involving both methods serve complementary roles in understanding the nature of vertical accelerations.

30.9.1 Dynamically active and dynamically inactive pressures

We here follow the formulation of the Boussinesq ocean equations from Section 29.1.1 to organize the pressure and gravity accelerations. For that purpose, introduce a constant reference density, $\rho_\circ$, along with a corresponding hydrostatically balanced reference pressure

$$p(\boldsymbol{x}, t) = p'(\boldsymbol{x}, t) + p_0(z) \quad \text{with} \quad \mathrm{d}p_0/\mathrm{d}z = -\rho_\circ\, g. \tag{30.84}$$

By decomposing pressure as $p = p_0 + p'$, we expose the dynamically active portion of the pressure field, p', by removing the dynamically inactive pressure, p_0, from the momentum equation. Note that the dynamical pressure, p', generally has both hydrostatic and non-hydrostatic contributions.

The decomposition (30.84) brings the pressure and gravity contributions on the right hand side of equation (30.83) into the form

$$\nabla p + \rho\, g\, \hat{\boldsymbol{z}} = \nabla p' - \rho_\circ\, b\, \hat{\boldsymbol{z}}. \tag{30.85}$$

In this equation we introduced the globally referenced Archimedean buoyancy computed relative to the globally constant reference density, $\rho_\circ$,

$$b = -g\, (\rho - \rho_\circ)/\rho_\circ = -g\, \rho'/\rho_\circ, \tag{30.86}$$

where

$$\rho' = \rho - \rho_\circ \tag{30.87}$$

is the density deviation relative to the reference density.

30.9.2 Hydrostatic and non-hydrostatic pressures

The second decomposition of the pressure and gravity forces in equation (30.83) is based on splitting into a local hydrostatic pressure, p_{h}, and a non-hydrostatic pressure, p_{nh},

$$p = p_{\mathsf{h}} + p_{\mathsf{nh}} \quad \text{with} \quad \partial p_{\mathsf{h}}/\partial z = -\rho\, g. \tag{30.88}$$

This decomposition is particularly useful when concerned with deviations from a local hydrostatic balance, which is central to the current analysis. However, it does not remove the global hydrostatic background pressure (i.e., the dynamically inactive pressure, $p_0(z)$), which can be seen by the identity

$$\partial p_{\mathsf{h}}/\partial z = \mathrm{d}p_0(z)/\mathrm{d}z - \rho'\, g = \mathrm{d}p_0(z)/\mathrm{d}z + \rho_\circ\, b. \tag{30.89}$$

With the pressure decomposition (30.88), the pressure and gravity contributions to the equation of motion take on the form

$$\nabla p + \rho\, g\, \hat{\boldsymbol{z}} = \nabla(p_{\text{h}} + p_{\text{nh}}) + \rho\, g\, \hat{\boldsymbol{z}} \tag{30.90a}$$
$$= \nabla_{\text{h}}(p_{\text{h}} + p_{\text{nh}}) + (\partial_z p_{\text{nh}} + \partial_z p_{\text{h}} + \rho\, g)\, \hat{\boldsymbol{z}} \tag{30.90b}$$
$$= \nabla_{\text{h}} p + \hat{\boldsymbol{z}}\, \partial_z p_{\text{nh}} \tag{30.90c}$$
$$= \nabla p_{\text{nh}} + \nabla_{\text{h}} p_{\text{h}}. \tag{30.90d}$$

Be mindful that the non-hydrostatic pressure is operated on by the full gradient operator, ∇, whereas the hydrostatic pressure has just the horizontal gradient, ∇_{h}.

30.9.3 Momentum equation for the Boussinesq ocean

To further study how pressure and gravity lead to vertical motion, we find it convenient to assume a Boussinesq ocean so that the momentum equation (30.83) takes the form of equation (29.65)

$$\rho_{\circ}\, \mathrm{D}\boldsymbol{v}/\mathrm{D}t + 2\, \boldsymbol{\Omega} \times \rho_{\circ}\, \boldsymbol{v} = -\nabla p - \rho\, g\, \hat{\boldsymbol{z}} + \rho_{\circ}\, \boldsymbol{F} \tag{30.91a}$$
$$= -\nabla p' + \rho_{\circ}\, b\, \hat{\boldsymbol{z}} + \rho_{\circ}\, \boldsymbol{F} \tag{30.91b}$$
$$= -\nabla p_{\text{nh}} - \nabla_{\text{h}} p_{\text{h}} + \rho_{\circ}\, \boldsymbol{F}. \tag{30.91c}$$

Focusing on the vertical velocity equation exposes processes leading to vertical accelerations of a fluid element (i.e., the vertical Lagrangian acceleration, $\mathrm{D}w/\mathrm{D}t$)

$$\rho_{\circ}\, \mathrm{D}w/\mathrm{D}t + \hat{\boldsymbol{z}} \cdot (2\, \boldsymbol{\Omega} \times \rho_{\circ}\, \boldsymbol{v}) = -\partial_z p - \rho\, g + \rho_{\circ}\, \boldsymbol{F} \cdot \hat{\boldsymbol{z}} \tag{30.92a}$$
$$= -\partial_z p' + \rho_{\circ}\, b + \rho_{\circ}\, \boldsymbol{F} \cdot \hat{\boldsymbol{z}} \tag{30.92b}$$
$$= -\partial_z p_{\text{nh}} + \rho_{\circ}\, \boldsymbol{F} \cdot \hat{\boldsymbol{z}}, \tag{30.92c}$$

In addition to the Coriolis acceleration on the left hand side, equation (30.92b) reveals that the vertical Lagrangian acceleration has contributions from the globally referenced Archimedean buoyancy, b, along with vertical gradients in the dynamical pressure, p'. From equation (30.92c) we see that the vertical Lagrangian acceleration has an inviscid contribution that arises solely from vertical derivatives in the non-hydrostatic pressure, p_{nh}. Note that when making either the tangent plane approximation (Section 24.5) or the Traditional approximation (Section 27.1.3), the Coriolis acceleration is absent from the vertical momentum equation since the rotating reference frame has an angular velocity oriented according to the local vertical, $\boldsymbol{\Omega} = \Omega\, \hat{\boldsymbol{z}}$.

30.10 Test fluid elements in a homogeneous fluid

In this section we study the motion of a test fluid elements with nonzero Archimedean buoyancy and in the absence of mixing.[20] We assume a tangent plane so that the Coriolis acceleration does not appear in the vertical momentum equation. Also, to avoid questions about local versus global buoyancy, and the associated questions about neutral directions, we assume the fluid environment has a constant and uniform density, ρ. A net buoyant force acts on the test fluid element arise if the fluid element has a density distinct from the environmental density.

In pursuing this analysis it is important to appreciate the nature of the corresponding thought experiments. Namely, we place a test fluid element somewhere in a prescribed fluid environment and examine how the environment forces affect its motion. Importantly, we assume the environment is unaffected by the test fluid element, so that the contact forces remain fixed

[20] As noted in Section 17.2.4, in the absence of mixing, a fluid element is the same as a fluid parcel.

and prescribed. That is, the pressure and frictional forces are unaffected by the test fluid element. This assumption is mechanically inconsistent since all fluid regions, no matter how small, affect the surroundings. Even so, results from the analysis are borne out for situations where we can safely ignore the environmental perturbations of real fluid elements. The analysis offers a useful warm-up to the study of effective buoyancy in Section 30.11.

30.10.1 Equations of motion

The equation of motion for a fluid element is given by

$$\rho \, \mathrm{D}\boldsymbol{v}/\mathrm{D}t + 2\,\Omega\,\hat{\boldsymbol{z}} \times \rho\,\boldsymbol{v} = -\nabla p - g\,\rho\,\hat{\boldsymbol{z}} + \rho\,\boldsymbol{F}, \tag{30.93}$$

whereas the equation of motion for a test fluid element is

$$\rho^{\text{tfe}}\,\dot{\boldsymbol{v}}^{\text{tfe}} + 2\,\Omega\,\hat{\boldsymbol{z}} \times \rho^{\text{tfe}}\,\boldsymbol{v}^{\text{tfe}} = -\nabla p - g\,\rho^{\text{tfe}}\,\hat{\boldsymbol{z}} + \rho^{\text{tfe}}\,\boldsymbol{F}, \tag{30.94}$$

where ρ^{tfe} is the density of the test fluid element, $\boldsymbol{v}^{\text{tfe}}$ is its velocity, and $\dot{\boldsymbol{v}}^{\text{tfe}}$ is its acceleration.[21] As per our assumption stated earlier, both the pressure gradient and friction vector are the same for the fluid element and the test fluid element.

30.10.2 Exact hydrostatic environment

Consider a test fluid element in a fluid that is in exact hydrostatic equilibrium, so that there is no fluid motion. The test fluid element can only move vertically, with the vertical component of equation (30.94) yielding

$$\rho^{\text{tfe}}\,\dot{w}^{\text{tfe}} = -\mathrm{d}p/\mathrm{d}z - g\,\rho^{\text{tfe}}. \tag{30.95}$$

The assumed exact hydrostatic background pressure gradient satisfies $\mathrm{d}p/\mathrm{d}z = -\rho\,g$, so that the test fluid element accelerates vertically according to

$$\rho^{\text{tfe}}\,\dot{w}^{\text{tfe}} = b\,\rho, \tag{30.96}$$

where we introduced the Archimedean buoyancy for the test fluid element, computed relative to the environmental fluid,

$$b = -g\,(\rho^{\text{tfe}} - \rho)/\rho. \tag{30.97}$$

Evidently, the test fluid element accelerates upward if it is lighter than the environment ($b > 0$), downward if heavier ($b < 0$), and remains stationary if neutrally buoyant ($b = 0$). This result accords with the study of Archimedean buoyancy from Section 30.2.

30.10.3 An accelerating yet non-rotating environment

In Section 11.3 we studied particle mechanics as viewed from an accelerated reference frame that is not rotating, such as for motion viewed in an accelerating train moving along a straight track. Here we place a tank of fluid (e.g., a tank of water) on a train car that experiences acceleration, $\boldsymbol{A}^{\text{tank}}$, such as depicted in Figure 30.8. Following equation (11.48), the equation of motion for the fluid in the tank is

$$\rho \, \mathrm{D}\boldsymbol{v}/\mathrm{D}t = -\nabla p - \rho\,(g\,\hat{\boldsymbol{z}} + \boldsymbol{A}^{\text{tank}}) + \rho\,\boldsymbol{F}. \tag{30.98}$$

We refer to $-\boldsymbol{A}^{\text{tank}}$ as the *non-inertial acceleration* that arises from the tank acceleration, and with $-\rho\,\boldsymbol{A}^{\text{tank}}$ the *non-inertial force* per volume acting on the fluid.[22] As a result of the

[21] We write the acceleration as $\dot{\boldsymbol{v}}^{\text{tfe}}$ rather than $\mathrm{D}\boldsymbol{v}^{\text{tfe}}/\mathrm{D}t$ since we are concerned with the motion of just a single test fluid element rather than a field of fluid elements.

[22] The minus sign accords with being pushed backward into a seat when a vehicle accelerates forward.

non-inertial force, fluid piles up on the back side of the tank and is depleted from the front.

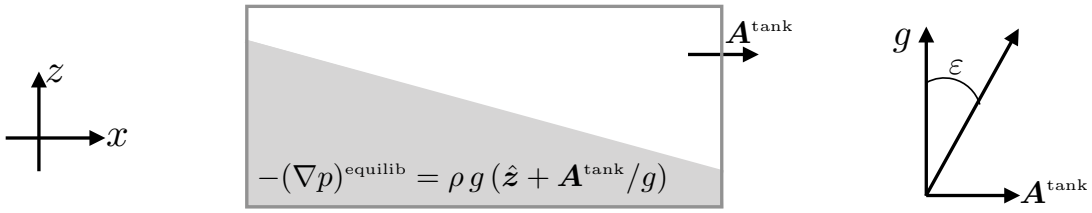

FIGURE 30.8: Left panel: A tank of homogeneous water on a train accelerating along a horizontal straight track, thus resulting in a pile up of the water at the back of the tank and depletion in the front. The water reaches a static equilibrium ($\boldsymbol{v} = 0$) when the pressure gradient acceleration balances both the gravitational acceleration and the train acceleration, $-(\nabla p)^{\rm equilib} = \rho\, g\, (\hat{\boldsymbol{z}} + \boldsymbol{A}^{\rm tank}/g)$. Right panel: Vector diagram for a positively buoyant test fluid element, with contributions from vertical buoyant acceleration and horizontal pressure gradient acceleration. The net acceleration on the test element acts at an angle to the vertical that is determined by the gravitational and train acceleration, making a slope, $\tan\varepsilon = |\boldsymbol{A}^{\rm tank}|/g$, with the vertical. Notably, the positively buoyant test fluid element is accelerated vertically upward and horizontally in the *same* direction as the train's acceleration, whereas a negatively buoyant test fluid element is accelerated vertically downward and horizontally in the *opposite* direction as the acceleration. This thought experiment is readily verified by a helium balloon tied to the floor of an accelerating car, or a pendulum tied to the ceiling of the car.

The difference in fluid depth within the tank leads to a horizontal pressure gradient, with higher pressure at the back of the tank and lower in the front. There is no fluid motion (relative to the tank) if there is a balance between the horizontal pressure gradient and the tank acceleration, as well as a balance between the vertical pressure gradient and gravity,

$$-(\nabla p)^{\rm equilib} = \rho\, g\, (\hat{\boldsymbol{z}} + \boldsymbol{A}^{\rm tank}/g). \tag{30.99}$$

We can consider this result as exact hydrostatic balance but with a modified gravitational acceleration.[23]

Motion of the test fluid element satisfies the equation

$$\rho^{\rm tfe}\, \dot{\boldsymbol{v}}^{\rm tfe} = -\nabla p - \rho^{\rm tfe}\, (g\, \hat{\boldsymbol{z}} + \boldsymbol{A}^{\rm tank}) + \rho^{\rm tfe}\, \boldsymbol{F}. \tag{30.100}$$

Now consider the test fluid element that feels the equilibrated pressure gradient according to equation (30.99), in which case

$$\rho^{\rm tfe}\, \dot{\boldsymbol{v}}^{\rm tfe} = (\rho - \rho^{\rm tfe})\, (g\, \hat{\boldsymbol{z}} + \boldsymbol{A}^{\rm tank}) = b\, \rho\, (\hat{\boldsymbol{z}} + \boldsymbol{A}^{\rm tank}/g) = -(b/g)\, (\nabla p)^{\rm equilib}. \tag{30.101}$$

Note that there is no frictional acceleration when there is no fluid motion, thus allowing us to set $\boldsymbol{F} = 0$. Evidently, the test fluid element accelerates along a line that is perpendicular to surfaces of constant pressure, thus making an angle with the vertical given by

$$\tan\varepsilon = |\boldsymbol{A}^{\rm tank}|/g. \tag{30.102}$$

Acceleration of a positively buoyant test fluid element is sloped in the same direction as the accelerating train, with this result readily verified by attaching a helium balloon to the floor of a train or car. Acceleration of the negatively buoyant test fluid element is sloped in the opposite direction as the accelerating train. This result accords with the discussion in Section 11.3.3, in which a pendulum at rest in the accelerated train slopes opposite to the acceleration.

[23] The Principle of Equivalence from general relativity says we cannot distinguish between the acceleration of a reference frame and the acceleration from gravity. The result (30.99) supports this equivalence.

30.10.4 Rotating tank

In Section 27.5 we studied the motion of a homogeneous fluid in a rotating tank, whose equation of motion in the rotating reference frame is given by equation (27.98)

$$\rho \frac{\mathrm{D}\boldsymbol{v}}{\mathrm{D}t} + 2\,\Omega\,\hat{\boldsymbol{z}} \times \rho\,\boldsymbol{v} = -\nabla\left[p + g\,z\,\rho - \Omega^2\,\rho\,(x^2+y^2)/2\right] + \rho\,\boldsymbol{F}. \tag{30.103}$$

The analogous equation for the test fluid element, again written in the rotating reference frame, is given by

$$\rho^{\text{tfe}}\,\dot{\boldsymbol{v}}^{\text{tfe}} + 2\,\Omega\,\hat{\boldsymbol{z}} \times \rho^{\text{tfe}}\,\boldsymbol{v}^{\text{tfe}} = -\nabla\left[p + g\,z\,\rho^{\text{tfe}} - \Omega^2\,\rho^{\text{tfe}}\,(x^2+y^2)/2\right] + \rho^{\text{tfe}}\,\boldsymbol{F}, \tag{30.104}$$

where we evaluate the position, $\boldsymbol{x} = \hat{\boldsymbol{x}}\,x + \hat{\boldsymbol{y}}\,y + \hat{\boldsymbol{z}}\,z$, according to the position of the test fluid element. At mechanical equilibrium, the fluid rotates as a rigid-body ($\boldsymbol{v} = 0$) with a parabolic free surface where the free surface is higher at the outer rim of the tank and lowest at the center. Furthermore, as the motion is rigid-body, the viscous friction vanishes. We thus find that the pressure gradient in the rigid-body rotating equilibrium satisfies

$$-(\nabla p)^{\text{equilb}} = \rho\,\nabla[g\,z - \Omega^2\,(x^2+y^2)/2] = g\,\rho\,[\hat{\boldsymbol{z}} - \Omega^2\,(x\,\hat{\boldsymbol{x}} + y\,\hat{\boldsymbol{y}})/g] \equiv -\rho\,\boldsymbol{g}^{\text{rotate}}, \tag{30.105}$$

where the final equality defined the gravitational vector, $\boldsymbol{g}^{\text{rotate}}$, arising from the sum of the geopotential (central earth gravity plus planetary centrifugal) plus the centrifugal acceleration from the rotating tank. When placed in this mechanically equilibrated fluid environment, the test fluid element equation of motion (30.104) becomes

$$\rho^{\text{tfe}}\,\dot{\boldsymbol{v}}^{\text{tfe}} + 2\,\Omega\,\hat{\boldsymbol{z}} \times \rho^{\text{tfe}}\,\boldsymbol{v}^{\text{tfe}} = b\,\rho\,[\hat{\boldsymbol{z}} - \Omega^2\,(\hat{\boldsymbol{x}}\,x + \hat{\boldsymbol{y}}\,y)/g] = -(\rho - \rho^{\text{tfe}})\,\boldsymbol{g}^{\text{rotate}}. \tag{30.106}$$

Evidently, a positively buoyant test fluid element accelerates upward and toward the center of the tank. Furthermore, as it moves horizontally toward the tank center, the test fluid element picks up a Coriolis acceleration that deflects it to the right for counter-clockwise rotating tanks.

For the test fluid element, the ratio of the magnitudes of its Coriolis acceleration to the centrifugal acceleration is

$$\frac{\text{Coriolis}}{\text{centrifugal}} = \frac{2\,\rho^{\text{tfe}}}{\rho}\,\frac{g}{b}\,\frac{|\boldsymbol{u}^{\text{tfe}}|}{\Omega\sqrt{x^2+y^2}} = \frac{2\,\rho^{\text{tfe}}}{\rho - \rho^{\text{tfe}}}\,\frac{|\boldsymbol{u}^{\text{tfe}}|}{\Omega\sqrt{x^2+y^2}}. \tag{30.107}$$

Heavy test fluid elements, with small buoyancy, move toward the outer edge of the tank due to dominance of the centrifugal acceleration, whereas lighter test fluid elements concentrate toward the center. We can further reduce the influence of the Coriolis acceleration by changing the geometry to that of a long test tube to thus reduce $|\boldsymbol{u}^{\text{tfe}}|$, with this geometry used for *centrifuges*.

Is there is a dynamically consistent motion in which the test fluid element has exactly zero horizontal material acceleration, $\dot{\boldsymbol{u}}^{\text{tfe}} = 0$? For this motion to occur requires a balance between the Coriolis and centrifugal accelerations

$$2\,\Omega\,\rho^{\text{tfe}}\,(\hat{\boldsymbol{z}} \times \boldsymbol{u}^{\text{tfe}}) = -(b\,\rho\,\Omega^2/g)\,(\hat{\boldsymbol{x}}\,x + \hat{\boldsymbol{y}}\,y) \Longrightarrow \boldsymbol{u}^{\text{tfe}} = [b\,\rho/(2\,g\,\rho^{\text{tfe}})]\,(\boldsymbol{\Omega} \times \boldsymbol{x}). \tag{30.108}$$

However, this velocity field does not, in fact, have a zero acceleration since

$$\dot{\boldsymbol{u}}^{\text{tfe}} = [b\,\rho/(2\,g\,\rho^{\text{tfe}})]\,(\boldsymbol{\Omega} \times \boldsymbol{u}^{\text{tfe}}) \neq 0. \tag{30.109}$$

We conclude that there is no self-consistent free motion with $\dot{\boldsymbol{u}}^{\text{tfe}} = 0$, much like the case of the test fluid element moving in the accelerating train studied in Section 30.10.3.

30.11 Effective buoyancy and vertical accelerations

In this section, we extend the discussion of Archimedean buoyancy by focusing on the vertical forces acting on a real fluid element, or more generally a finite sized fluid region, rather than on a test fluid element. To do so requires us to study, in some detail, the various forces appearing in the momentum equation. As a means to conceptually organize these forces, we introduce *static forces*, which are those forces not associated with fluid motion, plus *motional forces*, which are forces not associated with density inhomogeneities. Motional forces are specific to details of the velocity field, whereas static forces are deduced just from knowledge of the density field.

Effective buoyancy arises from the static forces acting on a fluid element. Although the effective buoyancy is in part comprised of Archimedean buoyancy, there are distinctions that arise through interactions between the fluid element and its surrounding environment. These interactions depend on the shape of the fluid region. As shown in this section (see in particular Figure 30.9), we find that fluid regions of different geometric shape can have different effective buoyancy even while they have the same Archimedean buoyancy.

To facilitate the analysis in this section, we consider a Boussinesq ocean, with the analysis also directly relevant to an anelastic atmosphere as considered by *Jeevanjee and Romps* (2015b). As explored in Section 29.3, pressure in a Boussinesq ocean constrains the velocity field to remain non-divergent. Furthermore, Boussinesq ocean pressure satisfies an elliptic boundary value problem (Poisson equation from Section 6.5). This boundary value problem is linear for the pressure field. Linearity is exploited for conceptual purposes by decomposing the pressure sources into physically distinct processes and studying the associated pressure field. The task for this section is to derive the Poisson equations according to the various pressure sources, and then to discuss the physics of their associated vertical accelerations.

30.11.1 Poisson equations for $p' = p'_{\text{buoy}} + p'_{\text{flow}}$

The two decompositions of pressure described in Sections 30.9.1 and 30.9.2, as reflected in the Boussinesq velocity equations from Section 30.9.3, render two sets of corresponding Poisson equations for pressure. We here focus on the decomposition (30.91b), where the pressure and gravity accelerations appear in terms of the Archimedean buoyancy plus perturbation pressure. We defer until Section 30.11.3 an examination of the alternative decomposition into the local hydrostatic and non-hydrostatic pressures given by equation (30.91c).

Boundary value problem for the perturbation pressure, p'

We start by considering the Boussinesq momentum equation (30.91b)

$$\rho_o \, (\partial_t + \boldsymbol{v} \cdot \nabla) \, \boldsymbol{v} + 2 \, \boldsymbol{\Omega} \times \rho_o \, \boldsymbol{v} = -\nabla p' + \rho_o \, b \, \hat{\boldsymbol{z}} + \rho_o \, \boldsymbol{F}. \tag{30.110}$$

As detailed in Section 29.3.1, the time tendency is eliminated by computing the divergence of this equation to render the Poisson equation for the perturbation pressure

$$-\nabla^2 p' = \rho_o \, \nabla \cdot \boldsymbol{G}' = \rho_o \, \nabla \cdot [(\boldsymbol{v} \cdot \nabla) \, \boldsymbol{v} + 2 \, \boldsymbol{\Omega} \times \boldsymbol{v} - b \, \hat{\boldsymbol{z}} - \boldsymbol{F}], \tag{30.111}$$

where we introduced the vector,

$$\boldsymbol{G}' = (\boldsymbol{v} \cdot \nabla) \, \boldsymbol{v} + 2 \, \boldsymbol{\Omega} \times \boldsymbol{v} - b \, \hat{\boldsymbol{z}} - \boldsymbol{F}, \tag{30.112}$$

whose divergence renders a source for the pressure field. We find it convenient to carry around a minus sign on the Laplacian operator since a positive source, $\rho_o \nabla \cdot \boldsymbol{G}' > 0$, leads to a locally positive pressure signal (see Section 29.3.1 for more details on this point).

We require boundary conditions to fully specify the pressure, and for simplicity we assume material boundaries. In this case, the analysis considered in Section 29.3.2 renders the Neumann boundary condition

$$\hat{\boldsymbol{n}} \cdot \nabla p' = -\rho_\circ \, \hat{\boldsymbol{n}} \cdot \boldsymbol{G}', \tag{30.113}$$

where $\hat{\boldsymbol{n}}$ is the outward normal along the boundary. We further simplify the analysis by assuming flat and rigid top and bottom boundaries along with horizontal boundaries that are either doubly periodic or infinite. Hence, along the top boundary, where $\hat{\boldsymbol{n}} = \hat{\boldsymbol{z}}$, pressure satisfies the Neumann boundary condition

$$\partial_z p' = -\rho_\circ \, \hat{\boldsymbol{z}} \cdot \boldsymbol{G}' = \rho_\circ \, (b + \boldsymbol{F} \cdot \hat{\boldsymbol{z}}) \qquad \text{top boundary.} \tag{30.114}$$

To reach this result we noted that

$$\hat{\boldsymbol{z}} \cdot [(\boldsymbol{v} \cdot \nabla) \, \boldsymbol{v}] = (\boldsymbol{v} \cdot \nabla) \, (\hat{\boldsymbol{z}} \cdot \boldsymbol{v}) = 0, \tag{30.115}$$

since $\hat{\boldsymbol{z}} \cdot \boldsymbol{v} = w = 0$ along a rigid and material flat surface. The analogous result holds along the bottom boundary where $\hat{\boldsymbol{n}} = -\hat{\boldsymbol{z}}$ so that

$$\partial_z p' = \rho_\circ \, \hat{\boldsymbol{z}} \cdot \boldsymbol{G}' = -\rho_\circ \, (b + \boldsymbol{F} \cdot \hat{\boldsymbol{z}}) \quad \text{bottom boundary.} \tag{30.116}$$

Buoyancy induced pressure and flow induced pressure

The Laplacian operator is linear, with linearity affording the freedom to decompose the source in the Poisson equation (30.111), $\rho_\circ \, \nabla \cdot \boldsymbol{G}'$, into physically distinct processes and then studyinig the pressures resulting from these processes.[24] For this purpose we choose the following decomposition

$$-\nabla^2 p' \equiv -\nabla^2 (p'_{\text{buoy}} + p'_{\text{flow}}) \tag{30.117a}$$

$$-\nabla^2 p'_{\text{buoy}} = -\rho_\circ \, \partial_z b \tag{30.117b}$$

$$-\nabla^2 p'_{\text{flow}} = \rho_\circ \, \nabla \cdot [(\boldsymbol{v} \cdot \nabla) \, \boldsymbol{v} + 2 \, \boldsymbol{\Omega} \times \boldsymbol{v} - \boldsymbol{F}]. \tag{30.117c}$$

The source term for the buoyancy pressure, p'_{buoy}, only involves the vertical derivative of the Archimedean buoyancy. Hence, there is no direct contribution from fluid motion on p'_{buoy}, with fluid motion only affecting p'_{buoy} indirectly through effects on $\partial_z b$. The converse holds for the pressure perturbation, p'_{flow}, which is sourced by fluid motion that gives rise to accelerations from self-advection, Coriolis, and friction. Hence, there is no direct impact from Archimedean buoyancy on p'_{flow}. The Neumann boundary conditions for these two pressures follows from the boundary conditions (30.114) and (30.116). For example, along the top boundary we have

$$\partial_z p'_{\text{buoy}} = \rho_\circ \, b \quad \text{and} \quad \partial_z p'_{\text{flow}} = \rho_\circ \, \hat{\boldsymbol{z}} \cdot \boldsymbol{F} \qquad \text{top boundary conditions,} \tag{30.118}$$

with the same conditions holding along the bottom yet with a minus sign on the right hand side.

30.11.2 Accelerations from effective buoyancy and fluid motion

Having established the Poisson equations for the variety of pressures in Section 30.11.1, we now examine contributions to the vertical Lagrangian acceleration as given by equations (30.92b) and (30.92c). Emulating the decomposition used for pressure, we here decompose the vertical acceleration into conceptually distinct contributions from buoyancy and from fluid flow.

[24] We exploited this superposition property when studying Green's functions in Chapter 9.

Vertical acceleration from effective buoyancy

Effective buoyancy is the first contribution to vertical Lagrangian acceleration, which is the vertical acceleration arising solely from the instantaneous mass/density field. Operationally, we deduce the effective buoyancy by instantaneously setting velocity to zero everywhere in the expression for the vertical acceleration

$$b_{\text{eff}} \equiv \left.\frac{\mathrm{D}w}{\mathrm{D}t}\right|_{\boldsymbol{v}=0} . \tag{30.119}$$

Two conclusions follow directly from the operational definition of b_{eff}. First, as viscous friction only arises when there is relative fluid motions that lead to strains (Section 25.8.6), viscous friction does not contribute to the effective buoyancy. Next, we observe that any direct role for pressure in b_{eff} arises solely from the buoyancy pressure, p'_{buoy}. We make this conclusion since the Poisson equation (30.120) for the buoyancy pressure has a source that only depends on the instantaneous Archimedean buoyancy field, whereas it ignores all contributions from fluid flow. This dependence is precisely that defined for b_{eff}.

From the definition (30.119) we make use of equations (30.92b) and (30.92c) to unpack the variety of contributions to effective buoyancy

$$\rho_{\circ}\, b_{\text{eff}} = \rho_{\circ}\, b - \partial_z p'\big|_{\boldsymbol{v}=0} = -\,\partial_z p_{\text{nh}}|_{\boldsymbol{v}=0}\,. \tag{30.120}$$

The first equality identifies the difference between the effective buoyancy and the Archimedean buoyancy

$$\rho_{\circ}\,(b_{\text{eff}} - b) = -\partial_z p'_{\text{buoy}}, \tag{30.121}$$

in which we set

$$\partial_z p'\big|_{\boldsymbol{v}=0} = \partial_z p_{\text{buoy}} \tag{30.122}$$

as per the discussion below equation (30.119). So equation (30.121) states that in the presence of a vertical gradient in the buoyancy pressure, then the Archimedean buoyancy is an incomplete description of the vertical acceleration associated with the density field.

Equation (30.120) also reveals that the effective buoyancy is associated with that portion of the vertical gradient in the non-hydrostatic pressure that remains when $\boldsymbol{v} = 0$

$$\rho_{\circ}\, b_{\text{eff}} = -\,\partial_z p_{\text{nh}}|_{\boldsymbol{v}=0}\,. \tag{30.123}$$

This equation provides a generalization of the local hydrostatic balance, $\rho_{\circ}\, b = \partial_z(p_{\text{h}} - p_0)$ (equation (30.89)), so that we have the correspondence

$$\underbrace{\rho_{\circ}\, b = \partial_z(p_{\text{h}} - p_0)}_{\text{hydrostatic}} \longleftrightarrow \underbrace{\rho_{\circ}\, b_{\text{eff}} = -\,\partial_z p_{\text{nh}}|_{\boldsymbol{v}=0}}_{\text{non-hydrostatic}}\,. \tag{30.124}$$

Vertical acceleration from fluid flow

If one introduces an Archimedean buoyancy anomaly in a static fluid, then the initial vertical acceleration acting on the anomaly is given by its effective buoyancy, with this result following from the definition of effective buoyancy in equation (30.119). However, as the anomaly evolves, fluid motion is generated, at which point effective buoyancy is an incomplete measure of vertical acceleration. So in the presence of fluid motion we must also consider another term referred to as the *flow induced or motional vertical acceleration*. Operationally, we deduce the motional vertical acceleration by setting the density to a constant within the expression for the vertical

acceleration

$$A_{\text{flow}} \equiv \left.\frac{\mathrm{D}w}{\mathrm{D}t}\right|_{\rho=\rho_{\circ}} . \tag{30.125}$$

As for the effective buoyancy in equation (30.119), the right hand side of equation (30.125) is evaluated using the full flow field at an instant, but with the accelerations evaluated with constant density at that instance. Since the Archimedean buoyancy vanishes when density has the uniform value, we know that

$$\rho_{\circ}\, A_{\text{flow}} = -\left.\partial_z p'\right|_{\rho=\rho_{\circ}} + \rho_{\circ}\, \boldsymbol{F}\cdot\hat{\boldsymbol{z}} = -\left.\partial_z p_{\text{nh}}\right|_{\rho=\rho_{\circ}} + \rho_{\circ}\, \boldsymbol{F}\cdot\hat{\boldsymbol{z}}. \tag{30.126}$$

Consequently, when the density field is uniform, $\rho = \rho_{\circ}$, then the vertical gradient of p' and p_{nh} are identical

$$\left.\partial_z p'\right|_{\rho=\rho_{\circ}} = \left.\partial_z p_{\text{nh}}\right|_{\rho=\rho_{\circ}} . \tag{30.127}$$

Furthermore, we identify the vertical gradient in $\left.\partial_z p'\right|_{\rho=\rho_{\circ}}$ with the vertical gradient in the flow induced pressure, p'_{flow}, that satisfies the Poisson equation (30.117c). We thus have the identities

$$\left.\partial_z p'\right|_{\rho=\rho_{\circ}} = \partial_z p'_{\text{flow}} = \left.\partial_z p_{\text{nh}}\right|_{\rho=\rho_{\circ}} . \tag{30.128}$$

30.11.3 Boundary value problems for the accelerations

Following from the discussion in Section 30.11.2, we here derive the boundary value problems for the effective buoyancy and the flow induced acceleration.

Poisson equations for b_{eff} and A_{flow}

From equation (30.121) for the effective buoyancy and from the Poisson equation (30.117b) for the buoyancy pressure, we arrive at the Poisson equation for the effective buoyancy

$$\rho_{\circ}\, b_{\text{eff}} = \rho_{\circ}\, b - \partial_z p'_{\text{buoy}} \quad \text{and} \quad -\nabla^2 p'_{\text{buoy}} = -\rho_{\circ}\, \partial_z b \Longrightarrow -\nabla^2 b_{\text{eff}} = -\nabla_{\text{h}}^2 b. \tag{30.129}$$

Hence, the source for the effective buoyancy is the horizontal Laplacian of the Archimedean buoyancy. Correspondingly, the source for the difference, $b_{\text{eff}} - b$, is the vertical curvature of the Archimedean buoyancy

$$-\nabla^2 (b_{\text{eff}} - b) = \partial_{zz} b. \tag{30.130}$$

We similarly derive the Poisson equation for the motional acceleration by making use of its operational definition (30.126) as well as the Poisson equation (30.117c) for the flow pressure

$$\begin{aligned} \rho_{\circ}\, A_{\text{flow}} = -\partial_z p'_{\text{flow}} + \rho_{\circ}\, \boldsymbol{F}\cdot\hat{\boldsymbol{z}} \quad \text{and} \quad -\nabla^2 p'_{\text{flow}} &= \rho_{\circ}\, \nabla\cdot\left[(\boldsymbol{v}\cdot\nabla)\,\boldsymbol{v} + 2\,\boldsymbol{\Omega}\times\boldsymbol{v} - \boldsymbol{F}\right] \\ \Longrightarrow -\nabla^2 A_{\text{flow}} &= -\partial_z \nabla\cdot\left[(\boldsymbol{v}\cdot\nabla)\,\boldsymbol{v} + 2\,\boldsymbol{\Omega}\times\boldsymbol{v} - \boldsymbol{F}\right] - \nabla^2(\boldsymbol{F}\cdot\hat{\boldsymbol{z}}). \end{aligned} \tag{30.131}$$

Boundary conditions

To completely specify the decomposition of vertical acceleration requires boundary conditions for the effective buoyancy, b_{eff}, and the motional acceleration, A_{flow}. Following our discussion of the Poisson equations in Section 30.11.1, we here only consider rigid and flat material upper and lower boundaries with no boundaries for the horizontal domain (either periodic or infinite horizontal domain). At the upper and lower boundaries we have $\mathrm{D}w/\mathrm{D}t = 0$, and this boundary condition holds whether $\boldsymbol{v} = 0$ or $\rho = \rho_{\circ}$, so that

$$b_{\text{eff}} = 0 \quad \text{and} \quad A_{\text{flow}} = 0 \quad \text{on rigid and flat boundaries.} \tag{30.132}$$

We are thus ensured that the net vertical acceleration is indeed the sum

$$\frac{\mathrm{D}w}{\mathrm{D}t} = A_{\text{flow}} + b_{\text{eff}}. \tag{30.133}$$

Poisson equation for the local non-hydrostatic pressure

We can also arrive at the above results by considering the momentum equation (30.91c) written using the decomposition of pressure into is local non-hydrostatic and local hydrostatic components

$$\rho_\circ \left(\partial_t + \boldsymbol{v}\cdot\nabla\right)\boldsymbol{v} + 2\,\boldsymbol{\Omega}\times\rho_\circ\,\boldsymbol{v} = -\nabla p_{\text{nh}} - \nabla_{\text{h}} p_{\text{h}} + \rho_\circ\,\boldsymbol{F}. \tag{30.134}$$

A divergence of this equation leads to the Poisson equation for the non-hydrostatic pressure

$$-\nabla^2 p_{\text{nh}} = \nabla_{\text{h}}^2 p_{\text{h}} + \rho_\circ\,\nabla\cdot[(\boldsymbol{v}\cdot\nabla)\,\boldsymbol{v} + 2\,\boldsymbol{\Omega}\times\boldsymbol{v} - \boldsymbol{F}]. \tag{30.135}$$

Taking a vertical derivative and use of the hydrostatic relation leads to the Poisson equation for the vertical derivative of the non-hydrostatic pressure

$$-\nabla^2(\partial_z p_{\text{nh}}) = -g\,\nabla_{\text{h}}^2\rho + \rho_\circ\,\partial_z\nabla\cdot[(\boldsymbol{v}\cdot\nabla)\,\boldsymbol{v} + 2\,\boldsymbol{\Omega}\times\boldsymbol{v} - \boldsymbol{F}]. \tag{30.136}$$

Setting $\boldsymbol{v}=0$ in equation (30.135) renders the Poisson equation

$$-(\nabla^2 p_{\text{nh}})_{\boldsymbol{v}=0} = \nabla_{\text{h}}^2 p_{\text{h}}. \tag{30.137}$$

This equation says that the static portion of the non-hydrostatic pressure is sourced by the horizontal Laplacian of the hydrostatic pressure. Equivalently, the convergence of $(\nabla p_{\text{nh}})_{\boldsymbol{v}=0}$ is balanced by the divergence of the horizontal hydrostatic pressure gradient, $\nabla_{\text{h}} p_{\text{h}}$. Furthermore, setting $\boldsymbol{v}=0$ in equation (30.136) yields the Poisson equation for the effective buoyancy

$$-\rho_\circ\nabla^2 b_{\text{eff}} = g\nabla_{\text{h}}^2\rho \Longleftrightarrow \nabla^2 b_{\text{eff}} = \nabla_{\text{h}}^2 b, \tag{30.138}$$

which accords with equation (30.129).

30.11.4 Relative scales for effective and Archimedean buoyancies

One way to emphasize the distinction between the effective buoyancy equation (30.138) and that for the Archimedean buoyancy is to compare their two elliptic equations

$$-\rho_\circ\nabla^2 b = g\,\nabla^2\rho \quad \text{and} \quad -\rho_\circ\nabla^2 b_{\text{eff}} = g\,\nabla_{\text{h}}^2\rho, \tag{30.139}$$

with the first equality following trivially by definition of Archimedean buoyancy, $b = -(g/\rho_\circ)\,(\rho - \rho_\circ)$. The different Laplacian operators acting on the source terms for b_{eff} and b are crucial. Namely, the difference means that these two buoyancy fields have different scales.

As an example of the distinct scaling for b_{eff} and b, consider a cylindrically shaped Archimedean buoyancy anomaly (Figure 30.9) of scale B and with diameter D and height H. Given this information we seek a corresponding scale for the effective buoyancy, B_{eff}. Using the relation (30.138), and the cylindrical-polar coordinate version of the Laplacian operator (equation (4.197b)), we have

$$\nabla^2 b_{\text{eff}} = \frac{1}{r}\frac{\partial}{\partial r}\left[r\,\frac{\partial b_{\text{eff}}}{\partial r}\right] + \frac{1}{r^2}\frac{\partial^2 b_{\text{eff}}}{\partial\vartheta^2} + \frac{\partial^2 b_{\text{eff}}}{\partial z^2} \quad \text{and} \quad \nabla_{\text{h}}^2 b = \frac{1}{r}\frac{\partial}{\partial r}\left[r\,\frac{\partial b}{\partial r}\right] + \frac{1}{r^2}\frac{\partial^2 b}{\partial\vartheta^2}, \tag{30.140}$$

where r is the radial distance from the cylinder axis, z the vertical coordinate along the cylinder

axis, and ϑ the polar coordinate. We thus find the scalings

$$\nabla^2 b_{\text{eff}} \sim B_{\text{eff}} \, (D^{-2} + H^{-2}) \quad \text{and} \quad \nabla_{\text{h}}^2 b \sim B \, D^{-2}, \tag{30.141}$$

so that for a given Archimedean buoyancy anomaly scale, B, we find an associated effective buoyancy scale

$$B_{\text{eff}} = \frac{B}{1 + D^2/H^2}. \tag{30.142}$$

Evidently, the effective buoyancy scale is smaller than the Archimedean buoyancy scale. The effective buoyancy scale is smaller due to the pressure contribution that slows down any buoyant fluid element, with this pressure induced environmental back-reaction missing from the Archimedean buoyancy. Also observe that the effective buoyancy decreases when the ratio D/H increases. As a result, wide and flat "pancake" shaped buoyancy anomalies rise slower (with $B > 0$) than narrow "rocket shaped" anomalies. This result follows since a flat pancake anomaly must push aside more surrounding fluid as it moves vertically, whereas the narrow rocket shaped anomaly is more streamlined and thus more readily rises or falls.

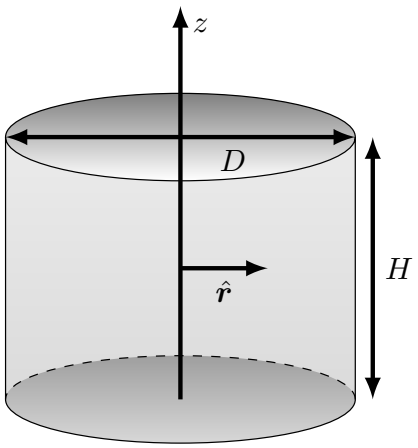

FIGURE 30.9: An Archimedean buoyancy anomaly of scale B here configured in the shape of a cylinder with diameter D and height H. Also shown are the vertical, z, and radial, r, axes for cyclindrical-polar coordinates from Section 4.22. In equation (30.142) we find the effective buoyancy for this anomaly scales as $B_{\text{eff}} = B/(1 + D^2/H^2)$, so that the effective buoyancy has a smaller magnitude than the Archimedean buoyancy. Also note that the magnitude of the effective buoyancy decreases as the diameter increases. This behavior reflects the need for a wide and flat buoyancy anomaly to push aside more surrounding fluid as it moves vertically, whereas a narrow and tall anomaly is more streamlined and so has less resistance to vertical motion.

As a buoyant fluid element moves vertically, it must displace the surrounding environmental fluid. The pressure contribution to the effective buoyancy accounts for the back-reaction of the environmental fluid on the buoyant fluid element. Since the Archimedean buoyancy ignores the back-reaction, it generally over estimates the magnitude of the vertical acceleration. By accounting for the pressure forces acting on the element from the surrounding fluid, the effective buoyancy offers a more accurate measure of the static vertical forces arising from density inhomogeneities.

30.11.5 Thought experiments for effective buoyancy

We here present some thought experiments for the purpose of developing an understanding of effective buoyancy. The thought experiments are somewhat trivial physically and yet they

require us to confront basic assumptions, which is generally a useful exercise.

Horizontally unstratified density

Consider a horizontally unstratified density, $\rho = \rho(z)$, on a horizontally periodic domain with the fluid in hydrostatic equilibrium. By construction, the Archimedean buoyancy, $b = -g\,(\rho - \rho_o)/\rho_o$, exactly balances the vertical pressure gradient, $\mathrm{d}(p - p_0)/\mathrm{d}z = b\,\rho_o$. In the absence of horizontal density gradients, the effective buoyancy is everywhere a harmonic function since $\nabla^2 b_{\text{eff}} = 0$. With vanishing Dirichlet boundary conditions at the rigid bottom and top of the domain, $z = 0, H$, then $b_{\text{eff}} = 0$ everywhere, signaling the absence of any vertical acceleration.

It is notable that this result holds for an arbitrary vertical profile of density, even if the density is gravitationally unstable (Section 30.5). The assumed horizontal symmetry is the key point. This assumption precludes any vertical motion since no fluid element at a single horizontal position can be vertically displaced without breaking the assumption of horizontal symmetry. The only way to maintain volume conservation ($\nabla \cdot \boldsymbol{v} = 0$) with vertical motion is for some fluid to move up while other fluid moves down, and for that to happen requires breaking horizontal symmetry. Once a tiny seed of horizontal asymmetry is presented to the fluid, effective buoyancy is sourced by $\nabla_{\text{h}}^2 \rho \neq 0$, which in turn allows the gravitational instability to grow.

Vertically unstratified density

Now consider a vertically unstratified density field, $\rho = \rho(x, y)$, so that the Archimedean buoyancy has no depth dependence. This vertically "neutrally buoyant" case commonly means that a fluid element can move vertically without feeling any buoyancy forces. Indeed, such is the case when referring to Archimedean buoyancy. What about effective buoyancy?

If density is a linear function of horizontal position then the effective buoyancy is a harmonic function so that $b_{\text{eff}} = 0$. If density is a nonlinear function of the horizontal then the effective buoyancy is nonzero. Yet is there vertical motion? Again we must confront the boundary conditions to answer this question. Here, the rigid top and bottom boundaries preclude movement of fluid across these boundaries by imparting a boundary pressure acting throughout the fluid to counteract the effective buoyancy. As a result, the fluid remains static. If instead we allow for a free surface, then the effective buoyancy would cause vertical motion that then leads to horizontal convergences, thus leading to further motion. Alternatively, if we allow for depth dependence of the density, then fluid can move laterally as well as vertically.

Localized source of Archimedean buoyancy

Although useful to garner some understanding of effective buoyancy, the previous examples are not realistic. More realistic applications are concerned with Archimedean buoyancy sources localized in both the horizontal and vertical directions. In this case the nonzero buoyancy source, $\nabla_z^2 \rho \neq 0$, along with the boundary conditions lead to a nontrivial structure for the effective buoyancy as found by solving the Poisson equation. Studies listed in Section 30.11.6 offer examples, both analytical and numerical, to further an understanding of how effective buoyancy offers a more complete description of vertical acceleration than Archimedean buoyancy.

30.11.6 Comments and further study

Studies from *Davies-Jones* (2003b), *Doswell and Markowski* (2004), *Jeevanjee and Romps* (2015a,b) and *Tarshish et al.* (2018), point to the use of the effective buoyancy and the limitations of Archimedean buoyancy when studying buoyancy dominated motion, such as the early stages of a buoyant thermal in the atmosphere. Much of the material in this section was gleaned from these papers, particularly from *Jeevanjee and Romps* (2015a,b). Chapter 2 of *Markowski and*

Richardson (2010) provides a pedagogical foundation for understanding pressure forces leading to vertical motion.

The structure of b_{eff} is distinct from the Archimedean buoyancy, b, with *Jeevanjee and Romps* (2015a) and *Tarshish et al.* (2018) providing examples where b and b_{eff} can even have opposite signs. Furthermore, *Tarshish et al.* (2018) made use of an analogy between the Poisson equation for b_{eff} and the Poisson equation for certain magnetostatics problems. The analogy allows for analytical expressions of b_{eff} for spherical and elliptical Archimedean buoyancy sources.

30.12 Exercises

EXERCISE 30.1: EXAMPLES OF BUOYANCY PERIOD
Using approximate but realistic values for the observed stratification, determine the buoyancy period ($T_{\text{b}} = 2\pi/N$) for

- mid-latitude troposphere
- stratosphere
- ocean thermocline
- ocean abyss.

Express the period in units of minutes, and provide references for where you obtained the observed stratification. Hint: for both the atmosphere and ocean, it is sufficient to assume stratification is dominated by potential temperature (or Conservative Temperature).

EXERCISE 30.2: BUOYANCY FREQUENCY FOR AN IDEAL GAS
Derive equation (30.38) for the squared buoyancy frequency of an ideal gas. Hint: first derive the expression for the potential density and then take its vertical derivative as per equation (30.37).

EXERCISE 30.3: VERTICAL INTEGRAL OF N^2
The expression for squared buoyancy frequency

$$N^2 = -g \left[\frac{\partial \ln \varrho}{\partial z} \right]_{p_{\text{ref}}=p} \tag{30.143}$$

makes is tempting to consider its vertical integral according to

$$-g^{-1} \int_{-H}^{\eta} N^2 \, \mathrm{d}z \stackrel{?}{=} [\ln \varrho]_{\eta} - [\ln \varrho]_{-H} \, . \tag{30.144}$$

Discuss what is wrong with this equation. Under what conditions is it correct?

EXERCISE 30.4: WATER LEVEL OF A BOAT WITH AND WITHOUT A STONE
Consider a boat of mass M_{b} floating in constant density water, ρ_{w}, contained in a tank with vertical sidewalls and cross-sectional area A. Place a stone of mass M_{s} and density $\rho_{\text{s}} > \rho_{\text{w}}$ in the boat and measure the water level on the tank wall, h_1. Then throw the stone into the water. What is the new water level, h_2, as a function of h_1 and the other properties listed above? Does the water level rise or fall along the sides of the tank as a result of throwing the stone over the side? Hint: Watch this Physics Girl video.

EXERCISE 30.5: ICEBERG FLIPPING INSTABILITY
This exercise has yet to be worked through.

(a) Consider an iceberg with constant density ρ_{berg} that is floating in ocean water with constant density ρ_{ocn}. Let the iceberg have a square solid shape with vertical thickness H and horizontal length $L \gg H$. What fraction of the iceberg sits above the ocean surface?

(b) Consider an iceberg with non-uniform density, $\rho_{\text{berg}}(z)$, where $0 \leq z \leq H$ measures the position along the vertical axis of the iceberg. A non-uniform density might occur for cases where rocks are frozen into the ice. Depending on the density profile, the iceberg can be unstable to horizontal forces that cause the iceberg to flip over, particularly if L decreases to be on the order of H. Develop the stability criteria for this "flipping instability" using Archimedes' principle and the mechanics of angular momentum and torques.

Chapter 31

GEOSTROPHY AND THERMAL WIND

Large-scale and low frequency flows in the atmosphere and ocean are stongly affected by planetary rotation. The inviscid balance for such flows is termed *geostrophy*, in which the planetary Coriolis acceleration balances the pressure gradient acceleration in the horizontal, while the vertical balance is hydrostatic. In this chapter, we introduce salient features of geostrophically balanced flow and the associated *thermal wind balance*. These two diagnostic relations involve no time derivatives, and so cannot be used to predict the fluid flow evolution. However, they provide a very powerful framework for interpreting large-scale and low frequency flow in the atmosphere and ocean.

After studying the basic elements of rotating flow, we study the distinctive nature of isopycnal form stresses associated with geostrophically balanced eddy motions. Such form stresses are a key feature of the earth's planetary energy balance, whereby positive buoyancy in the tropics is, in part, transported meridionally through the action of geostrophic eddies.

READER'S GUIDE TO THIS CHAPTER

This chapter assumes an understanding of the primitive equations from Chapter 27 and the Coriolis acceleration from Chapters 13 and 14. The material in this chapter is fundamental to understanding the mechanics of large-scale flow in the atmosphere and ocean, so that we make great use of this chapter in the remainder of the book. We are not explicitly concerned with sphericity in this chapter, thus enabling the use of Cartesian vector calculus.

31.1 Loose threads

- Max Nikurashin's work on topographic form stress in the Southern Ocean, and the lack of a direct connection to interfacial form stress. Unsure if this material is better here or in Chapter 28.

31.2 Primitive equations

Throughout this chapter we make use of the inviscid hydrostatic primitive equations derived in Section 27.1

$$[\partial_t + (\boldsymbol{v} \cdot \nabla)]\, \boldsymbol{u} + f\, \hat{\boldsymbol{z}} \times \boldsymbol{u} = -\rho^{-1}\, \nabla_h p \tag{31.1a}$$

$$\partial p / \partial z = -g\, \rho \tag{31.1b}$$

$$\mathrm{D}\rho/\mathrm{D}t = -\rho\, \nabla \cdot \boldsymbol{v}, \tag{31.1c}$$

where the velocity vector is written using Cartesian coordinates

$$\boldsymbol{v} = \boldsymbol{u} + \hat{\boldsymbol{z}}\, w = \hat{\boldsymbol{x}}\, u + \hat{\boldsymbol{y}}\, v + \hat{\boldsymbol{z}}\, w, \tag{31.2}$$

and the horizontal gradient operator is

$$\nabla_h = \hat{\boldsymbol{x}}\, \partial_x + \hat{\boldsymbol{y}}\, \partial_y. \tag{31.3}$$

For some of the scale analysis in this chapter we assume a Boussinesq ocean (Section 29.1), in which case the mass continuity equation (31.1c) becomes the non-divergent condition on the velocity

$$\nabla \cdot \boldsymbol{v} = 0. \tag{31.4}$$

Furthermore, ρ in the Boussinesq horizontal momentum equation (31.1a) is converted to a constant reference density, ρ_o, and yet it retains its full form when appearing in the hydrostatic equation since it is there multiplied by the gravitational acceleration.

31.3 The Rossby number

Large-scale geophysical fluid flows are strongly influenced by the earth's rotation. Indeed, the earth can be considered a rapidly rotating planet for much of the observed large-scale motion of the ocean and atmosphere. There are two points to emphasize in this regard. First, much of the ocean and atmosphere motion is close to rigid-body rotation, in which weather patterns

and ocean circulation are best viewed in the terrestrial reference frame on the rotating earth (a non-inertial reference frame) rather than from an inertial reference frame fixed in space. Second, length scales directly experienced by humans are generally far too small to take a direct notice of the planetary rotation. This point is quantified by considering the *Rossby number*, which includes a horizontal length scale, a velocity scale, and angular rotation speed.

31.3.1 Scaling for the Rossby number

The Rossby number measures the ratio of the horizontal material acceleration (acceleration of a fluid particle) to the Coriolis acceleration. The material acceleration has two contributions: one from local time tendencies and one from advection. We expose typical characteristic scales for the horizontal acceleration of a fluid particle by writing

$$\frac{\partial \boldsymbol{u}}{\partial t} + (\boldsymbol{v} \cdot \nabla)\, \boldsymbol{u} \sim \frac{U}{T} + \frac{U^2}{L} + \frac{WU}{H}, \tag{31.5}$$

where U, W are typical horizontal and vertical velocity scales, L, H are typical horizontal and vertical length scales, and T is a typical time scale (recall a similar scale analysis for the hydrostatic balance in Section 27.2). Likewise, the Coriolis acceleration scales as

$$f\, \hat{\boldsymbol{z}} \times \boldsymbol{u} \sim f_\circ U, \tag{31.6}$$

where $f_\circ$ is the scale for the Coriolis parameter. From the continuity equation for non-divergent flow ($\nabla \cdot \boldsymbol{v} = 0$) we see that the vertical and horizontal velocity scales are related by[1]

$$W/H \sim U/L \Longrightarrow W \sim U\,(H/L). \tag{31.7}$$

We are interested in flows where the ratio of the vertical to horizontal length scales, referred to as the *aspect ratio*, is small

$$\alpha_{\text{aspect}} = H/L \ll 1, \tag{31.8}$$

as per the hydrostatic approximation discussed in Section 27.2. Consequently, the vertical velocity scale is much less than the horizontal

$$W \ll U. \tag{31.9}$$

31.3.2 Ratio of material acceleration to Coriolis acceleration

Taking the ratio of the advection scale to the Coriolis scale leads to our first expression for the Rossby number

$$\text{Ro} = \frac{U^2/L}{f_\circ U} = \frac{U}{f_\circ L}. \tag{31.10}$$

For fixed scales U and L, the latitudinal variation of the Coriolis parameter makes the Rossby number smaller in magnitude near the poles than in the tropics.

31.3.3 Ratio of local time tendency to Coriolis acceleration

A complementary way to understand the Rossby number is to consider it as the ratio of the horizontal velocity's local time tendency to the Coriolis acceleration

$$\text{Ro} = \frac{U/T}{U f_\circ} = \frac{1/T}{f_\circ}. \tag{31.11}$$

[1] For divergent flows we can replace W with the scale for motion across hydrostatic pressure surfaces.

Hence, the Rossby number is small for motions that have a frequency, T^{-1}, that is small compared to the *inertial frequency*, f_c. In both expressions (31.10) and (31.11) for the Rossby number, we associate $\text{Ro} < 1$ with flow regimes where the earth's rotation plays a crucial role in the dynamics. With small Rossby number, both the local time derivative and the advective acceleration are smaller than the Coriolis acceleration.

31.3.4 Rossby number for a kitchen sink

Consider flow in a kitchen sink (left panel of Figure 31.1). Here, the length scale is $L = 1$ m (sink size) and the velocity scale is $U = 0.01 - 0.1$ m s^{-1}, thus giving a typical time scale for sink motion of $L/U \approx 10$ s $- 100$ s. Hence, at 30° latitude, where $f = 2\Omega \sin\phi = \Omega$, the Rossby number for fluid motion in a sink is

$$\text{Ro}_{\text{sink}} \approx 10^2 - 10^3. \tag{31.12}$$

The effects from planetary rotation are tiny on these length scales, so that the Coriolis force is negligible for kitchen sink fluid dynamics. Correspondingly, it is extremely difficult to experimentally determine a correlation between the hemisphere (northern or southern) to the rotational direction of water leaving a sink drain.

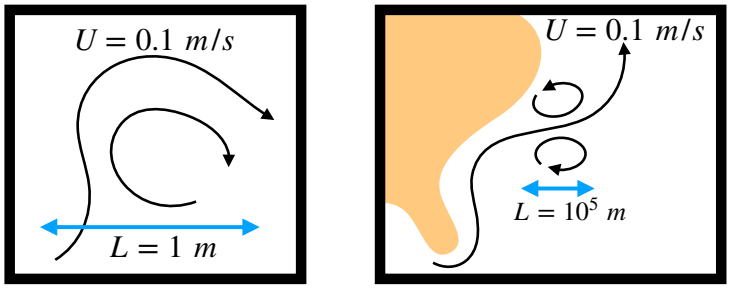

FIGURE 31.1: Estimating the Rossby number for flow in a kitchen sink (left panel) and rings spawned from the Gulf Stream (right panel). The kitchen sink has velocity scales on the order of $U \sim 0.01 - 0.1$ m s^{-1} whereas Gulf Stream rings have velocity scales on the order $U \sim 0.1 - 1.0$ m s^{-1}. Their length scales are much more distinct, with the scale for a sink $L \sim 1$ m whereas for the Gulf Stream rings $L \sim 10^5$ m. Taking the Coriolis parameter at 30° leads to $\text{Ro}_{\text{sink}} \sim 10^2 - 10^3$ and $\text{Ro}_{\text{ring}} \sim 10^{-2} - 10^{-1}$. The planetary Coriolis acceleration is central to Gulf Stream ring dynamics whereas it is utterly negligible for the kitchen sink.

31.3.5 Rossby number for a Gulf Stream ring

For a Gulf Stream ring (right panel of Figure 31.1), the typical length scale is $L = 10^5$ m and velocity scale is $U = 0.1 - 1.0$ m s^{-1}, thus leading to a time scale $L/U \approx 10^5 - 10^6$ s. At 30° latitude the Rossby number is

$$\text{Ro}_{\text{ring}} \approx 10^{-2} - 10^{-1}. \tag{31.13}$$

Flow features of such large length scales can feel the planetary rotation so that the Coriolis acceleration is central to dynamics of Gulf Stream rings, as reflected in the small magnitude of the associated Rossby number.

31.4 Geostrophic balance

Under the influence of horizontal pressure forces, a fluid accelerates down the pressure gradient (movement from high pressure to low pressure). In the presence of rotation, a nonzero horizontal velocity couples to the earth's rotation via the Coriolis parameter, f, thus giving rise to a nonzero

horizontally oriented Coriolis acceleration $-f\,\hat{\boldsymbol{z}} \times \boldsymbol{u}$. The Coriolis acceleration acts perpendicular to the fluid motion

$$\boldsymbol{u} \cdot (\hat{\boldsymbol{z}} \times \boldsymbol{u}) = 0, \tag{31.14}$$

and as such it affects the fluid motion but does not alter kinetic energy; i.e., it does zero work on the fluid.[2] In the northern hemisphere where $f > 0$, the Coriolis acceleration acts to the right of the fluid motion. It follows that if the Coriolis and pressure gradient accelerations are balanced, then fluid flow is counter-clockwise around low pressure centers and clockwise around high pressure centers. In the southern hemisphere, where $f < 0$, the Coriolis acceleration acts in the opposite direction so that geostrophically balanced flow is oppositely oriented in the southern hemisphere relative to the north.

When the pressure acceleration balances the Coriolis acceleration, fluid motion is said to be in *geostrophic* balance. Geostrophically balanced flows in the atmosphere and ocean follow isobars (lines of constant pressure). Recall from Chapter 13 that point particles also experience a Coriolis acceleration when viewed in a rotating reference frame. However, geostrophic balance is not afforded to particles since particles do not experience a pressure force that can balance the Coriolis force. Hence, the geostrophic balance is a distinctly fluid mechanical phenomena. Even so, in Figure 31.2 we offer a particle model to help understand the orientation of geostrophic flow, in which for this model the pressure force acting on a fluid parcel is replaced by the gravitational force acting on the point particle.

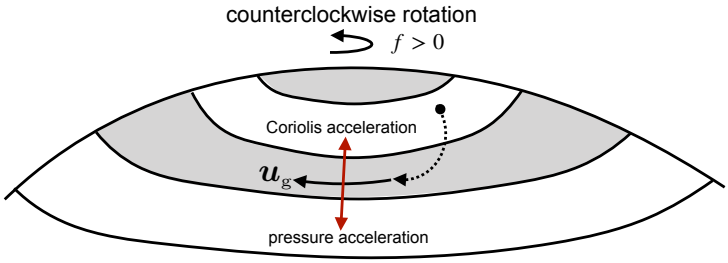

FIGURE 31.2: Geostrophy is a diagnostic relation where the pressure gradient acceleration balances the Coriolis acceleration so that the net acceleration acting on a fluid element is zero. Here we depict a particle on a rotating and frictionless hill (analogous to a high pressure center) as a conceptual model to help understand geostrophic balance. As the particle moves downhill it picks up a rightward component to its trajectory as a result of the Coriolis acceleration that couples to motion. Equilibrium arises when the downhill gravitational acceleration balances the oppositely directed Coriolis acceleration.

31.4.1 Geostrophic relation in geopotential coordinates

When the Rossby number is small and friction is negligible, the leading order dynamical balance in the horizontal momentum equation (31.1a) is between the Coriolis acceleration and horizontal pressure gradient acceleration

$$f\,\hat{\boldsymbol{z}} \times \boldsymbol{u}_g = -\rho^{-1}\,\nabla_h p, \tag{31.15}$$

with this equation known as *geostrophic balance*. The geostrophic balance equation leads to the expression for the geostrophic velocity[3]

$$\boldsymbol{u}_g = \frac{\hat{\boldsymbol{z}} \times \nabla p}{f\rho} \Longrightarrow u_g = -\frac{1}{f\rho}\frac{\partial p}{\partial y} \qquad \text{and} \qquad v_g = \frac{1}{f\rho}\frac{\partial p}{\partial x}. \tag{31.16}$$

[2] These characteristics of the Coriolis acceleration are directly analogous to the Lorentz force in electrodynamics (*Jackson*, 1975).

[3] We can write either ∇ or ∇_h in equation (31.16). The reason is that the $\hat{\boldsymbol{z}}\times$ operator selects only the horizontal portion of the gradient.

Note that the equator is special since the Coriolis parameter, $f = 2\,\Omega \sin\phi$, vanishes, thus precluding the relevance of geostrophy near the equator.

Equation (31.16) for the geostrophic velocity can be written as

$$\rho\, f\, \boldsymbol{u}_{\rm g} = \hat{\boldsymbol{z}} \times \nabla_{\rm h} p, \tag{31.17}$$

which suggests we interpret pressure as a streamfunction for $\rho\, f\, \boldsymbol{u}_{\rm g}$. For the particular case of a Boussinesq ocean on an f-plane, in which we set ρ to the reference density $\rho_{\rm o}$ and f is a constant, then we can write

$$\boldsymbol{u}_{\rm g} = \hat{\boldsymbol{z}} \times \nabla_{\rm h}[p/(\rho_{\rm o}\, f)]. \tag{31.18}$$

In this case $p/(\rho_{\rm o}\, f)$ is referred to as the *geostrophic streamfunction* for the f-plane Boussinesq geostrophic flow.

31.4.2 Cyclonic and anti-cyclonic flow orientation

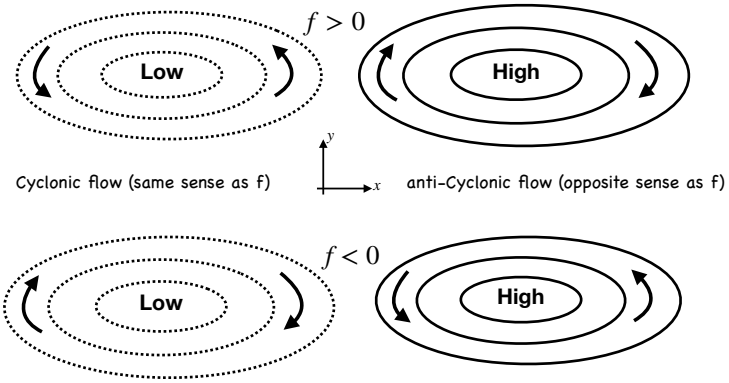

FIGURE 31.3: Geostrophic motion around low and high pressure centers in the northern hemisphere and southern hemisphere ($f = 2\,\Omega \sin\phi > 0$ in the north and $f < 0$ in the south). Upper panel: the counter-clockwise motion around the low pressure center in the northern hemisphere is in the same sense as the planetary rotation, and is thus termed *cyclonic*. Cyclonic motion around a low pressure in the southern hemisphere occurs in a clockwise direction, again corresponding to the direction of planetary rotation as viewed from the south. Geostrophic motion around a high pressure center is counter to the planetary rotation in both hemispheres, and is thus termed *anti-cyclonic*.

If oriented in the same sense as the earth's rotation (i.e., same sign of the Coriolis parameter), then rotational motion is said to be in a *cyclonic* sense. Oppositely oriented motion is *anti-cyclonic*. For example, geostrophic motion around a low pressure center in the northern hemisphere is counter-clockwise (Figure 31.3). Using the right hand rule, this motion represents a positively oriented rotation. Hence, with $f > 0$ in the north, counter-clockwise motion is cyclonic. In the southern hemisphere, geostrophic motion around a low pressure center is clockwise, which is a negatively oriented rotational motion (again, recall the right hand rule). In the south where $f < 0$, clockwise motion around a low pressure center represents cyclonic motion (Figure 31.3).

31.4.3 Gradients in the density and hydrostatic pressure

Horizontal momentum is affected by horizontal pressure gradient forces. Furthermore, the hydrostatic balance says that the vertical derivative of the horizontal pressure gradient is determined by horizontal density gradients

$$\frac{\partial(\nabla_{\rm h} p)}{\partial z} = -g \nabla_{\rm h} \rho. \tag{31.19}$$

Hence, in the presence of horizontal density gradients, the horizontal pressure gradient forces are depth dependent. Correspondingly, the horizontal velocity field experiences a depth dependent pressure force.

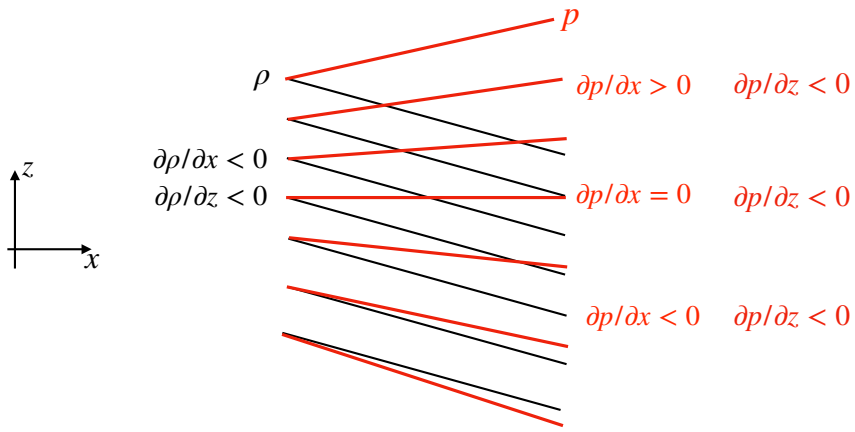

FIGURE 31.4: Horizontal density gradients support a vertical dependence to the horizontal gradient of the hydrostatic pressure via $\partial(\nabla_h p)/\partial z = -g\nabla_h \rho$. This figure depicts a vertically stable stratification of density ($\partial\rho/\partial z < 0$), along with pressure that decreases upward as per the hydrostatic balance ($\partial p/\partial z = -\rho\, g < 0$). Density is assumed to have a constant zonal gradient with $\partial\rho/\partial x < 0$, which leads to an increase in the zonal pressure gradient with height, $\partial(\partial p/\partial x)/\partial z > 0$. Depending on the thickness of the fluid column, the horizontal pressure gradient can change sign when moving up in the column, as shown here. Compare this figure to Figure 27.4, which discusses how to compute horizontal pressure gradients in a hydrostatic fluid.

We illustrate this depth dependence in Figure 31.4 with a depth independent horizontal density gradient, $\partial\rho/\partial x = \text{constant} < 0$. This density gradient leads to a depth dependent horizontal gradient in the hydrostatic pressure. This figure also illustrates how the sign of the horizontal pressure gradient can change when moving in the vertical, depending on the value of the gradient at depth. It also illustrates how horizontal density gradients that are mis-aligned with pressure gradients lead to a nonzero *baroclinicity* vector

$$\boldsymbol{B} = \frac{\nabla\rho \times \nabla p}{\rho^2}. \tag{31.20}$$

As shown in Section 40.4, a nonzero baroclinicity (i.e., a mis-alignment of the density and pressure surfaces) imparts a "torque" on fluid elements that acts as a source for vorticity.

Depth dependence to the horizontal pressure gradient leads to a vertical shear in the horizontal geostrophic velocity

$$\frac{\partial(\rho\, f\, \boldsymbol{u}_g)}{\partial z} = \hat{\boldsymbol{z}} \times \nabla(\partial p/\partial z) = -g\, \hat{\boldsymbol{z}} \times \nabla\rho. \tag{31.21}$$

This connection between horizontal density gradients and vertical shears in the geostrophic velocity is known as the *thermal wind balance*, which we return to in Section 31.6.

31.4.4 Geostrophic relation in pressure coordinates

The hydrostatic balance

$$\partial p/\partial z = -\rho\, g \tag{31.22}$$

can be used to eliminate density from the geostrophic balance (31.15) to render

$$f\, \hat{\boldsymbol{z}} \times \boldsymbol{u}_g = \frac{g\nabla_h p}{\partial p/\partial z}. \tag{31.23}$$

The right hand side is minus the lateral gradient of the geopotential, $\Phi = g\,z$, as computed along surfaces of constant pressure[4]

$$f\,\hat{\boldsymbol{z}} \times \boldsymbol{u}_{\mathrm{g}} = -\nabla_p \Phi \implies f\,\boldsymbol{u}_{\mathrm{g}} = \hat{\boldsymbol{z}} \times \nabla_p \Phi. \tag{31.24}$$

This is a useful expression of geostrophy for the compressible atmosphere.

31.4.5 Further study

Visualizations from rotating tank experiments offer a useful complement to the mathematical expressions presented here. For example, start around the 10 minute mark in this video from Prof. Fultz.

31.5 Planetary geostrophic mechanics

We here introduce the planetary geostrophic (PG) equations, which have found great use in describing elements of the large-scale laminar ocean circulation. We state the equations and discuss their physical implications, deferring a systematic derivation for later. In particular, the shallow water planetary geostrophic equations are derived in Section 43.4 and the continuously stratified planetary geostrophic equations are derived in Section 44.1.

31.5.1 Planetary geostrophic equations

The governing equations for planetary geostrophy are based on the hydrostatic Boussinesq equations stated in Section 29.1.7, with the assumption of a steady, linear, and frictional/geostrophic balance for the horizontal momentum

$$\rho_{\circ}\, f\, (\hat{\boldsymbol{z}} \times \boldsymbol{u}) = -\nabla p - \rho\, g\, \hat{\boldsymbol{z}} + \partial \boldsymbol{\tau}/\partial z \tag{31.25a}$$

$$\nabla_{\mathrm{h}} \cdot \boldsymbol{u} + \partial w/\partial z = 0 \tag{31.25b}$$

$$\mathrm{D}b/\mathrm{D}t = \dot{b}. \tag{31.25c}$$

The stress vector, $\boldsymbol{\tau}$, acts just in the horizontal directions so that the vertical component of the momentum equation (31.25a) is the hydrostatic balance

$$\partial p/\partial z = -\rho\, g. \tag{31.26}$$

We now list some of the key physical attributes captured by these equations.

Velocity is determined by buoyancy

The only time derivative appearing in the planetary geostrophic equations appears in the buoyancy equation (31.25c). All other equations are diagnostic. As the buoyancy evolves, the hydrostatic pressure changes and so too does the geostrophic velocity. Hence, the velocity is determined by the buoyancy field.

Planetary geostrophy admits no turbulence

The momentum equation is linear since planetary geostrophy drops the nonlinear advection of momentum. Turbulence relies on the nonlinear momentum advection. Hence, there is no

[4] See Section 63.12.2 for details of computing derivatives using generalized vertical coordinates. In particular, the formalism in that section reveals that $(\partial p/\partial x)_{y,z}/(\partial p/\partial z)_{x,y} = -(\partial z/\partial x)_{y,p} = -g^{-1}\,(\partial \Phi/\partial x)_{x,p}$, and likewise for the meridional derivative.

turbulent flow described by the planetary geostrophic equations. Instead, planetary geostrophy is used to describe laminar ocean circulation at the large-scales.

Vertical transfer of horizontal momentum and subgrid scale parameterizations

We introduced a horizontal stress vector (dimensions of force per area) into the momentum equation

$$\boldsymbol{\tau} = (\tau^x, \tau^y, 0). \tag{31.27}$$

This stress is associated with vertical transfer of horizontal momentum in the ocean interior through vertical viscosity, as well as vertical transport of momentum from the atmosphere to the ocean. The stress is enhanced by waves and turbulent features. However, such transient processes are not represented by planetary geostrophy. Hence, they must be parameterized, which generally leads to an enhanced vertical viscosity relative to that from molecular viscosity.

In general, all models, either analytical or numerical, that are focused on planetary scale circulations do not resolve the scales over which molecular viscosity dominates the frictional dissipation. Consequently, it is necessary to provide *subgrid-scale (SGS) parameterizations* for the variety of physical processes that are unresolved by the model. We have more to say about the parameterization of vertical transfer of horizontal momentum in Section 71.3.5.

31.5.2 Planetary geostrophic vorticity equation

The vertical component of relative vorticity is

$$\zeta = \partial v/\partial x - \partial u/\partial y. \tag{31.28}$$

We study the many facets of vorticity in Part VII of this book. Here, we form the relative vorticity budget for the planetary geostrophic system by taking the curl of the momentum equation. Doing so provides insights into the mechanics of planetary geostrophic flow, which we deduce by considering various limits of the vorticity equation.

Curl of the PG momentum equation

Taking the curl of the momentum equation (31.25a), and rearranging terms, leads to the planetary geostrophic vorticity equation

$$-\rho_o f \frac{\partial \boldsymbol{u}}{\partial z} + \hat{\boldsymbol{z}}\, \rho_o \nabla \cdot (f\, \boldsymbol{u}) = -g\, \nabla \times (\hat{\boldsymbol{z}}\, \rho) + \frac{\partial(\nabla \times \boldsymbol{\tau})}{\partial z}. \tag{31.29}$$

Note that $\nabla \cdot (f\, \boldsymbol{u}) = \nabla_h \cdot (f\, \boldsymbol{u})$ since $\boldsymbol{u}$ is the horizontal velocity vector. Introducing the Archimedean buoyancy (Section 29.1.2)

$$b = -g\, (\rho - \rho_o)/\rho_o \tag{31.30}$$

leads to

$$-f \frac{\partial \boldsymbol{u}}{\partial z} + \hat{\boldsymbol{z}}\, \nabla_h \cdot (f\, \boldsymbol{u}) = \nabla \times (\hat{\boldsymbol{z}}\, b) + \frac{1}{\rho_o} \frac{\partial(\nabla \times \boldsymbol{\tau})}{\partial z}, \tag{31.31}$$

whose horizontal and vertical components are the following

$$\rho_o f\, \partial_z \boldsymbol{u} = \hat{\boldsymbol{z}} \times \nabla b \tag{31.32a}$$

$$\rho_o \nabla \cdot (f\, \boldsymbol{u}) = \partial_z [\hat{\boldsymbol{z}} \cdot (\nabla \times \boldsymbol{\tau})]. \tag{31.32b}$$

In this section as well as Section 31.6 we study these equations when making a variety of simplifying assumptions.

Relative vorticity is absent from the PG vorticity equation

It is notable that there is no appearance of the relative vorticity, $\zeta = \partial_x v - \partial_y u$, in the planetary geostrophic vorticity equation (31.25a). The reason is that we dropped the material time derivative of velocity when forming the planetary geostrophic momentum equation (31.25a). By doing so, we eliminate ζ from the vorticity equation. Planetary geostrophy is valid for those cases where

$$|\zeta| \ll |f|, \tag{31.33}$$

which means the absolute vorticity (sum of planetary vorticity plus relative vorticity) is dominated by the planetary vorticity. We encounter more complete versions of the vorticity equation in Chapter 40 where we do not make the planetary geostrophic assumption.

Rather than taking the curl of the planetary geostrophic momentum equation, we could have also derived the vorticity equation (31.31) by taking planetary geostrophic scaling in the full vorticity equation. We choose here the path through the planetary geostrophic momentum equation since we have yet to discuss the full vorticity equation (Chapter 40).

31.5.3 Taylor-Proudman and vertical stiffening

Examination of the momentum equation (31.25a) reveals that inviscid planetary geostrophic flow on an f-plane is horizontally non-divergent

$$\nabla_h \cdot \boldsymbol{u} = 0 \qquad f\text{-plane geostrophy.} \tag{31.34}$$

Use of the continuity equation (31.25b) means there is no vertical stretching of a vertical material line element (Section 18.8.3)

$$\partial w/\partial z = 0. \tag{31.35}$$

As shown in Chapter 40, a vortex tube exhibits the same kinematics as a material line element described in Section 18.6. Hence, $\partial w/\partial z = 0$ means there is no vertical stretching of a vortex tube in the inviscid planetary geostrophic fluid. This result has important implications that we now describe.

Flat bottom boundary and columnar motion

If there is a solid flat bottom to the domain, then the vertical velocity vanishes at that surface. With $\partial_z w = 0$ in the interior as well, then w vanishes throughout the domain. Hence, the fluid has zero vertical velocity, and motion occurs on horizontal planes perpendicular to the rotation axis; i.e., the flow is two-dimensional. We furthermore assume zero horizontal buoyancy gradients (i.e., homogeneous fluid), so that the horizontal portion of the vorticity equation (31.32a) implies that the horizontal velocity has zero vertical shear

$$\partial \boldsymbol{u}/\partial z = 0 \qquad f\text{-plane and homogeneous density.} \tag{31.36}$$

This result is known as the *Taylor-Proudman effect*, with Figure 31.5 providing an illustration.[5]

Relevance to the ocean and atmosphere

In the ocean and atmosphere, the assumptions leading to the Taylor-Proudman effect are rarely satisfied due to the presence of stratification (i.e., vertical density variations), and a sloping solid earth bottom. Nonetheless, there is a tendency for vertical velocities to be quite small due to the effects of rotation; even smaller than the non-divergent flow scaling $W/H \sim U/L$ would

[5]The time-dependent establishment of the Taylor-Proudman effect is mediated by inertial waves, with a discussion provided in Section 53.5.

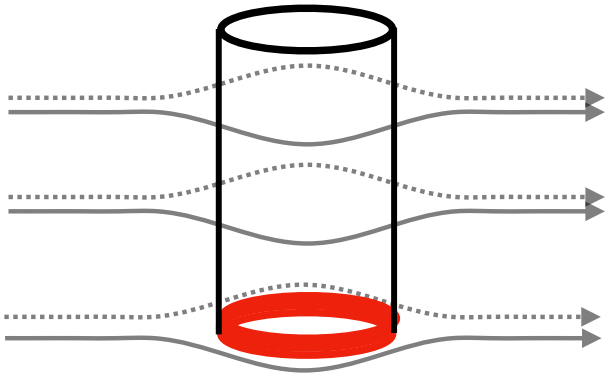

FIGURE 31.5: The Taylor-Proudman effect, summarized by equation (31.36), says that steady horizontal flow is depth-independent when it occurs in a homogeneous and rapidly rotating fluid (i.e., geostrophically balanced flow) over a flat bottom (where $w = 0$). Hence, when the geostrophic flow encounters an obstacle anywhere in the column, such as the red ring shown here at the bottom, then flow throughout the full depth coherently moves around the obstacle. The result is a vertically stiffened motion known as a *Taylor column*.

indicate (see Section 31.3.1). Additionally, for unstratified or linearly stratified fluids, there is a tendency for geostrophic turbulence to cascade energy into the *gravest vertical mode*; i.e., the largest vertical scale. This largest vertical scale mode is termed the *barotropic* mode, and motion of this mode is predominantly horizontal and depth independent. Smaller vertical scales of variation are captured by an infinite hierarchy of *baroclinic* modes. The process of moving energy to the barotropic mode is referred to as *barotropization*.

31.5.4 Meridional motion in response to vortex stretching and stress curls

The vertical component to the vorticity balance is given by equation (31.32b), which can be written

$$\beta\, v = -f\, \nabla_{\!h} \cdot \boldsymbol{u} + (1/\rho_o)\, \partial_z [\hat{\boldsymbol{z}} \cdot (\nabla \times \boldsymbol{\tau})], \tag{31.37}$$

where

$$\beta = \partial_y f \tag{31.38}$$

is the meridional derivative of the planetary vorticity.[6] The continuity equation (31.25b) can be used to yield the following expression of the vorticity balance

$$\beta\, v = f\, \partial_z w + (1/\rho_o)\, \partial_z [\hat{\boldsymbol{z}} \cdot (\nabla \times \boldsymbol{\tau})]. \tag{31.39}$$

The left hand side is the meridional advection of planetary vorticity, with $\beta > 0$ over the globe. The first term on the right hand side arises from vortex stretching by planetary vorticity; i.e., planetary induction or the β-effect discussed in Section 40.6.2. The second term is the vertical divergence of the curl of the frictional stress.

Reading the vorticity equation (31.39) from right to left indicates that any process leading to a vorticity source via vortex stretching or vertically dependent frictional stress curls must be balanced by meridional motion. That is, the fluid responds to vortex stretching and vertically dependent stress curls by moving meridionally through the planetary vorticity field. In the frictional planetary geostrophic theory, meridional movement is the only means for fluid to respond to vorticity input since the fluid's vorticity is set by planetary vorticity (recall that for this theory, the relative vorticity is far smaller in magnitude than planetary vorticity). Reading equation (31.39) from left to right reveals that any meridional motion must be balanced by vortex stretching/squashing plus stress curls. For example, in the absence of the frictional stress

[6] As studied in Part VII of this book, planetary rotation provides a vorticity, $\omega_{\text{planetary}} = f$, to fluids. Hence, the Coriolis parameter, f, is commonly referred to as the *planetary vorticity*.

term, poleward flow is balanced by stretching of a fluid column ($\partial w/\partial z > 0$), whereas equatorial flow is balanced by squashing a column ($\partial w/\partial z < 0$). In Section 44.3, we provide a detailed study of the depth integrated vorticity equation (31.39), where we see how the depth integrated meridional flow is affected by stretching imparted by boundary torques. To get an initial taste for that study, we consider the Sverdrup balance in Section 31.5.5.

31.5.5 The Sverdrup balance

Depth integrating the vorticity balance (31.39) over the full depth of an ocean column leads to

$$\beta\, V = f\,[w(\eta) - w(\eta_b)] + \hat{\boldsymbol{z}} \cdot \nabla \times [\boldsymbol{\tau}(\eta) - \boldsymbol{\tau}(\eta_b)]/\rho_o, \tag{31.40}$$

where

$$V = \int_{\eta_b}^{\eta} v\, dz \tag{31.41}$$

is the depth integrated meridional velocity. For the large-scale we generally assume the surface vertical velocity is relatively small, with $w(\eta) = 0$ when making the *rigid lid approximation*. Further assuming a flat bottom allows us to drop the vertical velocity at the ocean bottom, $w(\eta_b) = 0$. Additionally, the surface turbulent stress from winds is often far larger than the bottom turbulent stress. These assumptions then lead to the *Sverdrup balance*, which is a balance between the depth integrated meridional motion and the curl of the surface turbulent stress

$$\rho_o\, \beta\, V_{\text{Sverdrup}} = \hat{\boldsymbol{z}} \cdot \nabla \times \boldsymbol{\tau}(\eta) \qquad \text{Sverdrup balance.} \tag{31.42}$$

Evidently, for Sverdrup balanced flow, vertically integrated meridional transport (left hand side) balances the wind stress curl (right hand side). In particular, a positive wind stress curl leads to northward vertically integrated flow.

As further discussed in Section 40.9.4, the most unrealistic aspect of the Sverdrup balance (31.42) concerns the assumption of vanishing $w(\eta_b)$, since $w(\eta_b)$ is generally non-negligible in regions with sloping bottom boundaries and sizable bottom flows. Even so, the Sverdrup balance (31.42) is a useful place to start when studying the connection between wind stress curls and vertically integrated meridional transport. We also discuss a variant of the Sverdrup balance, known as the *geostrophic Sverdrup balance*, in Section 44.4.

31.5.6 Further study

Much of the material in this section and Section 31.6.2 forms the basis for laminar theories of the large-scale ocean circulation. We further pursue these theories in Chapter 44 by taking a rather deep dive into the study of planetary geostrophic vorticity budgets. Further discussion of phenomenology is given in Chapter 7 of *Marshall and Plumb* (2008). *Greenspan* (1969), *Pedlosky* (1996), *Samelson* (2011), and chapters 19-22 of *Vallis* (2017) present ocean circulation theory making use of fundamental concepts from geophysical fluid dynamics. A compelling discussion of the cascade of energy from the baroclinic modes to barotropic mode is offered by *Smith and Vallis* (2001). *Gill* (1982) provides a discussion of the depth of no motion problem arising in dynamic oceanography.

Rotating tank laboratory experiments offer a powerful means to explore the variety of rotating fluid mechanics relevant to the atmosphere and oceans. The following resources exemplify the Taylor-Proudman effect (31.36) and the associated vertical stiffening of rotating fluids.

- One means to test Taylor-Proudman is to insert a dye into a rapidly rotating tank of unstratified water. After a few rotation periods the dye forms vertical sheets known as *Taylor curtains* whose center is along the rotation axis. The fluid is said to have a *vertical*

stiffness due to the effects of rotation. Vertical stiffening in turn means that flow over a small obstacle is deflected throughout the column rather than just near the bump. This situation is depicted in Figure 31.5 and more vividly illustrated in this video from the UCLA SpinLab.

- Near the 20 minute mark of this video, also from UCLA, we see how vortices in a rotating fluid maintain their coherency much more than in a non-rotating fluid.

- Another laboratory test shown in this video from Prof. Fultz shows that a buoyant object (a ping pong ball) placed into a rotating tank rises much slower than in a non-rotating tank. The reason for the slower rise is that the ball must push up against the vertically stiffened fluid column when rotating, thus slowing its rise relative to when in a non-rotating fluid. Later in the same video, near the 16 minute mark, we see Taylor curtains in rotating fluids.

31.6 Thermal wind balance

Focusing now on the horizontal portion of the inviscid vorticity equation, as given by equation (31.32a), leads to the *thermal wind balance* (remember that $\nabla b = -(g/\rho_o)\,\nabla\rho$)

$$f\,\partial \boldsymbol{u}/\partial z = -\nabla \times (\hat{\boldsymbol{z}}\, b) = \hat{\boldsymbol{z}} \times \nabla b = -(g/\rho_o)\,\hat{\boldsymbol{z}} \times \nabla \rho, \tag{31.43}$$

which takes on the component form

$$f\,\partial_z u = -\partial_y b = (g/\rho_o)\,\partial_y \rho \quad \text{and} \quad f\,\partial_z v = \partial_x b = -(g/\rho_o)\,\partial_x \rho. \tag{31.44}$$

As seen already in Section 31.4.3, these relations can also be derived directly by taking the vertical derivative of the horizontal momentum equation (31.25a) and then using the horizontal gradient of the hydrostatic balance (31.26). In either case, the thermal wind balance (31.43) says that the horizontal geostrophic velocity possesses a vertical shear where the buoyancy field has a horizontal gradient. Buoyancy with a horizontal gradient is termed *baroclinic* since it leads to a nonzero baroclinicity vector that provides a source for vorticity (discussed in Section 40.7.2). Correspondingly, it is only the baroclinic (depth dependent) piece of geostrophic velocity that is related to horizontal buoyancy gradients. The depth-independent flow is not constrained by horizontal buoyancy gradients.

The thermal wind shear (31.43) is rotated by $\pi/2$ relative to the direction of ∇b. For the northern hemisphere ($f > 0$), the rotation is counter-clockwise so that, for example, with buoyancy increasing southward towards the equator, then the thermal wind increases upwards to the east. That is, the zonal geostrophic flow picks up a more eastward component moving upward. We illustrate this orientation in Figure 31.6, and consider further facets of this flow in Section 31.6.2.

31.6.1 Relevant portion of density needed for thermal wind

The cross product $\hat{\boldsymbol{z}} \times \nabla b = -(g/\rho_o)\,\hat{\boldsymbol{z}} \times \nabla \rho$ means that the thermal wind shear (31.43) depends only on the horizontal gradient of buoyancy or density. As seen in Section 31.6.4 for the atmosphere, Section 31.6.5 for the Boussinesq ocean, and Section 31.6.6 for the non-Boussinesq ocean, this property of the thermal wind shear means that we should focus on horizontal gradients of T computed on constant p surfaces (for the atmosphere), or on horizontal gradients of S and Θ (on constant z surfaces for the Boussinesq ocean and constant p surfaces for non-Boussinesq ocean). Consequently, when assessing the ability of a particular density field to drive thermal wind flow, we examine the T, S, and/or Θ fields rather than the *in situ* density field. Equivalently

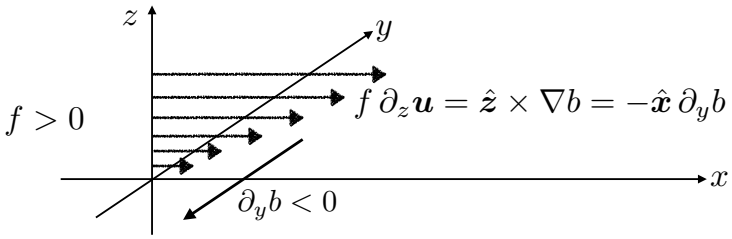

FIGURE 31.6: Orientation of the thermal wind shear for the northern hemisphere ($f > 0$). We depict a buoyancy that decreases to the north, so that $\nabla b = \hat{\boldsymbol{y}}\,\partial_y b = -\hat{\boldsymbol{y}}|\partial_y b|$. The corresponding geostrophic flow becomes more eastward moving vertically upward, as per the thermal wind relation $f\,\partial_z \boldsymbol{u} = \hat{\boldsymbol{z}} \times \nabla b = \hat{\boldsymbol{x}}\,|\partial_y b|$. More generally, for a northern hemisphere geostrophic flow, the thermal wind shear is oriented with fluid of greater buoyancy to the right when facing in the direction of the shear, and fluid of lesser buoyancy to the left. For the southern hemisphere, the orientation is opposite given $f < 0$, so that a southern hemisphere geostrophic flow has a thermal wind shear oriented with fluid of greater buoyancy to the left. Evidently, in both hemispheres if there is more buoyant fluid towards the equator then that yields a corresponding geostrophic flow that becomes more eastward moving vertically upward.

for the ocean, we examine the potential density (Section 30.3.4), with reference pressure taken at the local pressure.

These points are worth emphasizing since surfaces of constant T, S, and Θ in a compressible fluid generally have larger horizontal variability than constant *in situ* density surfaces. As such, one reaches misleading conclusions about the thermal wind flow if focusing on the *in situ* density field, whose quasi-horizontal surfaces might otherwise lead one to incorrectly conclude that the thermal wind shears are smaller than they actually are. We provide the necessary mathematical details to support these points in Sections 31.6.4, 31.6.5 and 31.6.6.

31.6.2 Atmospheric jet stream and the Antarctic Circumpolar Current

Due to the increased solar radiation reaching the equator relative to the poles, the zonal averaged temperature generally reduces when moving poleward. This poleward reduction in temperature corresponds to a poleward reduction in buoyancy. Also, for a stably stratified fluid, buoyancy increases upward. Figure 31.7 illustrates this situation.

A zonal average around a zonally symmetric solid earth boundary eliminates zonal derivatives and so renders the zonally averaged thermal wind relation

$$f \frac{\partial \overline{u}}{\partial z} = \frac{g}{\rho_o} \frac{\partial \overline{\rho}}{\partial y} = -\frac{\partial \overline{b}}{\partial y} > 0, \tag{31.45}$$

where $\overline{(\ )}$ is the zonal mean operator. In the northern hemisphere, $\partial_y \overline{b} < 0$ (zonal mean buoyancy decreases towards the north), so that the zonal averaged thermal wind shear is positive, $\partial_z \overline{u} > 0$. For example, a westerly zonal wind (blowing to the east) strengthens with height (easterly thermal wind shear). In the Southern Hemisphere, $f < 0$, one finds a poleward decreasing buoyancy, $\partial_y \overline{b} > 0$. This buoyancy gradient corresponds to a eastward thermal wind shear, just like for the northern hemispere. Note that poleward movement, where $|f|$ increases, leads to a smaller thermal wind shear given the same buoyancy gradient.

31.6.3 Diagnosing geostrophic velocity from buoyancy

Vertical integration of the thermal wind relation (31.43) between two constant depth surfaces leads to

$$\boldsymbol{u}(z) = \boldsymbol{u}(z_{\text{ref}}) - f^{-1} \nabla \times \hat{\boldsymbol{z}} \int_{z_{\text{ref}}}^{z} b \, \mathrm{d}z. \tag{31.46}$$

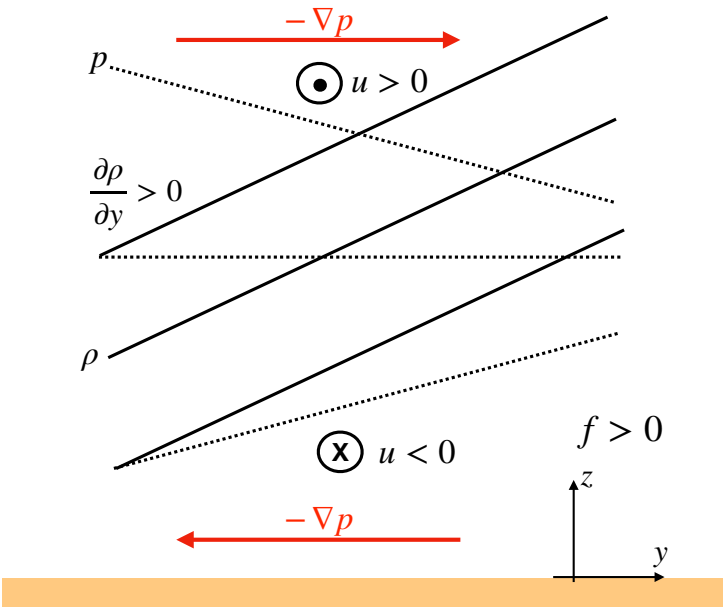

FIGURE 31.7: Schematic of the density (as per the discussion in Section 31.6.1) and hydrostatic pressure fields and the associated thermal wind balanced flow in the northern hemisphere ($f > 0$) with north to the right and east out of the page. We show surfaces of constant density (solid lines) and constant pressure (isobars; dashed lines). Density increases poleward ($\partial\rho/\partial y > 0$) so that, according to the discussion surrounding Figure 31.4, the meridional pressure gradient decreases when moving upward, $\partial(\partial p/\partial y)/\partial z = -g\,\partial_y \rho < 0$. We illustrate isobars with an equatorward directed downgradient pressure force at lower elevations ($-\partial p/\partial y < 0$) and poleward directed pressure force at higher elevations ($-\partial p/\partial y > 0$). The zonal geostrophic wind is in geostrophic balance with these pressure gradients, with a westward zonal flow at lower elevations (easterly winds) and eastward flow at higher elevations (westerly winds). This flow configuration creates an eastward vertical shear of the zonal geostrophic winds, $\partial u/\partial z > 0$.

Hence, knowledge of the buoyancy field (e.g., through hydrographic measurements of temperature and salinity in the ocean), along with knowledge of the geostrophic velocity at a single depth, $\boldsymbol{u}(z_{\text{ref}})$, allows for determination of the full geostrophic velocity in terms of density. Unfortunately, specification of the unknown reference velocity is unavailable just from hydrographic measurements. This is the origin of the *depth of no motion* problem in oceanography.

31.6.4 Thermal wind balance for the atmosphere

The large-scale atmosphere is compressible and approximately in hydrostatic balance. The expression for geostrophic balance (31.24) in pressure coordinates is a suitable starting point to derive thermal wind for the atmosphere. For this purpose, we take the pressure derivative, $\partial/\partial p$, of (31.24) to render

$$f \frac{\partial \boldsymbol{u}}{\partial p} = \hat{\boldsymbol{z}} \times \nabla_p \left[\frac{\partial \Phi}{\partial p} \right], \tag{31.47}$$

with $\Phi = g\,z$ the geopotential. The hydrostatic relation $\partial p/\partial z = -\rho\, g$ takes the form

$$\frac{\partial p}{\partial \Phi} = -\rho \Rightarrow \frac{\partial \Phi}{\partial p} = -1/\rho \tag{31.48}$$

in which case

$$f \frac{\partial \boldsymbol{u}}{\partial p} = -\hat{\boldsymbol{z}} \times \nabla_p (1/\rho). \tag{31.49}$$

Ideal gas atmosphere

The specific volume takes the following form for an ideal gas atmosphere (see Section 23.4.1)

$$\rho^{-1} = R^{\mathrm{M}}\, T/p. \tag{31.50}$$

Since the horizontal derivative in the thermal wind relation (31.49) is along pressure surfaces, we have

$$f\, \frac{\partial \boldsymbol{u}}{\partial p} = -\frac{R^{\mathrm{M}}}{p}\, [\hat{\boldsymbol{z}} \times \nabla_p T]\,. \tag{31.51}$$

This expression gives rise to the name "thermal wind", with vertical shears of the horizontal velocity generated by horizontal temperature gradients along isobars.

As for the ocean in equation (31.46), we vertically integrate the thermal wind expression (31.51), here between two pressure levels

$$\boldsymbol{u}(p_{\mathrm{A}}) - \boldsymbol{u}(p_{\mathrm{B}}) = f^{-1}\, R^{\mathrm{M}}\, \hat{\boldsymbol{z}} \times \nabla_p \left[\int_{p_{\mathrm{A}}}^{p_{\mathrm{B}}} \frac{T\, \mathrm{d}p}{p} \right], \tag{31.52}$$

where $p_{\mathrm{A}} < p_{\mathrm{B}}$, so that p_{A} is at a higher altitude than p_{B}. We define the thermal wind shear as the difference between the wind aloft (higher altitude and lower pressure) from that at a lower altitude (greater pressure)

$$\boldsymbol{u}_T = \boldsymbol{u}(p_{\mathrm{A}}) - \boldsymbol{u}(p_{\mathrm{B}}) \qquad \text{with } p_{\mathrm{A}} < p_{\mathrm{B}} \tag{31.53}$$

so that

$$\boldsymbol{u}_T = \frac{R^{\mathrm{M}}}{f}\, \hat{\boldsymbol{z}} \times \nabla_p \overline{T}^{\ln \mathrm{p}}, \tag{31.54}$$

where we introduced the log-pressure weighted temperature between the two pressure surfaces

$$\overline{T}^{\ln \mathrm{p}} = \int_{p_{\mathrm{A}}}^{p_{\mathrm{B}}} \frac{T\, \mathrm{d}p}{p}. \tag{31.55}$$

The relation (31.54) means that on the f-plane, R^{M}/f times the log-pressure weighted temperature serves as a streamfunction for the thermal wind shear. Reconsider the previous example where the polar regions are colder than tropics, so that in the northern hemisphere on pressure surfaces, $\partial \overline{T}^{\ln \mathrm{p}}/\partial y < 0$. Hence, the zonal westerly winds increase in magnitude with height. We depict this situation in Figure 31.8. Furthermore, the thermal wind shear points to the east. For a more general flow in the northern hemisphere, cold (less buoyant) air sits on the left side of the thermal wind shear and warm (buoyant) air on the right. The opposite orientation holds for the southern hemisphere since the Coriolis parameter is negative, $f < 0$.

Barotropic flow

Return to the thermal wind equation (31.49)

$$f\, \frac{\partial \boldsymbol{u}}{\partial p} = -\hat{\boldsymbol{z}} \times \nabla_p (1/\rho) = \frac{\hat{\boldsymbol{z}} \times \nabla_p \rho}{\rho^2}. \tag{31.56}$$

For the special case of density a function just of the pressure, $\rho = \rho(p)$, then $\nabla_p \rho = 0$. This situation defines a *barotropic* flow, which is characterized here by a horizontal geostrophic velocity with zero vertical variations. Note that we are here only concerned with the geostrophic flow. A density related to pressure through $\rho = \rho(p)$ can still support vertical variations of the ageostrophic flow.

We further discuss barotropic flow in Section 40.2 as part of our study of vorticity. As detailed

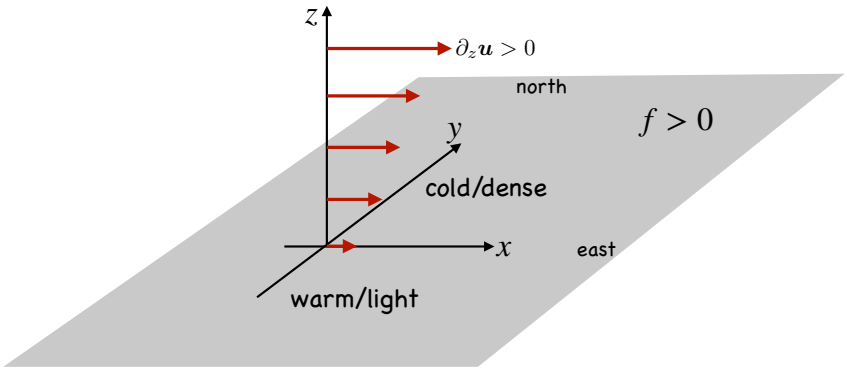

FIGURE 31.8: Thermal wind shear in the northern hemisphere ($f > 0$) middle latitude atmosphere, whereby cold/dense/less buoyant air sits to the north and warm/light/more buoyant air to the south. The zonal geostrophic winds increase to the east when rising in elevation, $\partial u/\partial z > 0$. We say that the zonal winds have an eastward thermal wind shear. In general, a geostrophic wind in the northern hemisphere atmosphere has cold/dense/less buoyant air to the left when facing downwind, whereas the opposite orientation holds for the southern hemisphere where $f < 0$.

in that discussion, the general definition of a barotropic flow is one whereby the *baroclinicity* vector vanishes, $\boldsymbol{B} = \nabla p \times \nabla(1/\rho) = 0$. The functional relation $\rho = \rho(p)$ (equivalently $p = p(\rho)$) is a sufficient condition for vanishing baroclinicity. As seen in Section 40.4, for a barotropic flow there is no generation of vorticity through the torques created when density isosurfaces deviate from pressure isosurfaces (isobars).

31.6.5 Thermal wind balance for a Boussinesq ocean

We here expose details for how to work with thermal wind in the ocean, accounting for the presence of both salinity and temperature in the equation of state, with this discussion following from that in Section 31.6.1. To start, consider the most general form of thermal wind according to equation (31.21)

$$f \frac{\partial(\rho \boldsymbol{u})}{\partial z} = -g \hat{\boldsymbol{z}} \times \nabla \rho. \tag{31.57}$$

Treatment of the *in situ* density depends on whether we consider a Boussinesq ocean (Chapter 29), as done for most of this section, versus a non-Boussinesq ocean. We here consider the Boussinesq ocean and then the non-Boussinesq ocean in Section 31.6.6.

For a Boussinesq ocean, the *in situ* density on the left hand side of equation (31.57) is set to the constant reference density, ρ_o, in which case the thermal wind relation is given by

$$f \rho_o \partial_z \boldsymbol{u} = -g \hat{\boldsymbol{z}} \times \nabla \rho. \tag{31.58}$$

Following from the discussion of Boussinesq energetics in Section 29.8.4, we know that the *in situ* density in a Boussinesq ocean takes the functional form of equation (29.212)

$$\rho = \rho[S(\boldsymbol{x}, t), \Theta(\boldsymbol{x}, t), p = -\rho_o \Phi(\boldsymbol{x}, t)]. \tag{31.59}$$

For geostrophic flows we are generally only concerned with the simple geopotential, $\Phi(\boldsymbol{x}, t) = g z$, which defines the local vertical direction, $\hat{\boldsymbol{z}}$. Hence, $\hat{\boldsymbol{z}} \times \nabla \rho$ picks out the horizontal derivatives of the *in situ* density along surfaces of constant geopotential

$$g \hat{\boldsymbol{z}} \times \nabla \rho = g \hat{\boldsymbol{z}} \times \nabla_h \rho. \tag{31.60}$$

We can thus express the horizontal *in situ* density gradient as

$$\nabla_h \rho = \left[\frac{\partial \rho}{\partial S}\right]_{\Theta,\Phi} \nabla_h S + \left[\frac{\partial \rho}{\partial \Theta}\right]_{S,\Phi} \nabla_h \Theta = \rho_o \, (\beta \, \nabla_h S - \alpha \, \nabla_h \Theta), \tag{31.61}$$

where we introduced the Boussinesq form of the haline contraction and thermal expansion coefficients

$$\beta = \frac{1}{\rho_o} \left[\frac{\partial \rho}{\partial S}\right]_{\Theta,\Phi} \qquad \text{and} \qquad \alpha = -\frac{1}{\rho_o} \left[\frac{\partial \rho}{\partial \Theta}\right]_{S,\Phi}. \tag{31.62}$$

These results lead to the oceanic Boussinesq form of the thermal wind relation

$$f \, \partial_z \boldsymbol{u} = -g \, \hat{\boldsymbol{z}} \times (\beta \, \nabla_h S - \alpha \, \nabla_h \Theta), \tag{31.63}$$

which decomposes the thermal wind shear into a contribution from horizontal gradients in S and from Θ. In some treatments, the right hand side contribution is referred to as the horizontal gradient of the locally referenced potential density (see Section 30.6.1). Correspondingly, one generally finds that vertical sections of the potential density (referenced to a pressure near to that where computing thermal wind) provide a useful means to determine the magnitude and direction of the thermal wind shears; more useful than sections of *in situ* density.

To help understand the geometry of the thermal wind equation (31.63), consider an ocean with a constant salinity and positive thermal expansion coefficient, so that

$$f \, \partial_z \boldsymbol{u} = g \, \alpha \, \hat{\boldsymbol{z}} \times \nabla_h \Theta \qquad \text{if } \nabla S = 0. \tag{31.64}$$

Hence, in the northern hemisphere ($f > 0$) the thermal wind shear is oriented with relatively warm water to the right of the shear, just like that shown for the atmosphere in Figure 31.8 and more generally as discussed in Figure 31.6. More generally, with a non-constant salinity the thermal wind shear is oriented with more buoyant waters to the right (in northern hemisphere), as per the vector, $\beta \, \nabla_h S - \alpha \, \nabla_h \Theta$, appearing on the right hand side of the thermal wind equation (31.63). This vector is proportional to the horizontal components of the dianeutral unit vector introduced in Section 30.5.3 and given by

$$\hat{\gamma} = \frac{-\alpha \, \nabla \Theta + \beta \, \nabla S}{|-\alpha \, \nabla \Theta + \beta \, \nabla S|} \qquad \text{so that} \qquad \hat{\gamma}_{\text{horz}} = \frac{-\alpha \, \nabla_h \Theta + \beta \, \nabla_h S}{|-\alpha \, \nabla \Theta + \beta \, \nabla S|}. \tag{31.65}$$

Evidently, the vertical shear of the horizontal geostrophic velocity is perpendicular to the horizontal projection of the dianeutral unit vector, with this orientation shown in Figure 31.9.

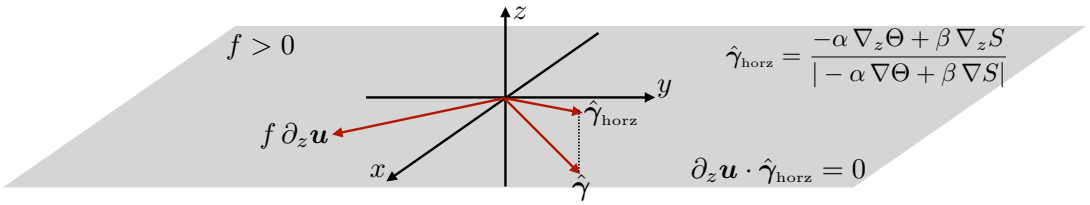

FIGURE 31.9: The thermal wind shear, $f \, \partial_z \boldsymbol{u}$, given by equation (31.63) is oriented perpendicular to the horizontal projection of the dianeutral unit vector given in equation (31.65). For example, with $\hat{\gamma}$ pointing towards less buoyant waters, the northern hemisphere thermal wind shear is oriented with more buoyant waters to the right when facing in the direction of the shear. For example, in an ocean with constant salinity, so that $\hat{\gamma}$ is normal to a constant Θ surface and pointing towards colder waters, then the thermal wind shear is oriented with warm water to the right of the shear. This orientation accords with that shown for the atmosphere in Figure 31.8 and more generally as per Figure 31.6.

31.6.6 Thermal wind for a non-Boussinesq hydrostatic ocean

We here expose details for how to work with thermal wind in a non-Boussinesq ocean, with this discussion following from that in Section 31.6.1. The formulation follows quite closely to a Boussinesq ocean, only now we start from the expression (31.49) for a compressible hydrostatic fluid using pressure as a vertical coordinate

$$\rho^2 f \frac{\partial \boldsymbol{u}}{\partial p} = \hat{\boldsymbol{z}} \times \nabla_p \rho. \tag{31.66}$$

For a non-Boussinesq ocean, we make use of the pressure dependence of the density so that

$$\rho = \rho[S(\boldsymbol{x}, t), \Theta(\boldsymbol{x}, t), p(\boldsymbol{x}, t)]. \tag{31.67}$$

The gradient operator in equation (31.66) is computed along surfaces of constant pressure so that

$$\nabla_p \rho = \left[\frac{\partial \rho}{\partial S}\right]_{\Theta,p} \nabla_p S + \left[\frac{\partial \rho}{\partial \Theta}\right]_{S,p} \nabla_p \Theta = \rho\,(\beta\,\nabla_p S - \alpha\,\nabla_p \Theta), \tag{31.68}$$

where we introduced the non-Boussinesq form of the haline contraction and thermal expansion coefficients

$$\beta = \frac{1}{\rho}\left[\frac{\partial \rho}{\partial S}\right]_{\Theta,p} \qquad \text{and} \qquad \alpha = -\frac{1}{\rho}\left[\frac{\partial \rho}{\partial \Theta}\right]_{S,p}. \tag{31.69}$$

In this manner we can write the thermal wind relation (31.66) as

$$\rho\, f \frac{\partial \boldsymbol{u}}{\partial p} = \hat{\boldsymbol{z}} \times (\beta\,\nabla_p S - \alpha\,\nabla_p \Theta). \tag{31.70}$$

This expression is directly analogous to the Boussinesq form given by equation (31.63). Indeed, we can go one step further by using the chain rule and the hydrostatic relation to write

$$\frac{\partial \boldsymbol{u}}{\partial p} = \frac{\partial \boldsymbol{u}}{\partial z}\frac{\partial z}{\partial p} = -(\rho\, g)^{-1} \frac{\partial \boldsymbol{u}}{\partial z}, \tag{31.71}$$

in which case the non-Boussinesq thermal wind takes on the form

$$f \frac{\partial \boldsymbol{u}}{\partial z} = -g\, \hat{\boldsymbol{z}} \times (\beta\,\nabla_p S - \alpha\,\nabla_p \Theta). \tag{31.72}$$

Now, the key distinction from the Boussinesq form (31.63) is the appearance of a constant pressure derivative, ∇_p, for the non-Boussinesq case, in contrast to the constant geopotential derivative, $\nabla_\hbar$, appearing in the Boussinesq case. Additionally, the non-Boussinesq case uses the slightly distinct form of α and β given by equation (31.69) rather than the Boussinesq form in equation (31.62).

31.7 Isopycnal form stress from geostrophic eddies

As introduced in Section 28.1, form stress is the horizontal stress arising from pressure acting on a sloped surface. The mathematical expression for the form stress acting on the top side of a surface is given by equation (28.6)

$$\boldsymbol{\Sigma}^{\text{form}} = p\,\nabla\eta, \tag{31.73}$$

with the opposite sign for the form stress on the bottom side of the surface. Here, $z = \eta(x, y, t)$ is the depth of the surface (see Figure 28.3 or Figure 31.10). The net horizontal force from form stress is the area integral over the surface.

In this section we examine the zonal mean zonal form stress acting on an isopycnal surface (Section 31.7.1) and on an isopycnal layer (Section 31.7.2), each for an adiabatic, Boussinesq, hydrostatic fluid in geostrophic balance and within a zonally periodic channel of length L. We furthermore assume the fluid density is a linear function of Θ to remove compressibility effects and focus on the dynamics rather than also consider the thermodynamics. As we show, the zonal mean zonal form stress arising from geostrophically balanced fluctuations provide an eastward acceleration to the fluid. At the same time, these *geostrophic eddies* transport buoyancy and thickness/volume meridionally.

Although the channel geometry is rather simple, it has applications to the middle latitude atmospheric circulation as well as for ocean circulation, particularly in the Southern Ocean where there is circumpolar channel-like flow within the Antarctic Circumpolar Current. Furthermore, the discussion exposes key elements of eddy-mean flow interactions, sharing points with the leading order generalized Lagrangian mean of Section 70.2 and the quasi-Stokes transport discussed in Section 71.3. Elements from this section rely on material discussed later in the book (we point to the relevant sections), so that it is best suited for those having some understanding of that material.

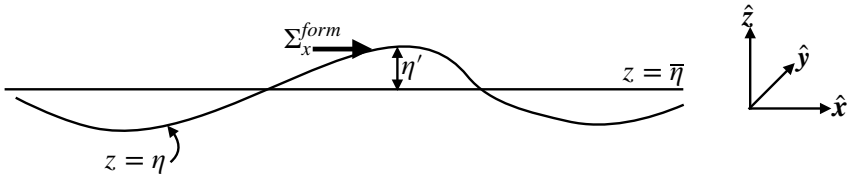

FIGURE 31.10: Schematic of the zonal form stress, $\Sigma_x^{\rm form}$, acting on a surface whose zonal mean vertical position is $z = \overline{\eta}(y,t)$ and whose vertical position relative to the zonal mean is $z = \overline{\eta}(y,t) + \eta'(x,y,t)$.

31.7.1 Zonal mean zonal form stress on an isopycnal surface

We are here interested in the form stress acting on an isopycnal surface. Before specializing to an isopycnal, we decompose the form stress according to the zonal mean depth and its deviation from zonal mean (see Figure 31.10). Thereafter, specialization to an isopycnal surface in an adiabatic fluid connects the zonal mean form stress to the meridional eddy flux of buoyancy.

Zonal form stress on an arbitrary surface in a channel

The zonal mean vertical position of a surface is written

$$\overline{\eta}(y,t) = \frac{1}{L} \int_0^L \eta(x,y,t)\, \mathrm{d}x \tag{31.74}$$

and its corresponding zonal fluctuation is

$$\eta' = \eta - \overline{\eta}. \tag{31.75}$$

The zonal component of the form stress acting on this surface is thus given by

$$\begin{aligned} p\, \partial_x \eta &= p(x, \overline{\eta} + \eta')\, \partial_x (\overline{\eta} + \eta') && \text{(31.76a)} \\ &= p(x, \overline{\eta} + \eta')\, \partial_x \eta' && \text{(31.76b)} \\ &\approx [p(x,\overline{\eta}) + \partial_z p(x,\overline{\eta})\, \eta']\, \partial_x \eta' && \text{(31.76c)} \\ &= p(x,\overline{\eta})\, \partial_x \eta' + \mathcal{O}(\eta')^2. && \text{(31.76d)} \end{aligned}$$

Hence, to second order in fluctuations, η', the zonal form stress acting on the surface equals to $p(x, \overline{\eta})\, \partial_x \eta'$, where it is important to note that pressure is evaluated at the zonal mean depth, $z = \overline{\eta}$.

To within the same accuracy, the zonal integral of the zonal form stress is given by

$$\int_0^L \Sigma_x^{\text{form}}\, \mathrm{d}x \approx \int_0^L p(\overline{\eta})\, (\partial \eta'/\partial x)\, \mathrm{d}x = -\int_0^L \eta'\, [\partial p(\overline{\eta})/\partial x]\, \mathrm{d}x. \tag{31.77}$$

The final equality follows from zonal periodicity, which allows us to introduce the dual form stress inside the integral.[7] Now assume the zonal pressure gradient at $\overline{\eta}$ is balanced by a meridional geostrophic velocity at the same vertical position

$$\partial p(\overline{\eta})/\partial x = f \rho_\circ\, v(\overline{\eta}). \tag{31.78}$$

We can now decompose $v(\overline{\eta})$ into a mean and fluctuation,

$$v(\overline{\eta}) = \overline{v}(\overline{\eta}) + v'(\overline{\eta}), \tag{31.79}$$

so that

$$\int_0^L \Sigma_x^{\text{form}}\, \mathrm{d}x = -\rho_\circ\, f \int_0^L \eta'\, v'\, \mathrm{d}x, \tag{31.80}$$

where we noted that the Coriolis parameter is independent of zonal position and so can be pulled outside of the zonal integral. Hence, there is a nonzero zonal mean zonal form stress when there is a nonzero zonal correlation between fluctuations in the meridional velocity and the depth of the surface

$$\overline{\Sigma}_x^{\text{form}} = -\rho_\circ\, f\, \overline{v'\, \eta'}. \tag{31.81}$$

Zonal mean zonal form stress acting on an isopycnal surface

To further unpack the correlation appearing in equation (31.81), specialize to the case of an isopycnal surface in an adiabatic fluid. As shown in our discussion of generalized Lagrangian mean averaging in Sections 70.2.6 and 70.4.7, vertical fluctuations in the position of the isopycnal surfaces, relative to the zonal mean $\overline{\eta}$, are related to zonal fluctuations in the density

$$\eta' \approx -\frac{\rho'}{\partial \overline{\rho}/\partial z} = -\frac{b'}{N^2}, \tag{31.82}$$

where we introduced the squared buoyancy frequency of the zonal mean state as well as the fluctuating buoyancy

$$N^2 = -\frac{g}{\rho_\circ}\frac{\partial \overline{\rho}}{\partial z} \qquad \text{and} \qquad b' = -\frac{g\, \rho'}{\rho_\circ}. \tag{31.83}$$

The zonally averaged zonal form stress thus takes the form

$$\overline{\Sigma}_x^{\text{form}} = \frac{\rho_\circ\, f}{N^2}\, \overline{v'\, b'}. \tag{31.84}$$

Again, the assumptions rendering the result (31.84) are (i) zonal periodicity, (ii) adiabatic and Boussinesq fluid, (iii) geostrophically balanced flow. Under these assumptions, the zonal mean zonal form stress acting on an isopycnal surface is proportional to the zonal correlation between fluctuations in the meridional velocity and the buoyancy. It is a general property of unstable

[7] We discussed the relation between form stress and dual form stress in Section 28.4.4. The dual form stress here appears because the channel is zonally periodic. Hence, a zonal integral of the form stress equals (with a minus sign) to the zonal integral of the dual form stress.

quasi-geostrophic eddies in the atmosphere and ocean to transport positive buoyancy (e.g., warm air/water) poleward and negative buoyancy (e.g., cold air/water) equatorward, thus ameliorating the equator-to-pole buoyancy difference setup by solar radiation that preferentially warms the tropics. More generally, as shown in Section 62.9, unstable quasi-geostrophic disturbances, such as those associated with *baroclinic instability*, transport buoyancy down the horizontal buoyancy gradient. Evidently, with buoyancy decreasing poleward, such disturbances transport buoyancy poleward. In turn, this property of geostrophic eddies leads to a positive zonal mean zonal form stress

$$\overline{\Sigma}_x^{\text{form}} > 0. \tag{31.85}$$

Hence, in addition to transporting buoyancy poleward, geostrophic eddies provide a positive zonal mean force through zonal integrated form stress that accelerates the fluid in the eastward direction. These two properties of geostrophic eddies (poleward flux of positive buoyancy anomalies along with an eastward acceleration from form stress) are fundamental to the middle latitude atmospheric circulation as well as for ocean circulation, particularly within the channel-like Antarctic Circumpolar Current.

31.7.2 Zonal mean zonal form stress acting on an isopycnal layer

We here offer another lens to understand the zonal mean zonal form stress by examining the form stress acting on a constant density layer of adiabatic Boussinesq fluid such as shown in Figure 31.11. This layered/isopycnal analysis anticipates some of the development considered for the stacked shallow water model in Chapters 35 and 36 as well as for isopycnal models in Section 66.2.

The net form stress acting on the upper and lower layer interfaces in Figure 31.11 is given by

$$\begin{aligned}
\boldsymbol{\Sigma}^{\text{layer form}} &= p_1 \nabla \eta_1 - p_2 \nabla \eta_2 && \text{(31.86a)}\\
&= p(\eta + h/2)\, \nabla(\eta + h/2) - p(\eta - h/2)\, \nabla(\eta - h/2) && \text{(31.86b)}\\
&\approx [p(\eta) - \rho\, g\, h/2]\, \nabla(\eta + h/2) - [p(\eta) + \rho\, g\, h/2]\, \nabla(\eta - h/2) && \text{(31.86c)}\\
&= p\, \nabla h - \rho\, g\, h\, \nabla \eta && \text{(31.86d)}\\
&= \nabla(p\, h) - h\, \nabla(p + \rho\, g\, \eta) && \text{(31.86e)}\\
&= \nabla(p\, h) - \rho_o\, h\, \nabla M. && \text{(31.86f)}
\end{aligned}$$

In this relation we set $z = \eta$ for the vertical position at the center of the layer, introduced the Montgomery potential from Section 66.2.1

$$M \rho_o = p + \rho\, g\, \eta, \tag{31.87}$$

and noted that ρ is a uniform constant layer density so that it commutes with the horizontal gradient operator computed along ρ surfaces. We also made use of the hydrostatic balance to approximate the interface pressures as

$$\begin{aligned}
p(\eta + h/2) &\approx p(\eta) + \frac{\partial p}{\partial z}\frac{h}{2} = p(\eta) - \rho\, g\, h/2 && \text{(31.88a)}\\
p(\eta - h/2) &\approx p(\eta) - \frac{\partial p}{\partial z}\frac{h}{2} = p(\eta) + \rho\, g\, h/2. && \text{(31.88b)}
\end{aligned}$$

The zonal mean of the zonal layer form stress is thus given by the correlation between the layer thickness fluctuations and fluctuations in the zonal derivative of the Montgomery potential

$$\overline{\Sigma}_x^{\text{layer form}} = -\rho_o\, \overline{h'\, \partial M'/\partial x}, \tag{31.89}$$

where we set $\overline{\partial M/\partial x} = 0$ due to zonal periodicity. As seen in Section 66.2.1, the Montgomery potential is the geostrophic streamfunction in isopycnal coordinates, so that the fluctuating meridional geostrophic velocity is given by

$$f\, v' = \partial_x M'. \tag{31.90}$$

Consequently, the zonal mean zonal form stress acting on the layer equals to the correlation between the thickness fluctuations and fluctuations in the meridional geostrophic velocity

$$\overline{\Sigma}_x^{\text{layer form}} = -\rho_o\, f\, \overline{v'\, h'}. \tag{31.91}$$

Hence, as the geostrophic eddies provide a net eastward acceleration to the layer (equation (31.85)), they also move volume meridionally within isopycnal layers, moving positive thickness fluctuations equatorward.

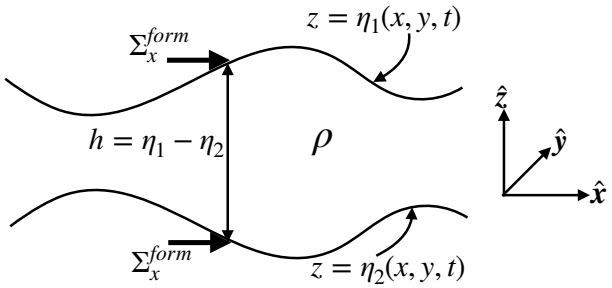

FIGURE 31.11: Schematic of a constant density layer of an adiabatic, hydrostatic, Boussinesq fluid with thickness $h(x, y, t) = \eta_1(x, y, t) - \eta_2(x, y, t) = (\eta + h/2) - (\eta - h/2)$, and uniform density $\rho =$ constant. East points to the right and north is oriented into the page. The zonal form stress, Σ_x^{form}, acting on the upper and lower interfaces at a horizontal position (x, y) are shown by the thick horizontal vectors. The zonal form stress is the horizontal component of the pressure force per area acting on the layer interfaces, with the sign of the form stress determined by the slope of the layer interface. For a zonally periodic fluid layer, the net zonal pressure force acting on the layer arises from the zonal form stress integrated over the layer interfaces.

To further understand the physics of the form stress in equation (31.91), parameterize the velocity-thickness eddy correlation, $\overline{v'\, h'}$, by downgradient diffusion of thickness

$$\overline{v'\, h'} = -\kappa\, \partial_y \overline{h}, \tag{31.92}$$

where $\kappa > 0$ is a nonzero kinematic diffusivity (dimensions of squared length per time). This parameterization is suggested by the work of *Gent and McWilliams* (1990) as discussed in Section 71.3.6. As noted there, thickness diffusion as a parameterization reflects the general tendency of geostrophic eddies to reduce horizontal gradients in layer thickness as they reduce the available potential energy of the flow. In this case the zonal mean zonal form stress is

$$\overline{\Sigma}_x^{\text{layer form}} = \rho_o\, f\, \kappa\, \partial_y \overline{h}. \tag{31.93}$$

So in the northern hemisphere in regions where the zonal mean layer thickness increases to the north, $\partial_y \overline{h} > 0$, there is a corresponding eastward zonal mean zonal form stress arising from parameterized geostrophic eddies acting on layer thickness. This situation corresponds to the case in Section 31.7.1, where we saw that geostrophic eddies preferentially transport positive buoyancy anomalies poleward and negative buoyancy anomalies equatorward. In the present analysis, meridional changes to the layer thickness correspond to a nonzero thermal wind shear. If layer thickness increases poleward, as for the case of weaker vertical stratification in the high latitudes, then the zonal velocity has a positive vertical shear, thus contributing an eastward zonal mean form stress.

31.7.3 Comments and further study

A key feature of geostrophic eddies exposed by this discussion concerns the connection between zonal form stress (providing an eastward force on the zonally periodic channel flow) and meridional eddy transport of buoyancy (positive buoyancy anomalies are transported poleward) and thickness (positive thickness anomalies are transported equatorward). The periodic channel domain is highly idealized. Nonetheless, the basic ideas form the roots for much of how we think about geostrophic eddies in the middle latitude atmosphere and the Southern Ocean. Further generalizations lead to the generalized Lagrangian mean, whose kinematic rudiments are discussed in Section 70.2, as well as the thickness weighted average, discussed in Chapter 67.

The fundamental role of form stress in geostrophic turbulent flows is pedagogically treated by *Vallis* (2017). See, in particular, his Chapter 21 for a thorough and insightful discussion of circulation in the Southern Ocean. We also return to form stress within the shallow water fluid in Section 36.4. That discussion complements the presentation given here, with a focus on a layer of shallow water fluid. We also touch on the notions of form stress when discussing the *Gent and McWilliams* (1990) mesoscale eddy parameterization in Section 71.3.

31.8 Exercises

EXERCISE 31.1: SMALL ROSSBY NUMBER AT HUMAN SCALES
Consider motion of a car at a speed $U \sim 10^5$ m hour^{-1} and a length scale of $L \sim 10$ m. Furthermore, assume the car is moving at 30°N latitude so that $f_{\text{human}} = 2\,\Omega_{\text{human}} \sin\phi = \Omega_{\text{human}}$.

(a) What is the rotation rate of the planet and corresponding rotation period, $T_{\text{human}} = 2\pi/\Omega_{\text{human}}$, required to render a unit Rossby number (Ro = 1) for the given "human" sized scales? Give resulting rotation rate in units of inverse seconds and period in seconds.

(b) If the earth rotated at the angular speed Ω_{human}, what would be the rigid-body speed for a point at rest on the earth's surface at the equator? Give result in units of meter per second.

(c) How does the rigid-body speed compare to the speed of sound at standard atmospheric conditions? What about the root-mean-square speed for air molecules? Hint: read Section 16.3.4.

(d) Discuss an astronomical object that has a very large rotational speed. Hint: 1993 Nobel Prize in physics.

EXERCISE 31.2: THE BETA SPIRAL
Consider a steady state Boussinesq planetary geostrophic fluid in the absence of mixing. Write the geostrophic velocity as

$$u = |\boldsymbol{u}| \cos\Delta \qquad v = |\boldsymbol{u}| \sin\Delta, \tag{31.94}$$

where Δ is the angle measured counter-clockwise from east. Use thermal wind and the steady state perfect fluid buoyancy equation to determine an expression for $\partial\Delta/\partial z$. Show that for $f > 0$ (northern hemisphere) and $\partial b/\partial z = N^2 > 0$ (gravitationally stable fluid column; see Section 30.5), then $\partial\Delta/\partial z$ has opposite sign from the vertical velocity, w. This spiralling of the geostrophic velocity is known as the *beta spiral* in oceanography.

EXERCISE 31.3: ALTERNATIVE FORM OF THERMAL WIND
Consider a fluid with density a function of pressure and potential temperature

$$\rho = \rho(\theta, p). \tag{31.95}$$

A physical realization of this equation of state is a lake. Show that the thermal wind shear for a hydrostatic and *compressible* fluid with this equation of state can be written in the form

$$\frac{\partial \boldsymbol{u}}{\partial z} = \left[\frac{N^2}{f\,\rho\,g}\right](\hat{\boldsymbol{z}} \times \nabla_\theta p), \tag{31.96}$$

where

$$N^2 = -\frac{g}{\rho}\frac{\partial \rho}{\partial \theta}\frac{\partial \theta}{\partial z} = g\,\alpha_\theta\,\frac{\partial \theta}{\partial z} > 0 \tag{31.97}$$

is the squared buoyancy frequency, assumed positive so that the fluid is gravitationally stable in the vertical (see Section 30.6). The term α_θ is the thermal expansion coefficient written in terms of potential temperature (Section 30.3.4),

$$\alpha_\theta = -(1/\rho)\,\partial\rho/\partial\theta > 0. \tag{31.98}$$

Finally, the horizontal gradient projected onto constant θ surfaces is given by (see Section 63.12.2)

$$\nabla_\theta = \hat{\boldsymbol{x}}\left[\frac{\partial}{\partial x}\right]_{y,\theta} + \hat{\boldsymbol{y}}\left[\frac{\partial}{\partial y}\right]_{x,\theta} \tag{31.99a}$$

$$= \nabla_h - \left[\frac{\nabla_h \theta}{\partial\theta/\partial z}\right]\frac{\partial}{\partial z}. \tag{31.99b}$$

Hint: This exercise requires careful use of the chain rule and the hydrostatic relation, along with the equations given in the problem statement. Furthermore, assume the fluid is fully compressible.

Hint: Some may wish to "warm-up" by showing that the result holds for the simpler equation of state $\rho = \rho(\theta)$. Some of the steps used for the simpler case are relevant for the case with $\rho = \rho(\theta, p)$.

Chapter 32

TANGENT PLANE FLOW BALANCES

We here consider a variety of inviscid tangent plane (horizontal) flow regimes characterized by a balance between a subset of terms appearing in the horizontal momentum equation. This discussion allows us to directly compare the geostrophically balanced flow of Chapter 31 to a variety of other balanced flows such as gradient wind, inertial motion, and cyclostrophic balance. We provide a categorization of the flow following *natural coordinates* or *intrinsic coordinates*, which offer a concise means to compare the relative magnitudes of the Coriolis, pressure, and centrifugal accelerations acting on a fluid element moving horizontally.[1]

READER'S GUIDE TO THIS CHAPTER

We make use of the hydrostatic primitive equations from Section 27.1, along with the Boussinesq aporoximation from Section 29.1. We also assume an understanding of the geostrophic balance from Chapter 31, and use of some geometric notions discussed in Chapter 5, though most of the salient math points are revisited here so that Chapter 5 is an option rather than a requirement. Throughout this chapter we assume a tangent plane geometry and associated equations from Section 24.5, thus allowing for Cartesian coordinates. Also, we ignore all vertical motion. Some of this material is used in subsequent chapters, in particular Chapter 33 on Ekman dynamics as well as Chapters 43 and 45 on quasi-geostrophy.

[1] It is important to recall from Section 13.10.4 that motion on a geopotential incorporates the acceleration from both the central gravitational field and the planetary centrifugal acceleration. This property holds for the tangent plane approximation assumed in this chapter, whereby a geopotential is assumed to be horizontal. Consequently, planetary centrifugal acceleration is absorbed by the geopotential and so it does not appear here.

32.1 Loose ends

- How to determine whether the velocity field is divergent or non-divergent for the cyclostrophic and gradient wind motions?
- Exercises needed for this chapter.

32.2 Horizontal flow described by natural coordinates

In this section we decompose the horizontal Boussinesq momentum equation into motion parallel to and motion perpendicular to the instantaneous trajectory of a fluid element moving along a constant geopoential surface. That is, we characterize the velocity and acceleration according to the local flow direction. Furthermore, we are only concerned with motion on a constant geopotetial using the tangent plane approximation; i.e., horizontal motion.[2] The *natural coordinates* arising from this description exposes the centripetal/centrifugal acceleration that arises from curvature in the trajectory as measured by the radius of curvature. This non-inertial acceleration is distinct from the centrifugal acceleration that arises from planetary rotation, with planetary centrifugal acceleration already contained within the effective gravitational acceleration that acts in the local vertical direction (see Section 13.8.1). We also decompose the accelerations from pressure, friction, and Coriolis into their natural coordinate components.

32.2.1 Natural coordinates

Natural coordinates for horizontal motion are defined by a locally orthogonal set of unit vectors (see Figure 32.1)

$$\hat{\boldsymbol{z}} = \hat{\boldsymbol{u}} \times \hat{\boldsymbol{n}} = \text{vertical direction} \tag{32.1a}$$
$$\hat{\boldsymbol{u}} = \hat{\boldsymbol{n}} \times \hat{\boldsymbol{z}} = \text{tangent to horizontal velocity} \tag{32.1b}$$
$$\hat{\boldsymbol{n}} = \hat{\boldsymbol{z}} \times \hat{\boldsymbol{u}} = \text{normal direction to the left of motion.} \tag{32.1c}$$

The unit vector, $\hat{\boldsymbol{u}}$, is tangent to the velocity vector (which is horizontal), so that

$$\boldsymbol{u} = |\boldsymbol{u}|\, \hat{\boldsymbol{u}} = \frac{\mathrm{D}s}{\mathrm{D}t}\, \hat{\boldsymbol{u}}, \tag{32.2}$$

where s is the arc-length measured along the trajectory as introduced in Section 2.4. The unit vector, $\hat{\boldsymbol{n}}$, is perpendicular to the velocity and points to the left of the trajectory facing downstream.

[2]The two-dimensional motion considered here can be generalized to three-dimensional motion through use of the *Frénet equations* from differential geometry. An introduction to this approach for fluid motion is provided by Section 20 of *Serrin* (1959) and Section 15.3.4 of *Dahlen and Tromp* (1998).

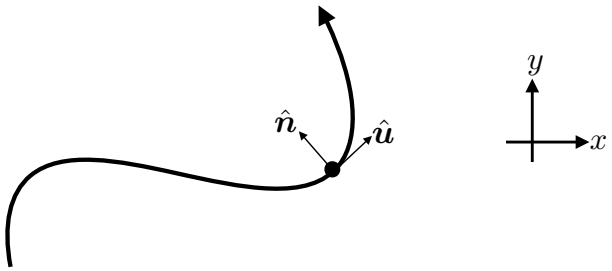

FIGURE 32.1: Illustrating the decomposition of horizontal motion of a fluid element into natural coordinate directions. These directions are defined by a unit tangent vector, $\hat{\boldsymbol{u}}$, pointing in the direction of the fluid element motion, and a unit normal vector, $\hat{\boldsymbol{n}}$, pointing to the left of the motion facing downstream.

32.2.2 Material acceleration

When writing the velocity according to equation (32.2), we decompose the acceleration into the change in speed and change in direction

$$\frac{\mathrm{D}\boldsymbol{u}}{\mathrm{D}t} = \frac{\mathrm{D}|\boldsymbol{u}|}{\mathrm{D}t}\,\hat{\boldsymbol{u}} + |\boldsymbol{u}|\,\frac{\mathrm{D}\hat{\boldsymbol{u}}}{\mathrm{D}t}. \tag{32.3}$$

Following our discussion of rigid-body rotational motion in Section 11.2 (see Figure 11.2), the magnitude of the direction change can be written in terms of the infinitesimal angle swept out by the motion as the fluid element moves along a trajectory

$$|\delta\hat{\boldsymbol{u}}| = |\delta\vartheta|. \tag{32.4}$$

The infinitesimal angle swept out by the trajectory is related to the radius of curvature, R (Figure 32.2), and the arc-length increment, δs, traversed by the trajectory

$$\delta\vartheta = \frac{\delta s}{R}. \tag{32.5}$$

Finally, the infinitesimal change in tangent, $\delta\hat{\boldsymbol{u}}$, is directed normal to the motion, which we see by noting

$$\hat{\boldsymbol{u}}\cdot\hat{\boldsymbol{u}} = 1 \Longrightarrow \delta\hat{\boldsymbol{u}}\cdot\hat{\boldsymbol{u}} = 0. \tag{32.6}$$

That is, $\delta\hat{\boldsymbol{u}}$ is orthogonal to $\hat{\boldsymbol{u}}$, so that it points either parallel or anti-parallel to $\hat{\boldsymbol{n}}$. We detailed this property of rotating unit vectors in Section 2.1.4 (see Figure 2.2). Our convention is that $\hat{\boldsymbol{n}}$ points to the left of $\hat{\boldsymbol{u}}$, so that if the trajectory turns to the left, then $\delta\hat{\boldsymbol{u}}$ points parallel to $\hat{\boldsymbol{n}}$, whereas if the trajectory turns to the right then $\delta\hat{\boldsymbol{u}}$ points anti-parallel to $\hat{\boldsymbol{n}}$. That is, $\delta\hat{\boldsymbol{u}}$ always points towards the center of the circle used to compute the radius of curvature as in Figure 32.2.

Bringing these results together leads to the expression for the infinitesimal unit vector change

$$\delta\hat{\boldsymbol{u}} = \hat{\boldsymbol{n}}\,\frac{\delta s}{R}. \tag{32.7}$$

Our sign convention takes $R > 0$ for a fluid element turning in the direction of $\hat{\boldsymbol{n}}$ (to the left facing downstream) and $R < 0$ when turning opposite to $\hat{\boldsymbol{n}}$ (to the right facing downstream). Hence, the material time change is

$$\frac{\mathrm{D}\hat{\boldsymbol{u}}}{\mathrm{D}t} = \frac{\mathrm{D}\hat{\boldsymbol{u}}}{\mathrm{D}s}\,\frac{\mathrm{D}s}{\mathrm{D}t} = \frac{\hat{\boldsymbol{n}}}{R}\,\frac{\mathrm{D}s}{\mathrm{D}t} = \frac{\hat{\boldsymbol{n}}}{R}\,|\boldsymbol{u}|, \tag{32.8}$$

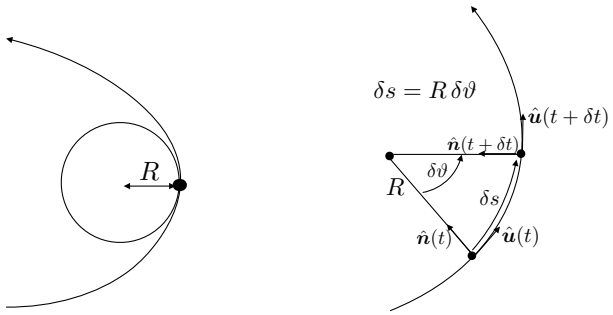

FIGURE 32.2: The left panel illustrates the radius of curvature associated with turning motion of a fluid element. The radius of curvature equals to the radius of a tangent circle (the *curvature circle*) that approximates, to second order accuracy, the trajectory at a particular point. The radius is smaller in magnitude when the trajectory is highly curved, and $|R| = \infty$ when the trajectory is straight. The radius is positive when the trajectory turns into the normal direction as depicted here (to the left; concave as defined by $\hat{\boldsymbol{n}}$) and negative when turning in the opposite direction (to the right; convex as defined by $\hat{\boldsymbol{n}}$). See Section 5.2 for more details on curvature, with Figure 5.4 offering more details for how to determine the radius of curvature. The right panel shows the time evolution of the unit vectors, $\hat{\boldsymbol{u}}$ and $\hat{\boldsymbol{n}}$, along a trajectory, with these unit vectors oriented along ($\hat{\boldsymbol{u}}$) and to the left ($\hat{\boldsymbol{n}}$) of the motion. For simplicity, we depict motion on a circle, so that the radius of curvature, R, remains constant and is equal to the circle's radius. In general, the radius also changes along the trajectory.

where the speed is given by the time change of the arc-length along the trajectory

$$|\boldsymbol{u}| = \frac{\mathrm{D}s}{\mathrm{D}t}. \tag{32.9}$$

Combining these results renders the acceleration

$$\frac{\mathrm{D}\boldsymbol{u}}{\mathrm{D}t} = \frac{\mathrm{D}|\boldsymbol{u}|}{\mathrm{D}t}\,\hat{\boldsymbol{u}} + \frac{|\boldsymbol{u}|^2}{R}\,\hat{\boldsymbol{n}} = \frac{\mathrm{D}^2 s}{\mathrm{D}t^2}\,\hat{\boldsymbol{u}} + \frac{|\boldsymbol{u}|^2}{R}\,\hat{\boldsymbol{n}}. \tag{32.10}$$

The acceleration has thus been decomposed into the change in speed of the fluid element along the direction of the motion, plus the centripetal acceleration due to curvature of the trajectory. In Section 32.2.3 we justify referring to $\hat{\boldsymbol{n}}\,|\boldsymbol{u}|^2/R$ as the *centripetal* acceleration.

32.2.3 Centripetal and centrifugal accelerations

The centripetal acceleration points towards the concave side of a turning trajectory: "centripetal" means "towards the center." Its opposing partner, the centrifugal ("away from center") acceleration points to the convex side (see Figure 32.3). So how do we interpret $\hat{\boldsymbol{n}}\,|\boldsymbol{u}|^2/R$? For motion turning to the left, towards $\hat{\boldsymbol{n}}$, the radius of curvature is positive, $R > 0$, so that $\hat{\boldsymbol{n}}\,|\boldsymbol{u}|^2/R$ points to the concave side of the trajectory (left side). For a trajectory turning to the right then $R < 0$, which again means that $\hat{\boldsymbol{n}}\,|\boldsymbol{u}|^2/R$ points to the concave side (now on the right). We conclude that the acceleration $\hat{\boldsymbol{n}}\,|\boldsymbol{u}|^2/R$ indeed represents a centripetal acceleration and $-\hat{\boldsymbol{n}}\,|\boldsymbol{u}|^2/R$ is the centrifugal acceleration.

32.2.4 Coriolis and pressure gradient

The Coriolis acceleration takes the following form in natural coordinates

$$-f\,\hat{\boldsymbol{z}} \times \boldsymbol{u} = -(\hat{\boldsymbol{z}} \times \hat{\boldsymbol{u}})\,f\,|\boldsymbol{u}| = -\hat{\boldsymbol{n}}\,f\,|\boldsymbol{u}|, \tag{32.11}$$

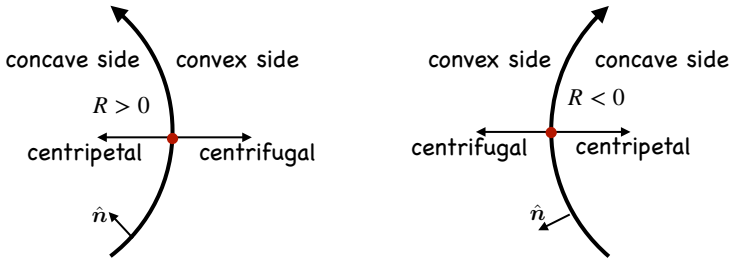

FIGURE 32.3: Centripetal acceleration of a turning fluid element, $\hat{\boldsymbol{n}} |\boldsymbol{u}|^2/R$, points to the concave side of the curve (towards the center) whereas the centrifugal acceleration, $-\hat{\boldsymbol{n}} |\boldsymbol{u}|^2/R$, points to the convex side (away from the center). The centripetal and centrifugal accelerations are paired action/reaction accelerations. The normal unit vector, $\hat{\boldsymbol{n}}$, always points to the left of the motion, whereas the radius of curvature, R, is positive or negative depending on the direction of the turning motion. For a left turning trajectory (in direction of $\hat{\boldsymbol{n}}$), the concave side is on the left and has positive radius of curvature, $R > 0$, whereas for the right turning trajectory (opposite direction of $\hat{\boldsymbol{n}}$) the concave side is to the right with $R < 0$. To help remember the signs, note that centrifugal means "away from the center" whereas centripetal means "towards the center". It is the centrifugal acceleration that pulls one away from the center of a merry-go-round whereas one's arms and hands provide the balancing centripetal acceleration.

so that the Coriolis acceleration always points to the right of the flow direction for $f > 0$. In contrast, the pressure gradient has two components

$$\nabla p = \hat{\boldsymbol{u}} \, (\hat{\boldsymbol{u}} \cdot \nabla p) + \hat{\boldsymbol{n}} \, (\hat{\boldsymbol{n}} \cdot \nabla p) = \hat{\boldsymbol{u}} \, \frac{\partial p}{\partial s} + \hat{\boldsymbol{n}} \, \frac{\partial p}{\partial n}, \tag{32.12}$$

one pointing along the flow direction and one normal to the direction.

32.2.5 Horizontal momentum equation and local Rossby number

Bringing the above results together leads to the horizontal momentum equation as decomposed into natural coordinates

$$\frac{\mathrm{D}|\boldsymbol{u}|}{\mathrm{D}t} = -\frac{1}{\rho_o} \frac{\partial p}{\partial s} + \boldsymbol{F} \cdot \hat{\boldsymbol{u}} \qquad \text{motion in } \hat{\boldsymbol{u}} \text{ direction} \tag{32.13a}$$

$$\frac{|\boldsymbol{u}|^2}{R} + f \, |\boldsymbol{u}| = -\frac{1}{\rho_o} \frac{\partial p}{\partial n} + \boldsymbol{F} \cdot \hat{\boldsymbol{n}} \qquad \text{motion in } \hat{\boldsymbol{n}} \text{ direction (perpendicular to } \hat{\boldsymbol{u}}), \tag{32.13b}$$

where $\boldsymbol{F}$ is the frictional acceleration and ρ_o is the reference density for the Boussinesq ocean. These equations decompose the accelerations into those acting parallel to and normal to the trajectory. It is notable that the equation for the normal component is purely diagnostic; there is no time derivative in equation (32.13b). Instead, it is a balance containing accelerations from centripetal, Coriolis, normal pressure gradient, and normal component of friction. In the next few sections we consider certain limiting cases as revealed by the equations of motion (32.13a) and (32.13b). Friction remains zero in this chapter but is nonzero for the discussion of Ekman mechanics in Chapter 33.

Steady frictionless flow

The frictionless balanced motions considered in this chapter all occur with a fixed velocity magnitude for the fluid element, so that the along-trajectory component of the momentum equation (32.13a) for frictionless motion reduces to

$$\frac{\mathrm{D}|\boldsymbol{u}|}{\mathrm{D}t} = -\frac{1}{\rho_o} \frac{\partial p}{\partial s} = 0. \tag{32.14}$$

Hence, there is no pressure gradient along the direction of the fluid element motion. Correspondingly, the frictionless fluid motion preserves its kinetic energy

$$\frac{1}{2}\frac{\mathrm{D}(\boldsymbol{u}\cdot\boldsymbol{u})}{\mathrm{D}t} = |\boldsymbol{u}|\,\frac{\mathrm{D}|\boldsymbol{u}|}{\mathrm{D}t} = 0. \tag{32.15}$$

Local Rossby number

As discussed in Section 31.3, the Rossby number is the ratio of the acceleration from velocity advection to the Coriolis acceleration. In the normal component to the momentum equation (32.13b), we have the advection term manifest as the local centrifugal term. Following Chapter 1 of *van Heijst* (2010) we define the *local Rossby number* as the ratio of the centrifugal acceleration to the Coriolis acceleration

$$\mathrm{Ro}_{\mathrm{local}} = \frac{|\boldsymbol{u}|^2/R}{f/|\boldsymbol{u}|} = \frac{|\boldsymbol{u}|}{R\,f}, \tag{32.16}$$

where, again, R is the radius of curvature for the motion. In this chapter we consider flow regimes as determined by values of the local Rossby number.

32.2.6 Decomposition of the acceleration

The horizontal equations of motion (32.13a) and (32.13b) offer a relatively simple and insightful description of the motion. We here provide a connection with the traditional Eulerian form of the equations of motion.

Advective form of the acceleration

The standard form of the material time derivative for horizontal motion is given by

$$\frac{\partial \boldsymbol{u}}{\partial t} + (\boldsymbol{u}\cdot\nabla)\,\boldsymbol{u} = \frac{\mathrm{D}|\boldsymbol{u}|}{\mathrm{D}t}\,\hat{\boldsymbol{u}} + \frac{|\boldsymbol{u}|^2}{R}\,\hat{\boldsymbol{n}}, \tag{32.17}$$

so that

$$\hat{\boldsymbol{u}}\cdot\left[\frac{\partial \boldsymbol{u}}{\partial t} + (\boldsymbol{u}\cdot\nabla)\,\boldsymbol{u}\right] = \frac{\mathrm{D}|\boldsymbol{u}|}{\mathrm{D}t} = -\frac{1}{\rho_\circ}\frac{\partial p}{\partial s} + \boldsymbol{F}\cdot\hat{\boldsymbol{u}} \tag{32.18a}$$

$$\hat{\boldsymbol{n}}\cdot\left[\frac{\partial \boldsymbol{u}}{\partial t} + (\boldsymbol{u}\cdot\nabla)\,\boldsymbol{u}\right] = \frac{|\boldsymbol{u}|^2}{R} = -f\,|\boldsymbol{u}| - \frac{1}{\rho_\circ}\frac{\partial p}{\partial n} + \boldsymbol{F}\cdot\hat{\boldsymbol{n}}. \tag{32.18b}$$

Depending on the information provided by a field measurement or numerical simulation, one might more readily diagnose the kinematic expressions on the left side of these equations or the force balances on the right side.

Expressions for the radius of curvature

The radius of curvature is an emergent property of the flow. From equation (32.18b), we find two means to diagnose the radius of curvature, given either the flow field itself or the forces contributing to the flow

$$R^{-1} = \underbrace{\frac{\hat{\boldsymbol{n}}\cdot[\partial\boldsymbol{u}/\partial t + (\boldsymbol{u}\cdot\nabla)\,\boldsymbol{u}]}{|\boldsymbol{u}|^2}}_{\text{kinematic method}} = \underbrace{\frac{-f\,|\boldsymbol{u}| - \rho_\circ^{-1}\,\partial p/\partial n + \boldsymbol{F}\cdot\hat{\boldsymbol{n}}}{|\boldsymbol{u}|^2}}_{\text{dynamic method}}. \tag{32.19}$$

A particularly elegant form for the kinematic expression arises for steady flow, in which case

$$|\boldsymbol{u}|^2 R^{-1} = \hat{\boldsymbol{n}} \cdot [(\boldsymbol{u} \cdot \nabla) \boldsymbol{u}]. \tag{32.20}$$

This expression reveals how the normal projection of the self-advection operator is identical, for steady flows, to the magnitude of the centrifugal acceleration arising from the curved trajectory. If we furthermore assume the steady flow also occurs with constant speed, then

$$\mathrm{D}|\boldsymbol{u}|/\mathrm{D}t = (\boldsymbol{u} \cdot \nabla)|\boldsymbol{u}| = 0, \tag{32.21}$$

in which case the inverse radius of curvature is given by

$$R^{-1} = \hat{\boldsymbol{n}} \cdot [(\hat{\boldsymbol{u}} \cdot \nabla) \hat{\boldsymbol{u}}]. \tag{32.22}$$

Vector invariant form of the acceleration

We can transform the self-advection term using the vector identity (see Section 2.3.4)

$$(\boldsymbol{u} \cdot \nabla) \boldsymbol{u} = \nabla K - \boldsymbol{u} \times \zeta \hat{\boldsymbol{z}}, \tag{32.23}$$

where $K = \boldsymbol{u} \cdot \boldsymbol{u}/2$ is the kinetic energy per mass in the horizontal flow, and $\zeta = \partial_x v - \partial_y u$ is the vertical component to the relative vorticity (see Chapter 37). The acceleration, $\boldsymbol{u} \times \zeta \hat{\boldsymbol{z}}$, is known as the *Magnus acceleration* and was discussed in Section 24.4. Projecting into the $\hat{\boldsymbol{u}}$ and $\hat{\boldsymbol{n}}$ directions leads to

$$\hat{\boldsymbol{u}} \cdot \frac{\partial \boldsymbol{u}}{\partial t} = -\frac{\partial (p/\rho_\circ + K)}{\partial s} + \boldsymbol{F} \cdot \hat{\boldsymbol{u}} \tag{32.24a}$$

$$\hat{\boldsymbol{n}} \cdot \frac{\partial \boldsymbol{u}}{\partial t} = -(f + \zeta)\,|\boldsymbol{u}| - \frac{\partial (p/\rho_\circ + K)}{\partial n} + \boldsymbol{F} \cdot \hat{\boldsymbol{n}}. \tag{32.24b}$$

The local acceleration along the direction of the flow is affected by both pressure and the *dynamical pressure* afforded by the kinetic energy per mass. The Magnus acceleration appears only in the normal component equation, which is expected since it acts just as the Coriolis acceleration to deflect the trajectory in a perpendicular direction. Following the example in Figure 24.1, consider a positive relative vorticity, $\zeta > 0$. For this case, the Magnus acceleration points to the right of the flow; i.e., opposite to the normal direction, which points to the left as per our convention in Figure 32.1.

32.2.7 Further study

Chapter 8 in *Zdunkowski and Bott* (2003) and Section 3.2 of *Holton and Hakim* (2013) detail the use of natural coordinates for geophysical flows, with a similar decomposition provided in Section 7.10 of *Gill* (1982) and Section 2.9 of *Vallis* (2017). Natural coordinates are also used in describing flows in non-rotating reference frames as in Section 20 of *Serrin* (1959) and as illustrated in this video.

32.3 Exact geostrophic balance

Frictionless flow parallel to pressure contours experiences no pressure gradient ($\partial p/\partial s = 0$), so that the speed of a fluid element remains constant. Furthermore, if this motion occurs with an infinite radius of curvature (straight line motion parallel to pressure contours), then the force balance is between the normal pressure gradient and Coriolis. In this case the local Rossby

number (32.16) vanishes

$$\mathrm{Ro}_{\mathrm{local}} = \frac{|\boldsymbol{u}|}{R\,f} = 0 \quad \text{if } |R| = \infty. \tag{32.25}$$

More precisely, exact geostrophic balance occurs under the following conditions.

- Fluid moves on a straight line so that the radius of curvature is infinite, $|R| = \infty$, thus making the centripetal acceleration and local Rossby number both vanish;
- Fluid moves along lines of constant pressure so that $\partial p/\partial s = 0$;
- Friction is zero.

In this case the equations of motion (32.13a) and (32.13b) take the form

$$\frac{\mathrm{D}|\boldsymbol{u}|}{\mathrm{D}t} = 0 \tag{32.26a}$$

$$f\,|\boldsymbol{u}| = -\frac{1}{\rho_\circ}\frac{\partial p}{\partial n}. \tag{32.26b}$$

Equation (32.26a) says that the speed of a fluid element is constant, so that the horizontal kinetic energy likewise is constant. Equation (32.26b) says that the pressure gradient normal to the motion balances the Coriolis acceleration. We refer to this flow, depicted in Figure 32.4, as *exact geostrophic balance* since it is an exact solution under the above assumptions.

Writing the horizontal advection of speed in the form

$$\boldsymbol{u}\cdot\nabla|\boldsymbol{u}| = |\boldsymbol{u}|\,\hat{\boldsymbol{u}}\cdot\nabla|\boldsymbol{u}| = |\boldsymbol{u}|\,\frac{\partial|\boldsymbol{u}|}{\partial s}, \tag{32.27}$$

allows us to write the material constancy of the flow speed as

$$\frac{\partial|\boldsymbol{u}|}{\partial t} + |\boldsymbol{u}|\,\frac{\partial|\boldsymbol{u}|}{\partial s} = 0. \tag{32.28}$$

Hence, a steady flow speed, with $\partial|\boldsymbol{u}|/\partial t = 0$, only holds for the exact geostrophic balance if the flow speed is fixed along each trajectory path

$$\frac{\partial|\boldsymbol{u}|}{\partial s} = 0 \Longrightarrow \frac{\partial|\boldsymbol{u}|}{\partial t} = 0. \tag{32.29}$$

What is required for this condition to hold? We examine two cases, again restricted to a tangent plane.

32.3.1 Steady f-plane flow

Geostrophic motion on an f-plane is horizontally non-divergent (Section 31.4)

$$\nabla\cdot\boldsymbol{u} = \nabla\cdot(\hat{\boldsymbol{u}}\,|\boldsymbol{u}|) = 0. \tag{32.30}$$

Flow in a straight line, with each trajectory parallel to one another, has the trajectory direction independent of space. Hence, the non-divergent condition means that

$$0 = \nabla\cdot(\hat{\boldsymbol{u}}\,|\boldsymbol{u}|) = (\hat{\boldsymbol{u}}\cdot\nabla)\,|\boldsymbol{u}| = \frac{\partial|\boldsymbol{u}|}{\partial s}, \tag{32.31}$$

which proves that exact geostrophic flow on an f-plane is steady.

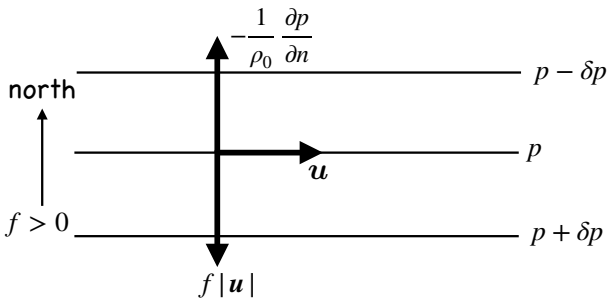

FIGURE 32.4: Exact geostrophic balance on a tangent plane occurs when the flow is horizontal, frictionless, straight, and follows contours of constant pressure. For this case the pressure gradient exactly balances the Coriolis acceleration so that the motion is perpendicular to both of these accelerations. We here depict motion assuming $f > 0$ as for the northern hemisphere. If flow is on an f-plane then the exact geostrophic balance is steady for any arbitrary flow direction. On a β-plane, steady exact geostrophic balance holds only for zonal flow.

32.3.2 Steady β-plane flow

The geostrophic velocity in the presence of a meridional gradient of the Coriolis parameter, $f = f(y)$, satisfies (Section 31.4)

$$\nabla \cdot (f\,\boldsymbol{u}) = 0. \tag{32.32}$$

Making use of $\nabla \cdot \hat{\boldsymbol{u}} = 0$ for straight line trajectories leads to

$$\nabla \cdot (f\,\boldsymbol{u}) = \frac{\partial (f\,|\boldsymbol{u}|)}{\partial s} = 0. \tag{32.33}$$

We conclude that $\partial|\boldsymbol{u}|/\partial s = 0$ holds only for trajectories that are parallel to latitude lines, in which case $\partial f/\partial s = \partial f/\partial x = 0$. Therefore, exact geostrophic motion on the β-plane is steady only for trajectories that follow constant latitude lines; i.e., zonal trajectories as depicted in Figure 32.4.

32.3.3 What about geostrophic balance with curved motion?

The geostrophically balanced flows discussed in Chapter 31 generally have curvature, such as for the geostrophic motion around a pressure center as shown in Figure 31.3. But as emphasized by the natural coordinate decomposition as per equations (32.13a) and (32.13b), curved motion has an associated centrifugal acceleration. So when speaking of geostrophic balance for flow that has a nonzero curvature, then the local Rossby number (32.16) is not precisely zero. Rather, its magnitude is small but nonzero

$$|\mathrm{Ro}_{\mathrm{local}}| \ll 1 \quad \text{approximate geostrophic flow.} \tag{32.34}$$

In this limit it is accurate to ignore the centrifugal acceleration, which is commonly the case for large-scale flows. Even so, it is an approximation, with the centrifugal acceleration identically zero only for straight line motion on a plane.

32.4 Inertial motion

Inertial motion occurs under the following conditions:

- vanishing pressure gradient
- vanishing friction,

so that the equations of motion (32.13a) and (32.13b) take the form

$$\frac{\mathrm{D}|\boldsymbol{u}|}{\mathrm{D}t} = 0 \tag{32.35a}$$

$$\frac{|\boldsymbol{u}|^2}{R} + f\,|\boldsymbol{u}| = 0. \tag{32.35b}$$

Equation (32.35a) says that inertial motion occurs with constant speed, whereas equation (32.35b) says that the motion maintains the balance between Coriolis and centrifugal accelerations

$$f\,|\boldsymbol{u}| = -\frac{|\boldsymbol{u}|^2}{R}. \tag{32.36}$$

Hence, local Rossby number has a unit magnitude

$$|\mathrm{Ro}_{\mathrm{local}}| = \frac{|\boldsymbol{u}|}{|R|\,|f|} = 1. \tag{32.37}$$

32.4.1 Anti-cyclonic circular motion on f-plane

To further understand inertial motion, rearrange equation (32.36) so that

$$f = -\frac{|\boldsymbol{u}|}{R}, \tag{32.38}$$

in which case the radius for the inertial circle is

$$R = -|\boldsymbol{u}|/f. \tag{32.39}$$

Equation (32.38) can be satisfied in the northern hemisphere ($f > 0$) only for motion turning to the right (in which $R < 0$). The opposite orientation occurs in the southern hemisphere, where inertial motion turns to the left so that the radius of curvature is positive, $R = -|\boldsymbol{u}|/f > 0$ (see Figure 32.2 for the sign convention on the radius of curvature). Hence, inertial motion is oriented anti-cyclonically (orientated opposite to the earth's rotation). If the Coriolis parameter is constant, then the motion is circular, as depicted in Figure 32.5.

To emphasize the balance, return to equation (32.36) and recall that the Coriolis acceleration in the northern hemisphere points to the right when facing downstream, as per equation (32.11). Hence, the balance (32.36) is between the Coriolis acceleration pointing to the right and the centrifugal acceleration pointing to the left. That is, the Coriolis acceleration provides the centripetal acceleration to balance the centrifugal acceleration.

32.4.2 Period for inertial motion

Equation (32.39) says that the speed of a fluid element is given by the radius of curvature times the magnitude of the Coriolis parameter

$$|\boldsymbol{u}| = |R\,f|. \tag{32.40}$$

The time for a fluid element to traverse an inertial circle is given by the circumference of the circle, $2\pi|R|$, divided by the constant speed, thus yielding the inertial period

$$T_{\mathrm{inertial}} = \frac{2\pi|R|}{|\boldsymbol{u}|} = \frac{2\pi}{|f|}. \tag{32.41}$$

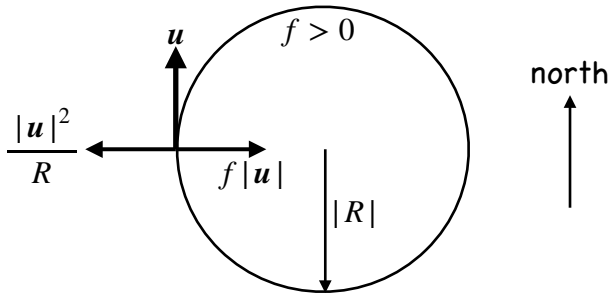

FIGURE 32.5: Inertial motion of a fluid on a plane occurs when the flow is horizontal, frictionless, and the centrifugal acceleration balances the Coriolis in the presence of zero pressure gradient. We here depict motion assuming $f > 0$ as for the northern hemisphere, revealing that inertial motion is an anti-cyclonic circular motion with radius $|R| = |\boldsymbol{u}|/|f|$. When turning to the right as in the northern hemisphere, the radius of curvature for the inertial circle is negative (see Figure 32.2 for sign convention), so that $R = -|\boldsymbol{u}|/f < 0$.

We encountered this inertial period in Section 14.4 when considering inertial oscillations for a point particle.

32.4.3 Observing inertial motion

Inertial motion is rarely observed in the atmosphere since fluid motion nearly always occurs in the presence of a pressure gradient. In contrast, surface ocean flow is commonly generated by wind stresses that setup motion even in the absence of ocean pressure gradients. The moving fluid then engenders a Coriolis acceleration, in which case there can be a balance between centrifugal and Coriolis for the moving ocean fluid. As a result, the observed surface ocean currents have nontrivial power within the inertial frequency band, rivaling energy contained in frequencies associated with astronomical tides (e.g., see Figure 3.3 of *Holton and Hakim* (2013)).

How large is an inertial circle? Consider a surface ocean current speed of $|\boldsymbol{u}| \sim 0.1$ m s^{-1}, which is not atypical of current speeds outside of strong boundary currents or mesoscale eddies, and assume the Coriolis parameter $f = 10^{-4}$ s^{-1}. In this case the inertial radius is

$$R_{\text{inertial}} \approx 10^3 \text{ m}. \tag{32.42}$$

Observations of inertial motion, such as that reproduced in Figure 8.3 of *Gill* (1982), confirm that the radii are indeed on the order of a few kilometers.

32.4.4 Inertial motion is Lagrangian

The analysis in this section concerns a fluid element moving without feeling the impacts from pressure forces. The fluid thus exhibits the same force balance as the point particle discussed in Section 14.4. So although we can measure inertial motion at a fixed point in space, the present considerations are Lagrangian in nature, focusing on motion of fluid elements. Furthermore, the inertial period refers to the time it takes for a fluid element to move around the inertial circle at its constant speed. It does not refer to the period of a wave, for example, and yet there are inertial waves (Chapter 53) with this period as well as inertia-gravity waves that have periods close to the inertial period (Section 55.8),

32.4.5 "Inertial" motion does not refer to an inertial reference frame

We make use of the term "inertial" when referring to inertial motion since both the Coriolis and centrifugal accelerations are nonzero only in the presence of motion; i.e., they require the inertia obtained by a moving massive body. Hence, as noted in Section 14.4.5, "inertial motion" in this context does *not* refer to the motion viewed in an inertial reference frame.

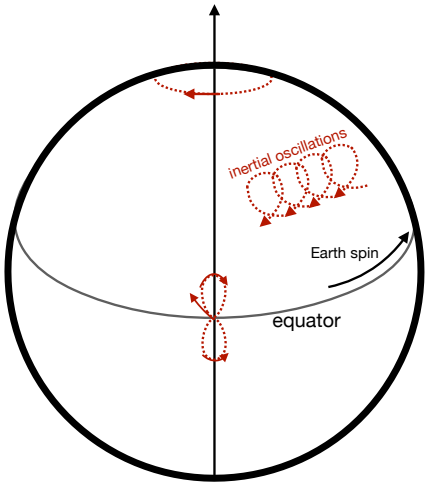

FIGURE 32.6: Depicting inertial motion on a sphere. As the fluid element moves poleward, f increases so that the radius of curvature decreases. Correspondingly, the fluid motion does not close, but instead the path drifts to the west. This westward drift holds for both hemispheres, where the sense of the motion is anti-cyclonic. The only closed and circular inertial motions are those that encircle the pole. Fluid elements that cross the equator exhibit a figure-eight pattern that also drifts to the west. This figure is taken after Figure 4-14 of *von Arx* (1962).

32.4.6 Inertial motion on a sphere

In the analysis thus far, we have assumed an f-plane so that inertial motion is circular. Without solving the spherical equations for inertial motion we can anticipate what happens when such motion occurs on a sphere. As a fluid element moves to higher latitudes the magnitude of the Coriolis parameter increases, thus decreasing the radius of curvature. The opposite happens when moving equatorward. This effect of planetary sphericity leads to an egg-shaped pattern that does not close but instead drifts to the west. Now consider inertial motion that spans the equator. As the fluid crosses the equator, where $f = 0$, the radius of curvature is infinite so that the motion is straight. When moving away from the equator the Coriolis parameter increases in magnitude, which causes a fluid element to turn and close its path, again with a drift to the west. Motion north of the equator turns to the right whereas motion to the south turns left, so that inertial motion that spans the equator forms a figure-eight path. We illustrate this motion in Figure 32.6.

32.5 Cyclostrophic balance

Cyclostrophic balance occurs under the following conditions:

- fluid elements move along lines of constant pressure so that $\partial p/\partial s = 0$;
- vanishing Coriolis acceleration;
- vanishing friction.

The resulting equations of motion (32.13a) and (32.13b) take the form

$$\frac{\mathrm{D}|\boldsymbol{u}|}{\mathrm{D}t} = 0 \tag{32.43a}$$

$$\frac{|\boldsymbol{u}|^2}{R} = -\frac{1}{\rho_\circ}\frac{\partial p}{\partial n}. \tag{32.43b}$$

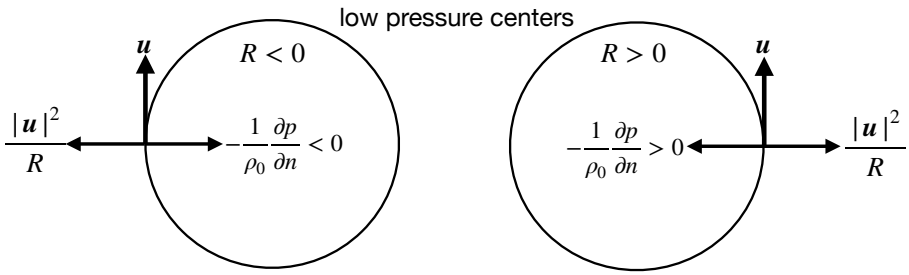

FIGURE 32.7: Cyclostrophic motion of a fluid element on a tangent plane occurs when the flow is horizontal, non-rotating, frictionless, with constant speed, and where the centrifugal acceleration balances the pressure gradient normal to the flow direction. We here depict motion for clockwise and counter-clockwise cyclostrophic flow, both around a low pressure center. Left panel: clockwise motion with radius of curvature, $R < 0$, and the pressure gradient pointing in the direction of the normal, $\partial p/\partial n > 0$. Right panel: counter-clockwise motion with radius of curvature, $R > 0$, and the pressure gradient pointing opposite to the direction of the normal, $\partial p/\partial n < 0$. Cyclostrophic balance does not occur for flow around a high pressure center. The reason is that if both the pressure and centrifugal accelerations point away from the center, then they are unable to balance one another.

With a vanishing Coriolis acceleration we see that cyclostrophic balance corresponds to local Rossby number that has an infinite magnitude

$$|\mathrm{Ro}_{\mathrm{local}}| = \infty \quad \text{if } f = 0. \tag{32.44}$$

Approxiate cyclostrophic balance holds when $|\mathrm{Ro}_{\mathrm{local}}| \gg 1$, but less than infinite.

Again, equation (32.43a) says that the speed is constant following a material fluid element. Equation (32.43b) says that cyclostrophic flow occurs when the centrifugal acceleration balances the pressure gradient, with the squared speed given by

$$|\boldsymbol{u}|^2 = -\frac{R}{\rho_\circ}\frac{\partial p}{\partial n}. \tag{32.45}$$

This equation can be satisfied for either clockwise or counter-clockwise motion around a low pressure center, as shown in Figure 32.7. For clockwise flow, the radius of curvature is negative, $R < 0$, whereas $\partial p/\partial n > 0$. The signs are swapped for counter-clockwise flow. Cyclostrophic balance cannot be maintained around a high pressure center. The reason is that if both the pressure and centrifugal accelerations point away from the circle's center, then they are unable to balance one another.

Cyclostrophic balance is relevant for scales on the order of a tornado, with a radius on the order of 300 m where tangential speeds are on the order of 30 m s^{-1} (see Section 3.2.4 of *Holton and Hakim* (2013)). For this flow scale, the Rossby number is on the order of 1000 at middle latitudes, thus justifying neglect of the Coriolis acceleration. Although tornadoes in cyclostrophic balance can rotate either clockwise or counter-clockwise, they are more often observed rotating cyclonically given that they are generally embedded within cyclonic storm systems. In contrast, smaller motions such as dust devils and water spouts are quite often seen rotating in either direction.

32.6 Gradient wind balance

Gradient wind balance occurs under the following conditions:

- fluid elements move along lines of constant pressure so that $\partial p/\partial s = 0$;
- vanishing friction.

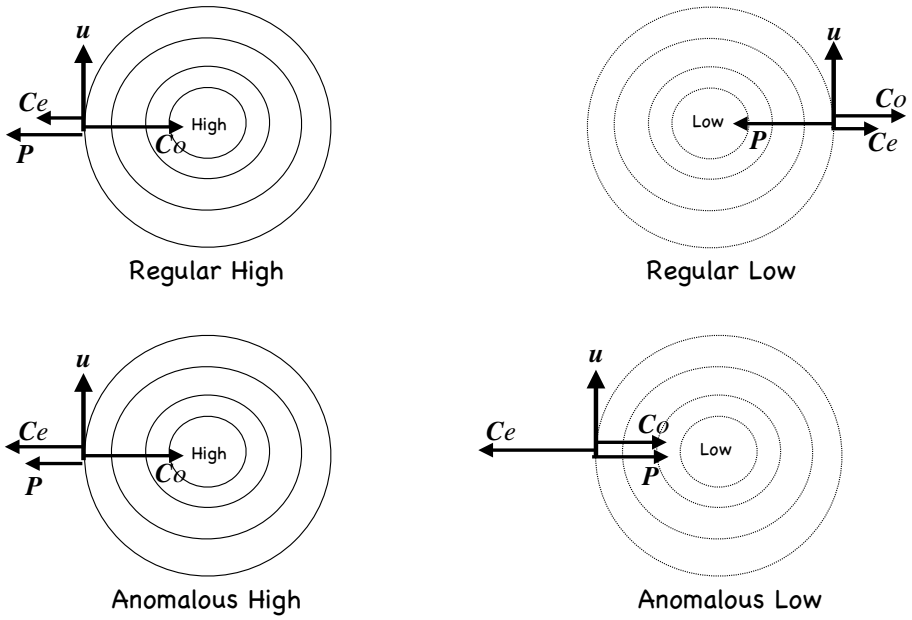

FIGURE 32.8: The variety of gradient wind balances available in the northern hemisphere ($f > 0$). Gradient wind balance occurs when the flow is horizontal, frictionless, with constant speed, and where the centrifugal, pressure, and Coriolis accelerations balance under a variety of magnitudes. To reduce clutter, we use the following shorthand for the accelerations: $P = -\rho_0^{-1}\,\partial p/\partial n$, $Co = f\,|\boldsymbol{u}|$, and $Ce = |\boldsymbol{u}|^2/R$. Upper left panel: motion around a regular high pressure center, whereby the centrifugal acceleration helps the pressure acceleration to balance the Coriolis acceleration. The pressure acceleration is larger in magnitude than the centrifugal. This flow is termed "regular" as it directly corresponds to geostrophic flow around a high pressure center. Lower left panel: motion around an anomalous high pressure center, whereby the centrifugal acceleration helps the pressure acceleration to balance the Coriolis acceleration, with the pressure acceleration smaller in magnitude than the centrifugal. This flow is termed "anomalous" as the pressure acceleration is subdominant to the centrifugal, in contrast to the case of geostrophic flow. Upper right panel: motion around a regular low pressure center, whereby the Coriolis and centrifugal accelerations balance the pressure acceleration. Lower right panel: motion around an anomalous low pressure center, whereby the Coriolis and pressure accelerations balance the centrifugal acceleration. Note the opposite flow orientation between the regular and anomalous lows, whereas the regular and anomalous highs have the same flow orientation.

The resulting equations of motion (32.13a) and (32.13b) take the form

$$\frac{\mathrm{D}|\boldsymbol{u}|}{\mathrm{D}t} = 0 \tag{32.46a}$$

$$\frac{|\boldsymbol{u}|^2}{R} + f\,|\boldsymbol{u}| = -\frac{1}{\rho_0}\frac{\partial p}{\partial n}, \tag{32.46b}$$

Again, equation (32.46a) says that the speed is constant following a material fluid element. Equation (32.46b) says that gradient wind balanced flow occurs when the centrifugal and Coriolis accelerations balance the pressure gradient acting normal to the motion.

The local Rossby number is order unity for the gradient wind balance

$$|\mathrm{Ro}_{\mathrm{local}}| = \frac{|\boldsymbol{u}|}{|R|\,|f|} \sim 1, \tag{32.47}$$

meaning that both centrifugal and Coriolis accelerations are important as they balance the pressure gradient. Recall that the inertial motion from Section 32.4 has $|\mathrm{Ro}_{\mathrm{local}}| = 1$, which arises when the pressure gradient vanishes so that the Coriolis and centrifugal terms have equal but opposite magnitudes. The nonzero pressure gradient makes gradient wind flow fundamentally distinct from inertial motion.

32.6.1 Constraints on gradient wind flow

The quadratic formula leads to the following expression for the speed of gradient wind flow

$$|\boldsymbol{u}| = \frac{R}{2}\left[f \pm \sqrt{f^2 - \frac{4}{R}\frac{1}{\rho_o}\frac{\partial p}{\partial n}}\right]. \tag{32.48}$$

The speed is a real number if the pressure gradient, Coriolis parameter, and radius of curvature satisfy

$$f^2 > \frac{4}{R}\frac{1}{\rho_o}\frac{\partial p}{\partial n} \Longrightarrow \frac{1}{\rho_o}\left|\frac{\partial p}{\partial n}\right| \leq \frac{|R|\, f^2}{4}. \tag{32.49}$$

This relation has direct implications for the structure of the pressure field depending on the sign of the radius of curvature. In particular, as seen in the following, this constraint implies that the pressure gradient at the center of a high pressure region must go to zero as the radius of curvature vanishes, which renders the pressure field relatively flat near the center of highs. In contrast, there is no analogous limit for the magnitude of the pressure gradient approaching a low pressure center. This asymmetry between high and low pressures manifests in atmospheric flow with low pressure centers (cyclonic lows) having stronger magnitude than high pressure centers (anti-cyclonic highs).

32.6.2 The variety of gradient wind flows

We now identify the following force balances available with a gradient wind balance, with illustrations provided in Figure 32.8.

Regular high pressure center (right turn with high pressure on right)

A *regular high pressure* occurs with $R < 0$ and $\partial p/\partial n \leq 0$. This case occurs with the centrifugal and pressure accelerations pointing away from the center, and these balance the Coriolis acceleration pointing to the high pressure center (upper left panel of Figure 32.8).

The inequality (32.49) provides a bound to the size of the pressure gradient since

$$\frac{1}{\rho_o}\frac{\partial p}{\partial n} \leq \frac{R\, f^2}{4} \;\text{ with }\; R \leq 0 \;\text{ and }\; \frac{\partial p}{\partial n} \leq 0 \Longrightarrow \frac{1}{\rho_o}\left|\frac{\partial p}{\partial n}\right|_{\max} = \frac{|R|\, f^2}{4}. \tag{32.50}$$

That is, the pressure gradient for a regular high cannot be larger than this bound in order for there to be a gradient wind solution. Since $R \to 0$ as the center is approached, the normal pressure gradient, $\partial p/\partial n$, in turn must vanish towards the center. *Holton and Hakim* (2013) identifies two subcases for this balance depending on the relative size of the pressure and centrifugal accelerations, with the anomalous high the case where the pressure gradient acceleration is weaker than the centrifugal (lower left panel of Figure 32.8).

Regular low (left turn with low pressure on left)

This flow occurs with $R \geq 0$ and $\partial p/\partial n \leq 0$, so that the inequality (32.49) is always satisfied

$$\frac{1}{\rho_o}\frac{\partial p}{\partial n} \leq \frac{R\, f^2}{4} \;\text{ with }\; R \geq 0 \;\text{ and }\; \frac{\partial p}{\partial n} \leq 0 \Longrightarrow \text{arbitrary size to } \left|\frac{\partial p}{\partial n}\right|. \tag{32.51}$$

Hence, there is no constraint imposed by gradient wind balance on the size of the pressure gradient magnitude, $|\partial p/\partial n|$. So the low pressure center can be arbitrarily strong and still maintain a gradient wind balance. Furthermore, the Coriolis and centrifugal accelerations point

away from the low pressure center, and these two accelerations balance the pressure acceleration that points toward the center (upper right panel of Figure 32.8).

Anomalous low (right turn with low pressure on right)

This flow occurs with $R < 0$ and $\partial p/\partial n \geq 0$. This case occurs with the Coriolis and pressure accelerations pointing toward the low pressure center, and these two accelerations balance the centrifugal acceleration pointing away from the center (lower right panel of Figure 32.8). As with the regular low, the inequality (32.49) provides no bound to the magnitude of the low pressure. Note the opposite orientation for the flow around an anomalous low relative to the regular low.

Left turn with high pressure on left

In this case $R > 0$ and $\partial p/\partial n > 0$. There is no solution for the northern hemisphere since all accelerations point to the right of the motion thus disallowing any balance.

32.6.3 Comments

As noted in Section 3.2 of *Holton and Hakim* (2013), the difference between gradient wind speeds and geostrophic wind speeds is no more than 10% to 20% in middle latitude synoptic atmosphere flow. In the tropics, where geostrophy becomes less relevant, it is important to apply the gradient wind relation to capture the balanced flow states. Furthermore, *van Heijst* (2010) and Chapter 18 of *Cushman-Roisin and Beckers* (2011) make use of a gradient wind analysis for the study of ocean vortices. The deviations from geostrophy become important when considering relatively small ocean vortices and/or tropical vortices.

Chapter 33

EKMAN MECHANICS

A *boundary layer* is a region of the fluid flow that is directly affected by boundaries. For geophysical applications we have in mind the solid-earth boundary that interacts with both the ocean and atmosphere; the ocean-atmosphere boundary; the ocean-cryosphere boundary; and the atmosphere-cryosphere boundary. The fluid flow in geophysical boundary layers is generally very turbulent, thus causing rapid mixing and the transfer of properties within the boundary layer, along with the transport of properties between the boundary layer and the less turbulent fluid interior. Boundary layer physics is a well developed discipline for geophysical as well as engineering applications. Our treatment is relatively superficial by comparison to the focused treatments given by books such as *Tennekes and Lumley* (1972), *Stull* (1988), and *Thorpe* (2005).

Here, we are particularly focused on the rudiments of *Ekman mechanics*, which is concerned with flow affected by accelerations from horizontal pressure gradients, vertical friction, and Coriolis, with particular attention given to regions near boundaries where friction is especially large and *Ekman boundary layers* form. The leading role for Coriolis acceleration causes Ekman boundary layers to exhibit behaviors quite distinct from their non-rotating cousins mentioned in Section 25.10.7. In particular, Ekman boundary layer flows are horizontally divergent, thus leading to the vertical exchange of mass, tracers, momentum, and vorticity between the boundary layer and the fluid region outside of the boundary layer (i.e., the fluid interior). In so doing, the Ekman layer flow imparts a stretching and squeezing of interior fluid columns that strongly couples the boundary layer to vorticity and circulation of the fluid interior. This role for Ekman layers is especially crucial for the ocean general circulation.

READER'S GUIDE TO THIS CHAPTER

To introduce the subject we exhibit the role of friction in producing a down pressure gradient component to the flow, making use of natural coordinates from Chapter 32 for this purpose. The remainder of the chapter focuses on the mechanics of Ekman boundary layers, with this study greatly extending our understanding of strongly rotating flows from Chapter 31. Indeed, the addition of friction to an otherwise geostrophically balanced flow provides a surprising level of richness that motivates the variety of perspectives presented in this chapter.

Ekman boundary layers are a key element in the study of ocean circulation, particularly the wind-driven circulation. We here borrow liberally from the material in Section 9.2 of *Gill* (1982), Section 6.2 of *Apel* (1987), Section 7.4 of *Marshall and Plumb* (2008), Chapter 8 of *Cushman-Roisin and Beckers* (2011), Section 5.7 of *Vallis* (2017), and materials from *Thorpe* (1988) and *Thorpe* (2005). A presentation consistent with engineering boundary layers can be found in Section 5.3 of *Tennekes and Lumley* (1972).

33.1 The dynamical balances

Throughout this chapter we make use of a steady, linear, Boussinesq, hydrostatic primitive equations that maintain a balance between the horizontal accelerations from Coriolis, pressure, and friction

$$f\,\hat{\boldsymbol{z}} \times \boldsymbol{u} = -\frac{1}{\rho_o}\nabla_h p + \boldsymbol{F}. \tag{33.1}$$

This balance is most relevant over large horizontal length scales as per the planetary geostrophic equations of Section 31.5.

The frictional acceleration, $\boldsymbol{F}$, of interest in this chapter arises from the vertical exchange of horizontal momentum between fluid layers. Turbulence induced viscous exchange is especially large in boundary regions such as the ocean surface, the atmospheric planetary boundary layer (i.e., atmosphere/land boundary), and the ocean bottom boundary layer. In such turbulent boundary layer regions we make use of the eddy viscosity, which is much larger than molecular values

$$\nu^{\text{eddy}} \gg \nu. \tag{33.2}$$

We have more to say regarding the mathematical form of the friction operator in Section 33.3.1.

For conceptual and mathematical convenience, we find it useful to separate the horizontal velocity into two components. The first is the geostrophic velocity defined by a balance between the pressure gradient and Coriolis accelerations

$$f\,\hat{\boldsymbol{z}} \times \boldsymbol{u}_g = -\frac{1}{\rho_o}\nabla_h p \implies \boldsymbol{u}_g = \frac{1}{f\rho_o}\,\hat{\boldsymbol{z}} \times \nabla_h p. \tag{33.3}$$

In some treatments, $\boldsymbol{u}_g$ is referred to as the *pressure driven velocity*. The second is an *ageostrophic*

or Ekman component defined by a balance between the frictional and Coriolis accelerations

$$f\,\hat{\boldsymbol{z}}\times\boldsymbol{u}_{\rm e}=\boldsymbol{F}\Longrightarrow\boldsymbol{u}_{\rm e}=-f^{-1}\,\hat{\boldsymbol{z}}\times\boldsymbol{F}, \tag{33.4}$$

so that $\boldsymbol{u}_{\rm e}$ is the *frictional driven velocity*.

This velocity decomposition has the appearance of superposing linearly independent flows, one geostrophic (pressure driven) and one ageostrophic (friction driven). However, the flows are coupled and thus not linearly independent. Namely, ageostrophic motions alter the pressure field which in turn affects the geostrophic flow. So the presence of friction and the associated ageostrophic flows lead to geostrophic flows differing from the inviscid case. Conversely, geostrophic flows affect the level of friction. Hence, the above decomposition does not reflect a physical decoupling of geostrophic and ageostrophic flows. Rather, it is only meant to help conceptually understand and describe the flow and the various force balances.

33.2 Horizontal balances in natural coordinates

Motion in Ekman boundary layers is both horizontal and vertical. Here, we introduce the role of friction in rotating flows by just focusing on the horizontal motion on a tangent plane. In particular, we study balances occuring in horizontal flows that maintain a frictional geostrophic balance. As per the definition (33.3), geostrophic motion occurs along lines of constant pressure, with frictionally induced deviations crossing isobars and providing a down pressure gradient component to the fluid trajectory. Motivated by the discussion in Chapter 32, we make use of natural coordinates for the kinematics.

33.2.1 Natural coordinates according to isobars

We represent the horizontal flow according to natural coordinates defined along an arbitrary geopotential surface. Instead of defining the natural coordinates according to the flow direction, as done in Section 32.2 for the frictionless case, we here decompose the motion according to pressure contours (isobars). The unit vector, $\hat{\boldsymbol{s}}$, is defined tangent to isobars in the horizontal plane and directed along the direction of geostrophic flow. We define the direction, $\hat{\boldsymbol{n}}$, to be perpendicular to isobars and oriented down the horizontal pressure gradient

$$\hat{\boldsymbol{n}}=-\frac{\nabla_{\rm h}p}{|\nabla_{\rm h}p|}. \tag{33.5}$$

As illustrated in Figure 33.1, in the northern hemisphere $\hat{\boldsymbol{n}}$ points to the left of the geostrophic velocity, whereas it is to the right in the southern hemisphere. We thus have the northern hemisphere triplet of unit vectors

NORTHERN HEMISPHERE TRIPLET OF DIRECTIONS

$$\hat{\boldsymbol{z}}=\hat{\boldsymbol{s}}\times\hat{\boldsymbol{n}}=\text{vertical direction} \tag{33.6a}$$

$$\hat{\boldsymbol{n}}=\hat{\boldsymbol{z}}\times\hat{\boldsymbol{s}}=\text{down pressure gradient direction} \tag{33.6b}$$

$$\hat{\boldsymbol{s}}=\hat{\boldsymbol{n}}\times\hat{\boldsymbol{z}}=\text{tangent to isobar in direction of geostrophic flow.} \tag{33.6c}$$

In the southern hemisphere, since $\hat{\boldsymbol{n}}$ points to the right of $\hat{\boldsymbol{s}}$, the triplet of directions becomes

SOUTHERN HEMISPHERE TRIPLET OF DIRECTIONS

$$\hat{\boldsymbol{z}}=\hat{\boldsymbol{n}}\times\hat{\boldsymbol{s}}=\text{vertical direction} \tag{33.7a}$$

$$\hat{\boldsymbol{n}}=\hat{\boldsymbol{s}}\times\hat{\boldsymbol{z}}=\text{down pressure gradient direction} \tag{33.7b}$$

$$\hat{\boldsymbol{s}}=\hat{\boldsymbol{z}}\times\hat{\boldsymbol{n}}=\text{tangent to isobar in direction of geostrophic flow.} \tag{33.7c}$$

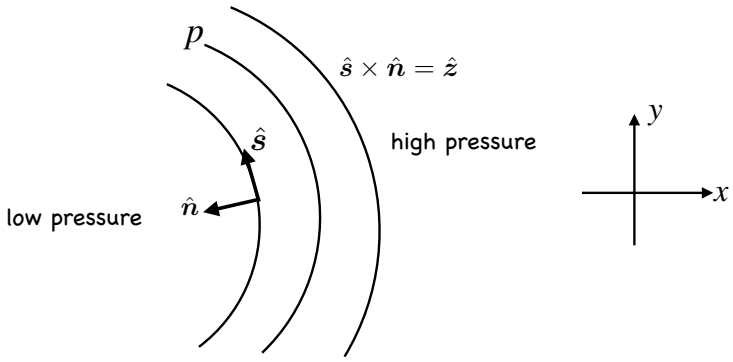

FIGURE 33.1: Natural coordinates defined along an arbitrary geopotential surface according to isobars in the horizontal plane, here depicted for the northern hemisphere. The normal direction, $\hat{\boldsymbol{n}} = -\nabla_h p / |\nabla_h p|$, is oriented down the horizontal pressure gradient so that it points to the left of the geostrophic velocity (facing downstream) in the northern hemisphere and to the right in the southern hemisphere. The tangent direction, $\hat{\boldsymbol{s}}$, points along the isobar in the direction of the geostrophic velocity.

33.2.2 Geostrophic and Ekman balances

As found when studying the geostrophic balance in Section 32.3, the geostrophic velocity flows along isobars and so only has a component in the $\hat{\boldsymbol{s}}$ direction

$$\hat{\boldsymbol{s}} \cdot \boldsymbol{u}_{\rm g} = -\frac{1}{f \rho_{\rm o}} \frac{\partial p}{\partial n} \quad \text{and} \quad \hat{\boldsymbol{n}} \cdot \boldsymbol{u}_{\rm g} = 0 \tag{33.8}$$

In contrast, the Ekman velocity has a component both along and across isobars. For the northern and southern hemispheres we have

$$\hat{\boldsymbol{s}} \cdot \boldsymbol{u}_{\rm e} = |f|^{-1} \, \hat{\boldsymbol{n}} \cdot \boldsymbol{F} \quad \text{and} \quad \hat{\boldsymbol{n}} \cdot \boldsymbol{u}_{\rm e} = -|f|^{-1} \, \hat{\boldsymbol{s}} \cdot \boldsymbol{F}. \tag{33.9}$$

As expected, the Ekman velocity vanishes when the frictional acceleration vanishes, in which case the flow reduces to the geostrophic flow that moves along isobars so that $\hat{\boldsymbol{s}} = \hat{\boldsymbol{u}}$. However, when there is a nonzero friction aligned along isobars, that drives an Ekman velocity across isobars. Conversely, friction aligned across isobars drives Ekman velocities along isobars.

We arrive at a complementary perspective on the origin of cross-isobar flow through the following considerations. Without friction, the Coriolis and pressure gradient accelerations balance when the flow is geostrophic. In the presence of friction, the velocity is slowed so that the Coriolis acceleration weakens. If the pressure gradient acceleration is retained, as occurs if it is determined by large scale balances outside of the Ekman layer, then the Coriolis acceleration no longer balances the pressure gradient. Consequently, flow is diverted from isobars and develops a component down the pressure gradient.

33.2.3 Rayleigh drag

The relative simplicity of Rayleigh drag facilitates analytical expressions for the Ekman velocity using natural coordinates, written in terms of the geostrophic velocity (equation (33.8)). In doing so we are afforded an explicit illustration of how friction provides a cross-isobar component to the flow in the direction down the pressure gradient. Before developing the Ekman flows we here summarize elements of Rayleigh drag.

In Section 26.3.3 we studied how Rayleigh drag affects the kinetic energy budget. As a reminder, consider a frictional acceleration in the form of a Rayleigh drag acting on the velocity field

$$\boldsymbol{F} = -\frac{U_{\rm fric} \, \boldsymbol{u}}{\delta} = -\gamma \, \boldsymbol{u}, \tag{33.10}$$

where δ is a vertical scale and U_{fric} is a friction velocity scale with dimensions L/T. The ratio

$$\gamma = \frac{U_{\text{fric}}}{\delta} \tag{33.11}$$

has dimensions T^{-1} and is an inverse spin-down time. That is, if only Rayleigh drag affected changes to the horizontal momentum, $\partial_t \boldsymbol{u} = -\gamma\, \boldsymbol{u}$, then the flow would exponentially come to a halt with an e-folding time, γ^{-1}. The drag is relatively large over rough surfaces, thus leading to a small e-folding time. In particular, drag on the lower atmospheric winds is larger over land than over the ocean. The reason is that trees, cities, and mountains dissipate more of the atmosphere's mechanical energy than interactions with the relatively smooth ocean surface.

Rayleigh drag dissipates all flow features regardless of their spatial structure. That is, Rayleigh drag does not prefer any particular length scales in the fluid flow. This lack of scale selectivity contrasts to the Laplacian friction discussed in Section 33.3.1, with Laplacian friction dissipating small spatial scales more strongly than large scales. Correspondingly, Rayleigh drag does not generally provide the means to produce a boundary layer.[1] Hence, when studying physics within the Ekman boundary layer in Section 33.3 we make use of Laplacian friction. But for now, Rayleigh drag provides a means to analytically illustrate the role of friction in producing spiral flows with non-zero horizontal divergence.

33.2.4 Cross isobar flow driven by Rayleigh drag

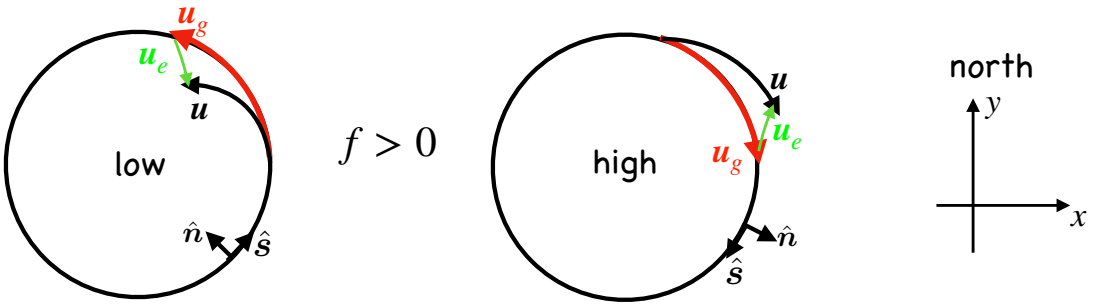

FIGURE 33.2: Illustrating frictional geostrophic flow in the northern hemisphere ($f > 0$). Left panel: geostrophic flow, $\boldsymbol{u}_{\text{g}}$, around a low pressure center is counter-clockwise and aligned with pressure isobars. Friction aligned along the isobars drives Ekman flow, $\boldsymbol{u}_{\text{e}}$, that has a component down the pressure gradient (normal to the geostrophic flow) as well as a component that is directed opposite the geostrophic flow. Consequently, the total velocity, $\boldsymbol{u}_{\text{g}} + \boldsymbol{u}_{\text{e}}$, spirals into the low pressure center. Right panel: the opposite oriented flow occurs around high pressure centers, where fluid spirals away from the high due to the cross-isobar flow driven by friction. By the definition given by equation (33.6b), the normal direction, $\hat{\boldsymbol{n}}$, is directed down the pressure gradient, whereas $\hat{\boldsymbol{s}}$ is tangent to the isobar and directed along the geostrophic flow direction.

Making use of the Rayleigh drag (33.10) brings the northern hemisphere expressions (33.9) for the Ekman velocity into the form

$$\hat{\boldsymbol{s}} \cdot \boldsymbol{u}_{\text{e}} = f^{-1}\, \hat{\boldsymbol{n}} \cdot \boldsymbol{F} = -(\gamma/f)\, \hat{\boldsymbol{n}} \cdot \boldsymbol{u} = -(\gamma/f)\, \hat{\boldsymbol{n}} \cdot \boldsymbol{u}_{\text{e}} \tag{33.12a}$$

$$\hat{\boldsymbol{n}} \cdot \boldsymbol{u}_{\text{e}} = -f^{-1}\, \hat{\boldsymbol{s}} \cdot \boldsymbol{F} = (\gamma/f)\, \hat{\boldsymbol{s}} \cdot \boldsymbol{u} = (\gamma/f)\, \hat{\boldsymbol{s}} \cdot (\boldsymbol{u}_{\text{e}} + \boldsymbol{u}_{\text{g}}). \tag{33.12b}$$

Similar considerations for the southern hemisphere lead to the general result for both hemispheres

$$\hat{\boldsymbol{s}} \cdot \boldsymbol{u}_{\text{e}} = -(\gamma/|f|)\, \hat{\boldsymbol{n}} \cdot \boldsymbol{u}_{\text{e}} \tag{33.13a}$$

[1] In Section 33.3.3 we provide further discussion of what is needed mathematically and physically to produce a boundary layer.

$$\hat{\boldsymbol{n}} \cdot \boldsymbol{u}_{\mathrm{e}} = (\gamma/|f|)\, \hat{\boldsymbol{s}} \cdot (\boldsymbol{u}_{\mathrm{e}} + \boldsymbol{u}_{\mathrm{g}}). \tag{33.13b}$$

Rearrangement of these equations allows us to express the Ekman velocity in terms of the geostrophic velocity (equation (33.8)), with results for both hemispheres given by

$$\hat{\boldsymbol{n}} \cdot \boldsymbol{u}_{\mathrm{e}} = \hat{\boldsymbol{s}} \cdot \boldsymbol{u}_{\mathrm{g}} \left[\frac{\gamma\, |f|}{f^2 + \gamma^2} \right] \tag{33.14a}$$

$$\hat{\boldsymbol{s}} \cdot \boldsymbol{u}_{\mathrm{e}} = -\hat{\boldsymbol{s}} \cdot \boldsymbol{u}_{\mathrm{g}} \left[\frac{\gamma^2}{\gamma^2 + f^2} \right], \tag{33.14b}$$

where equation (33.8) expresses the geostrophic velocity in terms of the normal pressure gradient. Equation (33.14a) says that the normal component to the Ekman velocity is directed down the pressure gradient. Equation (33.14b) says that the component of the Ekman velocity along the pressure isobar is directed opposite to the geostrophic velocity. We provide an example of an Ekman velocity in Figure 33.2 for the northern hemisphere.

Bringing all pieces together leads to the components for the total velocity, $\boldsymbol{u} = \boldsymbol{u}_{\mathrm{g}} + \boldsymbol{u}_{\mathrm{e}}$, and its squared magnitude

$$\hat{\boldsymbol{s}} \cdot \boldsymbol{u}_{\mathrm{g}} = -\frac{1}{f\rho_{\circ}} \frac{\partial p}{\partial n} \qquad \text{geostrophic velocity (aligned along isobars)} \tag{33.15a}$$

$$\hat{\boldsymbol{s}} \cdot \boldsymbol{u} = \hat{\boldsymbol{s}} \cdot \boldsymbol{u}_{\mathrm{g}} \left[\frac{f^2}{f^2 + \gamma^2} \right] \qquad \text{isobaric velocity component} \tag{33.15b}$$

$$\hat{\boldsymbol{n}} \cdot \boldsymbol{u} = (\gamma/|f|)\, \hat{\boldsymbol{s}} \cdot \boldsymbol{u} \qquad \text{normal velocity component} \tag{33.15c}$$

$$(\hat{\boldsymbol{s}} \cdot \boldsymbol{u})^2 + (\hat{\boldsymbol{n}} \cdot \boldsymbol{u})^2 = \frac{(\hat{\boldsymbol{s}} \cdot \boldsymbol{u}_{\mathrm{g}})^2}{1 + (\gamma/f)^2} \qquad \text{horizontal kinetic energy per mass.} \tag{33.15d}$$

The cross-isobar flow (equation (33.15c)) is directly driven by the Rayleigh drag, and it is directed down the normal pressure gradient so long as the flow has a positive projection onto the tangent direction

$$\hat{\boldsymbol{s}} \cdot \boldsymbol{u} > 0 \Longrightarrow \hat{\boldsymbol{n}} \cdot \boldsymbol{u} > 0. \tag{33.16}$$

When flow is moving counter-clockwise around a low pressure in the northern hemisphere, where $\hat{\boldsymbol{n}}$ points towards the low pressure center, then Rayleigh drag causes the fluid to spiral into the low pressure center. Conversely, when flow is moving clockwise around a high pressure, with $\hat{\boldsymbol{n}}$ pointing away from the high pressure center, then Rayleigh drag causes the fluid to spiral away from the high pressure center. We depict these cases in Figure 33.2. Furthermore, equation (33.15d) shows that when $\gamma \neq 0$ the magnitude of the total flow is reduced relative to the geostrophic flow, thus reflecting the dissipation of kinetic energy arising from Rayleigh drag.[2]

33.2.5 Horizontal spiral plus vertical rising/sinking

Thus far, we have focused on the horizontal spiral motion as shown in Figure 33.2. Through continuity we infer a corresponding vertical motion induced by the convergence of mass into the low pressure center and the divergence of mass away from the high pressure center. Figure 33.3 illustrates the vertical motion in a bottom Ekman boundary layer of either the atmosphere or ocean whereby mass rises above a low pressure center in response to the horizontal convergence of mass in the Ekman layer. Conversely, mass diverges from the high pressure Ekman layer, with this divergence inducing a sinking motion over the high pressure to replace the diverging mass. In subsequent sections of this chapter we develop the formalism needed to compute the mass transport into and out of the Ekman boundary layer.

[2] See Section 26.3.3 for more on frictional dissipation of kinetic energy.

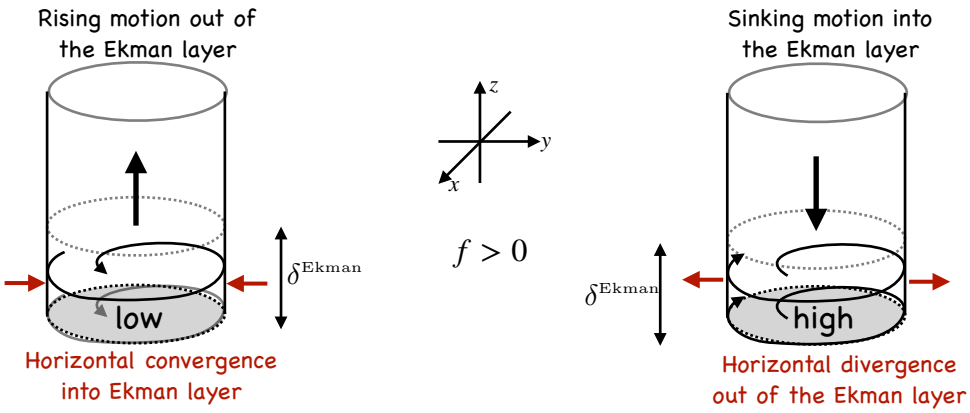

FIGURE 33.3: Illustrating the three-dimensional flow associated with Ekman layers in the northern hemisphere ($f > 0$) next to a bottom boundary. Left panel: flow spiralling into a low pressure center creates convergence of mass into the Ekman layer. Mass continuity means that flow must vertically leave the Ekman layer to thus enter the interior fluid above. Right panel: flow spiralling away from a high pressure center creates divergence of mass away from the Ekman layer. Mass continuity means that flow must vertically sink into the Ekman layer from above. The Ekman layer thickness is denoted by δ^{Ekman} (Section 33.3). An analogous picture holds for the surface Ekman layer in the ocean, yet with the Ekman layer at the top of the column rather than the bottom.

33.2.6 Further study

Our discussion of Ekman velocity arising from Rayleigh drag follows a similar treatment in Section 7.4 of *Marshall and Plumb* (2008).

33.3 Ekman number and Ekman layer thickness

Friction that is most prominent near surface and bottom boundaries arises from vertical shears in the horizontal velocity, with shears leading to flow instabilities and the development of turbulence and associated turbulent friction. There is no deductive theory for turbulent friction so we must rely on empirical expressions. These expressions are typically based on a Laplacian viscous operator, partly motivated by the form arising from kinetic theory of gases briefly mentioned in Chapter 16. Most notably, this operator supports the development of a boundary layer through maintenance of both the no-slip (homogeneous Dirichlet) and stress (Neumann) boundary conditions.

33.3.1 Laplacian vertical friction

We introduced the Laplacian friction operator in Section 25.8.6 when studying stress in fluids. The Laplacian friction operator considered here is given in terms of the vertical shear of the horizontal stress vector

$$\boldsymbol{F}^{\text{viscous}} = \frac{1}{\rho_o}\frac{\partial \boldsymbol{\tau}}{\partial z} = \frac{\partial}{\partial z}\left[\nu^{\text{eddy}}\,\frac{\partial \boldsymbol{u}}{\partial z}\right], \tag{33.17}$$

with $\nu^{\text{eddy}} > 0$ a turbulent kinematic viscosity with dimensions $\text{L}^2\ \text{T}^{-1}$. This form of the friction operator emulates the Laplacian operator representing molecular viscous friction (equation (25.88)). It is also the form most commonly used in theoretical and numerical models that focus on boundary layers where rotation is important.

Expanding the derivative in equation (33.17) reveals that the Laplacian friction is nonzero where there is curvature in the vertical profile of the horizontal velocity, and where there is

vertical dependence to the viscosity and velocity

$$\boldsymbol{F}^{\text{viscous}} = \frac{\partial \nu^{\text{eddy}}}{\partial z} \frac{\partial \boldsymbol{u}}{\partial z} + \nu^{\text{eddy}} \frac{\partial^2 \boldsymbol{u}}{\partial z^2}. \tag{33.18}$$

The turbulent viscosity generally has a vertical dependence, with larger values in the boundary layer where turbulence is most energetic. This form of the friction preferentially acts on velocity exhibiting nontrivial vertical structure, thus acting to smooth any vertical dependence. In Section 68.4 we discuss further mathematical properties of Laplacian friction.

33.3.2 Non-dimensionalization

We non-dimensionalize the equations to isolate non-dimensional numbers affecting the flow regime. In particular, we identify the Ekman number as a measure of the importance of friction relative to rotation, with friction important where the Ekman number is order unity or larger, and unimportant where the Ekman number is much smaller than unity.[3]

We make use of the following scales and associated non-dimensional quantities

$$(x, y) = L\,(\hat{x}, \hat{y}) \qquad z = H\,\hat{z} \qquad (u, v) = U\,(\hat{u}, \hat{v}) \qquad f = f_\circ\,\hat{f} \qquad p = P\,\hat{p} \tag{33.19}$$

where the hat terms are non-dimensional,[4] and we introduced typical scales for horizontal length (L), vertical length (H), velocity (U), Coriolis parameter ($f_\circ$), and pressure (P). For the pressure scale we assume it follows geostrophic scaling so that it can be writen[5]

$$P = f_\circ\,\rho_\circ\,U\,L. \tag{33.20}$$

Inserting the relations (33.19) into equation (33.1) leads to the non-dimensional frictional geostrophic equation

$$\hat{\boldsymbol{f}} \times \hat{\boldsymbol{u}} = -\hat{\nabla}\hat{p} + \frac{\boldsymbol{F}}{f_\circ\,U}. \tag{33.21}$$

33.3.3 Defining the Ekman number and layer thickness

The *Ekman number* is a non-dimensional measure of the relative importance of the frictional acceleration due to vertical shears versus the Coriolis acceleration

$$\text{Ek} = \frac{\text{frictional acceleration from vertical shears}}{\text{Coriolis acceleration}}. \tag{33.22}$$

The Ekman number increases when there is more boundary layer turbulence, in which case the eddy viscosity, ν^{eddy}, is large relative to its small values in the interior region outside of the boundary layer. Additionally, the Ekman number increases when moving towards the equator, where the Coriolis parameter reduces.[6]

For the viscous stress form of Laplacian vertical frictional acceleration (equation (33.17))

$$\boldsymbol{F}^{\text{viscous}} = \frac{\nu^{\text{eddy}}\,U}{H^2} \frac{\partial^2 \hat{\boldsymbol{u}}}{\partial \hat{z}^2}, \tag{33.23}$$

[3]For flows unaffected by rotation, the Reynolds number is the key non-dimensional number (Section 25.9) determining where viscous friction is important.

[4]In Section 32.2.1 we defined $\hat{\boldsymbol{u}}$ as the unit vector pointing along the trajectory of a fluid element. In contrast, we here let $\hat{\boldsymbol{u}}$ be the non-dimensional horizontal velocity. The duplication of notation is unfortunate.

[5]Recall that in Section 29.2.3 we considered pressure in a non-rotating system to scale according to the dynamical pressure scale, U^2, where U is a horizontal flow speed scale. In the presence of planetary rotation, the large-scale pressure field scales according to the geostrophic balance as per equation (33.20).

[6]When getting very close to the equator, our assumption of a frictional geostrophic balance breaks down so that other terms in the momentum equation, such as advection, become important.

the Ekman number is given by

$$\mathrm{Ek} = \frac{\nu^{\mathrm{eddy}}}{f_\circ H^2}, \tag{33.24}$$

and the horizontal velocity equation (33.21) takes on the form

$$\hat{\boldsymbol{f}} \times \hat{\boldsymbol{u}} = -\hat{\nabla}\hat{p} + \mathrm{Ek}\,\frac{\partial^2 \hat{\boldsymbol{u}}}{\partial \hat{z}^2}. \tag{33.25}$$

If we take the vertical scale, H, equal to the length scale over which interior flow processes occur, then the Ekman number will be very small, even if the eddy viscosity is relatively large. In this case we conclude that friction is negligible, as indeed it is for many purposes where the boundary layer is not of concern.

However, the Ekman number multiplies the highest derivative in equation (33.25). So setting the Ekman number to zero represents a *singular limit*, whose mathematial meaning is that we change the order of the differential equation when setting $\mathrm{Ek} = 0$. Reducing the order of the differential equation means we can only satisfy a reduced number of boundary conditions relative to the $\mathrm{Ek} > 0$ case. In particular, with $\mathrm{Ek} = 0$ we can no longer satisfy the no-slip condition at the solid-fluid boundary. In contrast, with any non-zero value of $\mathrm{Ek} > 0$, no matter how small but nonzero, viscosity drags the flow to zero within a *boundary layer* where friction is leading order. We expect a boundary layer to form within a boundary layer thickness, $H = \delta^{\mathrm{Ekman}}$, in which the Ekman number is order unity so where friction is of leading order importance

$$H = \delta^{\mathrm{Ekman}} \Longrightarrow \mathrm{Ek} = \frac{\nu^{\mathrm{eddy}}}{f_\circ\,(\delta^{\mathrm{Ekman}})^2} = 1. \tag{33.26}$$

Turning this equation around we see that the vertical scale, δ^{Ekman}, defines the viscous Ekman boundary layer thickness as a function of the eddy viscosity and Coriolis parameter

$$\mathrm{Ek} = 1 \Longrightarrow \delta^{\mathrm{Ekman}} = \delta^{\mathrm{viscous}} = \sqrt{\nu^{\mathrm{eddy}}/f_\circ}. \tag{33.27}$$

33.3.4 Estimates for the vertical eddy viscosity

The eddy viscosity is not readily available from direct measurements or first principles. However, measuring the boundary layer thickness provides a means to infer a bulk viscosity for the boundary layer

$$\nu^{\mathrm{eddy}} = f_\circ\,(\delta^{\mathrm{Ekman}})^2. \tag{33.28}$$

In the atmosphere, the boundary layer thickness is order 1000 m, so that at mid-latitudes, with $f_\circ = 10^{-4}$ s^{-1}, we expect

$$\nu^{\mathrm{eddy}}_{\mathrm{atmos}} \sim 10^2 \text{ m}^2 \text{ s}^{-1}. \tag{33.29}$$

In the ocean, the upper ocean boundary layer depth, outside of the deep convection regions, is roughly 50 m, in which case

$$\nu^{\mathrm{eddy}}_{\mathrm{ocean}} \sim 0.25 \text{ m}^2 \text{ s}^{-1}. \tag{33.30}$$

33.4 Ocean surface Ekman layer

It is possible to establish integrated mass transport properties of the Ekman layer even without specifying details of the friction (i.e., the viscosity) or the stratification. The key ingredient is the boundary stress. This stress is commonly estimated for the surface ocean given information about the wind speed and atmospheric stratification. Hence, Ekman theory has found much application to studies of the wind-driven ocean circulation, with the integrated properties the

most consequential results from Ekman theory. We here focus on the ocean surface Ekman layer and then consider bottom Ekman boundaries for the atmosphere and ocean in Section 33.5.

Before starting, we emphasize that the stress is the key ingredient in computing properties of the Ekman layer. And yet, determining the stress is a nontrivial exercise in boundary layer physics, which is outside our scope. Additionally, the turbulent boundary stress exchanged between the fluid and its boundary (either another fluid, ice, or the solid earth) arises within Ekman boundary layers, where flow spirals relative to the geostrophic flow in the fluid interior (outside the Ekman boundary layer). So the boundary stress is generally rotated some amount relative to the interior geostrophic flow. We consider an analytic example of this rotation when studying the bottom Ekman layer in Section 33.5. For now, we simply recognize that the story is relatively simple when assuming the stress is given, but the stress itself can be rather difficult to accurately determine.

33.4.1 Horizontal mass transport within the Ekman layer

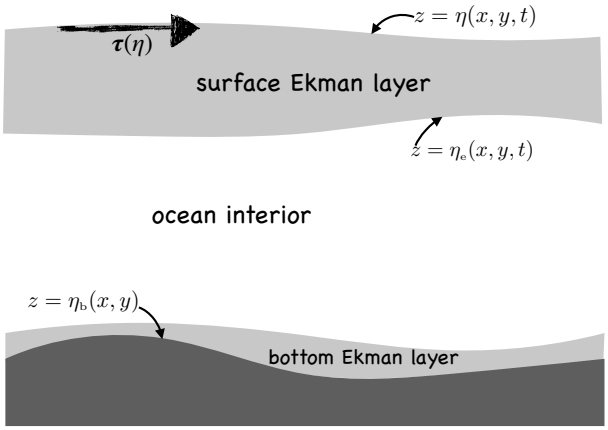

FIGURE 33.4: Ekman layer at the ocean surface, defined for vertical position $\eta_e(x,y,t) \leq z \leq \eta(x,y,t)$, with η_e specifying the Ekman layer bottom and η the free surface vertical position. Boundary stress from winds and/or sea ice imparts horizontal momentum to the upper ocean that is transmitted throughout the Ekman layer via the vertical divergence of turbulent horizontal shear stresses. As studied in Section 33.6, there is also a bottom Ekman layer created by stresses active next to the ocean bottom.

We are concerned with the mass budget for the ocean surface Ekman layer sitting between the Ekman layer bottom and the ocean free surface

$$\eta_e(x,y,t) \leq z \leq \eta(x,y,t), \tag{33.31}$$

as depicted in Figure 33.4. Knowledge of the mass budget has implications for how mechanical energy imparted to the boundary layer drives circulation well within the interior of the ocean. This transport and associated circulation are how Ekman mechanics, limited to the boundary layer, affect large-scale ocean circulation throughout the fluid column.

Integrating the horizontal Ekman balance (33.4) over the vertical scale of the Ekman layer leads to

$$\boldsymbol{M}_e = \int_{\eta_e}^{\eta} \rho_o \, \boldsymbol{u}_e \, dz \Longrightarrow f \, \hat{\boldsymbol{z}} \times \boldsymbol{M}_e = \int_{\eta_e}^{\eta} \rho_o \, \boldsymbol{F} \, dz, \tag{33.32}$$

with $\boldsymbol{M}_e$ the vertically integrated ageostrophic horizontal mass transport within the Ekman boundary layer. Assuming friction to be in the form of a vertical stress divergence as in equation (33.17) leads to the horizontal Ekman mass transport

$$\boldsymbol{M}_e = -f^{-1} \, \hat{\boldsymbol{z}} \times [\boldsymbol{\tau}(\eta) - \boldsymbol{\tau}(\eta_e)]. \tag{33.33}$$

Stress at the bottom of the Ekman layer, $\boldsymbol{\tau}(\eta_{\rm e})$, matches to the stress in the ocean interior. The stress in the fluid interior is generally much smaller than stress in the turbulent upper ocean surface, $\boldsymbol{\tau}(\eta)$, so that we can neglect $\boldsymbol{\tau}(\eta_{\rm e})$ when computing the mass transport. We are thus led to the expression for the surface stress induced ageostrophic horizontal mass transport within the upper ocean Ekman layer

$$\boldsymbol{M}_{\rm e} = -f^{-1}\, \hat{\boldsymbol{z}} \times \boldsymbol{\tau}(\eta) = f^{-1}\, [\hat{\boldsymbol{x}}\, \tau^y(\eta) - \hat{\boldsymbol{y}}\, \tau^x(\eta)]. \tag{33.34}$$

The surface stress induced mass transport given by equation (33.34) is very useful in practice. Notably, we do not need to know the thickness of the Ekman layer. Rather, the mass transport is determined solely by the surface boundary stress.[7] Furthermore, the horizontal mass transport within the Ekman layer is directed at right angles to the surface stress, as depicted in Figure 33.5, with mass transport to the right of the surface stress in the northern hemisphere and to the left in the southern hemisphere.

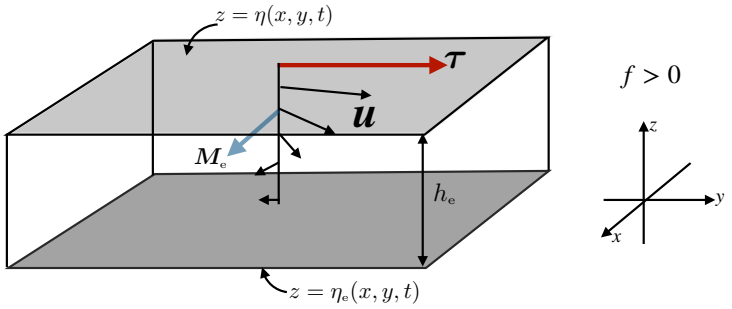

FIGURE 33.5: Horizontal transport integrated over the thickness of the surface ocean Ekman layer in the region $\eta_{\rm e}(x,y,t) \le z \le \eta(x,y,t)$. The net mass transport is directed perpendicular to the boundary stress, oriented to the right in the northern hemisphere and to the left in the southern hemisphere. Here, the boundary stress, $\boldsymbol{\tau}$, is shown directed to the north so that in the northern hemisphere ($f > 0$), the vertically integrated horizontal Ekman transport, $\boldsymbol{M}_{\rm e}$, is to the east. This perpendicular mass transport is the result of the vertically spiralling Ekman flow. The Ekman mass transport resulting from boundary stress is independent of the assumptions made about ocean friction within the ocean boundary layer, and it is independent of the stratification assumed for the Ekman layer.

33.4.2 Example Ekman mass transports

Consider an example with an eastward zonal boundary stress, $\boldsymbol{\tau}(\eta) = |\tau|\, \hat{\boldsymbol{x}}$ (i.e., westerly winds). In this case, the Ekman transport in the upper ocean is meridional

$$\boldsymbol{M}_{\rm e} = -(|\tau|/f)\, \hat{\boldsymbol{y}}, \tag{33.35}$$

which points equatorward in both hemispheres. Conversely, in the equatorial region where winds are predominantly from the east (easterly winds) so that $\boldsymbol{\tau}(\eta) = -|\tau|\, \hat{\boldsymbol{x}}$, then the horizontal Ekman mass transport causes waters to move poleward away from (diverge from) the equator. Mass continuity is then satisfied by upwelling waters along the equator within the Ekman layer. We sketch the elements of this flow in Figure 33.6. Exercise 33.1 considers an analogous situation for a channel in the southern hemisphere, thus illustrating a basic feature of the wind-driven overturning circulation in the Southern Ocean.

[7] As noted at the start of this section, determining the stress, $\boldsymbol{\tau}(\eta)$, transferred to the ocean requires information about the boundary layer processes in both the ocean and the adjoining media (either the atmosphere or cryosphere). Nevertheless, by expressing the mass transport, $\boldsymbol{M}_{\rm e}$, in terms of the boundary stress provides a clear delineation of the causes for boundary layer transport. It has thus offered an important foundation for theories of wind-driven ocean circulation.

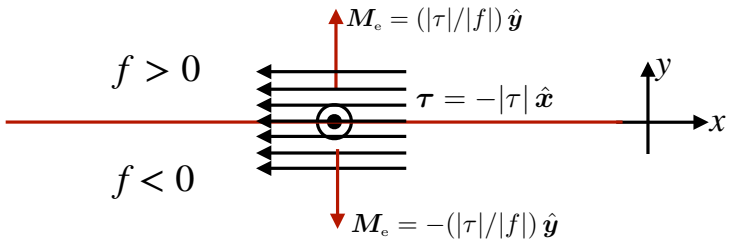

FIGURE 33.6: Easterly winds along the equator drive poleward horizontal mass transport within the upper ocean Ekman layer, as per equation (33.35). Furthermore, as discussed in Section 33.4.3, a steady state Ekman layer mass budget is typically realized by the upwelling of interior waters into the Ekman layer.

A second example concerns the case of a wind stress with a component aligned with a coastline as depicted in Figure 33.7. When the horizontal Ekman mass transport is directed away from the coast, a steady mass balance in the Ekman layer is associated with the upwelling of waters from beneath the Ekman layer. Conversely when the horizontal mass transport is directed toward the coast, steady mass balance is realized by coastal downwelling. This process is very important for coastal physical and biological oceanography.

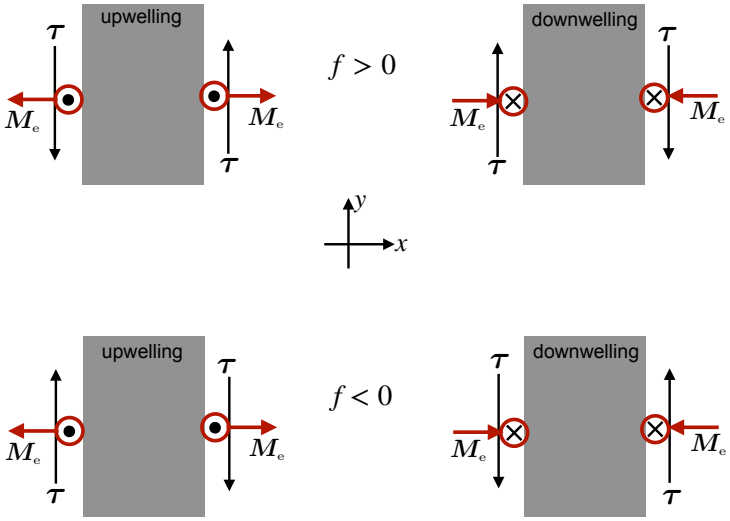

FIGURE 33.7: Wind stresses with a component that is parallel to coastlines lead to horizontal mass transport away from or towards the coast. Mass continuity then leads to coastal upwelling or downwelling of waters into or out of the Ekman layer. Here we depict the various scenarios for the northern hemisphere (top row) and southern hemisphere (bottom row), with the gray regions representing land, the black vectors the wind stresses, and the red arrows the horizontal wind induced mass transports in the Ekman layer. This figure is adapted from Figure 4-24 of *von Arx* (1962).

33.4.3 Mass budget for the Ekman layer

As seen in Figure 33.3, the horizontal transport of fluid within the Ekman layer induces a vertical transport into or out of the Ekman layer. To obtain a mathematical expression for the vertical transport, integrate the continuity equation $\nabla \cdot \boldsymbol{v} = 0$ over the vertical extent of the Ekman layer

$$\frac{\partial}{\partial x}\left[\int_{\eta_e}^{\eta} u\,dz\right] + \frac{\partial}{\partial y}\left[\int_{\eta_e}^{\eta} v\,dz\right] + [w(\eta) - \boldsymbol{u}(\eta)\cdot\nabla\eta] - [w(\eta_e) - \boldsymbol{u}(\eta_e)\cdot\nabla\eta_e] = 0. \tag{33.36}$$

For a Boussinesq ocean, the kinematic boundary condition at the ocean free surface is given by equation (21.5)

$$w + Q_m/\rho_o = \partial_t\eta + \boldsymbol{u}\cdot\nabla\eta \qquad \text{at } z = \eta(x,y,t). \tag{33.37}$$

Similarly, at the bottom of the Ekman layer we measure the volume transport through this layer by computing the dia-surface transport, $w^{(\dot{\eta}_e)}$, according to equation (64.38)

$$w^{(\dot{\eta}_e)} = w - (\partial_t z + \boldsymbol{u} \cdot \nabla z) \qquad \text{at } \; z = \eta_e(x, y, t). \tag{33.38}$$

The sign convention is such that $w^{(\dot{\eta}_e)} > 0$ means that volume enters (entrains into) the surface Ekman layer through its base, whereas $w^{(\dot{\eta}_e)} < 0$ means that volume leaves (detrains from) the surface Ekman layer base.

Using the kinematic boundary conditions (33.37) and (33.38) in the vertically integrated volume budget (33.36), and rearranging, leads to the Ekman layer mass budget

$$\rho_o \, w^{(\dot{\eta}_e)} + Q_m = \rho_o \, \partial h_e / \partial t + \nabla \cdot \boldsymbol{M}. \tag{33.39}$$

In this equation we wrote

$$h_e = \eta - \eta_e \tag{33.40}$$

for the thickness of the Ekman layer and

$$\boldsymbol{M} = \rho_o \int_{\eta_e}^{\eta} \boldsymbol{u} \, dz \tag{33.41}$$

for the Ekman layer integrated horizontal mass transport. As a check on the above manipulations, let the Ekman layer go to the ocean bottom (so that $w^{(\dot{\eta}_e)} = 0$ and $\eta_e = \eta_b$), in which case the mass budget equation (33.39) correctly reduces to the kinematic free surface equation for the full ocean column as given by equation (21.81)

$$\rho_o \, \partial_t \eta = Q_m - \rho_o \, \nabla \cdot \boldsymbol{U}, \tag{33.42}$$

with $\boldsymbol{U} = \int_{\eta_b}^{\eta} \boldsymbol{u} \, dz$ the vertically integrated horizontal velocity.

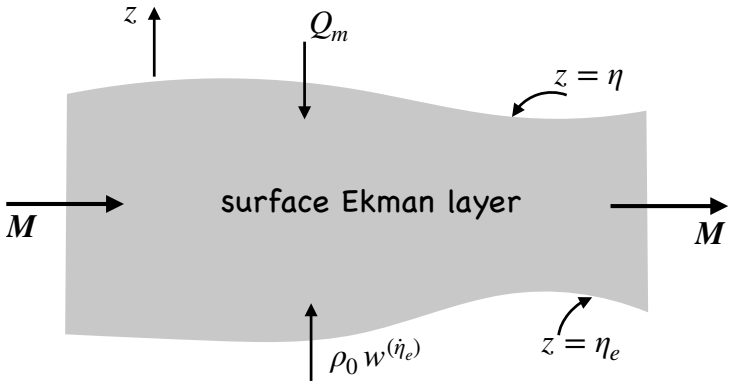

FIGURE 33.8: Mass budget over the surface Ekman layer of the ocean, with contributions from the surface mass flux, Q_m, flux through the bottom of the layer, $w^{(\dot{\eta}_e)}$, and vertically integrated horizontal flux, $\boldsymbol{M}$, within the layer. If there are any imbalances then the layer thickness will have a nonzero time tendency, $\partial_t h_e \neq 0$. Our sign convention is such as $w^{(\dot{\eta}_e)} > 0$ corresponds to water entering (entraining into) the Ekman layer (vertically upward motion) through the Ekman layer base at $z = \eta_e$, and likewise $Q_m > 0$ correspondes to water entering the Ekman layer through the free surface at $z = \eta$. Entrainment through the base of the Ekman layer is referred to as *Ekman suction* or *Ekman upwelling*. The opposite case is referred to as *Ekman pumping* or *Ekman downwelling* when water leaves the Ekman layer and enters the ocean interior.

The horizontal mass transport given by equation (33.41) has a contribution from both the Ekman transport and remaining processes, such as geostrophic flow and ageostrophic flows not associated with Ekman. We write this mass transport in the form

$$\boldsymbol{M} = \boldsymbol{M}_e + \boldsymbol{M}_{\text{other}}. \tag{33.43}$$

The horizontal Ekman transport is determined by the boundary stress according to equation (33.34), with its divergence given by

$$\nabla \cdot \boldsymbol{M}_{\rm e} = \hat{\boldsymbol{z}} \cdot [\nabla \times (\boldsymbol{\tau}/f)]. \tag{33.44}$$

This result brings the Ekman layer mass budget (33.39) into the form

$$\rho_{\circ}\, w^{(\dot{\eta}_{\rm e})} + Q_{\rm m} = \rho_{\circ}\, \partial_t h_{\rm e} + \nabla \cdot \boldsymbol{M}_{\rm other} + \hat{\boldsymbol{z}} \cdot [\nabla \times (\boldsymbol{\tau}/f)]. \tag{33.45}$$

The left hand side measures the mass transport crossing the bottom of the Ekman layer, $\rho_{\circ}\, w^{(\dot{\eta}_{\rm e})}$, plus the transport crossing the free surface, $Q_{\rm m}$. This transport balances a time change in the Ekman layer thickness (first right hand side term), plus the horizontal divergence of mass within the layer (associed with non-Ekman and Ekman). A steady state Ekman layer thickness, $\partial h_{\rm e}/\partial t = 0$, is realized if the horizontal divergence of mass within the Ekman layer is exactly balanced by mass entering the Ekman layer through the top and/or bottom of the layer. We illustrate this budget in Figure 33.8. For example, in the equatorial case of Figure 33.6, the diverging horizontal Ekman layer flow induced by easterly winds (poleward Ekman transport on both sides of the equator) is balanced by water upwelling into the Ekman layer through the base, $w^{(\dot{\eta}_{\rm e})} > 0$, along with a generally smaller effects from surface mass fluxes through $Q_{\rm m}$ and possible other contributions through $\nabla \cdot \boldsymbol{M}_{\rm other}$.

33.4.4 Ekman layer coupled to the geostrophic interior

The effects from boundary stress curl in equation (33.45) warrant particular attention whereby

$$\rho_{\circ}\, w^{(\dot{\eta}_{\rm e})}_{\rm Ekman} \equiv \nabla \cdot \boldsymbol{M}_{\rm e} = \hat{\boldsymbol{z}} \cdot [\nabla \times (\boldsymbol{\tau}/f)]. \tag{33.46}$$

The stress curl, as well as changes in f on the sphere, drive vertical motion through the base of the Ekman layer. The flow crossing the Ekman layer boundary acts to stretch or compress vertical fluid columns in the adjoining fluid interior. Interior fluid columns in a rotating fluid are stiffened through the effects of Taylor-Proudman (Section 31.5.3). From our understanding of vorticity (studied in Chapter 40), particularly the notions of vortex stretching, we see that the Ekman induced stretching/compression of interior fluid columns leads to a change in vorticity of the fluid interior, and can then lead to meridional motion due to the beta effect (see discussion of Sverdrup balance in Section 31.5.4).

Consider an example with $\nabla \cdot \boldsymbol{M}_{\rm e} = \hat{\boldsymbol{z}} \cdot [\nabla \times (\boldsymbol{\tau}/f)] > 0$, so that winds induce a divergence within the Ekman layer. In a steady state, the interior flow accommodates this Ekman layer mass divergence by upwelling water through the Ekman layer base, $w^{(\dot{\eta}_{\rm e})} > 0$. This process of entraining interior water into the Ekman layer is known as *Ekman suction* or *Ekman upwelling*. For the opposite case with $\hat{\boldsymbol{z}} \cdot [\nabla \times (\boldsymbol{\tau}/f)] < 0$, water leaves (detrains) from the Ekman layer and moves into the interior region sitting below the boundary layer. Water detraining from the Ekman layer is known as *Ekman pumping* or *Ekman downwelling*. As water diverges it produces a local low pressure so that the induced flow in the geostrophic interior is cyclonic around a region of Ekman divergence/upwelling. Conversely, the induced interior geostrophic flow is anti-cyclonic around a region of Ekman convergence/downwelling. Figure 33.9 provides an illustration for the variety of cases found in the northern and southern hemispheres.

In the language of vorticity, developed in Part VII of this book, Ekman upwelling with $w^{(\dot{\eta}_{\rm e})} > 0$ leads to vortex stretching of interior fluid columns, whereas Ekman downwelling with $w^{(\dot{\eta}_{\rm e})} < 0$ squashes the interior fluid columns. Vertical stiffening through Taylor-Proudman within the geostrophic interior, coupled to Ekman induced vortex stretching/squashing, makes what happens within the Ekman boundary layer of primary importance to the interior geostrophic flow. This boundary-interior coupling forms a key mechanism for how mechanical forcing from

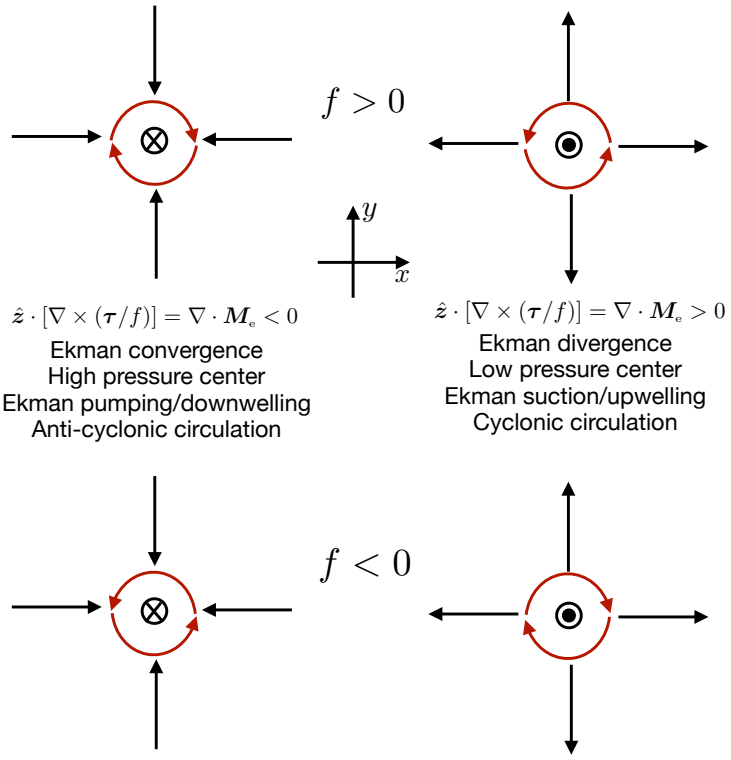

FIGURE 33.9: Plan view depicting the steady state horizontal and vertical transport in the surface ocean Ekman layer (ignoring the possible transport across the ocean surface from Q_m). The left column shows horizontal wind-induced convergence in the Ekman layer that induces vertical pumping/downwelling, where $\nabla \cdot \boldsymbol{M}_e = \hat{\boldsymbol{z}} \cdot [\nabla \times (\boldsymbol{\tau}/f)] < 0$. The right column shows the horizontal divergence within the Ekman layer that is balanced by suction/upwelling, where $\nabla \cdot \boldsymbol{M}_e = \hat{\boldsymbol{z}} \cdot [\nabla \times (\boldsymbol{\tau}/f)] > 0$. The top row is for the northern hemisphere, with $f > 0$, and the bottom row is for the southern hemisphere. The red arrows depict the sense for the induced geostrophic circulation in the interior just below the Ekman layer. Note that the horizontal Ekman transport is to the right of the red circulating flow in the northern hemisphere and to the left in the southern. Ekman pumping is associated with anti-cyclonic circulation (clockwise in the northern hemisphere and anti-clockwise in southern hemisphere). In contrast, Ekman suction is associated with cyclonic circulation. The circulation is supported by pressure gradients, with high pressure in regions of Ekman convergence, $\nabla \cdot \boldsymbol{M}_e < 0$, due to the accumulation of mass towards the center, thus giving rise to anti-cyclonic geostrophic flow in the interior. The opposite holds for regions of Ekman divergence, $\nabla \cdot \boldsymbol{M}_e > 0$, where water leaves the region thus leaving a low pressure center and inducing a cyclonic interior geostrophic flow.

surface boundary stress creates the *wind driven* ocean circulation. It is notable that the coupling between boundary layer and interior flow is absent from non-rotating boundary layer flows. In Figure 33.10 we offer a highly idealized schematic of the circulation implied by Ekman dynamics in a homogeneous fluid on an f-plane, thus illustrating the coupling of the upper surface Ekman layer to the geostrophic interior and then to the bottom Ekman layer. We also discuss the *geostrophic Sverdrup balance* in Section 44.4, which builds on the ideas in this section.

33.4.5 Further study

The following videos offer visuals to help develop further intuition for Ekman boundary flows.

- This 4-minute video from Science Primer provides an overview of how Ekman transport affects ocean circulation features near the coast and in open ocean gyres.

- This video from MIT Earth, Atmospheric, and Planetary Sciences illustrates the spiral flow found within an Ekman layer as realized in a rotating tank experiment.

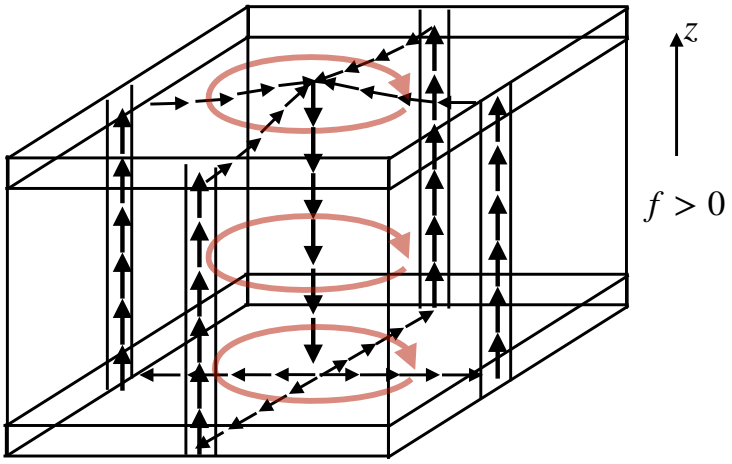

FIGURE 33.10: Schematic ocean Ekman gyre circulation in a rectangular box in the northern hemisphere on an f-plane as forced by an anti-cyclonic wind stress curl. The wind stress curl causes fluid to pile up in the center of the gyre and develop an anti-cyclonic flow. The horizontal convergence of mass towards the center of the gyre leads to downwelling into the gyre interior below the Ekman layer (as per the upper left panel of Figure 33.9). This downwelling water enters the geostrophic interior and further into the bottom Ekman layer. As discussed in Section 33.5, the downwelling water in the bottom Ekman layer causes a horizontal divergence of mass. Assuming the domain has fixed vertical side walls, continuity requires an upwelling along the outer portion of the gyre. If the wind stress is symmetric about the center of the domain, then so is the flow. However, as studied in Section 39.7, the axial symmetry is broken on the β-plane, in which flow is stronger on the western side of the gyre even if the wind remains symmetric about the domain center. This figure is adapted from Figure 6-15 of *von Arx* (1962).

- This video from the UCLA SpinLab, near the 18 minute mark, shows how Ekman transport helps to explain the garbage patches found near the center of the ocean's sub-tropical gyres.
- This video from the University of Chicago, starting near the 23 minute mark, provides examples of Ekman layers in a rotating tank. The other portions of this video exhibit many other novel aspects of rotating fluids and is highly recommended.

33.5 Bottom Ekman layer

In this section we study the mechanics of a bottom Ekman boundary layer. For the mass transport, we merely translate the results from the upper ocean Ekman layer considered in Section 33.4, whereby the mass transports are specified by the bottom boundary stress. We go further in this analysis by also providing an analytic expression for the velocity profile within the Ekman layer, with the velocity profile allowing us to diagnose the bottom boundary stress according to the Neumann boundary condition placed on the horizontal velocity (equation (33.59) below).

33.5.1 Horizontal mass transport within the Ekman layer

Turning the derivation from Section 33.4.1 upside-down leads to a bottom horizontal Ekman mass transport

$$\boldsymbol{M}_{\mathrm{e}} = \int_{\eta_{\mathrm{b}}}^{\eta_{\mathrm{e}}} \rho_{\circ}\, \boldsymbol{u}_{\mathrm{e}}\, \mathrm{d}z = -f^{-1}\, \hat{\boldsymbol{z}} \times [\boldsymbol{\tau}(\eta_{\mathrm{e}}) - \boldsymbol{\tau}(\eta_{\mathrm{b}})] \approx f^{-1}\, \hat{\boldsymbol{z}} \times \boldsymbol{\tau}(\eta_{\mathrm{b}}). \tag{33.47}$$

Note the sign swap relative to the upper Ekman layer transport in equation (33.34). Hence, the Ekman transport is directed to the left of the bottom stress in the northern hemisphere and to the right in the southern hemisphere. Care must be exercised when determining the stress, with

examples given below, including an analytic example given in Section 33.5.3. In general, the stress is not aligned with the interior geostrophic flow, but is instead rotated by some amount.

Atmosphere-ocean Ekman layers

Consider the case where the bottom Ekman layer is the bottom of the atmosphere sitting over the ocean. The stress imparted to the bottom of the atmosphere is equal in magnitude yet oppositely directed to the stress acting on the upper ocean.[8] Hence, the frictional stress induced mass transport (33.34) for the upper ocean Ekman layer is equal and opposite to the frictional stress induced mass transport in the atmosphere Ekman layer

$$\boldsymbol{M}_{\mathrm{e}}^{\mathrm{ocn}} = -\boldsymbol{M}_{\mathrm{e}}^{\mathrm{atm}} \Longrightarrow \boldsymbol{M}_{\mathrm{e}}^{\mathrm{ocn}} + \boldsymbol{M}_{\mathrm{e}}^{\mathrm{atm}} = 0. \tag{33.48}$$

Since the density of the atmosphere and ocean are quite different, the equal Ekman mass transports correspond to very different volume transports.

Ocean-solid earth or atmosphere-solid earth Ekman layer

Consider the bottom Ekman layer next to the solid earth. Just like the atmosphere-ocean case, the stress imparted by the fluid on the earth is equal and opposite to the stress by the earth on the fluid. It is not generally simple to determine this stress, though we provide an example in Section 33.5.3 based on assuming information about the vertical viscosity profile within the boundary layer. From that example, we see that the stress is not directly aligned with the interior geostrophic flow just above the boundary layer. Instead, the stress is $\pi/4$ rotated to the left of the interior flow. The rotation is due to the spiralling structure of the boundary layer flow that gives rise to the stress.

33.5.2 Mass budget for the bottom Ekman layer

Following the derivation of the Ekman layer mass budget in Section 33.4.3, and assuming no mass enters through the solid earth, we are led to the mass budget for the bottom Ekman boundary layer[9]

$$\rho_{\mathrm{o}}\, w^{(\dot{\eta}_{\mathrm{e}})} = \rho_{\mathrm{o}}\, \partial_t h_{\mathrm{e}} - \nabla \cdot \boldsymbol{M} \tag{33.49}$$

where $z = \eta_{\mathrm{e}}(x, y, t)$ is the vertical position for the top of the bottom Ekman layer, and

$$h_{\mathrm{e}} = \eta_{\mathrm{e}} - \eta_{\mathrm{b}} \tag{33.50}$$

is the Ekman layer thickness. For a steady state, the budget equation (33.49) says that the horizontal convergence of mass into the bottom Ekman boundary layer leads to a detrainment of mass from the Ekman layer into the interior fluid above (upwelling). Conversely, when fluid horizontally diverges from the bottom Ekman layer there is a balance from an entrainment (downwelling) of fluid from the interior into the Ekman layer. This orientation for the mass transport is illustrated in Figure 33.3 as part of our earlier discussion.

33.5.3 An analytic bottom Ekman spiral velocity

When studying the bottom boundary layer for the atmosphere or the surface boundary layer for the ocean, we are generally afforded an estimate of the frictional boundary stress, $\boldsymbol{\tau}(\eta)$. In turn,

[8] Recall our discussion of stress in Chapter 25, whereby stress on one side of an interface matches that on the other, which is a result following from Newton's third law.

[9] Note the sign swap in the budget (33.49) in front of the horizontal transport term as compared to the surface boundary layer mass budget (33.39).

we can estimate the boundary stress induced mass transport and its divergence, and we can do so without making assumptions about the density profile or viscous stresses within the boundary layer. However, this estimate is less directly accessible for the ocean bottom Ekman layer, where we need $\boldsymbol{\tau}(\eta_b)$ to determine the mass transport. We here take an alternative approach that produces an analytic profile for the velocity within the Ekman layer, so long as we know the viscosity within the boundary layer. Knowing the velocity profile then affords an estimate of the boundary stress. This approach requires a few assumptions that are not always met, in particular it requires the viscosity. Even so, it provides physical insights that further our understanding of Ekman mechanics thus motivating the analysis.

Physical configuration

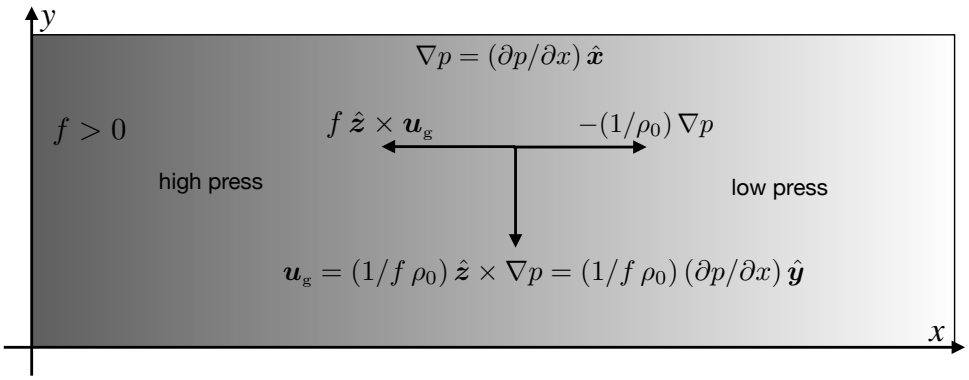

FIGURE 33.11: A southward geostrophic flow in the northern hemisphere ($f > 0$) induced by an eastward pressure gradient acceleration (low pressure to the east; $\partial p/\partial x < 0$) that balances a westward Coriolis acceleration.

We assume flow above the boundary layer is geostrophic and supported by a prescribed vertically independent pressure gradient

$$f\,\rho_o\,\boldsymbol{u}_g = \hat{\boldsymbol{z}} \times \nabla p. \tag{33.51}$$

A specific example is given by Figure 33.11, where a southward geostrophic flow in the northern hemisphere has an eastward pressure gradient acceleration (low pressure to the east) balanced by a westward Coriolis acceleration.

For flow within the bottom boundary layer, viscous stresses exchange horizontal momentum vertically between the inviscid geostrophic interior and the bottom no-slip condition. This viscous exchange slows the boundary layer velocity relative to the interior geostrophic velocity above the boundary layer. Since the pressure gradient is assumed to be vertically independent and prescribed, the slower velocity within the boundary layer means that the Coriolis acceleration is unable to balance the pressure gradient acceleration. This imbalance between pressure acceleration and Coriolis acceleration leads to a down pressure gradient component to the boundary layer velocity. As a result, the velocity spirals downward toward the bottom.

The key assumptions required to produce an analytic Ekman spiral velocity are: (i) the fluid within the Ekman layer has a constant density, ρ_o; (ii) the Coriolis parameter is a constant as per the f-plane; (iii) the prescribed pressure gradient is vertically independent so that the associated geostrophic velocity is vertically independent; (iv) the eddy viscosity is constant within the boundary layer and zero in the interior region above the boundary layer; (v) the flow is steady. The homogeneous density assumption is motivated by the rather small vertical scale of the bottom Ekman layer (tens of meters) relative to the horizontal scales over which density varies in the ocean bottom (tens to hundreds of kilometers). A constant viscosity is not always realistic since the turbulent viscosity is generally inhomogeneous within boundary layers. Even

so, by assuming sufficient time for statistics to become stationary we can expect to make good use of the time averaged viscosity.

Velocity profile within the Ekman layer

Bringing the above assumptions into the frictional geostrophic equations (33.1) leads to

$$f\,\hat{\boldsymbol{z}}\times\boldsymbol{u} = -(1/\rho_{\circ})\,\nabla p + \nu^{\text{eddy}}\,\partial_{zz}\boldsymbol{u} \qquad \text{frictional geostrophy} \tag{33.52a}$$

$$\partial_z(\nabla_{\!\mathsf{h}} p) = 0 \qquad z\text{-independent horizontal pressure gradient} \tag{33.52b}$$

$$\boldsymbol{u}(\eta_{\mathsf{b}}) = 0 \qquad \text{no-slip bottom boundary condition} \tag{33.52c}$$

$$\boldsymbol{u}(\infty) = \boldsymbol{u}_{\mathrm{g}} \qquad \text{matching to geostrophic interior.} \tag{33.52d}$$

Decomposing the velocity into its geostrophic and ageostrophic components

$$\boldsymbol{u} = \boldsymbol{u}_{\mathrm{g}} + \boldsymbol{u}_{\mathrm{e}}, \tag{33.53}$$

leads to

$$f\,\hat{\boldsymbol{z}}\times\boldsymbol{u}_{\mathrm{e}} = \nu^{\text{eddy}}\,\partial_{zz}\boldsymbol{u}_{\mathrm{e}} \tag{33.54a}$$

$$\boldsymbol{u}_{\mathrm{e}}(\eta_{\mathsf{b}}) = 0 \tag{33.54b}$$

$$\boldsymbol{u}_{\mathrm{e}}(\infty) = 0. \tag{33.54c}$$

To reach this result we noted that the geostrophic velocity is vertically independent within the boundary layer where the density is constant, so that the geostrophic velocity does not contribute to the viscous friction operator. These coupled second order differential equations are equivalent to the two uncoupled fourth order differential equations

$$(f^2 + \nu^2\,\partial_{zzzz})\,\boldsymbol{u}_{\mathrm{e}} = 0 \tag{33.55a}$$

$$\boldsymbol{u}_{\mathrm{e}}(\eta_{\mathsf{b}}) = 0 \tag{33.55b}$$

$$\boldsymbol{u}_{\mathrm{e}}(\infty) = 0. \tag{33.55c}$$

A solution to these equations renders the Ekman boundary layer profile

$$u(z) = u_{\mathrm{g}}\left[1 - e^{-\Delta z/h_{\mathrm{e}}}\cos(\Delta z/h_{\mathrm{e}})\right] - v_{\mathrm{g}}\,e^{-\Delta z/h_{\mathrm{e}}}\sin(\Delta z/h_{\mathrm{e}}) \tag{33.56a}$$

$$v(z) = v_{\mathrm{g}}\left[1 - e^{-\Delta z/h_{\mathrm{e}}}\cos(\Delta z/h_{\mathrm{e}})\right] + u_{\mathrm{g}}\,e^{-\Delta z/h_{\mathrm{e}}}\sin(\Delta z/h_{\mathrm{e}}) \tag{33.56b}$$

$$h_{\mathrm{e}}^2 = 2\,\nu^{\text{eddy}}/|f| \tag{33.56c}$$

$$\Delta z = z - \eta_{\mathsf{b}}. \tag{33.56d}$$

Properties of the Ekman spiral

The spiral velocity profile (33.56a)-(33.56b) vanishes at the bottom, $z = \eta_{\mathsf{b}} \Longrightarrow \Delta z = 0$, reflecting the no-slip bottom boundary condition. It also reduces to the interior geostrophic velocity at $\Delta z = \infty$. In moving downward through the boundary layer, the boundary layer current deflects to the left of the interior geostrophic current (deflection is to the right in the southern hemisphere). This deflection is consistent with the schematic in Figure 33.10. Making use of the integral identities

$$\int_{\eta_{\mathsf{b}}}^{\infty} e^{-\Delta z/h_{\mathrm{e}}}\cos(\Delta z/h_{\mathrm{e}})\,\mathrm{d}\Delta z = h_{\mathrm{e}}/2 \quad \text{and} \quad \int_{\eta_{\mathsf{b}}}^{\infty} e^{-\Delta z/h_{\mathrm{e}}}\sin(\Delta z/h_{\mathrm{e}})\,\mathrm{d}\Delta z = -h_{\mathrm{e}}/2 \tag{33.57}$$

leads to the frictionally induced mass transport within the Ekman layer

$$\boldsymbol{M}_{\mathrm{e}} = \rho_{\circ} \int_{\eta_{\mathrm{b}}}^{\infty} \boldsymbol{u}_{\mathrm{e}} \, \mathrm{d}z \tag{33.58a}$$

$$= (h_{\mathrm{e}} \, \rho_{\circ}/2) \, [-\hat{\boldsymbol{x}} \, (u_{\mathrm{g}} + v_{\mathrm{g}}) + \hat{\boldsymbol{y}} \, (u_{\mathrm{g}} - v_{\mathrm{g}})] \tag{33.58b}$$

$$= f^{-1} \, \hat{\boldsymbol{z}} \times \boldsymbol{\tau}(\eta_{\mathrm{b}}), \tag{33.58c}$$

where we introduced the bottom stress according to equation (33.47). Furthermore, this stress is given by the Neumann boundary condition placed on the horizontal velocity

$$\boldsymbol{\tau}(\eta_{\mathrm{b}}) = \rho_{\circ} \, \nu^{\mathrm{eddy}} \left[\frac{\partial \boldsymbol{u}_{\mathrm{e}}}{\partial z} \right]_{z=\eta_{\mathrm{b}}} = (f \, h_{\mathrm{e}}/2) \, [\hat{\boldsymbol{x}} \, (u_{\mathrm{g}} - v_{\mathrm{g}}) + \hat{\boldsymbol{y}} \, (u_{\mathrm{g}} + v_{\mathrm{g}})]. \tag{33.59}$$

Following from equation (33.49) we see that the bottom stress induced mass transport across the top of the bottom Ekman boundary layer is

$$\rho_{\circ} \, w^{(\dot{\eta}_{\mathrm{e}})}_{\mathrm{Ekman}} = -\nabla \cdot \boldsymbol{M}_{\mathrm{e}} = -\nabla \cdot [f^{-1} \, \hat{\boldsymbol{z}} \times \boldsymbol{\tau}(\eta_{\mathrm{b}})] = (h_{\mathrm{e}}/2) \, \zeta_{\mathrm{g}}, \tag{33.60}$$

where we made use of the f-plane assumption to set $\nabla \cdot \boldsymbol{u}_{\mathrm{g}} = 0$ and introduced the relative vorticity of the geostrophic flow

$$\zeta_{\mathrm{g}} = \partial_x v_{\mathrm{g}} - \partial_y u_{\mathrm{g}}. \tag{33.61}$$

Hence, the relative vorticity of the interior geostrophic flow equals to the divergence to the horizontal mass transport within the bottom Ekman layer. We illustrate the Ekman mass transport and bottom stress in Figure 33.12.

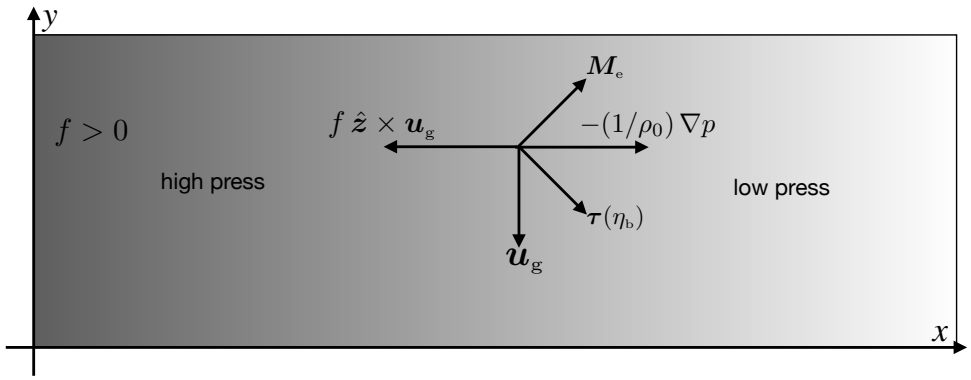

FIGURE 33.12: Mass transport and bottom stress in a homogeneous bottom Ekman layer on an f-plane in the northern hemisphere. Note how the boundary layer stress is directed $\pi/4$ radians to the left of the prescribed interior geostrophic velocity. Furthermore, the horizontal Ekman transport is itself $\pi/2$ radians to the left of the stress, which is then $3\pi/4$ to the left of the geostrophic velocity.

33.5.4 Comments

The Ekman spiral is a striking solution to the linear frictional geostrophic equations in a homogeneous fluid next to a flat no slip boundary. Section 5.7 of *Vallis* (2017) provides further discussion of the Ekman spiral solution discussed here. The spiral profile has been measured in the atmosphere and can be produced in the laboratory. However, it has proven difficult to measure in the ocean (see *Gnanadesikan and Weller* (1995) for an example). Even so, the effects from Ekman transport are robust features of the theory developed in this chapter, with those results independent of details for the vertical viscosity.

33.6 Arrested bottom Ekman flows

When studying the vertical velocity profile within the bottom boundary layer in Section 33.5, we assumed the density to be uniform within the boundary layer. A uniform density is commonly assumed for Ekman layers. However, *MacCready and Rhines* (1991, 1993), and *Garrett et al.* (1993) questioned that assumption in their study of bottom boundary layers in the presence of a nonzero vertical density stratification next to sloping topography. They point out the remarkable possibility of a vanishing frictional stress within the sloping bottom boundary layer. That is, rather than nonzero friction leading to a zero flow next to the bottom, flow is arrested by a compensation of pressure gradient accelerations. The vanishing frictional stress motivates the term *slippery Ekman layers*, whereas the equivalent term *arrested Ekman layer* refers to the zero boundary layer flow. We here briefly describe the arrested Ekman layer by studying Figure 33.13.

33.6.1 Description of the adjustment

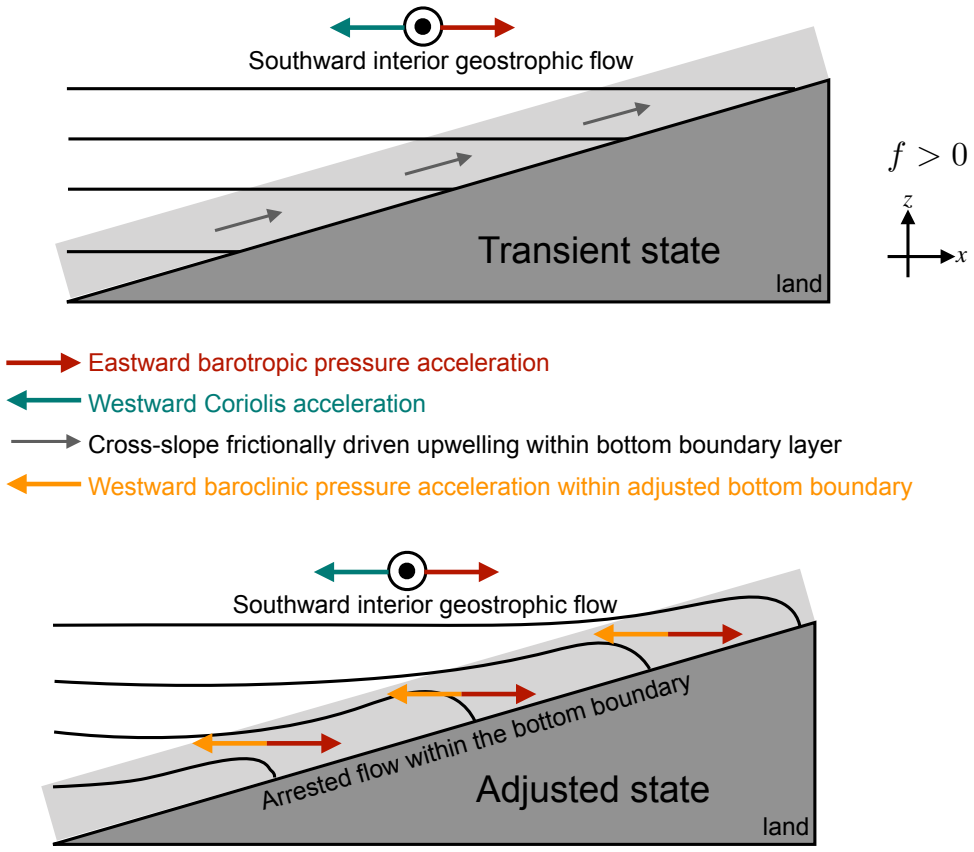

FIGURE 33.13: In both panels we depict a prescribed barotropic pressure acceleration that acts eastward and has a corresponding southward geostrophic flow and westward Coriolis acceleration. The solid black lines depict surfaces of constant buoyancy, also known as isopycnals (see Chapter 30). Top panel: As the flow enters the bottom boundary layer it slows so that its Coriolis acceleration no longer balances the barotropic pressure, thus sending water cross slope in the down pressure gradient direction. Bottom panel: The cross-slope movement of density creates a baroclinic pressure acceleration that counteracts the barotropic pressure acceleration. The steady state is realized when the two pressure accelerations balance, in which case flow within the boundary layer halts. In this halted state there are no frictional stresses since the flow halts due to pressure effects rather than friction. Note that isopycnals are shown intersecting the solid boundary in a perpendicular direction, which is implied by the no-flux bottom boundary condition (in the absence of geothermal heating) as discussed in Section 20.4.2. Geostrophic flow in the opposite direction leads to downwelling along the bottom rather than upwelling. This figure is adapted from Figure 5 of *Wåhlin et al.* (2012).

In both panels of Figure 33.13 we depict a prescribed vertically independent (barotropic) pressure acceleration that acts eastward and has a corresponding southward geostrophic flow ($f > 0$) and westward Coriolis acceleration. This configuration is identical to that shown in Figure 33.11 when studying the bottom Ekman spiral over a flat bottom. As the flow enters the bottom boundary layer it slows so that its Coriolis acceleration no longer balances the barotropic pressure gradient acceleration (we have seen this imbalance throughout this chapter). The bottom Ekman layer flow sends water cross-slope in the direction down the barotropic pressure gradient. In the configuration shown here, the cross-slope flow advects denser water upslope. In so doing, a horizontal depth-dependent (baroclinic) pressure acceleration develops adjacent to the bottom boundary layer, with the baroclinic pressure acceleration pointing opposite to the barotropic pressure acceleration. A steady state is realized when the two pressure accelerations balance, in which case flow within the boundary layer halts.

It is remarkable that the dynamical balance for the arrested bottom boundary layer flow does not involve friction. Rather, arrest happens when the two pressure gradients balance and the Coriolis acceleration vanishes. That is, referring to the frictional geostrophic equation (33.1), each term separately vanishes in the arrested state.

33.6.2 Applications

MacCready and Rhines (1991, 1993) and *Garrett et al.* (1993) study the transient adjustment leading to the arrested state. They derive the expression for the time scale for adjustment to the arrest state

$$T_{\text{arrest}} = \frac{|f|}{N^2 s^2}, \tag{33.62}$$

where s is the slope of the bottom topography and N^2 is the squared buoyancy frequency of the ambient water. The time is less in regions of strong stratification (N^2 relatively large), large topographic slopes (s^2 large), and low latitudes (f small). Conversely, the infinite time for either $N^2 = 0$ or $s^2 = 0$ indicates the need for both stratification and topographic slopes to render an arrest. Finally, we note the absence of any dissipation parameters (e.g., viscosity) from the time scale. Friction is needed to support the Ekman layer where flow crosses isobars, but the time to reach the arrested state is independent of friction.

Wåhlin et al. (2012) interpreted observations from the Amundsen Sea according to the arrested Ekman boundary layer and found T_{arrest} to be just a few hours. Additionally, the numerical model studies from *Spence et al.* (2017) and *Webb et al.* (2019) point to the ability of barotropic shelf waves around Antarctica to provide an onshore directed barotropic pressure acceleration. Through the arrested Ekman layer mechanism described here, they find that the barotropic pressure is compensated through an upslope transport of relatively warm deep water in regions of the Antarctic Peninsula. Extensions and refinements of these ideas support an active area of ongoing research (e.g., *Ruan et al.*, 2021; *Peterson and Callies*, 2022).

33.7 Exercises

EXERCISE 33.1: EKMAN MASS TRANSPORT IN A SOUTHERN CHANNEL

Consider a southern hemisphere zonally periodic channel (e.g., an idealized Southern Ocean) with a zonal wind stress that has a meridional dependence such as shown in Figure 33.14. Following the discussion in Sections 33.4.1 and 33.4.4, sketch the sense for the horizontal and vertical Ekman mass transport arising from this wind stress. Show the transport for regions to the north and to the south of the wind stress maximum. Ignore the β contribution by assuming

the channel is not very wide and by noting that β is smaller in the high latitudes (as relevant to the Southern Ocean).

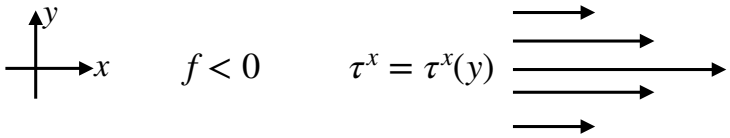

FIGURE 33.14: Zonal wind stress in a southern hemisphere zonally periodic channel with a maximum flanked by lower winds. What is the sense for the associated horizontal and vertical Ekman mass transport following from the discussion in Sections 33.4.1 and 33.4.4?

EXERCISE 33.2: RELATING EKMAN, ROSSBY, AND REYNOLDS NUMBERS

Under certain scalings, we can connect the Ekman number to the Rossby and Reynolds numbers. In detail, we have

$$\text{Ro} = \frac{U}{f_\circ L} \qquad \text{and} \qquad \text{Ek} = \frac{\nu^{\text{eddy}}}{f_\circ H^2} \qquad \text{and} \qquad \text{Re} = \frac{W H}{\nu^{\text{eddy}}}, \tag{33.63}$$

where

$$H = \text{vertical length scale} \tag{33.64a}$$
$$L = \text{horizonal length scale} \tag{33.64b}$$
$$U = \text{horizonal velocity scale} \tag{33.64c}$$
$$W = \text{vertical velocity scale.} \tag{33.64d}$$

and we defined the Reynolds number (Section 25.9) in terms of the vertical viscosity, vertical length scale, and vertical velocity scale. What is the ratio of the Rossby number to Reynolds if the flow is non-divergent?

EXERCISE 33.3: EKMAN BOUNDARY LAYERS AND RAYLEIGH DRAG

Rayleigh drag described in Section 33.2.3 allowed us to study the effects of friction on fluid trajectories. However, Rayleigh drag has no spatial derivatives, which contrasts to the Laplacian friction from Section 33.3.1 and used elsewhere in this chapter. Comment on whether Rayleigh drag can support the no-slip boundary condition and the corresponding development of a boundary layer.

Chapter 34

SPACE AND TIME DEPENDENT GRAVITY

We here formulate the dynamical equations for a geophysical fluid in the presence of a space and time dependent gravitational acceleration. This formulation has application to the study of astronomical tides in the ocean, thus motivating a discussion of the astronomical tidal forcing that follows the treatment given in Chapter 3 of *Pugh* (1987) and Section 5.15 of *Apel* (1987), with Chapter 2 of *Brown* (1999) and Section 17.4 of *Stewart* (2008) useful pedagogical supplements. Besides tides, a topic of interest to climate science concerns the study of how ocean sea level responds to changes in mass distributions associated with melting land ice. The nontrivial impact that melting land glaciers has on the earth's geoid and earth's rotation (*Farrell and Clark*, 1976; *Mitrovica et al.*, 2001; *Kopp et al.*, 2010) further motivates developing the dynamical equations of a liquid ocean in the presence of a space-time dependent gravity.

READER'S GUIDE TO THIS CHAPTER

This chapter assumes an understanding of the equations of motion derived in Chapter 24 as well as the gravitational and planetary centrifugal accelerations from Section 13.10. We dispense with tensor notation in this chapter, with subscripts used here as descriptive labels rather than tensor indices. No other chapter depends on the material in this chapter.

34.1 Gravitational potential

In this section we summarize elements of the gravitational force, including the case with a non-constant gravitational acceleration such as occurs from astronomical tidal forcing and changes to the mass distribution of the planet.

34.1.1 Simple geopotential

As detailed in Section 13.10, the effective gravitational field incorporates the effects from the planetary centrifugal acceleration. The effective gravitational field is conservative, so that the gravitational acceleration of a fluid element can be represented as the gradient of a scalar (see Section 13.10.4),

$$\boldsymbol{g} = -\nabla \Phi, \tag{34.1}$$

with Φ the geopotential. In most applications of this book, the local vertical direction is denoted by

$$z = r - R_{\rm e}, \tag{34.2}$$

with $z = 0$ the geopotential surface corresponding to a resting ocean and $R_{\rm e} = 6.367 \times 10^6$ m the average radius of the earth (Section 13.1). The geopotential in this case is given by

$$\Phi = \Phi_0 = g\, z, \tag{34.3}$$

with $g \approx 9.8\, \mathrm{m\, s^{-2}}$ the typical value used for the gravitational acceleration at the earth's surface.

34.1.2 General geopotential

Consider a generalized geopotential written in the form

$$\Phi = \Phi_0(r) + \Phi_1(r, \lambda, \phi, t), \tag{34.4}$$

where $\Phi_0(r)$ is the geopotential given by equation (34.3), and Φ_1 incorporates perturbations to the geopotential. For the study of ocean tides, the structure of Φ_1 arises from astronomical perturbations to the earth's gravity field. The calculation of ocean tides arising from astronomical forcing is formulated with a space-time dependent geopotential as in equation (34.4), with the radial dependence of Φ_1 neglected (e.g., Section 9.8 in *Gill*, 1982). *Arbic et al.* (2004) provide a discussion of global tide modelling.

Nontrivial Φ_1 variations also arise from perturbations in terrestrial masses, such as the melting of land ice such as that occurring on Greenland or Antarctica due to climate warming. These mass distribution changes lead to changes in the earth's gravitational field, its rotational moment of inertia, and the deformation of the crust (GRD as in *Gregory et al.* (2019)). Each of these effects lead to modifications in the *static equilibrium sea level*. In contrast to ocean tides, GRD perturbations associated with melting land ice are not periodic nor readily predictable. Furthermore, as evidenced by Figure 1 in *Mitrovica et al.* (2001), the amplitude of static equilibrium sea level changes can be far greater than typical open ocean tide fluctuations.

34.2 Momentum equation

As detailed in Section 24.2.3, the inviscid momentum equation for a rotating fluid in a gravitational field is given by

$$\rho \frac{\mathrm{D}\boldsymbol{v}}{\mathrm{D}t} + 2\, \boldsymbol{\Omega} \times \rho\, \boldsymbol{v} = -\nabla p - \rho\, \nabla \Phi. \tag{34.5}$$

In writing the momentum equation in the form (34.5), we have chosen to retain an orientation afforded by the unperturbed geopotential, $\Phi_0(r)$, which are surfaces of constant z. This approach reflects that commonly used to study ocean tides. In the presence of a perturbed geopotential, Φ_1, the "horizontal" directions defined by surfaces of constant z are no longer parallel to geopotential surfaces. We thus may interpret the sum $\nabla_{\rm h} p + \rho\, \nabla_{\rm h} \Phi$ as an orientation of the pressure gradient along surfaces of constant geopotential, where the geopotential is determined by $\Phi = \Phi_0 + \Phi_1$, rather than just the unperturbed geopotential Φ_0.

34.3 Hydrostatic primitive equations

As detailed in Section 27.1, the hydrostatic primitive equations reduce the vertical momentum equation to its static inviscid form, which is the hydrostatic balance

$$\frac{\partial p}{\partial z} = -\rho \frac{\partial \Phi}{\partial z} = -\rho \, (g + \partial_z \Phi_1). \tag{34.6}$$

The hydrostatic balance is modified from its traditional form for cases where the perturbation geopotential Φ_1 exhibits nontrivial depth dependence. Correspondingly, the horizontal momentum equation (making the Traditional Approximation from Section 27.1) takes the form

$$\rho \frac{\mathrm{D}\boldsymbol{u}}{\mathrm{D}t} + \hat{\boldsymbol{z}} \, f \times \rho \, \boldsymbol{u} = -(\rho \, \nabla_{\!\mathsf{h}} \Phi_1 + \nabla_{\!\mathsf{h}} p) \tag{34.7}$$

where $\nabla_{\!\mathsf{h}}$ is the horizontal gradient taken on surfaces of constant z. In their oceanic Boussinesq form (Chapter 29), the inviscid horizontal momentum equation becomes

$$\frac{\mathrm{D}\boldsymbol{u}}{\mathrm{D}t} + \hat{\boldsymbol{z}} \, f \times \boldsymbol{u} = -(1/\rho_{\circ}) \, (\rho_{\circ} \, \nabla_{\!\mathsf{h}} \Phi_1 + \nabla_{\!\mathsf{h}} p) \tag{34.8}$$

where $\rho_{\circ}$ is the constant reference density for a Boussinesq fluid. The Boussinesq form makes the addition of a perturbed geopotential quite straightforward, in which it is gradients in $\rho_{\circ} \, \Phi_1 + p$ that take the place of gradients in pressure p.

34.4 Depth independent perturbed geopotential

A particularly simple form of Φ_1 occurs when it is depth independent,

$$\Phi_1 = \Phi_1(\lambda, \phi, t), \tag{34.9}$$

in which case the hydrostatic balance (34.6) returns to its traditional form $\partial_z p = -\rho \, g$. This form is motivated by the scale analysis in Section 34.5.3 where we find that the radial component of the earth's gravitational field greatly exceeds that from the moon or other celestial bodies, so that it is the lateral variation in the gravitational acceleration that drive tidal motions. In this case it is convenient to write the geopotential as

$$\Phi_1 = -g \, h, \tag{34.10}$$

with $h = h(\lambda, \phi, t)$ the perturbed geopotential height field. The full geopotential is thus written

$$\Phi = g \, (z - h), \tag{34.11}$$

with this form revealing that the zero of the geopotential is now set by $z = h$ rather than $z = 0$. In the study of ocean tides, h is referred to as the *equilibrium tide*. In geodesy, h is referred to as the *static equilibrium sea level*.

Since the perturbed geopotential is depth independent, it only affects the depth integrated horizontal momentum, and it does so through the term

$$-\int_{\eta_{\mathsf{b}}}^{\eta} \nabla_{\!\mathsf{h}} \Phi_1 \, \mathrm{d}z = g \int_{\eta_{\mathsf{b}}}^{\eta} \nabla_{\!\mathsf{h}} h \, \mathrm{d}z = g \, (-\eta_{\mathsf{b}} + \eta) \, \nabla_{\!\mathsf{h}} h. \tag{34.12}$$

Hence, modifications to the geopotential as embodied by the perturbed geopotential height field, $h = h(\lambda, \phi, t)$, are isolated to their impacts on the horizontal pressure gradients acting on the depth integrated horizontal momentum.

34.5 Forces contributing to ocean tides

We here describe the rudiments of forces that contribute to ocean tides as well as solid-earth tides. For simplicity we focus just on the earth-moon system, though note that the sun also plays an analogous role for observed tidal motion.

34.5.1 Tidal acceleration in a spherically symmetric gravity field

Before considering the earth-moon system, we introduce the notion of *tidal acceleration*, which arises on a finite sized body placed within a non-uniform gravitational field. Figure 34.1 depicts this situation where the finite sized body is a narrow rod whose axis points towards the center of a spherically symmetric massive body. One end of the rod experiences a different gravitational acceleration than the other since the gravitational field falls off as the inverse squared distance from the center of the sphere. It is this differential gravitational acceleration that we refer to as the tidal acceleration. As we will see, its key property is that the tidal acceleration falls off as the inverse cube of the distance rather than the more familiar inverse square.

To develop a mathematical expression for the tidal acceleration, focus on the spherically symmetric gravitational field in which the gravitational acceleration at a point is given by (Section 13.10.2)

$$\boldsymbol{g} = -\frac{GM}{r^2}\,\hat{\boldsymbol{r}}, \tag{34.13}$$

where r is the distance from the sphere's center, G is Newton's gravitational constant, M is the mass of the sphere, and $\hat{\boldsymbol{r}}$ is the radial unit vector. The minus sign indicates that the gravitational acceleration points toward the center of the sphere. For the rod in Figure 34.1, the difference between the gravitational acceleration acting at a point nearest to the sphere (point B) and a point furthest from the sphere (point A) is given by

$$\boldsymbol{g}(r_B) - \boldsymbol{g}(r_A) = \boldsymbol{g}(r_0 - L/2) - \boldsymbol{g}(r_0 + L/2), \tag{34.14}$$

where r_0 is the distance from the sphere's center to the center of the rod. Assuming the rod is not long, we can expand this difference in a Taylor series about the rod center at r_0, thus leading to an expression for the tidal acceleration

$$\boldsymbol{g}(r_B) - \boldsymbol{g}(r_A) \approx -L\,\frac{\partial \boldsymbol{g}}{\partial r} = -2L\,\frac{GM}{r_0^3}\,\hat{\boldsymbol{r}} = (2\,L/r_0)\,\boldsymbol{g}(r_0). \tag{34.15}$$

The key point to conclude from this example is that the tidal acceleration is proportional to the inverse cube of the distance to the center of the sphere. We see this property again when considering in Section 34.5.3 the gravitational acceleration generated from a remote body (e.g., the moon) acting on the surface of a sphere (e.g., the earth).

34.5.2 Heuristics of tidal acceleration on the surface of a sphere

We now consider the tidal acceleration acting on the surface of a smooth massive sphere due to a spherically symmetric gravitational field generated by a neighboring massive body. Figure 34.2 depicts this system, which we consider an idealized earth-moon system where each body is assumed homogeneous and spherical. Given that they gravitationally attract one another, it is not astronomically possible for the two bodies to remain spatially fixed. Instead, they orbit around their common center of mass while conserving their angular momentum.

A central question of tidal studies is why there are generally two ocean tides per day (semi-diurnal tides) rather than just one (diurnal tides). We here offer two complementary arguments. The first is based on extending the tidal acceleration discussion of Section 34.5.1, whereas the

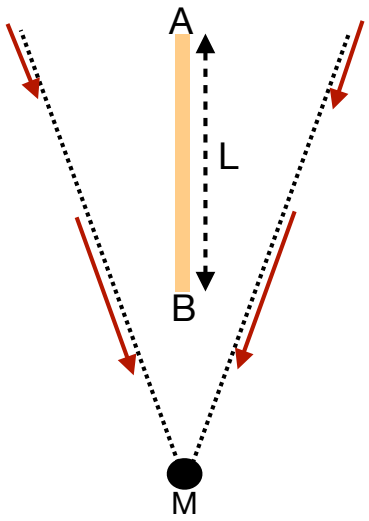

FIGURE 34.1: *Tidal acceleration* is the acceleration that acts on a finite sized object placed in a non-uniform gravitational field. The finite object is here depicted as a narrow rod of length L placed in the gravity field of a spherically symmetric body of mass M. That portion of the rod closer to the gravitating sphere (end B) experiences a stronger gravitational acceleration than the end that is further away (end A). The gradient in the gravitational acceleration constitutes the tidal acceleration acting on the rod.

second follows the more traditional account by considering a balance between gravitational and centrifugal accelerations.

General ideas

Every point on the surface of the earth is attracted to the earth's center by the earth's gravitational field. For a spherical earth, this attractive force is purely radial, so that it cannot lead to lateral motion on the surface of the perfect sphere. We thus conclude that the radial gravitational field is not the cause of tidal motion. Instead, tidal motion arises from a non-radial gravitational field.

The earth-moon gravitational field accelerates the earth and moon toward one another along the axis connecting their centers. Additionally, the spatial dependence of the moon's gravitational field over the earth leads to lateral forces along the earth's surface, thus providing the ingredient for ocean tidal motion. To capture the essence of this force, we examine how the moon's gravitational field acts on a point on the earth relative to its action at the center of the earth.

Sample tidal accelerations on the sphere

Again, we are tasked with computing the tidal acceleration from the moon's gravitational field for selected points on the earth, and we are computing these accelerations relative to the earth center. As for the rod in Figure 34.1, the tidal acceleration at point B relative to the center of the earth is given by

$$\boldsymbol{g}(r_B) - \boldsymbol{g}(R_{\text{em}}) = (2R_{\text{e}}/R_{\text{em}})\, \boldsymbol{g}(R_{\text{em}}). \tag{34.16}$$

This acceleration points towards the moon. In contrast, the tidal acceleration at point A relative to the center of the earth is given by

$$\boldsymbol{g}(r_A) - \boldsymbol{g}(R_{\text{em}}) = -(2R_{\text{e}}/R_{\text{em}})\, \boldsymbol{g}(R_{\text{em}}), \tag{34.17}$$

which is of equal magnitude but points away from the moon.

The tidal accelerations at points A and B act radially away from the earth's center. Hence, as noted above, these radial forces do not directly lead to tidal motion at those points. However,

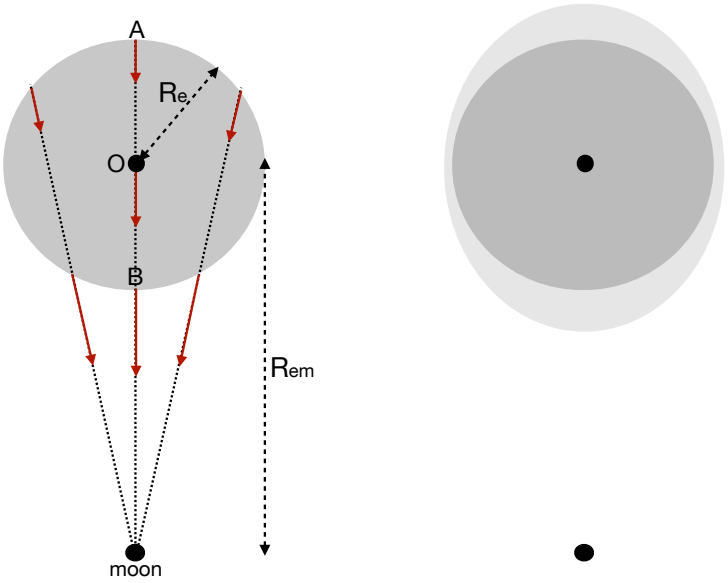

FIGURE 34.2: Illustrating the tidal force on the surface of a sphere. The sphere is an ideal depiction of the earth and the smaller massive object is the moon. The distance between the center of the earth and moon is R_{em}, and the radius of the earth is R_{e}. The left panel shows representative moon-generated gravitational field lines. Two points along these field lines on the surface of the earth represent the two ends of an imaginary rod as depicted in Figure 34.1. The tidal acceleration acting at point B, relative to the earth's center, points toward the moon (equation (34.16)). In contrast, the tidal acceleration at point A, relative to the earth's center, points in the opposite direction (equation (34.17)). Points on the earth surface between A and B have tidal accelerations with a non-zero component directed along the surface of the earth. Symmetry of the configuration allows us to conclude that a layer of water on the surface of the sphere will accumulate to produce two bulges as shown in the right panel. It is the lateral component of the gravitational acceleration that causes the water to accumulate to produce tidal bulges at points A and B. In contrast, the radial component to the moon's gravitational field has no contribution to the tides. Note that as shown in Section 34.5.3, the bulge shown in the right panel is greatly exaggerated.

through symmetry of the configuration, points on the surface of the sphere between A and B have a tidal acceleration from the moon's gravitational field with a nonzero lateral component. These lateral forces lead to the accumulation of water at points A and B. We can compute the gravitational acceleration at intermediate points. However, the trigonometry is somewhat complex and we prefer to compute the forces in Section 34.5.3 through use of the gravitational potential. For the current discussion we appeal to symmetry to conclude that the lateral tidal accelerations act to pile up water at both points A and B as depicted in the second panel of Figure 34.2. This argument, though heuristic, provides the means to understand how a water covered spherical planet has two bulges, rather than one, due to spatial gradients in the moon's gravitational field. We confirm this argument in Section 34.5.3 by explicitly computing the gravitational potential for this idealized earth-moon system and then taking the gradient to compute the gravitational acceleration (see Figure 34.4).

Including orbital motion

Thus far we have ignored the orbital motion of the earth-moon system around their common center of mass. As we will see, there are no fundamental changes to the above arguments when allowing for orbital motion.

In the absence of dissipation, as assumed here, the earth-moon distance remains constant due to their angular momentum conserving orbital motion. From a force-balance perspective, the two spherical bodies remain in a fixed orbit since the gravitational acceleration acting at their centers is balanced by their respective centrifugal accelerations, where the centrifugal acceleration is

computed relative to the center of mass of the two-body system. The gravitational acceleration from the moon, acting at the center of the earth, is given by the *free fall* value $\boldsymbol{g}(R_{\text{em}})$, which has magnitude $GM_{\text{m}}/R_{\text{em}}^2$ and is directed along the axis connecting the earth and moon centers.

Furthermore, when a body exhibits orbital motion, each point on the body exhibits the same orbital motion and has the same linear velocity. Consequently, each point on the earth possess the same centrifugal acceleration

$$\boldsymbol{a}_{\text{orbital centrifugal}} = -\boldsymbol{g}(R_{\text{em}}). \tag{34.18}$$

This property of orbital motion is distinct from the spinning motion of a planet rotating about its axis, whereby points further from the rotational axis have larger centrifugal acceleration (see Section 13.10). To help understand orbital motion, move your hand in a circle while maintaining the arm in a single direction so that the hand exhibits an orbital motion rather than a spinning motion. Notice that all parts of the hand move with the same linear velocity and exhibit the same orbital motion. Hence, each point on the hand has the same centrifugal acceleration.

We can now ask about the acceleration felt by a point on the surface of the earth. The acceleration giving rise to tidal motions is the sum of the gravitational acceleration from the moon plus the centrifugal acceleration due to orbital motion. However, this calculation is identical to that considered previously, which led, for example, to the tidal accelerations for points B and A as given by equations (34.16) and (34.17). We are thus led to the same result as before.

34.5.3 Gravitational potential for an idealized earth-moon system

We now perform a more thorough calculation of the gravitational acceleration by computing the gradient of the gravitational potential. First recall the discussion of Newton's gravitational law in Section 13.10.2, whereby the gravitational potential for a point at distance r from the center of a spherical earth is given by

$$\Phi_{\text{e}}(r) = -\frac{GM_{\text{e}}}{r}, \tag{34.19}$$

where M_{e} is the mass of the earth. The corresponding radial gravitational acceleration is given by

$$\boldsymbol{g}_{\text{e}} = -\nabla\Phi_{\text{e}} = -\frac{GM_{\text{e}}\,\hat{\boldsymbol{r}}}{r^2}. \tag{34.20}$$

The same considerations hold for the moon's gravitational potential. Hence, referring to Figure 34.3, the moon's gravitational potential evaluated at a distance L from the moon's center is given by

$$\Phi_{\text{m}}(L) = -\frac{GM_{\text{m}}}{L}. \tag{34.21}$$

Trigonometry leads to the law of cosines relation

$$L^2 = (R_{\text{em}} - r\cos\psi)^2 + (r\sin\psi)^2 = R_{\text{em}}^2 + r^2 - 2\,r\,R_{\text{em}}\cos\psi, \tag{34.22}$$

where again r is the distance to the earth's center and ψ is the polar angle relative to the $\hat{\boldsymbol{x}}$ axis pointing between the earth and moon centers (see Figure 34.3).

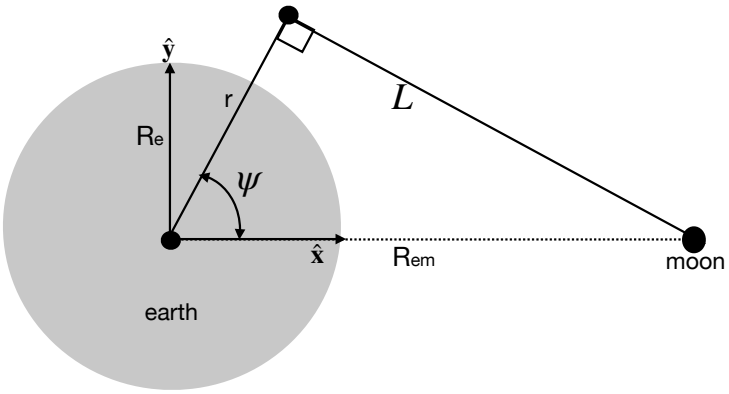

FIGURE 34.3: Geometry of an idealized earth-moon system. The center of the earth is a distance $R_{\rm em}$ from the center of the moon; the moon has a mass $M_{\rm m}$; and the earth has a radius $R_{\rm e}$. An arbitrary test point is shown a distance L from the center of the moon, r from the center of the earth, and with a polar angle ψ relative to the $\hat{\boldsymbol{x}}$ axis, where the $\hat{\boldsymbol{x}}$ axis points from the earth center to the moon center. Relative to the earth's center, the test point has Cartesian coordinates $(x, y) = r\,(\cos\psi, \sin\psi)$. See Section 4.22 for details on relating polar and Cartesian coordinates.

Identifying the leading order contributions

Assuming the test point in Figure 34.3 is closer to the earth than to the moon, we can perform a Taylor series expansion in the small parameter $r/R_{\rm em}$ to render

$$\Phi_{\rm m}(L) = -\frac{GM_{\rm m}}{L} = -\frac{GM_{\rm m}}{R_{\rm em}}\left[1 + \frac{r\cos\psi}{R_{\rm em}} + \frac{r^2}{2R_{\rm em}^2}\,(3\cos^2\psi - 1) + \mathcal{O}(r/R_{\rm em})^3\right]. \tag{34.23}$$

We thus identify the leading three terms to the geopotential

$$\Phi_{\rm m}^{(0)} = -\frac{GM_{\rm m}}{R_{\rm em}} \tag{34.24}$$

$$\Phi_{\rm m}^{(1)} = -\frac{GM_{\rm m}}{R_{\rm em}^2}\, r\cos\psi \tag{34.25}$$

$$\Phi_{\rm m}^{(2)} = -\frac{GM_{\rm m}}{2R_{\rm em}^3}\, r^2\,(3\cos^2\psi - 1). \tag{34.26}$$

Assuming the distance between the earth and moon remains fixed, the zeroth order term $\Phi_{\rm m}^{(0)}$ is a spatial constant and thus leads to no gravitational acceleration. We now examine the gravitational accelerations from the other two terms.

Acceleration maintaining the orbiting earth-moon system

For the first order term, $\Phi_{\rm m}^{(1)}$, we introduce the Cartesian coordinate as in Figure 34.3 to write

$$\Phi_{\rm m}^{(1)} = -\frac{GM_{\rm m}\, x}{R_{\rm em}^2}, \tag{34.27}$$

where $x = r\cos\psi$ is the distance along $\hat{\boldsymbol{x}}$. Hence, the gradient of $\Phi_{\rm m}^{(1)}$ leads to the gravitational acceleration

$$\boldsymbol{g}_{\rm m}^{(1)} = -\nabla\Phi_{\rm m}^{(1)} = \hat{\boldsymbol{x}}\,\frac{GM_{\rm m}}{R_{\rm em}^2}. \tag{34.28}$$

This gravitational acceleration has a constant magnitude at every point in space and it everywhere points in a direction parallel to the earth-moon axis. Furthermore, the magnitude of $\boldsymbol{g}_{\rm m}^{(1)}$ equals to that of the moon's gravitational acceleration, $\boldsymbol{g}_{\rm m}$, when evaluated at the earth's center. As

seen in Section 34.5.2, the acceleration $\boldsymbol{g}_{\mathrm{m}}^{(1)}$ maintains the earth in orbit about the center of mass for the earth-moon system; i.e., this is the free fall acceleration towards the moon. Notably, at the earth's surface, the magnitude of $\boldsymbol{g}_{\mathrm{m}}^{(1)}$ is tiny relative to the gravitational acceleration from the earth itself, with their ratios given by

$$\frac{M_{\mathrm{m}}/R_{\mathrm{em}}^2}{M_{\mathrm{e}}/R_{\mathrm{e}}^2} \approx 3.4 \times 10^{-6}, \tag{34.29}$$

where we set

$$M_{\mathrm{e}} = 5.97 \times 10^{24} \text{ kg} \qquad M_{\mathrm{m}} = 7.35 \times 10^{22} \text{ kg} = (1/81.2)\, M_{\mathrm{e}} \tag{34.30a}$$

$$R_{\mathrm{e}} = 6.367 \times 10^{6} \text{ m} \qquad R_{\mathrm{em}} = 3.84 \times 10^{8} \text{ m} = 60.3\, R_{\mathrm{e}}. \tag{34.30b}$$

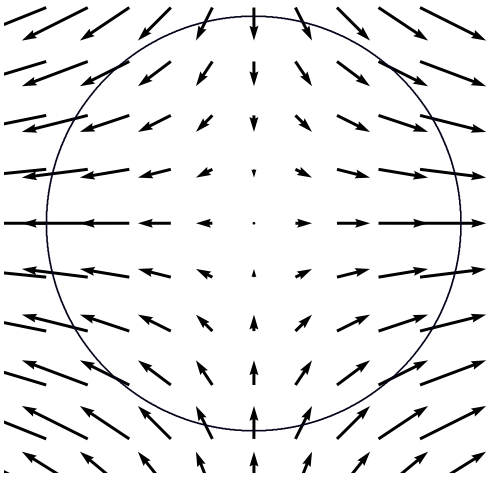

FIGURE 34.4: The tide producing gravitational acceleration $\boldsymbol{g}_{\mathrm{m}}^{(2)}$ given by equation (34.34). The moon is assumed to be positioned in the equatorial plane of the earth.

Tide producing geopotential

The main tide producing acceleration results from $\Phi_{\mathrm{m}}^{(2)}$. Introducing the second Cartesian coordinate, $y = r \sin\psi$, leads to

$$\Phi_{\mathrm{m}}^{(2)} = -\frac{GM_{\mathrm{m}}}{2R_{\mathrm{em}}^3}\, r^2\, (3\cos^2\psi - 1) = -\frac{GM_{\mathrm{m}}}{2R_{\mathrm{em}}^3}\, (2\,x^2 - y^2). \tag{34.31}$$

The corresponding perturbed geopotential height field (see equation (34.11)) is given by

$$h = -\frac{\Phi_{\mathrm{m}}^{(2)}}{g} = \frac{R_{\mathrm{e}}^2}{2\,R_{\mathrm{em}}^3}\, \frac{M_{\mathrm{m}}}{M_{\mathrm{e}}}\, r^2\, (3\cos^2\psi - 1). \tag{34.32}$$

Placing the test point on the earth surface, $r = R_{\mathrm{e}}$, renders

$$h = \frac{R_{\mathrm{e}}^4}{2\,R_{\mathrm{em}}^3}\, \frac{M_{\mathrm{m}}}{M_{\mathrm{e}}}\, (3\cos^2\psi - 1) \approx 2.8 \times 10^{-8}\, R_{\mathrm{e}}\, (3\cos^2\psi - 1). \tag{34.33}$$

Plugging in numbers for the earth-moon system suggests that the maximum perturbation to the geopotential height arising from the moon's gravity field is roughly 36 cm. Correspondingly, the bulge shown in Figure 34.2 is greatly exaggerated. Note that ocean tidal amplitudes can get much larger (order meters) than this "equilibrium tide" amplitude due to resonances from ocean

geometry, with the Bay of Fundy in Nova Scotia a particularly striking example.

Tide producing acceleration

The gravitational acceleration arising from the tidal potential is determined by the gradient of the tidal geopotential

$$\boldsymbol{g}_{\mathrm{m}}^{(2)} = -\nabla \Phi_{\mathrm{m}}^{(2)} = \frac{G M_{\mathrm{m}}}{R_{\mathrm{em}}^3} (2\, x\, \hat{\boldsymbol{x}} - y\, \hat{\boldsymbol{y}}). \tag{34.34}$$

We illustrate the vector field $\boldsymbol{g}_{\mathrm{m}}^{(2)}$ in Figure 34.4. Note how the accelerations lead to two bulges on opposite sides of the planet. We can write this acceleration using polar coordinates by introducing the polar unit vectors $\hat{\boldsymbol{r}}$ and $\hat{\boldsymbol{\psi}}$ according to Section 4.22.2

$$\hat{\boldsymbol{r}} = \hat{\boldsymbol{x}} \cos\psi + \hat{\boldsymbol{y}} \sin\psi \tag{34.35a}$$

$$\hat{\boldsymbol{\psi}} = -\hat{\boldsymbol{x}} \sin\psi + \hat{\boldsymbol{y}} \cos\psi \tag{34.35b}$$

thus rendering

$$\boldsymbol{g}_{\mathrm{m}}^{(2)} = \frac{G M_{\mathrm{m}} R_{\mathrm{e}}}{R_{\mathrm{em}}^3} \left[\hat{\boldsymbol{r}} \, (3\cos^2\psi - 1) - (3/2)\, \hat{\boldsymbol{\psi}} \, \sin 2\psi \right], \tag{34.36}$$

where we evaluated the acceleration at the earth surface so that $r = R_{\mathrm{e}}$. Evaluating the acceleration at $\psi = 0, \pi$ verifies the heuristic calculation performed in Section 34.5.2 for points on the earth surface nearest and furthest from the moon. We can further gauge the magnitude of the tidal acceleration by introducing the acceleration due to the earth's gravity field

$$\boldsymbol{g}_{\mathrm{m}}^{(2)} = g_{\mathrm{e}} \frac{M_{\mathrm{m}}}{M_{\mathrm{e}}} \frac{R_{\mathrm{e}}^3}{R_{\mathrm{em}}^3} \left[\hat{\boldsymbol{r}} \, (3\cos^2\psi - 1) - (3/2)\, \hat{\boldsymbol{\psi}} \, \sin 2\psi \right], \tag{34.37}$$

where $g_{\mathrm{e}} = G\, M_{\mathrm{e}}/R_{\mathrm{e}}^2$ is the acceleration at the earth's surface from the earth's gravity field. The dimensional prefactor has magnitude $\approx 5.6 \times 10^{-8}\, g_{\mathrm{e}}$, so that the tidal acceleration is tiny relative to that from the earth's gravity field. It is for this reason that the radial component of the tidal acceleration is largely irrelevant since it is dominated by the far larger radial component of the earth's gravity field. However, the angular component of the tidal acceleration, although small relative to the earth's radial gravitational acceleration, is able to move water along the surface of the planet as indicated by Figure 34.4, thus leading to tidal motion.

34.5.4 Concerning realistic tides

Our discussion of tides has been rather terse, aiming to identify key aspects of the tidal accelerations but giving little attention to details that impact real ocean tides. Here are a few points that must be considered for these purposes.

- As the earth spins under the tidal bulges, there are two high and two low tides per day. Additional orbital motion of the moon adds roughly 50 minutes per day to the diurnal (daily) tide and 25 minutes to the semi-diurnal (twice daily).

- The moon orbits the earth at a latitude of roughly $28.5^\circ N$ rather than within the equatorial plane, so that the tidal bulges are offset from the equator. As the earth spins under the bulges, one of the high tides is generally larger than the other due to the offset. This offset in turn introduces a diurnal component to the tides in addition to the semi-diurnal.

- The sun contributes to tides in a manner similar to the moon. The sun is more massive than the moon, yet it is further away, so that the ratio of the magnitudes for the tidal

producing accelerations is given by

$$\frac{\text{moon tidal acceleration}}{\text{sun tidal acceleration}} = \frac{M_{\rm m}/R_{\rm em}^3}{M_{\rm s}/R_{\rm es}^3} \approx 2.2 \tag{34.38}$$

where we set

$$M_{\rm s} = 1.99 \times 10^{30} \text{ kg} \qquad R_{\rm es} = 23460\, R_{\rm e}. \tag{34.39}$$

Hence, the moon has an impact on tides that is somewhat more than double that of the sun.

- The gravitational acceleration that leads to the tidal bulge moves around the mid-latitudes at roughly 330 m s^{-1}, which is faster than the $\approx$ 200 m s^{-1} wave speed for shallow water gravity waves. Hence, the ocean tidal motion is never equilibrated to the *equilibrium tides* defined by the tidal acceleration. In contrast, solid-earth waves are much faster and so the solid-earth tidal motions are mostly equilibrated with the equilibrium tidal acceleration. Solid-earth tides have an amplitude on the order of 10 cm with wavelengths spanning the planet. Hence, an accurate treatment of ocean tides must take into account the solid-earth tides.

- The movement of ocean mass modifies the earth's gravity field and the domain within with the ocean moves, and these effects are referred to as *self attraction and loading* (SAL). The loading term arises from alterations in the mass felt by the solid earth that leads the crust to expand or compress. Self-attraction arises from modifications to the gravity field due to self-gravity of both the load-deformed solid earth and the ocean tide itself. Locally, SAL can contribute to roughly 20% of the ocean tide amplitude, so that accurate tide modeling must include SAL. *Barton et al.* (2022) provide an example of global ocean tide modeling that includes a discussion of how to compute the SAL terms online during a simulation.

- Geometry of the ocean plays a leading role in determining tides at a particular location. We have incomplete information about the geometry of ocean basins, such as the presence of deep ridges, troughs, and seamounts. In lieu of such information we can garner useful information based on the analysis of past tides, with that information used to fit sinusoidal waves to the measured time series for use in projecting forward in time.

34.5.5 Comments

A key feature of the tidal producing forces is that it is the lateral (along-earth) component of the moon's tidal gravitational force that produces the earth's tides. These lateral forces cause water to accumulate at the point nearest to and furthest from the moon (points A and B in Figure 34.2), thus producing the characteristic double-bulge pattern. Notably, many common literature presentations make it appear that it is the radial (i.e., pointing to the earth's center) component of the moon's gravitational force, and its gradient across the earth, that leads to the earth's tidal bulges. But as discussed in Section 34.5.2, radial gravitational forces cannot lead to tidal motions; what is needed is a force that leads to lateral motion. These key notions are nicely emphasized in this Space Time video.

Part VI

Shallow water flows

Adiabatic shallow water models consist of constant density homogeneous fluid layers whose interfaces are material; i.e., no matter is transferred between the immiscible layers. Thermodynamic processes are absent from the system, thus allowing us to focus on the dynamics of fluid layers. Pressure is hydrostatic, which means that motion occurs in columns whereby horizontal velocity is independent of the vertical position within a layer, whereas the column can expand and contract so that there is vertical motion within a layer. Horizontal momentum is transferred between shallow water layers via pressure form stresses (Chapter 28) that act on sloping layer interfaces. Furthermore, we make the approximations arising from the primitive equations in Section 27.1, so that the Coriolis acceleration is based on just the local vertical component to the planetary rotation. Our goal in this part of the book is to develop an understanding of the shallow water model fundamentals and to study some basic dynamical features as realized in the model. We have further use of the shallow water model in the study of vorticity in Part VII, balanced flows in Part VIII, waves in Part X, and generalized vertical coordinates in Part XII.

The shallow water model provides a versatile theoretical toolbox for deducing how flow is affected by rotation and (when multiple layers are used) stratification. Consequently, the shallow water model is featured in many areas of geophysical fluid mechanics as well as in ocean and atmosphere applications. Additionally, there is a direct analogy between shallow water flow and compressible fluid flow, in which the *in situ* density of a compressible fluid corresponds to the layer thickness of a shallow water fluid. In particular, the acoustic waves of compressible flow (Chapter 51) are directly analogous to the gravity waves of shallow water flow (Section 55.5). However, shallow water flow is somewhat simpler than compressible three-dimensional flow, since shallow water flow is horizontal within a layer. For these reasons, the shallow water model has found great use both inside and outside of geophysical fluid mechanics.

The shallow water model is a vertically discrete realization of a continuously stratified fluid described by the isopyncal coordinates of Chapter 66. However, the mathematical formalism of generalized vertical coordinates developed in Part XII of this book, and needed to formulate the fluid equations using isopycnal coordinates, is largely unnecessary when working with the shallow water model. The reason for the simplification is that columnar motion within a shallow water layer means that lateral gradients of properties need not be projected along the slope of the layer. In contrast, this projection is needed for a continuously stratified fluid described by generalized vertical coordinates (e.g., see Figure 63.4). So although there is beauty and power in the methods of generalized vertical coordinates for studying continuously stratified flows, it is liberating to avoid that formalism while still capturing much of the underlying physics associated with stratification (albeit discretely stratified). This feature of the shallow water model greatly adds to its allure and accessibility.

Chapter 35

FORMULATING SHALLOW WATER MODELS

In this chapter we formulate the mechanical equations for a suite of shallow water models. For this purpose we develop the equations describing motion of a single shallow water layer; multiple shallow water layers (stacked shallow water); and reduced gravity models (models with one layer that is dynamically inactive). In mathematically formulating these models we also expose their physical basis.

READER'S GUIDE TO THIS CHAPTER

We make use of fluid kinematics and dynamics described in a variety of earlier chapters, with the presentation inspired by Chapter 3 of *Vallis* (2017) as well as various sections in *Salmon* (1998). We make use of the formulation for further study of the shallow water fluid mechanics, including dynamical balances in Chapter 36, vorticity mechanics in Chapter 39, and wave mechanics Chapter 55. This video offers a pedagogical introduction to shallow water flows. We commonly make use of oceanographic language and refer to the fluid as water. Even so, the shallow water model has many applications to the study of large-scale atmospheric flows.

The fluid density is constant within a shallow water layer, so that mass conservation is the same as volume conservation. Hence, the terms "mass conservation" and "volume conservation" are commonly used interchangeably when working with shallow water models. The horizontal velocity is vertically uniform within a shallow water layer, whereas the vertical velocity and hydrostatic pressure are linear functions of vertical position within the layer. When acting on a property that is vertically uniform within a layer, the gradient operator, ∇, results in a horizontal vector. To minimize notational clutter, we typically write ∇ for brevity, rather than ∇^{k} or ∇_{h} (with k the layer index). The meaning of the resulting vector equations are clear from the functional dependencies of the fields present in the equations.

35.1 Loose threads

- Internal and external mode as per Raymond's notes.

35.2 A single shallow water layer

Consider a homogeneous layer of fluid in a uniform effective gravitational field (gravity plus planetary centrifugal as in Section 13.10.4), bounded from below by solid walls. If there are no lateral force imbalances, then the fluid remains static. Now perturb the fluid so that it has a nonuniform layer thickness, say with a bump in a particular region. Conservation of fluid mass (which translates into volume conservation for a uniform density layer) means that thicker fluid regions must be exactly compensated by thinner fluid regions. Furthermore, layer thickness gradients create pressure differences (thicker fluid layer has larger hydrostatic pressure than thinner layer), which in turn drives fluid motion. If the fluid has much larger lateral extent than vertical, then the lateral motion occurs as an expanding and contracting column with no vertical dependence to the horizontal pressure forces and thus the horizontal motion is vertically independent.

The essence of a perfect fluid (i.e., no irreversible processes such as mixing) shallow water flow concerns the motion of fluid columns accelerated by pressure gradients created by layer thickness undulations, and the associated conservation of mass ensuring that the accumulation of fluid in one region is balanced by the depletion of fluid in another. Pressure gradients act to homogenize the layer thickness. However, planetary rotation and the corresponding Coriolis acceleration allows for layer thickness to be non-constant even in a steady state.

35.2.1 Pressure gradient force within the fluid layer

Figure 35.1 shows a single shallow water layer with a generally non-flat bottom and an undulating free surface height. We assume that each column of fluid within the layer is in hydrostatic

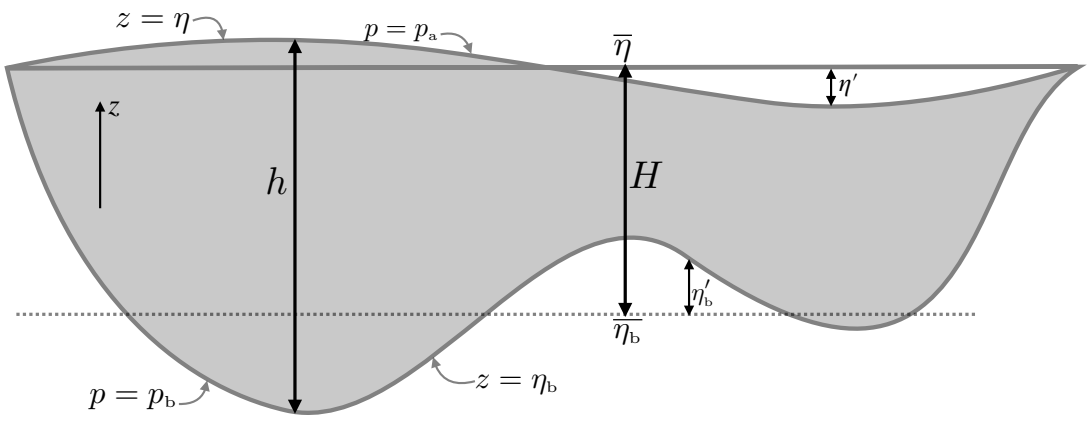

FIGURE 35.1: A single layer of shallow water fluid with thickness $h = \eta - \eta_b$ that extends from the bottom at $z = \eta_b$ to the free surface at $z = \eta$. The area averaged thickness is defined by $H = \overline{h} = A^{-1} \int h \, dx \, dy = A^{-1} \int (\eta - \eta_b) \, dx \, dy = \overline{\eta} - \overline{\eta_b}$, where $A = \int dx \, dy$ is the horizontal area of the layer. The deviation of the free surface from $\overline{\eta}$ is given by $\eta' = \eta - \overline{\eta} = \eta - (\overline{\eta_b} + H)$ so that $\eta(x, y, t) = \eta_b(x, y) + h(x, y, t) = \overline{\eta_b} + H + \eta'(x, y, t)$. Likewise, the deviation of the bottom from $\overline{\eta_b}$ is given by $\eta'_b = \eta_b - \overline{\eta_b}$, so that $h = \eta - \eta_b = H + \eta' - \eta'_b$. Volume conservation for the layer is maintained in the absence of volume boundary fluxes, in which case $\overline{\eta'} = 0$. Note that the position of the reference height, $z = 0$, is arbitrary. Atmospheric conventions typically set $z = 0$ so that $\overline{\eta_b} = 0$, $\eta = H + \eta'$, and $\overline{\eta} = H$. Oceanic conventions typically choose $\overline{\eta} = 0$ so that $\eta = \eta'$ and $\overline{\eta_b} = -H$. We are only concerned with fluctuations that leave the free surface monotonic; i.e., we do not consider overturns or breaking waves. This assumption is implied by assuming that each column extending from $\eta_b \leq z \leq \eta$ maintains hydrostatic balance.

balance, so that the vertical momentum equation reduces to

$$\frac{\partial p}{\partial z} = -\rho \, g. \tag{35.1}$$

Recall from Section 27.2 that the hydrostatic balance is consistent with lateral length scales much larger than vertical (small vertical to horizontal aspect ratio), which is satisfied by large-scale geophysical fluid motion. Hence, a shallow water fluid is a relevant idealization if we are considering horizontal flow scales that are very large relative to vertical flow scales.

Since the fluid density is assumed constant (i.e., the fluid is a homogeneous layer), we can integrate the hydrostatic balance from the surface to an arbitrary vertical position within the layer

$$p(x, y, z, t) = p_a(x, y, t) + g \, \rho \int_z^\eta dz = p_a(x, y, t) + g \, \rho \, [\eta(x, y, t) - z], \tag{35.2}$$

where $p_a(x, y, t)$ is the pressure applied to the layer free surface, say from the overlying atmosphere. Furthermore, the horizontal pressure gradient thus takes the form

$$\nabla_h p = \nabla_h p_a + g \, \rho \nabla_h \eta. \tag{35.3}$$

This pressure gradient is vertically independent within the layer, as depicted in Figure 35.2.

For the left hand side of the pressure gradient in equation (35.3), it is useful to write ∇_h since the pressure within a layer is a function of z (equation (35.2)), whereas for the horizontal momentum equation we only want the horizontal pressure gradient. For the right hand side, p_a and η are independent of z, so that there is no need to expose the z subscript on the gradient operator. We thus drop the subscript when no ambiguity results, as per our convention noted at the start of the chapter.

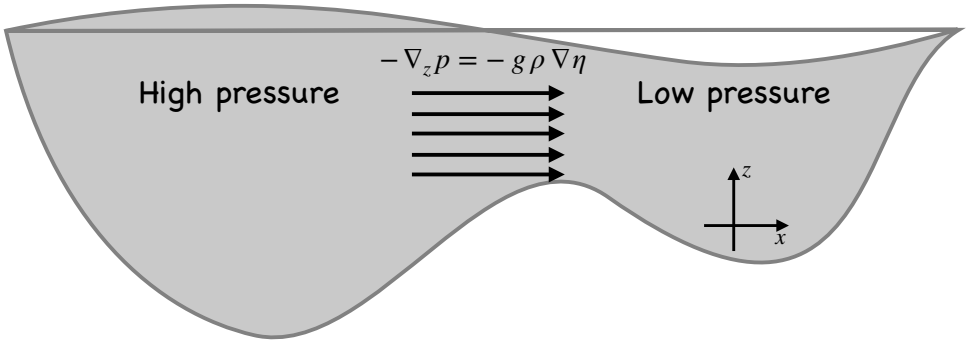

FIGURE 35.2: The horizontal pressure gradient within a shallow water layer is independent of the vertical position within that layer. In this schematic we assume here are zero horizontal gradients in the applied surface pressure, $\nabla p_a = 0$, in which case the horizontal acceleration from pressure within a single shallow water fluid layer is determined solely by the surface height, $-\nabla_h p = -g\rho\nabla_h\eta$. The acceleration is uniform throughout the layer and points from regions of high free surface height to regions of low free surface height (e.g., sea level highs towards sea level lows). Although bottom topography interacts with the flow and thus affects the shape of the free surface, the topography does not appear explicitly in the horizontal pressure gradient (though the bottom shape does affect bottom form stresses as per the discussion in Sections 28.1 and 36.4). Instead, we only need to know the shape of the free surface (and the applied pressure p_a) to know the horizontal pressure force throughout the layer.

The pressure gradient force is vertically independent within a layer

Although hydrostatic pressure within a shallow water layer is vertically dependent as per equation (35.2), the horizontal pressure gradient, as given by equation (35.3), has no vertical dependence within the layer. The acceleration from this hydrostatic pressure force points from highs in the effective sea level to lows in the effective sea level (see Figure 35.2). The vertical independence of the pressure gradient within a shallow water layer holds also for multiple shallow water layers as discussed in Section 35.4, in which case the horizontal velocity has no vertical structure within any layer.

Pressure gradient force only depends on layer interface gradients

It is notable that the horizontal pressure gradient is solely determined by properties at the upper interface of the layer. That is, we only need to know the shape of the free surface, $z = \eta$, and the applied pressure, p_a, to know the horizontal pressure force acting throughout the layer. There is no explicit dependence on the shape of the bottom topography. The result also holds for the stacked shallow water model discussed in Section 35.4, whereby horizontal pressure gradients are determined by gradients in the layer interfaces and with no appearance of the bottom topography. This characteristic is specific to the use of a pressure gradient body force to describe the role of pressure on the layer momentum. As a complement, we saw in Chapter 28 how to formulate the pressure contact force. It is through the contact force perspective that we see, in Section 36.4, how bottom topography appears in the momentum balance of a shallow water layer. In particular, this perspective exposes the topographic form stresses that mechanically exchange momentum between the layer and the solid earth bottom.

35.2.2 Effective sea level and the inverse barometer sea level

When considering a nonzero atmospheric pressure, we sometimes find it useful to introduce an *effective free surface height* or *effective sea level*

$$\eta^{\text{eff}} = \eta + p_a/(\rho g), \tag{35.4}$$

with gradients in the effective sea level leading to horizontal motion. However, when considering motions on time scales longer than a few days, the ocean free surface adjusts under atmospheric loading towards an *inverse barometer sea level*. An inverse barometer sea level compensates the atmospheric pressure so that there is no net horizontal pressure gradient, and so there is no motion induced by the atmospheric pressure. Hence, all that matters for motion are deviations from the inverse barometer sea level.[1]

We expose details to support the above comments by writing pressure within the shallow water layer as

$$p(z) = p_a + \rho\, g\, (\eta - z) \tag{35.5a}$$
$$= \overline{p_a} + (p_a - \overline{p_a}) + \rho\, g\, (\eta - z) \tag{35.5b}$$
$$= \overline{p_a} + \rho\, g\, (\eta - \eta^{ib} - z). \tag{35.5c}$$

In these equations we introduced the area mean atmospheric pressure, $\overline{p_a}$, as well as the inverse barometer sea level

$$\rho\, g\, \eta^{ib} = \overline{p_a} - p_a. \tag{35.6}$$

The inverse barometer sea level is defined according to deviations of the atmospheric pressure from its area mean. Hence, when the atmospheric pressure is higher than the area mean, $p_a > \overline{p_a}$, then the inverse barometer sea level is negative, $\eta^{ib} < 0$, reflecting the downward depression of the inverse barometer sea level. In contrast, $\eta^{ib} > 0$ for anomalously low pressures, $p_a < \overline{p_a}$.

Introducing the inverse barometer sea level brings the horizontal pressure gradient to the form

$$\nabla_h p = \nabla p_a + g\, \rho\, \nabla \eta = \rho\, g\, \nabla \eta^{eff} = \rho\, g\, \nabla(\eta - \eta^{ib}). \tag{35.7}$$

If sea level adjusts to the atmospheric pressure so that $\nabla \eta = \nabla \eta^{ib}$, then there is no horizontal pressure gradient in the shallow water layer, in which case there is no induced motion from the atmospheric pressure. It follows that for dynamical purposes, we can seamlessly incorporate atmospheric pressure into the formalism by working with deviations of sea level from the inverse barometer sea level, $\eta - \eta^{ib}$.

35.2.3 Further comments on pressure in a homogeneous layer

Vertical independence of the horizontal pressure gradient within the shallow water layer is a direct result of the assumed hydrostatic nature of pressure within the layer. To emphasize this point, we certainly can imagine a homogeneous fluid layer in which the horizontal velocity has a vertical shear. For example, in Section 52.3 we study surface gravity waves in a homogeneous fluid layer. Such waves have an amplitude that exponentially decays moving downward from the ocean surface, and so the horizontal and vertical fluid motion associated with the waves have a non-zero vertical shear. Such motion cannot be caused by a horizontal gradient in the hydrostatic pressure since this gradient has no vertical dependence throughout the homogeneous layer

$$\partial_z(\nabla_h p_{\text{hydrostatic}}) = 0. \tag{35.8}$$

Hence, in a homogeneous fluid layer, hydrostatic pressure gradients can only drive a horizontal flow that is vertically independent within that layer. So if the vertically sheared horizontal flow is found within a homogeneous fluid layer, and if pressure gradients cause this flow, then it can only be through gradients in the *non-hydrostatic pressure*. As discussed in Section 52.2.4, surface

[1] The discussion in this section follows Appendix C to *Griffies and Greatbatch* (2012), where further details are provided. In particular, they allow for continuously stratified density rather than the shallow water model considered here. Even so, the key points about the inverse barometer gleaned from the shallow water discussion also hold for the case of a continuously stratified fluid.

gravity waves indeed involve non-hydrostatic pressure forces that drive the vertical dependence to the wave amplitude.

Moving beyond the homogeneous layer assumption, we saw in Section 27.4.1 that a horizontal gradient in the density leads to a vertically dependent hydrostatic pressure gradient $\partial_z(\nabla_h p_{\text{hydrostatic}}) \neq 0$. This hydrostatic pressure force can impart vertical shears to the horizontal flow. Thermal wind shear is the canonical example whereby vertical shears in the horizontal velocity are present in geostrophically balanced fluids as driven by horizontal density gradients (Section 31.4.3). We encounter the shallow water version of thermal wind in Section 36.2.2.

35.2.4 Momentum equation

If there is no friction anywhere in the fluid, including at the upper and lower boundaries, then the horizontal momentum is effected only by the Coriolis and pressure forces. Following our discussion of the Traditional Approximation in Section 27.1.3, we retain only the local vertical component to the Coriolis acceleration, which is compatible with the hydrostatic approximation. We are thus led to the horizontal velocity equation

$$\frac{\mathrm{D}\boldsymbol{u}}{\mathrm{D}t} + f\,\hat{\boldsymbol{z}} \times \boldsymbol{u} = -\nabla(g\,\eta + p_{\mathrm{a}}/\rho), \tag{35.9}$$

where

$$\boldsymbol{v} = \boldsymbol{u} + w\,\hat{\boldsymbol{z}} \tag{35.10}$$

splits out the horizontal velocity vector, $\boldsymbol{u}$, from the vertical velocity component, w.

The Coriolis parameter, $\boldsymbol{f} = f\,\hat{\boldsymbol{z}}$, is vertically independent, as is the horizontal pressure force from gradients in the free surface and applied pressure. Consequently, if the horizontal velocity for the initial flow state is vertically independent, it remains so for all time. The material time derivative thus only has contributions from the local time derivative and from horizontal advection

$$\frac{\mathrm{D}\boldsymbol{u}}{\mathrm{D}t} = \left[\frac{\partial}{\partial t} + u\,\frac{\partial}{\partial x} + v\,\frac{\partial}{\partial y}\right]\boldsymbol{u} \tag{35.11}$$

so that the shallow water velocity equation (35.9) takes on the form

$$(\partial_t + u\,\partial_x + v\,\partial_y)\boldsymbol{u} + f\,\hat{\boldsymbol{z}} \times \boldsymbol{u} = -\nabla(g\,\eta + p_{\mathrm{a}}/\rho). \tag{35.12}$$

35.2.5 Thickness equation

The mass of a shallow water layer is constant in the absence of sources, sinks, or boundary fluxes. Hence, changes in mass at a particular region in the fluid must arise from mass fluxed across the region boundaries, leaving one region and accumulating in another. For simplicity, we assume that no mass crosses the fluid top (the free surface) or the bottom (the solid earth). We consider the more general case of boundary mass transport in Section 35.6.

Consider an infinitesimally thin (in horizontal cross-section) vertical column of shallow water fluid that is fixed in space and extending from $\eta_{\mathrm{b}} \leq z \leq \eta$. Let the horizontal cross-sectional area be written as $\mathrm{d}A$ and the thickness be $h = \eta - \eta_{\mathrm{b}}$ (see Figure 35.3). The total mass of fluid in this column is given by

$$M = \int_{\text{column}} \left[\int_{\eta_{\mathrm{b}}}^{\eta} \rho\,\mathrm{d}z\right]\mathrm{d}A = \rho \int_{\text{column}} (\eta - \eta_{\mathrm{b}})\,\mathrm{d}A = \rho \int_{\text{column}} h\,\mathrm{d}A. \tag{35.13}$$

Time changes in the column mass thus arise from time changes in the layer thickness integrated

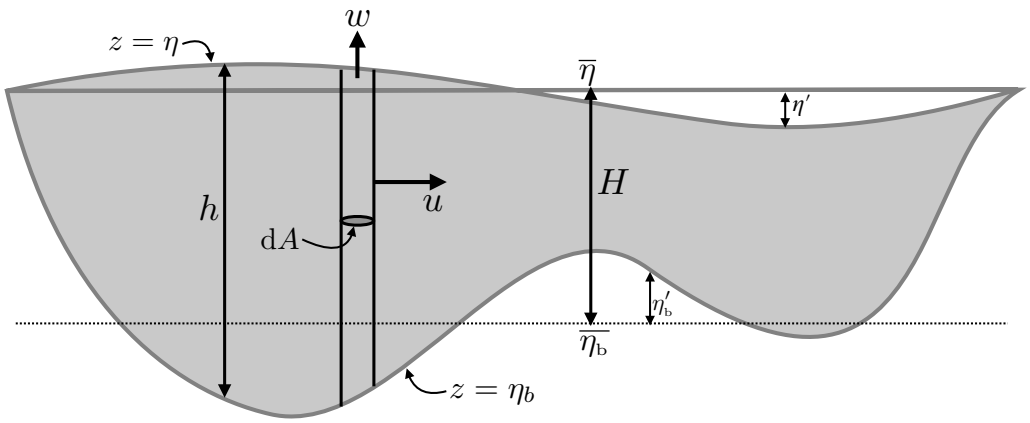

FIGURE 35.3: Mass budget for a column of shallow water fluid with fixed cross-sectional area, $\mathrm{d}A$, constant density, ρ, and layer thickness, $h(x, y, t)$. The column mass is affected only by horizontal transport (transport within the layer) in the absence of boundary mass fluxes through the top, $z = \eta$, or bottom, $z = \eta_{\mathrm{b}}$. Note that since the density of the layer is constant, then mass equals to the constant density times the volume.

over the horizontal area of the column

$$\frac{\mathrm{d}M}{\mathrm{d}t} = \rho \int_{\text{column}} \frac{\partial h}{\partial t} \, \mathrm{d}A, \tag{35.14}$$

where

$$\frac{\partial h}{\partial t} = \frac{\partial \left(\eta - \eta_{\mathrm{b}}\right)}{\partial t} = \frac{\partial \eta}{\partial t}, \tag{35.15}$$

since the bottom topography at $z = \eta_{\mathrm{b}}(x, y)$ is static.

General derivation

The mass within a fluid column changes due to mass crossing the column boundaries. Aagain, we assume here that no mass crosses the top or bottom interfaces. Hence, we only consider mass moving horizontally across the vertical boundaries of the column

$$\text{mass per time entering column} = -\rho \oint_{\text{column}} \boldsymbol{u} \cdot \hat{\boldsymbol{n}} \, \mathrm{d}\mathcal{S}, \tag{35.16}$$

where $\hat{\boldsymbol{n}}$ is the outward normal at the column boundary, and $\mathrm{d}\mathcal{S}$ is the area element along the column boundary. The area integral computed over the column boundary involves a vertical integral and a circumferential line integral

$$\text{mass per time entering column} = -\rho \oint_{\text{column}} \left[\int \boldsymbol{u} \cdot \hat{\boldsymbol{n}} \, \mathrm{d}z \right] \mathrm{d}l, \tag{35.17}$$

where $\mathrm{d}l$ is the infinitesimal line element around the column circumference. Since $\hat{\boldsymbol{n}} \cdot \boldsymbol{u}$ is vertically independent, we can perform the vertical integral to render

$$-\rho \oint_{\text{column}} \left[\int \boldsymbol{u} \cdot \hat{\boldsymbol{n}} \, \mathrm{d}z \right] \mathrm{d}l = -\rho \oint_{\text{column}} h \, \boldsymbol{u} \cdot \hat{\boldsymbol{n}} \, \mathrm{d}l = -\rho \int_{\text{column}} \nabla \cdot (h \, \boldsymbol{u}) \, \mathrm{d}A, \tag{35.18}$$

where the second equality follows from the divergence theorem applied to the horizontal cross-sectional area of the column. Equating this result to the mass time tendency (35.14), and noting that the horizontal cross-sectional area is arbitrary, yields an equation for the layer thickness

$$\partial_t h + \nabla \cdot (h \, \boldsymbol{u}) = 0. \tag{35.19}$$

This result means that the thickness of fluid at a fixed location increases if there is a convergence of thickness onto that location, and decreases if thickness diverges from the location.

We may also write the thickness equation (35.19) using the material time derivative

$$\frac{\mathrm{D}h}{\mathrm{D}t} = -h\,\nabla\cdot\boldsymbol{u}. \tag{35.20}$$

Hence, thickness of a material fluid column increases in regions where the horizontal flow converges and it decreases where the horizontal flow diverges. As for the horizontal velocity in equation (35.11), the material time derivative arises from the local time tendency plus horizontal advection

$$\frac{\mathrm{D}}{\mathrm{D}t} = \frac{\partial}{\partial t} + u\,\frac{\partial}{\partial x} + v\,\frac{\partial}{\partial y}., \tag{35.21}$$

Special case with a rectangular column

To further our understanding of the second step in equation (35.18), consider the special case of a rectangular column, for which the mass per time of fluid entering the column is given by

$$\text{mass per time entering column} = -\rho\int_{\text{column}} [(u\,h)_{\text{east}} - (u\,h)_{\text{west}}]\,\mathrm{d}y - \rho\int_{\text{column}} [(v\,h)_{\text{north}} - (v\,h)_{\text{south}}]\,\mathrm{d}x. \tag{35.22}$$

Taking the limit as the horizontal cross-section of the column becomes infinitesimal leads to

$$\text{mass per time entering column} = -\rho\int_{\text{column}} \left[\frac{\partial(u\,h)}{\partial x} + \frac{\partial(v\,h)}{\partial y}\right]\mathrm{d}x\,\mathrm{d}y = -\rho\int_{\text{column}} \nabla\cdot(h\,\boldsymbol{u})\,\mathrm{d}A, \tag{35.23}$$

thus recovering the result (35.18).

35.2.6 Bottom kinematic boundary condition

Kinematic boundary conditions arise from geometric constraints placed on the fluid system. We consider here the kinematic boundary condition at the bottom interface in the case where there is no flow through this interface, and follow in Section 35.2.7 with the surface kinematic boundary condition.[2]

The ocean bottom is located at a vertical position, $z = \eta_{\mathrm{b}}(x, y)$. This location can equivalently be specified mathematically by the surface

$$s(x, y, z) = z - \eta_{\mathrm{b}}(x, y) = 0. \tag{35.24}$$

The outward normal (pointing from the fluid into the rock) at this surface is given by

$$\hat{\boldsymbol{n}} = -\frac{\nabla s}{|\nabla s|} = \frac{\nabla\eta_{\mathrm{b}} - \hat{\boldsymbol{z}}}{\sqrt{1 + \nabla\eta_{\mathrm{b}}\cdot\nabla\eta_{\mathrm{b}}}}. \tag{35.25}$$

If the bottom is impenetrable to fluid then the velocity field is constrained to satisfy the no-normal

[2] From the discussion of fluid kinematics in Part III, we use the term *material surface* for any continuous surface or interface that is impenetrable to the flow of matter or thermal energy (mechanical energy can be transferred via pressure forces). In Section 19.6 we derived the kinematic boundary conditions for a fluid at interfaces. We here apply those ideas to the shallow water system, so that the presentation in Sections 35.2.6 and 35.2.7 offer a review of Section 19.6 as applied to a shallow water layer.

flow boundary condition

$$\boldsymbol{v} \cdot \hat{\boldsymbol{n}} = 0 \qquad \text{at } z = \eta_{\mathrm{b}}. \tag{35.26}$$

Making use of the bottom outward normal (35.25) leads to

$$w = \boldsymbol{u} \cdot \nabla \eta_{\mathrm{b}} \qquad \text{at } z = \eta_{\mathrm{b}}. \tag{35.27}$$

For a flat bottom, with $\nabla \eta_{\mathrm{b}} = 0$, the no-normal flow condition means that $w(\eta_{\mathrm{b}}) = 0$. For the case of nontrivial bottom topography, $w(\eta_{\mathrm{b}}) = 0$ remains if flow occurs along lines of constant topography; i.e., along isobaths, in which case $\boldsymbol{u} \cdot \nabla \eta_{\mathrm{b}} = 0$. But more generally, sloping bottoms lead to a nonzero vertical velocity component. Dynamically, a nonzero bottom vertical velocity arises from forces at the bottom that cause the horizontal velocity to cross isobaths, $\boldsymbol{u} \cdot \nabla \eta_{\mathrm{b}} \neq 0$.

The kinematic result (35.27) is written in an Eulerian sense, with the velocity constrained to satisfy this relation at each point along the bottom interface. It has a dual material interpretation based on acknowledging that the bottom interface is a material surface. A fluid element on the bottom at $s = z - \eta_{\mathrm{b}} = 0$ will thus remain there; it does not cross the bottom interface. Rather, it can at most move tangentially to the bottom.[3] We can ensure the no-normal flow constraint by setting

$$\frac{\mathrm{D}s}{\mathrm{D}t} = \frac{\mathrm{D}\left(z - \eta_{\mathrm{b}}\right)}{\mathrm{D}t} = 0 \qquad \text{at } z = \eta_{\mathrm{b}}. \tag{35.28}$$

Rearrangement of this result leads to the Eulerian constraint (35.27). Equivalently, we can write this boundary condition in the form

$$w = \frac{\mathrm{D}\eta_{\mathrm{b}}}{\mathrm{D}t} \qquad \text{at } z = \eta_{\mathrm{b}}. \tag{35.29}$$

Since $\eta_{\mathrm{b}} = \eta_{\mathrm{b}}(x, y)$, this expression of the kinematic boundary condition is identical to equation (35.27).

35.2.7 Surface kinematic boundary condition

We here assume the surface boundary is a material interface and thus derive the surface kinematic boundary condition. In Section 35.6 we consider the slightly more general case of volume crossing this surface. As a material surface, the surface kinematic boundary condition follows analogously to the bottom. However, there is a fundamentally new feature in that the layer's upper free surface is a time dependent moving boundary. We studied such boundaries in Section 19.6.2 when detailing the kinematic boundary conditions for a material surface. We here review some of that discussion.

The free surface is located at a vertical position $z = \eta(x, y, t)$. Equivalently, the free surface can be specified by a surface of constant s, where

$$s(x, y, z, t) = z - \eta(x, y, t) = 0. \tag{35.30}$$

The outward normal to the free surface is thus given by

$$\hat{\boldsymbol{n}} = \frac{\nabla s}{|\nabla s|} = \frac{\hat{\boldsymbol{z}} - \nabla \eta}{\sqrt{1 + \nabla \eta \cdot \nabla \eta}}. \tag{35.31}$$

We must account for motion of the surface when formulating the no-normal flow condition.

[3] Details of the tangential motion along a material boundary require dynamical information such as boundary stresses (see Chapter 25). We are not concerned with such dynamical information here, rather our concern is solely with kinematics.

To do so, write the no-normal flow condition as

$$(\boldsymbol{v} - \boldsymbol{v}^{(s)}) \cdot \hat{\boldsymbol{n}} = 0 \qquad \text{at } z = \eta(x, y, t), \tag{35.32}$$

where $\boldsymbol{v}^{(s)}$ is the velocity of a point on the ocean surface. The velocity of a point fixed on an arbitrary surface with specified s satisfies

$$\frac{\partial s}{\partial t} + \boldsymbol{v}^{(s)} \cdot \nabla s = 0. \tag{35.33}$$

As defined, $\boldsymbol{v}^{(s)}$ advects a fluid element in a manner to always keep the element fixed on the constant s surface. With $\hat{\boldsymbol{n}} = \nabla s / |\nabla s|$, we have

$$\boldsymbol{v}^{(s)} \cdot \hat{\boldsymbol{n}} = -\frac{\partial_t s}{|\nabla s|} = \frac{\partial_t \eta}{\sqrt{1 + \nabla \eta \cdot \nabla \eta}}. \tag{35.34}$$

Hence, if the surface remains static, then $\boldsymbol{v}^{(s)} \cdot \hat{\boldsymbol{n}} = 0$. But more generally, the surface is moving, and that movement is fundamental to the surface kinematic boundary condition.

Making use of the result (35.34) in the no-normal flow constraint (35.32) then leads to the surface kinematic boundary condition

$$\partial_t \eta = w - \boldsymbol{u} \cdot \nabla \eta \qquad \text{at } z = \eta. \tag{35.35}$$

As for the bottom kinematic boundary condition written as (35.28), we can interpret the surface kinematic condition (35.35) materially, in which case

$$\frac{\mathrm{D}s}{\mathrm{D}t} = \frac{\mathrm{D}\,(z - \eta)}{\mathrm{D}t} = 0 \qquad \text{at } z = \eta. \tag{35.36}$$

That is, in the absence of flow across the surface boundary, that surface remains material. We can write this boundary condition in the equivalent form

$$w = \frac{\mathrm{D}\eta}{\mathrm{D}t} = (\partial_t + \boldsymbol{u} \cdot \nabla)\, \eta \qquad \text{at } z = \eta. \tag{35.37}$$

35.2.8 Column stretching and the vertical velocity

Since the fluid has constant density, we know that the velocity has zero three-dimensional divergence

$$\nabla \cdot \boldsymbol{u} + \partial_z w = 0 \Longrightarrow \partial_z w = -\nabla \cdot \boldsymbol{u}. \tag{35.38}$$

This result also follows since material fluid elements in the constant density shallow water layer maintain a constant volume (see Section 21.2). Furthermore, since the horizontal velocity has no vertical dependence, we can vertically integrate the continuity equation (35.38) from the bottom to an arbitrary vertical position within the layer to render

$$w(z) = w(\eta_{\mathrm{b}}) - (z - \eta_{\mathrm{b}})\, \nabla \cdot \boldsymbol{u}, \tag{35.39}$$

so that the vertical velocity is a linear function of the vertical position within a shallow water layer. Applying this equation at the upper surface, $z = \eta(x, y, t)$, yields

$$w(\eta) = w(\eta_{\mathrm{b}}) - (\eta - \eta_{\mathrm{b}})\, \nabla \cdot \boldsymbol{u}. \tag{35.40}$$

Eliminating the horizontal convergence between equations (35.39) and (35.40) leads to

$$w(z) - w(\eta_\mathrm{b}) = \left[\frac{z-\eta_\mathrm{b}}{\eta-\eta_\mathrm{b}}\right] [w(\eta) - w(\eta_\mathrm{b})]. \tag{35.41}$$

Making use of the surface kinematic boundary condition (35.37) and bottom kinematic boundary condition (35.29) renders the material form

$$\frac{1}{z-\eta_\mathrm{b}}\left[\frac{\mathrm{D}(z-\eta_\mathrm{b})}{\mathrm{D}t}\right] = \frac{1}{\eta-\eta_\mathrm{b}}\left[\frac{\mathrm{D}(\eta-\eta_\mathrm{b})}{\mathrm{D}t}\right]. \tag{35.42}$$

Finally, introducing the layer thickness $h = \eta - \eta_\mathrm{b}$ yields the material conservation law

$$\frac{\mathrm{D}}{\mathrm{D}t}\left[\frac{z-\eta_\mathrm{b}}{h}\right] = 0. \tag{35.43}$$

Again, $h = \eta - \eta_\mathrm{b}$ is the layer thickness and $z - \eta_\mathrm{b}$ is the height of a fluid element from the bottom interface (see Figure 35.1). Consequently, equation (35.43) means that the ratio of the fluid element height above the bottom to the layer thickness remains constant as the fluid element moves through the shallow water fluid. That is, a vertical column of shallow water fluid stretches or squeezes coherently within a shallow water layer, so that the relative vertical position remains fixed for a point within the column. Shallow water mechanics thus comprises the mechanics of coherent vertical fluid columns moving within a fluid layer. This constrained behavior results from the linear z dependence of the vertical velocity, which itself is a result of the vertical independence of the horizontal velocity, and which follows from the vertical independence of the horizontal gradient of hydrostatic pressure.

35.2.9 Tracer concentration equation

Suppose there is a material substance, a tracer, contained within a shallow water layer.[4] We expect the tracer concentration, ψ, to have a non-uniform vertical structure within the layer, in addition to having horizontal structure: $\psi = \psi(x, y, z, t)$. If the tracer is advected through the layer without any diffusion, then the concentration satisfies the perfect fluid tracer equation (i.e., the *advection equation*)

$$\partial_t \psi + \boldsymbol{u} \cdot \nabla_\mathrm{h} \psi + w\, \partial_z \psi = 0. \tag{35.44}$$

For a shallow water layer, where the horizontal velocity has no vertical dependence within a layer, we find it sufficient to study the vertically averaged tracer concentration within the layer,

$$C(x, y, t) \equiv \frac{1}{h}\int_{\eta_\mathrm{b}}^{\eta} \psi(x, y, z, t)\, \mathrm{d}z. \tag{35.45}$$

To develop the evolution equation for C, we vertically integrate the tracer equation (35.44) over the layer and make use of Leibniz's rule (Section 20.2.4)

$$\int_{\eta_\mathrm{b}}^{\eta} \frac{\partial \psi}{\partial t}\, \mathrm{d}z = \partial_t(h\, C) - \psi(\eta)\, \partial_t \eta \tag{35.46a}$$

$$\int_{\eta_\mathrm{b}}^{\eta} \boldsymbol{u} \cdot \nabla \psi\, \mathrm{d}z = \nabla \cdot (h\, C\, \boldsymbol{u}) - \psi(\eta)\, \boldsymbol{u}(\eta) \cdot \nabla \eta + \psi(\eta_\mathrm{b})\, \boldsymbol{u}(\eta_\mathrm{b}) \cdot \nabla \eta_\mathrm{b} - h\, C\, \nabla \cdot \boldsymbol{u} \tag{35.46b}$$

$$\int_{\eta_\mathrm{b}}^{\eta} w\, \partial_z \psi\, \mathrm{d}z = w(\eta)\, \psi(\eta) - w(\eta_\mathrm{b})\, \psi(\eta_\mathrm{b}) - h\, C\, \partial_z w. \tag{35.46c}$$

[4] We developed the theory of material tracers in Chapter 20.

For these equations we made use of the z independence of $\boldsymbol{u}$ and $\partial_z w$ within the layer. Use of the kinematic boundary conditions from Sections 35.2.6 and 35.2.7, and the three dimensional continuity equation, $\nabla \cdot \boldsymbol{u} + \partial_z w = 0$, renders the equation for the layer vertically averaged tracer concentration

$$\frac{\partial (h\, C)}{\partial t} + \nabla \cdot (h\, C\, \boldsymbol{u}) = 0 \Longleftrightarrow \frac{\partial C}{\partial t} + \boldsymbol{u} \cdot \nabla C = \frac{\mathrm{D}C}{\mathrm{D}t} = 0. \tag{35.47}$$

As a self-consistency check, note that if the tracer concentration has a horizontally uniform value, then the flux-form of the tracer equation (35.47) reduces to the thickness equation (35.19).

35.2.10 Summary comments

Key physical assumptions for the shallow water fluid

The shallow water fluid model is based on the following two assumptions.

- The fluid layer has a uniform density, which then means the fluid is incompressible.
- The pressure is hydrostatic.

Since the pressure gradient is vertically independent within the layer, an initial horizontal velocity that is vertically independent will remain vertically independent. That is, the fluid moves as columns within the layer, with the columns stretching and squashing depending on the divergence or convergence of volume towards the column.

The term "shallow" refers to the small vertical to horizontal aspect ratio, $H/L \ll 1$, which in turn is consistent with the hydrostatic approximation (Section 27.2). The term "water" refers to the incompressible nature of the fluid, which is a more relevant approximation for the ocean than for the atmosphere (see Section 29.1). Nonetheless, the shallow water model has direct applications to many features of both the atmosphere and ocean circulation, and as such it is widely used across the atmosphere and ocean sciences.

Shallow water fluid columns are not Taylor columns

The columnar motion of fluid within a shallow water layer is reminscent of the Taylor columns discussed in Section 31.5.3. However, the columnar motion of fluid within a Taylor column holds for homogeneous fluids undergoing rapid rotation. The horizontal fluid velocity within a Taylor column is non-divergent so that there is no vertical motion of the fluid. These properties allow one to interpret a Taylor column as a fluid mechanical realization of a column of rigid matter much like a solid body.

In contrast, shallow water fluid columns do not rely on rotation, but instead arise from the hydrostatic balance (small aspect ratio flow) maintained within each homogeneous layer. Additionally, shallow water columns are not rigid. Rather, they stretch and squash in the presence of nonzero divergence in the horizontal flow, thus leading to vertical motion of fluid within the column. Finally, shallow water columns remain coherent even as they move over topography, and yet, again, they can stretch and squash. In Section 53.5.4, we further discuss the connections and distinctions between vertically coherent flow present in the small aspect ratio shallow water layer versus that for the rapidly rotating flow leading to the Taylor-Proudman effect.

35.3 Reduced gravity model for the upper ocean

The *reduced gravity model* describes an active layer of uniform density, ρ_1, above a stagnant layer of density, ρ_2, and below a fluid of zero density, $\rho_0 = 0$. It is often referred to as the 1.5 layer

model. This theoretical model has been used, to some success, as an idealization of the upper ocean circulation whereby an active layer (e.g., the region above the ocean pycnocline), sits above an inactive layer (the abyss) of much smaller motion (here assumed to be zero motion). In this way, we introduce the *level of no motion*, below which (baroclinic) currents vanish.

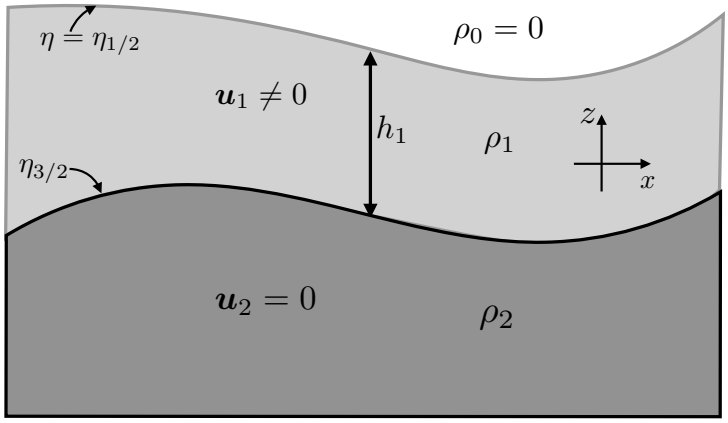

FIGURE 35.4: Reduced gravity model of shallow water fluid. The lower layer with density ρ_2 is dynamically inactive and thus has a zero velocity. The upper layer is dynamically active with thickness, $h = \eta_{1/2} - \eta_{3/2}$, and density, ρ_1. The dynamically active layer is bounded above by a zero density atmosphere, $\rho_0 = 0$. The lower inactive layer is assumed to be infinitely deep so that its continuity equation can be ignored; i.e., even though there are zero currents within this layer, the layer thickness can still undulate. The reduced gravity between the two layers is defined by $g'_{3/2} = g\,(\rho_2 - \rho_1)/\rho_{\text{ref}} \ll g$, whereas the reduced gravity at the top interface is given by $g'_{1/2} = g$.

35.3.1 Momentum and thickness equations for the active layer

We develop the momentum equations for the reduced gravity model by making use of the hydrostatic balance, in which pressure at a vertical position, z, in the upper layer is computed as (see Figure 35.4)

$$p_1(x, y, z, t) = p_{1/2}(x, y, t) + g\,\rho_1\,[\eta_{1/2}(x, y, t) - z], \tag{35.48}$$

where we denote an interface value by a half-index, so that $\eta_{1/2}$ and $p_{1/2}$ are the interface height and pressure at the upper layer interface.[5] Since the fluid above the upper layer is assumed to have zero density, we set

$$p_{1/2} = 0. \tag{35.49}$$

The horizontal momentum equation for the upper (active) layer is given by

$$\rho_{\text{ref}} \left[\frac{\mathrm{D}\boldsymbol{u}_1}{\mathrm{D}t} + f\,\hat{\boldsymbol{z}} \times \boldsymbol{u}_1 \right] = -g\,\rho_1\,\nabla\eta_{1/2}, \tag{35.50}$$

where the z dependent term in the pressure (35.48) drops out when computing the horizontal pressure gradient. Setting the reference density equal to the top layer density, $\rho_{\text{ref}} = \rho_1$, leads to the more tidy equation

$$\frac{\mathrm{D}\boldsymbol{u}_1}{\mathrm{D}t} + f\,\hat{\boldsymbol{z}} \times \boldsymbol{u}_1 = -g\nabla\eta_{1/2}. \tag{35.51}$$

[5]There is no general consensus on this notation, with some treatments, such as *Vallis* (2017) and *Cushman-Roisin and Beckers* (2011) using an integer to label an interface quantity, whereas some numerical model papers (e.g., *Griffies et al.* (2020)) use the half-index. We prefer the half-index since it removes any ambiguity concerning the ordering of the interfaces relative to the layer.

The equations for the upper layer are completed by volume conservation in the form of the thickness equation

$$\frac{\mathrm{D}h_1}{\mathrm{D}t} = -h_1 \, \nabla \cdot \boldsymbol{u}_1. \tag{35.52}$$

35.3.2 Relating undulations of the top and bottom layer interfaces

The pressure in the lower stagnant layer is given by the weight per horizontal area of fluid above it, and it can be written

$$p_2(x,y,z,t) = g\,\rho_1\,(\eta_{1/2} - \eta_{3/2}) + g\,\rho_2\,(\eta_{3/2} - z) \tag{35.53a}$$

$$= g\,\rho_1\,\eta_{1/2} + g\,(\rho_2 - \rho_1)\,\eta_{3/2} - g\,\rho_2\,z \tag{35.53b}$$

$$= \rho_{\text{ref}}\,(g'_{1/2}\,\eta_{1/2} + g'_{3/2}\,\eta_{3/2}) - g\,\rho_2\,z. \tag{35.53c}$$

In this equation we introduced the reference density and *reduced gravities*

$$\rho_{\text{ref}} = \rho_1 \quad \text{and} \quad g'_{1/2} = g \quad \text{and} \quad g'_{3/2} = g\,(\rho_2 - \rho_1)/\rho_{\text{ref}} \ll g. \tag{35.54}$$

Taking the reference density as the top layer density is common for Boussinesq shallow water models, and will be assumed in our formulations with multiple layers in Section 35.4. We employ the half-index notation for the reduced gravities since they are computed by differencing the densities between two adjacent layers, and as such they are considered an interface property. Additionally, the reduced gravities multiply a corresponding interface gradient, which also uses the half-integer notation.

For the reduced gravity model we assume the lower layer is motionless. To maintain zero motion in the lower layer requires the lower layer horizontal pressure gradient to vanish

$$\rho_{\text{ref}}^{-1}\,\nabla_{\text{h}} p_2 = g'_{1/2}\,\nabla\eta_{1/2} + g'_{3/2}\,\nabla\eta_{3/2} = 0. \tag{35.55}$$

This constraint links the undulations of the top and bottom interfaces of the dynamically active layer

$$\nabla\eta_{1/2} = -\frac{g'_{3/2}}{g'_{1/2}}\,\nabla\eta_{3/2} = -[(\rho_2 - \rho_1)/\rho_{\text{ref}}]\,\nabla\eta_{3/2} \Longrightarrow \eta_{1/2} = -\eta_{3/2}\,[(\rho_2 - \rho_1)/\rho_{\text{ref}}] + \text{constant}. \tag{35.56}$$

The density ratio, $(\rho_2 - \rho_1)/\rho_{\text{ref}}$, is positive but typically much smaller than unity. Hence, the relation (35.56) means that undulations of the free surface, $\eta_{1/2}$, are of opposite sign to and of much smaller amplitude than the undulations in the lower interface, $\eta_{3/2}$. This behavior is typical for undulations of the pycnocline region of the ocean and the free surface as depicted in Figure 35.5.

35.3.3 Momentum equation with reduced gravity

Relation (35.55) can be used to write the momentum equation (35.51) in the form

$$\frac{\mathrm{D}\boldsymbol{u}_1}{\mathrm{D}t} + f\,\hat{\boldsymbol{z}} \times \boldsymbol{u}_1 = g'_{3/2}\,\nabla\eta_{3/2}. \tag{35.57}$$

It is common to make use of the momentum equation in the form (35.57), rather than the original form (35.51). The reason is that historically, ocean hydrography measurements[6] have allowed for an estimate of the pycnocline slope, $\nabla\eta_{3/2}$, whereas it was not until precise satellite

[6] In oceanography, hydrography refers to measurements of temperature, salinity, and pressure; see *Talley et al.* (2011).

altimetry measurements starting in the 1990s that we could estimate the far smaller sea level slope, $\nabla\eta_{1/2}$.

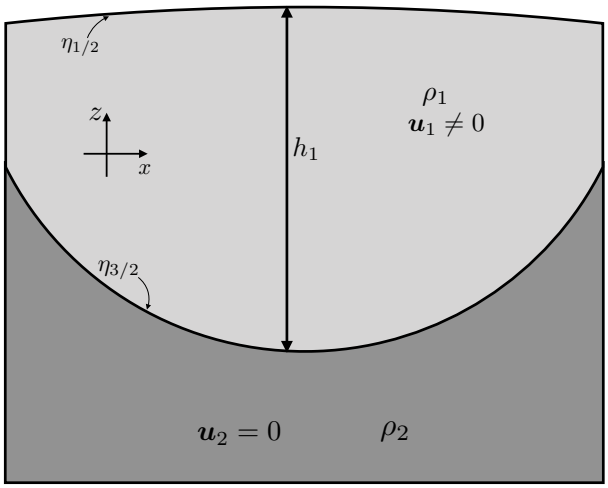

FIGURE 35.5: A vertical slice through a reduced gravity, or 1.5 layer, ocean in hydrostatic balance. Shown here is a plug of dynamically active light water, as may occur in a warm core eddy to the subtropical gyres, sitting on top of heavy water of zero motion. The free surface corresponds to $\eta_{1/2}$ in Figure 35.4, whereas the pycnocline (heavy black line) corresponds to the lower interface $\eta_{3/2}$ of Figure 35.4. The sea surface experiences an applied pressure $p = p_a$, assumed to be uniform for this idealized situation. Note how sea level is a maximum above the pycnocline minimum, with this geometry reflected in equation (35.56). In the ocean, the slope of the pycnocline is about 100-300 times larger than the slope of the sea level. That is, sea level may show undulations on the order of a metre, whereas the pycnocline undulations are on the order of 100-300 m.

35.3.4 Reduced gravity and relative buoyancy

Equation (35.55)

$$g\,\nabla\eta_{1/2} = -g^r_{3/2}\,\nabla\eta_{3/2}, \tag{35.58}$$

says that with $g^r_{3/2} \ll g$, the free surface slopes are much smaller than interior slopes

$$|\nabla\eta_{1/2}| \ll |\nabla\eta_{3/2}|. \tag{35.59}$$

We thus infer that the interior interface has less resistance to vertical motion than the free surface. To help understand this result, recall the study of Archimedean buoyancy in Section 30.4. We see that the reduced gravity, $g^r_{3/2}$, is the Archimedean buoyancy of layer 1 relative to layer 2, with normalization given by the reference density as per the Boussinesq approximation

$$\text{buoyancy layer 1 relative to layer 2} = -g\,(\rho_1 - \rho_2)/\rho_{\text{ref}} = g^r_{3/2}. \tag{35.60}$$

A small relative buoyancy between two density layers renders little resistence for motion of the layer interface. Indeed, as the density difference vanishes, so too does the buoyant resistance to motion of the layer interface. For the upper free surface, the buoyancy of layer 0 (a zero mass atmosphere) relative to layer 1 equals to the full gravitational acceleration.

$$\text{buoyancy layer 0 relative to layer 1} = -g\,(\rho_0 - \rho_1)/\rho_{\text{ref}} = g, \tag{35.61}$$

where we assumed that $\rho_{\text{ref}} = \rho_1$ and $\rho_0 = 0$. Evidently, the relative buoyancy between the top shallow water layer and the atmosphere is given by the full gravity acceleration, which indicates the large buoyant resistence to vertical motion of the free surface.

It is for this reason that the interior interface is more flexible than the free surface, as

depicted in Figure 35.5. Even for an atmosphere with mass, so that $\rho_0 > 0$, the upper interface's reduced gravity is close to g since the atmosphere is roughly 1000 times less dense than seawater. This result holds in general, whereby increasing the reduced gravity between density layers, and thus increasing the vertical density stratification, increases the resistance to motion of the layer interface and thus reduces the interface's flexibility.

35.3.5 Further study

The material in this section is inspired by Section 3.2 of *Vallis* (2017). *Tomczak and Godfrey* (1994) make use of the reduced gravity model for interpretating aspects of the observed ocean. Additional use is made by *Griffies et al.* (2014) for interpreting large-scale sea level patterns.

35.4 Stacked shallow water equations

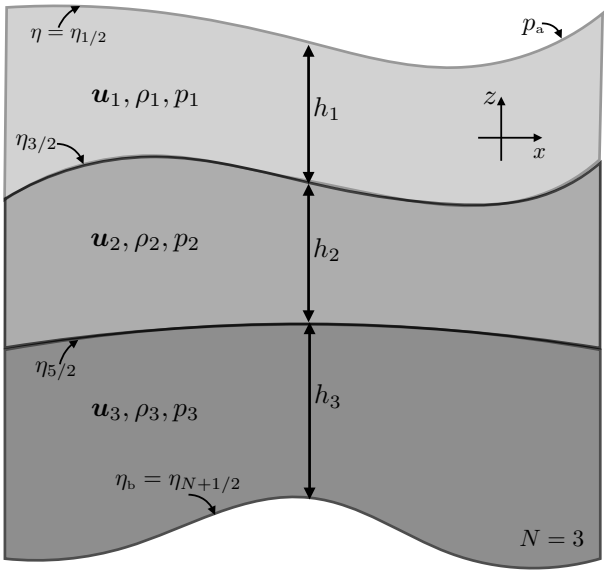

FIGURE 35.6: Three dynamically active layers of stacked shallow water fluid ($N = 3$). The notation corresponds to that for the reduced gravity model of Figure 35.4, yet here with three dynamically active layers. In particular, $\eta_{1/2}$ is the free surface, $\eta_{1/2} = \eta$, whereas $\eta_{N+1/2} = \eta_b$ is the bottom interface. Hence, the total thickness of a column is $h_1 + h_2 + h_3 = \eta_{1/2} - \eta_b$. The "atmosphere" above the layers is assumed to apply a pressure, p_a, to the upper surface. The horizontal velocity is vertically independent within each layer, as is the horizontal pressure gradient, so that both are discontinuous across a layer interface. In contrast, the pressure is a linear function of z within a layer and is continuous across a layer interface. Finally, the vertical velocity is also a linear function of z within a layer but it is discontinuous across a layer interface. The reduced gravity defined between each layer is given by $g'_{k+1/2} = g\,(\rho_{k+1} - \rho_k)/\rho_{ref}$. We take the reference density as $\rho_{ref} = \rho_1$, which results in a tidy set of layer equations.

In studies of shallow water fluids, much of the formalism developed for a single layer can be readily extended to an arbitrary number of layers. We here pursue this extension and thereby expose the underlying kinematics and dynamics of stacked shallow water models. We assume the layers are immiscible so that matter and thermal properties are not exchanged between the layers. Consequently, the layers couple only through mechanical forces arising from pressure form stress (Chapter 28). Furthermore, we continue to assume that the horizontal velocity has no vertical dependence within each shallow water layer, which in turn means the horizontal pressure gradient is vertically independent within each layer. The notation for our derivations is depicted in Figure 35.6 in the case of three active layers.

In Section 66.2 we develop the equations for a continuosly stratified Boussinesq fluid making use of isopycnal vertical coordinates. Although the vertical stratification is continuous in that case, we find that the isopycnal equations are isomorphic to the stacked shallow water equations. Hence, besides being of intrinsic interest as a versatile theoretical model, the stacked shallow water model offers a suitable step towards studies of a continuously stratified fluid using isopycnal coordinates.

35.4.1 Formulation of a 2-layer model

We here display the equations for two layers, thus offering the seeds for an extension to N layers in Section 35.4.2.

Thickness and tracer equations

Each shallow water layer satisfies its own independent thickness equation and tracer equation, representing the conservation of volume and tracer content for each layer

$$\frac{\partial h_1}{\partial t} + \nabla \cdot (h_1 \, \boldsymbol{u}_1) = 0 \tag{35.62a}$$

$$\frac{\partial h_2}{\partial t} + \nabla \cdot (h_2 \, \boldsymbol{u}_2) = 0 \tag{35.62b}$$

$$\frac{\partial (h_1 \, C_1)}{\partial t} + \nabla \cdot (h_1 \, C_1 \, \boldsymbol{u}_1) = 0 \tag{35.62c}$$

$$\frac{\partial (h_2 \, C_2)}{\partial t} + \nabla \cdot (h_2 \, C_2 \, \boldsymbol{u}_2) = 0. \tag{35.62d}$$

We emphasize that there is no explicit coupling between these equations, as each layer separately must satisfy volume conservation and tracer conservation. However, the velocities are coupled through the pressure force, as we now discuss.

Pressure within a layer

To compute the pressure within a layer, we make use of the hydrostatic balance and integrate down from the surface, which results in the pressure fields

$$p_1 = \rho_1 \, g \, (\eta_{1/2} - z) + p_\mathsf{a} \tag{35.63}$$

$$p_2 = \rho_1 \, g \, (\eta_{1/2} - \eta_{3/2}) + \rho_2 \, g \, (\eta_{3/2} - z) + p_\mathsf{a}. \tag{35.64}$$

As for the reduced gravity model in equation (35.53c), it is convenient to write pressure in layer-two using the reduced gravity, which leads to

$$p_2 - p_\mathsf{a} = \rho_1 \, g \, (\eta_{1/2} - \eta_{3/2}) + \rho_2 \, g \, (\eta_{3/2} - z) \tag{35.65a}$$

$$= g \, \eta_{1/2} \, \rho_1 + g \, (\rho_2 - \rho_1) \, \eta_{3/2} - g \, \rho_2 \, z \tag{35.65b}$$

$$= \rho_\mathsf{ref} \, (g^\mathsf{r}_{1/2} \, \eta_{1/2} + g^\mathsf{r}_{3/2} \, \eta_{3/2}) - g \, \rho_2 \, z \tag{35.65c}$$

with the Boussinesq reference density and reduced gravities given by

$$\rho_\mathsf{ref} = \rho_1 \quad \text{and} \quad g^\mathsf{r}_{1/2} = g \quad \text{and} \quad g^\mathsf{r}_{3/2} = g \, (\rho_2 - \rho_1) / \rho_\mathsf{ref} \ll g. \tag{35.66}$$

As for the reduced gravity model in equation (35.54), we set the reference density equal to the top layer density. As per the discussion around equation (35.76), $\rho_\mathsf{ref} = \rho_1$ results in a somewhat tidier set of layer velocity equations.

Boussinesq reference density and the reduced gravity

We are formulating the shallow water model according to Boussinesq ocean equations from Chapter 29, whereby fluid elements conserve their volume rather than their mass. According to our discussion of the Boussinesq momentum equation in Section 29.1.2, density is set to a constant reference density when measuring the inertial mass of a fluid element, yet density remains the *in situ* density when measuring weight of a fluid element. For the shallow water model, we multiply the inertial acceleration and Coriolis acceleration with a reference density,

$$\rho_{\mathsf{ref}} = \text{shallow water reference density}, \tag{35.67}$$

whereas pressure and potential energy maintain the density, ρ_{k}, of the shallow water layer.

We further make use of the Boussinesq ocean when computing the buoyancy frequency (Section 30.6). Namely, with ϱ the potential density, the Boussinesq form of the squared buoyancy frequency is

$$N^2 = -g \left[\frac{1}{\rho_{\mathsf{ref}}} \frac{\partial \varrho}{\partial z} \right] \approx -\frac{g}{\rho_{\mathsf{ref}}} \frac{\Delta \rho}{\Delta z} = -g^{\mathsf{r}}/\Delta z. \tag{35.68}$$

It is for this reason that we take ρ_{ref} for the denominator of the reduced gravity throughout all of the shallow water layers, thus defining

$$g^{\mathsf{r}}_{\mathsf{k}-1/2} = g\,(\rho_{\mathsf{k}} - \rho_{\mathsf{k}-1})/\rho_{\mathsf{ref}} \quad \text{and} \quad g^{\mathsf{r}}_{1/2} = g. \tag{35.69}$$

Horizontal velocity equations

The horizontal velocity equations for the two layers take the form

$$\rho_{\mathsf{ref}} \left[\frac{\mathrm{D}_1 \boldsymbol{u}_1}{\mathrm{D}t} + f\,\hat{\boldsymbol{z}} \times \boldsymbol{u}_1 \right] = -\nabla p_1 \tag{35.70a}$$

$$\rho_{\mathsf{ref}} \left[\frac{\mathrm{D}_2 \boldsymbol{u}_2}{\mathrm{D}t} + f\,\hat{\boldsymbol{z}} \times \boldsymbol{u}_2 \right] = -\nabla p_2, \tag{35.70b}$$

where we introduced the layer material time derivatives

$$\frac{\mathrm{D}_k}{\mathrm{D}t} = \frac{\partial}{\partial t} + \boldsymbol{u}_k \cdot \nabla \quad \text{for } k = 1, 2. \tag{35.71}$$

Making use of expressions (35.63) and (35.65c) for layer pressures leads to the horizontal momentum equations

$$\rho_{\mathsf{ref}} \left[\frac{\mathrm{D}_1 \boldsymbol{u}_1}{\mathrm{D}t} + f\,\hat{\boldsymbol{z}} \times \boldsymbol{u}_1 \right] = -g\,\rho_1\,\nabla[\eta_{1/2} + p_{\mathsf{a}}/(g\,\rho_1)] \tag{35.72a}$$

$$\rho_{\mathsf{ref}} \left[\frac{\mathrm{D}_2 \boldsymbol{u}_2}{\mathrm{D}t} + f\,\hat{\boldsymbol{z}} \times \boldsymbol{u}_2 \right] = -g\,\rho_1\,\nabla[\eta_{1/2} + p_{\mathsf{a}}/(g\,\rho_1)] - g^{\mathsf{r}}_{3/2}\,\rho_{\mathsf{ref}}\,\nabla \eta_{3/2}. \tag{35.72b}$$

It is convenient to express the interface heights in terms of layer thicknesses, h_1 and h_2, since the layer thicknesses are the prognostic fields determined by time stepping the thickness equations (35.62a) and (35.62b). We thus write

$$\eta_{1/2} = \eta_{\mathsf{b}} + h_1 + h_2 \qquad \text{and} \qquad \eta_{3/2} = \eta_{\mathsf{b}} + h_2, \tag{35.73}$$

so that

$$p_1 - p_{\mathsf{a}} = \rho_1\,g\,(\eta_{\mathsf{b}} + h_1 + h_2) - g\,\rho_1\,z \tag{35.74a}$$

$$p_2 - p_\mathsf{a} = \rho_1\, g\,(\eta_\mathsf{b} + h_1 + h_2) + \rho_\mathsf{ref}\, g'_{3/2}\,(\eta_\mathsf{b} + h_2) - g\,\rho_2\, z, \tag{35.74b}$$

thus resulting in the horizontal momentum equations

$$\rho_\mathsf{ref}\left[\frac{\mathrm{D}_1\boldsymbol{u}_1}{\mathrm{D}t} + f\,\hat{\boldsymbol{z}}\times\boldsymbol{u}_1\right] = -\rho_1\, g\,\nabla[\eta_\mathsf{b} + h_1 + h_2 + p_\mathsf{a}/(g\,\rho_1)] \tag{35.75a}$$

$$\rho_\mathsf{ref}\left[\frac{\mathrm{D}_2\boldsymbol{u}_2}{\mathrm{D}t} + f\,\hat{\boldsymbol{z}}\times\boldsymbol{u}_2\right] = -\rho_1\, g\,\nabla[\eta_\mathsf{b} + h_1 + h_2 + p_\mathsf{a}/(g\,\rho_1)] - \rho_\mathsf{ref}\, g'_{3/2}\,\nabla(\eta_\mathsf{b} + h_2). \tag{35.75b}$$

Notice how layer thickness from one layer appears in the other layer's pressure gradient. In this way, changes in the thickness of one layer have a direct impact on pressure forces and flow in the adjacent layer. Also notice how the bottom topography appears in the bottom pressure gradient, which arises due to our switch from layer interfaces to layer thicknesses.

As already noted, it is common for a stacked shallow water model to choose

$$\rho_\mathsf{ref} = \rho_1. \tag{35.76}$$

We here see why taking this choice is desirable, since doing so brings the layer velocity equations (35.75a) and (35.75b) into the more tidy forms

$$\frac{\mathrm{D}_1\boldsymbol{u}_1}{\mathrm{D}t} + f\,\hat{\boldsymbol{z}}\times\boldsymbol{u}_1 = -g\nabla[\eta_\mathsf{b} + h_1 + h_2 + p_\mathsf{a}/(g\,\rho_1)] \tag{35.77a}$$

$$\frac{\mathrm{D}_2\boldsymbol{u}_2}{\mathrm{D}t} + f\,\hat{\boldsymbol{z}}\times\boldsymbol{u}_2 = -g\nabla[\eta_\mathsf{b} + h_1 + h_2 + p_\mathsf{a}/(g\,\rho_1)] - g'_{3/2}\nabla(\eta_\mathsf{b} + h_2). \tag{35.77b}$$

Vertical shear in horizontal velocities between layers

The difference in layer velocities, $\boldsymbol{u}_1 - \boldsymbol{u}_2$, represents the vertical shear in the layers. This difference is affected by a pressure gradient arising just from bottom topography and the interior layer thickness, h_2

$$\frac{\mathrm{D}_1\boldsymbol{u}_1}{\mathrm{D}t} - \frac{\mathrm{D}_2\boldsymbol{u}_2}{\mathrm{D}t} + f\,\hat{\boldsymbol{z}}\times(\boldsymbol{u}_1 - \boldsymbol{u}_2) = g'_{3/2}\nabla\,(\eta_\mathsf{b} + h_2). \tag{35.78}$$

That is, the vertical shear does not directly feel undulations of the free surface, $\eta_{1/2}$, or the applied pressure, p_a. Rather, it feels these surface undulations only indirectly via nonlinear terms appearing in the advection on the left hand side. We further discuss this result in Section 36.2.2 by introducing thermal wind and the Margules' Relation.

35.4.2 N-layer model equations

The 2-layer equations from Section 35.4.1 can be generalized to N-layers. The thickness equation and tracer equation represent volume and tracer conservation for each layer

$$\frac{\partial h_\mathsf{k}}{\partial t} + \nabla\cdot(\boldsymbol{u}_\mathsf{k}\, h_\mathsf{k}) = 0 \tag{35.79a}$$

$$\frac{\partial (h_\mathsf{k}\, C_\mathsf{k})}{\partial t} + \nabla\cdot(\boldsymbol{u}_\mathsf{k}\, h_\mathsf{k}\, C_\mathsf{k}) = 0, \tag{35.79b}$$

where $\mathsf{k} = 1, N$ is the discrete layer index and there is no implied summation on this label.[7]

[7] To help distinguish the layer index, k, from a tensor index, k, we write the layer index using an upright Roman font whereas a tensor index is slanted.

Expressions for the pressure

Some work is needed to generalize the pressure gradient appearing in the velocity equation. For that purpose, write the interface height as

$$\eta_{k+1/2} = \eta_b + \sum_{j=k+1}^{N} h_j \quad \text{with } \eta_{N+1/2} = \eta_b \text{ and } \eta_{1/2} = \eta. \tag{35.80}$$

For example, the layer interfaces with $N = 3$ layers are given by

$$\eta_{1/2} = \eta_b + h_1 + h_2 + h_3 \qquad \eta_{3/2} = \eta_b + h_2 + h_3 \qquad \eta_{5/2} = \eta_b + h_3 \qquad \eta_{7/2} = \eta_b. \tag{35.81}$$

In turn, the hydrostatic pressure within layer-k is given by

$$p_k = -g\,\rho_k\,z + p_a + \rho_{ref} \sum_{j=0}^{k-1} g'_{j+1/2}\,\eta_{j+1/2} = p_{k-1/2} + g\,\rho_k\,(\eta_{k-1/2} - z), \tag{35.82}$$

where the reduced gravities are defined according to equation (35.69)

$$g'_{j-1/2} = g\,(\rho_j - \rho_{j-1})/\rho_{ref} > 0 \quad \text{with} \quad g'_{1/2} = g. \tag{35.83}$$

As an example, the layer pressures for $N = 3$ are given by

$$p_1 = p_a + g\,\rho_1\,(\eta_{1/2} - z) \qquad p_2 = p_{3/2} + g\,\rho_2\,(\eta_{3/2} - z) \qquad p_3 = p_{5/2} + g\,\rho_3\,(\eta_{5/2} - z). \tag{35.84}$$

The half-integer pressures are evaluated on the corresponding interface, and the hydrostatic balance yields the pressure difference

$$p_{k+1/2} - p_{k-1/2} = g\,\rho_k\,h_k = g\,\rho_k\,(\eta_{k-1/2} - \eta_{k+1/2}). \tag{35.85}$$

Summary of the thickness weighted velocity equation

The velocity equation for an arbitrary layer-k is given by

$$\rho_{ref}\left[\frac{D_k \boldsymbol{u}_k}{Dt} + f\,\hat{\boldsymbol{z}} \times \boldsymbol{u}_k\right] = -\nabla p_k \iff [\partial_t + (\boldsymbol{u}_k \cdot \nabla)]\boldsymbol{u}_k + f\,\hat{\boldsymbol{z}} \times \boldsymbol{u}_k = -\rho_{ref}^{-1}\,\nabla p_k. \tag{35.86}$$

Use of the layer thickness equation (35.79a) readily leads to the thickness-weighted momentum equation

$$\partial_t(h_k\,\boldsymbol{u}_k) + \nabla \cdot (h_k\,\boldsymbol{u}_k \otimes \boldsymbol{u}_k) + f\,\hat{\boldsymbol{z}} \times h_k\,\boldsymbol{u}_k = -(h_k/\rho_{ref})\,\nabla p_k. \tag{35.87}$$

We study the thickness-weighted momentum equation in Section 36.3, where we find it offers a more suitable framework than the velocity equation for studying the pressure form stresses acting at layer interfaces.

35.4.3 Dynamic pressure and the Montgomery potential

The term $g\,\rho_k\,z$ appearing in the layer pressures (35.82) has a zero horizontal gradient. Hence, it does not contribute to the horizontal pressure gradient acceleration acting on a layer. As a result, it is a "do nothing" pressure that motivates us to introduce the *shallow water dynamic pressure* (e.g., equation (3.44) of *Vallis* (2017))

$$p_k + g\,\rho_k\,z = p_a + \rho_{ref} \sum_{j=0}^{k-1} g'_{j+1/2}\,\eta_{j+1/2} \equiv p_a + p_k^{dyn} \implies \nabla p_k = \nabla p_a + \nabla p_k^{dyn}, \tag{35.88}$$

The term "dynamic" is motivated since $p_{\mathsf{k}}^{\text{dyn}}$ gradients directly lead to accelerations. Notably, the dynamic pressure is vertically independent within a layer, so that it has a jump moving across a layer interface. Also note that $p_{\mathsf{k}}^{\text{dyn}}$ is related to the shallow water *Montgomery potential* via

$$M_{\mathsf{k}}^{\text{dyn}} = \rho_{\text{ref}}^{-1} \, p_{\mathsf{k}}^{\text{dyn}} = \sum_{\mathsf{j}=0}^{\mathsf{k}-1} g_{\mathsf{j}+1/2}^{\mathsf{r}} \, \eta_{\mathsf{j}+1/2} \tag{35.89}$$

(e.g., Section 12.2 of *Cushman-Roisin and Beckers* (2011)), with the continuous Montgomery potential defined by equation (66.4). When studying the mechanical energy budget in Section 36.6, we find that $p_{\mathsf{k}}^{\text{dyn}}$ naturally appears since the energy budget is derived using the pressure gradient body force. The difference of the dynamic pressure between two layers is given by

$$p_{\mathsf{k}}^{\text{dyn}} - p_{\mathsf{k}+1}^{\text{dyn}} = -\rho_{\text{ref}} \, g_{\mathsf{k}+1/2}^{\mathsf{r}} \, \eta_{\mathsf{k}+1/2} \iff M_{\mathsf{k}}^{\text{dyn}} - M_{\mathsf{k}+1}^{\text{dyn}} = -g_{\mathsf{k}+1/2}^{\mathsf{r}} \, \eta_{\mathsf{k}+1/2}, \tag{35.90}$$

which is an expression of the hydrostatic balance for shallow water layers.

We often find it useful to study pressure contributions to the momentum equation via the duality between the pressure gradient body force and the pressure contact force as when studying form stress in Chapter 28, and further applied to the shallow water in Section 36.4 and in Chapter 67. For those purposes, we do not use $p_{\mathsf{k}}^{\text{dyn}}$ since it is not the hydrostatic pressure measured within a shallow water layer, so that $p_{\mathsf{k}}^{\text{dyn}}$ cannot be directly used to convert the pressure gradient body force to the pressure contact force. Instead, we must use the pressure, p_{k}.

35.4.4 Properties of the vertical velocity

From Section 19.6.2 we know that

$$w = \frac{\mathrm{D}\eta}{\mathrm{D}t} \tag{35.91}$$

provides an expression for the vertical velocity of a fluid parcel at a point on an impermeable surface, $z = \eta(x, y, t)$. We made use of this equation in Section (35.2.7) when studying the surface kinematic boundary condition for a single shallow water layer. We make use of this equation in this section to further an understanding of the vertical velocity in a shallow water model. In particular, we find that the jump in horizontal velocity across the interface leads to a jump in the vertical velocity.

Jump condition for the vertical velocity across a layer interface

Consider two shallow water layers labelled by k and $\mathsf{k}+1$ that are separated by an interface at $z = \eta_{\mathsf{k}+1/2}(x, y, t)$. Define the vertical velocity at the $z = \eta_{\mathsf{k}+1/2}$ interface according to the material kinematic condition

$$w^{(\mathsf{k})}(\eta_{\mathsf{k}+1/2}) = w_{\mathsf{k}+1/2}^{(\mathsf{k})} = (\partial_t + \boldsymbol{u}_{\mathsf{k}} \cdot \nabla) \, \eta_{\mathsf{k}+1/2}. \tag{35.92}$$

Evidently, $w_{\mathsf{k}+1/2}^{(\mathsf{k})}$ is the vertical velocity for a fluid parcel on the top side of the $z = \eta_{\mathsf{k}+1/2}$ interface. Similarly, define the vertical velocity for a fluid parcel on the lower side of the $z = \eta_{\mathsf{k}+1/2}$ interface according to

$$w_{\mathsf{k}+1/2}^{(\mathsf{k}+1)} = (\partial_t + \boldsymbol{u}_{\mathsf{k}+1} \cdot \nabla) \, \eta_{\mathsf{k}+1/2}. \tag{35.93}$$

Taking the difference leads to the jump condition

$$w^{(\mathsf{k})}(\eta_{\mathsf{k}+1/2}) - w^{(\mathsf{k}+1)}(\eta_{\mathsf{k}+1/2}) = (\boldsymbol{u}_{\mathsf{k}} - \boldsymbol{u}_{\mathsf{k}+1}) \cdot \nabla \eta_{\mathsf{k}+1/2} \neq 0. \tag{35.94}$$

As advertised, the vertical velocity has a jump across the interface that arises from the jump in the horizontal velocity. In Section 36.2.2 we derive the shallow water expression (36.9) for thermal wind balance maintained by geostrophic flow, known as the *Margules' relation*. In that special case there is no jump in the vertical velocity since $\hat{\boldsymbol{z}} \times (\boldsymbol{u}_{\mathsf{k}} - \boldsymbol{u}_{\mathsf{k}+1})$ is parallel to $\nabla\eta_{\mathsf{k}+1/2}$, so that $(\boldsymbol{u}_{\mathsf{k}} - \boldsymbol{u}_{\mathsf{k}+1}) \cdot \nabla\eta_{\mathsf{k}+1/2} = 0$. We thus conclude that the vertical velocity jump arises from ageostrophic contributions to the horizontal flow.

It is tempting to introduce a sub-region that smoothly connects the horizontal velocity between the layers, thus removing the jump condition for both $\boldsymbol{u}$ and w. Doing so enhances the realism of the stacked layers, since a physical realization of fluid layers will have a finite sized region that interpolates between the layer properties. However, adding this transition zone moves us beyond the stacked shallow water model, and so requires analysis that falls outside shallow water theory. Hence, we do not pursue that avenue. Instead, in this chapter we remain withing the shallow water theory while acknowledging it has limitations, including jumps in the horizontal velocity across layer interfaces.

Preservation of the relative vertical position within a column

Following the approach from Section 35.2.8, we compute the vertical velocity within a layer by vertically integrating the non-divergence condition, $\nabla \cdot \boldsymbol{v} = 0$. For layer k we have

$$w^{(\mathsf{k})}(z) = w^{(\mathsf{k})}_{\mathsf{k}+1/2} - (z - \eta_{\mathsf{k}+1/2})\, \nabla \cdot \boldsymbol{u}_{\mathsf{k}}, \tag{35.95}$$

where $w^{(\mathsf{k})}(z)$ is the vertical velocity at a vertical position, z, that is located within layer k so that $\eta_{\mathsf{k}+1/2} \leq z \leq \eta_{\mathsf{k}-1/2}$. Equation (35.95) generalizes the single-layer equation (35.39), thus revealing that the vertical velocity within an arbitrary shallow water layer is a linear function of the vertical position. Now evaluate equation (35.95) at the upper interface for the layer, $z = \eta_{\mathsf{k}-1/2}$, in which case

$$w^{(\mathsf{k})}_{\mathsf{k}-1/2} = w^{(\mathsf{k})}_{\mathsf{k}+1/2} - h_{\mathsf{k}}\, \nabla \cdot \boldsymbol{u}_{\mathsf{k}}, \tag{35.96}$$

where

$$h_{\mathsf{k}} = \eta_{\mathsf{k}-1/2} - \eta_{\mathsf{k}+1/2} \tag{35.97}$$

is the layer thickness. Eliminating the horizontal convergence between equations (35.95) and (35.96) renders

$$\frac{w^{(\mathsf{k})}_{\mathsf{k}-1/2} - w^{(\mathsf{k})}_{\mathsf{k}+1/2}}{h_{\mathsf{k}}} = \frac{w^{(\mathsf{k})}(z) - w^{(\mathsf{k})}_{\mathsf{k}+1/2}}{z - \eta_{\mathsf{k}+1/2}}. \tag{35.98}$$

Making use of the kinematic boundary condition at the two interfaces allows us to write

$$w^{(\mathsf{k})}_{\mathsf{k}-1/2} = \frac{\mathrm{D}^{(\mathsf{k})}\eta_{\mathsf{k}-1/2}}{\mathrm{D}t} = (\partial_t + \boldsymbol{u}_{\mathsf{k}} \cdot \nabla)\, \eta_{\mathsf{k}-1/2} \tag{35.99a}$$

$$w^{(\mathsf{k})}_{\mathsf{k}+1/2} = \frac{\mathrm{D}^{(\mathsf{k})}\eta_{\mathsf{k}+1/2}}{\mathrm{D}t} = (\partial_t + \boldsymbol{u}_{\mathsf{k}} \cdot \nabla)\, \eta_{\mathsf{k}+1/2}, \tag{35.99b}$$

which then brings equation (35.98) to the form

$$\frac{1}{h_{\mathsf{k}}} \frac{\mathrm{D}^{(\mathsf{k})} h_{\mathsf{k}}}{\mathrm{D}t} = \frac{1}{z - \eta_{\mathsf{k}+1/2}} \frac{\mathrm{D}^{(\mathsf{k})}(z - \eta_{\mathsf{k}+1/2})}{\mathrm{D}t} \implies \frac{\mathrm{D}^{(\mathsf{k})}}{\mathrm{D}t} \left[\frac{z - \eta_{\mathsf{k}+1/2}}{h_{\mathsf{k}}} \right] = 0 \tag{35.100}$$

Just like for a single layer of shallow water fluid, vertical columns within each layer are stretched and squeezed in a manner that preserves the relative vertical position for a point within the column.

Averaged vertical velocity for a layer

Since the vertical velocity is a linear function of z within a layer, its layer averaged value is the average of the vertical velocity at the upper and lower layer interfaces. It is a useful exercise of the formalism to prove this result

$$\begin{aligned}
\overline{w}_{\mathsf{k}} &= \frac{1}{h_{\mathsf{k}}} \int_{\eta_{\mathsf{k}+1/2}}^{\eta_{\mathsf{k}-1/2}} w^{(\mathsf{k})}(z)\,\mathrm{d}z && \text{(35.101a)}\\
&= \frac{1}{h_{\mathsf{k}}} \int_{\eta_{\mathsf{k}+1/2}}^{\eta_{\mathsf{k}-1/2}} \left[w^{(\mathsf{k})}_{\mathsf{k}+1/2} - (z - \eta_{\mathsf{k}+1/2})\,\nabla\cdot\boldsymbol{u}_{\mathsf{k}} \right] \mathrm{d}z && \text{(35.101b)}\\
&= w^{(\mathsf{k})}_{\mathsf{k}+1/2} + \eta_{\mathsf{k}+1/2}\,\nabla\cdot\boldsymbol{u}_{\mathsf{k}} - 1/(2h_{\mathsf{k}})\,(\eta^2_{\mathsf{k}-1/2} - \eta^2_{\mathsf{k}+1/2})\,\nabla\cdot\boldsymbol{u}_{\mathsf{k}} && \text{(35.101c)}\\
&= w^{(\mathsf{k})}_{\mathsf{k}+1/2} - (h_{\mathsf{k}}/2)\,\nabla\cdot\boldsymbol{u}_{\mathsf{k}} && \text{(35.101d)}\\
&= (w^{(\mathsf{k})}_{\mathsf{k}+1/2} + w^{(\mathsf{k})}_{\mathsf{k}-1/2})/2, && \text{(35.101e)}
\end{aligned}$$

where the final step made use of the identity (35.96). Note that we can also write the layer averaged vertical velocity as

$$\overline{w}_{\mathsf{k}} = (w^{(\mathsf{k})}_{\mathsf{k}+1/2} + w^{(\mathsf{k})}_{\mathsf{k}-1/2})/2 = \frac{\mathrm{D}^{(\mathsf{k})}\overline{\eta}_{\mathsf{k}}}{\mathrm{D}t}, \tag{35.102}$$

where

$$\overline{\eta}_{\mathsf{k}} = (\eta_{\mathsf{k}+1/2} + \eta_{\mathsf{k}-1/2})/2 \tag{35.103}$$

is the average of the interface height for the layer.

35.4.5 Rigid lid shallow water models

Throughout this section we formulated the equations for an N-layer shallow water model where $\eta_{1/2}$ is the undulating free surface. For some applications of large-scale oceanography, it is useful to remove the external gravity waves from the model, where these gravity waves are associated with linear fluctuations of the upper free surface.[8] To remove these gravity waves we can, by fiat, set the upper ocean interface to a rigid constant, conventionally taken as $\eta_{1/2} = 0$. This assumption is known as the *rigid lid*. There is good justification for this approximation given that undulations of the free surface are far smaller than undulations of interior interfaces, as seen for the reduced gravity model in Section 35.3.

If there is no applied pressure, $p_{\mathsf{a}} = 0$, then there is no horizontal pressure gradient in the upper layer, much like an inverted reduced gravity model (see Exercise 35.5). A dynamically more interesting case arises when there is an applied pressure, $p_{\mathsf{a}} \neq 0$, so that motion is generated in layer one, which in turn induces motion throughout all layers. Indeed, as seen when studying the horizontally non-divergent barotropic model in Chapter 38, there *must* be a nonzero applied surface pressure in order to constrain the free surface to be flat and fixed. This pressure is referred to as the *lid pressure*

A rigid lid constrains the vertically integrated flow to be horizontally non-divergent. We see this property by summing the thickness equation over all of the shallow water layers

$$\partial_t \eta_{1/2} + \sum_{\mathsf{k}=1}^{N} \nabla\cdot(\boldsymbol{u}_{\mathsf{k}}\, h_{\mathsf{k}}) = 0 \quad \text{where} \quad \sum_{\mathsf{k}=1}^{N} \partial_t h_{\mathsf{k}} = \partial_t(\eta_{1/2} - \eta_{\mathsf{b}}) = \partial_t \eta_{1/2}. \tag{35.104}$$

[8] In Section 55.5 we study gravity waves in a single shallow water layer.

For the rigid lid, $\partial_t \eta_{1/2} = 0$, which then leads to the non-divergence condition

$$\sum_{\mathsf{k}=1}^{N} \nabla \cdot (\boldsymbol{u}_{\mathsf{k}} \, h_{\mathsf{k}}) = \nabla \cdot \sum_{\mathsf{k}=1}^{N} \boldsymbol{u}_{\mathsf{k}} \, h_{\mathsf{k}} = \nabla \cdot \boldsymbol{U} = 0 \quad \text{with} \quad \boldsymbol{U} = \sum_{\mathsf{k}=1}^{N} \boldsymbol{u}_{\mathsf{k}} \, h_{\mathsf{k}}. \tag{35.105}$$

Note that velocity in the upper layer remains horizontally divergent since the $\eta_{3/2}$ interface is not generally rigid. Even so, fixing $\eta_{1/2}$ to be rigid serves to remove the relatively fast external gravity waves from the stacked shallow water model. We return to the rigid lid assumption when discussing the horizontal non-divergent barotropic model in Chapter 38 (see in particular Section 38.4).

35.4.6 Comments on vanishing layers

Interior layer interfaces can intersect either the surface, referred to as *outcropping*, or the solid bottom, referred to as *incropping*. In this manner, any particular layer may only exist over a sub-region of the full horizontal domain. Treatment of such geometries is actually quite subtle when numerically discretizing the equations of motion, since it requires methods to allow for layers to vanish and appear as a function of time. The thickness weighted equations developed in this section offer one means to handle these situations. They do so by ensuring that terms properly vanish as $h \to 0$ (see the end of Section 35.6.1 for more on this point). We also considered some of the related conceptual subtleties in Section 29.9 when studying available potential energy in a continuously stratified Boussinesq ocean. *Griffies et al.* (2020) present a primer on finite volume numerical methods that support vanishing layers.

35.5 Vector-invariant velocity equation

Following the discussion in Section 24.4 for a continuously stratified fluid, we here derive the vector-invariant form of the shallow water velocity equation. This formulation proves useful in the kinetic energy budget of Section 36.6.3 and for vorticity in Section 39.1.

35.5.1 Basic manipulations

The following manipulations hold for each shallow water layer, so it is convenient to drop layer indices to reduce clutter. Start by introducing vorticity for the full velocity field

$$\begin{aligned}
\boldsymbol{\omega} &= \nabla \times \boldsymbol{v} && \text{(35.106a)} \\
&= \hat{\boldsymbol{x}} \, (\partial_y w - \partial_z v) + \hat{\boldsymbol{y}} \, (\partial_z u - \partial_x w) + \hat{\boldsymbol{z}} \, (\partial_x v - \partial_y u) && \text{(35.106b)} \\
&= \hat{\boldsymbol{x}} \, \partial_y w - \hat{\boldsymbol{y}} \, \partial_x w + \hat{\boldsymbol{z}} \, (\partial_x v - \partial_y u) && \text{(35.106c)} \\
&= -\hat{\boldsymbol{z}} \times \nabla w + \hat{\boldsymbol{z}} \, (\partial_x v - \partial_y u), && \text{(35.106d)}
\end{aligned}$$

where we set

$$\partial_z u = \partial_z v = 0, \tag{35.107}$$

which holds for the horizontal velocity within a shallow water layer. We also find it convenient to introduce the vorticity associated with the horizontal velocity field

$$\boldsymbol{\omega}^* = \nabla \times \boldsymbol{u} = -\hat{\boldsymbol{x}} \, \partial_z v + \hat{\boldsymbol{y}} \, \partial_z u + \hat{\boldsymbol{z}} \, (\partial_x v - \partial_y u) = \hat{\boldsymbol{z}} \, (\partial_x v - \partial_y u). \tag{35.108}$$

The vertical component to vorticity is particularly important for geophysical flows, in which case we write

$$\zeta = \hat{\boldsymbol{z}} \cdot \boldsymbol{\omega} = \hat{\boldsymbol{z}} \cdot \boldsymbol{\omega}^* = \partial_x v - \partial_y u. \tag{35.109}$$

The vector identity (see Section 2.3.4)

$$(\boldsymbol{u}\cdot\nabla)\,\boldsymbol{u} = (1/2)\,\nabla(\boldsymbol{u}\cdot\boldsymbol{u}) - \boldsymbol{u}\times(\nabla\times\boldsymbol{u}) = (1/2)\,\nabla(\boldsymbol{u}\cdot\boldsymbol{u}) + \boldsymbol{\omega}^*\times\boldsymbol{u} \tag{35.110}$$

brings the inviscid shallow water velocity equation (35.86)

$$\frac{\partial \boldsymbol{u}}{\partial t} + (\boldsymbol{u}\cdot\nabla)\,\boldsymbol{u} + f\hat{\boldsymbol{z}}\times\boldsymbol{u} = -\rho_{\text{ref}}^{-1}\,\nabla p \tag{35.111}$$

into its *vector invariant* form

$$\frac{\partial \boldsymbol{u}}{\partial t} + (f+\zeta)\,\hat{\boldsymbol{z}}\times\boldsymbol{u} = -\nabla\left(p/\rho_{\text{ref}} + \boldsymbol{u}\cdot\boldsymbol{u}/2\right). \tag{35.112}$$

Again, this equation holds separately for each layer, so that by reintroducing layer indices we have

$$\frac{\partial \boldsymbol{u}_{\text{k}}}{\partial t} + (f+\zeta_{\text{k}})\,\hat{\boldsymbol{z}}\times\boldsymbol{u}_{\text{k}} = -\nabla(p_{\text{k}}/\rho_{\text{ref}} + \boldsymbol{u}_{\text{k}}\cdot\boldsymbol{u}_{\text{k}}/2). \tag{35.113}$$

35.5.2 Dynamical pressure and the Magnus acceleration

As in our discussion in Section 24.4 of the vector invariant velocity equation for continuously stratified flows, the velocity equation (35.113) exposes two physical processes that lend insight into the motion in the shallow water fluid.

Dynamical pressure from kinetic energy per mass

The kinetic energy per mass, $\boldsymbol{u}\cdot\boldsymbol{u}/2$, adds a *dynamical pressure* to the mechanical pressure associated with the free surface undulations. Gradients in the kinetic energy thus drive accelerations towards regions of smaller kinetic energy; i.e., down the kinetic energy gradient.[9]

Magnus acceleration

As discussed in Sections 24.4 and 32.2.6, the Magnus acceleration is a body acceleration defined by the nonlinear term

$$\boldsymbol{A}_{\text{magnus}} = -\boldsymbol{\omega}^*\times\boldsymbol{u} = \zeta\,(\boldsymbol{u}\times\hat{\boldsymbol{z}}), \tag{35.114}$$

appearing in the vector-invariant velocity equation (35.113). There is a non-zero Magnus acceleration when a shallow water fluid column spins while it moves, with this acceleration acting to deflect the spinning column perpendicular to its trajectory. As for the example in Figure 24.1, consider a shallow water fluid column moving zonally, in which case the Magnus acceleration is

$$\boldsymbol{A}_{\text{magnus}} = u\,\zeta\,(\hat{\boldsymbol{x}}\times\hat{\boldsymbol{z}}) = -\hat{\boldsymbol{y}}\,u\,\zeta. \tag{35.115}$$

With a positive relative vorticity, $\zeta > 0$, the Magnus acceleration is directed to the right of the motion, which is in the same direction as the Coriolis acceleration in the northern hemisphere. For large-scale geophysical flows, the Magnus acceleration is sub-dominant to the Coriolis acceleration. However, the Magnus acceleration is a crucial facet of large (order unity or larger) Rossby number motions in which relative vorticity is sizable.

[9] The dynamical pressure afforded by the kinetic energy should not be confused with the shallow water dynamic pressure introduced by equation (35.88). They are distinct.

35.6 Non-conservative processes

Much of the focus on shallow water mechanics in this book concerns the inviscid and adiabatic case in which shallow water layers are immiscible and there are no frictional or boundary stresses within or between layers. Even so, we find occasion to consider the transfer of volume between layers via irreversible dia-surface fluxes, as well as momentum transfer associated with viscous friction and boundary stresses, and tracer transfer via diffusion. Such non-conservative exchanges are central to many applications of shallow water models, thus prompting us to formulate the stacked shallow water equations that include such processes. The discussion offers a vertically discrete version of the continuous isopycnal model primitive equations detailed in Chapter 66.

35.6.1 Volume transfer across layer interfaces (dia-surface transport)

Consider the case of dia-surface transfer as occurs across the ocean surface through evaporation, precipitation, and river runoff, or as occurs for interior layers in the presence of irreversible mixing processes. Let $w^{(\dot\eta)}$ measure the volume per time per horizontal area of fluid crossing the surface interface of the shallow water layer, with $w^{(\dot\eta)}$ having dimensions of length per time. As shown in Figure 35.7, we choose a sign convention so that $w^{(\dot\eta)}_{k-1/2} > 0$ means volume leaves shallow layer k through its upper interface, whereas $w^{(\dot\eta)}_{k+1/2} > 0$ means that volume enters the layer through its lower interface.

Surface kinematic boundary condition for a single shallow water layer

The kinematic boundary condition (35.36) expresses the material nature of the free surface in the absence of boundary volume flux. In the presence of a non-zero boundary flux, $w^{(\dot\eta)} \neq 0$, we follow the formulation of the kinematic boundary condition for the ocean free surface with a mass flux (equation (19.94)), which renders the boundary condition

$$\frac{\mathrm{D}(z-\eta)}{\mathrm{D}t} = w^{(\dot\eta)} \qquad \text{at } z = \eta. \tag{35.116}$$

In effect, this relation defines the surface boundary flux, and this boundary condition can be written in the equivalent form

$$\frac{\mathrm{D}\eta}{\mathrm{D}t} = w(\eta) - w^{(\dot\eta)}. \tag{35.117}$$

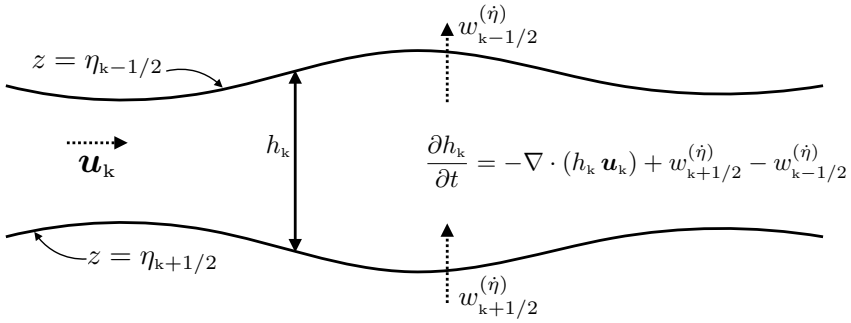

FIGURE 35.7: Dia-surface transport across the upper interface, $w^{(\dot\eta)}_{k-1/2}$, and lower interface, $w^{(\dot\eta)}_{k+1/2}$, of shallow water layer k. The sign convention is that $w^{(\dot\eta)}_{k+1/2} > 0$ for fluid entering layer k through its lower interface, and $w^{(\dot\eta)}_{k-1/2} > 0$ for fluid leaving layer k through its upper interface. The evolution of layer thickness at a horizontal position is given by equation (35.120), with a thickness time tendency due to the convergence of horizontal thickness transport within a layer, and the net transport of fluid moving across the layer interfaces.

Layer thickness equation for a single shallow water layer

Following through the derivation of the thickness equation in Section 35.2.5, we are trivially led to the following generalization in the presence of volume moving through the upper interface

$$\frac{\partial h}{\partial t} + \nabla \cdot (h\, \boldsymbol{u}) = -w^{(\dot\eta)}, \tag{35.118}$$

or equivalently

$$\frac{\mathrm{D}h}{\mathrm{D}t} = -h\, \nabla \cdot \boldsymbol{u} - w^{(\dot\eta)}. \tag{35.119}$$

As volume leaves the layer through its upper interface, $w^{(\dot\eta)} > 0$, equation (35.118) says that the layer thickness decreases, and conversely the layer thickness increases when volume is added via $w^{(\dot\eta)} < 0$.

Thickness equation for a stacked shallow water model

It is straightforward to generalize the thickness equation (35.118) to the case of a stacked shallow water model, in which

$$\frac{\partial h_{\mathrm{k}}}{\partial t} + \nabla \cdot (h_{\mathrm{k}}\, \boldsymbol{u}_{\mathrm{k}}) = -(w^{(\dot\eta)}_{\mathrm{k}-1/2} - w^{(\dot\eta)}_{\mathrm{k}+1/2}). \tag{35.120}$$

In this way, a positive volume flux coming through the lower layer interface, $w^{(\dot\eta)}_{\mathrm{k}+1/2} > 0$, leads to an increase in h_{k}, whereas a positive flux leaving through the upper interface, $w^{(\dot\eta)}_{\mathrm{k}-1/2} > 0$, decreases the layer thickness. The right hand side is written as the thickness weighted convergence of the cross-layer transport. Finally, the flux-form equation (35.120) takes on its material evolution form

$$\frac{\mathrm{D}_{\mathrm{k}} h_{\mathrm{k}}}{\mathrm{D}t} = -h_{\mathrm{k}}\, \nabla \cdot \boldsymbol{u}_{\mathrm{k}} - (w^{(\dot\eta)}_{\mathrm{k}-1/2} - w^{(\dot\eta)}_{\mathrm{k}+1/2}). \tag{35.121}$$

Evidently, the material evolution of layer thickness is affected by the convergence of the horizontal flow as well as the transfer of volume across the layer interfaces.

Vanishing layers and transfer across the top and bottom of the stacked layers

A shallow water layer can vanish at any horizontal position, so that it need not be defined for all horizontal positions in the domain. Such vanishing layers are elegantly handled by working with the thickness weighted tracer and momentum budgets, as doing so avoids dividing by a zero layer thickness when computing vertical transfer across layer interfaces. It also means that the transfer of material and momentum across the top and bottom of a stacked shallow water model occurs via the layer adjacent to these boundaries. That is, boundary fluxes are incorporated via cross-layer fluxes entering or leaving the layer that sits at the surface layer or bottom.

35.6.2 Subgrid scale advective volume tranport within layers

In the presence of subgrid scale processes, there can be an additional advective transport of volume within a layer beyond that arising from the resolved flow field, $\boldsymbol{u}$. Such *subgrid scale transport* from a velocity, $\boldsymbol{u}^{\mathrm{sgs}}_{\mathrm{k}}$, is commonly found when studying the effects of turbulent eddies on ocean and atmospheric flows, with the papers by *Gent and McWilliams* (1990) and *Gent et al.* (1995) offering the canonical ocean example (see Section 71.3 for more on this topic). For present purposes, we are not concerned with how to compute this subgrid flow. Rather, we are concerned with how to account for this flow in a manner that conserves volume, tracer, and momentum. For the thickness equation the extra transport simply represents a term added to

the resolved flow, so that the thickness equation takes on the form

$$\partial_t h_k + \nabla \cdot [(h_k \, (\boldsymbol{u}_k + \boldsymbol{u}_k^{\text{sgs}})] = -(w^{(\dot\eta)}_{k-1/2} - w^{(\dot\eta)}_{k+1/2}), \tag{35.122}$$

where $\boldsymbol{u}_k^{\text{sgs}}$ is the subgrid scale flow. Volume for the layer is conserved in the presence of $\boldsymbol{u}_k^{\text{sgs}}$ so long as $\boldsymbol{u}_k^{\text{sgs}}$ satisfies the same no-flow kinematic boundary conditions as $\boldsymbol{u}$. Bringing the subgrid scale contribution to the right hand side renders

$$\partial_t h_k + \nabla \cdot (h_k \, \boldsymbol{u}_k) = -(w^{(\dot\eta)}_{k-1/2} - w^{(\dot\eta)}_{k+1/2}) - \nabla \cdot (h_k \, \boldsymbol{u}_k^{\text{sgs}}). \tag{35.123}$$

As shown in the following sections, the presence of both the dia-surface transport and the subgrid scale along-layer transport lead to corresponding terms in the tracer and momentum equations, with such terms required for conservation of tracer and momentum.

35.6.3 Tracer equation

Tracer content is transferred into or out of layer k in the presence of a nonzero volume flux, $w^{(\dot\eta)}_{k\pm1/2} \neq 0$. Likewise, tracer is transferred within a layer due to advection by $\boldsymbol{u}_k + \boldsymbol{u}_k^{\text{sgs}}$. To formulate the tracer budget admitting such transfer, we work with the thickness weighted tracer equation so to work with an extensive quantity. Namely, the tracer content per horizontal area, $h_k \, C_k$, which satisfies a relatively straightforward budget.

Tracer equation with cross-layer transport and subgrid advection

We ensure self-consistency between the tracer equation and thickness equation (35.120) by writing the tracer budget, in the presence of cross-layer transfer and subgrid scale along-layer advection, as

$$\partial_t(h_k \, C_k) + \nabla \cdot (h_k \, C_k \, \boldsymbol{u}_k^{\text{eff}}) = -[(w^{(\dot\eta)} \, C)_{k-1/2} - (w^{(\dot\eta)} \, C)_{k+1/2}], \tag{35.124}$$

where we introduced the shorthand for the effective flow

$$\boldsymbol{u}_k^{\text{eff}} = \boldsymbol{u}_k + \boldsymbol{u}_k^{\text{sgs}}. \tag{35.125}$$

The tracer fluxes on the right hand side, $(w^{(\dot\eta)} \, C)_{k\pm1/2}$, are evaluated at the layer interfaces. Evidently, a positive flux at the lower interface, $(w^{(\dot\eta)} \, C)_{k+1/2} > 0$, contributes to an increase in the tracer content for layer k, whereas $(w^{(\dot\eta)} \, C)_{k-1/2} > 0$ signals tracer leaving through the upper interface.

To estimate the tracer concentration at the layer interface, we make use of the *upwind advective flux*. For the flux $(w^{(\dot\eta)} \, C)_{k+1/2}$, the upwind method uses C_{k+1} if $w^{(\dot\eta)}_{k+1/2} > 0$, whereas the flux uses C_k if $w^{(\dot\eta)}_{k+1/2} < 0$

$$(w^{(\dot\eta)} \, C)_{k+1/2} = w^{(\dot\eta)}_{k+1/2} \begin{cases} C_{k+1} & \text{if } w^{(\dot\eta)}_{k+1/2} > 0 \\ C_k & \text{if } w^{(\dot\eta)}_{k+1/2} < 0, \end{cases} \tag{35.126}$$

with the same approach used for other interfaces. This method ensures that integrated tracer content is conserved for the full domain, since the tracer content that enters one layer leaves an adjacent layer.

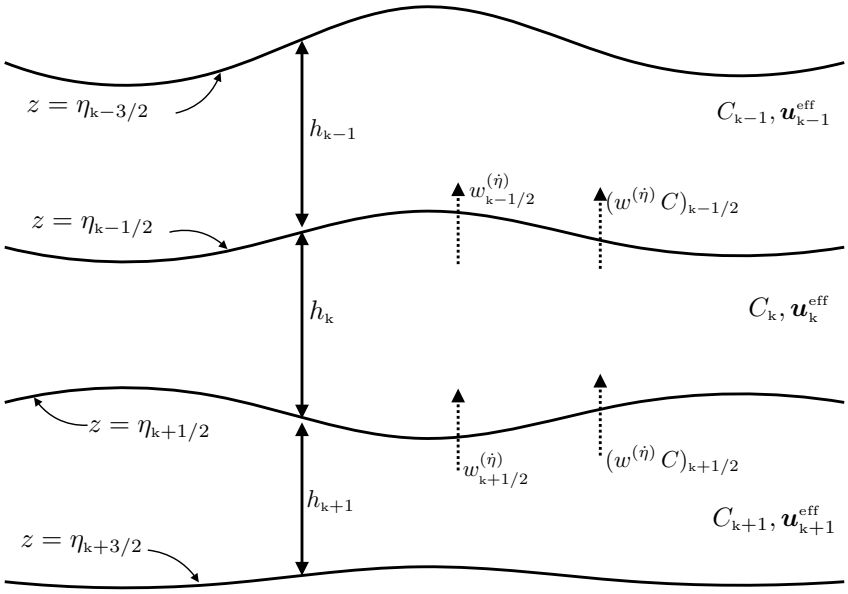

FIGURE 35.8: Depicting the tracer budget within a shallow water layer according to the thickness weighted tracer equation (35.124) and in the presence of dia-layer transport as in Figure 35.7. The cross-layer tracer fluxes, $(w^{(\dot\eta)}\, C)_{k\pm1/2}$, are computed according to an upwind method (35.126).

Consistency of the thickness weighted tracer equation and tracer concentration equation

As a consistency check, note that the thickness weighted tracer equation (35.124) reduces to the thickness equation (35.122) upon setting the tracer concentration to a space-time constant. As a second consistency check, use the product rule in equation (35.124) to have

$$C_k\,[\partial_t h_k + \nabla\cdot(h_k\,\boldsymbol{u}^{\text{eff}}_k)] + h_k\,(\partial_t C_k + \boldsymbol{u}^{\text{eff}}_k\cdot\nabla C_k) = -[(w^{(\dot\eta)}\,C)_{k-1/2} - (w^{(\dot\eta)}\,C)_{k+1/2}]. \quad (35.127)$$

Use of the thickness equation (35.122) and rearrangement renders the advective form tracer concentration equation

$$h_k\,(\partial_t + \boldsymbol{u}^{\text{eff}}_k\cdot\nabla)C_k = -\big[[(w^{(\dot\eta)}\,C)_{k-1/2} - C_k\,w^{(\dot\eta)}_{k-1/2}] - [(w^{(\dot\eta)}\,C)_{k+1/2} - C_k\,w^{(\dot\eta)}_{k+1/2}]\big]. \quad (35.128)$$

The tracer concentration equation (35.128) is self-consistent since both sides vanish when C_k is a space-time constant.

The particular case of $w^{(\dot\eta)}_{k-1/2} > 0$ and $w^{(\dot\eta)}_{k+1/2} > 0$, and use of upwind tracer fluxes (35.126), leads to the tracer concentration equation

$$h_k\,(\partial_t + \boldsymbol{u}^{\text{eff}}_k\cdot\nabla)C_k = -w^{(\dot\eta)}_{k+1/2}\,(C_k - C_{k+1}). \quad (35.129)$$

Evidently, again with $w^{(\dot\eta)}_{k+1/2} > 0$, the tracer concentration in layer k increases if $C_{k+1} > C_k$ and decreases if $C_{k+1} < C_k$. This is the expected behavior, thus further supporting self-consistency of both the thickness weighted tracer equation and the tracer concentration equation.

Including tracer diffusion

The addition of a cross-layer diffusive flux, with a kinematic diffusivity $\kappa_{cr} > 0$, and an along-layer diffusive flux, with a kinematic diffusivity $\kappa_{al} > 0$, leads to the shallow water thickness-weighted advection-diffusion equation

$$\partial_t(h_{\mathsf{k}}\, C_{\mathsf{k}}) + \nabla \cdot [h_{\mathsf{k}}\, (C_{\mathsf{k}}\, \boldsymbol{u}_{\mathsf{k}}^{\text{eff}} - \kappa_{\mathsf{al}} \nabla C_{\mathsf{k}})] \\ = -[(w^{(\dot\eta)}\, C - \kappa_{\mathsf{cr}}\, \partial_z C)_{\mathsf{k}-1/2} - (w^{(\dot\eta)}\, C - \kappa_{\mathsf{cr}}\, \partial_z C)_{\mathsf{k}+1/2}]. \quad (35.130)$$

In this equation, $(-\kappa_{\mathsf{cr}}\, \partial_z C)_{\mathsf{k}\pm 1/2}$ is the downgradient cross-layer diffusive tracer flux evaluated at the $\mathsf{k} \pm 1/2$ interface, and $-\kappa_{\mathsf{al}} \nabla C_{\mathsf{k}}$ is the downgradient along-layer diffusive flux within layer k. Both diffusivities, κ_{cr} and κ_{al}, can be functions of space and time. Finally, notice that the diffusive fluxes arise from gradients in the tracer concentration, not gradients in the thickness weighted tracer. Consequently, the presence of tracer diffusion does not affect self-consistency with the thickness equation, since the diffusive fluxes all vanish when the tracer concentration is a space-time constant.

Thickness weighted tracer equation or tracer concentration equation?

As suggested at the start of this section, the thickness weighted tracer equation offers a straightforward means to ensure that tracer content is conserved when including further physical processes, such as cross-layer transport, along-layer subgrid scale advection, and tracer diffusion. The reason is that this equation provides a budget for the tracer content per horizontal area within the shallow water layer. In contrast, tracer concentration, as an intrinsic property, does not satisfy a budget equation. We thus recommend using the thickness weighted tracer budget as the foundation for self-consistently including new physical processes. The tracer concentration is then simply diagnosed through division

$$C_{\mathsf{k}} = \frac{(h_{\mathsf{k}}\, C_{\mathsf{k}})}{h_{\mathsf{k}}}. \quad (35.131)$$

Additionally, the thickness weighted tracer equation can be converted to the tracer concentration equation through use of the product rule and the thickness equation.

35.6.4 Viscous frictional stresses acting within the layer

As discussed in Chapter 25, accelerations from friction appear in the momentum equation via the divergence of the frictional stress tensor. For a shallow water fluid we may choose to include a frictional stress proportional to lateral shears within each layer, much like the friction operators discussed in Section 25.8. The thickness weighted velocity equation (35.87) is given for a layer in the form

$$\partial_t(h_{\mathsf{k}}\, \boldsymbol{u}_{\mathsf{k}}) + \nabla \cdot (h_{\mathsf{k}}\, \boldsymbol{u}_{\mathsf{k}} \otimes \boldsymbol{u}_{\mathsf{k}}) + f\, \hat{\boldsymbol{z}} \times h_{\mathsf{k}}\, \boldsymbol{u}_{\mathsf{k}} = -(h_{\mathsf{k}}/\rho_{\mathsf{ref}})\, \nabla p_{\mathsf{k}} + h_{\mathsf{k}}\, \boldsymbol{F}_{\mathsf{k}}, \quad (35.132)$$

where $\boldsymbol{F}_{\mathsf{k}}$ is an acceleration arising from viscous friction. For a Laplacian operator arising from within-layer strains, we make use of the generalized vertical coordinate discussion in Section 63.15.2 to write

$$h_{\mathsf{k}}\, \boldsymbol{F}_{\mathsf{k}} = \nabla \cdot (h_{\mathsf{k}}\, \nu_{\mathsf{k}}\, \nabla \boldsymbol{u}_{\mathsf{k}}), \quad (35.133)$$

where $\nu_{\mathsf{k}} > 0$ is the along-layer kinematic viscosity (dimensions $\mathrm{L}^2\ \mathrm{T}^{-1}$), which can generally be a function of the flow. Notice how the thickness appears inside the divergence operator on the right hand side of equation (35.133). It accords with the treatment of along-layer tracer diffusion in equation (35.130). Like for the tracer, we note that the friction arises from shears in the velocity, not shears in the thickness weighted velocity.[10] Treatment of the Laplacian viscous

[10] Placement of thickness inside the divergence operator in equation (35.133) is consistent with the continuum treatment of generalized vertical coordinates in Section 63.15.2. As noted by *Gent* (1993), this placement of the thickness is often ignored in the shallow water literature. Instead, one often finds $\boldsymbol{F}_{\mathsf{k}} = \nabla \cdot (\nu_{\mathsf{k}} \nabla \boldsymbol{u}_{\mathsf{k}})$, which is appropriate only when the layer thickness is a constant, as for the two-dimensional non-divergent barotropic model of Chapter 38. For the shallow water model, in which thickness is generally not constant, then use of a

operator (35.133) is directly analogous to treatment of Laplacian tracer diffusion in Section 35.6.3. However, when the viscosity is a function of space, the direct analog holds only for the Cartesian coordinates used here. More general coordinates (e.g., spherical) require a distinct treatment to ensure symmetries are respected by the friction operator so to conserve angular momentum as discussed in Section 25.4. The appendix to *Griffies and Hallberg* (2000) and Part 5 of *Griffies* (2004) offer details for both the Laplacian and biharmonic friction operators.

35.6.5 Parameterized interfacial stresses

We now consider parameterized stresses at the layer interfaces. One application concerns the treatment of winds at the top of the shallow water column, and bottom friction at the interface with the solid-earth bottom. For this purpose, consider the Boussinesq form (Section 29.7.2) of the vertical stress divergence appearing in the momentum equation

$$\boldsymbol{F} = \frac{1}{\rho_o} \frac{\partial \boldsymbol{\tau}}{\partial z}, \tag{35.134}$$

where $\boldsymbol{\tau}$ is the horizontal stress vector acting on the layer interface. We discretize this stress divergence for the shallow water layer as

$$\boldsymbol{F}_{\mathsf{k}} = \frac{1}{\rho_{\mathsf{ref}}} \frac{\boldsymbol{\tau}_{\mathsf{k}-1/2} - \boldsymbol{\tau}_{\mathsf{k}+1/2}}{h_{\mathsf{k}}}. \tag{35.135}$$

In this expression, h_k is the layer thickness, $\boldsymbol{\tau}_{\mathsf{k}-1/2}$ is the stress vector acting at the upper layer interface and $\boldsymbol{\tau}_{\mathsf{k}+1/2}$ is the stress vector at the lower layer interface. Since a shallow water layer is homogeneous, the interface stress is, in effect, applied uniformly throughout the layer as a layer body stress.

Wind stress

Stress at the top interface of the top layer arises from winds, so that

$$\boldsymbol{\tau}_{k_{\mathrm{top}}} = \boldsymbol{\tau}_{\mathsf{wind}}, \tag{35.136}$$

where k_{top} is the index for the layer that sits at the top of the column at the particular horizontal position. We have $k_{\mathrm{top}} = 1$ for horizontal positions where that top layer exists. Yet it is possible for this layer to vanish, such as when a lower layer outcrops, in which case $k_{\mathrm{top}} \neq 1$. Furthermore, it is important to apply this boundary stress over a nontrivial layer thickness, which for thin upper layers can mean the boundary stress is applied to more than one layer. Doing so ensures that the boundary stress does not over-accelerate a layer that happens to be very thin.

Bottom drag

At the bottom interface of the lowest layer, $\mathsf{k} = k_{\mathrm{bot}}$, bottom drag is commonly applied as a means to include dissipation, in which case[11]

$$\boldsymbol{\tau}_{k_{\mathrm{bot}}} = \boldsymbol{\tau}_{\mathsf{bot}} = \rho_{\mathsf{ref}}\, C_{\mathsf{D}}\, |\boldsymbol{u}|_{k_{\mathrm{bot}}}\, \boldsymbol{u}_{k_{\mathrm{bot}}}, \tag{35.137}$$

where C_{D} is a dimensionless drag coefficient (typically with values on the order of 10^{-3}), and $\boldsymbol{u}_{k_{\mathrm{bot}}}$ is the velocity in the layer adjacent to the bottom. Generally we expect $k_{\mathrm{bot}} = \mathsf{K}$, yet it will differ in regions of incropping layers along the botton.

friction operator in the form $\boldsymbol{F}_{\mathsf{k}} = \nabla \cdot (\nu_{\mathsf{k}} \nabla \boldsymbol{u}_{\mathsf{k}})$ does *not* correspond to the divergence of a symmetric stress tensor (Section 25.8), and as such it is physically inconsistent.

[11] Be aware that the bottom drag coefficient, C_{D}, is distinct from tracer concentration, C_{k}.

Viscous stress

Finally, we may wish to consider a viscous stress that acts between layers and takes on the form

$$\boldsymbol{\tau}_{\mathrm{k}\pm 1/2} = -\rho_{\mathsf{ref}} \, (\mu \, \partial_z \boldsymbol{u})_{\mathrm{k}\pm 1/2}, \tag{35.138}$$

where $\mu > 0$ is a vertical kinematic viscosity (dimensions $\mathrm{L}^2 \, \mathrm{T}^{-1}$) and $(\mu \, \partial_z \boldsymbol{u})_{\mathrm{k}\pm 1/2}$ is the viscous stress evaluated at the $\mathrm{k} \pm 1/2$ interface.

35.6.6 Transfer of horizontal momentum from inter-layer volume transfer

A transfer of volume across the layer interface gives rise to a transfer of horizontal momentum. In a manner directly akin to the treatment of tracers in Section 35.6.3, we have the thickness weighted velocity equation given by

$$\begin{aligned} \partial_t(h_{\mathrm{k}} \, \boldsymbol{u}_{\mathrm{k}}) + \nabla \cdot (h_{\mathrm{k}} \, \boldsymbol{u}_{\mathrm{k}} \otimes \boldsymbol{u}_{\mathrm{k}}) + f \, \hat{\boldsymbol{z}} \times h_{\mathrm{k}} \, \boldsymbol{u}_{\mathrm{k}} &= -(h_{\mathrm{k}}/\rho_{\mathsf{ref}}) \, \nabla p_{\mathrm{k}} + \nabla \cdot (h_{\mathrm{k}} \, \nu_{\mathrm{k}} \, \nabla \boldsymbol{u}_{\mathrm{k}}) \\ &\quad - [(w^{(\dot{\eta})} \, \boldsymbol{u} - \mu \, \partial_z \boldsymbol{u})_{\mathbf{k}-1/2} - (w^{(\dot{\eta})} \, \boldsymbol{u} - \mu \, \partial_z \boldsymbol{u})_{\mathbf{k}+1/2}] + \delta_{\mathbf{k},\mathrm{k_{top}}} \, \boldsymbol{\tau}_{\mathsf{wind}} - \delta_{\mathbf{k},\mathrm{k_{bot}}} \, \boldsymbol{\tau}_{\mathsf{bot}}. \end{aligned} \tag{35.139}$$

In this equation, $(w^{(\dot{\eta})} \, \boldsymbol{u})_{\mathrm{k}+1/2}$ is the transfer of horizontal momentum across the lower layer interface, and $(w^{(\dot{\eta})} \, \boldsymbol{u})_{\mathrm{k}-1/2}$ is the transfer across the upper layer interface. To estimate the horizontal velocity at the interface, we can take an upwind approach just as for the tracers in equation (35.126)

$$(w^{(\dot{\eta})} \, \boldsymbol{u})_{\mathrm{k}+1/2} = w^{(\dot{\eta})}_{\mathrm{k}+1/2} \begin{cases} \boldsymbol{u}_{\mathrm{k}+1} & \text{if } w^{(\dot{\eta})}_{\mathrm{k}+1/2} > 0 \\ \boldsymbol{u}_{\mathrm{k}} & \text{if } w^{(\dot{\eta})}_{\mathrm{k}+1/2} < 0, \end{cases} \tag{35.140}$$

Gent (1993) notes that some realizations of the shallow water equations in the presence of $w^{(\dot{\eta})} \neq 0$ fail to incorporate the transfer of horizontal momentum between the layers present in equation (35.139). As such, these realizations are not self-consistent and thus do not correspond to a discrete realization of a continuous isopycnal model.[12]

35.6.7 Inclusion of subgrid along-layer volume transport

In Section 35.6.2, we introduced a subgrid scale advective volume tranport within layers, and then included that transport in the tracer equation in Section 35.6.3. To see how to do so for the linear momentum equation, it is sufficient to focus on the case without friction or viscosity, Unlike the thickness weighted tracer equation (35.124), here we do not have a straightforward consistency check with the thickness equation (35.122) to determine a unique form for including the effects from $\boldsymbol{u}^{\mathrm{sgs}}_{\mathrm{k}}$ into the momentum equation. We thus consider the following formulations.

Absence of $\boldsymbol{u}^{sgs}_{\mathrm{k}}$ in the thickness weighted velocity equation

In this formulation we assume there is no appearance of $\boldsymbol{u}^{\mathrm{sgs}}_{\mathrm{k}}$ in the thickness weighted velocity equation, so that

$$\begin{aligned} \partial_t(h_{\mathrm{k}} \, \boldsymbol{u}_{\mathrm{k}}) + \nabla \cdot (h_{\mathrm{k}} \, \boldsymbol{u}_{\mathrm{k}} \otimes \boldsymbol{u}_{\mathrm{k}}) + f \, \hat{\boldsymbol{z}} \times h_{\mathrm{k}} \, \boldsymbol{u}_{\mathrm{k}} &= -(h_{\mathrm{k}}/\rho_{\mathsf{ref}}) \, \nabla p_{\mathrm{k}} \\ &\quad - [(w^{(\dot{\eta})} \, \boldsymbol{u})_{\mathrm{k}-1/2} - (w^{(\dot{\eta})} \, \boldsymbol{u})_{\mathrm{k}+1/2}]. \end{aligned} \tag{35.141}$$

[12] We formulate the continuous isopycnal model equations in Chapter 66.

Use of the product rule gives

$$h_{\mathsf{k}}\left[\partial_t \boldsymbol{u}_{\mathsf{k}} + (\boldsymbol{u}_{\mathsf{k}} \cdot \nabla)\,\boldsymbol{u}_{\mathsf{k}}\right] + \boldsymbol{u}_{\mathsf{k}}\left[\partial_t h_{\mathsf{k}} + \nabla \cdot (h_{\mathsf{k}}\,\boldsymbol{u}_{\mathsf{k}})\right] + f\,\hat{\boldsymbol{z}} \times h_{\mathsf{k}}\,\boldsymbol{u}_{\mathsf{k}} = -(h_{\mathsf{k}}/\rho_{\mathsf{ref}})\,\nabla p_{\mathsf{k}} \\ - \left[(w^{(\dot{\eta})}\,\boldsymbol{u})_{\mathsf{k}-1/2} - (w^{(\dot{\eta})}\,\boldsymbol{u})_{\mathsf{k}+1/2}\right], \quad (35.142)$$

with the thickness equation (35.123) then rendering

$$h_{\mathsf{k}}\left[\partial_t \boldsymbol{u}_{\mathsf{k}} + (\boldsymbol{u}_{\mathsf{k}} \cdot \nabla)\,\boldsymbol{u}_{\mathsf{k}}\right] + f\,\hat{\boldsymbol{z}} \times h_{\mathsf{k}}\,\boldsymbol{u}_{\mathsf{k}} = -(h_{\mathsf{k}}/\rho_{\mathsf{ref}})\,\nabla p_{\mathsf{k}} \\ - \left[(w^{(\dot{\eta})}\,\boldsymbol{u})_{\mathsf{k}-1/2} - (w^{(\dot{\eta})}\,\boldsymbol{u})_{\mathsf{k}+1/2}\right] + \boldsymbol{u}_{\mathsf{k}}\left[\nabla \cdot (h_{\mathsf{k}}\,\boldsymbol{u}^{\mathrm{sgs}}_{\mathsf{k}}) + w^{(\dot{\eta})}_{\mathsf{k}-1/2} - w^{(\dot{\eta})}_{\mathsf{k}+1/2}\right]. \quad (35.143)$$

This formulation is unsatisfying since the velocity is advected by the velocity, $\boldsymbol{u}_{\mathsf{k}}$, whereas tracer is advected by $\boldsymbol{u}^{\mathrm{eff}}_{\mathsf{k}}$ as seen in equations (35.124) and (35.128).

Absence of $\boldsymbol{u}^{sgs}_{\mathsf{k}}$ in the velocity equation

As noted by *Jansen et al.* (2024), certain layered ocean models (such as MOM6 *Adcroft et al.* (2019)), are formulated with no appearance of $\boldsymbol{u}^{\mathrm{sgs}}_{\mathsf{k}}$ in the velocity equation, so that

$$h_{\mathsf{k}}\left[\partial_t \boldsymbol{u}_{\mathsf{k}} + (\boldsymbol{u}_{\mathsf{k}} \cdot \nabla)\boldsymbol{u}_{\mathsf{k}}\right] + f\,\hat{\boldsymbol{z}} \times h_{\mathsf{k}}\,\boldsymbol{u}_{\mathsf{k}} = -(h_{\mathsf{k}}/\rho_{\mathsf{ref}})\,\nabla p_{\mathsf{k}} - \left[(w^{(\dot{\eta})}\,\boldsymbol{u})_{\mathsf{k}-1/2} - (w^{(\dot{\eta})}\,\boldsymbol{u})_{\mathsf{k}+1/2}\right]. \quad (35.144)$$

Use of the product rule and thickness equation (35.123) leads to the thickness weighted velocity equation

$$\partial_t(h_{\mathsf{k}}\,\boldsymbol{u}_{\mathsf{k}}) + \nabla \cdot (h_{\mathsf{k}}\,\boldsymbol{u}_{\mathsf{k}} \otimes \boldsymbol{u}_{\mathsf{k}}) + f\,\hat{\boldsymbol{z}} \times h_{\mathsf{k}}\,\boldsymbol{u}_{\mathsf{k}} = -(h_{\mathsf{k}}/\rho_{\mathsf{ref}})\,\nabla p_{\mathsf{k}} \\ - \left[(w^{(\dot{\eta})}\,\boldsymbol{u})_{\mathsf{k}-1/2} - (w^{(\dot{\eta})}\,\boldsymbol{u})_{\mathsf{k}+1/2}\right] - \boldsymbol{u}_{\mathsf{k}}\left[\nabla \cdot (h_{\mathsf{k}}\,\boldsymbol{u}^{\mathrm{sgs}}_{\mathsf{k}}) + w^{(\dot{\eta})}_{\mathsf{k}-1/2} - w^{(\dot{\eta})}_{\mathsf{k}+1/2}\right]. \quad (35.145)$$

This equation is unsatisfying for the same reason as the velocity equation (35.143). Namely, both formulations have the advection of velocity determined by the velocity, $\boldsymbol{u}_{\mathsf{k}}$, whereas tracer is advected by $\boldsymbol{u}^{\mathrm{eff}}_{\mathsf{k}}$, as seen in equations (35.124) and (35.128).

Advection by $\boldsymbol{u}^{eff}_{\mathsf{k}}$ in the velocity equation and thickness weighted velocity equation

Next consider the case where advection occurs with $\boldsymbol{u}^{\mathrm{eff}}_{\mathsf{k}}$, just like for tracers as in equation (35.124), so that the thickness weighted velocity equation is written in the form

$$\partial_t(h_{\mathsf{k}}\,\boldsymbol{u}_{\mathsf{k}}) + \partial_i[h\,u^{\mathrm{eff}}_i\,\boldsymbol{u}]_{\mathsf{k}} + f\,\hat{\boldsymbol{z}} \times h_{\mathsf{k}}\,\boldsymbol{u}_{\mathsf{k}} = -(h_{\mathsf{k}}/\rho_{\mathsf{ref}})\,\nabla p_{\mathsf{k}} - \left[(w^{(\dot{\eta})}\,\boldsymbol{u})_{\mathsf{k}-1/2} - (w^{(\dot{\eta})}\,\boldsymbol{u})_{\mathsf{k}+1/2}\right], \quad (35.146)$$

where we exposed the Cartesian tensor index, i, on the left hand side. The thickness equation (35.122) leads to the identity

$$\partial_t(h_{\mathsf{k}}\,\boldsymbol{u}_{\mathsf{k}}) + \partial_i[h\,u^{\mathrm{eff}}_i\,\boldsymbol{u}]_{\mathsf{k}} = h_{\mathsf{k}}\left[\partial_t \boldsymbol{u}_{\mathsf{k}} + (\boldsymbol{u}^{\mathrm{eff}}_{\mathsf{k}} \cdot \nabla)\,\boldsymbol{u}_{\mathsf{k}}\right] + \boldsymbol{u}_{\mathsf{k}}\left[\partial_t h_{\mathsf{k}} + \nabla \cdot (h_{\mathsf{k}}\,\boldsymbol{u}^{\mathrm{eff}}_{\mathsf{k}})\right] \quad (35.147a)$$

$$= h_{\mathsf{k}}\left[\partial_t \boldsymbol{u}_{\mathsf{k}} + (\boldsymbol{u}^{\mathrm{eff}}_{\mathsf{k}} \cdot \nabla)\,\boldsymbol{u}_{\mathsf{k}}\right] - \boldsymbol{u}_{\mathsf{k}}\,(w^{(\dot{\eta})}_{\mathsf{k}-1/2} - w^{(\dot{\eta})}_{\mathsf{k}+1/2}), \quad (35.147b)$$

which, when inserted to equation (35.146), gives the velocity equation

$$h_{\mathsf{k}}\left[\partial_t \boldsymbol{u}_{\mathsf{k}} + (\boldsymbol{u}^{\mathrm{eff}}_{\mathsf{k}} \cdot \nabla)\,\boldsymbol{u}_{\mathsf{k}}\right] + f\,\hat{\boldsymbol{z}} \times h_{\mathsf{k}}\,\boldsymbol{u}_{\mathsf{k}} = -(h_{\mathsf{k}}/\rho_{\mathsf{ref}})\,\nabla p_{\mathsf{k}} \\ - \left[(w^{(\dot{\eta})}\,\boldsymbol{u})_{\mathsf{k}-1/2} - w^{(\dot{\eta})}_{\mathsf{k}-1/2}\,\boldsymbol{u}_{\mathsf{k}}\right] + \left[(w^{(\dot{\eta})}\,\boldsymbol{u})_{\mathsf{k}+1/2} - w^{(\dot{\eta})}_{\mathsf{k}+1/2}\,\boldsymbol{u}_{\mathsf{k}}\right]. \quad (35.148)$$

This form for the velocity equation corresponds to the tracer concentration equation (35.128), with both equations having advection determined by the effective velocity, $\boldsymbol{u}^{\mathrm{eff}}$. Rearrangement

renders the equivalent form

$$h_{\mathrm{k}}\left[\partial_t \boldsymbol{u}_{\mathrm{k}} + (\boldsymbol{u}_{\mathrm{k}}\cdot\nabla)\,\boldsymbol{u}_{\mathrm{k}}\right] + f\,\hat{\boldsymbol{z}}\times h_{\mathrm{k}}\,\boldsymbol{u}_{\mathrm{k}} = -(h_{\mathrm{k}}/\rho_{\mathrm{ref}})\,\nabla p_{\mathrm{k}} \\ - \left[(w^{(\dot\eta)}\,\boldsymbol{u})_{\mathrm{k}-1/2} - (w^{(\dot\eta)}\,\boldsymbol{u})_{\mathrm{k}+1/2}\right] + \left[w^{(\dot\eta)}_{\mathrm{k}-1/2} - w^{(\dot\eta)}_{\mathrm{k}+1/2} - h_{\mathrm{k}}\,(\boldsymbol{u}^{\mathrm{sgs}}_{\mathrm{k}}\cdot\nabla)\right]\boldsymbol{u}_{\mathrm{k}}. \quad (35.149)$$

35.6.8 Further study

Elements of the discrete stacked shallow water model formulation given in this section are considered by *Jansen et al.* (2024) for the case of a continuous vertical coordinate.

35.7 Exercises

EXERCISE 35.1: RELATIONS FOR VERTICAL VELOCITY (EXERCISE (3.2) OF *Vallis* (2006))
Show that the vertical velocity within a shallow water system is given by

$$w = \left[\frac{z-\eta_{\mathrm{b}}}{h}\right]\frac{\mathrm{D}h}{\mathrm{D}t} + \frac{\mathrm{D}\eta_{\mathrm{b}}}{\mathrm{D}t}, \quad (35.150)$$

where η_{b} is the position of the bottom topography (see Figure 35.1). Interpret the result, showing that it gives sensible answers at the top and bottom of the fluid layer.

EXERCISE 35.2: STRETCHING OF A VERTICAL COLUMN WITH LAYER VOLUME EXCHANGE
Show that if there is transport across the surface interface of a single shallow water layer, as per the thickness equation (35.118), then the column stretching equation (35.43) becomes

$$\frac{\mathrm{D}}{\mathrm{D}t}\left[\ln\left(\frac{z-\eta_b}{h}\right)\right] = \frac{w^{(\dot\eta)}}{h}. \quad (35.151)$$

Evidently, in the presence of a surface boundary volume flux, a column of shallow water fluid no longer stretches or squeezes uniformly. Instead, for $w^{(\dot\eta)} < 0$, a fluid parcel moves down within the column as more fluid is added to the top of the layer, and conversely when volume leaves the layer.

EXERCISE 35.3: DERIVING THE SHALLOW WATER TRACER EQUATION (35.47)
Show all steps needed to derive equations (35.46a)-(35.46c) and then show the steps leading to the shallow water tracer equation (35.47). Hint: use the z independence of $\boldsymbol{u}$ and $\partial_z w$ within the shallow water layer.

EXERCISE 35.4: SHALLOW WATER EQUATIONS WITH TIDES
In Chapter 34 we derive the equations for a primitive equation ocean in the presence of astronomical forcing that leads to tides. Specialize the general results from that chapter to derive the thickness and momentum equations for a single layer of shallow water fluid in the presence of astronomical tidal forcing. As in Section 34.4, assume the perturbation geopotential is vertically independent.

EXERCISE 35.5: INVERTED REDUCED GRAVITY MODEL
Derive the shallow water equations for a single moving layer of fluid of density ρ_2 above a rigid floor, with this moving layer below a stagnant fluid of density ρ_1, with $\rho_1 < \rho_2$, and with the upper stagnant layer assumed to have infinite thickness (as per the upper ocean reduced gravity model in Figure 35.4). Assume $\nabla p_{\mathrm{a}} = 0$. Discuss the constraint placed on the interface $\eta_{1/2}$ to maintain a stagnant upper layer. Show that as $\rho_1/\rho_2 \to 0$ with $\rho_{\mathrm{ref}} = \rho_2$, then the single layer

shallow water equations emerge. Make use of notation from the three-layer system shown in Figure 35.6. This model might be used to study flow in the atmosphere well above the boundary layer, or the abyssal ocean well below the pycnocline. Hint: invert the approach taken in Section 35.3 for the reduced gravity model of the upper ocean.

Chapter 36

SHALLOW WATER DYNAMICS

In this chapter we further our dynamical understanding of the shallow water fluid model. The study includes geostrophy, thermal wind (as expressed by Margules' relation), momentum budgets, form stress, kinetic energy, gravitational potential energy, available potential energy, and mechanical energy. We also develop the following case studies to exemplify the fundamentals: the steady force balance in a zonally reentrant channel, and the angular momentum dynamics of a rotating tank of shallow water fluid. We offer many details to support those aiming to become nimble with the equations describing the momentum and energy dynamics of a stacked shallow water model.

READER'S GUIDE TO THIS CHAPTER

This chapter builds from the formulations in Chapter 35 as well as the geostrophic mechanics from Chapter 31 and the pressure form stress from Chapter 28. We make use of the dynamical results in this chapter for many of the subsequent chapters. Notationally, we follow the same convention for the gradient operator noted at the start of Chapter 35.

36.1 Loose threads

- Some more interpretation of the N-layer mechanical energy equations and their connections to the continuous case.
- More schematics
- Consider adding a diabatic term to the energy budgets in Sections 36.5 and 36.6.

36.2 Geostrophic balance and thermal wind

As described in Chapter 31, geostrophic balance arises from neglecting the material time derivative in the inviscid horizontal momentum equation, which is a sensible assumption when the Rossby number is small. The resulting balance between Coriolis and pressure accelerations constitutes the geostrophic balance. We consider here the implications of geostrophy for one and two-layer shallow water systems.

36.2.1 Geostrophy for a single layer

Ignoring the applied pressure ($p_a = 0$) leads to the geostrophic balance for a single shallow water layer

$$f\,\hat{\boldsymbol{z}} \times \boldsymbol{u}_g = -g\,\nabla\eta \implies f\,\boldsymbol{u}_g = g\,\hat{\boldsymbol{z}} \times \nabla\eta, \tag{36.1}$$

or in component form

$$u_g = -\frac{g}{f}\frac{\partial\eta}{\partial y} \qquad \text{and} \qquad v_g = \frac{g}{f}\frac{\partial\eta}{\partial x}. \tag{36.2}$$

Consequently, the shallow water layer geostrophic current is balanced by the gradient of the free surface (sea level). In the northern hemisphere, where $f > 0$, geostrophic shallow water currents flow counter-clockwise around negative sea level anomalies (low pressure) and clockwise around

positive sea level anomalies (high pressure). The opposite orientation holds in the southern hemisphere, where $f < 0$. Figure 36.1 shows a schematic of geostrophic balance for a single shallow water layer.

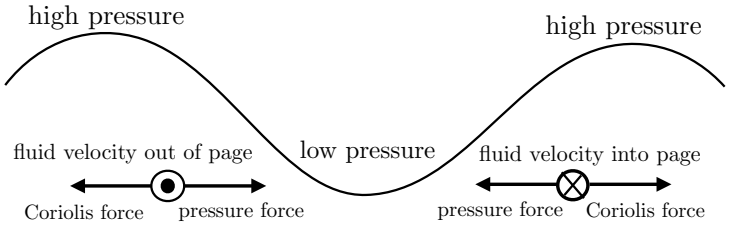

FIGURE 36.1: Side view of geostrophic balance for a single shallow water layer, here shown with two high pressure centers surrounding a low pressure center. A fluid particle path follows isolines of the free surface (constant pressure surface), with the Coriolis force balancing the pressure gradient force. In the northern hemisphere, where $f > 0$, geostrophic flow is counter-clockwise around a low pressure center and clockwise around a high pressure center, so that the Coriolis force acts to the right of the flow and it is balanced by a pressure gradient acting to the left. For the southern hemisphere, geostrophic flow is in the opposite direction since $f < 0$, so that the pressure gradient acts to the right of the flow and Coriolis to the left.

36.2.2 Margules' relation for two layers

Now consider two shallow water layers as in Figure 35.6. Recall the layer pressure equations (35.63) and (35.64), which leads to the pressure difference

$$p_1 - p_2 = g\,\eta_{3/2}\,(\rho_1 - \rho_2) + g\,z\,(\rho_2 - \rho_1) = g'_{3/2}\,\rho_{\text{ref}}\,(z - \eta_{3/2}), \tag{36.3}$$

where the reduced gravity is given by equation (35.69)

$$g'_{3/2} = g\,(\rho_2 - \rho_1)/\rho_{\text{ref}} > 0, \tag{36.4}$$

where ρ_{ref} is the shallow water Boussinesq reference density (35.67). The density difference, $\rho_2 - \rho_1$, is generally much smaller than either density, so that $g'_{3/2} \ll g$. For the Boussinesq shallow water system, the momentum equations are given by

$$\frac{\mathrm{D}^{(1)}\boldsymbol{u}_1}{\mathrm{D}t} + f\,\hat{\boldsymbol{z}} \times \boldsymbol{u}_1 = -\rho_{\text{ref}}^{-1}\,\nabla p_1 \tag{36.5a}$$

$$\frac{\mathrm{D}^{(2)}\boldsymbol{u}_2}{\mathrm{D}t} + f\,\hat{\boldsymbol{z}} \times \boldsymbol{u}_2 = -\rho_{\text{ref}}^{-1}\,\nabla p_2, \tag{36.5b}$$

where we introduced the material time derivatives for each layer (we introduced this notation in Section 35.4.4)

$$\frac{\mathrm{D}^{(\mathsf{k})}}{\mathrm{D}t} = \frac{\partial}{\partial t} + \boldsymbol{u}_{\mathsf{k}} \cdot \nabla. \tag{36.6}$$

Making use of the pressure difference (36.3) renders

$$\frac{\mathrm{D}_1\boldsymbol{u}_1}{\mathrm{D}t} - \frac{\mathrm{D}_2\boldsymbol{u}_2}{\mathrm{D}t} + f\,\hat{\boldsymbol{z}} \times \Delta\boldsymbol{u} = -\rho_{\text{ref}}^{-1}\,\nabla(p_1 - p_2) = g'_{3/2}\,\nabla\eta_{3/2}, \tag{36.7}$$

where

$$\Delta\boldsymbol{u} = \boldsymbol{u}_1 - \boldsymbol{u}_2 \tag{36.8}$$

is the vertical difference of the layer horizontal velocities. We see that the difference in the geostrophic velocities for the two layers is proportional to the slope of the interface between the

two layers

$$f\,\hat{\boldsymbol{z}} \times \Delta \boldsymbol{u}_{\mathrm{g}} = g^{r}_{3/2}\,\nabla \eta_{3/2} \Longrightarrow \Delta u_{\mathrm{g}} = +(g^{r}_{3/2}/f)\,\partial_y \eta_{3/2} \quad \text{and} \quad \Delta v_{\mathrm{g}} = -(g^{r}_{3/2}/f)\,\partial_x \eta_{3/2}. \tag{36.9}$$

These equations are known as the *Margules' relation*. It applies at any interface between two shallow water fluid layers. It says that the vertical difference between the layer geostrophic velocities is proportional to the interface slope. When the slope is large, the vertical difference in the geostrophic velocity is large. Also, the velocity difference is large when the reduced gravity is large; i.e., when the density difference is large. We illustrate this relation in Figure 36.2. The Margules relation is a discrete (two-layer) version of the thermal wind relation discussed in Section 31.6.

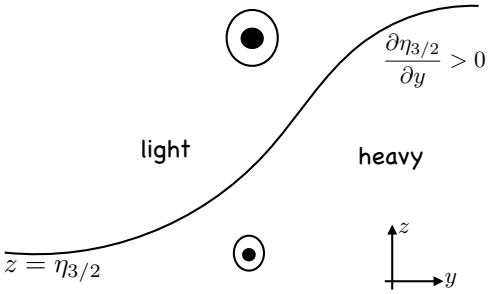

FIGURE 36.2: Illustrating Margules' relation for the northern hemisphere ($f > 0$). Here we show the interface between a two-layer shallow water model with a heavy layer to the right and a light layer to the left. The slope of the interface is positive, $\partial \eta_{3/2}/\partial y > 0$, thus leading to an increase in the eastward zonal geostrophic velocity moving upward, as depicted by the circles with a dot. This orientation corresponds to the northern hemisphere atmospheric jet stream, whereby the interface between cold/heavy air to the north and warm/light air to the south leads to a zonal thermal wind jet. This figure is directly comparable to the continuously stratified case shown in Figure 31.7.

36.2.3 Geostrophic transport within layers

We are often interested in computing the net volume transport within a layer of fluid in order to measure how much the fluid is moving across a particular region. For an N-layer shallow water fluid this transport is written

$$\boldsymbol{U} = \int \boldsymbol{u}\,\mathrm{d}z = \sum_{\mathsf{k}=1}^{N} \boldsymbol{u}_{\mathsf{k}}\,h_{\mathsf{k}}, \tag{36.10}$$

where $\boldsymbol{u}_{\mathsf{k}}$ is the layer horizontal velocity and h_{k} the layer thickness. For many purposes it is sufficient to compute the transport due to the geostrophic motion, in which case

$$\boldsymbol{u}_{\mathsf{k}} = (\rho_{\mathsf{ref}}\,f)^{-1}\,\hat{\boldsymbol{z}} \times \nabla p_{\mathsf{k}}, \tag{36.11}$$

so that the geostrophic transport is

$$\boldsymbol{U}_{\mathrm{g}} = \int_{\eta_{\mathsf{b}}}^{\eta} \boldsymbol{u}_{\mathrm{g}}\,\mathrm{d}z = (\rho_{\mathsf{ref}}\,f)^{-1}\,\hat{\boldsymbol{z}} \times \sum_{\mathsf{k}=1}^{N} h_{\mathsf{k}} \nabla p_{\mathsf{k}}. \tag{36.12}$$

For the pressure gradient we can make use of the expression (35.88)

$$\nabla p_{\mathsf{k}} = \nabla p_{\mathsf{a}} + \nabla p^{\mathrm{dyn}}_{\mathsf{k}} = \nabla p_{\mathsf{a}} + \rho_{\mathsf{ref}} \sum_{\mathsf{j}=1}^{\mathsf{k}} g^{r}_{\mathsf{j}-1/2}\,\nabla \eta_{\mathsf{j}-1/2} = \nabla p_{\mathsf{k}-1} + \rho_{\mathsf{ref}}\,g^{r}_{\mathsf{k}-1/2}\,\nabla \eta_{\mathsf{k}-1/2}, \tag{36.13}$$

thus revealing the cascade of contributions from each of the layer interfaces.

As an exercise, let us write the geostrophic transport for $N = 3$ layers, in which the layer pressure gradients are

$$\nabla p_1 = \nabla p_{\mathsf{a}} + \rho_{\mathsf{ref}}\, g\, \nabla \eta_{1/2} \tag{36.14a}$$

$$\nabla p_2 = \nabla p_1 + \rho_{\mathsf{ref}}\, g^{\mathsf{r}}_{3/2}\, \nabla \eta_{3/2} \tag{36.14b}$$

$$\nabla p_3 = \nabla p_2 + \rho_{\mathsf{ref}}\, g^{\mathsf{r}}_{5/2}\, \nabla \eta_{5/2}. \tag{36.14c}$$

We see here the utility of setting

$$\rho_{\mathsf{ref}} = \rho_1, \tag{36.15}$$

in which case the geostrophic transport within the three layers is

$$h_1\, \boldsymbol{u}_{1\mathrm{g}} = \frac{h_1}{f}\, \hat{\boldsymbol{z}} \times \nabla(g^{\mathsf{r}}_{1/2}\, \eta_{1/2}) \tag{36.16a}$$

$$h_2\, \boldsymbol{u}_{2\mathrm{g}} = \frac{h_2}{f}\, \hat{\boldsymbol{z}} \times \nabla(g^{\mathsf{r}}_{1/2}\, \eta_{1/2} + g^{\mathsf{r}}_{3/2}\, \eta_{3/2}) \tag{36.16b}$$

$$h_3\, \boldsymbol{u}_{3\mathrm{g}} = \frac{h_3}{f}\, \hat{\boldsymbol{z}} \times \nabla(g^{\mathsf{r}}_{1/2}\, \eta_{1/2} + g^{\mathsf{r}}_{3/2}\, \eta_{3/2} + g^{\mathsf{r}}_{5/2}\, \eta_{5/2}), \tag{36.16c}$$

so that the vertically integrated geostrophic transport is

$$\boldsymbol{U}_{\mathrm{g}} = f^{-1}\, \hat{\boldsymbol{z}} \times \Big[h_1 \nabla(g\, \eta) + h_2 \nabla(g\, \eta + g^{\mathsf{r}}_{3/2}\, \eta_{3/2}) + h_3 \nabla(g\, \eta + g^{\mathsf{r}}_{3/2}\, \eta_{3/2} + g^{\mathsf{r}}_{5/2}\, \eta_{5/2}) \Big]. \tag{36.17}$$

This expression for $\boldsymbol{U}_{\mathrm{g}}$ displays the cascade of contributions from each of the layer interfaces and their corresponding reduced gravities. Evidently, the geostrophic transport is directly related to the slopes for the layer interfaces, with more transport associated with larger magnitudes in the slopes as well as larger reduced gravities.

36.2.4 Flow within a geostrophic eddy

The ocean and atmosphere are highly turbulent fluids, with turbulent features extending from the small scales (millimeters) to large scales (hundreds to thousands of kilometers). The larger scale *macro-turbulent* features feel the earth's rotation and thus maintain a force balance close to geostrophic.[1] We here outline some features of an ocean *geostrophic eddy* as idealized using the reduced gravity model of Section 35.3. Figure 36.3 shows a vertical-zonal slice through the upper portion of an ocean eddy in the middle latitude northern hemisphere ($f > 0$). The central region consists of a geostrophic eddy, sometimes also referred to as an *ocean mesoscale eddy*. The signature of the eddy is a depression in the free surface height and upward deformation of the pycnocline. The lateral scale of the eddy is on the order of the internal deformation scale (see Exercise 36.10).

The ocean eddy in Figure 36.3 is an anomalously dense cyclonic mesoscale eddy with the dense water causing the pycnocline to deviate upward. If density is dominated by temperature, as it typically is within the middle to lower latitude oceans, then the eddy is a *cold core eddy*, meaning that the core of the eddy is cold. Under geostrophic balance, water circulates counter-clockwise in the northern hemisphere within the upper portion of the cold core eddy, in the region where the pressure gradient force is dominated by the free surface undulation. In this case we see say the eddy is cyclonic. According to the reduced gravity model from Section 35.3 (see in particular

[1] As noted in Section 32.6, the gradient wind balance provides a more accurate approximation to flows in ocean and atmospheric eddies by also including the centrifugal acceleration associated with the curved motion. Even so, the geostrophic balance provides a sufficient approximation for many purposes and it will be used here, along with thermal wind.

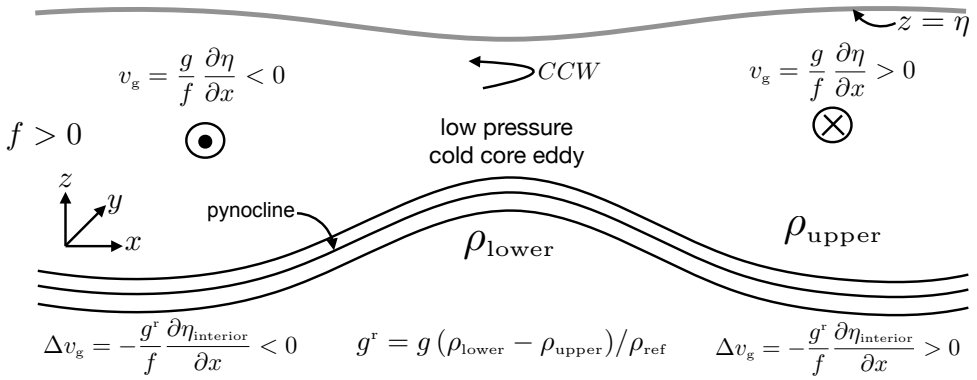

FIGURE 36.3: Vertical-zonal slice through a northern hemisphere mid-latitude cold-core ocean eddy looking from the south to the north (north is into the page). The ocean free surface is depressed down in the middle so that geostrophic flow is cyclonic (counter-clockwise in north) within the upper portion of the eddy where $\rho = \rho_{\text{upper}}$. The pycnocline (region of enhanced vertical density gradient) is deformed upward, and the baroclinic flow implied by Margules' relation (36.9) is indicated, making use of the reduced gravity $g^r = g\,(\rho_{\text{lower}} - \rho_{\text{upper}})/\rho_{\text{ref}}$. Note that $\Delta v_g = v_{\text{upper}} - v_{\text{lower}}$, so that $\Delta v_g > 0$ means that the meridional flow increases in the $+\hat{\boldsymbol{y}}$-direction when moving from the lower to upper layer, and conversely when $\Delta v_g < 0$.

Figure 35.5), the ratio of the free surface undulation to the pynocline undulation scales like the reduced gravity, so that a meter undulation of the free surface corresponds to roughly 100 m undulation of the pynocline. The same ideas hold for a *warm core eddy*, such as that depicted in Figure 36.4, with undulations complementing those in the cold core and thus supporting anti-cyclonic thermal wind flow.

In presenting the idealized rendition of an ocean eddy in Figure 36.3, we are assuming a reduced gravity model is sufficient and that the atmosphere has no significant horizontal pressure gradients over the scale of the eddy. Under these assumptions, we make use of the Margules' relation (36.9) to deduce the thermal wind flow in the upper layer relative to the layer below; i.e., the vertical shear in the geostrophic flow. For the left side of the eddy, where $\partial \eta_{\text{interior}}/\partial x > 0$, the vertical shear in the meridional geostrophic velocity is southward, consistent with orientation of the flow implied by the sea surface gradient. Conversely, on the right side of the eddy, where $\partial \eta_{\text{interior}}/\partial x < 0$, the vertical shear in the meridional flow is northward.

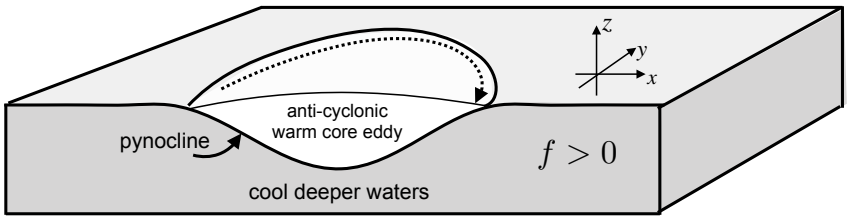

FIGURE 36.4: Schematic of a warm core (light water) geostrophic ocean eddy as idealized by a reduced gravity model. The geostrophic/thermal wind flow is anti-cyclonic within the eddy, which contrasts to the cyclonic flow for a cold core eddy as depicted in Figure 36.3. The eddy is characterized by a slight expansion of the free surface (high pressure) and a relatively larger depression of the pycnocline.

36.3 Thickness weighted momentum equation

Throughout our discussion of the shallow water model, we made use of the prognostic equation for the velocity of a layer. Here, we study the momentum equation as determined by the vertically integrated velocity within a shallow water layer. This formulation proves particularly useful

when studying forces acting on the layer, such as those from pressure contact forces (including form stresses) as well as kinetic stresses due to the fluid motion.[2]

For a shallow water model with just a single layer, the water column extends from the surface to the bottom of the layer (see Figure 36.5)

$$\int_{\eta_b}^{\eta} \boldsymbol{u}\, dz = \boldsymbol{u}\, h, \tag{36.18}$$

so that the column momentum equals to $\boldsymbol{u}\, h\, \rho\, dx\, dy$. The resulting momentum equation is written in its flux form. In Section 36.7 we illustrate the momentum budget for a zonal channel. We also show in Section 36.4.2 that the N-layer equations are isomorphic to the single layer, thus allowing for concepts developed for a single layer to be readily extended to multiple layers.

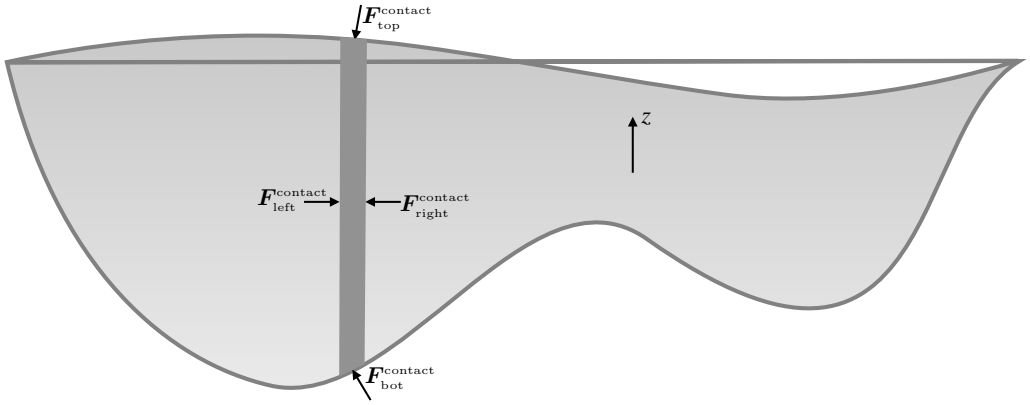

FIGURE 36.5: Momentum of a column of a single layer shallow water fluid is affected by contact forces at the column boundaries (pressure and friction), as well as body forces acting throughout the column (Coriolis and gravity).

36.3.1 Single layer equations

Recall the velocity and thickness equations written using the material time operator

$$\frac{D\boldsymbol{u}}{Dt} + f\, \hat{\boldsymbol{z}} \times \boldsymbol{u} = -g \nabla \eta \qquad \text{and} \qquad \frac{Dh}{Dt} = -h\, \nabla \cdot \boldsymbol{u}. \tag{36.19}$$

Combining these two equations allows us to write the thickness weighted material acceleration as

$$h \frac{D\boldsymbol{u}}{Dt} = h \frac{D\boldsymbol{u}}{Dt} + \boldsymbol{u} \left[\frac{Dh}{Dt} + h\, \nabla \cdot \boldsymbol{u} \right] = \partial_t (h\, \boldsymbol{u}) + \nabla \cdot [h\, \boldsymbol{u} \otimes \boldsymbol{u}], \tag{36.20}$$

so that the thickness weighted equation takes the vector form

$$\partial_t (h\, \boldsymbol{u}) + \nabla \cdot [h\, \boldsymbol{u} \otimes \boldsymbol{u}] + f\, \hat{\boldsymbol{z}} \times (h\, \boldsymbol{u}) = -g\, h\, \nabla \eta. \tag{36.21}$$

The Cartesian tensor form of the *outer product* (also called the *tensor product*) is[3]

$$[\boldsymbol{u} \otimes \boldsymbol{u}]_{mn} = u_m\, u_n \qquad \text{for } m, n = 1, 2, \tag{36.22}$$

[2] This formulation is of particular use for studies of rotating hydraulics such as pursued in the book by *Pratt and Whitehead* (2008).

[3] Equation (36.22) is the only place in this chapter where a subscript refers to a tensor label. Otherwise, subscripts refer to a shallow water layer index as in Section 36.4.2.

with $-h\,\rho\,\boldsymbol{u}\otimes\boldsymbol{u}$ the specialization to the shallow water system of the *kinetic stress* appearing in the continuously stratified momentum equation (25.61). The component form of the thickness weighted momentum equation (36.21) is

$$\partial_t(h\,u)+\partial_x(h\,u^2)+\partial_y(h\,u\,v)-v\,h\,f=-\,g\,h\,\partial_x\eta \tag{36.23a}$$
$$\partial_t(h\,v)+\partial_x(h\,u\,v)+\partial_y(h\,v^2)+u\,h\,f=-\,g\,h\,\partial_y\eta. \tag{36.23b}$$

Note that when the bottom is flat then $\nabla h=\nabla\eta$ so that

$$\partial_t(h\,u)+\partial_x(h\,u^2+g\,h^2/2)+\partial_y(h\,u\,v)-v\,h\,f=0 \tag{36.24a}$$
$$\partial_t(h\,v)+\partial_x(h\,u\,v)+\partial_y(h\,v^2+g\,h^2/2)+u\,h\,f=0. \tag{36.24b}$$

36.3.2 Geostrophic and ageostrophic contributions

Bringing the Coriolis terms to the right hand side of equations (36.23a) and (36.23b) renders

$$\partial_t(h\,u)+\partial_x(h\,u^2)+\partial_y(h\,u\,v)=h\,(-g\,\partial_x\eta+v\,f) \tag{36.25a}$$
$$\partial_t(h\,v)+\partial_x(h\,u\,v)+\partial_y(h\,v^2)+u\,h\,f=h\,(-g\,\partial_y\eta-u\,f). \tag{36.25b}$$

In the absence of rotation, the right hand side has contributions only from the thickness weighted pressure gradient. For the case of rotation it sometimes proves useful to decompose velocity into its geostrophic and ageostrophic components

$$f\,u=f\,(u_{\mathrm{a}}+u_{\mathrm{g}})=f\,u_{\mathrm{a}}-g\,\partial\eta/\partial y \tag{36.26a}$$
$$f\,v=f\,(v_{\mathrm{a}}+v_{\mathrm{g}})=f\,v_{\mathrm{a}}+g\,\partial\eta/\partial x, \tag{36.26b}$$

in which case equations (36.25a) and (36.25b) become

$$\partial_t(h\,u)+\partial_x(h\,u^2)+\partial_y(h\,u\,v)=h\,f\,v_{\mathrm{a}} \tag{36.27a}$$
$$\partial_t(h\,v)+\partial_x(h\,u\,v)+\partial_y(h\,v^2)=-h\,f\,u_{\mathrm{a}}. \tag{36.27b}$$

One should be careful *not* to take the $f=0$ limit of these equations since one might spuriously conclude there is no free surface contribution. Instead, equations (36.25a) and (36.25b) should be the basis for the $f=0$ limit.

36.3.3 Form stresses acting on a shallow water column

The kinetic stress contributes to momentum evolution in equations (36.23a) and (36.23b) via its divergence. In contrast, the pressure stress contributes as a thickness weighted pressure gradient body stress. In this subsection, and in all of Section 36.4, we formulate pressure as a contact stress, in which case it also contributes to momentum evolution as a divergence. In so doing, we provide a flux-form conservation law for momentum that supports analysis and interpretation.

Reintroducing atmospheric pressure to symmetrize the forces acting on the layer

To expose both the surface and bottom form stresses, we reintroduce the atmospheric pressure, p_{a}, and thus make use of the effective sea level (35.4)

$$\eta^{\mathrm{eff}}=\eta+p_{\mathrm{a}}/(\rho\,g)=\eta_{\mathrm{b}}+h+p_{\mathrm{a}}/(\rho\,g), \tag{36.28}$$

with the corresponding thickness weighted horizontal momentum equation

$$\partial_t(h\,\boldsymbol{u})+\nabla\cdot[h\,\boldsymbol{u}\otimes\boldsymbol{u}]+f\,\hat{\boldsymbol{z}}\times(h\,\boldsymbol{u})=-g\,h\,\nabla\eta^{\mathrm{eff}}. \tag{36.29}$$

Exposing the contact pressure stresses

The free surface height equals $\eta = \eta_\mathsf{b} + h$, in which case the momentum equation (36.29) is

$$\partial_t(h\,\boldsymbol{u}) + \nabla\cdot[h\,\boldsymbol{u}\otimes\boldsymbol{u}] + f\,\hat{\boldsymbol{z}}\times(h\,\boldsymbol{u}) = -(g/2)\nabla h^2 - g\,h\,\nabla[\eta_\mathsf{b} + p_\mathsf{a}/(\rho\,g)]. \tag{36.30}$$

To help interpret this equation it is convenient to write the boundary terms on the right hand side as

$$\begin{aligned} -g\,h\,\nabla[\eta_\mathsf{b} + p_\mathsf{a}/(\rho\,g)] &= -\nabla(h\,p_\mathsf{a}/\rho) + (p_\mathsf{a}/\rho)\,\nabla(\eta-\eta_\mathsf{b}) - g\,h\,\nabla\eta_\mathsf{b} && \text{(36.31a)}\\ &= -\nabla(h\,p_\mathsf{a}/\rho) + (p_\mathsf{a}/\rho)\,\nabla\eta - (g\,h + p_\mathsf{a}/\rho)\,\nabla\eta_\mathsf{b} && \text{(36.31b)}\\ &= -\nabla(h\,p_\mathsf{a}/\rho) + \rho^{-1}\,(p_\mathsf{a}\nabla\eta - p_\mathsf{b}\nabla\eta_\mathsf{b}), && \text{(36.31c)} \end{aligned}$$

so that

$$-(g/2)\nabla h^2 - g\,h\,\nabla[\eta_\mathsf{b} + p_\mathsf{a}/(\rho\,g)] = -\nabla[(g/2)\,h^2 + h\,p_\mathsf{a}/\rho] + \rho^{-1}\,(p_\mathsf{a}\nabla\eta - p_\mathsf{b}\nabla\eta_\mathsf{b}). \tag{36.32}$$

The first term on the right hand side is the gradient of the layer integrated hydrostatic pressure

$$P \equiv \int_{\eta_\mathsf{b}}^{\eta} [p_\mathsf{a} + \rho\,g\,(\eta - z)]\,\mathrm{d}z = h\,(\rho\,g\,h/2 + p_\mathsf{a}), \tag{36.33}$$

and the second term exposes the form stresses acting at the surface and bottom of the layer. With these expressions, the horizontal thickness weighted momentum equation (36.30) becomes

$$\frac{\partial(h\,\boldsymbol{u})}{\partial t} + \nabla\cdot[h\,\boldsymbol{u}\otimes\boldsymbol{u} + \mathbb{I}\,P/\rho] + f\,\hat{\boldsymbol{z}}\times(h\,\boldsymbol{u}) = (p_\mathsf{a}\nabla\eta - p_\mathsf{b}\nabla\eta_\mathsf{b})/\rho, \tag{36.34}$$

where $\mathbb{I}$ is the unit tensor. Exposing the zonal and meridional components renders

$$\begin{aligned} \partial_t(h\,u) + \partial_x(h\,u^2 + P/\rho) + \partial_y(h\,u\,v) - v\,h\,f &= (p_\mathsf{a}\,\partial_x\eta - p_\mathsf{b}\,\partial_x\eta_\mathsf{b})/\rho && \text{(36.35a)}\\ \partial_t(h\,v) + \partial_x(h\,u\,v) + \partial_y(h\,v^2 + P/\rho) + u\,h\,f &= (p_\mathsf{a}\,\partial_y\eta - p_\mathsf{b}\,\partial_y\eta_\mathsf{b})/\rho. && \text{(36.35b)} \end{aligned}$$

The horizontal pressure gradient appears as a continuous operator since we assumed an infinitesimal horizontal cross-sectional area for the fluid column. In contrast, the pressure form stresses appear as a vertical finite difference across the layer interfaces, which results since we are integrating over the thickness of a finite layer. Furthermore, note how the vertically integrated pressure contributions appear in a flux-form, which contrasts to the body force version that appears as thickness weighted pressure gradient.

Kinetic stresses and contact pressure stresses combined into a momentum flux

To anticipate the thickness weighted momentum equation for the stacked shallow water model in Section 36.4, write the finite difference of the form stresses as

$$p_\mathsf{a}\nabla\eta - p_\mathsf{b}\nabla\eta_\mathsf{b} = p_{1/2}\nabla\eta_{1/2} - p_{3/2}\nabla\eta_{3/2} \equiv \delta_\mathsf{k}(p_{\mathsf{k}-1/2}\nabla\eta_{\mathsf{k}-1/2}). \tag{36.36}$$

We here introduced the layer interface difference operator

$$\delta_\mathsf{k}(\Psi_{\mathsf{k}-1/2}) = \Psi_{\mathsf{k}-1/2} - \Psi_{\mathsf{k}+1/2} = -(\Psi_{\mathsf{k}+1/2} - \Psi_{\mathsf{k}-1/2}), \tag{36.37}$$

with the backward difference motivated since k increases downward whereas $\hat{\boldsymbol{z}}$ points upward. In the following, we choose to define the difference operator to only act on interface fields. Hence,

any layer quantity, such as the layer thickness, commutes with the interface operator

$$\delta_{\mathrm{k}}(h\, A_{\mathrm{k}-1/2}) = h\, (A_{\mathrm{k}-1/2} - A_{\mathrm{k}+1/2}). \tag{36.38}$$

Also note that the thickness itself is the difference between the layer interfaces

$$h = \eta - \eta_{\mathrm{b}} = \delta_{\mathrm{k}} \eta_{\mathrm{k}-1/2}, \tag{36.39}$$

where $\eta_{1/2} = \eta$ and $\eta_{3/2} = \eta_{\mathrm{b}}$.

With the above notation, the component momentum equations (36.35a) and (36.35b) take on the matrix-vector form

$$\begin{bmatrix} \partial_t(h\,u) - h\,f\,v \\ \partial_t(h\,v) + h\,f\,u \end{bmatrix} = -\begin{bmatrix} \partial_x & \partial_y & h^{-1}\,\delta_{\mathrm{k}} \end{bmatrix} \begin{bmatrix} D_1^{(\mathrm{u})} & D_1^{(\mathrm{v})} & 0 \\ D_2^{(\mathrm{u})} & D_2^{(\mathrm{v})} & 0 \\ D_3^{(\mathrm{u})} & D_3^{(\mathrm{v})} & 0 \end{bmatrix}. \tag{36.40}$$

The 3×3 matrix is a second order tensor with the first and second columns consisting of the layer thickness weighted momentum fluxes

$$\rho\, \boldsymbol{D}^{(\mathrm{u})} = (\rho\, h\, u^2 + P)\, \hat{\boldsymbol{x}} + \rho\, h\, u\, v\, \hat{\boldsymbol{y}} - p_{\mathrm{k}-1/2}\, \partial_x \eta_{\mathrm{k}-1/2}\, h\, \hat{\boldsymbol{z}} \tag{36.41a}$$

$$\rho\, \boldsymbol{D}^{(\mathrm{v})} = \rho\, h\, u\, v\, \hat{\boldsymbol{x}} + (\rho\, h\, v^2 + P)\, \hat{\boldsymbol{y}} - p_{\mathrm{k}-1/2}\, \partial_y \eta_{\mathrm{k}-1/2}\, h\, \hat{\boldsymbol{z}}, \tag{36.41b}$$

where we suppressed unnecessary layer indices. The horizontal flux components are given by minus the thickness weighted kinetic stress, $\rho\, h\, \boldsymbol{u} \otimes \boldsymbol{u}$, plus the vertically integrated contact pressure acting on the vertical sides of the shallow water column. The vertical flux component contains the pressure form stresses acting on the top and bottom interfaces, with these interfacial form stresses leading to the vertical transfer of horizontal form stresses across the layer boundaries. These fluxes allow us to write the thickness weighted zonal and meridional momentum equations as

$$\partial_t(h\,u) - v\, h\, f = -(\hat{\boldsymbol{x}}\, \partial_x + \hat{\boldsymbol{y}}\, \partial_y + \hat{\boldsymbol{z}}\, h^{-1} \delta_{\mathrm{k}}) \cdot \boldsymbol{D}^{(\mathrm{u})} \tag{36.42a}$$

$$\partial_t(h\,v) + u\, h\, f = -(\hat{\boldsymbol{x}}\, \partial_x + \hat{\boldsymbol{y}}\, \partial_y + \hat{\boldsymbol{z}}\, h^{-1} \delta_{\mathrm{k}}) \cdot \boldsymbol{D}^{(\mathrm{v})}. \tag{36.42b}$$

In this form of the momentum equation, contributions from contact stresses (kinetic stresses and form stresses) appear as the convergence of these stresses. Note that the divergence operator is built as combination of the continuous horizontal gradient operator along with a finite difference vertical operator. The third column of the tensor (36.40) is identically zero and so it can be readily dropped. However, we include it to connect with the *Eliassen-Palm flux tensor* as detailed by *Maddison and Marshall* (2013). We return to equations (36.42a) and (36.42b) in Section 36.4.9 for the stacked shallow water model.

36.3.4 Comments on the two pressure force formulations

The momentum equations (36.42a) and (36.42b) are written as a flux-form conservation law, with only the Coriolis force appearing as a body force. This formulation follows that for Cauchy's equation of motion as discussed in Section 24.2.3. We make use of these flux-form momentum equations in Section 36.7 when discussing force balances in a zonally periodic channel, as well as in Chapter 67 when formulating the thickness weighted averaged shallow water equations. Before doing so, we focus in Section 36.4 by further unpacking the contact force version of pressure as it appears in the shallow water model.

What has been gained by writing the momentum equation as the thickness weighted forms (36.42a) and (36.42b) versus the non-flux form velocity equation (36.19)? Indeed, the thickness

weighted formulation is arguably less elegant and takes more effort to derive. A key reason we consider the thickness weighted equations is that they provide a venue to study how pressure contact forces alter momentum of a shallow water fluid column through interactions with the bottom, the surface, and adjacent vertical columns. We put this perspective to use in Section 36.7 when studying the force balances on a zonally reentrant channel. Additionally, in Section 36.4 we further pursue the contact force perspective by studying how pressure form stresses appear within a stacked shallow water model.

36.4 Contact pressure forces in shallow water layers

For a finite region of fluid, if the boundary area integrated contact pressure stress is nonzero, then pressure accelerates the region. In this section we study the physics and maths of contact pressure forces as they appear in the stacked shallow water model. As revealed by this study, the columnar motion of the shallow water fluid is fundamental to the analysis. Namely, the contact pressure approach is realized by studying the thickness weighted velocity equations of motion, which determine evolution of the momentum per horizontal area of a shallow water fluid column. We introduced the thickness weighted approach in Section 36.3 for a single shallow water layer, and it led to the flux-form momentum equations (36.42a) and (36.42b). The single layer results are reproduced here for the stacked shallow water model, yet only after furthering our understanding of how pressure forces act to move momentum through shallow water layers.

36.4.1 Pressure contact force and pressure body force

As discussed in Section 25.2.3, the connection between the body force and contact force expressions of the pressure force arise through an application of Gauss's divergence theorem to scalar fields (see Section 2.7.2)

$$\boldsymbol{F}^{\text{press}}_{\mathcal{R}} = -\int_{\mathcal{R}} \nabla p \, \mathrm{d}V = -\oint_{\partial\mathcal{R}} p \, \hat{\boldsymbol{n}} \, \mathrm{d}\mathcal{S}. \tag{36.43}$$

The first expression on the right hand side is a volume integral of the pressure gradient over the fluid region, $\mathcal{R}$. This expression provides the body force version of the pressure force. The second expression is a surface area integral over the region boundary, $\partial\mathcal{R}$, whose outward normal is $\hat{\boldsymbol{n}}$. This second expression provides the contact force version of the pressure force. Neither expression is more or less fundamental. Instead, they offer complementary insights into how pressure acts to modify the momentum of a fluid, with general notions of this complementarity the topic of Chapter 28. We here pursue the contact force perspective as a means to understand the *pressure form stress* or *interfacial form stress* acting between layers of a shallow water fluid. There is also a pressure form stress acting between a fluid layer and the solid earth (topographic form stress), as well as between a fluid layer and the overlying atmosphere when the atmosphere has a non-zero mass (atmosphere form stress).

36.4.2 N-layer equations

We start this section with the N-layer shallow water thickness and velocity equations derived in Section 35.4.2

$$\frac{\partial h_{\mathsf{k}}}{\partial t} + \nabla \cdot (h_{\mathsf{k}} \, \boldsymbol{u}_{\mathsf{k}}) = 0 \quad \text{and} \quad [\partial_t + (\boldsymbol{u}_{\mathsf{k}} \cdot \nabla)]\boldsymbol{u}_{\mathsf{k}} + f \, \hat{\boldsymbol{z}} \times \boldsymbol{u}_{\mathsf{k}} = -(1/\rho_{\mathsf{ref}}) \, \nabla p_{\mathsf{k}}, \tag{36.44}$$

where $\mathsf{k} = 1, N$ is the layer index with no implied summation over this index, ρ_{ref} is the Boussinesq reference density (often chosen as $\rho_{\mathsf{ref}} = \rho_1$), and equation (35.82) gives the horizontal pressure gradient acceleration. Equations (36.44) are isomorphic to the single layer equations considered

in Section 36.3.1. Hence, the thickness weighted velocity equation is a simple generalization of the single layer equation (36.21)

$$\frac{\partial(h_{\mathsf{k}}\,\boldsymbol{u}_{\mathsf{k}})}{\partial t} + \nabla\cdot[h_{\mathsf{k}}\,\boldsymbol{u}_{\mathsf{k}}\otimes\boldsymbol{u}_{\mathsf{k}}] + f\,\hat{\boldsymbol{z}}\times(h_{\mathsf{k}}\,\boldsymbol{u}_{\mathsf{k}}) = -(h_{\mathsf{k}}/\rho_{\mathsf{ref}})\,\nabla p_{\mathsf{k}}, \tag{36.45}$$

where, again, there is no implied summation over the layer index, k. We commonly refer to the thickness weighted equation (36.45) as the momentum equation since $\rho\,\mathrm{d}x\,\mathrm{d}y\,h_{\mathsf{k}}\,\boldsymbol{u}_{\mathsf{k}}$ is the horizontal momentum of a shallow water fluid column,

36.4.3 Contact pressure force along vertical sides

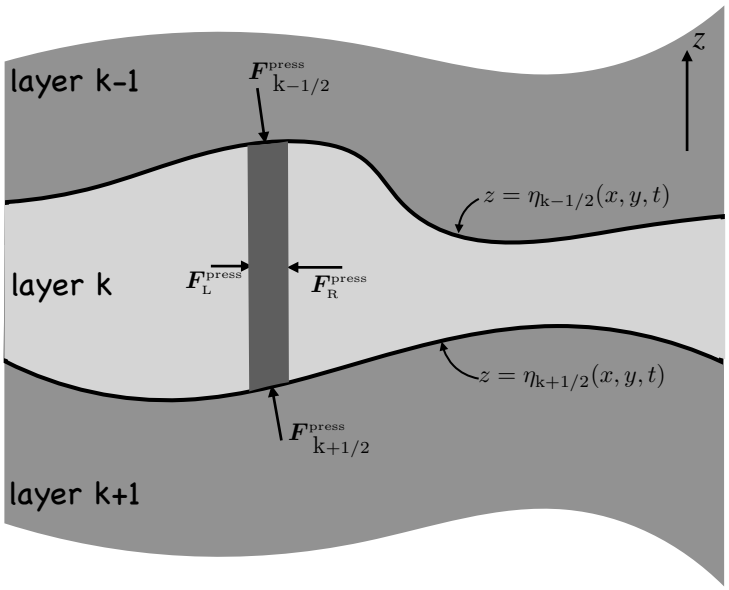

FIGURE 36.6: A schematic of the contact pressure force per area acting on the boundaries of a vertical column region within a shallow water layer of density ρ_{k}. Since fluid moves as vertical columns in a shallow water layer, we focus on the pressure forces acting on this column. The horizontal cross-sectional area of the column is vertically independent. The interface at the lower boundary is at the vertical position $z=\eta_{\mathsf{k}+1/2}$, and the upper interface is at $z=\eta_{\mathsf{k}-1/2}$. In accordance with Newton's third law, pressures are continuous across each of the $\eta_{\mathsf{k}\pm1/2}$ layer interfaces so that the pressure forces are equal in magnitude yet oppositely directed on the opposite sides to the interfaces. The layer thickness is the difference between the interface positions, $h_{\mathsf{k}}=\eta_{\mathsf{k}-1/2}-\eta_{\mathsf{k}+1/2}$. The boundaries of the columnar region feel a contact pressure force from the surrounding fluid that acts inward. The left side of the column experiences a pressure p_L; the right side experiences p_R; the upper interface has a pressure $p_{\mathsf{k}-1/2}$ acting between the layer $\mathsf{k}-1$ and layer k, and the lower interface has a pressure $p_{\mathsf{k}+1/2}$ acting between the layer $\mathsf{k}+1$ and layer k. The net pressure force acting on the column is computed as the area integral of the pressure acting around the full extent of the column boundaries. The horizontal components of the stress are known as *interfacial form stresses*. This figure is identical to Figure 28.5 used to discuss the general notions of pressure form stress.

We now build up our understanding of pressure form stresses acting in a stacked shallow water fluid, with the essence of this discussion following that encountered for the single layer in Section 36.3.3. Our interest concerns the pressure acting on the boundaries of a fluid column within a shallow water layer, such as shown in Figure 36.6.

The pressure at a vertical position within the shallow water layer-k is given by

$$p_{\mathsf{k}}(z) = \rho_{\mathsf{k}}\,g\,(\eta_{\mathsf{k}-1/2}-z) + p_{\mathsf{k}-1/2}. \tag{36.46}$$

Integrating this pressure over the layer thickness yields

$$P_{\mathsf{k}} \equiv \int_{\eta_{\mathsf{k}+1/2}}^{\eta_{\mathsf{k}-1/2}} p_{\mathsf{k}}(z)\,\mathrm{d}z \tag{36.47a}$$

$$= g\,\rho_{\mathsf{k}}\left[\eta_{\mathsf{k}-1/2}\,h_{\mathsf{k}} - (1/2)\,(\eta_{\mathsf{k}-1/2}^2 - \eta_{\mathsf{k}+1/2}^2)\right] + p_{\mathsf{k}-1/2}\,h_{\mathsf{k}} \tag{36.47b}$$

$$= h_{\mathsf{k}}\,(g\,\rho_{\mathsf{k}}\,h_{\mathsf{k}}/2 + p_{\mathsf{k}-1/2}). \tag{36.47c}$$

Since pressure is a linear function of z within a layer, the vertically averaged hydrostatic pressure within a layer, $P_{\mathsf{k}}/h_{\mathsf{k}}$, equals to the pressure at the upper interface, $p_{\mathsf{k}-1/2}$, plus one-half the weight per area of the layer, $g\,\rho_{\mathsf{k}}\,h_{\mathsf{k}}/2$.

The zonal pressure force acting on the column sides is the difference between the pressure integrated across the left and right zonal faces of the column. Assuming the fluid column to have an infinitesimal horizontal cross-sectional area $\mathrm{d}x\,\mathrm{d}y$, we find the zonal pressure force is given by

$$\mathrm{d}y \int_{\eta_{\mathsf{k}+1/2}}^{\eta_{\mathsf{k}-1/2}} (p_L - p_R)\,\mathrm{d}z = -\mathrm{d}x\,\mathrm{d}y\,\left[(g/2)\,\rho_{\mathsf{k}}\,\frac{\partial h_{\mathsf{k}}^2}{\partial x} + \frac{\partial (h_{\mathsf{k}}\,p_{\mathsf{k}-1/2})}{\partial x}\right] \tag{36.48a}$$

$$= -\mathrm{d}x\,\mathrm{d}y\,\partial_x\left[(g/2)\,\rho_{\mathsf{k}}\,h_{\mathsf{k}}^2 + h_{\mathsf{k}}\,p_{\mathsf{k}-1/2}\right] \tag{36.48b}$$

$$= -\mathrm{d}x\,\mathrm{d}y\,\partial_x P_{\mathsf{k}}. \tag{36.48c}$$

The analogous result holds for the meridional direction, thus rendering the net contact pressure force acting on the vertical sides of the column

$$\boldsymbol{F}_{\text{sides}}^{\text{press}} = -\mathrm{d}x\,\mathrm{d}y\,\nabla P_{\mathsf{k}}. \tag{36.49}$$

Hence, the contact force on the vertical sides of the column is given by the gradient of the layer vertically integrated pressure, with the vertical integral given by equation (36.47c). It is notable that this semi-discrete exercise reveals no more information than already contained within the integral theorem (36.43). Nonetheless, it is useful to see how the integral theorem manifests within discrete shallow water layers.

36.4.4 Contact pressure force along the top and bottom interfaces

Now consider the contact pressure force acting on the top interface. This interface is generally sloped, so that the contact force has a component in both the vertical and horizontal directions. The vertical component to the pressure force maintains hydrostatic balance with the contact pressure at the lower boundary interface. The horizontal component provides a horizontal acceleration, with this acceleration (sign and magnitude) determined by the slope of the interface. Following our discussion in Section 28.3, we term the horizontal pressure acting on the sloped interface the *interfacial form stress*.

To mathematically characterize the pressure force on the top interface, $z = \eta_{\mathsf{k}-1/2}$, requires the outward normal

$$\hat{\boldsymbol{n}}_{\mathsf{k}-1/2} = \frac{\nabla\,(z - \eta_{\mathsf{k}-1/2})}{|\nabla\,(z - \eta_{\mathsf{k}-1/2})|} = \frac{\hat{\boldsymbol{z}} - \nabla\eta_{\mathsf{k}-1/2}}{\sqrt{1 + (\nabla\eta_{\mathsf{k}-1/2})^2}}. \tag{36.50}$$

Temporarily assume the interface slope to have a zero projection in the $\hat{\boldsymbol{y}}$ direction. In this case,

the outward normal is

$$\hat{\boldsymbol{n}}_{\mathsf{k}-1/2} = \frac{\hat{\boldsymbol{z}} - \hat{\boldsymbol{x}}\, \partial_x \eta_{\mathsf{k}-1/2}}{\sqrt{1 + (\partial_x \eta_{\mathsf{k}-1/2})^2}} \tag{36.51a}$$

$$= \frac{\hat{\boldsymbol{z}} - \hat{\boldsymbol{x}}\, \tan\varphi_{\mathsf{k}-1/2}}{\sqrt{1 + \tan^2 \varphi_{\mathsf{k}-1/2}}} \tag{36.51b}$$

$$= (\hat{\boldsymbol{z}} - \hat{\boldsymbol{x}}\, \tan\varphi_{\mathsf{k}-1/2}) \cos\varphi_{\mathsf{k}-1/2}, \tag{36.51c}$$

where we defined the interface slope as

$$\frac{\partial \eta_{\mathsf{k}-1/2}}{\partial x} = \tan\varphi_{\mathsf{k}-1/2}, \tag{36.52}$$

with $\varphi_{\mathsf{k}-1/2}$ the angle between the horizontal plane and the interface. Trigonometry leads to an expression for the area of the top of the column[4]

$$\mathrm{d}\mathcal{S}_{\mathsf{k}-1/2} = \frac{\mathrm{d}x\, \mathrm{d}y}{\cos\varphi_{\mathsf{k}-1/2}}, \tag{36.53}$$

so that the product of the area and the outward normal is given by

$$\hat{\boldsymbol{n}}_{\mathsf{k}-1/2}\, \mathrm{d}\mathcal{S}_{\mathsf{k}-1/2} = \mathrm{d}x\, \mathrm{d}y\, (\hat{\boldsymbol{z}} - \hat{\boldsymbol{x}}\, \partial_x \eta_{\mathsf{k}-1/2}). \tag{36.54}$$

This result generalizes to an interface slope that projects into both horizontal directions

$$\hat{\boldsymbol{n}}_{\mathsf{k}-1/2}\, \mathrm{d}\mathcal{S}_{\mathsf{k}-1/2} = \mathrm{d}x\, \mathrm{d}y\, (\hat{\boldsymbol{z}} - \nabla \eta_{\mathsf{k}-1/2}), \tag{36.55}$$

so that the contact pressure force acting on layer-k at its top interface is given by

$$\boldsymbol{F}^{\text{press}}_{\text{top}} = -\mathrm{d}x\, \mathrm{d}y\, (\hat{\boldsymbol{z}} - \nabla \eta_{\mathsf{k}-1/2})\, p_{\mathsf{k}-1/2}. \tag{36.56}$$

Analogous considerations lead to the contact pressure force acting on layer-k at the bottom of the column

$$\boldsymbol{F}^{\text{press}}_{\text{bot}} = \mathrm{d}x\, \mathrm{d}y\, (\hat{\boldsymbol{z}} - \nabla \eta_{\mathsf{k}+1/2})\, p_{\mathsf{k}+1/2}. \tag{36.57}$$

36.4.5 Form stress

As noted earlier, form stress is the horizontal projection of the contact pressure acting on the sloped top or bottom interface of the fluid column (Chapter 28). The corresponding forces acting on layer-k is the horizontal area element multiplied by the form stress

$$\boldsymbol{F}^{\text{form stress}}_{\text{top face}} = \mathrm{d}x\, \mathrm{d}y\, (p_{\mathsf{k}-1/2} \nabla \eta_{\mathsf{k}-1/2}) \tag{36.58}$$

$$\boldsymbol{F}^{\text{form stress}}_{\text{bot face}} = -\mathrm{d}x\, \mathrm{d}y\, (p_{\mathsf{k}+1/2} \nabla \eta_{\mathsf{k}+1/2}). \tag{36.59}$$

These forces render a mechanically reversible vertical exchange of horizontal momentum. This momentum exchange occurs without any exchange of matter. Rather, it an inviscid exchange that occurs according to Newton's third law (the action/reaction law).

For a specific case, consider a $\mathsf{k} - 1/2$ interface that slopes upward in the $\hat{\boldsymbol{x}}$ direction (e.g., see Figure 36.6). Form stress acting at the interface provides a $+\hat{\boldsymbol{x}}$ directed acceleration on the column. For the $\mathsf{k} + 1/2$ interface, a negatively sloped interface also experiences a $+\hat{\boldsymbol{x}}$ directed

[4] Equation (36.53) was also found in Section 19.6.3 when developing the kinematic boundary condition for a material interface.

acceleration.

36.4.6 Net contact pressure force on a shallow water column

Summing the contact pressure forces (36.49), (36.56), and (36.57), and dividing by the horizontal area, leads to the net pressure force per horizontal area acting on a column within layer-k

$$\frac{\boldsymbol{F}^{\text{press}}_{\text{net},\mathsf{k}}}{\mathrm{d}x\,\mathrm{d}y} = -\nabla P_{\mathsf{k}} - (\hat{\boldsymbol{z}} - \nabla\eta_{\mathsf{k}-1/2})\, p_{\mathsf{k}-1/2} + (\hat{\boldsymbol{z}} - \nabla\eta_{\mathsf{k}+1/2})\, p_{\mathsf{k}+1/2} \tag{36.60a}$$

$$= \rho_{\mathsf{k}}\, g\, h_k\, \hat{\boldsymbol{z}} - \nabla P_{\mathsf{k}} + p_{\mathsf{k}-1/2}\nabla\eta_{\mathsf{k}-1/2} - p_{\mathsf{k}+1/2}\nabla\eta_{\mathsf{k}+1/2}. \tag{36.60b}$$

To reach this result we made use of the hydrostatic relation for the vertical pressure difference across a layer

$$p_{\mathsf{k}+1/2} - p_{\mathsf{k}-1/2} = \rho_{\mathsf{k}}\, g\, h_{\mathsf{k}}. \tag{36.61}$$

The vertical component of the net contact pressure force balances the weight of the column within the layer, which is expected since the shallow water fluid is in hydrostatic balance. The horizontal contact pressure force arises from a horizontal gradient plus the form stress at the surface and bottom interfaces. The gradient term is removed when integrating horizontally over the full domain given that the thickness of the layer vanishes upon reaching the coastlines (e.g., see Figure 28.6). The resulting net force on the full domain arises just from the weight of the fluid acting in the vertical, plus form stress at the surface and bottom. We discuss this point more in Section 36.4.7.

36.4.7 Contact pressure force summed over all layers

Summing the contact pressure force (36.60b) over all layers reveals the contact forces on the interior layer interfaces vanish, as per Newton's third law (see Section 28.1), thus leaving just the form stress at the surface and bottom and the contact pressure force acting on the vertical sides. Dividing by the horizonal area of the column leads to the net pressure force per area

$$\frac{1}{\mathrm{d}x\,\mathrm{d}y}\sum_{\mathsf{k}=1}^{N} \boldsymbol{F}^{\text{press}}_{\text{net},\mathsf{k}} = \hat{\boldsymbol{z}}\, g \sum_{\mathsf{k}=1}^{N} \rho_{\mathsf{k}}\, h_{\mathsf{k}} + p_{\mathsf{a}}\nabla\eta_{1/2} - p_{\mathsf{b}}\nabla\eta_{\mathsf{b}} - \sum_{\mathsf{k}=1}^{N} \nabla P_{\mathsf{k}} \tag{36.62a}$$

$$= (p_{\mathsf{b}} - p_{\mathsf{a}})\, \hat{\boldsymbol{z}} + p_{\mathsf{a}}\nabla\eta_{1/2} - p_{\mathsf{b}}\nabla\eta_{\mathsf{b}} - \sum_{\mathsf{k}=1}^{N} \nabla P_{\mathsf{k}}, \tag{36.62b}$$

where we wrote the total weight per area within the column as the difference between the bottom pressure and applied surface pressure

$$g \sum_{\mathsf{k}=1}^{N} \rho_{\mathsf{k}}\, h_{\mathsf{k}} = p_{\mathsf{b}} - p_{\mathsf{a}}. \tag{36.63}$$

The horizontal components to the applied and bottom pressure terms in equation (36.62b) arise from pressure form stresses applied to the interfaces at the top and bottom of the column. The vertical component arises from the net weight per area of the fluid. The summation term is the horizontal gradient of the vertically integrated contact pressure applied along the vertical sides of the column.

36.4.8 Horizontal pressure force with potential energy gradients

There is another means to express the horizontal pressure force. Here, we expose the gravitational potential energy per horizontal area for a column of fluid within a shallow water layer

$$\mathscr{P}_\mathsf{k} = g\,\rho_\mathsf{k} \int_{\eta_{\mathsf{k}+1/2}}^{\eta_{\mathsf{k}-1/2}} z\,\mathrm{d}z = (g\,\rho_\mathsf{k}/2)\,(\eta_{\mathsf{k}-1/2}^2 - \eta_{\mathsf{k}+1/2}^2). \tag{36.64}$$

Use of the layer gravitational potential energy brings the layer vertical integral of the hydrostatic pressure from Section 36.4.3 into

$$\int_{\eta_{\mathsf{k}+1/2}}^{\eta_{\mathsf{k}-1/2}} p_\mathsf{k}(z)\,\mathrm{d}z = g\,\rho_\mathsf{k}\,h_\mathsf{k}^2/2 + h_\mathsf{k}\,p_{\mathsf{k}-1/2} = \mathscr{P}_\mathsf{k} - g\,\rho_\mathsf{k}\,h_\mathsf{k}\,\eta_{\mathsf{k}+1/2} + h_\mathsf{k}\,p_{\mathsf{k}-1/2}. \tag{36.65a}$$

Making use of this result in equation (36.60b), along with a few lines of algebra, yields the net horizontal contact pressure force acting on a shallow water column

$$-\nabla P_\mathsf{k} + \delta_\mathsf{k}(p_{\mathsf{k}-1/2}\nabla\eta_{\mathsf{k}-1/2}) = -\nabla\mathscr{P}_\mathsf{k} - \delta_\mathsf{k}(\eta_{\mathsf{k}-1/2}\nabla p_{\mathsf{k}-1/2}). \tag{36.66}$$

To reach the identity (36.66) requires the hydrostatic relation, $p_{\mathsf{k}+1/2} - p_{\mathsf{k}-1/2} = g\,\rho_\mathsf{k}\,h_\mathsf{k}$, and the the layer thickness, $h_\mathsf{k} = \eta_{\mathsf{k}-1/2} - \eta_{\mathsf{k}+1/2}$. A consistency check notes that the curl of both sides to equation (36.66) are the same. The identity (36.66) suggests we define the form stress and its dual

$$\boldsymbol{F}^{\text{form}} = p\nabla\eta \quad \text{and} \quad \boldsymbol{F}^{\text{dual form}} = -\eta\nabla p, \tag{36.67}$$

with both $\boldsymbol{F}^{\text{form}}$ and $\boldsymbol{F}^{\text{dual form}}$ defined on layer interfaces. These two stresses have the same curl, and thus impart the same pressure torque on a column of fluid (Chapter 39)

$$\nabla \times (p\nabla\eta) = \nabla \times (-\eta\nabla p). \tag{36.68}$$

However, these stresses are distinct and as such cannot be arbitrarily interchanged.[5]

36.4.9 Momentum equation with contact pressure forces

Comparing the body force version and the contact force version

Recall that the thickness weighted velocity equation (36.45), as written in terms of the pressure gradient body force, is given by[6]

$$\frac{\partial(h_\mathsf{k}\,\boldsymbol{u}_\mathsf{k})}{\partial t} + \nabla\cdot[h_\mathsf{k}\,\boldsymbol{u}_\mathsf{k}\otimes\boldsymbol{u}_\mathsf{k}] + f\,\hat{\boldsymbol{z}}\times(h_\mathsf{k}\,\boldsymbol{u}_\mathsf{k}) = -(h_\mathsf{k}/\rho_{\mathsf{ref}})\,\nabla_\mathsf{h} p_\mathsf{k}, \tag{36.69}$$

again with no implied summation over the layer label, k. Alternatively, we can make use of the net contact pressure force (36.60b) so that

$$\frac{\partial(h_\mathsf{k}\,\boldsymbol{u}_\mathsf{k})}{\partial t} + \nabla\cdot(h_\mathsf{k}\,\boldsymbol{u}_\mathsf{k}\otimes\boldsymbol{u}_\mathsf{k} + \mathbb{I}\,P_\mathsf{k}/\rho_{\mathsf{ref}}) + f\,\hat{\boldsymbol{z}}\times(h_\mathsf{k}\,\boldsymbol{u}_\mathsf{k}) = \delta_\mathsf{k}(p_{\mathsf{k}-1/2}\nabla\eta_{\mathsf{k}-1/2})/\rho_{\mathsf{ref}}, \tag{36.70}$$

[5] As noted in Section 28.1.3, much of the literature refers to $-\eta\nabla p$ as the form stress rather than the dual form stress. This usage presumably originates from the common application of zonal averages for studying atmospheric motions, whereby $\overline{\eta\,\partial_x p}^x = -\overline{p\,\partial_x\eta}^x$. But this identity does not hold for arbitrary averaging operators, such as the ensemble averages commonly used for turbulence studies. So it is generally necessary to distinguish the form stress from the dual form stress.

[6] In equation (36.69) we wrote the gradient on the pressure as ∇_h since we are only interested in the horizontal gradient acting on $p_\mathsf{k}(x,y,z)$. All other objects in equation (36.69) are just a function of horizontal position within a layer, so that ∇ acting on them reduces to ∇_h. Hence, the subscript on the gradient operator, ∇_h, is exposed only when it acts on a function of z, such as for $p_\mathsf{k}(x,y,z)$. Since $p_\mathsf{k}(x,y,z)$ is a linear function of z, its horizontal gradient is vertically independent within the layer, as illustrated in Figure 35.1.

where $\mathbb{I}$ is the identity tensor, P_k is the layer integrated pressure given by equation (36.47c), and δ_k is the difference operator defined by equation (36.37). Choosing the contact pressure force as in equation (36.66) to expose the potential energy brings the momentum equation (36.70) into the alternative form

$$\frac{\partial(h_k\,\boldsymbol{u}_k)}{\partial t} + \nabla\cdot[h_k\,\boldsymbol{u}_k\otimes\boldsymbol{u}_k + \mathbb{I}\,\mathcal{P}_k/\rho_{ref}] + f\,\hat{\boldsymbol{z}}\times(h_k\,\boldsymbol{u}_k) = -\delta_k(\eta_{k-1/2}\nabla p_{k-1/2})/\rho_{ref}. \tag{36.71}$$

Equations (36.69), (36.70), and (36.71) allow us to identify the body force and contact force versions of the thickness weighted horizontal pressure acceleration

$$-h_k\nabla_h p_k = -\nabla P_k + \delta_k(p_{k-1/2}\nabla\eta_{k-1/2}) = -\nabla\mathcal{P}_k - \delta_k(\eta_{k-1/2}\nabla p_{k-1/2}). \tag{36.72}$$

The balance of pressure torques acting on a shallow water column

A necessary (but not sufficient) check of the identity (36.72) can be found by verifying that the curl agrees for each expression

$$\begin{aligned}
-\nabla\times\delta_k(\eta_{k-1/2}\nabla p_{k-1/2}) &= \nabla\times\delta_k(p_{k-1/2}\nabla\eta_{k-1/2}) && \text{(36.73a)}\\
&= \delta_k[\nabla\times(p_{k-1/2}\nabla\eta_{k-1/2})] && \text{(36.73b)}\\
&= \delta_k[\nabla p_{k-1/2}\times\nabla\eta_{k-1/2}] && \text{(36.73c)}\\
&= \nabla p_{k-1/2}\times\nabla\eta_{k-1/2} - \nabla(p_{k-1/2}+g\,\rho_k\,h_k)\times\nabla\eta_{k+1/2} && \text{(36.73d)}\\
&= \nabla p_{k-1/2}\times\nabla h_k - g\,\rho_k\nabla h_k\times\nabla\eta_{k+1/2} && \text{(36.73e)}\\
&= \nabla(p_{k-1/2}+g\,\rho_k\,\eta_{k+1/2})\times\nabla h_k && \text{(36.73f)}\\
&= \nabla(p_{k-1/2}-g\,\rho_k\,h_k+g\,\rho_k\,\eta_{k-1/2})\times\nabla h_k && \text{(36.73g)}\\
&= \nabla_h[p_{k-1/2}+g\,\rho_k\,(\eta_{k-1/2}-z)]\times\nabla h_k && \text{(36.73h)}\\
&= \nabla_h p_k\times\nabla h_k && \text{(36.73i)}\\
&= -\nabla\times(h_k\nabla_h p_k), && \text{(36.73j)}
\end{aligned}$$

which concurs with the curl of the left hand side of equation (36.72). To reach this result we set $h_k = \eta_{k-1/2} - \eta_{k+1/2}$ and used equation (36.46) for the pressure within a shallow water layer: $p_k(z) = \rho_k\,g\,(\eta_{k-1/2} - z) + p_{k-1/2}$.

Anticipating our discussion of vorticity for the shallow water fluid in Section 39.1, we observe that the identity derived above,

$$\nabla\times\delta_k(p_{k-1/2}\nabla\eta_{k-1/2}) = -\nabla\times(h_k\nabla_h p_k), \tag{36.74}$$

says that the difference between the interfacial pressure torques acting on the top and bottom of a shallow water layer precisely balances minus the torque arising from the thickness weighted horizontal pressure gradient acting within the layer. This rather remarkable fine tuning of the interfacial and interior pressure torques is a direct consequence of assuming that the fluid motion is restricted to extensible vertical columns within each shallow water layer. This balance is not maintained within a three dimensional fluid, where fluid columns can generally tilt and bend (Chapter 40).

Layer summed momentum equation

Taking the vertical sum of the layer-k momentum equation (36.70) leads to the column integrated horizontal momentum equation

$$\frac{\partial \boldsymbol{U}}{\partial t} + f\,\hat{\boldsymbol{z}} \times \boldsymbol{U} + \nabla \cdot \left[\sum_{\mathsf{k}=1}^{N} (h_{\mathsf{k}}\, \boldsymbol{u}_{\mathsf{k}} \otimes \boldsymbol{u}_{\mathsf{k}} + \mathbb{I}\, P_{\mathsf{k}}/\rho_{\mathsf{ref}}) \right] = [p_a \nabla \eta_{1/2} - p_{\mathsf{b}} \nabla \eta_{\mathsf{b}}]/\rho_{\mathsf{ref}}, \tag{36.75}$$

where $\boldsymbol{U}$ is the vertically integrated horizontal velocity given by equation (36.10). The same vertical sum for equation (36.71) leads to

$$\frac{\partial \boldsymbol{U}}{\partial t} + f\,\hat{\boldsymbol{z}} \times \boldsymbol{U} + \nabla \cdot \left[\sum_{\mathsf{k}=1}^{N} (h_{\mathsf{k}}\, \boldsymbol{u}_{\mathsf{k}} \otimes \boldsymbol{u}_{\mathsf{k}} + \mathbb{I}\, \mathscr{P}_{\mathsf{k}}/\rho_1) \right] = [-\eta_{1/2} \nabla p_a + \eta_{\mathsf{b}} \nabla p_{\mathsf{b}}]/\rho_{\mathsf{ref}}. \tag{36.76}$$

The right hand side of equation (36.75) exposes the pressure form stresses acting on the ocean surface and bottom, whereas the right hand side of equation (36.76) exposes the dual form stress acting on the ocean surface and bottom.

Decomposing into vertically averaged and vertical deviation velocities

For detailed analyses of the vertically integrated (layer summed) momentum and vorticity budgets, it is of interest to introduce the vertical averaging operator along with the deviation from the average,

$$\overline{\Phi}^{\mathsf{z}} = \frac{\sum_{\mathsf{k}=1}^{N} h_{\mathsf{k}}\, \Phi_{\mathsf{k}}}{\sum_{\mathsf{k}=1}^{N} h_{\mathsf{k}}} \quad \text{and} \quad \Phi'_{\mathsf{k}} = \Phi_{\mathsf{k}} - \overline{\Phi}^{\mathsf{z}}, \tag{36.77}$$

so that the vertically integrated kinetic stress in equation (36.75) is

$$\sum_{\mathsf{k}=1}^{N} h_{\mathsf{k}}\, \boldsymbol{u}_{\mathsf{k}} \otimes \boldsymbol{u}_{\mathsf{k}} = D\, [\overline{\boldsymbol{u}}^{\mathsf{z}} \otimes \overline{\boldsymbol{u}}^{\mathsf{z}} + \overline{\boldsymbol{u}' \otimes \boldsymbol{u}'}^{\mathsf{z}}] \quad \text{where } D = \textstyle\sum_{\mathsf{k}=1}^{N} h_{\mathsf{k}}. \tag{36.78}$$

The velocity, $\boldsymbol{u}'_{\mathsf{k}}$, is the deviation of the layer-k velocity from the vertically average velocity, and we refer to it as the *internal velocity*, whereas the vertically averaged velocity, $\overline{\boldsymbol{u}}^{\mathsf{z}}$, is the *external velocity*.[7] The identity (36.78) reveals that the vertically integrated kinetic stress can be decomposed into a stress arising from internal-internal velocity interactions plus external-external velocity interactions. By construction, there are no cross-terms (i.e., no internal-external terms) appearing in this vertically integrated stress.

Momentum fluxes

Following the single layer discussion in Section 36.3.3, we write the momentum equation (36.70) in the form

$$\frac{\partial (h\, u)}{\partial t} - v\, h\, f = -(\hat{\boldsymbol{x}}\, \partial_x + \hat{\boldsymbol{y}}\, \partial_y + \hat{\boldsymbol{z}}\, h^{-1} \delta_{\mathsf{k}}) \cdot \boldsymbol{D}^{(\mathrm{u})} \tag{36.79a}$$

$$\frac{\partial (h\, v)}{\partial t} + u\, h\, f = -(\hat{\boldsymbol{x}}\, \partial_x + \hat{\boldsymbol{y}}\, \partial_y + \hat{\boldsymbol{z}}\, h^{-1} \delta_{\mathsf{k}}) \cdot \boldsymbol{D}^{(\mathrm{v})}, \tag{36.79b}$$

[7] It is also common in the oceanography literature to refer to $\boldsymbol{u}'_{\mathsf{k}}$ as the *baroclinic velocity* and $\overline{\boldsymbol{u}}^{\mathsf{z}}$ as the *barotropic velocity*.

where we dropped the k label for brevity and introduced the layer momentum fluxes

$$\boldsymbol{D}^{(\mathrm{u})} = (h\,u^2 + P/\rho_{\mathsf{ref}})\,\hat{\boldsymbol{x}} + h\,u\,v\,\hat{\boldsymbol{y}} - (p_{\mathsf{k}-1/2}\,\partial_x \eta_{\mathsf{k}-1/2}/\rho_{\mathsf{ref}})\,h\,\hat{\boldsymbol{z}} \tag{36.80a}$$

$$\boldsymbol{D}^{(\mathrm{v})} = h\,u\,v\,\hat{\boldsymbol{x}} + (h\,v^2 + P/\rho_{\mathsf{ref}})\,\hat{\boldsymbol{y}} - (p_{\mathsf{k}-1/2}\,\partial_y \eta_{\mathsf{k}-1/2}/\rho_{\mathsf{ref}})\,h\,\hat{\boldsymbol{z}}. \tag{36.80b}$$

Likewise, we can write the momentum equation (36.71) in the component form

$$\frac{\partial(h\,u)}{\partial t} - v\,h\,f = -(\hat{\boldsymbol{x}}\,\partial_x + \hat{\boldsymbol{y}}\,\partial_y + \hat{\boldsymbol{z}}\,h^{-1}\delta_{\mathsf{k}}) \cdot \boldsymbol{E}^{(\mathrm{u})} \tag{36.81a}$$

$$\frac{\partial(h\,v)}{\partial t} + u\,h\,f = -(\hat{\boldsymbol{x}}\,\partial_x + \hat{\boldsymbol{y}}\,\partial_y + \hat{\boldsymbol{z}}\,h^{-1}\delta_{\mathsf{k}}) \cdot \boldsymbol{E}^{(\mathrm{v})}, \tag{36.81b}$$

where the dual layer momentum fluxes are given by

$$\boldsymbol{E}^{(\mathrm{u})} = (h\,u^2 + \mathscr{P}/\rho_{\mathsf{ref}})\,\hat{\boldsymbol{x}} + h\,u\,v\,\hat{\boldsymbol{y}} + (\eta_{\mathsf{k}-1/2}\,\partial_x p_{\mathsf{k}-1/2}/\rho_{\mathsf{ref}})\,h\,\hat{\boldsymbol{z}} \tag{36.82a}$$

$$\boldsymbol{E}^{(\mathrm{v})} = h\,u\,v\,\hat{\boldsymbol{x}} + (h\,v^2 + \mathscr{P}/\rho_{\mathsf{ref}})\,\hat{\boldsymbol{y}} + (\eta_{\mathsf{k}-1/2}\,\partial_y p_{\mathsf{k}-1/2}/\rho_{\mathsf{ref}})\,h\,\hat{\boldsymbol{z}}. \tag{36.82b}$$

Besides swapping the vertically integrated pressure, P, for the potential energy, $\mathscr{P}$, the dual momentum fluxes, $\boldsymbol{E}^{(\mathrm{u})}$ and $\boldsymbol{E}^{(\mathrm{v})}$, make use of the dual form stress, $\eta_{\mathsf{k}-1/2}\,\nabla p_{\mathsf{k}-1/2}$, rather than the form stress, $-p_{\mathsf{k}-1/2}\,\nabla\eta_{\mathsf{k}-1/2}$. Upon performing an eddy-mean flow decomposition as in Section 67.6, the eddy correlation portion of the fluxes (36.82a) and (36.82b) lead to the shallow water *Eliassen-Palm* fluxes, which are rows in the Eliassen-Palm flux tensor.

36.4.10 Further reading

Ward and Hogg (2011) and *Barthel et al.* (2017) offer pedagogical treatments of the stacked shallow water equations in the context of idealized simulations that lend insight into the dynamical balances. *Maddison and Marshall* (2013) study the Eliassen-Palm flux tensor for continuously stratified quasi-geostrophy as well as the Boussinesq hydrostatic equations.

36.5 Energetics for a single layer

In this section we develop budgets for gravitational potential energy, kinetic energy, and mechanical energy for a single shallow water layer sitting on top of a non-flat bottom. Since the shallow water model has no internal energy, the total energy of the fluid is just that arising from the mechanical energy of the macroscopic motion. As part of this discussion we also consider the available potential energy (APE).

Motion within a shallow water layer occurs in vertical columns, so that we consider the energy of the layer integrated motion. The gravitational potential energy of a shallow water column is affected by vertical movement of the top and bottom of the column within the gravitational field. The kinetic energy is affected by pressure work, with this work, as seen in Sections 36.3 and 36.4, expressed either as a gradient body force or a contact force. Furthermore, pressure work leading to vertical motion manifests as buoyancy work. Our goal in this section is to study these energetic transformations and their mathematical expressions. We then extend the energetic analysis from the single layer to multiple layers in Section 36.6, though note that much of our work for the single layer is sufficient for multiple layers.

Before diving into details, we note that shallow water energetics can be derived from a layer integration of the continuously stratified Boussinesq energy equations from Section 29.6. That approach offers a somewhat more telescopic presentation than given here. However, we choose to present the derivations in a manner that supports skills in manipulating the shallow water equations, and further exposes the physical concepts arising from the motion of shallow water

fluid columns.

36.5.1 Gravitational potential energy

The gravitational potential energy per horizontal area of a shallow water fluid is given by[8]

$$\mathscr{P}^{\text{sw}} = g\,\rho \int_{\eta_{\text{b}}}^{\eta} z\,\mathrm{d}z = \frac{g\,\rho}{2}\,(\eta^2 - \eta_{\text{b}}^2) = \rho\,g\,h\,\overline{\eta}, \tag{36.83}$$

where the final equality introduced the layer thickness, h, and average of the layer interface heights

$$h = \eta - \eta_{\text{b}} \quad \text{and} \quad \overline{\eta} = (\eta + \eta_{\text{b}})/2. \tag{36.84}$$

Notice how the gravitational potential energy vanishes when $\eta^2 = \eta_{\text{b}}^2$. For the case $\eta = \eta_{\text{b}}$, there is no fluid in the column and so we expect the potential energy to vanish. For the case $\eta = -\eta_{\text{b}} > 0$, there is the same amount of fluid above $z = 0$ as below, in which case the potential energy for the column vanishes since we are computing it relative to the $z = 0$ reference state. Furthermore, in the flat bottom case, $\eta_{\text{b}} = 0$ so that $h = \eta - \eta_{\text{b}} = \eta$, in which case the potential energy (36.83) reduces to $\mathscr{P}^{\text{sw}}_{\text{flat}} = g\,\rho\,\eta^2/2$.

Material time derivative of gravitational potential energy

Taking the material time derivative of the gravitational potential energy in equation (36.83) yields

$$\frac{\mathrm{D}\mathscr{P}^{\text{sw}}}{\mathrm{D}t} = g\,\rho\left[\eta\,\frac{\mathrm{D}\eta}{\mathrm{D}t} - \eta_{\text{b}}\,\frac{\mathrm{D}\eta_{\text{b}}}{\mathrm{D}t}\right] \tag{36.85a}$$

$$= g\,\rho\,[\eta\,w(\eta) - \eta_{\text{b}}\,w(\eta_{\text{b}})] \tag{36.85b}$$

$$= g\,\rho\,h\,[w(\eta_{\text{b}}) - \eta\,\nabla\cdot\boldsymbol{u}] \tag{36.85c}$$

$$= g\,\rho\,h\,[w(\eta) - \eta_{\text{b}}\,\nabla\cdot\boldsymbol{u}], \tag{36.85d}$$

where we used equations for the vertical velocity component from Section 35.2.8, and for the final equality we used equation (35.96) to write

$$w(\eta) - w(\eta_{\text{b}}) = -h\,\nabla\cdot\boldsymbol{u}. \tag{36.86}$$

Evidently, the potential energy changes according to how the thickness of the layer increases through vertical motion along the top and bottom interfaces, and as weighted by the position of these interfaces relative to $z = 0$. Finally, it is useful to write equation (36.85d) in its flux-form, which is given by

$$\partial_t \mathscr{P}^{\text{sw}} + \nabla\cdot(\boldsymbol{u}\,\mathscr{P}^{\text{sw}}) = \mathscr{P}^{\text{sw}}\,\nabla\cdot\boldsymbol{u} + g\,\rho\,h\,[w(\eta) - \eta_{\text{b}}\,\nabla\cdot\boldsymbol{u}]. \tag{36.87}$$

The source term on the right hand side can be written as a buoyancy work term, which we show next.

[8] We include the "sw" superscript to distinguish the shallow water energetic terms, which we consider in their thickness weighted form so their dimensions are energy per area. In other areas of this book, we consider the energy per mass, such as in Chapters 26 and 29.

Exposing the role of buoyancy work

An alternative expression for the potential energy evolution is found by working with the final expression for potential energy in equation (36.83), whose material time derivative is

$$\frac{\mathrm{D}\mathscr{P}^{\mathrm{sw}}}{\mathrm{D}t} = g\,\rho\,\overline{\eta}\,\frac{\mathrm{D}h}{\mathrm{D}t} + g\,\rho\,h\,\frac{\mathrm{D}\overline{\eta}}{\mathrm{D}t} = -\mathscr{P}^{\mathrm{sw}}\,\nabla\cdot\boldsymbol{u} + \rho\,g\,h\,\overline{w}, \tag{36.88}$$

where we introduced the averaged vertical velocity for the layer according to equation (35.102)

$$\overline{w} = \frac{\mathrm{D}\overline{\eta}}{\mathrm{D}t} = \frac{1}{2}\,\frac{\mathrm{D}(\eta+\eta_{\mathrm{b}})}{\mathrm{D}t}. \tag{36.89}$$

The flux-form version of the potential energy equation (36.88) thus takes on the form

$$\partial_t\mathscr{P}^{\mathrm{sw}} + \nabla\cdot(\boldsymbol{u}\,\mathscr{P}^{\mathrm{sw}}) = g\,\rho\,h\,\overline{w}. \tag{36.90}$$

This equation is the shallow water analog to the gravitational potential energy budget (26.5) for a continuously stratified fluid. In particular, we see that the buoyancy work term, $g\,\rho\,h\,\overline{w}$, alters potential energy when there is vertical motion through the gravity field. As a check on the manipulations, we verify that the potential energy budgets (36.87) and (36.90) are indeed self-consistent by noting that

$$\begin{aligned}
\mathscr{P}^{\mathrm{sw}}\,\nabla\cdot\boldsymbol{u} + \rho\,g\,h\,[w(\eta) - \eta_{\mathrm{b}}\,\nabla\cdot\boldsymbol{u}] &= \rho\,g\,h\,[(\overline{\eta}-\eta_{\mathrm{b}})\,\nabla\cdot\boldsymbol{u} + w(\eta)] && \text{(36.91a)}\\
&= \rho\,g\,h\,[(h/2)\,\nabla\cdot\boldsymbol{u} + w(\eta)] && \text{(36.91b)}\\
&= \rho\,g\,h\,[-(1/2)\,\mathrm{D}h/\mathrm{D}t + w(\eta)] && \text{(36.91c)}\\
&= \rho\,g\,h\,\overline{w}. && \text{(36.91d)}
\end{aligned}$$

36.5.2 Kinetic energy and work from pressure gradients

The kinetic energy per horizontal area is

$$\mathscr{K}^{\mathrm{sw}} = \frac{1}{2}\int_{\eta_{\mathrm{b}}}^{\eta}\rho\,\boldsymbol{u}\cdot\boldsymbol{u}\,\mathrm{d}z = \frac{1}{2}\,\rho\,h\,\boldsymbol{u}\cdot\boldsymbol{u}. \tag{36.92}$$

Its material time derivative is given by

$$\begin{aligned}
\frac{\mathrm{D}\mathscr{K}^{\mathrm{sw}}}{\mathrm{D}t} &= \rho\,h\,\boldsymbol{u}\cdot\frac{\mathrm{D}\boldsymbol{u}}{\mathrm{D}t} + \frac{1}{2}\,\rho\,\boldsymbol{u}\cdot\boldsymbol{u}\,\frac{\mathrm{D}h}{\mathrm{D}t} && \text{(36.93a)}\\
&= -h\,\boldsymbol{u}\cdot\nabla p + \rho\,h\,\boldsymbol{u}\cdot\boldsymbol{F} + \frac{\mathscr{K}^{\mathrm{sw}}}{h}\,\frac{\mathrm{D}h}{\mathrm{D}t} && \text{(36.93b)}\\
&= -h\,\boldsymbol{u}\cdot\nabla p + \rho\,h\,\boldsymbol{u}\cdot\boldsymbol{F} - \mathscr{K}^{\mathrm{sw}}\,\nabla\cdot\boldsymbol{u}, && \text{(36.93c)}
\end{aligned}$$

where we made use of the velocity equation (35.9) along with the addition of a frictional acceleration, $\boldsymbol{F}$ (see Section 35.6.5), and we used the thickness equation (35.20). Rearrangement of equation (36.93c) leads to the flux-form budget for layer integrated kinetic energy

$$\partial_t\mathscr{K}^{\mathrm{sw}} + \nabla\cdot(\boldsymbol{u}\,\mathscr{K}^{\mathrm{sw}}) = -h\,\boldsymbol{u}\cdot\nabla p + \rho\,h\,\boldsymbol{u}\cdot\boldsymbol{F}. \tag{36.94}$$

The first term on the right hand side is the projection of the horizontal velocity onto the horizontal pressure gradient acceleration, thus indicating that kinetic energy for the fluid column increases if the velocity has a component that is directed down the horizontal pressure gradient. This term arises from the work done by the horizontal pressure gradient force acting on the moving fluid columns. The second right hand side term is the projection of the velocity onto the

thickness weighted horizontal friction, which accounts for work done by friction and/or boundary stresses on the moving fluid.

For a slight modification to the budget equation (36.94), write the layer pressure as

$$p = p_a + \rho\, g\, (\eta - z) = \rho\, g\, (\eta^{\text{eff}} - z), \tag{36.95}$$

where we introduced the effective free surface from equation (35.4)

$$\eta^{\text{eff}} = \eta + p_a/(\rho\, g). \tag{36.96}$$

The thickness weighted pressure work thus takes the form

$$-h\, \boldsymbol{u} \cdot \nabla p = -h\, \rho\, g\, \boldsymbol{u} \cdot \nabla \eta^{\text{eff}}, \tag{36.97}$$

so that the kinetic energy equation (36.94) becomes

$$\partial_t \mathcal{K}^{\text{sw}} + \nabla \cdot [\boldsymbol{u}\, (\mathcal{K}^{\text{sw}} + \rho\, g\, h\, \eta^{\text{eff}})] = \rho\, g\, \eta^{\text{eff}}\, \nabla \cdot (h\, \boldsymbol{u}) + \rho\, h\, \boldsymbol{u} \cdot \boldsymbol{F}. \tag{36.98}$$

36.5.3 Kinetic energy and buoyancy work

Following the second formulation of gravitational potential energy in Section 36.5.1, we here expose the buoyancy work that is contained in the term $\rho\, g\, \eta^{\text{eff}}\, \nabla \cdot (h\, \boldsymbol{u})$ appearing in equation (36.98). For this purpose, make use of the thickness equation, $\partial_t h = -\nabla \cdot (\boldsymbol{u}\, h)$, to write

$$\rho\, g\, \eta^{\text{eff}}\, \nabla \cdot (h\, \boldsymbol{u}) = -\rho\, g\, \eta^{\text{eff}}\, \partial_t h = -\rho\, g\, \eta^{\text{eff}}\, \partial_t(\delta_k \eta_{k-1/2}) = -\delta_k(\rho\, g\, \eta^{\text{eff}}\, \partial_t \eta_{k-1/2}). \tag{36.99}$$

For the final two equations we introduced the layer index, with $k = 1$ for the single layer and with the layer interfaces $\eta_{1/2} = \eta$ and $\eta_{3/2} = \eta_b$. Additionally, δ_k is the finite difference operator (36.37) so that

$$h = \eta - \eta_b = \eta_{1/2} - \eta_{3/2} = \delta_k \eta_{k-1/2}. \tag{36.100}$$

We inserted $\rho\, g\, \eta^{\text{eff}}$ into the difference operator in equation (36.99) since this term is vertically independent across the layer.

For the next step, we make use of equation (36.95) for the layer pressure, $p = \rho\, g\, (\eta^{\text{eff}} - z)$, in which case[9]

$$-\delta_k(\rho\, g\, \eta^{\text{eff}}\, \partial_t \eta_{k-1/2}) = -\delta_k[(p + \rho\, g\, z)\, \partial_t \eta_{k-1/2}] \tag{36.101a}$$

$$= -\delta_k(p_{k-1/2}\, \partial_t \eta_{k-1/2}) - \delta_k(\rho\, g\, \eta_{k-1/2}\, \partial_t \eta_{k-1/2}). \tag{36.101b}$$

This step is somewhat subtle since we replaced $\rho\, g\, \eta^{\text{eff}}$, which is vertically independent within a layer, with the sum $p + \rho\, g\, z$, where both p and $\rho\, g\, z$ are functions of z. For equation (36.101b) we replaced p and z with their interface values since the argument of the difference operator is evaluated on the layer interfaces. Observe that $\partial_t \eta_b = 0$, and yet it is convenient to carry this term through the manipulations to retain symmetry of the equations, and to anticipate the same formulation for the stacked shallow water energetics in Section 36.6.

We now make use of the potential energy in Section 36.5.1 by writing

$$-\delta_k(\rho\, g\, \eta_{k-1/2}\, \partial_t \eta_{k-1/2}) = -(\rho\, g/2)\, \partial_t(\eta^2 - \eta_b^2) = -\partial_t \mathcal{P}^{\text{sw}} = \nabla \cdot (\boldsymbol{u}\, \mathcal{P}^{\text{sw}}) - g\, \rho\, h\, \overline{w}, \tag{36.102}$$

where the final step used the potential energy equation (36.90). As advertised, this formulation exposes the buoyancy work term, $-g\, \rho\, h\, \overline{w}$, which then allows us to bring the kinetic energy

[9] Equations (36.101a) and (36.101b) are inspired by some unpublished notes from Christopher Wolfe.

equation (36.98) to the form

$$\partial_t \mathcal{K}^{\text{sw}} + \nabla \cdot [\boldsymbol{u}\,(\mathcal{K}^{\text{sw}} - \mathcal{P}^{\text{sw}} + \rho\, g\, h\, \eta^{\text{eff}})] + \delta_{\text{k}}(p_{\text{k}-1/2}\, \partial_t \eta_{\text{k}-1/2}) = -g\, \rho\, h\, \overline{w} + \rho\, h\, \boldsymbol{u} \cdot \boldsymbol{F}. \quad (36.103)$$

We can simplify the advective flux by writing

$$-\mathcal{P}^{\text{sw}} + \rho\, g\, h\, \eta^{\text{eff}} = -\rho\, g\, h\, \overline{\eta} + \rho\, g\, \eta + h\, p_{\text{a}} = h\,(\rho\, g\, h/2 + p_{\text{a}}) = P, \quad (36.104)$$

where the final equality introduced the layer integrated pressure

$$P = \int_{\eta_{\text{b}}}^{\eta} p(z)\, \mathrm{d}z = \rho\, g \int_{\eta_{\text{b}}}^{\eta} (\eta^{\text{eff}} - z)\, \mathrm{d}z = h\,(\rho\, g\, h/2 + p_{\text{a}}). \quad (36.105)$$

The kinetic energy equation (36.103) thus takes the form

$$\partial_t \mathcal{K}^{\text{sw}} + \nabla \cdot [\boldsymbol{u}\,(\mathcal{K}^{\text{sw}} + P)] + \delta_{\text{k}}(p_{\text{k}-1/2}\, \partial_t \eta_{\text{k}-1/2}) = -g\, \rho\, h\, \overline{w} + \rho\, h\, \boldsymbol{u} \cdot \boldsymbol{F}. \quad (36.106)$$

The term $\delta_{\text{k}}(p_{\text{k}-1/2}\, \partial_t \eta_{\text{k}-1/2})$ on the left hand side is a vertical transfer that, as seen in Section 36.5.4, arises in part from pressure form stresses acting on the boundary of the fluid column.

36.5.4 Kinetic energy and pressure form stress

As a final form of the kinetic energy equation, we recombine the vertical transfer term and the buoyancy work term in equation (36.106) to have

$$-g\, \rho\, h\, \overline{w} - \delta_{\text{k}}(p_{\text{k}-1/2}\, \partial_t \eta_{\text{k}-1/2}) = -g\, \rho\, h\, \overline{w} - p_{\text{a}}\,[w(\eta) - \boldsymbol{u} \cdot \nabla \eta] + p_{\text{b}}\,[w(\eta_{\text{b}}) - \boldsymbol{u} \cdot \nabla \eta_{\text{b}}]. \quad (36.107)$$

Introducing the bottom pressure and vertically integrated pressure

$$p_{\text{b}} = p_{\text{a}} + \rho\, g\, h \quad \text{and} \quad P = h\,(p_{\text{a}} + \rho\, g\, h/2), \quad (36.108)$$

leads to

$$\begin{aligned}
-g\, \rho\, h\, \overline{w} - \delta_{\text{k}}(p_{\text{k}-1/2}\, \partial_t \eta_{\text{k}-1/2}) &= (P/h)\,[w(\eta_{\text{b}}) - w(\eta)] + \boldsymbol{u} \cdot (p_{\text{a}}\, \nabla \eta - p_{\text{b}}\, \nabla \eta_{\text{b}}) && (36.109a)\\
&= \frac{P}{h}\, \frac{\mathrm{D}(\eta_{\text{b}} - \eta)}{\mathrm{D}t} + \boldsymbol{u} \cdot (p_{\text{a}}\, \nabla \eta - p_{\text{b}}\, \nabla \eta_{\text{b}}) && (36.109b)\\
&= -\frac{P}{h}\, \frac{\mathrm{D}h}{\mathrm{D}t} + \boldsymbol{u} \cdot (p_{\text{a}}\, \nabla \eta - p_{\text{b}}\, \nabla \eta_{\text{b}}) && (36.109c)\\
&= P\, \nabla \cdot \boldsymbol{u} + \boldsymbol{u} \cdot (p_{\text{a}}\, \nabla \eta - p_{\text{b}}\, \nabla \eta_{\text{b}}), && (36.109d)
\end{aligned}$$

so that the kinetic energy equation (36.106) can be written

$$\partial_t \mathcal{K}^{\text{sw}} + \nabla \cdot (\boldsymbol{u}\, \mathcal{K}^{\text{sw}}) = \boldsymbol{u} \cdot (-\nabla P + p_{\text{a}}\, \nabla \eta - p_{\text{b}}\, \nabla \eta_{\text{b}}) + \rho\, h\, \boldsymbol{u} \cdot \boldsymbol{F}. \quad (36.110)$$

We have thus exposed the work done by pressure form stresses acting on the vertical side of an expanding or contracting shallow water column, plus those form stresses acting on the top and bottom layer interfaces.

A somewhat more direct way to derive the kinetic energy equation (36.110) is to return to the kinetic energy equation (36.94) and make use of the identity (36.72). This identity equates the thickness weighted horizontal pressure gradient acting on a shallow water column, to the pressure form stresses acting over the boundary of the column, and for a single shallow water layer this identity is

$$-h\, \nabla p = -\nabla P + p_{\text{a}}\, \nabla \eta - p_{\text{b}}\, \nabla \eta_{\text{b}}. \quad (36.111)$$

Nonetheless, we chose the more tedious derivation as it provides a check on the correctness of the transfer term and the buoyancy work term in the kinetic energy budget (36.106).

36.5.5 Mechanical energy budget

The mechanical energy per horizontal area for the shallow water layer is given by

$$\mathcal{M}^{\text{sw}} = \mathcal{K}^{\text{sw}} + \mathcal{P}^{\text{sw}} = (\rho/2)\,[h\,\boldsymbol{u}\cdot\boldsymbol{u} + g\,(\eta^2 - \eta_{\text{b}}^2)] = \rho\,h\,(\boldsymbol{u}\cdot\boldsymbol{u}/2 + g\,\overline{\eta}). \tag{36.112}$$

To form a budget equation for the mechanical energy we simply add the budgets for the gravitational potential energy and kinetic energy.

Summary of the potential and kinetic energy budgets

We here summarize the flux-form budgets for potential energy and kinetic energy (equations (36.90), (36.94), (36.98), (36.106), and (36.110)):

$$\partial_t \mathcal{P}^{\text{sw}} + \nabla\cdot(\boldsymbol{u}\,\mathcal{P}^{\text{sw}}) = g\,\rho\,h\,\overline{w} \tag{36.113a}$$

$$\partial_t \mathcal{K}^{\text{sw}} + \nabla\cdot(\boldsymbol{u}\,\mathcal{K}^{\text{sw}}) = -h\,\boldsymbol{u}\cdot\nabla p + \rho\,h\,\boldsymbol{u}\cdot\boldsymbol{F}. \tag{36.113b}$$

$$\partial_t \mathcal{K}^{\text{sw}} + \nabla\cdot[\boldsymbol{u}\,(\mathcal{K}^{\text{sw}} + \rho\,g\,h\,\eta^{\text{eff}})] = \rho\,g\,\eta^{\text{eff}}\,\nabla\cdot(h\,\boldsymbol{u}) + \rho\,h\,\boldsymbol{u}\cdot\boldsymbol{F}. \tag{36.113c}$$

$$\partial_t \mathcal{K}^{\text{sw}} + \nabla\cdot[\boldsymbol{u}\,(\mathcal{K}^{\text{sw}} + P)] + \delta_{\text{k}}(p_{\text{k}-1/2}\,\partial_t\eta_{\text{k}-1/2}) = -g\,\rho\,h\,\overline{w} + \rho\,h\,\boldsymbol{u}\cdot\boldsymbol{F} \tag{36.113d}$$

$$\partial_t \mathcal{K}^{\text{sw}} + \nabla\cdot(\boldsymbol{u}\,\mathcal{K}^{\text{sw}}) = \boldsymbol{u}\cdot(-\nabla P + p_{\text{a}}\,\nabla\eta - p_{\text{b}}\,\nabla\eta_{\text{b}}) + \rho\,h\,\boldsymbol{u}\cdot\boldsymbol{F}. \tag{36.113e}$$

Example forms of the mechanical energy budget

Adding equations (36.113a) and (36.113b) leads to the mechanical energy budget

$$\partial_t \mathcal{M}^{\text{sw}} + \nabla\cdot(\boldsymbol{u}\,\mathcal{M}^{\text{sw}}) = g\,\rho\,h\,\overline{w} - h\,\boldsymbol{u}\cdot\nabla p + \rho\,h\,\boldsymbol{u}\cdot\boldsymbol{F}, \tag{36.114}$$

whereas the sum of equations (36.113a) and (36.113d) leads to

$$\partial_t \mathcal{M}^{\text{sw}} + \nabla\cdot[\boldsymbol{u}\,(\mathcal{M}^{\text{sw}} + P)] + \delta_{\text{k}}(p_{\text{k}-1/2}\,\partial_t\eta_{\text{k}-1/2}) = \rho\,h\,\boldsymbol{u}\cdot\boldsymbol{F}. \tag{36.115}$$

As we discuss in Section 36.6, equations (36.114) and (36.115) hold also for the mechanical energy in a N-layer shallow water model.

Specializing to the single layer

Making use of the identity (see equation (36.104))

$$\mathcal{M}^{\text{sw}} + P = \rho\,h\,(\boldsymbol{u}\cdot\boldsymbol{u}/2 + g\,\eta^{\text{eff}}), \tag{36.116}$$

brings the mechanical energy budget (36.115) to the form

$$\partial_t \mathcal{M}^{\text{sw}} + \nabla\cdot[h\,\boldsymbol{u}\,(\rho\,\boldsymbol{u}\cdot\boldsymbol{u}/2 + \rho\,g\,\eta + p_{\text{a}})] + \delta_{\text{k}}(p_{\text{k}-1/2}\,\partial_t\eta_{\text{k}-1/2}) = \rho\,h\,\boldsymbol{u}\cdot\boldsymbol{F}. \tag{36.117}$$

Further note that $\partial_t\eta_{\text{b}} = 0$ so that

$$\nabla\cdot(h\,\boldsymbol{u}\,p_{\text{a}}) + \delta_{\text{k}}(p_{\text{k}-1/2}\,\partial_t\eta_{\text{k}-1/2}) = \nabla\cdot(h\,\boldsymbol{u}\,p_{\text{a}}) + p_{\text{a}}\,\partial_t\eta = h\,\boldsymbol{u}\cdot\nabla p_{\text{a}}, \tag{36.118}$$

where $\partial_t\eta + \nabla\cdot(h\,\boldsymbol{u}) = 0$. We are thus led to single layer mechanical energy budget

$$\partial_t \mathcal{M}^{\text{sw}} + \nabla\cdot[h\,\boldsymbol{u}\,(\boldsymbol{u}\cdot\boldsymbol{u}/2 + g\,\eta)] = -h\,\boldsymbol{u}\cdot\nabla p_{\text{a}} + \rho\,h\,\boldsymbol{u}\cdot\boldsymbol{F}. \tag{36.119}$$

which proves of use when studying the mechanical energy of shallow water waves in Section 55.3.2.

Shallow water form of the Bernoulli theorem

It is notable that in the steady state of an unforced perfect shallow water fluid (so with $p_\mathsf{a} = 0$ and $\boldsymbol{F} = 0$), equation (36.117) becomes

$$\boldsymbol{u} \cdot \nabla(\boldsymbol{u} \cdot \boldsymbol{u} + g\,h) = 0, \tag{36.120}$$

which is an expression of the Bernoulli theorem (Section 26.9) for steady shallow water flow.

Domain integrated mechanical energy

The budget equations (36.114) or (36.115) have already been layer integrated. So to study the domain integrated energetics requires only an area integral. The budget equation (36.115) is ideally suited for this purpose since all terms, except the non-conservative acceleration (e.g., friction), are written as a flux divergence and so they represent transfer processes. The domain integral of the flux-form mechanical energy equation (36.115) is

$$\int \partial_t \mathcal{M}^\mathsf{sw}\, \mathrm{d}\mathcal{S} = -\oint_{\partial\mathcal{S}} (\mathcal{M}^\mathsf{sw} + P)\, \boldsymbol{u} \cdot \hat{\boldsymbol{n}}\, \mathrm{d}l + \int_{\mathcal{S}} (-p_\mathsf{a}\, \partial_t \eta + h\, \rho\, \boldsymbol{u} \cdot \boldsymbol{F})\, \mathrm{d}\mathcal{S}, \tag{36.121}$$

where we set $\partial_t \eta_\mathsf{b} = 0$. The boundary integral on the right hand side is computed as a line integral around the edge of the layer. We consider three options for the layer geometry as illustrated in Figure 28.6. First, the thickness vanishes at the edge of the domain as in the case of shorelines, in which case the boundary integral vanishes since each term in the integral is thickness weighted (and thickness vanishes at the shoreline edge). Second, we assume the layer is bounded by vertical sidewalls, in which case $\boldsymbol{u} \cdot \hat{\boldsymbol{n}} = 0$ at the sidewall boundaries. Third, the domain has periodicity in one or both directions (e.g., a zonal channel), in which case the boundary integral again vanishes in the periodic directions.

Evidently, for either of the three types of domain boundaries considered above, the boundary integral in equation (36.121) vanishes, in which case the domain integrated mechanical energy budget reduces to

$$\int_{\mathcal{S}} \partial_t \mathcal{M}^\mathsf{sw}\, \mathrm{d}\mathcal{S} = \int_{\mathcal{S}} (-p_\mathsf{a}\, \partial_t \eta + h\, \rho\, \boldsymbol{u} \cdot \boldsymbol{F})\, \mathrm{d}\mathcal{S} = -\int_{\mathcal{S}} h\, \boldsymbol{u} \cdot (\nabla p_\mathsf{a} - \rho\, \boldsymbol{F})\, \mathrm{d}\mathcal{S}. \tag{36.122}$$

To reach the second equality we wrote

$$-\int_{\mathcal{S}} p_\mathsf{a}\, \partial_t \eta\, \mathrm{d}\mathcal{S} = \int_{\mathcal{S}} p_\mathsf{a}\, \nabla \cdot (h\, \boldsymbol{u})\, \mathrm{d}\mathcal{S} = -\int_{\mathcal{S}} h\, \boldsymbol{u} \cdot \nabla p_\mathsf{a}\, \mathrm{d}\mathcal{S}, \tag{36.123}$$

where we set

$$\int \nabla \cdot (p_\mathsf{a}\, h\, \boldsymbol{u})\, \mathrm{d}\mathcal{S} = 0, \tag{36.124}$$

which follows from the same reasoning used for the boundary integral in equation (36.121). Evidently, there is a nonzero domain integrated atmospheric pressure work only if there is a nonzero time tendency for the layer thickness. Furthermore, if p_a is a spatial constant, volume conservation for the full layer means that

$$\int_{\mathcal{S}} \partial_t \eta\, \mathrm{d}\mathcal{S} = -\int_{\mathcal{S}} \nabla \cdot (h\, \boldsymbol{u})\, \mathrm{d}\mathcal{S} = 0, \tag{36.125}$$

in which case we find that equation (36.122) is indeed self-consistent.

If the domain is bounded by sloping sides, then the mechanical energy vanishes at the horizontal boundaries, so that the time derivative acting on $\mathcal{M}^{\text{sw}}$ commutes with the area integral on the left hand side of equation (36.121). Alternatively, if the layer is bounded by fixed vertical walls, or is periodic in one or both directions, then the horizontal domain boundaries are static, again meaning that the time derivative commutes with the horizontal integral. In each case we can write the domain integrated mechanical energy equation as

$$\frac{\mathrm{d}}{\mathrm{d}t} \int_{\mathcal{S}} \mathcal{M}^{\text{sw}} \, \mathrm{d}\mathcal{S} = - \int_{\mathcal{S}} h \, \boldsymbol{u} \cdot (\nabla p_{\text{a}} - \rho \, \boldsymbol{F}) \, \mathrm{d}\mathcal{S}. \tag{36.126}$$

In the absence of work on the layer from atmospheric pressure, then the total mechanical energy is affected only via non-conservative forces, such as those from viscous friction. It then follows that for a perfect and unforced shallow water fluid, then the domain integrated mechanical energy remains constant, in which case there is an exact exchange between the domain integrated gravitational potential energy and kinetic energy.

36.5.6 Available potential energy

As discussed in Section 29.9, a huge portion of the gravitational potential energy is not realizable as kinetic energy, merely because the minimum potential energy state is when the fluid is at rest with some fluid parcels sitting above others. Available potential energy measures the gravitational potential energy that can be converted to kinetic energy through a reversible rearrangement of the fluid. We here display the available potential energy for a single shallow water layer in a simply connected domain, thus specializing the more general discussion given in Section 29.9 for a continuously stratified Boussinesq ocean.

Taking $z = 0$ as the reference level, the domain integrated gravitational potential energy for a single shallow water layer is

$$\int \mathcal{P}^{\text{sw}} \, \mathrm{d}\mathcal{S} = g \, \rho \int \mathrm{d}\mathcal{S} \int_{\eta_b}^{\eta} z \, \mathrm{d}z = \frac{g \, \rho}{2} \int (\eta^2 - \eta_b^2) \, \mathrm{d}\mathcal{S}. \tag{36.127}$$

We define a background or reference state potential energy as the potential energy contained in the fluid at rest, so that the free surface interface has its uniform area average value. Write the area average free surface height as

$$\langle \eta \rangle = \frac{1}{A} \int \eta \, \mathrm{d}\mathcal{S}, \tag{36.128}$$

where

$$A = \int \mathrm{d}\mathcal{S} \tag{36.129}$$

is the horizontal area integral over the full domain of the fluid. Hence, the reference state gravitational potential energy is realized when the surface height is flat at $z = \langle \eta \rangle$, so that

$$\int \mathcal{P}^{\text{sw}}_{\text{ref}} \, \mathrm{d}\mathcal{S} = \frac{g \, \rho}{2} \int (\langle \eta \rangle^2 - \eta_b^2) \, \mathrm{d}\mathcal{S}. \tag{36.130}$$

The available potential energy is defined by the difference

$$E_{\text{APE}} = \int (\mathcal{P}^{\text{sw}} - \mathcal{P}^{\text{sw}}_{\text{ref}}) \, \mathrm{d}\mathcal{S} = \frac{g \, \rho}{2} \int (\eta^2 - \langle \eta \rangle^2) \, \mathrm{d}\mathcal{S} = \frac{g \, \rho}{2} \int (\eta')^2 \, \mathrm{d}\mathcal{S} \geq 0, \tag{36.131}$$

where

$$\eta' = \eta - \langle \eta \rangle \tag{36.132}$$

is the anomalous free surface. Note how the bottom topography cancelled out from E_{APE} since η_{b}^2 appears in both $\mathscr{P}^{\text{sw}}$ and $\mathscr{P}^{\text{sw}}_{\text{ref}}$. Also note that to reach the final equality in equation (36.131) required the identity

$$\int (\eta - \langle\eta\rangle)^2 \, \mathrm{d}\mathcal{S} = \int (\eta^2 - 2\,\langle\eta\rangle\,\eta + \langle\eta\rangle^2) \, \mathrm{d}\mathcal{S} \tag{36.133a}$$

$$= \int \eta^2 \, \mathrm{d}\mathcal{S} + A\,\langle\eta\rangle^2 - 2\,\langle\eta\rangle \int \eta \, \mathrm{d}\mathcal{S} \tag{36.133b}$$

$$= \int \eta^2 \, \mathrm{d}\mathcal{S} - \langle\eta\rangle^2 \, A \tag{36.133c}$$

$$= \int (\eta^2 - \langle\eta\rangle^2) \, \mathrm{d}\mathcal{S}. \tag{36.133d}$$

Equation (36.131) shows that the available potential energy is non-negative for the shallow water layer. That is, any slope to the shallow water layer represents a store of positive available potential energy. We derive the available potential energy in Section 36.6.1 for the N-layer shallow water model, showing that it too is non-negative.

36.6 Energetics for N layers

We here generalize the single layer mechanical energy analysis from Section 36.5 to N-layers, making use of the N-layer equations from Section 35.4.

36.6.1 Potential energy and available potential energy

Here we develop the equation for potential energy in a form that naturally leads to the expression for the available potential energy.

Potential energy for N-layers

To derive the gravitational potential energy per horizontal area in a stacked shallow water model, first consider the case with $N = 3$ (Figure 35.6), in which the potential energy per horizontal area is

$$\mathscr{P}^{\text{sw}} = g \int_{\eta_{\mathsf{b}}}^{\eta} z\,\rho \, \mathrm{d}z = g\,\rho_3 \int_{\eta_{\mathsf{b}}}^{\eta_{5/2}} z \, \mathrm{d}z + g\,\rho_2 \int_{\eta_{5/2}}^{\eta_{3/2}} z \, \mathrm{d}z + g\,\rho_1 \int_{\eta_{3/2}}^{\eta} z \, \mathrm{d}z, \tag{36.134}$$

which then leads to

$$2\,\mathscr{P}^{\text{sw}} = g\,\rho_3\,(\eta_{5/2}^2 - \eta_{\mathsf{b}}^2) + g\,\rho_2\,(\eta_{3/2}^2 - \eta_{5/2}^2) + g\,\rho_1\,(\eta^2 - \eta_{3/2}^2) \tag{36.135a}$$

$$= g\,\eta_{5/2}^2\,(\rho_3 - \rho_2) + g\,\eta_{3/2}^2\,(\rho_2 - \rho_1) + g\,\eta_{1/2}^2\,\rho_1 - g\,\rho_3\,\eta_{\mathsf{b}}^2 \tag{36.135b}$$

$$= \rho_{\mathsf{ref}}\,(g^{\mathsf{r}}_{5/2}\,\eta_{5/2}^2 + g^{\mathsf{r}}_{3/2}\,\eta_{3/2}^2 + g^{\mathsf{r}}_{1/2}\,\eta_{1/2}^2) - g\,\rho_3\,\eta_{\mathsf{b}}^2, \tag{36.135c}$$

where $g^{\mathsf{r}}_{1/2} = g$ and $\eta_{1/2} = \eta$. Generalizing this expression to an arbitrary number of layers leads to

$$\mathscr{P}^{\text{sw}} = \frac{1}{2}\left[-g\,\rho_N\,\eta_{\mathsf{b}}^2 + \rho_{\mathsf{ref}} \sum_{\mathsf{k}=0}^{N-1} g^{\mathsf{r}}_{\mathsf{k}+1/2}\,\eta^2_{\mathsf{k}+1/2}\right], \tag{36.136}$$

with $\eta_{N+1/2} = \eta_{\mathsf{b}}$ (see Figure 35.6). The first term is a constant and so does not contribute to time changes of the potential energy, and so it is commonly ignored in the literature.

Available potential energy for N-layers

The time dependent terms in equation (36.136) are positive definite, so that potential energy increases when the reduced gravity increases and/or the layer interfaces deviate in either direction from their resting values. This behavior motivates us to introduce the available potential energy by decomposing the layer interface heights into their area mean and deviations, just as for the single layer in Section 36.5.6

$$\eta'_{\mathsf{k}\pm 1/2} = \eta_{\mathsf{k}\pm 1/2} - \langle \eta_{\mathsf{k}\pm 1/2} \rangle. \tag{36.137}$$

Volume conservation for each layer implies that the area mean, $\langle \eta_{\mathsf{k}-1/2} \rangle$, is a space and time constant. Substituting $\eta_{\mathsf{k}\pm 1/2} = \langle \eta_{\mathsf{k}\pm 1/2} \rangle + \eta'_{\mathsf{k}\pm 1/2}$ into equation (36.136) leads to

$$\begin{aligned} \mathcal{P}^{\mathsf{sw}} = \frac{1}{2} \left[-g\, \rho_N\, \eta_{\mathsf{b}}^2 + \rho_{\mathsf{ref}} \sum_{\mathsf{k}=0}^{N-1} g^{\mathsf{r}}_{\mathsf{k}+1/2}\, \langle \eta_{\mathsf{k}+1/2} \rangle^2 \right] \\ + \frac{\rho_{\mathsf{ref}}}{2} \left[2 \sum_{\mathsf{k}=0}^{N-1} g^{\mathsf{r}}_{\mathsf{k}+1/2}\, \langle \eta_{\mathsf{k}+1/2} \rangle\, \eta'_{\mathsf{k}+1/2} + \sum_{\mathsf{k}=0}^{N-1} g^{\mathsf{r}}_{\mathsf{k}+1/2}\, (\eta'_{\mathsf{k}+1/2})^2 \right]. \end{aligned} \tag{36.138}$$

The first bracketed term is a constant in time, and it measures the potential energy of the system when all interfaces sit at their area mean values, for which $\eta'_{\mathsf{k}1/2} = 0$. When performing an area integral over the full domain, the term with $\langle \eta_{\mathsf{k}+1/2} \rangle\, \eta'_{\mathsf{k}+1/2}$ vanishes since the area integral of $\eta'_{\mathsf{k}+1/2}$ vanishes. We thus define the available potential energy for the N-layer shallow water fluid

$$E_{\mathrm{APE}} = \frac{\rho_{\mathsf{ref}}}{2} \int \sum_{\mathsf{k}=0}^{N-1} g^{\mathsf{r}}_{\mathsf{k}+1/2}\, (\eta'_{\mathsf{k}+1/2})^2 \, \mathrm{d}\mathcal{S} \geq 0. \tag{36.139}$$

This expression generalizes the single layer form given by equation (36.131). As expected, the available potential energy increases whether a layer interface moves up or down, and it vanishes when all interfaces heights equal to their area mean values.

Time evolution of the potential energy

To derive an evolution equation for the potential energy, we take the time derivative of equation (36.136)

$$\partial_t \mathcal{P}^{\mathsf{sw}} = \rho_{\mathsf{ref}} \sum_{\mathsf{k}=0}^{N-1} g^{\mathsf{r}}_{\mathsf{k}+1/2}\, \eta_{\mathsf{k}+1/2}\, \partial_t \eta_{\mathsf{k}+1/2} = \rho_{\mathsf{ref}} \sum_{\mathsf{k}=0}^{N-1} g^{\mathsf{r}}_{\mathsf{k}+1/2}\, \eta_{\mathsf{k}+1/2} \sum_{\mathsf{j}=\mathsf{k}+1}^{N} \partial_t h_{\mathsf{j}}, \tag{36.140}$$

where the second equality made use of equation (35.80) to relate the interface height and the layer thickness. We can collapse the double sum through the following identities

$$\begin{aligned} \sum_{\mathsf{k}=0}^{N-1} g^{\mathsf{r}}_{\mathsf{k}+1/2}\, \eta_{\mathsf{k}+1/2} \sum_{\mathsf{j}=\mathsf{k}+1}^{N} \partial_t h_{\mathsf{j}} \\ = \partial_t h_N \sum_{\mathsf{j}=0}^{N-1} g^{\mathsf{r}}_{\mathsf{j}+1/2}\, \eta_{\mathsf{j}+1/2} + \partial_t h_{N-1} \sum_{\mathsf{j}=0}^{N-2} g^{\mathsf{r}}_{\mathsf{j}+1/2}\, \eta_{\mathsf{j}+1/2} + \ldots + \partial_t h_1\, g^{\mathsf{r}}_{1/2}\, \eta_{1/2}. \end{aligned} \tag{36.141}$$

The product of reduced gravity and interface height can be written in terms of the shallow water dynamic pressure from equation (35.88)

$$p_{\mathsf{k}}^{\mathrm{dyn}} = \rho_{\mathsf{ref}} \sum_{\mathsf{j}=0}^{\mathsf{k}-1} g'_{\mathsf{j}+1/2}\, \eta_{\mathsf{j}+1/2}, \tag{36.142}$$

in which case we have the potential energy budget

$$\partial_t \mathscr{P}^{\mathrm{sw}} = \sum_{\mathsf{k}=1}^{N} p_{\mathsf{k}}^{\mathrm{dyn}}\, \partial_t h_{\mathsf{k}} = -\sum_{\mathsf{k}=1}^{N} p_{\mathsf{k}}^{\mathrm{dyn}}\, \nabla \cdot (\boldsymbol{u}_{\mathsf{k}}\, h_{\mathsf{k}}), \tag{36.143}$$

where the second equality made use of the layer thickness equation (35.79a). Rearrangement brings this equation to its flux-form expression

$$\partial_t \mathscr{P}^{\mathrm{sw}} + \nabla \cdot \sum_{\mathsf{k}=1}^{N} p_{\mathsf{k}}^{\mathrm{dyn}}\, h_{\mathsf{k}}\, \boldsymbol{u}_{\mathsf{k}} = \sum_{\mathsf{k}=1}^{N} h_{\mathsf{k}}\, \boldsymbol{u}_{\mathsf{k}} \cdot \nabla p_{\mathsf{k}}^{\mathrm{dyn}}. \tag{36.144}$$

36.6.2 Potential energy and buoyancy work

Potential energy for N-layers

Following the method for the single layer in Section 36.5.1, we write the gravitational potential energy for a column of shallow water fluid as

$$\mathscr{P}^{\mathrm{sw}} = g \int_{\eta_{\mathrm{b}}}^{\eta} z\, \rho\, \mathrm{d}z = g \sum_{\mathsf{k}=1}^{N} \rho_{\mathsf{k}}\, h_{\mathsf{k}}\, \overline{\eta}_{\mathsf{k}} = \sum_{\mathsf{k}=1}^{N} \mathscr{P}_{\mathsf{k}}^{\mathrm{sw}}, \tag{36.145}$$

where, again,

$$h_{\mathsf{k}} = \eta_{\mathsf{k}-1/2} - \eta_{\mathsf{k}+1/2} \quad \text{and} \quad \overline{\eta}_{\mathsf{k}} = (\eta_{\mathsf{k}-1/2} + \eta_{\mathsf{k}+1/2})/2 \tag{36.146}$$

makes use of the layer thickness, h_{k}, and the average interface height, $\overline{\eta}_{\mathsf{k}}$. We can think of equation (36.145) as building the potential energy using layer properties, whereas the alternative expression (36.136) is built using interface properties.

Time evolution of the potential energy

Taking the time derivative of the potential energy (36.145) leads to

$$\begin{aligned}
\partial_t \mathscr{P}_{\mathsf{k}}^{\mathrm{sw}} &= g\, \rho_{\mathsf{k}}\, \partial_t (h_{\mathsf{k}}\, \overline{\eta}_{\mathsf{k}}) && \text{(36.147a)}\\
&= g\, \rho_{\mathsf{k}} (\partial_t h_{\mathsf{k}}\, \overline{\eta}_{\mathsf{k}} + h_{\mathsf{k}}\, \partial_t \overline{\eta}_{\mathsf{k}}) && \text{(36.147b)}\\
&= g\, \rho_{\mathsf{k}} \left[-\overline{\eta}_{\mathsf{k}}\, \nabla \cdot (\boldsymbol{u}_{\mathsf{k}}\, h_{\mathsf{k}}) + h_{\mathsf{k}}\, (\overline{w}_{\mathsf{k}} - \boldsymbol{u}_{\mathsf{k}} \cdot \nabla \overline{\eta}_{\mathsf{k}}) \right] && \text{(36.147c)}\\
&= g\, \rho_{\mathsf{k}}\, h_{\mathsf{k}}\, \overline{w}_{\mathsf{k}} - g\, \nabla \cdot (\rho_{\mathsf{k}}\, \overline{\eta}_{\mathsf{k}}\, h_{\mathsf{k}}\, \boldsymbol{u}_{\mathsf{k}}) && \text{(36.147d)}\\
&= g\, \rho_{\mathsf{k}}\, h_{\mathsf{k}}\, \overline{w}_{\mathsf{k}} - \nabla \cdot (\boldsymbol{u}_{\mathsf{k}}\, \mathscr{P}_{\mathsf{k}}^{\mathrm{sw}}), && \text{(36.147e)}
\end{aligned}$$

so that the flux-form budget is given by

$$\partial_t \mathscr{P}_{\mathsf{k}}^{\mathrm{sw}} + \nabla \cdot (\boldsymbol{u}\, \mathscr{P}_{\mathsf{k}}^{\mathrm{sw}}) = g\, \rho_{\mathsf{k}}\, h_{\mathsf{k}}\, \overline{w}_{\mathsf{k}}. \tag{36.148}$$

This budget is identical to equation (36.90) that we discussed for a single layer, with the buoyancy work term exposed on the right hand side.

36.6.3 Kinetic energy

Kinetic energy and work from pressure gradients

Following our treatment in Section 36.5.2, consider the kinetic energy per horizontal area contained in a shallow water layer

$$\mathcal{K}^{\text{sw}}_{\text{k}} = \frac{1}{2}\int_{\eta_{\text{k}+1/2}}^{\eta_{\text{k}-1/2}} \rho_{\text{ref}}\, \boldsymbol{u}_{\text{k}} \cdot \boldsymbol{u}_{\text{k}}\, \mathrm{d}z = \frac{1}{2}\, \rho_{\text{ref}}\, h_{\text{k}}\, \boldsymbol{u}_{\text{k}} \cdot \boldsymbol{u}_{\text{k}}. \tag{36.149}$$

Note that we set the density equal to the reference density as per the Boussinesq ocean, whereby the inertial mass is determined by the reference density (Section 29.1).

To derive an evolution equation for kinetic energy, multiply the thickness equation (35.79a) by $\boldsymbol{u}_{\text{k}} \cdot \boldsymbol{u}_{\text{k}}$, and take the dot product of the vector-invariant velocity equation (35.113) with $h_{\text{k}}\, \boldsymbol{u}_{\text{k}}$,

$$(\boldsymbol{u}_{\text{k}} \cdot \boldsymbol{u}_{\text{k}})\, \partial_t h_{\text{k}} = -(\boldsymbol{u}_{\text{k}} \cdot \boldsymbol{u}_{\text{k}})\, \nabla \cdot (h_{\text{k}}\, \boldsymbol{u}_{\text{k}}) \tag{36.150a}$$

$$h_{\text{k}}\, \boldsymbol{u}_{\text{k}} \cdot \partial_t \boldsymbol{u}_{\text{k}} = -h_{\text{k}}\, \boldsymbol{u}_{\text{k}} \cdot \nabla(p_{\text{k}}/\rho_{\text{ref}} + \boldsymbol{u}_{\text{k}} \cdot \boldsymbol{u}_{\text{k}}/2) + h_{\text{k}}\, \boldsymbol{u}_{\text{k}} \cdot \boldsymbol{F}_{\text{k}}, \tag{36.150b}$$

where we included an acceleration, $\boldsymbol{F}_{\text{k}}$, arising from friction or boundary stresses, as discussed in Section 35.6.5. Making use of these expressions leads to the time derivative of the kinetic energy per area, $\mathcal{K}^{\text{sw}}_{\text{k}} = \rho_{\text{ref}}\, h_{\text{k}}\, \boldsymbol{u}_{\text{k}} \cdot \boldsymbol{u}_{\text{k}}/2$, of a shallow water layer

$$(2/\rho_{\text{ref}})\, \partial_t \mathcal{K}^{\text{sw}}_{\text{k}} = \partial_t(h_{\text{k}}\, \boldsymbol{u}_{\text{k}} \cdot \boldsymbol{u}_{\text{k}}) \tag{36.151a}$$

$$= (\boldsymbol{u}_{\text{k}} \cdot \boldsymbol{u}_{\text{k}})\, \partial_t h_{\text{k}} + 2\, h_{\text{k}}\, \boldsymbol{u}_{\text{k}} \cdot \partial_t \boldsymbol{u}_{\text{k}} \tag{36.151b}$$

$$= -(\boldsymbol{u}_{\text{k}} \cdot \boldsymbol{u}_{\text{k}})\, \nabla \cdot (h_{\text{k}}\, \boldsymbol{u}_{\text{k}}) - 2\, h_{\text{k}}\, \boldsymbol{u}_{\text{k}} \cdot \nabla(p_{\text{k}}/\rho_{\text{ref}} + \boldsymbol{u}_{\text{k}} \cdot \boldsymbol{u}_{\text{k}}/2) + 2\, h_{\text{k}}\, \boldsymbol{u}_{\text{k}} \cdot \boldsymbol{F}_{\text{k}} \tag{36.151c}$$

$$= -2\, \nabla \cdot [\boldsymbol{u}_{\text{k}}\, \mathcal{K}^{\text{sw}}_{\text{k}}/\rho_{\text{ref}}] - 2\, h_{\text{k}}\, \boldsymbol{u}_{\text{k}} \cdot \nabla(p_{\text{k}}/\rho_{\text{ref}}) + 2\, h_{\text{k}}\, \boldsymbol{u}_{\text{k}} \cdot \boldsymbol{F}_{\text{k}}, \tag{36.151d}$$

which then leads to the equivalent forms for the layer integrated kinetic energy budget

$$\partial_t \mathcal{K}^{\text{sw}}_{\text{k}} + \nabla \cdot (\boldsymbol{u}_{\text{k}}\, \mathcal{K}^{\text{sw}}_{\text{k}}) = -h_{\text{k}}\, \boldsymbol{u}_{\text{k}} \cdot [\nabla p_{\text{k}} - \rho_{\text{ref}}\, \boldsymbol{F}_{\text{k}}], \tag{36.152a}$$

$$\partial_t \mathcal{K}^{\text{sw}}_{\text{k}} + \nabla \cdot [\boldsymbol{u}_{\text{k}}\, (\mathcal{K}^{\text{sw}}_{\text{k}} + h_{\text{k}}\, p_{\text{k}})] = p_{\text{k}}\, \nabla \cdot (h_{\text{k}}\, \boldsymbol{u}_{\text{k}}) + \rho_{\text{ref}}\, h_{\text{k}}\, \boldsymbol{u}_{\text{k}} \cdot \boldsymbol{F}_{\text{k}}. \tag{36.152b}$$

Recall that the pressure gradient is given by equation (35.88)

$$\nabla p_{\text{k}} = \nabla p_{\text{a}} + \nabla p^{\text{dyn}}_{\text{k}} = \nabla p_{\text{a}} + \rho_{\text{ref}}\, \nabla M^{\text{dyn}}_{\text{k}}, \tag{36.153}$$

which arises from gradients in the applied atmospheric pressure plus the dynamic pressure, and where $M^{\text{dyn}}_{\text{k}} = \rho_{\text{ref}}\, p^{\text{dyn}}_{\text{k}}$ is the Montgomery potential from Section 35.4.3. The budget equation (36.152b) corresponds to the single layer equation (36.98), where we identify the dynamic pressure for shallow water model with just a single layer

$$p^{\text{dyn}}_{\text{k}=1} = \rho\, g\, \eta^{\text{eff}} = p_{\text{a}} + \rho\, g\, \eta. \tag{36.154}$$

Kinetic energy and buoyancy work

The single layer discussion in Section 36.5.3 fully anticipated the N-layer case, so that we can immediately translate equation (36.106) to an arbitrary layer

$$\partial_t \mathcal{K}^{\text{sw}}_{\text{k}} + \nabla \cdot [\boldsymbol{u}\, (\mathcal{K}^{\text{sw}}_{\text{k}} + P_{\text{k}})] + \delta_{\text{k}}(p_{\text{k}-1/2}\, \partial_t \eta_{\text{k}-1/2}) = -g\, \rho_{\text{k}}\, h_{\text{k}}\, \overline{w}_{\text{k}} + \rho_{\text{k}}\, h_{\text{k}}\, \boldsymbol{u}_{\text{k}} \cdot \boldsymbol{F}_{\text{k}}. \tag{36.155}$$

36.6.4 Comments and further study

The discussion of mechanical energy for the single shallow water layer in Section 36.5.5 directly transfers to the N-layer case, thus making it unnecessary for us to develop the theory any further.

Elements of the discussion in this section are motivated by the energetic analysis of *Loose et al.* (2022), who detail the mechanical energy in a stacked shallow water model and decompose the energy budget into mean and transient eddy contributions.

36.7 Momentum balance in a zonal channel

In this section we study the vertically integrated steady momentum budget for a single shallow water layer of density ρ in a zonally re-entrant channel, such as depicted in Figure 36.7. Such shallow water models have been used to garner insights into adiabatic aspects of Southern Ocean circulation, and we keep this application in mind for the following (so that $f < 0$). We are particularly interested in the force balances required to reach a steady flow in the presence of a prescribed constant wind stress acceleration, $\boldsymbol{\tau}/\rho$. The channel has arbitrary topography, including northern and southern bounds with sloping shelves and shorelines. Applying a zonal surface stress inserts zonal momentum to the fluid through the ocean surface. For simplicity we set the atmospheric pressure to zero, $p_{\mathrm{a}} = 0$, so that the bottom pressure is $p_{\mathrm{b}} = \rho\, g\, h$, and there is no form stress acting on the layer's upper surface.

A similar analysis was presented in Section 28.5 for the vertically integrated axial angular momentum budget in a continuously stratified fluid. Following from that analysis, we ignore the role of internal viscous friction. However, we consider bottom frictional stresses written as a quadratic bottom drag

$$\boldsymbol{F}^{\mathrm{drag}} = -C_{\mathrm{d}}\, \boldsymbol{u}\, |\boldsymbol{u}|, \tag{36.156}$$

where $C_{\mathrm{d}} > 0$ is a dimensionless bottom drag coefficient.

The horizontal areal extent of the domain is a function of space and time since the shallow water layer rises up and down the northern and southern shorelines as motion occurs. Even so, since layer thickness vanishes at the shoreline edge, the horizontal boundary conditions for the shallow water layer are easy to apply when working with the thickness weighted equations. That is, all thickness weighted fields vanish at the shoreline edge merely since the thickness vanishes at the edge. Indeed, working with thickness weighted fields allows us to handle any degree of vanishing layer thicknesses, including if the topography in the center of the channel becomes an island rather than a submerged seamount. We also made use of this property of thickness weighted budgets in Section 28.5 where we also considered sloping sides rather than the commonly considered, yet less realistic, vertical sides.

36.7.1 Volume transport for steady flow

Before considering the steady force balance, we establish a constraint based on volume conservation by considering the steady thickness equation

$$\nabla \cdot (h\, \boldsymbol{u}) = 0. \tag{36.157}$$

As discussed for non-divergent flow in Chapter 21, this non-divergence condition means that there is zero net steady transport crossing any simply connected closed contour in the fluid. A particularly interesting closed contour is one that is periodic and extends across the full zonal extent of the channel (see Figure 36.7), in which case

$$\oint h\, \boldsymbol{u} \cdot \hat{\boldsymbol{n}}\, \mathrm{d}s = 0, \tag{36.158}$$

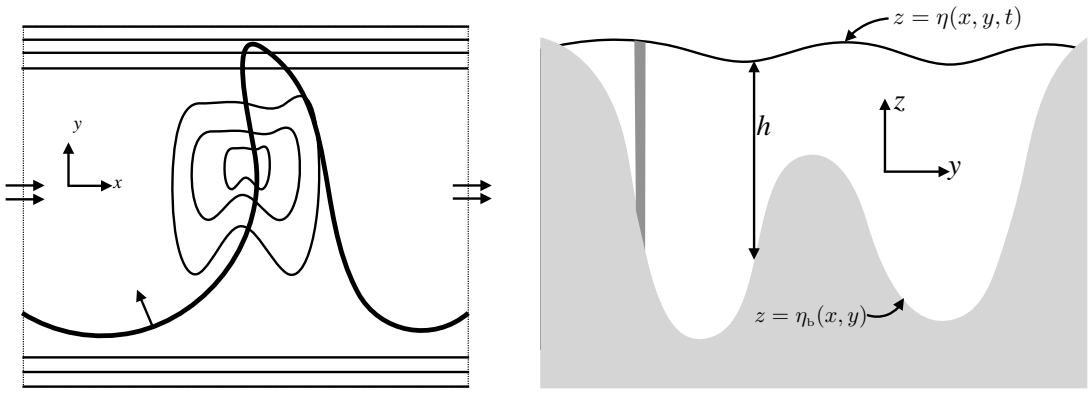

FIGURE 36.7: A zonally periodic/re-entrant southern hemisphere channel with northern and southern shelves and arbitrary seamount topography. Flow that leaves either the east or west boundary is assumed to re-enter the other side, so that the topology is periodic zonally. Left panel: horizontal (plan) view, showing the contours of the shelves and the topography, with flow leaving one of the zonal ends re-entering the other. The arbitrary dark solid contour extends across the zonal extent of the channel and is periodic, with a unit vector, $\hat{\boldsymbol{n}}$, depicted normal to a point along the contour. In a steady state, the net fluid transport crossing this contour vanishes: $\oint h\, \boldsymbol{u} \cdot \hat{\boldsymbol{n}}\, \mathrm{d}s = 0$, meaning that there is no accumulation of fluid within any region of the channel. Right panel: meridional-vertical view through an arbitrary longitude, along with a sample vertical column of water extending from the bottom to the surface. The shoreline edges occur where the layer thickness vanishes on the northern and southern shelves. So although the position of the shoreline edge is a function of space and time (since the fluid moves up and down the shoreline slope), the vanishing layer thickness found at the edge renders a simple treatment of boundary conditions for the thickness weighted equations.

where $\oint$ denotes a periodic line integral across the zonal extent of the channel, $\hat{\boldsymbol{n}}$ is a unit vector normal to the contour, and $\mathrm{d}s$ is the arc-length line element along the contour. The constraint (36.158) reflects the inability of the steady flow to build up or deplete the fluid on one region of the channel at the expense of another. In particular, if the contour follows a constant latitude line, then we see that for a steady state there is no net meridional transport across a latitude circle

$$\oint h\, \boldsymbol{u} \cdot \hat{\boldsymbol{y}}\, \mathrm{d}x = \oint h\, v\, \mathrm{d}x = 0 \qquad \text{steady flow.} \tag{36.159}$$

This result means that the thickness weighted Coriolis acceleration appearing in the zonal momentum equation vanishes when integrated zonally

$$\oint f\, h\, v\, \mathrm{d}x = f \oint h\, v\, \mathrm{d}x = 0 \qquad \text{steady flow.} \tag{36.160}$$

We make use of this result in Section 36.7.3.

36.7.2 Steady meridional balances

Consider the thickness weighted meridional momentum equation (36.35b) in the presence of a wind stress and bottom drag

$$\partial_t(h\, v) + \partial_x(h\, u\, v) + \partial_y(h\, v^2 + g\, h^2/2) + u\, h\, f = -(p_b/\rho)\, \partial_y \eta_b + \tau^y/\rho - C_d\, v\, |\boldsymbol{u}|. \tag{36.161}$$

Integrating zonally over the channel removes the zonal transport term, $\partial_x(h\, u\, v)$, due to periodicity

$$\oint \left[\partial_t(h\, v) + \partial_y(h\, v^2 + g\, h^2/2) + u\, h\, f\right] \mathrm{d}x = \oint \left[-(p_b/\rho)\, \partial_y \eta_b + \tau^y/\rho - C_d\, v\, |\boldsymbol{u}|\right] \mathrm{d}x. \tag{36.162}$$

We can pull the time derivative outside of the zonal integral since the domain is zonally periodic, in which case the time changes to the net meridional transport across a latitude circle are given by

$$\frac{\mathrm{d}}{\mathrm{d}t} \oint v\, h \,\mathrm{d}x = \oint \left[-\partial_y (h\, v^2 + g\, h^2/2) - u\, h\, f - (p_{\mathrm{b}}/\rho)\, \partial_y \eta_{\mathrm{b}} + \tau^y/\rho - C_{\mathrm{d}}\, v\, |\boldsymbol{u}| \right] \mathrm{d}x. \tag{36.163}$$

Correspondingly, a steady state along a latitude circle is realized by the balance

$$\oint \left[\partial_y (h\, v^2 + g\, h^2/2) + u\, h\, f \right] \mathrm{d}x = \oint \left[-(p_{\mathrm{b}}/\rho)\, \partial_y \eta_{\mathrm{b}} + \tau^y/\rho - C_{\mathrm{d}}\, v\, |\boldsymbol{u}| \right] \mathrm{d}x. \tag{36.164}$$

The right hand side represents forcing by the topographic form stress, meridional wind stress, and bottom drag. That forcing, integrated over a latitude circle, balances the left hand side, which is the Coriolis acceleration arising from zonal motion, plus the meridional divergence of meridional momentum advection plus layer integrated pressure.

We can eliminate the nonlinear term on the left hand side of the balance (36.164) by integrating meridionally across the channel. Since $h = 0$ at the shoreline edges we know that $h\, v^2 + g\, h^2/2$ vanishes at the boundaries, thus leaving

$$\int \left[\oint u\, h\, f \,\mathrm{d}x \right] \mathrm{d}y = \int \left[\oint \left[-(p_{\mathrm{b}}/\rho)\, \partial_y \eta_{\mathrm{b}} + \tau^y/\rho - C_{\mathrm{d}}\, v\, |\boldsymbol{u}| \right] \mathrm{d}x \right] \mathrm{d}y. \tag{36.165}$$

This is a balance between the integrated meridional Coriolis force on the left hand side with pressure form stress, winds, and bottom drag on the right hand side.

36.7.3 Steady zonal balance

Now consider the thickness weighted zonal momentum equation (36.35a), here with bottom drag and wind stress contributions

$$\partial_t (h\, u) + \partial_x (h\, u^2 + g\, h^2/2) + \partial_y (h\, u\, v) - v\, h\, f = -(p_{\mathrm{b}}/\rho)\, \partial_x \eta_{\mathrm{b}} + \tau^x/\rho - C_{\mathrm{d}}\, u\, |\boldsymbol{u}|. \tag{36.166}$$

Assuming a steady state and integrating along a latitude circle leads to

$$\rho \oint \partial_y (h\, u\, v) \mathrm{d}x = \oint \left[-p_{\mathrm{b}}\, \partial_x \eta_{\mathrm{b}} + \tau^x - C_{\mathrm{d}}\, \rho\, u\, |\boldsymbol{u}| \right] \mathrm{d}x, \tag{36.167}$$

where we dropped the Coriolis acceleration as per volume conservation in equation (36.160). For flows that are quasi-linear, the nonlinear term $\partial_y (h\, u\, v)$ will be subdominant to the wind stress and topographic form stress, thus leading to the approximate balance along each latitude circle

$$\oint p_{\mathrm{b}}\, \partial_x \eta_{\mathrm{b}} \,\mathrm{d}x \approx \oint \left[\tau^x - C_{\mathrm{d}}\, \rho\, u\, |\boldsymbol{u}| \right] \mathrm{d}x \qquad \text{nonlinear term small.} \tag{36.168}$$

We realize an exact balance over the full channel domain by meridionally integrating the latitude balance (36.167), in which the nonlinear term $\partial_y (h\, u\, v)$ drops out since $h = 0$ at the northern and southern shoreline edges

$$\int \left[\oint \tau^x \,\mathrm{d}x \right] \mathrm{d}y = \int \left[\oint \left[p_{\mathrm{b}}\, \partial_x \eta_{\mathrm{b}} + C_{\mathrm{d}}\, \rho\, u\, |\boldsymbol{u}| \right] \mathrm{d}x \right] \mathrm{d}y. \tag{36.169}$$

Again, this is an exact steady state balance realized by integrating the zonal thickness weighted momentum equation over the full domain channel. It is a balance between the zonal momentum input from the winds (left hand side) to the full domain, and the integrated bottom form stress

plus bottom frictional drag (right hand side).

36.7.4 The role of frictional bottom drag

Consider a flat bottom channel, in which case the area integrated balance (36.169) is between winds and bottom drag

$$\int \left[\oint \tau^x \, dx \right] dy = \int \left[\oint C_d \, \rho \, u \, |\boldsymbol{u}| \, dx \right] dy \Longrightarrow \rho^{-1} \langle \tau^x \rangle = C_d \, \langle u \, |\boldsymbol{u}| \rangle, \tag{36.170}$$

where the angle brackets denote a channel area mean. Typical empirical values for the dimensionless bottom drag coefficient are

$$C_d \approx 2 \times 10^{-3}. \tag{36.171}$$

An area mean eastward zonal wind stress of $\langle \tau^x \rangle = 0.1$ N m^{-2} leads to a root-mean-square zonal velocity of

$$\sqrt{\langle u \, |\boldsymbol{u}| \rangle} \approx \sqrt{\langle u^2 \rangle} \approx 0.2 \text{ m s}^{-1}, \tag{36.172}$$

where the first approximation follows from assuming the zonal velocity dominates over the meridional velocity. How realistic is this number for the Southern Ocean? Field measurements from the Southern Ocean suggest that vertically and area averaged velocities are far smaller than this value. Furthermore, if this value occurred in a channel 4000 m deep and 2000 km wide (a rough idealization of the Antarctic Circumpolar Current), then this vertically averaged velocity would yield a zonal volume transport of $\approx 1500 \times 10^6$ m^3 s^{-1}, which is about ten times larger than the measured transport through the Drake Passage.

Munk and Palmén (1951) identified the problematic aspect of assuming a bottom frictional stress balance for the Southern Ocean. In brief, the field measurements do not support a frictional balance, either from bottom drag or from internal turbulent viscous friction. By inference, they proposed that topographic form stress is the dominant term that balances wind stress in the Southern Ocean. They supported that inference through estimates based on topographic features encountered by the Antarctic Circumpolar Current in its transit of the Southern Ocean. Subsequent studies using theory, field measurements, and numerical models support their conclusion. Indeed, in numerical models one finds that so long as there is only a modest degree of bottom slope, the bottom topographic form stress dominates over bottom drag. Given these considerations, we dispense with bottom drag for the remainder of this section.

36.7.5 Correlation between surface height and topographic slope

Given the minor role for bottom drag in establishing a steady channel flow in the Southern Ocean, the balance (36.169) says that an eastward area integrated wind stress must be balanced by a westward topographic form stress

$$\int \left[\oint \tau^x \, dx \right] dy = \int \left[\oint p_b \, \partial_x \eta_b \, dx \right] dy. \tag{36.173}$$

What is required to establish a westward topographic form stress? Quite simply, in the area mean, there must be an anomalously large bottom pressure in regions where $\partial_x \eta_b > 0$ and an anomalously small bottom pressure in regions where $\partial_x \eta_b < 0$. Bottom pressure in a shallow water layer is determined by the column thickness. Hence, to establish the anomalous bottom pressures requires an anomalously thick fluid column upstream of topographic bumps and thin fluid column downstream. This situation is illustrated in Figure 36.8 described in Section 36.7.7.

To further reveal the correlation between surface height and bottom topography, write

$p_\flat = \rho\, g\, h$ and use $\eta = h + \eta_\flat$ so that

$$p_{\rm bot}\, \partial_x \eta_\flat = \rho\, g\, (\eta - \eta_\flat)\, \partial_x \eta_\flat = \rho\, g\, \eta\, \partial_x \eta_\flat - (g\, \rho/2)\, \partial_x \eta_\flat^2. \tag{36.174}$$

The balance (36.173) thus becomes

$$\langle \tau^x \rangle = \rho\, g \langle \eta\, \partial_x \eta_\flat \rangle. \tag{36.175}$$

Furthermore, due to zonal periodicity, it is only the zonal anomalies in η and $\eta_\flat$ that contribute so that

$$\langle \tau^x \rangle = \rho\, g \langle \eta'\, \partial_x \eta_\flat' \rangle, \tag{36.176}$$

where

$$\eta = \eta' + L^{-1} \oint \eta\, {\rm d}x \qquad \text{and} \qquad \eta_\flat = \eta_b' + L^{-1} \oint \eta_\flat\, {\rm d}x, \tag{36.177}$$

with $L = \oint {\rm d}x$ the zonal length of the channel. With $\langle \tau^x \rangle > 0$, we see that surface height anomalies must be positively correlated with the bottom slope, $\int \eta'\, \partial_x \eta_\flat'\, {\rm d}x\, {\rm d}y > 0$. That is, the surface height is high where topography slopes are positive and low where topography slopes are negative.

As noted above, we must have a positive correlation between surface height anomalies and topographic slope, as in equation (36.176). It follows that a nonzero zonal integrated topographic form stress requires a nonzero phase shift between surface height anomalies and the bottom topography anomalies. That is, if the surface height and bottom topography were perfectly aligned along a latitude circle, then $\oint \eta'\, \partial_x \eta_\flat'\, {\rm d}x = 0$, in which case there is a zero zonal integrated topographic form stress along that latitude. The required phase shift between the free surface and bottom topography has the free surface shifted ahead (i.e., to the west) of the topography. We consider an explicit example in Section 36.7.7 to help in our understanding.

36.7.6 Connection to meridional geostrophic transport

Zonal periodicity allows us to swap the zonal derivative in the balance (36.176) so that

$$\langle \tau^x \rangle = -\rho\, g \langle \partial_x \eta'\, \eta_\flat' \rangle \tag{36.178}$$

For the large scale flows under consideration here, we can assume that $g\, \partial_x \eta'$ is associated with an anomalous meridional geostrophic velocity

$$g\, \partial_x \eta' = f\, v_{\rm g}' \tag{36.179}$$

so that the balance (36.178) is

$$\langle \tau^x \rangle = -\rho\, \langle f\, v_{\rm g}'\, \eta_\flat' \rangle. \tag{36.180}$$

Hence, the steady balance is realized with anomalous meridional geostrophic transport correlated with topographic anomalies. Note that periodicity means that the steady meridional geostrophic transport has a zero zonal integral

$$\oint v_{\rm g}'\, {\rm d}x = (g/f) \oint \partial_x \eta'\, {\rm d}x = 0, \tag{36.181}$$

which follows from the steady volume balance discussed in Section 36.7.1.

36.7.7 Sinusoidal example

To help further our understanding of the balance (36.176), and the phase shift required to develop nonzero zonal integrated topographic form stress, consider a sinusoidal topography that

is a function only of the zonal direction. Also assume that the free surface has a sinusoidal shape (though we do not specify the dynamical mechanism for it to reach this shape). With these assumptions the anomalous surface height and bottom topography can be written

$$\eta' = \eta_o \sin(\kappa\, x + \varphi) \qquad \text{and} \qquad \eta'_{\rm b} = D \sin(\kappa\, x) \tag{36.182}$$

where $\eta_o > 0$ is a constant amplitude for the free surface undulations, $D > 0$ is the constant amplitude for the bottom undulations, $\kappa = 2\,\pi\, n/L$ is the wavenumber for the undulations, $n > 0$ is an integer, L is the size of the zonal channel, and φ is a phase shift between the topography and the free surface. The corresponding meridional geostrophic flow is given by

$$f\, v'_{\rm g} = g\, \partial_x \eta' = g\, \kappa\, \eta_o \cos(\kappa\, x + \varphi). \tag{36.183}$$

Plugging into the balance (36.176) leads to

$$\sin\varphi = \left[\frac{L\, \langle \tau^x \rangle}{D\, \rho\, g\, \eta_o\, \pi\, n} \right]. \tag{36.184}$$

For $\langle \tau^x \rangle > 0$ we see that the free surface undulations are, as expected, shifted to the west of the bottom topography undulations. As an explicit example from an idealized channel configuration, set

$$L = 10^7 \text{ m} \qquad D = 10^3 \text{ m} \qquad \eta_o = 1 \text{ m} \qquad \tau^x = 1 \text{ N m}^{-2}, \tag{36.185}$$

in which case

$$\sin\varphi \approx (\pi\, n)^{-1}. \tag{36.186}$$

For $n = 1$, which corresponds to just one topographic bump, then we have a phase shift of $\varphi \approx 18^\circ$, and this case is depicted in Figure 36.8 for the southern hemisphere. If there are two bumps, then the phase shift is reduced to $\varphi \approx 9^\circ$ since each bump shares half the burden of balancing the wind stress.

Summarizing the dependencies

We here highlight the various dependencies in the phase equation (36.184).

- The phase shift increases with both larger wind stress and larger zonal extent to the domain. This dependency arises since with enhanced wind stress and an enhanced zonal *fetch* (distance over which the winds blow), there is an increase in zonal momentum inserted to the ocean that must be absorbed by the bottom. The larger phase shift increases this topographic form stress, thus enabling the balance.

- Conversely, the phase shift decreases for larger topography D, and larger undulations in the free surface, η_o, in which case the free surface becomes more aligned with the topographic ridges. This result follows since the topographic form stress is larger for larger topography, thus requiring less phase shift in the surface wave patterns to affect a bottom pressure anomaly.

- Phase shifts decrease when there are more topographic bumps in the channel, with n the parameter setting the number of bumps. For the Southern Ocean, *Munk and Palmén* (1951) identified around four or five large-scale topographic features that provide the dominant balance for the zonal wind stress.

- What if the parameters are such that the right hand side of equation (36.184) has a magnitude larger than unity (e.g., huge winds, very long fetch, small topography, small surface height amplitude)? This situation signals that topographic form stress is insufficient

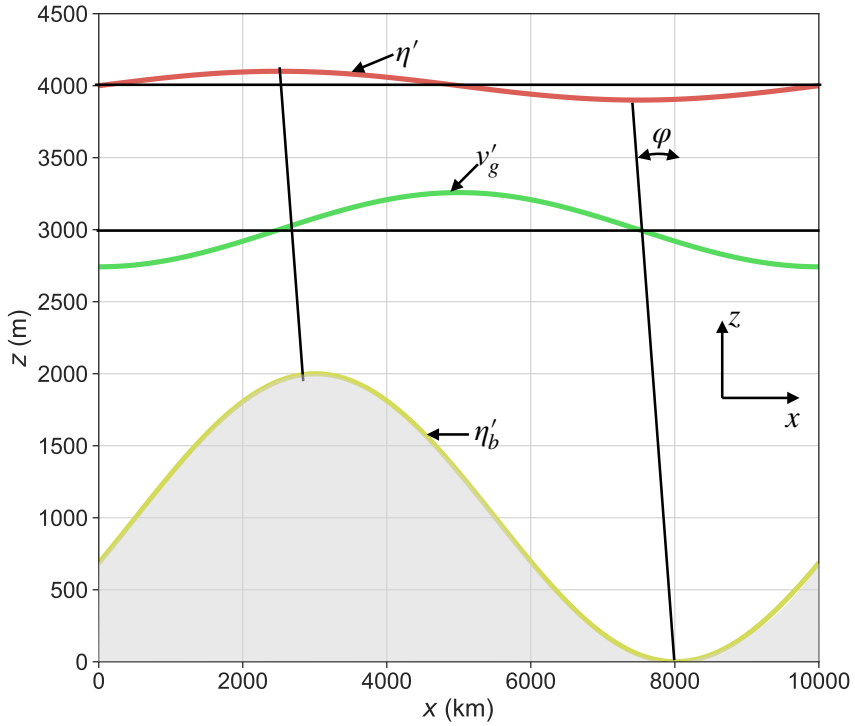

FIGURE 36.8: Zonal-vertical view of the wind stress and bottom pressure acting on a steady state layer of shallow water fluid flowing over a sinusoidal bump (north is directed into the page and east is to the right). The eastward surface stress acts in the $+\hat{\boldsymbol{x}}$ direction and it is balanced by a westward topographic form stress. To establish this form stress when integrated over the zonal extent of the channel requires the sea surface undulations to be phase shifted to the west of the bottom topography undulations, with the phase shift, φ, given by equation (36.184). To better visualize the sea surface, the surface undulations are in units of cm whereas the bottom topography undulations are in units of m. In general, for the topographic form stress to balance the wind stress, the bottom pressure must be anomalously large where $\partial\eta_b/\partial x > 0$ and small where $\partial\eta_b/\partial x < 0$, thus leading to the anomalously thick fluid column upstream of the bump and thin column downstream. This correlation also leads to a corresponding meridional geostrophic flow as shown here by the green curve for the southern hemisphere where $f < 0$, with $v_g > 0$ (northward) when shown above the horizontal line and $v_g < 0$ (southward) when below the line. Compare this figure to the analogous schematic in Figure 28.8.

to balance the winds. In a numerical model, one can merely increase the topograhic wavenumber, n, to increase the topographic form stress. Yet where topography is fixed, such as in Nature, then bottom frictional stresses come into play to help reach a force balance (see Section 36.7.4).

Distinguishing steady motion from zero motion

Why is the phase shift (36.184) independent of the fluid depth? One might suspect that to reach a force balance would require more form stress if there is more fluid. Instead, the force balance, as reflected in the phase shift, depends on the zonal anomalies of the surface height and bottom topography. The depth of the fluid is absent.

The answer to this question is that we are seeking a force balance. When forces are balanced there is no acceleration and thus, as per Newton's second law, the fluid maintains a constant velocity relative to the laboratory reference frame. If we instead wished to stop the fluid, then we would need to decelerate all fluid elements to zero velocity. Determining the forces needed to stop the fluid requires the total fluid mass and thus its depth (as well as the time over which the fluid is to stop). If the fluid is in motion, then halting the motion requires a net force, and that is a very different consideration than the case of zero net force. So in brief, a steady state refers

to the absence of time dependence in the fluid from the perspective of an Eulerian (laboratory) observer, with a steady state *not* necessarily a static state.

36.7.8 Comments and further study

Gyres and channels

The dominance of topographic form stress for the steady Southern Ocean balance contrasts to many of the frictional theories for gyre circulations, such as the classic solutions discussed in Section 39.7. In those theories, based on flat bottom and vertical side configurations, the curl of the wind stress is balanced by torques created by friction.[10] One is thus led to conclude that zonally re-entrant channels exhibit a fundamentally distinct steady force balance from gyres. However, as discussed in Section 28.5.11, *Hughes and de Cueves* (2001) showed how topographic form stresses associated with sloping sides can lead to an inviscid balance for gyres. That is, friction is far less important so long as the bottom can support topographic torques. In this manner, gyres and channels share much in common so long as they both contain topography and sloping sides.

The case with vertical stratification

The analysis of a single shallow water layer has direct relevance to flow in a stratified fluid. The reason is that when integrating over the full depth of the fluid, internal interfacial form stresses cancel pairwise.[11] The resulting net balance for contact forces is concerned with just those acting on the boundaries at the surface and the bottom. This property of contact forces was also implicit in Section 28.5 where we developed the angular momentum budget for a continuously stratified fluid. In that discussion we encountered the correlation between bottom pressure and bottom topography slope for steady flow in a channel as realized by a balance between wind stress and bottom form stress (see Figure 28.8). This correlation also holds for the single shallow water layer.

Although the single layer provides a direct connection to the vertically integrated momentum in a continuously stratified fluid, the direct connection between undulations in the sea surface height and bottom pressure is more nuanced when allowing for stratification. We here outline some of the considerations that arise with flow in a stratified channel with a topographic bump. Our presentation is rather incomplete, with a more thorough analysis supported by numerical simulations.

Following the analysis of Section 27.2, we decompose the horizontal gradient of bottom pressure according to equation (27.48)

$$\nabla_{\mathrm{h}} p_{\mathrm{b}} = \underbrace{\nabla_{\mathrm{h}} p_{\mathrm{a}} + g\,\rho(\eta)\,\nabla_{\mathrm{h}}\eta}_{\text{external contribution}} \; - \; \underbrace{\rho 0 \int_{\eta_{\mathrm{b}}}^{\eta} \nabla_{\mathrm{h}} b \, \mathrm{d}z'}_{\text{internal contribution}} \equiv \nabla_{\mathrm{h}} p_{\mathrm{bext}} + \nabla_{\mathrm{h}} p_{\mathrm{bint}}, \tag{36.187}$$

where $b = -g\,(\rho - \rho_{\mathrm{o}})/\rho_{\mathrm{o}}$ is the Archimedean buoyancy from Chapter 30. The external pressure gradient is all that is available for a single shallow water layer, so that there is a direct correlation between bottom topography and surface pressure in the steady channel flow where bottom form stress balances wind stress. In contrast, for a continuously stratified fluid, or for a stacked shallow water fluid, the internal contribution to the pressure gradient is nonzero since buoyancy generally has a horizontal gradient.

As discussed in Section 16.4 of *Olbers et al.* (2012), watermasses in the Southern Ocean generally align themselves with lighter water on the upstream side of topographic features (to

[10] We encounter such balances in Chapter 39 when studying vorticity.

[11] We discussed this property of interfacial form stresses in Sections 25.2, 28.3, and 36.4.

the west), and heavy water on the downstream side. This configuration means that the internal pressure is lower upstream of a topographic bump and higher downstream, thus leading to a westward internal pressure gradient force. To realize a steady flow with a balance between bottom pressure form stress and wind stress requires the external contribution to the bottom pressure gradient to counteract the internal contribution. Hence, the free surface height must have larger undulations in the presence of vertical stratification than without, with high values upstream of the bump and low values downstream. We depict this configuration in Figure 36.9, with the caption offering further details. *Zhang et al.* (2024) further detail the facets of the dynamical balances, including transient adjustments towards the steady balances discussed here. They offer a particularly clear distinction between the barotropic dynamics (as realized by a single shallow water layer) and baroclinic dynamics. Furthermore, they emphasize the central role of the barotropic dynamics for maintaining the momentum balance even for stratified fluid.

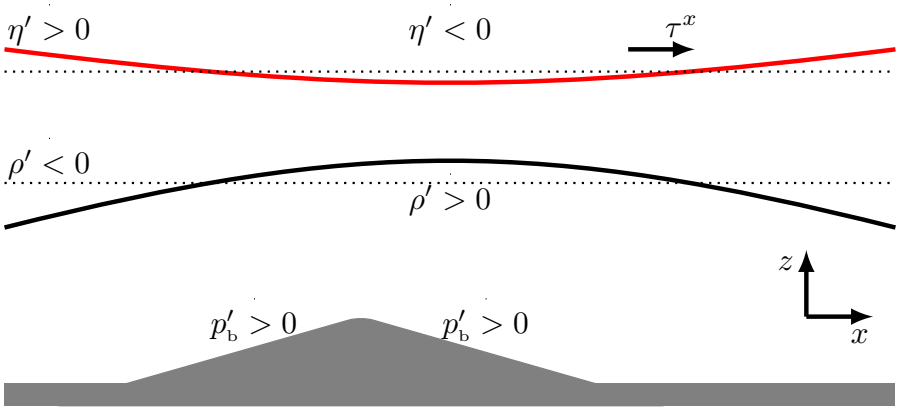

FIGURE 36.9: A schematic of steady flow in a two-layer zonally periodic channel with a topographic bump and with bottom pressure form stress balancing zonal wind stress. To realize this balance requires anomalously high bottom pressure on the upstream side of the bump and anomalously low bottom pressure on the downstream side, where anomalies are relative to the zonal mean. Such anomalous bottom pressure is just as for a single shallow water layer. However, for a stratified fluid the bottom pressure is established by the sum of effects from the external and internal pressure fields. The internal pressure field arises from density, here shown with anomalously light water on the upstream side of the bump and heavy water downstream, such as occurs in the Southern Ocean. This density field leads to a westward contribution to the bottom pressure gradient force; i.e., anomalously low bottom pressure on the upstream side of the bump and high bottom pressure on the downstream. The external pressure field arises from the free surface undulations (red line), with a high upstream of the bump and low downstream. This free surface field leads to an eastward contribution to the bottom pressure gradient force; i.e., anomalously high bottom pressure on the upstream side of the bump and low bottom pressure on the downstream. For the bottom pressure form stress to balance the wind stress, we must have the external pressure gradient dominate the internal pressure gradient. Note that undulations of the free surface height are roughly 100-300 times smaller than those of the density field, with the relative undulations set according to the reduced gravity as described in Section 35.3.

Meridional overturning circulation

The balances in this section are modified when allowing for the vertical transfer of volume between the layers as required to admit a meridional-vertical overturning circulation. In this case, there can be net meridional motion along a latitude circle to thus add the Coriolis force to the steady force balance, including an Ekman transport (balance between Coriolis and surface stress as in Section 33.1) for the layer feeling the zonal surface stress. Section 21.7 of *Vallis* (2017) as well as Chapter 16 of *Olbers et al.* (2012) provide pedagogical discussions of flow in the Antarctic Circumpolar Current, in which interfacial pressure form stress developed from

baroclinic eddies provides a mechanism for vertically redistributing horizontal momentum. The studies from *Webb and de Cueves* (2007) and *Zhang et al.* (2024) detail how the barotropic dynamics, which act over days and weeks, continue to play the dominant role in balancing the surface wind stress and topographic form stress, even in the case of a stratified ocean with eddy form stresses, which have a time scale of years.

36.8 Angular momentum in a rotating tank

As our second case study for this chapter, we study angular momentum for a layer of shallow water fluid in a rotating cylindrical tank. This system was first discussed in Section 27.5, where we developed the horizontal equation of motion

$$\frac{\mathrm{D}\boldsymbol{u}}{\mathrm{D}t} + f\,\hat{\boldsymbol{z}} \times \boldsymbol{u} = -\nabla\left(p/\rho + g_e\, z - \Omega^2\, r^2/2\right), \tag{36.188}$$

where $r^2 = x^2 + y^2$ is the radial distance from the rotational axis,

$$\Omega = f/2 \tag{36.189}$$

is the constant angular rotation rate, and the vertical component to the right hand side is the hydrostatic balance, $\partial p/\partial z = -\rho\, g_e$. Where convenient, we make use of the polar coordinates (see Chapter 4.22) in the following, whereby

$$x = r\,\cos\vartheta \tag{36.190a}$$

$$y = r\,\sin\vartheta, \tag{36.190b}$$

with the polar angle ϑ measured counter-clockwise from the positive x-axis.

36.8.1 Angular momentum for a column of shallow water fluid

The angular momentum for a column of shallow water fluid, computed with respect to the vertical rotational axis, is given by (see Sections 14.5 and 24.7)

$$L^z = \delta M\,[\boldsymbol{x} \times (\boldsymbol{u} + \boldsymbol{U}_{\text{rigid}})] \cdot \hat{\boldsymbol{z}}, \tag{36.191}$$

where $\boldsymbol{x} = x\,\hat{\boldsymbol{x}} + y\,\hat{\boldsymbol{y}} = r\,\hat{\boldsymbol{r}}$ is the position vector relative to the rotational axis, $\delta M = \rho\, h\, \delta A$ is the constant mass for the fluid column, and the rigid-body rotation velocity is

$$\boldsymbol{U}_{\text{rigid}} = (f/2)\,\hat{\boldsymbol{z}} \times \boldsymbol{x} = r\,\Omega\,\hat{\boldsymbol{\vartheta}}, \tag{36.192}$$

where $\hat{\boldsymbol{z}} \times \hat{\boldsymbol{r}} = \hat{\boldsymbol{\vartheta}}$ is the azimuthal unit vector pointing counter-clockwise around the origin.

We can further massage the expression for the angular momentum by writing

$$\boldsymbol{x} \times \boldsymbol{u} = (x\,v - y\,u)\,\hat{\boldsymbol{z}} = r^2 \dot{\vartheta}\,\hat{\boldsymbol{z}}, \tag{36.193}$$

where $\dot{\vartheta} = \mathrm{D}\vartheta/\mathrm{D}t$ is the angular velocity. Likewise, we have

$$\boldsymbol{x} \times \boldsymbol{U}_{\text{rigid}} = r^2\,\Omega\,\hat{\boldsymbol{z}}, \tag{36.194}$$

so that the angular momentum can be written

$$L^z = \delta M\,[\boldsymbol{x} \times (\boldsymbol{u} + \boldsymbol{U}_{\text{rigid}})] \cdot \hat{\boldsymbol{z}} = \delta M\, r^2\,(\dot{\vartheta} + \Omega). \tag{36.195}$$

36.8.2 Material time evolution of the angular momentum

The material time evolution for the angular momentum is given by

$$\frac{\mathrm{D}L^z}{\mathrm{D}t} = \delta M \left[\boldsymbol{u} \times (\boldsymbol{u} + \boldsymbol{U}_{\text{rigid}})\right] \cdot \hat{\boldsymbol{z}} + \delta M \left[\boldsymbol{x} \times \left(\frac{\mathrm{D}\boldsymbol{u}}{\mathrm{D}t} + \frac{\mathrm{D}\boldsymbol{U}_{\text{rigid}}}{\mathrm{D}t}\right)\right] \cdot \hat{\boldsymbol{z}}. \tag{36.196}$$

Note that we set

$$\frac{\mathrm{D}(\delta M)}{\mathrm{D}t} = \rho\, \mathrm{D}(\mathrm{h}\, \delta \mathrm{A})\mathrm{D}t = 0 \tag{36.197}$$

since the shallow water fluid columns each have constant volume as they move with the horizontal flow (Section 35.2.5). Using the rigid-body rotation velocity given by equation (36.192), and with a constant rotation rate, yields

$$\boldsymbol{u} \times \boldsymbol{U}_{\text{rigid}} + \boldsymbol{x} \times \frac{\mathrm{D}\boldsymbol{U}_{\text{rigid}}}{\mathrm{D}t} = \boldsymbol{u} \times (\boldsymbol{\Omega} \times \boldsymbol{x}) + \boldsymbol{x} \times (\boldsymbol{\Omega} \times \boldsymbol{u}) \tag{36.198a}$$

$$= (\boldsymbol{x} \cdot \boldsymbol{u})\, f\, \hat{\boldsymbol{z}}. \tag{36.198b}$$

Making use of the material evolution of the horizontal velocity given by equation (36.188) renders

$$\left[\boldsymbol{x} \times \frac{\mathrm{D}\boldsymbol{u}}{\mathrm{D}t}\right] \cdot \hat{\boldsymbol{z}} = \left(\boldsymbol{x} \times \left[-f\, \hat{\boldsymbol{z}} \times \boldsymbol{u} - \nabla\left(p/\rho + g_{\mathrm{e}}\, z - \Omega^2\, r^2/2\right)\right]\right) \cdot \hat{\boldsymbol{z}} \tag{36.199a}$$

$$= -f\, (\boldsymbol{x} \cdot \boldsymbol{u}) - (\boldsymbol{x} \times g\, \nabla\eta) \cdot \hat{\boldsymbol{z}}. \tag{36.199b}$$

The centrifugal term dropped out since

$$\boldsymbol{x} \times \nabla r^2 = 2\, \boldsymbol{x} \times r\, \hat{\boldsymbol{r}} = 2\, \boldsymbol{x} \times \boldsymbol{x} = 0. \tag{36.200}$$

The gravitational term dropped out since

$$(\boldsymbol{x} \times \nabla z) \cdot \hat{\boldsymbol{z}} = (\boldsymbol{x} \times \hat{\boldsymbol{z}}) \cdot \hat{\boldsymbol{z}} = 0, \tag{36.201}$$

as does the vertical component to the pressure gradient. We are thus left with

$$\frac{1}{\delta M}\frac{\mathrm{D}L^z}{\mathrm{D}t} = -g\, (\boldsymbol{x} \times \nabla\eta) \cdot \hat{\boldsymbol{z}}. \tag{36.202}$$

Consequently, the axial angular momentum for a fluid column is modified by the torque from the horizontal pressure gradient caused by undulations in the free surface height. Note how there is no contribution from the Coriolis acceleration, so that the evolution of angular momentum is the same whether viewed in the laboratory frame or rotating frame.

We can bring the expression (36.202) into a more transparent form by switching to polar coordinates

$$\boldsymbol{x} \times \nabla\eta = r\, \hat{\boldsymbol{r}} \times \left[\hat{\boldsymbol{r}}\, \frac{\partial\eta}{\partial r} + \hat{\boldsymbol{\vartheta}}\, \frac{1}{r}\, \frac{\partial\eta}{\partial\vartheta}\right] = \frac{\partial\eta}{\partial\vartheta}\, \hat{\boldsymbol{z}}, \tag{36.203}$$

so that

$$\frac{1}{\delta M}\frac{\mathrm{D}L^z}{\mathrm{D}t} = -g\, \frac{\partial\eta}{\partial\vartheta}. \tag{36.204}$$

This result is directly analogous to the angular momentum evolution for a fluid moving around a sphere as derived in Section 24.7. Namely, in the presence of angular pressure gradients, the fluid experiences a torque that in turn leads to a change in the angular momentum relative to the vertical rotation axis.

36.8.3 Materially invariant angular momentum

The angular momentum for a fluid column is materially invariant (i.e., a constant on a material fluid parcel) if

$$\frac{\mathrm{D}L^z}{\mathrm{D}t} = 0 \Longleftrightarrow \frac{\partial \eta}{\partial \vartheta} = 0. \tag{36.205}$$

For a flat bottom, equation (27.106) says that the free surface takes on a radial parabolic shape when the fluid is in rigid-body rotation. In this case, $\nabla\eta$ is in the radial direction, in which case $\boldsymbol{x} \times \nabla\eta = 0$. Consequently, when the fluid is in rigid-body rotation, the angular momentum for each fluid column remains materially constant.

36.8.4 Comments

The material evolution equation (36.202) also holds for a fluid on the f-plane tangent to a sphere. The f-plane formulation is slightly simpler than the tank since the centrifugal term is absorbed into the geopotential (see Section 13.10.4). However, the tank is arguably more pedagogical as it is simpler to visualize and to conduct laboratory experiments. See Section 6.6.4 of *Marshall and Plumb* (2008) for more discussion of rotating tank experiments. Also, we return to this physical system in Section 59.3 when studying centrifugal instability of cyclostrophically balanced flow.

36.9 Exercises

EXERCISE 36.1: POTENTIAL TEMPERATURE SLOPES IN ATMOSPHERE AND OCEAN
Use the two-layer thermal wind relations from Section 36.2.2, also known as Margules' relation, to estimate the slope of the potential temperature surfaces in the atmosphere and ocean. This question is based on exercise 3.2 of *Vallis* (2006).

(a) Model the atmosphere as two immiscible shallow water layers of different density stacked one above the other. Using reasonable values for any required physical parameters, estimate the vertical displacement of the interfacial surface associated with a pole-to-equator temperature difference of 40K. You may wish to consult *Wallace and Hobbs* (2006) or *Marshall and Plumb* (2008) for physical scales.

(b) Estimate a vertical interfacial displacement in the ocean thermocline associated with a temperature difference of 20K over a horizontal distance of 4000 km. The interface between the two shallow water layers offers a crude representation of the main oceanic thermocline. Ignore salinity effects so that temperature and density are directly proportional.

Double-check your results by examining some atmosphere and ocean latitude-height profiles for potential temperature (e.g., Figure 5.8 of *Marshall and Plumb* (2008)).

EXERCISE 36.2: CIRCULAR STEADY GEOSTROPHIC FLOW
Consider a single layer of shallow water fluid in steady geostrophic balance on a f-plane so that

$$f\,\hat{\boldsymbol{z}} \times \boldsymbol{u}_{\mathrm{g}} = -g\,\nabla\eta. \tag{36.206}$$

Assume $f > 0$ and that the free surface has a circular Gaussian shape

$$\eta = \eta_0\, e^{-r^2/(2\,\sigma^2)} \tag{36.207}$$

where $r^2 = x^2 + y^2$ is the squared radial position and σ is the standard deviation of the Gaussian.

(a) Determine the horizontal geostrophic velocity components corresponding to this free surface undulation. Write the solution in both Cartesian coordinates and polar coordinates. Is the flow oriented cyclonic or anti-cyclonic?

(b) Determine the streamlines for the flow. Hint: recall the discussion in Section 17.7.2. What is the geometric shape of a streamline?

EXERCISE 36.3: STEADY STATE MOMENTUM AND GEOSTROPHY

Consider a single layer of shallow water fluid with zero boundary mass fluxes through the surface. Assume the lateral boundaries are solid. All boundaries are thus material. The domain integrated horizontal momentum (within the rotating reference frame) is defined by

$$\boldsymbol{P} = \int \rho\, \boldsymbol{u}\, \mathrm{d}V = \int \rho\, h\, \boldsymbol{u}\, \mathrm{d}\mathcal{S}. \tag{36.208}$$

Show that for tangent plane motion (Section 24.5)

$$\frac{\mathrm{d}\boldsymbol{P}}{\mathrm{d}t} = 0 \tag{36.209}$$

can be realized either by (A) zero flow everywhere, (B) flow that is in geostrophic balance at each point, or (C) flow that is in geostrophic balance as a global integral.

EXERCISE 36.4: THICKNESS WEIGHTED MOMENTUM FOR TWO LAYERS

Following the methods from Section 36.3, derive the thickness weighted momentum equation for an inviscid two-layer stacked shallow water fluid. That is, derive the evolution equation for $h_1\, \boldsymbol{u}_1 + h_2\, \boldsymbol{u}_2$, thus providing the two-layer version of equation (36.21).

EXERCISE 36.5: CONTACT PRESSURE FORCE ON A SINGLE LAYER

As a check on our calculation of the contact pressure force (36.60b), consider a single shallow water layer under a massless atmosphere. Show that the contact pressure force per mass is given by

$$\frac{\boldsymbol{F}^{\text{press}}_{\text{net}}}{M} = g\, \hat{\boldsymbol{z}} - g \nabla \eta. \tag{36.210}$$

As expected, the horizontal component of this force equals to the pressure gradient body force per mass detailed in Section 35.2.1. The vertical pressure force balances the weight of the fluid as per the hydrostatic balance.

EXERCISE 36.6: TOPOGRAPHIC FORM STRESS FOR A RIDGE

As in Section 36.7, apply a constant eastward zonal wind to a zonally reentrant channel with a single shallow water layer. Let the layer flow over a topographic ridge of height H above the surrounding flat bottom, and let the ridge be a function just of zonal position, $\eta'_{\text{b}}(x)$. Furthermore, assume the ridge has a constant slope on both the upstream (west) side, S_{up}, and downstream (east) side, S_{dn}. An example is depicted in Figure 36.10. Following the force balance (36.176), derive an expression for the free surface height zonally averaged over the upstream side of the ridge, minus the free surface height zonally averaged over the downstream sides of the ridge,

$$\Delta\eta' = (\overline{\eta'})_{\text{up}} - (\overline{\eta'})_{\text{dn}}, \tag{36.211}$$

where

$$(\overline{\eta'})_{\text{up}} = \frac{\int_{x_{\text{up}}}^{x_0} \eta'\, \mathrm{d}x}{L_{\text{up}}} \qquad \text{and} \qquad (\overline{\eta'})_{\text{dn}} = \frac{\int_{x_0}^{x_{\text{dn}}} \eta'\, \mathrm{d}x}{L_{\text{dn}}}. \tag{36.212}$$

Show that the expression for $\Delta\eta'$ is independent of the two slopes. Instead, the only geometric property that determines $\Delta\eta'$ is the ridge height, H. Discuss this result.

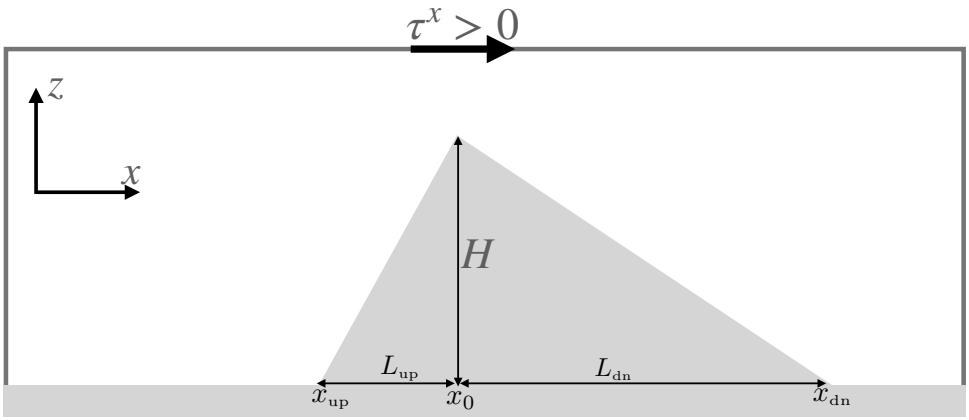

FIGURE 36.10: Zonal-vertical view of a single layer of shallow water fluid moving in a zonally re-enetrant channel for use in Exercise 36.6. The domain has a topographic ridge that is a function just of the zonal direction and has constant slopes on its western and eastern sides. There is a constant eastward zonal wind stress.

EXERCISE 36.7: GEOSTROPHIC TRANSPORT

Consider a zonal-vertical section of shallow water flow in the middle latitude northern hemisphere. Let the section be 1000 m deep and away from side and bottom boundaries. Assume the sea level is 1 cm higher at the eastern end of the section than the western end. Estimate the mass transport (kg/sec) of constant density seawater going through the section. What direction is the transport? Hint: Assume geostrophic balance; choose a representative constant seawater density; and note that the zonal width of the section cancels out so it is not needed.

EXERCISE 36.8: APE FOR TWO SHALLOW WATER LAYERS

Compute the APE for two shallow water layers using the notation from Figure 35.6 with nontrivial bottom topography, $z = \eta_{\rm b}(x, y)$. Show that the APE is non-negative. Assume the domain is simply connected. Hint: The answer is given by specializing the arbitrary N results in equation (36.139) to the special case of the $N = 2$. However, for this exercise you should not merely quote that result. Instead, show all steps starting from the potential energy for an $N = 2$ layer model.

EXERCISE 36.9: RATIO OF KE TO APE FOR SINGLE LAYER f-PLANE GEOSTROPHY

Consider a single layer of shallow water fluid in geostrophic balance on an f-plane with a flat bottom. Show that the ratio of kinetic energy to available potential energy scales like

$$\frac{E_{\rm KE}}{E_{\rm APE}} \sim \left[\frac{L_{\rm d}^{\rm ext}}{L}\right]^2 . \tag{36.213}$$

In this equation, L is the horizontal length scale for the fluctuation of the free surface η (i.e., $\nabla\eta \sim \eta'/L$), and

$$L_{\rm d}^{\rm ext} = \frac{\sqrt{g\,H}}{f} \tag{36.214}$$

is the external deformation radius. The scaling (36.213) means that for scales larger than the external deformation radius, $L_{\rm d}$, the available potential energy is larger than the kinetic energy. The converse holds for scales smaller than $L_{\rm d}$.

EXERCISE 36.10: RATIO OF KE TO APE FOR 1.5 LAYER f-PLANE GEOSTROPHY

Consider a reduced gravity system (Section 35.3) in geostrophic balance on an f-plane. Show

that the ratio of kinetic energy to available potential energy scales like

$$\frac{E_{\text{KE}}}{E_{\text{APE}}} \sim \left[\frac{L_{\text{d}}^{\text{int}}}{L}\right]^2. \tag{36.215}$$

In this equation, L is the horizontal length scale for the fluctuation of the internal interface $\eta_{3/2}$ (i.e., $\nabla\eta_{3/2} \sim \eta'_{3/2}/L$), and

$$L_{\text{d}}^{\text{int}} = \frac{\sqrt{g'_{3/2}\,\overline{h}}}{f} \tag{36.216}$$

is the internal deformation radius with $g'_{3/2} = g\,(\rho_2 - \rho_1)/\rho_{\text{ref}}$ the reduced gravity and $h = A^{-1}\int(\eta_{1/2} - \eta_{3/2})\,\mathrm{d}\mathcal{S}$ the area averaged layer thickness (see Figure 35.4). The scaling (36.215) means that for scales larger than the internal deformation radius, $L_{\text{d}}^{\text{int}}$, the available potential energy is larger than the kinetic energy, and conversely for scales smaller than $L_{\text{d}}^{\text{int}}$.

To solve this exercise you must make use of the following.

- Derive the APE for two layers with a flat bottom.
- Assume the contribution to the APE from free surface undulations, is much smaller than from the interior interface. So that the APE is roughly due just to undulations of the interior interface. This assumption follows from Figure 35.5.
- The scaling (36.215) is identical to that found for the quasi-geostrophic system in Section 45.9.4. However, to solve this exercise it is not sufficient to merely reproduce the scaling discussed in Section 45.9.4. Instead, use here the expressions for APE and KE appropriate for the shallow water system.

EXERCISE 36.11: NON-DIMENSIONALIZED LINEAR SHALLOW WATER EQUATIONS
For the linear equations (55.147a)-(55.147b), introduce

$$\boldsymbol{x} = L\,\hat{\boldsymbol{x}}, \quad \boldsymbol{u}' = U\,\hat{\boldsymbol{u}}, \quad t = \frac{L\,\hat{t}}{U}, \quad f = \hat{f}\,T^{-1}, \quad \eta' = H\,\hat{\eta}, \tag{36.217}$$

where L is a horizontal length scale, $T = L/U$ is an advective time scale, U is a velocity scale, and $H \ll L$ is the resting layer thickness. All variables with hats are non-dimensional and not to be confused with unit vectors. Substitute into equations (55.147a)-(55.147b) and identify the non-dimensional ratio of the advective velocity scale to the non-rotating gravity wave speed

$$\text{Fr} \equiv \frac{U}{\sqrt{g\,H}}. \tag{36.218}$$

This non-dimensional number is known as the *Froude number*. As seen in our brief discussion of non-rotating hydraulics in Section 55.5.4, the fluid can experience an instability known as an *hydraulic jump* when the Froude number is greater than unity.

Part VII

Vorticity and potential vorticity

Vorticity locally measures the spin of a fluid element. For geophysical flows, external forces, ultimately due to differential heating over the planet, resupply vorticity in the face of dissipation. The addition of planetary vorticity, arising from motion on a rotating spherical planet, also renders a nonzero vorticity to geophysical fluids even when the fluid is at rest in the rotating earth reference frame. Vorticity thus plays a central role in characterizing geophysical fluid motions, even for relatively sluggish and laminar flow, since motion on a rotating planet always involves vorticity.

Besides offering a key method for flow characterization, vorticity evolution and its steady balances provide the means to mechanically understand how flows respond under changes to forces. Surprisingly, it does so even without needing to directly compute forces acting on the fluid. We thus encounter examples where vorticity mechanics offers a more direct and focused explanation for flow behavior than momentum or energy mechanics. This practical feature of vorticity mechanics represents the central reason it is so essential to the theoretical machinery of geophysical fluid mechanics.

Potential vorticity is a strategically chosen component of vorticity whose evolution is simpler than the full vorticity vector, thus helping to identify key facets of geophysical flows, their forcing, and constraints. Indeed, under certain assumptions of balance (considered in Part VIII of this book), knowledge of potential vorticity offers the means to deduce all prognostic information about certain rotating and stratified flows. For these and other reasons explored in this part of the book, potential vorticity has found great use for understanding and predicting geophysical fluid flows. Indeed, the central importance of potential vorticity for the study of atmospheric and oceanic flows helps to distinguish geophysical fluid mechanics from other areas of fluid mechanics.

OUTLINE FOR THIS PART OF THE BOOK

We start this part of the book by introducing vorticity and circulation in Chapter 37, making use of Stokes' Theorem to show that the area integral of vorticity over a finite region yields the circulation around the region's boundary. In Chapter 38 we study vorticity in a horizontal flow that is non-divergent, thus leading to the study of non-divergent barotropic flow. This flow is fully described by the vorticity field, and it offers many insights into large-scale vortical flows in the atmosphere and ocean. Chapter 39 then introduces the mechanics of vorticity and potential vorticity within a shallow water fluid. It was for the shallow water system that *Rossby* (1940) revealed the power of potential vorticity conservation for understanding geophysical fluid flow patterns.

In Chapter 40 we fully dive into the fundamentals of vorticity and circulation. It is here that we encounter Kelvin's circulation theorem, which identifies the materially conserved nature of circulation around an arbitrary simply closed loop in a perfect barotropic flow. In Chapter 41 we explore the foundations of potential vorticity and then in Chapter 42 develop differential and integral potential vorticity budget equations. Our study of potential vorticity budgets exposes the remarkable impermeability property of the potential vorticity flux vector.

Chapter 37

VORTICITY AND CIRCULATION

Vorticity measures the angular motion contained in a fluid flow at each point within the fluid; i.e., it is a measure of spin. Vorticity generalizes to continuum mechanics the notion of angular momentum that is central to the study of rigid body mechanics. We here relate the two, showing that flows with a nonzero strain lead to distinctions between vorticity and angular momentum. Circulation measures the fluid flow computed over a closed line integral (circuit) within the fluid. Helmholtz was an early proponent of vorticity whereas Kelvin introduced circulation to help understand vorticity. These two flow properties are connected through Stokes' theorem, with the study of vortex lines and vortex tubes clearly exposing the connections.

CHAPTER GUIDE

We here study kinematic properties of vorticity and circulation, making use of vector calculus with Cartesian coordinates and Cartesian tensors as detailed in Chapter 2. The concepts and methods introduced in this chapter are fundamental to the remaining chapters throughout this part of the book.

37.1 Loose threads

- Write up the solution to Exercise 37.7.
- Write up the solution to Exercise 37.9.

37.2 Vorticity

Vorticity is the curl of the velocity field

$$\boldsymbol{\omega} = \nabla \times \boldsymbol{v}. \tag{37.1}$$

Vorticity measures the rotation or spin of fluid flow at each point and, unlike angular momentum, it does so without reference to an origin. In this manner, vorticity is an intrinsic property of the flow. In addition to writing vorticity as the curl of the velocity, we may choose to use the equivalent expression

$$\boldsymbol{\omega} = [\nabla \cdot (\boldsymbol{v} \times \hat{\boldsymbol{x}})]\,\hat{\boldsymbol{x}} + [\nabla \cdot (\boldsymbol{v} \times \hat{\boldsymbol{y}})]\,\hat{\boldsymbol{y}} + [\nabla \cdot (\boldsymbol{v} \times \hat{\boldsymbol{z}})]\,\hat{\boldsymbol{z}}. \tag{37.2}$$

That is, a vorticity component in a particular coordinate direction is the divergence of the velocity field after being rotated by $-\pi/2$ around the coordinate axis direction. For example, the vector $\boldsymbol{v} \times \hat{\boldsymbol{z}}$ is the result of rotating the velocity by $-\pi/2$ radians around the $\hat{\boldsymbol{z}}$ axis, with the identity

$$\hat{\boldsymbol{z}} \cdot (\nabla \times \boldsymbol{v}) = \nabla \cdot (\boldsymbol{v} \times \hat{\boldsymbol{z}}) = \partial_x v - \partial_y u \tag{37.3}$$

leading to the vertical component of the vorticity in equation (37.2).

Being the curl of a vector, the vorticity transforms as a vector under coordinate rotations. However, vorticity changes sign under mirror symmetry, thus making it a pseudo-vector (Section 1.7.2). A simple means to understand this property is to note that the spinning earth rotates counter-clockwise when viewed from above the north pole and clockwise when viewed from below the south pole (see Figure 4.3).

Figure 37.1 provides an example zonal flow with a meridional strain (shear). The vertical component to the vorticity is negative for this flow, as per the right hand rule

$$\zeta = \hat{\boldsymbol{z}} \cdot (\nabla \times \boldsymbol{v}) = \partial_x v - \partial_y u < 0. \tag{37.4}$$

Furthermore, an imaginary test "paddle wheel" placed anywhere within this flow spins clockwise about its axis. The nonzero spin of a test paddle wheel is a fundamental property of fluid flow with nonzero vorticity.

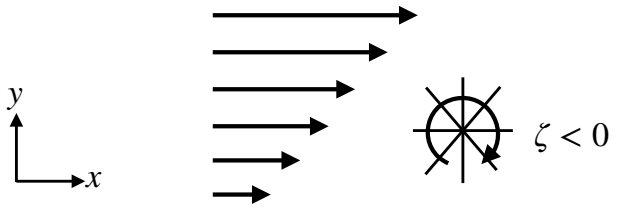

FIGURE 37.1: An example zonal flow with a meridional shear, $\boldsymbol{v} = u(y)\,\hat{\boldsymbol{x}}$, and a corresponding vertical vorticity component that is negative: $\zeta = \hat{\boldsymbol{z}} \cdot (\nabla \times \boldsymbol{v}) = \partial v/\partial x - \partial u/\partial y = -\partial u/\partial y < 0$. The clockwise arrow surrounds a test "paddle wheel" that exhibits a clockwise spin about its axis when placed in this flow. Such test paddle wheels only spin when there is nonzero vorticity. The right hand rule determines the sign of the vorticity, which for this example is into the page (negative $\hat{\boldsymbol{z}}$).

37.2.1 Rotation of line elements

In Section 18.6 we considered the kinematics of a material line element, $\delta\boldsymbol{x}$, whose evolution is given by equation (18.85)

$$\frac{\mathrm{D}(\delta x_m)}{\mathrm{D}t} = \delta x_n \frac{\partial v_m}{\partial x_n} \Longrightarrow \frac{\mathrm{D}(\delta \boldsymbol{x})}{\mathrm{D}t} = (\delta \boldsymbol{x} \cdot \nabla)\,\boldsymbol{v}. \tag{37.5}$$

This equation says that the material line element evolves according to the velocity gradient tensor $\partial_n v_m$. The symmetric portion of this tensor is the strain rate tensor,

$$\mathbb{S}_{mn} = (\partial_n v_m + \partial_m v_n)/2, \tag{37.6}$$

whose action generates changes in the distance between the fluid particles (Section 18.8.4). The anti-symmetric portion to the velocity gradient tensor is known as the rotation tensor,

$$\mathbb{R}_{mn} = (\partial_n v_m - \partial_m v_n)/2. \tag{37.7}$$

The rotation tensor is related to vorticity via equation (18.102)

$$\mathbb{R}_{mn} = -\epsilon_{mnp}\,\omega_p/2 \Longleftrightarrow \mathbb{R} = \frac{1}{2}\begin{bmatrix} 0 & -\omega_3 & \omega_2 \\ \omega_3 & 0 & -\omega_1 \\ -\omega_2 & \omega_1 & 0 \end{bmatrix}, \tag{37.8}$$

so that

$$2\,\mathbb{R}_{mn}\,\delta x_n = -\epsilon_{mnp}\,\omega_p\,\delta x_n \Longrightarrow 2\,\mathbb{R} \cdot \delta\boldsymbol{x} = \boldsymbol{\omega} \times \delta\boldsymbol{x}. \tag{37.9}$$

From our discussion of rotation in Section 11.2.3, this equation means that vorticity in a fluid generates a rigid rotation of a material line element around the instantaneous axis defined by the vorticity (Section 18.8.5). This result accords with Figure 37.1, whereby vorticity leads to the spin of a test paddle wheel; i.e., the rotation of line elements.

37.2.2 Rotating reference frame

For another means to understand the kinematics of vorticity, view the flow field from a reference frame that rotates with a constant angular velocity, $\boldsymbol{\Gamma}$, analogous to the case of observing geophysical flows from the non-inertial terrestrial reference frame. Following equation (13.42e), we know that the velocity observed in the non-rotating or absolute reference frame, $\boldsymbol{v}_{\mathrm{a}}$, is related to the rotating reference frame velocity, $\boldsymbol{v}$, via

$$\boldsymbol{v}_{\mathrm{a}} = \boldsymbol{v} + \boldsymbol{\Gamma} \times \boldsymbol{x}. \tag{37.10}$$

The vorticity measured in the absolute reference frame, $\boldsymbol{\omega}_{\text{a}}$, is related to the relative vorticity measured in the rotating reference frame, $\boldsymbol{\omega}$, via

$$\boldsymbol{\omega}_{\text{a}} = \nabla \times \boldsymbol{v}_{\text{a}} = \nabla \times \boldsymbol{v} + \nabla \times (\boldsymbol{\Gamma} \times \boldsymbol{x}) = \boldsymbol{\omega} + 2\,\boldsymbol{\Gamma}. \tag{37.11}$$

If there is a point in the fluid whereby the rotating reference frame's angular velocity equals to one-half the absolute vorticity at that point, $\boldsymbol{\Gamma} = \boldsymbol{\omega}_{\text{a}}/2$, then the rotating reference frame's vorticity (the relative vorticity) vanishes at that point

$$\boldsymbol{\Gamma} = \boldsymbol{\omega}_{\text{a}}/2 \Longrightarrow \boldsymbol{\omega} = 0. \tag{37.12}$$

Hence, we may interpret $\boldsymbol{\omega}_{\text{a}}/2$ as twice the local and instantaneous angular velocity of the fluid. Correspondingly, if the absolute vorticity, $\boldsymbol{\omega}_{\text{a}}$, is spatially constant, then we can move to a rotating reference frame in which the relative vorticity vanishes everywhere, with such flow referred to as *irrotational*.

37.2.3 There are no vorticity sources

Vorticity has zero divergence

$$\nabla \cdot \boldsymbol{\omega} = \nabla \cdot (\nabla \times \boldsymbol{v}) = 0. \tag{37.13}$$

This property is akin to the non-divergent nature of the velocity vector in an incompressible flow (see Chapter 21). However, vorticity is non-divergent for both compressible and incompressible flow. Consequently, there are no interior sources or sinks of vorticity for any fluid. This very basic kinematic property plays an important role in developing some further properties of vorticity in Chapter 40.

37.2.4 Further study

This video from 3Blue1Brown provides some compelling graphics to help develop intuition for the divergence and curl of a vector, with examples drawn from fluid flow.

37.3 Irrotational flows

Most geophysical flows have nonzero vorticity. Indeed, even when at rest on the earth, a geophysical fluid carries the vorticity of the rotating planet. However, if we can ignore the planetary vorticity component, as when focused on motions too small to feel the Coriolis acceleration, we can find some geophysically relevant flows with vanishing vorticity. Linear gravity waves in the absence of planetary rotation provide a particularly relevant example (Section 55.3.3). There are also many examples from engineering flows.

37.3.1 Characterizing irrotational flows

Irrotational fluid flow is characterized by a zero vorticity

$$\boldsymbol{\omega} = 0 = \text{irrotational flow}. \tag{37.14}$$

Since the curl of a gradient vanishes, irrotational flow has a velocity field equal to the gradient of a velocity potential

$$\nabla \times \boldsymbol{v} = 0 \Longrightarrow \boldsymbol{v} = \nabla \Psi. \tag{37.15}$$

Irrotational flow is therefore sometimes call *potential flow*. Figure 37.2 illustrates a two-dimensional flow field generated by taking the gradient of a scalar potential so that the flow has

zero vorticity. In this case, the vertical component of the vorticity vanishes at each point since $\partial v/\partial x = \partial u/\partial y$.

If the flow is non-divergent, as in a Boussinesq ocean (Section 29.1), then the velocity potential is a harmonic function since it satisfies Laplace's equation

$$\nabla \cdot \boldsymbol{v} = 0 \Longrightarrow \nabla^2 \Psi = 0. \tag{37.16}$$

The study of harmonic functions is a very mature area of mathematical physics, thus providing a great deal of analytic power towards the study of potential / non-divergent flows.

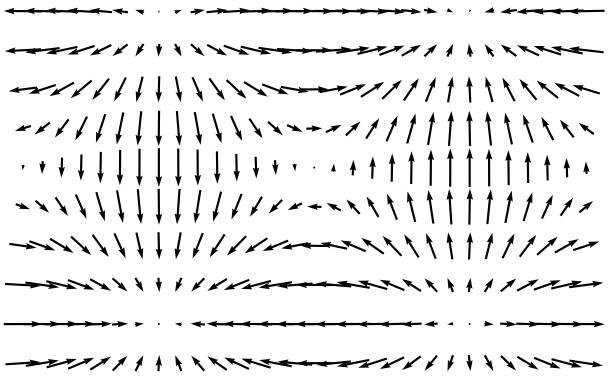

FIGURE 37.2: An example horizontal flow based on a potential, $\Psi = \sin(x/5)\sin(y/5)$. The flow has zero vorticity, $\boldsymbol{\omega} \cdot \hat{\boldsymbol{z}} = \zeta = \partial v/\partial x - \partial u/\partial y = 0$, since the flow is based on a scalar potential: $\boldsymbol{\omega} = \nabla \times \boldsymbol{v} = \nabla \times \nabla\Psi = 0$. This example illustrates how irrotational flow may have nontrivial structure even though a test paddle wheel will not spin anywhere in the flow, since there is zero vorticity given that $\partial v/\partial x = \partial u/\partial y$.

37.3.2 Comments

This book does not discuss turbulence in any depth. Nevertheless, we here note that three dimensional turbulence fundamentally relies on vorticity. Hence, irrotational flows, though they may exhibit chaotic motions, are not turbulent since they do not allow for the nonlinear cascade of energy to small spatial scales, with this cascade a fundamental characteristic of three dimensional turbulence. As we see in Section 40.3, vorticity evolves from sources that tilt and stretch vortex tubes. Vortex stretching is the key source for the turbulent cascade in three dimensional turbulence. Section 3.3 of *Tennekes and Lumley* (1972) provides a pedagogical discussion of vorticity in the context of three-dimensional turbulence.

37.4 Circulation of the velocity field

The velocity circulation, or more briefly the *circulation*, is defined as the oriented closed loop line integral of velocity as projected onto the unit tangent of the path

$$\mathcal{C} \equiv \oint_{\partial \mathcal{S}} \boldsymbol{v} \cdot \mathrm{d}\boldsymbol{x}, \tag{37.17}$$

with Figure 37.3 offering a schematic. The line element, $\mathrm{d}\boldsymbol{x}$, is oriented in the counter-clockwise direction around the circuit $\partial\mathcal{S}$. More precisely, let $\boldsymbol{x}(\varphi)$ be an expression for the position of a point on the circuit, with $\varphi(x, y, z, t)$ a parameter that measures the distance along the closed circuit (see Section 2.4). The difference between two very close positions along the circuit defines the increment

$$\mathrm{d}\boldsymbol{x} = \boldsymbol{x}(\varphi + \delta\varphi) - \boldsymbol{x}(\varphi). \tag{37.18}$$

By construction, $\mathrm{d}\boldsymbol{x}$ is tangent to the circuit so that $\boldsymbol{v} \cdot \mathrm{d}\boldsymbol{x}$ picks out the component of the velocity that is tangent to the path.

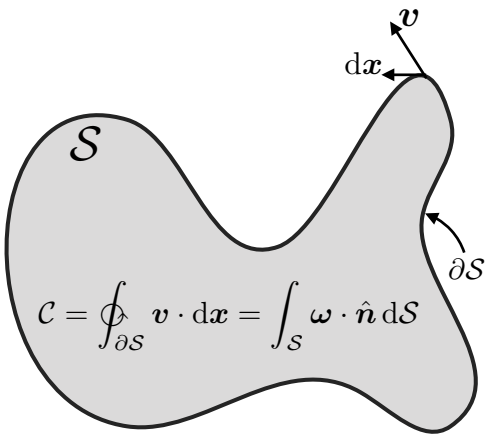

FIGURE 37.3: The velocity circulation around the boundary of a surface, $\partial\mathcal{S}$, is determined by the line integral of the velocity projected into the direction of the line integral, $\boldsymbol{v} \cdot \mathrm{d}\boldsymbol{x}$. Stokes' theorem shows that the velocity circulation computed as a line integral is identical to the normal projection of the vorticity integrated over the area of the region, $\mathcal{C} = \oint_{\partial\mathcal{S}} \boldsymbol{v} \cdot \mathrm{d}\boldsymbol{x} = \int_{\mathcal{S}} \boldsymbol{\omega} \cdot \hat{\boldsymbol{n}} \, \mathrm{d}\mathcal{S}$.

Stokes' theorem (Section 2.6) renders the very important identity

$$\mathcal{C} = \oint_{\partial\mathcal{S}} \boldsymbol{v} \cdot \mathrm{d}\boldsymbol{x} = \int_{\mathcal{S}} (\nabla \times \boldsymbol{v}) \cdot \hat{\boldsymbol{n}} \, \mathrm{d}\mathcal{S} = \int_{\mathcal{S}} \boldsymbol{\omega} \cdot \hat{\boldsymbol{n}} \, \mathrm{d}\mathcal{S}, \tag{37.19}$$

where $\hat{\boldsymbol{n}}$ is the outward unit normal vector orienting the area according to the right-hand rule applied to the bounding circuit. The area integral expression motivates interpreting velocity circulation as the "integrated flux of vorticity" that penetrates the surface. Stokes' theorem provides the means to connect the vorticity theories promoted by Helmholtz to the circulation theories of Kelvin.

37.5 The free vortex

Consider a two-dimensional rotating fluid in the x-y plane with angular velocity given by

$$\boldsymbol{\Omega} = \frac{\boldsymbol{x} \times \boldsymbol{v}}{r^2} = \frac{K \, \hat{\boldsymbol{z}}}{r^2}. \tag{37.20}$$

The constant K has dimensions $L^2 \, T^{-1}$, and $r^2 = x^2 + y^2$ is the squared distance from the axis of rotation with $\hat{\boldsymbol{z}}$ the unit vector normal to the x-y plane. The angular velocity falls off as the squared distance from the center, whereas it is singular at the origin. As shown in this section, the fluid flow associated with this *free vortex* has zero vorticity and zero circulation for all points except the origin. Yet the same points with zero vorticity and zero circulation have a constant angular momentum relative to the origin. As shown by Exercise 37.5, and pursued in more detail in Section 37.9, nonzero angular momentum can arise in a fluid with zero circulation so long as there is a nonzero strain within the fluid, such as the flow arising from the free vortex.

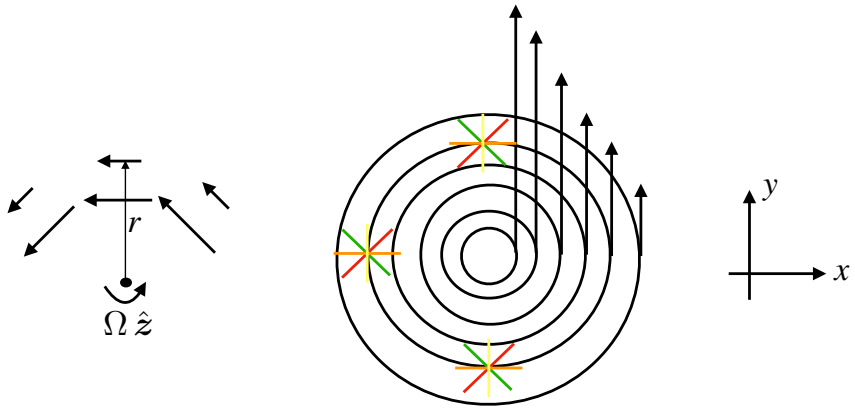

FIGURE 37.4: Irrotational counter-clockwise planar flow in the presence of a free vortex with velocity $\boldsymbol{v} = (K/r)\,\hat{\boldsymbol{\vartheta}}$. The tangential velocity decays as $1/r$ from the origin and the vorticity, $\nabla \times \boldsymbol{v}$, vanishes for all points except the origin. Test paddle wheels (colored line segments) do not spin when placed anywhere except at the origin. The free vortex has constant angular momentum per mass (computed relative to the origin), since the tangential velocity falls off as $1/r$ thus canceling the moment-arm distance r.

37.5.1 Velocity

Fluid flows in a circular orbit when in the free vortex flow field. Hence, the velocity of a fluid particle is perpendicular to its position vector, $\boldsymbol{x} = x\,\hat{\boldsymbol{x}} + y\,\hat{\boldsymbol{y}}$, with respect to the origin

$$\boldsymbol{v} \cdot \boldsymbol{x} = 0. \tag{37.21}$$

The velocity for pure rotational flow is given by (see Section 11.2.3)

$$\boldsymbol{v} = \boldsymbol{\Omega} \times \boldsymbol{x} = \frac{K\,(-y\,\hat{\boldsymbol{x}} + x\,\hat{\boldsymbol{y}})}{r^2} = \frac{K\hat{\boldsymbol{\vartheta}}}{r}, \tag{37.22}$$

where $\hat{\boldsymbol{\vartheta}}$ is the polar angle unit vector oriented in the counter-clockwise direction (see Section 4.22). We illustrate the velocity field (37.22) in Figure 37.4, which reveals the $1/r$ behavior with a singularity at the origin.

37.5.2 Vorticity

Away from the origin the vorticity vector vanishes

$$\boldsymbol{\omega} = \nabla \times \boldsymbol{v} = 0, \tag{37.23}$$

whereas it is singular at the origin. It is useful to expose a few details of this calculation by considering the vertical component to the vorticity, as computed using the polar coordinate curl (4.199c), in which

$$\hat{\boldsymbol{z}} \cdot (\nabla \times \boldsymbol{v}) = r^{-1}\,\partial_r(r\,v^{\vartheta}) - r^{-1}\,\partial_{\vartheta} v^r. \tag{37.24}$$

Since $v^r = 0$ there is a contribution only from the first term. Yet for the velocity (37.22) we have $r\,v^{\vartheta} = K$, so that $\partial_r(r\,v^{\vartheta}) = 0$. It is further insightful to perform the product rule to render

$$\hat{\boldsymbol{z}} \cdot (\nabla \times \boldsymbol{v}) = v^{\vartheta}/r + \partial_r v^{\vartheta} = K/r^2 - K/r^2 = 0, \tag{37.25}$$

which reveals that zero vorticity arises from an exact compensation between the curvature induced vorticity, v^ϑ/r, and the normal shear induced vorticity, $\partial_r v^\vartheta$

$$v^\vartheta/r = -\partial_r v^\vartheta = K/r^2. \tag{37.26}$$

We return to this result in Section 37.8, where we present a general means to decompose the vorticity into that arising from curvature in the flow plus that arising from normal shears (see Figure 37.10). The free vortex is a special case where these two contributions exactly counteract one another, thus leaving zero net vorticity.

In Figure 37.4 we exhibit a test paddle wheel in various positions around the free vortex. As the paddle wheel center moves counter-clockwise with the flow, the marked paddle wheel blades remain oriented at the same fixed angle. That is, the paddle wheel orbits around the vortex center but it does not spin since the vorticity vanishes in the region bounded away from the origin. Again, the vorticity vanishes in this case since the curvature induced vorticity exactly counteracts the normal shear induced vorticity, as per equation (37.26).

37.5.3 Angular momentum

Although vorticity is zero everywhere, except at the origin, the angular momentum (computed relative to the origin) is nonzero, as expected since the fluid is rotating around the vortex center. The angular momentum arises just from the nonzero strain in the flow field (see Exercise 37.5), with the strain causing fluid particles to move relative to one another. The angular momentum per unit mass, relative to the center of the vortex, is constant and pointed vertically

$$\boldsymbol{x} \times \boldsymbol{v} = r\,\hat{\boldsymbol{r}} \times (K/r)\,\hat{\boldsymbol{\vartheta}} = K\,\hat{\boldsymbol{z}}. \tag{37.27}$$

This result follows since the velocity falls of as $1/r$ to cancel the moment-arm distance, r. Hence, the angular momentum per mass is the same for all fluid particles in the presence of a free vortex, no matter what radial distance the particles have from the vortex center.

37.5.4 Circulation

The circulation vanishes for any circuit bounded away from the origin since vorticity vanishes away from the origin. However, the circulation is nonzero for any circuit enclosing the origin

$$\mathcal{C} = \oint_{\partial S} \boldsymbol{v} \cdot \mathrm{d}\boldsymbol{x} = \int_0^{2\pi} \boldsymbol{v} \cdot \hat{\boldsymbol{\vartheta}}\, r\, \mathrm{d}\vartheta = 2\pi K. \tag{37.28}$$

To reach this result, we set the line element to

$$\mathrm{d}\boldsymbol{x} = \hat{\boldsymbol{\vartheta}}\, r\, \mathrm{d}\vartheta \tag{37.29}$$

and inserted the velocity (37.22) represented in cylindrical polar coordinates, $\boldsymbol{v} \cdot \hat{\boldsymbol{\vartheta}} = K/r$. Hence, the singular point vortex at $r = 0$ induces a nonzero circulation for all circuits that enclose the origin.

37.6 Translation and rigid-body rotation

Rigid-body fluid motion occurs when all fluid particles are rigidly locked into their relative positions. There are two kinds of rigid body motion: translation and rotation. The velocity field for this motion is given by

$$\boldsymbol{v} = \boldsymbol{U} + \boldsymbol{\Gamma} \times \boldsymbol{x}, \tag{37.30}$$

where $\boldsymbol{x}$ is the position vector relative to the origin, $\boldsymbol{U}$ is a translation velocity, and $\boldsymbol{\Gamma}$ is an angular velocity. For rigid body motion, both $\boldsymbol{U}$ and $\boldsymbol{\Gamma}$ are spatially uniform, but can in general be time dependent. The strain rate tensor vanishes for uniform translation or rigid-body motion (see Exercise 18.2)

$$S_{mn} = \frac{1}{2}(\partial_m v_n + \partial_n v_m) = 0. \tag{37.31}$$

A zero strain rate tensor is expected since strain measures the relative motion between fluid particles, and for a rigid-body motion there is no such motion. Even so, the vorticity for rigid-body flow is nonzero (see Exercise 37.2)

$$\boldsymbol{\omega} = \nabla \times (\boldsymbol{\Gamma} \times \boldsymbol{x}) = 2\,\boldsymbol{\Gamma}. \tag{37.32}$$

We encountered this vorticity in Section 37.2.2 when connecting vorticity and angular velocity. In the remainder of this section, we set the rotation rate to that of the planet, $\boldsymbol{\Gamma} = \boldsymbol{\Omega}$, and assume it to be constant in space and time.

37.6.1 Absolute vorticity

For planetary fluid mechanics, planetary rotation imparts *planetary vorticity* to fluids. Hence, the total or *absolute* vorticity of a fluid is the vector sum of the *relative vorticity*, $\boldsymbol{\omega}$, plus the planetary vorticity

$$\boldsymbol{\omega}_{\rm a} = \boldsymbol{\omega}_{\rm planet} + \boldsymbol{\omega}. \tag{37.33}$$

In this equation,

$$\boldsymbol{\omega}_{\rm planet} = 2\,\boldsymbol{\Omega}_{\rm planet} \tag{37.34}$$

is the planetary vorticity associated with rigid-body motion of a fluid particle stationary with respect to the planet, and

$$\boldsymbol{\omega} = \nabla \times \boldsymbol{v} \tag{37.35}$$

is the relative vorticity. The relative vorticity measures the vorticity of the fluid due to motion relative to the rotating sphere, with $\boldsymbol{v}$ the velocity relative to the rotating sphere.

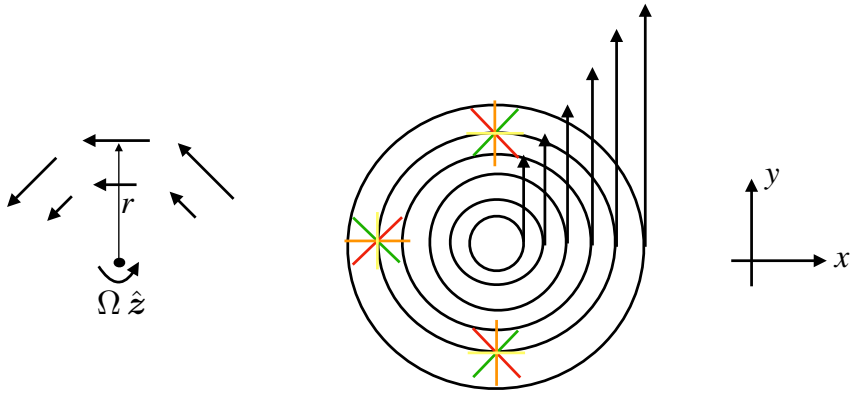

FIGURE 37.5: Rigid body fluid motion, whereby the fluid velocity is: (A) purely tangential and linearly proportional to the radial distance from the vortex center, $\boldsymbol{v} = |\Omega|\, r\, \hat{\boldsymbol{\vartheta}}$; (B) fluid particles maintain a fixed relative position; (C) and vorticity is constant and points perpendicular to the page, $\boldsymbol{\omega} = 2\,\boldsymbol{\Omega} = 2\,|\Omega|\,\hat{\boldsymbol{z}}$. Test paddle wheels rigidly move around the center, and they exhibit a spin about their axis that manifests the nonzero vorticity.

37.6.2 Rigid-body rotation on a plane

Consider the circular rigid-body rotation on a plane shown in Figure 37.5, in which the velocity is purely tangential and linearly proportional to the distance from the center

$$\boldsymbol{v} = \boldsymbol{\Omega} \times \boldsymbol{x} = |\Omega| \, (-y \, \hat{\boldsymbol{x}} + x \, \hat{\boldsymbol{y}}) = |\Omega| \, r \, \hat{\boldsymbol{\vartheta}}. \tag{37.36}$$

Assuming the center of mass to be at the circle center, the angular momentum for the flow is the same as that for a rigid-body. Even though the motion of each fluid particle is rigidly fixed relative to all other particles, there is a nonzero vorticity in this flow as illustrated by the spin of colored test paddle wheels in Figure 37.5.

37.6.3 Circulation for rigid-body rotation

For rigid-body rotation, the velocity circulation around a circular path of radius R is given by

$$\mathcal{C} = \oint \boldsymbol{v} \cdot \mathrm{d}\boldsymbol{x} = \oint (\boldsymbol{\Omega} \times \boldsymbol{x}) \cdot \mathrm{d}\boldsymbol{x} = R^2 \, |\Omega| \oint \mathrm{d}\vartheta = 2\pi R^2 \, |\Omega| = 2A \, |\Omega|, \tag{37.37}$$

where $A = \pi R^2$ is the area of the circle. Hence, the circulation per area for rigid-body rotating fluid flow is twice the angular rotation rate, which is the magnitude of the vorticity

$$\mathcal{C}/A = |\boldsymbol{\omega}| = 2 \, |\boldsymbol{\Omega}|. \tag{37.38}$$

37.6.4 Comments

As seen in Section 37.5, fluid flow in the presence of a free vortex has zero vorticity for all points except the origin of the vortex. However, the same points also have a constant angular momentum relative to the origin, and they experience a nonzero strain. In contrast, constant rigid-body rotating fluid flow has a nonzero vorticity, nonzero angular momentum, yet a zero strain. Section 37.9 details the connection between vorticity, strain, and angular momentum, where we see that angular momentum can be nonzero if either vorticity or strain are nonzero. These ideas are illustrated in this 3-minute video as well as in this 10 minute video from the Open University.

37.7 Kinematics of vortex lines and vortex tubes

We here develop the basics of vortex kinematics, with this discussion closely following from the kinematics of material line elements discussed in Section 18.6.3.

37.7.1 Vortex lines and vortex tubes

A *vortex line* is a curve in the fluid that is instantaneously tangent to the vorticity at each point along the curve.[1] That is, the collection of vortex lines provides the collection of integral curves for the vorticity field. A vortex line is mathematically parameterized just like any other curve, whereby we write the spatial coordinates along the curve as a function of a suitable parameter φ (e.g., the arc-length)

$$\boldsymbol{x}(\varphi) = x(\varphi) \, \hat{\boldsymbol{x}} + y(\varphi) \, \hat{\boldsymbol{y}} + z(\varphi) \, \hat{\boldsymbol{z}}. \tag{37.39}$$

[1] As noted in Section 1.4 of *Saffman* (1992), a *vortex filament* is a vortex tube surrounded by irrotational fluid, which contrasts to the more general concept of a vortex line.

Correspondingly, the tangent vector for the curve is given by

$$\frac{\mathrm{d}\boldsymbol{x}(\varphi)}{\mathrm{d}\varphi} = \frac{\mathrm{d}x(\varphi)}{\mathrm{d}\varphi}\,\hat{\boldsymbol{x}} + \frac{\mathrm{d}y(\varphi)}{\mathrm{d}\varphi}\,\hat{\boldsymbol{y}} + \frac{\mathrm{d}z(\varphi)}{\mathrm{d}\varphi}\,\hat{\boldsymbol{z}}. \tag{37.40}$$

The three coordinates of the vortex line are constrained so that the tangent is parallel to vorticity at each point

$$\frac{\mathrm{d}\boldsymbol{x}(\varphi)}{\mathrm{d}\varphi} \times \boldsymbol{\omega} = 0, \tag{37.41}$$

which is satisfied by the following constraint

$$\frac{\mathrm{d}x/\mathrm{d}\varphi}{\omega_x} = \frac{\mathrm{d}y/\mathrm{d}\varphi}{\omega_y} = \frac{\mathrm{d}z/\mathrm{d}\varphi}{\omega_z}. \tag{37.42}$$

These equations are directly analogous to those satisfied by velocity streamlines as discussed in Section 17.7.2. Notably, the velocity is not constant along a velocity streamline, nor is vorticity constant along a vortex line. In a steady state, streamlines map the trajectory of a fluid particle (see Section 17.7). However, a vortex line does not offer an interpretation in terms of trajectories.

A *vortex tube* is a bundle of vortex lines that pass through a simple closed curve such as that illustrated in Figure 37.6. By definition, the sides of the vortex tube are parallel to the vorticity field, since the sides are constructed from vortex lines.[2]

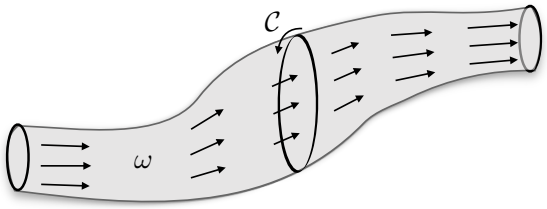

FIGURE 37.6: A vortex line is a line in the fluid that is everywhere tangent to the vorticity vector. A vortex tube is the accumulation of vortex lines passing through a closed loop. A related, but distinct, concept arises when a vortex tube is surrounded by irrotational flow, with such tubes referred to as *vortex filaments* (see Section 1.4 of *Saffman* (1992)). We here depict a vortex tube and circulation computed around the tube $\mathcal{C} = \oint_{\partial\mathcal{S}} \boldsymbol{v} \cdot \mathrm{d}\boldsymbol{x} = \int \boldsymbol{\omega} \cdot \hat{\boldsymbol{n}}\,\mathrm{d}\mathcal{S}$. Since vorticity has zero divergence, the circulation is the same for any loop embracing the vortex tube (Helmholtz's first theorem from Section 37.7.3). A uniform circulation along the tube means that the magnitude of the vorticity is larger in regions where the tube has a small area and conversely the circulation magnitude is smaller where the tube has a large area. Note that orientation of the circulation integral must accommodate the oppositely directed outward normals on the tube end caps. That is, circulation is computed around a counter-clockwise orientated path, with this orientation determined relative to the outward normal.

37.7.2 Kinematic properties

Vorticity has zero divergence

$$\nabla \cdot \boldsymbol{\omega} = \nabla \cdot (\nabla \times \boldsymbol{v}) = 0, \tag{37.43}$$

[2]We defined a similar notion, the streamtube, for a non-divergent velocity in Figure 17.5.

which follows since the divergence of a curl vanishes. Integrating the non-divergence relation over an arbitrary closed volume within the fluid leads to

$$\int_{\mathscr{R}} \nabla \cdot \boldsymbol{\omega} \, dV = \oint_{\partial \mathscr{R}} \boldsymbol{\omega} \cdot \hat{\boldsymbol{n}} \, d\mathcal{S} = 0, \tag{37.44}$$

where we made use of Gauss's divergence theorem to reach the surface integral expression, with $\hat{\boldsymbol{n}} \, d\mathcal{S}$ the oriented area element on the boundary of the volume, $\partial \mathscr{R}$, and $\hat{\boldsymbol{n}}$ the outward normal on the boundary. This result means there is no net vorticity entering or leaving an arbitrary closed region. That is, there is a vanishing net integrated "flux" of vorticity across the surface bounding a closed region. Consequently, there are no sources or sinks of vorticity within the fluid, meaning there is no accumulation nor depletion of vorticity within any arbitrary closed region within the fluid.

Now specialize the surface integral in equation (37.44) to a volume along a chosen vortex tube such as in Figure 37.6. The two ends of the tube generally have different cross-sectional areas. The integral over the sides of the vortex tube vanishes since vorticity is parallel to the sides of the tube. Hence, the surface integral only picks up contributions from the two ends of the tube[3]

$$\int_{\mathrm{A}} \boldsymbol{\omega} \cdot \hat{\boldsymbol{n}} \, d\mathcal{S}_A + \int_{\mathrm{B}} \boldsymbol{\omega} \cdot \hat{\boldsymbol{n}} \, d\mathcal{S}_B = 0. \tag{37.45}$$

The outward normals point in the opposite direction so that the flux of vorticity is independent of position along the tube. Stoke's theorem transfers the vorticity constraint to a constraint on the circulation around the circumference of the tube

$$\oint_{\mathrm{A}} \boldsymbol{v} \cdot d\boldsymbol{x} + \oint_{\mathrm{B}} \boldsymbol{v} \cdot d\boldsymbol{x} = 0. \tag{37.46}$$

Hence, the circulation around the vortex tube is the same no matter where it is computed. The circulation constraints (37.45) and (37.46) are kinematic, holding for any vorticity field. We now consider some consequences of this constraint.

37.7.3 Helmholtz's theorems

There are a few basic properties of vorticity that follow from its vanishing divergence. These properties are known as Helmholtz's theorems.

Helmholtz's first theorem

Since the cross-sectional slices used to derive the circulation constraint (37.46) are arbitrary, the constraint holds throughout the full extent of the vortex tube. Hence, as noted following equation (37.46), the circulation is the same for any position along the vortex tube; i.e., the strength of a vortex tube is the same value along its length (see Figure 37.6). This result is known as *Helmholtz's first theorem.*

As a corollary, we refer to the vorticity constraint (37.45) to note that any process that changes in the vortex tube cross-sectional area is compensated by changes in vorticity. For example, let the vortex tube shrink over some region. To maintain constant circulation along the tube, the vorticity magnitude must increase where the area decreases, which in turn means that the velocity circulating around the tube increases in magnitude as the area reduces. Think of a tornado as in Figure 37.7, which is a natural expression of a vortex tube. Near the ground, the cross-sectional area of the tornado is small, with the tangential velocity of a fluid particle

[3] In Exercise 21.9, we developed a similar set of results for a streamtube in a non-divergent velocity field.

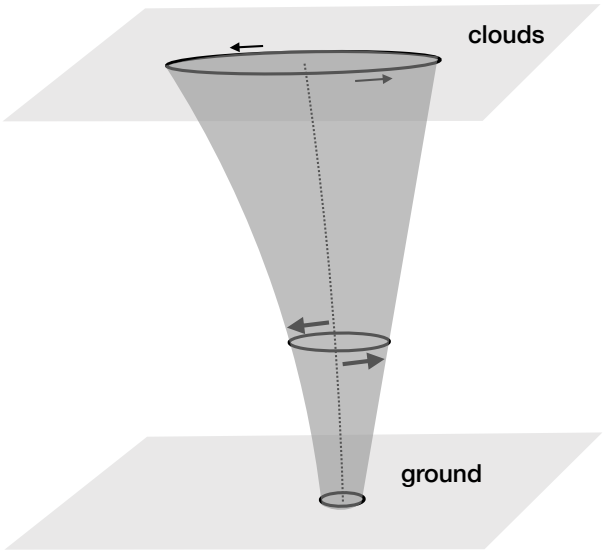

FIGURE 37.7: A vortex tube idealization of a tornado. Since the circulation around the tube is uniform (Helmholtz's first theorem), the tangential velocity of a fluid particle has a larger magnitude in regions where the vortex area is smaller, such as near the ground. As the tornado reaches into the clouds, it generally has a larger cross-sectional area and thus a smaller magnitude for the tangential velocity.

within the tube relatively large. Near the tornado top, the cross-sectional area is large so the tangential velocity is relatively small.

Helmholtz's second theorem

The vorticity constraint (37.45) cannot be satisfied by a finite vorticity if the area of a vortex tube vanishes anywhere. Hence, a vortex tube cannot begin or end within the fluid. This result follows from the absence of vortex sources and sinks within the fluid. Hence, a vortex tube can only loop with itself (e.g., a smoke ring as in Figure 37.8), or intersect a boundary (as for a tornado in Figure 37.7, where the ground and clouds form the boundary).

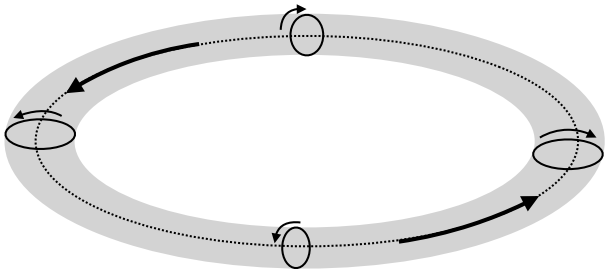

FIGURE 37.8: A vortex ring (torus) is a vortex tube that closes on itself. We here depict a vortex ring with vorticity pointing counter-clockwise around the ring. The tangential velocity is oriented as shown so that the vorticity points according to the right hand rule. That is, orient the fingers on the right hand according to the tangential velocity. The thumb of the right hand then points in the direction of the vorticity vector.

Helmholtz's third theorem

Helmholtz's third theorem states that an unforced inviscid barotropic fluid that has zero vorticity remains irrotational forever. This theorem is a special case of Kelvin's circulation theorem that is studied in Section 40.2.

37.7.4 Further study

A particularly insightful and pedagogical discussion of the ideas in this section can be found in Chapter 5 of *Acheson* (1990). Additionally, the following videos offer laboratory demonstrations of vorticity in non-rotating and rotating flows.

- Helmholtz's theorems are vividly exhibited by this video from the *Physics Girl* of flow generated by a paddle in a swimming pool. She also discusses vortex rings in this video.
- Vorticity and Helmholtz's theorems are also described by this classic video from Prof. Shapiro.
- A rotating tank experiment shown near the 15 minute mark of this video from Prof. Fultz shows how vorticity is affected by vortex stretching.
- This video offers a classic tutorial on vorticity in non-rotating fluids from Prof. Shapiro.

37.8 Relative vorticity from curvature and shear

In this section we decompose the vorticity into two terms: one arising from curvature in the flow and another arising from shears in the direction normal to the flow. This decomposition is formulated for horizontal flows, but can be generalized to arbitrary flow. It offers yet another means to understand the kinematic properties of vorticity.

37.8.1 Circular flow

Before treating the general case, consider a two-dimensional velocity that locally takes the form of an angular flow

$$\boldsymbol{u} = u^{\vartheta}(r, \vartheta)\, \hat{\boldsymbol{\vartheta}}, \tag{37.47}$$

where ϑ is the polar angle. Circulation around the circular wedge shown in Figure 37.9 has zero contributions from the two radial segments since these segments are perpendicular to the angular flow. The circulation is thus given by

$$\begin{aligned}
\mathcal{C} &= \oint_{\text{wedge}} \boldsymbol{u} \cdot \mathrm{d}\boldsymbol{x} && \text{(37.48a)}\\
&= \int_{\vartheta}^{\vartheta+\delta\vartheta} u^{\vartheta}(r+\delta r, \vartheta')\,(r+\delta r)\,\mathrm{d}\vartheta' + \int_{\vartheta+\delta\vartheta}^{\vartheta} u^{\vartheta}(r, \vartheta')\, r\,\mathrm{d}\vartheta' && \text{(37.48b)}\\
&= \int_{\vartheta}^{\vartheta+\delta\vartheta} \Big[u^{\vartheta}(r+\delta r, \vartheta')\,(r+\delta r) - r\,u^{\vartheta}(r, \vartheta')\Big]\,\mathrm{d}\vartheta' && \text{(37.48c)}\\
&\approx \int_{\vartheta}^{\vartheta+\delta\vartheta} \left[u^{\vartheta}(r, \vartheta')\,\delta r + \frac{\partial u^{\vartheta}}{\partial r}\, r\,\delta r\right]\mathrm{d}\vartheta' && \text{(37.48d)}\\
&= r\,\delta r \int_{\vartheta}^{\vartheta+\delta\vartheta} \left[\frac{u^{\vartheta}}{r} + \frac{\partial u^{\vartheta}}{\partial r}\right]\mathrm{d}\vartheta', && \text{(37.48e)}
\end{aligned}$$

where the approximation holds when $\delta r \to 0$. Taking the further limit $\delta\vartheta \to 0$ renders

$$\mathcal{C} \approx \zeta\,\delta A = \zeta\, r\,\delta r\,\delta\vartheta = \left[\frac{u^{\vartheta}}{r} + \frac{\partial u^{\vartheta}}{\partial r}\right] r\,\delta r\,\delta\vartheta \Longrightarrow \zeta = \frac{u^{\vartheta}}{r} + \frac{\partial u^{\vartheta}}{\partial r}. \tag{37.49}$$

The first term in the vorticity arises from the nonzero radius of curvature of the circular flow whereas the second term arises from radial shear.

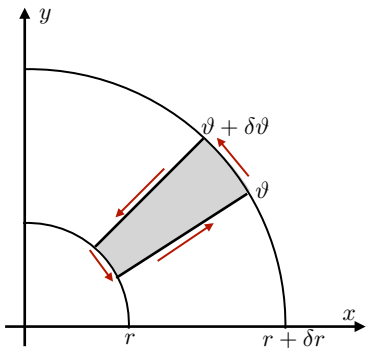

FIGURE 37.9: Circulation around the circular wedge $[r, r + \delta r] \otimes [\vartheta, \vartheta + \delta\vartheta]$.

37.8.2 Generalization to natural coordinates

The decomposition (37.49) can be generalized to arbitrary horizontal flow by making use of the natural coordinates from Section 32.2. Here, we introduce the locally orthogonal coordinates, (s, n), with s the arc-length defined along the trajectory of a fluid element and n measuring the distance normal to the trajectory. We make the convention that the unit tangent direction, $\hat{\boldsymbol{u}}$, is aligned along the local flow direction whereas the unit normal direction, $\hat{\boldsymbol{n}}$, is to the left facing downstream. Furthermore, the radius of curvature at a point along a trajectory (see Section 5.2.3) is positive if the flow turns into the positive $\hat{\boldsymbol{n}}$ direction (left turn) and negative for oppositely curved flow (right turn) (see Figures 32.2 and 32.3). Finally, the radius of curvature is infinite for straight flow.

For the counter-clockwise circuit in Figure 37.9, a left turn occurs with $\hat{\boldsymbol{n}} = -\hat{\boldsymbol{r}}$ so that equation (37.49) takes on the general form

$$\zeta = \underbrace{\frac{|\boldsymbol{u}|}{R}}_{\text{curvature}} - \underbrace{\frac{\partial|\boldsymbol{u}|}{\partial n}}_{\text{shear}} = \zeta_{\text{curv}} + \zeta_{\text{shear}}. \tag{37.50}$$

Again, the first term arises from curvature in the flow, with R the radius of curvature. This *curvature vorticity* is sometimes also called the *orbital vorticity*. A trajectory turning to the left has $R > 0$ and this curved trajectory contributes to a positive vorticity; conversely for a trajectory turning to the right. The second term in equation (37.50) arises from shears computed normal to the flow direction. If the flow speed decreases in the normal direction (e.g., towards the center of the circle in Figure 37.9), then that too contributes to a positive vorticity. Furthermore, flow with $\zeta = 0$ arises if there is an exact compensation between the curvature-induced vorticity with the shear-induced vorticity

$$\zeta = 0 \Longrightarrow \frac{|\boldsymbol{u}|}{R} = \frac{\partial|\boldsymbol{u}|}{\partial n}. \tag{37.51}$$

37.8.3 Example vorticities

Rigid body vortex and free vortex

To help further understand the decomposition (37.50), consider the case of rigid-body rotation (Figure 37.5) where $\boldsymbol{v} = \Omega\, r\, \hat{\boldsymbol{\vartheta}}$ and $\hat{\boldsymbol{n}} = -\hat{\boldsymbol{r}}$. For a circle the radius of curvature equals to the radius of the circle, so that

$$\zeta_{\text{curv}} = \frac{\Omega\, r}{r} = \Omega \quad \text{and} \quad \zeta_{\text{shear}} = -\partial_n|\boldsymbol{u}| = \partial_r(\Omega\, r) = \Omega, \tag{37.52}$$

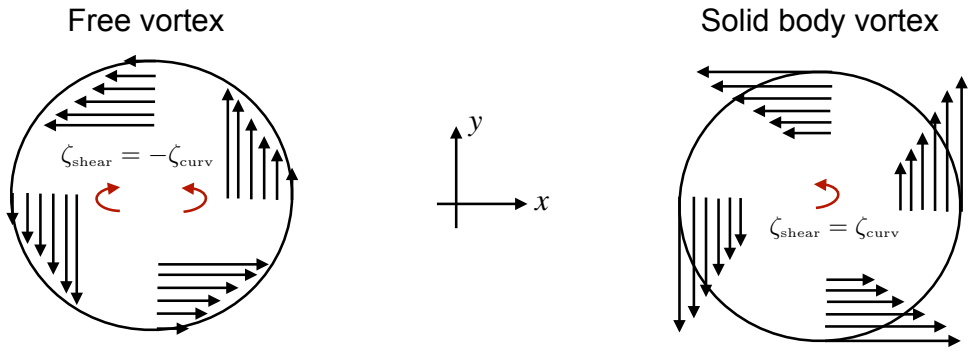

FIGURE 37.10: Decomposing the relative vorticity into its contributions from curvature and normal shear. Left panel: the free vortex from Figure 37.4 has $\zeta_{\text{curv}} = -\zeta_{\text{shear}} = K/r^2$ so that $\zeta = \zeta_{\text{curv}} + \zeta_{\text{shear}} = 0$. Right panel: the rigid-body vortex from Figure 37.5 has $\zeta_{\text{curv}} = \zeta_{\text{shear}} = \Omega$ so that $\zeta = 2\,\Omega$.

in which case

$$\zeta = \zeta_{\text{curv}} + \zeta_{\text{shear}} = 2\,\Omega = \hat{\boldsymbol{z}} \cdot (\nabla \times \boldsymbol{v}), \tag{37.53}$$

as depicted in the right panel of Figure 37.10. Likewise, for the free vortex (Figure 37.4) we have $\boldsymbol{v} = (K/r)\,\hat{\boldsymbol{\vartheta}}$ so that

$$\zeta_{\text{curv}} = K/r^2 \quad \text{and} \quad \zeta_{\text{shear}} = \partial|\boldsymbol{u}|/\partial r = -K/r^2, \tag{37.54}$$

which yields zero relative vorticity

$$\zeta = \zeta_{\text{curv}} + \zeta_{\text{shear}} = 0, \tag{37.55}$$

as depicted in the left panel of Figure 37.10.

Gaussian jet moving along a line and around a circle

Next consider a Gaussian jet moving along a straight line in the meridional direction with velocity field

$$\boldsymbol{v}(x) = v(x)\,\hat{\boldsymbol{y}} = v_0\,\exp[-(x - x_{\text{max}})^2/L^2]\,\hat{\boldsymbol{y}}, \tag{37.56}$$

where v_0 is the velocity scale, L is the e-folding length scale for the jet, and x_{max} is the position of the jet maximum. The corresponding vorticity of the jet is given by

$$\zeta_{\text{line}} = \partial_x v = -2\,[(x - x_{\text{max}})/L^2]\,v(x). \tag{37.57}$$

We depict the velocity (37.56) and vorticity (37.57) in the top row of Figure 37.11. Note the symmetry of the vorticity around the jet maximum at $x = x_{\text{max}}$, with the vorticity extrema corresponding to inflection points of the jet.[4]

Now assume the same jet is moving counter-clockwise around a circle so that the velocity field is given by

$$\boldsymbol{v}(r) = v(r)\,\hat{\boldsymbol{\vartheta}} = v_0\,\exp[-(r - r_{\text{max}})^2/L^2]\,\hat{\boldsymbol{\vartheta}}, \tag{37.58}$$

where we made use of the polar coordinates from Section 4.22 with $r^2 = x^2 + y^2$ the squared radial distance from the center, and $\hat{\boldsymbol{\vartheta}}$ the unit vector pointing in the counter-clockwise direction from the $\hat{\boldsymbol{x}}$ axis. Making use of the curl operation in polar coordinates given by equation (4.199c)

[4]Inflection points are where the curvature vanishes and has opposite signs on either side. For a function of a single variable, an inflection point is where the second derivative vanishes and changes sign when moving to either side.

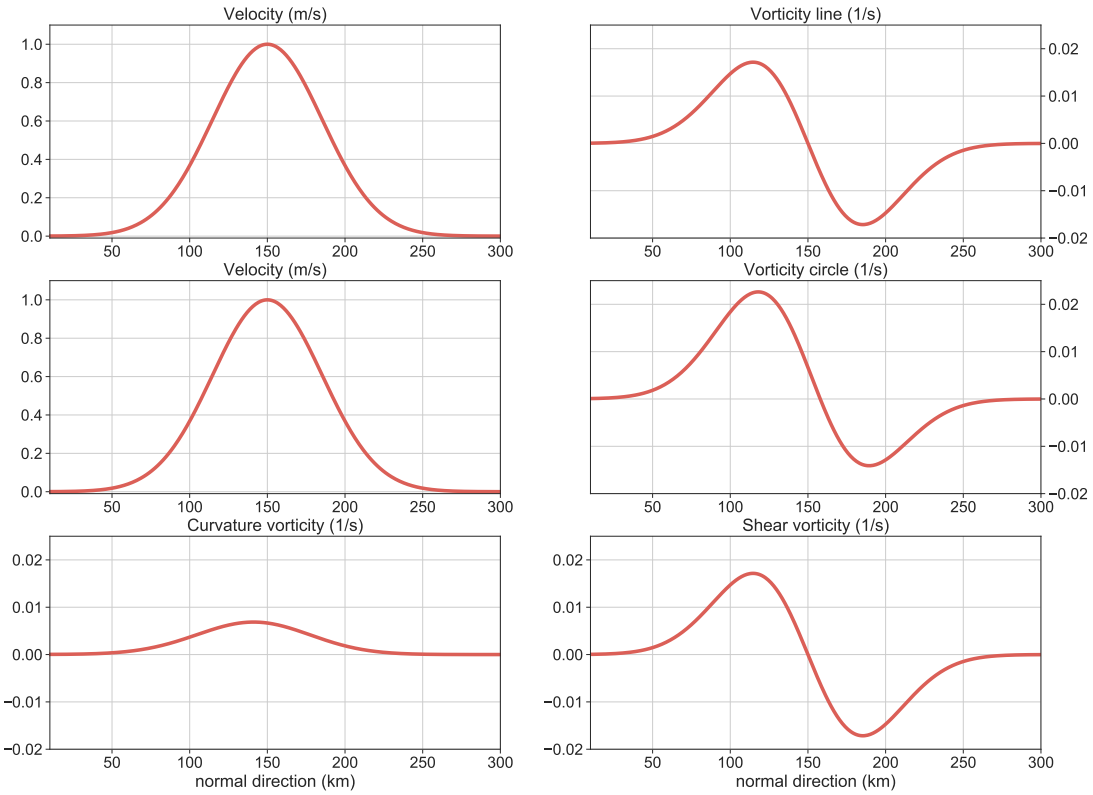

FIGURE 37.11: Top row: velocity and vorticity within a Gaussian jet that is moving along a straight line according to equations (37.56) and (37.57). We set the jet e-folding scale as $L = 50$ km, jet maximum at $x_{\max} = 150$ km, and velocity scale as $v_0 = 1$ m s^{-1}. Note the symmetry of the vorticity relative to the jet maximum, with the vorticity extrema corresponding to the inflection points of the Gaussian velocity field. Middle left: the same Gaussian velocity profile only now for a jet that is moving counter-clockwise around a circle so that $\boldsymbol{v} = v(r)\,\hat{\boldsymbol{\vartheta}}$ according to equation (37.58). To avoid a singularity of the curvature vorticity at $r = 0$ (infinite curvature) we assume the velocity field vanishes within a small distance from the origin. Middle right: vorticity for the Gaussian jet moving around the circle, with $\zeta = r^{-1}\,\partial_r(r\,v)$. Notice how the vorticity is not symmetric relative to the jet maximum. Rather, the zero vorticity occurs to the right of the jet maximum, and the vorticity on the inside of the jet maximum is larger in magnitude than the outer vorticity. Lower left: vorticity due to the curvature of the jet as it moves around the circle, $\zeta_{\text{curve}} = v(r)/r$. Lower right: vorticity due to the radial shear in the Gaussian jet, $\zeta_{\text{shear}} = -2\,(r - r_{\max})\,v(r)/L^2$.

renders the vorticity

$$\zeta = r^{-1}\,\partial_r(r\,v) = \frac{v}{r} - \frac{2\,(r - r_{\max})\,v}{L^2} = \zeta_{\text{curve}} + \zeta_{\text{shear}}. \tag{37.59}$$

We depict these terms in the third row of Figure 37.11. Note how the vorticity, ζ, has the amplitude of its maximum increased, whereas the amplitude of its minimum is decreased. Correspondingly, the vorticity is not symmetric about the jet maximum, with its zero crossing to the outside of the jet maximum. Asymmetry of the vorticity arises from the curvature vorticity, $\zeta_{\text{curve}} = v/r$, which has its peak inside the jet maximum. So although the shear vorticity, ζ_{curve}, is symmetric around the jet axis, the curvature vorticity causes a movement of vorticity towards the center of the circle.

37.9 Relating angular momentum to vorticity and strain

As noted in Section 37.6.4, fluid flow in the presence of a free vortex (Section 37.5) has zero vorticity for all points except the origin of the vortex. However, the same points with zero

vorticity also have a constant angular momentum relative to the origin, and they experience a nonzero strain. In contrast, rigid-body fluid flow (Section 37.6) has a nonzero vorticity, nonzero angular momentum, yet a zero strain rate. In this section we study the connection between vorticity, strain rate, and angular momentum for a fluid. We here show that angular momentum and vorticity are fundamentally distinct in a fluid that has straining motion between fluid elements. In contrast, angular momentum and vorticity are directly proportional (through the moment of inertia tensor) when the fluid exhibits rigid-body motion in which the strain rate tensor vanishes.

In this section we make use of the Lagrangian description from Section 18.2, whereby we write the trajectory of a fluid particle as in equation (18.2) using the motion field. Namely, by fixing the material coordinate, $\boldsymbol{a}$, the motion field provides the spatial position, $\boldsymbol{x}$, of the fluid particle as a function of the Lagrangian time, T

$$\boldsymbol{x} = \boldsymbol{X}(\boldsymbol{a}, T). \tag{37.60}$$

37.9.1 Linear momentum

Consider the velocity and linear momentum of a simply connected material fluid region denoted by $\mathcal{R}(\boldsymbol{v})$, with each point of the region moving with the fluid velocity. Let an arbitrary fluid particle within this region be marked with the material label, $\boldsymbol{a}$, so that its position vector is $\boldsymbol{X}(\boldsymbol{a}, T)$ and its velocity is

$$\boldsymbol{v}^{\mathrm{L}}(\boldsymbol{a}, T) = \partial_T \boldsymbol{X}(\boldsymbol{a}, T), \tag{37.61}$$

where the time derivative is computed holding the material label fixed, and where the "L" superscript signals a Lagrangian velocity. Since the fluid particle is within a finite material region, we can decompose its motion into the sum of the region's center of mass motion plus motion of the particle relative to the center of mass

$$\begin{aligned}
\boldsymbol{v}^{\mathrm{L}}(\boldsymbol{a}, T) &= \partial_T \boldsymbol{X}(\boldsymbol{a}, T), && \text{(37.62a)}\\
&= \partial_T [\overline{\boldsymbol{X}}(T) + \boldsymbol{X}'(\boldsymbol{a}, T)] && \text{(37.62b)}\\
&= \overline{\boldsymbol{v}^{\mathrm{L}}}(T) + \boldsymbol{v}^{\mathrm{L}'}(\boldsymbol{a}, T). && \text{(37.62c)}
\end{aligned}$$

The velocity, $\boldsymbol{v}^{\mathrm{L}'}(\boldsymbol{a}, T)$, is defined relative to the region's center of mass velocity, $\overline{\boldsymbol{v}^{\mathrm{L}}}(T)$. Furthermore, the center of mass velocity is given by

$$\begin{aligned}
\overline{\boldsymbol{v}^{\mathrm{L}}} &= \frac{\mathrm{d}\overline{\boldsymbol{X}}}{\mathrm{d}T} && \text{(37.63a)}\\
&= \frac{\mathrm{d}}{\mathrm{d}T}\left[\frac{\int_{\mathcal{R}(\boldsymbol{v})} \boldsymbol{x}\,\rho\,\mathrm{d}V}{\int_{\mathcal{R}(\boldsymbol{v})} \rho\,\mathrm{d}V}\right] && \text{(37.63b)}\\
&= \frac{1}{M}\int_{\mathcal{R}(\boldsymbol{v})} \frac{\mathrm{D}\boldsymbol{x}}{\mathrm{D}t}\,\rho\,\mathrm{d}V && \text{(37.63c)}\\
&= \frac{1}{M}\int_{\mathcal{R}(\boldsymbol{v})} \boldsymbol{v}\,\rho\,\mathrm{d}V. && \text{(37.63d)}
\end{aligned}$$

The identity (37.63c) follows since the material region maintains a constant mass,

$$M = \int_{\mathcal{R}(\boldsymbol{v})} \rho\,\mathrm{d}V \implies \frac{\mathrm{d}M}{\mathrm{d}t} = 0, \tag{37.64}$$

allowing the denominator to come outside the Lagrangian time derivative. Additionally, each of the fluid parcels in the region maintains constant mass. As per Reynold's transport theorem

(Section 19.5), the time derivative moves across the integral to act materially on the position vector. The final equality, (37.63d), follows since the material time derivative of a particle trajectory, when evaluated at a point, $\boldsymbol{x}$, equals to the velocity field at that point

$$\boldsymbol{v}(\boldsymbol{x}, t) = \frac{\mathrm{D}\boldsymbol{x}}{\mathrm{D}t}. \tag{37.65}$$

It follows that the linear momentum for the material fluid region is given by

$$\boldsymbol{P} = \int_{\mathcal{R}(\boldsymbol{v})} \boldsymbol{v}\, \rho \, \mathrm{d}V = M\, \overline{\boldsymbol{v}^{\mathrm{L}}}. \tag{37.66}$$

We conclude that the total linear momentum of an material fluid region equals to that of a point particle of mass, $M = \int_{\mathcal{R}(\boldsymbol{v})} \rho \, \mathrm{d}V$, moving with the center of mass velocity, $\overline{\boldsymbol{v}^{\mathrm{L}}}$. The analogous result was derived in Section 11.5 for a system of discrete point particles.

37.9.2 Angular momentum

Consider angular momentum for a material fluid region, which is determined by the material integral of the angular momentum for each fluid parcel

$$\boldsymbol{L} = \int_{\mathcal{R}(\boldsymbol{v})} (\boldsymbol{x} \times \boldsymbol{v})\, \rho \, \mathrm{d}V. \tag{37.67}$$

Our goal is to expose how physically distinct aspects of the fluid motion contribute to the angular momentum. To proceed, decompose the position vector of a point within the region into the center of mass position plus a deviation, $\boldsymbol{x} = \overline{\boldsymbol{x}} + \boldsymbol{x}'$, where $\overline{\boldsymbol{x}} = \overline{X}$ is the instantaneous position of the moving center of mass. The angular momentum thus takes the form

$$\begin{aligned}
\boldsymbol{L} &= \int_{\mathcal{R}(\boldsymbol{v})} (\boldsymbol{x} \times \boldsymbol{v})\, \rho \, \mathrm{d}V && \text{(37.68a)}\\
&= \int_{\mathcal{R}(\boldsymbol{v})} [(\overline{\boldsymbol{x}} + \boldsymbol{x}') \times \boldsymbol{v}]\, \rho \, \mathrm{d}V && \text{(37.68b)}\\
&= \overline{\boldsymbol{X}} \times \left[\int_{\mathcal{R}(\boldsymbol{v})} \boldsymbol{v}\, \rho \, \mathrm{d}V \right] + \int_{\mathcal{R}(\boldsymbol{v})} (\boldsymbol{x}' \times \boldsymbol{v})\, \rho \, \mathrm{d}V && \text{(37.68c)}\\
&= (\overline{\boldsymbol{X}} \times \boldsymbol{P}) + \int_{\mathcal{R}(\boldsymbol{v})} (\boldsymbol{x}' \times \boldsymbol{v})\, \rho \, \mathrm{d}V. && \text{(37.68d)}
\end{aligned}$$

The final equality introduced the linear momentum for the fluid region, $\boldsymbol{P}$, in the form of equation (37.66). The first term in equation (37.68d) is the angular momentum of the region with respect to the position of the center of mass. The second term arises from deviations of fluid particle positions relative to the center of mass.

We now focus on how the deviation term, $\int_{\mathcal{R}(\boldsymbol{v})} (\boldsymbol{x}' \times \boldsymbol{v})\, \rho \, \mathrm{d}V$, contributes to the angular momentum (37.67). As we will see, this analysis exposes how angular momentum of the extended material fluid region is affected by vorticity and strain rate in the fluid flow. To facilitate some of the manipulations, we make use of basic Cartesian tensor analysis from Chapter 1, including the summation convention whereby repeated indices are summed over their range.

37.9.3 Taylor expanding the velocity

We perform a Taylor expansion of the velocity $\boldsymbol{v}(\boldsymbol{x})$ around the instantaneous center of mass position, $\overline{\boldsymbol{x}} = \overline{X}$, and truncate the expansion to the leading order term[5]

$$\boldsymbol{v}(\boldsymbol{x}) = \boldsymbol{v}(\overline{\boldsymbol{x}} + \boldsymbol{x}') \approx \boldsymbol{v}(\overline{\boldsymbol{x}}) + (\boldsymbol{x}' \cdot \nabla)\, \boldsymbol{v}|_{\boldsymbol{x}=\overline{\boldsymbol{x}}}. \tag{37.69}$$

We are thus left with

$$\boldsymbol{L} = (\overline{\boldsymbol{X}} \times \boldsymbol{P}) + \int_{\mathcal{R}(\boldsymbol{v})} (\boldsymbol{x}' \times \boldsymbol{v})\, \rho \, \mathrm{d}V \tag{37.70a}$$

$$= (\overline{\boldsymbol{X}} \times \boldsymbol{P}) + \int_{\mathcal{R}(\boldsymbol{v})} [\boldsymbol{x}' \times \boldsymbol{v}(\overline{\boldsymbol{x}})]\, \rho \, \mathrm{d}V + \int_{\mathcal{R}(\boldsymbol{v})} [\boldsymbol{x}' \times (\boldsymbol{x}' \cdot \nabla)\, \boldsymbol{v}(\overline{\boldsymbol{x}})]\, \rho \, \mathrm{d}V. \tag{37.70b}$$

The velocity, $\boldsymbol{v}(\overline{\boldsymbol{x}})$, can be removed from the integration since it is evaluated at the center of mass point. Hence, the second term in equation (37.70b) vanishes

$$\int_{\mathcal{R}(\boldsymbol{v})} [\boldsymbol{x}' \times \boldsymbol{v}(\overline{\boldsymbol{x}})]\, \rho \, \mathrm{d}V = \left[\int_{\mathcal{R}(\boldsymbol{v})} \boldsymbol{x}' \, \rho \, \mathrm{d}V \right] \times \boldsymbol{v}(\overline{\boldsymbol{x}}) = 0, \tag{37.71}$$

where $\int_{\mathcal{R}(\boldsymbol{v})} \boldsymbol{x}' \, \rho \, \mathrm{d}V = 0$ by definition of the center of mass. The angular momentum is thus given by the two terms

$$\boldsymbol{L} = (\overline{\boldsymbol{X}} \times \boldsymbol{P}) + \int_{\mathcal{R}(\boldsymbol{v})} [\boldsymbol{x}' \times (\boldsymbol{x}' \cdot \nabla)\, \boldsymbol{v}(\overline{\boldsymbol{x}})]\, \rho \, \mathrm{d}V. \tag{37.72}$$

The $m'th$ component of the second right hand side term can be written

$$\int_{\mathcal{R}(\boldsymbol{v})} [\boldsymbol{x}' \times (\boldsymbol{x}' \cdot \nabla)\, \boldsymbol{v}(\overline{\boldsymbol{x}})]_m \, \rho \, \mathrm{d}V = \epsilon_{mnp} \int_{\mathcal{R}(\boldsymbol{v})} x'_n \, [(\boldsymbol{x}' \cdot \nabla)\, \boldsymbol{v}(\overline{\boldsymbol{x}})]_p \, \rho \, \mathrm{d}V \tag{37.73a}$$

$$= \epsilon_{mnp} \int_{\mathcal{R}(\boldsymbol{v})} x'_n \, x'_q \, \partial_q v_p(\overline{\boldsymbol{x}}) \, \rho \, \mathrm{d}V \tag{37.73b}$$

$$= \epsilon_{mnp} \left[\int_{\mathcal{R}(\boldsymbol{v})} x'_n \, x'_q \, \rho \, \mathrm{d}V \right] \partial_q v_p(\overline{\boldsymbol{x}}). \tag{37.73c}$$

We removed the velocity derivatives

$$\partial_q v_p(\overline{\boldsymbol{x}}) = \left[\frac{\partial v_p}{\partial x_q} \right]_{\boldsymbol{x}=\overline{\boldsymbol{x}}} \tag{37.74}$$

from the integral, since they are evaluated at the center of mass point and so do not participate in the integration.

37.9.4 Angular momentum, strain rate, and vorticity

Following from the discussion in Section 18.8, we know that the velocity derivatives, $\partial_q v_p$, appearing in equation (37.73c) form the components to a second order tensor known as the *velocity gradient tensor*, which can be decomposed into the strain rate tensor, $\mathbb{S}$, and the rotation tensor, $\mathbb{R}$. Introducing these two tensors brings the angular momentum for a continuum fluid

[5] The velocity field evaluated at the center of mass position, $\boldsymbol{v}(\overline{\boldsymbol{x}})$, is not equal to the center of mass velocity: $\boldsymbol{v}(\overline{\boldsymbol{x}}) \neq \overline{\boldsymbol{v}^{\mathrm{L}}}$.

region into the form

$$L_m = (\overline{\boldsymbol{X}} \times \boldsymbol{P})_m + \epsilon_{mnp} \left[\int_{\mathcal{R}(\boldsymbol{v})} x'_n \, x'_q \, \rho \, \mathrm{d}V \right] \mathbb{S}_{qp} + \epsilon_{mnp} \left[\int_{\mathcal{R}(\boldsymbol{v})} x'_n \, x'_q \, \rho \, \mathrm{d}V \right] \mathbb{R}_{qp} \tag{37.75a}$$

$$= (\overline{\boldsymbol{X}} \times \boldsymbol{P})_m + \epsilon_{mnp} \left[\int_{\mathcal{R}(\boldsymbol{v})} x'_n \, x'_q \, \rho \, \mathrm{d}V \right] \mathbb{S}_{qp} + \frac{1}{2} \, \epsilon_{mnp} \, \epsilon_{sqp} \left[\int_{\mathcal{R}(\boldsymbol{v})} x'_n \, x'_q \, \rho \, \mathrm{d}V \right] \omega_s \tag{37.75b}$$

$$= \underbrace{(\overline{\boldsymbol{X}} \times \boldsymbol{P})_m}_{\text{center of mass}} + \underbrace{\epsilon_{mnp} \left[\int_{\mathcal{R}(\boldsymbol{v})} x'_n \, x'_q \, \rho \, \mathrm{d}V \right] \mathbb{S}_{qp}}_{\text{strain rate contribution}} + \underbrace{\frac{1}{2} \left[\int_{\mathcal{R}(\boldsymbol{v})} (\boldsymbol{x}' \cdot \boldsymbol{x}' \, \delta_{ms} - x'_m \, x'_s) \, \rho \, \mathrm{d}V \right] \omega_s}_{\text{vorticity contribution}} . \tag{37.75c}$$

Since each point in the fluid continuum can be considered the center of mass for an arbitrary material region, the decomposition (37.75c) holds in general.

- Center of mass angular momentum: The first term on the right hand side of equation (37.75c) arises from the angular momentum of the material region as measured with respect to the center of mass position. It has the form of angular momentum for a point particle (see equation (11.39)).

- Strains: The second contribution is proportional to fluid deformations studied in Section 18.8. At each point of the fluid, deformations are measured by the strain rate tensor, $\mathbb{S}_{qp}$. A rigid body moves by uniform translations and/or rigid-body rotations, with the strain rate tensor vanishing for rigid-body motions (see Section 37.6). The contribution from strain rates is weighted by an integral of fluid particle position relative to the center of mass position. A closed form expression for this integral is available only for special shapes.

- Vorticity: The third contribution to angular momentum (37.75c) contains the vorticity as weighted by the moment of inertia tensor

$$I_{ms} \equiv \int_{\mathcal{R}(\boldsymbol{v})} (\boldsymbol{x}' \cdot \boldsymbol{x}' \, \delta_{ms} - x'_m \, x'_s) \, \rho \, \mathrm{d}V. \tag{37.76}$$

  Since the material region is evolving and is not rigid, the moment of inertia tensor is time dependent. Even so, the contribution

$$L_m^{\text{vorticity}} \equiv \frac{1}{2} \, I_{ms} \, \omega_s \tag{37.77}$$

  has the same form as angular momentum for a rigid body, with one-half the vorticity playing the role of angular velocity (see equation (11.41a) for the point particle expression). Evidently, vorticity in fluid flow contributes to angular momentum for a material region via its product with the moment of inertia tensor for the region.

37.9.5 Comments and further reading

Angular momentum is computed relative to a chosen origin, whereas vorticity is an intrinsic property measuring the spin of the fluid at a point. So although they both offer measures of the rotational properties of fluid motion, they are distinct when the fluid experiences a nonzero strain rate. It is only for the special case of a rigid-body motion that the strain rate vanishes, in which case the angular momentum of a fluid region is directly related to vorticity.

Further discussion of the material in this section can be found in *Chatwin* (1973), Section 2.3.1 of *Davidson* (2015), and the online notes "The Vorticity Equation and Conservation of

Angular Momentum" from A.J. DeCaria. See also Section 1.2 of the vorticity monograph by *Saffman* (1992).

37.10 Exercises

EXERCISE 37.1: VORTICITY AT A STATIC NO-SLIP BOUNDARY
Show that $\boldsymbol{\omega} \cdot \hat{\boldsymbol{n}} = 0$ at a static no-slip boundary, such as a solid wall. Here, $\hat{\boldsymbol{n}} = 0$ is the outward normal at the boundary. Hint: make use of Stoke's theorem and the adherence condition, $\boldsymbol{v} = 0$, at a static no-slip boundary.

EXERCISE 37.2: VORTICITY FOR RIGID-BODY ROTATION
A fluid in rigid-body rotation has an angular velocity

$$\boldsymbol{v}_{\text{rigid-body}} = \boldsymbol{\Omega} \times \boldsymbol{x}, \tag{37.78}$$

with $\boldsymbol{x}$ the position vector of a point in the fluid. Show that this fluid velocity has a corresponding vorticity given by

$$\nabla \times \boldsymbol{v}_{\text{rigid-body}} = 2\,\boldsymbol{\Omega}. \tag{37.79}$$

There are a few methods to prove this result. Display one method and be sure it is fully explained.

EXERCISE 37.3: PLANETARY ROTATION IS NON-DIVERGENT
Show that a fluid in rigid-body rotation with angular velocity

$$\boldsymbol{v}_{\text{rigid-body}} = \boldsymbol{\Omega} \times \boldsymbol{x}, \tag{37.80}$$

has zero divergence

$$\nabla \cdot \boldsymbol{v}_{\text{rigid-body}} = 0. \tag{37.81}$$

Consequently, rotation of the planet imparts zero divergence to fluid motion. We make use of this result in part to justify our study of non-rotating fluid kinematics in Part III of this book.

EXERCISE 37.4: VELOCITY POTENTIAL FOR THE FREE VORTEX
What is the velocity potential (37.15) for the free vortex whose velocity field is given by equation (37.22)? Hint: The problem is two-dimensional and rotationally symmetric, so it is convenient to make use of polar coordinates $x = r\cos\vartheta$ and $y = r\sin\vartheta$ as in Section 4.22.

EXERCISE 37.5: STRAIN TENSOR FOR THE FREE VORTEX
Determine all components to the strain rate tensor (Section 18.8)

$$S_{pq} = \begin{bmatrix} S_{11} & S_{12} \\ S_{21} & S_{22} \end{bmatrix} = \begin{bmatrix} \frac{\partial u}{\partial x} & \frac{1}{2}\left[\frac{\partial u}{\partial y} + \frac{\partial v}{\partial x}\right] \\ \frac{1}{2}\left[\frac{\partial v}{\partial x} + \frac{\partial u}{\partial y}\right] & \frac{\partial v}{\partial y} \end{bmatrix} \tag{37.82}$$

for the free vortex as specified by the velocity field (37.22). Present the answer in the form of a 2×2 matrix.

EXERCISE 37.6: VANISHING VISCOUS FRICTION FOR RIGID-BODY MOTION
As discussed in Section 25.8.6, viscous effects from molecular viscosity in a non-divergent flow appear in the momentum equation as a Laplacian weighted by a constant molecular viscosity

$$\text{viscous force per mass} = \nu\,\nabla^2 \boldsymbol{v}, \tag{37.83}$$

where $\nu > 0$ is the molecular kinematic viscosity, which is a constant that is a property of the fluid. Show that the viscous operator vanishes for a non-divergent flow in rigid-body rotation. That is, rigid-body motion engenders no frictional dissipation. This result reflects the lack of frictional interaction in a strain-free flow.

EXERCISE 37.7: MOMENT OF INERTIA FOR CYLINDER AND SPHERE

The moment of inertia for a continuous distribution of matter is defined by equation (37.76). In this exercise we compute the moment of inertia for two matter distributions with constant density but with different shapes. The results can be found through Google, so be sure to check your answer.

(a) Determine the moment of inertia for a right circular cylinder, where the moment is computed relative to the axis through the center of the cylinder. For simplicity, use cylindrical-polar coordinates and orient the vertical axis through the center of the cylinder.

(b) Determine the moment of inertia for a sphere computed around an axis through the center of the sphere.

EXERCISE 37.8: VORTICITY FOR A C-GRID NUMERICAL MODEL

Vorticity is commonly diagnosed in numerical model simulations. In this exercise we consider how one might determine a discrete equation for the vertical vorticity when the horizontal velocity is arranged according to the Arakawa C-grid (*Arakawa and Lamb*, 1977) commonly used in ocean models, and as depicted in Figure 37.12. Derive an expression for the area averaged vorticity over the shaded grid cell region centered at the vorticity point, $q_{i,j}$. Make use of Stokes' theorem with the surrounding C-grid velocity components and the corresponding grid distances.

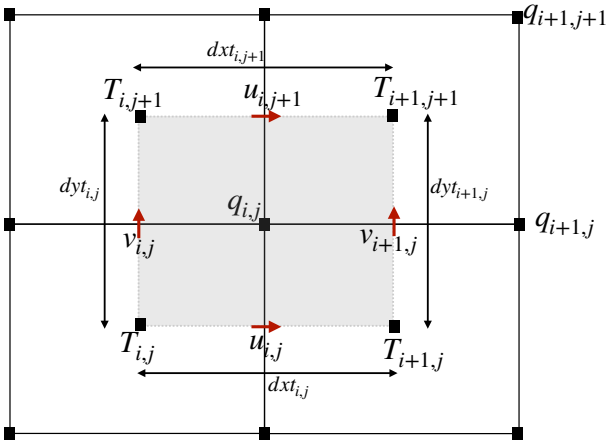

FIGURE 37.12: Layout for velocity on a discrete Arakawa C-grid for use in Exercise 37.8. The central T-point is labeled $T_{i,j}$ and its corresponding vorticity point, $q_{i,j}$, is located to its northeast. This exercise aims to determine the area averaged vorticity for the shaded region. The zonal velocity, $u_{i,j}$, is arranged on the east face of the T-cell, whereas the meridional velocity, $v_{i,j}$, is on the north face. The zonal and meridional grid distances are indicated, thus measuring distances between adjacent tracer points and so measuring the sides of the shaded region.

EXERCISE 37.9: PARTICLE TRAJECTORIES FROM A POINT VORTEX AND POINT DIVERGENCE

Consider a two-dimensional (horizontal) flow resulting from a point vortex as well as a point divergence, both at $\boldsymbol{x} = 0$,

$$\hat{\boldsymbol{z}} \cdot (\nabla \times \boldsymbol{u}) = \mathcal{C}\, \delta(\boldsymbol{x}) \tag{37.84a}$$

$$\nabla \cdot \boldsymbol{u} = \mathcal{D}\, \delta(\boldsymbol{x}). \tag{37.84b}$$

We here introduced the constants, $\mathcal{C} > 0$ and $\mathcal{D} > 0$, as well as the Dirac delta, $\delta(\boldsymbol{x}) = \delta(x)\,\delta(y)$. From Chapter 7 recall that the Dirac delta satisfies the normalization condition, $\int_{\mathcal{S}} \delta(\boldsymbol{x})\,\mathrm{d}\mathcal{S} = 1$, for any region, $\mathcal{S}$, that includes the origin, $\boldsymbol{x} = 0$. Consequently, the Dirac delta has physical dimensions of inverse area.

Throughout this exercise we ignore boundaries, so that the flow is considered on an infinite plane. Also, the reference frame is not rotating. Furthermore, the flow resulting from each point source is axially symmetric, so that the only functional dependence is radial; i.e., distance from the origin. You are thus asked to use polar coordinates from Section 4.22 throughout this exercise.

(a) Given the dimensions of the Dirac delta and those for the vorticity and divergence, then what are the physical dimensions of $\mathcal{C}$ an $\mathcal{D}$?

(b) What is the horizontal velocity field resulting from the point vortex ($\mathcal{C} > 0$ and $\mathcal{D} = 0$)? Sketch this field.

(c) What is the expression for the fluid particle trajectory within the velocity field generated by the point vortex?

(d) What is the horizontal velocity field resulting from the point divergence ($\mathcal{C} = 0$ and $\mathcal{D} > 0$)? Sketch this field.

(e) What is the expression for the fluid particle trajectory within the velocity field generated by the point divergence?

(f) Compute the fluid particle trajectories when the divergence source picks up an oscillatory time dependence, so that

$$\hat{\boldsymbol{z}} \cdot (\nabla \times \boldsymbol{u}) = \mathcal{C}\,\delta(\boldsymbol{x}) \tag{37.85a}$$

$$\nabla \cdot \boldsymbol{u} = \mathcal{D}\,\delta(\boldsymbol{x}) \sin(\omega_{\mathrm{d}}\, t). \tag{37.85b}$$

What parameter settings ensure that radial oscillations of the particle position are small relative to the initial radial distance? Only derive the angular position, $\vartheta(t)$, assuming these parameter settings.

(g) Now also include an oscillatory behavior to the vortex source, so that

$$\hat{\boldsymbol{z}} \cdot (\nabla \times \boldsymbol{u}) = \mathcal{C}\,\delta(\boldsymbol{x}) \cos(\omega_{\mathrm{c}}\, t) \tag{37.86a}$$

$$\nabla \cdot \boldsymbol{u} = \mathcal{D}\,\delta(\boldsymbol{x}) \sin(\omega_{\mathrm{d}}\, t). \tag{37.86b}$$

Compute the fluid particle trajectories assuming the condition from the previous part of this exercise is met. That is, assume the parameter settings ensure that radial oscillations of the particle position are small relative to the initial radial distance.

You may choose to consider the following hints.

- We are only concerned with horizontal motion in this exercise.
- In Section 38.2.8 we study point vortices in the horizontally non-divergent fluid. The velocity field for the point vortex is derived there.
- When both sources are turned on, the velocity field is the linear superposition of the velocity from the point vortex and that from the point divergence. The reason is that we are ignoring any back-reaction of the flow from one source onto the other source.

- It is useful to recall the discussion of fluid particle trajectories from Section 17.7.1.

Chapter 38

Two-dimensional non-divergent barotropic flow

A single layer of homogeneous shallow water fluid is among the simplest conceptual models available for the study of fluid motion. In the language of vorticity as described in Chapter 40, a single shallow water layer is a barotropic fluid since it has zero baroclinicity (Section 40.4). Notably, the shallow water layer has constant density, and so the flow has zero three-dimensional divergence ($\nabla \cdot \boldsymbol{v} = 0$). Yet the layer thickness fluctuates as a result of a nonzero divergence to the horizontal flow ($\nabla_{\mathrm{h}} \cdot \boldsymbol{u} \neq 0$), so that the single shallow water layer is a *horizontally divergent barotropic model*.

For some geophysical fluid studies, we are primarily interested in the vortical (Rossby wave) motions (Chapters 55 and 54), with these motions having far lower frequency than the gravity wave motions associated with horizontal divergence (Section 55.5 and Chapter 57). The two-dimensional *non-divergent barotropic model* focuses on vortical motion by assuming the horizontal velocity has zero divergence, with that assumption serving to filter out all gravity waves. We here study the non-divergent barotropic model with a flat free surface (i.e., *rigid lid*). For this flow the vertical fluid columns have a fixed thickness, which contrasts to the extensible columns found in the shallow water model. To retain a flat upper boundary requires the imposition of a *lid pressure*. Indeed, it is the lid pressure that provides the force generating fluid motion. We study the nature of these pressure forces, and in so doing garner insights into the pressure gradient force.

For many purposes, we do not need to compute the lid pressure since the relative vorticity is the primary dynamical field in the non-divergent barotropic model. That is, knowledge of the vorticity is sufficient to determine the streamfunction (through solving an elliptic boundary value problem), which then renders the velocity. Furthermore, the absolute vorticity is materially invariant in the absence of irreversible processes such as friction. Hence, meridional motion of a fluid column is associated with an exchange of vorticity between the fluid and the rotating reference frame (i.e., the rotating planet). This exchange constrains the flow, and we examine case studies to illustrate how this constraint affects motion. In particular, this constraint, in its linearized form, provides the physical mechanism for Rossby waves, which we study in Section 54.3.

CHAPTER GUIDE

We here develop some properties of the non-divergent barotropic model, and use this model to exemplify basic features of geophysical flows constrained by conservation of absolute vorticity. The model served as the basis for the pioneering numerical weather prediction model of *Charney et al.* (1950), and it has become a valued theoretical model for large-scale dynamics. It is also useful for studies of coherent vortex structures, with Chapter 3 of *McWilliams* (2006) exploring analytical vortex solutions. We return to this model in Sections 54.2 and 54.3 when studying Rossby waves.

Since all fields in this chapter are a spatial function only of the horizontal position, the vector gradient operator is itself two-dimensional; e.g., $\nabla\psi = \nabla_h\psi$. Furthermore, we retain the use of Cartesian coordinates as per the tangent plane approximation, with extensions to general coordinates following the tensor analysis methods from Chapter 4.

38.1 Basic equations and their properties

The non-divergent barotropic model arises from the following assumptions.

- The flow occurs in a single homogeneous fluid layer.
- The horizontal velocity is non-divergent: $\nabla \cdot \boldsymbol{u} = \partial_x u + \partial_y v = 0$, which means that the thickness of the layer is time independent.

The second property provides rather strict constraints on the flow relative to flow in the horizontally divergent shallow water layer from Part VI of this book. In this section we exhibit the governing equations and derive some of their properties.

38.1.1 Equations for velocity

The velocity equation for the non-divergent barotropic model follows in a manner akin to the shallow water model from Chapter 35. Namely, the fluid is a homogeneous (uniform and constant density) layer so that the horizontal velocity satisfies

$$\frac{\mathrm{D}\boldsymbol{u}}{\mathrm{D}t} + f\,\hat{\boldsymbol{z}} \times \boldsymbol{u} = -\nabla\varphi \qquad \text{and} \qquad \nabla \cdot \boldsymbol{u} = 0, \tag{38.1}$$

where the pressure is normalized according to

$$\varphi = p/\rho \tag{38.2}$$

with ρ the constant layer density, and where material evolution occurs with the two-dimensional non-divergent flow

$$\frac{\mathrm{D}}{\mathrm{D}t} = \frac{\partial}{\partial t} + \boldsymbol{u} \cdot \nabla. \tag{38.3}$$

All fields are depth independent and there is no vertical motion ($w = 0$), so that the flow occurs in rigid fluid columns. Making use of the vector identity (2.44)

$$(\boldsymbol{u} \cdot \nabla)\boldsymbol{u} = \zeta\,\hat{\boldsymbol{z}} \times \boldsymbol{u} + \nabla(\boldsymbol{u}^2/2), \tag{38.4}$$

brings the velocity equation (38.1) into its vector-invariant form

$$\partial_t \boldsymbol{u} + (f + \zeta)\,\hat{\boldsymbol{z}} \times \boldsymbol{u} = -\nabla(\varphi + \boldsymbol{u} \cdot \boldsymbol{u}/2), \tag{38.5}$$

which is a useful starting point in Section 38.2 for deriving the equation for the vorticity

$$\zeta = \hat{\boldsymbol{z}} \cdot (\nabla \times \boldsymbol{u}) = \partial_x v - \partial_y u. \tag{38.6}$$

The horizontal non-divergent flow can be described by a streamfunction

$$\boldsymbol{u} = \hat{\boldsymbol{z}} \times \nabla\psi \quad \Longrightarrow \quad u = -\partial_y \psi \quad \text{and} \quad v = \partial_x \psi. \tag{38.7}$$

Making use of the identities

$$\nabla\psi = -\hat{\boldsymbol{z}} \times \boldsymbol{u} \Longrightarrow \boldsymbol{u} \cdot \nabla\psi = 0 \tag{38.8}$$

brings the vector-invariant velocity equation (38.5) into the form

$$\partial_t \boldsymbol{u} - (f + \zeta)\, \nabla\psi = -\nabla(\varphi + \boldsymbol{u}\cdot\boldsymbol{u}/2). \tag{38.9}$$

38.1.2 Kinetic energy of the flow

Taking the scalar product of the velocity with the velocity equation (38.9) yields the kinetic energy equation

$$\partial_t \mathcal{K} = -\nabla\cdot[\boldsymbol{u}\,(\mathcal{K}+\varphi)] \Longrightarrow \frac{\mathrm{D}\mathcal{K}}{\mathrm{D}t} = -\nabla\cdot(\boldsymbol{u}\,\varphi), \tag{38.10}$$

where we introduced the kinetic energy per mass

$$\mathcal{K} = \boldsymbol{u}\cdot\boldsymbol{u}/2 = (u^2+v^2)/2 = \nabla\psi\cdot\nabla\psi/2. \tag{38.11}$$

The gravitational potential energy is constant since the fluid density is a uniform constant (so the buoyancy vanishes) and the vertical velocity vanishes. Hence, mechanical energy transformation only involves kinetic energy. Furthermore, the domain integrated kinetic energy is a constant (for the inviscid case), as shown in Exercise 38.5.

38.1.3 Kinematics of rigid fluid columns

Recall the thickness equation (35.20) for a shallow water layer

$$\frac{\mathrm{D}h}{\mathrm{D}t} = -h\,\nabla\cdot\boldsymbol{u}, \tag{38.12}$$

where $h = \eta - \eta_\mathrm{b}$ is the column thickness, $z = \eta(x,y,t)$ is the upper layer interface (the free surface), and $z = \eta_\mathrm{b}(x,y)$ is the lower interface (the bottom topography) (see Figure 35.1). With zero divergence in the horizontal velocity, the thickness of a fluid column is constant

$$(\partial_t + \boldsymbol{u}\cdot\nabla)\, h = \partial_t(\eta-\eta_\mathrm{b}) + \boldsymbol{u}\cdot\nabla(\eta-\eta_\mathrm{b}) = 0. \tag{38.13}$$

Choosing $\eta = 0$ to satisfy the thickness equation

We *choose* to satisfy the thickness equation (38.13) by setting the upper surface to be static and flat

$$\eta = 0, \tag{38.14}$$

so that the column thickness is constant at each point in space

$$\partial_t h = \partial_t(\eta-\eta_\mathrm{b}) = 0. \tag{38.15}$$

By setting $\eta = 0$ we constrain the horizontal flow to follow the bottom topography so that

$$\boldsymbol{u}\cdot\nabla\eta_\mathrm{b} = (\nabla\psi\times\nabla\eta_\mathrm{b})\cdot\hat{\boldsymbol{z}} = 0. \tag{38.16}$$

The case of a flat bottom offers no constraint, since $\nabla\eta_\mathrm{b} = 0$. However, for the case with nontrivial bottom topography, the constraint (38.16) is satisfied only if the flow streamfunction, ψ, is a function of the bottom topography,

$$\psi = \psi(\eta_\mathrm{b}), \tag{38.17}$$

so that the streamfunction is a constant along isolines of constant topography. Taking the limit as the sides become vertical, this boundary condition means that ψ is a constant along vertical

sidewalls so that

$$\boldsymbol{u} \cdot \hat{\boldsymbol{n}} = (\hat{\boldsymbol{z}} \times \nabla\psi) \cdot \hat{\boldsymbol{n}} = \hat{\boldsymbol{t}} \cdot \nabla\psi = 0, \tag{38.18}$$

where $\hat{\boldsymbol{n}}$ is the horizontal outward unit vector at the boundary, and $\hat{\boldsymbol{t}} = \hat{\boldsymbol{n}} \times \hat{\boldsymbol{z}}$ is the unit tangent vector along the boundary.

Streamfunction for the thickness-weighted velocity

With rigid columns, the thickness equation (38.12) reduces to the non-divergence condition,

$$\nabla \cdot (h\,\boldsymbol{u}) = 0. \tag{38.19}$$

We can thus introduce a streamfunction, Ψ, for the thickness weighted horizontal velocity

$$h\,\boldsymbol{u} = \hat{\boldsymbol{z}} \times \nabla\Psi = \hat{\boldsymbol{z}} \times h\nabla\psi. \tag{38.20}$$

Ψ has physical dimensions of $\mathrm{L}^3\ \mathrm{T}^{-1}$, whereas the velocity streamfunction, ψ, has physical dimensions of $\mathrm{L}^2\ \mathrm{T}^{-1}$.

Summary

We formulate the two-dimensional non-divergent flow within a homogeneous fluid layer, for which a fluid column does not expand or contract, vertical motion vanishes (as explored in Section 38.1.4), and the flow is constrained to move along lines of constant topography so that the streamfunction depends only on the bottom topography.

38.1.4 Vertical velocity

Vanishing vertical velocity

With zero horizontal divergence and with a flat free surface ($\eta = 0$), there is identically zero vertical motion within the layer

$$w = 0. \tag{38.21}$$

Another manner to deduce this property is by noting that the surface kinematic boundary condition for a static and flat free surface leads to

$$w(\eta) = \partial_t\eta + \boldsymbol{u} \cdot \nabla\eta = 0 + 0, \tag{38.22}$$

so that the vertical velocity at $z = \eta = 0$ vanishes. With $w(0) = 0$, and with $\nabla \cdot \boldsymbol{u} = 0$ for the horizontal velocity, then $w = 0$ throughout the layer. Correspondingly, this constraint means that the no-normal flow bottom kinematic condition (Section 19.6.1) renders a horizontal velocity that is aligned with the topography, $\boldsymbol{u} \cdot \nabla\eta_{\mathrm{b}} = 0$, which is a property we already encountered in Section 38.1.3. Since the vertical velocity is zero, the gravitational potential energy is a uniform constant, so that the mechanical energy budget involves only the kinetic energy.

But can there be a non-vanishing vertical velocity?

In Section 38.1.3 we chose to satisfy the thickness equation by setting $\partial_t\eta = 0$ and $\nabla\eta = 0$, in which case the vertical velocity vanishes so long as the horizontal flow follows the bottom topography. A static and flat upper boundary is a sufficient condition, yet it is not necessary for satisfying the thickness equation. Is there a viable alternative?

Another approach to satisfying the thickness equation (38.13) is to consider a static yet non-flat free surface ($\eta \neq 0$) with horizontal flow constrained so that

$$\boldsymbol{u} \cdot \nabla(\eta - \eta_{\mathsf{b}}) = 0. \tag{38.23}$$

The surface and bottom kinematic boundary conditions then result in a vertical velocity at the surface and bottom

$$w(\eta) = -\boldsymbol{u} \cdot \nabla\eta \quad \text{and} \quad w(\eta_{\mathsf{b}}) = -\boldsymbol{u} \cdot \nabla\eta_{\mathsf{b}}. \tag{38.24}$$

These two boundary velocities must be equal to ensure $\partial_z w = 0$. If the bottom topography is flat, $\nabla\eta_{\mathsf{b}} = 0$, then $w(\eta_{\mathsf{b}}) = w(\eta) = 0$, in which case $\nabla\eta = 0$, so that the upper surface is flat. If the bottom is not flat, then the kinematic constraints lead to

$$\nabla\eta = \nabla\eta_{\mathsf{b}}, \tag{38.25}$$

so that the upper surface slope equals to the slope of the bottom topography. In the ocean, it is generally the case that the upper ocean surface undulates far less than the bottom topography. Hence, $\nabla\eta = \nabla\eta_{\mathsf{b}}$ is not generally a realistic behavior, though one may study this case particularly with weakly sloping bottom topography.

For the remainder of this chapter we follow the conventional approach whereby $w = 0$ everywhere. Hence, the upper boundary is static and flat, and we set $\eta = 0$. In the presence of a non-flat bottom, then the horizontal flow follows lines of constant bottom topography so that $\boldsymbol{u} \cdot \nabla\eta_{\mathsf{b}} = 0$.

38.1.5 Velocity self-advection and the kinetic stress tensor

The velocity self-advection appearing in the velocity equation (38.1) can be written as the divergence of a 2×2 symmetric tensor

$$-(\boldsymbol{u} \cdot \nabla)\,\boldsymbol{u} = \nabla \cdot \mathbb{E} \Longleftrightarrow -u_m \partial_m u_n = -\partial_m(u_m\, u_n) = \partial_m \mathbb{E}_{mn}, \tag{38.26}$$

where

$$\mathbb{E}_{mn} = -u_m\, u_n \longleftrightarrow \mathbb{E} = -\boldsymbol{u} \otimes \boldsymbol{u} = \begin{bmatrix} -u^2 & -u\,v \\ -u\,v & -v^2 \end{bmatrix}, \tag{38.27}$$

thus bringing the momentum equation (38.1) to the Eulerian form

$$\partial_t \boldsymbol{u} + f\,\hat{\boldsymbol{z}} \times \boldsymbol{u} = -\nabla\varphi + \nabla \cdot \mathbb{E}. \tag{38.28}$$

We refer to

$$\rho\,\mathbb{E} = -\rho\,\boldsymbol{u} \otimes \boldsymbol{u} \tag{38.29}$$

as the *kinetic stress tensor*, with its three-dimensional form introduced in Section 25.6.

In anticipation of our study of vorticity in Section 38.2, we find it useful to decompose the kinetic stress tensor into its horizontally isotropic and horizontally anisotropic components[1]

$$\mathbb{E} = \begin{bmatrix} -u^2 & -u\,v \\ -u\,v & -v^2 \end{bmatrix} = -\mathcal{K} \begin{bmatrix} 1 & 0 \\ 0 & 1 \end{bmatrix} + \begin{bmatrix} -(u^2 - v^2)/2 & -u\,v \\ -u\,v & (u^2 - v^2)/2 \end{bmatrix} \equiv -\mathcal{K}\,\mathbb{I} + \mathbb{F}, \tag{38.30}$$

where we introduced the kinetic energy per mass according to equation (38.11), as well as the trace-free anisotropic portion of the kinetic stress tensor

$$\mathbb{F} = \mathcal{K}\,\mathbb{I} + \mathbb{E} = \begin{bmatrix} -(u^2 - v^2)/2 & -u\,v \\ -u\,v & (u^2 - v^2)/2 \end{bmatrix} \Longleftrightarrow \mathbb{F}_{mn} = \mathcal{K}\,\delta_{mn} - u_m\,u_n. \tag{38.31}$$

[1] Recall our discussion of isotropy in Section 1.11.

Making use of the decomposition (38.30) brings the velocity equation (38.32) to the form

$$\partial_t \boldsymbol{u} + f\,\hat{\boldsymbol{z}} \times \boldsymbol{u} = \nabla \cdot [\mathbb{F} - \mathbb{I}(\mathcal{K} + \varphi)]. \tag{38.32}$$

Comparing to the vector-invariant velocity equation (38.5) allows us to infer the identity

$$\nabla \cdot \mathbb{F} = -\zeta\,(\hat{\boldsymbol{z}} \times \boldsymbol{u}). \tag{38.33}$$

We provide an alternative derivation of this identity in Exercise (38.1).

38.1.6 Further reading

As discussed by *Hoskins et al.* (1983), *Waterman and Hoskins* (2013) and *Waterman and Lilly* (2015), the decomposition (38.30) is useful for developing a geometric interpretation of eddying flow features.

38.2 Vorticity

For the two-dimensional non-divergent flow with a vanishing vertical velocity, the vertical component of the relative vorticity is the only nonzero vorticity component, and it is given by the Laplacian of the streamfunction

$$\zeta = \hat{\boldsymbol{z}} \cdot (\nabla \times \boldsymbol{u}) = \partial_x v - \partial_y u = \nabla^2 \psi = \nabla \cdot (h^{-1}\,\nabla \Psi). \tag{38.34}$$

We here derive basic features of the vorticity for this fluid on the β-plane whereby the Coriolis parameter is (Section 24.5)

$$f = f_\circ + \beta\,(y - y_0). \tag{38.35}$$

38.2.1 Vorticity equation

To form the dynamical equation for the vorticity, take the zonal derivative of the meridional momentum equation (see equation (38.1)), the meridional derivative of the zonal momentum equation, and then subtract

$$\frac{\partial}{\partial t}\left(\frac{\partial v}{\partial x} - \frac{\partial u}{\partial y}\right) + \frac{\partial}{\partial x}\left[\nabla \cdot (\boldsymbol{u}\,v)\right] - \frac{\partial}{\partial y}\left[\nabla \cdot (\boldsymbol{u}\,u)\right] + f \nabla \cdot \boldsymbol{u} + \beta\, v = 0. \tag{38.36}$$

The pressure gradient dropped out since there is zero *baroclinicity* for a barotropic flow.[2] We now make use of the identity

$$\frac{\partial}{\partial x}\left[\nabla \cdot (\boldsymbol{u}\,v)\right] - \frac{\partial}{\partial y}\left[\nabla \cdot (\boldsymbol{u}\,u)\right] = \frac{\partial \boldsymbol{u}}{\partial x} \cdot \nabla v - \frac{\partial \boldsymbol{u}}{\partial y} \cdot \nabla u + \boldsymbol{u} \cdot \nabla \zeta = \boldsymbol{u} \cdot \nabla \zeta, \tag{38.37}$$

where we used the non-divergence condition, $\partial_x u + \partial_y v = 0$, thus rendering

$$\frac{\partial \boldsymbol{u}}{\partial x} \cdot \nabla v - \frac{\partial \boldsymbol{u}}{\partial y} \cdot \nabla u = \frac{\partial u}{\partial x}\frac{\partial v}{\partial x} + \frac{\partial v}{\partial x}\frac{\partial v}{\partial y} - \frac{\partial u}{\partial y}\frac{\partial u}{\partial x} - \frac{\partial v}{\partial y}\frac{\partial u}{\partial y} \tag{38.38a}$$

$$= -\frac{\partial v}{\partial y}\frac{\partial v}{\partial x} + \frac{\partial v}{\partial x}\frac{\partial v}{\partial y} + \frac{\partial u}{\partial y}\frac{\partial v}{\partial y} - \frac{\partial v}{\partial y}\frac{\partial u}{\partial y} \tag{38.38b}$$

$$= 0. \tag{38.38c}$$

[2] We discuss baroclinicity in Section 40.4.

We are thus led to the vorticity equation

$$\frac{\partial \zeta}{\partial t} + \nabla \cdot (\boldsymbol{u}\, \zeta) = -\beta\, v \quad \text{and} \quad \frac{\mathrm{D}\zeta}{\mathrm{D}t} = -\beta\, v. \tag{38.39}$$

Evidently, the material evolution of relative vorticity in a horizontally non-divergent barotropic fluid is only affected by meridional advection of planetary vorticity. Since $\beta > 0$ over the globe, northward flow ($v > 0$) produces a negative source (clockwise tendency) for relative vorticity following a fluid parcel. This source term is the *beta effect* that we study in Section 40.6.

38.2.2 Constraints from material invariance of absolute vorticity

Since f is time independent, we can write the vorticity equation (38.39) in the form

$$(\partial_t + \boldsymbol{u} \cdot \nabla)\zeta_{\mathsf{a}} = 0 \Longleftrightarrow \frac{\mathrm{D}\zeta_{\mathsf{a}}}{\mathrm{D}t} = 0, \tag{38.40}$$

where

$$\zeta_{\mathsf{a}} = \zeta + f \tag{38.41}$$

is the vertical component of the *absolute vorticity*. Equation (38.40) is a relatively simple version of the vorticity equation encountered in this book. It is simple because there are no sources on the right hand side, with nonzero sources studied in Chapter 40. In particular, there is no stretching or tilting of fluid columns in the non-divergent barotropic fluid.[3]

To maintain a materially constant absolute vorticity requires the relative vorticity to change oppositely to that of the planetary vorticity. For example, in the northern hemisphere the relative vorticity must decrease in value ($\zeta \downarrow$) for fluid particles moving northward. This change in the relative vorticity is needed to counteract the increasing planetary vorticity ($f \uparrow$) when moving northward. This result accords with the $-\beta\, v$ source found in the relative vorticity equation (38.39). Furthermore, it is a reflection of the beta effect studied in Section 40.6.2. We further pursue these invariance properties in Section 38.5.

38.2.3 Rossby potential vorticity

According to the kinematic boundary condition (38.16), horizontal flow is aligned with isobaths (lines of constant bathymetry or topography). Flow moving along constant isobaths generally crosses latitude lines, and in so doing the relative vorticity must change precisely to maintain $f + \zeta$ materially constant. As shown here, we can combine the absolute vorticity with the bottom topography to render a materially conserved object, the *Rossby potential vorticity*, which further helps to understand constraints on the flow (see Section 38.6 for an example).

As noted in Section 41.1.6 (see equation (41.24)), the absolute vorticity is the form of *Ertel's potential vorticity* for the horizontally non-divergent barotropic model. Additionally, since fluid columns are rigid so that $\mathrm{D}h/\mathrm{D}t = 0$, the *Rossby potential vorticity* is materially conserved (in the absence of non-conservative processes)

$$\frac{\mathrm{D}Q}{\mathrm{D}t} = 0 \quad \text{with } Q = (\zeta + f)/h. \tag{38.42}$$

As discussed in Section 39.3, this form of potential vorticity conservation also holds for the inviscid shallow water equations, yet where h is no longer rigid so that flow can cross isobaths.

[3] In Section 40.5, we see how stretching and tilting of fluid columns provides a sources of vorticity for more general fluid flow.

38.2.4 Jacobian forms of vorticity advection

In some contexts it is convenient to write the advection operator acting on relative vorticity as

$$\begin{aligned}
\boldsymbol{u} \cdot \nabla \zeta &= u\, \partial_x \zeta + v\, \partial_y \zeta && \text{(38.43a)} \\
&= -\partial_y \psi\, \partial_x \zeta + \partial_x \psi\, \partial_y \zeta && \text{(38.43b)} \\
&= \hat{\boldsymbol{z}} \cdot (\nabla \psi \times \nabla \zeta) && \text{(38.43c)} \\
&\equiv J(\psi, \zeta), && \text{(38.43d)}
\end{aligned}$$

where J is the Jacobian operator

$$J(A, B) = \hat{\boldsymbol{z}} \cdot (\nabla A \times \nabla B) = \frac{\partial A}{\partial x}\frac{\partial B}{\partial y} - \frac{\partial A}{\partial y}\frac{\partial B}{\partial x}. \tag{38.44}$$

We can also make use of the Jacobian for the advection of absolute vorticity[4]

$$\boldsymbol{u} \cdot \nabla \zeta_{\mathsf{a}} = \hat{\boldsymbol{z}} \cdot (\nabla \psi \times \nabla \zeta_{\mathsf{a}}) \equiv J(\psi, \zeta + f). \tag{38.45}$$

38.2.5 Taylor-Bretherton identity

An equivalent means to write the vorticity equation is to start from the velocity equation in the form (38.32). Taking the curl and projecting onto the vertical direction then leads to

$$\partial_t \zeta = -\beta\, v + \hat{\boldsymbol{z}} \cdot [\nabla \times \nabla \cdot \mathbb{F}]. \tag{38.46}$$

The nonlinear forcing from the anisotropic portion of the kinetic stress can be written

$$\begin{aligned}
\hat{\boldsymbol{z}} \cdot [\nabla \times \nabla \cdot \mathbb{F}] &= \hat{\boldsymbol{z}}_n\, \epsilon_{npq}\, \partial_p (\partial_m \mathbb{F}_{mq}) && \text{(38.47a)} \\
&= \partial_m \partial_p (\epsilon_{npq}\, \hat{\boldsymbol{z}}_n\, \mathbb{F}_{mq}) && \text{(38.47b)} \\
&= -\partial_m \partial_p (\epsilon_{pnq}\, \hat{\boldsymbol{z}}_n\, \mathbb{F}_{qm}) && \text{(38.47c)} \\
&= -\partial_m \partial_p (\hat{\boldsymbol{z}} \times \mathbb{F})_{pm} && \text{(38.47d)} \\
&= -\nabla \cdot [\nabla \cdot (\hat{\boldsymbol{z}} \times \mathbb{F})], && \text{(38.47e)}
\end{aligned}$$

where we used symmetry of the anisotropic kinetic tensor, $\mathbb{F}_{mq} = \mathbb{F}_{qm}$.

Taylor-Bretherton identity for relative vorticity

Comparing to the vorticity equation in the form (38.39) reveals the identity

$$\nabla \cdot (\boldsymbol{u}\, \zeta) = \nabla \cdot [\nabla \cdot (\hat{\boldsymbol{z}} \times \mathbb{F})] \Longrightarrow \boldsymbol{u}\, \zeta = \nabla \cdot (\hat{\boldsymbol{z}} \times \mathbb{F}). \tag{38.48}$$

This equation says that the advective vorticity flux equals to the divergence of the counter-clockwise rotated anisotropic kinetic stress tensor. Equation (38.48) is a special form of the *Taylor-Bretherton identity* that provides a connection between the vorticity flux and the momentum flux. We encounter the shallow water form of this identity in Chapter 67 when studying the decomposition of eddy and mean flows.

Verifying the Taylor-Bretherton identity

The divergence expression on the left hand side of equation (38.48) can be satisfied by $\hat{\boldsymbol{z}} \times \nabla \Upsilon + \nabla \cdot (\hat{\boldsymbol{z}} \times \mathbb{F})$, with Υ an arbitrary gauge function. However, $\Upsilon = 0$ is zero for the anisotropic

[4] The Jacobian operator corresponds to the Poisson bracket used in Hamiltonian mechanics.

kinetic tensor (38.31), as seen by

$$\begin{aligned}
[\nabla \cdot (\hat{\boldsymbol{z}} \times \mathbb{F})]_1 &= \partial_m(\epsilon_{mnp}\, \hat{\boldsymbol{z}}_n\, \mathbb{F}_{p1}) && \text{(38.49a)}\\
&= \epsilon_{m3p}\, \partial_m \mathbb{F}_{p1} && \text{(38.49b)}\\
&= -\epsilon_{3mp}\, \partial_m \mathbb{F}_{p1} && \text{(38.49c)}\\
&= -\epsilon_{312}\, \partial_1 \mathbb{F}_{21} - \epsilon_{321}\, \partial_2 \mathbb{F}_{11} && \text{(38.49d)}\\
&= -\partial_x \mathbb{F}_{21} + \partial_y \mathbb{F}_{11} && \text{(38.49e)}\\
&= \partial_x(u\, v) + \partial_y(-u^2 + v^2)/2 && \text{(38.49f)}\\
&= v\, \partial_x u + u\, \partial_x v - u\, \partial_y u + v\, \partial_y v && \text{(38.49g)}\\
&= u\, \zeta, && \text{(38.49h)}
\end{aligned}$$

and likewise

$$[\nabla \cdot (\hat{\boldsymbol{z}} \times \mathbb{F})]_2 = \partial_y \mathbb{F}_{12} - \partial_x \mathbb{F}_{22} = v\, \zeta. \tag{38.50}$$

Taylor-Bretherton identity for potential vorticity

Building from the development for relative vorticity, we can readily connect the potential vorticity flux, $\boldsymbol{u}\, q = \boldsymbol{u}\, \zeta_{\mathsf{a}}$, to the anisotropic kinetic stress. We do so by considering the two equivalent forms for the potential vorticity equation

$$\partial_t q = -\nabla \cdot (\boldsymbol{u}\, q) \quad \text{and} \quad \partial_t q = -\nabla \cdot [\boldsymbol{u}\, f + \nabla \cdot (\hat{\boldsymbol{z}} \times \mathbb{F})]. \tag{38.51}$$

Hence, the Taylor-Bretherton identity for potential vorticity in the two dimensional non-divergent flow is given by

$$\boldsymbol{u}\, q = \boldsymbol{u}\, f + \nabla \cdot (\hat{\boldsymbol{z}} \times \mathbb{F}). \tag{38.52}$$

38.2.6 Poisson equation for the streamfunction

Given boundary conditions, the barotropic vorticity equation (38.40) allows us to determine the evolution of vorticity. We can in turn invert the Poisson equation[5]

$$\nabla^2 \psi = \zeta \tag{38.53}$$

to determine the streamfunction and then the velocity field, $\boldsymbol{u} = \hat{\boldsymbol{z}} \times \nabla \psi$. This inversion requires information about the boundary conditions for the streamfunction, as discussed in Section 38.1.3. By this method, time integration of the absolute vorticity equation is sufficient to fully specify time evolution of the horizontal velocity. Notably, we do not need to explicitly determine pressure to determine the flow.

38.2.7 Zonal flow as an exact geostrophic solution

An arbitrary zonal velocity with a meridional shear, $\boldsymbol{u} = U(y)\, \hat{\boldsymbol{x}}$, is an exact solution of the inviscid non-divergent barotropic model. We see this property by plugging into the velocity equation (38.1) and noting that $\mathrm{D}\boldsymbol{u}/\mathrm{D}t = 0$. Hence, this flow is an exact geostrophic solution whose pressure field is itself also just a function of latitude and whose meridional gradient is determined by

$$f\, \hat{\boldsymbol{z}} \times \boldsymbol{u} = -\nabla \varphi \implies \partial_y \varphi = -f(y)\, U(y). \tag{38.54}$$

Furthermore, each term in the vorticity equation (38.39) identically vanishes, so that the vorticity

$$\zeta = -\partial_y U \tag{38.55}$$

[5] See Section 6.5 for a study of the Poisson equation.

remains constant in time at each point in space. These properties make $\boldsymbol{u} = U(y)\,\hat{\boldsymbol{x}}$ a common choice for a background flow in the study of Rossby waves (Section 54.3).

38.2.8 A point vortex and the free space Green's function

Consider an axially symmetric vortex centered at the origin, $\boldsymbol{x} = 0$, and in an infinite free space so there are no boundaries. Making use of polar coordinates from Section 4.22, we know that the relative vorticity for this vortex is related to the velocity via

$$\zeta = \hat{\boldsymbol{z}} \cdot (\nabla \times \boldsymbol{u}) = r^{-1}\,\partial_r(r\,u^{\vartheta}), \tag{38.56}$$

with r the distance from the origin and ϑ the polar angle. The identity (38.56) holds since all of the flow fields have axial symmetry, meaning that all fields are a function only of the radial distance from the origin. Now further assume the vorticity is given by

$$\zeta^{\text{point}} = -\alpha\,\delta(\boldsymbol{x}), \tag{38.57}$$

where α is a constant, and we use equation (7.66) to write the Dirac delta in polar coordinates

$$\delta(\boldsymbol{x}) = r^{-1}\,\delta(r)\,\delta(\vartheta). \tag{38.58}$$

In this manner we assume the vortex has zero extent yet infinite strength.[6] We can connect the constant, α, to the circulation by considering an arbitrary circuit that encloses the origin

$$\mathcal{C} = \oint_{\partial\mathcal{S}} \boldsymbol{u} \cdot \mathrm{d}\boldsymbol{r} = \int_{\mathcal{S}} \zeta^{\text{point}}\,\mathrm{d}\mathcal{S} = -\alpha, \tag{38.59}$$

so that

$$\zeta^{\text{point}} = \mathcal{C}\,\delta(\boldsymbol{x}) = (\mathcal{C}/r)\,\delta(r)\,\delta(\vartheta). \tag{38.60}$$

Referring to the Green's function discussion in Section 9.2, we see that the streamfunction for the point vortex (again, in the absence of boundaries) is the free space Green's functions for the Laplace operator. Equation (9.5b) provides an expression for this Green's function in the two-dimensional space of the barotropic model, which then leads to the point vortex streamfunction

$$\nabla^2\psi^{\text{point}} = \mathcal{C}\,\delta(\boldsymbol{x}) \Longleftrightarrow \psi^{\text{point}} = (\mathcal{C}/2\pi)\ln(r/r_0). \tag{38.61}$$

We introduced the arbitrary constant, r_0, to ensure the argument to the natural log is dimensionless. But r_0 merely adds a constant to the streamfunction, and so its precise value is physically irrelevant and so it is ignored in the following. The flow associated with the point vortex is given by

$$\boldsymbol{u} = \hat{\boldsymbol{z}} \times \nabla\psi^{\text{point}} = \frac{\mathcal{C}\,\hat{\boldsymbol{\vartheta}}}{2\,\pi\,r}. \tag{38.62}$$

Evidently, the flow is a purely angular swirling motion around the point vortex that falls off as the inverse distance from the vortex.

Though highly idealized, the flow field arising from the point vortex is aligned with that in the far field for realistic localized vorticies, thus making the point vortex a physically relevant theoretical idealization. The discussion here briefly touched upon the theoretical richness of point vorticies in fluid mechanics, with chapter 3 of *McWilliams* (2006) offering a more thorough study, also in the context of two dimensional non-divergent flow.

[6] See Chapter 7 for properties of the Dirac delta.

38.2.9 Green's function solution

Since the Poisson equation for the streamfunction is a linear partial differential equation, we can use the principle of superposition to have the point vortex solution (38.61) build up the streamfunction arising from an arbitrary vorticity. This approach makes use of the Green's function method from Chapter 9. For brevity, we only consider the case without boundaries, with the more general case including boundaries detailed in Sections 9.3 and 9.4.

We seek a streamfunction that satisfies the Poisson equation

$$\nabla^2\psi = \zeta, \tag{38.63}$$

with ζ a given vorticity that is localized in space. Making use of the free space Green's function (9.5b) leads to

$$\psi(\boldsymbol{x}) = \frac{1}{2\pi}\int \zeta(\boldsymbol{y})\ln(|\boldsymbol{x}-\boldsymbol{y}|)\,\mathrm{d}\mathcal{S}_{\boldsymbol{y}} \tag{38.64}$$

where $\mathrm{d}\mathcal{S}_{\boldsymbol{y}}$ is the area element for the horizontal integral over $\boldsymbol{y}$. This streamfunction is built by convolving the vorticity source with the free space Green's function. The corresponding velocity is given by

$$\boldsymbol{u}(\boldsymbol{x}) = \hat{\boldsymbol{z}}\times\nabla\psi(\boldsymbol{x}) = \frac{1}{2\pi}\int \zeta(\boldsymbol{y})\frac{\hat{\boldsymbol{z}}\times(\boldsymbol{x}-\boldsymbol{y})}{|\boldsymbol{x}-\boldsymbol{y}|^2}\,\mathrm{d}\mathcal{S}_{\boldsymbol{y}}. \tag{38.65}$$

As a check, we see that if the vorticity source is chosen to be a point vortex at the origin, $\zeta(\boldsymbol{y}) = \mathcal{C}\,\delta(\boldsymbol{y})$, then $\boldsymbol{u}$ correctly reduces to the point vortex velocity (38.62). The expression (38.65) is sometimes referred to as the two-dimensional *Biot-Savart law*, which arises from the analog in electromagnetism.[7]

38.3 Connection to equivalent barotropic flow[8]

In many cases, flows respecting the assumptions of quasi-geostrophy (Section 43.5) possess a vertical profile that can be separated from the horizontal. In this case we write the horizontal velocity as

$$\boldsymbol{u}(x,y,z,t) = \Gamma(z)\,\boldsymbol{u}^{\mathrm{eb}}(x,y,t), \tag{38.66}$$

where $\Gamma > 0$ is a single-signed non-dimensional structure function that has a unit vertical average, $\langle\Gamma\rangle = 1$, when computed over the fluid layer thickness, and where $\boldsymbol{u}^{\mathrm{eb}}(x,y,t)$ carries the horizontal spatial dependence of the flow. With $\Gamma > 0$, the horizontal flow remains in the same direction throughout the fluid column; i.e., eastward flow at the top of the column remains eastward at the bottom. This orientation of the flow is generally referred to as *equivalent barotropic*.

38.3.1 Vorticity equation for the depth averaged flow

To connect the very particular form (38.66) for the flow with the non-divergent barotropic model, we anticipate a discussion in Section 45.2.2 in which the quasi-geostrophic vorticity equation is shown to be

$$\frac{\partial\zeta_{\mathrm{g}}}{\partial t} + \boldsymbol{u}_{\mathrm{g}}\cdot\nabla\zeta_{\mathrm{g}} = -\beta\,\zeta_{\mathrm{g}} + f_{\mathrm{o}}\frac{\partial w}{\partial z}, \tag{38.67}$$

[7] See, for example, Section 5.2 of *Jackson* (1975) or Section 5.2 of *Griffiths* (1981) for an electromagnetism discussion of the Biot-Savart law. Note, however, that the more common expression of the Biot-Savart law is given in three-dimensions, where the magnetic field has a $(\boldsymbol{x}-\boldsymbol{y})/|\boldsymbol{x}-\boldsymbol{y}|^3$ dependence rather than the $(\boldsymbol{x}-\boldsymbol{y})/|\boldsymbol{x}-\boldsymbol{y}|^2$ dependence found in two-dimensions as in equation (38.65).

[8] Section 38.3 requires a basic understanding of quasi-geostrophic theory as discussed in Section 43.5. So this discussion here can be readily skipped on first reading, then returned to after studying quasi-geostrophy in Chapter 45.

where $\boldsymbol{u}_{\text{g}}$ is the horizontally non-divergent geostrophic velocity, and $\zeta_{\text{g}} = \hat{\boldsymbol{z}} \cdot (\nabla \times \boldsymbol{u}_{\text{g}})$ is the geostrophic relative vorticity. We see that the quasi-geostrophic vorticity is affected by both the beta-effect and by vertical stretching of fluid columns (the $\partial w/\partial z$ term), whereas vertical stretching is absent from the vorticity equation (38.39) for the horizontally non-divergent barotropic fluid. There are occasions in which it is sensible to assume the vertical velocity for a quasi-geostrophic flow vanishes at the top and bottom of the fluid domain, such as when considering flow in the absence of topography. In this case, performing the decomposition (38.66) for the horizontal flow and then taking a vertical average of the quasi-geostrophic vorticity equation (38.67) leads to

$$\frac{\partial \zeta_{\text{g}}^{\text{eb}}}{\partial t} + \langle \Gamma^2 \rangle \, \boldsymbol{u}_{\text{g}}^{\text{eb}} \cdot \nabla \zeta_{\text{g}}^{\text{eb}} = -\beta \, v_{\text{g}}^{\text{eb}}. \tag{38.68}$$

This equation motivates us to define

$$\boldsymbol{u}^* = \langle \Gamma^2 \rangle \, \boldsymbol{u}_{\text{g}}^{\text{eb}} \quad \text{and} \quad \zeta^* = \langle \Gamma^2 \rangle \, \zeta_{\text{g}}^{\text{eb}}, \tag{38.69}$$

which are the original geostrophic fields, $\boldsymbol{u}_{\text{g}}(x, y, z, t)$ and $\zeta_{\text{g}}(x, y, z, t)$, when evaluated at a depth where $\Gamma(z^*) = \langle \Gamma^2 \rangle$. The depth, z^*, is known as the *equivalent barotropic depth*. Introduction of the starred fields then brings the vorticity equation (38.68) into the form of the non-divergent barotropic vorticity equation

$$\frac{\partial \zeta^*}{\partial t} + \boldsymbol{u}^* \cdot \nabla \zeta^* = -\beta \, v^*. \tag{38.70}$$

38.3.2 Comments

Charney et al. (1950) justified their study of the non-divergent barotropic vorticity model by noting its connection to the commonly observed equivalent barotropic stucture of the large-scale middle latitude atmosphere. The equivalent barotropic model has been a very useful analysis and prediction tool for meteorologists, and it formed the basis of many numerical weather prediction models into the 1980s. Section 7.1 of *Haltiner and Williams* (1980) offers further details on such numerical models.

One hypothesis for why quasi-geostrophic flows tend towards an equivalent barotropic profile relates to movement of energy in rotationally dominant turbulent flows, whereby energy cascades to the larger scales. As discussed in *Smith and Vallis* (2001) and *Venaille et al.* (2012), among others, this *inverse* energy cascade pumps mechanical energy into a vertically uniform or "barotropic" stucture. In a realistic flow, including topography, stratification, and variable forcing, this cascade is never realized completely, thus rendering a flow that approaches an equivalent barotropic structure but never quite gets there fully.

The case of $f = 0$ with flat bottom is referred to as *two-dimensional turbulence* (*Kraichnan and Montgomery*, 1980). This model has a history of key theoretical results that presaged their analog in quasi-geostrophic turbulence. See chapters 11 and 12 of *Vallis* (2017) for further discussion of this model and its relevance to geostrophic turbulence of the ocean and atmosphere.

38.4 The externally applied lid pressure

Recall the velocity equation (38.1) for the two-dimensional non-divergent flow

$$[\partial_t + (\boldsymbol{u} \cdot \nabla)] \, \boldsymbol{u} + f \, \hat{\boldsymbol{z}} \times \boldsymbol{u} = -\nabla \varphi. \tag{38.71}$$

As noted in Section 38.2.6, we do not need to determine the lid pressure, φ, to determine the evolution of the flow. Instead, we can determine the flow by time stepping vorticity and then inverting the elliptic problem to get the streamfunction. Furthermore, the free surface is

absolutely flat even in the presence of topography. Hence, there is no pressure generated by undulations of the free surface. So how is there flow in this model?!

We answer this question by studying the *lid pressure*. It is the lid pressure that maintains a flat *rigid lid* upper surface in the two-dimensional non-divergent barotropic model. The lid pressure is imposed by some external means (whose details are not important), thus ensuring that the flow remains horizontally non-divergent. In turn, it is the lid pressure that provides the force to drive flow. We here expose details to help understand the fundamental, yet somewhat hidden, role for the lid pressure.

To further motivate the analysis, we again emphasize the strong constraints placed on the horizontal flow, which must satisfy the following conditions at each space and time point

$$\nabla \cdot \boldsymbol{u} = 0 \quad \text{and} \quad \boldsymbol{u} \cdot \nabla \eta_{\mathrm{b}} = 0 \quad \text{and} \quad w = 0. \tag{38.72}$$

Kinematics of the constrained flow induce a depth-independent pressure that enforces these constraints. Examining the resulting pressure field furthers our understanding of the forces acting in the moving fluid. This role for pressure as an enforcer of non-divergence is shared by the three-dimensional non-divergent flow found in a Boussinesq ocean (see Section 29.3). It is simpler to visualize fields in the two dimensional non-divergent barotropic model, thus facilitating understanding and insights that are also useful for the three dimensional case.

38.4.1 Poisson equation for pressure

We derive the pressure equation by using the two-dimensional non-divergence property of the horizontal flow and then developing a diagnostic relation. We can eliminate the time derivative from equation (38.1) by taking $\partial/\partial x$ on the zonal equation and $\partial/\partial y$ on the meridional equation, then adding. The result is a diagnostic relation for the Laplacian of the pressure[9]

$$-\nabla^2 \varphi = \partial_x [\nabla \cdot (\boldsymbol{u}\, u)] + \partial_y [\nabla \cdot (\boldsymbol{u}\, v)] - f\, \zeta + \beta\, u, \tag{38.73}$$

where we set

$$\nabla \cdot \partial_t \boldsymbol{u} = \partial_t \nabla \cdot \boldsymbol{u} = 0 \Longrightarrow \partial_x (\partial_t u) = -\partial_y (\partial_t v). \tag{38.74}$$

Making use of the boundary conditions discussed in Section 38.1.3, the elliptic partial differential equation (38.73) can be inverted to find the pressure field (Section 6.5). As for the three-dimensional Boussinesq ocean, or for a three-dimensional incompressible fluid, pressure is the force that instantaneously constrains the velocity to remain non-divergent.

Numerically inverting an elliptic operator in equation (38.73) is straightforward on simple domains, such as flat bottom rectangular regions or a smooth sphere. However, when the bottom is not flat, or when there are islands (i.e., the domain is not simply connected), then the elliptic inversion can be numerically difficult to perform. This algorithmic complexity is one reason numerical barotropic models are less commonly used for realistic numerical experimentation than the more general shallow water models. Even so, as pursued in the remainder of this section, we can make use of idealized configurations to garner insight into how pressure maintains the flow constraints.

38.4.2 Gradient wind balance

For two-dimensional non-divergent flow we can write the contribution to the pressure equation (38.73) from self-advection in terms of the streamfunction, or equivalently as the Jacobian of the

[9] We maintain the minus sign on the left hand side of equation (38.73) so that a positive source on the right hand side leads to a positive φ. We can readily understand the sign by taking a Fourier transform, whereby the Laplacian operator picks up a minus sign when converted to Fourier space. We follow the same sign convention when studying the Green's function for the Poisson equation in Chapter 9.

velocity field. We do so through the following manipulations

$$\begin{aligned}
\partial_x[\nabla\cdot(\boldsymbol{u}\,u)]+\partial_y[\nabla\cdot(\boldsymbol{u}\,v)] &= \nabla\cdot(\partial_x\boldsymbol{u}\,u)+\nabla\cdot(\boldsymbol{u}\,\partial_x u)+\nabla\cdot(\partial_y\boldsymbol{u}\,v)+\nabla\cdot(\boldsymbol{u}\,\partial_y v) && \text{(38.75a)}\\
&= \partial_x\boldsymbol{u}\cdot\nabla u+\partial_y\boldsymbol{u}\cdot\nabla v && \text{(38.75b)}\\
&= (\partial_x u)^2+(\partial_y v)^2+2\,\partial_x v\,\partial_y u && \text{(38.75c)}\\
&= 2\,[(\partial_x u)^2+\partial_x v\,\partial_y u] && \text{(38.75d)}\\
&= 2\,[(\partial_{xy}\psi)^2-\partial_{xx}\psi\,\partial_{yy}\psi] && \text{(38.75e)}\\
&= 2\,\hat{\boldsymbol{z}}\cdot(\partial_x\nabla\psi\times\partial_y\nabla\psi) && \text{(38.75f)}\\
&= -2\,J(\partial_x\psi,\partial_y\psi), && \text{(38.75g)}\\
&= 2\,J(v,u), && \text{(38.75h)}
\end{aligned}$$

where we introduced the Jacobian operator from equation (38.39). The pressure equation (38.73) thus takes on the form

$$-\nabla^2\varphi = 2\,J(u,v)-\nabla\cdot(f\,\nabla\psi), \tag{38.76}$$

where we also wrote

$$-\nabla\cdot(f\,\nabla\psi) = -f\,\nabla^2\psi-\beta\,\partial_y\psi = -f\,\zeta+\beta\,u. \tag{38.77}$$

We refer to equation (38.76) as a *gradient wind balance* in analog to the gradient wind balance discussed in Section 32.6. Here, the Jacobian term accounts for the centrifugal acceleration of the curved fluid motion, and the $\nabla\cdot(f\,\nabla\psi)$ term accounts for the Coriolis acceleration, both for the f-plane and β-plane. Equation (38.76) thus offers a more accurate diagnostic relation for the pressure field than provided by assuming a geostrophically balanced flow.

38.4.3 Pressure source from self-advection

We introduce yet another way to examine the self-advection source appearing in the pressure equation (38.73), and do so by writing it as

$$\partial_x[\nabla\cdot(\boldsymbol{u}\,u)]+\partial_y[\nabla\cdot(\boldsymbol{u}\,v)] = \mathbb{S}_{mn}\,\mathbb{S}_{mn}-\mathbb{R}_{mn}\,\mathbb{R}_{mn}, \tag{38.78}$$

where the strain rate tensor, $\mathbb{S}$, and rotation tensor, $\mathbb{R}$, have components given by equations (18.90a) and (18.90b)

$$\mathbb{S}_{mn} = (\partial_n v_m+\partial_m v_n)/2 = \mathbb{S}_{nm} \qquad \text{strain rate tensor} \tag{38.79}$$

$$\mathbb{R}_{mn} = (\partial_n v_m-\partial_m v_n)/2 = -\mathbb{R}_{nm} \qquad \text{rotation tensor.} \tag{38.80}$$

For two-dimensional flow the rotation tensor is related to the relative vorticity via

$$\mathbb{R}_{mn} = -\epsilon_{mn}\,\zeta/2 = -\epsilon_{mn}\,\nabla^2\psi/2, \tag{38.81}$$

where ϵ_{mn} is the anti-symmetric Levi-Civita permutation symbol (see Section 1.7.1)

$$\epsilon_{mn} = \begin{bmatrix} \epsilon_{11} & \epsilon_{12} \\ \epsilon_{21} & \epsilon_{22} \end{bmatrix} = \begin{bmatrix} 0 & 1 \\ -1 & 0 \end{bmatrix}, \tag{38.82}$$

which leads to the double contraction of the rotation tensor

$$\mathbb{R}_{mn}\,\mathbb{R}_{mn} = \zeta^2/2. \tag{38.83}$$

The identity (38.78) indicates that the squared strain rate (sometimes referred to as the *splat*) provides a positive source to the Poisson equation (38.73) whereas squared vorticity provides a negative source. Bringing these results together leads to the pressure equation

$$-\nabla^2\varphi = \mathbb{S}_{mn}\,\mathbb{S}_{mn} - \zeta^2/2 - \nabla\cdot(f\,\nabla\psi) = 2\,[(\partial_{xy}\psi)^2 - \partial_{xx}\psi\,\partial_{yy}\psi] - \nabla\cdot(f\,\nabla\psi), \tag{38.84}$$

where the second equality made use of equation (38.75e) to write the pressure source fully in terms of the streamfunction.

In the following sections, we present two examples to help understand how pressure gradients arise in a two-dimensional barotropic flow, with the pressure gradients maintaining a non-divergent two-dimensional velocity field. We start by assuming a non-rotating reference frame, so that it is sufficient to examine how pressure responds to the nonlinear source term $\mathbb{S}_{mn}\,\mathbb{S}_{mn} - \zeta^2/2$. Thereafter we include sources from the rotating reference frame.

38.4.4 Pressure source from circular rigid-body flow

Consider a velocity field in a flat domain that is initialized in circular rigid-body motion (Figure 38.1)

$$\boldsymbol{u} = \boldsymbol{\Omega}\times\boldsymbol{x} = \Omega\,(-y\,\hat{\boldsymbol{x}} + x\,\hat{\boldsymbol{y}}), \tag{38.85}$$

where $\boldsymbol{\Omega} = \Omega\,\hat{\boldsymbol{z}}$ is a constant angular velocity. This flow has zero strain (as do all rigid-body flows) yet constant vorticity

$$\hat{\boldsymbol{z}}\cdot(\nabla\times\boldsymbol{u}) = \zeta = 2\,\Omega \implies -\mathbb{R}_{mn}\,\mathbb{R}_{mn} = -2\,\Omega^2. \tag{38.86}$$

The velocity time tendency from the self-advection acceleration is

$$-(\boldsymbol{u}\cdot\nabla)\,\boldsymbol{u} = \Omega^2\,\boldsymbol{x}, \tag{38.87}$$

which is the outward directed centrifugal acceleration associated with the circular rigid-body motion.[10] The velocity equation (38.71) thus takes the form (recall we are considering $f = 0$ for now)

$$\partial_t\boldsymbol{u} = \Omega^2\,\boldsymbol{x} - \nabla\varphi. \tag{38.88}$$

Pressure gradient acceleration exactly balances centrifugal acceleration

If acting alone, the centrifugal acceleration would create a velocity field that diverges from the origin. However, the velocity is constrained to remain non-divergent at each instance, so the centrifugal acceleration cannot be the full story. Indeed, to maintain a non-divergent flow we find a pressure gradient that exactly balances the centrifugal acceleration. This pressure gradient is established instantaneously as per the solution to the elliptic pressure equation. We thus infer that there is a low pressure at the origin so that the pressure gradient force points inward, thus balancing the centrifugal acceleration.

We can extrapolate from this example to conclude that vorticity provides a source of low pressure in a non-divergent flow. Furthermore, since the centrifugal acceleration from the velocity self-advection is exactly balanced by the pressure gradient acceleration, the rigid-body flow is an exact steady solution for the non-divergent and non-rotating (zero Coriolis) barotropic system. This result holds even in the presence of viscosity, since the rigid-body flow has no strain and hence it does not support viscous stresses (see Section 25.8).

[10] We considered the more general case in Section 32.2.2 when decomposing the material acceleration for two-dimensional flow into natural coordinates.

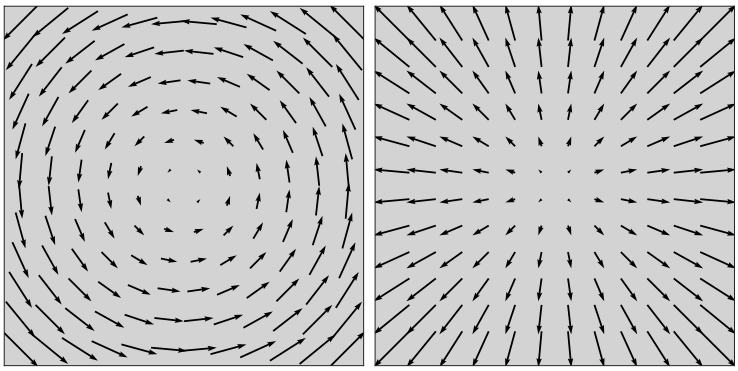

FIGURE 38.1: Left panel: example flow field from rigid-body rotation, $\boldsymbol{u} = \boldsymbol{\Omega} \times \boldsymbol{x} = \Omega\,(-y, x)$, which has vorticity $\nabla \times \boldsymbol{u} = 2\,\boldsymbol{\Omega}$ and zero strain. Right panel: corresponding acceleration from self-advection, $-(\boldsymbol{u} \cdot \nabla)\,\boldsymbol{u} = \Omega^2\,\boldsymbol{x}$, which is a centrifugal acceleration. The centrifugal acceleration from self-advection is exactly compensated by the pressure gradient force: $-(\boldsymbol{u} \cdot \nabla)\,\boldsymbol{u} - \nabla\varphi = 0$, thus allowing for the rigid-body motion to be an exact steady solution to two-dimensional non-divergent flow. The units are arbitrary.

Rotationally symmetric pressure field

We can support the above general statements by deriving an explicit expression for the pressure field, and we do so by solving the pressure Poisson equation (38.73). Since we have assumed zero planetary rotation ($f = 0$), equation (38.73) reduces to

$$-\nabla^2\varphi = -2\,\Omega^2, \tag{38.89}$$

which also follows from taking the divergence of equation (38.88) and noting that $\nabla \cdot \boldsymbol{x} = 2$. Furthermore, the solid-body flow is assumed to be rotationally symmetric so that all fields have only radial dependence. In this case, pressure satisfies the ordinary differential equation

$$r^{-1}\,\partial_r(r\,\partial_r\varphi) = 2\,\Omega^2, \tag{38.90}$$

where r is the radial distance from the origin and we used the polar coordinate version of the Laplacian given by equation (4.197b). The solution to the pressure equation (38.90) is given by

$$\varphi = (\Omega\,r)^2/2 \quad \text{and} \quad -\nabla\varphi = -\Omega^2\,\boldsymbol{x} = (\boldsymbol{u} \cdot \nabla)\,\boldsymbol{u}, \tag{38.91}$$

where we set $\varphi(r = 0) = 0$. Evidently, the pressure grows parabolically moving radially away from the center.

The pressure field in relation to rigid-body rotating shallow water

To help understand the physics of the pressure field (38.91), recall the analysis in Section 27.5 of a rigid-body rotating homogeneous shallow water fluid layer in a cylindrical tank. In contrast to the barotropic system, the horizontal velocity in a homogeneous fluid layer, such as in a shallow water fluid, is divergent so that the layer thickness is not constrained to remain flat. Hence, the centrifugal acceleration causes the velocity to diverge from the center so that the layer thickness increases radially outward, with the layer bounded by the tank wall. At steady state, the homogeneous fluid layer has a parabolic free surface with a minimum at the center (see equation (27.106)). The parabolic free surface creates a pressure field that precisely corresponds to the pressure field (38.91) in the non-divergent barotropic system. Note that the dynamical adjustment of a homogeneous shallow water fluid layer contain linear fluctuations in the form of gravity waves such as discussed in Chapter 36. In contrast, the adjustment required to reach a steady state occurs instantaneously in the non-divergent barotropic fluid.

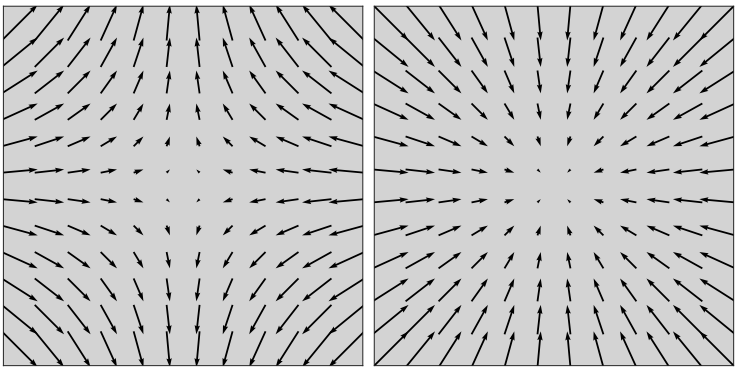

FIGURE 38.2: Left panel: example purely strained flow field with zero vorticity, $\boldsymbol{u} = \Omega\,(-x\,\hat{\boldsymbol{x}} + y\,\hat{\boldsymbol{y}})$. Right panel: corresponding converging acceleration from self-advection, $-(\boldsymbol{u}\cdot\nabla)\,\boldsymbol{u} = -\Omega^2\,\boldsymbol{x}$. The units are arbitrary.

38.4.5 Pressure source from irrotational (pure strain) flow

Consider the following pure strain flow (Figure 38.2)

$$\boldsymbol{u} = \Omega\,(-x\,\hat{\boldsymbol{x}} + y\,\hat{\boldsymbol{y}}), \tag{38.92}$$

whose vorticity vanishes and whose self-advection acceleration is given by

$$-(\boldsymbol{u}\cdot\nabla)\,\boldsymbol{u} = -\Omega^2\,\boldsymbol{x} \Longrightarrow \mathbb{S}_{mn}\,\mathbb{S}_{mn} = 2\,\Omega^2, \tag{38.93}$$

thus leading to a velocity equation (again, $f = 0$ is assumed)

$$\partial_t \boldsymbol{u} = -\Omega^2\,\boldsymbol{x} - \nabla\varphi. \tag{38.94}$$

The acceleration (38.93) is exactly the opposite of that produced by the rigid rotation studied in the previous example (equation (38.87)). Hence, to maintain a horizontally non-divergent barotropic flow, a pressure field is established with a high pressure at the center that exactly counteracts the converging self-advection acceleration present in the pure strain flow

$$\varphi = -(\Omega\,r)^2/2 \quad \text{and} \quad -\nabla\varphi = \Omega^2\,\boldsymbol{x} = (\boldsymbol{u}\cdot\nabla)\,\boldsymbol{u}. \tag{38.95}$$

This example illustrates how strain provides a source for high pressure in a non-divergent flow. Furthermore, we see that this flow, in the absence of viscosity, is an exact steady solution for non-divergent barotropic flow in a non-rotating reference frame. However, in contrast to the rigid-body flow in Section 38.4.4, the purely strained flow (38.92) supports viscous friction, so that this flow does not remain steady in the presence of viscosity.

38.4.6 Pressure source from Coriolis acceleration

In addition to the self-advection source, pressure is affected by a source from the Coriolis acceleration

$$-\nabla^2\varphi_{\text{geostrophy}} \equiv \nabla\cdot(f\,\hat{\boldsymbol{z}}\times\boldsymbol{u}) = -\nabla\cdot(f\,\nabla\psi) = \beta\,u - \zeta\,f. \tag{38.96}$$

As such, we can write the pressure gradient as[11]

$$-\nabla\varphi_{\text{geostrophy}} = f\,\hat{\boldsymbol{z}}\times\boldsymbol{u}. \tag{38.97}$$

[11] Formally, we can add an arbitrary gauge function to the right hand side of equation (38.97), with this term of the form $\hat{\boldsymbol{z}}\times\nabla\chi$. However, since we derived the pressure Poisson equation from the velocity equation, then we know there is no gauge function arising in equation (38.97).

Consider cyclonic flow around an arbitrary point. What is the pressure field induced by this flow? As in our discussion in Section 38.4.4 of the rigid-body rotating flow, a cyclonic flow has an associated centrifugal acceleration that points outward. To counteract the centrifugal acceleration, and thus to maintain a non-divergent flow, requires an inward pointing pressure force; i.e., a low pressure center. Hence, cyclonic circulation induces, through the Coriolis acceleration, a negative pressure source whereas anti-cyclonic circulation induces a positive pressure source. This is indeed an interesting perspective on geostrophic balance!

38.4.7 Pressure source from friction

Consider flow with friction, in which case the velocity equation (38.1) takes the form

$$\frac{\mathrm{D}\boldsymbol{u}}{\mathrm{D}t} + f\,\hat{\boldsymbol{z}} \times \boldsymbol{u} = -\nabla\varphi + \boldsymbol{F}, \tag{38.98}$$

with $\boldsymbol{F}$ a frictional acceleration. In this case we have yet another source for pressure given by

$$-\nabla^2\varphi_{\text{friction}} \equiv -\nabla \cdot \boldsymbol{F}. \tag{38.99}$$

As discussed in Section 25.8, viscous friction is generally associated with a nonzero strain rate. We see that the frictional acceleration induces a high pressure source in regions where frictional accelerations converge, $-\nabla \cdot \boldsymbol{F} > 0$, with this source acting to maintain non-divergent flow in the presence of converging frictional acceleration.

38.4.8 Comments and further study

- The pressure equation (38.73) is elliptic, and elliptic equations need boundary conditions. In the presence of topography the boundary conditions are modified relative to the flat bottom case. Hence, pressure knows about topography through its boundary conditions. The resulting pressure force keeps the flow non-divergent and the flow aligned with topography as per the kinematic conditions in Section 38.1.3.

- The discussion of pressure induced by self-advection in Sections 38.4.4 and 38.4.5 is based on a similar presentation in Appendix B of *Jeevanjee and Romps* (2015a).

- *Bryan* (1969) provided the first working numerical algorithm to simulate the ocean general circulation. Bryan's method made use of the rigid lid approximation of Section 38.4 so that the depth integrated velocity is non-divergent. However, the vorticity in Bryan's ocean model is affected by more than just the beta-effect. The reason is that the depth integrated velocity equation includes contributions from baroclinic processes, and such processes affect the barotropic vorticity in a baroclinic fluid. We detail such effects in Sections 44.5 and 44.6.

  The rigid lid method was used for large-scale ocean circulation modeling until the late 1990s. Free surface methods, allowing divergence in the depth integrated flow, have largely displaced the rigid lid as a practical method for time stepping ocean models (e.g., see chapter 12 of *Griffies* (2004)).

38.5 Constraints from material invariance of absolute vorticity

Following from Section 38.2.2, we here examine constraints on the flow imposed by material invariance of absolute vorticity, which holds for two-dimensional non-divergent flow when there

is no dissipation

$$\frac{\mathrm{D}(\zeta + f)}{\mathrm{D}t} = 0. \tag{38.100}$$

These constraints offer insights into the flow behavior and allow us to predict responses to perturbations. Notably, these predictions arise even without direct information about the forces giving rise to the responses. Rather, we deduce the responses based on vorticity constraints alone.

We frame the discussion in terms of the decomposition (37.50) of relative vorticity into a curvature (or orbital) term and normal shear term

$$\zeta = \frac{|\boldsymbol{u}|}{R} - \frac{\partial |\boldsymbol{u}|}{\partial n} \equiv \zeta_{\text{curv}} + \zeta_{\text{shear}}, \tag{38.101}$$

so that

$$\frac{\mathrm{D}(\zeta_{\text{curv}} + \zeta_{\text{shear}} + f)}{\mathrm{D}t} = 0. \tag{38.102}$$

When the flow turns, the curvature term contributes with R the radius of curvature.[12] If the flow develops shears in the direction normal to the flow, then the shear term contributes. In the presence of $\beta = \partial_y f$, meridional motion through the planetary vorticity field requires a compensating response from relative vorticity. In general each of the three terms contribute to the relative vorticity, yet for pedagogical purposes we consider cases where one term is subdominant and so can be ignored.

38.5.1 Relative vorticity from curvature and planetary beta

According to the decomposition (38.101), fluid flow that curves to the left (facing downstream) picks up a positive relative vorticity from flow curvature, $R > 0 \Rightarrow \zeta > 0$, as depicted in Figure 38.3. The oppositely curved flow has a negative radius of curvature so flow curving to the right picks up a negative relative vorticity, $R < 0 \Rightarrow \zeta < 0$. We focus here on the case where the normal shear induced relative vorticity can be neglected so that we are only concerned with curvature induced vorticity plus planetary vorticity (beta effect).

Consider a flow that is initially zonal with zero relative vorticity. If the flow turns meridionally then it experiences a change in relative vorticity both through the curvature term plus a change in planetary vorticity since f changes. To maintain constant absolute vorticity, a fluid column that moves meridionally requires the relative vorticity induced by the curved flow path to counteract the change in planetary vorticity. As we now discuss, the constraint of fixed absolute vorticity, in the absence of induced normal shears, means that eastward flow (westerly winds) cannot turn meridionally while maintaining fixed absolute vorticity, whereas westward flow (easterly winds) can turn (see Figure 38.3).

Consider westward flow in the northern hemisphere ($f > 0$). If the flow turns to the north (to the right facing downstream) then this flow picks up a curvature-induced negative relative vorticity, $\zeta < 0$, and an increase in the planetary vorticity (f increases). Likewise, a westward flowing fluid column that turns equatorward (to the left) has a positive curvature-induced relative vorticity ($\zeta > 0$) and a reduction in planetary vorticity (f decreases). Hence, westward flow in the northern hemisphere can turn either poleward (to the north) or equatorward (to the south) and still maintain constant absolute vorticity, so long as the curved motion induces the proper relative vorticity to counteract the changes to f. The same arguments also hold in the southern hemisphere, so that the general scenarios are depicted in Figure 38.3.

[12] As discussed in Section 32.2, we take the convention whereby the normal direction is to the left of flow when facing downstream. Flow turning into the normal direction (to the left) has a positive radius of curvature, $R > 0$, and flow turning opposite to the normal direction (to the right) has $R < 0$.

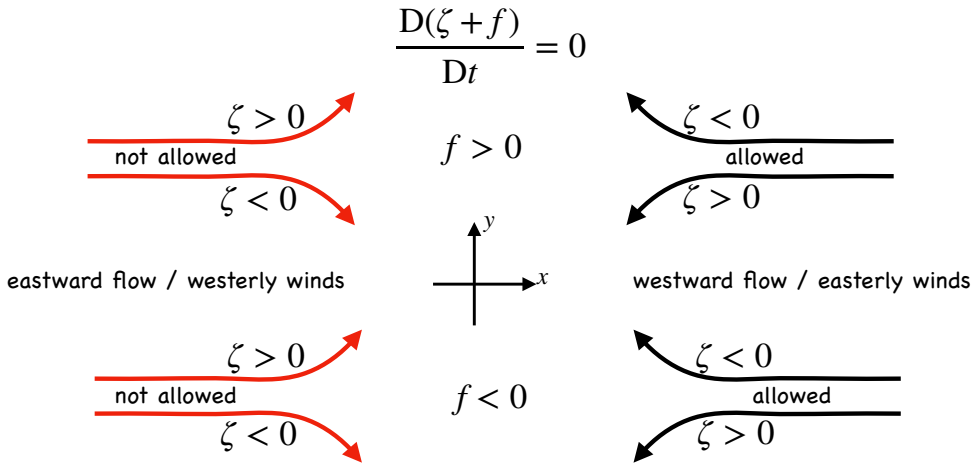

FIGURE 38.3: Illustrating the constraints on a two dimensional non-divergent flow imposed by material invariance of absolute vorticity: $\zeta + f =$ constant. We assume flow is over a flat region and assume there is only curvature induced relative vorticity (no shear-induced relative vorticity; $\partial|\boldsymbol{u}|/\partial n = 0$) as per the decomposition in equation (38.101). In each of the four cases depicted, the entering flow has zero relative vorticity, which means that absolute vorticity must remain constant at the initial Coriolis parameter, $\zeta + f = f_{\text{initial}}$. The red eastward flow (westerly winds) that turns meridionally picks up a curvature vorticity that supports the change in planetary vorticity, thus precluding material invariance of absolute vorticity. Hence, the meridional turning of eastward flow is not allowed so that flow must remain zonal for absolute vorticity to remain invariant. In contrast, the oppositely directed westward flow (easterly winds) can deviate either to the north or south and still retain a constant absolute vorticity. We illustrate flows for both the northern and southern hemispheres. This figure is adapted from Figure 4.13 of *Holton and Hakim* (2013).

The situation is different for eastward flow. Consider again flow in the northern hemisphere. A poleward (to the left) turning fluid column is associated with a positive curvature-induced relative vorticity, $\zeta > 0$, as well as an increase in the planetary vorticity. Hence, this motion changes the absolute vorticity and as such it is not allowed if the absolute vorticity is constrained to remain constant. Likewise, an equatorward (to the right) turning eastward fluid column induces a negative curvature-induced relative vorticity, $\zeta < 0$, and a decrease in planetary vorticity, again leading to a change in absolute vorticity. Hence, eastward flow (westerly winds) in either hemisphere must remain zonal to maintain a constant absolute vorticity.

As an application of these results, consider the situation depicted in Figure 38.4, whereby inviscid flow in the interior of an ocean domain moves westward into a frictional western boundary layer. The constraints imposed by absolute vorticity invariance allow for this flow to occur, whereas the opposite is disallowed whereby eastward inviscid flow cannot enter an eastern boundary. We return to this example in Section 39.7 when discussing western intensification of ocean gyres.

38.5.2 Relative vorticity from curvature and normal shears

Now consider the case in which the meridional displacements are small so that the beta effect can be neglected. In this case there is an exchange between relative vorticity arising from curvature and relative vorticity from normal shears, thus leaving their sum materially invariant

$$\frac{\mathrm{D}(\zeta_{\text{curv}} + \zeta_{\text{shear}})}{\mathrm{D}t} = 0. \tag{38.103}$$

We depict an example in Figure 38.5 whereby a vortex undergoes a left turn facing downstream. While on the curve, the relative vorticity of the vortex is in part due to the positive curvature vorticity, $\zeta_{\text{curv}} > 0$. If the relative vorticity is positive on the straight portion of the trajectory,

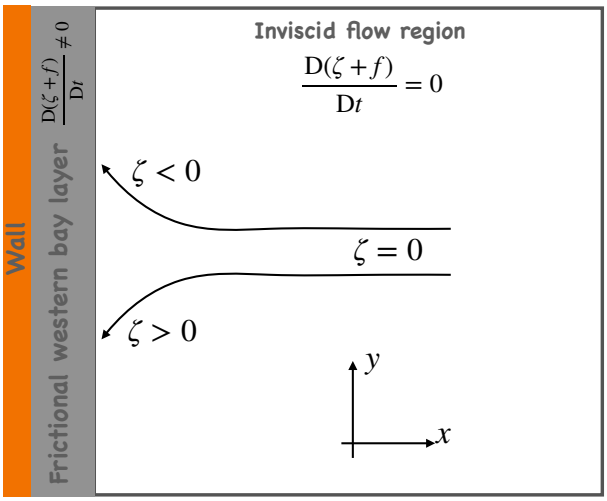

FIGURE 38.4: Illustrating the constraints on a homogeneous and constant thickness fluid layer imposed by material invariance of absolute vorticity: $\zeta + f =$ constant. As per the results from Figure 38.3, inviscid flow with initially zero relative vorticity can enter a western boundary layer as depicted here, whereas it cannot enter an eastern boundary layer. This conclusion assumes that there is no shear-induced relative vorticity ($\partial|\boldsymbol{u}|/\partial n = 0$) that can overcome changes in the vorticity induced by changes to f and by curvature-induced relative vorticity (see Section 37.8.2). This figure is adapted from Figure 19.12 of *Vallis* (2017).

then when on the curve the shear vorticity must lose some of its strength in order to compensate for the curvature vorticity. Conversely, if the relative vorticity is negative on the straight portion of the trajectory, then when on the curve the shear vorticity gains in strength to allow for the positive curvature vorticity.

38.5.3 Curvature, shear, and planetary contributions

We now consider all three terms appearing in the vorticity equation (38.102). Let us consider again the eastward flow that turns to the north in the northern hemisphere. Such flow is not allowed if the only source for relative vorticity is curvature. However, if the eastward flow, as it turns, picks up a shear that induces a nonzero negative relative vorticity, then such flow can turn so long as the shear-induced negative relative vorticity balances the positive absolute vorticity from increases in f and the curvature-induced vorticity. Writing this condition for the shear-induced relative vorticity yields

$$\zeta_{\text{shear}} = -\Delta f - \zeta_{\text{curv}} = -(f_{\text{final}} - f_{\text{init}}) - \zeta_{\text{curv}} < 0, \tag{38.104}$$

where f_{init} and f_{final} are the initial and final Coriolis parameters. Conversely, if the flow deviates towards the equator then it can do so only if there is a positive shear-induced relative vorticity

$$\zeta_{\text{shear}} = -(f_{\text{final}} - f_{\text{init}}) - \zeta_{\text{curv}} > 0. \tag{38.105}$$

38.5.4 Beta drift

In Exercise 24.6 we introduced the *Rossby effect* (*Rossby*, 1948), in which a circular cyclonic vortex experiences an area integrated Coriolis acceleration that is directed poleward, and with the integrated acceleration vanishing on the f-plane. Hence, this poleward drift arises from the beta effect. Following *Rossby* (1948), we did not consider the pressure field associated with the vortex, so it is unclear whether such a vortex would actually drift due northward. Indeed, subsequent studies showed that motion of an initially circular vortex sets up a secondary flow

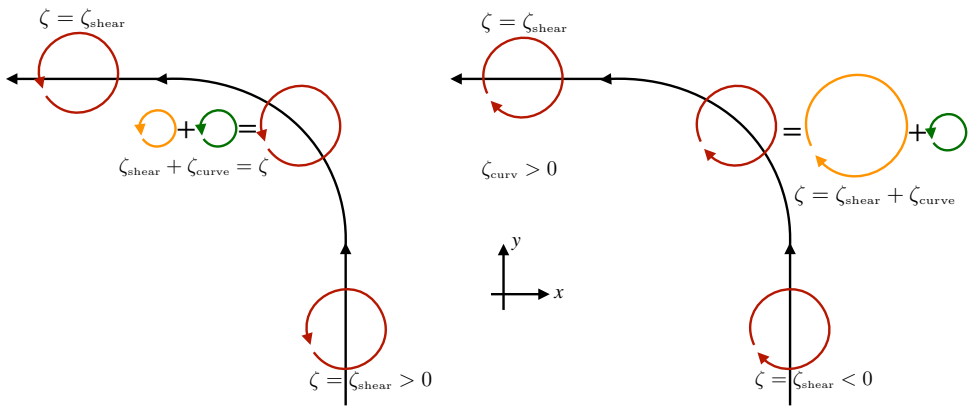

FIGURE 38.5: Material invariance of relative vorticity, $\mathrm{D}\zeta/\mathrm{D}t = \mathrm{D}(\zeta_{\text{curv}} + \zeta_{\text{shear}})/\mathrm{D}t = 0$, means that as a vortex moves around a curve its shear vorticity is modified to keep the total relative vorticity invariant. On the straight portion of these trajectories, the relative vorticity is due only to shear vorticity, $\zeta = \zeta_{\text{shear}}$ since $\zeta_{\text{curve}} = 0$. However, when the vortex enters the curve, maintaining a constant relative vorticity requires an exchange of shear vorticity with the curvature vorticity. In this example we illustrate a steady flow that turns to the left so that the vortex picks up a positive curvature vorticity when on the curve, $\zeta_{\text{curve}} > 0$. Left panel: a vortex that enters the left turn with a positive relative vorticity must give some of its shear vorticity to the curvature vorticity in order to maintain ζ constant along the trajectory. Right panel: a vortex that enters the curve with a negative relative vorticity sees its shear vorticity increase in magnitude to compensate for the positive curvature vorticity.

that renders a poleward+westward *beta drift*; i.e., northwestward in the northern hemisphere and southwestward in the southern hemisphere. As for the other motions considered in this section, we describe the mechanism for beta drift by invoking conservation of absolute vorticity respected by an inviscid non-divergent barotropic flow. This discussion reflects similar ideas encountered when studying Rossby waves in Section 54.3.

Consider a circularly symmetric northern hemisphere cyclonic monopole as shown in Figure 38.6. The monopole flow has positive circulation and thus positive relative vorticity. On an f-plane this circulation is stationary, whereas parcels moving around the monopole on the β-plane pick up anomalous relative vorticity according to the beta effect: $\mathrm{D}\zeta/\mathrm{D}t = -\beta\, v$. On the west side of the monopole, fluid elements are moving southward and thus pick up a positive anomalous relative vorticity ($-\beta\, v > 0$), whereas on the east side the northward flow picks up a negative relative vorticity anomaly. We note that the material evolution of relative vorticity is also reflected in the local time changes, since for an initially circular monopole, the only contribution to the local evolution is given by the beta effect. We see this property by writing the vorticity equation using polar coordinates (see Section 4.22)

$$\partial_t \zeta = -\beta\, v - \boldsymbol{u} \cdot \nabla \zeta = -\beta\, v - (\dot{r}\, \partial_r + \dot{\vartheta}\, \partial_\vartheta)\, \zeta, \tag{38.106}$$

where r is the radial coordinate and ϑ is the angular coordinate measured counter-clockwise from the x-axis. By assumption, the flow is initially moving only in the angular direction, so that $\dot{r} = 0$. Additionally, the monopole is symmetric in the angular direction, so that $\partial_\vartheta \zeta = 0$. As a result, $\partial_t \zeta = -\beta\, v$.

From the above analysis, we see that throughout the western side of the monopole, beta induces a positive anomalous vorticity, whereas beta induces a negative vorticity anomaly throughout the eastern side. When combined with the vorticity from the monopole, we see that the beta induced anomalous vorticity leads to a westward drift of the location for the maximum vorticity; i.e., the monopole maximum drifts to the west. Yet that is not the full story.

In addition to the westward drift of the monopole maximum, the positive vorticity anomaly on the western side induces a positive gyre-like circulation referred to as a *beta gyre*. Likewise, the negative vorticity on the eastern side induces a negative beta gyre. The beta gyre circulations

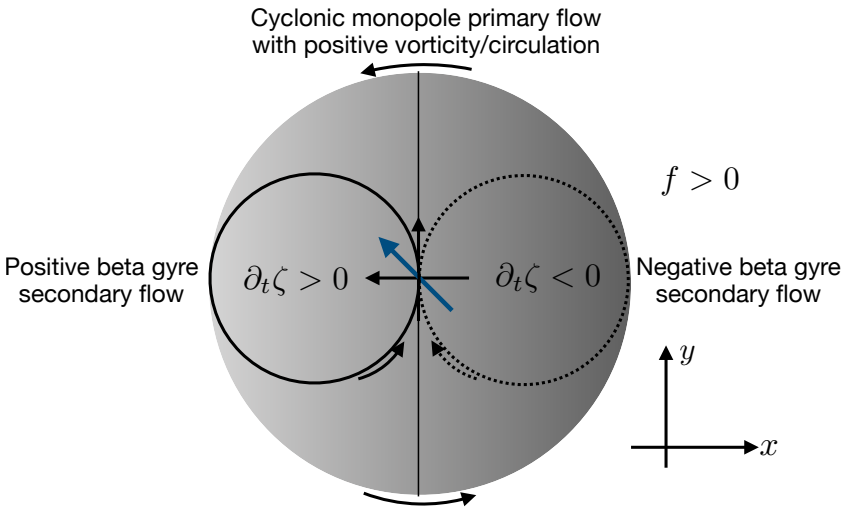

FIGURE 38.6: Schematic cyclonic and circularly symmetric northern hemisphere ($f > 0$) monopole flow in a two-dimensional non-divergent barotropic flow. The monopole has positive circulation and thus positive relative vorticity. On the β-plane, parcels moving around the monopole pick up anomalous relative vorticity according to the beta effect: $\mathrm{D}\zeta/\mathrm{D}t = -\beta\, v$. On the western side, parcels move southward and thus pick up a positive relative vorticity anomaly ($-\beta\, v > 0$), whereas on the eastern side the northward flow picks up a negative relative vorticity anomaly. The beta effect thus induces a westward drift of the monopole maximum, towards where the relative vorticity is increasing. Additionally, the positive anomaly on the western side of the monopole induces a secondary circulation known as a *beta gyre*, with this gyre rotating counter-clockwise, whereas there is an oppositely oriented beta gyre on the eastern side. The secondary circulation from the counter-rotating beta gyres induces a northward drift to the monopole. The combined effect of the westward beta induced drift and the northward drift from the beta gyres leads to a net northwestward *beta drift* for the monopole.

are referred to as *secondary circulations* since they arise in response to the anomalies induced by motion through the primary monopole circulation. Furthermore, the counter-rotating beta gyres induce a northward drift of the monopole. The combined westward drift induced by beta acting on the primary monopole circulation, plus the northward drift from the secondary beta gyre circulations, leads to an overall northwestward drift of the monopole. More generally, a cyclonic monopole experiences a poleward and westward beta drift, whereas for anti-cyclonic monopoles the beta drift is equatorward and westward.

The extent to which beta drift is respected by more realistic monopoles depends on many factors, such as the strength and radius of the monopole, strength of the background planetary vorticity gradient, and stability of the monopole. The literature on these topics makes use of numerical models to probe the nonlinearities associated with these relatively strong, and sometimes unstable, flow regimes. Some of the papers are motivated by motion of coherent ocean eddies (e.g., *McWilliams and Flierl*, 1979; *Carnevale et al.*, 1991), and others are motivated by motion of atmospheric tropical cyclones (e.g., *Holland*, 1983; *Smith*, 1993). For tropical cyclones born off the coast of Africa in the tropical Atlantic, beta drift gives the cyclones a general tendency to move northwestward toward North America (absent environmental flows that can counteract the beta drift). More recently, *Gavriel and Kaspi* (2021) employed these concepts to help understand vortices found in the polar regions of the Jovian atmosphere.

38.5.5 Understanding and prediction

The examples in this section illustrate the power of vorticity constraints for the purpose of predicting flow responses. The power largely rests on our ability to determine flow responses without directly determining forces causing the response. Even so, without determining the forces acting in the fluid, our understanding of the dynamics remains incomplete even if our ability to predict is complete. So when one can determine the forces (it is not always as simple

as the examples in Section 38.4), then doing so offers further physical insights into the nature of the flow.

38.6 Steady flow and the β-plume

In this section we consider the steady solution to the horizontally non-divergent barotropic model in the planetary geostrophic regime (Section 31.5 and Chapter 44). For this purpose, we return to the Rossby potential vorticity (38.42) and add a Rayleigh drag (Section 25.8.5) along with a frictional stress vector, $\boldsymbol{\tau}$.

38.6.1 The Rossby potential vorticity equation

Introducing the Rayleigh drag and frictional stresses into the velocity equation (38.1) leads to

$$\frac{\mathrm{D}\boldsymbol{u}}{\mathrm{D}t} + f\,\hat{\boldsymbol{z}}\times\boldsymbol{u} = -\nabla\varphi - \gamma\,\boldsymbol{u} + \boldsymbol{F}. \tag{38.107}$$

In this equation, $\gamma \geq 0$ is the constant Rayleigh drag coefficient (with dimensions of inverse time), and

$$\boldsymbol{F} = \frac{\boldsymbol{\tau}^{\text{wind}} - \boldsymbol{\tau}^{\text{bot}}}{h\,\rho_o} \tag{38.108}$$

is the acceleration arising from difference between the surface wind stress, $\boldsymbol{\tau}^{\text{wind}}$, and bottom stress, $\boldsymbol{\tau}^{\text{bot}}$ (see equation (35.135)). Carrying the Rayleigh drag and boundary stresses through the derivation of the Rossby potential vorticity equation (38.42) yields

$$h\,\frac{\mathrm{D}Q}{\mathrm{D}t} = -\gamma\,\zeta + \hat{\boldsymbol{z}}\cdot(\nabla\times\boldsymbol{F}) \quad \text{with } Q = (f+\zeta)/h. \tag{38.109}$$

Evidently, potential vorticity is no longer materially conserved in the presence of either Rayleigh drag or boundary stresses.

38.6.2 Steady flow balances

For steady flow, the potential vorticity equation (38.109) reads

$$h\,\boldsymbol{u}\cdot\nabla Q = -\gamma\,\zeta + \hat{\boldsymbol{z}}\cdot(\nabla\times\boldsymbol{F}), \tag{38.110}$$

which takes on the following form in terms of the transport streamfunction, $h\,\boldsymbol{u} = \hat{\boldsymbol{z}}\times\nabla\Psi$ (equation (38.20)),

$$(\hat{\boldsymbol{z}}\times\nabla Q)\cdot\nabla\Psi = -\gamma\,\nabla\cdot(h^{-1}\,\nabla\Psi) + \hat{\boldsymbol{z}}\cdot(\nabla\times\boldsymbol{F}), \tag{38.111}$$

where the potential vorticity is

$$h\,Q = f + \zeta = f + \nabla\cdot(h^{-1}\nabla\Psi). \tag{38.112}$$

Use of the product rule on the Rayleigh drag term, and rearrangement, leads to

$$(h\,\hat{\boldsymbol{z}}\times\nabla Q + \gamma\,\nabla\ln h)\cdot\nabla\Psi = \gamma\,\nabla^2\Psi + h\,\hat{\boldsymbol{z}}\cdot(\nabla\times\boldsymbol{F}). \tag{38.113}$$

To help intrepret this streamfunction equation, introduce

$$\boldsymbol{A} \equiv h\,\hat{\boldsymbol{z}}\times\nabla Q + \gamma\,\nabla\ln h, \tag{38.114}$$

which is a horizontally divergent vector ($\nabla \cdot \boldsymbol{A} \neq 0$) with physical dimensions $\mathrm{L}^{-1}\,\mathrm{T}^{-1}$ (the same dimensions as $\beta = \partial_y f$). In this case the streamfunction equation (38.113) takes on the form of a steady advective-diffusive-source equation[13]

$$\underbrace{\boldsymbol{A} \cdot \nabla \Psi}_{\text{advection}} = \underbrace{\gamma\, \nabla^2 \Psi}_{\text{diffusion}} + \underbrace{h\, \hat{\boldsymbol{z}} \cdot (\nabla \times \boldsymbol{F})}_{\text{source}}. \tag{38.115}$$

The vector, $\boldsymbol{A}$, serves as an advection "velocity" that acts to align the streamfunction along integral paths defined by $\boldsymbol{A}$; i.e., the streamfunction is "advected" by $\boldsymbol{A}$. For example, in the absence of non-conservative process and boundary stresses, isolines of constant streamfunction and Rossby potential vorticity are aligned,

$$(\hat{\boldsymbol{z}} \times \nabla Q) \cdot \nabla \Psi = (\nabla Q \times \nabla \Psi) \cdot \hat{\boldsymbol{z}} = 0 \quad \text{if } \gamma = 0 \text{ and } \boldsymbol{F} = 0. \tag{38.116}$$

In this case, the streamfunction functionally depends only on the potential vorticity, $\Psi = \Psi(Q)$, which is another way of stating that the steady unforced and inviscid flow is along lines of constant Q. The presence of boundary stresses, $\hat{\boldsymbol{z}} \cdot (\nabla \times \boldsymbol{F}) \neq 0$, causes the steady flow to deviate from Q isolines, with the stresses providing a source to the streamfunction equation (38.115). Finally, the presence of Rayleigh drag ($\gamma > 0$) acts to diffuse or spread the streamfunction isolines.

38.6.3 Planetary geostrophic flow and the effective beta

We develop more insights into the steady flow by linearizing the streamfunction equation (38.115), which is done by assuming the flow maintains a planetary geostrophic balance (Section 31.5 and Chapter 44). In this case the potential vorticity is independent of the streamfunction and takes on the form

$$Q^{\text{pg}} = f/h. \tag{38.117}$$

Correspondingly, $\boldsymbol{A}$ is now independent of the streamfunction and is given by

$$\boldsymbol{A} = -\beta\, \hat{\boldsymbol{x}} - Q^{\text{pg}}\, \hat{\boldsymbol{z}} \times \nabla h + \gamma\, \nabla \ln h \tag{38.118a}$$

$$= \hat{\boldsymbol{x}}\, [-\beta + Q^{\text{pg}}\, \partial_y h + (\gamma/h)\, \partial_x h] + \hat{\boldsymbol{y}}\, [-Q^{\text{pg}}\, \partial_x h + (\gamma/h)\, \partial_y h]. \tag{38.118b}$$

In the special case of a uniform layer thickness ($\nabla h = 0$), we find $\boldsymbol{A} = -\beta\, \hat{\boldsymbol{x}}$, so that the streamlines are advected to the west according to planetary beta. The more general advection is somewhat more complex. Even so, below we find interesting cases in which the advection remains zonal.

The advection velocity, $\boldsymbol{A}$, is purely zonal if

$$h\, Q^{\text{pg}}\, \partial_x h = \gamma\, \partial_y h \Longrightarrow f\, \partial_x h = \gamma\, \partial_y h, \tag{38.119}$$

which then leads to

$$\boldsymbol{A} = -\beta^{\text{eff}}\, \hat{\boldsymbol{x}} \quad \text{with } \beta^{\text{eff}} = \beta + \partial_y h\, (f^2 + \gamma^2)/(h\, f). \tag{38.120}$$

Stated in terms of the topographic slopes, the advective streamfunction transport is zonal if the topography satisfies

$$\nabla \ln h = \frac{(\beta^{\text{eff}} - \beta)\, (\gamma\, \hat{\boldsymbol{x}} + f\, \hat{\boldsymbol{y}})}{f^2 + \gamma^2}. \tag{38.121}$$

[13] We study the physics of advection and diffusion in Chapter 69. We here only require a few basic features of this equation.

The effective beta parameter, β^{eff}, is comprised of three contributions:

$$\beta^{\text{planetary}} = \beta \qquad = \partial_y f \tag{38.122a}$$
$$\beta^{\text{topog}} = f\,\partial_y \ln h \qquad = Q^{\text{pg}}\,\partial_y h \tag{38.122b}$$
$$\beta^{\text{Rayleigh}} = (\gamma^2/f)\,\partial_y \ln h = (\gamma^2/f^2)\,Q^{\text{pg}}\,\partial_y h. \tag{38.122c}$$

The first term, $\beta^{\text{planetary}}$, is the planetary beta that arises from meridional dependence of the planetary Coriolis parameter, $\beta = \partial_y f$. The second term, β^{topog}, arises from meridional dependence of the bottom topography in the presence of planetary rotation. The third term, β^{Rayleigh}, arises from meridional dependence of the bottom topography in the presence of Rayleigh drag and planetary rotation.

Note that β^{eff} is not sign-definite, and it passes through zero if

$$Q^{\text{pg}}\,\partial_y h^{\text{zero}} = -\frac{\beta\, f^2}{f^2+\gamma^2} < 0. \tag{38.123}$$

In this case the planetary potential vorticity has an opposite sign from the meridional topographic slope, with $Q^{\text{pg}}\,\partial_y h^{\text{zero}} = -\beta$ for case of vanishing Rayleigh drag.

38.6.4 The beta plume Green's function

(LOOK AT *Belmadani et al.* (2013) for further insights)

With a zonal advective transport, the streamfunction equation (38.115) reduces to the linear partial differential equation[14]

$$-(\beta^{\text{eff}}\,\partial_x + \gamma\,\nabla^2)\Psi = h\,\hat{\boldsymbol{z}}\cdot(\nabla\times\boldsymbol{F}). \tag{38.124}$$

It is notable that the linear differential operator on the left hand side is not self-adjoint, in a manner akin to the diffusion operator introduced in Section 6.6. We can make use of Green's function methods from Chapter 9 to write an expression for the streamfunction. Ignoring boundaries (i.e., assume an infinite β-plane) brings about the solution from Section 9.5

$$\Psi(\boldsymbol{x}) = \int h\,\hat{\boldsymbol{z}}\cdot(\nabla\times\boldsymbol{F})\,\mathcal{G}^{\ddagger}(\boldsymbol{x}|\boldsymbol{x}_0)\,\mathrm{d}\mathcal{S}_0, \tag{38.125}$$

where $\mathcal{G}^{\ddagger}(\boldsymbol{x}|\boldsymbol{x}_0)$ is the adjoint free space Green's function that satisfies

$$-(-\beta^{\text{eff}}\,\partial_x + \gamma\,\nabla^2)\mathcal{G}^{\ddagger}(\boldsymbol{x}|\boldsymbol{x}_0) = \delta(\boldsymbol{x}-\boldsymbol{x}_0), \tag{38.126}$$

where $\delta(\boldsymbol{x}-\boldsymbol{x}_0)$ is the Dirac delta with source at $\boldsymbol{x}=\boldsymbol{x}_0$ (see Chapter 7). Following the derivation of reciprocity in Section 9.5.7, we can relate the adjoint free space Green's function, $\mathcal{G}^{\ddagger}(\boldsymbol{x}|\boldsymbol{x}_0)$ to the free space Green's function, $\mathcal{G}(\boldsymbol{x}|\boldsymbol{x}_0)$, through

$$\mathcal{G}^{\ddagger}(\boldsymbol{x}|\boldsymbol{x}_0) = \mathcal{G}(\boldsymbol{x}_0|\boldsymbol{x}), \tag{38.127}$$

where $\mathcal{G}(\boldsymbol{x}|\boldsymbol{x}_0)$ satisfies

$$-(\beta^{\text{eff}}\,\partial_x + \gamma\,\nabla^2)\mathcal{G}(\boldsymbol{x}|\boldsymbol{x}_0) = \delta(\boldsymbol{x}-\boldsymbol{x}_0). \tag{38.128}$$

Since the Dirac delta is a positive point source, it provides a positive point source to for the Green's function equation (38.128). We refer to the Green's function, $\mathcal{G}(\boldsymbol{x}|\boldsymbol{x}_0)$, as the *beta plume*, with this name motivated by the sketch in Figure 38.7. That is, consider the case of $\beta^{\text{eff}} > 0$, so

[14] We encounter equation (38.124) again in Section 39.7.5 when studying the western intensification of ocean gyres. Namely, the analysis of *Stommel* (1948) leads to the Stommel equation (39.100) for the streamfunction, which is the same as the beta plume equation (38.124).

that the beta plume streamlines extend to the west of the Dirac delta source. The Rayleigh drag, $\gamma > 0$, causes the streamlines to spread both zonally and meridionally westward away from the source.

We can determine an analytical expression for the Green's function, $\mathcal{G}(\boldsymbol{x}|\boldsymbol{x}_0)$, through the substitution

$$\mathcal{G}(\boldsymbol{x}|\boldsymbol{x}_0) = \mathrm{e}^{-(x-x_0)/L_s}\, \Phi(\boldsymbol{x}|\boldsymbol{x}_0), \tag{38.129}$$

where we introduced the length scale

$$L_s \equiv 2\,\gamma/\beta^{\text{eff}}. \tag{38.130}$$

It is notable that this length scale increases when increasing the Rayleigh drag, which reflects the contribution of the Rayleigh drag to the westward spreading of the streamlines. The substitution (38.129) brings the Green's function problem (38.128) into the form

$$-(\nabla^2 - L_s^{-2})\, \Phi(\boldsymbol{x}|\boldsymbol{x}_0) = \delta(\boldsymbol{x} - \boldsymbol{x}_0)/\gamma, \tag{38.131}$$

which is the two-dimensional version of the screened Poisson equation discussed in Section 9.2.6. Note that for the right hand side we set $\delta(\boldsymbol{x} - \boldsymbol{x}_0)\, \mathrm{e}^{-(x-x_0)/L_s} = \delta(\boldsymbol{x} - \boldsymbol{x}_0)$, since the exponential factor equals unity at $x = x_0$ and so it does not alter the Dirac delta (see Section 7.8 for more details).

The solution to equation (38.131) is proportional to the Hankel function of the first kind and zeroth order, $H_0^{(1)}$, with the argument a pure imaginary number.[15] Reintroducing the exponential scaling from equation (38.129) then renders the beta plume Green's function

$$\mathcal{G}(\boldsymbol{x}|\boldsymbol{x}_0) = \frac{\mathrm{i}}{4\,\gamma}\, H_0^{(1)}(\mathrm{i}\, r/L_s)\, \mathrm{e}^{-(x-x_0)/L_s}, \tag{38.132}$$

where $\mathrm{i} = \sqrt{-1}$. We plot the magnitude of this Green's function in Figure 38.7. The exponential scaling makes the beta plume highly asymmetric, with more amplitude to the west of the Dirac source. The Dirac source in equation (38.128) provides a positive point source, so that the circulation is counter-clockwise around the source point.

38.6.5 Further study

Much from this section follows *Rhines* (1980) and *Haine and Fuller* (2016). *Welander* (1968) suggested interpreting the steady streamfunction equation (38.113) in terms of a steady advective-diffusive-source balance, and we pursue a similar interpretation for the steady shallow water planetary geostrophic flow in Section (39.7.8).

38.7 Exercises

EXERCISE 38.1: VORTICITY IDENTITY IN A TWO-DIMENSIONAL NON-DIVERGENT BAROTROPIC FLOW

Directly prove the identity (38.33) holding for the two-dimensional non-divergent barotropic flow.

EXERCISE 38.2: ALTERNATIVE FORM OF THE VORTICITY FLUX

[15] The Hankel function with an imaginary argument is sometimes referred to as *MacDonalds' function*.

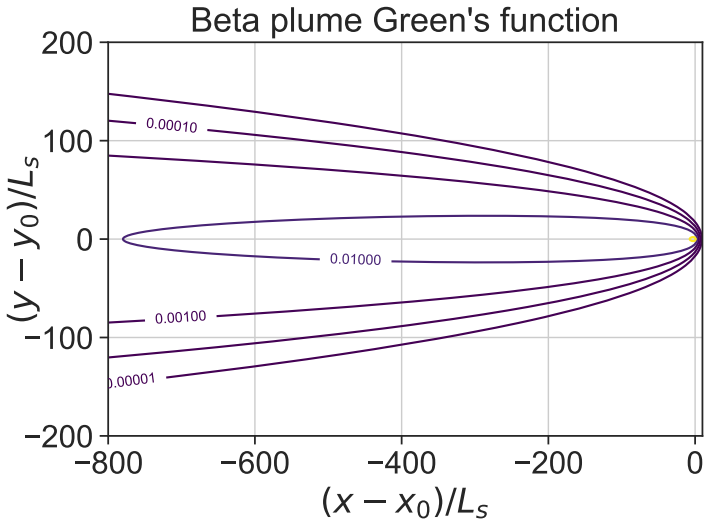

FIGURE 38.7: Sketch of the magnitude for the non-dimensional beta plume Green's function, $\gamma\, \mathcal{G}(\boldsymbol{x}|\boldsymbol{x}_0)$, given by equation (38.132) and here shown with $\beta^{\text{eff}} = 1.62 \times 10^{-11}$ m^{-1} s^{-1}, which is equal to the planetary β at latitude $\pi/4$. We furthermore choose the Rayleigh drag of $\gamma = (2\,\text{year})^{-1}$, and scale the coordinate axes by the length, $L_s = 2\,\gamma/\beta^{\text{eff}} \approx 2$ km, from equation (38.130).

Show that the vorticity flux can be written

$$\boldsymbol{u}\,\zeta = u\,\nabla v - v\,\nabla u + \hat{\boldsymbol{z}} \times \nabla \mathcal{K}, \tag{38.133}$$

so that the vorticity equation (38.39) can be written in the alternative form

$$\frac{\partial \zeta}{\partial t} + \nabla \cdot (u\,\nabla v - v\,\nabla u) = -\beta\, v. \tag{38.134}$$

As a corollary, we see that steady f-plane flow satisfies the constraint

$$\nabla \cdot (u\,\nabla v - v\,\nabla u) = u\,\nabla^2 v - v\,\nabla^2 u = 0. \tag{38.135}$$

EXERCISE 38.3: EXAMPLE TWO-DIMENSIONAL NON-DIVERGENT FLOW
Consider a perfect two-dimensional non-divergent flow in a non-rotating reference frame

$$\frac{\mathrm{D}\boldsymbol{u}}{\mathrm{D}t} = -\nabla\varphi \quad \text{and} \quad \nabla \cdot \boldsymbol{u} = 0. \tag{38.136}$$

Let the velocity be given by the steady flow

$$\boldsymbol{u} = U\,[\hat{\boldsymbol{x}}\sin(k\,y) + \hat{\boldsymbol{y}}\sin(k\,x)], \tag{38.137}$$

where U is a constant with dimensions L T^{-1} and k is a wavenumber with dimensions L^{-1}. We provide a sketch of this flow in Figure 38.8.

(a) Compute the streamfunction, ψ, so that $\boldsymbol{u} = \hat{\boldsymbol{z}} \times \nabla\psi$.

(b) Compute the self-advection, $(\boldsymbol{u} \cdot \nabla)\,\boldsymbol{u}$ and show that $\nabla \times [(\boldsymbol{u} \cdot \nabla)\,\boldsymbol{u}] = \boldsymbol{0}$.

(c) Compute the vorticity, $\zeta = \hat{\boldsymbol{z}} \cdot (\nabla \times \boldsymbol{u})$.

(d) Compute the pressure, to within an arbitrary constant.

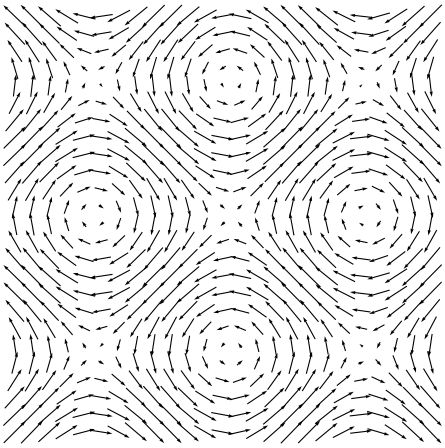

FIGURE 38.8: A sketch of the steady two-dimensional non-divergent sinusoidal flow (38.137), as given by $\boldsymbol{u} = U\,[\hat{\boldsymbol{x}}\sin(k\,y) + \hat{\boldsymbol{y}}\sin(k\,x)]$. The units are arbitrary. This flow is considered in Exercise 38.3.

EXERCISE 38.4: VELOCITY ARISING FROM A GIVEN VORTICITY
Following the discusson in Section 38.2.8, consider an axially symmetric two-dimensional non-divergent flow with a single vortex of the form

$$\zeta(r) = \begin{bmatrix} \zeta_0 & \text{for } r < r_0 \\ 0 & \text{for } r > r_0. \end{bmatrix} \tag{38.138}$$

(a) What is the velocity field corresponding to this vorticity?

(b) What is the circulation around a circular circuit with radius $r < r_0$? Assume the velocity is non-singular at the origin.

(c) What is the circulation around a circular circuit with radius $r > r_0$?

(d) For both the circular circuits with $r < r_0$ and $r > r_0$, write the circulation in terms of the velocity.

EXERCISE 38.5: INTEGRAL PROPERTIES OF THE INVISCID 2D NON-DIVERGENT FLOW
In this exercise, we establish some domain integrated conservation properties for inviscid two-dimensional non-divergent flow on a β-plane. Assume the geometry is a flat plane defined over a finite region, $\mathcal{S}$, with static material boundary, $\partial\mathcal{S}$. Many of the properties derived here are discussed in Section 3.1 of *McWilliams* (2006).

(a) Show that the domain integrated kinetic energy per mass remains constant in time

$$\frac{\mathrm{d}}{\mathrm{d}t}\int_{\mathcal{S}} \mathcal{K}\,\mathrm{d}\mathcal{S} = \frac{1}{2}\frac{\mathrm{d}}{\mathrm{d}t}\int_{\mathcal{S}} \boldsymbol{u}\cdot\boldsymbol{u}\,\mathrm{d}\mathcal{S} = 0, \tag{38.139}$$

where the horizontal integral extends over the full fluid domain $\mathcal{S}$.

(b) Why is the mechanical energy budget only associated with kinetic energy? What about the gravitational potential energy?

(c) Show that the domain integrated relative vorticity (equal also to the relative circulation) is constant in time

$$\frac{\mathrm{d}\mathcal{C}}{\mathrm{d}t} = \frac{\mathrm{d}}{\mathrm{d}t}\int_{\mathcal{S}} \zeta\,\mathrm{d}\mathcal{S} = 0. \tag{38.140}$$

(d) Show that the domain integrated enstrophy is constant in time for f-plane motion ($\beta = 0$)

$$\frac{\mathrm{dZ}^{(\zeta)}}{\mathrm{d}t} = \frac{\mathrm{d}}{\mathrm{d}t}\int_{\mathcal{S}} \zeta^2 \,\mathrm{d}\mathcal{S} = 0. \tag{38.141}$$

(e) Show that the domain integrated potential enstrophy is constant in time even with $\beta \neq 0$

$$\frac{\mathrm{dZ}^{(q)}}{\mathrm{d}t} = \frac{\mathrm{d}}{\mathrm{d}t}\int_{\mathcal{S}} q^2 \,\mathrm{d}\mathcal{S} = 0. \tag{38.142}$$

EXERCISE 38.6: ALTERNATIVE EXPRESSION FOR THE DOMAIN INTEGRATED KINETIC ENERGY
For a simply connected region, $\mathcal{S}$, with static material boundary, $\partial\mathcal{S}$, show that the globally integrated kinetic energy per mass can be written

$$\int_{\mathcal{S}} \mathcal{K} \,\mathrm{d}\mathcal{S} = \frac{1}{2}\int_{\mathcal{S}} \boldsymbol{u}\cdot\boldsymbol{u}\,\mathrm{d}\mathcal{S} = \frac{1}{2}\int_{\mathcal{S}} \zeta\,(\psi_{\mathfrak{b}} - \psi)\,\mathrm{d}\mathcal{S} = \frac{1}{2}\big[\psi_{\mathfrak{b}}\,\mathcal{C} - \int_{\mathcal{S}} \psi\,\zeta\,\mathrm{d}\mathcal{S}\big], \tag{38.143}$$

where $\boldsymbol{u} = \hat{\boldsymbol{z}}\times\nabla\psi$ is the horizontally non-divergent velocity, ψ is the streamfunction, $\psi_{\mathfrak{b}}$ is the streamfunction on the boundary, and $\zeta = \nabla^2\psi$ is the vorticity. Hint: recall from Section 21.4.2 that the streamfunction for two-dimensional non-divergent flow is a constant on material boundaries.

EXERCISE 38.7: CIRCULATION IN A 2D BAROTROPIC FLOW
Consider a non-divergent barotropic flow on a β-plane in the presence of a biharmonic friction operator, where the governing vorticity equation is

$$\frac{\partial\zeta}{\partial t} + J(\psi, \zeta + \beta y) = -\nu\nabla^4\zeta, \tag{38.144}$$

with $\nu > 0$ a constant biharmonic viscosity with dimensions of $\mathrm{L}^4\ \mathrm{T}^{-1}$. Show that the circulation around a fixed material area, $\mathcal{S}$, in the fluid evolves according to

$$\frac{\mathrm{d}\mathcal{C}}{\mathrm{d}t} = -\oint_{\partial\mathcal{S}} \left[\psi\frac{\partial q}{\partial s} + \nu\frac{\partial(\nabla^2\zeta)}{\partial n}\right]\mathrm{d}s, \tag{38.145}$$

where s is the arc-length along the boundary of the region and n is a coordinate normal to the boundary.

EXERCISE 38.8: KINEMATICS OF VORTICITY GRADIENTS
For many purposes it is of interest to develop equations describing the evolution of scalar gradients. We developed a general expression in Exercise 17.4. Here, we derive a similar equation for the gradient of relative vorticity in a non-divergent barotropic flow. For this purpose, consider the inviscid barotropic vorticity equation on an f-plane

$$\frac{\partial\zeta}{\partial t} + J(\psi, \zeta) = 0. \tag{38.146}$$

(a) Show that the material evolution of the vorticity gradient is given by

$$\frac{\mathrm{D}(\nabla\zeta)}{\mathrm{D}t} = -J(\nabla\psi, \zeta). \tag{38.147}$$

(b) Show that the material evolution of the squared vorticity gradient is given by

$$\frac{\mathrm{D}|\nabla\zeta|^2}{\mathrm{D}t} = 2\,J(\zeta, \nabla\psi)\cdot\nabla\zeta. \tag{38.148}$$

EXERCISE 38.9: ANGULAR MOMENTUM FOR BAROTROPIC FLOW IN A BASIN

The exercise derives some equations presented in *Holloway and Rhines* (1991), who offer a specialized example of the shallow water angular momentum discussed in Section 36.8.

As in Section 36.8.1, the relative angular momentum for a region of fluid is given by

$$\boldsymbol{L} = \int \mathrm{d}\mathcal{S} \int (\boldsymbol{x} \times \boldsymbol{v})\, \rho\, \mathrm{d}z, \tag{38.149}$$

where $\boldsymbol{x}$ is the position vector and the relative angular momentum is that due to the motion of the fluid with respect to the rigid-body. For a barotropic fluid of constant density and constant thickness, and correspondingly a zero vertical velocity, the relative angular momentum reduces to

$$\boldsymbol{L} = \rho\, H \int_{\mathcal{S}} (\boldsymbol{x} \times \boldsymbol{u})\, \mathrm{d}\mathcal{S}, \tag{38.150}$$

with $\boldsymbol{u}$ the horizontal velocity and $\mathcal{S}$ the horizontal region. For barotropic motion on a tangent plane we are interested in the vertical component of the relative angular momentum

$$L^z = \rho\, H \int_{\mathcal{S}} \hat{\boldsymbol{z}} \cdot (\boldsymbol{x} \times \boldsymbol{u})\, \mathrm{d}\mathcal{S}. \tag{38.151}$$

Show for a simply connected and bounded region, L^z can be written

$$L^z = 2\, \rho\, H \int_{\mathcal{S}} (\psi_b - \psi)\, \mathrm{d}\mathcal{S} \tag{38.152}$$

where ψ is the streamfunction satisfying $\boldsymbol{u} = \hat{\boldsymbol{z}} \times \nabla\psi$, and ψ_b is the value of the streamfunction evaluated on the region boundary. Hint: note that $\nabla \cdot \boldsymbol{x} = 2$ for a horizontal position vector. Also recall from Section 21.4.2 that the streamfunction equals to a spatial constant when evaluated along the domain boundary.

EXERCISE 38.10: STEADY AXIALLY SYMMETRIC FLOW

Consider a two-dimensional non-divergent velocity

$$\boldsymbol{v} = \hat{\boldsymbol{z}} \times \nabla\psi. \tag{38.153}$$

Assume the streamfunction is static and depends only on the radial distance from an arbitrary origin,

$$\psi = \psi(r), \tag{38.154}$$

where $r = \sqrt{x^2 + y^2}$, and assume the velocity is a solution to the steady inviscid non-divergent barotropic dynamics on an f-plane.

(a) Show that the velocity only has an angular component

$$\boldsymbol{v} = v^{\varphi}\, \hat{\boldsymbol{\varphi}}, \tag{38.155}$$

where $\hat{\boldsymbol{\varphi}}$ is the angular unit vector oriented counter-clockwise from the $\hat{\boldsymbol{x}}$ axis.[16] Express v^{φ} in terms of the streamfunction ψ. Hint: see Figure 4.2 and Section 4.22 for a reminder of polar coordinates.

(b) Write the relative vorticity in terms of the streamfunction using polar coordinates.

[16] The azimuthal angular coordinate, φ, that appears in $\boldsymbol{v} = v^{\varphi}\, \hat{\boldsymbol{\varphi}}$, is not the same as the density normalized pressure, $\varphi = p/\rho$, defined by equation (38.2) and used throughout this chapter.

(c) Consider the circulation

$$\mathcal{C} = \oint_{\partial\mathcal{S}} \boldsymbol{v} \cdot \mathrm{d}\boldsymbol{r}, \tag{38.156}$$

where $\mathcal{S}$ is a circular region in the x-y plane centered at $r = 0$. Express the circulation in terms of v^φ and the radius of the circle.

(d) Write the pressure gradient acceleration in terms of v^φ, f, and r. Hint: remember that $\hat{\boldsymbol{\varphi}}$ is a function of the polar angle φ.

(e) Interpret the steady balance of accelerations in terms of the balanced dynamics in Chapter 32.

(f) Why is this axial symmetric solution only valid for an f-plane? Hint: show that if $\beta \neq 0$ that there is an inconsistency in the velocity equation.

EXERCISE 38.11: GALILEAN TRANSFORMATION OF PV ADVECTION AND THE APV METHOD
In Section 17.5 we established the invariance of the material time derivative operator under a Galilean transformation

$$\overline{\boldsymbol{x}} = \boldsymbol{x} + \boldsymbol{U}\, t \quad \text{and} \quad \overline{\boldsymbol{u}} = \boldsymbol{u} + \boldsymbol{U}, \tag{38.157}$$

where $\boldsymbol{U}$ is a constant. Here we study the Galilean transformation properties of the non-divergent barotropic model on a β-plane.

(a) Determine the Galilean transformation properties of the potential vorticity equation

$$\frac{\partial q}{\partial t} + \boldsymbol{u} \cdot \nabla q = \frac{\partial q}{\partial t} + J(\psi, q) = 0, \tag{38.158}$$

where $q = \zeta + f$, $\hat{\boldsymbol{z}} \times \psi = \boldsymbol{u}$, and J is the Jacobian operator.

(b) Determine the Galilean transformation properties of the relative vorticity equation (38.39)

$$\frac{\partial \zeta}{\partial t} + \boldsymbol{u} \cdot \nabla \cdot \zeta = -\beta\, v. \tag{38.159}$$

Discuss why there is Galilean invariance *only* for zonal Galilean boosts, $\boldsymbol{U} = \hat{\boldsymbol{x}}\, U$.

(c) An Euler forward time stepping scheme for the PV equation leads to

$$q^{n+1} = q^n - \Delta t\, \boldsymbol{u}^n \cdot \nabla q^n, \tag{38.160}$$

where Δt is the discrete time step and the integer n represents the discrete time label. Inspired by this time discrete expression, *Sadourny and Basdevant* (1985) proposed the *anticipated potential vorticity* (APV) method for parameterizing subgrid scale processes. The simplest form of APV is given by

$$\frac{\partial q}{\partial t} = -\boldsymbol{u} \cdot \nabla[q - \tau\, \boldsymbol{u} \cdot \nabla q] = -J[\psi, q - \tau\, J(\psi, q)], \tag{38.161}$$

with τ a constant time scale. From the time discrete expression (38.160), we see that the APV method makes use of an estimate for the future value of PV in computing the advection operator, thus motivating the term "anticipated" in the method's name.

Show that $\tau \neq 0$ breaks Galilean invariance for the equation (38.161). Provide a discussion of why invariance is broken. Hint: *Vallis and Hua* (1988) offer a technical reason for why Galilean invariance is broken, making use of the streamfunction and Jacobian form. You do not necessarily need to follow their approach. Rather, it is sufficient to merely note how velocity appears in the APV operator.

EXERCISE 38.12: ELEMENTS OF THE FOFONOFF GYRE

A Fofonoff gyre is an unforced inviscid solution in a flat bottom bounded domain with a rigid lid. For a single layer of homogeneous fluid with constant thickness, the absolute vorticity is materially invariant, $\mathrm{D}(\zeta + f)/\mathrm{D}t = 0$. An explicit solution is derived in Section 19.5.3 of *Vallis* (2017) for quasi-geostrophic flow using the method of matched asymptotics. We depict elements of a double Fofonoff gyre in Figure 38.9. Provide a narrative for this flow based on material conservation of absolute vorticity. In particular, discuss how the flow enters and leaves the side boundaries and conversely how it leaves and enters the interior region. We are not concerned with how this flow is established. Instead, assume the flow exists and discuss how its existence is consistent with $\mathrm{D}(\zeta + f)/\mathrm{D}t = 0$. Hint: recall our discussion of Figure 38.3.

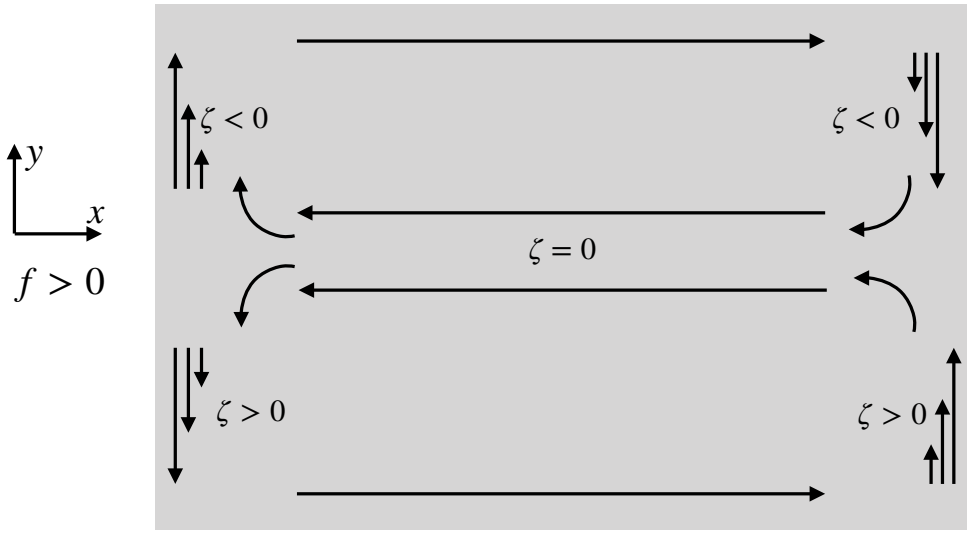

FIGURE 38.9: A Fofonoff gyre is an unforced inviscid flow in a bounded domain where $\mathrm{D}(\zeta + f)/\mathrm{D}t = 0$. We here depict elements of this double-gyre flow in the northern hemisphere as part of Exercise 38.12.

EXERCISE 38.13: PRESSURE EQUATION WITH $w \neq 0$

Equation (38.73) or equation (38.76) provide equivalent expressons for the pressure Poisson equation with $\nabla\eta = 0$ and, correspondingly, with $w = 0$. However, in Section 38.1.4 we considered the possibility of $\nabla\eta = \nabla\eta_b$, thus providing a solution with $w \neq 0$. In this case, derive the Poisson equation for pressure as decomposed according to $\varphi = g\,\eta + \varphi'$.

Chapter 39

SHALLOW WATER VORTICITY AND POTENTIAL VORTICITY

In this chapter we study vorticity and potential vorticity within the shallow water system. We start by deriving the evolution equation for vorticity by taking the curl of the velocity equation. Combining vorticity evolution with mass continuity then renders the evolution equation for potential vorticity. Potential vorticity is a material invariant for inviscid shallow water motion, thus providing a mechanical constraint on the fluid flow. After developing the basic concepts and equations, we consider a variety of flow regimes and case studies, mostly with an ocean focus. These case studies illustrate where the study of vorticity, potential vorticity, and circulation enhances our understanding of geophysical fluid mechanics.

CHAPTER GUIDE

The shallow water fluid offers a fruitful conceptual model to introduce the dynamics of vorticity and potential vorticity while requiring a relatively modest level of mathematical sophistication. Even so, we require vector calculus identities for Cartesian coordinates as detailed in Chapter 2. We also require an understanding of shallow water mechanics from Chapters 35 and 36, as well as the vorticity kinematics introduced in Chapter 37. The concepts and methods developed in this chapter are fundamental to the remaining chapters in this part of the book.

As anticipated in Section 38.2.3, the form of potential vorticity encountered here is sometimes referred to as *Rossby potential vorticity* or *shallow water potential vorticity*. Its connection to the more general *Ertel potential vorticity* (Chapter 41) is postponed until Chapter 66, where we study the Boussinesq ocean equations using isopycnal coordinates. As we see there, the shallow water equations provide a discrete representation of the isopycnal equations. Correspondingly, the Ertel potential vorticity expressed using isopycnal coordinates has its discrete form given by shallow water potential vorticity.

39.1 Shallow water vorticity equation

In this section we formulate the vorticity equation for the shallow water fluid, starting with a single layer and then extending to multiple layers. We sometimes make use of the vertical component to the absolute vorticity from equation (35.108)

$$\boldsymbol{\omega}_{\mathrm{a}}^{*} = (\zeta + f)\,\hat{\boldsymbol{z}} = \zeta_{\mathrm{a}}\,\hat{\boldsymbol{z}}, \tag{39.1}$$

which is the sum of the relative vorticity of the horizontal flow, $\boldsymbol{\omega}^{*} = \zeta\,\hat{\boldsymbol{z}}$, plus the rigid-body vorticity, $f\,\hat{\boldsymbol{z}}$, due to motion of the rotating reference frame (recall Section 37.6.1). The absolute vorticity appears in the vector-invariant velocity equation (35.113), which is valid for each of the layers in a shallow water fluid

$$\partial_t \boldsymbol{u} + \boldsymbol{\omega}_{\mathrm{a}}^{*} \times \boldsymbol{u} = -\nabla(p/\rho_{\mathrm{ref}} + \boldsymbol{u}\cdot\boldsymbol{u}/2). \tag{39.2}$$

This equation forms the starting point for deriving the shallow water vorticity equation.

39.1.1 Vorticity equation for a single layer

We make use of the vector identity from Section 2.3.4 to express the curl of the Magnus acceleration plus Coriolis acceleration in the form

$$\nabla \times (\boldsymbol{\omega}_{\mathrm{a}}^* \times \boldsymbol{u}) = \boldsymbol{\omega}_{\mathrm{a}}^* (\nabla \cdot \boldsymbol{u}) + (\boldsymbol{u} \cdot \nabla) \boldsymbol{\omega}_{\mathrm{a}}^* - \boldsymbol{u} (\nabla \cdot \boldsymbol{\omega}_{\mathrm{a}}^*) - (\boldsymbol{\omega}_{\mathrm{a}}^* \cdot \nabla) \boldsymbol{u} \tag{39.3a}$$

$$= \boldsymbol{\omega}_{\mathrm{a}}^* (\nabla \cdot \boldsymbol{u}) + (\boldsymbol{u} \cdot \nabla) \boldsymbol{\omega}_{\mathrm{a}}^*, \tag{39.3b}$$

so that

$$\hat{\boldsymbol{z}} \cdot [\nabla \times (\boldsymbol{\omega}_{\mathrm{a}}^* \times \boldsymbol{u})] = \nabla \cdot (\boldsymbol{u}\, \zeta_{\mathsf{a}}) \tag{39.4}$$

Equation (39.3b) required setting

$$\nabla \cdot \boldsymbol{\omega}_{\mathrm{a}}^* = \nabla \cdot \boldsymbol{\omega}^* + \nabla \cdot (f\, \hat{\boldsymbol{z}}) = 0, \tag{39.5}$$

which follows since this expression involves the divergence of a curl (first right hand side term) and since f has no z dependence. We furthermore set

$$(\boldsymbol{\omega}_{\mathrm{a}}^* \cdot \nabla) \boldsymbol{u} = \zeta_{\mathsf{a}}\, \partial_z \boldsymbol{u} = 0, \tag{39.6}$$

which follows since the horizontal velocity in a shallow water fluid is depth independent within a layer (see Section 35.2).

Applying the curl operator, $\hat{\boldsymbol{z}} \cdot (\nabla\times)$, onto the vector-invariant velocity equation (39.2) annihilates the gradient of pressure and kinetic energy, with the identity (39.4) leading to the flux-form evolution equation for absolute vorticity

$$\partial_t \zeta_{\mathsf{a}} + \nabla \cdot (\boldsymbol{u}\, \zeta_{\mathsf{a}}) = 0. \tag{39.7}$$

This equation says that the vertical component to the absolute vorticity, ζ_{a}, at a point in the inviscid shallow water fluid changes according to the horizontal convergence of vorticity advected to that point

$$\partial_t \zeta_{\mathsf{a}} = -\nabla \cdot (\boldsymbol{u}\, \zeta_{\mathsf{a}}). \tag{39.8}$$

We can write the vorticity equation (39.7) in the material form

$$\frac{\mathrm{D}\zeta_{\mathsf{a}}}{\mathrm{D}t} = -\zeta_{\mathsf{a}}\, \nabla \cdot \boldsymbol{u}, \tag{39.9}$$

where the material time derivative for the shallow water fluid includes advection just by the horizontal flow

$$\frac{\mathrm{D}}{\mathrm{D}t} = \frac{\partial}{\partial t} + \boldsymbol{u} \cdot \nabla = \frac{\partial}{\partial t} + u\, \partial_x + v\, \partial_y. \tag{39.10}$$

The material evolution equation (39.9) means that the absolute vorticity of a shallow water fluid column, moving with the horizontal flow, changes according to the horizontal convergence of the fluid flow as multiplied by the absolute vorticity. For comparison, recall the horizontally non-divergent barotropic fluid has $\nabla \cdot \boldsymbol{u} = 0$, so that the absolute vorticity in that flow is materially invariant (see equation (38.40)). In contrast, the shallow water fluid supports horizontal flow convergence, and with the flow convergence providing a source to the vorticity.

39.1.2 Vorticity equation for N-layers

The previous results for a single layer are readily extended to N-layers, simply because the velocity for layer-k evolves according to equation (39.2), now with a subscript k to denote the layer

$$\partial_t \boldsymbol{u}_{\mathsf{k}} + (f + \zeta_{\mathsf{k}})\, \hat{\boldsymbol{z}} \times \boldsymbol{u}_{\mathsf{k}} = -\nabla(p_{\mathsf{k}}/\rho_{\mathsf{ref}} + \boldsymbol{u}_{\mathsf{k}} \cdot \boldsymbol{u}_{\mathsf{k}}/2), \tag{39.11}$$

where $\zeta_k = \hat{\boldsymbol{z}} \cdot (\nabla \times \boldsymbol{u}_k)$ is the vertical component to the layer-k relative vorticity. Taking the curl and making use of the mathematical identities used for single layer in Section 39.1.1 renders the vorticity equation for layer-k

$$\partial_t \zeta_{ak} + \nabla \cdot (\boldsymbol{u}_k \, \zeta_{ak}) = 0 \iff \frac{\mathrm{D}_k \zeta_{ak}}{\mathrm{D}t} = -\zeta_{ak} \, \nabla \cdot \boldsymbol{u}_k \tag{39.12}$$

where

$$\zeta_{ak} = f + \zeta_k \tag{39.13}$$

is the vertical component to the absolute vorticity of layer-k. Hence, the vorticity equation for an arbitrary layer in a stacked shallow water model is the same as that for a single shallow water layer.

39.1.3 Vorticity flux divergence and curl of nonlinear advection

We revisit the manipulations from Section 39.1.1 to explicitly identify a connection between the nonlinear terms in the vorticity equation. Start by writing the velocity equation in the advective form and the vector invariant form

$$\partial_t \boldsymbol{u} + (\boldsymbol{u} \cdot \nabla) \, \boldsymbol{u} + f \hat{\boldsymbol{z}} \times \boldsymbol{u} = -g \, \nabla \eta \tag{39.14a}$$

$$\partial_t \boldsymbol{u} + (f + \zeta) \, \hat{\boldsymbol{z}} \times \boldsymbol{u} = -\nabla \left(g \, \eta + \boldsymbol{u} \cdot \boldsymbol{u} / 2 \right). \tag{39.14b}$$

Taking their curl yields two expressions of the vorticity equation

$$\partial_t \boldsymbol{\omega}^* + \nabla \times [(\boldsymbol{u} \cdot \nabla) \, \boldsymbol{u}] + \nabla \times [f \hat{\boldsymbol{z}} \times \boldsymbol{u}] = 0 \tag{39.15a}$$

$$\frac{\partial \boldsymbol{\omega}^*}{\partial t} + \nabla \times [(f + \zeta) \, \hat{\boldsymbol{z}} \times \boldsymbol{u}] = 0, \tag{39.15b}$$

whose equality leads to

$$\nabla \times [(\boldsymbol{u} \cdot \nabla) \, \boldsymbol{u} - \zeta \, \hat{\boldsymbol{z}} \times \boldsymbol{u}] = 0. \tag{39.16}$$

Making use of the identity

$$\hat{\boldsymbol{z}} \cdot [\nabla \times (\zeta \, \hat{\boldsymbol{z}} \times \boldsymbol{u})] = \nabla \cdot (\boldsymbol{u} \, \zeta) \tag{39.17}$$

renders the relation

$$\hat{\boldsymbol{z}} \cdot \nabla \times [(\boldsymbol{u} \cdot \nabla) \, \boldsymbol{u}] = \nabla \cdot (\boldsymbol{u} \, \zeta). \tag{39.18}$$

We thus see that the divergence of the advective vorticity flux (right hand side) equals to the curl of the nonlinear advection (left hand side). This identity holds for each layer in an N-layer shallow water model.

39.2 Potential vorticity for a rotating cylinder

To introduce the concept of shallow water potential vorticity, consider a fluid cylinder of constant mass M, constant density ρ, variable radius R, and variable height h, and assume the cylinder rotates about its central axis. Furthermore, assume the fluid particles within the cylinder rotate as a rigid-body, meaning there are no strains in the fluid, and yet allow the cylinder radius and height to change. This analysis offers a useful (albeit incomplete) conceptual picture for a coherently rotating column of a shallow water layer, in which time derivatives in the following are interpreted as material derivatives.

39.2.1 Mass conservation

With a constant density, mass conservation for the material cylinder means that its volume is fixed. Hence, mass conservation constrains the relative changes to the radius and height of the cylinder. Namely, a materially constant cylinder mass

$$M = \pi R^2 h \rho \tag{39.19}$$

implies

$$\frac{2}{R}\frac{\mathrm{D}R}{\mathrm{D}t} = -\frac{1}{h}\frac{\mathrm{D}h}{\mathrm{D}t}. \tag{39.20}$$

That is, mass conservation means that the relative height decreases as twice the relative radius increases. So if the cylinder is squashed (h decreases) then it thickens (R increases). Conversely, the cylinder thins (R decreases) as it extends (h increases).

39.2.2 Angular momentum conservation

A second constraint arises from angular momentum conservation. Choose the center of mass coordinate axes through the center of the cylinder, with the z-axis along the central line of the cylinder and with $z = 0$ at the cylinder mid-point. The angular rotation vector is thus given by

$$\boldsymbol{\Omega} = \Omega \hat{\boldsymbol{z}}. \tag{39.21}$$

With this axis orientation, rotation occurs about the center of mass so that the angular momentum of the center of mass vanishes. The moment of inertia tensor for a cylinder with this axis orientation is given by[1]

$$I_{mn} = \delta_{mn}\frac{MR^2}{2}. \tag{39.22}$$

The moment of inertia is a measure of the rotational inertia of a moving continuous body. For the cylinder it is directly related to the cylinder mass (assumed fixed here) and the radius (which can change). Notably, the moment of inertia about the central vertical axis is not a function of the cylinder height. The reason is that the moment measures the inertia relative to the rotational axis, which is here along the central vertical axis. The angular momentum for the cylinder is thus given by

$$\boldsymbol{L} = \frac{MR^2}{2}\Omega \hat{\boldsymbol{z}}. \tag{39.23}$$

The familiar *ice skater* example occurs when the cylinder radius changes and thus changes the moment of inertia (e.g., the ice skater's arms are brought in toward the central axis of the body or out away from the body). Maintaining constant angular momentum and constant mass means that the angular velocity, Ω, increases in magnitude (rotates faster) when the cylinder radius decreases, and vice versa. Explicitly for the cylinder we have $\mathrm{d}\boldsymbol{L}/\mathrm{d}t = 0$ and $\mathrm{d}M/\mathrm{d}t = 0$ thus rendering

$$\frac{2}{R}\frac{\mathrm{D}R}{\mathrm{D}t} = -\frac{1}{\Omega}\frac{\mathrm{D}\Omega}{\mathrm{D}t}. \tag{39.24}$$

We see that reducing the moment of inertia for a constant mass body by bringing its mass distribution towards the central axis (converging mass) leads, through angular momentum conservation, to an increase in rotation speed. The opposite occurs when mass diverges from a region, thus reducing the rotation speed.

Although the angular momentum constraint means that the spin rate changes when changing the moment of inertia, it does not impose a preferred direction. For example, no matter what

[1] See *Marion and Thornton* (1988) or other classical mechanics texts for a discussion of the moment of inertia for a variety of bodies.

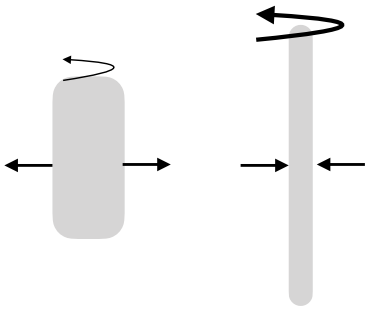

FIGURE 39.1: Illustrating the conservation of angular momentum for a spinning constant mass cylinder of shallow water fluid rotating around its central axis. Fluid particles within the cylinder are assumed to rotate as a rigid-body, meaning there are no strains in the fluid, and yet the cylinder radius and height are allowed to change. The moment of inertia (relative to the central axis) for the left cylinder is larger since more of its mass is distributed away from the central axis than in the right configuration. If the initial spin for the left cylinder is counterclockwise, then the two configurations have identical angular momentum if the right cylinder spins more rapidly than the left, since the moment of inertia for the right cylinder is smaller. This example exemplifies the familiar ice skater experience, whereby the skater's spin rate increases when bringing arms (mass) inward towards the central axis of the body (depicted by the inward arrows on the right panel), whereas the skater's rotation slows when extending arms outward (depicted by the outward arrows on the left panel).

direction a skater is rotating, decreasing the moment of inertia increases the spin rate in that particular direction. Yet when placing the spinning column on a rotating planet, the planetary rotation breaks the symmetry and thus prescribes the direction for the spin changes. The reason is that planetary rotation contributes to the spin of the column, even if the column has no spin relative to the rotating planetary reference frame. We encounter this additional part of the story in Section 39.3.

39.2.3 Material invariance of potential vorticity

Combining angular momentum conservation (39.24) with mass conservation (39.20) leads to the material conservation law

$$\frac{\mathrm{D}(\Omega/h)}{\mathrm{D}t} = 0. \tag{39.25}$$

Equation (39.25) means that the potential vorticity is constant for a material fluid column, with potential vorticity for the cylinder given by

$$Q \equiv \Omega/h. \tag{39.26}$$

For example, if the column thickens then the rotational velocity increases in order to maintain $Q = \Omega/h$ constant. Equivalently, if the column cross-sectional area decreases, the column thickness increases according to volume conservation, which in turn results in an increase in the spin according to angular momentum conservation.

39.2.4 Connecting angular momentum and vorticity

When allowing the shallow water fluid to exhibit motion that is more general than a rigid-body cylinder rotation (i.e., when allowing for strains in the fluid), then the angular rotation rate appearing in the potential vorticity (39.26) is generalized to the absolute vorticity, and we consider this generalization in Section 39.3. Furthermore, as shown in Section 37.6, the vorticity equals to twice the rotation rate, $2\,\boldsymbol{\Omega}$. Hence, the numerator for the potential vorticity of the rigid-body rotating cylinder equals to one-half the vorticity.

39.2.5 Comments and further study

The discussion in this section is motivated by Section 2.4 of *Salmon* (1998). The rotating cylinder succintly identifies the two mechanical properties contributing to the potential vorticity conservation law (39.25): a kinematic property (mass conservation) and a dynamic property (angular momentum conservation). For the rotating cylinder, the implications of potential vorticity conservation are well gleaned from the separate mass and angular momentum conservation principles. Hence, potential vorticity conservation lends little novel insight for the cylinder. However, the material invariance of potential vorticity is of fundamental use for studies of rotating and stratified fluids where the flow generally has strains that make vorticity distinct from angular momentum (Section 37.9).

Another important element missing from this discussion is the *beta effect*, which accounts for the changes in planetary vorticity when moving on a rotating spherical planet. We encounter this effect in the following sections.

39.3 Shallow water (Rossby) potential vorticity

We now consider the potential vorticity for a single layer of shallow water fluid. The form of the shallow water potential vorticity is sometimes referred to as the *Rossby potential vorticity*. The derivation here makes use of fluid mechanical equations rather than those from rigid-body mechanics, thus allowing for the added feature of strains in the fluid that distinguish vorticity from angular momentum. We present two derivations: one based on manipulations of the mass and momentum equations, and one based on the small aspect ratio limit of Kelvin's circulation theorem, with Kelvin's theorem more thoroughly studied in Chapter 40.

Figure 39.2 summarizes key elements leading to potential vorticity conservation for a shallow water fluid layer. Namely, as shown in this section, shallow water potential vorticity conservation arises from combining the kinematic constraint of mass conservation (material invariance of $h\,A$) with either the vorticity equation or Kelvin's circulation theorem for a small aspect ratio fluid.

In the absence of non-conservative processes, we show that shallow water potential vorticity for a material column of fluid remains constant. We often refer to this conservation property as *material invariance*, since the property remains invariant (constant) when following material fluid columns. This terminology was introduced in Section 17.4.5.

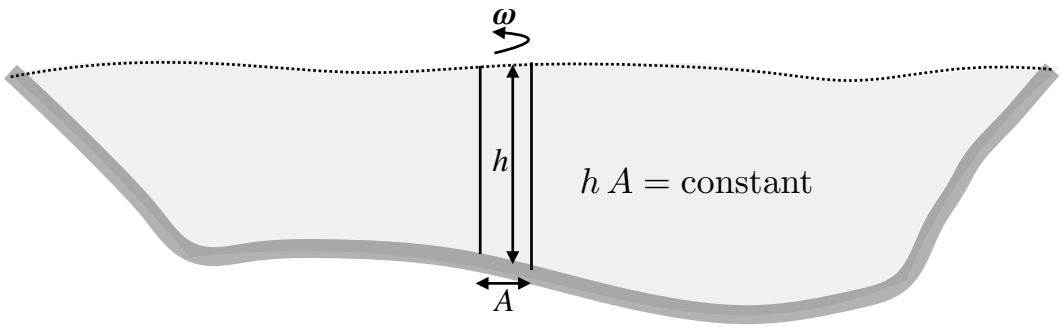

FIGURE 39.2: Illustrating the material invariance of potential vorticity for a layer of shallow water fluid column. Material invariance results from merging mass conservation (material invariance of the column volume, $h\,A$), to either the vorticity equation or Kelvin's circulation theorem for a small aspect ratio fluid (material invariance of $\zeta\,A$).

39.3.1 Mass conservation plus the vorticity equation

To derive the potential vorticity equation, we here make use of the vorticity equation (39.9) and combine it with mass conservation.

Shallow water vorticity and vortex stretching

Mass conservation in the form of the material thickness equation (35.20) leads to the following expression for the divergence of the horizontal velocity

$$\nabla \cdot \boldsymbol{u} = -\frac{1}{h}\frac{\mathrm{D}h}{\mathrm{D}t}. \tag{39.27}$$

Making use of this result in the vorticity equation (39.9) allows us to eliminate the horizontal convergence

$$\frac{\mathrm{D}\zeta_a}{\mathrm{D}t} = -\zeta_a \nabla \cdot \boldsymbol{u} = \frac{\zeta_a}{h}\frac{\mathrm{D}h}{\mathrm{D}t}. \tag{39.28}$$

This equation says that material changes in shallow water absolute vorticity arise only from material changes in the layer thickness; i.e., absolute vorticity increases in magnitude if the column stretches and decreases if the column compresses. We refer to this process as *vortex stretching*.

We see in Section 40.5.3 that vorticity in continuously stratified fluids is affected by vortex stretching and *vortex tilting*, as well as torques from baroclinicity. In contrast, equation (39.28) says that the material evolution of absolute vorticity for a shallow water fluid is affected only through vortex stretching. This behavior is a result of the depth independence of the horizontal velocity within a shallow water layer and the associated vertical columnar motion of fluid within the layer. On a related note, we see in Section 39.3.3 that vortex tubes in a shallow water layer are nearly vertical, so that we are only concerned with the vertical component of shallow water vorticity. Correspondingly, shallow water vortex tubes never close.

Material invariance of shallow water potential vorticity

Equation (39.28) can be written as an expression of the material invariance of the shallow water potential vorticity

$$\frac{\mathrm{D}Q}{\mathrm{D}t} = 0, \tag{39.29}$$

where

$$Q = \frac{\zeta_a}{h} = \frac{\zeta + f}{h} \tag{39.30}$$

is the shallow water potential vorticity. As defined, shallow water potential vorticity is the ratio of absolute vorticity to the thickness of the fluid layer. The material conservation law (39.29) says that this ratio remains constant for the shallow water layer in the absence of non-conservative processes such as friction.

39.3.2 Motivating the name

Material invariance of the shallow water potential vorticity in equation (39.30) is most practically a statement about how the relative vorticity, ζ, changes when changing column thickness or latitude. That is, by maintaining Q fixed, ζ must change when either the column thickness, h, changes or when the column moves meridionally and thus alters the planetary vorticity, f. By focusing on relative vorticity we are offered insights into how the fluid motion is constrained and thus a means to predict changes in that motion. In turn, these changes in ζ motivate the name "potential vorticity" as we now see.

Potential vorticity measures the ability for a shallow water fluid column to either spin up or spin down (change its relative vorticity) relative a standard configuration. For example, let the standard configuration be defined by an arbitrary standard thickness, h_s, at the equator (where $f = 0$). Now move an off-equatorial shallow water fluid column with zero relative vorticity to the equator and stretch/compress the column to the standard thickness. Material invariance of the column's potential vorticity allows us to deduce the column's relative vorticity at the equator, given information about the initial column thickness and initial Coriolis parameter (see Figure 39.3). Hence, potential vorticity, as an invariant material property, provides the "potential" for a fluid column to manifest a particular value of the relative vorticity when moved and stretched into a standard configuration. In this manner, the use of "potential" in "potential vorticity" is directly analogous to the use of "potential" in "potential temperature" as described in Section 23.3, or gravitational potential energy as discussed in Section 26.2.

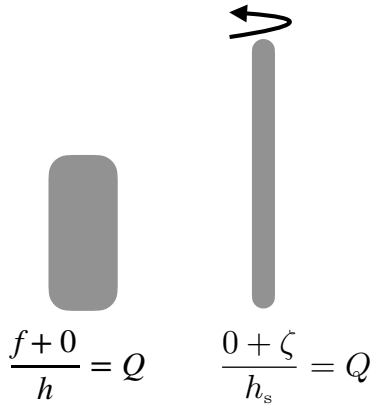

FIGURE 39.3: Left panel: an arbitrary shallow water column with zero relative vorticity and potential vorticity $Q = f/h$, with $f > 0$ assumed for this figure (northern hemisphere). Right panel: the same fluid column moved to the equator (where $f = 0$) and stretched to have the standard thickness, $h_s > h$. The relative vorticity of the column at the equator is given by $\zeta = f\,(h_s/h)$, where f is the Coriolis parameter at the original latitude where $f > 0$. Potential vorticity thus provides a means to deduce the relative vorticity that can be realized by moving any particular configuration to a standard location and with a standard thickness. This property motivates the "potential" used in the name.

39.3.3 Mass conservation + Kelvin's circulation theorem

Although we have yet to discuss Kelvin's theorem (Section 40.2), we here invoke it to illustrate another way to derive the material invariance of shallow water potential vorticity. As we see, this derivation provides a direct analog to the rotating cylinder discussed in Section 39.2.

When applied to an infinitesimal circuit in an inviscid and constant density fluid, Kelvin's theorem says that

$$\frac{\mathrm{D}\left(\boldsymbol{\omega}_a \cdot \hat{\boldsymbol{n}}\, \delta\mathcal{S}\right)}{\mathrm{D}t} = 0, \tag{39.31}$$

where $\boldsymbol{\omega}_a$ is the absolute vorticity

$$\boldsymbol{\omega}_a = \boldsymbol{\omega} + f\,\hat{\boldsymbol{z}}, \tag{39.32}$$

$\hat{\boldsymbol{n}}\,\delta\mathcal{S}$ is the infinitesimal surface area enclosed by the closed circuit, with $\hat{\boldsymbol{n}}$ the unit outward normal to the surface. Hence, equation (39.31) says that the projection of the absolute vorticity onto the local normal of an area element, multiplied by that area element, remains materially constant. This identity offers a very strong constraint on the flow.

To make use of equation (39.31) for the shallow water layer, decompose absolute vorticity into

$$\boldsymbol{\omega}_a = \hat{\boldsymbol{z}}\,(\zeta + f) + \boldsymbol{\omega}_h, \tag{39.33}$$

where

$$\boldsymbol{\omega}_{\rm h} = -\hat{\boldsymbol{z}} \times \nabla w = \hat{\boldsymbol{x}}\, \partial_y w - \hat{\boldsymbol{y}}\, \partial_x w \tag{39.34}$$

is the horizontal component to the shallow water relative vorticity from equation (35.106d) (recall the expression for $\boldsymbol{\omega}_{\rm h}$ follows since the horizontal velocity components have no vertical dependence within a shallow water layer: $\partial u/\partial z = \partial v/\partial z = 0$). Inserting the absolute vorticity (39.33) into Kelvin's theorem (39.31) leads to

$$\frac{\mathrm{D}}{\mathrm{D}t}\left[(\zeta + f)\, \delta A + \boldsymbol{\omega}_{\rm h} \cdot \hat{\boldsymbol{n}}\, \delta \mathcal{S}\right] = 0, \tag{39.35}$$

where the horizontal area element, δA, is the projection of the surface area element onto the vertical direction

$$\delta A = \hat{\boldsymbol{z}} \cdot \hat{\boldsymbol{n}}\, \mathrm{d}\mathcal{S}. \tag{39.36}$$

Shallow water fluid mechanics arises from considering a constant density fluid layer whose flow respects the small aspect ratio limit: $H/L \ll 1$, with H the vertical length scale of the flow, and L the horizontal length scale of the flow. Under this limit, the second term in equation (39.35) is much smaller than the first. It is further reduced in size since $\hat{\boldsymbol{n}}$ is nearly vertical, so that $\hat{\boldsymbol{n}} \cdot \hat{\boldsymbol{x}} \approx 0$ and $\hat{\boldsymbol{n}} \cdot \hat{\boldsymbol{y}} \approx 0$, in which case we are led to the scaling

$$\frac{|\boldsymbol{\omega}_{\rm h} \cdot \hat{\boldsymbol{n}}\, \delta \mathcal{S}|}{|(\zeta + f)\, \delta A|} \ll 1. \tag{39.37}$$

This result is consistent with our earlier comment in Section 39.3.1 that shallow water vortex tubes never close. Rather, they are nearly vertical, running from the bottom of a shallow water layer to the top. With the scaling (39.37), we find

$$\frac{\mathrm{D}}{\mathrm{D}t}\left[\left(\frac{\zeta + f}{h}\right) h\, \delta A\right] = 0, \tag{39.38}$$

where h is the layer thickness and $h\, \delta A$ is the volume of a fluid column extending through the shallow water layer. Given the incompressible nature of the fluid in a shallow water layer, the column volume is materially constant

$$\frac{\mathrm{D}\,(h\, \delta A)}{\mathrm{D}t} = 0, \tag{39.39}$$

so that equation (39.38) yields material invariance of shallow water potential vorticity

$$\frac{\mathrm{D}}{\mathrm{D}t}\left[\frac{\zeta + f}{h}\right] = \frac{\mathrm{D}Q}{\mathrm{D}t} = 0, \tag{39.40}$$

where $Q = (\zeta + f)/h$ is the same shallow water potential vorticity derived above in Section 39.3.1.

39.3.4 A fluid column with constant $f \neq 0$

Some of the essential features of shallow water potential vorticity material conservation are depicted in Figure 39.4 for the case of a fluid column with constant $f \neq 0$. In the left panel, the column thickness increases (column is stretched). Volume conservation for the column means that the column radius decreases. As the material in the column moves radially inward toward the center, it experiences a Coriolis deflection to the right in the northern hemisphere and to the left in the southern. Both of these deflections renders a cyclonic tendency to the relative vorticity, creating a positive relative vorticity tendency in the northern hemisphere and negative

relative vorticity tendency in the southern hemisphere.

An equivalent way to understand the cyclonic tendency is to consider the angular momentum of the fluid column, assuming the column moves coherently as a rigid-body as in Section 39.2.[2] As the radius of the column decreases so too does its moment of inertia. Angular momentum conservation means that the column picks up a tendency that causes its spin to increase. The direction of this spin increase accords with the background f of the environment. Returning to the skater analog in Figure 39.1, we consider f to be the initial spin of the skater so that when the moment of inertia decreases the column picks up a spin in the same direction as f; i.e., a cyclonic tendency.[3]

In both hemispheres, the Coriolis deflection, or equivalently angular momentum conservation, creates a cyclonic relative vorticity tendency when the column stretches, thus maintaining $Q = (f+\zeta)/h$ fixed. Again, the cyclonic relative vorticity adds to the magnitude of the planetary vorticity to ensure that the absolute vorticity magnitude increases in accord with the column thickness increase, thus keeping $Q = \zeta_a/h$ constant. The converse holds when the column is flattened/squashed, whereby the relative vorticity picks up an anti-cyclonic tendency (negative relative vorticity tendency in the northern hemisphere and positive relative vorticity tendency in the southern). Doing so reduces the magnitude of the absolute vorticity in accord with the reduced column thickness.

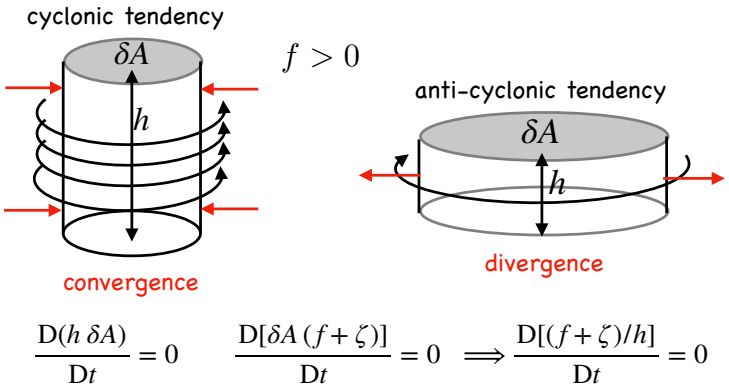

FIGURE 39.4: Material invariance for shallow water potential vorticity results from combining material invariance of the volume of a coherent fluid column with the material invariance of the area weighted absolute vorticity. As the cross-sectional area of the column decreases, as in a converging flow, the thickness of the fluid must increase in order to maintain constant volume. Furthermore, potential vorticity material invariance can be maintained by changing the fluid spin, as measured by the relative vorticity, or by changing the latitude and thus changing its planetary vorticity (the β-effect discussed in Section 40.6). We here depict the case with $f > 0$ constant (so that $\beta = 0$). Flow converging toward the center of the column picks up a Coriolis acceleration that creates a cyclonic tendency in the relative vorticity, just like the spinning cylinder in Figure 39.1. Equivalently, as the radius of the column decreases so too does its moment of inertia so that the column must pick up a cyclonic tendency to conserve angular momentum. Conversely, as the cross-sectional area increases, the diverging flow creates an anti-cyclonic tendency in the relative vorticity.

[2]Recall that in Section 39.2, the column rotates as a rigid-body, meaning there is no strain in the fluid, and yet the radius and thickness are allowed to change.

[3]The connection between the Coriolis acceleration and angular momentum conservation was discussed for particle mechanics in Section 14.6.

39.3.5 Material invariance of an arbitrary function of PV

The material invariance of shallow water potential vorticity, equation (39.29), means that any function, $F(Q)$ is also materially constant. We see this property through the chain rule

$$\frac{\mathrm{D}F}{\mathrm{D}t} = \frac{\mathrm{d}F}{\mathrm{d}Q}\frac{\mathrm{D}Q}{\mathrm{D}t} = 0. \tag{39.41}$$

Since F is arbitrary, there are an infinite number of material invariants corresponding to distinct functions F. This result holds for all materially invariant scalar properties of the fluid.

39.3.6 N-layer potential vorticity

The thickness equation (35.79a) and the vorticity equation (39.12) for an N-layer shallow water model are given by

$$\frac{\mathrm{D}_{\mathsf{k}} h_{\mathsf{k}}}{\mathrm{D}t} = -h_{\mathsf{k}}\,\nabla\cdot\boldsymbol{u}_{\mathsf{k}} \quad \text{and} \quad \frac{\mathrm{D}_{\mathsf{k}}\zeta_{\mathsf{ak}}}{\mathrm{D}t} = -\zeta_{\mathsf{ak}}\,\nabla\cdot\boldsymbol{u}_{\mathsf{k}}, \tag{39.42}$$

where there is no implied summation over the layer index k. These forms are isomorphic to the single layer equations so that the potential vorticity of layer-k is given by

$$Q_{\mathsf{k}} = \frac{f+\zeta_{\mathsf{k}}}{h_{\mathsf{k}}}, \tag{39.43}$$

and for a perfect shallow water fluid this layer potential vorticity is materially constant

$$\frac{\mathrm{D}_{\mathsf{k}} Q_{\mathsf{k}}}{\mathrm{D}t} = \frac{\partial Q_{\mathsf{k}}}{\partial t} + \boldsymbol{u}_{\mathsf{k}}\cdot\nabla Q_{\mathsf{k}} = 0, \tag{39.44}$$

where, again, there is no implied summation over k.

39.3.7 Further study

The shallow water potential vorticity (39.30) was introduced by *Rossby* (1940) and as such it is sometimes referred to as the *Rossby potential vorticity*. Non-rotating shallow water potential vorticity, ζ/h, is illustratated in this video from Prof. Shapiro at around the 11 minute mark. Note that he does not use the term "potential vorticity", instead invoking mass conservation and angular momentum conservation to describe the motion.

39.4 Potential vorticity with non-conservative processes

In this section we consider the role of a non-conservative acceleration, $\boldsymbol{F}$, with this term arising from friction and boundary stresses (Section 35.6.5). Additionally, we allow for the presence of a boundary volume source, $w^{(\dot\eta)}$ (as in precipitation minus evaporation), thus changing the volume in the layer. We introduced such processes in Section 35.6, in which case the shallow water equations take on the form

$$\frac{\mathrm{D}\boldsymbol{u}}{\mathrm{D}t} + f\,\hat{\boldsymbol{z}}\times\boldsymbol{u} = -g\,\nabla\eta + \boldsymbol{F} \qquad \text{and} \qquad \frac{\mathrm{D}h}{\mathrm{D}t} + h\,\nabla\cdot\boldsymbol{u} = w^{(\dot\eta)}. \tag{39.45}$$

39.4.1 Material time evolution of potential vorticity

In the presence of non-conservative forces, the absolute vorticity equation (39.7) becomes

$$\partial_t\zeta_{\mathsf{a}} + \nabla\cdot(\boldsymbol{u}\,\zeta_{\mathsf{a}}) = \hat{\boldsymbol{z}}\cdot(\nabla\times\boldsymbol{F}) \Longrightarrow \frac{\mathrm{D}\zeta_{\mathsf{a}}}{\mathrm{D}t} + \zeta_{\mathsf{a}}\,\nabla\cdot\boldsymbol{u} = \hat{\boldsymbol{z}}\cdot(\nabla\times\boldsymbol{F}), \tag{39.46}$$

so that vorticity is now affected by the curl of $\boldsymbol{F}$. As before, we make use of the thickness equation to replace the horizontal divergence according to

$$\nabla \cdot \boldsymbol{u} = \frac{1}{h}\left[-\frac{\mathrm{D}h}{\mathrm{D}t} + w^{(\dot{\eta})}\right]. \tag{39.47}$$

The presence of $w^{(\dot{\eta})}$ modifies the divergence of the horizontal velocity beyond that for a conservative fluid. We are thus led to the potential vorticity equation

$$h\,\frac{\mathrm{D}Q}{\mathrm{D}t} = -Q\,w^{(\dot{\eta})} + \hat{\boldsymbol{z}} \cdot (\nabla \times \boldsymbol{F}). \tag{39.48}$$

Hence, with $w^{(\dot{\eta})} \neq 0$ and/or $\hat{\boldsymbol{z}} \cdot (\nabla \times \boldsymbol{F}) \neq 0$, shallow water potential vorticity is no longer materially invariant.

39.4.2 The potential vorticity flux

Deriving the flux-form equation

We can convert the potential vorticity equation (39.48) into a flux-form conservation equation by making use of the thickness equation

$$h\,\frac{\mathrm{D}Q}{\mathrm{D}t} = h\left[\frac{\partial Q}{\partial t} + \boldsymbol{u} \cdot \nabla Q\right] + Q\left[\frac{\partial h}{\mathrm{D}t} + \nabla \cdot (h\,\boldsymbol{u}) - w^{(\dot{\eta})}\right] = \frac{\partial (h\,Q)}{\partial t} + \nabla \cdot (\boldsymbol{u}\,h\,Q) - Q\,w^{(\dot{\eta})}, \tag{39.49}$$

thus rendering

$$\partial_t (h\,Q) + \nabla \cdot (h\,\boldsymbol{u}\,Q) = \hat{\boldsymbol{z}} \cdot (\nabla \times \boldsymbol{F}). \tag{39.50}$$

As a final step, make use of the identity

$$\hat{\boldsymbol{z}} \cdot (\nabla \times \boldsymbol{F}) = -\nabla \cdot (\hat{\boldsymbol{z}} \times \boldsymbol{F}), \tag{39.51}$$

so that the thickness weighted potential vorticity equation (39.50) can be written

$$\partial_t (h\,Q) = -\nabla \cdot (h\,Q\,\boldsymbol{u} + \hat{\boldsymbol{z}} \times \boldsymbol{F}). \tag{39.52}$$

Note how the volume source term, $w^{(\dot{\eta})}$, does not explicitly appear in the flux-form equation (39.52) since the effects from $w^{(\dot{\eta})}$ are captured by the divergence, $\nabla \cdot \boldsymbol{u}$, as per equation (39.47).

For the shallow water fluid, the thickness weighted potential vorticity equals to the absolute vorticity

$$h\,Q = \zeta_{\mathsf{a}}. \tag{39.53}$$

Consequently, the flux-form conservation form of the potential vorticity equation (39.52) is identical to equation (39.46) for the absolute vorticity

$$\partial_t (h\,Q) = -\nabla \cdot (h\,Q\,\boldsymbol{u} + \hat{\boldsymbol{z}} \times \boldsymbol{F}) \Longleftrightarrow \partial_t \zeta_{\mathsf{a}} = -\nabla \cdot (\zeta_{\mathsf{a}}\,\boldsymbol{u} + \hat{\boldsymbol{z}} \times \boldsymbol{F}). \tag{39.54}$$

Potential vorticity flux vector

It is remarkable that even with non-conservative forcing, the thickness weighted potential vorticity (equivalently, the absolute vorticity) has its Eulerian evolution determined by the convergence of a flux,

$$\boldsymbol{J}^{\mathrm{Q}} = h\,Q\,\boldsymbol{u} + \hat{\boldsymbol{z}} \times \boldsymbol{F}. \tag{39.55}$$

Observe that this potential vorticity flux is oriented in the horizontal direction. As detailed in Chapters 42 and 66, the potential vorticity flux never crosses the interface between two shallow

water layers, even in the presence of non-conservative processes such as mixing and friction. This result is a special case of the more general *impermeability theorem* that holds for continuously stratified fluids (Section 42.2).

A kinematic expression for the potential vorticity flux vector

The flux convergence evolution for the potential vorticity equation (39.54) is a kinematic result of the definition of potential vorticity. Namely,

$$h\,Q - f = \zeta = \nabla \cdot (\boldsymbol{u} \times \hat{\boldsymbol{z}}) \tag{39.56}$$

so that

$$\partial_t (h\,Q) = \nabla \cdot (\partial_t \boldsymbol{u} \times \hat{\boldsymbol{z}}) \equiv -\nabla \cdot \boldsymbol{J}^{\text{kin}}, \tag{39.57}$$

where we defined the kinematic potential vorticity flux vector

$$\boldsymbol{J}^{\text{kin}} \equiv -\partial_t \boldsymbol{u} \times \hat{\boldsymbol{z}}. \tag{39.58}$$

We can relate the kinematic potential vorticity flux vector to $\boldsymbol{J}^{\text{Q}}$ through the following. Take the cross product of the vector invariant velocity equation (39.2) with $\hat{\boldsymbol{z}}$ to find

$$\partial_t \boldsymbol{u} \times \hat{\boldsymbol{z}} + \zeta_{\text{a}}\,\boldsymbol{u} = -\nabla(g\,\eta + \boldsymbol{u} \cdot \boldsymbol{u}/2) \times \hat{\boldsymbol{z}} + \boldsymbol{F} \times \hat{\boldsymbol{z}}. \tag{39.59}$$

Now write

$$\zeta_{\text{a}}\,\boldsymbol{u} = h\,Q\,\boldsymbol{u} = \boldsymbol{J}^{\text{Q}} - \hat{\boldsymbol{z}} \times \boldsymbol{F} \tag{39.60}$$

to have

$$\boldsymbol{J}^{\text{kin}} = \boldsymbol{J}^{\text{Q}} + \nabla \times [\hat{\boldsymbol{z}}\,(g\,\eta + \boldsymbol{u} \cdot \boldsymbol{u}/2)]. \tag{39.61}$$

Since the two potential vorticity fluxes differ by a curl; i.e., a rotational term, their divergences are identical

$$\nabla \cdot \boldsymbol{J}^{\text{kin}} = \nabla \cdot \boldsymbol{J}^{\text{Q}}, \tag{39.62}$$

so that their convergence leads to the same evolution of $h\,Q$. Stated more formally, $\boldsymbol{J}^{\text{kin}}$ and $\boldsymbol{J}^{\text{Q}}$ differ by a gauge, with the gauge function given by $g\,\eta + \boldsymbol{u} \cdot \boldsymbol{u}/2$.

39.5 Example implications of material PV invariance

The material invariance of shallow water potential vorticity constrains the shallow water motion by stating that f, h, ζ cannot change independently of the other. Rather, the combination $Q = (f + \zeta)/h$ must remain materially invariant (in the absence of non-conservative processes). There are a variety of situations that induce changes in one or two of the terms, with the third term constrained to ensure Q remains unchanged. We here consider some thought experiments to garner experience with shallow water PV-thinking.

39.5.1 Topographic beta effect

Changes in the topography affect the potential vorticity by changing the thickness of a fluid column via (see Figure 35.1)

$$h = H + \Delta\eta - \Delta\eta_{\text{b}}, \tag{39.63}$$

with $H = \overline{h}$ the area mean layer thickness, $\Delta\eta = \eta - \overline{\eta}$ the deviation of the free surface from its area mean, and $\Delta\eta_{\text{b}} = \eta_{\text{b}} - \overline{\eta_{\text{b}}}$ the deviation of the bottom from its area mean. For relative vorticity, we note that spatial changes in the topography act to drive a vertical velocity at the

layer bottom as per equation (35.29),

$$w = \frac{\mathrm{D}\eta_{\mathrm{b}}}{\mathrm{D}t} \quad \text{at } z = \eta_{\mathrm{b}}, \tag{39.64}$$

which then leads to vortex stretching and hence to a change in relative vorticity. In this subsection we highlight the analog between topographic slopes and planetary beta to thus motivate the term *topographic beta effect*.

To mathematically exhibit the topographic beta effect, consider a fluid column whose vorticity is dominated by planetary vorticity and with bottom topography having a small and linear slope in the meridional direction

$$\Delta\eta_{\mathrm{b}} = \delta\, y, \tag{39.65}$$

where $|\delta| \ll 1$ is the topographic slope. Assuming the free surface undulations are small relative to the resting layer thickness, $\Delta\eta \ll H$, we can expand the potential vorticity according to

$$\begin{aligned} Q &= \frac{f + \zeta}{h} && \text{(39.66a)} \\ &= \frac{f_{\circ} + \beta\, y + \zeta}{H + \Delta\eta - \delta\, y} && \text{(39.66b)} \\ &\approx \frac{f_{\circ} + \beta\, y + \zeta}{H} \left[1 - H^{-1}\,(\Delta\eta - \delta\, y)\right] && \text{(39.66c)} \\ &\approx \frac{f_{\circ} + \beta\, y + \zeta}{H} - \frac{f_{\circ}}{H^2}\,(\Delta\eta - \delta\, y). && \text{(39.66d)} \end{aligned}$$

Setting $\mathrm{D}Q/\mathrm{D}t = 0$ and rearranging leads to the material evolution of relative vorticity

$$\frac{\mathrm{D}\zeta}{\mathrm{D}t} = -v\,(\beta + f_{\circ}\delta/H) + \frac{f_{\circ}\, w(\eta)}{H}. \tag{39.67}$$

The second term on the right hand side is the vortex stretching associated with vertical motion at the top of the layer, where

$$w(\eta) = \frac{\mathrm{D}(\Delta\eta)}{\mathrm{D}t} = \frac{\mathrm{D}\eta}{\mathrm{D}t}, \tag{39.68}$$

according to the surface kinematic boundary condition (35.37). The first term on the right hand side is vortex stretching arising from both planetary beta and topographic slopes. It is written in a form revealing the parallels between these two contributions, and it is readily generalized to the following for arbitrary topography

$$\beta^{\mathsf{eff}} = (H - \eta_{\mathrm{b}})\,\nabla[f/(H - \eta_{\mathrm{b}})] \approx \beta\,\hat{\boldsymbol{y}} + (f_{\circ}/H)\nabla\eta_{\mathrm{b}}. \tag{39.69}$$

One of the more prominant roles for topographic beta is in supporting topographic Rossby waves, which are analogous to the Rossby waves supported by planetary beta (see Section 54.3). We also encounter the topographic beta effect in Section 43.6.1 in our study of the quasi-geostrophic shallow water model.

39.5.2 Planetary geostrophic potential vorticity and f/H contours

As introduced in Section 31.5, planetary geostrophy (PG) is used to study the large-scale laminar ocean circulation where relative vorticity is ignored. Furthermore, as shown in Section 43.4, the inviscid and adiabatic PG system materially preserves the PG potential vorticity, $Q = f/h$, so that

$$\frac{\mathrm{D}(f/h)}{\mathrm{D}t} = 0. \tag{39.70}$$

Consequently, fluid particles respecting the inviscid planetary geostrophic equations follow contours of constant f/h. These contours are referred to as *geostrophic contours* since the flow is under geostrophic balance. In Section 39.7.3 we offer a geometrical interpretation of $Q = f/h$ material invariance in terms of the Taylor-Proudman effect.

Example f/H contours

If we assume the free surface undulations are negligible compared to the bottom topography (a useful assumption for planetary geostrophic flow), then shallow water columns follow contours of constant f/H, where $z = -H(x, y) = \eta_b(x, y)$ is the vertical position of the bottom topography. In Figure 39.5 we illustrate f/H contours for a topographic seamount (bump), a topographic depression (bowl), and a shelf/slope along the western boundary. We see that f/H contours are diverted equatorward when depth decreases, whereas they are diverted poleward when encountering deeper water. Furthermore, those contours near to either a bump or bowl are closed, so that fluid columns following these contours are trapped around the topographic feature.

For the shelf/slope region in Figure 39.5, the f/H contours are horizontal where the topography is flat, which for this example is on the shelf and in the open ocean, whereas they are steered toward the equator as they pass from the shelf toward the coast. In this example, the difference between the shelf and deep ocean is only around 200 m, so that this example corresponds to upper ocean columns interacting with the continental slope. Part of the reason for choosing this geometry is that thicker fluid columns from the open ocean are unable to reach the continental shelf. The reason is that thick columns, as they reach the slope, have their f/H contours reach the equator along the slope before they reach the shelf. That is, the f/H contours for thick open ocean columns are almost entirely southward when reaching the continental slope, so that they cannot climb to shallower depths on the shelf.

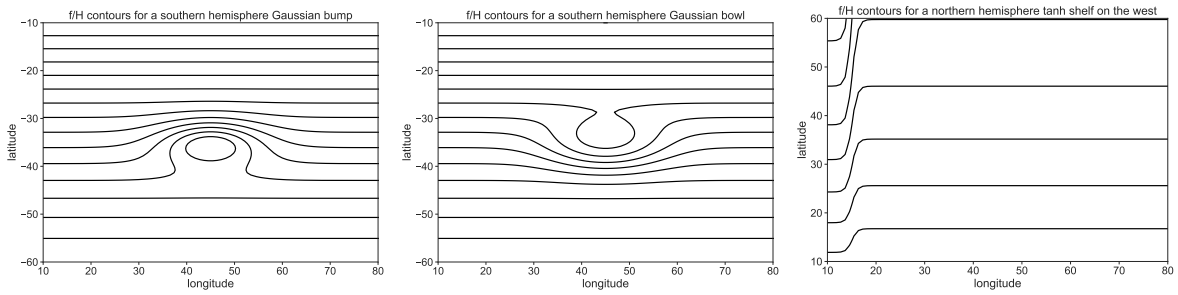

FIGURE 39.5: When a shallow water fluid is governed by the inviscid and adiabatic planetary geostrophic equations and there is no external forcing, then shallow water fluid columns maintain fixed planetary geostrophic potential vorticity, $\mathrm{D}(f/h)/\mathrm{D}t = 0$. Ignoring free surface undulations relative to changes in the bottom depth means that f/H remains fixed following the inviscid geostrophic flow, where $z = -H(x, y) = \eta_b(x, y)$ is the bottom topography. We illustrate these *geostrophic contours* for three topographic features: a Gaussian seamount or bump and a Gaussian bowl, both in the southern hemisphere; and a western boundary continental slope and shelf in the northern hemisphere. Contours of f/H follow lines of constant latitude when H is constant, f/H contours are steered equatorward when moving into a region of shoaling water (H decreases), and steered poleward when moving into deeper water (H increases). Futhermore, note that contours near the seamount and bowl can close, in which case the associated geostrophic contours are trapped next to the topographic features.

How planetary β affects f/H contours

The shelf example in Figure 39.5 reveals that for a given change in depth, the latitudinal diversion of an f/H contour is larger in magnitude for poleward contours relative to equatorward contours. We here show that this property of the f/H contours arises from planetary β.

For this purpose, consider a particular f/H contour, on which the latitude and depth change so as to keep f/H fixed so that

$$\delta(f/H) = 0, \tag{39.71}$$

where δ is a differential operator following the f/H contour. With $f = 2\,\Omega \sin\phi$, the constraint (39.71) relates deviations in latitude, $\delta\phi$, to deviations in depth, δH, along an f/H contour

$$\delta\phi = (\delta H/H) \tan\phi = \frac{f/H}{2\,\Omega \cos\phi} = \frac{f}{H}\,\frac{\delta H}{R_e\,\beta} \Longrightarrow \frac{\delta\phi}{\delta H} = \frac{f}{H}\,\frac{1}{R_e\,\beta}, \tag{39.72}$$

where we introduced planetary β according to

$$\beta = \partial_y f = (2\,\Omega/R_e) \cos\phi. \tag{39.73}$$

For a particular f/H contour, we see that $\delta\phi/\delta H$ is proportional to β^{-1}. Consequently, the magnitude of $\delta\phi/\delta H$ increases moving poleward, as β decreases toward zero.

39.5.3 Spin up of converging flow

Consider the flow shown in Figure 39.6, whereby mass in the shallow water layer converges into a region. Just as described in the potential vorticity derivation Figure 39.4, increasing the column thickness, without substantially altering the planetary vorticity (e.g., f-plane), requires $\partial\zeta/\partial t > 0$ in order to maintain $Q = (\zeta + f)/h$ materially constant. Following our discussion of the rotating column in Section 39.2, note that convergence of mass reduces the moment of inertia relative to the center of the region. Angular momentum conservation requires the fluid to rotate faster thus picking up a positive relative vorticity. This dynamical process is embedded in the material invariance of potential vorticity. Finally, note that the opposite occurs in a region of diverging fluid, whereby potential vorticity material invariance implies that the relative vorticity has a negative tendency ($\partial\zeta/\partial t < 0$) (see also Figure 39.4).

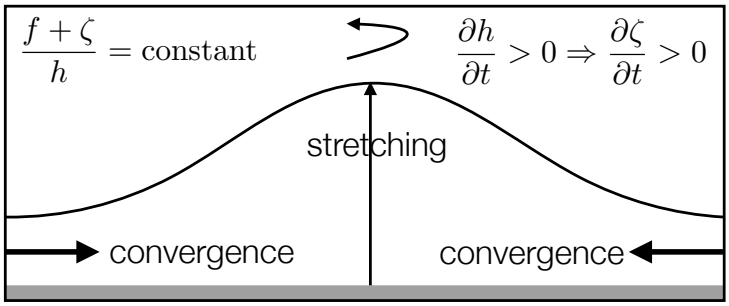

FIGURE 39.6: Illustrating the implications of potential vorticity material invariance for a shallow water fluid on an f-plane. If mass converges into a region, thus stretching the fluid column, then potential vorticity material invariance implies the relative vorticity increases, $\partial\zeta/\partial t > 0$. This result is directly analogous to the rotating cylinder example considered in Figures 39.1 and 39.4. Namely, converging a region of constant mass reduces its moment of inertia so that angular momentum conservation leads to an increase in spin.

39.5.4 Further study

Section 4.5 of *Holton and Hakim* (2013) discusses the case of flow over topography where the full shallow water potential vorticity is materially invariant, $\mathrm{D}(f + \zeta)/\mathrm{D}t = 0$. In that case there is a dramatic difference between easterly and westerly flows. In the northern hemisphere, westerly winds (eastward flow) deflects over the topography and downstream it undulates as topographic leewaves. A rotating tank offers a useful controlled setting to observe leewaves, such as shown

near the 20 minute mark in this video from Prof. Fultz. Easterly winds (westward flow) do not exhibit a wavelike pattern, instead following a trajectory similar to the f/H contours of planetary geostrophic case, though modified by relative vorticity. In general, the study of flow near topography, either in the shallow water or continuously stratified, introduces a wealth of dynamical behaviors where material invariance of potential vorticity provides an important tool to help unravel mechanisms.

39.6 Circulation with non-conservative processes

We follow the discussion in Section 39.4 to study the evolution of circulation in the presence of non-conservative processes such as dia-surface transport and boundary stresses (Section 35.6). For this purpose, consider the velocity circulation around a closed horizontal area, $\mathcal{S}$ (see Figure 39.7)

$$\mathcal{C} = \int_{\mathcal{S}} \zeta \, \mathrm{d}\mathcal{S} = \oint_{\partial \mathcal{S}} \boldsymbol{u} \cdot \hat{\boldsymbol{t}} \, \mathrm{d}\ell. \tag{39.74}$$

In this equation, $\hat{\boldsymbol{t}} \, \mathrm{d}\ell$ is the vector line increment around the contour, and $\hat{\boldsymbol{t}}$ is the tangent vector orienting the contour integral in a counterclockwise direction. We assume the circulation contour extends vertically through the non-vanishing fluid layer[4] so that the unit outward normal, $\hat{\boldsymbol{n}}$, to the contour is strictly horizontal, as is the tangent vector, $\hat{\boldsymbol{t}}$. We now seek an evolution equation for this circulation by making use of the vorticty equation (39.54).

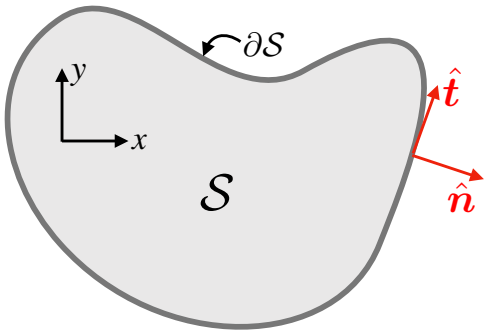

FIGURE 39.7: Illustrating the calculation of circulation around the contour, $\partial\mathcal{S}$, of a static horizontal area, $\mathcal{S}$, within a layer of shallow water fluid. The circulation theorem (39.78) provides the means to compute the time changes in circulation as a function of the advection of absolute vorticity crossing the contour plus the circulation of friction. Note that the contour has a vertical extent throughout the shallow water layer, so that the unit outward normal, $\hat{\boldsymbol{n}}$, and the unit tangent direction, $\hat{\boldsymbol{t}}$, are both horizontal vectors.

To develop an evolution equation for $\mathcal{C}$, integrate the vorticity equation (39.54) over the area $\mathcal{S}$ to yield

$$\int_{\mathcal{S}} \frac{\partial \zeta}{\partial t} \, \mathrm{d}\mathcal{S} = \int_{\mathcal{S}} [-\nabla \cdot (\zeta_a \, \boldsymbol{u} + \hat{\boldsymbol{z}} \times \boldsymbol{F})] \, \mathrm{d}\mathcal{S} = - \oint_{\partial \mathcal{S}} [\zeta_a \, \boldsymbol{u} + \hat{\boldsymbol{z}} \times \boldsymbol{F})] \cdot \hat{\boldsymbol{n}} \, \mathrm{d}\ell, \tag{39.75}$$

where $\oint$ symbolizes an integral around the contour. To reach this equation we used the divergence theorem on the right hand side, with $\hat{\boldsymbol{n}}$ the *horizontal* unit outward normal vector along the contour, $\partial\mathcal{S}$, and $\mathrm{d}\ell$ is the line increment along the contour. We also set $\partial f/\partial t = 0$ as part of

[4] The case of a vanishing layer thickness, such as occurs when allowing for sloped side boundaries as per a seashore, is handled by studying the thickness weighted velocity equation and the corresponding column vorticity. We consider this topic in Section 39.8.

the time derivative of the absolute vorticity. The non-conservative forcing term can be written

$$(\hat{\boldsymbol{z}} \times \boldsymbol{F}) \cdot \hat{\boldsymbol{n}} = (\hat{\boldsymbol{n}} \times \hat{\boldsymbol{z}}) \cdot \boldsymbol{F} = -\hat{\boldsymbol{t}} \cdot \boldsymbol{F}, \tag{39.76}$$

thus leading to

$$\int_{\mathcal{S}} \frac{\partial \zeta}{\partial t} \, \mathrm{d}\mathcal{S} = -\oint_{\partial \mathcal{S}} \zeta_{\mathrm{a}} \, \boldsymbol{u} \cdot \hat{\boldsymbol{n}} \, \mathrm{d}\ell + \oint_{\partial \mathcal{S}} \boldsymbol{F} \cdot \hat{\boldsymbol{t}} \, \mathrm{d}\ell, \tag{39.77}$$

where $\oint$ is the counter-clockwise oriented closed contour integral. We next assume the area $\mathcal{S}$ is constant in time, so that the Eulerian time derivative can be pulled across the integral to render

$$\frac{\mathrm{d}\mathcal{C}}{\mathrm{d}t} = -\oint_{\partial \mathcal{S}} \zeta_{\mathrm{a}} \, \boldsymbol{u} \cdot \hat{\boldsymbol{n}} \, \mathrm{d}\ell + \oint_{\partial \mathcal{S}} \boldsymbol{F} \cdot \hat{\boldsymbol{t}} \, \mathrm{d}\ell. \tag{39.78}$$

The first term on the right hand side arises from the horizontal advection of absolute vorticity across the contour. This term is not oriented and so the integral sign has no arrow. The second term arises from the counter-clockwise oriented circulation of any non-conservative accelerations. We refer to equation (39.78) as a *circulation theorem*. It has many uses under specific cases, some of which are described in the remainder of this chapter.

39.6.1 Circulation around a closed streamline in steady flow

As a particular example of the circulation theorem (39.78), consider a steady flow in the absence of boundary volume sources ($w^{(\hat{\eta})} = 0$). In this case, the thickness equation (35.19) reduces to $\nabla \cdot (h \, \boldsymbol{u}) = 0$ so that we can introduce a transport streamfunction, Ψ (with dimensions of $\mathrm{L}^3 \, \mathrm{T}^{-1}$)

$$h \, \boldsymbol{u} = \hat{\boldsymbol{z}} \times \nabla \Psi. \tag{39.79}$$

In a bounded domain, the streamlines (contours of constant Ψ) are closed. Furthermore, the unit outward normal to a closed streamline is perpendicular to the velocity, $\boldsymbol{u} \cdot \hat{\boldsymbol{n}} = 0$. We thus see that the steady state expression of the circulation theorem (39.78), computed around a closed streamline, leads to the following constraint on the non-conservative forces

$$\oint_{\text{streamline}} \boldsymbol{F} \cdot \hat{\boldsymbol{t}} \, \mathrm{d}\ell = \int_{\text{streamline area}} (\nabla \times \boldsymbol{F}) \cdot \hat{\boldsymbol{z}} \, \mathrm{d}\mathcal{S} = 0, \tag{39.80}$$

where the second equality follows from Stokes' theorem applied over the area bounded by the streamline. Equation (39.80) provides a constraint on the non-conservative forcing that must be satisfied to enable a steady flow. For example, when integrated around a closed streamline, the wind stress forcing must balance dissipation. If the constraint (39.80) is not satisfied, then the flow cannot reach a steady state. Although we may not know explicit details of the streamlines, we can still make use of this constraint if we assume the flow is steady. The analysis in Section 39.7 offers an example application of these ideas for studies of circulation in steady ocean gyres.

39.6.2 Circulation from wind stress and Rayleigh drag

A particularly simple form for the non-conservative acceleration is given by

$$\boldsymbol{F} = -\gamma \, \boldsymbol{u} + \boldsymbol{\tau}^{\text{wind}}/(h \, \rho) \equiv -\gamma \, \boldsymbol{u} + \boldsymbol{F}^{\text{wind}}. \tag{39.81}$$

The first term is referred to as *Rayleigh drag* with $\gamma > 0$ a constant with dimensions of inverse time.[5] Rayleigh drag damps all flow to rest with γ^{-1} the e-folding time for the damping. The

[5] See Section 33.2.4 for more discussion of Rayleigh drag in the context of Ekman mechanics.

second term in equation (39.81) is the acceleration on the layer from wind stress,

$$\boldsymbol{F}^{\text{wind}} = \frac{\boldsymbol{\tau}^{\text{wind}}}{h\,\rho}, \tag{39.82}$$

with this form following from the discussion of boundary stresses in Section 35.6.5. Namely, homogeneity of the shallow water layer renders the contact stress from winds into a body stress applied throughout the layer.

Plugging the acceleration (39.81) into the time dependent circulation theorem (39.78) leads to

$$(\mathrm{d}/\mathrm{d}t + \gamma)\,\mathcal{C} = -\int_{\partial\mathcal{S}} \zeta_{\mathsf{a}}\,\boldsymbol{u}\cdot\hat{\boldsymbol{n}}\,\mathrm{d}\ell + \oint_{\partial\mathcal{S}} \boldsymbol{F}^{\text{wind}}\cdot\hat{\boldsymbol{t}}\,\mathrm{d}\ell. \tag{39.83}$$

Specializing to a steady state and choosing the contour as a closed streamline (along which $\boldsymbol{u}\cdot\hat{\boldsymbol{n}} = 0$), renders

$$\mathcal{C} = \gamma^{-1}\oint_{\text{streamline}} \boldsymbol{F}^{\text{wind}}\cdot\hat{\boldsymbol{t}}\,\mathrm{d}\ell = (\gamma\,\rho)^{-1}\oint_{\text{streamline}} (\boldsymbol{\tau}^{\text{wind}}/h)\cdot\hat{\boldsymbol{t}}\,\mathrm{d}\ell. \tag{39.84}$$

This equation says that velocity circulation around a closed streamline is determined by wind stress circulation around that streamline plus knowledge of the Rayleigh drag damping time scale γ^{-1}. This result supports our expectation that the steady circulation around a closed streamline is oriented with the same sense as the applied wind stress.

39.7 A primer on steady ocean gyres

Large-scale gyres are a prominent feature of ocean circulation, with the North Atlantic and North Pacific middle-latitude gyres two canonical examples. It is particularly remarkable that ocean gyres are not symmetric in the east-west direction, with a prominent western side where poleward flow is stronger than the more sluggish equatorward flow in the interior. As shown in this section, gyre zonal asymmetry is not a response to the wind forcing, with the asymmetry found even without any zonal variations in the boundary forcing. Instead, it is a manifestation of the beta effect present for flow on a rotating spherical planet (or idealized as the β-plane from Section 24.5). The role of

$$\beta = \partial_y f > 0 \tag{39.85}$$

in western intensification was first articulated by *Stommel* (1948), with β encapsulating the leading order role of the earth's sphericity on large-scale flows in the atmosphere and ocean.

We have the basic tools in hand to understand the physical balances leading to western intensification in steady ocean gyres. We follow the traditional approach by focusing on vorticity balance, which offer a more direct path towards understanding western intensification than the momentum or axial angular momentum balances used to explore channel flow in Sections 28.5 and 36.7. Furthermore, observe that with western intensification fundamentally relying on $\beta > 0$, then the arguments given below hold for both hemispheres; i.e., gyres are western intensified in both hemispheres and with either signed wind stress curl. So although we orient the discussion according to a northern hemisphere anti-cyclonic gyre, the arguments hold in general.

39.7.1 Steady and large-scale vorticity balance

The steady circulation theorem (39.84) holds regardless the bottom topography or surface height undulations. Again, it says that circulation around a closed streamline is in the same sense as the wind circulation. However, we need more information to see how western intensification emerges as a property of the flow in ocean gyres. For that purpose, consider the steady absolute

vorticity equation (39.54), again in the presence of wind forcing and Rayleigh drag

$$\nabla \cdot (\boldsymbol{u}\, \zeta_a) = -\gamma\, \zeta + \hat{\boldsymbol{z}} \cdot (\nabla \times \boldsymbol{F}^{\text{wind}}). \tag{39.86}$$

Introducting the shallow water potential vorticity, $Q = \zeta_a/h$, allows us to write

$$\nabla \cdot (\boldsymbol{u}\, \zeta_a) = \nabla \cdot (h\, \boldsymbol{u}\, Q). \tag{39.87}$$

The steady state thickness equation (35.19) means that $\nabla \cdot (h\, \boldsymbol{u}) = 0$, so that the vorticity equation (39.86) takes the form

$$h\, \boldsymbol{u} \cdot \nabla Q = -\gamma\, \zeta + \hat{\boldsymbol{z}} \cdot (\nabla \times \boldsymbol{F}^{\text{wind}}). \tag{39.88}$$

This equation says that in the absence of the Rayleigh friction ($\gamma = 0$) and with a zero wind stress curl, the steady horizontal flow is aligned with potential vorticity contours. This result follows directly from the material invariance of potential vorticity in the absence of non-conservative processes. However, in the presence of Rayleigh drag and/or wind stress curl, the potential vorticity is modified when following the flow so that $\boldsymbol{u} \cdot \nabla Q \neq 0$, in which case the circulation does not follow Q contours.

39.7.2 Planetary geostrophic flow and the Sverdrup balance

For large-scale flow away from lateral boundaries, the flow has an absolute vorticity that is dominated by planetary vorticity so that

$$Q \approx Q^{\text{pg}} = f/h, \tag{39.89}$$

which is the potential vorticity for shallow water planetary geostrophic flow introduced in Section 39.5.2 and studied more thoroughly in Sections 31.5 and 43.4. In this flow the only means for changing potential vorticity arise from changes to planetary vorticity (changes to f) and changes to layer thickness, h.

Away from boundaries we also assume the Rayleigh drag term is negligible since the relative vorticity is small. In this case, the potential vorticity equation (39.88) takes the form

$$h\, \boldsymbol{u} \cdot \nabla Q^{\text{pg}} = \hat{\boldsymbol{z}} \cdot (\nabla \times \boldsymbol{F}^{\text{wind}}). \tag{39.90}$$

Expanding the left hand side and introducing the planetary vorticity gradient renders the *shallow water Sverdrup balance*

$$\beta\, v = Q^{\text{pg}}\, \boldsymbol{u} \cdot \nabla h + \hat{\boldsymbol{z}} \cdot (\nabla \times \boldsymbol{F}^{\text{wind}}) \qquad \text{shallow water Sverdrup balance.} \tag{39.91}$$

This balance states how horizontal advection of layer thickness (first right hand side term) plus the wind stress curl (second term) balance meridional motion for flow on a rotating sphere (beta effect on left hand side). Gradients in the layer thickness arise from free surface undulations as well as gradients in the bottom topography (see Figure 35.1). The traditional *Sverdrup balance* arises when we assume the flow takes place over a flat bottom and the free surface undulations are negligible, in which case $\nabla h = 0$ so that

$$\beta\, v = \hat{\boldsymbol{z}} \cdot (\nabla \times \boldsymbol{F}^{\text{wind}}) \qquad \text{traditional Sverdrup balance.} \tag{39.92}$$

This balance is also suited to a stratified ocean in regions where the upper ocean flow does not interact with the bottom, such as in regions far from the continental shelves, or in regions where vertical stratification (i.e., the pynocline) shields the upper ocean flows from bottom topography.

39.7.3 Taylor-Proudman, Sverdrup balance, and f/h invariance

Material invariance of planetary geostrophic potential vorticity, $Q^{\rm pg} = f/h$, has a geometric interpretation in terms of the Taylor-Proudman vertical stiffening discussed in Section 31.5.3. As shown in Figure 39.8, since $Q^{\rm pg}$ is materially conserved then so is the stiffness distance, $h^{\rm stiff} = h/\sin\phi = 2\,\Omega/Q^{\rm pg}$, where we wrote the Coriolis parameter as $f = 2\,\Omega\sin\phi$. Material invariance of $h^{\rm stiff}$ manifests the Taylor-Proudman effect, whereby geostrophically balanced fluid columns are stiffened in the direction of the rotation axis. Here, the rotation axis is the planetary axis through the poles.

Vertical fluid columns respecting the planetary geostrophic balance are stiffened in a direction that parallels the planetary rotation axis. As a result, processes that cause the layer thickness, h, to squash/compress must occur with equatorward movement, whereas expansion/stretching of layer thickness occurs with poleward movement. Figure 39.8 provides a geometric lens for understanding the shallow water Sverdrup balance (39.91) discussed in Section 39.7.2, with boundary stresses and nonlinear advection leading to changes in layer thickness and so leading to meridional motion. This geometrical view makes it clear that Sverdrup balance requires planetary curvature.

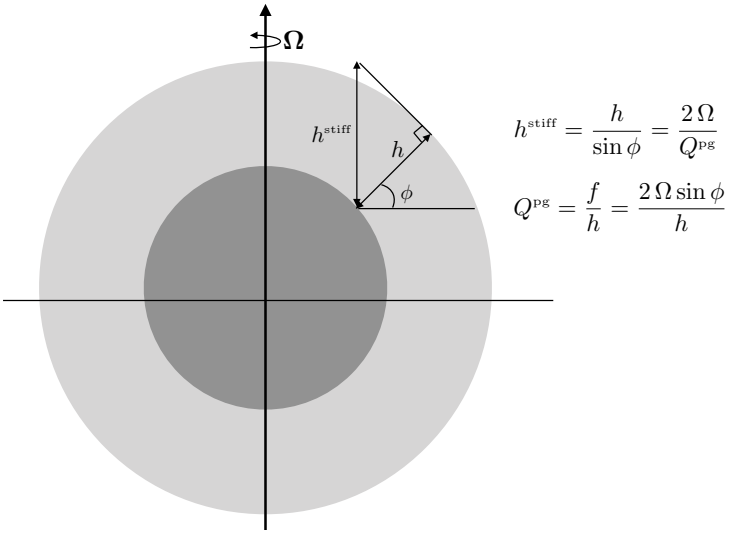

FIGURE 39.8: This figure depicts a homogeneous layer of shallow water fluid (light gray shell; not drawn to scale!) covering a rotating planet, with h the fluid layer thickness. Material invariance of planetary geostrophic potential vorticity, $Q^{\rm pg} = f/h = 2\,\Omega\sin\phi/h$, also means that the distance, $h^{\rm stiff} = h/\sin\phi = 2\,\Omega/Q^{\rm pg}$, is materially conserved. Material conservation of $h^{\rm stiff}$ reflects the vertical stiffening along the rotational axis that occurs for geostrophic flows as per the Taylor-Proudman effect (Section 31.5.3). Processes that change the layer thickness correspond to meridional movement of the fluid column in such a manner to maintain material invariance of $h^{\rm stiff}$. Namely, a process that causes h to squash/compress leads to equatorward movement whereas expanding/stretching h leads to poleward movement. This constrained motion extends to multiple shallow water layers, yet with the interior interfaces allowed to expand or contract. This figure is inspired by Figure 1 of *Rhines* (1980).

39.7.4 Sverdrup flow in a closed domain with anti-cyclonic wind stress

Consider a closed northern hemisphere middle latitude β-plane domain driven by an anti-cyclonic wind stress

$$\hat{\boldsymbol{z}} \cdot (\nabla \times \boldsymbol{F}^{\rm wind}) < 0 \qquad \text{northern hemisphere anti-cyclonic wind stress.} \tag{39.93}$$

This situation is depicted in Figure 39.9, where we also illustrate a commonly used wind stress profile that is purely zonal and has a co-sinusoidal meridional structure that is symmetric about

the central latitude of the domain

$$\boldsymbol{F}^{\text{wind}} = -\hat{\boldsymbol{x}}\, A \cos[\pi\,(y - y_0 + L/2)/L] \tag{39.94a}$$

$$\hat{\boldsymbol{z}} \cdot (\nabla \times \boldsymbol{F}^{\text{wind}}) = -(\pi\, A/L) \sin[\pi\,(y - y_0 + L/2)/L]. \tag{39.94b}$$

In these equations, $A > 0$ is the magnitude of the wind stress acceleration applied to the layer, and the domain extends meridionally from $y_0 - L/2 \leq y \leq y_0 + L/2$ with $y = y_0$ the central latitude. This wind stress has westerlies on the poleward side of the domain and easterlies (trade winds) on the equatorward side so that $\hat{\boldsymbol{z}} \cdot (\nabla \times \boldsymbol{\tau}) < 0$ throughout the domain.

The Sverdrup balance (39.92) indicates that an anti-cyclonic wind stress curl drives an equatorward Sverdrup flow. We emphasize that this flow is *not* the result of meridional winds pushing the fluid to the south. Instead, it arises in response to the constraints of vorticity balance with an anti-cyclonic wind stress curl in the presence of the beta effect. Indeed, for the idealized wind stress (39.94a) there is no meridional wind component. Although fluid satisfying Sverdrup balance flows south, all the fluid in the domain cannot be moving to the south. Rather, volume conservation requires a poleward return flow somewhere outside the region of Sverdrup balance.

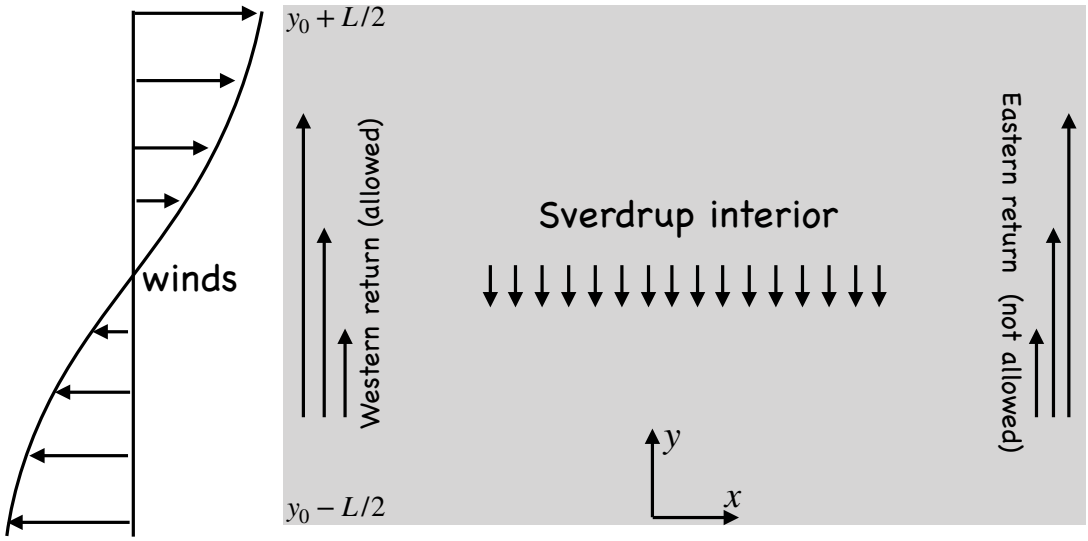

FIGURE 39.9: Illustrating the southward Sverdrup flow in response to an anti-cyclonic wind stress forcing in a bounded northern hemisphere domain. A northward return flow is required to satisfy volume conservation. As seen in Section 39.7.5, a linear vorticity balance between beta, winds, and friction lead to a western boundary return flow and corresponding western intensification. An analogous eastern intensification is not dynamically allowed.

39.7.5 Western intensification and the role of beta

Volume conservation is a kinematic constraint that requires a return flow on either the eastern or western side of the domain, outside the region of Sverdrup balance. But what side? We offer the following arguments for the western side, with these arguments representing the basic elements to the *Stommel model*.

Inertial entry into a boundary layer region

Recall the discussion of Figure 38.4 where we considered how inviscid flow of a two-dimensional non-divergent fluid over a flat bottom region materially preserves absolute vorticity in the

presence of a meridional barrier. To materially preserve absolute vorticity (and ignoring free surface undulations relative to the depth of the fluid), the flow can deviate meridionally, either northward or southward, when encountering a western wall. In contrast, such meridional deviation is prohibited for absolute vorticity preserving flow that encounters an eastern wall. So in referring to Figure 39.9, southward flow can make a turn westward towards the western boundary, enter the boundary layer, and move northward within the boundary layer. It cannot do so for the eastern side. The central limitation of this argument concerns the presence of dissipation in the boundary, in which absolute vorticity is no longer materially preserved. Even so, the argument offers a useful first suggestion for the flow favoring the western side.

Steady vorticity balance and a role for dissipation

Even if the western side is the preferred region for the return flow, we still need an argument for intensification of that flow. To develop an argument, recall that the return flow region is not in Sverdrup balance. To see what terms can break that balance, consider again the steady vorticity balance (39.88). Continuing to assume a flat bottom and rigid lid surface leads to

$$\beta\, v = -\gamma\, \zeta + \hat{\boldsymbol{z}} \cdot (\nabla \times \boldsymbol{F}^{\text{wind}}), \tag{39.95}$$

where we dropped the nonlinear advection term $\boldsymbol{u} \cdot \nabla\zeta$ (the "inertial" term) since we wish to determine whether a linear balance can give rise to western intensification (we return to this assumption in Section 39.7.9). The Rayleigh drag on the right hand side breaks the Sverdrup balance in regions where the relative vorticity is nontrivial. Since we know there must be a return flow somewhere in the domain, we know there must be a region where dissipation is sufficiently strong to break Sverdrup balance.

What is required for the steady and linear dissipative vorticity balance (39.95) to be maintained in the northward return flow region? To answer this question, expose the signs on the terms in equation (39.95)

$$\underbrace{\beta\, v}_{\text{positive}} + \underbrace{\gamma\, \zeta}_{\text{unspecified}} = \underbrace{\hat{\boldsymbol{z}} \cdot (\nabla \times \boldsymbol{F}^{\text{wind}})}_{\text{negative}}. \tag{39.96}$$

We have $\beta\, v > 0$ since we are concerned with the region of northward return flow, and $\hat{\boldsymbol{z}} \cdot (\nabla \times \boldsymbol{F}^{\text{wind}}) < 0$ by assumption of anti-cyclonic wind stress over the full domain. Hence, for the balance (39.96) to be realized requires $\zeta < 0$, with the value large enough to balance both the winds and the meridional advection of planetary vorticity

$$\underbrace{\gamma\, \zeta}_{\text{negative}} = \underbrace{-\beta\, v}_{\text{negative}} + \underbrace{\hat{\boldsymbol{z}} \cdot (\nabla \times \boldsymbol{F}^{\text{wind}})}_{\text{negative}}. \tag{39.97}$$

For anti-cyclonic gyre flow, as required by the circulation condition (39.84), the only way to realize $\zeta < 0$ of sufficient magnitude is to have an intensified flow along the western side of the gyre. In this region, $\zeta \approx \partial v/\partial x < 0$ can become sufficiently large in magnitude. Furthermore, since the wind stress is applied throughout the domain, all streamlines feel the winds and must pass through the western boundary region where vorticity is enhanced and Rayleigh drag is able to balance the winds and planetary advection. The required boundary current flow is depicted in Figure 39.9.

The importance of beta

In the absence of beta, there would be no interior region in Sverdrup balance driving southward flow. The flow would thus only be subject to the circulation condition (39.84) whereby linear flow can symmetrically dissipate the wind stress. Hence, the beta effect is the fundamental

element that causes poleward flow to intensify along the western side of the gyre in response to the equatorward interior flow.

Western intensification regardless the sense for the wind stress curl

The steady circulation theorem (39.84) means that the flow circulation is in the same sense as the wind circulation. The arguments offered above for western intensification focused on the anti-cyclonic winds, as per the middle latitude gyres in the northern hemisphere Atlantic and Pacific oceans. What if the winds were cyclonic? In that case, the steady circulation theorem (39.84) means that the circulation is also cyclonic. Even so, the arguments based on the beta effect still result in western intensification. Namely, with cyclonic winds the interior Sverdrup flow is northward, so that the return flow must be southward. For this case, equation (39.97) now takes the form

$$\underbrace{\gamma\,\zeta}_{\text{positive}} = \underbrace{-\beta\,v}_{\text{positive}} + \underbrace{\hat{\boldsymbol{z}}\cdot(\nabla\times\boldsymbol{F}^{\text{wind}})}_{\text{positive}}. \tag{39.98}$$

Again, we find that vorticity arguments lead to western intensifiction of the cyclonic gyre.

The Stommel equation for the streamfunction

By assuming a rigid lid and homogeneous fluid layer, the fluid velocity is horizontally non-divergent and so it can be written in terms of a streamfunction

$$\nabla\cdot(h\,\boldsymbol{u}) = h\,\nabla\cdot\boldsymbol{u} = 0 \Longrightarrow \boldsymbol{u} = \hat{\boldsymbol{z}}\times\nabla\psi = h^{-1}\,\hat{\boldsymbol{z}}\times\nabla\Psi, \tag{39.99}$$

where Ψ is the streamfunction for the thickness weighted velocity from equation (39.79). Introducing the streamfunction into the linearized vorticity balance (39.95) leads to

$$(\gamma\,\nabla^2 + \beta\,\partial_x)\,\psi = \hat{\boldsymbol{z}}\cdot(\nabla\times\boldsymbol{F}^{\text{wind}}). \tag{39.100}$$

We encountered this linear partial differential equation in Section 38.6.4 when studying the beta plume. The two problems describe steady gyre circulations in the presence of Rayleigh drag, the beta effect, and wind stress curl. For the beta plume we ignored boundaries and solved for the free space Green's function shown in Figure 38.7. Here, the western boundary is a fundamental feature of the problem, with further analysis prompting the use of rudimentary boundary layer theory to match the interior Sverdrup solution to the boundary region. That analysis is summarized in Section 19.1.3 of *Vallis* (2017).

39.7.6 A role for bottom pressure torques

Recall the shallow water Sverdrup balance (39.91), here with the addition of Rayleigh drag

$$\beta\,v = Q^{\text{pg}}\,\boldsymbol{u}\cdot\nabla h - \gamma\,\zeta + \hat{\boldsymbol{z}}\cdot(\nabla\times\boldsymbol{F}^{\text{wind}}). \tag{39.101}$$

For the right hand side, we have thus far considered a flat bottom and ignored free surface undulations, in which case $\nabla h = 0$. In this case, the only way to balance meridional motion on a beta plane is to invoke non-conservative processes either from wind stress or Rayleigh drag.

Spatial variations in the bottom topography open up the possibility for an inviscid balance

$$\beta\,v = Q^{\text{pg}}\,\boldsymbol{u}\cdot\nabla h, \tag{39.102}$$

or more generally a balance where frictional vorticity sinks are unimportant except for regions very close to the boundary. For example, consider northward flow in the northern hemisphere along a shallow western continental shelf. Assume the bottom topography only has variations in

the zonal direction, with $\partial_x h > 0$ reflecting deeper water to the east of the shelf. The inviscid vorticity balance (39.102) thus takes the form

$$\beta\, v = (f/h)\, u\, \partial_x h. \tag{39.103}$$

Since $\beta\, v > 0$ and $(f/h)\, \partial_x h > 0$, we must have $u > 0$. Hence, flow departs from purely northward motion by leaving the shelf and moving into deeper waters. This behavior is also revealed by the western shelf example in Figure 39.5, where the f/H contours deviate from contours of constant depth when there is a nonzero β. As examined in this section, the bottom pressure torque, arising from bottom topographic form stress, plays the lead role in the corresponding vorticity balance.

Curl of the form stresses

In the present analysis, we are only concerned with that portion of $\boldsymbol{u} \cdot \nabla h$ directly arising from pressure gradients. We thus consider just the geostrophic flow to arrive at

$$\boldsymbol{u} \cdot \nabla h = (g/f)\, \nabla h \cdot (\hat{\boldsymbol{z}} \times \nabla \eta) = (g/f)\, \hat{\boldsymbol{z}} \cdot (\nabla \eta \times \nabla h). \tag{39.104}$$

It is this term that contains the various pressure torques arising from form stresses. But before unpacking those torques, briefly return to the above shelf example and note that with $\nabla h = \hat{\boldsymbol{x}}\, \partial_x h$ then there is a nonzero $\boldsymbol{u} \cdot \nabla h$ only with a nonzero $\partial_y \eta$, which in turn means there is a nonzero zonal geostrophic flow. As noted above, this zonal flow is a consequence of the sloping bottom topography.

Pressure torques

Returning to the general situation, we determine the expressions for the pressure torques contained in the term $\boldsymbol{u} \cdot \nabla h$ by making use of the hydrostatic relation $p_{\mathrm{b}} = p_{\mathrm{a}} + \rho\, g\, h$, and the layer thickness, $h = \eta - \eta_{\mathrm{b}}$ (see Figure 35.1), in which case

$$\begin{aligned}
\boldsymbol{u} \cdot \nabla h &= (g/f)\, \hat{\boldsymbol{z}} \cdot (\nabla \eta \times \nabla h) && \text{(39.105a)}\\
&= 1/(\rho\, f)\, \hat{\boldsymbol{z}} \cdot [\nabla \times (p_{\mathrm{a}} \nabla \eta) + \nabla \eta \times \nabla p_{\mathrm{b}}] && \text{(39.105b)}\\
&= 1/(\rho\, f)\, \hat{\boldsymbol{z}} \cdot [\nabla \times (p_{\mathrm{a}} \nabla \eta) - \nabla \times (p_{\mathrm{b}} \nabla \eta_{\mathrm{b}}) + \nabla h \times \nabla p_{\mathrm{b}}] && \text{(39.105c)}\\
&= 1/(\rho\, f)\, \hat{\boldsymbol{z}} \cdot [\nabla \times (p_{\mathrm{a}} \nabla \eta) - \nabla \times (p_{\mathrm{b}} \nabla \eta_{\mathrm{b}}) + \nabla p_{\mathrm{b}} \times \nabla p_{\mathrm{a}}/(\rho\, g)]\,. && \text{(39.105d)}
\end{aligned}$$

The first and second terms are the curls of the pressure form stresses applied to the surface (atmospheric) and bottom boundaries (Section 28.2), respectively, which we refer to as the atmospheric and bottom pressure torques. The third term is a torque arising from misalignment of the applied pressure and bottom pressure. Inserting equation (39.105d) in the vorticity balance (39.101) leads to the steady balance

$$\beta\, \rho\, h\, v = \hat{\boldsymbol{z}} \cdot [\nabla \times (p_{\mathrm{a}} \nabla \eta) - \nabla \times (p_{\mathrm{b}} \nabla \eta_{\mathrm{b}}) + \nabla p_{\mathrm{b}} \times \nabla p_{\mathrm{a}}/(\rho\, g)] + \rho\, h\, [-\gamma\, \zeta + \hat{\boldsymbol{z}} \cdot (\nabla \times \boldsymbol{F}^{\mathrm{wind}})]\,. \tag{39.106}$$

We consider a few special cases to see how the pressure torques affect the meridional flow in a gyre circulation, with a focus on bottom pressure torque since this term is generally far larger than those torques involving the atmospheric pressure.

Inviscid balance between meridional flow and bottom pressure torque

In the absence of friction and wind forcing, and with a uniform atmospheric pressure ($\nabla p_{\mathrm{a}} = 0$), then β times the depth integrated meridional mass transport in equation (39.106) is balanced

by the bottom pressure torque (i.e., curl of the topographic form stress)

$$\beta \rho h v = -\hat{\boldsymbol{z}} \cdot (\nabla \times p_{\mathrm{b}} \nabla \eta_{\mathrm{b}}) \qquad \text{linear inviscid and unforced.} \tag{39.107}$$

Again consider the example of northward flow along a western continental shelf. In this case, $\nabla \eta_{\mathrm{b}} = \hat{\boldsymbol{x}}\, \partial_x \eta_{\mathrm{b}} < 0$, so that the balance (39.107) reduces to

$$\beta \rho h v = \partial_y p_{\mathrm{b}}\, \partial_x \eta_{\mathrm{b}}. \tag{39.108}$$

This balance says that if the bottom depth increases eastward away from the shelf, so that $\partial_x \eta_{\mathrm{b}} < 0$, then northward flow corresponds to a northward decrease in the bottom pressure, $\partial_y p_{\mathrm{b}} < 0$. That is, the northward flow is directed down the bottom pressure gradient.

Association rather than causality

The inviscid planetary geostrophic balance (39.107) does not express causality. Rather, it expresses a balance or association that is maintained by steady linear flows in the presence of sloping topography. Hence, it is incorrect to say that bottom pressure torque gives rise to (i.e., causes) inviscid planetary geostrophic flow. Rather, the balance (39.107) says for planetary geostrophic flow, there is no bottom pressure torque without a meridional flow, and conversely there is no meridional flow without bottom pressure torque.

Vanishing topographic form stress curl for geostrophic f-plane motion

From the balance (39.107), we find that a linear inviscid and unforced geostrophic flow on an f-plane satisfies

$$\hat{\boldsymbol{z}} \cdot (\nabla \times p_{\mathrm{b}} \nabla \eta_{\mathrm{b}}) = \hat{\boldsymbol{z}} \cdot (\nabla p_{\mathrm{b}} \times \nabla \eta_{\mathrm{b}}) = 0 \quad \beta = 0. \tag{39.109}$$

When we can ignore the applied surface pressure, $p_{\mathrm{a}} = 0$, then the bottom pressure is given by $p_{\mathrm{b}} = g \rho h = g \rho (\eta - \eta_{\mathrm{b}})$, in which case $\hat{\boldsymbol{z}} \cdot (\nabla p_{\mathrm{b}} \times \nabla \eta_{\mathrm{b}}) = \hat{\boldsymbol{z}} \cdot (\nabla \eta \times \nabla \eta_{\mathrm{b}})$. Evidently, linear inviscid and unforced geostrophic flow on an f-plane means that $\hat{\boldsymbol{z}} \cdot (\nabla \eta \times \nabla \eta_{\mathrm{b}}) = 0$. That is, isolines of surface height align with isolines of bottom topography. Conversely, surface height contours that deviate from bottom topography contours signal the role of friction and/or β acting on the planetary geostrophic flow.

Local generation of bottom pressure torque

The beta effect provides an inviscid means to balance a misalignment between the surface height and the bottom topography, with misalignment required to generate a nonzero topographic form stress curl, which we have been referring to as the bottom pressure torque. We discussed an analogous misalignment is Section 36.7 when studying the force balances in a steady zonally re-entrant channel with bottom topography. Wind stress forcing and dissipation offer another means to balance $(\eta, \eta_{\mathrm{b}})$-misalignment, as seen merely by rewriting the vorticity balance (39.106) as an expression for the bottom pressure torque

$$\begin{aligned} &\hat{\boldsymbol{z}} \cdot (\nabla \times p_{\mathrm{b}} \nabla \eta_{\mathrm{b}}) = \\ &\quad - \beta \rho h v + \hat{\boldsymbol{z}} \cdot [\nabla \times (p_{\mathrm{a}} \nabla \eta) + \nabla p_{\mathrm{b}} \times \nabla p_{\mathrm{a}} / (\rho g)] + \rho h \left[-\gamma \zeta + \hat{\boldsymbol{z}} \cdot (\nabla \times \boldsymbol{F}^{\mathrm{wind}}) \right]. \end{aligned} \tag{39.110}$$

In our discussion of western intensification in Section 39.7.5, we ignored the role of bottom pressure torque. However, as seen by this balance, bottom pressure torque plays a role when topography and surface height are misaligned, with that role in some locations more important than friction. Ssee *Becker and Salmon* (1997), *Hughes* (2000), *Hughes and de Cueves* (2001), *Jackson et al.* (2006) and *Patmore et al.* (2019) for examples.

39.7.7 Properties of area integrated bottom pressure torques

Consider a simply connected fluid domain bounded by an isobath. Stokes' theorem reveals that the integral of the bottom pressure torque, $\hat{\boldsymbol{z}} \cdot (\nabla \times p_b \nabla \eta_b)$, vanishes when computed over the area bounded by any isobath

$$\int_{\mathcal{S}} \hat{\boldsymbol{z}} \cdot (\nabla \times p_b \nabla \eta_b) \, d\mathcal{S} = \oint_{\partial \mathcal{S}} p_b \nabla \eta_b \cdot \hat{\boldsymbol{t}} \, d\ell = 0. \tag{39.111}$$

The integrand for the line integral vanishes pointwise since, by construction, the boundary, $\partial \mathcal{S}$, is determined by an isobath so its the tangent vector, $\hat{\boldsymbol{t}}$, is orthogonal to $\nabla \eta_b$. The identical argument holds for an area bounded by an isobar of bottom pressure since, for any region,

$$\int_{\mathcal{S}} \hat{\boldsymbol{z}} \cdot (\nabla \times p_b \nabla \eta_b) \, d\mathcal{S} = -\int_{\mathcal{S}} \hat{\boldsymbol{z}} \cdot (\nabla \times \eta_b \nabla p_b) \, d\mathcal{S} = -\oint_{\partial \mathcal{S}} \eta_b \nabla p_b \cdot \hat{\boldsymbol{t}} \, d\ell. \tag{39.112}$$

Now if the region is bounded by an isobar, then $\nabla p_b \cdot \hat{\boldsymbol{t}} = 0$ at each point along the region boundary. With a bit more work, we can show that the area integral of the bottom pressure torque vanishes for an annular region bounded by any two isobaths or any two bottom pressure isobars. The proof is presented in the caption to Figure 39.10.

These mathematical identities mean that bottom pressure torque plays no role in the area integrated vorticity budget for regions bounded by isobaths or bottom pressure isobars. In particular, taking a contour that encircles the global ocean reveals that bottom pressure torque does not alter the global area integrated vorticity. Equivalently, topographic form stresses integrated around a closed contour defined by an isobath or isobar do not alter the circulation around that contour. Evidently, topographic form stress cannot spin-up or spin-down the circulation around a contour determined by isobaths or bottom pressure isobars. Other processes, such as flow nonlinearities, viscous friction, and/or boundary stresses, must play role in determining the circulation since their contour integrals are unconstrained. As studied by *Stewart et al.* (2021), these very special properties of bottom pressure torque and topographic form stress introduce a variety of nuances when interpreting the area integrated vorticity budget.

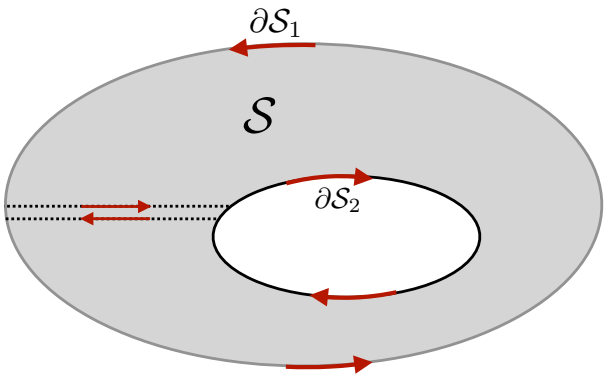

FIGURE 39.10: Stokes' theorem is generally applicable in a simply connected region. However, an annulus region, $\mathcal{S}$, is not simply connected since it has a hole. To apply Stokes' theorem over an annulus we imagine snipping the outer contour, $\partial\mathcal{S}_1$, and inner contour, $\partial\mathcal{S}_2$, and then connecting the two ends of the snipped contours as shown here. In this manner we convert the non-simply connected annulus into a simply connected region, over which we can apply Stokes' theorem in the naive manner. Importantly, we see that the the two segments connecting the inner and outer contour are traversed in opposite directions when performing the contour integral. Assuming all functions are smooth, we can take the limit as these two contours get infinitesimally close, in which they cancel identically. This limit also recovers the connected outer and inner contours. If the outer and inner contours are defined by isobaths or bottom pressure isobars, then the bottom pressure torque identically vanishes on the contours. In this manner we have proven that the bottom pressure torque vanishes within the annulus region. We make use of this method in Exercise 40.10 when considering the circulation in an ocean domain with islands.

39.7.8 Advection-diffusion of the steady streamfunction[6]

Since the steady state flow satisfies $\nabla \cdot (h\,\boldsymbol{u}) = 0$, we can introduce a streamfunction

$$h\,\boldsymbol{u} = \hat{\boldsymbol{z}} \times \nabla \Psi, \tag{39.113}$$

in which case the relative vorticity becomes

$$\zeta = \hat{\boldsymbol{z}} \cdot (\nabla \times \boldsymbol{u}) = \nabla \cdot (h^{-1}\, \nabla \psi), \tag{39.114}$$

and the steady vorticity equation (39.88) can be written

$$\hat{\boldsymbol{z}} \cdot (\nabla \Psi \times \nabla Q) = -\gamma\, \nabla \cdot (h^{-1}\, \nabla \Psi) + \hat{\boldsymbol{z}} \cdot (\nabla \times \boldsymbol{F}^{\text{wind}}). \tag{39.115}$$

Following *Welander* (1968), we interpret equation (39.115) as a steady advection-diffusion equation for Ψ. Namely, introduce the horizontally non-divergent vector

$$\boldsymbol{u}^{(\mathrm{Q})} = \hat{\boldsymbol{z}} \times \nabla Q, \tag{39.116}$$

in which case the streamfunction equation (39.115) becomes

$$\boldsymbol{u}^{(\mathrm{Q})} \cdot \nabla \Psi = \gamma\, \nabla \cdot (h^{-1}\, \nabla \Psi) - \hat{\boldsymbol{z}} \cdot (\nabla \times \boldsymbol{F}^{\text{wind}}). \tag{39.117}$$

With zero wind stress curl and zero Rayleigh drag, the contours of the steady streamfunction are aligned with $\boldsymbol{u}^{(\mathrm{Q})}$; that is, Ψ and Q contours are parallel. In the presence of Rayleigh drag, the streamfunction deviates from the Q contours, as it does in the presence of a wind stress curl.

These results represent a mere repackaging of results found earlier. Even so, the advection-diffusion interpretation offers complementary insights into the patterns of the steady streamfunction. Indeed, as we see in Section 39.9, the advective-diffusive interpretation proves very useful when studying patterns of steady sea level in planetary geostrophic gyres.

39.7.9 Comments and further study

Friction is needed to close the vorticity budget in a flat bottom linear ocean

This video from SciencePrimer provides a concise summary of the dynamics of ocean gyres and western boundary intensification due to the beta effect. Chapter 19 of *Vallis* (2017) provides a lucid treatment of ocean gyre dynamics by working through the key features of the *Stommel* (1948) model, as well as variants such as that from *Munk* (1950), who considered a viscous closure (most important next to side boundaries) rather than the Rayleigh drag used by Stommel. The Stommel model and its variants are themselves very idealized renditions of the ocean gyres occuring in Nature. Notable further factors become important in studying Nature's gyres, such as topography (briefly discussed in Section 39.7.6), flow nonlinearities and instabilities (recall we dropped the inertial term in Section 39.7.5, thus focusing on linear balances), turbulent boundary layers, and coupled air-sea processes. Each of these processes render the study of western boundary currents one of the most complex and timeless areas of physical oceanography.

Distinguishing beta-induced western boundary currents from frictional boundary layers

Western intensification of the gyre, implied by $\beta > 0$, is distinct from a frictional boundary layer, implied by a no-slip side boundary (e.g., Section 25.8). Namely, a frictional western boundary layer, supported by a no-slip solid earth boundary, leads to cyclonic flow within the boundary

[6] We study the physics of advection and diffusion in Chapter 69. For Section 39.7.8 we only require a few basic features of this equation.

layer. In contrast, as discussed in this section, planetary β-induced western intensification gives rise to anti-cyclonic flow in the western boundary current. This distinction emphasizes the importance of the side boundary condition, be it no-slip, free-slip, or partial slip. Namely, the free-slip boundary does not support the cyclonic boundary layer of the no-slip. As explored in *Kiss* (2002) and *Kiss* (2004), these distinct boundary conditions lead to distinct boundary current properties, with impacts on the dynamics of how the boundary current separates from the side.

Topographic form stress reduces the fundamental role of friction

Friction plays a central role in the Stommel and Munk models of western intensification. As described in Chapter 19 of *Vallis* (2017), there have been attempts to produce an inviscid (and unforced) gyre solution, with the study from *Fofonoff* (1954) of particular note. We consider elements of the Fofonoff gyre in Exercise 38.12. Additionally, we raised the importance of sloping sides in Section 39.7.6 and in the earlier discussion of axial angular momentum in Section 28.5. Sloping sides enable bottom topographic form stress and bottom pressure torques to dominate over bottom turbulent stresses and turbulent torques. In so doing, sloping sides play a leading role in gyre balances, though we did note in the discussion surrounding equation (39.111) that friction remains essential to close the vorticity balance integrated around the gyre. The role of sloping sides for gyre circulations was emphasized by *Hughes* (2000), *Hughes and de Cueves* (2001), with *Stewart et al.* (2021) identifying further nuances related to the integrated properties in Section 39.7.7.

Flow nonlinearities also reduce the role of friction

Furthermore, we ignored the role of nonlinearities, which generally require the use of numerical models to investigate. Indeed, one of the first numerical simulations was from *Bryan* (1963), who showed that western boundary currents in a flat bottom gyre generally experience hydrodynamical instabilities when the flows become strong enough. *Becker and Salmon* (1997) and *Becker* (1999) further studied the case of a nonlinear gyre circulation in the presence of a sloping side shelf, thus allowing for the role of both nonlinearities and topographic form stress in the vorticity balance. These, and many other, studies allow for inviscid contributions to the vorticity balance, thus alleviating the need for invoking strong frictional effects found in the models of Stommel and Munk.

39.8 Column vorticity

Throughout this chapter we have focused on vorticity as defined by the curl of the horizontal velocity, $\zeta = \hat{\boldsymbol{z}} \cdot (\nabla \times \boldsymbol{u})$. Since flow within a shallow water layer moves in coherent and extensible vertical columns (Section 35.2), the shallow water vorticity measures the spin of a shallow water column.

We can also measure the column spin by considering the curl of the thickness weighted velocity

$$\Sigma = \hat{\boldsymbol{z}} \cdot \nabla \times (h\, \boldsymbol{u}) = h\, \zeta + \hat{\boldsymbol{z}} \cdot \nabla h \times \boldsymbol{u}. \tag{39.118}$$

We refer to Σ as the *column vorticity*, though note that it has the dimensions of a velocity due to the thickness weighting. In addition to the thickness weighted relative vorticity, the column vorticity measures the misalignment between the layer thickness gradient and the velocity, with $\hat{\boldsymbol{z}} \cdot \nabla h \times \boldsymbol{u}$ generally nonzero especially for geostrophic flows. Hence, the second term offers an extra measure of the spin for the fluid column beyond the relative vorticity measure.[7] The

[7] Exercise 39.8 offers a particular example of a geostrophic flow that is aligned perpendicular to ∇h, as found

layer thickness factor ensures that Σ directly probes stresses acting at the layer interfaces, as well as stresses within the fluid layer. Besides its intrinsic interest, this analysis is motivated by studies of the depth integrated flow commonly pursued in oceanography, with examples studied in Chapter 44. It also provides a venue for studying vorticity in those situations where the shallow water layer thickness vanishes, such as for a shallow water layer along a sloping side boundary.

39.8.1 Formulating the column vorticity equation

To formulate the dynamical equation for Σ, we start from the momentum equation (36.29)

$$\frac{\partial(h\,\boldsymbol{u})}{\partial t} + \nabla\cdot(h\,\boldsymbol{u}\otimes\boldsymbol{u}) + f\,\hat{\boldsymbol{z}}\times(h\,\boldsymbol{u}) = -g\,h\,\nabla\eta^{\text{eff}} + \boldsymbol{f}^{\text{nc}} \tag{39.119}$$

where

$$\boldsymbol{f}^{\text{nc}} = h\,\boldsymbol{F} \tag{39.120}$$

is the thickness weighted acceleration (dimension of squared velocity) arising from non-conservative processes, such as from horizontal strains in the presence of viscosity and the boundary transfer of turbulent momentum such as through winds and bottom drag (see Section 35.6). For example, recall the acceleration given by equation (39.81), which is built from Rayleigh drag plus wind stress, in which case

$$\boldsymbol{f}^{\text{nc}} = -\gamma\,h\,\boldsymbol{u} + \boldsymbol{\tau}^{\text{wind}}/\rho = -\gamma\,h\,\boldsymbol{u} + h\,\boldsymbol{F}^{\text{wind}}. \tag{39.121}$$

Taking the vertically projected curl of equation (39.119) leads to

$$\partial_t\Sigma + \hat{\boldsymbol{z}}\cdot\nabla\times[\nabla\cdot(h\,\boldsymbol{u}\otimes\boldsymbol{u})] + \nabla\cdot(f\,h\,\boldsymbol{u}) = -g\,\hat{\boldsymbol{z}}\cdot(\nabla h\times\nabla\eta^{\text{eff}}) + \hat{\boldsymbol{z}}\cdot(\nabla\times\boldsymbol{f}^{\text{nc}}). \tag{39.122}$$

Let us now examine each of these terms and offer physical interpretations.

Frictional torques and boundary pressure torques

The term $\hat{\boldsymbol{z}}\cdot(\nabla\times\boldsymbol{f}^{\text{nc}})$ in equation (39.122) provides a torque from boundary stresses and interior viscous stresses. The term $g\,\nabla h\times\nabla\eta^{\text{eff}}$ provides a torque whenever the thickness gradients are not aligned with the gradients in the effective surface height. We can write this term in the equivalent form based on the following identities

$$\begin{aligned}
\rho\,g\,\nabla h\times\nabla\eta^{\text{eff}} &= \rho\,g\,\nabla h\times\nabla\eta + \nabla h\times\nabla p_{\text{a}} && \text{(39.123a)}\\
&= -\nabla p_{\text{a}}\times\nabla\eta + \nabla p_{\text{b}}\times\nabla\eta + \nabla(p_{\text{b}}-p_{\text{a}})\times\nabla p_{\text{a}}/(\rho\,g) && \text{(39.123b)}\\
&= -\nabla p_{\text{a}}\times\nabla\eta + \nabla p_{\text{b}}\times\nabla[\eta + p_{\text{a}}/(\rho\,g)] && \text{(39.123c)}\\
&= -\nabla p_{\text{a}}\times\nabla\eta + \nabla p_{\text{b}}\times\nabla[\eta_{\text{b}} + h + p_{\text{a}}/(\rho\,g)] && \text{(39.123d)}\\
&= -\nabla p_{\text{a}}\times\nabla\eta + \nabla p_{\text{b}}\times\nabla\eta_{\text{b}} && \text{(39.123e)}\\
&= \nabla\times(-p_{\text{a}}\,\nabla\eta + p_{\text{b}}\,\nabla\eta_{\text{b}}), && \text{(39.123f)}
\end{aligned}$$

where we made use of the hydrostatic relation $p_{\text{b}} = p_{\text{a}} + \rho\,g\,h$. We thus see that $-g\,\nabla h\times\nabla\eta^{\text{eff}} = \rho^{-1}\nabla\times(p_{\text{a}}\,\nabla\eta - p_{\text{b}}\,\nabla\eta_{\text{b}})$ arises from pressure torques acting on the surface and bottom interfaces of the shallow water layer. These torques spin the column if there is a misalignment between the boundary pressure gradients and the boundary surface slopes. Notably, it is commonly the case that the torque associated with the applied surface pressure is far smaller than that from the bottom pressure, in which case

$$-g\,\nabla h\times\nabla\eta^{\text{eff}} \approx -\rho^{-1}\nabla\times(p_{\text{b}}\,\nabla\eta_{\text{b}}) = -\rho^{-1}\nabla p_{\text{b}}\times\nabla\eta_{\text{b}}. \tag{39.124}$$

in a geostrophic shallow water front.

Torque from the nonlinear transport

The nonlinear term $\hat{\boldsymbol{z}} \cdot \nabla \times [\nabla \cdot (h\,\boldsymbol{u} \otimes \boldsymbol{u})]$ can be written

$$\begin{aligned}
\hat{\boldsymbol{z}} \cdot \nabla \times [\nabla \cdot (h\,\boldsymbol{u} \otimes \boldsymbol{u})] &= \hat{z}_m\, \epsilon_{mst}\, \partial_s[\partial_n\,(h\,u_n\,u_t)] && \text{(39.125a)}\\
&= \partial_n\, \partial_s[(h\,u_n)\, \epsilon_{mst}\, \hat{z}_m\, u_t] && \text{(39.125b)}\\
&= \partial_n[\partial_s(h\,u_n)\, \epsilon_{mst}\, \hat{z}_m\, u_t + h\,u_n\,\zeta] && \text{(39.125c)}\\
&= -\partial_n[\epsilon_{smt}\, \hat{z}_m\, u_t\, \partial_s(h\,u_n)] + \nabla \cdot (h\,\zeta\,\boldsymbol{u}), && \text{(39.125d)}
\end{aligned}$$

which exposes the divergence of the thickness weighted advective flux of relative vorticity. Further manipulations lead to

$$\begin{aligned}
-\partial_n[\epsilon_{smt}\, \hat{z}_m\, u_t\, \partial_s(h\,u_n)] &= -\partial_n[\epsilon_{smt}\, \hat{z}_m\, u_t\, u_n\, \partial_s h + \epsilon_{smt}\, \hat{z}_m\, u_t\, h\, \partial_s u_n] && \text{(39.126a)}\\
&= \partial_n[\hat{z}_m\, (\epsilon_{mst}\, \partial_s h\, u_t)\, u_n - h\, \epsilon_{smt}\, \hat{z}_m\, u_t\, \partial_s u_n] && \text{(39.126b)}\\
&= \nabla \cdot [\hat{\boldsymbol{z}} \cdot (\nabla h \times \boldsymbol{u})\, \boldsymbol{u}] - \partial_n[h\, (\hat{\boldsymbol{z}} \times \boldsymbol{u}) \cdot \nabla u_n] && \text{(39.126c)}\\
&= \nabla \cdot [\hat{\boldsymbol{z}} \cdot (\nabla h \times \boldsymbol{u})\, \boldsymbol{u}] + \nabla \cdot [h\, (v\, \partial_x - u\, \partial_y) \boldsymbol{u}], && \text{(39.126d)}
\end{aligned}$$

so that the nonlinear term takes the form

$$\hat{\boldsymbol{z}} \cdot \nabla \times [\nabla \cdot (h\,\boldsymbol{u} \otimes \boldsymbol{u})] = \nabla \cdot [\Sigma\, \boldsymbol{u} + h\, (v\, \partial_x - u\, \partial_y)\, \boldsymbol{u}] = \nabla \cdot [\Sigma\, \boldsymbol{u} + h\, (\boldsymbol{u}_{\rm clock} \cdot \nabla)\, \boldsymbol{u}]. \quad \text{(39.127)}$$

The first term inside the square bracket is the advective flux of Σ. The second term is the thickness weighted transport of $\boldsymbol{u}$ by the clockwise rotated horizontal velocity

$$\boldsymbol{u}_{\rm clock} = -\hat{\boldsymbol{z}} \times \boldsymbol{u}. \quad \text{(39.128)}$$

39.8.2 Summary of the column vorticity equation

The above manipulations bring the Σ equation (39.122) into the flux-form

$$\partial_t \Sigma = -\nabla \cdot \boldsymbol{J}^{\Sigma} + \rho^{-1}\, \hat{\boldsymbol{z}} \cdot \nabla \times [-p_{\rm a} \nabla \eta + p_{\rm b} \nabla \eta_{\rm b} + \rho\, \boldsymbol{f}^{\rm nc}], \quad \text{(39.129)}$$

where

$$\boldsymbol{J}^{\Sigma} \equiv [h\, f + \Sigma + h\, (v\, \partial_x - u\, \partial_y)]\, \boldsymbol{u} = h\, \zeta_{\rm a}\, \boldsymbol{u} + [v\, (\partial_x h + h\, \partial_x) - u\, (\partial_y h + h\, \partial_y)]\, \boldsymbol{u} \quad \text{(39.130)}$$

is the total flux of Σ. The corresponding material time derivative form of equation (39.129) is given by

$$\frac{\mathrm{D}\Sigma}{\mathrm{D}t} + \Sigma\, \nabla \cdot \boldsymbol{u} + \nabla \cdot [h\, f\, \boldsymbol{u} + h\, (v\, \partial_x - u\, \partial_y)\, \boldsymbol{u}] = \rho^{-1}\, \hat{\boldsymbol{z}} \cdot \nabla \times [-p_{\rm a} \nabla \eta + p_{\rm b} \nabla \eta_{\rm b} + \rho\, \boldsymbol{f}^{\rm nc}]. \quad \text{(39.131)}$$

The thickness equation (35.119)

$$\frac{\mathrm{D}h}{\mathrm{D}t} = -h\, \nabla \cdot \boldsymbol{u} + w^{(\dot{\eta})}, \quad \text{(39.132)}$$

brings equation (39.131) into the form

$$h\, \frac{\mathrm{D}(\Sigma/h)}{\mathrm{D}t} + \nabla \cdot [h\, f\, \boldsymbol{u} - h\, \hat{\boldsymbol{z}} \cdot (\boldsymbol{u} \times \nabla)\, \boldsymbol{u}] = -\frac{\Sigma\, w^{(\dot{\eta})}}{h} + \rho^{-1}\, \hat{\boldsymbol{z}} \cdot \nabla \times [-p_{\rm a} \nabla \eta + p_{\rm b} \nabla \eta_{\rm b} + \rho\, \boldsymbol{f}^{\rm nc}], \quad \text{(39.133)}$$

where we wrote

$$v\, \partial_x - u\, \partial_y = -\hat{\boldsymbol{z}} \cdot (\boldsymbol{u} \times \nabla). \quad \text{(39.134)}$$

39.8.3 Steady linear column vorticity balance and the island rule

To garner experience with the column vorticity equation (39.129), consider the steady state and assume $\boldsymbol{J}^{\Sigma}$ is dominated by the planetary vorticity

$$\boldsymbol{J}^{\Sigma} \approx h\, f\, \boldsymbol{u}, \tag{39.135}$$

in which case the budget equation (39.129) reduces to the balance

$$\nabla \cdot (h\, f\, \boldsymbol{u}) = \rho^{-1}\, \hat{\boldsymbol{z}} \cdot \nabla \times [-p_{\mathsf{a}} \nabla \eta + p_{\mathsf{b}} \nabla \eta_{\mathsf{b}} + \rho\, \boldsymbol{f}^{\mathrm{nc}}]. \tag{39.136}$$

Hence, torques due to interface pressures and turbulent stresses are balanced by the divergence of the thickness weighted advective flux of planetary vorticity. Furthermore, since $\nabla \cdot (h\, \boldsymbol{u}) = 0$ in the steady state, equation (39.136) takes the form

$$\rho\, h\, \beta\, v = \hat{\boldsymbol{z}} \cdot \nabla \times (-p_{\mathsf{a}} \nabla \eta + p_{\mathsf{b}} \nabla \eta_{\mathsf{b}} + \rho\, \boldsymbol{f}^{\mathrm{nc}}), \tag{39.137}$$

which connects to the discussion of pressure torques given in Section 39.7.6. It says that for planetary geostrophic flow, meridional transport in the presence of $\beta \neq 0$ is balanced by the torques arising from atmospheric and bottom form stresses, as well as from non-conservative processes such as wind stress, viscous friction, and bottom drag.

Formulating an integral balance

The local balance (39.136) holding for planetary geostrophic flow leads to an integral balance through an area integral computed over an arbitrary closed domain

$$\oint_{\mathcal{S}} \nabla \cdot (h\, f\, \boldsymbol{u})\, \mathrm{d}\mathcal{S} = \rho^{-1} \oint_{\mathcal{S}} \hat{\boldsymbol{z}} \cdot \nabla \times [-p_{\mathsf{a}} \nabla \eta + p_{\mathsf{b}} \nabla \eta_{\mathsf{b}} + \rho\, \boldsymbol{f}^{\mathrm{nc}}]\, \mathrm{d}\mathcal{S}. \tag{39.138}$$

Making use of Gauss' divergence theorem on the left hand side and Stokes' curl theorem on the right hand side renders

$$\oint_{\partial \mathcal{S}} h\, f\, \boldsymbol{u} \cdot \hat{\boldsymbol{n}}\, \mathrm{d}\ell = \rho^{-1} \oint_{\partial \mathcal{S}} [-p_{\mathsf{a}} \nabla \eta + p_{\mathsf{b}} \nabla \eta_{\mathsf{b}} + \rho\, \boldsymbol{f}^{\mathrm{nc}}] \cdot \hat{\boldsymbol{t}}\, \mathrm{d}\ell. \tag{39.139}$$

The left hand side is a contour integral with $\hat{\boldsymbol{n}}$ the unit outward normal along the contour. The right hand side is also a contour integral, yet with $\hat{\boldsymbol{t}}$ the unit tangent along the contour oriented in the counter-clockwise sense. The integral balance (39.139) says that the advective transport of planetary vorticity leaving the closed region (left hand side) is balanced by the oriented contour integral of the pressure and turbulent stresses.

The integral balance (39.139) is a rather remarkable statement that equates the transport leaving a region (left hand side) to pressure and turbulent stresses integrated along the region boundary (right hand side). For example, if the contour used to compute the integrals in equation (39.139) follows a closed streamline, on which $\boldsymbol{u} \cdot \hat{\boldsymbol{n}} = 0$, then the left hand side vanishes, which in turn means that the right hand side contour integral must also vanish. *Godfrey* (1989) chose another contour, such as that depicted in Figure 39.11, and made some assumptions about the stresses along the contour. His assumptions allow for an estimate of the transport, with this estimate having proven quite useful for many purposes. We present the arguments next.

Assumptions about the stresses

A portion of the red contour in Figure 39.11 traverses the eastern boundary on both Island A and Island B. As shown in Section 39.7, friction in the eastern boundary region of an ocean

gyre is much less than the western boundary, motivating us to ignore friction (either viscous or bottom drag) along the eastern boundary portions of the contour. Likewise, friction is generally small for the open ocean portion along the two latitudinal lines. Hence, wind stress is the only non-conservative process that affects the right hand side of equation (39.139).

Godfrey (1989) furthermore ignored pressure form stresses and their associated torques. This assumption is reasonable for the atmospheric form stress, $-p_{\mathrm{a}} \nabla \eta$, which is generally quite small (it is zero for a rigid lid approximation). However, the bottom form stress, $p_{\mathrm{b}} \nabla \eta_{\mathrm{b}}$, and the associated bottom pressure torque, can be larger than the wind stress and wind stress curl, especially near the continential margins and with strong currents. Hence, ignoring bottom pressure torque is an unsatisfying assumption.

The island rule

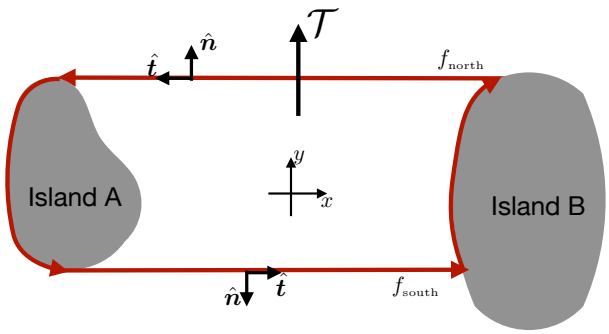

FIGURE 39.11: Illustrating the island rule with two land masses ("islands"). The red contour surrounds all of Island A and traverses along the eastern side of both Island A and Island B. The northern contour extends along a constant latitude line with a corresponding Coriolis parameter f_{north}, whereas the southern contour has Coriolis parameter f_{south}. Ignoring any precipitation or evaporation crossing the surface, steady state volume conservation means that the same meridional transport, $\mathcal{T}$, crosses both the southern and northern contours. Godfrey's island rule (39.142) provides an estimate for this transport when given the wind stress along the contour.

The islands are material surfaces so that $\boldsymbol{u} \cdot \hat{\boldsymbol{n}} = 0$ along those portions of the contour that are adjacent to the coasts. Integrating along the northern latitude, with $\hat{\boldsymbol{n}} = \hat{\boldsymbol{y}}$, yields

$$f_{\mathrm{north}} \int_{y_{\mathrm{north}}} h\, v \, \mathrm{d}x \equiv f_{\mathrm{north}}\, \mathcal{T}, \tag{39.140}$$

where $\mathcal{T}$ is the meridional transport. Ignoring any volume transport through the layer surface (e.g., $w^{(\dot{\eta})} = 0$), the steady transport crossing the northern boundary equals to that crossing the southern boundary, so that

$$f_{\mathrm{south}} \int_{y_{\mathrm{south}}} h\, v \, \mathrm{d}x \equiv f_{\mathrm{south}}\, \mathcal{T}. \tag{39.141}$$

Making use of these results in the integral balance (39.139), and following the above assumptions about the boundary stresses, leads to *Godfrey's island rule*

$$\rho \mathcal{T} = \frac{1}{f_{\mathrm{north}} - f_{\mathrm{south}}} \oint_{\partial \mathcal{S}} \boldsymbol{\tau}^{\mathrm{wind}} \cdot \hat{\boldsymbol{t}} \, \mathrm{d}\ell, \tag{39.142}$$

where $\boldsymbol{\tau}^{\mathrm{wind}}$ is the wind stress, and where the minus sign on f_{south} arises since $\hat{\boldsymbol{n}} = -\hat{\boldsymbol{y}}$ along the southern latitude contour. This expression provides an approximation to the flow around Island A, noting that the only nonzero flow normal to the contour is through the two latitudinal segments.

39.8.4 Further study

Godfrey (1989) applied the island rule (39.142) to estimate transport around Austral-Asia, New Zealand, and Malagasy. Further discussion of Godfrey's island rule can be found in *Tomczak and Godfrey* (1994), *Pedlosky et al.* (1997), and *Klinger and Haine* (2019).

39.9 Free surface patterns in steady ocean gyres

We here consider basic features of steady free surface patterns realized by a shallow water fluid. The basic question is how to relate the free surface near the coast to that in the interior of an ocean gyre. We formulate the steady linear case with sloping bottom topography.

39.9.1 Formulating the free surface equation

We make use of the steady frictional geostrophic equations, with the velocity equation given by the linearized version of equation (39.119)

$$f\,\hat{\boldsymbol{z}} \times h\,\boldsymbol{u} = -g\,h\,\nabla\eta + \boldsymbol{f}^{\rm nc}. \tag{39.143}$$

Here, $\boldsymbol{f}^{\rm nc}$ is the thickness weighted acceleration from non-conservative processes, such as the wind stress, viscous friction, and bottom drag, with details provided in Section 39.8.1. Since the flow is steady, the layer thickness equation (35.20) leads to the non-divergence condition

$$\nabla \cdot (h\,\boldsymbol{u}) = 0. \tag{39.144}$$

We now formulate a vorticity-like equation. Yet rather than taking the curl of equation (39.143), thus emulating the work from Section 39.8, we first divide equation (39.143) by the Coriolis parameter to write

$$\hat{\boldsymbol{z}} \times h\,\boldsymbol{u} = -(g\,h/f)\,\nabla\eta + \boldsymbol{f}^{\rm nc}/f, \tag{39.145}$$

so that the curl leads to

$$\hat{\boldsymbol{z}} \cdot [\nabla(g\,h/f) \times \nabla\eta] = \hat{\boldsymbol{z}} \cdot \nabla \times (\boldsymbol{f}^{\rm nc}/f), \tag{39.146}$$

where we used the non-divergence condition (39.144). Dividing by the Coriolis parameter limits the analysis to regions bounded away from the equator, which is not a problem for our focus on middle or high latitude planetary geostrophic ocean gyres. We are motivated to pursue this formulation since it supports the use of equation (39.146) next to sloping boundaries, in which the layer thickness vanishes ($h = 0$) at the shoreline edge of the domain.

39.9.2 Advecting the free surface

To help interpret the conservative portion of the free surface equation (39.146), we introduce the streamfunction[8]

$$\psi^{(\eta)} \equiv -g\,h/f, \tag{39.147}$$

so that equation (39.146) takes the form

$$\boldsymbol{u}^{(\eta)} \cdot \nabla\eta = -\hat{\boldsymbol{z}} \cdot \nabla \times (\boldsymbol{f}^{\rm nc}/f), \quad \text{with} \quad \boldsymbol{u}^{(\eta)} = \hat{\boldsymbol{z}} \times \nabla\psi^{(\eta)} = -\hat{\boldsymbol{z}} \times \nabla(g\,h/f). \tag{39.148}$$

[8]We follow the sign convention of *Wise et al.* (2018) by introducing $\psi^{(\eta)} = -g\,h/f$ in equation (39.147). The alternative choice of $\psi^{(\eta)} = +g\,h/f$ is less convenient for interpreting the direction of the velocity induced by topographic slopes. Additionally, in equation (39.155) we introduce Rayleigh drag and interpret the resulting equation as an advective-diffusion balance. If we take $\psi^{(\eta)} = +g\,h/f$ then it would be an advective-anti-diffusive balance, which is far less physically satisfying.

The left hand side is written as the advection of the free surface by the horizontally non-divergent velocity, $\boldsymbol{u}^{(\eta)}$. That is, the velocity, $\boldsymbol{u}^{(\eta)}$, advects the free surface, whereas the fluid velocity, $\boldsymbol{u}$, advects matter. In the absence of non-conservative forces ($\boldsymbol{f}^{\text{nc}} = 0$), the free surface is aligned with isolines of $h/f = 1/Q^{\text{pg}}$, or equivalently with lines of constant planetary geostrophic potential vorticity, Q^{pg} (recall that $Q^{\text{pg}} = f/h$ as defined by equation (39.89)). For free surface contours to deviate from Q^{pg} contours requires non-conservative forces, such as those from wind stresses and frictional dissipation. This discussion is related to that given in Section 39.5.2 where we introduced the notion of f/H contours for planetary geostrophic flow.

The advection operator

The layer thickness is the difference between the free surface and bottom topography, $h = \eta - \eta_{\text{b}} \geq 0$ (see Figure 35.1), in which case the advection operator takes on the form

$$\nabla\psi^{(\eta)} \times \nabla\eta = -(g/f)\,\nabla(\eta - \eta_{\text{b}}) \times \nabla\eta + (g\,h/f^2)\,\beta\,\hat{\boldsymbol{y}} \times \nabla\eta \tag{39.149a}$$

$$= (g/f)\,[\nabla\eta_{\text{b}} + (h\,\beta/f)\,\hat{\boldsymbol{y}}] \times \nabla\eta. \tag{39.149b}$$

This result motivates decomposing $\boldsymbol{u}^{(\eta)}$ into two terms

$$\boldsymbol{u}^{(\text{b})} = (g/f)\,\hat{\boldsymbol{z}} \times \nabla\eta_{\text{b}} = (g/f)\,(-\hat{\boldsymbol{x}}\,\partial_y\eta_{\text{b}} + \hat{\boldsymbol{y}}\,\partial_x\eta_{\text{b}}) \tag{39.150a}$$

$$\boldsymbol{u}^{(\beta)} = \hat{\boldsymbol{z}} \times (g\,h\,\beta/f^2)\,\hat{\boldsymbol{y}} = -(g\,h\,\beta/f^2)\,\hat{\boldsymbol{x}}, \tag{39.150b}$$

so that the free surface equation (39.148) takes on the form

$$(\boldsymbol{u}^{(\text{b})} + \boldsymbol{u}^{(\beta)}) \cdot \nabla\eta = -\hat{\boldsymbol{z}} \cdot \nabla \times (\boldsymbol{f}^{\text{nc}}/f). \tag{39.151}$$

As so defined, $\boldsymbol{u}^{(\text{b})}$ arises from gradients in the bottom topography and it is directed with shallow water to the right in the northern hemisphere and to the left in the southern hemisphere (just as the phase velocity for a coastally trapped Kelvin wave; see Section 55.7). The velocity, $\boldsymbol{u}^{(\beta)}$, arises from the planetary vorticity gradient and is always directed to the west, just as the phase velocity of a Rossby wave (Section 55.9). Notably, $\boldsymbol{u}^{(\eta)}$ has a meridional component only so long as there is a zonal topographic slope, $\partial_x\eta_{\text{b}} \neq 0$.

Free surface trajectories in the absence of non-conservative forcing

In the absence of non-conservative forces the steady free surface equation (39.151) is

$$(\boldsymbol{u}^{(\text{b})} + \boldsymbol{u}^{(\beta)}) \cdot \nabla\eta = 0 \Longrightarrow [\hat{\boldsymbol{z}} \times \nabla\eta_{\text{b}} - (h\,\beta/f)\,\hat{\boldsymbol{x}}] \cdot \nabla\eta = 0. \tag{39.152}$$

For the case of a flat bottom domain, so that $\boldsymbol{u}^{(\text{b})} = 0$, free surface contours are purely zonal ($\partial_x\eta = 0$). Conversely, on an f-plane, so that $\boldsymbol{u}^{(\beta)} = 0$, free surface contours are aligned with the bottom topography, $\hat{\boldsymbol{z}} \cdot (\nabla\eta_{\text{b}} \times \nabla\eta) = 0$. In the general case, the unforced steady free surface contours are aligned according to the interplay between planetary beta and bottom topography according to equation (39.152).

It is instructive to imagine a free surface "trajectory" as defined by integral curves of $\boldsymbol{u}^{(\eta)}$. Consider one such trajectory that moves from the interior of a northern hemisphere gyre onto the continental shelf, such as in the example depicted in Figure 39.5. In the interior we assume the bottom topography is nearly flat, so that $\boldsymbol{u}^{(\text{b})} \approx 0$ and the corresponding free surface trajectory is along a constant latitude line. As we reach the continental slope, the trajectory becomes southwestward with a trajectory slope determined by the zonal slope of the topography. Finally, as the continental shelf is reached, which is relatively flat, the trajectory returns to a near constant latitude contour.

39.9.3 Rayleigh drag and free surface diffusion

The free surface equation (39.151) indicates that any non-conservative acceleration, $\boldsymbol{f}^{\rm nc}$, causes the free surface to deviate from contours of constant streamfunction, $\psi^{(\eta)} = -g\,h/f$. The dominant contribution to $\boldsymbol{f}^{\rm nc}$ arises from wind stress. Here, we consider the role of a thickness weighted Rayleigh drag assumed to take the form given by equation (39.121)

$$\boldsymbol{f}^{\rm nc} = -\gamma\, h\, \boldsymbol{u}_{\rm g}, \tag{39.153}$$

where γ has dimensions of inverse time and $\boldsymbol{u}_{\rm g}$ is the geostrophic flow given by

$$\boldsymbol{u}_{\rm g} = (g/f)\, \hat{\boldsymbol{z}} \times \nabla\eta. \tag{39.154}$$

Substituting into the free surface equation (39.151) leads to

$$\underbrace{(\boldsymbol{u}^{\rm (b)} + \boldsymbol{u}^{(\beta)}) \cdot \nabla\eta}_{\text{advection}} = \underbrace{\nabla \cdot [(\gamma\, h\, g/f^2)\, \nabla\eta]}_{\text{diffusion}} \; \underbrace{-\hat{\boldsymbol{z}} \cdot \nabla \times [\boldsymbol{\tau}^{\rm wind}/(\rho\, f)]}_{\text{source from } \nabla \times \boldsymbol{\tau}^{\rm wind}/f}. \tag{39.155}$$

In the absence of a wind stress, the free surface satisfies a steady advective-diffusive balance.[9] Evidently, the Rayleigh drag, acting as a sink to the geostrophic momentum, also acts to diffuse the free surface and so to cause the free surface contours to deviate or spread out from contours of constant $g\,h/f$. Notice that the diffusion coefficient,

$$\kappa = \gamma\, h\, g/f^2 = -(\gamma/f)\, \psi^{(\eta)}, \tag{39.156}$$

gets larger moving toward the equator. Hence, free surface contours can more readily deviate from contours of constant $\psi^{(\eta)}$ when moving towards the equator.

39.9.4 Further study

Inspiration for this section follows from *Minobe et al.* (2017), *Wise et al.* (2018), *Wise et al.* (2020a) and *Wise et al.* (2020b). Also note that the advection-diffusion interpretation of the streamfunction equation follows *Welander* (1968), and was already introduced in Section 39.7.8 and used in Section 38.6 for the study of beta plumes. We formulated the steady linear case following *Wise et al.* (2018), who considered sloping bottom topography rather than the vertical walls assumed by *Minobe et al.* (2017). The transient case, which involves coastal boundary waves, is considered by *Hughes et al.* (2019), *Wise et al.* (2020a) and *Wise et al.* (2020b).

39.10 Exercises

EXERCISE 39.1: FLOW NEAR A TOPOGRAPHIC BUMP IN A REDUCED GRAVITY MODEL
Elements of this exercise are motivated by Figure 2 from *Adcock and Marshall* (2000) and Figure 1 from *Marshall et al.* (2012), where we consider a reduced gravity model with a dynamic lower layer and stagnant upper layer. Place a topographic bump (e.g., seamount or mountain) fully within the lower layer as shown in Figure 39.12.

(a) Following Exercise 35.5, derive the momentum and thickness equations for a reduced gravity model with a stagnant upper layer. Then derive the potential vorticity equation for the dynamical layer.

[9] We study advection and diffusion in Chapter 69.

(b) Now assume an f-plane. If the lower layer potential vorticity is (somehow) horizonally homogenized (e.g., some form of mixing produces a horizontally constant potential vorticity), draw the resulting layer interface $\eta_{3/2}$. Assume the relative vorticity is negligible compared to the planetary vorticity so that the flow satisfies the planetary geostrophic scaling introduced in Section 39.5.2 and further pursued in Section 43.4. Also, ignore any non-steady processes; we are only interested here in the steady flow.

(c) For the case of horizontally homogenized potential vorticity from the previous part, what is the direction for a geostrophically balanced flow: cyclonic or anti-cyclonic? Hint: make use of Exercise 35.5 for the momentum equation of an inverted reduced gravity model.

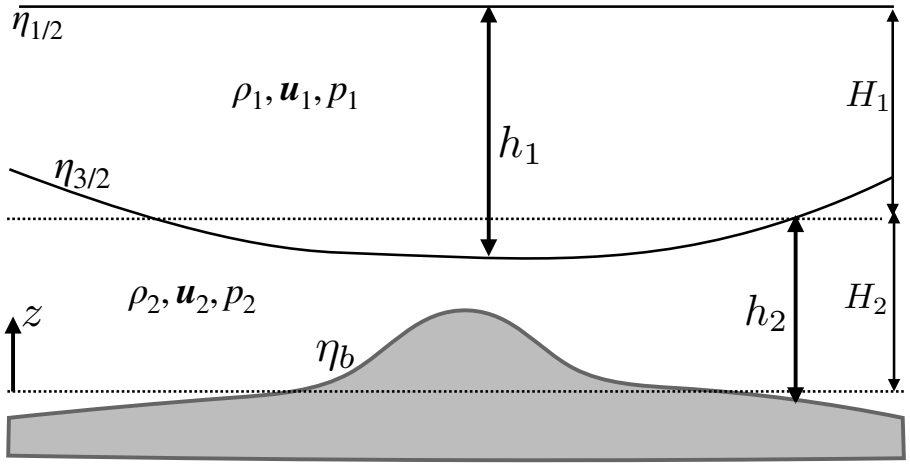

FIGURE 39.12: A reduced gravity model (see Section 35.3) with a stagnant upper layer and a dynamic lower layer as in Exercise 35.5. A seamount sits fully within the lower layer.

EXERCISE 39.2: POTENTIAL VORTICITY FOR TWO SHALLOW WATER LAYERS
Consider the inviscid Boussinesq two-layer shallow water model as discussed in Section 35.4. Derive the potential vorticity equation for each layer, showing the mathematical steps used in the derivation. Hint: the answer is given in Section 39.3.6.

EXERCISE 39.3: AVERAGE VORTICITY IN A SHALLOW WATER LAYER
Consider a single layer of shallow water fluid on a rotating plane with rotation rate $\boldsymbol{\Omega} = \hat{\boldsymbol{z}}\,\Omega$. Assume the fluid is contained in an arbitrary horizontal region and that it has a constant total volume given by

$$\mathcal{V} = \int \left[\int \mathrm{d}z \right] \mathrm{d}\mathcal{S} = \int h \, \mathrm{d}\mathcal{S} = \int (H + \Delta\eta - \eta_{\mathrm{b}}) \, \mathrm{d}\mathcal{S} = H \, \mathcal{S}, \tag{39.157}$$

where $\mathcal{S}$ is the horizontal area of the domain, $h(x,y,t) = H + \Delta\eta(x,y,t) - \eta_{\mathrm{b}}(x,y)$ is the layer thickness, H is the resting depth relative to $z = 0$, $\Delta\eta$ is the sea level deviation from resting, and η_{b} is the undulation of the bottom topography (see Figure 35.1). Additionally, recall that $z = 0$ is set according to

$$\int \eta_{\mathrm{b}} \, \mathrm{d}\mathcal{S} = 0, \tag{39.158}$$

and volume conservation ensures that

$$\int \Delta\eta \, \mathrm{d}\mathcal{S} = 0. \tag{39.159}$$

(a) Determine the volume average of the vorticity $\hat{\boldsymbol{z}} \cdot \boldsymbol{\omega}_{\text{rigid}}$ arising from the rigid-body rotation

$$\langle \hat{\boldsymbol{z}} \cdot \boldsymbol{\omega}_{\text{rigid}} \rangle = \mathcal{V}^{-1} \int \hat{\boldsymbol{z}} \cdot \boldsymbol{\omega}_{\text{rigid}} \, \mathrm{d}V. \tag{39.160}$$

(b) Determine the area average of the relative vorticity,

$$\overline{\zeta} = \mathcal{S}^{-1} \int \hat{\boldsymbol{z}} \cdot \boldsymbol{\omega} \, \mathrm{d}\mathcal{S}, \tag{39.161}$$

in terms of the circulation around the boundary of the domain.

(c) Determine the volume average of the relative vorticity

$$\langle \zeta \rangle = \mathcal{V}^{-1} \int \hat{\boldsymbol{z}} \cdot \boldsymbol{\omega} \, \mathrm{d}V. \tag{39.162}$$

Write the expression in terms of the area average vorticity, $\overline{\zeta}$, and the correlation, $\overline{\zeta' h'}$, where primes are deviations from the area mean.

EXERCISE 39.4: APPLICATION OF THE MATERIAL INVARIANCE OF POTENTIAL VORTICITY
In an adiabatic shallow water fluid in a rotating reference frame, show that the potential vorticity satisfies

$$\frac{\mathrm{D}}{\mathrm{D}t} \left[\frac{\zeta + f}{\eta - \eta_b} \right] = 0, \tag{39.163}$$

where η is the height of the free surface and η_b is the height of the bottom topography (see Figure 35.1). For both of the following questions, assume constant volume for the fluid column. Also, assume the column rotates coherently about its axis.

(a) A cylindrical column of air at 30° latitude with radius 100 km expands horizontally to twice its original radius. If the air is initially at rest, what is the mean tangential velocity at the perimeter after the expansion?

(b) An air column at 60°N with zero relative vorticity ($\zeta = 0$) stretches from the surface to the tropopause, which we assume is a rigid lid at 10 km. The air column moves zonally onto a plateau 2.5 km high. What is its relative vorticity? Suppose it then moves southward along the plateau to 30°N, starting from the relative vorticity it obtained from the plateau. What is its new relative vorticity?

EXERCISE 39.5: APPLICATION OF THE MATERIAL INVARIANCE OF POTENTIAL VORTICITY
An air column at 60°N with $\zeta = 0$ initially reaches from the surface to a fixed tropopause at 10 km height. If the air column moves across a mountain 2.5 km high at 45°N, what is its absolute vorticity and relative vorticity as it passes the mountaintop? Hint: Use the material invariance of shallow water potential vorticity, and assume the top of the column remains at 10 km.

EXERCISE 39.6: STEADY SHALLOW WATER FLOW IN A ROTATING CHANNEL
In Figure 39.13 we depict a single layer of shallow water fluid moving within a zonal channel on a northern hemisphere f-plane with meridional extent $y = y_0 - L/2$ and $y = y_0 + L/2$, where y_0 is the latitude of the f-plane. The fluid moves in the zonal direction under the influence of an imposed pressure gradient and under a rigid lid at $z = H$. The lower boundary that starts at $z = 0$ and transitions to $z = d$ at some upstream position. Assume the fluid moves without frictional dissipation so that all solid surfaces are free-slip. As a hint to this exercise, refer to Section 2.4 of *Stern* (1975).

(a) Assuming a non-rotating reference frame, determine the velocity in the far downstream where the fluid thickness is $H - d$.

(b) Now assume an f-plane and determine the meridional profile of the zonal velocity at a distance far downstream.

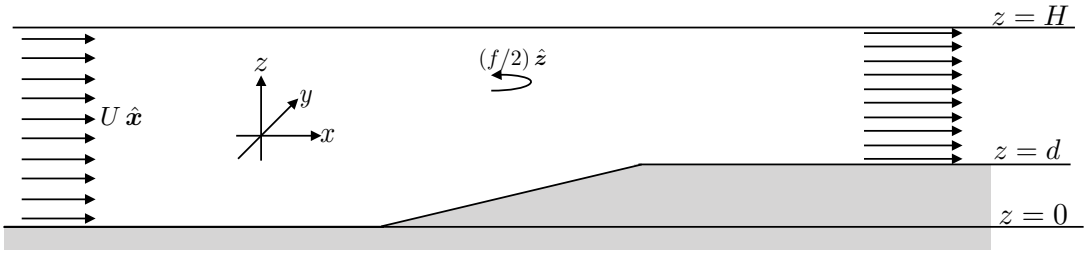

FIGURE 39.13: A single layer of shallow water fluid flows in a free-slip zonal channel on a northern hemisphere f-plane with vertical walls at $y = y_0 \pm L/2$ and rigid upper surface at $z = H$. An imposed pressure gradient causes the fluid to flow from left to right, with $\boldsymbol{u} = U\,\hat{\boldsymbol{x}}$ the velocity in the far upstream direction given.

EXERCISE 39.7: PROPERTIES OF THE STEADY STATE SHALLOW WATER FLUID

Consider a single layer of shallow water fluid in steady state (i.e., all Eulerian time derivatives vanish).

(a) Show that there exists a streamfunction for the steady state thickness weighted horizontal flow

$$h\,\boldsymbol{u} = \hat{\boldsymbol{z}} \times \nabla\Psi. \tag{39.164}$$

(b) What are the physical dimensions of Ψ?

(c) Show that the shallow water potential vorticity is a constant along the steady state streamlines of the thickness weighted flow

$$Q = Q(\Psi). \tag{39.165}$$

(d) Show that the Bernoulli function,

$$B = g\,\eta + \boldsymbol{u}\cdot\boldsymbol{u}/2 \tag{39.166}$$

is also a constant along the same streamlines; i.e.,

$$B = B(\Psi). \tag{39.167}$$

(e) What is the functional relation between the Bernoulli function and the potential vorticity? Hint: make use of the physical dimensions for Q, B, and Ψ to be sure that your solution is dimensionally consistent.

EXERCISE 39.8: ZONALLY SYMMETRIC SHALLOW WATER FRONT

Consider a single layer of shallow water fluid on a β-plane ($f = f_\circ + \beta\,y$) with a flat bottom. Assume all fields possess zonal symmetry as in the zonal front shown in Figure 39.14. Since the zonal pressure gradient vanishes under the assumption of zonal symmetry, the geostrophic portion of the meridional velocity vanishes. However, there is generally a non-zero ageostrophic component to this velocity, and we retain that possibility throughout this exercise.

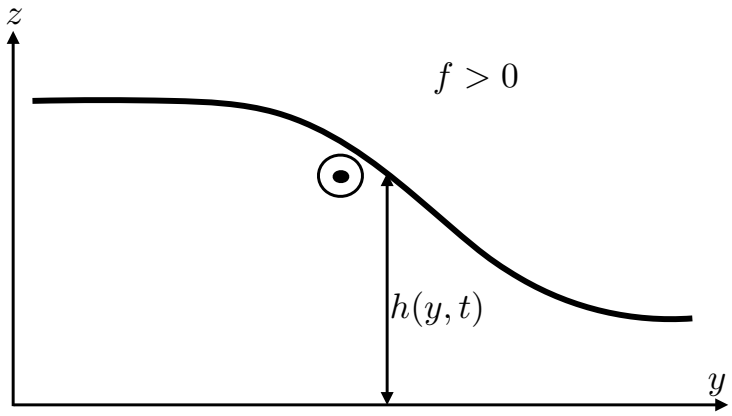

FIGURE 39.14: Schematic of a zonally symmetric front in a shallow water layer in the northern hemisphere ($f > 0$), here used for Exercise 39.8. The thickness decreases to the north. If the zonal flow is in geostrophic balance, then the northward pressure gradient is in geostrophic balance with a southward Coriolis acceleration arising from an eastward (out of the page) geostrophic current (see also Figure 36.1). The geostrophic component of the meridional flow vanishes due to zonal symmetry, but the full meridional flow need not vanish if there are ageostrophic processes. We allow for the possibility of a nonzero meridional velocity throughout this exercise.

(a) Write the potential vorticity, Q, assuming the zonal flow is in geostrophic balance. Write Q terms of meridional derivatives of the layer thickness.

(b) From the shallow water equations, explicitly show that the potential vorticity is materially constant (i.e., it is a Lagrangian invariant). To do so, work through the usual shallow water potential vorticity material conservation derivation yet make use of the zonally symmetric equations of motion. Allow for a nonzero ageostrophic meridional flow. Show all relevant steps.

(c) Show that the potential vorticity can be written as $Q = -(\partial_y M)/h$, where h is the layer thickness. What is the expression for M? Hint: recall our discussion of potential momentum in Section 14.3.

(d) Potential vorticity is not the only material constant for this system. Due to the zonal symmetry, Noether's Theorem indicates there is another. Show that M is materially constant. Again, continue to allow for a nonzero meridional velocity component.

EXERCISE 39.9: RAYLEIGH DRAG AND GALILEAN INVARIANCE

Recall the discussion of Galilean invariance from Section 17.5. Is the Rayleigh drag used in equation (39.81) Galilean invariant? Why? If not, then should that be of concern for its use in studying flow in a closed and bounded domain?

EXERCISE 39.10: GYRES IN THE PRESENCE OF CYCLONIC WINDS

Consider the ocean gyre discussion in Section 39.7. Rather than anti-cyclonic winds, now apply a cyclonic wind stress to the domain. As per the circulation theorem (39.84), the gyre flow will have a cyclonic sense. Will the resulting gyre exhibit eastern intensification or western? Appeal to whatever arguments you wish.

EXERCISE 39.11: SHALLOW WATER EQUATIONS WITH DIVERGENCE-DAMPING

When breaking the continuous symmetry of the equations of motion, a discretized numerical simulation admits unphysical flow features sometimes referred to as *computational modes*. Some computational modes can evolve in time with energy accumulating at high wave numbers, in which case the numerical simulation produces unphysical grid noise and becomes of little physical use. To suppress grid noise, numerical models commonly introduce numerical dissipation, even if the continuous equations have zero dissipation. The formulation of numerical dissipation is

largely an art guided by the dual needs of suppressing grid noise without otherwise damaging physical properties of the simulated flow. We here consider physical properties of a specific form of numerical dissipation known as *divergence-damping*. We work within the framework of the continuous equations so to develop generic physical properties of the divergence-damping operator. No knowledge of numerical methods is required to solve this problem.

Divergence-damping is motivated by the desire to leave the vorticity equation untouched while damping divergent motion that can arise in numerical simulations. This motivation is based on noting that much of the large-scale circulation in a rotating fluid has a nontrivial absolute vorticity yet a relatively small horizontal divergence. For example, geostrophic flow on an f-plane has vorticity dominated by planetary vorticity f, while it is has zero horizontal divergence (see Section 31.4 or the 2d barotropic equation in Section 38.1). The divergence-damping operator is thus designed to reduce the magnitude of the horizontal divergence while leaving the vorticity untouched.

We here examine the impacts of divergence-damping on mechanical energy and angular momentum. For this purpose, consider a single layer of shallow water fluid with divergence-damping. This system is described by the momentum and thickness equations

$$\frac{\mathrm{D}\boldsymbol{u}}{\mathrm{D}t} + f\,\hat{\boldsymbol{z}} \times \boldsymbol{u} = -\nabla\,(g\,\eta + \alpha\,\Gamma) \tag{39.168a}$$

$$\frac{\mathrm{D}h}{\mathrm{D}t} = -h\,\nabla \cdot \boldsymbol{u}. \tag{39.168b}$$

The parameter $\alpha > 0$ is a constant and the field Γ is given by the Laplacian of the horizontal flow divergence

$$\Gamma = \nabla^2 \mathcal{D}, \tag{39.169}$$

where

$$\mathcal{D} = \nabla \cdot \boldsymbol{u}. \tag{39.170}$$

The divergence has physical dimensions of inverse time (T^{-1}), so that its Laplacian, Γ, has dimensions of $L^{-2}\,T^{-1}$, and the coefficient α has dimensions $L^4\,T^{-1}$.

Divergence damping leads to a modification to the horizontal pressure gradient. We may think of this modification as arising from the horizontal gradient of a modified free surface height

$$\tilde{\eta} = \eta + \frac{\alpha\,\Gamma}{g}. \tag{39.171}$$

Notably, mass conservation remains the same since the thickness equation is unchanged. Hence, momentum evolution is modified by changing the pressure gradient, yet the thickness equation remains the same.

(a) Show that the vorticity equation (39.9) remains unchanged in the presence of divergence-damping.

(b) Show that the potential vorticity equation (39.29) remains unchanged in the presence of divergence-damping.

(c) Show that the horizontal divergence evolves according to

$$\frac{\partial \mathcal{D}}{\partial t} = \left[\frac{\partial \mathcal{D}}{\partial t}\right]_{\alpha=0} - \alpha \nabla^2 \Gamma. \tag{39.172}$$

(d) Show that the evolution of gravitational potential energy per horizontal area

$$\mathscr{P} = g\,\rho \int_{\eta_b}^{\eta} z\,\mathrm{d}z \tag{39.173}$$

remains unchanged from that determined in Section 36.5.1.

(e) Show that the kinetic energy per horizontal area evolves according to

$$\frac{\partial \mathcal{K}}{\partial t} + \nabla \cdot (\boldsymbol{u}\,\mathcal{K}) = -h\rho\, g\, \boldsymbol{u} \cdot \nabla \tilde{\eta}, \tag{39.174}$$

where

$$\mathcal{K} = \frac{1}{2} \int_{\eta_b}^{\eta} \rho\, \mathbf{u}^2\,\mathrm{d}z = \rho\, h\, \mathbf{u}^2/2, \tag{39.175}$$

is the horizontal kinetic energy per area (Section 36.5.2).

(f) Determine the evolution equation for global integrated kinetic energy

$$\frac{\partial}{\partial t}\left[\int \mathcal{K}\,\mathrm{d}A\right] = \frac{\partial}{\partial t}\left[\int \int_{\eta_b}^{\eta} (\rho\,\boldsymbol{u}\cdot\boldsymbol{u}/2)\,\mathrm{d}z\,\mathrm{d}A\right]. \tag{39.176}$$

Hint: drop all lateral boundary terms by assuming either solid lateral walls or periodicity.

(g) Consider a single shallow water layer in a rotating tank as in Section 36.8. Show that the material evolution of angular momentum relative to the vertical rotational axis is given by

$$\frac{1}{\delta M}\frac{\mathrm{D}L^z}{\mathrm{D}t} = -g\,\frac{\partial \eta}{\partial \phi} + \mathcal{T}. \tag{39.177}$$

What is the mathematical form for $\mathcal{T}$? Hint: check your answer with the next part of this exercise.

(h) Show that the domain integrated angular momentum satisfies the equation

$$\frac{\partial}{\partial t}\int L^z = \alpha\,\rho \int \Gamma\,\frac{\partial \eta}{\partial \phi}\,\mathrm{d}A. \tag{39.178}$$

where we assume the bottom topography is flat so that $h = \eta$.

(i) The linearized thickness equation (see Section 55.5) for a flat bottom is given by

$$\frac{\partial \eta}{\partial t} + H\,\nabla \cdot \boldsymbol{u} = 0, \tag{39.179}$$

where H is the thickness of the resting fluid layer. Show that the time change for the global integrated angular momentum is given by

$$\frac{\partial}{\partial t}\int L^z = -\frac{\alpha\,\rho}{H}\int \left[\frac{\partial}{\partial t}\nabla^2 \eta\right]\frac{\partial \eta}{\partial \phi}\,\mathrm{d}A. \tag{39.180}$$

Chapter 40

VORTICITY AND CIRCULATION MECHANICS

In this chapter we study the kinematics and dynamics of vorticity and circulation, extending our introductory study in earlier chapters in this part of the book. An understanding of vorticity mechanics offers many insights into the nature of fluid flow and how that flow is constrained. In making use of vorticity for geophysical fluids, it can be useful to move beyond the vorticity of a fluid element as defined by the curl of the velocity field. For example, as a means to summarize facets of the vorticity contained within a three-dimensional fluid, we study the depth integral of the vorticity equation in Section 40.8 for a hydrostatic and Boussinesq fluid and in Section 44.3 for a planetary geostrophic flow. This analysis is particularly useful in understanding facets of ocean circulation. Relatedly, there are occasions to study vorticity of the depth integrated flow (i.e., vorticity of the transport) or depth averaged flow (i.e., vorticity of the barotropic flow), and we do so in Section 40.9. Such studies emphasize the importance of boundary forces and their curls ("torques") for the vorticity of a fluid column. Details of the terms affecting such vorticities depend on the form of the vorticity, with somewhat complementary features emphasized.

CHAPTER GUIDE

This chapter assumes an understanding of vorticity developed in earlier chapters in this part of the book. We also make use of fluid kinematics from Part III and fluid dynamics from Part V. As for the shallow water vorticity discussed in Chapter 39, we here make use of vector calculus identities for Cartesian coordinates as detailed in Chapter 2. The concepts and methods developed in this chapter are fundamental to the notions of vorticity and circulation, with elements encountered in the remainder of this part of the book as well as in the study of balanced models in Part VIII.

Throughout this chapter, when considering spherical geometry, we make use of the planetary Cartesian coordinates from Figure 4.3. Since the sphere is assumed to be embedded in Euclidean space, we can naively perform integrals of vectors over the Euclidean space.

40.1 Loose threads

- Rewrite Section 40.8 using the full vertical vorticity equation derived in Section 40.3.4. The only difference is the presence of a component of baroclinicity, $-\hat{\boldsymbol{z}} \times \rho^{-1} \nabla p$.

- Summarize the various forms of the vorticity budget as per *McWilliams et al.* (2024) Section 2.

40.2 Kelvin's circulation theorem

In this section we study the evolution of circulation around a closed loop that follows the flow, or equivalently (through Stokes' theorem) with the change in vorticity penetrating the area enclosed by the loop

$$\frac{\mathrm{d}\mathcal{C}}{\mathrm{d}t} = \frac{\mathrm{d}}{\mathrm{d}t}\oint_{\partial\mathcal{S}(\boldsymbol{v})} \boldsymbol{v}\cdot\mathrm{d}\boldsymbol{x} = \frac{\mathrm{d}}{\mathrm{d}t}\int_{\mathcal{S}(\boldsymbol{v})} \boldsymbol{\omega}\cdot\hat{\boldsymbol{n}}\,\mathrm{d}\mathcal{S}, \tag{40.1}$$

where $\mathcal{S}(\boldsymbol{v})$ designates a surface whose points all move with the fluid flow. We here consider the case of a non-rotating reference frame, with the straightforward extension to rotating reference frames in Section 40.6. Kelvin's theorem refers to the special case of a perfect barotropic fluid, whereas the treatment here considers how circulation evolves for more general flows.

We emphasize that our concern is with circulation computed around closed loops that follow the flow. For single-component fluids, such loops are material (i.e., the same fluid particles are fixed to the loop). Correspondingly, we can make use of Kelvin's circulation theorem for any material loop, including loops next to static material boundaries such as that considered in Exercise 40.11. For multi-component fluids there is no perfectly material loop in the presence of diffusion, and yet we can still make use of Kelvin's theorem for loops that follow the barycentric velocity, $\boldsymbol{v}$ (see Section 20.1 for a discussion of the barycentric velocity in the context of tracer mechanics).

40.2.1 Formulation

Since the circulation is computed for a closed circuit following the flow, the time derivative in equation (40.1) moves inside the integral as a material/Lagrangian time derivative[1]

$$\frac{\mathrm{d}\mathcal{C}}{\mathrm{d}t} = \frac{\mathrm{d}}{\mathrm{d}t}\oint_{\partial\mathcal{S}(\boldsymbol{v})} \boldsymbol{v}\cdot\mathrm{d}\boldsymbol{x} = \oint_{\partial\mathcal{S}(\boldsymbol{v})} \frac{\mathrm{D}(\boldsymbol{v}\cdot\mathrm{d}\boldsymbol{x})}{\mathrm{D}t}. \tag{40.2}$$

The material evolution of $\boldsymbol{v}$ is determined by Newton's law of motion, which for a non-rotating reference frame is given by (see Section 26.13)

$$\frac{\mathrm{D}\boldsymbol{v}}{\mathrm{D}t} = -\frac{1}{\rho}\nabla p - \nabla\Phi + \boldsymbol{F}. \tag{40.3}$$

In this equation, p is the pressure, ρ is the mass density, Φ is the geopotential (and/or the potential for any conservative force), and $\boldsymbol{F}$ is the acceleration from any non-conservative forces such as from viscous stresses and/or boundary stresses.

The material time derivative of the differential line element moving around the circuit equals to the differential of the velocity on the circuit

$$\frac{\mathrm{D}(\mathrm{d}\boldsymbol{x})}{\mathrm{D}t} = \mathrm{d}\boldsymbol{v}. \tag{40.4}$$

This result follows since all points along the circuit follow the flow, by construction. Consequently, evolution of circulation following a loop becomes

$$\frac{\mathrm{d}\mathcal{C}}{\mathrm{d}t} = \oint_{\partial\mathcal{S}(\boldsymbol{v})} \left[\left(-\rho^{-1}\nabla p - \nabla\Phi + \boldsymbol{F}\right)\cdot\mathrm{d}\boldsymbol{x} + \boldsymbol{v}\cdot\mathrm{d}\boldsymbol{v}\right] \tag{40.5a}$$

$$= \oint_{\partial\mathcal{S}(\boldsymbol{v})} \left[\left(-\rho^{-1}\nabla p + \boldsymbol{F}\right)\cdot\mathrm{d}\boldsymbol{x} + \mathrm{d}(-\Phi + \boldsymbol{v}\cdot\boldsymbol{v}/2)\right] \tag{40.5b}$$

[1] In Section 20.2, we studied how to take derivatives of flow-following integrals.

$$= \oint_{\partial\mathcal{S}(\boldsymbol{v})} (-\rho^{-1}\,\nabla p + \boldsymbol{F}) \cdot \mathrm{d}\boldsymbol{x} \tag{40.5c}$$

$$= \int_{\mathcal{S}(\boldsymbol{v})} \left[-\nabla \times \left(\rho^{-1}\,\nabla p\right) + \nabla \times \boldsymbol{F}\right] \cdot \hat{\boldsymbol{n}}\,\mathrm{d}\mathcal{S} \tag{40.5d}$$

$$= \int_{\mathcal{S}(\boldsymbol{v})} (\boldsymbol{B} + \nabla \times \boldsymbol{F}) \cdot \hat{\boldsymbol{n}}\,\mathrm{d}\mathcal{S}. \tag{40.5e}$$

We noted that when integrating over space at a particular time, $\nabla\Phi \cdot \mathrm{d}\boldsymbol{x} = \mathrm{d}\Phi$ is an exact spatial differential, and so is $\mathrm{d}\boldsymbol{v}^2$. Hence, they both have a zero line integral around a closed circuit in space[2]

$$\oint_{\partial\mathcal{S}(\boldsymbol{v})} \mathrm{d}\Phi = 0 \quad \text{and} \quad \oint_{\partial\mathcal{S}(\boldsymbol{v})} \mathrm{d}\boldsymbol{v}^2 = 0. \tag{40.6}$$

40.2.2 Two processes affecting circulation

Equation (40.5e) says that the circulation around a flow-following loop is affected by two processes, whose form depends on whether considering their line integral or surface integral expressions. The contribution from non-conservative forces take the form

$$\oint_{\partial\mathcal{S}(\boldsymbol{v})} \boldsymbol{F} \cdot \mathrm{d}\boldsymbol{x} = \int_{\mathcal{S}(\boldsymbol{v})} (\nabla \times \boldsymbol{F}) \cdot \hat{\boldsymbol{n}}\,\mathrm{d}\mathcal{S}. \tag{40.7}$$

The line integral form expresses the mechanical work per unit mass (acceleration times distance) done by the non-conservative forces around the closed loop.[3] If the force is associated with friction, then friction acts to dissipate kinetic energy (see Section 26.3.3), with friction also leading, in general, to a reduction of the circulation magnitude. The surface integral form expresses the curl of friction as integrated over the surface.

The pressure gradient acceleration appears in equation (40.5e), and it provides a reversible mechanical process affecting circulation

$$\oint_{\partial\mathcal{S}(\boldsymbol{v})} (-\rho^{-1}\,\nabla p) \cdot \mathrm{d}\boldsymbol{x} = \int_{\mathcal{S}(\boldsymbol{v})} \rho^{-2} (\nabla\rho \times \nabla p) \cdot \hat{\boldsymbol{n}}\,\mathrm{d}\mathcal{S} = \int_{\mathcal{S}(\boldsymbol{v})} \boldsymbol{B} \cdot \hat{\boldsymbol{n}}\,\mathrm{d}\mathcal{S}. \tag{40.8}$$

As for friction, the line integral form expresses the mechanical work per unit mass (acceleration times distance) done by the pressure gradient acceleration as integrated around the circuit. The vector $\boldsymbol{B}$ is referred to as the *baroclinicity*

$$\boldsymbol{B} = -\nabla \times (\rho^{-1}\,\nabla p) = \rho^{-2}\,\nabla\rho \times \nabla p, \tag{40.9}$$

and it has physical dimensions of inverse squared time, T^{-2}. Its appearance in the circulation theorem arises from the non-alignment of density and pressure isolines.

Work done by pressure around an arbitrary loop does not generally vanish, nor does it have a specific sign. However, there are a variety of special loops around which the pressure work does vanish. For example, the pressure work vanishes for closed contours on surfaces of constant density or constant pressure. However, such contours are generally not flow-following, and so their circulation is not considered as part of Kelvin's theorem. In the remainder of this section, we consider some further cases where baroclinicity vanishes.

[2] See Section 2.8 for more on exact differentials.

[3] We introduced the notions of mechanical work in Section 11.1.4.

40.2.3 Barotropic flow

The solenoidal/baroclinicity vector vanishes for a constant density fluid, in which $\nabla\rho = 0$ such as for a single layer of shallow water fluid. More generally, the baroclinicity vector vanishes for barotropic flow, in which

$$p = p(\rho) \implies \text{barotropic flow.} \tag{40.10}$$

Kelvin's circulation theorem then follows, which states that for inviscid barotropic flow the circulation around any closed flow-following circuit remains constant

$$\frac{\mathrm{d}\mathcal{C}}{\mathrm{d}t} = \frac{\mathrm{d}}{\mathrm{d}t} \oint_{\partial\mathcal{S}(\boldsymbol{v})} \boldsymbol{v} \cdot \mathrm{d}\boldsymbol{x} = \frac{\mathrm{d}}{\mathrm{d}t} \int_{\mathcal{S}(\boldsymbol{v})} \boldsymbol{\omega} \cdot \hat{\boldsymbol{n}}\, \mathrm{d}\mathcal{S} = 0 \qquad \Longleftarrow \text{inviscid barotropic flow.} \tag{40.11}$$

That is, the circulation around any closed flow-following circuit in a perfect barotropic fluid remains materially constant. This remarkable result greatly constrains the flow and thus provides a wealth of insights into the nature of the flow field.

Another way to recognize that baroclinicity vanishes for a barotropic flow is to note that the curl of the pressure gradient acceleration vanishes

$$\nabla \times (\rho^{-1}\, \nabla p) = -\rho^{-2}\, \nabla\rho \times \nabla p = -\rho^{-2}\, (\partial p/\partial\rho)\, \nabla\rho \times \nabla\rho = 0. \tag{40.12}$$

Hence, for a barotropic fluid there is a scalar potential whereby

$$\nabla\Phi_{\mathrm{p}} = \rho^{-1}\nabla p. \tag{40.13}$$

This identity means that the pressure gradient acceleration for a barotropic flow is an exact spatial differential

$$\rho^{-1}\nabla p \cdot \mathrm{d}\boldsymbol{x} = \rho^{-1}\, \mathrm{d}p \equiv \mathrm{d}\Phi_{\mathrm{p}}, \tag{40.14}$$

with integration leading to

$$\Phi_{\mathrm{p}} = \int_{p_0}^{p} \frac{\mathrm{d}p'}{\rho(p')}, \tag{40.15}$$

where p_0 is an arbitrary reference pressure. Since the closed loop integral of an exact differential vanishes, we again see that the pressure gradient acceleration has no impact on circulation around flow-following loops in a barotropic flow. Stated alternatively, with $\nabla\Phi_{\mathrm{p}} = \rho^{-1}\nabla p$, then the Euler equation takes on the form

$$\frac{\mathrm{D}\boldsymbol{v}}{\mathrm{D}t} = -\nabla(\Phi_{\mathrm{p}} + \Phi), \tag{40.16}$$

which renders a materially constant circulation.

40.2.4 Pressure contribution to circulation in an ideal gas

Building on the notions from a barotropic flow in Section 40.2.3, we here determine a class of contours for an ideal gas where baroclinicity vanishes even if the flow is not barotropic. To start, recall from Exercise 23.3 that we derived equation (23.106) for an ideal gas

$$\rho^{-1}\, \nabla p = \theta\, \nabla\Pi, \tag{40.17}$$

where θ is the potential temperature (equation (23.92)) and Π is the Exner function (equation (23.93)). This equation says that the pressure gradient acceleration, for an ideal gas, is equal to the potential temperature times the gradient of the Exner function. We can thus write the

pressure gradient acceleration contribution in equation (40.5c) as

$$-\oint_{\partial\mathcal{S}(\boldsymbol{v})} \rho^{-1}\,\nabla p\cdot \mathrm{d}\boldsymbol{x} = -\oint_{\partial\mathcal{S}(\boldsymbol{v})} \theta\,\nabla\Pi\cdot \mathrm{d}\boldsymbol{x} = -\oint_{\partial\mathcal{S}(\boldsymbol{v})} \theta\,\mathrm{d}\Pi = \oint_{\partial\mathcal{S}(\boldsymbol{v})} \Pi\,\mathrm{d}\theta, \tag{40.18}$$

where the final step noted that the closed loop integral of an exact differential vanishes

$$\oint_{\partial\mathcal{S}(\boldsymbol{v})} \mathrm{d}(\theta\,\Pi) = 0. \tag{40.19}$$

Hence, the contribution from baroclinicity (i.e., pressure gradient acceleration) vanishes for closed contours drawn either on a constant Π surface or a constant θ surface. For an ideal gas, changes in θ are directly related to changes in specific entropy (see equation (26.200) from Exercise 26.4). Hence, for a perfect fluid flow of an ideal gas, where specific entropy is materially invariant, so too is potential temperature: $\mathrm{D}\theta/\mathrm{D}t = 0$. It follows that a contour drawn on a potential temperature surface remains a flow-following contour for a perfect fluid. We have thus deduced that isentropic flow of an ideal gas has a flow-following circulation that is unaffected by baroclinicity.

40.2.5 Circulation around a loop with constant entropy and concentration

We here make use of the expression (26.69) for the pressure gradient acceleration in terms of thermodynamic functions

$$-\rho^{-1}\,\nabla p = -\nabla\mathcal{H} + T\,\nabla\mathcal{S} + \mu\,\nabla C, \tag{40.20}$$

where $\mathcal{H}$ is the specific enthalpy, $\mathcal{S}$ is the specific entropy, T is the thermodynamic (Kelvin) *in situ* temperature, C is the material tracer concentration, and μ is the chemical potential for a binary fluid such as commonly assumed for the ocean (freshwater and salt) and atmosphere (dry air and water vapor). Equation (40.20) holds for a compressible fluid, in which the thermodynamic pressure and mechanical pressure are the same (Section 25.8.1).

The identity (40.20) brings the pressure gradient contribution to Kelvin's circulation theorem (40.5e) into

$$-\oint_{\partial\mathcal{S}(\boldsymbol{v})} \rho^{-1}\,\nabla p\cdot \mathrm{d}\boldsymbol{x} = \oint_{\partial\mathcal{S}(\boldsymbol{v})} (T\,\nabla\mathcal{S} + \mu\,\nabla C)\cdot \mathrm{d}\boldsymbol{x}, \tag{40.21}$$

where we set

$$\oint_{\partial\mathcal{S}(\boldsymbol{v})} \nabla\mathcal{H}\cdot \mathrm{d}\boldsymbol{x} = 0, \tag{40.22}$$

which holds since $\mathcal{H}$ is a state function so that for any time instance,

$$\nabla\mathcal{H}\cdot \mathrm{d}\boldsymbol{x} = \mathrm{d}\mathcal{H} \tag{40.23}$$

is an exact spatial differential. The decomposition (40.21) reveals that the pressure contribution to circulation vanishes when computing circulation for an isentropic and constant concentration loop[4]

$$\oint_{\partial\mathcal{S}(\boldsymbol{v})} \rho^{-1}\,\nabla p\cdot \mathrm{d}\boldsymbol{x} = 0 \quad \text{if } \mathrm{d}\mathcal{S} = 0 \text{ and } \mathrm{d}C = 0. \tag{40.24}$$

Such loops follow the flow in those cases where specific entropy and matter concentration are materially invariant

$$\frac{\mathrm{D}\mathcal{S}}{\mathrm{D}t} = 0 \quad \text{and} \quad \frac{\mathrm{D}C}{\mathrm{D}t} = 0. \tag{40.25}$$

[4]For the ocean, an isentropic and constant salt concentration process maintains a constant Conservative Temperature.

It follows that for the special case of a homogeneous fluid (C = constant) undergoing isentropic quasi-static changes, pressure plays no role in the circulation computed around an isentropic loop.

40.2.6 Circulation around a loop with constant S and Θ

Rather than invoking the gradient form of the fundamental thermodynamic relation (40.20), consider an ocean application where equation (30.10) says that the *in situ* density, ρ, takes on the functional form

$$\rho = \rho(S, \Theta, p), \tag{40.26}$$

with S the salinity and Θ the Conservative Temperature. It follows that along a contour that maintains fixed S and Θ, the pressure gradient acceleration is a function just of the pressure, in which case we write

$$\rho^{-1} \nabla p \cdot \mathrm{d}\boldsymbol{x} = \rho^{-1}(S_{\text{const}}, \Theta_{\text{const}}, p)\, \mathrm{d}p \equiv \mathrm{d}\Psi_{\mathrm{p}} \quad \text{if } S = S_{\text{const}} \text{ and } \Theta = \Theta_{\text{const}}, \tag{40.27}$$

where we followed the barotropic case of equation (40.15) to write

$$\Psi_{\mathrm{p}}(S_{\text{const}}, \Theta_{\text{const}}, p) = \int_{p_0}^{p} \frac{\mathrm{d}p'}{\rho(S_{\text{const}}, \Theta_{\text{const}}, p')}, \tag{40.28}$$

with p_0 an arbitrary reference pressure. As in Section 40.2.5, we conclude that pressure plays no role in affecting circulation around loops with fixed S and Θ

$$\oint_{\partial\mathcal{S}(\boldsymbol{v})} \rho^{-1} \nabla p \cdot \mathrm{d}\boldsymbol{x} = \oint_{\partial\mathcal{S}(\boldsymbol{v})} \mathrm{d}\Psi_{\mathrm{p}}(S, \Theta, p) = 0 \quad \text{if } S = S_{\text{const}} \text{ and } \Theta = \Theta_{\text{const}}, \tag{40.29}$$

which follows since $\mathrm{d}\Psi_{\mathrm{p}}$ is an exact spatial differential. Such closed loop contours follow the flow if S and Θ are materially invariant

$$\frac{\mathrm{D}S}{\mathrm{D}t} = 0 \quad \text{and} \quad \frac{\mathrm{D}\Theta}{\mathrm{D}t} = 0, \tag{40.30}$$

which is the case in the absence of mixing and/or sources of S and Θ.

40.2.7 Comments and further reading

There is no guarantee that the closed flow-following contours discussed in Sections 40.2.5 and 40.2.6 exist in any particular flow. Rather, all we showed is that *if* such closed contours exist, and if the flow maintains materially invariant specific entropy and concentration (Section 40.2.5) or salinity and Conservative Temperature (Section 40.2.6), then the circulation around such loops is unaffected by the pressure gradient acceleration.

Our presentation of Kelvin's circulation theorem anticipates analogous considerations encountered with potential vorticity in Chapter 41, with portions of the discussion motivated by our study of *Kooloth et al.* (2022) given in Section 41.6.

40.3 Vorticity dynamics

We now study the time evolution of vorticity and the processes leading to this evolution. We considered this question in Chapter 39 when focused on shallow water vorticity, and in Chapter 38 for the horizontally non-divergent barotropic flow. Here, we consider the general case of a stratified flow with non-conservative forces. As for Kelvin's theorem, we make use of Newton's

law of motion, written here in the form for a rotating fluid (see Section 26.13)

$$\frac{\mathrm{D}\boldsymbol{v}}{\mathrm{D}t} + 2\,\boldsymbol{\Omega} \times \boldsymbol{v} = -\rho^{-1}\,\nabla p - \nabla\Phi + \boldsymbol{F}, \tag{40.31}$$

where $\boldsymbol{\Omega}$ is the angular velocity of the rotating reference frame.

40.3.1 Vector-invariant velocity equation

As for the shallow water fluid in Section 39.1, we find it useful to convert the advective-form momentum equation to vector-invariant velocity equation. For this purpose, make use of the vector identity (see Section 2.3.4)

$$\boldsymbol{\omega} \times \boldsymbol{v} = -(1/2)\,\nabla(\boldsymbol{v} \cdot \boldsymbol{v}) + (\boldsymbol{v} \cdot \nabla)\,\boldsymbol{v} \tag{40.32}$$

to eliminate velocity self-advection in favor of vorticity and kinetic energy

$$\partial_t \boldsymbol{v} + \boldsymbol{\omega}_{\mathrm{a}} \times \boldsymbol{v} = -\rho^{-1}\,\nabla p - \nabla(\boldsymbol{v}^2/2 + \Phi) + \boldsymbol{F}. \tag{40.33}$$

We here introduced the absolute vorticity

$$\boldsymbol{\omega}_{\mathrm{a}} = \nabla \times (\boldsymbol{v} + \boldsymbol{\Omega} \times \boldsymbol{x}) = \boldsymbol{\omega} + 2\,\boldsymbol{\Omega}, \tag{40.34}$$

which is the curl of the absolute (inertial frame) velocity, and which equals to the sum of the relative vorticity plus the planetary vorticity (see Section 37.6.1).

40.3.2 Basic form of the vorticity equation

Taking the curl of the vector-invariant momentum equation (40.33) removes the mechanical energy per mass, $\boldsymbol{v}^2/2 + \Phi$, thus leaving

$$\partial_t \boldsymbol{\omega} + \nabla \times (\boldsymbol{\omega}_{\mathrm{a}} \times \boldsymbol{v}) = \rho^{-2}\,(\nabla\rho \times \nabla p) + \nabla \times \boldsymbol{F}. \tag{40.35}$$

For geophysical fluid mechanics, we generally assume that $\boldsymbol{\Omega}$ has zero time tendency so that

$$\partial_t \boldsymbol{\omega}_{\mathrm{a}} = \partial_t\,(\boldsymbol{\omega} + 2\,\boldsymbol{\Omega}) = \partial_t \boldsymbol{\omega}, \tag{40.36}$$

in which case equation (40.35) can be written as an equation for absolute vorticity

$$\partial_t \boldsymbol{\omega}_{\mathrm{a}} + \nabla \times (\boldsymbol{\omega}_{\mathrm{a}} \times \boldsymbol{v}) = \boldsymbol{B} + \nabla \times \boldsymbol{F}, \tag{40.37}$$

where $\boldsymbol{B}$ is the baroclinicity vector given by equation (40.9).

40.3.3 Massaged form of the vorticity equation

Physical interpretation of the term $\nabla \times (\boldsymbol{\omega}_{\mathrm{a}} \times \boldsymbol{v})$ appearing in the prognostic equation (40.37) can be made more transparent by using the following vector identity

$$\nabla \times (\boldsymbol{\omega}_{\mathrm{a}} \times \boldsymbol{v}) = (\boldsymbol{v} \cdot \nabla)\boldsymbol{\omega}_{\mathrm{a}} - (\boldsymbol{\omega}_{\mathrm{a}} \cdot \nabla)\boldsymbol{v} + \boldsymbol{\omega}_{\mathrm{a}}\,\nabla \cdot \boldsymbol{v} - \boldsymbol{v}\,\nabla \cdot \boldsymbol{\omega}_{\mathrm{a}} \tag{40.38a}$$

$$= (\boldsymbol{v} \cdot \nabla)\boldsymbol{\omega}_{\mathrm{a}} - (\boldsymbol{\omega}_{\mathrm{a}} \cdot \nabla)\boldsymbol{v} - \frac{\boldsymbol{\omega}_{\mathrm{a}}}{\rho}\frac{\mathrm{D}\rho}{\mathrm{D}t}. \tag{40.38b}$$

The second equality required the continuity equation

$$\frac{\mathrm{D}\rho}{\mathrm{D}t} = -\rho\,\nabla \cdot \boldsymbol{v}, \tag{40.39}$$

and the non-divergent nature of the absolute vorticity

$$\nabla \cdot \boldsymbol{\omega}_{\mathrm{a}} = \nabla \cdot (\nabla \times \boldsymbol{v} + 2\,\boldsymbol{\Omega}) = 0. \tag{40.40}$$

Equation (40.37) thus takes the form

$$\frac{\mathrm{D}\boldsymbol{\omega}_{\mathrm{a}}}{\mathrm{D}t} - \frac{\boldsymbol{\omega}_{\mathrm{a}}}{\rho}\frac{\mathrm{D}\rho}{\mathrm{D}t} = (\boldsymbol{\omega}_{\mathrm{a}} \cdot \nabla)\boldsymbol{v} + \frac{1}{\rho^2}(\nabla\rho \times \nabla p) + \nabla \times \boldsymbol{F}, \tag{40.41}$$

which can be written

$$\rho\,\frac{\mathrm{D}(\boldsymbol{\omega}_{\mathrm{a}}/\rho)}{\mathrm{D}t} = (\boldsymbol{\omega}_{\mathrm{a}} \cdot \nabla)\,\boldsymbol{v} + \boldsymbol{B} + \nabla \times \boldsymbol{F}. \tag{40.42}$$

Each term on the right hand side of the material evolution equation (40.42) represents a distinct physical process that affects $\boldsymbol{\omega}_{\mathrm{a}}/\rho$ of a fluid element. The first term, $(\boldsymbol{\omega}_{\mathrm{a}} \cdot \nabla)\,\boldsymbol{v}$, embodies stretching and twisting and is explored in Section 40.5 in the simplified context of a barotropic fluid. The second term arises from baroclinicity as introduced in equation (40.9) and given a mechanical interpretation in Section 40.4. The third term arises from the curl of the non-conservative forces (e.g., friction). Such forces contribute especially in boundary layer regions where friction curls are relatively large in magnitude.

40.3.4 Evolution of Cartesian vorticity components

Terms appearing on the right hand side of the vorticity equation (40.42) provide sources for the vorticity of a fluid element. Here we derive flux-form conservation equations that are separately satisfied by each of the vorticity components. We find that each vorticity component has an Eulerian time derivative determined by the convergence of a corresponding flux.

Vertical component to the absolute vorticity

Consider the material evolution equation for the vertical component of the absolute vorticity

$$\rho\,\frac{\mathrm{D}(\zeta_{\mathrm{a}}/\rho)}{\mathrm{D}t} = (\boldsymbol{\omega}_{\mathrm{a}} \cdot \nabla)\,w + \hat{\boldsymbol{z}} \cdot (\boldsymbol{B} + \nabla \times \boldsymbol{F}) \quad \text{with } \zeta_{\mathrm{a}} = \hat{\boldsymbol{z}} \cdot \boldsymbol{\omega}_{\mathrm{a}}. \tag{40.43}$$

Making use of the identities[5]

$$\rho\,\frac{\mathrm{D}(\zeta_{\mathrm{a}}/\rho)}{\mathrm{D}t} = \frac{\partial \zeta_{\mathrm{a}}}{\partial t} + \nabla \cdot (\boldsymbol{v}\,\zeta_{\mathrm{a}}) \tag{40.44a}$$

$$(\boldsymbol{\omega}_{\mathrm{a}} \cdot \nabla)\,w = \nabla \cdot (\boldsymbol{\omega}_{\mathrm{a}}\,w) \tag{40.44b}$$

$$\hat{\boldsymbol{z}} \cdot \boldsymbol{B} = -\hat{\boldsymbol{z}} \cdot [\nabla \times (\rho^{-1}\,\nabla p)] = \nabla \cdot (\hat{\boldsymbol{z}} \times \rho^{-1}\,\nabla p) \tag{40.44c}$$

$$\hat{\boldsymbol{z}} \cdot (\nabla \times \boldsymbol{F}) = -\nabla \cdot (\hat{\boldsymbol{z}} \times \boldsymbol{F}), \tag{40.44d}$$

brings equation (40.43) into the flux-form

$$\partial_t \zeta_{\mathrm{a}} = -\nabla \cdot \boldsymbol{J}^{\zeta_{\mathrm{a}}} \quad \text{with} \quad \boldsymbol{J}^{\zeta_{\mathrm{a}}} = \boldsymbol{v}\,\zeta_{\mathrm{a}} - \boldsymbol{\omega}_{\mathrm{a}}\,w - \hat{\boldsymbol{z}} \times \rho^{-1}\,\nabla p + \hat{\boldsymbol{z}} \times \boldsymbol{F}. \tag{40.45}$$

This budget equation says that ζ_{a} evolves at a point according to the convergence of a vorticity flux, $\boldsymbol{J}^{\zeta_{\mathrm{a}}}$. The vorticity flux is comprised of the following terms:

- advective flux of vertical vorticity: $\boldsymbol{v}\,\zeta_{\mathrm{a}}$,

[5] Exercise 40.1 asks for a proof of the identity (40.44a), which follows from use of the mass continuity equation in the form of equation (19.10). For equation (40.44d) we can use $\hat{\boldsymbol{z}} \cdot (\nabla \times \boldsymbol{F}) = \nabla z \cdot (\nabla \times \boldsymbol{F}) = \nabla \cdot [z\,\nabla \times \boldsymbol{F}] = \nabla \cdot [\nabla \times (z\,\boldsymbol{F}) - \nabla z \times \boldsymbol{F}] = -\nabla \cdot (\hat{\boldsymbol{z}} \times \boldsymbol{F})$.

- absolute vorticity transported vertically: $-\boldsymbol{\omega}_{\mathrm{a}}\, w$,
- pressure gradient acceleration rotated clockwise by $\pi/2$ radians around the vertical axis: $-\hat{\boldsymbol{z}} \times \rho^{-1}\, \nabla p$,
- $\pi/2$ counter-clockwise rotated friction acceleration, $\hat{\boldsymbol{z}} \times \boldsymbol{F}$.

Note that there is no vertical component to the vorticity flux:

$$\hat{\boldsymbol{z}} \cdot \boldsymbol{J}^{\zeta_{\mathrm{a}}} = \hat{\boldsymbol{z}} \cdot [\boldsymbol{v}\, \zeta_{\mathrm{a}} - \boldsymbol{\omega}_{\mathrm{a}}\, w - \hat{\boldsymbol{z}} \times \rho^{-1}\, \nabla p + \hat{\boldsymbol{z}} \times \boldsymbol{F}] = 0, \tag{40.46}$$

so that ζ_{a} is only affected by the convergence of a purely horizontal flux. We offer a schematic of this property in Figure 40.1.

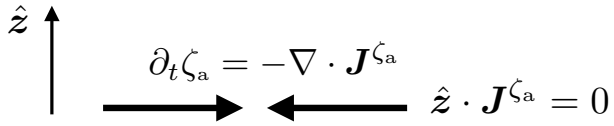

FIGURE 40.1: Tendency for the vertical component to the absolute vorticity arises from convergence of the vorticity flux, $\boldsymbol{J}^{\zeta_{\mathrm{a}}}$, given by equation (40.45). This vorticity flux is strictly horizontal, $\hat{\boldsymbol{z}} \cdot \boldsymbol{J}^{\zeta_{\mathrm{a}}} = 0$. This result generalizes for any arbitrary Cartesian component of the absolute vorticity, whereby the corresponding vorticity flux is orthogonal to its vorticity component. Generalization of this result leads to the impermeability theorem of potential vorticity studied in Section 42.2.

Flux for the other Cartesian directions

Mathematically, there is nothing special about the vertical vorticity component. Hence, we readily find that the horizontal vorticity components also satisfy their own respective flux-form conservation equations, thus leading to the general result

$$\partial_t (\hat{\boldsymbol{e}} \cdot \boldsymbol{\omega}_{\mathrm{a}}) = -\nabla \cdot [\boldsymbol{v}\, (\hat{\boldsymbol{e}} \cdot \boldsymbol{\omega}_{\mathrm{a}}) - \boldsymbol{\omega}_{\mathrm{a}}\, (\hat{\boldsymbol{e}} \cdot \boldsymbol{v}) - \hat{\boldsymbol{e}} \times \rho^{-1}\, \nabla p + \hat{\boldsymbol{e}} \times \boldsymbol{F}], \tag{40.47}$$

where $\hat{\boldsymbol{e}}$ is any one of the Cartesian unit vectors $\hat{\boldsymbol{x}}, \hat{\boldsymbol{y}}, \hat{\boldsymbol{z}}$. Furthermore, we readily see that the vorticity flux satisfies

$$\hat{\boldsymbol{e}} \cdot [\boldsymbol{v}\, (\hat{\boldsymbol{e}} \cdot \boldsymbol{\omega}_{\mathrm{a}}) - \boldsymbol{\omega}_{\mathrm{a}}\, (\hat{\boldsymbol{e}} \cdot \boldsymbol{v}) - \hat{\boldsymbol{e}} \times \rho^{-1}\, \nabla p + \hat{\boldsymbol{e}} \times \boldsymbol{F}] = 0, \tag{40.48}$$

so that the time tendency for $\hat{\boldsymbol{e}} \cdot \boldsymbol{\omega}_{\mathrm{a}}$ is affected by a flux in the directions orthogonal to $\hat{\boldsymbol{e}}$. This property of the vorticity flux is generalized via the impermeability theorem of potential vorticity studied in Section 42.2, with particular connection to the present discussion given in Section 42.2.2.

The kinematic vorticity flux

Following our study of vorticity for the shallow water fluid in Section 39.4.2, we here show that there is a kinematic reason that each Cartesian component of vorticity has a time tendency given by the convergence of a flux. For this purpose, recall the identity (37.2), in which the vertical component to the relative vorticity is written as the divergence of the velocity rotated by $\pi/2$ in the clockwise direction around the vertical axis

$$\zeta = \nabla \cdot (\boldsymbol{v} \times \hat{\boldsymbol{z}}). \tag{40.49}$$

It follows, quite trivially, that

$$\partial_t \zeta_{\mathsf{a}} = \nabla \cdot (\partial_t \boldsymbol{v} \times \hat{\boldsymbol{z}}) \equiv -\nabla \cdot \boldsymbol{J}^{\text{kin}}. \tag{40.50}$$

The kinematic flux,

$$\boldsymbol{J}^{\text{kin}} = -\partial_t \boldsymbol{v} \times \hat{\boldsymbol{z}}, \tag{40.51}$$

differs from $\boldsymbol{J}^{\zeta_{\mathsf{a}}}$ by a total curl, so that their convergences are identical. We prove this assertion by returning to the vector-invariant velocity equation (40.33), which leads to the identity

$$-\partial_t \boldsymbol{v} \times \hat{\boldsymbol{z}} = (\boldsymbol{\omega}_{\mathrm{a}} \times \boldsymbol{v}) \times \hat{\boldsymbol{z}} + \nabla \times [\hat{\boldsymbol{z}} \, (\Phi + \boldsymbol{v} \cdot \boldsymbol{v}/2)] - \hat{\boldsymbol{z}} \times \rho^{-1} \nabla p + \hat{\boldsymbol{z}} \times \boldsymbol{F}, \tag{40.52}$$

which then renders

$$\boldsymbol{J}^{\text{kin}} = \boldsymbol{J}^{\zeta_{\mathsf{a}}} + \nabla \times [\hat{\boldsymbol{z}} \, (\Phi + \boldsymbol{v} \cdot \boldsymbol{v}/2)]. \tag{40.53}$$

The rotational term equals to the mechanical energy per mass, which was also found for the shallow water case given by equation (39.61).

40.3.5 Evolution of the normal component of absolute vorticity

As a further examination of vorticity components, we here consider the material evolution of vorticity projected onto the unit normal vector, $\hat{\boldsymbol{n}}$, for an infinitesimal material area, $\delta\mathcal{S}$. This discussion leads to an infinitesimal version of Kelvin's circulation theorem, thus explicitly linking the evolution equations for vorticity and circulation. In the process we make use of some kinematics from Chapter 18.

The unit normal vector to a material surface evolves according to equation (18.130e)

$$\frac{\mathrm{D}\hat{n}_m}{\mathrm{D}t} = -\hat{\boldsymbol{n}} \cdot \partial_m^{\text{surf}} \boldsymbol{v}, \tag{40.54}$$

where the surface derivative, and corresponding surface divergence, are given from equation (18.126)

$$\partial_m^{\text{surf}} = \partial_m - \hat{n}_m \, (\hat{\boldsymbol{n}} \cdot \nabla) \quad \text{and} \quad \nabla^{\text{surf}} = \nabla - \hat{\boldsymbol{n}} \, (\hat{\boldsymbol{n}} \cdot \nabla). \tag{40.55}$$

Making use of the vorticity equation in the form (40.41), along with the continuity equation (40.39), leads to

$$\hat{\boldsymbol{n}} \cdot \frac{\mathrm{D}\boldsymbol{\omega}_{\mathrm{a}}}{\mathrm{D}t} = -(\hat{\boldsymbol{n}} \cdot \boldsymbol{\omega}_{\mathrm{a}}) \, \nabla \cdot \boldsymbol{v} + \hat{n}_j \, (\boldsymbol{\omega}_{\mathrm{a}} \cdot \nabla) \, v_j + \hat{\boldsymbol{n}} \cdot (\boldsymbol{B} + \nabla \times \boldsymbol{F}). \tag{40.56}$$

Likewise, taking the dot product of $\boldsymbol{\omega}_{\mathrm{a}}$ with the evolution equation (40.54) yields

$$\boldsymbol{\omega}_{\mathrm{a}} \cdot \frac{\mathrm{D}\hat{\boldsymbol{n}}}{\mathrm{D}t} = \hat{n}_j \, [-(\boldsymbol{\omega}_{\mathrm{a}} \cdot \nabla) + (\hat{\boldsymbol{n}} \cdot \boldsymbol{\omega}_{\mathrm{a}}) \, (\hat{\boldsymbol{n}} \cdot \nabla)] \, v_j. \tag{40.57}$$

Adding these two equations renders the material time evolution

$$\frac{\mathrm{D}(\boldsymbol{\omega}_{\mathrm{a}} \cdot \hat{\boldsymbol{n}})}{\mathrm{D}t} = -(\boldsymbol{\omega}_{\mathrm{a}} \cdot \hat{\boldsymbol{n}}) \, \nabla^{\text{surf}} \cdot \boldsymbol{v} + \hat{\boldsymbol{n}} \cdot (\boldsymbol{B} + \nabla \times \boldsymbol{F}). \tag{40.58}$$

The surface divergence of the velocity measures, via equation (18.127), evolution of the material surface area

$$\frac{1}{\delta S} \frac{\mathrm{D}\delta\mathcal{S}}{\mathrm{D}t} = \nabla^{\text{surf}} \cdot \boldsymbol{v}, \tag{40.59}$$

so that the material evolution equation for the $\hat{\boldsymbol{n}}$ component of absolute vorticity is

$$\frac{\mathrm{D}(\boldsymbol{\omega}_{\mathrm{a}} \cdot \hat{\boldsymbol{n}})}{\mathrm{D}t} = -\frac{(\boldsymbol{\omega}_{\mathrm{a}} \cdot \hat{\boldsymbol{n}})}{\delta S} \frac{\mathrm{D}\delta\mathcal{S}}{\mathrm{D}t} + \hat{\boldsymbol{n}} \cdot (\boldsymbol{B} + \nabla \times \boldsymbol{F}). \tag{40.60}$$

The area term arises from the familiar "ice-skater" effect that reflects angular momentum conservation for the column (Section 39.2.2), whereas the other terms are the projection of the baroclinicity and friction curl onto $\hat{\boldsymbol{n}}$. Bringing the area term onto the left hand side then renders the infinitesimal form of Kelvin's circulation theorem (40.5e)

$$\frac{\mathrm{D}}{\mathrm{D}t}(\boldsymbol{\omega}_{\mathrm{a}} \cdot \hat{\boldsymbol{n}}\, \mathrm{d}\mathcal{S}) = (\boldsymbol{B} + \nabla \times \boldsymbol{F}) \cdot \hat{\boldsymbol{n}}\, \mathrm{d}\mathcal{S}. \tag{40.61}$$

Note the presence of the absolute vorticity, $\boldsymbol{\omega}_{\mathrm{a}}$, in equation (40.60) rather than the relative vorticity considered in Section 40.2. We return in Section 40.6 to the question of circulation arising from planetary rotation, where we derive the finite version of the circulation theorem (40.60).

40.3.6 Vorticity, angular momentum, and torques

Both vorticity and angular momentum offer measures of the rotational motion of a fluid flow. However, there are key distinctions as detailed in Section 37.9. Perhaps the most fundamental distinction is that vorticity measures the rotation or spin without reference to an origin, whereas angular momentum is computed relative to a subjectively chosen origin. Vorticity is thus an intrinsic property of the fluid flow, whereas angular momentum depends on the chosen origin and is affected by fluid strains. Consequently, there is a direct connection between angular momentum and vorticity only for the special case of flow exhibiting rigid-body motion.

Angular momentum of motion relative to an origin changes in the presence of torques computed about the chosen origin, with the torque equal to the crosss product of the position vector of a point and the force vector acting at that point. In contrast, vorticity at a point is affected by the curl of the force per mass acting at the point. Furthermore, angular momentum is a property of any mechanical system, including point particles and rigid bodies, whereas vorticity is a property only of a continuous media where we can compute spatial derivatives of the velocity field.

When the curl of a force per mass is applied to a fluid and thus changes its vorticity, we commonly use the term "torque" in reference to this force curl. For example, in Section 40.4 we explore baroclinicity, which is the key mechanism for how inviscid torques from pressure modify vorticity. In that discussion, we see that baroclinicity provides a vorticity source when the pressure force acting on a fluid element does not pass through the center of mass of that element. When there is baroclinicity, the pressure force spins the fluid element thus affecting vorticity. Analogous inviscid and viscous force curls act on boundaries, such as when a fluid interacts with the solid earth. It is within this context that we use the term "torque" when referring to a vorticity source. Correspondingly, the torques providing a vorticity source have the dimension of force per mass per length, whereas the torques altering angular momentum have the dimension of force times length.[6]

40.4 Mechanics of baroclinicity

Baroclinicity is present in most geophysical flows, thus affecting the material evolution of circulation and vorticity. Flow with a nonzero baroclinicity vector is generally referred to as

[6] See Section 2 of *Hughes* (2000) for a similar perspective on usage of the term "torque" for processes affecting vorticity.

baroclinic flow, whereas *barotropic* flows have zero baroclinicity. We illustrate the basic distinction between barotropic and baroclinic fluids in Figure 40.2. We observe that a baroclinic fluid is associated with fluid motion that is a function of the vertical direction. In contrast, a barotropic fluid in the special case of pressure and density surfaces aligned with geopotentials, supports no motion. We further develop these points as we explore the mechanics of baroclinicity.

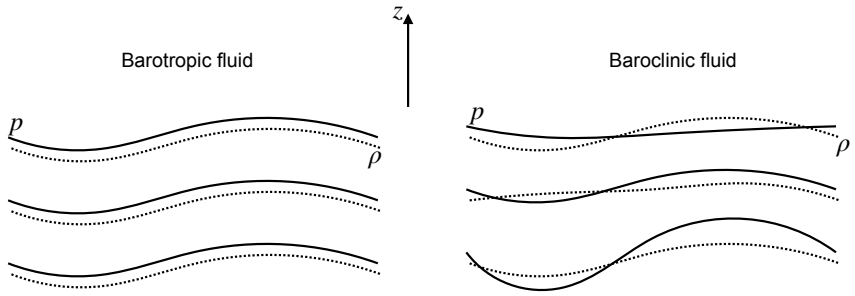

FIGURE 40.2: Left panel: a barotropic fluid, whereby density is a function just of pressure, $\rho = \rho(p)$, so that density surfaces (dashed lines) and pressure surfaces (solid lines) are parallel. Horizontal density and pressure surfaces in a barotropic fluid support no motion. Right panel: a baroclinic fluid, whereby density and pressure surfaces generally differ so that density is a function of more than just the pressure. A baroclinic fluid is associated with fluid motion that is a function of the vertical direction.

40.4.1 Curl of the pressure gradient body force

Baroclinicity is the curl of the pressure gradient body force

$$\boldsymbol{B} = \nabla \times \boldsymbol{F}_{\text{press}} = \nabla \times (-\rho^{-1} \nabla p) = -\nabla \rho^{-1} \times \nabla p = \frac{\nabla \rho \times \nabla p}{\rho^2}. \tag{40.62}$$

As discussed in Section 40.3.6, the curl of a force provides a torque that spins the fluid, thus rendering a vorticity source. Geometrically, baroclinicity arises when there is nonzero change in pressure along contours of constant density, or conversely changes in density along contours of constant pressure.[7] It can be useful to introduce the notion of a *solenoid*, which is a tube region in the fluid that is perpendicular to both $\nabla \rho$ and ∇p. There are no solenoids for barotropic flows, whereby $p = p(\rho)$ (see equation (40.10)). For baroclinic flow, solenoids are associated with a torque that affects vorticity.

To further understand the mechanical interpretation of solenoids in terms of a torque, consider the cross product

$$\rho \boldsymbol{B} = \boldsymbol{F}^{\text{press}} \times \nabla \rho = (-\rho^{-1} \nabla p) \times \nabla \rho. \tag{40.63}$$

The first term on the right hand side is the pressure gradient acceleration that is oriented down the pressure gradient. Now consider a tiny fluid element such as shown in Figure 40.3. By construction, the pressure force acts at the geometric center of the element. However, the nonzero density gradient means that the center of mass for the fluid element is not at the geometric center. In this case, the pressure gradient force does not pass through the center of mass, so that it imparts a torque to the fluid element. This torque then modifies the vorticity and hence the circulation around the boundary of the element. As an example, consider a horizontal pressure gradient acting in a fluid that is vertically stratified so $\partial_z \rho \neq 0$. There is a non-zero baroclinicity pointing in the horizontal direction (perpendicular to the horizontal pressure gradient and vertical density gradient), with this horizontal baroclinicity vector providing a source for horizontal vorticity. It is only if the pressure gradient force is aligned with the density gradient (barotropic

[7] See Exercise 5.1 for a two-dimensional example of this geometry.

flow), or if the density is spatially uniform (e.g., constant density homogeneous fluid), that we find the pressure gradient force passing through the center of mass and thus inducing no vorticity.

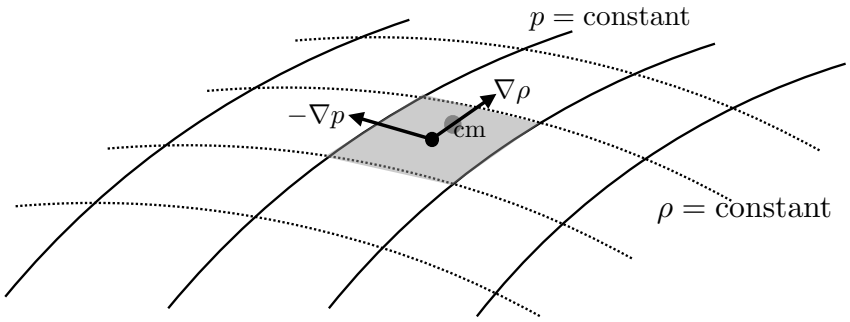

FIGURE 40.3: A mechanical interpretation of the baroclinicity vector. We consider a tiny fluid element bounded by surfaces of constant pressure and density. By construction, the pressure gradient force acts at the geometric center of the element, whereas the center of mass for the element is off-center due to the density gradient across the element. The pressure gradient force thus provides a torque for the fluid element, with the moment-arm for the torque determined by the distance between the geometric center and the center of mass. This torque modifies the vorticity of the fluid element, and in turn modifies the circulation computed around the element's boundary. As depicted here, the baroclinicity vector points into the page (right hand rule for $(-\rho^{-1}\,\nabla p) \times \nabla\rho$), so that this baroclinicity spins-up a clockwise circulation around the element, or equivalently a clockwise vorticity. This figure is adapted from Figure 14.9 of *Thorne and Blandford* (2017).

40.4.2 Kelvin's circulation theorem and contact pressure forces

We are afforded another means to understand baroclinicity by returning to the formulation of Kelvin's circulation theorem in Section 40.2.1. Focusing just on the baroclinicity contribution in equation (40.5e) we have

$$\left[\frac{\mathrm{d}\mathcal{C}}{\mathrm{d}t}\right]_{\text{baroclinicity}} = \oint_{\partial\mathcal{S}(\boldsymbol{v})} -\rho^{-1}\,\nabla p\cdot\mathrm{d}\boldsymbol{x} = \oint_{\partial\mathcal{S}(\boldsymbol{v})} \rho^{-2}\,(-p\,\nabla\rho)\cdot\mathrm{d}\boldsymbol{x}, \tag{40.64}$$

which follows since, at any particular instance,

$$\oint_{\partial\mathcal{S}(\boldsymbol{v})} \nabla(p/\rho)\cdot\mathrm{d}\boldsymbol{x} = \oint_{\partial\mathcal{S}(\boldsymbol{v})} \mathrm{d}(p/\rho) = 0. \tag{40.65}$$

The term $-p\,\nabla\rho$ in equation (40.64) is proportional to the compressive contact pressure force (Section 25.2) acting normal to a constant density surface. Consequently, if the material surface on which we are computing circulation happens to be parallel to a constant density surface, then pressure cannot generate any circulation around that material circuit. The left circuit in Figure 40.4 illustrates this situation. For the more general case where a material surface crosses constant density surfaces, pressure modifies circulation computed around such circuits (right circuit in Figure 40.4).

40.4.3 Bottom pressure contributions at the solid-earth boundary

As an application of the above ideas, consider a fluid region that intersects the solid-earth boundary. The solid-earth boundary is material so that we can apply Kelvin's circulation theorem to a circuit on the boundary. Consider the situation in Figure 40.5, which shows a vertical slice next to a sloping bottom with constant density surfaces intersecting the bottom. As in our considerations in Section 40.4.2, any material circuit that sits within the bottom

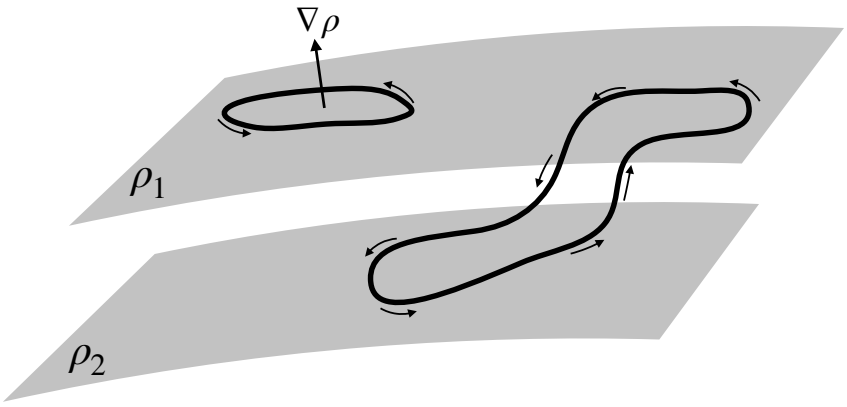

FIGURE 40.4: The material circuit on the left is assumed to be within a constant density surface. In this case, $\nabla\rho \cdot \mathrm{d}\boldsymbol{x} = 0$ so that pressure cannot modify the circulation around this circuit. However, if a material circuit is not contained fully within constant density surface, such as depicted on the right, then pressure is able to modify the circulation computed around the circuit.

boundary crosses density surfaces, in which case circulation is affected by the bottom pressure. Indeed, even if the bottom is flat, so long as density is not constant along the bottom, then a material circuit within the bottom has circulation modified by bottom pressure.

To develop the mathematics of the above ideas, write the differential line element within the bottom circuit as

$$\mathrm{d}\boldsymbol{x} = \hat{\boldsymbol{x}}\,\mathrm{d}x + \hat{\boldsymbol{y}}\,\mathrm{d}y + \hat{\boldsymbol{z}}\,\mathrm{d}z = (\hat{\boldsymbol{x}} + \hat{\boldsymbol{z}}\,\partial_x\eta_{\mathrm{b}})\mathrm{d}x + (\hat{\boldsymbol{y}} + \hat{\boldsymbol{z}}\,\partial_y\eta_{\mathrm{b}})\mathrm{d}y. \tag{40.66}$$

To reach this result we set $z = \eta_{\mathrm{b}}(x, y)$ since the circuit is along the bottom boundary, which in turn means that[8]

$$\mathrm{d}z = \mathrm{d}\eta_{\mathrm{b}} = \nabla\eta_{\mathrm{b}} \cdot (\hat{\boldsymbol{x}}\,\mathrm{d}x + \hat{\boldsymbol{y}}\,\mathrm{d}y) = \nabla\eta_{\mathrm{b}} \cdot \mathrm{d}\boldsymbol{x}_{\mathrm{horz}}. \tag{40.67}$$

Consequently, the projection of the density gradient onto the circuit is given by

$$\nabla\rho \cdot \mathrm{d}\boldsymbol{x} = (\nabla_{\mathrm{h}}\rho + \partial_z\rho\,\nabla\eta_{\mathrm{b}}) \cdot \mathrm{d}\boldsymbol{x}_{\mathrm{horz}}. \tag{40.68}$$

Making use of this result in Kelvin's circulation theorem and focusing on the pressure contribution, as in equation (40.64), leads to

$$\left[\frac{\mathrm{d}C}{\mathrm{d}t}\right]_{\mathrm{bottom}} = -\oint_{\partial\mathcal{S}_{\mathrm{bottom}}} p\,\rho^{-2}\,\nabla\rho \cdot \mathrm{d}\boldsymbol{x} = -\oint_{\partial\mathcal{S}_{\mathrm{bottom}}} \frac{p_{\mathrm{b}}}{\rho^2}(\nabla_{\mathrm{h}}\rho + \partial_z\rho\,\nabla\eta_{\mathrm{b}}) \cdot \mathrm{d}\boldsymbol{x}_{\mathrm{horz}}. \tag{40.69}$$

There are two contributions to the circulation changes revealed by equation (40.69). The first arises from the sloped density surfaces next to the bottom, and the second arises from the sloped bottom multiplied by the vertical density gradient. These two contributions are weighted by the bottom pressure, p_{b}, which is normalized by the squared density. Circulation modifications are enhanced by increased horizontal density gradients next to the bottom, as well as increased topographic slopes. For the special case of flat topography and flat density there are no bottom pressure-induced changes to the circulation around a bottom material circuit.

40.4.4 Further study

This video from Prof. Shapiro provides a lucid discussion of baroclinicity and its role in affecting vorticity and circulation.

[8] Since $\eta_{\mathrm{b}} = \eta_{\mathrm{b}}(x, y)$, its gradient is horizontal: $\nabla\eta_{\mathrm{b}} = \hat{\boldsymbol{x}}\,\partial_x\eta_{\mathrm{b}} + \hat{\boldsymbol{y}}\,\partial_y\eta_{\mathrm{b}}$.

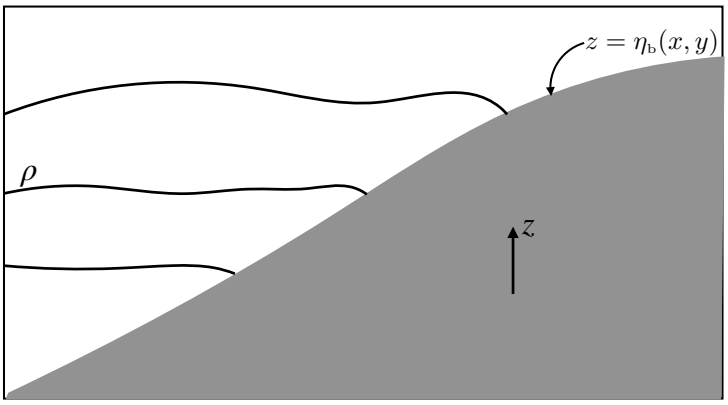

FIGURE 40.5: Constant density surfaces intersecting a sloped solid-earth boundary. Any circuit that sits along the boundary is material since the bottom is material. For circuits that cross density surfaces, the bottom pressure acts to modify circulation computed for this circuit.

40.5 Vortex lines and material lines

We here study the physics of the source term

$$(\boldsymbol{\omega}_{\rm a} \cdot \nabla)\, \boldsymbol{v} = f\, \partial_z \boldsymbol{v} + (\boldsymbol{\omega} \cdot \nabla)\, \boldsymbol{v} \tag{40.70}$$

appearing in the vorticity equation (40.42). The contribution from $\hat{\boldsymbol{z}}\, f\, \partial_z w$ to the first term is further explored when studying the planetary geostrophic equations in Sections 31.5 and 44.2, given its importance for large-scale meridional motion on a spherical planet. The second term, $(\boldsymbol{\omega} \cdot \nabla)\, \boldsymbol{v}$, is the focus of this section.

40.5.1 Vortex lines evolve through the strain rate tensor

To help unpack the physics of the source, $(\boldsymbol{\omega} \cdot \nabla)\, \boldsymbol{v}$, write it in the following form found by exposing Cartesian tensor labels

$$\omega_m\, \partial_m v_n = (\omega_m/2)\, [(\partial_m v_n + \partial_n v_m) + (\partial_m v_n - \partial_n v_m)] \tag{40.71a}$$

$$= \omega_m\, \mathbb{S}_{mn} - \omega_m\, \mathbb{R}_{mn}, \tag{40.71b}$$

where $\mathbb{S}_{mn} = (1/2)\, (\partial_n v_m + \partial_m v_n)$ are components to the strain rate tensor and $\mathbb{R}_{mn} = (1/2)\, (\partial_n v_m - \partial_m v_n)$ are components to the rotation tensor. These tensors were introduced in Section 18.6 when studying the kinematics of line elements. As shown in that discussion, the rotation tensor is related to the vorticity by the identity (18.102), whose use leads to

$$2\, \omega_m\, \mathbb{R}_{mn} = -\omega_m\, \epsilon_{mnp}\, \omega_p = \epsilon_{nmp}\, \omega_m\, \omega_p = (\boldsymbol{\omega} \times \boldsymbol{\omega})_n = 0. \tag{40.72}$$

Recalling that the rotation tensor generates rotations about the axis defined by vorticity, we can understand why $\boldsymbol{\omega} \cdot \mathbb{R} = 0$. Namely, there is no rotation generated when a vector is rotated about its own axis. We are thus left just with

$$(\boldsymbol{\omega} \cdot \nabla)\, \boldsymbol{v} = \boldsymbol{\omega} \cdot \mathbb{S}. \tag{40.73}$$

That is, the source, $(\boldsymbol{\omega} \cdot \nabla)\, \boldsymbol{v}$, appearing in the vorticity equation is determined by the projection of the vorticity onto the strain rate tensor. This result highlights the fundamental role of flow strains in affecting vorticity.

40.5.2 Frozen-in nature of vorticity

Consider an inviscid barotropic fluid in the absence of planetary rotation and whose flow is non-divergent, in which case the vorticity equation (40.42) reduces to

$$\frac{\mathrm{D}\boldsymbol{\omega}}{\mathrm{D}t} = (\boldsymbol{\omega}\cdot\nabla)\,\boldsymbol{v}, \tag{40.74}$$

and recall the evolution equation for a material line element as detailed in Section 18.6

$$\frac{\mathrm{D}(\delta\boldsymbol{x})}{\mathrm{D}t} = (\delta\boldsymbol{x}\cdot\nabla)\,\boldsymbol{v}. \tag{40.75}$$

Now recall from Section 37.7.1 that a vortex line is a line drawn through the fluid that is everywhere parallel to the vorticity. Such a line connects material fluid particles, so that a vortex line constitutes a particular case of a material line. At some initial time, $t = 0$, let the vorticity on an infinitesimal vortex line be related to the material line element according to

$$\delta\boldsymbol{x}(0) = \Gamma\,\boldsymbol{\omega}(\boldsymbol{x}, 0), \tag{40.76}$$

where Γ has dimensions $L\,T$ and is determined by the initial vorticity and initial line element. Since the vorticity equation (40.74) has precisely the same mathematical form as the material line element equation (40.75), the difference vector

$$\boldsymbol{A} \equiv \delta\boldsymbol{x} - \Gamma\,\boldsymbol{\omega}, \tag{40.77}$$

evolves according to

$$\frac{\mathrm{D}\boldsymbol{A}}{\mathrm{D}t} = (\boldsymbol{A}\cdot\nabla)\boldsymbol{v}. \tag{40.78}$$

But since $\boldsymbol{A}$ vanishes at $t = 0$, we conclude that it vanishes for all time

$$\frac{\mathrm{D}\boldsymbol{A}}{\mathrm{D}t} = 0. \tag{40.79}$$

Consequently, the relation (40.76) holds for all time with Γ a constant. That is, the vortex line and its corresponding line element remain parallel as they both evolve according to their projection onto the strain rate tensor. We thus say that vorticity is a *frozen-in* property as illustrated by Figure 40.6. Although we established this property only for the case of an inviscid, barotropic fluid with non-divergent flow, it offers insight into the more general situation occuring in real fluids.

40.5.3 Stretching and tilting of vortex tubes

Vorticity responds when vortex lines or tubes are stretched or bent by the strain rate tensor. To help understand the response, consider again the perfect fluid barotropic vorticity equation with a non-divergent flow (equation (40.74)) and focus on the material evolution of the vertical vorticity component

$$\frac{\mathrm{D}\omega_z}{\mathrm{D}t} = \omega_x\frac{\partial w}{\partial x} + \omega_y\frac{\partial w}{\partial y} + \omega_z\frac{\partial w}{\partial z} = \boldsymbol{\omega}\cdot\nabla w = \nabla\cdot(w\,\boldsymbol{\omega}). \tag{40.80}$$

The following discussion closely emulates that given for a material line element in Section 18.8.3.

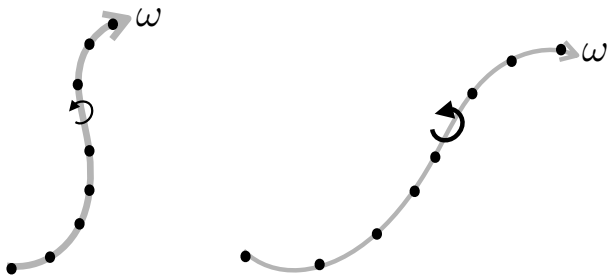

FIGURE 40.6: For the non-divergent flow of a perfect barotropic fluid, vortex lines are also material lines. This property means that for an arbitrary vortex line drawn in the fluid, the fluid particles that are initially on the vortex line remain on the line as it moves through the fluid according to the strain rate tensor. We here show two instances of the same vortex line along with sample test fluid particles. The left configuration stretches into the right configuration, with the vorticity increasing as the vortex line stretches according to the discussion in Section 40.5.3. This property of a vortex line is known as its *frozen-in nature*. The frozen-in nature of vortex lines strictly holds only for perfect barotropic fluid exhibiting non-divergent flow, yet it offers useful insights into the vortex dynamics of more general fluids.

Stretching

Consider the vortex tube to be initially aligned with the $\hat{\boldsymbol{z}}$-axis, so that $\omega_x = \omega_y = 0$, in which case there is only a single term impacting the material evolution of vertical vorticity[9]

$$\frac{\mathrm{D}\omega_z}{\mathrm{D}t} = \omega_z \frac{\partial w}{\partial z}. \tag{40.81}$$

Since the flow is non-divergent, the volume of an infinitesimal portion of the vortex tube is materially constant

$$\frac{\mathrm{D}(\delta V)}{\mathrm{D}t} = 0, \tag{40.82}$$

which means that the vertical extent, δz, and cross-sectional area, δA, are constrained

$$\frac{1}{\delta z}\frac{\mathrm{D}(\delta z)}{\mathrm{D}t} + \frac{1}{\delta A}\frac{\mathrm{D}(\delta A)}{\mathrm{D}t} = 0. \tag{40.83}$$

As the tube stretches vertically, its horizontal area reduces, and vice versa. Making use of the expression for the evolution of a material line segment (equation (40.75)) allows us to write

$$\frac{1}{\delta z}\frac{\mathrm{D}(\delta z)}{\mathrm{D}t} = \frac{\partial w}{\partial z}, \tag{40.84}$$

so that the vorticity equation (40.81) becomes

$$\frac{\mathrm{D}\omega_z}{\mathrm{D}t} = \omega_z \frac{\partial w}{\partial z} = \omega_z \left[\frac{1}{\delta z}\frac{\mathrm{D}(\delta z)}{\mathrm{D}t}\right] = -\omega_z \left[\frac{1}{\delta A}\frac{\mathrm{D}(\delta A)}{\mathrm{D}t}\right]. \tag{40.85}$$

Rearrangement leads to

$$\frac{\mathrm{D}(\omega_z\, \delta A)}{\mathrm{D}t} = 0, \tag{40.86}$$

which is an expression of Kelvin's circulation theorem (equation (40.11)) for a horizontal cross-section of the vortex tube.

The above manipulations suggest the following interpretation for the *stretching* term, $\omega_z\,(\partial w/\partial z)$, appearing in the vertical vorticity equation (40.80) and illustrated in Figure 40.7.

[9] Be mindful to distinguish the symbols for the vertical component of vorticity, ω_z, and the vertical component of velocity, w.

Namely, as the vortex tube is stretched and its cross-sectional area is compressed, the vorticity magnitude increases so to maintain a constant circulation around the tube, as per Kelvin's theorem (or equivalently as per Helmholtz's first theorem discussed in Section 37.7.3). Stretching a vortex tube increases the magnitude of the vorticity in the direction of the stretching whereas compressing a tube reduces the vorticity magnitude. This result accords with our understanding of angular momentum conservation as discussed for the rotating cylinder in Section 39.2.2 and depicted by Figure 39.1.

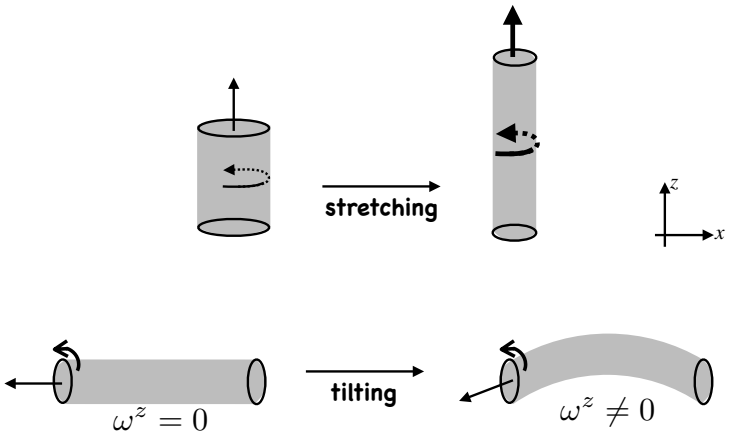

FIGURE 40.7: Illustrating how stretching and tilting of a vortex tube impacts on the vorticity. Top panels: As the cross-sectional area of the vortex tube shrinks, and the vertical extent of the tube stretches, the magnitude of the vorticity along the axis of the tube increases. This result accords with our understanding of angular momentum conservation as discussed for the rotating cylinder in Section 39.2.2 and depicted by Figure 39.1, as well as with Helmholtz's first theorem in Section 37.7.3 and Figure 37.7. Lower panels: The initial vortex tube is assumed to be aligned parallel to the x-axis, so that it has zero projection in the vertical direction. A horizontal shear of the vertical velocity ($\partial w/\partial x \neq 0$) deforms the vortex tube. Upon deforming (or tilting), the tube picks up a nonzero projection in the vertical, which means that it now has a nonzero vertical component to vorticity.

Tilting

Now consider an initially horizontal vortex tube as in the lower left panel of Figure 40.7 so that $\omega_z = 0$. Furthermore, to focus on just one of the two horizontal directions we set $\omega_y = 0$ so that equation (40.80) for the vertical vorticity becomes

$$\frac{\mathrm{D}\omega_z}{\mathrm{D}t} = \omega_x \frac{\partial w}{\partial x}. \tag{40.87}$$

If there is no horizontal shear in the vertical velocity ($\partial w/\partial x = 0$), then the vortex tube remains horizontal. However, in the presence of $\partial w/\partial x \neq 0$, the vorticity vector picks up a nonzero vertical projection. To help visualize this process, recall the frozen-in nature of vortex lines, and consider the evolution of an infinitesimal line segment on the vortex tube. With the vortex tube initially aligned parallel to the x-axis, the evolution of a material line segment (equation (40.75)) is given by

$$\frac{\mathrm{D}(\delta \boldsymbol{x})}{\mathrm{D}t} = \delta x \frac{\partial \boldsymbol{v}}{\partial x}. \tag{40.88}$$

The initially horizontal line segment thus picks up a projection in the vertical so long as $\partial w/\partial x \neq 0$. Correspondingly, the vorticity picks up a vertical component. We can think of this process as a tilting or deforming of the initially horizontal vortex tube, with the tilted tube having a nonzero vertical projection.

40.5.4 Shallow water vorticity revisited

We here revisit our discussion of the shallow water vorticity from Chapter 39 in light of the vorticity equation (40.42). Notably, an inviscid shallow water fluid has zero baroclinicity, so that only stretching and tilting affect shallow water vorticity.

Vortex tubes never close in a shallow water layer

The absolute vorticity vector in a shallow water layer is given by equation (35.106d)

$$\boldsymbol{\omega}_{\mathrm{a}} = \nabla \times \boldsymbol{v} + \hat{\boldsymbol{z}}\, f = \boldsymbol{\omega}_{\mathrm{h}} + \hat{\boldsymbol{z}}\,(\zeta + f) = \hat{\boldsymbol{x}}\,\partial_y w - \hat{\boldsymbol{y}}\,\partial_x w + \hat{\boldsymbol{z}}\,\zeta_{\mathrm{a}} = -\hat{\boldsymbol{z}} \times \nabla w + \hat{\boldsymbol{z}}\,\zeta_{\mathrm{a}}, \tag{40.89}$$

where we set $\partial_z u = \partial_z v = 0$ for the horizontal velocity within a shallow water layer. Since the shallow water fluid is hydrostatic, the horizontal vorticity component is much smaller in magnitude than the vertical component,

$$|\partial_x w, \partial_y w| \ll |\zeta|. \tag{40.90}$$

Vortex tubes in a shallow water fluid do not close, since to close requires breaking this inequality. Hence, shallow water vortex tubes reach from the bottom of the layer to the top, with only a slight tilt relative to the vertical.

Material time evolution of shallow water vorticity

To determine how shallow water vorticity evolves, we make use of the stretching and tilting term in the form of equation (40.73) so that

$$\frac{\mathrm{D}\boldsymbol{\omega}_{\mathrm{a}}}{\mathrm{D}t} = (\boldsymbol{\omega}_{\mathrm{a}} \cdot \nabla)\,\boldsymbol{v} \implies \frac{\mathrm{D}\omega_{\mathrm{a}n}}{\mathrm{D}t} = \omega_{\mathrm{a}m}\,\mathbb{S}_{mn}. \tag{40.91}$$

The strain rate tensor for the shallow water fluid is

$$\mathbb{S} = \frac{1}{2}\begin{bmatrix} 2\,\partial_x u & \partial_y u + \partial_x v & \partial_z u + \partial_x w \\ \partial_x v + \partial_y u & 2\,\partial_y v & \partial_z v + \partial_y w \\ \partial_x w + \partial_z u & \partial_y w + \partial_z v & 2\,\partial_z w \end{bmatrix} = \frac{1}{2}\begin{bmatrix} 2\,\partial_x u & \partial_y u + \partial_x v & \partial_x w \\ \partial_x v + \partial_y u & 2\,\partial_y v & \partial_y w \\ \partial_x w & \partial_y w & 2\,\partial_z w \end{bmatrix}, \tag{40.92}$$

so that material time evolution of the vertical vorticity component, is given by

$$\begin{aligned} \frac{\mathrm{D}(\zeta + f)}{\mathrm{D}t} &= \omega_1\,\mathbb{S}_{13} + \omega_2\,\mathbb{S}_{23} + \hat{\boldsymbol{z}} \cdot \boldsymbol{\omega}_{\mathrm{a}}\,\mathbb{S}_{33} && \text{(40.93a)} \\ &= (1/2)\,(\omega_1\,\partial_x w + \omega_2\,\partial_y w) + \omega_{\mathrm{a}3}\,\partial_z w && \text{(40.93b)} \\ &= (\zeta + f)\,\partial_z w && \text{(40.93c)} \\ &= -(\zeta + f)\,\nabla \cdot \boldsymbol{u}, && \text{(40.93d)} \end{aligned}$$

which agrees with the shallow water vorticity equation (39.9). For the zonal vorticity component we have

$$\begin{aligned} \frac{\mathrm{D}\omega_1}{\mathrm{D}t} &= \omega_1\,\mathbb{S}_{11} + \omega_2\,\mathbb{S}_{21} + \hat{\boldsymbol{z}} \cdot \boldsymbol{\omega}_{\mathrm{a}}\,\mathbb{S}_{31} && \text{(40.94a)} \\ &= \omega_1\,\partial_x u + \omega_2\,(\partial_x v + \partial_y u)/2 + \omega_3\,\partial_x w, && \text{(40.94b)} \end{aligned}$$

and a similar expression for the meridional component.

Flux-form evolution of Cartesian vorticity components

In Section 40.3.4, we showed how each of the three Cartesian vorticity components evolves according to a flux-form equation. For the vertical component to the vorticity, the vorticity flux, $\boldsymbol{J}^{\zeta_a}$, is given by equation (40.45) and it takes on the following form for a shallow water layer

$$\boldsymbol{J}^{\zeta_a} = \boldsymbol{v}\,\zeta_a - w\,\boldsymbol{\omega}_a = \boldsymbol{u}\,\zeta_a - w\,\boldsymbol{\omega}_h = \boldsymbol{u}\,\zeta_a + w\,\hat{\boldsymbol{z}}\times\nabla w = \boldsymbol{u}\,\zeta_a + \hat{\boldsymbol{z}}\times\nabla w^2/2. \tag{40.95}$$

The term

$$\hat{\boldsymbol{z}}\times\nabla w^2/2 = -\nabla\times\hat{\boldsymbol{z}}\,w^2/2 \tag{40.96}$$

has a zero divergence and so has no contribution to the convergence of the vorticity flux. Hence, the vorticity flux, $\boldsymbol{J}^{\zeta_a}$, derived here differs by a gauge from the purely advective flux, $\boldsymbol{u}\,\zeta_a$, considered in the shallow water vorticity equation (39.7).

For the zonal component to the vorticity, the vorticity flux, $\boldsymbol{J}^{\omega_1}$, is given by equation (40.47) and it takes on the following form for a shallow water layer

$$\boldsymbol{J}^{\omega_1} = \boldsymbol{v}\,\omega_{a1} - u\,\boldsymbol{\omega}_a = (\hat{\boldsymbol{y}}\,v + \hat{\boldsymbol{z}}\,w)\,\omega_1 - \hat{\boldsymbol{y}}\,\omega_2 - \hat{\boldsymbol{z}}\,(\zeta+f) = \hat{\boldsymbol{y}}\,(v\,\omega_1 - u\,\omega_2) + \hat{\boldsymbol{z}}\,[w\,\omega_1 - u\,(\zeta+f)], \tag{40.97}$$

with a similar form for the flux of the meridional vorticity component, $\boldsymbol{J}^{\omega_2}$.

40.5.5 Concerning three-dimensional turbulence

As a vortex tube is stretched in the presence of straining motion, it spins faster as its radius decreases. Hence, its kinetic energy moves from larger to smaller spatial scales. This process of downscale energy cascade (i.e., the movement of kinetic energy from large to small scales) is a fundamental property of three dimensional turbulence, and vortex stretching is the dominant mechanism for the cascade. In contrast, two dimensional turbulence, which occurs in horizontal non-divergent flows, does not support vortex stretching and consequently does not support the downscale energy cascade. Instead, two dimensional turbulence supports an inverse cascade whereby there is a net flow of energy to larger scales, with that flow related to the material conservation of vorticity in two dimensional non-divergent flows (see Chapter 38). *Vallis* (2017) provides a lucid discussion of energy cascades in both two and three dimesional turbulence.

40.6 Circulation viewed in a rotating reference frame

We here tie up an important loose end by studying circulation and vorticity for fluids in a rotating reference frame, such as those on a rotating planet. It turns out that incorporating rotation is straightforward, and yet the implications are quite profound for the motion of geophysical fluids. In this section we are careful to make use of planetary Cartesian coordinates, whereby the origin of the coordinate system is at the center of the planet (see Figure 4.3).

Start by recalling the expression from Section 13.7.1 for the inertial or absolute velocity (i.e., velocity measured in an inertial frame)

$$\boldsymbol{v}_a = \boldsymbol{v} + \boldsymbol{\Omega}\times\boldsymbol{x}, \tag{40.98}$$

where $\boldsymbol{v}$ is the velocity measured in the rotating frame (relative velocity), and $\boldsymbol{x}$ is the position vector relative to the origin (e.g., center of earth). The absolute circulation around an arbitrary circuit (a circuit that is not necessarily material) is thus given by

$$\mathcal{C}_a = \oint_{\partial\mathcal{S}} (\boldsymbol{v} + \boldsymbol{\Omega}\times\boldsymbol{x})\cdot \mathrm{d}\boldsymbol{x} = \mathcal{C} + \mathcal{C}_{\text{planet}}, \tag{40.99}$$

where the circulation measured in the rotating reference frame is

$$\mathcal{C} = \oint_{\partial\mathcal{S}} \boldsymbol{v} \cdot \mathrm{d}\boldsymbol{x} \tag{40.100}$$

and the circulation associated with the rotating planet is

$$\mathcal{C}_{\text{planet}} = \oint_{\partial\mathcal{S}} (\boldsymbol{\Omega} \times \boldsymbol{x}) \cdot \mathrm{d}\boldsymbol{x}. \tag{40.101}$$

A fluid element at rest in the rotating reference frame still has a nonzero absolute circulation as given by the planetary circulation. Making use of Stokes' theorem leads to the equivalent forms for the circulations

$$\mathcal{C} = \oint_{\partial\mathcal{S}} \boldsymbol{v} \cdot \mathrm{d}\boldsymbol{x} = \int_{\mathcal{S}} \boldsymbol{\omega} \cdot \hat{\boldsymbol{n}}\, \mathrm{d}\mathcal{S} \qquad \text{relative circulation} \tag{40.102a}$$

$$\mathcal{C}_{\text{planet}} = \oint_{\partial\mathcal{S}} (\boldsymbol{\Omega} \times \boldsymbol{x}) \cdot \mathrm{d}\boldsymbol{x} = \int_{\mathcal{S}} \boldsymbol{\omega}_{\text{planet}} \cdot \hat{\boldsymbol{n}}\, \mathrm{d}\mathcal{S} \qquad \text{planetary circulation} \tag{40.102b}$$

$$\mathcal{C}_{\text{a}} = \oint_{\partial\mathcal{S}} \boldsymbol{v}_{\text{a}} \cdot \mathrm{d}\boldsymbol{x} = \int_{\mathcal{S}} \boldsymbol{\omega}_{\text{a}} \cdot \hat{\boldsymbol{n}}\, \mathrm{d}\mathcal{S} \qquad \text{absolute circulation,} \tag{40.102c}$$

where

$$\boldsymbol{\omega} = \nabla \times \boldsymbol{v} \qquad \text{relative vorticity} \tag{40.103a}$$

$$\boldsymbol{\omega}_{\text{planet}} = \nabla \times (\boldsymbol{\Omega} \times \boldsymbol{x}) = 2\,\boldsymbol{\Omega} \qquad \text{planetary vorticity} \tag{40.103b}$$

$$\boldsymbol{\omega}_{\text{a}} = \nabla \times (\boldsymbol{v} + \boldsymbol{\Omega} \times \boldsymbol{x}) = \boldsymbol{\omega} + \boldsymbol{\omega}_{\text{planet}} \qquad \text{absolute vorticity.} \tag{40.103c}$$

Thus far we have merely substituted in the expression (40.98) for the inertial velocity and then decomposed the vorticity and circulation into its relative and planetary components. Next we consider how circulation evolves, in which case we see how the relative and planetary circulations interact.

40.6.1 Material evolution of absolute circulation

Consider how the absolute circulation evolves for a material circuit that moves with the fluid

$$\frac{\mathrm{d}\mathcal{C}_{\text{a}}}{\mathrm{d}t} = \frac{\mathrm{d}}{\mathrm{d}t} \oint_{\partial\mathcal{S}(\boldsymbol{v})} \boldsymbol{v}_{\text{a}} \cdot \mathrm{d}\boldsymbol{x} = \frac{\mathrm{d}}{\mathrm{d}t} \oint_{\partial\mathcal{S}(\boldsymbol{v})} (\boldsymbol{v} + \boldsymbol{\Omega} \times \boldsymbol{x}) \cdot \mathrm{d}\boldsymbol{x}. \tag{40.104}$$

We measure fluid motion in the rotating frame so that the material time derivative is computed with the velocity, $\boldsymbol{v}$, rather than the absolute velocity, $\boldsymbol{v}_{\text{a}}$. Following the derivation of Kelvin's circulation theorem in a non-rotating reference frame from Section 40.2 leads to

$$\frac{\mathrm{d}\mathcal{C}_{\text{a}}}{\mathrm{d}t} = \frac{\mathrm{d}}{\mathrm{d}t} \oint_{\partial\mathcal{S}(\boldsymbol{v})} (\boldsymbol{v} + \boldsymbol{\Omega} \times \boldsymbol{x}) \cdot \mathrm{d}\boldsymbol{x} \tag{40.105a}$$

$$= \oint_{\partial\mathcal{S}(\boldsymbol{v})} \left[\frac{\mathrm{D}\boldsymbol{v}}{\mathrm{D}t} + \boldsymbol{\Omega} \times \frac{\mathrm{D}\boldsymbol{x}}{\mathrm{D}t} \right] \cdot \mathrm{d}\boldsymbol{x} + \oint_{\partial\mathcal{S}(\boldsymbol{v})} (\boldsymbol{v} + \boldsymbol{\Omega} \times \boldsymbol{x}) \cdot \mathrm{d}\boldsymbol{v} \tag{40.105b}$$

$$= \oint_{\partial\mathcal{S}(\boldsymbol{v})} \left[\frac{\mathrm{D}\boldsymbol{v}}{\mathrm{D}t} + \boldsymbol{\Omega} \times \boldsymbol{v} \right] \cdot \mathrm{d}\boldsymbol{x} + \oint_{\partial\mathcal{S}(\boldsymbol{v})} (\boldsymbol{\Omega} \times \boldsymbol{x}) \cdot \mathrm{d}\boldsymbol{v} \tag{40.105c}$$

$$= \oint_{\partial\mathcal{S}(\boldsymbol{v})} \left[\frac{\mathrm{D}\boldsymbol{v}}{\mathrm{D}t} + 2\,\boldsymbol{\Omega} \times \boldsymbol{v} \right] \cdot \mathrm{d}\boldsymbol{x}. \tag{40.105d}$$

To reach this result we set

$$\boldsymbol{v} = \frac{\mathrm{D}\boldsymbol{x}}{\mathrm{D}t}, \tag{40.106}$$

for the velocity of a fluid particle on the circuit. We also used the identity

$$\oint_{\partial\mathcal{S}(\boldsymbol{v})} \boldsymbol{v}\cdot\mathrm{d}\boldsymbol{v} = \frac{1}{2}\oint_{\partial\mathcal{S}(\boldsymbol{v})} \mathrm{d}(\boldsymbol{v}\cdot\boldsymbol{v}) = 0 \tag{40.107}$$

as well as

$$\oint_{\partial\mathcal{S}(\boldsymbol{v})} (\boldsymbol{\Omega}\times\boldsymbol{x})\cdot\mathrm{d}\boldsymbol{v} = \oint_{\partial\mathcal{S}(\boldsymbol{v})} \mathrm{d}\left[(\boldsymbol{\Omega}\times\boldsymbol{x})\cdot\boldsymbol{v}\right] - \oint_{\partial\mathcal{S}(\boldsymbol{v})} (\boldsymbol{\Omega}\times\mathrm{d}\boldsymbol{x})\cdot\boldsymbol{v} = \oint_{\partial\mathcal{S}(\boldsymbol{v})} (\boldsymbol{\Omega}\times\boldsymbol{v})\cdot\mathrm{d}\boldsymbol{x}, \tag{40.108}$$

where we set

$$\oint_{\partial\mathcal{S}(\boldsymbol{v})} \mathrm{d}\left[(\boldsymbol{\Omega}\times\boldsymbol{x})\cdot\boldsymbol{v}\right] = 0 \tag{40.109}$$

since, as for equation (40.107), the closed loop integral of an exact spatial differential vanishes. We also noted that $\boldsymbol{\Omega}$ is a constant vector so that $\mathrm{d}\boldsymbol{\Omega} = 0$. Now insert the momentum equation (40.31) into equation (40.105d) to yield

$$\frac{\mathrm{d}\mathcal{C}_{\mathrm{a}}}{\mathrm{d}t} = \oint_{\partial\mathcal{S}(\boldsymbol{v})} \left[\frac{\mathrm{D}\boldsymbol{v}}{\mathrm{D}t} + 2\,\boldsymbol{\Omega}\times\boldsymbol{v}\right]\cdot\mathrm{d}\boldsymbol{x}. \tag{40.110a}$$

$$= \oint_{\partial\mathcal{S}(\boldsymbol{v})} \left[-\frac{1}{\rho}\nabla p - \nabla\Phi + \boldsymbol{F}\right]\cdot\mathrm{d}\boldsymbol{x}. \tag{40.110b}$$

$$= \oint_{\partial\mathcal{S}(\boldsymbol{v})} \left[-\frac{\mathrm{d}p}{\rho} + \boldsymbol{F}\cdot\mathrm{d}\boldsymbol{x}\right]. \tag{40.110c}$$

Making use of Stokes' theorem leads to the evolution of absolute circulation around a material loop

$$\frac{\mathrm{d}\mathcal{C}_{\mathrm{a}}}{\mathrm{d}t} = \oint_{\partial\mathcal{S}(\boldsymbol{v})} \left[-\frac{\mathrm{d}p}{\rho} + \boldsymbol{F}\cdot\mathrm{d}\boldsymbol{x}\right] = \int_{S(\boldsymbol{v})} (\boldsymbol{B} + \nabla\times\boldsymbol{F})\cdot\hat{\boldsymbol{n}}\,\mathrm{d}\mathcal{S}, \tag{40.111}$$

where $\boldsymbol{B} = \rho^{-2}\,\nabla\rho\times\nabla p$ is the baroclinicity vector from equation (40.62).

The circulation theorem (40.111) is the same as obtained for Kelvin's circulation theorem in a non-rotating reference frame as discussed in Section 40.2 (see equation (40.5e)). As such, we find that time changes to the absolute circulation are affected by the work applied by pressure and friction when integrated around the material circuit. Evidently, the formalism confirms that absolute circulation is a frame invariant property of the fluid, in which its evolution is unchanged when moving to a non-inertial rotating frame.

40.6.2 The beta effect

As given by equation (40.99), the absolute circulation around an arbitrary circuit equals to the circulation of fluid measured in the rotating frame (relative circulation) plus circulation of the rotating frame itself (planetary circulation)

$$\mathcal{C}_{\mathrm{a}} = \mathcal{C} + \mathcal{C}_{\mathrm{planet}} = \mathcal{C} + 2\int_{\mathcal{S}} \boldsymbol{\Omega}\cdot\hat{\boldsymbol{n}}\,\mathrm{d}\mathcal{S} \Longleftrightarrow \frac{\mathrm{d}\mathcal{C}_{\mathrm{a}}}{\mathrm{d}t} = \frac{\mathrm{d}\mathcal{C}}{\mathrm{d}t} + \frac{\mathrm{d}\mathcal{C}_{\mathrm{planet}}}{\mathrm{d}t}. \tag{40.112}$$

We can determine the processes that affect the absolute circulation around a material loop by using the circulation theorem (40.111)

$$\frac{\mathrm{d}\mathcal{C}}{\mathrm{d}t} = -\frac{\mathrm{d}\mathcal{C}_{\mathrm{planet}}}{\mathrm{d}t} + \frac{\mathrm{d}\mathcal{C}_{\mathrm{a}}}{\mathrm{d}t} \tag{40.113a}$$

$$= -2 \frac{\mathrm{d}}{\mathrm{d}t} \left[\int_{\mathcal{S}(\boldsymbol{v})} \boldsymbol{\Omega} \cdot \hat{\boldsymbol{n}} \, \mathrm{d}\mathcal{S} \right] + \int_{\mathcal{S}(\boldsymbol{v})} (\boldsymbol{B} + \nabla \times \boldsymbol{F}) \cdot \hat{\boldsymbol{n}} \, \mathrm{d}\mathcal{S}. \tag{40.113b}$$

We generally assume that the planetary rotation is a constant in time and points through the north pole of the sphere[10] $\boldsymbol{\Omega} = \Omega \, \hat{\boldsymbol{Z}}$, so that

$$\int_{\mathcal{S}(\boldsymbol{v})} \boldsymbol{\Omega} \cdot \hat{\boldsymbol{n}} \, \mathrm{d}\mathcal{S} = \Omega \int_{\mathcal{S}(\boldsymbol{v})} \hat{\boldsymbol{Z}} \cdot \hat{\boldsymbol{n}} \, \mathrm{d}\mathcal{S} = \Omega \, A_\perp. \tag{40.114}$$

The area, $A_\perp$, is the projection of the spherical area enclosed by the circuit onto the horizontal equatorial plane, with Figure 40.8 illustrating the geometry. This result has profound impact on large scale geophysical fluid motion, whereby relative circulation around a material circuit in the rotating frame changes according to

$$\frac{\mathrm{d}\mathcal{C}}{\mathrm{d}t} = \underbrace{-2 \, \Omega \, \frac{\mathrm{d}A_\perp}{\mathrm{d}t}}_{\text{beta effect}} + \underbrace{\int_{\mathcal{S}} (\boldsymbol{B} + \nabla \times \boldsymbol{F}) \cdot \hat{\boldsymbol{n}} \, \mathrm{d}\mathcal{S}(\boldsymbol{v})}_{\text{baroclinicity plus friction curl}}. \tag{40.115}$$

Equation (40.115) is sometimes referred to as the *Bjerknes circulation theorem* (see *Holton and Hakim* (2013) equation (4.5)). The second term, comprised of baroclinicity and friction, also appears in case of a non-rotating reference frame that we studied in Sections 40.2 and 40.4.

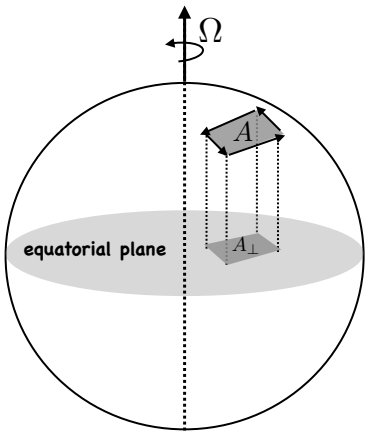

FIGURE 40.8: Geometry of the beta effect on a rotating sphere. According to the Bjerknes circulation theorem (40.115), the circulation for a material loop on the surface of a rotating sphere is affected by baroclinicity and friction, as for a non-rotating sphere, as well as latitudinal motion of the loop. The latitudinal motion alters the area of the loop as projected onto the equatorial plane, with the projected area increasing as the loop moves poleward. When multiplied by the magnitude of the planetary vorticity, $2\,\Omega$, the area contribution is termed *planetary induction* (i.e., relative circulation is induced by latitudinal motion), or more commonly it is called the *beta effect*. The beta effect requires both rotation ($2\,\Omega$) and curvature of the sphere ($\partial_y f = \beta$); it is therefore absent on the f-plane.

The first term in the circulation theorem (40.115) is fundamentally new. It is nonzero in the presence of both rotation and curvature of the sphere. The spherical effect arises from latitudinal movement of a material circuit, with the area, $A_\perp$, changing under such motion. When the circuit moves poleward, the projected area, $A_\perp$, increases whereas it decreases to zero as it moves equatorward. The material change in $A_\perp$, when multiplied by the planetary vorticity, modifies the relative circulation around the material circuit. We refer to *planetary induction* as

[10] We follow the notational conventions of Figure 4.3 with one exception. Here, the vertical Cartesian direction through the north pole is written $\hat{\boldsymbol{Z}}$ to avoid confusion with the local vertical direction $\hat{\boldsymbol{z}}$ determined by the geopotential.

the process whereby relative circulation is modified by latitudinal motion of a material circuit on a rotating sphere. Or more commonly, planetary induction is referred to as the *beta effect*, given its connection to the latitudinal gradient of the Coriolis parameter, $\beta = \partial_y f$. Notably, longitudinal motion of the circuit has no impact on $A_\perp$, so that longitudinal motion imparts no planetary induction of relative circulation.

In theories of large-scale laminar planetary flows, the baroclinicity and friction terms are typically sub-dominant. For these flows, the material evolution of relative circulation is dominated by the beta effect. Planetary geostrophic flow is the canonical example of such flow, as studied in Section 31.5 as well as Chapters 43 and 44. In such flows, forces that lead to meridional motion also give rise to changes in the relative circulation. Conversely, forces that change the circulation around a material loop affect meridional motion of the loop.

40.6.3 The case of two-dimensional non-divergent flow

To garner further insight into the nature of the beta effect, consider a perfect (i.e., inviscid) two-dimensional and non-divergent flow (zero vertical velocity) on a rotating sphere. In this case there is only a vertical component to vorticity and baroclinicity vanishes. Hence, relative vorticity is affected only via the beta effect. In addition, the fluid flow materially preserves the area of any material region. This *two-dimensional non-divergent barotropic flow* is discussed in more detail in Chapter 38. We here use it as an example to expose essential features of the beta effect (see also Section 38.2.2).

In the rotating frame, circulation around an infinitesimal closed material loop is

$$\mathcal{C} = A\,\zeta, \tag{40.116}$$

where ζ is the relative vorticity and A is the area enclosed by the loop. Because the fluid flow is non-divergent, the loop area A remains constant even as the loop becomes contorted (see Section 21.6). This area preservation property simplifies the evolution equation for the circulation, which is given by

$$\frac{\mathrm{D}\mathcal{C}}{\mathrm{D}t} = \frac{\mathrm{D}(A\,\zeta)}{\mathrm{D}t} = A\,\frac{\mathrm{D}\zeta}{\mathrm{D}t}. \tag{40.117}$$

Equating this result to the circulation change implied by Bjerknes' circulation theorem (40.115) renders

$$\frac{\mathrm{D}\mathcal{C}}{\mathrm{D}t} = A\,\frac{\mathrm{D}\zeta}{\mathrm{D}t} = -2\,\Omega\,\frac{\mathrm{D}A_\perp}{\mathrm{D}t}. \tag{40.118}$$

Let the material circuit be at a latitude, ϕ, so that the projection of the loop area onto the equatorial plane is (see Figure 40.8)

$$A_\perp = A\sin\phi. \tag{40.119}$$

Hence, material evolution of the circulation is

$$\begin{aligned}
\frac{\mathrm{D}\mathcal{C}}{\mathrm{D}t} &= A\,\frac{\mathrm{D}\zeta}{\mathrm{D}t} && \text{(40.120a)}\\
&= -2\,\Omega\,\frac{\mathrm{D}A_\perp}{\mathrm{D}t} && \text{(40.120b)}\\
&= -2\,A\,\Omega\,\frac{\mathrm{D}\sin\phi}{\mathrm{D}t} && \text{(40.120c)}\\
&= -2\,A\,\Omega\,\cos\phi\,\frac{\mathrm{D}\phi}{\mathrm{D}t} && \text{(40.120d)}\\
&= -A\left[\frac{2\,\Omega\,\cos\phi}{R}\right]\left[R\frac{\mathrm{D}\phi}{\mathrm{D}t}\right] && \text{(40.120e)}\\
&= -A\,\beta\,v, && \text{(40.120f)}
\end{aligned}$$

where we introduced the meridional velocity component

$$v = R \frac{\mathrm{D}\phi}{\mathrm{D}t} \tag{40.121}$$

and the meridional derivative of the planetary vorticity

$$\beta = \frac{\mathrm{d}f}{\mathrm{d}y} = \frac{1}{R}\frac{\mathrm{d}}{\mathrm{d}\phi}(2\,\Omega\,\sin\phi) = \frac{2\,\Omega\,\cos\phi}{R}. \tag{40.122}$$

The result (40.120f)

$$\frac{1}{A}\frac{\mathrm{D}\mathcal{C}}{\mathrm{D}t} = \frac{\mathrm{D}\zeta}{\mathrm{D}t} = -\beta\, v, \tag{40.123}$$

shows how meridional motion on a rotating sphere induces relative circulation, and thus relative vorticity. It furthermore motivates the name *beta effect* for the planetary induction.

40.6.4 Planetary circulation, planetary vorticity, and the Coriolis acceleration

From equation (40.103b) we know that the planetary vorticity is given by the constant vector

$$\boldsymbol{\omega}_{\text{planet}} = \nabla \times (\boldsymbol{\Omega} \times \boldsymbol{x}) = 2\,\boldsymbol{\Omega}. \tag{40.124}$$

As a constant vector, it is the same everywhere in space. However, its impact on the fluid circulation and vorticity depends on what latitude the rotation vector is sampled. We here focus on the radial component of the planetary vorticity by measuring the circulation per area for fixed radius circuits, with reference to Figure 40.9.

Planetary circulation centered on the pole and on the equator

Equation (40.114) leads to the planetary circulation

$$\mathcal{C}_{\text{planet}} = 2\,\Omega\,A_\perp, \tag{40.125}$$

for an arbitrary constant radius circuit. Stokes' theorem then says that the planetary vorticity, as projected onto the local radial direction (outward normal to the surface), has value

$$\boldsymbol{\omega}_{\text{planet}} \cdot \hat{\boldsymbol{n}} \approx \mathcal{C}_{\text{planet}}/\mathcal{S} = 2\,\Omega\,A_\perp/\mathcal{S}, \tag{40.126}$$

where $\mathcal{S} = \int_{\mathcal{S}} \mathrm{d}\mathcal{S}$ is the area enclosed by the circuit. In the limit that the circuit becomes infinitesimal, then $A_\perp \to \mathcal{S}$ when the circuit is centered on the north pole, whereas $A_\perp \to 0$ for an equatorially centered circuit. Correspondingly, the planetary vorticity, when projected into the radial direction, is $2\,\Omega$ at the north pole (and $-2\,\Omega$ at the south pole), whereas it vanishes at the equator. We emphasize that it is not the planetary vorticity that vanishes at the equator, which is obvious since $\boldsymbol{\omega}_{\text{planet}} = 2\,\boldsymbol{\Omega}$ is a constant vector. Rather, it is the radial projection, $\boldsymbol{\omega}_{\text{planet}} \cdot \hat{\boldsymbol{r}}$, that vanishes at the equator.

Comments on the Coriolis acceleration

Although $\boldsymbol{\omega}_{\text{planet}} \cdot \hat{\boldsymbol{r}} = 0$ at the equator, the Coriolis acceleration does not generally vanish there. That is, recall the discussion in Section 13.9.8 where the Coriolis acceleration in spherical coordinates is written

$$\boldsymbol{A}_{\text{Coriolis}} = -2\,\Omega\left[\hat{\boldsymbol{\lambda}}\,(w\cos\phi - v\sin\phi) + \hat{\boldsymbol{\phi}}\,u\sin\phi - \hat{\boldsymbol{r}}\,u\cos\phi\right], \tag{40.127}$$

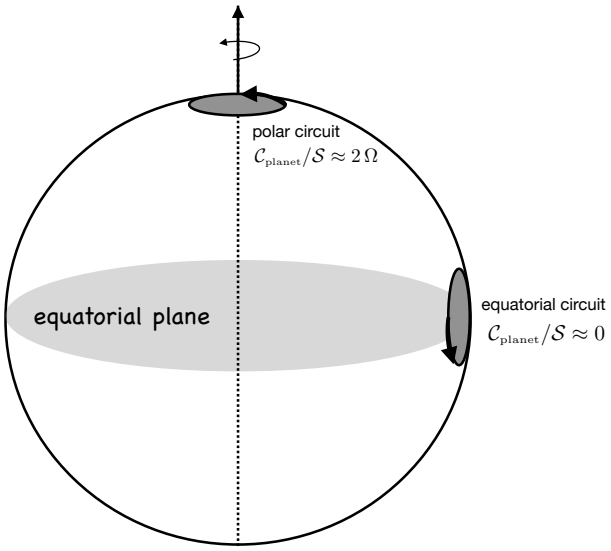

FIGURE 40.9: Area mean of the planetary vorticity as computed around two closed circular loops with area $\mathcal{S}$. One circuit is centered on the north pole, in which case the area mean planetary circulation, $\mathcal{C}_{\text{planet}}/\mathcal{S} \approx 2\,\Omega$. The other circuit is centered on the equator so that $\mathcal{C}_{\text{planet}}/\mathcal{S} \approx 0$. Stokes' theorem says that the planetary vorticity, as projected onto the local radial direction (outward normal), has value $\boldsymbol{\omega}_{\text{planet}} \cdot \hat{\boldsymbol{r}} \approx \mathcal{C}_{\text{planet}}/\mathcal{S}$. Hence, the planetary vorticity equals $2\,\Omega$ at the north pole (and $-2\,\Omega$ at the south pole), whereas it vanishes at the equator.

which, at $\phi = 0$, is

$$\boldsymbol{A}_{\text{Coriolis}}(\phi = 0) = -2\,\Omega\,(w\,\hat{\boldsymbol{\lambda}} - u\,\hat{\boldsymbol{r}}). \tag{40.128}$$

Evidently, a nonzero Coriolis acceleration at the equator arises since it depends on $\boldsymbol{\Omega} = \boldsymbol{\omega}_{\text{planet}}/2$ rather than just its radial projection, $\boldsymbol{\omega}_{\text{planet}} \cdot \hat{\boldsymbol{r}}$. For large-scale flows, we commonly ignore $\boldsymbol{A}_{\text{Coriolis}}(\phi = 0)$ since its radial term is tiny relative to the gravitational acceleration, and the longitudinal term is small for large-scale flows where the vertical velocity is typically small.[11] Indeed, these points were made in Section 13.9.8, whereby the Coriolis acceleration for large-scale planetary flows is approximated by equation (13.99)

$$\boldsymbol{A}^{\text{large-scale}}_{\text{Coriolis}} \equiv -2\,\Omega \sin\phi\,(-\hat{\boldsymbol{\lambda}}\,v + \hat{\boldsymbol{\phi}}\,u) \equiv -f\,\hat{\boldsymbol{r}} \times \boldsymbol{v}. \tag{40.129}$$

This approximate Coriolis acceleration does vanish at the equator, and it is the form resulting from the Traditional Approximation used for the hydrostatic primitive equations in Section 27.1.3.

40.6.5 Further study

The beta effect and its role in vorticity is nicely summarized in this video from Science Primer in the context of Rossby waves.

40.7 Vorticity budget for a primitive equation Boussinesq ocean

In this section we develop the vorticity budget for a hydrostatic primitive equation Boussinesq ocean in the presence of diabatic sources and frictional forcing. This system is of particular importance for ocean circulation models. The governing primitive equations, as derived in

[11] *Stewart and Dellar* (2011) argue for the importance of the full expression of the Coriolis acceleration (40.127) for the dynamics of cross-equatorial abyssal ocean flows.

Section 29.1.6, are given by

$$\frac{\mathrm{D}\boldsymbol{u}}{\mathrm{D}t} + f\,\hat{\boldsymbol{z}} \times \boldsymbol{v} = -\nabla_{\!\mathrm{h}}\varphi + \boldsymbol{F} \tag{40.130a}$$

$$\partial_z \varphi = b \tag{40.130b}$$

$$\nabla \cdot \boldsymbol{v} = 0 \tag{40.130c}$$

$$\frac{\mathrm{D}b}{\mathrm{D}t} = \dot{b}, \tag{40.130d}$$

with the non-divergent velocity field written

$$\boldsymbol{v} = (\boldsymbol{u}, w) = \boldsymbol{u} + w\,\hat{\boldsymbol{z}}. \tag{40.131}$$

The perturbation pressure is given by

$$\rho_{\circ}\,\varphi = \delta p = p - p_0, \tag{40.132}$$

with the reference pressure, $p_0 = p_0(z)$, in hydrostatic balance with the constant reference density

$$\frac{\mathrm{d}p_0}{\mathrm{d}z} = -g\,\rho_{\circ}, \tag{40.133}$$

and p the hydrostatic pressure satisfying the local hydrostatic balance

$$\partial_z p = -g\,\rho. \tag{40.134}$$

The globally referenced Archimedean buoyancy is given by

$$b = -g\,(\rho - \rho_{\circ})/\rho_{\circ}, \tag{40.135}$$

with this field discussed in Section 30.4.2. As mentioned at the end of Section 40.6.4, we here assume the Coriolis acceleration of the form relevant to the Traditional approximation (Section 27.1.3), in which we are only concerned with the local vertical component of planetary rotation so that

$$f\,\hat{\boldsymbol{z}} \times \boldsymbol{v} = f\,\hat{\boldsymbol{z}} \times \boldsymbol{u}. \tag{40.136}$$

Finally, the friction acceleration vector is horizontal

$$\boldsymbol{F} = (F^x, F^y, 0) \tag{40.137}$$

and the gradient operator is decomposed into its horizontal plus vertical contribution.

$$\nabla = \nabla_{\!\mathrm{h}} + \hat{\boldsymbol{z}}\,\partial_z. \tag{40.138}$$

40.7.1 Deriving the vorticity equation

Vector invariant velocity equation

To derive the vorticity equation, it is useful to combine the horizontal momentum equation with the hydrostatic balance, in which case

$$\frac{\mathrm{D}\boldsymbol{u}}{\mathrm{D}t} + f\,\hat{\boldsymbol{z}} \times \boldsymbol{v} = -\nabla\varphi + b\,\hat{\boldsymbol{z}} + \boldsymbol{F}. \tag{40.139}$$

As for the non-hydrostatic case (Section 40.3.1), we rewrite the self-advection operator, $(\boldsymbol{v}\cdot\nabla)\,\boldsymbol{u}$, before taking the curl. In turn, we introduce the hydrostatic relative vorticity given by the curl

of the horizontal velocity

$$\boldsymbol{\omega}^{\text{hy}} = \nabla \times \boldsymbol{u} = \hat{\boldsymbol{z}} \times \partial_z \boldsymbol{u} + \hat{\boldsymbol{z}}\, \zeta = -\hat{\boldsymbol{x}}\, \partial_z v + \hat{\boldsymbol{y}}\, \partial_z u + \hat{\boldsymbol{z}}\, \zeta, \tag{40.140}$$

where

$$\zeta = \partial_x v - \partial_y u \tag{40.141}$$

is the vertical component to the relative vorticity, and the hydrostatic vorticity is non-divergent

$$\nabla \cdot \boldsymbol{\omega}^{\text{hy}} = 0. \tag{40.142}$$

It is then straightforward to show that

$$\boldsymbol{\omega}^{\text{hy}} \times \boldsymbol{v} = \hat{\boldsymbol{x}}\, (w\, \partial_z u - v\, \partial_x v + v\, \partial_y u) + \hat{\boldsymbol{y}}\, (w\, \partial_z v - u\, \partial_y u + u\, \partial_x v) - \hat{\boldsymbol{z}}\, \partial_z (u^2 + v^2)/2 \tag{40.143a}$$

$$= w\, \partial_z \boldsymbol{u} + \zeta\, (-v\, \hat{\boldsymbol{x}} + u\, \hat{\boldsymbol{y}}) - \hat{\boldsymbol{z}}\, \partial_z (u^2 + v^2)/2, \tag{40.143b}$$

in which case

$$\nabla(\boldsymbol{u}^2/2) + \boldsymbol{\omega}^{\text{hy}} \times \boldsymbol{v} = \nabla\, (u^2 + v^2)/2 - \hat{\boldsymbol{z}}\, \partial_z\, (u^2 + v^2)/2 + w\, \partial_z \boldsymbol{u} + \zeta\, (-v\, \hat{\boldsymbol{x}} + u\, \hat{\boldsymbol{y}}) \tag{40.144a}$$

$$= (u\, \partial_x + v\, \partial_y + w\, \partial_z)\, \boldsymbol{u} \tag{40.144b}$$

$$= (\boldsymbol{v} \cdot \nabla)\, \boldsymbol{u}. \tag{40.144c}$$

The material time derivative of the horizontal velocity can thus be written

$$\frac{\mathrm{D}\boldsymbol{u}}{\mathrm{D}t} = \partial_t \boldsymbol{u} + (\boldsymbol{v} \cdot \nabla)\, \boldsymbol{u} = \partial_t \boldsymbol{u} + \boldsymbol{\omega}^{\text{hy}} \times \boldsymbol{v} + \nabla(\boldsymbol{u}^2/2), \tag{40.145}$$

which then leads to the vector invariant horizontal velocity equation

$$\partial_t \boldsymbol{u} + (f\, \hat{\boldsymbol{z}} + \boldsymbol{\omega}^{\text{hy}}) \times \boldsymbol{v} = -\nabla(\varphi + \boldsymbol{u}^2/2) + b\, \hat{\boldsymbol{z}} + \boldsymbol{F}, \tag{40.146}$$

which can be written in the equivalent form[12]

$$(\partial_t + w\, \partial_z)\, \boldsymbol{u} + (f + \zeta)\, \hat{\boldsymbol{z}}\, \times \boldsymbol{u} = -\nabla_{\!\text{h}}\, (\varphi + \boldsymbol{u}^2/2) - (\partial_z \varphi - b)\, \hat{\boldsymbol{z}} + \boldsymbol{F}. \tag{40.147}$$

Curl of the velocity equation to render the vorticity equation

Now take the curl of the vector invariant velocity equation (40.146), and make use of the identity

$$\nabla \times (\boldsymbol{\omega}_{\text{a}}^{\text{hy}} \times \boldsymbol{v}) = (\boldsymbol{v} \cdot \nabla)\, \boldsymbol{\omega}_{\text{a}}^{\text{hy}} - (\boldsymbol{\omega}_{\text{a}}^{\text{hy}} \cdot \nabla)\, \boldsymbol{v}, \tag{40.148}$$

where we introduced the absolute vorticity for a hydrostatic fluid

$$\boldsymbol{\omega}_{\text{a}}^{\text{hy}} = f\, \hat{\boldsymbol{z}} + \boldsymbol{\omega}^{\text{hy}}. \tag{40.149}$$

The result is the vorticity equation

$$\partial_t \boldsymbol{\omega}^{\text{hy}} + (\boldsymbol{v} \cdot \nabla)\, \boldsymbol{\omega}_{\text{a}}^{\text{hy}} = (\boldsymbol{\omega}_{\text{a}}^{\text{hy}} \cdot \nabla)\, \boldsymbol{v} + \nabla \times \hat{\boldsymbol{z}}\, b + \nabla \times \boldsymbol{F}. \tag{40.150}$$

[12] As discussed in *Griffies et al.* (2020), the form (40.147) is commonly used for Boussinesq and hydrostatic ocean models.

Since the Coriolis parameter is time independent, we can add it to the time derivative to yield and equation for absolute vorticity

$$\frac{\mathrm{D}\boldsymbol{\omega}_{\mathrm{a}}^{\mathrm{hy}}}{\mathrm{D}t} = \underbrace{(\boldsymbol{\omega}_{\mathrm{a}}^{\mathrm{hy}} \cdot \nabla)\, \boldsymbol{v}}_{\text{stretching + tilting}} + \underbrace{\nabla \times \hat{\boldsymbol{z}}\, b}_{\text{baroclinicity}} + \underbrace{\nabla \times \boldsymbol{F}}_{\text{friction curl}}. \tag{40.151}$$

It is notable that the pressure gradient is eliminated from the Boussinesq vorticity equation. Even so, the vorticity is affected by baroclinicity as manifested through horizontal gradients in the buoyancy field, which we discuss next.

40.7.2 Boussinesq baroclinicity

Let us compare the Boussinesq vorticity equation (40.151) to the vorticity equation (40.42) for a non-hydrostatic and non-Boussinesq fluid. One difference concerns the form of the vorticity, which differs due to the use of only the horizontal velocity, $\boldsymbol{\omega}^{\mathrm{hy}} = \nabla \times \boldsymbol{u}$, for the hydrostatic fluid whereas the full velocity is used for the non-hydrostatic case, $\boldsymbol{\omega} = \nabla \times \boldsymbol{v}$. Even so, both vorticity equations have a vorticity source due to stretching and tilting, and both have a source due to the curl of friction. The key difference arises in the form of the baroclinicity vector. Namely, the Boussinesq baroclinicity does not involve the Boussinesq pressure gradient acceleration since it has zero curl. Instead, Boussinesq baroclinicity is given by[13]

$$\boldsymbol{B}_{\mathrm{bouss}} = \nabla \times \hat{\boldsymbol{z}}\, b = \nabla b \times \hat{\boldsymbol{z}}. \tag{40.152}$$

Boussinesq baroclinicity has a somewhat simpler form than baroclinicity in a compressible fluid, as given by equation (40.62)

$$\boldsymbol{B} = (\nabla \rho \times \nabla p)/\rho^2 = -\nabla \times (\rho^{-1} \nabla p). \tag{40.153}$$

Again, the fundamental difference arises since the Boussinesq pressure gradient acceleration is annihilated when taking the curl of the velocity equation to produce the Boussinesq vorticity equation. So rather than arise from the misalignment of pressure and density isolines, Boussinesq baroclinicity arises from the misalignment of the gravity field and density gradients.

One practical feature of the Boussinesq baroclinicity (40.152) is that we can readily deduce the presence of baroclinicity (either for the non-hydrostatic or hydrostatic Boussinesq ocean) merely by noting whether there is a slope to the buoyancy surfaces relative to the horizontal (e.g., Figure 40.10). That is, a sloping buoyancy surface provides a vorticity source for the Boussinesq ocean.

Boussinesq baroclinicity only affects a horizontal vorticity tendency

Given that the Boussinesq baroclinicity (40.152) does not involve the pressure gradient acceleration, we must modify the physical interpretation offered in Section 40.4. In particular, the curl of the non-Boussinesq pressure acceleration has components in all three directions so that the non-Boussinesq baroclinicity affects a source for each of the three vorticity components. In contrast, the Boussinesq baroclinicity is the curl of the Archimedean buoyant acceleration and this acceleration acts only in the vertical. Consequently, the Boussinesq baroclinicity has no direct affect on the vertical component to absolute vorticity

$$\hat{\boldsymbol{z}} \cdot \boldsymbol{B}_{\mathrm{bouss}} = \hat{\boldsymbol{z}} \cdot (\nabla \times \hat{\boldsymbol{z}}\, b) = 0. \tag{40.154}$$

[13] We see in Exercise 41.2 that the baroclinicity vector (40.152) also applies for the non-hydrostatic Boussinesq ocean.

Rather, Boussinesq baroclinicity only acts directly as a source for horizontal vorticity. Thus, Boussinesq baroclinicity can only indirectly affect vertical vorticity through the effects of baroclinicity on vertical velocity and the corresponding vertical stretching.

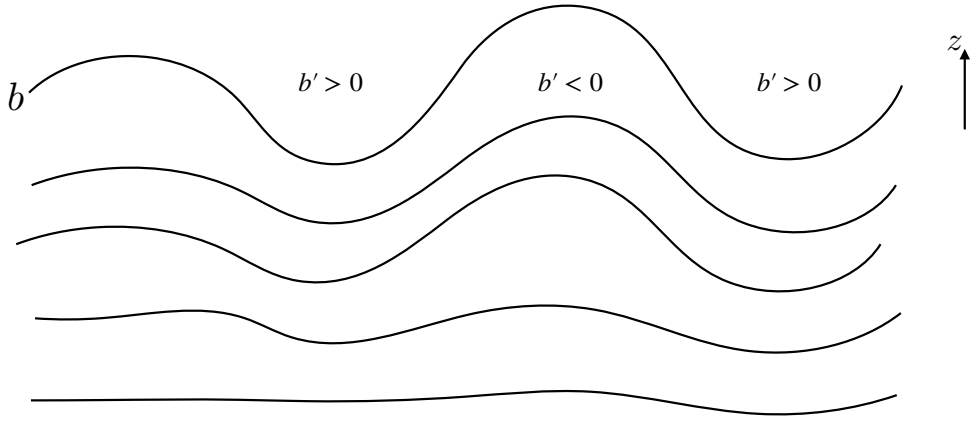

FIGURE 40.10: Baroclinicity in a Boussinesq ocean is manifest by nonzero horizontal gradients in the buoyancy field. Here we depict a region of relatively strong baroclinicity above a region of weaker baroclinicity. A sloping buoyancy surface is therefore synonymous with a nontrivial baroclinic structure. We label anomalously positive ($b' > 0$) and negative buoyancy ($b' < 0$), where the prime denotes anomalies relative to a horizontal average. Furthermore, as per equation (40.154), baroclinicity in a Boussinesq ocean only acts as a source for horizontal vorticity.

Comments on shallow water vorticity

In Chapter 39, we studied vorticity in the shallow water fluid. As noted in Section 39.3.3, we are only concerned with the vertical component to vorticity in the shallow water fluid, since the horizontal components are tiny by comparison. Furthermore, equation (39.28) says that the vertical component to shallow water absolute vorticity is materially altered only through material changes to the layer thickness. There is no impact from baroclinicity on the shallow water vorticity. The absence of baroclinicity follows trivially from the absence of any horizontal buoyancy gradients within the shallow water layer. In this manner, the shallow water layer is barotropic.

40.7.3 Vertical vorticity equation

Following the discussion in Section 40.3.4 for the unapproximated vorticity, we here examine the vertical component of the hydrostatic and Boussinesq vorticity equation (40.151)

$$\frac{\mathrm{D}\zeta_{\mathrm{a}}}{\mathrm{D}t} = (\boldsymbol{\omega}_{\mathrm{a}}^{\mathrm{hy}} \cdot \nabla)\, w + \hat{\boldsymbol{z}} \cdot (\nabla \times \boldsymbol{F}), \tag{40.155}$$

with the absence of baroclinicity noted above in Section 40.7.2. The stretching, tilting, and friction curl appearing on the right hand side provide vorticity sources that affect the left hand side's material time evolution. We see this evolution more fully by expanding the terms to render

$$\partial_t \zeta_{\mathrm{a}} + (\boldsymbol{v} \cdot \nabla)\, \zeta + \beta\, v = \hat{\boldsymbol{z}} \cdot (\partial_z \boldsymbol{u} \times \nabla_{\mathrm{h}} w) + (\zeta + f)\, \partial_z w + \hat{\boldsymbol{z}} \cdot (\nabla \times \boldsymbol{F}). \tag{40.156}$$

Planetary geostrophic limit

The linearized, inviscid, and steady version of the vorticity equation (40.156) leads to the linear vorticity balance studied in Section 31.5.4 and Chapter 44

$$\beta\, v = f\, \partial_z w. \tag{40.157}$$

This relation comprises the inviscid vorticity equation for the planetary geostrophic equations. It represents a kinematic balance since no forces are exposed here to explicitly cause motion, though such forces do appear in the momentum equation. Reading the balance from right to left indicates that any process generating vorticity via vortex stretching must be balanced by meridional motion. That is, the fluid responds to vortex stretching by moving meridionally through the planet's vorticity field. Since the vorticity of a planetary geostrophic fluid is solely determined by planetary vorticity, meridional movement is the only means for the fluid to balance vortex sources. Conversely, reading the equality from left to right reveals that any meridional motion itself must be balanced by vortex stretching.

Vorticity flux vector

We can write the vorticity equation (40.156) in an alternative form by making use of $\nabla \cdot \boldsymbol{v} = \nabla \cdot \boldsymbol{\omega}_{\mathrm{a}}^{\mathrm{hy}} = 0$ to yield

$$\partial_t \zeta_{\mathrm{a}} = -\nabla \cdot (\boldsymbol{v}\, \zeta_{\mathrm{a}} - w\, \boldsymbol{\omega}_{\mathrm{a}}^{\mathrm{hy}}) + \hat{\boldsymbol{z}} \cdot (\nabla \times \boldsymbol{F}). \tag{40.158}$$

Furthermore, we can use equation (40.44d) for the friction curl, $\hat{\boldsymbol{z}} \cdot (\nabla \times \boldsymbol{F}) = -\nabla \cdot (\hat{\boldsymbol{z}} \times \boldsymbol{F})$. Hence, the vertical component of the Boussinesq vorticity evolves according to the convergence of the vorticity flux

$$\partial_t \zeta_{\mathrm{a}} = -\nabla \cdot \boldsymbol{J}^{\zeta_{\mathrm{a}}} \qquad \text{with} \qquad \boldsymbol{J}^{\zeta_{\mathrm{a}}} = \boldsymbol{v}\, \zeta_{\mathrm{a}} - w\, \boldsymbol{\omega}_{\mathrm{a}}^{\mathrm{hy}} + \hat{\boldsymbol{z}} \times \boldsymbol{F}, \tag{40.159}$$

which can be compared to the vorticity flux (40.45) for the compressible nonhydrostatic fluid. Again, the main difference arises from the absence of a baroclinicity contribution for the hydrostatic Boussinesq ocean.

The identity $\boldsymbol{\omega}_{\mathrm{a}}^{\mathrm{hy}} = \hat{\boldsymbol{z}} \times \partial_z \boldsymbol{u} + \hat{\boldsymbol{z}}\, \zeta_{\mathrm{a}}$ allows us to write

$$\boldsymbol{v}\, \zeta_{\mathrm{a}} - w\, \boldsymbol{\omega}_{\mathrm{a}}^{\mathrm{hy}} = \boldsymbol{u}\, \zeta_{\mathrm{a}} - w\, \hat{\boldsymbol{z}} \times \partial_z \boldsymbol{u}, \tag{40.160}$$

which is a horizontal vector. Furthermore, note that $\hat{\boldsymbol{z}} \times \boldsymbol{F}$ is a horizontal vector, which then means that there is no vertical contribution to the vorticity flux vector, $\boldsymbol{J}^{\zeta_{\mathrm{a}}} \cdot \hat{\boldsymbol{z}} = 0$. We previously encountered this property in Section 40.3.4 when discussing the vorticity flux for the non-Boussinesq fluid, with Figure 40.1 providing a schematic.

40.8 Evolution of depth integrated vertical vorticity

In this section we study the depth integral of the vertical vorticity equation (40.45)

$$\partial_t \zeta_{\mathrm{a}} = -\nabla \cdot \boldsymbol{J}^{\zeta_{\mathrm{a}}} \quad \text{with} \quad \boldsymbol{J}^{\zeta_{\mathrm{a}}} = \boldsymbol{v}\, \zeta_{\mathrm{a}} - \boldsymbol{\omega}_{\mathrm{a}}\, w - \hat{\boldsymbol{z}} \times \rho^{-1} \nabla p + \hat{\boldsymbol{z}} \times \boldsymbol{F}. \tag{40.161}$$

We perform the depth integral over the full depth of the ocean from its bottom at $z = \eta_{\mathrm{b}}(x, y)$ to the ocean surface at $z = \eta(x, y, t)$ (see Figure 35.1). Studies of the depth integrated vorticity equation allow us to focus on the two dimensional budgets with particular attention to how boundary torques alter the budget. This section anticipates analysis of the depth integrated planetary geostrophic vorticity equation in Section 44.3, with that analysis of use for understanding the role of topography in forcing the large-scale ocean circulation. We also

consider the vorticity of the depth integrated flow in Section 40.9, which is commonly considered in numerical applications. Notably, the discussion in the present section does not assume pressure is approximatly hydrostatic, so that all results hold for the general case of a non-hydrostatic flow.

40.8.1 Comments on the role of baroclinicity

Results of the analysis in this section can be readily specialized to the Boussinesq and hydrostatic case given by equation (40.159). The key distinction, as noted in Section 40.7.2, is that Boussinesq baroclinicity does not directly affect changes to the vertical component of the Boussinesq vorticity (whether hydrostatic or non-hydrostatic; see Exercise 41.2). This property of the Boussinesq baroclinicity means that the boundary pressure torques discussed in Sections 40.8.3 and 40.8.4 play no direct role in the Boussinesq vorticity equation. However, these boundary pressure torques play a direct role in vertical motion next to the boundaries, especially next to the bottom, with such motion affecting a source to vorticity through stretching. We have much to say in Section 44.3 concerning how boundary pressure torques affect vertical motion for vorticity for the planetary geostrophic fluid. Additionally, as seen in Section 40.9, boundary pressure torques do play a direct role in affecting vorticity of the depth integrated flow in both the Boussinesq and non-Boussinesq fluids.

This discussion exemplifies the sometimes subtle differences between vorticity sources depending on the precise nature of the vorticity, whether it be vorticity for a fluid element as discussed in this section, vorticity of the depth integrated flow in Section 40.9, or vorticity of the depth averaged flow in Section 40.9.7. When studying flavors of vorticity, it is important to be clear on details of their evolution equations since the details color the physical interpretations.

40.8.2 Leibniz rule expressions

The necessary manipulations are typical for the analysis of depth integrated budgets, such as considered for the depth integrated momentum in Section 28.4 and depth integrated angular momentum in Section 28.5. For vorticity we are interested in manipulating following equation

$$\int_{\eta_b}^{\eta} \frac{\partial \zeta_a}{\partial t} \, dz = - \int_{\eta_b}^{\eta} \nabla \cdot \boldsymbol{J}^{\zeta_a} \, dz, \tag{40.162}$$

where $\boldsymbol{J}^{\zeta_a}$ is the vorticity flux given by equation (40.161). We make use of Leibniz's rule (Section 20.2.4) to move the time and space derivatives from inside the integrals to outside[14]

$$\int_{\eta_b}^{\eta} \frac{\partial \zeta_a}{\partial t} \, dz = -[\zeta_a \, \partial_t \eta]_{z=\eta} + \frac{\partial}{\partial t} \int_{\eta_b}^{\eta} \zeta_a \, dz \tag{40.163}$$

$$- \int_{\eta_b}^{\eta} \nabla_h \cdot \boldsymbol{J}^{\zeta_a} \, dz = [\nabla_h \eta \cdot \boldsymbol{J}^{\zeta_a}]_{z=\eta} - [\nabla_h \eta_b \cdot \boldsymbol{J}^{\zeta_a}]_{z=\eta_b} - \nabla_h \cdot \int_{\eta_b}^{\eta} \boldsymbol{J}^{\zeta_a} \, dz \tag{40.164}$$

$$- \int_{\eta_b}^{\eta} \frac{\partial (\hat{\boldsymbol{z}} \cdot \boldsymbol{J}^{\zeta_a})}{\partial z} \, dz = -[\hat{\boldsymbol{z}} \cdot \boldsymbol{J}^{\zeta_a}]_{z=\eta} + [\hat{\boldsymbol{z}} \cdot \boldsymbol{J}^{\zeta_a}]_{z=\eta_b}. \tag{40.165}$$

These results then lead to

$$\frac{\partial}{\partial t} \int_{\eta_b}^{\eta} \zeta_a \, dz = \Big[\zeta_a \, \partial_t \eta - \nabla(z-\eta) \cdot \boldsymbol{J}^{\zeta_a}\Big]_{z=\eta} + \Big[\nabla(z-\eta_b) \cdot \boldsymbol{J}^{\zeta_a}\Big]_{z=\eta_b} - \nabla_h \cdot \int_{\eta_b}^{\eta} \boldsymbol{J}^{\zeta_a} \, dz. \tag{40.166}$$

[14] Recall that since $\eta(x,y,t)$ is a spatial function just of the horizontal position, there is no difference between $\nabla\eta$ and $\nabla_h\eta$. The same point holds for $\eta_b(x,y)$ as well.

The time tendency for the depth integral of the vertical component of absolute vorticity, for a fluid column at a fixed horizontal position (left hand side) is determined by a suite of boundary contributions due to baroclinicity, vortex stretching and friction, plus the convergence of the depth integrated vorticity flux (final term on right hand side). We next massage the boundary contributions to expose their associated physical processes.

40.8.3 Bottom boundary contribution

The bottom boundary contribution to the vorticity equation (40.166) takes on the form

$$\nabla(z-\eta_{\mathrm{b}})\cdot\boldsymbol{J}^{\zeta_{\mathrm{a}}} = \nabla(z-\eta_{\mathrm{b}})\cdot\big[\boldsymbol{v}\,\zeta_{\mathrm{a}} - \boldsymbol{\omega}_{\mathrm{a}}\,w - \hat{\boldsymbol{z}}\times\rho^{-1}\,\nabla p + \hat{\boldsymbol{z}}\times\boldsymbol{F}\big]_{z=\eta_{\mathrm{b}}} \tag{40.167a}$$

$$= -|\nabla(z-\eta_{\mathrm{b}})|\,\hat{\boldsymbol{n}}\cdot\big[-\boldsymbol{\omega}_{\mathrm{a}}\,w - \hat{\boldsymbol{z}}\times\rho^{-1}\,\nabla p + \hat{\boldsymbol{z}}\times\boldsymbol{F}\big]_{z=\eta_{\mathrm{b}}}, \tag{40.167b}$$

where we made use of the no-normal flow bottom kinematic boundary condition, $\hat{\boldsymbol{n}}\cdot\boldsymbol{v}=0$ (Section 19.6.1), and where

$$\hat{\boldsymbol{n}} = -\left[\frac{\nabla(z-\eta_{\mathrm{b}})}{|\nabla(z-\eta_{\mathrm{b}})|}\right] = -\left[\frac{\hat{\boldsymbol{z}}-\nabla_{\mathrm{h}}\eta_{\mathrm{b}}}{\sqrt{1+\nabla_{\mathrm{h}}\eta_{\mathrm{b}}\cdot\nabla_{\mathrm{h}}\eta_{\mathrm{b}}}}\right] \tag{40.168}$$

is the outward unit normal at the bottom.

Vortex stretching by vertical flow along a sloping bottom

The first term in the bottom boundary flux (40.167b) provides an inviscid vertical transport of the normal component of the absolute vorticity at the boundary. This term contributes through the action of vertical motion next to a sloping bottom, thus providing a vertical transfer of the vorticity component that is perpendicular to the bottom. This motion provides a form of vortex stretching that vanishes for a flat bottom, in which case $w(\eta_{\mathrm{b}})=0$. It also vanishes for flow that parallels the bottom, whereby $\boldsymbol{u}\cdot\nabla\eta_{\mathrm{b}}=0$ so that $w(\eta_{\mathrm{b}})=0$ according to the bottom kinematic boundary condition (19.56).

Bottom pressure torques

The second term in the bottom boundary flux (40.167b) arises from baroclinicity next to the bottom, in which case we consider the following term

$$\hat{\boldsymbol{n}}\cdot[\hat{\boldsymbol{z}}\times(\rho^{-1}\,\nabla p)]_{z=\eta_{\mathrm{b}}} = [\rho^{-1}\,\nabla p]_{z=\eta_{\mathrm{b}}}\cdot(\hat{\boldsymbol{n}}\times\hat{\boldsymbol{z}}) \equiv [\rho^{-1}\,\nabla p]_{z=\eta_{\mathrm{b}}}\cdot\boldsymbol{t}, \tag{40.169}$$

where we introduced the tangent direction

$$\boldsymbol{t} = \hat{\boldsymbol{n}}\times\hat{\boldsymbol{z}} = \left[\frac{\nabla\eta_{\mathrm{b}}\times\hat{\boldsymbol{z}}}{|\nabla(z-\eta_{\mathrm{b}})|}\right]. \tag{40.170}$$

The vector $\boldsymbol{t}$ is horizontal and it points along isolines of constant topography in a direction with land to the left pointing in the direction of $\boldsymbol{t}$, as depicted in Figure 40.11. Since $\hat{\boldsymbol{z}}$ and $\hat{\boldsymbol{n}}$ are not orthogonal, $\boldsymbol{t}$ is not normalized so that it is not adorned with a hat.

Let us decompose the pressure gradient at the bottom according to

$$\nabla p = \hat{\boldsymbol{n}}\,(\hat{\boldsymbol{n}}\cdot\nabla p) + \hat{\boldsymbol{t}}\,(\hat{\boldsymbol{t}}\cdot\nabla p) \qquad z=\eta_{\mathrm{b}}, \tag{40.171}$$

where $\hat{\boldsymbol{t}}=\boldsymbol{t}/|\boldsymbol{t}|$ is the normalized horizontal tangent vector. Evidently, for the boundary condition (40.169) we only need the $\hat{\boldsymbol{t}}\,(\hat{\boldsymbol{t}}\cdot\nabla p)$ term. But that term is simply the gradient of the bottom pressure

$$\hat{\boldsymbol{t}}\,(\hat{\boldsymbol{t}}\cdot\nabla p) = \nabla p_{\mathrm{b}}. \tag{40.172}$$

We can provide a bit more thorough derivation of this result by using the methods of generalized vertical coordinates from Section 63.12, whereby

$$\nabla p = (\hat{\boldsymbol{z}} - \nabla_\sigma z)\, \partial_z p + \nabla_\sigma p, \tag{40.173}$$

where σ is an arbitrary generalized vertical coordinate. Evaluating the pressure gradient (40.173) at the ocean bottom ($z = \eta_\mathrm{b}$), and letting σ align with the bottom, leads to

$$[\nabla p]_{z=\eta_\mathrm{b}} = (\hat{\boldsymbol{z}} - \nabla \eta_\mathrm{b})\, \partial_z p + \nabla p_\mathrm{b}. \tag{40.174}$$

As before, we conclude that ∇p_b is the horizontal component of $[\nabla p]_{z=\eta_\mathrm{b}}$ in the direction tangent to the bottom.

We thus find the contribution from baroclinicity at the ocean bottom takes the form

$$\nabla(z - \eta_\mathrm{b}) \cdot \boldsymbol{J}_\zeta^{\text{baroclinicity}} = \rho^{-1} \nabla p_\mathrm{b} \cdot (\nabla \eta_\mathrm{b} \times \hat{\boldsymbol{z}}) = \rho^{-1} \hat{\boldsymbol{z}} \cdot [\nabla p_\mathrm{b} \times \nabla \eta_\mathrm{b}] = \rho^{-1} \hat{\boldsymbol{z}} \cdot [\nabla \times (p_\mathrm{b} \nabla \eta_\mathrm{b})]. \tag{40.175}$$

Evidently, the contribution from baroclinicity next to the bottom arises from the bottom pressure torque due to bottom pressure isolines that are not parallel to bottom topography isolines. We have more to say concerning boundary pressure torques in Section 40.9.3 as they also affect vorticity of the depth integrated flow.

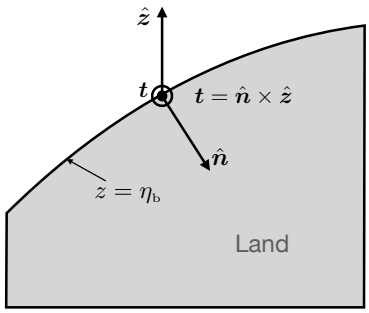

FIGURE 40.11: Orientation of the unit vectors next to the bottom of the fluid. The vertical unit vector, $\hat{\boldsymbol{z}}$, points vertically upward and the outward unit vector, $\hat{\boldsymbol{n}}$, points downward into the rock (shaded gray). The along-topography horizontal vector, $\boldsymbol{t} = \hat{\boldsymbol{n}} \times \hat{\boldsymbol{z}}$, points along lines of constant topography with land to the left when facing in the direction of $\boldsymbol{t}$; in this figure it points out from the page. The vector $\boldsymbol{t}$ is not necessarily a unit vector since it is not orthogonal to $\hat{\boldsymbol{n}}$.

Torques from bottom friction

The third term in the boundary flux (40.167b) is the contribution from friction along the bottom

$$-\hat{\boldsymbol{n}} \cdot (\hat{\boldsymbol{z}} \times \boldsymbol{F}) = -\boldsymbol{F} \cdot (\hat{\boldsymbol{n}} \times \hat{\boldsymbol{z}}) \equiv -\boldsymbol{F} \cdot \boldsymbol{t}. \tag{40.176}$$

Hence, contributions to the vertical vorticity evolution arise from the component of friction that projects onto the direction that parallels isobaths. To further our understanding of this result, consider a bottom friction written as a Rayleigh drag (e.g., Section 33.2.3) so that $\boldsymbol{F} = -\gamma\, \boldsymbol{u}$ and

$$-\boldsymbol{F} \cdot \boldsymbol{t} = \gamma\, \boldsymbol{u} \cdot \boldsymbol{t}, \tag{40.177}$$

with γ an inverse time scale. If the flow is oriented with shallow water to the right; e.g., into the page in Figure 40.11, then $-\boldsymbol{F} \cdot \boldsymbol{t} < 0$, thus contributing a negative vorticity tendency. In general, the bottom friction acts to damp the depth integrated vorticity, which is expected since bottom friction does not spontaneously spin-up the flow.

40.8.4 Surface boundary contribution

The surface boundary contribution to the vorticity equation (40.166) takes on a similar form to the bottom, with the new feature that the free surface is both moving and permeable (Section 19.6.3). This boundary term is given by

$$\zeta_a \, \partial_t \eta - \nabla(z-\eta) \cdot \boldsymbol{J}^{\zeta_a} = \zeta_a \, \partial_t \eta - \nabla(z-\eta) \cdot \left[\boldsymbol{v} \, \zeta_a - w \, \boldsymbol{\omega}_a - \hat{\boldsymbol{z}} \times \rho^{-1} \nabla p + \hat{\boldsymbol{z}} \times \boldsymbol{F} \right]_{z=\eta} \tag{40.178a}$$

$$= \zeta_a \left[\partial_t \eta + \boldsymbol{u} \cdot \nabla_h \eta - w \right]_{z=\eta} + \nabla(z-\eta) \cdot \left[w \, \boldsymbol{\omega}_a + \hat{\boldsymbol{z}} \times \rho^{-1} \nabla p - \hat{\boldsymbol{z}} \times \boldsymbol{F} \right]_{z=\eta} \tag{40.178b}$$

$$= \zeta_a \, Q_m / \rho + |\nabla(z-\eta)| \, \hat{\boldsymbol{n}} \cdot \left[w \, \boldsymbol{\omega}_a + \hat{\boldsymbol{z}} \times \rho^{-1} \nabla p - \hat{\boldsymbol{z}} \times \boldsymbol{F} \right]_{z=\eta}, \tag{40.178c}$$

where we made use of the surface kinematic boundary condition (19.94) to introduce the surface mass flux Q_m, and where

$$\hat{\boldsymbol{n}} = \frac{\nabla(z-\eta)}{|\nabla(z-\eta)|} = \frac{\nabla_h \eta + \hat{\boldsymbol{z}}}{\sqrt{1 + \nabla_h \eta \cdot \nabla_h \eta}} \tag{40.179}$$

is the outward unit normal at the surface. The first term in the surface boundary flux (40.178c) provides transport of boundary vorticity due to the transfer of mass across the boundary. The second term provides an inviscid vertical transport of absolute vorticity at the surface boundary, thus acting as a vortex stretching contribution. The third term provides a torque due to misalignments between the applied pressure isobars and the free surface isolines

$$|\nabla(z-\eta)| \, \hat{\boldsymbol{n}} \cdot (\hat{\boldsymbol{z}} \times \rho^{-1} \nabla p_a) = \rho^{-1} \nabla p_a \cdot (\nabla \eta \times \hat{\boldsymbol{z}}) = \rho^{-1} \, \hat{\boldsymbol{z}} \cdot (\nabla p_a \times \nabla \eta) = \rho^{-1} \, \hat{\boldsymbol{z}} \cdot [\nabla \times (p_a \nabla \eta)], \tag{40.180}$$

where the density, ρ, is evaluated at the ocean surface. Note that we made use of the same kinematics as for the bottom, thus allowing us to write

$$\hat{\boldsymbol{n}} \cdot [\hat{\boldsymbol{z}} \times \rho^{-1} \nabla p]_{z=\eta} = \hat{\boldsymbol{n}} \cdot (\hat{\boldsymbol{z}} \times \rho^{-1} \nabla p_a), \tag{40.181}$$

which is directly analogous to the bottom pressure equation (40.173). The fourth term in equation (40.178c) provides the corresponding contribution from the friction along the upper surface, with friction acting to reduce the magnitude of the surface boundary vorticity. For a rigid lid surface, $w(0) = 0$, $\eta = 0$, and $Q_m = 0$ so that the only surface boundary contribution arises from friction.

40.8.5 Comments

The depth integrated vorticity budget as derived in this section is perhaps the most physically straightforward of the suite of depth integrated vorticity budgets. However, in the practice of ocean modeling, this budget is generally not used since it requires an online coding of the vorticity equation and then its depth integral. As ocean models generally time step the velocity rather than the vorticity, it is common to form a vorticity budget based on the depth integrated flow or the depth averaged flow. We develop these budgets in the following section.

40.9 Vorticity for depth integrated hydrostatic flow

In this section we develop dynamical equations for vorticity of the depth integrated flow in a hydrostatic primitive equation fluid. A compelling application of these ideas comes from the study of large-scale ocean circulation. The leading order impacts from bottom pressure torques has emerged from research during recent decades, thus pointing to the fundamental role of bottom topography and flows next to sloping bottom (rather than vertical sidewalls) in affecting the ocean circulation. This recognition contrasts to traditional theories whereby the wind stress curl balances meridional motion through the beta effect. In particular, numerical model studies

reveal that wind stress curl is sub-dominant in any region with nontrivial bottom velocities.[15] In this section we introduce the basics and provide more discussion in Sections 44.5 and 44.6 when studying vorticity dynamics for the planetary geostrophic system.

40.9.1 Comparing the two vorticities

In Section 40.8 we derived the evolution equation for the depth integral of the vertical component to the absolute vorticity,

$$\int_{\eta_b}^{\eta} \zeta_a \, dz = \int_{\eta_b}^{\eta} (f + \hat{\boldsymbol{z}} \cdot \nabla \times \boldsymbol{u}) \, dz. \tag{40.182}$$

In this section we study the evolution equation for the relative vorticity in the depth integrated horizontal flow

$$\hat{\boldsymbol{z}} \cdot \nabla \times \boldsymbol{U}^{\rho} = \hat{\boldsymbol{z}} \cdot \nabla \times \int_{\eta_b}^{\eta} \boldsymbol{u} \, \rho \, dz, \tag{40.183}$$

where we introduced the depth integrated horizontal mass flux

$$\boldsymbol{U}^{\rho} = \int_{\eta_b}^{\eta} \rho \, \boldsymbol{u} \, dz. \tag{40.184}$$

For a Boussinesq ocean we set the density to a constant, in which case the difference between the two relative vorticities is[16]

$$\hat{\boldsymbol{z}} \cdot \nabla \times \left[\int_{\eta_b}^{\eta} \boldsymbol{u} \, dz \right] - \int_{\eta_b}^{\eta} \hat{\boldsymbol{z}} \cdot \nabla \times \boldsymbol{u} \, dz = \hat{\boldsymbol{z}} \cdot [\nabla \eta \times \boldsymbol{u}(\eta) - \nabla \eta_b \times \boldsymbol{u}(\eta_b)] \, . \tag{40.185}$$

Flows along boundaries generally have a nontrivial projection in the direction parallel to boundary isosurfaces, in which case the cross products are nonzero thus leading to differences in the two relative vorticities.

40.9.2 Evolution of vorticity for the depth integrated horizontal flow

In Section 28.4 we developed the depth integrated horizontal momentum equation for a hydrostatic fluid, as given by equation (28.50)

$$(\partial_t + f \, \hat{\boldsymbol{z}} \times) \, \boldsymbol{U}^{\rho} = \boldsymbol{u}(\eta) \, Q_m - \eta \nabla_h p_a + \eta_b \nabla_h p_b - \nabla_h \mathscr{P} + \boldsymbol{D} + \nabla_h \cdot \left[\int_{\eta_b}^{\eta} \mathbb{T}^{\text{kinetic}}_{\text{hor}} \, dz \right] . \tag{40.186}$$

We here introduced the potential energy per horizontal area of the fluid column (equation (28.40)), the depth integrated horizontal friction (equation (28.51)), and the divergence of the horizontal kinetic stress tensor (equation (28.33))

$$\mathscr{P} = \int_{\eta_b}^{\eta} g \, \rho \, z \, dz \quad \text{and} \quad \boldsymbol{D} = \int_{\eta_b}^{\eta} \rho \, \boldsymbol{F}_{\text{horz}} \, dz \quad \text{and} \quad \mathbb{T}^{\text{kinetic}}_{\text{hor}} = -\rho \, \boldsymbol{u} \otimes \boldsymbol{u}. \tag{40.187}$$

[15] The natural ocean has no distinction between side and bottom. Rather, as discussed in Figure 28.6, the ocean has a sloping bottom that reaches to the surface along its boundary at the "beach." *Hallberg and Rhines* (1996), *Hughes and de Cueves* (2001), and many subsequent studies emphasize that theoretical and numerical models using vertical sides and a flat bottom exhibit somewhat unnatural dynamical balances, whereas models with sloping bottoms better capture effects from topography consistent with the theory presented in this chapter.

[16] As noted in footnote 14, we can reduce notational clutter by writing ∇ rather than ∇_h when operating on functions that are independent of z, such as η, p_a, η_b and p_b. Since these fields are independent of z, then $\nabla_h \eta = \nabla \eta$, and likewise for p_a, η_b and p_b. We sometimes make use of this notation, though write ∇_h where it can help to reduce ambiguity.

All terms on the right hand side of equation (40.186) provide a stress that drives changes in $\boldsymbol{U}^\rho$. Hence, the curl of these terms provides a torque, in which case we have

$$\hat{\boldsymbol{z}} \cdot \partial_t (\nabla \times \boldsymbol{U}^\rho) = -\nabla \cdot (f \boldsymbol{U}^\rho) + \hat{\boldsymbol{z}} \cdot \nabla \times \left[\boldsymbol{u}(\eta)\, Q_{\mathsf{m}} - \eta \nabla_{\mathsf{h}} p_{\mathsf{a}} + \eta_{\mathsf{b}} \nabla_{\mathsf{h}} p_{\mathsf{b}} + \Delta \boldsymbol{\tau} + \boldsymbol{D} + \nabla_{\mathsf{h}} \cdot \left(\int_{\eta_{\mathsf{b}}}^{\eta} \mathbb{T}^{\text{kinetic}}_{\text{hor}} \, \mathrm{d}z \right) \right], \quad (40.188)$$

where we used the vector identity

$$\hat{\boldsymbol{z}} \cdot \nabla \times (f\, \hat{\boldsymbol{z}} \times \boldsymbol{U}^\rho) = \nabla \cdot (f \boldsymbol{U}^\rho), \quad (40.189)$$

as well as $\nabla \times \nabla_{\mathsf{h}} \mathscr{P} = 0$. We now discuss the various physical processes appearing in the vorticity equation (40.188).

Beta effect

The first term on the right hand side of the vorticity equation (40.188) arises from the convergence of mass within a fluid column due to depth integrated horizontal flow. We can further decompose the effects from this term by performing the product rule

$$-\nabla \cdot (f \boldsymbol{U}^\rho) = -f \nabla \cdot \boldsymbol{U}^\rho - \beta V^\rho. \quad (40.190)$$

The contribution from βV^ρ arises from the beta effect as discussed in Section 40.6.2. For the first term, the weighting by the Coriolis parameter means that mass convergence at higher latitudes has more impact on vorticity changes than at lower latitudes. We can understand this weighting by noting that vertical fluid columns are more aligned with the planetary rotation at the high latitudes. Hence, when the mass of vertical columns converges at the higher latitudes, there is more impact on changes to the vorticity of the depth integrated flow.

Mass transfer, turbulent momentum transfer, and nonlinear effects

The term $\nabla \times [\boldsymbol{u}(\eta)\, Q_{\mathsf{m}}]$ appearing in in equation (40.191) accounts for vorticity crossing the ocean surface as affected by the mass flux. The term $\nabla \times \Delta \boldsymbol{\tau}$ is the torque from turbulent stresses at the ocean surface and bottom, and $\hat{\boldsymbol{z}} \cdot \nabla \times \boldsymbol{D}$ is the torque from horizontal frictional stresses in the fluid interior. The final term arises from the nonlinear kinetic stresses, $\mathbb{T}^{\text{kinetic}}_{\text{hor}}$, that account for curls in the self-advection operator.

40.9.3 Boundary pressure torques

The pressure terms in equation (40.188)

$$\hat{\boldsymbol{z}} \cdot \nabla \times (-\eta \nabla p_{\mathsf{a}} + \eta_{\mathsf{b}} \nabla p_{\mathsf{b}}) = \hat{\boldsymbol{z}} \cdot \nabla \times (p_{\mathsf{a}} \nabla \eta - p_{\mathsf{b}} \nabla \eta_{\mathsf{b}}) \quad (40.191)$$

arise from curls of the pressure form stresses (see Chapter 28) at the ocean surface and bottom, and these contributions are referred to as *pressure torques*. When the fluid is a column of ocean water, then the surface pressure contribution is the *atmospheric pressure torque* and the bottom pressure term is the *bottom pressure torque*.

Geometry of boundary pressure torques

Geometrically, there is a nonzero atmospheric pressure torque when the applied pressure, p_{a}, has a gradient when moving along contours of constant free surface. Likewise, there is a nonzero bottom pressure torque when bottom pressure, p_{b}, changes along contours of constant bottom

topography. Mathematically, we reveal these properties through use of either Exercise 5.1 or 40.14. For example, the bottom pressure torque along an isobath (contour of constant η_b) can be written

$$\hat{\boldsymbol{z}} \cdot \nabla \eta_b \times \nabla p_b = -(\hat{\boldsymbol{n}} \cdot \nabla \eta_b)\, (\hat{\boldsymbol{t}} \cdot \nabla p_b), \tag{40.192}$$

where $\hat{\boldsymbol{t}}$ is a unit tangent vector directed along the isobath, and $\hat{\boldsymbol{n}}$ is a unit vector that points to the left of $\hat{\boldsymbol{t}}$ (see Figure 40.12). Both $\hat{\boldsymbol{t}}$ and $\hat{\boldsymbol{n}}$ are horizontal vectors.[17] Hence, $\hat{\boldsymbol{n}} \cdot \nabla \eta_b$ measures the slope of the bottom topography in the direction normal to an isobath, and $\hat{\boldsymbol{t}} \cdot \nabla p_b$ measures the change of the bottom pressure along the isobath. There is a nonzero bottom pressure torque along an isobath so long as there is a slope to the bottom pressure along the isobath, and there is a change in bottom pressure moving along the isobath.

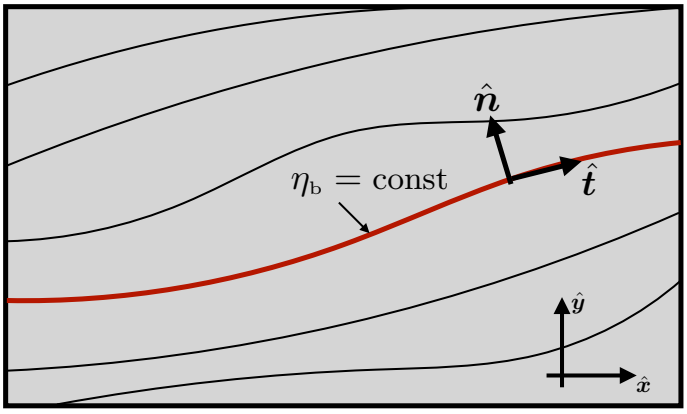

FIGURE 40.12: Geometry depicting a contour along a particular line of constant topography (i.e., an isobath), $\eta_b(x, y)$. The along-contour direction is $\hat{\boldsymbol{t}} = \mathrm{d}\boldsymbol{x}/\mathrm{d}s$, with s the arc length along the contour. The unit direction pointing to the left of $\hat{\boldsymbol{t}}$ is written $\hat{\boldsymbol{n}}$, with $\hat{\boldsymbol{n}} \cdot \hat{\boldsymbol{t}} = 0$ and $\hat{\boldsymbol{t}} \times \hat{\boldsymbol{n}} = \hat{\boldsymbol{z}}$. Both $\hat{\boldsymbol{n}}$ and $\hat{\boldsymbol{t}}$ are horizontal unit vectors. There is a nonzero bottom pressure torque if bottom pressure changes when following an isobath.

Geostrophic velocity associated with the bottom pressure torque

To further our understanding of the pressure torques in equation (40.191), focus on the bottom pressure and introduce a geostrophic velocity[18]

$$\rho_o\, f\, \boldsymbol{u}_g = \hat{\boldsymbol{z}} \times (\nabla_h p)_{z=\eta_b} = \hat{\boldsymbol{z}} \times [\nabla p_b + g\, \rho(\eta_b)\, \nabla \eta_b], \tag{40.193}$$

where the second equality made use of equation (27.60b) to express the horizontal pressure gradient at the bottom, $(\nabla_h p)_{z=\eta_b}$, in terms of the gradient of bottom pressure and gradient of bottom topography. Hence,

$$\nabla p_b = -\rho_o\, f\, \hat{\boldsymbol{z}} \times \boldsymbol{u}_g - g\, \rho(\eta_b)\, \nabla \eta_b, \tag{40.194}$$

so that the bottom pressure torque takes the form

$$\hat{\boldsymbol{z}} \cdot \nabla \times (\eta_b \nabla p_b) = \hat{\boldsymbol{z}} \cdot (\nabla \eta_b \times \nabla p_b) = -\rho_o\, f\, \boldsymbol{u}_g \cdot \nabla \eta_b. \tag{40.195}$$

[17] It is important to note that $\hat{\boldsymbol{n}}$ is not the outward normal direction to the bottom, contrary to its usage in Section 40.8. Here, $\hat{\boldsymbol{n}}$ it is the horizontal direction within the bottom surface that is normal to contours of constant topography.

[18] The geostrophic velocity is a balance between the Coriolis acceleration and the *horizontal* pressure gradient. We thus need to decompose the horizontal pressure gradient into the bottom pressure gradient and the gradient of the botom slope, as per equation (27.60b).

This equation is merely a replacement of the bottom pressure gradient with a corresponding geostrophic velocity. However, if this geostrophic velocity is assumed to satisfy the kinematic boundary condition (19.56), then we reach the equality[19]

$$\hat{\boldsymbol{z}} \cdot \nabla \eta_{\mathrm{b}} \times \nabla p_{\mathrm{b}} = -\rho_{\circ} f w_{\mathrm{g}}, \tag{40.196}$$

which links the bottom pressure torque to vertical vortex stretching by the vertical component to the geostrophic velocity. Evidently, if the bottom geostrophic velocity is negative ($w_{\mathrm{g}} < 0$), then that induces vortex stretching and a corresponding positive tendency for vorticity of the depth integrated flow. The opposite holds with $w_{\mathrm{g}} > 0$, in which vortex squashing induces a negative tendency for vorticity of the depth integrated flow.

The equality (40.196) is sometimes used to infer the bottom pressure torque by diagnosing the bottom vertical velocity, $w(\eta_{\mathrm{b}})$ (*Spence et al.*, 2012). Although this diagnostic is suitable for some studies, there are important caveats. Namely, the bottom vertical velocity is generally affected by bottom frictional effects and thus can have a nontrivial Ekman component.[20] Nonlinear effects can also be important especially when considering motions with sizable Rossby numbers. Neither the Ekman component nor nonlinear terms are directly related to the bottom pressure torque. We thus expect $\rho_{\circ} f w(\eta_{\mathrm{b}})$ to be distinct from $\hat{\boldsymbol{z}} \cdot \nabla \eta_{\mathrm{b}} \times \nabla p_{\mathrm{b}}$ in regions of sizable deep flows where bottom friction and/or nonlinear effects are of leading order importance.[21] The studies from *Gula et al.* (2015) and *LeCorre et al.* (2020) illustrate these points from numerical simulations of the subpolar North Atlantic circulation.

40.9.4 Steady state vorticity budget

The steady state form of the vorticity budget (40.188) leads to the balance

$$\begin{aligned} \beta V^{\rho} = &-f \nabla \cdot \boldsymbol{U}^{\rho} \\ &+ \hat{\boldsymbol{z}} \cdot \nabla \times \left[\boldsymbol{u}(\eta)\, Q_{\mathsf{m}} - \eta \nabla_{\mathrm{h}} p_{\mathrm{a}} + \eta_{\mathrm{b}} \nabla_{\mathrm{h}} p_{\mathrm{b}} + \Delta \boldsymbol{\tau} + \boldsymbol{D} + \nabla_{\mathrm{h}} \cdot \left(\int_{\eta_{\mathrm{b}}}^{\eta} \mathbb{T}^{\mathrm{kinetic}}_{\mathrm{hor}}\, \mathrm{d}z \right) \right]. \end{aligned} \tag{40.197}$$

Writing the balance in this manner reveals how the beta affect affords a steady meridional mass transport as a balance with the variety of terms on the right hand side.

Specializing the budget to expose a variety of balanced flow regimes

Let us further specialize to the case appropriate for many studies of the large-scale circulation, whereby we make the following assumptions.

- Uniform mass atmosphere so that p_{a} is a constant.
- The frictional stresses from horizontal strains within the fluid interior, $\boldsymbol{D}$, can be neglected.
- Zero boundary mass transport so that $Q_{\mathsf{m}} = 0$ and, correspondingly, the steady depth integrated mass budget (19.103) means that $\nabla \cdot \boldsymbol{U}^{\rho} = 0$ when $Q_{\mathsf{m}} = 0$.

[19] The velocity, $\boldsymbol{v}$, satisfies the kinematic boundary condition (19.56), in which $\boldsymbol{v}(\eta_{\mathrm{b}}) \cdot \hat{\boldsymbol{n}} = 0$. Decomposing the velocity into its geostrophic and ageostrophic components, $\boldsymbol{v} = \boldsymbol{v}_{\mathrm{g}} + \boldsymbol{v}_{\mathrm{a}}$, does not generally imply that $\boldsymbol{v}_{\mathrm{g}}$ and $\boldsymbol{v}_{\mathrm{a}}$ separately satisfy the kinematic boundary condition. Rather, we must make that assumption in order to reach the equality (40.196).

[20] Recall our discussion of Ekman boundary layers in Chapter 33.

[21] In addition to the Ekman and nonlinear effects noted here, diagnosing $w(\eta_{\mathrm{b}})$ in a numerical model can be frought with difficulties related to the discrete grid stencil given that grids can be quite coarse in the deep ocean with many ocean model configurations.

These simplifications bring the balance (40.197) to the form

$$\beta V^\rho = \hat{\boldsymbol{z}} \cdot \nabla \times \left[\eta_b \nabla_h p_b + \Delta \boldsymbol{\tau} + \nabla_h \cdot \left(\int_{\eta_b}^{\eta} \mathbb{T}^{\text{kinetic}}_{\text{hor}} \, dz \right) \right] \tag{40.198a}$$

$$\text{MERIDIONAL TRANSPORT} = \text{BOTTOM PRESS TORQUE} + \text{BOUNDARY STRESS} + \text{NONLINEAR}. \tag{40.198b}$$

This steady balance reveals distinct flow regimes depending on which of the terms dominate, and as such it serves as a useful framework for analysis.

Topographic nonlinear balance

Jackson et al. (2006), *Patmore et al.* (2019), and *LeCorre et al.* (2020) emphasize the importance of the nonlinear term in equation (40.198b) when flows are especially strong. The bottom pressure torque contribution is particularly strong where flows are strong near the bottom. Such nonlinear flow regimes generally have variations over length scales much smaller than that of the wind stress. Hence, if the horizontal friction is small, as it is even for strong flows not directly adjacent to solid boundaries, and the bottom frictional drag is small, then the vorticity balance (40.198a) in the nonlinear inviscid regime takes on the form

$$\beta V^\rho = \hat{\boldsymbol{z}} \cdot \nabla \times \left[\eta_b \nabla_h p_b + \nabla_h \cdot \left(\int_{\eta_b}^{\eta} \mathbb{T}^{\text{kinetic}}_{\text{hor}} \, dz \right) \right] \qquad \text{topographic nonlinear balance.} \tag{40.199}$$

Observe that the nonlinear term and bottom pressure torque have derivatives wherease there are none on the βV^ρ term. These derivatives make the right hand side terms have variations at smaller scales than βV^ρ. We infer that the smaller scales present in the bottom pressure torque and the nonlinear term nearly balance, and with any residual leading to the broader scale meridional transport. Figure 6 in *LeCorre et al.* (2020) provides a striking example of this balance in a numerical simulation of the North Atlantic subpolar gyre.

Linear regime of planetary geostrophy

For the linear regime of planetary geostrophic flow (Chapter 44), the nonlinear term from the kinetic stress is small, so that the balance is between meridional transport, bottom pressure torque, and curl of turbulent boundary stresses. The *Sverdrup balance* is one particular example of a planetary geostrophic balance, with Sverdrup balance ignoring the bottom pressure torque and bottom turbulent stresses, and thus focuses just on the balance between meridional transport with the turbulent surface stresses largely arising from winds

$$\beta V^\rho = \hat{\boldsymbol{z}} \cdot \nabla \times \boldsymbol{\tau}^\eta \qquad \text{Sverdrup balance.} \tag{40.200}$$

However, as emphasized by *Hallberg and Rhines* (1996) and *Hughes and de Cueves* (2001), as well as more recent studies, contributions from bottom pressure torques are of leading order importance in the presence of flow next to sloping side boundaries, thus making the traditional Sverdrup balance mostly relevant in the open ocean away from boundaries. A more general balance is known as *topographic Sverdrup balance*

$$\beta V^\rho = \hat{\boldsymbol{z}} \cdot \nabla \times (\eta_b \nabla_h p_b + \boldsymbol{\tau}^\eta) \qquad \text{topographic Sverdrup balance.} \tag{40.201}$$

We further study these balances of planetary geostrophy in Sections 44.3, 44.5, and 44.6.

40.9.5 Integral balances satisfied by steady flows

Reconsider the steady vorticity balance (40.197), here written in the form

$$\nabla \cdot (f \boldsymbol{U}^\rho) = \hat{\boldsymbol{z}} \cdot \nabla \times \boldsymbol{M} \tag{40.202}$$

where we introduced the stress vector

$$\boldsymbol{M} = \boldsymbol{u}(\eta)\, Q_{\mathsf{m}} - \eta \nabla_{\mathsf{h}} p_{\mathsf{a}} + \eta_{\mathsf{b}} \nabla_{\mathsf{h}} p_{\mathsf{b}} + \Delta \boldsymbol{\tau} + \boldsymbol{D} + \nabla_{\mathsf{h}} \cdot \left(\int_{\eta_{\mathsf{b}}}^{\eta} \mathbb{T}^{\text{kinetic}}_{\text{hor}} \, \mathrm{d}z \right). \tag{40.203}$$

Now integrate equation (40.202) over an area, $\mathcal{S}$, with Gauss's divergence theorem on the left hand side leading to

$$\int_{\mathcal{S}} \nabla \cdot (f \boldsymbol{U}^\rho) \, \mathrm{d}\mathcal{S} = \oint_{\partial \mathcal{S}} f \boldsymbol{U}^\rho \cdot \hat{\boldsymbol{n}} \, \mathrm{d}s, \tag{40.204}$$

where $\hat{\boldsymbol{n}}$ is the horizontal outward unit normal on the boundary, $\partial \mathcal{S}$, and $\mathrm{d}s$ is the arc-length increment along the boundary. This term is the mass transport crossing the boundary as weighted by the Coriolis parameter.

Use of Stokes' curl theorem on the right hand side of equation (40.202) leads to

$$\int_{\mathcal{S}} \hat{\boldsymbol{z}} \cdot \nabla \times \boldsymbol{M} \, \mathrm{d}\mathcal{S} = \oint_{\partial \mathcal{S}} \boldsymbol{M} \cdot \hat{\boldsymbol{t}} \, \mathrm{d}s, \tag{40.205}$$

where $\hat{\boldsymbol{t}}$ is the horizontal unit tangent vector along the boundary, and the integral is oriented in the counter-clockwise direction. To help interpret the closed loop integral in equation (40.205), consider just the contribution from bottom pressure

$$\oint_{\partial \mathcal{S}} \boldsymbol{M}_{\text{bottom press}} \cdot \hat{\boldsymbol{t}} \, \mathrm{d}s = \oint_{\partial \mathcal{S}} \eta_{\mathsf{b}} \, \nabla p_{\mathsf{b}} \cdot \hat{\boldsymbol{t}} \, \mathrm{d}s = - \oint_{\partial \mathcal{S}} p_{\mathsf{b}} \, \nabla \eta_{\mathsf{b}} \cdot \hat{\boldsymbol{t}} \, \mathrm{d}s, \tag{40.206}$$

which is the work done by bottom topographic form stress around the closed contour. The other terms in equation (40.202) have interpretations as the work arising from integrating stresses from mass transport through the surface, atmospheric form stress, turbulent boundary stresses, interior frictional stresses, and nonlinear kinetic stress. Observe that the integral of bottom pressure torque in equation (40.206) vanishes if the closed contour follows either an isobath or a bottom pressure isobar. The vanishing of this integral means that bottom pressure torques have zero net circulation around isobaths or bottom isobars. An analogous property is satisfied by the atmospheric pressure torque when integrated around closed contours of constant atmospheric pressure, p_{a}, or constant surface height, η.

Bringing the above results together renders the general balance around the boundray of an arbitrary closed region

$$\oint_{\partial \mathcal{S}} f \boldsymbol{U}^\rho \cdot \hat{\boldsymbol{n}} \, \mathrm{d}s = \oint_{\partial \mathcal{S}} \boldsymbol{M} \cdot \hat{\boldsymbol{t}} \, \mathrm{d}s. \tag{40.207}$$

We thus see that transport across the closed boundary, as weighted by the Coriolis parameter, arises from a nonzero net work around the boundary by the variety of stresses comprising $\boldsymbol{M}$. We are afforded a key simplification if $\boldsymbol{U}^\rho \cdot \hat{\boldsymbol{n}} = 0$ at each point along the boundary. For example, if $\nabla \cdot \boldsymbol{U}^\rho = 0$, which generally also requires $Q_{\mathsf{m}} = 0$, then contours along which $\boldsymbol{U}^\rho \cdot \hat{\boldsymbol{n}} = 0$ correspond to closed streamlines of the steady $\boldsymbol{U}^\rho$. Hence, we find the following balance holds around any closed streamline

$$\oint_{\partial \mathcal{S}} \boldsymbol{M} \cdot \hat{\boldsymbol{t}} \, \mathrm{d}s = 0. \quad \text{for } \partial \mathcal{S} \text{ a closed streamline of } \boldsymbol{U}^\rho. \tag{40.208}$$

Closed streamlines do not always exist. But when they do, such as for steady ocean gyre circulations, this balance holds. In Section 44.5.3, we consider the planetary geostrophic version of this balance.

40.9.6 Formulation based on the vector-invariant velocity equation

In formulating the budget equation (40.188) for vorticity of the depth integrated flow, we started with the depth integrated momentum in Section 28.4.5. However, many numerical models are formulated using the vector invariant form of the horizontal velocity equation (40.147), here written in the equivalent form for a Boussinesq ocean

$$\underbrace{\partial_t \boldsymbol{u} + f\,\hat{\boldsymbol{z}}\times\boldsymbol{u} + \nabla_h p/\rho_o - \boldsymbol{F}}_{\text{linear terms plus friction}} = \underbrace{-\zeta\,\hat{\boldsymbol{z}}\times\boldsymbol{u} - w\,\partial_z\boldsymbol{u} - \nabla_h \boldsymbol{u}^2/2.}_{\text{Magnus + vertical advection + kinetic energy}} \tag{40.209}$$

The three nonlinear terms on the right hand side arise from expanding the nonlinear self-advection term, $(\boldsymbol{v}\cdot\nabla)\,\boldsymbol{u}$, following the manipulations in Section 40.7.1. Much of the formulation to follow emulates that considered thus far, with the exception of the nonlinear terms and elements of the boundary contributions.

We take the vertical integral of equation (40.209)

$$\int_{\eta_b}^{\eta} [\partial_t \boldsymbol{u} + f\,\hat{\boldsymbol{z}}\times\boldsymbol{u} + \nabla_h p/\rho_o - \boldsymbol{F}]\,dz = -\int_{\eta_b}^{\eta} \left(\zeta\,\hat{\boldsymbol{z}}\times\boldsymbol{u} + w\,\partial_z\boldsymbol{u} + \nabla_h \boldsymbol{u}^2/2\right) dz, \tag{40.210}$$

and then the curl

$$\nabla\times\int_{\eta_b}^{\eta} (\partial_t \boldsymbol{u} + f\,\hat{\boldsymbol{z}}\times\boldsymbol{u} + \nabla_h p/\rho_o - \boldsymbol{F})\,dz = -\nabla\times\int_{\eta_b}^{\eta} (\zeta\,\hat{\boldsymbol{z}}\times\boldsymbol{u} + w\,\partial_z\boldsymbol{u} + \nabla_h \boldsymbol{u}^2/2)\,dz. \tag{40.211}$$

Making use of the following identities

$$\hat{\boldsymbol{z}}\cdot\left[\nabla\times\int_{\eta_b}^{\eta} \partial_t \boldsymbol{u}\,dz\right] = \hat{\boldsymbol{z}}\cdot\partial_t(\nabla\times\boldsymbol{U}) - \hat{\boldsymbol{z}}\cdot\nabla\times[\boldsymbol{u}(\eta)\,\partial_t\eta] \tag{40.212a}$$

$$\hat{\boldsymbol{z}}\cdot\left[\nabla\times\int_{\eta_b}^{\eta} f\,\hat{\boldsymbol{z}}\times\boldsymbol{u}\,dz\right] = \nabla\cdot(f\,\boldsymbol{U}) \tag{40.212b}$$

$$\hat{\boldsymbol{z}}\cdot\left[\nabla\times\int_{\eta_b}^{\eta} \nabla_h p\,dz\right] = \hat{\boldsymbol{z}}\cdot\nabla\times(\eta\nabla p_a - \eta_b\nabla p_b) \tag{40.212c}$$

$$\hat{\boldsymbol{z}}\cdot\left[\nabla\times\int_{\eta_b}^{\eta} \zeta\,\hat{\boldsymbol{z}}\times\boldsymbol{u}\,dz\right] = \nabla\cdot\left[\int_{\eta_b}^{\eta} \zeta\,\boldsymbol{u}\,dz\right] \tag{40.212d}$$

$$\hat{\boldsymbol{z}}\cdot\left[\nabla\times\int_{\eta_b}^{\eta} \rho_o\,\boldsymbol{F}\,dz\right] = \hat{\boldsymbol{z}}\cdot\nabla\times(\Delta\boldsymbol{\tau} + \boldsymbol{D}), \tag{40.212e}$$

leads to

$$\begin{aligned}\hat{\boldsymbol{z}}\cdot\partial_t(\nabla\times\boldsymbol{U}) &= -\nabla\cdot\left[f\,\boldsymbol{U} + \int_{\eta_b}^{\eta} \zeta\,\boldsymbol{u}\,dz\right] \\ &+ \hat{\boldsymbol{z}}\cdot\nabla\times\left[\boldsymbol{u}(\eta)\,\partial_t\eta - \eta\nabla p_a + \eta_b\nabla p_b + (\Delta\boldsymbol{\tau} + \boldsymbol{D})/\rho_o - \int_{\eta_b}^{\eta} (w\,\partial_z\boldsymbol{u} + \nabla_h \boldsymbol{u}^2/2)\,dz\right].\end{aligned} \tag{40.213}$$

The left hand side is the time tendency of the vorticity of the depth integrated horizontal flow, with this time tendency driven by the various linear and nonlinear terms on the right hand side. This evolution equation should be compared to equation (40.188) as derived from the advective form of the momentum equation. Likewise, we derive a steady state balance by setting the time

tendencies to zero to yield

$$\beta V = -f \nabla \cdot \boldsymbol{U} - \nabla \cdot \left[\int_{\eta_b}^{\eta} \zeta \, \boldsymbol{u} \, dz \right] + \hat{\boldsymbol{z}} \cdot \nabla \times \left[\boldsymbol{u}(\eta) \, \partial_t \eta - \eta \nabla p_a + \eta_b \nabla p_b + (\Delta \boldsymbol{\tau} + \boldsymbol{D})/\rho_o - \int_{\eta_b}^{\eta} (w \, \partial_z \boldsymbol{u} + \nabla_h \boldsymbol{u}^2/2) \, dz \right], \quad (40.214)$$

which should be compared to equation (40.197).

40.9.7 Vorticity of the depth averaged flow

The vorticity of the depth averaged flow is given by $\hat{\boldsymbol{z}} \cdot \nabla \times \overline{\boldsymbol{u}}$, where $\overline{\boldsymbol{u}}$ is given by equation (28.34) for a compressible non-Boussinesq fluid, and which takes on the following form for a Boussinesq ocean

$$\overline{\boldsymbol{u}} = \frac{\int_{\eta_b}^{\eta} \boldsymbol{u} \, dz}{\eta - \eta_b} = \frac{\boldsymbol{U}}{\eta - \eta_b}. \quad (40.215)$$

The difference is given by

$$\nabla \times \boldsymbol{U} - (\eta - \eta_b) \nabla \times \overline{\boldsymbol{u}} = \nabla(\eta - \eta_b) \times \overline{\boldsymbol{u}}, \quad (40.216)$$

so that the two vorticities are the same in the special case of a depth averaged flow that is parallel to $\nabla(\eta - \eta_b)$. Quite trivially, $\nabla(\eta - \eta_b) \times \overline{\boldsymbol{u}} = 0$ occurs for a rigid lid and flat bottom ocean, in which $\nabla \eta = \nabla \eta_b = 0$. More generally, $\nabla(\eta - \eta_b) \times \overline{\boldsymbol{u}} \neq 0$, particularly in the presence of topography. We further study the budgets for these two vorticities, for planetary geostrophic flow, in Sections 44.5 and 44.6.

40.9.8 Comments and further study

The diagnostic budgets derived in this section have appeared in many studies of ocean vorticity. When diagnosing the budget terms in a numerical model, the choice for how to mathematically formulate the diagnostic balances is largely driven by physical transparency as well as by numerical precision. Concerning numerical precision, it is useful to note that vorticity, as the derivative of velocity, has more power at the high spatial wave numbers than does velocity. In a numerical model, such power can manifest as grid scale noise. It is thus of use to perform much of the calculation online to enable the most accurate available diagnostic. Even so, further spatial smoothing is generally required, especially in realistic models, to extract physically interpretable signals.

40.10 Exercises

EXERCISE 40.1: FILLING IN DETAILS TO A DERIVATION
Fill in the mathematical details to prove the identity (40.44a)

$$\rho \frac{D(\zeta_a/\rho)}{Dt} = \frac{\partial \zeta_a}{\partial t} + \nabla \cdot (\boldsymbol{v} \, \zeta_a) \quad (40.217)$$

Hint: make use of mass continuity in the form of equation (19.10).

EXERCISE 40.2: RELATING THE INTEGRAL OF DIVERGENCE AND VORTICITY
For some purposes, it is useful to consider evolution of the flow divergence as well as the vorticity.

In this chapter we focused on the vorticity. Here are to prove, using Cartesian tensors, that

$$\int_{\mathcal{R}} (\boldsymbol{v}\,\nabla\cdot\boldsymbol{v} + \boldsymbol{\omega}\times\boldsymbol{v})\,\mathrm{d}V = \oint_{\partial\mathcal{R}} [\boldsymbol{v}\,(\boldsymbol{v}\cdot\hat{\boldsymbol{n}}) - \hat{\boldsymbol{n}}\,\mathcal{K}]\,\mathrm{d}\mathcal{S}, \tag{40.218}$$

where $\mathcal{K} = \boldsymbol{v}\cdot\boldsymbol{v}/2$ is the kinetic energy per mass. Hint: make use of the vector identity (40.32) as well as the scalar form of Gauss's divergence theorem given by equation (2.84).

EXERCISE 40.3: STRAIN AND ROTATION FOR STRETCHING AND TILTING
In this exercise we write the 3×3 strain rate tensor, $\mathbb{S}$, and rotation tensor, $\mathbb{R}$, for the examples of vortex stretching and vortex tilting considered in Section 40.5.3. Recall that elements of $\mathbb{S}$ are given by equation (18.90a) and $\mathbb{R}$ have elements given by equation (18.90b). Hint: there is no unique answer for the strain rate tensors, so offer a simple example that renders the desired behavior of a vortex line.

(a) Write a strain rate tensor corresponding to vortex stretching as per equation (40.81) along with $\omega^x = \omega^y = 0$, and write the corresponding vorticity source term $\boldsymbol{\omega}\cdot\mathbb{S}$.

(b) Write the rotation tensor for vortex stretching as per equation (40.81) and verify that $\omega_m \cdot \mathbb{R}_{mn} = 0$.

(c) Write a strain rate tensor corresponding to vortex tilting as per equation (40.87) along with $\omega^y = \omega^z = 0$.

(d) Write the rotation tensor for vortex tilting as per equation (40.87) and verify that $\omega_m\,\mathbb{R}_{mn} = 0$.

EXERCISE 40.4: FRICTION IN THE VORTICITY EQUATION
Assume a viscous friction operator of the form

$$\boldsymbol{F} = \nu\nabla^2\boldsymbol{v}, \tag{40.219}$$

with ν a constant molecular kinematic viscosity. Assuming Cartesian coordinates, write the vorticity equation (40.42) with this term included.

EXERCISE 40.5: FRICTION FOR NON-DIVERGENT FLOWS
Consider a non-divergent flow with a Laplacian frictional acceleration

$$\boldsymbol{F} = \nu\nabla^2\boldsymbol{v} \quad \text{with} \quad \nabla\cdot\boldsymbol{v} = 0, \tag{40.220}$$

with ν a constant molecular kinematic viscosity. Write this expression in terms of the vorticity. Hint: check that $\nabla\times\boldsymbol{F}$ equals to the friction appearing in the vorticity equation derived in exercise 40.4. Further hint: the derivation is given in Section 25.8.9.

EXERCISE 40.6: VORTICITY FOR STEADY NON-DIVERGENT y-z CIRCULATION
This exercise is based on exercise (1) in Section 1.1 of *Pratt and Whitehead* (2008). Consider inviscid, constant density, and non-divergent flow in the y-z (meridional-vertical) plane and in a non-rotating reference frame

$$\rho\,(\partial_t + v\,\partial_y + w\,\partial_z)v = -\partial_y p \tag{40.221a}$$
$$\rho\,(\partial_t + v\,\partial_y + w\,\partial_z)w = -\partial_z p - \rho\,g \tag{40.221b}$$
$$\partial_y v + \partial_z w = 0. \tag{40.221c}$$

(a) Show that the zonal component of the relative vorticity is materially constant following the y-z flow

$$(\partial_t + v\,\partial_y + w\,\partial_z)\,\omega^x = 0 \quad \text{with} \quad \omega^x = \hat{\boldsymbol{x}}\cdot(\nabla\times\boldsymbol{v}) = \partial_y w - \partial_z v. \tag{40.222}$$

(b) Introduce the y-z (meridional-vertical) overturning streamfunction

$$(v, w) = \hat{\boldsymbol{x}} \times \nabla\psi = -\hat{\boldsymbol{y}}\partial_z\psi + \hat{\boldsymbol{z}}\,\partial_y\psi, \tag{40.223}$$

so that the vorticity is the Laplacian of the streamfunction

$$\omega^x = (\partial_{yy} + \partial_{zz})\,\psi. \tag{40.224}$$

Write the vorticity equation (40.222) in terms of the streamfunction. Check your answer by showing that the steady vorticity equation implies that the Jacobian of the streamfunction with the vorticity vanishes

$$J(\psi, \omega^x) = \partial_y\psi\,\partial_z\omega^x - \partial_z\psi\,\partial_y\omega^x = 0. \tag{40.225}$$

(c) Following from the previous part, show that for steady flow that the vorticity is a function just of the streamfunction,

$$\omega^x = F(\psi), \tag{40.226}$$

where the function, F, is determined by the value of the vorticity along the streamlines.

Hint: we already know that $\omega^x = (\partial_{yy} + \partial_{zz})\,\psi$, even for time dependent flow, which follows from the non-divergent nature of the y-z overturning circulation. What equation (40.226) says is that for steady flow, the vorticity is a function just of the streamfunction. Consequently, if we specify the vorticity at any point along a streamline, then we know the vorticity everywhere along the streamline since it remains constant. Furthermore, it means that the streamfunction satisfies the elliptic problem

$$(\partial_{yy} + \partial_{zz})\,\psi = F(\psi). \tag{40.227}$$

EXERCISE 40.7: BAROCLINICITY WITH $\rho_o(z)$

Recall the discussion of the Boussinesq momentum equation in Section 29.1.2. The form given by equation (29.8) is written with the reference density, $\rho_o = \rho_o(z)$. We then stated that the form of the baroclinicity vector appearing in the Boussinesq vorticity equation is greatly simplified by setting ρ_o to a global constant, and thus dropping the z dependence. Derive the second term in the baroclinicity

$$\boldsymbol{B} = \nabla\left[b - \frac{\delta p}{\rho_o^2}\frac{\mathrm{d}\rho_o}{\mathrm{d}z}\right] \times \hat{\boldsymbol{z}}, \tag{40.228}$$

so that $\boldsymbol{B} = \nabla b \times \hat{\boldsymbol{z}}$ when ρ_o is assumed to be a global constant. Hint: write the vector-invariant form of equation (29.8) with $\rho_o(z)$. Then take the curl.

EXERCISE 40.8: GENERATION OF VORTICITY BY BAROCLINICITY

Consider a body of water with a flat bottom and rigid sides. Let the top surface be at $z = 0$ and bottom at $z = -H$, and assume zero pressure applied at the top surface. Let the density have a horizontal structure given by

$$\rho(x) = \rho_o\,(1 - \gamma\,x) \tag{40.229}$$

where ρ_o and γ are positive constants (with dimensions of density and inverse length, respectively). We furthermore assume that $\gamma|x| \ll 1$ so that the density is XFstrictly positive. Note that a study of Figure 40.3 helps with this exercise.

As posed, the fluid is not in mechanical equilibrium since there is a horizontal density gradient. Hence, the fluid will adjust as a result of the nonzero horizontal pressure gradient force. Our aim here is to compute the baroclinicity contained in the fluid to garner a sense for the initial

adjustment of vorticity.

(a) Compute the density gradient $\nabla\rho$ and draw a schematic.

(b) Compute the pressure gradient, ∇p, assuming approximate hydrostatic balance so that $\partial p/\partial z = -\rho\, g$. Draw a schematic at $x = 0$.

(c) Compute the baroclinicity/solenoidal vector $\boldsymbol{B} = \rho^{-2}\,(\nabla\rho \times \nabla p)$. Draw a schematic.

(d) Describe the vorticity induced by the baroclinicity vector.

EXERCISE 40.9: GENERATION OF CIRCULATION BY BAROCLINICITY IN AN IDEAL GAS

In this exercise we examine the baroclinicity vector for a simple ideal gas, which is described by the equation of state (23.48)

$$\rho = \frac{p\, M_{\text{mole}}}{T\, R^{\text{g}}} \equiv \frac{p}{T\, R^{\text{M}}}, \tag{40.230}$$

where R^{g} is the universal gas constant and R^{M} is the specific gas constant. We also assume the atmosphere is in approximate hydrostatic balance (Section 27.2), and we ignore rotation (relatively small lateral region of the atmosphere). For further hints to this exercise, see Section 4.1 of *Holton and Hakim* (2013) or Section 2.4.3 of *Markowski and Richardson* (2010), where they discuss circulation generated by differences in land-sea temperatures, thus leading to a sea breeze.

(a) Express the baroclinicity vector, $\boldsymbol{B}$, in terms of pressure and temperature gradients.

(b) Express the baroclinicity vector in terms of pressure and potential temperature gradients. Hint: see Section 23.4.11 for potential temperature in an ideal gas.

(c) Consider an ideal gas atmosphere straddling the ocean and flat land as in Figure 40.13. Let the daytime air be relatively cool over the ocean and relatively warm over the land. Furthermore, assume the sea level pressure is the same value over land and ocean. Ignoring rotation, draw isolines of constant temperature and constant pressure. Assume the horizontal temperature gradient is constant with height. Here are some hints.

- Temperature decreases from land to ocean and decreases when ascending into the atmosphere.
- Pressure is assumed to be horizontally constant at sea level and it decreases upward. Use the ideal gas law to determine the sense for the horizontal pressure gradient as one ascends. Consult the discussion in Section 23.4.10 for geopotentials in an ideal gas atmosphere.
- We are only concerned with a qualitative sense for the isolines in the lower atmosphere and over a horizontal region small enough that rotation can be ignored.

(d) Describe the sense for the circulation induced by the baroclinicity. Does circulation correspond to your experience at a sunny beach day as the air warms over the land faster than over the adjacent ocean? What force causes air to rise and to fall?

EXERCISE 40.10: CIRCULATION WITH ISLANDS

Our discussion of Stokes' theorem has been thus far restricted to a simply connected domain, in which

$$\oint_{\partial\mathcal{S}} \boldsymbol{v} \cdot \mathrm{d}\boldsymbol{x} = \int_{\mathcal{S}} \boldsymbol{\omega} \cdot \hat{\boldsymbol{n}}\, \mathrm{d}\mathcal{S}. \tag{40.231}$$

For a simply connected domain, the closed contour can be shrunk to a point without leaving the domain.

FIGURE 40.13: Setup for the sea breeze Exercise 40.9. We here depict a vertical-zonal crossection of the atmosphere where the lower boundary straddles the ocean and land. The atmosphere over the ocean is assumed to be cooler than the atmosphere over the land, as typically occurs on a sunny afternoon with solar radiation warming land faster than the ocean.

A more general topology consists of a region with holes, whereby closed contours cannot in general be shrunk to a point without leaving the region. In an oceanographic context, the "holes" are islands or continents and the circulation is that for the depth integrated flow. Figure 40.14 shows a region of the ocean containing three arbitrarily shaped impenetrable islands, with the three islands surrounded by a contour. The contour cannot be shrunk to a point without crossing over the islands, thus making this region of the ocean multiply-connected. The presence of islands thus adds a level of complexity to the World Ocean that is absent an AquaPlanet or the global atmosphere.

Derive the following expression for the circulation in multiply-connected regions

$$\oint_{\partial\mathcal{S}} \boldsymbol{v} \cdot \mathrm{d}\boldsymbol{x} = \sum_{n=1}^{N} \left(\oint_{\partial\mathcal{S}_n} \boldsymbol{v} \cdot \mathrm{d}\boldsymbol{x} \right) + \int_{\mathcal{S}} \boldsymbol{\omega} \cdot \hat{\boldsymbol{n}} \, \mathrm{d}\mathcal{S}, \tag{40.232}$$

where N is the number of islands, $\mathcal{S}_n$ is the contour surrounding each island, and $\mathcal{S}$ is the region of water that excludes the islands. In words, this result says that the circulation around a region equals to the circulation around the islands within the region, plus the normal component of the vorticity integrated over the area within the fluid region. Removing the islands allows the island contours to be shrunk to zero size, in which case we recover the simply connected result (40.231). As part of your solution, make use of the contour integral method detailed in Figure 39.10.

EXERCISE 40.11: EVOLUTION OF CIRCULATION AROUND ISLANDS

The momentum equation for a homogeneous layer of inviscid shallow water fluid on a tangent plane is given by

$$\partial_t \boldsymbol{u} + (\boldsymbol{u} \cdot \nabla) \, \boldsymbol{u} + f \, \hat{\boldsymbol{z}} \times \boldsymbol{u} = -g \, \nabla \eta. \tag{40.233}$$

In this equation, $\boldsymbol{u} = (u, v)$ is the horizontal velocity, f is the Coriolis parameter (need not be constant), g is the effective gravitational acceleration, and η is the deviation of the free surface from its horizontal resting position. All spatial derivatives are horizontal, so that

$$\boldsymbol{u} \cdot \nabla = u \, \partial_x + v \, \partial_y. \tag{40.234}$$

Use of a vector identity allows us to write

$$\partial_t \boldsymbol{u} + (f + \zeta) \, \hat{\boldsymbol{z}} \times \boldsymbol{u} = -\nabla \, (\boldsymbol{u}^2/2 + g \, \eta), \tag{40.235}$$

where

$$\zeta = \hat{\boldsymbol{z}} \cdot (\nabla \times \boldsymbol{u}) \tag{40.236}$$

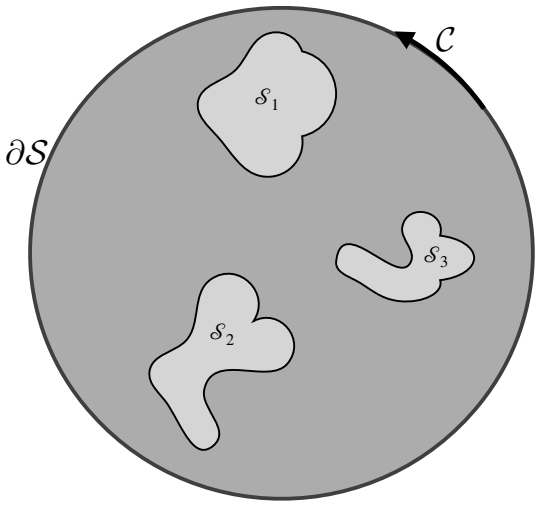

FIGURE 40.14: A region of the ocean consisting of three islands, $\mathcal{S}_1$, $\mathcal{S}_2$, and $\mathcal{S}_3$, each with boundaries $\partial\mathcal{S}_n$ and with the closed contour, $\partial\mathcal{S}$, drawn around the three islands. The contour $\partial\mathcal{S}$ cannot be shrunk to a point without crossing over the islands, thus indicating that the domain is multiply connected. Exercise 40.10 is concerned with deriving an expression for the circulation of the depth-integrated flow as defined along the closed contour, $\partial\mathcal{S}$. In that derivation we can make use of the contour initegral method detailed in Figure 39.10.

is the vorticity of the shallow water fluid.

Consider an island, such as one shown in Figure 40.14. Each island is static and impenetrable to fluid flow, which means that

$$\boldsymbol{u} \cdot \hat{\boldsymbol{n}} = 0 \tag{40.237}$$

where $\hat{\boldsymbol{n}}$ is the outward normal on an island boundary. For simplicity, assume this island outward normal is horizontal; i.e., the island is bounded by a vertical side. This no-normal flow constraint means that the velocity just next to an island is parallel to the island[22]

$$\boldsymbol{u} \times \mathrm{d}\boldsymbol{x} = 0. \tag{40.238}$$

Equivalently, the island represents a solid material boundary across which no flow passes.

Show that the inviscid shallow-water circulation around an island remains constant in time

$$\frac{\mathrm{d}}{\mathrm{d}t} \oint_I \boldsymbol{u} \cdot \mathrm{d}\boldsymbol{x} = 0. \tag{40.239}$$

Recall that Kelvin's circulation theorem is formulated for a material circuit in an inviscid fluid, with the circuit moving with the flow. This exercise shows that the circulation theorem also holds for a material circuit enclosing a static solid boundary.

EXERCISE 40.12: HELICITY FOR A PERFECT BAROTROPIC FLUID IN A GRAVITY FIELD AND NON-ROTATING REFERENCE FRAME

Consider a closed material volume, $\mathcal{R}$, of a perfect single-constituent barotropic fluid ($\rho = \rho(p)$) in a gravity field ($\boldsymbol{g} = -\nabla\Phi$) and in a non-rotating reference frame ($\boldsymbol{\Omega} = 0$). Let this material volume have a boundary that is always tangent to the fluid vorticity, $\boldsymbol{\omega}$. Hence, the outward normal to the region boundary is orthogonal to the vorticity,

$$\hat{\boldsymbol{n}} \cdot \boldsymbol{\omega} = 0. \tag{40.240}$$

[22]This boundary condition is valid only for inviscid fluids such as that considered here. For a real fluid with nonzero viscosity, all components of the velocity vector vanish at solid boundaries due to the no-slip condition discussed in Section 25.8.8.

Such volumes define closed vortex tubes, such as a smoke ring or linked smoke rings. The *helicity* of the fluid within the vortex tube volume is defined as the integration of the helicity density, $\boldsymbol{v} \cdot \boldsymbol{\omega}$, over the closed volume

$$\mathbb{H} = \int_{\mathcal{R}(\boldsymbol{v})} \boldsymbol{v} \cdot \boldsymbol{\omega} \, \mathrm{d}V, \tag{40.241}$$

where the volume $\mathcal{R}(\boldsymbol{v})$ is material. In Cartesian coordinates, the helicity density takes the form

$$\boldsymbol{v} \cdot \boldsymbol{\omega} = u \, (\partial_y w - \partial_z v) + v \, (\partial_z u - \partial_x w) + w \, (\partial_x v - \partial_y u). \tag{40.242}$$

Although the helicity density vanishes for some common examples, such as for a fluid in rigid-body rotation, it need not vanish in general.

(a) Show that helicity is materially constant following the material volume

$$\frac{\mathrm{d}\mathbb{H}}{\mathrm{d}t} = 0. \tag{40.243}$$

(b) Discuss why helicity is not defined for a shallow water fluid.

Use the following hints.

- Make use of Φ_{p} that satisfies equation (40.13).
- The shallow water fluid model is based on the small aspect ratio limit, in which the fluid depth is much smaller than its lateral extent. In this limit, the vertical component of vorticity dominates over the horizontal. See further discussion in Section 40.5.4.

EXERCISE 40.13: DISCRETE CALCULATION OF BOTTOM PRESSURE TORQUE

In many diagnostic studies with numerical models it is of interest to compute pressure torques affecting vorticity. One particularly common diagnostic concers the bottom pressure torque arising in equation (40.191). Derive a discrete expression for the area averaged bottom pressure torque

$$\overline{\mathrm{BPT}} = A^{-1} \int_{\mathcal{S}} \hat{\boldsymbol{z}} \cdot \nabla \times (\eta_{\mathrm{b}} \nabla p_{\mathrm{b}}) \, \mathrm{d}\mathcal{S} = A^{-1} \oint_{\partial \mathcal{S}} \eta_{\mathrm{b}} \nabla p_{\mathrm{b}} \cdot \hat{\boldsymbol{t}} \, \mathrm{d}\ell, = -A^{-1} \oint_{\partial \mathcal{S}} p_{\mathrm{b}} \nabla \eta_{\mathrm{b}} \cdot \hat{\boldsymbol{t}} \, \mathrm{d}\ell, \tag{40.244}$$

over the shaded region depicted in Figure 40.15, with $A = \int_{\mathcal{S}} \mathrm{d}\mathcal{S}$ the horizontal area of this region. Hint: this exercise shares much with the area averaged vorticity in Exercise 37.8, although the final result is distinct. Note: given that the bottom pressure torque is generally the small difference between large numbers, it is very useful to perform the diagnostic calculation online so that full computational precision can be maintained.

EXERCISE 40.14: DYNAMICAL PORTION OF THE TOPOGRAPHIC FORM STRESS

We discussed bottom topographic form stress in Chapter 28, with its curl leading to the bottom pressure torque in equation (40.191). As noted in Section 28.1.3, the dominant portion of the bottom topographic form stress acting on the ocean has little to do with fluid motion. Rather, it merely holds the ocean fluid within the basin, much as water is held within a drinking container through pressure imparted by the container sides.

(a) To help isolate the dynamically relevant portion of the bottom bottom pressure, show that we can write the horizontal gradient of the bottom pressure for a hydrostatic fluid according to

$$\nabla_{\mathrm{h}} p_{\mathrm{b}} = g \, [\rho(\eta) \, \nabla_{\mathrm{h}} \eta - \rho(\eta_{\mathrm{b}}) \, \nabla_{\mathrm{h}} \eta_{\mathrm{b}}] + g \int_{\eta_{\mathrm{b}}}^{\eta} \nabla_{\mathrm{h}} \rho \, \mathrm{d}z. \tag{40.245}$$

where we ignore the applied surface pressure, p_{a}, for simplicity.

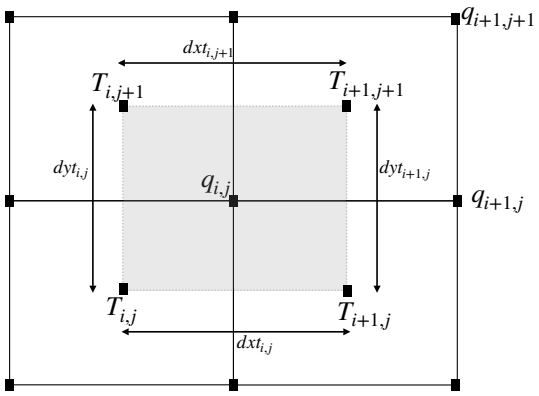

FIGURE 40.15: Discrete grid layout for variables needed to compute the bottom pressure torque as averaged over the shaded vorticity region. The bottom topography and bottom pressure are both known at the tracer points.

(b) Hence, show that the bottom pressure torque takes the form

$$\hat{\boldsymbol{z}} \cdot \nabla_h \eta_b \times \nabla_h p_b = g\, \hat{\boldsymbol{z}} \cdot \nabla_h \eta_b \times \left[\rho(\eta) \nabla_h \eta + \int_{\eta_b}^{\eta} \nabla_h \rho \, dz \right] \equiv \hat{\boldsymbol{z}} \cdot \nabla \eta_b \times \nabla p_b^*, \tag{40.246}$$

where

$$\nabla_h p_b^* = g\, \rho(\eta)\, \nabla_h \eta + g \int_{\eta_b}^{\eta} \nabla_h \rho \, dz. \tag{40.247}$$

Note how $\nabla_h p_b^*$ has no contribution from the potentially very large term, $-g\, \rho(\eta_b)\, \nabla_h \eta_b$, arising from gradients in the bottom topography.

(c) *Molemaker et al.* (2015) and *Gula et al.* (2015) assume knowledge of the bottom pressure torque along contours of constant topography. Given that knowledge they then make use of the following diagnostic expression for p_b^*

$$p_b^*(s) - p_b^*(s_0) = - \int_{s_0}^{s} \frac{\hat{\boldsymbol{z}} \cdot (\nabla \eta_b \times \nabla p_b)}{\hat{\boldsymbol{n}} \cdot \nabla \eta_b} \, ds, \tag{40.248}$$

with $p_b^*(s_0)$ the value at the arbitrary starting point for the contour. Derive equation (40.248), with the following information of possible use.

- As depicted in Figure 40.12, s is the arc length along the chosen contour of constant η_b, with s increasing in the tangent direction, $\hat{\boldsymbol{t}}$. Likewise, $\hat{\boldsymbol{n}}$ is a unit vector pointing to the left of the contour so that $\hat{\boldsymbol{n}} \cdot \hat{\boldsymbol{t}} = 0$ and $\hat{\boldsymbol{t}} \times \hat{\boldsymbol{n}} = \hat{\boldsymbol{z}}$.
- Along any contour of constant $\eta_b(x, y)$ we have

$$0 = d\eta_b = \nabla \eta_b \cdot d\boldsymbol{x} = \nabla \eta_b \cdot \frac{d\boldsymbol{x}}{ds} \, ds = \nabla \eta_b \cdot \hat{\boldsymbol{t}} \, ds. \tag{40.249}$$

- The main mathematics of this exercise are contained in Exercise 5.1.

Equation (40.248) provides a means to compute the anomalous p_b^* [anomalous relative to $p_b^*(s_0)$] along a constant topography contour. Mapping $p_b^*(s) - p_b^*(s_0)$ for a suite of contours then provides the means to determine the dynamically relevant portion of the bottom pressure and then, when multiplying by the bottom slope, compute the dynamically relevant portion of the form stress.

Chapter 41

POTENTIAL VORTICITY MECHANICS

Potential vorticity (PV) is a dynamical tracer of immense importance to the study of geophysical fluid mechanics. One application of potential vorticity concerns its direct connection to the flow field in certain balanced models (e.g., geostrophically balanced models), with *Hoskins* (1991) providing an insightful starting point for this perspective. Potential vorticity is also useful as a tracer whose structure signals a variety of dynamical interactions, particularly with boundaries, and that can be directly tied to flow stability properties. In this chapter we establish fundamental properties of potential vorticity and its time evolution. The potential vorticity we consider here is sometimes referred to as *Ertel* potential vorticity (*Ertel*, 1942), which is the most basic of the many potential vorticities encountered in geophysical fluids mechanics.

The barotropic fluid forms a pedagogically useful starting point for our study. However, realistic geophysical flows are baroclinic, and it is the baroclinic fluid where "PV thinking" is arguably the most useful and powerful. The general method exploited for the construction of potential vorticity is to choose a scalar field to strategically orient the absolute vorticity. If the scalar is a material invariant, and it annihilates the baroclinicity vector, then the corresponding potential vorticity is a material invariant in the absence of irreversible processes. For a barotropic fluid, the choice of scalar field is rather arbitrary, with preference given to one that is materially invariant. For a baroclinic fluid we are more restricted since the scalar must orient vorticity in a direction that annihilates the torque from baroclinicity and, ideally, be itself materially invariant in the absence of irreversible processes. Even in the presence of irreversible processes, potential vorticity remains an important flow property that constrains the motion and provides insights into the mechanics of that motion.

CHAPTER GUIDE

This chapter requires an understanding of vorticity from Chapter 40 as well as skills with vector calculus identities for Cartesian coordinates as detailed in Chapter 2. The concepts and methods developed in this chapter are fundamental to the notions of potential vorticity, and are essential for the budget equations developed in Chapter 42. We also encounter potential vorticity when studying balanced models in Part VIII of this book.

41.1 Potential vorticity in perfect fluids

In this section we derive the material invariance of potential vorticity (PV) for a perfect homogeneous fluid.[1] We make use of Kelvin's circulation theorem for an infinitesimal closed loop, in which case the primary object of interest is a particular component of the absolute vorticity.

41.1.1 Perfect barotropic fluid

Consider a perfect barotropic fluid. As for the shallow water discussion in Section 39.3.3, we can apply Kelvin's circulation theorem (Section 40.2.3) to an infinitesimal material circuit within the fluid (Figure 41.1) to render the material invariance

$$\frac{\mathrm{D}}{\mathrm{D}t}(\boldsymbol{\omega}_{\mathrm{a}} \cdot \hat{\boldsymbol{n}}\, \delta\mathcal{S}) = 0, \tag{41.1}$$

with $\delta\mathcal{S}$ the area enclosed by the circuit. The conservation of potential vorticity is built from specializing this result. For that purpose, introduce a materially invariant field

$$\frac{\mathrm{D}\chi}{\mathrm{D}t} = 0. \tag{41.2}$$

In most applications, χ is a scalar field such as tracer concentration, globally referenced Archimedean buoyancy, Conservative Temperature, or specific entropy. However, in equation (41.21) we consider the non-standard case of $\chi = z$, which is relevant for two-dimensional non-divergent barotropic fluids. The one key assumption we make is that χ is a smooth field that is not a spatial constant, so that $|\nabla\chi| \neq 0$.

[1] A perfect homogeneous fluid has zero viscosity (inviscid) and a single material component. There can be no mixing of matter in this fluid since every fluid element has the same homogeneous concentration. So without viscosity, the homogeneous fluid is perfect.

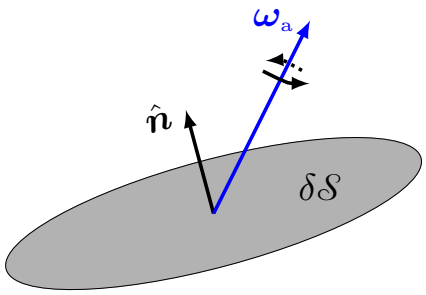

FIGURE 41.1: The projection of the absolute vorticity, $\boldsymbol{\omega}_a$, onto the normal direction of an infinitesimal moving surface, $\hat{\boldsymbol{n}}\,\delta\mathcal{S}$.

41.1.2 Cylinder between two constant χ surfaces

We make use of isosurfaces of χ to orient a material circuit used to compute circulation and hence to orient the vorticity. In particular, referring to Figure 41.2, let the circuit bound a small cylinder whose ends sit on isosurfaces with concentrations $\chi - \delta\chi/2$ and $\chi + \delta\chi/2$. We can consider this cylinder to be a portion of a vortex tube that is bounded by the two χ isosurfaces. The cylinder's volume is given by

$$\delta V = \delta\mathcal{S}\,\delta h, \tag{41.3}$$

where δh is the distance between the χ isosurfaces. The unit normal direction orienting the area, $\delta\mathcal{S}$, is given by

$$\hat{\boldsymbol{n}} = \nabla\chi/|\nabla\chi|. \tag{41.4}$$

It is the need to define $\hat{\boldsymbol{n}}$ that requires us to assume $|\nabla\chi| \neq 0$. The distance, δh, between the two isosurfaces is related to the χ increment, $\delta\chi$, through

$$\delta\chi = \nabla\chi \cdot \delta\boldsymbol{x} = |\nabla\chi|\,\hat{\boldsymbol{n}} \cdot \delta\boldsymbol{x} = |\nabla\chi|\,\delta h. \tag{41.5}$$

This result takes on the equivalent form

$$\delta\chi = |\nabla\chi|\,\delta h = (\hat{\boldsymbol{n}} \cdot \nabla\chi)\,\delta h, \tag{41.6}$$

so that the distance (or thickness) between the two isosurfaces is

$$\delta h = \delta\chi/|\nabla\chi|. \tag{41.7}$$

As seen in Figure 41.2, the spatial separation between the two isosurfaces is relatively small in regions of strong scalar gradients (large $|\nabla\chi|$), whereas the separation is relatively large in regions of small $|\nabla\chi|$.

41.1.3 Material invariance

We now have the necessary pieces to write the normal projection of the absolute vorticity according to the following

$$\begin{aligned}
\boldsymbol{\omega}_a \cdot \hat{\boldsymbol{n}}\,\delta\mathcal{S} &= \frac{\boldsymbol{\omega}_a \cdot \nabla\chi}{|\nabla\chi|}\,\delta\mathcal{S} && \text{equation (41.4)} && \text{(41.8a)}\\
&= \frac{\boldsymbol{\omega}_a \cdot \nabla\chi}{|\nabla\chi|}\,\frac{\delta V}{\delta h} && \text{equation (41.3)} && \text{(41.8b)}\\
&= (\boldsymbol{\omega}_a \cdot \nabla\chi)\,\frac{\delta V}{\delta\chi} && \text{equation (41.7)} && \text{(41.8c)}
\end{aligned}$$

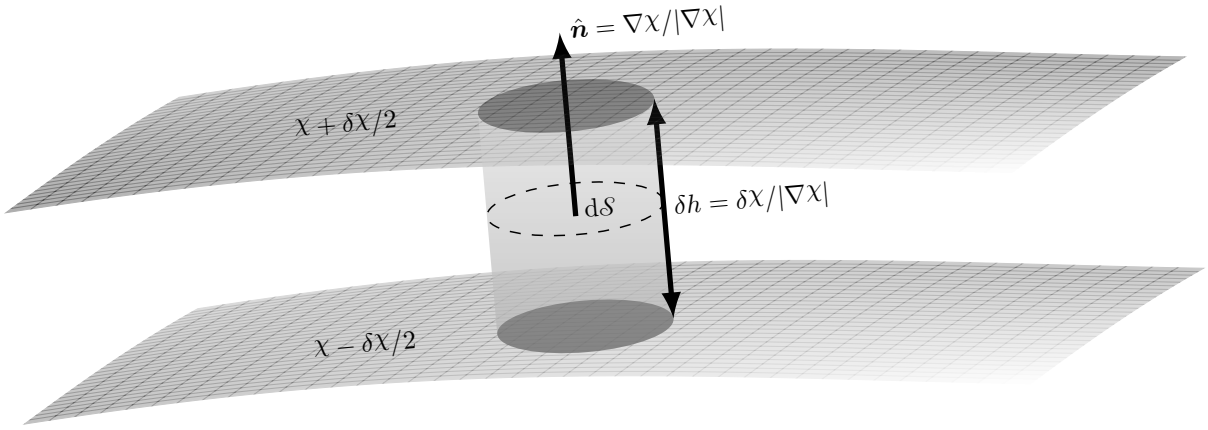

FIGURE 41.2: Illustrating the geometry of a cylindrical region of fluid between two iso-surfaces of a field χ, separated by the infinitesimal amount $\delta\chi$. The volume of the cylinder is $\delta V = \delta\mathcal{S}\,\delta h$, with δh the thickness and $\delta\mathcal{S}$ the area. By convention, the unit normal vector, $\hat{\boldsymbol{n}} = \nabla\chi/|\nabla\chi|$, points towards larger values of χ. It is here depicted at the center of the cylinder, which differs by an infinitesimal amount from the normal computed on either $\chi + \delta\chi/2$ or $\chi - \delta\chi/2$. If χ is a material invariant so that $\mathrm{D}\chi/\mathrm{D}t = 0$, then so too is its infinitesimal increment, $\mathrm{D}(\delta\chi)/\mathrm{D}t = 0$. As per equation (41.7), the geometric thickness between the isosurfaces is related to the field increment by $\delta h = \delta\chi/|\nabla\chi|$, so that the larger the magnitude of the gradient in the scalar field, the smaller the layer thickness. For a baroclinic fluid, material invariance of potential vorticity in a perfect fluid holds if we can find a field such that $\hat{\boldsymbol{n}} \cdot \boldsymbol{B} = 0$, with baroclinicity $\boldsymbol{B} = (\nabla\rho \times \nabla p)/\rho^2$. The cylindrical tube acts as a vortex tube for that component of absolute vorticity, $\boldsymbol{\omega}_\mathrm{a} \cdot \hat{\boldsymbol{n}}$, that is parallel to the tube.

$$= \frac{\boldsymbol{\omega}_\mathrm{a} \cdot \nabla\chi}{\rho} \frac{\rho\,\delta V}{\delta\chi} \qquad \text{multiply by } \rho/\rho. \tag{41.8d}$$

Mass is materially invariant so that

$$\frac{\mathrm{D}(\rho\,\delta V)}{\mathrm{D}t} = 0. \tag{41.9}$$

Likewise, by assumption χ is materially invariant so that the increment between two χ isosurfaces is materially invariant

$$\frac{\mathrm{D}(\delta\chi)}{\mathrm{D}t} = 0. \tag{41.10}$$

Bringing these elements into Kelvin's circulation theorem (41.1) leads us to conclude that the potential vorticity, Q, is also materially invariant

$$Q \equiv \frac{\boldsymbol{\omega}_\mathrm{a} \cdot \nabla\chi}{\rho} = \frac{\nabla \cdot (\boldsymbol{\omega}_\mathrm{a}\chi)}{\rho} \quad \text{with} \quad \frac{\mathrm{D}Q}{\mathrm{D}t} = 0. \tag{41.11}$$

This expression for the potential vorticity is the most general form and it is often referred to as the *Ertel potential vorticity* (*Ertel*, 1942). The first expression shows the numerator as the projection of the absolute vorticity into the direction normal to χ isosurfaces. Conversely, it is a measure of the χ stratification in the direction of the absolute vorticity vector. The second expression follows since the absolute vorticity has zero divergence so that the numerator is a total divergence. This divergence form of the potential vorticity numerator has important implications for the potential vorticity budgets studied in Section 41.4 and throughout Chapter 42.

41.1.4 Perfect baroclinic fluid

Consider the case of a perfect baroclinic fluid, in which Kelvin's circulation theorem for an infinitesimal circuit takes the form

$$\frac{\mathrm{D}}{\mathrm{D}t}(\boldsymbol{\omega}_{\mathrm{a}} \cdot \hat{\boldsymbol{n}}\, \delta\mathcal{S}) = \boldsymbol{B} \cdot \hat{\boldsymbol{n}}\, \delta\mathcal{S}. \tag{41.12}$$

The source on the right hand side involves the baroclinicity vector, $\boldsymbol{B}$, discussed in Sections 40.2 and 40.4, which is the curl of the pressure gradient acceleration

$$\boldsymbol{B} = \nabla \times (-\rho^{-1}\, \nabla p) = \rho^{-2}\, \nabla\rho \times \nabla p. \tag{41.13}$$

Now assume there exists a materially invariant field, $\mathrm{D}\chi/\mathrm{D}t = 0$, that also annihilates the baroclinicity vector as in Figure 41.3, so that

$$\boldsymbol{B} \cdot \hat{\boldsymbol{n}} = \frac{\boldsymbol{B} \cdot \nabla\chi}{|\nabla\chi|} = 0. \tag{41.14}$$

In that case, the derivation detailed earlier for the barotropic fluid follows directly for the baroclinic case, in which case we conclude that potential vorticity remains materially invariant

$$\frac{\mathrm{D}Q}{\mathrm{D}t} = 0 \qquad \text{where} \qquad Q = \frac{\boldsymbol{\omega}_{\mathrm{a}} \cdot \nabla\chi}{\rho}. \tag{41.15}$$

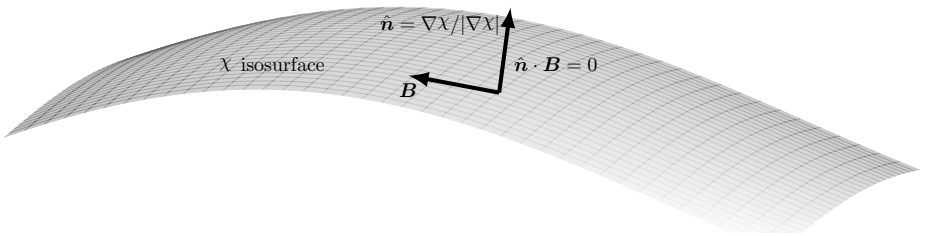

FIGURE 41.3: Material invariance of potential vorticity is ensured for perfect fluids that admit a materially invariant field that also annihilates the baroclinicity vector. Mathematically, this property means that $\hat{\boldsymbol{n}} \cdot \boldsymbol{B} = 0$ where $\hat{\boldsymbol{n}} = \nabla\chi/|\nabla\chi|$ is the unit normal direction for the surface. In this figure we depict the baroclinicity vector, $\boldsymbol{B}$, that is aligned with χ isosurfaces.

The existence of a materially invariant potential vorticity for perfect baroclinic fluids depends on the existence of a materially invariant scalar field that annihilates the baroclinicity vector. Buoyancy is the most common choice for this field in geophysical fluid applications, with buoyancy typically measured by specific entropy or potential temperature in the atmosphere and potential density in the ocean. We have more to say on the chosen field in the remainder of this chapter as well as in Section 42.3.

41.1.5 A variety of materially invariant potential vorticities

The material invariant statement

$$\frac{\mathrm{D}Q}{\mathrm{D}t} = \frac{\mathrm{D}(\rho^{-1}\, \boldsymbol{\omega}_{\mathrm{a}} \cdot \nabla\chi)}{\mathrm{D}t} = 0 \tag{41.16}$$

generates a number of further materially invariant fields. First, consider any function of Q, whereby

$$\frac{\mathrm{D}\mathcal{F}(Q)}{\mathrm{D}t} = \frac{\mathrm{d}\mathcal{F}}{\mathrm{d}Q}\, \frac{\mathrm{D}Q}{\mathrm{D}t} = 0, \tag{41.17}$$

which follows since $\mathrm{D}Q/\mathrm{D}t = 0$. Among the infinite number of possible functions, $\mathcal{F}(Q)$, the most commonly considered is $\mathcal{F}(Q) = Q^2$, whose global integral is referred to as the *potential enstrophy*.

Second, consider the *iterated potential vorticity* defined according to

$$Q^{(1)} = \rho^{-1}\, \boldsymbol{\omega}_{\mathrm{a}} \cdot \nabla\chi \quad \text{and} \quad Q^{(n)} = \boldsymbol{\omega}_{\mathrm{a}} \cdot \nabla Q^{(n-1)} \quad \text{for } n = 2, 3, 4... \tag{41.18}$$

As defined, $Q^{(1)}$ is the familiar Ertel potential vorticity, whereas higher iterations replace the field, χ, with $Q^{(n-1)}$. Since $Q^{(n-1)}$ is materially invariant, so too is $Q^{(n)}$. Consider the example

$$Q^{(2)} = \boldsymbol{\omega}_{\mathrm{a}} \cdot \nabla Q^{(1)} = \boldsymbol{\omega}_{\mathrm{a}} \cdot \nabla(\rho^{-1}\, \boldsymbol{\omega}_{\mathrm{a}} \cdot \nabla\chi) = \nabla \cdot [\boldsymbol{\omega}_{\mathrm{a}}\, \rho^{-1}\, (\boldsymbol{\omega}_{\mathrm{a}} \cdot \nabla\chi)], \tag{41.19}$$

which reveals that there are n powers of absolute vorticity for $Q^{(n)}$.

41.1.6 Some remarks about potential vorticity

Perfect fluid PV material invariance ↔ Kelvin's circulation theorem

Kelvin's circulation theorem from Section 40.2.3 is at the heart of the derivations presented in this section, with the theorem applied to a strategically chosen infinitesimal loop. Because the loop is tiny, we use Stokes' theorem to convert the line integral expression of Kelvin's theorem into a statement about the material evolution of absolute vorticity projected onto the normal direction of the loop, and multiplied by the loop area. We further specialize the theorem to a cylindrical region between two isosurfaces of a materially invariant field. For the perfect barotropic fluid, we require the mass of the cylinder to be materially invariant, as well as the scalar field. In this case there is a potential vorticity that is also materially invariant. For a baroclinic fluid, material invariance of potential vorticity requires a field that is both materially invariant *and* that annihilates the baroclinicity vector. We have more to say regarding the availability of such fields in the remainder of this chapter.

There are numerous forms for potential vorticity

The expression (41.11) is, on first glance, quite distinct from the shallow water (Rossby) potential vorticity, $Q = (\zeta + f)/h$, studied in Chapter 39 (see equation (39.30)). However, as shown in Section 66.3, they are closely related for the special case of entropic potential vorticity in a Boussinesq ocean when formulated using isopycnal/isentropic coordinates. Even so, there are a variety of other forms for potential vorticity, with the forms (and physical dimensions) depending on the dynamical and thermodynamical properties. We encounter some further forms of potential vorticity in the remainder of this chapter, as well as in the oceanic potential vorticity discussions of Chapter 66 and in our study of balanced models in Part VIII. The review paper by *Müller* (1995) offers a lucid presentation of potential vorticity and its many forms encountered in physical oceanography.

Motivating the adjective "potential"

In Section 39.3.2 we motivated the advective "potential" for the shallow water potential vorticity. We do so here for Ertel's potential vorticity. For that purpose, write potential vorticity in the form

$$Q = \frac{\boldsymbol{\omega}_{\mathrm{a}} \cdot \hat{\boldsymbol{n}}}{\rho}\, |\nabla\chi| \qquad \text{with} \qquad \hat{\boldsymbol{n}} = \frac{\nabla\chi}{|\nabla\chi|}. \tag{41.20}$$

In cases where ρ is roughly a constant (e.g., Boussinesq ocean), and when Q is materially invariant, the component of the absolute vorticity increases in the direction parallel to $\nabla\chi$ when the fluid parcel moves into a region where $|\nabla\chi|$ decreases. Hence, there is a "release" of

absolute vorticity aligned with $\nabla\chi$ in regions where χ isosurfaces are spread. We conceive of this increased vorticity as through the stretching of the cylindrical tube extending between χ isosurfaces along the $\hat{\boldsymbol{n}}$ direction, with this tube acting as a vortex tube for that component of vorticity parallel to the tube. In contrast, when the χ isosurfaces are tightly packed, then the vortex tube is squashed and so too is the vorticity. We thus conceive of potential vorticity as the "potential" for releasing absolute vorticity that is oriented in the direction parallel to $\nabla\chi$.

Potential vorticity as a dynamical tracer

We refer to potential vorticity as a *dynamical tracer* since it depends directly on the velocity field through the vorticity. It also depends on the scalar field, χ, which is commonly taken as a thermodynamic tracer such as the potential temperature, θ. In these cases, potential vorticity embodies both dynamical and thermodynamical information. In contrast, material tracers such as salinity, and thermodynamic tracers such as θ, are properties of the fluid whose distribution is affected by the velocity but whose local measurement does not require knowledge of the flow.

Entropic potential vorticity as the grand unifier

Entropic potential vorticity provides a connection between vorticity (mechanics) and stratification (thermodynamics). By connecting these two basic facets of geophysical fluid flows, the study of potential vorticity and its conservation properties provides a powerful and unique lens to help rationalize the huge variety of geophysical flow regimes, and to predict their response to changes in forcing. It is for this reason that potential vorticity is sometimes considered the grand unifying concept in geophysical fluid mechanics.

Potential vorticity as a diagnostic tracer

Suppose we have an initial flow field in which $\rho\, Q = \boldsymbol{\omega}_{\text{a}} \cdot \nabla\chi = 0$, which means that the absolute vorticity is aligned with surfaces of constant χ. In an inviscid and adiabatic fluid, material conservation of Q means that $\boldsymbol{\omega}_{\text{a}}$ remains within constant χ surfaces for all time. We infer from this particular example that if we know the evolution of χ, then we know the evolution of vortex lines defined by $\boldsymbol{\omega}_{\text{a}}$, which in turn allows for the inference of a number of further flow properties. This particular example offers a hint at the multiple applications of "PV thinking" to understand and predict fluid motion, with *Hoskins* (1991) providing an elegant survey of such thinking.

Potential vorticity versus momentum

Momentum is affected by pressure, and pressure fluctuations propagate at the speed of sound (Chapter 51) for compressible flows (including the Boussinesq ocean; see Section 29.1.9), whereas they move with infinite speed for incompressible fluids. In contrast, potential vorticity, for those cases where we can remove the effects of the baroclinicity vector, does not directly feel the impacts from pressure fluctuations. Hence, potential vorticity, much like vorticity in a barotropic fluid, evolves much slower and more locally than momentum. This dynamical difference offers a key reason that potential vorticity offers added insights into fluid flows beyond that afforded by momentum.

Potential vorticity for horizontally non-divergent barotropic flow

A non-standard, but relevant, choice for the function χ used to define potential vorticity is given by the vertical coordinate

$$\chi = z, \tag{41.21}$$

in which case

$$\rho\, Q = \boldsymbol{\omega}_{\rm a} \cdot \hat{\boldsymbol{z}} = \zeta_{\rm a}. \tag{41.22}$$

In Chapter 38, we consider the two-dimensional non-divergent barotropic model, in which case ρ is a constant and

$$w = \frac{\mathrm{D}z}{\mathrm{D}t} = 0. \tag{41.23}$$

The corresponding materially invariant potential vorticity is the vertical component of the absolute vorticity divided by the constant density. Ignoring the constant density factor leads us to identify the absolute vorticity as the Ertel potential vorticity for this flow

$$q = \zeta_{\rm a} = \zeta + f. \tag{41.24}$$

As discussed in Section 38.2.3, the horizontally non-divergent barotropic flow also maintains material constancy (in the absence of non-conservative processes) of the Rossby potential vorticity, $(\zeta + f)/h$, with this property holding since $\mathrm{D}h/\mathrm{D}t = 0$ for this flow.

41.2 Potential vorticity and seawater

As seen in Section 41.1, material invariance of potential vorticity for a perfect fluid requires a materially invariant scalar field to annihilate the baroclinicity vector. There is no such scalar field for the ocean with a realistic seawater equation of state. Nonetheless, there are important approximate cases that allow for material potential vorticity invariance, and we explore such cases in this section.

41.2.1 Baroclinicity vector

Recall the baroclinicity vector given by (Sections 40.2 and 40.4)

$$\boldsymbol{B} = \frac{\nabla\rho \times \nabla p}{\rho^2}. \tag{41.25}$$

If we take the *in situ* density as the scalar field to define potential vorticity, then $\boldsymbol{B} \cdot \nabla\rho = 0$. However, *in situ* density is not a conserved scalar in the ocean due to pressure effects. Namely, with *in situ* density having the function dependence $\rho = \rho(S, \Theta, p)$ (see Section 30.3), its material time derivative is

$$\frac{\mathrm{D}\rho}{\mathrm{D}t} = \frac{\partial\rho}{\partial S}\frac{\mathrm{D}S}{\mathrm{D}t} + \frac{\partial\rho}{\partial\Theta}\frac{\mathrm{D}\Theta}{\mathrm{D}t} + \frac{\partial\rho}{\partial p}\frac{\mathrm{D}p}{\mathrm{D}t}. \tag{41.26}$$

Even when salinity and Conservative Temperature are materially constant, $\mathrm{D}S/\mathrm{D}t = 0$ and $\mathrm{D}\Theta/\mathrm{D}t = 0$, the *in situ* density has a nonzero material time derivative due to material pressure changes, $\mathrm{D}p/\mathrm{D}t \neq 0$. Material changes in the pressure of a fluid element arise even in the absence of irreversible processes such as mixing. In general, such *mechanical changes* arise due to the gradients in the pressure field that the fluid element feels. Given that pressure affects *in situ* density, with such effects occuring even in a perfect fluid, we conclude that *in situ* density is not an appropriate scalar for developing a materially invariant potential vorticity. For the same reason, we do not consider pressure as a suitable scalar field.

41.2.2 Potential vorticity based on potential density, ϱ

Potential density is commonly used in oceanography (see Section 30.3.4), with potential density the *in situ* density referenced to a chosen pressure.[2] We write potential density as in equation

[2] Oceanographers often choose the reference pressure as the standard atmospheric sea level pressure. However, that is not required for the following formalism to hold, with any reference pressure suitable.

(30.18)

$$\varrho(S, \Theta) = \rho(S, \Theta, p = p_{\text{ref}}), \tag{41.27}$$

so that its material time derivative is

$$\frac{\mathrm{D}\varrho}{\mathrm{D}t} = \frac{\partial \varrho}{\partial S}\frac{\mathrm{D}S}{\mathrm{D}t} + \frac{\partial \varrho}{\partial \Theta}\frac{\mathrm{D}\Theta}{\mathrm{D}t}, \tag{41.28}$$

which vanishes in the absence of irreversible material changes to salinity and Conservative Temperature. When using potential density as the scalar field for potential vorticity, the baroclinicity vector projects onto the diapycnal direction according to

$$\begin{aligned}
\rho^2 \boldsymbol{B} \cdot \nabla \varrho &= (\nabla \rho \times \nabla p) \cdot \nabla \varrho && \text{(41.29a)}\\
&= (\nabla \varrho \times \nabla \rho) \cdot \nabla p && \text{(41.29b)}\\
&= [(\varrho_S \nabla S + \varrho_\Theta \nabla \Theta) \times (\rho_S \nabla S + \rho_\Theta \nabla \Theta + \rho_p \nabla p)] \cdot \nabla p && \text{(41.29c)}\\
&= [(\varrho_S \nabla S + \varrho_\Theta \nabla \Theta) \times (\rho_S \nabla S + \rho_\Theta \nabla \Theta)] \cdot \nabla p && \text{(41.29d)}\\
&= [\varrho_S \nabla S \times \rho_\Theta \nabla \Theta + \varrho_\Theta \nabla \Theta \times \rho_S \nabla S] \cdot \nabla p && \text{(41.29e)}\\
&= (\varrho_S \rho_\Theta - \varrho_\Theta \rho_S)(\nabla S \times \nabla \Theta) \cdot \nabla p, && \text{(41.29f)}
\end{aligned}$$

where we used the shorthand notation for partial derivatives

$$\rho_S = \frac{\partial \rho}{\partial S} \quad \text{and} \quad \varrho_S = \frac{\partial \varrho}{\partial S} \tag{41.30a}$$

$$\rho_\Theta = \frac{\partial \rho}{\partial \Theta} \quad \text{and} \quad \varrho_\Theta = \frac{\partial \varrho}{\partial \Theta}. \tag{41.30b}$$

Note that the triple product, $(\nabla S \times \nabla \Theta) \cdot \nabla p$, also appears in the discussion of neutral helicity in Section 30.7 (see equation (30.65)). Equation (41.29f) allows us to identify cases where the baroclinicity vector is annihilated, $\boldsymbol{B} \cdot \nabla \varrho = 0$, thus yielding a materially invariant potential vorticity in the absence of irreversible processes.

- UNIFORM SALINITY OR UNIFORM CONSERVATIVE TEMPERATURE: If salinity or Conservative Temperature are spatially uniform, then $\boldsymbol{B} \cdot \nabla \varrho = 0$.

- ADDITIVE PRESSURE DEPENDENCE TO THE *in situ* DENSITY: There is a materially invariant potential vorticity with a vanishing thermodynamic pre-factor in equation (41.29f), $\varrho_S \rho_\Theta - \varrho_\Theta \rho_S$. This term does not generally vanish since the ocean has a pressure dependent equation of state, and this pressure dependence generally means that $\boldsymbol{B} \cdot \nabla \varrho \neq 0$. Even so, we can annihilate the baroclinicity vector if the *in situ* density has a pressure dependence that is additive, in which case we can write

  $$\rho(S, \Theta, p) = \varrho(S, \Theta) + F(p) - F(p_{\text{ref}}) \Longrightarrow \varrho_S \rho_\Theta - \varrho_\Theta \rho_S = 0. \tag{41.31}$$

  Notably, we did not assume a linear equation of state; only that it has the special functional form in equation (41.31). For some cases, we may assume F to be a constant, in which case there is no pressure dependence so that *in situ* density is the same as potential density.

41.2.3 An example EOS admitting a materially invariant PV

An explicit realization of the equation of state (41.31) can be found by taking a Taylor series expansion of the *in situ* density around the reference pressure, and evaluating the derivatives in the expansion in terms of a chosen reference pressure, reference salinity, and

reference Conservative Temperature

$$\rho(S,\Theta,p) \approx \varrho(S,\Theta) + \underbrace{(p-p_{\rm ref})\left[\frac{\partial\rho}{\partial p}\right]_{S=S_{\rm ref},\Theta=\Theta_{\rm ref},p=p_{\rm ref}}}_{F(p)-F(p_{\rm ref})} + H.O.T. \tag{41.32}$$

where

$$\varrho(S,\Theta) = \rho(S,\Theta,p_{\rm ref}) \tag{41.33}$$

is the potential density referenced to $p = p_{\rm ref}$, and where $H.O.T.$ symbolizes higher order terms. This approach ignores the salinity and Conservative Temperature dependence of terms in the Taylor series expansion. Ignoring this dependence is a rather good approximation for many purposes since the ocean sound speed is not far from a constant

$$c_{\rm s}^{-2} = \frac{\partial\rho}{\partial p} \approx \text{constant}. \tag{41.34}$$

In this case, the equation of state takes the form

$$\rho(S,\Theta,p) \approx \varrho(S,\Theta) + \frac{p-p_{\rm ref}}{c_{\rm s}^2}, \tag{41.35}$$

41.2.4 Further reading

The presentation given here follows that given in Section 4.5.4 of *Vallis* (2017). *Straub* (1999) focuses on the source of potential vorticity arising from a nonzero thermobaricity parameter, $\mathcal{T} = \partial_p(\alpha/\beta)$ (see Section 72.3.4). In Section 41.6 we reconsider the notions presented here by suggesting the relevance of an alternative potential vorticity field that is attached to a finite sized region rather than to a fluid particle.

41.3 Potential vorticity evolution in real fluids

Thus far we have considered perfect fluids, with the use of Kelvin's circulation theorem a suitable framework to derive the material invariance of potential vorticity. In this section we consider a real fluid that contains non-conservative processes. Potential vorticity is no longer materially invariant when exposed to non-conservative processes such as mixing, friction, and diabatic sources.

To develop the potential vorticity budget in the presence of non-conservative processes, we pursue an algebraic approach that starts from the vorticity equation (40.42)

$$\rho\,\frac{\mathrm{D}(\boldsymbol{\omega}_{\rm a}/\rho)}{\mathrm{D}t} = (\boldsymbol{\omega}_{\rm a}\cdot\nabla)\,\boldsymbol{v} + \boldsymbol{B} + \nabla\times\boldsymbol{F}, \tag{41.36}$$

where $\boldsymbol{F}$ is the acceleration from non-conservative forces and $\boldsymbol{B}$ the baroclinicity vector. Furthermore, we introduce a scalar field that generally has a nonzero material evolution

$$\frac{\mathrm{D}\chi}{\mathrm{D}t} = \dot{\chi}, \tag{41.37}$$

with $\dot{\chi}$ arising from diffusion, sources, boundary fluxes, or other processes that lead to material evolution of χ.

As part of the manipulations in this section, we make use of the identity

$$(\boldsymbol{\omega}_{\rm a}\cdot\nabla)\,\frac{\mathrm{D}\chi}{\mathrm{D}t} = \boldsymbol{\omega}_{\rm a}\cdot\frac{\mathrm{D}\,(\nabla\chi)}{\mathrm{D}t} + [(\boldsymbol{\omega}_{\rm a}\cdot\nabla)\,\boldsymbol{v}]\cdot\nabla\chi, \tag{41.38}$$

which is readily proven by expanding terms and assuming Cartesian coordinates. Rearrangement, and use of the scalar equation (41.37), leads to

$$\boldsymbol{\omega}_{\text{a}} \cdot \frac{\text{D}\,(\nabla\chi)}{\text{D}t} = (\boldsymbol{\omega}_{\text{a}} \cdot \nabla)\,\dot{\chi} - [(\boldsymbol{\omega}_{\text{a}} \cdot \nabla)\,\boldsymbol{v}] \cdot \nabla\chi. \tag{41.39}$$

Now project the vorticity equation (41.36) onto the direction normal to the χ isosurfaces

$$\rho\,\nabla\chi \cdot \frac{\text{D}(\boldsymbol{\omega}_{\text{a}}/\rho)}{\text{D}t} = \nabla\chi \cdot [(\boldsymbol{\omega}_{\text{a}} \cdot \nabla)\,\boldsymbol{v}] + \nabla\chi \cdot (\boldsymbol{B} + \nabla \times \boldsymbol{F}). \tag{41.40}$$

The sum of equations (41.39) and (41.40) leads to

$$\rho\,\frac{\text{D}(\nabla\chi \cdot \boldsymbol{\omega}_{\text{a}}/\rho)}{\text{D}t} = (\boldsymbol{\omega}_{\text{a}} \cdot \nabla)\,\dot{\chi} + \nabla\chi \cdot (\boldsymbol{B} + \nabla \times \boldsymbol{F}). \tag{41.41}$$

This equation is general so that it applies to any scalar field.

To simplify the source terms on the right hand side of equation (41.41), follow the discussion from Section 41.1.4 by assuming that χ annihilates the baroclinicity vector.[3] This scalar field is typically given by potential temperature, specific entropy, buoyancy, or potential density. We thus have

$$\nabla\chi \cdot \boldsymbol{B} = 0, \tag{41.42}$$

which in turn leads to the potential vorticity equation in the presence of irreversible processes such as friction and mixing

$$\rho\,\frac{\text{D}Q}{\text{D}t} = (\boldsymbol{\omega}_{\text{a}} \cdot \nabla)\,\dot{\chi} + \nabla\chi \cdot (\nabla \times \boldsymbol{F}), \tag{41.43}$$

where the potential vorticity is again given by

$$Q = \rho^{-1}\,\boldsymbol{\omega}_{\text{a}} \cdot \nabla\chi. \tag{41.44}$$

If χ is a thermodynamic scalar such as potential entropy, then the material evolution of potential vorticity is affected by diabatic processes (heating and cooling) as well as friction. Hence, the potential vorticity of a fluid element can be either generated or destroyed depending on details of these irreversible process. Such processes are often localized to areas of mixing as well as to boundaries where strong mechanical and/or buoyant processes are active. The study of how potential vorticity is materially modified by irreversible processes forms an important area of research in potential vorticity dynamics. We have more to say on this notion when studying finite volume budgets of potential vorticity in Chapter 42.

41.4 Flux-form potential vorticity budget

The material invariance of potential vorticity is an example of a material or Lagrangian conservation property of perfect fluids, with the material conservation statement $\rho\,\text{D}Q/\text{D}t = 0$ having its flux-form expression

$$\partial_t(\rho\,Q) + \nabla \cdot (\rho\,\boldsymbol{v}\,Q) = 0 \qquad \text{perfect fluid}, \tag{41.45}$$

which is derived through use of mass conservation (19.10). Following the formalism established for material tracers in Section 20.2, the flux-form local conservation law (41.45) leads to conservation properties over finite regions, which we refer to as *global conservation* laws. In this section

[3] In Section 42.3 we study what happens when no such scalar exists.

we examine the flux-form budget in the presence of non-conservative processes. In particular, we show that the Eulerian evolution of potential vorticity continues to be determined by the convergence of a flux, thus allowing for natural extensions to global conservation laws and budget analyses. These properties were observed earlier in our study of shallow water potential vorticity in Section 39.4.2 and absolute vorticity in Section 40.3.4. These common features of the various vorticity budgets relate to the ability to write components of the absolute vorticity (including the potential vorticity) as the divergence of a vector.

41.4.1 Deriving the flux-form potential vorticity budget

To transform the material evolution equation (41.43) into a flux-form equation we make use of the following identities

$$\frac{\mathrm{D}}{\mathrm{D}t} = \frac{\partial}{\partial t} + \boldsymbol{v}\cdot\nabla \qquad \text{relating material and Eulerian time changes} \tag{41.46a}$$

$$\frac{\mathrm{D}\rho}{\mathrm{D}t} = -\rho\,\nabla\cdot\boldsymbol{v} \qquad \text{mass conservation} \tag{41.46b}$$

$$(\boldsymbol{\omega}_{\mathrm{a}}\cdot\nabla)\,\dot{\chi} = \nabla\cdot(\boldsymbol{\omega}_{\mathrm{a}}\,\dot{\chi}) \qquad \text{absolute vorticity is non-divergent: } \nabla\cdot\boldsymbol{\omega}_{\mathrm{a}} = 0 \tag{41.46c}$$

$$\nabla\chi\cdot(\nabla\times\boldsymbol{F}) = \nabla\cdot(\boldsymbol{F}\times\nabla\chi) \qquad \text{divergence of curl vanishes.} \tag{41.46d}$$

The identity (41.46d) follows from

$$\nabla\chi\cdot(\nabla\times\boldsymbol{F}) = \nabla\cdot(\chi\,\nabla\times\boldsymbol{F}) = \nabla\cdot[\nabla\times(\chi\,\boldsymbol{F}) - \nabla\chi\times\boldsymbol{F}] = \nabla\cdot(\boldsymbol{F}\times\nabla\chi), \tag{41.47}$$

where a vanishing divergence of a curl is needed to reach the first and third equalities. These identities then lead to the material evolution equation

$$\rho\,\frac{\mathrm{D}Q}{\mathrm{D}t} = \nabla\cdot(\boldsymbol{\omega}_{\mathrm{a}}\,\dot{\chi} + \boldsymbol{F}\times\nabla\chi). \tag{41.48}$$

Now converting the material time derivative into its Eulerian expression, and making use of mass conservation, renders the flux-form potential vorticity budget equation

$$\partial_t(\rho\,Q) + \nabla\cdot[\rho\,Q\,\boldsymbol{v} - \boldsymbol{\omega}_{\mathrm{a}}\,\dot{\chi} - \boldsymbol{F}\times\nabla\chi] = 0. \tag{41.49}$$

41.4.2 PV-substance and the potential vorticity flux

The budget equation (41.49) says that the density-weighted potential vorticity,

$$\rho\,Q = \boldsymbol{\omega}_{\mathrm{a}}\cdot\nabla\chi, \tag{41.50}$$

has a local time tendency determined by the convergence of the potential vorticity flux vector

$$\partial_t(\rho\,Q) = -\nabla\cdot\boldsymbol{J}^{\mathrm{Q}} \qquad \text{with} \qquad \boldsymbol{J}^{\mathrm{Q}} = \rho\,Q\,\boldsymbol{v} - \boldsymbol{\omega}_{\mathrm{a}}\,\dot{\chi} + \nabla\chi\times\boldsymbol{F}. \tag{41.51}$$

The potential vorticity flux vector, $\boldsymbol{J}^{\mathrm{Q}}$, compares to that found for shallow water potential vorticity given by equation (39.55). The budget (41.49) follows a form similar to material tracers detailed in Chapter 20, though here with some particularly specific terms in the potential vorticity flux vector, $\boldsymbol{J}^{\mathrm{Q}}$. The correspondence suggests that one consider equation (41.49) as the local budget for *PV-substance*, with Q the concentration of PV-substance and $\boldsymbol{J}^{\mathrm{Q}}$ its flux. This interpretation is pursued further in Chapter 42 when exposing the rather novel properties of budgets for PV-substance when integrated over regions bounded by isentropes.

The first term in the PV-substance flux vector (41.51) arises from the advection of PV-substance; the second contribution arises from processes leading to material evolution of χ; and

the third from any non-conservative acceleration, $\boldsymbol{F}$, that is not parallel to $\nabla\chi$. Note that the form of the non-conservative contribution, $\nabla\chi \times \boldsymbol{F}$, suggests that we think of $\boldsymbol{F}$ as contributing to a torque that rotates the χ isosurfaces as it modifies the PV-substance (see Figure 41.4).

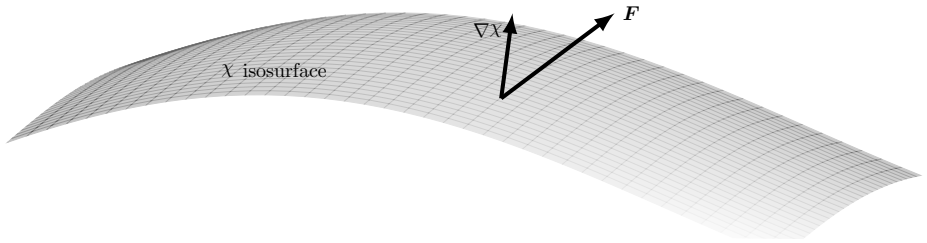

FIGURE 41.4: The contribution from any non-conservative acceleration (e.g., friction) to the potential vorticity flux is given by $\boldsymbol{J}_{\text{friction}} = \nabla\chi \times \boldsymbol{F}$. This cross product is nonzero only when $\boldsymbol{F}$ is not fully aligned with $\nabla\chi$, so that non-conservative forces create potential vorticity by rotating χ isosurfaces. Hence, if $\boldsymbol{F}$ is aligned with $\nabla\chi$, or when there is no spatial structure to $\nabla\chi \times \boldsymbol{F}$ (i.e., zero divergence), then non-conservative accelerations do not contribute to potential vorticity evolution. This interpretation is analogous to that given to the effects from baroclinicity on vorticity given in Section 40.4.

41.4.3 Gauge freedom in $\boldsymbol{J}^{\mathrm{Q}}$ and the kinematic flux

As seen by the potential vorticity equation (41.51), the time tendency for PV-substance, $\partial_t(\rho Q)$, is unchanged by adding the curl of a vector to the flux, $\boldsymbol{J}^{\mathrm{Q}}$. This ambiguity manifests a *gauge freedom*. We here exhibit the gauge freedom associated with $\boldsymbol{J}^{\mathrm{Q}}$, and then in Section 41.4.4 expose yet another gauge freedom associated with the potential vorticity itself.[4]

Kinematic potential vorticity flux

Consider the identity

$$\rho Q = \nabla\chi \cdot \boldsymbol{\omega}_{\mathrm{a}} = \nabla \cdot (\chi\, \boldsymbol{\omega}_{\mathrm{a}}), \tag{41.52}$$

which means that

$$\partial_t(\rho Q) = \partial_t[\nabla \cdot (\chi\, \boldsymbol{\omega}_{\mathrm{a}})] = \nabla \cdot [\partial_t(\chi\, \boldsymbol{\omega}_{\mathrm{a}})] = -\nabla \cdot \boldsymbol{J}^{\mathrm{kin}}, \tag{41.53}$$

where the time derivative commutes with the divergence operator. The final equality introduced the kinematic potential vorticity flux

$$\boldsymbol{J}^{\mathrm{kin}} \equiv -\partial_t(\chi\, \boldsymbol{\omega}_{\mathrm{a}}), \tag{41.54}$$

which compares to the shallow water version given by equation (39.58). We conclude that the two potential vorticity fluxes, $\boldsymbol{J}^{\mathrm{kin}}$ and $\boldsymbol{J}^{\mathrm{Q}}$, have equal divergence

$$\nabla \cdot \boldsymbol{J}^{\mathrm{kin}} = \nabla \cdot \boldsymbol{J}^{\mathrm{Q}}, \tag{41.55}$$

and so they differ at most by the curl of a vector

$$\boldsymbol{J}^{\mathrm{kin}} = \boldsymbol{J}^{\mathrm{Q}} + \nabla \times \boldsymbol{A}, \tag{41.56}$$

[4]We offer more discussion of gauge freedom in Section 21.5.1 and further the use of gauge freedom for the study of potential vorticity in Section 41.5 as well as throughout Chapter 42.

with $\boldsymbol{A}$ referred to as a *gauge function*. There are a variety of potential vorticity fluxes encountered in the study of potential vorticity, with each flux differing by the curl of a gauge function.

Relating the potential vorticity fluxes $\boldsymbol{J}^{kin}$ and $\boldsymbol{J}^{Q}$

We determine the relation between $\boldsymbol{J}^{\text{kin}}$ and $\boldsymbol{J}^{\text{Q}}$ through the following steps starting from

$$\boldsymbol{J}^{\text{kin}} = -\partial_t(\chi\,\boldsymbol{\omega}_{\text{a}}) = -\partial_t\chi\,\boldsymbol{\omega}_{\text{a}} - \chi\,(\nabla\times\partial_t\boldsymbol{v}). \tag{41.57}$$

To reach this result required the identity

$$\partial_t\boldsymbol{\omega}_{\text{a}} = \nabla\times\partial_t(\boldsymbol{v}+\boldsymbol{\Omega}\times\boldsymbol{x}) = \nabla\times\partial_t\boldsymbol{v}, \tag{41.58}$$

which follows since $\boldsymbol{\Omega}$ is time independent, and $\partial_t\boldsymbol{x}=0$ since the Eulerian time derivative is computed at a fixed space point. We next use the identity

$$-\chi\,(\nabla\times\partial_t\boldsymbol{v}) = -\nabla\times(\chi\,\partial_t\boldsymbol{v}) + \nabla\chi\times\partial_t\boldsymbol{v}, \tag{41.59}$$

so that the kinematic flux from equation (41.57) becomes

$$\boldsymbol{J}^{\text{kin}} = -\partial_t\chi\,\boldsymbol{\omega}_{\text{a}} + \nabla\chi\times\partial_t\boldsymbol{v} - \nabla\times(\chi\,\partial_t\boldsymbol{v}). \tag{41.60}$$

Next recall the vector-invariant form of the velocity equation (40.33), here written in the form

$$\partial_t\boldsymbol{v} + \boldsymbol{\omega}_{\text{a}}\times\boldsymbol{v} = -\rho^{-1}\,\nabla p - \nabla\mathcal{M} + \boldsymbol{F}, \tag{41.61}$$

where we introduced the mechanical energy per mass

$$\mathcal{M} = \boldsymbol{v}\cdot\boldsymbol{v}/2 + \Phi. \tag{41.62}$$

Equation (41.61) then leads to the cross product

$$\nabla\chi\times\partial_t\boldsymbol{v} = \rho\,Q\,\boldsymbol{v} - (\dot\chi - \partial_t\chi)\,\boldsymbol{\omega}_{\text{a}} - \nabla\chi\times\rho^{-1}\nabla p - \nabla\times(\chi\,\nabla\mathcal{M}) + \nabla\chi\times\boldsymbol{F}, \tag{41.63}$$

where we used the identities

$$(\boldsymbol{\omega}_{\text{a}}\times\boldsymbol{v})\times\nabla\chi = (\nabla\chi\cdot\boldsymbol{\omega}_{\text{a}})\,\boldsymbol{v} - (\nabla\chi\cdot\boldsymbol{v})\,\boldsymbol{\omega}_{\text{a}} = \rho\,Q\,\boldsymbol{v} - (\dot\chi-\partial_t\chi)\,\boldsymbol{\omega}_{\text{a}}. \tag{41.64}$$

Making use of equation (41.63) brings the kinematic flux (41.60) into the form

$$\boldsymbol{J}^{\text{kin}} = \rho\,Q\,\boldsymbol{v} - \dot\chi\,\boldsymbol{\omega}_{\text{a}} - \nabla\chi\times\rho^{-1}\nabla p + \nabla\chi\times\boldsymbol{F} - \nabla\times(\chi\,\nabla\mathcal{M} + \chi\,\partial_t\boldsymbol{v}). \tag{41.65}$$

Comparing to equation (41.51) for $\boldsymbol{J}^{\text{Q}}$ leads to the relation

$$\boldsymbol{J}^{\text{kin}} = \boldsymbol{J}^{\text{Q}} - \chi\,\boldsymbol{B} + \nabla\times[\chi\,(\partial_t\boldsymbol{v} + \rho^{-1}\,\nabla p + \nabla\mathcal{M})], \tag{41.66}$$

where we introduced the baroclinicity vector, $\boldsymbol{B} = \nabla\times(-\rho^{-1}\,\nabla p)$. Although the term $-\chi\,\boldsymbol{B}$ does not appear in the form of a curl, it does have a zero divergence

$$\nabla\cdot(\chi\,\boldsymbol{B}) = \nabla\chi\cdot\boldsymbol{B} + \chi\,\nabla\cdot\boldsymbol{B} = 0+0, \tag{41.67}$$

where we set $\nabla\chi\cdot\boldsymbol{B}=0$, and noted that the baroclinicity has zero divergence, $\nabla\cdot\boldsymbol{B} = \nabla\cdot[\nabla\times(-\rho^{-1}\nabla p)] = 0$. As a result, we have shown that $\nabla\cdot\boldsymbol{J}^{\text{kin}} = \nabla\cdot\boldsymbol{J}^{\text{Q}}$, which means that each flux has the same affect on the time evolution of $\rho\,Q$.

41.4.4 Gauge freedom resulting from $\nabla \cdot \boldsymbol{\omega}_{\mathrm{a}} = 0$

The divergence form of PV-substance given by equation (41.52) reveals that ρQ remains unchanged if we add a total curl to the argument of the divergence operator. In particular, consider the identities[5]

$$\chi \boldsymbol{\omega}_{\mathrm{a}} = \chi (\nabla \times \boldsymbol{v} + 2\boldsymbol{\Omega}) \qquad \text{since } \boldsymbol{\omega}_{\mathrm{a}} = \boldsymbol{\omega} + 2\boldsymbol{\Omega} \tag{41.68a}$$

$$= \nabla \times (\chi \boldsymbol{v}) - \nabla\chi \times \boldsymbol{v} + \chi 2\boldsymbol{\Omega} \qquad \text{move gradient operator.} \tag{41.68b}$$

We have thus moved the curl operation acting on the velocity field (to compute relative vorticity) onto a gradient of the scalar field, with a total curl making up the difference. Since $\nabla \cdot [\nabla \times (\chi \boldsymbol{v})] = 0$, we are led to the equivalent expressions for PV-substance

$$\rho Q = \nabla\chi \cdot \boldsymbol{\omega}_{\mathrm{a}} = \nabla \cdot (\chi 2\boldsymbol{\Omega} + \chi \boldsymbol{\omega}) = \nabla \cdot (2\boldsymbol{\Omega}\chi - \nabla\chi \times \boldsymbol{v}) = \nabla\chi \cdot (2\boldsymbol{\Omega}) - \nabla \cdot (\nabla\chi \times \boldsymbol{v}). \tag{41.69}$$

The result of these manipulations is an expression for the Ertel potential vorticity that does not involve the relative vorticity, but is instead written as the convergence of a vector

$$\rho Q = -\nabla \cdot (-2\boldsymbol{\Omega}\chi + \nabla\chi \times \boldsymbol{v}). \tag{41.70}$$

This form involves the component of the velocity that is parallel to χ isosurfaces since

$$(\nabla\chi \times \boldsymbol{v}) \cdot \nabla\chi = 0. \tag{41.71}$$

Besides offering a curious expression for potential vorticity that does not require the relative vorticity, we show in Section 42.4 how the formulation (41.70) can be especially useful for developing budgets of integrated PV-substance.

In the manipulations (41.68a)-(41.68b), we did not touch the planetary vorticity term. We certainly could do so, in which case

$$\chi 2\boldsymbol{\Omega} = \chi \nabla \times (\boldsymbol{\Omega} \times \boldsymbol{x}) = \nabla \times (\chi \boldsymbol{\Omega} \times \boldsymbol{x}) - \nabla\chi \times (\boldsymbol{\Omega} \times \boldsymbol{x}). \tag{41.72}$$

The term $\nabla \times (\chi \boldsymbol{\Omega} \times \boldsymbol{x})$ drops out when taking the divergence. However, the term $\boldsymbol{\Omega} \times \boldsymbol{x}$ requires us to evaluate the position vector, $\boldsymbol{x}$, for each point in the fluid, and doing so is not generally convenient. For this reason, we do not modify the planetary vorticity contribution to the potential vorticity, preferring to keep the form $\chi 2\boldsymbol{\Omega}$ in equation (41.70).

41.5 A hydrostatic primitive equation and Boussinesq ocean

Building on the vorticity budget in Section 40.7, we here develop the PV-substance budget for a hydrostatic primitive equation Boussinesq ocean in the presence of diabatic processes and non-conservative forces such as friction. For that purpose, recall the vorticity equation for a hydrostatic and Boussinesq ocean (40.151)

$$\frac{\mathrm{D}\boldsymbol{\omega}_{\mathrm{a}}^{\mathrm{hy}}}{\mathrm{D}t} = \underbrace{(\boldsymbol{\omega}_{\mathrm{a}}^{\mathrm{hy}} \cdot \nabla)\, \boldsymbol{v}}_{\text{stretching + tilting}} + \underbrace{\nabla \times \hat{\boldsymbol{z}}\, b}_{\text{baroclinicity}} + \underbrace{\nabla \times \boldsymbol{F}}_{\text{friction curl}}, \tag{41.73}$$

where b is the Archimedean buoyancy used in our discussion of the Boussinesq ocean in Chapter 29, and

$$\boldsymbol{\omega}_{\mathrm{a}}^{\mathrm{hy}} = \boldsymbol{\omega}^{\mathrm{hy}} + f\,\hat{\boldsymbol{z}} = \nabla \times \boldsymbol{u} + f\,\hat{\boldsymbol{z}} \tag{41.74}$$

[5] We encounter similar mathematical manipulations in Section 69.4 when studying the connection between advection and skew diffusion in the tracer equation.

is the absolute vorticity for the hydrostatic fluid with $\boldsymbol{u}$ the horizontal velocity (see equations (40.140) and (40.149)).

41.5.1 Potential vorticity

Baroclinicity is eliminated from the vorticity equation (41.73) by projecting the absolute vorticity onto the direction normal to buoyancy surfaces

$$\nabla b \cdot \frac{\mathrm{D}\boldsymbol{\omega}_{\mathrm{a}}^{\mathrm{hy}}}{\mathrm{D}t} = \nabla b \cdot [(\boldsymbol{\omega}_{\mathrm{a}}^{\mathrm{hy}} \cdot \nabla)\, \boldsymbol{v}] + \nabla b \cdot (\nabla \times \boldsymbol{F}), \tag{41.75}$$

where we used

$$\nabla b \cdot (\nabla \times \hat{\boldsymbol{z}}\, b) = \nabla b \cdot (\nabla b \times \hat{\boldsymbol{z}}) = 0. \tag{41.76}$$

We next make use of the identity

$$\frac{\mathrm{D}(\partial b/\partial x^i)}{\mathrm{D}t} = \frac{\partial}{\partial x^i}\left[\frac{\mathrm{D}b}{\mathrm{D}t}\right] - \nabla b \cdot \frac{\partial \boldsymbol{v}}{\partial x^i} = \frac{\partial \dot{b}}{\partial x^i} - \nabla b \cdot \frac{\partial \boldsymbol{v}}{\partial x^i}, \tag{41.77}$$

so that

$$\boldsymbol{\omega}_{\mathrm{a}}^{\mathrm{hy}} \cdot \left[\frac{\mathrm{D}\,\nabla b}{\mathrm{D}t}\right] = \boldsymbol{\omega}_{\mathrm{a}}^{\mathrm{hy}} \cdot \nabla \dot{b} - \nabla b \cdot [(\boldsymbol{\omega}_{\mathrm{a}}^{\mathrm{hy}} \cdot \nabla)\, \boldsymbol{v}]. \tag{41.78}$$

Making use of this result in equation (41.75) renders

$$\nabla b \cdot \frac{\mathrm{D}\boldsymbol{\omega}_{\mathrm{a}}^{\mathrm{hy}}}{\mathrm{D}t} + \boldsymbol{\omega}_{\mathrm{a}}^{\mathrm{hy}} \cdot \frac{\mathrm{D}\nabla b}{\mathrm{D}t} = \boldsymbol{\omega}_{\mathrm{a}}^{\mathrm{hy}} \cdot \nabla \dot{b} + \nabla b \cdot (\nabla \times \boldsymbol{F}), \tag{41.79}$$

which leads to

$$\frac{\mathrm{D}Q}{\mathrm{D}t} = (\boldsymbol{\omega}_{\mathrm{a}}^{\mathrm{hy}} \cdot \nabla)\, \dot{b} + \nabla b \cdot (\nabla \times \boldsymbol{F}) \tag{41.80}$$

where

$$Q = \boldsymbol{\omega}_{\mathrm{a}}^{\mathrm{hy}} \cdot \nabla b = \boldsymbol{\omega}^{\mathrm{hy}} \cdot \nabla b + f\, \partial_z b \tag{41.81}$$

is the potential vorticity for a rotating hydrostatic Boussinesq ocean. Potential vorticity is materially invariant for the inviscid and adiabatic case, in which $\boldsymbol{F} = 0$ and $\dot{b} = 0$.

It is sometimes useful to split the hydrostatic vorticity into its vertical and horizontal terms as per equation (40.140). In this way, potential vorticity takes on the form

$$Q = \frac{\partial u}{\partial z}\frac{\partial b}{\partial y} - \frac{\partial v}{\partial z}\frac{\partial b}{\partial x} + (\zeta + f)\frac{\partial b}{\partial z} = \hat{\boldsymbol{z}} \cdot \left[\frac{\partial \boldsymbol{u}}{\partial z} \times \nabla b\right] + (\zeta + f)\frac{\partial b}{\partial z}. \tag{41.82}$$

This expression plays an important role in characterizing flows with order unity Rossby number, where the term $\hat{\boldsymbol{z}} \cdot (\partial_z \boldsymbol{u} \times \nabla b)$ can become comparable to $(\zeta + f)\, \partial_z b$, particularly in regions of strong horizontal buoyancy fronts such as those studied by *Thomas et al.* (2008) and *Thomas et al.* (2013).

41.5.2 Potential vorticity flux vector

The material form of the potential vorticity equation (41.80) is converted into its flux-form via

$$\partial_t Q + \nabla \cdot (\boldsymbol{v}\, Q) = \boldsymbol{\omega}_{\mathrm{a}}^{\mathrm{hy}} \cdot \nabla \dot{b} + \nabla b \cdot (\nabla \times \boldsymbol{F}) \tag{41.83a}$$

$$= \nabla \cdot [\dot{b}\, \boldsymbol{\omega}_{\mathrm{a}}^{\mathrm{hy}} + b\, (\nabla \times \boldsymbol{F})] \tag{41.83b}$$

$$= \nabla \cdot [\dot{b}\, \boldsymbol{\omega}_{\mathrm{a}}^{\mathrm{hy}} + \nabla \times (b\, \boldsymbol{F}) - \nabla b \times \boldsymbol{F}] \tag{41.83c}$$

$$= \nabla \cdot (\dot{b}\, \boldsymbol{\omega}_{\mathrm{a}}^{\mathrm{hy}} - \nabla b \times \boldsymbol{F}), \tag{41.83d}$$

where we used

$$\nabla \cdot \boldsymbol{v} = 0 \qquad \text{Boussinesq flow is non-divergent} \tag{41.84a}$$
$$\nabla \cdot \boldsymbol{\omega}_{\mathrm{a}}^{\mathrm{hy}} = 0 \qquad \text{vorticity always has zero divergence} \tag{41.84b}$$
$$\nabla \cdot (\nabla \times \boldsymbol{F}) = 0 \qquad \text{divergence of curl vanishes} \tag{41.84c}$$
$$\nabla \cdot [\nabla \times (b\,\boldsymbol{F})] = 0 \qquad \text{divergence of curl vanishes.} \tag{41.84d}$$

The conservation equation (41.83d) allows us to identify a potential vorticity flux vector for the hydrostatic Boussinesq ocean

$$\boldsymbol{J}^{\mathrm{Q}} = \boldsymbol{v}\,Q - \dot{b}\,\boldsymbol{\omega}_{\mathrm{a}}^{\mathrm{hy}} + \nabla b \times \boldsymbol{F}, \tag{41.85}$$

so that the potential vorticity equation takes the form

$$\partial_t Q + \nabla \cdot \boldsymbol{J}^{\mathrm{Q}} = 0. \tag{41.86}$$

The potential vorticity flux (41.85) compares directly to the potential vorticity flux (41.51) suited to the non-hydrostatic and non-Boussinesq fluid. As such, it is comprised of an advective term

$$\boldsymbol{J}_{\text{advective}} = \boldsymbol{v}\,Q, \tag{41.87}$$

and non-advective terms arising from diabatic processes and non-conservative accelerations (e.g., friction)

$$\boldsymbol{J}_{\text{non-advective}} = -\dot{b}\,\boldsymbol{\omega}_{\mathrm{a}}^{\mathrm{hy}} + \nabla b \times \boldsymbol{F}. \tag{41.88}$$

41.5.3 Kinematic derivation of the potential vorticity flux

Following the discussion in Section 41.4.3, we consider a kinematic derivation of the potential vorticity flux vector for the hydrostatic and Boussinesq ocean. For that purpose, write the hydrostatic Boussinesq potential vorticity (41.81) in the form

$$Q = \boldsymbol{\omega}_{\mathrm{a}}^{\mathrm{hy}} \cdot \nabla b = \nabla \cdot (b\,\boldsymbol{\omega}_{\mathrm{a}}^{\mathrm{hy}}), \tag{41.89}$$

which follows since $\nabla \cdot \boldsymbol{\omega}_{\mathrm{a}}^{\mathrm{hy}} = 0$. Taking the Eulerian time derivative then leads to

$$\partial_t Q = -\nabla \cdot \boldsymbol{J}^{\mathrm{kin}} \tag{41.90}$$

where we defined the kinematic potential vorticity flux

$$\boldsymbol{J}^{\mathrm{kin}} = -\partial_t (b\,\boldsymbol{\omega}_{\mathrm{a}}^{\mathrm{hy}}). \tag{41.91}$$

The kinematic potential vorticity flux (41.91) is directly analogous to the potential vorticity flux (41.54) appearing in the non-hydrostatic and non-Boussinesq fluid.

Manifesting impermeability

The potential vorticity flux (41.91) manifests the impermeability property of Chapter 42 since

$$\hat{\boldsymbol{n}} \cdot \boldsymbol{J}^{\mathrm{kin}}/Q = -\frac{1}{|\nabla b|}\frac{\partial b}{\partial t} = \hat{\boldsymbol{n}} \cdot \boldsymbol{v}_{b\perp}, \tag{41.92}$$

where $\hat{\boldsymbol{n}} = \nabla b/|\nabla b|$ is the outward unit normal for a buoyancy surface, and with $\boldsymbol{v}_{b\perp}$ the velocity of a point on the isopycnal that satisfies

$$(\partial_t + \boldsymbol{v}_{b\perp} \cdot \nabla)\, b = 0. \tag{41.93}$$

We return in Chapter 42 to help clarify this particular point about impermeability.

Relating $\boldsymbol{J}^{Q}$ and $\boldsymbol{J}^{kin}$

We relate the two potential vorticity fluxes, $\boldsymbol{J}^{\mathrm{Q}}$ and $\boldsymbol{J}^{\mathrm{kin}}$, just like in Section 41.4.3 for the non-hydrostatic and non-Boussinesq fluid. Although the steps are exactly analogous, it is good practice to work through the details. For that purpose, start with the kinematic flux to write

$$\boldsymbol{J}^{\mathrm{kin}} = -\partial_t(b\,\boldsymbol{\omega}_{\mathrm{a}}^{\mathrm{hy}}) = -\partial_t b\,\boldsymbol{\omega}_{\mathrm{a}}^{\mathrm{hy}} - b\,(\nabla \times \partial_t \boldsymbol{u}), \tag{41.94}$$

where we used

$$\partial_t \boldsymbol{\omega}_{\mathrm{a}}^{\mathrm{hy}} = \partial_t \boldsymbol{\omega}^{\mathrm{hy}} = \nabla \times \partial_t \boldsymbol{u}. \tag{41.95}$$

Next use the identity

$$-b\,(\nabla \times \partial_t \boldsymbol{u}) = -\nabla \times (b\,\partial_t \boldsymbol{u}) + \nabla b \times \partial_t \boldsymbol{u}, \tag{41.96}$$

so that the kinematic flux from equation (41.94) becomes

$$\boldsymbol{J}^{\mathrm{kin}} = -\partial_t b\,\boldsymbol{\omega}_{\mathrm{a}}^{\mathrm{hy}} + \nabla b \times \partial_t \boldsymbol{u} - \nabla \times (b\,\partial_t \boldsymbol{u}). \tag{41.97}$$

Next recall the vector-invariant form of the hydrostatic and Boussineq velocity equation (40.146)

$$\partial_t \boldsymbol{u} + \boldsymbol{\omega}_{\mathrm{a}}^{\mathrm{hy}} \times \boldsymbol{v} = -\nabla(\varphi + \boldsymbol{u}^2/2) + b\,\hat{\boldsymbol{z}} + \boldsymbol{F}, \tag{41.98}$$

This equation then leads to the cross product

$$\nabla b \times \partial_t \boldsymbol{u} = Q\,\boldsymbol{v} - (\dot{b} - \partial_t b)\,\boldsymbol{\omega}_{\mathrm{a}}^{\mathrm{hy}} - \nabla \times [b\,\nabla(\varphi + \boldsymbol{u}\cdot\boldsymbol{u}/2) - (b^2/2)\,\hat{\boldsymbol{z}}] + \nabla b \times \boldsymbol{F}, \tag{41.99}$$

where we used the identities

$$(\boldsymbol{\omega}_{\mathrm{a}}^{\mathrm{hy}} \times \boldsymbol{v}) \times \nabla b = (\nabla b \cdot \boldsymbol{\omega}_{\mathrm{a}}^{\mathrm{hy}})\,\boldsymbol{v} - (\nabla b \cdot \boldsymbol{v})\,\boldsymbol{\omega}_{\mathrm{a}}^{\mathrm{hy}} = Q\,\boldsymbol{v} - (\dot{b} - \partial_t b)\,\boldsymbol{\omega}_{\mathrm{a}}^{\mathrm{hy}}. \tag{41.100}$$

Bringing everything together leads to the kinematic potential vorticity flux

$$\begin{aligned}
\boldsymbol{J}^{\mathrm{kin}} &= -\partial_t b\,\boldsymbol{\omega}_{\mathrm{a}}^{\mathrm{hy}} + \nabla b \times \partial_t \boldsymbol{u} - \nabla \times (b\,\partial_t \boldsymbol{u}) && \text{(41.101a)}\\
&= Q\,\boldsymbol{v} - \dot{b}\,\boldsymbol{\omega}_{\mathrm{a}}^{\mathrm{hy}} + \nabla b \times \boldsymbol{F} + \nabla \times [-b\,\nabla(\varphi + \boldsymbol{u}\cdot\boldsymbol{u}/2) + b^2\,\hat{\boldsymbol{z}} - b\,\partial_t \boldsymbol{u}] && \text{(41.101b)}\\
&= \boldsymbol{J}^{\mathrm{Q}} + \nabla \times [-b\,\nabla(\varphi + \boldsymbol{u}\cdot\boldsymbol{u}/2) + b^2\,\hat{\boldsymbol{z}} - b\,\partial_t \boldsymbol{u}]. && \text{(41.101c)}
\end{aligned}$$

We have thus verified that $\boldsymbol{J}^{\mathrm{kin}}$ and $\boldsymbol{J}^{\mathrm{Q}}$ differ by the curl of a vector, so that their divergences are indeed equal.

41.5.4 A potential vorticity flux vector suited to steady flows

Schär (1993) provided a generalization of Bernoulli's theorem for understanding steady geophysical flows, with *Marshall* (2000), *Marshall et al.* (2001), and *Polton and Marshall* (2007) applying this theorem to oceanic contexts within a hydrostatic and Boussinesq ocean.[6] We here derive their potential vorticity flux vector for the hydrostatic and Boussinesq ocean. The manipulations share similarities with those in Section 41.5.3, yet we present the details for further developing

[6] We studied the Bernoulli potential and Bernoulli theorem in Section 26.9.3.

an appreciation of the various manipulations, which are a central facet of working with potential vorticity. The presentation here is a warm-up to the non-Boussinesq and non-hydrostatic case studied in Section 42.3.1, where we also provide example uses for the formulation.

Momentum equation

We start by exposing the Boussinesq form of the Bernoulli potential within the vector-invariant velocity equation. For this purpose, return to the horizontal momentum equation (40.146), and expand the expressions for perturbation pressure and the buoyancy

$$\begin{aligned}
\partial_t \boldsymbol{u} + (\boldsymbol{f} + \boldsymbol{\omega}^{\text{hy}}) \times \boldsymbol{v} &= -\nabla (\varphi + |\boldsymbol{u}|^2/2) + \hat{\boldsymbol{z}}\, b + \boldsymbol{F} && \text{(41.102a)} \\
&= -\nabla (|\boldsymbol{u}|^2/2) - \nabla(p - p_0)/\rho_\circ - \hat{\boldsymbol{z}}\, g\, (\rho - \rho_\circ)/\rho_\circ + \boldsymbol{F} && \text{(41.102b)} \\
&= -\nabla (|\boldsymbol{u}|^2/2) - \nabla(p/\rho_\circ) - \hat{\boldsymbol{z}}\, g\, \rho/\rho_\circ + \boldsymbol{F} && \text{(41.102c)} \\
&= -\nabla(|\boldsymbol{u}|^2/2 + p/\rho_\circ) - \hat{\boldsymbol{z}} \left[\frac{g\,\rho - g\,\rho_o + g\,\rho_\circ}{\rho_\circ} \right] + \boldsymbol{F} && \text{(41.102d)} \\
&= -\nabla(|\boldsymbol{u}|^2/2 + p/\rho_\circ + g\, z) - \hat{\boldsymbol{z}}\, g\, (\rho - \rho_o)/\rho_\circ + \boldsymbol{F} && \text{(41.102e)} \\
&= -\nabla \mathcal{B} + \hat{\boldsymbol{z}}\, b + \boldsymbol{F}, && \text{(41.102f)}
\end{aligned}$$

where we introduced the Bernoulli potential for a hydrostatic and Boussinesq fluid[7]

$$\mathcal{B} = |\boldsymbol{u}|^2/2 + p/\rho_\circ + g\, z. \tag{41.103}$$

Potential vorticity flux

The flux-form potential vorticity conservation statement remains as given by equation (41.83d), and the PV-substance flux is given by equation (41.85). However, we can make use of the gauge invariance of the potential vorticity flux to write it in a manner conducive to analyzing steady state conditions. For this purpose, operate with $\nabla b \times$ on the velocity equation (41.102f) to have

$$\nabla b \times \partial_t \boldsymbol{u} + \nabla b \times (\boldsymbol{\omega}_{\text{a}}^{\text{hy}} \times \boldsymbol{v}) = -\nabla b \times \nabla \mathcal{B} + \nabla b \times \hat{\boldsymbol{z}}\, b + \nabla b \times \boldsymbol{F}. \tag{41.104}$$

Now make use of the identity

$$\nabla b \times (\boldsymbol{\omega}_{\text{a}}^{\text{hy}} \times \boldsymbol{v}) = (\nabla b \cdot \boldsymbol{v})\, \boldsymbol{\omega}_{\text{a}}^{\text{hy}} - (\boldsymbol{\omega}_{\text{a}}^{\text{hy}} \cdot \nabla b)\, \boldsymbol{v} \tag{41.105}$$

in equation (41.104) to yield

$$(\boldsymbol{v} \cdot \nabla b)\, \boldsymbol{\omega}_{\text{a}}^{\text{hy}} - (\boldsymbol{\omega}_{\text{a}}^{\text{hy}} \cdot \nabla b)\, \boldsymbol{v} = -\nabla b \times \partial_t \boldsymbol{u} - \nabla b \times \nabla \mathcal{B} + \nabla b \times \hat{\boldsymbol{z}}\, b + \nabla b \times \boldsymbol{F}. \tag{41.106}$$

We next make use of this identity for the purpose of manipulating the potential vorticity flux given by equation (41.85)

$$\begin{aligned}
\boldsymbol{J}^{\text{Q}} &= \boldsymbol{v}\, Q - \dot{b}\, \boldsymbol{\omega}_{\text{a}}^{\text{hy}} + \nabla b \times \boldsymbol{F} && \text{(41.107a)} \\
&= \boldsymbol{v}\, (\boldsymbol{\omega}_{\text{a}}^{\text{hy}} \cdot \nabla b) - [\partial_t b + \boldsymbol{v} \cdot \nabla b]\, \boldsymbol{\omega}_{\text{a}}^{\text{hy}} + \nabla b \times \boldsymbol{F} && \text{(41.107b)} \\
&= [\boldsymbol{v}\, (\boldsymbol{\omega}_{\text{a}}^{\text{hy}} \cdot \nabla b) - (\boldsymbol{v} \cdot \nabla b)\, \boldsymbol{\omega}_{\text{a}}^{\text{hy}}] - \partial_t b\, \boldsymbol{\omega}_{\text{a}}^{\text{hy}} + \nabla b \times \boldsymbol{F} && \text{(41.107c)} \\
&= [\nabla b \times \partial_t \boldsymbol{u} + \nabla b \times \nabla \mathcal{B} - \nabla b \times \hat{\boldsymbol{z}}\, b - \nabla b \times \boldsymbol{F}] - \partial_t b\, \boldsymbol{\omega}_{\text{a}}^{\text{hy}} + \nabla b \times \boldsymbol{F} && \text{(41.107d)} \\
&= \nabla b \times \partial_t \boldsymbol{u} - \partial_t b\, \boldsymbol{\omega}_{\text{a}}^{\text{hy}} + \nabla b \times \nabla \mathcal{B} - \nabla b \times \hat{\boldsymbol{z}}\, b && \text{(41.107e)} \\
&= \nabla b \times [\partial_t \boldsymbol{u} + \nabla \mathcal{B}] - \partial_t b\, \boldsymbol{\omega}_{\text{a}}^{\text{hy}} - \nabla \times (\hat{\boldsymbol{z}}\, b^2/2). && \text{(41.107f)}
\end{aligned}$$

[7] See Section 26.9 for the non-Boussinesq Bernoulli potential.

Dropping the rotational (gauge) term, $-\nabla \times (\hat{\boldsymbol{z}}\, b^2/2)$, leads to the flux vector

$$\boldsymbol{J}^{\text{ss}} = \nabla b \times (\partial_t \boldsymbol{u} + \nabla \mathcal{B}) - \partial_t b\, \boldsymbol{\omega}_{\text{a}}^{\text{hy}} \tag{41.108}$$

We have now reached our goal whereby the steady state version of the potential vorticity flux (41.108) takes the rather elegant form

$$\boldsymbol{J}^{\text{ss}} = \nabla b \times \nabla \mathcal{B} = \nabla \times b \nabla \mathcal{B} = -\nabla \times \mathcal{B} \nabla b \qquad \text{steady state.} \tag{41.109}$$

Hence, the steady state potential vorticity flux is aligned with the intersection of surfaces of constant buoyancy and Bernoulli potential

$$\nabla b \cdot \boldsymbol{J}^{\text{ss}} = 0 \quad \text{and} \quad \nabla \mathcal{B} \cdot \boldsymbol{J}^{\text{ss}} = 0 \qquad \text{steady state.} \tag{41.110}$$

Recalling our discussion of vector streamfunctions in Section 21.5.3, where here see that the buoyancy and Bernoulli potential serve as the two scalar functions that build the vector streamfunction for the steady state potential vorticity flux. Mapping surfaces of constant buoyancy and constant Bernoulli potential, and determining their intersections, then determines the pathways for potential vorticity flux operating in a steady state. Figure 41.5 offers a schematic based on the analogous situation for a velocity streamfunction shown in Figure 21.3. This result is the Boussinesq/hydrostatic form of the more general non-Boussinesq/non-hydrostatic case derived in Section 42.3.3.

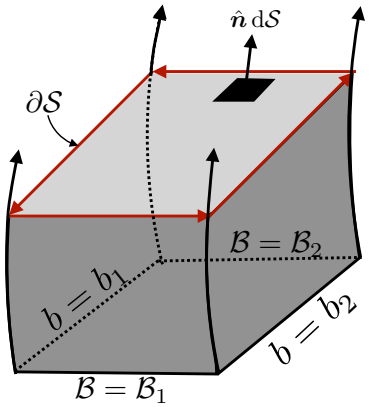

FIGURE 41.5: Isosurfaces of constant buoyancy, b, and Bernoulli potential, $\mathcal{B}$, serving as the two scalar functions building the vector streamfunction for potential vorticity flux, $\boldsymbol{J}^{\text{Q}}_{\text{ss}}$, in the steady state (see equation (41.110)). Streamlines are defined by the intersections of the b and $\mathcal{B}$ isosurfaces, as shown by four streamlines along the corners of this particular volume. The transport of PV-substance through the surface, $\mathcal{S}$, is determined by the line integral, $\oint_{\partial\mathcal{S}} \mathcal{B}\, \mathrm{d}b = -\oint_{\partial\mathcal{S}} b\, \mathrm{d}\mathcal{B} = (\mathcal{B}_1 - \mathcal{B}_2)\,(b_2 - b_1)$, around the boundary circuit.

41.6 Potential vorticity over finite regions

In Section 41.2, we detailed why there is no materially invariant potential vorticity for a realistic equation of state for seawater, in which $\rho = \rho(S, \Theta, p)$. A similar limitation holds for the atmosphere, where the specific entropy is a function of pressure, density, and moisture concentration. We here build from our discussion of Kelvin's circulation theorem in Section 40.2 to consider a finite volume *pancake potential vorticity*. Rather than being a property carried by each fluid particle, the pancake potential vorticity is carried by a finite fluid region and it is materially invariant for perfect fluid flows, even for a realistic equation of state. The discussion here follows that given by *Kooloth et al.* (2022).

41.6.1 Differential relations

The starting point is the potential vorticity equation written as in equation (41.41)

$$\rho \frac{\mathrm{D}Q}{\mathrm{D}t} = (\boldsymbol{\omega}_{\mathrm{a}} \cdot \nabla)\, \dot{\chi} + \nabla\chi \cdot [\nabla \times (-\rho^{-1} \nabla p)] + \nabla\chi \cdot (\nabla \times \boldsymbol{F}) \quad \text{with} \quad Q = \rho^{-1} \nabla\chi \cdot \boldsymbol{\omega}_{\mathrm{a}}. \tag{41.111}$$

The key step in the derivation is to replace the pressure gradient acceleration with its equivalent in terms of specific enthalpy and its partial derivatives.[8] For this purpose, write the specific enthalpy as a function of Conservative Temperature, salinity, and pressure

$$\mathcal{H} = \mathcal{H}(\Theta, S, p), \tag{41.112}$$

which leads to the spatial gradient[9]

$$\nabla\mathcal{H} = \rho^{-1} \nabla p + \left[\frac{\partial \mathcal{H}}{\partial \Theta}\right]_{p,S} \nabla\Theta + \left[\frac{\partial \mathcal{H}}{\partial S}\right]_{\Theta,p} \nabla S, \tag{41.113}$$

which then leads to the expression for the pressure gradient acceleration

$$-\rho^{-1} \nabla p = -\nabla\mathcal{H} + \mathcal{H}_\Theta \nabla\Theta + \mathcal{H}_S \nabla S, \tag{41.114}$$

where we introduced the shorthand notation

$$\mathcal{H}_\Theta = \left[\frac{\partial \mathcal{H}}{\partial \Theta}\right]_{p,S} \quad \text{and} \quad \mathcal{H}_S = \left[\frac{\partial \mathcal{H}}{\partial S}\right]_{\Theta,p}. \tag{41.115}$$

Use of the identity (41.114) within the potential vorticity equation (41.111) leads to

$$\rho \frac{\mathrm{D}Q}{\mathrm{D}t} = (\boldsymbol{\omega}_{\mathrm{a}} \cdot \nabla)\, \dot{\chi} + \nabla\chi \cdot \nabla \times [\mathcal{H}_\Theta \nabla\Theta + \mathcal{H}_S \nabla S + \boldsymbol{F}], \tag{41.116}$$

where we set $\nabla \times \nabla\mathcal{H} = 0$. Now make use of the following vector identity, with $\boldsymbol{C}$ an arbitrary vector,

$$\nabla\chi \cdot (\nabla \times \boldsymbol{C}) = \nabla \cdot (\chi \nabla \times \boldsymbol{C}) = \nabla \cdot [\nabla \times (\chi \boldsymbol{C}) - \nabla\chi \times \boldsymbol{C}] = -\nabla \cdot (\nabla\chi \times \boldsymbol{C}), \tag{41.117}$$

to bring the potential vorticity equation (41.116) to

$$\rho \frac{\mathrm{D}Q}{\mathrm{D}t} = \nabla \cdot \left[\boldsymbol{\omega}_{\mathrm{a}}\, \dot{\chi} - \nabla\chi \times (\mathcal{H}_\Theta \nabla\Theta + \mathcal{H}_S \nabla S + \boldsymbol{F})\right]. \tag{41.118}$$

41.6.2 Integral relations

Equation (41.118) is quite general. To reduce by one the terms on the right hand side, we can either choose $\chi = \Theta$ or $\chi = S$. Let us choose $\chi = \Theta$, in which case

$$\rho \frac{\mathrm{D}Q^{(\Theta)}}{\mathrm{D}t} = \nabla \cdot \left[\mathcal{H}_S \nabla S \times \nabla\Theta + \boldsymbol{F} \times \nabla\Theta + \boldsymbol{\omega}_{\mathrm{a}}\, \dot{\Theta}\right] \quad \text{with} \quad Q^{(\Theta)} = \rho^{-1} \nabla\Theta \cdot \boldsymbol{\omega}_{\mathrm{a}}. \tag{41.119}$$

We still have the reversible term, $\mathcal{H}_S \nabla S \times \nabla\Theta$, contributing to the material time evolution of $Q^{(\Theta)}$, and this term vanishes only for particularly idealized forms of the fluid thermodynamics. Rather than pursue material invariance for potential vorticity along a fluid particle, consider an

[8] We made use of a similar approach when studying circulation in Section 40.2.5.

[9] We performed a similar manipulation in Section 26.6.2.

integration of $Q^{(\Theta)}$ over a finite region that moves with the flow, and take its time derivative

$$\frac{\mathrm{d}}{\mathrm{d}t}\int_{\mathcal{R}(\boldsymbol{v})} \rho\, Q^{(\Theta)}\, \mathrm{d}V = \int_{\mathcal{R}(\boldsymbol{v})} \rho\, \frac{\mathrm{D}Q^{(\Theta)}}{\mathrm{D}t}\, \mathrm{d}V \tag{41.120a}$$

$$= \int_{\mathcal{R}(\boldsymbol{v})} \nabla\cdot\Big[\mathcal{H}_S\, \nabla S\times\nabla\Theta + \boldsymbol{F}\times\nabla\Theta + \boldsymbol{\omega}_{\mathrm{a}}\,\dot{\Theta}\Big]\, \mathrm{d}V \tag{41.120b}$$

$$= \oint_{\partial\mathcal{R}(\boldsymbol{v})} \Big[\mathcal{H}_S\, \nabla S\times\nabla\Theta + \boldsymbol{F}\times\nabla\Theta + \boldsymbol{\omega}_{\mathrm{a}}\,\dot{\Theta}\Big]\cdot\hat{\boldsymbol{n}}\, \mathrm{d}\mathcal{S}. \tag{41.120c}$$

The first and second terms on the right hand side vanish if we choose a volume whose boundary has an outward unit normal vector, $\hat{\boldsymbol{n}}$, parallel to $\nabla\Theta$ at every point around the closed region. This sort of Θ-bubble is uncommon in a stably stratified fluid, though it may occur over relatively small scales in turbulent flows.

For another arrangement, consider the case of salinity with closed contours on Conservative Temperature surfaces. We thus take a pancake/disk region with $\hat{\boldsymbol{n}}$ parallel to $\nabla\Theta$ on its top and bottom and $\hat{\boldsymbol{n}}$ parallel to ∇S on the sides.[10] For this region, the $\nabla S\times\nabla\Theta$ contribution vanishes along all the boundaries, and the contribution from $\boldsymbol{F}$ only appears on the sides where $\hat{\boldsymbol{n}}$ is parallel to ∇S. We can take a complementary approach by setting $\chi = S$, in which case the previous discussion holds yet with Θ and S interchanged. Either of these pancake regions preserves the materially integrated potential vorticity for inviscid flows with S and Θ both materially invariant.

41.7 Exercises

EXERCISE 41.1: POTENTIAL VORTICITY FOR A PERFECT NON-HYDROSTATIC BOUSSINESQ OCEAN

Consider a perfect tangent plane Boussinesq ocean whose governing equations are given by

$$\frac{\mathrm{D}\boldsymbol{v}}{\mathrm{D}t} + f\,(\hat{\boldsymbol{z}}\times\boldsymbol{v}) = -\nabla\varphi + b\,\hat{\boldsymbol{z}} \tag{41.121}$$

$$\nabla\cdot\boldsymbol{v} = 0 \tag{41.122}$$

$$\frac{\mathrm{D}b}{\mathrm{D}t} = 0 \tag{41.123}$$

$$b = -\frac{g\,(\rho-\rho_\circ)}{\rho_\circ} = g\,\alpha\,\theta, \tag{41.124}$$

where θ is the potential temperature and $\alpha > 0$ is a constant thermal expansion coefficient, and we assumed a linear equation of state for density whereby

$$\rho = \rho_\circ\,(1-\alpha\,\theta). \tag{41.125}$$

Further details are provided in Section 29.1.6. Some of this exercise follows the hydrostatic Boussinesq discussion in Section 41.5, though they differ in important places, so be careful!

(a) Derive the equation for the material time evolution of potential vorticity in this fluid system. Show all steps in the derivation.

[10] The geometry is similar to that shown in Figure 41.5 when discussing the steady state potential vorticity flux.

(b) The baroclinicity vector appearing in the Boussinesq vorticity equation is $\boldsymbol{B} = \nabla \times \hat{\boldsymbol{z}}\, b = \nabla b \times \hat{\boldsymbol{z}}$ (see Section 40.7.1 to check the derivation in part (a) above). Show that this vector results upon making the Boussinesq approximation to the non-Boussinesq expression $\boldsymbol{B} = (\nabla\rho \times \nabla p)/\rho^2$. Hint: drop the $\delta\rho$ and δp product given that it is a higher order quantity.

(c) Show that the vertical portion of Q^{bouss} can be written

$$Q^{\text{bouss}}_{\text{vert}} = (\zeta + f)\, N^2 \tag{41.126}$$

where $\zeta = \partial_x v - \partial_y u$ is the vertical component to the relative vorticity and $N^2 = \partial b/\partial z$ is the squared buoyancy frequency (Section 30.6). Hint: this is not tough to show; there is no trick.

(d) If flow maintains hydrostatic and geostrophic balance, show that the horizontal portion of Q^{bouss} can be written

$$Q^{\text{bouss}}_{\text{horz}} = \boldsymbol{\omega} \cdot \nabla_{\!\text{h}} b \approx -f^{-1} |\nabla_{\!\text{h}} b|^2. \tag{41.127}$$

Hint: recall that for hydrostatic and geostrophic flow, the vertical velocity is much smaller than horizontal.

EXERCISE 41.2: POTENTIAL VORTICITY FOR DIABATIC AND FRICTIONAL NON-HYDROSTATIC BOUSSINESQ OCEAN

Reconsider Exercise 41.1 in the presence of irreversible forces (e.g., friction) and buoyancy sources so that the governing tangent plane equations are

$$\frac{\mathrm{D}\boldsymbol{v}}{\mathrm{D}t} + f\,(\hat{\boldsymbol{z}} \times \boldsymbol{v}) = -\nabla\varphi + b\,\hat{\boldsymbol{z}} + \boldsymbol{F} \tag{41.128}$$

$$\nabla \cdot \boldsymbol{v} = 0 \tag{41.129}$$

$$\frac{\mathrm{D}b}{\mathrm{D}t} = \dot{b} \tag{41.130}$$

$$b = -\frac{g\,(\rho - \rho_{\circ})}{\rho_{\circ}} = g\,\alpha\,\theta. \tag{41.131}$$

In these equations we assumed a linear equation of state for density whereby

$$\rho = \rho_{\circ}\,(1 - \alpha\,\theta), \tag{41.132}$$

with $\alpha > 0$ a constant thermal expansion coefficient. Hence, material time changes to the buoyancy are given by

$$\frac{\mathrm{D}b}{\mathrm{D}t} = \dot{b} = g\,\alpha\,\dot{\theta}, \tag{41.133}$$

where $\dot{\theta}$ is a diabatic heating source/sink. We also included $\boldsymbol{F}$ to the velocity equation (41.128), which represents a non-conservative acceleration such as from friction or boundary stresses.

(a) Derive the equation for the material time evolution of potential vorticity in this fluid system, including the irreversible contributions from non-conservative accelerations and from heating.

(b) Derive an equation for the potential vorticity time tendency (i.e., Eulerian time derivative), written in the form

$$\partial_t Q = -\nabla \cdot \boldsymbol{J}^{\mathrm{Q}}. \tag{41.134}$$

What is the potential vorticity flux $\boldsymbol{J}^{\mathrm{Q}}$? Note that your answer is unique up to the curl of an arbitrary vector (gauge symmetry). Also note that for a Boussinesq flow we drop the constant reference density in the definition of $\boldsymbol{J}^{\mathrm{Q}}$.

(c) A common diabatic process is written in the form of a damping source

$$\dot{b} = -\mu\,(b - b^*), \tag{41.135}$$

where μ is a constant Newtonian damping coefficient (dimensions of inverse time), and b^* is a specified buoyancy profile. This form of a buoyancy source acts to damp the buoyancy towards a specified profile b^*. Show that Newtonian damping of buoyancy corresponds to potential vorticity damping towards $Q^* = \boldsymbol{\omega}_{\mathrm{a}} \cdot \nabla b^*$.

(d) A form for the friction operator is given by Rayleigh drag

$$\boldsymbol{F} = -\gamma\,\boldsymbol{v}, \tag{41.136}$$

with γ a constant Rayleigh damping coefficient with dimension of inverse time. Show that Rayleigh drag in the momentum equation, which acts to damp velocity towards zero, corresponds to a damping of potential vorticity towards its planetary geostrophic form, $Q^{\mathrm{pg}} = f\,N^2$, where $N^2 = \partial b/\partial z$ is the squared buoyancy frequency.

(e) Discuss the balance needed between forcing terms in $\boldsymbol{J}^{\mathrm{Q}}$ to arrive at a steady state (i.e., zero Eulerian time tendency). Continue to assume the friction is in the form of Rayleigh drag and heating is in the form of Newtonian damping.

Chapter 42

POTENTIAL VORTICITY BUDGETS

In Chapter 41 we studied properties of the *Ertel potential vorticity*, $Q = \rho^{-1}\,\boldsymbol{\omega}_{\mathrm{a}} \cdot \nabla\chi$, which is the specific volume times the projection of the absolute vorticity, $\boldsymbol{\omega}_{\mathrm{a}}$, onto the gradient of a scalar field, $\nabla\chi$. For a perfect fluid (i.e., no friction, heating, or diffusion) with $\nabla\chi$ orthogonal to the baroclinicity vector, $\boldsymbol{B} = \rho^{-2}\,\nabla\rho \times \nabla p$, and if χ is itself materially invariant, then Q is a material invariant: $\mathrm{D}Q/\mathrm{D}t = 0$, meaning that Q remains constant when following a fluid particle. In geophysical fluid mechanics, it is common to define potential vorticity with χ equal to the specific entropy (for the atmosphere) or Archimedean buoyancy (for the ocean). Specific entropy and buoyancy are thermodynamic tracers that are a function of the fluid state (e.g., temperature, pressure, salinity), whereas potential vorticity is a function of the flow (via the absolute vorticity). It is remarkable that a materially invariant property of the fluid can, if it annihilates baroclinicity, generate a materially invariant property of the flow.

In this chapter we develop finite volume budgets for *potential vorticity substance*, $\int_{\mathcal{R}} Q\,\rho\,\mathrm{d}V$, with such budgets fundamentally affected by the *impermeability theorem* respected by the potential vorticity flux, $\boldsymbol{J}^{\mathrm{Q}}$. Impermeability says that there is identically zero potential vorticity flux crossing χ-isosurfaces, with this property holding even when there are mass and thermal fluxes crossing χ-isosurfaces. Such generality signals the kinematic nature of impermeability, which ultimately follows from the non-divergent nature of vorticity. It offers further insight into why, as developed in Section 42.4, the volume integrated PV-substance, $\int_{\mathcal{R}} Q\,\rho\,\mathrm{d}V$, changes only when χ surfaces intersect a boundary.

Impermeability and material invariance are two aspects of potential vorticity that are easily confused. Here we summarize their basic elements that are explored within this chapter.

- The potential vorticity flux, $\boldsymbol{J}^{\mathrm{Q}}$, does not cross χ isosurfaces, and this property is referred to as impermeability. Impermeability holds for all flows, even with irreversible processes and with $\mathrm{D}\chi/\mathrm{D}t \neq 0$. Hence, any closed volume, $\mathcal{R}_\chi$, moving with velocity, $\boldsymbol{v}_Q = \boldsymbol{J}^{\mathrm{Q}}/(\rho\,Q)$, maintains a constant $\int_{\mathcal{R}_\chi} \rho\,Q\,\mathrm{d}V$, so that the addition or removal of mass to the region only dilutes or concentrates the potential vorticity substance. This finite domain conservation of potential vorticity substance is a kinematic property that follows from the non-divergent nature of absolute vorticity, or, equivalently, since $\rho\,Q = \boldsymbol{\omega}_{\mathrm{a}} \cdot \nabla\chi = \nabla \cdot (\boldsymbol{\omega}_{\mathrm{a}}\,\chi)$ equals to a divergence.

- Material invariance of potential vorticity, $\mathrm{D}Q/\mathrm{D}t = 0$, holds for a perfect fluid and for Q that is defined according to a materially constant scalar field, χ, that annihilates baroclinicity via $\rho^{-2}\,(\nabla\rho \times \nabla p) \cdot \nabla\chi = 0$. Material conservation of potential vorticity is a local property holding for each fluid particle, and as such it is a far more restrictive property than impermeability and the associated finite volume conservation of potential vorticity substance.

CHAPTER GUIDE

The goal of this chapter is to fill in the conceptual and technical details needed to understand the above two bullet points about finite volume and local conservation properties of potential vorticity. We build from the potential vorticity mechanics introduced in Chapter 41, and make use of vector calculus summarized in Chapter 2. This chapter is an essential read for those interested in potential vorticity theory and potential vorticity budgets. Further study of these topics are summarized by *Müller* (1995).

42.1 Loose threads

- Make a table with PV and PV fluxes. They can get rather confusing.

- *Callies and Ferrari* (2018) and bottom mixing induced circulation. Connect the thermal wind next to the bottom, inducing flow counter to Kelvin waves, to the potential vorticity boundary fluxes in Section 42.5.3. Discuss the spin up experiment in Section 4 of *Callies and Ferrari* (2018) from a potential vorticity perspective. Note the role of bottom friction in enabling the bottom buoyancy mixing to impart potential vorticity to the flow. without friction then there would be no way to introduce potential vorticity to the flow. That then couples the buoyancy mixing to the friction. *Callies and Ferrari* (2018) also note that to satisfy $\hat{\boldsymbol{n}} \cdot \nabla b = 0$ requires friction. I do not understand that fully, but must be related to this potential vorticity argument.

42.2 Variations on the impermeability theorem

In this section we derive the impermeabity theorem satisfied by the potential vorticity flux vector. We illustrate the theorm for a variety of potential vorticity flux vectors that differ by a gauge function. So although these fluxes have identical divergences, the physical content of the fluxes is distinct. Consequently, one may choose to use a particular flux depending on the context of their use. We return to this point in Section 42.5.6.

42.2.1 Impermeability for the Haynes-McIntyre potential vorticity flux

We start with the flux-form evolution equation for PV-substance given by equation (41.49)

$$\partial_t(\rho\, Q) + \nabla\cdot \boldsymbol{J}^{\mathrm{Q}} = 0 \qquad \text{with} \qquad \boldsymbol{J}^{\mathrm{Q}} = \rho\, \boldsymbol{v}\, Q - \dot{\chi}\, \boldsymbol{\omega}_{\mathrm{a}} + \nabla\chi \times \boldsymbol{F}, \tag{42.1}$$

with $\dot{\chi} = \mathrm{D}\chi/\mathrm{D}t$, and with the PV-substance flux vector, $\boldsymbol{J}^{\mathrm{Q}}$, given in the form examined in *Haynes and McIntyre* (1987).[1] Following the derivation in *Haynes and McIntyre* (1987), we decompose the velocity into two components, one oriented parallel to constant χ surfaces and one oriented perpendicular

$$\boldsymbol{v}_{\parallel} = \boldsymbol{v} - \hat{\boldsymbol{n}}\,(\boldsymbol{v}\cdot\hat{\boldsymbol{n}}) \qquad \text{and} \qquad \boldsymbol{v}_{\perp} = -\frac{\hat{\boldsymbol{n}}\,\partial\chi/\partial t}{|\nabla\chi|} \qquad \Longrightarrow \boldsymbol{v} = \boldsymbol{v}_{\parallel} + \boldsymbol{v}_{\perp} + \frac{\hat{\boldsymbol{n}}\,\dot{\chi}}{|\nabla\chi|} \tag{42.2}$$

where

$$\hat{\boldsymbol{n}} = \nabla\chi/|\nabla\chi| \tag{42.3}$$

is the unit normal vector for χ-isosurfaces. By construction, the velocity $\boldsymbol{v}_{\perp}$ satisfies

$$(\partial_t + \boldsymbol{v}_{\perp}\cdot\nabla)\,\chi = 0. \tag{42.4}$$

Hence, according to the kinematics detailed in Section 19.6.2,

$$\boldsymbol{v}_{\perp}\cdot\hat{\boldsymbol{n}} = \boldsymbol{v}_{\chi}\cdot\hat{\boldsymbol{n}}, \tag{42.5}$$

where $\boldsymbol{v}_{\chi}$ is the velocity of a point fixed on a constant χ surface. That is, $\boldsymbol{v}_{\perp}$ provides a measure of the velocity for a point following a constant χ surface, even as that surface moves through the fluid. We make use of this key identity below.

With the velocity decomposition (42.2), the PV-substance flux vector takes the form

$$\begin{aligned}
\boldsymbol{J}^{\mathrm{Q}} &= \rho\, \boldsymbol{v}\, Q - \dot{\chi}\, \boldsymbol{\omega}_{\mathrm{a}} + \nabla\chi\times\boldsymbol{F} && \text{(42.6a)}\\
&= \left[\boldsymbol{v}_{\parallel} + \boldsymbol{v}_{\perp} + \frac{\dot{\chi}\,\nabla\chi}{|\nabla\chi|^2}\right]\rho\, Q - \dot{\chi}\,\boldsymbol{\omega}_{\mathrm{a}} + \nabla\chi\times\boldsymbol{F} && \text{(42.6b)}\\
&= (\boldsymbol{v}_{\parallel} + \boldsymbol{v}_{\perp})\,\rho Q - \dot{\chi}\,[\boldsymbol{\omega}_{\mathrm{a}} - (\boldsymbol{\omega}_{\mathrm{a}}\cdot\hat{\boldsymbol{n}})\,\hat{\boldsymbol{n}}] + \nabla\chi\times\boldsymbol{F} && \text{(42.6c)}\\
&= (\boldsymbol{v}_{\parallel} + \boldsymbol{v}_{\perp})\,\rho Q - \dot{\chi}\,(\boldsymbol{\omega}_{\mathrm{a}})_{\parallel} + \nabla\chi\times\boldsymbol{F} && \text{(42.6d)}\\
&= \underbrace{\boldsymbol{v}_{\perp}\,\rho\, Q}_{\boldsymbol{J}_{\perp}} + \underbrace{\left[\rho\, Q\,\boldsymbol{v}_{\parallel} - \dot{\chi}\,(\boldsymbol{\omega}_{\mathrm{a}})_{\parallel}\right] + \nabla\chi\times\boldsymbol{F}}_{\boldsymbol{J}_{\parallel}} && \text{(42.6e)}\\
&\equiv \boldsymbol{J}_{\perp} + \boldsymbol{J}_{\parallel}, && \text{(42.6f)}
\end{aligned}$$

where

$$(\boldsymbol{\omega}_{\mathrm{a}})_{\parallel} = \boldsymbol{\omega}_{\mathrm{a}} - (\boldsymbol{\omega}_{\mathrm{a}}\cdot\hat{\boldsymbol{n}})\,\hat{\boldsymbol{n}} = \boldsymbol{\omega}_{\mathrm{a}} - \left[\frac{\boldsymbol{\omega}_{\mathrm{a}}\cdot\nabla\chi}{|\nabla\chi|^2}\right]\nabla\chi = \boldsymbol{\omega}_{\mathrm{a}} - \frac{\rho\, Q}{|\nabla\chi|}\,\hat{\boldsymbol{n}}. \tag{42.7}$$

[1] Following *Haynes and McIntyre* (1987), we set the gauge function, $\boldsymbol{A}$, to zero in equation (42.1).

The above results motivate us to write the PV-substance budget equation (42.1) in the form

$$\partial_t(\rho\, Q) + \nabla \cdot (\boldsymbol{v}_{\mathrm{Q}}\, \rho\, Q) = 0, \tag{42.8}$$

where

$$\begin{aligned}
\boldsymbol{v}_{\mathrm{Q}} &\equiv \frac{\boldsymbol{J}^{\mathrm{Q}}}{\rho\, Q} && \text{definition of } \boldsymbol{v}_{\mathrm{Q}} && \text{(42.9a)}\\
&= \boldsymbol{v} + \frac{-\dot{\chi}\, \boldsymbol{\omega}_{\mathrm{a}} + \nabla\chi \times \boldsymbol{F}}{\rho\, Q} && \text{equation (42.1)} && \text{(42.9b)}\\
&= \boldsymbol{v}_{\perp} + \boldsymbol{v}_{\parallel} + \frac{-\dot{\chi}\, (\boldsymbol{\omega}_{\mathrm{a}})_{\parallel} + \nabla\chi \times \boldsymbol{F}}{\rho\, Q} && \text{equation (42.6e)}, && \text{(42.9c)}
\end{aligned}$$

so that $\boldsymbol{v}_{\mathrm{Q}}$ is the velocity that advects the PV-substance through the fluid. A direct calculation shows that $\boldsymbol{v}_{\mathrm{Q}}$ satisfies the following property

$$\boldsymbol{v}_{\mathrm{Q}} \cdot \hat{\boldsymbol{n}} = \boldsymbol{v}_{\perp} \cdot \hat{\boldsymbol{n}} = \boldsymbol{v}_{\chi} \cdot \hat{\boldsymbol{n}}, \tag{42.10}$$

where the final equality made use of the identity (42.5). As a result, $\boldsymbol{v}_{\mathrm{Q}}$ has a normal component that is identical to that of the velocity of a point fixed on the χ surface

$$(\partial_t + \boldsymbol{v}_{\mathrm{Q}} \cdot \nabla)\, \chi = 0. \tag{42.11}$$

We depict this result in Figure 42.1, whereby the PV-substance flux never crosses the χ-isosurface, even as the surface moves and even in the presence of processes that allow for matter and thermal properties to cross the surface. This result holds since the χ-isosurface moves in a way to precisely track the PV-substance flux. In general, χ surfaces are permeable to matter and thermal properties but, as we have just shown, are impermeable to PV-substance. This is a rather remarkable kinematic result that has important implications for budgets of PV-substance within regions bounded by constant χ surfaces.

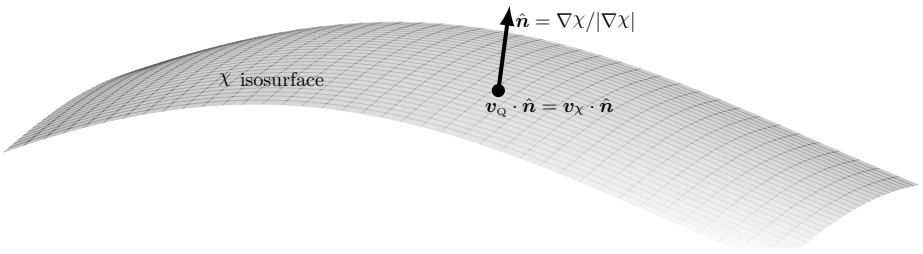

FIGURE 42.1: The flux, $\boldsymbol{J}^{\mathrm{Q}}$, of PV-substance, $\rho\, Q = \nabla \cdot (\chi\, \boldsymbol{\omega}_{\mathrm{a}})$, does not penetrate a surface of constant χ. This kinematic result follows since the effective velocity of PV-substance, $\boldsymbol{v}_{\mathrm{Q}} = \boldsymbol{J}^{\mathrm{Q}}/(\rho\, Q)$, has the same normal component as a point fixed on a χ surface, $\boldsymbol{v}_{\mathrm{Q}} \cdot \hat{\boldsymbol{n}} = \boldsymbol{v}_{\chi} \cdot \hat{\boldsymbol{n}}$. Consequently, the χ surface moves in a manner so that no flux of PV-substance crosses the surface, even in the presence of irreversible processes. This result is known as the impermeability theorem since χ surfaces are impermeable to the flux of PV-substance, even though they are permeable to matter and thermal properties.

42.2.2 A kinematic derivation of impermeability

The derivation of impermeability in Section 42.2.1 follows that given by *Haynes and McIntyre* (1987). We now complement that derivation by an alternative that emphasizes the kinematic origins of impermeability. For that purpose, we make no use of the vorticity equation or the equation for χ. Instead, we merely use the definition of potential vorticity and the non-divergence property of absolute vorticity. This derivation follows our discussion of gauge freedom introduced in Section 41.4.3, as well as the discussion of potential vorticity for a hydrostatic Boussinesq ocean in Section 41.5.

The key identity we need was already given by equation (41.11)

$$\rho Q = \boldsymbol{\omega}_a \cdot \nabla \chi = \nabla \cdot (\boldsymbol{\omega}_a \chi), \tag{42.12}$$

thus revealing that ρQ is a pure divergence. Taking the Eulerian time derivative then leads to

$$\partial_t (\rho Q) = -\nabla \cdot \boldsymbol{J}^{\text{kin}}, \tag{42.13}$$

where

$$\boldsymbol{J}^{\text{kin}} = -\partial_t (\boldsymbol{\omega}_a \chi) \tag{42.14}$$

is the kinematic form of the PV-substance flux. By construction, this flux vanishes in the steady state

$$\boldsymbol{J}^{\text{kin}} = 0 \qquad \text{in steady state,} \tag{42.15}$$

which certainly contrasts to the steady state Haynes-McIntyre flux given by equation (42.1).

Introducing the velocity seen from an inertial reference frame (also called the absolute velocity (Section 13.7.1)

$$\boldsymbol{v}_a = \boldsymbol{v} + \boldsymbol{\Omega} \times \boldsymbol{x} \tag{42.16}$$

leads to

$$-(\partial_t \boldsymbol{\omega}_a)\chi = -\partial_t (\nabla \times \boldsymbol{v}_a)\chi = -(\nabla \times \partial_t \boldsymbol{v}_a)\chi = -\nabla \times (\partial_t \boldsymbol{v}_a \chi) + \nabla\chi \times \partial_t \boldsymbol{v}_a. \tag{42.17}$$

Dropping the total curl (which amounts to choosing a gauge function) yields the modified kinematic form for the PV-substance flux

$$\widetilde{\boldsymbol{J}}^{\text{kin}} = -\partial_t \boldsymbol{v}_a \times \nabla\chi - \boldsymbol{\omega}_a \, \partial_t \chi. \tag{42.18}$$

It follows that

$$\widetilde{\boldsymbol{v}}^{\text{kin}} \cdot \hat{\boldsymbol{n}} = \frac{\widetilde{\boldsymbol{J}}^{\text{kin}} \cdot \hat{\boldsymbol{n}}}{\rho Q} = -\frac{\boldsymbol{\omega}_a \cdot \nabla\chi}{\rho Q} \frac{\partial \chi}{\partial t} \frac{1}{|\nabla\chi|} = -\frac{\partial \chi}{\partial t} \frac{1}{|\nabla\chi|} = \boldsymbol{v}_\chi \cdot \hat{\boldsymbol{n}}, \tag{42.19}$$

which is the same result (42.10) as found for the Haynes-McIntyre flux. This result allows us to conclude that $\widetilde{\boldsymbol{J}}^{\text{kin}}$ satisfies the impermeability theorem. We again emphasize that there has been no use of the dynamical equations for vorticity or for χ. Instead, this expression of impermeability only used the definition of potential vorticity, along with the non-divergent nature of vorticity, $\nabla \cdot \boldsymbol{\omega}_a = 0$.

Throughout this discussion, we assumed χ to be an arbitrary smooth scalar field. Hence, *any* scalar field used to project out a component of the absolute vorticity has its iso-surfaces impenetrable to the flux of the corresponding component of absolute vorticity. This result trivializes the impermeability theorem from a mathematical perspective. In Section 40.3.4 we somewhat anticipated this result when studying the Cartesian components of the absolute vorticity (see also Section 5 of *Haynes and McIntyre* (1987)). This trivial mathematical result does not reduce the importance of the entropic potential vorticity impermeability theorem for

studying stratified fluid flows. The importance holds since this particular potential vorticity has direct connection to dynamics and thermodynamics.

42.2.3 Comments

The impermeability theorem was introduced by *Haynes and McIntyre* (1987). Their paper was met by some confusion thus prompting them to write *Haynes and McIntyre* (1990). Besides exposing the purely kinematic aspects of impermeability, the presentation in this section reveals that there are multiple potential vorticity flux vectors that satisfy impermeability, with the vectors differing by a gauge transformation. Which flux vector is prefered depends on the application, with *Bretherton and Schär* (1993), *Davies-Jones* (2003a), and *Marshall et al.* (2001) proposing criteria favoring one form over another. We pursue such considerations in Section 42.3.

42.3 Impermeability theorem for seawater

As seen from Section 42.2.2, impermeability holds for any component of vorticity and the corresponding scalar isosurface. In contrast, material invariance of potential vorticity requires a materially conserved scalar to annihilate the baroclinicity vector (e.g., Section 41.1.4). Consequently, material invariance is much tougher to satisfy than impermeability. Indeed, as shown in Section 41.2, there is no materially invariant potential vorticity for an ocean with a realistic nonlinear equation of state (EOS). Hence, there is no materially invariant potential vorticity for the ocean even in the absence of irreversible processes. Nevertheless, one can define an ocean potential vorticity according to any scalar field, such as potential density, and still make use of the impermeability theorem when performing a potential vorticity budget. We here expose the details.

42.3.1 Ocean potential vorticity in terms of potential density

Following *Marshall et al.* (2001), we introduce an ocean potential vorticity field according to

$$Q^{\text{ocn}} = \rho^{-1} \nabla b \cdot \boldsymbol{\omega}_{\text{a}}, \tag{42.20}$$

where the Archimedean buoyancy field, b, is approximated by a chosen potential density (see Section 30.3.4). As shown in Section 41.2, a globally defined buoyancy does not annihilate the baroclinicity vector for a realistic seawater equation of state

$$\boldsymbol{B} \cdot \nabla b = [-\nabla(1/\rho) \times \nabla p] \cdot \nabla b \neq 0. \tag{42.21}$$

Consequently, $\mathrm{D}Q^{\text{ocn}}/\mathrm{D}t \neq 0$ even in the absence of irreversible processes. Nonetheless, the Eulerian budget for PV-substance satisfies

$$\partial_t(\rho\, Q^{\text{ocn}}) = -\nabla \cdot \widetilde{\boldsymbol{J}}^{\text{Q-ocn}}, \tag{42.22}$$

and $\widetilde{\boldsymbol{J}}^{\text{Q-ocn}}$ satisfies the impermeability theorem for b-surfaces. A flux-form budget equation greatly facilitates the study of budgets for PV-substance even within an ocean with a realistic equation of state. Derivation of the flux-form equation (42.22) follows from the discussion in Section 42.2.2, where we know that the kinematic flux

$$\widetilde{\boldsymbol{J}}^{\text{Q-ocn}} = -\partial_t \boldsymbol{v}_{\text{a}} \times \nabla b - \boldsymbol{\omega}_{\text{a}}\, \partial_t b = -\partial_t \boldsymbol{v} \times \nabla b - \boldsymbol{\omega}_{\text{a}}\, \partial_t b \tag{42.23}$$

satisfies the impermeability theorem for b-surfaces and whose convergence drives the time tendency for the PV-substance. Note that the second equality in equation (42.23) follows since

$$\partial_t \boldsymbol{v}_{\mathrm{a}} = \partial_t(\boldsymbol{v} + \boldsymbol{\Omega} \times \boldsymbol{x}) = \partial_t \boldsymbol{v}, \tag{42.24}$$

given that the Eulerian time derivative is computed at a fixed position, $\boldsymbol{x}$, and the planetary rotation is assumed constant, $\partial_t \boldsymbol{\Omega} = 0$.

42.3.2 A modified PV-substance flux

The kinematic flux (42.23) vanishes in the steady state. We here motivate a gauge transformed flux that leads to the same flux divergence yet that renders a nonzero steady state flux. For this purpose, make use of the vector-invariant velocity equation (equation (40.33))

$$\partial_t \boldsymbol{v} + \boldsymbol{\omega}_{\mathrm{a}} \times \boldsymbol{v} = -\rho^{-1} \nabla p - \nabla \mathcal{M} + \boldsymbol{F}, \tag{42.25}$$

where

$$\mathcal{M} = \boldsymbol{v} \cdot \boldsymbol{v}/2 + \Phi \tag{42.26}$$

is the mechanical energy per mass of a fluid element. Bringing the pressure term inside of the gradient operator leads to

$$\partial_t \boldsymbol{v} + \boldsymbol{\omega}_{\mathrm{a}} \times \boldsymbol{v} = p \nabla(1/\rho) - \nabla(\mathcal{M} + p/\rho) + \boldsymbol{F}. \tag{42.27}$$

Following our treatment of the hydrostatic Boussinesq ocean in Section 41.5.4, we introduce the Bernoulli function[2]

$$B = \mathcal{M} + p/\rho. \tag{42.28}$$

The vector-invariant velocity equation (42.27) thus leads to the cross-product

$$\begin{aligned}
\partial_t \boldsymbol{v} \times \nabla b &= -(\boldsymbol{\omega}_{\mathrm{a}} \times \boldsymbol{v}) \times \nabla b + [p \nabla(1/\rho) - \nabla(\mathcal{M} + p/\rho) + \boldsymbol{F}] \times \nabla b && \text{(42.29a)} \\
&= -(\nabla b \cdot \boldsymbol{\omega}_{\mathrm{a}})\, \boldsymbol{v} + (\nabla b \cdot \boldsymbol{v})\, \boldsymbol{\omega}_{\mathrm{a}} + [p \nabla(1/\rho) - \nabla(\mathcal{M} + p/\rho) + \boldsymbol{F}] \times \nabla b && \text{(42.29b)} \\
&= -\boldsymbol{v}\, \rho\, Q^{\mathrm{ocn}} + (\dot{b} - \partial_t b)\, \boldsymbol{\omega}_{\mathrm{a}} + [p \nabla(1/\rho) - \nabla(\mathcal{M} + p/\rho) + \boldsymbol{F}] \times \nabla b. && \text{(42.29c)}
\end{aligned}$$

Use of this result leads to the flux (42.23)

$$\begin{aligned}
\widetilde{\boldsymbol{J}}^{\text{Q-ocn}} &= -\partial_t \boldsymbol{v} \times \nabla b - \boldsymbol{\omega}_{\mathrm{a}}\, \partial_t b && \text{(42.30a)} \\
&= \boldsymbol{v}\, \rho\, Q^{\mathrm{ocn}} - \dot{b}\, \boldsymbol{\omega}_{\mathrm{a}} - \boldsymbol{F} \times \nabla b + [\nabla(\mathcal{M} + p/\rho) - p \nabla(1/\rho)] \times \nabla b && \text{(42.30b)} \\
&= \boldsymbol{J}^{\mathrm{Q}} + [\nabla(\mathcal{M} + p/\rho) - p \nabla(1/\rho)] \times \nabla b, && \text{(42.30c)}
\end{aligned}$$

where $\boldsymbol{J}^{\mathrm{Q}}$ is the Haynes-McIntyre form of the PV-substance flux given by equation (42.1). The term

$$\nabla(\mathcal{M} + p/\rho) \times \nabla b = \nabla \times [(\mathcal{M} + p/\rho) \nabla b] \tag{42.31}$$

is a total curl and as such it can be moved around without altering the evolution of PV-substance. Furthermore, since it is parallel to buoyancy isosurfaces it does not alter the impermeability properties of the PV-substance flux.

Marshall et al. (2001) focused attention on the flux

$$\boldsymbol{J}^{\mathrm{marshall}} = \widetilde{\boldsymbol{J}}^{\text{Q-ocn}} - \nabla(\mathcal{M} + p/\rho) \times \nabla b = -[\partial_t \boldsymbol{v} + \nabla(\mathcal{M} + p/\rho)] \times \nabla b - \boldsymbol{\omega}_{\mathrm{a}}\, \partial_t b. \tag{42.32}$$

[2]The Bernoulli potential, $\mathcal{B}$, arises from an analysis of the total energy budget as in equation (26.104), where we see that the Bernoulli potential in a compressible (non-Boussinesq) fluid, $\mathcal{B} = \mathcal{M} + p/\rho + \mathcal{I}$, also includes the internal energy per mass, $\mathcal{I}$. However, the internal energy is missing from equation (42.28), thus motivating our use of the terminology "a Bernoulli function" rather than "the Bernoulli potential".

Since $\boldsymbol{J}^{\text{marshall}}$ differs from $\widetilde{\boldsymbol{J}}^{\text{Q-ocn}}$ by a total curl, their divergences are equal. Diagnostically desirable features of $\boldsymbol{J}^{\text{marshall}}$ include the following:

- $\nabla b \cdot \boldsymbol{J}^{\text{marshall}}/(\rho\, Q) = \partial_t b$, thus satisfying the impermeability theorem.
- $\boldsymbol{J}^{\text{marshall}}$ has no explicit reference to irreversible processes. Consequently, in some cases it can be simpler to diagnose than the Haynes-McIntyre flux, $\boldsymbol{J}^{\text{Q}}$.
- In a steady state, the flux is given by

$$\boldsymbol{J}^{\text{marshall}} = \nabla b \times \nabla(\mathcal{M} + p/\rho) = \nabla \times [b\, \nabla(\mathcal{M} + p/\rho)]. \tag{42.33}$$

  Consequently, $\mathcal{M} + p/\rho$ provides a streamfunction for the steady state flux on buoyancy surfaces. As emphasized by *Schär* (1993), this result holds even when there are irreversible processes, thus providing useful diagnostics even in the presence of dissipation.

42.3.3 Integral constraints for steady state

The steady state PV-substance flux in the form (42.33) can be used to develop some integral constraints on the steady flow. For this purpose consider the steady form of $\boldsymbol{J}^{\text{marshall}}$ and integrate over an arbitrary simply connected area making use of Stokes' theorem

$$\int_{\mathcal{S}} \nabla \times [b\, \nabla B] \cdot \hat{\boldsymbol{n}}\, \mathrm{d}\mathcal{S} = \oint_{\partial \mathcal{S}} b\, \nabla B \cdot \mathrm{d}\boldsymbol{r} = \oint_{\partial \mathcal{S}} b\, \mathrm{d}B = -\oint_{\partial \mathcal{S}} B\, \mathrm{d}b. \tag{42.34a}$$

The first equality made use of Stokes' theorem; the second make use of the identity for exact differentials

$$\nabla B \cdot \mathrm{d}\boldsymbol{r} = \mathrm{d}B; \tag{42.35}$$

and the final equality made use of

$$b\, \mathrm{d}B = \mathrm{d}(b\, B) - B\, \mathrm{d}b \tag{42.36}$$

and noted that the closed loop integral of an exact differential vanishes, so that

$$\oint_{\partial \mathcal{S}} \mathrm{d}(B\, b) = 0. \tag{42.37}$$

If we can find a closed contour where either B is a constant ($\mathrm{d}B = 0$), or the buoyancy is a constant ($\mathrm{d}b = 0$), then we have the steady state constraint

$$\int_{\mathcal{S}} \boldsymbol{J}^{\text{marshall}} \cdot \hat{\boldsymbol{n}}\, \mathrm{d}\mathcal{S} = 0 \qquad \text{area enclosed by contour with } \mathcal{M} + p/\rho \text{ constant or } b \text{ constant.} \tag{42.38}$$

In regions where there are such closed contours, this constraint offers useful insight into the steady state balances. *Marshall* (2000) and *Polton and Marshall* (2007) make particular use of closed B contours on constant depth surfaces (so that $\hat{\boldsymbol{n}} = \hat{\boldsymbol{z}}$) in a Boussinesq ocean.

42.3.4 Further study

Marshall et al. (2001) builds from the generalized Bernoulli theorem of *Schär* (1993) and *Bretherton and Schär* (1993). We also consider these topics for a hydrostatic Boussinesq ocean in Section 41.5.4.

42.4 Integrated potential vorticity substance

In this section we derive some properties of integrated potential vorticity, with these properties merely the result of how potential vorticity is defined. We write potential vorticity using a global buoyancy field, b, as in our discussion of ocean potential vorticity in Section 42.3

$$\rho Q = \boldsymbol{\omega}_{\mathrm{a}} \cdot \nabla b = \nabla \cdot (\boldsymbol{\omega}_{\mathrm{a}}\, b) = \nabla \cdot [(\boldsymbol{\omega} + 2\,\boldsymbol{\Omega})\, b]. \tag{42.39}$$

The following points are central to the results derived in this section, and they all follow from the non-divergent nature of the absolute vorticity.

- The divergence form given in the second and third equalities of equation (42.39) is the starting point for the derivations in this section. Indeed, as emphasized by *Morel et al.* (2019), the divergence form is appropriate for deriving discrete approximations since in this case the discrete potential vorticity also satisfies the properties developed in this section.
- As emphasized in Section 42.2, the properties in this section hold for any smooth scalar field that is used to define the potential vorticity.
- The properties in this section hold even when there is no materially invariant potential vorticity since we only make use of the non-divergent nature of the absolute vorticity.

42.4.1 The primary role of boundaries

Integral in terms of boundary vorticity and boundary buoyancy

We consider Q to be an intensive fluid propery measuring the amount of PV-substance per unit mass (i.e., the concentration of PV-substance), and correspondingly with ρQ the amount of PV-substance per volume.[3] With this interpretation, the amount of PV-substance within an arbitrary finite region is determined by the volume integral of ρQ

$$\mathcal{I} = \int_{\mathcal{R}} Q\, \rho \, \mathrm{d}V = \int_{\mathcal{R}} \nabla \cdot (\boldsymbol{\omega}_{\mathrm{a}}\, b)\, \mathrm{d}V = \oint_{\partial \mathcal{R}} b\, \boldsymbol{\omega}_{\mathrm{a}} \cdot \hat{\boldsymbol{n}}\, \mathrm{d}\mathcal{S}, \tag{42.40}$$

where the final equality used Gauss's divergence theorem. Hence, the volume integrated PV-substance in a region is determined solely by values of the absolute vorticity and buoyancy on the region boundary. This property is strikingly distinct from material tracers. In practice it can be useful to decompose the absolute vorticity into the relative vorticity plus planetary vorticity

$$\mathcal{I} = \int_{\mathcal{R}} Q\, \rho \, \mathrm{d}V = \oint_{\partial \mathcal{R}} b\, \boldsymbol{\omega}_{\mathrm{a}} \cdot \hat{\boldsymbol{n}}\, \mathrm{d}\mathcal{S} = \oint_{\partial \mathcal{R}} b\, \boldsymbol{\omega} \cdot \hat{\boldsymbol{n}}\, \mathrm{d}\mathcal{S} + \oint_{\partial \mathcal{R}} b\, 2\,\boldsymbol{\Omega} \cdot \hat{\boldsymbol{n}}\, \mathrm{d}\mathcal{S}. \tag{42.41}$$

Integral in terms of boundary velocity and boundary buoyancy gradient

We follow *Morel et al.* (2019) by deriving an alternative expression for $\mathcal{I}$ in equation (42.41), with this alternative expression more convenient in some cases. For this purpose we write

$$b\,\boldsymbol{\omega} = b\,\nabla \times \boldsymbol{v} = \nabla \times (b\,\boldsymbol{v}) - \nabla b \times \boldsymbol{v}, \tag{42.42}$$

and use the divergence theorem to eliminate the total curl term (see Section 2.7.6)

$$\oint_{\partial \mathcal{R}} \nabla \times (b\,\boldsymbol{v}) \cdot \hat{\boldsymbol{n}}\, \mathrm{d}\mathcal{S} = \int_{\mathcal{R}} \nabla \cdot [\nabla \times (b\,\boldsymbol{v})]\, \mathrm{d}V = 0. \tag{42.43}$$

[3] Recall our discussion of extensive and intensive fluid properties in Section 20.2.1.

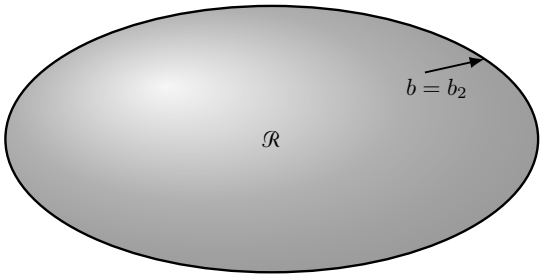

FIGURE 42.2: Integrating PV-substance over regions bounded by constant buoyancy surfaces that do not intersect the ground. Here we show a single buoyancy surface, $b = b_2$, bounding the bubble-like fluid region, $\mathcal{R}$. Notably, the region inside the bubble generally has a nontrivial buoyancy distribution. The only assumption is that it is wholly contained inside the $b = b_2$ contour. There is identically zero domain integrated potential vorticity in $\mathcal{R}$. Hence, if there is any nontrivial distribution of potential vorticity somewhere in the domain, there must be as much integrated positive values as there are negative.

We are thus led to the equivalent expressions for the integrated potential vorticity substance

$$\mathcal{I} = \int_{\mathcal{R}} Q\,\rho\,\mathrm{d}V = \oint_{\partial\mathcal{R}} b\,\boldsymbol{\omega}\cdot\hat{\boldsymbol{n}}\,\mathrm{d}\mathcal{S} + 2\oint_{\partial\mathcal{R}} b\,\boldsymbol{\Omega}\cdot\hat{\boldsymbol{n}}\,\mathrm{d}\mathcal{S} = -\oint_{\partial\mathcal{R}} (\nabla b\times\boldsymbol{v})\cdot\hat{\boldsymbol{n}}\,\mathrm{d}\mathcal{S} + 2\oint_{\partial\mathcal{R}} b\,\boldsymbol{\Omega}\cdot\hat{\boldsymbol{n}}\,\mathrm{d}\mathcal{S}. \tag{42.44}$$

In effect, the alternative forms move the derivative operator between the boundary velocity (for computing the relative vorticity) and the boundary buoyancy. One formulation may be more convenient than the other, depending on the boundary conditions. We emphasize that once a particular formulation is chosen, it is necessary to use that formulation for all of the domain boundaries. We must do so since the curl term that moves us from one form to the other vanishes only when integrating over the full domain boundary.

42.4.2 Region bounded by a single buoyancy surface

Consider a volume of fluid bounded by a single buoyancy surface as shown in the bubble-like region in Figure 42.2. Since the outer boundary of the region is set by a constant b-surface, we can pull b outside of the surface integral in equation (42.44) so that

$$\mathcal{I} = \oint_{\partial\mathcal{R}} \boldsymbol{\omega}_{\mathrm{a}}\,b\cdot\hat{\boldsymbol{n}}\,\mathrm{d}\mathcal{S} = b_2\oint_{\partial\mathcal{R}} \boldsymbol{\omega}_{\mathrm{a}}\cdot\hat{\boldsymbol{n}}\,\mathrm{d}\mathcal{S}. \tag{42.45}$$

We can now use the divergence theorem to return to the volume integral, only now with b outside of the integral

$$\mathcal{I} = b_2\int_{\mathcal{R}} \nabla\cdot\boldsymbol{\omega}_{\mathrm{a}}\,\mathrm{d}V = 0, \tag{42.46}$$

where $\nabla\cdot\boldsymbol{\omega}_{\mathrm{a}} = 0$ led to the final equality. Equivalently, we can use Stokes' theorem to convert the closed area integral, $\oint_{\partial\mathcal{R}} \boldsymbol{\omega}_{\mathrm{a}}\cdot\hat{\boldsymbol{n}}\,\mathrm{d}\mathcal{S}$, to a line integral around the boundary. However, there is no boundary for the closed area since it covers the sphere, thus again showing that $\mathcal{I} = 0$ (see also Section 2.7.6).

Yet another way to derive the identity (42.46) is to make use of the alternative expression for $\mathcal{I}$ given by equation (42.44)

$$\mathcal{I} = -\oint_{\partial\mathcal{R}} (\nabla b\times\boldsymbol{v})\cdot\hat{\boldsymbol{n}}\,\mathrm{d}\mathcal{S} + 2\oint_{\partial\mathcal{R}} b\,\boldsymbol{\Omega}\cdot\hat{\boldsymbol{n}}\,\mathrm{d}\mathcal{S}. \tag{42.47}$$

Since the domain is bounded by a constant b surface, the outward normal is parallel to ∇b so that the first integral vanishes. Furthermore, since b is a constant in the second integral we are

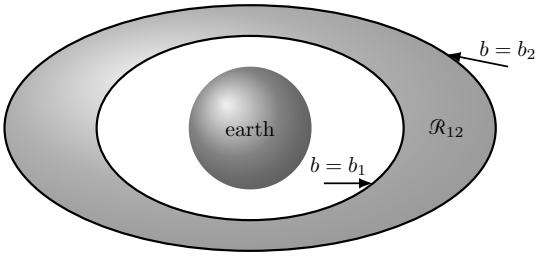

FIGURE 42.3: Integrating PV-substance over regions bounded by constant buoyancy surfaces that do not intersect the ground. Here we show a buoyancy layer or shell, $\mathcal{R}_{12}$, bounded by two buoyancy isosurfaces, $b_1 < b_2$, surrounding the earth, with neither surface intersecting the ground. There is identically zero domain integrated potential vorticity in $\mathcal{R}_{12}$. Hence, if there is any nontrivial distribution of potential vorticity somewhere in the domain, there must be as much integrated positive values as there are negative.

led to consider

$$\oint_{\partial\mathcal{R}} 2\,\boldsymbol{\Omega}\cdot\hat{\boldsymbol{n}}\,\mathrm{d}\mathcal{S} = \oint_{\partial\mathcal{R}} [\nabla\times(\boldsymbol{\Omega}\times\boldsymbol{x})]\cdot\hat{\boldsymbol{n}}\,\mathrm{d}\mathcal{S} = \int_{\mathcal{R}} \nabla\cdot[\nabla\times(\boldsymbol{\Omega}\times\boldsymbol{x})]\,\mathrm{d}V = 0, \tag{42.48}$$

which made use of the divergence theorem and the vanishing divergence of a curl.

The identity (42.46) says that there is zero integrated PV-substance contained within any region bounded by a single buoyancy surface; i.e., a bubble. The result holds whether there are reversible or irreversible processes acting on the buoyancy surface, and it holds if the b-surface is moving in space. Hence, within the domain there is just as much positive PV-substance as there is negative PV-substance. So if potential vorticity changes locally within the domain, then somewhere else it must experience an oppositely signed change so to leave a zero net integrated PV-substance. We emphasize that this result holds at each time instance.

42.4.3 Region bounded by two buoyancy surfaces

The identity (42.46) has a corollary, in which we consider a region bounded by two b-surfaces such as the region $\mathcal{R}_{12}$ shown in Figure 42.3. The above arguments hold for that region as well, since we can decompose the surface integral into two integrals separately over b_1 and b_2

$$\mathcal{I} = \int_{\mathcal{R}_{12}} \nabla\cdot(\boldsymbol{\omega}_{\mathrm{a}}\,b)\,\mathrm{d}V = \int_{\mathcal{R}_2} \nabla\cdot(\boldsymbol{\omega}_{\mathrm{a}}\,b)\,\mathrm{d}V - \int_{\mathcal{R}_1} \nabla\cdot(\boldsymbol{\omega}_{\mathrm{a}}\,b)\,\mathrm{d}V, \tag{42.49}$$

where the domain $\mathcal{R}_1$ extends from the ground up to b_1 and $\mathcal{R}_2$ extends from the ground up to b_2. Integration over the region below b_1 cancels through the subtraction. Indeed, the region below b_1 could be anything without changing the result. So let that region be filled with fluid throughout (i.e., ignore the earth) to allow us to extend both integrals throughout the spherical region just like in the buoyancy bubble $\mathcal{R}$ in Figure 42.3. Invoking the buoyancy bubble result we see that both integrals separately vanish. We are thus led to a vanishing integral for the layer

$$\mathcal{I} = \int_{\mathcal{R}_{12}} \nabla\cdot(\boldsymbol{\omega}_{\mathrm{a}}\,b)\,\mathrm{d}V = 0. \tag{42.50}$$

Again, the key assumption is that no buoyancy surface intersects land, in which case we are able to ignore the presence of land altogether and thus make use of the buoyancy bubble result. The identity (42.50) also follows from the second form of equation (42.44).

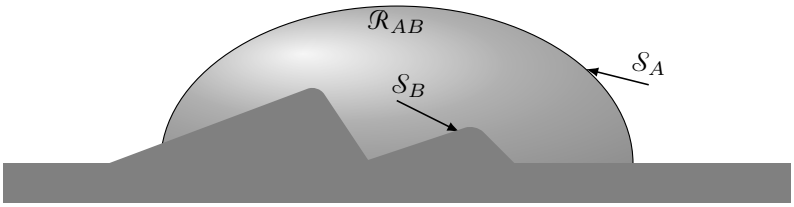

FIGURE 42.4: A fluid region, $\mathcal{R}_{AB}$, bounded by two buoyancy surfaces, $\mathcal{S}_A$ and $\mathcal{S}_B$. The upper surface, $\mathcal{S}_A$, is defined by a buoyancy isosurface, $b = b_A$, with this surface intersecting the ground. The lower surface, $\mathcal{S}_B$, is along the ground (which is generally not flat, as shown here) and has a buoyancy that is a function of space and time, $b = b_B(\boldsymbol{x}, t)$.

42.4.4 Region bounded by land and a buoyancy surface

We now consider a domain consisting of fluid bounded by a buoyancy surface that intersects (incrops) the ground, such as the region shown in Figure 42.4. This atmospheric example can be turned over to produce an ocean example with buoyancy surfaces outcropping at the ocean surface. Using the vorticity form of the integrated potential vorticity in equation (42.44) leads to

$$\mathcal{I} = \int_{\mathcal{R}_{AB}} \nabla \cdot (\boldsymbol{\omega}_{\rm a}\, b)\, \mathrm{d}V \tag{42.51a}$$

$$= \int_{\mathcal{S}_A} \boldsymbol{\omega}_{\rm a}\, b \cdot \hat{\boldsymbol{n}}\, \mathrm{d}\mathcal{S} + \int_{\mathcal{S}_B} \boldsymbol{\omega}_{\rm a}\, b \cdot \hat{\boldsymbol{n}}\, \mathrm{d}\mathcal{S} \tag{42.51b}$$

$$= b_A \int_{\mathcal{S}_A} \boldsymbol{\omega}_{\rm a} \cdot \hat{\boldsymbol{n}}\, \mathrm{d}\mathcal{S} + \int_{\mathcal{S}_B} b\, \boldsymbol{\omega}_{\rm a} \cdot \hat{\boldsymbol{n}}\, \mathrm{d}\mathcal{S} \tag{42.51c}$$

$$= b_A \left[\int_{\mathcal{S}_A} \boldsymbol{\omega}_{\rm a} \cdot \hat{\boldsymbol{n}}\, \mathrm{d}\mathcal{S} + \int_{\mathcal{S}_B} \boldsymbol{\omega}_{\rm a} \cdot \hat{\boldsymbol{n}}\, \mathrm{d}\mathcal{S} - \int_{\mathcal{S}_B} \boldsymbol{\omega}_{\rm a} \cdot \hat{\boldsymbol{n}}\, \mathrm{d}\mathcal{S} \right] + \int_{\mathcal{S}_B} b\, \boldsymbol{\omega}_{\rm a} \cdot \hat{\boldsymbol{n}}\, \mathrm{d}\mathcal{S} \tag{42.51d}$$

$$= b_A \int_{\mathcal{R}_{AB}} \nabla \cdot \boldsymbol{\omega}_{\rm a}\, \mathrm{d}V + \int_{\mathcal{S}_B} (b - b_A)\, \boldsymbol{\omega}_{\rm a} \cdot \hat{\boldsymbol{n}}\, \mathrm{d}\mathcal{S} \tag{42.51e}$$

$$= \int_{\mathcal{S}_B} (b - b_A)\, (\boldsymbol{\omega} + 2\,\boldsymbol{\Omega}) \cdot \hat{\boldsymbol{n}}\, \mathrm{d}\mathcal{S}, \tag{42.51f}$$

where we made use of $\nabla \cdot \boldsymbol{\omega}_{\rm a} = 0$ to reach the final equality. As both the ground and the ocean surface have buoyancy gradients, they contribute to the PV-substance within the region they bound.

For this domain it can be quite useful to use the second form of the integral in equation (42.44). For this purpose we write

$$\int_{\mathcal{S}_B} (b - b_A)\, \boldsymbol{\omega} \cdot \hat{\boldsymbol{n}}\, \mathrm{d}\mathcal{S} = \int_{\mathcal{S}_B + \mathcal{S}_A} (b - b_A)\, \boldsymbol{\omega} \cdot \hat{\boldsymbol{n}}\, \mathrm{d}\mathcal{S} \tag{42.52a}$$

$$= - \int_{\mathcal{S}_B + \mathcal{S}_A} (\nabla b \times \boldsymbol{v}) \cdot \hat{\boldsymbol{n}}\, \mathrm{d}\mathcal{S} \tag{42.52b}$$

$$= - \int_{\mathcal{S}_B} (\nabla b \times \boldsymbol{v}) \cdot \hat{\boldsymbol{n}}\, \mathrm{d}\mathcal{S}. \tag{42.52c}$$

Equation (42.52a) follows from

$$\int_{\mathcal{S}_A} (b - b_A)\, \boldsymbol{\omega} \cdot \hat{\boldsymbol{n}}\, \mathrm{d}\mathcal{S} = 0 \qquad \text{since } b = b_A \text{ on } \mathcal{S}_A. \tag{42.53}$$

Equation (42.52b) follows from the divergence theorem

$$\int_{\mathcal{S}_B+\mathcal{S}_A} \nabla \times [(b-b_A)\,\boldsymbol{v}] \cdot \hat{\boldsymbol{n}}\,\mathrm{d}\mathcal{S} = \int_{\mathcal{R}_{AB}} \nabla \cdot (\nabla \times [(b-b_A)\,\boldsymbol{v}])\,\mathrm{d}V = 0. \tag{42.54}$$

And equation (42.52c) holds since $\hat{\boldsymbol{n}} \times \nabla b = 0$ along $\mathcal{S}_A$. The expression (42.52c) is particularly convenient for the case of a no-slip boundary condition (Section 25.10.3), whereby the velocity vanishes along $\mathcal{S}_B$ so that we are left with the rather tidy expression

$$\mathcal{I} = 2 \int_{\mathcal{S}_B} (b-b_A)\,\boldsymbol{\Omega} \cdot \hat{\boldsymbol{n}}\,\mathrm{d}\mathcal{S} \qquad \text{no-slip condition on } \mathcal{S}_B. \tag{42.55}$$

42.4.5 A layer outcropping at the ocean surface

Figure 42.5 depicts a buoyancy layer that outcrops at the ocean surface at both of its ends. Following the derivation in Section 42.4.4 leads to the integrated PV-substance

$$\mathcal{I}_A \equiv \int_{\mathcal{S}_1+\mathcal{S}_2+\mathcal{S}_3+\mathcal{S}_A} b\,\boldsymbol{\omega}_{\mathrm{a}} \cdot \hat{\boldsymbol{n}}\,\mathrm{d}\mathcal{S} = \int_{\mathcal{S}_1+\mathcal{S}_2+\mathcal{S}_3} (b-b_A)\,\boldsymbol{\omega}_{\mathrm{a}} \cdot \hat{\boldsymbol{n}}\,\mathrm{d}\mathcal{S} \tag{42.56a}$$

$$\mathcal{I}_B \equiv \int_{\mathcal{S}_2+\mathcal{S}_B} b\,\boldsymbol{\omega}_{\mathrm{a}} \cdot \hat{\boldsymbol{n}}\,\mathrm{d}\mathcal{S} = \int_{\mathcal{S}_2} (b-b_B)\,\boldsymbol{\omega}_{\mathrm{a}} \cdot \hat{\boldsymbol{n}}\,\mathrm{d}\mathcal{S}, \tag{42.56b}$$

with the difference leading to the integrated potential vorticity within the layer $\mathcal{R}_{AB}$

$$\mathcal{I}_{AB} \equiv \mathcal{I}_A - \mathcal{I}_B = \int_{\mathcal{R}_{AB}} \rho\, Q\,\mathrm{d}V = \int_{\mathcal{S}_1+\mathcal{S}_3} (b-b_A)\,\boldsymbol{\omega}_{\mathrm{a}} \cdot \hat{\boldsymbol{n}}\,\mathrm{d}\mathcal{S} + (b_B-b_A) \int_{\mathcal{S}_2} \boldsymbol{\omega}_{\mathrm{a}} \cdot \hat{\boldsymbol{n}}\,\mathrm{d}\mathcal{S}. \tag{42.57}$$

The relation (42.57) requires information about the absolute vorticity over the region $\mathcal{S}_2$ that lies outside the outcrop regions. To instead only make use of information over the outcrop areas, $\mathcal{S}_1$ and $\mathcal{S}_3$, we consider buoyancy gradients when considering the contributions from the relative vorticity

$$\begin{aligned} \int_{\mathcal{S}_1+\mathcal{S}_2+\mathcal{S}_3+\mathcal{S}_A} b\,\boldsymbol{\omega} \cdot \hat{\boldsymbol{n}}\,\mathrm{d}\mathcal{S} - \int_{\mathcal{S}_2+\mathcal{S}_B} b\,\boldsymbol{\omega} \cdot \hat{\boldsymbol{n}}\,\mathrm{d}\mathcal{S} \\ = -\int_{\mathcal{S}_1+\mathcal{S}_2+\mathcal{S}_3+\mathcal{S}_A} (\nabla b \times \boldsymbol{v}) \cdot \hat{\boldsymbol{n}}\,\mathrm{d}\mathcal{S} + \int_{\mathcal{S}_2+\mathcal{S}_B} (\nabla b \times \boldsymbol{v}) \cdot \hat{\boldsymbol{n}}\,\mathrm{d}\mathcal{S}. \end{aligned} \tag{42.58}$$

We can drop the integrals along $\mathcal{S}_A$ and $\mathcal{S}_B$ since their respective normals are parallel to ∇b, in which case

$$\int_{\mathcal{S}_1+\mathcal{S}_2+\mathcal{S}_3+\mathcal{S}_A} b\,\boldsymbol{\omega} \cdot \hat{\boldsymbol{n}}\,\mathrm{d}\mathcal{S} - \int_{\mathcal{S}_2+\mathcal{S}_B} b\,\boldsymbol{\omega} \cdot \hat{\boldsymbol{n}}\,\mathrm{d}\mathcal{S} = -\int_{\mathcal{S}_1+\mathcal{S}_3} (\nabla b \times \boldsymbol{v}) \cdot \hat{\boldsymbol{n}}\,\mathrm{d}\mathcal{S}. \tag{42.59}$$

We are thus led to write the layer integrated PV-substance in the form

$$\mathcal{I}_{AB} = -\int_{\mathcal{S}_1+\mathcal{S}_3} (\nabla b \times \boldsymbol{v}) \cdot \hat{\boldsymbol{n}}\,\mathrm{d}\mathcal{S} + \int_{\mathcal{S}_1+\mathcal{S}_3} (b-b_A)\,2\,\boldsymbol{\Omega} \cdot \hat{\boldsymbol{n}}\,\mathrm{d}\mathcal{S} + (b_B-b_A) \int_{\mathcal{S}_2} 2\,\boldsymbol{\Omega} \cdot \hat{\boldsymbol{n}}\,\mathrm{d}\mathcal{S}. \tag{42.60}$$

As desired, this alternative formulation only requires information about the flow field and buoyancy field over the outcrop surfaces, $\mathcal{S}_1$ and $\mathcal{S}_3$. For the region between the outcrops, we only need to know its area and outward normal, with $\hat{\boldsymbol{n}} \approx \hat{\boldsymbol{z}}$ an accurate approximation.

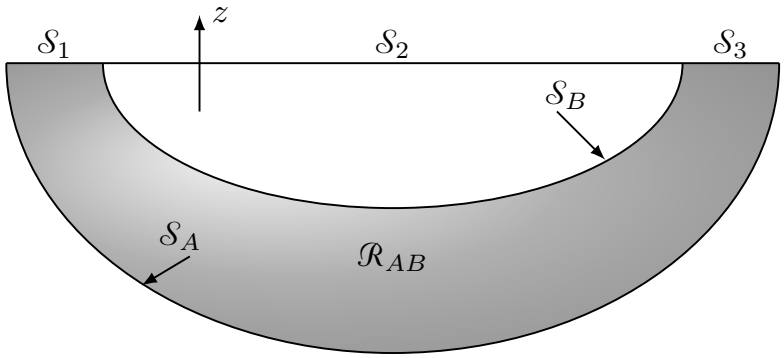

FIGURE 42.5: This figure depicts a buoyancy layer in the ocean that outcrops at both ends of the layer. The boundaries for the layer are given by the following surfaces. Surfaces $\mathcal{S}_A$ and $\mathcal{S}_B$ are defined by buoyancy isosurfaces with $b_A < b_B$. The sea surface is decomposed into three regions, $\mathcal{S}_1, \mathcal{S}_2$, and $\mathcal{S}_3$ according to the outcrop locations of $\mathcal{S}_A$ and $\mathcal{S}_B$.

42.4.6 Further study

Section 4.8 of *Vallis* (2017) discusses the integrated PV-substance in terms of the vorticity formulation, whereas *Morel et al.* (2019) introduced the dual perspective based on the buoyancy gradient formulation. *Morel et al.* (2019) also provide details for the practical diagnosis of potential vorticity in a numerical ocean model or from observational based measurements.

42.5 Boundary fluxes of PV-substance

In Section 42.4 we developed kinematic expressions for the PV-substance integrated over a selection of volumes. That discussion illustrated how the volume integrated potential vorticity has contributions only from boundaries; e.g., where an atmospheric region intersects the ground or ocean, and where an oceanic region intersects the ground or the atmosphere. In this section we further our understanding of budgets for PV-substance by examining a buoyancy layer within the ocean that intersects the bottom on one side and the atmosphere on the other (Figure 42.6). We garner further understanding of the physical processes affecting changes to the PV-substance by here unpacking the boundary fluxes.

A buoyancy layer generally moves as it expands and contracts due to both reversible and irreversible processes (waves, currents, mixing). The impermeability theorem means that the total potential vorticity substance for the layer changes only through exchanges at the boundaries, including the bottom (boundary between the solid earth and the fluid) and air-sea boundaries. Removing interior interfaces from the layer PV-substance budget simplifies the budget analysis, as already revealed in Section 42.4. As per the discussion of Section 42.3, the results in this section apply even when there is no materially invariant potential vorticity. All we require is a flux-form budget along with the impermeability theorem, which holds for potential vorticity defined according to an arbitrary smooth scalar field (Section 42.2.2).

42.5.1 Layer integrated budget

In addition to waves, currents, mixing, and sources affecting the layer interfaces, there is movement of the intersection of the layer with the side boundaries, thus changing the vertical and horizontal extents of these intersections. As a formulational framework, we derive the layer potential vorticity budget making use of the Leibniz-Reynolds transport theorem derived in Section 20.2.4. Just as for the layer integrated tracer budget considered in Section 20.4, applying

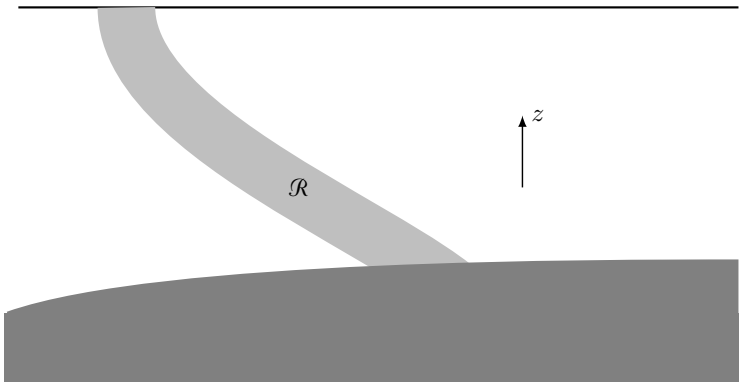

FIGURE 42.6: A buoyancy layer of seawater denoted by $\mathcal{R}$, with the layer intersecting bottom topography on one side and the atmosphere on the other. The interior boundaries of the layer are formed by constant buoyancy surfaces.

Leibniz-Reynolds to the layer integrated potential vorticity budget renders

$$\frac{\mathrm{d}}{\mathrm{d}t}\left[\int_{\mathcal{R}} \rho\, Q\, \mathrm{d}V\right] = \int_{\mathcal{R}} \partial_t(\rho\, Q)\, \mathrm{d}V + \oint_{\partial\mathcal{R}} \rho\, Q\, \dot{\boldsymbol{x}} \cdot \hat{\boldsymbol{n}}\, \mathrm{d}\mathcal{S}, \tag{42.61}$$

where $\mathcal{R}$ is the domain defined by the layer (Figure 42.6), $\partial\mathcal{R}$ is its boundary, and

$$\dot{\boldsymbol{x}} = \frac{\mathrm{d}\boldsymbol{x}}{\mathrm{d}t} \tag{42.62}$$

is the velocity for a point on the boundary. Making use of the potential vorticity equation,

$$\partial_t(\rho\, Q) = -\nabla \cdot \boldsymbol{J}^{\mathrm{Q}}, \tag{42.63}$$

and the divergence theorem renders

$$\frac{\mathrm{d}}{\mathrm{d}t}\left[\int_{\mathcal{R}} \rho\, Q\, \mathrm{d}V\right] = \oint_{\partial\mathcal{R}} (-\boldsymbol{J}^{\mathrm{Q}} + \rho\, Q\, \dot{\boldsymbol{x}}) \cdot \hat{\boldsymbol{n}}\, \mathrm{d}\mathcal{S}. \tag{42.64}$$

This result holds around the full domain boundary. Now we decompose that boundary into portions defined by layer interfaces and those along the air-sea and land-sea boundaries.

42.5.2 Impermeability across interior layer interfaces

Rather than invoking the impermeability theorem derived in Section 42.2, we rederive it within the present context to further our confidence in its use. We thus consider the following for interior layer interfaces, here making use of the Haynes-McIntyre form (42.1) of the potential vorticity flux vector

$$\begin{aligned}
[-\boldsymbol{J}^{\mathrm{Q}} + \rho\, Q\, \dot{\boldsymbol{x}}] \cdot \hat{\boldsymbol{n}} &= \Big[\rho\, Q\, (\dot{\boldsymbol{x}} - \boldsymbol{v}) + \dot{b}\, \boldsymbol{\omega}_{\mathrm{a}} - \nabla b \times \boldsymbol{F}\Big] \cdot \hat{\boldsymbol{n}} && \text{(42.65a)} \\
&= \Big[(\boldsymbol{\omega}_{\mathrm{a}} \cdot \nabla b)\, (\dot{\boldsymbol{x}} - \boldsymbol{v}) + \dot{b}\, \boldsymbol{\omega}_{\mathrm{a}}\Big] \cdot \hat{\boldsymbol{n}} && \text{(42.65b)} \\
&= [(\boldsymbol{\omega}_{\mathrm{a}} \cdot \nabla b)\, (\dot{\boldsymbol{x}} - \boldsymbol{v}) + (\partial_t b + \boldsymbol{v} \cdot \nabla b)\, \boldsymbol{\omega}_{\mathrm{a}}] \cdot \hat{\boldsymbol{n}} && \text{(42.65c)} \\
&= [(\boldsymbol{\omega}_{\mathrm{a}} \cdot \nabla b)\, \dot{\boldsymbol{x}} + \boldsymbol{\omega}_{\mathrm{a}}\, \partial_t b] \cdot \hat{\boldsymbol{n}}, && \text{(42.65d)}
\end{aligned}$$

where

$$\hat{\boldsymbol{n}} = \nabla b / |\nabla b| \tag{42.66}$$

is the outward unit normal vector pointing to regions of higher buoyancy. Now recall that the velocity of a point fixed on an layer interface has a normal component that satisfies equation (42.10) (here applied to buoyancy surfaces)

$$\dot{\boldsymbol{x}} \cdot \hat{\boldsymbol{n}} = -\partial_t b / |\nabla b|. \tag{42.67}$$

This result then leads to the impermeability statement for isopycnal interfaces in the fluid interior

$$(-\boldsymbol{J}^{\mathrm{Q}} + \rho Q \, \dot{\boldsymbol{x}}) \cdot \hat{\boldsymbol{n}} = 0. \tag{42.68}$$

We thus conclude that changes to the layer integrated potential vorticity occur only via transfer across the land-sea boundary and the air-sea boundary

$$\frac{\mathrm{d}}{\mathrm{d}t} \left[\int_{\mathscr{R}} \rho Q \, \mathrm{d}V \right] = \int_{\text{land-sea}} [-\boldsymbol{J}^{\mathrm{Q}} + \rho Q \, \dot{\boldsymbol{x}}] \cdot \hat{\boldsymbol{n}} \, \mathrm{d}\mathcal{S} + \int_{\text{air-sea}} [-\boldsymbol{J}^{\mathrm{Q}} + \rho Q \, \dot{\boldsymbol{x}}] \cdot \hat{\boldsymbol{n}} \, \mathrm{d}\mathcal{S}. \tag{42.69}$$

We now separately consider these two boundaries.

42.5.3 Potential vorticity flux at a land-sea boundary

We here evaluate the potential vorticity flux from equation (42.6a) at a land-sea boundary

$$-\boldsymbol{J}^{\mathrm{Q}} + \rho Q \, \dot{\boldsymbol{x}} = \rho Q \, (\dot{\boldsymbol{x}} - \boldsymbol{v}) + \dot{b} \, \boldsymbol{\omega}_{\mathrm{a}} - \nabla b \times \boldsymbol{F}. \tag{42.70}$$

At a solid and static boundary, the no-normal flow boundary condition (Section 19.6.1) means that $\hat{\boldsymbol{n}} \cdot \boldsymbol{v} = 0$. Likewise, the velocity of a point along the boundary moves along the tangent to the boundary so that $\dot{\boldsymbol{x}} \cdot \hat{\boldsymbol{n}} = 0$. Hence, the bottom boundary condition is solely comprised of irreversible processes

$$(-\boldsymbol{J}^{\mathrm{Q}} + \rho Q \, \dot{\boldsymbol{x}}) \cdot \hat{\boldsymbol{n}} = (\dot{b} \, \boldsymbol{\omega}_{\mathrm{a}} - \nabla b \times \boldsymbol{F}) \cdot \hat{\boldsymbol{n}}. \tag{42.71}$$

If this boundary flux is positive, then it acts to increase the integrated PV-substance of the region, and conversely if the boundary flux is negative.

In many parts of the ocean bottom, geothermal heating is negligible so that there is no buoyancy input at the bottom, thus leaving just the contribution from friction

$$\text{no geothermal heating} \implies (-\boldsymbol{J}^{\mathrm{Q}} + \rho Q \, \dot{\boldsymbol{x}}) \cdot \hat{\boldsymbol{n}} = -(\nabla b \times \boldsymbol{F}) \cdot \hat{\boldsymbol{n}} = (\nabla b \times \hat{\boldsymbol{n}}) \cdot \boldsymbol{F}. \tag{42.72}$$

Furthermore, in the absence of geothermal heating the buoyancy satisfies a no-flux boundary condition, which can be ensured by having the buoyancy satisfying

$$\text{no geothermal heating} \implies \hat{\boldsymbol{n}} \cdot \nabla b = 0. \tag{42.73}$$

Buoyancy isolines thus intersect the bottom parallel to the bottom outward normal, as shown in Figure 42.7.[4] Correspondingly, $(\nabla b \times \hat{\boldsymbol{n}}) \cdot \boldsymbol{F}$ projects onto that component of the friction vector pointing parallel to the bottom. Assuming buoyancy increases upward along the sloping bottom, as per a stably stratified fluid, then $\nabla b \times \hat{\boldsymbol{n}}$ points counter-clockwise around bowls and clockwise around bumps (see Figure 42.7).

[4]There is ongoing research aimed at determining the thickness of the region over which the boundary condition (42.73) is accurate. The boundary condition presumably holds within a molecular sublayer. But the question is whether larger scale motions near the ocean bottom allow for this condition to hold over a thicker region. See the review chapter by *Polzin and McDougall* (2021) for discussion.

Within the bottom boundary layer, quadratic bottom drag is a common parameterization of the acceleration associated with turbulent frictional processes

$$\boldsymbol{F} = -C_{\rm d} \, |\boldsymbol{u}| \, \boldsymbol{u}, \tag{42.74}$$

where $C_{\rm d}$ is a non-dimensional drag coefficient and $\boldsymbol{u}$ is the horizontal velocity. In this case the boundary condition for potential vorticity takes the form

$$(-\boldsymbol{J}^{\mathrm{Q}} + \rho \, Q \, \dot{\boldsymbol{x}}) \cdot \hat{\boldsymbol{n}} = (\nabla b \times \hat{\boldsymbol{n}}) \cdot \boldsymbol{F} = -C_{\rm d} \, |\boldsymbol{u}| \, (\nabla b \times \hat{\boldsymbol{n}}) \cdot \boldsymbol{u}. \tag{42.75}$$

We see that the sign of the bottom boundary potential vorticity flux depends on the relative orientation of the bottom flow and the vector $\nabla b \times \hat{\boldsymbol{n}}$. To help understand the sign, consider an abyssal bowl with buoyancy increasing upward along the sloping bottom, in which case $\nabla b \times \hat{\boldsymbol{n}}$ points counter-clockwise around the bowl. A bottom boundary flow that is also oriented counter-clockwise carries a positive curvature relative vorticity (Section 37.8). This positive relative vorticity is damped by the bottom friction, which corresponds to the negative potential vorticity source as per equation (42.75). Conversely, a bottom boundary flow that is oriented clockwise around the abyssal bowl carries a negative curvature relative vorticity. This negative relative vorticity is damped by the bottom friction, which corresponds to the positive potential vorticity source as per equation (42.75).

Consider a component to the bottom flow that is parallel to ∇b. Theis flow provides a zero potential vorticity source since $\nabla b \times \boldsymbol{F} = 0$ (again, assuming $\boldsymbol{F} = -C_{\rm d} \, |\boldsymbol{u}| \, \boldsymbol{u}$). This result is expected from the discussion in Section 41.4 and Figure 41.4, where we note that friction changes potential vorticity by rotating buoyancy surfaces, with that rotation realized only when friction is not aligned with ∇b.

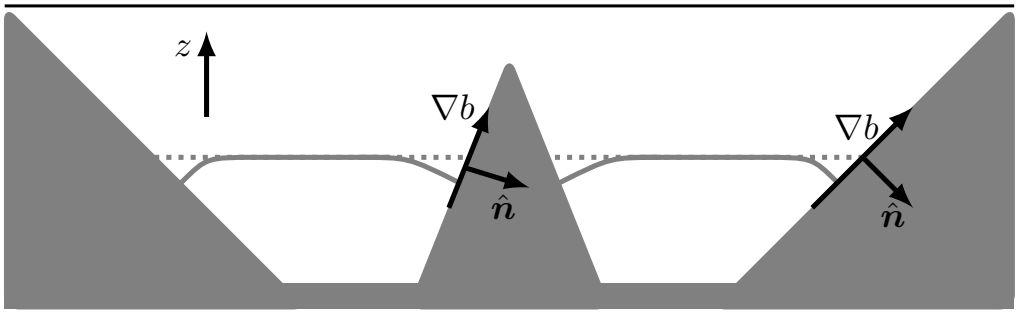

FIGURE 42.7: Depicting a buoyancy isosurface that intersects the bottom. As discussed in Section 20.4 and depicted in Figure 20.5, in the absence of geothermal heating, a buoyancy isosurface satisfies the no-normal flux bottom boundary condition, $\hat{\boldsymbol{n}} \cdot \nabla b = 0$. This boundary condition requires buoyancy isosurfaces to be orthogonal to the bottom. Assuming buoyancy increases upward along the sloping bottom, then $\nabla b \times \hat{\boldsymbol{n}}$ points counterclockwise around bowls and clockwise around bumps (when viewed from above). This structure for the buoyancy surfaces affects how friction impacts on the layer-integrated potential vorticity budget, with details provided in Section 42.5.3.

42.5.4 Potential vorticity flux at the air-sea boundary

For the permeable air-sea boundary, we make use of the kinematic boundary condition derived in Section 19.6.3, where the boundary condition (19.78) leads to

$$\rho \, \hat{\boldsymbol{n}} \cdot (\dot{\boldsymbol{x}} - \boldsymbol{v}) = \mathcal{Q}_{\rm m} \qquad \text{air-sea boundary}, \tag{42.76}$$

with $\mathcal{Q}_{\rm m}$ the mass per time per surface area of matter that crosses the air-sea boundary. We are thus led to the air-sea boundary condition

$$(-\boldsymbol{J}^{\rm Q} + \rho\, Q\, \dot{\boldsymbol{x}}) \cdot \hat{\boldsymbol{n}} = Q\, \mathcal{Q}_{\rm m} + (\dot{b}\, \boldsymbol{\omega}_{\rm a} - \nabla b \times \boldsymbol{F}) \cdot \hat{\boldsymbol{n}}. \tag{42.77}$$

Besides the irreversible processes, potential vorticity is affected at the air-sea interface by the transfer of matter across the boundary via the term $Q\, \mathcal{Q}_{\rm m}$. We can think of this term as an advection of potential vorticity across the boundary via the boundary mass transport. More generally, we can think of the full boundary flux (42.77) as acting to stretch/compress the fluid column so to alter vorticity and hence the potential vorticity.

To help interpret the friction term appearing in the flux (42.77), write

$$(\dot{b}\, \boldsymbol{\omega}_{\rm a} - \nabla b \times \boldsymbol{F}) \cdot \hat{\boldsymbol{n}} = (\boldsymbol{\omega}_{\rm a} \cdot \hat{\boldsymbol{n}})\, (\partial_t b + \boldsymbol{v} \cdot \nabla b) + (\hat{\boldsymbol{n}} \times \boldsymbol{F}) \cdot \nabla b \tag{42.78a}$$

$$= (\boldsymbol{\omega}_{\rm a} \cdot \hat{\boldsymbol{n}})\, [\partial_t b + (\boldsymbol{v} - \boldsymbol{v}_{\rm E}) \cdot \nabla b]\,, \tag{42.78b}$$

where we introduced the *generalized Ekman velocity*

$$\boldsymbol{v}_{\rm E} \equiv \frac{\boldsymbol{F} \times \hat{\boldsymbol{n}}}{\boldsymbol{\omega}_{\rm a} \cdot \hat{\boldsymbol{n}}}, \tag{42.79}$$

thus bringing the air-sea boundary potential vorticity flux (42.77) to the form

$$(-\boldsymbol{J}^{\rm Q} + \rho\, Q\, \dot{\boldsymbol{x}}) \cdot \hat{\boldsymbol{n}} = Q\, \mathcal{Q}_{\rm m} + (\boldsymbol{\omega}_{\rm a} \cdot \hat{\boldsymbol{n}})\, [\partial_t b + (\boldsymbol{v} - \boldsymbol{v}_{\rm E}) \cdot \nabla b]\,. \tag{42.80}$$

Note that for the special case of a vertical outward normal, $\hat{\boldsymbol{n}} = \hat{\boldsymbol{z}}$, and weak relative vorticity, $f + \zeta \approx f$, we have

$$\boldsymbol{v}_{\rm E} \approx f^{-1}\, \boldsymbol{F} \times \hat{\boldsymbol{z}}, \tag{42.81}$$

which is the Ekman velocity given by equation (33.4). We thus see that the sign of the $(\boldsymbol{\omega}_{\rm a} \cdot \hat{\boldsymbol{n}})$ portion of the potential vorticity flux is determined by whether the surface buoyancy is increasing or decreasing in time following the velocity difference, $\boldsymbol{v} - \boldsymbol{v}_{\rm E}$, along the air-sea boundary. We can interpret $\boldsymbol{v} - \boldsymbol{v}_{\rm E}$ as the inviscid portion of the velocity since it removes that portion arising from friction.[5]

42.5.5 Thought experiments

The surface potential vorticity flux (42.77), or its rewritten form in equation (42.80), provide an explicit expression for how surface boundary fluxes affect the potential vorticity budget within a buoyancy layer outcropping at the ocean surface. It contains a wealth of physics that can be explored via thought experiments.

Potential vorticity generation in a fluid with zero initial baroclinicity

Consider a fluid region initially with zero baroclinicity and zero flow so that the initial potential vorticity is given by $f\, N^2$, with N^2 the squared buoyancy frequency. The surface potential vorticity flux (42.77) creates potential vorticity via the mass flux term and through heating/cooling. If this term alone affected the potential vorticity, and it did so uniformly in space, then it would alter potential vorticity only via changes in the vertical stratification. More generally, both the mass term and the diabatic term create horizontal buoyancy gradients, which then generate currents and vorticity that generate further contributions to the potential vorticity flux.

[5]The velocity difference, $\boldsymbol{v} - \boldsymbol{v}_{\rm E}$, is not equal to the inviscid velocity that would appear in an inviscid (perfect) fluid. Rather, $\boldsymbol{v} = \boldsymbol{v}_{\rm E} + (\boldsymbol{v} - \boldsymbol{v}_{\rm E})$ is an interpretational decomposition akin to that studied in Chapter 33 for Ekman mechanics. See the comment after equation (33.4) for more on this point.

Potential vorticity generation in a fluid that is initially homogeneous

Consider an initially homogenous box of seawater with zero potential vorticity. In this case it is only the buoyancy term, $\dot{b}\, f$, that contributes to initial changes in potential vorticity. Northern hemisphere ($f > 0$) surface cooling ($\dot{b} < 0$) adds negative potential vorticity to the box. Cooling also initiates gravitational instability that mixes the water and in turn spreads the negative potential vorticity boundary source throughout the fluid. Cooling adds structure to the buoyancy field by inflating the formerly zero thickness buoyancy layers, with layer inflation originating from the boundary. Once inflated, the impermeability theorem dictates that the layer integrated PV-substance changes only via boundary interactions, whereas stirring and mixing transport potential vorticity into the fluid interior. Notably, a region with $f\, Q < 0$ is locally unstable to symmetric instability, with the generated symmetric instability acting to locally bring the flow towards a state with zero potential vorticity. However, the constraints from impermeability mean that the net PV-substance remains unchanged within a buoyancy layer, even in the presence of mixing.

42.5.6 Is there a preferred form of the PV-substance flux?

Analysis in this section made use of the Haynes-McIntyre form of the PV-substance flux (equation (42.1))

$$\boldsymbol{J}^{\mathrm{Q}} = \rho\, \boldsymbol{v}\, Q - \dot{b}\, \boldsymbol{\omega}_{\mathrm{a}} + \nabla b \times \boldsymbol{F}. \tag{42.82}$$

We could have instead chosen to work with the Marshall form (equation (42.32))

$$\boldsymbol{J}^{\mathrm{marshall}} = -\left[\partial_t \boldsymbol{v} + \nabla(\mathcal{M} + p/\rho)\right] \times \nabla b - \boldsymbol{\omega}_{\mathrm{a}}\, \partial_t b, \tag{42.83}$$

or the modified kinematic form (equation (42.18))

$$\widetilde{\boldsymbol{J}}^{\mathrm{kin}} = -\partial_t \boldsymbol{v}_{\mathrm{a}} \times \nabla b - \boldsymbol{\omega}_{\mathrm{a}}\, \partial_t b. \tag{42.84}$$

These fluxes differ by a gauge choice and yet they each satisfy the impermeability theorem. Subjective choices determine which one is preferred. Importantly, once chosen, we can use only a single form of the flux throughout the budget analysis in order to remain self-consistent with the form of the total curl that is removed by the divergence operator.

The PV-substance budget, though invariant to the choice of flux, has distinct physical pictures depending on the choice of the flux. As a particularly clear example consider a steady state budget in which the fluxes take the form

$$\boldsymbol{J}^{\mathrm{Q}} = \rho\, \boldsymbol{v}\, Q - (\boldsymbol{v} \cdot \nabla b)\, \boldsymbol{\omega}_{\mathrm{a}} + \nabla b \times \boldsymbol{F} \tag{42.85}$$

$$\boldsymbol{J}^{\mathrm{marshall}} = -\nabla(\mathcal{M} + p/\rho) \times \nabla b \tag{42.86}$$

$$\widetilde{\boldsymbol{J}}^{\mathrm{kin}} = 0. \tag{42.87}$$

The physical picture for $\widetilde{\boldsymbol{J}}^{\mathrm{kin}}$ is rather trivial, whereby the PV-substance stays constant within buoyancy layers and there are zero PV-substance fluxes across *all* boundaries of the layer. In contrast, a steady state budget when working with $\boldsymbol{J}^{\mathrm{Q}}$ or $\boldsymbol{J}^{\mathrm{marshall}}$ afford a physical picture of PV-substance entering, leaving, and transported through the buoyancy layers. *Marshall et al.* (2001) developed a rather elegant analysis framework using $\boldsymbol{J}^{\mathrm{marshall}}$ for steady budgets, and we explore facets of that approach in Section 41.5 for the special case of a Boussinesq hydrostatic fluid.

Nevertheless, our use of the Haynes-McIntyre PV-substance flux in the present section is motivated by its utility for describing how boundary forcing can change the sign of the potential vorticity. Such forcing exposes the flow to a variety of local instabilities (e.g., symmetric,

centrifugal, gravitational). *Thomas et al.* (2008) offer a pedagogical review for the ocean; *Thomas et al.* (2013) provides a thorough study of the upper reaches of the Gulf Stream; and *Naveira Garabato et al.* (2019) provide evidence for such boundary forcing in regions of strong abyssal flows. Each of these studies points to the need to further understand details of the boundary potential vorticity flux and to furthermore ensure it is properly formulated within numerical models (e.g., *Hallberg and Rhines* (1996)).

42.5.7 Further study

The study of boundary potential vorticity fluxes generally requires careful analysis of the multitude of processes active in boundary layers. The interested reader can find ocean examples of these analyses in *Benthuysen and Thomas* (2012) and *Wenegrat et al.* (2018), and the references therein.

Part VIII

Nearly geostrophic flows

Fluid motion dominated by rotation is characterized by a small Rossby number. To zeroth order in an asymptotic expansion in Rossby number, the flow maintains geostrophic balance, which is a balance between the Coriolis acceleration and pressure gradient acceleration. As seen in Chapter 31, the geostrophic balance is diagnostic, which means it offers no means to compute time evolution of the motion. To obtain a prognostic equation requires going to next order in Rossby number within the asymptotic expansion. For quasi-geostrophy (QG), the resulting prognostic equation makes use of ageostrophic motions, though only as an intermediate step towards an evolution equation involving just zeroth order geostrophically balanced fields. For planetary geostrophy (PG), the prognostic equation arises from mass (or volume) conservation, whereas fluid motion is a directly determined by evolution of the mass field.

The nuts and bolts of this part of the book involve methods of scaling analysis and asymptotic analysis via perturbation series. In Chapter 43, we use these tools to derive equations for both planetary geostrophy and quasi-geostrophy within shallow water flows, and then extend that discussion to continuously stratified flows in Chapters 44 and 45. Planetary geostrophy and quasi-geostrophy are both very useful theoretical models lending insights into ocean and atmosphere fluid mechanics. In particular, planetary geostrophy is often the foundation for theories of large-scale laminar ocean circulation. Quasi-geostrophy serves as a theoretical model for studies of both oceanic and atmospheric flows at or near the deformation radius, particularly when concerned with transient features such as Rossby waves, baroclinic instability, and geostrophic turbulence.

One central property of balanced flow is that knowledge of the relevant balanced version of potential vorticity is sufficient to determine the flow field. A way to appreciate this property is to consider a horizontally non-divergent barotropic flow (Chapter 38), in which the Laplacian of the streamfunction gives the relative vorticity, $\zeta = \nabla^2 \psi$. Conversely, if we know the vorticity then we can invert the Laplacian (with suitable boundary conditions) to yield the streamfunction and hence the velocity.[6] In our discussion of quasi-geostrophy in Chapter 45, we extend this result to three-dimensional quasi-geostrophic flow, where the prognostic fields are the horizontal components to the geostrophic flow, plus the buoyancy field. Such methods of *potential vorticity inversion* are routinely used to study atmospheric flows given maps of potential vorticity (see *Hoskins* (1991) for a review).

[6] Recall the study of Green's function methods in Chapter 9 for examples of inverting the partial differential equation to determine the solution to an elliptic boundary value problem.

Chapter 43

Models of nearly geostrophic flows

Planetary rotation, and the corresponding Coriolis acceleration, is a primary feature of geophysical fluid flows. To probe the physics of such flows, it is useful to develop mathematical models where rotation of the reference frame is a prominent facet of the equations of motion. Systematically deriving such models is the focus of this chapter, where we develop the mechanical equations for planetary geostrophy (PG) and quasi-geostrophy (QG) within the shallow water fluid. We also work through non-dimensionalization of the stratified Boussinesq equations, thus providing the foundations for the equations of stratified planetary geostrophy in Chapter 44 and stratified quasi-geostrophy in Chapter 45.

READER'S GUIDE FOR THIS CHAPTER

This chapter makes use of dimensional analysis, scale analysis, and asymptotic methods to derive approximate geostrophic equations. As such, the chapter is technical in nature and with mathematical derivations offered in detail. We assume an understanding of the equations for a single layer of shallow water fluid as derived in Chapter 35, as well as the Boussinesq ocean equations from Chapter 29. We follow this work with studies of continuously stratified planetary geostrophy in Chapter 44 and continuously stratified quasi-geostrophy in Chapter 45.

43.1 Loose threads

- External and internal modes for QG two layers in Section 43.6.10.

43.2 Scale analysis and the Buckingham-Π theorem

Scale analysis is ubiquitous in physics, with geophysical fluid mechanics no exception. We find it useful to distinguish two classes of scales. *External scales* are prescribed as part of the physical system under consideration, and they can be considered to be under "control" of the physicist. Examples include planetary rotation rate, gravitational acceleration, and domain geometry. *Internal scales* emerge from the flow itself, such as the length and time scales of the flow, and as such internal scales are only indirectly controlled by the physicist.

The Buckingham-Π theorem provides a useful framework for organizing dimensions and scales. The theorem states that the number of dimensionless parameters characterizing a physical system is a function of the number of dimensional parameters or scales, K_{scales} (e.g., scales for the velocity, rotation rate, pressure force, friction force, gravitational acceleration) and the number of physical dimensions, $K_{\text{dimensions}}$ (e.g., time, length, mass). Precisely, Buckingham-Π states that the number of dimensionless parameters is

$$N_{\text{dimensionless}} = K_{\text{scales}} - K_{\text{dimensions}}. \tag{43.1}$$

Different physical systems possessing the same suite of dimensionless parameters are isomorphic. For example, a laboratory study of flow around a cylinder contains two dimensionless parameters: the drag coefficient, C_{d}, and the Reynolds number, Re. If the problem is scaled up to a building with the same shape, then so long as the values for the dimensionless parameters are the same (e.g., same drag coefficient and same Reynolds number), one can make use of the laboratory analog for determining suitability of the building architecture. Similar isomorphisms exist between flows in a rotating tank and flows in the ocean and atmosphere.

The Buckingham-Π theorem does not provide the form of the dimensionless parameters. Nor does the theorem determine their values. This information comes only after introducing physical prejudices surrounding a regime of chosen interest. Additionally, Buckingham-Π does not offer information about how the dimensionless parameters might be related. Instead, any such relations arise from the mechanical and thermodynamical equations describing the system.

Consequently, mechanical and thermodynamical equations generally mean that fewer than $N_{\text{dimensionless}}$ non-dimensional numbers are independent.

We focus in this chapter on the regime of large-scale atmospheric and oceanic flow where the shallow water fluid is close to geostrophic balance. That choice then guides the length and time scales, which in turn determines the size of the dimensionless parameters. In many cases, one is able to identify dimensionless parameters that are large or small in particular regimes, which in turn suggests asymptotic analyses to render equations specific to the regime of interest.

43.3 Shallow water equations

A single-layer of inviscid shallow water fluid of thickness h is governed by the velocity and thickness equations (Chapter 35)

$$\partial_t \boldsymbol{u} + (\boldsymbol{u} \cdot \nabla)\, \boldsymbol{u} + \boldsymbol{f} \times \boldsymbol{u} = -g \nabla \eta \tag{43.2a}$$

$$\partial_t h + \nabla \cdot (h\, \boldsymbol{u}) = 0, \tag{43.2b}$$

where $\boldsymbol{u}$ is the horizontal velocity that is independent of depth within the layer ($\partial_z \boldsymbol{u} = 0$). The vertical bounds for the layer are specified by the free surface height, $z = \eta(x, y, t)$, and bottom topography, $z = \eta_{\mathrm{b}}(x, y)$ (see Figure 35.1). They are related according to

$$\eta = \eta_{\mathrm{b}} + h = H + \overline{\eta_{\mathrm{b}}} + \eta' = \overline{h} + \overline{\eta_{\mathrm{b}}} + \eta', \tag{43.3}$$

where $H = \overline{h}$ is the area average layer thickness, $\overline{\eta_{\mathrm{b}}}$ is the area average of the bottom topography, $\eta' = \eta - \overline{\eta}$ is the deviation of the surface height from its area average, $\overline{\eta} = \overline{\eta_{\mathrm{b}}} + H$. We also find occasion to write the layer thickness in the form

$$h = \eta - \eta_{\mathrm{b}} = H + (\overline{\eta_{\mathrm{b}}} - \eta_{\mathrm{b}}) + \eta' = \overline{h} - \eta'_{\mathrm{b}} + \eta' = \overline{h} + h', \tag{43.4}$$

where $\eta'_{\mathrm{b}} = \eta_{\mathrm{b}} - \overline{\eta_{\mathrm{b}}}$ is the deviation of the bottom topography from its area average, and we introduced the thickness deviation

$$h' = h - \overline{h} = \eta' - \eta'_{\mathrm{b}}. \tag{43.5}$$

Dexterity with the geometrical relations (43.3)-(43.5) is assumed in the following.

43.3.1 Dimensional scales

We identify the following nine dimensional scales for the shallow water layer.

- LENGTH SCALES
  - ⋆ H = depth scale of the fluid layer. Given that the layer is homogeneous, we take H equal to the area average layer thickness (see Figure 35.1).
  - ⋆ L = horizontal/lateral length scale of flows under consideration. We assume both horizontal directions to have the same flow length scale. This assumption is not necessarily appropriate on a rotating planet, where flows in the zonal (east-west) direction typically have length scales longer than meridional (north-south) flow scales. Nonetheless, this choice does not preclude the dynamical emergence of anisotropic length scales, and so it serves our uses for the present analysis.
  - ⋆ R_{e} = prescribed radius of the planet. We include this scale anticipating that for length scales small compared to the earth's radius, the Coriolis parameter may be approximated by a constant (f-plane) or linear function of latitude (β-plane).

  - ⋆ $\mathcal{H}$ = length scale for deviations of the free surface height, η, relative to its area average, $\overline{\eta}$, so that $\eta' = \eta - \overline{\eta} \sim \mathcal{H}$.
  - ⋆ $\mathcal{B}$ = prescribed length scale for deviations of the bottom topography, η_b, relative to its area average, $\overline{\eta_b}$, so that $\eta'_b = \eta_b - \overline{\eta_b} \sim \mathcal{B}$.

- VELOCITY SCALES
  - ⋆ U = velocity scale for horizontal fluid particle motion; i.e., the speed for horizontal flows.
  - ⋆ c = scale for wave speeds. For the shallow water model, the wave speed is given by the shallow water gravity wave (Section 55.5.1)

$$c = \sqrt{g\,H}. \tag{43.6}$$

    We introduce the wave speed anticipating the presence of distinct flow regimes depending on whether the fluid particle speed is larger or smaller than the wave speed. The ratio of the fluid particle speed (advection speed) to the wave speed is known as the *Froude number* (Section 43.3.4).

- BODY FORCES: There are two body forces acting on the fluid; one from gravity and one from Coriolis. These two forces are scaled according to the following prescribed parameters:
  - ⋆ g = gravitational acceleration
  - ⋆ f = Coriolis frequency.

If we were interested in other forces, such as electromagnetic or frictional forces, then we add further dimensional parameters corresponding to these forces.

43.3.2 Physical dimensions

There are two physical dimensions in the shallow water system: length, L, and time, T. Notably, there is no mass in the shallow water system. The reason is that the fluid density is assumed uniform within a shallow water layer so that mass is described by area times thickness

$$M = \int \rho \,\mathrm{d}V \;[\equiv]\; L^2 H\,\rho, \tag{43.7}$$

where $[\equiv]$ is read "has dimensions".

43.3.3 Number of non-dimensional parameters

The Buckingham-Π theorem says there are

$$N_{\text{dimensionless}} = 9 - 2 = 7 \tag{43.8}$$

non-dimensional parameters that characterize the flow within a single shallow water layer. So we expect to find seven non-dimensional parameters as part of the analysis.

How do we know that we properly counted the physical dimensions or the dimensional scales? Fortunately, the process of determining the non-dimensional parameters is largely self-correcting. Namely, if a physical dimension or a physical scale is omitted, then it would appear somewhere in the subsequent analysis. Indeed, such omissions often are only found at the point of a mathematical or physical inconsistency. Hence, the analyst must remain cognizant of the need to self-correct when performing dimensional analysis.

43.3.4 Choosing the non-dimensional parameters

There is no unique choice for the non-dimensional parameters. Our choice is guided by experience, interest, and what parameters might be available to experimental control or measurement.

1. VERTICAL TO HORIZONTAL/LATERAL ASPECT RATIO: The ratio of the vertical scale of the layer to the horizontal/lateral scale of the flow[1] defines the aspect ratio

$$\delta_{\text{vertical/horizontal}} = \frac{\text{vertical length scale}}{\text{horizontal length scale}} = \frac{H}{L}. \tag{43.9}$$

2. RATIO OF HORIZONTAL/LATERAL SCALE TO PLANETARY SCALE: The ratio of the horizontal length scale of the flow to the planetary radius is

$$\delta_{\text{horizontal/planet}} = \frac{\text{horizontal length scale}}{\text{planetary length scale}} = \frac{L}{R_e}. \tag{43.10}$$

3. RATIO OF FREE SURFACE UNDULATION TO VERTICAL LENGTH SCALE: The ratio of the free surface undulations that emerge from the flow, to the vertical length scale of the layer is

$$\delta_{\text{free surface/depth}} = \frac{\text{free surface undulation scale}}{\text{vertical length scale}} = \frac{\mathcal{H}}{H}. \tag{43.11}$$

4. RATIO OF BOTTOM TOPOGRAPHY UNDULATION TO VERTICAL LENGTH: The ratio of the prescribed bottom topography undulation scale to the vertical length scale is

$$\delta_{\text{bottom/depth}} = \frac{\text{bottom topography undulation scale}}{\text{vertical length scale}} = \frac{\mathcal{B}}{H}. \tag{43.12}$$

5. FROUDE NUMBER: The Froude number is the ratio of the fluid particle speed emerging from the flow, to the gravity wave speed determined by geophysical parameters. For the shallow water system, this ratio is

$$\text{Fr} = \frac{U}{c} = \frac{U}{\sqrt{g\,H}}. \tag{43.13}$$

6. ROSSBY NUMBER: The Rossby number is the ratio of the fluid particle acceleration scale to the Coriolis acceleration scale, both of which emerge from the flow

$$\text{Ro} = \frac{\text{particle acceleration}}{\text{Coriolis acceleration}}. \tag{43.14}$$

   The particle acceleration scale is determined by the local time tendency plus advection

$$\text{particle acceleration} = \frac{\partial \boldsymbol{u}}{\partial t} + (\boldsymbol{u}\cdot\nabla)\,\boldsymbol{u} \sim \frac{U}{T} + \frac{U^2}{L}. \tag{43.15}$$

   The local time tendency and advection generally have distinct scales, thus leading to the potential for two Rossby numbers

$$\text{Ro}^{\text{tendency}} = \frac{1}{T\,f} \quad \text{and} \quad \text{Ro}^{\text{advection}} = \frac{U}{L\,f}. \tag{43.16}$$

[1] The terms "lateral" and "horizontal" are used interchangeably, referring to motion at constant vertical position either on the sphere or on the plane.

In the following we consider these two Rossby numbers to have the same scale, which is realized by advective contributions to material time evolution being comparable to local time changes. We refer to this choice as an *advective time scale*, whereby

$$T = \frac{L}{U} \Longrightarrow \frac{U^2}{L} = \frac{U}{T}, \tag{43.17}$$

so that there is only one Rossby number

$$\mathrm{Ro} = \frac{1}{f\,T} = \frac{U}{f\,L}. \tag{43.18}$$

Another interpretation for the Rossby number is the ratio of the relative vorticity to the planetary vorticity

$$\mathrm{Ro} = \frac{\text{relative vorticity}}{\text{planetary vorticity}}. \tag{43.19}$$

With the relative vorticity scaling as U/L and the planetary vorticity scaling as f, we recover the expression (43.18) for the Rossby number.

7. GEOSTROPHIC NUMBER: We define the geostrophic number as the ratio of the Coriolis acceleration scale to the scale of the pressure gradient acceleration

$$\mathrm{Ge} = \frac{\text{Coriolis acceleration}}{\text{pressure gradient acceleration}}. \tag{43.20}$$

The Coriolis acceleration scales as

$$\text{Coriolis acceleration} \sim f\,U, \tag{43.21}$$

whereas the pressure gradient acceleration, $-g\,\nabla\eta$, scales as

$$\text{pressure gradient acceleration} \sim \frac{g\,\mathcal{H}}{L}, \tag{43.22}$$

so that

$$\mathrm{Ge} = \frac{\text{Coriolis acceleration}}{\text{pressure gradient acceleration}} = \frac{f\,U}{(g/L)\,\mathcal{H}}. \tag{43.23}$$

43.3.5 Assumed values for the non-dimensional parameters

We now enumerate the assumed values for the non-dimensional parameters. These values are based on the preconceived topic of the analysis as determined by a chosen range of external and internal scales. Here, those scales arise from our interest in large scale flows in the atmosphere and ocean.

1. SMALL VERTICAL TO HORIZONTAL ASPECT RATIO: The aspect ratio is generally small for large-scale atmospheric and oceanic fluid systems

$$\delta_{\text{vertical/horizontal}} = H/L \ll 1. \tag{43.24}$$

This assumption was made when formulating the shallow water system, which is based on hydrostatic balance (see Section 35.2). We thus retain this assumption as we further scale the shallow water system.

2. SMALL OR ORDER ONE RATIO OF HORIZONTAL/LATERAL TO PLANETARY SCALES: The ratio of the lateral length scale to the planet radius is small for quasi-geostrophic systems

and order unity for planetary geostrophy

$$\delta_{\text{horizontal/planet}} = L/R_e \ll 1 \quad \text{quasi-geostrophy} \tag{43.25a}$$
$$\delta_{\text{horizontal/planet}} = L/R_e \sim 1 \quad \text{planetary geostrophy.} \tag{43.25b}$$

3. RATIO OF FREE SURFACE UNDULATION TO VERTICAL LENGTH SCALE: The ratio $\mathscr{H}/H$ is implied below by assuming a unit geostrophic number.

4. RATIO OF BOTTOM TOPOGRAPHY UNDULATION TO VERTICAL LENGTH SCALE: For quasi-geostrophy, we assume that undulations in the bottom topography are small relative to the vertical length scale, whereas there is no restriction for planetary geostrophy. "Small" in the present context is determined by the Rossby number, in which case

$$\delta_{\text{bottom/depth}} = \mathscr{B}/H = \text{Ro} \quad \text{for quasi-geostrophy.} \tag{43.26}$$

5. FROUDE NUMBER: We find that the Froude number is implied by scales assumed for the other non-dimensional numbers.

6. SMALL ROSSBY NUMBER: The Rossby number is assumed small

$$\text{Ro} = U/(f\,L) \ll 1, \tag{43.27}$$

which means that the Coriolis acceleration is a leading order term in the horizontal velocity equation (43.2a).

7. UNIT GEOSTROPHIC NUMBER: The geostrophic number is assumed to be order unity

$$\text{Ge} \sim 1. \tag{43.28}$$

This assumption means that the Coriolis acceleration and pressure gradient acceleration scale together

$$f\,U \sim (g/L)\,\mathscr{H}. \tag{43.29}$$

Making use of the velocity equation (43.2a), we see that this scaling is consistent only so long as the Rossby number is small, $\text{Ro} \ll 1$. Furthermore, this scaling constrains the scale of the free surface undulation, $\mathscr{H}$, as we discuss in Section 43.3.6.

43.3.6 Deformation radius and the free surface undulation scale

We determine the scale for the free surface height undulation, $\mathscr{H}$, by making use of the assumed order unity geostrophic number. For this purpose, start from the geostrophic scaling of Coriolis and pressure gradient accelerations, equation (43.29), to express the free surface undulation scale according to

$$\eta' \sim \mathscr{H} = \frac{f\,U\,L}{g} = \text{Ro}\,\frac{f^2\,L^2}{g} = \text{Ro}\,H\,\frac{f^2\,L^2}{g\,H} = \text{Ro}\,H\left[\frac{L}{L_d}\right]^2. \tag{43.30}$$

In the final equality we introduced the *deformation radius*

$$L_d = \sqrt{g\,H}/f = c_{\text{grav}}/f, \tag{43.31}$$

where $c_{\text{grav}} = \sqrt{g\,H}$ is the shallow water gravity wave speed (Section 55.5.1). The deformation radius distinguishes flows where the Coriolis force is important, $L \geq L_d$, from those where the Coriolis can be neglected, $L \ll L_d$. Since the deformation radius decreases toward the poles,

rotational effects are felt by smaller scales in the high latitudes than in the tropics. The shallow water deformation radius is an external scale that we find in Section 43.6.2 acts as a regime boundary between relative vorticity and vortex stretching for the quasi-geostrophic potential vorticity. We again encounter the shallow water deformation radius when discussing shallow water waves in Chapter 55.

We can use L_d to rewrite the Froude number as

$$\text{Fr} = U/\sqrt{g\,H} = U/(f\,L_\mathsf{d}) = \text{Ro}\,(L/L_\mathsf{d}), \tag{43.32}$$

where the second equality wrote the Froude number as the ratio of the advection speed, U, to the rotation speed, $f\,L_\mathsf{d}$. Furthermore, the squared ratio of the deformation radius to the lateral length scale of the flow is termed the *Burger number*

$$\text{Bu} = (L_\mathsf{d}/L)^2. \tag{43.33}$$

Use of the Burger number allows us to write the Froude number in terms of the Rossby number and Burger number

$$\text{Fr} = \text{Ro}/\sqrt{\text{Bu}}. \tag{43.34}$$

Likewise, the free surface height undulation scale can be written

$$\mathscr{H} = H\,\text{Ro}\,(L/L_\mathsf{d})^2 = H\,\text{Ro}/\text{Bu} = H\,\text{Fr}^2/\text{Ro}. \tag{43.35}$$

Hence, the ratio of the free surface undulations to the layer thickness (depth) scale is given by

$$\delta_{\text{free surface/depth}} = \mathscr{H}/H = \text{Ro}\,(L/L_\mathsf{d})^2 = \text{Ro}/\text{Bu} = \text{Fr}^2/\text{Ro}. \tag{43.36}$$

Again, this scaling is implied by making the dynamical assumption of a unit geostrophic number, which means that the pressure gradient acceleration scales according to the Coriolis acceleration.

43.3.7 Non-dimensional shallow water equations

To non-dimensionalize the shallow water equations we introduce non-dimensional variables for time, space, velocity, and Coriolis parameter. Non-dimensional variables are adorned with a widehat[2]

$$t = T\,\widehat{t}, \quad (x,y) = L\,(\widehat{x},\widehat{y}), \quad \partial_t = \partial_{\widehat{t}}/T, \quad \nabla = \widehat{\nabla}/L, \quad (u,v) = U\,(\widehat{u},\widehat{v}), \quad f = f_\circ\,\widehat{f}, \tag{43.37}$$

where $f_\circ$ is the Coriolis parameter at the central latitude for the β-plane approximation (Section 24.5). We also require non-dimensional variables for the surface and bottom undulations

$$\eta' = \mathscr{H}\,\widehat{\eta}, \quad \eta'_\mathsf{b} = \mathscr{B}\,\widehat{\eta}_\mathsf{b}, \quad h = H + \eta' - \eta'_\mathsf{b} = H + \mathscr{H}\,\widehat{\eta} - \mathscr{B}\,\widehat{\eta}_\mathsf{b}, \tag{43.38}$$

where we used equation (43.4) for the layer thickness. Importantly, we assume that the non-dimensional variables (the widehat variables) are order unity. That assumption is critical for organizing terms in the asymptotic expansion.

[2]The LaTeX widehat symbol is used for non-dimensional variables, such as the non-dimensional velocity, $\widehat{\boldsymbol{u}}$. The widehat is distinguished from the hat used for unit vectors, such as for the vertical unit vector, $\hat{\boldsymbol{z}}$. We also use widehats for thickness weighted means in Chapter 67, but that usage is completely distinct from the non-dimensionalization usage in the present chapter.

Non-dimensional velocity equation

Introducing the above variables into the shallow water velocity equation (43.2a) renders

$$\frac{U}{T}\frac{\partial \widehat{\boldsymbol{u}}}{\partial \widehat{t}} + \frac{U^2}{L}\left(\widehat{\boldsymbol{u}}\cdot\widehat{\nabla}\right)\widehat{\boldsymbol{u}} + f_\circ U\left(\widehat{\boldsymbol{f}}\times\widehat{\boldsymbol{u}}\right) = -\frac{g\,\mathscr{H}}{L}\widehat{\nabla}\widehat{\eta}. \tag{43.39}$$

As before, we assume the time scale is given by the advection time

$$T = L/U = 1/(\mathrm{Ro}\, f_\circ), \tag{43.40}$$

so that dividing by $f_\circ U$ leads to

$$\mathrm{Ro}\left[\frac{\partial \widehat{\boldsymbol{u}}}{\partial \widehat{t}} + \left(\widehat{\boldsymbol{u}}\cdot\widehat{\nabla}\right)\widehat{\boldsymbol{u}}\right] + \left(\widehat{\boldsymbol{f}}\times\widehat{\boldsymbol{u}}\right) = -\left[\frac{g\,H}{f_\circ L\,U}\frac{\mathrm{Ro}}{\mathrm{Bu}}\right]\widehat{\nabla}\widehat{\eta}, \tag{43.41}$$

where we set $\mathscr{H} = H\,(\mathrm{Ro}/\mathrm{Bu})$ according to equation (43.36). We simplify the factor on the right hand side according to

$$\frac{g\,H}{f_\circ L\,U}\frac{\mathrm{Ro}}{\mathrm{Bu}} = \frac{g\,H}{f_\circ L\,U}\frac{U}{f_\circ L}\frac{L^2}{L_\mathrm{d}^2} = \frac{g\,H}{f_\circ L\,U}\frac{U}{f_\circ L}\frac{L^2 f_\circ^2}{g\,H} = 1. \tag{43.42}$$

Hence, the non-dimensional inviscid shallow water velocity equation takes on the rather elegant form

$$\mathrm{Ro}\left[\frac{\partial \widehat{\boldsymbol{u}}}{\partial \widehat{t}} + \left(\widehat{\boldsymbol{u}}\cdot\widehat{\nabla}\right)\widehat{\boldsymbol{u}}\right] + \widehat{\boldsymbol{f}}\times\widehat{\boldsymbol{u}} = -\widehat{\nabla}\widehat{\eta}. \tag{43.43}$$

Introducing the non-dimensional material time derivative

$$\frac{\mathrm{D}}{\mathrm{D}\widehat{t}} = \frac{\partial}{\partial \widehat{t}} + \widehat{\boldsymbol{u}}\cdot\widehat{\nabla} \tag{43.44}$$

brings the velocity equation to

$$\mathrm{Ro}\,\frac{\mathrm{D}\widehat{\boldsymbol{u}}}{\mathrm{D}\widehat{t}} + \widehat{\boldsymbol{f}}\times\widehat{\boldsymbol{u}} = -\widehat{\nabla}\widehat{\eta}. \tag{43.45}$$

The velocity equation is consistent with a unit geostrophy number (i.e., Coriolis acceleration balances pressure gradient acceleration) if and only if the Rossby number is small, thus eliminating the material acceleration. We noted this point earlier when studying geostrophic motion, such as in Chapter 31. Even so, it is reassuring to see it emerge from the process of non-dimensionalization and scaling.

Non-dimensional thickness equation

The thickness equation (43.2b) can be written

$$\frac{\partial \eta'}{\partial t} + \nabla\cdot\left[\left(H + \eta' - \eta'_\mathrm{b}\right)\boldsymbol{u}\right] = 0, \tag{43.46}$$

which takes on the non-dimensional form

$$\frac{\mathscr{H}}{T}\frac{\partial \widehat{\eta}}{\partial \widehat{t}} + \frac{U\,H}{L}\widehat{\nabla}\cdot\left[\left(1 + \widehat{\eta}\,\mathscr{H}/H - \widehat{\eta}_\mathrm{b}\,\mathscr{B}/H\right)\widehat{\boldsymbol{u}}\right] = 0. \tag{43.47}$$

The advective time scaling $T = L/U$ brings the thickness equation to

$$\frac{\mathscr{H}}{H}\frac{\partial \widehat{\eta}}{\partial \widehat{t}} + \widehat{\nabla} \cdot [(1 + \widehat{\eta}\,\mathscr{H}/H - \widehat{\eta}_{\mathrm{b}}\,\mathscr{B}/H)\,\widehat{\boldsymbol{u}}] = 0. \tag{43.48}$$

We further specialize this equation in the following, as determined by the assumed horizontal length scale of the flow.

43.4 Shallow water planetary geostrophy

We make use of the non-dimensional equations derived in Section 43.3.7 to derive the mechanical equations for planetary geostrophy. We already encountered facets of planetary geostrophy for the continuously stratified case in Section 31.5 and for the shallow water in Sections 39.7, 39.9, and 39.8. We further pursue the continuously stratified theory in Chapter 44, developing a variety of vorticity analyses for use in understanding the large-scale ocean circulation. For these reasons, our presentation here is rather brief.

Planetary geostrophy is realized by dropping the fluid particle acceleration from the momentum equation (43.45), given that it is one order of Rossby number smaller than the Coriolis and pressure gradient accelerations. This assumption means that the velocity equation reduces to the geostrophic balance

$$\widehat{\boldsymbol{f}} \times \widehat{\boldsymbol{u}} = -\widehat{\nabla}\widehat{\eta}. \tag{43.49}$$

We furthermore assume that the Rossby number and Burger number scale together

$$\mathrm{Ro} \sim \mathrm{Bu} = (L_{\mathrm{d}}/L)^2 \ll 1, \tag{43.50}$$

so that the horizontal length scale for the planetary geostrophic flow is much larger than the deformation radius

$$L \gg L_{\mathrm{d}}. \tag{43.51}$$

This assumption is consistent with dropping material acceleration in the velocity equation. Although the velocity equation is greatly simplified, we make no assumption concerning the thickness equation. Consequently, the free surface and bottom undulations are unconstrained with planetary geostrophic flows, so long as the flow maintains the hydrostatic balance.

In summary, the thickness equation for the planetary geostrophic fluid retains its full unapproximated form, whereas the velocity equation reduces to geostrophy. Reintroducing dimensions leads to the planetary geostrophic equations

$$f\,\hat{\boldsymbol{z}} \times \boldsymbol{u} = -g\,\nabla\eta \quad \text{and} \quad \frac{\mathrm{D}h}{\mathrm{D}t} = -h\,\nabla \cdot \boldsymbol{u} \quad \text{and} \quad h = \eta - \eta_{\mathrm{b}}. \tag{43.52}$$

Since the Coriolis parameter retains its spatial dependence, and so includes the beta effect, the horizontal velocity field is divergent

$$f\,\nabla \cdot \boldsymbol{u} = -\beta\,(g/f)\,\partial_x \eta = -\beta\, v. \tag{43.53}$$

As shown in Exercise 43.1, the shallow water planetary geostrophic equations are equivalent to

$$f\,\hat{\boldsymbol{z}} \times \boldsymbol{u} = -g\,\nabla\eta \quad \text{and} \quad \frac{\mathrm{D}Q}{\mathrm{D}t} = 0 \quad \text{with} \quad Q = f/h. \tag{43.54}$$

As seen in Chapter 44, the planetary geostrophic potential vorticity, $Q = f/h$, plays a huge role in the mechanical interpretation of large scale flows in the ocean.

43.5 Shallow water quasi-geostrophy

In this section we develop the quasi-geostrophic equations for a single shallow water layer. Doing so requires far more work than for the planetary geostrophic equations. In particular, we use rudimentary asymptotic methods with the Rossby number acting as the relvant small non-dimensional parameter.

43.5.1 Quasi-geostrophic scaling

Quasi-geostrophic scaling is based on the following assumptions, with the first and second shared with planetary geostrophy whereas the remaining are distinct.

1. SMALL ROSSBY NUMBER: $\text{Ro} \ll 1$, which is fundamental to geostrophic scaling.

2. ADVECTIVE TIME SCALE: $T \sim L/U$; that is, the time scale is determined by horizontal advection of the horizontal flow, which is how we scale time throughout this chapter. Notably, we do not distinguish between the two horizontal directions, so that L and U are scales for both the zonal and meridional flow. This assumption will be jettisoned when considering the dynamics of fronts in Section 59.9, which then leads to the *semi-geostrophic* equations.

3. ORDER ROSSBY NUMBER BETA EFFECT: $|\beta L| \ll |f_\circ|$, which means that the Coriolis frequency does not vary much from its central value. To incorporate this assumption into the asymptotics, we expand the non-dimensional Coriolis parameter in terms of the Rossby number[3]
$$\widehat{f} = f/f_\circ = (1 + \beta\, y/f_\circ) \equiv (\widehat{f}_0 + \text{Ro}\, \widehat{\beta}\, \widehat{y}). \tag{43.55}$$
Making use of the advective scaling for time as in equation (43.40) renders[4]
$$\widehat{\beta}\, \widehat{y} = \beta\, y/(\text{Ro}\, f_\circ) = T\, \beta\, y \quad \text{and} \quad \widehat{f}_0 = f_\circ/f_\circ = 1. \tag{43.56}$$
The non-dimensional Coriolis parameter (43.55) and the scaling (43.56) are motivated by assuming the horizontal scales of motion are on the same order as the deformation radius, and that the Coriolis parameter does not vary much from its central value. Quasi-geostrophy is thus formulated within the beta plane approximation discussed in Section 24.5.

4. BURGER NUMBER ORDER ONE: $\text{Bu} \sim 1$, which means that the horizontal scales of motion for the quasi-geostrophic flows are on the same order as the deformation radius, $L \sim L_\text{d}$.

5. ORDER ROSSBY NUMBER FREE SURFACE UNDULATIONS: From equation (43.36), an order unity Burger number means that undulations of the free surface height scale according to the Rossby number: $\mathcal{H}/H = \text{Ro}$, so that free surface height undulations are small.

6. ORDER ROSSBY NUMBER BOTTOM TOPOGRAPHY UNDULATIONS: As seen in Section 43.6.4, for the quasi-geostrophic potential vorticity to correspond to the small Rossby number version of the shallow water potential vorticity requires the topography undulations to scale as $\mathcal{B}/H = \text{Ro}$. The assumed scaling for the bottom topography undulation pairs with that for the free surface, so that the layer thickness undulations, $h' = \eta' - \eta'_\text{b}$, also scale as Ro. We are thus able to take a sensible Ro expansion of the $1/h$ factor appearing in the shallow

[3] One could conceive of another small parameter that scales the beta effect, but the resulting asymptotics would be more difficult to manage given the need to keep track of two small parameters.

[4] Although $\widehat{f}_0 = 1$ in equation (43.56), it is useful to retain this term as a placeholder in the manipulations to follow. In particular, it helps when reintroducing dimensions in Section 43.6.1.

water potential vorticity (Section 43.6.4). It is useful to maintain a direct connection to the shallow water model as doing so helps to ensure that the resulting asymptotic theory is self-consistent. In particular, it ensures that quasi-geostrophic energetics are physically sensible since there is a direct lineage to the shallow water energetics.

The $\mathcal{B}/H = \text{Ro}$ scaling is consistent with the assumption that the planetary beta effect is small. Together, the two scalings

$$\mathcal{B}/H = \text{Ro} \quad \text{and} \quad \mathcal{H}/H = \text{Ro} \tag{43.57}$$

mean that the effective beta effect (arising from both planetary and topographic variations; see Section 43.6.1 below) are small.

43.5.2 Outlining the asymptotic method

To derive equations for the quasi-geostrophic shallow water model, we employ an asymptotic method with the Rossby number as the small parameter. Furthermore, we stop at the first nontrivial order. For this purpose, recall the non-dimensional shallow water equations from Section 43.3.7, and make use of the assumed $\text{Bu} \sim 1$ scaling

$$\text{Ro} \frac{\text{D}\widehat{\boldsymbol{u}}}{\text{D}\widehat{t}} + (\widehat{\boldsymbol{f}} \times \widehat{\boldsymbol{u}}) = -\widehat{\nabla}\widehat{\eta} \tag{43.58a}$$

$$\text{Ro} \left[\frac{\partial(\widehat{\eta} - \widehat{\eta}_\text{b})}{\partial \widehat{t}} + \widehat{\nabla} \cdot [(\widehat{\eta} - \widehat{\eta}_\text{b}) \widehat{\boldsymbol{u}}] \right] = -\widehat{\nabla} \cdot \widehat{\boldsymbol{u}}. \tag{43.58b}$$

We brought the time independent bottom topography, $\widehat{\eta}_\text{b}$, into the time derivative for the thickness equation, as doing so provides some symmetry with $\widehat{\eta}$.[5]

Asymptotic expansion of the prognostic fields

Asymptotic methods are ideally suited for non-dimensional equations since we can unambiguously determine scales via the size of non-dimensional parameters. We here assume the Rossby number to be small, in which case we are led to perform an asymptotic expansion of the prognostic fields in terms of the Rossby number. There are three prognostic fields, $\widehat{u}, \widehat{v}, \widehat{\eta}$, and corresponding vertical velocity, $\widehat{w}$, which we assume can be written as an asymptotic series

$$\widehat{u} = \widehat{u}_0 + \text{Ro}\, \widehat{u}_1 + \text{Ro}^2\, \widehat{u}_2 + \ldots \tag{43.59a}$$

$$\widehat{v} = \widehat{v}_0 + \text{Ro}\, \widehat{v}_1 + \text{Ro}^2\, \widehat{v}_2 + \ldots \tag{43.59b}$$

$$\widehat{w} = \widehat{w}_0 + \text{Ro}\, \widehat{w}_1 + \text{Ro}^2\, \widehat{w}_2 + \ldots \tag{43.59c}$$

$$\widehat{\eta} = \widehat{\eta}_0 + \text{Ro}\, \widehat{\eta}_1 + \text{Ro}^2\, \widehat{\eta}_2 + \ldots \tag{43.59d}$$

We thus refer to the zeroth, first, second, etc. order of the asymptotic expansion. The three components of the velocity satisfy the non-divergence condition at each order

$$\nabla \cdot \widehat{\boldsymbol{v}}_n = 0 \quad \forall\, n. \tag{43.60}$$

Practical goal

The practical goal of asymptotic analysis is to develop a closed set of prognostic equations for functions appearing in the asymptotic expansions (43.59a)-(43.59d). For our purposes, we are

[5] Also recall our nomenclature, whereby $\boldsymbol{u}$ is the horizontal velocity, so that $-\widehat{\nabla} \cdot \widehat{\boldsymbol{u}}$ is the non-dimensionalized horizontal convergence of the horizontal velocity. Also, since η is a function just of the horizontal directions (and time), $\widehat{\nabla}\widehat{\eta}$ is the non-dimensionalized horizontal gradient of the free surface.

content to stop at the lowest nontrivial order, meaning the point at which there is a prognostic equation that provides a means to move the system forward in time. Motivation for asymptotic analysis is to produce an equation set offering a means to focus analysis on dynamics most active under the regime determined by the chosen non-dimensional parameters. Each higher order in asymptotic expansion generally produces more accurate solutions, and yet requires more complex algebraic manipulations. Hence, pursuit of higher order expansions should be undertaken only after first determining that the lower order equation set remains physically lacking.

Enabling the machinery

At this point we enable the machinery by "turning the crank". To do so, insert the asymptotic expansions (43.59a)-(43.59d) into the non-dimensional partial differential equations (43.58a) and (43.58b). Since the Rossby number, Ro, is arbitrarily small, and all non-dimensional fields are order unity regardless their order, the only means to maintain self-consistency is for terms to balance at equal order in Rossby number. Hence, we do not mix terms from different orders of Rossby number. This point is fundamental to asymptotic methods.

Again, our goal is to establish a set of prognostic equations that allows us to evolve a state that is arbitrarily close to geostrophic balance. We anticipate that at zeroth order, the asymptotic method offers us just the geostrophic balance, which has no prognostic value. Hence, we need to go at least to order Ro^1, and hopefully no further since the algebraic tedium increases with order. With that anticipation and hope (and prior knowledge of what is sufficient), we only keep track of terms of order Ro^0 and Ro^1, in which the momentum and continuity equations become

$$\mathrm{Ro}\,\frac{\mathrm{D}_0\widehat{\boldsymbol{u}}_0}{\mathrm{D}\widehat{t}} + (\widehat{f}_0 + \mathrm{Ro}\,\widehat{\beta}\,\widehat{y})\,\hat{\boldsymbol{z}}\times(\widehat{\boldsymbol{u}}_0 + \mathrm{Ro}\,\widehat{\boldsymbol{u}}_1) = -\widehat{\nabla}(\widehat{\eta}_0 + \mathrm{Ro}\,\widehat{\eta}_1) \tag{43.61a}$$

$$\mathrm{Ro}\left[\frac{\partial\widehat{\eta}_0}{\partial\widehat{t}} + \widehat{\nabla}\cdot[(\widehat{\eta}_0 - \widehat{\eta}_\mathrm{b})\,\widehat{\boldsymbol{u}}_0] + \widehat{\nabla}\cdot\widehat{\boldsymbol{u}}_1\right] = -\widehat{\nabla}\cdot\widehat{\boldsymbol{u}}_0. \tag{43.61b}$$

Note that the material time derivative in equation (43.61a) makes use of *only* the zeroth order geostrophic horizontal velocity

$$\frac{\mathrm{D}_0}{\mathrm{D}\widehat{t}} = \frac{\partial}{\partial\widehat{t}} + \widehat{\boldsymbol{u}}_0\cdot\widehat{\nabla}. \tag{43.62}$$

43.5.3 Order Ro^0 asymptotic equations

Terms in equations (43.61a) and (43.61b) balancing at order Ro^0 are given by

$$\widehat{\boldsymbol{f}}_0\times\widehat{\boldsymbol{u}}_0 = -\widehat{\nabla}\widehat{\eta}_0 \tag{43.63a}$$

$$\widehat{\nabla}\cdot\widehat{\boldsymbol{u}}_0 = 0. \tag{43.63b}$$

The zeroth order velocity equation (43.63a) is the f-plane geostrophic balance. Furthermore, the vertical component to the curl of equation (43.63a) leads to the horizontal non-divergence condition, $\widehat{\nabla}\cdot\widehat{\boldsymbol{u}}_0 = 0$, which is identical to the zeroth order thickness equation (43.63b). Hence, the zeroth order horizontal velocity is given by f-plane geostrophy within a single shallow water layer.

The geostrophic streamfunction

Given the non-divergence condition (43.63b), the zeroth order velocity field can be written in terms of a *geostrophic streamfunction*

$$\widehat{u}_0 = -\partial_{\widehat{y}}\widehat{\psi}_0 \qquad \text{and} \qquad \widehat{v}_0 = \partial_{\widehat{x}}\widehat{\psi}_0 \qquad \text{and} \qquad \widehat{\zeta}_0 = \widehat{\nabla}^2\widehat{\psi}_0, \tag{43.64}$$

where the zeroth order streamfunction is the ratio of the zeroth order surface height to zeroth order Coriolis parameter

$$\widehat{\psi}_0 = \widehat{\eta}_0 / \widehat{f}_0, \tag{43.65}$$

and we introduced the non-dimensional sgeostrophic relative vorticity

$$\widehat{\zeta}_0 = \partial_{\widehat{x}} \widehat{v}_0 - \partial_{\widehat{y}} \widehat{u}_0. \tag{43.66}$$

The corresponding dimensionful quantities are

$$\psi = (U\,L)\,\widehat{\psi}_0 \quad \text{and} \quad \zeta = (U/L)\,\widehat{\zeta}_0. \tag{43.67}$$

We dropped the asymptotic label on the dimensional geostrophic streamfunction since it is the only streamfunction considered in quasi-geostrophy.[6]

Horizontally non-divergent flow with an undulating free surface

Recall the discussion of horizontally non-divergent flow in Chapter 38, where the vertical velocity vanishes and the lid pressure renders a surface interface that is rigid and flat. We here also have a horizontally non-divergent flow, and yet it is within a single shallow water layer with a free surface that is not flat and that provides a pressure gradient in geostrophic balance with the Coriolis acceleration. Geostrophy and horizontal non-divergence enforces a free surface (and hence pressure field) that is related to relative vorticity through the Laplacian operator in equation (43.64). Furthermore, in the absence of horizontal convergence, there is no means for the flow to generate a vertical velocity, so that at this order we have

$$\widehat{w}_0 = 0 \tag{43.68}$$

for shallow water quasi-geostrophy.

43.5.4 Order Ro^1 asymptotic equations

Time derivatives appear at order Ro^1, with the velocity and thickness equations given by

$$\frac{\mathrm{D}_0 \widehat{\boldsymbol{u}}_0}{\mathrm{D}\widehat{t}} + \widehat{f}_0\, \hat{\boldsymbol{z}} \times \widehat{\boldsymbol{u}}_1 + \widehat{\beta}\, \widehat{y}\, \hat{\boldsymbol{z}} \times \widehat{\boldsymbol{u}}_0 = -\widehat{\nabla} \widehat{\eta}_1 \tag{43.69a}$$

$$\frac{\mathrm{D}_0 (\widehat{\eta}_0 - \widehat{\eta}_{\mathrm{b}})}{\mathrm{D}\widehat{t}} = -\widehat{\nabla} \cdot \widehat{\boldsymbol{u}}_1. \tag{43.69b}$$

These equations appear to be unclosed because the evolution equation for zeroth order (geostrophic) terms is dependent on first order (ageostrophic) terms. However, the ageostrophic terms can be eliminated using two steps. First, we produce the vorticity equation from the momentum equation, which removes the ageostrophic pressure gradient, $-\widehat{\nabla}\widehat{\eta}_1$. Second, combining the vorticity equation and continuity equation eliminates the horizontal convergence of the ageostrophic velocity, $-\widehat{\nabla} \cdot \widehat{\boldsymbol{u}}_1$. The second step leads to the quasi-geostrophic potential vorticity equation. Although details are specific to the present study of shallow water quasi-geostrophy, similar steps are encountered in other balanced geophysical fluid systems.

[6] In some of our discussions, it is useful to introduce "g" or "ag" subscripts to distinguish $\mathcal{O}(\mathrm{Ro}^0)$ geostrophic terms from $\mathcal{O}(\mathrm{Ro}^1)$ ageostrophic terms.

The geostrophic vorticity equation

Taking the curl of the momentum equation (43.69a) eliminates the ageostrophic pressure gradient, $\widehat{\nabla}\widehat{\eta}_1$, thus producing the vorticity equation

$$\partial_{\widehat{t}}\widehat{\zeta}_0 + (\widehat{\boldsymbol{u}}_0 \cdot \widehat{\nabla})\,(\widehat{\zeta}_0 + \widehat{\beta}\,\widehat{y}) = -\widehat{f}_0\,\widehat{\nabla}\cdot\widehat{\boldsymbol{u}}_1. \tag{43.70}$$

The right hand side term arises from stretching in the presence of planetary rotation, which can be seen by using continuity to express the right hand side as

$$-\widehat{f}_0\,\widehat{\nabla}\cdot\widehat{\boldsymbol{u}}_1 = \widehat{f}_0\,\partial_{\widehat{z}}\widehat{w}_1. \tag{43.71}$$

Evidently, to this order in Rossby number, stretching arises just from the planetary vorticity, with stretching due to relative vorticity appearing at a higher order. Since $\widehat{\beta}\,\widehat{y}$ is time independent, we can write the vorticity equation (43.70) using the geostrophic material time derivative

$$\frac{\mathrm{D}_0\,(\widehat{\zeta}_0 + \widehat{\beta}\,\widehat{y})}{\mathrm{D}\widehat{t}} = -\widehat{f}_0\,\widehat{\nabla}\cdot\widehat{\boldsymbol{u}}_1. \tag{43.72}$$

The quasi-geostrophic potential vorticity equation

We need one more step to close the system since the evolution of zeroth order vorticity in equations (43.70) and (43.72) depends on vortex stretching induced by convergence of the first order velocity. To eliminate $\widehat{\nabla}\cdot\widehat{\boldsymbol{u}}_1$, we substitute from the thickness equation (43.69b), thus leading to a prognostic equation involving just zeroth order terms

$$\frac{\partial[\widehat{\zeta}_0 + \widehat{\beta}\,\widehat{y} - \widehat{f}_0\,(\widehat{\eta}_0 - \widehat{\eta}_\mathrm{b})]}{\partial\widehat{t}} + \widehat{\boldsymbol{u}}_0\cdot\widehat{\nabla}[\widehat{\zeta}_0 + \widehat{\beta}\,\widehat{y} - \widehat{f}_0\,(\widehat{\eta}_0 - \widehat{\eta}_\mathrm{b})] = 0, \tag{43.73}$$

which can be written in the material form

$$\frac{\mathrm{D}_0}{\mathrm{D}\widehat{t}}\Big[\widehat{\zeta}_0 + \widehat{\beta}\,\widehat{y} - \widehat{f}_0\,(\widehat{\eta}_0 - \widehat{\eta}_\mathrm{b})\Big] = 0. \tag{43.74}$$

Finally, we introduce the geostrophic streamfunction $\widehat{\psi}_0 = \widehat{\eta}_0/\widehat{f}_0$ (equation (43.65)) to render

$$\frac{\mathrm{D}_0}{\mathrm{D}\widehat{t}}\Big[\widehat{\nabla}^2\,\widehat{\psi}_0 + \widehat{\beta}\,\widehat{y} + \widehat{f}_0\,\widehat{\eta}_\mathrm{b} - \widehat{f}_0^2\,\widehat{\psi}_0\Big] = 0. \tag{43.75}$$

Equation (43.75) is a statement of the material conservation of quasi-geostrophic potential vorticity (in its non-dimensional form), where material evolution is defined by the horizontal geostrophic currents (equation (43.62)). This equation is the culmination of our quest to derive a prognostic equation for the evolution of geostrophic flow. It enables us to evolve the geostrophic velocity and geostrophic free surface by accessing, but not explicitly determining, the leading order ageostrophic motions. Practical use of the quasi-geostrophic method is based on time stepping the quasi-geostrophic potential vorticity, and then inverting the potential vorticity equation to diagnose the streamfunction to then determine the geostrophic velocity and free surface. That inversion requires solving an elliptic boundary value problem (see Chapters 6 and 9), and we present further remarks on inversion in Section 43.6.5.

43.6 Elements of shallow water quasi-geostrophy

The asymptotic analysis of Section 43.5 worked with non-dimensional quantities, which are suitable for determining the scales required for organizing terms in the asymptotic expansion.

Now that we have worked through the details, we can make use of that effort to further expose the physical content of shallow water quasi-geostrophy theory. For that purpose, it is useful to reintroduce physical dimensions.

43.6.1 Dimensional potential vorticity and streamfunction

To introduce physical dimensions, we invert the relations used in Section 43.3.7

$$\widehat{t} = t/T \qquad (\widehat{x},\widehat{y}) = (x,y)/L \qquad \partial_{\widehat{t}} = T\,\partial_t \qquad \widehat{\nabla} = L\,\nabla \qquad (\widehat{u},\widehat{v}) = (u,v)/U \tag{43.76a}$$

$$\widehat{\eta} = \eta'/\mathcal{H} \qquad \widehat{\eta}_{\mathsf{b}} = \eta'_{\mathsf{b}}/\mathcal{B} \qquad \mathcal{H} = H\,\mathrm{Ro} \qquad \mathcal{B} = H\,\mathrm{Ro} \tag{43.76b}$$

$$\widehat{f_0} = f_o/f_o \qquad \widehat{\beta}\,\widehat{y} = \beta\,y/(\mathrm{Ro}\,f_o) = (L/U)\,\beta\,y \qquad \widehat{\zeta} = (L/U)\,\zeta = L^2\,\nabla^2\psi. \tag{43.76c}$$

We often drop asymptotic subscripts on dimensional terms to help reduce clutter, though at times it is useful to introduce a g or ag subscript to distinguish the geostrophic and ageostrophic components (e.g., see Section 43.6.6).

Starting from the non-dimensional quasi-geostrophic potential vorticity (43.74), the reintroduction of dimensions leads to

$$\widehat{q} = \widehat{\zeta}_0 + \widehat{\beta}\,\widehat{y} + \widehat{f}_0\,\widehat{\eta}_{\mathsf{b}} - \widehat{f}_0\,\widehat{\eta}_0 \tag{43.77a}$$

$$= \frac{L}{U}\,(\zeta + \beta\,y) + \frac{\eta'_{\mathsf{b}}}{\mathcal{B}} - \frac{\eta'}{\mathcal{H}} \tag{43.77b}$$

$$= \frac{L}{U}\,(\zeta + \beta\,y) + \frac{\eta'_{\mathsf{b}}}{H\,Ro} - \frac{\eta'}{H\,Ro} \tag{43.77c}$$

$$= \frac{L}{U}\left[\zeta + \beta\,y - \frac{f_o\,(\eta' - \eta'_{\mathsf{b}})}{H}\right] \tag{43.77d}$$

$$= \frac{L}{U}\left[\zeta + \beta\,y - \frac{g\,(\eta' - \eta'_{\mathsf{b}})}{f_o}\,\frac{1}{L_{\mathsf{d}}^2}\right] \tag{43.77e}$$

$$= \frac{L}{U}\left[\zeta + \beta\,y - L_{\mathsf{d}}^{-2}\,(\psi - \psi_{\mathsf{b}})\right], \tag{43.77f}$$

where $L_{\mathsf{d}} = \sqrt{g\,H}/f$ is the shallow water deformation radius (equation (43.31)), and we introduced the geostrophic streamfunction[7]

$$\psi = (g/f_o)\,\eta'. \tag{43.78}$$

We also wrote the contribution from topography as

$$\psi_{\mathsf{b}} = (g/f_o)\,\eta'_{\mathsf{b}}, \tag{43.79}$$

which is a static field. We are thus led to the dimensionful quasi-geostrophic potential vorticity for a single shallow water layer

$$q = f_o\,(1 + \mathrm{Ro}\,\widehat{q}) = (\zeta + f) - L_{\mathsf{d}}^{-2}\,(\psi - \psi_{\mathsf{b}}) = f + \psi_{\mathsf{b}}\,L_{\mathsf{d}}^{-2} + (\nabla^2 - L_{\mathsf{d}}^{-2})\,\psi. \tag{43.80}$$

We took the liberty of adding the constant, f_o, to the QG potential vorticity, which does not alter the dynamics but does allow us to introduce the planetary vorticity, $f = f_o + \beta\,y$. Evidently, the dynamically relevant portions of q appear at order Ro, as expected since the zeroth order theory is f-plane geostrophy, which provides no prognostic capability.

[7] The geostrophic streamfunction is arbitrary up to a constant. For example, *Vallis* (2017) defines the geostrophic streamfunction in his equation (5.69) as $\psi_{\mathrm{vallis}} = g\,\eta/f_o = \psi + g\,H/f_o$, which differs by the constant $g\,H/f_o$.

43.6.2 Contributions to quasi-geostrophic potential vorticity

The quasi-geostrophic potential vorticity (43.80) has three main contributions

$$q = f + \zeta - f_o\, h'/H, \tag{43.81}$$

where we wrote

$$L_d^{-2}\,(\psi - \psi_b) = f_o^2/(g\,H)\,(g/f_o)\,(\eta' - \eta_b') = f_o\, h'/H, \tag{43.82}$$

with h' the undulations in the layer thickness due to undulations in the free surface and bottom topography. Heuristically, we can connect q to the shallow water $Q = (f+\zeta)/h$ by

$$(f+\zeta)/h \approx (f+\zeta)\,(1 - h'/H) \approx H^{-1}\,(f + \zeta - f_o\, h'/H), \tag{43.83}$$

where we assumed $\beta\, y$, ζ, and h' are order Ro whereas f_o is order unity. We pursue this expansion more formally in Section 43.6.4.

It is notable that the quasi-geostrophic potential vorticity, q, is determined by the free surface height, the bottom topography, and the Coriolis parameter. That is, once f, η_b, and η are known, then we have q and thus, through inversion, the geostrophic flow is determined. This is a rather remarkable result that embodies the following variety of physical processes contributing to potential vorticity, and hence to quasi-geostrophic dynamics.

- PLANETARY VORTICITY: The contribution $f = f_o + \beta\, y$ arises from planetary vorticity, with the dynamically relevant contribution for quasi-geostrophy arising just from the $\beta\, y$ term. The difference, $q - f$, is sometimes referred to as the *relative potential vorticity*, in analog to the relative vorticity, $\zeta = \zeta_a - f$.

- GEOSTROPHIC RELATIVE VORTICITY: $\zeta = \nabla^2\psi = (g/f_o)\,\nabla^2\eta$ is the relative vorticity of the geostrophic flow. The Laplacian operator emphasizes small spatial scales, so that the relative vorticity is most important at scales at or smaller than the deformation radius.

- EFFECTIVE BETA: The contribution from the gradient of planetary vorticity is given by $\beta\, y = \boldsymbol{x}\cdot\nabla f$. Likewise, the contribution from topography is given by

  $$\psi_b\, L_d^{-2} = f_o\, \eta_b'/H = (f_o/H)\,(\eta_b - \overline{\eta_b}) \approx (f_o/H)\,\boldsymbol{x}\cdot\nabla\eta_b, \tag{43.84}$$

  where the approximate expression made use of a Taylor series. These two contributions can be combined into an effective beta

  $$\beta\, y + \psi_b\, L_d^{-2} = \boldsymbol{x}\cdot\nabla(f + f_o\,\eta_b/H) \approx \boldsymbol{x}\cdot(H - \eta_b)\,\nabla[f/(H-\eta_b)], \tag{43.85}$$

  with the final approximate expression connecting to the effective beta discussed in Section 39.5.1.

- VERTICAL STRETCHING: As discussed in Section 35.2, shallow water fluids move as vertical columns that can expand (stretch) and contract (squash). Hence, the term $(f_o/H)\,h'$ accounts for the contribution to potential vorticity from column stretching and squashing. It is most important for scales at or larger than those where the relative vorticity is important; i.e., at or larger than the deformation radius.

- FLOW REGIMES RELATIVE TO THE DEFORMATION RADIUS: The term $(\nabla^2 - L_d^{-2})\,\psi$ signals two regimes as determined by the deformation radius. For lateral scales on the order of the deformation radius, both the relative vorticity and vortex stretching make equal contributions to the potential vorticity. For smaller scales, relative vorticity is more important whereas for larger scales vortex stretching dominates.

43.6.3 Connecting to background (resting state) potential vorticity

For some purposes, particularly when studying Rossby waves in Section 55.9, we find it useful to unpack the material time derivative,

$$\mathrm{D}q/\mathrm{D}t = \partial_t q + \hat{\boldsymbol{z}} \cdot (\nabla\psi \times \nabla q), \tag{43.86}$$

to expose the role of the potential vorticity contained in a resting fluid. For this purpose, expand the gradient

$$\nabla q = \nabla(\nabla^2\psi) - \nabla\psi/L_\mathrm{d}^2 + \nabla f + \nabla\psi_\mathrm{b}/L_\mathrm{d}^2, \tag{43.87}$$

so that

$$\nabla\psi \times \nabla q = \nabla\psi \times \nabla(\nabla^2\psi) + \nabla\psi \times (\nabla f + \nabla\psi_\mathrm{b}/L_\mathrm{d}^2). \tag{43.88}$$

The second term on the right hand side can be written in terms of the resting state potential vorticity

$$\nabla f + \nabla\psi_\mathrm{b}/L_\mathrm{d}^2 = \nabla f + (f_\circ/H)\,\nabla\eta'_\mathrm{b} = \nabla f - (f_\circ/H)\,\nabla(H - \eta'_\mathrm{b}) \approx H\,\nabla(f/H_\mathrm{r}) = H\,\nabla Q_\mathrm{r}, \tag{43.89}$$

where $H_\mathrm{r} = H - \eta'_\mathrm{b}$ is the thickness of the resting fluid, and Q_r is the potential vorticity of the resting fluid. The approximation in the penultimate step follows from assuming $\eta'_\mathrm{b}/H = \mathcal{O}(\mathrm{Ro})$, as per the quasi-geostrophic scaling in Section 43.5.1.

Bringing the pieces together leads us to write the material time evolution of quasi-geostrophic potential vorticity as

$$(f_\circ/g)\,\mathrm{D}q/\mathrm{D}t = \partial_t\,[(L_\mathrm{d}^{-2} - \nabla^2)\,\eta'] - H\,\hat{\boldsymbol{z}} \cdot (\nabla\eta' \times \nabla Q_\mathrm{r}) - (g/f_\circ)\,\hat{\boldsymbol{z}} \cdot [\nabla\eta' \times \nabla(\nabla^2\eta')]. \tag{43.90}$$

The second term on the right hand side arises from geostrophic advection of the potential vorticity in the resting fluid. This linear term is fundamental to the Rossby wave dispersion relation studied in Section 55.9. The nonlinear term on the right hand side arises from advection of the geostrophic relative vorticity by the geostrophic velocity. This term is generally ignored when studying small amplitude wave fluctuations. Furthermore, it is notable that this term vanishes identically for plane waves (see Section 55.9.2 for more discussion).

43.6.4 Connecting to Rossby's shallow water potential vorticity

We here determine how potential vorticity for shallow water quasi-geostrophy relates to Rossby's shallow water potential vorticity studied in Chapter 39. For that purpose, recall that the potential vorticity for a single layer of shallow water fluid is (Section 39.3)

$$Q = \frac{f + \zeta}{h}, \tag{43.91}$$

where $h = H + \eta' - \eta'_\mathrm{b}$ (equation (43.4)) is the layer thickness.

To connect to the quasi-geostrophic potential vorticity, we non-dimensionalize the potential vorticity and then perform an asymptotic expansion to order Ro^1. For this purpose, use the scaling relations from Section 43.3.7 to write the geostrophic relative vorticity as

$$\zeta = \nabla^2\psi = (g/f_\circ)\,\nabla^2\eta' = (g\,\mathscr{H})/(f_\circ\,L^2)\,\widehat{\nabla}^2\widehat{\eta} = (g\,H\,\mathrm{Ro})/(f_\circ\,L^2)\,\widehat{\zeta}_0 = f_\circ\,\mathrm{Ro}\,(L_\mathrm{d}/L)^2\,\widehat{\zeta}_0, \tag{43.92}$$

as well as

$$h = H + H\,\mathrm{Ro}\,(\widehat{\eta} - \widehat{\eta}_\mathrm{b}) \tag{43.93a}$$

$$f = f_\circ\,(\widehat{f}_0 + \mathrm{Ro}\,\widehat{\beta}\,\widehat{y}). \tag{43.93b}$$

Taking the ratio and expanding to order Ro^1 leads to

$$\frac{f+\zeta}{h} = \frac{f_\circ}{H}\left[\frac{\widehat{f}_0 + \mathrm{Ro}\,(L_\mathsf{d}/L)^2\,\widehat{\zeta}_0 + \mathrm{Ro}\,\widehat{\beta}\,\widehat{y}}{1+\mathrm{Ro}\,(\widehat{\eta}-\widehat{\eta}_\mathsf{b})}\right] \tag{43.94a}$$

$$\approx \frac{f_\circ}{H} + \frac{f_\circ\,\mathrm{Ro}}{H}\left[-\widehat{f}_0\,(\widehat{\eta}-\widehat{\eta}_\mathsf{b}) + (L_\mathsf{d}/L)^2\,\widehat{\zeta}_0 + \widehat{\beta}\,\widehat{y}\right] \tag{43.94b}$$

$$= \frac{f_\circ}{H} + \frac{f_\circ\,\mathrm{Ro}}{H}\left[(L_\mathsf{d}/L)^2\,\widehat{\zeta}_0 + \widehat{\beta}\,\widehat{y} - \widehat{f}_0\,(\widehat{\eta}-\widehat{\eta}_\mathsf{b})\right] \tag{43.94c}$$

$$= \frac{f_\circ}{H} + \frac{f_\circ\,\mathrm{Ro}}{H}\left[\frac{\zeta}{f_\circ\,\mathrm{Ro}} + \frac{\beta\,y}{f_\circ\,\mathrm{Ro}} - \frac{\eta'}{\mathscr{H}} + \frac{\eta'_\mathsf{b}}{\mathscr{B}}\right] \tag{43.94d}$$

$$= \frac{1}{H}\left[\zeta + f_\circ + \beta\,y - \frac{f_\circ\,(\eta'-\eta'_\mathsf{b})}{H}\right] \tag{43.94e}$$

$$= \widehat{q}\,U/(H\,L) \tag{43.94f}$$

$$= q/H. \tag{43.94g}$$

We are thus led to the relation between the shallow water potential vorticity and the quasi-geostrophic shallow water potential vorticity

$$\frac{f+\zeta}{h} = \frac{q}{H}\left[1+\mathcal{O}(\mathrm{Ro}^2)\right]. \tag{43.95}$$

As noted in Section 43.5.1, this connection between the potential vorticities only holds when assuming deviations in *both* the bottom topography and free surface scale according to the Rossby number, $\eta' = \mathscr{H}\,\mathrm{Ro}$ and $\eta'_\mathsf{b} = \mathscr{B}\,\mathrm{Ro}$, thus allowing us to combine $\widehat{\eta}$ and $\widehat{\eta}_\mathsf{b}$ in the thickness equation (43.93a). That is, we must assume that both the planetary beta and topographic beta are on the order of Ro^1.

The identity (43.95) is a consequence of the asymptotic expansion of the velocity and thickness equations. We could alternatively invert our development of quasi-geostrophy by using the quasi-geostrophic potential vorticity as the basis for deriving the governing equations. We pursue that approach to derive the layered quasi-geostrophic equations in Section 43.6.10.

43.6.5 Geostrophic flow via potential vorticity inversion

Here are the key pieces to single layer shallow water quasi-geostrophic theory:

$$\boldsymbol{u} = \hat{\boldsymbol{z}}\times\nabla\psi \quad\text{and}\quad \zeta = \hat{\boldsymbol{z}}\cdot\nabla\times\boldsymbol{u} = \nabla^2\psi \quad\text{and}\quad q = f+\zeta - L_\mathsf{d}^{-2}\,(\psi-\psi_\mathsf{b}) \tag{43.96a}$$

$$\psi = (g/f_\circ)\,\eta' \quad\text{and}\quad \psi_\mathsf{b} = (g/f_\circ)\,\eta'_\mathsf{b} \quad\text{and}\quad L_\mathsf{d} = \sqrt{g\,H}/f_\circ. \tag{43.96b}$$

Note that we can choose to use the full free surface height, $\eta = \eta' + \overline{\eta}$, and bottom topography, $\eta_\mathsf{b} = \eta'_\mathsf{b} - \overline{\eta_\mathsf{b}}$, since doing so only adds a dynamically irrelevant constant to ψ, ψ_b, and q.

As seen in Section 43.5.4, evolution of the geostrophic flow is determined by material evolution of the quasi-geostrophic potential vorticity following the horizontal geostrophic flow. This evolution equation takes on the dimensional form

$$\frac{\mathrm{D}q}{\mathrm{D}t} = (\partial_t + \boldsymbol{u}\cdot\nabla)\,q = \partial_t q + \hat{\boldsymbol{z}}\cdot(\nabla\psi\times\nabla q) = \partial_t q + J(\psi,q), \tag{43.97}$$

where the final equality introduced the Jacobian operator

$$J(\psi,q) = \hat{\boldsymbol{z}}\cdot(\nabla\psi\times\nabla q) = \partial_x\psi\,\partial_y q - \partial_y\psi\,\partial_x q. \tag{43.98}$$

For a perfect fluid, the quasi-geostrophic potential vorticity is materially constant, whereas more

general flows have forcing and dissipation so that

$$\frac{\mathrm{D}q}{\mathrm{D}t} = \text{forcing} - \text{dissipation}. \tag{43.99}$$

As a method to evolve the quasi-geostrophic state forward in time, we first update the potential vorticity to a new time step. Thereafter, we must diagnose the streamfunction, $\psi = g\,\eta/f_\circ$, by solving the elliptic boundary value problem for ψ,

$$(\nabla^2 - L_\mathsf{d}^{-2})\,\psi = q - f - \psi_\mathsf{b}/L_\mathsf{d}^2, \tag{43.100}$$

at which point we have the updated free surface and updated velocity. This same inversion method was outlined for time stepping the two-dimensional non-divergent barotropic model in Section 38.2.6. It is here referred to as *potential vorticity inversion*.

The streamfunction equation (43.100) is a forced *Helmholtz equation* (Section 6.7.3), which is an elliptic partial differential equation.[8] While q results from taking derivatives of ψ, the streamfunction results from taking integrals of q. Consequently, maps of the potential vorticity have more structure at the high wave numbers (small scales) relative to the streamfunction. Writing the potential vorticity in equation (43.100) as

$$(\nabla^2 - L_\mathsf{d}^{-2})\,(\psi - \psi_\mathsf{b}) = q - f - L_\mathsf{d}^{-2}\,\nabla^2\psi_\mathsf{b} \tag{43.101}$$

offers us further interpretations, based on properties of the horizontal Laplacian operator. Namely, regions of relatively low $\psi - \psi_\mathsf{b}$ correspond to regions of relatively high $q - f - L_\mathsf{d}^{-2}\,\nabla^2\psi_\mathsf{b}$, and vice versa. For a flat bottom where ψ_b is a constant, relatively low sea level regions (low pressure regions) correspond to regions of relatively high $q - f$. Finally, on the f-plane with a flat bottom, relatively low pressure regions correspond to relatively high potential vorticity regions.

43.6.6 Evolution of quasi-geostrophic vorticity, velocity, and free surface

When making use of the potential vorticity inversion method from Section 43.6.5, we are unconcerned with the velocity equation and the free surface equation. Rather, it is sufficient to invert the potential vorticity equation (43.100) to find the streamfunction, from which both the velocity and the free surface are diagnosed. Even so, there are physical insights resulting from analysis of the quasi-geostrophic velocity, vorticity, and free surface. We here discuss these equations and identify a notable ambiguity in their specification.

Quasi-geostrophic absolute vorticity equation

Reintroducing dimensions to the non-dimensional quasi-geostrophic vorticity equation (43.70) leads to

$$(\partial_t + \boldsymbol{u}_\mathsf{g}\cdot\nabla)\,(\zeta_\mathsf{g} + f) = -f_\circ\,\nabla\cdot\boldsymbol{u}_\mathsf{ag}, \tag{43.102}$$

which takes on the equivalent form using the geostrophic material time derivative[9]

$$\frac{\mathrm{D}_\mathsf{g}(\zeta_\mathsf{g} + f)}{\mathrm{D}t} = -f_\circ\,\nabla\cdot\boldsymbol{u}_\mathsf{ag} \quad \text{with} \quad \frac{\mathrm{D}_\mathsf{g}}{\mathrm{D}t} = \partial_t + \boldsymbol{u}_\mathsf{g}\cdot\nabla. \tag{43.103}$$

[8] We can mathematically formulate the inversion problem using the Green's function method for elliptic operators studied in Chapter 9.

[9] It is important to remember our notation for the velocity, in which $\boldsymbol{u}_\mathsf{g}$ is horizontal so that $\boldsymbol{u}_\mathsf{g}\cdot\nabla = u_\mathsf{g}\,\partial_x + v_\mathsf{g}\,\partial_y$. See also equation (43.106).

In these equations we introduced subscripts to distinguish the geostrophic velocity and corresponding free surface height,

$$f_o \, \hat{\boldsymbol{z}} \times \boldsymbol{u}_g = -g \, \nabla \eta_g, \tag{43.104}$$

from the ageostrophic velocity, $\boldsymbol{u}_{ag}$, and ageostrophic free surface height, η_{ag}. We have already discussed the vorticity equation (43.103) in its non-dimensional form. There, we emphasized the central role of the horizontal convergence of the ageostrophic flow in providing a source for the geostrophic material time evolution of the geostrophic absolute vorticity.

Quasi-geostrophic velocity and free surface equations: Version I

The velocity and free surface equations are determined by the order Ro^1 equations derived in Section 43.5.4. These equations take on the following dimensional form

$$\partial_t \boldsymbol{u}_g + (\boldsymbol{u}_g \cdot \nabla) \, \boldsymbol{u}_g + (f_o + \beta \, y) \, \hat{\boldsymbol{z}} \times \boldsymbol{u}_g + f_o \, \hat{\boldsymbol{z}} \times \boldsymbol{u}_{ag} = -g \, \nabla(\eta_g + \eta_{ag}) \tag{43.105a}$$

$$\partial_t(\eta_g - \eta_b) + (\boldsymbol{u}_g \cdot \nabla) \, (\eta_g - \eta_b) = -H \, \nabla \cdot \boldsymbol{u}_{ag}. \tag{43.105b}$$

The ageostrophic velocity generally has a nonzero horizontal convergence. Even so, it is three dimensionally non-divergent since the fluid layer has constant density. Hence, vertical component to the ageostrophic velocity satisfies

$$\boldsymbol{v}_{ag} = \boldsymbol{u}_{ag} + \hat{\boldsymbol{z}} \, w_{ag} \quad \text{with} \quad \nabla \cdot \boldsymbol{v}_{ag} = \partial_x u_{ag} + \partial_y v_{ag} + \partial_z w_{ag} = 0. \tag{43.106}$$

Cancelling the geostrophic balance (43.104) from the velocity equation (43.105a), making use of continuity (43.106), and introducing the geostrophic material time derivative (equation (43.103)) leads to

$$\frac{\mathrm{D}_g \boldsymbol{u}_g}{\mathrm{D}t} + (\beta \, y) \, \hat{\boldsymbol{z}} \times \boldsymbol{u}_g + f_o \, \hat{\boldsymbol{z}} \times \boldsymbol{u}_{ag} = -g \, \nabla \eta_{ag} \tag{43.107a}$$

$$\frac{\mathrm{D}_g(\eta_g - \eta_b)}{\mathrm{D}t} = H \, \partial_z w_{ag}. \tag{43.107b}$$

Quasi-geostrophic velocity and free surface equations: Version II

As seen in Section 43.5.4, we eliminate the ageostrophic pressure gradient, $-g \, \nabla \eta_{ag}$, by forming the quasi-geostrophic vorticity equation. The resulting source term arises from convergence of the ageostrophic flow, $-f_o \, \nabla \cdot \boldsymbol{u}_{ag}$, with continuity equating this vorticity source to vortex stretching by the ageostrophic flow in a rotating reference frame, $-f_o \, \nabla \cdot \boldsymbol{u}_{ag} = f_o \, \partial_z w$ (see equation (43.103)). Evidently, the vorticity equation is unchanged if the ageostrophic free surface is modified by an arbitrary scalar function, since that function is annihilated when taking the curl to form the vorticity equation. Likewise, the ageostrophic velocity is arbitrary up to a horizontally non-divergent velocity, since that extra non-divergent velocity also plays no role in the vorticity equation.

The ambiguity in specifying η_{ag} and $\boldsymbol{u}_{ag}$ is constrained, as revealed by taking the divergence of the velocity equation (43.107a) and noting that $\nabla \cdot \boldsymbol{u}_g = 0$, in which case

$$g \, \nabla^2 \eta_{ag} = 2 \, J(u_g, v_g) + \beta \, (y \, \zeta_g - u_g) + f_o \, \zeta_{ag}, \tag{43.108}$$

where we used

$$\nabla \cdot (\beta \, y \, \hat{\boldsymbol{z}} \times \boldsymbol{u}_g) = -\beta \, y \, \zeta_g + \beta \, u_g \tag{43.109a}$$

$$\nabla \cdot (f_o \, \hat{\boldsymbol{z}} \times \boldsymbol{u}_{ag}) = -f_o \, \zeta_{ag} \tag{43.109b}$$

$$\nabla \cdot \partial_t \boldsymbol{u}_g = \partial_t (\nabla \cdot \boldsymbol{u}_g) = 0 \tag{43.109c}$$

$$\nabla \cdot [\partial_t \boldsymbol{u}_{\mathrm{g}} + (\boldsymbol{u}_{\mathrm{g}} \cdot \nabla)\, \boldsymbol{u}_{\mathrm{g}}] = -2\, J(u_{\mathrm{g}}, v_{\mathrm{g}}), \tag{43.109d}$$

with

$$\zeta_{\mathsf{ag}} = \partial_x v_{\mathsf{ag}} - \partial_y u_{\mathsf{ag}} \tag{43.110}$$

the relative vorticity contained in the horizontal ageostrophic flow. The constraint (43.108) means that adding a horizontally non-divergent velocity, $\widetilde{\boldsymbol{u}}$, to the ageostrophic velocity, $\boldsymbol{u}_{\mathsf{ag}}$, requires a corresponding modification to the free surface via $\widetilde{\eta}$ added to η_{ag}, in which $\widetilde{\eta}$ satisfies the Poisson equation

$$g\, \nabla^2 \widetilde{\eta} = f_{\circ}\, \hat{\boldsymbol{z}} \cdot (\nabla \times \widetilde{\boldsymbol{u}}). \tag{43.111}$$

Again, these ambiguities arise in quasi-geostrophy since potential vorticity inversion is sufficient to specify evolution of the flow and free surface, with η_{ag} and $\boldsymbol{u}_{\mathsf{ag}}$ having no affect on the quasi-geostrophic potential vorticity. We refer to this freedom as a *gauge* freedom. Following Section 6.3 of *Holton and Hakim* (2013), a convenient gauge choice sets $\eta_{\mathsf{ag}} = 0$ so that all ageostrophic effects live within the ageostrophic flow, $\boldsymbol{u}_{\mathsf{ag}} + \hat{\boldsymbol{z}} w_{\mathsf{ag}}$. In this case the momentum equation (43.107a) takes on the particularly tidy form

$$\frac{\mathrm{D}_{\mathrm{g}} \boldsymbol{u}_{\mathrm{g}}}{\mathrm{D}t} + (\beta\, y)\, \hat{\boldsymbol{z}} \times \boldsymbol{u}_{\mathrm{g}} + f_{\circ}\, \hat{\boldsymbol{z}} \times \boldsymbol{u}_{\mathsf{ag}} = 0, \tag{43.112}$$

so that the f-plane ageostrophic Coriolis acceleration is the only means for the ageostrophic flow to affect the geostrophic flow. The $\eta_{\mathsf{ag}} = 0$ gauge choice amounts to expanding the velocity fields in the asymptotic series (43.59a)–(43.59c), whereas the free surface appears only at zeroth order.[10] The corresponding divergence equation (43.108) reveals that the ageostrophic relative vorticity is diagnosed from the geostrophic flow according to

$$f_{\circ}\, \zeta_{\mathsf{ag}} = -2\, J(u_{\mathrm{g}}, v_{\mathrm{g}}) - \beta\, (y\, \zeta_{\mathrm{g}} - u_{\mathrm{g}}). \tag{43.113}$$

43.6.7 Unpacking quasi-geostrophic evolution

Evolution of the quasi-geostrophic state occurs via the geostrophic material evolution of potential vorticity and then potential vorticity inversion (Section 43.6.5). This perspective is complete and elegant, and it encompasses a wealth of processes. To help expose those processes, and thus to reveal the fine tuned nature of quasi-geostrophic evolution, consider the evolution equation (43.112) for the geostropic velocity along with equation (43.107b) for the free surface, written in the form

$$\frac{\mathrm{D}_{\mathrm{g}} \boldsymbol{u}_{\mathrm{g}}}{\mathrm{D}t} = -(\beta\, y)\, \hat{\boldsymbol{z}} \times \boldsymbol{u}_{\mathrm{g}} - f_{\circ}\, \hat{\boldsymbol{z}} \times \boldsymbol{u}_{\mathsf{ag}} \tag{43.114a}$$

$$\frac{\mathrm{D}_{\mathrm{g}} \eta_{\mathrm{g}}}{\mathrm{D}t} = \frac{\mathrm{D}_{\mathrm{g}} \eta_{\mathrm{b}}}{\mathrm{D}t} + H\, \partial_z w_{\mathsf{ag}}. \tag{43.114b}$$

The quasi-geostrophic flow retains a geostrophically balanced state, $f_{\circ}\, \hat{\boldsymbol{z}} \times \boldsymbol{u}_{\mathrm{g}} = -g\, \nabla \eta_{\mathrm{g}}$, at each point in space and for each time instance.[11] Consequently, geostrophic balance is maintained for an observer following a fluid particle moving with the horizontal geostrophic velocity, $\boldsymbol{u}_{\mathrm{g}}$, so that

$$\frac{\mathrm{D}_{\mathrm{g}}}{\mathrm{D}t} (f_{\circ}\, \hat{\boldsymbol{z}} \times \boldsymbol{u}_{\mathrm{g}} + g\, \nabla \eta_{\mathrm{g}}) = 0. \tag{43.115}$$

Performing the material time derivatives in equation (43.115), and making use of the evolution

[10] We know of no other gauge choice discussed in the literature.

[11] Maintaining geostrophic balance at each point in space and time is a constraint analogous to the non-divergent flow condition maintained by a Boussinesq ocean. In that case, the pressure field satisfies an elliptic partial differential equation that ensures the flow satisfies non-divergence (see Section 29.3).

equations (43.114a) and (43.114b), lead to the balance

$$\underbrace{f_o\,\beta\,y\,\boldsymbol{u}_g + g\,\boldsymbol{Q}^{(\eta_g)} + g\,\nabla\,(\boldsymbol{u}_g\cdot\nabla\eta_b)}_{\text{geostrophic}} + \underbrace{f_o^2\,\boldsymbol{u}_{ag} + g\,H\,\nabla\partial_z w_{ag}}_{\text{ageostrophic}} = 0, \tag{43.116}$$

where we used

$$\mathrm{D}_g(\nabla\eta_g)/\mathrm{D}t = \nabla\,(\mathrm{D}_g\eta_g/\mathrm{D}t) + \boldsymbol{Q}^{(\eta_g)} = \nabla\,(\boldsymbol{u}_g\cdot\nabla\eta_b) + H\,\nabla(\partial_z w_{ag}) + \boldsymbol{Q}^{(\eta_g)}. \tag{43.117}$$

$\boldsymbol{Q}^{(\eta_g)}$ is a vector arising from the nonlinear coupling of horizontal shears in the geostrophic flow with gradients in the free surface

$$\begin{aligned} g\,\boldsymbol{Q}^{(\eta_g)} &= -g\,\hat{\boldsymbol{x}}\,\partial_x\boldsymbol{u}_g\cdot\nabla\eta_g - g\,\hat{\boldsymbol{y}}\,\partial_y\boldsymbol{u}_g\cdot\nabla\eta_g && \text{(43.118a)}\\ &= f_o\,\hat{\boldsymbol{x}}\,[\partial_x\boldsymbol{u}_g\cdot(\hat{\boldsymbol{z}}\times\boldsymbol{u}_g)] + f_o\,\hat{\boldsymbol{y}}\,[\partial_y\boldsymbol{u}_g\cdot(\hat{\boldsymbol{z}}\times\boldsymbol{u}_g)] && \text{(43.118b)}\\ &= f_o\,\hat{\boldsymbol{x}}\,[\hat{\boldsymbol{z}}\cdot(\boldsymbol{u}_g\times\partial_x\boldsymbol{u}_g)] + f_o\,\hat{\boldsymbol{y}}\,[\hat{\boldsymbol{z}}\cdot(\boldsymbol{u}_g\times\partial_y\boldsymbol{u}_g)], && \text{(43.118c)}\end{aligned}$$

where the second equality used the geostrophic balance. If any process contributes to changes in one of the terms in the balance (43.116), then the other terms compensate to retain the balance and thus to retain geostrophy.

The special case of a flat bottom β-plane is of particular interest, in which case the nonlinear geostrophic term, $\boldsymbol{Q}^{(\eta_g)}$, balances the ageostrophic terms

$$g\,\boldsymbol{Q}^{(\eta_g)} = -[f_o^2\,\boldsymbol{u}_{ag} + g\,H\,\nabla\partial_z w_{ag}]. \tag{43.119}$$

For example, if $\boldsymbol{Q}^{(\eta_g)}$ grows, say from a wave or instability, ageostrophic processes arise to compensate, thus preserving the balance (43.119) and, by extension, preserving geostrophy. From its definition (43.118a), for $\boldsymbol{Q}^{(\eta_g)}$ to be nonzero requires the geostrophic flow to not be parallel to its horizontal shear. For example, geostrophic flow along a straight front (say, with $\boldsymbol{u}_g = \hat{\boldsymbol{x}}\,u_g(y)$ and $\nabla\eta_g = \hat{\boldsymbol{y}}\,\partial_y\eta_g$) has $\boldsymbol{Q}^{(\eta_g)} = 0$, whereas $\boldsymbol{Q}^{(\eta_g)} \neq 0$ for fronts with curvature. *Hoskins* (1975) and Section 6.5 of *Holton and Hakim* (2013) provide a thorough discussion of this term and its role in the dynamics of atmospheric fronts.

43.6.8 Energetics of quasi-geostrophic flows

To derive the energetic balances within an unforced quasi-geostrophic shallow water flow, we start by multiplying the potential vorticity equation by the streamfunction

$$\psi\,\partial_t q + \psi\,\boldsymbol{u}\cdot\nabla q = 0. \tag{43.120}$$

The time tendency term can be written

$$\begin{aligned} \psi\,\partial_t q &= \psi\,(\partial_t\zeta - L_d^{-2}\,\partial_t\psi) && \text{(43.121a)}\\ &= \psi\,\nabla\cdot(\nabla\partial_t\psi) - (1/2)L_d^{-2}\,\partial_t(\psi)^2 && \text{(43.121b)}\\ &= \nabla\cdot(\psi\,\nabla\partial_t\psi) - \nabla\psi\cdot\nabla(\partial_t\psi) - (1/2)L_d^{-2}\,\partial_t(\psi)^2 && \text{(43.121c)}\\ &= \nabla\cdot(\psi\,\nabla\partial_t\psi) - \partial_t(\boldsymbol{u}\cdot\boldsymbol{u} + L_d^{-2}\,\psi^2)/2, && \text{(43.121d)}\end{aligned}$$

whereas the advection term can be written

$$\psi\,\boldsymbol{u}\cdot\nabla q = \psi\,\nabla\cdot(\boldsymbol{u}\,q) = \nabla\cdot(\psi\,\boldsymbol{u}\,q) - \nabla\psi\cdot\boldsymbol{u}\,q = \nabla\cdot(\psi\,\boldsymbol{u}\,q), \tag{43.122}$$

where we used

$$\nabla\psi\cdot\boldsymbol{u} = \nabla\psi\cdot(\hat{\boldsymbol{z}}\times\nabla\psi) = 0. \tag{43.123}$$

We are thus led to the energy equation for shallow water quasi-geostrophy

$$\partial_t(\boldsymbol{u}\cdot\boldsymbol{u} + L_{\mathrm{d}}^{-2}\,\psi^2)/2 = \nabla\cdot(\psi\,\nabla\partial_t\psi + \boldsymbol{u}\,q\,\psi). \tag{43.124}$$

The first term on the left hand side is the kinetic energy per mass. The second term is the available potential energy per mass, where the available potential energy is proportional to the free surface height undulation (Section 36.5.6)

$$L_{\mathrm{d}}^{-2}\,\psi^2 = f_{\circ}^2/(g\,H)\,(g^2/f_{\circ}^2)\,(\eta')^2 = (g/H)\,(\eta')^2 = c_{\mathrm{grav}}^2\,(\eta'/H)^2, \tag{43.125}$$

where the final step introduced the shallow water gravity wave speed $c_{\mathrm{grav}} = \sqrt{g\,H}$.

43.6.9 Considering topography to be $\mathcal{O}(\mathrm{Ro}^0)$

In our treatment of quasi-geostrophy, we assumed the topographic undulations to be on the order of Ro. Doing so ensured asymptotic consistency by combining η' and η'_{b} into an order Rossby number fluctuation of the layer thickness. We just encountered this need in Section 43.6.4 when connecting quasi-geostrophic potential vorticity to Ertel potential vorticity (see also Section 43.5.1). What happens if we allow for arbitrarily large topographic undulations? It is not uncommon to examine how an asymptotic theory performs when outside of its formal regime of validity, particularly with the advent of numerical codes to facilitate such studies. In many cases the theories continue to provide provocative, and sometimes physically relevant, information.

To see what happens, consider the quasi-geostrophic PV equation

$$(\partial_t + \boldsymbol{u}\cdot\nabla)\,[\zeta + \beta\,y + L_{\mathrm{d}}^{-2}\,(\psi_{\mathrm{b}} - \psi)] = 0. \tag{43.126}$$

If ψ_{b} order Ro^0, whereas the other terms are order Ro, then to leading order the potential vorticity is given by the static term, $L_{\mathrm{d}}^{-2}\,\psi_{\mathrm{b}}$, so that material conservation of potential vorticity reduces to

$$\boldsymbol{u}\cdot\nabla\psi_{\mathrm{b}} = 0 \Longrightarrow \boldsymbol{u}\cdot\nabla\eta_{\mathrm{b}} = 0. \tag{43.127}$$

This constraint means that the f-plane geostrophic flow is constrained to flow along lines of constant topography (isobaths), in which case the geostrophic streamfunction satisfies

$$(f/g)\,\boldsymbol{u}\cdot\nabla\eta_{\mathrm{b}} = \hat{\boldsymbol{z}}\cdot(\nabla\eta\times\nabla\eta_{\mathrm{b}}) \equiv J(\eta,\eta_{\mathrm{b}}) = 0. \tag{43.128}$$

Evidently, the order unity bottom topography undulations provide a constraint on the quasi-geostrophic flow, making the flow align with the bottom topography and in turn aligning surface height undulations with bottom undulations. We uncovered this constraint in our analysis of topographic form stress in Section 39.7.6. We also discussed this flow as a particular realization of the two-dimensional non-divergent barotropic flow in Section 38.1.4.

43.6.10 Two layer quasi-geostrophy

In Section 35.4 we developed the equations for an adiabatic stacked shallow water model. We here specialize those equations to a two-layer quasi-geostrophic model, with extensions to multiple layers following straightforwardly. Rather than pursue the formal asymptotic methods used previously, we here make use of our observation in Section 43.6.4 concerning the connection between shallow water and quasi-geostrophic potential vorticities.

To get started, recall from Section 39.3.6 that the shallow water potential vorticity for an

arbitrary layer, labelled by the index k, is given by

$$Q_{\mathsf{k}} = \frac{f + \zeta_{\mathsf{k}}}{h_{\mathsf{k}}}, \tag{43.129}$$

As in Section 43.6.2, we assume $\beta\, y$, ζ_{k}, and h'_{k} scale as Ro, in which case we have the quasi-geostrophic potential vorticity for each layer

$$q_{\mathsf{k}} = f + \zeta_{\mathsf{k}} - f_{\circ}\, h'_{\mathsf{k}}/H, \tag{43.130}$$

where ζ_{k} is here the geostrophic relative vorticity for layer k.

From our asymptotic analysis earlier in this section, the toughest part of that analysis concerned derivation of the quasi-geostrophic potential vorticity equation. In the present approach, we already have the potential vorticity for each layer via equation (43.130). What we need is the velocity field to advect it. Again, we know what that velocity is: it is the f-plane geostrophic velocity for each layer. The 2-layer velocity equations are given by equations (35.75a) and (35.75b), with their geostrophic components determined by

$$f_{\circ}\, \hat{\boldsymbol{z}} \times \boldsymbol{u}_1 = -g\, \nabla(\eta'_{\mathsf{b}} + h'_1 + h'_2) \tag{43.131a}$$

$$f_{\circ}\, \hat{\boldsymbol{z}} \times \boldsymbol{u}_2 = -\nabla \left[g'_{1/2}\, (\eta'_{\mathsf{b}} + h'_1 + h'_2) + g'_{3/2}\, (\eta'_{\mathsf{b}} + h'_2) \right]. \tag{43.131b}$$

In these equations we set the applied atmospheric pressure to a constant, and made use of the reduced gravities at the layer interfaces are

$$g'_{1/2} = g\, (\rho_1 - \rho_{\mathsf{atm}})/\rho_{\mathsf{ref}} \approx g \quad \text{and} \quad g'_{3/2} = g\, (\rho_2 - \rho_1)/\rho_{\mathsf{ref}}, \tag{43.132}$$

with the Boussinesq reference density taken as $\rho_{\mathsf{ref}} = \rho_1$. Furthermore, we assume $\rho_{\mathsf{atm}} \ll \rho_{\mathsf{ref}}$ so that the top interface reduced gravity is well approximated by the full gravity. From equations (43.131a) and (43.131b) we can identify the geostrophic streamfunctions

$$\psi_1 = (g/f_{\circ})\, (\eta'_{\mathsf{b}} + h'_1 + h'_2) \tag{43.133a}$$

$$\psi_2 = (1/f_{\circ}) \left[g'_{1/2}\, (\eta'_{\mathsf{b}} + h'_1 + h'_2) + g'_{3/2}\, (\eta'_{\mathsf{b}} + h'_2) \right], \tag{43.133b}$$

so that the layer geostrophic velocities are given by

$$\boldsymbol{u}_1 = \hat{\boldsymbol{z}} \times \nabla \psi_1 \quad \text{and} \quad \boldsymbol{u}_2 = \hat{\boldsymbol{z}} \times \nabla \psi_2. \tag{43.134}$$

We thus proceed with the usual quasi-geostrophic method, whereby evolution is determined by the material time changes of the potential vorticity with advection given by the layer geostrophic flow

$$(\partial_t + \boldsymbol{u}_{\mathsf{k}} \cdot \nabla) q_{\mathsf{k}} = 0. \tag{43.135}$$

43.6.11 Rigid lid shallow water quasi-geostrophy

We studied the horizontally non-divergent barotropic model in Chapter 38, whereby the full velocity field has zero horizontal divergence, thus leading to a rigid surface boundary. Gradients in the lid pressure drive the flow, with the lid pressure required to maintain the non-divergence constraint on the horizontal flow. For a single layer of quasi-geostrophic shallow water fluid, the rigid lid approximation means that the external deformation radius goes to infinity, so that the quasi-geostrophic potential vorticity reduces to the absolute geostrophic vorticity

$$L_{\mathsf{d}} \to \infty \Longrightarrow q = \zeta + f. \tag{43.136}$$

That is, the single rigid layer reduces to the non-divergent barotropic model in Chapter 38.

For more than one layer, we follow the rigid lid stacked shallow water model discussed in Section 35.4.5. In this case, the rigid upper surface means that $\eta'_{1/2} = 0$ so that fluctuations in the upper layer are given just by that of its lower interface

$$h'_1 = \eta'_{1/2} - \eta'_{3/2} = -\eta'_{3/2}. \tag{43.137}$$

As a result, the upper layer potential vorticity is given by

$$q_1 = f + \zeta_1 - f_\circ h'_1/H = f + \zeta_1 + f_\circ \eta'_{3/2}/H. \tag{43.138}$$

43.6.12 Further study

Section 6.4 of *Holton and Hakim* (2013) provides an insightful discussion of potential vorticity inversion for example atmospheric flows.

43.7 Non-dimensional Boussinesq ocean equations

In this section we non-dimensionalize the continuously stratified Boussinesq ocean equations. As part of this process we identify a variety of non-dimensional numbers that characterize the flow. As for the shallow water system in Section 43.4, continuously stratified planetary geostrophy is rather simple to derive, so that the detailed work in this section is arguably not necessary. However, the details here are essential for systematically deriving the continuously stratified quasi-geostrophic theory pursued in Chapter 45.

Our starting point is the perfect fluid stratified hydrostatic Boussinesq equations (Section 29.1.6)

$$\frac{\mathrm{D}\boldsymbol{u}}{\mathrm{D}t} + f\,\hat{\boldsymbol{z}} \times \boldsymbol{u} = -\nabla_{\!\mathrm{h}}\varphi \tag{43.139a}$$

$$\frac{\partial \varphi}{\partial z} = b \tag{43.139b}$$

$$\frac{\mathrm{D}b}{\mathrm{D}t} = 0 \tag{43.139c}$$

$$\nabla \cdot \boldsymbol{v} = 0, \tag{43.139d}$$

where $\boldsymbol{v} = (\boldsymbol{u}, w)$ is the three-dimensional velocity written using Cartesian coordinates, $b = -g\,(\rho - \rho_\circ)/\rho_\circ$ is the Archimedian buoyancy relative to a constant reference density, $\rho_\circ$, with ρ the density. We also write $\varphi = \delta p/\rho_\circ$ for the dynamic pressure (dimensions of $\mathrm{L}^2\ \mathrm{T}^{-2}$), and $\nabla_{\!\mathrm{h}} = (\partial_x, \partial_y, 0)$ for the horizontal gradient operator. We separate a background vertical buoyancy profile from a space-time fluctuating buoyancy

$$b = \tilde{b}(z) + b'(x, y, z, t), \tag{43.140}$$

and introduce the corresponding background squared buoyancy frequency

$$N^2(z) = \frac{\mathrm{d}\tilde{b}(z)}{\mathrm{d}z}. \tag{43.141}$$

The background stratification is not determined by the quasi-geostrophic theory. Rather, it is assumed to be a prescribed function.

With the above decomposition, the buoyancy equation (43.139c) takes the form

$$\frac{\mathrm{D}b'}{\mathrm{D}t} + w\,N^2 = 0. \tag{43.142}$$

We also introduce an associated decomposition of the hydrostatic pressure

$$\varphi = \tilde{\varphi}(z) + \varphi'(x, y, z, t) \tag{43.143}$$

where $\tilde{\varphi}$ is hydrostatically balanced by $\tilde{b}$

$$\frac{\mathrm{d}\tilde{\varphi}}{\mathrm{d}z} = \tilde{b}, \tag{43.144}$$

and the fluctuating pressure, φ', is hydrostatically balanced by b'

$$\frac{\partial \varphi'}{\partial z} = b'. \tag{43.145}$$

43.7.1 Dimensional parameters

As for the shallow water discussion in Section 43.3.1, we have the following dimensional parameters for the perfect Boussinesq fluid.

- LENGTH SCALES
  - ⋆ H = length scale of a typical vertical structure in the fluid (e.g., the depth of the ocean pycnocline or height of the atmospheric tropopause). This scale is affected by the prescribed vertical stratification, $N(z)$.
  - ⋆ L = horizontal/lateral length scale of the flow (e.g., Gulf Stream rings, atmospheric synoptic weather pattern, ocean gyre).
  - ⋆ R_{e} = radius of the planet.
- VELOCITY SCALES
  - ⋆ U = horizontal velocity scale for fluid motion.
  - ⋆ W = vertical velocity scale for fluid motion.
- PRESSURE AND BUOYANCY SCALES: Pressure is a contact force, acting on the boundary of an arbitrary fluid region, and buoyancy arises from the gravitational force that acts to raise or lower a fluid element depending on its density relative to the environment. They have scales given by the following.
  - ⋆ Φ = scale for pressure fluctuations, φ' (dimensions of pressure divided by density = length scale × acceleration).
  - ⋆ B = scale of buoyancy fluctuations, b' (dimensions of acceleration).
- BODY FORCES: There are two body forces acting on the fluid, one from gravity and one from Coriolis.
  - ⋆ g = gravitational acceleration
  - ⋆ f = Coriolis frequency.

Contrary to the shallow water discussion in Section 43.3.1, we do not introduce a wave speed since it does not affect the asymptotics considered here. Also, we do not introduce a scale for

the bottom topography undulations, since for planetary geostrophy there is no constraint on topographic undulations. However, for quasi-geostrophy in Chapter 45 we follow the approach used for shallow water in Section 43.3.5 by assuming topographic undulations scale like the Rossby number. Further details of the bottom boundary conditions and their scaling are detailed in Section 45.6.

43.7.2 Physical dimensions and non-dimensional parameters

There are two physical dimensions in the Boussinesq system: length, L, and time, T. As for the shallow water system, there is no need to consider a mass dimension since mass is determined by the density (buoyancy) and volume. The Buckingham-Π theorem then says there are

$$N_{\text{dimensionless}} = 9 - 2 = 7 \tag{43.146}$$

non-dimensional parameters.

43.7.3 Choosing the non-dimensional parameters

Following the shallow water discussion in Section 43.3.4, we choose the following non-dimensional parameters.

1. VERTICAL TO HORIZONTAL ASPECT RATIO: The ratio of the vertical length scale to the horizontal length scale of the flow defines the aspect ratio

$$\delta_{\text{vertical/horizontal}} = \frac{\text{vertical length scale}}{\text{horizontal length scale}} = \frac{H}{L}. \tag{43.147}$$

2. RATIO OF HORIZONTAL SCALE TO PLANETARY SCALE: The ratio of the horizontal length scale of the flow to the planetary radius is given by

$$\delta_{\text{horizontal/planet}} = \frac{\text{horizontal length scale}}{\text{planetary length scale}} = \frac{L}{R_e}. \tag{43.148}$$

3. RATIO VERTICAL TO HORIZONTAL VELOCITY SCALES: The ratio of the vertical to horizontal velocity scales is given by

$$\frac{\text{vertical velocity scale}}{\text{horizontal velocity scale}} = \frac{W}{U}. \tag{43.149}$$

4. HYDROSTATIC NUMBER: The hydrostatic number is the ratio of the pressure fluctuation scale to the buoyancy fluctuation scale,

$$\frac{\text{pressure fluctuations}}{\text{buoyancy fluctuations}} = \frac{\Phi/H}{B}. \tag{43.150}$$

5. ROSSBY NUMBER: The Rossby number is the ratio of the fluid particle acceleration scale to the Coriolis acceleration

$$\text{Ro} = \frac{\text{particle acceleration}}{\text{Coriolis acceleration}} = \frac{U}{f\,L}. \tag{43.151}$$

As in Section 43.3.4, we assume that the time scale is advective

$$T \sim L/U \Longrightarrow \text{Ro} = U/(f\,L) = (f\,T)^{-1}. \tag{43.152}$$

6. GEOSTROPHIC NUMBER: The ratio of the Coriolis acceleration to the pressure gradient acceleration defines the geostrophic number

$$\text{Ge} = \frac{\text{Coriolis acceleration}}{\text{pressure gradient acceleration}}. \tag{43.153}$$

The Coriolis acceleration scales as

$$\text{Coriolis acceleration} \sim f\,U \tag{43.154}$$

whereas the pressure gradient acceleration from the fluctuating pressure, φ', scales as

$$\text{pressure gradient acceleration} \sim \Phi/L, \tag{43.155}$$

so that

$$\text{Ge} = \frac{\text{Coriolis acceleration}}{\text{pressure gradient acceleration}} = \frac{f\,U}{(\Phi/L)}. \tag{43.156}$$

7. RATIO OF FLUCTUATING STRATIFICATION TO BACKGROUND STRATIFICATION: The ratio of the buoyancy frequency arising from the fluctuating buoyancy, B/H, to the background squared buoyancy frequency, $N^2(z)$, is given by

$$\frac{\text{fluctuating squared buoyancy frequency}}{\text{background squared buoyancy frequency}} = \frac{B/H}{N^2(z)}. \tag{43.157}$$

43.7.4 Relating the buoyancy scale to the Coriolis acceleration scale

The fluctuating buoyancy, b', and fluctuating pressure, φ', have scales related through the hydrostatic balance. Hence, taking a unit hydrostatic number from equation (43.150) renders

$$B = \Phi/H. \tag{43.158}$$

Additionally, assuming geostrophic scaling as per equation (43.156) means that the fluctuating pressure has a scale related to the Coriolis acceleration scale according to

$$\Phi = U\,f\,L. \tag{43.159}$$

Evidently, the scale for the fluctuating buoyancy is given by

$$B = f\,U\,(L/H). \tag{43.160}$$

We emphasize that the scale for pressure fluctuation, $\Phi = U\,f\,L$, is distinct from the non-rotating case considered in Section 29.2.3, where $\Phi = U^2$.

43.7.5 Richardson number and QG/PG flow regimes

The *Richardson number* provides a measure of the stabilizing effects from vertical stratification versus the destabilizing effects from vertical shear

$$\text{Ri} = \frac{\text{vertical stratification}}{\text{vertical shear}}. \tag{43.161}$$

More precisely, the Richardson number is given by the ratio of the squared buoyancy frequency to the squared vertical shear of the horizontal velocity

$$\mathrm{Ri} = \frac{N^2}{|\partial_z \mathbf{u}|^2}. \tag{43.162}$$

In regions where $\mathrm{Ri} < 1$, the vertical shear is stronger than the stabilizing effects from vertical stratification. In regions with small Richardson numbers, there is enough kinetic energy in the vertical shear to extract potential energy from the stratification, and this extraction process occurs via a vertical shear instability as studied in Chapter 61. In contrast, for large-scale highly stratified flow, the Richardson number is quite large, with $\mathrm{Ri} \sim 100$ common. Large Richardson number flow regimes are where quasi-geostrophy is relevant (Chapter 45).

Given the fundamental role of the Richardson number for stratified fluid motions, it is useful to introduce it as one of our dimensionless parameters. Namely, we define the vertically dependent Richardson number scale as

$$\mathrm{Ri}(z) = \frac{N^2(z)}{(U/H)^2}, \tag{43.163}$$

where we set the vertical length scale to H, the horizontal velocity scale to U, and the squared buoyancy frequency to the background value, $N^2(z)$, introduced by equation (43.141). Retaining vertical dependence to the background buoyancy frequency means that the Richardson number scale is also vertically dependent.

The Richardson number scale can be related to the Rossby and Burger numbers through

$$\mathrm{Bu}(z) = \left[\frac{L_{\mathrm{d}}(z)}{L}\right]^2 = \left[\frac{N(z)\,H}{f\,L}\right]^2 = \frac{U^2\,\mathrm{Ri}(z)}{U^2/(\mathrm{Ro})^2} = (\mathrm{Ro})^2\,\mathrm{Ri}(z). \tag{43.164}$$

Evidently, vertical dependence to the prescribed background buoyancy frequency makes the Burger number and Richardson number vertically dependent, as well as the deformation radius.

One further way to write the Burger number is by introducing the angle φ defined by the vertical and horizontal length scales

$$\tan\varphi \equiv H/L \tag{43.165}$$

in which case

$$\mathrm{Bu} = \left[\frac{L_{\mathrm{d}}}{L}\right]^2 = \left[\frac{N\,H}{f\,L}\right]^2 = (\mathrm{Ro})^2\,\mathrm{Ri} = [(N/f)\,\tan\varphi]^2. \tag{43.166}$$

When $\tan^2\varphi$ is set according to the slope of the ocean bottom, then $[(N/f)\,\tan\varphi]^2$ is known as the *slope Burger number* (*MacCready and Rhines*, 1993; *Peterson and Callies*, 2022).

The horizontal length scales, L, for quasi-geostrophic flows are assumed to be on the order of the deformation radius, L_{d}, in which case the Burger number is close to unity. The relation (43.164) means that the Richardson number scales as

$$\mathrm{Ri} \sim (\mathrm{Ro})^{-2} \qquad \text{quasi-geostrophic flow regime.} \tag{43.167}$$

For atmospheric flows with a Rossby number order 1/10, quasi-geostrophic flow regimes are realized with a Richardson number ~ 100. For the ocean, the Rossby number can be even smaller, in which case quasi-geostrophic flows are characeterized by an even larger Richardson number. For planetary geostrophy, the Burger number is small. Hence, planetary geostrophic flows are characterized by somewhat smaller Richardson numbers than quasi-geostrophic flows.

43.7.6 The Rossby deformation radius

The combined effects of buoyancy and rotation yield the richness of continuously stratified planetary geostrophic and quasi-geostrophic motions. Hence, the buoyancy frequency and the Coriolis parameter play central role in characterizing these flow regimes. The ratio of these two frequencies, N/f, in regions of nontrivial vertical stratification is typically around 100. Hence, rotational inertial oscillations (usually just called *inertial oscillations*; Section 14.4) have about 100 times longer period, $2\pi/f$, than buoyancy oscillations with period $2\pi/N$.

Letting the squared buoyancy frequency, N^2, refer to a value typical of a particular flow regime, one can define the Rossby deformation radius

$$L_{\mathsf{d}} = H\,(N/f). \tag{43.168}$$

As defined, the deformation radius is the vertical length scale multiplied by the ratio of the buoyancy frequency to the Coriolis frequency. The ratio, f/N, appears frequently in rotating/stratified fluids, and is sometimes called the *Prandtl ratio*

$$\text{Prandtl ratio} = f/N. \tag{43.169}$$

With $H \approx 1$ km and $N/f \approx 100$, the Rossby deformation radius is roughly 100 km. This length scale measures the relative importance of stratification and rotation. Depending on the ratio L/L_{d}, we can have large or small stratification fluctuations relative to the background stratification. Furthermore, as studied in Chapter 62, the deformation radius sets the scale for unstable baroclinic waves leading to baroclinically unstable flow.

For some context, recall the shallow water deformation radius is given by equation (43.31), $L_{\mathsf{d}} = \sqrt{g\,H}/f$, which is the ratio of the gravity wave speed to Coriolis frequency. With $N = 100\,f = 10^{-2}$ s^{-1} and $H = 10^3$ m, the shallow water deformation radius is about an order of magnitude larger than the internal deformation radius. This scale difference means that the characteristic length scales, as set by L_{d}, are much larger in a single layer of shallow water fluid than in a stratified fluid.

43.7.7 Assumed values for the non-dimensional parameters

We now enumerate the assumed values for the non-dimensional parameters, again following the choices made for the shallow water layer in Section 43.3.5. These assumptions are guided by the flow regimes of interest.

1. SMALL VERTICAL TO HORIZONTAL ASPECT RATIO: The aspect ratio is generally small for large-scale atmospheric and oceanic flows

$$\delta_{\text{vertical/horizontal}} \ll 1. \tag{43.170}$$

   This assumption is part of the hydrostatic approximation (Section 27.2), and as such it is a necessary scaling for any asymptotic theory based on a hydrostatic starting point.

2. SMALL OR ORDER ONE RATIO OF HORIZONTAL TO PLANETARY SCALES: The ratio of the horizontal length scale of the flow to the planetary radius is small for quasi-geostrophic systems, whereas the ratio is order unity for planetary geostrophy

$$\delta_{\text{horizontal/planet}} \ll 1 \qquad \text{quasi-geostrophy} \tag{43.171a}$$
$$\delta_{\text{horizontal/planet}} \sim 1 \qquad \text{planetary geostrophy.} \tag{43.171b}$$

   For example, the vertical length scale could be determined by the averaged depth of the pycnocline in the ocean, or the averaged height of the tropopause in the atmosphere. For

the horizontal length scale in quasi-geostrophic theory, we might choose the scale of a Gulf Stream ring in the ocean or synoptic weather pattern in the atmosphere. Alternatively, we might choose the laterial scale of an ocean gyre for planetary geostrophy.

3. SMALL RATIO OF VERTICAL TO HORIZONTAL VELOCITY SCALES: The continuity equation implies
$$W/H = U/L, \tag{43.172}$$
so that
$$W = U\,(H/L). \tag{43.173}$$
As noted above, for a hydrostatic fluid the vertical to horizontal aspect ratio, H/L, is small, so that the vertical velocity scale is smaller than the horizontal velocity scale. Furthermore, when the fluid is close to geostrophically balanced, the vertical velocity scale is even smaller, by a factor of Ro. We see that factor emerge in the following scale analysis.

4. UNIT HYDROSTATIC NUMBER: The hydrostatic balance (43.139b) means that the scales for a buoyancy fluctuation and pressure fluctuation are related by (see equation (43.150))
$$\Phi = H\,B. \tag{43.174}$$

5. SMALL ROSSBY NUMBER: The Rossby number is assumed small
$$\mathrm{Ro} = U/(f\,L) = (f\,T)^{-1} \ll 1, \tag{43.175}$$
where we set the time scale for the motion according to advection, $T = L/U$.

6. UNIT GEOSTROPHIC NUMBER: The geostrophic number is assumed to be order unity
$$\mathrm{Ge} \sim 1, \tag{43.176}$$
which means that the Coriolis acceleration and pressure gradient acceleration scale together
$$f\,U \sim \Phi/L \Longrightarrow \Phi \sim U\,f\,L. \tag{43.177}$$
This scaling is consistent with the momentum equation (43.139a) so long as the Rossby number is small, $\mathrm{Ro} \ll 1$.

7. STRATIFICATION FLUCTUATIONS COMPARED TO BACKGROUND STRATIFICATION: Making use of the assumed unit geostrophic number, the ratio of the buoyancy frequency arising from the fluctuating buoyancy to the background buoyancy frequency is given by
$$\frac{B/H}{N^2} = \frac{\Phi}{H^2\,N^2} = \frac{f\,U\,L}{H^2\,N^2} = \frac{U}{f\,L}\,\frac{L^2\,f^2}{H^2\,N^2} = \mathrm{Ro}\,\frac{L^2}{L_{\mathrm{d}}^2} = \frac{\mathrm{Ro}}{\mathrm{Bu}^2(z)}, \tag{43.178}$$
where we introduced the deformation radius (43.168) $L_{\mathrm{d}} = H\,(N/f)$, which is a function of vertical position through the prescribed background buoyancy frequency, $N(z)$. We also introduced the Burger number, $\mathrm{Bu}(z) = (L_{\mathrm{d}}(z)/L)^2$, as per equation (43.33). It is important to keep the depth dependence of $N^2, \mathrm{Bu}(z)$, and $L_{\mathrm{d}}(z)$, when returning to dimensional fields, particularly for the quasi-geostrophic equations derived in Section 45.3.7.

43.7.8 Non-dimensional Boussinesq equations

Following the shallow water approach in Section 43.3.7, we introduce non-dimensional variables according to

$$t = T\,\widehat{t} \quad (x,y) = L\,(\widehat{x},\widehat{y}) \quad \partial_t = \partial_{\widehat{t}}/T \quad \nabla_{\!\mathrm{h}} = \widehat{\nabla}_{\!\mathrm{h}}/L \quad \partial_z = \partial_{\widehat{z}}/H \quad f = f_\circ\,\widehat{f} \tag{43.179a}$$

$$(u,v) = U\,(\widehat{u},\widehat{v}) \qquad w = W\,\widehat{w} \qquad \varphi' = f_\circ\,U\,L\,\widehat{\varphi} \quad b' = B\,\widehat{b} = (f_\circ\,U\,L/H)\,\widehat{b}. \tag{43.179b}$$

For the second equality in the buoyancy scale, we made use of equation (43.160) to connect the buoyancy fluctuation scale to the Coriolis acceleration scale. We also make use of the following relations between scales

$$T = L/U \qquad \text{advective scaling for } T \tag{43.180}$$

$$W = U\,(H/L) \qquad \text{continuity scaling for } W \tag{43.181}$$

$$\mathrm{Ro} = U/(f_\circ\,L) = (T\,f_\circ)^{-1} \qquad \text{advective scaling for } T. \tag{43.182}$$

The first relation assumes the time scale is determined by the advection time, $T = L/U$, which then means that the Rossby number is the ratio of the advective frequency, $1/T$, to the Coriolis frequency, $f_\circ$. Furthermore, we assume a vertical velocity scale according to the continuity equation, $W = U\,(H/L)$. This continuity scaling for W is actually an over-estimate, where we find below that W instead scales like $W = \mathrm{Ro}\,U\,(H/L)$.

Non-dimensional momentum equation

Introducing the dimensionless variables and dimensionful scales into the Boussinesq momentum equation (43.139a) renders

$$\frac{U}{T}\frac{\partial\widehat{\boldsymbol{u}}}{\partial\widehat{t}} + \frac{U^2}{L}\,(\widehat{\boldsymbol{u}}\cdot\widehat{\nabla}_{\!\mathrm{h}})\,\widehat{\boldsymbol{u}} + \frac{W\,U}{H}\,\widehat{\boldsymbol{w}}\,\frac{\partial\widehat{\boldsymbol{u}}}{\partial\widehat{z}} + f_\circ\,U\,(\widehat{\boldsymbol{f}}\times\widehat{\boldsymbol{u}}) = -f_\circ\,U\,\widehat{\nabla}_{\!\mathrm{h}}\,\widehat{\varphi}, \tag{43.183}$$

and dividing by $f_\circ U$ leads to

$$\mathrm{Ro}\left[\frac{\partial\widehat{\boldsymbol{u}}}{\partial\widehat{t}} + (\widehat{\boldsymbol{u}}\cdot\widehat{\nabla}_{\!\mathrm{h}})\,\widehat{\boldsymbol{u}} + \widehat{w}\,\frac{\partial\widehat{\boldsymbol{u}}}{\partial\widehat{z}}\right] + (\widehat{\boldsymbol{f}}\times\widehat{\boldsymbol{u}}) = -\widehat{\nabla}_{\!\mathrm{h}}\,\widehat{\varphi}. \tag{43.184}$$

The non-dimensional hydrostatic balance is given by

$$\frac{\partial\widehat{\varphi}}{\partial\widehat{z}} = \widehat{b}, \tag{43.185}$$

and the non-dimensional continuity equation is

$$\widehat{\nabla}\cdot\widehat{\boldsymbol{v}} = 0. \tag{43.186}$$

Non-dimensional buoyancy equation

The buoyancy equation (43.142) requires a bit more work to non-dimensionalize. The material time derivative takes the form

$$\frac{\mathrm{D}b'}{\mathrm{D}t} = \frac{B}{T}\frac{\mathrm{D}\widehat{b}}{\mathrm{D}\widehat{t}} = \frac{U}{L}\frac{f_\circ\,U\,L}{H}\frac{\mathrm{D}\widehat{b}}{\mathrm{D}\widehat{t}} = \frac{f_\circ\,U^2}{H}\frac{\mathrm{D}\widehat{b}}{\mathrm{D}\widehat{t}}, \tag{43.187}$$

where we made use of the advective scaling $T = L/U$ and continuity scaling $W = U\,(H/L)$. The vertical advection of background stratification is given by

$$N^2\, w = N^2\, W\, \widehat{w} = N^2\, U\, (H/L)\, \widehat{w} = L_{\mathsf{d}}^2\, \frac{U\, f_{\mathsf{o}}^2}{H\, L}\, \widehat{w}, \tag{43.188}$$

where we introduced the deformation radius, $L_{\mathsf{d}} = H(N/f)$, from equation (43.168). Bringing these two pieces together leads to

$$\mathrm{Ro}\, \frac{\mathrm{D}\widehat{b}}{\mathrm{D}\widehat{t}} + \mathrm{Bu}\, \widehat{w} = 0, \tag{43.189}$$

where we introduced the Burger number, $\mathrm{Bu} = (L_{\mathsf{d}}/L)^2$.

43.7.9 Comments

As stated earlier, the material in this section serves as the starting point for a systematic derivation of the continuously stratified planetary geostrophic equations in Chapter 44, and the continuously stratified quasi-geostrophic equations in Chapter 45. Particularly for the quasi-geostrophic equations, we make use of asymptotic methods as for the shallow water quasi-geostrophic equations in Section 43.5.

43.8 Exercises

EXERCISE 43.1: PV CONSERVATION FOR PLANETARY GEOSTROPHY
Show that the planetary geostrophic equations

$$\boldsymbol{f} \times \boldsymbol{u} = -g\, \nabla \eta \qquad \text{and} \qquad \frac{\mathrm{D}h}{\mathrm{D}t} = -h \nabla \cdot \boldsymbol{u} \qquad \text{with} \qquad \eta = \eta_{\mathsf{b}} + h \tag{43.190}$$

are equivalent to

$$\boldsymbol{f} \times \boldsymbol{u} = -g\, \nabla \eta \qquad \text{and} \qquad \frac{\mathrm{D}Q}{\mathrm{D}t} = 0 \qquad \text{with} \qquad Q = \frac{f}{h}. \tag{43.191}$$

This result shows that the shallow water PG equations may be written as an evolution equation for an approximated version of the shallow water potential vorticity, $(f + \zeta)/h \approx f/h$. This limit holds when the Rossby number is small.

EXERCISE 43.2: CONSTRAINTS ON STEADY STATE PLANETARY GEOSTROPHIC FLOW
Consider a shallow water fluid satisfying the planetary geostrophic equations developed in Section 43.4. Assume the flow is in steady state.

(a) In what manner does potential vorticity conservation constrain the velocity field?

(b) Consider an initially zonal geostrophic flow. In what direction (poleward or equatorward) will a fluid parcel deviate when encountering a seamount (i.e., a region of relatively shallow depth)?

(c) Describe the geostrophic contours (i.e., path of fluid particles following the geostrophic flow) for the case where the ocean sea surface height undulations, η', are far smaller than undulations in the bottom topography, η'_{b} (see Figure 35.1 for notation).

(d) For the special case of an f-plane, show that the velocity is aligned with isolines of bottom topography.

(e) For the special case of a flat bottom and latitudinally dependent Coriolis parameter, $f(y)$, show that there is no meridional geostrophic velocity. That is, the flow is zonally aligned.

Chapter 44

Planetary geostrophic vorticity analysis

The planetary geostrophic equations consist of steady and linear frictional geostrophic flow coupled to the non-steady and nonlinear buoyancy evolution. Consequently, the fluid state evolves through the buoyancy equation, whereas the flow is diagnosed from frictional geostrophy and continuity. Furthermore, there is no turbulence in planetary geostrophy since the momentum equation is linear and steady. Evidently, planetary geostrophy is focused on large-scale flow of a stably stratified laminar fluid whose vorticity is dominated by planetary rotation in the presence of planetary beta and topographic beta.

We already studied various physical properties of planetary geostrophy in Chapter 31, such as geostrophy, vorticity, thermal wind, and Taylor-Proudman. We also made use of planetary geostrophy to study western boundary current intensification for a shallow water layer in Section 39.7. We were able to present those studies earlier in the book since, as seen in Section 43.4 for the shallow water, derivation of the planetary geostrophic equations is a very simple task, thus allowing the equations to be plausibly written down without needing any formal asymptotics.

The stratified planetary geostrophic equations form the foundation for theories of the large-scale ocean circulation, with vorticity constraints providing a key reason for the central role of planetary geostrophy. The central role for vorticity motivates a focus in this chapter on the mathematical and physical basis for planetary geostrophic vorticity analysis. It is notable that in a planetary geostrophic flow, we are only concerned with planetary vorticity, and thus ignore relative vorticity. Consequently, we ignore vorticity sources from baroclinicity and tilting. Instead, we focus on how vertical stretching modifies a fluid's planetary vorticity, and how the fluid responds by moving meridionally to adjust its planetary vorticity in response to stretching.

After summarizing the planetary geostrophic equation set, we derive the planetary geostrophic potential vorticity budget and determine how the impermeability theorem from Section 42.2 appears in planetary geostrophy. We then study a suite of vorticity budgets arrived at through vertical integration the fluid from its bottom to top, with particular focus on ocean applications. Each of the resulting two-dimensional vorticity budgets offers insights into how large-scale ocean flow is constrained by rotation and the beta effect. In particular, these budgets render insights into how forces and the curl of forces generate vertical flow next to the boundaries as well as meridional flow for the full fluid column.

CHAPTER GUIDE

We here extend the shallow water discussions from Chapter 43 to develop an understanding of the continuously stratified planetary geostrophic equations. We make use of stratified geophysical fluid dynamics from Chapters 24 and 31, vorticity and the planetary beta effect from Chapter 40, and potential vorticity from Chapter 41. Physical properties of stratified geostrophic mechanics were considered in Chapter 31, with an understanding of that material assumed here.

44.1 Equations for planetary geostrophy

Just like for the shallow water model in Section 43.4, the planetary geostrophic model for the stratified Boussinesq ocean is a rather simple asymptotic theory. For this case, we assume the horizontal scales are large compared to the deformation radius, so that

$$\mathrm{Ro}/\mathrm{Bu} \sim 1 \implies \mathrm{Ro}\, L^2 \sim L_\mathrm{d}^2. \tag{44.1}$$

With this scaling, and with a small Rossby number, the momentum equation (43.184) reduces to geostrophic balance. However, the continuity and buoyancy equations retain their unapproximated Boussinesq form. Hence, in dimensional form, the perfect (adiabatic and inviscid) planetary geostrophic equations for a stratified Boussinesq ocean are

$$\frac{\mathrm{D}b'}{\mathrm{D}t} + w\, N^2 = 0 \quad \text{and} \quad f\, \hat{\boldsymbol{z}} \times \boldsymbol{u} = -\nabla_\mathrm{h} \varphi' \quad \text{and} \quad \frac{\partial \varphi'}{\partial z} = b' \quad \text{and} \quad \nabla \cdot \boldsymbol{v} = 0. \tag{44.2}$$

44.1.1 Common form of the equations

We could just as well write the planetary geostrophic equations (44.2) in terms of the full buoyancy

$$b = \tilde{b}(z) + b', \tag{44.3}$$

and full pressure,

$$p = p_0(z) + \rho_\circ\, \varphi. \tag{44.4}$$

Additionally, it is quite useful to include non-conservative terms such as buoyancy mixing, $\dot{b}$, to allow for the study of how stratification evolves, as well as horizontal frictional accelerations and/or boundary accelerations, $\boldsymbol{F}$, to include boundary stress driven circulations through Ekman

layers (Chapter 33). For these reasons, we take the frictional and diabatic planetary geostrophic equations as the basis for discussions in this chapter

$$f\,\hat{\boldsymbol{z}} \times \boldsymbol{u} = -\rho_0^{-1}\,\nabla_{\!\mathrm{h}} p + \boldsymbol{F} \qquad \text{frictional geostrophy} \tag{44.5a}$$

$$(\partial_t + \boldsymbol{u} \cdot \nabla_{\!\mathrm{h}})\, b + N^2\, w = \dot{b} \qquad \text{diabatic buoyancy equation} \tag{44.5b}$$

$$\partial_z p = -\rho\, g \qquad \text{hydrostatic balance} \tag{44.5c}$$

$$\nabla \cdot \boldsymbol{v} = \nabla_{\!\mathrm{h}} \cdot \boldsymbol{u} + \partial_z w = 0 \qquad \text{non-divergent flow} \tag{44.5d}$$

$$N^2 = \partial_z b \qquad \text{squared buoyancy frequency} \tag{44.5e}$$

$$b = -g\,(\rho - \rho_o)/\rho_o \qquad \text{Archimedean buoyancy.} \tag{44.5f}$$

Note that the material time derivative in planetary geostrophy makes use of advection by the three velocity components, $\boldsymbol{v} = (\boldsymbol{u}, w)$, as seen in the buoyancy equation (44.5b), with the horizontal velocity components determined by the frictional geostrophic balance (44.5a). This situation contrasts to quasi-geostrophy, where it is only the horizontal advection by the geostrophic flow that contributes to material time evolution (Section 45.2).

As for the Boussinesq ocean equations discussed in Section 29.1.6, we sometimes find it convenient to combine the horizontal velocity equation with the hydrostatic balance to write

$$f\,\hat{\boldsymbol{z}} \times \boldsymbol{u} = -\nabla\varphi + b\,\hat{\boldsymbol{z}} + \boldsymbol{F}. \tag{44.6}$$

Furthermore, it is common to assume an equation of state that is independent of pressure, so that material time changes in buoyancy arise only from changes in Conservative Temperature and/or salinity

$$\dot{b} = \frac{\partial b}{\partial S}\,\dot{S} + \frac{\partial b}{\partial \Theta}\,\dot{\Theta}. \tag{44.7}$$

The partial derivatives, $\partial b/\partial\Theta$ and $\partial b/\partial S$, are commonly assumed constant in idealized studies.

44.1.2 Planetary geostrophic energetics

Since the velocity is diagnostic in planetary geostrophy, it is determined by the buoyancy field. In turn, there is a prognostic equation for potential energy that arises from the buoyancy equation, whereas kinetic energy is diagnostic. The energetics are thus a special case of the Boussinesq energetics studied in Section 29.6. We here consider just the basics.

General considerations

Multiplying the buoyancy equation (44.5b) by z leads to the potential energy equation

$$\partial_t P + \nabla \cdot (\boldsymbol{v}\, P) + w\, b = -z\, \dot{b}, \tag{44.8}$$

where we introduced the potential energy per mass relative to the reference density[1]

$$P = -z\, b = z\, g\,(\rho - \rho_o)/\rho_o. \tag{44.9}$$

Equation (44.8) says that the potential energy at a point in the planetary geostrophic fluid is affected by advective transport, buoyancy work, and diabatic processes. As we will see, diabatic processes such as diffusion provide a local source for potential energy, whereas buoyancy work transfers potential energy to kinetic energy.

[1] We considered this same form for the potential energy in Section 29.7 as well as Exercise 29.5 as part of the Boussinesq ocean chapter.

Projecting the geostrophic/hydrostatic balance equation (44.6) onto the velocity leads to the diagnostic balance between pressure work, buoyancy work, and friction

$$\boldsymbol{v} \cdot \nabla \varphi - w\, b = \boldsymbol{u} \cdot \boldsymbol{F}. \tag{44.10}$$

We can add this balance to the potential energy equation (44.8) to eliminate the buoyancy work term, $w\, b$, thus yielding

$$\partial_t P + \nabla \cdot (\boldsymbol{v}\, P + \boldsymbol{v}\, \varphi) = \boldsymbol{u} \cdot \boldsymbol{F} - z\, \dot{b}, \tag{44.11}$$

where we used $\nabla \cdot \boldsymbol{v} = 0$ to bring $\boldsymbol{v}\, \varphi$ inside the divergence. We thus see that potential energy at a point in the planetary geostrophic fluid is affected by reversible transport processes from advection and pressure work, along with irreversible processes from friction and material buoyancy changes.

Diffusively driven flow

It is revealing to consider the special case of a constant volume domain with static and rigid boundaries and with no boundary fluxes. We also assume that buoyancy is irreversibly modified through diffusion

$$\dot{b} = \nabla \cdot (\kappa\, \nabla b), \tag{44.12}$$

with $\kappa > 0$ an isotropic kinematic diffusivity that can be a function of space and time. Integrating the potential energy equation (44.11) over the domain leads to

$$\partial_t \langle P \rangle = \langle \boldsymbol{u} \cdot \boldsymbol{F} \rangle + \langle \kappa\, N^2 \rangle, \tag{44.13}$$

where the angle brackets signify volume means. To reach this identity we made use of

$$z\, \dot{b} = z\, \nabla \cdot (\kappa\, \nabla b) = \nabla \cdot (z\, \kappa\, \nabla b) - \kappa\, \partial_z b = \nabla \cdot (z\, \kappa\, \nabla b) - \kappa\, N^2, \tag{44.14}$$

with $\nabla \cdot (z\, \kappa\, \nabla b)$ integrating to zero in the absence of boundary fluxes. The global mean potential energy equation (44.13) indicates that diffusion increases volume mean potential energy for a stably stratified fluid ($N^2 > 0$), whereas friction generally dissipates potential energy since $\langle \boldsymbol{u} \cdot \boldsymbol{F} \rangle < 0$ (Section 26.3.3). So diffusion is the only source for potential energy, with spatial variations in potential energy leading to motion through the geostrophic balance. In the steady state this *diffusively driven flow* leads to the global mean balance between diffusion and friction

$$\langle \kappa\, N^2 \rangle = -\langle \boldsymbol{u} \cdot \boldsymbol{F} \rangle \qquad \text{steady state.} \tag{44.15}$$

44.2 Planetary geostrophic potential vorticity

In Section 41.5 we developed the potential vorticity equation for the hydrostatic Boussinesq ocean in the presence of horizontal friction in the momentum equation and diabatic terms in the buoyancy equation. Here we specialize that result to the case of planetary geostrophic system written in the form of equations (44.5a)-(44.5e).

44.2.1 Derivation

Derivation of the potential vorticity equation proceeds much like that for the hydrostatic Boussinesq ocean. The first step requires the planetary geostrophic vorticity equation as determined by taking the curl of the momentum equation (44.5a). The vertical component of this vorticity equation is given by (see also Section 31.5.2)

$$\beta\, v = f\, \partial_z w + \hat{\boldsymbol{z}} \cdot (\nabla_h \times \boldsymbol{F}) \qquad \text{with} \qquad \beta = \partial_y f. \tag{44.16}$$

Next, make use of frictional thermal wind balance

$$f\,\partial_z \boldsymbol{u} = \hat{\boldsymbol{z}} \times \nabla_h - \partial_z(\hat{\boldsymbol{z}} \times \boldsymbol{F}) \tag{44.17}$$

as well as the identities

$$N^2 \frac{\mathrm{D}f}{\mathrm{D}t} = N^2\,\beta\,v \tag{44.18a}$$

$$f \frac{\mathrm{D}N^2}{\mathrm{D}t} = f\,\frac{\partial \dot{b}}{\partial z} - f\,\nabla b \cdot \frac{\partial \boldsymbol{v}}{\partial z} \tag{44.18b}$$

$$f\,\nabla b \cdot \frac{\partial \boldsymbol{v}}{\partial z} = f\,N^2 \frac{\partial w}{\partial z} - \frac{\partial(\hat{\boldsymbol{z}} \times \boldsymbol{F})}{\partial z} \cdot \nabla_h b, \tag{44.18c}$$

to render

$$\frac{\mathrm{D}(f\,N^2)}{\mathrm{D}t} = N^2\,\beta\,v + f\,\frac{\partial \dot{b}}{\partial z} - f\,\nabla b \cdot \frac{\partial \boldsymbol{v}}{\partial z} \tag{44.19a}$$

$$= N^2 \left[f\,\frac{\partial w}{\partial z} + \hat{\boldsymbol{z}} \cdot (\nabla_h \times \boldsymbol{F}) \right] + f\,\frac{\partial \dot{b}}{\partial z} - f\,N^2 \frac{\partial w}{\partial z} + \frac{\partial(\hat{\boldsymbol{z}} \times \boldsymbol{F})}{\partial z} \cdot \nabla_h b \tag{44.19b}$$

$$= f\,\frac{\partial \dot{b}}{\partial z} + \nabla b \cdot (\nabla \times \boldsymbol{F}) \tag{44.19c}$$

$$= \nabla \cdot (f\,\dot{b}\,\hat{\boldsymbol{z}} + \boldsymbol{F} \times \nabla b). \tag{44.19d}$$

We thus identify the planetary geostrophic potential vorticity

$$Q^{\mathrm{pg}} = f\,N^2, \tag{44.20}$$

which is materially invariant in the absence of diabatic processes and friction

$$\frac{\mathrm{D}Q^{\mathrm{pg}}}{\mathrm{D}t} = 0 \qquad \text{if } \dot{b} = 0 \text{ and } \boldsymbol{F} = 0. \tag{44.21}$$

We can write the general budget equation in the form of an Eulerian flux-form expression

$$\partial_t Q^{\mathrm{pg}} + \nabla \cdot \boldsymbol{J}_{\mathrm{pg}} = 0, \tag{44.22}$$

where the planetary geostrophic potential vorticity flux is given by

$$\boldsymbol{J}_{\mathrm{pg}} = \boldsymbol{v}\,Q^{\mathrm{pg}} - \dot{b}\,f\,\hat{\boldsymbol{z}} + \nabla b \times \boldsymbol{F} + \nabla \times \boldsymbol{A}. \tag{44.23}$$

The vector $\boldsymbol{A}$ is an arbitrary gauge function that has no impact on the potential vorticity evolution. Comparing to the hydrostatic Boussinesq ocean expression (41.85), we see that the planetary geostrophic result follows by approximating the absolute vorticity by just the planetary vorticity.

44.2.2 Impermeability theorem

Following the discussion in Section 42.2.2, we verify that the potential vorticity flux vector (44.23) satisfies the impermeability theorem for buoyancy isosurfaces. We do so for the particular case of a zero gauge function ($\boldsymbol{A} = 0$), in which case

$$\boldsymbol{v}_{\mathrm{pg}} \cdot \nabla b = (\boldsymbol{J}_{\mathrm{PG}}/Q) \cdot \nabla b = \boldsymbol{v} \cdot \nabla b - \dot{b} = -\partial_t b, \tag{44.24}$$

so that

$$(\partial_t + \boldsymbol{v}_{\text{pg}} \cdot \nabla) b = 0. \tag{44.25}$$

Evidently, there is zero flux of PV-substance crossing buoyancy isosurfaces, even in the presence of irreversible processes that allow matter and buoyancy to cross those surfaces. As shown in the next subsection, we identify two more forms of the PV-substance flux vector that also satisfy impermeability, with these alternative forms differing by gauge transformations.

44.2.3 A kinematic PV flux satisfying impermeability

Following the discussion of impermeability for the Ertel potential vorticity in Section 42.2.2, we expose a purely kinematic means to derive the impermeability theorem for the planetary geostrophic potential vorticity. This derivation follows by computing the time tendency of the potential vorticity

$$\frac{\partial Q}{\partial t} = \frac{\partial}{\partial t} \nabla \cdot (f\, b\, \hat{\boldsymbol{z}}) = \nabla \cdot \left[f\, \frac{\partial b}{\partial t}\, \hat{\boldsymbol{z}} \right] \equiv -\nabla \cdot \tilde{\boldsymbol{J}}_{\text{pg}}, \tag{44.26}$$

where

$$\tilde{\boldsymbol{J}}_{\text{pg}} = -f\, \partial_t b\, \hat{\boldsymbol{z}}. \tag{44.27}$$

This form of the PV-substance flux also satisfies impermeability since

$$\tilde{\boldsymbol{v}}_{\text{pg}} \cdot \nabla b = (\tilde{\boldsymbol{J}}_{\text{pg}}/Q) \cdot \nabla b = -\partial_t b, \tag{44.28}$$

so that

$$(\partial_t + \tilde{\boldsymbol{v}}_{\text{pg}} \cdot \nabla) b = 0. \tag{44.29}$$

The PV-substance flux, $\tilde{\boldsymbol{J}}_{\text{pg}}$, vanishes in the steady state, whereas the steady state form of the alternative flux, $\boldsymbol{J}_{\text{PG}}$, is nonzero. Following the discussion in Section 42.3.2, we may choose to introduce a gauge transformation to the kinematic flux, $\tilde{\boldsymbol{J}}_{\text{pg}}$, so that it does not vanish in the steady state. Taking the small Rossby number limit of the flux (42.32) renders

$$\boldsymbol{J}_{\text{Q}}^{\text{marshall PG}} = -\nabla(g\, z + \varphi) \times \nabla b - f\, \partial_t b\, \hat{\boldsymbol{z}}. \tag{44.30}$$

This flux differs from $\tilde{\boldsymbol{J}}_{\text{pg}}$ by a curl

$$\nabla(g\, z + \varphi) \times \nabla b = \nabla \times [(g\, z + \varphi)\, \nabla b], \tag{44.31}$$

and it also satisfies the impermeability theorem. As discussed in Section 42.5.6, there are a variety of motivations for using one form of the PV-substance flux versus another. Some applications prefer a nonzero steady flux that also does not expose any irreversible processes, with $\boldsymbol{J}_{\text{Q}}^{\text{marshall PG}}$ satisfying these desires.

44.3 Depth integrated vorticity budget

In a planetary geostrophic flow, vorticity arises just from planetary vorticity since relative vorticity is negligible by comparison. With planetary vorticity a function just of latitude, a budget for the planetary geostrophic vorticity reveals how the curl of forces imparted to the fluid cause meridional motion as the fluid meets the constraints imposed by the vorticity equation. As per our discussion in Section 40.3.6, we refer to a force curl as a "torque" in our study of vorticity sources. However, one must keep in mind that more common usage in physics refers to a torque as affecting changes to angular momentum, with angular momentum generally distinct from vorticity (see Section 37.9 for a discussion of the distinction).

In this section we study the depth integrated vorticity budget for the planetary geostrophic fluid and derive implications for the meridional flow. For this purpose we focus on frictional and boundary accelerations that take the form of a vertical divergence of horizontal turbulent stress vector

$$\boldsymbol{F} = \partial_z \boldsymbol{\tau}. \tag{44.32}$$

The curl of this stress, as well as pressure forces, provide torques that generate meridional motion as revealed by the planetary geostrophic vorticity budget.

44.3.1 The β-effect, stretching, and meridional transport

In Section 31.5.2 we derived the vorticity equation for planetary geostrophy. We also encountered this equation when deriving the potential vorticity budget in Section 44.2.1. With friction written as a vertical divergence of horizontal turbulent stresses (equation (44.32)), the vertical component of the planetary geostrophic vorticity equation takes the form

$$\rho_\circ \, \beta \, v = \partial_z \left[\rho_\circ \, f \, w + \hat{\boldsymbol{z}} \cdot (\nabla \times \boldsymbol{\tau}) \right]. \tag{44.33}$$

Vertical integration from the ocean bottom at $z = \eta_\flat(x, y)$ to sea surface at $z = \eta(x, y, t)$ leads to[2]

$$\rho_\circ \, \beta \, V = \underbrace{\rho_\circ \, f \, [w(\eta) - w(\eta_\flat)]}_{\text{column stretching}} + \underbrace{\hat{\boldsymbol{z}} \cdot (\nabla \times \Delta \boldsymbol{\tau})}_{\text{boundary stresses}}, \tag{44.34}$$

where

$$V = \int_{\eta_\flat}^{\eta} v \, \mathrm{d}z \tag{44.35}$$

is the depth-integrated meridional flow, and

$$\Delta \boldsymbol{\tau} = \boldsymbol{\tau}(\eta) - \boldsymbol{\tau}(\eta_\flat) \tag{44.36}$$

is the difference in boundary stresses applied at the ocean surface and ocean bottom. Note that $\Delta \boldsymbol{\tau}$ is just a function of horizontal position and time.

For a planetary geostrophic flow, absolute vorticity is approximated by just the planetary vorticity

$$\zeta_\mathrm{a} = \zeta + f \approx f. \tag{44.37}$$

As revealed by the vorticity equation (44.34), vorticity sources in a planetary geostrophic fluid lead to meridional motion, with meridional motion the only way a planetary geostrophic fluid can modify its vorticity in response to vorticity sources.

The first term on the right hand side of the vorticity equation (44.34) arises from vertical stretching of the depth integrated column, as measured by differences in the vertical velocity at the ocean surface and bottom. For example, vertical stretching caused by positive surface velocity, $w(\eta) > 0$, or a negative bottom velocity, $w(\eta_\flat) < 0$, lead to poleward motion of the fluid column. Conversely, vertical squashing leads to equatorward motion. We emphasize that when studying the motion of the depth integrated flow, we are only concerned with vertical stretching from differences in the boundary vertical velocity rather than the vertical velocity within the fluid interior.

The second term in the vorticity equation (44.34) arises from differences in the vorticity imparted by surface and bottom boundary stresses. Positive vorticity is imparted to the fluid through a positive curl of wind stresses, $\hat{\boldsymbol{z}} \cdot [\nabla \times \boldsymbol{\tau}(\eta)] > 0$, or by a negative curl of bottom

[2] As a means to unclutter notation, we write ∇, rather than $\nabla_\hbar$, whenever acting on a field that is just a function of horizontal position, such as $p_\mathrm{a}, p_\flat, \eta_\flat$ and $\Delta \boldsymbol{\tau}$. We can do so since, for example, $\nabla p_\flat = \nabla_\hbar p_\flat$, since $\partial_z p_\flat = 0$.

stresses, $\hat{\boldsymbol{z}} \cdot [\nabla \times \boldsymbol{\tau}(\eta_b)] < 0$, with such stress curls leading to poleward motion of the fluid column. The opposite motion occurs from the converse curls.

The β-effect (Section 40.6.2) is a fundamental element of the depth integrated vorticity equation (44.34). Namely, as fluid columns are stretched or squashed, they must move meridionally to maintain vorticity balance for a planetary geostrophic fluid on a rotating spherical earth. The planetary geostrophic vorticity equation restricts attention to vertical stretching through vertical motion (the w terms) and through the vorticity imparted by the curl of boundary stresses. Notably, the curl of boundary stresses also imparts vertical motion through surface and bottom Ekman layer dynamics (see Chapter 33). Hence, the right hand side of the vorticity equation (44.34) is fundamentally related to vortex stretching.

Equation (44.34) is central to mechanical descriptions of large-scale ocean circulation. For many flow regimes, the curl of the surface wind stress dominates, thus allowing us to ignore the vertical velocity terms as well as bottom frictional stresses. Formally, we isolate the wind stress when studying a flat bottom rigid lid model, whereby $w(\eta) = w(\eta_b) = 0$. However, there can be nontrivial impacts from bottom pressure torques when flow interacts with sloping topography, with the North Atlantic and Southern Ocean providing important case studies. Other processes can be important in various flow regimes, thus prompting us to derive a full diagnostic framework to identify where these processes are important. To pursue that framework, we make use of the kinematic boundary conditions and the horizontal momentum equation to unpack the vertical velocity terms. Doing so reveals the forces and their curls that drive vertical motion at the boundaries for a planetary geostrophic flow.

44.3.2 Bottom kinematics and dynamics

The bottom kinematic boundary condition applied at $z = \eta_b(x, y)$ (Section 19.6.1) is given by

$$w = \boldsymbol{u} \cdot \nabla \eta_b \qquad \text{at } z = \eta_b(x, y). \tag{44.38}$$

This relation expresses the no-normal flow condition, $\hat{\boldsymbol{n}} \cdot \boldsymbol{v} = 0$, at the ocean bottom, with

$$\hat{\boldsymbol{n}} = -\frac{\nabla(z - \eta_b)}{|\nabla(z - \eta_b)|} = -\left[\frac{\hat{\boldsymbol{z}} - \nabla \eta_b}{\sqrt{1 + \nabla \eta_b \cdot \nabla \eta_b}}\right] \tag{44.39}$$

the outward unit normal to the bottom. The boundary condition constrains the flow so that any horizontal motion next to a sloping bottom that is oriented either up or down the slope must have an associated vertical motion. As we see in this section, such vertical motion next to the bottom boundary arises from force curls acting to stretch or squash a fluid column. In turn, through the vorticity equation (44.34), vertical motion at the bottom leads to meridional motion of the full fluid column.

Expressions for bottom vertical velocity

The bottom kinematic boundary condition holds for all dynamical flow regimes. For the particular case of planetary geostrophy, we garner insight into the forces that drive vertical flow near the bottom by making use of the planetary geostrophic momentum equation (44.5a). Evaluating the horizontal components of this equation at the ocean bottom yields[3]

$$\rho_o f \hat{\boldsymbol{z}} \times \boldsymbol{u} = -(\nabla p)_{z=\eta_b} + \boldsymbol{F}_b, \tag{44.40}$$

[3]Recall that since $p_b = p_b(x, y, t)$, we have $\nabla p_b = \nabla_h p_b$. As noted in the footnote on page 1267, we drop the z script to reduce notational clutter.

where $(\nabla p)_{z=\eta_b}$ is the horizontal pressure gradient evaluated at the ocean bottom and $\boldsymbol{F}_b(x, y, t)$ is the bottom friction. For the special case of a no-slip bottom, all velocity components vanish at $z = \eta_b$. In that case, we consider $\boldsymbol{u}$ in equation (44.40) to be the horizontal velocity averaged within the bottom boundary layer, and w the corresponding vertical velocity leaving the boundary layer.

It is convenient to decompose the bottom horizontal velocity into its geostrophic and Ekman[4] components via

$$\rho_o f \hat{\boldsymbol{z}} \times \boldsymbol{u}_g = -(\nabla p)_{z=\eta_b} \qquad \text{and} \qquad \rho_o f \hat{\boldsymbol{z}} \times \boldsymbol{u}_e = \boldsymbol{F}_b, \tag{44.41}$$

so that

$$\boldsymbol{u}_g = \frac{\hat{\boldsymbol{z}} \times (\nabla p)_{z=\eta_b}}{\rho_o f} \qquad \text{and} \qquad \boldsymbol{u}_e = -\frac{\hat{\boldsymbol{z}} \times \boldsymbol{F}_b}{\rho_o f}. \tag{44.42}$$

For the horizontal horizontal pressure gradient at the ocean bottom, we make use of equation (27.60b) to write

$$(\nabla_h p)_{z=\eta_b} = \nabla_h p_b + g\, \rho(\eta_b)\, \nabla_h \eta_b. \tag{44.43}$$

The corresponding bottom vertical velocity components are determined by inserting equations (44.42) and (44.43) into the bottom kinematic boundary condition (44.38)

$$w_g = \frac{\hat{\boldsymbol{z}} \cdot (-\nabla \eta_b \times \nabla p_b)}{\rho_o f} \qquad \text{and} \qquad w_e = \frac{\hat{\boldsymbol{z}} \cdot (\nabla \eta_b \times \boldsymbol{F}_b)}{\rho_o f}. \tag{44.44}$$

These equations reveal how the curl of pressure forces and boundary frictional forces drive a nonzero vertical motion next to the bottom, while maintaining the bottom kinematic boundary condition (44.38). As seen by these equations, is only the projection of ∇p_b and $\boldsymbol{F}_b$ onto the isobath direction that contributes to a nonzero vertical velocity. These along-isobath forces are needed to render a horizontal velocity that is itself misaligned with isobaths, thus satisfying the kinematic requirement for vertical motion.[5]

To further understand the bottom pressure term, we write it as

$$w_g = \frac{\hat{\boldsymbol{z}} \cdot (-\nabla \eta_b \times \nabla p_b)}{\rho_o f} = \frac{\hat{\boldsymbol{z}} \cdot [\nabla \times p_b \nabla \eta_b]}{\rho_o f}. \tag{44.45}$$

The numerator is the curl of the horizontal projection of the pressure contact force along the bottom, $p_b \nabla \eta_b$. This term is the topographic form stress discussed in Section 28.2 for a general fluid and in Section 39.7.6 for the shallow water. We thus conclude that vertical geostrophic motion next to the bottom arises from the curl of the topographic form stress. This is an important result that will appear again within this section as well as in Sections 44.5 and 44.6.

Comments on the bottom vertical geostrophic velocity

A large part of the bottom pressure gradient driving the horizontal geostrophic flow in equation (44.42) arises from changes in bottom depth. However, that portion of the bottom pressure gradient has no impact on w_g, since it only drives horizontal flow along isobaths. We see this property by writing

$$p_b = -\rho_o\, g\, \eta_b + p_b' \Longrightarrow w_g = \frac{\hat{\boldsymbol{z}} \cdot (-\nabla \eta_b \times \nabla p_b')}{\rho_o f}. \tag{44.46}$$

When there is misalignment between isolines of bottom pressure and bottom topography, the geostrophic flow in a fluid column crosses isobaths. Correspondingly, with the pressure force misaligned with topographic gradients, the fluid column experiences a twisting action akin

[4] Recall our discussion of Ekman mechanics in Chapter 33.

[5] Note that we derived the expression (44.44) for w_g in equation (40.196) when studying vorticity mechanics.

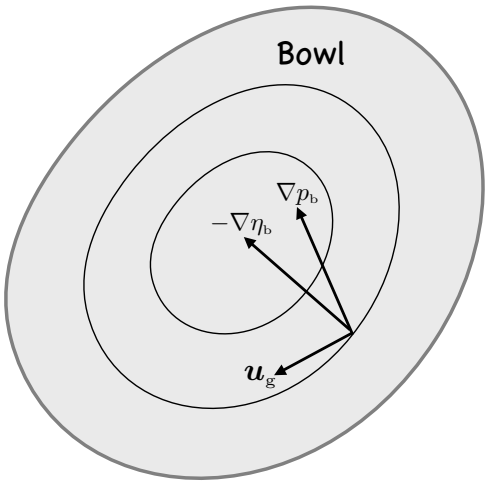

FIGURE 44.1: Depicting how bottom pressure gradients create vertical motion in planetary geostrophic flow next to a sloping bottom according to equations (44.44) and (44.46). Here we show a bowl or depression (local maximum in the depth) with $-\eta_b$ increasing inward toward the bowl center. Only those portions of ∇p_b and $\boldsymbol{F}_b$ that are aligned parallel to the topographic slope contribute to vertical motion. We illustrate here a case where the bottom pressure gradient leads to $-\nabla \eta_b \cdot \boldsymbol{u}_g > 0$ so that $w_g < 0$ in the northern hemisphere and $w_g > 0$ in the southern hemisphere.

to how baroclinicity spins a fluid element if the pressure force does not act through the fluid element's center of mass (see Section 40.4).

To illustrate the above, consider the topographic bowl in Figure 44.1, with sides steep enough so that the bottom pressure gradient is dominated by the topographic slopes. Along the bottom the pressure increases moving down (increasing depth) towards the bowl center. The corresponding bottom geostrophic flow is anti-cyclonic within the bowl and largely follows isobaths. As already noted, if the geostrophic flow exactly follows isobaths, then there is no corresponding vertical component to the bottom velocity. A vertical velocity arises only in the presence of an anomalous bottom pressure gradient, $\nabla p_b'$, that is misaligned with the bottom slope, $\nabla \eta_b$. This bottom pressure gradient balances a geostrophic flow that deviates from isobaths thus giving rise to a nonzero w_g. Similar geometric analysis holds for the bottom friction vector, $\boldsymbol{F}_b$, and how it gives rise to a nonzero vertical Ekman velocity, w_e.

What causes misalignment between p_b and η_b?

As we just discussed, misalignment of p_b and η_b lead to vertical geostrophic motion along the bottom. In Section 44.3.3 we will see a similar relation for vertical geostrophic motion at the ocean surface. But what causes such misalignment? The answer to this question is circular when working within planetary geostrophy since its momentum equation is diagnostic. Even so, we can offer some insight by returning to the depth-integrated vorticity balance (44.34) and rewriting it as an expression for vertical motion

$$\rho_o f [w(\eta_b) - w(\eta)] = -\rho_o \beta V + \hat{\boldsymbol{z}} \cdot (\nabla \times \Delta \boldsymbol{\tau}). \tag{44.47}$$

Hence, vertical motion at the surface and bottom balance meridional motion in the presence of planetary beta, plus the curl of surface and bottom stresses. The absence of planetary beta, and the absence of boundary stress curls, realizes $w(\eta_b) = w(\eta)$.

44.3.3 Surface kinematics and dynamics

For purposes of large-scale circulation studies using planetary geostrophy, it is generally sufficient to assume a rigid lid upper boundary condition, whereby $w(\eta) = w(0) = 0$. Even so, we find it revealing to present the results for a free surface in which there is the possibility of nonzero surface mass fluxes. This situation is commonly encountered in general circulation models. The surface kinematic boundary condition for a Boussinesq fluid (Section 21.3) is given by

$$w = -Q_{\mathrm{m}}/\rho_{\circ} + (\partial_t + \boldsymbol{u} \cdot \nabla)\eta \qquad \text{at } z = \eta(x, y, t). \tag{44.48}$$

We retain the sea surface time tendency, $\partial_t \eta$, even though for transient solutions the time tendency is many orders of magnitude smaller than the typical vertical velocity under the planetary geostrophic regime.[6] Evaluating the horizontal planetary geostrophic momentum equation (31.25a) at the ocean surface renders

$$\rho_{\circ}\, f\, \hat{\boldsymbol{z}} \times \boldsymbol{u} = -(\nabla_{\mathrm{h}} p)_{z=\eta} + \boldsymbol{F}_{\eta}, \tag{44.49}$$

where $\boldsymbol{F}_{\eta}$ is the horizontal friction vector at the surface, and (see equation (27.60a))

$$(\nabla_{\mathrm{h}} p)_{z=\eta} = \nabla_{\mathrm{h}} p_{\mathrm{a}} + g\, \rho(\eta)\, \nabla_{\mathrm{h}} \eta \tag{44.50}$$

is the horizontal pressure gradient at the ocean surface. Like the bottom, we decompose the horizontal velocity into a geostrophic component and an Ekman component via

$$\rho_{\circ}\, f\, \hat{\boldsymbol{z}} \times \boldsymbol{u}_{\mathrm{g}} = -(\nabla_{\mathrm{h}} p)_{z=\eta} \qquad \text{and} \qquad \rho_{\circ}\, f\, \hat{\boldsymbol{z}} \times \boldsymbol{u}_{\mathrm{e}} = \boldsymbol{F}_{\eta}, \tag{44.51}$$

so that

$$\boldsymbol{u}_{\mathrm{g}} = \frac{\hat{\boldsymbol{z}} \times (\nabla_{\mathrm{h}} p)_{z=\eta}}{\rho_{\circ}\, f} \qquad \text{and} \qquad \boldsymbol{u}_{\mathrm{e}} = -\frac{\hat{\boldsymbol{z}} \times \boldsymbol{F}_{\eta}}{\rho_{\circ}\, f}. \tag{44.52}$$

The corresponding vertical velocity components are determined by inserting into the surface kinematic boundary condition (44.48)

$$w_{\mathrm{Q}\eta} = -\frac{Q_{\mathrm{m}}}{\rho_{\circ}} + \frac{\partial \eta}{\partial t} \qquad \text{and} \qquad w_{\mathrm{g}} = \frac{\hat{\boldsymbol{z}} \cdot (-\nabla \eta \times \nabla p_{\mathrm{a}})}{\rho_{\circ}\, f} \qquad \text{and} \qquad w_{\mathrm{e}} = \frac{\hat{\boldsymbol{z}} \cdot (\nabla \eta \times \boldsymbol{F}_{\eta})}{\rho_{\circ}\, f}, \tag{44.53}$$

where we introduced a vertical velocity, $w_{\mathrm{Q}\eta}$, associated with the boundary mass flux and transient sea level fluctuations. As for the bottom, the second and third of these equations reveal how the curl of inviscid pressure forces and boundary frictional forces drive a nonzero vertical motion at the ocean surface, all while maintaining the surface kinematic boundary condition (44.48). Furthermore, it is only the projection of ∇p_{a} and $\boldsymbol{F}_{\eta}$ onto the direction parallel to sea surface height contours that contributes to a nonzero vertical velocity. This orientation of the surface forces is needed to render a horizontal velocity that is itself misaligned with sea surface height contours, thus satisfying the kinematics required to render vertical motion.

44.3.4 Summary of force curls driving depth integrated meridional flow

Plugging expressions (44.44), (44.46), and (44.53) into equation (44.34) renders the depth integrated planetary vorticity balance

$$\rho_{\circ}\, \beta\, V = f\, (-Q_{\mathrm{m}} + \rho_{\circ}\, \partial_t \eta) + \hat{\boldsymbol{z}} \cdot \left[\nabla \eta \times (\boldsymbol{F}_{\eta} - \nabla p_{\mathrm{a}}) - \nabla \eta_{\mathrm{b}} \times (\boldsymbol{F}_{\mathrm{b}} - \nabla p'_{\mathrm{b}}) + \nabla \times \Delta \boldsymbol{\tau}\right]. \tag{44.54}$$

[6] See Section 3.3 of *Samelson* (2011) for more details on this scaling of the planetary geostrophic equations.

Evidently, the force curls are symmetrically applied at the surface and bottom, which is part of the motivation for exposing the surface terms even though they are generally subdominant. In general, equation (44.54) shows that the depth integrated meridional flow, within the planetary geostrophic regime, is driven by the following processes.

Surface mass transport plus sea surface fluctuations

The term $f \rho_o (-Q_m/\rho_o + \partial_t \eta)$ arises from mass transport across the ocean surface plus fluctuations in the sea surface height. For example, as sea surface height increases or as water leaves the ocean surface, they impart a positive surface vertical velocity, $w(\eta) > 0$, thus causing column stretching and poleward meridional depth integrated flow. In the steady state, where it is just the mass flux term that contributes, the meridional circulation is known as the Goldsbrough-Stommel circulation (see *Huang and Schmitt* (1993) for a review).

Curl of turbulent boundary stresses

The term $\hat{\boldsymbol{z}} \cdot (\nabla \times \Delta \boldsymbol{\tau})$ arises from the curl of the turbulent wind stress and turbulent bottom stress. The wind stress term is generally larger than the bottom turbulent stress, with many theories for ocean circulation, particularly those with a flat bottom, almost exclusively focused on the role of surface stress in forcing planetary geostrophic vorticity. We comment more on this case in Section 44.4 where we discuss the *Sverdrup balance*.

Atmospheric pressure torque

The term

$$\nabla p_a \times \nabla \eta = \nabla \times (p_a \nabla \eta) = -\nabla \times (\eta \nabla p_a) \tag{44.55}$$

arises from differences in lines of constant atmospheric pressure and lines of constant sea surface height. Such misalignments create a torque akin to the baroclinicity detailed in Section 40.4, with these misalignments driving vertical motion and a corresponding depth integrated meridional flow.

Bottom pressure torque

The term

$$\nabla p'_b \times (-\nabla \eta_b) = \nabla \times (-p'_b \nabla \eta_b) = \nabla \times (\eta_b \nabla p'_b) \tag{44.56}$$

arises from differences in lines of constant bottom pressure and lines of constant bottom topography. That is, bottom pressure torque requires a gradient of bottom pressure along isobaths, thus producing a bottom geostrophic flow that deviates from isobaths. As for the atmospheric pressure torques, such misalignments create a torque that drives a depth integrated meridional flow, with this term vanishing when the bottom topography is flat. In many cases with strong flow next to sloping bottoms, this term can contribute more to the vorticity budget than the turbulent bottom stress. Indeed, in some cases it can rival contributions from the surface wind stress. We sketched out such cases for the shallow water when discussing western boundary currents in Section 39.7.6.

Surface frictional acceleration

The term

$$\hat{\boldsymbol{z}} \cdot (\nabla \eta \times \boldsymbol{F}_\eta) = \hat{\boldsymbol{z}} \cdot [\nabla \eta \times \partial_z \boldsymbol{\tau}_\eta] \tag{44.57}$$

arises from evaluating the vertical divergence of the frictional stress at the sea surface. A finite volume boundary layer treatment of this term prompts us to integrate the stress divergence over

the extent of the surface Ekman layer to render the alternative expression

$$\hat{\boldsymbol{z}} \cdot \int_{-h_{\text{e-surf}}}^{\eta} [\nabla \eta \times \partial_z \boldsymbol{\tau}] \, \mathrm{d}z = \hat{\boldsymbol{z}} \cdot [\nabla \eta \times \boldsymbol{\tau}(\eta)], \tag{44.58}$$

where we assumed $\boldsymbol{\tau}$ is negligible at the base of the surface Ekman layer, $z = -h_{\text{e-surf}}(x, y, t)$. The term $\hat{\boldsymbol{z}} \cdot [\nabla \eta \times \boldsymbol{\tau}(\eta)]$ creates a torque from that component of the surface turbulent stress that is aligned with isolines of the sea surface height.

Bottom frictional acceleration

The term

$$\hat{\boldsymbol{z}} \cdot (-\nabla \eta_{\mathrm{b}} \times \boldsymbol{F}_{\mathrm{b}}) = \hat{\boldsymbol{z}} \cdot \left[-\nabla \eta_{\mathrm{b}} \times \frac{\partial \boldsymbol{\tau}_{\mathrm{b}}}{\partial z} \right] \tag{44.59}$$

arises from evaluating the vertical divergence of the frictional stress at the ocean bottom. As for the analogous term for the surface, we offer a finite volume Ekman boundary layer treatment to render the alternative expression

$$\hat{\boldsymbol{z}} \cdot \int_{\eta_{\mathrm{b}}}^{h_{\text{e-bot}}} \left[-\nabla \eta_{\mathrm{b}} \times \frac{\partial \boldsymbol{\tau}}{\partial z} \right] \mathrm{d}z = \hat{\boldsymbol{z}} \cdot [-\nabla \eta_{\mathrm{b}} \times \boldsymbol{\tau}(\eta_{\mathrm{b}})], \tag{44.60}$$

where we assumed $\boldsymbol{\tau}$ is negligible at the top of the bottom Ekman layer, $z = -\eta_{\mathrm{b}} + h_{\text{e-bot}}$. The term $\hat{\boldsymbol{z}} \cdot [-\nabla \eta_{\mathrm{b}} \times \boldsymbol{\tau}(\eta_{\mathrm{b}})]$ creates a torque from that component of the bottom turbulent stress that is aligned with isobaths.

44.3.5 Integral constraints

The atmospheric and bottom pressure torques appearing in the depth integrated planetary vorticity balance (44.54) satisfy an integral constraint that follows from Stokes' curl theorem. To illustrate this constraint, consider the bottom pressure torque integrated over an arbitrary area along the bottom

$$\int (\nabla \eta_{\mathrm{b}} \times \nabla p'_{\mathrm{b}}) \cdot \hat{\boldsymbol{z}} \, \mathrm{d}A = \int [\nabla \times (\eta_{\mathrm{b}} \nabla p'_{\mathrm{b}})] \cdot \hat{\boldsymbol{z}} \, \mathrm{d}A \tag{44.61a}$$

$$= \oint \eta_{\mathrm{b}} \nabla p'_{\mathrm{b}} \cdot \hat{\boldsymbol{t}} \, \mathrm{d}s \tag{44.61b}$$

$$= - \oint p'_{\mathrm{b}} \nabla \eta_{\mathrm{b}} \cdot \hat{\boldsymbol{t}} \, \mathrm{d}s. \tag{44.61c}$$

We see that the bottom pressure torque vanishes when integrated around a closed loop that follows either an isobath or a bottom isobar, since the integrand vanishes identically. A similar constraint holds for the atmospheric pressure torque, whereas there is generally no analogous constraint satisfied by the turbulent boundary stresses.

One exception for the turbulent stresses occurs for f-plane flow ($\beta = 0$) where the depth integrated flow is non-divergent

$$\partial_t \eta - Q_{\mathrm{m}}/\rho_{\mathrm{o}} = -\nabla \cdot \boldsymbol{U} = 0, \tag{44.62}$$

and where the interior friction vanishes at the surface and bottom boundaries, $\boldsymbol{F}_\eta = \boldsymbol{F}_{\mathrm{b}} = 0$. From equation (44.54), we see that a steady state is realized only if there is a balance between pressure torques and turbulent boundary stresses

$$\hat{\boldsymbol{z}} \cdot (\nabla \eta \times \nabla p_{\mathrm{a}} - \nabla \eta_{\mathrm{b}} \times \nabla p'_{\mathrm{b}}) = \hat{\boldsymbol{z}} \cdot (\nabla \times \Delta \boldsymbol{\tau}). \tag{44.63}$$

Consider even further specialization in which the atmospheric pressure torque vanishes, and the bottom turbulent stress is negligible, in which case a steady state balance requires a balance between bottom pressure torques and torques from surface turbulent wind stress

$$-\hat{\boldsymbol{z}} \cdot (\nabla \eta_{\rm b} \times \nabla p'_{\rm b}) = \hat{\boldsymbol{z}} \cdot [\nabla \times \boldsymbol{\tau}(\eta)]. \tag{44.64}$$

Integration over either an isobath or bottom pressure isobar then requires, for a steady state, the following identity

$$\int [\nabla \times \boldsymbol{\tau}(\eta)] \cdot \hat{\boldsymbol{z}} \, \mathrm{d}A = \oint \boldsymbol{\tau}(\eta) \cdot \hat{\boldsymbol{t}} \, \mathrm{d}s = 0 \quad f\text{-plane closed isobath or closed isobar.} \tag{44.65}$$

Deviation from this identity leads to non-steady flow on the f-plane. In contrast, the β-plane has no such steady state constraint since meridional flow can balance the circulation imparted by turbulent wind stresses.

44.4 Sverdrup balance and geostrophic Sverdrup balance

The balance (44.54) exposes the many processes that affect meridional flow in a planetary geostrophic fluid. However, when confronted with minimal information from ocean measurements, we are motivated to examine just the main contributors to this balance.

The *Sverdrup balance* is a very simplified form of the balance (44.54), and it was first encountered in Section 31.5.5

$$\rho_{\circ} \, \beta \, V_{\rm Sverdrup} = \hat{\boldsymbol{z}} \cdot [\nabla \times \boldsymbol{\tau}(\eta)] \qquad \text{Sverdrup balance.} \tag{44.66}$$

This balance arises from dropping the vertical velocity at both the ocean surface and ocean bottom; ignoring horizontal frictional stresses; and assuming $\partial_t \eta = -Q_{\rm m}/\rho_{\circ} = 0$ as per a rigid lid flow in which $\nabla \cdot \boldsymbol{U} = 0$. The Sverdrup balance offers a null hypothesis for the large-scale and low frequency meridional ocean circulation away from sloping sides; i.e., in regions where bottom pressure torques can be ignored.

To derive the Sverdrup balance (44.66), we performed a depth integral of the planetary geostrophic vorticity equation (44.33) from the ocean bottom to the free surface. This integral encompasses both the geostrophic interior and the ageostrophic Ekman flow in the top and bottom Ekman layers. In some treatments we focus exclusively on contributions from the geostrophic interior, in which case the depth integral extends from the top of the bottom Ekman layer, $z = \eta_{\rm eb}$, to the bottom of the top Ekman layer, $z = \eta_{\rm et}$, thus leading to the depth integrated geostrophic transport

$$V_{\rm g} \equiv \int_{\eta_{\rm eb}}^{\eta_{\rm et}} v \, \mathrm{d}z. \tag{44.67}$$

Integrating the planetary geostrophic vorticity balance (44.33) over this depth range, and ignoring contributions from friction since we are concerned just with the geostrophic interior, leads to

$$\rho_{\circ} \, \beta \, V_{\rm g} = f \, [w(\eta_{\rm et}) - w(\eta_{\rm eb})]. \tag{44.68}$$

This equation provides a balance between the depth integrated meridional transport within the geostrophic interior (left hand side), with the vertical vortex stretching within this depth range (right hand side).

We now make use of the Ekman theory from Chapter 33 to approximate the vertical velocities in equation (44.68). For this purpose we neglect both the time tendency for the vertical position of the Ekman layer and the slope of the Ekman layer, in which case the kinematic identity

(33.38), applied at the Ekman base, $z = \eta_{\rm e}(x, y, t)$, is approximated by

$$w^{(\dot\eta_{\rm e})} = w - (\partial_t z + \boldsymbol{u} \cdot \nabla z) \approx w \qquad \text{at } \; z = \eta_{\rm e}(x, y, t), \tag{44.69}$$

where $z = \eta_{\rm e}$ is ths vertical position of the Ekman layer. We now make use of the Ekman layer mass budgets to determine the entrainment velocity, $w^{(\dot\eta_{\rm e})}$. In particular, equation (33.45) is used for $w(\eta_{\rm et})$ to give

$$w(\eta_{\rm et}) \approx w^{(\dot\eta_{\rm e})}_{\text{Ekman-top}} = (1/\rho_{\rm o})\, \hat{\boldsymbol{z}} \cdot [\nabla \times (\boldsymbol{\tau}(\eta)/f)]. \tag{44.70}$$

with a similar treatment for the bottom leading to

$$w(\eta_{\rm eb}) \approx w^{(\dot\eta_{\rm e})}_{\text{Ekman-bot}} = (1/\rho_{\rm o}) f\, \hat{\boldsymbol{z}} \cdot [\nabla \times (\boldsymbol{\tau}(\eta_{\rm b})/f)]. \tag{44.71}$$

Bringing these results into equation (44.68) leads to

$$\rho_{\rm o}\, \beta\, V_{\rm g} = f\, \hat{\boldsymbol{z}} \cdot \nabla \times [\boldsymbol{\tau}(\eta)/f - \boldsymbol{\tau}(\eta_{\rm b})/f]. \tag{44.72}$$

Since the bottom turbulent stress is generally much smaller than the surface, it is typically ignored, in which case we reach the *geostrophic Sverdrup balance*

$$\rho_{\rm o}\, \beta\, V_{\rm g} = f\, \hat{\boldsymbol{z}} \cdot \nabla \times [\boldsymbol{\tau}(\eta)/f] \qquad \text{geostrophic Sverdrup balance.} \tag{44.73}$$

The geostrophic Sverdrup balance relates the meridional geostrophic transport to the curl of $\boldsymbol{\tau}/f$ due to upper ocean mechanical stresses from boundary processes; i.e., wind stress and ice-ocean stresses. It is differs from the full Sverdrup balance in equation (44.66) by the presence of the f outside of the curl and $1/f$ inside the curl. *Gray and Riser* (2014) assess the geostrophic Sverdrup balance based on ocean measurements.

44.5 Vorticity of the depth integrated velocity

In Section 44.3 we studied the depth integrated vorticity budget for planetary geostrophic flow. We were led to see how boundary torques (i.e., the curl of boundary forces) lead to vertical motion and in turn, through the β-effect, lead to meridional motion of the depth integrated flow. In this section we present another analysis of vorticity in the planetary geostrophic regime, here focusing on vorticity of the depth integrated velocity. Elements of this material were discussed in Section 40.9 without making the planetary geostrophic assumption. By assuming planetary geostrophy we can further constrain the flow by focusing just on vortex stretching.

44.5.1 Depth integrated velocity equation

The depth integrated horizontal velocity equation (44.5a) is given by

$$\rho_{\rm o}\, f\, \hat{\boldsymbol{z}} \times \boldsymbol{U} = -\int_{\eta_{\rm b}}^{\eta} \nabla_{\rm h} p \, {\rm d}z + \Delta\boldsymbol{\tau} \tag{44.74}$$

where

$$\boldsymbol{U} = \int_{\eta_{\rm b}}^{\eta} \boldsymbol{u} \, {\rm d}z \tag{44.75}$$

is the depth integrated horizontal velocity, and we assumed friction in the form of the vertical divergence of a horizontal turbulent stress as in equation (44.32). For the depth integrated

pressure gradient, we follow the decomposition in Section 28.4.4 by writing

$$\int_{\eta_b}^{\eta} p \, dz = \int_{\eta_b}^{\eta} [d(p\, z) - z \, dp] = p_a \, \eta - p_b \, \eta_b + \mathscr{P}, \tag{44.76}$$

where we used the hydrostatic balance to write $dp = -g \, \rho \, dz$, which is valid for each fluid column. We also introduced the potential energy per horizontal area of a fluid column

$$\mathscr{P} = \int_{\eta_b}^{\eta} g \, \rho \, z \, dz = (g \, \rho_o/2) \, (\eta^2 - \eta_b^2) + \int_{\eta_b}^{\eta} g \, \rho' \, z \, dz, \tag{44.77}$$

where

$$\rho' = \rho - \rho_o \tag{44.78}$$

is the density deviation from the background reference density. These results then lead to the depth integrated horizontal pressure gradient

$$\begin{aligned}
\int_{\eta_b}^{\eta} \nabla_h p \, dz &= \nabla_h \left[\int_{\eta_b}^{\eta} p \, dz \right] - p_a \nabla_h \eta + p_b \nabla_h \eta_b && \text{(44.79a)} \\
&= \nabla_h \left[p_a \, \eta - p_b \, \eta_b + \mathscr{P} \right] - p_a \nabla_h \eta + p_b \nabla_h \eta_b && \text{(44.79b)} \\
&= \eta \nabla_h p_a - \eta_b \nabla_h p_b + \nabla_h \mathscr{P}, && \text{(44.79c)} \\
&= \eta \nabla p_a - \eta_b \nabla p_b + \nabla \mathscr{P}, && \text{(44.79d)}
\end{aligned}$$

where the final equality follows since p_a, η_b, p_b, and $\mathscr{P}$, are functions just of horizontal position and time. We are thus led to the depth integrated planetary geostrophic momentum balance

$$\rho_o \, f \, \hat{\boldsymbol{z}} \times \boldsymbol{U} = -\eta \, \nabla p_a + \eta_b \nabla p_b - \nabla \mathscr{P} + \Delta \boldsymbol{\tau}. \tag{44.80}$$

The depth integrated balance is here written in terms of gradients in the surface and bottom pressures, the gradient of the potential energy per area, and the difference in turbulent stresses at the top and bottom boundaries, $\Delta \boldsymbol{\tau} = \boldsymbol{\tau}(\eta) - \boldsymbol{\tau}(\eta_b)$.

44.5.2 Vorticity budget

Taking the curl of the depth integrated balance (44.80) annihilates the potential energy term, thus leaving

$$\rho_o \, \beta \, V = -\rho_o \, f \, \nabla \cdot \boldsymbol{U} + \hat{\boldsymbol{z}} \cdot \nabla \times [p_a \nabla \eta + \boldsymbol{\tau}(\eta) - p_b \nabla \eta_b - \boldsymbol{\tau}(\eta_b)]. \tag{44.81}$$

From Section 21.8, we know that the divergence of the depth-integrated flow for a steady Boussinesq fluid is given by

$$\rho_o \nabla \cdot \boldsymbol{U} = Q_m, \tag{44.82}$$

so that

$$\rho_o \, \beta \, V = -f \, Q_m + \hat{\boldsymbol{z}} \cdot \nabla \times [p_a \nabla \eta + \boldsymbol{\tau}(\eta) - p_b \nabla \eta_b - \boldsymbol{\tau}(\eta_b)]. \tag{44.83}$$

This is the vorticity equation for the depth integrated planetary geostrophic fluid. It is quite similar to the vorticity balance for a shallow water fluid as given by equation (39.106) (which considered zero atmospheric pressure). In the presence of β, meridional mass transport for the fluid column is balanced by surface mass fluxes, $Q_m \neq 0$; the curl of surface form stresses and surface turbulent stresses; and the curl of topographic form stresses and bottom turbulent stresses. This result follows quite naturally when recognizing that the forces acting on a depth integrated fluid column arise from the depth integrated stresses acting on the column sides plus those acting on the top and bottom boundaries. In the absence of interior friction stresses due to horizontal strains (as assumed here), it is only the depth integrated pressure that acts on the

column sides, and this term has zero curl. We are thus left just with the curl of the surface and bottom boundary form stresses and turbulent stresses, along with a contribution from boundary mass transport.

The Sverdrup balance (44.66) is a special case of the more complete vorticity budget (44.81). Furthermore, the *topographic Sverdrup balance* results when meridional transport balances the curl of the wind plus bottom pressure form stress

$$\rho_o \, \beta \, V_{\text{topo-Sverdrup}} = \hat{\boldsymbol{z}} \cdot \nabla \times (\boldsymbol{\tau}(\eta) - p_b \nabla \eta_b) \qquad \text{topographic Sverdrup balance.} \tag{44.84}$$

In the presence of flows interacting with topography, where bottom pressure torques are sizable, this balance is generally much more accurate than the Sverdrup balance.

44.5.3 Integral balances for steady flows

Following the discussion in Section 40.9.5, we write the vorticity balance (44.81) in the form

$$\rho_o \, \nabla \cdot (f \, \boldsymbol{U}) = \hat{\boldsymbol{z}} \cdot \nabla \times [p_a \nabla \eta + \boldsymbol{\tau}(\eta) - p_b \nabla \eta_b - \boldsymbol{\tau}(\eta_b)]. \tag{44.85}$$

Integrating over a horizontal area, $\mathcal{S}$, leads to

$$\rho_o \oint_{\partial \mathcal{S}} f \, \boldsymbol{U} \cdot \hat{\boldsymbol{n}} \, ds = \oint_{\partial \mathcal{S}} [p_a \nabla \eta + \boldsymbol{\tau}(\eta) - p_b \nabla \eta_b - \boldsymbol{\tau}(\eta_b)] \cdot \hat{\boldsymbol{t}} \, ds. \tag{44.86}$$

To reach this result we used Gauss's divergence theorem for the left hand side and Stokes' curl theorem for the right hand side. The unit vector $\hat{\boldsymbol{n}}$ points horizontally outward from the boundary of the area, whereas the unit vector $\hat{\boldsymbol{t}}$ is the counter-clockwise oriented tangent to the closed contour around the boundary. For the special case of $Q_m = 0$ we are afforded a steady state streamfunction for the depth-integrate flow since $\nabla \cdot \boldsymbol{U} = 0$. Choosing the area, $\mathcal{S}$, to be bounded by a closed streamline allows us to set $\boldsymbol{U} \cdot \hat{\boldsymbol{n}} = 0$ along that streamline. We thus see that for steady planetary geostrophic flow with $\nabla \cdot \boldsymbol{U} = 0$, any closed streamline of the flow must maintain the following work balance around the streamline

$$\oint_{\partial \mathcal{S}} [p_a \nabla \eta + \boldsymbol{\tau}(\eta) - p_b \nabla \eta_b - \boldsymbol{\tau}(\eta_b)] \cdot \hat{\boldsymbol{t}} \, ds = 0. \tag{44.87}$$

This equation is a simplified form of equation (40.208) that was formulated for a more general flow. We can rearrange equation (44.87) to display an integrated balance between the work done by boundary pressure form stresses around a closed streamline, and work done by boundary turbulent stresses around the same streamline

$$\oint_{\partial \mathcal{S}} (p_a \nabla \eta - p_b \nabla \eta_b) \cdot \hat{\boldsymbol{t}} \, ds = - \oint_{\partial \mathcal{S}} [\boldsymbol{\tau}(\eta) - \boldsymbol{\tau}(\eta_b)] \cdot \hat{\boldsymbol{t}} \, ds. \tag{44.88}$$

44.5.4 Comments

Yeager (2015) connects torques acting on the depth integrated horizontal flow in the North Atlantic to buoyancy forces affecting the Atlantic meridional overturning circulation, thus illustrating how the formulation in this section can be of use for the analysis of an ocean circulation model.

44.6 Vorticity equation for the depth averaged velocity

In some numerical models, it is more common to have access to the depth averaged velocity

$$\overline{\boldsymbol{u}} = \frac{1}{D} \int_{\eta_b}^{\eta} \boldsymbol{u} \, dz \qquad \text{with} \qquad D = \eta - \eta_b. \tag{44.89}$$

We thus find it useful to develop a budget for the vorticity of the depth averaged velocity. In this discussion we encounter a distinct means for describing how bottom topography, in the presence of baroclinicity, generates meridional flow.

44.6.1 Relating the depth average velocity to boundary velocities

Before studying the vorticity equation, we here relate the depth averaged velocity, $\overline{\boldsymbol{u}}(x, y, t)$, to the surface velocity, $\boldsymbol{u}(x, y, z = \eta, t)$, and bottom velocity, $\boldsymbol{u}(x, y, z = \eta_b, t)$. This analysis exposes some general features of how the boundary flows are driven away from the depth average.

The starting point is the identity

$$\int_{\eta_b}^{\eta} \boldsymbol{u} \, dz = (\eta - \eta_b) \, \boldsymbol{u}(\eta) - \int_{\eta_b}^{\eta} \frac{\partial \boldsymbol{u}}{\partial z} \, (z - \eta_b) \, dz, \tag{44.90}$$

which, along with the analogous identity for the bottom flow, leads to

$$\overline{\boldsymbol{u}} - \boldsymbol{u}(\eta) = - \int_{\eta_b}^{\eta} \frac{\partial \boldsymbol{u}}{\partial z} \left[\frac{z - \eta_b}{\eta - \eta_b} \right] dz \qquad \text{and} \qquad \overline{\boldsymbol{u}} - \boldsymbol{u}(\eta_b) = \int_{\eta_b}^{\eta} \frac{\partial \boldsymbol{u}}{\partial z} \left[\frac{\eta - z}{\eta - \eta_b} \right] dz. \tag{44.91}$$

Note that $\boldsymbol{u}(\eta) - \boldsymbol{u}(\eta_b) = \int_{\eta_b}^{\eta} (\partial \boldsymbol{u}/\partial z) \, dz$ serves as a useful check on the manipulations leading to equation (44.91). We see that the difference between the depth averaged flow and the surface flow, $\overline{\boldsymbol{u}} - \boldsymbol{u}(\eta)$, is determined by the integral of the weighted vertical shear, with the weight linearly decreasing from unity at the surface to zero at the bottom. The minus sign in front of the integral for $\overline{\boldsymbol{u}} - \boldsymbol{u}(\eta)$ follows because if the flow increases in the positive direction from the bottom to the surface, then the depth averaged flow will have a smaller magnitude than the surface flow. The converse weighting holds for computing the difference $\overline{\boldsymbol{u}} - \boldsymbol{u}(\eta_b)$.

The identities (44.91) hold for arbitrary horizontal velocity fields. Assuming the flow satisfies frictional geostrophy as per equation (44.5a) leads to the frictional thermal wind relation

$$f \, \boldsymbol{u} = \rho_o^{-1} \, \hat{\boldsymbol{z}} \times \nabla p - \hat{\boldsymbol{z}} \times \boldsymbol{F} \Longrightarrow f \, \partial_z \boldsymbol{u} = -(g/\rho_o) \, \hat{\boldsymbol{z}} \times \nabla \rho - \hat{\boldsymbol{z}} \times \partial_z \boldsymbol{F}, \tag{44.92}$$

so that the velocity differences are given by

$$f \, [\overline{\boldsymbol{u}} - \boldsymbol{u}(\eta)] = \int_{\eta_b}^{\eta} [(g/\rho_o) \, \hat{\boldsymbol{z}} \times \nabla \rho - \hat{\boldsymbol{z}} \times \partial_z \boldsymbol{F}] \left[\frac{z - \eta_b}{\eta - \eta_b} \right] dz \tag{44.93a}$$

$$f \, [\overline{\boldsymbol{u}} - \boldsymbol{u}(\eta_b)] = - \int_{\eta_b}^{\eta} [(g/\rho_o) \, \hat{\boldsymbol{z}} \times \nabla \rho - \hat{\boldsymbol{z}} \times \partial_z \boldsymbol{F}] \left[\frac{\eta - z}{\eta - \eta_b} \right] dz. \tag{44.93b}$$

Hence, differences between the depth averaged flow and the boundary flows are determined by weighted integrals of the baroclinicity and vertical friction shears.

44.6.2 Formulation of the vorticity equation

To develop the vorticity equation, we start by deriving the momentum equation for the depth averaged flow. For that purpose, rearrange the depth integrated momentum budget (44.80)

according to

$$\rho_o f \hat{\boldsymbol{z}} \times \boldsymbol{U} = -\eta \nabla_h (p_a - p_b) - D \nabla p_b - \nabla \mathscr{P} + \Delta \boldsymbol{\tau}, \tag{44.94}$$

and then divide by the column thickness, $D = \eta - \eta_b$, to render

$$\rho_o f \hat{\boldsymbol{z}} \times \overline{\boldsymbol{u}} = -(\eta/D) \nabla (p_a - p_b) - \nabla p_b + (1/D)(-\nabla \mathscr{P} + \Delta \boldsymbol{\tau}). \tag{44.95}$$

Taking the curl then leads to

$$\rho_o \nabla \cdot (f \overline{\boldsymbol{u}}) = -\hat{\boldsymbol{z}} \cdot \nabla \times [(\eta/D) \nabla (p_a - p_b)] + D^{-2} \hat{\boldsymbol{z}} \cdot [\nabla \times (D \nabla \mathscr{P})] + \hat{\boldsymbol{z}} \cdot [\nabla \times (D^{-1} \Delta \boldsymbol{\tau})] \tag{44.96a}$$

$$= \hat{\boldsymbol{z}} \cdot \nabla \times [(p_a - p_b) \nabla (\eta/D)] - D^{-2} \hat{\boldsymbol{z}} \cdot [\nabla \times (\mathscr{P} \nabla D)] + \hat{\boldsymbol{z}} \cdot [\nabla \times (D^{-1} \Delta \boldsymbol{\tau})]. \tag{44.96b}$$

The vorticity budget (44.96) is a bit less tidy than that for the depth integrated budget (44.83). Nonetheless, it offers some novel insights concerning the flow, which can be seen by writing the left hand side in the form

$$\nabla \cdot (f \overline{\boldsymbol{u}}) = \nabla \cdot [(f/D) \boldsymbol{U}], \tag{44.97}$$

with f/D reminiscient of the shallow water potential vorticity for the planetary geostrophic flow (Section 43.4). Motivated by this analog, we write the vorticity equation (44.96) in the form

$$\rho_o \boldsymbol{U} \cdot \nabla (f/D) = -\rho_o (f/D) \nabla \cdot \boldsymbol{U} + \hat{\boldsymbol{z}} \cdot \nabla \times [(p_a - p_b) \nabla (\eta/D)] \\ - D^{-2} \hat{\boldsymbol{z}} \cdot [\nabla \times (\mathscr{P} \nabla D)] + \hat{\boldsymbol{z}} \cdot [\nabla \times (D^{-1} \Delta \boldsymbol{\tau})]. \tag{44.98}$$

Contrary to the shallow water case, we here see that even for a perfect planetary geostrophic fluid, the depth-integrated flow does not generally follow contours of constant f/D. Even so, it is of interest to examine how the processes on the right hand side contribute to flow deviations from f/D contours. For that purpose we simplify the flow even more by making the rigid lid approximation.

44.6.3 Rigid lid approximation and the role of JEBAR

The rigid lid approximation is commonly made for studies of large-scale circulation. Indeed, it was the basis for many ocean general circulation models following the work of *Bryan* (1969). A fluid satisfying the rigid lid approximation has a vanishing horizontal divergence for the depth integrated flow

$$\text{rigid lid approximation} \implies \nabla \cdot \boldsymbol{U} = 0. \tag{44.99}$$

Furthermore, as part of the rigid lid approximation we assume the free surface undulations are much smaller than the resting ocean depth so that

$$|\eta| \ll |\eta_b| \implies \eta/D \approx 0 \tag{44.100a}$$

$$1/(\eta - \eta_b) \approx 1/(-\eta_b) = 1/\mathtt{H}. \tag{44.100b}$$

We introduced

$$\mathtt{H} = -\eta_b \tag{44.101}$$

to correspond to the literature for rigid lid models and the JEBAR term.[7] Hence, with the rigid lid approximation the vorticity equation (44.98) takes the simplified form

$$\boldsymbol{U} \cdot \nabla(f/\mathtt{H}) = \rho_o^{-1}\, \hat{\boldsymbol{z}} \cdot [\nabla \times (\mathscr{P}\, \nabla \mathtt{H}^{-1}) + \nabla \times (\mathtt{H}^{-1}\, \Delta \boldsymbol{\tau})]. \tag{44.102}$$

Each term in this equation has dimensions of inverse squared time, T^{-2}.

JEBAR drives deviations from $f/\mathtt{H}$ aligned flow

The first term on the right hand side of the vorticity equation (44.102) is referred to as the Joint Effect of Baroclinicity and Relief (JEBAR)

$$\text{JEBAR} \equiv \rho_o^{-1}\, \hat{\boldsymbol{z}} \cdot [\nabla \times (\mathscr{P}\, \nabla \mathtt{H}^{-1})] = \rho_o^{-1}\, \hat{\boldsymbol{z}} \cdot [\nabla \mathscr{P} \times \nabla \mathtt{H}^{-1}]. \tag{44.103}$$

This name arises since JEBAR is nonzero only in the presence of non-flat topography ("relief") and (as shown below) when density is not a constant (i.e., for baroclinic flow). In addition to contributions from boundary stresses, equation (44.102) says that misalignment of $f/\mathtt{H}$ contours with the depth-integrated steady rigid lid flow is driven by misalignments of isobaths and isolines of the depth integrated potential energy.

Contributions to JEBAR arise only from the component of the potential energy that deviates from a constant density reference state. To show that property, note that in the rigid lid approximation, the potential energy in a column, as given by equation (44.77), takes the form

$$\mathscr{P} = (1/2)\, g\, \rho_o\, \mathtt{H}^2 + g \int_{-\mathtt{H}}^{0} \rho'\, z\, \mathrm{d}z, \tag{44.104}$$

where $\rho' = \rho - \rho_o$. With $\nabla \mathtt{H}^2 \times \nabla(1/\mathtt{H}) = 0$, we are left with just the contribution from ρ'

$$\text{JEBAR} = \rho_o^{-1}\, \hat{\boldsymbol{z}} \cdot \left[\nabla \left(g \int_{-\mathtt{H}}^{0} \rho'\, z\, \mathrm{d}z \right) \times \nabla \mathtt{H}^{-1} \right]. \tag{44.105}$$

JEBAR vanishes for a homogeneous density field, where ρ' is a constant, but is nonzero with a nonzero ρ'. In a Boussinesq ocean, a nonzero ρ' is associated with baroclinicity (Figure 40.10).

Relating JEBAR to pressure

JEBAR as given by equation (44.103) has the appearance of the curl of a form stress, and yet it is not. The reason is that $\mathscr{P}$ is the potential energy of the fluid column rather than bottom pressure. We make this point explicit by recalling the decomposition (44.76), here specialized to the rigid lid in which

$$\mathscr{P} = \mathtt{H}\, (\overline{p} - p_b) \qquad \text{with} \qquad \overline{p} = \mathtt{H}^{-1} \int_{-\mathtt{H}}^{0} p\, \mathrm{d}z = (-\eta_b)^{-1} \int_{\eta_b}^{0} p\, \mathrm{d}z. \tag{44.106}$$

Plugging into the vorticity equation (44.102) leads to

$$\rho_o\, \boldsymbol{U} \cdot \nabla(f/\mathtt{H}) = \mathtt{H}^{-1}\, \hat{\boldsymbol{z}} \cdot [\nabla \mathtt{H} \times \nabla(\overline{p} - p_b)] + \hat{\boldsymbol{z}} \cdot \nabla \times (\mathtt{H}^{-1}\, \Delta \boldsymbol{\tau})]. \tag{44.107}$$

Evidently, JEBAR is nonzero where the depth averaged pressure deviates from the bottom pressure

$$\text{JEBAR} = \rho_o^{-1}\, \hat{\boldsymbol{z}} \cdot [\nabla \mathscr{P} \times \nabla \mathtt{H}^{-1})] = (\rho_o\, \mathtt{H})^{-1}\, \hat{\boldsymbol{z}} \cdot [\nabla \mathtt{H} \times \nabla(\overline{p} - p_b)]. \tag{44.108}$$

[7] Note that H is the vertical depth scale, which is a constant, and it is distinct from $\mathtt{H}(x,y) = -\eta_b(x,y)$, which is a function of horizontal position.

We can go one more step in exposing the pressure difference through use of equation (44.91), here applied to hydrostatic pressure, in which case (remember that $\mathtt{H} = -\eta_b$)

$$\overline{p} - p_b = \int_{\eta_b}^{0} \frac{\partial p}{\partial z} \frac{z}{\eta_b} \, dz = (g/\mathtt{H}) \int_{-\mathtt{H}}^{0} z \, \rho \, dz = \mathtt{H}^{-1} \, \mathscr{P}, \tag{44.109}$$

so that[8]

$$\nabla_h(\overline{p} - p_b) = -g \, \rho(z = -\mathtt{H}) \, \nabla_h \mathtt{H} + g \int_{-\mathtt{H}}^{0} \nabla_h(\rho \, z/\mathtt{H}) \, dz. \tag{44.110}$$

The first term arises from slopes in the bottom topography as weighted by the bottom density, whereas the second term arises from the integral of horizontal gradients in the $z/\mathtt{H}$ weighted density.

Alternatively, we can introduce a geostrophic velocity associated with the gradient of the bottom pressure as well as the vertically averaged pressure

$$\rho_o \, f \, \hat{\boldsymbol{z}} \times \boldsymbol{u}_{gb} = -\nabla p_b \quad \text{and} \quad \rho_o \, f \, \hat{\boldsymbol{z}} \times \overline{\boldsymbol{u}}_g = -\nabla \overline{p} \Longrightarrow \nabla(\overline{p} - p_b) = \rho_o \, f \, \hat{\boldsymbol{z}} \times (\boldsymbol{u}_{gb} - \overline{\boldsymbol{u}}_g). \tag{44.111}$$

Doing so brings JEBAR from equation (44.108) into the form

$$\text{JEBAR} = (\rho_o \, \mathtt{H})^{-1} \, \hat{\boldsymbol{z}} \cdot [\nabla \mathtt{H} \times \nabla(\overline{p} - p_b)] = -f \, \mathtt{H}^{-1} \, \nabla \mathtt{H} \cdot (\overline{\boldsymbol{u}}_g - \boldsymbol{u}_{gb}). \tag{44.112}$$

JEBAR thus arises from a nonzero projection onto the bottom slope of the difference between the geostrophic velocity arising from the bottom pressure and the geostrophic velocity arising from the depth averaged pressure.

Equation (44.83) provides the budget for vorticity of the depth integrated flow, in which we find the curl of the topographic form stress leads to vortex stretching. For the vorticity of the depth averaged flow, we instead encounter the JEBAR term in equation (44.107), which is not a pure vortex stretching term. Instead, it accounts for the fact that it is the horizontal velocity flowing across isobaths, $\boldsymbol{u}(z = \eta_b)$, rather than depth averaged horizontal velocity, $\overline{\boldsymbol{u}}$, that leads to vortex stretching. Hence, when studying vorticity of the depth averaged velocity, $\overline{\boldsymbol{u}}$, accounting for the role of vortex stretching requires us to include JEBAR.

Integral balances

Since the depth integrated flow is assumed to be non-divergent in the rigid lid approximation, $\nabla \cdot \boldsymbol{U} = 0$, we know there exists a streamfunction for this flow. Consider a region where there are closed streamlines. Following the steps in Section (44.5.3), we integrate the steady vorticity equation (44.102) around the streamline. Noting that $\boldsymbol{U} \cdot \hat{\boldsymbol{n}} = 0$ along the streamline, where $\hat{\boldsymbol{n}}$ is the horizontal unit normal to the streamline, thus renders the steady balance

$$\oint_{\partial \mathcal{S}_{\text{streamline}}} (\mathscr{P} \, \nabla \mathtt{H}^{-1} + \mathtt{H}^{-1} \, \Delta \boldsymbol{\tau}) \cdot \hat{\boldsymbol{t}} \, ds = 0. \tag{44.113}$$

44.6.4 Further study

Mertz and Wright (1992) discuss the physics of how JEBAR relates to the curl of the topographic form stress as well as other mathematically equivalent forms. *Cane et al.* (1998) as well as Section 2.5 of *Drijfhout et al.* (2013) discusses how JEBAR can be physically misleading. For this reason, recent studies of vorticity budgets in ocean models generally eschew JEBAR, instead favoring an analysis of vorticity of the depth integrated flow as in Section 44.5 or the depth integrated

[8] We reintroduced the notation, ∇_h, given the presence of z and $\rho(z)$ in the integral in equation (44.110).

vorticity from Section 44.3. *Waldman and Giordani* (2023) provide a review of vorticity analysis for the ocean.

Chapter 45

FOUNDATIONS OF QUASI-GEOSTROPHY

Quasi-geostrophy (QG) is the canonical *balanced model* in geophysical fluid mechanics whereby the quasi-geostrophic potential vorticity is the sole prognostic field. All other fields, such as the velocity and buoyancy, are diagnosed from potential vorticity. The process of diagnosing the allied fields requires solving an elliptic boundary value problem to compute the geostrophic streamfunction with potential vorticity acting as the source. This connection between potential vorticity and streamfunction represents an *invertibility* principle, with the mathematical technology required for inversion shared with many other elliptic problems in mathematical physics.[1]

Quasi-geostrophy is an elegant theory of mathematical physics that offers physical and mathematical insights into the workings of geophysical fluid motions where rotation and stratification play leading roles. Our goal in this chapter is to provide a taste of its continuously stratified realization, offering a detailed derivation that builds from Chapters 43 and 44. We also sample some of its physical and mathematical content.

CHAPTER GUIDE

In this chapter we extend to continuously stratified fluids the shallow water discussion of quasi-geostrophy in Chapter 43. Continuously stratified quasi-geostrophy is not concerned with the processes that affect stratification, but instead with the processes that slightly perturb that stratification. We make use of stratified geophysical fluid dynamics from Chapters 24 and 31, as well as potential vorticity from Chapter 41. This chapter is essential for the study of Rossby waves and baroclinic instability in Chapter 62.

[1] See Section 6.5 for a summary of elliptic partial differential equations, and Chapter 9 for solution methods based on Green's functions.

45.1 Loose threads

- Solution needed for Exercise 45.4.

45.2 Non-dimensional equations of quasi-geostrophy

In deriving the quasi-geostrophic potential vorticity equation, we proceed much like for the single layer of shallow water fluid in Section 43.5. In particular, quasi-geostrophic scaling from Section 43.5.1 is relevant for both the shallow water and for the continuously stratified fluid. We employ an asymptotic expansion in the Rossby number and stop at the first nontrivial order, which (as for the shallow water) is Ro^1. For this purpose, recall the non-dimensional momentum and continuity equations from Section 43.7.8

$$\mathrm{Ro}\left[\frac{\partial \widehat{\boldsymbol{u}}}{\partial \widehat{t}} + (\widehat{\boldsymbol{u}}\cdot\widehat{\nabla}_{\widehat{z}})\,\widehat{\boldsymbol{u}} + \widehat{w}\frac{\partial \widehat{\boldsymbol{u}}}{\partial \widehat{z}}\right] + \widehat{\boldsymbol{f}}\times\widehat{\boldsymbol{u}} = -\widehat{\nabla}_z\,\widehat{\varphi} \tag{45.1a}$$

$$\frac{\partial \widehat{\varphi}}{\partial \widehat{z}} = \widehat{b} \tag{45.1b}$$

$$\widehat{\nabla}\cdot\widehat{\boldsymbol{v}} = 0 \tag{45.1c}$$

$$\frac{\mathrm{Ro}}{\mathrm{Bu}}\frac{\mathrm{D}\widehat{b}}{\mathrm{D}\widehat{t}} + \widehat{w} = 0. \tag{45.1d}$$

We expand all fields in an asymptotic series in Rossby number

$$\widehat{u} = \widehat{u}_0 + \mathrm{Ro}\,\widehat{u}_1 + \mathrm{Ro}^2\,\widehat{u}_2 + \ldots \tag{45.2a}$$

$$\widehat{v} = \widehat{v}_0 + \mathrm{Ro}\,\widehat{v}_1 + \mathrm{Ro}^2\,\widehat{v}_2 + \ldots \tag{45.2b}$$

$$\widehat{w} = \widehat{w}_0 + \mathrm{Ro}\,\widehat{w}_1 + \mathrm{Ro}^2\,\widehat{w}_2 + \ldots \tag{45.2c}$$
$$\widehat{b} = \widehat{b}_0 + \mathrm{Ro}\,\widehat{b}_1 + \mathrm{Ro}^2\,\widehat{b}_2 + \ldots \tag{45.2d}$$
$$\widehat{\varphi} = \widehat{\varphi}_0 + \mathrm{Ro}\,\widehat{\varphi}_1 + \mathrm{Ro}^2\,\widehat{\varphi}_2 + \ldots \tag{45.2e}$$

along with the expansion (43.55) for the Coriolis parameter

$$\widehat{f} = \widehat{f}_0 + \mathrm{Ro}\,\widehat{\beta}\,\widehat{y}, \tag{45.3}$$

and where (equation (43.56))

$$\widehat{\beta}\,\widehat{y} = \frac{\beta\, y}{\mathrm{Ro}\, f_\circ} = T\,\beta\, y. \tag{45.4}$$

As noted in Section 43.5.2, the velocity field is non-divergent at each order of Rossby number, so that

$$\nabla \cdot \widehat{\boldsymbol{v}}_n = 0 \quad \forall\, n. \tag{45.5}$$

The Burger number is order unity since the horizontal length scales of the flow considered here are on the order of the deformation radius

$$\mathrm{Bu} \sim 1 \Longrightarrow L \sim L_\mathrm{d}, \tag{45.6}$$

where we introduced the *internal deformation radius* from Section 43.7.6

$$L_\mathrm{d}(z) = H\,[N(z)/f_\circ]. \tag{45.7}$$

It is important to retain the depth dependence of the Burger number through its dependence on the background stratification $N^2(z)$

$$\mathrm{Bu}(z) = \left[\frac{L_\mathrm{d}}{L}\right]^2 = N^2(z)\left[\frac{H}{L\, f_\circ}\right]^2, \tag{45.8}$$

which motivates the name *Burger function* for continuously stratified quasi-geostrophy. Importantly, the Burger function does not commute with the vertical derivative operator.

45.2.1 Zeroth order asymptotic equations

The zeroth order asymptotic equations are

$$\widehat{\boldsymbol{f}}_0 \times \widehat{\boldsymbol{u}}_0 = -\widehat{\nabla}_z\, \widehat{\varphi}_0 \tag{45.9a}$$
$$\partial_{\widehat{z}} \widehat{\varphi}_0 = \widehat{b}_0 \tag{45.9b}$$
$$\widehat{\nabla}_z \cdot \widehat{\boldsymbol{u}}_0 + \partial_{\widehat{z}} \widehat{w}_0 = 0 \tag{45.9c}$$
$$\widehat{w}_0 = 0. \tag{45.9d}$$

The first equation represents f-plane geostrophy, which means that the horizontal velocity has zero divergence

$$\widehat{\nabla}_z \cdot \widehat{\boldsymbol{u}}_0 = 0. \tag{45.10}$$

Equation (45.9b) means the zeroth order buoyancy determines the zeroth order hydrostatic pressure. Since the horizontal velocity has zero divergence, the continuity equation (45.9c) means that the vertical velocity is depth independent

$$\partial_{\widehat{z}} \widehat{w}_0 = 0. \tag{45.11}$$

If it vanishes somewhere, such as a solid horizontal bottom boundary, then it vanishes everywhere. This is a manifestation of the Taylor-Proudman theorem (see Section 31.5.3). Indeed, a vanishing $\widehat{w}_0$ is required by the zeroth-order buoyancy equation (45.9d) even if the bottom is not flat. Hence, the non-dimensional velocity has a nonzero contribution only at order Ro^1

$$\widehat{w} = \mathrm{Ro}\,\widehat{w}_1 + \mathrm{Ro}^2\,\widehat{w}_2 + \ldots, \tag{45.12}$$

thus manifesting the vertical stiffening of fluid columns found in rotating fluids. Correspondingly, the dimensionful vertical velocity has the asymptotic expansion

$$w = W\widehat{w} = W\,\mathrm{Ro}\,(\widehat{w}_1 + \mathrm{Ro}\,\widehat{w}_2 + \ldots), \tag{45.13}$$

so that to leading to order Ro^1

$$\widehat{w}_1 = \frac{w}{W\,\mathrm{Ro}}. \tag{45.14}$$

Since the zeroth-order horizontal velocity is non-divergent, we can introduce a geostrophic streamfunction

$$\widehat{u}_0 = -\partial_{\widehat{y}}\widehat{\psi}_0 \qquad \text{and} \qquad \widehat{v}_0 = \partial_{\widehat{x}}\widehat{\psi}_0 \qquad \text{and} \qquad \widehat{\zeta}_0 = \widehat{\nabla}^2\widehat{\psi}_0, \tag{45.15}$$

where the zeroth-order streamfunction is the ratio of the zeroth order pressure to zeroth order Coriolis parameter

$$\widehat{\psi}_0 = \widehat{\varphi}_0/\widehat{f}_0. \tag{45.16}$$

Note also that the zeroth-order system satisfies the thermal wind balance

$$\widehat{\boldsymbol{f}}_0 \times \partial_{\widehat{z}}\widehat{\boldsymbol{u}}_0 = -\widehat{\nabla}_z\,\widehat{b}_0. \tag{45.17}$$

Finally, note that the zeroth order buoyancy is determined by the streamfunction through the hydrostatic balance

$$\widehat{b}_0 = \partial_{\widehat{z}}\widehat{\varphi}_0 = \widehat{f}_0\,\partial_{\widehat{z}}\widehat{\psi}_0. \tag{45.18}$$

45.2.2 First order asymptotic equations

For a prognostic equation we must consider equations at order Ro^1

$$\frac{\mathrm{D}_0\widehat{\boldsymbol{u}}_0}{\mathrm{D}\widehat{t}} + \widehat{\boldsymbol{f}}_0 \times \widehat{\boldsymbol{u}}_1 + \widehat{\beta}\,\widehat{y}\,\hat{\boldsymbol{z}} \times \widehat{\boldsymbol{u}}_0 = -\widehat{\nabla}_z\widehat{\varphi}_1 \tag{45.19a}$$

$$\partial_{\widehat{z}}\widehat{\varphi}_1 = \widehat{b}_1 \tag{45.19b}$$

$$\widehat{\nabla}_z \cdot \widehat{\boldsymbol{u}}_1 + \partial_{\widehat{z}}\widehat{w}_1 = 0 \tag{45.19c}$$

$$\frac{1}{\mathrm{Bu}}\frac{\mathrm{D}_0\widehat{b}_0}{\mathrm{D}\widehat{t}} + \widehat{w}_1 = 0. \tag{45.19d}$$

The first order terms are often referred to as the *ageostrophic* components, though note that all contributions higher than zeroth order constitute ageostrophic contributions.

At order Ro^1, the material time derivative makes use *only* of the zeroth order horizontal geostrophic velocity

$$\frac{\mathrm{D}_0}{\mathrm{D}\widehat{t}} = \frac{\partial}{\partial\widehat{t}} + \widehat{\boldsymbol{u}}_0 \cdot \widehat{\nabla}. \tag{45.20}$$

To close this set of equations, we produce the vorticity equation from the momentum equation, and then combine the vorticity equation and buoyancy equation to produce the quasi-geostrophic potential vorticity equation. In Section 43.5, we performed the same procedure for deriving the shallow water quasi-geostrophic equations.

Taking the curl of the momentum equation (45.19a) eliminates the pressure gradient, $\widehat{\nabla}\widehat{\varphi}_1$, thus producing the vorticity equation

$$\partial_{\widehat{t}}\widehat{\zeta}_0 + (\widehat{\boldsymbol{u}}_0 \cdot \widehat{\nabla})\,(\widehat{\zeta}_0 + \widehat{\beta}\,\widehat{y}) = -\widehat{f}_0\,\widehat{\nabla}_z \cdot \widehat{\boldsymbol{u}}_1. \tag{45.21}$$

We make use of the continuity equation (45.19c) to eliminate the horizontal convergence

$$\partial_{\widehat{t}}\widehat{\zeta}_0 + (\widehat{\boldsymbol{u}}_0 \cdot \widehat{\nabla})\,(\widehat{\zeta}_0 + \widehat{\beta}\,\widehat{y}) = \widehat{f}_0\,\partial_{\widehat{z}}\widehat{w}_1. \tag{45.22}$$

The right hand side represents the contribution to vorticity evolution from stretching by the ageostrophic vertical velocity acting in a rotating reference frame. We can eliminate the ageostrophic vertical velocity through use of the buoyancy equation (45.19d). When doing so, it is important to keep the depth dependence of the Burger function, $\mathrm{Bu}(z)$, according to equation (45.8), with this depth dependence arising from the prescribed background stratification, $N^2(z)$. The resulting vorticity equation is

$$\partial_{\widehat{t}}\widehat{\zeta}_0 + (\widehat{\boldsymbol{u}}_0 \cdot \widehat{\nabla})\,(\widehat{\zeta}_0 + \widehat{\beta}\,\widehat{y}) = -\widehat{f}_0\,\frac{\partial}{\partial \widehat{z}}\left[\frac{1}{\mathrm{Bu}}\,\frac{\mathrm{D}_0\widehat{b}_0}{\mathrm{D}\widehat{t}}\right]. \tag{45.23}$$

We now use the identity

$$\frac{\partial}{\partial \widehat{z}}\left[\frac{1}{\mathrm{Bu}}\,\frac{\mathrm{D}_0\widehat{b}_0}{\mathrm{D}\widehat{t}}\right] = \frac{\partial}{\partial \widehat{z}}\left[\frac{1}{\mathrm{Bu}}\left(\frac{\partial}{\partial \widehat{t}} + \widehat{\boldsymbol{u}}_0 \cdot \widehat{\nabla}\right)\widehat{b}_0\right] \tag{45.24a}$$

$$= \frac{\mathrm{D}_0}{\mathrm{D}\widehat{t}}\left[\frac{\partial}{\partial \widehat{z}}\left(\frac{\widehat{b}_0}{\mathrm{Bu}}\right)\right] + \frac{1}{\mathrm{Bu}}\,\frac{\partial \widehat{\boldsymbol{u}}_0}{\partial \widehat{z}} \cdot \widehat{\nabla}_z\widehat{b}_0 \tag{45.24b}$$

$$= \frac{\mathrm{D}_0}{\mathrm{D}\widehat{t}}\left[\frac{\partial}{\partial \widehat{z}}\left(\frac{\widehat{b}_0}{\mathrm{Bu}}\right)\right], \tag{45.24c}$$

where we set

$$\partial_{\widehat{z}}\widehat{\boldsymbol{u}}_0 \cdot \widehat{\nabla}_z\widehat{b}_0 = 0 \tag{45.25}$$

since the zeroth-order velocity maintains thermal wind balance (45.17). Bringing terms together then leads to the material conservation equation for quasi-geostrophic potential vorticity

$$\frac{\mathrm{D}_0}{\mathrm{D}\widehat{t}}\left[\widehat{\zeta}_0 + \widehat{\beta}\,\widehat{y} + \widehat{f}_0\,\frac{\partial}{\partial \widehat{z}}\left(\frac{\widehat{b}_0}{\mathrm{Bu}}\right)\right] = 0. \tag{45.26}$$

45.3 Dimensionful equations of quasi-geostrophy

To expose physical elements to the continusously stratified quasi-geostrophic theory, we reintroduce physical dimensions as done for shallow water quasi-geostrophy in Section 43.6. For that purpose, we write

$$\boldsymbol{u} \equiv \boldsymbol{u}_{\mathrm{g}} + \boldsymbol{u}_{\mathrm{ag}} = U\,(\widehat{\boldsymbol{u}}_0 + \mathrm{Ro}\,\widehat{\boldsymbol{u}}_1) \tag{45.27a}$$

$$w \equiv w_{\mathrm{ag}} = \mathrm{Ro}\,W\,\widehat{w}_1 \tag{45.27b}$$

$$b \equiv b_{\mathrm{g}} + B_{\mathrm{ag}} = B\,(\widehat{b}_0 + \mathrm{Ro}\,\widehat{b}_1) \tag{45.27c}$$

$$\varphi \equiv \varphi_{\mathrm{g}} + \varphi_{\mathrm{ag}} = f_\circ\,U\,L\,(\widehat{\varphi}_0 + \mathrm{Ro}\,\widehat{\varphi}_1). \tag{45.27d}$$

Reintroducing dimensions is straightforward but a bit tedious.

45.3.1 Hydrostatic balance

Hydrostatic balance is maintained for terms at each Rossby number order, so that we have the dimensional equations

$$\partial_z \varphi_{\mathrm{g}} = b_{\mathrm{g}} \quad \text{and} \quad \partial_z \varphi_{\mathrm{ag}} = B_{\mathrm{ag}}. \tag{45.28}$$

45.3.2 Continuity equation

The three dimensional velocity is non-divergent at each order in Rossby number. The zeroth order (geostrophic) flow is horizontally non-divergent so that

$$\nabla \cdot \boldsymbol{u}_{\mathrm{g}} = 0, \tag{45.29}$$

whereas the next order (ageostrophic) flow satisfies

$$\nabla \cdot \boldsymbol{v}_{\mathrm{ag}} = \nabla \cdot \boldsymbol{u}_{\mathrm{ag}} + \partial_z w_{\mathrm{ag}} = 0. \tag{45.30}$$

45.3.3 Geostrophic balance

The non-dimensional geostrophic balance for the zeroth order fields

$$\widehat{\boldsymbol{f}}_0 \times \widehat{\boldsymbol{u}}_0 = -\widehat{\nabla}_z \, \widehat{\varphi}_0 \tag{45.31}$$

takes on the dimensional form

$$\hat{\boldsymbol{z}} \times \boldsymbol{u}_{\mathrm{g}}/U = -L \, \nabla_{\mathrm{h}} \varphi_{\mathrm{g}}/(f_{\mathrm{o}} \, U \, L). \tag{45.32}$$

Canceling factors leads to the expected form of f-plane geostrophy

$$f_{\mathrm{o}} \, \hat{\boldsymbol{z}} \times \boldsymbol{u}_{\mathrm{g}} = -\nabla_{\mathrm{h}} \varphi_{\mathrm{g}}. \tag{45.33}$$

45.3.4 Material time derivative

For the material time derivative operator we write

$$\begin{aligned}
\mathrm{D}/\mathrm{D}t &= \partial_t + \boldsymbol{u} \cdot \nabla + w \, \partial_z && \text{(45.34a)} \\
&= (1/T) \, \partial_{\widehat{t}} + (U/L) \, \widehat{\boldsymbol{u}} \cdot \widehat{\nabla} + (W/H) \, \widehat{w} \, \partial_{\widehat{z}} && \text{(45.34b)} \\
&= (1/T) \, (\partial_{\widehat{t}} + \widehat{\boldsymbol{u}} \cdot \widehat{\nabla} + \widehat{w} \, \partial_{\widehat{z}}) && \text{(45.34c)} \\
&= (1/T) \, (\partial_{\widehat{t}} + \widehat{\boldsymbol{u}}_0 \cdot \widehat{\nabla}_z) + (\mathrm{Ro}/T) \, (\widehat{\boldsymbol{u}}_0 \cdot \widehat{\nabla}_z + \widehat{w}_1 \, \partial_{\widehat{z}}) && \text{(45.34d)} \\
&= \partial_t + \boldsymbol{u}_{\mathrm{g}} \cdot \nabla_{\mathrm{h}} + \boldsymbol{u}_{\mathrm{ag}} \cdot \nabla_{\mathrm{h}} + w_{\mathrm{ag}} \, \partial_z && \text{(45.34e)} \\
&\equiv \mathrm{D}_{\mathrm{g}}/\mathrm{D}t + \boldsymbol{u}_{\mathrm{ag}} \cdot \nabla_{\mathrm{h}} + w_{\mathrm{ag}} \partial_z, && \text{(45.34f)}
\end{aligned}$$

where time scales according to advection, $T = L/U$, vertical velocity scales according to continuity, $W = H \, U/L$, and we introduced the geostrophic material time derivative operator

$$\mathrm{D}_{\mathrm{g}}/\mathrm{D}t \equiv \partial_t + \boldsymbol{u}_{\mathrm{g}} \cdot \nabla_{\mathrm{h}}. \tag{45.35}$$

45.3.5 Buoyancy equation

The buoyancy equation requires a bit more work. For that purpose, split buoyancy into a depth dependent static background and a deviation from the background

$$b = \tilde{b}(z) + b'(x, y, z, t), \tag{45.36}$$

with its vertical derivative

$$\partial_z b = \mathrm{d}\tilde{b}/\mathrm{d}z + \partial_z b' = N^2 + \partial_z b', \tag{45.37}$$

where $N^2(z)$ is the squared buoyancy frequency for the prescribed background buoyancy field. In this manner, the adiabatic buoyancy equation is

$$\frac{\partial b'}{\partial t} + \boldsymbol{u} \cdot \nabla b' + w\,(N^2 + \partial_z b') = 0. \tag{45.38}$$

We non-dimensionalize this equation by making use of the following relations between the scales

$$B = f_\circ\, U\, L/H \qquad W = H\,(U/L) \qquad \mathrm{Ro} = U/(f_\circ\, L) \qquad \mathrm{Bu} = (N\,H)^2/(f_\circ\, L)^2, \tag{45.39}$$

in which case the buoyancy equation takes the form

$$\partial_t b' + \boldsymbol{u} \cdot \nabla b' + w\,(N^2 + \partial_z b') = \frac{B}{T}\frac{\partial \widehat{b}}{\partial \widehat{t}} + \frac{U\,B}{L}\,\widehat{\boldsymbol{u}} \cdot \widehat{\nabla}_z \widehat{b} + W\,\widehat{w}\,N^2 + \frac{W\,B}{H}\,\widehat{w}\,\partial_{\widehat{z}}\widehat{b} = 0. \tag{45.40}$$

We find it useful to divide by $f_\circ\, N^2$, so that

$$\frac{1}{f_\circ\, N^2}\left[\partial_t b' + \boldsymbol{u} \cdot \nabla b' + w\,(N^2 + \partial_z\, b')\right] = \frac{H\,\mathrm{Ro}^2}{\mathrm{Bu}}\left[\partial_{\widehat{t}}\widehat{b} + \widehat{\boldsymbol{u}} \cdot \widehat{\nabla}\widehat{b} + \widehat{w}\,\partial_{\widehat{z}}\widehat{b}\right] + \mathrm{Ro}\,\widehat{w} = 0. \tag{45.41}$$

The vertical velocity component, $\widehat{w}$, is nonzero only at order Ro^1, so the term $\mathrm{Ro}\,\widehat{w}$ is order Ro^2 (recall equation (45.27b)). For the material time derivative term, we drop the vertical velocity term, $\widehat{w}\,\partial_{\widehat{z}}\widehat{b}$, since it is order Ro^1 smaller than the other terms in the material time operator. We thus retain only the zeroth order buoyancy contribution, $\widehat{b}_0$. Reintroducing physical dimensions then leads to the dimensional form of the quasi-geostrophic buoyancy equation

$$(\partial_t + \boldsymbol{u}_\mathrm{g} \cdot \nabla_\mathrm{h})\, b_\mathrm{g} + w_\mathrm{ag}\, N^2 = \frac{\mathrm{D}_\mathrm{g} b_\mathrm{g}}{\mathrm{D}t} + w_\mathrm{ag}\, N^2 = 0. \tag{45.42}$$

This equation means that the geostrophic transport of the geostrophic buoyancy is affected by a source due to the ageostrophic vertical advection of background buoyancy

$$\frac{\mathrm{D}_\mathrm{g} b_\mathrm{g}}{\mathrm{D}t} = -w_\mathrm{ag}\, N^2 \quad \text{with} \quad b_\mathrm{g} = f_\circ\, \partial_z \psi. \tag{45.43}$$

45.3.6 Vorticity equation

Reintroducing dimensions to the vorticity equation (45.22) yields[2]

$$\partial_{\widehat{t}}\widehat{\zeta}_0 + (\widehat{\boldsymbol{u}}_0 \cdot \widehat{\nabla}_\mathrm{h})\,(\widehat{\zeta}_0 + \widehat{\beta}\,\widehat{y}) - \widehat{f}_0\,\partial_{\widehat{z}}\widehat{w}_1 = T^2\,[\partial_t \zeta + \boldsymbol{u}_\mathrm{g} \cdot \nabla_\mathrm{h}(\zeta + \beta\, y)] - \frac{H}{W\,\mathrm{Ro}}\,\partial_z w_\mathrm{ag}. \tag{45.44}$$

The identity $H/(W\,\mathrm{Ro}) = f_\circ\, T^2$ leads to the order Ro^1 vorticity equation

$$\partial_t \zeta_\mathrm{a} + J(\psi, \zeta_\mathrm{a}) = f_\circ\, \partial_z w_\mathrm{ag}, \tag{45.45}$$

with the absolute vorticity given by the sum of the geostrophic relative vorticity plus the planetary beta contribution

$$\zeta_\mathrm{a} = \zeta_\mathrm{g} + \beta\, y. \tag{45.46}$$

Hence, the absolute geostrophic vorticity is advected by the geostrophic flow, and it has a source (right hand side of equation (45.45)) due to vertical stretching by the ageostrophic flow.

[2] Recall from equation (45.27b) that to order Ro^1 we have $W\,\widehat{w} = \mathrm{Ro}\,W\,\widehat{w}_1 = w_\mathrm{ag}$.

Expanding the Jacobian and introducing the geostrophic velocity, $\boldsymbol{u}_{\text{g}} = \hat{\boldsymbol{z}} \times \nabla\psi$, leads to the geostrophic relative vorticity equation

$$(\partial_t + \boldsymbol{u}_{\text{g}} \cdot \nabla_{\text{h}})\, \zeta_{\text{g}} = -\beta\, v_{\text{g}} + f_{\circ}\, \partial_z w_{\text{ag}}. \tag{45.47}$$

We thus see that the beta effect from the geostrophic flow, plus vertical stretching by the ageostrophic flow, provide local sources for geostrophic relative vorticity.

45.3.7 Potential vorticity

From equation (45.26), we identify the non-dimensional quasi-geostrophic potential vorticity

$$\widehat{q} = \widehat{\zeta}_0 + \widehat{\beta}\,\widehat{y} + \widehat{f}_0\, \frac{\partial(\widehat{b}_0/\text{Bu})}{\partial \widehat{z}}. \tag{45.48}$$

Introducing dimensional quantities to the right hand side yields[3]

$$\widehat{q} = \frac{L}{U}\,[\zeta_{\text{g}} + \beta\, y] + \frac{\partial}{\partial z}\left[\frac{H\, b_{\text{g}}}{B\,\text{Bu}}\right] \tag{45.49a}$$

$$= (1/(f_{\circ}\,\text{Ro})\,(\zeta_{\text{g}} + \beta\, y) + \frac{H}{B}\,\frac{\partial}{\partial z}\left[\frac{b_{\text{g}}}{\text{Bu}}\right]. \tag{45.49b}$$

The scale for the fluctuating buoyancy is given by equation (43.160), $B = f_{\circ}\, U\, L/H$, and the inverse Burger function is given by equation (45.8), $\text{Bu}^{-1} = [(L\, f_{\circ})/(H\, N)]^2$, so that

$$\widehat{q} = (1/(f_{\circ}\,\text{Ro})\,(\zeta_{\text{g}} + \beta\, y) + \frac{H^2}{f_{\circ}\, U\, L}\,\frac{L^2\, f_{\circ}^2}{H^2}\,\frac{\partial}{\partial z}\left[\frac{b_{\text{g}}}{N^2}\right] \tag{45.50a}$$

$$= (1/(f_{\circ}\,\text{Ro})\,(\zeta_{\text{g}} + \beta\, y) + \text{Ro}^{-1}\,\partial_z(b_{\text{g}}/N^2). \tag{45.50b}$$

Introducing the geostrophic streamfunction,

$$\boldsymbol{u}_{\text{g}} = \hat{\boldsymbol{z}} \times \nabla_{\text{h}}\psi \quad \text{and} \quad \zeta = \hat{\boldsymbol{z}} \cdot (\nabla \times \boldsymbol{u}_{\text{g}}) = \nabla_{\text{h}}^2\psi \quad \text{and} \quad b_{\text{g}} = f_{\circ}\,\partial_z\psi, \tag{45.51}$$

leads to

$$q \equiv f_{\circ}\,\text{Ro}\,\widehat{q} = \beta\, y + \zeta_{\text{g}} + \frac{\partial}{\partial z}\left[\frac{f_{\circ}^2}{N^2}\,\frac{\partial\psi}{\partial z}\right]. \tag{45.52}$$

Just as for the shallow water case in Section 43.6.1, the potential vorticity (45.52) scales as $f_{\circ}\,\text{Ro}$. The order Ro scaling is expected since it is only at this order that we realize a prognostic set of equations. We sometimes choose to add the constant $f_{\circ}$ to q, which has no effect on the dynamics but reveals the beta plane planetary vorticity

$$q = \underbrace{f_{\circ} + \beta\, y}_{\text{planetary vorticity}} + \underbrace{\nabla_{\text{h}}^2\psi}_{\text{relative vorticity}} + \underbrace{\frac{\partial}{\partial z}\left[\frac{f_{\circ}^2}{N^2}\,\frac{\partial\psi}{\partial z}\right]}_{\text{stretching by } f}. \tag{45.53}$$

Evidently, there are three contributions to the quasi-geostrophic potential vorticity.

- PLANETARY VORTICITY: The planetary vorticity contribution, $f_{\circ} + \beta\, y$, arises from rotation of the reference frame. As noted above, the $\beta\, y$ term is the only dynamically relevant contribution, so that we can equally well drop the $f_{\circ}$ contribution.

[3] Recall $\widehat{f}_0 = 1$ and $\widehat{\beta}\,\widehat{y} = T\,\beta\, y = (L/U)\,\beta\, y$.

- GEOSTROPHIC RELATIVE VORTICITY: The vertical component of the geostrophic relative vorticity, $\zeta = \hat{\boldsymbol{z}} \cdot (\nabla \times \boldsymbol{u}) = \nabla_{\mathrm{h}}^2 \psi$, acts to bring out the smaller scale features in the streamfunction.

- VERTICAL STRETCHING: The final contribution arises from vertical stretching in the presence of a rotating planet. Equation (45.22) helps to remind us why this term arises from vortex stretching.

Material evolution of quasi-geostrophic potential vorticity follows the horizontal geostrophic flow

$$(\partial_t + \boldsymbol{u}_{\mathrm{g}} \cdot \nabla_{\mathrm{h}})\, q = 0. \tag{45.54}$$

Geostrophic material constancy of q represents a balance, following the geostrophic flow, of time changes for the planetary vorticity, relative vorticity, and vertical stretching. This is a remarkable property of quasi-geostrophic flows. It packs in a wealth of physical processes that act to evolve the geostrophic flow while maintaining an exact geostrophic balance at each point in space and time.

45.3.8 Velocity equation

The prognostic velocity equation arises from the first order asymptotic equation (45.19a)

$$\frac{\mathrm{D}_0 \widehat{\boldsymbol{u}}_0}{\mathrm{D}\widehat{t}} + \widehat{\boldsymbol{f}}_0 \times \widehat{\boldsymbol{u}}_1 + \widehat{\beta}\, \widehat{y}\, \hat{\boldsymbol{z}} \times \widehat{\boldsymbol{u}}_0 = -\widehat{\nabla}_z \widehat{\varphi}_1. \tag{45.55}$$

Our skills with reintroducing dimensional quantities should be sufficient to write down the dimensional velocity equation by inspection

$$(\partial_t + \boldsymbol{u}_{\mathrm{g}} \cdot \nabla)\, \boldsymbol{u}_{\mathrm{g}} + \beta\, y\, \hat{\boldsymbol{z}} \times \boldsymbol{u}_{\mathrm{g}} + f_{\mathrm{o}}\, \hat{\boldsymbol{z}} \times \boldsymbol{u}_{\mathrm{ag}} = -\nabla_{\mathrm{h}}\, \varphi_{\mathrm{ag}}. \tag{45.56}$$

We can also choose to add the geostrophic balanced flow that holds at order Ro^0, $f_{\mathrm{o}}\, \hat{\boldsymbol{z}} \times \boldsymbol{u}_{\mathrm{g}} = -\nabla_{\mathrm{h}}\, \varphi_{\mathrm{g}}$, so to have the equivalent equation

$$(\partial_t + \boldsymbol{u}_{\mathrm{g}} \cdot \nabla)\, \boldsymbol{u}_{\mathrm{g}} + \beta\, y\, \hat{\boldsymbol{z}} \times \boldsymbol{u}_{\mathrm{g}} + f_{\mathrm{o}}\, \hat{\boldsymbol{z}} \times (\boldsymbol{u}_{\mathrm{g}} + \boldsymbol{u}_{\mathrm{ag}}) = -\nabla_{\mathrm{h}}\, (\varphi_{\mathrm{g}} + \varphi_{\mathrm{ag}}). \tag{45.57}$$

Observe that from equation (45.27d) that

$$\varphi_{\mathrm{ag}} = f_{\mathrm{o}}\, U\, L\, \mathrm{Ro}\, \widehat{\varphi}_1 = U^2\, \widehat{\varphi}_1, \tag{45.58}$$

so that the ageostrophic portion of the pressure scales according to pressure in a non-rotating fluid as discussed in Section 29.2.3.

45.3.9 Concerning the ageostrophic state in quasi-geostrophy

Following the shallow water discussion in Section 43.6.6, we here expose an ambiguity (i.e., *gauge freedom*) associated with the ageostrophic pressure, buoyancy, and velocity within quasi-geostrophy. This gauge freedom arises since the quasi-geostrophic potential vorticity equation remains unchanged upon adding an arbitrary horizontally non-divergent velocity to $\boldsymbol{u}_{\mathrm{ag}}$, along with an arbitrary gradient of a scalar to φ_{ag}. The freedom to modify these ageostrophic fields is constrained by taking the divergence of the velocity equation (45.56) to find (compare to equation (43.108) for shallow water quasi-geostrophy)

$$\nabla_{\mathrm{h}}^2 \varphi_{\mathrm{ag}} = 2\, J(u_{\mathrm{g}}, v_{\mathrm{g}}) + \beta\, (y\, \zeta_{\mathrm{g}} - u_{\mathrm{g}}) + f_{\mathrm{o}}\, \zeta_{\mathrm{ag}}, \tag{45.59}$$

where

$$\zeta_{\text{ag}} = \partial_x v_{\text{ag}} - \partial_y u_{\text{ag}} \tag{45.60}$$

is the relative vorticity contained in the horizontal ageostrophic flow. The constraint (45.59) means that adding a horizontally non-divergent velocity, $\widetilde{\boldsymbol{u}}$, to the ageostrophic velocity, $\boldsymbol{u}_{\text{ag}}$, requires a corresponding modification to the pressure via $\widetilde{\varphi}$ added to φ_{ag}, in which $\widetilde{\varphi}$ satisfies the Poisson equation

$$\nabla_{\text{h}}^2 \widetilde{\varphi} = f_{\text{o}}\, \hat{\boldsymbol{z}} \cdot (\nabla \times \widetilde{\boldsymbol{u}}). \tag{45.61}$$

Given the gauge freedom, we follow Section 6.3 of *Holton and Hakim* (2013) by choosing $\varphi_{\text{ag}} = 0$ (and thus $b_{\text{ag}} = 0$) so that all ageostrophic effects live within the velocity, $\boldsymbol{u}_{\text{ag}} + \hat{\boldsymbol{z}} w_{\text{ag}}$. In this case, the quasi-geostrophic velocity equation (45.56) simplifies to

$$(\partial_t + \boldsymbol{u}_{\text{g}} \cdot \nabla)\, \boldsymbol{u}_{\text{g}} + \beta\, y\, \hat{\boldsymbol{z}} \times \boldsymbol{u}_{\text{g}} + f_{\text{o}}\, \hat{\boldsymbol{z}} \times \boldsymbol{u}_{\text{ag}} = 0. \tag{45.62}$$

Evidently, the Coriolis acceleration, $f_{\text{o}}\, \hat{\boldsymbol{z}} \times \boldsymbol{u}_{\text{ag}}$, provides the only place that ageostrophic effects couple to the geostrophic velocity equation.

45.4 Constraints on quasi-geostrophic evolution

How is it that quasi-geostrophic flow retains a geostrophically balanced state, $f_{\text{o}}\, \hat{\boldsymbol{z}} \times \boldsymbol{u}_{\text{g}} = -\nabla_{\text{h}} \varphi_{\text{g}}$, while allowing that state to evolve? The discussion thus far provides an operational means to answer that question via time integration of the quasi-geostrophic potential vorticity equation. Alternatively, let us consider the velocity equation and in so doing to expose a diagnostic balance of geostrophic and ageostrophic flow processes, with this balance ensuring that geostrophy is maintained. We derive this balance closely following that considered for shallow water quasi-geostrophy in Section 43.6.7.[4]

45.4.1 A balance between geostrophic and ageostrophic processes

Geostrophic balance is maintained for an observer following a fluid particle moving with the horizontal geostrophic velocity, so that

$$\frac{\mathrm{D}_{\text{g}}}{\mathrm{D}t}(f_{\text{o}}\, \hat{\boldsymbol{z}} \times \boldsymbol{u}_{\text{g}} + \nabla_{\text{h}} \varphi_{\text{g}}) = 0. \tag{45.63}$$

Performing the material time derivative, and making use of equation (45.62) for the geostrophic velocity and equation (45.43) for buoyancy, here written as

$$\frac{\mathrm{D}_{\text{g}} \boldsymbol{u}_{\text{g}}}{\mathrm{D}t} = -(\beta\, y)\, \hat{\boldsymbol{z}} \times \boldsymbol{u}_{\text{g}} - f_{\text{o}}\, \hat{\boldsymbol{z}} \times \boldsymbol{u}_{\text{ag}} \tag{45.64a}$$

$$\frac{\mathrm{D}_{\text{g}} b_{\text{g}}}{\mathrm{D}t} = -w_{\text{ag}}\, N^2, \tag{45.64b}$$

leads to the balance

$$f_{\text{o}}\, \beta\, y\, \boldsymbol{u}_{\text{g}} + f_{\text{o}}^2\, \boldsymbol{u}_{\text{ag}} + \frac{\mathrm{D}_{\text{g}}(\nabla_{\text{h}} \varphi_{\text{g}})}{\mathrm{D}t} = 0. \tag{45.65}$$

We can derive a diagnostic balance (i.e., an equation without a time derivative) by taking the vertical derivative of equation (45.65) and using the hydrostatic balance and the buoyancy

[4] Enforcing geostrophy even while the flow evolves is analogous to constraints arising from non-divergent flow condition, $\nabla \cdot \boldsymbol{v} = 0$, in an evolving flow. As seen in Section 29.3, pressure in a Boussinesq ocean enforces flow non-divergence at each point in space and time.

equation. For that purpose we need

$$\partial_z[\mathrm{D}_{\mathrm{g}}(\nabla_{\mathrm{h}}\varphi)/\mathrm{D}t] = \mathrm{D}_{\mathrm{g}}(\nabla_{\mathrm{h}}b_{\mathrm{g}})/\mathrm{D}t) + (\partial_z \boldsymbol{u}_{\mathrm{g}} \cdot \nabla_{\mathrm{h}})\nabla_{\mathrm{h}}\varphi_{\mathrm{g}} \tag{45.66a}$$

$$= \nabla_{\mathrm{h}}(\mathrm{D}_{\mathrm{g}}b_{\mathrm{g}}/\mathrm{D}t) + \mathbf{Q} + (\partial_z \boldsymbol{u}_{\mathrm{g}} \cdot \nabla_{\mathrm{h}})\nabla_{\mathrm{h}}\varphi_{\mathrm{g}} \tag{45.66b}$$

$$= -\nabla_{\mathrm{h}}(N^2\, w_{\mathrm{ag}}) + \mathbf{Q} + (\partial_z \boldsymbol{u}_{\mathrm{g}} \cdot \nabla_{\mathrm{h}})\, \nabla_{\mathrm{h}}\varphi_{\mathrm{g}}, \tag{45.66c}$$

where we introduced the vector arising from the coupling of horizontal shears in the geostrophic flow with horizontal gradients in the geostrophic buoyancy

$$\mathbf{Q} = -\hat{\boldsymbol{x}}\, \partial_x \boldsymbol{u}_{\mathrm{g}} \cdot \nabla_{\mathrm{h}} b_{\mathrm{g}} - \hat{\boldsymbol{y}}\, \partial_y \boldsymbol{u}_{\mathrm{g}} \cdot \nabla_{\mathrm{h}} b_{\mathrm{g}}. \tag{45.67}$$

We can further simplify by use of thermal wind to write

$$\mathbf{Q} = -\hat{\boldsymbol{x}}\, \partial_x \boldsymbol{u}_{\mathrm{g}} \cdot (f_{\mathrm{o}}\, \hat{\boldsymbol{z}} \times \partial_z \boldsymbol{u}_{\mathrm{g}}) - \hat{\boldsymbol{y}}\, \partial_y \boldsymbol{u}_{\mathrm{g}} \cdot (f_{\mathrm{o}}\, \hat{\boldsymbol{z}} \times \partial_z \boldsymbol{u}_{\mathrm{g}}) \tag{45.68a}$$

$$= f_{\mathrm{o}}\, \hat{\boldsymbol{x}}\, (-\partial_x u\, \partial_z v + \partial_x v\, \partial_z u) + f_{\mathrm{o}}\, \hat{\boldsymbol{x}}\, (-\partial_y u\, \partial_z v + \partial_y v\, \partial_z u), \tag{45.68b}$$

and geostrophy to write

$$(\partial_z \boldsymbol{u}_{\mathrm{g}} \cdot \nabla_{\mathrm{h}})\, \nabla_{\mathrm{h}}\varphi_{\mathrm{g}} = f_{\mathrm{o}}\, (\partial_z \boldsymbol{u}_{\mathrm{g}} \cdot \nabla_{\mathrm{h}})\, (-v_{\mathrm{g}}\, \hat{\boldsymbol{x}} + u_{\mathrm{g}}\, \hat{\boldsymbol{y}}) \tag{45.69a}$$

$$= f_{\mathrm{o}}\, \hat{\boldsymbol{x}}\, (-\partial_x u\, \partial_z v + \partial_x v\, \partial_z u) + f_{\mathrm{o}}\, \hat{\boldsymbol{x}}\, (-\partial_y u\, \partial_z v + \partial_y v\, \partial_z u) \tag{45.69b}$$

$$= \mathbf{Q}, \tag{45.69c}$$

so that

$$\partial_z[\mathrm{D}_{\mathrm{g}}(\nabla_{\mathrm{h}}\varphi)/\mathrm{D}t] = 2\, \mathbf{Q}. \tag{45.70}$$

Bringing terms together leads to the diagnostic balance

$$\underbrace{f_{\mathrm{o}}\, \beta\, y\, \partial_z \boldsymbol{u}_{\mathrm{g}} + 2\, \mathbf{Q}}_{\text{geostrophic}} + \underbrace{f_{\mathrm{o}}^2\, \partial_z \boldsymbol{u}_{\mathrm{ag}} - N^2\, \nabla_{\mathrm{h}} w_{\mathrm{ag}}}_{\text{ageostrophic}} = 0, \tag{45.71}$$

where we noted that the buoyancy frequency is a function only of the vertical. Equation (45.71) summarizes a wealth of geostrophic and ageostrophic processes that, when taken together, maintain geostrophy and thermal wind for evolving quasi-geostrophic flows. Note that when considered in isolation, each process acts to move the flow away from geostrophic balance (e.g., see *Hoskins* (1975) and Section 6.5 of *Holton and Hakim* (2013), who emphasize the nonlinear geostrophic term, $\mathbf{Q}$). It is only when all terms are considered together that they render an evolving flow respecting geostrophy.

45.4.2 Vertical motion and the ω-equation

As we discovered in this chapter, for quasi-geostrophy the vertical component to the velocity is non-zero only at first order in Rossby number, hence it is part of the ageostrophic flow. In contrast, the zeroth order flow is horizontally non-divergent and geostrophically balanced. To evolve the horizontal geostrophic flow it is not necessary to explicitly compute the ageostrophic vertical velocity. However, there are cases where vertical ageostrophic velocity is of interest. Since the vertical motion is relatively small, it is important to formulate the calculation of this motion in a manner that avoids computing small differences between large numbers. Namely, even if we knew the horizontal ageostrophic flow, vertically integrating the continuity equation, $\partial_z w_{\mathrm{ag}} = -(\partial_x u_{\mathrm{ag}} + \partial_y v_{\mathrm{ag}})$, is prone to errors since the horizontal convergence is typically the small difference of relatively large numbers. We here derive a more suitable means to diagnose w_{ag}, with the diagnostic equation known as the ω-equation. The name for this equation originates from the atmospheric community where ω is the common symbol for mass transport across pressure

surfaces (using pressure vertical coordinates rather than geopotential). Here, we make use of the Boussinesq ocean equations so that the vertical velocity component is across geopoential surfaces.

It turns out that we have done most of the work needed to derive an equation for w_{ag} as part of our derivation of the balance (45.71). Namely, by simply taking horizontal the divergence of (45.71) and noting that $\nabla \cdot \boldsymbol{u}_g = 0$, we have

$$(f_o^2\, \partial_{zz} + N^2\, \nabla_h^2) w_{ag} = (\nabla_h + \hat{\boldsymbol{z}} \partial_z) \cdot (2\, \mathbf{Q} + \hat{\boldsymbol{z}}\, f_o\, \beta\, v_g), \tag{45.72}$$

which corresponds to the second form of the ω-equation first derived by *Hoskins et al.* (1978). We identify the following convenient features of this ω-equation. First, the right hand side is determined solely from knowledge of the geostrophic flow, which contrasts to the approach from continuity. Second, the linear operator acting on w_{ag} is elliptic, so that w_{ag} is a smoothed version of the geostrophic forcing on the right hand side of equation (45.72). Third, maps of the vector field, $\mathbf{Q} + \hat{\boldsymbol{z}}\, f_o\, \beta\, v_g$, provide insights into regions where w_{ag} is prone to have large values. For example, where the divergence on the right hand side is positive, the vertical velocity is negative.[5]

45.4.3 Another derivation of the ω-equation

One commonly finds an alternative derivation in the literature. Here, we write the dimensional buoyancy equation (45.42) and vorticity equation (45.45) in the form

$$f_o\, \partial_{tz} \psi + J(\psi, b_g) + N^2\, w_{ag} = 0 \tag{45.73a}$$

$$\partial_t (\nabla_h^2 \psi) + J(\psi, \nabla_z^2 \psi + \beta\, y) - f_o\, \partial_z w_{ag} = 0. \tag{45.73b}$$

Taking the horizontal Laplacian of equation (45.73a) and subtracting it from f_o times the vertical derivative of equation (45.73b) allows us to cancel the time derivative and thus to render the Boussinesq form of the quasi-geostrophic ω-equation

$$(N^2 \nabla_h^2 + f_o^2\, \partial_{zz})\, w_{ag} = f_o\, \partial_z [J(\psi, \zeta_g + \beta\, y)] - \nabla_h^2 J(\psi, b_g). \tag{45.74}$$

The operator on the left hand side is a generalized Laplacian and all terms on the right hand side are known from the geostrophic streamfunction, including the vorticity, $\zeta_g = \nabla_h^2 \psi$, and buoyancy, $b_g = f_o\, \partial_z \psi$. This equation is thus in the form of a generalized Poisson equation, whose solution renders an expression for the vertical velocity valid to order Ro^1. Note that the right hand side can be written as the convergence of a flux

$$f_o\, \partial_z [J(\psi, \zeta_g + \beta\, y)] - \nabla_h^2 J(\psi, b_g) = -\nabla_h \cdot [\nabla_h\, J(\psi, b_g)] + f_o\, \partial_z [J(\psi, \zeta_g + \beta\, y)] \tag{45.75a}$$

$$= -\nabla \cdot \boldsymbol{G}, \tag{45.75b}$$

where the geostrophic forcing vector is given by

$$\boldsymbol{G} = \nabla_h J(\psi, b_g) - f_o\, \partial_z [J(\psi, \zeta_g + \beta\, y)]\, \hat{\boldsymbol{z}}. \tag{45.76}$$

It is a useful exercise to show that equations (45.74) and (45.72) are identical.

[5] Elliptic operators generally swap signs, which can be readily seen upon assuming a single Fourier mode solution to w_{ag}.

45.5 Connecting to Ertel potential vorticity

Following our treatment for the shallow water system in Section 43.6.4, we here determine how quasi-geostrophic potential vorticity relates to the Ertel potential vorticity from Chapter 41. For this purpose, consider the continuously stratified hydrostatic Boussinesq fluid and make use of the Ertel potential vorticity derived in Exercise 41.1

$$Q = (\boldsymbol{\omega} + \hat{\boldsymbol{z}}\, f) \cdot \nabla b = \frac{\partial u}{\partial z}\frac{\partial b}{\partial y} - \frac{\partial v}{\partial z}\frac{\partial b}{\partial x} + (\zeta + f)\,\frac{\partial b}{\partial z}. \tag{45.77}$$

In a perfect fluid we have the material conservation

$$(\partial_t + \boldsymbol{u} \cdot \nabla_{\!\mathrm{h}} + w\,\partial_z)\, Q = 0. \tag{45.78}$$

Our strategy in this section is to non-dimensionalize both Q and the material time operator, and then to organize terms in equation (45.78) according to the Rossby number. We then show that material conservation of Ertel potential vorticity, when expanded asymptotically to order Ro^1, leads to the geostrophic material conservation of quasi-geostrophic potential vorticity. The continuous stratification makes the derivation more involved than for the shallow water potential vorticity in Section 43.6.4, prompting us to expose the details.

45.5.1 Non-dimensionalizing the Ertel potential vorticity

As above for the buoyancy, we are led to write the Ertel potential vorticity in the form

$$\frac{Q - f_\circ\, N^2}{f_\circ\, N^2} = \frac{1}{f_\circ\, N^2}\left[\frac{\partial u}{\partial z}\frac{\partial b'}{\partial y} - \frac{\partial v}{\partial z}\frac{\partial b'}{\partial x}\right] + \frac{1}{N^2}\,\frac{\partial b'}{\partial z} + \frac{\beta\, y + \zeta}{f_\circ}\left[1 + \frac{1}{N^2}\,\frac{\partial b'}{\partial z}\right]. \tag{45.79}$$

with non-dimensionalization leading to

$$\frac{1}{f_\circ\, N^2}\left[\frac{\partial u}{\partial z}\frac{\partial b'}{\partial y} - \frac{\partial v}{\partial z}\frac{\partial b'}{\partial x}\right] = \frac{B\,U}{f_\circ\, N^2\, H\, L}\left[\frac{\partial \widehat{u}}{\partial \widehat{z}}\frac{\partial \widehat{b}}{\partial \widehat{y}} - \frac{\partial \widehat{v}}{\partial \widehat{z}}\frac{\partial \widehat{b}}{\partial \widehat{x}}\right] = \frac{\mathrm{Ro}^2}{\mathrm{Bu}}\left[\frac{\partial \widehat{u}}{\partial \widehat{z}}\frac{\partial \widehat{b}}{\partial \widehat{y}} - \frac{\partial \widehat{v}}{\partial \widehat{z}}\frac{\partial \widehat{b}}{\partial \widehat{x}}\right] \tag{45.80a}$$

$$\frac{1}{N^2}\,\frac{\partial b'}{\partial z} = \frac{B}{H\, N^2}\,\frac{\partial \widehat{b}}{\partial \widehat{z}} = \frac{\mathrm{Ro}}{\mathrm{Bu}}\,\frac{\partial \widehat{b}}{\partial \widehat{z}} \tag{45.80b}$$

$$\frac{\beta\, y + \zeta}{f_\circ} = \mathrm{Ro}\,(\widehat{\beta}\,\widehat{y} + \widehat{\zeta}). \tag{45.80c}$$

The order Ro^2 terms appearing in equation (45.80a) are dropped since they do not contribute to the quasi-geostrophic potential vorticity, which involve terms only up to order Ro^1. For the order Ro^1 term, we only retain the zeroth order buoyancy, $\widehat{b}_0 = b_{\mathrm{g}}/B$, and likewise we just retain the zeroth order relative vorticity, $\widehat{\zeta}_0 = (L/U)\,\zeta_{\mathrm{g}}$. Hence, the Ertel potential vorticity is given by

$$Q = N^2\,(f_\circ + q_*) + \mathcal{O}(\mathrm{Ro}^2) \tag{45.81}$$

where q_* is the order Ro^1 term

$$q_* = \mathrm{Ro}\, f_\circ\left[\frac{1}{\mathrm{Bu}}\,\frac{\partial \widehat{b}_0}{\partial \widehat{z}} + \widehat{\beta}\,\widehat{y} + \widehat{\zeta}_0\right] = \frac{f_\circ}{N^2}\,\frac{\partial b_{\mathrm{g}}}{\partial z} + \beta\, y + \zeta_{\mathrm{g}}. \tag{45.82}$$

45.5.2 Material conservation of Ertel PV to order Ro^1

The material conservation of Ertel PV now takes the form

$$(\partial_t + \boldsymbol{u}_g \cdot \nabla_h + w_{ag}\,\partial_z)\,(f_o\,N^2 + q_*\,N^2) = f_o\,w_{ag}\,\partial_z N^2 + N^2\,\mathrm{D}_g q_*/\mathrm{D}t = 0. \tag{45.83a}$$

We dropped the $w_{ag}\,\partial_z$ contribution to the advection of q_* since ageostrophic vertical advection of q_* is an order Ro^2 term. To eliminate the vertical ageostrophic velocity we make use of the buoyancy equation (45.42) so that

$$\frac{\mathrm{D}_g q_*}{\mathrm{D}t} + \frac{w_{ag}}{N^2}\,\frac{\partial N^2}{\partial z} = \frac{\mathrm{D}_g q_*}{\mathrm{D}t} - \frac{f_o}{N^4}\,\frac{\mathrm{D}_g b_g}{\mathrm{D}t}\,\frac{\partial N^2}{\partial z} = 0. \tag{45.84}$$

Writing

$$\frac{\partial}{\partial z}\left[\frac{1}{N^2}\right] = -\frac{1}{N^4}\frac{\partial N^2}{\partial z} \tag{45.85}$$

leads to

$$\frac{\mathrm{D}_g q_*}{\mathrm{D}t} + f_o\left[\frac{\partial N^{-2}}{\partial z}\right]\,\frac{\mathrm{D}_g b_g}{\mathrm{D}t} = 0. \tag{45.86}$$

Since the geostrophic material time derivative operator only involves horizontal advection, we can merge these two terms to render

$$\begin{aligned}
\frac{\mathrm{D}_g q_*}{\mathrm{D}t} + f_o\left[\frac{\partial N^{-2}}{\partial z}\right]\,\frac{\mathrm{D}_g b_g}{\mathrm{D}t} &= \frac{\mathrm{D}_g}{\mathrm{D}t}\left[q_* + f_o\,b_g\left(\frac{\partial N^{-2}}{\partial z}\right)\right] && \text{(45.87a)}\\
&= \frac{\mathrm{D}_g}{\mathrm{D}t}\left[\beta\,y + \zeta + \frac{f_o}{N^2}\left(\frac{\partial b_g}{\partial z}\right) + f_o\,b_g\left(\frac{\partial N^{-2}}{\partial z}\right)\right] && \text{(45.87b)}\\
&= \frac{\mathrm{D}_g}{\mathrm{D}t}\left[\beta\,y + \zeta + f_o\,\frac{\partial}{\partial z}\left(\frac{b_g}{N^2}\right)\right] && \text{(45.87c)}\\
&= \frac{\mathrm{D}_g q}{\mathrm{D}t} && \text{(45.87d)}\\
&= 0. && \text{(45.87e)}
\end{aligned}$$

In the penultimate step we introduced the quasi-geostrophic potential vorticity given by equation (45.53)

$$q = \beta\,y + \zeta + f_o\,\frac{\partial}{\partial z}\left[\frac{b_g}{N^2}\right] = q_* + f_o\,b_g\frac{\partial N^{-2}}{\partial z}. \tag{45.88}$$

We have thus established how material conservation of Ertel potential vorticity, when expanded asymptotically to order Ro^1, leads to the geostrophic material conservation of quasi-geostrophic potential vorticity.

45.6 Boundary conditions

We need boundary conditions on the geostrophic streamfunction, ψ, to invert the elliptic quasi-geostrophic PV equation (45.53), with boundary conditions the focus of this section.

45.6.1 Concerning doubly-periodic QG models

For lateral boundaries, we may choose to set the normal component of the flow to zero for the inviscid case, in which case ψ is a constant along material boundaries as discussed in Section 21.4.2. More commonly (at least for idealized studies), we remove the lateral boundaries altogether by assuming a doubly periodic domain. The value of the Coriolis parameter does

not appear in the potential vorticity equation (45.54). Rather, it is only $\partial_y f = \beta$ that appears. So even though the Coriolis parameter, $f = f_o + \beta\, y$, is not meridionally periodic, we can still consider a horizontally doubly-periodic domain in which there is periodicity in flow properties in both the zonal and meridional directions.

Furthermore, we can study quasi-geostrophic flows in doubly periodic domains in the presence of certain idealized background flows. Namely, for a prescribed depth-independent thermal wind flow, the corresponding buoyancy that supports this flow plays no role in the quasi-geostrophic potential vorticity. For example, if the buoyancy has the form

$$b = \underbrace{M^2\, y + N^2\, z}_{\text{prescribed background}} + b'(x, y, z, t), \tag{45.89}$$

with M and N constant frequencies, then the corresponding quasi-geostrophic potential vorticity is independent of M. In this manner, the background buoyancy, though not meridionally periodic, prescribes a background thermal wind shear that is constant and so is trivially periodic.

45.6.2 Buoyancy equation

To develop the vertical boundary conditions on the streamfunction, consider the quasi-geostrophic buoyancy equation (45.42)

$$\mathrm{D}_g b_g / \mathrm{D}t + w_{ag}\, N^2 = (\partial_t + \boldsymbol{u}_g \cdot \nabla)\, b_g + w_{ag}\, N^2 = 0, \tag{45.90}$$

where the buoyancy is related to the geostrophic streamfunction via

$$b_g = f_o\, \partial_z \psi, \tag{45.91}$$

which leads to the equivalent form of the buoyancy equation

$$(\partial_t + \boldsymbol{u}_g \cdot \nabla_h)\, (f_o\, \partial_z \psi) + w_{ag}\, N^2 = 0. \tag{45.92}$$

We now consider how the buoyancy equation appears at the top and bottom boundaries.

45.6.3 Top boundary condition

Assuming the top boundary is a material surface, we are led to the kinematic boundary condition (19.66)

$$w = (\partial_t + \boldsymbol{u}_g \cdot \nabla_h)\, \eta. \tag{45.93}$$

How does this vertical velocity compare to that associated with motion in the fluid interior? To answer that question we assume an advective scaling for time derivatives so that the vertical velocity at the free surface scales as

$$w_{\text{surf}} \sim U\, \eta / L \sim U\, p / (\rho_o\, g\, L) \sim U^2\, f_o / g, \tag{45.94}$$

where L is the horizontal length scale, and we scaled the surface pressure gradient according to the free surface gradient. A point in the fluid interior has a vertical velocity that scales according to the buoyancy equation (45.90),

$$w_{\text{interior}} \sim U\, b / (N^2\, L) \sim f_o\, U^2 / (H\, N^2), \tag{45.95}$$

where H is the vertical scale over which the thermal wind shear is sizable, and which scales the buoyancy frequency according to

$$N^2 \sim (g/\rho_o)\, \Delta\rho / H, \tag{45.96}$$

where $\Delta\rho \ll \rho_o$ is the scale for the density difference setting the size of the buoyancy frequency. The ratio of the two vertical velocities is thus given by

$$w_{\text{surf}}/w_{\text{interior}} = H\, N^2/g = \Delta\rho/\rho_o \ll 1. \tag{45.97}$$

Evidently, we can set the surface boundary condition to that of a rigid lid, in which $w_{ag} = 0$. In this case, the top boundary condition reduces to geostrophic advection of boundary buoyancy

$$(\partial_t + \boldsymbol{u}_g \cdot \nabla_h)\,(f_o\, \partial_z \psi) = (\partial_t + \boldsymbol{u}_g \cdot \nabla_h)\, b_g = 0 \quad \text{at top boundary where } w_{ag} = 0. \tag{45.98}$$

That is, the geostrophic buoyancy at the surface is a material constant when advected by the surface geostrophic flow.

45.6.4 Bottom boundary condition

With a nonzero slope in the bottom topography, $\nabla\eta_b \neq 0$, the bottom kinematic boundary condition (Section 19.6.1) says that velocity is constrained so that

$$\boldsymbol{v} \cdot \hat{\boldsymbol{n}} = 0 \Longrightarrow w = \boldsymbol{u} \cdot \nabla\eta_b, \tag{45.99}$$

where $\hat{\boldsymbol{n}} = -\nabla(z - \eta_b)/|\nabla(z - \eta_b)|$ is the boundary's outward normal. Expanding this kinematic boundary condition leads to

$$w_{ag} = (\boldsymbol{u}_g + \boldsymbol{u}_{ag}) \cdot \nabla\eta_b, \tag{45.100}$$

which means there is vertical ageostrophic motion at the bottom so long as the horizontal motion is not aligned with isobaths. To be clear on the implications of this boundary condition, it is useful to examine the asymptotics by non-dimensionalizing[6]

$$\boldsymbol{u}_g = U\, \widehat{\boldsymbol{u}}_0 \tag{45.101a}$$
$$w_{ag} = W\, \text{Ro}\, \widehat{w}_1 \tag{45.101b}$$
$$\boldsymbol{u}_{ag} = U\, \text{Ro}\, \widehat{\boldsymbol{u}}_1 \tag{45.101c}$$
$$\nabla\eta_b = (\mathcal{B}/L)\, \widehat{\nabla}\widehat{\eta}_b = (H\, \text{Ro}/L)\, \widehat{\nabla}\widehat{\eta}_b, \tag{45.101d}$$

which brings the kinematic boundary condition (45.100) to

$$f_o\, H\, \text{Ro}^2\, (\widehat{\boldsymbol{u}}_0 + \text{Ro}\, \widehat{\boldsymbol{u}}_1) \cdot \widehat{\nabla}\widehat{\eta}_b = W\, \text{Ro}\, \widehat{w}_1 \Longrightarrow (\widehat{\boldsymbol{u}}_0 + \text{Ro}\, \widehat{\boldsymbol{u}}_1) \cdot \widehat{\nabla}\widehat{\eta}_b = \widehat{w}_1. \tag{45.102}$$

Asymptotic consistency implies that

$$\widehat{\boldsymbol{u}}_0 \cdot \widehat{\nabla}\widehat{\eta}_b = \widehat{w}_1 \Longrightarrow \boldsymbol{u}_g \cdot \nabla\eta_b = w_{ag}. \tag{45.103}$$

Hence, for quasi-geostrophic flow, any projection of the horizontal geostrophic velocity in a direction not aligned with isobaths leads to an ageostrophic vertical velocity at the bottom.

Use of the bottom kinematic boundary condition (45.103) in the buoyancy equation (45.92) leads to the bottom boundary evolution of buoyancy

$$\partial_t(f_o\, \partial_z\psi) + \boldsymbol{u}_g \cdot \nabla_h \left[f_o\, \partial_z\psi + N^2\, \eta_b\right] = 0 \quad \text{at } z = \overline{\eta_b}, \tag{45.104}$$

which can be written in terms of the geostrophic buoyancy

$$\partial_t b_g + \boldsymbol{u}_g \cdot \nabla_h (b_g + N^2\, \eta_b) = 0 \quad \text{at } z = \overline{\eta_b}, \tag{45.105}$$

[6]The bottom topography slope is non-dimensionalized according to the shallow water discussion in Section 43.3.4.

The boundary condition is evaluated at the horizontally averaged bottom positin, $z = \overline{\eta_b}$, since the more precise boundary location, $z = \eta_b(x, y)$, is higher order in Rossby number. Since $N^2 \, \eta_b$ is time independent, the boundary condition (45.105) can be written as a material conservation statement for buoyancy at the bottom

$$(\partial_t + \boldsymbol{u}_g \cdot \nabla_h)(b_g + N^2 \, \eta_b) = \frac{D_g(b_g + N^2 \, \eta_b)}{Dt} = 0 \quad \text{at } z = \overline{\eta_b}. \tag{45.106}$$

When η_b is a constant, and since N^2 is just a function of z, then the bottom boundary condition becomes a statement about the material conservation of buoyancy along the bottom boundary

$$\frac{D_g b_g}{Dt} = 0 \quad \text{at } z = \overline{\eta_b} = 0, \tag{45.107}$$

which is the bottom analog of the top boundary condition (45.98) that holds when making the rigid lid approximation. The more general case of a nonzero bottom slope renders a source for bottom buoyancy

$$\frac{D_g b_g}{Dt} = -N^2 \, \boldsymbol{u}_g \cdot \nabla \eta_b = -N^2 \, w_{ag} \quad \text{at } z = \overline{\eta_b}. \tag{45.108}$$

In this manner we see that a material evolution of bottom buoyancy is associated with vertical ageostrophic flow at the bottom, and correspondingly to horizontal geostrophic flow that deviates from the contours of constant topography.

Finally, since N^2 is a function only of z, this boundary condition can be written in terms of the stretching term appearing in the potential vorticity

$$\frac{D_g}{Dt}\left[\frac{f_o \, b_g}{N^2}\right] = -f_o \, \boldsymbol{u}_g \cdot \nabla \eta_b \quad \text{at } z = \overline{\eta_b}. \tag{45.109}$$

Evidently, material evolution of vertical stretching is coupled to bottom geostrophic flow that crosses lines of constant topography.

45.7 Potential vorticity with Dirac delta sheets

Based on the boundary conditions derived in Section 45.6, we know that quasi-geostrophic theory is comprised of the material conservation of potential vorticity in the interior, along with material evolution of buoyancy at the boundaries, with the material evolution determined by the horizontal geostrophic velocity

$$\frac{D_g q}{Dt} = 0 \qquad \text{for } \overline{\eta_b} < z < 0 \tag{45.110a}$$

$$\frac{D_g b_g}{Dt} = 0 \qquad \text{for } z = 0 \tag{45.110b}$$

$$\frac{D_g b_g}{Dt} = -N^2 \, \boldsymbol{u}_g \cdot \nabla \eta_b \quad \text{for } z = \overline{\eta_b}, \tag{45.110c}$$

where the geostrophic velocity, buoyancy, material time derivative, and quasi-geostrophic potential vorticity are written in terms of the geostrophic streamfunction

$$\boldsymbol{u}_g = \hat{\boldsymbol{z}} \times \nabla \psi \tag{45.111a}$$

$$b_g = f_o \, \partial_z \psi \tag{45.111b}$$

$$D_g/Dt = \partial_t + \boldsymbol{u}_g \cdot \nabla \tag{45.111c}$$

$$q = f_o + \beta \, y + \nabla_h^2 \psi + \frac{\partial}{\partial z}\left[\frac{f_o^2}{N^2}\frac{\partial \psi}{\partial z}\right] = f_o + \beta \, y + \nabla_h^2 \psi + \frac{\partial}{\partial z}\left[\frac{f_o \, b_g}{N^2}\right]. \tag{45.111d}$$

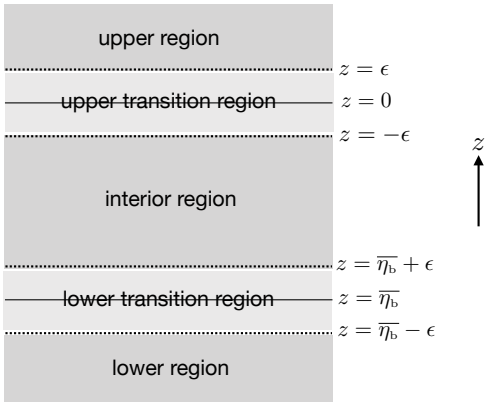

FIGURE 45.1: Geometry for the transition layers associated with the Dirac delta sheets at the upper and lower boundaries of the domain.

Studying the dynamics of boundary buoyancy constitutes the focus of *surface quasi-geostrophy*, as exemplified by *Held et al.* (1995) and whose mathematical foundations were examined by *Yassin and Griffies* (2022). In this section we focus on how to understand the transition from the interior to the boundaries. We follow the method of *Bretherton* (1966), where he noted that it can be conceptually convenient to bring the boundary conditions into the potential vorticity, much like when studying Green's functions for elliptic operators as in Chapter 9. In this manner, the boundary and interior terms can be placed on equal footing and thus their contribution to the potential vorticity directly compared.[7]

45.7.1 Transition between the interior and the boundaries

The transition from the interior to the boundary occurs over an infinitesimal region surrounding each boundary. There is a corresponding jump in the buoyancy as it moves from the domain interior to the boundaries. To help understand the nature of the jump it is useful to expand the infinitesimal thickness into a tiny but finite layer whose thickness, $\Delta z = \epsilon$, is later taken to vanish. For notational brevity introduce

$$S = b_{\mathrm{g}}/N^2, \tag{45.112}$$

and, with reference to the geometry in Figure 45.1, the full domain extent of this function is written

$$S^{\mathrm{ext}}(z) = \underbrace{S(\overline{\eta_{\mathrm{b}}} - \epsilon)\, \mathcal{H}(\overline{\eta_{\mathrm{b}}} - \epsilon - z)}_{\text{lower region}} + \underbrace{S(z)\, [\mathcal{H}(z - \overline{\eta_{\mathrm{b}}} - \epsilon) - \mathcal{H}(z + \epsilon)]}_{\text{interior region}} + \underbrace{S(\epsilon)\, \mathcal{H}(z - \epsilon)}_{\text{upper region}}, \tag{45.113}$$

where $\mathcal{H}$ is the Heaviside step function detailed in Section 7.5. Values within the outer edge of the transition regions (i.e., $S(\epsilon)$ and $S(\overline{\eta_{\mathrm{b}}} - \epsilon)$) are constructs whose values must be set consistent with the boundary conditions (45.110b) and (45.110c). We furthermore choose these values to be static, since we have no way to determine their evolution since they are outside the domain. The upper boundary satisfies the homogeneous boundary condition

$$(\partial_t + \boldsymbol{u}_{\mathrm{g}} \cdot \nabla) b_{\mathrm{g}} = 0, \tag{45.114}$$

which allows us to set

$$b_{\mathrm{g}}(\epsilon) = 0. \tag{45.115}$$

[7] See also Section 5.4.3 of *Vallis* (2017) for general comments on this approach.

Likewise, the lower boundary condition

$$(\partial_t + \boldsymbol{u}_\mathrm{g} \cdot \nabla) b_\mathrm{g} = -N^2 \, \boldsymbol{u}_\mathrm{g} \cdot \nabla \eta_\mathrm{b}, \tag{45.116}$$

is consistent with the choice

$$S(\overline{\eta_\mathrm{b}} - \epsilon) = -\eta_\mathrm{b}. \tag{45.117}$$

45.7.2 Calculating the stretching term over the extended domain

Since the derivative of a Heaviside step function yields a Dirac delta (Section 7.5), we have

$$\begin{aligned}\partial_z S^\mathrm{ext}(z) = \partial_z S(z) \, [\mathcal{H}(z - \overline{\eta_\mathrm{b}} - \epsilon) - \mathcal{H}(z + \epsilon)] + S(z) \, \delta(z - \overline{\eta_\mathrm{b}} - \epsilon) \\ - S(\overline{\eta_\mathrm{b}} - \epsilon) \, \delta(\overline{\eta_\mathrm{b}} - \epsilon - z) + S(\epsilon) \, \delta(z - \epsilon) - S(z) \, \delta(z + \epsilon),\end{aligned} \tag{45.118}$$

whose $\epsilon \to 0$ limit is

$$\partial_z S^\mathrm{ext}(z) = \partial_z S(z) \, [\mathcal{H}(z - \overline{\eta_\mathrm{b}}) - \mathcal{H}(z)] + [S(z) - S(\overline{\eta_\mathrm{b}} - \epsilon)] \, \delta(z - \overline{\eta_\mathrm{b}}) + [S(\epsilon) - S(z)] \, \delta(z). \tag{45.119}$$

Reintroducing the definition of S as per equation (45.112) yields the stretching term contribution to the potential vorticity, now defined over the full vertical extent of the domain (i.e., the domain interior and its boundaries)

$$\begin{aligned}\partial_z (f_\mathrm{o} \, b_\mathrm{g}/N^2)^\mathrm{ext} = \partial_z (f_\mathrm{o} \, b_\mathrm{g}/N^2) \, [\mathcal{H}(z - \overline{\eta_\mathrm{b}}) - \mathcal{H}(z)] \\ + \delta(z - \overline{\eta_\mathrm{b}}) \left[\frac{f_\mathrm{o} \, b_\mathrm{g}}{N^2} \right]_{z=\overline{\eta_\mathrm{b}}^-}^{z=\overline{\eta_\mathrm{b}}^+} + \delta(z) \left[\frac{f_\mathrm{o} \, b_\mathrm{g}}{N^2} \right]_{z=0^-}^{z=0^+},\end{aligned} \tag{45.120}$$

where the square bracket terms measure the jump in the stretching term taking place across the respective boundaries. The Heaviside term is nonzero only within the interior of the domain, whereas the two Dirac delta terms fire at their respective boundaries.

45.7.3 The extended potential vorticity

Making use of the extended stretching term (45.120) for the potential vorticity allows us to collapse the three equations (45.110a)-(45.110c) into the single equation valid over the domain interior as well as the domain boundaries

$$\frac{\mathrm{D}_\mathrm{g} q^\mathrm{ext}}{\mathrm{D}t} = 0 \quad \text{for } \overline{\eta_\mathrm{b}} \leq z \leq 0. \tag{45.121}$$

Bringing the above results together leads to the extended potential vorticity[8]

$$q^\mathrm{ext} = \underbrace{f_\mathrm{o} + \beta \, y + \nabla_\mathrm{h}^2 \psi + \frac{\partial}{\partial z} \left[\frac{f_\mathrm{o} \, b_\mathrm{g}}{N^2} \right]}_{\text{interior}} + \underbrace{\delta(z) \left[\frac{f_\mathrm{o} \, b_\mathrm{g}}{N^2} \right]_{z=0^-}^{z=0^+} + \delta(z - \overline{\eta_\mathrm{b}}) \left[\frac{f_\mathrm{o} \, b_\mathrm{g}}{N^2} \right]_{z=\overline{\eta_\mathrm{b}}^-}^{z=\overline{\eta_\mathrm{b}}^+}}_{\text{boundary contributions}}. \tag{45.122}$$

Note that the Dirac deltas have dimensions of inverse length (see Section 7.3), thus making this equation dimensionally consistent. We can make use of the transition region values (45.115) and

[8] We drop the Heaviside terms in equation (45.122) for brevity.

(45.117) to evaluate the jump conditions

$$\left[\frac{f_o\, b_g}{N^2}\right]_{z=0^-}^{z=0^+} = \left[\frac{f_o\, b_g}{N^2}\right]_{z=0} \tag{45.123a}$$

$$\left[\frac{f_o\, b_g}{N^2}\right]_{z=\overline{\eta_b}^-}^{z=\overline{\eta_b}^+} = \left[\frac{f_o\, b_g}{N^2}\right]_{z=\overline{\eta_b}} + f_o\, \eta_b, \tag{45.123b}$$

in which case the extended potential vorticity is

$$q^{ext} = \underbrace{f_o + \beta\, y + \nabla_h^2 \psi + \frac{\partial}{\partial z}\left[\frac{f_o\, b_g}{N^2}\right]}_{\text{interior}} + \underbrace{\delta(z)\,(f_o\, b_g/N^2) + f_o\, \delta(z-\overline{\eta_b})\,(b_g/N^2 + \eta_b)}_{\text{boundary contributions}}. \tag{45.124}$$

For some studies it is useful to ignore the buoyancy contribution at the two boundaries by setting them to zero, in which case the potential vorticity is

$$q^{ext} = \underbrace{f_o + \beta\, y + \nabla_h^2 \psi + \frac{\partial}{\partial z}\left[\frac{f_o\, b_g}{N^2}\right]}_{\text{interior}} + \underbrace{f_o\, \eta_b\, \delta(z-\overline{\eta_b})}_{\text{bottom topog}}. \tag{45.125}$$

Dropping the boundary buoyancy contributions allows one to focus on contributions from the bottom topography and interior processes, in isolation from the boundary buoyancy.

45.8 Mathematical expressions of the theory

In this section we sample various mathematical expressions of quasi-geostrophic theory.

45.8.1 The Jacobian form of geostropic advection

The geostrophic velocity, as a horizontally non-divergent field, can be written in terms of the quasi-geostrophic streamfunction

$$\boldsymbol{u}_g = \hat{\boldsymbol{z}} \times \nabla \psi. \tag{45.126}$$

We can thus write the following equivalent forms for the material time derivative of quasi-geostrophic PV

$$\frac{Dq}{Dt} = \partial_t q + \boldsymbol{u}_g \cdot \nabla q \tag{45.127a}$$

$$= \partial_t q + (\hat{\boldsymbol{z}} \times \nabla \psi) \cdot \nabla q \tag{45.127b}$$

$$= \partial_t q + (\nabla \psi \times \nabla q) \cdot \hat{\boldsymbol{z}} \tag{45.127c}$$

$$= \partial_t q + J(\psi, q). \tag{45.127d}$$

The final equality introduced the Jacobian operator

$$J(\psi, q) = (\nabla \psi \times \nabla q) \cdot \hat{\boldsymbol{z}}, \tag{45.128}$$

which is a notation commonly used in the geophysical fluids literature.[9]

For a perfect fluid, in which $Dq/Dt = 0$, a steady state (zero Eulerian time derivative) is realized when

$$\boldsymbol{u}_g \cdot \nabla\, q = (\nabla \psi \times \nabla q) \cdot \hat{\boldsymbol{z}} = J(\psi, q) = 0, \tag{45.129}$$

[9] Recall that we also encountered the Jacobian form for horizontally non-divergent two-dimensional advection in Section 38.2.4, as part of our study of the non-divergent barotropic flows.

which means that the steady velocity is parallel to surfaces of constant q. We are ensured that these equalities hold if the streamfunction is a function only of the potential vorticity

$$\psi = \psi(q) \Longrightarrow (\nabla\psi \times \nabla q) \cdot \hat{\boldsymbol{z}} = J(\psi, q) = 0. \tag{45.130}$$

As the steady state is of physical interest, this functional relation between streamfunction and potential vorticity commonly arises in applications.

45.8.2 The case of constant background buoyancy frequency

Consider the quasi-geostrophic potential vorticity for the special case of a constant background buoyancy frequency, $N^2 = \text{constant}$, in which the relative potential vorticity (45.52) takes on the form

$$q - \beta\, y = \nabla_{\mathsf{h}}^2 \psi + \frac{\partial}{\partial z}\left[\frac{f_{\mathsf{o}}^2}{N^2}\frac{\partial\psi}{\partial z}\right] \tag{45.131a}$$

$$= \frac{\partial^2\psi}{\partial x^2} + \frac{\partial^2\psi}{\partial y^2} + \frac{f_{\mathsf{o}}^2}{N^2}\frac{\partial^2\psi}{\partial z^2} \tag{45.131b}$$

$$= [\partial_{xx} + \partial_{yy} + \partial_{\tilde{z}\tilde{z}}]\psi. \tag{45.131c}$$

For the final equality we introduced the vertical coordinate

$$z = (f/N)\,\tilde{z} \Longleftrightarrow \tilde{z} = (N/f)\,z, \tag{45.132}$$

where f/N is the Prandtl ratio introduced by equation 43.169. Since $|N/f| >> 1$ the stably stratified flows considered in QG, $\tilde{z}$ is a *stretched* vertical coordinate so that the Laplacian operator acting on ψ is anisotropic. The linear operator acting on ψ remains elliptic even in the more general case of a depth dependent stratification, thus warranting the use of elliptical solvers when performing the inversion numerically.

45.8.3 Potential vorticity induction and impermeability

Outside of boundaries, the potential vorticity equation is the sole prognostic equation required to evolve the quasi-geostrophic flow. Consequently, one often ignores the quasi-geostrophic velocity and buoyancy equations. Even so, we found it useful to consider the buoyancy equation in Section 45.3.5 as part of connecting quasi-geostrophic potential vorticity to Ertel potential vorticity. Likewise, there are occasions when it is useful to examine the velocity equation, with a similar discussion provided in Section 43.6.6. In this section we directly connect the velocity and buoyancy equations and then reveal their connection to the potential vorticity equation.

Combining the velocity and buoyancy equations

Consider the quasi-geostrophic velocity and buoyancy equations derived in Section 45.3

$$(\partial_t + \boldsymbol{u}_{\mathsf{g}} \cdot \nabla)\boldsymbol{u}_{\mathsf{g}} + \hat{\boldsymbol{z}} \times (\beta\, y\, \boldsymbol{u}_{\mathsf{g}} + f_{\mathsf{o}}\, \boldsymbol{u}_{\mathsf{ag}}) = -\nabla_{\mathsf{h}}\, \varphi_{\mathsf{ag}} + \boldsymbol{F} \tag{45.133a}$$

$$(\partial_t + \boldsymbol{u}_{\mathsf{g}} \cdot \nabla_{\mathsf{h}})b_{\mathsf{g}} + w_{\mathsf{ag}}\, N^2 = \dot{b} \tag{45.133b}$$

$$f_{\mathsf{o}}\, \hat{\boldsymbol{z}} \times \boldsymbol{u}_{\mathsf{g}} + \nabla_{\mathsf{h}}\varphi_{\mathsf{g}} = 0 \tag{45.133c}$$

$$\nabla \cdot \boldsymbol{u}_{\mathsf{g}} = \partial_x u_{\mathsf{g}} + \partial_y v_{\mathsf{g}} = 0 \tag{45.133d}$$

$$\nabla \cdot \boldsymbol{v}_{\mathsf{ag}} = \nabla \cdot \boldsymbol{u}_{\mathsf{ag}} + \partial_z w_{\mathsf{ag}} = 0, \tag{45.133e}$$

where we added a non-conservative force per mass, $\boldsymbol{F}$ (e.g., friction, wind stress), and irreversible buoyancy source, $\dot{b}$ (e.g., diffusion, boundary fluxes). Taking $-\hat{\boldsymbol{z}}\times$ on the velocity equation[10] and multiplying the buoyancy equation by $f_\circ/N^2$ leads to

$$(\partial_t + \boldsymbol{u}_\mathrm{g}\cdot\nabla)(-\hat{\boldsymbol{z}}\times\boldsymbol{u}_\mathrm{g}) + \beta\, y\, \boldsymbol{u}_\mathrm{g} + f_\circ\, \boldsymbol{u}_\mathrm{ag} = \hat{\boldsymbol{z}}\times\nabla_\mathrm{h}\varphi_\mathrm{ag} - \hat{\boldsymbol{z}}\times\boldsymbol{F} \tag{45.134a}$$

$$(\partial_t + \boldsymbol{u}_\mathrm{g}\cdot\nabla_\mathrm{h})(f_\circ\, b_\mathrm{g}/N^2) + f_\circ\, w_\mathrm{ag} = f_\circ\, \dot{b}/N^2. \tag{45.134b}$$

Introduce the following vector fields

$$\boldsymbol{D} \equiv -\hat{\boldsymbol{z}}\times\boldsymbol{u}_\mathrm{g} + (f_\circ/N^2)\, b_\mathrm{g}\, \hat{\boldsymbol{z}} = \nabla_\mathrm{h}\psi + (f_\circ/N)^2\, \partial_z\psi\, \hat{\boldsymbol{z}} \tag{45.135a}$$

$$\boldsymbol{R} \equiv -\hat{\boldsymbol{z}}\times\boldsymbol{F} + (f_\circ/N^2)\, \dot{b}\, \hat{\boldsymbol{z}}, \tag{45.135b}$$

with $\boldsymbol{D}$ built from both the velocity and buoyancy fields and $\boldsymbol{R}$ built from the corresponding non-conservative tendencies. These vectors allow us to combine the velocity and buoyancy equations into a single vector equation

$$(\partial_t + \boldsymbol{u}_\mathrm{g}\cdot\nabla)\, \boldsymbol{D} + \beta\, y\, \boldsymbol{u}_\mathrm{g} + f_\circ\, \boldsymbol{v}_\mathrm{ag} = \hat{\boldsymbol{z}}\times\nabla_\mathrm{h}\varphi_\mathrm{ag} + \boldsymbol{R}. \tag{45.136}$$

Potential vorticity induction

The divergence of $\boldsymbol{D}$ yields the relative quasi-geostrophic potential vorticity

$$\nabla\cdot\boldsymbol{D} = q - (f_\circ + \beta\, y), \tag{45.137}$$

where we made use of the expression (45.53) for the potential vorticity. In analogy to Gauss's law of electromagnetism, we refer to $\boldsymbol{D}$ as the quasi-geostrophic potential vorticity *induction vector*.[11] Additionally, the potential vorticity equation can be written (see Exercise 45.3)

$$(\partial_t + \boldsymbol{u}_\mathrm{g}\cdot\nabla)\, q = \nabla\cdot\boldsymbol{R}, \tag{45.138}$$

so that the quasi-geostrophic potential vorticity flux vector

$$\boldsymbol{J}^\mathrm{q} = \boldsymbol{u}_\mathrm{g}\, q - \boldsymbol{R} \tag{45.139}$$

allows us to write the potential vorticity equation in the Eulerian flux-form

$$\partial_t q = -\nabla\cdot\boldsymbol{J}^\mathrm{q}. \tag{45.140}$$

Kinematic PV flux and impermeability

Taking the Eulerian time derivative of the potential vorticity induction equation (45.137) renders

$$\partial_t q = \partial_t(\nabla\cdot\boldsymbol{D}) = \nabla\cdot(\partial_t\boldsymbol{D}) \equiv -\nabla\cdot\boldsymbol{J}^\mathrm{q\text{-}kin}, \tag{45.141}$$

where we introduced the kinematic form of the potential vorticity flux

$$\boldsymbol{J}^\mathrm{q\text{-}kin} \equiv -\partial_t\boldsymbol{D} = \boldsymbol{J}^\mathrm{q} + \nabla\times\boldsymbol{A}, \tag{45.142}$$

with $\boldsymbol{A}$ a gauge function. This equation is analogous to the kinematic Ertel PV flux discussed in Section 42.2.2. We determine the explicit expression for the gauge function in Exercise 45.4.

[10] The operation $-\hat{\boldsymbol{z}}\times$ acts to rotate by $\pi/2$ in the clockwise direction.

[11] This connection between potential vorticity dynamics and electromagnetism was pointed out by *Schneider et al.* (2003) and further examined by *Maddison and Marshall* (2013).

45.9 Energetics for quasi-geostrophic flow

Consider a quasi-geostrophic fluid configured with flat upper (rigid lid) and lower boundaries, and assume the lateral boundaries are periodic or material solid boundaries. These restrictive assumptions allow us to more readily study energetics within the fluid, sans the impacts from nontrivial boundary effects. To study energetics we make use of the quasi-geostrophic buoyancy equation (45.42) and relative vorticity equation (45.47)

$$(\partial_t + \boldsymbol{u} \cdot \nabla)\, b = -w\, N^2 \tag{45.143a}$$
$$(\partial_t + \boldsymbol{u} \cdot \nabla)\, \zeta = -\beta\, v + f_\circ\, \partial_z w, \tag{45.143b}$$

where all labels are dropped from the variables to reduce clutter, and where

$$\frac{\mathrm{D}}{\mathrm{D}t} = \partial_t + \boldsymbol{u} \cdot \nabla \qquad b = f_\circ\, \partial_z \psi \qquad u = -\partial_y \psi \qquad v = \partial_x \psi \qquad \zeta = \nabla_{\mathrm{h}}^2 \psi. \tag{45.144}$$

45.9.1 Kinetic energy

The kinetic energy per mass for the total fluid domain is given by the integral

$$\mathcal{K} = \frac{1}{2} \int \boldsymbol{u} \cdot \boldsymbol{u}\, \mathrm{d}V = \frac{1}{2} \int \nabla_{\mathrm{h}} \psi \cdot \nabla_{\mathrm{h}} \psi\, \mathrm{d}V, \tag{45.145}$$

and its time derivative is

$$\frac{\mathrm{d}\mathcal{K}}{\mathrm{d}t} = \int \nabla_{\mathrm{h}} \psi \cdot \nabla_{\mathrm{h}} (\partial_t \psi)\, \mathrm{d}V. \tag{45.146}$$

For the kinetic energy time derivative we noted that the fluid domain has a constant volume to allow the time derivative to move inside the integral without introducing boundary terms. Manipulation renders

$$\frac{\mathrm{d}\mathcal{K}}{\mathrm{d}t} = \int \nabla_{\mathrm{h}} \psi \cdot \nabla_{\mathrm{h}} (\partial_t \psi)\, \mathrm{d}V \tag{45.147a}$$
$$= \int \left[\nabla_{\mathrm{h}} \cdot [\psi\, \nabla_{\mathrm{h}} (\partial_t \psi)] - \psi\, \partial_t (\nabla_{\mathrm{h}}^2 \psi) \right] \mathrm{d}V \tag{45.147b}$$
$$= -\int \psi\, \partial_t \zeta\, \mathrm{d}V, \tag{45.147c}$$

where we dropped the lateral boundary term and introduced relative vorticity. Use of the vorticity equation (45.143b) yields

$$\frac{\mathrm{d}\mathcal{K}}{\mathrm{d}t} = -\int \psi\, \partial_t \zeta\, \mathrm{d}V = \int \psi\, [\boldsymbol{u} \cdot \nabla_{\mathrm{h}} \zeta + \beta\, v - f_\circ\, \partial_z w]\, \mathrm{d}V. \tag{45.148}$$

The first and second terms vanish since

$$\int \psi\, (\boldsymbol{u} \cdot \nabla_{\mathrm{h}} \zeta + \beta\, v)\, \mathrm{d}V = \int \psi\, \boldsymbol{u} \cdot \nabla_{\mathrm{h}} (\zeta + f)\, \mathrm{d}V \tag{45.149a}$$
$$= \int \psi\, \nabla_{\mathrm{h}} \cdot (\boldsymbol{u}\, \zeta_{\mathrm{a}})\, \mathrm{d}V \tag{45.149b}$$
$$= \int [\nabla_{\mathrm{h}} \cdot (\psi\, \boldsymbol{u}\, \zeta_{\mathrm{a}}) - \nabla_{\mathrm{h}} \psi \cdot \boldsymbol{u}\, \zeta_{\mathrm{a}}]\, \mathrm{d}V = 0. \tag{45.149c}$$

The final equality holds since the boundary term vanishes, and $\boldsymbol{u} \cdot \nabla_{\mathrm{h}} \psi = 0$ since ψ is the streamfunction for the horizontal geostrophic flow. We are thus left with the expression for the

kinetic energy evolution

$$\frac{\mathrm{d}\mathcal{K}}{\mathrm{d}t} = -f_\circ \int \psi\, \partial_z w \,\mathrm{d}V. \tag{45.150}$$

Since the top and bottom are assumed flat and rigid, the vertical velocity vanishes on these boundaries so that

$$\frac{\mathrm{d}\mathcal{K}}{\mathrm{d}t} = -f_\circ \int \psi\, \partial_z w \,\mathrm{d}V = -f_\circ \int [\partial_z(w\,\psi) - w\,\partial_z\psi]\,\mathrm{d}V = f_\circ \int w\,\partial_z\psi \,\mathrm{d}V. \tag{45.151}$$

Introducing the quasi-geostrophic buoyancy through $b = f_\circ\, \partial_z\psi$ leads to

$$\frac{\mathrm{d}\mathcal{K}}{\mathrm{d}t} = \int w\, b \,\mathrm{d}V. \tag{45.152}$$

Kinetic energy thus increases when vertical motion is positively correlated with buoyancy. For example, upward motion ($w > 0$) of a positive buoyancy anomaly (relatively light water has $b > 0$) increases kinetic energy, as does downward motion of a negative buoyancy anomaly. This behavior is also reflected in the full fluid system discussed in Section 26.4.

45.9.2 Available potential energy

Available potential energy was introduced in Section 29.9 within the context of the Boussinesq ocean. An approximate form of the APE is given by equation (29.236), which we here write as

$$\mathcal{A}_{\text{bouss}} \approx \frac{1}{2}\int (b/N)^2 \mathrm{d}V = \frac{1}{2}\int [(f_\circ/N)\,\partial_z\psi]^2 \,\mathrm{d}V, \tag{45.153}$$

where we set $b = f_\circ\, \partial\psi/\partial z$ for the second equality. Taking a time derivative leads to

$$\frac{\mathrm{d}\mathcal{A}}{\mathrm{d}t} = \int (f_\circ/N)^2\, \partial_z\psi\, \partial_{tz}\psi \,\mathrm{d}V = \int (f_\circ/N)^2\, \partial_z\psi \left[-w\, N^2 - \nabla_{\!\mathrm{h}} \cdot (\boldsymbol{u}\, b)\right] \mathrm{d}V, \tag{45.154}$$

where we used the buoyancy equation (45.143a) for the second equality. The second term vanishes since

$$\int (f_\circ/N)^2\, \partial_z\psi\, [\nabla_{\!\mathrm{h}} \cdot (\boldsymbol{u}\, b)]\,\mathrm{d}V = \int \left[(f_\circ/N)^2\, \partial_z\psi\right] \boldsymbol{u} \cdot \nabla_{\!\mathrm{h}}\, (\partial_z\psi)\,\mathrm{d}V \tag{45.155a}$$

$$= \frac{1}{2}\int \nabla_{\!\mathrm{h}} \cdot \left[\boldsymbol{u}\, \left((f_\circ/N)\,\partial_z\psi\right)^2\right] \mathrm{d}V \tag{45.155b}$$

$$= 0. \tag{45.155c}$$

Consequently, the quasi-geostrophic APE has a time derivative given by

$$\frac{\mathrm{d}\mathcal{A}}{\mathrm{d}t} = -\int w\, f_\circ\, \partial_z\psi \,\mathrm{d}V = -\int w\, b \,\mathrm{d}V, \tag{45.156}$$

so that the APE evolves oppositely to the kinetic energy.

45.9.3 Exchange of mechanical energy

We refer to the term

$$\text{buoyancy work} = \int w\, f_\circ\, \partial_z\psi \,\mathrm{d}V = \int w\, b \,\mathrm{d}V, \tag{45.157}$$

as the buoyancy work conversion term. It has the same form as that encountered for the conversion between potential energy and kinetic energy in the unapproximated equations studied in Section 26.4.

The evolution of kinetic energy involves the relative vorticity equation, whereas evolution of the APE involves the buoyancy equation. However, their sum remains constant in time. The reason for the exact exchange of energy is that, when the kinetic energy increases through buoyancy work, the available potential energy decreases

$$\frac{\mathrm{d}(\mathcal{K} + \mathcal{A})}{\mathrm{d}t} = 0. \tag{45.158}$$

This is a relatively simple mechanical energy budget equation reminscent of a classical point particle discussed in Section 14.7. In particular, note the absence of a pressure work term that appears in the mechanical energy budget for other fluids such as for the Euler equations (Section 26.4) and Boussinesq ocean (Sections 29.6 and 29.8). We anticipate the absence of pressure work since knowledge of potential vorticity is sufficient to know all quasi-geostrophic dynamical fields, and yet pressure plays no explicit role in potential vorticity evolution.

45.9.4 Scaling APE and KE

The scale for kinetic energy in a quasi-geostrophic flow is given by

$$\mathcal{K} = \frac{1}{2} \int (\nabla_{\mathrm{h}} \psi \cdot \nabla_{\mathrm{h}} \psi) \, \mathrm{d}V \sim L^{-2} \, \Psi^2 \, V \tag{45.159}$$

and the scale for the APE is

$$\mathcal{A} = \frac{1}{2} \int \left[\frac{f_\circ}{N} \frac{\partial \psi}{\partial z} \right]^2 \mathrm{d}V \sim H^{-2} \, (f_\circ / N)^2 \Psi^2 \, V = L_{\mathrm{d}}^{-2} \, \Psi^2 \, V, \tag{45.160}$$

where we wrote Ψ for the streamfunction scale, V for the domain volume, and $L_{\mathrm{d}} = H \, (N/f_\circ)$ is the deformation radius (see equation (45.7)). Taking the ratio yields

$$\frac{\mathcal{K}}{\mathcal{A}} \sim \left[\frac{L_{\mathrm{d}}}{L} \right]^2 = \left[\frac{H}{L} \right]^2 \left[\frac{N}{f_\circ} \right]^2 = \mathrm{Bu}. \tag{45.161}$$

Hence, the Burger number is the ratio of the scale for quasi-geostrophic kinetic energy to the scale for quasi-geostrophic available potential energy. A large Burger number means that the horizontal scales of the flow are smaller than the deformation radius, in which case the quasi-geostrophic dynamics is dominated by its kinetic energy. In contrast, for scales larger than the deformation radius (not much larger, as then the flow would not satisfy quasi-geostrophic scaling), the Burger number is less than unity, in which case the quasi-geostrophic dynamics is dominated by available potential energy.

45.10 Exercises

EXERCISE 45.1: A VARIETY OF POTENTIAL VORTICITIES
Give the mathematical expressions for dimensionful potential vorticity in the following fluid models. Define all terms in the respective expressions. Give the physical dimensions and/or SI units for the potential vorticity. Hint: the answers can be found somewhere in this book.

(a) Ertel potential vorticity for compressible fluid in a rotating reference frame using potential temperature as the tracer.

(b) Ertel potential vorticity for a Boussinesq ocean in a rotating reference frame using Archimedean buoyancy as the tracer.

(c) Single shallow water layer on a beta plane

(d) Continuously stratified planetary geostrophy

(e) Continously stratified quasi-geostrophy on a beta plane

EXERCISE 45.2: QUASI-GEOSTROPHIC PV EVOLUTION WITH VERTICAL FRICTION

The first part of this exercise involves elements of the asymptotic method used for deriving the quasi-geostrophic equations, only now with the advent of a non-zero friction. Use is made to incorporate the non-dimensionalization detailed in Section 33.1, which provides a detailed discussion of the Ekman number and Ekman layers. The second part of this exercise makes use of the thermal wind balance to connect horizontal buoyancy transfer to the vertical viscous transfer of horizontal momentum.

(a) Derive the material evolution equation for quasi-geostrophic potential vorticity in a continuously stratified Boussinesq fluid in the presence of friction, $\boldsymbol{F}$. Assume the Ekman number is on the order of the Rossby number, so that the zeroth order asymptotic solution satisfies the usual inviscid f-plane geostrophic balance. Friction only appears in the first order equations.

(b) Assume friction arises just from vertical shears in the horizontal velocity, so that

$$\boldsymbol{F} = \frac{\partial}{\partial z}\left[\nu \frac{\partial \boldsymbol{u}}{\partial z}\right], \tag{45.162}$$

where $\nu = \nu(z)$ is a vertical eddy viscosity that is a function of depth (dimensions of squared length per time). Also assume an approximate form of quasi-geostrophic potential vorticity in which we drop relative vorticity (i.e., quasi-geostrophic potential vorticity is dominated by planetary vorticity and stretching). Determine the form for the vertical eddy viscosity so that the approximate form of quasi-geostrophic PV is laterally diffused via

$$\frac{\mathrm{D}q^{\text{approx}}}{\mathrm{D}t} = A \nabla_z^2 q^{\text{approx}}, \tag{45.163}$$

where A is a constant eddy diffusivity for the potential vorticity.

Hint: to leading order, the friction operator is a function just of the geostrophic velocity.

EXERCISE 45.3: QGPV FLUX-FORM EQUATION WITH NON-CONSERVATIVE PROCESSES

Derive the quasi-geostrophic potential vorticity equation (45.138). Show all the relevant steps. Hint: the key step requires showing that

$$\nabla \cdot [(\boldsymbol{u}_{\text{g}} \cdot) \boldsymbol{D}] = (\boldsymbol{u}_{\text{g}} \cdot) \nabla \cdot \boldsymbol{D}. \tag{45.164}$$

To do so, it is useful to express $\boldsymbol{u}_{\text{g}}$ and b_{g} in terms of the geostrophic streamfunction.

EXERCISE 45.4: QGPV GAUGE FUNCTION

Derive the gauge function, $\boldsymbol{A}$, that connects the two forms of the quasi-geostrophic flux vector as per equation (45.142).

Part IX

Hamilton's principle for fluid flows

In this part of the book we add a new layer to the conceptual foundations of fluid mechanics, and we do so by making use of *Hamilton's variational principle* to develop the equations for continuum motion. To appreciate the various aspects of Hamilton's principle requires revisiting a number of foundational topics and making use of distinct mathematical methods. Hamilton's principle is applicable to conservative physical systems, so that we only consider perfect fluids in this part of the book (i.e., single-component fluids without diffusion, conduction, or friction). Even so, Hamilton's principle provides a satisfying means to unify across the variety of physical content within perfect fluid mechanics. On a practical side, it offers a useful framework to develop approximate theories. Namely, by developing approximations within the action, one is ensured that the associated Euler-Lagrange equations satisfy corresponding conservation laws. In a nutshell, this part of the book will appeal to those interested in understanding the whys of fluid mechanics as a complement to the hows.

The continuum expression of Hamilton's variational principle, and the associated continuum *Euler-Lagrange field equations*, are the foundations for both classical and quantum field theory. Among the most celebrated payoffs for developing the variational formalism, we are afforded the origin story for differential conservation laws (e.g., linear momentum, angular momentum, mechanical energy, potential vorticity) that is otherwise obscure using alternative approaches (i.e., by inspired manipulations of the dynamical equations). It does so by directly connecting continuous space-time symmetries of the action to differential conservation laws through use of the celebrated *Noether's theorem* (*Noether*, 1918; *Noether and Tavel*, 2018). We used Noether's theorem in our study of analytical particle mechanics in Chapter 12. Noether's original work concerned field theory, so our use of Noether's theorem for continuum mechanics is directly connected to her work.

Hamilton's principle and Lagrangian kinematics

Many practitioners of fluid mechanics are neither aware of, nor concerned with, the use of Hamilton's variational principle for continuum mechanics. One reason for the intellectual distance arises from success of the Eulerian description of fluid mechanics, in which there is no concern for the flow map induced by the motion field, nor for the corresponding trajectories of fluid particles (see Chapter 18). Rather, the Eulerian approach focuses on the fluid velocity as a classical field, and the enumeration of forces acting on a fluid element that lead to accelerations via Newton's law. This approach offers a sufficient means to formulate the suite of fluid dynamical equations. Even so, there is more to the story that is revealed through the paired use of Hamilton's principle and Noether's theorem.

The absence of trajectories in Eulerian fluid mechanics distinguishes it from point particle mechanics and, it turns out, makes Hamilton's principle less transparent when formulated using Eulerian kinematics. In particular, Eulerian kinematics introduces nuances to Hamilton's principle related to the need to employ constraint fields not encountered with Lagrangian kinematics. These features of the Eulerian approach to Hamilton's principle have, whether fairly or unfairly, turned many practitioners away from Hamilton's principle. The nature of an Eulerian formulation of Hamilton's principle was clarified by *Salmon* (1988), who provided a systematic connection between Eulerian and Lagrangian formulations. Nonetheless, the direct connection between Lagrangian fluid kinematics to the kinematics of point particles offers a relatively straightforward extension (both conceptually and technically) of Hamilton's principle to fluid mechanics. It also more closely aligns to the methods used in continuum mechanics and quantum field theory. It is for these reasons that we embrace Lagrangian kinematics in our study of Hamilton's principle in this part of the book.[12]

[12] It is notable that in solid mechanics, Hamilton's principle is more routinely used (e.g., see Chapter 2 of *Tromp* (2025a)), presumably since Lagrangian kinematics is more routinely used in solid mechanics. Those interested in the Eulerian approach will find Chapter 8 of *Salmon* (1998) a valuable introduction.

Harmonic oscillator versus the motion field

We start this part of the book in Chapter 46 by focusing on Hamilton's principle for a continuous scalar field, following approaches standard in the quantum field theory literature (e.g., *Quigg* (1983); *Ryder* (1985); *Ramond* (1990)). In this treatment, we establish the Euler-Lagrange field equations by taking the continuum limit of a discrete version of Hamilton's principle applied to coupled simple harmonic oscillators. As such, we are afforded a pedagogical introduction to Hamilton's principle for a continuum that builds from the earlier work with particles in Chapters 12 and 15. This approach then lends the conceptual picture of the continuous field as representing small amplitude (linear) fluctuations relative to an equilibrium state.

In Chapter 47, we meld the classical field theory from Chapter 46 to the Lagrangian kinematics of continuum matter from Chapters 18 and 19. Doing so offers a suitable framework to use Hamilton's principle for describing fluid flows. Notably, through the advent of the motion field, $\varphi(\boldsymbol{a}, T)$, appearing in Lagrangian kinematics, we appreciate that continuum mechanics is a fundamentally nonlinear field theory and thus it is not generally amenable to the harmonic oscillator paradigm that forms the foundation for much of classical and quantum field theory.[13] That is, motion of continuum matter is not restricted to small fluctuations relative to an equilibrated state. So to examine the gamut of fluid motions, in Chapter 47 we apply Hamilton's principle to the fluid motion field, $\boldsymbol{\varphi}$. We thus develop a field theory for the motion field as it appears in Lagrangian space-time. Even given this distinction between the scalar field theory from Chapter 46 to the Lagrangian space-time of the motion field, it is remarkable that the perfect fluid Euler-Lagrange equation (47.43a) is mathematically identical to equation (46.43) formulated for the continuous scalar field.

Concerning local field theory

In our studies of continuum mechanics in general, or fluid mechanics in particular, we rely on *local fields* to formulate the equations describing motion of continuous matter. Namely, all fields (e.g., temperature, velocity, energy) depend locally on positions in Galilean space-time. The use of fields and the corresponding local approach were discussed in Chapter 16 in the context of the continuum approximation. Local field theories embody the inability for information to transfer at speeds faster than light or, for our studies that ignore electromagnetism, for signals to travel faster than acoustic waves. Furthermore, local field theories are ubiquitous in physics in part since they offer a robust conceptual and operational foundation that is simpler than non-local approaches.[14] As noted on page 24 of *Ramond* (1990), local field theories are so well trusted that they are commonly used for describing non-local phenomena. For our study of fluid mechanics, we make use of both the Lagrangian and Eulerian reference frames. The Eulerian approach considers fields that are local in the Eulerian $\boldsymbol{x}$-space, whereas the Lagrangian approach considers fields that are local in the material $\boldsymbol{a}$-space.

These remarks about the relevance of local field theory might seem obvious, with action-at-a-distance phenomena absent from any fundamental processes in classical physics. Even so, there are approximate theories where we assume a wave speed to be infinite, thus transitioning from a hyperbolic system to an elliptic system. The primary example occurs when assuming a non-divergent fluid flow, as in the Boussinesq ocean. For this case, the pressure is purely mechanical (i.e., it is not related to internal energy via a thermodynamic derivative), and it solves an elliptic boundary value problem to enforce the non-divergence nature of the flow. That is, for non-divergent flow, pressure is the Lagrange multiplier that ensure the constraint of $\nabla \cdot \boldsymbol{v} = 0$ is maintained at each point in space and time, with the acoustic wave speed assumed

[13] The study of linear waves in Part X is one area where the harmonic oscillator paradigm is suited for fluid mechanics.

[14] Chapter 1 of *Morse and Feshbach* (1953) provides an insightful discussion of fields and their use in physics.

infinite. In general, if encountering a non-local process in classical physics, we must inquire about the corresponding unapproximated process in order to determine if the non-local theory is a physically sensible approximation to a local theory. If not, then the non-local theory is not a viable theory of classical continuum mechanics.

Chapter 46

Scalar field theory in Galilean space-time

In this chapter we study *classical scalar field theory* in Galilean space-time from the perspective of *Hamilton's principle* of stationary action. We motivate this study by considering the continuum limit of a system of coupled simple harmonic oscillators, which provides the canonical example of how to extend Lagrangian particle mechanics to Lagrangian continuum mechanics. We then develop the equations of motion within the continuum and make use of Noether's theorem to derive dynamical conservation laws connected to space-time symmetries.

CHAPTER GUIDE

This chapter relies on the formulation of Lagrangian mechanics and Hamilton's principle from Chapter 12 and 15. We also make use of general tensor formalism from Chapters 1 through 4. The use of general tensors here anticipates their use for the perfect fluid in Chapter 47. This chapter serves as the foundations for applying Hamilton's variational principle for fluid mechanics in Chapter 47, for potential flow in Section 52.2.9, and various topics in wave mechanics found in Part X.

46.1 Continuum limit of coupled harmonic oscillators

Further study of the discrete coupled oscillator system from Section 15.7 involves the introduction of discrete normal modes and the examination of energy moving through discrete waves (e.g., see Section 24 of *Fetter and Walecka* (2003)). However, that analysis takes us somewhat outside the main topic of this book. Instead, we here examine the continuum limit of the oscillator system. The purpose of this study is to extend discrete Lagrangian mechanics and Hamilton's principle to the continuum, thus providing a direct connection to fluid mechanics and classical field theory.

46.1.1 Continuum limit

We work in a classical physics universe, so that we have no concern for the quantum nature of matter. As such, the continuum limit is here considered as a mere mathematical transition from discrete classical matter to continuous classical matter. This approach is physically naive in the face of the molecular and atomic nature of matter as described by quantum mechanics. Even so, it provides a suitable mathematical framework for studying the classical mechanics of continuous media, and as such it serves the needs of this book. See Chapter 16 for more discussion of the physical basis for the continuum limit.

The continuum limit for the coupled harmonic oscillator system is realized by the following (see Section 15.7 for notation):

$$\Delta \to \mathrm{d}x \qquad \text{equilibrium distance betwen particles becomes infinitesimal} \tag{46.1a}$$

$$N \to \infty \qquad \text{infinite number of particles} \tag{46.1b}$$

$$(N+1)\,\Delta = \ell \qquad \text{equilibrium length remains constant} \tag{46.1c}$$

$$m/\Delta = \sigma \qquad \text{mass per length} \tag{46.1d}$$

$$\Gamma\,\Delta = \tau \qquad \text{compressive/expansive force} \tag{46.1e}$$

$$\mathsf{n}\,\Delta = x \qquad \text{continuous coordinate for equilibrium position} \tag{46.1f}$$

$$\xi_{\mathsf{n}}(t) \to \xi(x,t) \qquad \text{displacement becomes function of space and time.} \tag{46.1g}$$

The displacement function, $\xi(x,t)$, measures the displacement of an infinitesimal piece of matter whose equilibrium position is x. As such, the coordinate x acts as a parameter that labels an infinitesimal piece of matter whose equilibrium position is x and whose instantaneous position is $x + \xi(x,t)$.[1]

We take the continuum limit starting from two different perspectives. First we focus on the equation of motion (15.146) for the coupled oscillators, which is the topic of Section 46.1.2. Alternatively, we take the continuum limit of the Lagrangian and then derive the corresponding Euler-Lagrange equations, with this approach considered in Section 46.1.3. The second approach is aligned with the approach in classical field theory used in later sections.

[1]The displacement field, $\xi(x,t)$, is a one-dimensional version of the vector field, $\boldsymbol{\xi}(\boldsymbol{x},t)$, used for the *generalized Lagrangian mean* of Section 70.2.

46.1.2 Continuum limit and the wave equation

Introducing the notation from equations (46.1a)-(46.1g), yet without taking the continuum limit, brings the coupled oscillator equation (15.146) into the form

$$\ddot{\xi}_{\mathsf{n}} = \frac{\Gamma}{m}\left(\xi_{\mathsf{n}+1} - 2\,\xi_{\mathsf{n}} + \xi_{\mathsf{n}-1}\right) \tag{46.2a}$$

$$= \frac{\Gamma\,\Delta}{m/\Delta}\,\frac{\xi_{\mathsf{n}+1} - 2\,\xi_{\mathsf{n}} + \xi_{\mathsf{n}-1}}{\Delta^2} \tag{46.2b}$$

$$= \frac{\tau}{\sigma}\left[\frac{\xi_{\mathsf{n}+1} - 2\,\xi_{\mathsf{n}} + \xi_{\mathsf{n}-1}}{\Delta^2}\right]. \tag{46.2c}$$

To take the continuum limit, note that the finite difference on the right hand side approximates the second order spatial derivative operator, so that in the continuum limit we recover the one dimensional *wave equation*

$$(\partial_{tt} - c^2\,\partial_{xx})\,\xi = 0, \tag{46.3}$$

with the wave speed given by

$$c = (\tau/\sigma)^{1/2}. \tag{46.4}$$

We studied the mathematics of the wave equation (46.3) in Section 6.7 in the context of hyperbolic partial differential equations. A general solution is given by

$$\xi(x,t) = A(x - c\,t) + B(x + c\,t), \tag{46.5}$$

where A and B are arbitrary smooth functions determined by the initial conditions and boundary conditions. The solution $A(x - c\,t)$ is a signal moving in the $+\hat{\boldsymbol{x}}$ direction, whereas $B(x - c\,t)$ is a signal moving in the $-\hat{\boldsymbol{x}}$ direction, both moving at speed c.

We have restricted attention to motion constrained to a line whereby the harmonic oscillators render a series of alternative rarefactions and compressions that lead to wave-like motions along that line. Upon taking the continuum limit, we find that each piece of the continuum oscillates about its equilibrium position, again with the oscillations in a direction aligned with the waves. Such motions are the defining characteristic of *longitudinal waves*. The longitudinal waves resulting from the continuum limit of coupled harmonic oscillators offers a prototype for the acoustic waves studied in Chapter 51.

46.1.3 Continuum limit of the Lagrangian

Rather than taking the continuum limit of the equation of motion, we here consider the continuum limit of the Lagrangian and then derive the corresponding Euler-Lagrange equation of motion. This approach accords with the methods of classical field theory and it will serve many purposes in this book.

Recall the discrete Lagrangian given by equation (15.155)

$$L = \sum_{\mathsf{n}=1}^{N+1}\left[\frac{m}{2}\,(\dot{\xi}_{\mathsf{n}})^2 - \frac{\Gamma}{2}\,(\xi_{\mathsf{n}} - \xi_{\mathsf{n}-1})^2\right]. \tag{46.6}$$

The continuum limit from Section 46.1.2 brings the kinetic energy to

$$\frac{m}{2}\sum_{\mathsf{n}=1}^{N+1}(\dot{\xi}_{\mathsf{n}})^2 = \frac{\sigma}{2}\sum_{\mathsf{n}=1}^{N+1}(\dot{\xi}_{\mathsf{n}})^2\,\Delta \longrightarrow \frac{\sigma}{2}\int_0^{\ell}(\partial_t\xi)^2\,\mathrm{d}x, \tag{46.7}$$

where we set $m = \sigma\,\Delta$ according to equation (46.1d), and made the correspondence

$$\sum_{n=1}^{N+1} \Delta \longrightarrow \int_0^\ell dx. \tag{46.8}$$

Similarly, the continuum limit of the potential energy yields

$$\frac{\Gamma}{2}\sum_{n=1}^{N+1}(\xi_n - \xi_{n-1})^2 = \frac{\Gamma\,\Delta}{2}\sum_{n=1}^{N+1}\frac{(\xi_n - \xi_{n-1})^2}{\Delta^2}\,\Delta \longrightarrow \frac{\tau}{2}\int_0^\ell (\partial_x\xi)^2\,dx, \tag{46.9}$$

where we set $\Gamma\,\Delta = \tau$ according to equation (46.1e). As a result, the Lagrangian has the continuum limit

$$L = \sum_{n=1}^{N+1}\left[\frac{m}{2}(\dot\xi_n)^2 - \frac{\Gamma}{2}(\xi_n - \xi_{n-1})^2\right] \longrightarrow \frac{1}{2}\int_0^\ell [\sigma\,(\partial_t\xi)^2 - \tau\,(\partial_x\xi)^2]\,dx \equiv \int_0^\ell \mathcal{L}\,dx, \tag{46.10}$$

where we defined the *Lagrangian density*

$$\mathcal{L} = [\sigma\,(\partial_t\xi)^2 - \tau\,(\partial_x\xi)^2]/2. \tag{46.11}$$

Now observe that

$$\frac{\partial}{\partial t}\frac{\partial \mathcal{L}}{\partial(\partial_t\xi)} + \frac{\partial}{\partial x}\frac{\partial \mathcal{L}}{\partial(\partial_x\xi)} = \sigma\,\partial_{tt}\xi - \tau\,\partial_{xx}\xi = \sigma\,(\partial_{tt}\xi - c^2\,\partial_{xx}\xi) = 0. \tag{46.12}$$

This result hints at a means to derive the Euler-Lagrange equation using a continuum version of Hamilton's principle, which is the topic of Section 46.2.

46.1.4 Further study

In transitioning from the discrete harmonic oscillators to the continuum field theory, we are inspired by treatments from *Fetter and Walecka* (2003) (chapters 4, 6, and 8), chapter 12 of *Goldstein* (1980), chapter 9 of *José and Saletan* (1998), and Chapter 2 of *Soper* (2008). Note that some of these treatments (e.g., Chapter 4 of *Fetter and Walecka* (2003)) works through the continuum limit of a string, which accords quite closely to the continuum limit of simple harmonic oscillators considered here.

46.2 Hamilton's principle and the Euler-Lagrange equations

The continuum limit considered in Section 46.1 suggests that we can study the mechanics of continuous media using the methods of Lagrangian mechanics and Hamilton's principle, and that we can pursue this approach without concern for the discrete nature of matter. In this section we explore the rudiments of the resulting field theory for scalar fields. For simplicity, we focus here on the case of one space dimension, along with time. Generalizations to higher space dimensions are straightforward, in which case the space-time domain, R, includes higher dimensional region of space, $\mathcal{R}$, along with a time interval.

46.2.1 The action for a continuous field

In Section 12.6 we applied Hamilton's principle to the trajectories of discrete particles moving through space, with the spatial position specified by generalized coordinates and the position along a trajectory parameterized by time. Hamilton's principle states that the physically realized

trajectory is that trajectory that makes the action stationary. Here we postulate that Hamilton's principle for point particles can be extended to continuous matter whose mechanics is described by space-time fields. Many steps in the derivation here are straightforward extensions of the discrete particle discussion.

Consider a 1+1 dimensional field, $\psi = \psi(x,t)$, that is a function of one Cartesian space coordinate, x, and time, t. For example, $\psi(x,t)$ can represent the displacement field, $\xi(x,t)$, introduced by the continuum limit of the oscillators studied in Section 46.1. In this manner, the continuum extension of the discrete particle action defined by equation (12.63) is here given by the space-time integral

$$\mathcal{S}[t_{\mathsf{A}}, x_{\mathsf{A}}, t_{\mathsf{B}}, x_{\mathsf{B}}, \psi] = \int_{t_{\mathsf{A}}}^{t_{\mathsf{B}}} L \, \mathrm{d}t = \int_{t_{\mathsf{A}}}^{t_{\mathsf{B}}} \left[\int_{x_{\mathsf{A}}}^{x_{\mathsf{B}}} \mathcal{L}(\psi, \partial_t \psi, \partial_x \psi, x, t) \, \mathrm{d}x \right] \mathrm{d}t, \tag{46.13}$$

where $\mathcal{L}$ is the *Lagrangian density*[2] and the physical system lives on a space domain, $x \in [x_{\mathsf{A}}, x_{\mathsf{B}}]$, and evolves over the time range, $t \in [t_{\mathsf{A}}, t_{\mathsf{B}}]$. We refer to this space-time domain as

$$\mathrm{R} \equiv x \in [x_{\mathsf{A}}, x_{\mathsf{B}}] \oplus t \in [t_{\mathsf{A}}, t_{\mathsf{B}}], \tag{46.14}$$

and its boundary is $\partial\mathrm{R}$. On the left hand side of equation (46.13) we exposed the dependence of the action on the space and time endpoints, as well as the function, ψ. We generally omit such dependence for brevity in notation.

Note the presence of both space and time derivatives inside the action in equation (46.13), as per the use of both space and time as independent variables for the field, ψ. Evidently, the Lagrangian density, $\mathcal{L}$, is a functional[3] of the field, ψ, and its derivatives, $\partial_t \psi$ and $\partial_x \psi$. Since ψ is a function of (x,t), then the Lagrangian density, $\mathcal{L}$, is an implicit function of (x,t) through its dependence on $\psi(x,t)$, $\partial_t \psi(x,t)$, and $\partial_x \psi(x,t)$. Furthermore, we allow for $\mathcal{L}$ to be an explicit function of (x,t), which may arrive via other prescribed functions that contribute to the Lagrangian (e.g., a space-time dependent background field through which waves propagate, as studied in Chapter 50). In Section 46.3.1 we emphasize the importance of being mindful of the variety of explicit and implicit dependencies of the Lagrangian density.

46.2.2 Functional variation of the field

In the action (46.13), it is the field, $\psi(x,t)$, that is the continuum extension of the generalized coordinates used in the discrete particle mechanics action (12.63). Correspondingly, it is the field that is varied when varying the continuum action. Let $\psi(x,t)$ be the physically realized field and introduce a virtual variation around that field according to

$$\psi(x,t|\epsilon) = \psi(x,t) + \epsilon \, \chi(x,t) = \psi(x,t) + \delta\psi(x,t). \tag{46.15}$$

The first equality introduced a non-dimensional parameter, ϵ, that scales the perturbation field, χ, thus defining a one-parameter family of functions, $\psi(x,t|\epsilon)$. The second equality in equation (46.15) introduced the δ notion commonly used for variations (see Section 12.6). We emphasize that it is the field that is varied, so that the field parameters, (x,t), are the same across the two equalities in equation (46.15). Consequently, the δ operator commutes with space and time derivatives.

Figure 46.1 illustrates the field variation (46.15). There is a nonzero variation, $\delta\psi(x,t) = \epsilon \, \chi(x,t)$, for space-time points that are not on the space-time boundary, $(x,t) \notin \partial\mathrm{R}$. In contrast, the field is specified along $\partial\mathrm{R}$ to be the physically realized field, so that on the space-time

[2] We commonly refer to $\mathcal{L}$ as the "Lagrangian", thus omitting the "density" qualifier.
[3] A functional is a "function of a function".

boundary there is no variation

$$\delta\psi(x,t) = 0 \quad \forall\ (x,t) \in \partial\mathrm{R} \iff \frac{\partial\psi(x,t|\epsilon)}{\partial\epsilon} = 0 \quad \forall\ (x,t) \in \partial\mathrm{R}. \tag{46.16}$$

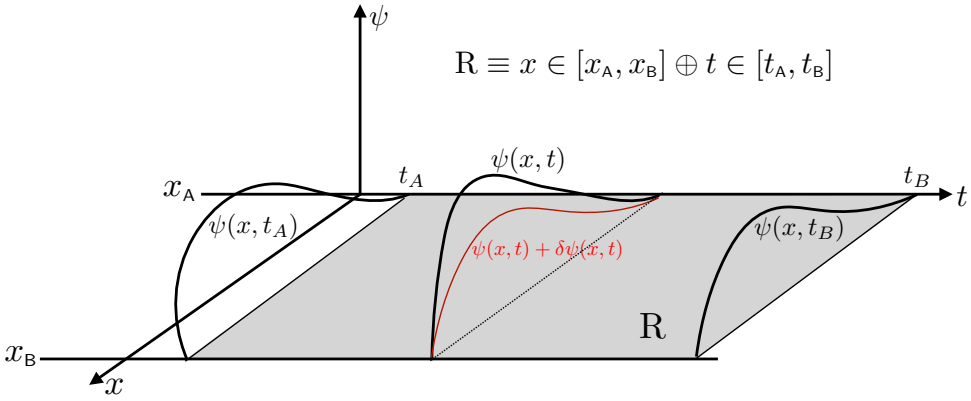

FIGURE 46.1: Illustrating the variation of a field for use in Hamilton's principle for continuous media. The field, $\psi(x,t)$, is specified along the space-time boundary of the domain, $\partial\mathrm{R}$, where R is the space domain $x \in [x_\mathrm{A}, x_\mathrm{B}]$ plus a time domain $t \in [t_\mathrm{A}, t_\mathrm{B}]$. When not on $\partial\mathrm{R}$, then there is a nonzero, $\delta\psi(x,t)$, whereas $\delta\psi = 0$ on the boundary, $\partial\mathrm{R}$. This figure is inspired by Figure 25.3 of *Fetter and Walecka* (2003).

46.2.3 Variation of the action

Hamilton's principles says that the physically realized field, $\psi(x,t|\epsilon = 0)$, makes the action stationary, which is mathematically stated as

$$\text{Hamilton's principle} \implies \left[\frac{\mathrm{d}\mathcal{S}}{\mathrm{d}\epsilon}\right]_{\epsilon=0} = \left[\frac{\mathrm{d}}{\mathrm{d}\epsilon}\int_\mathrm{R} \mathcal{L}\,\mathrm{d}x\,\mathrm{d}t\right]_{\epsilon=0} = 0. \tag{46.17}$$

Making use of the δ shorthand leads to

$$\text{Hamilton's principle} \implies \delta\mathcal{S} = \delta\left[\int_\mathrm{R} \mathcal{L}\,\mathrm{d}x\,\mathrm{d}t\right] = 0 \quad \text{with} \quad \delta = [\mathrm{d}/\mathrm{d}\epsilon]_{\epsilon=0}\,. \tag{46.18}$$

In varying the action we only vary the field and its derivatives, with the space-time domain, R, unchanged. Hence, the variation operator commutes with the space-time integral

$$\delta\mathcal{S} = \int_\mathrm{R} \delta\mathcal{L}\,\mathrm{d}x\,\mathrm{d}t. \tag{46.19}$$

Variation of the Lagrangian density is computed according to the chain rule

$$\delta\mathcal{L} = \left[\frac{\partial\mathcal{L}}{\partial\psi}\right]_{\partial_t\psi,\partial_x\psi}\delta\psi + \left[\frac{\partial\mathcal{L}}{\partial(\partial_t\psi)}\right]_{\psi,\partial_x\psi}\delta(\partial_t\psi) + \left[\frac{\partial\mathcal{L}}{\partial(\partial_x\psi)}\right]_{\psi,\partial_t\psi}\delta(\partial_x\psi). \tag{46.20}$$

We exposed subscripts to denote which terms are held fixed during the partial functional derivative operation. This equation makes it clear that variation of the Lagrangian density occurs at a fixed space-time point, which explains why there are no $(\partial\mathcal{L}/\partial t)\,\delta t$ nor $(\partial\mathcal{L}/\partial x)\,\delta x$ terms. Correspondingly, under this variation we consider (x,t) as space-time parameters so that the ∂_x and ∂_t operators acting on ψ commute with the variation operator

$$\delta\mathcal{L} = \frac{\partial\mathcal{L}}{\partial\psi}\,\delta\psi + \frac{\partial\mathcal{L}}{\partial(\partial_t\psi)}\,\partial_t(\delta\psi) + \frac{\partial\mathcal{L}}{\partial(\partial_x\psi)}\,\partial_x(\delta\psi). \tag{46.21}$$

Further rearranging the space-time operators leads to the equivalent expression

$$\delta\mathscr{L} = \left[\frac{\partial\mathscr{L}}{\partial\psi} - \frac{\partial}{\partial t}\frac{\partial\mathscr{L}}{\partial(\partial_t\psi)} - \frac{\partial}{\partial x}\frac{\partial\mathscr{L}}{\partial(\partial_x\psi)}\right]\delta\psi + \frac{\partial}{\partial t}\left[\frac{\partial\mathscr{L}}{\partial(\partial_t\psi)}\,\delta\psi\right] + \frac{\partial}{\partial x}\left[\frac{\partial\mathscr{L}}{\partial(\partial_x\psi)}\,\delta\psi\right]. \tag{46.22}$$

46.2.4 Euler-Lagrange field equations

Plugging the result (46.22) into the action variation (46.19) leads to

$$\delta\mathcal{S} = \int_{\mathrm{R}} \delta\psi\left(\frac{\partial\mathscr{L}}{\partial\psi} - \frac{\partial}{\partial t}\frac{\partial\mathscr{L}}{\partial(\partial_t\psi)} - \frac{\partial}{\partial x}\frac{\partial\mathscr{L}}{\partial(\partial_x\psi)}\right)\mathrm{d}x\,\mathrm{d}t + \int_{\mathrm{R}}\left(\frac{\partial}{\partial t}\left[\frac{\partial\mathscr{L}}{\partial(\partial_t\psi)}\,\delta\psi\right] + \frac{\partial}{\partial x}\left[\frac{\partial\mathscr{L}}{\partial(\partial_x\psi)}\,\delta\psi\right]\right)\mathrm{d}x\,\mathrm{d}t. \tag{46.23}$$

As noted earlier, we are assuming the field variation vanishes on the space-time boundary, so that $\delta\psi = 0$ for points on $\partial\mathrm{R}$. Doing so eliminates the second integral since both terms integrate to boundary contributions. Furthermore, since $\delta\psi$ is an arbitary variation of the field within the interior of the domain, a general satisfaction of Hamilton's principle, $\delta\mathcal{S} = 0$, only holds if the integrand in the first integral vanishes for each space and time point, which thus leads to the continuum *Euler-Lagrange equations*

$$\delta\mathcal{S} = 0 \Longrightarrow \frac{\partial\mathscr{L}}{\partial\psi} - \frac{\partial}{\partial t}\left[\frac{\partial\mathscr{L}}{\partial(\partial_t\psi)}\right] - \frac{\partial}{\partial x}\left[\frac{\partial\mathscr{L}}{\partial(\partial_x\psi)}\right] = 0. \tag{46.24}$$

We emphasize here an important practical point related to computation of the partial derivatives. Namely, when performing the partial derivative on $\mathscr{L}$ with respect to ψ and its derivatives, $\partial_t\psi$ and $\partial_x\psi$, each of the other variables in the Lagrangian density are held fixed. However, when performing the space and time partial derivatives, ∂_x and ∂_t, we only maintain the complement space and time variable fixed, so that we need to employ the chain rule to extract all places where ∂_x and ∂_t affect. We offer details in Section 46.3.1 on these points about computing the partial derivatives.

46.2.5 Example Lagrangian densities

We have many opportunities in this book to use a Lagrangian density to derive the correspondingly Euler-Lagrange equations. Here we provide a few examples that lead to wave equations.

Acoustic wave equation

As studied in Section 46.1, the Lagrangian density

$$\mathscr{L} = [\sigma\,(\partial_t\psi)^2 - \tau\,(\partial_x\psi)^2]/2, \tag{46.25}$$

with σ and τ constants, renders the wave equation as the Euler-Lagrange equation

$$(\partial_{tt} - c^2\,\partial_{xx})\,\psi = 0, \tag{46.26}$$

where the wave speed is $c = \sqrt{\tau/\sigma}$ (equation (46.4)). Notice that the dimensions of $\mathscr{L}$ are energy per length, which accords with this being a wave equation in a single spatial dimension. The Lagrangian (46.25) and wave equation (46.26) also hold for the more general case of a tension that is a function of time, $\tau = \tau(t)$, and a mass density that is a function of space, $\sigma = \sigma(x)$, in which case the wave speed is a function of space and time

$$c^2(x,t) = \tau(t)/\sigma(x). \tag{46.27}$$

We derived the Lagrangian density (46.25) in Section 46.1 by taking the continuum limit of coupled harmonic oscillators, where $\psi(x,t)$ represents the $\hat{\boldsymbol{x}}$-displacement of a particle from its equilibrium position, so that linear fluctuations are *longitudinal waves* (wave motion in the same direction of the particle displacement). An analogous derivation leads to the same Lagrangian density for a tight string, with $\psi(x,t)$ now measuring the transverse displacements of the string from its equilibrium position (see Section 25 in *Fetter and Walecka* (2003)), and with linear oscillations leading to *transverse waves*.

Returning to the continuum harmonic oscillator, we note that it is directly related to the study of acoustic waves in a fluid. We pursue this study in Chapter 51, thus encountering the Lagrangian density

$$\mathscr{L} = [c_{\text{s}}^{-2}\,(\partial_t p')^2 - (\nabla p')^2]/(2\,\rho_{\text{e}}), \tag{46.28}$$

where ρ_{e} is the mass density of the background fluid state, c_{s} is the sound speed in the fluid, and p' is the perturbation pressure. In this case the Euler-Lagrange equation is the acoustic wave equation

$$\partial_t[(\rho_{\text{e}}\,c_{\text{s}}^2)^{-1}\,\partial_t p'] - \nabla\cdot(\rho_{\text{e}}^{-1}\,\nabla p') = 0, \tag{46.29}$$

which, in the special case of ρ_{e} and c_{s} independent of space and time, gives the wave equation

$$(\partial_{tt} - c_{\text{s}}^2\,\nabla^2)\,p' = 0. \tag{46.30}$$

Note that the physical dimensions of the Lagrangian density (46.28) are not energy per volume, so that the terms in the Lagrangian are thought of as pseudo-energy densities.

Sine-Gordon and Klein-Gordon wave equations

For another example, consider

$$\mathscr{L} = [\sigma\,(\partial_t\psi)^2 - \tau\,(\partial_x\psi)^2]/2 - \sigma\,\Gamma^2\,(1-\cos\psi), \tag{46.31}$$

where ψ is here a non-dimensional field. The corresponding Euler-Lagrange equation is known as the *sine-Gordon equation*

$$\partial_{tt}\psi - c^2\,\partial_{xx}\psi + \Gamma^2\sin\psi = 0. \tag{46.32}$$

As shown in Section 9.1.1 of *José and Saletan* (1998), the sine-Gordon equation is the continuum limit of a coupled pendulum-spring system, with Γ proportional to the gravitational acceleration. For small ψ, the sine-Gordon Lagrangian (46.31) and wave equation (46.32) reduce to the *Klein-Gordon* Lagrangian and Klein-Gordon equation

$$\mathscr{L} = [\sigma\,(\partial_t\psi)^2 - \tau\,(\partial_x\psi)^2]/2 + \sigma\,\Gamma^2\,\psi^2 \quad \text{and} \quad (\partial_{tt} - c^2\,\partial_{xx} + \Gamma^2)\,\psi = 0. \tag{46.33}$$

The Klein-Gordon equation forms the starting point for scalar quantum field theories (e.g., *Ryder* (1985)).

46.3 Operational aspects of Hamilton's principle

We here summarize a number of points about the formalism that are particularly relevant when performing the many operational steps with Hamilton's principle.

46.3.1 Care with the partial derivative operations

As noted in Section 46.2, the Lagrangian density, $\mathscr{L}$, is a functional of the field, ψ, as well as its space and time derivatives,

$$\frac{\partial\psi(x,t)}{\partial t} = \left[\frac{\partial\psi(x,t)}{\partial t}\right]_x \quad \text{and} \quad \frac{\partial\psi(x,t)}{\partial x} = \left[\frac{\partial\psi(x,t)}{\partial x}\right]_t , \tag{46.34}$$

where the subscripts on the right hand side of these equations indicate those variables held fixed while performing the partial derivative. We typically do not need this extra adornment for partial derivatives acting on functions of space and time. But the Lagrangian density is a rather loaded object, and so it is important to clarify what is meant by its derivatives.

With ψ and its derivatives explicit functions of (x,t), then $\mathscr{L}$ is an implicit function of (x,t). There are additional physical systems where the Lagrangian density picks up an explicit space and time dependence, such as when waves move through a space and time dependent background media (Section 50.5). Such added space and time dependence does not alter the derivation of the Euler-Lagrange field equation, since in that derivation we only vary the field and its derivatives. However, the distinction between implicit versus explicit functional dependence can easily lead to confusion when performing partial derivative manipulations involving ∂_t and ∂_x operations, such as when deriving the continuum conservation laws in Section 46.4. We thus find it useful to here write these derivatives for the record.

The partial time derivative of $\mathscr{L}$, computed at a fixed x position, is given by

$$\left[\frac{\partial\mathscr{L}}{\partial t}\right]_x = \left[\frac{\partial\mathscr{L}}{\partial\psi}\right]_{\partial_t\psi,\partial_x\psi}\frac{\partial\psi}{\partial t} + \left[\frac{\partial\mathscr{L}}{\partial(\partial_t\psi)}\right]_{\psi,\partial_x\psi}\frac{\partial^2\psi}{\partial t^2} + \left[\frac{\partial\mathscr{L}}{\partial(\partial_x\psi)}\right]_{\psi,\partial_t\psi}\frac{\partial^2\psi}{\partial x\partial t} + \left[\frac{\partial\mathscr{L}}{\partial t}\right]_{\psi,\partial_t\psi,\partial_x\psi,x} . \tag{46.35}$$

Exposing the subscripts on the $\mathscr{L}$ partial derivatives helps to distinguish the time derivative on the left hand side from the time derivative appearing in the final term on the right hand side. Namely, the $(\partial\mathscr{L}/\partial t)_x$ on the left hand side only holds x fixed, whereas the $(\partial\mathscr{L}/\partial t)_{\psi,\partial_t\psi,\partial_x\psi,x}$ on the right hand side holds the full gamut, $\psi, \partial_t\psi, \partial_x\psi, x$, fixed while computing the time derivative. Distinguishing these two derivatives is the primary point of confusion, so that for it is commonly sufficient to abbreviate this equation with the more succinct expression

$$\frac{\partial\mathscr{L}}{\partial t} = \frac{\partial\mathscr{L}}{\partial\psi}\frac{\partial\psi}{\partial t} + \frac{\partial\mathscr{L}}{\partial(\partial_t\psi)}\frac{\partial^2\psi}{\partial t^2} + \frac{\partial\mathscr{L}}{\partial(\partial_x\psi)}\frac{\partial^2\psi}{\partial x\partial t} + \left[\frac{\partial\mathscr{L}}{\partial t}\right]_{\psi,\partial_t\psi,\partial_x\psi,x} . \tag{46.36}$$

A similar expression holds for the partial space derivative computed at a fixed time,

$$\left[\frac{\partial\mathscr{L}}{\partial x}\right]_t = \left[\frac{\partial\mathscr{L}}{\partial\psi}\right]_{\partial_t\psi,\partial_x\psi}\frac{\partial\psi}{\partial x} + \left[\frac{\partial\mathscr{L}}{\partial(\partial_t\psi)}\right]_{\psi,\partial_x\psi}\frac{\partial^2\psi}{\partial t\partial x} + \left[\frac{\partial\mathscr{L}}{\partial(\partial_x\psi)}\right]_{\psi,\partial_t\psi}\frac{\partial^2\psi}{\partial x^2} + \left[\frac{\partial\mathscr{L}}{\partial x}\right]_{\psi,\partial_t\psi,\partial_x\psi,t} , \tag{46.37}$$

which also has the succinct form[4]

$$\frac{\partial\mathscr{L}}{\partial x} = \frac{\partial\mathscr{L}}{\partial\psi}\frac{\partial\psi}{\partial x} + \frac{\partial\mathscr{L}}{\partial(\partial_t\psi)}\frac{\partial^2\psi}{\partial t\partial x} + \frac{\partial\mathscr{L}}{\partial(\partial_x\psi)}\frac{\partial^2\psi}{\partial x^2} + \left[\frac{\partial\mathscr{L}}{\partial x}\right]_{\psi,\partial_t\psi,\partial_x\psi,t} . \tag{46.38}$$

[4]Note that some authors (e.g., chapter 12 of *Goldstein* (1980)), write $\mathrm{d}/\mathrm{d}t$ and $\mathrm{d}/\mathrm{d}x$ for the left hand side operators in equations (46.35) and (46.37), referring to these derivatives as "total time" and "total space" derivatives. We do not follow that nomenclature here.

46.3.2 Generalized spatial coordinates

As when studying discrete particle mechanics, we often find that Cartesian space coordinates are less suited to symmetry of the physical configuration. This point is particularly relevant for Chapter 47 when working with the Lagrangian space-time field theory relevant to fluids, in which we coordinate lines are attached to fluid particles. We thus now allow for the spatial coordinates, $x^a (a = 1, 2, 3)$, to be arbitrary general coordinates rather than restricted to Cartesian. To do so requires results from general tensor analysis in Chapters 3 and 4. In particular, we need the invariant volume element given by equation (4.60)

$$\mathrm{d}V = g \, \mathrm{d}^3 x, \tag{46.39}$$

where g is the square root of the spatial metric tensor's determinant as represented by the arbitrary spatial coordinates (see Sections 4.5.2 and 4.5.3), and

$$\mathrm{d}^3 x = \mathrm{d}x^1 \, \mathrm{d}x^2 \, \mathrm{d}x^3 \tag{46.40}$$

is a shorthand for the spatial coordinate element. Note that g can generally be a function of space and time.

We are thus led to a variation of the action[5]

$$\delta \mathcal{S} = \int_{\mathrm{R}} (\delta \mathcal{L}) \, g \, \mathrm{d}^3 x \, \mathrm{d}t. \tag{46.41}$$

Generalizing the Cartesian coordinate derivation requires us now to keep track of g, so that

$$\int_{\mathrm{R}} \delta\psi \left[\frac{\partial \mathcal{L}}{\partial \psi} - \frac{1}{g} \frac{\partial}{\partial t} \left[g \, \frac{\partial \mathcal{L}}{\partial (\partial_t \psi)} \right] - \frac{1}{g} \frac{\partial}{\partial x^a} \left[g \, \frac{\partial \mathcal{L}}{\partial (\partial_a \psi)} \right] \right] g \, \mathrm{d}^3 x \, \mathrm{d}t. \tag{46.42}$$

Setting $\delta \mathcal{S} = 0$ leads to the Euler-Lagrange equation

$$\frac{\partial \mathcal{L}}{\partial \psi} - \frac{1}{g} \frac{\partial}{\partial t} \left[g \, \frac{\partial \mathcal{L}}{\partial (\partial_t \psi)} \right] - \frac{1}{g} \frac{\partial}{\partial x^a} \left[g \, \frac{\partial \mathcal{L}}{\partial (\partial_a \psi)} \right] = 0. \tag{46.43}$$

From our discussion in Section 4.15, we see that the covariant divergence of a vector natually appears in this formulation. Namely, from equation (4.134) we have the covariant divergence

$$\nabla_a \left[\frac{\partial \mathcal{L}}{\partial (\partial_a \psi)} \right] = \frac{1}{g} \frac{\partial}{\partial x^a} \left[g \, \frac{\partial \mathcal{L}}{\partial (\partial_a \psi)} \right], \tag{46.44}$$

where ∇_a is the covariant derivative operator. For the remainder of this chapter we make use of general spatial coordinates since they are necessary for the study of fluids in Chapter 47 using Lagrangian space-time.

46.3.3 Natural spatial boundary conditions

As seen in Section 46.2.4, the Euler-Lagrange field equations arise by setting the field variation, $\delta\psi$, to zero on both the space and times boundaries. This assumption is typical of many treatments given that it offers a sensible generalization of the discrete case in Section 12.6, in which the variation vanishes at the initial and final times. It is also relevant for the case without boundaries, with all terms assumed to vanish at infinity. However, for geophysical fluid

[5]The variation (46.41) only varies the field, ψ, which means there is no variation of the space-time element, $g \, \mathrm{d}^3 x \, \mathrm{d}t$. In Section 46.5 we allow for coordinates to be varied, in which case we must consider variations of $g \, \mathrm{d}^3 x \, \mathrm{d}t$.

mechanics the question of spatial boundary conditions is often of primary importance. We thus investigate alternatives to setting $\delta\psi = 0$ on the spatial boundaries.[6]

In particular, consider a situation where the fluid is bounded by a static material boundary, $\partial\mathcal{R}$. All fields, whether the actual physical field or variations around this field, must satisfy the relevant kinematic boundary conditions. In terms of the Lagrangian density, the natural boundary condition is given by

$$\hat{\boldsymbol{n}} \cdot \frac{\partial \mathscr{L}}{\partial(\nabla\psi)} = \hat{n}_a \frac{\partial \mathscr{L}}{\partial(\partial_a\psi)} = 0 \quad \text{on } \partial\mathcal{R}, \tag{46.45}$$

where $\hat{\boldsymbol{n}}$ is the outward normal along the spatial boundary, $\partial\mathcal{R}$. The boundary condition (46.45) means that there is no generalized forces acting on the physical field at the boundaries. If this boundary condition is satisfied, then the Euler-Lagrange equation (46.24) follows even without specifying how $\delta\psi$ behaves on the spatial boundaries.

What if the boundary is dynamical and thus feels forces, such as occurs in free boundary problems? For example, the boundary could represent the material interface between the ocean and atmosphere, in which forces are imparted at the boundary. In this case the boundary itself is dynamical and so it too must be incorporated into Hamilton's principle. This situation is more subtle than when the boundary is static, and we explore an example in Section 52.2 when studying potential flow in a homogeneous fluid layer with a dynamical free surface.

46.3.4 Galilean space-time notation

In certain places in the following, it proves useful to streamline the notation by making use of the space-time tensor notation from Section 3.5.4. Here, we introduce the Greek index, $\alpha = 0, 1, 2, 3$ with $\alpha = 0$ corresponding to the time index and $\alpha = 1, 2, 3$ for space. In this manner the Euler-Lagrange field equation

$$\frac{\partial \mathscr{L}}{\partial \psi} - \frac{1}{g}\frac{\partial}{\partial t}\left[\frac{\partial \mathscr{L}}{\partial(\partial_t\psi)}\right] - \frac{1}{g}\frac{\partial}{\partial x^a}\left[\frac{\partial \mathscr{L}}{\partial(\partial_a\psi)}\right] = 0, \tag{46.46}$$

takes on the more compact form

$$\frac{\partial \mathscr{L}}{\partial \psi} - \frac{1}{g}\frac{\partial}{\partial x^\alpha}\left[\frac{\partial \mathscr{L}}{\partial(\partial_\alpha\psi)}\right] = 0, \tag{46.47}$$

or even more succinct by making use of the covariant space-time divergence

$$\frac{\partial \mathscr{L}}{\partial \psi} - \nabla_\alpha\left[\frac{\partial \mathscr{L}}{\partial(\partial_\alpha\psi)}\right] = 0. \tag{46.48}$$

Integrals over space and time take on the form

$$\int \int_{\mathscr{R}} g \, \mathrm{d}^3x \, \mathrm{d}t = \int_{\mathrm{R}} g \, \mathrm{d}^4x, \tag{46.49}$$

so that the action is written

$$\mathcal{S} = \int_{\mathrm{R}} \mathscr{L}(\psi, \partial_\alpha\psi, x^\alpha) \, g \, \mathrm{d}^4x. \tag{46.50}$$

Additionally, for brevity we sometimes write x rather than x^α when there is no need to expose the coordinate labels.

In the study of continuum conservation laws from Noether's theorem (Sections 46.4 and

[6] See Section 41 of *Fetter and Walecka* (2003) for similar considerations.

46.5), we encounter continuity equations of the form

$$\nabla_\alpha J^\alpha = g^{-1}\left[\partial_t(g\,J^0) + \partial_a(g\,J^a)\right] = 0, \tag{46.51}$$

where J^α is a Galilean four-vector. Integration over the global spatial domain renders,

$$\int_{\mathcal{R}} \nabla_\alpha J^\alpha \; g\,\mathrm{d}^3x = 0, \tag{46.52}$$

which for a time-independent domain yields the global conservation law

$$\frac{\mathrm{d}}{\mathrm{d}t}\int_{\mathcal{R}} J^0\, g\,\mathrm{d}^3x = -\int_{\partial\mathcal{R}} J^a\,\hat{n}_a\, g\,\mathrm{d}\mathcal{S}. \tag{46.53}$$

If the boundary integral vanishes then we have a global constant of integration, which corresponds to a symmetry of the action.

46.3.5 Mechanical equivalence of Lagrangians

In Section 12.6.6 we noted that the mechanics of discrete particles is unchanged if the Lagrangian for a particle system is modified by a total time derivative of a function of the generalized coordinates. Analogously, the mechanics of a continuum field remains unchanged if the Lagrangian density is modified by a space and/or time derivative of functions that have zero variation along the boundaries. More specifically, consider the two Lagrangian densities and briefly return to Cartesian coordinates in 1+1 dimensions

$$\mathscr{L}^{\mathsf{new}} = \mathscr{L}^{\mathsf{old}} + \partial_t\Gamma(\psi,\partial_t\psi,\partial_x\psi,x,t) + \partial_x\Sigma(\psi,\partial_t\psi,\partial_x\psi,x,t), \tag{46.54}$$

where Γ and Σ are arbitrary functions of the field, ψ, its derivatives, $\partial_t\psi, \partial_x\psi$, as well as the space and time positions. To examine mechanical equivalance, consider a space-time domain $\mathrm{R} = [x_\mathsf{A}, x_\mathsf{B}] \oplus [t_\mathsf{A}, t_\mathsf{B}]$, so that the action transforms into

$$\begin{aligned}\mathcal{S}^{\mathsf{new}} = \mathcal{S}^{\mathsf{old}} &+ \int_{x_\mathsf{A}}^{x_\mathsf{B}} \left(\Gamma[\psi(t_\mathsf{B}),\partial_t\psi(t_\mathsf{B}),\partial_x\psi(t_\mathsf{B}),x,t_\mathsf{B}] - \Gamma[\psi(t_\mathsf{A}),\partial_t\psi(t_\mathsf{A}),\partial_x\psi(t_\mathsf{A}),x,t_\mathsf{A}]\right)\mathrm{d}x \\ &+ \int_{t_\mathsf{A}}^{t_\mathsf{B}} \left(\Sigma[\psi(x_\mathsf{B}),\partial_t\psi(x_\mathsf{B}),\partial_x\psi(x_\mathsf{B}),x_\mathsf{B},t] - \Sigma[\psi(x_\mathsf{A}),\partial_t\psi(x_\mathsf{A}),\partial_x\psi(x_\mathsf{A}),x_\mathsf{A},t]\right)\mathrm{d}t.\end{aligned} \tag{46.55}$$

The added terms in the first integral are evaluated at the time boundaries, t_A and t_B, whereas the second integral is evaluated at the space boundaries, x_A and x_B. So mechanical equivalence depends arises if the field has zero variation along the space and time boundaries, in which case

$$\delta\mathcal{S}^{\mathsf{new}} = \delta\mathcal{S}^{\mathsf{old}}, \tag{46.56}$$

which then means that the associated Euler-Lagrange equation is unchanged.

A more general approach, allowing for arbitrary coordinates, is given by

$$\mathscr{L}^{\mathsf{new}} = \mathscr{L}^{\mathsf{old}} + \nabla_\alpha J^\alpha, \tag{46.57}$$

where $\nabla_\alpha J^\alpha$ is a Galilean space-time divergence of a four-vector, J^α. In this case the action changes by

$$\mathcal{S}^{\mathsf{new}} = \mathcal{S}^{\mathsf{old}} + \int_{\partial\mathrm{R}} J^\alpha\,\hat{n}_\alpha\,\mathrm{d}\mathcal{S}, \tag{46.58}$$

where we made use of the space-time form of the divergence theorem from Section 4.19, thus rendering a boundary integral of the flux projected onto the space-time boundary. Mechanical

equivalence thus depends on how J^α behaves along the space-time boundaries. Details depend on specifics of the variation, in particular whether we are considering Hamilton's principle to derive the Euler-Lagrange equations, or whether we are probing symmetries of the dynamical system to determine conservation laws. We further pursue these points when studying symmetries in Sections 46.4 and 46.5, as well as in Section 52.2.9 when using Hamilton's principle for potential flow.

46.3.6 The absence of second or higher derivatives in the Lagrangian

It is notable that the Lagrangian in equation (46.13) is a functional of the field, ψ, and its first derivatives, $\partial_\alpha \psi$. We were originally motivated to consider just the field and its first derivatives based on the continuum limit of coupled oscillators from Section 46.1, where the discrete Lagrangian (46.6) only includes the displacement field and its first time derivative. But when moving away from the discrete limit, we might wish to include higher derivatives for continuum fields. Yet, as noted in Section 1.5 of *Ramond* (1990), higher derivatives in the Lagrangian can lead to non-causal behavior in the corresponding Euler-Lagrange field equations, with the Lorentz-Dirac equation of electrodynamics an example. Heading Ramond's warning motivates us to also restrict Lagrangians to have no second or higher order derivatives.

46.4 Space-time symmetry and stress-energy-momentum

An experiment conducted on a mechanically closed and isolated physical system does not care about the origin of space or time. That is, an experiment conducted in London in the year 1900 yields the same results as when done in New York in the year 2000, assuming all relevant conditions are the same. This observation can be formalized by deriving conservation laws that arise from the absence of a dependence on the space-time origin. Operationally, we expose the equations describing the physical system to a coordinate variation, δx^α, that represents a bulk shift of every point within the physical system. *Noether's theorem* (*Noether*, 1918; *Noether and Tavel*, 2018) provides the means to derive a corresponding conservation law.

In this section we derive conservation laws arising from symmetry in the space-time position. These conservation laws are maintained by the physically realized field, ψ, that satisfy the Euler-Lagrange equation. As noted in Section 12.9 when studying classical point particles, to connect a symmetry to a conservation law it is sufficient to focus on the Lagrangian as it encapsulates the mechanics. In this section we identify cyclic coordinates in the Lagrangian density, with these coordinates then reflecting a symmetry of the physical system that leads to a corresponding conservation law. We consider an alternative approach in Section 46.5 that focuses on the action.

46.4.1 Time symmetry and the Hamiltonian density

Consider a physical system that respects time homogeneity. What does this symmetry imply about the dynamical fields? To answer this question, return to the partial time derivative in equation (46.36)

$$\frac{\partial \mathscr{L}}{\partial t} = \frac{\partial \mathscr{L}}{\partial \psi} \frac{\partial \psi}{\partial t} + \frac{\partial \mathscr{L}}{\partial (\partial_\alpha \psi)} \frac{\partial}{\partial x^\alpha} \frac{\partial \psi}{\partial t} + \left[\frac{\partial \mathscr{L}}{\partial t} \right]_{\psi, \partial_\alpha \psi, x^a}. \tag{46.59}$$

Now make use of the Euler-Lagrange equation (46.48) to have

$$\frac{\partial \mathscr{L}}{\partial \psi} \frac{\partial \psi}{\partial t} = \nabla_\alpha \left[\frac{\partial \mathscr{L}}{\partial (\partial_\alpha \psi)} \right] \frac{\partial \psi}{\partial t} = g^{-1} \frac{\partial}{\partial x^\alpha} \left[g \frac{\partial \mathscr{L}}{\partial (\partial_\alpha \psi)} \right] \frac{\partial \psi}{\partial t}, \tag{46.60}$$

which then leads to

$$\frac{\partial \mathscr{L}}{\partial t} = g^{-1} \frac{\partial}{\partial x^\alpha} \left[g \frac{\partial \mathscr{L}}{\partial(\partial_\alpha \psi)} \frac{\partial \psi}{\partial t} \right] + \left[\frac{\partial \mathscr{L}}{\partial t} \right]_{\psi, \partial_t \psi, \partial_x \psi, \boldsymbol{x}}. \tag{46.61}$$

We now assume spatial coordinates whose representation of the metric tensor is time-independent so that

$$\partial_t g = 0. \tag{46.62}$$

This assumption holds for Eulerian coordinates and for Lagrangian coordinates used in fluid mechanics (with the time derivative taken holding the corresponding spatial coordinates fixed).[7] With this assumption we have

$$\frac{\partial}{\partial t} \left[\frac{\partial \mathscr{L}}{\partial(\partial_t \psi)} \frac{\partial \psi}{\partial t} - \mathscr{L} \right] + \nabla_a \left[\frac{\partial \mathscr{L}}{\partial(\partial_a \psi)} \frac{\partial \psi}{\partial t} \right] = - \left[\frac{\partial \mathscr{L}}{\partial t} \right]_{\psi, \partial_t \psi, \partial_x \psi, \boldsymbol{x}}. \tag{46.63}$$

Following the discrete case discussed in Section 12.10, introduce the *generalized (or canonical) momentum density*, $\mathscr{P}$, and the *Hamiltonian density*, $\mathscr{H}$, along with the energy flux, $\boldsymbol{\mathscr{F}}$,

$$\mathscr{P} \equiv \frac{\partial \mathscr{L}}{\partial(\partial_t \psi)} \quad \text{and} \quad \mathscr{H} = \mathscr{P}\, \partial_t \psi - \mathscr{L} \quad \text{and} \quad \mathscr{F}^a = \frac{\partial \mathscr{L}}{\partial(\partial_a \psi)} \frac{\partial \psi}{\partial t}. \tag{46.64}$$

These definitions bring equation (46.63) to the form of a budget equation for the Hamiltonian density

$$\partial_t \mathscr{H} + \nabla \cdot \boldsymbol{\mathscr{F}} = - \left[\frac{\partial \mathscr{L}}{\partial t} \right]_{\psi, \partial_t \psi, \partial_x \psi, \boldsymbol{x}}. \tag{46.65}$$

Evidently, the Hamiltonian density at a point in space evolves according to the covariant convergence of the flux, $\boldsymbol{\mathscr{F}}$, along with a source term due to any explicit time dependence of the Lagrangian density.

When the Lagrangian density has no explicit time dependence, so that

$$\mathscr{L} = \mathscr{L}(\psi, \partial_t \psi, \partial_a \psi, x^a), \tag{46.66}$$

then the budget equation (46.65) reduces to the *Hamiltonian density continuity equation*

$$\partial_t \mathscr{H} + \nabla \cdot \boldsymbol{\mathscr{F}} = 0. \tag{46.67}$$

This equation is written in the form of a continuum conservation law, with such conservation laws encountered throughout this book.[8] Evidently, for the special case of a time independent spatial domain, and with the flux, $\boldsymbol{\mathscr{F}}$, having zero area integrated normal projection at the domain boundary, we are led to the conservation of the domain integrated Hamiltonian

$$\frac{\mathrm{d}H}{\mathrm{d}t} = 0 \quad \text{with} \quad H = \int_{\mathscr{R}} \mathscr{H}\, \mathrm{d}V = \int_{\mathscr{R}} \mathscr{H}\, g\, \mathrm{d}^3 x, \tag{46.68}$$

where $\mathscr{R}$ is the spatial domain. This result constitutes an expression of Noether's theorem arising from time symmetry.

[7] The metric tensor is generally time dependent when represented using generalized vertical coordinates considered in Part XII of this book. We return to this point in Part XII when formulating a Hamilton's principle with generalized vertical coordinates.

[8] See Section 26.12 for more discussion on such continuum conservation laws.

46.4.2 Stress-energy-momentum tensor

The derivation in Section 46.4.1 can be generalized to yield a budget equation built from elements of the *stress-energy-momentum tensor*. The space-time derivative of the Lagrangian density is given by (again, being careful with partial derivatives as discussed in Section 46.3.1)

$$\frac{\partial \mathscr{L}}{\partial x^\beta} = \frac{\partial \mathscr{L}}{\partial \psi} \frac{\partial \psi}{\partial x^\beta} + \frac{\partial \mathscr{L}}{\partial (\partial_\alpha \psi)} \frac{\partial}{\partial x^\alpha} \frac{\partial \psi}{\partial x^\beta} + \left[\frac{\partial \mathscr{L}}{\partial x^\beta} \right]_{\psi, \partial_\alpha \psi, x^{\alpha \neq \beta}}. \tag{46.69}$$

Use of the Euler-Lagrange equation (46.48) leads to

$$\frac{\partial \mathscr{L}}{\partial x^\beta} = g^{-1} \frac{\partial}{\partial x^\alpha} \left[g \frac{\partial \mathscr{L}}{\partial (\partial_\alpha \psi)} \frac{\partial \psi}{\partial x^\beta} \right] + \left[\frac{\partial \mathscr{L}}{\partial x^\beta} \right]_{\psi, \partial_\alpha \psi, x^{\alpha \neq \beta}}. \tag{46.70}$$

Now assume the metric determinant is independent of coordinate x^β so that

$$\partial g / \partial x^\beta = 0, \tag{46.71}$$

in which case we have

$$g^{-1} \frac{\partial}{\partial x^\alpha} \left[-g \, \delta^\alpha{}_\beta \, \mathscr{L} + g \frac{\partial \mathscr{L}}{\partial (\partial_\alpha \psi)} \frac{\partial \psi}{\partial x^\beta} \right] = - \left[\frac{\partial \mathscr{L}}{\partial x^\beta} \right]_{\psi, \partial_\alpha \psi, x^{\alpha \neq \beta}}. \tag{46.72}$$

Introducing the *stress-energy-momentum tensor*

$$T^\alpha{}_\beta = -\delta^\alpha{}_\beta \, \mathscr{L} + \frac{\partial \mathscr{L}}{\partial (\partial_\alpha \psi)} \frac{\partial \psi}{\partial x^\beta}, \tag{46.73}$$

brings equation (46.72) to the form

$$g^{-1} \, \partial_\alpha (g \, T^\alpha{}_\beta) = - \left[\frac{\partial \mathscr{L}}{\partial x^\beta} \right]_{\psi, \partial_\alpha \psi, x^{\alpha \neq \beta}}, \tag{46.74}$$

For each value of β, this equation says that the four-divergence of $T^\alpha{}_\beta$ is determined by the partial derivative of the Lagrangian with respect to x^β. Integrating over the global space domain, and assuming the domain is time-independent, leads to

$$\frac{\mathrm{d}}{\mathrm{d}t} \int_{\mathscr{R}} T^0{}_\beta \, g \, \mathrm{d}^3 x = - \int_{\partial \mathscr{R}} T^a{}_\beta \, \hat{n}_a \, \mathrm{d}\mathcal{S} - \int_{\mathscr{R}} \left[\frac{\partial \mathscr{L}}{\partial x^\beta} \right]_{\psi, \partial_\alpha \psi, x^{\alpha \neq \beta}} g \, \mathrm{d}^3 x, \tag{46.75}$$

where we used the general coordinate version of the divergence theorem from Section 4.19. If the Lagrangian is not an explicit function of x^β, and we have a vanishing boundary integral of the flux, $T^a{}_\beta$, projected onto the outward normal, then there is a global conserved quantity

$$\frac{\mathrm{d}}{\mathrm{d}t} \int_{\mathscr{R}} T^0{}_\beta \, g \, \mathrm{d}^3 x = 0 \quad \Longleftarrow x^\beta \text{ is a cyclic coordinate.} \tag{46.76}$$

In the study of analytical mechanics in Section 12.10.1, we referred to x^β as a *cyclic* coordinate. Cyclic coordinates arise from a symmetry of the physical system, and the coordinates used to represent the system, along the direction defined by the cyclic coordinate. This symmetry then leads to a conservation law, as we just showed. This result represents an example implication of Noether's theorem: any symmetry gives rise to a conservation law. We offer more on Noether's theorem in Section 46.5. Note that when $\beta = 0$, the budget equation (46.74) includes equation

(46.65) for Hamiltonian density

$$\mathcal{H} = T^0{}_0 = -\mathcal{L} + \frac{\partial \mathcal{L}}{\partial(\partial_t \psi)} \frac{\partial \psi}{\partial t} \qquad \text{Hamiltonian density} \tag{46.77a}$$

$$\mathcal{F}^a = T^a{}_0 = \frac{\partial \mathcal{L}}{\partial(\partial_a \psi)} \frac{\partial \psi}{\partial t} \qquad \text{Hamiltonian density flux,} \tag{46.77b}$$

and for $\beta = b > 0$ we define

$$T^0{}_b = \frac{\partial \mathcal{L}}{\partial_t \psi} \frac{\partial \psi}{\partial x^b} \qquad \text{momentum density} \tag{46.78a}$$

$$T^a{}_b = -\mathcal{L}\, \delta^a{}_b + \frac{\partial \mathcal{L}}{\partial_a \psi} \frac{\partial \psi}{\partial x^b} \qquad \text{stress tensor.} \tag{46.78b}$$

46.4.3 An auxiliary functional for deriving conservation laws

Hayes (1970) introduced an alternative method for computing conservation laws, with particular application to the wave-action conservation law (see Section 50.5). In this method we introduce the functional

$$\mathcal{E}(\psi, \Phi) = \frac{\partial \mathcal{L}}{\partial(\partial_\alpha \psi)} \frac{\partial \Phi}{\partial x^\alpha} + \frac{\partial \mathcal{L}}{\partial \psi} \Phi \tag{46.79a}$$

$$= \frac{\partial \mathcal{L}}{\partial(\partial_\alpha \psi)} \frac{\partial \Phi}{\partial x^\alpha} + g^{-1} \frac{\partial}{\partial x^\alpha} \left[g \frac{\partial \mathcal{L}}{\partial(\partial_\alpha \psi)} \right] \Phi \tag{46.79b}$$

$$= g^{-1} \frac{\partial}{\partial x^\alpha} \left[g \frac{\partial \mathcal{L}}{\partial(\partial_\alpha \psi)} \Phi \right] \tag{46.79c}$$

$$= \nabla_\alpha \left[\frac{\partial \mathcal{L}}{\partial(\partial_\alpha \psi)} \Phi \right], \tag{46.79d}$$

where we used the Euler-Lagrange equation (46.48) for ψ, and where $\Phi(\boldsymbol{x}, t)$ is an arbitrary function yet to be specified. As a four-divergence, the functional, $\mathcal{E}$, has a spatial domain integral depending on the boundary conditions.

Separating the space and time derivative terms, and introducing the canonical momentum from equation (46.64), leads to

$$\mathcal{E}(\psi, \Phi) = g^{-1}\, \partial_t (g\, \Phi\, \mathcal{P}) + g^{-1} \frac{\partial}{\partial x^a} \left[g\, \Phi\, \frac{\partial \mathcal{L}}{\partial(\partial_a \psi)} \right]. \tag{46.80}$$

Now we specify $\Phi = \partial\psi/\partial t$ to render

$$\mathcal{E} = g^{-1} \left[\frac{\partial [g\, (\mathcal{H} + \mathcal{L})]}{\partial t} \right]_{\boldsymbol{x}} + \nabla_a \mathcal{F}^a = \left[\frac{\partial \mathcal{L}}{\partial t} \right]_{\boldsymbol{x}} - \left[\frac{\partial \mathcal{L}}{\partial t} \right]_{\psi, \partial_t \psi, \partial_x \psi, \boldsymbol{x}}, \tag{46.81}$$

where $\mathcal{F}^a$ are components to the energy flux (46.64), we introduced the Hamiltonian density, $\mathcal{H}$, also given by equation (46.64), and made use of equation (46.61) to introduce the partial time derivatives. If the metric is independent of time, then the $[\partial \mathcal{L}/\partial t]_{\boldsymbol{x}}$ term cancels on both sides, which then renders the Hamiltonian continuity equation (46.65). We can likewise derive the momentum conservation equations from Section 46.4.2 through setting $\Phi = \partial_a \psi$. In Section 50.5 we introduce yet another choice useful for the study of waves.

46.4.4 Summary of the cyclic coordinate method

A physical system has no dependence on cyclic coordinates, so there is an arbitrariness associated with the value of the coordinate. This arbitrariness then leads to a corresponding differential conservation law in the form of a continuity equation. We here summarize the cyclic coordinate method used in this section to construct conservation laws. Generalizing the discussion of *mechanical equivalence* from Section 46.3.5, we know that a space-time variation has no impact on the physical system if the Lagrangian density changes only by a total divergence

$$\delta\mathcal{L} = \mathcal{L}[\psi(x'), \partial_\alpha\psi(x'), x'] - \mathcal{L}[\psi(x), \partial_\alpha\psi(x), x] = \delta x^\alpha\, \partial_\alpha\mathcal{L}. \tag{46.82}$$

If the Lagrangian has no explicit dependence on any of the space-time coordinates, x^α, then

$$\delta\mathcal{L} = \delta x^\alpha\, \partial_\alpha\mathcal{L} = \delta x^\alpha \left[\frac{\partial\mathcal{L}}{\partial\psi}\,\frac{\partial\psi}{\partial x^\alpha} + \frac{\partial\mathcal{L}}{\partial(\partial_\beta\psi)}\,\frac{\partial}{\partial x^\beta}\frac{\partial\psi}{\partial x^\alpha}\right]. \tag{46.83}$$

Thus far we have not used the Euler-Lagrange equations, so that equation (46.83) results solely due to the absence of an explicit dependence of $\mathcal{L}$ on the space-time coordinates, x^α. An alternative approach to computing the variation is found by writing

$$\delta\mathcal{L} = \frac{\partial\mathcal{L}}{\partial\psi}\,\delta\psi + \frac{\partial\mathcal{L}}{\partial(\partial_\alpha\psi)}\,\delta(\partial_\alpha\psi), \tag{46.84}$$

where we again assumed $\mathcal{L}$ has no explicit dependence on any of the space-time coordinates, x^α. We now make use of the Euler-Lagrange equation (46.48) to bring equation (46.84) into the form

$$\delta\mathcal{L} = g^{-1}\,\frac{\partial}{\partial x^\alpha}\left[g\,\frac{\partial\mathcal{L}}{\partial(\partial_\alpha\psi)}\,\delta\psi\right] = g^{-1}\,\delta x^\beta\,\frac{\partial}{\partial x^\alpha}\left[g\,\frac{\partial\mathcal{L}}{\partial(\partial_\alpha\psi)}\,\frac{\partial\psi}{\partial x^\beta}\right], \tag{46.85}$$

where we made use of the variation of the field and its derivative

$$\delta\psi = \psi(x') - \psi(x) = \delta x^\beta\,\partial_\beta\psi(x) \tag{46.86a}$$

$$\delta(\partial_\alpha\psi) = \partial_\alpha[\psi(x') - \psi(x)] = \delta x^\beta\,\partial_\beta\partial_\alpha\psi(x), \tag{46.86b}$$

and remembered that δx^β is a constant. Setting $\delta\mathcal{L}$ from equation (46.83) equal to $\delta\mathcal{L}$ from equation (46.85) leads to

$$\delta x^\beta\, g^{-1}\,\partial_\alpha(g\,T^\alpha{}_\beta) = 0, \tag{46.87}$$

where we introduced the stress-energy-momentum tensor from equation (46.73)

$$T^\alpha{}_\beta = -\delta^\alpha{}_\beta\,\mathcal{L} + \frac{\partial\mathcal{L}}{\partial(\partial_\alpha\psi)}\,\frac{\partial\psi}{\partial x^\beta}. \tag{46.88}$$

We have thus established four conservation laws (one for each value of $\beta = 0, 1, 2, 3$) that correspond to the space-time shift symmetry

$$\nabla_\alpha T^\alpha{}_\beta = g^{-1}\,\partial_\alpha(g\,T^\alpha{}_\beta) = 0. \tag{46.89}$$

There is no conservation law for those coordinates that have an explicit appearance in the Lagrangian. For example, if the Lagrangian has an explicit time dependence, such as when considering astronomical tidal forcing on the ocean, then the total energy of the system (as measured by the globally integrated Hamiltonian density) is not a constant. Instead, the system's energy is affected by the astronomical forces whose dynamics is described by another Lagrangian density that sits outside of the ocean that serves to modify the gravitational force. That is, a non-constant energy is generally a consequence of a physical system being mechanically open.

Similarly, if the Lagrangian is a function of one of the spatial coordinates, then that indicates the absence of spatial symmetry in that direction and so the absence of a global conservation law.

46.5 Noether's theorem and symmetries of the action

In Section 46.4 we derived dynamical conservation laws by identifying cyclic coordinates in the Lagrangian density. Here we further our understanding of how symmetries give rise to conservation laws by introducing a few more concepts and methods. Central to these concepts is the notion of a transformation, and we are only concerned with smooth and continuous transformations rather than discrete. To determine physical implications of a continuous transformation, it is sufficient to examine how the action varies under an infinitesimal transformation, which we refer to as a *variation*. This treatment is convenient since deriving the implications of infinitesimal variations is simpler mathematically than finite transformations. In effect, we only need to work to leading order in a Taylor expansion to deduce the differential conservation laws.

46.5.1 Distinctions beween Noether and Hamilton

Recall from Section 46.2 that we derived the Euler-Lagrange equation of motion by examining how the action changes when confronted with a functional variation of the field, $\psi \to \psi + \delta\psi$, with $\delta\psi$ vanishing along the time boundary. Setting to zero the corresponding variation of the action, $\delta\mathcal{S} = 0$, is the statement of Hamilton's principle that leads to the Euler-Lagrange equation (along with natural spatial boundary conditions) that are satisfied by the physically realized dynamical system. The variations are never physically realized. Hamilton's realized that by probing these unphysical realizations renders a novel perspective (relative to Newton) on the physically realized system.

To deduce conservation laws using Noether's theorem requires a conceptual approach that builds from that used for Hamilton's principle. For Hamilton's principle we postulate that variation of the action vanishes when considering a variation in the field in the interior of the space-time domain. For Noether's theorem we work exclusively with the physical system that satisfies the Euler-Lagrange equations that arise from invoking Hamilton's principle. Noether's theorem then exposes the differential conservation laws arising from symmetries, as probed by variations to the space-time, that leave the physically realized action unchanged (or mechanically equivalent).

46.5.2 Active transformations

There are two complementary perspectives we take when considering a transformation (and its infinitesimal version referred to as a *variation*): the *active transformation* (*active variation*) and the *passive transformation* (*passive variation*). Active transformations arise from moving the physical system through space-time, whereas a passive transformation modifies the space-time coordinates while keeping the physical system unchanged. We here discuss active transformations with Section 46.5.3 considering the passive.[9] Notably, they lead to the same mathematical result, and yet conceptually it can be useful to take one or the other perspective when studying variations to physical systems.

Active transformations and Noether's first theorem

Operationally, an active transformation arises from confronting the action with a variation of the physical fields (to probe *internal symmetries*) and/or a variation of the space-time position

[9] Chapter 3 in *José and Saletan* (1998) provides a thorough discussion of active and passive transformations.

of the system (to probe space-time symmetries). With these variations considered in their active sense, we imagine the physical system to be transformed (e.g., moved or rotated) whereas the space-time coordinate system used to describe the physical system remain unchanged. Moving an experimental apparatus from one side of the laboratory to another is an example active transformation, as is rotating the apparatus by some angle. Those active transformations that leave the action unchanged are symmetries of the physical system that directly lead to differential conservation laws. This connection between active symmetries and conservation laws constitutes *Noether's first theorem.*

Active transformations leave the coordinate system unchanged

As note above, the coordinate system used to describe the physical system is unchanged when performing an active transformation. Instead, an active transformation results in the modification to the space-time position of a point within the physical system

$$x^\alpha \to x'^\alpha = x^\alpha + \delta x^\alpha, \tag{46.90}$$

where δx^α is a tiny coordinate variation so that the space-time point, x', is very close to the point, x. Since the coordinate lines remain fixed under an active transformation, we do not introduce a new set of coordinates, which are typically expressed as $x^{\overline{\alpha}}$ in this book. Instead, we kept the same coordinates, and wrote x^α for the original space-time point and x'^α for the displaced space-time point.

Galilean space-time active transformations and Noether's first theorem

The space-time symmetries we focus on are taken from Galilean space-time, which is relevant for studies of geophysical fluid mechanics.[10] In particular, we consider a uniform space-time translation plus a rigid rotation. For a space and time coordinate translation, the new point has a coordinate position relative to the original point according to the coordinate variation

$$\delta x^\alpha = h^\alpha, \tag{46.91}$$

where h^α is a constant coordinate variation that is scaled by a tiny non-dimensional number to ensure that δx^α is tiny. To investigate spatial rotations we examine the coordinate variation determined by a small spatial rotation of the physical system as given by

$$\delta x^a = \mathcal{R}^a{}_b \, x^b \quad \text{and} \quad \delta x^0 = 0. \tag{46.92}$$

Here we introduced the anti-symmetric rotation matrix

$$\mathcal{R}^a{}_b = \epsilon^a{}_{bc} \, \Omega^c, \tag{46.93}$$

with $\boldsymbol{\Omega} = \widehat{\boldsymbol{\Omega}} \, |\boldsymbol{\Omega}|$ a vector that orients the rotation and with $|\boldsymbol{\Omega}| \ll 1$ a tiny angle. Bringing both the translation and rotation together into a single active variation leads to

$$x'^\alpha = x^\alpha + \delta x^\alpha = x^\alpha + h^\alpha + \mathcal{R}^\alpha{}_\beta \, x^\beta, \tag{46.94}$$

where $\mathcal{R}^\alpha{}_\beta = 0$ if either $\alpha = 0$ or $\beta = 0$.

[10] In other areas of physics, such as electrodynamics and quantum field theory, symmetries are examined within the Lorentzian space-time of special relativity.

Variations to the volume element under an active transformation

The spatial coordinate measure, d^3x, remains unchanged since the coordinate lines are fixed under an active transformation. However, since we are moving the physical system to a new space-time position and/or modifying its spatial orientation, the spatial metric tensor is generally modified. We here assume the metric is time independent, and consider the effects on the volume element under an active transformation. The volume element appearing within the action integral has a variation

$$\delta(g\,\mathrm{d}^3x) = \delta(g)\,\mathrm{d}^3x, \tag{46.95}$$

so we must determine a variation of the square root of the metric tensor determinant, g. It is a bit simpler to work with the determinant of the metric, g^2, which is a function only of the metric tensor elements, g_{ab}, so that

$$\delta g^2 = \frac{\partial g^2}{\partial g_{ab}}\,\delta g_{ab} = g^2\,g^{ab}\,\delta g_{ab}, \tag{46.96}$$

where the second equality follows from equation (4.75) holding for determinants.[11] We thus find that an active transformation leads to the variation of the spatial volume element

$$\delta(g\,\mathrm{d}^3x) = (g\,\mathrm{d}^3x)\,g^{ab}\,\delta g_{ab}/2 \iff \delta(\mathrm{d}V) = \mathrm{d}V\,g^{ab}\,\delta g_{ab}/2. \tag{46.97}$$

To determine the variation of the metric tensor components, we proceed much like in Section 18.8.8 where we determined the material evolution of the Cauchy-Green strain tensor, thus resulting in[12]

$$g^{ab}\,\delta g_{ab} = 2\,g^{ab}\,\nabla_a(\delta x_b) = 2\,\nabla^b(\delta x_b) = 2\,\nabla_a(\delta x^a), \tag{46.98}$$

so that

$$\delta(g\,\mathrm{d}^3x) = (g\,\mathrm{d}^3x)\,\nabla_a(\delta x^a) \iff \delta(\mathrm{d}V) = \mathrm{d}V\,\nabla_a(\delta x^a). \tag{46.99}$$

Evidently, under an active transformation, the relative variation of the volume element is determined by the covariant divergence of the coordinate variation, so that the active transformation is volume perserving if the covariant divergence vanishes

$$\nabla_a(\delta x^a) = 0 \implies \text{volume preserving active transformation.} \tag{46.100}$$

This result corresponds to that found using alternative methods in Chapters 18 and 19 when studying how fluid flow divergence affects the volume of a fluid element (e.g., see equation (19.18)). Indeed, we could have appealed to those earlier results to immediately write equation (46.99). Furthermore, we know that one physical way to alter the volume of a fluid region is to apply pressure work.

Variations to the mass element under an active transformation

In continuum mechanics we generally follow mass conserving parcels of matter. It is thus relevant to determine if the mass changes under an active transformation, in which we investigate

$$\delta(\rho\,\mathrm{d}V) = \rho\,\delta(\mathrm{d}V) + \delta\rho\,\mathrm{d}V \tag{46.101a}$$

$$= \mathrm{d}V\,(\rho\,\nabla_a(\delta x^a) + \delta x^a\,\partial_a\rho) \tag{46.101b}$$

[11] In words, equation (46.96) says that the derivative of the determinant, with respect to one of its elements (here g_{ab}), equals to the determinant times the component of the inverse matrix corresponding to the element (here g^{ab}).

[12] A more general approach makes use of *Lie derivatives* to compute the variation of the metric along the congruence of curves defined by the variation, δx^α. Here, we largely appeal to the intuition of the result (46.99). Section F.3 of *Tromp* (2025a) provides a lucid discussion of Lie derivatives.

$$= \mathrm{d}V\,(g^{-1}\,\rho\,\partial_a(g\,\delta x^a) + \delta x^a\,\partial_a\rho) \tag{46.101c}$$
$$= \mathrm{d}V\,\nabla_a(\rho\,\delta x^a). \tag{46.101d}$$

Evidently, the mass of a region of matter remains unchanged if the covariant divergence of the density weighted variation vanishes

$$\nabla_a(\rho\,\delta x^a) = 0 \Longrightarrow \text{mass preserving active transformation.} \tag{46.102}$$

This sort of transformation requires the volume of the region to reduce while the density increases, and vice versa, thus keeping the mass unchanged. Conversely, a nonzero covariant divergence, $\nabla_a(\rho\,\delta x^a) \neq 0$, is the signal of a modification to the mass of an infinitesimal region.

46.5.3 Passive transformations

A *passive transformation* keeps the physical system untouched while it alters its coordinate representation. For example, the transformation between Cartesian coordinates and spherical coordinates is passive, as is the transformation between Eulerian and Lagrangian coordinates. Passive transformations have been discussed extensively in this book in the context of tensor analysis, whereby tensors are considered objective geometric objects whose coordinate representations leave a tensor unchanged whereas the tensor's representation is changed (see Chapters 1 through 4). Equations written in a manner that remain form invariant under coordinate transformations are said to satisfy *coordinate covariance*. In the context of symmetry principles, if we can find a continuous transformation of the coordinates that leaves the physical action unchanged, then this passive transformation leads, through *Noether's second theorem*, to a local conservation law (sometimes referred to as a *Bianchi identity*). The particle relabeling symmetry detailed in Section 47.7 is an example of a passive transformation applied to fluid flow as represented using Lagrangian kinematics.

An infinitesimal passive transformation is a coordinate variation of the form

$$x^{\overline{\alpha}} = \delta^{\overline{\alpha}}{}_{\alpha}\,(x^\alpha + \delta x^\alpha), \tag{46.103}$$

which should be compared to the active variation in equation (46.90). The transformation matrix arising from the coordinate variation (46.103) is given by

$$\Lambda^{\overline{\alpha}}{}_{\beta} = \partial x^{\overline{\alpha}}/\partial x^\beta = \delta^{\overline{\alpha}}{}_{\alpha}\,[\delta^\alpha{}_\beta + \partial_\beta(\delta x^\alpha)], \tag{46.104}$$

and its Jacobian determinant is, to leading order in variation, given by

$$\det(\Lambda^{\overline{\alpha}}{}_{\beta}) \approx 1 + \partial_\alpha(\delta x^\alpha). \tag{46.105}$$

Consequently, the space-time coordinate measure transforms according to

$$\mathrm{d}^4\overline{x} = \det(\Lambda^{\overline{\alpha}}{}_{\beta})\,\mathrm{d}^4x = [1 + \partial_\alpha(\delta x^\alpha)]\,\mathrm{d}^4x \Longrightarrow \delta(\mathrm{d}^4x) = (\partial_\alpha(\delta x^\alpha)\,\mathrm{d}^4x. \tag{46.106}$$

Assuming the metric tensor is time independent, we find that the spatial volume element transforms as

$$\delta(\mathrm{d}V) = \delta(g\,\mathrm{d}^3x) = [g^{-1}\,\delta x^a\,\partial_a g + \partial_a(\delta x^a)]\,g\,\mathrm{d}^3x = (\nabla_a\delta x^a)\,\mathrm{d}V. \tag{46.107}$$

Hence, a volume conserving passive transformation arises from the same non-divergence condition (46.100) holding for the active transformation. In a similar manner, we find that the mass transforms under a passive transformation just as for the active transformation (46.101d), so that the mass is unchanged if $\nabla_a(\rho\,\delta x^a) = 0$.

46.5.4 Total variation of the field

In Section 46.2.2 we defined the functional variation of the field, $\delta\psi$. The functional variation affects a change just to the function, with the space-time point unchanged

$$\delta\psi(x^\alpha) = \psi'(x^\alpha) - \psi(x^\alpha), \tag{46.108}$$

where each term is evaluated at the same space-time point using the coordinate, x^α. This is the sort of variation considered for Hamilton's principle. Focusing here on active transformations, we find it useful to define the *total variation*, which considers both a functional change as well as a change to the space-time point, so that (dropping the α label on $\psi(x^\alpha)$ for brevity)

$$\begin{aligned}
\Delta\psi(x) &\equiv \psi'(x') - \psi(x) && \text{(46.109a)}\\
&= [\psi'(x') - \psi(x')] + [\psi(x') - \psi(x)] && \text{(46.109b)}\\
&\approx \delta\psi(x') + \delta x^\alpha\, \partial_\alpha\psi(x) && \text{(46.109c)}\\
&\approx \delta\psi(x) + \delta x^\alpha\, \partial_\alpha\psi(x). && \text{(46.109d)}
\end{aligned}$$

For the final equality we set

$$\delta\psi(x') \approx \delta[\psi(x) + \delta x^\alpha\, \partial_\alpha\psi(x)] = \delta\psi(x) + \mathcal{O}(\delta^2), \tag{46.110}$$

with second order terms ignored. Evidently, to first order in δ, the total variation of the field is given by

$$\Delta\psi(x) = (\delta + \delta x^\alpha\, \partial_\alpha)\, \psi(x). \tag{46.111}$$

The first term on the right hand side is the functional variation, $\delta\psi$, and the second term is a transport term that arises from translation and/or rotation of the coordinates, $\delta x^\alpha\, \partial_\alpha\psi$. Note that when we are just probing space-time symmetries, then $\Delta\psi = 0$ so that $\delta\psi = -\delta x^\alpha\, \partial_\alpha\psi$.

46.5.5 Variation of the action under an active transformation

We here consider the variation of the action under an active transformation

$$\delta\mathcal{S} = \mathcal{S}' - \mathcal{S} = \int_{\mathrm{R}} \mathcal{L}[\psi'(x'), \partial_\alpha\psi'(x'), x'^\alpha]\, g'\, \mathrm{d}^4x' - \int_{\mathrm{R}} \mathcal{L}[\psi(x), \partial_\alpha\psi(x), x^\alpha]\, g\, \mathrm{d}^4x. \tag{46.112}$$

Making use of equation (46.107) for the volume element renders, to first order in variation,

$$\delta\mathcal{S} = \int_{\mathrm{R}} [\delta + \nabla_\alpha(\delta x^\alpha)]\, \mathcal{L}[\psi(x), \partial_\alpha\psi(x), x^\alpha]\, g\, \mathrm{d}^4x. \tag{46.113}$$

The chain rule yields the variation

$$\begin{aligned}
\delta\mathcal{L} + \mathcal{L}\, \nabla_\alpha(\delta x^\alpha) &= \frac{\partial\mathcal{L}}{\partial\psi}\, \delta\psi + \frac{\partial\mathcal{L}}{\partial(\partial_\alpha\psi)}\, \delta(\partial_\alpha\psi) + \frac{\partial\mathcal{L}}{\partial x^\alpha}\, \delta x^\alpha + g^{-1}\, \mathcal{L}\, \partial_\alpha(\delta x^\alpha) && \text{(46.114a)}\\
&= \frac{\partial\mathcal{L}}{\partial\psi}\, \delta\psi + \frac{\partial\mathcal{L}}{\partial(\partial_\alpha\psi)}\, \delta(\partial_\alpha\psi) + \nabla_\alpha(\mathcal{L}\, \delta x^\alpha), && \text{(46.114b)}
\end{aligned}$$

with the Euler-Lagrange equation (46.47) substituted in for $\partial\mathcal{L}/\partial\psi$ rendering the very tidy result

$$\delta\mathcal{L} + \mathcal{L}\, \nabla_\alpha(\delta x^\alpha) = \nabla_\alpha \left[\frac{\partial\mathcal{L}}{\partial(\partial_\alpha\psi)}\, \delta\psi + \mathcal{L}\, \delta x^\alpha \right]. \tag{46.115}$$

Now introduce the total variation, $\Delta\psi$, from equation (46.109d), and the stress-energy-momentum tensor from equation (46.73) to find

$$\delta\mathcal{L} + \mathcal{L}\,\nabla_\alpha(\delta x^\alpha) = \nabla_\alpha\left[\frac{\partial\mathcal{L}}{\partial(\partial_\alpha\psi)}\,\Delta\psi - T^\alpha{}_\beta\,\delta x^\beta\right], \tag{46.116}$$

which then leads to the variation of the action under and active transformation

$$\delta\mathcal{S} = \int_{\mathrm{R}}[\delta + \nabla_\alpha(\delta x^\alpha)]\,\mathcal{L}\,\mathrm{d}^4x = \int_{\mathrm{R}}\nabla_\alpha J^\alpha\,g\,\mathrm{d}^4x = \int_{\partial\mathrm{R}} J^\alpha\,\hat{n}_\alpha\,\mathrm{d}\mathcal{S}, \tag{46.117}$$

where $\hat{n}_\alpha\,\mathrm{d}\mathcal{S}$ is the oriented area element on the space-time boundary, and we introduced the space-time flux[13]

$$J^\alpha \equiv \frac{\partial\mathcal{L}}{\partial(\partial_\alpha\psi)}\,\Delta\psi - T^\alpha{}_\beta\,\delta x^\beta. \tag{46.118}$$

We conclude that if the total variation, $\Delta\psi$, reflects a symmetry of the physical system, then the action must have a zero variation, in which case we have the local conservation law (continuity equation)

$$\nabla_\alpha J^\alpha = 0, \tag{46.119}$$

where J^α is given by equation (46.118). This result constitutes Noether's first theorem.

46.5.6 Angular momentum and space isotropy

In Section 46.4 we considered the space-time symmetry associated with the absence of dependence on an origin, and we assumed the total field variation vanishes,

$$\Delta\psi = \psi'(x') - \psi(x) = 0 \Longrightarrow \delta\psi = -\delta x^\alpha\,\partial_\alpha\psi. \tag{46.120}$$

In this case the conservation law reduces to a statement about the stress-energy-momentum tensor (see Section 46.4.2). Namely, if there is no special space or time origin, then linear momentum and mechanical energy are conserved. Here we display the angular momentum conservation law arising from the absence of a dependence on the orientation of the spatial coordinates. We also consider $\Delta\psi = 0$, but specify the spatial variation according to the rotation (46.93) so that the active variation is

$$\delta x^0 = 0 \quad \text{and} \quad \delta x^a = \mathcal{R}^a{}_b\,x^b = \epsilon^a{}_{bc}\,\Omega^c\,x^b, \tag{46.121}$$

where Ω^c are the components to a spatial vector whose magnitude, $|\boldsymbol{\Omega}|$, is small. The space-time flux, J^α, from equation (46.118) thus has the components

$$-J^\beta = T^\beta{}_\alpha\,\delta x^\alpha = T^\beta{}_a\,\epsilon^a{}_{bc}\,\Omega^c\,x^b. \tag{46.122}$$

At this point we assume Cartesian coordinates, so that the covariant derivative is a partial derivative, and the four-convergence of the flux is

$$-\partial_\beta J^\beta = \partial_\beta T^\beta{}_a\,\epsilon^a{}_{bc}\,\Omega^c\,x^b + T^\beta{}_a\,\epsilon^a{}_{\beta c}\,\Omega^c. \tag{46.123}$$

If the physical system has no concern for the origin of space, then we know from Section 46.4.4 that $\partial_\beta T^\beta{}_a = 0$ for each of the $a = 1, 2, 3$ spatial coordinates. If the physical system likewise has no concern for the orientation of space (i.e., it is spatially isotropic), then we must have rotational symmetry. For that property to manifest in a conservation law requires the

[13] In the quantum field theory literature, J^α is referred to as a *current*, in analog to an electrical current. Here we refer to it as a flux to correspond to the nomenclature in flud mechanics.

stress-energy-momentum tensor to be symmetric so that

$$T^{\beta}{}_{a}\,\epsilon^{a}{}_{\beta c} = 0 \Longleftrightarrow T^{\beta}{}_{a} = T_{a}{}^{\beta} = (T^{\beta}{}_{a})^{\mathrm{T}}. \tag{46.124}$$

We encountered this same condition in Section 25.4 arising from similar considerations.[14]

46.5.7 Comments

The space-time symmetries considered in this section and Section 46.4 are generally broken in realistic physical systems. For example, in Chapter 47 we study the motion of a perfect fluid moving around a rotating and gravitating planet, with spatial symmetry reduced to axial symmetry around the rotation axis (assuming a smooth planet). When considering motion of a geophysical fluid on a realistic planet with non-smooth boundaries (i.e., mountains, land-sea boundaries), we have no spatial symmetry and so no momentum conservation. Even so, by examining the properties of closed fluid systems moving in spaces of particular symmetry, we reveal the conservation laws forming the foundation for the physical theory. Doing so provides a valuable conceptual and operational baseline for then examining how processes and boundary conditions break symmetry.

We have thus far only considered space-time symmetries, so that we assumed the total field variation vanishes,

$$\Delta\psi = \psi'(x') - \psi(x) = 0 \Longrightarrow \delta\psi = -\delta x^{\alpha}\,\partial_{\alpha}\psi, \tag{46.125}$$

which means that the field is a scalar. But the formalism developed in this section also allows for probing symmetries in the space of fields, in which $\Delta\psi \neq 0$. If the action remains unchanged under a $\Delta\psi \neq 0$, then that reflects an *internal symmetry* that is not associated with space and time symmetries. Such internal symmetries are the basis for *gauge theories* of particle physics, as discussed in *Quigg* (1983), *Ryder* (1985), *Ramond* (1990), and many other texts.

46.5.8 Further study

The treatment of Noether's theorem in this section was inspired by Chapter 2 of *Quigg* (1983), Section E.1 of *Wald* (1984), Section 3.2 of *Ryder* (1985), Section 1.5 of *Ramond* (1990), and Section 2.6 of *Tromp* (2025a).

[14] There are some Lagrangian densities that do not produce a symmetric stress-energy-momentum tensor when evaluating equation (46.73). However, we can add a term, $\partial_{\lambda}F^{\lambda\alpha}{}_{\beta}$, to $T^{\alpha}{}_{\beta}$ without affecting the conservation law (46.89), so long as $F^{\lambda\alpha}{}_{\beta} = -F^{\alpha\lambda}{}_{\beta}$. This gauge degree of freedom allows us to always work with a symmetrized stress-energy-momentum tensor. See Section E.1 of *Wald* (1984) or Section 3.2 of *Ryder* (1985) for more discussion on this point, which is of particular relevance to general relativity.

Chapter 47

HAMILTON'S PRINCIPLE FOR PERFECT FLUIDS

In this chapter we derive the momentum equation (Euler equation) for a single-component perfect fluid using *Hamilton's variational principle* rather than Newton's laws. To do so, we couple the field theory of Chapter 46 with the Lagrangian kinematics of the motion field, $\boldsymbol{\varphi}(\boldsymbol{a}, T)$, thus deriving a field theory for $\boldsymbol{\varphi}$ in Lagrangian space-time. Hamilton's principle is concerned with conservative physical systems, such as a single component perfect fluid in a static gravitational field with each fluid parcel only experiencing reversible processes (i.e., no diffusion, friction, or conduction), which means that the fluid is contained within a materially and thermally closed domain. The fluid parcels feel conservative body forces from gravity, as well as, in a rotating terrestrial frame, the planetary Coriolis and planetary centrifugal forces are present. Interactions between the parcels are limited to mechanical contact forces from pressure, with pressure forces performing work on fluid parcels by modifying their volume (for non-Boussinesq fluids).

READER'S GUIDE FOR THIS CHAPTER

Mathematical elements of variational principles are presented in Chapter 10, along with a suite of examples. We make use of arbitrary material coordinates ($\boldsymbol{a}$-space), thus requiring the general tensor analysis as detailed in Chapters 3 and 4. We use general Eulerian ($\boldsymbol{x}$-space) coordinates up to the point of deriving the variation of the internal energy, at which point we assume Cartesian Eulerian coordinates. We make full use of the Lagrangian kinematics from Chapters 17, 18, and 19, and require a rudimentary understanding of thermodynamics as considered in Part IV. Development and use of Hamilton's principle are provided in Chapters 12 and 15 for discrete systems and in Chapter 46 for continuous fields.

Salmon (1988) is the canonical reference for Hamilton's principle in fluid mechanics (see also *Müller* (1995), chapter 7 in *Salmon* (1998) and *Badin and Crisciani* (2018)). *Soper* (2008) provides a treatment based on the Lorentz space-time of special relativity, though with some non-relativistic limiting cases to connect with the Galilean space-time of terrestrial motion. *Jezierski and Kijowski* (1990) and *Sieniutycz* (1994) target a unification of thermodynamics with continuum mechanics using variational methods. Our presentation makes use of general tensor notation for working in Lagrangian space-time, and offers a particular emphasis on the motion field, $\boldsymbol{\varphi}(\boldsymbol{a}, T)$, following from the treatment of continuum mechanics in Chapters 1 and 2 of *Tromp* (2025a).

47.1 Loose threads

- Referential flow and deviations from that flow
- Clean up notation and presenation, particularly in the particle relabeling Section 47.7.
- It would be nice not to need the Cartesian Eulerian assumption to compute the variation of the internal energy. Is there a simple way to generalize?

47.2 Motion and velocity

We here summarize salient points concerning the motion field studied in Chapters 17 and 18.

47.2.1 The motion field, flow map, deformation matrix, and velocity

We conceive of fluid flow as the smooth movement through space of a matter continuum, with this movement measured by the three-component *motion field*, $\boldsymbol{\varphi}$. Mathematically, the motion field provides the *flow map* that takes the matter continuum from its reference state (e.g., some spatial configuration at time $T = t_{\mathsf{R}}$) to the state at time $T > t_{\mathsf{R}}$. Assuming $\boldsymbol{x}$ is the position of a point in Euclidean space, the motion field provides a point transformation,

$$\boldsymbol{x} = \boldsymbol{\varphi}(\boldsymbol{a}, T) \quad \text{and} \quad t = T, \tag{47.1}$$

between the Eulerian ($\boldsymbol{x}$-position space) reference frame to the Lagrangian ($\boldsymbol{a}$-material space) reference frame. The motion field enables a 1-to-1 and invertible mapping (a *diffeomorphism*) between Eulerian and Lagrangian space-time. Transformation of tensors between Eulerian and Lagrangian space is provided by the *deformation matrix* (Section 18.4), with components to this matrix given by the partial derivatives

$$F^i{}_I = \frac{\partial \varphi^i}{\partial a^I} = \partial_I \varphi^i, \tag{47.2}$$

where lowercase indices are reserved for Eulerian space coordinates, x^i, and upper case for Lagrangian coordinates, a^I. The components to the inverse of the deformation matrix are written $F^I{}_i$, so that

$$F^i{}_J \, F^J{}_j = \delta^i{}_j \quad \text{and} \quad F^I{}_i F^i{}_J = \delta^I{}_J. \tag{47.3}$$

We also have use for the determinant of the transformation matrix (the Jacobian of transformation), which is written

$$\det(F^i{}_I) = \frac{\partial \boldsymbol{\varphi}}{\partial \boldsymbol{a}} \tag{47.4}$$

Evaluating the motion field for a particular value for the material coordinate, $\boldsymbol{a}$, and allowing time to progress, provides the space-time trajectory, $\boldsymbol{X}$, of the fluid particle labeled by $\boldsymbol{a}$

$$\boldsymbol{X}(\boldsymbol{a}, T) = \boldsymbol{\varphi}(\boldsymbol{a}, T). \tag{47.5}$$

The velocity of a material fluid particle is determined by the material time derivative of the motion

$$\boldsymbol{v}^{\mathsf{L}}(\boldsymbol{a}, T) = \partial_T \boldsymbol{\varphi}(\boldsymbol{a}, T) \Longleftrightarrow (v^{\mathsf{L}})^i = \partial_T \varphi^i. \tag{47.6}$$

We include the L superscript to emphasize that $\boldsymbol{v}^{\mathsf{L}}$ is sampled on a fluid particle and so it is a function of $(\boldsymbol{a}, T)$. Consequently, we commonly refer to $\boldsymbol{v}^{\mathsf{L}}$ as the "Lagrangian velocity". Even so, we see below (equation (47.8)) another candidate for this same name that is more precise from a tensor analysis perspective. The velocity $\boldsymbol{v}^{\mathsf{L}}$ has a dual Eulerian velocity, $\boldsymbol{v}(\boldsymbol{x}, t)$, that is equal to the Lagrangian velocity for the fluid particle that passes through $\boldsymbol{x}$ at time t

$$\boldsymbol{v}(\boldsymbol{x}, t) = \boldsymbol{v}^{\mathsf{L}}(\boldsymbol{a}, T) \quad \text{for } \boldsymbol{x} = \boldsymbol{\varphi}(\boldsymbol{a}, T) \text{ and } t = T. \tag{47.7}$$

This self-evident relation is reflected in all other properties of the continuum.

The Lagrangian velocity, $\boldsymbol{v}^{\mathsf{L}}(\boldsymbol{a}, T)$, and Eulerian velocity, $\boldsymbol{v}(\boldsymbol{x}, t)$, are generally distinct functions of their respective coordinates, thus prompting use of the distinct symbols, $\boldsymbol{v}^{\mathsf{L}}$ versus $\boldsymbol{v}$. For example, we might choose one of the material coordinates to be the specific entropy since for a perfect fluid the specific entropy is constant on fluid particles. For this case it is clear that $\boldsymbol{v}^{\mathsf{L}}(\boldsymbol{a}, T)$ and $\boldsymbol{v}(\boldsymbol{x}, t)$ are distinct mathematical functions. Even so, as tensors, both $\boldsymbol{v}^{\mathsf{L}}$ and $\boldsymbol{v}$ carry Eulerian space-time indices, $(v^{\mathsf{L}})^i$ and v^i. A representation of the velocity that carries Lagrangian space-time indices is realized through use of the inverse transformation matrix,

$$v^I = F^I{}_i \, (v^{\mathsf{L}})^i. \tag{47.8}$$

We encounter this *tensorially Lagrangian* representation of the velocity when studying the fluid particle relabeling symmetry in Section 47.7.

47.2.2 Including planetary rotation

As detailed in Section 13.6, the inertial frame representation for the velocity of a fluid particle moving on the rotating planet is given by

$$\boldsymbol{v}_{\text{inertial}} = \boldsymbol{v} + \boldsymbol{\Omega} \times \boldsymbol{x}, \tag{47.9}$$

where $\boldsymbol{v}$ is the particle velocity relative to the rotating planet, $\boldsymbol{\Omega}$ is the time-independent angular velocity of the rotating planet, $\boldsymbol{x}$ is the position vector of the particle relative to an origin, and $\boldsymbol{\Omega} \times \boldsymbol{x}$ is the velocity arising from the rigid body rotation of the planetary reference frame. The corresponding Eulerian velocity field for fluid motion on a rotating planet is thus given by

$$\boldsymbol{v}_{\text{inertial}}(\boldsymbol{x}, t) = \boldsymbol{v}(\boldsymbol{x}, t) + \boldsymbol{\Omega} \times \boldsymbol{x}, \tag{47.10}$$

and the Lagrangian velocity is

$$\boldsymbol{v}^{\text{L}}_{\text{inertial}}(\boldsymbol{a}, T) = \partial_T \boldsymbol{\varphi}(\boldsymbol{a}, T) + \boldsymbol{\Omega} \times \boldsymbol{\varphi}(\boldsymbol{a}, T). \tag{47.11}$$

As studied in Chapter 13, planetary rotation gives rise to the planetary Coriolis acceleration and planetary centrifugal acceleration when describing motion in the rotating terrestrial reference frame.

47.3 Mass, density, and specific volume

We here recall elements of fluid kinematics related to the mass and volume of infinitesimal material fluid parcels, and for finite sized spatial material domains denoted by $\mathcal{R}$. Since the region is material, it is time independent when expressed in terms of Lagrangian coordinates, $\mathcal{R}(\boldsymbol{a})$, whereas it is time dependent when expressed in terms of Eulerian coordinates, $\mathcal{R}(t)$.

47.3.1 Expressions for mass over a material region

From the discussion of mass conservation in Section 19.4.4, the mass over a material region can be written in either the Eulerian or Lagrangian integral expressions

$$M = \int_{\mathcal{R}(t)} \rho(\boldsymbol{x}, t)\, g^{\text{E}}(\boldsymbol{x})\, \mathrm{d}^3 x = \int_{\mathcal{R}(\boldsymbol{a})} \rho^{\text{L}}(\boldsymbol{a}, T)\, g^{\text{L}}(\boldsymbol{a}, T)\, \mathrm{d}^3 a. \tag{47.12}$$

The first expression for mass makes use of arbitrary Eulerian coordinates and thus represents the volume integral of mass density over the moving material region. The square root of the metric determinant, $g^{\text{E}}(\boldsymbol{x})$, is independent of Eulerian time, by construction of Eulerian coordinates, whereas the Lagrangian analog, $g^{\text{L}}(\boldsymbol{a}, T)$, is generally a function of the Lagrangian time. The second expression for mass in equation (47.12) makes use of Lagrangian coordinates, with the material coordinate element given by

$$\mathrm{d}^3 a = \mathrm{d}a^1\, \mathrm{d}a^2\, \mathrm{d}a^3, \tag{47.13}$$

which has physical dimensions determined by those of the material coordinates, (a^1, a^2, a^3). The products $g^{\text{E}}(\boldsymbol{x})\, \mathrm{d}^3 x$ and $g^{\text{L}}(\boldsymbol{a}, T)\, \mathrm{d}^3 a$ have dimensions of volume (L^3), so that they are expressions for the same invariant volume element studied in Section 18.7

$$\mathrm{d}V = g^{\text{E}}(\boldsymbol{x})\, \mathrm{d}^3 x = g^{\text{L}}(\boldsymbol{a}, T)\, \mathrm{d}^3 a. \tag{47.14}$$

This equation then leads to the identity (see equation (18.45)) for the Jacobian of transformation between Eulerian and Lagrangian coordinates

$$\frac{\partial \boldsymbol{x}}{\partial \boldsymbol{a}} = \frac{\partial \boldsymbol{\varphi}}{\partial \boldsymbol{a}} = \det(F^i{}_I) = \frac{g^{\mathsf{L}}}{g^{\mathsf{E}}}. \tag{47.15}$$

47.3.2 Constant mass fluid parcels

From Section 19.4.2, the mass of a fluid parcel remains constant when its center of mass follows a fluid particle trajectory, so that

$$\mathrm{d}M = \rho^{\mathsf{L}}(\boldsymbol{a}, T)\, g^{\mathsf{L}}(\boldsymbol{a}, T)\, \mathrm{d}^3 a \tag{47.16}$$

is a material constant. The element, $\mathrm{d}^3 a$, measures the material coordinate volume and it is fixed within material space. Hence, mass conservation for material parcels means that $\rho^{\mathsf{L}}(\boldsymbol{a}, T)\, g^{\mathsf{L}}(\boldsymbol{a}, T)$ is independent of material time,

$$\partial_T [\rho^{\mathsf{L}}(\boldsymbol{a}, T)\, g^{\mathsf{L}}(\boldsymbol{a}, T)] = 0. \tag{47.17}$$

We can thus set its value at any convenient time instance, which we choose as the $T = t_{\mathsf{R}}$ conditions and write

$$\mathring{\rho}^{\mathsf{L}}(\boldsymbol{a})\, \mathring{g}^{\mathsf{L}}(\boldsymbol{a}) = \rho^{\mathsf{L}}(\boldsymbol{a}, T = t_{\mathsf{R}})\, g^{\mathsf{L}}(\boldsymbol{a}, T = t_{\mathsf{R}}) = \rho^{\mathsf{L}}(\boldsymbol{a}, T)\, g^{\mathsf{L}}(\boldsymbol{a}, T), \tag{47.18}$$

with the corresponding mass of the material region

$$M = \int_{\mathscr{R}(\boldsymbol{a})} \mathring{\rho}^{\mathsf{L}}(\boldsymbol{a})\, \mathring{g}^{\mathsf{L}}(\boldsymbol{a})\, \mathrm{d}^3 a. \tag{47.19}$$

Evidently, $\mathring{\rho}^{\mathsf{L}}$, $\mathring{g}^{\mathsf{L}}$, and $\mathrm{d}^3 a$ are each set at the initial time, and thus are unaltered when considering the variation of trajectories when varying the action for Hamilton's principle in Section 47.5. They can be changed, however, when varying coordinates as per the discussion of particle relabeling in Section 47.7.

47.3.3 Cartesian Eulerian for when varying internal energy

We need the specific volume for working with the internal energy in Section 47.4.4, which from equations (47.18) and (47.15) yield

$$\nu_{\mathsf{s}}^{\mathsf{L}}(\boldsymbol{a}, T) = 1/\rho^{\mathsf{L}}(\boldsymbol{a}, T) = \frac{g^{\mathsf{L}}(\boldsymbol{a}, T)}{\mathring{\rho}^{\mathsf{L}}(\boldsymbol{a})\, \mathring{g}^{\mathsf{L}}(\boldsymbol{a})} = \frac{g^{\mathsf{E}}(\boldsymbol{x})}{\mathring{\rho}^{\mathsf{L}}(\boldsymbol{a})\, \mathring{g}^{\mathsf{L}}(\boldsymbol{a})} \frac{\partial \boldsymbol{\varphi}(\boldsymbol{a}, T)}{\partial \boldsymbol{a}}. \tag{47.20}$$

When varying the internal energy, we find it convenient to choose Cartesian coordinates for describing Eulerian $\boldsymbol{x}$-space. For this case we have $g^{\mathsf{E}} = 1$ so that

$$\nu_{\mathsf{s}}^{\mathsf{L}}(\boldsymbol{a}, T) = \frac{1}{\mathring{\rho}^{\mathsf{L}}(\boldsymbol{a})\, \mathring{g}^{\mathsf{L}}(\boldsymbol{a})} \frac{\partial \boldsymbol{\varphi}(\boldsymbol{a}, T)}{\partial \boldsymbol{a}} \Longleftarrow \text{Cartesian Eulerian coordinates with } g^{\mathsf{E}}(\boldsymbol{x}) = 1 \tag{47.21a}$$

$$\frac{\partial \boldsymbol{\varphi}(\boldsymbol{a}, T)}{\partial \boldsymbol{a}} = g^{\mathsf{L}}(\boldsymbol{a}, T) \Longleftarrow \text{Cartesian Eulerian coordinates with } g^{\mathsf{E}}(\boldsymbol{x}) = 1. \tag{47.21b}$$

47.3.4 Concerning mass-labeling/unimodular coordinates

The material time independence of $\mathring{\rho}^{\mathsf{L}}\,\mathring{g}^{\mathsf{L}}$ motivate some authors to assume the material coordinates are *unimodular*, which is also sometimes called *mass-labeling*. In this case, one sets

$$\mathring{\rho}^{\mathsf{L}}(\boldsymbol{a})\,\mathring{g}^{\mathsf{L}}(\boldsymbol{a}) = 1 \quad \text{mass-labeling (or unimodular) } \boldsymbol{a}\text{-space coordinates.} \tag{47.22}$$

These coordinates are used by, for example, *Salmon* (1988), *Jezierski and Kijowski* (1990), *Müller* (1995), and *Salmon* (1998). Furthermore, for $\boldsymbol{a}$-space mass-labeling coordinates and $\boldsymbol{x}$-space Cartesian coordinates, the specific volume from equation (47.21a) reduces to the Jacobian

$$\nu^{\mathsf{L}}_{\mathsf{s}}(\boldsymbol{a}, T) = \frac{\partial \boldsymbol{\varphi}(\boldsymbol{a}, T)}{\partial \boldsymbol{a}} \quad \text{Cartesian } \boldsymbol{x}\text{-space and mass-labeling } \boldsymbol{a}\text{-space.} \tag{47.23}$$

Although rather convenient for many purposes, we do not choose mass-labeling $\boldsymbol{a}$-space coordinates for the following reasons. First, doing so makes it awkward to use dimensional analysis as a check on the equations.[1] Second, it hides the fundamentally non-Cartesian nature of material space coordinates by hiding $\mathring{g}^{\mathsf{L}}$. This concern is mild, since one can readily assume the initial coordinate layout sets $\mathring{g}^{\mathsf{L}} = 1$. Third, we wish to maintain a connection between the perfect fluid field theory of this chapter to the continuum mechanics of *Tromp* (2025a), as well as the scalar field theory from Chapter 46, with unimodular coordinates obscuring that connection since it absorbs the density factor into the coordinates.

47.4 Energetics and entropy

In this section we develop equations for domain integrated kinetic energy, gravitational potential energy, and internal energy for a perfect fluid in a thermally and materially closed domain, $\mathcal{R}$, and as viewed from a rotating planetary reference frame.

47.4.1 Kinetic energy

Building on the two expressions for mass in equation (47.12) leads to the corresponding expressions for the kinetic energy within the material domain, first written using Cartesian Eulerian coordinates

$$E_{\text{KE}} = \frac{1}{2}\int_{\mathcal{R}(t)} (\boldsymbol{v} + \boldsymbol{\Omega}\times\boldsymbol{x})\cdot(\boldsymbol{v} + \boldsymbol{\Omega}\times\boldsymbol{x})\,\rho\, g^{\mathsf{E}}\,\mathrm{d}^3x, \tag{47.24}$$

and with the equivalent expression using arbitrary Lagrangian coordinates

$$E_{\text{KE}} = \frac{1}{2}\int_{\mathcal{R}(\boldsymbol{a})} (\partial_T\boldsymbol{\varphi} + \boldsymbol{\Omega}\times\boldsymbol{\varphi})\cdot(\partial_T\boldsymbol{\varphi} + \boldsymbol{\Omega}\times\boldsymbol{\varphi})\,\mathring{\rho}^{\mathsf{L}}\,\mathring{g}^{\mathsf{L}}\,\mathrm{d}^3a. \tag{47.25}$$

47.4.2 Gravitational potential energy

The gravitational potential, Φ_{e}, accounts for the potential energy per mass from the earth's gravity field (Section 13.10.2). As such, its domain integral measures the total gravitational potential energy of the fluid

$$E_{\text{GPE}} = \int_{\mathcal{R}(t)} \Phi_{\mathsf{e}}(\boldsymbol{x}, t)\,\rho\, g^{\mathsf{E}}\,\mathrm{d}^3x = \int_{\mathcal{R}(\boldsymbol{a})} \Phi_{\mathsf{e}}(\boldsymbol{\varphi}, T)\,\mathring{\rho}^{\mathsf{L}}\,\mathring{g}^{\mathsf{L}}\,\mathrm{d}^3a. \tag{47.26}$$

[1] Throughout this book we exploit the dimensional nature of physical quantities to enable the use of dimensional analysis in debugging mathematical equations. Unimodular or mass-labeling coordinates make that process difficult.

For most applications in this book, we assume the gravitational potential is time independent, which is required for a mechanically closed system as assumed here.[2]

47.4.3 Specific entropy is materially constant

As seen in Section 26.6.8, the specific entropy is materially constant for a perfect fluid. Consequently, each fluid parcel has a specific entropy equal to the value at its initial condition

$$\mathcal{S}(\boldsymbol{a}, T) = \mathcal{S}(\boldsymbol{a}, T = t_{\mathsf{A}}) = \mathring{\mathcal{S}}(\boldsymbol{a}). \tag{47.27}$$

With the density satisfying equation (47.18), the constancy of specific entropy means that the entropy content of a fluid parcel can be written

$$\mathcal{S}(\boldsymbol{a}, T)\, \rho^{\mathsf{L}}(\boldsymbol{a}, T)\, g^{\mathsf{L}}(\boldsymbol{a}, T)\, \mathrm{d}^3 a = \mathring{\mathcal{S}}(\boldsymbol{a})\, \mathring{\rho}^{\mathsf{L}}(\boldsymbol{a})\, \mathring{g}^{\mathsf{L}}(\boldsymbol{a})\, \mathrm{d}^3 a. \tag{47.28}$$

When applying Hamilton's principle, the fluid particle trajectories are unaltered at their temporal boundaries. Hence, any field that is independent of time, such as the the specific entropy, $\mathring{\mathcal{S}}(\boldsymbol{a})$, has zero variation under changes to the fluid particle trajectories. However, when varying the material coordinates, such as when studying particle relabeling in Section 47.7, then we find a nonzero $\delta\mathring{\mathcal{S}}(\boldsymbol{a})$.

47.4.4 Internal energy

As encountered in the study of thermodynamics in Part IV of this book, as well as the thermohydrodynamics in Chapter 26, *internal energy* is that portion of the total energy for a region of the continuum that is not accounted for by the mechanical energy of macroscopic motion (kinetic energy) nor the mechanical energy arising from being in an external force field (gravitational potential energy). The fundamental thermodynamic relation (22.62) for a single component fluid renders the natural functional dependency of specific internal energy (dimensions of energy per mass, which equals squared length per squared time)

$$\mathcal{I} = \mathcal{I}(\mathcal{S}, \nu_{\mathsf{s}}) = \mathcal{I}(\mathring{\mathcal{S}}(\boldsymbol{a}), \nu_{\mathsf{s}}), \tag{47.29}$$

with $\mathcal{S}$ the specific entropy and $\nu_{\mathsf{s}} = 1/\rho$ the specific volume. We also made use of results from Section 47.4.3 by setting $\mathcal{S}(\boldsymbol{a}, T) = \mathring{\mathcal{S}}(\boldsymbol{a})$ since the specific entropy remains materially constant. For the specific volume we make use of equation (47.21a), which assumes the Eulerian coordinates are Cartesian. In turn, it is just the Jacobian, $\partial\boldsymbol{\varphi}(\boldsymbol{a}, T)/\partial\boldsymbol{a}$, portion of the specific volume that is affected by variations in the trajectories. Bringing the above results together renders the integrated internal energy for the material fluid domain

$$E_{\mathsf{IE}} = \int_{\mathscr{R}(t)} \mathcal{I}(\boldsymbol{x}, t)\, \rho(\boldsymbol{x}, t)\, g^{\mathsf{E}}(\boldsymbol{x})\, \mathrm{d}^3 x = \int_{\mathscr{R}(\boldsymbol{a})} \mathcal{I}[\mathring{\mathcal{S}}(\boldsymbol{a}), \nu_{\mathsf{s}}^{\mathsf{L}}(\boldsymbol{a}, T)]\, \mathring{\rho}^{\mathsf{L}}(\boldsymbol{a})\, \mathring{g}^{\mathsf{L}}(\boldsymbol{a})\, \mathrm{d}^3 a. \tag{47.30}$$

47.5 Variation of the action and Euler-Lagrange equations

The action for the perfect fluid is given by the space-time integral of the kinetic energy minus the gravitational energy and minus the internal energy[3]

$$\mathsf{S}^{\backslash} = \int_{t_{\mathcal{A}}}^{t_{\mathcal{B}}} \int_{\mathscr{R}(\boldsymbol{a})} \left[\tfrac{1}{2}\, (\partial_T \boldsymbol{\varphi} + \boldsymbol{\Omega} \times \boldsymbol{\varphi}) \cdot (\partial_T \boldsymbol{\varphi} + \boldsymbol{\Omega} \times \boldsymbol{\varphi}) - \Phi_{\mathsf{e}} - \mathcal{I}\right] \mathring{\rho}^{\mathsf{L}}\, \mathring{g}^{\mathsf{L}}\, \mathrm{d}^3 a\, \mathrm{d}T. \tag{47.31}$$

[2] One exception concerns the study of a space-time dependent gravitational acceleration in Chapter 34.

[3] We write $\mathcal{S}^{\text{action}}$ for the action to distinguish it from the specific entropy, $\mathcal{S}$. Also note that the lower time bound for the action, t_{A}, is not necessarily the same as the time bound, t_{R}, used to define the base manifold.

We here focus on the action written in terms of Lagrangian coordinates rather than the Eulerian coordinates, with functional dependencies given by

$$\boldsymbol{\varphi}(\boldsymbol{a},T) \quad \text{and} \quad \Phi(\boldsymbol{\varphi}(\boldsymbol{a},T),T) \quad \text{and} \quad \mathcal{I}(\mathring{\mathcal{S}}(\boldsymbol{a}),\nu_{\mathsf{s}}^{\mathsf{L}}(\boldsymbol{a},T)). \tag{47.32}$$

Making use of Lagrangian kinematics provides a direct link between Hamilton's principle applied here to continuum matter and Hamilton's principle applied to the discrete particle systems in Chapters 12 and 15. Namely, we here examine a variation of the continuum motion field (i.e., trajectories) that vanishes at the temporal bounds (just like we did for particle mechanics)

$$\boldsymbol{\varphi}(\boldsymbol{a},T) \to \boldsymbol{\varphi}(\boldsymbol{a},T) + \delta\boldsymbol{\varphi}(\boldsymbol{a},T) \quad \text{with} \quad \delta\boldsymbol{\varphi}(\boldsymbol{a},t_{\mathsf{A}}) = \delta\boldsymbol{\varphi}(\boldsymbol{a},t_{\mathsf{B}}) = 0. \tag{47.33}$$

Hamilton's principle says that when varying the action by varying the motion, the physically realized motion extremizes the action so that

$$\text{Hamilton's principle} \implies \delta\mathcal{S}^{\text{action}} = 0. \tag{47.34}$$

Extremizing the action leads to the *Euler-Lagrange* equation satisfied by the Lagrangian. As derived in this section, the Euler-Lagrange equation is a partial differential equation satisfied by each component, φ^i, of the motion field. That is, we derive a Lagrangian space-time field theory for the three component motion field, $\boldsymbol{\varphi}(\boldsymbol{a},T)$.

We now summarize the operational task at hand to apply Hamilton's principle to the action (47.31). First, apply the variation operator, δ, to vary the motion field and compute the variation of the action. The variation operator acts solely on the motion field via equation (47.33). Hence, δ has no affect on space and time points, which means the variation operator commutes with $(\boldsymbol{a},T)$ and its differential operators.[4] We organize the varied integrand to isolate $\delta\varphi^i$, and we do so via integrating by parts and setting $\delta\varphi^i$ to zero on the temporal boundaries. Invoking Hamilton's principle renders the Euler-Lagrange differential equations and natural boundary conditions on the material space boundaries.

47.5.1 General expression for the Euler-Lagrange equation

We here directly follow the procedure used for the scalar field theory in Section 46.2. Here we have three fields for the three components to the motion field, with these fields living in Lagrangian space time. Following the approach in Section 46.2, we find it convenient to write the action (47.31) in the form

$$\mathcal{S}^{\text{action}} = \int_{t_{\mathsf{A}}}^{t_{\mathsf{B}}} \int_{\mathcal{R}(\boldsymbol{a})} \mathscr{L}\, \mathring{g}^{\mathsf{L}}\, \mathrm{d}^3a\, \mathrm{d}T \implies \delta\mathcal{S}^{\text{action}} = \int_{t_{\mathsf{A}}}^{t_{\mathsf{B}}} \int_{\mathcal{R}(\boldsymbol{a})} (\delta\mathscr{L})\, \mathring{g}^{\mathsf{L}}\, \mathrm{d}^3a\, \mathrm{d}T, \tag{47.35}$$

where we defined the *Lagrangian density* (dimensions of energy per material coordinate volume, d^3a)

$$\mathscr{L}[\boldsymbol{\varphi},\partial_T\boldsymbol{\varphi},\partial_I\boldsymbol{\varphi},\boldsymbol{a},T] = \mathring{\rho}^{\mathsf{L}}\left[\tfrac{1}{2}\left(\partial_T\boldsymbol{\varphi} + \boldsymbol{\Omega}\times\boldsymbol{\varphi}\right)\cdot\left(\partial_T\boldsymbol{\varphi} + \boldsymbol{\Omega}\times\boldsymbol{\varphi}\right) - \Phi_{\mathsf{e}} - \mathcal{I}(\mathring{\mathcal{S}},\nu_{\mathsf{s}}^{\mathsf{L}})\right]. \tag{47.36}$$

Note that varying the trajectories has no affect on $\mathring{g}^{\mathsf{L}}\,\mathrm{d}^3a$ since these terms are fixed at $T = t_{\mathsf{R}}$, and the same holds for $\mathring{\rho}^{\mathsf{L}}$.

[4] This commutation property holds when applying δ to the action for Hamilton's principle. However, as seen in Section 46.5, δ affects a variation of the space-time points when developing conservation laws using the methods of Noether's theorem. We emphasized these distinct variations in Section 46.5.1.

Use of the chain rule renders a variation of the Lagrangian density[5]

$$\mathring{g}^{\mathsf{L}}\,\delta\mathscr{L} = \mathring{g}^{\mathsf{L}}\,\frac{\partial\mathscr{L}}{\partial\varphi^i}\,\delta\varphi^i + \mathring{g}^{\mathsf{L}}\,\frac{\partial\mathscr{L}}{\partial(\partial_T\varphi^i)}\,\delta(\partial_T\varphi^i) + \mathring{g}^{\mathsf{L}}\,\frac{\partial\mathscr{L}}{\partial(\partial_I\varphi^i)}\,\delta(\partial_I\varphi^i), \tag{47.37}$$

where the summation convention is followed for the motion field indices, so that repeated indices are summed over their range, $i = 1, 2, 3$. Since the variation operator, δ, commutes with $(\boldsymbol{a}, T)$ derivative operators, we can write the equivalent expression

$$\mathring{g}^{\mathsf{L}}\,\delta\mathscr{L} = \mathring{g}^{\mathsf{L}}\,\frac{\partial\mathscr{L}}{\partial\varphi^i}\,\delta\varphi^i + \mathring{g}^{\mathsf{L}}\,\frac{\partial\mathscr{L}}{\partial(\partial_T\varphi^i)}\,\partial_T(\delta\varphi^i) + \mathring{g}^{\mathsf{L}}\,\frac{\partial\mathscr{L}}{\partial(\partial_I\varphi^i)}\,\partial_I(\delta\varphi^i). \tag{47.38}$$

We now bring the time and space derivative operators onto the full term and subtract the remainder. Doing so for the time derivative leads to

$$\mathring{g}^{\mathsf{L}}\,\frac{\partial\mathscr{L}}{\partial(\partial_T\varphi^i)}\,\frac{\partial(\delta\varphi^i)}{\partial T} = \frac{\partial}{\partial T}\left[\mathring{g}^{\mathsf{L}}\,\frac{\partial\mathscr{L}}{\partial(\partial_T\varphi^i)}\,\delta\varphi^i\right] - \frac{\partial}{\partial T}\left[\mathring{g}^{\mathsf{L}}\,\frac{\partial\mathscr{L}}{\partial(\partial_T\varphi^i)}\right]\delta\varphi^i. \tag{47.39}$$

When plugging this term into the action variation (47.35), the total time derivative on the right hand side vanishes since we assume $\delta\varphi^i$ vanishes at temporal boundaries as per equation (47.33). Similar manipulations lead to the material space derivative expression

$$\mathring{g}^{\mathsf{L}}\,\frac{\partial\mathscr{L}}{\partial(\partial_I\varphi^i)}\,\frac{\partial(\delta\varphi^i)}{\partial a^I} = \frac{\partial}{\partial a^I}\left[\mathring{g}^{\mathsf{L}}\,\frac{\partial\mathscr{L}}{\partial(\partial_I\varphi^i)}\,\delta\varphi^i\right] - \frac{\partial}{\partial a^I}\left[\mathring{g}^{\mathsf{L}}\,\frac{\partial\mathscr{L}}{\partial(\partial_I\varphi^i)}\right]\delta\varphi^i. \tag{47.40}$$

When plugging this term into the action variation (47.35), the total space derivative term vanishes if we assume the following natural boundary condition

$$\frac{\partial\mathscr{L}}{\partial(\partial_I\varphi^i)}\,\hat{n}_I = 0 \quad \text{at material boundaries,} \tag{47.41}$$

where $\hat{n}_I$ are components to the outward normal one-form along the material boundary. We encountered a similar version of the natural boundary conditions in Section 46.3.3 when studying Hamilton's principle for a scalar field.

Bringing terms together leads to the variation of the action (47.35) taking the form

$$\delta\mathcal{S}^{\mathsf{action}} = \int_{t_{\mathsf{A}}}^{t_{\mathsf{B}}}\int_{\mathscr{R}(\boldsymbol{a})}\left(\frac{\partial\mathscr{L}}{\partial\varphi^i} - \frac{1}{\mathring{g}^{\mathsf{L}}}\,\frac{\partial}{\partial T}\left[\mathring{g}^{\mathsf{L}}\,\frac{\partial\mathscr{L}}{\partial(\partial_T\varphi^i)}\right] - \frac{1}{\mathring{g}^{\mathsf{L}}}\,\frac{\partial}{\partial a^I}\left[\mathring{g}^{\mathsf{L}}\,\frac{\partial\mathscr{L}}{\partial(\partial_I\varphi^i)}\right]\right)\delta\varphi^i\,\mathring{g}^{\mathsf{L}}\,\mathrm{d}^3a\,\mathrm{d}T, \tag{47.42}$$

Variation of the motion, $\delta\varphi^i$, is arbitrary everywhere except at the temporal boundaries. Setting the variation of the action to zero as per Hamilton's principle requires the Lagrangian density to satisfy the Euler-Lagrange equation as well as the natural kinematic boundary condition, with both satisfied by each of the $i = 1, 2, 3$ components of the motion field

$$\frac{\partial\mathscr{L}}{\partial\varphi^i} = \frac{1}{\mathring{g}^{\mathsf{L}}}\,\frac{\partial}{\partial T}\left[\mathring{g}^{\mathsf{L}}\,\frac{\partial\mathscr{L}}{\partial(\partial_T\varphi^i)}\right] + \frac{1}{\mathring{g}^{\mathsf{L}}}\,\frac{\partial}{\partial a^I}\left[\mathring{g}^{\mathsf{L}}\,\frac{\partial\mathscr{L}}{\partial(\partial_I\varphi^i)}\right] \tag{47.43a}$$

$$\frac{\partial\mathscr{L}}{\partial(\partial_I\varphi^i)}\,\hat{n}_I = 0 \quad \text{at material boundaries.} \tag{47.43b}$$

The presence of $1/\mathring{g}^{\mathsf{L}}(\boldsymbol{a})$ on the outside of the derivatives, and $\mathring{g}^{\mathsf{L}}(\boldsymbol{a})$ on the inside, allows us to identify a covariant divergence (based on $\mathring{g}^{\mathsf{L}}$) on the right hand side of the Euler-Lagrange equation (47.43a). The $\mathring{g}^{\mathsf{L}}(\boldsymbol{a})$ term cancels for the time derivative term, since $\mathring{g}^{\mathsf{L}}(\boldsymbol{a})$ is independent

[5] When integrating by parts, we must keep track of the metric tensor determinant, $\mathring{g}^{\mathsf{L}}$, since it is a function of the material coordinates. We follow the approach in Section 46.3.2.

of material time. However, it is an essential piece for the space derivative term given that Lagrangian space coordinates are not Cartesian.

The Euler-Lagrange equation (47.43a) and boundary conditions (47.43b) are identical to those derived in Section 46.2.4 when studying scalar field theory. The only operational difference is that here we have $i = 1, 2, 3$ fields whereas there we had a single scalar field. We also note that here the field theory is in Lagrangian space-time, $(\boldsymbol{a}, T)$, rather than Eulerian space-time, $(\boldsymbol{x}, t)$, and the dynamical field is the motion field, $\boldsymbol{\varphi}(\boldsymbol{a}, T)$. As noted earlier in this section, the Lagrangian kinematic formulation of Hamilton's principle is directly connected to the discrete particle mechanics treatment of Hamilton's principle. In particular, by tracking the fluid motion field (i.e., fluid particle trajectories), we are afforded a straitghtforward means to constrain variations to vanish at the temporal boundaries. An Eulerian formulation does not follow fluid particles and requires Lagrange multipliers to constrain material coordinates to remain constant along trajectories (see Section 3 of *Salmon* (1988) for details).

In the remainder of this section we derive the Euler-Lagrange equations for the perfect fluid using the Lagrangian density (47.36). Rather than compute partial derivatives of the Lagrangian density as per the Euler-Lagrange equation (47.43a), we find it slightly more pedagogical to work directly from the action variation in equation (47.35).

47.5.2 Variation of the kinetic energy

Starting with the kinetic energy appearing in the Lagrangian density (47.36), we have

$$\tfrac{1}{2}\,(\partial_T \boldsymbol{\varphi}+\boldsymbol{\Omega}\times\boldsymbol{\varphi})\cdot(\partial_T \boldsymbol{\varphi}+\boldsymbol{\Omega}\times\boldsymbol{\varphi}) = \tfrac{1}{2}\,\partial_T\boldsymbol{\varphi}\cdot\partial_T\boldsymbol{\varphi}+\partial_T\boldsymbol{\varphi}\cdot(\boldsymbol{\Omega}\times\boldsymbol{\varphi})+\tfrac{1}{2}\,(\boldsymbol{\Omega}\cdot\boldsymbol{\Omega})\,(\boldsymbol{\varphi}\cdot\boldsymbol{\varphi})-\tfrac{1}{2}\,(\boldsymbol{\Omega}\cdot\boldsymbol{\varphi})^2, \tag{47.44}$$

which made use of the identity (1.73c). Use of the chain rule leads to the variation

$$\begin{aligned}&\delta\,[\tfrac{1}{2}\,(\partial_T\boldsymbol{\varphi}+\boldsymbol{\Omega}\times\boldsymbol{\varphi})\cdot(\partial_T\boldsymbol{\varphi}+\boldsymbol{\Omega}\times\boldsymbol{\varphi})]\\ &\qquad = \partial_T(\delta\boldsymbol{\varphi})\cdot(\partial_T\boldsymbol{\varphi}+\boldsymbol{\Omega}\times\boldsymbol{\varphi})+\partial_T\boldsymbol{\varphi}\cdot(\boldsymbol{\Omega}\times\delta\boldsymbol{\varphi})+\Omega^2\,\boldsymbol{\varphi}\cdot\delta\boldsymbol{\varphi}-(\boldsymbol{\Omega}\cdot\boldsymbol{\varphi})\,(\boldsymbol{\Omega}\cdot\delta\boldsymbol{\varphi}),\end{aligned} \tag{47.45}$$

which can be rearranged to

$$\begin{aligned}&\delta\,[\tfrac{1}{2}\,(\partial_T\boldsymbol{\varphi}+\boldsymbol{\Omega}\times\boldsymbol{\varphi})\cdot(\partial_T\boldsymbol{\varphi}+\boldsymbol{\Omega}\times\boldsymbol{\varphi})]\\ &\qquad = \partial_T[(\partial_T\boldsymbol{\varphi}+\boldsymbol{\Omega}\times\boldsymbol{\varphi})\cdot\delta\boldsymbol{\varphi}]-[\partial_{TT}\boldsymbol{\varphi}+2\,\boldsymbol{\Omega}\times\partial_T\boldsymbol{\varphi}-\Omega^2\,\boldsymbol{\varphi}+(\boldsymbol{\Omega}\cdot\boldsymbol{\varphi})\,\boldsymbol{\Omega}]\cdot\delta\boldsymbol{\varphi}.\end{aligned} \tag{47.46}$$

Since the variations, $\delta\boldsymbol{\varphi}$, vanish at the initial and final times, as per equation (47.33), the total time derivative in equation (47.46) drops out when integrated over time as part of the action. We are thus left with the kinetic energy variation

$$\begin{aligned}&\tfrac{1}{2}\,\delta\int_{t_\mathsf{A}}^{t_\mathsf{B}}\int_{\mathcal{R}(\boldsymbol{a})}(\partial_T\boldsymbol{\varphi}+\boldsymbol{\Omega}\times\boldsymbol{\varphi})\cdot(\partial_T\boldsymbol{\varphi}+\boldsymbol{\Omega}\times\boldsymbol{\varphi})\,\mathring{\rho}^{\mathsf{L}}\,\mathring{g}^{\mathsf{L}}\,\mathrm{d}^3a\,\mathrm{d}T\\ &\qquad = -\int_{t_\mathsf{A}}^{t_\mathsf{B}}\int_{\mathcal{R}(\boldsymbol{a})}[\partial_{TT}\boldsymbol{\varphi}+2\,\boldsymbol{\Omega}\times\partial_T\boldsymbol{\varphi}+\boldsymbol{\Omega}\times(\boldsymbol{\Omega}\times\boldsymbol{\varphi})]\cdot\delta\boldsymbol{\varphi}\,\mathring{\rho}^{\mathsf{L}}\,\mathring{g}^{\mathsf{L}}\,\mathrm{d}^3a\,\mathrm{d}T,\end{aligned} \tag{47.47}$$

where we used equation (1.71g) to write

$$\boldsymbol{\Omega}\times(\boldsymbol{\Omega}\times\boldsymbol{\varphi}) = -\Omega^2\,\boldsymbol{\varphi}+(\boldsymbol{\Omega}\cdot\boldsymbol{\varphi})\,\boldsymbol{\Omega}. \tag{47.48}$$

Variation of the kinetic energy in equation (47.47) reveals the material acceleration, $\partial_{TT}\boldsymbol{\varphi}$, plus contributions from the planetary Coriolis and planetary centrifugal accelerations.

47.5.3 Variation of the gravitational potential energy

The gravitational potential energy (47.26) depends on the motion field, so that its variation follows from the chain rule

$$\delta\Phi_{\mathsf{e}} = \frac{\partial\Phi_{\mathsf{e}}}{\partial\varphi^i}\,\delta\varphi^i. \tag{47.49}$$

We thus have variation of the gravitational potential energy

$$\delta\int_{t_{\mathsf{A}}}^{t_{\mathsf{B}}}\int_{\mathcal{R}(\boldsymbol{a})}\Phi_{\mathsf{e}}\,\mathring{\rho}^{\mathsf{L}}\,\mathring{g}^{\mathsf{L}}\,\mathrm{d}^3a\,\mathrm{d}T = \int_{t_{\mathsf{A}}}^{t_{\mathsf{B}}}\int_{\mathcal{R}(\boldsymbol{a})}\frac{\partial\Phi_{\mathsf{e}}}{\partial\varphi^i}\,\delta\varphi^i\,\mathring{\rho}^{\mathsf{L}}\,\mathring{g}^{\mathsf{L}}\,\mathrm{d}^3a\,\mathrm{d}T. \tag{47.50}$$

47.5.4 Variation of the specific internal energy

As seen by equation (47.29), the specific internal energy is a function of the specific entropy and specific volume

$$\mathcal{I} = \mathcal{I}[\mathring{\mathcal{S}}(\boldsymbol{a}), \nu_{\mathsf{s}}^{\mathsf{L}}(\boldsymbol{a}, T)], \tag{47.51}$$

where $\mathring{\mathcal{S}}(\boldsymbol{a})$ is the specific entropy set by the initial conditions, and $\nu_{\mathsf{s}}^{\mathsf{L}}(\boldsymbol{a}, T)$ is related to the Jacobian of transformation between the Eulerian and Lagrangian coordinates, as given by equation (47.21a). It is through dependence on $\nu_{\mathsf{s}}^{\mathsf{L}}(\boldsymbol{a}, T)$ that the specific internal energy is a function of $\partial_I\varphi^i$, so that variation of the internal energy portion of the action is

$$\int_{t_{\mathsf{A}}}^{t_{\mathsf{B}}}\int_{\mathcal{R}(\boldsymbol{a})}\delta\mathcal{I}\,\mathring{\rho}^{\mathsf{L}}\,\mathring{g}^{\mathsf{L}}\,\mathrm{d}^3a\,\mathrm{d}T = \int_{t_{\mathsf{A}}}^{t_{\mathsf{B}}}\int_{\mathcal{R}(\boldsymbol{a})} -p^{\mathsf{L}}\,(\delta\nu_{\mathsf{s}}^{\mathsf{L}})\,\mathring{\rho}^{\mathsf{L}}\,\mathring{g}^{\mathsf{L}}\,\mathrm{d}^3a\,\mathrm{d}T, \tag{47.52}$$

where $p^{\mathsf{L}}(\boldsymbol{a}, T)$ is the pressure written as a function of the Lagrangian space-time coordinates, and it is related to the specific internal energy via the thermodynamic identity (22.64)

$$\delta\mathcal{I} = \left[\frac{\partial\mathcal{I}}{\partial\nu_{\mathsf{s}}}\right]_{\mathcal{S}}\delta\nu_{\mathsf{s}}^{\mathsf{L}} = -p^{\mathsf{L}}\,\delta\nu_{\mathsf{s}}^{\mathsf{L}}. \tag{47.53}$$

From equation (47.21a) we have

$$\nu_{\mathsf{s}}^{\mathsf{L}}\,\mathring{\rho}^{\mathsf{L}}\,\mathring{g}^{\mathsf{L}} = \partial\boldsymbol{\varphi}/\partial\boldsymbol{a} = \det(F^i{}_I) \tag{47.54}$$

so that

$$\mathring{\rho}^{\mathsf{L}}\,\mathring{g}^{\mathsf{L}}\,\delta\nu_{\mathsf{s}}^{\mathsf{L}} = \delta(\mathring{\rho}^{\mathsf{L}}\,\mathring{g}^{\mathsf{L}}\,\nu_{\mathsf{s}}^{\mathsf{L}}) = \delta(\partial\boldsymbol{\varphi}/\partial\boldsymbol{a}) = \delta\det(F^i{}_I). \tag{47.55}$$

We thus need to determine how the Jacobian varies when changing trajectories.

Since the Jacobian is only a function of the deformation matrix elements, $F^i{}_I = \partial_I\varphi^i$, the chain rule gives

$$\delta\det(F^i{}_I) = \frac{\partial\det(F^i{}_I)}{\partial F^l{}_L}\,\delta F^l{}_L = \frac{\partial\det(F^i{}_I)}{\partial F^l{}_L}\,\partial_L(\delta\varphi^l), \tag{47.56}$$

where the second equality noted that the trajectory variation operator commutes with the partial derivative operator. We now make use of the identity (4.75) to write the derivative of the Jacobian with respect to an element of the transformation matrix

$$\delta[\det(F^i{}_I)] = \det(F^i{}_I)\,F^L{}_l\,\partial_L(\delta\varphi^l) = \det(F^i{}_I)\,\partial_l(\delta\varphi^l), \tag{47.57}$$

where the final equality transformed from a Lagrangian partial derivative to an Eulerian partial derivative via

$$F^L{}_l\,\partial_L = \partial_l. \tag{47.58}$$

At the end of this chapter, we present an alternative derivation of equation (47.57) that does not make use of the identity (4.75). That derivation is far more tedious than the one presented

here, and yet it is presented for those wishing further exposure to index gymnastics.

Equation (47.57) says that the relative variation of the Jacobian determinant is directly determined by the $\boldsymbol{x}$-space divergence of the motion field's variation. This result is analogous to equation (18.148) that expresses the material time evolution of the Jacobian. We can understand its kinematical content by observing that an $\boldsymbol{x}$-space divergence of $\delta\boldsymbol{\varphi}$ leads to a variation in the $\boldsymbol{x}$-space volume of a fluid parcel, and thus to a variation in the Jacobian. Making use of the variation (47.57) in equation (47.52) yields the internal energy variation

$$\int_{t_{\mathsf{A}}}^{t_{\mathsf{B}}} \int_{\mathscr{R}(\boldsymbol{a})} \delta\mathcal{I}\, \mathring{\rho}^{\mathsf{L}}\, \mathring{g}^{\mathsf{L}}\, \mathrm{d}^3a\, \mathrm{d}T = -\int_{t_{\mathsf{A}}}^{t_{\mathsf{B}}} \int_{\mathscr{R}(\boldsymbol{a})} p^{\mathsf{L}}\, \frac{\partial(\delta\varphi^i)}{\partial x^i}\, \frac{\partial\boldsymbol{\varphi}}{\partial\boldsymbol{a}}\, \mathrm{d}^3a\, \mathrm{d}T. \tag{47.59}$$

47.5.5 How the pressure gradient appears

We now present two related methods for for how the pressure gradient appears within the integral (47.59).

Method I

Making use of the relations in Section 47.3 allows us to convert the right hand side of equation (47.59) to Cartesian Eulerian coordinates so that

$$\int_{\mathscr{R}(\boldsymbol{a})} p^{\mathsf{L}}\, \frac{\partial(\delta\varphi^i)}{\partial x^i}\, \frac{\partial\boldsymbol{\varphi}}{\partial\boldsymbol{a}}\, \mathrm{d}^3a = \int_{\mathscr{R}(t)} p\, \frac{\partial(\delta\varphi^i)}{\partial x^i}\, \mathrm{d}^3x, \tag{47.60}$$

with integration by parts yielding

$$\int_{\mathscr{R}(t)} p\, \frac{\partial(\delta\varphi^i)}{\partial x^i}\, \mathrm{d}^3x = \int_{\mathscr{R}(t)} \frac{\partial(p\,\delta\varphi^i)}{\partial x^i}\, \mathrm{d}^3x - \int_{\mathscr{R}(t)} \frac{\partial p}{\partial x^i}\, \delta\varphi^i\, \mathrm{d}^3x. \tag{47.61}$$

Assuming either zero mechanical forcing at the boundaries (e.g., free boundary with $p = 0$), or assuming $\delta\boldsymbol{\varphi}\cdot\hat{\boldsymbol{n}} = 0$ at the boundaries (i.e., rigid solid-earth boundary), allows us to drop the boundary term. We are thus left with the internal energy variation

$$\int_{\mathscr{R}(\boldsymbol{a})} \delta\mathcal{I}\, \mathring{\rho}^{\mathsf{L}}\, \mathring{g}^{\mathsf{L}}\, \mathrm{d}^3a = \int_{\mathscr{R}(t)} \frac{1}{\rho}\frac{\partial p}{\partial x^i}\, \delta\varphi^i\, \rho\, \mathrm{d}^3x = \int_{\mathscr{R}(\boldsymbol{a})} \frac{1}{\rho^{\mathsf{L}}}\frac{\partial p^{\mathsf{L}}}{\partial\varphi^i}\, \delta\varphi^i\, \mathring{\rho}^{\mathsf{L}}\, \mathring{g}^{\mathsf{L}}\, \mathrm{d}^3a, \tag{47.62}$$

with the final equality converting back to Lagrangian coordinates and making use of equation (47.18) for the density, $\mathring{\rho}^{\mathsf{L}}\, \mathring{g}^{\mathsf{L}}$.

Method II

Rather than convert to Cartesian Eulerian coordinates at the point done in equation (47.60), we write

$$p^{\mathsf{L}}\, \frac{\partial(\delta\varphi^i)}{\partial x^i}\, \frac{\partial\boldsymbol{\varphi}}{\partial\boldsymbol{a}} = p^{\mathsf{L}}\, \frac{\partial(\delta\varphi^i)}{\partial a^I}\, \frac{\partial a^I}{\partial x^i}\, \frac{\partial\boldsymbol{\varphi}}{\partial\boldsymbol{a}} = \frac{\partial}{\partial a^I}\left[p^{\mathsf{L}}\, \delta\varphi^i\, \frac{\partial a^I}{\partial x^i}\, \frac{\partial\boldsymbol{\varphi}}{\partial\boldsymbol{a}}\right] - \delta\varphi^i\, \frac{\partial}{\partial a^I}\left[p^{\mathsf{L}}\, \frac{\partial a^I}{\partial x^i}\, \frac{\partial\boldsymbol{\varphi}}{\partial\boldsymbol{a}}\right], \tag{47.63}$$

where the first equality made use of the chain rule and the second equality used the product rule. For the final term note that

$$\frac{\partial}{\partial a^I}\left[F^I{}_i\, \frac{\partial\boldsymbol{\varphi}}{\partial\boldsymbol{a}}\right] = \frac{\partial}{\partial a^I}\left[\frac{\partial a^I}{\partial x^i}\, \frac{\partial\boldsymbol{\varphi}}{\partial\boldsymbol{a}}\right] = 0, \tag{47.64}$$

which follows from the determinant identity (4.73) in which

$$\frac{\partial a^I}{\partial x^i}\,\frac{\partial \boldsymbol{\varphi}}{\partial \boldsymbol{a}} = \frac{1}{2}\,\epsilon^{IJK}\,\epsilon_{ijk}\,\frac{\partial \varphi^j}{\partial a^J}\,\frac{\partial \varphi^k}{\partial a^K}, \tag{47.65}$$

thus yielding equation (47.64) through anti-symmetry of ϵ^{IJK} and symmetry of the second partial derivatives ∂_{IK} and ∂_{IJ}. These results then bring equation (47.63) into the form

$$p^{\text{L}}\,\frac{\partial(\delta\varphi^i)}{\partial x^i}\,\frac{\partial \boldsymbol{\varphi}}{\partial \boldsymbol{a}} = \frac{\partial}{\partial a^I}\left[p^{\text{L}}\,\delta\varphi^i\,\frac{\partial a^I}{\partial x^i}\,\frac{\partial \boldsymbol{\varphi}}{\partial \boldsymbol{a}}\right] - \delta\varphi^i\,\frac{\partial p^{\text{L}}}{\partial a^I}\,\frac{\partial a^I}{\partial x^i}\,\frac{\partial \boldsymbol{\varphi}}{\partial \boldsymbol{a}}. \tag{47.66}$$

When integrated over the material domain, the ∂_I divergence term drops out due to the material boundary conditions. We are thus led to

$$\int_{\mathcal{R}(\boldsymbol{a})} \delta\mathcal{I}\,\mathring{\rho}^{\text{L}}\,\mathring{g}^{\text{L}}\,\mathrm{d}^3a = \int_{\mathcal{R}(\boldsymbol{a})} \frac{\partial p^{\text{L}}}{\partial a^I}\,\frac{\partial a^I}{\partial \varphi^i}\,\frac{\partial \boldsymbol{\varphi}}{\partial \boldsymbol{a}}\,\delta\varphi^i\,\mathrm{d}^3a \quad \text{equations (47.59) and (47.66)} \tag{47.67a}$$

$$= \int_{\mathcal{R}(\boldsymbol{a})} \frac{1}{\rho^{\text{L}}}\,\frac{\partial p^{\text{L}}}{\partial x^i}\,\delta\varphi^i\,\mathring{\rho}^{\text{L}}\,\mathring{g}^{\text{L}}\,\mathrm{d}^3a \quad \text{chain rule and equation (47.54)}, \tag{47.67b}$$

which agrees with equation (47.62).

47.5.6 The perfect fluid Euler-Lagrange equation

Making use of the variation of the kinetic energy portion of the action (47.47), the gravitational potential energy portion (47.50), and the internal energy portion (47.62), leads us to the variation of the action under variations in the trajectories that are fixed at the temporal boundaries

$$\delta\mathsf{S}^{\text{action}} = -\int_{t_{\text{A}}}^{t_{\text{B}}}\int_{\mathcal{R}(\boldsymbol{a})}\left[\partial_{TT}\boldsymbol{\varphi} + 2\,\boldsymbol{\Omega}\times\partial_T\boldsymbol{\varphi} + \boldsymbol{\Omega}\times(\boldsymbol{\Omega}\times\boldsymbol{\varphi}) + \frac{\partial\Phi_{\text{e}}}{\partial\boldsymbol{\varphi}} + \frac{1}{\rho^{\text{L}}}\frac{\partial p^{\text{L}}}{\partial\boldsymbol{\varphi}}\right]\cdot\delta\boldsymbol{\varphi}\,\mathring{\rho}^{\text{L}}\,\mathring{g}^{\text{L}}\,\mathrm{d}^3a\,\mathrm{d}T. \tag{47.68}$$

Hamilton's principle says that the physically realized action is stationary under variations to the motion, with that motion fixed at the temporal boundaries. Invoking this principle then leads to the Euler-Lagrange equation

$$\partial_{TT}\boldsymbol{\varphi} + 2\,\boldsymbol{\Omega}\times\partial_T\boldsymbol{\varphi} = -\frac{1}{\rho^{\text{L}}}\frac{\partial p^{\text{L}}}{\partial\boldsymbol{\varphi}} - \frac{\partial\Phi}{\partial\boldsymbol{\varphi}} \iff \partial_T\boldsymbol{v}^{\text{L}} + 2\,\boldsymbol{\Omega}\times\boldsymbol{v}^{\text{L}} = -\frac{1}{\rho^{\text{L}}}\frac{\partial p^{\text{L}}}{\partial\boldsymbol{\varphi}} - \frac{\partial\Phi}{\partial\boldsymbol{\varphi}}, \tag{47.69}$$

where we introduced the velocity in the rotating reference frame

$$\boldsymbol{v}^{\text{L}} = \partial_T\boldsymbol{\varphi}, \tag{47.70}$$

and the geopotential

$$\Phi = \Phi_{\text{e}} - (\boldsymbol{\Omega}\times\boldsymbol{\varphi})^2/2, \tag{47.71}$$

which is the sum of the gravitational potential and the planetary centrifugal potential (see Section 13.10.4).

The Euler-Lagrange equation (47.69) is written with spatial derivatives taken with respect to the motion field, $\boldsymbol{\varphi}$, and time derivatives with respect to Lagrangian time, T. Transforming this equation to an Eulerian perspective leads to the rotating perfect fluid Euler equation derived in Section 24.2.4. It is particularly notable that this transformation is rather trivial, simply requiring a swap of the motion field for an Eulerian position, $\boldsymbol{x}$. This transformation to the Eulerian reference frame removes all remnants of the motion field from the equations. A key reason for this rather simple result arises from the form of the internal energy, whose dependence on trajectories arises only via the Jacobian, $\partial\boldsymbol{\varphi}/\partial\boldsymbol{a}$. Different forms of the internal energy arise

in other areas of continuum mechanics, thus making the translation to an Eulerian perspective less convenient than found here for the perfect fluid.

47.5.7 Comments

Based on our experience with particle mechanics in Chapters 12 and 15, we expected to realize the same equations using Hamilton's principle as those found through Newton's laws. Even so, it is a remarkable result given the fundamentally distinct conceptual and operational perspectives. This agreement offers further confidence that the theoretical construct of continuum mechanics has a robust foundation beyond that afforded by the work of Euler and Cauchy in their applications of Newton's laws to the continuum.

47.6 Perfect fluid Hamiltonian continuity equation

As a means to illustrate the connection between symmetry and conservation within the perfect fluid, note that the Lagrangian density in equation (47.36) has no explicit dependence on time

$$\left[\frac{\partial \mathscr{L}}{\partial T}\right]_{\varphi^i,\partial_T\varphi^i,\partial_I\varphi^i,a^I} = 0, \tag{47.72}$$

where the subscripts on the derivative denote those terms that are held fixed in computing the partial derivative. According to the discussion of Noether's theorem in Sections 46.4 and 46.5, we know that the Hamiltonian density, $\mathscr{H}$, satisfies the Lagrangian space-time continuity equation (46.67)

$$\partial_T \mathscr{H} + \mathring{\nabla}_I \mathscr{F}^I = 0, \tag{47.73}$$

where

$$\mathring{\nabla}_I \mathscr{F}^I = (1/\mathring{g}^{\text{L}})\, \partial_I (\mathring{g}^{\text{L}}\, \mathscr{F}^I) \tag{47.74}$$

is the covariant divergence as defined by the geometry of the reference manifold at $T = t_{\text{R}}$.

The canonical momentum, Hamiltonian density, and the energy flux are given in equation (46.64) for the scalar field are generalized to the φ^i field theory of a perfect fluid

$$\mathscr{P}_i \equiv \frac{\partial \mathscr{L}}{\partial(\partial_T \varphi^i)} \quad \text{and} \quad \mathscr{H} = \mathscr{P}_i\, \partial_T \varphi^i - \mathscr{L} \quad \text{and} \quad \mathscr{F}^I = \frac{\partial \mathscr{L}}{\partial(\partial_I \varphi^i)}\, \frac{\partial \varphi^i}{\partial T}, \tag{47.75}$$

where the implied summation over the i index is the only distinction from the scalar field in considered in Section 46.4. We now determine an expression of this continuity equation for the perfect fluid. Doing so provides useful experience with the variety of tensor manipulations arising from this formalism.

47.6.1 Canonical momentum and Hamiltonian density

Making use of the perfect fluid Lagrangian density (47.36) renders the canonical momentum

$$\mathscr{P}_j = \mathring{\rho}^{\text{L}}\, [\partial_T \varphi^i + (\boldsymbol{\Omega} \times \boldsymbol{\varphi})^i]\, \delta_{ij}, \tag{47.76}$$

so that the Hamiltonian density is

$$\mathscr{H} = \mathring{\rho}^{\mathcal{L}}\, [\partial_T \varphi^i + (\boldsymbol{\Omega} \times \boldsymbol{\varphi})^i]\, \delta_{ij}\, \partial_T \varphi^j - \mathscr{L} = \mathring{\rho}^{\mathcal{L}}\, (\partial_T \boldsymbol{\varphi} \cdot \partial_T \boldsymbol{\varphi}/2 + \Phi + \mathcal{I}), \tag{47.77}$$

where we introduced the geopotential from equation (47.71). Evidently, the Hamiltonian density is the sum of the kinetic energy plus geopotential plus internal energy.

47.6.2 Energy flux and the covariant flux divergence

For the energy flux we need the derivative of the Lagrangian density with respect to the deformation matrix components, $F^i{}_I = \partial_I \varphi^i$, which appear only within the specific internal energy

$$\begin{aligned}
\frac{\partial \mathcal{L}}{\partial F^i{}_I} &= -\mathring{\rho}^{\text{L}} \frac{\partial \mathcal{I}}{\partial \nu_{\text{s}}} \frac{\partial \nu_{\text{s}}}{\partial F^i{}_I} && \text{chain rule with } \mathcal{I} = \mathcal{I}(\mathring{\mathcal{S}}, \nu_{\text{s}}) \text{ and } \mathring{\mathcal{S}} = \mathring{\mathcal{S}}(\boldsymbol{a}) && \text{(47.78a)}\\
&= \mathring{\rho}^{\text{L}}\, p^{\text{L}} \frac{\partial \nu_{\text{s}}}{\partial F^i{}_I} && \text{thermodynamic identity (47.53)} && \text{(47.78b)}\\
&= \frac{p^{\text{L}}}{\mathring{g}^{\text{L}}} \frac{\partial (\mathring{\rho}^{\text{L}}\, \mathring{g}^{\text{L}}\, \nu_{\text{s}}))}{\partial F^i{}_I} && \partial(\mathring{\rho}^{\text{L}}\, \mathring{g}^{\text{L}})/\partial F^i{}_I = 0 && \text{(47.78c)}\\
&= \frac{p^{\text{L}}}{\mathring{g}^{\text{L}}} \frac{\partial \det(F^i{}_I)}{\partial F^i{}_I} && \mathring{\rho}^{\text{L}}\, \mathring{g}^{\text{L}}\, \nu_{\text{s}} = \det(F^i{}_I) \text{ from equation (47.54)} && \text{(47.78d)}\\
&= (p^{\text{L}}/\mathring{g}^{\text{L}})\, \det(F^i{}_I)\, F^I{}_i && \text{determinant identity (4.75),} && \text{(47.78e)}
\end{aligned}$$

which yields the energy flux

$$\mathcal{F}^I = \frac{\partial \mathcal{L}}{\partial F^i{}_I} \frac{\partial \varphi^i}{\partial T} = (p^{\text{L}}/\mathring{g}^{\text{L}})\, \det(F^i{}_I)\, F^I{}_i\, \partial_T \varphi^i. \tag{47.79}$$

Making use of equation (4.134) for the covariant divergence, we have the $\boldsymbol{a}$-space covariant flux divergence

$$\mathring{\nabla}_I [\det(F^i{}_I)\, F^I{}_i\, (p^{\text{L}}/\mathring{g}^{\text{L}})\, \partial_T \varphi^i] = (1/\mathring{g}^{\text{L}})\, \partial_I [\det(F^i{}_I)\, F^I{}_i\, p^{\text{L}}\, \partial_T \varphi^i]. \tag{47.80}$$

The identity (47.64) says that $\partial_I [\det(F^i{}_I)\, F^I{}_i] = 0$, so that the covariant flux divergence is

$$\mathring{\nabla}_I [\det(F^i{}_I)\, F^I{}_i\, (p^{\text{L}}/\mathring{g}^{\text{L}})\, \partial_T \varphi^i] = (1/\mathring{g}^{\text{L}})\, \det(F^i{}_I)\, F^I{}_i\, \partial_I (p^{\text{L}}\, \partial_T \varphi^i). \tag{47.81}$$

Finally, we convert the $\boldsymbol{a}$-space derivative to an $\boldsymbol{x}$-space derivative using the deformation matrix

$$F^I{}_i\, \partial_I = \partial_i, \tag{47.82}$$

so that

$$\mathring{\nabla}_I [\det(F^i{}_I)\, F^I{}_i\, (p^{\text{L}}/\mathring{g}^{\text{L}})\, \partial_T \varphi^i] = (1/\mathring{g}^{\text{L}})\, \det(F^i{}_I)\, \partial_i (p^{\text{L}}\, \partial_T \varphi^i) = \mathring{\rho}^{\text{L}}\, \nu_{\text{s}}^{\text{L}}\, \partial_i (p^{\text{L}}\, \partial_T \varphi^i), \tag{47.83}$$

where the second equality used the determinant identity (47.21a) that says $\det(F^i{}_I) = \nu_{\text{s}}^{\text{L}}\, \mathring{\rho}^{\text{L}}\, \mathring{g}^{\text{L}}$.

47.6.3 Lagrangian and Eulerian Hamiltonian continuity equations

Bringing the pieces together leads the Hamiltonian density continuity equation (47.73) taking the following perfect fluid expression

$$\partial_T \left[\mathring{\rho}^{\mathcal{L}}\, (\partial_T \boldsymbol{\varphi} \cdot \partial_T \boldsymbol{\varphi}/2 + \Phi + \mathcal{I})\right] + \mathring{\rho}^{\text{L}}\, \nu_{\text{s}}^{\text{L}}\, \partial_i (p^{\text{L}}\, \partial_T \varphi^i) = 0. \tag{47.84}$$

The density $\mathring{\rho}^{\text{L}} = \mathring{\rho}^{\text{L}}(\boldsymbol{a})$ cancels from both terms, so that

$$\rho^{\mathcal{L}}\, \partial_T (\partial_T \boldsymbol{\varphi} \cdot \partial_T \boldsymbol{\varphi}/2 + \Phi + \mathcal{I}) + \partial_i (p^{\text{L}}\, \partial_T \varphi^i) = 0, \tag{47.85}$$

which has a corresponding Eulerian expression[6]

$$\rho \frac{\mathrm{D}(\boldsymbol{v}\cdot\boldsymbol{v}/2+\Phi+\mathcal{I})}{\mathrm{D}t} + \nabla\cdot(p\,\boldsymbol{v}) = 0. \tag{47.86}$$

This equation accords with the perfect fluid total energy budget equation (26.91) derived using very different methods. This agreement lends further confidence to our use of Hamilton's principle with Lagrangian kinematics for the perfect fluid.

47.7 Particle relabeling symmetry and potential vorticity

In this chapter we are working with a Lagrangian space-time field theory for the perfect fluid motion field, $\boldsymbol{\varphi}(\boldsymbol{a}, T)$. Hence, as just seen in Section 47.6 for the Hamiltonian density, space-time symmetries leading to conservation laws in the perfect fluid arise from variations in the position within the Lagrangian space-time. For the usual momentum conservation laws corresponding to spatial symmetry, we take the material coordinates equal to the Cartesian coordinates at some reference time. For a perfect geophysical fluid in motion around a rotating and gravitating planet, we no longer have the full symmetry of empty space considered in Chapter 46. Instead, we have axial symmetry around the planetary rotational axis. As a result, perfect planetary fluid motion only realizes differential conservation laws for axial angular momentum conservation along with the energy conservation of Section 47.6.

For momentum conservation, the *active transformation* (Section 46.5.2) is realized by shifting the material spatial position of each fluid particle by the same constant, and for energy each fluid particle has its material time shifted by the same constant. Here we examine whether there is a nontrivial *passive transformation* that leaves the action invariant. Recall from our discussion in Section 46.5.3, a passive transformation only affects a variation to the coordinate representation of a physical system. *Noether's second theorem* says that each passive symmetry gives rise to a *Bianchi identity* that corresponds to a local conservation law. Here we consider *particle relabeling* symmetry and the corresponding local (in $\boldsymbol{a}$-space) conservation of potential vorticity. Our presentation is inspired by *Salmon* (1988), *Müller* (1995), *Padhye and Morrison* (1996), and Chapter 7 of *Salmon* (1998).

47.7.1 Passive transformation of Lagrangian space coordinates

Consider a time dependent coordinate transformation of the material spatial coordinates

$$\boldsymbol{a}' = \boldsymbol{a}'(\boldsymbol{a}, T), \tag{47.87}$$

with an infinitesimal version of this transformation

$$\boldsymbol{a}' = \boldsymbol{a} + \delta\boldsymbol{a}(\boldsymbol{a}, T). \tag{47.88}$$

In this manner, each fluid particle experiences a distinct variation of its material coordinate. The transformation is passive (only affects coordinates) and so the fluid particle trajectories are unchanged. We do not expect particle labels to affect our ability to describe the physically realized trajectories, and this expectation is given the name *particle relabeling symmetry* (*Salmon*, 1988).

We consider a particular form of coordinate transformation that is assumed to vanish at the material space and time bounds. Furthermore, we assume that the coordinate transformation respects the constraint of mass conservation holding for each fluid parcel. As shown in Sections 46.5.2 and 46.5.3, a mass conserving transformation, δa^I, as a zero density weighted covariant

[6] Recall we are assuming Cartesian coordinates for $\boldsymbol{x}$-space.

divergence. Since the material coordinates, a^I, are set at the reference time, $T = t_{\mathsf{R}}$, the relevant density at that time is $\mathring{\rho}^{\mathsf{L}} = \rho^{\mathsf{L}}(\boldsymbol{a}, T = t_{\mathsf{R}})$, as is the metric determinant, $\mathring{g}^{\mathsf{L}}(\boldsymbol{a}) = g^{\mathsf{L}}(\boldsymbol{a}, T = t_{\mathsf{R}})$. Hence, the particular form of coordinate variation relevant to particle relabeling is given by

$$\delta\boldsymbol{a} = 0 \quad \text{at material space-time boundaries} \quad \text{and} \quad \mathring{\nabla}_I(\mathring{\rho}^{\mathsf{L}}\,\delta a^I) = 0. \tag{47.89}$$

Since δa^I is time dependent, trajectories have their material coordinate modified at each point that is not on the material space-time boundary, with the modification constrained by assuming that the mass of each fluid parcel is invariant.

To deduce the conservation resulting from particle relabeling symmetry, and to expose the key aspects of the derivation, it is sufficient to study flow in a non-rotating reference frame. Generalization to a rotating reference frame is straightforward. We thus consider the following perfect fluid action

$$\mathsf{S}^{\backslash} = \int_{t_{\mathcal{A}}}^{t_{\mathcal{B}}} \int_{\mathcal{R}(\boldsymbol{a})} \left(\tfrac{1}{2}\,\partial_T\boldsymbol{\varphi}\cdot\partial_T\boldsymbol{\varphi} - \Phi_{\mathsf{e}} - \mathcal{I}\right)\mathring{\rho}^{\mathsf{L}}\,\mathring{g}^{\mathsf{L}}\,\mathrm{d}^3a\,\mathrm{d}T. \tag{47.90}$$

47.7.2 Constraints from mass conservation

The spatial region where the fluid flows, $\mathcal{R}$, is material and each fluid parcel is material. Consequently, if particle relabeling is to render an equivalent description of the fluid, then the measurement of mass must remain unchanged using the new set of coordinates. Globally, mass conservation means that

$$\int_{\mathcal{R}(\boldsymbol{a})} \mathring{\rho}^{\mathsf{L}}\,\mathring{g}^{\mathsf{L}}\,\mathrm{d}^3a = \int_{\mathcal{R}'(\boldsymbol{a}')} \mathring{\rho}'^{\mathsf{L}}\,\mathring{g}'^{\mathsf{L}}\,\mathrm{d}^3a', \tag{47.91}$$

where $\mathcal{R}'(\boldsymbol{a}')$ is the functional expression for the domain when written in terms of the varied coordinates. Since the domain is not changed by the coordinate variation, we must have the functional expression for the domain when using coordinates $\boldsymbol{a}'$ equal to the functional expression for the domain when using coordinates $\boldsymbol{a}$, which is succinctly expressed as

$$\mathcal{R}'(\boldsymbol{a}') = \mathcal{R}(\boldsymbol{a}). \tag{47.92}$$

Likewise, since the mass of a fluid parcel is unchanged we have

$$\mathrm{d}M(\boldsymbol{a}) = \mathrm{d}M'(\boldsymbol{a}') \implies \mathring{\rho}^{\mathsf{L}}(\boldsymbol{a})\,\mathring{g}^{\mathsf{L}}(\boldsymbol{a})\,\mathrm{d}^3a = \mathring{\rho}'^{\mathsf{L}}(\boldsymbol{a}')\,\mathring{g}'^{\mathsf{L}}(\boldsymbol{a}')\,\mathrm{d}^3a'. \tag{47.93}$$

This result then means that the Jacobian of transformation between the two material coordinates is given by the volume ratio

$$\frac{\partial\boldsymbol{a}'}{\partial\boldsymbol{a}} = \frac{\mathring{\rho}^{\mathsf{L}}(\boldsymbol{a})\,\mathring{g}^{\mathsf{L}}(\boldsymbol{a})}{\mathring{\rho}'^{\mathsf{L}}(\boldsymbol{a}')\,\mathring{g}'^{\mathsf{L}}(\boldsymbol{a}')}, \tag{47.94}$$

which is a familiar result from coordinate transformations discussed in Section 18.7.

Specific volume is invariant

Making use of equation (47.21a) for the specific volume along with the mass conservation identity (47.94), we find

$$\nu_{\mathsf{s}}^{\mathsf{L}'}(\boldsymbol{a}', T) = \frac{1}{\mathring{\rho}'^{\mathsf{L}}(\boldsymbol{a}')\,\mathring{g}'^{\mathsf{L}}(\boldsymbol{a}')}\frac{\partial\boldsymbol{\varphi}}{\partial\boldsymbol{a}'} = \frac{1}{\mathring{\rho}^{\mathsf{L}}(\boldsymbol{a})\,\mathring{g}^{\mathsf{L}}(\boldsymbol{a})}\frac{\partial\boldsymbol{a}'}{\partial\boldsymbol{a}}\frac{\partial\boldsymbol{\varphi}}{\partial\boldsymbol{a}'} = \frac{1}{\mathring{\rho}^{\mathsf{L}}(\boldsymbol{a})\,\mathring{g}^{\mathsf{L}}(\boldsymbol{a})}\frac{\partial\boldsymbol{\varphi}}{\partial\boldsymbol{a}} = \nu_{\mathsf{s}}^{\mathsf{L}}(\boldsymbol{a}, T), \tag{47.95}$$

where the third equality made use of the chain rule identity (4.78) holding for determinants

$$\frac{\partial \boldsymbol{a}'}{\partial \boldsymbol{a}} \frac{\partial \boldsymbol{\varphi}}{\partial \boldsymbol{a}'} = \frac{\partial \boldsymbol{\varphi}}{\partial \boldsymbol{a}}. \tag{47.96}$$

Evidently, so long as the coordinate transformation from $\boldsymbol{a}$ to $\boldsymbol{a}'$ leaves the mass of a fluid parcel unchanged as per equation (47.93), then it also leaves its specific volume unchanged as per equation (47.95).

Zero covariant divergence of density weighted coordinate variation

So far we have only assumed the coordinate transformation is mass preserving. To determine a differential expression of that property, we make use of the discussion in Section 46.5.3 for infinitesimal coordinate transformations. Evidently, the mass conservation identity (47.93) means that, to second order in variation, the density weighted coordinate variation has a zero covariant divergence

$$\mathring{\nabla}_I(\mathring{\rho}^{\text{L}}\,\delta a^I) = (1/\mathring{g}^{\text{L}})\,\partial_I(\mathring{g}^{\text{L}}\,\mathring{\rho}^{\text{L}}\,\delta a^I) = 0. \tag{47.97}$$

This constraint is satisfied by setting $\mathring{\rho}^{\text{L}}\,\delta\boldsymbol{a}$ equal to the covariant curl of an arbitrary vector (see equation (4.146) in Section 4.18)

$$\mathring{\rho}^{\text{L}}\,\delta\boldsymbol{a} = \mathring{\text{curl}}(\boldsymbol{W}) \Longleftrightarrow \mathring{\rho}^{\text{L}}\,\delta a^I = \mathring{\varepsilon}^{IJK}\,\partial_J W_K = (1/\mathring{g}^{\text{L}})\,\epsilon^{IJK}\,\partial_J W_K, \tag{47.98}$$

where

$$\mathring{\varepsilon}^{IJK} = (1/\mathring{g}^{\text{L}})\,\epsilon^{IJK} \tag{47.99}$$

is the coordinate covariant Levi-Civita tensor discussed in Section 4.7.1, and $\boldsymbol{W} = \boldsymbol{W}(\boldsymbol{a}, T)$ is an arbitrary vector that parameterizates the coordinate variation.[7]

Summary from mass conservation

In summary, there are three conditions resulting from the constraint that mass remains invariant when performing a variation of the Lagrangian space coordinates: (1) we only need to vary the energy terms in the action, (2) the specific volume is invariant, and (3) the density weighted coordinate variation is a total curl

$$\delta\mathcal{S}^{\text{action}} = \int_{t_{\text{A}}}^{t_{\text{B}}} \int_{\mathcal{R}(\boldsymbol{a})} \delta\left(\tfrac{1}{2}\,\partial_T\boldsymbol{\varphi}\cdot\partial_T\boldsymbol{\varphi} - \Phi_{\text{e}} - \mathcal{I}\right)\mathring{\rho}^{\text{L}}\,\mathring{g}^{\text{L}}\,\mathrm{d}^3a\,\mathrm{d}T \tag{47.100a}$$

$$\delta\nu_{\text{s}}^{\text{L}} = 0 \tag{47.100b}$$

$$\mathring{\rho}^{\text{L}}\,\delta\boldsymbol{a} = \text{curl}(\boldsymbol{W}). \tag{47.100c}$$

47.7.3 The motion field is a scalar

The gravitational potential is a function of the spatial position as determined by the motion field

$$\Phi_{\text{e}} = \Phi_{\text{e}}(\boldsymbol{\varphi}), \tag{47.101}$$

so that the gravitational potential has a functional dependence

$$\Phi_{\text{e}} = \Phi_{\text{e}}[\boldsymbol{\varphi}(\boldsymbol{a}, T)]. \tag{47.102}$$

[7] Note that $W_K = \mathfrak{g}_{KL}\,W^L$, where $\mathfrak{g}_{KL} = F^k{}_K\,F^l{}_L\,g_{kl}$ is the Lagrangian representation of the metric tensor whereas g_{kl} is the Eulerian representation. Choosing Cartesian Eulerian coordinates so that $g_{kl} = \delta_{kl}$ means that $\mathfrak{g}_{KL}$ is the Cauchy-Green strain tensor (18.41).

For the coordinate variation (47.88) to keep the geopotential invariant requires the motion field to satisfy[8]

$$\boldsymbol{\varphi}'(\boldsymbol{a}', T) = \boldsymbol{\varphi}(\boldsymbol{a}, T). \tag{47.103}$$

This equality means that the motion field, $\boldsymbol{\varphi}'(\boldsymbol{a}', T)$, points to the same fluid particle as the motion field, $\boldsymbol{\varphi}(\boldsymbol{a}, T)$. This condition is consistent with the concept of a passive transformation. From the discussion in Section 1.5.1, we conclude that each component of the motion field transforms as a scalar (zeroth order tensor) under the particle relabeling coordinate transformation, so that the total variation (see Section 46.5.4) of each component vanishes

$$\Delta\boldsymbol{\varphi} = \boldsymbol{\varphi}'(\boldsymbol{a}', T) - \boldsymbol{\varphi}(\boldsymbol{a}, T) = 0. \tag{47.104}$$

47.7.4 The specific internal energy is a scalar

To retain the same specific internal energy, $\mathcal{I}$, when affecting the passive variation requires $\mathcal{I}$ to be a scalar under particle relabeling so that

$$\mathcal{I} = \mathcal{I}(\mathring{\mathcal{S}}(\boldsymbol{a}), \nu_{\mathsf{s}}) = \mathcal{I}'(\mathring{\mathcal{S}}'(\boldsymbol{a}'), \nu'_{\mathsf{s}}). \tag{47.105}$$

We already saw that mass conservation ensures that the specific volume remains a scalar under particle relabeling as per equation (47.100b). In order for relabeling to keep the specific entropy unchanged we must have

$$\mathring{\mathcal{S}}'(\boldsymbol{a}') = \mathring{\mathcal{S}}(\boldsymbol{a}). \tag{47.106}$$

To realize this symmetry requires the coordinate variation to be orthogonal to the $\boldsymbol{a}$-space gradient of the specific entropy

$$\delta\boldsymbol{a}^I\, \partial_I \mathring{\mathcal{S}} = \delta\boldsymbol{a} \cdot \nabla_{\boldsymbol{a}} \mathring{\mathcal{S}} = 0. \tag{47.107}$$

Namely, the relabeling must remain on a constant specific entropy surface. This condition reduces the coordinate variation to two degrees of freedom, and the constraint (47.107) can be readily realized by setting one of the material coordinates equal to the specific entropy. Alternatively, the constraint can be satisfied by writing the coordinate variation as

$$\mathring{\rho}^{\text{L}}\, \delta\boldsymbol{a} = \mathring{\text{curl}}(\boldsymbol{W}) = \mathring{\text{curl}}(A\, \nabla_{\boldsymbol{a}} \mathring{\mathcal{S}}) \iff \mathring{\rho}^{\text{L}}\, \delta a^I = \mathring{\varepsilon}^{IJK}\, \partial_J W_K = \mathring{\varepsilon}^{IJK}\, \partial_J (A\, \partial_K \mathring{\mathcal{S}}). \tag{47.108}$$

We have thus specified the particle relabeling variation up to an arbitrary function, $A(\boldsymbol{a}, T)$.

47.7.5 Coordinate variation of the kinetic energy

The coordinate variation of the kinetic energy per mass is

$$\delta(\partial_T \boldsymbol{\varphi} \cdot \partial_T \boldsymbol{\varphi}/2) = \partial_T \boldsymbol{\varphi} \cdot \delta(\partial_T \boldsymbol{\varphi}), \tag{47.109}$$

where the variation of the velocity is given by

$$\delta(\partial_T \boldsymbol{\varphi}) = \left.\frac{\partial \boldsymbol{\varphi}'(\boldsymbol{a}', T)}{\partial T}\right|_{\boldsymbol{a}'} - \left.\frac{\partial \boldsymbol{\varphi}(\boldsymbol{a}, T)}{\partial T}\right|_{\boldsymbol{a}}. \tag{47.110}$$

Note the distinct time derivatives on the right hand side, as per the need to hold distinct space coordinates fixed while computing the time derivatives. This derivative, to first order in variation,

[8] The geopotential arising in a rotating reference frame is the sum of the gravitational potential plus the planetary centrifugal potential (see equation (47.69)) $\Phi(\boldsymbol{\varphi}) = \Phi_{\mathsf{e}}(\boldsymbol{\varphi}) - (\boldsymbol{\Omega} \times \boldsymbol{\varphi})^2/2$. So if the motion field is a scalar under the coordinate variation as per equation (47.103), then so is the geopotential.

is given by

$$\left.\frac{\partial \boldsymbol{\varphi}'(\boldsymbol{a}', T)}{\partial T}\right|_{\boldsymbol{a}'} = \left.\frac{\partial \boldsymbol{\varphi}(\boldsymbol{a}, T)}{\partial T}\right|_{\boldsymbol{a}'} = \left.\frac{\partial \boldsymbol{\varphi}(\boldsymbol{a}, T)}{\partial T}\right|_{\boldsymbol{a}} + \left.\frac{\partial a^I}{\partial T}\right|_{\boldsymbol{a}'} \frac{\partial \boldsymbol{\varphi}(\boldsymbol{a}, T)}{\partial a^I}, \tag{47.111}$$

where the first equality follows from $\boldsymbol{\varphi}'(\boldsymbol{a}', T) = \boldsymbol{\varphi}(\boldsymbol{a}, T)$ as per equation (47.103), and the second equality follows from the chain rule. Next, make use of the coordinate variation (47.88) to write

$$\left.\frac{\partial a^I}{\partial T}\right|_{\boldsymbol{a}'} = \left.\frac{\partial (a'^I - \delta a^I)}{\partial T}\right|_{\boldsymbol{a}'} = -\left.\frac{\partial (\delta a^I)}{\partial T}\right|_{\boldsymbol{a}'} = -\left.\frac{\partial (\delta a^I)}{\partial T}\right|_{\boldsymbol{a}}, \tag{47.112}$$

where the second equality follows since the time derivative is computed with $\boldsymbol{a}'$ fixed, and the third equality drops terms that are second order in the coordinate variation. This result thus brings the velocity variation in equation (47.111) to

$$\delta(\partial_T \boldsymbol{\varphi}) = \left.\frac{\partial \boldsymbol{\varphi}'(\boldsymbol{a}', T)}{\partial T}\right|_{\boldsymbol{a}'} - \left.\frac{\partial \boldsymbol{\varphi}(\boldsymbol{a}, T)}{\partial T}\right|_{\boldsymbol{a}} = -\left.\frac{\partial (\delta a^I)}{\partial T}\right|_{\boldsymbol{a}} \frac{\partial \boldsymbol{\varphi}}{\partial a^I}, \tag{47.113}$$

so that

$$\delta(\partial_T \boldsymbol{\varphi} \cdot \partial_T \boldsymbol{\varphi}/2) = \partial_T \boldsymbol{\varphi} \cdot \delta(\partial_T \boldsymbol{\varphi}) = -\partial_T(\delta a^I)\, \partial_I \boldsymbol{\varphi} \cdot \partial_T \boldsymbol{\varphi} = -\partial_T(\delta a^I)\, v_I, \tag{47.114}$$

where every term is evaluated at the Lagrangian space-time point $(\boldsymbol{a}, T)$, and where we introduced the covariant expression for the Lagrangian velocity[9]

$$v_I = \partial_I \boldsymbol{\varphi} \cdot \partial_T \boldsymbol{\varphi} = F^i{}_I\, \delta_{ij}\, \partial_T \varphi^j = F^i{}_I\, v^{\text{L}}_i, \tag{47.115}$$

with Eulerian coordinates assumed Cartesian so that $\delta_{ij}\, (v^{\text{L}})^j = v^{\text{L}}_i$.

47.7.6 Lagrangian expression for the potential vorticity

As this point, the action (47.90) has a variation given only through variations in the kinetic energy as per equation (47.114)

$$\delta \mathcal{S}^{\text{action}} = -\int_{t_{\text{A}}}^{t_{\text{B}}} \int_{\mathcal{R}(\boldsymbol{a})} \partial_T(\delta a^I)\, v_I\, \mathring{\rho}^{\text{L}}\, \mathring{g}^{\text{L}}\, \mathrm{d}^3 a\, \mathrm{d}T = \int_{t_{\text{A}}}^{t_{\text{B}}} \int_{\mathcal{R}(\boldsymbol{a})} \delta a^I\, (\partial_T v_I)\, \mathring{\rho}^{\text{L}}\, \mathring{g}^{\text{L}}\, \mathrm{d}^3 a\, \mathrm{d}T, \tag{47.116}$$

where we assumed the coordinate variation vanishes at the temporal bounds

$$\delta a^I = 0 \quad \text{for } T = t_{\text{A}} \text{ and } T = t_{\text{B}}. \tag{47.117}$$

We next introduce equation (47.108) for the non-divergent coordinate variation, and use equation (47.99) to relate the Levi-Civita tensor to the permutation symbol, so that

$$\mathring{\rho}^{\text{L}}\, \mathring{g}^{\text{L}}\, \delta a^I = \epsilon^{IJK}\, \partial_J W_K, \tag{47.118}$$

which brings the action variation to

$$\delta \mathcal{S}^{\text{action}} = \int_{t_{\text{A}}}^{t_{\text{B}}} \int_{\mathcal{R}(\boldsymbol{a})} \epsilon^{IJK}\, \partial_J W_K\, \partial_T v_I\, \mathrm{d}^3 a\, \mathrm{d}T. \tag{47.119}$$

[9] Recall that equation (47.8) introduced the contravariant Lagrangian representation of the velocity, $v^I = F^I{}_i\, (v^{\text{L}})^i$.

Integrating by parts on the spatial derivative leads to

$$\delta\mathcal{S}^{\text{action}} = -\int_{t_A}^{t_B}\int_{\mathcal{R}(\boldsymbol{a})} \epsilon^{IJK}\, W_K\, \partial_J \partial_T v_I \,\mathrm{d}^3a\,\mathrm{d}T, \tag{47.120}$$

where we assumed the coordinate variation vanishes at the material boundaries

$$\delta a^I = 0 \quad \text{for } \boldsymbol{a} \in \partial\mathcal{R}(\boldsymbol{a}). \tag{47.121}$$

The time and space derivatives commute in equation (47.120), and the permutation symbol, ϵ^{IJK}, and specific entropy, $\mathring{\mathcal{S}}$, are both independent of material time so that (with $W_K = A\,\partial_K\mathring{\mathcal{S}}$)

$$\begin{aligned}
\delta\mathcal{S}^{\text{action}} &= -\int_{t_A}^{t_B}\int_{\mathcal{R}(\boldsymbol{a})} W_K\, \partial_T(\epsilon^{IJK}\,\partial_J v_I)\,\mathrm{d}^3a\,\mathrm{d}T && \text{(47.122a)}\\
&= -\int_{t_A}^{t_B}\int_{\mathcal{R}(\boldsymbol{a})} A\,\partial_T(\partial_K\mathring{\mathcal{S}}\,\epsilon^{IJK}\,\partial_J v_I)\,\mathrm{d}^3a\,\mathrm{d}T. && \text{(47.122b)}\\
&= -\int_{t_A}^{t_B}\int_{\mathcal{R}(\boldsymbol{a})} A\,\partial_T[(1/\mathring{\rho}^{\mathsf{L}})\,\partial_K\mathring{\mathcal{S}}\,\mathring{\varepsilon}^{IJK}\,\partial_J v_I]\,\mathring{\rho}^{\mathsf{L}}\,\mathring{g}^{\mathsf{L}}\,\mathrm{d}^3a\,\mathrm{d}T. && \text{(47.122c)}
\end{aligned}$$

At this point we assert that particle relabeling symmetry holds, so that the action has zero variation.[10] For a zero variation to be realized with an arbitrary A requires the material time invariance of the Lagrangian expression of *Ertel potential vorticity* (Section 41.1)

$$Q \equiv \frac{\nabla_{\boldsymbol{a}}\mathring{\mathcal{S}}\cdot\mathring{\mathrm{curl}}(\boldsymbol{v})}{\mathring{\rho}^{\mathsf{L}}} = \frac{\partial_K\mathring{\mathcal{S}}\,\mathring{\varepsilon}^{IJK}\,\partial_J v_I}{\mathring{\rho}^{\mathsf{L}}} = \frac{\partial_K\mathring{\mathcal{S}}\,\epsilon^{IJK}\,\partial_J v_I}{\mathring{g}^{\mathsf{L}}\,\mathring{\rho}^{\mathsf{L}}}. \tag{47.123}$$

47.7.7 Eulerian expression for the potential vorticity

Transforming the Lagrangian expression (47.7) of the potential vorticity into its Eulerian form offers useful experience with index gymnastics. First we transform the Lagrangian gradient of the specific entropy into its Eulerian gradient using the chain rule with the transformation matrix (47.2)

$$\partial_K\mathring{\mathcal{S}} = F^k{}_K\,\partial_k\mathcal{S}, \tag{47.124}$$

where $\mathcal{S} = \mathcal{S}(\boldsymbol{x},t)$ is the Eulerian expression for the specific entropy. Next, expand the Lagrangian expression of the relative vorticity according to (recall the Eulerian coordinates are Cartesian)

$$\begin{aligned}
\epsilon^{IJK}\,\partial_J v_I &= \epsilon^{IJK}\,\partial_J(F^i{}_I\,\partial_T\varphi^j\,\delta_{ij}) && \text{(47.125a)}\\
&= \epsilon^{IJK}\,\partial_J(\partial_I\varphi^i\,\partial_T\varphi^j\,\delta_{ij}) && \text{(47.125b)}\\
&= \epsilon^{IJK}\,\partial_I\varphi^i\,\partial_T\partial_J\varphi^j\,\delta_{ij} && \text{(47.125c)}\\
&= \epsilon^{IJK}\,F^i{}_I\,\partial_T F^j{}_J\,\delta_{ij} && \text{(47.125d)}\\
&= \epsilon^{IJK}\,F^i{}_I\,F^m{}_J\,\partial_m v^j\,\delta_{ij}, && \text{(47.125e)}
\end{aligned}$$

where we used equation (18.108) to write the material time evolution of the transformation matrix in terms of the Eulerian expression for the velocity gradient tensor

$$\partial_T F^j{}_J = F^m{}_J\,\partial_m v^j. \tag{47.126}$$

[10] A vanishing action variation is here not a result of invoking Hamilton's principle. Rather, it results from insisting that particle relabeling symmetry holds.

Now contract the relative vorticity (47.125e) with the gradient of the specific entropy

$$\partial_K \mathring{\mathcal{S}}\, \epsilon^{IJK}\, \partial_J v_I = \partial_k \mathcal{S}\, \epsilon^{IJK}\, F^i{}_I\, F^m{}_J\, F^k{}_K\, \partial_m v^j\, \delta_{ij}. \tag{47.127}$$

We can make this expression a bit more tidy through use of equation (4.71) for the determinant

$$\partial_K \mathring{\mathcal{S}}\, \epsilon^{IJK}\, \partial_J v_I = \partial_k \mathring{\mathcal{S}}\, \epsilon^{imk}\, \frac{\partial \boldsymbol{\varphi}}{\partial \boldsymbol{a}}\, \partial_m v^j\, \delta_{ij}. \tag{47.128}$$

Finally, using equation (47.21a) for the specific volume renders

$$\partial_K \mathring{\mathcal{S}}\, \epsilon^{IJK}\, \partial_J v_I = \partial_k \mathcal{S}\, \epsilon^{ijk}\, \partial_j(\delta_{im}\, v^m) = \mathring{g}^{\text{L}}\, \mathring{\rho}^{\text{L}}\, \frac{\nabla_{\boldsymbol{x}} \mathcal{S} \cdot \operatorname{curl}(\boldsymbol{v})}{\rho}, \tag{47.129}$$

which then leads us to the expected Eulerian expression for the potential vorticity, written entirely in terms of Eulerian quantities

$$Q = \frac{\nabla_{\boldsymbol{x}} \mathcal{S} \cdot \operatorname{curl}(\boldsymbol{v})}{\rho}. \tag{47.130}$$

47.7.8 Global versus local conservation

Space-time symmetries leading to the conservation of momentum and energy lead to differential conservation laws in the form of a continuity equation, such as equation (47.73) for the Hamiltonian density. A global spatial integration of the continuity equation leads to a constant of the motion (e.g., the globally integrated energy) in cases where the normal component of the corresponding fluxes vanish on the boundaries. Such differential conservation laws operationally arise when an active variation leads to a mechanically equivalent action, such as discussed in Section 46.4.4 for constant space-time shifts.

Rather than a mechanically equivalent Lagrangian, are there symmetries related to coordinate transformations (passive variations) that lead to unaltered actions? If so, then the corresponding Noether theorem conservation law does not appear as a continuity equation. Instead, it appears as a property that is a temporal constant everywhere in Lagrangian space-time. That is, it leads to a *local conservation law* rather than a *global conservation law*. As seen in this section, the material time independence of potential vorticity is just that local conservation law for a perfect fluid. That is, potential vorticity is constant for each point in the Lagrangian (material) space-time.

A more tedious calculation of the Jacobian variation (47.57)

To derive the variation of the Jacobian in equation (47.57), we made use of the identity (4.75) for the derivative of the Jacobian with respect to an element of the matrix. For fun, we here derive equation (47.57) yet do not make use of equation (4.75). The calculation is more tedious but it does serve to further our experience with index gymnastics, and is thus of use for those wishing to garner practice.

The first step makes use of the product rule

$$\delta\left[\frac{\partial \varphi^m}{\partial a^I}\,\frac{\partial \varphi^n}{\partial a^J}\,\frac{\partial \varphi^p}{\partial a^K}\right] = \frac{\partial(\delta\varphi^m)}{\partial a^I}\,\frac{\partial \varphi^n}{\partial a^J}\,\frac{\partial \varphi^p}{\partial a^K} + \frac{\partial(\delta\varphi^n)}{\partial a^J}\,\frac{\partial \varphi^m}{\partial a^I}\,\frac{\partial \varphi^p}{\partial a^K} + \frac{\partial(\delta\varphi^p)}{\partial a^K}\,\frac{\partial \varphi^m}{\partial a^I}\,\frac{\partial \varphi^n}{\partial a^J}. \tag{47.131}$$

We now introduce $\boldsymbol{x}$-space derivatives rather than sticking solely with $\boldsymbol{a}$-space derivatives, and

for this purpose we make use of the chain rule to write[11]

$$\frac{\partial(\delta\varphi^m)}{\partial a^I} = \frac{\partial(\delta\varphi^m)}{\partial x^q}\,\frac{\partial\varphi^q}{\partial a^I}, \qquad \frac{\partial(\delta\varphi^n)}{\partial a^J} = \frac{\partial(\delta\varphi^n)}{\partial x^q}\,\frac{\partial\varphi^q}{\partial a^J}, \qquad \frac{\partial(\delta\varphi^p)}{\partial a^K} = \frac{\partial(\delta\varphi^p)}{\partial x^q}\,\frac{\partial\varphi^q}{\partial a^K}, \tag{47.132}$$

where the $\boldsymbol{x}$-space derivatives of the variation, $\delta\boldsymbol{\varphi}$, are computed at the point $\boldsymbol{x} = \boldsymbol{\varphi}(\boldsymbol{a}, T)$. Making use of equations (47.132) renders the variation

$$\begin{aligned}\delta&\left[\frac{\partial\varphi^m}{\partial a^I}\,\frac{\partial\varphi^n}{\partial a^J}\,\frac{\partial\varphi^p}{\partial a^K}\right]\\ &= \frac{\partial(\delta\varphi^m)}{\partial x^q}\,\frac{\partial\varphi^q}{\partial a^I}\,\frac{\partial\varphi^n}{\partial a^J}\,\frac{\partial\varphi^p}{\partial a^K} + \frac{\partial(\delta\varphi^n)}{\partial x^q}\,\frac{\partial\varphi^q}{\partial a^J}\,\frac{\partial\varphi^m}{\partial a^I}\,\frac{\partial\varphi^p}{\partial a^K} + \frac{\partial(\delta\varphi^p)}{\partial x^q}\,\frac{\partial\varphi^q}{\partial a^K}\,\frac{\partial\varphi^m}{\partial a^I}\,\frac{\partial\varphi^n}{\partial a^J}.\end{aligned} \tag{47.133}$$

Now reintroduce the permutation symbols to yield

$$\begin{aligned}\delta&\left[\frac{1}{3!}\,\epsilon_{mnp}\,\epsilon^{IJK}\,\frac{\partial\varphi^m}{\partial a^I}\,\frac{\partial\varphi^n}{\partial a^J}\,\frac{\partial\varphi^p}{\partial a^K}\right]\\ &= \frac{1}{3!}\,\epsilon_{mnp}\,\epsilon^{IJK}\,\frac{\partial(\delta\varphi^m)}{\partial x^q}\left(\frac{\partial\varphi^q}{\partial a^I}\,\frac{\partial\varphi^n}{\partial a^J}\,\frac{\partial\varphi^p}{\partial a^K} - \frac{\partial\varphi^q}{\partial a^J}\,\frac{\partial\varphi^n}{\partial a^I}\,\frac{\partial\varphi^p}{\partial a^K} - \frac{\partial\varphi^q}{\partial a^K}\,\frac{\partial\varphi^p}{\partial a^I}\,\frac{\partial\varphi^n}{\partial a^J}\right),\end{aligned} \tag{47.134}$$

which can be simplified to

$$\delta\left[\frac{1}{3!}\,\epsilon_{mnp}\,\epsilon^{IJK}\,\frac{\partial\varphi^m}{\partial a^I}\,\frac{\partial\varphi^n}{\partial a^J}\,\frac{\partial\varphi^p}{\partial a^K}\right] = \frac{1}{2}\,\epsilon_{mnp}\,\epsilon^{IJK}\,\frac{\partial(\delta\varphi^m)}{\partial x^q}\left(\frac{\partial\varphi^q}{\partial a^I}\,\frac{\partial\varphi^n}{\partial a^J}\,\frac{\partial\varphi^p}{\partial a^K}\right). \tag{47.135}$$

The right hand side vanishes unless $m = q$, which can be seen by expanding the terms. The case with $m = q = 1$ is given by

$$\begin{aligned}\frac{1}{2}\,\epsilon_{1np}\,\epsilon^{IJK}\,\frac{\partial(\delta\varphi^1)}{\partial x^1}&\left(\frac{\partial\varphi^1}{\partial a^I}\,\frac{\partial\varphi^n}{\partial a^J}\,\frac{\partial\varphi^p}{\partial a^K}\right)\\ &= \frac{1}{2}\,\epsilon_{123}\,\epsilon^{IJK}\,\frac{\partial(\delta\varphi^1)}{\partial x^1}\left(\frac{\partial\varphi^1}{\partial a^I}\,\frac{\partial\varphi^2}{\partial a^J}\,\frac{\partial\varphi^3}{\partial a^K} - \frac{\partial\varphi^1}{\partial a^I}\,\frac{\partial\varphi^3}{\partial a^J}\,\frac{\partial\varphi^2}{\partial a^K}\right),\end{aligned} \tag{47.136}$$

which can be simplified to

$$\frac{1}{2}\,\epsilon_{1np}\,\epsilon^{IJK}\,\frac{\partial(\delta\varphi^1)}{\partial x^1}\left(\frac{\partial\varphi^1}{\partial a^I}\,\frac{\partial\varphi^n}{\partial a^J}\,\frac{\partial\varphi^p}{\partial a^K}\right) = \epsilon^{IJK}\,\frac{\partial(\delta\varphi^1)}{\partial x^1}\left(\frac{\partial\varphi^1}{\partial a^I}\,\frac{\partial\varphi^2}{\partial a^J}\,\frac{\partial\varphi^3}{\partial a^K}\right). \tag{47.137}$$

The cases $m = 2$ and $m = 3$ lead to corresponding results, in which case we are led to

$$\delta\left[\frac{\partial\boldsymbol{\varphi}}{\partial\boldsymbol{a}}\right] = \frac{\partial(\delta\varphi^i)}{\partial x^i}\,\epsilon^{IJK}\left(\frac{\partial\varphi^1}{\partial a^I}\,\frac{\partial\varphi^2}{\partial a^J}\,\frac{\partial\varphi^3}{\partial a^K}\right) \tag{47.138a}$$

$$= \frac{\partial(\delta\varphi^i)}{\partial x^i}\,\frac{1}{3!}\,\epsilon_{mnp}\,\epsilon^{IJK}\,\frac{\partial\varphi^m}{\partial a^I}\,\frac{\partial\varphi^n}{\partial a^J}\,\frac{\partial\varphi^p}{\partial a^K} \tag{47.138b}$$

$$= \frac{\partial(\delta\varphi^i)}{\partial x^i}\,\frac{\partial\boldsymbol{\varphi}}{\partial\boldsymbol{a}}, \tag{47.138c}$$

which is equation (47.57).

[11] At this point, it can be useful to be reminded of the notational conventions detailed in Section 18.4.

Chapter 48

Approximate theories from Hamilton's principle

In this chapter we derive some approximate theories for perfect fluids using *Hamilton's variational principle*.

READER'S GUIDE FOR THIS CHAPTER

This chapter is a direct follow-on from Chapter 47 that considered Hamilton's principle for a perfect fluid.

48.1 Loose threads

- Adiabatic Boussinesq in buoyancy coordinates
- Quasi-geostrophy
- Semi-geostrophy
- shallow water

48.2 Boussinesq ocean

We studied the Boussinesq ocean in Chapter 29, and here establish the Boussinesq equations of motion via Hamilton's principle. There are some novel conceptual and technical points to raise here relative to the non-Boussinesq fluid considered in Chapter 47, thus warranting a full discussion of the Boussinesq case.

48.2.1 Unit Jacobian for non-divergent flow

Following the approach earlier in this chapter, we use Cartesian Eulerian coordinates so that $\boldsymbol{x} = \boldsymbol{\varphi}(\boldsymbol{a}, T)$ provides the instantaneous Cartesian position of a fluid particle with material label, $\boldsymbol{a}$, and material time, T. Additionally, we here assume material coordinates are given by the

Cartesian initial positions of fluid particles, in which case the Jacobian is unity at the initial condition

$$\boldsymbol{a} = \mathring{\boldsymbol{x}} \implies \frac{\partial \boldsymbol{\varphi}}{\partial \mathring{\boldsymbol{x}}} = 1 \quad \text{at } T = t_0. \tag{48.1}$$

With this choice for the Eulerian and material coordinates, equation (18.77) means that the Jacobian is the ratio of the present fluid parcel volume to the initial parcel volume

$$\frac{\partial \boldsymbol{\varphi}}{\partial \mathring{\boldsymbol{x}}} = \frac{\mathrm{d}^3 x}{\mathrm{d}^3 \mathring{x}}. \tag{48.2}$$

From our study in Chapter 21, we know that non-divergent flows keep the volume of fluid parcels constant while following fluid particle trajectories, so that the Jacobian is a material constant

$$\partial_T (\partial \boldsymbol{\varphi} / \partial \mathring{\boldsymbol{x}}) = 0. \tag{48.3}$$

A unit initial value as per equation (48.1) along material constancy means that the Jacobian retains its unity value along each particle trajectory for all time

$$\partial \boldsymbol{\varphi} / \partial \mathring{\boldsymbol{x}} = 1 \; \forall \; T. \tag{48.4}$$

48.2.2 Boussinesq energetics

As described in Section 29.1.8, the Boussinesq ocean does not respect the principle of equivalence, since the mass used for the kinetic energy (inertial mass) is based on a constant reference density, $\rho_\circ$, whereas the mass used for the gravitational potential energy (gravitational mass) uses the *in situ* density, ρ. A constant reference density for kinetic energy means that the flow is non-divergent, whereas the *in situ* density for potential energy allows for buoyancy to affect motion via density gradients.

Now recall from Section 47.4.3 that the specific internal energy is a function of the specific entropy and specific volume. For the perfect fluid the specific entropy is a material constant. Equation (48.4) implies that the specific volume is also a material constant. Consequently, the specific internal energy for the Boussinesq ocean is a material constant. Evidently, there is a disconnect between between pressure and internal energy for the Boussinesq ocean. Stated otherwise, we know that in the absence of flow divergence, there can be no pressure work on a fluid parcel. Hence, pressure in the Boussinesq ocean has no thermodynamic connection to internal energy. Pressure instead plays a purely mechanical role, which we see in Section 48.2.3 via its role as a Lagrange multiplier that constrains the flow to remain non-divergent. We already described pressure as a constraint in Section 29.3, with the present discussion furthering that understanding through Hamilton's principle.

48.2.3 Action for the Boussinesq ocean

We follow the approach in Sections 13.11.3 and 15.5.2 by absorbing the centrifugal potential into the geopotential, thus writing

$$\Phi = g\, z. \tag{48.5}$$

In this manner we are led to the action for a Boussinesq ocean (recall that $\boldsymbol{a} = \mathring{\boldsymbol{x}}$)

$$\begin{aligned} \mathsf{S}^{\text{action}} = \int_{T_{\text{init}}}^{T_{\text{final}}} \int_{\mathscr{R}(\mathring{\boldsymbol{x}})} \left[\tfrac{1}{2}\, \partial_T \boldsymbol{\varphi} \cdot \partial_T \boldsymbol{\varphi} + \partial_T \boldsymbol{\varphi} \cdot (\boldsymbol{\Omega} \times \boldsymbol{\varphi}) \right] \rho_\circ \, \mathrm{d}^3 \mathring{x} \, \mathrm{d}T - \int_{T_{\text{init}}}^{T_{\text{final}}} \int_{\mathscr{R}(\mathring{\boldsymbol{x}})} \Phi \, \mathring{\rho} \, \mathrm{d}^3 \mathring{x} \, \mathrm{d}T \\ + \int_{T_{\text{init}}}^{T_{\text{final}}} \int_{\mathscr{R}(\mathring{\boldsymbol{x}})} p \, (\partial \boldsymbol{\varphi} / \partial \mathring{\boldsymbol{x}} - 1) \, \mathrm{d}^3 \mathring{x} \, \mathrm{d}T, \end{aligned} \tag{48.6}$$

where p is a Lagrange multiplier that plays the role of mechanical pressure. Notice that we used the constant Boussinesq reference density, $\rho_\circ$, for computing the kinetic energy, whereas the geopotential uses $\mathring{\rho}$. The use of distinct densities arises since the Boussinesq ocean does not respect the principle of equivalance.

48.2.4 Boussinesq Euler-Lagrange equation

We now vary the Boussinesq action (48.6) by independently varying the trajectories as well as the Lagrange multiplier, p. Varying the Lagrange multipler leads, as expected, to the non-divergence constraint (48.4)

$$\delta_p \mathcal{S}^{\text{act}} = 0 \Longrightarrow \partial\boldsymbol{\varphi}/\partial\mathring{\boldsymbol{x}} = 1. \tag{48.7}$$

We now detail results from varying the trajectories.

Kinetic energy variation arising from variation of the trajectories

Following the steps in Section 47.5.2, only now with density set to the constant reference density, $\rho_\circ$, leads to variation of the kinetic energy contribution to the action

$$\begin{aligned}\delta \int_{T_{\text{init}}}^{T_{\text{final}}} \int_{\mathscr{R}(\mathring{\boldsymbol{x}})} [\tfrac{1}{2}\, \partial_T \boldsymbol{\varphi} \cdot \partial_T \boldsymbol{\varphi} + \partial_T \boldsymbol{\varphi} \cdot (\boldsymbol{\Omega} \times \boldsymbol{\varphi})]\, \rho_\circ \, \mathrm{d}^3\mathring{x}\, \mathrm{d}T \\ = - \int_{T_{\text{init}}}^{T_{\text{final}}} \int_{\mathscr{R}(\mathring{\boldsymbol{x}})} [\partial_{TT} \boldsymbol{\varphi} + 2\, \boldsymbol{\Omega} \times \partial_T \boldsymbol{\varphi}] \cdot \delta\boldsymbol{\varphi}\, \rho_\circ \, \mathrm{d}^3\mathring{x}\, \mathrm{d}T.\end{aligned} \tag{48.8}$$

Geopotential energy variation arising from variation of the trajectories

The chain rule leads to variation of the integrated geopotential

$$\delta \int_{\mathscr{R}(\mathring{\boldsymbol{x}})} \Phi\, \mathring{\rho}\, \mathrm{d}^3\mathring{x} = \int_{\mathscr{R}(\mathring{\boldsymbol{x}})} \frac{\partial \Phi}{\partial \varphi^i}\, \delta\varphi^i\, \mathring{\rho}\, \mathrm{d}^3\mathring{x} = \int_{\mathscr{R}(\mathring{\boldsymbol{x}})} \frac{\partial \Phi}{\partial \varphi^i}\, \delta\varphi^i\, \rho^{\text{L}}\, \mathrm{d}^3\mathring{x}, \tag{48.9}$$

where the final equality made use of the identity (47.18) with a unit Jacobian

$$\mathring{\rho} = \rho^{\text{L}}\, \partial\boldsymbol{\varphi}/\partial\mathring{\boldsymbol{x}} = \rho^{\text{L}}. \tag{48.10}$$

Constraint variation arising from variation of the trajectories

Varying the trajectories leads to variation of the constraint

$$\int_{\mathscr{R}(\mathring{\boldsymbol{x}})} p\, \delta(\partial\boldsymbol{\varphi}/\partial\mathring{\boldsymbol{x}})\, \mathrm{d}^3\mathring{x} = \int_{\mathscr{R}(\mathring{\boldsymbol{x}})} p\, \frac{\partial(\delta\varphi^i)}{\partial x^i}\, \mathrm{d}^3\mathring{x} = - \int_{\mathscr{R}(\mathring{\boldsymbol{x}})} \frac{\partial p}{\partial x^i}\, \delta\varphi^i\, \mathrm{d}^3\mathring{x}, \tag{48.11}$$

where we used equation (47.138c) for the Jacobian variation in the presence of a unit Jacobian

$$\delta \left[\frac{\partial\boldsymbol{\varphi}}{\partial\mathring{\boldsymbol{x}}}\right] = \frac{\partial(\delta\varphi^i)}{\partial x^i}\, \frac{\partial\boldsymbol{\varphi}}{\partial\mathring{\boldsymbol{x}}} = \frac{\partial(\delta\varphi^i)}{\partial x^i}, \tag{48.12}$$

and assumed zero mechanical forcing at the domain boundaries.

The Euler-Lagrange equation for the Boussinesq ocean

Bringing terms together leads to the action variation under variation of the trajectories

$$\delta_{\boldsymbol{\varphi}} \mathcal{S}^{\text{act}} = -\int_{T_{\text{init}}}^{T_{\text{final}}} \int_{\mathcal{R}(\mathring{\boldsymbol{x}})} [\partial_{TT} \boldsymbol{\varphi} + 2\,\boldsymbol{\Omega} \times \partial_T \boldsymbol{\varphi}] \cdot \delta\boldsymbol{\varphi}\, \rho_{\circ}\, \mathrm{d}^3\mathring{x}\, \mathrm{d}T - \int_{T_{\text{init}}}^{T_{\text{final}}} \int_{\mathcal{R}(\mathring{\boldsymbol{x}})} \frac{\partial \Phi}{\partial \varphi^i}\, \delta\varphi^i\, \rho^{\text{L}}\, \mathrm{d}^3\mathring{x}\, \mathrm{d}T - \int_{T_{\text{init}}}^{T_{\text{final}}} \int_{\mathcal{R}(\mathring{\boldsymbol{x}})} \frac{\partial p}{\partial x^i}\, \delta\varphi^i\, \mathrm{d}^3\mathring{x}\, \mathrm{d}T. \quad (48.13)$$

Setting the variation to zero leads to the Boussinesq Euler-Lagrange equations

$$\partial_T \boldsymbol{v}^{\text{L}} + 2\,\boldsymbol{\Omega} \times \boldsymbol{v}^{\text{L}} = -\frac{1}{\rho_{\circ}} \frac{\partial p}{\partial \boldsymbol{\varphi}} - \frac{\rho^{\text{L}}}{\rho_{\circ}} \frac{\partial \Phi}{\partial \boldsymbol{\varphi}}, \quad (48.14)$$

which agrees with the perfect fluid Boussinesq ocean equations derived in Section 29.1.7 using Newtonian methods.

48.2.5 Comments

Absence of an equivalence principle for the Boussinesq ocean prompts a careful treatment of the density factors. Furthermore, note how the pressure, here appearing as a Lagrange multiplier, corresponds directly to the thermodynamic pressure for the non-Boussinesq fluid in Section 47.5. That correspondence is not a coincidence, with the sign of the constraint as written in equation (48.6) chosen to facilitate the agreement.

Part X

Linear wave mechanics

Waves and the central role of a dispersion relation

In this part of the book, we study the mechanics of non-dissipative linear waves appearing in geophysical fluids. This study of *wave mechanics* forms a key part of geophysical fluid mechanics in part since so much of the observed geophysical flows manifest waves in one form or another.[1] Waves in fluids manifest as fluctuations of fluid particles and associated fluid properties, with the fluctuations possessing coherency in both space and time. Linear waves exist dynamically due to a restoring force that provides the means for fluid particles to undergo simple harmonic oscillations. Kinematically, linear waves arise when a symmetry is mildly broken, with coherent fluctuations the collective response to the symmetry breaking. This *wave mechanics* forms a key part of observed geophysical fluid phenomena.[2]

Linear waves have spatial and temporal properties that are closely linked. This linkage relates the angular frequency, ω, which measures the temporal structure of a wave, to the wavevector, $\boldsymbol{k}$, which measures the spatial structure of a wave. The *dispersion relation* is the mathematical equation that specifies the linkage between ω and $\boldsymbol{k}$. Details of the dispersion relation are determined by the physical forces that give rise to the wave, such as compressibility for acoustic waves (Chapter 51), surface tension for capillary waves (Chapter 52), gravitational acceleration for gravity waves (Chapters 52, 55, and 57), the Coriolis acceleration for inertial waves (Chapters 53 and 55) and differential rotation (beta effect) for planetary Rossby waves (Chapters 54 and 55).

Linear waves satisfy the *superposition principle* that is generally respected by linear physical phenomena. As a result, interactions between linear waves are reversible, and consist of constructive and destructive *interferences*.[3] The superposition principle allows for the solution of a linear wave equation to be constructed from constituent elementary pieces. Linear superposition is the fundamental reason we can usefully examine properties of waves by examining the behavior of a single traveling wave. We use this property of linearity when deriving the dispersion relation for waves, and, in Part XI of this book, for determining stability properties.

Linearization to derive the wave equations

Derivation of a wave equation and corresponding dispersion relation requires us to linearize the nonlinear governing equations of fluid motion. After deriving the linearized equations, we study their salient properties to help understand the mechanics of their linear wave solutions and dispersion relations. Each wave system has unique properties depending on the underlying dynamical forces. Even so, many kinematical properties transcend details of the dynamics, with kinematics forming the focus for Chapters 49 and 50.

Wave energy transport versus matter transport

The movement of fluid particles within a fluid is associated with the movement of matter, including tracers, as well as other properties such as momentum, vorticity, enthalpy, entropy, etc. Although waves can lead to a net transfer of matter, through a process known as *Stokes drift*, the transfer of wave energy and momentum generally occurs without any net movement of fluid particles, where "net movement" refers to a time average over a wave period (i.e., the *phase average* from Section 8.1.2). As such, wave energy propagates at speeds that are unconstrained by fluid particle speeds. Indeed, wave energy in linear waves is generally transmitted many times

[1] "Wave mechanics" sometimes refers to that part of quantum mechanics based on Schrödinger's equation. We are instead here concerned with waves that occur in classical geophysical fluids.

[2] "Wave mechanics" sometimes refers to that part of quantum mechanics based on Schrödinger's equation. We are instead here concerned with waves that occur in classical geophysical fluids.

[3] Some authors prefer to consider reversible interactions as the absence of any interaction, since one can exactly distinguish individual linear waves through the Fourier decomposition of a wave field comprised of multiple waves.

faster than matter. We thus conceive of waves as organized disturbances on a background fluid state (sometimes called the base state or equilibrium state) that transmit energy from one part of the media to another. The speed and direction of wave energy is determined by the dispersion relation, thus making the dispersion relation a central feature of wave mechanics.

The scope of our study

The study of wave mechanics forms a central part of physics, engineering, and applied mathematics. We target the reader aiming to learn wave mechanics for the first time, while also providing selected material for the experienced physicist interested in geophysical fluid wave mechanics. For these purposes, we survey a suite of geophysical fluid waves and dive deep into particular special topics to support understanding and to develop mathematical methods. To help simplify the maths, we restrict attention to Cartesian waves (i.e., plane waves), leaving the geophysically relevant topic of spherical waves for more specialized treatments. Our presentation is not comprehensive. Instead, we aim to offer an intellectual platform for further study and research. Insights and skills working with waves requires practice, and we get plenty from the wide variety of geophysical fluid waves considered here.

Chapter 49

PLANE WAVES AND WAVE PACKETS

Forces acting in a fluid determine the *dispersion relation* satisfied by linear waves, with the dispersion relation connecting the wave angular frequency, ω, to the *wavevector*, $\boldsymbol{k}$. We write this relation in the functional form[1]

$$\omega = \varpi(\boldsymbol{k}), \tag{49.1}$$

where ϖ is generally a nonlinear function of the wavevector. The dispersion relation couples the space and time structure of a wave: once a wavevector is chosen then the angular frequency is specified. In this chapter we develop the foundations for *wave kinematics*, which focuses on wave properties arising from the existence of a dispersion relation yet is unconcerned with the forces that determine this relation.

The *wave function* plays a fundamental role in describing waves. Example wave functions include the velocity potential (acoustic and surface waves), the streamfunction (Rossby waves), and free surface height (shallow water waves). All other dynamical fields can be generated from the wave function, thus allowing us to focus on characterizing how the wave appears through study of the wave function. The wave function has both an $\boldsymbol{x}$-space (geographic/height space) representation as well as a $\boldsymbol{k}$-space (wavevector space) representation. These two representations offer complementary characterizations of wave properties, with the transformation between these representations provided by Fourier's integral theorem from Section 8.3.1. One of the more remarkable aspects of this complementarity arises through the *uncertainty relation*, which states that it is not possible to simultaneously specify the position of a wave packet with arbitrary precision in both $\boldsymbol{x}$-space and $\boldsymbol{k}$-space. That is, precision in one space corresponds to imprecision in the other. We derive this uncertainty relation through the study of Gaussian wave packets.

READER'S GUIDE TO THIS CHAPTER

We focus on plane waves in this chapter and so make use of Cartesian coordinates and Cartesian tensors (Chapters 1 and 2). Furthermore, we assume familiarity with the use of complex variables as well as Fourier transforms, both reviewed in Chapter 8. We restrict attention to a homogeneous background/base state upon which waves are supported. A homogeneous base state is rarely realized in geophysics, and yet it serves our pedagogical needs prior to moving onto the more realistic, and mathematically complex, case of an inhomogeneous base state in Chapter 50.

The presentation shares much with books and reviews covering topics in linear wave mechanics, such as *Bretherton* (1971), chapter 3 of *Acheson* (1990), chapters 1 and 2 of *Pedlosky* (2003), chapter 6 of *Olbers et al.* (2012), chapter 1 of *Sutherland* (2010), chapter 7 of *Thorne and Blandford* (2017), and chapter 6 of *Vallis* (2017). However, be mindful that not all authors agree on the conventions followed here and as summarized in Section 49.2.

[1] For waves moving on a space and time dependent background, the dispersion relation picks up space and time dependence. This topic is the focus of Chapter 50.

49.1 Loose threads

- Figures

- More on wave packets and Green's functions. Derive the Green's function equation from the packet equation plus the dispersion relation.

49.2 Nomenclature and conventions

Many readers have encountered wave kinematics in prior studies. Yet some of the conventions are not universal, so that it is useful to summarize salient points to expose the choices made in this book.

49.2.1 Types of waves

Table 49.1 summarizes the various types of waves considered in this book. We mostly encounter plane traveling waves, though also make use of standing waves (as for waves within a bounded domain) and stationary waves (when a wave has only spatial periodicity and no time dependence). The wave patterns in Table 49.1 can arise from any conceivable context, physical or otherwise (e.g., the wave produced by spectators in a large sporting event). The specifics of a physical system arises when enforcing that a wave function, Φ, satisfies a linear partial differential equation, and it is through this equation that we derive the dispersion relation.

We wish to emphasize the above points in a bit more mundane manner. Namely, there are many mathematical functions that give rise to oscillating patterns. However, these patterns correspond to particular solutions to a physical system only when they satisfy a partial differential equation such as equation (6.65). That is, there are more mathematial wave-like patterns than there are physical waves. For example, consider the function

$$\Phi(x,y,t) = A\cos(k_x\,x - \omega\,t)\cos(\omega\,t) = (A/2)\,[\cos(k_x\,x - 2\,\omega\,t) + \cos(k_x x)], \tag{49.2}$$

where A is a constant amplitude. The second expression reveals the sum of a traveling plane wave plus a stationary wave. It is notable that this function is *not* in the form of a Fourier component that constitutes the wave patterns in Table 49.1. Rather, it is simply the sum of two trigonometric functions having a particular space and time structure. Is this function a particular solution to the classic wave equation with operator $\partial_{tt} - c^2\,\partial_{xx}$? A quick calculation reveals that it is *not* a solution since

$$\partial_{tt}\Phi = -2\,A\,\omega^2\cos(k_x\,x - 2\,\omega\,t) \tag{49.3a}$$

$$\partial_{xx}\Phi = -k_x^2\,\Phi = -(k_x^2\,A/2)[\cos(k_x\,x - 2\,\omega\,t) + \cos(k_x x)], \tag{49.3b}$$

revealing that there is no way to relate $\partial_{tt}\Phi$ and $c^2\,\partial_{xx}\Phi$ at arbitrary space and time points. In turn, this function is *not* a suitable wave function ansatz for deriving a dispersion relation.[2]

NAME	SPACE-TIME STRUCTURE
monochromatic	$\mathrm{Re}[\Phi_0\,\mathrm{e}^{-\mathrm{i}\,\omega\,t}]$
traveling	$\mathrm{Re}[\mathcal{A}(\boldsymbol{k})\,\mathrm{e}^{\mathrm{i}\,(\boldsymbol{k}\cdot\boldsymbol{x}-\omega\,t)}]$
standing	$\mathrm{Re}[\mathcal{A}(\boldsymbol{k})\,\mathrm{e}^{\mathrm{i}\,\boldsymbol{k}\cdot\boldsymbol{x}}]\cos(\omega t)$
stationary	$\mathrm{Re}[\mathcal{A}(\boldsymbol{k})\,\mathrm{e}^{\mathrm{i}\,\boldsymbol{k}\cdot\boldsymbol{x}}]$

TABLE 49.1: Summarizing the variety of waves encountered in this book, with distinctions based on their space-time structure. The operator, Re, extracts the real part of its argument, so that, for example, $\mathrm{Re}[\mathrm{e}^{\mathrm{i}\,(\boldsymbol{k}\cdot\boldsymbol{x}-\omega\,t)}] = \cos(\boldsymbol{k}\cdot\boldsymbol{x} - \omega\,t)$. The first three patterns are monochromatic, which means they oscillate coherently with a single period, $2\pi/\omega$, where $\omega \geq 0$ is the angular frequency. However, note that $\mathrm{Re}[\Phi_0\,\mathrm{e}^{-\mathrm{i}\,\omega\,t}]$ is monochromatic and yet we cannot conclude whether it is a wave until we have further information about its spatial structure. Spatial dependence is introduced in the form $\mathrm{e}^{\mathrm{i}\boldsymbol{k}\cdot\boldsymbol{x}}$, where $\boldsymbol{k}$ is the wavevector that determines the direction of the wave and its wavelength. For a plane wave in three-dimensional space, $\boldsymbol{k}\cdot\boldsymbol{x} = k_x\,x + k_y\,y + k_z\,z$, whereas a plane wave in two dimensions has wavevector $\boldsymbol{k}\cdot\boldsymbol{x} = k_x\,x + k_y\,y$. Standing waves do not travel in space but oscillate in place. A stationary wave has an oscillatory spatial pattern but has no time dependence and so is static. The final three waves are *harmonic* since they have a regular spatial pattern.

[2] See Section 49.5.5 for a discussion of wave *ansatz*.

49.2.2 Types of dispersion relations

The dispersion relation (49.1) is the root of all wave properties since it links the space and time structure of the wave. Some waves encountered in this book have a dispersion relation in the slightly more restricted form

$$\omega = \varpi(|\boldsymbol{k}|), \tag{49.4}$$

where $|\boldsymbol{k}|$ is the *wavenumber*. Evidently, these waves have their angular frequency independent of the wave direction. Examples include acoustic waves (Chapter 51) and surface waves (Chapter 52). Inertial waves from Chapter 53 and internal gravity waves from Chapter 57 are the complement, with their dispersion relation independent of the wavenumber yet dependent on the wave direction,

$$\omega = \varpi(\hat{\boldsymbol{k}}) \quad \text{with} \quad \hat{\boldsymbol{k}} = \boldsymbol{k}/|\boldsymbol{k}|. \tag{49.5}$$

Finally, the Rossby waves introduced in Chapters 54 and 55 have a dispersion relation that depends on both the wavenumber and wave direction; i.e., on the wavevector, $\boldsymbol{k}$.

49.2.3 Conventions for space-time description of waves

The suite of dispersion relations encountered in geophysical fluids motivates the following conventions that form the basis for our space-time description of waves. Readers should be aware that certain of these conventions are not universally followed in the literature.

- ANGULAR FREQUENCY: Following *Bretherton* (1971), the angular frequency of a stable linear wave that results from the dispersion relation, $\omega = \varpi(\boldsymbol{k})$, is chosen as a non-negative real number,

  $$\omega \geq 0, \tag{49.6}$$

  so that the wave period, $2\pi/\omega$, is also a non-negative number and the wave advances forward in time with the wave direction determined by the wavevector.

  This convention is not universally followed in the literature. One reason to allow for a negative angular frequency is that dispersion relations typically lead to quadratic equations that have a positive and a negative root. For example, the one-dimensional acoustic wave equation has

  $$\omega^2(\boldsymbol{k}) = c_{\mathrm{s}}^2\, \boldsymbol{k}^2, \tag{49.7}$$

  which has roots $\omega = \pm c_{\mathrm{s}}|\boldsymbol{k}|$ (c_{s} is the acoustic wave speed; Section 51.5.1). When choosing both roots, one interprets them as representing oppositely moving waves. Even so, we follow a convention that always chooses the positive root, so that the wave direction is determined by the wavevector (see next point) rather than the sign of the angular frequency. Additionally, we are not generally interested in waves traveling backward in time, which is sometimes used to interpret waves with $\omega < 0$.

  One encounters a negative angular frequency when conducting time-frequency Fourier analysis in the complex plane, as in Section 8.4. In that context, the negative frequency is not physical, but instead is a mathematical expedient that allows one to work with a complex Fourier transform. There is nothing physical associated with the negative frequency in this context, since one could equivalently work with real Fourier sine and cosine transforms where the angular frequency is non-negative. See Section 8.4.1 for more discussion. Furthermore, if using complex Fourier analysis, then switching the sign of the angular frequency and the wavevector merely leads to the complex conjugate wave function. Since the physical wave is real in classical physics, the complex conjugate wave function is the same wave.

- WAVE DIRECTION: The direction of a wave is specified by the wavevector, $\boldsymbol{k}$ (Section 49.5), and its wavelength is $2\pi/|\boldsymbol{k}|$, where $|\boldsymbol{k}| \geq 0$ is the wavenumber.
- PHASE SPEED: The phase speed, C_p, is a non-negative number. It is not a vector so that we do not consider components to the phase speed. Rather, we consider components to the phase velocity vector, which is a vector whose direction is given by the wavevector and whose non-negative magnitude, along with the angular frequency, determine the phase speed (Section 49.5.2).

49.3 Two classes of linear waves

We distinguish two types of linear wave phenomena: non-dispersive waves and dispersive waves. In this section we present a mathematical overview of these waves, offering examples of each type of wave along with pointers to the physics and maths to come later.[3]

49.3.1 Non-dispersive waves

The canonical non-dispersive wave phenomena is described by "the" wave equation

$$(\partial_{tt} - c^2 \nabla^2)\Phi = 0, \tag{49.8}$$

where Φ is a wave function (e.g., velocity potential, streamfunction, surface height), and $c^2 > 0$ is the squared wave speed. As discussed in Section 6.7, this wave equation is hyperbolic and its wave solutions all transmit signals with speed, $c > 0$, without distortion. That is, waves satisfying equation (49.8) of arbitrary wavelengths travel at the same speed so that there is no mixing across the spectrum of wavevectors. We find that for non-dispersive waves the angular frequency divided by the wavenumber equals to a constant phase speed shared by all waves. The acoustic waves of Chapter 51 and the shallow water gravity waves of Chapter 55 are example non-dispersive waves considered in this book.

To expose some of the mathematical details, consider the wave equation (49.8) in one space dimension and written in the factored form

$$(\partial_t - c\,\partial_x)\,(\partial_t + c\,\partial_x)\Phi = 0. \tag{49.9}$$

As discussed in Section 6.7, the solution to this hyperbolic partial differential equation takes the form of two signals moving in opposite directions

$$\Phi(x,t) = F(x - c\,t) + G(x + c\,t), \tag{49.10}$$

where the functions F and G are specified by boundary and initial conditions. Their respectiive functional dependencies, $x \pm c\,t$, determine the propagation direction of the signal, with $F(x - c\,t)$ a signal propagating in the $+\hat{\boldsymbol{x}}$ direction whereas $G(x + c\,t)$ is a signal propagating in the $-\hat{\boldsymbol{x}}$ direction. A key point is that the signals all move with the same speed, with F and G arbitrary functions that may be built from a single linear wave or any number of waves (including an infinity of waves). Also note that the wave equation (49.9) has been factored into the product of two linear operators, so that a simpler hyperbolic wave equation is either of the two first order equations

$$(\partial_t \pm c\,\partial_x)\Phi = 0. \tag{49.11}$$

In other parts of this book this equation is referred to as the *advection equation* for a one-dimensional signal with constant advection velocity (e.g., see Sections 69.3 and 69.4).

[3] Chapter 1 of *Whitham* (1974) provides a thorough mathematical introduction to the variety of linear and nonlinear waves.

It is common to be introduced to wave physics through solutions to the hyperbolic wave equations (49.8) or (49.11). Correspondingly, much of our experience with waves is based on the non-dispersive nature of these waves. For example, when listening to a symphony, we hear the sounds from various instruments "in concert". That is, the speed that the acoustic waves propagate are independent of the wavelength. Indeed, imagine how difficult it would be for an audience spread throughout a concert hall to equally appreciate a symphonic performance if acoustic waves were dispersive!

49.3.2 Dispersive waves

Upon studying geophysical waves, we soon realize that non-dispersive waves are the exception rather than the norm. That is, most waves in geophysical fluids are dispersive, with their governing wave equations sometimes mathematically classified as hyperbolic though many are not. A dispersive wave is one that admits solutions of the form

$$\Phi(\boldsymbol{x}, t) = A\, \mathrm{e}^{\mathrm{i}\,(\boldsymbol{k}\cdot\boldsymbol{x} - \varpi\, t)} = A\, \mathrm{e}^{\mathrm{i}\,\boldsymbol{k}\cdot(\boldsymbol{x} - \hat{\boldsymbol{k}}\, C_{\mathrm{p}}\, t)} \tag{49.12}$$

where the speed of a surface with constant phase,

$$C_{\mathrm{p}} = \varpi(\boldsymbol{k})/|\boldsymbol{k}|, \tag{49.13}$$

is a function of the wavevector. As such, the movement of the dispersive wave signal (i.e., the *phase velocity*) depends on the wavelength of the wave. For example, if we prepare a packet of dispersive waves with a particular shape in space, the evolution of the packet is characterized by the dispersion of the packet.

Waves visible by eye on the surface of a pond or surface of the ocean offer a canonical example of dispersive waves. As explored in Section 52.5.3, long surface gravity waves (which also have low frequency) travel faster than short and high frequency surface gravity waves. Indeed, it is this dispersion for surface gravity waves that surfers appreciate when assessing the suitability of coastal surf conditions following an offshore storm.[4]

49.3.3 Comments about time derivatives

As noted when discussing the non-dispersive wave equation (49.9), the presence of two time derivatives provides the means for two wave signals to arise from solutions to this equation, where the waves move in opposite directions. This case occurs for acoustic waves, gravity waves, and inertial waves. It manifests as a dispersion relation written for the squared angular frequency. In contrast, when there is only one time derivative in the wave equation, then the dispersion relation is written for the angular frequency rather than its square. Furthermore, the system chooses a preferred direction for the wave signal, with the Rossby wave offering the canonical example of such anisotropic waves. Rossby waves also offer a clear example of how the non-negative angular frequency convention (Section 49.2.3) helps to understand the phase velocity.

49.4 Monochromatic patterns

A *monochromatic pattern* is a feature characterized by having all points maintain the same time periodic motion with single angular frequency, ω. Hence, all points within a *monochromatic wave* have the same angular frequency. The trigonometric functions, $\cos(\omega\, t)$ and $\sin(\omega\, t)$, both exhibit time periodic behavior, which explains the factors of 2π appearing throughout wave

[4] See *Butt et al.* (2004) for a scientific view on surface ocean waves geared towards surfing.

physics. As noted in Section 49.2.3, we choose the convention in which the angular frequency is a non-negative number, $\omega \geq 0$, so that the period of the oscillation is $2\pi/\omega$.

It is often convenient to make use of the *Euler identity*

$$\mathrm{e}^{-\mathrm{i}\,\omega\,t} = \cos(\omega\,t) - \mathrm{i}\,\sin(\omega\,t), \tag{49.14}$$

to thus write a time periodic *wave function* as[5]

$$\Phi = \mathrm{Re}[\Phi_0\,\mathrm{e}^{-\mathrm{i}\,\omega\,t}], \tag{49.15}$$

where Φ_0 is a complex function further specified below, and Re[ ] is an operator that returns the real part of its argument (see Section 8.1). For linear calculations we can safely omit the Re operation until the end of the calculations. However, for products of wave fields, such as when performing energetic analyses, more care is needed, with details given in Section 8.1.[6]

49.5 Free plane waves

Plane waves are characterized by a single wavevector and single angular frequency, with the wave exhibiting symmetry in directions perpendicular to the propagation direction (hence the "plane" in its name). Any linear wave, be it acoustic, gravity, Rossby, etc., can be decomposed into a sum or integral of plane waves with a suite of frequencies and wavevectors, and with modulation by an amplitude function.

The general form of a stationary plane wave function is given by

$$\Phi_0 = \mathscr{A}(\boldsymbol{k})\,\mathrm{e}^{\mathrm{i}\,\boldsymbol{k}\cdot\boldsymbol{x}}, \tag{49.16}$$

where $\mathscr{A}(\boldsymbol{k})$ is a complex wave amplitude and $\boldsymbol{k}$ is the *wavevector* or *wavenumber vector*. The wavevector has dimensions of inverse length and it characterizes the wavelength of the wave as well as the spatial direction of the wave propagation (as per travelling plane waves in Section 49.5.1). The magnitude of the wavevector, $|\boldsymbol{k}|$, is referred to as the *wavenumber* as it measures 2π times the number of waves per unit length (we further discuss this notion in Section 49.5.2). We allow the wave amplitude, $\mathscr{A}(\boldsymbol{k})$, to be a function of wavevector so that different plane waves can have distinct amplitudes. We also allow for $\mathscr{A}(\boldsymbol{k})$ to be complex so that different plane waves can have their phases shifted relative to one another (we discuss phases in Section 49.5.1).

Given that the plane wave possesses symmetry in planes perpendicular to $\boldsymbol{k}$, it is spatially dependent only on the direction parallel to the wavevector,[7]

$$\boldsymbol{k} = |\boldsymbol{k}|\,\hat{\boldsymbol{k}}. \tag{49.17}$$

We say that the plane wave function (49.16) is *free* since it exists throughout all of space and is unaffected by boundaries. Furthermore, we are uninterested in how the plane wave was formed. Indeed, since it is present throughout all of space, we imagine that the plane wave has existed for all time. Clearly these notions are not physically realizable. Even so, the mathematical simplicity of the plane wave, along with the superposition principle, affords it a central role in the study of wave mechanics. Furthermore, through the construct of wave packets studied in Sections 49.6 and 49.7, which are built via the superposition of plane waves, we can build wave

[5]The minus sign is motivated by convenience for when we consider a traveling wave and the phase velocity in Section 49.5.2. See in particular Figure 49.1.

[6]As noted when developing the basics of Fourier analysis in Chapter 8, we use complex variables solely for mathematical convenience, with all physical fields producing real numbers in this book.

[7]Caution: many authors write $\hat{\boldsymbol{k}}$ for the unit vertical direction, whereas in this book we write $\hat{\boldsymbol{z}}$ for the unit vertical direction whereas $\hat{\boldsymbol{k}}$ is the direction of a wave.

forms that are spatially and temporally localized and are thus physically realizable.

49.5.1 Traveling plane wave

Allowing for time to evolve renders the traveling monochromatic plane wave function

$$\Phi = \mathrm{Re}[\Phi_0\, \mathrm{e}^{-\mathrm{i}\,\omega\, t}] = \mathrm{Re}[\mathcal{A}(\boldsymbol{k})\, \mathrm{e}^{\mathrm{i}\,(\boldsymbol{k}\cdot\boldsymbol{x}-\omega\, t)}] = |\mathcal{A}(\boldsymbol{k})|\, \mathrm{Re}[\mathrm{e}^{\mathrm{i}\,(\boldsymbol{k}\cdot\boldsymbol{x}-\omega\, t+\alpha)}]. \tag{49.18}$$

We here wrote complex wave amplitude according to a real amplitude and a phase shift

$$\mathcal{A}(\boldsymbol{k}) = |\mathcal{A}(\boldsymbol{k})|\, \mathrm{e}^{\mathrm{i}\,\alpha} \quad \text{with} \quad \tan\alpha = \mathrm{Im}[\mathcal{A}(\boldsymbol{k})]/\,\mathrm{Re}[\mathcal{A}(\boldsymbol{k})]. \tag{49.19}$$

The traveling plane wave *phase* function is given by

$$\mathcal{P} = \boldsymbol{k}\cdot\boldsymbol{x} - \omega\, t + \alpha, \tag{49.20}$$

so that

$$\Phi = |\mathcal{A}(\boldsymbol{k})|\, \mathrm{Re}[\mathrm{e}^{\mathrm{i}\,\mathcal{P}}] = |\mathcal{A}(\boldsymbol{k})|\cos\mathcal{P}. \tag{49.21}$$

The traveling plane wave function, Φ, depends on the wavevector as well as the space and time point. It is also a function of the angular frequency, ω. However, recall that for the study of waves realized by a physical system, once the wavevector is known then the angular frequency is specified through the dispersion relation (49.1).

The phase factor on the wave amplitude in equation (49.19) is generally a function of wavevector, $\alpha = \alpha(\boldsymbol{k})$. However, for most applications it is taken as a constant, in which case it is referred to as the *standard phase*.

49.5.2 Characterizing the wave

Wave period

The wave function (49.18) for the traveling plane wave takes on the same value for all space and time points with a phase, $\mathcal{P}$, that is shifted by any integer multiple of 2π. By fixing a point in space, the plane wave is identical for all times, t_n, satisfying

$$\omega\, t_n = \omega\, t + 2\,\pi\, n = \omega\,(t + 2\,\pi\, n/\omega). \tag{49.22}$$

Hence, the wave period is given by

$$\text{wave period} = 2\,\pi/\omega. \tag{49.23}$$

Wavelength

By fixing time, we see that the plane wave is identical for all space points, $\boldsymbol{x}_n$, satisfying

$$\boldsymbol{k}\cdot\boldsymbol{x}_n = \boldsymbol{k}\cdot\boldsymbol{x} + 2\,\pi\, n = |\boldsymbol{k}|\,(\boldsymbol{x}\cdot\hat{\boldsymbol{k}} + 2\,\pi\, n/|\boldsymbol{k}|), \tag{49.24}$$

which allows us to identify $2\,\pi/|\boldsymbol{k}|$ as the *wavelength*, which we write as[8]

$$\Lambda = 2\,\pi/|\boldsymbol{k}| \Longrightarrow \boldsymbol{k} = 2\,\pi\,\hat{\boldsymbol{k}}/\Lambda. \tag{49.25}$$

Figure 49.1 provides an example cosine wave in one-dimension, illustrating the wavelength and traveling nature of the wave.

[8] We choose the uppercase, Λ, to denote wavelength rather than the more commonly used λ. We do so in order to distinguish the wavelength, Λ, from the longitude, λ, that commonly appears in this book.

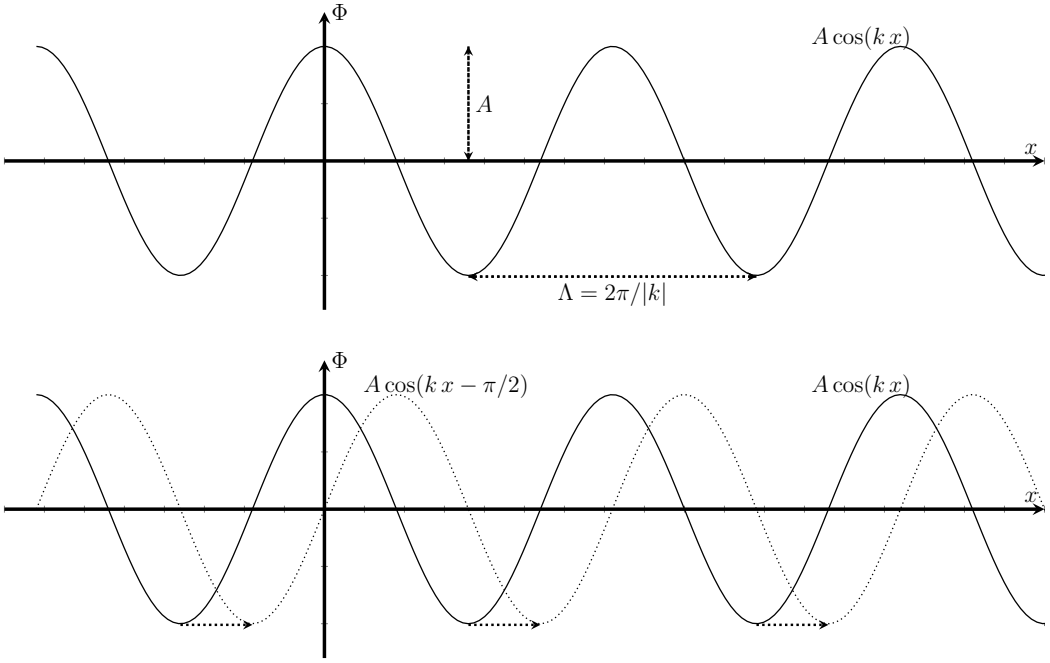

FIGURE 49.1: Top panel: a cosine wave, $\Phi = A\cos(k\,x - \omega\,t)$, along the x-axis at $t = 0$, with wavelength $\Lambda = 2\pi/|k|$, wavevector $\boldsymbol{k} = k\,\hat{\boldsymbol{x}}$, and real amplitude, A. Lower panel: two snapshots of a traveling cosine wave, one shown at $t = 0$ as in the top panel, and another shown a quarter period later, at $\omega\,t = \pi/2$. With $k > 0$ and $\omega\,t > 0$, as shown in this figure, a point with constant phase moves in the $+\hat{\boldsymbol{x}}$ direction. Correspondingly, as the phase becomes more negative (as time increases), the wave form moves to the right, in the direction of the wave propagation. If $k < 0$ then the phase propagates in the $-\hat{\boldsymbol{x}}$ direction.

Phase velocity and phase speed

When observing a traveling plane wave from a fixed point in space, one wavelength passes by the point within a single wave period. We refer to the *phase velocity*, $\boldsymbol{c}_{\text{p}}$, as the velocity of a point fixed on a phase surface and traveling in the direction of the wavevector. Its magnitude is the *phase speed*, C_{p}, which is the speed that the phase moves in the direction of the wavevector,

$$\boldsymbol{c}_{\text{p}} = C_{\text{p}}\,\hat{\boldsymbol{k}} = (\omega/|\boldsymbol{k}|)\,\hat{\boldsymbol{k}} \Longrightarrow C_{\text{p}} = \boldsymbol{c}_{\text{p}} \cdot \hat{\boldsymbol{k}} = (2\pi/|\boldsymbol{k}|)/(2\pi/\omega) = \omega/|\boldsymbol{k}| \geq 0, \tag{49.26}$$

which allows us to write the angular frequency as

$$\omega = \boldsymbol{c}_{\text{p}} \cdot \boldsymbol{k} = C_{\text{p}}\,|\boldsymbol{k}|. \tag{49.27}$$

Figure 49.2 provides an illustration of the phase velocity and phase speed.

An equivalent means to understand the phase velocity is to consider the time derivative, $\text{D}_{\text{p}}/\text{D}t$, defined to measure time changes within the reference frame of a point on a constant phase surface

$$\frac{\text{D}_{\text{p}}\mathcal{P}}{\text{D}t} \equiv \partial_t + \boldsymbol{c}_{\text{p}} \cdot \nabla, \tag{49.28}$$

in which case

$$\frac{\text{D}_{\text{p}}\mathcal{P}}{\text{D}t} = (\partial_t + \boldsymbol{c}_{\text{p}} \cdot \nabla)(\boldsymbol{x} \cdot \boldsymbol{k} - \omega\,t) = \boldsymbol{c}_{\text{p}} \cdot \boldsymbol{k} - \omega = 0. \tag{49.29}$$

We are thus led to the expression for the phase speed and angular frequency

$$C_{\mathrm{p}} = \hat{\boldsymbol{k}} \cdot \frac{\mathrm{D}_{\mathrm{p}}\boldsymbol{x}}{\mathrm{D}t} \quad \text{and} \quad \omega = \boldsymbol{c}_{\mathrm{p}} \cdot \boldsymbol{k} = \boldsymbol{k} \cdot \frac{\mathrm{D}_{\mathrm{p}}\boldsymbol{x}}{\mathrm{D}t}. \tag{49.30}$$

The wave phase time derivative (49.28) is directly analogous to the material time derivative,

$$\frac{\mathrm{D}}{\mathrm{D}t} = \partial_t + \boldsymbol{v} \cdot \nabla, \tag{49.31}$$

defined in the reference frame following the velocity of a fluid particle (Section 17.4). Likewise, in Section 50.3.2 we define the time derivative following the group velocity, $\boldsymbol{c}_{\mathrm{g}}$, in which case $\boldsymbol{c}_{\mathrm{p}}$ in equation (49.28) is replaced by $\boldsymbol{c}_{\mathrm{g}}$.

Phase distance

We can define the phase speed in another manner by introducing the projection of the position vector along the direction of the wavevector

$$S_{\hat{\boldsymbol{k}}} \equiv \hat{\boldsymbol{k}} \cdot \boldsymbol{x}, \tag{49.32}$$

which we refer to as the *phase distance*. Note that $S_{\hat{\boldsymbol{k}}}$ can be positive or negative, depending on the direction of the wavevector. The wavelength as defined by equation (49.24) takes on the form

$$\boldsymbol{k} \cdot \boldsymbol{x}_n = \boldsymbol{k} \cdot \boldsymbol{x} + 2\,\pi\,n = |\boldsymbol{k}|\,(S_{\hat{\boldsymbol{k}}} + 2\,\pi\,n/|\boldsymbol{k}|). \tag{49.33}$$

As such, the phase speed is the change in the position of the constant phase lines in the direction of the wavevector, so that

$$C_{\mathrm{p}} = \left[\frac{\partial S_{\hat{\boldsymbol{k}}}}{\partial t}\right]_{\mathcal{P}} = -\frac{\partial \mathcal{P}/\partial t}{\partial \mathcal{P}/\partial S_{\hat{\boldsymbol{k}}}} = \omega/|\boldsymbol{k}|. \tag{49.34}$$

For this equation we made use of some basic mathematics of generalized surfaces as detailed in Section 63.12.2. Finally, this notation allows us to write the phase function as

$$\mathcal{P} = \boldsymbol{k} \cdot \boldsymbol{x} - \omega\,t + \alpha = |\boldsymbol{k}|\,(S_{\hat{\boldsymbol{k}}} - C_{\mathrm{p}}\,t) + \alpha. \tag{49.35}$$

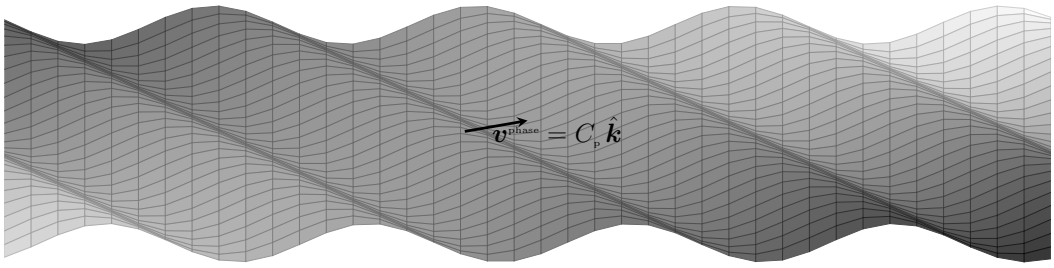

FIGURE 49.2: A mesh plot of a plane wave with phase velocity, $\boldsymbol{c}_{\mathrm{p}} = C_{\mathrm{p}}\,\hat{\boldsymbol{k}} = (\omega/|\boldsymbol{k}|)\,\hat{\boldsymbol{k}}$, pointing perpendicular to surfaces of constant phase.

49.5.3 Wavenumber and factors of 2π

The magnitude of the wavevector, $|\boldsymbol{k}|$, appears in many places in wave kinematics, such as in the definition (49.25) of the wavelength. As a shorthand terminology, we refer to $|\boldsymbol{k}|$ as the

wavenumber, with the wavenumber related to the wavelength via

$$|\boldsymbol{k}| = 2\pi/\Lambda. \tag{49.36}$$

The wavenumber measures 2π times the number of waves per unit length, so that the wavenumber measures the *spatial angular frequency* of a wave. In some contexts it is useful to introduce the *reduced wavelength*

$$\lambda\!\!\!^{-} = \Lambda/2\pi, \tag{49.37}$$

so that the wavenumber is given by the inverse reduced wavelength

$$|\boldsymbol{k}| = \lambda\!\!\!^{-1}. \tag{49.38}$$

Alternatively, it is sometimes convenient to work with the *reduced wavenumber* as introduced in Section 8.3.7 when discussing Fourier transforms

$$\bar{k} = |\boldsymbol{k}|/2\pi. \tag{49.39}$$

Hence, the reduced wavenumber is the inverse wavelength

$$\bar{k} = 1/\Lambda \tag{49.40}$$

so that $\bar{k}$ measures the number of waves per unit length.

In Section 8.3.7 we raised some issues about various conventions for placing 2π factors in Fourier analysis. We further those concerns by noting that the 2π factor associated with wavenumbers can be unclear in the literature. The ambiguity occurs when a particular length scale, L, is considered, yet it is not specified whether the length scale refers to a wavelength, in which case the corresponding wavenumber is $|\boldsymbol{k}| = 2\pi/L$, or to a reduced wavelength, in which case the corresponding wavenumber is $|\boldsymbol{k}| = 1/L$. The bottomline is that care is necessary to ensure the proper usage.

49.5.4 Superposition of plane waves

Through the principle of superposition respected by linear waves, realistic linear waves can be decomposed into the sum or integral of modulated plane waves. Indeed, this decomposition forms the mathematical basis for *Fourier analysis* detailed in Chapter 8. We here offer an illustration of this decomposition by considering how two plane waves combine, and then how three plane waves combine.

Consider the sum of two plane waves, each with same real amplitude of unity (in arbitrary units), and with distinct (but close) wavevectors and angular frequencies

$$\boldsymbol{k}_\pm = \boldsymbol{k} \pm \Delta\boldsymbol{k} \quad \text{and} \quad \omega_\pm = \omega \pm \Delta\omega \quad \text{with} \quad |\Delta\boldsymbol{k}|/|\boldsymbol{k}| \ll 1 \quad \text{and} \quad |\Delta\omega/\omega| \ll 1. \tag{49.41}$$

The resulting superposition of the two waves is given by

$$\text{Re}[\mathrm{e}^{\mathrm{i}\,(\boldsymbol{x}\cdot\boldsymbol{k}_+ - t\,\omega_+)} + \mathrm{e}^{\mathrm{i}\,(\boldsymbol{x}\cdot\boldsymbol{k}_- - t\,\omega_-)}] = 2\cos(\Delta\boldsymbol{k}\cdot\boldsymbol{x} - \Delta\omega\,t)\cos(\boldsymbol{k}\cdot\boldsymbol{x} - \omega\,t). \tag{49.42}$$

The $\cos(\Delta\boldsymbol{k}\cdot\boldsymbol{x} - \Delta\omega\,t)$ factor acts as a low wavenumber and low frequency modulation of the second factor, $\cos(\boldsymbol{k}\cdot\boldsymbol{x} - \omega\,t)$, which is much more rapidly varying in space and time. We illustrate this superposition of two plane waves in Figure 49.3 for time $t = 0$. Adding a third wave, also with unit amplitude, $\exp[\mathrm{i}\,(\boldsymbol{k}\cdot\boldsymbol{x} - \omega\,t)]$, renders the superposition

$$\text{Re}[\mathrm{e}^{\mathrm{i}\,(\boldsymbol{x}\cdot\boldsymbol{k}_+ - t\,\omega_+)} + \mathrm{e}^{\mathrm{i}\,(\boldsymbol{x}\cdot\boldsymbol{k} - t\,\omega)} + \mathrm{e}^{\mathrm{i}\,(\boldsymbol{x}\cdot\boldsymbol{k}_- - t\,\omega_-)}] \;=\; 4\cos^2[(\Delta\boldsymbol{k}\cdot\boldsymbol{x} - \Delta\omega\,t)/2]\cos(\boldsymbol{k}\cdot\boldsymbol{x} - \omega\,t). \tag{49.43}$$

The third wave serves to double the amplitude through constructive interference, while also broadening the width of the low amplitude destructive interference region. Additionally, the modulation function, $\cos^2[(\Delta \boldsymbol{k} \cdot \boldsymbol{x} - \Delta\omega\, t)/2]$, is rendered non-negative when adding the third wave. We also illustrate this superposition in Figure 49.3.

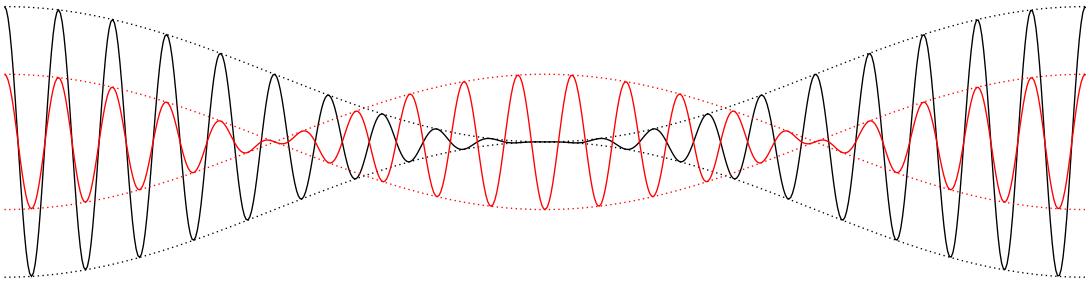

FIGURE 49.3: Superposition of two plane waves (red lines; equation (49.42)) and three plane waves (black lines; equation (49.43)), with all plane waves having equal real amplitudes and here shown for time $t = 0$. Notice how in both cases, a high wavenumber wave (short wave) is modulated by a low wavenumber wave (long wave). The units in this figure are arbitrary.

49.5.5 Wave ansatz

The principle of superposition allows us to study properties of a linear wave equation, in particular the dispersion relation, by inserting a single plane wave into the wave equation. In this manner we refer to the plane wave as an *ansatz*, which is a German word meaning "educated guess".

49.5.6 Summary of kinematic wave properties

In Table 49.2, we summarize the variety of kinematic properties of waves. In this book we work mostly with the angular frequency, ω, the wavevector, $\boldsymbol{k}$, and the wavenumber, $|\boldsymbol{k}|$. Even so, it is useful to be versed in the alternative choices.

NAME	MATH SYMBOL	DIMENSIONS	MATH RELATION
period	τ_{period}	T	$\tau_{\text{period}} = 2\pi/\omega$
angular frequency	ω	T^{-1}	$\omega = 2\pi/\tau_{\text{period}}$
frequency	f	T^{-1}	$f = \omega/2\pi = 1/\tau_{\text{period}}$
wavenumber	$\lvert\boldsymbol{k}\rvert$	L^{-1}	$\lvert\boldsymbol{k}\rvert = 2\pi/\Lambda$
wavevector	$\boldsymbol{k}$	L^{-1}	$\boldsymbol{k} = \lvert\boldsymbol{k}\rvert\, \hat{\boldsymbol{k}}$
reduced wavevector	$\bar{\boldsymbol{k}}$	L^{-1}	$\bar{\boldsymbol{k}} = \boldsymbol{k}/2\pi$
wavelength	Λ	L	$\Lambda = 2\pi/\lvert\boldsymbol{k}\rvert = 1/\lvert\bar{\boldsymbol{k}}\rvert$
reduced wavelength	$\lambda\!\!\!^{-}$	L	$\lambda\!\!\!^{-} = \Lambda/2\pi = 1/\lvert\boldsymbol{k}\rvert$

TABLE 49.2: Summarizing the variety of terms used to kinematically describe waves. In this book we mostly use the angular frequency, $\omega \geq 0$, the wavevector, $\boldsymbol{k}$, and the wavenumber, $|\boldsymbol{k}|$.

49.6 Free wave packets

The modulation of waves in Figure 49.3 serve to organize waves into $\boldsymbol{x}$-space regions known as *wave trains*. A *wave packet* is a train of free waves that are organized into a localized (and moving) region of $\boldsymbol{x}$-space. Localization is enabled by a *modulation function* and the plane wave

modes that are organized within the packet are known as *carrier waves*.[9] Wave trains and wave packets are generated by a *wavemaker*. For example, consider a wavemaker oscillating at a known frequency, ω_0. Ramping up the wavemaker amplitude for a period of time, and then ramping it down towards zero, then produces a group of waves that are localized in time and have angular frequency and wavenumber centered on ω_0 and $\boldsymbol{k}_0$, where $\boldsymbol{k}_0$ is determined by the dispersion relation given ω_0. In the laboratory, the wavemaker might be an oscillating piston placed in a tank of water, such as considered for acoustic waves in Section 51.8. In the natural environment, a wavemaker might be a storm that passes over the ocean and generates surface gravity waves, or an atmospheric convective event that generates atmospheric internal gravity waves.

Mathematically, wave packets are described by complementary wave functions in $\boldsymbol{k}$-space and $\boldsymbol{x}$-space. The $\boldsymbol{k}$-space representation, $\mathcal{A}(\boldsymbol{k}, t)$, is also called the amplitude function for the $\boldsymbol{x}$-space wave function, $\Phi(\boldsymbol{x}, t)$. In the world of mathematical abstraction, we prepare wave packets with a specified $\boldsymbol{k}$-space initial condition, $\mathcal{A}(\boldsymbol{k}, t = 0)$, that has a corresponding $\boldsymbol{x}$-space initial condition, $\Phi(\boldsymbol{x}, t = 0)$, determined by the inverse Fourier transform. Upon initializing the packets we study their evolution. Since the packets are constructed by linear plane waves, their evolution is determined by the superposed and evolving constituent plane waves. What distinguishes a packet of acoustic waves from a packet of gravity waves, for example, is the dispersion relation, which is specific to the physics describing the particular waves.

49.6.1 Phase velocity, group velocity, and the dispersion relation

Examination of Figure 49.3 suggests that the velocity of a wave packet's center is not directly related to the phase velocity of the constituent plane waves. Rather, it is determined by motion of the modulation function. For the one-dimensional examples of Figure 49.3, the packet motion is determined by $\Delta\omega/\Delta k$. In this section we generalize this result to the *group velocity* determined by[10]

$$\boldsymbol{c}_{\text{g}} = \nabla_{\boldsymbol{k}} \varpi(\boldsymbol{k}). \tag{49.44}$$

In this equation, we introduced the wave dispersion relation (49.1) that specifies how the angular frequency is functionally connected to the wavevector. We see that the group velocity is determined by the gradient of the dispersion relation in wavevector space, which prompted us to expose a wavevector subscript on the gradient operator. As defined, the group velocity points in the $\boldsymbol{k}$-space direction of maximum increase for the angular frequency. Figure 49.4 illustrates two dispersion relations for a one-dimensional wave.

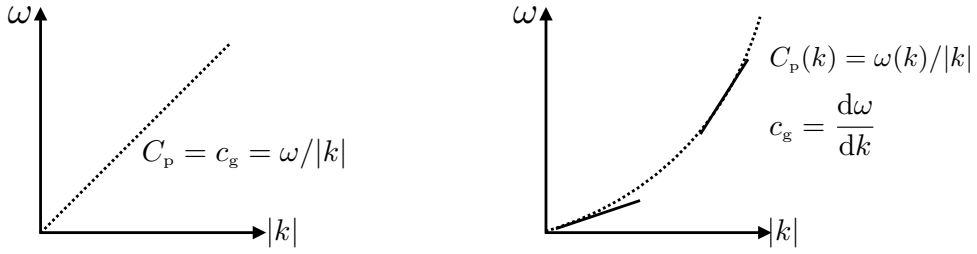

FIGURE 49.4: Example dispersion relations for one-dimensional waves. Left panel: a non-dispersive wave has a phase speed, C_{p}, that is a constant so that all waves, regardless their wavelength or angular frequency, move at the same speed. Right panel: a dispersive wave, here shown for a wave whose phase speed increases as the wave number increases, as does the group velocity.

[9] From an engineering perspective, the carrier wave carries the most useful information contained in the wave packet signal, hence the name.

[10] Many dispersion relations are naturally written as ω^2, in which case it is simpler to compute the group velocity according to $\nabla_{\boldsymbol{k}} \omega^2 = 2\,\omega\,\boldsymbol{c}_{\text{g}}$.

The dispersion relation for non-dispersive waves results in phase speeds that are independent of the wavenumber so that

$$\varpi = C_{\mathsf{p}} \, |\boldsymbol{k}|, \tag{49.45}$$

where $C_{\mathsf{p}} > 0$ is the constant phase speed. Evidently, the angular frequency is identical for all waves having the same wavenumber. That is, the angular frequency only cares about the wavelength of the non-dispersive wave and not about its direction. Furthermore, we see that the continuum of wavenumbers results in a continuum of angular frequencies, with higher wavenumbers rendering higher angular frequencies. This behavior is familiar for both electromagnetic and acoustic waves, which are both non-dispersive, in which waves of smaller wavelength (higher wavenumber) have higher frequencies. We depict this sort of dispersion relation in the left panel of Figure 49.4.

Dispersive waves are characterized by a dispersion relation with the phase speed a function of the wavevector

$$\varpi = C_{\mathsf{p}}(\boldsymbol{k}) \, |\boldsymbol{k}| > 0. \tag{49.46}$$

Again, the phase speed and angular frequency are positive, but now we find the phase speed depends on the wavenumber and possibly the wave direction. We provide an example for this sort of dispersion relation in the right panel of Figure 49.4.

49.6.2 A continuum of traveling plane waves

Consider the superposition of a continuum of traveling plane waves given by the integral expression for the wave function

$$\Phi(\boldsymbol{x}, t) = \frac{1}{(2\pi)^3} \int \mathscr{A}(\boldsymbol{k}) \, \mathrm{e}^{\mathrm{i} \, (\boldsymbol{k} \cdot \boldsymbol{x} - \varpi(\boldsymbol{k}) \, t)} \, \mathrm{d}\boldsymbol{k}. \tag{49.47}$$

The wave function, $\Phi(\boldsymbol{x}, t)$, is constructed through combining a continuum of traveling plane waves, with the amplitude function, $\mathscr{A}(\boldsymbol{k})$, determining which wavevectors contribute to the packet and by how much they contribute. The integral in equation (49.47) is computed over all the three-dimensional wavevector space ($\boldsymbol{k}$-space). For example, a Cartesian representation of a wavevector volume element is written

$$\mathrm{d}\boldsymbol{k} = \mathrm{d}k_x \, \mathrm{d}k_y \, \mathrm{d}k_z, \tag{49.48}$$

with the integration limits $k_x, k_y, k_z \in (-\infty, \infty)$, corresponding to waves traveling in all directions and spanning all wavenumbers. Furthermore, the angular frequency in equation (49.47) is specified by the dispersion relation,

$$\omega = \varpi(\boldsymbol{k}) \geq 0, \tag{49.49}$$

so that the wave function (49.47) is built from a continuum of wavevectors with corresponding angular frequencies.

49.6.3 The wave function is real

For brevity we often drop the Re operator on the wave function (49.47). Even so, it is critical to note that the wave function is real, which has implications for how we compute the $\boldsymbol{k}$-space amplitude function, $\mathscr{A}(\boldsymbol{k})$. For example, if the amplitude function is real[11]

$$\mathscr{A}(\boldsymbol{k}) = A(\boldsymbol{k}) = A^*(\boldsymbol{k}), \tag{49.50}$$

[11] The star is the complex conjugate operator.

then the wave function takes the form

$$\Phi(\boldsymbol{x},t) = \frac{1}{(2\pi)^3}\int A(\boldsymbol{k})\cos[\boldsymbol{k}\cdot\boldsymbol{x} - \varpi(\boldsymbol{k})\,t]\,\mathrm{d}\boldsymbol{k}. \tag{49.51}$$

However, there are cases where we need the extra phase degree of freedom afforded by a complex amplitude function, in which case the real part of equation (49.47) leads to

$$\Phi(\boldsymbol{x},t) = \mathrm{Re}\left[\frac{1}{(2\pi)^3}\int \mathcal{A}(\boldsymbol{k})\,\mathrm{e}^{\mathrm{i}\,(\boldsymbol{k}\cdot\boldsymbol{x}-\varpi(\boldsymbol{k})\,t)}\,\mathrm{d}\boldsymbol{k}\right] \tag{49.52a}$$

$$= \frac{1}{2\,(2\pi)^3}\int \left[\mathcal{A}(\boldsymbol{k})\,\mathrm{e}^{\mathrm{i}\,(\boldsymbol{k}\cdot\boldsymbol{x}-\varpi(\boldsymbol{k})\,t)} + \mathcal{A}^*(\boldsymbol{k})\,\mathrm{e}^{-\mathrm{i}\,(\boldsymbol{k}\cdot\boldsymbol{x}-\varpi(\boldsymbol{k})\,t)}\right]\mathrm{d}\boldsymbol{k}. \tag{49.52b}$$

Since the integral is over all of $\boldsymbol{k}$-space, we can write

$$\int \mathcal{A}^*(\boldsymbol{k})\,\mathrm{e}^{-\mathrm{i}\,(\boldsymbol{k}\cdot\boldsymbol{x}-\varpi(\boldsymbol{k})\,t)}\,\mathrm{d}\boldsymbol{k} = \int \mathcal{A}^*(-\boldsymbol{k})\,\mathrm{e}^{\mathrm{i}\,(\boldsymbol{k}\cdot\boldsymbol{x}+\varpi(-\boldsymbol{k})\,t)}\,\mathrm{d}\boldsymbol{k}, \tag{49.53}$$

in which case the wavefunction takes the form

$$\Phi(\boldsymbol{x},t) = \frac{1}{2\,(2\pi)^3}\int \mathrm{e}^{\mathrm{i}\,\boldsymbol{k}\cdot\boldsymbol{x}}\,[\mathcal{A}(\boldsymbol{k})\,\mathrm{e}^{-\mathrm{i}\,\varpi(\boldsymbol{k})\,t} + \mathcal{A}^*(-\boldsymbol{k})\,\mathrm{e}^{\mathrm{i}\,\varpi(-\boldsymbol{k})\,t}]\,\mathrm{d}\boldsymbol{k}, \tag{49.54}$$

and its time tendency is

$$\partial_t\Phi(\boldsymbol{x},t) = \frac{\mathrm{i}}{2\,(2\pi)^3}\int \mathrm{e}^{\mathrm{i}\,\boldsymbol{k}\cdot\boldsymbol{x}}\,[-\varpi(\boldsymbol{k})\,\mathcal{A}(\boldsymbol{k})\,\mathrm{e}^{-\mathrm{i}\,\varpi(\boldsymbol{k})\,t} + \varpi(-\boldsymbol{k})\,\mathcal{A}^*(-\boldsymbol{k})\,\mathrm{e}^{\mathrm{i}\,\varpi(-\boldsymbol{k})\,t}]\,\mathrm{d}\boldsymbol{k}. \tag{49.55}$$

49.6.4 Initializing the wave packet

We often consider wave packets in the context of initial value problems, whereby the packet is initialized according to some process such as described at the start of this section. We are concerned with freely moving wave packets, so that boundary conditions are not considered here. Thus, we consider three possibilities: initializing the packet's wave function, initializing its time tendency, or initializing both the wave function and its time tendency. To describe these initial conditions requires the use of complex $\boldsymbol{k}$-space amplitudes. Setting $t = 0$ in equation (49.54) for the wave function and equation (49.55) for the time tendency leads to

$$\Phi_0(\boldsymbol{x}) \equiv \Phi(\boldsymbol{x},0) = \frac{1}{2\,(2\pi)^3}\int \mathrm{e}^{\mathrm{i}\,\boldsymbol{k}\cdot\boldsymbol{x}}\,[\mathcal{A}(\boldsymbol{k}) + \mathcal{A}^*(-\boldsymbol{k})]\,\mathrm{d}\boldsymbol{k} \tag{49.56a}$$

$$\dot{\Phi}_0(\boldsymbol{x}) \equiv \partial_t\Phi(\boldsymbol{x},0) = \frac{\mathrm{i}}{2\,(2\pi)^3}\int \mathrm{e}^{\mathrm{i}\,\boldsymbol{k}\cdot\boldsymbol{x}}\,[-\varpi(\boldsymbol{k})\,\mathcal{A}(\boldsymbol{k}) + \varpi(-\boldsymbol{k})\,\mathcal{A}^*(-\boldsymbol{k})]\,\mathrm{d}\boldsymbol{k}. \tag{49.56b}$$

Inverting the Fourier transform for the initial condition (49.56a) and the initial tendency (49.56b) renders

$$\mathcal{A}(\boldsymbol{k}) + \mathcal{A}^*(-\boldsymbol{k}) = 2\int \Phi_0(\boldsymbol{x})\,\mathrm{e}^{-\mathrm{i}\,\boldsymbol{k}\cdot\boldsymbol{x}}\,\mathrm{d}\boldsymbol{x} \tag{49.57a}$$

$$-\varpi(\boldsymbol{k})\,\mathcal{A}(\boldsymbol{k}) + \varpi(-\boldsymbol{k})\,\mathcal{A}^*(-\boldsymbol{k}) = -2\,\mathrm{i}\int \dot{\Phi}_0(\boldsymbol{x})\,\mathrm{e}^{-\mathrm{i}\,\boldsymbol{k}\cdot\boldsymbol{x}}\,\mathrm{d}\boldsymbol{x}, \tag{49.57b}$$

which then leads to the $\boldsymbol{k}$-space amplitude

$$\mathcal{A}(\boldsymbol{k}) = \frac{2}{\varpi(\boldsymbol{k}) + \varpi(-\boldsymbol{k})}\int [\varpi(-\boldsymbol{k})\,\Phi_0(\boldsymbol{x}) + \mathrm{i}\,\dot{\Phi}_0(\boldsymbol{x})]\,\mathrm{e}^{-\mathrm{i}\,\boldsymbol{k}\cdot\boldsymbol{x}}\,\mathrm{d}\boldsymbol{x} \tag{49.58a}$$

$$\mathcal{A}^*(-\boldsymbol{k}) = \frac{2}{\varpi(\boldsymbol{k}) + \varpi(-\boldsymbol{k})} \int [\varpi(\boldsymbol{k})\, \Phi_0(\boldsymbol{x}) - \mathrm{i}\, \dot{\Phi}_0(\boldsymbol{x})]\, \mathrm{e}^{-\mathrm{i}\, \boldsymbol{k}\cdot\boldsymbol{x}}\, \mathrm{d}\boldsymbol{x}. \tag{49.58b}$$

Notice that

$$\mathcal{A}(\boldsymbol{k}) = \mathcal{A}^*(-\boldsymbol{k}) \quad \text{if } \dot{\Phi}_0 = 0, \tag{49.59}$$

which is referred to as *conjugate symmetry* when studying Fourier transforms in Section 8.3.2, whereas

$$\mathcal{A}(\boldsymbol{k}) = -\mathcal{A}^*(-\boldsymbol{k}) \quad \text{if } \Phi_0 = 0, \tag{49.60}$$

which we refer to as *conjugate anti-symmetry*.

Now substitute the amplitude functions (49.58a) and (49.58b) into the wave function (49.55), and rearrange to find

$$\begin{aligned}\Phi(\boldsymbol{x}, t) = \frac{1}{(2\pi)^3} \int \left[\int \frac{\mathrm{e}^{\mathrm{i}\, \boldsymbol{k}\cdot(\boldsymbol{x}-\boldsymbol{\xi})}\, [\varpi(-\boldsymbol{k})\, \mathrm{e}^{-\mathrm{i}\, \varpi(\boldsymbol{k})\, t} + \varpi(\boldsymbol{k})\, \mathrm{e}^{\mathrm{i}\, \varpi(-\boldsymbol{k})\, t}]}{\varpi(\boldsymbol{k}) + \varpi(-\boldsymbol{k})}\, \mathrm{d}\boldsymbol{k} \right] \Phi_0(\boldsymbol{\xi})\, \mathrm{d}\boldsymbol{\xi} \\ + \frac{\mathrm{i}}{(2\pi)^3} \int \left[\int \frac{\mathrm{e}^{\mathrm{i}\, \boldsymbol{k}\cdot(\boldsymbol{x}-\boldsymbol{\xi})}\, [\mathrm{e}^{-\mathrm{i}\, \varpi(\boldsymbol{k})\, t} - \mathrm{e}^{\mathrm{i}\, \varpi(-\boldsymbol{k})\, t}]}{\varpi(\boldsymbol{k}) + \varpi(-\boldsymbol{k})}\, \mathrm{d}\boldsymbol{k} \right] \dot{\Phi}_0(\boldsymbol{\xi})\, \mathrm{d}\boldsymbol{\xi}.\end{aligned} \tag{49.61}$$

This equation can be written as the convolution of the initial conditions with two kernel functions

$$\Phi(\boldsymbol{x}, t) = \int [\dot{G}(\boldsymbol{x} - \boldsymbol{\xi}, t)\, \Phi_0(\boldsymbol{\xi}) + G(\boldsymbol{x} - \boldsymbol{\xi}, t)\, \dot{\Phi}_0(\boldsymbol{\xi})]\, \mathrm{d}\boldsymbol{\xi}, \tag{49.62}$$

where the kernels are

$$G(\boldsymbol{x}, t) \equiv \frac{\mathrm{i}}{(2\pi)^3} \int \frac{\mathrm{e}^{\mathrm{i}\, \boldsymbol{k}\cdot\boldsymbol{x}}\, [\mathrm{e}^{-\mathrm{i}\, \varpi(\boldsymbol{k})\, t} - \mathrm{e}^{\mathrm{i}\, \varpi(-\boldsymbol{k})\, t}]}{\varpi(\boldsymbol{k}) + \varpi(-\boldsymbol{k})}\, \mathrm{d}\boldsymbol{k} \tag{49.63a}$$

$$\dot{G}(\boldsymbol{x}, t) \equiv \frac{1}{(2\pi)^3} \int \frac{\mathrm{e}^{\mathrm{i}\, \boldsymbol{k}\cdot\boldsymbol{x}}\, [\varpi(-\boldsymbol{k})\, \mathrm{e}^{-\mathrm{i}\, \varpi(\boldsymbol{k})\, t} + \varpi(\boldsymbol{k})\, \mathrm{e}^{\mathrm{i}\, \varpi(-\boldsymbol{k})\, t}]}{\varpi(\boldsymbol{k}) + \varpi(-\boldsymbol{k})}\, \mathrm{d}\boldsymbol{k}. \tag{49.63b}$$

In fact, the kernels are related by a time derivative, which can be seen by writing them in the following form[12]

$$G(\boldsymbol{x}, t) = -\frac{2}{(2\pi)^3} \int \frac{\sin[\boldsymbol{k}\cdot\boldsymbol{x} - \varpi(\boldsymbol{k})\, t]}{\varpi(\boldsymbol{k}) + \varpi(-\boldsymbol{k})}\, \mathrm{d}\boldsymbol{k} \tag{49.64a}$$

$$\dot{G}(\boldsymbol{x}, t) = \frac{2}{(2\pi)^3} \int \frac{\varpi(\boldsymbol{k}) \cos[\boldsymbol{k}\cdot\boldsymbol{x} - \varpi(\boldsymbol{k})\, t)]}{\varpi(\boldsymbol{k}) + \varpi(-\boldsymbol{k})}\, \mathrm{d}\boldsymbol{k} = \partial_t G(\boldsymbol{x}, t). \tag{49.64b}$$

Evidently, the kernels provide a wave mechanism to propagate information about the initial conditions outward in space as time moves forward. In this manner, these functions are *Green's functions* such as those studied in Chapter 9. Indeed, the solution (49.64b) corresponds to the Green's function (9.232), which was derived for the initial-boundary value problem with non-dispersive waves. Here, we are just concerned with the initial condition problem for free wave packets where the waves can be either non-dispersive or dispersive. It is satisfying that even dispersive waves allow us to write the wave packet evolution in terms of Green's functions as in equation (49.62).

49.6.5 The case of non-dispersive waves

To help further understand the nature of the wave packet equation (49.62), and to connect it to the non-dispersive Green's function (9.232), consider a packet of non-dispersive waves for $t \geq 0$

[12] To derive equation (49.64b), recall that the integral is over all of $\boldsymbol{k}$-space.

and in one space dimension.[13] For this case the dispersion relation takes the form

$$\varpi(\boldsymbol{k}) = C_{\mathsf{p}}\,|k| \implies \boldsymbol{k}\cdot\boldsymbol{x} - \varpi(\boldsymbol{k})\,t = k\,x - C_{\mathsf{p}}\,|k|\,t, \tag{49.65}$$

where $C_{\mathsf{p}} > 0$ is the constant phase speed. In this case we make use of the Dirac delta expression (8.113) in the form

$$\delta(x) = \frac{1}{2\pi}\int_{-\infty}^{\infty} \mathrm{e}^{\mathrm{i}\,k\,x}\,\mathrm{d}k = \frac{2}{2\pi}\int_{0}^{\infty} \cos(k\,x)\,\mathrm{d}k, \tag{49.66}$$

so that

$$\begin{aligned}
\dot{G}(x,t) &= \frac{1}{2\pi}\int_{-\infty}^{\infty} \cos(k\,x - C_{\mathsf{p}}\,|k|\,t)\,\mathrm{d}k && \text{(49.67a)}\\
&= \frac{1}{2\pi}\int_{-\infty}^{0} \cos(k\,x + C_{\mathsf{p}}\,k\,t)\,\mathrm{d}k + \frac{1}{2\pi}\int_{0}^{\infty} \cos(k\,x - C_{\mathsf{p}}\,k\,t)\,\mathrm{d}k && \text{(49.67b)}\\
&= \frac{1}{2\pi}\int_{0}^{\infty} \cos(k\,x + C_{\mathsf{p}}\,k\,t)\,\mathrm{d}k + \frac{1}{2\pi}\int_{0}^{\infty} \cos(k\,x - C_{\mathsf{p}}\,k\,t)\,\mathrm{d}k && \text{(49.67c)}\\
&= [\delta(x + C_{\mathsf{p}}\,t) + \delta(x - C_{\mathsf{p}}\,t)]/2. && \text{(49.67d)}\\
&= \delta(C_{\mathsf{p}}\,t - |x|)/2. && \text{(49.67e)}
\end{aligned}$$

Hence, $\dot{G}$ is built from two Dirac delta wave fronts that move in opposite directions at speed C_{p}. Its time integral leads to the Green's function as a Heaviside step function (see Section 7.5)

$$G(x,t) = \mathcal{H}(C_{\mathsf{p}}\,t - |x|)/(2\,C_{\mathsf{p}}). \tag{49.68}$$

To within a constant factor, the Green's function (49.68) is the causal free space Green's function (9.220a) derived for the one dimensional non-dispersive waves. Making use of these results in the wave packet equation (49.64b) leads to

$$\begin{aligned}
\Phi(x,t) &= \frac{1}{2}\int_{-\infty}^{\infty} \delta(C_{\mathsf{p}}\,t - |x-\xi|)\,\Phi_0(\xi)\,\mathrm{d}\xi + \frac{1}{2\,C_{\mathsf{p}}}\int_{-\infty}^{\infty} \mathcal{H}(C_{\mathsf{p}}\,t - |x-\xi|)\,\dot{\Phi}_0(\xi)\,\mathrm{d}\xi && \text{(49.69a)}\\
&= [\Phi_0(x - C_{\mathsf{p}}\,t) + \Phi_0(x + C_{\mathsf{p}}\,t)]/2 + \frac{1}{2\,C_{\mathsf{p}}}\int_{x-C_{\mathsf{p}}\,t}^{x+C_{\mathsf{p}}\,t} \dot{\Phi}_0(\xi)\,\mathrm{d}\xi. && \text{(49.69b)}
\end{aligned}$$

For the second equality we used

$$\begin{aligned}
\int_{-\infty}^{\infty} \mathcal{H}(C_{\mathsf{p}}\,t - |x-\xi|)\,\dot{\Phi}_0(\xi)\,\mathrm{d}\xi &= \int_{-\infty}^{\infty} \mathcal{H}(C_{\mathsf{p}}\,t - |y|)\,\dot{\Phi}_0(x+y)\,\mathrm{d}y && \text{(49.70a)}\\
&= \int_{-C_{\mathsf{p}}\,t}^{C_{\mathsf{p}}\,t} \dot{\Phi}_0(x+y)\,\mathrm{d}y && \text{(49.70b)}\\
&= \int_{x-C_{\mathsf{p}}\,t}^{x+C_{\mathsf{p}}\,t} \dot{\Phi}_0(\xi)\,\mathrm{d}\xi. && \text{(49.70c)}
\end{aligned}$$

Evidently, for non-dispersive waves the initial condition, $\Phi_0(x)$, splits in half as two signals that propagate without distortion in opposite directions, whereas the initial tendency, $\dot{\Phi}_0(x)$, contributes via an integral over the *domain of influence*, which is given by the spatial region $[x - C_{\mathsf{p}}\,t, x + C_{\mathsf{p}}\,t]$ (see Figure 6.3 for a discussion of the domain of influence).

[13] This case corresponds to the infinite string discussed in Section 7.8 of *Stakgold* (2000b). We also consider packets of non-dispersive waves in Section 49.7.7, with a focus on Gaussian packets.

49.6.6 Wave trains and wave packets

Consider a wave train initialized according to[14]

$$\Phi_0(\boldsymbol{x}) = \mathrm{Re}[a(\epsilon\,\boldsymbol{x})\,\mathrm{e}^{\mathrm{i}\,\boldsymbol{k}_0\cdot\boldsymbol{x}}] = a(\epsilon\,\boldsymbol{x})\cos(\boldsymbol{k}_0\cdot\boldsymbol{x}), \tag{49.71}$$

where a is a real $\boldsymbol{x}$-space modulation function and ϵ^{-1}, is a length scale that is large relative to the wavelength of the carrier wave; i.e., $\epsilon^{-1} \ll |\boldsymbol{k}_0|$. Figure 49.5 provides an example of such a wave train. A further modulation of the $\boldsymbol{x}$-space wave train into a wave packet can be realized by an amplitude that sets $\Phi_0(\boldsymbol{x})$ to zero (or exponentially close to zero) for length scales larger than ϵ^{-1}.

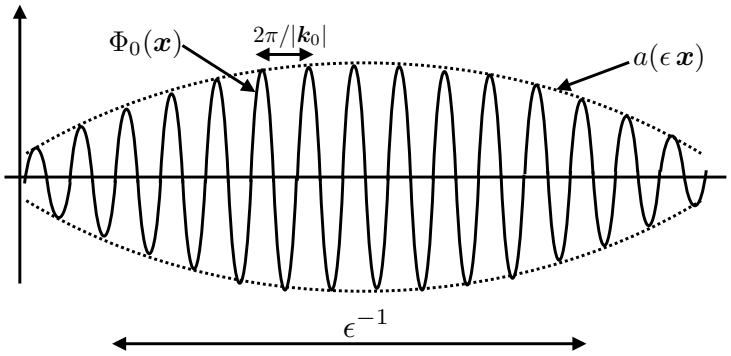

FIGURE 49.5: Example of a wave train comprised of a modulated amplitude function, $a(\epsilon\,\boldsymbol{x})$, acting on a carrier wave, $\mathrm{e}^{\mathrm{i}\,\boldsymbol{k}_0\cdot\boldsymbol{x}}$. The modulation function has a scale ϵ^{-1}, which is large relative to that of the wave length, $2\pi/|\boldsymbol{k}_0|$, so that $2\pi/\epsilon \ll |\boldsymbol{k}_0|$.

For either a wave train or wave packet to be dominated by a single carrier wave of wavenumber $\boldsymbol{k}_0$, the $\boldsymbol{k}$-space wave amplitude must vanish for wavevectors outside of an ϵ range of $\boldsymbol{k}_0$

$$|\mathcal{A}(\boldsymbol{k})| \approx 0 \quad \text{for } |\boldsymbol{k}-\boldsymbol{k}_0| > \epsilon. \tag{49.72}$$

As a result, evolution of the $\boldsymbol{x}$-space wave packet (49.47) is dominated by the dispersion relation centerd on $\boldsymbol{k}_0$, thus motivating a Taylor series

$$\begin{aligned}\boldsymbol{k}\cdot\boldsymbol{x} - \varpi(\boldsymbol{k})\,t &\approx \boldsymbol{k}\cdot\boldsymbol{x} - \varpi(\boldsymbol{k}_0)\,t - (k_a - k_{0a})\,[\partial_{k_a} + (1/2)\,(k_b - k_{0b})\,\partial_{k_a}\partial_{k_b}]\,\varpi(\boldsymbol{k}_0)\,t &\text{(49.73a)}\\ &= \boldsymbol{k}_0\cdot\boldsymbol{x} - \omega_0\,t + (\boldsymbol{k}-\boldsymbol{k}_0)\cdot[\boldsymbol{x} - \boldsymbol{c}_{\mathrm{g}}\,t - (t/2)\,(k_b - k_{0b})\,\partial_{k_b}\boldsymbol{c}_{\mathrm{g}}], &\text{(49.73b)}\end{aligned}$$

where we made use of the summation convention[15] and introduced the angular frequency, ω_0, and group velocity, $\boldsymbol{c}_{\mathrm{g}}$, as defined by the dispersion relation evaluated at $\boldsymbol{k}_0$

$$\omega_0 = \varpi(\boldsymbol{k}_0) \quad \text{and} \quad \boldsymbol{c}_{\mathrm{g}} = \nabla_{\boldsymbol{k}}\varpi(\boldsymbol{k}_0). \tag{49.74}$$

Plugging the Taylor expansion (49.73b) into the wave packet (49.47) renders

$$\Phi(\boldsymbol{x},t) = \mathrm{e}^{\mathrm{i}\,(\boldsymbol{k}_0\cdot\boldsymbol{x}-\omega_0\,t)}\,\frac{1}{(2\pi)^3}\int \mathcal{A}(\boldsymbol{k})\,\mathrm{e}^{\mathrm{i}\,(\boldsymbol{k}-\boldsymbol{k}_0)\cdot\tilde{\boldsymbol{x}}}\,\mathrm{d}\boldsymbol{k} = \mathrm{e}^{\mathrm{i}\,(\boldsymbol{k}_0\cdot\boldsymbol{x}-\omega_0\,t)}\,\mathcal{M}(\boldsymbol{x},t). \tag{49.75}$$

In this equation we introduced the moving position determined by the group velocity and its

[14] Note that the real operator, Re, will henceforth be dropped for brevity.

[15] We use the Cartesian version of the summation convention so there is no distinction between upstairs and downstairs indices.

derivative

$$\tilde{\boldsymbol{x}} = \boldsymbol{x} - \boldsymbol{c}_{\mathrm{g}}\, t - (t/2)\,(k_b - k_{0b})\,\partial_{k_b}\boldsymbol{c}_{\mathrm{g}} \Longleftrightarrow \tilde{x}^a = x^a - t\,\frac{\partial \varpi}{\partial k_a} - (t/2)\,(k_b - k_{0b})\,\frac{\partial^2 \varpi}{\partial_{k_a}\partial_{k_b}}. \tag{49.76}$$

The evolving packet in equation (49.75) represents a traveling plane carrier wave, $\mathrm{e}^{\mathrm{i}\,(\boldsymbol{k}_0\cdot\boldsymbol{x} - \omega_0\, t)}$, with the integral term providing a moving modulation function

$$\mathcal{M}(\boldsymbol{x}, t) \equiv \frac{1}{(2\pi)^3}\int \mathcal{A}(\boldsymbol{k})\,\mathrm{e}^{\mathrm{i}\,(\boldsymbol{k}-\boldsymbol{k}_0)\cdot\tilde{\boldsymbol{x}}}\,\mathrm{d}\boldsymbol{k}. \tag{49.77}$$

We follow this discussion in Section 49.7 by studying one-dimensional Gaussian wave packets, where we explicitly compute the $\boldsymbol{x}$-space modulation function, and find that it is peaked at a point following the group velocity,

$$\boldsymbol{x}_{\mathrm{peak}} = \boldsymbol{x} - \boldsymbol{c}_{\mathrm{g}}\, t, \tag{49.78}$$

whereas the term, $\partial_{k_j}\boldsymbol{c}_{\mathrm{g}}$, appearing in equation (49.76) gives rise to a spread or *dispersion* of the $\boldsymbol{x}$-space packet.

49.6.7 PDE for the wave packet modulation function

To further an understanding of wave packet evolution, we derive the partial differential equation satisfied by the modulation function. For this purpose, take the space and time derivatives of $\mathcal{M}(\boldsymbol{x}, t)$ from equation (49.77) to find

$$\frac{\partial \mathcal{M}}{\partial t} = \frac{-\mathrm{i}}{(2\pi)^3}\int \mathcal{A}(\boldsymbol{k})\,(k_a - k_{0a})\,(\partial_{k_a}\varpi + (1/2)\,(k_b - k_{0b})\,\partial_{k_b}\partial_{k_a}\varpi)\,\mathrm{e}^{\mathrm{i}\,(\boldsymbol{k}-\boldsymbol{k}_0)\cdot\tilde{\boldsymbol{x}}}\,\mathrm{d}\boldsymbol{k} \tag{49.79a}$$

$$\frac{\partial \mathcal{M}}{\partial x^a} = \frac{\mathrm{i}}{(2\pi)^3}\int \mathcal{A}(\boldsymbol{k})\,(k_a - k_{0a})\,\mathrm{e}^{\mathrm{i}\,(\boldsymbol{k}-\boldsymbol{k}_0)\cdot\tilde{\boldsymbol{x}}}\,\mathrm{d}\boldsymbol{k} \tag{49.79b}$$

$$\frac{\partial^2 \mathcal{M}}{\partial x^a \partial x^b} = -\frac{1}{(2\pi)^3}\int \mathcal{A}(\boldsymbol{k})\,(k_a - k_{0a})\,(k_b - k_{0b})\,\mathrm{e}^{\mathrm{i}\,(\boldsymbol{k}-\boldsymbol{k}_0)\cdot\tilde{\boldsymbol{x}}}\,\mathrm{d}\boldsymbol{k}, \tag{49.79c}$$

which then leads to

$$(\partial_t + \boldsymbol{c}_{\mathrm{g}}\cdot\nabla)\,\mathcal{M} = \frac{\mathrm{i}}{2}\,\frac{\partial^2 \varpi}{\partial k_a \partial k_b}\,\frac{\partial^2 \mathcal{M}}{\partial x^a \partial x^b}. \tag{49.80}$$

The left hand side reveals the time evolution of the modulation function following the group velocity, with the group velocity evaluated at the carrier wavevector, $\boldsymbol{k}_0$. The right hand side is a phase shifted (by $\pi/2$) transport of the modulation function by the *dispersion tensor*, $\mathbb{K}$, with the dispersion tensor determined by the second derivative of the dispersion relation evaluated at the carrier wavevector, $\boldsymbol{k}_0$

$$\mathbb{K}^{ab} = \left.\frac{\partial^2 \varpi}{\partial k_a \partial k_b}\right|_{\boldsymbol{k}=\boldsymbol{k}_0}. \tag{49.81}$$

The dispersion tensor is symmetric, as appropriate for a diffusion tensor (Chapter 69). However, there is no guarantee that it is positive-definite. Hence, dispersion can both broaden (as for diffusion) or sharpen (as for anti-diffusion) the wave packet.

It is important to emphasize that dispersion is distinct from dissipation. Indeed, dissipation is absent from this chapter. Evidently, modification of the modulation function arises from the dependence of the phase velocity on the wavevector, hence the name "dispersion." Dispersion is a property inherent in the waves and has nothing to do with dissipation.

49.6.8 Wave packets of non-dispersive waves

Much of the "interesting" behavior of wave packets appears for dispersive waves. Indeed, as we here show, packets of non-dispersive waves propagate their initial condition without modification, thus retaining their initial structure. We can understand this result by recalling that all waves comprising the packet move with the same phase velocity, so that the group and phase velocities are identical and constant. Hence, the packet maintains its initial organization of its waves as the packet evolves.

A vanishing dispersion tensor (49.81) is one signature that the wave packet moves coherently and without modification. As a result, the packet modulation function remains constant following the group velocity,

$$(\partial_t + \boldsymbol{c}_{\mathrm{g}} \cdot \nabla)\, \mathcal{M} = 0 \qquad \text{non-dispersive waves.} \tag{49.82}$$

The modulation function is given by equation (49.77) with a constant phase velocity

$$\mathcal{M}(\boldsymbol{x}, t) = \frac{1}{(2\pi)^3} \int \mathcal{A}(\boldsymbol{k})\, \mathrm{e}^{\mathrm{i}\,(\boldsymbol{k}-\boldsymbol{k}_0)\cdot(\boldsymbol{x}-\boldsymbol{c}_{\mathrm{g}}\,t)}\, \mathrm{d}\boldsymbol{k} = \mathcal{M}(\boldsymbol{x} - \boldsymbol{c}_{\mathrm{g}}\, t), \tag{49.83}$$

which means that the wave packet (49.75) evolves according to

$$\Phi(\boldsymbol{x}, t) = \mathrm{e}^{\mathrm{i}\,(\boldsymbol{k}_0\cdot\boldsymbol{x}-\omega_0\,t)}\, \mathcal{M}(\boldsymbol{x} - \boldsymbol{c}_{\mathrm{g}}\, t). \tag{49.84}$$

Indeed, returning to the original form (49.75) of the wave packet we find that for non-dispersive waves

$$\Phi(\boldsymbol{x}, t) = \mathrm{e}^{\mathrm{i}\,(\boldsymbol{k}_0\cdot\boldsymbol{x}-\omega_0\,t)}\, \frac{1}{(2\pi)^3} \int \mathcal{A}(\boldsymbol{k})\, \mathrm{e}^{\mathrm{i}\,(\boldsymbol{k}-\boldsymbol{k}_0)\cdot(\boldsymbol{x}-\boldsymbol{c}_{\mathrm{g}}\,t)}\, \mathrm{d}\boldsymbol{k} \tag{49.85a}$$

$$= \frac{1}{(2\pi)^3} \int \mathcal{A}(\boldsymbol{k})\, \mathrm{e}^{\mathrm{i}\,\boldsymbol{k}\cdot(\boldsymbol{x}-\boldsymbol{c}_{\mathrm{g}}\,t)}\, \mathrm{d}\boldsymbol{k} \tag{49.85b}$$

$$= \Phi_0(\boldsymbol{x} - \boldsymbol{c}_{\mathrm{g}}\, t), \tag{49.85c}$$

where we introduced the initial condition, Φ_0, from equation (49.56a). Evidently, packets of non-dispersive waves translate their initial condition without any alteration, with translation determined by the group velocity as determined by the carrier wavevector, $\boldsymbol{k}_0$. We make this result compatible with the one dimensional case found in equation (49.69b) by noting that here we only focus on the carrier wavenumber, whereas for the one dimensional packet in equation (49.69b) we considered both the carrier wavenumber, $k_\circ$, and its opposite, $-k_\circ$. However, for a wave packet, we generally focus only on the group velocity determined by the carrier wave since any other wavevectors outside the local neighborhood have an exponentially small amplitude. We consider this result for the specific case of a Gaussian wave packet in Section 49.7.7, with further comment in Section 49.7.9.

49.6.9 Wave function PDE implied by the dispersion relation

Typically when studying waves we start with a partial differential equation in space and time, linearize this equation, and then insert a plane wave ansatz to determine a dispersion relation. Here we follow in a manner analogous to that in Section 49.6.7 and seek the partial differential equation satisfied by the wave function, now assuming knowledge of the dispersion relation as might be provided by measurements of wave properties. The method is best illustrated by an example, here taken as that for a planetary Rossby wave for the horizontally non-divergent barotropic model (Section 54.3.4)

$$\varpi(\boldsymbol{k}) = -\beta\, k_x / |\boldsymbol{k}|^2, \tag{49.86}$$

where $\beta = \partial_y f \geq 0$ is the meridional derivative of the Coriolis parameter, and $\boldsymbol{k} = k_x\,\hat{\boldsymbol{x}} + k_y\,\hat{\boldsymbol{y}}$ is a two-dimensional wavevector. Now build a wave function from such waves, where the wave function is written as in equation (49.47)

$$\Phi(\boldsymbol{x},t) = \frac{1}{(2\pi)^3}\int \mathcal{A}(\boldsymbol{k})\,\mathrm{e}^{\mathrm{i}\,(\boldsymbol{k}\cdot\boldsymbol{x}-\varpi\,t)}\,\mathrm{d}\boldsymbol{k} = \frac{1}{(2\pi)^3}\int \mathcal{A}(\boldsymbol{k})\,\mathrm{e}^{\mathrm{i}\,(\boldsymbol{k}\cdot\boldsymbol{x}+t\,\beta\,k_x/|\boldsymbol{k}|^2)}\,\mathrm{d}\boldsymbol{k}. \tag{49.87}$$

What is the partial differential equation satisfied by this wave function?

To answer this question we proceed as in Section 49.6.7 for the modulation function by taking partial derivatives in space and time, and noting that the integral for the wave function is over $\boldsymbol{k}$-space so that space and time derivatives commute with the integral. Hence, the Laplacian of the wave function is given by

$$\nabla^2\Phi = -\frac{1}{(2\pi)^3}\int \mathcal{A}(\boldsymbol{k})\,|\boldsymbol{k}|^2\,\mathrm{e}^{\mathrm{i}\,(\boldsymbol{k}\cdot\boldsymbol{x}-\varpi\,t)}\,\mathrm{d}\boldsymbol{k}, \tag{49.88}$$

and its time derivative is

$$\partial_t(\nabla^2\Phi) = \frac{\mathrm{i}}{(2\pi)^3}\int \mathcal{A}(\boldsymbol{k})\,\varpi\,|\boldsymbol{k}|^2\,\mathrm{e}^{\mathrm{i}\,(\boldsymbol{k}\cdot\boldsymbol{x}-\varpi\,t)}\,\mathrm{d}\boldsymbol{k} \tag{49.89a}$$

$$= -\frac{\mathrm{i}\,\beta}{(2\pi)^3}\int \mathcal{A}(\boldsymbol{k})\,k_x\,\mathrm{e}^{\mathrm{i}\,(\boldsymbol{k}\cdot\boldsymbol{x}-\varpi\,t)}\,\mathrm{d}\boldsymbol{k} \tag{49.89b}$$

$$= -\beta\,\partial_x\Phi, \tag{49.89c}$$

which then leads to the linear partial differential equation

$$\partial_t(\nabla^2\Phi) + \beta\,\partial_x\Phi = 0. \tag{49.90}$$

As we see in Chapter 54, equation (49.90) is the linearized version of the vorticity equation (54.29) with zero background flow, and solutions of this equation are planetary Rossby waves. Consequently, equation (49.90) describes the evolution of a packet of planetary Rossby waves in a two-dimensional non-divergent barotropic fluid.

49.6.10 Standing wave packets

The wave packet (49.47) can be written in the form

$$\Phi^{(+)}(\boldsymbol{x},t) = \frac{1}{(2\pi)^3}\int \mathcal{A}(\boldsymbol{k})\,\mathrm{e}^{\mathrm{i}\,[\boldsymbol{k}\cdot\boldsymbol{x}-\varpi(\boldsymbol{k})\,t]}\,\mathrm{d}\boldsymbol{k} = \frac{1}{(2\pi)^3}\int \mathcal{A}(\boldsymbol{k})\,\mathrm{e}^{\mathrm{i}\,|\boldsymbol{k}|[S_{\hat{\boldsymbol{k}}}-C_\mathrm{p}\,t]}\,\mathrm{d}\boldsymbol{k}, \tag{49.91}$$

where

$$S_{\hat{\boldsymbol{k}}} = \hat{\boldsymbol{k}}\cdot\boldsymbol{x} \tag{49.92}$$

is the phase distance from equation (49.32), and $C_\mathrm{p} = \varpi(\boldsymbol{k})/|\boldsymbol{k}| > 0$ is the phase speed. As noted in Section 49.6.1, the phase speed is a constant for non-dispersive waves, whereas for dispersive waves it is a function of the wavevector, $C_\mathrm{p} = C_\mathrm{p}(\boldsymbol{k})$. We introduce the + notation on the packet (49.91) to distinguish from the oppositely traveling packet, $\Phi^{(-)}$, defined according to

$$\Phi^{(-)}(\boldsymbol{x},t) = \frac{1}{(2\pi)^3}\int \mathcal{A}(-\boldsymbol{k})\,\mathrm{e}^{-\mathrm{i}\,[\boldsymbol{k}\cdot\boldsymbol{x}+\varpi(\boldsymbol{k})\,t]}\,\mathrm{d}\boldsymbol{k}. \tag{49.93}$$

If the amplitude function has even parity

$$\mathcal{A}(-\boldsymbol{k}) = \mathcal{A}(\boldsymbol{k}), \tag{49.94}$$

then $\Phi^{(-)}(\boldsymbol{x},t) = \Phi^{(+)}(-\boldsymbol{x},t)$, in which case the sum of these two traveling packets is a standing wave packet

$$\Phi^{(-)}(\boldsymbol{x},t) + \Phi^{(+)}(\boldsymbol{x},t) = \frac{2}{(2\pi)^3}\int \mathcal{A}(\boldsymbol{k})\,\mathrm{e}^{-\mathrm{i}\,\varpi(\boldsymbol{k})\,t}\cos(\boldsymbol{k}\cdot\boldsymbol{x})\,\mathrm{d}\boldsymbol{k} \qquad \text{if } \mathcal{A}(-\boldsymbol{k}) = \mathcal{A}(\boldsymbol{k}), \quad (49.95)$$

and the initial condition is the inverse cosine transform of $\mathcal{A}(\boldsymbol{k})$

$$\Phi^{(-)}(\boldsymbol{x},t=0) + \Phi^{(+)}(\boldsymbol{x},t=0) = \frac{2}{(2\pi)^3}\int \mathcal{A}(\boldsymbol{k})\cos(\boldsymbol{k}\cdot\boldsymbol{x})\,\mathrm{d}\boldsymbol{k} \qquad \text{if } \mathcal{A}(-\boldsymbol{k}) = \mathcal{A}(\boldsymbol{k}). \quad (49.96)$$

Recall that to ensure the wave function is real, then the amplitude function must satisfy conjugate symmetry via equation (49.94). Hence, with the further assumption of even parity (49.94), then the amplitude function, $\mathcal{A}(\boldsymbol{k})$, is real, in which case we indeed see that $\Phi^{(-)}(\boldsymbol{x},t=0) + \Phi^{(+)}(\boldsymbol{x},t=0)$ is a real function.

As seen in Section 49.7.5, we generally consider Gaussian packets that include modulated traveling waves, so that such wave packets have amplitude functions that are not even functions of the wavevector, $\mathcal{A}(-\boldsymbol{k}) \neq \mathcal{A}(\boldsymbol{k})$. Even so, the present discussion identifies the general properties satisfied by standing waves, which occur, for example, in bounded regions (e.g., see Section 52.8 for standing gravity waves in a closed basin).

49.7 Wave packets in one-dimension

In this section we study a variety of packets moving in one space dimension.[16] Doing so provides a pedagogical means to explicitly reveal some of the general ideas developed in Section 49.6. We give particular attention to the Gaussian wave packet since it allows for analytic expressions that serve pedagogical needs.[17]

49.7.1 The positive wave packet

For a packet built from plane waves traveling in the $+\hat{\boldsymbol{x}}$ direction, we write the wavevector as $\boldsymbol{k} = k\,\hat{\boldsymbol{x}}$ with wavenumber $k \geq 0$ so that a positive-traveling packet takes the form

$$\Phi^{(+)}(x,t) = \frac{1}{2\pi}\int_0^\infty \mathcal{A}(k)\,\mathrm{e}^{\mathrm{i}\,(k\,x-\varpi\,t)}\,\mathrm{d}k. \quad (49.97)$$

49.7.2 The negative wave packet

A packet moving in the negative $\hat{\boldsymbol{x}}$ direction is built from plane waves with $\boldsymbol{k} = -k\,\hat{\boldsymbol{x}}$, again with wavenumber $k \geq 0$, so that

$$\Phi^{(-)}(x,t) = \frac{1}{2\pi}\int_0^\infty \mathcal{A}(-k)\,\mathrm{e}^{-\mathrm{i}\,[k\,x+\varpi\,t]}\,\mathrm{d}k. \quad (49.98)$$

Observe that $\Phi^{(-)}(x,t)$ can be written in the equivalent form

$$\Phi^{(-)}(x,t) = \frac{1}{2\pi}\int_0^\infty \mathcal{A}(-k)\,\mathrm{e}^{-\mathrm{i}\,[k\,x+\varpi\,t]}\,\mathrm{d}k = \frac{1}{2\pi}\int_{-\infty}^0 \mathcal{A}(k)\,\mathrm{e}^{\mathrm{i}\,[k\,x-\varpi\,t]}\,\mathrm{d}k, \quad (49.99a)$$

[16] Section 7.8 of *Stakgold* (2000b) provides a thorough discussion of one-dimensional waves, such as those propagating on a string.

[17] As a wave packet in one-dimension, the wave function Φ has dimensions of its amplitude function, $\mathcal{A}$, times inverse length. In three dimensions, in contrast, the wave function has dimensions of $\mathcal{A}$ times inverse volume as in equation (49.47).

where we assumed that the dispersion relation has even parity

$$\varpi(k) = \varpi(-k) > 0. \tag{49.100}$$

This assumption for the dispersion relation does not hold for all waves (e.g., Rossby waves). When it does hold, it means that a wave traveling to the right with wavenumber k has the same angular frequency as a wave traveling to the left with the same wavenumber. The equality (49.99a) allows us to interpret integration over negative wavenumbers to represent a wave packet traveling in a direction opposite to the sense suggested by the phase relation. That is, the phase $k\,x - \varpi\,t$ suggests a positive traveling packet, but the packet is actually a negative packet since the integration extends over negative wavenumbers.

49.7.3 The positive-negative wave packet

The sum of the positive packet (49.97) and negative packet (49.99a) leads us to define the positive-negative packet

$$\Phi^{(+-)}(x,t) = \Phi^{(+)}(x,t) + \Phi^{(-)}(x,t) = \frac{1}{2\pi}\int_{-\infty}^{\infty} \mathcal{A}(k)\,\mathrm{e}^{\mathrm{i}\,(k\,x - \varpi\,t)}\,\mathrm{d}k. \tag{49.101}$$

49.7.4 The positive-positive wave packet

This final wave packet is designed to travel in a single direction, which defines the positive-positive packet

$$\Phi^{(++)}(x,t) = \frac{1}{2\pi}\int_{-\infty}^{\infty} \mathcal{A}(k)\,\mathrm{e}^{\mathrm{i}\,k\,(x - C_\mathrm{p}\,t)}\,\mathrm{d}k, \tag{49.102}$$

where $C_\mathrm{p} = \varpi/|k| > 0$ is the phase speed. It is revealing to decompose this packet as[18]

$$\Phi^{(++)}(x,t) = \frac{1}{2\pi}\int_{-\infty}^{0} \mathcal{A}(k)\,\mathrm{e}^{\mathrm{i}\,k\,(x - \varpi\,t/|k|)}\,\mathrm{d}k + \frac{1}{2\pi}\int_{0}^{\infty} \mathcal{A}(k)\,\mathrm{e}^{\mathrm{i}\,k\,(x - \varpi\,t/|k|)}\,\mathrm{d}k \tag{49.103a}$$

$$= \frac{1}{2\pi}\int_{-\infty}^{0} \mathcal{A}(k)\,\mathrm{e}^{\mathrm{i}\,(k\,x + \varpi\,t)}\,\mathrm{d}k + \frac{1}{2\pi}\int_{0}^{\infty} \mathcal{A}(k)\,\mathrm{e}^{\mathrm{i}\,(k\,x - \varpi\,t)}\,\mathrm{d}k. \tag{49.103b}$$

The second integral equals to $\Phi^{(+)}(x,t)$, whereas the first is new. Again, both contributions to $\Phi^{(++)}(x,t)$ move in the $+\hat{\boldsymbol{x}}$ direction.

49.7.5 Initial uncertainty relation for a Gaussian packet

The initial condition for both $\Phi^{(+-)}$ and $\Phi^{(++)}$ are the same, which we write as

$$\Phi_0(x) = \Phi^{(+-)}(x,0) = \Phi^{(++)}(x,0) = \frac{1}{2\pi}\int_{-\infty}^{\infty} \mathcal{A}(k)\,\mathrm{e}^{\mathrm{i}\,k\,x}\,\mathrm{d}k. \tag{49.104}$$

The specific case of a Gaussian wave packet offers insight into the physics while allowing for analytically tractable expressions. Specifically, consider the $\boldsymbol{k}$-space representation of a wave packet with a Gaussian spread around a central wavevector, $\boldsymbol{k}_0 = k_\circ\,\hat{\boldsymbol{x}}$. We choose the wave amplitude as

$$\mathcal{A}(k) = A\,\mathrm{e}^{-\sigma(k-k_\circ)^2}, \tag{49.105}$$

where $A > 0$ is a real constant and $\sigma > 0$ has dimensions of squared length. If we choose the central wavenumber to be positive, $k_\circ > 0$, then the wave packet is dominated by plane

[18] In deriving equation (49.103b), it is important to remember that $\varpi > 0$ for all wavenumbers.

waves moving in the $+\hat{\boldsymbol{x}}$ direction. Referring to the discussion in Section 49.6.10, note that $\mathcal{A}(k) \neq \mathcal{A}(-k)$ when $k_\circ \neq 0$. As we will see, if $k_\circ = 0$ then we have a Gaussian packet without any modulated plane waves.

Width of the initial wave packet in $\boldsymbol{k}$-space

The squared modulus of the $\boldsymbol{k}$-space wave packet (49.105) provides a measure of the packet's intensity

$$|\mathcal{A}(k)|^2 = A^2\, \mathrm{e}^{-2\,\sigma (k-k_\circ)^2}, \tag{49.106}$$

with the intensity peaked at the wavenumber $k = k_\circ$ and declining to e^{-1} times the maximum for

$$k = k_\circ \pm (2\,\sigma)^{-1/2} \Longrightarrow \Delta k^{\text{e-fold}} \equiv 2\,(2\,\sigma)^{-1/2}, \tag{49.107}$$

where $\Delta k^{\text{e-fold}}$ measures the $\boldsymbol{k}$-space width of the wave packet. We say that the $\boldsymbol{k}$-space width of the packet is *narrow band* for σ large, in which the packet is concentrated around $k = k_\circ$ since $\Delta k^{\text{e-fold}} \to 0$.

The initial wave packet in $\boldsymbol{x}$-space

The inverse Fourier transform of the $\boldsymbol{k}$-space wave function (49.105) leads to the initial condition for the $\boldsymbol{x}$-space wave function (49.104)

$$\Phi_0(x) = \frac{A}{2\pi} \int_{-\infty}^{\infty} \mathrm{e}^{-\sigma\,(k-k_\circ)^2}\, \mathrm{e}^{\mathrm{i}\,k\,x}\, \mathrm{d}k = \frac{A\, \mathrm{e}^{\mathrm{i}\,k_\circ\,x}}{2\pi} \int_{-\infty}^{\infty} \mathrm{e}^{-\sigma\,q^2}\, \mathrm{e}^{\mathrm{i}\,q\,x}\, \mathrm{d}q, \tag{49.108}$$

with the corresponding initial conditions for the positive and negative wave packets

$$\Phi^{(+)}(x,0) = \frac{A}{2\pi} \int_{0}^{\infty} \mathrm{e}^{-\sigma\,(k-k_\circ)^2}\, \mathrm{e}^{\mathrm{i}\,k\,x}\, \mathrm{d}k = \frac{A\, \mathrm{e}^{\mathrm{i}\,k_\circ\,x}}{2\pi} \int_{-k_\circ}^{\infty} \mathrm{e}^{-\sigma\,q^2}\, \mathrm{e}^{\mathrm{i}\,q\,x}\, \mathrm{d}q \tag{49.109a}$$

$$\Phi^{(-)}(x,0) = \frac{A}{2\pi} \int_{-\infty}^{0} \mathrm{e}^{-\sigma\,(k-k_\circ)^2}\, \mathrm{e}^{\mathrm{i}\,k\,x}\, \mathrm{d}k = \frac{A\, \mathrm{e}^{\mathrm{i}\,k_\circ\,x}}{2\pi} \int_{-\infty}^{-k_\circ} \mathrm{e}^{-\sigma\,q^2}\, \mathrm{e}^{\mathrm{i}\,q\,x}\, \mathrm{d}q. \tag{49.109b}$$

With the central wavenumber assumed positive, $k_\circ > 0$, observe that the initial negative wave packet, $\Phi^{(-)}(x,0)$, has an exponentially small amplitude since the integral in equation (49.109b) never samples $q = k - k_\circ = 0$. In contrast, $\Phi^{(+)}(x,0)$ samples $q = 0$ so that

$$\Phi_0(x) = \Phi^{(+)}(x,0) + \Phi^{(-)}(x,0) \approx \Phi^{(+)}(x,0). \tag{49.110}$$

Although there is no exact closed form expression for the initial conditions, $\Phi^{(+)}(x,0)$ and $\Phi^{(-)}(x,0)$, we can evaluate the integral for $\Phi_0(x)$ in equation (49.108). First observe that

$$\int_{-\infty}^{\infty} \mathrm{e}^{-\sigma\,q^2}\, \sin(q\,x)\, \mathrm{d}q = 0, \tag{49.111}$$

since the Gaussian is symmetric under $q \to -q$, whereas $\sin(q\,x)$ switches sign. Hence, expanding the imaginary exponential in equation (49.108) according to Euler's identity leaves only the cosine contribution, so that[19]

$$\Phi_0(x) = \frac{A\, \mathrm{e}^{\mathrm{i}\,k_\circ\,x}}{2\pi} \int_{-\infty}^{\infty} \mathrm{e}^{-\sigma\,q^2}\, \cos(q\,x)\, \mathrm{d}q = \frac{A\, \mathrm{e}^{\mathrm{i}\,k_\circ\,x}}{2\pi} \sqrt{\frac{\pi}{\sigma}}\, \mathrm{e}^{-x^2/(4\sigma)}, \tag{49.112}$$

where we made use of an integral table for the final equality (e.g., integral 679 of *Beyer* (1973)).

[19]The integral in equation (49.112) is also encountered in Section 8.5.3 when studying Fourier transforms.

Evidently, the initial wave packet, $\Phi_0(x)$, in equation (49.112) consists of a single plane wave, $e^{i\,k_\circ\,x}$, modulated by the Gaussian, $e^{-x^2/(4\sigma)}$. In this manner the plane wave, which is defined for all space, has been localized in space by the Gaussian modulation function. In Figure 49.6 we illustrate a Gaussian wave packet of the form (49.112).

If we choose the central wavenumber to be zero, $k_\circ = 0$, then the wavenumber amplitude function has even parity, $\mathcal{A}(k) = \mathcal{A}(-k)$. The wave function, $\Phi_0(x)$, in equation (49.112) reduces to just the Gaussian modulation function without a carrier wave, so that Figure 49.6 reduces to just the positive Gaussian modulation function. Hence, the $k_\circ = 0$ limit results in a Gaussian signal, constructed with a continuum of plane waves, yet without any modulated carrier wave.

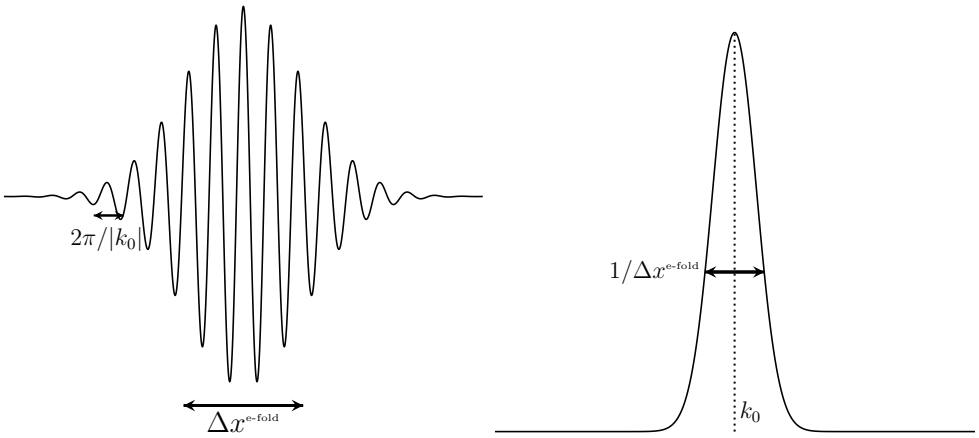

FIGURE 49.6: Left panel: example of a Gaussian wave packet, $\Phi_0(x)$, of the form given by the real part of equation (49.112), with $2\pi/|k_\circ|$ wavelength for the modulated carrier wave. From equation (49.113) we also show $\Delta x^{\text{e-fold}} = 2\,(2\,\sigma)^{1/2} \gg 2\pi/|k_\circ|$, which determines the e-folding width of the squared modulus of the packet. The plane wave, $e^{i\,k_\circ\,x}$, is referred to as the *carrier wave*. Right panel: the $\boldsymbol{k}$-space Gaussian amplitude function (49.105). Units are arbitrary in both panels.

The uncertainty relation

The squared modulus of the $\boldsymbol{x}$-space wave function (49.112) is proportional to $\exp[-x^2/(2\sigma)]$, which has an e-folding width

$$\Delta x^{\text{e-fold}} = 2\,(2\,\sigma)^{1/2}. \tag{49.113}$$

This $\boldsymbol{x}$-space wave function spread exactly complements its $\boldsymbol{k}$-space spread (49.107), so that their product is a constant

$$\Delta x^{\text{e-fold}}\,\Delta k^{\text{e-fold}} = 4. \tag{49.114}$$

The precise value of the constant is not important since it depends on the somewhat arbitrary choices made for defining Δx and Δk. What is important is that if we narrow the wavenumber band by increasing σ and thus making $\mathcal{A}(\boldsymbol{k})$ more sharply peaked, then we broaden the $\boldsymbol{x}$-space width of the wave function. That is, a narrow Gaussian wave packet in $\boldsymbol{k}$-space leads to a broad wave packet in $\boldsymbol{x}$-space. The complement holds, whereby a narrow packet in $\boldsymbol{x}$-space leads to a broad packet in $\boldsymbol{k}$-space. This tradeoff holds for general wave packets, whereby it is not possible to have a narrow packet in both $\boldsymbol{x}$-space and $\boldsymbol{k}$-space. We refer to equation (49.114) as an *uncertainty relation*. It is a fundamental feature of quantum wave mechanics, where it is known as the *Heisenberg uncertainty principle* (e.g., Chapter 3 of *Bohm* (1951) or Chapter 2 of *Gasiorowicz* (1974)). We also encountered this relation when studying the Fourier transform of a Gaussian function in Section 8.5.3.

49.7.6 Extreme examples of the uncertainty relation

The uncertainty relation is a bit odd on first encounter. Why is it impossible to know arbitrarily precise information about both the $\boldsymbol{k}$-space location and $\boldsymbol{x}$-space location of a wave packet? The answer fundamentally boils down to the dual relation between these two spaces. As a means to further exemplify this relation, and thus to build understanding, we consider the most extreme example of the uncertainty relation.[20]

First assume we know that the $\boldsymbol{k}$-space wave function is a single plane wave with just one wavevector, $\boldsymbol{k} = k_\circ \hat{\boldsymbol{x}}$. In this case the $\boldsymbol{k}$-space amplitude function is

$$\mathcal{A}(k) = a_0 \, \delta(k - k_\circ), \tag{49.115}$$

where a_0 is a constant and δ is the Dirac delta discussed in Chapter 7. Note that $\delta(k - k_\circ)$ has physical dimensions of length and is normalized so that

$$\int_{-\infty}^{\infty} \delta(k - k_\circ) \, \mathrm{d}k = 1. \tag{49.116}$$

The sifting property of the Dirac delta (Section 7.2) yields the $\boldsymbol{x}$-space wave function

$$\Phi_0(x) = \frac{a_0}{2\pi} \int_{-\infty}^{\infty} \delta(k - k_\circ) \, \mathrm{e}^{\mathrm{i}\, k\, x} \, \mathrm{d}k = \frac{a_0 \, \mathrm{e}^{\mathrm{i}\, k_\circ\, x}}{2\pi}. \tag{49.117}$$

So although we know the precise $\boldsymbol{k}$-space position, $k = k_\circ$, we have zero information about the wave function's $\boldsymbol{x}$-space position. That is, the wave function is a pure carrier wave without any modulation function so that the wave function is equally present throughout all space.

We turn the table by assuming precise $\boldsymbol{x}$-space information, in which case the modulation function is a Dirac delta

$$\Phi_0(x) = \phi_0 \, \delta(x - x_0), \tag{49.118}$$

where ϕ_0 is a constant and $\delta(x - x_0)$ is normalized so that

$$\int_{-\infty}^{\infty} \delta(x - x_0) \, \mathrm{d}x = 1. \tag{49.119}$$

We say that the modulation function has exactly specified the spatial position of this packet. Yet the price to pay for this precise x-space information is that there is zero information concerning the $\boldsymbol{k}$-space location since

$$\mathcal{A}(k) = \phi_0 \int_{-\infty}^{\infty} \delta(x - x_0) \, \mathrm{e}^{-\mathrm{i}\, k\, x} \, \mathrm{d}x = \phi_0 \, \mathrm{e}^{-\mathrm{i}\, k\, x_0}. \tag{49.120}$$

That is, the carrier wave can be any plane wave with arbitrary wavenumber, k. So although we know the precise $\boldsymbol{x}$-space position, $x = x_0$, we have zero information about the wave function's $\boldsymbol{k}$-space position. That is, the wave function carries precise $\boldsymbol{x}$-space information (delta modulated) yet zero $\boldsymbol{k}$-space information.

[20] For a similar example, see Section 8.5.1 where we discuss the Fourier transform of the Dirac delta.

49.7.7 Evolution of a non-dispersive Gaussian wave packet

We now study the evolution of the $\boldsymbol{x}$-space wave functions, $\Phi^{(+-)}(x,t)$ and $\Phi^{(++)}(x,t)$. Starting with the positive-negative wave function, recall that it evolves according to equation (49.101)

$$\Phi^{(+-)}(x,t) = \frac{1}{2\pi}\int_{-\infty}^{\infty} \mathcal{A}(k)\, \mathrm{e}^{\mathrm{i}\,(k\,x - \varpi\,t)}\,\mathrm{d}k = \frac{A}{2\pi}\int_{-\infty}^{\infty} \mathrm{e}^{-\sigma\,(k-k_\circ)^2}\,\mathrm{e}^{\mathrm{i}\,[k\,x - \varpi(k)\,t]}\,\mathrm{d}k. \tag{49.121}$$

This integral offers a complete space and time specification of $\Phi^{(+-)}(x,t)$. Even so, it is useful to massage the integral to garner insight into the physics of this evolving pattern. We do so in this section for the case of non-dispersive waves, where we show that the $\boldsymbol{x}$-space wave packet propagates the initial wave packet without alteration. This result is expected since non-dispersive waves are described by hyperbolic partial differential equations that translate initial patterns without alteration (Section 49.3.1). Furthermore, we already proved this result for a general packet of non-dispersive waves in Section 49.6.8. Even so, it is useful to expose the details in the context of the one dimensional Gaussian packets. Doing so offers insights into certain features of wave packets, and provides practice for the technically more challenging case of dispersive waves in Section 49.7.8.

Evolution of a Gaussian $\Phi^{(+-)}(x,t)$ packet of non-dispersive waves

As already encountered in this chapter, a non-dispersive wave is characterized by a dispersion relation with a constant phase speed

$$\omega = \varpi = C_{\mathsf{p}}\,|k|. \tag{49.122}$$

Such waves are said to be non-dispersive since waves with arbitrary wavenumber travel at the same phase speed. The absolute value sign in the dispersion relation (49.122) means that the relation has a continuous derivative only when $k \neq 0$. In that manner, it is a linear dispersion relation only when $k \neq 0$. Care must be exercised to account for the sign swap when moving across $k = 0$, with this movement corresponding to waves moving in opposite directions as seen earlier in Section 49.6.5.

The $\boldsymbol{x}$-space wave packet (49.121) propagates according to

$$\begin{aligned}
\Phi^{(+-)}(x,t) &= \frac{A}{2\pi}\int_{-\infty}^{\infty} \mathrm{e}^{-\sigma\,(k-k_\circ)^2}\,\mathrm{e}^{\mathrm{i}\,(k\,x - |k|\,C_{\mathsf{p}}\,t)}\,\mathrm{d}k && \text{(49.123a)}\\
&= \frac{A}{2\pi}\int_{0}^{\infty} \mathrm{e}^{-\sigma\,(k-k_\circ)^2}\,\mathrm{e}^{\mathrm{i}\,k\,(x - C_{\mathsf{p}}\,t)}\,\mathrm{d}k + \frac{A}{2\pi}\int_{-\infty}^{0} \mathrm{e}^{-\sigma\,(k-k_\circ)^2}\,\mathrm{e}^{\mathrm{i}\,k\,(x + C_{\mathsf{p}}\,t)}\,\mathrm{d}k && \text{(49.123b)}\\
&= \frac{A}{2\pi}\int_{0}^{\infty} \mathrm{e}^{-\sigma\,(k-k_\circ)^2}\,\mathrm{e}^{\mathrm{i}\,k\,(x - C_{\mathsf{p}}\,t)}\,\mathrm{d}k + \frac{A}{2\pi}\int_{0}^{\infty} \mathrm{e}^{-\sigma\,(k+k_\circ)^2}\,\mathrm{e}^{-\mathrm{i}\,k\,(x + C_{\mathsf{p}}\,t)}\,\mathrm{d}k && \text{(49.123c)}\\
&= \Phi^{(+)}(x - C_{\mathsf{p}}\,t, 0) + \Phi^{(-)}(x + C_{\mathsf{p}}\,t, 0), && \text{(49.123d)}
\end{aligned}$$

where we made use of equations (49.109a) and (49.109b) for the $\Phi^{(+)}$ and $\Phi^{(-)}$ initial conditions. Evidently, the x-space wave packet splits from its initial condition into positive and negative propagating wave packets, and the packets move without altering their respective initial conditions. However, as already discussed for the initial conditions leading up to equation (49.110), the wave packets are *not* symmetric reflections of each other if $k_\circ \neq 0$. In fact, $\Phi^{(-)}$ is exponentially smaller than $\Phi^{(+)}$ if $k_\circ > 0$.

Evolution of a Gaussian $\Phi^{(++)}(x,t)$ packet of non-dispersive waves

Now consider evolution of the $\Phi^{(++)}$ packet (49.102) built from non-dispersive waves. In this case we can perform the integral to produce

$$\Phi^{(++)}(x,t) = \frac{A}{2\pi}\int_{-\infty}^{\infty} \mathrm{e}^{-\sigma\,(k-k_\circ)^2}\,\mathrm{e}^{\mathrm{i}\,k\,(x-C_\mathsf{p}\,t)}\,\mathrm{d}k \tag{49.124a}$$

$$= \frac{A}{2\,\pi}\,\mathrm{e}^{\mathrm{i}\,k_\circ\,(x-C_\mathsf{p}\,t)}\,\mathrm{e}^{-(x-C_\mathsf{p}\,t)^2/(4\,\sigma)}\int_{-\infty}^{\infty}\mathrm{e}^{-\sigma\,[q-\mathrm{i}\,(x-C_\mathsf{p}\,t)/(2\,\sigma)]^2}\,\mathrm{d}q \tag{49.124b}$$

$$= \frac{A\,\mathrm{e}^{\mathrm{i}\,k_\circ\,(x-C_\mathsf{p}\,t)}}{2\,\pi}\sqrt{\frac{\pi}{\sigma}}\,\mathrm{e}^{-(x-C_\mathsf{p}\,t)^2/(4\,\sigma)}. \tag{49.124c}$$

The second equality resulted from completing the square in the exponential, and the final equality evaluated the integral using methods from complex analysis.[21] Comparing the expression in equation (49.124c) to the initial wave packet in equation (49.112) reveals that

$$\Phi^{(++)}(x,t) = \Phi^{(++)}(x-C_\mathsf{p}\,t,0) = \Phi_0(x-C_\mathsf{p}\,t). \tag{49.125}$$

As noted in Section 49.7.4, the initial condition for $\Phi^{(++)}(x,t)$ is propagated in the positive direction as a single coherent packet, which contrasts to the splitting found for the packet $\Phi^{(+-)}(x,t)$ in equation (49.123d).

49.7.8 Evolution of a dispersive Gaussian wave packet

Most geophysical waves are *dispersive*. As we see in the following, dispersive waves render a spreading of the $\boldsymbol{x}$-space wave packet as it evolves, along with a decay in its amplitude. Furthermore, the packet moves at the *group velocity*, which, for dispersive waves, is distinct from the phase velocity. To reveal these properties analytically, we here characterize evolution of the $\Phi^{(+-)}$ wave packet when constructed with dispersive waves, following steps taken for the general case in Section 49.6.6. Though straightforward, the maths is more tedious than for the non-dispersive packets from Section 49.7.7.

Taylor expanding the phase function

To examine the propagation of a dispersive wave packet, we Taylor expand the dispersion relation around the central wavenumber, $k = k_\circ$, and assume the packet is relatively narrow band in wavevector space. With these assumptions we truncate the Taylor series at second order

$$\varpi(k) \approx \varpi(k_\circ) + (k-k_\circ)\left[\frac{\mathrm{d}\varpi}{\mathrm{d}k}\right]_{k=k_\circ} + \frac{(k-k_\circ)^2}{2}\left[\frac{\mathrm{d}^2\varpi}{\mathrm{d}k^2}\right]_{k=k_\circ} \tag{49.126a}$$

$$\equiv \omega_0 + (k-k_\circ)\,c_\mathsf{g} + (k-k_\circ)^2\,\mu. \tag{49.126b}$$

We here introduced the one-dimensional group velocity evaluated at $k = k_\circ$

$$\boldsymbol{c}_\mathsf{g} = \hat{\boldsymbol{x}}\,c_\mathsf{g} = \hat{\boldsymbol{x}}\left[\frac{\mathrm{d}\varpi}{\mathrm{d}k}\right]_{k=k_\circ}. \tag{49.127}$$

Recall from its definition in equation (49.26) that the phase speed is positive by definition, $C_\mathsf{p} > 0$. In contrast, c_g can be positive or negative, or even zero, depending on the slope of the dispersion relation at $k = k_\circ$. In equation (49.126b) we also introduced one-half the second

[21] More precisely, it makes use of the calculus of residues, with Section G_I in *Cohen-Tannoudji et al.* (1977) providing a discussion and Appendix A9 of *Fetter and Walecka* (2003) providing a tutorial for physicists.

derivative of the dispersion relation (dimensions of L^2/T)

$$\mu = \frac{1}{2}\left[\frac{\mathrm{d}^2\varpi}{\mathrm{d}k^2}\right]_{k=k_\circ}. \tag{49.128}$$

As shown below, a nonzero μ leads to an $\boldsymbol{x}$-space modification of the wave packet shape, and generally leading to a reduction in the packet's amplitude (regardless the sign of μ).

Performing the integral

Making use of the Taylor expansion (49.126b) yields the approximate form of the phase function appearing in the $\boldsymbol{x}$-space wave packet (49.121)

$$k\,x - \varpi(k)\,t = (k-k_\circ)\,x + k_\circ\,x - t\,[\omega_0 + c_\mathrm{g}\,(k-k_\circ) + \mu\,(k-k_\circ)^2] \tag{49.129a}$$

$$= (k_\circ\,x - \omega_0\,t) + (x - c_\mathrm{g}\,t)\,(k-k_\circ) - t\,\mu\,(k-k_\circ)^2. \tag{49.129b}$$

As a result, the $\boldsymbol{x}$-space wave packet takes on the approximate form

$$\Phi^{(+-)}(x,t) \approx \frac{A\,\mathrm{e}^{\mathrm{i}\,(k_\circ\,x-\omega_0\,t)}}{2\pi}\int_{-\infty}^{\infty}\mathrm{e}^{-(\sigma+\mathrm{i}\,\mu\,t)\,(k-k_\circ)^2+\mathrm{i}\,(k-k_\circ)\,(x-c_\mathrm{g}\,t)}\,\mathrm{d}k \tag{49.130a}$$

$$= \frac{A\,\mathrm{e}^{\mathrm{i}\,(k_\circ\,x-\omega_0\,t)}}{2\pi}\int_{-\infty}^{\infty}\mathrm{e}^{-(\sigma+\mathrm{i}\,\mu\,t)\,q^2+\mathrm{i}\,q\,(x-c_\mathrm{g}\,t)}\,\mathrm{d}q, \tag{49.130b}$$

where the second equality made use of the same substitution, $q = k - k_\circ$, used when evaluating the integral for the initial value wave packet in Section 49.7.5. Introducing the shorthand

$$\alpha = x - c_\mathrm{g}\,t \quad \text{and} \quad \beta = \sigma + \mathrm{i}\,\mu\,t, \tag{49.131}$$

proves useful for completing the square in the integral exponential

$$-(\sigma+\mathrm{i}\,\mu\,t)\,q^2 + \mathrm{i}\,q\,(x-c_\mathrm{g}\,t) = -\beta\,[q - \mathrm{i}\,\alpha/(2\,\beta)]^2 - \alpha^2/(4\,\beta), \tag{49.132}$$

which brings the $\boldsymbol{x}$-space wave packet (49.130b) to the form[22]

$$\Phi^{(+-)}(x,t) = \frac{A\,\mathrm{e}^{\mathrm{i}\,(k_\circ\,x-\omega_0\,t)}\,\mathrm{e}^{-\alpha^2/(4\,\beta)}}{2\pi}\int_{-\infty}^{\infty}\mathrm{e}^{-\beta\,[q-\mathrm{i}\,\alpha/(2\,\beta)]^2}\,\mathrm{d}q \tag{49.133a}$$

$$= \frac{A\,\mathrm{e}^{\mathrm{i}\,(k_\circ\,x-\omega_0\,t)}}{2\pi}\sqrt{\frac{\pi}{\beta}}\,\mathrm{e}^{-\alpha^2/(4\,\beta)}. \tag{49.133b}$$

We next expose a complex exponential multiplied by a real exponential

$$\Phi^{(+-)}(x,t) = \frac{A\,\mathrm{e}^{\mathrm{i}\,(k_\circ\,x-\omega_0\,t)}}{2\sqrt{\pi}}\frac{\mathrm{e}^{-[(x-c_\mathrm{g}\,t)^2/(4\,(\sigma+\mathrm{i}\,\mu\,t))]}}{\sqrt{\sigma+\mathrm{i}\,\mu\,t}} \tag{49.134a}$$

$$= \frac{A\,\mathrm{e}^{\mathrm{i}\,(k_\circ\,x-\omega_0\,t)}}{2\sqrt{\pi}}\frac{\mathrm{e}^{\mathrm{i}\left[\frac{(x-c_\mathrm{g}\,t)^2\,\mu\,t}{4\,(\sigma^2+(\mu\,t)^2)}\right]}\,\mathrm{e}^{-\frac{(x-c_\mathrm{g}\,t)^2\,\sigma}{4\,(\sigma^2+(\mu\,t)^2)}}}{\sqrt{\sigma+\mathrm{i}\,\mu\,t}} \tag{49.134b}$$

$$= \frac{A\,\mathrm{e}^{\mathrm{i}\,(k_\circ\,x-\omega_0\,t)}}{2\sqrt{\pi}}\frac{\mathrm{e}^{\mathrm{i}\left[\frac{(x-c_\mathrm{g}\,t)^2\,\mu\,t}{4\,(\sigma^2+(\mu\,t)^2)}+\varphi/2\right]}\,\mathrm{e}^{-\frac{(x-c_\mathrm{g}\,t)^2\,\sigma}{4\,(\sigma^2+(\mu\,t)^2)}}}{[\sigma^2+(\mu\,t)^2]^{1/4}}, \tag{49.134c}$$

where $\tan\varphi = -\mu\,t/\sigma$.

[22] The integral in equation (49.133b) is evaluated using complex analysis as discussed in Section G_I of *Cohen-Tannoudji et al.* (1977) as well as Section 54 and Appendix A9 of *Fetter and Walecka* (2003).

Interpreting the wave packet

The phase factor in the $\boldsymbol{x}$-space wave packet (49.134c)

$$\mathcal{P} = (k_\circ\, x - \omega_0\, t) + \frac{(x - c_g\, t)^2\, \mu\, t}{4\,(\sigma^2 + (\mu\, t)^2)} + \varphi/2, \tag{49.135}$$

equals to that for a non-dispersive wave, $k_\circ\, x - \omega_0\, t$, plus a space and time dependent phase shift that is nonzero for dispersive waves ($\mu \neq 0$). The phase shift simplifies for points following the group velocity, $x = c_g\, t$, and it is here that the Gaussian exponential is maximized

$$\Phi^{(+-)}(x = c_g\, t, t) = \frac{A\, \mathrm{e}^{\mathrm{i}\,(k_\circ\, x - \omega_0\, t + \varphi/2)}}{2\sqrt{\pi}\,[\sigma^2 + (\mu\, t)^2]^{1/4}}. \tag{49.136}$$

Evidently, as the $\boldsymbol{x}$-space wave packet moves with the group velocity (which can be either signed), its amplitude declines according to $|\mu\, t|^{-1/2}$. The $t^{-1/2}$ decay of the packet amplitude is also found from the method of stationary phase for dispersive packets considered in Section 49.8.3.

Time dependent uncertainty relation

As for the $\boldsymbol{k}$-space packet in Section (49.7.5), we consider the squared modulus of the $\boldsymbol{x}$-space packet (49.134c) as a measure of its intensity

$$|\Phi^{(+-)}(x, t)|^2 = \frac{A^2\, \mathrm{e}^{-\frac{(x - c_g\, t)^2\, \sigma}{2\,(\sigma^2 + (\mu\, t)^2)}}}{4\pi\,[\sigma^2 + (\mu\, t)^2]^{1/2}}. \tag{49.137}$$

The e-folding width of $|\Phi(x, t)|^2$ is revealed by setting the decaying exponential to unity, which leads to

$$x = c_g\, t \pm (2\,\sigma)^{1/2}\left[1 + (\mu\, t/\sigma)^2\right]^{1/2} \Longrightarrow \Delta x^{\text{e-fold}} = 2\,(2\,\sigma)^{1/2}\left[1 + (\mu\, t/\sigma)^2\right]^{1/2}. \tag{49.138}$$

Multiplying by the time-independent $\boldsymbol{k}$-space packet width (49.107) leads to the time dependent uncertainty relation

$$\Delta x^{\text{e-fold}}\, \Delta k^{\text{e-fold}} = 2\,(2\,\sigma)^{1/2}\left[1 + (\mu\, t/\sigma)^2\right]^{1/2} 2\,(2\,\sigma)^{-1/2} = 4\left[1 + (\mu\, t/\sigma)^2\right]^{1/2}. \tag{49.139}$$

The time dependent uncertainty relation starts from its initial condition (49.114) at $t = 0$, and then grows as $t^{1/2}$. For non-dispersive waves ($\mu = 0$), the uncertainty relation is time-independent, which is expected since non-dispersive waves translate the initial packet without changing the properties of the packet.

49.7.9 The non-dispersive limit of a dispersive packet

We set the spreading parameter, μ, to zero for for non-dispersive waves, in which case $\mu = 0 \Longrightarrow \varphi = 0$. In this limit the wave packet (49.134c) takes on the form

$$\mu = 0 \Longrightarrow \Phi^{(+-)}(x, t) = \frac{A\, \mathrm{e}^{\mathrm{i}\, k_\circ\,(x - c_g\, t)}}{2\,\pi}\sqrt{\frac{\pi}{\sigma}}\, \mathrm{e}^{-(x - c_g\, t)^2/(4\,\sigma)}. \tag{49.140}$$

If we set $c_g = C_p$ then this result corresponds to equation (49.124c), which is the non-dispersive form of the packet $\Phi^{(++)}(x, t)$.

So why did the non-dispersive limit not reduce to equation (49.123d), which is the non-dispersive form of $\Phi^{(+-)}(x, t)$? The reason is that when performing the Taylor series expansion

for the dispersive packet, we only picked out the group velocity at the single wavenumber, $k = k_\circ$. Hence, we can only get one of the two packets comprising $\Phi^{(+-)}(x,t)$ in equation (49.123d). Namely, we ignore the exponentially small packet using the Taylor series approach. Furthermore, note that c_g can be positive or negative for dispersive waves (indeed, it can even be zero). In contrast, C_p is the phase speed and that is always positive. So in the case of $c_\mathrm{g} = -C_\mathrm{p} < 0$ then equation (49.140) is a negative moving wave packet.

So in summary, the non-dispersive limit of a dispersive packet does not exactly correspond to the purely non-dispersive packet due to a few subtleties. In particular, if one cares about the exponentially small packet exposed with the non-dispersive analysis in Section 49.7.7, then it is necessary to follow the approach taken in that section rather than taking the non-dispersive limit of dispersive waves as considered here.

49.7.10 Comments and further study

The study of wave packets in this section revealed properties that appear throughout the study of waves. First, there is the uncertainty relation, whereby a packet that is narrow banded in wavevector space is broad banded in position space, and conversely. Second, dispersive wave packets have a modulation function that is modified with time, thus producing a time dependent uncertainty relation. Regardless the sign of the dispersion coefficient, μ (equation (49.128)), the packet amplitude decays in time and the uncertainty grows. We see this behavior for generic wave packets when studying the stationary phase method in Section 49.8. Third, the center of the packet moves with the group velocity rather than phase velocity, with the two velocities distinct for dispersive waves. We also encountered this property in Section 49.6.7 when studying how the wave packet modulation function evolves. It will appear again in Chapter 50 when studying how energy (or more generally the wave action) propagates with the wave field.

The study of wave packets and their evolution is a central concern of quantum mechanics. Most books on the subject have a discussion of quantum wave packets at the level discussed here. In particular, we made use in this section of Chapter 3 of *Bohm* (1951), Chapter 2 of *Gasiorowicz* (1974), and Section G_I of *Cohen-Tannoudji et al.* (1977). We also followed Section 54 of *Fetter and Walecka* (2003), who consider wave packets built from surface gravity waves. However, it is notable that the distinctions we made here between positive and negative moving packets in Section 49.7.7 are not considered by this literature.

49.8 Method of stationary phase

As shown in Section 49.6.8, a packet of non-dispersive waves holds its initial condition unchanged as it propagates at the phase speed. This evolution is exact. Hence, we know everything about a packet of non-dispersive waves for all time, given the phase velocity and the initial conditions.

The situation is more complicated for packets of dispersive waves, whose modulation function changes its shape due to wave dispersion. We encountered such behavior when introducing wave trains and wave packets in Section 49.6.6, as well as when studying Gaussian wave packets of dispersive waves in Section 49.7. In the present section we study the long-time behavior for a packet of dispersive waves using the *method of stationary phase*. From the Gaussian wave packet study in Section 49.7.8, we expect the packet to decay according to $t^{-1/2}$, as revealed by the exact Gaussian packet results in Section 49.7. Here we show that this $t^{-1/2}$ behavior is generic for packets of dispersive waves.

For analytical simplicity we focus on a wave function in one space dimension, written as

$$\Phi(x,t) = \frac{1}{2\pi} \int_{k_\mathrm{a}}^{k_\mathrm{b}} \mathcal{A}(k)\, \mathrm{e}^{\mathrm{i}\, h(k)\, t}\, \mathrm{d}k, \tag{49.141}$$

where $\mathcal{A}(k)$ is the amplitude function, $h(k)$ is a real phase function, and we focus on a wavenumber interval $k \in [k_a, k_b]$. For example, with a plane wave we have

$$h(k) = k\,x/t - \varpi(k), \tag{49.142}$$

where $\varpi(k)$ is the dispersion relation. Note that for the integral in equation (49.141), x and t are considered parameters, so we only expose the k dependence to the phase function, $h(k)$. Finally, with a focus on dispersive waves we assume

$$\varpi''(k) \neq 0. \tag{49.143}$$

49.8.1 Riemann-Legesque lemma and center of the packet

As $t \to \infty$, the wave packet's integrand, $\mathcal{A}(k)\,\mathrm{e}^{\mathrm{i}\,h(k)\,t}$, oscillates faster. Consequently, terms in the integral cancel since the oscillations dominate any behavior of the amplitude (which is assumed smooth). Indeed, the *Riemann-Legesque lemma* states that the integral has a zero limit as $t \to \infty$, so long as the amplitude function is integrable and finite.

Contributions to the wave packet are maximized when two elements of the integrand align. First we want to maximize the amplitude, which for a wave packet is assumed to be maximized in a small interval surrounding a wavenumber, k_o or k_o. Next we want the phase function to be in a small neighborhood of an extrema, which is where $h'(k) = 0$. Aligning this phase extrema with the amplitude maximum means we want space-time locations where $h'(k_o) = 0$. For a packet built from plane waves, $h'(k_o) = 0$ occurs at a specific space-time point determined by the group velocity

$$h'(k_o) = x/t - c_g = 0 \Longrightarrow x/t = c_g, \tag{49.144}$$

where

$$c_g = c_g(k_o) = \varpi'(k_o) \tag{49.145}$$

is the group velocity for the packet as determined at the wavenumber, k_o, where the amplitude has its maximum. Evidently, the center of the wave packet (i.e., where the packet has its maximum amplitude) is located at

$$x_{\text{center}} = t\,c_g, \tag{49.146}$$

so that the center moves at the group velocity. This result for the packet center was previously found using different approaches in Sections 49.6.6, 49.7.7, and 49.7.8.

In addition to wanting information about the packet center, it is useful to know about its amplitude which, according to Riemann-Legesque, decays to zero as time increases. To get an expression for the amplitude modulation requires some work, which is the topic of the remainder of this section.

49.8.2 Wavenumber intervals with no phase extrema

Consider the case whereby the phase has no extrema within the chosen wavenumber interval, $k \in [k_a, k_b]$, so that $h'(k) \neq 0$. This assumption allows us to use integration by parts in the form

$$\int_{k_a}^{k_b} v\,\mathrm{d}u = [u\,v]\Big|_{k_a}^{k_b} - \int_{k_a}^{k_b} u\,\mathrm{d}v, \tag{49.147}$$

where

$$v = \mathcal{A}/h' \quad \text{and} \quad u = \mathrm{e}^{\mathrm{i}\,h\,t}/(\mathrm{i}\,t), \tag{49.148}$$

so that

$$v\,\mathrm{d}u = (\mathcal{A}/h')\,\mathrm{d}[\mathrm{e}^{\mathrm{i}\,h\,t}/(\mathrm{i}\,t)] = \mathcal{A}\,\mathrm{e}^{\mathrm{i}\,h\,t}\,\mathrm{d}k, \tag{49.149}$$

and

$$u\,\mathrm{d}v = [\mathrm{e}^{\mathrm{i}\,h\,t}/(\mathrm{i}\,t)]\,\mathrm{d}(\mathcal{A}/h'). \tag{49.150}$$

We can thus write the integral as

$$2\,\pi\,\Phi = \frac{1}{\mathrm{i}\,t}\left[(\mathcal{A}/h')\,\mathrm{e}^{\mathrm{i}\,h\,t}\Big|_{k_\mathrm{a}}^{k_\mathrm{b}} - \int_{k_\mathrm{a}}^{k_\mathrm{b}} \mathrm{e}^{\mathrm{i}\,h\,t}\,\mathrm{d}(g/h')\right] \sim \mathcal{O}(t^{-1}). \tag{49.151}$$

The key point is that the integral decays as t^{-1} for wavenumber intervals, $k \in [k_\mathrm{a}, k_\mathrm{b}]$, where the phase, $h(k)$, has no extrema.

49.8.3 Wavenumber interval including a phase extrema

We expect that contributions from regions near an extrema decay slower in time, since near those regions the phase does not oscillate so rapidly.[23] In particular, as noted in Section 49.8.1, we expect that the packet center follows a point in space determined by the group velocity. We thus consider the case where the phase has an extrema at the wavenumber $k_\circ$, which is now included in the interval: $k_\circ \in [k_\mathrm{a}, k_\mathrm{b}]$, in which case we Taylor expand the phase

$$h(k) = h(k_\circ) + h'(k_\circ)\,(k-k_\circ) + (k-k_\circ)^2\,h''(k_\circ)/2 + ... = h(k_\circ) + (k-k_\circ)^2\,h''(k_\circ)/2 + ..., \tag{49.152}$$

where we set

$$h'(k_\circ) = 0 \tag{49.153}$$

since it is an extrema. We showed in Section 49.8.2 that wavenumber regions where there is no extrema contribute terms of order $\mathcal{O}(t^{-1})$ to the integral. We now show that regions including an extrema decay like $\mathcal{O}(t^{-1/2})$, thus allowing us to focus on the region surrounding the packet center,

$$k_\circ - 1/\sqrt{2\sigma} \leq k \leq k_\circ + 1/\sqrt{2\sigma}. \tag{49.154}$$

We introduced $1/\sqrt{2\sigma}$ as a measure of the packet width, such as used for the Gaussian packet in equation (49.107). We thus have the integral

$$2\,\pi\,\Phi = \mathrm{e}^{\mathrm{i}\,t\,h(k_\circ)} \int_{k_\circ - 1/\sqrt{2\sigma}}^{k_\circ + 1/\sqrt{2\sigma}} \mathcal{A}(k)\,\mathrm{e}^{\mathrm{i}\,t\,(k-k_\circ)^2\,h''(k_\circ)/2}\,\mathrm{d}k + \mathcal{O}(t^{-1}). \tag{49.155}$$

Changing variables to a shifted wavenumber $\ell = k - k_\circ$ gives the expression

$$2\,\pi\,\Phi = \mathrm{e}^{\mathrm{i}\,t\,h(k_\circ)} \int_{-1/\sqrt{2\sigma}}^{1/\sqrt{2\sigma}} \mathcal{A}(\ell + k_\circ)\,\mathrm{e}^{\mathrm{i}\,t\,\ell^2\,h''(k_\circ)/2}\,\mathrm{d}\ell + \mathcal{O}(t^{-1}). \tag{49.156}$$

One more change in variables to $p = \ell\,\sqrt{t}$ renders the integral

$$2\,\pi\,\Phi = t^{-1/2}\,\mathrm{e}^{\mathrm{i}\,t\,h(k_\circ)} \int_{-1/\sqrt{2\sigma}}^{1/\sqrt{2\sigma}} \mathcal{A}(p\,t^{-1/2} + k_\circ)\,\mathrm{e}^{\mathrm{i}\,p^2\,h''(k_\circ)/2}\,\mathrm{d}p + \mathcal{O}(t^{-1}). \tag{49.157}$$

We simplify the integrand by performing a Taylor expansion

$$\mathcal{A}(p\,t^{-1/2} + k_\circ) = \mathcal{A}(p_0) + \mathcal{O}(t^{-1/2}), \tag{49.158}$$

[23] According to Section 11.3 of *Whitham* (1974), this insight is originally due to Lord Kelvin.

so that, keeping only terms of order $t^{-1/2}$, brings about the integral

$$2\,\pi\,\Phi = t^{-1/2}\,\mathcal{A}(k_\circ)\,\mathrm{e}^{\mathrm{i}\,t\,h(k_\circ)}\int_{-\sqrt{t/2\sigma}}^{\sqrt{t/2\sigma}}\mathrm{e}^{\mathrm{i}\,p^2\,h''(k_\circ)/2}\,\mathrm{d}p + \mathcal{O}(t^{-1}). \tag{49.159}$$

For a dispersive packet with non-zero $h''(k_\circ)$, the $t\to\infty$ limit allows us to extend the limit on the integral (49.159) to infinity so that

$$2\,\pi\,\Phi = t^{-1/2}\,\mathcal{A}(k_\circ)\,\mathrm{e}^{\mathrm{i}\,t\,h(k_\circ)}\int_{-\infty}^{\infty}\mathrm{e}^{\mathrm{i}\,p^2\,h''(k_\circ)/2}\,\mathrm{d}p + \mathcal{O}(t^{-1}). \tag{49.160}$$

The integral is in the form of a *Fresnal integral* and it can be done using methods from complex analysis to find

$$\int_{-\infty}^{\infty}\mathrm{e}^{\mathrm{i}\,p^2\,h''(k_\circ)/2}\,\mathrm{d}p = \sqrt{\frac{2\,\pi}{|h''(k_\circ)|}}\,\mathrm{e}^{\pm\,\mathrm{i}\pi/4}, \tag{49.161}$$

where the $\pm$ sign corresponds to the sign of $h''(k_\circ)$. We thus have the stationary phase expression for the wave function

$$\Phi(x,t) = \frac{\mathcal{A}(k_\circ)\,\mathrm{e}^{\mathrm{i}\,t\,h(k_\circ)\pm\mathrm{i}\,\pi/4}}{[2\,\pi\,t\,|h''(k_\circ)|]^{1/2}} + \mathcal{O}(t^{-1}). \tag{49.162}$$

As noted at the start of this section, a packet built from plane waves has

$$h(k_\circ)\,t = k_\circ\,x - \varpi(k_\circ)\,t, \tag{49.163}$$

so that the long-time behavior of the wave packet is given by

$$\Phi(x,t) = \mathcal{A}(k_\circ)\,\mathrm{e}^{\mathrm{i}\,(k_\circ\,x-\varpi(k_\circ)\,t)}\,\frac{\mathrm{e}^{\pm\mathrm{i}\,\pi/4}}{[2\,\pi\,t\,|\varpi''(k_\circ)|]^{1/2}} + \mathcal{O}(t^{-1}). \tag{49.164}$$

This wave function is built from a plane wave with wavenumber $k_\circ$ that is modulated by a function whose amplitude is decaying according to $t^{-1/2}$. The $t^{-1/2}$ decay accords with the exact solution of the dispersive Gaussian packet in Section 49.7.8. Furthermore, note how the strength of the $t^{-1/2}$ decay is affected by the size of $|\varpi''(k_\circ)|$.

As noted in Section 49.8.1, the packet is a maximum when sampled at the center, which is given by (equation (49.146)) $x_{\text{center}} = c_{\mathsf{g}}\,t$. At this point, the phase of the wave function (49.164) takes the form

$$k_\circ\,x_{\text{center}} - \varpi(k_\circ)\,t = k_\circ\,c_{\mathsf{g}}\,t - \varpi(k_\circ)\,t = k_\circ\,(c_{\mathsf{g}} - c_{\mathsf{p}})\,t, \tag{49.165}$$

where we introduced the phase velocity for the carrier wave

$$c_{\mathsf{p}} = \varpi(k_\circ)/k_\circ. \tag{49.166}$$

As a result, the wave function as evaluated at the packet center is given by

$$\Phi(x_{\text{center}},t) = \mathcal{A}(k_\circ)\,\mathrm{e}^{\mathrm{i}\,k_\circ\,(c_{\mathsf{g}}-c_{\mathsf{p}})\,t}\,\frac{\mathrm{e}^{\pm\mathrm{i}\,\pi/4}}{[2\,\pi\,t\,|\varpi''(k_\circ)|]^{1/2}} + \mathcal{O}(t^{-1}). \tag{49.167}$$

49.8.4 Comments and further study

If both the first and second derivatives vanish, $h'(k_\circ) = 0$ and $h''(k_\circ) = 0$, then the same procedure as used above must be pursued but to the next higher order in the Taylor series expansion. Also if there are multiple extrema, then each will add a contribution of the form given by equation (49.162).

Variations on the derivation given in this section can be found in section 11.3 of *Whitham* (1974), section 3.7 of *Lighthill* (1978), section 55 of *Fetter and Walecka* (2003) and section 1.C.2 of *Cohen-Tannoudji et al.* (1977).

49.9 Exercises

EXERCISE 49.1: PARSEVAL'S IDENTITY FOR WAVE PACKETS
Consider the expression (49.47) for a wave function

$$\Phi(\boldsymbol{x},t) = \frac{1}{(2\pi)^3}\int \mathcal{A}(\boldsymbol{k})\,\mathrm{e}^{\mathrm{i}\,(\boldsymbol{k}\cdot\boldsymbol{x}-\varpi\,t)}\,\mathrm{d}\boldsymbol{k}. \tag{49.168}$$

Prove the following expression of Parseval's identity (Section 8.3.6)

$$\int |\nabla\Phi|^2\,\mathrm{d}\boldsymbol{x} = \frac{1}{(2\pi)^3}\int |\boldsymbol{k}|^2\,|\mathcal{A}(\boldsymbol{k})|^2\,\mathrm{d}\boldsymbol{k}. \tag{49.169}$$

Notice that the right hand side is time-independent, so that the left hand side must be likewise. Hint: make use of the following representation of the Dirac delta from Section 8.5.1

$$\delta(\boldsymbol{k}-\boldsymbol{q}) = \frac{1}{(2\pi)^3}\int \mathrm{e}^{\mathrm{i}\,(\boldsymbol{k}-\boldsymbol{q})\cdot\boldsymbol{x}}\,\mathrm{d}\boldsymbol{x}. \tag{49.170}$$

EXERCISE 49.2: SQUARE WAVE PACKET (EXERCISE 2.1 OF *Gasiorowicz* (1974))
Consider a wave packet in one space dimension with real k-space amplitude function

$$A(k) = \begin{cases} 0 & k < -K \\ N & -K < k < K \\ 0 & k > K, \end{cases} \tag{49.171}$$

where $K > 0$.

(a) Find the $\boldsymbol{x}$-space wave function, which in one space dimension takes the form

$$\Phi_0(x) = \frac{1}{2\pi}\int_{-\infty}^{\infty} A(k)\,\mathrm{e}^{\mathrm{i}\,k\,x}\,\mathrm{d}k. \tag{49.172}$$

Hint: $\Phi_0(x)$ is the inverse Fourier transform of $A(k)$. The integral is simple to do.

(b) Find the value of N for which

$$\int_{-\infty}^{\infty} |\Phi_0(x)|^2\,\mathrm{d}x = 1. \tag{49.173}$$

Hint: massage the integral until it looks like one found in a standard integral table.

(c) Relate the above choice for N to one that makes

$$\int_{-\infty}^{\infty} |A(k)|^2\,\mathrm{d}k = 1. \tag{49.174}$$

(d) Show that a reasonable definition for Δx in part (a) yields the uncertainty relation

$$\Delta x \, \Delta k > 1. \tag{49.175}$$

Hint: this uncertainty relation holds independently of K.

EXERCISE 49.3: INVERSE SQUARED WAVE PACKET (EXERCISE 2.2 OF *Gasiorowicz* (1974))
Consider a wave packet in one space dimension with real k-space amplitude function

$$A(k) = \frac{N}{k^2 + \alpha^2} \tag{49.176}$$

with $\alpha > 0$.

(a) Find the $\boldsymbol{x}$-space wave function, which in one space dimension takes the form

$$\Phi_0(x) = \frac{1}{2\pi} \int_{-\infty}^{\infty} A(k) \, \mathrm{e}^{\mathrm{i}\, k\, x} \, \mathrm{d}k \tag{49.177}$$

Hint: $\Phi_0(x)$ is the inverse Fourier transform of $A(k)$. Massage the integral until it looks like one found in a standard integral table.

(b) Show that a reasonable definition for Δx in part (a) yields the uncertainty relation

$$\Delta x \, \Delta k > 1. \tag{49.178}$$

Hint: this relation holds independently of α.

EXERCISE 49.4: WAVE FUNCTION PDE DERIVED FROM THE DISPERSION RELATION
Follow the method from Section 49.6.9 to derive the partial differential equation satisfied by a wave function, $\Phi(\boldsymbol{x}, t)$, whose constituent waves satisfy the following dispersion relations, where for each case $\boldsymbol{k} = k_x \, \hat{\boldsymbol{x}} + k_y \, \hat{\boldsymbol{y}} + k_z \, \hat{\boldsymbol{z}}$ a three-dimensional wavevector.

(a) $\varpi^2 = c^2 \, |\boldsymbol{k}|^2$, with c a constant with dimensions L T^{-1}.

(b) $\varpi^2 = B^2 \, k_z^2 / |\boldsymbol{k}|^2$, with B a constant with dimensions T^{-1}.

Chapter 50

Waves in a gently varying background

We here study linear waves propagating through a prescribed gently varying (in space and time) background environment, such as for waves moving through a stratified ocean or atmosphere, or waves moving through a mean flow. We assume the relevance of space and time coherent wave patterns so that we can consider a wave phase function. However, the wavevector and angular frequency, as well as the wave amplitude, are here functions of space and time and as such we cannot use traditional Fourier analysis. Instead, asymptotic methods are needed, and we develop the leading order theory referred to in various contexts as *ray theory*, *geometric optics*, *eikonal approximation* or the *WKBJ approximation*.[1] Notably, we do *not* consider the back-reaction effects of waves on the background state, which is the subject matter of *waves and mean flow interaction* theory.

Given the more general background state, we must consider a wave ansatz that is more general than the plane wave Fourier ansatz from Chapter 49. We refer to the new ansatz as the *WKBJ wave ansatz* or equivalently the *eikonal wave ansatz* (the specific form is given by equation (50.54)). Plugging in this wave ansatz to the wave equation then leads to a suite of asymptotic equations that are used to build the wave function, ray equations, energy equation, etc. In principle this approach is straightforward, yet in practice it is tedious and uninspired. *Whitham's variational principle* provides an alterative that is both elegant and powerful. In brief, Whitham's principle is based on Hamilton's principle from classical continuum mechanics (Part IX of this book), only now applied to the leading order (in WKBJ expansion) phase averaged action. The resulting Euler-Lagrange equations render the dispersion relation and conservation equations for an energy-momentum-stress tensor. As part of these conservation equations, we encounter the *wave action*, which offers a generalization of wave energy, and the flux of wave action is determined by the group velocity.

READER'S GUIDE TO THIS CHAPTER

We assume familiarity with the material from Chapter 49, which considered wave kinematics for traveling plane waves on a static and homogeneous background state. We here make use of Cartesian coordinates and Cartesian tensors (Chapters 1 and 2). The wave energetics/action discussion makes use of Hamilton's principle for a continuum from Part IX of this book, in particular the material in Chapter 46. Much of the material here is inspired by the review chapter from *Bretherton* (1971), as well as *Bretherton and Garrett* (1969), chapter 11 of *Whitham* (1974), Part 2 in the Epilogue of *Lighthill* (1978), *Andrews and McIntyre* (1978b), chapter 9 of *Olbers et al.* (2012), and *Tracy et al.* (2014).

[1] WKBJ stands for Wentzel, Kramers, Brillouin, and Jeffreys, scientists who promoted the method in the 20th century for use in quantum mechanics. Often this method is referred to as WKB. In fact, the method was developed in the 19th century by Liouville and Green.

50.1 Loose threads

- Figures
- Adiabatic invariants as per Section 9.2 of *Olbers et al.* (2012) and Section 49 of *Landau and Lifshitz* (1976). See also *José and Saletan* (1998).

50.2 General phase functions

Throughout Chapter 49 , the phase of the wave function takes the linear plane wave form given by equation (49.20) (here written with zero phase shift)

$$\mathcal{P}(\boldsymbol{x}, t) = \boldsymbol{k} \cdot \boldsymbol{x} - \omega\, t = k_a\, x^a - \omega\, t, \tag{50.1}$$

where the wavevector, $\boldsymbol{k}$, and angular frequency, ω, are parameters of the wave that are independent of space and time. The second equality made use of the summation convention, with the wavevector components written with lower indices to accord with the upstairs spatial indices. The relatively simple form (50.1) of the phase function is suited only for background states that are homogeneous and static. In this chapter we consider a more general phase function that allows us to study waves moving through a background state that is inhomogeneous and/or time

dependent. The key restriction to our approach is that we retain the notion of a locally defined wavevector and angular frequency, which are now considered to be functions of space and time

$$\nabla\mathcal{P} \equiv \boldsymbol{k}(\boldsymbol{x},t) \quad \text{and} \quad -\partial_t\mathcal{P} \equiv \omega(\boldsymbol{x},t). \tag{50.2}$$

These expressions tacitly assume that the base state fluid properties are changing slowly in space and time relative to the wave phase, thus allowing us to generalize much of the wave kinematics holding for homogeneous/static media while locally considering the waves to be planar. For this assumption to hold, it is sufficient to make the following space and time scale separation, as assumed throughout this chapter

$$|\boldsymbol{k}| = |\nabla\mathcal{P}| \gg L^{-1} \quad \text{and} \quad \omega = -\partial_t\mathcal{P} \gg T^{-1}, \tag{50.3}$$

where L is a characteristic length scale defined by spatial variations in the background state, and T is the corresponding time scale for changes in the background state. In terms of the local measure of the wavelength, $\Lambda = 2\pi/|\boldsymbol{k}|$, and period, $2\pi/\omega$, we have

$$\Lambda \ll 2\pi\, L \quad \text{and} \quad 2\pi/\omega \ll T. \tag{50.4}$$

Values for L and T depend on details of the physical system defining the background state. For example, in Section 50.5.2 we consider L and T for a stretched string with time dependent tension and space dependent mass density, and in Section 51.9.5 we consider L for the case of acoustic waves moving through a spatially inhomogenous yet static background.

50.2.1 Path independence of phase difference

Given that the wavevector is defined as the gradient of the phase as per equation (50.2), it must satisfy the consistency condition

$$\nabla \times \boldsymbol{k} = \nabla \times \nabla\mathcal{P} = 0. \tag{50.5}$$

This property of the wavevector means that there are the same number of wave crests between any two points in the fluid at any particular time instance, no matter what path is taken to connect the two points. This property is trivially maintained by plane waves in a homogeneous media since $\boldsymbol{k}$ is a space-time constant vector. To prove it holds for the more general phase function, consider the difference in phase (at a fixed time) between points A and B within the fluid (see Figure 50.1). Compute this phase difference via a path, $\mathcal{C}_1$, that goes from point A to point B, and then via an alternative path, $\mathcal{C}_2$, that also goes from point A to point B

$$\Delta\mathcal{P}_{\mathcal{C}_1} = \int_{\mathcal{C}_1} \boldsymbol{k}\cdot \mathrm{d}\boldsymbol{x} \quad \text{and} \quad \Delta\mathcal{P}_{\mathcal{C}_2} = \int_{\mathcal{C}_2} \boldsymbol{k}\cdot \mathrm{d}\boldsymbol{x}. \tag{50.6}$$

The path $\mathcal{C}_1 - \mathcal{C}_2$ is a closed loop that is oriented in the counterclockwise direction. We can thus make use of Stokes' theorem to find

$$\Delta\mathcal{P}_{\mathcal{C}_1} - \Delta\mathcal{P}_{\mathcal{C}_2} = \oint_{\mathcal{C}_1-\mathcal{C}_2} \boldsymbol{k}\cdot \mathrm{d}\boldsymbol{x} = \oint (\nabla\times\boldsymbol{k})\cdot\hat{\boldsymbol{n}}\,\mathrm{d}\mathcal{S} = 0, \tag{50.7}$$

which proves the path independence of the phase difference.

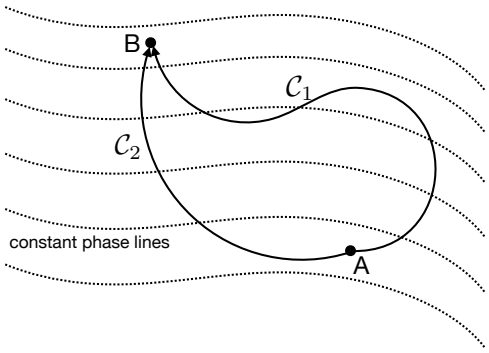

FIGURE 50.1: This figure illustrates the conservation of wave crests embodied by equation (50.9). Here we consider two paths in space, $\mathcal{C}_1$ and $\mathcal{C}_2$, that go from point A to point B. Both paths move across surfaces of constant phase, illustrated by the dotted lines and shown for a particular time instance. As shown by equation (50.7), the difference in phase computed along the two different paths is the same, and this property follows from $\nabla \times \boldsymbol{k} = 0$ and Stokes' theorem.

50.2.2 Conservation of wave crests

Because the mixed partial derivatives of the phase function commute, we have

$$\frac{\partial \omega}{\partial x^a} = -\frac{\partial^2 \mathcal{P}}{\partial t \, \partial x^a} \quad \text{and} \quad \frac{\partial k_a}{\partial t} = \frac{\partial^2 \mathcal{P}}{\partial x^a \, \partial t}, \tag{50.8}$$

which leads to the vector equation

$$\frac{\partial \boldsymbol{k}}{\partial t} + \nabla \omega = 0. \tag{50.9}$$

This equation says that the time change in wavevector, $\partial_t \boldsymbol{k}$, is exactly compensated by the spatial change in angular frequency, $\nabla\omega$. This self-consistency condition is referred to as the *conservation of wave crests*. Motivation for this name follows since the wavenumber, $|\boldsymbol{k}|$, is the number of wave crests per unit length at a fixed time. Likewise, the angular frequency, ω, is the number of wave crests passing a fixed location per unit time. Having their respective space and time derivatives match is a self-consistency condition for a coherent wave pattern to exist.

As a further means to understand the balance equation (50.9), and the name "conservation of wave crests", consider an integral between two points fixed in space taken along a fixed path in space, such as the path C_1 in Figure 50.1. The time tendency of the phase difference is given by

$$\partial_t(\Delta \mathcal{P}_{\mathcal{C}_1}) = \frac{\partial}{\partial t} \int_{\mathcal{C}_1} \boldsymbol{k} \cdot \mathrm{d}\boldsymbol{x} = \int_{\mathcal{C}_1} \partial_t \boldsymbol{k} \cdot \mathrm{d}\boldsymbol{x} = -\int_{\mathcal{C}_1} \nabla\omega \cdot \mathrm{d}\boldsymbol{x} = \omega(A) - \omega(B). \tag{50.10}$$

If the angular frequency is greater at point A than at point B, then that means that there is an accumulation of wave crests entering the region at point A relative to those leaving at point B; i.e., there is a convergence of wave crests between the two points. This convergence is associated with an increase in the wavenumber between the two points.

50.2.3 Phase velocity and phase speed

Consider an observer moving on a smooth trajectory through space and time defined by a fixed point on a constant phase surface, such as when the observer remains fixed on the crest of a traveling wave.[2] As such, we assume that the trajectory is aligned in the direction of $\nabla\mathcal{P}$, which

[2]Our formulation in this section emulates that used in Section 17.4 for the Lagrangian time derivative, which is concerned with measuring fluid properties following a fluid particle. Here, we are following a wave as defined by a surface of constant phase.

is the local direction of the wave

$$\hat{\boldsymbol{k}} \equiv \nabla\mathcal{P}/|\nabla\mathcal{P}| \equiv \boldsymbol{k}/|\boldsymbol{k}|, \tag{50.11}$$

with the local wavevector defined by equation (50.2).

To determine the velocity of the fixed-phase observer, consider an infinitesimal spatial increment, $\delta\boldsymbol{x}^{\text{phase}}$, that occurs over a small time increment, δt. Assuming this space increment follows the fixed-phase observer leads to the identity

$$\mathcal{P}(\boldsymbol{x} + \delta\boldsymbol{x}^{\text{phase}}, t + \delta t) = \mathcal{P}(\boldsymbol{x}, t). \tag{50.12}$$

Truncating a Taylor series expansion of this identity leads to the differential equation satisfied by the phase

$$(\partial_t + \boldsymbol{c}_{\text{p}} \cdot \nabla)\mathcal{P} = 0, \tag{50.13}$$

where we defined the *phase velocity*

$$\boldsymbol{c}_{\text{p}} = \delta\boldsymbol{x}^{\text{phase}}/\delta t. \tag{50.14}$$

The partial differential equation (50.13) specifies $\boldsymbol{c}_{\text{p}} \cdot \nabla\mathcal{P} = \boldsymbol{c}_{\text{p}} \cdot \boldsymbol{k}$ in terms of the time derivative of the phase

$$\boldsymbol{c}_{\text{p}} \cdot \boldsymbol{k} = \boldsymbol{c}_{\text{p}} \cdot \nabla\mathcal{P} = -\partial_t\mathcal{P}. \tag{50.15}$$

Indeed, since the observer is assumed to move along the direction of the wavevector, $\hat{\boldsymbol{k}}$, then $\boldsymbol{c}_{\text{p}} \cdot \hat{\boldsymbol{k}}$ is the only component of the phase velocity. We thus write the phase velocity as in our discussion of plane waves in Section 49.5.2

$$\boldsymbol{c}_{\text{p}} = (\boldsymbol{c}_{\text{p}} \cdot \hat{\boldsymbol{k}})\,\hat{\boldsymbol{k}} \equiv C_{\text{p}}\,\hat{\boldsymbol{k}}, \tag{50.16}$$

where $C_{\text{p}} > 0$ is the *phase speed*, which is the magnitude of the phase velocity. Figure 49.2 provides an illustration.

50.2.4 Angular frequency and wavelength

The time derivative, $\partial_t\mathcal{P}$, measures the time change of the phase at a fixed point in space, which we use to define the local angular frequency of the wave as per equation (50.2)

$$\omega = -\partial_t\mathcal{P}. \tag{50.17}$$

The differential equation (50.13) for the phase can thus be written in the equivalent manners

$$(\partial_t + \boldsymbol{c}_{\text{p}} \cdot \nabla)\mathcal{P} = 0 \iff \omega = \boldsymbol{c}_{\text{p}} \cdot \boldsymbol{k}, \tag{50.18}$$

which also leads to the relations

$$\boldsymbol{c}_{\text{p}} = C_{\text{p}}\,\hat{\boldsymbol{k}} = \frac{-\partial_t\mathcal{P}}{|\nabla\mathcal{P}|}\frac{\nabla\mathcal{P}}{|\nabla\mathcal{P}|}, \tag{50.19}$$

where $C_{\text{p}} \geq 0$ is the phase speed. We likewise identify the wavelength

$$\Lambda = 2\pi/|\boldsymbol{k}| \implies C_{\text{p}} = \omega\,\Lambda/2\pi. \tag{50.20}$$

Note that the relations (50.19) and (50.20) also hold for free plane waves moving through a homogeneous media, as discussed in Section 49.5.

50.3 Kinematics of rays

Recall that when studying wave packets in Section 49.6, we found the group velocity to be fundamental to the wave packet evolution. We show later in this chapter that the group velocity defines the paths along which wave action (wave energy divided by wave angular frequency) propagates. Such paths are referred to as *rays*. Given the prominence of rays, we find it useful to develop evolution equations for wave properties along rays. We here start that process, focusing on the wave phase, wavevector, and angular frequency. This material forms elements to *geometric optics*, which is a subject commonly taught in introductory physics courses by presenting a series of rules for how light reflects and refracts. In this section we derive those rules in the form of partial differential equations following from basic principles.

50.3.1 Eikonal equation

The dispersion relation provides the local value of the angular frequency as a function of space, time, and wavevector, where the wavevector itself is a function of space and time

$$\omega = \varpi(\boldsymbol{x}, t, \boldsymbol{k}(\boldsymbol{x}, t)) = \varpi(\boldsymbol{x}, t, \nabla\mathcal{P}). \tag{50.21}$$

As such, the dispersion relation is an explicit function of $(\boldsymbol{x}, t)$, as well as a function of a function, $\boldsymbol{k} = \boldsymbol{k}(\boldsymbol{x}, t)$, which makes ϖ also an implicit function of $(\boldsymbol{x}, t)$. This dependence is reminiscent of the Lagrangian and Hamiltonian densities encountered in Chapter 46. Just like for the Lagrangian density, it is crucial to account for this functional dependency when computing space and time derivatives.[3] A useful rule to remember is that the angular frequency, ω, is a function of space and time, $\omega = \omega(\boldsymbol{x}, t) = -\partial_t\mathcal{P}(\boldsymbol{x}, t)$. Yet when connected to a dispersion relation, $\varpi(\boldsymbol{x}, t, \boldsymbol{k}(\boldsymbol{x}, t))$, which links a wavevector to an angular frequency, then we must treat the dispersion relation as an explicit function of $\boldsymbol{x}, t$, *as well as* an implicit function through the wavevector dependence, $\boldsymbol{k} = \boldsymbol{k}(\boldsymbol{x}, t)$.

Recall from Section 50.2 that there is a relation between the wave phase, $\mathcal{P}$, the local angular frequency, $\omega = -\partial_t\mathcal{P}$, and the local wavevector, $\boldsymbol{k} = \nabla\mathcal{P}$. Inserting these identities into the local dispersion relation (50.21) leads to the *eikonal equation*, which is a nonlinear partial differential equation for the phase[4]

$$\partial_t\mathcal{P} + \varpi(\boldsymbol{x}, t, \nabla\mathcal{P}) = 0. \tag{50.22}$$

This equation is formally the same as the *Hamilton-Jacobi* equation of classical mechanics, yet with ϖ playing the role of the Hamiltonian (e.g., *Marion and Thornton* (1988) or *Goldstein* (1980)). That analogy offers suggestions for how to make use of this equation. Note that on *Olbers et al.* (2012) (see their page 168) write the eikonal equation in the alternative form

$$(\partial_t\mathcal{P})^2 = C_{\mathsf{p}}^2\,(\nabla\mathcal{P})^2, \tag{50.23}$$

which follows from the definition of the local phase speed in equation (50.19).

50.3.2 Rays are integral curves of the group velocity

A *ray* is an integral curve of the group velocity. Hence, the ray trajectory, $\boldsymbol{X}(t)$, follows a ray and is determined by solving the ordinary differential equation

$$\frac{\mathrm{D}_t\boldsymbol{X}}{\mathrm{D}t} = \boldsymbol{c}_{\mathsf{g}}. \tag{50.24}$$

[3] In Section 46.3.1 we provide a detailed discussion of these derivatives, with that discussion suited to the present discussion of geometric optics.

[4] As per page 362 of *Thorne and Blandford* (2017).

The time derivative, $\mathrm{D}_r/\mathrm{D}t$, determines time changes when following a ray, and so it is defined by this equation. Indeed, our specification of $\mathrm{D}_r/\mathrm{D}t$ and $\boldsymbol{c}_g$ correspond precisely to how we defined the trajectory of a fluid particle as the integral curve of the fluid velocity as per equation (17.66a). Introducing the dispersion relation leads to

$$\frac{\mathrm{D}_r \boldsymbol{X}}{\mathrm{D}t} = \boldsymbol{c}_g = \nabla_{\boldsymbol{k}} \varpi(\boldsymbol{x}, t, \boldsymbol{k}). \tag{50.25}$$

Writing this equation in component form

$$\frac{\mathrm{D}_r X^a}{\mathrm{D}t} = c_g^a = \left[\frac{\partial \varpi(\boldsymbol{x}, t, \boldsymbol{k})}{\partial k_a}\right]_{\boldsymbol{x},t} \tag{50.26}$$

emphasizes that the derivative is computed while holding the space and time point fixed while varying the wavevector.

50.3.3 Evolution of $\boldsymbol{k}$ along a ray

To determine the evolution of the wavevector and angular frequency along a ray, we start with the following identity that holds for the phase function, $\mathcal{P} = \mathcal{P}(\boldsymbol{x}, t)$, merely since the partial derivatives commute

$$\nabla(\partial_t \mathcal{P}) = \partial_t(\nabla \mathcal{P}). \tag{50.27}$$

The derivatives in this equation are taken with their complementary variables fixed, and this point is important when inserting the dispersion relation. Indeed, before working through the following manipulations it can be useful to reread Section 50.3.1 to be reminded of the various functional relationships.

Exposing subscripts for clarity, we start from equation (50.27) to write

$$\begin{aligned}
\frac{\partial}{\partial t}\Big]_{\boldsymbol{x}} \left[\frac{\partial \mathcal{P}}{\partial x^a}\right]_t &= \left[\frac{\partial k_a}{\partial t}\right]_{\boldsymbol{x}} && \text{equation (50.2)} && \text{(50.28a)}\\
&= -\left[\frac{\partial \omega(\boldsymbol{x}, t)}{\partial x^a}\right]_t && \text{equation (50.27)} && \text{(50.28b)}\\
&= -\left[\frac{\partial \varpi(\boldsymbol{x}, t, \boldsymbol{k})}{\partial x^a}\right]_t && \text{equation (50.21)} && \text{(50.28c)}\\
&= -\left[\frac{\partial \varpi(\boldsymbol{x}, t, \boldsymbol{k})}{\partial k_b}\right]_{\boldsymbol{x},t} \left[\frac{\partial k_b}{\partial x^a}\right]_t - \left[\frac{\partial \varpi(\boldsymbol{x}, t, \boldsymbol{k})}{\partial x^a}\right]_{\boldsymbol{k},t} && \text{chain rule} && \text{(50.28d)}\\
&= -c_g^b \left[\frac{\partial k_b}{\partial x^a}\right]_t - \left[\frac{\partial \varpi(\boldsymbol{x}, t, \boldsymbol{k})}{\partial x^a}\right]_{\boldsymbol{k},t} && \text{equation (50.25).} && \text{(50.28e)}
\end{aligned}$$

We can massage the first right hand side term in equation (50.28e) by commuting partial derivatives

$$\frac{\partial k_b}{\partial x^a} = \frac{\partial^2 \mathcal{P}}{\partial x^b \, \partial x^a} = \frac{\partial k_a}{\partial x^b}, \tag{50.29}$$

so that

$$\left[\frac{\partial k_a}{\partial t}\right]_{\boldsymbol{x}} = -(\boldsymbol{c}_g \cdot \nabla) k_a - \left[\frac{\partial \varpi(\boldsymbol{x}, t, \boldsymbol{k})}{\partial x^a}\right]_{\boldsymbol{k},t}. \tag{50.30}$$

Introducing the time derivative following a ray renders the wavevector evolution equation

$$\frac{\mathrm{D}_r k_a}{\mathrm{D}t} = -\left[\frac{\partial \varpi(\boldsymbol{x}, t, \boldsymbol{k})}{\partial x^a}\right]_{\boldsymbol{k},t}. \tag{50.31}$$

Evidently, if the dispersion relation has no explicit dependence on x^a, then the corresponding component of the wavevector remains constant when following a ray. However, if there is a dependence, then the wavevector evolves along the ray, with this evolution known as *refraction*.

50.3.4 Evolution of ω along a ray

Being a bit more streamlined than in Section 50.3.3, we compute the time derivative of the angular frequency

$$-\frac{\partial^2 \mathcal{P}}{\partial t^2} = \left[\frac{\partial \omega}{\partial t}\right]_{\boldsymbol{x}} \tag{50.32a}$$

$$= \left[\frac{\partial \varpi}{\partial t}\right]_{\boldsymbol{x}} \tag{50.32b}$$

$$= \left[\frac{\partial \varpi}{\partial k_b}\right]_{\boldsymbol{x},t} \left[\frac{\partial k_b}{\partial t}\right]_{\boldsymbol{x}} + \left[\frac{\partial \varpi}{\partial t}\right]_{\boldsymbol{x},\boldsymbol{k}} \tag{50.32c}$$

$$= -c_{\mathrm{g}}^b \left[\frac{\partial \omega}{\partial x^b}\right]_t + \left[\frac{\partial \varpi}{\partial t}\right]_{\boldsymbol{x},\boldsymbol{k}}, \tag{50.32d}$$

where the final step used

$$\left[\frac{\partial k_b}{\partial t}\right]_{\boldsymbol{x}} = \frac{\partial^2 \mathcal{P}}{\partial t\, \partial x^b} = \frac{\partial}{\partial x^b}\frac{\partial \mathcal{P}}{\partial t} = -\left[\frac{\partial \omega}{\partial x^b}\right]_t. \tag{50.33}$$

We are thus lead to the evolution equation for the angular frequency along a ray

$$\frac{\mathrm{D}_t \omega}{\mathrm{D}t} = \left[\frac{\partial \varpi}{\partial t}\right]_{\boldsymbol{x},\boldsymbol{k}}. \tag{50.34}$$

Evidently, if the dispersion relation has no explicit dependence on time, then the angular frequency is a constant following a ray. For example, this is the situation when gravity waves approach a beach, assuming the slope of the beach is static (considered in Section 52.7.1). For this example, the angular frequency of gravity waves remains constant following a ray, whereas the wavevector changes according to equation (50.31).

50.3.5 Changes in the phase following a ray

Considering the phase function to be a function of space and time, $\mathcal{P}(\boldsymbol{x}, t)$, we compute its time derivative along a ray according to

$$\mathrm{D}_r\mathcal{P}/\mathrm{D}t = (\partial_t + \boldsymbol{c}_{\mathrm{g}} \cdot \nabla)\,\mathcal{P} = -\omega + \boldsymbol{c}_{\mathrm{g}} \cdot \boldsymbol{k} = \boldsymbol{k} \cdot (-\boldsymbol{c}_{\mathrm{p}} + \boldsymbol{c}_{\mathrm{g}}), \tag{50.35}$$

where $\omega = -\partial_t \mathcal{P} = \boldsymbol{c}_{\mathrm{p}} \cdot \boldsymbol{k}$, as per equations (50.17) and (50.18), and $\boldsymbol{k} = \nabla_{\boldsymbol{x}} \mathcal{P}$ as per equation (50.2). Non-dispersive have a phase that remains unchanged when following a ray, which holds so long as

$$\boldsymbol{k} \cdot \boldsymbol{c}_{\mathrm{p}} = \boldsymbol{k} \cdot \boldsymbol{c}_{\mathrm{g}} \quad \text{non-dispersive waves.} \tag{50.36}$$

Otherwise, for dispersive waves the phase changes according to the source term, $\boldsymbol{k} \cdot (-\boldsymbol{c}_{\mathrm{p}} + \boldsymbol{c}_{\mathrm{g}})$.

50.3.6 Summary of the ray equations

We here summarize the evolution equations for wave properties derived thus far in this chapter, with these equations constituting *Hamilton's equations for rays*

$$\frac{\mathrm{D}_r \boldsymbol{X}}{\mathrm{D}t} = \boldsymbol{c}_\mathrm{g} \qquad \text{trajectory on a ray} \quad (50.37a)$$

$$\frac{\mathrm{D}_r \mathcal{P}}{\mathrm{D}t} = \boldsymbol{k}\cdot(-\boldsymbol{c}_\mathrm{p}+\boldsymbol{c}_\mathrm{g}) \iff \partial_t \mathcal{P} + \varpi(\boldsymbol{x},t,\nabla\mathcal{P}) = 0 \qquad \text{eikonal equation for phase} \quad (50.37b)$$

$$\frac{\mathrm{D}_r \boldsymbol{k}}{\mathrm{D}t} = -\left[\frac{\partial \varpi}{\partial \boldsymbol{x}}\right]_{t,\boldsymbol{k}} \qquad \boldsymbol{k} \text{ evolution on a ray} \quad (50.37c)$$

$$\frac{\mathrm{D}_r \omega}{\mathrm{D}t} = \left[\frac{\partial \varpi}{\partial t}\right]_{\boldsymbol{x},\boldsymbol{k}} \qquad \omega \text{ evolution on a ray} \quad (50.37d)$$

$$\frac{\mathrm{D}_r}{\mathrm{D}t} = \partial_t + \boldsymbol{c}_\mathrm{g}\cdot\nabla \qquad \text{time derivative on a ray} \quad (50.37e)$$

$$\omega = -\partial_t \mathcal{P} \qquad \omega \text{ defined} \quad (50.37f)$$

$$\boldsymbol{k} = \nabla\mathcal{P} \qquad \boldsymbol{k} \text{ defined} \quad (50.37g)$$

$$\nabla\times\boldsymbol{k} = 0 \qquad \boldsymbol{k} \text{ consistency condition} \quad (50.37h)$$

$$\partial_t \boldsymbol{k} + \nabla\omega = 0 \qquad \text{conservation of wave crests.} \quad (50.37i)$$

Equation (50.37a) defines the rays as integral lines of the group velocity, $\boldsymbol{c}_\mathrm{g}$. Equation (50.37b) is the eikonal equation that connects the local angular frequency to the dispersion relation

$$\omega = -\partial_t \mathcal{P} = \varpi(\boldsymbol{x},t,\nabla\mathcal{P}). \quad (50.38)$$

Each of the evolution equations (50.37b)–(50.37d) is hyperbolic, which is notable since this property holds even though the wave equation describing the evolution of the wave function is not generally hyperbolic (particularly for dispersive waves).

By definition, the phase remains constant when following along a constant wave phase so that

$$(\partial_t + \boldsymbol{c}_\mathrm{p}\cdot\nabla)\,\mathcal{P} = 0. \quad (50.39)$$

However, for dispersive waves, equation (50.37b) indicates that the phase does not stay fixed when following rays as defined by the group velocity. Hence, wave crests pass through a point following the group velocity, such as a point fixed within a wave packet. Conversely, equations (50.37c) and (50.37d) show that for dispersive waves, the wavevector and angular frequency are not constant when following a constant wave phase. Instead, they remain fixed when following the group velocity in media where the dispersion relation is independent of space and time. For more general media, both the wavevector and angular frequency evolve even when following the group velocity.

50.3.7 Comments and further study

Knowledge of the dispersion relation is sufficient to solve the ray equations (typically using numerical methods), thus mapping the rays and paths of wave packets, and determining the wavevector, angular frequency, and phase following a ray. This procedure works quite well to describe waves moving through smoothly varying media, and is familiar from the rays of light bending through water or glass. Failure of the method occurs when the background media no longer satisfies the "gently varying" assumptions that are formalized in Section 50.5.3 for the case of a stretched string. Breaking these assumptions often results in the intersection of rays which, in many fluid applications, signals a nonlinear process such as a fluid instability and

corresponding turbulent mixing. Chapter 11 of *Whitham* (1974), Chapters 3 and 4 of *Bühler* (2014a), and the bulk of *Tracy et al.* (2014) provide more details and insights.

50.4 Hamilton's principle and the Euler-Lagrange equation

The geometric optics discussion in Section 50.3 is largely kinematic, with the only piece of dynamical information arising from the dispersion relation. To develop a theory for the energetics of waves and wave packets moving through gently varying background states, we make use of Hamilton's principle, or more specifically Whitham's variational principle applying to the phase averaged equations. We pursue that study in Section 50.5, yet here first summarize salient points from Lagrangian field theory from Chapter 46.

50.4.1 Stationary action $\Longleftrightarrow$ Euler-Lagrange equation

The *action*, $\mathcal{S}$, for a continuous scalar field, $\psi(\boldsymbol{x},t)$, is given by equation (46.13)

$$\mathcal{S} = \int_R \mathscr{L}(\psi, \partial_t\psi, \nabla\psi, \boldsymbol{x}, t)\, g\, \mathrm{d}^3x\, \mathrm{d}t, \tag{50.40}$$

where R is a space-time domain, g is the square root of the metric tensor determinant, and $\mathscr{L}$ is the *Lagrangian density*. The Lagrangian density is a functional of the field and its space-time derivatives (i.e., $\mathscr{L}$ is a function of a function). There can also be additional explicit dependencies on the space and time position, which occurs, in particular, for waves moving through a media that is inhomogeneous in space and/or non-stationary in time, in which case $\mathscr{L}$ is an explicit function of $(\boldsymbol{x},t)$. *Hamilton's principle* as stated by equation (46.18) says that variation of the action is stationary (i.e., variation of the action vanishes) for the physically realized field. Hamilton's principle then leads to the *Euler-Lagrange field equation* (46.24)

$$\frac{\partial\mathscr{L}}{\partial\psi} - \frac{1}{g}\frac{\partial}{\partial x^\alpha}\left[g\,\frac{\partial\mathscr{L}}{\partial(\partial_\alpha\psi)}\right] = 0, \tag{50.41}$$

where $\alpha = 0,1,2,3$ is the space-time label. In performing the partial derivative with respect to ψ and its derivatives, $\partial_\alpha\psi$, each of the other variables in the Lagrangian density are held fixed. However, when performing the space and time partial derivatives, ∂_α, we only maintain the complement space and time variable fixed. This technical point is very important when taking derivatives of the Lagrangian density (see Section Section 46.3.1), and it is directly analogous to how we take derivatives of the dispersion relation in Section 50.3.

50.4.2 Hamiltonian density and energy of the continuum

In Section 46.4.1 we introduced the *generalized momentum density*, $\mathscr{P}$, and the *Hamiltonian density*,

$$\mathscr{P} = \frac{\partial\mathscr{L}}{\partial(\partial_t\psi)} \quad \text{and} \quad \mathscr{H} = \mathscr{P}\,\partial_t\psi - \mathscr{L}. \tag{50.42}$$

We then showed that the Hamiltonian density satisfies the budget equation

$$\partial_t\mathscr{H} + \nabla\cdot\boldsymbol{\mathscr{F}} = -(\partial\mathscr{L}/\partial t)_{\psi,\partial_\alpha\psi,\boldsymbol{x}}, \tag{50.43}$$

where the time derivative on the right hand side is computed while fixing ψ, its space and time derivatives, and the space position, $\boldsymbol{x}$. Equation (50.43) also introduced the flux vector, $\boldsymbol{\mathscr{F}}$, with components

$$\mathscr{F}^a = \frac{\partial\mathscr{L}}{\partial(\partial_a\psi)}\frac{\partial\psi}{\partial t}. \tag{50.44}$$

In those cases where the Lagrangian has no explicit time dependence, so that it has the functional dependence

$$\mathscr{L} = \mathscr{L}(\psi, \partial_t \psi, \nabla \psi, \boldsymbol{x}), \tag{50.45}$$

then the Hamiltonian equation (50.43) becomes a conservation equation for energy that follows from time symmetry and Noether's theorem

$$\partial_t \mathscr{H} + \nabla \cdot \mathscr{F} = 0. \tag{50.46}$$

50.4.3 Stress-energy-momentum tensor

As detailed in Section 46.4, the energy equation (50.43) is but one piece of the equation satisfied by the stress-energy-momentum tensor, $T^{\alpha}{}_{\beta}$. This equation is given by equation (46.74)

$$\partial_\alpha T^{\alpha}{}_{\beta} = -\left[\frac{\partial \mathscr{L}}{\partial x^\beta}\right]_{\psi, \partial_\alpha \psi, x^{\alpha \neq \beta}}. \tag{50.47}$$

where the *stress-energy-momentum tensor* is

$$T^{\alpha}{}_{\beta} = -\delta^{\alpha}{}_{\beta}\, \mathscr{L} + \frac{\partial \mathscr{L}}{\partial_\alpha \psi} \frac{\partial \psi}{\partial x^\beta}. \tag{50.48}$$

50.5 Whitham's variational principle

The Euler-Lagrange field equation (50.41) and associated energy equation (50.43) provide the foundation for the field theory of continuous classical matter. In this section we specialize the field theory formalism for the purpose of describing waves and the movement of wave energy through a prescribed background environment. Much of this formalism was proposed by Whitham (e.g., see Chapter 11 of *Whitham* (1974)), so that we refer to the method as *Whitham's variational principle*. In other treatments, such as Section 2.2 of *Tracy et al.* (2014), it is referred to as the *reduced variational principle*.

We anticipated much of the material in this section when studying a pendulum with variable length in Section 15.2. In that section we showed that the pendulum energy divided by its frequency is an *adiabatic invariant*; i.e., it is nearly constant. In the present section we show that the *wave action* is the corresponding adiabatic invariant for waves moving on a gently varying background, with the wave action also equal to the energy (or Hamiltonian) divided by the angular frequency.

50.5.1 Some motivation

One practical motivation for developing Whitham's variational principle is to describe the energetics of waves propagating on a non-homogeneous and non-stationary background, though the formalism is also quite useful for homogeneous and stationary backgrounds, particularly for dispersive waves. In the presence of a space dependent background properties, there are no simple sinusoidal (plane) wave solutions. That is, Fourier methods are insufficient. Even so, there are waves that are quite close to plane waves *if* the space and time scales for changes in the background state are well separated from those describing the wave properties (frequency and wavelength). This space-time scale separation constitutes a "gently varying" background state, which in turn enables analytical progress. We introduced the scaling for this gentle background at the start of Section 50.2, and follow up in Section 50.5.3 with more details.

Whitham's method starts by inserting a wave ansatz into the Lagrangian density. Phase averaging then produces the *phase averaged Lagrangian* and corresponding *phase averaged action*.

We maintain only the leading order term in this phase average Lagrangian, and Whitham's variational principle then states that the physically realized wave produces a stationary wave averaged action. There are two associated Euler-Lagrange fields, one arising from varying the wave amplitude and the other from varying the wave phase.

50.5.2 The stretched string

Following *Bretherton and Garrett* (1969) and *Bretherton* (1971), we use a stretched string as a case study for exploring Whitham variational method. In particular, recall from Section 46.2.5 the Lagrangian density for the stretched string whose tension[5] is a function of time, $\tau = \tau(t)$, and whose mass density (mass per length) is a function of space, $\sigma = \sigma(x)$, is given by

$$\mathscr{L} = (1/2)[\sigma\,(\partial_t\psi)^2 - \tau\,(\partial_x\psi)^2], \tag{50.49}$$

and whose Hamiltonian density (50.42) is

$$\mathscr{H} = (1/2)[\sigma\,(\partial_t\psi)^2 + \tau\,(\partial_x\psi)^2]. \tag{50.50}$$

Note that $\psi(x,t)$ measures transverse displacements of the string from its equilibrium position at $\psi = 0$. We furthermore assume that there are no longitudinal waves along the string, thus focusing exclusively on transverse motion.

The action for the stretched string is

$$\mathcal{S} = \int \mathscr{L}\,\mathrm{d}x\,\mathrm{d}t = \int (1/2)\,[\sigma\,(\partial_t\psi)^2 - \tau\,(\partial_x\psi)^2]\,\mathrm{d}x\,\mathrm{d}t, \tag{50.51}$$

and the Euler-Lagrange equation resulting from Hamilton's principle is the wave equation

$$\delta\mathcal{S} = \int (\delta\mathscr{L})\,\mathrm{d}x\,\mathrm{d}t = 0 \Longleftrightarrow (\partial_{tt} - c^2\,\partial_{xx})\psi = 0, \tag{50.52}$$

with the squared wave speed

$$c^2(x,t) = \tau(t)/\sigma(x). \tag{50.53}$$

Because the wave speed is a function of space and time, we cannot use traditional Fourier methods to find a wave solution. Hence, the mathematical goal of this section is to develop methods for use when there are space and time variations of the background state, in particular when such variations are "gentle". In this case we are afforded the *eikonal wave ansatz*[6]

$$\psi(x,t) = A(x,t)\cos[\mathcal{P}(x,t)], \tag{50.54}$$

where $A > 0$ is a space-time dependent real amplitude function, and $\mathcal{P}$ is the phase function introduced in equation (50.2). We have more comments on this form for the wave ansatz in Section 50.5.4. s

50.5.3 Space and time scale separation

To make analytical progress requires us to detail the space and time scale separation between the linear waves and the background state, following from our introduction to this scaling at the start of Section 50.2. Although we here focus on the string, the same sorts of assumptions must

[5]The dimensions of τ are force, M L T^{-2}, but we refer to it as a tension since it is an internal force within the string.

[6]The ansatz (50.54) is commonly used with the WKBJ asymptotic method, and so is sometimes referred to as the WKBJ wave ansatz.

be realized for other waves systems in order to make use of the methods of this section. For the time scale, we assume that changes in the string tension occur over time sales that are much longer than the period of the linear waves supported by the string, so that

$$|\partial_t \tau/\tau| \ll |\partial_t \mathcal{P}|/2\pi = \omega/2\pi. \tag{50.55}$$

Correspondingly, temporal changes in the angular frequency are assumed to be on the same scale as temporal changes to the string tension

$$|\partial_t \omega/\omega| \sim |\partial_t \tau/\tau| \Longrightarrow |\partial_t \omega| \ll \omega^2/2\pi, \quad \text{or equivalently} \quad |\partial_{tt}\mathcal{P}| \ll (\partial_t \mathcal{P})^2/2\pi. \tag{50.56}$$

Likewise, time changes to the wave amplitude are defined by the background state so that

$$|\partial_t A/A| \sim |\partial_t \tau/\tau|. \tag{50.57}$$

For the length scale, we assume spatial changes in the mass density occur over scales that are large compared to the wavelength

$$|\partial_x \sigma/\sigma| \ll |\partial_x \mathcal{P}|/2\pi = |k|/2\pi, \tag{50.58}$$

and that spatial changes to the wavenumber and wave amplitude are on the same scale as changes to string mass density

$$|\partial_x k/k| \sim |\partial_x \sigma/\sigma| \Longrightarrow |\partial_x k| \ll k^2/2\pi \quad \text{or equivalently} \quad |\partial_{xx}\mathcal{P}| \ll (\partial_x \mathcal{P})^2/2\pi. \tag{50.59}$$

Likewise, space changes to the wave amplitude are defined by the background state so that

$$|\partial_x A/A| \sim |\partial_x \sigma/\sigma|. \tag{50.60}$$

50.5.4 The leading order phase averaged action

The space and time scale separation from Section 50.5.3 motivate the wave ansatz (50.54). Note that a more general ansatz might also consider a space-time dependent phase shift. We do not consider a phase shift since we are concerned with leading order evolution of the wave amplitude, and the extra phase degree of freedom is not directly tied to the amplitude. Furthermore, we could have expanded the amplitude function into an asymptotic series. But again, we are only interested in the leading order, with the ansatz (50.54) sufficient for that purpose.[7]

Leading order contribution to $\sigma\,(\partial_t \psi)^2$

To determine the leading order terms contributing to the Lagrangian (50.49), we start with the squared time tendency of the wave function

$$(\partial_t \psi)^2 = (\partial_t A \cos \mathcal{P})^2 + (A\,\partial_t \mathcal{P} \sin \mathcal{P})^2 - 2\,(A\,\partial_t \mathcal{P}\,\partial_t A \sin \mathcal{P} \cos \mathcal{P}), \tag{50.61}$$

which has a phase average

$$\langle \sigma\,(\partial_t \psi)^2 \rangle = \sigma\,[(\partial_t A)^2 + (A\,\partial_t \mathcal{P})^2]/2. \tag{50.62}$$

To compute the phase average we assumed that σ, $\partial_t A$, and $\partial_t \mathcal{P} = -\omega$ are roughly constant over the course of a 2π change in the phase, with this assumption following from the scaling in

[7] See Section 4 of *Bretherton* (1971) for more details of the phase shift and amplitude expansion.

Section 50.5.3. Further use of the scaling in Section 50.5.3 leads to the leading order contribution

$$\langle \sigma \, (\partial_t \psi)^2 \rangle \approx \sigma \, (A \, \partial_t \mathcal{P})^2 / 2 = \sigma \, A^2 \, \omega^2 / 2. \tag{50.63}$$

Leading order contribution to $\tau \, (\partial_x \psi)^2$

Proceeding just as above, the squared space derivative term in the Lagrangian (50.49) is given by

$$(\partial_x \psi)^2 = (\partial_x A \cos \mathcal{P})^2 + (A \, \partial_x \mathcal{P} \sin \mathcal{P})^2 - 2 \, (A \, \partial_x \mathcal{P} \, \partial_x A \sin \mathcal{P} \cos \mathcal{P}), \tag{50.64}$$

whose phase average is

$$\langle \tau \, (\partial_x \psi)^2 \rangle = \tau \, [(\partial_x A)^2 + (A \, \partial_x \mathcal{P})^2] / 2. \tag{50.65}$$

To compute the phase average we assumed that τ, $\partial_x A$, and $\partial_x \mathcal{P} = k$ are roughly constant over the course of a 2π change in the phase, with this assumption following from the scaling in Section 50.5.3. Further using the scaling in Section 50.5.3 we are led to the leading order contribution

$$\langle \tau \, (\partial_x \psi)^2 \rangle \approx \tau \, (A \, \partial_x \mathcal{P})^2 / 2 = \tau \, A^2 \, k^2 / 2. \tag{50.66}$$

Leading order phase averaged action

The above discussion provides the leading order phase averaged action

$$\langle \mathcal{S} \rangle = \frac{1}{4} \int A^2 \, (\sigma \, \omega^2 - \tau \, k^2) \, \mathrm{d}x \, \mathrm{d}t = \int \langle \mathcal{L} \rangle \, \mathrm{d}x \, \mathrm{d}t. \tag{50.67}$$

This phase averaged Lagrangian is directly analogous to the phase averaged Lagrangian (15.44) for the pendulum whose length is slowly varying.

50.5.5 Whitham's variational principle for the string

Whitham's variational principle states that the phase averaged action, $\langle \mathcal{S} \rangle$, is stationary when $\psi = A \cos \mathcal{P}$ is the physically realized wave function. To find the associated Euler-Lagrange equations requires computing the variation of the action, which in turn requires varying the wave function. Variations in the wave function arise from arbitrary smooth and independent variations (with compact support) of the amplitude, A, and the phase, $\mathcal{P}$. Hence, the phase averaged action must be stationary with respect to independent variations in both A and $\mathcal{P}$. As we see in the following, the dispersion relation is the Euler-Lagrange equation resulting from $\delta_A \langle \mathcal{S} \rangle = 0$, whereas *wave action* conservation results from $\delta_{\mathcal{P}} \langle \mathcal{S} \rangle = 0$.

Vanishing variation with respect to A is equivalent to the dispersion relation

Variation of the phase averaged action (50.67) under variations in the wave amplitude is given by

$$\delta_A \langle \mathcal{S} \rangle = \frac{1}{2} \int (\sigma \, \omega^2 - \tau \, k^2) \, A \, \delta A \, \mathrm{d}x \, \mathrm{d}t, \tag{50.68}$$

and with a zero variation leading to

$$\delta_A \langle \mathcal{S} \rangle = 0 \iff \omega^2 = (\sigma / \tau)^2 \, k^2 = c^2 \, k^2. \tag{50.69}$$

Evidently, satisfying the dispersion relation is equivalent to a zero variation of the phase averaged action with respect to the wave amplitude. Furthermore, since $\langle \mathcal{L} \rangle$ is proportional to the squared wave amplitude, then satisfying the dispersion relation (50.69) means that the phase averaged

Lagrangian vanishes when evaluated with the physical solution,

$$\langle \mathcal{L} \rangle = A^2 \, (\sigma \, \omega^2 - \tau \, k^2)/4 = 0. \tag{50.70}$$

Vanishing variation with respect to $\mathcal{P}$

Variation of the phase averaged action (50.67) under variations in the wave phase function is given by

$$\delta_{\mathcal{P}} \langle \mathcal{S} \rangle = \frac{1}{2} \int A^2 \, (\sigma \, \omega \, \delta\omega - \tau \, k \, \delta k) \, \mathrm{d}x \, \mathrm{d}t = \frac{1}{2} \int A^2 \, [\sigma \, \partial_t \mathcal{P} \, \delta(\partial_t \mathcal{P}) - \tau \, \partial_x \mathcal{P} \, \delta(\partial_x \mathcal{P})] \, \mathrm{d}x \, \mathrm{d}t, \tag{50.71}$$

with rearrangement giving

$$\begin{aligned} \delta_{\mathcal{P}} \langle \mathcal{S} \rangle = \frac{1}{2} \int A^2 \, \left[\partial_t (A^2 \, \sigma \, \partial_t \mathcal{P} \, \delta\mathcal{P}) - \partial_x (A^2 \, \tau \, \partial_x \mathcal{P} \, \delta\mathcal{P}) \right] \mathrm{d}x \, \mathrm{d}t \\ - \frac{1}{2} \int A^2 \left[\partial_t (A^2 \, \sigma \, \partial_t \mathcal{P}) \, \delta\mathcal{P} - \partial_x (A^2 \, \tau \, \partial_x \mathcal{P}) \, \delta\mathcal{P} \right] \mathrm{d}x \, \mathrm{d}t. \end{aligned} \tag{50.72}$$

Assuming $\delta\mathcal{P}$ vanishes on the space-time boundaries, or that it has compact support in space and time, eliminates the first integral to leave

$$\delta_{\mathcal{P}} \langle \mathcal{S} \rangle = -\frac{1}{2} \int A^2 \left[\partial_t (A^2 \, \sigma \, \partial_t \mathcal{P}) - \partial_x (A^2 \, \tau \, \partial_x \mathcal{P}) \right] \delta\mathcal{P} \, \mathrm{d}x \, \mathrm{d}t, \tag{50.73}$$

with Whitham's principle $\delta_{\mathcal{P}} \langle \mathcal{S} \rangle = 0$ producing the conservation law

$$\delta_{\mathcal{P}} \langle \mathcal{S} \rangle = 0 \Longrightarrow \partial_t (A^2 \, \sigma \, \omega) + \partial_x (A^2 \, \tau \, k) = 0. \tag{50.74}$$

Interpretation of this conservation law follows from the discussion in the remainder of this Section.

50.5.6 Phase averaged Hamiltonian

Making use of the eikonal wave ansatz (50.54) renders the leading order phase averaged Hamiltonian (50.50)

$$\langle \mathcal{H} \rangle = A^2 \, (\sigma \, \omega^2 + \tau \, k^2)/4, \tag{50.75}$$

with the dispersion relation (50.69) yielding

$$\langle \mathcal{H} \rangle = A^2 \, \sigma \, \omega^2/2 = A^2 \, \tau \, k^2/2. \tag{50.76}$$

We can use these expressions to write the conservation law (50.74) as

$$\partial_t (\langle \mathcal{H} \rangle / \omega) + \partial_x (\langle \mathcal{H} \rangle / k) = 0. \tag{50.77}$$

This equation is nearly ready for interpretation, but it aided by the discussion in Section 50.5.7.

50.5.7 A general statement of Whitham's variational principle

To help interpret the conservation law (50.77), it is useful to provide a generic expression of Whitham's variational principle, which we write as

$$\delta \int \langle \mathcal{L} \rangle (A, \omega, k; \sigma, \tau) \, \mathrm{d}x \, \mathrm{d}t = \delta \int \langle \mathcal{L} \rangle (A, -\partial_t \mathcal{P}, \partial_x \mathcal{P}; \sigma, \tau) \, \mathrm{d}x \, \mathrm{d}t = \int \delta \langle \mathcal{L} \rangle \, \mathrm{d}x \, \mathrm{d}t = 0. \tag{50.78}$$

The resulting Euler-Lagrange equations follow through variations of the wave amplitude, A, and phase function, $\mathcal{P}$.

Varying the wave amplitude and the dispersion relation

The Euler-Lagrange equation resulting from varying the amplitude is written (see equation (50.41))

$$\frac{\delta \mathcal{S}}{\delta A} = \frac{\partial \langle \mathcal{L} \rangle}{\partial A} - \frac{\partial}{\partial t}\left[\frac{\partial \langle \mathcal{L} \rangle}{\partial (\partial_t A)}\right] - \frac{\partial}{\partial x}\left[\frac{\partial \langle \mathcal{L} \rangle}{\partial (\partial_x A)}\right] = 0. \tag{50.79}$$

Notably, for linear waves the wave amplitude appears in $\langle \mathcal{L} \rangle$ only via its square, A^2, so that the second and third terms in equation (50.79) vanish identically. As a result, the Euler-Lagrange equation resulting from varying A is

$$\frac{\partial \langle \mathcal{L} \rangle}{\partial A} = 0, \tag{50.80}$$

which, as we saw for the stretched string in Section 50.5.5, is equivalaent to the dispersion relation connecting the wave angular frequency to the wavevector. Another way to write the dispersion relation is to note that the phase averaged Lagrangian for linear waves satisfies

$$A\, \partial \langle \mathcal{L} \rangle / \partial A = 2 \langle \mathcal{L} \rangle, \tag{50.81}$$

so that

$$\langle \mathcal{L} \rangle = 0 \Longleftrightarrow \text{dispersion relation}. \tag{50.82}$$

Varying the phase function, group velocity, and conservation of wave action

For linear waves, the phase function only appears in terms of its space and time derivatives, so that $\partial \langle \mathcal{L} \rangle / \partial \mathcal{P} = 0$, in which case the Euler-Lagrange equation resulting from varying the phase function is given by

$$\frac{\delta \mathcal{S}}{\delta \mathcal{P}} = \frac{\partial}{\partial t}\left[\frac{\partial \langle \mathcal{L} \rangle}{\partial (\partial_t \mathcal{P})}\right] + \frac{\partial}{\partial x}\left[\frac{\partial \langle \mathcal{L} \rangle}{\partial (\partial_x \mathcal{P})}\right] = 0 \Longrightarrow -\frac{\partial}{\partial t}\left[\frac{\partial \langle \mathcal{L} \rangle}{\partial \omega}\right] + \frac{\partial}{\partial x}\left[\frac{\partial \langle \mathcal{L} \rangle}{\partial k}\right] = 0. \tag{50.83}$$

We can write this conservation equation in a slightly different form by introducing the group velocity. For this purpose, consider the implications for a zero variation of the phase averaged Lagrangian (another way to state Whitham's principle as in equation (50.78)) so that

$$0 = \delta \langle \mathcal{L} \rangle = \frac{\partial \langle \mathcal{L} \rangle}{\partial A}\, \delta A + \frac{\partial \langle \mathcal{L} \rangle}{\partial \omega}\, \delta \omega + \frac{\partial \langle \mathcal{L} \rangle}{\partial k}\, \delta k = \frac{\partial \langle \mathcal{L} \rangle}{\partial \omega}\, \delta \omega + \frac{\partial \langle \mathcal{L} \rangle}{\partial k}\, \delta k, \tag{50.84}$$

where $\partial \langle \mathcal{L} \rangle / \partial A = 0$ follows from equation (50.80). Rearrangement allows us to write the group velocity in terms of derivatives of the phase averaged Lagrangian

$$c_{\mathrm{g}} = \delta \omega / \delta k = -\frac{\partial \langle \mathcal{L} \rangle / \partial k}{\partial \langle \mathcal{L} \rangle / \partial \omega}, \tag{50.85}$$

so that the Euler-Lagrange equation (50.83) can be written in the form of a traditional conservation law

$$\partial_t \mathcal{A} + \partial_x (c_{\mathrm{g}}\, \mathcal{A}) = 0, \tag{50.86}$$

where we defined the *wave action*

$$\mathcal{A} \equiv \frac{\partial \langle \mathcal{L} \rangle}{\partial \omega}. \tag{50.87}$$

Note that for some applications it is more useful to write the wave action equation (50.86) following the group velocity, so that

$$\frac{\mathrm{D}_{\mathrm{r}}\mathcal{A}}{\mathrm{D}t} = -\mathcal{A}\,\partial_x c_{\mathrm{g}}. \tag{50.88}$$

Hence, the wave action evolves following a ray when moving through regions where the group velocity has a nonzero convergence.

50.5.8 Interpreting the string's wave action conservation equation

For the string, we find

$$\partial\langle\mathcal{L}\rangle/\partial\omega = A^2\,\sigma\,\omega/2 = \langle\mathscr{H}\rangle/\omega = \mathcal{A}, \tag{50.89}$$

so that the wave action conservation law (50.87) can be written in terms of the Hamiltonian

$$\partial_t(\langle\mathscr{H}\rangle/\omega) + \partial_x(c_{\mathrm{g}}\,\langle\mathscr{H}\rangle/\omega) = 0, \tag{50.90}$$

which accords with equation (50.77) given that the string is non-dispersive so that the group velocity is $c_{\mathrm{g}} = \omega/k$.

So in summary, the Euler-Lagrange equation arising from $\delta_{\mathcal{P}}\langle\mathcal{S}\rangle = 0$ leads to the wave action conservation law (50.90). This conservation law is associated with a symmetry of the phase averaged Lagrangian; namely, it is has no explicit dependence on the phase so that $\partial\langle\mathcal{L}\rangle/\partial\mathcal{P} = 0$. Whereas mechanical energy satisfies a conservation law when the background state is time-independent (i.e., the Lagrangian has no explicit time dependence), the wave action satisfies a conservation law since the phase averaged Lagrangian has no explicit dependence on the phase.

50.5.9 Comments

Although the presentation in this section used the relatively simple case of a stretched string, the underlying theory holds for all linear waves. As such, we expand our understanding of the theory when considering waves of more complexity in the following chapters. In particular, the theory proves quite useful for organizing our thinking about group velocity and wave energetics, particularly for dispersive waves whether on a stationary and homogeneous background or more generally.

50.6 Variational methods for self-adjoint wave operators

Our use of variational methods for waves is concerned with the propagation of wave packets through a gently varying and prescribed background state. We assume the packet is prepared at some initial time and fully known at the final time, so that variations of the wave function (as per Hamilton's principle) are nonzero only at intermediate times. Likewise, we assume the packet is specified at the spatial boundaries, so that its variation vanishes there as well. With these assumptions, we here detail a variational method that makes use of the self-adjoint nature of the wave operator. By exploiting the self-adjoint property, we can reformulate Whitham's variational principle from Section 50.5.

50.6.1 Self-adjoint linear wave operators

Assuming Cartesian coordinates, the Euler-Lagrange equations for the acoustic and Klein-Gordon wave equations from Section 46.2.5 can be written

$$\frac{\delta \mathcal{S}}{\delta \psi} = \frac{\partial \mathcal{L}}{\partial \psi} - \frac{\partial}{\partial x^\alpha}\left[\frac{\partial \mathcal{L}}{\partial(\partial_\alpha \psi)}\right] = \widehat{D}\psi = 0, \tag{50.91}$$

where $\widehat{D}$ is the linear partial differential operator,

$$\widehat{D} = -(\partial_{tt} - c^2\,\nabla^2 + \Gamma^2), \tag{50.92}$$

for the Klein-Gordon wave equation with constant c, and with $\Gamma = 0$ for the acoustic wave equation. This result allows us to write the action for this, and other, linear non-dissipative waves in the bilinear form

$$\mathcal{S} = \frac{1}{2}\int_{\mathrm{R}} \psi\,(\widehat{D}\psi)\,\mathrm{d}^3x\,\mathrm{d}t. \tag{50.93}$$

Notably, this action vanishes identically when ψ is a solution to the wave equation, as per equation (50.91), yet the action is non-zero for a general function.

50.6.2 Varying the action

Variation of the action (50.93) can be written

$$2\,\delta\mathcal{S} = \int_{\mathrm{R}} (\delta\psi)\,\widehat{D}\psi\,\mathrm{d}^3x\,\mathrm{d}t + \int_{\mathrm{R}} \psi\,(\widehat{D}\delta\psi)\,\mathrm{d}^3x\,\mathrm{d}t, \tag{50.94}$$

with integration by parts bringing the second right hand side term into the form

$$\begin{aligned}\int_{\mathrm{R}} \psi\,(\widehat{D}\delta\psi)\,\mathrm{d}^3x\,\mathrm{d}t &= \int_{\mathrm{R}} \delta\psi\,(\widehat{D}\psi)\,\mathrm{d}^3x\,\mathrm{d}t \\ &\quad - \int_{\mathrm{R}} \partial_t(\psi\,\partial_t\delta\psi - \delta\psi\,\partial_t\psi)\,\mathrm{d}^3x\,\mathrm{d}t + c^2\int_{\mathrm{R}} \delta^{ab}\partial_b(\psi\,\partial_a\delta\psi - \delta\psi\,\partial_a\psi)\,\mathrm{d}^3x\,\mathrm{d}t.\end{aligned} \tag{50.95}$$

For Hamilton's principle, we assume that $\delta\psi = 0$ at the temporal endpoints, so that

$$\int_{\mathrm{R}} \partial_t(\delta\psi\,\partial_t\psi)\,\mathrm{d}^3x\,\mathrm{d}t = 0. \tag{50.96}$$

Likewise, the term

$$\int_{\mathrm{R}} \delta^{ab}\partial_b(\delta\psi\,\partial_a\psi)\,\mathrm{d}^3x\,\mathrm{d}t = \int_{\mathrm{R}} \nabla\cdot(\delta\psi\,\nabla\psi)\,\mathrm{d}^3x\,\mathrm{d}t, \tag{50.97}$$

vanishes if $\delta\psi = 0$ on the spatial boundaries, or if the physically realized field satisfies the natural boundary conditions

$$\hat{\boldsymbol{n}}\cdot\nabla\psi = 0 \quad \text{for } \boldsymbol{x} \in \partial\mathcal{R}. \tag{50.98}$$

We are thus led to the variation

$$\int_{\mathrm{R}} \psi\,(\widehat{D}\delta\psi)\,\mathrm{d}^3x\,\mathrm{d}t = \int_{\mathrm{R}} \delta\psi\,(\widehat{D}\psi)\,\mathrm{d}^3x\,\mathrm{d}t + \int_{\mathrm{R}} [-\partial_t(\psi\,\partial_t\delta\psi) + c^2\,\delta^{ab}\,\partial_b(\psi\,\partial_a\delta\psi)]\,\mathrm{d}^3x\,\mathrm{d}t. \tag{50.99}$$

We can eliminate the remaining boundary terms as follows. The temporal boundary term vanishes if we assume either ψ or $\delta(\partial_t\psi)$ vanishes at temporal boundaries. We assume either of these conditions holds. Likewise, the spatial boundary term vanishes if ψ or $\delta(\partial_a\psi)$ vanishes at

the spatial boundaries.[8] Assuming the boundary conditions indeed vanish makes $\widehat{D}$ a self-adjoint wave operator, thus bringing about the action variation

$$\delta \mathcal{S} = \int_{\mathrm{R}} (\delta\psi)\, \widehat{D}\psi \, \mathrm{d}^3x \, \mathrm{d}t, \tag{50.100}$$

with Hamilton's principle, $\delta\mathcal{S} = 0$, again leading to the wave equation, $\widehat{D}\psi = 0$.

50.6.3 Comments on the method

The above presentation is a bit circular since we compute the wave operator, $\widehat{D}$, from the Euler-Lagrange equation, and the Euler-Lagrange equation requires the Lagrangian density, $\mathcal{L}$. However, the discussion suggests a complementary means to connect the variational framework of Hamilton's principle to the study of linear waves. Namely, all we need is the linear self-adjoint wave operator, $\widehat{D}$, rather than the Lagrangian density, $\mathcal{L}$. This approach is useful particularly for those cases where the Lagrangian is tricky to determine. For example, the Lagrangian for Rossby waves requires the introduction of auxiliary fields (see page 293 of *Olbers et al.* (2012)). So by writing the action in the form of equation (50.93), we directly connect the variational framework to the study of linear waves via knowledge of the wave operator rather than the wave Lagrangian. We offer examples throughout the chapters in this part of the book. One important caveat is that the action for some wave systems cannot be written in the bilinear form (50.93), such as the interface waves from Chapter 52, in which case distinct methods are needed (see Section 52.2.9).

We also note the need to assume boundary conditions that ensure the wave operator is self-adjoint. These boundary conditions are somewhat restrictive. Even so, they allow us to focus on the form of the waves in the interior of the space-time domain, rather than be concerned with initia-boundary conditions.

[8] In considering these boundary conditions when, recall that δ for Hamilton's principle commutes with space and time derivatives, as detailed in Section 46.2.2.

Chapter 51

Acoustic waves

In this chapter we study the physics of *acoustic waves* in fluids. When reaching the human ear we interpret acoustic waves as sound, hence the synonymous term *sound waves*. The pressure fluctuations associated with standard acoustic waves (those not damaging to the human ear) are a tiny fraction of those arising from, say, a weather disturbance or an atmospheric gravity wave (see Section 51.5.3 for details). Hence, acoustic waves play a negligible role in the geophysical fluid flows forming the focus of this book. Nonetheless, the relative simplicity of acoustic waves, and their ubiquitous presence in the natural environment, make them an ideal pedagogical introduction to the somewhat more complex geophysical waves considered in later chapters. Here, we study acoustic waves in a perfect compressible fluid where the only force arises from pressure, thus ignoring gravity, Coriolis, and viscous friction. We derive the acoustic wave equation using both Lagrangian and Eulerian viewpoints, and thereafter study various properties of acoustic waves, including their energetics.

READER'S GUIDE TO THIS CHAPTER

Development of the linear equations for acoustic waves relies on the momentum dynamics from Chapter 24, and the acoustic energetics makes use of thermodynamics from Chapters 22, 23, and 26. Furthermore, we assume an understanding of wave kinematics from Chapter 49. As a useful conceptual preface, see Sections 15.6 and 15.7 where we study simple harmonic oscillators, as well as Section 46.1 where we take the continuum limit of the oscillators to reveal the acoustic wave equation.

There are many treatments of acoustic waves in the literature, and we made use of Chapter VIII in *Landau and Lifshitz* (1987), Chapter 9 in *Fetter and Walecka* (2003), Section 15.2 of *Kundu et al.* (2016), and Section 16.5 in *Thorne and Blandford* (2017). Additionally, the second half of this video offers a pedagogical introduction to acoustic waves.

51.1 Loose threads

- Need the solution to Exercise 51.3.

51.2 Conceptual introduction to acoustic waves

Physical processes giving rise to acoustic waves

Consider a static background fluid state that is in mechanical and thermodynamic equilibrium. Acoustic waves involve four physical processes within this background state: (i) the density in a compressible fluid changes according to flow divergences and convergences; (ii) density fluctuations lead to pressure fluctuations; (iii) pressure fluctuations lead to fluid particle fluctuations; (iv) for small amplitude fluctuations, fluid particle displacements exhibit space-time coherent oscillatory motion known as linear acoustic waves. Small fluctuations correspond to a fluid particle speed that is much smaller than the acoustic wave speed, with the ratio known as the *Mach number* (we see this relation in Section 51.5.2). Hence, we are concerned only with small Mach number flow in this chapter. As such, acoustic wave properties such as the wave momentum and wave energy are transmitted at a much greater speed than the transport of properties arising from fluid particle motion (e.g., enthalpy and mass transport). Furthermore, we find that fluid particles feeling the passage of an acoustic wave oscillate in the direction of the wave, with the alignment of the fluid velocity and wave direction characterizing *longitudinal waves*.

The alternating compression and rarefaction of fluid elements within an acoustic wave give rise to alternating pressure work that affects the internal energy. For small Mach number flow, acoustic waves can be assumed to be isentropic, so that the pressure work is reversible. We make use of perfect fluid mechanics throughout this chapter, thus ignoring mixing and heating so that fluid elements maintain constant specific entropy. Indeed, we generally assume the fluid

has uniform specific entropy to further isolate the core physical features accounting for acoustic waves.

Comments on compressible, incompressible, and the Boussinesq ocean

All real fluids are compressible and thus support acoustic waves. When compressibility is reduced towards zero, so that the continuous media becomes more rigid, the acoustic wave speed increases. Hence, we generally find acoustic waves travel faster through solids than liquids, and faster through liquids than gases. Taking the mathematical limit of a fully incompressible fluid (where the fluid density is uniform and constant) results in an infinite acoustic wave speed, in which case acoustic waves are absent from incompressible fluid dynamics.

There are occasions where we study incompressible fluids in this book. For example, the shallow water models in Part VI of this book are comprised of incompressible fluid layers with three-dimensional motion, whereas the two-dimensional non-divergent barotropic model in Chapter 38 considers just a two-dimensional velocity (zero vertical motion). The Boussinesq ocean in Chapter 29 offers an important step towards a more realistic fluid. Namely, the Boussinesq ocean is quasi-compressible since the Boussinesq velocity is non-divergent even though the fluid density varies in space and time. The varying density in the Boussinesq ocean gives rise to a divergent velocity that supports acoustic waves. Even so, we commonly ignore the divergent velocity when working with the Boussinesq ocean since this velocity, and the associated acoustic waves, never couple to the Boussineq ocean dynamics that are the concern of the theory.

51.3 Lagrangian perspective

Consider a continuum fluid system whose motion is constrained to one space dimension, $\hat{\boldsymbol{x}}$. Assume that all fluid properties and flow properties are independent of the y and z directions. We assume the only forces acting on fluid elements arise from pressure, so that gravity, electromagnetism, and friction are ignored. Furthermore, all fluid motion remains close to a static background state, where the background state density and pressure are everywhere uniform with values ρ_{e} and p_{e}:

$$\rho_{\text{e}} = \text{background state density} \quad \text{and} \quad p_{\text{e}} = \text{background state pressure.} \tag{51.1}$$

Derivation of the equation for the acoustic waves proceeds in three steps. The first concerns the equation for mass conservation; the second arises from momentum conservation; and the third concerns the equation of state relating pressure, density, and specific entropy. Throughout the derivation in this section, we make use of the Lagrangian displacement field, $\xi(x,t)$, used in Section 46.1 when taking the continuum limit of coupled harmonic oscillators. Recall that this function measures the displacement, at time t, of a fluid element whose equilibrium position is x. We here also introduce the density, $\rho(x,t)$, as the density of a fluid element whose equilibrium position is x, and we maintain the same interpretation for the pressure field, $p(x,t)$.

51.3.1 Mass conservation

In Figure 51.1 we find two configurations for a fluid element, in which the first assumes the fluid is in mechanical equilibrium with constant density, ρ_{e}, and mass per unit area

$$M/A = \rho_{\text{e}}\, \delta x, \tag{51.2}$$

where A is the horizontal cross sectional area. The second configuration has been displaced by $\xi(x,t)$ a small amount so that the fluid element is out of mechanicial equilibrium. In this case its

density, $\rho(x,t)$, is found through mass conservation. Namely, the mass in the original rectangle equals to that in the displaced rectangle

$$\begin{aligned} M/A &= \rho_{\text{e}}\,\delta x && \text{(51.3a)}\\ &= \rho\,[x+\delta x+\xi(x+\delta x,t+\delta t)-x-\xi(x,t+\delta t)] && \text{(51.3b)}\\ &= \rho\,[\delta x+\xi(x+\delta x,t+\delta t)-\xi(x,t+\delta t)] && \text{(51.3c)}\\ &= \rho\,\delta x\left[1+\frac{\partial\xi(x^*,t)}{\partial x}\right] && \text{(51.3d)}\\ &\approx \rho\,\delta x\left[1+\frac{\partial\xi(x,t)}{\partial x}\right]. && \text{(51.3e)} \end{aligned}$$

The penultimate equality made use of the mean value theorem from differential calculus, where x^* is a point between x and $x+\delta x$, whereas the final step involves the approximation that arises when taking the infinitesimal limit allowing us to evaluate $\partial\xi/\partial x$ at the position x. We are thus led to the relation[1]

$$\rho(x,t) = \rho_{\text{e}}\,(1+\partial\xi/\partial x)^{-1} \approx \rho_{\text{e}}\,(1-\partial\xi/\partial x). \tag{51.4}$$

This equation says that the density of a fluid element, $\rho(x,t)$, whose equilibrium position is x, differs from its equilibrium density, ρ_{e}, according to whether the fluid element is expanded ($\partial\xi/\partial x>0$) or contracted ($\partial\xi/\partial x<0$).

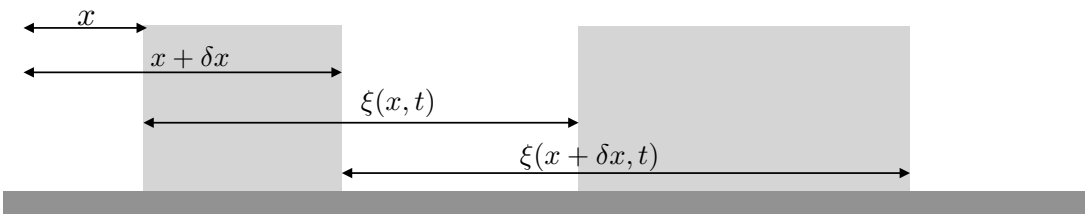

FIGURE 51.1: Schematic of a rectangular fluid element constrained to move just in the $\hat{\boldsymbol{x}}$ direction with uniform properties in the $\hat{\boldsymbol{y}}$ and $\hat{\boldsymbol{z}}$ directions. The fluid element has a constant mass, M, and with density uniform within the element. The equilibrium configuration in the left rectangle has a mass per unit area $M/A=\rho_{\text{e}}\,\delta x$, where A is the fixed cross sectional area, and ρ_{e} is the equilibrium density. The right rectangle shows the fluid element at a displaced non-equilibrium configuration where the density deviates from its equilibrium value. This density, $\rho(x,t)$, is the density of the displaced fluid element (specified by the displacement field $\xi(x,t)$) whose equilibrium position is x. The mass of the fluid element is identical for both the equilibrium and non-equilibrium configurations, which leads to $\rho(x,t)=\rho_{\text{e}}\,(1+\partial\xi/\partial x)^{-1}$. This relation means, for example, if $\partial\xi/\partial x>0$ (fluid element expands relative to equilibrium), then $\rho(x)<\rho_{\text{e}}$.

51.3.2 Momentum conservation

At equilibrium the fluid element experiences a pressure, p_{e}, that is assumed to be spatially uniform.[2] If fluid elements are displaced in a manner that produces nonzero density perturbations, then the pressure field is likewise modified, in which case fluid moves. Recall that we interpret $p(x,t)$ as the pressure acting on a fluid element whose equilibrium position is x. Hence, the net pressure force per area acting on the displaced fluid element is given by the gradient

$$\boldsymbol{F}^{\text{press}} = [-p(x+\delta x,t)+p(x,t)]\,\hat{\boldsymbol{x}} \approx -(\partial p(x,t)/\partial x)\,\delta x\,\hat{\boldsymbol{x}}. \tag{51.5}$$

[1] By assuming small perturbations relative to the background state, we disallow the extreme case where $\partial\xi/\partial x=-1$, in which the fluid becomes so rarefied (vanishing mass density) that we can no longer make use of the continuum description (see Chapter 16 for more on the continuum approximation).

[2] Recall we are ignoring gravity, so there is no hydrostatic pressure that would give rise to a pressure gradient.

The position of the fluid element is fully specified by the deviation function, $\xi(x,t)$, so that the acceleration is its second time derivative, $\partial_{tt}\xi(x,t)$, in which case Newton's equation of motion is given by

$$\frac{\partial}{\partial t}\left[\rho\,\frac{\partial \xi}{\partial t}\right] = -\frac{\partial p}{\partial x}. \tag{51.6}$$

51.3.3 Equation of state and acoustic wave equation

We now assume an equation of state whereby density is a function of pressure and specific entropy[3]

$$\rho = \rho(p, \mathcal{S}). \tag{51.7}$$

Assuming the fluctuations occur with constant specific entropy, $\mathcal{S}$, the equation of motion (51.6) takes the form

$$\frac{\partial}{\partial t}\left[\rho\,\frac{\partial \xi}{\partial t}\right] = -\left[\frac{\partial p}{\partial \rho}\right]_{\mathcal{S}}\frac{\partial \rho}{\partial x}. \tag{51.8}$$

Use of the continuity equation (51.4) allows us to eliminate density in favor of the displacement field

$$\frac{\partial}{\partial t}\left[\rho\,\frac{\partial \xi}{\partial t}\right] = \frac{\rho_{\mathsf{e}}\,c_{\mathsf{s}}^2}{(1+\partial\xi/\partial x)^2}\,\frac{\partial^2 \xi}{\partial x^2}, \tag{51.9}$$

where we introduced the inverse squared speed

$$c_{\mathsf{s}}^{-2} = \left[\frac{\partial \rho}{\partial p}\right]_{\mathcal{S}}, \tag{51.10}$$

where c_{s} is interpreted as the sound speed. We can linearize the acoustic equation (51.9) by dropping all terms with the products of the displacement field and assuming density is approximated by its equilibrium value, ρ_{e}, in which case we recover the acoustic wave equation

$$(\partial_{tt} - c_{\mathsf{s}}^2\,\partial_{xx})\,\xi = 0. \tag{51.11}$$

This equation says that the displacements of the fluid elements relative to their equilibrium position satisfy the linear wave equation, and the displacements travel with the sound speed.

51.3.4 Sound speed

It is important to observe that the pressure derivative in the sound speed equation (51.10) is computed with a fixed entropy, $\mathcal{S}$. We are thus treating acoustic waves as reversible adiabatic waves, which accords with our use of a perfect fluid throughout this chapter.[4] This approach is suitable for those cases where the speed of acoustic waves is much larger than the speed of fluid particles, so that an acoustic wave moves through a fluid far faster than the time for enthalpy to be transferred by fluid particles. In this case, acoustic waves are accurately treated as reversible adiabatic waves.

In Section 23.4.8 we consider the sound speed in an ideal gas, in which

$$c_{\mathsf{s}}^2 = (p/\rho)\,(c_{\mathsf{p}}/c_{\mathsf{v}}) = T\,R^{\mathsf{M}}\,(c_{\mathsf{p}}/c_{\mathsf{v}}), \tag{51.12}$$

where R^{M} is the specific gas constant given by equation (23.49), c_{v} is the specific heat capacity holding specific volume fixed (equation (23.59)), and $c_{\mathsf{p}} = c_{\mathsf{v}} + R^{\mathsf{M}}$ is the specific heat capacity holding pressure fixed. For air we have $c_{\mathsf{s}} \approx 350$ m s^{-1} for $T = 300$ K. We identify these waves as

[3] We study equations of state, including the ideal gas equation, in Chapters 23 and 30.

[4] Matter concentration is also held fixed when considering sound speeds in a fluid with multiple matter constituents.

acoustic (sound) waves due to the agreement of the wave speed (51.12) with the speed of sound measured in the laboratory. Note that LaPlace discovered the relevance of the specific heats ratio, c_p/c_v, in the expression (51.12) for the sound speed. This ratio arises when recognizing acoustic waves to be constant entropy waves, whereas Newton incorrectly assumed they were isothermal, in which case the specific heat ratio does not appear.

A more compressible media, such as the atmosphere, has a smaller sound speed ($c_s \approx 350$ m s^{-1}) than a less compressible media such as the ocean ($c_s \approx 1500$ m s^{-1}). Indeed, the sound speed is infinite when the media is fully incompressible, with the infinite speed a signature that the hyperbolic wave system has converted to an elliptic system (see Chapter 6). We offer further discussion of the sound speed in Sections 22.7.4 and 23.4.8 as part of our study of thermodynamics.

The *Mach number* is the ratio of the fluid particle speed to the sound speed. If a fluid is moving with Mach number greater than unity (supersonic), then there can be discontinuities (shocks) that break the continuum approximation (Chapter 16). In this case, the continuous fluid equations must be supplemented by other physical conditions such as those afforded by molecular dynamics. We have no occasion to study supersonic flow in this book.

51.3.5 Comments and further study

The original calculation of sound speed computed the density derivative holding temperature fixed rather than entropy. This mistake, originally made by Newton in his studies of sound, was corrected by LaPlace by noting that acoustic waves more closely maintain adiabatic conditions, which means they preserve specific entropy. It is perhaps a testament to the genius of Newton that even his mistakes took decades to centuries to correct, and often only after being considered in light of new areas of physics (e.g., thermodynamics) that were totally undeveloped during Newton's time.

Elements of this section were taken from Sections 2.1, 2.2, and 2.3 of *Towne* (1967) and Section 47-3 in Volume I of *Feynman et al.* (1963). See also Section 1.2 of *Lighthill* (1978) for more on the sound speed calculation.

51.4 Eulerian perspective

We here derive the acoustic wave equation using an Eulerian approach, thus offering a complement to the Lagrangian treatment in Section 51.3. Furthermore, we no longer restrict motion to one dimension, so that here the resulting acoustic waves travel in three space dimensions. We also generalize the background state, here allowing for the background density and specific entropy to be static functions of space.

51.4.1 Lagrangian wave equation

Consider a single component perfect fluid that does not feel gravity, Coriolis, or friction, so that the only acceleration acting on a fluid element arises from pressure gradients

$$\frac{\mathrm{D}\boldsymbol{v}}{\mathrm{D}t} = -\rho^{-1}\,\nabla p. \tag{51.13}$$

This expression of the *Euler equation* is coupled to the mass continuity equation (19.16)

$$\frac{\mathrm{D}\rho}{\mathrm{D}t} = -\rho\,\nabla\cdot\boldsymbol{v}, \tag{51.14}$$

that reflects the material constancy of mass following a fluid element. Furthermore, density and pressure are coupled through the equation of state (51.7), so that the density and pressure

material time derivatives are related by

$$\frac{\mathrm{D}\rho}{\mathrm{D}t} = \left[\frac{\partial\rho}{\partial p}\right]_{\mathcal{S}} \frac{\mathrm{D}p}{\mathrm{D}t} + \left[\frac{\partial\rho}{\partial \mathcal{S}}\right]_{p} \frac{\mathrm{D}\mathcal{S}}{\mathrm{D}t} = c_{\mathrm{s}}^{-2} \frac{\mathrm{D}p}{\mathrm{D}t}, \tag{51.15}$$

where we set $\mathrm{D}\mathcal{S}/\mathrm{D}t = 0$ due to the isentropic nature of the perfect fluid, and introduced the squared sound speed

$$c_{\mathrm{s}}^{-2} = \left[\frac{\partial\rho}{\partial p}\right]_{\mathcal{S}}. \tag{51.16}$$

Combining the continuity equation (51.14) and the material time derivative of the equation of state (51.15) renders

$$\frac{1}{\rho\, c_{\mathrm{s}}^2} \frac{\mathrm{D}p}{\mathrm{D}t} + \nabla\cdot\boldsymbol{v} = 0. \tag{51.17}$$

We can relate the velocity divergence to pressure by taking $\mathrm{D}/\mathrm{D}t$ of this equation and then using the Euler equation (51.13)

$$-\frac{\mathrm{D}(\nabla\cdot\boldsymbol{v})}{\mathrm{D}t} = -(\partial_t + v^n\partial_n)\,(\partial_m v^m) \tag{51.18a}$$

$$= -\nabla\cdot\frac{\mathrm{D}\boldsymbol{v}}{\mathrm{D}t} + \partial_m v^n\,\partial_n v^m \tag{51.18b}$$

$$= \nabla\cdot(\rho^{-1}\nabla p) + S^m{}_n\,S^n{}_m - R^m{}_n\,R^n{}_m. \tag{51.18c}$$

In the final equality we introduced components to the strain rate tensor, $\boldsymbol{S}$, and the rotation tensor, $\boldsymbol{R}$, both of which were introduced in Section 18.8 when studying the velocity gradient tensor. Furthermore, note that the combination, $S^m{}_n\,S^n{}_m - R^m{}_n\,R^n{}_m$, also appears in the elliptic pressure equation for the Boussinesq ocean in Section 29.3.4. Use of equation (51.18c) along with $\mathrm{D}/\mathrm{D}t$ of equation (51.17) leads to the pressure equation

$$\frac{\mathrm{D}}{\mathrm{D}t}\left[\frac{1}{\rho\, c_{\mathrm{s}}^2}\frac{\mathrm{D}p}{\mathrm{D}t}\right] - \nabla\cdot(\rho^{-1}\nabla p) = S^m{}_n\,S^n{}_m - R^m{}_n\,R^n{}_m. \tag{51.19}$$

The left hand side is a *Lagrangian wave equation*, which, when linearized, forms the more familiar acoustic wave equation to be described below. Equation (51.19) describes pressure fluctuations relative to the moving flow, with the nonlinear source on the right hand side arising from strain and rotation within the fluid flow. In Exercise 51.2 we consider the special case of pressure fluctuations when the background flow is a uniform constant.

The pressure equation (51.19) is nonlinear since pressure, density, and velocity are coupled. We garner insight into certain of the physical processes captured by this equation by linearizing around a static background state and examining small amplitude fluctuations, to which we now turn our attention.

51.4.2 Inhomogeneous background state

In Section 51.3 we assumed the background state has zero velocity, uniform density, uniform specific entropy, uniform pressure, and uniform sound speed. This trivial state is itself an exact solution to the perfect fluid equations of motion, thus serving as a suitable state from which to study linear fluctuations. Here we introduce a slightly less trivial background state that is also an exact solution to the equations of motion.

We continue to assume a trivial solution of the Euler equation with vanishing velocity (background $\boldsymbol{v} = 0$) and spatially uniform pressure (p_{e} constant). In this case, the continuity equation (51.14) can be satisfied by a background density that is time independent yet spatially inhomogeneous, $\rho_{\mathrm{e}} = \rho_{\mathrm{e}}(\boldsymbol{x})$. This inhomogeneous density is consistent with the equation of state

(51.7) if the specific entropy is itself inhomogeneous, $\mathcal{S}_e = \mathcal{S}_e(\boldsymbol{x})$, in which case

$$\rho(\boldsymbol{x}) = \rho[p = p_e, \mathcal{S} = \mathcal{S}_e(\boldsymbol{x})]. \tag{51.20}$$

By allowing ρ_e and $\mathcal{S}_e$ to be spatially dependent functions, we extend the applicability of the resulting wave equation to the study of acoustic waves propagating in a static inhomogeneous media. A geophysically relevant example concerns an ocean or atmosphere in exact hydrostatic balance (Section 24.6), with vanishing flow yet density and specific entropy that are functions of geopotential coordinate, z. *Pierce* (1990) considers the even more realistic case with a space and time dependent background flow, and a correspondingly nonuniform pressure field, in which case the acoustic wave equation is modified relative to that considered in this chapter.

51.4.3 Acoustic wave equation

We now linearize the Euler equation (51.13), along with the mass continuity equation in the form of equation (51.17), and perform the linearization relative to a background state of zero motion yet inhomogeneous density. We thus write pressure, density, and velocity as

$$p = p_e + p' \quad \text{and} \quad \rho = \rho_e(\boldsymbol{x}) + \rho' \quad \text{and} \quad \boldsymbol{v} = 0 + \boldsymbol{v}', \tag{51.21}$$

where the pressure and density perturbations are small relative to their background values $|p'| \ll p_e$ and $|\rho'| \ll \rho_e(\boldsymbol{x})$, and where the background density is generally a function of space. A positive p' arises from a local *compression* in the fluid, whereas a negative p' is a local expansion or *rarefaction*.

Wave equation with an inhomogeneous background state

Inserting the perturbations (51.21) into the Euler equation (51.13) leads to

$$(\rho_e + \rho')\,\partial_t \boldsymbol{v}' + (\rho_e + \rho')\,(\boldsymbol{v}' \cdot \nabla)\boldsymbol{v}' = -\nabla p', \tag{51.22}$$

and dropping all products of perturbation fields leads to the linearized Euler equation

$$\rho_e\,\partial_t \boldsymbol{v}' = -\nabla p'. \tag{51.23}$$

Likewise, the linearized continuity equation (51.17) takes the form

$$\partial_t p' + \rho_e\, c_s^2\, \nabla \cdot \boldsymbol{v}' = 0, \tag{51.24}$$

where the squared sound speed is here determined by compressibility of the equilibrum state

$$c_s^{-2} = \left[\left(\frac{\partial \rho}{\partial p}\right)_{\mathcal{S}}\right]_{p=p_e}. \tag{51.25}$$

Taking the divergence of the velocity equation (51.23) and making use of the continuity equation (51.24) renders the acoustic wave equation for the anomalous pressure

$$\frac{1}{\rho_e\, c_s^2}\,\frac{\partial^2 p'}{\partial t^2} - \nabla \cdot (\rho_e^{-1}\,\nabla p') = 0. \tag{51.26}$$

This linear wave equation compares to its fully nonlinear analog in equation (51.19). We can perform analogous manipulations to determine the following wave equation satisfied by the

velocity divergence

$$\partial_{tt}\mathcal{D}' - \nabla\cdot\left[\rho^{-1}\,\nabla(\rho\,c^2\,\mathcal{D}'\right] = 0 \qquad \text{with } \mathcal{D}' = \nabla\cdot\boldsymbol{v}'. \tag{51.27}$$

Finally, note that from the linearized Euler equation (51.23) that the density weighted velocity fluctuation has a static curl

$$\partial_t[\nabla\times(\rho_{\mathsf{e}}\,\boldsymbol{v}')] = 0. \tag{51.28}$$

Wave equation with a homogeneous background state

Equation (51.26) for the pressure, equation (51.27) for the velocity divergence, and equation (51.28) for the curl of the density weighted velocity constitute the suite of equations for acoustic waves in a static yet inhomogeneous background state. In the remainder of this section we study properties of the wave solutions to these equations, yet restricted to the homogeneous and static background state with ρ_{e} a uniform constant and with the sound speed also uniform, in which case we have the linear acoustic wave equations

$$(\partial_{tt}-c_{\mathsf{s}}^2\,\nabla^2)p' = 0 \quad\text{and}\quad (\partial_{tt}-c_{\mathsf{s}}^2\,\nabla^2)\mathcal{D}' = 0 \quad\text{and}\quad \partial_t(\nabla\times\boldsymbol{v}') = 0 \quad\text{with}\quad \mathcal{D}' = \nabla\cdot\boldsymbol{v}'. \tag{51.29}$$

The more realistic, yet complex, case of waves propagating through an inhomogeneous background state requires extra mathematical technology that we develop in Section 51.9.

51.4.4 The velocity potential and acoustic wave properties

The locally static curl (equation (51.29)) means that acoustic waves do not alter vorticity. Hence, if the linear system is initialized with zero vorticity then it stays that way.

Velocity potential for acoustic waves

Assuming zero initial vorticity, as appropriate when considering fluctuations around a state of rest, allows us to introduce a velocity potential (dimensions squared length per time), ψ, so that

$$\boldsymbol{v}' = -\nabla\psi. \tag{51.30}$$

The velocity equation (51.23) thus implies

$$\nabla(p' - \rho_{\mathsf{e}}\,\partial_t\psi) = 0 \Longrightarrow p' = \rho_{\mathsf{e}}\,(\partial_t\psi + K), \tag{51.31}$$

where $K(t)$ is an arbitrary function of time that is independent of space. The velocity potential is itself arbitrary up to a function of time. Hence, we can choose to work with a modified velocity potential, Ψ, that absorbs the function K

$$\Psi = \psi + \int^t K(t')\,\mathrm{d}t', \tag{51.32}$$

so that pressure is determined by the time derivative of Ψ and velocity is determined by the gradient

$$p' = \rho_{\mathsf{e}}\,\partial_t\Psi \quad\text{and}\quad \boldsymbol{v}' = -\nabla\Psi. \tag{51.33}$$

Note that the process of transforming from ψ to Ψ is referred to as a *gauge transformation*. The same approach is used in Section 52.2.2 when studying surface waves.

Making use of the relation (51.33) in the linearized continuity equation (51.24) renders the wave equation for the velocity potential

$$(\partial_{tt} - c_{\mathsf{s}}^2\,\nabla^2)\,\Psi = 0. \tag{51.34}$$

Furthermore, we can take the gradient of this equation to find that each of the three velocity components satisfies the acoustic wave equation

$$-(\partial_{tt} - c_{\mathsf{s}}^2 \nabla^2) \nabla \Psi = (\partial_{tt} - c_{\mathsf{s}}^2 \nabla^2) \boldsymbol{v}' = 0. \tag{51.35}$$

Density fluctuations in an acoustic wave

We determine the density perturbation within an acoustic wave by linearizing the equation of state (51.7) around the background state[5]

$$\rho = \rho(p, \mathcal{S}) \approx \rho_{\mathsf{e}} + c_{\mathsf{s}}^{-2} (p - p_{\mathsf{e}}), \tag{51.36}$$

so that

$$\rho' = \rho - \rho_{\mathsf{e}} = c_{\mathsf{s}}^{-2} p' = \rho_{\mathsf{e}} c_{\mathsf{s}}^{-2} \partial_t \Psi. \tag{51.37}$$

Taking the time derivative and using the wave equation (51.34) reveals the self-consistency of this result with the linearized mass continuity equation (51.24)

$$\partial_t \rho' = \rho_{\mathsf{e}} c_{\mathsf{s}}^{-2} \partial_{tt} \Psi = \rho_{\mathsf{e}} \nabla^2 \Psi = -\rho_{\mathsf{e}} \nabla \cdot \boldsymbol{v}'. \tag{51.38}$$

Temperature fluctuations in an acoustic wave

For an acoustic wave, a differential temperature increment arises just from changes to the pressure while holding entropy fixed

$$\mathrm{d}T = \left[\frac{\partial T}{\partial p}\right]_{\mathcal{S}} \mathrm{d}p. \tag{51.39}$$

In Section 23.2 we referred to this temperature partial derivative is the *adiabatic lapse rate*. Equation (23.26) provides a practical form of the lapse rate

$$\left[\frac{\partial T}{\partial p}\right]_{\mathsf{S}} = \frac{T_{\mathsf{e}} \alpha_{\mathrm{T}}}{\rho_{\mathsf{e}} c_{\mathsf{p}}}, \tag{51.40}$$

with T_{e} the background temperature, c_{p} the specific heat capacity (22.99), and α_T the thermal expansion coefficient (22.103) defined in terms of the *in situ* temperature (α_T and c_{p} are computed for the background state). We thus have a fluctuation of temperature given by

$$T - T_{\mathsf{e}} = T' = \frac{T_{\mathsf{e}} \alpha_{\mathrm{T}} p'}{\rho_{\mathsf{e}} c_{\mathsf{p}}} = (T_{\mathsf{e}} \alpha_{\mathrm{T}} / c_{\mathsf{p}}) \partial_t \Psi. \tag{51.41}$$

Hence, as an acoustic wave propagates it has an associated oscillation of the temperature field due to oscillations in pressure.

51.5 Dispersion relation and flow properties

We now characterize physical properties of acoustic waves, focusing on the properties as realized by a traveling acoustic plane wave in a homogeneous media (i.e., ρ_{e} is a uniform constant). These properties are determined largely through the acoustic wave *dispersion relation*, which provides a functional relation between the wave frequency and the wavevector. After determining the dispersion relation, we derive the pressure, density, and velocity fluctuations in an acoustic wave.

[5] Recall that $\mathcal{S}$ is assumed constant for the background state, so that it plays a passive role in the Taylor expansion (51.36).

51.5.1 Dispersion relation

Not every traveling plane wave is a solution to the acoustic wave equation (51.34). Rather, the wavevector and angular frequency must be related in a specific manner that is dependent on physics of the particular wave. This relation is known as the *dispersion relation*. Plugging in the traveling plane wave (49.18) into the acoustic wave equation (51.34) renders the acoustic wave dispersion relation

$$(\omega^2 - c_s^2 \boldsymbol{k}^2)\,\Psi = 0 \Longrightarrow \omega = c_s\,|\boldsymbol{k}| \Longrightarrow C_p = \omega/|\boldsymbol{k}| = c_s. \tag{51.42}$$

Note that we only consider the positive sign for the angular frequency since $\omega \geq 0$ corresponds to our convention for wave frequencies (Section 49.4). Traveling acoustic plane waves of a given wavevector have their angular frequency specified by the dispersion relation (51.42). The dispersion relation (51.42) reveals that the phase speed for acoustic waves, C_p, equals to the sound speed, c_s.

The sound speed is a function of the background fluid state; it is not a function of wave properties such as the wavelength or wave frequency. Hence, all acoustic waves, regardless their wavelength, travel at the same phase speed, $C_p = c_s$. Correspondingly, we say that acoustic waves are *non-dispersive*. This property accords with common experience, whereby the variety of sound waves with different frequencies from, say, an orchestra are heard together since all sound frequencies travel with the same speed. Furthermore, it is certainly possible for any particular point in space to be comprised of multiple acoustic waves. Since each wave satisfies the wave equation (51.34), and since the wave equation is linear, acoustic waves satisfy the *principle of superposition*. That is, the sum of multiple traveling acoustic waves is also an acoustic wave that satisfies the same wave equation with same speed, c_s.

51.5.2 Flow properties for acoustic plane waves

We here establish expressions for flow fields, such as velocity, pressure, and density, in the presence of an acoustic plane wave. We start with equation (51.33), which relates pressure and velocity to derivatives of the velocity potential. Following our discussion of traveling plane wave kinematics in Section 49.5.1, write the velocity potential for an acoustic plane wave as

$$\Psi(\boldsymbol{x}, t) = A\,\mathrm{Re}[e^{\mathrm{i}\,(\boldsymbol{k}\cdot\boldsymbol{x} - \omega\,t + \alpha)}] = A\cos(\boldsymbol{k}\cdot\boldsymbol{x} - \omega\,t + \alpha), \tag{51.43}$$

which leads to the corresponding pressure fluctuation

$$p' = \rho_e\,\partial_t \Psi = \rho_e\,\mathrm{Re}[-\mathrm{i}\,\omega\,\Psi] = \rho_e\,\omega\,A\sin(\boldsymbol{k}\cdot\boldsymbol{x} - \omega\,t + \alpha). \tag{51.44}$$

Hence, higher frequency acoustic plane waves have higher magnitude for their fluctuating pressure. Likewise, the fluctuating velocity of fluid particles takes on the form

$$\boldsymbol{v}' = -\nabla\Psi = -\,\mathrm{Re}[\mathrm{i}\,\boldsymbol{k}\,\Psi] = A\,\boldsymbol{k}\sin(\boldsymbol{k}\cdot\boldsymbol{x} - \omega\,t + \alpha). \tag{51.45}$$

This relation means that fluid particles moving in an acoustic plane wave have their velocity aligned with the wave direction

$$\boldsymbol{v}' \times \boldsymbol{k} = 0. \tag{51.46}$$

Furthermore, this relation follows since the vorticity of the linear fluctuations vanish (Section 51.4.4). The alignment of particle velocity and wave vector is a defining feature of *longitudinal waves*.[6] It also means that the squared magnitude of the particle velocity equals to the squared

[6] We later encounter waves in non-divergent flows, $\nabla\cdot\boldsymbol{v} = 0$, which are *transverse waves* whereby $\boldsymbol{k}\cdot\boldsymbol{v} = 0$. That is, for transverse waves the fluid particle motion is perpendicular to the wave direction, whereas for longitudinal

projection of this velocity onto the wave direction

$$|\boldsymbol{v}'|^2 = (\boldsymbol{v}' \cdot \hat{\boldsymbol{k}})^2 = [A\,|\boldsymbol{k}| \sin(\boldsymbol{k} \cdot \boldsymbol{x} - \omega\, t + \alpha)]^2. \tag{51.47}$$

Finally, the fluctuating density within an acoustic wave is given by the linearized equation of state (51.37), which takes the following form for an acoustic plane wave

$$\rho' = c_s^{-2}\, p' = c_s^{-2}\, \rho_e\, \omega\, A \sin(\boldsymbol{k} \cdot \boldsymbol{x} - \omega\, t + \alpha). \tag{51.48}$$

Equations (51.44), (51.45), and (51.48) imply the following relations between the fluctuating pressure, velocity, and density in an acoustic plane wave

$$\rho_e\, \omega\, \boldsymbol{v}' = p'\, \boldsymbol{k} \Longrightarrow p' = \rho_e\, c_s\, \boldsymbol{v}' \cdot \hat{\boldsymbol{k}} \Longrightarrow \rho' = \rho_e\, \boldsymbol{v}' \cdot \hat{\boldsymbol{k}}/c_s. \tag{51.49}$$

where we used the dispersion relation (51.42). These relations reveal that pressure, velocity, and density fluctuations are in-phase; i.e., they have the same phase. The density fluctuation in equation (51.49) reveals that its ratio with the background density equals to the ratio of the fluid particle speed to the sound speed. This ratio is the *Mach number*, so that for an acoustic plane wave we have

$$|p'|/(\rho_e\, c_s^2) = |\rho'|/\rho_e = |\boldsymbol{v}' \cdot \hat{\boldsymbol{k}}|/c_s = \mathrm{Ma} \ll 1. \tag{51.50}$$

Hence, small Mach number corresponds to small density fluctuation relative to the background density. We made use of this relation when introducing the Boussinesq ocean at the start of Chapter 29.

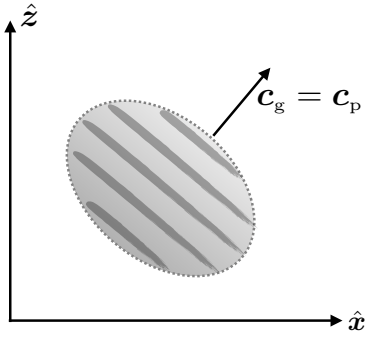

FIGURE 51.2: Example packet of acoustic waves, with the gray shaded lines denoting constant phase surfaces. Acoustic waves are non-dispersive, so that the group and phase velocities are equal, $\boldsymbol{c}_p = \boldsymbol{c}_g$, and all acoustic waves have phase speed given by the speed of sound, $C_p = c_s$. The fluid particle motion is parallel to the phase velocity according to equation (51.45), with such particle motion characterizing longitudinal waves.

51.5.3 Example acoustic pressure perturbations

We noted in the introduction to this chapter that acoustic waves, and their associated pressure perturbations, play a negligible role in large-scale geophysical fluid flows, such as those associated with atmospheric weather patterns. To support that contention, consider some common sounds and examine their pressure perturbations. For that purpose, we make use of the decibel scale (dB) for the sound pressure level (SPL)

$$\mathrm{SPL} = 20 \log_{10}(|p'|/p_{\mathrm{ref}}) \Longrightarrow |p'| = p_{\mathrm{ref}}\, 10^{\mathrm{SPL}/20}. \tag{51.51}$$

waves the particle motion is parallel to the wave direction.

It is conventional to choose the reference pressure, p_{ref}, so that 0 dB is a quiet sound at the threshold of human hearing, with

$$p_{\text{ref}} = 20 \times 10^{-6} \text{ Pa} = 20 \ \mu\text{Pa} \tag{51.52}$$

serving as the international convention. Following equation (51.50), we can determine the Mach number associated with a particular sound pressure level (assuming acoustic plane waves) according to

$$\text{Ma} = |p'|/(\rho_{\text{e}} \, c_{\text{s}}^2) = |p'|/[p \, (c_{\text{p}}/c_{\text{v}})], \tag{51.53}$$

where we made use of the ideal gas relation (23.70) for the sound speed

$$\rho_{\text{e}} \, c_{\text{s}}^2 = p \, c_{\text{p}}/c_{\text{v}}. \tag{51.54}$$

We evaluate the sound speed at the standard sea level atmospheric pressure, $p = p_{\text{stand}} = 101.325 \times 10^3$ Pa, and assume the specific heat capacity ratio, $c_{\text{p}}/c_{\text{v}} = 7/5$, which holds for an ideal diatomic gas, in which case

$$\rho_{\text{e}} \, c_{\text{s}}^2 = p_{\text{stand}} \, (c_{\text{p}}/c_{\text{v}}) = 140 \times 10^3 \text{ Pa}. \tag{51.55}$$

Table 51.1 tabulates the SPL, pressure perturbation, and Mach number for some common sounds. We see that even extremely loud sounds, relative to human hearing, have very small Mach numbers, thus justifying the use of linear acoustic wave dynamics for their description.

To gauge the size of these acoustic pressure fluctuations relative to typical atmospheric pressure fluctuations, consider a middle latitude geostrophic wind, in which case equation (31.15) gives

$$\rho \, f \, \hat{\boldsymbol{z}} \times \boldsymbol{u}_{\text{geostrophic}} = -\nabla p_{\text{geostrophic}} \Longrightarrow |p'_{\text{geostrophic}}| \sim \rho \, f \, U \, L, \tag{51.56}$$

where U is the scale of the geostrophic wind speed, and L is the horizontal length scale over which the winds vary. Taking $f = 10^{-4}$ s^{-1}, $U = 10$ m s^{-1}, $\rho = 1$ kg m^{-3}, and $L = 10^6$ m we find a typical pressure fluctuation

$$|p'_{\text{geostrophic}}| \approx 10^3 \text{ Pa}. \tag{51.57}$$

This pressure fluctuation is on the order of that found inside of an automobile exhaust system (see Table 51.1). However, the atmospheric fluctuation associated with this geostrophic wind extends over thousands of kilometers, whereas the sound waves inside of an exhaust system extend over a fraction of a meter. Hence, the energy contained in the atmospheric weather pattern is many orders larger than that for even the loudest sounds extending over typical human length scales. This example further emphasizes the irrelevance of acoustic waves for large-scale geophysical fluid flows.

51.6 Energetics

We here specialize the energetic analysis from Section 26.7 and 26.9 to study the energetics of an acoustic wave in a homogeneous background state. For an acoustic wave, the total energy is the sum of the kinetic energy of the oscillating fluid particles, plus the changes to internal energy of the fluid that arise from pressure work (recall we are ignoring gravity). We thus write the total energy per mass, $\mathcal{E}$, as the sum of the internal energy per mass, $\mathcal{I}$, plus kinetic energy per mass, $\mathcal{K}$,

$$\mathcal{E} = \mathcal{I} + \mathcal{K}. \tag{51.58}$$

SOUND	SPL (dB)	$\lvert p'\rvert$ (Pa)	$\lvert p'\rvert/\lvert p'_{\text{geostrophic}}\rvert$	Ma
soft whisper	30	6.3×10^{-4}	6.3×10^{-7}	4.5×10^{-9}
normal conversation	60	2×10^{-2}	2×10^{-5}	1.4×10^{-7}
noisy factory	90	0.63	6.3×10^{-4}	4.5×10^{-6}
rock concert	115	11	1.1×10^{-2}	8×10^{-5}
aircraft engine	130	63	6.3×10^{-2}	4.5×10^{-4}
automobile exhaust system	160	2×10^{3}	2	1.4×10^{-2}

TABLE 51.1: Acoustic properties of common sounds, following Example 15.2 from *Kundu et al.* (2016). The first column lists the sound, the second column the sound pressure level in dB, the third column the corresponding pressure fluctuation in Pa, the fourth column the ratio of the pressure fluctuation to a pressure fluctuation associated with a geostrophic atmospheric fluctuation, $|p'_{\text{geostrophic}}| \approx 10^3$ Pa (equation (51.57)), and the fifth column the Mach number assuming standard atmospheric sea level pressure, $p_{\text{stand}} = 1.01 \times 10^5$ Pa. Since the Mach number is far smaller than unity even for the loudest sound, we are justified in using linear acoustic wave theory to describe the propagation of these sounds.

The Eulerian form of the total energy equation is given by equation (26.102), which here takes the form

$$\frac{\partial(\rho\,\mathcal{E})}{\partial t} + \nabla\cdot[\rho\,\boldsymbol{v}\,(\mathcal{I} + \mathcal{K} + p/\rho)] = 0, \tag{51.59}$$

where $\mathcal{I} + p/\rho$ is the enthalpy per mass (Section 22.6.4)

$$\mathcal{H} = \mathcal{I} + p/\rho, \tag{51.60}$$

and we set the thermal and chemical fluxes to zero as per a perfect fluid. In the remainder of this section we specialize this energy equation to the case of linear acoustic wave fluctuations.

51.6.1 Expressions for the wave energies

To linearize terms in the energy equation (51.59) requires us to drop third order products of fluctuating quantities while keeping second, first, and zeroth order terms. This procedure is further supported by our ability to develop a self-consistent and closed energy budget for acoustic waves.

Kinetic energy of an acoustic wave

Since velocity is a first order quantity, the kinetic energy per volume is

$$\rho\,\mathcal{K} = (\rho_e + \rho')\,\boldsymbol{v}'\cdot\boldsymbol{v}'/2 \approx \rho_e\,\boldsymbol{v}'\cdot\boldsymbol{v}'/2. \tag{51.61}$$

Internal (potential) energy of an acoustic wave

For the internal energy, recall from Section 22.6.2 that its natural functional dependence for a single-component fluid is

$$\mathcal{I} = \mathcal{I}(\mathcal{S}, \rho). \tag{51.62}$$

Since entropy is held fixed in an acoustic wave, consider the following Taylor series approximation for the internal energy per volume as computed around the background state

$$\rho\,\mathsf{I} \approx \rho\,\mathsf{I}_e + (\rho - \rho_e)\left[\frac{\partial(\rho\,\mathcal{I})}{\partial\rho}\right]_{\rho=\rho_e} + \frac{(\rho-\rho_e)^2}{2}\left[\frac{\partial^2(\rho\,\mathcal{I})}{\partial\rho^2}\right]_{\rho=\rho_e}. \tag{51.63}$$

The first partial derivative is given by

$$\frac{\partial(\rho\,\mathcal{I})}{\partial\rho} = \mathcal{I} + \rho\,\frac{\partial\mathcal{I}}{\partial\rho} = \mathcal{I} + p/\rho = \mathcal{H}, \tag{51.64}$$

where we used identity (22.64) in the penultimate step. The second partial derivative is thus given by

$$\frac{\partial^2(\rho\,\mathcal{I})}{\partial\rho^2} = \frac{\partial\mathcal{H}}{\partial\rho} = \frac{\partial\mathcal{H}}{\partial p}\,\frac{\partial p}{\partial\rho} = c_{\mathrm{s}}^2/\rho, \tag{51.65}$$

where we used the identity (22.76) for the final step. We also used the equation of state (51.7) to convert the density derivative to a pressure derivative in the penultimate step.

Bringing these results together leads to the approximate internal energy per volume

$$\rho\,\mathsf{I} \approx \rho_{\mathrm{e}}\,\mathsf{I}_{\mathrm{e}} + \rho'\,\mathsf{H}_{\mathrm{e}} + (c_{\mathrm{s}}\,\rho')^2/(2\,\rho_{\mathrm{e}}). \tag{51.66}$$

The first term on the right hand side is a constant measuring the internal energy per volume of the background state, and it has no relation to the acoustic wave. The second term is the background enthalpy per mass times the fluctuating density. When integrating over the full domain, the fluctuating density vanishes due to mass conservation. That is, we assume the mass in the domain is the same in the background state as well as when there are acoustic waves, so that

$$\int_{\mathcal{R}} \rho\,\mathrm{d}V = \int_{\mathcal{R}} \rho_{\mathrm{e}}\,\mathrm{d}V \implies \int_{\mathcal{R}} \rho'\,\mathrm{d}V = 0. \tag{51.67}$$

Since the $\rho'\,\mathcal{H}_{\mathrm{e}}$ term drops out from a domain volume integral, it is common to drop this term when studying the energy density for an acoustic wave. However, we choose not to drop it at this point in the discussion. Rather, we find in Section 51.6.3 that $\rho'\,\mathcal{H}_{\mathrm{e}}$ naturally cancels from the flux-form acoustic energy budget equation, at which point we can confidently conclude that it has no significance to the energetic transfers within an acoustic wave. The third term in equation (51.66), $(c_{\mathrm{s}}\,\rho')^2/(2\,\rho_{\mathrm{e}})$, is a potential energy per volume in the acoustic wave that arises from fluid compressibility.

Total energy per volume of an acoustic wave

We conclude that the total energy per volume, accurate to second order in fluctuating acoustic wave fields, is given by

$$\rho\,\mathcal{E} = \rho'\,\mathsf{H}_{\mathrm{e}} + (\rho_{\mathrm{e}}/2)\,[(c_{\mathrm{s}}\,\rho'/\rho_{\mathrm{e}})^2 + \boldsymbol{v}'\cdot\boldsymbol{v}']. \tag{51.68}$$

As a final step, we make use of equations (51.33) and (51.37) to write the wave energy per volume in terms of the velocity potential

$$\rho\,\mathcal{E} = \rho'\,\mathsf{H}_{\mathrm{e}} + (\rho_{\mathrm{e}}/2)\,[(c_{\mathrm{s}}\,\rho'/\rho_{\mathrm{e}})^2 + \boldsymbol{v}'\cdot\boldsymbol{v}'] = \frac{\rho_{\mathrm{e}}}{2\,c_{\mathrm{s}}^2}\left[2\,\mathcal{H}_{\mathrm{e}}\,\partial_t\Psi + (\partial_t\Psi)^2 + c_{\mathrm{s}}^2\,\nabla\Psi\cdot\nabla\Psi\right]. \tag{51.69}$$

51.6.2 Equipartition of energy

Following our study of energy for a simple harmonic oscillator in Section 15.6.3, we here study how energy in an acoustic wave is partitioned between kinetic energy and potential energy. Recall that the simple harmonic oscillator equally partitions energy when time averaging over an oscillation period; i.e., performing the phase average of Section 8.1.2. That result follows from the *virial theorem* considered in Section 12.7.3. We here verify energy equipartition also holds for acoustic waves.

As for the oscillator, we expect energy equipartition for acoustic waves, thus reflecting the alternating exchange of energy between kinetic and potential. Mathematically, equipartition

arises since the potential energy is a homogeneous function of degree two, with details of this property discussed as part of the virial theorem from Section 12.7.3. Here, we show that energy equipartition holds instantaneously for a monochromatic traveling acoustic wave. However, for a general linear acoustic fluctuation, equipartition holds only when averaging over a wave period plus integrating over the closed spatial domain.

Equipartition for a monochromatic traveling acoustic wave

For an acoustic plane wave, the energy density simplifies through use of equation (51.49) to render

$$(c_s\,\rho'/\rho_e)^2 = (\boldsymbol{v}'\cdot\hat{\boldsymbol{k}})^2 = \boldsymbol{v}'\cdot\boldsymbol{v}', \tag{51.70}$$

where the second equality holds since the fluid particle velocity within the plane wave is aligned with the plane wave phase velocity. We thus find that the potential energy per volume and kinetic energy per volume contribute an equal amount to the acoustic plane wave's energy per volume

$$\rho\,\mathcal{E} = \rho'\,\mathsf{H}_e + (\rho_e/2)\,[(c_s\,\rho'/\rho_e)^2 + \boldsymbol{v}'\cdot\boldsymbol{v}'] = \rho'\,\mathcal{H}_e + 2\,\rho_e\,\mathcal{K}. \tag{51.71}$$

Equipartition for an arbitrary periodic linear fluctuation

The general expression (51.69) for the energy in a linear fluctuation does not render energy equipartition at each point in space and time. Rather, being inspired by the oscillator in Section 15.6.3, we here show that a phase and space averaged energy does possess equipartition. For the phase average we integrate the energy density over a single period, and doing so eliminates the background enthalpy term, $2\,\mathcal{H}_e\,\partial_t\Psi$, thus leaving

$$\int_0^{2\pi/\omega} \rho\,\mathcal{E}\,\mathrm{d}t = \frac{\rho_e}{2\,c_s^2}\int_0^{2\pi/\omega}\left[(\partial_t\Psi)^2 + c_s^2\,\nabla\Psi\cdot\nabla\Psi\right]\mathrm{d}t. \tag{51.72}$$

Now integrate by parts and make use of the wave equation (51.34) to find

$$\int_0^{2\pi/\omega} \rho\,\mathcal{E}\,\mathrm{d}t = \frac{\rho_e}{2\,c_s^2}\int_0^{2\pi/\omega}\left[-\Psi\,\partial_{tt}\Psi + c_s^2\,\nabla\Psi\cdot\nabla\Psi\right]\mathrm{d}t \tag{51.73a}$$

$$= \frac{\rho_e}{2}\int_0^{2\pi/\omega}\left[-\Psi\,\nabla^2\Psi + \nabla\Psi\cdot\nabla\Psi\right]\mathrm{d}t \tag{51.73b}$$

$$= \frac{\rho_e}{2}\int_0^{2\pi/\omega}\left[-\nabla\cdot(\Psi\,\nabla\Psi) + 2\,\nabla\Psi\cdot\nabla\Psi\right]\mathrm{d}t. \tag{51.73c}$$

We see that for an arbitrary linear and periodic fluctuation, energy equipartition is realized by time integrating over a wave period and then integrating over a spatially closed or spatially periodic domain

$$\int_{\mathcal{R}}\left[\int_0^{2\pi/\omega}\rho\,\mathcal{E}\,\mathrm{d}t\right]\mathrm{d}V = \rho_e\int_{\mathcal{R}}\left[\int_0^{2\pi/\omega}\nabla\Psi\cdot\nabla\Psi\,\mathrm{d}t\right]\mathrm{d}V = 2\,\rho_e\int_{\mathcal{R}}\left[\int_0^{2\pi/\omega}\mathcal{K}\,\mathrm{d}t\right]\mathrm{d}V. \tag{51.74}$$

This equation says that the phase and domain averaged flow contains an equal amount of kinetic energy as internal energy. This result holds for any periodic acoustic fluctuation, and is not specific to plane acoustic waves.

51.6.3 Energy budget equation

Taking the partial time derivative of the energy per volume, (51.69), leads to

$$\partial_t(\rho\,\mathcal{E}) = \frac{\rho_e}{c_s^2}\left[\partial_{tt}\Psi\,(\mathcal{H}_e + \partial_t\Psi) + c_s^2\,\nabla\Psi\cdot\nabla\partial_t\Psi\right] \tag{51.75a}$$

$$= \rho_e\left[\nabla^2\Psi\,(\mathcal{H}_e + \partial_t\Psi) + \nabla\Psi\cdot\nabla\partial_t\Psi\right] \tag{51.75b}$$

$$= \rho_e\,\nabla\cdot[(\mathcal{H}_e + \partial_t\Psi)\,\nabla\Psi] \tag{51.75c}$$

$$= -\rho_e\,\nabla\cdot[\boldsymbol{v}'\,(\mathcal{H}_e + p'/\rho_e)]. \tag{51.75d}$$

We can thus write the acoustic energy equation in terms of the velocity potential

$$\partial_t\left[2\,\mathsf{H}_e\,\partial_t\Psi + (\partial_t\Psi)^2 + c_s^2\,\nabla\Psi\cdot\nabla\Psi\right] = 2\,c_s^2\,\nabla\cdot[(\mathcal{H}_e + \partial_t\Psi)\,\nabla\Psi]. \tag{51.76}$$

The two $\mathcal{H}_e$ terms cancel identically through use of the wave equation (51.34), thus leaving the acoustic energy equation, here written in two equivalent forms

$$(1/2)\,\partial_t\left[(\partial_t\Psi)^2 + c_s^2\,\nabla\Psi\cdot\nabla\Psi\right] = c_s^2\,\nabla\cdot(\partial_t\Psi\,\nabla\Psi) \tag{51.77a}$$

$$(\rho_e/2)\,\partial_t\left[(c_s\,\rho'/\rho_e)^2 + \boldsymbol{v}'\cdot\boldsymbol{v}'\right] = -\nabla\cdot(\boldsymbol{v}'\,p'). \tag{51.77b}$$

The energy equation (51.77b) identifies $\boldsymbol{v}'\,p'$ as the energy flux for acoustic waves, whose convergence affects a local time change to the wave energy per volume. In this manner we have established the budget equations for acoustic energy, as summarized by[7]

$$\partial_t(\rho_e\,\mathcal{E}) = -\nabla\cdot\boldsymbol{J}_{\mathcal{E}} \tag{51.78a}$$

$$\mathcal{E} = [(c_s\,\rho'/\rho_e)^2 + \boldsymbol{v}'\cdot\boldsymbol{v}']/2 = [c_s^{-2}\,(\partial_t\Psi)^2 + \nabla\Psi\cdot\nabla\Psi]/2 \tag{51.78b}$$

$$\boldsymbol{J}_{\mathcal{E}} = \boldsymbol{v}'\,p' = -\rho_e\,\partial_t\Psi\,\nabla\Psi. \tag{51.78c}$$

Finally, for an acoustic plane wave, use of the relations (51.49) allows us to write the wave energy flux in terms of the wave energy density

$$\boldsymbol{J}_{\mathcal{E}} = \boldsymbol{v}'\,p' = \boldsymbol{v}'\,(\rho_e\,c_s\,\boldsymbol{v}'\cdot\hat{\boldsymbol{k}}) = c_s\,\rho_e\,(\boldsymbol{v}'\cdot\hat{\boldsymbol{k}})^2\,\hat{\boldsymbol{k}} = c_s\,\rho_e\,\mathcal{E}\,\hat{\boldsymbol{k}} = \rho_e\,\mathcal{E}\,\boldsymbol{c}_p \quad \Longleftarrow \text{plane wave.} \tag{51.79}$$

That is, for the acoustic plane wave, the flux of energy moves with the plane wave phase velocity. For dispersive waves in later chapters, we find that the energy flux moves with the group velocity rather than the phase velocity.

51.7 Wave momentum

The linear momentum in a fluid region, $\mathcal{R}$, is given by (see Section 24.2.3)

$$\boldsymbol{P} = \int_{\mathcal{R}} \rho\,\boldsymbol{v}\,\mathrm{d}V, \tag{51.80}$$

so that the linear momentum of acoustic waves is given by

$$\boldsymbol{P} = \int_{\mathcal{R}} (\rho_e + \rho')\,\boldsymbol{v}'\mathrm{d}V \tag{51.81a}$$

$$= -\rho_e\int_{\mathcal{R}} \nabla\Psi\,\mathrm{d}V + \int_{\mathcal{R}} \rho'\,\boldsymbol{v}'\,\mathrm{d}V \tag{51.81b}$$

[7] As shown following equation (51.76), the term $\rho'\,\mathcal{H}_e$ plays no role in energy transformations. Hence, we drop it from $\mathcal{E}$ in equation (51.78b).

$$= -\rho_e \oint_{\partial\mathcal{R}} \Psi\, \hat{\boldsymbol{n}}\, \mathrm{d}V + c_s^{-2} \int_{\mathcal{R}} \boldsymbol{J}_{\mathcal{E}}\, \mathrm{d}V. \tag{51.81c}$$

If the waves are localized to a finite region, such as in a wave packet rather than a plane wave, then we can drop the boundary integral so long as the boundary of the domain extends outside the region where the packet is located. In this case, the integrated energy flux equals to the squared wave speed times the linear momentum

$$c_s^2\, \boldsymbol{P} = \int_{\mathcal{R}} p'\, \boldsymbol{v}'\, \mathrm{d}V = \int_{\mathcal{R}} \boldsymbol{J}_{\mathcal{E}}\, \mathrm{d}V. \tag{51.82}$$

51.8 Acoustic waves radiated from a piston

In this section we introduce the study of acoustic wave radiation, here for the specific case of a circular piston in a flat wall (see Figure 51.3). In addition to exemplifying some of the physical ideas presented earlier in the chapter, this section illustrates the use of the Green's function for the Helmholtz equation that we originally studied in Section 9.6.8. We do not pursue the radiation problem to its entirety as doing so is quite an extensive exercise that is lucidly and thoroughly presented in section 51 of *Fetter and Walecka* (2003). Instead, our goal is mostly to illustrate the style of problems that can be solved using Green's functions for acoustics.

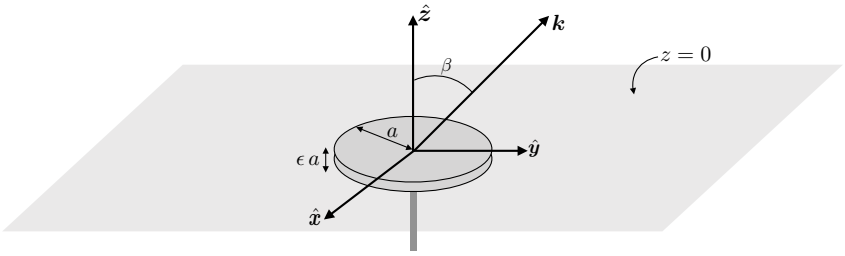

FIGURE 51.3: Illustrating the geometry of a piston radiating acoustic waves as studied in Section 51.8. The piston is circular with radius $r = a$ and situated within an infinite rigid wall along the $z = 0$ plane. We make use of cylindrical-polar coordinates from Section 4.22, with origin at the center of the piston and vertical axis through the origin. The piston oscillates along the vertical axis with a vertical position $z(t) = \epsilon\, a\, \mathrm{e}^{-\mathrm{i}\,\omega\, t}$, where $\epsilon \ll 1$ is small and ω is the angular frequency of the oscillations. The piston generates acoustic waves with angular frequency ω in the surrounding fluid. We depict a single acoustic wavevector, $\boldsymbol{k}$, making an angle, β, with respect to the vertical axis, though note that waves are radiated throughout space. Given the assumed small amplitude of the piston motion, we evaluate boundary conditions on the $z = 0$ plane, which is sufficiently accurate for linear analysis. Our focus concerns waves within the region $z > 0$.

51.8.1 Setting up the physics problem

We are interested in properties of acoustic waves radiated in the $z > 0$ half-plane as depicted in Figure 51.3. If the piston was at rest ($\omega = 0$) at $z = 0$, then we would merely be studying acoustic waves in the $z > 0$ half-plane as described by the boundary value problem for the velocity potential

$$(\partial_{tt} - c_s^2\, \nabla^2)\, \Psi = 0 \quad z > 0 \tag{51.83a}$$

$$\hat{\boldsymbol{z}} \cdot \nabla \Psi = 0 \quad z = 0. \tag{51.83b}$$

Indeed, if there is no wavemaker (i.e., no piston motion), then Ψ would be a space-time constant and so there would be no waves.

Now turn on the piston and write its vertical position as

$$z(t) = \begin{cases} \epsilon\, a\, \mathrm{e}^{-\mathrm{i}\omega t} & r \leq a \\ 0 & r > a, \end{cases} \tag{51.84}$$

where r is the radial distance from the vertical axis and $\epsilon \ll 1$ is a small positive and non-dimensional number. The corresponding vertical velocity of the piston is

$$\dot{z}(t) = \begin{cases} -\mathrm{i}\,\epsilon\, a\, \omega\, \mathrm{e}^{-\mathrm{i}\omega t} & r \leq a \\ 0 & r > a. \end{cases} \tag{51.85}$$

We are thus led to the boundary value problem for the velocity potential

$$(\partial_{tt} - c_{\mathrm{s}}^2\, \nabla^2)\, \Psi = 0 \qquad z > 0 \tag{51.86a}$$

$$\hat{\boldsymbol{z}} \cdot \nabla \Psi = 0 \qquad z = 0 \text{ and } r > a \tag{51.86b}$$

$$\hat{\boldsymbol{z}} \cdot \nabla \Psi = \mathrm{i}\,\epsilon\, a\, \omega\, \mathrm{e}^{-\mathrm{i}\omega t} \qquad z = 0 \text{ and } r \leq a. \tag{51.86c}$$

The time dependent boundary condition generates acoustic waves, and these waves manifest in the velocity potential. We restrict attention to times long enough after the initial setup that allows the wave field to be present throughout the fluid, in which case the velocity potential can be written as a monochromatic field

$$\Psi(\boldsymbol{x}, t) = \Phi(\boldsymbol{x})\, \mathrm{e}^{-\mathrm{i}\omega t}. \tag{51.87}$$

We thus find that the time-independent portion of the velocity potential satisfies the Helmholtz boundary value problem

$$[\nabla^2 + (\omega/c_{\mathrm{s}})^2]\, \Phi = 0 \qquad z > 0 \tag{51.88a}$$

$$\hat{\boldsymbol{z}} \cdot \nabla \Phi = 0 \qquad z = 0, r > a \tag{51.88b}$$

$$\hat{\boldsymbol{z}} \cdot \nabla \Phi = \mathrm{i}\,\epsilon\, a\, \omega \qquad z = 0, r \leq a. \tag{51.88c}$$

51.8.2 Solution in terms of the Green's function

Following our study in Chapter 9, we make use of a Green's function to determine the velocity potential resulting from the oscillating piston. In particular, introduce the Green's function, $G(\boldsymbol{x}|\boldsymbol{x}_0)$, that satisfies the Helmholtz equation with a Dirac source at $\boldsymbol{x}_0$ and a homogeneous Neumann boundary condition

$$[\nabla_{\boldsymbol{x}}^2 + (\omega/c_{\mathrm{s}})^2]\, G(\boldsymbol{x}|\boldsymbol{x}_0) = -\delta(\boldsymbol{x} - \boldsymbol{x}_0) \qquad z > 0 \tag{51.89a}$$

$$\hat{\boldsymbol{z}} \cdot \nabla_{\boldsymbol{x}} G(\boldsymbol{x}|\boldsymbol{x}_0) = 0 \qquad z = 0. \tag{51.89b}$$

Multiplying the Green's function equation (51.89a) by $\Phi(\boldsymbol{x})$ and integrating over $z \geq 0$ leads to

$$-\Phi(\boldsymbol{x}_0) = \int_{\mathscr{R}} \Phi(\boldsymbol{x})[\nabla_{\boldsymbol{x}}^2 + (\omega/c_{\mathrm{s}})^2]\, G(\boldsymbol{x}|\boldsymbol{x}_0)\, \mathrm{d}V_{\boldsymbol{x}}, \tag{51.90}$$

with integration by parts yielding

$$-\Phi(\boldsymbol{x}_0) = \int_{\mathscr{R}} \left[\nabla_{\boldsymbol{x}} \cdot (\Phi\, \nabla_{\boldsymbol{x}} G - G\, \nabla_{\boldsymbol{x}} \Phi) + G\, (\nabla^2 + (\omega/c)^2)\, \Phi\right] \mathrm{d}V_{\boldsymbol{x}}. \tag{51.91}$$

Setting $\nabla^2 + (\omega/c)^2)\Phi = 0$ as per the Helmholtz equation (51.88a), and use of the divergence theorem, renders

$$-\Phi(\boldsymbol{x}_0) = \int_{\partial\mathcal{R}} \hat{\boldsymbol{n}} \cdot (\Phi\, \nabla_{\boldsymbol{x}} G - G\, \nabla_{\boldsymbol{x}} \Phi)\, \mathrm{d}\mathcal{S}. \tag{51.92}$$

There are two boundaries to consider. The first is at $z = \infty$, at which we assume the fields vanishes so we can ignore this boundary. The second boundary is at $z = 0$, where $\hat{\boldsymbol{n}} = -\hat{\boldsymbol{z}}$ and the Neumann boundary conditions for G and Φ bring about the expression

$$-\Phi(\boldsymbol{x}_0) = \int_0^a \int_0^{2\pi} G\, \hat{\boldsymbol{z}} \cdot \nabla_{\boldsymbol{x}} \Phi\, r\, \mathrm{d}r\, \mathrm{d}\vartheta, \tag{51.93}$$

where ϑ is the polar angle. This is a very tidy result that says we merely need to determine the Green's function over the region of the piston, $r \leq a$ at $z = 0$, in order to determine the velocity potential and hence the acoustic wave field for the $z > 0$ half-space.

51.8.3 Method of images for the Green's function

We can make use of a special trick, known as the *method of images*, to determine the Green's function on the $z \geq 0$ half-space. For this purpose, recall the free space Green's function for the Helmholtz equation from Section 9.6.8, which satisfies

$$[\nabla^2 + (\omega/c)^2]\, \mathcal{G}(\boldsymbol{x}|\boldsymbol{x}_0) = -\delta(\boldsymbol{x} - \boldsymbol{x}_0), \tag{51.94}$$

and takes the form

$$\mathcal{G}(\boldsymbol{x}|\boldsymbol{x}_0) = \frac{\mathrm{e}^{\mathrm{i}\,|\boldsymbol{x}-\boldsymbol{x}_0|\,\omega/c}}{4\,\pi\,|\boldsymbol{x} - \boldsymbol{x}_0|}. \tag{51.95}$$

This Green's function does not satisfy the Neumann boundary condition at $z = 0$. However, to generate a Green's function that does, introduce another Dirac delta point source, $-\delta(\boldsymbol{x} - \overline{\boldsymbol{x}}_0)$, where the source is positioned at

$$\overline{\boldsymbol{x}}_0 = x_0\, \hat{\boldsymbol{x}} + y_0\, \hat{\boldsymbol{y}} - z_0\, \hat{\boldsymbol{z}}. \tag{51.96}$$

This Dirac source is at a position in the $z < 0$ half-space reflected across the $z = 0$ plane from the original source at $\boldsymbol{x}_0$. Notably, the new Dirac source never fires when the field point, $\boldsymbol{x}$, is in the upper, $z > 0$, half-space, just in the same manner that the original Dirac source, $\delta(\boldsymbol{x} - \boldsymbol{x}_0)$, never fires when the field point is in the $z < 0$ half space. Consequently, the Green's function resulting from these two Dirac sources satisfies the following equation set

$$[\nabla^2 + (\omega/c)^2]\, G(\boldsymbol{x}|\boldsymbol{x}_0) = -\delta(\boldsymbol{x} - \boldsymbol{x}_0) \quad z > 0 \tag{51.97a}$$

$$[\nabla^2 + (\omega/c)^2]\, G(\boldsymbol{x}|\boldsymbol{x}_0) = -\delta(\boldsymbol{x} - \overline{\boldsymbol{x}}_0) \quad z < 0 \tag{51.97b}$$

$$\hat{\boldsymbol{z}} \cdot \nabla G = 0 \quad z = 0, \tag{51.97c}$$

and it is given by the sum of the two free space Green's functions,

$$G(\boldsymbol{x}|\boldsymbol{x}_0) = \mathcal{G}(\boldsymbol{x}|\boldsymbol{x}_0) + \mathcal{G}(\boldsymbol{x}|\overline{\boldsymbol{x}}_0) = \frac{\mathrm{e}^{\mathrm{i}\,|\boldsymbol{x}-\boldsymbol{x}_0|\,\omega/c}}{4\,\pi\,|\boldsymbol{x} - \boldsymbol{x}_0|} + \frac{\mathrm{e}^{\mathrm{i}\,|\boldsymbol{x}-\overline{\boldsymbol{x}}_0|\,\omega/c}}{4\,\pi\,|\boldsymbol{x} - \overline{\boldsymbol{x}}_0|}. \tag{51.98}$$

The vanishing Neumann boundary condition (51.97c) results from taking the sum of the original free space Green's function and its image across the $z = 0$ plane, so that the vertical derivative of the two Green's functions cancel at $z = 0$. To verify this result, write

$$\partial_z[\mathcal{G}(\boldsymbol{x}|\boldsymbol{x}_0) + \mathcal{G}(\boldsymbol{x}|\overline{\boldsymbol{x}}_0)] = \partial_z[F(|\boldsymbol{x} - \boldsymbol{x}_0|) + F(|\boldsymbol{x} - |\overline{\boldsymbol{x}}_0|)] \tag{51.99a}$$

$$= F'(|\boldsymbol{x}-\boldsymbol{x}_0|)\frac{z-z_0}{|\boldsymbol{x}-\boldsymbol{x}_0|} + F'(|\boldsymbol{x}-\overline{\boldsymbol{x}}_0|)\frac{z-\overline{z}_0}{|\boldsymbol{x}-\overline{\boldsymbol{x}}_0|} \tag{51.99b}$$

$$= F'(|\boldsymbol{x}-\boldsymbol{x}_0|)\frac{z-z_0}{|\boldsymbol{x}-\boldsymbol{x}_0|} + F'(|\boldsymbol{x}-\overline{\boldsymbol{x}}_0|)\frac{z+z_0}{|\boldsymbol{x}-\overline{\boldsymbol{x}}_0|}, \tag{51.99c}$$

where F' is the derivative of the function. At $z=0$, the two distances are equal so that

$$|\boldsymbol{x}-\boldsymbol{x}_0| = |\boldsymbol{x}-\overline{\boldsymbol{x}}_0| \quad \text{and} \quad F'(|\boldsymbol{x}-\boldsymbol{x}_0|) = F'(|\boldsymbol{x}-\overline{\boldsymbol{x}}_0|) \quad \text{at } z=0, \tag{51.100}$$

which then yields the desired result

$$\partial_z G(\boldsymbol{x}|\boldsymbol{x}_0) = 0 \quad z=0. \tag{51.101}$$

Note that we are only interested in the boundary condition at $z=0$ and the behavior of the Green's function in the half-space $z>0$. We have no concern for what the Green's function does in the region $z<0$. So placement of an image source in the lower half-space is merely a trick to enable proper behavior in the $z\geq 0$ region of interest. This "method of images" constructed Green's function is indeed somewhat magical, as it produces precisely what we need yet without solving any new Green's function equation. Hence, it is a very useful method to construct the Green's function for certain highly symmetric configurations such as given here. However, it is not a general method, so we can only make use of it for certain very special cases. Even so, we accept such gifts when they are available, here providing the Green's function needed to determine the velocity potential, Φ, as per equation (51.93).

51.8.4 Velocity potential

Making use of the Green's function (51.98) within the expression (51.93) leads to the velocity potential

$$-\Phi(\boldsymbol{x}_0) = \frac{\mathrm{i}\,\epsilon\,a\,\omega}{2\pi}\int_0^a \int_0^{2\pi} \frac{\mathrm{e}^{\mathrm{i}\,|\boldsymbol{x}-\boldsymbol{x}_0|\,\omega/c}}{|\boldsymbol{x}-\boldsymbol{x}_0|}\, r\,\mathrm{d}r\,\mathrm{d}\vartheta, \tag{51.102}$$

where the integral is computed at $z=0$ within the region $r\leq a$ of the piston, and where we used the Neumann boundary condition (51.88c) for the velocity potential at $z=0$. Making use of the expression (51.87) for the velocity potential, Ψ, renders

$$\Psi(\boldsymbol{x}_0,t) = \Phi(\boldsymbol{x}_0)\,\mathrm{e}^{-\mathrm{i}\,\omega\,t} = -\frac{\mathrm{i}\,\epsilon\,a\,\omega}{2\pi}\int_0^a \int_0^{2\pi} \frac{\mathrm{e}^{\mathrm{i}\,(|\boldsymbol{x}-\boldsymbol{x}_0|\,\omega/c-\omega\,t)}}{|\boldsymbol{x}-\boldsymbol{x}_0|}\, r\,\mathrm{d}r\,\mathrm{d}\vartheta. \tag{51.103}$$

The velocity potential is constructed by integrating outgoing spherical waves over the area of the piston, with these waves having a strength that is proportional to the piston velocity. As shown in section 51 of *Fetter and Walecka* (2003), further evaluation of this integral reveals that the acoustic energy and power intensity display characteristic lobes as a function of the angle, β, relative to the vertical axis (see Figure 51.3).

51.8.5 Further study

This section is based on section 51 of *Fetter and Walecka* (2003). Further study of acoustic waves from a planar source can be found in section I.12 of *Lighthill* (1978).

51.9 Acoustic waves in a gently varying background

In Section 51.4.3 we developed the acoustic wave equations for linear waves propagating through a static yet inhomogeneous background state with both ρ_e and c_s functions of space. However,

subsequent analysis of acoustic waves was restricted to homogeneous background state whereby ρ_e and c_s are taken to be space and time constants. In this section we extend the geometric optics formalism from Section 50.3 to render equations for the propagation of acoustic wave energy through a spatially inhomogeneous yet static background.[8] We make use of the *WKBJ asymptotic method*, which is a powerful approach for a variety of purposes.[9] We also present Whitham's variational principle, which, as we show, offers a far more streamlined means to deriving the leading order equations. Both the WKBJ and variational methods make use of the *eikonal wave ansatz* (equation (51.124)) rather than a Fourier plane wave ansatz, with the more general ansatz needed since Fourier methods are not suited to inhomogeneous backgrounds.

51.9.1 Scalar potential for density-weighted velocity

Return to the derivation of the acoustic wave equation in Sections 51.4.3 and 51.4.4, now generalizing the velocity potential to include the spatially variable background density. Again, the linearized Euler equation (51.23), its curl, and the linearized continuity equation (51.24) are given by

$$\partial_t(\rho_e\,\boldsymbol{v}') = -\nabla p' \quad \text{and} \quad \partial_t[\nabla\times(\rho_e\,\boldsymbol{v}')] = 0 \quad \text{and} \quad \partial_t p' + \rho_e\, c_s^2\,\nabla\cdot\boldsymbol{v}' = 0. \tag{51.104}$$

Assuming a vanishing initial curl, $\nabla\times(\rho_e\,\boldsymbol{v}') = 0$, as appropriate for a static initial condition, allows us to focus on fluctuations that satisfy $\nabla\times(\rho_e\,\boldsymbol{v}') = 0$ for all time. We are thus led to introduce a scalar potential for the density-weighted velocity

$$\rho_e\,\boldsymbol{v}' = -\nabla\chi, \tag{51.105}$$

with χ having dimensions of density times squared length per time (compare to the velocity potential ψ in equation (51.30)). Use of χ in the linearized Euler equation (first of equation (51.104)) leads to

$$\nabla(\partial_t\chi - p') = 0. \tag{51.106}$$

Following the procedure from Section 51.4.4, we choose a gauge so that

$$p' = \partial_t\chi. \tag{51.107}$$

Using this expression for the pressure in the linearized continuity equation (third of equation (51.104)) renders the wave equation for the velocity potential

$$\frac{1}{\rho_e\,c_s^2}\frac{\partial^2\chi}{\partial t^2} - \nabla\cdot(\rho_e^{-1}\,\nabla\chi) = 0. \tag{51.108}$$

Once we have determined χ, then the pressure field is determined by taking the time derivative in equation (51.107), and the velocity is determined by taking the gradient according to equation (51.105).

51.9.2 Energetics

We studied the energetics of acoustic waves in Section 51.6. Here we provide a terse version of that discussion starting from the wave equation (51.108) and deriving the corresponding

[8] Restricting to static background simplifies the maths. Also, it is sufficient for many applications since acoustic waves are quite fast relative to the slower movement of fluid particles. Finally, as discussed by *Pierce* (1990), the acoustic wave equation picks up extra terms when moving through a time evolving background state, and we are only interested here in the familiar form of the acoustic wave equation.

[9] Chapter 10 of *Bender and Orszag* (1978) presents a thorough discussion of the WKBJ method from an applied mathematical perspective.

energy equation. Multiplying equation (51.108) by $\partial_t\chi$, and recalling that ρ_e and c_s are time independent, brings the first term to

$$[\rho_e\, c_s^2]^{-1}\, \partial_t\chi\, \partial_{tt}\chi = [2\,\rho_e\, c_s^2]^{-1}\, \partial_t(\partial_t\chi\, \partial_t\chi), \tag{51.109}$$

whereas the second term in equation (51.108) gives

$$-\partial_t\chi\, \nabla\cdot(\rho_e^{-1}\, \nabla\chi) = -\nabla\cdot(\rho_e^{-1}\, \partial_t\chi\, \nabla\chi) + \partial_t(\rho_e^{-1}\, \nabla\chi\cdot\nabla\chi)/2. \tag{51.110}$$

We are thus led to the energy conservation law

$$(1/2)\, \partial_t[(\rho_e\, c_s^2)^{-1}\, (\partial_t\chi)^2 + \rho_e^{-1}\, (\nabla\chi)^2] = \nabla\cdot(\rho_e^{-1}\, \partial_t\chi\, \nabla\chi), \tag{51.111}$$

which can be equivalently written

$$(1/2)\, \partial_t[(\rho_e\, c_s^2)^{-1}\, (p')^2 + \rho_e\, \boldsymbol{v}'\cdot\boldsymbol{v}'] = -\nabla\cdot(p'\, \boldsymbol{v}'), \tag{51.112}$$

which compares directly to the energy equation (51.77a) derived for fluctuations around a homogeneous background state.

51.9.3 Stress-energy-momentum tensor

As an aside, we here display the stress-energy-momentum tensor for acoustic waves, following the field theory formalism from Section 50.4.3. The Lagrangian density for acoustic waves can be written as

$$\mathscr{L} = (2\,\rho_e)^{-1}\, [c_s^{-2}\, (\partial_t\chi)^2 - (\nabla\chi)^2], \tag{51.113}$$

whose Euler-Lagrange field equation is the acoustic wave equation (51.108). The corresponding generalized momentum, Hamiltonian density, and energy flux (equation (46.64)) are given by

$$\mathscr{P} = \frac{\partial\mathscr{L}}{\partial(\partial_t\chi)} = (\rho_e\, c_s^2)^{-1}\, \partial_t\chi = p'/(\rho_e\, c_s^2) \tag{51.114a}$$

$$\mathscr{H} = \mathscr{P}\, \partial_t\chi - \mathscr{L} = (2\,\rho_e)^{-1}\, [c_s^{-2}\, (\partial_t\chi)^2 + (\nabla\chi)^2] = (1/2)\, [(\rho_e\, c_s^2)^{-1}\, (p')^2 + \rho_e\, \boldsymbol{v}'\cdot\boldsymbol{v}'] \tag{51.114b}$$

$$F^a = \frac{\partial\mathscr{L}}{\partial(\partial_{x^a}\chi)}\, \frac{\partial\chi}{\partial t} = -\rho_e^{-1}\, \nabla\chi\, \partial_t\chi = \boldsymbol{v}'\, p'. \tag{51.114c}$$

Since the Lagrangian has no explicit time dependence, the Hamiltonian satisfies a source-free continuity equation, which is equivalent to the wave energy equation (51.111)

$$\partial_t\mathscr{H} + \nabla\cdot\boldsymbol{F} = 0. \tag{51.115}$$

Likewise, for a background state that has no dependence on $x = x^1$, the corresponding wave momentum is conserved so that

$$\partial_t T^0{}_1 + \partial_a T^a{}_1 = 0. \tag{51.116}$$

Elements to the stress-energy-momentum tensor are generally given by equation (50.48) and take on the following form for acoustic waves

$$T^0{}_1 = (\rho_e\, c_s^2)^{-1}\, \partial_t\chi\, \partial_x\chi \tag{51.117a}$$

$$T^1{}_1 = -(2\,\rho_e)^{-1}\, [c_s^{-2}\, (\partial_t\chi)^2 - (\partial_x\chi)^2 + (\partial_y\chi)^2 + (\partial_z\chi)^2] \tag{51.117b}$$

$$T^2{}_1 = -(\rho_e)^{-1}\, \partial_y\chi\, \partial_x\chi \tag{51.117c}$$

$$T^3{}_1 = -(\rho_e)^{-1}\, \partial_z\chi\, \partial_x\chi, \tag{51.117d}$$

which can be written in the equivalent form

$$T^0{}_1 = -p'\,u'/c_s^2 \tag{51.118a}$$
$$T^1{}_1 = -[(\rho_e\,c_s^2)^{-1}\,(p')^2 - \rho_e\,(u')^2 + \rho_e\,(v')^2 + \rho_e\,(w')^2]/2 \tag{51.118b}$$
$$T^2{}_1 = -\rho_e\,u'\,v' \tag{51.118c}$$
$$T^3{}_1 = -\rho_e\,u'\,w'. \tag{51.118d}$$

In Exercise 51.3 we verify that the budget equation (51.116) holds for the acoustic waves using elements of the stress-energy-momentum tensor given by equations (51.118a)–(51.118d).

51.9.4 Alternative expression for the action

Following the observation in Sections 50.6 and 50.6, we write the action for acoustic waves in the form

$$\mathcal{S} = \frac{1}{2}\int_R \chi\,\hat{D}\chi\,\mathrm{d}V\,\mathrm{d}t, \tag{51.119}$$

where the acoustic linear operator, $\hat{D}$, is given by

$$-\hat{D} = (\rho_e\,c_s^2)^{-1}\,\partial_{tt} - \nabla(\rho_e^{-1})\cdot\nabla - \rho_e^{-1}\,\nabla^2. \tag{51.120}$$

To verify the expression (51.119), perform an integration by parts to find

$$2\,\mathsf{S} = -\int_R \partial_t[(\rho_e\,c_s^2)^{-1}\,\chi\,\partial_t\chi]\,\mathrm{d}V\,\mathrm{d}t + \int_R \nabla\cdot(\rho_e^{-1}\,\chi\,\nabla\chi)\,\mathrm{d}V\,\mathrm{d}t + 2\int_R \mathcal{L}\,\mathrm{d}V\,\mathrm{d}t, \tag{51.121}$$

where we introduced the Lagrangian density

$$\mathcal{L} = (2\,\rho_e)^{-1}\,[c_s^{-2}\,(\partial_t\chi)^2 - (\nabla\chi)^2], \tag{51.122}$$

from equation (51.113). Dropping boundary terms, which renders $\widehat{D}$ a self-adjoint wave operator, leads to the traditional form of the action

$$\mathcal{S} = \int_R \mathcal{L}\,\mathrm{d}V\,\mathrm{d}t. \tag{51.123}$$

51.9.5 Space and time scale separation

We are motivated by the hypothesis that waves moving through a gently varying inhomogeneous background are locally close to the plane wave form realized for homogeneous background. Asymptotic methods arising from this hypothesis were developed in Chapter 50, and here we apply it to acoustic waves. Rather the traveling plane wave ansatz (49.18) used for homogeneous media, we here consider the *eikonal wave ansatz*

$$\chi(\boldsymbol{x},t) = \mathrm{Re}[A(\boldsymbol{x},t)\,e^{\mathrm{i}\,\mathcal{P}(\boldsymbol{x},t)}] = A(\boldsymbol{x},t)\cos[\mathcal{P}(\boldsymbol{x},t)], \tag{51.124}$$

where $A > 0$ is the real amplitude and $\mathcal{P}$ is the phase introduced in Section 50.2. We assume that spatial variations of the wave amplitude scale according to the length scale, L, introduced by equation (50.3), so that

$$|\nabla A|/A \sim L^{-1} \sim |\nabla\rho_e|/\rho_e. \tag{51.125}$$

The complement assumption is that the phase function varies over a length scale that is much smaller than L, so that the local wavenumber satisfies equation (50.3), here written as

$$|\nabla \mathcal{P}| \gg L^{-1} \implies \frac{1/|\nabla \mathcal{P}|}{L} \ll 1. \tag{51.126}$$

Combined with the definition (51.125), the WKBJ approximation considers a wave amplitude and wave phase that satisfy

$$|\nabla A|/A \ll |\nabla \mathcal{P}| = |\boldsymbol{k}|. \tag{51.127}$$

The same arguments hold for the time scale of the waves, so that

$$|\partial_t A|/A \ll |\partial_t \mathcal{P}| = \omega. \tag{51.128}$$

In developing the WKBJ asymptotic equations from the eikonal wave ansatz, it can be useful to scale the phase by a small non-dimensional parameter, ϵ, in which case

$$\mathcal{P} = \varphi/\epsilon \quad \text{where} \quad |\nabla A|/A \sim |\nabla \varphi|, \tag{51.129}$$

and equation (51.127) then takes on the form

$$|\nabla A|/A \ll |\nabla \varphi|/\epsilon. \tag{51.130}$$

An equivalent means to organize similarly scaled terms is to write the wave function (51.124) in the form

$$\chi = A\, e^{\mathrm{i}\mathcal{P}/\sigma}, \tag{51.131}$$

where $\sigma = 1$ is used to organize the terms, with this approach used in Section 51.9.6.

51.9.6 The WKBJ asymptotic solution

We now plug in the eikonal wave ansatz (51.131) to the wave equation (51.133) to develop the WKBJ asymptotic equations that determine how the amplitude and phase evolve. The manipulations are straightforward but somewhat tedious and uninspired. We expose sufficient details to facilitate checking the maths.

Notation used for the WKBJ asymptotic expansion

In this subsection we find it useful to introduce the following notation

$$W = 1/(\rho_{\mathrm{e}}\, c_{\mathrm{s}}^2) \tag{51.132}$$

so that the wave equation (51.108) is written

$$W \frac{\partial^2 \chi}{\partial t^2} - \nabla \cdot (W\, c_{\mathrm{s}}^2\, \nabla \chi) = 0. \tag{51.133}$$

Likewise, the energy equation (51.111) takes on the form

$$(1/2)\, \partial_t \left[W\, (\partial_t \chi)^2 + W\, c_{\mathrm{s}}^2\, (\nabla \chi)^2 \right] = \nabla \cdot (W\, c_{\mathrm{s}}^2\, \partial_t \chi\, \nabla \chi), \tag{51.134}$$

so that the Hamiltonian density (i.e., the energy) and the energy flux are

$$\mathscr{H} = W\, [(\partial_t \chi)^2 + c_{\mathrm{s}}^2\, (\nabla \chi)^2]/2 \quad \text{and} \quad \boldsymbol{F} = -W\, c_{\mathrm{s}}^2\, \partial_t \chi\, \nabla \chi. \tag{51.135}$$

W does not appear in the dispersion relation derived below, thus motivating its introduction.

The derivatives

The derivatives are given by the following expressions, organized according to powers of σ:

$$e^{-\mathrm{i}\,\mathcal{P}/\sigma}\,\nabla\chi = (\mathrm{i}/\sigma)\,A\,\nabla\mathcal{P} + \nabla A \tag{51.136a}$$

$$e^{-\mathrm{i}\,\mathcal{P}/\sigma}\,\nabla^2\chi = -\sigma^{-2}\,A\,(\nabla\mathcal{P})^2 + (\mathrm{i}/\sigma)\,(2\,\nabla A\cdot\nabla\mathcal{P} + A\,\nabla^2\mathcal{P}) + \nabla^2 A \tag{51.136b}$$

$$e^{-\mathrm{i}\,\mathcal{P}/\sigma}\,\partial_{tt}\chi = -\sigma^{-2}\,A\,(\partial_t\mathcal{P})^2 + (\mathrm{i}/\sigma)\,(2\,\partial_t A\,\partial_t\mathcal{P} + A\,\partial_{tt}\mathcal{P}) + \partial_{tt}A, \tag{51.136c}$$

along with

$$\begin{aligned} e^{-\mathrm{i}\,\mathsf{P}/\sigma}\,\nabla\cdot(W\,c^2\,\nabla\chi) = W\,c_{\mathsf{s}}^2\,\big[-\sigma^{-2}\,A\,(\nabla\mathcal{P})^2 + (\mathrm{i}/\sigma)\,(2\,\nabla A\cdot\nabla\mathcal{P} + A\,\nabla^2\mathcal{P}) + \nabla^2 A\big] \\ + \nabla(W\,c_{\mathsf{s}}^2)\cdot[(\mathrm{i}/\sigma)\,A\,\nabla\mathcal{P} + \nabla A]. \end{aligned} \tag{51.137}$$

$\mathcal{O}(\sigma^{-2})$ terms

As for deriving the quasi-geostrophic equations in Part VIII of this book, when deriving asymptotic equations we balance terms according to powers of the expansion parameter, with σ the parameter for the present analysis. The $\mathcal{O}(\sigma^{-2})$ terms render

$$(\partial_t\mathcal{P})^2 = c_{\mathsf{s}}^2\,\nabla\mathcal{P}\cdot\nabla\mathcal{P} \Longrightarrow \omega^2 = c_{\mathsf{s}}^2\,|\boldsymbol{k}|^2. \tag{51.138}$$

This local dispersion relation is the same as the dispersion relation (51.42) holding for acoustic waves moving in a homogeneous media. Now, however, the angular frequency, wave speed, and wavenumber are each functions of the spatial position. This result accords with our original hypothesis that waves move through the inhomogeneous media with a local plane wave behavior. It also accords with the assumptions built into the ray theory studied in Sections 50.2 and 50.3.

$\mathcal{O}(\sigma^{-1})$ terms

The $\mathcal{O}(\sigma^{-1})$ balance yields

$$W\,(2\,\partial_t A\,\partial_t\mathcal{P} + A\,\partial_{tt}\mathcal{P}) = W\,c_{\mathsf{s}}^2\,(2\,\nabla A\cdot\nabla\mathcal{P} + A\,\nabla^2\mathcal{P}) + A\,\nabla\mathcal{P}\cdot\nabla(W\,c_{\mathsf{s}}^2), \tag{51.139}$$

which can be rearranged to the form

$$(\partial_t + \boldsymbol{c}_{\mathsf{p}}\cdot\nabla)A = -\frac{A}{2\,W\,\omega}\,[W\,\partial_t\omega + \nabla\cdot(\boldsymbol{k}\,W\,c_{\mathsf{s}}^2)]. \tag{51.140}$$

The left hand side is the time derivative of the amplitude computed by following the phase velocity,

$$\boldsymbol{c}_{\mathsf{p}} = c_{\mathsf{s}}\,\hat{\boldsymbol{k}} = (\omega/|\boldsymbol{k}|)\,\hat{\boldsymbol{k}}. \tag{51.141}$$

The right hand side of equation (51.140) is a source term that contributes to the amplitude change following the phase velocity. Furthermore, since the acoustic waves are non-dispersive, in which $\boldsymbol{c}_{\mathsf{p}} = \boldsymbol{c}_{\mathsf{g}}$, equation (51.140) can be written using the time derivative following a ray

$$-\frac{2\,\omega}{A}\,\frac{\mathrm{D}_t A}{\mathrm{D}t} = \partial_t\omega + \nabla\cdot(\boldsymbol{k}\,W\,c_{\mathsf{s}}^2)/W \tag{51.142a}$$

$$= \partial_t\omega + c_{\mathsf{s}}^2\,\nabla\cdot\boldsymbol{k} + \boldsymbol{k}\cdot\nabla c_{\mathsf{s}}^2 + c_{\mathsf{s}}^2\,\boldsymbol{k}\cdot(\nabla W)/W. \tag{51.142b}$$

Massaging the source terms

Terms on the right hand side of the amplitude equation (51.142b) provide sources for the wave amplitude along a ray. We find it useful to rearrange these terms by using the following expression

for the wavevector in an acoustic wave

$$\boldsymbol{k} = \boldsymbol{c}_{\mathsf{p}}\,|\boldsymbol{k}|/c_{\mathsf{s}} = \boldsymbol{c}_{\mathsf{p}}\,\omega/c_{\mathsf{s}}^2 = \boldsymbol{c}_{\mathsf{g}}\,\omega/c_{\mathsf{s}}^2, \tag{51.143}$$

so that

$$\nabla\cdot\boldsymbol{k} = (\omega/c_{\mathsf{s}}^2)\,\nabla\cdot\boldsymbol{c}_{\mathsf{g}} + \boldsymbol{c}_{\mathsf{g}}/c_{\mathsf{s}}^2\cdot\nabla\omega + \omega\,\boldsymbol{c}_{\mathsf{g}}\cdot\nabla c_{\mathsf{s}}^{-2}, \tag{51.144}$$

thus leading to

$$\partial_t\omega + c_{\mathsf{s}}^2\,\nabla\cdot\boldsymbol{k} + \boldsymbol{k}\cdot\nabla c_{\mathsf{s}}^2 = (\partial_t + \boldsymbol{c}_{\mathsf{g}}\cdot\nabla)\omega + \omega\,\nabla\cdot\boldsymbol{c}_{\mathsf{g}} + \omega\,c_{\mathsf{s}}^2\,\boldsymbol{c}_{\mathsf{g}}\cdot\nabla c_{\mathsf{s}}^{-2} + \boldsymbol{k}\cdot\nabla c_{\mathsf{s}}^2 \tag{51.145a}$$

$$= \frac{\mathrm{D}_{\mathsf{r}}\omega}{\mathrm{D}t} + \omega\,\nabla\cdot\boldsymbol{c}_{\mathsf{g}}, \tag{51.145b}$$

where we used

$$\omega\,c_{\mathsf{s}}^2\,\boldsymbol{c}_{\mathsf{g}}\cdot\nabla c_{\mathsf{s}}^{-2} = -2\,(\omega/c_{\mathsf{s}})\boldsymbol{c}_{\mathsf{g}}\cdot\nabla c_{\mathsf{s}} = -\omega\,c_{\mathsf{s}}^{-2}\,(c_{\mathsf{s}}^2\,\boldsymbol{k}/\omega)\cdot\nabla c_{\mathsf{s}}^2 = -\boldsymbol{k}\cdot\nabla c_{\mathsf{s}}^2. \tag{51.146}$$

These results then lead to the amplitude equation

$$\frac{1}{A}\,\frac{\mathrm{D}_{\mathsf{r}}A}{\mathrm{D}t} = -\frac{1}{2\,\omega}\,\frac{\mathrm{D}_{\mathsf{r}}\omega}{\mathrm{D}t} - \nabla\cdot(\boldsymbol{c}_{\mathsf{g}}\,W)/(2\,W). \tag{51.147}$$

The dispersion relation has no explicit time dependence given that the background state is time independent. As a result, equation (50.34) from geometric optics means that the angular frequency remains constant along a ray, so that $\mathrm{D}_{\mathsf{r}}\omega/\mathrm{D}t = 0$. Even so, we retain this term since it hints at the more general case holding for time dependent background states.

For the second term on the right hand side of equation (51.147) we set $W^{-1} = \rho_{\mathsf{e}}\,c_{\mathsf{s}}^2$ from equation (51.132) to have

$$-\nabla\cdot(\boldsymbol{c}_{\mathsf{g}}\,W)/(2\,W) = -(\rho_{\mathsf{e}}\,c_{\mathsf{s}}^2/2)\,\nabla\cdot(\boldsymbol{c}_{\mathsf{g}}/\rho_{\mathsf{e}}\,c_{\mathsf{s}}^2) = -\nabla\cdot\boldsymbol{c}_{\mathsf{g}}/2 + \boldsymbol{c}_{\mathsf{g}}\cdot\nabla(\rho_{\mathsf{e}}\,c_{\mathsf{s}}^2)/(2\,\rho_{\mathsf{e}}\,c_{\mathsf{s}}^2), \tag{51.148}$$

so that equation (51.147) takes the form

$$\frac{2}{A}\,\frac{\mathrm{D}_{\mathsf{r}}A}{\mathrm{D}t} + \frac{1}{\omega}\,\frac{\mathrm{D}_{\mathsf{r}}\omega}{\mathrm{D}t} = -\nabla\cdot\boldsymbol{c}_{\mathsf{g}} + \boldsymbol{c}_{\mathsf{g}}\cdot\nabla(\rho_{\mathsf{e}}\,c_{\mathsf{s}}^2)/(\rho_{\mathsf{e}}\,c_{\mathsf{s}}^2). \tag{51.149}$$

Since $\rho_{\mathsf{e}}\,c_{\mathsf{s}}^2$ is assumed to be time independent, we can write this equation as

$$\frac{2}{A}\,\frac{\mathrm{D}_{\mathsf{r}}A}{\mathrm{D}t} + \frac{1}{\omega}\,\frac{\mathrm{D}_{\mathsf{r}}\omega}{\mathrm{D}t} - \frac{\mathrm{D}_{\mathsf{r}}(\rho_{\mathsf{e}}\,c_{\mathsf{s}}^2)}{\mathrm{D}t} = -\nabla\cdot\boldsymbol{c}_{\mathsf{g}}, \tag{51.150}$$

which combines to read

$$\frac{\mathrm{D}_{\mathsf{r}}[(A^2\,\omega)/(\rho_{\mathsf{e}}\,c_{\mathsf{s}}^2)]}{\mathrm{D}t} = -(A^2\,\omega)/(\rho_{\mathsf{e}}\,c_{\mathsf{s}}^2)\,\nabla\cdot\boldsymbol{c}_{\mathsf{g}}, \tag{51.151}$$

which can be written as the flux-form conservation equation

$$\partial_t[A^2\,\omega/(\rho_{\mathsf{e}}\,c_{\mathsf{s}}^2)] + \nabla\cdot[\boldsymbol{c}_{\mathsf{g}}\,A^2\,\omega/(\rho_{\mathsf{e}}\,c_{\mathsf{s}}^2)] = 0. \tag{51.152}$$

In Section 51.9.7 we interpret this equation in terms of phase averaged energy and wave action.

51.9.7 Phase averaged energy

We here compute the phase averaged Hamiltonian (energy) consistent with the assumed scaling from Section 51.9.5. Working with the real expression (51.124) leads to

$$\partial_t \chi = A\,[A^{-1}\,\partial_t A \cos\mathcal{P} - \partial_t \mathcal{P} \sin\mathcal{P}] \approx A\,\omega \sin\mathcal{P}, \tag{51.153}$$

where $A^{-1}\,\partial_t A \ll \omega$ as per the assumed scaling (51.128), and $\omega = -\partial_t \mathcal{P}$ as per equation (50.2). Similarly, we compute the gradient as

$$\nabla \chi = A\,[A^{-1}\,\nabla A \cos\mathcal{P} - \nabla\mathcal{P} \sin\mathcal{P}] \approx -A\,\boldsymbol{k} \sin\mathcal{P}, \tag{51.154}$$

which follows from the scaling (51.127) and $\boldsymbol{k} = \nabla\mathcal{P}$ from equation (50.2). We thus have the expression for the Hamiltonian

$$\mathscr{H} = \frac{A^2 \sin^2\mathcal{P}\,(\omega^2 + c_{\mathrm{s}}^2\,|\boldsymbol{k}|^2)}{2\,\rho_{\mathrm{e}}\,c_{\mathrm{s}}^2} = \frac{\omega^2\,A^2 \sin^2\mathcal{P}}{\rho_{\mathrm{e}}\,c_{\mathrm{s}}^2}, \tag{51.155}$$

where we inserted the dispersion relation (51.138). Taking the phase average leads to

$$\langle\mathscr{H}\rangle = \frac{\omega^2\,A^2}{2\,\rho_{\mathrm{e}}\,c_{\mathrm{s}}^2}. \tag{51.156}$$

Making use of the phase averaged energy (51.156) in the amplitude equation (51.152) leads to

$$\partial_t(\langle\mathscr{H}\rangle/\omega) + \nabla\cdot(\boldsymbol{c}_{\mathrm{g}}\,\langle\mathscr{H}\rangle/\omega) = 0. \tag{51.157}$$

The quantity

$$\mathcal{A} = \langle\mathscr{H}\rangle/\omega \tag{51.158}$$

is the *wave action* that we studied in Section 50.5.

51.9.8 Whitham's variational principle

We studied Whitham's variational principle in Section 50.5, where we claimed that it offers a more streamlined means to derive the leading order phase averaged equations than the WKBJ method used in Sections 51.9.6 and 51.9.7. Taking the results from Section 50.5, we write the phase averaged acoustic Lagrangian (51.113)

$$\langle\mathscr{L}\rangle = (4\,\rho_{\mathrm{e}})^{-1}\,A^2\,(c_{\mathrm{s}}^{-2}\,\omega^2 - |\boldsymbol{k}|^2). \tag{51.159}$$

The dispersion relation arises from the Euler-Lagrange equation resulting from a variation of the wave amplitude,

$$\partial\langle\mathscr{L}\rangle/\partial A = 0 \Longrightarrow \omega^2 = c_{\mathrm{s}}^2\,|\boldsymbol{k}|^2. \tag{51.160}$$

Likewise, the Euler-Lagrange equation corresponding to varying the phase function yields the wave action conservation equation

$$\partial_t(\mathcal{A}) + \nabla\cdot(\boldsymbol{c}_{\mathrm{g}}\,\mathcal{A}) = 0, \tag{51.161}$$

where $\boldsymbol{c}_{\mathrm{g}} = c_{\mathrm{s}}\,\hat{\boldsymbol{k}}$ is the group velocity and the wave action is

$$\mathcal{A} = \partial\langle\mathscr{L}\rangle/\partial\omega = \frac{\omega\,A^2}{2\,\rho_{\mathrm{e}}\,c_{\mathrm{s}}^2} = \langle\mathscr{H}\rangle/\omega. \tag{51.162}$$

Evidently, we only needed the phase averaged Lagrangian to leading order when using Whitham's principle to derive both the dispersion relation and the wave action conservation equation. In contrast, the WKBJ method required one order higher in the asymptotics when working with the wave equation to derive wave action conservation, which required a relatively large amount of manipulation.

The relative simplicity of Whitham's variational principle, compared to the WKBJ method, is reminscent of analytic mechanics versus Newtonian mechanics. As shown through a variety of case studies in Chapter 15, analytical mechanics is far more powerful for the study of systems that are generally quite tedious, if not unavailable, using Newtonian mechanics. The price to pay is that analytical mechanics requires some relatively nontrivial theoretical work up front to establish the framework. But once established, exposure of the underlying symmetries and conservation laws is far more streamlined, if not trivial. Likewise, Whitham's variational principle requires some theoretical work up front to derive the framework (Section 50.5). The payoff is that the variational framework is optimized for capturing the leading order physics of phase averaged wave mechanics.

51.9.9 Further study

The WKBJ treatment here followed that given in Section 7.3 of *Thorne and Blandford* (2017). However, we limited attention to the case of a static background state since we only developed the physics for acoustic waves moving in a static inhomogenous background (Section 51.4.2). *Pierce* (1990) considers the more general case with a space and time dependent background, in which the acoustic wave equation contains further terms.

51.10 Exercises

EXERCISE 51.1: ACOUSTIC MODES IN RECTANGULAR CAVITY (PROBLEM 9.1 OF *Fetter and Walecka* (2003))
A rectangular cavity with dimensions $x \in [0, L_x]$, $y \in [0, L_y]$, and $z \in [0, L_z]$ is bounded by rigid material walls on all sides. The fluid is homogeneous within the cavity. Determine the eigenfrequencies and eigenfunctions for the acoustic normal modes in this cavity.

Hint: this exercise requires solving the acoustic wave equation in a closed domain with associated kinematic boundary conditions. The resulting acoustic modes are standing wave modes rather than traveling waves, and the wavenumbers are quantized rather than continuous. Note that standing wave modes can be thought of as the superposition of two oppositvely traveling waves with identical stucture. For example, the sum of a right and left moving wave with equal amplitude, wavenumber, and frequency is given by the standing wave pattern

$$A\cos(k\,x - \omega\,t) + A\cos(k\,x + \omega\,t) = 2\,A\cos(\omega\,t)\cos(k\,x). \tag{51.163}$$

EXERCISE 51.2: PRESSURE FLUCTUATIONS RELATIVE TO A UNIFORM FLOW (PROBLEM 9.4 OF *Fetter and Walecka* (2003))
Consider a homogeneous and compressible fluid with uniform flow, $\boldsymbol{v}$. Show that the pressure fluctuations relative to this fluid flow state satisfy

$$(\partial_t + \boldsymbol{v}\cdot\nabla)^2\,p - c_s^2\,\nabla^2 p = 0. \tag{51.164}$$

Hint: ths solution is a one-liner that results from linearizing equation (51.19) with a nonzero background flow.

EXERCISE 51.3: MOMENTUM BUDGET FOR ACOUSTIC WAVES

Verify that the budget equation (51.116) holds for the acoustic waves, with elements of the stress-energy-momentum tensor given by equations (51.118a)–(51.118d).

Chapter 52

INTERFACIAL WAVES ON POTENTIAL FLOW

In this chapter we study *interfacial waves*, which are waves occuring at the interface between two homogeneous (constant density) fluid layers. We limit the study to the case where the upper layer has zero density, with this idealization motivated by the study of waves on the surface of the ocean under a massless atmosphere, referred to here as *surface waves*. We are here concerned with two restoring forces that affect small amplitude motion relative to a static equilibrium base state. One force arises from gravitation in the presence of a density jump between the two fluid layers; i.e., the buoyancy studied in Chapter 30. The other force arises from surface tension due to molecular forces at the interface (see Section 25.11).

To help understand the basics of surface waves along the ocean's free surface, consider a water parcel that rises above its equilibrium level into an environment where it is heavier than the surrounding atmosphere, in which case the water parcel experiences a downward buoyancy force that returns it to its equilibrium level. However, this motion generally overshoots the equilibrium level, at which point the parcel feels an upward buoyancy force. This up and down motion results in the exchange between kinetic energy and potential energy for the parcel, with the spatio-temporal organization of the oscillations constituting a *surface gravity wave*. A similar picture holds for *capillary waves* that arise from surface tension acting as the restoring force. By ignoring planetary rotation we tacitly focus on ocean surface waves whose lateral extent is too short to be affected by the planetary Coriolis acceleration. That is, we are concerned with surface waves and capillary waves that can be visually observed.

The interfacial waves studied in this chapter do not carry vorticity within the fluid interior, thus enabling use of irrotational fluid mechanics. In this case, the fluid velocity can be written as the gradient of a scalar potential, thus leading to the term *potential flow*. We also pursued the methods of potential flow in Chapter 51 when studying acoustic waves. Yet here the surface waves appear in a fluid with a strictly constant density, thus removing any acoustic modes and rendering non-divergent flow. A flow that is both irrotational and non-divergent is described by a scalar potential that satisfies Laplace's equation (Section 6.5); i.e., the potential is a harmonic function. Waves arise solely through the role of the boundary condition placed at the interface. Furthermore, the waves propagate in the horizontal direction along the interface and exponentially decay in the vertical, with a vertical decay scale directly related to the horizontal wavenumber. Mathematically, this coupling of the horizontal and vertical length scales is a direct result of the scalar potential satisfying Laplace's equation.

Gravity waves along an interface are transverse in the horizontal direction, meaning fluid particles move perpendicular to the wave. Furthermore, the waves do not propagate vertically and they induce vertical particle motion whose amplitude exponentially vanishes with depth in the ocean layer. Although the surface gravity waves we study in this chapter are linear, the depth decay in their amplitude leads to a net drift of fluid particles and hence to the transport of matter. This matter transport is known as *Stokes drift*, which plays an important role in the transport of matter at the ocean surface. Stokes drift provides the canonical example of how averaging at a fixed point in space (Eulerian average) yields distinct behaviors from averaging

on a fixed fluid particle (Lagrangian average).[1]

READER'S GUIDE TO THIS CHAPTER

We make use of dynamical ideas from Chapter 24, elements of the filtered equations from Chapter 27, and salient features of wave kinematics from Chapter 49. The study of capillary waves requires an understanding of surface tension in Section 25.11. We also use ideas from partial differential equations introduced in Chapter 6. The mathematical description of Stokes drift requires an understanding of Eulerian and Lagrangian kinematic descriptions from Chapter 17. Generalizations of Stokes drift appear in Chapter 70 in our study of wave-mean flow interactions, isopycnal averaging, and the corresponding eddy-induced tracer transport. In this chapter we only consider waves at the upper surface of a single massive fluid layer, whereas in Chapter 60 we extend this analysis to the case of two massive fluid layers as part of a study of the Rayleigh-Taylor and Kelvin-Helmholtz instabilities. Finally, note that Chapter 10 in *Fetter and Walecka* (2003) and chapter 13 *Whitham* (1974) work through a number of examples, and in so doing they provide great practice in the mathematical physics of surface waves.

We use Cartesian coordinates throughout this chapter.

[1] Certain treatments of linear waves suggests that they affect a zero drift of matter. However, the Stokes drift by surface gravity waves provides an example where linear waves can transport matter. As noted in Section 52.11.5, the Lagrangian kinematics of particle trajectories introduces nonlinearites that lead to Stokes drift.

52.1 Loose threads

- Waves using Luke's variational principle as per *Miles* (1977) and *Milder* (1977).
- When can we naively use Eulerian coordinates for Hamilton's principle versus the introduction of auxiliary fields? I believe potential flow is quite forgiving on these matters.
- Build on the following ideas. Much more to think about here.

  Potential flow provides an example of a *scalar field theory*, which is distinctively less complex than the vector field theory encountered when the flow is less constrained. In particular, one need not worry about the Lagrangian approach, and can thus use Eulerian coordinates naively, much as done in other areas of field theory.

52.2 Potential flow in a homogeneous fluid layer

Throughout this chapter we assume the fluid is inviscid with constant density and with a flow that has zero vorticity.[2] These assumptions greatly simplify the expression for the velocity field, which is both non-divergent and irrotational. In this section we establish some general results for a perfect homogeneous fluid with a velocity that is non-divergent and irrotational; i.e., for *potential flow*.

We are concerned with a single layer of homogeneous fluid bounded below by a solid material surface and above by a free material surface, and refer to this layer as an "ocean". We depict the flat bottom case in Figure 52.1, showing the material free upper ocean surface at $z = \eta(x, y, t)$

[2] A more general approach can be considered in which the flow is decomposed into a potential flow (irrotational) and a vortical flow. However, for linear fluctuations these two flows are uncoupled. As we are unconcerned with vortical flow in this chapter, we set the vorticity to zero and thus focus on the potential flow.

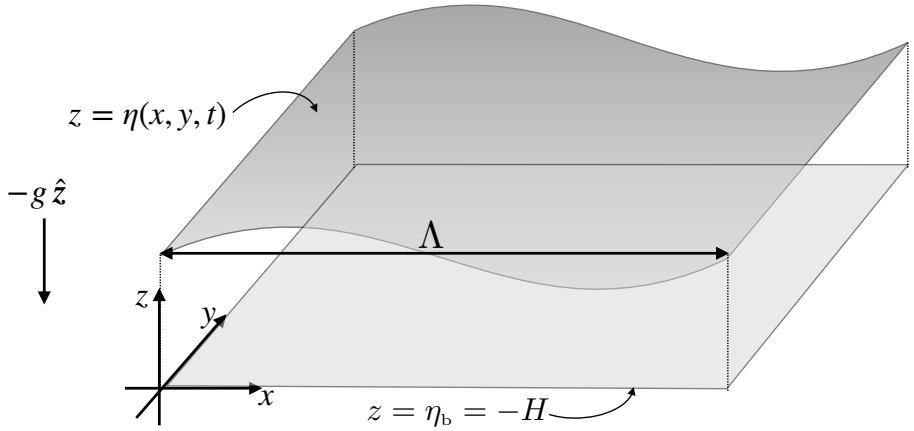

FIGURE 52.1: A depiction of an "ocean" comprised of a homogeneous (i.e., constant density) fluid with an upper free surface that is a moving material interface. The atmosphere applies a pressure to the ocean due to its mass; however, that mass is assumed to be uniform and static so that it does not affect surface motion. Linear fluctuations of the free surface exhibit gravity wave motion due to the restoring effects from a uniform gravitational field, $\boldsymbol{g} = -g\,\hat{\boldsymbol{z}}$, as well as capillary waves due to surface tension. We here depict a single wave with wavelength, Λ, with the wavevector parallel to the $\hat{\boldsymbol{x}}$ direction. We assume the fluid layer retains a fixed volume so that the domain integral of the free surface is constant, $\int \eta \, \mathrm{d}x \, \mathrm{d}y = \text{constant}$. This property follows from the assumption that the free surface is material.

separating a homogeneous ocean from a homogeneous atmosphere. The mass of the atmosphere is assumed to be horizontally uniform and static, even as its bottom boundary (the layer free surface) undulates. This approximation treatment means that atmospheric pressure does not contribute to motion of the ocean fluid layer. The ocean boundaries are material so that the mass of the ocean (equal to the ocean volume times the constant density, ρ) is fixed. Consequently, the domain integral of the free surface is constant,

$$\int \eta \, \mathrm{d}x \, \mathrm{d}y = \int \eta \, \mathrm{d}A = \text{constant}. \tag{52.1}$$

52.2.1 Motivating the irrotational assumption

We are familiar with the non-divergent flow assumption, which is part of the Boussinesq ocean studied in Chapter 29. However, we find it necessary to justify the assumption of irrotational flow, which also appeared in Chapter 51 when studying acoustic waves, and yet is not the case for most other geophysical waves encountered in this book. For this purpose, consider the equation of motion for a perfect non-rotating homogeneous fluid in a gravity field

$$\rho \, \mathrm{D}\boldsymbol{v}/\mathrm{D}t = -\nabla p - \rho \, \nabla \Phi, \tag{52.2}$$

where we assume the simple form of the geopotential (Section 13.10.4),

$$\Phi = g \, z, \tag{52.3}$$

with g the constant and uniform gravitational acceleration. As in our discussion of the Boussinesq ocean in Section 29.1.1, we remove the static background pressure by writing

$$p = -g \, \rho \, z + p_{\mathrm{d}} = -\rho \, \Phi + p_{\mathrm{d}}, \tag{52.4}$$

in which case the velocity equation (52.2) becomes

$$\rho \, \mathrm{D}\boldsymbol{v}/\mathrm{D}t = -\nabla p_{\mathrm{d}}. \tag{52.5}$$

When studying linear waves later in this chapter, this equation is linearized by dropping self-advection so that

$$\rho \, \partial_t \boldsymbol{v} = -\nabla p_{\mathrm{d}}. \tag{52.6}$$

The pressure gradient cannot impart any vorticity to the velocity time tendency since $\nabla \times \nabla p_{\mathrm{d}} = 0$. Evidently, if the velocity is initialized with zero vorticity, then the linearized equations of motion retain that zero vorticity. We thus examine linear fluctuations around a zero vorticity rest state, just as we did for the study of acoustic waves in Chapter 51.

This result offers motivation for studying properties of fluid flow with an irrotational velocity. In the remainder of this section we establish some general results for a perfect homogeneous fluid in non-rotating reference frame feeling a uniform gravity field and with an irrotational velocity. These results hold for the full nonlinear equations of motion and will later be specialized to the linear equations.

52.2.2 Harmonic scalar potential

A velocity field that has zero vorticity

$$\boldsymbol{\omega} = \nabla \times \boldsymbol{v} = 0, \tag{52.7}$$

can be written as the gradient of a scalar potential (see Section 2.3.2)[3]

$$\boldsymbol{v} = -\nabla \psi. \tag{52.8}$$

The scalar potential is unspecified up to an arbitrary function of time. The reason for this arbitrariness is that ψ and $\psi + F(t)$ yield the same velocity field, where $F(t)$ is any spatially constant function of time. We make use of this *gauge* degree of freedom in Section 52.2.3, just like we did for acoustic waves in Section 51.4.4.

Since the fluid is assumed to have uniform density, mass conservation in the form of the continuity equation (19.16) implies that the velocity field is non-divergent. Consequently, the scalar potential satisfies Laplace's equation (Section 2.3.3)

$$\nabla \cdot \boldsymbol{v} = -\nabla \cdot \nabla \psi = -\nabla^2 \psi = 0, \tag{52.9}$$

in which we say that ψ is a *harmonic function*. We develop salient mathematical properties for harmonic functions in Section 6.5.

Harmonic functions do not support spatial oscillations in all three directions since the sum of the curvature in each direction (i.e., second partial derivatives) must vanish. Correspondingly, we will find that the velocity potential supports traveling waves in the horizontal and exponentially decaying in the vertical, with decay when moving away from the surface boundary. It is remarkable that the wavenumber of the horizontally traveling waves also determines the vertical decay scale. That is, the structure of the horizontal waves directly determines the vertical structure.

52.2.3 Equation of motion and Bernoulli's principle

To fully specify the scalar potential requires boundary conditions, which enter the development via the equation of motion. The vector-invariant equation of motion (24.32) for a non-rotating,

[3] The minus sign in equation (52.8) is conventional.

irrotational, inviscid, uniform density fluid is given by

$$\partial_t \boldsymbol{v} = -\nabla(\Phi + \mathcal{K} + p/\rho), \tag{52.10}$$

with

$$\mathcal{K} = \boldsymbol{v} \cdot \boldsymbol{v}/2 \tag{52.11}$$

the kinetic energy per mass of a fluid element. Inserting the scalar potential, $\boldsymbol{v} = -\nabla\psi$, brings the equation of motion (52.10) to the form

$$\nabla \left(\Phi + \mathcal{K} + p/\rho - \partial_t \psi\right) = 0. \tag{52.12}$$

This equation means that everywhere in the fluid the dynamical fields satisfy

$$\Phi + \mathcal{K} + p/\rho - \partial_t \psi = C(t), \tag{52.13}$$

for some arbitrary time dependent function, $C(t)$. This equation is a particular expression of Bernoulli's theorem studied in Section 26.9.3.

We ascribe no physical significance to the arbitrary function, $C(t)$, appearing in equation (52.13). In fact, it can be completely removed by exploiting the gauge degree of freedom in the scalar potential as noted following equation (52.8). We do so by introducing a modified scalar potential

$$\Psi(\boldsymbol{x}, t) = \psi(\boldsymbol{x}, t) + \int_0^t C(t')\, \mathrm{d}t'. \tag{52.14}$$

Both ψ and Ψ lead to the same velocity vector

$$\boldsymbol{v} = -\nabla\psi = -\nabla\Psi, \tag{52.15}$$

and as such the two scalar potentials are physically indistinguishable. However, Ψ is more convenient for our use since it absorbs the arbitrary time dependent function, $C(t)$, thus rendering the simpler expression for the equation of motion

$$\partial_t \Psi = \Phi + \mathcal{K} + p/\rho. \tag{52.16}$$

In this manner we have dispensed with the need to compute $C(t)$ since it is sufficient to work with Ψ. In the following, we refer to equation (52.16) as the *Bernoulli equation of motion.*

52.2.4 Concerning the pressure field

We here explore facets of the pressure field as decomposed into either its hydrostatic and non-hydrostatic components, or its dynamically active and inactive components.

Two methods for decomposing pressure

In Section 52.2.1 we decomposed the pressure into its dynamically inactive component, $-\rho\, g\, z$, and dynamically active component, p_{d}. We can consider the alternative decomposition into hydrostatic and non-hydrostatic pressure components. As we will see, the dynamically active pressure is partly hydrostatic, due to motion of the free surface, and partly non-hydrostatic. We also considered these two decompositions of pressure when discussing effective buoyancy in Section 30.11, yet the discussion here is far simpler since the fluid has constant density.

Hydrostatic and non-hydrostatic pressures

The Bernoulli equation of motion (52.16) yields the vertical derivative of pressure

$$\partial_z p = -\rho\,\partial_z\Phi + \rho\,\partial_z(\partial_t\Psi - \mathcal{K}) = \partial_z p_{\text{h}} + \partial_z p_{\text{nh}}. \tag{52.17}$$

We here identified two contributions to the pressure. The hydrostatic pressure satisfies

$$\partial_z p_{\text{h}} = -\rho\,\partial_z\Phi = -\rho\,g \Longrightarrow p_{\text{h}} = -\rho\,g\,(z-\eta) = -\rho\,\Phi + \rho\,g\,\eta. \tag{52.18}$$

This expression reveals that part of the hydrostatic pressure is the dynamically inactive pressure, $-\rho\,\Phi = -\rho\,g\,z$, as discussed in Section 52.2.1, plus a dynamically active portion due to undulations of the free surface. The non-hydrostatic pressure has a vertical derivative given by

$$\partial_z p_{\text{nh}} = \rho\,\partial_z(\partial_t\Psi - \mathcal{K}). \tag{52.19}$$

Note that plugging in the hydrostatic pressure (52.18) into the Bernoulli equation of motion (52.16) leads to

$$\partial_t\Psi = \mathcal{K} + g\,\eta + p_{\text{nh}}/\rho, \tag{52.20}$$

whose vertical derivative yields equation (52.19) (recall $\eta = \eta(x,y,t)$ is depth independent).

Equation (52.19) indicates that depth variations in the kinetic energy and depth-time variations in the velocity potential lead the pressure to deviate from locally hydrostatic. We do not generally expect the flow to be hydrostatically balanced for two reasons: (i) the fluid layer has a uniform density so there is no stratification to suppress vertical accelerations that contribute to non-hydrostatic pressures; (ii) the fluid is nonrotating and so there is no vertical stiffening via the Taylor-Proudman result (Section 31.5.3), with vertical stiffening acting to suppress vertical accelerations that cause deviations from hydrostatic balance. Casual observations of surface ocean waves also supports the nontrivial vertical accelerations present in surface gravity waves, thus suggesting a key role for the non-hydrostatic pressure.

Comments on a hydrostatic shallow water layer

For the shallow water model we also consider a homogenous density layer. However, as emphasized in Chapter 35, the hydrostatic balance is fundamental to shallow water dynamics. Indeed, in Section 35.2 we see that the hydrostatic balance over a single homogeneous layer leads to horizontal motion that is depth independent throughout the layer. Hence, $\partial_z(\partial_t\Psi) = 0$ and the kinetic energy contained in the horizontal flow is depth independent, $\partial_z(u^2+v^2) = 0$. Furthermore, the vertical motion has a linear depth dependence across the shallow water layer (Section 35.2.8) and its magnitude is far smaller than horizontal motions. Therfore, we can drop all contributions to $\partial_z\mathcal{K}$ for the shallow water layer, in which case equation (52.17) reduces to the hydrostatic limit

$$\partial_z p = -\rho\,\partial_z\Phi = -\rho\,g \qquad \text{hydrostatic (shallow water) limit.} \tag{52.21}$$

This limit is relevant when the horizontal scales of motion are far larger than the vertical: $L \gg H$, in which case the flow is well approximated as hydrostatic.

So in summary, a homogeneous layer of fluid can have a depth dependence to its horizontal flow, and that depth dependence is driven through non-hydrostatic pressure forces. In contrast, hydrostatic pressure has a depth-independent horizontal gradient within a homogeneous layer

$$\partial_z(\nabla_{\text{h}} p_{\text{h}}) = -g\,\nabla_{\text{h}}\rho = 0 \qquad \text{homogeneous density layer.} \tag{52.22}$$

Consequently, a hydrostatic pressure cannot drive depth dependence to the horizontal velocity

field in a homogeneous fluid.

52.2.5 Bernoulli equation of motion and boundary conditions

Decompositions of the pressure discussed in Sections 52.2.1 and 52.2.4 render the following equivalent expressions for the Bernoulli equation of motion

$$\partial_t \Psi = \mathcal{K} + g\, z + p/\rho \qquad \text{full pressure form} \tag{52.23a}$$
$$\partial_t \Psi = \mathcal{K} + p_{\mathsf{d}}/\rho \qquad \text{dynamically active/inactive pressure split} \tag{52.23b}$$
$$\partial_t \Psi = \mathcal{K} + g\, \eta + p_{\mathsf{nh}}/\rho \qquad \text{hydrostatic/non-hydrostatic pressure split.} \tag{52.23c}$$

With the velocity given by $\boldsymbol{v} = -\nabla\Psi$, we take the gradient of equations (52.23a)-(52.23c) to render the velocity equations

$$\partial_t \boldsymbol{v} = -\nabla(\mathcal{K} + g\, z + p/\rho) \qquad \text{full pressure form} \tag{52.24a}$$
$$\partial_t \boldsymbol{v} = -\nabla(\mathcal{K} + p_{\mathsf{d}}/\rho) \qquad \text{dynamically active/inactive pressure split} \tag{52.24b}$$
$$\partial_t \boldsymbol{v} = -\nabla(\mathcal{K} + g\, \eta + p_{\mathsf{nh}}/\rho) \qquad \text{hydrostatic/non-hydrostatic pressure split.} \tag{52.24c}$$

A complete specification of the mathematical physics for this system requires the kinematic and dynamic boundary conditions given by the following.

Kinematic free surface boundary condition

The free surface is a moving material interface, so that its kinematics are described by the surface kinematic boundary condition (19.66) holding for a non-divergent flow at a material boundary

$$(\partial_t + \boldsymbol{u} \cdot \nabla)\eta = w \qquad \text{kinematic b.c. at } z = \eta(x, y, t). \tag{52.25}$$

When $\hat{\boldsymbol{n}}$ has a nonzero vertical component (always assumed to hold in this chapter), the surface kinematic boundary condition can be written in the equivalent form

$$\boldsymbol{v} \cdot \hat{\boldsymbol{n}} = \frac{\partial_t \eta}{|\nabla(z - \eta)|}, \tag{52.26}$$

where the outward normal is

$$\hat{\boldsymbol{n}} = \frac{\nabla(z - \eta)}{|\nabla(z - \eta)|} = \frac{\hat{\boldsymbol{z}} - \nabla\eta}{\sqrt{1 + \nabla\eta \cdot \nabla\eta}}. \tag{52.27}$$

It is furthermore convenient to make use of the relation between the area elements on the free surface given by equation (19.91)

$$\mathrm{d}\mathcal{S} = |\nabla(z - \eta)|\, \mathrm{d}A \quad \text{with} \quad \mathrm{d}A = \mathrm{d}x\, \mathrm{d}y, \tag{52.28}$$

where $\mathrm{d}A$ is the horizontal projection of $\mathrm{d}\mathcal{S}$. Consequently, we are led to the expression of the kinematic boundary condition

$$\boldsymbol{v} \cdot \hat{\boldsymbol{n}}\, \mathrm{d}\mathcal{S} = \boldsymbol{v} \cdot \nabla(z - \eta)\, \mathrm{d}A = \partial_t \eta\, \mathrm{d}A. \tag{52.29}$$

Dynamic free surface boundary condition

At the ocean free surface we assume zero atmospheric pressure,[4] in which case the ocean pressure must also vanish there. We are thus led to the following pressure boundary conditions

$$p = 0 \quad \text{and} \quad p_{\mathsf{d}} = g\,\eta\,\rho \quad \text{and} \quad p_{\mathsf{nh}} = 0 \quad \text{at } z = \eta, \tag{52.30}$$

each of which leads to the surface boundary condition for the velocity potential

$$\partial_t \Psi = \mathcal{K} + g\,\eta \quad \text{at } z = \eta. \tag{52.31}$$

Kinematic bottom boundary condition

The bottom is a rigid material surface so that the bottom kinematic boundary condition (Section 19.6.1) is the no-normal flow condition

$$\hat{\boldsymbol{n}} \cdot \boldsymbol{v} = -\nabla\Psi \cdot \hat{\boldsymbol{n}} = 0 \quad \text{at } z = \eta_{\mathsf{b}}(x, y). \tag{52.32}$$

When studying surface waves later in this chapter, we only consider the flat bottom ($\hat{\boldsymbol{n}} = -\hat{\boldsymbol{z}}$), in which case $w = 0$ at the bottom

$$w = -\partial_z \Psi = 0 \quad \text{at } z = \eta_{\mathsf{b}} = -H. \tag{52.33}$$

Dynamic bottom boundary condition

To develop the pressure boundary condition at the bottom, recall that a static material bottom has a static outward normal, $\hat{\boldsymbol{n}}$, so that

$$\hat{\boldsymbol{n}} \cdot \partial_t \boldsymbol{v} = \partial_t(\hat{\boldsymbol{n}} \cdot \boldsymbol{v}) = 0, \tag{52.34}$$

which then brings equations (52.24a)-(52.24c) to the form

$$\hat{\boldsymbol{n}} \cdot \nabla\mathcal{K} = -\hat{\boldsymbol{n}} \cdot \nabla(g\,z + p/\rho) \tag{52.35a}$$
$$\hat{\boldsymbol{n}} \cdot \nabla\mathcal{K} = -\hat{\boldsymbol{n}} \cdot \nabla p_{\mathsf{d}}/\rho \tag{52.35b}$$
$$\hat{\boldsymbol{n}} \cdot \nabla\mathcal{K} = -\hat{\boldsymbol{n}} \cdot \nabla(g\,\eta + p_{\mathsf{nh}}/\rho). \tag{52.35c}$$

Specializing to the flat bottom with $\hat{\boldsymbol{n}} = -\hat{\boldsymbol{z}}$ yields the bottom boundary conditions

$$\partial_z\mathcal{K} = -g - \rho^{-1}\,\partial_z p \tag{52.36a}$$
$$\partial_z\mathcal{K} = -\rho^{-1}\,\partial_z p_{\mathsf{d}} \tag{52.36b}$$
$$\partial_z\mathcal{K} = -\rho^{-1}\,\partial_z p_{\mathsf{nh}}, \tag{52.36c}$$

where $\partial_z\eta = 0$. In the linearized theory, $\partial_z\mathcal{K}$ is far smaller than g or $\rho^{-1}\,\partial_z p$, which means that the balance in equation (52.36a) must be hydrostatic, $\partial_z p = -\rho\,g$. This result then means that the non-hydrostatic boundary condition is $\partial_z p_{\mathsf{nh}} = 0$. Likewise, with $p = -\rho\,g\,z + p_{\mathsf{d}}$, and $\partial_z p = -\rho\,g$ at the bottom, we must have $\partial_z p_{\mathsf{nh}} = 0$. These results are thus summarized as

$$\partial_z p = -g\,\rho \quad \text{and} \quad \partial_z p_{\mathsf{d}} = 0 \quad \text{and} \quad \partial_z p_{\mathsf{nh}} = 0 \quad \text{at } z = \eta_{\mathsf{b}} = -H. \tag{52.37}$$

[4] In Section 52.3.2 we show that a uniform and constant atmospheric pressure plays no role in the physics of concern here since the fluid density is itself a uniform constant.

Comments on the need for two boundary conditions

Mathematically, the solution to Laplace's equation requires only a single boundary condition when posed in a domain with specified boundaries (e.g., see Section 6.5). For the current setup, however, the free surface is a moving boundary, thus offering one more dynamical degree of freedom that necessitates an extra boundary condition. Physically, there are two dynamical fields that describe the fluid layer, the velocity potential, Ψ, and the free surface height, η. Consequently, there are two boundary conditions that arise when specifying these fields: one from kinematics (the boundary interfaces are material) and one from dynamics (forces on both sides of the boundary interfaces must balance as per Newton's third law).

52.2.6 Local energetic balances

Since the fluid has a constant density, the only energy arises from mechanical energy due to motion (kinetic energy) plus the gravity field (gravitational potential energy)

$$\mathcal{E} = \mathcal{K} + \Phi = \boldsymbol{v} \cdot \boldsymbol{v}/2 + g\, z. \tag{52.38}$$

The internal energy is a constant and so plays no role in the energetic analysis. Also, we ignore dissipation and heat transfer so that energy is modified only through reversible processes. Local energetic budget equations are readily computed by taking the scalar product of the velocity with the velocity tendency. We consider here the three forms of the velocity equation (52.24a)-(52.23c) and their corresponding energy equations.

Velocity equation with unsplit pressure

With $\partial_t \boldsymbol{v}$ written in the form of equation (52.24a) we have

$$\partial_t \mathcal{K} = -\boldsymbol{v} \cdot \nabla(\mathcal{K} + \Phi + p/\rho) = -\nabla \cdot [\boldsymbol{v}\,(\mathcal{K} + \Phi + p/\rho)], \tag{52.39}$$

where we used $\nabla \cdot \boldsymbol{v} = 0$ for the second equality. Since the geopotential has a zero Eulerian time derivative, the kinetic energy equation readily leads to the total mechanical energy equation

$$\partial_t \mathcal{E} = -\nabla \cdot [\boldsymbol{v}\,(\mathcal{E} + p/\rho)] \Longrightarrow \rho\, \mathrm{D}\mathcal{E}/\mathrm{D}t = -\nabla \cdot (\boldsymbol{v}\, p). \tag{52.40}$$

Evidently, convergence of the pressure flux, $\boldsymbol{v}\, p$, leads to a material time change in the total energy.

Dynamically active/inactive pressure split

An equivalent form of the energy equation can be found by making use of the pressure split into dynamically active and inactive components according to the velocity equation (52.24b), which yields

$$\partial_t \mathcal{K} = -\nabla \cdot [\boldsymbol{v}\,(\mathcal{K} + p_{\mathsf{d}}/\rho)] \Longrightarrow \rho\, \mathrm{D}\mathcal{K}/\mathrm{D}t = -\nabla \cdot (\boldsymbol{v}\, p_{\mathsf{d}}). \tag{52.41}$$

We here find that convergence of the dynamic pressure flux, $\boldsymbol{v}\, p_{\mathsf{d}}$, leads to a material time change in the kinetic energy.

Hydrostatic/non-hydrostatic pressure split

We now develop the energetics with the hydrostatic/non-hydrostatic pressure decomposition (52.23c) to render

$$\partial_t \mathcal{K} = -\nabla \cdot [\boldsymbol{v}\,(\mathcal{K} + g\,\eta + p_{\mathsf{nh}}/\rho)]. \tag{52.42}$$

This form only lends itself to a total energy budget written in the form

$$\partial_t \mathcal{E} = -\nabla \cdot [\boldsymbol{v}\,(\mathcal{E} + p/\rho)] \Longrightarrow \rho\, \mathrm{D}\mathcal{E}/\mathrm{D}t = -\nabla \cdot [\boldsymbol{v}\,(p_{\mathsf{h}} + p_{\mathsf{nh}})]. \tag{52.43}$$

52.2.7 Expressions for the globally integrated kinetic energy

The kinetic energy per mass can be written in terms of the scalar potential

$$2\,\mathcal{K} = \boldsymbol{v} \cdot \boldsymbol{v} = \nabla\Psi \cdot \nabla\Psi = \nabla \cdot (\Psi\, \nabla\Psi), \tag{52.44}$$

where we used $\nabla^2\Psi = 0$ for the final equality. This divergence form of the kinetic energy means that its global integral is fully determined by properties at the boundaries.

Domain integrated kinetic energy is just due to surface properties

Integration of the kinetic energy in the form of equation (52.44) over the full ocean domain, $\mathcal{R}$, leads to the total kinetic energy

$$E_{\mathrm{KE}} = \int_{\mathcal{R}} \rho\, \mathcal{K}\, \mathrm{d}V = \frac{\rho}{2} \int_{\mathcal{R}} \nabla \cdot (\Psi\, \nabla\Psi)\, \mathrm{d}V = \frac{\rho}{2} \int_{\partial\mathcal{R}} \Psi\, \nabla\Psi \cdot \hat{\boldsymbol{n}}\, \mathrm{d}\mathcal{S}, \tag{52.45}$$

where we made use of the divergence theorem. The ocean bottom is material so that the flow satisfies the no-normal flow condition at each point along the bottom (Section 19.6.1)

$$\boldsymbol{v} \cdot \hat{\boldsymbol{n}} = -\nabla\Psi \cdot \hat{\boldsymbol{n}} = 0, \tag{52.46}$$

where $\hat{\boldsymbol{n}}$ is the outward normal on the rigid material boundaries. Lateral boundaries are either periodic or rigid material walls. We thus find the remarkable result that the domain integrated kinetic energy arises solely from properties integrated over the free surface

$$E_{\mathrm{KE}} = \frac{\rho}{2} \int_{z=\eta} \Psi\, \nabla\Psi \cdot \hat{\boldsymbol{n}}\, \mathrm{d}\mathcal{S} = -\frac{\rho}{2} \int_{z=\eta} \Psi\, \boldsymbol{v} \cdot \hat{\boldsymbol{n}}\, \mathrm{d}\mathcal{S}. \tag{52.47}$$

Evidently, contributions from interior motion play no role in the domain integrated kinetic energy. Furthermore, the kinetic energy is a non-negative number, so that the right hand side of equation (52.47) is non-negative although it is not obvious without noting that Ψ is a harmonic function in the domain interior. That is, the nature of the kinetic energy is fundamentally related to the harmonic nature of the velocity potential that allows the kinetic energy to be written as the total divergence in equation (52.44). We encountered a similar feature of harmonic functions in Section 6.5.2 when studying their mean-value property.

Gauge invariance of the domain integrated kinetic energy

The kinetic energy per mass, $\mathcal{K} = \nabla\Psi \cdot \nabla\Psi/2$, is manifestly gauge invariant since it remains unchanged if Ψ is shifted by a spatial constant. This property also holds for the domain integrated kinetic energy, (52.47), as follows from use of the divergence theorem and then the non-divergence of the velocity field

$$\int_{z=\eta} \boldsymbol{v} \cdot \hat{\boldsymbol{n}}\, \mathrm{d}\mathcal{S} = \int_{\partial\mathcal{R}} \boldsymbol{v} \cdot \hat{\boldsymbol{n}}\, \mathrm{d}\mathcal{S} = \int_{\mathcal{R}} \nabla \cdot \boldsymbol{v}\, \mathrm{d}V = 0. \tag{52.48}$$

Evidently, if the scalar potential is shifted by a function of time that is spatially independent, then the globally integrated kinetic energy (52.47) remains unchanged and so is gauge invariant. An alternative derivation makes use of the surface kinematic boundary condition (52.29) that

leads to the identity

$$\int_{z=\eta} \boldsymbol{v} \cdot \hat{\boldsymbol{n}} \, d\mathcal{S} = \int \partial_t \eta \, dA = - \int \nabla \cdot \boldsymbol{U} \, dA = 0, \tag{52.49}$$

where we set $\partial_t \eta = -\nabla \cdot \boldsymbol{U}$ as per the free surface equation (21.81) holding for a volume conserving fluid, with $\boldsymbol{U} = \int_{-H}^{\eta} \boldsymbol{u} \, dz$ the depth integrated horizontal velocity.[5]

Kinetic energy in terms of time tendencies

We write yet another form for the domain integrated kinetic energy, which proves of use when studying Hamilton's principle in Section 52.2.9. For this purpose, make use of the free surface kinematic boundary condition (52.29) to bring the kinetic energy equation (52.47) into the form

$$E_{\text{KE}} = -\frac{\rho}{2} \int_{z=\eta} \Psi \, \boldsymbol{v} \cdot \hat{\boldsymbol{n}} \, d\mathcal{S} = -\frac{\rho}{2} \int_{z=\eta} \Psi \, \partial_t \eta \, dA. \tag{52.50}$$

Now reintroduce the vertical integral via Leibniz's rule (Section 20.2.4) to write

$$\int_{z=\eta} \Psi \, \partial_t \eta \, dA = \int \left[\frac{\partial}{\partial t} \int_{\eta_b}^{\eta} \Psi \, dz \right] dA - \int \left[\int_{\eta_b}^{\eta} \partial_t \Psi \, dz \right] dA. \tag{52.51}$$

If the horizontal extent of the domain has a static extent, such as when the horizontal domain is periodic or it is bounded by rigid vertical walls (e.g., see Figure 28.6), then the time derivative commutes with the area integral so that equation (52.51) becomes

$$\int_{z=\eta} \Psi \, \partial_t \eta \, dA = \frac{d}{dt} \left[\int \int_{\eta_b}^{\eta} \Psi \, dz \, dA \right] - \int \int_{\eta_b}^{\eta} \partial_t \Psi \, dz \, dA = \frac{d}{dt} \int \Psi \, dV - \int \partial_t \Psi \, dV. \tag{52.52}$$

We make use of this identity in the discussion of Hamilton's principle in Section 52.2.9.

52.2.8 Kelvin's minimum kinetic energy theorem

The domain integrated kinetic energy equation (52.47) points to the central role of boundary conditions. We here expose a property of the kinetic energy associated with *Kelvin's minimum kinetic energy theorem*.

Basic formulation

Following Kelvin (as detailed in Section 45 of *Lamb* (1993)), consider a non-divergent flow, $\boldsymbol{v}^{\text{tot}}$, built from the sum of an irrotational and non-divergent velocity field (i.e., potential flow), $\boldsymbol{v}$, plus a non-divergent and rotational flow, $\boldsymbol{v}_{\text{r}}$

$$\boldsymbol{v}_{\text{tot}} = \boldsymbol{v} + \boldsymbol{v}_{\text{r}} \quad \text{with} \quad \nabla \cdot \boldsymbol{v} = \nabla \cdot \boldsymbol{v}_{\text{r}} = 0 \quad \text{and} \quad \nabla \times \boldsymbol{v}_{\text{tot}} = \nabla \times \boldsymbol{v}_{\text{r}}. \tag{52.53}$$

The domain integrated kinetic energy of this flow,

$$E^{\text{tot}}_{\text{KE}} = \frac{\rho}{2} \int_{\mathcal{R}} \boldsymbol{v}_{\text{tot}} \cdot \boldsymbol{v}_{\text{tot}} \, dV, \tag{52.54}$$

has three terms

$$E^{\text{tot}}_{\text{KE}} = \frac{\rho}{2} \int_{\mathcal{R}} \boldsymbol{v} \cdot \boldsymbol{v} \, dV + \frac{\rho}{2} \int_{\mathcal{R}} \boldsymbol{v}_{\text{r}} \cdot \boldsymbol{v}_{\text{r}} \, dV + \rho \int_{\mathcal{R}} \boldsymbol{v} \cdot \boldsymbol{v}_{\text{r}} \, dV. \tag{52.55}$$

[5] See also Exercise 21.10.

The domain integrated kinetic energy for the irrotational flow equals to the boundary integral from equation (52.47)

$$\frac{\rho}{2}\int_{\mathcal{R}} \boldsymbol{v}\cdot\boldsymbol{v}\,\mathrm{d}V = -\frac{\rho}{2}\int_{\partial\mathcal{R}} \Psi\,\boldsymbol{v}\cdot\hat{\boldsymbol{n}}\,\mathrm{d}\mathcal{S}. \tag{52.56}$$

The cross-term also takes the form of a boundary integral

$$\int_{\mathcal{R}} \boldsymbol{v}\cdot\boldsymbol{v}_{\mathrm{r}}\,\mathrm{d}V = -\int_{\mathcal{R}} \nabla\Psi\cdot\boldsymbol{v}_{\mathrm{r}}\,\mathrm{d}V = -\int_{\mathcal{R}} \nabla\cdot(\Psi\,\boldsymbol{v}_{\mathrm{r}})\,\mathrm{d}V = -\int_{\partial\mathcal{R}} \Psi\,\boldsymbol{v}_{\mathrm{r}}\cdot\hat{\boldsymbol{n}}\,\mathrm{d}\mathcal{S}, \tag{52.57}$$

so that the domain integrated kinetic energy is

$$E^{\mathrm{tot}}_{\mathrm{KE}} = \frac{\rho}{2}\int_{\mathcal{R}} (\boldsymbol{v}_{\mathrm{r}}\cdot\boldsymbol{v}_{\mathrm{r}} + \boldsymbol{v}\cdot\boldsymbol{v})\,\mathrm{d}V - \rho\int_{\partial\mathcal{R}} \Psi\,\boldsymbol{v}_{\mathrm{r}}\cdot\hat{\boldsymbol{n}}\,\mathrm{d}\mathcal{S} \tag{52.58a}$$

$$= \frac{\rho}{2}\int_{\mathcal{R}} \boldsymbol{v}_{\mathrm{r}}\cdot\boldsymbol{v}_{\mathrm{r}}\,\mathrm{d}V - \frac{\rho}{2}\int_{\partial\mathcal{R}} \Psi\,(\boldsymbol{v}+2\,\boldsymbol{v}_{\mathrm{r}})\cdot\hat{\boldsymbol{n}}\,\mathrm{d}\mathcal{S}. \tag{52.58b}$$

Kelvin's minimum kinetic energy theorem

Consider the case where the flow is irrotational and so it satisfies the boundary conditions appropriate for potential flow in a homogeneous fluid layer with a free surface

$$\boldsymbol{v}\cdot\hat{\boldsymbol{n}} = 0 \qquad \text{at solid bottom boundary, } z=\eta_{\mathrm{b}}(x,y) \tag{52.59a}$$

$$\boldsymbol{v}\cdot\hat{\boldsymbol{n}}\,\mathrm{d}\mathcal{S} = \partial_t\eta\,\mathrm{d}A \quad \text{at free surface boundary, } z=\eta(x,y,t). \tag{52.59b}$$

The free surface condition (52.59b) arises from equation (52.26) as well as the area relation in equation (52.28). Now add a rotational flow, and assume the rotational flow leaves the potential flow's boundary conditions (52.59a) and (52.59b) unaffected, which can be ensured if the rotational flow satisfies the no-normal flow condition at all boundaries

$$\boldsymbol{v}_{\mathrm{r}}\cdot\hat{\boldsymbol{n}} = 0 \quad \boldsymbol{x}\in\partial\mathcal{R}. \tag{52.60}$$

Kelvin's minimum kinetic energy theorem follows from equation (52.58a) with $\boldsymbol{v}_{\mathrm{r}}\cdot\hat{\boldsymbol{n}}=0$, in which case

$$E^{\mathrm{tot}}_{\mathrm{KE}} = \frac{\rho}{2}\int_{\mathcal{R}} (\boldsymbol{v}\cdot\boldsymbol{v} + \boldsymbol{v}_{\mathrm{r}}\cdot\boldsymbol{v}_{\mathrm{r}})\,\mathrm{d}V, \tag{52.61}$$

so that kinetic energy of the pure irrotational flow is less than that for the flow based on the same irrotational flow plus a rotational perturbation. Evidently, the irrotational flow minimizes the kinetic energy for the simply connected material domain.

In formulating the theorem (52.61), we considered the rotational component to the flow as a perturbation to the original irrotational flow, with the perturbation not altering the boundary conditions satisfied by the irrotational flow. In this manner, the rotational flow is akin to a variation added to the irrotational flow in the sense used for Hamilton's principle (e.g., Sections 46.2 and 52.2.9), in which variations do not touch boundary (or initial) conditions.

Material boundary condition for $\boldsymbol{v}_r + \boldsymbol{v}$

Now consider the material boundary conditions at the bottom and surface to be satisfied by the full flow

$$(\boldsymbol{v}+\boldsymbol{v}_{\mathrm{r}})\cdot\hat{\boldsymbol{n}} = 0 \qquad \text{at solid bottom boundary, } z=\eta_{\mathrm{b}}(x,y) \tag{52.62a}$$

$$(\boldsymbol{v}+\boldsymbol{v}_{\mathrm{r}})\cdot\hat{\boldsymbol{n}}\,\mathrm{d}\mathcal{S} = \partial_t\eta\,\mathrm{d}A \quad \text{at free surface boundary, } z=\eta(x,y,t), \tag{52.62b}$$

so that these boundary conditions couple the rotational and irrotational components. The kinetic energy equation (52.58b) now takes the form

$$E^{\text{tot}}_{\text{KE}} = \frac{\rho}{2}\int_{\mathscr{R}} \boldsymbol{v}_{\text{r}}\cdot\boldsymbol{v}_{\text{r}}\,\text{d}V - \frac{\rho}{2}\int_{z=\eta}\Psi\,\partial_t\eta\,\text{d}A - \frac{\rho}{2}\int_{\partial\mathscr{R}}\Psi\,\boldsymbol{v}_{\text{r}}\cdot\hat{\boldsymbol{n}}\,\text{d}\mathcal{S} \tag{52.63a}$$

$$= \frac{\rho}{2}\int_{\mathscr{R}}(\boldsymbol{v}_{\text{r}}\cdot\boldsymbol{v}_{\text{r}} - \boldsymbol{v}\cdot\boldsymbol{v})\,\text{d}V - \rho\int_{z=\eta}\Psi\,\partial_t\eta\,\text{d}A \tag{52.63b}$$

For a rigid material upper boundary, so that $\partial_t\eta = 0$, the domain integrated kinetic energy in the irrotational flow is less than that in the rotational flow. Any further general statements are unavailable for the case with a time dependent free surface. The absence of a general theorem can be traced to coupling between the rotational and irrotational flow as realized via the boundary conditions. This situation contrasts to the case of Kelvin's minimum kinetic energy theorem, where there we purposely disabled any coupling.

52.2.9 Hamilton's principle and Luke's variational principle

Following the discussion of classical field theory in Chapter 46, we here consider the Lagrangian density functional and the corresponding equations of motion that follow from *Hamilton's principle*. The special nature of the dynamical free surface boundary condition prompts a modified version of the action that allows for a treatment of both the interior potential flow and the nonlinear surface boundary conditions. This modification is due to *Luke* (1967), prompting the name *Luke's variational principle*.[6]

Conventional form of the Lagrangian density

The Lagrangian density (dimensions of energy per unit volume) is the kinetic energy per volume minus the gravitational potential energy per volume, which takes the following form for potential flow of a homogeneous fluid layer

$$\mathscr{L} = \rho\,(\boldsymbol{v}\cdot\boldsymbol{v}/2 - g\,z) = \rho\,(\nabla\Psi\cdot\nabla\Psi - g\,z)/2. \tag{52.64}$$

The corresponding action is

$$\mathcal{S} = \int_R \mathscr{L}\,\text{d}V\,\text{d}t, \tag{52.65}$$

where R is the space-time domain. Hamilton's principle says that variation of the action vanishes for the physically realized fields

$$\delta\mathcal{S} = \int_R \delta\mathscr{L}\,\text{d}V\,\text{d}t = 0, \tag{52.66}$$

where the variation operator, δ, does not touch space or time and so it commutes with integrals and derivatives (see Sections 46.2.2 and 46.2.3).

The puzzle we have, however, is that the free surface does not explicitly appear in the Lagrangian (52.64). Rather, it only appears as a boundary in the action integral (52.66). That is not a problem *per se*, but the problem is that varying the action using the Lagrangian (52.64) fails to produce the dynamical boundary condition at the free surface. To resolve this puzzle we follow *Luke* (1967) by transforming the action into a modified form that differs from the original action by a time derivative which, as shown in Section 46.3.5, does not alter the mechanics.

[6] Elements of this section follow from *Luke* (1967), Section 13.2 of *Whitham* (1974), and Exercise 10.14 of *Fetter and Walecka* (2003). See also *Miles* (1977) and *Milder* (1977).

Furthermore, the appropriate action turns out to be, quite remarkably, the space-time integral of the pressure.

Surface Lagrangian density

Before considering the approach of *Luke* (1967), observe that the Lagrangian density (52.64) can be written

$$\rho^{-1} \int_{\mathcal{R}} \mathcal{L} \, \mathrm{d}V = \int_{\mathcal{R}} (\boldsymbol{v} \cdot \boldsymbol{v}/2 - g\, z) \, \mathrm{d}V = -\frac{1}{2} \int [\Psi_{\mathrm{s}} \, \partial_t \eta + g \, (\eta^2 - \eta_{\mathrm{b}}^2)] \, \mathrm{d}A, \tag{52.67}$$

where we made use of the kinematic boundary conditions (52.59a) and (52.59b), in which case the action is

$$\mathsf{S} = -\frac{\rho}{2} \int [\Psi_{\mathrm{s}} \, \partial_t \eta + g \, (\eta^2 - \eta_{\mathrm{b}}^2)] \, \mathrm{d}A \, \mathrm{d}t \equiv \int \mathcal{L}_{\mathrm{s}} \, \mathrm{d}A \, \mathrm{d}t. \tag{52.68}$$

In this equation we introduced the velocity potential evaluated at the free surface

$$\Psi_{\mathrm{s}} = \Psi(x, y, z = \eta, t), \tag{52.69}$$

and the surface Lagrangian density (dimensions of energy per unit area)

$$\mathcal{L}_{\mathrm{s}} = -\rho [\Psi_{\mathrm{s}} \, \partial_t \eta + g \, (\eta^2 - \eta_{\mathrm{b}}^2)]/2. \tag{52.70}$$

This Lagrangian forms the starting point for *Milder* (1977).

Transforming the action into the integral of pressure

We transform the action through use of equation (52.52) for the kinetic energy, in which

$$\int \left[\int \nabla \Psi \cdot \nabla \Psi \, \mathrm{d}V \right] \mathrm{d}t = - \int \left[\int [\Psi \, \partial_t \eta]_{z=\eta} \, \mathrm{d}A \right] \mathrm{d}t \tag{52.71a}$$

$$= - \int \left[\frac{\partial}{\partial t} \int \Psi \, \mathrm{d}V \right] \mathrm{d}t + \int \partial_t \Psi \, \mathrm{d}V \, \mathrm{d}t. \tag{52.71b}$$

As noted in deriving equation (52.52), we assumed here that the horizontal bounds for the domain are static. For the more general case of sloping side boundaries (e.g., see Figure 28.6), then we need to introduce yet another dynamical field, namely the moving horizontal bounds. That added dynamical degree of freedom is not the focus here, so that we assume the domain has static horizontal boundaries, thus allowing the time derivative to commute with the area integral.

Use of equation (52.71b) brings the action to the form

$$\mathcal{S} = -\frac{\rho}{2} \int \left[\frac{\partial}{\partial t} \int \Psi \, \mathrm{d}V \right] \mathrm{d}t + \rho \int \left[\frac{1}{2} \frac{\partial \Psi}{\partial t} - g\, z \right] \mathrm{d}V \, \mathrm{d}t. \tag{52.72}$$

Following the discussion in Section 46.3.5, the first term on the right hand side is mechanically irrelevant since it evaluates to the time bounds, during which the velocity potential has zero variation. We can thus drop the first right hand side term in equation (52.72) to focus on the modified action

$$\mathcal{S}^{\mathrm{mod}} = \rho \int \left[\frac{1}{2} \frac{\partial \Psi}{\partial t} - g\, z \right] \mathrm{d}V \, \mathrm{d}t. \tag{52.73}$$

Making use again of equation (52.52) along with the mechanical equivalence (52.72) gives

$$\mathcal{S}^{\text{Luke}} = \rho \int \left[\frac{\partial \Psi}{\partial t} - \frac{1}{2} \frac{\partial \Psi}{\partial t} - g\, z \right] \mathrm{d}V\, \mathrm{d}t = \rho \int \left[\frac{\partial \Psi}{\partial t} - \frac{1}{2} \nabla \Psi \cdot \nabla \Psi - g\, z \right] \mathrm{d}V\, \mathrm{d}t. \tag{52.74}$$

Variation of the action with respect to η

Exposing the vertical integration limits on the action (52.74) yields

$$\mathsf{S}^{\text{Luke}} = \rho \int \int \int_{\eta_{\mathsf{b}}}^{\eta} \left[\frac{\partial \Psi}{\partial t} - \frac{1}{2} \nabla \Psi \cdot \nabla \Psi - g\, z \right] \mathrm{d}z\, \mathrm{d}A\, \mathrm{d}t, \tag{52.75}$$

so that the variation arising from $\delta\eta$ is straightforward to compute. In so doing we find

$$\frac{\delta \mathcal{S}^{\text{Luke}}}{\delta \eta} = 0 \Longrightarrow \partial_t \Psi = \frac{1}{2} \nabla \Psi \cdot \nabla \Psi + g\, \eta \quad \text{at } z = \eta, \tag{52.76}$$

which is the dynamic boundary condition (52.31).

Variation of the action with respect to Ψ

Variation of the action with respect to the velocity potential leads to

$$\delta_\Psi \mathcal{S}^{\text{Luke}} = \frac{\rho}{2} \int \partial_t(\delta \Psi)\, \mathrm{d}V\, \mathrm{d}t - \rho \int \delta \Psi\, \nabla \Psi \cdot \hat{\boldsymbol{n}}\, \mathrm{d}\mathcal{S}\, \mathrm{d}t + \rho \int \nabla^2 \Psi\, \delta \Psi\, \mathrm{d}V\, \mathrm{d}t, \tag{52.77}$$

where we noted that $\delta(\partial_t \Psi) = \partial_t(\delta \Psi)$, and integrated by parts to get the second and third terms on the right hand side. For the time derivative term we write

$$\int \partial_t(\delta \Psi)\, \mathrm{d}V = \int \left[\int_{\eta_{\mathsf{b}}}^{\eta} \partial_t(\delta \Psi)\, \mathrm{d}z \right] \mathrm{d}A = \int \left[\frac{\partial}{\partial t} \int_{\eta_{\mathsf{b}}}^{\eta} \delta \Psi\, \mathrm{d}z - \partial_t \eta\, \delta \Psi_{\mathrm{s}} \right] \mathrm{d}A, \tag{52.78}$$

whereas the kinematic boundary conditions (equations (52.59a) and (52.59b)) bring the spatial boundary term to

$$- \int \delta \Psi\, \nabla \Psi \cdot \hat{\boldsymbol{n}}\, \mathrm{d}\mathcal{S} = \int \partial_t \eta\, \delta \Psi_{\mathrm{s}}\, \mathrm{d}A, \tag{52.79}$$

thus leading to the action variation

$$\delta_\Psi \mathcal{S}^{\text{Luke}} = \int \nabla^2 \Psi\, \delta \Psi\, \mathrm{d}V\, \mathrm{d}t. \tag{52.80}$$

The action variation vanishes so long as $\nabla^2 \Psi = 0$ within the fluid domain. Bringing everything together leads to the boundary value problem for the velocity potential and the free surface

$$\nabla^2 \Psi = 0 \qquad \boldsymbol{x} \in \mathcal{R} \tag{52.81a}$$

$$\hat{\boldsymbol{n}} \cdot \nabla \Psi = 0 \qquad \boldsymbol{x} \in \partial \mathcal{R} \text{ kinematic rigid condition} \tag{52.81b}$$

$$(\nabla \eta - \hat{\boldsymbol{z}}) \cdot \nabla \Psi = \partial_t \eta \qquad z = \eta \text{ kinematic free surface condition} \tag{52.81c}$$

$$\partial_t \Psi = \frac{1}{2} \nabla \Psi \cdot \nabla \Psi + g\, \eta \qquad z = \eta \text{ dynamic free surface condition.} \tag{52.81d}$$

Comments

Remarkably, the Bernoulli equation of motion (52.16) means that the Lagrangian functional appearing in the action (52.74) equals to the pressure

$$\mathcal{S}^{\text{Luke}} = \rho \int \left[\frac{\partial \Psi}{\partial t} - \frac{1}{2} \nabla \Psi \cdot \nabla \Psi - g\, z \right] \mathrm{d}V\, \mathrm{d}t = \int p\, \mathrm{d}V\, \mathrm{d}t. \tag{52.82}$$

Starting from this form of the action, Hamilton's principle extremizes the space-time integral of the pressure. *Seliger and Whitham* (1968) provide some discussion of pressure as the action within the context of the Boussinesq approximation, where the same result holds.

A free surface certainly adds subtleties to the use of Hamilton's principle. The presentation given in this subsection proceeds in the opposite order to that given by *Luke* (1967) as well as section 13.2 of *Whitham* (1974). Here, we started with the conventional form of the Lagrangian (52.64) written as the difference between kinetic energy and potential energy, and then showed how to transform the action into the pressure action integral (52.82) that captures the dynamical boundary condition. In that transformation we made use of the kinematic boundary conditions at both the static bottom boundary (equation (52.59a)) and the free surface (equation (52.59b)). The alternative approach taken by *Luke* (1967) starts from the inspired guess of a pressure based action integral (52.82), and shows that it indeed produces the proper dynamical equations so long as the kinematic boundary conditions are satisfied. The present approach is thus offered as a complement to that from *Luke* (1967) and *Whitham* (1974)

52.3 Linearized dynamics

We here develop the boundary value problem describing linear surface gravity wave motions of the free surface, and characterize physical aspects of the waves. Surface tension is ignored so that pressure is continuous across the free surface. In Section 52.10 we remove this assumption by considering the pressure jump at the ocean surface due to surface tension, with this pressure jump leading to capillary waves. The fundamental parameter measuring nonlinearity concerns the ratio of the free surface undulation to the length of a wave disturbance. A small value for this non-dimensional ratio allows us to confidently make use of the linear equations.

Note that we focus on the velocity potential in our analysis of linear surface gravity waves. A directly analogous approach focuses on the dynamic pressure, p_{d}, which is a harmonic function for the linearized system (take the divergence of the linearized velocity equation (52.6)). Section 7.1 of *Vallis* (2017) takes the pressure approach. The two methods are equivalent, with the velocity potential and pressure closely connected.

52.3.1 Linear relations between the velocity potential and pressure

The Bernoulli equations of motion (52.23a)-(52.23c) provide an expression for the time tendency of the velocity potential. When linearizing the equations we drop the contribution from the kinetic energy since it is second order in the velocity field.[7] We are thus led to the linear relations

$$\partial_t \Psi = g\, z + p/\rho = p_{\text{d}}/\rho = g\, \eta + p_{\text{nh}}/\rho. \tag{52.83}$$

This equation provides the linearized relation between the velocity potential and the various pressure fields.

[7] We do *not* drop kinetic energy when studying the energetics of linear waves. But here we are studying their momentum, in which we linearize by dropping all second and higher order terms.

52.3.2 Dynamic boundary condition at the free surface

The equation of motion (52.16) applies to any point within the fluid and at any time. In particular, it applies at the free surface, $z = \eta(x, y, t)$, where pressure equals to the atmospheric pressure. As stated earlier, we assume that the atmospheric pressure is constant in space and time so that

$$g\,\eta + \mathcal{K} - \partial_t \Psi = -p_a/\rho = \text{constant}. \tag{52.84}$$

Without loss of generality we can set this constant to zero,[8] thus leaving the boundary condition

$$g\,\eta + \mathcal{K} - \partial_t \Psi = 0 \qquad \text{linearized dynamic b.c. at } z = \eta. \tag{52.85}$$

We now linearize relative to a state of rest with $\eta = 0$, $\boldsymbol{v} = 0$, and $\partial_t \Psi = 0$. Linear fluctuations about this rest state have small velocities. Consequently, the kinetic energy, which is second order in velocity, is small relative to the remaining terms and so we arrive at the linearized dynamic boundary condition

$$g\,\eta = \partial_t \Psi \qquad \text{linearized dynamic b.c. at } z = \eta. \tag{52.86}$$

This boundary condition directly connects the free surface to time tendencies of the velocity potential. The free surface fluctuates upward when the velocity potential has a positive tendency, and vice versa. Also note that we arrive at this boundary condition by making use of the pressure boundary conditions (52.30) within equation (52.83).

52.3.3 Kinematic boundary conditions

The free surface is assumed to be a material interface, meaning that there is no matter transported across this surface. Consequently, following the discussion of kinematic boundary conditions in Section 19.6.2, we have

$$(\partial_t + \boldsymbol{u} \cdot \nabla)\eta = w \qquad \text{kinematic b.c. at } z = \eta. \tag{52.87}$$

Linearizing this boundary condition about the state of rest, and introducing the scalar potential, leads to

$$\partial_t \eta = w = -\partial_z \Psi \qquad \text{linearized kinematic b.c. at } z = \eta. \tag{52.88}$$

This is yet another constraint that links the free surface to the velocity potential.

52.3.4 Summary of the linear equations

The boundary value problem for the velocity potential and free surface is given by

$$\boldsymbol{v} = -\nabla\Psi \qquad \text{velocity potential} \tag{52.89a}$$

$$\nabla^2 \Psi = 0 \qquad \text{irrotational and non-divergent velocity for } \boldsymbol{x} \in \text{ocean} \tag{52.89b}$$

$$\partial_t \Psi = g\,\eta \qquad \text{linearized dynamic b.c. at } z = \eta \tag{52.89c}$$

$$\partial_z \Psi = -\partial_t \eta \qquad \text{linearized kinematic b.c. at } z = \eta \tag{52.89d}$$

$$\hat{\boldsymbol{n}} \cdot \nabla\Psi = 0 \qquad \text{no-normal flow kinematic b.c. on rigid boundaries.} \tag{52.89e}$$

Equations (52.89a) and (52.89b) hold throughout the fluid whereas the remaining equations hold only at the boundaries.

Although the equations (52.89b)-(52.89e) were derived through linearization, there is one remaining nonlinearity that needs to be removed to enable a fully linear analytical treatment.

[8] Alternatively, can use a gauge transformation $\Psi' = \Psi - t\,(p_a/\rho)$ to eliminate the constant.

Namely, when combining the boundary conditions into a single equation we compute the time derivative of equation (52.89c) according to

$$g \frac{\partial \eta}{\partial t} = \left[\frac{\partial}{\partial t} + \frac{\partial \eta}{\partial t} \frac{\partial}{\partial z} \right] \frac{\partial \Psi}{\partial t}, \tag{52.90}$$

which follows since $\Psi = \Psi(x, y, z = \eta(x, y, t), t)$ at the surface boundary. Combining with equation (52.89d) renders

$$\left[\frac{\partial}{\partial t} + \frac{\partial \eta}{\partial t} \frac{\partial}{\partial z} \right] \frac{\partial \Psi}{\partial t} = -g \frac{\partial \Psi}{\partial z}. \tag{52.91}$$

With $w \approx \partial \eta / \partial t$ at the free surface, we identify $(\partial \eta / \partial t)\, \partial_z$ as a vertical advection operator. The corresponding term $(\partial \eta / \partial t)\, \partial_{zt} \Psi$ is nonlinear and second order in fluctuating fields. Hence, we drop this term as part of the linearization process. An equivalent means to realize this linearization is to evaluate the free surface boundary condition at $z = 0$ rather than at $z = \eta(x, y, t)$. For this approximation to be self-consistent requires the amplitude of free surface undulations to be much smaller than the typical wavelengths of the fluctuations, in which case

$$|\eta| / \Lambda \ll 1, \tag{52.92}$$

with this condition holding for the waves considered here.

In summary, the fully linearized equation set takes the form

$$\boldsymbol{v} = -\nabla \Psi \qquad \text{velocity potential} \tag{52.93a}$$

$$\nabla^2 \Psi = 0 \qquad \text{irrotational and non-divergent velocity for } \boldsymbol{x} \in \text{ocean} \tag{52.93b}$$

$$\partial_t \Psi = g\, \eta \qquad \text{linearized dynamic b.c. at } z = 0 \tag{52.93c}$$

$$\partial_z \Psi = -\partial_t \eta \qquad \text{linearized kinematic b.c. at } z = 0 \tag{52.93d}$$

$$\hat{\boldsymbol{n}} \cdot \nabla \Psi = 0 \qquad \text{no-normal flow kinematic b.c. on rigid boundaries.} \tag{52.93e}$$

Observe that these equations for surface gravity waves involve a harmonic scalar potential, Ψ, defined throughout the full fluid domain (equation (52.93b)), whereas the time tendencies are determined by the kinematic boundary condition (equation (52.93d)) and dynamic boundary condition (equation (52.93c)). Mathematically, the free surface, η, lives on a two-dimensional manifold of the surface interface, whereas the velocity potential, Ψ, lives on a three-dimensional manifold defined by the ocean domain. The velocity potential and free surface are coupled by the kinematic and dynamic boundary conditions, thus requiring the velocity potential to be determined throughout the three-dimensional ocean domain even if we might only care about fluctuations of the free surface. These features of surface gravity waves make them inherently more complex, and rich, than surface fluctuations of a membrane[9], or the volume fluctuations of a compressible fluid leading to acoustic waves (Chapter 51). The surface gravity wave system provides a canonical example of a surface boundary dynamical system, with surface quasi-geostrophy another prominent geophysical example.[10]

52.4 Energetics for the linearized equations

We here specialize the energetic analysis from Section 52.2.6 to study the energetics of the linearized equations in a manner analogous to the acoustic wave energetics considered in Section

[9] A drumhead provides the canonical example of a vibrating membrane. For determining waves moving on a drumhead, we focus exclusively on the drumhead without also considering dynamics of the surrounding fluid. See Chapter 8 of *Fetter and Walecka* (2003) for details.

[10] See *Held et al.* (1995) for a classic treatment of surface quasi-geostrophy. *Yassin* (2021) and *Yassin and Griffies* (2022) provide further studies of surface quasi-geostrophy in the context of normal mode theory.

51.6.

52.4.1 Domain integrated kinetic energy

The surface integral (52.50) for the domain integrated kinetic energy is computed at $z = \eta(x, y, t)$. For the linearized system, this integral is approximated at $z = 0$, so that the domain integrated kinetic energy is

$$E_{\text{KE}} = -\frac{\rho}{2} \int [\Psi \, \partial_t \eta]_{z=0} \, \mathrm{d}A = \frac{\rho}{2} \int [\Psi \, \partial_z \Psi]_{z=0} \, \mathrm{d}A = -\frac{\rho}{2} \int [\Psi \, w]_{z=0} \, \mathrm{d}A, \tag{52.94}$$

where we made use of the kinematic boundary condition (52.93d).

52.4.2 Domain integrated potential and available potential energies

Measuring the zero of gravitational potential energy at $z = -H$ (see Figure 52.1), yields the domain integrated gravitational potential energy

$$g \, \rho \int_{z=0} \left[\int_{-H}^{\eta} z \, \mathrm{d}z \right] \mathrm{d}A = \frac{g \, \rho}{2} \int (\eta^2 - H^2) \, \mathrm{d}A. \tag{52.95}$$

The available potential energy (see Sections 29.9 and 36.5.6) is the difference between the gravitational potential energy and that contained in an ocean at rest with $\eta = 0$, so that

$$E_{\text{APE}} = g \, \rho \int \left[\int_{-H}^{\eta} z \, \mathrm{d}z \right] \mathrm{d}A - g \, \rho \int \left[\int_{-H}^{0} z \, \mathrm{d}z \right] \mathrm{d}A = \frac{g \, \rho}{2} \int \eta^2 \, \mathrm{d}A = \frac{\rho}{2 \, g} \int (\partial_t \Psi)^2 \, \mathrm{d}A, \tag{52.96}$$

where the final step made use of the dynamic boundary condition (52.93c). Hence, a non-negative available potential energy is associated with any undulation of the free surface, whether the undulation is positive or negative.

In Section 36.5.6 we computed the available potential energy for a single layer of shallow water fluid. In that discussion we chose to set $z = 0$ at the resting free surface (Figure 35.1), whereas in the current discussion we chose $z = 0$ at the flat bottom (Figure 52.1). Even so, the available potential energy (52.96) is identical to the shallow water case, which we see by noting that the area average of η vanishes for the current choice in Figure 52.1 (due to volume conservation)

$$\overline{\eta} = \frac{1}{A_{\text{ocn}}} \int \eta \, \mathrm{d}A = 0, \tag{52.97}$$

where

$$A_{\text{ocn}} = \int \mathrm{d}A \tag{52.98}$$

is the surface area of the ocean. We thus find

$$E_{\text{APE}} = \frac{g \, \rho}{2} \int \eta^2 \, \mathrm{d}A = \frac{g \, \rho}{2} \int (\eta - \overline{\eta})^2 \, \mathrm{d}A = \frac{g \, \rho}{2} \int (\eta')^2 \, \mathrm{d}A, \tag{52.99}$$

which agrees with equation (36.131) derived for the shallow water layer. We expect the two energies to agree since the gravitational energy depends only on the density and the position within the gravity field; it has no concern for dynamical assumptions such as whether the fluid motion is approximately hydrostatic (as for the shallow water model) or general (as considered here).

52.4.3 Equipartition for the phase averaged domain integrated energies

The expression (52.96) for the available potential energy can be written

$$E_{\text{APE}} = \frac{\rho}{2} \int \eta \, \partial_t \Psi \, \mathrm{d}A = \frac{\rho}{2} \int [-\Psi \, \partial_t \eta + \partial_t(\eta \, \Psi)] \, \mathrm{d}A = E_{\text{KE}} + \frac{\rho}{2} \int \partial_t(\eta \, \Psi) \, \mathrm{d}A, \tag{52.100}$$

where we made use of equation (52.94) for the total kinetic energy. If the fields exhibit periodicity in time, such as for a surface gravity wave field, then integration over an integer multiple of the wave period results in an equipartition between the phase averaged available potential energy and phase averaged kinetic energy

$$\langle E_{\text{APE}} \rangle = \langle E_{\text{KE}} \rangle \quad \text{with} \quad \langle E_{\text{APE}} \rangle = \frac{\omega}{2\pi} \int_0^{2\pi/\omega} E_{\text{APE}} \, \mathrm{d}t, \tag{52.101}$$

where $2\pi/\omega$ is the wave period. We found a similar equipartition of energy in Section 51.6.2 for acoustic waves.

52.4.4 Energetics for the depth integrated linear flow

We here study the mechanical energy contained in the fluid layer within the linear theory. Notably, when computing the kinetic energy in the depth integrated flow, we only integrate to $z = 0$ since going to $z = \eta$ involves third order terms that are neglected in the linear theory. Hence, the time derivative of the depth integrated kinetic energy per mass is

$$\frac{\partial}{\partial t} \int_{-H}^{0} \mathcal{K} \, \mathrm{d}z = \frac{1}{2} \frac{\partial}{\partial t} \int_{-H}^{0} \nabla\Psi \cdot \nabla\Psi \, \mathrm{d}z = \int_{-H}^{0} \nabla(\partial_t \Psi) \cdot \nabla\Psi \, \mathrm{d}z, \tag{52.102}$$

which follows since the integral bounds are static so that the time derivative commutes with the integral. Note that we used the partial time derivative operator, $\partial/\partial t$, as it is computed holding the horizontal position fixed. We next make use of the harmonic nature of the velocity potential ($\nabla^2 \Psi = 0$) to write

$$\frac{\partial}{\partial t} \int_{-H}^{0} \mathcal{K} \, \mathrm{d}z = \int_{-H}^{0} \nabla \cdot (\partial_t \Psi \, \nabla\Psi) \, \mathrm{d}z = [\partial_t \Psi \, \partial_z \Psi]_{z=0} + \nabla_{\!\mathrm{h}} \cdot \int_{-H}^{0} \partial_t \Psi \, \nabla_{\!\mathrm{h}} \Psi \, \mathrm{d}z, \tag{52.103}$$

where we used the bottom kinematic boundary condition, $\partial_z \Psi = 0$ at $z = -H$, and noted that H is a constant (flat bottom) so that the horizontal derivative commutes with the integral. For the boundary term we use the linearized dynamic boundary condition (52.93c) and linearized kinematic boundary condition (52.93d) to yield

$$\frac{\partial}{\partial t} \int_{-H}^{0} \mathcal{K} \, \mathrm{d}z = -g \, \eta \, \partial_t \eta + \nabla_{\!\mathrm{h}} \cdot \int_{-H}^{0} \partial_t \Psi \, \nabla_{\!\mathrm{h}} \Psi \, \mathrm{d}z. \tag{52.104}$$

Observe that the boundary term is the time tendency of the depth integrated potential energy per mass

$$\int_{-H}^{\eta} \Phi \, \mathrm{d}z = \int_{-H}^{\eta} g \, z \, \mathrm{d}z = (g/2) \, (\eta^2 - H^2) \implies \frac{\partial}{\partial t} \int_{-H}^{\eta} g \, z \, \mathrm{d}z = g \, \eta \, \partial_t \eta. \tag{52.105}$$

The potential energy in the column is computed by integrating all the way to the free surface, even for the linear theory. That integration limit is needed since changes in the potential energy over a column of constant density fluid arise solely through changes in the free surface. Bringing the pieces together allows us to write the time derivative of the depth integrated mechanical

energy per mass in the linear theory

$$\frac{\partial}{\partial t}\left[\frac{1}{2}\int_{-H}^{0}\boldsymbol{v}\cdot\boldsymbol{v}\,\mathrm{d}z+\int_{-H}^{\eta}g\,z\,\mathrm{d}z\right]=\nabla_{\mathsf{h}}\cdot\int_{-H}^{0}\partial_t\Psi\,\nabla_{\mathsf{h}}\Psi\,\mathrm{d}z. \tag{52.106}$$

Finally, set $\boldsymbol{u}=-\nabla_{\mathsf{h}}\Psi$, and use the linear theory identity, $\partial_t\Psi=p_{\mathsf{d}}/\rho$ from equation (52.83), thus leading to

$$\frac{\partial}{\partial t}\left[\int_{-H}^{0}\rho\,\mathcal{K}\,\mathrm{d}z+\int_{-H}^{\eta}\rho\,\Phi\,\mathrm{d}z\right]=-\nabla_{\mathsf{h}}\cdot\int_{-H}^{0}p_{\mathsf{d}}\,\boldsymbol{u}\,\mathrm{d}z. \tag{52.107}$$

Evidently, it is the horizontal convergence of the layer integrated flux of dynamical pressure, $p_{\mathsf{d}}\,\boldsymbol{u}$, that affects a time change to the layer integrated mechanical energy for the linear theory. That is, the layer integrated mechanical energy has a time tendency due to work by the dynamical pressure. Recall we saw the importance of pressure work in Section 52.2.6 when considering the local energy balances for the fully nonlinear system. We also saw the importance of pressure work for acoustic wave energetics in Section 51.6.3. Other wave systems we encounter in this part of the book also have pressure work central to their energetics.

52.5 Traveling gravity waves in a flat domain

We now study a traveling plane wave solution to the equations (52.93b)-(52.93e) as posed in a flat bottom domain such as illustrated in Figure 52.1. The waves are assumed to travel horizontally, with the example in Figure 52.1 showing waves in the $\pm\hat{\boldsymbol{x}}$ direction. There are no lateral boundaries. The waves also contain a vertical profile that, as we shall see, exponentially decays from the surface into the interior.

Besides providing an explicit realization of surface gravity waves, our analysis offers experience with the *separation of variables* method for solving certain partial differential equations. In our analysis, we are not interested in the most general wave solution. Instead, we aim to determine a particular solution of sufficient generality to expose the underlying physics of the linear wave fluctuations, and in particular to expose the exponential decay of the wave amplitude with depth. Furthermore, given linearity, the *superposition principle* holds whereby the sum or integral of particular solutions are also solutions.

52.5.1 Horizontally traveling plane wave

We seek a traveling plane wave solution with angular frequency, $\omega>0$, and horizontal wavevector and wave direction

$$\boldsymbol{k}=k_x\,\hat{\boldsymbol{x}}+k_y\,\hat{\boldsymbol{y}}\quad\text{and}\quad\hat{\boldsymbol{k}}=\boldsymbol{k}/|\boldsymbol{k}|. \tag{52.108}$$

For this purpose we assume the waves appear in the velocity potential in the shape of a cosine modulated by a vertical structure function[11]

$$\Psi(x,y,z,t)=\Psi_0\,\Gamma(z)\cos(\boldsymbol{k}\cdot\boldsymbol{x}-\omega\,t). \tag{52.109}$$

Plugging this ansatz into Laplace's equation, $\nabla^2\Psi=0$, leads to the ordinary differential equation satisfied by the non-dimensional vertical structure function

$$\frac{\mathrm{d}^2\Gamma}{\mathrm{d}z^2}=|\boldsymbol{k}|^2\,\Gamma\qquad -H\le z\le 0 \tag{52.110a}$$

$$\frac{\mathrm{d}\Gamma}{\mathrm{d}z}=0\qquad\text{at } z=-H, \tag{52.110b}$$

[11] We could use complex exponentials for the traveling wave, as discussed in Chapter 49. We here work with the real trigonometric functions to exemplify their use.

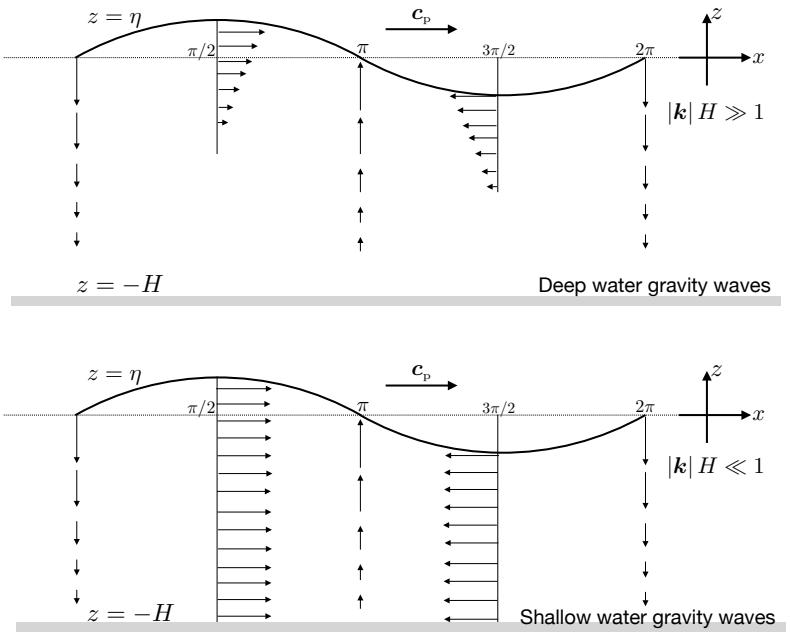

FIGURE 52.2: Snapshot of surface gravity waves over deep water ($|\boldsymbol{k}|\, H \gg 1$, top panel) and shallow water ($|\boldsymbol{k}|\, H \ll 1$, lower panel), with velocities computed according to equations (52.113a) and (52.113b). Shown here are the horizontal and vertical components to the velocity at a particular time instance, with the horizontal velocity in phase with the free surface undulations, and the vertical velocity $\pi/2$ out of phase. The horizontal axis along the top designates values for $\boldsymbol{k} \cdot \boldsymbol{x}$, with values of $0, \pi/2, \pi, 3\pi/2, 2\pi$ providing samples along the wave.

where the bottom boundary condition is required to satisfy the no-normal flow condition (52.93e). We write the solution in the form

$$\Psi = \Psi_0 \cosh[|\boldsymbol{k}|\,(z+H)] \cos(\boldsymbol{k} \cdot \boldsymbol{x} - \omega\, t) \tag{52.111a}$$

$$\Psi_0 = \frac{g\, \eta_0/\omega}{\cosh(|\boldsymbol{k}|\, H)}, \tag{52.111b}$$

so that the dynamic boundary condition (52.93c) renders the free surface height

$$\eta(\boldsymbol{x}, t) = \eta_0 \sin(\boldsymbol{k} \cdot \boldsymbol{x} - \omega\, t). \tag{52.112}$$

The corresponding fluid velocity field, $\boldsymbol{v} = -\nabla\Psi$, is given by

$$\boldsymbol{u} = \frac{g\, \eta_0\, \hat{\boldsymbol{k}}}{C_\mathrm{p}} \frac{\cosh[|\boldsymbol{k}|\,(z+H)] \sin(\boldsymbol{k} \cdot \boldsymbol{x} - \omega\, t)}{\cosh(|\boldsymbol{k}|\, H)} \tag{52.113a}$$

$$w = -\frac{g\, \eta_0}{C_\mathrm{p}} \frac{\sinh[|\boldsymbol{k}|\,(z+H)] \cos(\boldsymbol{k} \cdot \boldsymbol{x} - \omega\, t)}{\cosh(|\boldsymbol{k}|\, H)}, \tag{52.113b}$$

where the wave phase speed is given by

$$C_\mathrm{p} = \omega/|\boldsymbol{k}| > 0. \tag{52.114}$$

Figure 52.2 depicts the horizontal and vertical velocity in a snapshot of a deep water wave ($|\boldsymbol{k}|\, H \gg 1$) and shallow water wave ($|\boldsymbol{k}|\, H \ll 1$). We emphasize the following properties of these waves.

- The horizontal fluid particle velocity, $\boldsymbol{u}$, is parallel to the horizontal wavevector, $\boldsymbol{k}$. Hence, the gravity waves are horizontally longitudinal.

- The horizontal velocity is in phase with the free surface, η, whereas they are both $\pi/2$ out of phase with the vertical velocity.
- The vertical velocity vanishes at the bottom, $z = -H$, as needed to satisfy the no-normal flow boundary condition.
- The horizontal wave number, $|\boldsymbol{k}|$, both determines the horizontal wavelength, $2\pi/|\boldsymbol{k}|$, as well as the vertical decay scale, $|\boldsymbol{k}|$. This coupling of the horizontal to the vertical is a notable property of surface gravity waves.
- Letting time progress at a fixed space position reveals a clockwise progression of a fluid particle, as can be imagined by letting Figure 52.2 evolve in time. Further details of fluid particle trajectories are developed in Section 52.11 when studying Stokes drift.
- In the shallow water limit, $|\boldsymbol{k}|\, H \ll 1$, the horizontal velocity is depth independent. The vertical velocity is a linear function of depth and it is a factor of $|\boldsymbol{k}|\, H$ times smaller in magnitude than the horizontal velocity. We provide a focused study of such shallow water gravity waves in Section 55.5.

52.5.2 Domain integrated mechanical energy of a traveling wave

The domain integrated kinetic energy (52.94) contained in a traveling surface gravity wave is

$$E_{\text{KE}} = -\frac{\rho}{2} \int_{z=0} \Psi\, \partial_t \eta \, \mathrm{d}A \tag{52.115a}$$

$$= (\rho/2)\, \Psi_0\, \eta_0\, \omega \cosh(|\boldsymbol{k}|\, H) \int \cos^2(\boldsymbol{k} \cdot \boldsymbol{x} - \omega\, t)\, \mathrm{d}A \tag{52.115b}$$

$$= (\rho/2)\, g\, \eta_0^2 \int \cos^2(\boldsymbol{k} \cdot \boldsymbol{x} - \omega\, t)\, \mathrm{d}A, \tag{52.115c}$$

and likewise the domain integrated available potential energy (52.96) is

$$E_{\text{APE}} = (\rho/2)\, g\, \eta_0^2 \int \sin^2(\boldsymbol{k} \cdot \boldsymbol{x} - \omega\, t)\, \mathrm{d}A, \tag{52.116}$$

so that their sum is a space and time constant

$$E_{\text{KE}} + E_{\text{APE}} = A_{\text{ocn}}\, \rho\, g\, \eta_0^2/2, \tag{52.117}$$

where A_{ocn} is the total ocean area.[12] We also see that the phase average of the domain integrated kinetic energy and available potential energy manifest the equipartition property (52.101)

$$\langle E_{\text{APE}} \rangle = \langle E_{\text{KE}} \rangle = A_{\text{ocn}}\, \rho\, g\, \eta_0^2/4. \tag{52.118}$$

52.5.3 Dispersion relation

Combining the two $z = 0$ boundary conditions (52.93c) and (52.93d) yields

$$(\partial_{tt} + g\, \partial_z)\Psi = 0 \qquad \text{at } z = 0. \tag{52.119}$$

Substituting the traveling plane wave (52.111a) into this relation leads to the *dispersion relation*

$$\omega^2 = g\, |\boldsymbol{k}| \tanh(|\boldsymbol{k}|\, H) \Longrightarrow \omega = \sqrt{g\, |\boldsymbol{k}| \tanh(|\boldsymbol{k}|\, H)}. \tag{52.120}$$

[12] For the single traveling surface gravity wave to be a valid wave solution requires no lateral boundaries, in which case the ocean area is formally infinite.

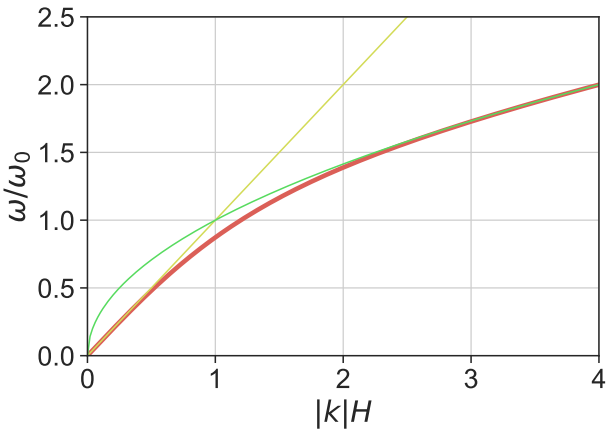

FIGURE 52.3: The dispersion relation (52.120) for surface gravity waves, plotted here as $\omega/\omega_0 = \sqrt{|\boldsymbol{k}|\,H\,\tanh(|\boldsymbol{k}|\,H)}$ (dark thick curved line), where $\omega_0^2 = g/H$ is the square of a fundamental frequency for surface gravity waves. We also show the dispersion relation for non-dispersive shallow water waves, $\omega/\omega_0 = |\boldsymbol{k}|\,H$ (straight line), which holds for $|\boldsymbol{k}|\,H \ll 1$, and the dispersive deep-water gravity waves, $\omega/\omega_0 = \sqrt{|\boldsymbol{k}|\,H}$, which holds for $|\boldsymbol{k}|\,H \gg 1$ (see Section 52.5.5).

The dispersion relation constrains those values available for the angular frequency, ω, and wavenumber, $|\boldsymbol{k}|$. That is, the surface gravity waves only exist if their frequency and wavenumber are related according to the dispersion relation (52.120). We depict the dispersion relation in Figure 52.3.

52.5.4 Alternative forms for the velocity potential and velocity

The dispersion relation (52.120) allows for a slight rewrite of the velocity potential (52.111a) and velocity field (52.113a) and (52.113b), with these variety of forms appearing in the literature

$$\eta = \eta_0 \sin(\boldsymbol{k}\cdot\boldsymbol{x} - \omega\,t) \tag{52.121a}$$

$$\Psi_0 = \frac{g\,\eta_0}{\omega\cosh(|\boldsymbol{k}|\,H)} = \frac{\eta_0\,C_{\mathsf{p}}}{\sinh(|\boldsymbol{k}|\,H)} \tag{52.121b}$$

$$\Psi = \frac{g\,\eta_0\cosh[|\boldsymbol{k}|\,(z+H)]\cos(\boldsymbol{k}\cdot\boldsymbol{x}-\omega\,t)}{\omega\cosh(|\boldsymbol{k}|\,H)} = \frac{\eta_0\,C_{\mathsf{p}}\cosh[|\boldsymbol{k}|\,(z+H)]\cos(\boldsymbol{k}\cdot\boldsymbol{x}-\omega\,t)}{\sinh(|\boldsymbol{k}|\,H)} \tag{52.121c}$$

$$\boldsymbol{u} = \frac{g\,\eta_0\,\hat{\boldsymbol{k}}}{C_{\mathsf{p}}}\,\frac{\cosh[|\boldsymbol{k}|\,(z+H)]\sin(\boldsymbol{k}\cdot\boldsymbol{x}-\omega\,t)}{\cosh(|\boldsymbol{k}|\,H)} = \frac{\eta_0\,\omega\,\hat{\boldsymbol{k}}\cosh[|\boldsymbol{k}|\,(z+H)]\sin(\boldsymbol{k}\cdot\boldsymbol{x}-\omega\,t)}{\sinh(|\boldsymbol{k}|\,H)} \tag{52.121d}$$

$$w = -\frac{g\,\eta_0}{C_{\mathsf{p}}}\,\frac{\sinh[|\boldsymbol{k}|\,(z+H)]\cos(\boldsymbol{k}\cdot\boldsymbol{x}-\omega\,t)}{\cosh(|\boldsymbol{k}|\,H)} = -\frac{\eta_0\,\omega\sinh[|\boldsymbol{k}|\,(z+H)]\cos(\boldsymbol{k}\cdot\boldsymbol{x}-\omega\,t)}{\sinh(|\boldsymbol{k}|\,H)}. \tag{52.121e}$$

52.5.5 Phase speed, group velocity, and angular frequency

We here characterize the phase speed, group velocity, and angular frequency for the surface gravity waves, and introduce the limits for deep water and shallow water waves.

Phase speed

The phase speed for the surface gravity wave is given by

$$C_{\mathsf{p}} = \omega/|\boldsymbol{k}| = \sqrt{(g/|\boldsymbol{k}|)\,\tanh(|\boldsymbol{k}|\,H)}. \tag{52.122}$$

We consider the two limits: $|\boldsymbol{k}|\,H \gg 1$ are known as shortwaves or deep water waves, and $|\boldsymbol{k}|\,H \ll 1$ are known as longwaves or shallow water waves. In these two limits the phase speed is given by

$$\omega \approx \sqrt{g\,|\boldsymbol{k}|} \qquad C_{\text{p}} \approx \sqrt{g/|\boldsymbol{k}|} \qquad |\boldsymbol{k}|\,H \gg 1 \qquad \text{shortwave/deep water} \tag{52.123a}$$

$$\omega \approx |\boldsymbol{k}|\,\sqrt{g\,H} \qquad C_{\text{p}} \approx \sqrt{g\,H} \qquad |\boldsymbol{k}|\,H \ll 1 \qquad \text{longwave/shallow water.} \tag{52.123b}$$

Observe that the shallow water gravity waves are non-dispersive since the phase speed is the same for all wave numbers, $C_{\text{p}} \approx \sqrt{g\,H}$. In contrast, the deep water gravity waves are dispersive, with the shorter (and higher frequency) waves having a slower phase speed than longer waves. To further emphasize the point about deep water waves, write the squared phase speed for the deep water waves as

$$C_{\text{p}}^2 = \frac{g}{|\boldsymbol{k}|} = \frac{g^2}{\omega^2} \Longrightarrow C_{\text{p}} = g/\omega. \tag{52.124}$$

Hence, so long as the deep water limit is maintained, higher frequency and shorter waves have smaller phase speed than lower frequency and longer waves.

Group velocity

As shown in Section 49.6, the group velocity, $\boldsymbol{c}_{\text{g}} = \nabla_{\boldsymbol{k}}\omega$, measures the direction and speed of a group of waves (e.g., a wave train or wave packet), with the group velocity for surface gravity waves given by

$$\boldsymbol{c}_{\text{g}} = \frac{g\,\hat{\boldsymbol{k}}}{2\,\omega}\left[\frac{|\boldsymbol{k}|\,H + \cosh(|\boldsymbol{k}|\,H)\sinh(|\boldsymbol{k}|\,H)}{\cosh^2(|\boldsymbol{k}|\,H)}\right]. \tag{52.125}$$

The ratio of the group speed to the phase speed is given by

$$\frac{\hat{\boldsymbol{k}}\cdot\boldsymbol{c}_{\text{g}}}{C_{\text{p}}} = \frac{g\,|\boldsymbol{k}|^2\,[|\boldsymbol{k}|\,H + \cosh(|\boldsymbol{k}|\,H)\sinh(|\boldsymbol{k}|\,H)]}{2\,\omega^2\,\cosh^2(|\boldsymbol{k}|\,H)} = \frac{1}{2}\left[1 + \frac{2\,|\boldsymbol{k}|\,H}{\sinh(2\,|\boldsymbol{k}|\,H)}\right]. \tag{52.126}$$

The shallow water limit, with $|\boldsymbol{k}|\,H \ll 1$, has phase speed and group speed equal, whereas the deep water waves have group speed one-half the phase speed. More precisely, we find the following limiting behaviors.

$$\omega \approx \sqrt{g\,|\boldsymbol{k}|} \qquad C_{\text{p}} \approx \sqrt{g/|\boldsymbol{k}|} \qquad \boldsymbol{c}_{\text{g}} \approx \boldsymbol{c}_{\text{p}}/2 \qquad |\boldsymbol{k}|\,H \gg 1 \qquad \text{shortwave/deep water} \tag{52.127a}$$

$$\omega \approx |\boldsymbol{k}|\,\sqrt{g\,H} \qquad C_{\text{p}} \approx \sqrt{g\,H} \qquad \boldsymbol{c}_{\text{g}} \approx \boldsymbol{c}_{\text{p}} \qquad |\boldsymbol{k}|\,H \ll 1 \qquad \text{longwave/shallow water.} \tag{52.127b}$$

For shallow water gravity waves, the group velocity equals to the phase velocity. In contrast, for deep water gravity waves, the group velocity magnitude is one-half the phase speed. When watching a packet of deep water gravity waves, we see the phase of the carrier waves appear at the back of the packet and move forward at twice the speed of the packet, only to then disappear at the front of the packet.

Angular frequency

The deep water limit, $|\boldsymbol{k}|\,H \gg 1$, and shallow water limit, $|\boldsymbol{k}|\,H \ll 1$, are set according to the wavenumber. These limits lead to a distinct frequency for the two waves. To compute the ratio of the corresponding angular frequencies, introduce two non-dimensional numbers according to

$$\Gamma_{\text{sw}} \equiv H\,|\boldsymbol{k}|_{\text{sw}} \ll 1 \quad \text{and} \quad \Gamma_{\text{dw}} \equiv H\,|\boldsymbol{k}|_{\text{dw}} \gg 1, \tag{52.128}$$

in which case

$$\frac{\omega_{\rm dw}^2}{\omega_{\rm sw}^2} = \frac{g\,|\boldsymbol{k}|_{\rm dw}}{|\boldsymbol{k}|_{\rm sw}^2\, c_{\rm grav}^2} = \frac{g\,H^{-1}\,\Gamma_{\rm dw}}{\Gamma_{\rm sw}^2\,H^{-2}\,g\,H} = \frac{\Gamma_{\rm dw}}{\Gamma_{\rm sw}^2} \gg 1. \tag{52.129}$$

We conclude that frequency of those short gravity waves whose extent is largely confined to the upper ocean (deep water waves) is much higher than the long gravity waves that extend throughout the water column (shallow water gravity waves). So although the shallow water waves and deep water waves feel the same gravitational acceleration, the huge scale for the shallow water waves leads to far lower frequency than for the deep water gravity waves.

52.5.6 Particle trajectories ignoring Stokes drift

Following the discussion in Section 17.7.1 of fluid particles and the motion of points within a continuum, we here determine the trajectory of a fluid particle labeled by the material coordinate, $\boldsymbol{a}$, and do so by time integrating the ordinary differential equation (Section 17.3.1)

$$\frac{\partial \boldsymbol{X}(\boldsymbol{a},T)}{\partial T} = \boldsymbol{v}[\boldsymbol{X}(\boldsymbol{a},T),T], \tag{52.130}$$

where $T = t$ is the material time label. In Section 52.11 we study the fluid particle motion within a surface gravity wave, noting that there is a net motion in the direction of the phase. This *Stokes drift* arises from the distinction between averaging at a fixed point in space versus averaging that follows a fluid particle. Here, we provide a step towards the Stokes drift discussion by considering the leading order motion of fluid particles found by ignoring the distinction between Eulerian and Lagrangian averaging. In effect, we time integrate equation (52.130) by fixing the particle trajectory on the right hand side to the value it had at an arbitrary initial time, $T = t_0$. Using the horizontal velocity (52.121d) and vertical velocity (52.121e) we have (now dropping the $\boldsymbol{a}$ label for brevity)

$$\frac{{\rm d}\boldsymbol{X}_{\rm h}}{{\rm d}T} = \frac{\eta_0\,\omega\,\hat{\boldsymbol{k}}\cosh[|\boldsymbol{k}|\,(z_0+H)]\sin(\boldsymbol{k}\cdot\boldsymbol{x}_0 - \omega\,T)}{\sinh(|\boldsymbol{k}|\,H)} \tag{52.131a}$$

$$\frac{{\rm d}Z}{{\rm d}T} = -\frac{\eta_0\,\omega\sinh[|\boldsymbol{k}|\,(z_0+H)]\cos(\boldsymbol{k}\cdot\boldsymbol{x}_0 - \omega\,T)}{\sinh(|\boldsymbol{k}|\,H)}, \tag{52.131b}$$

which integrates to the horizontal and vertical trajectories

$$\boldsymbol{X}_{\rm h} = \boldsymbol{x}_0 + \frac{\eta_0\,\hat{\boldsymbol{k}}\cosh[|\boldsymbol{k}|\,(z_0+H)]\cos(\boldsymbol{k}\cdot\boldsymbol{x}_0 - \omega\,T)}{\sinh(|\boldsymbol{k}|\,H)} \tag{52.132a}$$

$$Z = z_0 + \frac{\eta_0\,\sinh[|\boldsymbol{k}|\,(z_0+H)]\sin(\boldsymbol{k}\cdot\boldsymbol{x}_0 - \omega\,T)}{\sinh(|\boldsymbol{k}|\,H)}. \tag{52.132b}$$

Eliminating the time dependence leads to the equation for an ellipse in the horizontal-vertical plane

$$\frac{(\boldsymbol{X}_{\rm h}-\boldsymbol{x}_0)^2}{\cosh^2[|\boldsymbol{k}|\,(z_0+H)]} + \frac{(Z-z_0)^2}{\sinh^2[|\boldsymbol{k}|\,(z_0+H)]} = \frac{\eta_0^2}{\sinh^2(|\boldsymbol{k}|\,H)}. \tag{52.133}$$

In the deep water limit, with $|\boldsymbol{k}|\,H \gg 1$, the ellipse becomes circular and the radius exponentially decreases with depth, with short waves (large $\boldsymbol{k}|$) decaying over a shorter depth range. As a result, deep water waves have nearly circular particle trajectories such as those shown in Figure 52.4. In the shallow water limit, with $|\boldsymbol{k}|\,H \ll 1$, the vertical motion reduces to zero so that particles move horizontally. Furthermore, their horizontal excursions are independent of z, so that particles throughout the full column move coherently by the same amount.

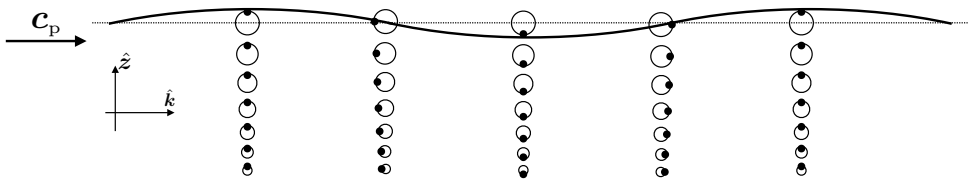

FIGURE 52.4: Motion of fluid particles in deep water waves. Shown here is a snapshot of the wave, with fluid particles denoted by black dots positioned at a point along their nearly circular orbits. The wavevector is directed to the right so that particles exhibit a clockwise orbital motion as the wave moves. Correspondingly, by moving ones eye to the left in this snapshot, then the series of fluid particles exhibit a clockwise rotation. As the horizontal motion is larger on the top of the orbit than the bottom, there is a net particle drift in the direction of the wave; this is *Stokes drift* discussed in Section 52.11. For these deep water waves, the particle motion becomes exponentially small when moving away from the interface. In contrast, for shallow water gravity waves, the particle orbits are elliptical and the horizontal major axis is depth independent whereas the vertical excursion vanishes at the bottom. This figure is taken after Figure 50 of *Lighthill* (1978).

52.5.7 Depth integrated mechanical energy of a traveling plane wave

In Section 52.4.4 we derived general expressions for the layer integrated mechanical energy budget. Here we specialize those results to the case of traveling plane surface gravity waves, and limit our focus to the phase averaged quantities.

Available potential energy

The layer integrated potential energy (per horizontal area) is given by

$$g\,\rho \int_{-H}^{\eta} z\,\mathrm{d}z = (\rho\, g\, \eta_0^2/2)\sin^2(\boldsymbol{k}\cdot\boldsymbol{x} - \omega\, t) - \rho\, g\, H^2/2. \tag{52.134}$$

We are concerned with the potential energy relative to the constant term, $-\rho\, g\, H^2/2$. That is, we focus on the available potential energy of the waves rather than the potential energy (see Section 52.5.2), in which we compute

$$g\,\rho \int_{-H}^{\eta} z\,\mathrm{d}z - g\,\rho \int_{-H}^{0} z\,\mathrm{d}z = g\,\rho \int_{0}^{\eta} z\,\mathrm{d}z = (\rho\, g\, \eta_0^2/2)\sin^2(\boldsymbol{k}\cdot\boldsymbol{x} - \omega\, t). \tag{52.135}$$

The phase average of the available potential energy (per horizontal area) is thus given by

$$\left\langle g\,\rho \int_{0}^{\eta} z\,\mathrm{d}z \right\rangle = \rho\, g\, \eta_0^2/4. \tag{52.136}$$

Evidently, the phase averaged and layer integrated available potential energy is proportional to the square of the amplitude of the free surface undulations, η_0^2.

Kinetic energy

Making use of the expression (52.113a) for the horizontal wave velocity leads to the layer integrated kinetic energy (per horizontal area) in the horizontal flow

$$\frac{\rho}{2}\int_{-H}^{0} \boldsymbol{u}^2\,\mathrm{d}z = \frac{\rho\,\Psi_0^2\,|\boldsymbol{k}|^2}{2}\int_{-H}^{0} \cosh^2[|\boldsymbol{k}|\,(z+H)]\sin^2(\boldsymbol{k}\cdot\boldsymbol{x} - \omega\, t)\,\mathrm{d}z, \tag{52.137}$$

which has the phase average

$$\left\langle \frac{\rho}{2}\int_{-H}^{0} \boldsymbol{u}^2\,\mathrm{d}z \right\rangle = \frac{\rho\,\Psi_0^2\,|\boldsymbol{k}|^2}{4}\int_{-H}^{0} \cosh^2[|\boldsymbol{k}|\,(z+H)]\,\mathrm{d}z. \tag{52.138}$$

Likewise, the phase averaged kinetic energy of the layer integrated vertical wave motion (52.113b) is given by

$$\left\langle \frac{\rho}{2} \int_{-H}^{0} w^2 \, \mathrm{d}z \right\rangle = \frac{\rho \, \Psi_0^2 \, |\boldsymbol{k}|^2}{4} \int_{-H}^{0} \sinh^2[|\boldsymbol{k}| \, (z+H)] \, \mathrm{d}z. \tag{52.139}$$

With $\cosh^2 y + \sinh^2 y = \cosh(2y)$, the phase average of the layer integrated kinetic energy per area of the wave is

$$\left\langle \frac{\rho}{2} \int_{-H}^{0} \boldsymbol{v}^2 \, \mathrm{d}z \right\rangle = \frac{\rho \, \Psi_0^2 \, |\boldsymbol{k}|^2}{4} \int_{-H}^{0} \cosh[2 \, |\boldsymbol{k}| \, (z+H)] \, \mathrm{d}z = (\Psi_0^2 \, |\boldsymbol{k}|/8) \sinh(2 \, |\boldsymbol{k}| \, H). \tag{52.140}$$

Making use of the expression (52.111b) for Ψ_0, as well as the dispersion relation (52.120) yields

$$\left\langle \frac{\rho}{2} \int_{-H}^{0} \boldsymbol{v}^2 \, \mathrm{d}z \right\rangle = \frac{\rho \, g^2 \, \eta_0^2 \, |\boldsymbol{k}|}{8 \, \omega^2} \frac{\sinh(2 \, |\boldsymbol{k}| \, H)}{\cosh^2(|\boldsymbol{k}| \, H)} = \rho \, g \, \eta_0^2/4, \tag{52.141}$$

which is identical to the phase averaged layer integrated available potential energy (52.136). We thus find, again, the equipartition of the phase averaged kinetic and available potential energies, here computed per horizontal area.

Energy flux vector

Now we determine the phase averaged horizontal flux of layer integrated mechanical energy. The general expression is given by equations (52.106) and (52.107), and is here specialized to the plane wave

$$\int_{-H}^{0} p_{\mathrm{d}} \, \boldsymbol{u} \, \mathrm{d}z = -\rho \int_{-H}^{0} \partial_t \Psi \, \nabla_{\!\mathrm{h}} \Psi \, \mathrm{d}z \tag{52.142a}$$

$$= (\rho \, \Psi_0^2 \, \boldsymbol{k} \, \omega) \sin^2(\boldsymbol{k} \cdot \boldsymbol{x} - \omega \, t) \int_{-H}^{0} \cosh^2[|\boldsymbol{k}| \, (z+H)] \, \mathrm{d}z, \tag{52.142b}$$

which has a phase average

$$\left\langle \int_{-H}^{0} p_{\mathrm{d}} \, \boldsymbol{u} \, \mathrm{d}z \right\rangle = \frac{\rho \, \Psi_0^2 \, \boldsymbol{k} \, \omega}{2} \int_{-H}^{0} \cosh^2[k \, (z+H)] \, \mathrm{d}z \tag{52.143a}$$

$$= \frac{\rho \, \Psi_0^2 \, \omega \, \hat{\boldsymbol{k}}}{4} \left[|\boldsymbol{k}| \, H + \sinh(|\boldsymbol{k}| \, H) \cosh(|\boldsymbol{k}| \, H) \right] \tag{52.143b}$$

$$= (\rho \, g \, \eta_0^2/2) \, \boldsymbol{c}_{\mathrm{g}}, \tag{52.143c}$$

where we used equation (52.125) for the group velocity and equation (52.111b) for Ψ_0. We thus see that the mechanical energy fluxed by the waves is, in the phase average and depth integral, equal to the mechanical energy times the group velocity

$$\left\langle \int_{-H}^{0} p_{\mathrm{d}} \, \boldsymbol{u} \, \mathrm{d}z \right\rangle = \rho \, \boldsymbol{c}_{\mathrm{g}} \left\langle \int_{-H}^{0} \mathcal{K} \, \mathrm{d}z + \int_{0}^{\eta} \Phi \, \mathrm{d}z \right\rangle. \tag{52.144}$$

This connection between wave energy flux and the group velocity provides yet another reason why the group velocity is more relevant to wave mechanics than the phase velocity.

Comments on group velocity and a single wave

The analysis in this subsection focused on energetics for a single wave with wavevector, $\boldsymbol{k}$. However, the group velocity is the wavevector space gradient of the dispersion relation, $c_{\mathrm{g}} = \nabla_{\boldsymbol{k}} \varpi$,

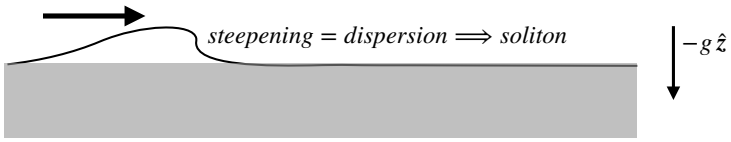

FIGURE 52.5: A soliton in the deep water limit results when the wave dispersion (long waves travel faster than short waves) balances the nonlinear steepening. The result is a soliton, which has an exact analytic expression following from the KdV equation (see *Drazin and Johnson* (1989)).

which tacitly considers more than a single wavevector. From our study of wavepackets in Section 49.6, we consider the packet to be localized in $\boldsymbol{k}$-space around a single wavevector, so that we can develop wave energetics by focusing on that single wave. When this wave forms the central carrier wave for a packet, then the group velocity serves as the velocity of the packet and it appears in the energy flux.

52.5.8 Further study

Further discussions of surface gravity waves, following that provided here, can be found in Section 54 of *Fetter and Walecka* (2003), Lectures 3 and 4 of *Pedlosky* (2003), and Section 7.1 of *Vallis* (2017).

52.6 Qualitative features of deep water waves

The shortwave/deep water waves are notable for having shorter waves travel slower than longer waves. In the event of a perturbation to the fluid, such as from a stone dropped into a pond or a storm on a lake or the ocean, deep water waves are energized. The dispersion relation (52.123a) means that longer waves spread away from the source faster than the shorter waves, leading to a self-organization of the wavelengths and corresponding wave packets.

Now imagine a deep water wave packet that somehow steepens and takes on a nonlinear form. Fourier decomposing this nonlinear wave into linear deep water modes requires more shortwave modes in the steep region, whereas the less steep portion of the wave requires longer deep water modes, which travel faster. If the nonlinear steepening on the wave face is exactly balanced by the faster dispersion of the long waves near the wave base and backside, then the wave pattern remains stable; it does not break. This balance of steepening and dispersion describes the fundamental features of a *soliton* as depicted in Figure 52.5, with a soliton a *nonlinear wave*.

52.7 Shallow water waves approaching a shore

The shallow water limit is notable for the absence of wave dispersion; i.e., shallow water gravity waves of all wavelengths travel at speed $\sqrt{g\,H}$. Tsunamis are the prototypical shallow water waves. The shallow water dispersion relation also means that shallow water gravity waves slow down when the ocean depth shoals, as when approaching a shoreline. Consequently, as waves reach the shoreline there is a tendency to accumulate wave energy as the deeper waves pile up behind the shallower waves. Furthermore, the steeper part of the wave, being part of a thicker region of the fluid and thus a larger effective H, travels slightly faster than the wave trough. As such, the steeper part of the wave overtakes the trough and, at some point, the assumptions of linearity breakdown and the shallow water waves break on the beach as depicted in Figure 52.6. In the remainder of this section, we provide some quantitative context for these remarks.

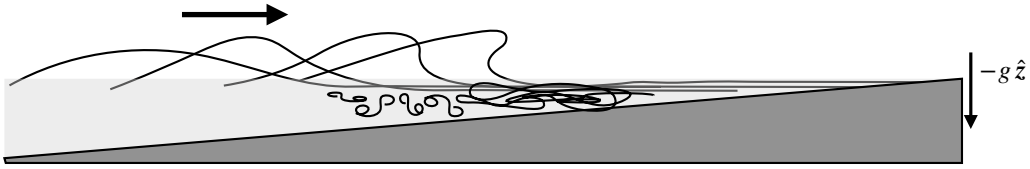

FIGURE 52.6: Shallow water waves approaching a shoreline steepen and eventually break. We can infer this behavior from the phase speed, $C_{\text{p}} = \sqrt{g\,H}$, whereby waves in deeper water move slightly faster than those in shallower water, so that the wave energy accumulates near the shore. Furthermore, water on the steeper part of the wave moves slightly faster than water in the trough, due to the difference in thickness of the water. This process causes water on the steeper portion of the wave to travel slightly faster than in the trough, leading to steepening of the waves. Nonlinearities eventually invalidate the assumptions made in deriving the linear waves. Even so, the qualitative characterization based on the linear analysis allows for a useful heuristic understanding of shallow water wave breaking on the beach. This video offers a pedagogical introduction to shallow water waves, with the 12-minute mark describing "compression" waves, in which waves steepen due to differences in the layer thickness, much like shallow water waves approaching a beach

52.7.1 Wavenumber changes

Consider the ray equations from Section 50.3 for a one-dimensional shallow water gravity wave approaching a beach with $\boldsymbol{k} = k\,\hat{\boldsymbol{x}}$ where $k > 0$. Let the resting depth be a function, $H(x)$, that decreases in the $+\hat{\boldsymbol{x}}$ direction, $\partial_x H < 0$. Since the background state is time-independent (i.e., the resting depth is static), the angular frequency remains fixed while following along a ray, so that[13]

$$\frac{\mathrm{D}_{\mathrm{r}}\varpi}{\mathrm{D}t} = 0. \tag{52.145}$$

With the local shallow water dispersion relation given by

$$\varpi(x) = k(x)\,\sqrt{g\,H(x)}, \tag{52.146}$$

we have

$$\frac{\mathrm{D}_{\mathrm{r}}\varpi}{\mathrm{D}t} = 0 \Longrightarrow \frac{1}{k}\,\frac{\mathrm{D}_{\mathrm{r}}k}{\mathrm{D}t} = -\frac{1}{2\,H}\,\frac{\mathrm{D}_{\mathrm{r}}H}{\mathrm{D}t} > 0. \tag{52.147}$$

The inequality holds since the shoreline gets shallower as the ray approaches the beach. Consequently, the wavenumber increases and the wavelength decreases for waves approaching the shore.

52.7.2 Wave energy and wave action

What happens to the wave energy as a wave approaches the shore? Common experience suggests that the wave energy increases since the amplitude increases when the wave moves into shallower water. To see this effect analytically, consider the wave action equation introduced in Section 50.5. Recall that the wave action, $\mathcal{A}$, equals to the phase averaged wave energy, $\langle \mathcal{H} \rangle$, divided by the angular frequency, ω. When following a ray, the wave action satisfies equation (50.88), which here takes the form

$$\frac{1}{\mathcal{A}}\,\frac{\mathrm{D}_{\mathrm{r}}\mathcal{A}}{\mathrm{D}t} = -\nabla \cdot \boldsymbol{c}_{\mathrm{g}}. \tag{52.148}$$

For the one-dimensional shallow water example considered here, the convergence of the group velocity is

$$-\nabla \cdot \boldsymbol{c}_{\mathrm{g}} = -\partial_x c_{\mathrm{g}} = -\partial_x (g\,H)^{1/2} = -(g\,H)^{1/2}\,\partial_x H/(2\,H) > 0. \tag{52.149}$$

Hence, the wave action increases along a ray moving towards a beach. Furthermore, as noted earlier, a static background environment means that the angular frequency remains constant

[13] Standing on a pier looking at a periodic wave field approaching the beach should reveal that the angular frequency is a constant even as the waves move into shallower water.

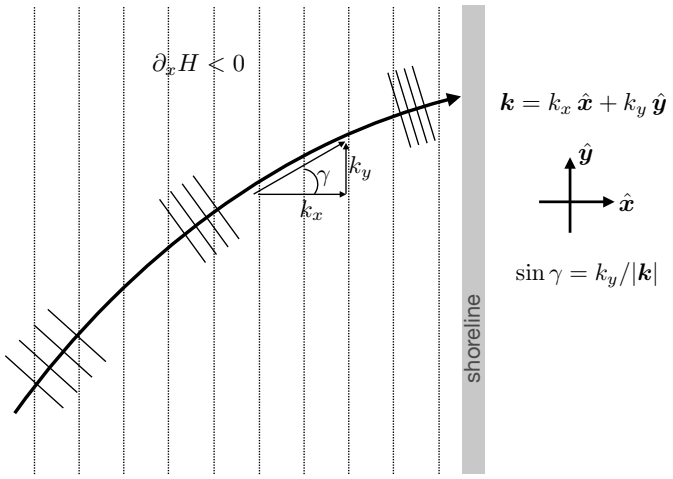

FIGURE 52.7: Depicting the refraction of shallow water gravity waves as a packet approaches the shoreline, thus causing the phase velocity to bend more directly into the shore and lines of constant phase to become more parallel to the shore. Refraction with the bottom shoaling ($\partial_x H > 0$) occurs by increasing k_x (wave length on a ray gets smaller approaching the shore) while keeping the angular frequency and k_y constant along a ray. In this manner, the angle, γ, reduces toward zero as the bottom shoals, simply through increasing k_x as a wave packet moves toward the shoreline. The dotted straight lines are lines of constant bottom depth, $H(x) =$ constant.

along a ray. Consequently, the increase in wave action following a ray onto the beach occurs since the phase averaged wave energy increases, which means that the wave amplitude is increasing. Eventually the linear analysis fails when the nonlinear effects amplify with increasing wave amplitude, as illustrated in Figure 52.6 where the waves eventually break. Even so, it is satisfying that the linear theory provides a clear picture of its ultimate demise as nonlinear effects take over.

52.7.3 Wave refraction

When distant from the shore, waves typically approach at an oblique angle, but, observations readily verify, waves bend as they start to feel the bottom, so that their phase velocity is nearly straight onto the shoreline upon reaching the beach. This bending of the wave phase lines is known as *refraction*, and the amount of refraction is a function of the bottom slope and rules for refraction are embodied in *Snell's law* from optics.

To introduce the notion of shallow water gravity wave refraction, return to the ray equation (50.37c), now with the wavevector two-dimensional,

$$\boldsymbol{k} = \hat{\boldsymbol{x}}\,k_x + \hat{\boldsymbol{y}}\,k_y. \tag{52.150}$$

If the bottom remains a function just of x, then the angular frequency remains constant along a ray, as does k_y. So writing the squared angular frequency as

$$\omega^2 = g\,H\,(k_x^2 + k_y^2), \tag{52.151}$$

it is only H and k_x that change when following along a ray. As the ray approaches the shore, $H(x)$ gets smaller. So to keep the angular frequency constant along the ray requires k_x to increase, which is the same result as in Section 52.7.1. However, now the increase in k_x means that the wave phase velocity turns into the coast so that phase lines become more parallel as the wave approaches the shore. Figure 52.7 illustrates the basic physics.

52.7.4 Further study

This video from Prof. A. Hogg provides a pedagogical introduction to shallow water wave breaking along with deep water solitons, both as realized in a laboratory. Also, section 2.2 of *Johnson* (1997) provides a thorough mathematical analysis of shallow water waves approaching a shoreline.

52.8 Standing gravity waves in a closed basin

We now consider the surface gravity wave equations (52.93a)-(52.93e) for a closed rectangular basin of constant depth and with horizontal dimensions $x \in [0, L_x]$ and $y \in [0, L_y]$. As we show, waves in a bounded domain are no longer traveling, but instead they are standing waves that oscillate in place rather than travel. We can think of such standing wave modes as a superposition of two oppositely traveling waves with the same frequency and wavenumber that are locked in-phase in a manner that satisfies the boundary conditions. For example, the sum of a right and left moving wave with equal amplitude, wavenumber, and frequency is given by the standing pattern

$$A\cos(k\,x - \omega\,t) + A\cos(-k\,x - \omega\,t) = 2\,A\cos(\omega\,t)\cos(k\,x). \tag{52.152}$$

We encountered a similar situation in Exercise 51.1 when considering acoustic waves in a closed rectangular cavity.

52.8.1 Solution for the standing waves

To satisfy the no-normal flow conditions at the four walls (equation (52.93e)) requires the horizontal wave numbers to be quantized. Correspondingly, the waves are not traveling plane waves since the flow is confined in a box. Rather, the solution is in the form of spatially standing wave that oscillates in time

$$\Psi(x, y, z, t) = \Psi_0\,\Gamma(z)\cos(k_m\,x)\cos(l_n\,y)\cos(\omega\,t), \tag{52.153}$$

where the quantized wave numbers are

$$k_m = m\,\pi/L_x \quad \text{and} \quad l_n = n\,\pi/L_y \quad \text{with} \quad m, n \text{ integers}. \tag{52.154}$$

The vertical structure function satisfies same differential equation as for the traveling waves in a channel from Section 52.5,

$$\frac{\mathrm{d}^2\Gamma}{\mathrm{d}z^2} = (k_m^2 + l_n^2)\,\Gamma \qquad -H \le z \le 0 \tag{52.155a}$$

$$\frac{\mathrm{d}\Gamma}{\mathrm{d}z} = 0 \qquad \text{at } z = -H, \tag{52.155b}$$

thus leading to the standing gravity wave solution

$$\Psi = \Psi_0\cosh[K_{m,n}\,(z + H)]\cos(k_m\,x)\cos(l_n\,y)\sin(\omega\,t) \tag{52.156a}$$

$$\Psi_0 = \frac{g\,\eta_0/\omega_{m,n}}{\cosh(K_{m,n}\,H)} \tag{52.156b}$$

$$\eta = \eta_0\cos(k_m\,x)\cos(l_n\,y)\cos(\omega_{m,n}\,t) \tag{52.156c}$$

$$u = \frac{g\,\eta_0\,k_m}{\omega_{m,n}}\,\frac{\cosh[K_{m,n}\,(z + H)]}{\cosh(K_{m,n}\,H)}\sin(k_m\,x)\cos(l_n\,y)\sin(\omega_{m,n}\,t) \tag{52.156d}$$

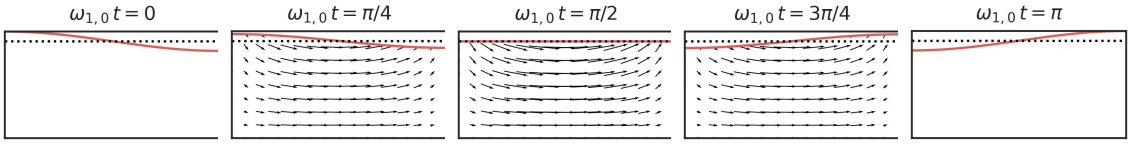

FIGURE 52.8: Flow in the $(m, n) = (1, 0)$ seiche mode, with panels corresponding to an increment of $\omega_{1,0}\, t = \pi/4$. Note that there is no flow at times $\omega_{1,0}\, t = 0$ and $\omega_{1,0}\, t = \pi$. Units are arbitrary.

$$v = \frac{g\,\eta_0\,l_n}{\omega_{m,n}}\,\frac{\cosh[K_{m,n}\,(z+H)]}{\cosh(K_{m,n}\,H)}\,\cos(k_m\,x)\,\sin(l_n\,y)\,\sin(\omega_{m,n}\,t) \tag{52.156e}$$

$$w = -\frac{g\,\eta_0\,K_{m,n}}{\omega_{m,n}}\,\frac{\sinh[K_{m,n}\,(z+H)]}{\cosh(K_{m,n}\,H)}\,\cos(k_m\,x)\,\cos(l_n\,y)\,\sin(\omega_{m,n}\,t) \tag{52.156f}$$

$$K_{m,n}^2 = k_n^2 + l_m^2. \tag{52.156g}$$

As for the channel, we find the dispersion relation by substituting the standing wave solution into the boundary condition equation (52.119), thus leading to the quantized angular frequencies

$$\omega_{m,n}^2 = g\,K_{m,n}\tanh(K_{m,n}\,H). \tag{52.157}$$

52.8.2 Gravest seiche mode as an example

The standing wave solutions are commonly referred to as *seiches*, and they can be found in enclosed lakes and ocean basins after strong and persistent winds. Winds, generally with large scale variations, tend to force the lowest or *gravest* seiche mode. For example, assume the wind blows in the zonal direction so that it excites the lowest zonal standing wave with frequency

$$\omega_{1,0}^2 = g\,K_{1,0}\tanh(K_{1,0}\,H) = (g\,\pi/L_x)\tanh(\pi\,H/L_x), \tag{52.158}$$

which has the shallow water limit $(H/L_x \to 0)$

$$\omega_{1,0}^2 \approx g\,H\,(\pi/L_x)^2. \tag{52.159}$$

As the winds relax, the seiche mode oscillates according to the angular frequency $\omega_{1,0}^2$. We depict such oscillations in Figure 52.8 over one-half a period.

52.8.3 Further study

More discussion of seiche modes can be found in Section 12.5 of *Cushman-Roisin and Beckers* (2011), Section 1.6.4 of *Brown* (1999), and Chapter 10 of *Neumann and Pierson* (1966).

52.9 Wave packets of surface gravity waves

In this section we derive expressions for surface gravity wave packets moving over a flat bottom domain, specializing the general approach considered in Section 49.6. It is sufficient to focus on the free surface, though note that the free surface packets are associated with packets of the velocity potential and velocity field, with amplitudes related by equations (52.121b)-(52.121e). We apply the wave packet technology from Sections 49.6 and 49.7 to write a free surface wave packet as

$$\eta(\boldsymbol{x}, t) = \frac{1}{(2\pi)^2}\int \mathcal{A}(\boldsymbol{k})\,\mathrm{e}^{\mathrm{i}\,[\boldsymbol{k}\cdot\boldsymbol{x} - \varpi(\boldsymbol{k})\,t]}\,\mathrm{d}\boldsymbol{k}. \tag{52.160}$$

In this equation, $\boldsymbol{k}$ is the horizontal wavevector, the wavevector integral extends over all of the horizontal wavevector space, and the amplitude function, $\mathcal{A}(\boldsymbol{k})$, is generally complex and peaked around a wavevector, $\boldsymbol{k}_0$. The surface gravity wave dispersion relation (52.120) specifies the angular frequency, $\omega = \varpi(\boldsymbol{k})$, as a function of the wavevector. Since the surface gravity wave dispersion relation is a function only of the wavevector magnitude, it satisfies

$$\varpi(\boldsymbol{k}) = \varpi(-\boldsymbol{k}) = \varpi(|\boldsymbol{k}|). \tag{52.161}$$

This property affects some simplification relative to the general discussion of wave packets in Section 49.6.

52.9.1 Initializing the packet and dispensing with conjugate symmetry

To initialize the packet we consider the possiblity of initializing the free surface, $\eta(\boldsymbol{x}, t = 0)$, and/or its time derivative, $\partial_t \eta(\boldsymbol{x}, t = 0)$. As shown here, by allowing for either possibility we must dispense with the conjugate symmetry property (8.67) otherwise assumed for the amplitudes of wave packets in Sections 49.6 and 49.7.

Given that the free surface height, η, is a real field, we can write its packet as one-half the sum of the real and imaginary parts of the integral (52.160) so that

$$\eta(\boldsymbol{x}, t) = \frac{1}{2\,(2\pi)^2} \int \left[\mathcal{A}(\boldsymbol{k})\, \mathrm{e}^{\mathrm{i}\,[\boldsymbol{k}\cdot\boldsymbol{x} - \varpi(\boldsymbol{k})\,t]} + \left(\mathcal{A}(\boldsymbol{k})\, \mathrm{e}^{\mathrm{i}\,[\boldsymbol{k}\cdot\boldsymbol{x} - \varpi(\boldsymbol{k})\,t]}\right)^*\right] \mathrm{d}\boldsymbol{k} \tag{52.162a}$$

$$= \frac{1}{2\,(2\pi)^2} \int \left[\mathcal{A}(\boldsymbol{k})\, \mathrm{e}^{\mathrm{i}\,[\boldsymbol{k}\cdot\boldsymbol{x} - \varpi(\boldsymbol{k})\,t]} + \mathcal{A}^*(\boldsymbol{k})\, \mathrm{e}^{-\mathrm{i}\,[\boldsymbol{k}\cdot\boldsymbol{x} - \varpi(\boldsymbol{k})\,t]}\right] \mathrm{d}\boldsymbol{k} \tag{52.162b}$$

$$= \frac{1}{2\,(2\pi)^2} \int \left[\mathcal{A}(\boldsymbol{k})\, \mathrm{e}^{\mathrm{i}\,[\boldsymbol{k}\cdot\boldsymbol{x} - \varpi(\boldsymbol{k})\,t]} + \mathcal{A}^*(-\boldsymbol{k})\, \mathrm{e}^{-\mathrm{i}\,[-\boldsymbol{k}\cdot\boldsymbol{x} - \varpi(-\boldsymbol{k})\,t]}\right] \mathrm{d}\boldsymbol{k} \tag{52.162c}$$

$$= \frac{1}{2\,(2\pi)^2} \int \mathrm{e}^{\mathrm{i}\,\boldsymbol{k}\cdot\boldsymbol{x}} \left[\mathcal{A}(\boldsymbol{k})\, \mathrm{e}^{-\mathrm{i}\,\varpi(\boldsymbol{k})\,t} + \mathcal{A}^*(-\boldsymbol{k})\, \mathrm{e}^{\mathrm{i}\,\varpi(\boldsymbol{k})\,t}\right] \mathrm{d}\boldsymbol{k}, \tag{52.162d}$$

where the second equality made use of the associative property (8.6b) of the complex conjugate operation, and the final equality used the property (52.161) of the surface gravity wave dispersion relation. We can compute the time derivative of the wave packet by differentiating equation (52.162d) to have

$$\partial_t \eta(\boldsymbol{x}, t) = \frac{\mathrm{i}}{2\,(2\pi)^2} \int \varpi(\boldsymbol{k})\, \mathrm{e}^{\mathrm{i}\,\boldsymbol{k}\cdot\boldsymbol{x}} \left[-\mathcal{A}(\boldsymbol{k})\, \mathrm{e}^{-\mathrm{i}\,\varpi(\boldsymbol{k})\,t} + \mathcal{A}^*(-\boldsymbol{k})\, \mathrm{e}^{\mathrm{i}\,\varpi(\boldsymbol{k})\,t}\right] \mathrm{d}\boldsymbol{k}. \tag{52.163}$$

It is now clear why we must dispense with the conjugate symmetry property (8.67), which says that $\mathcal{A}^*(-\boldsymbol{k}) = \mathcal{A}(\boldsymbol{k})$. Namely, if conjugate symmetry holds, then $\partial_t \eta(\boldsymbol{x}, t = 0) = 0$. If we instead choose conjugate anti-symmetry, whereby $\mathcal{A}^*(-\boldsymbol{k}) = -\mathcal{A}(\boldsymbol{k})$, then $\eta(\boldsymbol{x}, t = 0) = 0$. So to enable a nonzero initial free surface and/or a nonzero free surface time derivative requires an amplitude function that does not satisfy conjugate symmetry. If one is physically motivated to choose just one of these initial conditions, then either conjugate symmetry or conjugate anti-symmetry is available. For the current analysis, we do not constrain the amplitudes. Even so, η remains a real function given that it is written in equation (52.162a) as the sum of a complex number plus its complex conjugate.

52.9.2 Expressions for the amplitude function

Setting $t = 0$ in equation (52.160) for the free surface and equation (52.163) for its time derivative leads to

$$\eta(\boldsymbol{x}, 0) = \frac{1}{2\,(2\pi)^2} \int \mathrm{e}^{\mathrm{i}\,\boldsymbol{k}\cdot\boldsymbol{x}}\,[\mathcal{A}(\boldsymbol{k}) + \mathcal{A}^*(-\boldsymbol{k})]\;\mathrm{d}\boldsymbol{k} \tag{52.164a}$$

$$\partial_t\eta(\boldsymbol{x}, 0) = \frac{\mathrm{i}}{2\,(2\pi)^2} \int \varpi(\boldsymbol{k})\,\mathrm{e}^{\mathrm{i}\,\boldsymbol{k}\cdot\boldsymbol{x}}\,[-\mathcal{A}(\boldsymbol{k}) + \mathcal{A}^*(-\boldsymbol{k})]\;\mathrm{d}\boldsymbol{k}. \tag{52.164b}$$

Inverting these Fourier integral yields

$$[\mathcal{A}(\boldsymbol{k}) + \mathcal{A}^*(-\boldsymbol{k})]/2 = \int \eta(\boldsymbol{x}, 0)\,\mathrm{e}^{-\mathrm{i}\,\boldsymbol{k}\cdot\boldsymbol{x}}\,\mathrm{d}\boldsymbol{x} \tag{52.165a}$$

$$\mathrm{i}\,\varpi(\boldsymbol{k})\,[-\mathcal{A}(\boldsymbol{k}) + \mathcal{A}^*(-\boldsymbol{k})]/2 = \int \partial_t\eta(\boldsymbol{x}, 0)\,\mathrm{e}^{-\mathrm{i}\,\boldsymbol{k}\cdot\boldsymbol{x}}\,\mathrm{d}\boldsymbol{x}, \tag{52.165b}$$

which then provide expressions for the amplitude functions in terms of the prescribed initial conditions

$$\mathcal{A}(\boldsymbol{k}) = \int [\eta(\boldsymbol{x}, 0) + (\mathrm{i}/\varpi)\,\partial_t\eta(\boldsymbol{x}, 0)]\,\mathrm{e}^{-\mathrm{i}\,\boldsymbol{k}\cdot\boldsymbol{x}}\,\mathrm{d}\boldsymbol{x} \tag{52.166a}$$

$$\mathcal{A}^*(-\boldsymbol{k}) = \int [\eta(\boldsymbol{x}, 0) - (\mathrm{i}/\varpi)\,\partial_t\eta(\boldsymbol{x}, 0)]\,\mathrm{e}^{-\mathrm{i}\,\boldsymbol{k}\cdot\boldsymbol{x}}\,\mathrm{d}\boldsymbol{x}. \tag{52.166b}$$

Note that the $\boldsymbol{x}$-integral extends over all of the horizontal $\boldsymbol{x}$-space. As discussed in Section 52.9.1, we find that the amplitude function indeed does not satisfy conjugate symmetry

$$\mathcal{A}(\boldsymbol{k}) \neq \mathcal{A}^*(-\boldsymbol{k}). \tag{52.167}$$

52.9.3 Wave packet in terms of a propagator function

Making use of the amplitude functions (52.166a) and (52.166b) in the integral expansion (52.162d) leads to the expression for the free surface height

$$\eta(\boldsymbol{x}, t) = \frac{1}{2\,(2\pi)^2} \int\int \mathrm{e}^{\mathrm{i}\,\boldsymbol{k}\cdot(\boldsymbol{x}-\boldsymbol{\xi})-\mathrm{i}\,\varpi\,t}[\eta(\boldsymbol{\xi}, 0) + (\mathrm{i}/\varpi)\,\partial_t\eta(\boldsymbol{\xi}, 0)]\;\mathrm{d}\boldsymbol{k}\,\mathrm{d}\boldsymbol{\xi} \tag{52.168}$$

$$+ \frac{1}{2\,(2\pi)^2} \int\int \mathrm{e}^{\mathrm{i}\,\boldsymbol{k}\cdot(\boldsymbol{x}-\boldsymbol{\xi})+\mathrm{i}\,\varpi\,t}[\eta(\boldsymbol{\xi}, 0) - (\mathrm{i}/\varpi)\,\partial_t\eta(\boldsymbol{\xi}, 0)]\;\mathrm{d}\boldsymbol{k}\,\mathrm{d}\boldsymbol{\xi}. \tag{52.169}$$

Rearrangement then renders the tidy expression

$$\eta(\boldsymbol{x}, t) = \int [\partial_t G(\boldsymbol{x} - \boldsymbol{\xi}, t)\,\eta(\boldsymbol{\xi}, 0) + G(\boldsymbol{x} - \boldsymbol{\xi}, t)\,\partial_t\eta(\boldsymbol{\xi}, 0)]\mathrm{d}\boldsymbol{\xi}, \tag{52.170}$$

where we introduced the propagator function and its time derivative

$$G(\boldsymbol{x}, t) = \frac{1}{(2\pi)^2} \int \mathrm{e}^{\mathrm{i}\,\boldsymbol{k}\cdot\boldsymbol{x}}\,\frac{\sin((\varpi(|\boldsymbol{k}|)\,t)}{(\varpi(|\boldsymbol{k}|)}\,\mathrm{d}\boldsymbol{k} \quad \text{and} \quad \partial_t G(\boldsymbol{x}, t) = \frac{1}{(2\pi)^2} \int \mathrm{e}^{\mathrm{i}\,\boldsymbol{k}\cdot\boldsymbol{x}} cos(\varpi(|\boldsymbol{k}|)\,t)\,\mathrm{d}\boldsymbol{k}. \tag{52.171}$$

As written, the function, $G(\boldsymbol{x}, t)$, and its time derivative encapsulate all the temporal behavior of the wave packet, acting to propagate the initial conditions, $\eta(\boldsymbol{\xi}, 0)$ and $\partial_t\eta(\boldsymbol{\xi}, 0)$, forward in time. As noted in Section 49.6. equation (52.170) is quite elegant since $G(\boldsymbol{x}, t)$ is independent of details of the initial conditions. In this manner it acts like a Green's function (Chapter 9).

52.9.4 Further study

Elements of this section follow from Section 55 of *Fetter and Walecka* (2003).

52.10 Capillary-gravity waves

As studied in Section 25.11, surface tension exists at the interface between two media, such as a liquid and solid or liquid and gas. In this section we consider the effects from surface tension on surface waves, with surface tension providing the means to realize *capillary waves*.

52.10.1 Pressure jump across the air-sea surface

As studied in Section 25.11, surface tension on an interface between two fluids leads to a pressure jump across the interface. That is, the pressure on one side of the interface is different from the pressure on the other side. The pressure jump is given by the Young-Laplace formula (25.149), which when applied to the ocean free surface renders

$$p_{\text{a}} - p_{\text{ocn}} = \gamma \nabla^2 \eta \implies p_{\text{ocn}} = p_{\text{a}} - \gamma \nabla^2 \eta. \tag{52.172}$$

In this equation, $\gamma > 0$ is the surface tension (dimensions of force per length = M T^{-2}), p_{a} is the pressure on the atmospheric side of the free surface, and p_{ocn} is the pressure on the ocean side of the free surface. To help remember signs for the pressure jump, note that the Young-Laplace formula (52.172) says that pressure on the concave side of the interface is higher than on the convex side. For example, if the free surface extends upward then $p_{\text{ocn}} - p_{\text{a}} > 0$ since the ocean is on the concave side and so it has the higher pressure. This result also follows since $\nabla^2 \eta < 0$ for an upward extension, which leads to a local free surface maximum.[14]

52.10.2 Dynamic boundary condition with surface tension

We can continue to apply Bernoulli's theorem even in the presence of surface tension to determine the dynamic boundary condition. Hence, we proceed as in Section 52.3.2 to evaluate the Bernoulli potential at the free surface. Now, however, it is important to specify which side of the free surface we evaluate the Bernoulli potential. Being interested in ocean waves, we evaluate the Bernoulli potential on the ocean side, in which case equation (52.84) takes on the form

$$g\,\eta + \mathcal{K} - \partial_t \Psi = -p_{\text{ocn}}/\rho = -(p_{\text{a}} - \gamma \nabla^2 \eta)/\rho, \tag{52.173}$$

where the second equality follows from the Young-Laplace formula (52.172). We again assume the atmospheric pressure is a given constant that can be trivially absorbed by a gauge transformation (just like we did in Section 52.2.3 for surface gravity waves). We thus have the equation of motion

$$\partial_t \Psi = \rho^{-1} \left[g\,\rho - \gamma\,\nabla^2 \right] \eta + \mathcal{K}. \tag{52.174}$$

The surface tension term, $-(\gamma/\rho)\,\nabla^2 \eta$, is new relative to equation (52.84) holding for gravity waves.

52.10.3 Dispersion relation for capillary-gravity waves

In Section 52.3.4 we detailed the steps needed to derive the linear equations (52.93b)-(52.93e) for surface gravity waves. Those steps also hold for capillary-gravity waves, with the only difference

[14] The discussion in Section 25.11.4 considered bubbles, where the Young-Laplace formula shows that surface tension causes pressure inside of a bubble (concave side) to be larger than outside the bubble.

being a modification to the dynamic boundary condition arising from surface tension

$$\nabla^2 \Psi = 0 \qquad \text{irrotational and non-divergent velocity} \tag{52.175a}$$

$$\partial_t \Psi = \rho^{-1} \left[g\,\rho - \gamma\,\nabla^2 \right] \eta \qquad \text{linearized dynamic b.c. at } z = 0 \tag{52.175b}$$

$$\partial_z \Psi = -\partial_t \eta \qquad \text{linearized kinematic b.c. at } z = 0 \tag{52.175c}$$

$$\hat{\boldsymbol{n}} \cdot \nabla \Psi = 0 \qquad \text{no-normal flow kinematic b.c. on rigid boundaries.} \tag{52.175d}$$

The analysis in Section 52.5.1 concerns the interior harmonic scalar potential as well as the kinematic boundary condition. Both of these properties hold equivalently for surface gravity waves and for capillary-gravity waves. Hence, we can write the scalar potential for capillary-gravity waves as in equations (52.111a) and (52.111b), and the corresponding free surface as equation (52.112). The dispersion relation is derived by using these expressions for Ψ and η in the dynamic boundary condition (52.175b), with a few lines of algebra rendering

$$\omega^2 = g\,|\boldsymbol{k}|\,(1 + \Upsilon)\tanh(|\boldsymbol{k}|\,H) \quad \text{capillary-gravity waves,} \tag{52.176}$$

where we introduced the non-dimensional parameter

$$\Upsilon = |\boldsymbol{k}|^2\,\gamma/(g\,\rho). \tag{52.177}$$

The capillary-gravity wave dispersion relation (52.176) generalizes the gravity wave dispersion (52.120). The Υ parameter provides a regime boundary where capillary waves dominate ($\Upsilon \gg 1$) versus where gravity waves dominate ($\Upsilon \ll 1$).

52.10.4 Deep water capillary-gravity waves

The hydrostatic limit is not relevant for capillary waves since capillary waves are generally very small (as seen below) and thus do not satisfy hydrostatic scaling. Hence, we find it physically most interesting to examine the limit of deep water capillary-gravity waves, in which case $|\boldsymbol{k}|\,H \to \infty$ so that the dispersion relation (52.176) simplifies to

$$\omega^2 = g\,|\boldsymbol{k}|\,(1 + \Upsilon) \quad \text{deep water capillary-gravity waves.} \tag{52.178}$$

Phase speed

The phase speed for deep water capillary-gravity waves is given by

$$C_{\mathsf{p}} = \omega/|\boldsymbol{k}| = \sqrt{(g/|\boldsymbol{k}|)\,(1 + \Upsilon)} = \sqrt{g/|\boldsymbol{k}| + \gamma\,|\boldsymbol{k}|/\rho}, \tag{52.179}$$

which has the longwave and shortwave limits

$$C_{\mathsf{p}} \approx C_{\mathsf{p}}^{\text{dwg}} \quad \text{for } \Upsilon \ll 1 \quad \text{and} \quad C_{\mathsf{p}} \approx \sqrt{\gamma\,|\boldsymbol{k}|/\rho} \quad \text{for } \Upsilon \gg 1, \tag{52.180}$$

where we introduced the deep water gravity wave phase speed from equation (52.123a)

$$C_{\mathsf{p}}^{\text{dwg}} = \sqrt{g/|\boldsymbol{k}|}. \tag{52.181}$$

At both extremes the phase speed is unbounded, with gravity waves dominant for longwaves and capillary waves dominant for shortwaves.

Group velocity

The transport of energy within a packet of capillary-gravity waves is determined by the group velocity, $\boldsymbol{c}_{\mathrm{g}} = \nabla_{\boldsymbol{k}}\omega$, which takes the form

$$\boldsymbol{c}_{\mathrm{g}} = \frac{\hat{\boldsymbol{k}}\, C_{\mathrm{p}}^{\mathrm{dwg}}}{2}\, \frac{1+3\,\Upsilon}{(1+\Upsilon)^{1/2}} = \frac{\hat{\boldsymbol{k}}}{2}\left[\frac{g\,\gamma}{\rho}\right]^{1/4} \frac{1+3\,\Upsilon}{\sqrt{\Upsilon^{1/2}+\Upsilon^{3/2}}}. \tag{52.182}$$

The group velocity has the following shortwave and longwave limits

$$\boldsymbol{c}_{\mathrm{g}} \approx \hat{\boldsymbol{k}}\, C_{\mathrm{p}}^{\mathrm{dwg}}/2 \quad \text{for } \Upsilon \ll 1 \quad \text{and} \quad \boldsymbol{c}_{\mathrm{g}} \approx \frac{3}{2}\hat{\boldsymbol{k}}\left[\frac{|\boldsymbol{k}|\,\gamma}{\rho}\right]^{1/2} \quad \text{for } \Upsilon \gg 1. \tag{52.183}$$

As for the phase speed, we find that the group velocity is unbounded at both extremes, with gravity waves dominant for longwaves and capillary waves dominant at shortwaves.

Wavelength of the minimum group velocity

As seen above, there is a continuum of wavelengths for capillary-gravity waves, with gravity waves dominating for longwaves and capillary waves dominating for shortwaves. To delineate between shortwaves and longwaves, we seek the wavenumber where the group velocity is a minimum. To simplify the algebra, assume $\boldsymbol{k} = k\,\hat{\boldsymbol{x}}$ so that we reach an extrema of the group velocity when

$$\frac{\mathrm{d}c_{\mathrm{g}}}{\mathrm{d}k} = 0 \Longrightarrow 3\,\Upsilon_{\mathrm{min}}^2 + 6\,\Upsilon_{\mathrm{min}} - 1 = 0, \tag{52.184}$$

in which case

$$\Upsilon_{\mathrm{min}} = 2/\sqrt{3} - 1 \approx 0.1547 \tag{52.185a}$$

$$k_{\mathrm{min}} = (\Upsilon_{\mathrm{min}}\, g\,\rho/\gamma)^{1/2} \approx 0.393\,(g\,\rho/\gamma)^{1/2} \tag{52.185b}$$

$$(c_{\mathrm{g}})_{\mathrm{min}} \approx 1.086\,(g\,\gamma/\rho)^{1/4}. \tag{52.185c}$$

For an air-water interface we take $\gamma = 0.072$ N m^{-1} $= 0.072$ kg s^{-2}, along with the water density of $\rho = 10^3$ kg m^{-3} and gravitational acceleration $g = 9.8$ m s^{-2}, thus leading to

$$k_{\mathrm{min}} \approx 145 \text{ m}^{-1} \tag{52.186a}$$

$$\Lambda_{\mathrm{min}} \approx 4.3 \times 10^{-2} \text{ m} \tag{52.186b}$$

$$(c_{\mathrm{g}})_{\mathrm{min}} \approx 1.7 \times 10^{-1} \text{ m s}^{-1}. \tag{52.186c}$$

Evidently, for wavelengths smaller than roughly 4 cm the surface tension effects are important in their support of capillary waves. In contrast, larger wavelengths are dominated by gravity waves.

52.10.5 Comments and further study

As noted in Section 25.11.5, we can ignore the pressure jump induced by surface tension across the air-sea interface if the radius of curvature of the air-sea interface is larger than a few centimeters. Here, we also see that the boundary between gravity waves and capillary waves occurs for wavelengths of a few centimeters. It is for these reasons that capillary waves, and surface tension more generally, can be ignored when considering geophysical fluid motions with scales larger than a few centimeters. Even so, we highlight the importance of surface tension and capillary waves for the study of fundamental processes affecting air-sea exchanges of matter, energy, and momentum.

Much of the discussion in this section follows that in Section 54 of *Fetter and Walecka* (2003). We again encounter surface tension effects in Section 60.2 when studying the Rayleigh-Taylor instability in the presence of gravity and surface tension.

52.11 Particle trajectories and Stokes drift

We here consider the trajectories of fluid particles moving as part of a wave field, going to the next order in asymptotics beyond the leading order results from Section 52.5.6. With a spatially constant wave amplitude, a fluid particle periodically returns to its original position. However, in the presence of wave inhomogeneities, such as the surface gravity waves considered in Sections 52.3 and 52.5, fluid particles oscillate between regions where the undulation in one direction does not match that in the other direction. In effect, a fluid particle spends a bit more time in the forward moving part of the wave crest than the backward moving part of the wave trough. This asymmetry leads to a net drift of fluid particles in the direction of the wave. Figure 52.4 illustrates particle trajectories in a deep water wave for the case where the Stokes drift is ignored, in which case the particles exhibit periodic orbits. In this section we focus on the Stokes drift, in which case the particle orbits are nearly periodic, but not exactly, so that they do not return to their initial point.

To describe fluid particle drift induced by waves requires us to distinguish between an average computed at a fixed point in space (Eulerian mean), versus along a fixed fluid particle (Lagrangian mean). Their difference defines the *Stokes correction*

$$\text{Lagrangian mean} = \text{Eulerian mean} + \text{Stokes correction}. \tag{52.187}$$

When applied to the trajectory of fluid particles, the Stokes correction is referred to as the *Stokes drift*. In linear waves, Stokes drift arises when the wave field has spatial inhomogeneities that cause a particle to sample distinct portions of the wave that lead to a net, or rectified, transport. For the examples considered in this section, where there are no boundaries, then the Eulerian mean vanishes so that the Lagrangian mean particle position equals to the Stokes drift.

In this section we introduce the basic mathematics to support equation (52.187) when applied to the fluid particle position within a plane wave. These ideas form part of the rudiments for wave-mean flow interaction theory further studied in Chapter 70 and pursued in far more detail by *Bühler* (2014a).

52.11.1 Formulation of Stokes drift

Consider a three-dimensional particle trajectory written in Cartesian coordinates,

$$\boldsymbol{X}(\boldsymbol{a}, t) = X(\boldsymbol{a}, t)\, \hat{\boldsymbol{x}} + Y(\boldsymbol{a}, t)\, \hat{\boldsymbol{y}} + Z(\boldsymbol{a}, t)\, \hat{\boldsymbol{z}}. \tag{52.188}$$

In the analysis of waves, it is common to assume the material coordinate, $\boldsymbol{a}$, is the initial position of a fluid particle, which we here assume. As discussed in Section 17.7.1, the particle trajectory is determined by time integrating the particle velocity

$$\frac{\partial \boldsymbol{X}(\boldsymbol{a}, t)}{\partial t} = \boldsymbol{v}[\boldsymbol{X}(\boldsymbol{a}, t), t] \tag{52.189}$$

so that

$$\boldsymbol{X}(\boldsymbol{a}, t) = \boldsymbol{X}(\boldsymbol{a}, 0) + \int_0^t \boldsymbol{v}[\boldsymbol{X}(\boldsymbol{a}, t'), t']\, \mathrm{d}t'. \tag{52.190}$$

This equation is a trivial result of time integrating the particle velocity. Nonetheless, it is useful to express the content of this equation in words. It says that the position at time, t, of a fluid

particle labelled by the material coordinate, $\boldsymbol{a}$, is given by the initial position of the particle, $\boldsymbol{X}(\boldsymbol{a}, 0)$, plus the time integrated movement of the particle following the fluid flow.

Equation (52.190) provides the trajectory, but only by knowing the velocity following the trajectory. To produce a result that is more readily computed analytically, we develop a Taylor series computed relative to the initial position of the fluid particle. In this manner we make use of the approximate expression for the particle velocity at time t

$$v^n[\boldsymbol{X}(\boldsymbol{a}, t), t] \approx v^n[\boldsymbol{X}(\boldsymbol{a}, 0), t] + \nabla v^n[\boldsymbol{X}(\boldsymbol{a}, 0), t] \cdot [\boldsymbol{X}(\boldsymbol{a}, t) - \boldsymbol{X}(\boldsymbol{a}, 0)] \tag{52.191a}$$

$$= v^n[\boldsymbol{X}(\boldsymbol{a}, 0), t] + \nabla v^n[\boldsymbol{X}(\boldsymbol{a}, 0), t] \cdot \int_0^t \frac{\mathrm{d}\boldsymbol{X}(\boldsymbol{a}, t')}{\mathrm{d}t'} \, \mathrm{d}t' \tag{52.191b}$$

$$= v^n[\boldsymbol{X}(\boldsymbol{a}, 0), t] + \nabla v^n[\boldsymbol{X}(\boldsymbol{a}, 0), t] \cdot \int_0^t \boldsymbol{v}[\boldsymbol{X}(\boldsymbol{a}, t'), t'] \, \mathrm{d}t', \tag{52.191c}$$

where the Taylor series was truncated after terms linear in the particle displacement $\boldsymbol{X}(\boldsymbol{a}, t) - \boldsymbol{X}(\boldsymbol{a}, 0)$. We emphasize two points regarding equation (52.191c).

- The velocity, $v^n[\boldsymbol{X}(\boldsymbol{a}, 0), t]$, is the n'th component of the fluid velocity field evaluated at the initial point of the fluid particle trajectory, $\boldsymbol{X}(\boldsymbol{a}, 0)$, and at the time t. That is, $v^n[\boldsymbol{X}(\boldsymbol{a}, 0), t]$ is the Eulerian velocity evaluated at the fixed Eulerian point, $\boldsymbol{X}(\boldsymbol{a}, 0)$.

- What determines the accuracty of the Taylor series? A suitable non-dimensional expansion coefficient for the Taylor expansion is the ratio of the particle displacement to the wave length, L,

  $$\epsilon = \frac{|\boldsymbol{X}(\boldsymbol{a}, t) - \boldsymbol{X}(\boldsymbol{a}, 0)|}{L}. \tag{52.192}$$

  This ratio is small for the small amplitude waves considered here, whereby the particle displacements are far smaller than the wavelength.

The integrand on the right hand side of equation (52.191c) is the Lagrangian velocity integrated over the time interval. To within the same order of accuracy as maintained for writing equation (52.191c), we can use the Eulerian velocity evaluated at the initial position, thus rendering

$$v^n[\boldsymbol{X}(\boldsymbol{a}, t), t] \approx v^n[\boldsymbol{X}(\boldsymbol{a}, 0), t] + \nabla v^n[\boldsymbol{X}(\boldsymbol{a}, 0), t] \cdot \int_0^t \boldsymbol{v}[\boldsymbol{X}(\boldsymbol{a}, 0), t'] \, \mathrm{d}t', \tag{52.193}$$

with rearrangement leading to

$$v^n[\boldsymbol{X}(\boldsymbol{a}, t), t] - v^n[\boldsymbol{X}(\boldsymbol{a}, 0), t] \approx \nabla v^n[\boldsymbol{X}(\boldsymbol{a}, 0), t] \cdot \int_0^t \boldsymbol{v}[\boldsymbol{X}(\boldsymbol{a}, 0), t'] \, \mathrm{d}t'. \tag{52.194}$$

The left hand side is the difference between the velocity following a fluid particle (the Lagrangian velocity for the moving fluid particle) from the velocity at the initial particle point (the Eulerian velocity at the initial point of the trajectory). The right hand side terms are all evaluated at the initial position, $\boldsymbol{X}(\boldsymbol{a}, 0)$. Furthermore, the right hand side is non-zero where the velocity at the initial position has a nonzero gradient (i.e., it is spatially inhomogeneous), with its inhomogeneity projecting onto the time integrated velocity at that point. Equation (52.194) says that the velocity following a fluid particle is modified from the velocity at its initial position if the particle moves through an inhomogeneous velocity field.

Stokes drift of fluid particles is defined as the difference of the velocities in equation (52.194)

when phased averaged, which we write as[15]

$$(v^{(\mathsf{S})})^n[\boldsymbol{X}(\boldsymbol{a},0),t] = \langle v^n[\boldsymbol{X}(\boldsymbol{a},t),t] - v^n[\boldsymbol{X}(\boldsymbol{a},0),t]\rangle \tag{52.195a}$$

$$\approx \left\langle \nabla v^n[\boldsymbol{X}(\boldsymbol{a},0),t] \cdot \int_0^t \boldsymbol{v}[\boldsymbol{X}(\boldsymbol{a},0),t']\,\mathrm{d}t' \right\rangle. \tag{52.195b}$$

This expression holds for any arbitrary initial point in the fluid, so that we can write it in a concise Eulerian form that dispenses with trajectories

$$(v^{(\mathsf{S})})^n(\boldsymbol{x},t) \approx \left\langle \nabla v^n(\boldsymbol{x},t) \cdot \int_0^t \boldsymbol{v}(\boldsymbol{x},t')\,\mathrm{d}t' \right\rangle. \tag{52.196}$$

We can draw an analogy between Stokes drift and surfing. Namely, the more a fluid particle samples larger amplitude variations in the velocity field (the gradient term), the further it drifts (the integral term).

52.11.2 Particle trajectories in a homogeneous wave

The expression (52.196) for the Stokes drift is general and will be specialized in Section 52.11.4 for the case of surface gravity waves. Before doing so, in this section and in Section 52.11.3 we determine particle trajectories for the traveling plane wave

$$\frac{\mathrm{d}X}{\mathrm{d}t} = U\sin(k\,x - \omega\,t) \tag{52.197a}$$

$$\frac{\mathrm{d}Z}{\mathrm{d}t} = -U\cos(k\,x - \omega\,t). \tag{52.197b}$$

We here set the wavevector to $\boldsymbol{k} = k\,\hat{\boldsymbol{x}}$, so that it is purely zonal, let $U > 0$ be the speed of the particle motion, and wrote X and Z for the Cartesian components of the particle trajectory. To simplify the mathematics we perform the analysis in a frame moving with the waves so that the phase $k\,x - \omega\,t$ can be replaced by $-\omega\,t$, so that the particle trajectories satisfy

$$\frac{\mathrm{d}X}{\mathrm{d}t} = -U\sin(\omega\,t) \tag{52.198a}$$

$$\frac{\mathrm{d}Z}{\mathrm{d}t} = -U\cos(\omega\,t). \tag{52.198b}$$

Figure 52.4 shows a schematic of the particle trajectories appropriate for a deep water gravity wave, with the trajectories resulting from equations (52.198a) and (52.198b) directly analogous.

We start by examining particle motion in the case with a constant wave amplitude, $U = U_0$. Particle trajectories in this case are clockwise in the x-z plane around a circle with radius U_0/ω

$$X(t) - X_0 = (U_0/\omega)\,[\cos(\omega t) - 1] \tag{52.199a}$$

$$Z(t) - Z_0 = -(U_0/\omega)\sin(\omega t), \tag{52.199b}$$

where the initial position at time $t = 0$ is

$$\boldsymbol{X}(t = t_0) = \hat{\boldsymbol{x}}\,X_0 + \hat{\boldsymbol{z}}\,Z_0, \tag{52.200}$$

and the center of the circle is

$$\boldsymbol{X}_{\text{center}} = [X_0 - U_0/\omega]\,\hat{\boldsymbol{x}} + Z_0\,\hat{\boldsymbol{z}}. \tag{52.201}$$

[15] We introduced the phase average in Section 8.1.2. It is realized by averaging over a 2π extent of the wave phase. It can be performed via a time average over a period, a space average over a wavelength, or a combination.

There is no Stokes drift since the particles return to their initial position each wave period.

52.11.3 Stokes drift from an inhomogeneous wave

Now consider the case of a vertically dependent wave amplitude, $U = U(z)$. The canonical example is where the wave amplitude decreases with depth, as for the surface gravity waves from Section 52.5. In turn, we expect there to be a fluid particle drift in the zonal direction introduced by the vertical wave inhomogeneity. This drift is a particular realization of Stokes drift.

To compute the leading order expression for the Stokes drift, expand U in a Taylor series about the initial position

$$U \approx U_0 + \sigma\,(Z - Z_0) \tag{52.202}$$

where the vertical shear, σ, has units of inverse time and is given by

$$\sigma = \left[\frac{\mathrm{d}U}{\mathrm{d}Z}\right]_{Z=Z_0}. \tag{52.203}$$

The Taylor series (52.202) is valid so long as the vertical trajectories maintain the inequality

$$|\sigma|\,|Z - Z_0| \ll U_0, \tag{52.204}$$

which says that the vertical shear is small

$$|\sigma| \ll \frac{U_0}{|Z - Z_0|}. \tag{52.205}$$

We use the Taylor series expansion (52.202) to solve for the vertical trajectory as determined by

$$\frac{\mathrm{d}(Z - Z_0)}{\mathrm{d}t} = -[U_0 + \sigma\,(Z - Z_0)]\cos(\omega t). \tag{52.206}$$

Rearrangement leads to

$$\int_{Z_0}^{Z} \frac{\mathrm{d}(Z - Z_0)}{U_0 + \sigma\,(Z - Z_0)} = -\int_0^t \cos(\omega t)\,\mathrm{d}t. \tag{52.207}$$

The left hand side integral can be computed by changing variables

$$\Sigma = U_0 + \sigma\,(Z - Z_0) \Longrightarrow \mathrm{d}\Sigma = \sigma\,\mathrm{d}(Z - Z_0), \tag{52.208}$$

so that equation (52.207) becomes

$$\int_{U_0}^{\Sigma} \frac{\mathrm{d}\Sigma}{\Sigma} = -\sigma \int_0^t \cos(\omega t)\,\mathrm{d}t. \tag{52.209}$$

Performing the integrals and evaluating the end points renders

$$\ln\left[1 + \frac{\sigma}{U_0}(Z - Z_0)\right] = -\frac{\sigma \sin(\omega t)}{\omega}, \tag{52.210}$$

which yields the exponential solution

$$1 + \frac{\sigma}{U_0}(Z - Z_0) = \mathrm{e}^{-(\sigma/\omega)\sin(\omega t)} \Longrightarrow Z - Z_0 = \frac{U_0}{\sigma}\left[-1 + \mathrm{e}^{-(\sigma/\omega)\sin(\omega t)}\right]. \tag{52.211}$$

The vertical particle position is seen to oscillate around its initial position Z_0.

We next consider the zonal particle position, in which case

$$\frac{\mathrm{d}(X - X_0)}{\mathrm{d}t} = -U_0 \left[1 + \frac{\sigma}{U_0}(Z - Z_0)\right] \sin(\omega t) = -U_0 \, \mathrm{e}^{-(\sigma/\omega)\sin(\omega t)} \sin(\omega t), \tag{52.212}$$

where we used equation (52.211) for the vertical trajectory. To make progress, we expand the exponential assuming the ratio of inverse time scales, σ/ω, is small

$$|\sigma/\omega| \ll 1. \tag{52.213}$$

In this limit, the vertical trajectory retains its unperturbed form (52.199b), and the zonal trajectory satisfies

$$\frac{\mathrm{d}(X - X_0)}{\mathrm{d}t} \approx -U_0 \sin(\omega t) \left[1 - \frac{\sigma}{\omega} \sin(\omega t)\right], \tag{52.214}$$

where we dropped terms of order $(\sigma/\omega)^2$. We can understand the scaling in equation (52.213) by noting that the period for the circular motion is given by

$$\tau_{\text{circle}} = 2\,\pi/\omega. \tag{52.215}$$

The inverse time, σ, introduces a time scale for the drift, defined according to

$$\tau_{\text{drift}} = 2\,\pi/|\sigma|. \tag{52.216}$$

A small ratio $|\sigma/\omega|$ thus implies

$$|\sigma/\omega| = \tau_{\text{circle}}/\tau_{\text{drift}} \ll 1. \tag{52.217}$$

Hence, we are solving for the zonal trajectory in the limit where the time scale for the circular motion is small (i.e., fast oscillations around the circle) relative to the time scale for the drift (i.e., slow drift).

Returning now to the approximate zonal trajectory equation (52.214) yields

$$\frac{\mathrm{d}(X - X_0)}{\mathrm{d}t} = -U_0 \sin(\omega t) \left[1 - \frac{\sigma}{\omega} \sin(\omega t)\right] \tag{52.218a}$$

$$= -U_0 \sin(\omega t) + \frac{U_0\,\sigma}{2\,\omega}\,[1 - \cos(2\,\omega t)], \tag{52.218b}$$

which integrates to

$$X - X_0 = \left(\frac{U_0}{\omega}\right)\left[\cos(\omega\,t) - 1 - \frac{\sigma \sin(2\,\omega\,t)}{4\,\omega} + \frac{\sigma\,t}{2}\right] \tag{52.219a}$$

$$= \underbrace{\left(\frac{U_0}{\omega}\right)[\cos(\omega\,t) - 1]}_{\text{homogeneous}} + \underbrace{\frac{U_0\,\sigma\,t}{2\,\omega}}_{\text{Stokes drift}} - \underbrace{\frac{U_0\,\sigma \sin(2\,\omega\,t)}{4\,\omega^2}}_{\text{higher harmonic}} + \mathcal{O}(\sigma/\omega)^2. \tag{52.219b}$$

The leading order term is the homogeneous motion given by equation (52.199a). The next term is the Stokes drift, followed by a higher order harmonic and then further terms on the order of $(\sigma/\omega)^2$. There is no vertical Stokes drift to this order in (σ/ω), so that the Stokes drift velocity is given by

$$\left[\frac{\boldsymbol{X} - \boldsymbol{X}_0}{t}\right]^{\text{drift}} = \frac{\sigma\,U_0}{2\omega}\,\hat{\boldsymbol{x}}. \tag{52.220}$$

The circular motion of the parcels is therefore deformed by the zonal Stokes drift. The drift

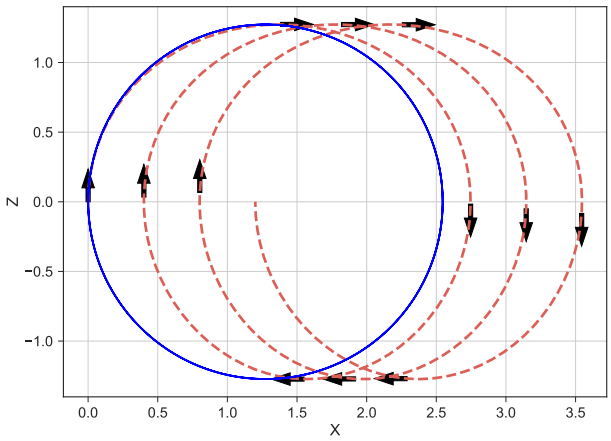

FIGURE 52.9: Example trajectories of fluid particles undergoing Stokes drift. Particle motion is clockwise in the x-z plane. For homogeneous waves, there is zero Stokes drift with circular trajectories given by equations (52.199a) and (52.199b), as depicted here by the blue trajectory. There is a Stokes drift in the presence of vertical derivative in the wave amplitude and thus in the particle velocity, with trajectories for this example given by equation (52.211) for the vertical component and equation (52.219b) for the horizontal component. We set the parameters as follows: $T = 2\pi/\omega = 60$ s, $U_0 = 0.1$ m s^{-1}, and $\sigma = \omega/10$ and exhibit trajectories over four minutes.

increases with larger wave amplitude (U_0 large); with larger vertical shear (σ large); and with longer period waves (ω small). Each of these wave properties affects the time that a fluid particle samples the wave as it moves forward versus backward, thus determining the magnitude of the Stokes drift. See Figure 52.9 for an illustration based on a particular choice for the dimensional parameters.

52.11.4 Stokes drift for surface gravity waves

The velocity field for surface gravity waves, given by equations (52.113a) and (52.113b), is far more complicated than the prototypical wave considered in Sections 52.11.2 and 52.11.3. For that reason we make use of the general expression (52.196) to determine the Stokes drift velocity for surface gravity waves in a flat channel, rather than directly integrate to determine the trajectories. Hence, we need to compute terms in the following equations for surface gravity waves

$$u^{(\mathsf{S})}(\boldsymbol{x}) \approx \left\langle \nabla u(\boldsymbol{x},t) \cdot \int_0^t \boldsymbol{v}(\boldsymbol{x},t')\,\mathrm{d}t' \right\rangle \tag{52.221a}$$

$$v^{(\mathsf{S})}(\boldsymbol{x}) \approx \left\langle \nabla v(\boldsymbol{x},t) \cdot \int_0^t \boldsymbol{v}(\boldsymbol{x},t')\,\mathrm{d}t' \right\rangle \tag{52.221b}$$

$$w^{(\mathsf{S})}(\boldsymbol{x}) \approx \left\langle \nabla w(\boldsymbol{x},t) \cdot \int_0^t \boldsymbol{v}(\boldsymbol{x},t')\,\mathrm{d}t' \right\rangle . \tag{52.221c}$$

The components to the velocity field for surface gravity waves are given by equations (52.113a) and (52.113b), repeated here to be self-contained

$$\boldsymbol{u} = \frac{g\,\eta_0\,\hat{\boldsymbol{k}}}{C_{\mathsf{p}}} \frac{\cosh[|\boldsymbol{k}|\,(z+H)]\sin(\mathcal{P})}{\cosh(|\boldsymbol{k}|\,H)} \tag{52.222a}$$

$$w = -\frac{g\,\eta_0}{C_{\mathsf{p}}} \frac{\sinh[|\boldsymbol{k}|\,(z+H)]\cos(\mathcal{P})}{\cosh(|\boldsymbol{k}|\,H)}, \tag{52.222b}$$

and their spatial gradients are given by

$$\nabla u = \frac{g\,\eta_0\,k_x\left[\hat{\boldsymbol{k}}\cos(\mathcal{P})\cosh[|\boldsymbol{k}|\,(z+H)] + \hat{\boldsymbol{z}}\sin(\mathcal{P})\sinh[|\boldsymbol{k}|\,(z+H)]\right]}{C_{\mathsf{p}}\cosh(|\boldsymbol{k}|\,H)} \tag{52.223a}$$

$$\nabla v = \frac{g\,\eta_0\,k_y\left[\hat{\boldsymbol{k}}\cos(\mathcal{P})\cosh[|\boldsymbol{k}|\,(z+H)] + \hat{\boldsymbol{z}}\sin(\mathcal{P})\sinh[|\boldsymbol{k}|\,(z+H)]\right]}{C_{\mathsf{p}}\cosh(|\boldsymbol{k}|\,H)} \tag{52.223b}$$

$$\nabla w = \frac{g\,\eta_0\,|\boldsymbol{k}|\left[\hat{\boldsymbol{k}}\sin(\mathcal{P})\sinh[|\boldsymbol{k}|\,(z+H)] - \hat{\boldsymbol{z}}\cos(\mathcal{P})\cosh[|\boldsymbol{k}|\,(z+H)]\right]}{C_{\mathsf{p}}\cosh(|\boldsymbol{k}|\,H)}, \tag{52.223c}$$

where we introduced the phase

$$\mathcal{P} = \boldsymbol{k}\cdot\boldsymbol{x} - \omega\,t \tag{52.224}$$

to produce more tidy expressions, and recall that

$$\hat{\boldsymbol{k}} = \boldsymbol{k}/|\boldsymbol{k}| = (\hat{\boldsymbol{x}}\,k_x + \hat{\boldsymbol{y}}\,k_y)/|\boldsymbol{k}| \tag{52.225}$$

is the wave direction in the horizontal plane. We also require the following time integrals

$$\int_0^t \sin(\boldsymbol{k}\cdot\boldsymbol{x} - \omega\,t')\,\mathrm{d}t' = \omega^{-1}\left[\cos(\boldsymbol{k}\cdot\boldsymbol{x} - \omega\,t) - \cos(\boldsymbol{k}\cdot\boldsymbol{x})\right] \tag{52.226a}$$

$$\int_0^t \cos(\boldsymbol{k}\cdot\boldsymbol{x} - \omega\,t')\,\mathrm{d}t' = -\omega^{-1}\left[\sin(\boldsymbol{k}\cdot\boldsymbol{x} - \omega\,t) - \sin(\boldsymbol{k}\cdot\boldsymbol{x})\right]. \tag{52.226b}$$

Use of these results in equations (52.221a)-(52.221c) leads to the horizontal Stokes drift velocity for surface gravity waves in a flat bottom domain, here written in three equivalent manners through use of the dispersion relation and the phase speed

$$\boldsymbol{v}^{(\mathsf{S})} = \frac{\boldsymbol{k}\,(g\,\eta_0)^2\cosh[2|\boldsymbol{k}|\,(z+H)]}{2\,\omega\,C_{\mathsf{p}}^2\cosh^2(|\boldsymbol{k}|\,H)} \tag{52.227a}$$

$$= \frac{\boldsymbol{k}\,\omega\,\eta_0^2\cosh[2\,|\boldsymbol{k}|\,(z+H)]}{2\sinh^2(|\boldsymbol{k}|\,H)} \tag{52.227b}$$

$$= \frac{\hat{\boldsymbol{k}}\,C_{\mathsf{p}}\,(|\boldsymbol{k}|\,\eta_0)^2\cosh[2\,|\boldsymbol{k}|\,(z+H)]}{2\sinh^2(|\boldsymbol{k}|\,H)}. \tag{52.227c}$$

The purely horizontal nature of the Stokes drift agrees with that found for the prototypical wave in Section 52.11.3.

The ratio of the Stokes speed at $z=0$ to that at $z=-H$ is given by

$$\frac{\hat{\boldsymbol{k}}\cdot\boldsymbol{v}^{(\mathsf{S})}(z=0)}{\hat{\boldsymbol{k}}\cdot\boldsymbol{v}^{(\mathsf{S})}(z=-H)} = \cosh(2\,|\boldsymbol{k}|\,H). \tag{52.228}$$

In the deep water limit, $k\,H \gg 1$, this ratio is much greater than unity, indicating a nontrivial vertical shear in the zonal Stokes velocity. In contrast, the ratio becomes unity in the shallow water limit, $|\boldsymbol{k}|\,H \ll 1$, so that there is no vertical shear to the Stokes velocity. In this case the Stokes speed takes on the depth-independent shallow water form

$$\boldsymbol{v}^{(\mathsf{S})}\cdot\hat{\boldsymbol{k}} \approx (C_{\mathsf{p}}/2)\,(\eta_0/H)^2 \quad \text{for } |\boldsymbol{k}|\,H \ll 1, \tag{52.229}$$

which has no dependence on the wavelength (other than $|\boldsymbol{k}|\,H \ll 1$). This speed is much smaller

than the deep water Stokes speed at $z = 0$, which we can see by computing

$$\hat{\boldsymbol{k}} \cdot \boldsymbol{v}^{(\mathsf{S})}(z=0) \approx \eta_0^2 \, g^{1/2} \, |\boldsymbol{k}|^{3/2}/4 \quad \text{for } |\boldsymbol{k}| \, H \gg 1 \tag{52.230a}$$

$$\hat{\boldsymbol{k}} \cdot \boldsymbol{v}^{(\mathsf{S})}(z=0) \approx (\eta_0/H)^2 \, \sqrt{g \, H} \quad \text{for } |\boldsymbol{k}| \, H \ll 1, \tag{52.230b}$$

so that the ratio of the deep water to shallow water Stokes speed at $z = 0$ is

$$\frac{\hat{\boldsymbol{k}} \cdot \boldsymbol{v}^{(\mathsf{S})\mathsf{dw}}(z=0)}{\hat{\boldsymbol{k}} \cdot \boldsymbol{v}^{(\mathsf{S})\mathsf{sw}}(z=0)} \approx |\boldsymbol{k} \, H|^{3/2}/4 \gg 1. \tag{52.231}$$

Since the phase average vanishes at a fixed point in space, the Eulerian mean vanishes so that the Lagrangian mean in equation (52.187) is given by the Stokes drift. Hence, the presence of Stokes drift indicates that there is a net movement of matter in the direction of the wave. In particular, for the shallow water case there is a steady column of fluid moving in the direction of the wave according to the Stokes drift expression (52.229). It is important to appreciate that this example is on an unbounded domain. If the domain is bounded so that the phase averaged center of mass for the fluid is fixed in space, then the Eulerian mean exactly compensates the Stokes drift to render a zero Lagrangian mean motion.

52.11.5 Comments and further study

Is Stokes drift a nonlinear phenomena? In answering this question we note that Stokes drift occurs with particle motion in linear waves, but the waves must be inhomogeneous such as the surface gravity waves studied in this chapter. Nonlinearity appears in the form of the particle-following (Lagrangian) average, as can be seen by the expression of Stokes drift given by equation (52.196)

$$(v^{(\mathsf{S})})^n(\boldsymbol{x}, t) \approx \left\langle \nabla v^n(\boldsymbol{x}, t) \cdot \int_0^t \boldsymbol{v}(\boldsymbol{x}, t') \, \mathrm{d}t' \right\rangle . \tag{52.232}$$

The dot product of the velocity gradient with the time integrated velocity (to give the time integrated position) is nonlinear. So although the waves are linear, the Lagrangian kinematics of particle trajectories introduces nonlinearites.

Stokes drift occurs in many guises when studying the motion of fluid particles within wave fields. We revisit elements of Stokes drift in Chapter 70 when studying the rudiments of eddy-induced tracer transport. This video from Prof. Hogg at Australian National University provides an overview of the discussion in this section along with some laboratory experiments to illustrate Stokes drift. Section 10.1.1 of *Bühler* (2014a) discusses Stokes corrections in the context of generalized Lagrangian mean.

52.12 Exercises

EXERCISE 52.1: UNIQUENESS THEOREM FOR POTENTIAL FLOW
Here we show that there is a unique potential flow that satisfies any given boundary condition. For that purpose, assume there are two potential flows, $\boldsymbol{v}_1$ and $\boldsymbol{v}_2$, that satisfy the same boundary conditions on $\partial\mathcal{R}$. Show that $\boldsymbol{v}_1 = \boldsymbol{v}_2$ throughout the domain. Hint: consider the domain integrated kinetic energy contained in the difference field, $\boldsymbol{V} = \boldsymbol{v}_1 - \boldsymbol{v}_2$, and make use of the results from Section 52.2.7.

EXERCISE 52.2: SURFACE GRAVITY WAVES ON THE VIDEO CHANNEL *Veritasium*
Veritasium is a science channel that has the following educational video on surface ocean waves.

However, the host makes a few minor errors in this video. Discuss the errors.

EXERCISE 52.3: SURFACE KINEMATIC BOUNDARY CONDITION
Show that for an irrotational and non-divergent flow, the surface kinematic boundary condition (52.25) can be written

$$\partial_t \eta = -\nabla \cdot [(z-\eta)\, \nabla \Psi] \quad \text{at } z = \eta. \tag{52.233}$$

Hint: read Section 21.3.

EXERCISE 52.4: GAUGE INVARIANCE OF KINETIC ENERGY
In Section 52.2.6 we argued that the gauge invariance of the globally integrated kinetic energy follows from equation (52.49): $\int \boldsymbol{v} \cdot \hat{\boldsymbol{n}}\, \mathrm{d}\mathcal{S} = 0$, which follows for the case where the free surface is a material interface so that $\partial_t \eta = -\nabla \cdot \boldsymbol{U}$. Discuss whether the kinetic energy remains gauge invariant if the upper free surface is not material, so that $\partial_t \eta = -\nabla \cdot \boldsymbol{U} + Q_{\mathsf{m}}/\rho$, where $Q_{\mathsf{m}} \neq 0$ is a mass flux crossing the free surface and with this mass flux having density equal to the constant layer density, ρ.

Hint: to write $\boldsymbol{v} = -\nabla \Psi$ requires $\nabla \times \boldsymbol{v} = 0$. Do we expect the flow to remain irrotational in the presence of nonzero Q_{m} when the density of Q_{m} equals to that of the homogeneous domain?

EXERCISE 52.5: ENERGETICS OF DEPTH INTEGRATED FLOW IN FULL NONLINEAR THEORY
In Section 52.4.4 we computed the energy budget for the depth integrated flow within the linearized theory. Derive the mechanical energy equation for the full nonlinear theory integrated over $-H \leq z \leq \eta$, thus providing the nonlinear analog to the energy equation (52.107) derived for the linear theory. Do not assume the bottom is flat for the nonlinear theory. Confirm that all terms missing from the energy budget (52.107) are third order or higher. Hint: make use of results from Section 52.2.6.

EXERCISE 52.6: ENERGETICS OF CAPILLARY-GRAVITY WAVES
In Section 52.4.4 we derived equations for the energetics of depth integrated linearized flow in absence of surface tension. Extend that discussion to include surface tension as discussed in Section 52.10. Specifically, derive the equation for the time tendency of the depth integrated sum of the kinetic plus gravitational potential energy. Interpret the extra term arising from surface tension. Hint: start at a point in the derivation from Section 52.4.4 that is valid whether surface tension is present or not. Thereafter, make use of the dynamic boundary condition that includes surface tension.

EXERCISE 52.7: STOKES DRIFT FOR ONE-DIMENSIONAL MONOCHROMATIC WAVE
Consider a one-dimensional monochromatic longitudinal wave with velocity

$$u = u_0 \sin(k\, x - \omega\, t), \tag{52.234}$$

where u_0 is the wave amplitude, $k = 2\pi/\Lambda > 0$ the wave number, Λ the wavelength, $\omega = 2\pi/T > 0$ the angular frequency, T the wave period, and $C_{\mathsf{p}} = \omega/k = \Lambda/T$ is the phase speed. A longitudinal wave is one whose particle motions are parallel to the wave vector, which in this exercise are both in the $\hat{\boldsymbol{x}}$ direction. Determine the wave period averaged Stokes velocity to first order accuracy in the small parameter

$$\epsilon = u_0/C_{\mathsf{p}} = u_0\, k/\omega = u_0\, T/\Lambda, \tag{52.235}$$

with this parameter the ratio of the wave amplitude to wave speed, or equivalently the ratio of the length scale of particle displacements to the wavelength. Hint: make use of the general result given by equation (52.196).

Chapter 53

INERTIAL WAVES ON THE f-PLANE

Inertial waves are dispersive waves that arise from the Coriolis acceleration. Fluid particles within inertial waves exhibit the anti-cyclonic *inertial oscillations* studied in Section 14.4. We study inertial waves in an inviscid, homogeneous (constant density), f-plane fluid, and examine traveling plane inertial waves in an unbounded domain as well as forced inertial waves in both unbounded domains and vertically bounded domains. Inertial waves provide the mechanism for vertical stiffness exhibited by the *Taylor-Proudman effect* (Section 31.5.3), and we discuss that role in this chapter.

READER'S GUIDE TO THIS CHAPTER

We assume a working knowledge of fluid mechanics in a rotational reference frame as studied in Chapter 31. Our study of inertial waves was inspired by Section 9.2 of *Davidson* (2015), who emphasizes the role of inertial waves in forming vertically stiff structures in rapidly rotating turbulent flows, as well as Section 2.2 of *Stern* (1975), the Epilogue of *Lighthill* (1978), and the concise review by *Mory* (1992). For a visualization of inertial waves, refer to the 18 minute mark from the rotating tank experiments of Prof. Fultz, which illustrates inertial oscillations within a bounded rotating homogeneous fluid. We again encounter inertial waves in Section 57.9 when studying free inertia-gravity waves, in which case the limit of zero buoyancy frequency reduces to the inertial waves of this chapter.[a]

[a] Some authors refer to Rossby waves as a type of inertial wave, since Rossby waves also owe their existence to the Coriolis acceleration. However, we consider *inertial waves* to be those waves occuring on an f-plane, where Rossby waves do not occur. We study Rossby waves in Chapters 54, 55, and 62.

53.1 Equations for a uniformly rotating homogeneous fluid

We study inertial motions in a homogeneous and unbounded inviscid fluid on an f-plane. To start that study, we here formulate the nonlinear equations for the fluid motion and follow up in Section 53.2 with the linearized equations. Recall that we also studied motion of surface waves in a homogeneous fluid in Chapter 52. One key distinction is that here we are concerned with motion away from any boundary, including a free surface. Additionally, we now work on the f-plane.

53.1.1 Velocity equation

A homogeneous inviscid fluid on the f-plane is governed by the momentum equation

$$[\partial_t + (\boldsymbol{v} \cdot \nabla)]\, \boldsymbol{v} + 2\, \boldsymbol{\Omega} \times \boldsymbol{v} = -\nabla p/\rho - g\, \hat{\boldsymbol{z}}, \tag{53.1}$$

where g is the effective gravitational acceleration that arises from central gravity and planetary centrifugal (Section 13.10.4), and

$$\boldsymbol{\Omega} = \Omega\, \hat{\boldsymbol{z}} = (f/2)\, \hat{\boldsymbol{z}} \tag{53.2}$$

is the constant angular frequency of the f-plane. Recall from Section 24.5 that the f-plane is based on assuming a locally flat geopotential, in which case the centrifugal acceleration from the rotating reference frame is incorporated into the effective gravitational acceleration. In this manner, each point on the f-plane experiences the same effects from rotation of the reference frame.

As when formulating the Boussinesq approximation in Section 29.1.1, we find it useful to decompose pressure according to a static background hydrostatic pressure, plus a dynamical pressure

$$p = p_0 + \rho\, \varphi \quad \text{where} \quad \mathrm{d}p_0/\mathrm{d}z = -\rho\, g, \tag{53.3}$$

with ρ the constant density and $p_0(z)$ the static background hydrostatic pressure that exactly balances the fluid weight. This decomposition brings the momentum equation 53.1 to the form

$$[\partial_t + (\boldsymbol{v} \cdot \nabla)]\, \boldsymbol{v} + 2\, \boldsymbol{\Omega} \times \boldsymbol{v} = -\nabla \varphi \tag{53.4}$$

There is no buoyancy since density is uniform (Chapter 30).

Furthermore, again since the density is uniform everywhere, and since we are ignoring all boundaries, there can be no hydrostatic pressure induced either by gradients of the density nor by gradients of the boundary[1] As a result, the dynamical pressure is fully non-hydrostatic for the system we are studying here.

[1] Recall that for surface waves in a homogeneous fluid layer, a hydrostatic pressure is generated through undulations of the free ocean surface as given by equation (52.18).

53.1.2 Vorticity equation

In addition to the velocity equation, we make use of the vorticity equation, whose nonlinear form is derived from the vector invariant velocity equation (see Section 40.3.1)

$$\partial_t \boldsymbol{v} + (2\,\boldsymbol{\Omega} + \boldsymbol{\omega}) \times \boldsymbol{v} = -\nabla(\varphi + \mathcal{K}), \tag{53.5}$$

where we introduced the kinetic energy per mass and the relative vorticity

$$\mathcal{K} = \boldsymbol{v} \cdot \boldsymbol{v}/2 \quad \text{and} \quad \boldsymbol{\omega} = \nabla \times \boldsymbol{v}. \tag{53.6}$$

The vorticity equation (40.42) takes on the following form in this constant density inviscid fluid

$$[\partial_t + (\boldsymbol{v} \cdot \nabla)]\,\boldsymbol{\omega}_{\text{a}} = (\boldsymbol{\omega}_{\text{a}} \cdot \nabla)\,\boldsymbol{v} \quad \text{with} \quad \boldsymbol{\omega}_{\text{a}} = 2\,\boldsymbol{\Omega} + \boldsymbol{\omega}. \tag{53.7}$$

Noting that $\boldsymbol{\Omega}$ is independent of space and time allows us to write the relative vorticity equation

$$\partial_t \boldsymbol{\omega} = [(2\,\boldsymbol{\Omega} + \boldsymbol{\omega}) \cdot \nabla]\,\boldsymbol{v}. \tag{53.8}$$

53.1.3 Energy equations

Taking the scalar product of $\boldsymbol{v}$ with the velocity equation (53.1) yields the equation for the kinetic energy per mass, $\mathcal{K} = \boldsymbol{v} \cdot \boldsymbol{v}/2$, and gravitational potential energy per mass, $\Phi = g\,z$ (i.e., the geopotential), and their sum (the mechanical energy per mass)

$$\frac{\mathrm{D}\mathcal{K}}{\mathrm{D}t} = -\boldsymbol{v} \cdot \nabla p/\rho - w\,g \tag{53.9a}$$

$$\frac{\mathrm{D}\Phi}{\mathrm{D}t} = w\,g \tag{53.9b}$$

$$\frac{\mathrm{D}(\mathcal{K} + \Phi)}{\mathrm{D}t} = -\boldsymbol{v} \cdot \nabla p/\rho. \tag{53.9c}$$

Since the fluid density is uniform and constant, the gravitational potential energy decouples from the kinetic energy through use of the pressure decomposition (53.3), thus leading to

$$\frac{\mathrm{D}\mathcal{K}}{\mathrm{D}t} = -\boldsymbol{v} \cdot \nabla\varphi = -\nabla \cdot (\boldsymbol{v}\,\varphi). \tag{53.10}$$

Hence, the kinetic energy is materially modified for flows where the velocity is misaligned with constant dynamic pressure surfaces (e.g., kinetic energy increases when flow is down the pressure gradients), or equivalently where there is a convergence of the dynamical pressure flux.

53.2 Linearized equations

We here formulate the linear equations for an inviscid homogeneous fluid moving on an f-plane, with these equations providing the basis for the study of inertial waves.

53.2.1 Linearized velocity equation

We are interested in small amplitude fluctuations relative to a state of zero motion. Linearization of the velocity equation (53.4) occurs by dropping the self-advection term, $(\boldsymbol{v} \cdot \nabla)\,\boldsymbol{v}$, thus leading to

$$\partial_t \boldsymbol{v} + 2\,\boldsymbol{\Omega} \times \boldsymbol{v} = -\nabla\varphi. \tag{53.11}$$

With $\boldsymbol{\Omega}$ independent of time, we see that the velocity projected onto $\boldsymbol{\Omega}$ satisfies

$$\partial_t(\boldsymbol{v} \cdot \boldsymbol{\Omega}) = -\boldsymbol{\Omega} \cdot \nabla\varphi. \tag{53.12}$$

Hence, if there is no pressure gradient along the direction of the rotation axis, then the velocity of the linear flow in that direction remains constant in time. For rotation around the vertical axis, $\boldsymbol{\Omega} = \Omega\,\hat{\boldsymbol{z}}$, and with no vertical dynamic pressure gradient, $\partial_z\varphi = 0$, then the vertical velocity is static, $\partial_t w = 0$.

53.2.2 Forced oscillator equation for the velocity

Taking a time derivative on the velocity equation (53.11) and back-substituting the velocity equation leads to

$$\partial_{tt}\boldsymbol{v} + 4\,\Omega^2\,\boldsymbol{v} - 4\,\boldsymbol{\Omega}\,(\boldsymbol{v} \cdot \boldsymbol{\Omega}) = 2\,\boldsymbol{\Omega} \times \nabla\varphi - \partial_t\nabla\varphi. \tag{53.13}$$

Now decompose the velocity according to the orientation of the rotation vector

$$\widehat{\boldsymbol{\Omega}} = \boldsymbol{\Omega}/|\boldsymbol{\Omega}| \tag{53.14a}$$
$$\boldsymbol{v} = \boldsymbol{v}_\perp + \boldsymbol{v}_\parallel \tag{53.14b}$$
$$\boldsymbol{v}_\perp = \boldsymbol{v} - \widehat{\boldsymbol{\Omega}}\,(\widehat{\boldsymbol{\Omega}} \cdot \boldsymbol{v}) \tag{53.14c}$$
$$\boldsymbol{v}_\parallel = \boldsymbol{v} - \boldsymbol{v}_\perp = \widehat{\boldsymbol{\Omega}}\,(\widehat{\boldsymbol{\Omega}} \cdot \boldsymbol{v}), \tag{53.14d}$$

which allows us to decompose equation (53.13) into an equation for the parallel velocity and one for the perpendicular velocity

$$\partial_t[\widehat{\boldsymbol{\Omega}} \cdot (\partial_t\boldsymbol{v} + \nabla\varphi)] = 0 \tag{53.15a}$$
$$(\partial_{tt} + 4\,\Omega^2)\,\boldsymbol{v}_\perp = 2\,\widehat{\boldsymbol{\Omega}} \times \nabla\varphi - \partial_t[\nabla\varphi - \widehat{\boldsymbol{\Omega}}\,(\widehat{\boldsymbol{\Omega}} \cdot \nabla\varphi)]. \tag{53.15b}$$

Equation (53.15a) says that the projection of $\partial_t\boldsymbol{v} + \nabla\varphi$ onto the rotation axis remains constant in time. With $\widehat{\boldsymbol{\Omega}} = \hat{\boldsymbol{z}}$ then

$$\partial_t(\partial_t w + \partial_z\varphi) = 0. \tag{53.16}$$

Equation (53.15b) is a forced simple harmonic oscillator equation for motion in the plane perpendicular to the rotation axis. The natural angular frequency is $2\,\Omega$ and the forcing arises from pressure gradients in the perpendicular plane. Again, with $\widehat{\boldsymbol{\Omega}} = \hat{\boldsymbol{z}}$, equation (53.15b) becomes

$$(\partial_{tt} + 4\,\Omega^2)\,\boldsymbol{u} = 2\,\Omega\,\hat{\boldsymbol{z}} \times \nabla\varphi - \partial_t\nabla_{\!\mathsf{h}}\varphi. \tag{53.17}$$

The appearance of an oscillator equation anticipates the simple harmonic oscillations of fluid particles within a linear wave.

53.2.3 Forced oscillator equation for $\nabla_{\!\mathsf{h}} \cdot \boldsymbol{u} = -\partial_z w$

We find it useful to determine expressions for the horizontal velocity divergence in the special case of $f = 2\,\boldsymbol{\Omega} = 2\,\Omega\,\hat{\boldsymbol{z}}$, in which case equation (53.17) has the two components

$$(\partial_{tt} + f^2)\,u = -f\,\partial_y\varphi - \partial_{xt}\varphi \tag{53.18a}$$
$$(\partial_{tt} + f^2)\,v = f\,\partial_x\varphi - \partial_{yt}\varphi. \tag{53.18b}$$

Taking ∂_x on the first equation and ∂_y on the second, and then adding leads to

$$(\partial_{tt} + f^2)\,\nabla_{\!\mathsf{h}} \cdot \boldsymbol{u} = -\nabla_{\!\mathsf{h}}(\partial_t\varphi) \Longleftrightarrow (\partial_{tt} + f^2)\,\partial_z w = \nabla_{\!\mathsf{h}}(\partial_t\varphi). \tag{53.19}$$

Evidently, if the vertical velocity is a linear function of z (as in the long wave limit), then the pressure is independent of z, which in turn from equations (53.18a) and (53.18b) mean that $\partial_z \boldsymbol{u} = 0$. We make use of this property in Section 53.5.2 when discussing inertial waves forced from a moving sinusoidal boundary.

53.2.4 Wave equation for the vertical velocity

Taking the vertical derivative of equation (53.19) and then using equation (53.16) renders the wave equation for the vertical velocity in the case that $\boldsymbol{\Omega} = \hat{\boldsymbol{z}}\,\Omega$

$$(\partial_{tt}\nabla^2 + f^2\,\partial_{zz})w = 0. \tag{53.20}$$

This equation provides the starting point for studies of inertial oscillations on an f-plane. In Section 53.2.6 we derive a slightly more general form of this equation for an arbitrary oriented rotation vector.

53.2.5 Linearized vorticity equation

Taking the curl of the linear velocity equation (53.11) eliminates the pressure gradient and yields the linear vorticity equation

$$\partial_t \boldsymbol{\omega} = 2\,(\boldsymbol{\Omega}\cdot\nabla)\,\boldsymbol{v}. \tag{53.21}$$

To reach this result requires the identity (2.39h) for the curl of a cross product. We also assumed $\boldsymbol{\Omega}$ has no spatial dependence so that all of its derivatives vanish.

The linear vorticity equation (53.21) can also be derived by linearizing the nonlinear vorticity equation (53.8) by dropping the contributions from nonlinear stretching and tilting, which are processes we studied in Section 40.5. So the only source for vorticity in the linear theory arises from stretching and tilting along the rotational axis. That is, from the derivative of velocity in a direction aligned with the rotational axis. With $\boldsymbol{\Omega} = \hat{\boldsymbol{z}}\,\Omega$, the vorticity evolves according to

$$\partial_t \boldsymbol{\omega} = 2\,\Omega\,\partial_z \boldsymbol{v}, \tag{53.22}$$

in which case the horizontal vorticity components evolve according to vertical tilting whereas the vertical component evolves according to vertical stretching[2]

$$\partial_t(\hat{\boldsymbol{x}}\cdot\boldsymbol{\omega}) = 2\,\Omega\,\partial_z u \quad \text{and} \quad \partial_t(\hat{\boldsymbol{y}}\cdot\boldsymbol{\omega}) = 2\,\Omega\,\partial_z v \quad \text{and} \quad \partial_t(\hat{\boldsymbol{z}}\cdot\boldsymbol{\omega}) = 2\,\Omega\,\partial_z w. \tag{53.23}$$

Evidently, inertial waves carry a non-zero vorticity, and that vorticity is directly generated by the rotation vector, $\boldsymbol{\Omega}$, in the presence of velocity gradients.

53.2.6 The inertial wave equation for general $\boldsymbol{\Omega}$

To develop a wave equation, we take a time derivative of the linear vorticity equation (53.21), and make use of the linearized momentum equation (53.11), thus leading to

$$\partial_{tt}\boldsymbol{\omega} = -2\,(\boldsymbol{\Omega}\cdot\nabla)\,(2\,\boldsymbol{\Omega}\times\boldsymbol{v} + \nabla\varphi). \tag{53.24}$$

To eliminate the pressure gradient we take another curl and again make use of the identity (2.39h) to write

$$\nabla\times\boldsymbol{\omega} = \nabla\times(\nabla\times\boldsymbol{v}) = \nabla(\nabla\cdot\boldsymbol{v}) - \nabla^2\boldsymbol{v} = -\nabla^2\boldsymbol{v}, \tag{53.25}$$

where $\nabla\cdot\boldsymbol{v} = 0$ since the fluid density is constant. We also make use of Cartesian tensor calculus from Chapter 2, remembering that $\boldsymbol{\Omega}$ and the permutation symbol are constants, to derive the

[2] We study vortex stretching and tilting in Section 40.5.3.

identity

$$
\begin{aligned}
(\nabla \times [(\boldsymbol{\Omega} \cdot \nabla)\,(\boldsymbol{\Omega} \times \boldsymbol{v})])^m &= \epsilon^{mnp}\,\partial_n[\Omega^s \partial_s\,(\boldsymbol{\Omega} \times \boldsymbol{v})_p] && \text{(53.26a)}\\
&= \epsilon^{mnp}\,\partial_n[\Omega^s \partial_s\,\epsilon_{pqr}\,\Omega^q\,v^r] && \text{(53.26b)}\\
&= \epsilon^{mnp}\,\epsilon_{qrp}\,\Omega^s\,\Omega^q\,\partial_n \partial_s v^r && \text{(53.26c)}\\
&= (\delta^m{}_q\,\delta^n{}_r - \delta^m{}_r\,\delta^n{}_q)\,\Omega^s\,\Omega^q\,\partial_n \partial_s v^r && \text{(53.26d)}\\
&= \Omega^s\,(\Omega^m\,\partial_r\,\partial_s v^r - \Omega^n\,\partial_n\,\partial_s\,v^m) && \text{(53.26e)}\\
&= -(\boldsymbol{\Omega} \cdot \nabla)^2\,v^m, && \text{(53.26f)}
\end{aligned}
$$

where we made use of the ϵ-tensor identity (1.69) as well as $\nabla \cdot \boldsymbol{v} = 0$. We are thus led to the wave equation for inertial waves, which is satisfied separately for each of the Cartesian components of the velocity field

$$
[\partial_{tt}\nabla^2 + (2\,\boldsymbol{\Omega} \cdot \nabla)^2]\,\boldsymbol{v} = 0 \Longleftrightarrow \partial_{tt}(\nabla \times \boldsymbol{\omega}) = (2\,\boldsymbol{\Omega} \cdot \nabla)^2\,\boldsymbol{v}. \tag{53.27}
$$

The vertical component of the first equation reduces to equation (53.20) when $\boldsymbol{\Omega} = \hat{\boldsymbol{z}}\,\Omega$. The second expression makes use of equation (53.25) that relates the curl of the vorticity to the Laplacian of the velocity.

53.3 Plane inertial waves

In this section we study the physics of plane inertial waves moving in an unbounded domain.

53.3.1 Dispersion relation for inertial waves

The inertial wave equation (53.27) provides the starting point for developing mechanical properties of inertial waves. To develop the dispersion relation we consider a traveling plane wave solution of the form

$$
\boldsymbol{v} = \tilde{\boldsymbol{v}}\,\mathrm{e}^{\mathrm{i}\,(\boldsymbol{k}\cdot\boldsymbol{x} - \omega\,t)} \quad \text{and} \quad \varphi = \tilde{\varphi}\,\mathrm{e}^{\mathrm{i}\,(\boldsymbol{k}\cdot\boldsymbol{x} - \omega\,t)}, \tag{53.28}
$$

with three-dimensional wavevector and wave direction unit vector

$$
\boldsymbol{k} = \hat{\boldsymbol{x}}\,k_x + \hat{\boldsymbol{y}}\,k_y + \hat{\boldsymbol{z}}\,k_z \quad \text{and} \quad \hat{\boldsymbol{k}} = (\hat{\boldsymbol{x}}\,k_x + \hat{\boldsymbol{y}}\,k_y + \hat{\boldsymbol{z}}\,k_z)/|\boldsymbol{k}|. \tag{53.29}
$$

We introduced complex amplitudes, $\tilde{\boldsymbol{v}}$ and $\tilde{\varphi}$, for the velocity and pressure. The angular frequency, $\omega \geq 0$, is determined as a function of the wavevector according to the dispersion relation (53.31) derived below.[3] As we are considering free space waves (no boundaries), there is no preferred length scale for the inertial waves.[4] Furthermore, since the flow is non-divergent and the waves have a three dimensional wavevector, the constraint $\nabla \cdot \boldsymbol{v} = 0$ means that the velocity of fluid particles is perpendicular to the wavevector

$$
\nabla \cdot \boldsymbol{v} = 0 \Longrightarrow \boldsymbol{v} \cdot \boldsymbol{k} = 0. \tag{53.30}
$$

This orientation of wavevector and fluid velocity characterizes *transverse waves*, in which lines of constant wave phase (e.g., wave crests and troughs) are everywhere perpendicular to $\boldsymbol{k}$. We illustrate this property of transverse waves in Figure 53.1.

Plugging the wave ansatz (53.28) into the inertial wave equation (53.27) leads to the *dispersion*

[3] Be careful to distinguish the angular frequency, ω, from the vorticity vector, $\boldsymbol{\omega}$.

[4] Inertial waves in a bounded domain will generally have quantized wavenumbers, as required by the boundary conditions.

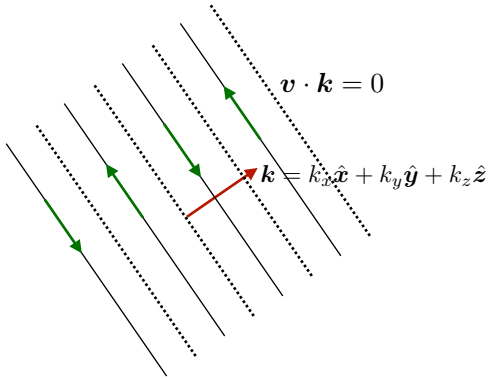

FIGURE 53.1: Illustrating the transverse nature of plane waves appearing in a homogeneous fluid with constant density, whereby $\boldsymbol{v} \cdot \boldsymbol{k} = 0$. The alternating solid-dotted lines depict lines of constant phase that differ by $\pi/2$ radians so that the velocity field switches sign between every π radians.

relation

$$\omega^2 = \varpi^2(\boldsymbol{k}) = (2\,\boldsymbol{\Omega} \cdot \boldsymbol{k})^2/|\boldsymbol{k}|^2 = (2\,\boldsymbol{\Omega} \cdot \hat{\boldsymbol{k}})^2. \tag{53.31}$$

As per our previous encounter with linear waves, we recognize that the disperson relation specifies the inertial wave's angular frequency, ω, once the wavevector is chosen.[5] We illustrate the basics of plane inertial waves in Figure 53.2.

The dispersion relation (53.31) means that the angular frequency of inertial waves is directly proportional to the orientation of the wavevector relative to the rotation vector. Furthermore, it is independent of the magnitude of the wave vector. One way to display these geometric properties is to write

$$\boldsymbol{\Omega} \cdot \hat{\boldsymbol{k}} = |\boldsymbol{\Omega}| \cos\alpha = |\boldsymbol{\Omega}| \sin\gamma \quad \text{with} \quad 0 \leq \alpha \leq \pi \quad \text{and} \quad -\pi/2 \leq \gamma \leq \pi/2, \tag{53.32}$$

where α is the angle between $\boldsymbol{\Omega}$ and $\boldsymbol{k}$, whereas γ is the complement angle. We mostly use α in this chapter, though switch to γ when discussing internal gravity waves and inertia-gravity waves in Chapter 57. The dispersion relation (53.31) thus takes on the particularly compact form

$$\omega^2 = (2\,\Omega\cos\alpha)^2 = (2\,\Omega\sin\gamma)^2. \tag{53.33}$$

Sweeping through the possible orientation angles, α, reveals that the angular frequency (which is a non-negative number) for free space inertial waves spans the continuum range

$$0 \leq \omega \leq 2\,|\Omega|. \tag{53.34}$$

Since the magnitude of the angular frequency is bounded above by $2\,|\Omega| = |f|$, such waves are referred to as *sub-inertial*.[6]

53.3.2 Interpreting the dispersion relation

Since inertial waves are transverse, $\boldsymbol{v} \cdot \boldsymbol{k} = 0$ (Figure 53.2), fluid particle motion associated with inertial waves is parallel to constant phase surfaces, and there is no particle motion in the direction of the wave vector.[7] Dynamical fields have the same geometric structure within a plane

[5] We write $\omega = \varpi(\boldsymbol{k})$ when aiming to distinguish the angular frequency, ω, from the function, ϖ, determining the angular frequency.

[6] In Section 55.8.5 we find that shallow water waves in the presence of gravity and rotation have their angular frequency bounded below by $|f|$, in which case these shallow water *inertia-gravity* waves are *super-inertial*.

[7] It is the oscillatory motion of the fluid particles in the transverse direction that constitutes motion of the phase, thus constituting the traveling wave. A fluid particle moves in the direction of a phase surface. However,

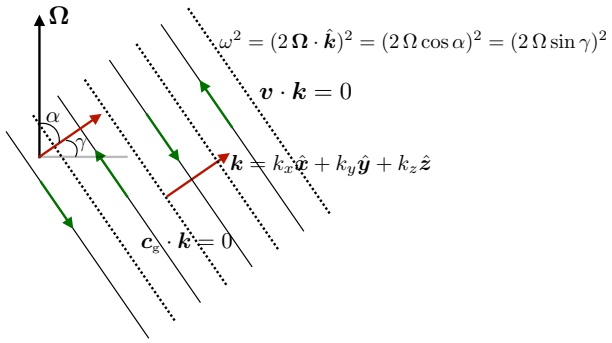

FIGURE 53.2: Illustrating the transverse nature of inertial waves, with their dispersion relation given by equation (53.31), whereby $\omega^2 = (2\,\boldsymbol{\Omega}\cdot\hat{\boldsymbol{k}})^2$. We show lines of constant phase separated by $\pi/2$ radians so that the fluid particle velocity switches sign every alternative line. Evidently, the frequency of inertial waves is maximized when the wavevector, $\boldsymbol{k}$, is aligned with the rotation vector, $\boldsymbol{\Omega}$, in which the angles $\alpha = 0$ and $\gamma = \pi/2$. In contrast, the angular frequency vanishes when the wavevector is orthogonal to $\boldsymbol{\Omega}$. The waves are transverse, $\boldsymbol{v}\cdot\boldsymbol{k} = 0$, so that fluid particle motion occurs within surfaces of constant phase. Maximum frequency waves with $\alpha = 0$ correspond to fluid particle motion on planes orthogonal to the rotation vector, whereby the particles exhibit pure inertial oscillations. Zero frequency waves (standing inertial waves) occur with $\alpha = \pi/2$ and $\gamma = 0$, whereby fluid particle motion is vertical. Vertical particle motion does not feel a Coriolis acceleration so that the wave frequency vanishes in this case. The group velocity is parallel to the fluid particle velocity since, according to equation (53.39), it satisfies $\boldsymbol{c}_g\cdot\boldsymbol{k} = 0$. Note that we make use of the angle α in this chapter, though switch to $\gamma = \pi/2 - \alpha$ when studying internal waves in Chapter 57.

wave, so that all fields are spatially constant along a phase surface. It follows that there is no spatial pressure gradient force along a constant phase surface at any particular time instance. Hence, fluid particles moving parallel to the phase surfaces feel the Coriolis acceleration arising from the projection, $\boldsymbol{k}\cdot\boldsymbol{\Omega}$, of the rotational vector along the wave vector.[8]

Recall that a particle moving in a rotating reference frame exhibits inertial oscillations (Section 14.4) when the particle does not feel any pressure forces. Evidently, fluid particle motion induced by inertial waves exhibits inertial oscillations in the phase plane orthogonal to the wavevector. If the wavevector is aligned parallel to the rotation vector, then a fluid particle feels the full extent of the Coriolis acceleration, whereby inertial oscillations have a squared angular frequency $(2\,\boldsymbol{\Omega}\cdot\hat{\boldsymbol{k}})^2$. This situation corresponds to a particle at either of the planetary poles.[9] When the wavevector is mis-aligned from the rotation vector, then only that portion of the rotation vector projected onto $\hat{\boldsymbol{k}}$ acts to produce inertial oscillations. Finally, if the wavevector is perpendicular to the rotation vector, then the particle feels no Coriolis acceleration, just like a particle on the equator feels no planetary Coriolis acceleration.

53.3.3 Group velocity

As seen from our discussion of wave packets in Section 49.6, the group velocity determines the speed and direction of wave energy propagation within a packet, with the group velocity given

the particle does not remain on a fixed phase surface since the phase travels in the $\hat{\boldsymbol{k}}$ direction and yet particles have $\boldsymbol{v}\cdot\hat{\boldsymbol{k}} = 0$ since the waves are transverse.

[8]The argument here holds either in an Eulerian reference frame, in which case we ignore the nonlinear self-advection contribution as per the linearized velocity equation (53.11), or in a Lagrangian reference frame, in which we are following a material fluid particle. In either case, motion of a fluid particle in an inertial wave, moving in a direction that parallels the constant phase surfaces, only feels the Coriolis acceleration; pressure forces are zero.

[9]From Figure 53.2 we note that the angle α is the co-latitude, so to connect to the planetary Coriolis parameter we set $\phi = \pi/2 - \alpha$ where ϕ is the latitude.

by the wavevector gradient of the dispersion relation

$$\boldsymbol{c}_{\mathrm{g}} = \nabla_{\boldsymbol{k}} \varpi = \hat{\boldsymbol{x}} \frac{\partial \varpi}{\partial k_x} + \hat{\boldsymbol{y}} \frac{\partial \varpi}{\partial k_y} + \hat{\boldsymbol{z}} \frac{\partial \varpi}{\partial k_z}. \tag{53.35}$$

Making use of the dispersion relation (53.31) renders

$$\boldsymbol{c}_{\mathrm{g}} = \frac{4\,(\boldsymbol{\Omega}\cdot\hat{\boldsymbol{k}})\,[\boldsymbol{\Omega} - \hat{\boldsymbol{k}}\,(\boldsymbol{\Omega}\cdot\hat{\boldsymbol{k}})]}{\omega\,|\boldsymbol{k}|} = \frac{(\boldsymbol{\Omega}\cdot\hat{\boldsymbol{k}})}{|\boldsymbol{\Omega}\cdot\hat{\boldsymbol{k}}|}\,\frac{\hat{\boldsymbol{k}}\times(2\,\boldsymbol{\Omega}\times\hat{\boldsymbol{k}})}{|\boldsymbol{k}|} \tag{53.36}$$

where we made use of the vector identity (1.71g). Since

$$\boldsymbol{\Omega}\cdot\hat{\boldsymbol{k}} = \pm|\boldsymbol{\Omega}\cdot\hat{\boldsymbol{k}}| \tag{53.37}$$

we can write the group velocity as

$$\boldsymbol{c}_{\mathrm{g}} = \pm\frac{\hat{\boldsymbol{k}}\times(2\,\boldsymbol{\Omega}\times\hat{\boldsymbol{k}})}{|\boldsymbol{k}|}. \tag{53.38}$$

This expression leads to a particularly remarkable property of the group velocity for inertial waves

$$\boldsymbol{k}\cdot\boldsymbol{c}_{\mathrm{g}} = 0. \tag{53.39}$$

Since the waves are transverse, $\boldsymbol{k}\cdot\boldsymbol{v} = 0$, so that the group velocity is aligned with the fluid particle velocity. The Coriolis acceleration acts perpendicular to the direction of a moving fluid particle. That orientation manifests for inertial waves via $\boldsymbol{k}\cdot\boldsymbol{c}_{\mathrm{g}} = 0$, so that inertial waves carry energy (via the group velocity) in a direction parallel to wave crests (perpendicular to $\boldsymbol{k}$), which is aligned with fluid particle motion. A second property of the group velocity is found by projecting it onto the direction of the rotational axis

$$\boldsymbol{c}_{\mathrm{g}}\cdot\boldsymbol{\Omega} = \pm 2\,[\Omega^2\,\boldsymbol{k}\cdot\boldsymbol{k} - (\boldsymbol{\Omega}\cdot\boldsymbol{k})^2]/|\boldsymbol{k}|^3 = \pm 2\,[\Omega^2 - (\omega/2)^2]/|\boldsymbol{k}| = \pm 2\,(\Omega^2/|\boldsymbol{k}|)\sin^2\alpha, \tag{53.40}$$

where we made use of the expressions (53.31) and (53.33) for the dispersion relation.

53.3.4 Polarization relations for the velocity components

The velocity amplitude, $\tilde{\boldsymbol{v}}$, is generally a complex number, which allows for there to be a variety of phase shifts between the velocity components. We here determine some general relations beween these amplitudes by returning to the linear velocity equation (53.11) and inserting the wave ansatz (53.28) to render

$$-\mathrm{i}\,\omega\,\tilde{u} - f\,\tilde{v} = -\mathrm{i}\,k_x\,\tilde{\varphi} \tag{53.41a}$$
$$-\mathrm{i}\,\omega\,\tilde{v} + f\,\tilde{u} = -\mathrm{i}\,k_y\,\tilde{\varphi} \tag{53.41b}$$
$$-\mathrm{i}\,\omega\,\tilde{w} = -\mathrm{i}\,k_z\,\tilde{\varphi}, \tag{53.41c}$$

where we set $2\,\boldsymbol{\Omega} = f\,\hat{\boldsymbol{z}}$, so that the vertical and horizontal wavenumbers are related by

$$k_z^2 = |\boldsymbol{k}|^2\cos^2\alpha \Longrightarrow k_z^2\sin^2\alpha = (k_x^2 + k_y^2)\cos^2\alpha. \tag{53.42}$$

Equations (53.41a), (53.41b), and (53.41c) define *polarization* relations that specify the relative phases for the velocity components and pressure. We have the freedom to choose how to reference the phases. In the following discussion of kinetic energy, we choose to measure phases relative to the pressure amplitude, which means $\tilde{\varphi}$ is a real amplitude.

53.3.5 Phase averaged kinetic energy

The phase averaged kinetic energy for a plane inertial wave is given by

$$\langle \mathcal{K} \rangle = \langle \mathrm{Re}(\boldsymbol{v}) \cdot \mathrm{Re}(\boldsymbol{v}) \rangle / 2 = (|\tilde{u}|^2 + |\tilde{v}|^2 + |\tilde{w}|^2)/4, \tag{53.43}$$

where we used equation (8.18) for the phase average of the square of a periodic function. To derive the squared amplitudes, multiply the zonal and meridional velocity equations (53.41a) and (53.41b) by $\mathrm{i}\,\omega$, and then back-substitute

$$\tilde{u}\,(f^2 - \omega^2) = -\tilde{\varphi}\,(k_x\,\omega + \mathrm{i} k_y\,f) \tag{53.44a}$$

$$\tilde{v}\,(f^2 - \omega^2) = \tilde{\varphi}\,(-k_y\,\omega + \mathrm{i} k_x\,f), \tag{53.44b}$$

so that

$$|\tilde{u}|^2 = \tilde{\varphi}^2\,\frac{(k_x\,\omega)^2 + (k_y\,f)^2}{(\omega^2 - f^2)^2} = \tilde{\varphi}^2\,\frac{(k_x \cos\alpha)^2 + k_y^2}{f^2 \sin^4\alpha} \tag{53.45a}$$

$$|\tilde{v}|^2 = \tilde{\varphi}^2\,\frac{(k_y\,\omega)^2 + (k_x\,f)^2}{(\omega^2 - f^2)^2} = \tilde{\varphi}^2\,\frac{(k_y \cos\alpha)^2 + k_x^2}{f^2 \sin^4\alpha}, \tag{53.45b}$$

where the second equalities made use of the dispersion relation

$$\omega^2 = f^2 \cos^2\alpha. \tag{53.46}$$

Likewise, equation (53.41c) renders the squared magnitude of the vertical velocity amplitude

$$|\tilde{w}|^2 = \tilde{\varphi}^2\,k_z^2/\omega^2. \tag{53.47}$$

Adding equations (53.45a), (53.45b), and (53.47) then leads to

$$\frac{\langle \mathcal{K} \rangle}{\tilde{\varphi}^2} = \frac{\omega^2\,(k_x^2 + k_y^2)(1 + \cos^2\alpha) + k_z^2\,f^2 \sin^4\alpha}{4\,f^2\,\omega^2 \sin^4\alpha} \tag{53.48a}$$

$$= \frac{f^2 \cos^2\alpha\,(k_x^2 + k_y^2)(1 + \cos^2\alpha) + k_z^2\,f^2 \sin^4\alpha}{4\,f^4 \cos^2\alpha \sin^4\alpha}. \tag{53.48b}$$

Use of equation (53.42) relating the horizontal and vertical wave numbers leads to

$$\langle \mathcal{K} \rangle = \frac{\tilde{\varphi}^2\,k_z^2}{2\,f^2 \cos^2\alpha \sin^2\alpha} = \frac{\tilde{\varphi}^2\,(k_x^2 + k_y^2)}{2\,f^2 \sin^4\alpha}. \tag{53.49}$$

Consider the two limiting cases of $\alpha = 0$ and $\alpha = \pi/2$, which we show are non-singular. A vertical inertial wave, with $\boldsymbol{k} = \hat{\boldsymbol{z}}\,k_z$, $\alpha = 0$, and $\omega^2 = f^2$, has zero vertical particle motion, $\tilde{w} = 0$, so that the pressure fluctuation vanishes, $\tilde{\varphi} = 0$, according to equation (53.41c). As discussed in Section 53.3.6, this case corresponds to free inertial oscillations in the horizontal plane. The complement case of a horizontal inertial wave, with $k_z = 0$, $\alpha = \pi/2$, and $\omega = 0$, has vertical particle motion and is discussed in Section 53.3.7.

53.3.6 High frequency inertial waves with $\omega \approx |f|$

The dispersion relation (53.33) leads to a maximum angular frequency magnitude for a wavevector aligned parallel or anti-parallel to the rotation axis,

$$\boldsymbol{k} \times \boldsymbol{\Omega} = 0 \Longrightarrow \omega = 2\,|\Omega| = |f|. \tag{53.50}$$

Recall that inertial waves are transverse so that $\boldsymbol{v} \cdot \boldsymbol{k} = 0$. This property, in combination with $\boldsymbol{k} \times \boldsymbol{\Omega} = 0$, means that high frequency inertial waves have fluid particle motion in a plane perpendicular to the rotation axis: $\boldsymbol{v} \cdot \boldsymbol{\Omega} = 0$. With a vertical rotation vector, then the wavevector only has a vertical component, $\boldsymbol{k} = k_z \, \hat{\boldsymbol{z}}$. In this case, the plane waves propagate vertically ($k_x = k_y = 0$) while fluid particle motion is restricted to the horizontal plane.

For inertial waves with $\omega = |f| > 0$ and $\boldsymbol{k} = k_z \, \hat{\boldsymbol{z}}$, the fluid velocity amplitude relations (53.41a) and (53.41b) indicate that

$$\tilde{u} = \mathrm{i} \, \tilde{v}, \tag{53.51}$$

so that the horizontal velocity of the wave is given by

$$\boldsymbol{u}/\tilde{u} = \hat{\boldsymbol{x}} \, \mathrm{e}^{\mathrm{i}(k_z z - |f| \, t)} + \hat{\boldsymbol{y}} \, \mathrm{e}^{\mathrm{i}(k_z z - |f| \, t - \pi/2)}, \tag{53.52}$$

which is a vertically propagating plane wave. Taking the real part renders

$$\boldsymbol{u}/\tilde{u} = \hat{\boldsymbol{x}} \cos(k_z z - |f| \, t) + \hat{\boldsymbol{y}} \sin(k_z z - |f| \, t). \tag{53.53}$$

With $k_x = k_y = 0$ in the velocity equations (53.41a) and (53.41b), we see that there is no coupling between the horizontal velocity components and pressure. Hence, the motion of fluid particles reduces to inertial oscillations in the horizontal plane just as we studied for point particle motion in Section 14.4, whereby fluid particle motion occurs with a balance between Coriolis acceleration and centrifugal acceleration (see Figure 14.2). Furthermore, since there is no dependence on the horizontal position (since $k_x = k_y = 0$), fluid particles move together in a coherent oscillation within each horizontal plane while the wave propagates vertically. As a check, we see that for a fixed vertical position, say $z = 0$, the velocity relation (53.53) for inertial waves is identical to the velocity relation (14.15b) for particles undergoing inertial oscillations in a circle with a constant radius

$$\boldsymbol{u}/\tilde{u} = \hat{\boldsymbol{x}} \cos(|f| \, t) - \hat{\boldsymbol{y}} \sin(|f| \, t) \quad \text{for } z = 0 \text{ and } \omega = |f|. \tag{53.54}$$

In oceanography, inertial waves with $\omega \approx |f|$ are referred to as *near inertial waves*, which refers to their angular frequency being close to the Coriolis frequency. Since near inertial waves have their wavevector oriented close to the rotation axis, equation (53.38) indicates that they also have a vanishingly small group velocity.

53.3.7 Low frequency inertial waves with $\omega \approx 0$

Low frequency inertial waves occur when the wavevector is nearly perpendicular to the rotation axis

$$\boldsymbol{\Omega} \cdot \boldsymbol{k} \approx 0 \implies \omega/\Omega \approx 0. \tag{53.55}$$

Hence, the wave number parallel to the rotation axis is vanishingly small. For example, if the rotation axis is vertical, then low frequency inertial waves have a vanishingly small vertical wave number,

$$k_z^2 \ll k_x^2 + k_y^2. \tag{53.56}$$

Correspondingly, for the velocity vector in the form given by equation (53.28), $\boldsymbol{\Omega} \cdot \boldsymbol{k} \approx 0$ means that

$$(\boldsymbol{\Omega} \cdot \nabla) \, \boldsymbol{v} = \mathrm{i} (\boldsymbol{\Omega} \cdot \boldsymbol{k}) \, \boldsymbol{v} \approx 0. \tag{53.57}$$

That is, the velocity vector for low frequency inertial waves is coherent in the direction aligned with the rotation axis. Furthermore, when $\boldsymbol{\Omega} \cdot \boldsymbol{k} \approx 0$, the group velocity (53.40) has a magnitude

$$|\boldsymbol{c}_{\mathrm{g}}| \approx 2 \, |\Omega| / |\boldsymbol{k}|. \tag{53.58}$$

Evidently, low frequency inertial waves with long wavelength (small wavenumber $|\boldsymbol{k}|$) quickly transmit their energy along the direction of the rotation axis. We return to this property in Section 53.5 when considering the Taylor-Proudman effect.

53.4 Radially symmetric high frequency inertial waves

To help further our understanding of inertial oscillations, consider a particularly simple case of a coherent axially symmetric fluid ring within a horizontal f-plane as depicted in Figure 53.3. Slightly perturb the ring by expanding its radius outward and then let the ring move freely. What happens? We study the motion using angular momentum arguments as well as Coriolis arguments, and assume zero pressure gradients throughout the discussion. As we show, the ring oscillates at frequency $\omega = f$ and thus displays a canonical form of inertial oscillations.

53.4.1 Qualitative presentation

The outward radial perturbation gives the ring a larger moment of inertia computed relative to the rotational axis. In Section 24.7, we studied a fluid ring looped around the planet. As in that case, the constraint imposed by angular momentum conservation (computed relative to the rotational axis) requires the ring to rotate anti-cyclonically (clockwise if $\Omega > 0$) in response to a perturbation that increases its radius.[10] Equivalently, radially outward motion induces a Coriolis acceleration that causes the ring to rotate clockwise (anti-cyclonic). In turn, as the ring rotates anti-cyclonically, each fluid particle within the ring experiences a radial Coriolis acceleration pointing towards the center of the ring (to the right of the particle motion). This Coriolis acceleration halts the outward perturbation and returns the ring towards a smaller radius, with the inward motion leading to a further Coriolis acceleration that causes the ring to rotate cyclonically (again, to the right of the inward particle motion). The whole process oscillates between radially outward and anti-cyclonic rotation, and radially inward and cyclonic rotation. The oscillations of a fluid ring exhibit the basic mechanism of inertial waves propagating along the rotational axis ($\boldsymbol{k} \times \boldsymbol{\Omega} = 0$) with frequency f (Section 53.3.6).

53.4.2 Radially symmetric inertial oscillations

The thought experiment in Figure 53.3 can be mathematically described by writing the linearized equation of motion using polar-coordinates from Section 4.22. We assume all fields are axially symmetric around any point, and all motion is two-dimensional on a horizontal plane. We also assume there is no horizontal dynamical pressure gradient acting on the fluid, so that motion is purely inertial. Decomposing the velocity equation (53.4) into radial and angular directions leads to

$$\frac{\mathrm{D}v^r}{\mathrm{D}t} - (f + \dot{\vartheta})\, v^\vartheta = 0 \quad \text{and} \quad \frac{\mathrm{D}v^\vartheta}{\mathrm{D}t} + (f + \dot{\vartheta})\, v^r = 0, \tag{53.59}$$

where we introduced the polar components to the velocity

$$\boldsymbol{v} = (\boldsymbol{v} \cdot \hat{\boldsymbol{r}})\, \hat{\boldsymbol{r}} + (\boldsymbol{v} \cdot \hat{\boldsymbol{\vartheta}})\, \hat{\boldsymbol{\vartheta}} + 0\, \hat{\boldsymbol{z}}, \tag{53.60}$$

and the radial and azimuthal unit vectors

$$\hat{\boldsymbol{r}} = \hat{\boldsymbol{x}} \cos\vartheta + \hat{\boldsymbol{y}} \sin\vartheta \quad \text{and} \quad \hat{\boldsymbol{\vartheta}} = -\hat{\boldsymbol{x}} \sin\vartheta + \hat{\boldsymbol{y}} \cos\vartheta. \tag{53.61}$$

[10] In Figure 24.3 we studied the angular momentum of an axially symmetric ring of fluid around the planet. Axial symmetry means there are no zonal pressure gradients so that axial angular momentum is materially constant for the earth spanning fluid ring. Here we are making use of the same angular momentum constraint for an axially symmetric ring of fluid in a rotating f-plane.

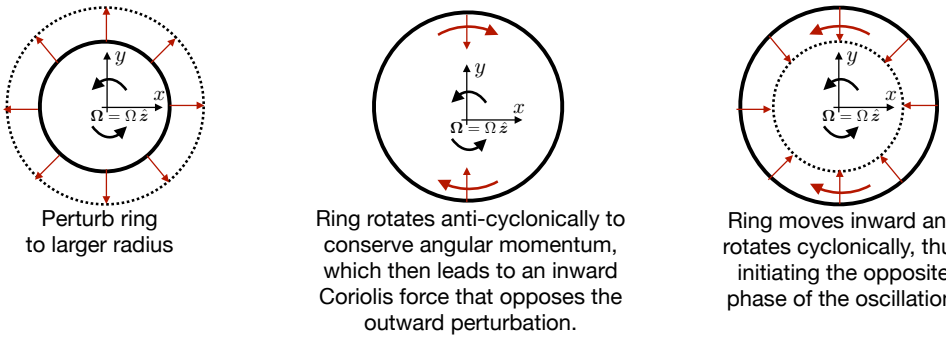

FIGURE 53.3: Schematic of inertial oscillations of an axially symmetric ring of fluid in the horizontal plane in the presence of rotation, $\boldsymbol{\Omega} = \Omega\,\hat{\boldsymbol{z}}$ with $\Omega > 0$, where the rotation axis extends through the ring center and out of the page. The left panel shows the ring perturbed outward, with this perturbation increasing the ring's moment of inertia about the vertical axis running through the center of the ring. To conserve angular momentum the ring must turn opposite to the sense of the rotating reference frame; that is, it rotates anti-cyclonically, as shown in the middle panel. As it turns anti-cyclonically the ring generates a Coriolis acceleration that points inward (to the right of the motion), thus causing the ring to oscillate back to a smaller radius (right panel), where the oscillation turns around. The physics depicted in this figure, representing a three-way balance between linear acceleration, Coriolis acceleration, and pressure gradient acceleration, is summarized by the linear velocity equation (53.11).

The presence of $\dot{\vartheta}$ along with the Coriolis parameter accounts for the centrifugal acceleration due to the fluid motion (as distinct from the planetary centrifugal acceleration). This is a nonlinear effect that is dropped in the linear analysis.

Linearizing the velocity equation (53.59) leads to

$$\partial_t v^r - f\,v^\vartheta = 0 \quad \text{and} \quad \partial_t v^\vartheta + f\,v^r = 0, \tag{53.62}$$

which then renders a linear oscillator equation satisfied by each velocity component

$$(\partial_{tt} + f^2)\,v^r = 0 \quad \text{and} \quad (\partial_{tt} + f^2)\,v^\vartheta = 0. \tag{53.63}$$

Assuming a monochromatic time dependence

$$v^r = \tilde{v}^r \mathrm{e}^{-\mathrm{i}\,\omega\,t} \quad \text{and} \quad v^\vartheta = \tilde{v}^\vartheta \mathrm{e}^{-\mathrm{i}\,\omega\,t} \tag{53.64}$$

leads to the dispersion relation

$$\omega^2 = f^2. \tag{53.65}$$

The linear velocity equation (53.62) ensures that the velocity components are $\pi/2$ out of phase with

$$\tilde{v}^r = \mathrm{i}\,\tilde{v}^\vartheta = \tilde{v}^\vartheta\,\mathrm{e}^{\mathrm{i}\,\pi/2}. \tag{53.66}$$

The motion is thus a coherent oscillation of the fluid consisting of vascillations between radial and angular motion whereby the Coriolis acceleration acts to turn the motion to the right (assuming $f > 0$). There is no preferred length scale in the horizontal plane. Indeed, since the flow is horizontally non-divergent (there is no vertical fluid particle motion so $\tilde{w} = 0$), and due to the assumed symmetry in the angular direction, there can be no radial dependence to the motion. That is, the radial wavenumber is zero. However, there can be vertical propagation of the waves, just as discussed in Section 53.3.6.

53.5 Low frequency inertial waves and vertical stiffening

We consider two more thought experiments focused on low frequency inertial waves and their connection to the vertical stiffening that arises either from a small aspect ratio flow (as in shallow

water theory) or in flow in a rapidly rotating reference frame (as in the Taylor-Proudman effect). The first experiment is treated heuristically whereas we include some mathematical analysis for the second one.

53.5.1 Slowly oscillating disk

Imagine a slowly oscillating disk that moves in a direction aligned with the axis of rotation, such as depicted in Figure 53.4. If the oscillation frequency is much slower than the rotation frequency, $\omega_{\text{disk}} \ll |\Omega|$, then the disk generates low frequency inertial waves at the frequency of the oscillating disk, $\omega = \omega_{\text{disk}}$. Following from our discussion in Section 53.3.7, we know that the low frequency inertial waves have a wavevector oriented perpendicular to the rotation axis, $\boldsymbol{\Omega} \cdot \boldsymbol{k} = 0$, as depicted in Figure 53.4. Since inertial waves have a group velocity that is itself perpendicular to the wavevector, the low frequency inertial waves have a group velocity parallel to the rotation axis: $\boldsymbol{\Omega} \times \boldsymbol{c}_{\text{g}} = 0$.

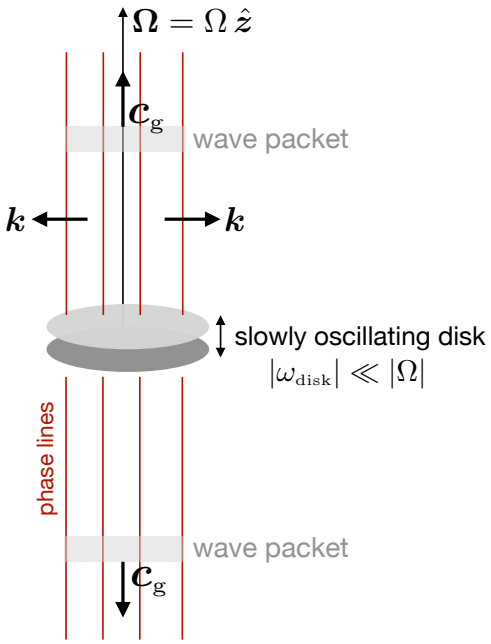

FIGURE 53.4: Schematic of inertial waves generated by a slowly oscillating disk in a rotating homogeneous fluid. The disk moves along the rotation axis (vertical axis) in small amplitude oscillations whose angular frequency is much smaller than the rotational angular frequency, $\omega_{\text{disk}} \ll |\Omega|$. The oscillating disk preferentially generates inertial waves whose frequency is close to ω_{disk}; i.e., low frequency inertial waves as discussed in Section 53.3.7. The phase lines and group velocity for these waves are parallel to the rotation axis, and the wavevector is perpendicular to the rotation axis. We depict two wave packets that send energy vertically away from the disk, with the long wave and low frequency waves having the highest magnitude for the group velocity. Since $\boldsymbol{\Omega} \cdot \boldsymbol{k} = 0$, the fluid particle velocity associated with the inertial waves is constant in the direction along the rotation axis: $(\boldsymbol{\Omega} \cdot \nabla)\,\boldsymbol{v} = \Omega\,\partial_z \boldsymbol{v} = 0$.

As seen by the equation (53.58) for the group velocity magnitude, information (i.e., energy) concerning the oscillating disk is most rapidly transmitted by long wavelength low frequency inertial waves. Such low frequency and long wavelength inertial waves generate fluid particle motion that is independent of the position along the rotational axis since $(\boldsymbol{\Omega} \cdot \nabla)\,\boldsymbol{v} = 0$. Hence, the particle motion is parallel to the rotational axis, and this motion is coherent. We conclude that inertial waves transmit information about stiffening along the rotation axis, thus providing a mechanism for the Taylor-Proudman effect from Section 31.5.3 found when the flow is strictly geostrophic.

53.5.2 Inertial waves from a moving sinusoidal boundary[11]

We here provide a bit more substance to the previous discussion by exploring the steady linear waves generated by a moving sinusoidal lower boundary, as depicted in Figure 53.5. In particular, consider a horizontally unbounded region of homogeneous fluid on an f-plane that is bounded above by a rigid lid at $z = H$ and bounded below by a moving sinusoidal boundary with vertical position

$$z = \eta_b(x,t) = h \sin(q\,x - U\,q\,t) = h \sin(q\,x - \omega_b\,t), \tag{53.67}$$

where we introduced the frequency set by the moving boundary

$$\omega_b = U\,q > 0. \tag{53.68}$$

The amplitude, h, of the lower boundary is assumed to be small compared to the wavenumber of the boundary

$$h\,q \ll 1, \tag{53.69}$$

which ensures that movement of the boundary generates linear waves. Because the fluid is homogeneous and on an f-plane, the undulating bottom boundary forces inertial waves. The excited inertial waves have a horizontal wavenumber given by that of the topography, q, and their vertical wavenumber is set according to the inertial wave equation (53.27). We also require the top and bottom boundary conditions to derive an expression for the vertical velocity

$$w(z=0) = \partial_t \eta_b = -h\,\omega_b \cos(q\,x - \omega_b\,t) \quad \text{and} \quad w(z=H) = 0. \tag{53.70}$$

The bottom boundary condition results from linearizing the kinematic boundary condition,

$$\partial_t \eta_b + \boldsymbol{u} \cdot \nabla \eta_b = w \Longrightarrow w(z=0) \approx \partial_t \eta_b. \tag{53.71}$$

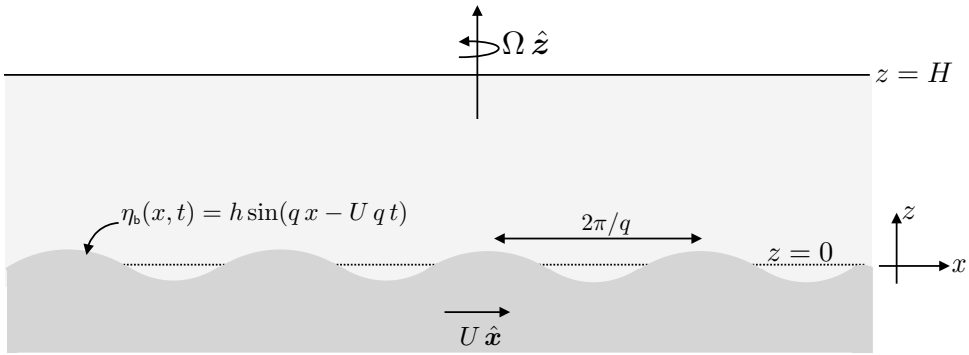

FIGURE 53.5: Schematic for the study of inertial waves generated by a moving sinusoidal lower boundary at $z(x,t) = h_0 \sin(q\,x - \omega_0\,t)$, with the frequency generated by the moving boundary given by $\omega_0 = U\,q$. The region is filled with a homogenous fluid of density ρ and bounded above by a rigid lid at $z = H$.

53.5.3 Stationary wave solution

We examine waves after they have reached a steady state, and as such they are *stationary*. Given the meridional symmetry, we are only concerned with inertial waves that have a zero meridional wavenumber, $k_y = 0$, so that

$$\boldsymbol{k} = k_x\,\hat{\boldsymbol{x}} + k_z\,\hat{\boldsymbol{z}} = q\,\hat{\boldsymbol{x}} + k_z\,\hat{\boldsymbol{z}}, \tag{53.72}$$

[11] This thought experiment comes from Section 2.2 of *Stern* (1975).

where we set $k_x = q$ given the forcing from the lower boundary.

Since the horizontal domain is unbounded, we consider the horizontal fluid velocity arising from a traveling plane wave

$$\boldsymbol{u}(\boldsymbol{x}, t) = \tilde{\boldsymbol{u}}\, \mathrm{e}^{\mathrm{i}\,(\boldsymbol{k}\cdot\boldsymbol{x} - \omega\, t)}. \tag{53.73}$$

Assuming the waves are indeed inertial with frequency, ω_{b}, and horizontal wavenumber, q, the dispersion relation (53.31) renders the corresponding vertical wavenumber

$$\omega_{\mathsf{b}}^2 = \frac{f^2\, k_z^2}{q^2 + k_z^2} \Longrightarrow k_z^2 = \frac{\omega_{\mathsf{b}}^2\, q^2}{f^2 - \omega_{\mathsf{b}}^2}. \tag{53.74}$$

Evidently, there are two distinct regimes for the excited fluctuations: one that leads to exponential decay away from the lower boundary, with these *evanescent* waves trapped next to the bottom. The other excitation appears as inertial waves

$$\omega_{\mathsf{b}}^2 > f^2 \quad \text{exponential decay away from lower boundary} \tag{53.75a}$$

$$\omega_{\mathsf{b}}^2 < f^2 \quad \text{inertial waves are excited.} \tag{53.75b}$$

We only consider the case of sub-inertial forcing so that $\omega_{\mathsf{b}}^2 < f^2$.

The structure of the vertical velocity associated this forced motion is determined by the following boundary value problem

$$[\partial_{tt}\nabla^2 + (2\,\boldsymbol{\Omega}\cdot\nabla)^2]\, w = 0 \tag{53.76a}$$

$$w(z=0) = -h\,\omega_{\mathsf{b}} \cos(q\,x - \omega_{\mathsf{b}}\, t) \tag{53.76b}$$

$$w(z=H) = 0. \tag{53.76c}$$

To find a particular solution we take the ansatz

$$w(x,t) = w(0)\,\Gamma(z), \tag{53.77}$$

with the non-dimensional structure function satisfying

$$\frac{\mathrm{d}^2\Gamma}{\mathrm{d}z^2} + k_z^2\,\Gamma = 0 \quad \text{for } 0 < z < H \quad \text{with} \quad \Gamma(0) = 1 \quad \text{and} \quad \Gamma(H) = 0, \tag{53.78}$$

which readily leads to the vertical fluid velocity

$$w(x,z,t) = w(0)\,\frac{\sin[k_z(H-z)]}{\sin(k_z H)} = -h\,\omega_{\mathsf{b}} \cos(q\,x - \omega_{\mathsf{b}}\, t)\,\frac{\sin[k_z(H-z)]}{\sin(k_z H)}. \tag{53.79}$$

53.5.4 Vertically coherent motion

Consider the longwave limit in which

$$\Gamma(z) = \lim_{k_z H \to 0} \frac{\sin[k_z(H-z)]}{\sin(k_z H)} = (H-z)/H, \tag{53.80}$$

so that the vertical velocity is a linear function of z

$$w(x,z,t) \approx -h\,\omega_{\mathsf{b}} \cos(q\,x - \omega_{\mathsf{b}}\, t)\,(H-z)/H. \tag{53.81}$$

As seen in equation (53.19), a linear vertical dependence to w means that the dynamic pressure is independent of z. Correspondingly, equations (53.18a) and (53.18b) reveal that $\partial_z \boldsymbol{u} = 0$, which means that horizontal fluid motion is vertically coherent. This motion corresponds to

the shallow water fluid from Part VI of this book. It also corresponds to the Taylor-Proudman effect discussed in Section 53.5.

To determine the non-dimensional scaling that leads to vertically coherent motion, return to equation (53.78) for the vertical structure function and introduce the non-dimensional vertical coordinate

$$\hat{z} = z/H, \tag{53.82}$$

in which equation (53.78) becomes

$$\frac{\mathrm{d}^2\Gamma}{\mathrm{d}\hat{z}^2} + (k_z\, H)^2\, \Gamma = 0. \tag{53.83}$$

The vertical structure of the vertical velocity is a linear function of $\hat{z}$ in the limit that $(k_z\, H)^2 \to 0$, which means

$$(k_z\, H)^2 \to 0 \Longrightarrow \frac{(q\, H)^2}{(f/U\, q)^2 - 1} \to 0. \tag{53.84}$$

This limit can be realized if

$$q\, H \ll 1 \quad \text{small aspect ratio (shallow water limit)} \tag{53.85a}$$

$$U\, q/f \ll 1 \quad \text{small Rossby number (Taylor-Proudman limit).} \tag{53.85b}$$

Evidently, a small aspect ratio, with a Rossby number bounded away from unity, leads to vertically coherent motion even if the fluid is not in a rotating reference frame. This motion corresponds to that of shallow water fluid studied in Part VI of this book. As emphasized in Section 35.2.10, the small aspect ratio shallow water fluid displays vertically coherent motion due to the fluid being homogeneous and hydrostatic. Alternatively, we realize vertically coherent columnar motion with a small Rossby number. This motion corresponds to the Taylor-Proudman effect for rotating fluids. It is notable that vertically coherent motion becomes more restricted (i.e., needs a smaller Rossby number) when the upper boundary moves far away, $H \to \infty$, thus moving to the deep water limit.

Chapter 54

BAROTROPIC VORTICITY WAVES

In this chapter we study *vorticity waves*, also called *Rossby waves* or *vortical modes*, which rely on the presence of a gradient in the base state potential vorticity field. We examine a particularly simple realization of Rossby waves as found in the inviscid two-dimensional non-divergent barotropic model on an unbounded β-plane. This model supports two general kinds of vorticity waves. One arises from the gradient of planetary vorticity (i.e., β-effect), which gives rise to *planetary Rossby waves*. The second arises from gradients in the vorticity of the base flow. *Edge waves* are a particularly simple kind of vorticity waves that arise from assuming a jump in the background vorticity field.

READER'S GUIDE TO THIS CHAPTER

We make extensive use of the horizontally non-divergent barotropic model from Chapter 38, as well as the wave kinematics from Chapter 49. Rossby waves are encountered again when discussing shallow water waves in Chapter 55, and edge waves are encountered when studying shear instability in Chapter 61 and baroclinic instability in Chapter 62.

54.1 Loose threads

- Hamilton/Whitham principle
- energetics
- Rossby wave particle velocity and trajectories
- Plot the dispersion relation for Rossby waves
- Rectification by Rossby waves that are radiated by a source; Section 5.4 of *McWilliams* (2006).
- Work through the Green's function problem as in *Haidvogel and Rhines* (1983) as well as Bill Young's Les Houches lectures.
- Stokes drift
- Rossby waves on a rotating planet as per continuum Lagrangian field theory
- Rossby wave packets in a non-constant background flow

54.2 A single plane wave in the non-divergent barotropic fluid

In this section we study properties of a single plane wave in an inviscid barotropic and horizontally non-divergent fluid on an unbounded beta plane. We then follow in Section 54.3 with a study of Rossby waves in this model.[1] Recall that the barotropic and horizontally non-divergent model was studied in Chapter 38, with the flow fully described by the vorticity equation

$$\frac{\mathrm{D}(\zeta + f)}{\mathrm{D}t} = (\partial_t + \boldsymbol{u} \cdot \nabla)(\zeta + f) = 0, \tag{54.1}$$

where the horizontal velocity is non-divergent and so can be written in terms of a streamfunction

$$\nabla \cdot \boldsymbol{u} = 0 \Longrightarrow \boldsymbol{u} = \hat{\boldsymbol{z}} \times \nabla\psi \quad \text{and} \quad \zeta = \hat{\boldsymbol{z}} \cdot (\nabla \times \boldsymbol{u}) = \nabla^2\psi. \tag{54.2}$$

As we show in this section, a single plane wave in this model exactly satisfies linear velocity and vorticity equations, with such equations summarized in Table 54.1. Since there are no nonlinear terms affecting the single plane wave, there is no need to linearize the equations of motion when studying properties of this wave. We emphasize, however, that this distinct property holds only for a single plane wave. In particular, the advection operator that vanishes for a single wave is nonzero when the flow has more than a single plane wave. Indeed, the nonlinear interactions between distinct wave modes provide the mechanism for the inverse turbulent cascade in this model (e.g., see Chapter 11 of *Vallis* (2017)).

[1] The edge waves studied in Section 54.5 are not plane waves, and so they do not satisfy the special properties described in this section.

NAME	GENERAL RELATION	SINGLE PLANE WAVE
streamfunction	ψ	$\psi = A \cos \mathcal{P}$
velocity	$\boldsymbol{u} = \hat{\boldsymbol{z}} \times \nabla \psi$	$\boldsymbol{u} = -(\hat{\boldsymbol{z}} \times \boldsymbol{k}) A \sin \mathcal{P}$
velocity tendency	$\partial_t \boldsymbol{u} = \hat{\boldsymbol{z}} \times \nabla(\partial_t \psi)$	$\partial_t \boldsymbol{u} = \omega (\hat{\boldsymbol{z}} \times \boldsymbol{k}) \psi$
non-divergence	$\nabla \cdot \boldsymbol{u} = 0$	$\boldsymbol{k} \cdot \boldsymbol{u} = 0$
relative vorticity	$\zeta = \nabla^2 \psi$	$\zeta = -\lvert\boldsymbol{k}\rvert^2 \psi$
β-plane vorticity equation	$(\partial_t + \boldsymbol{u} \cdot \nabla)\zeta = -v \beta$	$\partial_t \zeta = -v \beta$
pressure equation	$-\nabla \cdot (\nabla \varphi - f \nabla \psi) = \boldsymbol{S}^2 - \boldsymbol{R}^2$	$-\nabla \cdot (\nabla \varphi - f \nabla \psi) = 0$
Coriolis acceleration	$-f \hat{\boldsymbol{z}} \times \boldsymbol{u} = f \nabla \psi$	$-f A \boldsymbol{k} \sin \mathcal{P}$
velocity equation	$\partial_t \boldsymbol{u} + (f + \zeta) \hat{\boldsymbol{z}} \times \boldsymbol{u} = -\nabla(\varphi + \mathcal{K})$	$\partial_t \boldsymbol{u} + f \hat{\boldsymbol{z}} \times \boldsymbol{u} = -\nabla \varphi$
kinetic energy equation	$\mathrm{D}\mathcal{K}/\mathrm{D}t = -\nabla \cdot (\boldsymbol{u} \varphi)$	$\partial_t \mathcal{K} = -\nabla \cdot (\boldsymbol{u} \varphi)$

TABLE 54.1: Properties of the inviscid horizonally non-divergent barotropic model. The left column holds for a general flow whereas the right column holds for a single plane wave, with $\mathcal{P} = \boldsymbol{k} \cdot \boldsymbol{x} - \omega t$ the phase function. $\boldsymbol{S}$ is the strain rate tensor, with $\boldsymbol{S}^2 = S_{mn} S^{mn}$. Likewise, $\boldsymbol{R}$ is the rotation tensor, with $\boldsymbol{R}^2 = R_{mn} R^{mn}$. Both of these tensors are introduced in Section 18.8. This table highlights the remarkable properties of the single plane wave in the inviscid horizonally non-divergent barotropic model, in which the nonlinear terms in the velocity and vorticity equation vanish identically.

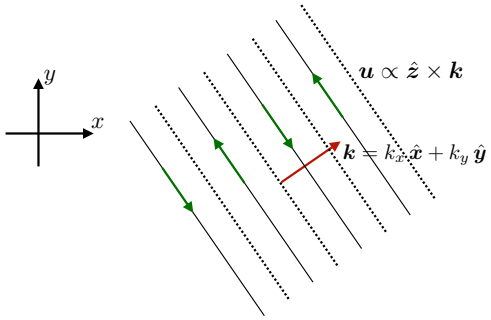

FIGURE 54.1: Illustrating the transverse nature of plane waves appearing in a horizontally non-divergent barotropic model, whereby $\boldsymbol{u} \cdot \boldsymbol{k} = 0$. The alternating solid-dotted lines depict lines of constant phase that differ by $\pi/2$ radians so that the velocity field switches sign between every π radians. Compare this figure to Figure 53.1, which illustrates transverse plane waves in three dimensions.

54.2.1 Transverse plane waves

Consider a plane wave ansatz for the streamfunction

$$\psi(\boldsymbol{x}, t) = A \cos(\boldsymbol{k} \cdot \boldsymbol{x} - \omega t) \quad \text{with} \quad \boldsymbol{k} = k_x \hat{\boldsymbol{x}} + k_y \hat{\boldsymbol{y}} \quad \text{and} \quad \mathcal{P} = \boldsymbol{k} \cdot \boldsymbol{x} - \omega t, \tag{54.3}$$

with A a constant amplitude. The velocity of fluid particles in the plane wave is thus given by

$$\boldsymbol{u} = -A (\hat{\boldsymbol{z}} \times \boldsymbol{k}) \sin(\boldsymbol{k} \cdot \boldsymbol{x} - \omega t), \tag{54.4}$$

which then leads to

$$\boldsymbol{k} \cdot \boldsymbol{u} = 0. \tag{54.5}$$

The horizontally propagating plane waves are transverse, as illustrated in Figure 54.1, which arises since the flow is horizontally non-divergent. This property compares to the three dimensional transverse inertial plane waves discussed in Section 53.3.1 and depicted in Figure 53.1.

54.2.2 Absence of inertial waves and gravity waves

Since there is no vertical motion in the two-dimensional non-divergent barotropic model, any wavevector must be horizontal and thus perpendicular to the vertically oriented rotation vector.

Hence, the inertial wave dispersion relation (53.31) only admits a zero frequency mode, which is geostrophic balance. Furthermore, gravity waves are absent from this model since gravity waves vanish with a flow that has zero horizontal divergence (see the discussion of shallow water gravity waves in Section 55.5). We thus conclude that the two-dimensional non-divergent barotropic model has neither inertial waves nor gravity waves.

As we will see, the only wave supported by this model occurs in the presence of a background or base state vorticity gradient, such as from planetary vorticity or the vorticity of a mean flow. In the absence of vorticity gradients, there are no linear waves in the two-dimensional non-divergent barotropic model. Such is the case, for example, in non-rotating and homogeneous two-dimensional flows, which are commonly used to study two-dimensional turbulence.

54.2.3 Zero advection for a single plane wave

Linearizing the equations of motion is a basic step in the development of a dispersion relation. For the vorticity equation appropriate for Rossby waves, linearization means neglecting the advection of relative vorticity. However, quite remarkably, there is no advection of relative vorticity for a plane wave in the horizontally non-divergent barotropic model. That is, the advection operator, $\boldsymbol{u} \cdot \nabla\zeta$, vanishes identically when $\boldsymbol{u}$ and ζ are built from a single plane wave. To see this property, consider a traveling plane wave streamfunction

$$\psi(x, y, t) = A \cos(\boldsymbol{k} \cdot \boldsymbol{x} - \omega\, t) \Longrightarrow \zeta = -|\boldsymbol{k}|^2\, \psi \quad \text{and} \quad \nabla\zeta = -|\boldsymbol{k}|^2\, \nabla\psi, \tag{54.6}$$

in which case we readily find

$$\boldsymbol{u} \cdot \nabla\zeta = (\hat{\boldsymbol{z}} \times \nabla\psi) \cdot (-|\boldsymbol{k}|^2\, \nabla\psi) = 0. \tag{54.7}$$

Evidently, for this model the velocity of fluid particles in a plane wave are aligned parallel to surfaces of constant relative vorticity of the wave. Equivalently, this model supports no nonlinear self-interactions for a single plane wave.

54.2.4 Pressure equation for a single plane wave

Recall the discussion in Section 38.4 where we showed that pressure in the horizontally non-divergent barotropic model satisfies the Poisson equation (38.84)

$$-\nabla \cdot (\nabla\varphi - f\, \nabla\psi) = 2\, [(\partial_{xy}\psi)^2 - \partial_{xx}\psi\, \partial_{yy}\psi]. \tag{54.8}$$

Making use of the traveling plane wave (54.6) readily reveals that the nonlinear source term vanishes identically

$$(\partial_{xy}\psi)^2 - \partial_{xx}\psi\, \partial_{yy}\psi = 0. \tag{54.9}$$

Although the plane wave supports a nonzero strain rate tensor and a nonzero rotation tensor, their respective squares cancel identically. As a result, the pressure source from a plane wave is due only to the Coriolis acceleration

$$-\nabla \cdot (\nabla\varphi - f\, \nabla\psi) = -\nabla \cdot (\nabla\varphi + f\, \hat{\boldsymbol{z}} \times \boldsymbol{u}) = 0. \tag{54.10}$$

Consequently,

$$\nabla\varphi + f\, \hat{\boldsymbol{z}} \times \boldsymbol{u} = -\hat{\boldsymbol{z}} \times \nabla\lambda, \tag{54.11}$$

where $\lambda(x, y, t)$ is a gauge function. In Section (54.2.5) we show that $\nabla\lambda = \nabla(\partial_t\psi)$.

54.2.5 Velocity equation for a single plane wave

So what velocity equation does a single plane wave satisfy for the inviscid horizontally non-divergent barotropic model? To answer that question we make use of the vector-invariant velocity equation (38.5) written in the form

$$\partial_t \boldsymbol{u} + f\,\hat{\boldsymbol{z}} \times \boldsymbol{u} + \nabla\varphi = -(\nabla\mathcal{K} + \hat{\boldsymbol{z}} \times \zeta\,\boldsymbol{u}) \quad \text{with} \quad \mathcal{K} = \boldsymbol{u}\cdot\boldsymbol{u}/2. \tag{54.12}$$

Introducing the streamfunction brings the right hand side terms into the form

$$\nabla\mathcal{K} + \hat{\boldsymbol{z}} \times \zeta\,\boldsymbol{u} = \hat{\boldsymbol{x}}\,(\partial_y\psi\,\partial_{xy}\psi - \partial_x\psi\,\partial_{yy}\psi) + \hat{\boldsymbol{y}}\,(\partial_x\psi\,\partial_{xy}\psi - \partial_y\psi\,\partial_{xx}\psi) \tag{54.13a}$$

$$= \hat{\boldsymbol{x}}\,[\hat{\boldsymbol{z}}\cdot(\partial_y\nabla\psi \times \nabla\psi)] + \hat{\boldsymbol{y}}\,[\hat{\boldsymbol{z}}\cdot(\partial_x\nabla\psi \times \nabla\psi)]. \tag{54.13b}$$

We readily find that each of these nonlinear terms vanishes when the streamfunction is given by the single plane wave function (54.3)

$$\partial_y\nabla\psi \times \nabla\psi = A^2\,k_y(\boldsymbol{k}\times\boldsymbol{k})\sin(\boldsymbol{k}\cdot\boldsymbol{x} - \omega\,t)\cos(\boldsymbol{k}\cdot\boldsymbol{x} - \omega\,t) = 0 \tag{54.14a}$$

$$\partial_x\nabla\psi \times \nabla\psi = A^2\,k_x(\boldsymbol{k}\times\boldsymbol{k})\sin(\boldsymbol{k}\cdot\boldsymbol{x} - \omega\,t)\cos(\boldsymbol{k}\cdot\boldsymbol{x} - \omega\,t) = 0. \tag{54.14b}$$

Evidently, a single plane wave in the horizontally non-divergent barotropic model exactly satisfies the linear velocity equation

$$\partial_t \boldsymbol{u} + f\,\hat{\boldsymbol{z}} \times \boldsymbol{u} = -\nabla\varphi. \tag{54.15}$$

Comparing to the result from the pressure equation (54.11) reveals that $\nabla\lambda = \nabla(\partial_t\psi)$. Furthermore, recall that we made no assumptions about f in arriving at equation (54.15), so that f can be a function of latitude as per the β-plane. Indeed, f can be an arbitrary function of space, $f(x, y)$. Finally, equation (54.15) indicates that a stationary plane wave ($\omega = 0$) is in exact geostrophic balance. We further discuss this result in Section 54.2.6 when studying the structure of a single plane wave.

54.2.6 Structure of a single plane wave

TERM	$\mathcal{P} = 0$	$\mathcal{P} = \pi/2$	$\mathcal{P} = \pi$	$\mathcal{P} = 3\pi/2$	$\mathcal{P} = 2\pi$
$\boldsymbol{u}$	0	$-A\,(\hat{\boldsymbol{z}} \times \boldsymbol{k})$	0	$A\,(\hat{\boldsymbol{z}} \times \boldsymbol{k})$	0
$-f\,\hat{\boldsymbol{z}} \times \boldsymbol{u}$	0	$-A\,f\,\boldsymbol{k}$	0	$A\,f\,\boldsymbol{k}$	0
$-\nabla\varphi$	$A\,\omega\,(\hat{\boldsymbol{z}} \times \boldsymbol{k})$	$A\,f\,\boldsymbol{k}$	$-A\,\omega\,(\hat{\boldsymbol{z}} \times \boldsymbol{k})$	$-A\,f\,\boldsymbol{k}$	$A\,\omega\,(\hat{\boldsymbol{z}} \times \boldsymbol{k})$
$\partial_t\boldsymbol{u}$	$A\,\omega\,(\hat{\boldsymbol{z}} \times \boldsymbol{k})$	0	$-A\,\omega\,(\hat{\boldsymbol{z}} \times \boldsymbol{k})$	0	$A\,\omega\,(\hat{\boldsymbol{z}} \times \boldsymbol{k})$

TABLE 54.2: Values for plane wave terms in the velocity equation as the phase, $\mathcal{P} = \boldsymbol{k}\cdot\boldsymbol{x} - \omega\,t$, moves from 0 to 2π. The time tendency, $\partial_t\boldsymbol{u}$, is always perpendicular to the wavevector, which accords with the transverse nature of the wave. Also note that the time tendency is $\pi/2$ out of phase with the velocity itself. When the time tendency vanishes, then the pressure gradient and Coriolis accelerations are in geostrophic balance, with this balance occuring every π radians.

In Table 54.1 we summarize the properties satisfied by a single plane wave in the horizontally non-divergent barotropic model. In particular, note that the pressure gradient has been decomposed into linearly independent directions parallel to the wave, $\hat{\boldsymbol{k}}$, and perpendicular to the wave, $\hat{\boldsymbol{z}} \times \hat{\boldsymbol{k}}$

$$-\nabla\varphi = A\,[\omega\,(\hat{\boldsymbol{z}} \times \boldsymbol{k})\cos\mathcal{P} + f\,\boldsymbol{k}\sin\mathcal{P}]. \tag{54.16}$$

Table 54.2 considers the values for each term in the velocity equation as the phase moves around the unit circle, and Figure 54.2 provides a schematic. Evidently, the transverse plane waves oscillate between geostrophic balance, with $\partial_t\boldsymbol{u} = 0$, and pressure driven tendency, where $\partial_t\boldsymbol{u} = -\nabla\varphi$.

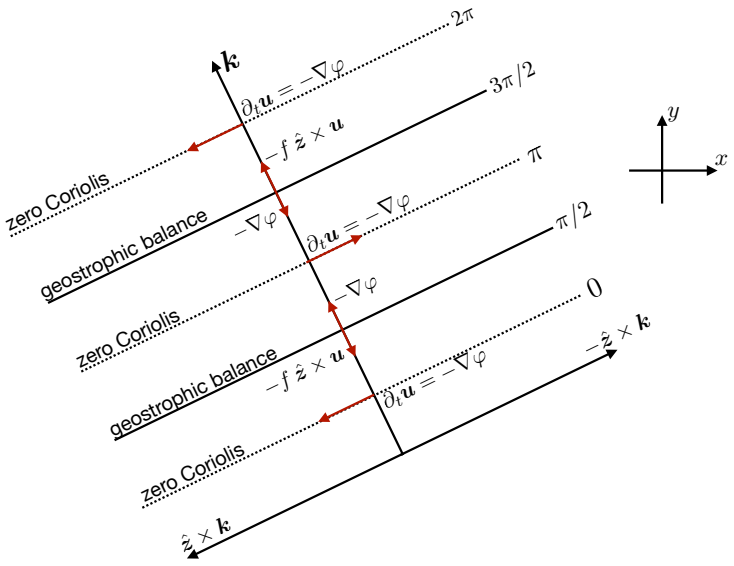

FIGURE 54.2: Schematic of the terms appearing in a horizontally propagating plane wave in the horizontally non-divergent barotropic model. We display terms as a function of the phase, $\mathcal{P} = (\boldsymbol{k}\cdot\boldsymbol{x} - \omega\, t)$, whose value is shown for $\mathcal{P} = 0, \pi/2, \pi, 3\pi/2, 2\pi$. The terms correspond to those given in Table 54.2. Note the oscillation between geostrophic balance, with zero time tendency, with a phase where there is a downgradient acceleration (i.e. ageostrophic motion). Also note that the pressure gradient rotates in a clockwise direction when the phase increases.

54.2.7 Kinetic energy of a single plane wave

Taking the scalar product of the velocity with the velocity equation (54.12) leads to the kinetic energy equation (38.10)

$$\frac{\mathrm{D}\mathcal{K}}{\mathrm{D}t} = -\nabla\cdot(\boldsymbol{u}\,\varphi). \tag{54.17}$$

Likewise, taking the scalar product with the linear velocity equation (54.15) satisfied by the single plane wave renders

$$\partial_t\mathcal{K} = -\nabla\cdot(\boldsymbol{u}\,\varphi). \tag{54.18}$$

As for the velocity, we see that the kinetic energy of the plane wave experiences no advection. Furthermore, making use of the wave ansatz (54.3) leads to the kinetic energy per mass within a single plane wave

$$\mathcal{K} = (A^2\,|\boldsymbol{k}|^2/2)\sin^2\mathcal{P}, \tag{54.19}$$

thus indicating more energy in higher wavenumber waves. In contrast, the gravitational potential energy is constant given that the fluid has a uniform density and rigid lid. Hence, as the kinetic energy fluctuates within a wave, there is no exchance with potential energy. Instead, there is an exchange with the external dynamical system that affects a rigid lid on the fluid.

The phase average of the kinetic energy (54.19) is

$$\langle\mathcal{K}\rangle = A^2\,|\boldsymbol{k}|^2/4. \tag{54.20}$$

Now consider the energy flux convergence, again as rendered by the single plane wave

$$-\nabla\cdot(\boldsymbol{u}\,\varphi) = -\boldsymbol{u}\cdot\nabla\varphi = \omega\,A^2|\boldsymbol{k}|^2\sin\mathcal{P}\cos\mathcal{P}, \tag{54.21}$$

where we made use of equation (54.16) for the pressure gradient. The phase average of this flux convergence vanishes

$$\langle\nabla\cdot(\boldsymbol{u}\,\varphi)\rangle = 0. \tag{54.22}$$

Evidently, the zero kinetic energy flux convergence arises since the plane wave is present throughout space, so that there is no means to converge phase averaged wave energy to any particular region. Only when there is a symmetry breaking, such as by modulating the plane wave into a localized packet, will there be a nonzero phase average flux convergence.

54.3 Barotropic and non-divergent Rossby waves

In this section we build on the general properties of the plane wave as developed in Section 54.2. The key new ingredient considered here is the dispersion relation that couples the wavevector to the wave angular frequency. As we see, the fluctuations are organized into *Rossby waves*, which are waves that carry a nonzero vorticity and are reliant on gradients in the background potential vorticity field.

54.3.1 The vorticity mechanism for planetary Rossby waves

Before developing the detailed properties of Rossby waves, we discuss the underlying mechanism for planetary Rossby waves. This discussion serves as both a motivation and guide for the mathematics to follow. The foundational principle is that fluctuations constrained by material conservation of potential vorticity organize into Rossby waves when they are presented with a background potential vorticity gradient. The background potential vorticity gradient can arise from the meridional gradient of the planetary vorticity (giving rise to planetary waves), gradients in the vorticity of the base flow (e.g., edge waves), and, in more general models, buoyancy gradients and topography gradients (topographic Rossby waves). Note that the seeds for these arguments were planted in Section 38.5 when studying vorticity constraints on the flow for the non-divergent barotropic model.

Westward phase propagation

In Figure 54.3 we display the essential physics of planetary Rossby waves as realized in the horizontally non-divergent barotropic model. As described in the figure caption, the constraint of absolute vorticity conservation for fluctuating fluid parcels, in the presence of $\beta > 0$, gives rise to the westward phase propagation of the planetary Rossby wave. As we see in Section 54.5.6, a pseudo-westward propagation arises for edge waves generated by vorticity jumps. This preferred direction for propagation is a canonical property of vorticity waves, and it distinguishes these waves from other waves whose phase propagation has no directional preference.

Vorticity and momentum arguments

The argument offered in Figure 54.3 does not consider forces. Rather, we make use of the constraint imposed by materical conservation of absolute vorticity and infer the motion of fluid parcels by noting how the relative vorticity anomaly induces flow of a particular orientation. Rossby waves carry vorticity, so vorticity arguments offer the natural means to understand their mechanism. Even so, a complementary approach to understanding Rossby waves considers the forces acting in the wave, and as such is referred to as a *momentum argument*. This argument is concerned with the nature of pressure fluctuations within the wave. We note in Section 54.2.5 that plane waves in an inviscid horizonally non-divergent barotropic model oscillate between a state with exact geostrophic balance and a state with zero Coriolis acceleration so that acceleration is down the pressure gradient.

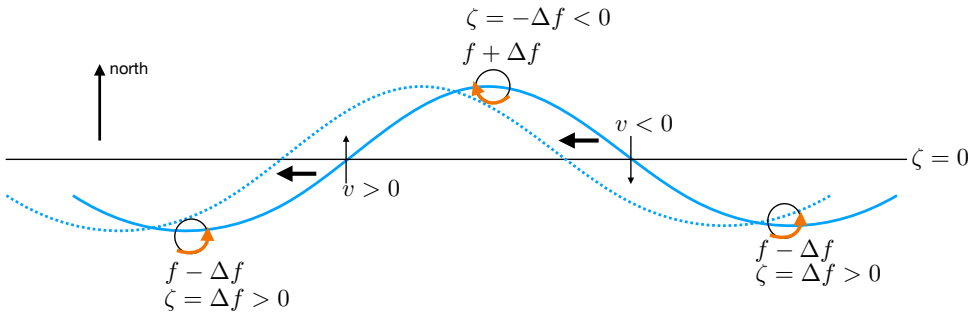

FIGURE 54.3: The westward phase propagation of a planetary Rossby wave arises from the presence of $\beta > 0$ and the constraint that absolute vorticity ($\zeta_a = f + \zeta$) is materially constant for a two-dimensional non-divergent and inviscid barotropic flow. In this figure we consider a material curve within the fluid in either the northern or southern hemispheres. The background flow is assumed to be static to allow us to focus on the role of the planetary vorticity gradient as measured by β. The relative vorticity is assumed to vanish for points on the straight constant latitude line, so that $\zeta_a = f$ must be maintained by any latitudinal perturbation. For a northward perturbation relative to the latitude line, a fluid parcel finds itself at a latitude with Coriolis parameter more positive than its original value ($f \to f + \Delta f > f$, with absolute vorticity conservation requiring the parcel to pick up a negative relative vorticity anomaly, $\zeta = -\Delta f < 0$. The opposite occurs for a southward perturbation. The counter-rotating secondary flow induced by the relative vorticity anomaly acts to move the wave pattern westward, so that the solid wave pattern is, at a future time, moved to the dashed wave pattern. We depict that the meridional motion induced by the wave as the pattern crosses the constant latitude line. In the absence of β, the meridional movement of parcels does not render a change in the planetary vorticity since in this case f is a constant. So for the f-plane there is no induced relative vorticity anomaly so there is no coherent movement of the wave pattern. We thus see the central role of $\beta \neq 0$ for planetary Rossby waves. We also see that the sign of the Coriolis parameter is not relevant; it is only $\beta > 0$ that determines the westward wave motion in both northern and southern hemispheres. A generic way to orient the phase is to note that when looking in the phase direction, higher planetary vorticity is to the right, with this rule holding for Rossby waves arising from potential vorticity gradients other than planetary β.

54.3.2 Flow relative to a zonal base state

We here examine wave fluctuations relative to a static base flow whose vorticity satisfies

$$\boldsymbol{u}_b \cdot \nabla(f + \zeta_b) = 0, \tag{54.23}$$

along with a corresponding velocity potential so that

$$\boldsymbol{u}_b = \hat{\boldsymbol{z}} \times \nabla \psi_b \quad \text{and} \quad \zeta_b = \nabla^2 \psi_b. \tag{54.24}$$

This base flow maintains a materially constant absolute vorticity, so that it is an exact static solution to the equations of motion for the inviscid two-dimensional non-divergent barotropic model, and thus serves as a suitable base flow to study wave fluctuations.[2]

We focus in this chapter on a static background zonal flow written in the form[3]

$$\boldsymbol{u}_b = \hat{\boldsymbol{x}}\, U(y) \quad \text{with} \quad \psi_b = -\int^y u_b(y')\, dy' \quad \text{and} \quad \zeta_b = -\partial_y u_b = \partial_{yy} \psi_b. \tag{54.25}$$

As we show, the base flow with constant $u_b = U$ (and thus with $\zeta_b = 0$) supports plane waves. The study of wave fluctuations on general base states requires more general methods, such as the asymptotics from Chapter 50. We encounter another case not admitting plane waves when studying edge waves in Section 54.5. Although not admitting plane waves, the edge waves do support interfacial waves similar to the surface waves in Chapter 52.

[2] Although we cannot generally determine an analytic expression for the base flow, we know that a pressure can be found that accords with the flow configuration and the non-divergent nature of the flow (see Section 38.4).

[3] Recall that the streamfunction is arbitrary up to a constant (Section 21.4). It is for this reason that we have no concern for the lower integration limit in equation (54.25).

54.3.3 Equations for the fluctuating vorticity and streamfunction

In the presence of a base state flow, we write the vorticity, velocity, and streamfunction in the form[4]

$$\zeta_{\text{full}} = \zeta + \zeta_{\text{b}} \quad \text{and} \quad \boldsymbol{u}_{\text{full}} = \boldsymbol{u} + \boldsymbol{u}_{\text{b}} \quad \text{and} \quad \psi_{\text{full}} = \psi + \psi_{\text{b}}, \tag{54.26}$$

with the vorticity equation

$$[\partial_t + (\boldsymbol{u} + \boldsymbol{u}_{\text{b}}) \cdot \nabla](\zeta + \zeta_{\text{b}} + f) = 0. \tag{54.27}$$

Again, from equation (54.23) we assume the static base state satisfies $\boldsymbol{u}_{\text{b}} \cdot \nabla(f + \zeta_{\text{b}}) = 0$, which means the vorticity equation (54.27) reduces to the equation for the fluctuating vorticity

$$\partial_t \zeta + (\boldsymbol{u} + \boldsymbol{u}_{\text{b}}) \cdot \nabla \zeta + \boldsymbol{u} \cdot \nabla(f + \zeta_{\text{b}}) = 0. \tag{54.28}$$

Introducing a streamfunction for the fluctuating flow, $\zeta = \nabla^2 \psi$, brings the vorticity equation (54.28) into the form

$$\partial_t(\nabla^2 \psi) + \hat{\boldsymbol{z}} \cdot [\nabla \psi \times \nabla(\nabla^2 \psi + f + \nabla^2 \psi_{\text{b}})] + \hat{\boldsymbol{z}} \cdot [\nabla \psi_{\text{b}} \times \nabla(\nabla^2 \psi)] = 0. \tag{54.29}$$

As we show below, this equation supports traveling plane vorticity waves. It is notable that it has only one time derivative, which contrasts to all the other wave equations we have encountered in this book (e.g., equation (51.34) for acoustic waves, equation (52.119) for surface gravity waves, and equation (53.27) for inertial waves). It leads to an asymmetric phase propagation of the linear wave fluctuations.

54.3.4 Rossby wave dispersion relation

To develop a dispersion relation we substitute the plane wave ansatz (54.3) into the vorticity equation (54.29). For the plane wave ansatz to lead to a self-consistent dispersion relation requires the background vorticity field to be extremely simple. In particular, the background velocity and background vorticity gradient must both be independent of space

$$\nabla f = \text{constant} \quad \text{and} \quad \boldsymbol{u}_{\text{b}} = U\,\hat{\boldsymbol{x}} \implies \zeta_{\text{b}} = 0, \tag{54.30}$$

with the first assumption holding for the β plane. In general, these assumptions ensure that the angular frequency for the plane wave is independent of space. In Section 54.5 we consider a slightly less trivial background state that supports edge waves rather than plane waves.

Given our focus on plane waves, assume a domain without boundaries and consider a horizontal traveling plane wave ansatz in the form of equation (54.6). Plugging this ansatz into the vorticity equation (54.29), and recalling that $\boldsymbol{u} \cdot \nabla \zeta = 0$ for a plane wave as discussed in Section 54.2.3, leads to

$$A \sin(\boldsymbol{k} \cdot \boldsymbol{x} - \omega\, t)[-\omega\, |\boldsymbol{k}|^2 + (\boldsymbol{k} \cdot \boldsymbol{u}_{\text{b}})\, |\boldsymbol{k}|^2 - (\hat{\boldsymbol{z}} \times \boldsymbol{k}) \cdot \nabla f] = 0. \tag{54.31}$$

This equation is generally satisfied only when the bracketed term vanishes, which gives the dispersion relation that expresses the angular frequency as a function of the wavevector, the base flow, and geophysical parameters

$$\varpi = \underbrace{\boldsymbol{k} \cdot \boldsymbol{u}_{\text{b}}}_{\text{Doppler}} \; \underbrace{+(\boldsymbol{k} \times \hat{\boldsymbol{z}}) \cdot \nabla f / |\boldsymbol{k}|^2}_{\text{planetary vorticity gradient}} = k_x\,(U - \beta/|\boldsymbol{k}|^2). \tag{54.32}$$

[4] An alternative notation is to write $\zeta = \zeta' + \zeta_{\text{b}}$, where ζ' is the fluctuating vorticity. We choose the notation in equation (54.26) to reduce the abundance of primes appearing in the equations.

As noted at the end of Section 54.3.2, the Rossby wave dispersion relation (54.32) results from a wave equation with only a single time derivative. We commented in Section 49.3.3 on such wave equations as being notable for possessing a preferred direction for wave propagation, which we see in Section 54.3.6 results in Rossby waves having a phase that moves westward.

Doppler shift from the base flow

The term

$$\varpi_{\text{Doppler}} \equiv \boldsymbol{k} \cdot \boldsymbol{u}_{\mathfrak{b}} = k_x U \tag{54.33}$$

provides a shift in the angular frequency relative to the case with zero base flow. If the wave direction is aligned with the base flow, then $\varpi_{\text{Doppler}} > 0$, so that the angular frequency of the wave is increased. In contrast, the wave frequency is decreased when the wave is directed anti-parallel to the base flow. This frequency shift is referred to as a *Doppler shift*. A Doppler shift is familiar from acoustic waves when, for example, the frequency of a train whistle received by a stationary listener is higher when the train approaches and lower when it is moving away.

Rossby waves supported by a gradient in the planetary vorticity

The planetary beta effect leads to the term

$$\varpi_\beta \equiv -(\hat{\boldsymbol{z}} \times \hat{\boldsymbol{k}}) \cdot \nabla f / |\boldsymbol{k}| = -\beta\, k_x / |\boldsymbol{k}|^2, \tag{54.34}$$

which gives rise to the *planetary wave* or *planetary Rossby wave*. We see that planetary Rossby waves rely on planetary curvature, in which case $\beta \neq 0$. Equivalently, planetary Rossby waves rely on a nonzero gradient in the planetary vorticity, $\nabla f = \beta\, \hat{\boldsymbol{y}}$, so that planetary Rossby waves do not exist on an f-plane.

The dispersion relation (54.34) reveals that long planetary waves (small wavenumber) have higher angular frequency than short planetary waves. The maximum angular frequency is given by the Rossby wave with zero meridional wavenumber

$$\omega_{\beta\text{-max}} = \beta / |k_x|. \tag{54.35}$$

This frequency corresponds to a purely zonal Rossby wave with no meridional structure. Correspondingly, the transverse nature of the waves means that fluid particles are moving meridionally in the presence of a zonal Rossby wave. Evidently, the frequency of the waves is directly related to the degree to which fluid particles move through the background potential vorticity field, with highest frequency for particles moving meridionally and zero frequency for particles moving zonally.

We compute the ratio of the maximum angular frequency for a Rossby wave to the central value of the Coriolis parameter, $f_\circ$, used for the beta-plane approximation (Section 24.5)

$$\omega_{\beta\text{-max}} / f_\circ = \beta / |k_x\, f_\circ| = \beta\, L_x / |f_\circ| \ll 1. \tag{54.36}$$

In this equation we set the zonal wavenumber equal to the inverse of a zonal length scale of the flow, $k_x = 1/L_x$. The ratio $\beta\, L_x / |f_\circ|$ is much less than unity so long as the β-plane approximation is accurate.[5] We thus see that the maximum angular frequency of the Rossby waves is much smaller than the Coriolis frequency, thus making the planetary Rossby wave a *sub-inertial wave*.

[5] See Section 24.5.4 for more on the β-plane approximation.

54.3.5 Extrinsic and intrinsic angular frequency

We here introduce some terminology sometimes applied to waves in the presence of a background mean flow. For this purpose, consider again the dispersion relation, ϖ, given by equation (54.32). This relation renders the angular frequency as measured by an observer stationary with respect to the moving frame. As such, it is sometimes referred to as the *ground-based frequency* or the *extrinsic frequency*

$$\text{extrinsic frequency} = \varpi = \boldsymbol{k} \cdot \boldsymbol{u}_{\text{b}} + (\boldsymbol{k} \times \hat{\boldsymbol{z}}) \cdot \nabla f / |\boldsymbol{k}|^2 = k_x \, (U - \beta / |\boldsymbol{k}|^2). \tag{54.37}$$

The frequency measured by an observer moving with the background flow does not have a Dopper contribution, motivating the name *intrinsic frequency*

$$\text{intrinsic frequency} = \varpi - \boldsymbol{k} \cdot \boldsymbol{u}_{\text{b}} = -\beta / |\boldsymbol{k}|^2. \tag{54.38}$$

The intrinsic frequency is also sometimes referred to as the *Doppler-shifted frequency*, but that name should perhaps more clearly be the "frequency with the Doppler shift removed".

The above definitions for extrinsic and intrinsic angular frequencies accord with the conventional definitions. However, it is notable than Section 6.2 of *Sutherland* (2010) offers the exact opposite definitions. One should thus be mindful of these different naming conventions.

54.3.6 Concerning the westward phase velocity

The phase velocity, $\boldsymbol{c}_{\text{p}} = (\omega / |\boldsymbol{k}|) \, \hat{\boldsymbol{k}}$ (see equation (49.26)), takes on the following form for a barotropic Rossby wave[6]

$$\boldsymbol{c}_{\text{p}} = \hat{\boldsymbol{k}} \left[\hat{\boldsymbol{k}} \cdot \boldsymbol{u}_{\text{b}} - (\hat{\boldsymbol{z}} \times \hat{\boldsymbol{k}}) \cdot \nabla f / |\boldsymbol{k}|^2 \right] = \hat{\boldsymbol{k}} \left[\hat{\boldsymbol{k}} \cdot \boldsymbol{u}_{\text{b}} + \hat{\boldsymbol{k}} \cdot (\hat{\boldsymbol{z}} \times \nabla f) / |\boldsymbol{k}|^2 \right] = \hat{\boldsymbol{k}} \, (\hat{\boldsymbol{k}} \cdot \hat{\boldsymbol{x}}) \, (U - \beta \, / |\boldsymbol{k}|^2). \tag{54.39}$$

The phase velocity arising from planetary beta

$$[\boldsymbol{c}_{\text{p}}]_\beta = -\beta \, \hat{\boldsymbol{k}} \, (\hat{\boldsymbol{x}} \cdot \hat{\boldsymbol{k}}) / |\boldsymbol{k}|^2 \tag{54.40}$$

has a sign-definite zonal component

$$\left[\boldsymbol{c}_{\text{p}} \cdot \hat{\boldsymbol{x}} \right]_\beta = -(\hat{\boldsymbol{x}} \cdot \hat{\boldsymbol{k}})^2 / |\boldsymbol{k}|^2 = -k_x^2 \, \beta / |\boldsymbol{k}|^4 < 0. \tag{54.41}$$

We depict this property of the Rossby wave phase velocity in Figure 54.4. This westward phase propagation holds for both hemispheres since $\beta \geq 0$ over the globe. Furthermore, the westward propagation is larger in magnitude at lower latitudes where β is larger, with a ratio given by

$$\frac{\left[\boldsymbol{c}_{\text{p}}(\phi_1) \cdot \hat{\boldsymbol{x}} \right]_\beta}{\left[\boldsymbol{c}_{\text{p}}(\phi_2) \cdot \hat{\boldsymbol{x}} \right]_\beta} = \frac{\cos \phi_1}{\cos \phi_2}. \tag{54.42}$$

For example, $\boldsymbol{c}_{\text{p}}(\phi_1) \cdot \hat{\boldsymbol{x}}$ at 60° latitude is one-half that at the equator. Both the westward phase propagation and the faster phase speed at lower latitudes are canonical features of planetary Rossby waves. These properties are readily seen in large-scale flow patterns in both the atmosphere and ocean.

[6] In this book, we eschew the notion of components to the phase speed since the phase speed is not a vector and so it has no components. Rather, as discussed in Section 49.5.2, the phase speed is the magnitude of the phase velocity, $C_{\text{p}} = \boldsymbol{c}_{\text{p}} \cdot \hat{\boldsymbol{k}} = \omega / |\boldsymbol{k}| \geq 0$, with the phase velocity $\boldsymbol{c}_{\text{p}} = C_{\text{p}} \, \hat{\boldsymbol{k}}$.

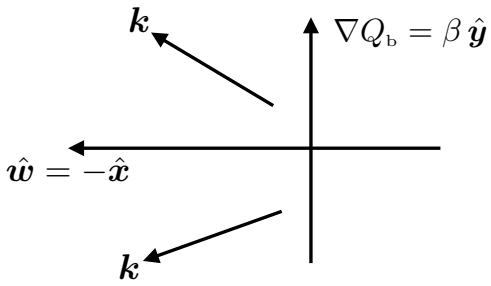

FIGURE 54.4: Illustrating the westward phase propagation of a planetary Rossby wave. In this case the westward unit vector is $\hat{\boldsymbol{w}} = -\hat{\boldsymbol{x}}$, and the phase velocity is projected in the westward direction, $\big[\boldsymbol{c}_{\mathrm{p}} \cdot \hat{\boldsymbol{w}}\big]_\beta > 0$. We show two possible wavevectors, $\boldsymbol{k} = k_x\,\hat{\boldsymbol{x}} + k_y\,\hat{\boldsymbol{y}}$, with $k_x < 0$ so the wavevector has a westward component, but the meridional component can be either positive or negative.

Westward phase velocity implied by positive angular frequency

Another indication that Rossby waves have a westward phase propagation is to recall that the angular frequency of a wave is positive (Section 49.2.3). This convention is maintained by noting that the direction of the phase propagation is carried by the wavevector

$$\boldsymbol{k} = \hat{\boldsymbol{x}}\,k_x + \hat{\boldsymbol{y}}\,k_y, \tag{54.43}$$

rather than allowing the angular frequency to be negative.[7] Planetary Rossby waves in two-dimensional non-divergetnt barotropic flow have the dispersion relation (54.34)

$$\varpi_\beta = -\beta\,k_x/|\boldsymbol{k}|^2. \tag{54.44}$$

The resulting angular frequency is positive if $k_x < 0$, meaning that propagating planetary waves have a westward component to the phase velocity.

The result (54.44) generalizes by considering the dispersion relation arising from a more general background potential vorticity[8]

$$\varpi_{\mathrm{base}+\beta} \equiv -(\hat{\boldsymbol{z}} \times \hat{\boldsymbol{k}}) \cdot \nabla Q_{\mathrm{b}}/|\boldsymbol{k}|, \tag{54.45}$$

with non-negative values assured only for wavevectors oriented in the pseudo-westward direction so that

$$(\hat{\boldsymbol{z}} \times \hat{\boldsymbol{k}}) \cdot \nabla Q_{\mathrm{b}} = -(\hat{\boldsymbol{z}} \times \nabla Q_{\mathrm{b}}) \cdot \hat{\boldsymbol{k}} = -(\hat{\boldsymbol{k}} \cdot \hat{\boldsymbol{w}})\,|\hat{\boldsymbol{z}} \times \nabla Q_{\mathrm{b}}| < 0, \tag{54.46}$$

where we introduced the *pseudo-westward* unit vector

$$\hat{\boldsymbol{w}} \equiv \frac{\hat{\boldsymbol{z}} \times \nabla Q_{\mathrm{b}}}{|\hat{\boldsymbol{z}} \times \nabla Q_{\mathrm{b}}|}. \tag{54.47}$$

Emphasizing the special nature of the westward phase velocity

The westward phase velocity is a very distinct feature of Rossby waves. As seen in Section 54.3.1, it results from the constraint of material conservation of potential vorticity in the presence of a background potential vorticity gradient. Other waves that we have studied, such as acoustic waves (Chapter 51), surface waves (Chapter 52), and inertial waves (Chapter 53), support an arbitrary orientation for their phase velocity. As a result, a source for these sorts of waves will

[7] Our use of a positive angular frequency is not universally maintained in the literature. For example, *Pedlosky* (2003) considers $\omega < 0$ for Rossby waves.

[8] For the angular frequency to be independent of spatial position (assumed for plane waves) requires ∇Q_{b} to be spatially independent. See discussion in Section 54.3.2 for more on the restrictions of the background flow enabling plane waves.

generate waves whose phases are oriented in directions constrained by details of the source rather than by any intrinsic property of the waves. In contrast, an arbitrary source for Rossby waves can only produce Rossby waves with a westward oriented phase. There are no Rossby waves with an eastward phase propagation. In this manner, Rossby waves are *anisotropic waves*.

54.3.7 Stationary Rossby waves

Stationary Rossby waves have zero phase velocity, which occurs if the base flow satisfies

$$\boldsymbol{c}_{\text{p}} = 0 \Longrightarrow \hat{\boldsymbol{k}} \cdot \hat{\boldsymbol{x}} \, (U - \beta/|\boldsymbol{k}|^2) = 0. \tag{54.48}$$

That is, the zonal portion of the Doppler shift exactly cancels the westward phase propagation from planetary β

$$U = \beta/|\boldsymbol{k}|^2. \tag{54.49}$$

The corresponding wavelength, $\Lambda = 2\pi/|\boldsymbol{k}|$, is given by

$$\Lambda_{\text{stationary}} = 2\pi \sqrt{U/\beta}. \tag{54.50}$$

For example, assuming an eastward base flow speed of $U = 1$ m s^{-1} (as in portions of the Antarctic Circumpolar Current) at $\phi = 60°$S, where $\beta = (2\,\Omega/R) \cos\phi \approx 1.14 \times 10^{-11}$ m^{-1} s^{-1}, renders a stationary barotropic Rossby wavelenth of $\Lambda_{\text{stationary}} \approx 1860$ km, whereas for the atmosphere with $\boldsymbol{u}_{\text{b}} \cdot \hat{\boldsymbol{x}} = 25$ m s^{-1} we find $\Lambda_{\text{stationary}} \approx 9300$ km. Evidently, at these large scales the Rossby waves feel the Coriolis acceleration and thus properly earn the name *planetary wave*.

54.3.8 Group velocity

If Rossby waves were non-dispersive, then the westward phase velocity would introduce a puzzle: how can all the wave energy propagate only in the westward direction? Since wave energy follows the group velocity (Section 49.6), would there be an unbounded accumulation of Rossby wave energy in the western side of a domain? In fact, this puzzle does not arise since Rossby waves are dispersive, with their group velocity not constrained to be westward. We here introduce the group velocity and then follow up in Sections 54.4.1 and 54.4.2 by focusing on the group and phase velocities for planetary Rossby waves.

The Rossby wave group velocity, $\boldsymbol{c}_{\text{g}} = \nabla_{\boldsymbol{k}} \varpi$, is given by

$$\boldsymbol{c}_{\text{g}} = \boldsymbol{u}_{\text{b}} + \frac{\hat{\boldsymbol{z}} \times \nabla f - 2\,\hat{\boldsymbol{k}}\,[\hat{\boldsymbol{k}} \cdot (\hat{\boldsymbol{z}} \times \nabla f)]}{|\boldsymbol{k}|^2} = U\,\hat{\boldsymbol{x}} - \frac{\beta\,[\hat{\boldsymbol{x}} - 2\,\hat{\boldsymbol{k}}\,(\hat{\boldsymbol{k}} \cdot \hat{\boldsymbol{x}})]}{|\boldsymbol{k}|^2}. \tag{54.51}$$

The presence of $U \neq 0$ signals the bulk transport of a Rossby wave packet by the base flow. The remaining terms can be related to the phase velocity (54.39) by projecting onto the wavevector direction

$$(\boldsymbol{c}_{\text{g}} - \boldsymbol{c}_{\text{p}}) \cdot \hat{\boldsymbol{k}} = 2\,\beta\,\hat{\boldsymbol{x}} \cdot \hat{\boldsymbol{k}}/|\boldsymbol{k}|^2. \tag{54.52}$$

Since wave dispersion is signaled by a difference between the phase velocity and group velocity, equation (54.52) indicates that Rossby wave dispersion arises from a nonzero gradient in the planetary vorticity, $\nabla Q_{\text{b}} = \nabla f = \beta\,\hat{\boldsymbol{y}}$, along with a nonzero projection of the wavevector onto the westward direction.

54.4 Geometry of planetary Rossby waves

We here focus on some special properties of planetary Rossby waves revealed by studying the geometry of the group velocity using a diagrammatic method developed by *Longuet-Higgins*

(1964).

54.4.1 Group and phase velocities for planetary Rossby waves

We start by focusing on the relation between group and phase velocities for planetary Rossby waves. The β contribution to the group velocity (54.51) is given by

$$[\boldsymbol{c}_{\text{g}}]_\beta = \frac{\beta\,[(k_x^2 - k_y^2)\,\hat{\boldsymbol{x}} + 2\,k_x\,k_y\,\hat{\boldsymbol{y}}]}{|\boldsymbol{k}|^4} \Longrightarrow [\boldsymbol{c}_{\text{g}} \cdot \boldsymbol{c}_{\text{g}}]_\beta = \beta^2/|\boldsymbol{k}|^4. \tag{54.53}$$

Recall the westward component of the phase velocity arising from planetary beta as discussed in Section 54.3.6. In contrast, the zonal component to the group velocity

$$[\boldsymbol{c}_{\text{g}} \cdot \hat{\boldsymbol{x}}]_\beta = \frac{\beta\,(k_x^2 - k_y^2)}{|\boldsymbol{k}|^4} = -[\boldsymbol{c}_{\text{p}} \cdot \hat{\boldsymbol{x}}]_\beta - \frac{\beta\,k_y^2}{|\boldsymbol{k}|^4}, \tag{54.54}$$

can be directed in either direction. Note that to reach this equality we used equation (54.41) for $[\boldsymbol{c}_{\text{p}} \cdot \hat{\boldsymbol{x}}]_\beta$.

Evidently, the group velocity (54.53) for planetary Rossby waves depends on the shape of the wave as characterized by $(k_x^2 - k_y^2)\,\hat{\boldsymbol{x}} + 2\,k_x\,k_y\,\hat{\boldsymbol{y}}$. Consequently, the group velocity has the following properties for its zonal component

$$[\boldsymbol{c}_{\text{g}} \cdot \hat{\boldsymbol{x}}]_\beta > 0 \quad \text{if } k_x^2 > k_y^2 \quad \Rightarrow \text{eastward } \boldsymbol{c}_{\text{g}} \text{ for short zonal planetary waves} \tag{54.55a}$$

$$[\boldsymbol{c}_{\text{g}} \cdot \hat{\boldsymbol{x}}]_\beta < 0 \quad \text{if } k_x^2 < k_y^2 \quad \Rightarrow \text{westward } \boldsymbol{c}_{\text{g}} \text{ for long zonal planetary waves} \tag{54.55b}$$

$$[(\boldsymbol{c}_{\text{g}} + \boldsymbol{c}_{\text{p}}) \cdot \hat{\boldsymbol{x}}]_\beta = 0 \quad \text{if } k_y = 0 \quad \Rightarrow \text{eastward } \boldsymbol{c}_{\text{g}} \text{ for } k_y = 0 \text{ planetary waves.} \tag{54.55c}$$

Wave energy moves eastward in packets of zonally short ($k_x^2 > k_y^2$) planetary Rossby waves, whereas wave energy is westward in zonally long ($k_x^2 < k_y^2$) planetary Rossby waves. That is, zonally elongated Rossby waves have westward group velocity whereas zonally compressed Rossby waves have eastward group velocity, where "elongated" and "compressed" are relative to the meridional structure. Indeed, if $k_y = 0$, in which case there is no meridional structure to the wave, then Rossby waves of any zonal wavenumber have eastward group velocity, even while the phase velocity is westward

$$[\boldsymbol{c}_{\text{g}} \cdot \hat{\boldsymbol{x}}]_\beta = -[\boldsymbol{c}_{\text{p}} \cdot \hat{\boldsymbol{x}}]_\beta > 0 \quad \text{if } k_y = 0. \tag{54.56}$$

This property is consistent with the ratio

$$\frac{[\boldsymbol{c}_{\text{p}} \cdot \boldsymbol{c}_{\text{p}}]_\beta}{[\boldsymbol{c}_{\text{g}} \cdot \boldsymbol{c}_{\text{g}}]_\beta} = \frac{k_x^2}{|\boldsymbol{k}|^2} = (\hat{\boldsymbol{k}} \cdot \hat{\boldsymbol{x}})^2, \tag{54.57}$$

which then allows us to write the dispersion relation in the form

$$[\omega^2]_\beta = |\boldsymbol{k}|^2\,[\boldsymbol{c}_{\text{p}} \cdot \boldsymbol{c}_{\text{p}}]_\beta = k_x^2\,[\boldsymbol{c}_{\text{g}} \cdot \boldsymbol{c}_{\text{g}}]_\beta. \tag{54.58}$$

54.4.2 Dispersion circle for planetary Rossby waves

Figure 54.5 illustrates the geometry of the phase and group velocity as realized for planetary Rossby waves. We refer to this diagram as the *dispersion circle*, and it arises from noting that the dispersion relation, $\omega = -\beta\,k_x/|\boldsymbol{k}|^2$, can be written as an equation for a circle in the (k_x, k_y) plane

$$[k_x + \beta/(2\,\omega)]^2 + k_y^2 = [\beta/(2\,\omega)]^2. \tag{54.59}$$

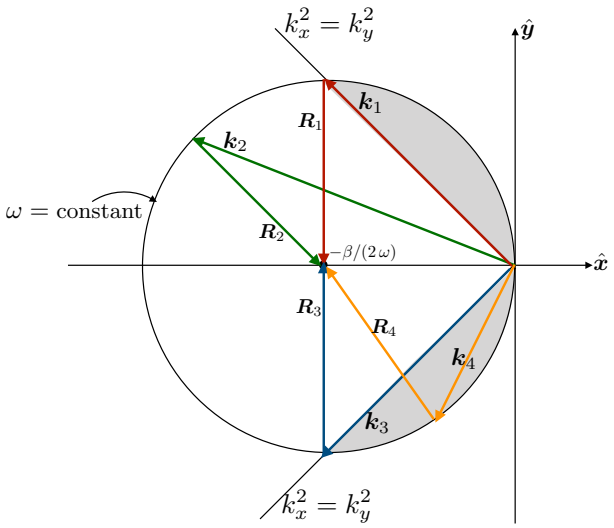

FIGURE 54.5: Dispersion circle for planetary Rossby waves, with this diagram orienting the group velocity and phase velocity in wavevector space, (k_x, k_y). The angular frequency, ω, determines a particular dispersion circle. We depict four example wavevectors, $\boldsymbol{k} = k_x\,\hat{\boldsymbol{x}} + k_y\,\hat{\boldsymbol{y}}$, that orient the phase velocity, $\boldsymbol{c}_\mathsf{p} = \hat{\boldsymbol{k}}\,\omega/|\boldsymbol{k}|$. Each wavevector extends from the origin to a point on the dispersion circle perimeter, $[k_x + \beta/(2\omega)]^2 + k_y^2 = [\beta/(2\omega)]^2$, with the circle having center at $\boldsymbol{k}_\text{center} = -\beta/(2\,\omega)\,\hat{\boldsymbol{x}}$ and radius $\beta/(2\,\omega)$. Each wavevector has an associated group velocity orientation vector, $\boldsymbol{R} = -\boldsymbol{k} - \beta/(2\,\omega)\,\hat{\boldsymbol{x}}$, that points from the circle perimeter to the circle center. The group velocity is westward for those wavevectors that intersect the circle perimeter within the gray-shaded region. Such wavevectors characterize Rossby waves with zonal wavenumbers that are smaller than their meridional wavenumbers; i.e., relatively long zonal Rossby waves. The group velocity has an eastward component for wavevectors outside the gray region, with the lines $k_x^2 = k_y^2$ separating these regions where the group velocity is eastward or westward. Such wavevectors characterize Rossby waves with zonal wavenumbers that are larger than their meridional wavenumbers; i.e., relatively short zonal Rossby waves. The group velocity for wavevector $\boldsymbol{k}_1$ is exactly southward; for $\boldsymbol{k}_2$ it is southeastward; for $\boldsymbol{k}_3$ it is exactly northward, and for k_4 it is northwestward. This figure is taken after *Longuet-Higgins* (1964).

The center of the circle is at the wavevector

$$\boldsymbol{k}_{\text{center}} = -\beta/(2\,\omega)\,\hat{\boldsymbol{x}}, \tag{54.60}$$

and with a radius equal to $\beta/(2\,\omega)$. The circle has angular frequency, ω, acting as a parameter, with lower frequency Rossby waves yielding larger circles. We further reveal the geometry of the group velocity (54.53) by writing it in the form

$$[\boldsymbol{c}_{\text{g}}]_\beta = \frac{\beta\,[(k_x^2 - k_y^2)\,\hat{\boldsymbol{x}} + 2\,k_x\,k_y\,\hat{\boldsymbol{y}}]}{|\boldsymbol{k}|^4} = -\frac{2\,\omega\,\big[[k_x + \beta/(2\,\omega)]\,\hat{\boldsymbol{x}} + k_y\,\hat{\boldsymbol{y}}\big]}{|\boldsymbol{k}|^2}. \tag{54.61}$$

Furthermore, we introduce the group velocity orientation vector

$$\boldsymbol{R} = -\boldsymbol{k} - \beta/(2\,\omega)\,\hat{\boldsymbol{x}} = -[k_x + \beta/(2\,\omega)]\,\hat{\boldsymbol{x}} - k_y\,\hat{\boldsymbol{y}} \quad \text{with} \quad |\boldsymbol{R}| = \beta/(2\omega), \tag{54.62}$$

so that the group velocity can be written in the rather tidy form

$$[\boldsymbol{c}_{\text{g}}]_\beta = 2\,\omega\,\boldsymbol{R}/|\boldsymbol{k}|^2. \tag{54.63}$$

Notice that $\boldsymbol{R}$ has magnitude equal to the radius of the circle. Furthermore, this vector points from the circle perimeter to the circle center, as seen since $\boldsymbol{R} + \boldsymbol{k} = -\beta/(2\,\omega)\,\hat{\boldsymbol{x}} = \boldsymbol{k}_{\text{center}}$.

The geometry depicted in Figure 54.5 partitions the group velocity according to the wavevector. Again, the phase velocity always has a westward component, yet the group velocity can be westward or eastward. Additionally, for each angular frequency there is one wave whose group velocity is precisely northward and another that is southward. The squared magnitude of the group velocity is given by equation (54.53)

$$[\boldsymbol{c}_{\text{g}} \cdot \boldsymbol{c}_{\text{g}}]_\beta = \beta^2/|\boldsymbol{k}|^4, \tag{54.64}$$

so that longer waves (smaller wavenumber) have higher group velocity magnitude.

54.4.3 Reflection of planetary Rossby waves

The diagrammatic method developed in Section 54.4.2 provides a basis to characterize the reflection of Rossby wave packets from a smooth solid boundary. In the left panel of Figure 54.6 we depict a straight and smooth wall sloped with angle γ in the counter-clockwise direction from the positive x-axis. An incident southwestward group velocity carries a Rossby wave packet to the wall at an angle, θ_{i}, relative to the wall's normal direction, $\hat{\boldsymbol{n}}$. We assume the group velocity represents a packet whose central carrier Rossby wave has a wavevector $\boldsymbol{k}_{\text{i}}$, and seek information about the reflected wave packet's carrier wavevector, $\boldsymbol{k}_{\text{r}}$. Geometric optics from Section 50.3 provides the foundation for the approach taken in the following, in which we describe a diagrammatic approach for understanding how the wave packet reflects. Details are summarized in the right panel of Figure 54.6. We assume that the waves reflect from the boundary without dissipation (i.e., perfectly smooth and straight wall), so that reflection only involves kinematic boundary conditions.

Kinematic boundary condition at the wall

The kinematic boundary condition along the wall requires the velocity of fluid particles in the wave to have zero normal component at the wall, so that the the streamfunction must be constant along the wall

$$\boldsymbol{u} \cdot \hat{\boldsymbol{n}} = (\hat{\boldsymbol{z}} \times \nabla\psi) \cdot \hat{\boldsymbol{n}} = (\hat{\boldsymbol{n}} \times \hat{\boldsymbol{z}}) \cdot \nabla\psi = -\hat{\boldsymbol{t}} \cdot \nabla\psi = 0, \tag{54.65}$$

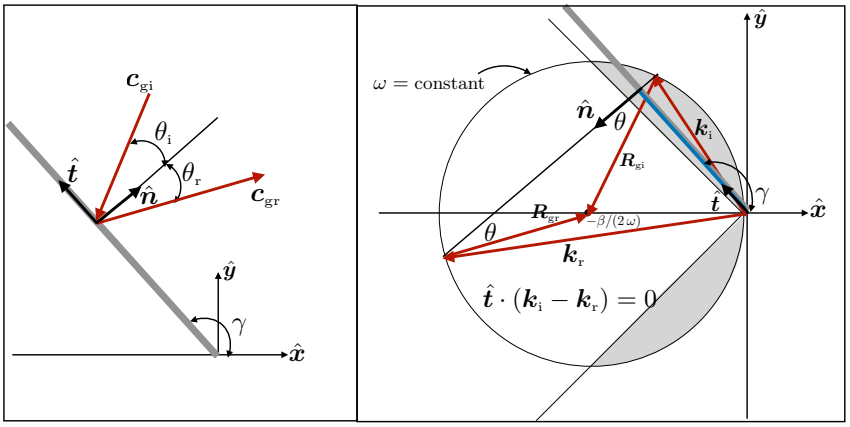

FIGURE 54.6: Depicting the reflection of a Rossby wave packet from a solid wall. The left panel shows the wall sloped at an angle, γ, relative to the positive x-axis. We orient the wall using both its tangential unit vector, $\hat{\boldsymbol{t}} = \hat{\boldsymbol{z}} \times \hat{\boldsymbol{n}} = \hat{\boldsymbol{x}} \cos\gamma + \hat{\boldsymbol{y}} \sin\gamma$, as well as its unit normal, $\hat{\boldsymbol{n}} = \hat{\boldsymbol{x}} \sin\gamma - \hat{\boldsymbol{y}} \cos\gamma$. The incident wave packet has group velocity $\boldsymbol{c}_{gi}$ directed to the southwest and reflected group velocity $\boldsymbol{c}_{gr}$ directed to the northeast. The angle of incidence equals to the angle of reflectance, $\theta_i = \theta_r = \theta$, as required by the kinematic boundary condition (54.67). The right panel shows the wave packet reflection using the dispersion diagram from Figure 54.5. Since the incident and reflected wave have the same angular frequency, we can use the same circle for deriving the wavevectors. The incident and reflected group velocities are oriented by the vectors $\boldsymbol{R}_{gi}$ (southwest) and $\boldsymbol{R}_{gr}$ (northeast) that point from the perimeter to the center of the ω-circle. They both make an angle of θ with respect to the wall's normal direction, $\hat{\boldsymbol{n}}$. The incident and reflected wavevectors satisfy equation (54.72), which says $(\boldsymbol{k}_i - \boldsymbol{k}_r) \cdot \hat{\boldsymbol{t}} = 0$. This relation provides the means to determine the reflected wavevector, $\boldsymbol{k}_r$ using the diagrammatic method illustrated here. Note that the right panel depicts the orientation of the western wall relative to the wavevectors and group velocities in wavevector space. One should not interpret this depiction as somehow making the western wall boundary into an eastern wall.

where we introduced the wall's unit tangent vector

$$\hat{\boldsymbol{t}} = \hat{\boldsymbol{z}} \times \hat{\boldsymbol{n}} = \hat{\boldsymbol{x}} \cos\gamma + \hat{\boldsymbol{y}} \sin\gamma. \tag{54.66}$$

The streamfunction can be any constant on the wall, which we take to be zero without loss of generality

$$\psi(\boldsymbol{x} = \boldsymbol{x}_{\text{wall}}, t) = 0, \tag{54.67}$$

with $\boldsymbol{x}_{\text{wall}}$ the coordinate for a point on the wall.

Relating incident and reflected wave properties

Write the velocity streamfunctions for the incident and reflected carrier waves as

$$\psi_i = A_i \cos(\boldsymbol{k}_i \cdot \boldsymbol{x} - \omega_i t) \quad \text{and} \quad \psi_r = A_r \cos(\boldsymbol{k}_r \cdot \boldsymbol{x} - \omega_r t), \tag{54.68}$$

where A_i and A_r are the real wave amplitudes, $\boldsymbol{k}_i$ and $\boldsymbol{k}_r$ are the wavevectors, and ω_i and ω_r are the angular frequencies. At any point in the fluid, the streamfunction is the sum of the streamfunctions for the incident and reflected waves

$$\psi(\boldsymbol{x}, t) = \psi_i(\boldsymbol{x}, t) + \psi_r(\boldsymbol{x}, t). \tag{54.69}$$

Satisfaction of the boundary condition (54.67) requires

$$A_i \cos(\boldsymbol{k}_i \cdot \boldsymbol{x}_{\text{wall}} - \omega_i t) + A_r \cos(\boldsymbol{k}_r \cdot \boldsymbol{x}_{\text{wall}} - \omega_r t) = 0. \tag{54.70}$$

For this equality to hold at each point along the wall and for all time requires

$$\omega_i = \omega_r \quad \text{equal incident and reflected angular frequency} \tag{54.71a}$$

$$A_i = -A_r \quad \text{equal wave amplitudes but opposite sign} \tag{54.71b}$$

$$(\boldsymbol{k}_i - \boldsymbol{k}_r) \cdot \hat{\boldsymbol{t}} = 0 \quad \text{equal projection of wavevectors onto } \hat{\boldsymbol{t}}. \tag{54.71c}$$

The final equality means that there is an equal projection of the incident and reflected wavevectors onto the wall's tangential direction. It arises by writing the position for a point on the wall as

$$\boldsymbol{x}_{\text{wall}} = |\boldsymbol{x}_{\text{wall}}| \, \hat{\boldsymbol{t}} \Longrightarrow \boldsymbol{k}_i \cdot \hat{\boldsymbol{t}} = \boldsymbol{k}_r \cdot \hat{\boldsymbol{t}}. \tag{54.72}$$

Considering the wall to be an extreme case of a static inhomogeneous media, we can connect these relations to the ray equations in Section 50.3.6. In that discussion we found that a wave packet moving through a static but inhomogeneous media maintains a constant angular frequency along a ray, whereas the wavevector changes.

Geometry of the reflection in wavevector space

Our considerations thus far have been generic, holding for any wave packet described by a wave function such as the velocity streamfunction. To determine further details of the reflected Rossby wavevector, return to the Rossby wave dispersion diagram in Figure 54.5, depicting the reflection process in wavevector space. We only need one dispersion circle since both the incident and reflected waves have the same angular frequency, as required by the kinematic boundary condition (54.70).

To construct the dispersion diagram we start with the known incident group velocity, $\boldsymbol{c}_{gi}$, which is assumed to be directed towards the southwest. Draw the corresponding group velocity orientation vector, $\boldsymbol{R}_{gi}$, from the circle perimeter to the center, also oriented in the same southwesterly direction. From knowledge of $\boldsymbol{R}_{gi}$, draw the incident carrier wavector, $\boldsymbol{k}_i$, extending from the origin to where $\boldsymbol{R}_{gi}$ meets the perimeter. Next make use of the kinematic condition (54.72) that allows us to compute the unique reflected carrier wavevector, $\boldsymbol{k}_r$, constructed by setting $\boldsymbol{k}_r \cdot \hat{\boldsymbol{t}} = \boldsymbol{k}_i \cdot \hat{\boldsymbol{t}}$. Finally, we can now compute the reflected group velocity orientation vector, $\boldsymbol{R}_{gr}$, which points to the center of the circle from the point where $\boldsymbol{k}_r$ hits the circle perimeter. It is through this construction that we find the incident and reflected group velocities make the same angle with the wall normal:

$$\theta_i = \theta_r = \theta. \tag{54.73}$$

Reflections that satisfy this property are known as *specular*.

Features of the incident and reflected waves

Both the incident and reflected carrier wavevectors have a westward component, as required for Rossby waves. However, the southwestward orientation of the incident group velocity is reflected at the wall into a northeastward group velocity. The reflected wave packet, moving eastward, has a larger zonal wavenumber than the incident wave packet:

$$|\boldsymbol{k}_r| > |\boldsymbol{k}_i|. \tag{54.74}$$

This increase in wavenumber arises from an increase in zonal wavevector component, so that the zonal wavelength of the waves within the reflected eastward wave packet are shorter than those in the the incident wave packet. The larger wavenumber decreases the group velocity, so that the northeastward reflected packet is slower than the southwestward incident packet. In a fluid with dissipation, such as through viscosity (see Section 25.8), we expect smaller scale features to

be dissipated more readily than larger scale features. Hence, the northeastward reflected wave packet is expected to be dissipated more readily than the southwestward incident packet.

The reflection of westerly moving Rossby wave packets off a western boundary hold in their converse for the reflection at easterly packets hitting an eastern wall. Namely, a slowly moving easterly wave packet, which is comprised of short wavelength Rossby waves, is reflected off the eastern wall as a faster moving westerly packet of longer wavelength Rossby waves. These results have particular relevance to the ocean, such as through middle latitude western boundary current intensification and the El Niño / Southern Oscillation phenomena in the tropics (see *Vallis* (2017) for further discussion).

54.4.4 Further study

In addition to working through the geometry of planetary waves on a β-plane, *Longuet-Higgins* (1964) studies planetary waves on a sphere, thus making use of spherical harmonics.

54.5 Edge waves

Edge waves are vorticity fluctuations that live on the interface separating two regions of different background vorticity.[9] As vorticity waves, the edge waves of this section share many features with planetary Rossby waves studied in Section 54.3. Additionally, edge waves share features with surface waves studied in Chapter 52, in that they travel along the interface while exponentially decaying in the direction away from the interface.

54.5.1 Base state and the meridionally modulated wave ansatz

Following the decomposition (54.26) we write the relative vorticity as

$$\zeta_{\text{full}} = \zeta + \zeta_{\text{b}} \tag{54.75}$$

where ζ_{b} is a static base state vorticity and ζ the vorticity fluctuating around the base state. The absolute vorticity equation thus takes the form

$$\mathrm{D}(\zeta + \zeta_{\text{b}} + f)/\mathrm{D}t = 0, \tag{54.76}$$

in which we see that the base state vorticity, ζ_{b}, plays a role directly analogous to planetary vorticity, f. This analog allows us to transfer concepts of planetary Rossby waves from Section 54.3 directly over to the edge waves of this section.

We are concerned with a base state comprised of a meridionally dependent zonal flow and corresponding vorticity

$$\boldsymbol{u}_{\text{b}} = \hat{\boldsymbol{x}}\, u_{\text{b}}(y) \quad \text{and} \quad \zeta_{\text{b}} = \zeta_{\text{b}}(y) = -\partial_y u_{\text{b}}. \tag{54.77}$$

In particular, to generate edge waves we assume in Section 54.5.3 that the background vorticity has a jump at $y = y_0$. The vorticity equation (54.28) describing fluctuations relative to the background flow (54.77) is given by

$$\partial_t \zeta + (\boldsymbol{u} + \hat{\boldsymbol{x}}\, u_{\text{b}}) \cdot \nabla\zeta + v\,(\beta + \partial_y \zeta_{\text{b}}) = 0, \tag{54.78}$$

which, when introducing the streamfunction $\zeta = \nabla^2\psi$, leads to

$$\partial_t(\nabla^2\psi) + \hat{\boldsymbol{z}} \cdot [\nabla\psi \times \nabla(\nabla^2\psi)] + u_{\text{b}}\, \partial_x(\nabla^2\psi) + \partial_x\psi\,(\beta + \partial_y\zeta_{\text{b}}) = 0. \tag{54.79}$$

[9] *Sutherland* (2010) in his section 2.6.2 refers to edge waves as *Rayleigh waves*.

If we substitute the plane wave ansatz (54.3) into the vorticity equation (54.79), assuming the angular frequency and wavevector are spatially independent, then we are led to

$$\omega = k_x\, u_{\mathrm{b}} - \frac{k_x\,(\beta + \partial_y u_{\mathrm{b}})}{|\boldsymbol{k}|^2} \qquad \text{inconsistent equation.} \tag{54.80}$$

This equation looks like a straightforward generalization of the Rossby wave dispersion relation (54.32). However, since the background flow, $u_{\mathrm{b}}(y)$, has a meridional dependence, the plane wave assumption that ω and $\boldsymbol{k}$ are spatial constants is, in fact, flawed. We conclude that the vorticity equation (54.79) does not admit a plane wave solution when the background flow is not a constant.

For the case of a background $u_{\mathrm{b}}(y)$ that is gently varying, we can make use of the asymptotic methods from Chapter 50. However, for the edge waves considered in this section we can make progress with a somewhat simpler approach, in which we assume the streamfunction is a zonal traveling wave modulated by a meridionally dependant amplitude

$$\psi(x, y, t) = \widetilde{\psi}(y) \cos(k\,x - \omega\,t). \tag{54.81}$$

We pursue this ansatz in the following.

54.5.2 Rayleigh-Kuo equation

The plane wave properties studied in Section 54.2 do not hold for the meridionally modulated wave (54.81). Consequently, to derive a dispersion relation requires us to linearize the vorticity equation (54.79), which takes the form

$$\partial_t(\nabla^2\psi) + u_{\mathrm{b}}\,\partial_x(\nabla^2\psi) + \partial_x\psi\,(\beta + \partial_y\zeta_{\mathrm{b}}) = 0. \tag{54.82}$$

Substituting the modulated wave ansatz (54.81) into the linearized vorticity equation (54.82) gives

$$\partial_t(\nabla^2\psi) = \omega\,(-k^2 + \partial_{yy})\widetilde{\psi}\sin(k\,x - \omega\,t) \tag{54.83a}$$

$$u_{\mathrm{b}}\,\partial_x(\nabla^2\psi) = -u_{\mathrm{b}}\,k\,(-k^2 + \partial_{yy})\widetilde{\psi}\sin(k\,x - \omega\,t) \tag{54.83b}$$

$$\partial_x\psi\,(\beta + \partial_y\zeta_{\mathrm{b}}) = -k\,(\beta + \partial_y\zeta_{\mathrm{b}})\widetilde{\psi}\sin(k\,x - \omega\,t), \tag{54.83c}$$

which then leads to the *Rayleigh-Kuo* equation for the meridional wave amplitude function[10]

$$(u_{\mathrm{b}} - c)\,(\partial_{yy} - k^2)\,\widetilde{\psi} + (\beta - \partial_{yy}u_{\mathrm{b}})\,\widetilde{\psi} = 0 \quad \text{with} \quad c = \omega/k, \tag{54.84}$$

which can also be written in the form

$$\partial_y[(u_{\mathrm{b}} - c)\,\partial_y\widetilde{\psi} - \widetilde{\psi}\,\partial_y u_{\mathrm{b}}] + [\beta - k^2\,(u_{\mathrm{b}} - c)]\,\widetilde{\psi} = 0. \tag{54.85}$$

The Rayleigh-Kuo equation is fundamental to our study of barotropic shear instability in Chapter 61. For current purposes we use it to derive the dispersion relation for edge waves.

[10] Kuo extended the original Rayleigh equation to account for the β effect. In the absence of β we refer to just the *Rayleigh equation*.

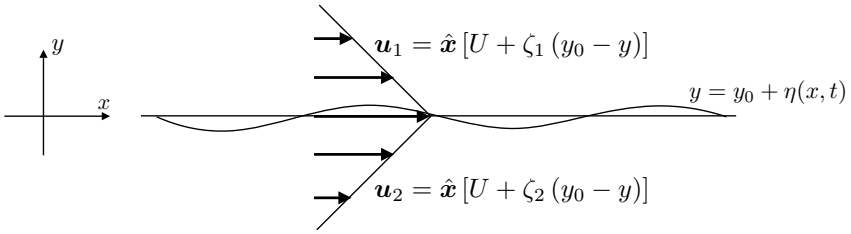

FIGURE 54.7: A zonal point jet in the horizontal x-y plane with the jet maxima at $y = y_0$. The velocity is linear on both sides of the maxima and there is a finite jump in the vorticity at the maxima. Vorticity in the upper region is given by $\zeta_1 = -\partial_y u_1$ and in the lower region $\zeta_2 = -\partial_y u_2$, with $\zeta_1 > 0$ and $\zeta_2 < 0$ depicted in this figure. Oscillations of the material interface, $y = y_0 + \eta(x,t)$, are known as *edge waves*, which exist due to the jump in the vorticity. The top half-plane is referred to as region 1 and the lower half-plane is region 2. Any surface with a finite vorticity jump supports edge waves, with the symmetric point jet shown in this figure a prototypical case.

54.5.3 The point jet

Figure 54.7 illustrates the zonal flow characterizing a *point jet*, in which there is a linear velocity profile on both sides of a maxima

$$\boldsymbol{u}_\mathrm{b} = u_\mathrm{b}(y)\,\hat{\boldsymbol{x}} \quad \text{with} \quad u_\mathrm{b}(y) = U + (y_0 - y) \begin{cases} \zeta_1 & \text{for } y > y_0 \\ \zeta_2 & \text{for } y < y_0, \end{cases} \tag{54.86}$$

where ζ_1 and ζ_2 are constants that measure the vorticity in the two half-planes

$$\zeta_\mathrm{b} = -\partial_y u_\mathrm{b} = \begin{cases} \zeta_1 & \text{for } y > y_0 \\ \zeta_2 & \text{for } y < y_0. \end{cases} \tag{54.87}$$

Because of the finite vorticity jump at $y = y_0$, the meridional derivative of the vorticity is proportional to the Dirac delta[11]

$$\partial_y \zeta_\mathrm{b}(y = y_0) = \lim_{\epsilon \to 0} \frac{\zeta_\mathrm{b}(y = y_0 + \epsilon/2) - \zeta_\mathrm{b}(y = y_0 - \epsilon/2)}{\epsilon} = (\zeta_1 - \zeta_2)\,\delta(y - y_0). \tag{54.88}$$

As a check on this expression, we take an integral across the interface to find

$$\int_{y_0-\epsilon/2}^{y_0+\epsilon/2} \partial_y \zeta_\mathrm{b}\,\mathrm{d}y = \zeta_\mathrm{b}(y_0 + \epsilon/2) - \zeta_\mathrm{b}(y_0 - \epsilon/2) = (\zeta_1 - \zeta_2) \int_{y_0-\epsilon/2}^{y_0+\epsilon/2} \delta(y - y_0)\,\mathrm{d}y. \tag{54.89}$$

Finally, note that the point yet is zonally symmetric so that the base flow only has a nonzero meridional pressure gradient

$$\nabla \varphi_\mathrm{b} = \hat{\boldsymbol{y}}\,\partial_y \varphi_\mathrm{b}. \tag{54.90}$$

We study waves traveling on the material vorticity interface at $y = y_0 + \eta(x,t)$, and written in the form

$$\eta(x,t) = \tilde{\eta} \cos(k\,x - \omega\,t). \tag{54.91}$$

To develop properties of the flow on each side of the interface requires us to develop the kinematic and dynamic boundary conditions at the interface. Furthermore, the amplitude, $\tilde{\eta}$, is assumed to be much smaller than the wavelength, thus allowing us to linearize the boundary conditions and to evaluate the conditions at $y = y_0$.[12] Note that we assume the interface undulation has the same phase as the streamfunction (54.81), and this assumption will be seen to be self-consistent.

[11] See Chapter 7 for more on the Dirac delta. In particular, note that the Dirac delta, $\delta(y)$, has dimensions of inverse length.

[12] We took the same approach for the surface gravity waves in Section 52.3.4.

54.5.4 Kinematic boundary condition at the interface

The material nature of the interface means that the meridional velocity of a fluid particle at the interface is given by[13]

$$v = \mathrm{D}\eta/\mathrm{D}t = (\partial_t + u\,\partial_x)\eta \approx (\partial_t + u_\mathrm{b}\,\partial_x)\eta, \tag{54.92}$$

where the approximation follows from linearization. This kinematic boundary condition holds on both sides of the interface so that

$$(\partial_t + u_1\,\partial_x)\eta = \partial_x\psi_1 \quad \text{and} \quad (\partial_t + u_2\,\partial_x)\eta = \partial_x\psi_2. \tag{54.93}$$

Applying this relation to the wave ansatz (54.91) for the interface, and the wave ansatz (54.81) for the streamfunction as evaluated at $y = y_0$, leads to

$$(u_1 - c)\,\tilde{\eta} = \widetilde{\psi}_1 \quad \text{and} \quad (u_2 - c)\,\tilde{\eta} = \widetilde{\psi}_2. \tag{54.94}$$

Since $u_1(y_0) = u_2(y_0) = U$, the kinematic boundary condition says that the streamfunctions match at the interface

$$\widetilde{\psi}_1 = \widetilde{\psi}_2 \quad \text{at } y = y_0. \tag{54.95}$$

54.5.5 Dynamic boundary condition at the interface

For the dynamic boundary condition we assume there is no surface tension on the interface, in which case pressure matches

$$\varphi_1 = \varphi_2 \quad \text{at } y = y_0. \tag{54.96}$$

To make use of this boundary condition, consider the zonal velocity equation (38.1) with the zonal flow decomposed as in equation (54.26)

$$\partial_t(u + u_\mathrm{b}) + (\boldsymbol{u} + \boldsymbol{u}_\mathrm{b}) \cdot \nabla(u + u_\mathrm{b}) - f\,v = -\partial_x\varphi, \tag{54.97}$$

which linearizes to

$$(\partial_t + u_\mathrm{b}\,\partial_x)\,u + v\,(\partial_y u_\mathrm{b} - f) = -\partial_x\varphi \implies (\partial_t + u_\mathrm{b}\,\partial_x)\,\partial_y\psi - \partial_x\psi\,(\partial_y u_\mathrm{b} - f) = \partial_x\varphi, \tag{54.98}$$

where we set $\partial_x\varphi_\mathrm{b} = 0$ as per the assumed zonal symmetry of the background state in equation (54.90). Consider an ansatz for the pressure in the same form as for the streamfunction

$$\varphi(x, y, t) = \widetilde{\varphi}(y)\cos(k\,x - \omega\,t), \tag{54.99}$$

which, along with the streamfunction ansatz (54.81), brings the velocity equation (54.98) to

$$[(u_\mathrm{b} - c)\,\partial_y + (f - \partial_y u_\mathrm{b})]\,\widetilde{\psi} = \widetilde{\varphi} \quad \text{at } y = y_0. \tag{54.100}$$

Invoking continuity of pressure at the interface yields

$$[(U - c)\,\partial_y + (f - \partial_y u_1)]\,\widetilde{\psi}_1 = [(U - c)\,\partial_y + (f - \partial_y u_2)]\,\widetilde{\psi}_2 \quad \text{at } y = y_0. \tag{54.101}$$

This dynamic boundary condition also follows from integrating the Rayleigh-Kuo equation (54.85) across the interface and noting that $[\beta - k^2\,(u_\mathrm{b} - c)]\,\widetilde{\psi}$ is continuous at the interface. We can further simplify the dynamic boundary condition (54.101) by making use of the kinematic

[13] Equation (54.92) is the direct analog of the kinematic boundary condition developed in Section 19.6.2 for vertical position of a material surface, $z = \eta(x, y, t)$.

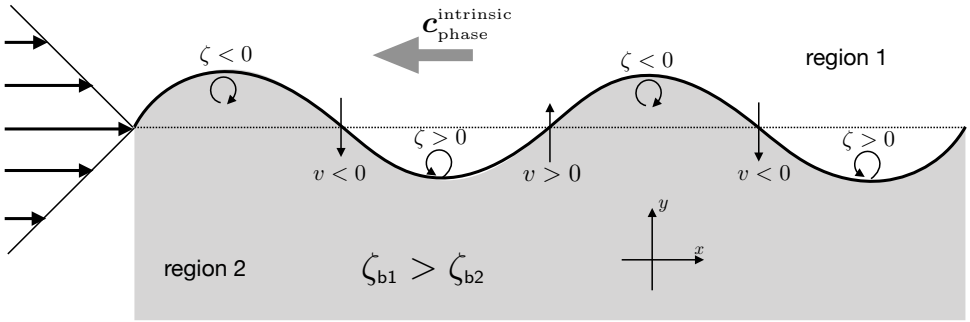

FIGURE 54.8: Depicting the *pseudo-westward* intrinsic phase propagation of an edge wave along a material surface separating two regions of vorticity. Here the larger background relative vorticity is oriented to the north, $\zeta_{b1} > \zeta_{b2}$, so that the intrinsic phase velocity for the edge wave propagates to the west. We also show the point jet velocity profile, whose relative vorticity jump supports the westward phase velocity of the edge wave. The variables, v and ζ, are the anomalies relative to the unperturbed reference state, as per the decomposition equation (54.26). The vorticity mechanism for the phase propagation is identical to that for planetary Rossby waves depicted in Figure 54.3, where the background vorticity jump from the point jet serves the same role as the planetary vorticity gradient. Consider a material line initially along $y = y_0$ and whose relative vorticity equals to that of the background point jet. A southward extension of this line leads to a local positive relative vorticity anomaly, $\zeta' > 0$, since the particle moves into a region with lower background relative vorticity. This anomaly is depicted by the counterclockwise induced secondary flow. Conversely, a northward extension leads to a local negative vorticity anomaly and associated clockwise secondary flow. The anomalous meridional motion is depicted every π radians, with maximal anomalies at wave nodes. The action of the coherent counter-rotating secondary vortices leads to westward propagation of the phase. In general, the phase moves with the higher vorticity to the right, which means that it moves from the convex side of the velocity profile towards the concave side.

boundary condition (54.95), $\widetilde{\psi}_1 = \widetilde{\psi}_2$ at $y = y_0$. Doing so eliminates the Coriolis term and yields

$$(U - c)\,(\partial_y \widetilde{\psi}_1 - \partial_y \widetilde{\psi}_2) = [\partial_y u_1 - \partial_y u_2]\,\widetilde{\psi} \quad \text{at } y = y_0. \tag{54.102}$$

54.5.6 Edge wave dispersion relation

Set $\beta = 0$ to focus on wave solutions arising just from the point jet, in which the Rayleigh-Kuo equation (54.84) simplifies to

$$(u_{\text{b}} - c)\,(\partial_{yy} - k^2)\,\widetilde{\psi} - \partial_{yy} u_{\text{b}}\,\widetilde{\psi} = 0. \tag{54.103}$$

Evaluating this equation on the two sides of the interface, and assuming the base flow is distinct from the phase velocity so that $u_{\text{b}} \neq c$, leads to

$$\widetilde{\psi} = \psi_0 \begin{cases} \mathrm{e}^{-|k|(y-y_0)} & \text{for } y > y_0 \\ \mathrm{e}^{+|k|(y-y_0)} & \text{for } y < y_0. \end{cases} \tag{54.104}$$

As anticipated, the edge wave exponentially decays away from the interface. Just like the surface waves in Chapter 52, the horizontal wave number, $|k|$, determines the exponential decay scale.

Using equation (54.104) in the dynamic boundary condition (54.102) yields the phase velocity[14]

$$c = \omega/k = U + \frac{\partial_y u_1 - \partial_y u_2}{2\,|k|} = \underbrace{U}_{\text{Doppler}} \underbrace{-\frac{(\zeta_1 - \zeta_2)}{2\,|k|}}_{\text{intrinsic}}. \tag{54.105}$$

The background zonal flow, U, provides a Doppler shift to the phase velocity. The second piece arises from the vorticity jump across the interface, and we refer to it as the *intrinsic* portion

[14]The phase of the edge wave only moves in the zonal direction, with $c > 0$ for a phase velocity in the $+\hat{\boldsymbol{x}}$ direction and $c < 0$ for a phase velocity in the $-\hat{\boldsymbol{x}}$ direction.

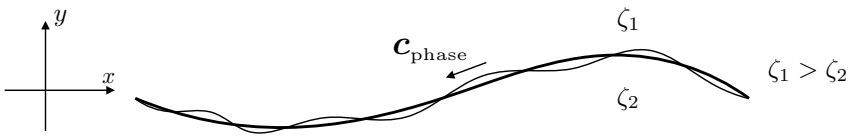

FIGURE 54.9: Edge waves moving along a jump in the background vorticity field, with the background vorticity equal to ζ_1 north of the jump and ζ_2 to the south. The phase velocity is oriented with the higher relative vorticity to the right when facing in the direction of the phase velocity.

to the phase velocity. If the vorticity increases northward, so that $\zeta_1 - \zeta_2 > 0$, then $c - U < 0$, thus signaling a westward phase velocity relative to the background flow. This behavior is precisely that found for planetary Rossby waves, thus prompting some to refer to edge waves as prototypical Rossby waves. In Figure 54.8, we summarize the vorticity mechanism for the *pseudo-westward* phase velocity, with the mechanism identical to the planetary Rossby wave in Figure 54.3. In general, the phase velocity for edge waves is directed so that the region of higher vorticity is to the right when facing in the direction of the phase velocity, with this orientation defining "pseudo-westward". This terminology is taken from the truly westward phase velocity corresponding to planetary waves, in which the larger planetary vorticity is to the north. Figure 54.9 provides a schematic for a curved vorticity jump line, whereby the edge waves propagate along the jump, again with the phase in the pseudo-westward direction.

54.5.7 Further study

A similar treatment of edge waves can be found in Section 3.12 of *Smyth and Carpenter* (2019) and Section 9.2.3 of *Vallis* (2017). As studied in Chapter 61, interactions between vorticity waves can lead to shear instabilities, with such instabilities forming a fundamental feature of unstable and turbulent geophysical flows.

54.6 Exercises

EXERCISE 54.1: ROSSBY WAVES IN A ZONAL CHANNEL

In Section 54.3 we examined the physics of Rossby waves on an unbounded β-plane. Here we consider a zonal channel on a β-plane, with the channel unbounded in the zonal direction but bounded meridionally. The meridional domain is given by $y_{\text{s}} \leq y \leq y_{\text{n}}$ where $y_{\text{n}} - y_{\text{s}} = L$, and with rigid material walls at the meridional boundaries. Everything else is just as in Section 54.3, with a zonal and constant base flow, $\boldsymbol{u}_{\text{b}} = U\,\hat{\boldsymbol{x}}$.

(a) Write a single plane wave mode that travels in the zonal direction but is standing in the meridional direction. Hint: the plane wave ansatz (54.6) should be modified so that $\hat{\boldsymbol{n}} \cdot (\hat{\boldsymbol{z}} \times \nabla\psi) = 0$ at the northern and southern walls. The boundary condition imposes a constraint on the meridional wavenumber. What is the constraint?

(b) What is the dispersion relation for the Rossby waves in this channel?

Hint: recall our study of standing gravity wave modes in Section 52.8, with such modes occuring when waves live in a bounded domain and thus can no longer travel freely. Instead, the wave modes must fit inside of the domain in a manner that satisfies the boundary conditions. We can think of such standing wave modes as a superposition of two oppositely traveling waves with the same frequency and wavenumber that are locked in-phase in a manner that satisfies

the boundary conditions. For example, the sum of a right and left moving wave with equal amplitude, wavenumber, and frequency is given by the standing pattern

$$A\cos(k\,x-\omega\,t)+A\cos(-k\,x-\omega\,t)=2\,A\cos(\omega\,t)\cos(k\,x). \tag{54.106}$$

EXERCISE 54.2: VORTEX MECHANISM FOR EDGE WAVES

Provide a sketch like Figure 54.8 but for edge waves in the case with $\zeta_1 < \zeta_2$. Hint: be sure to orient the wave so that it moves from the convex side of the velocity profile towards the concave side.

Chapter 55

SHALLOW WATER WAVES

In this chapter we develop the basic theory for waves appearing in the shallow water fluid. In the literature these waves are sometimes referred to as *long waves* since the shallow water approximation applies when the horizontal length scale is much larger than the vertical, in which case the horizontal wavelength is larger than the fluid depth. Our presentation focuses on the case of a single shallow water layer, but we offer brief discussions of two-layer cases to illustrate the generalizations to multiple layers. Notably, the algebraic tedium increases greatly when adding layers. Hence, for theoretical analysis concerned with the role of stratification, it is typically more fruitful to move to the continuous vertical stratification in Chapter 57, rather than study waves in more than two stacked shallow water layers.

We first consider general features of both the nonlinear and then the linear shallow water equations. For the linearized system, we develop a unified wave equation for the free surface. The derivation of this equation is rather detailed and the resulting linear equation somewhat complicated. Even so, it serves to unify across the full suite of linear shallow water waves on a rotating β-plane, and offers insights into both the methods used to derive wave equations and the scalings used to extract their core physical features. In unpacking this wave equation we pursue a focused study of gravity waves, inertia-gravity waves, and Rossby waves. We also consider the case of a Kelvin wave, which relies on a boundary in the presence of the Coriolis parameter.

READER'S GUIDE TO THIS CHAPTER

This chapter builds from the shallow water studies in Chapters 35 and 36, as well as other waves chapters in this part of the book. In Chapter 56 we extend the study of shallow water waves by considering a variety of case studies. The first half of this video offers a pedagogical introduction to non-rotating shallow water waves.

55.1 Loose threads

- Equatorial waves
- Energetics of Rossby waves as per Section 6.6 of *Vallis* (2017).

55.2 Shallow water equations

The shallow water equations of motion are given by the velocity equation (35.12) and thickness equation (35.19), written here in their Eulerian form and with zero atmospheric pressure

$$\partial_t \boldsymbol{u} + (\boldsymbol{u} \cdot \nabla)\, \boldsymbol{u} + f\, \hat{\boldsymbol{z}} \times \boldsymbol{u} = -g\, \nabla \eta \tag{55.1a}$$

$$\partial_t h + \nabla \cdot (h\, \boldsymbol{u}) = 0. \tag{55.1b}$$

In Section 55.3 we linearize these shallow water equations and study their properties in anticipation of later study of their wave fluctuations. Before doing so, however, we formulate a wave-like equation that holds for the nonlinear shallow water model. Doing so anticipates certain features of the linear equations while offering yet another view of the shallow water system beyond that provided in Chapters 35 and 36. We pursued the analogous manipulations for acoustic waves in Section 51.4.1.

55.2.1 Nonlinear wave equation

Consider the shallow water equations written using the material time derivative

$$\mathrm{D}\boldsymbol{u}/\mathrm{D}t + f\,\hat{\boldsymbol{z}} \times \boldsymbol{u} = -g\,\nabla\eta \quad \text{and} \quad \mathrm{D}h/\mathrm{D}t = -h\,\nabla\cdot\boldsymbol{u}. \tag{55.2}$$

Taking the material time derivative of the thickness equation, and then using the velocity equation, yields

$$\begin{aligned}
\frac{\mathrm{D}}{\mathrm{D}t}\left[\frac{1}{h}\frac{\mathrm{D}h}{\mathrm{D}t}\right] &= -\frac{\mathrm{D}(\nabla\cdot\boldsymbol{u})}{\mathrm{D}t} && \text{(55.3a)}\\
&= -\nabla\cdot\frac{\mathrm{D}\boldsymbol{u}}{\mathrm{D}t} + \partial_m u^n\,\partial_n u^m && \text{(55.3b)}\\
&= -\nabla\cdot(-f\,\hat{\boldsymbol{z}} \times \boldsymbol{u} - g\,\nabla\eta) + \boldsymbol{S}^m{}_n\,\boldsymbol{S}^n{}_m - \boldsymbol{R}^m{}_n\,\boldsymbol{R}^n{}_m, && \text{(55.3c)}
\end{aligned}$$

where $\boldsymbol{S}$ is the strain rate tensor and $\boldsymbol{R}$ is the rotation tensor (both are discussed in Section 18.8). Rearrangement then leads to

$$\frac{\mathrm{D}}{\mathrm{D}t}\left[\frac{1}{h}\frac{\mathrm{D}h}{\mathrm{D}t}\right] - g\,\nabla^2\eta = \nabla\cdot(f\,\hat{\boldsymbol{z}}\times\boldsymbol{u}) + \boldsymbol{S}^m{}_n\,\boldsymbol{S}^n{}_m - \boldsymbol{R}^m{}_n\,\boldsymbol{R}^n{}_m, \tag{55.4}$$

which corresponds to equation (51.19) holding for the compressible fluid. We interpret this equation as a generalized wave equation holding for movement following a shallow water fluid column. The second order material time operator acts on the thickness to propagate signals relative to the moving fluid. The linear terms, $g\,\nabla^2\eta$ and $\nabla\cdot(f\,\hat{\boldsymbol{z}}\times\boldsymbol{u})$, also appear in the linearized equations and will be discussed later, whereas $\boldsymbol{S}^m{}_n\,\boldsymbol{S}^n{}_m - \boldsymbol{R}^m{}_n\,\boldsymbol{R}^n{}_m$ is a nonlinear source arising from gradients in the fluid velocity. We drop the nonlinear source when working with the linearized equations, and likewise the material time derivative becomes a local time derivative.

55.2.2 Another form of the nonlinear wave equation

To align more closely with the linear wave equation derived in Section (55.3), we consider again the velocity and thickness equations in the form of equation (55.2) yet first determine the evolution equation for the divergence of the thickness flux. For this purpose, multiply the thickness equation by the velocity and the velocity equation by the thickness, and then add to find

$$\mathrm{D}(h\,\boldsymbol{u})/\mathrm{D}t = -f\,h\,\hat{\boldsymbol{z}}\times\boldsymbol{u} - g\,h\,\nabla\eta - (h\,\boldsymbol{u})\,\nabla\cdot\boldsymbol{u}. \tag{55.5}$$

Divergence of the left hand side of this equation is given by

$$\nabla\cdot[\mathrm{D}(h\,\boldsymbol{u})/\mathrm{D}t] = \mathrm{D}[\nabla\cdot(h\,\boldsymbol{u})]/\mathrm{D}t + (\partial_m\boldsymbol{u})\cdot\nabla(h\,u^m) = -\mathrm{D}(\partial_t h)/\mathrm{D}t + (\partial_m\boldsymbol{u})\cdot\nabla(h\,u^m), \tag{55.6}$$

where we used the thickness equation for the final equality. Combining with the divergence of the right hand side of equation (55.5) yields

$$-\mathrm{D}(\partial_t h)/\mathrm{D}t + \partial_m\boldsymbol{u}\cdot\nabla(h\,u^m) = -\nabla\cdot(f\,h\,\hat{\boldsymbol{z}}\times\boldsymbol{u}) - \nabla\cdot(g\,h\,\nabla\eta) - \nabla\cdot(h\,\boldsymbol{u}\,\nabla\cdot\boldsymbol{u}), \tag{55.7}$$

with rearrangement leading to the nonlinear wave equation

$$\frac{\mathrm{D}}{\mathrm{D}t}\frac{\partial \eta}{\partial t} - \nabla \cdot (g\, h\, \nabla \eta) = \nabla \cdot (f\, h\, \hat{\boldsymbol{z}} \times \boldsymbol{u}) + \partial_m \boldsymbol{u} \cdot \nabla (h\, u^m) + \nabla \cdot (h\, \boldsymbol{u}\, \nabla \cdot \boldsymbol{u}), \tag{55.8}$$

where we noted that $\partial_t h = \partial_t \eta$. This nonlinear equation corresponds directly to the linear wave equation (55.31) derived below. It is this alternative form that readily offers a direct decomposition of the various waves appearing in the shallow water fluid. Namely, in the linear equations we drop the nonlinear sources on the the right hand side, and convert the material time derivative to the local Eulerian time derivative.

55.2.3 Comments

This section stopped short of pursuing an analysis of nonlinear wave solutions. However, as in the analogous discussion of the compressible fluid in Section 51.4.1, these manipulations signal that wave-like equations are not restricted to linearized equations. Rather, they are basic to the nonlinear equations, though with a more complex mathematical structure that generally requires numerical or asymptotic methods to penetrate.

For the remainder of this chapter we focus on the linearized set of equations, thus enabling the use of linear analysis methods. Even though much simpler than the nonlinear equations, we uncover a rich and complex variety of linear wave phenomena within the shallow water model.

55.3 Linearized shallow water equations

In this section we linearize the shallow water velocity equation (55.1a) and thickness equation (55.1b) in a manner that supports subsequent analysis of small amplitude fluctuations. In the process we derive a linear wave equation for free surface undulations, with a number of source terms that support the variety of waves studied in later sections. This wave equation is the linearized version of the nonlinear shallow water equation (55.8).

55.3.1 Linearized thickness and velocity equations

We linearize the equations around a base state that is at rest and thus with a flat free surface. Referring to Figure 35.1 leads to the expressions for the layer thickness

$$h(x,y,t) = [\overline{\eta} + \eta'(x,y,t)] - [\overline{\eta_{\mathrm{b}}} + \eta'_{\mathrm{b}}(x,y)] = H + \eta'(x,y,t) - \eta'_{\mathrm{b}}(x,y), \tag{55.9}$$

along with the corresponding velocity

$$\boldsymbol{u}(x,y,t) = 0 + \boldsymbol{u}'(x,y,t). \tag{55.10}$$

The terms $\overline{\eta}$ and $\overline{\eta_{\mathrm{b}}}$ are area means for the free surface and bottom topography, whereas η' and η'_{b} are deviations from these means. We assume there are no boundary sources of volume so that $\overline{\eta}$ is constant in time. The prime on the velocity in equation (55.10) acts as a reminder that it is driven by gradients in the fluctuating free surface, η'.

We make the following assumptions about the terms comprising the layer thickness.

- The layer thickness is everywhere positive, $h > 0$, thus ensuring there is water at each point in the layer at each time. We make this assumption since a vanishing layer thickness represents a nontrivial change in the domain that requires the full nonlinear equations.
- A nonzero η'_{b} allows for local variations in the bottom topography. We assume these

variations are bounded by the mean thickness,

$$H_r \equiv H - \eta'_b > 0, \tag{55.11}$$

thus ensuring the resting thickness, H_r, is nonzero everywhere. This assumption does not place strong constraints on η'_b. In particular, we do not generally assume η'_b is small beyond assuming that $H_r > 0$. However, we do assume that η'_b is small when studying the quasi-geostrophic motion associated with Rossby waves in Sections 55.9.

- We assume the free surface undulations are much smaller than the resting thickness

$$|\eta'| \ll H_r. \tag{55.12}$$

This is the key assumption in the linearization process. It follows from our interest in studying linear wave fluctuations of the free surface.

The above assumptions lead to the linearized version of the thickness equation (55.1b)

$$\partial_t \eta' + \nabla \cdot (H_r \, \boldsymbol{u}') = 0. \tag{55.13}$$

This equation says that a time tendency of the free surface is driven by the convergence of a thickness flux, where the thickness is approximated by its resting value

$$h = H + \eta' - \eta'_b \approx H - \eta'_b = H_r. \tag{55.14}$$

We conclude from equation (55.13) that free surface transients (i.e., waves) require a nonzero horizontal convergence, $-\nabla \cdot (H_r \, \boldsymbol{u}') \neq 0$. It follows that waves in a flat bottom domain arise only when there is a nonzero convergence in the horizontal flow, $-\nabla \cdot \boldsymbol{u}' \neq 0$. Such horizontal convergences are fundamental to the shallow water fluid, and provide the key distinction from waves appearing in the horizontally non-divergent barotropic fluid from Chapter 54.

The linearized version of the shallow water velocity equation (55.1a) is

$$\partial_t \boldsymbol{u}' + f \, \hat{\boldsymbol{z}} \times \boldsymbol{u}' = -g \, \nabla \eta', \tag{55.15}$$

which is reached by dropping the nonlinear advection, $(\boldsymbol{u}' \cdot \nabla)\boldsymbol{u}'$. Advection is indeed smaller than the other terms since velocity tendencies are driven by the assumed small amplitude fluctuations in the free surface, thus making $(\boldsymbol{u}' \cdot \nabla)\boldsymbol{u}'$ second order in small terms.

55.3.2 Energetics

We studied energetics of a single layer of shallow water fluid in Section 36.5. We here summarize how the energetics appear for the linearized thickness equation (55.13) and velocity equation (55.15). As per the norm with energetics of linearized systems (e.g., see the study of acoustic energy in Section 51.6 and surface waves in Section 52.4), we work to second order accuracy in fluctuating fields.

The gravitational potential energy per horizontal area is given by

$$\mathcal{P}^{\text{sw}} = g \, \rho \int_{\eta_b}^{\eta} z \, \mathrm{d}z = (g \, \rho / 2) \, (\eta^2 - \eta_b^2), \tag{55.16}$$

and its time tendency is

$$\partial_t \mathcal{P}^{\text{sw}} = g \, \rho \, (\overline{\eta} + \eta') \, \partial_t \eta' \approx -g \, \rho \, (\overline{\eta} + \eta') \, \nabla \cdot (H_r \, \boldsymbol{u}'). \tag{55.17}$$

Likewise, the kinetic energy per area is

$$\mathcal{K}^{\text{sw}} = \frac{\rho}{2} \int_{\eta_{\text{b}}}^{\eta} \boldsymbol{u} \cdot \boldsymbol{u} \, \mathrm{d}z = (\rho/2) \, h \, \boldsymbol{u}' \cdot \boldsymbol{u}' \approx (\rho/2) \, H_{\text{r}} \, \boldsymbol{u}' \cdot \boldsymbol{u}', \tag{55.18}$$

and its time tendency is

$$\partial_t \mathcal{K}^{\text{sw}} = \rho \, H_{\text{r}} \, \boldsymbol{u}' \cdot \partial_t \boldsymbol{u}' = -g \, \rho \, H_{\text{r}} \, \boldsymbol{u}' \cdot \nabla \eta' = -g \, \rho \, H_{\text{r}} \, \boldsymbol{u}' \cdot \nabla(\overline{\eta} + \eta'). \tag{55.19}$$

The time tendency for the mechanical energy is thus given by

$$\partial_t (\mathcal{K}^{\text{sw}} + \mathcal{P}^{\text{sw}}) = -g \, \rho \, \nabla \cdot [H_{\text{r}} \, (\overline{\eta} + \eta') \, \boldsymbol{u}']. \tag{55.20}$$

This equation is a linearized version of the mechanical energy equation (36.119). Here, we only have the transfer of energy due to the advection of pressure, whereas the nonlinear equations also have the advection of kinetic energy and potential energy.

55.3.3 Potential vorticity

The shallow water potential vorticity (Section 39.3) is given by

$$Q = \frac{f + \zeta}{h} = \frac{f + \zeta}{H - \eta'_{\text{b}} + \eta'} \approx Q' \tag{55.21}$$

where, to first order in primed quantities,

$$Q' = \frac{f + \zeta'}{H_{\text{r}}} - \frac{f \, \eta'}{H_{\text{r}}^2} \approx \frac{f}{H} + \frac{H \, \zeta' + f \, (\eta'_{\text{b}} - \eta')}{H^2}, \tag{55.22}$$

with the approximation following from assuming $|\eta'| \ll H_{\text{r}} = H - \eta'_{\text{b}} \approx H$. That is, we assume both small amplitude free surface fluctuations, and small amplitude bottom topography variations. Note that for the f-plane, the f/H term can be dropped since it is a constant. Use of the linearized thickness equation (55.13) and linearized velocity equation (55.15), yields the time tendency for the linearized potential vorticity (see Exercise 55.1)

$$\partial_t Q' + \boldsymbol{u}' \cdot \nabla (f / H_{\text{r}}) = 0. \tag{55.23}$$

For a flat bottom f-plane domain, the linearized potential vorticity remains static at each point in the fluid, $\partial_t Q' = 0$. In contrast, nonzero gradients in f or H_{r} cause the linearized potential vorticity to be modified through advection of f/H_{r}, with f/H_{r} the potential vorticity of the background rest state. Hence, if f and/or H_{r} are spatially varying, solutions to the linear equations, including waves, have an evolving potential vorticity.

55.3.4 Traveling plane wave ansatz and $\nabla \cdot \boldsymbol{v} = 0$

To derive the dispersion relation for the various shallow water waves, we consider the traveling plane wave ansatz from Section 49.5, here written in the form

$$(u', v', \eta') = (\tilde{u}, \tilde{v}, \tilde{\eta}) \, \mathrm{e}^{\mathrm{i}(\boldsymbol{k} \cdot \boldsymbol{x} - \omega \, t)}, \tag{55.24}$$

where the real part of the right hand side is assumed. The amplitudes $(\tilde{u}, \tilde{v}, \tilde{\eta})$ are generally complex numbers that are independent of space and time. Recall from Section 35.2 that the horizontal velocity has no depth dependence in the shallow water layer, which follows from making the hydrostatic approximation in the homogeneous fluid layer. Hence, a plane wave solution to the shallow water wave equations must have a zero vertical component to the

wavevector, $k_z = 0$, so that

$$\boldsymbol{k} = \hat{\boldsymbol{x}}\, k_x + \hat{\boldsymbol{y}}\, k_y. \tag{55.25}$$

Evidently, the phase of shallow water plane waves (55.24) travels horizontally within a layer.

As a layer with a constant density, the fluid in the shallow water layer is incompressible so that $\nabla \cdot \boldsymbol{v} = 0$. For plane waves moving in three-dimensions, this non-divergence constraint means that the velocity of the plane waves satisfies, $\boldsymbol{k} \cdot \boldsymbol{u} + k_z\, w = 0$, (e.g., see our study of inertial waves in Chapter 53). However, for the shallow water system we saw above that $k_z = 0$, which would then seem to imply that $\boldsymbol{k} \cdot \boldsymbol{u} = 0$. Yet shallow water waves do *not* satisfy $\boldsymbol{k} \cdot \boldsymbol{u} = 0$ since they are horizontally divergent.

The resolution of this quandary concerns the vertical velocity in a shallow water layer. Namely, the vertical velocity component is diagnosed via the horizontal convergence, $\partial_z w = -\nabla \cdot \boldsymbol{u}$. The depth independence of the horizontal velocity leads to a linear depth-dependence of the vertical velocity component (equation (35.39))

$$\nabla \cdot \boldsymbol{u} + \partial_z w = 0 \Longrightarrow w(z) = w(\eta_\mathsf{b}) - (z - \eta_\mathsf{b})\, \nabla \cdot \boldsymbol{u}, \tag{55.26}$$

which for the plane wave (55.24) leads to

$$w(z) = w(\eta_\mathsf{b}) - \mathrm{i}\, (z - \eta_\mathsf{b})\, \boldsymbol{k} \cdot \tilde{\boldsymbol{u}}\, \mathrm{e}^{\mathrm{i}(\boldsymbol{k}\cdot\boldsymbol{x} - \omega\, t)}. \tag{55.27}$$

The factor of $\mathrm{i} = \sqrt{-1}$ out front means that the vertical velocity component is $\pi/2$ out of phase with the horizontal velocity. Also note that $|z - \eta_\mathsf{b}|\, |\boldsymbol{k}| \leq H\, |\boldsymbol{k}|$. Since $H\, |\boldsymbol{k}| \ll 1$ for shallow water flow, we see that the vertical velocity component has a much smaller magnitude than the horizontal velocity.

55.4 Unified shallow water wave equation

In this section we combine the linearized thickness equation (55.13) and linearized velocity equation (55.15) to render a unified wave equation for the free surface.[1] We start by closely following the steps taken for the nonlinear wave equation in Section 55.2.2. Yet we go much further for the purpose of obtaining a linear equation with the free surface as the only prognostic field. Although the unified wave equation is rather tedious, it does serve to unify the variety of waves supported by the rotating shallow water system. Once deriving this wave equation (equation (55.42)), we study its scaling for high frequency ($\omega^2 > f^2$; super-inertial) and low frequency ($\omega^2 < f^2$; sub-inertial) wave motion. That discussion anticipates analysis pursued in more depth in the remaining sections of this chaper.

55.4.1 Use of the divergence equation

We start by forming an equation for the evolution of the divergence of $H_\mathrm{r}\, \boldsymbol{u}'$, which is found by multiplying the linearized velocity equation (55.15) by H_r and then taking the divergence

$$\partial_t [\nabla \cdot (H_\mathrm{r}\, \boldsymbol{u}')] + \nabla \cdot (\hat{\boldsymbol{z}} \times f\, H_\mathrm{r}\, \boldsymbol{u}') = -\nabla \cdot (g\, H_\mathrm{r}\, \nabla \eta'), \tag{55.28}$$

where the divergence and time derivative commute. The thickness equation (55.13) can be used to eliminate the divergence, in which case we are led to

$$\partial_{tt} \eta' - \nabla \cdot (g\, H_\mathrm{r}\, \nabla \eta') = -\hat{\boldsymbol{z}} \cdot [\nabla \times (f\, H_\mathrm{r}\, \boldsymbol{u}')]. \tag{55.29}$$

[1] Many of the manipulations in this section follow Lecture 14 of *Pedlosky* (2003).

where we made use of the identity

$$\nabla \cdot (\hat{\boldsymbol{z}} \times f\, H_r\, \boldsymbol{u}') = -\hat{\boldsymbol{z}} \cdot [\nabla \times (f\, H_r\, \boldsymbol{u}')]. \tag{55.30}$$

The wave equation (55.29) is the linear analog of the nonlinear equation (55.8). We can expand the cross product on the right hand side to identify the variety of physical processes supporting shallow water waves

$$\partial_{tt}\eta' = \underbrace{\nabla \cdot (g\, H_r\, \nabla \eta')}_{\text{gravity waves}} \; \underbrace{-\hat{\boldsymbol{z}} \cdot (f\, H_r\, \nabla \times \boldsymbol{u}')}_{\text{inertial waves}} \; \underbrace{-\hat{\boldsymbol{z}} \cdot (H_r\, \nabla f \times \boldsymbol{u}')}_{\text{planetary Rossby waves}} \; \underbrace{-\hat{\boldsymbol{z}} \cdot (f\, \nabla H_r \times \boldsymbol{u}')}_{\text{topographic Rossby waves}}. \tag{55.31}$$

Although suggestive, it is useful to further manipulate this equation into one that involves a single prognostic field, here chosen to be the free surface. In so doing we provide a unified discussion of the dispersion relation for the various waves admitted by the shallow water model, and allow for a seamless decomposition of these motions in terms of space and time scales. We pursue the somewhat tedious manipulations in Section 55.4.2, but only after considering a heuristic discussion of the physical processes in equation (55.31).

Non-rotating gravity waves

Without rotation ($f = 0$) yet with gravity ($g \neq 0$), equation (55.31) reduces to the shallow water gravity wave equation

$$\partial_{tt}\eta' - \nabla \cdot (g\, H_r\, \nabla \eta') = 0. \tag{55.32}$$

With a flat bottom, these waves are non-dispersive plane gravity waves, whereas the case with a gently sloping bottom requires the WKBJ method developed in Section 51.9. These waves are sometimes referred to as *long gravity waves*, in contrast to the shorter waves that occur in deep water (see Section 52.6). We study shallow water gravity waves in Section 55.5.

Inertia-gravity waves

The wave equation

$$\partial_{tt}\eta' - \nabla \cdot (g\, H_r\, \nabla \eta') = -f\, H_r\, \zeta' \tag{55.33}$$

describes dispersive inertia-gravity waves in a shallow water layer. The inertial portion of the waves rely on both rotation ($f \neq 0$) and vorticity ($\zeta' \neq 0$). In Chapter 53 we studied inertial waves in a homogeneous fluid. The key difference here is that the shallow water fluid is hydrostatic, which, as we will see, alters the dispersion relation relative to that derived for the non-hydrostatic homogeneous fluid in Chapter 53. It furthermore motivates us to examine inertial waves along with gravity waves since a hydrostatic fluid only arises in a gravity field. Such *inertia-gravity* or *Poincaré waves*, as they appear in the shallow water fluid, are the topic of Section 55.8

Planetary and topographic Rossby waves

The remaining two terms on the right hand side of equation (55.31) lead to waves supported by a background vorticity gradient. The *planetary Rossby waves* rely on a nonzero planetary vorticity gradient (i.e., the β effect), whereas *topographic Rossby waves* rely on a nonzero gradient in the bottom topography. Both of these waves are dispersive, and both have frequencies lower than inertia-gravity waves. As shown in Section 55.4.6, and as already detailed for the horizontally non-divergent barotropic model in Section 54.3, the wave equation for Rossby waves has just a single time derivative acting on the free surface. This situation contrasts to the two time derivatives found for inertia-gravity waves and currently appearing in equation (55.31). Although

shallow water Rossby waves rely on a nonzero $\nabla(H_r f) \times \boldsymbol{u}'$, we postpone writing their wave equation until working through some more technical details.

In Chapter 54 we studied many properties of Rossby waves in the horizontally non-divergent barotropic fluid, with these waves also relying on a gradient in the background (potential) vorticity. It is thus not surprising that shallow water Rossby waves share key physical properties with Rossby waves in the non-divergent barotropic flow. We require more technical steps to extract the physics within the shallow water model, and to expose their key distinction from Rossby waves in the horizontally non-divergent barotropic model. Note also that the shallow water model supports topographic Rossby waves. In contrast, no such waves appear in the horizontally non-divergent barotropic model, since that flow is restricted to strictly move along constant depth contours, with no cross isobath motion.

55.4.2 Use of the vorticity equation

We now return to the wave equation (55.31) and perform some further manipulations in a quest to derive an equation that only has the free surface along with geophysical parameters. Start by writing the divergence equation (55.29) in its form that extracts the β term

$$\partial_{tt}\eta' - \nabla \cdot (g\, H_r\, \nabla\eta') = -f\, \hat{\boldsymbol{z}} \cdot [\nabla \times (H_r\, \boldsymbol{u}')] + \beta\, H_r\, u. \tag{55.34}$$

Next work with $\hat{\boldsymbol{z}} \cdot [\nabla \times (H_r\, \boldsymbol{u}')]$, which is the vorticity of the thickness (resting thickness) weighted velocity. To compute its time evolution, multiply the velocity equation (55.15) by H_r and take the curl

$$\begin{aligned} \nabla \times \partial_t(H_r\, \boldsymbol{u}') &= -\nabla \times (\hat{\boldsymbol{z}} \times f\, H_r\, \boldsymbol{u}') - g\, \nabla H_r \times \nabla\eta' && \text{(55.35a)} \\ &= -\hat{\boldsymbol{z}}\, [\nabla \cdot (f\, H_r\, \boldsymbol{u})] - g\, \nabla H_r \times \nabla\eta', && \text{(55.35b)} \end{aligned}$$

where the second equality made use of the identity

$$\nabla \times (\hat{\boldsymbol{z}} \times f\, H_r\, \boldsymbol{u}') = \hat{\boldsymbol{z}}\, [\nabla \cdot (f\, H_r\, \boldsymbol{u})]. \tag{55.36}$$

Now take the time derivative of the divergence equation (55.34) and use the vorticity equation (55.35b) to find

$$\begin{aligned} \partial_t\, [\partial_{tt}\eta' - \nabla \cdot (g\, H_r\, \nabla\eta')] &= -f\, \hat{\boldsymbol{z}} \cdot [\nabla \times \partial_t(H_r\, \boldsymbol{u}')] + \beta\, H_r\, \partial_t u' && \text{(55.37a)} \\ &= f\, \nabla \cdot (f\, H_r\, \boldsymbol{u}) + f\, g\, \hat{\boldsymbol{z}} \cdot (\nabla H_r \times \nabla\eta') + \beta\, H_r\, \partial_t u' && \text{(55.37b)} \\ &= -f^2\, \partial_t\eta' + f\, g\, \hat{\boldsymbol{z}} \cdot (\nabla H_r \times \nabla\eta') + \beta\, H_r\, (f\, v' + \partial_t u'). && \text{(55.37c)} \end{aligned}$$

Rearrangement leads to

$$\partial_t\, [\mathcal{L}(\eta') - \nabla \cdot (g\, H_r\, \nabla\eta')] = f\, g\, \hat{\boldsymbol{z}} \cdot (\nabla H_r \times \nabla\eta') + \beta\, H_r\, (f\, v' + \partial_t u'), \tag{55.38}$$

where we introduced the linear time operator as a shorthand

$$\mathcal{L} = \partial_{tt} + f^2. \tag{55.39}$$

This operator commutes with time derivatives but commutes with space derivatives only for the f-plane. For the case of $\beta = 0$, equation (55.38) only has the free surface height as a prognostic field. Hence, this equation is suited to developing the dispersion relation for gravity waves and inertial waves. Yet, as we show in the following, we need more work for sub-inertial Rossby waves.

55.4.3 The unified wave equation just with η'

The final step is to eliminate the term $f\,v' + \partial_t u'$ from equation (55.38) in favor of terms proportional to the free surface. The key step is to make use of the following identities derived in Exercise 55.2

$$\mathcal{L}(u') = -g\,(\partial_{xt}\eta' + f\,\partial_y\eta') \quad \text{and} \quad \mathcal{L}(v') = -g\,(\partial_{yt}\eta' - f\,\partial_x\eta'). \tag{55.40}$$

Acting with $\mathcal{L}$ on equation (55.38), and using the identities (55.40), yield

$$\partial_t\big[\mathcal{L}[\mathcal{L}(\eta') - \nabla\cdot(g\,H_r\,\nabla\eta')]\big] = f\,g\,\hat{\boldsymbol{z}}\cdot[\nabla H_r\times\nabla\mathcal{L}(\eta')] + \beta\,H_r\,f\,\mathcal{L}(v') + \beta\,H_r\,\partial_t\mathcal{L}(u'). \tag{55.41}$$

Expanding the linear operator and rearranging leads to the desired unified equation

$$\partial_t\big[\mathcal{L}[\mathcal{L}(\eta')-\nabla\cdot(g\,H_r\,\nabla\eta')]\big] = f\,g\,\hat{\boldsymbol{z}}\cdot[\nabla H_r\times\nabla\mathcal{L}(\eta')]+g\,\beta\,H_r\,(f^2\,\partial_x\eta'-2\,f\,\partial_{yt}\eta'-\partial_{xtt}\eta'). \tag{55.42}$$

As shown in the following sections, this linear partial differential equation encapsulates the full suite of linear wave processes active in a shallow water layer on a β-plane with topography. However, it is not so simple to parse in its current form, thus motivating the examination of limiting forms of this equation. In particular, we consider super-inertial waves ($\omega^2 > f^2$) versus sub-inertial waves ($\omega^2 < f^2$). In both cases we assume horizontal length scales according to the β-plane, along with small fluctuations of the topography.

55.4.4 Scaling for the β-plane with small topography

To help analyze the super-inertial and sub-interial wave motions contained in equation (55.42), introduce the following length and time scales of the motions

$$L = \text{horizontal scale} \quad \text{and} \quad \omega = \text{angular frequency}. \tag{55.43}$$

We work under the assumptions of a β-plane approximation (see equation (24.50)) so that the horizontal scales of motion satisfy

$$\beta\,L \ll |f_o|, \tag{55.44}$$

where we wrote the Coriolis parameter as $f = f_o + \beta\,y$. We also assume the topography undulation, η'_b, is much smaller than the mean layer thickness,

$$\eta'_b \ll H. \tag{55.45}$$

Both approximations (55.44) and (55.45) are familiar from the development of quasi-geostrophy theory in Section 43.5.1. Finally, assume $f > 0$ as per the northern hemisphere, with occurances of f changed to $|f|$ for southern hemisphere results.

Introducing the above scales into the wave equation (55.42) leads to

$$\partial_t\mathcal{L}^2(\eta') \sim \omega\,(\omega^2 + f^2)^2\,\eta' \tag{55.46a}$$

$$\partial_t\mathcal{L}[\nabla\cdot(g\,H_r\,\nabla\eta')] \sim \omega\,(\omega^2 + f^2)\,(g\,H_r/L^2)\,\eta' \tag{55.46b}$$

$$f\,g\,\nabla H_r\times\nabla\mathcal{L}(\eta') \sim (f\,g\,\eta'_b/L^2)\,(\omega^2 + f^2)\,\eta' \tag{55.46c}$$

$$g\,\beta\,H_r\,f^2\,\partial_x\eta' \sim (g\,\beta\,H_r\,f^2/L)\,\eta' \tag{55.46d}$$

$$-2\,\beta\,g\,H_r\,f\,\partial_{yt}\eta' \sim (\beta\,g\,H_r\,f\,\omega/L)\,\eta' \tag{55.46e}$$

$$\beta\,g\,H_r\,\partial_{xtt}\eta' \sim \beta\,g\,H_r\,(\omega^2/L)\,\eta'. \tag{55.46f}$$

Next, we separately examine the super-inertial regime, $\omega^2 > f^2$, and the sub-inertial regime, $\omega^2 < f^2$.

55.4.5 Super-inertial wave equation

In this subsection we derive an approximate wave equation relevant for super-inertial motions ($\omega^2 > f^2$).

Super-inertial scaling for the LHS of equation (55.42)

From equations (55.46a) and (55.46b), the two terms on the left hand side of the wave equation (55.42) scale as

$$\text{LHS} = \partial_t \mathcal{L}^2(\eta') - \partial_t \mathcal{L}[\nabla \cdot (g\, H_r\, \nabla \eta')] \sim \omega^3 \left[\omega^2 + g\, H_r / L^2\right] \eta'. \tag{55.47}$$

Assuming the horizontal length scale is given by the inverse wavenumber, $L = |\boldsymbol{k}|^{-1}$, yields

$$g\, H_r / L^2 \approx c_{\text{grav}}^2\, |\boldsymbol{k}|^2 \approx \omega^2 \implies L^2 \sim g\, H_r / \omega^2. \tag{55.48}$$

The first approximation follows from assuming $\eta_b' \ll H$ so that $g\, H_r \approx g\, H = c_{\text{grav}}^2$, and the second approximation follows from assuming a non-rotating gravity wave dispersion relation.[2] In essence, we are assuming the two terms in equation (55.47) scale the same, which holds so long as the length scale of the super-inertial waves satisfies $L^2 \sim g\, H_r / \omega^2$.

Ratio of RHS terms to the LHS

Now consider the magnitude for each term on the right hand side of the wave equation (55.42) relative to the left hand side terms just found in equation (55.47). The ratio for terms in equation (55.46c) satisfy

$$\frac{f\, g\, \nabla H_r \times \nabla \mathcal{L}(\eta')}{\text{LHS}} \sim \frac{\omega^2\, f\, g\, \eta_b' / L^2}{\omega^3\, g\, H_r / L^2} = \frac{f\, \eta_b'}{\omega\, H_r} \ll 1, \tag{55.49}$$

where the inequality follows from assuming that the bottom topography undulation is small as per equation (55.45). The ratio for the remaining three terms (equations (55.46d), (55.46e), and (55.46f)) are also much less than unity, with these inequalities following from the β-plane approximation (55.44)

$$\frac{g\, \beta\, H_r\, f^2\, \partial_x \eta'}{\text{LHS}} \sim \frac{g\, \beta\, H_r\, f^2 / L}{\omega^3\, g\, H_r / L^2} = (\beta\, L/\omega)\, (f/\omega)^2 < (\beta\, L/f)\, (f/\omega)^2 \ll 1 \tag{55.50a}$$

$$\frac{-2\, f\, \partial_{yt} \eta'}{\text{LHS}} \sim \frac{\beta\, g\, H_r\, f\, \omega / L}{\omega^3\, g\, H_r / L^2} = (\beta\, L/\omega)\, (f/\omega) < (\beta\, L/f)\, (f/\omega) \ll 1 \tag{55.50b}$$

$$\frac{\beta\, g\, H_r\, \partial_{xtt} \eta'}{\text{LHS}} \sim \frac{\beta\, g\, H_r\, (\omega^2 / L)}{\omega^3\, g\, H_r / L^2} = (\beta\, L/\omega) < (\beta\, L/f) \ll 1. \tag{55.50c}$$

Inertia-gravity wave equation for super-inertial waves

We thus conclude that for super-inertial waves on a β-plane and with small amplitude topography, then the two terms on the left hand side of equation (55.42) balance so that

$$\partial_t \mathcal{L}\left[\mathcal{L}(\eta') - \nabla \cdot (g\, H_r\, \nabla \eta')\right] \approx 0. \tag{55.51}$$

This relation can be maintained by setting

$$(\partial_{tt} + f_o^2)\, \eta' - \nabla \cdot (g\, H_r\, \nabla \eta') = 0, \tag{55.52}$$

[2] We derive the shallow water gravity wave dispersion relation in equation (55.80). Also, see the discussion of long surface gravity waves in Section 52.5.3.

which is the equation for inertia-gravity waves on an f-plane with small amplitude topography. Note that we put $f = f_o$ in equation (55.52) since the β effect is most crucial for sub-inertial wave motions as discussed in Section 55.4.6, rather than super-inertial motions. We study non-rotating gravity waves in Section 55.5 and inertia-gravity waves in Section 55.8.

55.4.6 Sub-inertial wave equation

We here derive an equation relevant for sub-inertial wave motions ($\omega^2 < f^2$). In fact, we further restrict the motion to those that are very low frequency so that

$$\omega/f \sim \beta\, L/f_o \sim \eta'_b/H \ll 1. \tag{55.53}$$

We also assume that the horizontal length scales are on the order of

$$L \sim L_d = c_{grav}/f = \sqrt{g\,H}/f, \tag{55.54}$$

which is known as the *deformation radius* for the shallow water layer, first introduced in Section 43.3.6 . This length scale appears throughout our discussion of rotating shallow water waves.

The assumed scalings (55.53) along with (55.54) are precisely those assumed for shallow water quasi-geostrophy as detailed in Section 43.5. The corresponding sub-inertial waves are referred to as *planetary Rossby waves* and *topographic Rossby waves*. We here derive the wave equation for these waves, with further details of their dispersion relation provided in Section 55.9.

Sub-inertial scaling for the LHS of equation (55.42)

For the sub-inertial scalings (55.53), the linear operator is order $\mathcal{L} \sim \mathcal{O}(f^2)$, so that the left hand side of the wave equation (55.42) scales as

$$\text{LHS} = \partial_t \mathcal{L}^2(\eta') + \partial_t \mathcal{L}[\nabla \cdot (g\,H_r\,\nabla\eta')] \sim \omega\, f^2\, [f^2 + g\,H_r/L^2]\,\eta'. \tag{55.55}$$

As for the super-inertial waves in Section 55.4.5, we assume the two terms in the right expression scale the same. To ensure that scaling holds, we focus on horizontal length scales satisfying

$$L^2 \sim g\,H_r/f^2 \sim g\,H/f^2 = c_{grav}^2/f^2 = L_d^2. \tag{55.56}$$

This assumption of deformation scale motions for sub-inertial waves can be compared to the super-inertial length scale in equation (55.48). We find that super-inertial motions are generally smaller than the deformation radius whereas sub-inertial motions are on the order or larger than the deformation radius.

With the above scaling (55.56) for the horizontal length, the left hand side of the wave equation (55.42) scales as

$$\text{LHS} \sim (\omega\, f\, g\, H_r/L^2)\,\eta'. \tag{55.57}$$

We will later replace f with f_o in equation (55.57), with that replacement warranted by the β-plane approximation, $\beta\, L \ll f_o$. For now, we reduce clutter by just writing f.

Ratio of RHS terms to the LHS

Now consider the magnitude for each term on the right hand side of the wave equation (55.42) relative to the left hand side terms just found in equation (55.57). The ratio for terms in equation

(55.46c) is given by

$$\frac{f\, g\, \nabla H_\mathsf{r} \times \nabla \mathcal{L}(\eta')}{\text{LHS}} \sim \frac{f^3\, g\, \eta'_\mathsf{b}/L^2}{\omega\, f^2\, g\, H_\mathsf{r}/L^2} = \frac{f\, \eta'_\mathsf{b}}{\omega\, H_\mathsf{r}} = \mathcal{O}(1), \tag{55.58}$$

with the final equality following from the assumed scales in equation (55.53). We also find that the ratio for terms in equation (55.46d) is given by

$$\frac{g\, \beta\, H_\mathsf{r}\, f^2\, \partial_x \eta'}{\text{LHS}} \sim \frac{g\, \beta\, H_\mathsf{r}\, f^2/L}{\omega\, f^2\, g\, H_\mathsf{r}/L^2} = \beta\, L/\omega = \mathcal{O}(1), \tag{55.59}$$

where we again made use of equation (55.53) for the final equality. In contrast to these order unity ratios, the ratios involving terms in equations (55.46e) and (55.46f) are much less than unity

$$\frac{-2\, f\, \partial_{yt} \eta'}{\text{LHS}} \sim \frac{\beta\, g\, H_\mathsf{r}\, f\, \omega/L}{\omega\, f^2\, g\, H_\mathsf{r}/L^2} = \beta\, L/f \ll 1 \tag{55.60a}$$

$$\frac{\beta\, g\, H_\mathsf{r}\, \partial_{xtt} \eta'}{\text{LHS}} \sim \frac{\beta\, g\, H_\mathsf{r}\, (\omega^2/L)}{\omega\, f^2\, g\, H_\mathsf{r}/L^2} = (\beta\, L/f)\, (\omega/f) \ll 1. \tag{55.60b}$$

The first inequality follows from the β-plane approximation (55.44), and the second follows also from the β-plane approximation as well as the low frequency assumption, $\omega^2 \ll f^2$.

Shallow water planetary and topographic Rossby wave equation

The above scalings lead to the approximate wave equation for sub-inertial waves moving on a β-plane with small amplitude bottom topography

$$\partial_t \left[f^2\, \eta' - \nabla \cdot (g\, H\, \nabla \eta') \right] = f\, g\, \hat{\boldsymbol{z}} \cdot (\nabla H_\mathsf{r} \times \nabla \eta') + g\, H\, \beta\, \partial_x \eta'. \tag{55.61}$$

Note that we set $H_\mathsf{r} = H$ everywhere except where it is differentiated, with this replacement consistent with the assumed $\eta'_\mathsf{b} \ll H$ (equation (55.53)). A slightly more tidy version arises by introducing the squared gravity wave speed $c^2_\mathsf{grav} = g\, H$ and the deformation radius, $L_\mathsf{d} = c_\mathsf{grav}/f$, so that

$$\partial_t \left[(L_\mathsf{d}^{-2} - \nabla^2)\, \eta' \right] = (f/H)\, \hat{\boldsymbol{z}} \cdot (\nabla H_\mathsf{r} \times \nabla \eta') + \beta\, \partial_x \eta'. \tag{55.62}$$

The first term on the right hand side gives rise to topographic Rossby waves, whereas the second term gives rise to planetary Rossby waves. It is notable that this equation has only a single time derivative, which contrasts with the super-inertial wave equation (55.52).

Rossby waves are supported by potential vorticity gradients

We can write the right hand side of equation (55.62) in the following equivalent form

$$\partial_t \left[(L_\mathsf{d}^{-2} - \nabla^2)\, \eta' \right] = H\, \hat{\boldsymbol{z}} \cdot (\nabla \eta' \times \nabla Q_\mathsf{r}). \tag{55.63}$$

In this manner we see that both planetary Rossby waves and topographic Rossby waves are supported by gradients in the resting fluid's potential vorticity[3]

$$Q_\mathsf{r} = f/H_\mathsf{r}. \tag{55.64}$$

[3]When studying waves in the horizontally non-divergent barotropic fluid (Section 54.3), we also noted the need for a background potential vorticity gradient to support Rossby wave modes.

Equation (55.63) reveals that shallow water Rossby waves arise from a mis-alignment between contours of constant resting state potential vorticity and contours of constant surface height.

The effective β vector

We offer one further expression for the Rossby wave equation

$$\partial_t \left[(L_{\mathrm{d}}^{-2} - \nabla^2)\, \eta' \right] = \hat{\boldsymbol{z}} \cdot (\nabla \eta' \times \boldsymbol{\beta}_{\mathrm{eff}}), \tag{55.65}$$

where we introduced the effective beta vector that combines the planetary vorticity gradient with the topographic gradient

$$\boldsymbol{\beta}_{\mathrm{eff}} = \nabla f - Q_{\mathrm{r}} \nabla H_{\mathrm{r}} = \beta\, \hat{\boldsymbol{y}} - Q_{\mathrm{r}} \nabla H_{\mathrm{r}}. \tag{55.66}$$

Again, this form exhibits the parallel role of both planetary beta and topographic slopes in supporting Rossby waves. Equation (55.65) says that shallow water Rossby waves arise from a mis-alignment between the effective beta vector and free surface height gradients.

55.4.7 Comments on bottom topography

Throughout this section we allowed for the bottom topography, as defined by $H_{\mathrm{r}} = H - \eta'_{\mathrm{b}}$ (equation (55.11)), to have arbitrary (x, y) spatial dependence. In the following sections we make simplifications to the topography, thus facilitating the study of plane waves, planetary waves, and topographically trapped waves. The study of waves with more general bottom topographies requires the asymptotic methods from Chapter 50.

55.5 Shallow water gravity waves

In this section we study shallow water gravity waves in the absence of planetary rotation ($f = 0$). We already encountered features of these waves in Chapter 52 when studying surface gravity waves. Even so, it is useful to start from the shallow water equations to directly derive the properties of the non-dispersive gravity waves. Additionally, we here do not introduce a velocity potential as done for the surface gravity waves, even though the non-rotating shallow water gravity waves are irrotational. We do not introduce the velocity potential since the other waves studied in this chapter carry vorticity, thus making the velocity potential an incomplete description for those cases.

55.5.1 Flat bottom gravity waves

Setting $\eta'_{\mathrm{b}} = 0$ in equation (55.32) yields the shallow water gravity wave equation holding for a flat bottom domain

$$(\partial_{tt} - c_{\mathrm{grav}}^2 \nabla^2)\, \eta' = 0, \tag{55.67}$$

where the gravity wave speed is determined by the two geophysical properties of the system

$$c_{\mathrm{grav}} = \sqrt{g\, H}. \tag{55.68}$$

To help emphasize a few key properties, we return to the linear thickness equation (55.13) and linear velocity equation (55.15), now written with $f = 0$ and $\eta'_{\mathrm{b}} = 0$

$$\partial_t \eta' = -H\, \nabla \cdot \boldsymbol{u}' \quad \text{and} \quad \partial_t \boldsymbol{u}' = -g\, \nabla \eta'. \tag{55.69}$$

Taking the time derivative of the thickness equation and then using the velocity equation readily yields the wave equation (55.67). Conversely, taking the horizontal divergence of the velocity equation yields

$$\partial_t(\nabla \cdot \boldsymbol{u}') = -g\,\nabla^2\eta', \tag{55.70}$$

so that time changes in the horizontal divergence are driven by curvature in the free surface. Taking the time derivative of this equation, and using the thickness equation, reveals that the horizontal divergence also satisfies the wave equation

$$(\partial_{tt} - c_{\text{grav}}^2\nabla^2)\,(\nabla \cdot \boldsymbol{u}') = 0. \tag{55.71}$$

Hence, both the free surface and the horizontal divergence travel as non-dispersive gravity waves in the flat bottom non-rotating shallow water layer.

Finally, observe that the linearized potential vorticity equation (55.23), in the presence of $f = 0$ and $\eta_{\text{b}}' = 0$, means that the relative vorticity is static at each point in the fluid

$$\partial_t\zeta' = 0. \tag{55.72}$$

Hence, these gravity wave fluctuations do not alter the flow vorticty. In particular, if the flow starts with zero vorticity then shallow water gravity wave fluctuations retain the zero vorticity.

55.5.2 Structure of the gravity wave

Substituting the plane wave ansatz (55.24) into the linearized thickness and velocity equation (55.69) allows us to connect the wave amplitudes for the free surface and velocity

$$\omega\,\tilde{\boldsymbol{u}} = g\,\boldsymbol{k}\,\tilde{\eta} \Longrightarrow \boldsymbol{k} \times \tilde{\boldsymbol{u}} = 0 \qquad \text{and} \qquad \omega\,\tilde{\eta} = H\,\boldsymbol{k} \cdot \tilde{\boldsymbol{u}}. \tag{55.73}$$

The identity $\boldsymbol{k} \times \tilde{\boldsymbol{u}} = 0$ for the plane wave means that the fluid particle's horizontal velocity is oriented parallel to the horizontal wave vector, so that

$$\tilde{\boldsymbol{u}} = \hat{\boldsymbol{k}}\,(\hat{\boldsymbol{k}} \cdot \tilde{\boldsymbol{u}}) \quad \text{with} \quad \hat{\boldsymbol{k}} = \boldsymbol{k}/|\boldsymbol{k}|. \tag{55.74}$$

This alignment of the horizontal velocity with the wavevector is a direct result of the irrotational nature of the gravity waves, which was already noted when discussing the linearized vorticity equation (55.72). Additionally, with a real wavevector and real angular frequency, the amplitude relation $\omega\,\tilde{\boldsymbol{u}} = g\,\boldsymbol{k}\,\tilde{\eta}$ also holds for the traveling plane wave velocity and free surface so that

$$\omega\,\boldsymbol{u} = g\,\boldsymbol{k}\,\eta \Longrightarrow \boldsymbol{k} \cdot \boldsymbol{u} = g|\boldsymbol{k}|^2\eta/\omega \quad \text{and} \quad \boldsymbol{u} = \hat{\boldsymbol{k}}\,(g/c_{\text{grav}})\,\tilde{\eta}\cos\mathcal{P}, \tag{55.75}$$

where

$$\mathcal{P} = \boldsymbol{k} \cdot \boldsymbol{x} - \omega\,t \tag{55.76}$$

is the phase.

Alignment of the horizontal fluid particle velocity with the wavevector (equation (55.75)) indicates that motion in the shallow water gravity wave is horizontally longitudinal. However, as noted in Section 55.3.4, a shallow water fluid has a nonzero vertical velocity component that is a linear function of depth, as given by equations (55.26) and (55.27). The presence of vertical motion within the wave means that the waves are not longitudinal in three dimensions. Rather, a fluid particle moves horizontally in the direction of the wavevector but the particle also moves vertically, thus tracing out an elliptical path in the vertical-horizontal plane.

To describe the vertical particle motion in the wave, make use of equation (55.27) for the

vertical velocity and equation (55.75) for the horizontal velocity, thus leading to

$$w = -\mathrm{i}\,(z - \eta_{\mathsf{b}})\,\boldsymbol{k}\cdot\tilde{\boldsymbol{u}}\,\mathrm{e}^{\mathrm{i}(\boldsymbol{k}\cdot\boldsymbol{x}-\omega\,t)} = (z-\eta_{\mathsf{b}})\,(g\,|\boldsymbol{k}|^2\,\tilde{\eta}/\omega)\,(-\mathrm{i}\cos\mathcal{P} + \sin\mathcal{P}), \tag{55.77}$$

where we set $w(\eta_{\mathsf{b}}) = 0$ for a flat bottom. Taking the real part renders the vertical velocity within the shallow water gravity wave

$$w = (z-\eta_{\mathsf{b}})\,(g\,|\boldsymbol{k}|^2/\omega)\,\tilde{\eta}\sin\mathcal{P} = (z-\eta_{\mathsf{b}})\,|\boldsymbol{k}|\,(g/c_{\mathsf{grav}})\,\tilde{\eta}\sin\mathcal{P} \tag{55.78}$$

The vertical velocity is $\pi/2$ out of phase with both the free surface and the horizontal velocity. Furthermore, the ratio of the maximum magnitude for the vertical and horizontal velocities is given by

$$\frac{|w|_{\max}}{|\boldsymbol{u}|_{\max}} = (z-\eta_{\mathsf{b}})\,|\boldsymbol{k}|. \tag{55.79}$$

Shallow water gravity waves are characterized by wavelengths that are long relative to the fluid depth. Hence, even at the free upper surface, the ratio (55.79) is much less than unity. As a result, the elliptical particle paths are longer in the horizontal direction than vertical direction. Furthermore, since the horizontal motion is depth-independent, the elliptical particle trajectories have the same excursion along the major axis (the horizontal axis) throughout the layer depth. This behavior contrasts to the deepwater gravity waves studied in Chapter 52, whose amplitude in all directions decreases with depth. In Figure 55.1, we depict the motion of fluid particles with a shallow water gravity wave. In Section 52.11.4 we study the Stokes drift resulting from the phase averaged particle motion in these waves.

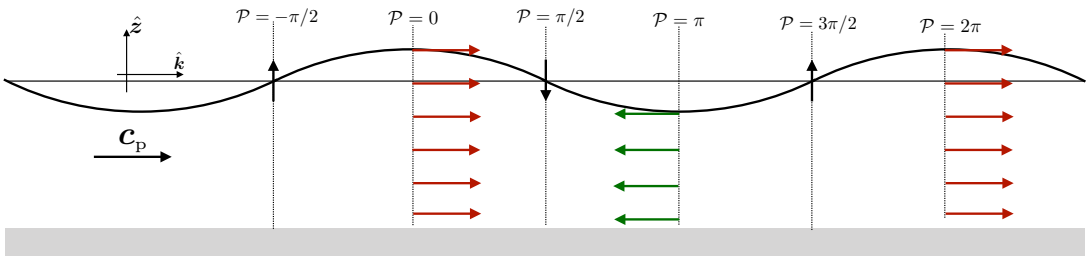

FIGURE 55.1: Illustrating motion within a shallow water gravity wave over a flat bottom, here depicted at a fixed point in time with the phase velocity to the right. The horizontal arrows are the horizontal velocity as per equation (55.75), and the vertical arrows are for the vertical velocity as per equation (55.78). The horizontal and vertical velocity components are $\pi/2$ out of phase, so that the vertical velocity vanishes when the horizontal velocity has maximum magnitude, and vice versa. This figure is a slightly simplified version of the lower panel in Figure 52.2.

55.5.3 Dispersion relation

Substitution of the plane wave ansatz (55.24) into the wave equation (55.67) leads to

$$\omega^2 = g\,H\,|\boldsymbol{k}|^2 = c_{\mathsf{grav}}^2\,|\boldsymbol{k}|^2. \tag{55.80}$$

Taking the positive square root then leads to the shallow water gravity wave dispersion relation[4]

$$\omega = |\boldsymbol{k}|\,c_{\mathsf{grav}} \Longrightarrow C_{\mathsf{p}} = \omega/|\boldsymbol{k}| = c_{\mathsf{grav}}, \tag{55.81}$$

[4]Recall that we always consider the angular frequency of waves to be non-negative (Section 49.2), hence we only take the positive root for the dispersion relation (55.81).

where we identified the phase speed as the gravity wave speed

$$C_{\mathsf{p}} = c_{\mathsf{grav}} = \sqrt{g\,H}. \tag{55.82}$$

Each wavevector propagates at the same speed since the phase speed is only dependent on geophysical parameters (gravitational acceleration and the resting layer thickness). Equivalently, higher wavenumber waves have correspondingly higher frequency, and the relation between the two is linear. We conclude that non-rotating shallow water gravity waves are *non-dispersive*.

55.5.4 Steady one-dimensional flow over an obstacle

Consider a steady one-dimensional inviscid flow of a single shallow water layer of fluid in a channel with a varying bottom, $z = \eta_{\mathsf{b}}(x)$, such as depicted in Figure 55.2. This flow approximates that in a straight canal as water moves over a *weir*. The thicker water upstream of the weir creates a pressure gradient that speeds up the flow as it moves over the weir. Throughout the analysis we assume the fluid has a positive layer thickness, $h > 0$, so that there is no region where the fluid layer vanishes.

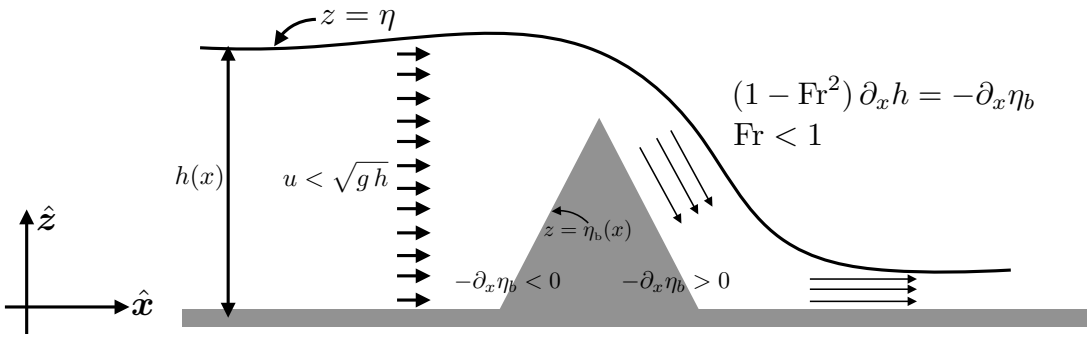

FIGURE 55.2: One-dimensional flow of a shallow water fluid layer in a channel with an obstacle. This flow approximates that for water flowing over a weir in a straight canal. If a fluid particle moves faster than the locally defined gravity wave speed, $u > \sqrt{g\,h}$ or $\mathrm{Fr} > 1$, then the flow is said to undergo a *hydraulic jump*, which typically occurs first at the peak of the weir with $u = \sqrt{g\,h}$ or $\mathrm{Fr} = 1$. Flow that is faster than the gravity wave speed is said to be *super-critical*, whereas slower flow is *sub-critical*. We here depict sub-critical flow where the local Froude number is everywhere less than unity, $\mathrm{Fr} < 1$. The fluid is thicker upstream than downstream of the weir as per equation (55.89), thus enabling a higher pressure upstream to create a pressure drop across the weir.

The steady, one-dimensional, non-rotating shallow water equations take the form

$$u\,\partial_x u = -g\,\partial_x(\eta_{\mathsf{b}} + h) \tag{55.83a}$$

$$u\,\partial_x h + h\,\partial_x u = 0, \tag{55.83b}$$

where we wrote the free surface height, η, as the sum of the bottom topography position plus the layer thickness (see Figure 35.1)

$$\eta = \eta_{\mathsf{b}} + h. \tag{55.84}$$

The momentum equation can be written in the form of a mechanical energy equation

$$\partial_x(u^2/2 + g\,h) = -g\,\partial_x \eta_{\mathsf{b}}. \tag{55.85}$$

We see that the mechanical energy, $u^2/2 + g\,h$, has spatial variations according to the variations in the bottom topography. Otherwise, the mechanical energy is a spatial constant.

Writing the steady state thickness equation (55.83b) in the form

$$\partial_x u = -(u/h)\,\partial_x h, \tag{55.86}$$

allows us to write the momentum equation (55.83a) as

$$(g - u^2/h)\,\partial_x h = -g\,\partial_x \eta_{\mathfrak{b}}. \tag{55.87}$$

Introducing the local *Froude number*,

$$\text{Fr} = u/\sqrt{g\,h}, \tag{55.88}$$

then leads to

$$(1 - \text{Fr}^2)\,\partial_x h = -\partial_x \eta_{\mathfrak{b}}. \tag{55.89}$$

The bottom is flat in regions away from the weir, so that $\partial_x \eta_b = 0$, in which case the left hand side of equation (55.89) must vanish. The left hand side vanishes if $\partial_x h = 0$, in which the free surface is flat, such as depicted for the region away from the weir in Figure 55.2. The left hand side also vanishes if the Froude number is unity, Fr = 1. A unit Froude number means that the particle velocity equals to the local gravity wave speed

$$u^2 = g\,h. \tag{55.90}$$

Flow moving at speeds less than the gravity wave speed is called *sub-critical*, such as flow upstream of the weir. Flow whose speed equals the gravity wave speed is said to be under *hydraulic control*, which commonly occurs near the peak of the weir in Figure 55.2. Flow that is faster than the local gravity wave speed is said to be *super-critical*, with the steady assumptions going into equation (55.89) breaking down for super-critical flow. Super-critical flow is found to exhibit a *hydraulic jump*, which is an instability with flow seemingly overtaking itself since it cannot "see" where it is going. The situation is akin to the sonic boom occuring in a compressible fluid moving at speeds greater than the acoustic wave speed.

The discussion here is rather descriptive, with more analysis required to deductively support the presentation, particularly for super-critical flow. Chapter 1 of *Pratt and Whitehead* (2008) considers this topic in more detail. The remaining chapters in *Pratt and Whitehead* (2008) consider planetary rotation, thus developing the subject of *rotating hydraulics*, which is particularly important for describing geophysical flows moving over topographic slopes.

55.6 Gravity waves in two layers

When adding more shallow water layers, how much can we use from the single layer results? To help answer that question, consider the linearized equations for two shallow water layers. The equations can be generalized to multiple layers, though with increased algebraic complexity. Indeed, even the two-layer case with rotation proves to be algebraically tedious, thus motivating us to examine just the case of gravity waves without rotation. For more general depth dependence, we find it simpler analytically to study the continuously stratified fluid in Chapter 57.

55.6.1 Linearized two-layer equations

We derived the equations for a stacked shallow water model in Section 35.4, and focused on two layers in Section 35.4.1. With reference to Figure 35.6 for notation, write the layer thicknesses in the form

$$h_1 = H_1 + h_1' = \eta_{1/2} - \eta_{3/2} = (\overline{\eta_{1/2}} - \overline{\eta_{3/2}}) + (\eta_{1/2}' - \eta_{3/2}') \tag{55.91a}$$

$$h_2 = H_2 + h_2' = \eta_{3/2} - \eta_{\mathfrak{b}} = (\overline{\eta_{3/2}} - \overline{\eta_{\mathfrak{b}}}) + (\eta_{3/2}' - \eta_{\mathfrak{b}}'), \tag{55.91b}$$

where we introduced the resting layer thicknesses

$$H_1 = \overline{\eta_{1/2}} - \overline{\eta_{3/2}} \quad \text{and} \quad H_2 = \overline{\eta_{3/2}} - \overline{\eta_{\mathfrak{b}}} \quad \text{and} \quad H = H_1 + H_2, \tag{55.92}$$

with the overbar representing the area mean, and with the half-integer labels representing interface fields. This notation leads to the linearized version of the thickness equations (35.62a) and (35.62b)

$$\partial_t h'_1 + H_1 \, \nabla \cdot \boldsymbol{u}'_1 = 0 \tag{55.93a}$$
$$\partial_t h'_2 + H_2 \, \nabla \cdot \boldsymbol{u}'_2 = 0, \tag{55.93b}$$

where $\boldsymbol{u}'_1$ and $\boldsymbol{u}'_2$ are the horizontal velocities in the two layers. Likewise, assuming a zero atmospheric pressure leads to the linearized version of velocity equations (35.77a) and (35.77b)

$$\partial_t \boldsymbol{u}'_1 + f \, \hat{\boldsymbol{z}} \times \boldsymbol{u}'_1 = -g \nabla \eta'_{1/2} \tag{55.94a}$$
$$\partial_t \boldsymbol{u}'_2 + f \, \hat{\boldsymbol{z}} \times \boldsymbol{u}'_2 = -g \nabla \eta'_{1/2} - g^{\mathrm{r}}_{3/2} \nabla \eta'_{3/2}. \tag{55.94b}$$

For the linearized equations, the only layer coupling occurs through undulations of the free surface impacting on the pressure felt in the lower layer.

55.6.2 Gravity wave equations

We restrict further analysis to the case with zero Coriolis acceleration so that the layer equations take the form

$$\partial_t(\eta'_{1/2} - \eta'_{3/2}) + H_1 \, \nabla \cdot \boldsymbol{u}'_1 = 0 \quad \text{and} \quad \partial_t \boldsymbol{u}'_1 = -g \, \nabla \eta'_{1/2} \tag{55.95a}$$
$$\partial_t \eta'_{3/2} + H_2 \, \nabla \cdot \boldsymbol{u}'_2 = 0 \quad \text{and} \quad \partial_t \boldsymbol{u}'_2 = -g \, \nabla \eta'_{1/2} - g^{\mathrm{r}} \, \nabla \eta'_{3/2}, \tag{55.95b}$$

where we introduced the reduced gravity for the interior layer interface

$$g^{\mathrm{r}} = g^{\mathrm{r}}_{3/2} = g \, (\rho_2 - \rho_1)/\rho_1. \tag{55.96}$$

Taking time derivatives of the thickness equations and substituting the divergence of the velocity equations leads to the matrix-vector equation

$$\begin{bmatrix} (\partial_{tt} - g \, H_1 \nabla^2) & -\partial_{tt} \\ -g \, H_2 \, \nabla^2 & (\partial_{tt} - g^{\mathrm{r}} \, H_2 \nabla^2) \end{bmatrix} \begin{bmatrix} \eta'_{1/2} \\ \eta'_{3/2} \end{bmatrix} = \begin{bmatrix} 0 \\ 0 \end{bmatrix}. \tag{55.97}$$

This equation has non-trivial solutions if the determinant of the matrix vanishes, and we use that property to derive the dispersion relation.

55.6.3 Dispersion relation

To derive the dispersion relation, consider the plane wave ansatz for the free surface undulation in each layer

$$\eta'_{1/2} = \tilde{\eta}_{1/2} \, \mathrm{e}^{\mathrm{i} \, (\boldsymbol{k} \cdot \boldsymbol{x} - \omega \, t)} \quad \text{and} \quad \eta'_{3/2} = \tilde{\eta}_{3/2} \, \mathrm{e}^{\mathrm{i} \, (\boldsymbol{k} \cdot \boldsymbol{x} - \omega \, t)}. \tag{55.98}$$

Note that we assume each layer has the same wavevector and same angular frequency. However, the amplitudes, $\tilde{\eta}_{1/2}$ and $\tilde{\eta}_{3/2}$, are generally complex so that the phase of the layers can differ. The corresponding velocity for the two layers is given by

$$\boldsymbol{u}'_1 = \tilde{\boldsymbol{u}}_1 \, \mathrm{e}^{\mathrm{i} \, (\boldsymbol{k} \cdot \boldsymbol{x} - \omega \, t)} \quad \text{and} \quad \boldsymbol{u}'_2 = \tilde{\boldsymbol{u}}_2 \, \mathrm{e}^{\mathrm{i} \, (\boldsymbol{k} \cdot \boldsymbol{x} - \omega \, t)}. \tag{55.99}$$

Plugging the wave ansatz (55.98) into equation (55.97) converts the differential operators to algebraic expressions

$$\begin{bmatrix} (-\omega^2 + g\,H_1|\boldsymbol{k}|^2) & \omega^2 \\ g\,H_2\,|\boldsymbol{k}|^2 & (-\omega^2 + g^{\mathrm{r}}\,H_2\,|\boldsymbol{k}|^2) \end{bmatrix} \begin{bmatrix} \tilde{\eta}_{1/2} \\ \tilde{\eta}_{3/2} \end{bmatrix} = \begin{bmatrix} 0 \\ 0 \end{bmatrix}. \tag{55.100}$$

Setting the determinant to zero leads to the quadratic equation in ω^2

$$(\omega^2 - g\,H_1\,|\boldsymbol{k}|^2)\,(\omega^2 - g^{\mathrm{r}}\,H_2\,|\boldsymbol{k}|^2) - g\,H_2\,|\boldsymbol{k}|^2\,\omega^2 = 0. \tag{55.101}$$

Solving for the squared phase speed ($C_{\mathsf{p}}^2 = \omega^2/|\boldsymbol{k}|^2$) leads to

$$2\,\omega^2/|\boldsymbol{k}|^2 = (g\,H + g^{\mathrm{r}}\,H_2) \pm \sqrt{(g\,H + g^{\mathrm{r}}\,H_2)^2 - 4\,g\,g^{\mathrm{r}}\,H_1\,H_2}. \tag{55.102}$$

Introducing the small non-dimensional parameter,

$$\epsilon = g^{\mathrm{r}}\,H_2/(g\,H) = g^{\mathrm{r}}\,H_2/c_{\mathsf{grav}}^2 \ll 1, \tag{55.103}$$

and expanding the dispersion relation (55.102) to expose the leading order behavior, yields the squared phase speeds

$$C_{\mathsf{p}}^2 \approx c_{\mathsf{grav}}^2 = g\,H \qquad \text{squared barotropic phase speed} \tag{55.104a}$$

$$C_{\mathsf{p}}^2 \approx c_{\mathsf{grav}}^2\,g^{\mathrm{r}}\,H_1\,H_2/(g\,H^2) = g^{\mathrm{r}}\,H_1\,H_2/H \qquad \text{squared baroclinic phase speed.} \tag{55.104b}$$

We motivate the names *barotropic mode* and *baroclinic mode* in the following, based on our study of vorticity in Section 40.7.2 for a Boussinesq fluid. Note that the phase speed for the barotropic mode is roughly given by the gravity wave speed for a single layer of fluid with resting thickness $H = H_1 + H_2$. This speed is much greater than that for the baroclinic mode since $g^{\mathrm{r}} \ll g$.

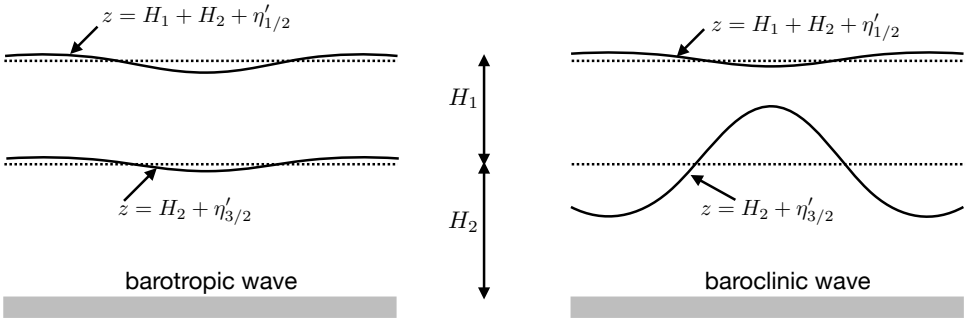

FIGURE 55.3: Illustrating the interface displacements for a two-layer shallow water gravity wave as discussed in Section 55.6.4. The left panel depicts a barotropic wave, where the undulations are both relatively small, in-phase, and on the same order of magnitude. The right panel shows a baroclinic wave, where the undulations of the free surface are small whereas those of the interior interface are much larger (order g/g^{r}) and the two undulations are π radians out of phase. For the baroclinic mode, recall that the same structure occurs for the reduced gravity model shown in Figure 35.5.

55.6.4 Structure of a plane gravity wave

In this subsection we examine the structure of a plane gravity wave by relating the wave amplitudes. To start, we relate interface height amplitudes by making use of equation (55.100) to write

$$\frac{\tilde{\eta}_{1/2}}{\tilde{\eta}_{3/2}} = \frac{\omega^2}{\omega^2 - g\,H_1\,|\boldsymbol{k}|^2} = \frac{\omega^2 - g^{\mathrm{r}}\,H_2\,|\boldsymbol{k}|^2}{g\,H_2\,|\boldsymbol{k}|^2}. \tag{55.105}$$

Since the right hand side is real, so too is the ratio of the amplitudes. Hence, the interfaces undulate either in phase or π radians out of phase. Correspondingly, we can, without loss of generality, take the interface height amplitudes to be real.

We relate the velocity amplitude to the interface amplitude by evaluating the linearized velocity equations (55.95a) and (55.95b) for plane waves, in which

$$\omega\,\tilde{\boldsymbol{u}}_1 = \boldsymbol{k}\,g\,\tilde{\eta}_{1/2} \quad \text{and} \quad \omega\,\tilde{\boldsymbol{u}}_2 = \boldsymbol{k}\,(g'\,\tilde{\eta}_{1/2} + g\,\tilde{\eta}_{3/2}). \tag{55.106}$$

Since the interface height amplitudes are real, so too are the velocity amplitudes. Evidently, the fluid particle velocity in each layer is aligned with the phase velocity, so that the gravity waves are horizontally longitudinal. Correspondingly, the ratio of the velocity amplitudes is found by taking the scalar product of equation (55.106) with the wavevector to find

$$\omega\,\tilde{\boldsymbol{u}}_1 \cdot \boldsymbol{k} = |\boldsymbol{k}|^2\,g\,\tilde{\eta}_{1/2} \quad \text{and} \quad \omega\,\tilde{\boldsymbol{u}}_2 \cdot \boldsymbol{k} = |\boldsymbol{k}|^2\,(g' + g\,H_2/H)\,\tilde{\eta}_{1/2}, \tag{55.107}$$

whose ratio is

$$\frac{\tilde{\boldsymbol{u}}_1 \cdot \boldsymbol{k}}{\tilde{\boldsymbol{u}}_2 \cdot \boldsymbol{k}} = \frac{g\,\tilde{\eta}_{1/2}}{g'\,\tilde{\eta}_{1/2} + g\,\tilde{\eta}_{3/2}}. \tag{55.108}$$

Structure of the barotropic mode

For the barotropic mode we set $\omega^2 \approx g\,H\,|\boldsymbol{k}|^2$ within equation (55.105) to render the amplitude ratio

$$\tilde{\eta}_{1/2}/\tilde{\eta}_{3/2} \approx H/H_2 > 1. \tag{55.109}$$

This inteface height ratio then leads, through equation (55.108), to the velocity amplitude

$$\frac{\tilde{\boldsymbol{u}}_1 \cdot \boldsymbol{k}}{\tilde{\boldsymbol{u}}_2 \cdot \boldsymbol{k}} \approx \tilde{\eta}_{1/2}/\tilde{\eta}_{3/2} \approx H/H_2. \tag{55.110}$$

Evidently, the two interfaces undulate in-phase and with the surface interface fluctuating more than the interior interface. Likewise, the horizontal velocities move in-phase with the interface heights, and with an amplitude ratio that concurs with the interface height ratio. We depict this wave motion in the left panel of Figure 55.3.

Structure of the baroclinic wave mode

For the baroclinic mode, setting $\omega^2 \approx g'\,H_1\,H_2\,|\boldsymbol{k}|^2/H$ within equation (55.100) leads to the amplitude ratio

$$\tilde{\eta}_{1/2}/\tilde{\eta}_{3/2} \approx -g'\,H_2/(g\,H). \tag{55.111}$$

Hence, the two interfaces undulate oppositely (i.e., π radians out of phase) and with the amplitude of the upper interface far less than the interior interface

$$|\tilde{\eta}_{1/2}/\tilde{\eta}_{3/2}| \ll 1. \tag{55.112}$$

That is, the free surface is nearly rigid relative to the interior interface, as depicted in the right panel of Figure 55.3. For the velocity amplitude, we make use of equation (55.108) along with the interface height amplitude ratio (55.111), so that

$$\frac{\tilde{\boldsymbol{u}}_1 \cdot \boldsymbol{k}}{\tilde{\boldsymbol{u}}_2 \cdot \boldsymbol{k}} \approx -\frac{g'\,H_2}{g\,H}, \tag{55.113}$$

so that the velocities are π radians out of phase and their ratio is identical to that for the interface heights.

Evidently, the baroclinic mode consists of layer velocities and interface heights that oscillate π radians out of phase, and with the velocity and surface height in the upper layer undulating much less than in the interior layer. Indeed, to leading order the upper interface is rigid and the corresponding flow stagnant. In contrast, the lower interface fluctuates as a gravity wave with the squared phase speed, $g^r\, H_1\, H_2/H$. This wave speed is far less than the $\approx \sqrt{g\, H}$ speed of the barotropic mode.

55.6.5 Energetic scaling for the waves

We here examine the relative amounts of phase averaged kinetic and available potential energies contained in the waves. From Section 36.6.3, we write the linearized layer integrated kinetic energy per area

$$\mathcal{K} = (\rho_o/2)\,(H_1\, \boldsymbol{u}_1' \cdot \boldsymbol{u}_1' + H_2\, \boldsymbol{u}_2' \cdot \boldsymbol{u}_2'), \tag{55.114}$$

whose phase average is

$$\langle \mathcal{K} \rangle = (\rho_o/4)\,(H_1\, |\tilde{\boldsymbol{u}}_1|^2 + H_2\, |\tilde{\boldsymbol{u}}_2|^2). \tag{55.115}$$

Within the gravity wave, the velocity amplitudes are related to the interface amplitudes via equation (55.106), so that the phase averaged kinetic energy per horizontal area is

$$\langle \mathcal{K} \rangle = (\rho_o/4)\,(|\boldsymbol{k}|/\omega)^2\,[H_1\,(g\,\tilde{\eta}_{1/2})^2 + H_2\,(g^r\,\tilde{\eta}_{1/2} + g\,\tilde{\eta}_{3/2})^2]. \tag{55.116}$$

For the available potential energy, we make use of the phase averaged version of equation (36.139) to write the phase averaged available potential energy per area as

$$\langle \mathcal{A} \rangle = (\rho_o/4)\,(g\,\tilde{\eta}_{1/2}^2 + g^r\,\tilde{\eta}_{3/2}^2). \tag{55.117}$$

Scaling within a barotropic gravity wave

For the barotropic gravity wave, the interface height undulations are related by equation (55.109). Hence, the phase averaged kinetic energy and available potential energy are given by the approximate expressions

$$\langle \mathcal{K} \rangle \approx \frac{\rho_o\, \tilde{\eta}_{1/2}^2}{4\, g\, H}\,[H_1\, g^2 + H_2\,(g^r + g\, H_2/H)^2] \tag{55.118a}$$

$$\langle \mathcal{A} \rangle \approx (\rho_o/4)\,\tilde{\eta}_{1/2}^2\,(g + g^r\, H_2^2/H^2), \tag{55.118b}$$

and their ratio is

$$\frac{\langle \mathcal{K} \rangle}{\langle \mathcal{A} \rangle} = \frac{1}{g\, H}\,\frac{H_1\, H^2\, g^2 + H_2\,(g^r\, H + g\, H_2)^2}{g\, H^2 + g^r\, H_2^2}. \tag{55.119}$$

This ratio is on the order of unity, with specific values determined by the layer thickness and reduced gravity. Hence, for the barotropic wave there is roughly the same amount of energy contained in the kinetic energy as in the available potential energy.

Scaling within a baroclinic gravity wave

For the baroclinic gravity wave, the interface height undulations are related by equation (55.111). Hence, the phase averaged kinetic energy and available potential energy are given by the approximate expressions

$$\langle \mathcal{K} \rangle \approx \frac{\rho_o\, \tilde{\eta}_{1/2}^2}{4\, C_{\mathsf{p}}^2}\,(H_1\, g^2 + H_2\,[g^r - (g^2\, H)/(g^r\, H_2)]^2) \approx \frac{\rho_o\, \tilde{\eta}_{1/2}^2}{4\, C_{\mathsf{p}}^2}\,\frac{g^2\, H^2}{(g^r)^2\, H_2} \tag{55.120}$$

$$\langle \mathcal{A} \rangle \approx (\rho_\circ/4)\, \tilde{\eta}_{1/2}^2\, \frac{g^2\, H^2}{g^{\mathrm{r}}\, H_2^2}. \tag{55.121}$$

Use of equation (55.104b) for the squared phase speed in the baroclinic mode leads to the energy ratio

$$\frac{\langle \mathcal{K} \rangle}{\langle \mathcal{A} \rangle} \approx \frac{1}{C_{\mathrm{p}}^2}\, \frac{g^2\, H_2}{g^{\mathrm{r}}} = \frac{g^2\, H}{(g^{\mathrm{r}})^2\, H_1} \gg 1. \tag{55.122}$$

This ratio is generally much larger than unity, indicating that the baroclinic gravity wave carries far more kinetic energy than available potential energy.

Comparing the available potential energies between the waves

Making use of the above results leads to the ratio of the available potential energies contained in the barotropic gravity wave and baroclinic gravity wave

$$\frac{\langle \mathcal{A}^{\mathrm{bt}} \rangle}{\langle \mathcal{A}^{\mathrm{bc}} \rangle} \approx \frac{g^{\mathrm{r}}\, H_2^2}{g\, H^2}\, \frac{(\tilde{\eta}_{1/2}^2)^{\mathrm{bt}}}{(\tilde{\eta}_{1/2}^2)^{\mathrm{bc}}} \approx \frac{g\, H^2}{g^{\mathrm{r}}\, H_2^2}\, \frac{(\tilde{\eta}_{3/2}^2)^{\mathrm{bt}}}{(\tilde{\eta}_{3/2}^2)^{\mathrm{bc}}}. \tag{55.123}$$

The ratio thus depends on the assumed ratio of the undulations found in the two waves. In general we expect that

$$\frac{(\tilde{\eta}_{1/2}^2)^{\mathrm{bt}}}{(\tilde{\eta}_{1/2}^2)^{\mathrm{bc}}} \gg 1 \quad \text{and} \quad \frac{(\tilde{\eta}_{3/2}^2)^{\mathrm{bt}}}{(\tilde{\eta}_{3/2}^2)^{\mathrm{bc}}} \ll 1. \tag{55.124}$$

Even so, we cannot make any general statements about the ratio of available potential energies without further information. That is, we cannot *a priori* state that the barotropic wave requires more or less available potential energy than the baroclinic wave. Whereas the baroclinic wave involves large undulations of the interior interface, these undulations are coupled to the relatively small reduced gravity ($g^{\mathrm{r}} \ll g$), thus ameliorating the available potential energy cost. In contrast, the barotropic wave involves a relatively small undulation of the interior interface and somewhat larger free surface undulation (larger than for the baroclinic mode). The free surface motion is coupled to the relatively large buoyancy through $g \gg g^{\mathrm{r}}$, thus enhancing the potential energy cost for the free surface undulation, making the barotropic wave available potential energy comparable to that of the baroclinic wave.

55.6.6 The depth averaged velocity and the velocity difference

There are occasions in which it is useful to combine the layer velocity equations in a manner that directly approximates the barotropic and baroclinic motions. For this purpose we introduce the depth averaged velocity[5]

$$H\, \overline{\boldsymbol{u}} = H_1\, \boldsymbol{u}_1' + H_2\, \boldsymbol{u}_2', \tag{55.125}$$

with $H = H_1 + H_2$, along with the layer deviations from the depth average

$$\boldsymbol{u}_{1\mathrm{b}} = \boldsymbol{u}_1' - \overline{\boldsymbol{u}} \quad \text{and} \quad \boldsymbol{u}_{2\mathrm{b}} = \boldsymbol{u}_2' - \overline{\boldsymbol{u}}. \tag{55.126}$$

Making use of the linearized equations (55.94a) and (55.94b) (here returning to the case with rotation) leads to the equations of motion (see Exercise 55.3)

$$\partial_t \overline{\boldsymbol{u}} + f\, \hat{\boldsymbol{z}} \times \overline{\boldsymbol{u}} = -g\, \nabla \eta_{1/2}' - (H_2\, g^{\mathrm{r}}/H)\, \nabla \eta_{3/2}' \tag{55.127a}$$

$$\partial_t \boldsymbol{u}_{1\mathrm{b}} + f\, \hat{\boldsymbol{z}} \times \boldsymbol{u}_{1b} = (g^{\mathrm{r}}\, H_2/H)\, \nabla \eta_{3/2}' \tag{55.127b}$$

$$\partial_t \boldsymbol{u}_{2\mathrm{b}} + f\, \hat{\boldsymbol{z}} \times \boldsymbol{u}_{2b} = -(g^{\mathrm{r}}\, H_1/H)\, \nabla \eta_{3/2}'. \tag{55.127c}$$

[5]We study vorticity of the depth averaged velocity for a continuous fluid in Section 40.9.7.

Notice that the two deviation velocities, $\boldsymbol{u}_{1\mathrm{b}}$ and $\boldsymbol{u}_{2\mathrm{b}}$, are independent of the free surface fluctuations. Furthermore, a layer integration of these two velocities vanishes

$$H_1 \, \boldsymbol{u}_{1\mathrm{b}} + H_2 \, \boldsymbol{u}_{2\mathrm{b}} = 0, \tag{55.128}$$

which is consistent with a vanishing integral for their equations of motion

$$H_1(\partial_t \boldsymbol{u}_{1\mathrm{b}} + f \, \hat{\boldsymbol{z}} \times \boldsymbol{u}_{1\mathrm{b}}) + H_2(\partial_t \boldsymbol{u}_{2\mathrm{b}} + f \, \hat{\boldsymbol{z}} \times \boldsymbol{u}_{2\mathrm{b}}) = 0. \tag{55.129}$$

Finally, introduce the vertical shear velocity

$$\boldsymbol{u}_{\mathrm{s}} = \boldsymbol{u}_1 - \boldsymbol{u}_2 = \boldsymbol{u}_{1\mathrm{b}} - \boldsymbol{u}_{2\mathrm{b}} \tag{55.130}$$

whose equation of motion is

$$\partial_t \boldsymbol{u}_{\mathrm{s}} + f \, \hat{\boldsymbol{z}} \times \boldsymbol{u}_{\mathrm{s}} = g^{\mathrm{r}} \nabla \eta'_{3/2}. \tag{55.131}$$

For the barotropic wave, whereby both layer interfaces undulate in phase and with a relatively small amplitude (Figure 55.3), then the shear velocity is nearly zero since the pressure gradient, $g^{\mathrm{r}} \nabla \eta'_{3/2}$ in equation (55.131) is small for the barotropic wave. In contrast, the depth averaged velocity described by equation (55.127a) is dominated by the larger (in magnitude) pressure gradient arising from free surface height undulations, $-g \nabla \eta'_{1/2}$. For the baroclinic wave, the depth averaged velocity is far smaller in magnitude than found in the barotropic wave, and the pressure gradient is dominated by interior interface undulations via $g^{\mathrm{r}} \nabla \eta'_{3/2}$. These behaviors motivate the oceanographic colloquial terminology whereby the depth averaged velocity is referred to as the *barotropic velocity* and the shear velocity is referred to as the *baroclinic velocity*.

55.6.7 Comments

As noted at the start of this section, the addition of further layers greatly increases the algebraic complexity of the analysis, thus motivating the use of numerical models for studies with $N > 2$ layers. One generally finds that each layer adds another wave mode, with N layers realizing N modes (one barotropic mode and $N - 1$ baroclinic modes). We further the study of gravity waves in Chapter 57 by studying internal gravity waves, with such waves corresponding here to a continuum of baroclinic modes.

55.7 Kelvin waves

The Kelvin wave is a non-dispersive gravity wave. It arises from the combined presence of a boundary and the Coriolis acceleration. The boundary considered here is a solid vertical wall. Additionally, Kelvin waves occur along the equator, with the equator acting as a boundary due to the change in sign of the Coriolis parameter, f.

55.7.1 Wave solutions with a southern boundary

To expose the key points about the shallow water Kelvin wave, it is sufficient to orient the f-plane with a boundary at $y = y_0$ and to consider flow in the region $y > y_0$. The meridional velocity component must vanish at $y = y_0$ to satisfy the no-normal flow condition. We are thus motivated to seek nontrivial solutions with $v' = 0$ everywhere, in which case the linearized

f-plane thickness and velocity equations are

$$\partial_t \eta' = -H\, \partial_x u' \tag{55.132a}$$
$$\partial_t u' = -g\, \partial_x \eta' \tag{55.132b}$$
$$f\, u' = -g\, \partial_y \eta'. \tag{55.132c}$$

It is notable that the meridional velocity equation (55.132c) expresses geostrophic balance between the Coriolis acceleration, $f\, u'$, and meridional pressure gradient, $-g\, \partial_y \eta'$.

Taking the time derivative of the zonal velocity equation (55.132b) and making use of the free surface equation (55.132a) leads to the one-dimensional wave equation for the zonal velocity

$$(\partial_{tt} - c_{\text{grav}}^2\, \partial_{xx})\, u' = 0, \tag{55.133}$$

where

$$c_{\text{grav}} = \sqrt{g\, H} \tag{55.134}$$

is the shallow water gravity wave speed. Likewise, a time derivative of the free surface equation (55.132a) and substitution of zonal velocity equation (55.132b) recovers the same wave equation satisfied by the free surface

$$(\partial_{tt} - c_{\text{grav}}^2\, \partial_{xx})\, \eta' = 0. \tag{55.135}$$

55.7.2 Kelvin wave solutions

In Section 6.7 we studied how to solve the wave equations (55.133) and (55.135), in which we write the general solutions in the form

$$u'(x, y, t) = F_1(x^{\text{L}}(t), y) + F_2(x^{\text{R}}(t), y), \tag{55.136a}$$
$$\eta'(x, y, t) = E_1(x^{\text{L}}(t), y) + E_2(x^{\text{R}}(t), y). \tag{55.136b}$$

In these expressions, F_1, E_1, F_2, E_2 are functions of space that are specified by the initial conditions, and

$$x^{\text{L}}(t) = x + c_{\text{grav}}\, t \quad \text{and} \quad x^{\text{R}}(t) = x - c_{\text{grav}}\, t \tag{55.137}$$

are points along the x-axis that, as time increases, move to the left and right, respectively, at the gravity wave speed. Evidently, the wave signal transmits, without distortion, the F_1 and E_1 patterns in the negative $\hat{\boldsymbol{x}}$-direction, and the F_2 and E_2 patterns propagate in the positive $\hat{\boldsymbol{x}}$-direction.

The free surface height and zonal velocity are coupled via the equations of motion (55.132a)–(55.132c), so that the functions F_1, F_2 are related to E_1, E_2. To determine this relation we use the velocity equation (55.132b) along with the chain rule

$$\frac{\partial F_1}{\partial t} = \frac{\partial F_1(x^{\text{L}}, y)}{\partial x^{\text{L}}} \frac{\mathrm{d}x^{\text{L}}}{\mathrm{d}t} = \frac{\partial F_1(x^{\text{L}}, y)}{\partial x^{\text{L}}}\, c_{\text{grav}} \tag{55.138a}$$
$$\frac{\partial F_2}{\partial t} = \frac{\partial F_2(x^{\text{R}}, y)}{\partial x^{\text{R}}} \frac{\mathrm{d}x^{\text{R}}}{\mathrm{d}t} = -\frac{\partial F_2(x^{\text{R}}, y)}{\partial x^{\text{R}}}\, c_{\text{grav}}, \tag{55.138b}$$

in which case

$$\partial_t u' = c_{\text{grav}}\, (\partial F_1 / \partial x^{\text{L}} - \partial F_2 / \partial x^{\text{R}}) = -g\, \partial_x \eta' = -g\, (\partial E_1 / \partial x^{\text{L}} - \partial E_2 / \partial x^{\text{R}}), \tag{55.139}$$

so that

$$\eta'(x, y, t) = (c_{\text{grav}}/g)\, \big[-F_1(x + c_{\text{grav}}\, t, y) + F_2(x - c_{\text{grav}}\, t, y)\big]. \tag{55.140}$$

To determine the meridional dependence to the wave solutions requires the geostrophic

balance (55.132c), with the free surface equation (55.140) and zonal velocity equation (55.136a) leading to

$$\partial_y F_1 = f\, F_1 / c_{\text{grav}} \quad \text{and} \quad \partial_y F_2 = -f\, F_2 / c_{\text{grav}}, \tag{55.141}$$

whose solutions take the form

$$F_1 = F(x + c_{\text{grav}}\, t)\, \mathrm{e}^{(y-y_0)/L_{\text{d}}} \quad \text{and} \quad F_2 = G(x - c_{\text{grav}}\, t)\, \mathrm{e}^{-(y-y_0)/L_{\text{d}}}, \tag{55.142}$$

where

$$L_{\text{d}} = c_{\text{grav}} / f \tag{55.143}$$

is the shallow water deformation radius defined in equation (43.31) (and used in Section 55.4.6). We also introduced the functions F and G, which are functions of a single space coordinate. To ensure boundedness in the region $y > y_0$, where the fluid is assumed to exist, we drop the F_1 solution, thus leaving the free surface

$$\eta' = (H/g)^{1/2}\, \mathrm{e}^{-(y-y_0)/L_{\text{d}}}\, G(x - c_{\text{grav}}\, t), \tag{55.144}$$

and the horizontal velocity components

$$u' = \mathrm{e}^{-(y-y_0)/L_{\text{d}}}\, G(x - c_{\text{grav}}\, t) \quad \text{and} \quad v' = 0. \tag{55.145}$$

For the vertical velocity component we return to equation (55.26) to write

$$w'(z) = w'(z = -H) - (z + H)\, \partial_x u' \tag{55.146a}$$

$$= w'(z = -H) + H^{-1}\, (z + H)\, \partial_t \eta' \tag{55.146b}$$

$$= w'(z = -H) - (z + H)\, \mathrm{e}^{-(y-y_0)/L_{\text{d}}}\, \frac{\mathrm{d}G(x^{\text{R}})}{\mathrm{d}x^{\text{R}}}, \tag{55.146c}$$

where the second equality used the linearized thickness equation (55.132a), and the third equality used the chain rule.

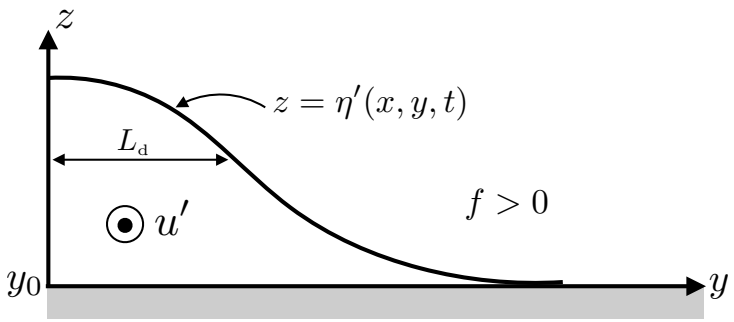

FIGURE 55.4: Illustrating free surface and zonal velocity for a northern hemisphere Kelvin wave with a solid boundary on the south. The free surface exponentially decays away from the boundary with a decay scale set by the deformation radius, L_{d}. With $f > 0$ the Kelvin wave propagates with the boundary on the right, so that for this orientation the wave phase velocity is coming out of the page.

These non-dispersive gravity wave signals propagate in the positive $\hat{\boldsymbol{x}}$ direction, in which case the boundary $y = y_0$ is on the right. This orientation holds for any boundary orientation in the northern hemisphere, whereby Kelvin waves propagate with the solid boundary on the right when looking in the direction of wave phase velocity. For the southern hemisphere, Kelvin waves propagate with the boundary to the left of the wave motion. Hence, Kelvin waves propagate cyclonically around a closed basin. In Figure 55.4 we illustrate the free surface and velocity for the Kelvin wave solution just derived.

55.8 Inertia-gravity waves

In this section we set the Coriolis parameter, f, to a nonzero constant while retaining a flat bottom and removing all side boundaries. We also retain a nonzero gravity, which is consistent with the shallow water being in hydrostatic balance. The linearized thickness equation (55.13), velocity equation (55.15), and potential vorticity equation (55.23) take the form

$$\partial_t \eta' = -H \nabla \cdot \boldsymbol{u}' \tag{55.147a}$$

$$\partial_t \boldsymbol{u}' + f \hat{\boldsymbol{z}} \times \boldsymbol{u}' = -g \nabla \eta' \tag{55.147b}$$

$$\partial_t Q' = 0, \tag{55.147c}$$

where the linear flat bottom f-plane shallow water potential vorticity is given from equation (55.22)

$$Q' = \zeta'/H - f \eta'/H^2, \tag{55.148}$$

where we dropped the constant f since it plays no dynamical role.

55.8.1 Forced oscillator equation for horizontal velocity

Taking a time derivative of the horizontal velocity equation (55.147b), and then back-substituting the velocity equation, leads to

$$(\partial_{tt} + f^2)\boldsymbol{u}' = -g\,(\partial_t \nabla \eta' - f \hat{\boldsymbol{z}} \times \nabla \eta'). \tag{55.149}$$

This equation for the horizontal velocity is in the form of a forced oscillator, with forcing from gradients in the free surface. We make use of this equation when developing the mathematical expressions for plane inertia-gravity waves in Section 55.8.9.

55.8.2 Free wave equation and potential vorticity

For the case of a flat bottom on an f-plane, we can write the wave equation (55.31) as

$$(\partial_{tt} - c_{\text{grav}}^2 \nabla^2)\eta' = -H f \zeta'. \tag{55.150}$$

This equation describes a forced shallow water gravity wave with forcing from relative vorticity coupled to the Coriolis parameter. Recall that this coupling between Coriolis and relative vorticity is fundamental to the inertial waves studied in Chapter 53. We can now use the vorticity equation as in Section 55.4.2 to eliminate ζ' to reveal a free wave equation. Equivalently, in equation (55.38) we set f to a constant and the bottom to be flat, thus leading to

$$\partial_t \left[\partial_{tt}\eta' + f^2 \eta' - c_{\text{grav}}^2 \nabla^2 \eta'\right] = 0. \tag{55.151}$$

The linear fluctuations described by this equation are known as shallow water *inertia-gravity* or *Poincaré waves*. The name "inertia-gravity" is due to the presence of both the Coriolis frequency, f, and gravitational acceleration, g, with both playing a role as restoring forces to support the waves.

The wave equation (55.151) is in the form of a local conservation law where the term in square brackets is static. We already know about another static field, namely the potential vorticity, Q', given by equation (55.148). We here show that the wave equation (55.151) is indeed identical to the potential vorticity equation (55.147c). For this purpose, substitute the expression (55.148) for the potential vorticity into the forced wave equation (55.150), which readily yields

$$f H^2 Q' = -(\partial_{tt} + f^2 - c_{\text{grav}}^2 \nabla^2)\,\eta'. \tag{55.152}$$

We thus find that

$$\partial_t Q' = 0 \Longrightarrow \partial_t \left[\partial_{tt} \eta' + f^2 \, \eta' - c_{\text{grav}}^2 \nabla^2 \eta' \right] = 0, \tag{55.153}$$

so that the wave equation (55.151) for inertia-gravity waves is identical to the conservation equation for linear shallow water potential vorticity. We saw a similar connection between potential vorticity conservation and waves in our study of Rossby waves in Section 54.3 for the horizontally non-divergent barotropic fluid, and will see the connection yet again for shallow water Rossby waves in Section 55.9.

55.8.3 Dispersion relation

Substituting the wave ansatz (55.24) into equations (55.147a)-(55.147b) renders the homogeneous matrix-vector equation

$$\begin{bmatrix} -\mathrm{i}\,\omega & -f & \mathrm{i}\,g\,k_x \\ f & -\mathrm{i}\,\omega & \mathrm{i}\,g\,k_y \\ \mathrm{i}\,H\,k_x & \mathrm{i}\,H\,k_y & -\mathrm{i}\,\omega \end{bmatrix} \begin{bmatrix} \tilde{u} \\ \tilde{v} \\ \tilde{\eta} \end{bmatrix} = \begin{bmatrix} 0 \\ 0 \\ 0 \end{bmatrix}. \tag{55.154}$$

This equation has a nontrivial solution only when the determinant of the matrix vanishes. The real part of the determinant cancels exactly, thus leaving just the imaginary part. Setting the imaginary part to zero yields the dispersion relation

$$\omega \left[\omega^2 - f^2 - g\,H\,|\boldsymbol{k}|^2 \right] = 0. \tag{55.155}$$

We can derive the same dispersion relation by substituting the wave ansatz into the wave equation (55.153). There are three solutions to this cubic equation described in the following subsections.

55.8.4 Zero frequency geostrophic mode

The zero frequency solution to the dispersion relation (55.155) corresponds to f-plane geostrophic motion. Such motion is static so that the linearized continuity equation (55.147a) means that the flow is horizontally non-divergent, $\nabla \cdot \boldsymbol{u}' = 0$. Furthermore, the geostrophic solution corresponds to a static yet non-zero potential vorticity

$$f\,\hat{\boldsymbol{z}} \times \boldsymbol{u}' = -g\,\nabla\eta' \Longrightarrow (f/g)\,Q' = (\nabla^2 - L_{\mathsf{d}}^{-2})\,\eta' \neq 0, \tag{55.156}$$

where we introduced the deformation radius, $L_{\mathsf{d}} = c_{\text{grav}}/f$, from equation (55.54). Turning equation (55.156) around, we see that if the potential vorticity is known, then the geostrophically balanced free surface can be found by inverting the elliptic operator, $\nabla^2 - L_{\mathsf{d}}^{-2}$.

The static geostrophic mode with nonzero potential vorticity is decoupled, in the linear theory, from the ageostrophic inertia-gravity wave whose potential vorticity is identically zero and yet whose relative vorticity and free surface are time dependent. For this reason we can separately study the two linear modes without concern for interactions.

55.8.5 Inertia-gravity wave modes

The $\omega \neq 0$ solution to the dispersion relation (55.155) satisfies the dispersion relation

$$\omega^2 = f^2\,(1 + L_{\mathsf{d}}^2\,|\boldsymbol{k}|^2). \tag{55.157}$$

Recall from Section 49.2 that we consider the angular frequency of waves to be non-negative. Hence, we only take the positive root

$$\omega = |f| \sqrt{1 + L_\mathsf{d}^2 \, |\boldsymbol{k}|^2}, \tag{55.158}$$

with Figure 55.5 depicting this relation.

The $\omega > 0$ modes satisfying the dispersion relation (55.158) are inertia-gravity waves. These waves have an angular frequency greater than or equal to the inertial frequency

$$\omega \geq |f|, \tag{55.159}$$

and are thus said to be *super-inertial waves*.[6] Furthermore, they carry zero potential vorticity (equation (55.152))

$$f \, H^2 \, Q' = -(\partial_{tt} + f^2 - c_\mathsf{grav}^2 \, \nabla^2) \, \eta' = 0, \tag{55.160}$$

where we verify this property holds for plane inertia-gravity waves in Exercise 55.5. With $Q' = 0$, equation (55.148) for the potential vorticity shows that the inertia-gravity waves carry a relative vorticity given by

$$\zeta' = f \, \eta' / H. \tag{55.161}$$

Since $|\eta'|/H \ll 1$, we see that the relative vorticity carried by shallow water inertia-gravity waves is small relative to the planetary vorticity

$$|\zeta'| \ll |f|. \tag{55.162}$$

55.8.6 Group velocity

Taking the $\boldsymbol{k}$-space gradient of the dispersion relation (55.158) leads to the group velocity for the shallow water inertia-gravity waves

$$\boldsymbol{c}_\mathsf{g} = \nabla_{\boldsymbol{k}} \varpi(\boldsymbol{k}) = \frac{c_\mathsf{grav}^2 \, \boldsymbol{k}}{\omega} = \frac{\boldsymbol{c}_\mathsf{p} \, c_\mathsf{grav}^2}{|\boldsymbol{c}_\mathsf{p}|^2} = \frac{\boldsymbol{c}_\mathsf{p}}{1 + (L_\mathsf{d} \, |\boldsymbol{k}|)^{-2}}, \tag{55.163}$$

where the phase velocity is $\boldsymbol{c}_\mathsf{p} = (\omega / |\boldsymbol{k}|) \, \hat{\boldsymbol{k}}$. Evidently, the group velocity is parallel to the phase velocity and the ratio of their magnitudes is given by

$$\frac{|\boldsymbol{c}_\mathsf{g}|}{|\boldsymbol{c}_\mathsf{p}|} = \frac{c_\mathsf{grav}^2}{|\boldsymbol{c}_\mathsf{p}|^2} = \frac{1}{1 + (L_\mathsf{d} \, |\boldsymbol{k}|)^{-2}}. \tag{55.164}$$

In the non-rotating case, where $f = 0$ so that $L_\mathsf{d}^{-2} = (c_\mathsf{grav}/f)^{-2} = 0$, the group and phase velocities are equal, which we expect since the non-rotating shallow water gravity waves from Section 55.5 are non-dispersive. The inertia-gravity waves approach the non-dispersive limit for wavelengths much smaller than the deformation radius, in which the waves are too small to feel the effects from the Coriolis acceleration (we further discuss the shortwave limit in Section 55.8.7). But for the general case with dispersion, the Coriolis acceleration causes the group velocity to be smaller in magnitude than the phase velocity. Hence, the wave energy, which is carried by the group velocity (see Section 55.8.10 on energetics), is more slowly transmitted than the phase.

[6] The inertial waves considered in Chapter 53, which we studied in a homogeneous fluid, have their angular frequency bounded by $\omega^2 < f^2$. These are *sub-inertial* waves. They are again encountered in Section 57.9.1 as a special case of a rotating internal gravity wave in the limit where the reference fluid state is homogeneous. They are distinct from the shallow water inertial waves since the shallow water fluid is hydrostatic whereas the inertial waves in Chapter 53 rely on non-hydrostatic pressure.

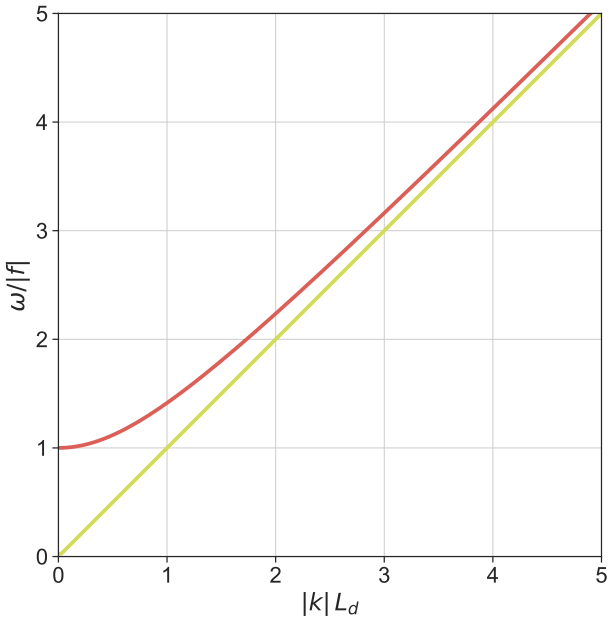

FIGURE 55.5: Illustrating the dispersion relation for shallow water inertia-gravity waves. The red hyperbolic curve is the dispersion relation (55.157), which asymptotes at high wavenumber (small wavelength) to the straight line for the non-rotating case. The angular frequency, ω, is scaled by the magnitude of the Coriolis frequency, $|f|$, and the horizontal wavenumber, $|\boldsymbol{k}|$, is multiplied by the deformation radius $L_{\text{d}} = \sqrt{gH}/f = c_{\text{grav}}/f$. For small wave numbers ($|\boldsymbol{k}|\, L_{\text{d}} \ll 1$ or $\Lambda \gg 2\,\pi\, L_{\text{d}}$), the inertial-gravity wave frequency approaches the inertia frequency, f, with this behavior seen at the minimum of the dispersion curve. We expect this result since waves large relative to the deformation radius feel the Coriolis acceleration. At the opposite extreme of high wave numbers ($\Lambda \ll 2\,\pi\, L_{\text{d}}$), the wave frequency approaches the non-rotating gravity wave frequency, shown here by the linear dispersion relation $\omega = |\boldsymbol{k}|\,\sqrt{g\,H} = |\boldsymbol{k}| c_{\text{grav}}$. Waves small relative to the deformation radius do not feel the Coriolis acceleration and thus converge to non-rotating gravity waves. Since all shallow water inertia-gravity waves satisfy $\omega^2 \geq f^2$, they are said to be *super-inertial* waves; i.e., waves whose frequency is larger in magnitude than the inertial frequency.

55.8.7 Shortwave limit for inertia-gravity waves

The shortwave limit is in the regime where

$$|\boldsymbol{k}|^2\, L_{\text{d}}^2 \gg 1, \tag{55.165}$$

so that the shortwave limit occurs when the wavelength is much shorter than the deformation radius, in which case the waves do not feel the effects from the Coriolis acceleration. For example, consider a middle latitude shallow water gravity wave in a layer with $H = 10^3$ m and $f = 10^{-4}$ s^{-1}, in which case the shallow water deformation radius is $L_{\text{d}} = \sqrt{g\,H}/f = 10^3$ km. Maintaining the constraint (55.165) means that the wavelength of the gravity wave, $\Lambda = 2\pi/|\boldsymbol{k}|$, must satisfy

$$\Lambda \ll 2\pi\, L_{\text{d}}. \tag{55.166}$$

Within the shortwave limit, however, the wavelength cannot be too small since the flow must retain the hydrostatic balance as per a shallow water model. As discussed in Section 27.2, maintaining the hydrostatic balance means that the flow retains a small vertical to horizontal aspect ratio. In terms of the wavenumber for gravity waves, the hydrostatic balance implies

$$|\boldsymbol{k}|\, H \ll 1 \quad \Longleftarrow \text{hydrostatic balance.} \tag{55.167}$$

We conclude that the shortwave limit for shallow water gravity waves is given by the regime

$$L_{\text{d}}^{-1} \ll |\boldsymbol{k}| \ll H^{-1} \Longleftrightarrow 2\pi\, H \ll \Lambda \ll 2\pi\, L_{\text{d}}. \tag{55.168}$$

Although considered short from the perspective of the shallow water model, these waves are hydrostatic and thus considered long gravity waves from the perspective of the surface gravity waves studied in Chapter 52.

Finally, for the shortwave limit, the dispersion relation (55.157) reduces to the dispersion relation (55.81)

$$\omega \approx |\boldsymbol{k}|\, c_{\text{grav}}. \tag{55.169}$$

Such waves are only weakly affected by the Coriolis acceleration so that their dispersion relation reduces to linear and non-dispersive gravity waves of Section 55.5.

55.8.8 Longwave limit for inertia-gravity waves

The longwave limit occurs when

$$|\boldsymbol{k}|^2\, L_{\text{d}}^2 \ll 1, \tag{55.170}$$

so the waves are much longer than the deformation radius. In this limit the wave is strongly affected by the Coriolis acceleration. Indeed, the wave dispersion relation becomes

$$\omega^2 = f^2, \tag{55.171}$$

in which fluid particles exhibit inertial oscillations (Sections 55.8.9 and 14.4).

55.8.9 Polarization relations for a plane inertia-gravity wave

As for the gravity waves in Section 55.5, we study the behavior of the traveling plane wave ansatz (55.24). In contrast to the case with $f = 0$, here we require the complex nature of the wave amplitudes $(\tilde{u}, \tilde{v}, \tilde{\eta})$ in order to realize nontrivial inertia-gravity wave solutions. Such complex amplitudes mean there are differences in phase between the velocity and free surface, with phase differences arising from the Coriolis parameter.

Polarization relations for the wave

Substituting the traveling plane wave ansatz (55.24) into the forced oscillator equation (55.149) leads to the amplitude relation

$$(-\omega^2 + f^2)\, \tilde{\boldsymbol{u}} = -g\, (\omega\, \boldsymbol{k} - \mathrm{i}\, f\, \hat{\boldsymbol{z}} \times \boldsymbol{k})\, \tilde{\eta}. \tag{55.172}$$

Without loss of generality, we assume the free surface amplitude, $\tilde{\eta}$, is real, which then leads to the free surface height

$$\eta' = \tilde{\eta} \cos(\boldsymbol{k} \cdot \boldsymbol{x} - \omega\, t), \tag{55.173}$$

and the fluid velocity within a plane wave

$$\boldsymbol{u}' = \frac{g\, |\boldsymbol{k}|\, \tilde{\eta}}{\omega^2 - f^2} \left[\underbrace{\omega\, \hat{\boldsymbol{k}} \cos(\boldsymbol{k} \cdot \boldsymbol{x} - \omega\, t)}_{\text{horizontally longitudinal}} + \underbrace{f\, (\hat{\boldsymbol{z}} \times \hat{\boldsymbol{k}}) \sin(\boldsymbol{k} \cdot \boldsymbol{x} - \omega\, t)}_{\text{horizontally transverse}} \right] \tag{55.174a}$$

$$= \frac{\tilde{\eta}}{|\boldsymbol{k}|\, H} \left[\underbrace{\omega\, \hat{\boldsymbol{k}} \cos(\boldsymbol{k} \cdot \boldsymbol{x} - \omega\, t)}_{\text{horizontally longitudinal}} + \underbrace{f\, (\hat{\boldsymbol{z}} \times \hat{\boldsymbol{k}}) \sin(\boldsymbol{k} \cdot \boldsymbol{x} - \omega\, t)}_{\text{horizontally transverse}} \right], \tag{55.174b}$$

where the unit vector

$$\hat{\boldsymbol{k}} = \boldsymbol{k}/|\boldsymbol{k}| \tag{55.175}$$

points in the direction of the wave, and equation (55.174b) follows from use of the dispersion relation (55.157) in equation (55.174a). The vanishing potential vorticity in these waves means

that they carry a nonzero relative vorticity as given by equation (55.161), so that

$$\zeta' = f\,\eta'/H = (f\,\tilde{\eta}/H)\cos(\boldsymbol{k}\cdot\boldsymbol{x} - \omega\,t). \tag{55.176}$$

Hence, in the northern hemisphere the relative vorticity is in-phase with the free surface, whereas in the southern hemisphere it is π radians out of phase.

These mathematical expressions for the fields within a wave are sometimes referred to as *polarization relations*. Observe that the horizontally transverse component of the velocity vector is $\pi/2$ out of phase from the horizontally longitudinal component. Furthermore, the transverse component corresponds to fluid particle motion that is perpendicular to the wavevector, in which case we say that the transverse component is *polarized* perpendicular to the wavevector.

Drawing the polarization relations

To draw the free surface (55.173), vorticity (55.176), and velocity (55.174b) we assume that $f > 0$ for the northern hemisphere, and recall that $\omega^2 \geq f^2$ since shallow water inertia-gravity waves are super-inertial. We also find it convenient to write the velocity as

$$\frac{\boldsymbol{u}'\,|\boldsymbol{k}|\,H}{\tilde{\eta}\,f} = (\omega/f)\,\hat{\boldsymbol{k}}\cos(\boldsymbol{k}\cdot\boldsymbol{x} - \omega\,t) + (\hat{\boldsymbol{z}}\times\hat{\boldsymbol{k}})\sin(\boldsymbol{k}\cdot\boldsymbol{x} - \omega\,t). \tag{55.177}$$

Consider a point fixed in space and let time progress so that the phase,

$$\mathcal{P} = \boldsymbol{k}\cdot\boldsymbol{x} - \omega\,t, \tag{55.178}$$

decreases. Consequently, the velocity vector rotates in a clockwise direction, forming an ellipse with the major axis along the longitudinal direction, $\hat{\boldsymbol{k}}$, and minor axis along the transverse direction, $(\hat{\boldsymbol{z}}\times\hat{\boldsymbol{k}})$. This motion corresponds to the inertial oscillations studied in Section 14.4 (where $\omega^2 = f^2$). Now consider a fixed time and sample the velocity field in the direction of the wave. In this case the phase increases as we move in the wave direction, so that the sampled velocity progresses counter-clockwise around the ellipse. Figure 55.6 offers three depictions of the wave field.

55.8.10 Energetics

In Section 55.3.2 we considered the general form of energy balances for the linearized shallow water equations integrated over the shallow water layer. For the special case of a flat bottom domain (with $\eta_\mathrm{b} = 0$ for simplicity), these equations take the form

$$\partial_t(\mathcal{K}^{\mathrm{sw}} + \mathcal{P}^{\mathrm{sw}}) = -g\,\rho\,H\,\nabla\cdot[(\overline{\eta} + \eta')\,\boldsymbol{u}'] \tag{55.179a}$$

$$\mathcal{P}^{\mathrm{sw}} = (\rho/2)\,g\,\eta^2 \tag{55.179b}$$

$$\mathcal{K}^{\mathrm{sw}} = (\rho/2)\,H\,\boldsymbol{u}'\cdot\boldsymbol{u}'. \tag{55.179c}$$

Here we consider the energy carried by a plane inertia-gravity wave, and focus on the phase averaged energetics. Note that since the waves are present throughout space (as per the plane wave assumption), we do not expect to have energy accumulate in any particular region when phase averaged. Instead, we expect the phase averaged energy to remain constant. So our question then concerns how that energy is partitioned according to kinetic energy and potential energy, and how the energy moves or is fluxed.

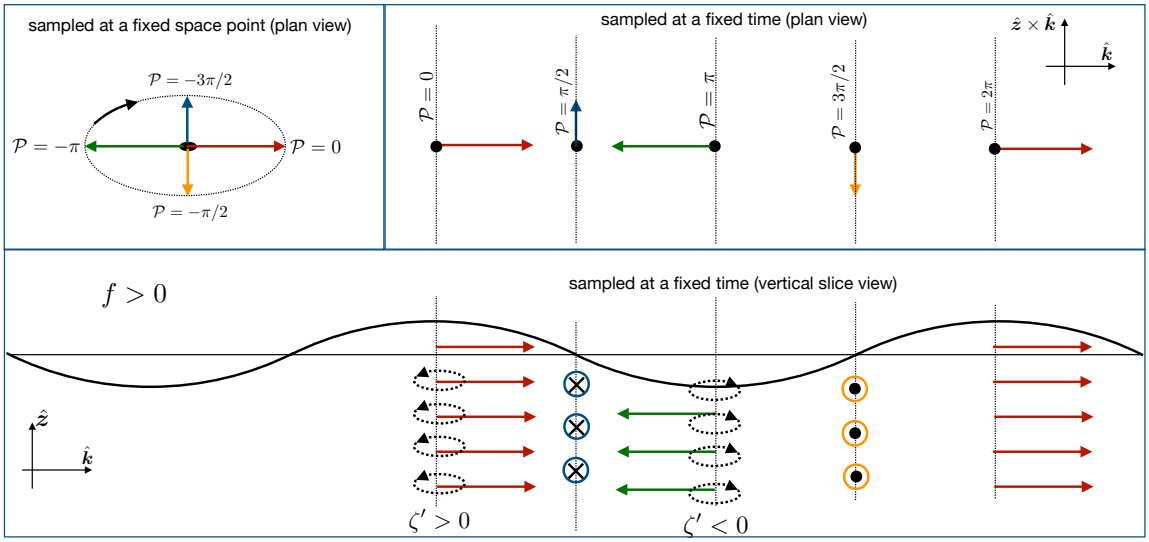

FIGURE 55.6: Illustrating the shallow water inertia gravity wave from three perspectives, with $\mathcal{P} = \boldsymbol{k} \cdot \boldsymbol{x} - \omega\, t$ the phase and $f > 0$. The upper left panel shows the horizontal velocity vector at a fixed point in space as time increases and so the phase decreases (becomes more negative). The resulting velocity vector rotates clockwise and exhibits inertial oscillations. The upper right panel shows the horizontal velocity vector sampled along the wave direction, $\hat{\boldsymbol{k}}$, at a fixed time from a plan (horizontal) view, in which case the phase increases moving in the $\hat{\boldsymbol{k}}$ direction. The lower panel shows the horizontal velocity, relative vorticity, and free surface as viewed from a vertical slice aligned with the wavevector direction. Note that the relative vorticity is the vertical component, ζ', so that the arrowed ellipses on the lower panel are in the horizontal plane.

Kinetic and potential energies contained in a plane wave

Writing the free surface as in equation (55.173) and the horizontal velocity as in equations (55.174a) and (55.174b) leads to the potential energy and kinetic energy carried by the wave field

$$\mathscr{P}^{\text{sw}} = \frac{\rho\, g\, \tilde{\eta}^2}{2} \cos^2(\boldsymbol{k} \cdot \boldsymbol{x} - \omega\, t) \tag{55.180a}$$

$$\mathscr{K}^{\text{sw}} = \frac{\rho\, \tilde{\eta}^2}{|\boldsymbol{k}|^2\, H^2} \left[\omega^2 \cos^2(\boldsymbol{k} \cdot \boldsymbol{x} - \omega\, t) + f^2 \sin^2(\boldsymbol{k} \cdot \boldsymbol{x} - \omega\, t)\right], \tag{55.180b}$$

with a corresponding phase average given by

$$\langle \mathscr{P}^{\text{sw}} \rangle = \frac{\rho\, g\, \tilde{\eta}^2}{4} \tag{55.181a}$$

$$\langle \mathscr{K}^{\text{sw}} \rangle = \frac{\rho\, \tilde{\eta}^2\, (\omega^2 + f^2)}{2\, |\boldsymbol{k}|^2\, H^2} = \frac{\rho\, g\, \tilde{\eta}^2}{4} \frac{\omega^2 + f^2}{\omega^2 - f^2}. \tag{55.181b}$$

Evidently, for non-rotating shallow water gravity waves, $f = 0$, there is an equipartition between phase averaged potential and kinetic energy. However, for the general case with rotation, the phase averaged kinetic energy is larger than the potential energy

$$\frac{\langle \mathscr{K}^{\text{sw}} \rangle}{\langle \mathscr{P}^{\text{sw}} \rangle} = \frac{\omega^2 + f^2}{\omega^2 - f^2} = 1 + 2\, (L_{\text{d}}\, |\boldsymbol{k}|)^{-2}, \tag{55.182}$$

with equipartition approached only for wave lengths smaller than the deformation radius (high wave numbers).

Mechanical energy and energy flux contained in a plane wave

The phase averaged mechanical energy contained in a plane wave is given by

$$\langle \mathscr{P}^{\text{sw}} \rangle + \langle \mathscr{K}^{\text{sw}} \rangle = \langle \mathscr{P}^{\text{sw}} \rangle \left[1 + \frac{\omega^2}{\omega^2 - f^2} \right] = 2 \langle \mathscr{P}^{\text{sw}} \rangle \frac{|\boldsymbol{c}_{\text{p}}|^2}{c_{\text{grav}}^2} = \frac{\rho\, g\, \tilde{\eta}^2}{2} \frac{|\boldsymbol{c}_{\text{p}}|}{|\boldsymbol{c}_{\text{g}}|}, \tag{55.183}$$

where we made use of equation (55.164) for the ratio of the group velocity magnitude to the phase velocity magnitude. For the flux of energy contained in the wave, we return to the energy equation (55.179a) and only consider the phase averaged flux, which takes the form

$$g\, \rho\, H\, \langle \eta'\, \boldsymbol{u}' \rangle = \frac{g\, \rho\, \tilde{\eta}^2\, \omega\, \boldsymbol{k}}{2\, |\boldsymbol{k}|^2} = \frac{g\, \rho\, \tilde{\eta}^2\, \boldsymbol{c}_{\text{p}}}{2} = \frac{g\, \rho\, \tilde{\eta}^2\, \boldsymbol{c}_{\text{g}}}{2} \frac{|\boldsymbol{c}_{\text{p}}|}{|\boldsymbol{c}_{\text{g}}|} = \boldsymbol{c}_{\text{g}} \left(\langle \mathscr{P}^{\text{sw}} \rangle + \langle \mathscr{K}^{\text{sw}} \rangle \right). \tag{55.184}$$

Hence, the phase averaged mechanical energy flux contained in the plane wave is given by the group velocity times the phase averaged mechanical energy. This is a standard result that we have seen before in the study of other linear waves.

55.9 Rossby waves

We now focus on the sub-inertial wave equation (55.62) derived in Section (55.4.6)

$$\partial_t \left[(L_{\text{d}}^{-2} - \nabla^2)\, \eta' \right] = H\, \hat{\boldsymbol{z}} \cdot (\nabla \eta' \times \nabla Q_{\text{r}}), \tag{55.185}$$

where

$$Q_{\text{r}} = f / H_{\text{r}} \tag{55.186}$$

is the potential vorticity in the resting fluid. Equation (55.185) describes shallow water *Rossby waves*.

55.9.1 Dispersion relation

Making use of the plane wave ansatz (55.24) in the wave equation (55.185) readily leads to the shallow water Rossby wave dispersion relation

$$\omega = \frac{H\, (\boldsymbol{k} \times \hat{\boldsymbol{z}}) \cdot \nabla Q_{\text{r}}}{k_{\text{d}}^2 + |\boldsymbol{k}|^2} \tag{55.187}$$

For the angular frequency to be independent of space, ∇Q_{r} must be spatially independent. We can ensure this property by assuming a β-plane along with linear and gently varying topography

$$\nabla H_{\text{r}}^{-1} = -H_{\text{r}}^{-2}\, \nabla H_{\text{r}} = H_{\text{r}}^{-2}\, \nabla \eta_{\text{b}}' \approx H^{-2}\, \nabla \eta_{\text{b}}', \tag{55.188}$$

where $\nabla \eta_{\text{b}}'$ is spatially independent with linear topography. More general (but gently varying) bottom topography requires the asymptotic methods from Chapter 50.

The dispersion relation (55.187) compares directly to equation (54.32) for Rossby waves in the horizontally non-divergent barotropic model. The sole difference concerns the presence of the deformation radius, L_{d} from equation (55.54), and its associated wavenumber

$$k_{\text{d}} = L_{\text{d}}^{-1} = f / c_{\text{grav}}, \tag{55.189}$$

which is present in the shallow water dispersion relatio. This term is missing from the non-divergent barotropic model since c_{grav} is formally infinite (there are no gravity waves in that model), in which case $L_{\text{d}}^{-2} = k_{\text{d}}^2 = 0$.

55.9.2 Connecting to quasi-geostrophic potential vorticity

When deriving the sub-inertial equations in Section 55.4.6, we noted that the assumptions made in that derivation are identical to the assumptions made when deriving shallow water quasi-geostrophy in Section 43.5. Indeed, the Rossby wave equation (55.185) is the linearized equation for the material evolution of shallow water quasi-geostrophic potential vorticity. We see this equality by recalling the discussion in Section (43.6.3), where we derived equation (43.90)

$$(f_\circ/g)\,\mathrm{D}q/\mathrm{D}t = \partial_t\left[(L_\mathrm{d}^{-2} - \nabla^2)\,\eta'\right] - H\,\hat{\boldsymbol{z}}\cdot(\nabla\eta'\times\nabla Q_\mathrm{r}) - (g/f_\circ)\,\hat{\boldsymbol{z}}\cdot[\nabla\eta'\times\nabla(\nabla^2\eta')], \quad (55.190)$$

where q is the quasi-geostrophic potential vorticity. For an inviscid fluid, $\mathrm{D}q/\mathrm{D}t = 0$, and for small amplitude fluctuations the nonlinear term in equation (55.190) (final term on the right hand side) is neglected. In this case we see that the linearized equation for material evolution of quasi-geostrophic potential vorticity is identical to the Rossby wave equation (55.185).

The nonlinear term in equation (55.190) arises from the geostrophic advection of geostrophic relative vorticity. Although it is small for small amplitude fluctuations, and thus commonly dropped when deriving the dispersion relation, we note that it vanishes identically for a plane wave. It does so in precisely the same way as it vanishes for the non-divergent barotropic vorticity equation in Section 54.2.3. Namely, this result follows since for a plane wave, $\nabla(\nabla^2\eta') = -|\boldsymbol{k}|^2\nabla\eta'$, so that it follows immediately that $\nabla\eta'\times\nabla(\nabla^2\eta') = 0$. Hence, a plane Rossby wave is an exact solution to the shallow water quasi-geostrophic potential vorticity equation in an inviscid fluid.

55.9.3 Vorticity mechanism

In Section 54.3 we studied Rossby waves in the horizontally non-divergent barotropic model, with a vorticity mechanism for the waves presented in Figure 54.3. This mechanism follows from the material evolution of absolute vorticity in the horizontally non-divergent barotropic model. The identical mechanism holds for the shallow water fluid yet with quasi-geostrophic potential vorticity replacing absolute vorticity. Hence, all conceptual points from Figure 54.3 also hold for the shallow water fluid.

55.9.4 Dispersion circle for planetary Rossby waves

In Section 54.4.2 we described a geometric method to help interpret the dispersion relation for planetary Rossby waves in the horizontally non-divergent barotropic model. That method also proved useful in Section 54.4.3 for describing the reflection of Rossby waves from a smooth and flat wall. Here we extend the geometric method to shallow water planetary Rossby waves, in which the dispersion relation is given by the β portion of the general dispersion relation (55.187)

$$\varpi_\beta = -\frac{\beta\,k_x}{k_\mathrm{d}^2 + |\boldsymbol{k}|^2}. \quad (55.191)$$

This equation compares to the β portion of the dispersion relation (54.32) holding for the non-divergent barotropic model. Again, the sole distinction is that the shallow water Rossby wave dispersion has a nonzero deformation wavenumber, $k_\mathrm{d} \neq 0$.

Dispersion circle

Following the geometric approach from Section 54.4, we write the dispersion relation (55.191) as the equation of a circle in wavevector space

$$(k_x + \beta/2\omega)^2 + k_y^2 = (\beta/2\omega)^2 - k_\mathrm{d}^2. \quad (55.192)$$

As written, the angular frequency, ω, is a parameter for the circle whose center is

$$\boldsymbol{k}_{\text{center}} = -(\beta/2\omega)\,\hat{\boldsymbol{x}} \tag{55.193}$$

and squared radius is $(\beta/2\omega)^2 - k_{\mathsf{d}}^2$. The deformation wavenumber appearing on the right hand side of the circle equation (55.192) places an upper bound on the angular frequency allowed for propagating Rossby waves

$$\omega \leq \omega_{\max} = \beta/(2\,k_{\mathsf{d}}) = \beta\,L_{\mathsf{d}}/2. \tag{55.194}$$

The shallow water model supports gravity waves that render $k_{\mathsf{d}} \neq 0$, thus imposing an upper bound on the shallow water Rossby wave angular frequency. In contrast, for the horizontally non-divergent barotropic model, $k_{\mathsf{d}} = 0$ since there are no gravity waves, in which case there is no maximum frequency for Rossby waves. Note that for the β-plane scaling used to derive the Rossby waves,

$$\omega_{\max}/f_{\mathsf{o}} = \beta\,L_{\mathsf{d}}/(2\,f_{\mathsf{o}}) \ll 1, \tag{55.195}$$

thus confirming that the shallow water Rossby waves are strictly sub-inertial.

Group velocity

The group velocity, $\boldsymbol{c}_{\mathsf{g}} = \nabla_{\boldsymbol{k}}\varpi$, is given by

$$\boldsymbol{c}_{\mathsf{g}} = \frac{\beta\,[(k_x^2 - k_y^2 - k_{\mathsf{d}}^2)\,\hat{\boldsymbol{x}} + 2\,k_x\,k_y\,\hat{\boldsymbol{y}}]}{(|\boldsymbol{k}|^2 + k_{\mathsf{d}}^2)^2} = -\frac{2\,\omega\,\boldsymbol{R}}{|\boldsymbol{k}|^2 + k_{\mathsf{d}}^2}, \tag{55.196}$$

where we introduced the group velocity orientation vector

$$\boldsymbol{R} = -\boldsymbol{k} - \beta/(2\,\omega)\,\hat{\boldsymbol{x}} = -[k_x + \beta/(2\,\omega)]\,\hat{\boldsymbol{x}} - k_y\,\hat{\boldsymbol{y}} \quad \text{with} \quad |\boldsymbol{R}|^2 = (\beta/2\omega)^2 - k_{\mathsf{d}}^2. \tag{55.197}$$

As for the orientation vector (54.62) in the horizontally non-divergent barotropic model, the vector $\boldsymbol{R}$ points from the perimeter of the dispersion circle to the center (its magnitude equals to the radius of the circle). We thus conclude that the dispersion geometry for shallow water planetary waves directly carries over from the horizontally non-divergent barotropic model detailed in Section 54.4.2. We illustrate the dispersion geometry for shallow water Rossby waves in Figure 55.7, with many details provided in the figure and its caption.

55.9.5 Comments

A more streamlined approach to deriving the Rossby wave dispersion relation starts directly from the quasi-geostrophic potential vorticity equation. That approach makes use of the quasi-geostrophic theory derived in in Section 43.5. Even so, the longer approach taken in the current section benefits by exposing the direct connection to other shallow water waves through the unified shallow water equation (55.42).

In Chapter 62 we study waves in a continuous quasi-geostrophic fluid, thus returning to some of the material in this section while extending it to continuous stratification.

55.10 Exercises

EXERCISE 55.1: STEPS IN DERIVING THE LINEAR PV EQUATION
Fill in the mathematical details needed to derive the linearized potential vorticity equation (55.23). Hint: form the linearized relative vorticity equation as an intermediate step.

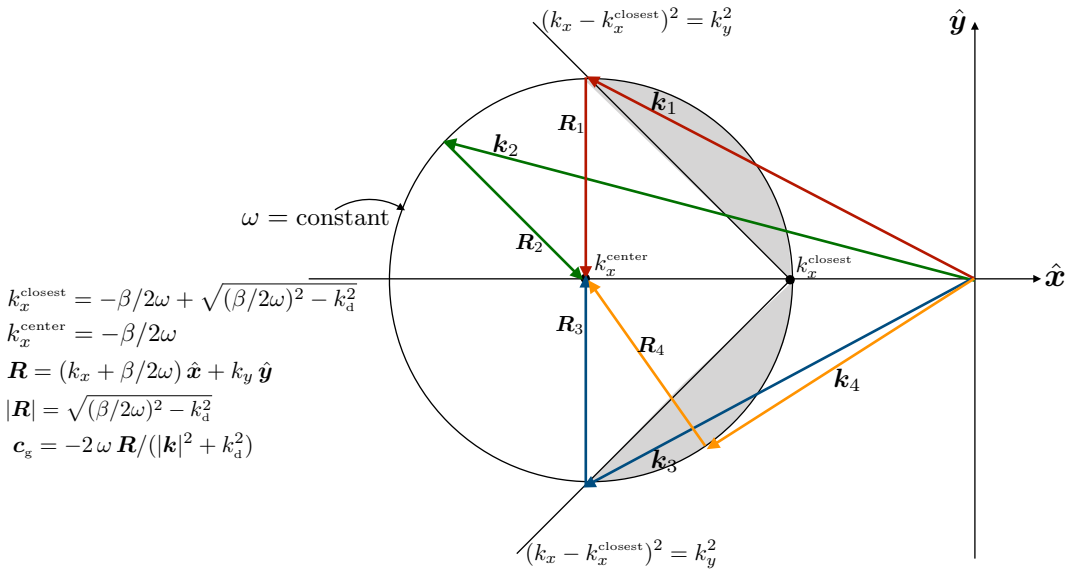

FIGURE 55.7: Dispersion circle for shallow water planetary Rossby waves as depicted by a circle in wavevector space, (k_x, k_y), parameterized by the angular frequency, ω. The center of the circle is at $\boldsymbol{k}_{\text{center}} = -(\beta/2\omega)\,\hat{\boldsymbol{x}}$ and the squared radius is $(\beta/2\omega)^2 - k_d^2$. A positive radius requires the angular frequency to be less than the maximum, $\omega_{\text{max}} = \beta/(2\,k_d)$. We depict four sample wavevectors, $\boldsymbol{k} = k_x\,\hat{\boldsymbol{x}} + k_y\,\hat{\boldsymbol{y}}$, that orient the phase velocity, $\boldsymbol{c}_p = \hat{\boldsymbol{k}}\,\omega/|\boldsymbol{k}|$. Each wavevector extends from the origin to a point on the circle. Each wavevector has an associated group velocity orientation vector, $\boldsymbol{R} = -\boldsymbol{k} - \beta/(2\,\omega)\,\hat{\boldsymbol{x}}$, that points from the circle perimeter to the circle center. The group velocity is westward for those wavevectors that intersect the circle perimeter within the gray-shaded region, which generally includes Rossby waves with low zonal wavenumbers. The group velocity is eastward for wavevectors outside the gray region, with the lines $(k_x - k_x^{\text{closest}})^2 = k_y^2$ separating these regions where the group velocity is westward or eastward. In particular, the group velocity for wavevector $\boldsymbol{k}_1$ is southward; for $\boldsymbol{k}_2$ it is southeastward; for $\boldsymbol{k}_3$ it is northward, and for $\boldsymbol{k}_4$ it is northwestward. This dispersion circle directly compares to Figure 54.5 constructed for the horizontally non-divergent barotropic model, with the key difference being $k_d \neq 0$ for the shallow water so that the dispersion circle does not touch the origin at $\boldsymbol{k} = 0$.

EXERCISE 55.2: STEPS IN DERIVING EQUATION (55.40)
Derive equation (55.40) from the linearized velocity equation (55.15).

EXERCISE 55.3: EQUATIONS FOR BAROTROPIC AND BAROCLINIC VELOCITIES
Fill in the details for deriving the equations (55.127a)-(55.127c) for the depth averaged and depth-deviation velocities.

EXERCISE 55.4: GRAVITY WAVES ON A CONSTANT REFERENCE FLOW
Consider a one-dimensional shallow water layer moving with a constant zonal speed, $U > 0$, over a flat bottom and in a non-rotating reference frame. We here examine the linear gravity wave disturbances on this constant background flow, thus generalizing the case from Section 55.5 for gravity waves propagating on a stationary background.

(a) Determine a general expression for the free surface wave fluctuation. Hint: perform a Galilean transformation (Section 17.5) to a reference frame moving with the constant background flow.

(b) Determine a general expression for the zonal velocity wave fluctuation.

(c) Making use of the ideas from hydraulic control in Section 55.5.4, discuss the cases where $U < c_{\text{grav}}$ (subcritical flow), $U > c_{\text{grav}}$ (supercritical flow), and $U = c_{\text{grav}}$ (critical flow).

EXERCISE 55.5: VANISHING POTENTIAL VORTICITY FOR INERTIA-GRAVITY WAVES
Verify that the linearized potential vorticity, $H\,Q' = \zeta' - f\,\eta'/H$, vanishes for the plane shallow water inertia-gravity waves (f-plane) given by the polarization relations in Section 55.8.9.

Chapter 56

SHALLOW WATER WAVES: CASE STUDIES

In this chapter we examine some case studies in shallow waves, thus furthering our study of shallow water wave mechanics.

READER'S GUIDE TO THIS CHAPTER

This chapter is a direct extension of the shallow water wave theory studied in Chapter 55.

56.1 Loose threads

- WKBJ approximation for shallow water gravity waves so to compute the change in the amplitude of the wave. Need to reinterpret the acoustic amplitude equation 50.37c for shallow water.

- Salmon class notes Chapter 9 on shallow water waves induced by an earthquake: solving the initial value problem.

- String function discussion from *Tyler and Käse* (2000) and *Tyler and Käse* (2001).

- non-Doppler for long Rossby waves as on page 14 of Liu's notes.

56.2 Waves excited by flow over topography

Consider the f-plane flow of a single layer of shallow water fluid with a static and prescribed reference flow, $\boldsymbol{u}_{\text{R}}$, and let this flow pass over a non-flat bottom with vertical position

$$\eta_{\text{b}}(x, y) = \overline{\eta_{\text{b}}} + \eta'_{\text{b}}(x, y). \tag{56.1}$$

If the topographic amplitude is much smaller than the resting layer thickness, $|\eta'_{\text{b}}| \ll H$, then the motion consists of linear waves, and with the principle of superposition allowing Fourier analysis to construct the linear wave fields generated by arbitrary (small amplitude) topography. Additionally, the linearized form of shallow water potential vorticity conservation constrains the waves. Indeed, it provides the wave equation. This section works through many elements of the kinematics and dynamics encountered in a variety of forced wave problems, here with the special restrictions imposed by the vertically columnar motion of a shallow water layer.[1]

56.2.1 Linearized governing equations

Following the linearization process detailed in Section 55.3, here with a nonzero reference flow, leads to the thickness and velocity decomposition

$$h = H + \eta' - \eta'_{\text{b}} = H + h' \quad \text{and} \quad \boldsymbol{u} = \boldsymbol{u}_{\text{R}} + \boldsymbol{u}'. \tag{56.2}$$

The reference flow is assumed to be in geostrophic balance with a prescribed pressure gradient generated by a static free surface,

$$f_{\circ}\, \hat{\boldsymbol{z}} \times \boldsymbol{u}_{\text{R}} = -g\, \nabla \eta_{\text{R}}. \tag{56.3}$$

Making use of equations (56.2) and (56.3) in the shallow water equations (55.1a) and (55.1b) leads to the linearized governing equations

$$[\partial_t + \gamma + (\boldsymbol{u}_{\text{R}} \cdot \nabla)]\boldsymbol{u}' + f\, \hat{\boldsymbol{z}} \times \boldsymbol{u}' = -g\, \nabla \eta' \tag{56.4a}$$

$$(\partial_t + \boldsymbol{u}_{\text{R}} \cdot \nabla) h' = -H\, \nabla \cdot \boldsymbol{u}'. \tag{56.4b}$$

The constant, $\gamma \geq 0$, is the inverse time scale for a Rayleigh drag (Section 25.8.5). We include Rayleigh drag since in many wave problems it is used to retain a finite solution in the presence of resonances. Even so, we drop it when examining the structure of the waves generated in the presence of flow over topography.

Taking the curl of the velocity equation (56.4a) and then making use of the thickness equation (56.4b) leads to the linearized version of the potential vorticity equation

$$(\partial_t + \boldsymbol{u}_{\text{R}} \cdot \nabla) Q' = -\gamma\, \zeta'/H, \tag{56.5}$$

where $\zeta' = \partial_x v' - \partial_y u'$ is the relative vorticity of the perturbation, and

$$Q' = f/H + \zeta'/H - f\, h'/H^2 \tag{56.6}$$

is the linearized potential vorticity (equation (55.22)), with f/H a constant for the f-plane examined here. Equation (56.5) reveals that the linearized potential vorticity locally evolves according to dissipation from Rayleigh drag acting on the relative vorticity.

[1] The setup is analogous to that considered for inertial waves in Section 53.5.2, which considered inertial waves generated in a resting flow forced by moving topography.

56.2.2 Galilean transformation to the frame of the reference flow

The reference flow is constant in space and time, so that a Galilean transformation to the frame moving with this flow acts to remove advection from the equations of motion (56.4a)-(56.4b). For this purpose, consider the Galilean transformation

$$\bar{t} = t \qquad \text{and} \qquad \overline{\boldsymbol{x}} = \boldsymbol{x} - \boldsymbol{u}_{\mathsf{R}}\, t. \tag{56.7}$$

Following our discussion of Galilean transformations in Section 17.5, we know that the derivative operators transform according to

$$\partial_{\bar{t}} = \partial_t + \boldsymbol{u}_{\mathsf{R}} \cdot \nabla \quad \text{and} \quad \partial_{\overline{x}} = \partial_x \quad \text{and} \quad \partial_{\overline{y}} = \partial_y, \tag{56.8}$$

which then brings the linear equations (56.4a), (56.4b), and (56.5) to

$$(\partial_{\bar{t}} + \gamma)\boldsymbol{u}' + f\,\hat{\boldsymbol{z}} \times \boldsymbol{u}' = -g\,\nabla\eta' \tag{56.9a}$$

$$\partial_{\bar{t}} h' = -H\,\nabla \cdot \boldsymbol{u}' \tag{56.9b}$$

$$\partial_{\bar{t}} Q' = -\gamma\,\zeta'/H. \tag{56.9c}$$

Whereas the reference flow moves with the velocity $\boldsymbol{u}_{\mathsf{R}}$ relative to the topography, the topography moves with a velocity $-\boldsymbol{u}_{\mathsf{R}}$ relative to the reference flow. Correspondingly, by moving to the boosted frame of the reference flow, the topography, which is independent of the rest frame time, t, is a function of time as measured in the boosted frame, $\bar{t}$.

56.2.3 Forced wave equation and potential vorticity

To derive a wave equation, take $\partial_{\bar{t}}$ of the thickness equation (56.9b) to render

$$\partial_{\bar{t}\bar{t}} h' = -H\,\nabla \cdot \partial_{\bar{t}}\boldsymbol{u}'. \tag{56.10}$$

Replacing $\partial_{\bar{t}}\boldsymbol{u}'$ using the linearized velocity equation (56.9a) leads to the forced wave equation

$$\partial_{\bar{t}}\left[(\partial_{\bar{t}} + \gamma)\, h'\right] - c_{\mathsf{grav}}^2\,\nabla^2\eta' = -f\,H\,\zeta', \tag{56.11}$$

where we introduced the squared shallow water gravity wave speed

$$c_{\mathsf{grav}}^2 = g\,H. \tag{56.12}$$

Following the approach in Section 55.8.2, make use of the linearized potential vorticity, Q' (equation (56.6)) to replace ζ', in which

$$f\,H^2\,Q' = -(\partial_{\bar{t}\bar{t}} + \gamma\,\partial_{\bar{t}} + f^2)h' + c_{\mathsf{grav}}^2\,\nabla^2\eta', \tag{56.13}$$

which agrees with equation (55.152) for the case with $\boldsymbol{u}_{\mathsf{R}} = 0$, $\gamma = 0$, and $\eta'_{\mathsf{b}} = 0$. Equation (56.13) brings the potential vorticity evolution equation (56.9c) to the form

$$\partial_{\bar{t}}[(\partial_{\bar{t}\bar{t}} + \gamma\,\partial_{\bar{t}} + f^2)h' - c_{\mathsf{grav}}^2\,\nabla^2\eta'] = f\,H\,\gamma\,\zeta', \tag{56.14}$$

which can be rewritten to isolate a forced wave equation for η'

$$\partial_{\bar{t}}[(\partial_{\bar{t}\bar{t}} + f^2)\eta' - c_{\mathsf{grav}}^2\,\nabla^2\eta'] = \gamma\,[f\,H\,\zeta' - \partial_{\bar{t}\bar{t}}(\eta' - \eta'_{\mathsf{b}})] + \partial_{\bar{t}}[(\partial_{\bar{t}\bar{t}} + f^2)\eta'_{\mathsf{b}}]. \tag{56.15}$$

In the absence of dissipation ($\gamma = 0$) and for a flat bottom ($\eta'_{\mathsf{b}} = 0$), this equation has solutions given by the free inertia-gravity wave modes discussed in Section 55.8.

For the remainder of this section we set $\gamma = 0$ to focus on responses of a non-dissipative flow moving over small amplitude topography. In this case equation (56.15) simplifies to

$$\partial_{\bar{t}}[(\partial_{\bar{t}\bar{t}} + f^2)\eta' - c_{\text{grav}}^2 \nabla^2 \eta'] = \partial_{\bar{t}}[(\partial_{\bar{t}\bar{t}} + f^2)\eta'_{\text{b}}]. \tag{56.16}$$

Furthermore, consistent with our treatment of free inertia-gravity waves in Section 55.8, we focus on wave solutions with zero potential vorticity, which leads to the forced linear wave equation

$$(\partial_{\bar{t}\bar{t}} + f^2)\eta' - c_{\text{grav}}^2 \nabla^2 \eta' = (\partial_{\bar{t}\bar{t}} + f^2)\eta'_{\text{b}}. \tag{56.17}$$

Finally, since the bottom topography is independent of time, t, the source on the right hand side takes the form

$$(\partial_{\bar{t}\bar{t}} + f^2)\eta' - c_{\text{grav}}^2 \nabla^2 \eta' = [(\boldsymbol{u}_{\text{R}} \cdot \nabla)^2 + f^2]\eta'_{\text{b}}. \tag{56.18}$$

This is a forced linear wave equation for a shallow water layer moving in a uniform background flow over topography.

56.2.4 Monochromatic topography

We consider bottom topography in the form of a monochromatic wave

$$\eta'_{\text{b}} = \eta_{\text{o}}\, \mathrm{e}^{\mathrm{i}\boldsymbol{k}_{\text{b}} \cdot \boldsymbol{x}} = \eta_{\text{o}}\, \mathrm{e}^{\mathrm{i}\boldsymbol{k}_{\text{b}} \cdot (\bar{\boldsymbol{x}} + \boldsymbol{u}_{\text{R}}\, \bar{t})} = \eta_{\text{o}}\, \mathrm{e}^{\mathrm{i}(\boldsymbol{k}_{\text{b}} \cdot \bar{\boldsymbol{x}} - \omega_{\text{R}}\, \bar{t})}, \tag{56.19}$$

where η_{o} is a constant real amplitude, $\boldsymbol{k}_{\text{b}}$ is the topography wavevector, and

$$\omega_{\text{R}} = -\boldsymbol{k}_{\text{b}} \cdot \boldsymbol{u}_{\text{R}} > 0 \tag{56.20}$$

is the angular frequency implied by the reference flow that moves over the topography. Since the wave response is assumed to be linear, the response to more complex topography can be built using Fourier analysis.[2]

The topography (56.19) is stationary in the rest frame, but it moves in the direction opposite to the reference flow when viewed in the boosted frame. This direction swap is reflected in the choice $\boldsymbol{k}_{\text{b}} \cdot \boldsymbol{u}_{\text{R}} < 0$, which orients the topography wavevector, $\boldsymbol{k}_{\text{b}}$, according to the reference flow, $\boldsymbol{u}_{\text{R}}$. For example, a zonal referential flow, $\boldsymbol{u}_{\text{R}} = U\, \hat{\boldsymbol{x}}$, with $U > 0$, has a topography wavevector $\boldsymbol{k}_{\text{b}} = -|\boldsymbol{k}_{\text{b}}|\, \hat{\boldsymbol{x}}$, in which case the topography (56.19) takes the form

$$\eta'_{\text{b}} = \eta_{\text{o}}\, \mathrm{e}^{-\mathrm{i}|\boldsymbol{k}_{\text{b}}| x} = \eta_{\text{o}}\, \mathrm{e}^{-\mathrm{i}|\boldsymbol{k}_{\text{b}}|\, (\bar{x} + U\, \bar{t})}. \tag{56.21}$$

Evidently, a boosted frame observer rides along with the reference flow while the topography moves as a plane wave in the $-\hat{\boldsymbol{x}}$ direction. Conversely, a rest frame observer sees static topography with the reference flow moving in the $+\hat{\boldsymbol{x}}$ direction.

56.2.5 Stationary waves and causality

Before considering the non-stationary (or non-steady) wave response in Section 56.2.7, we determine the stationary response from a uniform flow moving over the monochromatic topography (56.21). Notably, stationary flow (also steady flow) refers to stationary in the rest frame of the topography, so that

$$\partial_t = 0 \Longrightarrow \partial_{\bar{t}} = \boldsymbol{u}_{\text{R}} \cdot \nabla. \tag{56.22}$$

In effect, we assume all transient (traveling) waves have propagated far away from the region of interest, leaving just the stationary wave response to the forcing. For flow over topography, the

[2] We illustrate the Fourier analysis approach in Section 58.3 for stationary internal gravity waves generaged by flow over a single mountain.

forcing angular frequency is $\omega_\mathsf{R} = -\boldsymbol{u}_\mathsf{R} \cdot \boldsymbol{k}_\mathsf{b} > 0$, whereas this frequency might have a different origin in other systems, such as the frequency of a piston in a laboratory experiment.

Causality and the non-negative forcing frequency

Stationary waves are generally simpler to mathematically determine than their transient cousins. Furthermore, stationary waves are often of primary physical interest when concerned with long term wave responses. However, there are subtleties related to *causality* that must be kept in mind when studying stationary solutions. Namely, the stationary equations have time symmetry merely because all fields are time independent (in the rest frame). However, stationary waves result from equilibration of transients that arise from a particular forcing. For example, with flow over topography the stationary wave solution knows about the direction of the reference flow, thus respecting causality (e.g., waves are swept downstream not upstream). So although there are no time derivatives in the stationary equations, we build in causality through specifying the forcing frequency, $\omega_\mathsf{R} = -\boldsymbol{u}_\mathsf{R} \cdot \boldsymbol{k}_\mathsf{b} > 0$ (equation (56.20)). Our choice to insist on a positive forcing angular frequency provides a robust means to maintain causality. It also accords with our choice in this book to only consider non-negative angular frequencies (see Section 49.2.3).

Free surface and velocity for the stationary flow

We insert the topography Fourier mode (56.19) into the potential vorticity equation (56.16), and take a plane wave ansatz for the free surface

$$\eta' = \widetilde{\eta}\, \mathrm{e}^{\mathrm{i}(\boldsymbol{k}\cdot\overline{\boldsymbol{x}} - \overline{\omega}\,\overline{t})}, \tag{56.23}$$

where $\overline{\omega}$ is the angular frequency seen in the boosted reference frame. This substitution yields

$$\overline{\omega}\,(-\overline{\omega}^2 + f^2 + c_\mathsf{grav}^2\,|\boldsymbol{k}|^2)\,\widetilde{\eta}\,\mathrm{e}^{\mathrm{i}(\boldsymbol{k}\cdot\overline{\boldsymbol{x}} - \overline{\omega}\,\overline{t})} = \omega_\mathsf{R}\,(-\omega_\mathsf{R}^2 + f^2)\,\eta_\circ\,\mathrm{e}^{\mathrm{i}(\boldsymbol{k}_\mathsf{b}\cdot\overline{\boldsymbol{x}} - \omega_\mathsf{R}\,\overline{t})}. \tag{56.24}$$

Since the fluctuations are assumed to be linear, we expect the reference flow over the topography to excite linear waves. Furthermore, in the steady state we expect the wavevector and angular frequency to be set by the flow and topography

$$\overline{\omega}^2 = \omega_\mathsf{R}^2 = (\boldsymbol{k}_\mathsf{b} \cdot \boldsymbol{u}_\mathsf{R})^2 \quad \text{and} \quad |\boldsymbol{k}|^2 = |\boldsymbol{k}_\mathsf{b}|^2, \tag{56.25}$$

in which case equation (56.24) yields the amplitude ratio

$$\frac{\widetilde{\eta}}{\eta_\circ} = \frac{\omega_\mathsf{R}^2 - f^2}{\omega_\mathsf{R}^2 - f^2 - c_\mathsf{grav}^2\,|\boldsymbol{k}_\mathsf{b}|^2}, \tag{56.26}$$

and the corresponding free surface wave form

$$\eta' = \widetilde{\eta}\,\mathrm{e}^{\mathrm{i}\boldsymbol{k}_\mathsf{b}\cdot\boldsymbol{x}} = \frac{(\omega_\mathsf{R}^2 - f^2)\;\eta_\circ\,\mathrm{e}^{\mathrm{i}\boldsymbol{k}_\mathsf{b}\cdot\boldsymbol{x}}}{\omega_\mathsf{R}^2 - f^2 - c_\mathsf{grav}^2\,|\boldsymbol{k}_\mathsf{b}|^2} = \left[\frac{\omega_\mathsf{R}^2 - f^2}{\omega_\mathsf{R}^2 - f^2 - c_\mathsf{grav}^2\,|\boldsymbol{k}_\mathsf{b}|^2}\right] \eta'_\mathsf{b}, \tag{56.27}$$

with an example given by Figure 56.1. Evidently, the stationary solution has a free surface and bottom topography that are either in-phase (same sign) or π radians out of phase (opposite sign), depending on properties of the reference flow, the topography, the gravity wave speed, and the Coriolis parameter. The stationary velocity field can be found just like for the free inertia-gravity waves in Section 55.8.9 through use of the linear velocity equation (56.9a) (with the Rayleigh drag, $\gamma = 0$), in which

$$\boldsymbol{u}' = \widetilde{\boldsymbol{u}}\,\mathrm{e}^{\mathrm{i}\,\boldsymbol{k}_\mathsf{b}\cdot\boldsymbol{x}} \tag{56.28}$$

with the complex amplitude

$$\widetilde{\boldsymbol{u}} = \frac{g\,\widetilde{\eta}\,(-\boldsymbol{k}_\mathsf{b}\,\omega_\mathsf{R} - \mathrm{i}\,f\,\hat{\boldsymbol{z}}\times\boldsymbol{k}_\mathsf{b})}{\omega_\mathsf{R}^2 - f^2} = \frac{g\,\eta_\circ\,(-\boldsymbol{k}_\mathsf{b}\,\omega_\mathsf{R} - \mathrm{i}\,f\,\hat{\boldsymbol{z}}\times\boldsymbol{k}_\mathsf{b})}{\omega_\mathsf{R}^2 - f^2 - c_\mathsf{grav}^2\,|\boldsymbol{k}_\mathsf{b}|^2}. \tag{56.29}$$

These waves are not the free inertia-gravity waves studied in Section 55.8 since $\omega_\mathsf{R}^2 \neq f^2\,(1 + L_\mathsf{d}^2\,|\boldsymbol{k}_\mathsf{b}|^2)$. Rather, they are stationary waves forced by the motion of the shallow water fluid over the sinusoidal topography. Even so, they share many properties with inertia-gravity waves, including the polarization relation exhibited by equation (56.29), which directly compares to the free inertia-gravity wave in equation (55.174b).

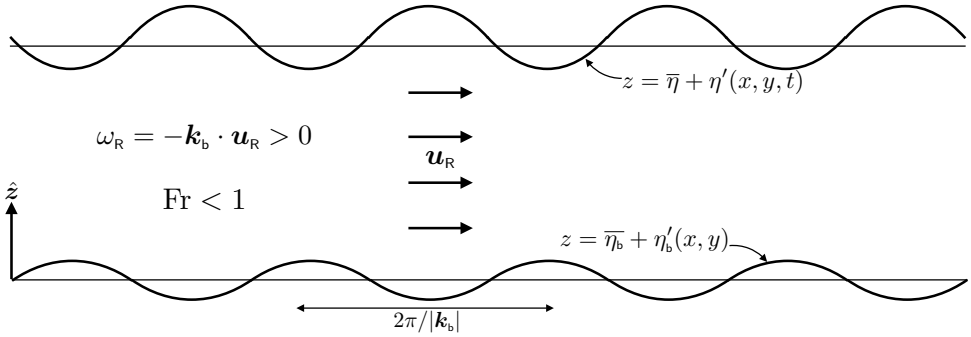

FIGURE 56.1: A shallow water fluid layer with reference flow that moves over a sinusoidal bottom topography for the sub-critical case ($\mathrm{Fr} < 1$) from equation (56.33) with $f = 0$. The stationary gravity waves have amplitude, $\widetilde{\eta} = -\eta_\circ\,\mathrm{Fr}^2/(1-\mathrm{Fr}^2)$, that is opposite to that of the topography. Note that the specification, $\boldsymbol{k}_\mathsf{b}\cdot\boldsymbol{u}_\mathsf{R} < 0$, orients the topography wavevector, $\boldsymbol{k}_\mathsf{b}$, according to the reference flow, $\boldsymbol{u}_\mathsf{R}$. This orientation ensures that the topography observed in the boosted frame moves in the opposite direction to the reference flow as viewed in the rest frame. It also builds in causality as discussed in Section 56.2.5.

Flow regimes and free surface deflections

To help understand the amplitude ratio (56.26), consider the special case of zonal reference flow with $\boldsymbol{u}_\mathsf{R} = U\,\hat{\boldsymbol{x}}$, so that the squared frequency is

$$\omega_\mathsf{R}^2 = U^2\,|\boldsymbol{k}_\mathsf{b}|^2. \tag{56.30}$$

We also find it useful to introduce the Froude number, shallow water deformation radius, and period of an inertial oscillation

$$\mathrm{Fr} = U/c_\mathsf{grav} \quad \text{and} \quad L_\mathsf{d} = c_\mathsf{grav}/f \quad \text{and} \quad T_\mathsf{inertial} = 2\pi/f. \tag{56.31}$$

We can thus write the amplitude ratio (56.26) in the equivalent forms

$$\frac{\widetilde{\eta}}{\eta_\circ} = \frac{\omega_\mathsf{R}^2 - f^2}{\omega_\mathsf{R}^2 - f^2 - c_\mathsf{grav}^2\,|\boldsymbol{k}_\mathsf{b}|^2} = \frac{U^2 - f^2\,|\boldsymbol{k}_\mathsf{b}|^{-2}}{U^2 - f^2\,|\boldsymbol{k}_\mathsf{b}|^{-2} - c_\mathsf{grav}^2} = \frac{\mathrm{Fr}^2 - (L_\mathsf{d}\,|\boldsymbol{k}_\mathsf{b}|)^{-2}}{\mathrm{Fr}^2 - (L_\mathsf{d}\,|\boldsymbol{k}_\mathsf{b}|)^{-2} - 1}, \tag{56.32}$$

with the first a ratio of angular frequencies, the second a ratio of speeds, and the third a ratio of non-dimensional numbers.

There are three regimes for the amplitude as determined by

$$\frac{\widetilde{\eta}}{\eta_\circ} = \begin{cases} > 0 & \text{if} \quad \omega_\mathsf{R}^2 > f^2 + c_\mathsf{grav}^2\,|\boldsymbol{k}_\mathsf{b}|^2 \\ < 0 & \text{if} \quad f^2 < \omega_\mathsf{R}^2 < f^2 + c_\mathsf{grav}^2\,|\boldsymbol{k}_\mathsf{b}|^2 \\ > 0 & \text{if} \quad \omega_\mathsf{R}^2 < f^2, \end{cases} \tag{56.33}$$

as well as their equivalent forms in terms of speeds and non-dimensional numbers. Actually, it is simplest to start by considering the $f = 0$ case, in which there are just two regimes as determined by

$$\left[\frac{\widetilde{\eta}}{\eta_\circ}\right]_{\text{non-rotating}} = \begin{cases} > 0 & \text{if} \quad \text{Fr} > 1 \\ < 0 & \text{if} \quad \text{Fr} < 1. \end{cases} \tag{56.34}$$

With $\text{Fr} > 1$, the free surface is in-phase with the topography, so that the free surface rises when the bottom rises, and vice versa. As discussed in Section 55.5.4, the $\text{Fr} > 1$ flow is a state of hydraulic control and is generally unstable (the fluid particle speed is greater than the gravity wave speed, and the flow generally breaks down into turbulence). For the sub-critical flow with $\text{Fr} < 1$, the free surface falls when the topography rises, and vice versa. Equation (56.33) shows that the addition of a non-zero Coriolis parameter, and thus a finite deformation radius and finite inertial oscillation period, introduces a third regime for in-phase free surface and topography, while it modifies the sub-critical and super-critical regimes.

56.2.6 Free stationary inertia-gravity waves

Consider the special case of

$$\omega_{\mathsf{R}}^2 = (\boldsymbol{k}_{\mathsf{b}} \cdot \boldsymbol{u}_{\mathsf{R}})^2 = f^2, \tag{56.35}$$

in which case the topographic forcing vanishes on the right hand side of the potential vorticity equation (56.24). This case allows for any free inertia-gravity wave to fit within the domain so that

$$\omega^2 = f^2 \, (1 + L_{\mathsf{d}}^2 \, |\boldsymbol{k}|^2). \tag{56.36}$$

That is, the free inertia-gravity wave can exist just as in the case of the flat bottom domain examined in Section 55.8. Transforming the free surface back to the rest frame yields

$$\eta' = \widetilde{\eta} \, \mathrm{e}^{\mathrm{i}(\boldsymbol{k} \cdot \overline{\boldsymbol{x}} - \overline{\omega} \, \overline{t})} = \widetilde{\eta} \, \mathrm{e}^{\mathrm{i}[\boldsymbol{k} \cdot \boldsymbol{x} - (\boldsymbol{k} \cdot \boldsymbol{u}_{\mathsf{R}} + \overline{\omega}) \, t]} = \widetilde{\eta} \, \mathrm{e}^{\mathrm{i}(\boldsymbol{k} \cdot \boldsymbol{x} - \omega \, t)}, \tag{56.37}$$

where we related the boosted frame frequency, $\overline{\omega}$, according to the *Doppler shift* relative to the rest frame frequency, ω,

$$\overline{\omega} = \omega - \boldsymbol{u}_{\mathsf{R}} \cdot \boldsymbol{k}. \tag{56.38}$$

Furthermore note that the free surface amplitude is unconstrained since these waves are invisible to the topography. We have thus identified a free wave solution, which arises for the special case of topography and reference flow satisfying $\omega_{\mathsf{R}}^2 = f^2 > 0$ so that $\omega^2 / f^2 = 1 + (|\boldsymbol{k}| \, L_{\mathsf{d}})^2$, which is the flat bottom frequency for free traveling inertia-gravity waves found in Section 55.8.

56.2.7 Non-stationary gravity wave adjustment

So far we have focused on the stationary waves that result after allowing for transient non-stationary waves to propagate away from the area of interest (formally, to propagate out to infinity). We here consider the case of non-stationary gravity waves ($f = 0$) generated by flow over topography. We assume the free surface fluctuation, η', is initially equal to the bottom topography and to have a zero initial tendency. With a zonal reference flow ($\boldsymbol{u}_{\mathsf{R}} = U \, \hat{\boldsymbol{x}}$) and zonally dependent bottom topography, $\eta'_{\mathsf{b}} = \eta'_{\mathsf{b}}(x)$, we are led to the initial value problem from equation (56.18)

$$(\partial_{\overline{t}\overline{t}} - c_{\mathsf{grav}}^2 \, \partial_{\overline{x}\overline{x}}) \eta' = U^2 \, \partial_{\overline{x}\overline{x}} \eta'_{\mathsf{b}} \tag{56.39a}$$

$$\eta'(\overline{x}, \overline{t} = 0) = \eta'_{\mathsf{b}}(\overline{x}) \tag{56.39b}$$

$$\partial_t \eta'(\overline{x}, \overline{t} = 0) = 0. \tag{56.39c}$$

This is an initial value problem formulated using the boosted reference frame coordinates, $(\overline{x}, \overline{t}) = (x - U\,t, t)$ from Section 56.2.2. Additionally, as shallow water gravity waves are non-dispersive, we can naively allow the bottom topography to be arbitrarily shaped.[3]

We do not expect the initial condition to remain fixed for all time. Rather, we expect the flow (in the limit of linear behavior) to adjust through gravity waves that propagate in both directions. Additionally, we expect this propagation to occur in the presence of the stationary solution from Section 56.2.5. This expectation motivates the ansatz

$$\eta'(\overline{x}, \overline{t}) = \eta'_{\text{stationary}}(\overline{x}) + \eta'_{\text{transient}}(\overline{x}, \overline{t}) = \frac{\text{Fr}^2}{\text{Fr}^2 - 1}\,\eta'_{\text{b}}(x) + \eta'_{\text{transient}}(\overline{x}, \overline{t}), \tag{56.40}$$

where we wrote the stationary solution in terms of the rest frame coordinates, (x, t), which is the frame where $\eta'_{\text{stationary}}$ is stationary. The transient solution embodies linear gravity waves propagating in both directions, and it satisfies equation (56.39a) with zero forcing and with initial conditions set according to equations (56.39b) and (56.39c)

$$(\partial_{\overline{t}\,\overline{t}} - c^2_{\text{grav}}\,\partial_{\overline{x}\,\overline{x}})\eta'_{\text{transient}} = 0 \tag{56.41a}$$

$$\eta'_{\text{transient}}(\overline{x}, \overline{t} = 0) = -\eta'_{\text{transient}}(\overline{x}, \overline{t} = 0) \tag{56.41b}$$

$$\partial_{\overline{t}}\eta'_{\text{transient}}(\overline{x}, \overline{t} = 0) = 0. \tag{56.41c}$$

The solution to the non-dispersive wave equation (56.41a) is given by the D'Alembert formula from Section 6.7.1, which takes the form

$$\eta'_{\text{transient}} = A\,\eta'_{\text{b}}(\overline{x} - c_{\text{grav}}\,\overline{t}) + B\,\eta'_{\text{b}}(\overline{x} + c_{\text{grav}}\,\overline{t}) \tag{56.42a}$$

$$= A\,\eta'_{\text{b}}[x - t\,(U + c_{\text{grav}})] + B\,\eta'_{\text{b}}[x - t\,(U - c_{\text{grav}})] \tag{56.42b}$$

$$= A\,\eta'_{\text{b}}(x - c_{(+)}\,t) + B\,\eta'_{\text{b}}(x - c_{(-)}\,t), \tag{56.42c}$$

where

$$c_{(\pm)} = U \pm c_{\text{grav}} \tag{56.43}$$

are the gravity wave speeds relative to the reference flow. The constants A and B are set according to the initial conditions (56.41b) and (56.41c), which yields

$$\eta'(x, t) = \frac{\text{Fr}^2}{\text{Fr}^2 - 1}\,\eta'_{\text{b}}(x) + \frac{1}{2}\left[\frac{\eta'_{\text{b}}(x - c_{(-)}\,t)}{1 - \text{Fr}} + \frac{\eta'_{\text{b}}(x - c_{(+)}\,t)}{1 + \text{Fr}}\right]. \tag{56.44}$$

For subcritical flow, with $U < c_{\text{grav}}$, we have

$$\text{subcritical} \Longrightarrow c_{(+)} = U + c_{\text{grav}} > 0 \quad \text{and} \quad c_{(-)} = U - c_{\text{grav}} < 0. \tag{56.45}$$

Since $|c_{(-)}| < |c_{(+)}|$, we find the transient solution consists of a relatively fast rightward moving signal, $\eta'_{\text{b}}(x - c_{(+)}\,t)/[2\,(1 + \text{Fr})]$, plus a relatively slow leftward moving signal, $\eta'_{\text{b}}(x - c_{(-)}\,t)/[2\,(1 - \text{Fr})]$. Since $\text{Fr} < 1$, the amplitude of the right moving signal is smaller than the left moving signal according to the ratio $0 < (1 - \text{Fr})/(1 + \text{Fr}) < 1$. The stationary solution has a negative amplitude of relatively absolute value. We depict an example in the left panel of Figure 56.2 for the case of a single Gaussian mountain with $\text{Fr} = 1/4$. We can make use of a Gaussian shaped mountain rather than a single Fourier mode since the linear responses are non-dispersive gravity waves that travel at the same speed. Hence, we can sum any number of non-dispersive gravity wave modes to render the Gaussian shaped wave response that remains coherent.

[3] We consider dispersive internal gravity waves in Section 58.3, which requires Fourier analysis methods to account for wave dispersion.

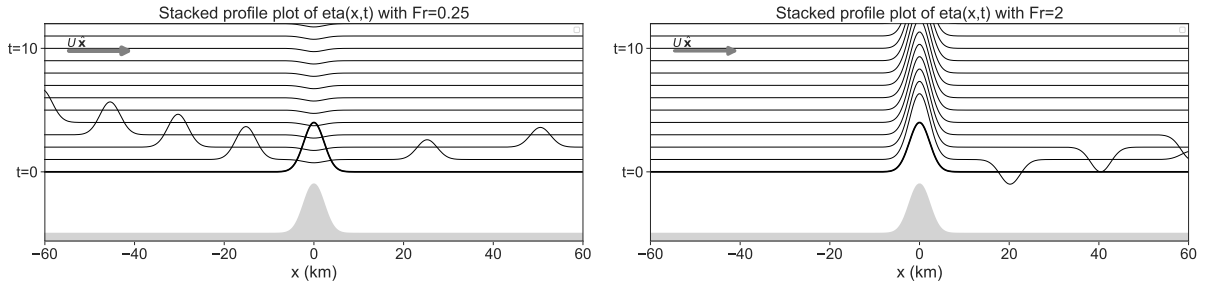

FIGURE 56.2: Stacked profiles of the free surface height that depicts the transient linear gravity wave adjustment of a shallow water layer flowing over a mountain, with the reference flow moving from left to right, $\boldsymbol{u}_{\text{R}} = U\,\hat{\boldsymbol{x}}$ with $U > 0$. Each line represents the free surface incremented in time (moving upward) by the amount $\Delta t = 20 \times 10^3$ m/$\sqrt{1000 \text{ m } 9.8 \text{ m s}^{-2}} \approx 200$ s. The left panel shows results for subcritical flow with Fr $= 1/4$, and the right panel shows supercritical flow with Fr $= 2$, both according to the solution (56.44). The initial condition for the free surface, $\eta'(\overline{x}, \overline{t} = 0) = \eta'_{\text{b}}(\overline{x})$, is shown as a thick black line. For the subcritical flow, the stationary solution has a relatively small and negative amplitude, whereas for the supercritical flow the stationary solution has a large a positive amplitude. The subcritical case reveals leftward and rightward moving gravity waves that propagate away from the mountain, with the leftward wave having a relatively large amplitude and slow speed. The supercritical case has both waves moving to the right, with the relatively small amplitude positive signal moving much faster than the larger amplitude negative signal.

For supercritical flow, with $U > c_{\text{grav}}$, have

$$\text{supercritical} \implies c_{(+)} = U + c_{\text{grav}} > 0 \quad \text{and} \quad c_{(-)} = U - c_{\text{grav}} > 0. \tag{56.46}$$

Since $c_{(\pm)} > 0$, both signals move to the right. The slower signal, $\eta'_{\text{b}}(x - c_{(-)}\,t)/[2\,(1 - \text{Fr})]$, has a negative amplitude since Fr > 1, with this amplitude larger in absolute sense than the faster signal, $\eta'_{\text{b}}(x - c_{(+)}\,t)/[2\,(1 + \text{Fr})]$, whose amplitude is positive. Furthermore, the stationary solution has a positive amplitude. We depict an example supercritical response in the right panel of Figure 56.2 for the case of a single Gaussian mountain with Fr $= 2$.

It is notable that the potential energy of the stationary state for subcritical flow is less than that of the initial condition, given the depressed free surface height, whereas the potential energy of the supercritical flow's stationary state is greater than the initial condition. We cannot perform a closed energy budget since the reference flow is assumed to be fixed. Even so, we understand the ability of the supercritical reference flow to lift the full column of shallow water fluid up and over the mountain, given its relatively large source of kinetic energy. In contrast, the subcritical reference flow insufficient kinetic energy to lift the free surface over the mountain.

56.2.8 Comments and further study

There is no vertical wave propagation in a shallow water layer (see Section 55.3.4). Hence, the layer responds to movement of the reference flow over variable bottom topography by conforming to the constraints from shallow water potential vorticity conservation. It is for this reason that we focused on the linearized potential vorticity equation (56.9c). A further focus on fluctuations with zero potential vorticity, $Q' = 0$, leads to the wave equation (56.18), just as for the free inertia-gravity waves in Section 55.8. In Section 58.2 we study the generation of internal inertia-gravity waves by flow over topography. That study extends the work done here for the shallow water fluid, and it reveals a richer phenomenology that is supported by continuous stratification and non-hydrostatic pressure. Chapter 5 of *Sutherland* (2010) works through a variety of examples for shallow water fluid layers moving over topography, including a study of the initial value problem that we considered in Section 56.2.7.

56.3 Geostrophic adjustment

The geostrophic balance presented in Sections 31.4 and 36.2 is very well maintained by the observed large-scale atmosphere and ocean. Hence, geostrophy (and the associated thermal wind) is a powerful diagnostic. In this section, we examine how a flow state that is initially not in geostrophic balance evolves towards geostrophy. We thus study the dynamical processes associated with the *geostrophic adjustment* problem. As we see, the adjustment occurs through the propagation of linear inertia-gravity waves.

A single shallow water layer on a flat f-plane is sufficient to introduce the main physical ideas of geostrophic adjustment. Furthermore, we focus on linear perturbations so that the governing equations are those derived in Section 55.8 when studying inertia-gravity waves. The adjustment consists of linear inertia-gravity waves that maintain a locally static potential vorticity (equation (55.23)). For brevity in notation, we here drop all primes on the linear fluctuating terms.

56.3.1 Potential vorticity inversion

Before studying the geostrophic adjustment problem, we offer a few comments about *potential vorticity inversion,* which generally refers to the process of determining the flow field given information about the potential vorticity. In a shallow water layer, the potential vorticity is given by

$$Q = h^{-1} (f + \zeta) = h^{-1} (f + \partial_x v - \partial_y u). \tag{56.47}$$

If we further assume the flow to be in geostrophic balance (Section 36.2), then

$$Q = \frac{f}{h} + \frac{1}{h} \left[\frac{\partial}{\partial x} \left(\frac{g}{f} \frac{\partial \eta}{\partial x} \right) + \frac{\partial}{\partial y} \left(\frac{g}{f} \frac{\partial \eta}{\partial y} \right) \right]. \tag{56.48}$$

Assuming we know Q throughout the domain; assuming f and Q are uniformly of the same sign within the domain; and assuming we know boundary conditions for η, then equation (56.48) is a nonlinear elliptic boundary value problem (Section 6.5) for η. Nonlinearities come from the $h^{-1} = (\eta - \eta_b)^{-1}$ pre-factor, as well as the boundary conditions discussed below. Linearizing by setting $h^{-1} \approx H^{-1}$ and simplifying the boundary conditions (see below) allows equation (56.48) to be solved for η. This solution process is referred to as *inverting* the elliptic operator, so that this particular inversion process is referred to as *potential vorticity inversion.*

General boundary conditions for η can be rather complex to handle mathematically. Namely, in a domain with a sloping bottom, such as in Figure 35.1, the free surface deviation equals to the bottom deviation, $\eta = \eta_b$, along the domain boundaries since the layer thickness vanishes there. Furthermore, the horizontal position of the domain boundary is a function of time since the layer moves up and down the sloping bottom. Vanishing layers and the associated moving boundaries are intrinsically nonlinear; i.e., there is no way to linearize the process without removing it altogether. Instead, to facilitate the use of linear physics requires us to assume the layer thickness remains nonzero throughout the domain. Furthermore, we assume the layer thickness deviates only a small amount from the layer averaged thickness: $h/H \approx 1$. These assumptions are made in the following discussion of geostrophic adjustment.

56.3.2 Posing the initial value problem

We solve for the $t > 0$ evolution of surface height and velocity by making use of the linearized equations from Section 55.3[4]

$$\partial_t \boldsymbol{u} + f \, \hat{\boldsymbol{z}} \times \boldsymbol{u} = -g \, \nabla \eta \tag{56.49a}$$

[4]Recall that to reduce notational clutter, we drop primes on the fluctuation variables in this section.

$$\partial_t \eta + H\,\nabla\cdot\boldsymbol{u} = 0 \tag{56.49b}$$

$$\zeta - f\,\eta/H = H\,Q(x,y). \tag{56.49c}$$

$Q(x,y)$ is the linearized potential vorticity that is static for the flat bottom f-plane and so it is fully determined by the initial conditions (Section 55.3.3). To illustrate the geostrophic adjustment in an analytically tractable manner, consider the following step initial conditions for the surface height

$$\eta(x,t=0) = \begin{cases} +\eta_\circ & x<0 \\ -\eta_\circ & x>0, \end{cases} \tag{56.50}$$

which can be written

$$\eta(x,t=0) = \eta_\circ\,[1-2\,\mathcal{H}(x)] = -\eta_\circ\,\mathrm{sgn}(x), \tag{56.51}$$

where the sign-function is given by

$$\mathrm{sgn}(x) = \begin{cases} -1 & \text{if } x<0 \\ 0 & \text{if } x=0 \\ 1 & \text{if } x>0, \end{cases} \tag{56.52}$$

which can also be written in terms of the Heaviside step function

$$\mathrm{sgn}(x) = 2\,\mathcal{H}(x) - 1, \tag{56.53}$$

where[5]

$$\mathcal{H}(x) = \begin{cases} 0 & \text{if } x<0 \\ 1/2 & \text{if } x=0 \\ 1 & \text{if } x>0. \end{cases} \tag{56.54}$$

The velocity is assumed to be zero initially

$$\boldsymbol{u}(x,y,t=0) = 0. \tag{56.55}$$

Correspondingly, the initial relative vorticity vanishes so that the linearized potential vorticity (equation (56.49c)) is

$$Q(x,y) = \frac{f\eta_\circ}{H^2}\,\mathrm{sgn}(x). \tag{56.56}$$

Since $\partial Q/\partial t = 0$ (equation (55.23)), the potential vorticity (56.56) is maintained at each point in space throughout the adjustment process. The velocity and surface height adjustment is thus constrained to keep potential vorticity static. This rather basic point is key to determining evolution of the velocity and surface height, and thus in determining the final (equilibrium) state for these fields.

56.3.3 Adjustment with $f = 0$

In the absence of planetary rotation ($f=0$), relative vorticity is constant at each grid point. With a zero initial velocity, relative vorticity remains zero throughout the adjustment. The adjustment is thus quite simple. Namely, it consists of linear gravity waves, which carry zero relative vorticity (equation (55.72)). These gravity waves propagate away from the initial step, converting the potential energy of the step into kinetic energy of waves that propagate to infinity. As the linear gravity waves are non-dispersive, they carry the initial pulse out to infinity without distortion in the wave form

$$\eta(x,t) = -\frac{\eta_\circ}{2}\left[\,\mathrm{sgn}(x + c_{\text{grav}}\,t) + \mathrm{sgn}(x - c_{\text{grav}}\,t)\right]. \tag{56.57}$$

[5] We discuss the Heaviside step function in Section 7.5.

The meridional velocity remains zero, whereas the zonal velocity equation

$$\partial_t u = -g\,\partial_x \eta, \tag{56.58}$$

leads to

$$u(x,t) = \frac{g\,\eta_o}{2\,c_{grav}}\left[\operatorname{sgn}(x + c_{grav}\,t) - \operatorname{sgn}(x - c_{grav}\,t)\right]. \tag{56.59}$$

After the transient waves have passed, the steady solution is a flat surface height with zero velocity. This steady solution is familiar from the case of a rock dropped into a still pond. After dropping the rock into the pond, the surface gravity waves radiate outward from the rock and are eventually damped upon reaching the shore. In equilibrium, the pond returns to a state of rest with a flat surface height.[6]

56.3.4 Adjustment on the f-plane

On a rotating f-plane, the transient solution consists of the inertia-gravity waves studied in Section 55.8, with these waves transmitting information about the initial surface height perturbation out to infinity. After the transient waves have passed, we might guess that the steady solution is either the trivial solution with flat surface height (as for the $f = 0$ case), or a nontrivial solution that is in geostrophic balance

$$f\hat{\boldsymbol{z}} \times \boldsymbol{u} = -g\,\nabla\eta \qquad \text{and} \qquad \nabla \cdot \boldsymbol{u} = 0 \qquad \text{and} \qquad Q = H^{-2}\,f\,\eta_o \operatorname{sgn}(x). \tag{56.60}$$

Conservation of potential vorticity chooses the geostrophic solution, so that a steady solution of no-motion is not allowed by potential vorticity conservation. This is a profound distinction from the adjustment with $f = 0$.

Computing the steady state

As the steady flow is geostrophic on an f-plane, we make use of the geostrophic streamfunction

$$\psi = g\,\eta/f. \tag{56.61}$$

The steady state is written in terms of the streamfunction according to

$$u = -\partial_y \psi \qquad \text{and} \qquad v = \partial_x \psi \qquad \text{and} \qquad \zeta = \nabla^2 \psi. \tag{56.62}$$

Making use of these expressions for the linearized potential vorticity (56.49c) leads to the elliptic partial differential equation for the streamfunction

$$\left[\nabla^2 - L_d^{-2}\right]\psi = H\,Q(x,y), \tag{56.63}$$

where we introduced the shallow water deformation radius, $L_d = c_{grav}/f$, from equation (55.54).

The initial condition (56.51) has no y-dependence. Furthermore, there is nothing in the adjustment process that breaks meridional symmetry. Hence, the steady state is a function only of x, in which case the streamfunction satisfies the ordinary differential equation

$$\frac{\mathrm{d}^2\psi}{\mathrm{d}x^2} - L_d^{-2}\,\psi = \frac{f\eta_o}{H}\operatorname{sgn}(x). \tag{56.64}$$

We solve this equation separately for $x > 0$ and $x < 0$ and match the function and its first derivative at $x = 0$, and furthermore constrain the streamfunction to vanish at $\pm\infty$. The $x > 0$

[6] For most ponds, waves are better studied using deep water equations rather than shallow water equations; see Section 52.3. Even so, the key physical points in this example are maintained.

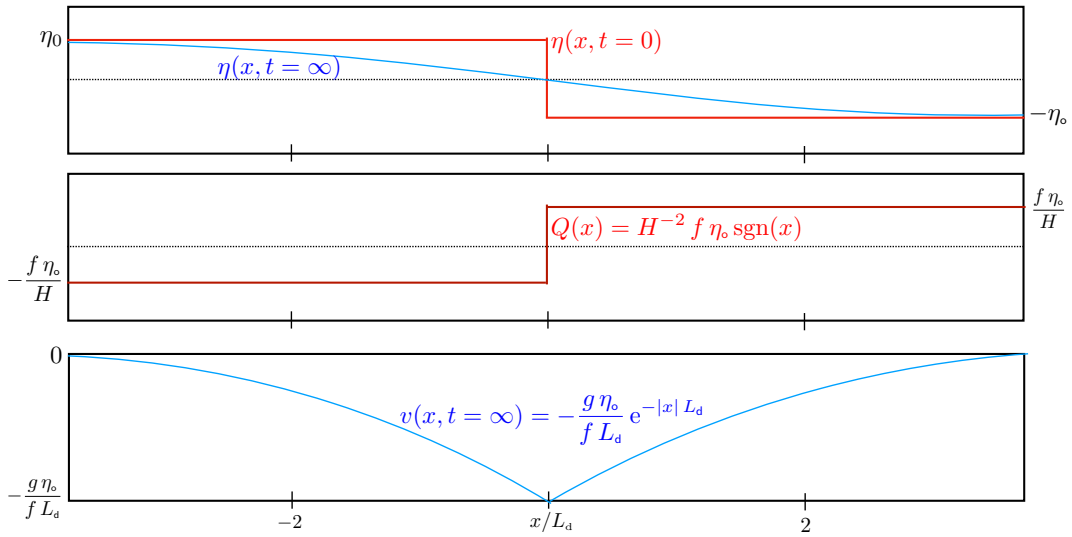

FIGURE 56.3: Depicting solutions to the linear geostrophic adjustment of a rotating shallow water layer on an f-plane. The top panel shows the initial (step-function) surface height (56.51) and the steady state (exponential) surface height (56.70). The second panel shows the static (step-function) potential vorticity (56.60). The third panel shows the steady state (exponential) meridional velocity (56.71) comprised of a jet centered at $x = 0$. The horizontal axis is scaled according to the shallow water deformation radius, $L_\mathrm{d} = f^{-1}\sqrt{g\,H}$. This figure is adapted from figure 3.10 of *Vallis* (2017).

streamfunction satisfies

$$\frac{\mathrm{d}^2\psi}{\mathrm{d}x^2} - L_\mathrm{d}^{-2}\,\psi = \frac{f\eta_\circ}{H}. \tag{56.65}$$

The particular solution is

$$\psi_\mathrm{p} = -L_\mathrm{d}^2\,H\,Q = -L_\mathrm{d}^2\,f\,\eta_\circ/H = -g\,\eta_\circ/f, \tag{56.66}$$

and the homogeneous solution is

$$\psi_\mathrm{h} = (g\,\eta_\circ/f)\,\mathrm{e}^{-x/L_\mathrm{d}}, \tag{56.67}$$

so that

$$\psi = -\frac{g\,\eta_\circ}{f}\left[1 - \mathrm{e}^{-x/L_\mathrm{d}}\right]. \tag{56.68}$$

The $x < 0$ solution is found similarly, so that the full solution is

$$\psi = \frac{g\,\eta_\circ}{f}\begin{cases} -\left(1 - \mathrm{e}^{-x/L_\mathrm{d}}\right) & x > 0 \\ \left(1 - \mathrm{e}^{x/L_\mathrm{d}}\right) & x < 0, \end{cases} \tag{56.69}$$

which means that the steady state surface height is

$$\eta = \eta_\circ\begin{cases} -\left(1 - \mathrm{e}^{-x/L_\mathrm{d}}\right) & x > 0 \\ \left(1 - \mathrm{e}^{x/L_\mathrm{d}}\right) & x < 0. \end{cases} \tag{56.70}$$

Note that the streamfunction vanishes at $x = 0$ and has a first derivative of $-\eta_\circ\sqrt{gH}/H$. Since the streamfunction only has a zonal dependence, the steady state velocity is purely meridional

$$u = 0 \qquad \text{and} \qquad v = -\frac{g\,\eta_\circ}{f\,L_\mathrm{d}}\,\mathrm{e}^{-|x|/L_\mathrm{d}}. \tag{56.71}$$

The steady state velocity thus consists of a jet that is perpendicular to the surface height front.

56.3.5 Concerning the deformation radius

As illustrated in Figure 56.3, the steady state profiles for the surface height and velocity both have an exponential decay, with decay length scale given by the deformation radius. The deformation radius is this length scale over which a signal can propagate before being affected or "deformed" by the Coriolis acceleration, thus motivating the name *deformation radius*. More precisely, the deformation radius measures the horizontal length scale over which a wave can propagate within the time $|f|^{-1}$ (the *inertial period* is $2\pi/|f|$), before feeling the effects of the Coriolis acceleration, thus making

$$L_{\text{d}} |f| = \sqrt{g H}. \tag{56.72}$$

In the $f = 0$ limit, the deformation radius is infinity and the steady solution returns to the case considered in Section 56.3.3, whereby the steady state free surface is flat and there is no flow. A key feature of the $f \neq 0$ case is that some of the potential energy contained within the initial perturbed free surface remains part of the steady state geostrophic flow. Conservation of potential vorticity constrains the flow so that all the initial potential energy cannot be converted to kinetic energy. Rather, the adjustment occurs only within a deformation radius distance from the initial perturbation.

We can extend the ideas introduced in this single-layer adjustment to a two-layer system as depicted in Figure 56.4, with the figure caption summarizing the physics. Again, adjustment leads to geostrophic flow when the lateral extent of the flow reaches the deformation scale. In this case, the deformation scale is much smaller than the single-layer fluid given that it is the reduced gravity that determines the velocity scale rather than the gravity.[7] The slower internal wave speeds propagate the internal wave signal a shorter distance before feeling the effects from Coriolis

$$L_{\text{d}} |f| = \sqrt{g' H} \ll \sqrt{g H}. \tag{56.73}$$

56.3.6 Comments and further reading

Our study of shallow water geostrophic adjustement shares some features with that of the gravity wave adjustment to flow over topography as studied in Section 56.2.7. For the topographic case we considered $f = 0$, whose linear gravity waves carry zero relative vorticity, whereas for the geostrophic adjustment we allow for $f \neq 0$, whose linear inertia-gravity waves carry zero potential vorticity. Transients for both cases consist of linear waves carrying information out to "infinity", leaving behind a stationary flow. For the topographic case the stationary flow is set according to the topography and the Froude number, whereas for the geostrophic case the stationary flow is set according to the Coriolis acceleration and initial conditions.

Section 3.9 of *Vallis* (2017) presents a far more thorough discussion of this linear geostrophic adjustment problem, including an elegant variational approach. Chapter 3 of *Pratt and Whitehead* (2008) provide a thorough discussion for both linear and nonlinear geostrophic adjustment.

56.4 Exercises

EXERCISE 56.1: DEFORMATION RADIUS

The deformation radius appears in many contexts within rotating fluid dynamics. Here, we compute this length scale for selective geophysical flow regimes at $30^\circ N$ latitude, where $f = 7.3 \times 10^{-5}$ s^{-1}.

[7] Recall from Section 55.6 that we study gravity waves in two shallow water layers, where we indeed find the reduced gravity determines the baroclinic phase speed.

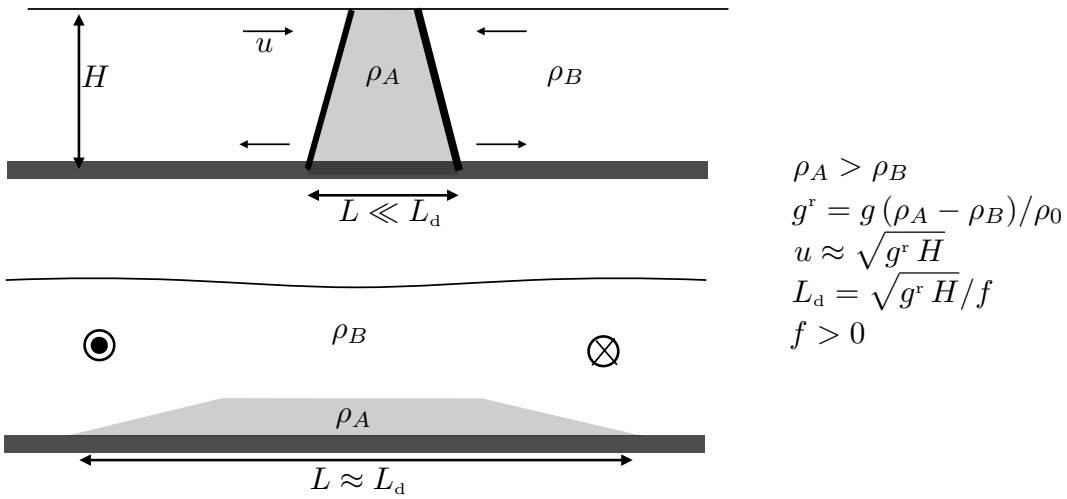

FIGURE 56.4: Two regions of uniform density fluid used to illustrate the adjustment under gravity acceleration and Coriolis acceleration in the absence of mixing. Top panel: two fluid layers each have uniform density with $\rho_A > \rho_B$ and with the heavy fluid sitting between two regions of the lighter fluid, with the fluids separated by a barrier. Lower panel: upon releasing the barrier, gravity causes the heavy fluid to slump under the lighter fluid. This process halts when the lateral scale of the heavier fluid reaches the deformation scale, $L_d = \sqrt{g^r\,H}/f$, where $\sqrt{g^r\,H} \approx N\,H$ is the speed of the internal gravity wave signal appearing in a two-layer fluid. The adjusted state reaches two-layer geostrophic balance as discussed in Section 36.2.2, whereby the difference in geostrophic flow in the two layers is proportional to the slope of the interface between the layers. By extension, if the initial region of heavy fluid had an initial lateral extent on the order of the deformation scale, then there will be minimal change in the lateral extent after the barrier is removed since the Coriolis acceleration will balance the pressure gradients to render a geostrophic flow. See Figure 15.4 of *Cushman-Roisin and Beckers* (2011) for more examples of geostrophic adjustment.

(a) Compute the shallow water deformation radius for an ocean continental shelf of depth 500 m.

(b) Compute the shallow water deformation radius for the deep ocean with depth 5000 m.

(c) The deformation radius defined in this chapter is sometimes called the *external deformation radius* as it makes use of the full depth of the fluid and the gravitational acceleration. In contrast, the deformation radius defined in terms of internal layer thickness and reduced gravity, g^r, leads to the internal deformation radius. The internal deformation radius, $L_d^{\text{int}} = \sqrt{g^r\,h}/f$ is the appropriate rotational length scale for density layers in the interior of the ocean or isentropic layers in the interior of the atmosphere. Compute the deformation radius for a density layer of thickness $h = 200$ m and reduced gravity of $g^r = g/1000$.

EXERCISE 56.2: GEOSTROPHIC ADJUSTMENT (BASED ON EXERCISE 4.6 OF *Vallis* (2019))
Consider the linear geostrophic adjustment problem on an f-plane with a single layer of shallow water fluid over a flat bottom. Rather than assume an initial free surface profile, as we did in Section 56.3, here we assume an initial meridional velocity profile given by

$$v(x, t = 0) = v_0\,\text{sgn}(x) = v_0\,(2\,\mathcal{H}(x) - 1), \tag{56.74}$$

where $v_0 > 0$ is a constant, sgn is the sign-function (equation (56.52)), and $\mathcal{H}$ is the Heaviside step function (equation (56.54)). The free surface is assumed to be initially flat.

(a) Show that the linearized potential vorticity, $H\,Q' = \zeta' - f\,\eta'/H$, is given by

$$H\,Q'(x) = 2\,v_0\,\delta(x), \tag{56.75}$$

where $\delta(x)$ is the Dirac delta with dimensions L^{-1}.

(b) As we did in Section 56.3, solve for the geostrophic streamfunction $\psi = g\,\eta/f$.

(c) Discuss the geostrophically adjusted streamfunction and velocity, and draw a sketch of ψ and v.

Here are some hints.

- We discuss properties of the Dirac delta in Chapter 7. However, to answer the first part of this question it is sufficient to know that the derivative of the Heaviside step function (a dimensionless step function) is the Dirac delta

$$\delta(x) = \frac{\mathrm{d}\mathcal{H}(x)}{\mathrm{d}x}, \tag{56.76}$$

  so that the Dirac delta has dimensions of inverse length.

- For the second part, note that the streamfunction is exponentially decaying on either side of the $x = 0$ according to $\psi = \psi_0\,\mathrm{e}^{-|x|/L_\mathrm{d}}$, which then leads to a jump in the derivative approaching the origin from each side. Carefully use equations (56.63) and (56.76) to determine ψ_0.

Chapter 57

INTERNAL INERTIA-GRAVITY WAVES

In this chapter we continue the study of how gravity affects wave motion in geophysical fluids, here focusing on gravity waves realized in a continuously stratified fluid. As part of anticipating this discussion, recall Section 55.6 where we studied gravity waves in two shallow water layers and decomposed the motion into two modes: the *barotropic mode* and *baroclinic mode*. When moving to a continuously stratified fluid we encounter an infinity of baroclinic modes. These modes are associated with motion of interior stratification surfaces, and have very little projection onto motion of the upper free surface. Consequently, these waves are generally referred to as internal gravity waves.

Although the shallow water system anticipated some features of gravity waves in a continuous system, there are many properties revealed only when moving to continuous stratification. In particular, the dispersion relation for internal gravity waves presents the peculiar feature of having a group velocity that is perpendicular to the phase velocity. In fact, this property was already encountered in Chapter 53 when studying inertial waves in a homogeneous fluid. We here focus most attention on the case of internal gravity waves in a non-rotating reference frame. Extending to the case of an f-plane is relatively straightforward and builds on the inertial wave material from Chapter 53 as well as the shallow water inertia-gravity waves studied in Section 55.8.

READER'S GUIDE TO THIS CHAPTER

We build on the prior wave mechanics chapters and assume familiarity with the equations for a Boussinesq ocean in Chapter 29 and the concept of Archimedean buoyancy from Chapter 30. Chapter 58 continues our study of internal inertia-gravity waves by focusing on a variety of geophysical mechanisms for the forcing of such waves.

Further resources for material in this chapter can be found in *Lighthill* (1978), *Gill* (1982), *Pedlosky* (2003), *Sutherland* (2010), *Cushman-Roisin and Beckers* (2011), *Kundu et al.* (2016), and *Vallis* (2017). The second half of this video offers some pedagogical visualizations of stratified flow phenomena, and this video provides more visualizations from simulations and laboratory tank experiments.

57.1 Loose threads

- energetic balances for reflected waves.
- Is there a general means to determine $\boldsymbol{c}_g \cdot \boldsymbol{k} = 0$ without going through the process of computing the group velocity? Why do some waves have this property but others do not?
- Vertical normal modes in Section 57.7 as per Lecture 9 of *Pedlosky* (2003) or Section 6.10 of *Gill* (1982).

57.2 Boussinesq ocean and its linearization

Throughout this chapter we work with the Boussinesq ocean equations in their inviscid/adiabatic limit, and linearize the governing equations around a rest state in exact hydrostatic balance. In

this section we review the governing equations from Chapter 29 and perform the linearization.

57.2.1 Boussinesq ocean equations

We make use of the governing equations for an adiabatic and inviscid Boussinesq ocean written in the form (see Section 29.1.7)

$$\rho_\circ \left[\partial_t \boldsymbol{v} + (\boldsymbol{v}\cdot\nabla)\,\boldsymbol{v} + 2\,\boldsymbol{\Omega}\times\boldsymbol{v}\right] = -\nabla p - \rho\, g\,\hat{\boldsymbol{z}} \quad \text{inviscid velocity equation} \tag{57.1a}$$

$$\nabla\cdot\boldsymbol{v} = 0 \quad \text{non-divergent flow} \tag{57.1b}$$

$$(\partial_t + \boldsymbol{v}\cdot\nabla)\,\rho = 0 \quad \text{adiabatic density equation} \tag{57.1c}$$

$$\rho = -\rho_\circ\,\alpha_\Theta\,\Theta \quad \text{linear equation of state.} \tag{57.1d}$$

The density field contains a nontrivial spatial structure

$$\rho = \rho(\boldsymbol{x}, t), \tag{57.2}$$

with the Boussinesq reference density, $\rho_\circ$, a constant, and we furthermore assume the thermal expansion coefficient, α_Θ, is a constant. Hence, the density and Conservative Temperature, Θ, are linearly proportional, with the adiabatic density equation (57.1c) meaning that Conservative Temperature is materially constant. The velocity field resolved by the Boussinesq ocean is non-divergent so that it does not support acoustic waves.[1] The inhomogeneous density field couples to the gravity field to render a nonzero buoyancy that appears in the velocity equation (57.1a). Buoyancy is the essential ingredient for the internal gravity waves studied in this chapter. Finally, we make use of the Traditional Approximation (Section 27.1.3) and tangent plane approximation (Section 24.5) with the planetary rotation approximated by

$$2\,\boldsymbol{\Omega} \approx f_\circ\,\hat{\boldsymbol{z}}, \tag{57.3}$$

where $f_\circ$ is the planetary vorticity set either to zero or a nonzero constant.

57.2.2 The prescribed reference state

We consider a three-component decomposition of density into a constant Boussinesq reference density, $\rho_\circ > 0$, plus a prescribed static reference density, $\rho_{\mathsf{R}}(z) > 0$, and a perturbation density, $\rho'(\boldsymbol{x}, t)$,

$$\rho(\boldsymbol{x}, t) = \rho_\circ + \rho_{\mathsf{R}}(z) + \rho'(\boldsymbol{x}, t). \tag{57.4}$$

We assume the following inequalities hold

$$\rho_{\mathsf{R}} \ll \rho_\circ \quad \text{and} \quad |\rho'| \ll \rho_{\mathsf{R}}, \tag{57.5}$$

with the first inequality following from the Boussinesq ocean approximation, and the second inequality supporting linearization in Section 57.2.4. The buoyancy is decomposed according to the density decomposition (57.4), so that

$$b = -g\,(\rho - \rho_\circ)/\rho_\circ = -g\,(\rho_{\mathsf{R}} + \rho')/\rho_\circ = b_{\mathsf{R}} + b'. \tag{57.6}$$

Likewise, we decompose pressure so that

$$p = p_\circ(z) + p_{\mathsf{R}}(z) + p'(\boldsymbol{x}, t), \tag{57.7}$$

[1] See Section 51.2 for more on how we interpret the quasi-compressible properties of the Boussinesq ocean.

where

$$\mathrm{d}p_{\circ}(z)/\mathrm{d}z = -\rho_{\circ}\, g \quad \text{and} \quad \mathrm{d}p_{\mathsf{R}}(z)/\mathrm{d}z = -\rho_{\mathsf{R}}(z)\, g, \tag{57.8}$$

so that $p_{\circ}$ and p_{R} are both hydrostatic base state pressures given by

$$p_{\circ}(z) = -\rho_{\circ}\, g\, z \quad \text{and} \quad p_{\mathsf{R}}(z) = g \int_{z}^{0} \rho_{\mathsf{R}}(z')\, \mathrm{d}z'. \tag{57.9}$$

The corresponding pressure and gravity contributions to the velocity equation (57.1a) take the form

$$-\nabla p - \rho\, g\, \hat{\boldsymbol{z}} = -\rho_{\circ}\, \nabla\varphi' - \rho'\, g\, \hat{\boldsymbol{z}} = -\rho_{\circ}\, (\nabla\varphi' - b'\, \hat{\boldsymbol{z}}), \tag{57.10}$$

where we introduced the normalized dynamic pressure (with dimensions of squared velocity)

$$\varphi' = p'/\rho_{\circ}. \tag{57.11}$$

Introducing the reference state into the velocity equation (57.1a) and density equation (57.1c) leads to

$$\partial_t \boldsymbol{v} + (\boldsymbol{v}\cdot\nabla)\, \boldsymbol{v} + f_{\circ}\, \hat{\boldsymbol{z}} \times \boldsymbol{v} = -\nabla\varphi' + b'\, \hat{\boldsymbol{z}} \quad \text{decomposed velocity equation} \tag{57.12a}$$

$$(\partial_t + \boldsymbol{v}\cdot\nabla)\, b' = -w\, N_{\mathsf{R}}^2 \quad \text{decomposed buoyancy equation.} \tag{57.12b}$$

In the buoyancy equation we introduced the reference state's squared buoyancy frequency

$$N_{\mathsf{R}}^2 = -\frac{g}{\rho_{\circ}} \frac{\mathrm{d}\rho_{\mathsf{R}}}{\mathrm{d}z}. \tag{57.13}$$

It is notable that the velocity equation (57.12a) is mathematically identical to the original velocity equation (57.1a). However, the fluctuating buoyancy equation (57.12b) is distinct from the original buoyancy equation (57.1c). Namely, the reference state squared buoyancy frequency couples to the vertical velocity to provide a source, $-w\, N_{\mathsf{R}}^2$, for the material evolution of the perturbation buoyancy.

57.2.3 Buoyancy frequency compared to surface gravity waves

As revealed in this chapter, the buoyancy frequency of the background state, N_{R}, sets the time scale for the internal gravity wave motions. To garner a sense for its scale, we compare this frequency to that found for the deep water surface gravity waves studied in Section 52.5.5. Making use of equation (52.123a) for deep water gravity waves leads to the ratio

$$\frac{N_{\mathsf{R}}^2}{\omega_{\mathrm{dww}}^2} = \frac{N_{\mathsf{R}}^2}{g\, |\boldsymbol{k}|_{\mathrm{dww}}} = \left| \frac{g}{\rho_{\circ}} \frac{\mathrm{d}\rho_{\mathsf{R}}}{\mathrm{d}z} \frac{\Lambda_{\mathrm{dww}}}{2\,\pi\, g} \right| = \left| \frac{\Delta\rho_{\mathsf{R}}}{2\,\pi\,\rho_{\circ}} \right|. \tag{57.14}$$

In the final step we took the deep water wave length, Λ_{dww}, as the vertical scale over which to measure the vertical density difference, $\Delta\rho_{\mathsf{R}}$. Now the deep water wavelength is just a few meters, which means that $|\Delta\rho_{\mathsf{R}}| \lll \rho_{\circ}$. We conclude that the buoyancy frequency is much less than the frequency of deep water surface gravity waves. We can understand this result by noting that the gravitational restoring force acting on deep water surface waves is far stronger than the reduced gravity acting on internal waves, so we expect the deep water waves to oscillate much faster.

Now consider the same calculation for shallow water surface gravity waves by making use of

the dispersion relaation (52.123b) to yield

$$\frac{N_{\mathsf{R}}^2}{\omega_{\text{sww}}^2} = \frac{N_{\mathsf{R}}^2}{|\boldsymbol{k}|_{\text{sww}}^2 \, c_{\text{grav}}^2} = \left| \frac{g}{\rho_{\circ}} \frac{\mathrm{d}\rho_{\mathsf{R}}}{\mathrm{d}z} \frac{\Lambda_{\text{sww}}}{2\,\pi\,|\boldsymbol{k}|_{\text{sww}}\, g\, H} \right| = \left| \frac{\Delta\rho_{\mathsf{R}}}{\rho_{\circ}} \frac{1}{2\,\pi\,|\boldsymbol{k}|_{\text{sww}}\, H} \right|. \tag{57.15}$$

In this case the density difference, $\Delta\rho_{\mathsf{R}}$, is computed over a vertical length scale equal to the wavelength, Λ_{sww}. But since $|\boldsymbol{k}|_{\text{sww}}\, H \ll 1$ for shallow water gravity waves, we take $\Delta\rho_{\mathsf{R}}$ over the full depth of the ocean. Even so, the density ratio remains small, $\Delta\rho_{\mathsf{R}}/\rho_{\circ} \ll 1$. Yet now this ratio is divided by the small number $2\,\pi\,|\boldsymbol{k}|_{\text{sww}}\, H = (2\,\pi)^2\, H/\Lambda_{\text{sww}} \ll 1$. We thus find that the internal gravity wave frequency can be on the order of the shallow water gravity wave frequency. So although the shallow water waves feel the full gravitational acceleration, just like deep water gravity waves, the huge scale for shallow water waves leads to far slower wave motion than the deep water gravity waves. As a result, the frequency for shallow water waves is on the order of that for internal waves.

57.2.4 Linearization around the background state of rest

The second of the density inequalities (57.5) implies the buoyancy inequality

$$|b'| \ll b_{\mathsf{R}}. \tag{57.16}$$

Evidently, fluctuations in the buoyancy field, which can be positive or negative, are far smaller in magnitude than the reference state buoyancy. These small fluctuations in buoyancy lead to correspondingly small fluctuations in dynamic pressure, φ', and small fluctuations in the velocity, $\boldsymbol{v}'$. The linearized velocity equation (57.12a) and buoyancy equation (57.12b) are obtained by dropping nonlinear product of fluctuating fields

$$\partial_t \boldsymbol{u}' + f_{\circ}\, \hat{\boldsymbol{z}} \times \boldsymbol{u}' = -\nabla_{\mathsf{h}} \varphi' \qquad \text{linearized horizontal velocity equation} \tag{57.17a}$$

$$\partial_t w' = -\partial_z \varphi' + b' \qquad \text{linearized vertical-velocity equation} \tag{57.17b}$$

$$\partial_t b' = -w'\, N_{\mathsf{R}}^2 \qquad \text{linearized buoyancy equation} \tag{57.17c}$$

$$\nabla \cdot \boldsymbol{v}' = 0 \qquad \text{continuity for velocity fluctuations.} \tag{57.17d}$$

The final equation expresses the non-divergent nature of the fluctuating velocity field.[2] These three linear equations are the linearized governing equations used in this chapter.

57.2.5 Energetics

We studied the energetics of the nonlinear equation set (57.1a)-(57.1d) in Section 29.6. We here revisit that discussion and then derive energetics for the linearized equations (57.17a)-(57.17d).

Adiabatic inviscid Boussinesq ocean

The kinetic energy per volume and potential energy per volume in a Boussinesq ocean are given by

$$\rho_{\circ}\, \mathcal{K} = \rho_{\circ}\, \boldsymbol{v} \cdot \boldsymbol{v}/2 \quad \text{and} \quad \rho\, \Phi = \rho\, g\, z, \tag{57.18}$$

where we introduced the kinetic energy per mass and potential energy per mass (i.e., the geopotential)

$$\mathcal{K} = \boldsymbol{v} \cdot \boldsymbol{v}/2 \quad \text{and} \quad \Phi = g\, z. \tag{57.19}$$

[2] The velocity has been decomposed into its background state flow, $\boldsymbol{v}_{\mathsf{R}}$, which is assumed here to be zero, plus a fluctuation around the background flow, $\boldsymbol{v}'$. Since $\nabla \cdot \boldsymbol{v} = 0$ and $\boldsymbol{v}_{\mathsf{R}} = 0$, we see that $\nabla \cdot \boldsymbol{v}' = 0$.

Material evolution of the kinetic energy is derived by making use of the velocity equation (57.1a), in which

$$\rho_o \, \mathrm{D}\mathcal{K}/\mathrm{D}t = -\nabla \cdot (\boldsymbol{v}\, p) - \rho\, g\, w. \tag{57.20}$$

Material evolution of the potential energy per volume for an adiabatic Boussinesq ocean is given by

$$\mathrm{D}(\rho\, \Phi)/\mathrm{D}t = g\, \rho\, w. \tag{57.21}$$

We are thus led to the mechanical energy equation for the adiabatic and inviscid Boussinesq ocean

$$\rho_o \, \mathrm{D}\mathcal{K}/\mathrm{D}t + \rho\, \mathrm{D}\Phi/\mathrm{D}t = -\nabla \cdot (\boldsymbol{v}\, p), \tag{57.22}$$

so that mechanical energy following a fluid element is modified by convergence of the pressure flux. We thus identify $\boldsymbol{v}\, p$ as the flux of mechanical energy in the Boussinesq ocean.

Linearized adiabatic inviscid Boussinesq ocean

In the process of deriving the linearized equation set (57.17a)-(57.17d), we gave no attention to the energetic balances. Hence, it is not *a priori* clear that a sensible energetic balance exists for these linear equations. However, as we now show, there is indeed an energetic balance that manifests a physically relevant exchange of mechanical energy between its kinetic and potential forms. For the kinetic energy per mass, $\mathcal{K}' = \boldsymbol{v}' \cdot \boldsymbol{v}'/2$, use of the velocity equation (57.17a) readily yields

$$\partial_t \mathcal{K}' = -\nabla \cdot (\boldsymbol{v}'\, \varphi') + w'\, b'. \tag{57.23}$$

The potential energy is a bit less straightforward. Namely, multiplying the linear buoyancy equation (57.17c) by b' readily finds

$$\partial_t \mathcal{A}' = -w'\, b' \quad \text{with} \quad \mathcal{A}' = (b'/N_{\mathsf{R}})^2/2. \tag{57.24}$$

Recall the discussion in Section 29.9.4, where $\mathcal{A}$ is identified as a measure of the available potential energy contained in small amplitude fluctuations of buoyancy surfaces.[3] Evidently, the linearized Boussinesq ocean has a mechanical energy budget given by

$$\partial_t(\mathcal{K}' + \mathcal{A}') = -\nabla \cdot (\boldsymbol{v}'\, \varphi'). \tag{57.25}$$

Hence, a time tendency for the sum of the kinetic energy plus the available potential energy is driven by convergences in the dynamic pressure flux, $\boldsymbol{v}'\, \varphi'$.

57.3 Buoyancy oscillations

As a starting point to studying small amplitude flow features emerging from the linearized Boussinesq ocean equations (57.17a)-(57.17d), consider $\boldsymbol{\Omega} = 0$ (flow in a non-rotating reference frame), in which the buoyancy equation and vertical velocity equation are

$$\partial_t b' + w'\, N_{\mathsf{R}}^2 = 0 \quad \text{and} \quad \partial_t w' = -\partial_z \varphi' + b'. \tag{57.26}$$

The time derivative of the velocity equation and use of the buoyancy equation, along with the complement operations, yield

$$(\partial_{tt} + N_{\mathsf{R}}^2)\, w' = -\partial_{tz} \varphi' \quad \text{and} \quad (\partial_{tt} + N_{\mathsf{R}}^2)\, b' = N_{\mathsf{R}}^2\, \partial_z \varphi'. \tag{57.27}$$

[3] In Section 57.5.14 we offer a further interpretation of the available potential energy as it appears for an internal gravity wave.

Each of these equations describes a forced oscillator with angular frequency given by the buoyancy frequency, N_{R}. We determine the forcing by determining the pressure, which satisfies the Poisson equation

$$-\nabla^2\varphi' = -\partial_z b', \tag{57.28}$$

along with boundary conditions specific to the domain. As studied in Sections 29.3 and 30.11, this pressure equation results from taking the divergence of the velocity equation (57.17a) (with $\boldsymbol{\Omega} = 0$) and using the continuity equation, $\nabla \cdot \boldsymbol{v}' = 0$. In the absence of any vertical structure to the buoyancy (i.e., $\partial_z b' = 0$), the pressure satisfies Laplace's equation, $\nabla^2\varphi' = 0$, which renders a zero pressure fluctuation in the absence of boundary effects.

57.3.1 Unforced buoyancy oscillations

Ignoring the pressure forcing in the forced oscillator equations (57.27) leads to free oscillations for the buoyancy and vertical velocity

$$(\partial_{tt} + N_{\mathsf{R}}^2)w'_{\text{free}} = 0 \quad \text{and} \quad (\partial_{tt} + N_{\mathsf{R}}^2)b'_{\text{free}} = 0. \tag{57.29}$$

Evidently, both the vertical velocity and the buoyancy exhibit simple harmonic oscillations with angular frequency, N_{R}. Such free oscillations occur when the pressure field has zero vertical gradient, $\partial_z\varphi' = 0$, in which case there is no resistance to free oscillations in the vertical.

By ignoring the pressure fluctuations, we are in effect ignoring the impact of the buoyancy fluctuation on pressure. This approach is not dynamically self-consistent. However, it is a common approach, sometimes referred to as the *parcel method*, whereby we consider the motion of a test fluid element that is assumed to have no impact on the surrounding fluid.[4] We considered the pros and cons of this approach when studying Archimedean buoyancy in Section 30.4 and effective buoyancy in Section 30.11.

As seen in Section 57.5.11, fluid particles exhibit free oscillations when they move in directions that parallel the surfaces of constant phase for internal gravity waves *if* the phase surfaces are not horizontal. On constant phase surfaces the pressure is spatially constant so that the only force acting on the fluid particle arises from gravity in a vertically stratified fluid; i.e., buoyancy. We return to this conceptual picture in Section 57.5.11 as it is fundamental to the forces acting within an internal gravity wave.

57.3.2 The lack of oscillations with horizontal homogeneity

When discussing buoyancy oscillations one sometimes finds it convenient to consider a horizontally homogenous fluid and conceive of the oscillations moving horizontal stratification surfaces up and down. However, there are caveats to this conceptual picture that offer further hints at the physics of gravity waves.

Horizontal homogeneity means that the horizontal pressure gradient vanishes, and thus the horizontal velocity vanishes (remember we are assuming a non-rotating reference frame so that $\boldsymbol{\Omega} = 0$). To maintain continuity for the Boussinesq ocean requires $\partial_z w' = 0$, which means, with zero horizontal motion, that $w' = 0$ throughout the domain. It follows that for a Boussinesq ocean there can be no buoyancy fluctuation with $\boldsymbol{v}' = 0$. Although this conclusion might be clear enough, we step through the details to further support an undestanding of the linear equations.

A vanishing vertical velocity in the forced oscillator equation (57.27) means that the vertical pressure gradient is time independent, $\partial_t(\partial_z\varphi') = 0$. Furthermore, horizontal homogeneity for the pressure equation (57.28) means that

$$\partial_z(\partial_z\varphi' - b') = 0, \tag{57.30}$$

[4] See Sections 17.2.5 and 30.4 for more on test fluid elements.

so that $\partial_z \varphi' - b' = B(t)$, where B is an arbitrary function of time. Taking a time derivative, and using $\partial_t(\partial_z \varphi') = 0$, leads to $\partial_t b' = -\partial_t B$, which means that the buoyancy fluctuation is vertically independent. A vertically independent buoyancy in the forced buoyancy oscillator equation (57.27) means that $N_{\mathsf{R}}^2 \, \partial_z \varphi'$ is also vertically independent, which can be satisfied if $\partial_z \varphi' = 0$. But then $w' = 0$ and $\partial_z \varphi' = 0$ in the vertical velocity equation (57.29) then means that $b' = 0$. We are thus led to conclude that the horizontally homogeneous linear Boussinesq system is dynamically consistent only with the trivial solution: $\boldsymbol{v}' = 0$ and $b' = 0$. That is, horizontal homogeneity means exact hydrostatic balance in which, for a Boussinesq fluid, there is zero motion and zero buoyancy oscillations.[5]

As we see in the following sections, the study of internal gravity waves leads to fluctuations that have both horizontal and vertical spatial variations, thus allowing for nontrivial wave motions. Now a surface of constant phase for a plane wave has homogeneous flow properties, in which case fluid particles exhibit free buoyant oscillations along these surfaces.[6] Yet as seen in the following, such buoyancy oscillations exist only if the phase surfaces are sloped relative to the horizontal plane, thus allowing the background buoyancy to produce buoyancy oscillations along the phase surfaces. No internal gravity waves occur if the phase surface is strictly horizontal, with this result consistent with the above arguments. We further detail this physical picture in Section 57.5.11.

57.4 The linear Boussinesq ocean with $f = 0$

We here study properties of the linearized Boussinesq equations (57.17a)-(57.17d) in a non-rotating reference frame

$$\partial_t \boldsymbol{v}' = -\nabla \varphi' + b' \, \hat{\boldsymbol{z}} \quad \text{linearized } \boldsymbol{\Omega} = 0 \text{ velocity equation} \tag{57.31a}$$

$$\partial_t b' = -w' \, N_{\mathsf{R}}^2 \quad \text{linearized buoyancy equation} \tag{57.31b}$$

$$\nabla \cdot \boldsymbol{v}' = 0 \quad \text{continuity for velocity fluctuations.} \tag{57.31c}$$

57.4.1 Relative vorticity

Taking the curl of the velocity equation (57.31a) leads to the evolution equation for the relative vorticity[7]

$$\partial_t (\nabla \times \boldsymbol{v}') = \nabla \times b' \, \hat{\boldsymbol{z}} \implies \partial_t \boldsymbol{\omega}' = -\hat{\boldsymbol{z}} \times \nabla b'. \tag{57.32}$$

The right hand side is the baroclinicity vector (40.152) for a Boussinesq fluid. Hence, in the linearized Boussinesq equations for a fluid in a non-rotating reference frame, relative vorticity has a local time tendency driven by baroclinicity. In the absence of a buoyancy gradient, the vorticity vector in the linear theory is static and remains zero if initialized to zero.

As noted in Section 40.7.2, baroclinicity in a Boussinesq fluid only affects vorticity in the

[5] A non-Boussinesq fluid can exhibit vertical motion even if the fluid has its density modified in a manner that does not introduce horizontal density gradients. For example, a horizontally homogeneous heating in an ocean with constant salinity will reduce the density and expand the water column, without introducing any horizontal inhomogeneities. This expansion results from the divergent nature of the flow field in a non-Boussinesq fluid. However, this expansion is not represented by a Boussinesq ocean. Namely, the Boussinesq ocean has a prognostic flow field that is non-divergent, so that a uniform heating is not directly felt by the flow. In Section 72.7.6 we discuss implications of this limitation of the Boussinesq ocean for the study of global mean sea level.

[6] This conclusion follows since internal gravity waves in a Boussinesq ocean are transverse waves, so that fluid particles move along constant phase surfaces.

[7] Be careful to distinguish the relative vorticity vector, $\boldsymbol{\omega}' = \nabla \times \boldsymbol{v}'$, from the angular frequency, ω, of a plane wave, and from the vertical component of the velocity vector, $\boldsymbol{v} = \hat{\boldsymbol{x}} \, u + \hat{\boldsymbol{y}} \, v + \hat{\boldsymbol{z}} \, w$.

horizontal directions, here seen for the linearized vorticity equation (57.32) since

$$\hat{\boldsymbol{z}} \cdot (\hat{\boldsymbol{z}} \times \nabla b') = 0. \tag{57.33}$$

One interpretation of internal gravity waves is that they arise from oscillations of the baroclinicity vector that leads to an oscillation of the horizontal components of the relative vorticity.[8] Since the vertical component to the vorticity is unaffected by baroclinicity, in the linear theory the vertical vorticity is locally static

$$\partial_t \zeta' = 0 \quad \text{with} \quad \zeta' = \hat{\boldsymbol{z}} \cdot (\nabla \times \boldsymbol{v}'). \tag{57.34}$$

So if the flow starts with a zero vertical vorticity, then the linearized Boussinesq ocean maintains $\zeta' = 0$. In Section 55.5.1 we also found a static vertical component of relative vorticity holds for the shallow water gravity waves in a non-rotating reference frame (see equation (55.72)).

57.4.2 Wave equation for the vertical velocity

In Section 57.3 we derived the forced harmonic oscillator equation (57.27) for the vertical velocity

$$(\partial_{tt} + N_{\mathsf{R}}^2) w' = -\partial_{tz} \varphi'. \tag{57.35}$$

We find it useful to derive a wave equation solely in terms of w', which is then used to derive the dispersion relation for internal gravity waves. To eliminate pressure, start by taking the horizontal divergence of the horizontal components to the velocity equation (57.31a)

$$\partial_t (\nabla_{\mathsf{h}} \cdot \boldsymbol{u}') = -\nabla_{\mathsf{h}}^2 \varphi', \tag{57.36}$$

where we introduced the horizontal gradient operator and horizontal Laplacian operator

$$\nabla_{\mathsf{h}} = \hat{\boldsymbol{x}}\, \partial_x + \hat{\boldsymbol{y}}\, \partial_y \quad \text{and} \quad \nabla_{\mathsf{h}}^2 = \nabla_{\mathsf{h}} \cdot \nabla_{\mathsf{h}} = \partial_{xx} + \partial_{yy}. \tag{57.37}$$

Equation (57.36) says that time evolution of the horizonal velocity divergence is driven by the negative horizontal Laplacian acting on the dynamic pressure. Since the full velocity is non-divergent, $\nabla \cdot \boldsymbol{v}' = \nabla_{\mathsf{h}} \cdot \boldsymbol{u}' + \partial_z w' = 0$, equation (57.36) becomes an equation for the vertical divergence of the vertical velocity

$$\partial_t (\partial_z w') = \nabla_{\mathsf{h}}^2 \varphi'. \tag{57.38}$$

Taking the horizontal Laplacian of the forced oscillator equation (57.35) (recall $N_{\mathsf{R}} = N_{\mathsf{R}}(z)$) yields

$$(\partial_{tt} + N_{\mathsf{R}}^2) \nabla_{\mathsf{h}}^2 w' = -\partial_{tz} \nabla_{\mathsf{h}}^2 \varphi', \tag{57.39}$$

and then using equation (57.38) leads to the wave equation for the vertical velocity

$$(\partial_{tt} \nabla^2 + N_{\mathsf{R}}^2 \nabla_{\mathsf{h}}^2)\, w' = 0. \tag{57.40}$$

There is anisotropy in this equation due to the gravity force that distinguishes the vertical direction from the horizontal. The anisotropy manifests by the fully three dimensional Laplacian, ∇^2, in the first term in equation (57.40), whereas just the horizontal Laplacian, ∇_{h}^2, appears in the second term. We furthermore observe that the wave equation (57.40) shares features with the wave equation (53.27) satisfied by the inertial waves in a homogeneous fluid in a constantly rotating reference frame. Gravity, coupled to nonzero density gradients, breaks symmetry in the Boussinesq ocean by introducing the buoyancy acceleration that then supports internal gravity waves. Analogously, a rotating reference frame breaks symmetry of the homogeneous fluid by

[8] For example, see the 16 minute mark of this video from Prof. Long.

introducing the Coriolis acceleration that then supports inertial waves.

57.4.3 Linearized boundary conditions

For much of this chapter, we study freely traveling internal inertia-gravity waves in the absence of boundaries. However, we do have occasions to study waves within a bounded or semi-bounded domain, in which case we need to apply boundary conditions. Hence, we here formulate the linearized boundary conditions for these cases. To be specific, we orient the domain with $z = 0$ the vertical position of a resting upper free surface boundary, such as for a resting ocean domain. However, when studying waves generated by bottom topography in Section 58.2, we place $z = 0$ at the position of a flat bottom domain.

Kinematic boundary conditions

Since the reference flow is assumed to vanish, the kinematic no-normal flow boundary condition holds for the fluctuating flow

$$\boldsymbol{v}' \cdot \hat{\boldsymbol{n}} = 0 \quad \text{at solid boundaries.} \tag{57.41}$$

At a moving material boundary (Section 19.6.2), such as the ocean free surface at $z = \eta(x, y, t)$, the kinematic boundary condition (19.66)

$$(\partial_t + \boldsymbol{u} \cdot \nabla)\eta = w' \quad \text{at } z = \eta \tag{57.42}$$

is linearized to

$$\partial_t \eta = w' \quad \text{at } z = \eta. \tag{57.43}$$

In fact, we must go one step further to fully linearize this boundary condition. The reason is that $w(\eta)$ is nonlinear, as seen by a Taylor expansion about the resting $z = 0$ free surface position

$$w'(z = \eta) \approx w'(z = 0) + \eta\, \partial_z w'. \tag{57.44}$$

The term, $\eta\, \partial_z w'$, and all higher order terms, are nonlinear and so are dropped for the linear theory. We are thus led to the linearized surface kinematic boundary condition

$$\partial_t \eta = w' \quad \text{at } z = 0. \tag{57.45}$$

We made use of this same boundary condition linearization in Section 52.3.4 when studying linear surface gravity waves and surface capillary waves, in which we also evaluate boundary terms at $z = 0$ rather than $z = \eta$.

Dynamic boundary condition for pressure

Following our treatment of stresses acting at an interface in Section 25.10, we make use of Newton's third law to set the pressure boundary condition at the free surface. Namely, pressure, in the absence of surface tension (which we ignore here), is continuous across the free surface. We find it useful to determine a boundary condition for the pressure written as the decomposition (57.7)

$$p(\boldsymbol{x}, t) = p_{\circ}(z) + p_{\mathsf{R}}(z) + p'(\boldsymbol{x}, t) = -\rho_{\circ}\, g\, z + g \int_z^0 \rho_{\mathsf{R}}(z')\, \mathrm{d}z' + p'(\boldsymbol{x}, t). \tag{57.46}$$

Assuming the atmospheric pressure applied on the free surface is a constant, which we take to be zero without loss of generality, leads to

$$0 = -\rho_o \, g \, \eta + g \int_\eta^0 \rho_R(z') \, dz' + p'(x, y, z = \eta, t). \tag{57.47}$$

Since the free surface height is small for linear waves, we Taylor expand the reference density around $z' = 0$ so that the integral becomes

$$\int_\eta^0 \rho_R(z') \, dz' \approx \int_\eta^0 \left[\rho_R(0) + (d\rho_R/dz)_{z=0} \, z'\right] dz' = -\eta \, \rho_R(0) - (\eta^2/2) \, (d\rho_R/dz)_{z=0}. \tag{57.48}$$

Dropping the term η^2 since it is nonlinear then leads to the boundary condition for the dynamic pressure evaluated at the free surface

$$\varphi'(x, y, z = \eta, t) = g \, \eta \, [\rho_o + \rho_R]/\rho_o \quad \text{at } z = \eta. \tag{57.49}$$

We fully linearize by evaluating the pressure at $z = 0$ and note that $\rho_R \ll \rho_o$ so that the boundary condition becomes

$$\varphi' = g \, \eta \quad \text{at } z = 0. \tag{57.50}$$

Evidently, the dynamic pressure at the ocean surface is determined by the free surface height. This boundary condition is identical to that used for the surface gravity waves as derived in Sections 52.3.2 and 52.3.3. Here, we needed to work a bit harder than for surface gravity waves. The reason is that here the fluid is stratified whereas we studied surface gravity waves at the surface of a homogeneous ocean that resulted in irrotational motion, and thus a rather simple expression of Bernoulli's theorem (Section 52.3).

Vertical velocity boundary condition

We further combine the pressure boundary condition (57.50) with the linearized surface kinematic boundary condition (57.45) to eliminate the free surface in favor of the vertical velocity

$$\partial_t \varphi' = g \, w' \quad \text{at } z = 0. \tag{57.51}$$

When studying vertical normal modes in an ocean domain in Section 57.7, we find it more convenient to have a boundary condition just for the vertical velocity. To eliminate the pressure we take the divergence of the horizontal velocity equation, $\partial_t \boldsymbol{u}' = -\nabla_h \varphi'$, and use the non-divergence condition on the velocity to yield

$$\partial_{tz} w' = \nabla_h^2 \varphi'. \tag{57.52}$$

Taking another time derivative and evaluating the expression at $z = 0$ yields

$$\partial_{ttz} w' = \nabla_h^2 \partial_t \varphi' \implies \partial_{ttz} w' = g \, \nabla_h^2 w' \quad \text{at } z = 0, \tag{57.53}$$

where we used the boundary condition (57.51) to eliminate pressure in favor of the vertical velocity.

57.5 Free internal gravity waves with constant stratification

Thus far we have assumed that the reference state buoyancy frequency is a function of the vertical direction. We now specialize to the case of a constant frequency, N_R, in which case we study free plane internal gravity waves. We return in Section 58.4 to the more realistic case of vertically varying buoyancy frequency, $N_R(z)$, which requires the WKBJ approximation.

57.5.1 Plane wave ansatz

To examine the physics of internal gravity waves in a fluid with constant buoyancy frequency, we introduce a traveling plane wave ansatz for the velocity, dynamic pressure, and buoyancy

$$\boldsymbol{v}' = \widetilde{\boldsymbol{v}}\, \mathrm{e}^{\mathrm{i}\,(\boldsymbol{k}\cdot\boldsymbol{x} - \omega\, t)} \quad \text{and} \quad \varphi' = \widetilde{\varphi}\, \mathrm{e}^{\mathrm{i}\,(\boldsymbol{k}\cdot\boldsymbol{x} - \omega\, t)}, \quad \text{and} \quad b' = \widetilde{b}\, \mathrm{e}^{\mathrm{i}\,(\boldsymbol{k}\cdot\boldsymbol{x} - \omega\, t)}, \tag{57.54}$$

where the amplitudes, $\widetilde{\boldsymbol{v}}$, $\widetilde{\varphi}$, and $\widetilde{b}$, are generally complex numbers, and where we write the three dimensional and horizontal wavevectors as

$$\boldsymbol{k} = k_x\, \hat{\boldsymbol{x}} + k_y\, \hat{\boldsymbol{y}} + k_z\, \hat{\boldsymbol{z}} \quad \text{and} \quad \boldsymbol{k}_{\mathrm{h}} = k_x\, \hat{\boldsymbol{x}} + k_y\, \hat{\boldsymbol{y}}. \tag{57.55}$$

Substitution of the ansatz (57.54) into the linearized Boussinesq equations (57.31a)-(57.31c) allows us to determine relations between the velocity, pressure, and buoyancy for a traveling plane wave. These relations are referred to as *polarization* relations. Furthermore, as part of developing polarization relations we derive the dispersion relation (Section 57.5.7) that connects the wavevector, $\boldsymbol{k}$, to the wave angular frequency, ω.

57.5.2 Transverse nature of internal gravity waves

The non-divergence condition holding for the Boussinesq ocean flow, $\nabla \cdot \boldsymbol{v}' = 0$, means that internal gravity waves are transverse, so that the velocity amplitude satisfies

$$\boldsymbol{k} \cdot \widetilde{\boldsymbol{v}} = \boldsymbol{k}_{\mathrm{h}} \cdot \widetilde{\boldsymbol{u}} + k_z\, \widetilde{w} = 0. \tag{57.56}$$

Consequently, fluid particles within a plane internal gravity wave move within the planes defined by constant phase, and these planes are perpendicular to the wavevector. Recall from Chapter 53 that plane inertial waves are also transverse.

57.5.3 Relative vorticity

The relative vorticity vector satisfies equation (57.32), which for a plane wave takes on the form

$$\omega\, \boldsymbol{k} \times \widetilde{\boldsymbol{v}} = -\mathrm{i}\, \widetilde{b}\, (\hat{\boldsymbol{z}} \times \boldsymbol{k}) \Longrightarrow \boldsymbol{k} \times (\omega\, \widetilde{\boldsymbol{v}} - \mathrm{i}\, \hat{\boldsymbol{z}}\, \widetilde{b}) = 0. \tag{57.57}$$

Evidently, the vector, $\omega\, \widetilde{\boldsymbol{v}} - \mathrm{i}\, \hat{\boldsymbol{z}}\, \widetilde{b}$, is parallel to the wavevector. Taking the dot product of the $\boldsymbol{k}$-space relative vorticity equation (57.57) with $\hat{\boldsymbol{z}}$ leads to

$$\hat{\boldsymbol{z}} \cdot (\boldsymbol{k} \times \widetilde{\boldsymbol{v}}) = 0, \tag{57.58}$$

which is the $\boldsymbol{k}$-space expression for a zero vertical component to the relative vorticity, $\zeta' = 0$. This constraint means that the plane waves maintain $\zeta' = 0$ since the horizontal velocity amplitudes are related by

$$k_x\, \widetilde{v} = k_y\, \widetilde{u}. \tag{57.59}$$

57.5.4 Amplitude of pressure fluctuations

Substitution of the plane wave ansatz into the pressure equation (57.28) renders

$$\widetilde{\varphi}/\widetilde{b} = -\mathrm{i}\, k_z/|\boldsymbol{k}|^2. \tag{57.60}$$

Hence, the pressure and buoyancy in the plane wave are $\pi/2$ radians out of phase. Observe that the pressure amplitude vanishes for a horizontal wavevector, in which $k_z = 0$. We expect this

result for a free wave since vertical structure in the fluctuating buoyancy (i.e., $k_z \neq 0$) provides the source for pressure fluctuations as per the pressure Poisson equation (57.28).

57.5.5 Vertical velocity component

For the vertical velocity component, make use of the forced oscillator equation (57.35) to render a relation between the vertical velocity amplitude and amplitude of the dynamic pressure

$$\widetilde{w}/\widetilde{\varphi} = -\frac{k_z\,\omega}{N_{\mathsf{R}}^2 - \omega^2}. \tag{57.61}$$

We can also relate the vertical velocity amplitude to the buoyancy amplitude through use of the pressure equation (57.60)

$$\widetilde{w}/\widetilde{b} = \frac{\mathrm{i}\,k_z^2\,\omega}{|\boldsymbol{k}|^2\,(N_{\mathsf{R}}^2 - \omega^2)}. \tag{57.62}$$

Evidently, the vertical velocity is either in phase or π radians out of phase with the pressure (depending on the sign of k_z), whereas the vertical velocity is $\pi/2$ out of phase with buoyancy.

57.5.6 Horizontal velocity

The horizontal portion of the velocity equation (57.31a) leads to the relation satisfied by the plane wave

$$\omega\,\boldsymbol{k}_{\mathsf{h}} \cdot \widetilde{\boldsymbol{u}} = \widetilde{\varphi}\,|\boldsymbol{k}_{\mathsf{h}}|^2 = -\mathrm{i}\,\widetilde{b}\,k_z\,|\boldsymbol{k}_{\mathsf{h}}|^2/|\boldsymbol{k}|^2, \tag{57.63}$$

where we used the pressure equation (57.60) for the second equality. Equivalently, we can use the transverse nature of the wave as per equation (57.56) to write

$$\omega\,\boldsymbol{k}_{\mathsf{h}} \cdot \widetilde{\boldsymbol{u}} = -\omega\,k_z\,\widetilde{w} = -\frac{\mathrm{i}\,k_z^3\,\omega^2\,\widetilde{b}}{|\boldsymbol{k}|^2\,(N_{\mathsf{R}}^2 - \omega^2)}, \tag{57.64}$$

where we used equation (57.62) for the vertical velocity.

57.5.7 Dispersion relation

Equating equations (57.63) and (57.64) yields the dispersion relation for internal gravity waves

$$\omega^2 = |\boldsymbol{k}_{\mathsf{h}}|^2\,N_{\mathsf{R}}^2/|\boldsymbol{k}|^2 = N_{\mathsf{R}}^2\cos^2\gamma \Longrightarrow 0 \leq \omega \leq N_{\mathsf{R}}. \tag{57.65}$$

In the second equality we introduced the angle between the wavevector and the horizontal plane

$$\cos\gamma = |\boldsymbol{k}_{\mathsf{h}}|/|\boldsymbol{k}|, \tag{57.66}$$

with the geometry illustrated in Figure 57.1. An alternative means to write the dispersion relation (57.65) is given by

$$\frac{N_{\mathsf{R}}^2 - \omega^2}{\omega^2} = \frac{k_z^2}{|\boldsymbol{k}_{\mathsf{h}}|^2} = \tan^2\gamma. \tag{57.67}$$

This expression makes it clear that internal gravity waves with maximum frequency, $\omega = N_{\mathsf{R}}$, correspond to a horizontal phase velocity, $k_z = 0$ and $\gamma = 0$. Conversely, the angular frequency goes to zero when $\gamma = \pi/2$ whereby the waves have a purely vertical phase velocity, $\boldsymbol{k}_{\mathsf{h}} = 0$.

The dispersion relation (57.65) can be directly derived from the wave equation (57.40) satisfied by the vertical velocity

$$(\partial_{tt}\nabla^2 + N_{\mathsf{R}}^2\,\nabla_{\mathsf{h}}^2)\,w' = 0 \Longrightarrow \omega^2\,|\boldsymbol{k}|^2 - N_{\mathsf{R}}^2\,|\boldsymbol{k}_{\mathsf{h}}|^2 = 0. \tag{57.68}$$

Furthermore, note that if we only extract the horizontal and time harmonic portion of w', so that

$$w' = W(z)\, e^{i\,(\boldsymbol{k}_h \cdot \boldsymbol{x} - \omega\, t)}, \tag{57.69}$$

then the vertical structure function, $W(z)$, satisfies the ordinary differential equation

$$\left[\frac{d^2}{dz^2} + \frac{|\boldsymbol{k}_h|^2\,(N_R^2 - \omega^2)}{\omega^2}\right] W = 0 \Longrightarrow \left[\frac{d^2}{dz^2} + k_z^2\right] W = 0. \tag{57.70}$$

This equation is satisfied if $W = e^{i\,k_z\,z}$, which is what we use for the constant N_R case now being studied. However, in Section 58.4 we find that equation (57.70) is generalized for the case with the background buoyancy frequency a function of the vertical, $N_R = N_R(z)$, in which case $W \neq e^{i\,k_z\,z}$.

57.5.8 Concerning the upper limit on the frequency

The internal gravity wave dispersion relation (57.65) says that no internal gravity waves exist with angular frequency greater than the buoyancy frequency of the background reference state, $\omega \leq N_R$. What happens if a stratified fluid is agitated at a frequency $\omega_{source} > N_R$? In this case, fluid particles do not have time to exhibit buoyancy oscillations. Instead, the fluid particles follow whatever displacements are forced on them by the external forcing, and with fluid particles in phase with the forcing. No propagating internal gravity waves are formed, and any energy imparted to the fluid stays local to the agitation. Indeed, with enough agitation the fluid becomes a forced turbulent soup.[9] For a mechanical analog, consider a forced linear pendulum where the forcing frequency is greater than the pendulum's natural frequency. In this case, the forcing fails to generate a natural oscillation, but instead it causes an incoherent and non-periodic back and forth motion of the pendulum.

57.5.9 Unpacking the dispersion relation

The angular frequency for an internal gravity wave only depends on the buoyancy frequency and the cosine of the angle the wavevector makes with the horizontal plane, whereas it is independent of the wavenumber, $|\boldsymbol{k}|$, and thus of the wavelength, $2\pi/|\boldsymbol{k}|$. Furthermore, the angular frequency possesses rotational (azimuthal) symmetry around the vertical direction. As such, the angular frequency is the same along the surface of a cone for wavevectors extending out from the origin along the $\hat{\boldsymbol{z}}$ axis in either direction. Figure 57.1 provides an illustration for the two cones associated with a particular γ. The upper cone has $k_z > 0$ and so waves on this code have an upward phase velocity, whereas waves on the lower cone, with $k_z < 0$, have a downward phase velocity.

57.5.10 Group velocity

The dispersion relation (57.65) leads to the group velocity, $\boldsymbol{c}_g = \nabla_{\boldsymbol{k}} \varpi(\boldsymbol{k})$, which for internal gravity waves is given by

$$\boldsymbol{c}_g = \frac{N_R\, k_z}{|\boldsymbol{k}|^3\, |\boldsymbol{k}_h|}\,(k_z\, \boldsymbol{k}_h - |\boldsymbol{k}_h|^2\, \hat{\boldsymbol{z}}). \tag{57.71}$$

In this section we identify a number of properties satisfied by the group velocity and summarize these properties in Figure 57.2.

[9] See Section 13.2 of *Cushman-Roisin and Beckers* (2011) for further discussion on this point.

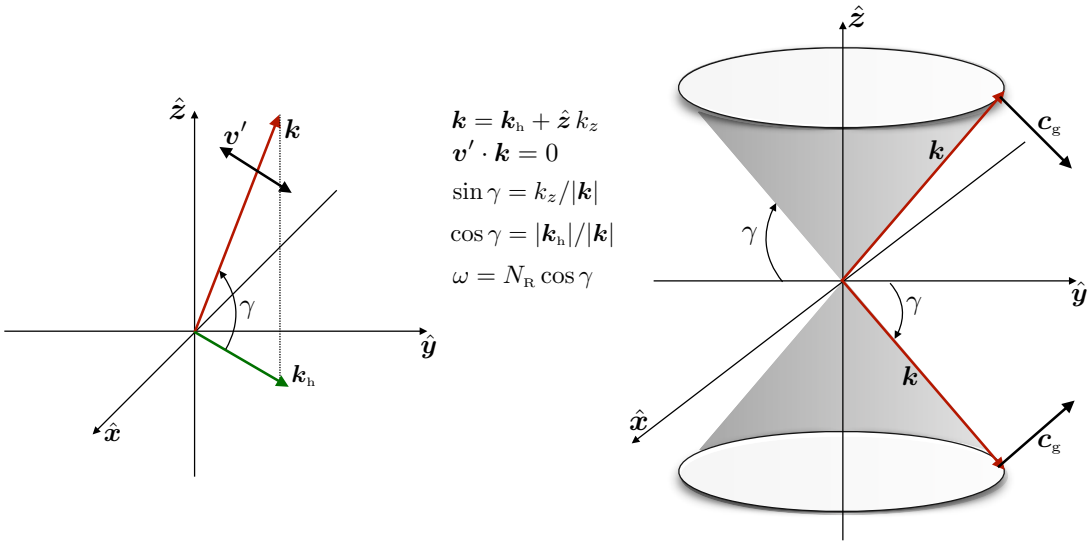

FIGURE 57.1: Left panel: A sample wavevector, $\boldsymbol{k} = \boldsymbol{k}_\mathrm{h} + \hat{\boldsymbol{z}}\, k_z$, for a plane internal gravity wave. The wave is transverse so that the velocity of fluid particles is orthogonal to the wavevector, $\boldsymbol{k} \cdot \boldsymbol{v}' = 0$. The dispersion relation, $\omega = N_\mathrm{R} \cos\gamma$, is independent of the wavenumber, $|\boldsymbol{k}|$, but instead only depends on the cosine of the angle made with the horizontal plane, $\cos\gamma = |\boldsymbol{k}_\mathrm{h}|/|\boldsymbol{k}|$. Right panel: another depiction of the dispersion relation. The angular frequency is the same for all wavevectors on the surface of an ω-cone extending from the origin along the $\hat{\boldsymbol{z}}$ axis and with arbitrary magnitude. Correspondingly, with the phase velocity given by $\boldsymbol{c}_\mathrm{p} = \hat{\boldsymbol{k}}\,(\omega/|\boldsymbol{k}|)$, higher wavenumber waves along a particular ω-cone have slower phase speeds than lower wavenumber waves. Cones with $k_z > 0$ correspond to internal gravity waves with an upward phase velocity, and those with $k_z < 0$ are downward. The group velocity, $\boldsymbol{c}_\mathrm{g} = \nabla_{\boldsymbol{k}} \varpi(\boldsymbol{k})$, points in the $\boldsymbol{k}$-space direction of steepest ascent for the angular frequency, and so it is orthogonal to surfaces of constant ω. For internal gravity waves, the group velocity is orthogonal to the phase velocity ($\boldsymbol{c}_\mathrm{g} \cdot \hat{\boldsymbol{k}} = 0$), and the group velocity points towards the horizontal plane (i.e., smaller $|\gamma|$) since that is the direction of increasing angular frequency. Hence, waves with an upward phase velocity have a downward group velocity, and downward phase velocity waves have an upward group velocity. Evidently, internal wave energy is directed away from the inside of the ω-cone and thus toward the horizontal plane.

Group velocity is orthogonal to the phase velocity

The internal wave group velocity (57.71) is orthogonal to the phase velocity

$$\boldsymbol{c}_\mathrm{g} \cdot \boldsymbol{c}_\mathrm{p} = 0, \tag{57.72}$$

where the phase velocity is

$$\boldsymbol{c}_\mathrm{p} = (\omega/|\boldsymbol{k}|)\, \hat{\boldsymbol{k}}. \tag{57.73}$$

Hence, the group velocity is aligned parallel to constant phase surfaces, as with motion of fluid particles within an internal gravity wave. Recall that these properties also hold for inertial waves discussed in Section 53.3.3.

We geometrically understand the orientation of the phase and group velocities as follows. The phase velocity is aligned with the wavevector, $\boldsymbol{k}$. All wavevectors emanating from the origin that make an angle, γ, have the same angular frequency and so form points along a particular ω-cone (Figure 57.1). Consequently, surfaces of constant angular frequency are parallel to all these wavevectors. Now the group velocity, $\boldsymbol{c}_\mathrm{g} = \nabla_{\boldsymbol{k}} \varpi(\boldsymbol{k})$, points in the $\boldsymbol{k}$-space direction of steepest ascent for the angular frequency, so that the group velocity is normal to surfaces of constant angular frequency. Hence, the group velocity points in a direction normal to the ω-cone, and as such it is orthogonal to the phase velocity, $\boldsymbol{c}_\mathrm{p} \cdot \boldsymbol{c}_\mathrm{g} = 0$.

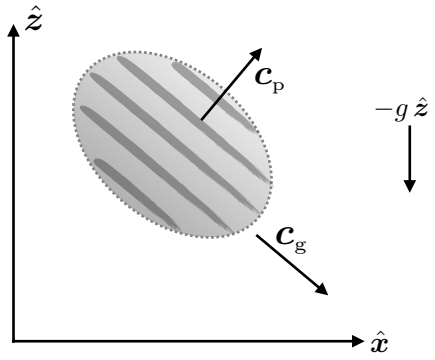

FIGURE 57.2: An example elliptical packet of internal gravity waves, with the packet moving down to the right according to the group velocity, $\boldsymbol{c}_{\mathrm{g}}$, whereas phase lines move upward to the right. The packet moves parallel to the phase lines, with the phase velocity, $\boldsymbol{c}_{\mathrm{p}}$, directed up and to the right.

The phase velocity and group velocity have opposing vertical components

The vertical component to the group velocity has the opposite sign of the vertical component to the phase velocity, which is seen by

$$(\boldsymbol{c}_{\mathrm{p}} \cdot \hat{\boldsymbol{z}})\,(\boldsymbol{c}_{\mathrm{g}} \cdot \hat{\boldsymbol{z}}) = -\frac{\omega\, k_z}{|\boldsymbol{k}|^2}\,\frac{N_{\mathsf{R}}\, k_z\, |\boldsymbol{k}_{\mathrm{h}}|}{|\boldsymbol{k}|^3} = -\frac{\omega^2 \sin^2\gamma}{|\boldsymbol{k}|^2} < 0. \tag{57.74}$$

The phase velocity is directed away from the $\gamma = 0$ horizontal plane, whereas the group velocity is directed toward the horizontal plane. This property is depicted in Figures 57.1 and 57.4. Evidently, the internal gravity wave energy, which is fluxed in the direction of the group velocity, is directed away from the inside of the ω-cone and towards the horizontal plane.

The group velocity magnitude

The squared magnitude of the group velocity is given by

$$\boldsymbol{c}_{\mathrm{g}} \cdot \boldsymbol{c}_{\mathrm{g}} = \frac{N_{\mathsf{R}}^2\, k_z^2}{|\boldsymbol{k}|^4} = \frac{N_{\mathsf{R}}^2 \sin^2\gamma}{|\boldsymbol{k}|^2} \quad \text{where} \quad \sin\gamma = k_z/|\boldsymbol{k}|. \tag{57.75}$$

To help understand this expression it is useful to consider two extreme cases.

The group velocity vanishes when the wavevector is horizontal ($k_z = 0$ and $\gamma = 0$). As a result, no wave energy is propagated when the wavevector is horizontal.[10] When the wavevector is horizontal, all fluid particle motion in the wave is vertical, with fluid particles exhibiting vertical buoyancy oscillations at the maximum allowable gravity wave frequency, $\omega = N_{\mathsf{R}}$. So even though the wave has energy when it has a horizontal phase velocity, the wave energy is not propagated since $\boldsymbol{c}_{\mathrm{g}} = 0$. Rather, the wave energy is stationary as fluid particles exhibit vertical buoyancy oscillations.

At the opposite extreme, when the phase velocity is vertical, so that $\boldsymbol{k}_{\mathrm{h}} = 0$ and $\gamma = \pi/2$, the fluid particles move along a horizontal plane in an arbitrary horizontal direction. The group velocity is also horizontal and takes the form

$$\boldsymbol{c}_{\mathrm{g}} = (N_{\mathsf{R}}/|k_z|)\,\hat{\boldsymbol{k}}_{\mathrm{h}} \quad \text{with } \boldsymbol{k}_{\mathrm{h}} = 0, \tag{57.76}$$

where $\hat{\boldsymbol{k}}_{\mathrm{h}}$ is any horizontal direction. The angular frequency (57.65) vanishes ($\omega = 0$) so that the wave is stationary; i.e., phase lines do not move when $\gamma = \pi/2$.

[10] In Section 57.5.14 we see that the mechanical energy flux of an internal gravity wave is proportional to the group velocity, which is the case for any linear waves (see Chapter 50).

Relating the dispersion relation for internal gravity waves and inertial waves

The internal gravity wave dispersion relation (57.65) shares features with that for inertial waves, whose dispersion relation is given by equation (53.33), so that we have

$$\omega_{\text{igw}}^2 = N_{\text{R}}^2 \cos^2\gamma \quad \text{and} \quad \omega_{\text{inertial}}^2 = f^2 \sin^2\gamma. \tag{57.77}$$

Both dispersion relations are independent of the wavenumber, depending only on the wave's orientation. For the gravity wave, the vertical is a special direction since it is the direction of the gravitational acceleration, whereas for the inertial wave, the horizontal direction is special since is the direction of the Coriolis acceleration. Indeed, the switch from $\cos^2\gamma$ to $\sin^2\gamma$ arises since gravitation acts in the vertical whereas the Coriolis acts in the horizontal.[11] Both angular frequencies have an upper bound, with inertial waves having angular frequencies no larger than the Coriolis frequency, $|f|$, and internal gravity waves having angular frequencies no larger than the buoyancy frequency, N_{R}.

57.5.11 Force balance within an internal gravity wave

To help further understand the internal gravity wave dispersion relation (57.65), consider a test fluid element that moves with the wave in the transverse direction; i.e., parallel to surfaces of constant phase. As discussed in Section 17.2.5, a test fluid element is assumed to have zero impact on the surrounding fluid, in particular it has no impact on the pressure. This assumption is broken when considering real fluid elements, since all fluid elements affect the surrounding fluid. However, the pressure is spatially constant along a constant phase direction. Hence, for a particle displaced in this direction it only feels the change in buoyancy. So our critique of the test fluid elements in Section 57.3.1 is tempered when considering motion along directions that parallel phase surfaces. In the following, we refer to the test fluid element as a fluid particle both for brevity and to accord with the literature.

Fluid particle displacement vector

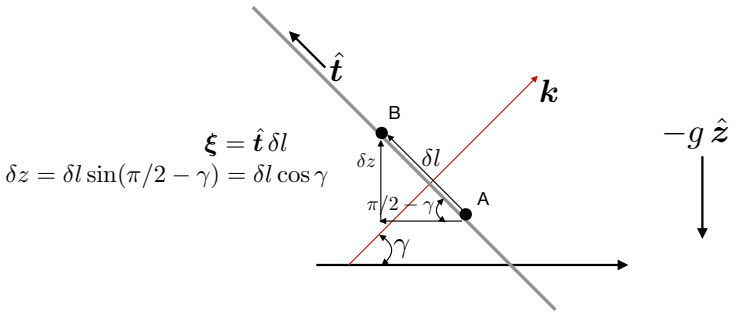

FIGURE 57.3: Depicting the displacement of a fluid particle along a direction transverse to a constant phase surface for a plane internal gravity wave whose wavevector makes an angle γ with the horizontal. We write the displacement vector as $\boldsymbol{\xi}(\boldsymbol{x}, t) = \delta l\, \hat{\boldsymbol{t}}$, with the local tangent vector, $\hat{\boldsymbol{t}}$, pointing in a transverse direction orthogonal to the wavevector, $\boldsymbol{k}$. The displacement of the fluid particle from point A to point B occurs over a distance, δl, with a corresponding change in vertical position given by $\delta z = \delta l \cos\gamma$.

As depicted in Figure 57.3, we measure a fluid particle's position relative to its equilibrium position through a displacement field,

$$\boldsymbol{\xi}(\boldsymbol{x}, t) = \hat{\boldsymbol{x}}\,\delta x + \hat{\boldsymbol{y}}\,\delta y + \hat{\boldsymbol{z}}\,\delta z. \tag{57.78}$$

[11] We discuss the force balances for an internal gravity wave in Section 57.5.11 and then for an intertia-gravity wave in Section 57.9.3.

The displacement field vanishes when the fluid particle is at its equilibrium position, and it has a time tendency that equals to the velocity of a fluid particle[12]

$$\partial_t \boldsymbol{\xi}(\boldsymbol{x}, t) = \boldsymbol{v}'(\boldsymbol{x}, t). \tag{57.79}$$

Evidently, since the plane wave is transverse,

$$\boldsymbol{v}' \cdot \boldsymbol{k} = (\partial_t \boldsymbol{\xi}) \cdot \boldsymbol{k} = 0. \tag{57.80}$$

If the fluid particle moves in the vertical, it moves through the background reference density field, $\rho_{\mathsf{R}}(z)$. Referring to Figure 57.3, assume the fluid particle starts at point A with local buoyancy equal to the reference buoyancy. As it rises an infinitesimal amount to point B, its buoyancy referenced to the local environment is negative since it started from a denser level. As such, the fluid particle wants to return to its deeper level. We can express the locally referenced buoyancy anomaly felt at point B in terms of the particle displacement

$$b' = -\boldsymbol{\xi} \cdot \nabla b_{\mathsf{R}} = -\delta z \, (\mathrm{d}b_{\mathsf{R}}/\mathrm{d}z) = -\delta z \, N_{\mathsf{R}}^2. \tag{57.81}$$

As a check on this expression, we find that if $\delta z > 0$, so that the fluid particle rises, then the buoyancy anomaly is negative, $b' < 0$, since it started from a deeper level where the density is larger. Hence, there is a buoyant acceleration back to the deeper level. Also observe that the time derivative of equation (57.81) leads to

$$\partial_t b' = -w' \, N_{\mathsf{R}}^2, \tag{57.82}$$

which is the linearized buoyancy equation (57.17c).

Equation of motion

We now make use of the result (57.81) in the equation of motion (57.31a). More precisely, we project that equation onto the transverse direction, $\hat{\boldsymbol{t}}$. This direction is fixed in time for a plane wave so that we have

$$\partial_t(\hat{\boldsymbol{t}} \cdot \boldsymbol{v}') = \hat{\boldsymbol{t}} \cdot (-\nabla \varphi' + b' \, \hat{\boldsymbol{z}}). \tag{57.83}$$

As noted above, there is no spatial gradient of flow properties along a constant phase surface. Hence, the tangential component of the pressure gradient vanishes

$$\hat{\boldsymbol{t}} \cdot \nabla \varphi' = 0, \tag{57.84}$$

which means pressure has no affect on fluid particles moving in the direction transverse to the wavevector. We write δl for the displacement along the phase surface, so that

$$\hat{\boldsymbol{t}} \cdot \boldsymbol{v}' = \partial_t(\delta l), \tag{57.85}$$

which brings the equation of motion (57.83) to the form

$$\partial_{tt}(\delta l) - \hat{\boldsymbol{z}} \cdot \hat{\boldsymbol{t}} \, b' = 0. \tag{57.86}$$

[12]We make use of a one dimensional displacement field in Section 51.3 when considering acoustic waves using a Lagrangian perspective. We also make use of fluid particle displacement vectors when studying the generalized Lagrangian mean in Section 70.2, as well as for tracer kinematics in Section 70.3. The present discussion is heuristic and skims over details explored in these other sections. We can afford some degree of informality since all perturbations here are small.

Noting that $\hat{\boldsymbol{z}} \cdot \hat{\boldsymbol{t}} = \cos\gamma$ and making use of equation (57.81) for the buoyancy anomaly leads to

$$\partial_{tt}(\delta l) + \cos\gamma\, N_{\mathsf{R}}^2\, \delta z = 0. \tag{57.87}$$

Finally, we set $\delta z = \delta l \cos\gamma$ to render the simple harmonic oscillator equation for displacements along the constant phase line

$$(\partial_{tt} + N_{\mathsf{R}}^2 \cos^2\gamma)\, \delta l = 0. \tag{57.88}$$

The angular frequency of the oscillations, $N_{\mathsf{R}} \cos\gamma$, is precisely that arising from the internal gravity wave dispersion relation (57.65).

Summary of the physical picture for internal gravity waves

The above analysis suggests the following physical picture for internal gravity waves. Namely, the waves consist of fluid particle motion in directions that parallel the constant phase surfaces, which accords with the property of all transverse waves. As the particles move along the transverse direction, $\hat{\boldsymbol{t}}$, they sample the background buoyancy field and thus experience buoyancy accelerations that act to return the particle to its neutral buoyancy position. The buoyancy force acting on the particles only depends on the angle of the phase lines relative to the horizontal. Oscillatory motion arises from over-shooting the neutral buoyancy position, with the oscillations having an angular frequency, $N_{\mathsf{R}} \cos\gamma$. The oscillations have their maximum angular frequency when the angle, $\gamma = 0$, which arises since the particles are moving vertically and thus fully sampling the background buoyancy field. In contrast, there are no oscillations when the particles move along a horizontal phase surface ($\gamma = \pi/2$ so that $\hat{\boldsymbol{k}} = \hat{\boldsymbol{z}}$) since horizontal surfaces sample the same background buoyancy. The vanishing of oscillations with $\gamma = \pi/2$ accords with our discussion in Section 57.3.2. The force balance dependence on the angle, γ, explains the geometry of the ω-cones in Figure 57.1, which, in turn, explains why the group velocity is perpendicular to the phase velocity.

We emphasize that although the fluid particles are moving in a direction that parallels the constant phase surfaces, they are *not* moving with those surfaces. Rather, the fluid particles are oscillating in the transverse direction, and it is their oscillation that gives rise to the wave itself and thus to the movement of the phase surfaces through the fluid.

57.5.12 Forced internal gravity wave packets

A further remark about the dispersion relation written as in equation (57.67) concerns the case where we know the frequency of the wave and the buoyancy frequency, in which case the angle γ is specified. For example, consider a local source (say an oscillating disk) with angular frequency, ω_{source}, moving with a small amplitude in a stratified fluid with $\omega_{\text{source}} < N_{\mathsf{R}}$. This source preferentially forces internal waves of angular frequency $\omega = \omega_{\text{source}}$. Consequently, the left hand side of the dispersion relation (57.67) is specified.

Gravity wave packets extend outward from the oscillating source and define the group velocity direction (not the phase velocity direction). Consequently, the group velocity extends outward from the source at an angle $\pi/2 - \gamma$ from the horizontal. The reason the source defines the group velocity is that energy is input to the wave field by the oscillating source, and the wave energy propagates along the group velocity direction with the wave packets (we discuss internal gravity wave energy in Section 57.5.14). The phase velocity is directed perpendicular to the group velocity and it makes an angle γ with the horizontal. Hence, as the source angular frequency approaches the buoyancy frequency, γ approaches zero so that the group velocity "cross" pattern steepens toward the vertical axis. Figure 57.4 provides a schematic of the experiment along with links to videos illustrating the remarkable wave patterns in a laboratory setting as well as a

numerical simulation.[13]

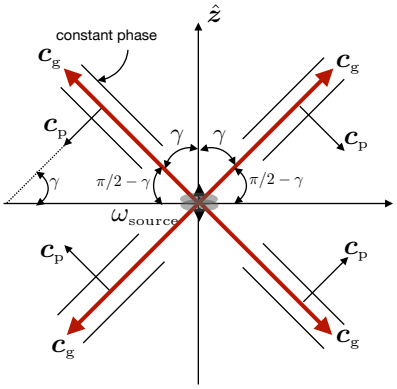

$$\omega_\mathrm{source} < N_\mathrm{R}$$
$$\tan^2\gamma = \frac{N_\mathrm{R}^2 - \omega_\mathrm{source}^2}{\omega_\mathrm{source}^2}$$
$$\boldsymbol{c}_\mathrm{p}\cdot\boldsymbol{c}_\mathrm{g} = 0$$
$$(\boldsymbol{c}_\mathrm{p}\cdot\hat{\boldsymbol{z}})(\boldsymbol{c}_\mathrm{g}\cdot\hat{\boldsymbol{z}}) < 0$$

FIGURE 57.4: A small amplitude oscillating source in a stratified fluid with angular frequency, $\omega_\mathrm{source} < N_\mathrm{R}$. If the source has small amplitude then it generates linear internal gravity waves with $\omega = \omega_\mathrm{source}$. These waves radiate wave packets with group velocity, $\boldsymbol{c}_\mathrm{g}$, away from the source and with an angle, $\pi/2-\gamma$, from the horizontal. The angle, γ, is determined by the dispersion relation through $\tan^2\gamma = (N_\mathrm{R}^2 - \omega_\mathrm{source}^2)/\omega_\mathrm{source}^2$. The group velocity is parallel to lines of constant phase and perpendicular to the phase velocity so that $\boldsymbol{c}_\mathrm{p}\cdot\boldsymbol{c}_\mathrm{g} = 0$. Furthermore, the phase and group velocities are oriented so that $(\boldsymbol{c}_\mathrm{g}\cdot\hat{\boldsymbol{z}})(\boldsymbol{c}_\mathrm{p}\cdot\hat{\boldsymbol{z}}) < 0$, so that if the group velocity is directed upward then the phase velocity is directed downward, and vice versa. As the source angular frequency approaches the buoyancy frequency, γ approaches zero so that the group velocity "cross" pattern steepens toward the vertical axis. The pattern is sometimes referred to as *St. Andrew's cross*. This video and this video, both from the geophysical fluids laboratory at The Australian National University, as well as this video from Prof. Rhines' lab at the University of Washington, illustrate the phenomena in a laboratory settings, whereas this animation from Prof. Durran's website at the University of Washington illustrates the phenomena in a numerical simulation. *Sutherland* (2010) in his Chapter 5 works through the boundary value problems arising from both an oscillating cylinder and a sphere, thus illustrating the analytical methods available to solve for the generated internal gravity wave fields.

Internal gravity waves have an angular frequency that is bounded above by the buoyancy frequency: $0 \le \omega \le N_\mathrm{R}$. There are no internal gravity waves with frequency larger than the buoyancy frequency of the background reference state. This limit exists since internal gravity waves are coherent patterns of buoyancy oscillations, with the angular frequency of that oscillation taken from the background stratification (see Section 57.5.11 for more on this perspective).

57.5.13 Polarization relations and structure of a plane wave

We now piece together the polarization relations to provide expressions for the velocity, pressure, and buoyancy within a wave. We first express all fields in terms of the buoyancy amplitude, $\widetilde{b}$, and then in terms of the pressure amplitude, $\widetilde{\varphi}$. These amplitudes are related via the pressure equation from Section 57.5.4, whereby

$$\widetilde{\varphi}/\widetilde{b} = -\mathrm{i}\,k_z/|\boldsymbol{k}|^2 = -\mathrm{i}\sin\gamma/|\boldsymbol{k}|. \tag{57.89}$$

Neither is more fundamental, and yet one amplitude might be more readily available than the other so it is useful to provide both expressions.

[13] It is notable that this video from Prof. Rhines' lab shows both a St. Andrew's cross, which is well described by linear theory, as well as horizontal phase lines indicative of $\gamma = \pi/2$ vertical phase propagation and horizontal group propagation. Paraphrasing from an email discussion with Prof. Rhines, the horizontal phase lines are in part the result of mixing (a nonlinear process) at the oscillating circular cylinder, which affects the background buoyancy frequency enough to alter the linear waves a bit. This mixing causes a diffusive drift away from the source that excites low frequency internal waves, which move rapidly ahead of the turbulently mixed fluid.

Vertical velocity component

The dispersion relation in the form of equation (57.67) brings the vertical velocity expressions (57.61) and (57.62) into the tidy forms

$$\widetilde{w}/\widetilde{\varphi} = -\frac{k_z\,\omega}{N_{\mathsf{R}}^2 - \omega^2} = -\frac{|\boldsymbol{k}_{\mathsf{h}}|^2}{\omega\,k_z} \tag{57.90a}$$

$$\widetilde{w}/\widetilde{b} = \frac{\mathrm{i}\,k_z^2\,\omega}{|\boldsymbol{k}|^2\,(N_{\mathsf{R}}^2 - \omega^2)} = \frac{\mathrm{i}\,|\boldsymbol{k}_{\mathsf{h}}|^2}{\omega\,|\boldsymbol{k}|^2} = \frac{\mathrm{i}\cos\gamma}{N_{\mathsf{R}}}. \tag{57.90b}$$

Notice how the vertical velocity and pressure are in phase (or π out of phase), whereas the vertical velocity and buoyancy are $\pi/2$ out of phase.

Horizontal velocity

For the horizontal velocity we use the transverse nature of the wave (Section 57.5.2) to relate the horizontal components to the vertical

$$\boldsymbol{k}_{\mathsf{h}} \cdot \widetilde{\boldsymbol{u}} = -k_z\,\widetilde{w}, \tag{57.91}$$

as well as the zero vertical component of the relative vorticity (Section 57.5.3) so that

$$k_x\,\widetilde{v} = k_y\,\widetilde{u}. \tag{57.92}$$

These two relations, along with the vertical velocity amplitude equations (57.90a) and (57.90b), lead to

$$\widetilde{\boldsymbol{u}} = -\frac{\mathrm{i}\,\widetilde{b}\,\boldsymbol{k}_{\mathsf{h}}\sin\gamma}{N_{\mathsf{R}}\,|\boldsymbol{k}_{\mathsf{h}}|}. \tag{57.93}$$

As for the vertical velocity, we here find that the horizontal velocity is $\pi/2$ out of phase with the buoyancy.

Wave solutions in terms of the buoyancy amplitude

Bringing the previous results together allows us to express the solutions for the velocity, pressure, and buoyancy within a freely propagating internal gravity wave. The solutions in terms of a real buoyancy amplitude, $\widetilde{b}$, are given by

$$b' = \widetilde{b}\cos(\boldsymbol{k}\cdot\boldsymbol{x} - \omega\,t) \tag{57.94a}$$

$$\varphi' = \frac{\widetilde{b}\sin\gamma}{|\boldsymbol{k}|}\sin(\boldsymbol{k}\cdot\boldsymbol{x} - \omega\,t) \tag{57.94b}$$

$$\boldsymbol{u}' = \frac{\widetilde{b}\,\boldsymbol{k}_{\mathsf{h}}\sin\gamma}{N_{\mathsf{R}}\,|\boldsymbol{k}_{\mathsf{h}}|}\sin(\boldsymbol{k}\cdot\boldsymbol{x} - \omega\,t) \tag{57.94c}$$

$$w' = -\frac{\widetilde{b}\cos\gamma}{N_{\mathsf{R}}}\sin(\boldsymbol{k}\cdot\boldsymbol{x} - \omega\,t) \tag{57.94d}$$

$$\boldsymbol{v}' = \frac{\boldsymbol{c}_{\mathrm{g}}\,\widetilde{b}\,|\boldsymbol{k}|^2}{N_{\mathsf{R}}^2\,k_z}\sin(\boldsymbol{k}\cdot\boldsymbol{x} - \omega\,t). \tag{57.94e}$$

Equation (57.94e) for $\boldsymbol{v}'$ made use of equation (57.71) for the group velocity, thus exposing the parallel nature of the particle velocity and group velocity for plane internal gravity waves. Note that the buoyancy is $\pi/2$ out of phase with the pressure along with the three components of the velocity.

Wave solutions in terms of the pressure amplitude

An alternative suite of wave solutions arises when assuming a real pressure amplitude, $\widetilde{\varphi}$, which leads to

$$\varphi' = \widetilde{\varphi} \cos(\boldsymbol{k} \cdot \boldsymbol{x} - \omega\, t) \tag{57.95a}$$

$$b' = -\frac{\widetilde{\varphi}\, |\boldsymbol{k}|^2}{k_z} \sin(\boldsymbol{k} \cdot \boldsymbol{x} - \omega\, t) \tag{57.95b}$$

$$\boldsymbol{u}' = \frac{\widetilde{\varphi}\, \boldsymbol{k}_{\text{h}}}{\omega} \cos(\boldsymbol{k} \cdot \boldsymbol{x} - \omega\, t) \tag{57.95c}$$

$$w' = -\frac{\widetilde{\varphi}\, |\boldsymbol{k}_{\text{h}}|^2}{\omega\, k_z} \cos(\boldsymbol{k} \cdot \boldsymbol{x} - \omega\, t) \tag{57.95d}$$

$$\boldsymbol{v}' = \frac{\boldsymbol{c}_{\text{g}}\, \widetilde{\varphi}\, |\boldsymbol{k}|^4}{N_{\text{R}}^2\, k_z^2} \cos(\boldsymbol{k} \cdot \boldsymbol{x} - \omega\, t). \tag{57.95e}$$

57.5.14 Energetics of a plane internal gravity wave

In Section 57.2.5 we derived the energetics for the linearized Boussinesq ocean equations and were led to the energy equation (57.25)

$$\partial_t(\mathcal{K}' + \mathcal{A}') = -\nabla \cdot (\boldsymbol{v}'\, \varphi') \quad \text{with} \quad \mathcal{K}' = \boldsymbol{v}' \cdot \boldsymbol{v}'/2 \quad \text{and} \quad \mathcal{A}' = (b'/N_{\text{R}})^2/2, \tag{57.96}$$

where $\mathcal{K}'$ is the kinetic energy per mass of the linear fluctuation, and $\mathcal{A}'$ is the corresponding available potential energy per mass. We only consider energetics of a plane internal wave. This idealized physical system has rather trivial energetics since for a plane wave there is no spatial convergence of the phase averaged energy flux, which means that the phase averaged energy is fixed in time. Even so, it is useful to work through the maths to gain practice in developing the phase averaged energy relations.

Interpreting the available potential energy

We saw in Section 57.2.5 that $\mathcal{A}' = (b'/N_{\text{R}})^2/2$ measures the available potential energy per mass arising from the small amplitude buoyancy fluctuation. When those fluctuations are part of a plane wave we can introduce the fluid particle displacement as in equation (57.81), in which

$$\mathcal{A}' = (b'/N_{\text{R}})^2/2 = (\delta z\, N_{\text{R}})^2/2. \tag{57.97}$$

This expression is identical to the potential energy (15.131) that we encountered for a point mass connected to a spring, where here the spring constant per mass equals to N_{R}^2.

Mechanical energy in the wave field

Assuming the small amplitude fluctuations are given by the wave relations (57.95a)-(57.95d) leads to

$$\mathcal{K}' = \frac{\widetilde{\varphi}^2\, |\boldsymbol{k}|^4}{2\, N_{\text{R}}^2\, k_z^2} \cos^2(\boldsymbol{k} \cdot \boldsymbol{x} - \omega\, t) \tag{57.98a}$$

$$\mathcal{A}' = \frac{\widetilde{\varphi}^2\, |\boldsymbol{k}|^4}{2\, N_{\text{R}}^2\, k_z^2} \sin^2(\boldsymbol{k} \cdot \boldsymbol{x} - \omega\, t), \tag{57.98b}$$

so that

$$\mathcal{K}' + \mathcal{A}' = \frac{\widetilde{\varphi}^2\, |\boldsymbol{k}|^4}{2\, N_{\text{R}}^2\, k_z^2} = \frac{\widetilde{\varphi}^2\, |\boldsymbol{k}_{\text{h}}|^2\, |\boldsymbol{k}|^2}{2\, \omega^2\, k_z^2}. \tag{57.99}$$

It is notable that the wave's mechanical energy, $\mathscr{K}' + \mathscr{A}'$, is independent of the space and time position. Furthermore, the phase averaged kinetic energy equals to that of the available potential energy

$$\langle \mathscr{K}' \rangle = \langle \mathscr{A}' \rangle, \tag{57.100}$$

which manifests equipartition for the wave field.[14] We can relate the total mechanical energy to the phase average of the squared vertical velocity through use of equation (57.95d), which yields

$$\mathscr{K}' + \mathscr{A}' = \langle w' \, w' \rangle \, |\boldsymbol{k}|^2 / |\boldsymbol{k}_\mathsf{h}|^2 = \langle w' \, w' \rangle / \cos^2 \gamma. \tag{57.101}$$

Note that the first expression in equation (57.99) indicates that for vertical waves, where $\gamma = \pi/2$, the sum $\mathscr{K}' + \mathscr{A}'$ is non-singular since $(w')^2$ vanishes. More precisely, we set $\boldsymbol{k}_\mathsf{h} = 0$ in equation (57.99) and find that a vertical phase velocity wave has mechanical energy

$$\mathscr{K}' + \mathscr{A}' = \frac{\widetilde{\varphi}^2 \, k_z^2}{2 \, N_\mathsf{R}^2} \quad \text{if } \boldsymbol{k}_\mathsf{h} = 0. \tag{57.102}$$

Energy flux and group velocity

The flux of mechanical energy can be written as

$$\boldsymbol{v}' \, \varphi' = \frac{\widetilde{\varphi}^2 \cos^2(\boldsymbol{k} \cdot \boldsymbol{x} - \omega \, t)}{k_z \, \omega} \, (k_z \, \boldsymbol{k}_\mathsf{h} - \hat{\boldsymbol{z}} \, |\boldsymbol{k}_\mathsf{h}|^2) = \frac{\boldsymbol{c}_\mathsf{g} \, \widetilde{\varphi}^2 |\boldsymbol{k}|^4 \cos^2(\boldsymbol{k} \cdot \boldsymbol{x} - \omega \, t)}{N_\mathsf{R}^2 k_z^2}, \tag{57.103}$$

where we used equation (57.71) for the group velocity. Taking the phase average then leads to

$$\langle \boldsymbol{v}' \, \varphi' \rangle = \frac{\boldsymbol{c}_\mathsf{g} \, \widetilde{\varphi}^2 |\boldsymbol{k}|^4}{2 \, N_\mathsf{R}^2 k_z^2} = \boldsymbol{c}_\mathsf{g} \, (\mathscr{K}' + \mathscr{A}'). \tag{57.104}$$

We thus confirm that the phase averaged flux of mechanical energy contained in an internal gravity wave equals to the group velocity times the total mechanical energy. This result accords with both the group velocity and the particle velocity being parallel to lines of constant phase and hence perpendicular to the wavevector

$$\boldsymbol{c}_\mathsf{g} \cdot \boldsymbol{k} = \boldsymbol{v}' \cdot \boldsymbol{k} = 0. \tag{57.105}$$

Energetics in terms of buoyancy amplitude

The above energetics made use of the polarization relations (57.95a)-(57.95e), written in terms of the pressure amplitude, $\widetilde{\varphi}$. Here we briefly expose the results making use of equations (57.94a)-(57.94e), in which we write the fields in terms of the buoyancy amplitude, $\widetilde{b}$. For this purpose we write for the kinetic energy

$$\mathscr{K}' = \frac{\boldsymbol{c}_\mathsf{g} \cdot \boldsymbol{c}_\mathsf{g} \, \widetilde{b}^2 \, |\boldsymbol{k}|^4}{2 \, N_\mathsf{R}^4 \, k_z^2} \sin^2(\boldsymbol{k} \cdot \boldsymbol{x} - \omega \, t) = \frac{\widetilde{b}^2}{2 \, N_\mathsf{R}^2} \sin^2(\boldsymbol{k} \cdot \boldsymbol{x} - \omega \, t), \tag{57.106}$$

where we used equation (57.75) for $\boldsymbol{c}_\mathsf{g} \cdot \boldsymbol{c}_\mathsf{g}$. The corresponding available potential energy is

$$\mathscr{A}' = (b'/N_\mathsf{R})^2/2 = \frac{\widetilde{b}^2}{2 \, N_\mathsf{R}^2} \cos^2(\boldsymbol{k} \cdot \boldsymbol{x} - \omega \, t), \tag{57.107}$$

[14] See Section 12.7.3 for the underlying reason for the equipartition of energy within linear waves, which is related to the virial theorem of classical mechanics.

so that the total mechanical energy is

$$\mathcal{K}' + \mathcal{A}' = \frac{\widetilde{b}^2}{2\,N_{\mathsf{R}}^2}, \tag{57.108}$$

and the phase averaged energy flux is

$$\langle \boldsymbol{v}'\,\varphi' \rangle = \frac{\boldsymbol{c}_{\mathrm{g}}\,\widetilde{b}^2}{2\,N_{\mathsf{R}}^2} = \boldsymbol{c}_{\mathrm{g}}\,(\mathcal{K}' + \mathcal{A}'). \tag{57.109}$$

57.6 Reflection of gravity waves

In Section 54.4.3 we studied the reflection of planetary Rossby wave packets from a smooth solid surface. That approach made use of some methods from geometric optics, in which we assume the waves reflect from the boundary without dissipation. Consequently, we only need to invoke the kinematic boundary condition to derive relations between incident and reflected waves. Here we pursue a similar study for internal gravity waves. Rossby waves (and many other waves such as acoustic waves and electromagnetic waves) exhibit specular reflection, whereby the angle the incident wave packet makes with the surface is preserved upon reflection. In contrast, the dispersion relation for internal gravity waves leads to a distinctly *non-specular* property. Namely, the angle the wave makes with the horizontal plane remains unchanged, rather than the angle the wave makes with the surface of reflection. Correspondingly, we encounter a particularly striking ability for the internal gravity wave, hitting the plane surface at a critical angle, to have an unbounded (infinite) wavenumber upon reflection.

57.6.1 Reflection conditions

Consider a packet of internal gravity waves with group velocity, $\boldsymbol{c}_{\mathrm{gi}}$, that is incident on a plane solid boundary, with the boundary making an angle, β, with the horizontal (see Figure 57.5). Let the carrier wave in the wave packet have an angular frequency, ω_{i}, and wavevector, $\boldsymbol{k}_{\mathrm{i}}$, with $\boldsymbol{c}_{\mathrm{gi}} \cdot \boldsymbol{k}_{\mathrm{i}} = 0$. Since the velocity of fluid particles is parallel to the group velocity for internal waves, we write the velocity of fluid particles in the carrier wave as

$$\boldsymbol{v}_{\mathrm{i}}' = \boldsymbol{c}_{\mathrm{gi}}\,A_{\mathrm{i}} \cos(\boldsymbol{k}_{\mathrm{i}} \cdot \boldsymbol{x} - \omega_{\mathrm{i}}\,t), \tag{57.110}$$

with the amplitude,

$$A_{\mathrm{i}} = A_{\mathrm{i}}(\boldsymbol{k}_{\mathrm{i}}) \tag{57.111}$$

a shorthand for the amplitudes in either equation (57.94e) or (57.95e). As such, A_{i} is a function of the incident wavevector, $\boldsymbol{k}_{\mathrm{i}}$, and the buoyancy frequency, N_{R}. The same considerations hold for the velocity of fluid particles in the reflected wave, so that

$$\boldsymbol{v}_{\mathrm{r}}' = \boldsymbol{c}_{\mathrm{gr}}\,A_{\mathrm{r}} \cos(\boldsymbol{k}_{\mathrm{r}} \cdot \boldsymbol{x} - \omega_{\mathrm{r}}\,t), \tag{57.112}$$

with $A_{\mathrm{r}} = A_{\mathrm{r}}(\boldsymbol{k}_{\mathrm{r}})$, $\boldsymbol{k}_{\mathrm{r}}$, and ω_{r}, the amplitude, wavevector, and angular frequency of the velocity of the reflected wave.

Now consider a steady state situation in which there are both incident and reflected waves, so that the fluid velocity at any given point in the fluid is given by the sum[15]

$$\boldsymbol{v}' = \boldsymbol{v}_{\mathrm{i}}' + \boldsymbol{v}_{\mathrm{r}}'. \tag{57.113}$$

[15]Recall that steady state does not mean static. Here, we assume steady state in the sense that the incident and reflected waves are fully established, so that our concern is not with the initial value problem. Instead, we are concerned with the boundary value problem.

The no-normal flow boundary condition at a solid boundary couples the incident and reflected wave properties, in which case

$$\boldsymbol{v}' \cdot \hat{\boldsymbol{n}} = (\boldsymbol{v}'_{\text{i}} + \boldsymbol{v}'_{\text{r}}) \cdot \hat{\boldsymbol{n}} = 0 \quad \text{at } \boldsymbol{x} = \boldsymbol{x}_{\text{w}}. \tag{57.114}$$

In these equations, $\hat{\boldsymbol{n}}$ is the outward normal on the solid boundary and $\boldsymbol{x}_{\text{w}} = |\boldsymbol{x}_{\text{w}}| \, \hat{\boldsymbol{t}}$ is a point on the boundary with $\hat{\boldsymbol{t}}$ the unit vector pointing tangent to the boundary so that $\hat{\boldsymbol{n}} \cdot \hat{\boldsymbol{t}} = 0$.

As for Rossby wave reflection considered in Section 54.4.3, the boundary condition (57.114) leads to the reflection conditions for the angular frequency and wavevectors

$$\omega_{\text{i}} = \omega_{\text{r}} \quad \text{and} \quad (\boldsymbol{k}_{\text{i}} - \boldsymbol{k}_{\text{r}}) \cdot \hat{\boldsymbol{t}} = 0. \tag{57.115}$$

These conditions hold so long as the velocity amplitude and the group velocity satisfy

$$A_{\text{i}} \, \boldsymbol{c}_{\text{gi}} \cdot \hat{\boldsymbol{n}} = -A_{\text{r}} \, \boldsymbol{c}_{\text{gr}} \cdot \hat{\boldsymbol{n}}. \tag{57.116}$$

57.6.2 Specializing to internal gravity waves

The wavevector condition in equation (57.115) means that there is an equal projection onto the tangent direction of the incident and reflected wavevectors. This same condition holds for other waves, such as we found when studying Rossby wave reflection in Section 54.4.3 and as found for inertial waves in Exercise 57.1. Even so, the angular frequency condition, $\omega_{\text{i}} = \omega_{\text{r}}$, when coupled to the internal gravity wave dispersion relation (57.65), leads to non-specular wave reflection. The reason is that specification of the angular frequency and the background buoyancy frequency fixes the angle of the gravity wave relative to the horizontal plane. Hence, the angle that a reflected internal gravity wave makes relative to the solid boundary is generally different from the angle made by the incident wave. To prove this result requires trigonometry based on the boundary conditions (57.115), with details provided in Figure 57.5.

Non-specular nature of internal gravity wave reflection

For internal gravity waves, the frequency condition in equation (57.115) means that the angle the wavevector makes with the horizontal, γ, remains unchanged upon reflection

$$\omega_{\text{i}} = \omega_{\text{r}} = N_{\text{R}} \cos\gamma. \tag{57.117}$$

This relation holds no matter what angle, β, the solid wall makes with the horizontal. This identity is depicted in Figure 57.5, where the angle α_{i}, which is the angle the incident packet makes with the horizontal, equals to the reflected angle, α_{r}. It follows that the angle that the wave packet makes relative to the solid surface is different for the incident and reflected waves. This property is referred to as *non-specular*. For the example of Figure 57.5, the reflected wave is more nearly parallel to the solid boundary than the incident wave. Reversing the sense for the wave packet provides an example of a reflected packet that is less aligned with the boundary than the incident packet.

Basic identities for internal gravity wave reflection

The frequency identity (57.117), the wavevector relation (57.115), along with some basic vector and trigonometric analysis, lead to the following identities

$$\hat{\boldsymbol{t}} = \hat{\boldsymbol{h}} \cos\beta + \hat{\boldsymbol{z}} \sin\beta \tag{57.118a}$$

$$\hat{\boldsymbol{k}}_{\text{i}} = \hat{\boldsymbol{h}} \cos\gamma + \hat{\boldsymbol{z}} \sin\gamma \tag{57.118b}$$

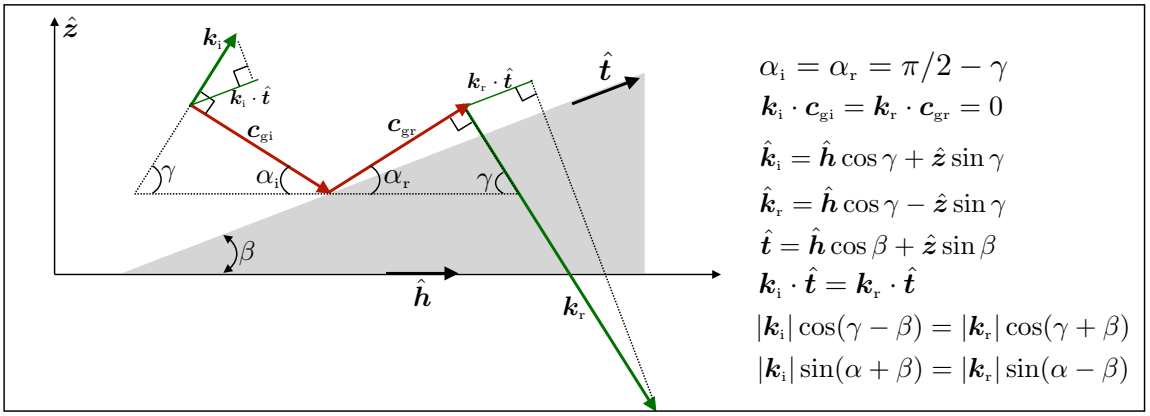

FIGURE 57.5: Depicting the reflection of an internal gravity wave packet as viewed within the geometrical optics approximation. Here the packet reflects from a planar inclined solid boundary that makes an angle, β, with the horizontal direction, $\hat{\boldsymbol{h}}$. The downward incident wave packet has a group velocity, $\boldsymbol{c}_{\rm gi}$, and an upward carrier wavevector, $\boldsymbol{k}_{\rm i}$, with $\boldsymbol{c}_{\rm gi} \cdot \boldsymbol{k}_{\rm i} = 0$. The incident group velocity makes an angle, $\alpha_{\rm i} = \pi/2 - \gamma$, with the horizontal, whereas $\boldsymbol{k}_{\rm i}$ makes an angle, γ, with the horizontal. The upward reflected wave packet has group velocity, $\boldsymbol{c}_{\rm gr}$, and a downward carrier wavevector, $\boldsymbol{k}_{\rm r}$, with $\boldsymbol{c}_{\rm gr} \cdot \boldsymbol{k}_{\rm r} = 0$. The angular frequency of the incident carrier wave is the same as the reflected wave, $\omega_{\rm i} = \omega_{\rm r} = \omega = N_{\rm R}\cos\gamma$, which then means that $\boldsymbol{k}_{\rm r}$ makes an angle, γ, with the horizontal. Consequently, the reflected group velocity makes an angle $\alpha_{\rm r} = \pi/2 - \gamma$, which is the same as the incident wave, $\alpha_{\rm r} = \alpha_{\rm i}$. The projection of the incident wavevector onto the surface tangent direction equals to that of the reflected wavevector, $\boldsymbol{k}_{\rm i} \cdot \hat{\boldsymbol{t}} = \boldsymbol{k}_{\rm r} \cdot \hat{\boldsymbol{t}}$, which means that $|\boldsymbol{k}_{\rm i}|\cos(\gamma - \beta) = |\boldsymbol{k}_{\rm r}|\cos(\gamma + \beta)$, or equivalently, $|\boldsymbol{k}_{\rm i}|\sin(\alpha + \beta) = |\boldsymbol{k}_{\rm r}|\sin(\alpha - \beta)$. For this example, the reflected wave has a larger wavenumber, $|\boldsymbol{k}_{\rm r}|$, than the incident wave, $|\boldsymbol{k}_{\rm i}|$, since $\alpha - \beta$ is smaller than $\alpha + \beta$. Indeed, for a packet with incident group velocity angle equal to the boundary angle, $\alpha = \beta$, then the reflected wave has an infinite wavenumber, which is an indication that the linear theory breaks down. To the right of the schematic we list the basic relations between the incident and reflected waves.

$$\hat{\boldsymbol{k}}_{\rm r} = \hat{\boldsymbol{h}}\cos\gamma - \hat{\boldsymbol{z}}\sin\gamma \tag{57.118c}$$

$$\hat{\boldsymbol{k}}_{\rm i} \cdot \hat{\boldsymbol{t}} = \cos\gamma\cos\beta + \sin\gamma\sin\beta = \cos(\gamma - \beta) = \sin(\alpha + \beta) \tag{57.118d}$$

$$\hat{\boldsymbol{k}}_{\rm r} \cdot \hat{\boldsymbol{t}} = \cos\gamma\cos\beta - \sin\gamma\sin\beta = \cos(\gamma + \beta) = \sin(\alpha - \beta), \tag{57.118e}$$

where $\hat{\boldsymbol{h}}$ is a unit vector in the horizontal. With these results we find that the wavevector boundary condition, $\boldsymbol{k}_{\rm i} \cdot \hat{\boldsymbol{t}} = \boldsymbol{k}_{\rm r} \cdot \hat{\boldsymbol{t}}$, (equation (57.115)) leads to the equivalent relations

$$|\boldsymbol{k}_{\rm i}|\cos(\gamma - \beta) = |\boldsymbol{k}_{\rm r}|\cos(\gamma + \beta) \tag{57.119a}$$

$$|\boldsymbol{k}_{\rm i}|\sin(\alpha + \beta) = |\boldsymbol{k}_{\rm r}|\sin(\alpha - \beta). \tag{57.119b}$$

Critical reflection of internal gravity waves

The identity (57.119b) makes it clear that a most remarkable result holds when the incident packet hits the boundary at an angle that equals to the solid wall angle, $\alpha = \beta$. In this case the reflected wavenumber, $|\boldsymbol{k}_{\rm r}|$, is unbounded, which means that the reflected waves have arbitrarily small wavelength. In a real fluid such small wavelength waves will eventually feel the impacts from viscous dissipation (e.g., Section 25.8), and/or they will break. In either case, such *critical reflection* of internal gravity waves provides an important mechanism for the transfer of energy from large to small scales, with the small scale features more prone to dissipative mixing.

57.6.3 Comments and further reading

Figure 57.5 provides an example where the reflected wave has a higher wavenumber than the incident wave. We can reverse all vectors to provide an example where a reflected wave has a smaller wavenumber than the incident wave. However, in a real fluid the reflections are not

generally reversible since higher wavenumber waves are more subject to irreversible mixing, either through viscous dissipation or breaking. These, and other, wave-induced ocean mixing processes are reviewed in *MacKinnon et al.* (2013), *MacKinnon et al.* (2017), and *Buijsman et al.* (2019).

57.7 Vertical normal modes

We here look for gravity waves in an ocean domain that is bounded below by a flat bottom at $z = -H$ and free surface at $z = \eta$. Since the bottom is flat we assume the waves are traveling only in the horizontal, in which we consider an ansatz of the form

$$w' = W(z)\, \mathrm{e}^{\mathrm{i}\,(k_x\, x + k_y\, y - \omega\, t)}. \tag{57.120}$$

Plugging this ansatz into the wave equation (57.40) for the vertical velocity leads to the eigenvalue problem for the vertical structure function

$$\left[\frac{\mathrm{d}^2}{\mathrm{d}z^2} + \frac{|\boldsymbol{k}_\mathrm{h}|^2\,(N_\mathrm{R}^2 - \omega^2)}{\omega^2}\right] W = 0 \qquad -H < z < 0 \tag{57.121a}$$

$$W = 0 \qquad \text{at } z = -H \tag{57.121b}$$

$$\omega^2 \mathrm{d}W/\mathrm{d}z = g\,|\boldsymbol{k}_\mathrm{h}|^2\, W \qquad \text{at } z = 0, \tag{57.121c}$$

where we used the flat bottom kinematic boundary condition at $z = -H$, and the upper ocean boundary condition (57.53) for equation (57.121c).

INCOMPLETE.

57.8 Linear Boussinesq ocean on an f-plane

We here establish some general properties of the linear Boussinesq ocean on an f-plane as described by equations (57.17a)-(57.17d)

$$\partial_t \boldsymbol{u}' + f\,\hat{\boldsymbol{z}} \times \boldsymbol{u}' = -\nabla_\mathrm{h}\varphi' \qquad \text{horizontal velocity equation} \tag{57.122a}$$

$$\partial_t w' = -\partial_z \varphi' + b' \qquad \text{vertical velocity equation} \tag{57.122b}$$

$$\partial_t b' = -w'\, N_\mathrm{R}^2 \qquad \text{buoyancy equation} \tag{57.122c}$$

$$\nabla \cdot \boldsymbol{v}' = 0 \qquad \text{continuity equation.} \tag{57.122d}$$

Since we are only concerned with f-plane motion, Rossby waves are not included in the physical system. As we see, the discussion reveals many forced oscillator equations satisfied by the linear fields, thus providing insight into the workings of the inertia-gravity waves discussed in Section 57.9. These oscillator equations also prove of use when developing the polarization relations for the plane inertia-gravity wave in Section 57.9.5.

57.8.1 Forced oscillator equation for horizontal velocity

Taking the time derivative of the horizontal velocity equation (57.122a) and back-substituting in the horizontal velocity tendency leads to

$$(\partial_{tt} + f^2)\, \boldsymbol{u}' = f\,\hat{\boldsymbol{z}} \times \nabla_\mathrm{h}\varphi' - \partial_t(\nabla_\mathrm{h}\varphi'). \tag{57.123}$$

This equation takes the form of a forced harmonic oscillator with natural angular frequency, f, and with forcing from the horizontal pressure gradient. Evidently, if we know the horizontal pressure gradient then that is sufficient to determine the horizontal velocity. Note that this is

the same forced oscillator equation as (53.17) found for inertial oscillations in a homogeneous fluid.

57.8.2 Vertical component to the relative vorticity

Evolution of the vertical component to the relative vorticity is derived by taking the curl of the horizontal velocity equation (57.122a) and projecting onto the vertical, in which we find

$$\partial_t \zeta' = f \, \partial_z w'. \tag{57.124}$$

Hence, relative vorticity evolves when there is vertical stretching in the presence of planetary rotation. This property accords with the more general understanding of vortex mechanics studied in Section 40.7.3. It also reduces to the $f = 0$ case, in which ζ' is static since $f = 0$ (Section 57.4.1). Finally, we can derive a forced oscillator equation for relative vorticity by taking the curl of the velocity equation (57.123) to find

$$(\partial_{tt} + f^2) \, \zeta' = f \, \nabla_{\mathsf{h}}^2 \varphi'. \tag{57.125}$$

Evidently, the relative vorticity exhibits forced inertial oscillations, with the forcing proportional to the horizontal Laplacian of the pressure field as weighted by the Coriolis parameter.

57.8.3 Forced oscillator and free wave equations for vertical velocity

Taking the divergence of the horizontal velocity equation (57.122a), and then using the continuity equation (57.122d), leads to

$$\partial_t (\nabla_{\mathsf{h}} \cdot \boldsymbol{u}') - f \, \zeta' = -\nabla_{\mathsf{h}}^2 \varphi' \implies \partial_{tz} w' + f \, \zeta' = \nabla_{\mathsf{h}}^2 \varphi'. \tag{57.126}$$

Now taking a time derivative and using the relative vorticity stretching equation (57.124) leads to the forced inertial oscillator equation for the vertical derivative of the vertical velocity

$$(\partial_{tt} + f^2) \partial_z w' = \partial_t \nabla_{\mathsf{h}}^2 \varphi'. \tag{57.127}$$

This equation says that when the horizontal flow has a nonzero divergence in the presence of rotation, then it experiences a forced inertial oscillation. Notice that if the pressure is constant in the horizontal direction, then the inertial oscillations are unforced.

We can derive another forced oscillator equation, this one for w'. To do so, take the time derivative of the vertical velocity equation (57.122b) and then use the linearized buoyancy equation (57.122c), which yields the forced buoyancy oscillator equation

$$\partial_{tt} w' = -\partial_{tz} \varphi' + \partial_t b' \implies (\partial_{tt} + N_{\mathsf{R}}^2) \, w' = -\partial_{tz} \varphi'. \tag{57.128}$$

We already encountered this equation in Section (57.3) when studying buoyancy oscillations. It says that vertical motion in the presence of a buoyancy field leads to forced buoyancy oscillations. Furthermore, if the pressure is constant in the vertical then the buoyancy oscillations are unforced.

Just like in the case of a non-rotating reference frame in Section 57.4.2, we can derive a free wave equation for w' by taking the vertical derivative of equation (57.127), the horizontal Laplacian of equation (57.128), and then adding to cancel the pressure contribution

$$(\partial_{tt} \, \nabla^2 + N_{\mathsf{R}}^2 \, \nabla_{\mathsf{h}}^2 + f^2 \, \partial_{zz}) \, w' = 0. \tag{57.129}$$

This is the fundamental wave equation for internal inertia-gravity waves. The build-up to this equation offers signatures of the forces acting within these waves. Namely, $\partial_z w'$ exhibits forced

inertial oscillations with natural angular frequency f (equation (57.127)). Such oscillations are associated, through continuity, with horizontally diverging flow that feels the Coriolis acceleration. Likewise, w' exhibits forced buoyancy oscillations with natural angular frequency N_{R} (equation (57.128)). These oscillations are associated with vertical motion that feels the effects from the background vertical stratification and associated buoyancy. By eliminating the pressure forcing the two complementary modes of oscillation, we reveal a free wave equation for w'. The free wave equation exposes the roles for Coriolis and buoyancy accelerations, yet hides the intermediate role of pressure accelerations that force the oscillations.

57.8.4 Forced oscillator equation for buoyancy

Since the flow is non-divergent at each time instant, we know that

$$\nabla \cdot \partial_t \boldsymbol{v}' = \partial_t \nabla \cdot \boldsymbol{v}' = 0. \tag{57.130}$$

Hence, taking the divergence of the horizontal velocity equation (57.122a) and adding to the vertical derivative of the vertical velocity equation (57.122b) leads to the pressure equation

$$-\nabla^2 \varphi' = -(f\,\zeta' + \partial_z b'). \tag{57.131}$$

Evidently, a source for the dynamic pressure arises from vertical buoyancy gradients along with relative vorticity. We characterized the phyics of these sources in Section 29.3.4 when studying the pressure equation in a Boussinesq ocean.

Taking the time derivative of the pressure equation (57.131) and using the stretching relative vorticity equation (57.124) leads to

$$f^2\,\partial_z w' = \partial_t(\nabla^2 \varphi' - \partial_z b'). \tag{57.132}$$

One more time derivative and use of the vertical velocity equation (57.122b) yields the forced inertial oscillator equation for the vertical derivative of buoyancy

$$(\partial_{tt} + f^2)\,\partial_z b' = (\partial_{tt}\nabla^2 + f^2\,\partial_{zz})\,\varphi'. \tag{57.133}$$

57.8.5 An equation for pressure

We now consider an equation for pressure that is based on taking the time derivative of the forced inertial oscillator equation (57.133) for $\partial_z b'$. Focusing on the left hand side we find

$$\begin{aligned}
\partial_t[(\partial_{tt} + f^2)\,\partial_z b'] &= \partial_z[(\partial_{tt} + f^2)\,\partial_t b'] && \text{swap } \partial_z \text{ and } \partial_t && (57.134a)\\
&= -\partial_z[(\partial_{tt} + f^2)\,w'\,N_{\mathsf{R}}^2] && \text{equation (57.122c)} && (57.134b)\\
&= -\partial_z N_{\mathsf{R}}^2\,(\partial_{tt} + f^2)\,w' - N_{\mathsf{R}}^2\,(\partial_{tt} + f^2)\,\partial_z w' && \text{product rule} && (57.134c)\\
&= -\partial_z N_{\mathsf{R}}^2\,(\partial_{tt} + f^2)\,w' - N_{\mathsf{R}}^2\,\partial_t \nabla_{\mathsf{h}}^2 \varphi' && \text{equation (57.127)} && (57.134d)
\end{aligned}$$

Combining with the time derivative on the right hand side of equation (57.133) leads to the pressure equation

$$\partial_t[(\partial_{tt}\nabla^2 + f^2\,\partial_{zz} + N_{\mathsf{R}}^2\,\nabla_{\mathsf{h}}^2)\,\varphi'] = -\partial_z N_{\mathsf{R}}^2\,(\partial_{tt} + f^2)\,w'. \tag{57.135}$$

In the special case of a constant background stratification we find

$$\partial_t[(\partial_{tt}\nabla^2 + f^2\,\partial_{zz} + N_{\mathsf{R}}^2\,\nabla_{\mathsf{h}}^2)\,\varphi'] = 0 \quad \text{if } \partial_z N_{\mathsf{R}} = 0, \tag{57.136}$$

which is nearly the same as the free wave equation (57.129) for w'.[16]

57.8.6 Potential vorticity

Although inertia-gravity waves modify relative vorticity, we here show they retain the linearized potential vorticity unchanged. For this purpose, use the relative vorticity equation (57.124) and the buoyancy equation (57.122c) to find[17]

$$\partial_t[\zeta' + f\,\partial_z(b'/N_{\mathsf{R}}^2)] = 0 \Longrightarrow \partial_t Q' = 0 \quad \text{with} \quad Q' = \zeta' + f\,\partial_z(b'/N_{\mathsf{R}}^2). \tag{57.137}$$

Hence, an inertia-gravity wave does not alter the potential vorticity, at least to linear order. This means that any vortical portion of the flow (i.e., flow with $Q' \neq 0$), such as a background static geostrophic flow, can exist without either the waves or the background flow affecting one another. Furthermore, we observe that the linearized potential vorticity (57.137) accords with the relative vorticity and buoyancy contribution to the quasi-geostrophic potential vorticity (45.53). In the present case, however, we are concerned with the f-plane rather than the β-plane considered for quasi-geostrophy. Another difference is that the potential vorticity (57.137) is locally static, $\partial_t Q' = 0$, whereas the quasi-geostrophic potential vorticity remains constant when following the geostrophic flow.

Potential vorticity and layer thickness

For yet another way to interpret the linear potential vorticity (57.137), write the buoyancy fluctuation in terms of the particle displacement as in equation (57.81)

$$\delta z = -b'/N_{\mathsf{R}}^2, \tag{57.138}$$

which brings the linearized potential vorticity to the form

$$Q' = \zeta' + f\,\partial_z(b'/N_{\mathsf{R}}^2) = \zeta' - f\,\partial_z(\delta z). \tag{57.139}$$

Since Q' is a static field, the presence of $\partial_z(\delta z)$ leads in a rotating reference frame to a compensating relative vorticity. In an internal gravity wave, δz measures the periodic compression and expansion of the vertical distance between constant buoyancy surfaces. This layer interpretation of potential vorticity accords with our understanding of potential vorticity from shallow water theory in Section 39.3, as well as potential vorticity in isopycnal/buoyancy coordinate models in Section 66.3.

Connection to pressure and buoyancy

The various harmonic oscillator equations established thus far in this section are not satisfied by Q' since it is a static field. However, we can derive an expression for Q' in terms of pressure and buoyancy through the following manipulations

$$(\partial_{tt} + f^2)\,Q' = f^2\,Q' \tag{57.140a}$$

$$= (\partial_{tt} + f^2)[\zeta' + f\,\partial_z(b'/N_{\mathsf{R}}^2)] \tag{57.140b}$$

$$= f\,\nabla_{\mathsf{h}}^2\varphi' + N_{\mathsf{R}}^{-2}\,(\partial_{tt}\nabla^2 + f^2\,\partial_{zz})\,\varphi' + \partial_z(N_{\mathsf{R}}^{-2})\,(\partial_{tt} + f^2)\,b', \tag{57.140c}$$

[16] See Lecture 11 in *Pedlosky* (2003) for connection between the pressure equation (57.136) to the potential vorticity equation in the case of constant N_{R}.

[17] Note that in this chapter we define potential vorticity with dimensions of inverse time, T^{-1}, as for the continuously stratified quasi-geostrophic potential vorticity in Section 45.3.7. In contrast, in our study of shallow water waves in Chapter 55, we defined Q' in Section 55.3.3 to have dimensions of $L^{-1}\,T^{-1}$.

where equation (57.140a) follows since $\partial_t Q' = 0$, equation (57.140b) used the definition of Q' from equation (57.137), and equation (57.140c) used the forced harmonic oscillator equations (57.125) and (57.127). Multiplying by N_{R}^2 leads to

$$f\, N_{\mathsf{R}}^2\, Q' = (\partial_{tt}\nabla^2 + N_{\mathsf{R}}^2\, \nabla_{\mathsf{h}}^2 + f^2\, \partial_{zz})\, \varphi' + N_{\mathsf{R}}^2\, \partial_z(N_{\mathsf{R}}^{-2})\, (\partial_{tt} + f^2)\, b'. \tag{57.141}$$

Decomposing vortical and divergent motions for constant vertical stratification

In the special case of a constant N_{R}, we see that the potential vorticity can be written entirely in terms of the pressure

$$f\, N_{\mathsf{R}}^2\, Q' = (\partial_{tt}\nabla^2 + N_{\mathsf{R}}^2\, \nabla_{\mathsf{h}}^2 + f^2\, \partial_{zz})\, \varphi' \quad \text{if } \partial_z N_{\mathsf{R}} = 0. \tag{57.142}$$

Evidently, for constant background stratification the static nature of the potential vorticity is equivalent to the wave equation (57.136)

$$\partial_t Q' = 0 \Longrightarrow \partial_t[(\partial_{tt}\nabla^2 + N_{\mathsf{R}}^2\, \nabla_{\mathsf{h}}^2 + f^2\, \partial_{zz})\, \varphi'] = 0 \quad \text{if } \partial_z N_{\mathsf{R}} = 0. \tag{57.143}$$

We found the same connection between the potential vorticity equation and the wave equation in Section 55.8.2 when studying shallow water inertia-gravity waves (see equation (55.153)). As for the shallow water, we conclude that for the case of constant stratification the vortical motions associated with f-plane geostrophy (hence with zero vertical velocity) are decoupled from the divergent motions associated with inertia-gravity waves. Hence, we can describe the fluid motion by a static potential vorticity whose non-zero value is set by f-plane geostrophic (vortical) flow, plus a zero potential vorticity flow arising from inertia-gravity waves. In the linear theory, and for constant vertical stratification, there is no exchange of potential vorticity between the vortical flow and divergent waves. As a practical matter, one often has knowledge of the static potential vorticity arising from the geostrophic motion. We can obtain the associated geostrophic pressure field from inverting the elliptic operator in equation (57.142).

57.9 Free inertia-gravity waves

In this section we study the free *inertia-gravity* waves that arise under small amplitude fluctuations in a continuously stratified fluid on an f-plane. To enable plane wave solutions we assume the stratification is constant.

57.9.1 Dispersion relation

Returning to the wave equation (57.129) for w'

$$(\partial_{tt}\, \nabla^2 + N_{\mathsf{R}}^2\, \nabla_{\mathsf{h}}^2 + f^2\, \partial_{zz})\, w' = 0, \tag{57.144}$$

we take the plane wave ansatz

$$w' = \widetilde{w}\, \mathrm{e}^{\mathrm{i}\,(\boldsymbol{k}\cdot\boldsymbol{x} - \omega\, t)} \tag{57.145}$$

which readily leads to the dispersion relation

$$\varpi^2(\boldsymbol{k}) = \frac{N_{\mathsf{R}}^2\, |\boldsymbol{k}_{\mathsf{h}}|^2 + f^2\, k_z^2}{|\boldsymbol{k}|^2}. \tag{57.146}$$

Just like the case of internal gravity waves studied in Section 57.5, the dispersion relation is only a function of the wave direction. To manifest this property we introduce the angle, γ, between

the wavevector and the horizontal plane

$$\varpi^2(\boldsymbol{k}) = N_{\mathsf{R}}^2 \cos^2\gamma + f^2 \sin^2\gamma = (N_{\mathsf{R}}^2 - f^2)\cos^2\gamma + f^2 = N_{\mathsf{R}}^2 - (N_{\mathsf{R}}^2 - f^2)\sin^2\gamma. \tag{57.147}$$

The dispersion relation reduces to that for internal gravity waves when $f = 0$ given as by equation (57.65).

57.9.2 Near-inertial waves

In stably stratified geophysical fluids we typically find the squared buoyancy frequency is larger than the squared Coriolis frequency, $N_{\mathsf{R}}^2 > f^2$. In this case the plane inertia-gravity wave angular frequency is bounded by

$$f^2 \leq \omega^2 \leq N_{\mathsf{R}}^2 \quad \text{when } N_{\mathsf{R}}^2 > f^2. \tag{57.148}$$

Indeed, in many cases we have $f^2 \ll N_{\mathsf{R}}^2$. Even so, there are weakly stratified regions with $N_{\mathsf{R}}^2 < f^2$, in which case the opposite frequency range holds whereby $N_{\mathsf{R}}^2 \leq \omega^2 \leq f^2$. In the limit with $N_{\mathsf{R}} = 0$, then the inertia-gravity waves reduce to the *inertial waves* studied in Chapter 53, which are waves appearing for motion on the f-plane within a fluid with homogeneous density ($N_{\mathsf{R}} = 0$).

Inertia-gravity waves typically have horizontal scales much larger than vertical, in which case $|\boldsymbol{k}_{\mathsf{h}}|^2 \ll k_z^2$. As discussed in Exercise 57.2, such waves satisfy hydrostatic scaling in which

$$\frac{\text{vertical scales in the waves}}{\text{horizontal scales in the waves}} = \frac{|\boldsymbol{k}_{\mathsf{h}}|}{|k_z|} \ll 1 \Longleftarrow \text{hydrostatic motion.} \tag{57.149}$$

The reason for this anisotropy in the waves is related to the processes forcing the waves. In particular, for the ocean the forcing by winds occurs with large horizontal patterns characteristic of the atmosphere. With $|\boldsymbol{k}_{\mathsf{h}}|^2 \ll k_z^2$, the phase velocity for the waves is nearly vertical so that $\gamma \approx \pi/2$. We thus find that the dominant forcing frequency for inertia-gravity waves is near that of the Coriolis frequency

$$\omega^2 = f^2 + (N_{\mathsf{R}}^2 - f^2)\cos^2\gamma \gtrsim f^2. \tag{57.150}$$

Such waves are referred to as *near-inertial waves*.

57.9.3 Force balance in an inertia-gravity wave

In Section 57.5.11 we studied the buoyancy forces acting on a fluid particle that moves transverse to the constant phase surfaces in a gravity wave. We pursue the same analysis here with the added feature of the Coriolis acceleration. This analysis offers a force balance interpretation of the dispersion relation (57.147).

For a phase surface that has a nonzero slope in the vertical, the displaced fluid particle moving parallel to the phase surface feels the effects from buoyancy forces. Likewise, when including the Coriolis acceleration on an f-plane, a horizontal displacement of a fluid particle induces a Coriolis acceleration. Given the nature of the Coriolis acceleration, the particle turns in the horizontal. Hence, a fluid particle moving in the direction of contant phase surfaces feels the effects of the buoyant acceleration when it moves vertically plus the Coriolis acceleration when it moves horizontally. For small amplitude motion, these forces give rise to simple harmonic oscillator motion, and they represent the essential features of an an inertia-gravity wave. We here detail the mechanics of this motion.

Particle displacements and Coriolis acceleration

Following the approach in Section 57.5.11, we make use of the fluid particle displacement field, $\boldsymbol{\xi}(\boldsymbol{x}, t)$, whose time derivative yields the velocity of the fluid particle in a small amplitude wave

$$\partial_t \boldsymbol{\xi}(\boldsymbol{x}, t) = \boldsymbol{v}'(\boldsymbol{x}, t). \tag{57.151}$$

To understand the role of the Coriolis acceleration, consider an inertial particle that satisfies the equation of motion

$$\partial_t \boldsymbol{v}' + f\, \hat{\boldsymbol{z}} \times \boldsymbol{v}' = 0 \Longrightarrow \partial_t \left(\partial_t \boldsymbol{\xi} + f\, \hat{\boldsymbol{z}} \times \boldsymbol{\xi} \right) = 0. \tag{57.152}$$

Hence, in terms of particle displacements, the inertial particle satisfies

$$\partial_t \boldsymbol{\xi} + f\, \hat{\boldsymbol{z}} \times \boldsymbol{\xi} = \text{constant}, \tag{57.153}$$

with the constant determined by initial conditions, which can be set to zero without loss of generality. Evidently, an inertial particle in a rotating reference frame, displaced in a direction perpendicular to the rotation axis (horizontal direction here), induces a time tendency for motion in the orthogonal horizontal direction

$$\partial_t \boldsymbol{\xi} = -f\, \hat{\boldsymbol{z}} \times \boldsymbol{\xi}. \tag{57.154}$$

Particle displacements with buoyancy and Coriolis

The linearized equation of motion that includes the effects from pressure, Coriolis, and buoyancy, is given by

$$\partial_t \boldsymbol{v}' + f\, \hat{\boldsymbol{z}} \times \boldsymbol{v}' = -\nabla \varphi' + b'\, \hat{\boldsymbol{z}}. \tag{57.155}$$

Focusing on a fluid particle in the presence of a transverse wave, we project the equation of motion onto the transverse direction, $\hat{\boldsymbol{t}}$, with this direction static for a plane wave. Doing so eliminates the pressure gradient since it is constant along a surface of constant phase, so that fluid particle motion in the transverse direction satisfies

$$\partial_t (\hat{\boldsymbol{t}} \cdot \boldsymbol{v}') + f\, \hat{\boldsymbol{t}} \cdot (\hat{\boldsymbol{z}} \times \boldsymbol{v}') = b'\, \hat{\boldsymbol{t}} \cdot \hat{\boldsymbol{z}}. \tag{57.156}$$

Introducing the particle displacement yields

$$\hat{\boldsymbol{t}} \cdot \boldsymbol{v}' = \partial_t (\hat{\boldsymbol{t}} \cdot \boldsymbol{\xi}) = \partial_t \delta l \tag{57.157a}$$

$$b'\, \hat{\boldsymbol{t}} \cdot \hat{\boldsymbol{z}} = -N_{\mathsf{R}}^2\, \delta z \cos\gamma = -N_{\mathsf{R}}^2\, \delta l \cos^2\gamma, \tag{57.157b}$$

with the buoyancy expression in equation (57.157b) following from equation (57.81) derived when studying internal gravity waves ($f = 0$). For the Coriolis acceleration we make use of equation (57.154) to write

$$f\, \hat{\boldsymbol{t}} \cdot (\hat{\boldsymbol{z}} \times \boldsymbol{v}') = f\, \boldsymbol{v}' \cdot (\hat{\boldsymbol{t}} \times \hat{\boldsymbol{z}}) \tag{57.158a}$$

$$= f\, \partial_t \boldsymbol{\xi} \cdot (\hat{\boldsymbol{t}} \times \hat{\boldsymbol{z}}) \tag{57.158b}$$

$$= -f^2\, (\hat{\boldsymbol{z}} \times \boldsymbol{\xi}) \cdot (\hat{\boldsymbol{t}} \times \hat{\boldsymbol{z}}) \tag{57.158c}$$

$$= f^2\, \delta l \sin^2\gamma, \tag{57.158d}$$

where we used the vector identity (1.73c) and set $\hat{\boldsymbol{z}} \cdot \hat{\boldsymbol{t}} = \sin\gamma$.

Bringing the above results together leads to the equation of motion for particle displacements

$$(\partial_{tt} + N_{\mathsf{R}}^2 \cos^2\gamma + f^2 \sin^2\gamma)\, \delta l = 0. \tag{57.159}$$

This is an equation for a simple harmonic oscillator with angular frequency

$$\omega^2 = N_{\mathsf{R}}^2 \cos^2\gamma + f^2 \sin^2\gamma, \tag{57.160}$$

which is the dispersion relation derived in Section 57.9.1 through use of the plane wave ansatz.

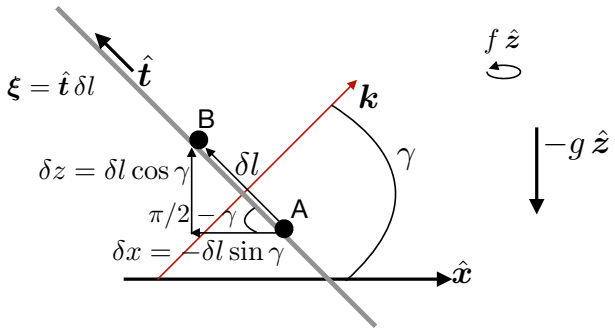

FIGURE 57.6: An extension of Figure 57.3 to now allow for a fluid particle to feel accelerations from both buoyancy and Coriolis as it moves in the direction transverse to the plane waves. The wavevector makes an angle, γ, with the horizontal. We show a view in the x-z plane with the particle displacement vector, $\boldsymbol{\xi}(\boldsymbol{x}, t) = \delta l\, \hat{\boldsymbol{t}}$. The local transverse unit vector, $\hat{\boldsymbol{t}}$, points in a direction that is orthogonal to the wavevector, $\boldsymbol{k}$. The displacement of the fluid particle from point A and point B occurs over a distance, δl, with a corresponding change in vertical position given by $\delta z = \delta l \cos\gamma$ and horizontal position changes by $\delta x = -\delta l \sin\gamma$. This displacement causes the fluid particle to experience accelerations from both buoyancy and Coriolis.

57.9.4 Group velocity

The wavevector gradient of the dispersion relation (57.160) yields the group velocity for inertia-gravity waves

$$\boldsymbol{c}_{\mathsf{g}} = \frac{(N_{\mathsf{R}}^2 - f^2)\, k_z}{|\boldsymbol{k}|^4\, \omega}\, (k_z\, \boldsymbol{k}_{\mathsf{h}} - |\boldsymbol{k}_{\mathsf{h}}|^2\, \hat{\boldsymbol{z}}). \tag{57.161}$$

As for internal gravity waves in equation (57.71), we find that the group velocity is perpendicular to the phase velocity ($\boldsymbol{c}_{\mathsf{p}} = \hat{\boldsymbol{k}}\, \omega/|\boldsymbol{k}|$)

$$\boldsymbol{c}_{\mathsf{g}} \cdot \boldsymbol{c}_{\mathsf{p}} = 0. \tag{57.162}$$

We also find that

$$(\boldsymbol{c}_{\mathsf{g}} \cdot \hat{\boldsymbol{z}})\, (\boldsymbol{c}_{\mathsf{p}} \cdot \hat{\boldsymbol{z}}) = -\frac{(N_{\mathsf{R}}^2 - f^2)\, k_z^2\, |\boldsymbol{k}_{\mathsf{h}}|^2}{|\boldsymbol{k}|^4\, \omega}, \tag{57.163}$$

so that

$$(\boldsymbol{c}_{\mathsf{g}} \cdot \hat{\boldsymbol{z}})\, (\boldsymbol{c}_{\mathsf{p}} \cdot \hat{\boldsymbol{z}}) < 0 \quad \text{if } f^2 < N_{\mathsf{R}}^2 \tag{57.164a}$$

$$(\boldsymbol{c}_{\mathsf{g}} \cdot \hat{\boldsymbol{z}})\, (\boldsymbol{c}_{\mathsf{p}} \cdot \hat{\boldsymbol{z}}) > 0 \quad \text{if } f^2 > N_{\mathsf{R}}^2. \tag{57.164b}$$

The usual case for the atmosphere and ocean finds $f^2 < N_{\mathsf{R}}^2$, so that if the group velocity is upward then the phase velocity is downward, and vice versa. However, if $f^2 > N_{\mathsf{R}}^2$, as for inertial waves where $N_{\mathsf{R}} = 0$ (Chapter 53, Exercise 57.1), or more generally for inertia-gravity waves in very weak vertical stratification, then the group and phase velocities have the same orientation with respect to the vertical.

57.9.5 Polarization relations for a plane wave

We now make use of the plane wave ansatz (57.54) to derive the polarization relations that determine the structure of a plane wave. For this purpose we make use of the various forced harmonic oscillator equations from Section 57.8 to express the velocity and buoyancy in terms

of a real pressure amplitude, $\widetilde{\varphi}$, where pressure is assumed to take the form

$$\varphi' = \widetilde{\varphi} \cos(\boldsymbol{k} \cdot \boldsymbol{x} - \omega\, t). \tag{57.165}$$

We also make use of the dispersion relation (57.147) to write the polarization relations in a variety of forms. In the limit with $f = 0$, each of the expressions below reduce to the gravity wave polarization relations (57.90a)-(57.90b) derived in Section 57.5.13.

Buoyancy

Buoyancy satisfies the forced oscillator equation (57.133), which for a plane wave takes the form

$$(-\omega^2 + f^2)\, \mathrm{i}\, k_z\, \widetilde{b} = (\omega^2\, |\boldsymbol{k}|^2 - f^2\, k_z^2)\, \widetilde{\varphi}. \tag{57.166}$$

Various forms of the dispersion relation given in Section 57.9.1 lead to the identities

$$\omega^2\, |\boldsymbol{k}|^2 - f^2\, k_z^2 = N_{\mathsf{R}}^2\, |\boldsymbol{k}_{\mathsf{h}}|^2 \tag{57.167a}$$

$$\omega^2 - f^2 = (N_{\mathsf{R}}^2 - f^2)\, |\boldsymbol{k}_{\mathsf{h}}|^2 / |\boldsymbol{k}|^2 = (N_{\mathsf{R}}^2 - \omega^2)\, |\boldsymbol{k}_{\mathsf{h}}|^2 / k_z^2 \tag{57.167b}$$

so that the ratio of amplitudes can be written in the equivalent manners

$$\widetilde{b}/\widetilde{\varphi} = \frac{\mathrm{i}\, (\omega^2\, |\boldsymbol{k}|^2 - f^2\, k_z^2)}{k_z\, (\omega^2 - f^2)} = \frac{\mathrm{i}\, N_{\mathsf{R}}^2\, |\boldsymbol{k}_{\mathsf{h}}|^2}{k_z\, (\omega^2 - f^2)} = \frac{\mathrm{i}\, N_{\mathsf{R}}^2\, |\boldsymbol{k}|^2}{k_z\, (N_{\mathsf{R}}^2 - f^2)} = \frac{\mathrm{i}\, N_{\mathsf{R}}^2\, k_z}{N_{\mathsf{R}}^2 - \omega^2}, \tag{57.168}$$

which means that the real buoyancy wave is given by

$$b'/\widetilde{\varphi} = -\frac{N_{\mathsf{R}}^2\, |\boldsymbol{k}_{\mathsf{h}}|^2 \sin(\boldsymbol{k} \cdot \boldsymbol{x} - \omega\, t)}{k_z\, (\omega^2 - f^2)} = -\frac{N_{\mathsf{R}}^2\, k_z \sin(\boldsymbol{k} \cdot \boldsymbol{x} - \omega\, t)}{N_{\mathsf{R}}^2 - \omega^2}. \tag{57.169}$$

Vertical velocity component

From Section 57.8.3 we know that the vertical velocity satisfies the two forced oscillator equations (57.127) and (57.128)

$$(\partial_{tt} + f^2)\partial_z w' = \partial_t \nabla_{\mathsf{h}}^2 \varphi' \quad \text{and} \quad (\partial_{tt} + N_{\mathsf{R}}^2)\, w' = -\partial_{tz} \varphi'. \tag{57.170}$$

For a plane wave these equations lead to

$$\widetilde{w}/\widetilde{\varphi} = -\frac{\omega\, |\boldsymbol{k}_{\mathsf{h}}|^2}{k_z\, (\omega^2 - f^2)} = -\frac{\omega\, k_z}{N_{\mathsf{R}}^2 - \omega^2} = -\frac{\omega\, |\boldsymbol{k}|^2}{k_z\, (N_{\mathsf{R}}^2 - f^2)}, \tag{57.171}$$

so that the real wave takes on the form

$$w'/\widetilde{\varphi} = -\frac{\omega\, |\boldsymbol{k}_{\mathsf{h}}|^2 \cos(\boldsymbol{k} \cdot \boldsymbol{x} - \omega\, t)}{k_z\, (\omega^2 - f^2)} = -\frac{\omega\, k_z \cos(\boldsymbol{k} \cdot \boldsymbol{x} - \omega\, t)}{N_{\mathsf{R}}^2 - \omega^2} = -\frac{\omega\, |\boldsymbol{k}|^2 \cos(\boldsymbol{k} \cdot \boldsymbol{x} - \omega\, t)}{k_z\, (N_{\mathsf{R}}^2 - f^2)}. \tag{57.172}$$

Horizontal velocity

Equation (57.123) for the horizontal velocity leads to the relation for the plane wave amplitude

$$\widetilde{\boldsymbol{u}}/\widetilde{\varphi} = \frac{\omega\, \boldsymbol{k}_{\mathsf{h}} - \mathrm{i}\, f\, (\hat{\boldsymbol{z}} \times \boldsymbol{k}_{\mathsf{h}})}{\omega^2 - f^2}, \tag{57.173}$$

so that the real plane wave polarization relation is given by

$$\boldsymbol{u}/\widetilde{\varphi} = \frac{\omega\, \boldsymbol{k}_{\mathsf{h}} \cos(\boldsymbol{k}\cdot\boldsymbol{x} - \omega\, t) + f\, (\hat{\boldsymbol{z}} \times \boldsymbol{k}_{\mathsf{h}}) \sin(\boldsymbol{k}\cdot\boldsymbol{x} - \omega\, t)}{\omega^2 - f^2}, \tag{57.174}$$

which compares directly to the shallow water polarization relation (55.174a).

57.9.6 Energetics of a plane inertia-gravity wave

We here extend the energetic analysis of plane internal gravity waves in Section 57.5.14 to the case of plane inertia-gravity waves, making use of the polarization relations from Section 57.9.5. Each of the expressions found here reduce to the internal gravity waves case when taking $f = 0$.

Instantaneous energetics

The plane inertia-gravity wave has squared velocity components

$$\boldsymbol{u}' \cdot \boldsymbol{u}'/\widetilde{\varphi}^2 = \frac{\omega^2\, |\boldsymbol{k}_{\mathsf{h}}|^2 \cos^2(\boldsymbol{k}\cdot\boldsymbol{x} - \omega\, t) + f^2\, |\boldsymbol{k}_{\mathsf{h}}|^2 \sin^2(\boldsymbol{k}\cdot\boldsymbol{x} - \omega\, t)}{(\omega^2 - f^2)^2} \tag{57.175a}$$

$$(w')^2/\widetilde{\varphi}^2 = \frac{\omega^2\, |\boldsymbol{k}_{\mathsf{h}}|^4 \cos^2(\boldsymbol{k}\cdot\boldsymbol{x} - \omega\, t)}{k_z^2\, (\omega^2 - f^2)^2}, \tag{57.175b}$$

so that the wave's kinetic energy is

$$\mathcal{K}' = \frac{\widetilde{\varphi}^2\, |\boldsymbol{k}_{\mathsf{h}}|^2}{2\, (\omega^2 - f^2)^2} \big[\omega^2\, (1 + |\boldsymbol{k}_{\mathsf{h}}|^2/k_z^2) \cos^2(\boldsymbol{k}\cdot\boldsymbol{x} - \omega\, t) + f^2 \sin^2(\boldsymbol{k}\cdot\boldsymbol{x} - \omega\, t)\big], \tag{57.176}$$

which can be written in the more tidy form through use of the dispersion relation (57.147)

$$\mathcal{K}' = \frac{\widetilde{\varphi}^2\, |\boldsymbol{k}_{\mathsf{h}}|^2 [f^2 + (N_{\mathsf{R}}^2 \cot^2\gamma) \cos^2(\boldsymbol{k}\cdot\boldsymbol{x} - \omega\, t)]}{2\, (\omega^2 - f^2)^2}, \tag{57.177}$$

where we set

$$\cot\gamma = |\boldsymbol{k}_{\mathsf{h}}|/k_z. \tag{57.178}$$

Likewise, the available potential energy is given by

$$\mathcal{A}' = \frac{\widetilde{\varphi}^2\, (|\boldsymbol{k}_{\mathsf{h}}|^2\, N_{\mathsf{R}}^2 \cot^2\gamma) \sin^2(\boldsymbol{k}\cdot\boldsymbol{x} - \omega\, t)}{2\, (\omega^2 - f^2)^2}. \tag{57.179}$$

Taking the sum leads to the total mechanical energy in a plane inertia-gravity wave

$$\mathcal{K}' + \mathcal{A}' = \frac{\widetilde{\varphi}^2\, |\boldsymbol{k}_{\mathsf{h}}|^2\, (f^2\, k_z^2 + N_{\mathsf{R}}^2\, |\boldsymbol{k}_{\mathsf{h}}|^2)}{2\, k_z^2\, (\omega^2 - f^2)^2} \tag{57.180}$$

Time independence of mechanical energy for the plane inertia-gravity wave accords with the result (57.99) for the plane internal gravity wave.

Phase averaged energetics

Taking the phase averages on the kinetic energy and available potential energy leads to

$$\langle \mathcal{K}' \rangle = \frac{\widetilde{\varphi}^2\, |\boldsymbol{k}_{\mathsf{h}}|^2\, (\omega^2\, |\boldsymbol{k}|^2 + f^2\, k_z^2)}{4\, k_z^2\, (\omega^2 - f^2)^2} \quad \text{and} \quad \langle \mathcal{A}' \rangle = \frac{\widetilde{\varphi}^2\, N_{\mathsf{R}}^2\, |\boldsymbol{k}_{\mathsf{h}}|^4}{4\, k_z^2\, (\omega^2 - f^2)^2}, \tag{57.181}$$

whose sum is

$$\langle \mathcal{K}' + \mathcal{A}' \rangle = \frac{\widetilde{\varphi}^2 \, |\boldsymbol{k}_{\mathsf{h}}|^2 \, (\omega^2 \, |\boldsymbol{k}|^2 + f^2 \, k_z^2 + N_{\mathsf{R}}^2 \, \boldsymbol{k}_{\mathsf{h}}^2)}{4 \, k_z^2 \, (\omega^2 - f^2)^2} = \frac{\widetilde{\varphi}^2 \, |\boldsymbol{k}_{\mathsf{h}}|^2 \, (f^2 \, k_z^2 + N_{\mathsf{R}}^2 \, \boldsymbol{k}_{\mathsf{h}}^2)}{2 \, k_z^2 \, (\omega^2 - f^2)^2} \tag{57.182}$$

and ratio is

$$\frac{\langle \mathcal{K}' \rangle}{\langle \mathcal{A}' \rangle} = 1 + 2 \, (f/N_{\mathsf{R}})^2 \tan^2 \gamma = \frac{\omega^2 \, |\boldsymbol{k}|^2 + f^2 \, k_z^2}{N_{\mathsf{R}}^2 \, |\boldsymbol{k}_{\mathsf{h}}|^2}. \tag{57.183}$$

It is notable that the ratio is bounded below by unity, so that the kinetic energy is never less than the available potential energy. The ratio is unity when the phase velocity is horizontal ($\gamma = 0$), in which fluid particles have vertical trajectories and thus exhibit purely vertical buoyancy oscillations. This equipartition of kinetic and available potential energies (again, holding with$\gamma = 0$) was found for the internal gravity wave in Section 57.5.14. When the phase velocity is vertical, so that $\gamma = \pi/2$, the plane waves have no available potential energy since the fluid particles are exhibiting horizontal inertial oscillations and do not sample the background buoyancy field.

Phase averaged mechanical energy flux

The phase averaged mechanical energy flux is given by

$$\frac{\langle \boldsymbol{v}' \, \varphi' \rangle}{\widetilde{\varphi}^2} = \frac{\omega \, (k_z \, \boldsymbol{k}_{\mathsf{h}} - \hat{\boldsymbol{z}} \, |\boldsymbol{k}_{\mathsf{h}}|^2)}{2 \, k_z \, (\omega^2 - f^2)} \tag{57.184a}$$

$$= \frac{\omega^2 \, |\boldsymbol{k}|^4 \, \boldsymbol{c}_{\mathsf{g}}}{2 \, k_z^2 \, (N_{\mathsf{R}}^2 - f^2) \, (\omega^2 - f^2)} \tag{57.184b}$$

$$= \frac{\boldsymbol{c}_{\mathsf{g}} \, |\boldsymbol{k}_{\mathsf{h}}|^2 \, (f^2 \, k_z^2 + N_{\mathsf{R}}^2 \, |\boldsymbol{k}_{\mathsf{h}}|^2)}{2 \, k_z^2 \, (\omega^2 - f^2)^2}, \tag{57.184c}$$

where we made use of the inertia-gravity wave group velocity (57.161). Now the phase averaged mechanical energy is given by equation (57.182), so that the plane inertia-gravity waves exhibit the group velocity property also found for internal gravity waves in equation (57.104)

$$\langle \boldsymbol{v}' \, \varphi' \rangle = \boldsymbol{c}_{\mathsf{g}} \, (\mathcal{K}' + \mathcal{A}'). \tag{57.185}$$

That is, a plane inertia-gravity wave has a phase averaged mechanical energy flux equal to the group velocity times the phase averaged mechanical energy.

57.9.7 Comments

The inertial waves studied in Chapter 53 are the $N_{\mathsf{R}} = 0$ limit of inertia-gravity waves studied in the present section. It is notable that in the presence of any nonzero vertical stratification, the squared angular frequency of propagating inertia-waves is super-inertial, $\omega^2 \geq f^2$, whereas when $N_{\mathsf{R}} = 0$ the waves are sub-inertial, $\omega^2 \leq f^2$. If an inertial wave from an unstratified region, with $\omega^2 \leq f^2$, encounters stratification, then this low frequency wave cannot propagate into the stratified region.

57.10 Exercises

EXERCISE 57.1: REFLECTION CONDITIONS FOR INERTIAL WAVES
Inertial waves studied in Chapter 53 are the $N^2 = 0$ limit of inertia-gravity waves from Section

57.9. Emulating the analysis in Section 57.6.2 for internal gravity waves, determine the reflection conditions for packets of plane inertial waves. Figure 57.5 is drawn for internal gravity waves. Redraw this figure for inertial waves.

EXERCISE 57.2: INERTIA-GRAVITY WAVES IN A HYDROSTATIC FLUID

Throughout this chapter we studied inertia-gravity waves as they appear in a non-hydrostatic flow that satisfies the linear Boussineseq equations (57.17a)-(57.17d). However, inertia-gravity waves also exist in flows maintaining an approximate hydrostatic balance, and in this exercise we derive their dispersion relation and discuss the relation to the non-hydrostatic waves. Hint: see Section 57.9.2 as well as page 280 of *Vallis* (2017).

(a) Write the hydrostatic version of the linear Boussinesq equations (57.17a)-(57.17d).

(b) Following the methods from Section 57.9, derive the free wave equation satisfied by the vertical velocity, w', in a hydrostatic flow. That is, derive the hydrostatic version of equation (57.129). Show all steps.

(c) Derive the dispersion relation for inertia-gravity waves in a hydrostatic flow with a constant reference buoyancy frequency, N_{R}.

(d) Start from the dispersion relation for inertia-gravity waves in a non-hydrostatic flow. Discuss the maths and physics of the length scale limiting process that results in the dispersion relation for inertia-gravity waves in a hydrostatic flow.

(e) What does the hydrostatic limit say about the angular frequency of inertia-gravity waves relative to non-hydrostatic inertia-gravity waves?

Chapter 58

INTERNAL GRAVITY WAVES: CASE STUDIES

In this chapter we consider some case studies that help further our understanding of internal gravity waves as they appear in geophysical fluids. Sections 58.2 and 58.3 consider the generation of internal gravity waves via flow over topography, thus giving rise to *mountain waves*. Mountain waves arise when stratified fluid flows over topography in both the atmosphere (hence their name) and the ocean. We limit the analysis to *stationary waves*, which are time independent in the rest frame. Doing so allows us to avoid some of the more mathematical questions of transient adjustment. Even so, the discussion exposes us to some mathematical methods commonly used to study waves. It also deepens our understanding of gravity wave mechanics within a geophysical context.

Section 58.4 examines gravity waves within a gently varying stratification, making use of the ray theory presented in Chapter 50.

READER'S GUIDE TO THIS CHAPTER

This chapter is a natural extension of material studied in Chapter 57. Further resources for this chapter can be found in *Lighthill* (1978), *Pedlosky* (2003), *Sutherland* (2010), *Cushman-Roisin and Beckers* (2011), *Kundu et al.* (2016), *Vallis* (2017), and *Buijsman et al.* (2019). The second half of this video offers some pedagogical visualizations of stratified flow phenomena, and this video provides more visualizations from simulations and laboratory tank experiments.

58.1 Loose threads

- Work through the examples Legg notes, as well as material from *Vallis* (2017).
- Expand the ray theory in Section 58.4. Follow elements from Chapter 6 of *Sutherland* (2010).

58.2 Gravity waves from a sinusoidal mountain range

Following the discussion for inertial waves in Section 53.5.2, and for shallow water inertia-gravity waves in Section 56.2, we here consider a prescribed and fixed constant horizontal reference (background) flow on a stratified f-plane that moves over small amplitude topography (e.g., mountains) in an otherwise unbounded domain. The flow over a non-flat bottom provides a forcing of vertical motion as imposed by the bottom kinematic boundary condition, with a vertically moving fluid parcel sampling the continuously stratified reference buoyancy. As such, flow over topography in a continuously stratified fluid serves as a forcing for internal inertia-gravity waves. Those waves that propagate do so both vertically and horizontally throughout the domain. The horizontal wavenumber of the waves is set by the horizontal wavenumber of the topography. The angular frequency of stationary waves is fully determined by the Doppler shift from the moving reference flow, which is set by the wavevector of the topography and the flow speed. The vertical wavenumber of stationary waves is determined by the dispersion relation. As for surface gravity waves in Chapter 52, waves with high horizontal wavenumber are exponentially trapped near the mountains, whereas waves with lower horizontal wavenumber propagate vertically. The transition between evanescence and propagation is set by the ratio of the reference stratification to the reference flow.

The *mountain waves* studied in this section represent a rich area of geophysical fluid mechanics of primary importance for waves and mixing in the ocean and atmosphere. For the ocean, barotropic (depth independent) tidal motions offers an important source for the reference flow, with barotropic tidal motions generating internal waves that are referred to as *internal tides*. Our goal is to introduce some of the richness of this geophysical system by mathematically formulating the generation of linear internal waves and studying their properties. For simplicity, we focus on the *stationary waves* that arise from a fully developed wave field.[1] Some of the formulation in this section is analogous to that of the shallow water in Section 56.2, yet with two key distinctions. First, the fluid here is continuously stratified, and second, the flow is non-hydrostatic. Both of these properties support a rich wave field that is not constrained by the columnar motion found in hydrostatic shallow water layers.

58.2.1 Linearized equations with constant reference flow

Figure 58.1 depicts the physical system studied in this section, in which we consider a reference flow whose velocity is given by

$$\boldsymbol{v} = \boldsymbol{u}_{\mathrm{R}} + \boldsymbol{v}', \tag{58.1}$$

[1] Recall from Section 49.2 that stationary waves have no time dependence in the rest frame. We here encounter stationary waves as the steady solution to the propagating internal gravity wave equations. The initial value problem requires more mathematical machinery beyond our scope.

where $\boldsymbol{u}_{\mathsf{R}}$ is a prescribed space-time constant horizontal reference flow, and $\boldsymbol{v}'$ is the space-time dependent flow relative to this reference. Furthermore, we assume that the steady reference flow is in geostrophic balance with a prescribed reference pressure field

$$f_{\circ}\,\hat{\boldsymbol{z}} \times \boldsymbol{u}_{\mathsf{R}} = -\nabla\varphi_{\mathsf{R}}. \tag{58.2}$$

Alternatively, for the case with $f_{\circ} = 0$, we simply assume the reference flow is down the prescribed gradient of the reference pressure. In either case we have no concern for how the reference pressure field is maintained, only that it supports the steady reference flow.

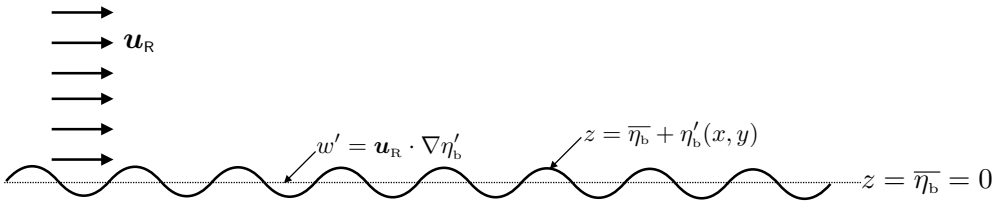

FIGURE 58.1: Schematic of a constant reference flow, $\boldsymbol{u}_{\mathsf{R}}$, moving over small amplitude monochromatic bottom topography, $z = \overline{\eta_{\mathsf{b}}} + \eta'_{\mathsf{b}}(x,y) = 0 + \eta_{\circ}\,\mathrm{e}^{\boldsymbol{k}_{\mathsf{b}}\cdot\boldsymbol{x}}$, where we assume $\overline{\eta_{\mathsf{b}}} = 0$, and with $\eta_{\circ}$ a real amplitude, and $\boldsymbol{k}_{\mathsf{b}}$ a horizontal wavevector. We choose to orient the topography wavevector so that $\boldsymbol{u}_{\mathsf{R}} \cdot \boldsymbol{k}_{\mathsf{b}} < 0$, which is based on noting that the reference flow, $\boldsymbol{u}_{\mathsf{R}}$, when viewed in the rest frame, is equivalent to topography moving in the direction opposite to $\boldsymbol{u}_{\mathsf{R}}$ when viewed in the boosted frame. We assume the topography has a small amplitude in the sense that $\eta_{\circ}\,|\boldsymbol{k}_{\mathsf{b}}| \ll 1$, thus ensuring that the generated waves are linear. There is no upper boundary nor side boundary, so waves generated by flow over the bottom are free to propagate horizonally and vertically. At the bottom, the full flow must satisfy the kinematic boundary condition, $w = \boldsymbol{u} \cdot \nabla\eta_{\mathsf{b}}$. Linearizing this boundary condition brings about its evaluation at $z = \overline{\eta_{\mathsf{b}}} = 0$ rather than at $z = \eta_{\mathsf{b}}(x,y)$. Additionally, with η'_{b} of small amplitude, the linearized bottom boundary condition is $w' = \boldsymbol{u}_{\mathsf{R}} \cdot \nabla\eta'_{\mathsf{b}} = \mathrm{i}\,(\boldsymbol{u}_{\mathsf{R}} \cdot \boldsymbol{k}_{\mathsf{b}})\,\eta'_{\mathsf{b}}$ at $z = 0$.

Following the steps in Section 57.2, we decompose the density and pressure according to

$$\rho(\boldsymbol{x},t) = \rho_{\circ} + \rho_{\mathsf{R}}(\boldsymbol{x}) + \rho'(\boldsymbol{x},t), \tag{58.3}$$

where the reference density, ρ_{R}, is a function of all three spatial coordinates, and where we consider two static pressures, $p_{\circ}$ and p_{R}, that are in hydrostatic balance with their corresponding densities

$$\frac{\mathrm{d}p_{\circ}}{\mathrm{d}z} = -\rho_{\circ}\,g \quad \text{and} \quad \frac{\partial p_{\mathsf{R}}}{\partial z} = -\rho_{\mathsf{R}}\,g. \tag{58.4}$$

Inserting this density and pressure decomposition in the Boussinesq equations (57.1a)-(57.1d), and then linearizing, leads to the linearized governing equations

$$(\partial_t + \boldsymbol{u}_{\mathsf{R}} \cdot \nabla)\boldsymbol{u}' + f_{\circ}\,\hat{\boldsymbol{z}} \times \boldsymbol{u}' = -\nabla_{\mathsf{h}}\varphi' \qquad \text{linear horizontal velocity equation} \tag{58.5a}$$

$$(\partial_t + \boldsymbol{u}_{\mathsf{R}} \cdot \nabla)w' = -\partial_z\varphi' + b' \qquad \text{linear vertical velocity equation} \tag{58.5b}$$

$$(\partial_t + \boldsymbol{u}_{\mathsf{R}} \cdot \nabla)b' = -w'\,N_{\mathsf{R}}^2 \qquad \text{linear buoyancy equation} \tag{58.5c}$$

$$\nabla \cdot \boldsymbol{v}' = 0 \qquad \text{continuity for velocity fluctuations,} \tag{58.5d}$$

which reduce to equations (57.17a)-(57.17d) when $\boldsymbol{u}_{\mathsf{R}} = 0$.

58.2.2 Bottom topography and bottom boundary condition

As for the shallow water case studied in Section 56.2 (in particular, see Section 56.2.4), we consider the domain to be bounded from below with monochromatic bottom topography undulations given by

$$\eta'_{\mathsf{b}}(x,y) = \eta_{\circ}\mathrm{e}^{\mathrm{i}\,\boldsymbol{k}_{\mathsf{b}}\cdot\boldsymbol{x}}, \tag{58.6}$$

such as depicted in Figure 58.1. In this expression, $\eta_\circ$ is the real and constant amplitude of the topography and $\boldsymbol{k}_\flat$ is a horizontal wave number that specifies the direction and wavelength of the topography. Linearity of the waves generated by the topography is ensured by assuming

$$\eta_\circ \, |\boldsymbol{k}_\flat| \ll 1, \tag{58.7}$$

so that the amplitude of the topography is small on the length scale set by the topography's wavelength.

We orient the topography's wavevector, $\boldsymbol{k}_\flat$, to be opposite that of the reference flow, so that

$$\omega_\mathsf{R} = -\boldsymbol{u}_\mathsf{R} \cdot \boldsymbol{k}_\flat \geq 0, \tag{58.8}$$

where ω_R is an angular frequency of the bottom boundary forcing induced by the flow over the topography. As discussed in Section 56.2.5 when studying shallow water waves generated by topography, the sign for the inequality (58.8) reflects the fact that topography is stationary in the rest frame but it moves in the direction opposite to the reference flow when viewed in the frame following the reference flow. This inequality can be considered a causality condition and it is central to the phase functions encountered in the following.[2]

The no-flow bottom kinematic boundary condition for the full nonlinear flow takes the form (Section 19.6.1)

$$w = \boldsymbol{u} \cdot \nabla \eta_\flat \quad \text{at } z = \eta_\flat(x, y). \tag{58.9}$$

Inserting the velocity decomposition (58.1) and the bottom topography,

$$z = \overline{\eta_\flat} + \eta'_\flat(x, y), \tag{58.10}$$

leads to

$$w' = (\boldsymbol{u}' + \boldsymbol{u}_\mathsf{R}) \cdot \nabla(\overline{\eta_\flat} + \eta'_\flat) = (\boldsymbol{u}' + \boldsymbol{u}_\mathsf{R}) \cdot \nabla \eta'_\flat \approx \boldsymbol{u}_\mathsf{R} \cdot \nabla \eta'_\flat \quad \text{at } z = 0, \tag{58.11}$$

where the approximation arises from dropping the relatively small term, $\boldsymbol{u}' \cdot \nabla \eta'_\flat$.

58.2.3 Galilean transformation to the moving flow's reference frame

Following the shallow water case from Section 56.2.2, we transform to the moving frame of the constant reference flow by introducing the boosted (moving reference frame) coordinates

$$\overline{t} = t \quad \text{and} \quad \overline{\boldsymbol{x}} = \boldsymbol{x} - \boldsymbol{u}_\mathsf{R} \, t \quad \text{and} \quad \overline{\boldsymbol{v}} = \boldsymbol{v} - \boldsymbol{u}_\mathsf{R}. \tag{58.12}$$

Observers in the rest frame see the topography at rest and the reference flow moving with velocity, $\boldsymbol{u}_\mathsf{R}$. In contrast, observers in the boosted reference frame see the topography moving with velocity $-\boldsymbol{u}_\mathsf{R}$ whereas the reference flow is at rest. Since the flow is constant in space and time, the two observers are inertial, so the transformation between the two reference frames is Galilean (Section 17.5). Following the discussion in Section 17.5, the Galilean transformation (58.12) leads to the transformed differential operators

$$\partial_{\overline{t}} = \partial_t + \boldsymbol{u}_\mathsf{R} \cdot \nabla \quad \text{and} \quad \overline{\nabla} = \nabla, \tag{58.13}$$

and the corresponding transformation of the linearized governing equations (58.5a)-(58.5d)

$$\partial_{\overline{t}} \boldsymbol{u}' + f_\circ \, \hat{\boldsymbol{z}} \times \boldsymbol{u}' = -\overline{\nabla}_\mathsf{h} \varphi' \tag{58.14a}$$

[2] We are considering the steady state flow where one generally has time symmetry. However, keeping in mind the transient situation where time symmetry is broken, we here break time symmetry through acknowledging a directionality to the reference flow (left to right) and by insisting that the forcing angular frequency, ω_R, is positive.

$$\partial_{\bar{t}} w' = -\partial_{\bar{z}} \varphi' + b' \tag{58.14b}$$

$$\partial_{\bar{t}} b' = -w' \, N_{\mathsf{R}}^2 \tag{58.14c}$$

$$\overline{\nabla} \cdot \boldsymbol{v}' = 0. \tag{58.14d}$$

Notice how transformation to the moving frame removed advection by the reference flow from the horizontal velocity equation.

58.2.4 Free space dispersion relation with moving reference flow

Before considering the case of a lower boundary, we here establish some basic results for waves moving in a uniform flow in free space. For that purpose, note that equations (58.14a)-(58.14d) are mathematically identical to the linear equations (57.17a)-(57.17d) that apply to the case of zero reference flow, only here with the time derivative computed in the boosted reference frame, $\partial_{\bar{t}}$, rather than the rest frame time derivative, ∂_t. Consequently, when assuming a constant reference state buoyancy frequency, the equation for the vertical velocity in the boosted reference frame is given by equation (57.144) with boosted coordinates

$$(\partial_{\bar{t}\bar{t}} \, \overline{\nabla}^2 + N_{\mathsf{R}}^2 \, \overline{\nabla_{\mathsf{h}}^2} + f^2 \, \partial_{\bar{z}\bar{z}}) \, w' = 0. \tag{58.15}$$

In the absence of any boundaries, the phase function for linear waves is written[3]

$$\boldsymbol{k} \cdot \boldsymbol{x} - \omega \, t = \boldsymbol{k} \cdot (\overline{\boldsymbol{x}} + \boldsymbol{u}_{\mathsf{R}} \, t) - \omega \, t = \boldsymbol{k} \cdot \overline{\boldsymbol{x}} - (\omega - \boldsymbol{u}_{\mathsf{R}} \cdot \boldsymbol{k}) \, \bar{t} = \boldsymbol{k} \cdot \overline{\boldsymbol{x}} - \overline{\omega} \, \bar{t}, \tag{58.16}$$

where the final equality introduced[4]

$$\overline{\omega} = \omega - \boldsymbol{u}_{\mathsf{R}} \cdot \boldsymbol{k}, \tag{58.17}$$

which relates the angular frequency in the boosted frame, $\overline{\omega}$, to that in the rest frame, ω. The frequency shift, $-\boldsymbol{u}_{\mathsf{R}} \cdot \boldsymbol{k}$, is known as the *Doppler shift*, which vanishes when the phase is directed orthogonal to the reference flow, $\boldsymbol{u}_{\mathsf{R}} \cdot \boldsymbol{k} = 0$. Furthermore, the boosted frame's angular frequency, $\overline{\omega}$, vanishes for waves whose Doppler shift satisfies $\omega = \boldsymbol{u}_{\mathsf{R}} \cdot \boldsymbol{k}$. For these waves, the boosted reference frame rides along a fixed wave and so there is no propagation within this reference frame.

Critical levels

Plugging the free wave ansatz,

$$w' = \widetilde{w} \, \mathrm{e}^{\mathrm{i} \, (\boldsymbol{k} \cdot \overline{\boldsymbol{x}} - \overline{\omega} \, \bar{t})}, \tag{58.18}$$

into the vertical velocity equation (58.15) leads to the dispersion relation

$$\overline{\omega}^2 = (\omega - \boldsymbol{u}_{\mathsf{R}} \cdot \boldsymbol{k})^2 = N_{\mathsf{R}}^2 \cos^2 \gamma + f_{\mathsf{o}}^2 \sin^2 \gamma = [(N_{\mathsf{R}} \, \boldsymbol{k}_{\mathsf{h}})^2 + (f_{\mathsf{o}} \, k_z)^2] / |\boldsymbol{k}|^2. \tag{58.19}$$

This is a straightforward extension of the frequency from the rest frame value, ω, to the moving frame.

[3] Throughout this book we are working with particle and wave speeds that are far smaller than the speed of light, thus enabling the use of Galilean space-time rather than Lorentz space-time. Hence, we do not encounter the special relativistic effects from length contraction, and so there are no changes to the wavelength when moving to the Galilean boosted reference frame. Consequently, movement to the Galilean boosted reference frame leaves the wavevector, $\boldsymbol{k}$, unchanged.

[4] We introduced the same angular frequency relation in equation (56.38) for shallow water waves generated by flow over topography.

Wave energy propagates according to the group velocity, which we compute from the wavevector gradient

$$\nabla_{\boldsymbol{k}}\overline{\omega}^2 = 2\,\overline{\omega}\,\nabla_{\boldsymbol{k}}\overline{\omega} = 2\,\overline{\omega}\,(\nabla_{\boldsymbol{k}}\omega - \boldsymbol{u}_{\mathsf{R}}) = 2\,\overline{\omega}\,(\boldsymbol{c}_{\mathsf{g}} - \boldsymbol{u}_{\mathsf{R}}), \tag{58.20}$$

where $\boldsymbol{c}_{\mathsf{g}} = \nabla_{\boldsymbol{k}}\omega$ is the group velocity (57.161) as measured in the rest frame, and $\boldsymbol{c}_{\mathsf{g}} - \boldsymbol{u}_{\mathsf{R}}$ is that in the moving frame. Computing $\nabla_{\boldsymbol{k}}\overline{\omega}^2$ yields

$$\boldsymbol{c}_{\mathsf{g}} - \boldsymbol{u}_{\mathsf{R}} = \frac{(N_{\mathsf{R}}^2 - f^2)\,k_z}{\overline{\omega}\,|\boldsymbol{k}|^4}\,(k_z\,\boldsymbol{k}_{\mathsf{h}} - |\boldsymbol{k}_{\mathsf{h}}|^2\,\hat{\boldsymbol{z}}). \tag{58.21}$$

It is particularly revealing to consider gravity waves with $f_{\mathsf{o}} = 0$, in which we find the vertical component to the group velocity

$$\hat{\boldsymbol{z}} \cdot \boldsymbol{c}_{\mathsf{g}} = -(\omega - \boldsymbol{u}_{\mathsf{R}} \cdot \boldsymbol{k})\,k_z/|\boldsymbol{k}|^2. \tag{58.22}$$

The group velocity slows down, and halts, as the wave frequency approaches $\boldsymbol{u}_{\mathsf{R}} \cdot \boldsymbol{k}$. Although derived here for a constant reference flow, this equation holds to leading order for gently varying reference flows using WKBJ methods as in Section 58.4. In such cases we can find the vertical component of the group velocity vanish at certain *critical levels*, which are levels where waves can deposit their energy to the mean flow.

58.2.5 Wavenumbers for stationary inertial-gravity waves

Now consider the case of a monochromatic bottom (mountains) as depicted in Figure 58.1, with bottom topography of the form

$$\eta'_{\mathsf{b}} = \eta_{\mathsf{o}}\,\mathrm{e}^{\mathrm{i}\,\boldsymbol{k}_{\mathsf{b}}\cdot\boldsymbol{x}} = \eta_{\mathsf{o}}\,\mathrm{e}^{\mathrm{i}\,(\boldsymbol{k}_{\mathsf{b}}\cdot\overline{\boldsymbol{x}} - \omega_{\mathsf{R}}\,\overline{t})}. \tag{58.23}$$

The topography is static in the rest frame, whereas it is a traveling plane wave in the boosted frame with angular frequency $\omega_{\mathsf{R}} = -\boldsymbol{u}_{\mathsf{R}} \cdot \boldsymbol{k}_{\mathsf{b}} \geq 0$ given from equation (58.8). In the presence of topography, the waves are not free in all three directions. Rather, they must satisfy the bottom boundary condition (58.11), which takes on the following form for a monochromatic mountain range

$$w'(z=0) = \boldsymbol{u}_{\mathsf{R}} \cdot \nabla\eta'_{\mathsf{b}} = \mathrm{i}\,(\boldsymbol{u}_{\mathsf{R}} \cdot \boldsymbol{k}_{\mathsf{b}})\,\eta'_{\mathsf{b}} = -\mathrm{i}\,\omega_{\mathsf{R}}\,\eta'_{\mathsf{b}}. \tag{58.24}$$

For waves that are stationary in the rest frame ($\omega = 0$ so that $\overline{\omega} = \omega_{\mathsf{R}}$), we satisfy the boundary condition (58.24) by setting the vertical velocity to

$$w' = -\mathrm{i}\,\omega_{\mathsf{R}}\,\eta_{\mathsf{o}}\,\mathrm{e}^{\mathrm{i}\,(\boldsymbol{k}_{\mathsf{b}}\cdot\overline{\boldsymbol{x}} + k_z\,\overline{z} - \omega_{\mathsf{R}}\,\overline{t})} = -\mathrm{i}\,\omega_{\mathsf{R}}\,\eta_{\mathsf{o}}\,\mathrm{e}^{\mathrm{i}\,(\boldsymbol{k}_{\mathsf{b}}\cdot\boldsymbol{x} + k_z\,z)}, \tag{58.25}$$

which has a real part given by

$$w' = \omega_{\mathsf{R}}\,\eta_{\mathsf{o}}\sin(\boldsymbol{k}_{\mathsf{b}} \cdot \boldsymbol{x} + k_z\,z). \tag{58.26}$$

Notably, the horizontal wavevector is set by the topography,

$$\boldsymbol{k}_{\mathsf{h}} = \boldsymbol{k}_{\mathsf{b}}. \tag{58.27}$$

With constant N_{R}, we can use the stationary form of the dispersion relation (58.19),

$$\overline{\omega}^2 = \omega_{\mathsf{R}}^2 = (\boldsymbol{u}_{\mathsf{R}} \cdot \boldsymbol{k})^2 = N_{\mathsf{R}}^2\cos^2\gamma + f_{\mathsf{o}}^2\sin^2\gamma = [(N_{\mathsf{R}}\,|\boldsymbol{k}_{\mathsf{h}}|)^2 + (f_{\mathsf{o}}\,k_z)^2]/|\boldsymbol{k}|^2, \tag{58.28}$$

to find the squared vertical wavenumber for the stationary inertia-gravity waves (again, $\boldsymbol{k}_{\mathsf{h}} = \boldsymbol{k}_{\mathsf{b}}$

via equation (58.27))

$$k_z^2 = \frac{|\boldsymbol{k}_\mathsf{b}|^2 \, (N_\mathsf{R}^2 - \omega_\mathsf{R}^2)}{\omega_\mathsf{R}^2 - f_\circ^2}, \tag{58.29}$$

with the vertical wavenumber either real or imaginary according to

$$k_z^2 = \begin{cases} < 0 & \text{if } \omega_\mathsf{R}^2 < f_\circ^2 \\ > 0 & \text{if } f_\circ^2 < \omega_\mathsf{R}^2 < N_\mathsf{R}^2 \\ < 0 & \text{if } \omega_\mathsf{R}^2 > N_\mathsf{R}^2. \end{cases} \tag{58.30}$$

The cases with $k_z^2 < 0$ lead to stationary waves that are oscillating in the horizontal yet exponentially trapped in the vertical, much like the surface gravity waves studied in Chapter 52 or the edge waves studied in 54.5. In contrast, with $k_z^2 > 0$ there are stationary waves extending throughout the vertical. The regime of vertically extended stationary waves is given by

$$2\pi / N_\mathsf{R} < \Lambda_\mathsf{b} / U < 2\pi / f_\circ, \tag{58.31}$$

where

$$\Lambda_\mathsf{b} = 2\pi / |\boldsymbol{k}_\mathsf{b}| \tag{58.32}$$

is the topography's wavelength. In the atmosphere, typical values for the reference state are $N_\mathsf{R} = 10^{-2}$ s^{-1}, $U = 10$ m s^{-1}, and $f_\circ = 10^{-4}$ s^{-1}, in which case there are vertically extended inertia-gravity waves for mountains having wavelengths within the range

$$2\pi \, U / N_\mathsf{R} < \Lambda_\mathsf{b} < 2\pi \, U / f_\circ \implies 2\pi \times 10^3 \text{ m} < \Lambda_\mathsf{b} < 2\pi \times 10^5 \text{ m}. \tag{58.33}$$

For the deep ocean we take $N_\mathsf{R} = 10^{-3}$ s^{-1}, $U = 10^{-1}$ m s^{-1} (barotropic tidal speeds), and $f_\circ = 10^{-4}$ s^{-1}, so that there are vertically extended stationary inertia-gravity waves for undersea mountains having wavelengths within the range

$$2\pi \times 10^2 \text{ m} < \Lambda_\mathsf{b} < 2\pi \times 10^3 \text{ m}. \tag{58.34}$$

These numbers are only meant to give an impression of the approximate scales of mountain forcing that generate vertically extended internal inertia-gravity waves. One key point is the roughly one order smaller scales for the ocean relative to the atmosphere.

58.2.6 Stationary mountain waves with $f_\circ^2 < \omega_\mathsf{R}^2 < N_\mathsf{R}^2$

For $f_\circ^2 < \omega_\mathsf{R}^2 < N_\mathsf{R}^2$, we have stationary inertia-gravity waves with $k_z^2 > 0$ according to equation (58.29). As the reference flow interacts with the mountains at the lower boundary, internal inertia-gravity waves propagate energy upwards according to the group velocity. As seen in Section 57.5.10, an upward group velocity means a downward phase velocity, so that we take the negative root from equation (58.29)

$$k_z = -|\boldsymbol{k}_\mathsf{b}| \sqrt{\frac{N_\mathsf{R}^2 - \omega_\mathsf{R}^2}{\omega_\mathsf{R}^2 - f_\circ^2}} = -|k_z| < 0, \tag{58.35}$$

which renders the stationary vertical velocity in the wave[5]

$$w' = -\mathrm{i} \, \omega_\mathsf{R} \, \eta_\circ \, \mathrm{e}^{\mathrm{i} \, (\boldsymbol{k}_\mathsf{b} \cdot \boldsymbol{x} - |k_z| \, z)}. \tag{58.36}$$

[5]In equation (58.35), and elsewhere in this chapter, we find it useful to introduce the absolute value around a wavenumber in order to clearly expose the sign of the wavenumber. Doing so can greatly help in capturing the proper phase relations for the waves.

For the specific case of zonal reference flow, $\boldsymbol{u}_{\mathsf{R}} = U\,\hat{\boldsymbol{x}}$ with $U > 0$, we have $\boldsymbol{k}_{\mathsf{b}} = -|\boldsymbol{k}_{\mathsf{b}}|\,\hat{\boldsymbol{x}}$, so that

$$\omega_{\mathsf{R}} = -\boldsymbol{u}_{\mathsf{R}} \cdot \boldsymbol{k}_{\mathsf{b}} = U\,|\boldsymbol{k}_{\mathsf{b}}| \implies w' = -\mathrm{i}\,U\,|\boldsymbol{k}_{\mathsf{b}}|\,\eta_{\circ}\,\mathrm{e}^{-\mathrm{i}\,(|\boldsymbol{k}_{\mathsf{b}}|\,x + |k_z|\,z)}, \tag{58.37}$$

which has real part

$$w' = \widetilde{w}\sin(|\boldsymbol{k}_{\mathsf{b}}|\,x + |k_z|\,z) = -U\,|\boldsymbol{k}_{\mathsf{b}}|\,\eta_{\circ}\sin(|\boldsymbol{k}_{\mathsf{b}}|\,x + |k_z|\,z), \tag{58.38}$$

where we defined the vertical velocity amplitude

$$\widetilde{w} = -U\,|\boldsymbol{k}_{\mathsf{b}}|\,\eta_{\circ}. \tag{58.39}$$

Evidently, the vertical velocity amplitude is directly related to the reference flow magnitude, the topography wavenumber, and the topography amplitude.

To determine polarization relations for the other fields, we can return to those derived earlier for the free waves in Section 58.2.4, specializing to the case with $\omega = \omega_{\mathsf{R}}$. Alternatively, we can set $\partial_t = 0$ in the linear governing equations (58.5a)-(58.5d). This work is considered in Exercise 58.1 and follows a method similar to that taken for stationary mountain gravity waves in Section 58.2.7.

58.2.7 Stationary mountain waves with $0 < \omega_{\mathsf{R}}^2 < N_{\mathsf{R}}^2$

We now specialize to $f_{\circ} = 0$, such as appropriate for mountain waves that are small enough laterally to not feel the impacts from Coriolis. Also, continue to assume a zonal reference flow, $\boldsymbol{u}_{\mathsf{R}} = U\,\hat{\boldsymbol{x}}$ with $U > 0$ and $\boldsymbol{k}_{\mathsf{b}} = -|\boldsymbol{k}_{\mathsf{b}}|\,\hat{\boldsymbol{x}}$. The vertical velocity is still given by equation (58.38)

$$w' = -U\,|\boldsymbol{k}_{\mathsf{b}}|\,\eta_{\circ}\sin(|\boldsymbol{k}_{\mathsf{b}}|\,x + |k_z|\,z), \tag{58.40}$$

yet here with the angular frequency for stationary waves given by

$$\omega_{\mathsf{R}} = N_{\mathsf{R}}\,|\boldsymbol{k}_{\mathsf{b}}|/|\boldsymbol{k}| = U\,|\boldsymbol{k}_{\mathsf{b}}| \implies U = N_{\mathsf{R}}/|\boldsymbol{k}|, \tag{58.41}$$

and the vertical wavenumber corresponding to an upward directed group velocity

$$k_z = -|\boldsymbol{k}_{\mathsf{b}}|\sqrt{(N_{\mathsf{R}}/\omega_{\mathsf{R}})^2 - 1} = -\sqrt{(N_{\mathsf{R}}/U)^2 - |\boldsymbol{k}_{\mathsf{b}}|^2} < 0. \tag{58.42}$$

As discussed in Exercise 58.2, the frequency ratio,

$$\mathrm{Fr}(|\boldsymbol{k}_{\mathsf{b}}|) = \frac{\omega_{\mathsf{R}}}{N_{\mathsf{R}}} = \frac{U\,|\boldsymbol{k}_{\mathsf{b}}|}{N_{\mathsf{R}}}, \tag{58.43}$$

can be considered a wavenumber dependent Froude number. Inserting this Froude number into equation (58.42) yields

$$k_z = -|\boldsymbol{k}_{\mathsf{b}}|\sqrt{\mathrm{Fr}^{-2} - 1}, \tag{58.44}$$

so that the Froude number distinguishes vertically propagating stationary gravity waves ($\mathrm{Fr} < 1$) from vertically evanescent waves ($\mathrm{Fr} > 1$).

Lines of constant phase

For the vertical propagating waves ($\mathrm{Fr} < 1$), the vertical velocity (58.40) is constant along phase lines that satisfy

$$|\boldsymbol{k}_{\mathsf{b}}|\,x + |k_z|\,z = \text{constant}. \tag{58.45}$$

These phase lines have a slope

$$\frac{\mathrm{d}z}{\mathrm{d}x} = -|\boldsymbol{k}_\mathrm{b}|/|k_z|, \tag{58.46}$$

which indicates that the phase lines slope up to the left such as depicted in Figure 58.2. Evidently, the phase lines tilt into the reference flow.

Polarization relations

The polarization relations for the stationary waves are determined by the steady linear governing equations (58.5a)-(58.5d) with $f_\circ = 0$ and $\partial_t = 0$

$$(\boldsymbol{u}_\mathrm{R} \cdot \nabla)\boldsymbol{u}' = -\nabla_\mathrm{h}\varphi' \qquad \text{steady linearized horizontal velocity equation} \tag{58.47a}$$
$$(\boldsymbol{u}_\mathrm{R} \cdot \nabla)w' = -\partial_z\varphi' + b' \qquad \text{steady linearized vertical velocity equation} \tag{58.47b}$$
$$(\boldsymbol{u}_\mathrm{R} \cdot \nabla)b' = -w'\, N_\mathrm{R}^2 \qquad \text{steady linearized buoyancy equation} \tag{58.47c}$$
$$\nabla \cdot \boldsymbol{v}' = 0 \qquad \text{continuity for velocity fluctuations.} \tag{58.47d}$$

All motion is in the x-z plane, so that the continuity equation (58.47d) gives the zonal velocity

$$u' = -(|k_z|/|\boldsymbol{k}_\mathrm{b}|)\, w' \Longrightarrow u'\, \frac{\mathrm{d}z}{\mathrm{d}x} = w' \quad \text{and} \quad u' = U\, |k_z|\, \eta_\circ \sin(|\boldsymbol{k}_\mathrm{b}|\, x + |k_z|\, z), \tag{58.48}$$

where we used the slope relation (58.46). The steady buoyancy equation (58.47c) yields

$$U\, \partial_x b' = N_\mathrm{R}^2\, U\, |\boldsymbol{k}_\mathrm{b}|\, \eta_\circ \sin(|\boldsymbol{k}_\mathrm{b}|\, x + |k_z|\, z) \Longrightarrow b' = -\eta_\circ\, N_\mathrm{R}^2 \cos(|\boldsymbol{k}_\mathrm{b}|\, x + |k_z|\, z). \tag{58.49}$$

Likewise, the steady horizontal velocity equation (58.47a) gives the wave pressure

$$\varphi' = -U\, u' = -\eta_\circ\, |k_z|\, U^2 \sin(|\boldsymbol{k}_\mathrm{b}|\, x + |k_z|\, z). \tag{58.50}$$

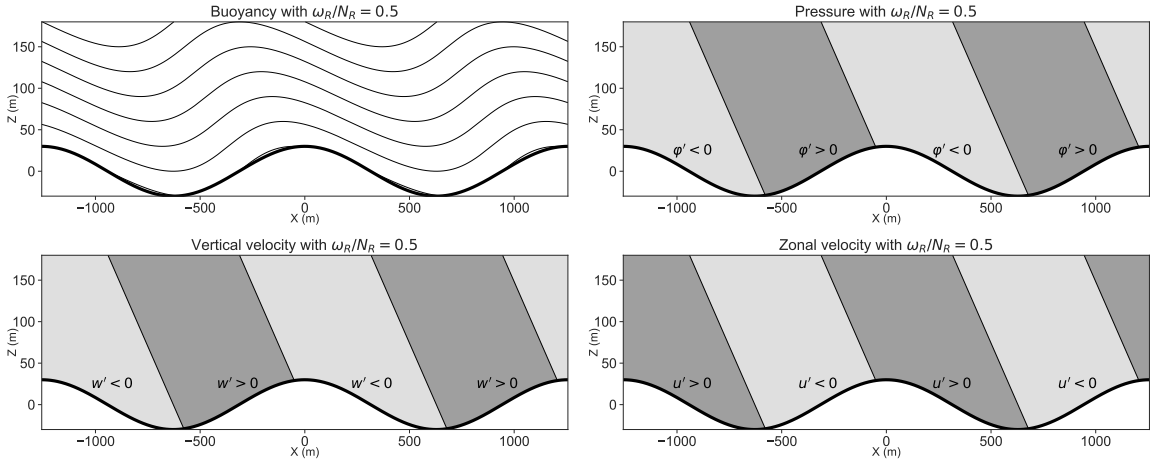

FIGURE 58.2: Stationary mountain gravity waves generated by an eastward reference flow, $\boldsymbol{u}_\mathrm{R} = U\,\hat{\boldsymbol{x}}$, over monochromatic topography. We set the parameters according to ocean values, with $\eta_\circ = 30$ m, $U = 0.1$ m s^{-1}, $N_\mathrm{R} = 10^{-3}$ s^{-1}, and $\Lambda_\mathrm{b} = 2\pi \times 200$ m, so that $\omega_\mathrm{R}/N_\mathrm{R} = 0.5$. Top left panel: contours of the buoyancy field, $b = b_\mathrm{R} + b'$, with $b_\mathrm{R} = N_\mathrm{R}^2\, z$ and $b' = -\eta_\circ\, N_\mathrm{R}^2 \cos(|\boldsymbol{k}_\mathrm{b}|\, x + |k_z|\, z)$ from equation (58.49). Top right panel: perturbation pressure field, $\varphi' = -U\, u' = U\, w'\, |k_z|/|\boldsymbol{k}_\mathrm{b}|$, from equation (58.50). Lower left panel: the vertical velocity anomaly, $w' = -U\, |\boldsymbol{k}_\mathrm{b}|\, \eta_\circ \sin(|\boldsymbol{k}_\mathrm{b}|\, x + |k_z|\, z)$ from equation (58.40). Lower right panel: the zonal velocity anomaly, $u' = -|k_z|/|\boldsymbol{k}_\mathrm{b}|\, w'$ from equation (58.48). The color scale is set to highlight just the sign of the field. The phase shift, whereby high pressures are on the windward side of the mountains and low pressures on the lee side, leads to a topographic pressure form stress acting on the fluid according to equation (58.51).

Wave induced topographic form stress

In Figure 58.2 we illustrate the buoyancy, pressure, vertical velocity, and zonal velocity within a stationary gravity wave for a particular set of parameters. Note the phase lines that are tilted into the mean flow with the positive pressure perturbation on the upwind side of the mountains. This orientation is reflective of the general discussion surrounding Figure 28.8 when studying pressure form stress acting between the fluid and the solid lower boundary. From that discussion we know that a positive pressure anomaly on the upwind side of a mountain renders an eastward form stress from the fluid to the solid, and a corresponding (through Newton's third law) westward topographic form stress directed from the solid to the fluid.

From the discussion in Section 28.2.2, we write the topographic form stress acting on the fluid as $-p \nabla \eta_\mathrm{b}$. The pressure is evaluated at the solid-fluid boundary for the nonlinear case, whereas for linear waves we evaluate the topographic form stress at $z = 0$, with a phase average yielding

$$\langle -\varphi' \, \partial_x \eta_\mathrm{b} \rangle = -U^2 \, \eta_\mathrm{o}^2 \, |\boldsymbol{k}_\mathrm{b}| \, |k_z|/2. \tag{58.51}$$

This westward topographic form stress acts from the solid onto the fluid, with a corresponding eastward form stress of the same magnitude from the fluid to the solid. The stress is directly related to the square of the reference flow speed and the square of the topography amplitude. It is also linearly related to the vertical wavenumber of the gravity wave and the vertical wavenumber of the topography. Since the stress is directed contrary to the reference flow direction, it is commonly referred to as a *mountain drag*.

Wave energy flux

From Section 57.5.14 we know that the energy flux carried by a gravity wave is given by $\boldsymbol{v}' \, \varphi'$. For stationary mountain waves in the x-z plane we have

$$\boldsymbol{v}' \, \varphi' = -(\hat{\boldsymbol{x}} \, u' + \hat{\boldsymbol{z}} \, w') \, U \, u' = \frac{U \, w' \, w' \, |k_z|}{|\boldsymbol{k}_\mathrm{b}|^2} \, (-|k_z| \, \hat{\boldsymbol{x}} + |\boldsymbol{k}_\mathrm{b}| \, \hat{\boldsymbol{z}}). \tag{58.52}$$

Now the group velocity for internal gravity waves is given by equation (57.71), which takes on the following form for the forced stationary waves

$$\boldsymbol{c}_\mathrm{g} = \frac{N_\mathsf{R} \, k_z}{|\boldsymbol{k}|^3 \, |\boldsymbol{k}_\mathrm{b}|} \, (k_z \, \boldsymbol{k}_\mathrm{b} - |\boldsymbol{k}_\mathrm{b}|^2 \, \hat{\boldsymbol{z}}) \tag{58.53a}$$

$$= \frac{N_\mathsf{R} \, |k_z|}{|\boldsymbol{k}|^3} \, (-|k_z| \, \hat{\boldsymbol{x}} + |\boldsymbol{k}_\mathrm{b}| \, \hat{\boldsymbol{z}}) \tag{58.53b}$$

$$= \frac{U \, |k_z|}{|\boldsymbol{k}|^2} \, (-|k_z| \, \hat{\boldsymbol{x}} + |\boldsymbol{k}_\mathrm{b}| \, \hat{\boldsymbol{z}}), \tag{58.53c}$$

where the second equality set $\boldsymbol{k}_\mathrm{b} = -|\boldsymbol{k}_\mathrm{b}| \, \hat{\boldsymbol{x}}$ and $k_z = -|k_z| < 0$, and the third equality set $U = N_\mathsf{R}/|\boldsymbol{k}|$ from equation (58.41). Next, we make use of equation (57.101) to write the mechanical energy within the stationary internal gravity wave

$$\mathcal{K}' + \mathcal{A}' = \langle w' \, w' \rangle \, |\boldsymbol{k}|^2/|\boldsymbol{k}_\mathrm{b}|^2 = \tfrac{1}{2} \, \eta_\mathrm{o}^2 \, U^2 \, |\boldsymbol{k}|^2 = \tfrac{1}{2} \, \eta_\mathrm{o}^2 \, N_\mathsf{R}^2, \tag{58.54}$$

which then brings the phase averaged energy flux to the standard form holding for a linear wave

$$\langle \boldsymbol{v}' \, \varphi' \rangle = \boldsymbol{c}_\mathrm{g} \, (\mathcal{K}' + \mathcal{A}'). \tag{58.55}$$

58.2.8 Trapped mountain waves with $\omega_{\mathsf{R}} > N_{\mathsf{R}}$

For the case with mountain forcing at a frequency greater than buoyancy frequency, $\omega_{\mathsf{R}} > N_{\mathsf{R}}$, the vertical wavenumber becomes imaginary

$$k_z = \mathrm{i}\sqrt{|\boldsymbol{k}_{\mathsf{b}}|^2 - (N_{\mathsf{R}}/U)^2} = \mathrm{i}\,|k_z|, \tag{58.56}$$

which yields a wave solution that is exponentially decaying away from the mountains (see equation (58.36) and remember that $\boldsymbol{k}_{\mathsf{b}} = -|\boldsymbol{k}_{\mathsf{b}}|\,\hat{\boldsymbol{x}}$ and $\omega_{\mathsf{R}} = U\,|\boldsymbol{k}_{\mathsf{b}}| > 0$)

$$w' = -\mathrm{i}\,\omega_{\mathsf{R}}\,\eta_{\mathsf{o}}\,\mathrm{e}^{\mathrm{i}\,\boldsymbol{k}_{\mathsf{b}}\cdot\boldsymbol{x} - |k_z|\,z} \xrightarrow{\text{Re}} -U\,|\boldsymbol{k}_{\mathsf{b}}|\,\eta_{\mathsf{o}}\sin(|\boldsymbol{k}_{\mathsf{b}}|\,x)\,\mathrm{e}^{-|k_z|\,z}. \tag{58.57}$$

We refer to these fluctuations as *vertically evanescent* or *vertically trapped* gravity waves. The corresponding zonal velocity, buoyancy, and pressure fields are

$$u' = U\,|k_z|\,\eta_{\mathsf{o}}\cos(|\boldsymbol{k}_{\mathsf{b}}|\,x)\,\mathrm{e}^{-|k_z|\,z} \tag{58.58a}$$

$$b' = -\eta_{\mathsf{o}}\,N_{\mathsf{R}}^2\cos(|\boldsymbol{k}_{\mathsf{b}}|\,x)\,\mathrm{e}^{-|k_z|\,z} \tag{58.58b}$$

$$\varphi' = -U^2\,|k_z|\,\eta_{\mathsf{o}}\cos(|\boldsymbol{k}_{\mathsf{b}}|\,x)\,\mathrm{e}^{-|k_z|\,z}. \tag{58.58c}$$

Zero energy propagation and zero topographic form stress

Since the vertical velocity (58.57) and pressure (58.58c) are $\pi/2$ radians out of phase, vertically trapped waves generate no vertical propagation of phase averaged wave energy

$$\langle w'\,\varphi'\rangle = 0. \tag{58.59}$$

Likewise, there is no topographic form stress since there is no phase shift between the topography and the pressure

$$\langle \varphi'\,\partial_x \eta_{\mathsf{b}}\rangle = 0. \tag{58.60}$$

Limit where $\omega_{\mathsf{R}} \gg N_{\mathsf{R}}$

The case of $\omega_{\mathsf{R}} \gg N_{\mathsf{R}}$ corresponds to large topographic frequency and/or small buoyancy frequency. In this limit the vertical wavenumber has a magnitude $|k_z| \approx |\boldsymbol{k}_{\mathsf{b}}|$ so that N_{R} drops out from the system. This case corresponds to the surface gravity waves studied in Chapter 52 where stratification was completely ignored. In that case, as well as here, the exponential trapping is determined by the horizontal wavenumber, $|\boldsymbol{k}_{\mathsf{b}}|$. Furthermore, in the case with vertical length scales, H, such that $|k_z|\,H \approx |\boldsymbol{k}_{\mathsf{b}}|\,H \ll 1$, then the vertical velocity becomes a linear function of z. This case corresponds to the shallow water inertia-gravity waves studied in Section 56.2

Comments on exponential trapping

As discussed in Section 57.5.8, forcing a stratified fluid at a frequency greater than the buoyancy frequency does not lead to propagating internal gravity waves. For the case of mountain gravity waves, we see that exponential trapping arises when the topographic forcing has a frequency, ω_{R}, greater than the maximum frequency of the buoyancy oscillations, N_{R}. In this case, motion induced by the forcing is too fast for fluid particles to exhibit buoyancy oscillations. The result is fluid particles largely following whatever displacements are imposed on them by the external forcing, with exponential damping when moving away from the forcing and with fluid particles in phase with the forcing. In this case, no propagating internal gravity waves are formed, and energy imparted to the fluid stays local to the topographic forcing.

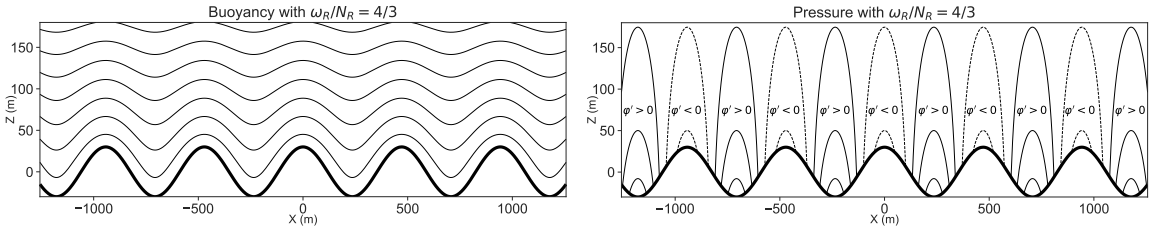

FIGURE 58.3: Stationary trapped mountain gravity waves generated by an eastward reference flow, $\boldsymbol{u}_{\mathsf{R}} = U\,\hat{\boldsymbol{x}}$, over monochromatic topography. We set the parameters according to ocean values, with $\eta_{\circ} = 30$ m, $U = 0.1$ m s^{-1}, $N_{\mathsf{R}} = 10^{-3}$ s^{-1}, and $\Lambda_{\mathsf{b}} = 2\pi \times 75$ m (we used the larger wavelength of $\Lambda_{\mathsf{b}} = 2\pi \times 200$ m in Figure 58.2), so that $\omega_{\mathsf{R}}/N_{\mathsf{R}} = 4/3$. These waves are exponentially trapped near the topography with e-folding scale $|k_z|^{-1} = 1/\sqrt{(N_{\mathsf{R}}/U)^2 - |\boldsymbol{k}_{\mathsf{b}}|^2} \approx 110$ m. Left panel: contours of the buoyancy field, $b = b_{\mathsf{R}} + b'$, with $b_{\mathsf{R}} = N_{\mathsf{R}}^2\, z$ and $b' = -\eta_{\circ}\, N_{\mathsf{R}}^2 \cos(|\boldsymbol{k}_{\mathsf{b}}|\, x)\, \mathrm{e}^{-|k_z|\, z}$ from equation (58.58c). Right panel: perturbation pressure field, $\varphi' = -U^2\, |\boldsymbol{k}_{\mathsf{b}}|\, \eta_{\circ} \cos(|\boldsymbol{k}_{\mathsf{b}}|\, x)\, \mathrm{e}^{-|k_z|\, z}$ from equation (58.58c). Note how the pressure is anomously high over the valleys (solid contours with $\varphi' > 0$) and low over the crests (dashed contours with $\varphi' < 0$). We chose the horizontal extent to be the same as in Figure 58.2, thus emphasizing how the smaller scale topography in this figure can lead to exponentially trapped waves, whereas the larger scale topography in Figure 58.2 allows for vertical propagation. Since there is no phase shift with height for the vertically trapped waves, there is no topographic form stress, which we see in equation (58.60).

58.2.9 Comments on the phenomenology

Gravity waves are ubiquitous in the ocean and atmosphere, with flow over topography one of the key means for generating such waves. As seen in this section, the flow speed, $U > 0$, and mountain wavenumber, $|\boldsymbol{k}_{\mathsf{b}}|$, together define the angular frequency for the forcing, $\omega_{\mathsf{R}} = U\,|\boldsymbol{k}_{\mathsf{b}}| > 0$. This forcing generates propagating gravity waves if $\omega_{\mathsf{R}} < N_{\mathsf{R}}$, or evanescent (trapped) gravity waves if $\omega_{\mathsf{R}} > N_{\mathsf{R}}$. That is, fast flow and/or high wavenumber mountains produce gravity waves that are trapped next to the mountain, whereas slower flow or lower wavenumber mountains generate gravity waves that propagate vertically.

Consider the case of an atmosphere with $N_{\mathsf{R}} = 10^{-2}$ s^{-1} and $U = 10$ m s^{-1}. Propagating gravity waves are generated for mountains with a horizontal wavelength ($|\boldsymbol{k}_{\mathsf{b}}| = 2\pi/\Lambda$) larger than $\Lambda = 2\pi \times 10^3$ m. For the deep ocean, with $N_{\mathsf{R}} = 10^{-3}$ m and $U = 10^{-2}$ m s^{-1}, propagating gravity waves are generated for abyssal mountains with wavelengths larger than $\Lambda = 2\pi \times 10^1$ m. These numbers suggest that all topographic features larger than a minimal scale will generate gravity waves. However, there is an upper bound on the scale imposed by the Coriolis parameter. Namely, for large enough scales the flow feels the Coriolis acceleration, thus requiring us to recall from Section 57.9.1 that propagating inertia-gravity waves have a dispersion relation (57.147)

$$\omega^2 = N_{\mathsf{R}}^2 \cos^2\gamma + f^2 \sin^2\gamma \implies f^2 < \omega^2 < N_{\mathsf{R}}^2, \tag{58.61}$$

where we here assume the Coriolis frequency is less than the buoyancy frequency. Hence, the condition for an upper bound on the forcing frequency, set by the buoyancy frequency, is coupled to a lower bound set by the Coriolis frequency. For the atmosphere at middle latitudes with $|f| = 10^{-4}$ s^{-1}, we find $2\pi \times 10^3$ m $< \Lambda < 2\pi \times 10^5$ m, whereas the ocean requires $2\pi \times 10^1$ m $< \Lambda < 2\pi \times 10^2$ m.

58.3 Gravity waves from a Lorentzian mountain

In this section we examine stationary mountain waves resulting from constant zonal flow, $\boldsymbol{u}_{\mathsf{R}} = U\,\hat{\boldsymbol{x}}$, moving over arbitrary (x-dependent) topography. This analysis extends our study of waves emanating from flow over monochromatic topography considered in Section 58.2. To handle arbitrary topography, we make use of Fourier analysis from Chapter 8 by exploiting the zonal symmetry of the reference flow and geometry. For pedagogy, we find it especially useful to

carefully step through the formulation, with a particular realization given by a mountain in the shape of a Lorentzian function.

58.3.1 Mathematical formulation using Fourier methods

Following our discussion in Section 8.3, we here introduce the Fourier transform and inverse Fourier transform for the bottom topography, velocity, buoyancy, and pressure. Furthermore, from our discussion of causality in Section 56.2.5, and with the reference flow $\boldsymbol{u}_{\mathsf{R}} = U\,\hat{\boldsymbol{x}}$ with $U > 0$, we build in causality by only considering $k_x \leq 0$, so that the forcing frequency is non-negative

$$\omega_{\mathsf{R}} = -\boldsymbol{u}_{\mathsf{R}} \cdot \boldsymbol{k}_{\mathsf{b}} = -U\,k_x \geq 0 \implies k_x \leq 0. \tag{58.62}$$

These considerations lead to the Fourier transform pairs

$$\widehat{\eta}_{\mathsf{b}}(k_x) = \int_{-\infty}^{\infty} \eta'_{\mathsf{b}}(x)\,\mathrm{e}^{-\mathrm{i}\,k_x\,x}\,\mathrm{d}x \qquad \eta'(x) = \frac{1}{2\pi}\int_{-\infty}^{0} \widehat{\eta}_{\mathsf{b}}(k_x)\,\mathrm{e}^{\mathrm{i}\,k_x\,x}\,\mathrm{d}k_x \tag{58.63a}$$

$$\widehat{u}(k_x,z) = \int_{-\infty}^{\infty} u'(x,z)\,\mathrm{e}^{-\mathrm{i}\,k_x\,x}\,\mathrm{d}x \qquad u'(x,z) = \frac{1}{2\pi}\int_{-\infty}^{0} \widehat{u}(k_x,z)\,\mathrm{e}^{\mathrm{i}\,k_x\,x}\,\mathrm{d}k_x \tag{58.63b}$$

$$\widehat{w}(k_x,z) = \int_{-\infty}^{\infty} w'(x,z)\,\mathrm{e}^{-\mathrm{i}\,k_x\,x}\,\mathrm{d}x \qquad w'(x,z) = \frac{1}{2\pi}\int_{-\infty}^{0} \widehat{w}(k_x,z)\,\mathrm{e}^{\mathrm{i}\,k_x\,x}\,\mathrm{d}k_x \tag{58.63c}$$

$$\widehat{b}(k_x,z) = \int_{-\infty}^{\infty} b'(x,z)\,\mathrm{e}^{-\mathrm{i}\,k_x\,x}\,\mathrm{d}x \qquad b'(x,z) = \frac{1}{2\pi}\int_{-\infty}^{0} \widehat{b}(k_x,z)\,\mathrm{e}^{\mathrm{i}\,k_x\,x}\,\mathrm{d}k_x \tag{58.63d}$$

$$\widehat{\varphi}(k_x,z) = \int_{-\infty}^{\infty} \varphi'(x,z)\,\mathrm{e}^{-\mathrm{i}\,k_x\,x}\,\mathrm{d}x \qquad \varphi'(x,z) = \frac{1}{2\pi}\int_{-\infty}^{0} \widehat{\varphi}(k_x,z)\,\mathrm{e}^{\mathrm{i}\,k_x\,x}\,\mathrm{d}k_x, \tag{58.63e}$$

where we only perform the x direction Fourier transform since the domain has a lower boundary and so is not symmetric in z. The hatted Fourier transform fields have an extra length dimension relative to their $\boldsymbol{x}$-space partners.

Now write the stationary linear equations (58.47a)-(58.47d) using the reference flow, $\boldsymbol{u}_{\mathsf{R}} = U\,\hat{\boldsymbol{x}}$,

$$U\,\partial_x u' = -\partial_x \varphi' \tag{58.64a}$$

$$U\,\partial_x w' = -\partial_z \varphi' + b' \tag{58.64b}$$

$$U\,\partial_x b' = -w'\,N_{\mathsf{R}}^2 \tag{58.64c}$$

$$\partial_x u' + \partial_z w' = 0, \tag{58.64d}$$

where we set $v' = 0$ and $\partial_y = 0$. Operating on these equations with $\int_{-\infty}^{\infty} \mathrm{e}^{-\mathrm{i}\,k_x\,x}$, and assuming all boundary terms vanish, brings about the Fourier space equations

$$U\,\widehat{u} = -\widehat{\varphi} \tag{58.65a}$$

$$\mathrm{i}\,k_x\,U\,\widehat{w} = -\partial_z \widehat{\varphi} + \widehat{b} \tag{58.65b}$$

$$\mathrm{i}\,k_x\,U\,\widehat{b} = -\widehat{w}\,N_{\mathsf{R}}^2 \tag{58.65c}$$

$$\mathrm{i}\,k_x\,\widehat{u} + \partial_z \widehat{w} = 0, \tag{58.65d}$$

along with the Fourier space version of the linearized bottom boundary condition (58.11)

$$\widehat{w}(k_z, z=0) = \mathrm{i}\,k_x\,U\,\widehat{\eta}(k_x). \tag{58.66}$$

58.3.2 Wave solution in (k_x, z)-space

To satisfy the bottom kinematic boundary condition (58.66), we follow the approach from Section 58.2.5 used for the monochromatic topography by writing

$$\widehat{w} = \mathrm{i}\, k_x\, U\, \widehat{\eta}_\mathsf{b}\, \mathrm{e}^{\mathrm{i}\, k_z\, z}. \tag{58.67}$$

The vertical wavenumber is determined through use of the stationary gravity wave dispersion relation as in Section 58.2.7

$$k_z = -\sqrt{(N_\mathsf{R}/U)^2 - k_x^2}. \tag{58.68}$$

The negative sign ensures that $k_z < 0$ for long horizontal waves with $k_x < N_\mathsf{R}/U$, thus ensuring that gravity wave energy, which follows the group velocity, propagates vertically upward (away from the mountains), thus satisfying causality. The Fourier space continuity equation (58.65d) leads to the zonal velocity Fourier transform

$$\widehat{u} = -\mathrm{i}\, k_z\, U\, \widehat{\eta}_\mathsf{b}\, \mathrm{e}^{\mathrm{i}\, k_z\, z}, \tag{58.69}$$

which, with the pressure equation (58.65a), leads to

$$\widehat{\varphi} = \mathrm{i}\, k_z\, U^2\, \widehat{\eta}_\mathsf{b}\, \mathrm{e}^{\mathrm{i}\, k_z\, z}. \tag{58.70}$$

Finally, we make use of the buoyancy equation (58.65c) to find

$$\widehat{b} = \frac{\mathrm{i}\, \widehat{w}\, N_\mathsf{R}^2}{U\, k_x} = -N_\mathsf{R}^2\, \widehat{\eta}_\mathsf{b}\, \mathrm{e}^{\mathrm{i}\, k_z\, z}. \tag{58.71}$$

58.3.3 Wave solution in (x, z)-space

Making use of the inverse Fourier transforms from equations (58.63a)-(58.63e) renders the (x, z)-space expressions

$$\eta'(x) = \frac{1}{2\pi} \int_{-\infty}^{0} \widehat{\eta}_\mathsf{b}\, \mathrm{e}^{\mathrm{i}\, k_x\, x}\, \mathrm{d}k_x \tag{58.72a}$$

$$u'(x,z) = \frac{-\mathrm{i}\, U}{2\pi} \int_{-\infty}^{0} k_z\, \widehat{\eta}_\mathsf{b}\, \mathrm{e}^{\mathrm{i}\,(k_x\, x + k_z\, z)}\, \mathrm{d}k_x \tag{58.72b}$$

$$w'(x,z) = \frac{\mathrm{i}\, U}{2\pi} \int_{-\infty}^{0} k_x\, \widehat{\eta}_\mathsf{b}\, \mathrm{e}^{\mathrm{i}\,(k_x\, x + k_z\, z)}\, \mathrm{d}k_x \tag{58.72c}$$

$$b'(x,z) = \frac{-N_\mathsf{R}^2}{2\pi} \int_{-\infty}^{0} \widehat{\eta}_\mathsf{b}\, \mathrm{e}^{\mathrm{i}\,(k_x\, x + k_z\, z)}\, \mathrm{d}k_x \tag{58.72d}$$

$$\varphi'(x,z) = \frac{\mathrm{i}\, U^2}{2\pi} \int_{-\infty}^{0} k_z\, \widehat{\eta}_\mathsf{b}\, \mathrm{e}^{\mathrm{i}\,(k_x\, x + k_z\, z)}\, \mathrm{d}k_x. \tag{58.72e}$$

Again, the vertical wavenumber is given by equation (58.68), in terms of the horizontal wavenumber and the prescribed background stratification and reference flow speed. Evidently, stationary gravity waves with relatively low horizontal wavenumber ($k_x^2 < (N_\mathsf{R}/U)^2$) are vertically propagating ($k_z^2 > 0$), whereas higher horizontal wavenumber waves are exponentially trapped next to the mountains ($k_z^2 < 0$).

58.3.4 Lorentzian topography

Consider the case of topography given by the *Lorentzian* form

$$\eta_{\mathsf{b}}'(x) = \frac{\eta_{\circ}\,\ell^2}{x^2+\ell^2} = \frac{\eta_{\circ}}{1+(x/\ell)^2}, \tag{58.73}$$

where $\ell > 0$ is a length scale and $\eta_{\circ} > 0$ is an amplitude. The Fourier transform of the Lorentzian topography is given by

$$\widehat{\eta}_{\mathsf{b}}(k_x) = \pi\,\eta_{\circ}\,\ell\,\mathrm{e}^{-|k_x|\,\ell}. \tag{58.74}$$

When $\ell \to 0$, the topography sharpens in x-space whereas the k_x-space distribution broadens, with the high $|k_x|$ waves exponentially trapped near the mountain ($k_z^2 < 0$). Conversely, when $\ell \to \infty$, the topography flattens in x-space whereas the k_x-space distribution sharpens around $k_x = 0$, with such long horizontal waves vertically propagating ($k_z^2 > 0$).

Pressure in vertically propagating stationary waves

Getting the signs correct for the inverse Fourier transform can be a bit tricky, so let us work through the case of pressure with some care. First consider the case of vertically propagating stationary waves so that

$$k_z^2 > 0 \quad \text{and} \quad k_z = -\sqrt{(N_{\mathsf{R}}/U)^2 - k_x^2} < 0, \tag{58.75}$$

in which the pressure equation (58.72e) takes the form

$$\varphi'_{\text{prop}}(x,z) = \frac{\mathrm{i}\,U^2}{2\pi}\int_{-\infty}^{0} k_z(k_x)\,\widehat{\eta}_{\mathsf{b}}(k_x)\,\mathrm{e}^{\mathrm{i}\,(k_x\,x + k_z\,z)}\,\mathrm{d}k_x \tag{58.76a}$$

$$= \frac{\mathrm{i}\,U^2}{2\pi}\int_{0}^{\infty} k_z(-k_x)\,\widehat{\eta}_{\mathsf{b}}(-k_x)\,\mathrm{e}^{\mathrm{i}\,(-k_x\,x + k_z\,z)}\,\mathrm{d}k_x \tag{58.76b}$$

$$= \frac{\mathrm{i}\,U^2}{2\pi}\int_{0}^{\infty} k_z(k_x)\,\widehat{\eta}_{\mathsf{b}}(k_x)\,\mathrm{e}^{\mathrm{i}\,(-k_x\,x + k_z\,z)}\,\mathrm{d}k_x, \tag{58.76c}$$

where the final step noted that k_z is an even function of k_x, as is $\widehat{\eta}_{\mathsf{b}}(k_x)$ for the Lorentzian topography according to equation (58.74). Next make use of causality with $k_z = -|k_z| < 0$, so that

$$\varphi'_{\text{prop}}(x,z) = -\frac{\mathrm{i}\,U^2}{2\pi}\int_{0}^{\infty} |k_z|\,\widehat{\eta}_{\mathsf{b}}\,\mathrm{e}^{-\mathrm{i}\,(k_x\,x + |k_z|\,z)}\,\mathrm{d}k_x. \tag{58.77}$$

Assuming the Fourier transform of the topography is real (as for the Lorentzian in equation (58.74)), and taking the real part of the pressure field, renders the vertically propagating pressure

$$\varphi'_{\text{prop}}(x,z) = -\frac{U^2}{2\pi}\int_{0}^{\infty} |k_z|\,\widehat{\eta}_{\mathsf{b}}\sin(|k_x|\,x + |k_z|\,z)\,\mathrm{d}k_x, \tag{58.78}$$

which accords with equation (58.50) found for a monochromatic topography. Finally, we insert the Fourier transform (58.74) to have

$$\varphi'_{\text{prop}}(x,z) = -\frac{U^2\,\eta_{\circ}\,\ell}{2}\int_{0}^{N_{\mathsf{R}}/U} |k_z|\,\mathrm{e}^{-|k_x|\,\ell}\sin(|k_x|\,x + |k_z|\,z)\,\mathrm{d}k_x, \tag{58.79}$$

where we cutoff the upper limit in recognition that $|k_x < N_{\mathsf{R}}/U$ for vertically propagating waves.

Pressure in vertically trapped waves

With an imaginary vertical wavenumber,

$$k_z^2 < 0 \quad \text{and} \quad k_z = \mathrm{i}\sqrt{k_x^2 - (N_\mathsf{R}/U)^2} = \mathrm{i}\,|k_z|, \tag{58.80}$$

the pressure equation (58.72e) takes the form

$$\varphi'_{\text{trap}}(x,z) = -\frac{U^2}{2\pi}\int_{-\infty}^{0} |k_z(k_x)|\,\widehat{\eta}_\mathsf{b}(k_x)\,\mathrm{e}^{\mathrm{i}\,k_x\,x - |k_z|\,z}\,\mathrm{d}k_x \tag{58.81a}$$

$$= -\frac{U^2}{2\pi}\int_{0}^{\infty} |k_z(-k_x)|\,\widehat{\eta}_\mathsf{b}(-k_x)\,\mathrm{e}^{-\mathrm{i}\,k_x\,x - |k_z|\,z}\,\mathrm{d}k_x \tag{58.81b}$$

$$= -\frac{U^2}{2\pi}\int_{0}^{\infty} |k_z(k_x)|\,\widehat{\eta}_\mathsf{b}(k_x)\cos(k_x\,x)\,\mathrm{e}^{-|k_z|\,z}\,\mathrm{d}k_x, \tag{58.81c}$$

where the final step took the real part and made use of $|k_z(-k_x)| = |k_z(k_x)|$, as well as $\widehat{\eta}_\mathsf{b}(-k_x) = \widehat{\eta}_\mathsf{b}(k_x)$ and its reality. This expression for the trapped pressure accords with equation (58.58c) for the case of monochromatic topography. Making use of the Fourier transform (58.74) renders

$$\varphi'_{\text{trap}}(x,z) = -\frac{U^2\,\eta_\circ\,\ell}{2}\int_{N_\mathsf{R}/U}^{\infty} |k_z|\,\cos(k_x\,x)\,\mathrm{e}^{-|k_z|\,z}\,\mathrm{d}k_x, \tag{58.82}$$

where we set the lower limit to N_R/U in recognition that the waves are trapped with $|k_x| > N_\mathsf{R}/U$.

Summary expression for the pressure field

Bringing the two pieces together yields the pressure field

$$\varphi'(x,z) = -\frac{U^2\,\eta_\circ\,\ell}{2}\int_{0}^{N_\mathsf{R}/U} |k_z|\,\mathrm{e}^{-|k_x|\,\ell}\sin(|k_x|\,x + |k_z|\,z)\,\mathrm{d}k_x$$
$$- \frac{U^2\,\eta_\circ\,\ell}{2}\int_{N_\mathsf{R}/U}^{\infty} |k_z|\,\cos(k_x\,x)\,\mathrm{e}^{-|k_z|\,z}\,\mathrm{d}k_x. \tag{58.83}$$

We provide two examples in Figure 58.4, one with a relatively sharp mountain and one that is broader. Note that the sharp mountain exhibits oscillatory features on the lee side of the mountain, which are referred to as *lee waves*.

58.4 Gravity waves in gently varying stratification

In Section 57.5 and 57.6 we assumed a constant background buoyancy frequency, N_R, thus enabling us to study plane internal gravity waves. However, for geophysical fluids it is common for reference state stratification to be a function of the vertical, $N_\mathsf{R}(z)$. Indeed, such vertical dependence was considered in Sections 57.2, 57.3, and 57.4 when studying properties of the linear Boussinesq equations before specializing to plane waves in Sections 57.5 and 57.6. In this section we make use of the WKBJ approximation also used for acoustic waves in Section 51.9 (see Chapter 50 for a more general discussion), here using it to study internal gravity waves in the presence of $N_\mathsf{R}(z)$. Our fundamental assumption is that the background reference density, which is static, displays vertical variations over a vertical scale that is much larger than the vertical wavelength of the gravity waves. This scale separation is essential to use WKBJ methods.

We can anticipate the basic results of this analysis by noting that if a propagating internal gravity wave, with frequency $\omega < N_\mathsf{R}$, moves into a region where $\omega > N_\mathsf{R}$, then it can no longer propagate. Instead, it becomes an exponentially damped or *evanescent* wave. In this case, the

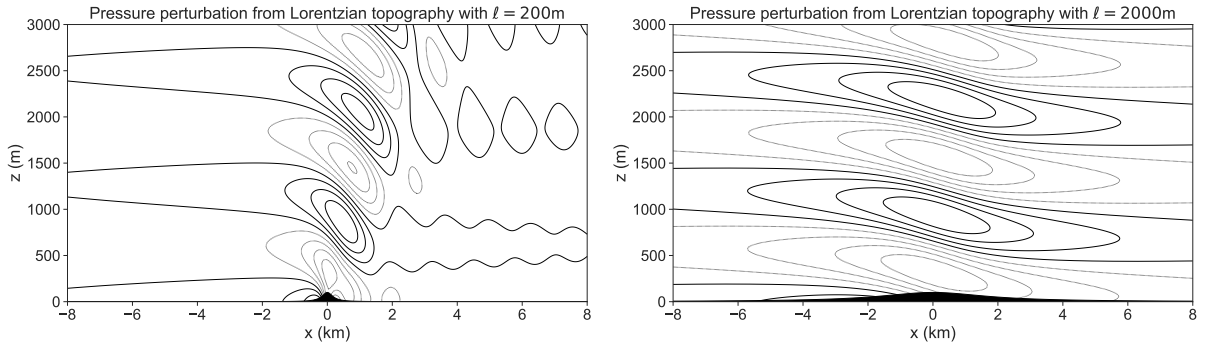

FIGURE 58.4: Stationary gravity waves over a Lorentzian mountain as seen in the pressure field, and as generated with buoyancy frequency, $N = 0.005\,\mathrm{s}^{-1}$, reference flow speed $U = 1\,\mathrm{m\,s}^{-1}$ (flow from left to right), and topographic amplitude, $\eta_\circ = 100$ m. The left panel makes use of the Lorentzian mountain (58.73) with $\ell = U/N = 200$ m, whereas the right panel uses $\ell = 10\,U/N = 2000$ m. Dotted contours depict negative pressure anomalies (such as those adjacent to the mountain) and solid contours are positive anomalies. The pressure field resulting from the relatively sharp mountain (left panel) exhibits oscillatory features on the lee side of the mountain, which are referred to as *lee waves*. These solutions were generated using a trapezoidal numerical integration to compute the integrals in equation (58.83).

propagating wave can reflect back to regions where propagation is available. Alternatively, if the region of evanescence is narrow, then the wave can tunnel through such regions.

58.4.1 The two length scale assumption

We introduced the WKBJ formalism in Section 51.9 for acoustic waves moving in a fluid with a spatially dependent equilibrium density. For internal gravity waves we consider the somewhat simpler case with vertical variations in the background density stratification, rather than the fully three dimensional variations considered for acoustic waves. We thus introduce the length scale for vertical variations in the stably stratified background density field

$$L \equiv |\partial_z \rho_\mathsf{R}/\rho_\mathsf{R}|^{-1} = (\rho_\circ\, N_\mathsf{R}^2/(g\,\rho_\mathsf{R}))^{-1}. \tag{58.84}$$

We assume that the internal gravity waves have a phase that has a vertical wavevector component that is a function of vertical position, $k_z = k_z(z)$, which satisfies the following scaling

$$L \gg |k_z|^{-1} \Longrightarrow |k_z| \gg \rho_\circ\, N_\mathsf{R}^2/(g\,\rho_\mathsf{R}). \tag{58.85}$$

This assumption means that we are concerned with a vertical length scale of the waves, as measured by $|k_z(z)|^{-1}$, that is much smaller than the length scale, L. Furthermore, we assume that the vertical variations of k_z^{-1} occur over the length scale L, so that

$$\left|\mathrm{d}k_z^{-1}/\mathrm{d}z\right| = |k_z\,L|^{-1} \ll 1. \tag{58.86}$$

In addition to having k_z now a function of vertical, we allow the wave amplitude to slowly vary with z. Writing $A(z)$ for that amplitude we assume, as for $k_z(z)$, that

$$|\mathrm{d}A/\mathrm{d}z| = |A/L|, \tag{58.87}$$

which implies that

$$|A^{-1}\,\mathrm{d}^2A/\mathrm{d}z^2| = L^{-2} \ll k_z^2. \tag{58.88}$$

58.4.2 The wave equation with the WKBJ ansatz

The wave equation (57.40) for the vertical velocity holds for $N_{\mathsf{R}}(z)$, so we focus our WKBJ analysis on that equation, rewritten here in the form

$$(\partial_{tt}\,\nabla^2 + N_{\mathsf{R}}^2\,\nabla_{\mathsf{h}}^2)\,w' = \partial_{tt}\partial_{zz}w' + (\partial_{tt} + N_{\mathsf{R}}^2)\,\nabla_{\mathsf{h}}^2 w' = 0. \tag{58.89}$$

Recall the plane wave ansatz (57.54) assumed for constant background density, which for the vertical velocity is given by

$$w'(\boldsymbol{x},t) = \widetilde{w}\,\mathrm{e}^{\mathrm{i}\,(\boldsymbol{k}\cdot\boldsymbol{x}-\omega\,t)} = (\widetilde{w}\,\mathrm{e}^{\mathrm{i}\,k_z\,z})\,\mathrm{e}^{\mathrm{i}\,(k_x\,x+k_y\,y-\omega\,t)} \quad \text{for constant } N_{\mathsf{R}}. \tag{58.90}$$

For the case with $N_{\mathsf{R}}(z)$ we generalize this ansatz to the form

$$w'(\boldsymbol{x},t) = A(z)\,\mathrm{e}^{\mathrm{i}\,(k_x\,x+k_y\,y+\sigma(z)-\omega\,t)} \quad \text{for vertically varying } N_{\mathsf{R}}(z), \tag{58.91}$$

with the real amplitude, $A(z)$, and real phase, $\sigma(z)$, each of which are to be determined. For the ansatz (58.91), we took a horizontal wavevector, $\boldsymbol{k}_{\mathsf{h}} = k_x\,\hat{\boldsymbol{x}} + k_y\,\hat{\boldsymbol{y}}$, and angular frequency, ω, just as for the constant N_{R} waves. This form is motivated by the geometric optics results in Section 50.3. Namely, when following a ray, a wavevector component is constant if the background structure is constant in its corresponding direction, and the angular frequency is constant if the background state is time independent. Given that the only spatial dependence of the background state is in the vertical, it is only the vertical wavenumber that has a vertical dependence.

Making use of the WKBJ wave ansatz (58.91) in the wave equation (58.89) leads to the following expressions

$$\partial_{zz}w'/w' = A^{-1}\,\partial_{zz}A - (\mathrm{d}\sigma/\mathrm{d}z)^2 + \mathrm{i}\,[\mathrm{d}^2\sigma/\mathrm{d}z^2 + 2\,A^{-1}\,(\mathrm{d}\sigma/\mathrm{d}z)\,(\mathrm{d}A/\mathrm{d}z)] \tag{58.92a}$$

$$\nabla_{\mathsf{h}}^2 w'/w' = -|\boldsymbol{k}_{\mathsf{h}}|^2 \tag{58.92b}$$

$$\partial_{tt}w'/w' = -\omega^2, \tag{58.92c}$$

which brings the wave equation (58.89) to the form

$$\left[\partial_{zz} + k_z^2(z)\right] w' = 0, \tag{58.93}$$

where we defined

$$k_z^2(z) = \frac{|\boldsymbol{k}_{\mathsf{h}}|^2\,(N_{\mathsf{R}}^2(z) - \omega^2)}{\omega^2}. \tag{58.94}$$

This expression for $k_z(z)$ is identical to the case with a constant N_{R} (see equation (57.67)), only now it holds with $N_{\mathsf{R}}(z)$ a function of vertical position. Equation (58.93) generalizes equation (57.70) that holds when N_{R} is a spatial constant.

58.4.3 WKBJ solution for the vertical velocity

Making use of equation (58.92a) for $\partial_{zz}w'$ in equation (58.94), and setting the real and imaginary parts to zero, leads to

$$k_z^2 - (\mathrm{d}\sigma/\mathrm{d}z)^2 = A^{-1}\,\mathrm{d}^2A/\mathrm{d}z^2 \tag{58.95a}$$

$$\mathrm{d}^2\sigma/\mathrm{d}z^2 + 2\,A^{-1}\,(\mathrm{d}\sigma/\mathrm{d}z)\,(\mathrm{d}A/\mathrm{d}z) = 0. \tag{58.95b}$$

Recall the amplitude scaling (58.88), which says that $A^{-1}\,\mathrm{d}^2A/\mathrm{d}z^2 \ll k_z^2$. Equation (58.95a) thus leads to the vertical phase function

$$\mathrm{d}\sigma/\mathrm{d}z = k_z \implies \sigma(z) = \int_{z_0}^{z} k_z(z')\,\mathrm{d}z'. \tag{58.96}$$

The vertical position, z_0, is generally ignored since it results only in an overall shift in the phase. Equation (58.95b) can be written in the form of a total derivative

$$\frac{\mathrm{d}}{\mathrm{d}z}\left[A\left(\frac{\mathrm{d}\sigma}{\mathrm{d}z}\right)^{1/2}\right] = 0, \tag{58.97}$$

which means that the wave amplitude is related to the vertical wavenumber via

$$A \propto (\mathrm{d}\sigma/\mathrm{d}z)^{-1/2} = |k_z|^{-1/2}. \tag{58.98}$$

Bringing the pieces together leads to the WKBJ solution for the vertical velocity component

$$w'(\boldsymbol{x},t) = C\,|k_z|^{-1/2}\,\mathrm{e}^{\mathrm{i}\,(k_x\,x + k_y\,y + \sigma(z) - \omega\,t)}. \tag{58.99}$$

Assuming the constant C is real leads to

$$w'(\boldsymbol{x},t) = C\,|k_z|^{-1/2}\,\cos(k_x\,x + k_y\,y + \sigma(z) - \omega\,t) \tag{58.100a}$$

$$k_z(z) = (|\boldsymbol{k}_\mathsf{h}|/\omega)\,\sqrt{N_\mathsf{R}^2(z) - \omega^2} \tag{58.100b}$$

$$\sigma(z) = \int^{z} k_z(z')\,\mathrm{d}z' \tag{58.100c}$$

$$\omega = N_\mathsf{R}(z)\cos\gamma(z) \tag{58.100d}$$

$$C\ [=]\ L^{1/2}/T. \tag{58.100e}$$

In equation (58.100b) for the vertical component to the wavevector, we exposed its z dependence along with that for the buoyancy frequency, $N_\mathsf{R}(z)$. However, recall that the angular frequency, ω, and the horizontal wavevector, $\boldsymbol{k}_\mathsf{h}$, are both spatially independent. Consequently, equation (58.100d) means that the angle, $\gamma(z)$, changes as the buoyancy frequency changes in order to keep $N_\mathsf{R}(z)\cos\gamma(z)$ constant, with this property an essential feature of the wave guides discussed in Section 58.4.5. Furthermore, note that the vertical wavenumber, k_z, becomes imaginary in regions where $\omega^2 > N_\mathsf{R}^2(z)$. So if a propagating wave enters such a region of relatively low vertical stratification, then it becomes *evanescent*, which means that the wave exponentially decays when moving into the region. This behavior is exemplified by the wave guide discussed in Section 58.4.5.

58.4.4 Structure of an internal gravity wave

The WKBJ expressions (58.100a)-(58.100e) are sufficient to construct the full structure of an internal gravity wave moving through a region with non-constant background stratification. To do so requires making use of the linear relations from Section 57.4 in a manner similar to what we did in Section 57.5 for plane waves with N_R constant. We start with equation (57.17c) that relates buoyancy and vertical velocity via

$$\partial_t b' = -w'\,N_\mathsf{R}^2. \tag{58.101}$$

Time integrating the vertical velocity in equation (58.100a) leads to the buoyancy field

$$b' = \mathrm{i}\, C\, N_{\mathsf{R}}^2/(\omega\,|k_z|^{1/2})\, \mathrm{e}^{\mathrm{i}\,(\boldsymbol{k}_{\mathsf{h}}\cdot\boldsymbol{x}+\sigma(z)-\omega\,t)}, \tag{58.102}$$

where

$$\boldsymbol{k}_{\mathsf{h}}\cdot\boldsymbol{x} = k_x\,x + k_y\,y. \tag{58.103}$$

For the horizontal velocity we use the non-divergence condition, $\nabla\cdot\boldsymbol{v}' = 0$ (Section 57.5.2), as well as the vanishing vertical component to the relative vorticity, $\partial_x v' = \partial_y u'$ (Section 57.5.3), to find

$$\boldsymbol{u}' = -\frac{C\,\boldsymbol{k}_{\mathsf{h}}}{|2\,k_z|^{1/2}\,|\boldsymbol{k}_{\mathsf{h}}|^2}\big[(k_z^{-1}\,\partial_z k_z)\sin(\boldsymbol{k}_{\mathsf{h}}\cdot\boldsymbol{x}+\sigma(z)-\omega\,t) + 2\,k_z\cos(\boldsymbol{k}_{\mathsf{h}}\cdot\boldsymbol{x}+\sigma(z)-\omega\,t)\big]. \tag{58.104}$$

58.4.5 Wave packets within a wave guide

We here highlight a particularly special property of internal gravity waves moving in a region with vertically varying stratification. This property results from having the angular frequency remain constant within the dispersion relation (58.100d). Again, the constancy of the angular frequency follows from our discussion of geometric optics in Section 50.3, with the angular frequency of a wave a space-time constant if the base state is static. For the angular frequency to remain constant within a varying $N_{\mathsf{R}}(z)$ requires the phase angle, $\gamma(z)$, to compensate. For example, if a wave packet moves from a region of large vertical stratification to a region with small stratification, then $\gamma(z)$ must get smaller in magnitude so to keep ω constant. At some point if $N_{\mathsf{R}}(z)$ continues to get smaller then $\gamma(z)$ will vanish, $\gamma = 0$, which means that the waves only have a vertical wavenumber. So what happens beyond that point?

To answer this question recall equation (57.71) for the group velocity, which can be written in the form

$$\boldsymbol{c}_{\mathsf{g}} = \frac{N_{\mathsf{R}}\,k_z}{|\boldsymbol{k}|^3\,|\boldsymbol{k}_{\mathsf{h}}|}\,(k_z\,\boldsymbol{k}_{\mathsf{h}} - |\boldsymbol{k}_{\mathsf{h}}|^2\,\hat{\boldsymbol{z}}) = \frac{N_{\mathsf{R}}\,k_z}{|\boldsymbol{k}|^2}\,(\widehat{\boldsymbol{k}_{\mathsf{h}}}\sin\gamma - \hat{\boldsymbol{z}}\cos\gamma), \tag{58.105}$$

where $\widehat{\boldsymbol{k}_{\mathsf{h}}} = \boldsymbol{k}_{\mathsf{h}}/|\boldsymbol{k}_{\mathsf{h}}|$ is the unit vector pointing in the direction of the horizontal wavector. As the wave becomes horizontal to compensate for the reduced $N_{\mathsf{R}}(z)$, the group velocity vanishes, which we already noted by equation (57.75) for the group velocity magnitude. Yet the second form of equation (58.105) reveals that the horizontal component to the group velocity vanishes before the vertical component. Hence, as the wave packet approaches the region of weak stratification its ray forms a vertical cusp as the packet stalls. Since the packet cannot propagate into a region with $\omega^2 > N_{\mathsf{R}}^2$, which is a region of evanescence, then the wave reflects back into the region where $\omega^2 < N_{\mathsf{R}}^2$. If the propagation region with $\omega^2 < N_{\mathsf{R}}^2$ sits between two regions with weak stratification with $\omega^2 > N_{\mathsf{R}}^2$, then the bounded relatively high stratification region forms a *wave guide* for the internal gravity waves. We depict an idealized example of a wave guide in Figure 58.5.

We can compute an analytic expression for the wave packet ray (i.e., its trajectory) as it rises to a *turning level*, at $z = z_{\mathsf{t}}$, defined as the level where $N_{\mathsf{R}}(z = z_{\mathsf{t}}) = \omega$. We do so by taking a Taylor series for the squared buoyancy frequency for points close to the turning level

$$N_{\mathsf{R}}^2(z) \approx N_{\mathsf{R}}^2(z_{\mathsf{t}}) + (\mathrm{d}N_{\mathsf{R}}/\mathrm{d}z)\,(z - z_{\mathsf{t}}) = \omega^2 - |\mathrm{d}N_{\mathsf{R}}/\mathrm{d}z|\,(z - z_{\mathsf{t}}) = \omega^2 + |\mathrm{d}N_{\mathsf{R}}/\mathrm{d}z|\,(z_{\mathsf{t}} - z), \tag{58.106}$$

where we note that N_{R}^2 is a decreasing function as z increases towards z_{t}, which means that $\mathrm{d}N_{\mathsf{R}}^2/\mathrm{d}z = -|\mathrm{d}N_{\mathsf{R}}^2/\mathrm{d}z|$. Assuming the packet is moving in the x-z plane, we obtain the ray equation from the group velocity (58.105) and the dispersion relation (58.100b)

$$\frac{\mathrm{d}z}{\mathrm{d}x} = -\frac{|\boldsymbol{k}_{\mathsf{h}}|}{k_z} = -\frac{\omega}{\sqrt{N_{\mathsf{R}}^2 - \omega^2}} = -\frac{\omega}{\sqrt{|\mathrm{d}N_{\mathsf{R}}^2/\mathrm{d}z|\,(z_{\mathsf{t}} - z)}}. \tag{58.107}$$

We integrate along the ray as the packet moves from a point (x, z) to the turning level at (x_t, z_t) (see Figure 58.5), which yields the expression for the ray trajectory

$$(z_t - z)^{3/2} = \frac{(3\,\omega/2)\,(x_t - x)}{\sqrt{|\mathrm{d}N_R^2/\mathrm{d}z|}} \Longrightarrow z_t - z = \left[\frac{(3\,\omega/2)\,(x_t - x)}{\sqrt{|\mathrm{d}N_R^2/\mathrm{d}z|}}\right]^{2/3}. \tag{58.108}$$

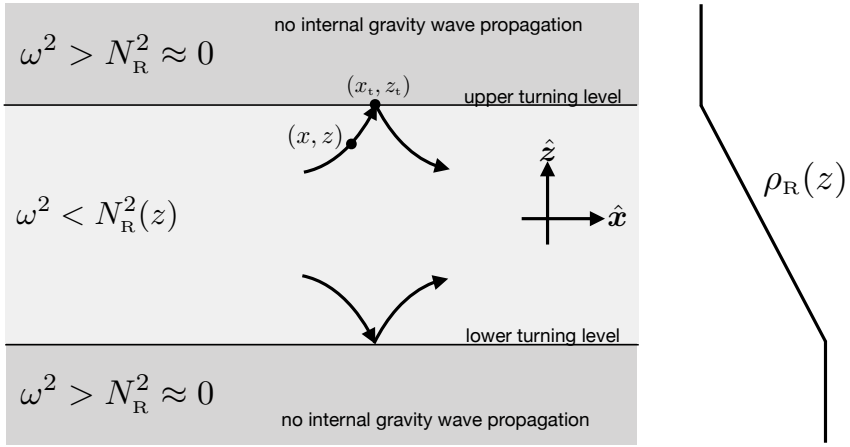

FIGURE 58.5: A waveguide for internal gravity waves, here depicted by two low stratification regions ($N_R^2 \approx 0$) bounding a higher stratification region ($N_R^2 > 0$). The density profile on the right provides an idealized realization of such a guide. The levels where $N_R = \omega$ are referred to as *turning levels*. We depict sample rays approaching and leaving the turning levels, with the rays computed from the group velocity and dispersion relation. For example, a ray approaching the upper turning is computed from (x, t) to (x_t, zt), with the cusp-like trajectory given by equation (58.108).

58.4.6 Comments and further study

See Lecture 9 of *Pedlosky* (2003) or Section 7.5 of *Vallis* (2017) for similar presentations. Note that there remains ongoing research to understand details of what happens to internal gravity waves when they reach a turning level. For an ocean application, concerning how gravity waves interact with the upper ocean boundary layer, see *Shakespeare et al.* (2021).

58.5 Exercises

EXERCISE 58.1: POLARIZATION RELATIONS FOR STATIONARY INERTIA-GRAVITY WAVES ON A MEAN FLOW

Following the discussion in Section 58.2.6, determine the polarization relations for stationary inertia-gravity waves in the presence of a constant reference flow, $\boldsymbol{u}_R = U\,\hat{\boldsymbol{x}}$ and with $\omega_R = -\boldsymbol{u}_R \cdot \boldsymbol{k}_b > 0$. Assume $f_o^2 < \omega_R^2 < N_R^2$ so that the waves extend throughout the vertical. Write expressions for u', v', w', b', and φ' in terms of the vertical velocity amplitude, $\widetilde{w}$, as given by equation (58.39). Confirm that setting $f_o = 0$ reduces the intertia-gravity results to the gravity wave case derived in Section 58.2.7.

EXERCISE 58.2: MOUNTAIN GRAVITY WAVE FROUDE NUMBER BASED ON FREQUENCIES

Consider the non-dimensional *Froude number* for forced mountain gravity waves ($f_o = 0$)

$$\mathrm{Fr} = \frac{|\boldsymbol{u}_R \cdot \boldsymbol{k}_b|}{N_R} = \frac{\omega_R}{N_R}, \tag{58.109}$$

which is the ratio of the forcing frequency (from flow over the monochromatic mountains) to the buoyancy frequency.

(a) Write the squared vertical wavenumber (58.42) for mountain gravity waves in terms of Fr.

(b) Write Fr as the ratio of two time scales. Provide an interpretation for why mountain waves are vertically trapped when one of those time scales is greater than the other, and vertically propagating for the alternative.

Hint: see Section 5.4.2 of *Sutherland* (2010) for a discussion of this non-dimensional number. The second part of this exercise is mostly meant to be answered in words.

EXERCISE 58.3: MECHANICAL ENERGY OF A TRAPPED MOUNTAIN GRAVITY WAVE

We studied the energetics of propagating mountain gravity waves in Section 58.2.7. Here we consider the energetics of trapped mountain waves.

(a) Compute the mechanical energy for the trapped mountain gravity waves from Section 58.2.8.

(b) Compute the phase averaged mechanical energy.

(c) Evaluate the phase averaged mechanical energy at the ground (approximated by $z = 0$ in the linear theory), and compare this energy to the phase averaged mechanical energy in a propagating mountain wave.

Part XI

Flow instabilities

Part X of this book is concerned with small amplitude wave fluctuations that move on the background of a prescribed exact solution to the fluid equations. For example, in studying acoustic waves in Chapter 51, the background state is static and uniform, whereas when studying internal gravity waves in Chapter 57, the background is static yet stably stratified according to gravity. In each of these cases, the background state is stable to small perturbations so that the wave fluctuations do not lead to waves of growing amplitude. In Part XI of the book we examine conditions required to ensure stability of background flow states, or conversely, what properties of the background state are necessary (and sometimes sufficient) to support instabilities.

What enables an instability?

As noted in Section 2 of the authoritative book by *Drazin and Reid* (2004), flow instabilities occur when a disturbance leads to the disequilibrium of forces within the fluid, and with this disequilibrium enabling the disturbance to grow. We explore numerous mechanisms for the growth of disturbances that manifest positive feedbacks energized by the background state. Examples include the kinetic energy that supports shear instability, the potential energy that supports baroclinic instability, and the angular momentum that supports centrifugal instability. A central goal of instability theory is to develop a physical understanding and mathematical recipe to determine what constitutes an unstable flow state. Furthermore, a flow state might be unstable, but not all disturbances "tickle" the instability. This situation motivates the study of conditions required of the disturbance for it to manifest the instability.

We focus on mechanisms that lead to a variety of geophysical flow instabilities, and in so doing develop associated mathematical analysis methods. Instabilities are the norm for geophysical flows rather than the exception, and they play a fundamental role in establishing properties of planetary circulations in both the atmosphere and ocean. Furthermore, most of the instabilities occuring in geophysical fluids are primarily understood in the absence of viscous dissipation, thus prompting us to focus exclusively on the inviscid equations.

Distinguishing two classes of flow instabilities

We distinguish two general classes of fluid flow instabilities: *local* (or *parcel*) instabilities and *global* (or *wave*) instabilities. Local/parcel instabilities afford a local necessary and sufficient condition to determine whether the background flow state is unstable. For example, in the study of gravitational instability (in the absence of surface tension), we can measure the local squared buoyancy frequency: if $N^2 < 0$ then the fluid is gravitationally unstable at the location where $N^2 < 0$. The study of symmetric instabilities in Chapter 59 explores a broader class of local instabilities, in which angular momentum and potential vorticity are central to determining stability conditions. Stability conditions are generally derived by considering an imagined displacement of a fluid parcel within the environment of the prescribed background state. If the forces acting on the parcel lead to furthering the displacement, then that signals a positive feedback indicating that the background state is unstable. The result of such local instabilities is a catastrophic breakdown of the background state without concern for any special space and/or time scale for the breakdown.

Global/wave instabilities arise from the interference of waves that lead to mutually constructive positive feedbacks, thus constituting the *wave resonance* interpretation of such instabilities. The stability analysis is generally referred to as the *method of normal modes*. We do not seek the most general solution to the linearized equations. Instead we ask if a single wave can go unstable, and if so then what properties of such waves enable the instability to manifest? Determining properties of the unstable waves (e.g., the most unstable wavelength, wave velocity, and the growth rate) requires solving an eigenvalue problem where boundary conditions often play a fundamental role. Shear instabilities of Chapter 61 and baroclinic instabilities of Chapter 62

are canonical examples of this sort of instability. Operationally, the means to reveal a global instability is similar to that used to study linear waves in Part X of this book. Namely, we determine a dispersion relation for small amplitude fluctuations, only now allowing the possibility of the wave frequency or wavevector to be complex. Temporally unstable waves occur with a complex wave frequency and real wavevector, whereas spatial instabilities arise with real wave frequency and complex wavevector. Finally, observe that local instabilities can be considered wave instabilities in which all waves are unstable.

Flow instabilities lead to a stable end state

Flow instabilities are energized by the background state and, through the process of creating the instability and allowing it to grow to a nonlinear stage, act to eliminate the source for the instability. For example, the catastrophic vertical motion of a gravitationally unstable fluid column serves to remove the potential energy source of the instability, with the resulting equilibrium state gravitationally stable. In geophysical fluids, there are external forces (ultimately arising from solar heating, geothermal heating, or astronomical tides) that return the background state to an unstable condition, thus allowing for the fluid to undergo a multitude of successive instabilities. Through such successive instabilities, or further secondary instabilities that feed off the primary instability, the fluid generally evolves into an extremely complex state of linear and nonlinear waves, instabilities, and turbulence. The resulting fluid flow is comprised of a wide suite of space and time scales whose mathematical description requires methods from statistics and stochastics. We do not pursue the study of wave turbulence or fully developed turbulence in this book, but do appreciate that instabilities are the central means for geophysical fluids to transition into a turbulent state. Hence, understanding the mechanisms for flow instabilities offers insights into the nature of the associated turbulence.

We do not examine the effects of instabilities on the background state

Throughout this study, we do not examine evolution of the prescribed background state. Ignoring changes to the background state is a sensible assumption when studying the motion of stable linear waves, whose amplitudes remain bounded and so offer only a tiny perturbation to the background state. However, for unstable flows, the assumption of a fixed background proves untenable when fluctuations become large enough to engage flow nonlinearities and thus to nontrivially impact the background state. It is for this reason that our analysis focuses exclusively on the early stages of an instability, whereby small amplitude assumptions allow for a focus on linear mechanisms leading to growth of a disturbance, rather than enable the rich complexities of interactions (some stable and some unstable) between the disturbance and an evolving background state.

Seek out visualizations of flow instabilities to help develop understanding

This video from Prof. Mollo-Christensen provides an insightful introduction to the topic of fluid mechanical instabilities. This and many other videos from laboratory studies and numerical simulations offer useful, if not essential, visual impressions to complement the somewhat intricate mathematical analysis in this part of the book.

Chapter 59

SYMMETRIC FLOWS

In this chapter we study the stability of fluid flows exhibiting either axial symmetry (e.g., rotating fluid column) or spatial symmetry in one horizontal direction (e.g., f-plane geostrophic fronts). This analysis supports the study of frontal features in geophysical fluids, where a front is a region of strong buoyancy gradients that leads to a jet-like geostrophic flow. Because of the assumed symmetry in the base flow state and the perturbation, the instabilities in this chapter are generically referred to as *symmetric instabilities*. However, the terminology is not universal, with flavors of symmetric instability often referred to as *centrifugal*, *inertial*, and *symmetric*.

We make use of three methods for stability analysis in this chapter. One consists of an energetic approach due to Rayleigh (*energetic stability analysis*); one is Lagrangian and considers force balances acting on a test fluid parcel (*parcel stability analysis*); and one is Eulerian and considers wave perturbations (*modal stability analysis*). For the instabilities considered in this chapter, each method leads to the same stability condition, which is here measured by local properties of the flow so that we refer to the method as *local stability* analysis. As part of the analysis we make use of material invariants, such as angular momentum, potential momentum, buoyancy, and potential vorticity. We restrict attention to the f-plane since that allows us to make use of potential momentum as a material invariant. It is notable that the flows considered in this chapter generally exhibit secondary overturning circulations, with such circulations studied here using the rudiments of *semi-geostrophy*.

Energetic and parcel methods probe the base state flow by perturbing test fluid parcels. A test parcel is assumed to have no impact on the flow state itself, meaning that the pressure field remains unchanged even as the parcel is moved. In effect, the test fluid parcel stability analysis makes the tacit assumption that pressure responses to a perturbation can be neglected for the purpose of detecting an unstable flow state. Ignoring the impacts on pressure is consistent with the notion of a test fluid element introduced in Section 17.2.5.[1] However, we questioned that approach when studying buoyancy in Section 30.11, where we computed the pressure response to the perturbation and found that the response has an important impact on the effective buoyancy felt by a finite fluid region. Acknowledging this limitation motivates us to complement the parcel approach with an Eulerian linear stability analysis using plane waves. This approach is dynamically consistent, and yet it works within the limitations of the linearized equations.

READER'S GUIDE FOR THIS CHAPTER

We make use of the shallow water system from Chapters 35 and 36, in particular the study of angular momentum in Section 36.8 (see also Section 27.5). We also assume an understanding of geostrophic flow as studied in Chapter 31, as well as the continuously stratified Boussinesq ocean from Chapter 29.

Gravitational instability is the canonical local instability and it is signaled by $N^2 < 0$.

[1] Since the concern here is with perfect fluids, the test fluid element from Section 17.2.5 is the same as a test fluid parcel.

However, we do not consider gravitational instability in this chapter, with this instability introduced in Chapter 30 when studying buoyancy, and Chapter 60 when studying the Rayleigh-Taylor instability.

59.1 Loose threads

- Work through symmetric instability in two shallow water layers. Does it work? Do we need to have mixing of the layers?
- Write the full oscillator equation for (59.75), including Δx and Δz motion.
- Energy analysis for each instability as per Chapter 8 of *Smyth and Carpenter* (2019), who use a modal approach and linearize the equations. Include energetics of gravitational instability.
- Maximum growth rate for symmetric instability in chapter 8 of *Smyth and Carpenter* (2019).
- Include more in Section 59.9.7 concerning stable and unstable symmetric fronts.
- More closely connect the ageostrophic overturning from Section 59.9 to symmetric instability. Make the case that the overturning is either stable or unstable, with the unstable form leading to symmetric instability.
- More about the growth of the squared buoyancy gradient in equation (59.170). Can that equation be written in a more revealing manner?
- Pursue the coordinate transformation from *Hoskins* (1975), in which case the discussion of semi-geostrophy could form a separate chapter.
- What is the potential vorticity for the linearized perturbations in Section 59.8?

59.2 Instabilities in this chapter

The instabilities studied in this chapter are termed *local* since they are detected through a local condition that yields a necessary and sufficient condition for instability. The physical features of the flow instabilities considered here are quite similar, thus making it convenient to study them together. For centrifugal and horizontal inertial instabilities, we develop the stability conditions using both energetic and parcel analysis methods. For symmetric instability we use the parcel and modal methods.

59.2.1 Summary of the instabilities studied in this chapter

Before diving into the details, we here offer a summary of the instabilities studied in this chapter.

Centrifugal instability of cyclostrophic balanced flow

Consider an equilibrium flow state under inviscid cyclostrophic balance. As studied in Section 32.5, cyclostrophic balance arises when pressure and centrifugal accelerations are balanced, with centrifugal accelerations arising from curvature in the fluid particle trajectory. The angular momentum is materially invariant when the equilibrium state is rotationally symmetric, as in an ideal circular vortex or a rotating circular tank (Section 36.8). Flow stability can be probed by horizontally displacing a rotationally symmetric circular ring of fluid parcels, with each parcel retaining its original angular momentum. If the parcels are displaced to a position where pressure and centrifugal accelerations further support the displacement, then the base state is unstable to centrifugal instability.

Horizontal inertial instability of f-plane geostrophic flow

Consider an equilibrium flow state in a barotropic fluid under inviscid geostrophic balance on an f-plane, whereby pressure and Coriolis accelerations are balanced (Chapter 31). The potential momentum is materially invariant when the equilibrium state is symmetric in a horizontal direction, as in a zonally or meridionally symmetric f-plane front. Flow stability is probed by horizontally displacing a symmetric line of fluid parcels, with each parcel retaining its original potential momentum. If the parcels are displaced to a position where pressure and Coriolis accelerations further support the displacement, then the base state is unstable to horizontal inertial instability.

Isentropic inertial instability (symmetric instability) for f-plane flow

Consider an equilibrium flow state under inviscid f-plane geostrophic balance in a baroclinic fluid. Potential momentum in the direction of the front as well as buoyancy are materially invariant when the base state is symmetric in a horizontal direction. Flow stability of the base flow is probed by isentropically displacing a symmetric line of fluid parcels, with each parcel retaining its original potential momentum and buoyancy. If the parcels are displaced to a position where pressure and Coriolis accelerations further support the displacement, then the base state is unstable to isentropic inertial instability, which we call *symmetric* instability.

59.2.2 Nature of the base state and the perturbations

For the study of centrifugal instability, we make use of the shallow water model from Chapters 35 and 36, whereas we consider the continuously stratified Boussinesq ocean (Chapter 29) for the horizontal and isentropic inertial instabilities. When the fluid is continuosly stratified and inviscid, all motion occurs along isentropes. However, when probing for centrifugal or horizontal inertial instabilities using parcel arguments, we examine stability to perturbations along geopotential surfaces. Such horizontal displacements generally cross isentropic surfaces in a baroclinic fluid. The isentropic inertial instability analysis in Section 59.6 maintains the adiabatic nature of displacements when probing for instabilities. Even so, these perturbations do not maintain a materially invariant potential vorticity. So what is it about these perturbations that makes them relevant to stability analysis?

The stability thought experiment using test fluid parcels assumes the parcels maintain their materially invariant property (e.g., buoyancy, angular momentum, potential momentum) as they probe stability of the surrounding fluid flow. That is the nature of the test parcels, as they do not directly interact with nor alter the surrounding fluid environment. Local flow stability is examined by having test parcels cross surfaces of constant materially invariant properties. For example, gravitational stability is probed by test parcels moving across buoyancy surfaces (Section 30.6). Likewise, entering the *wedge of instability* for symmetrically unstable flow requires a test parcel to leave its constant buoyancy and constant potential momentum surfaces (Section 59.6).

59.2.3 Comments

Section 7.1 of *Holton and Hakim* (2013) distinguishes between *parcel* and *wave* instabilities. Analogously, *Cushman-Roisin and Beckers* (2011) use the terms *local* and *global*. Canonical examples of global instabilities are Kelvin-Helmholtz and baroclinic. We are not concerned with those instabilities in this chapter. Rather, the three instabilities considered here are examples of parcel or local instabilities.

Because of the rather close similarities between centrifugal and inertial instability, the oceanographic literature often uses the term centrifugal instability when referring to the inertial

instability considered here (e.g., see *Thomas et al.* (2013) and *McWilliams* (2016)). However, we do not follow that usage since the inertial instability in this chapter is *not* associated with centrifugal accelerations. Rather, inertial instability is associated with Coriolis accelerations. We choose to follow the terminology of the atmospheric literature as detailed in the texts by *Holton and Hakim* (2013) and *Markowski and Richardson* (2010), which also follows the fluid mechanics terminology used by *Drazin and Reid* (1981). So in brief, we use the term *centrifugal instability* for an axisymmetric base state in cyclostrophic balance, and *inertial instability* for a two-dimensional base state in geostrophic balance.

59.3 Centrifugal instability of cyclostrophic flow

Consider flow of a single shallow water fluid layer in a rotating cylindrical tank with rotation about its vertical axis.[2] Throughout this analysis we assume all flow features maintain rotational symmetry (Figure 59.1). Hence, all dynamical fields are a spatial function only of the radial distance from the rotational axis (*axisymmetric*). We are interested in questions concerning flow stability as a function of the radial distribution of the angular momentum per mass, $l^z(r)$. In particular, we examine stability of *cyclostrophically balanced* flow, defined by flow whose radial acceleration vanishes so that the radial pressure gradient balances the centrifugal acceleration (Section 32.5). Furthermore, we examine stability under perturbations that also maintain axial symmetry. We find that such cyclostrophic flow is stable to rotationally symmetric perturbations so long as the squared angular momentum increases radially outward. This system provides a pedagogical introduction to the stability of rotating vortices in the ocean and atmosphere, and it establishes analysis methods we later use for inertial and symmetric instabilities arising in two-dimensional frontal regions. The stability condition for angular momentum is reflected in observed stable vortices in both the atmosphere and ocean.

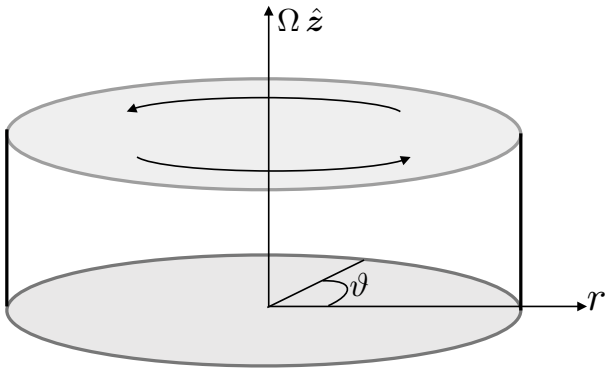

FIGURE 59.1: Rotating tank of shallow water fluid used to discuss centrifugal instability. We make use of cylindrical-polar coordinates from Section 4.22 to describe the flow. All flow features are assumed to be rotationally symmetric, including both the cyclostrophic balanced state and perturbations relative to the balanced state.

The centrifugal instability described here does *not* rely on baroclinic structure. Rather, it arises from the imbalances between centrifugal and pressure forces along a geopotential surface.[3] By using the shallow water fluid to study this instability, we directly connect to Section 36.8,

[2] The same ideas can be formulated for rotating Couette flow, in which fluid is placed between two rotating cylinders. We prefer the shallow water tank since it is a system considered elsewhere in this book as a laboratory model for rotating fluid mechanics.

[3] One may conceive of centrifugal instability in a baroclinic flow where parcel displacements maintain their angular momentum and buoyancy. That analysis would lead to isentropic centrifugal instability, which is directly analogous to the isentropic inertial instability discussed in Section 59.6. See *Buckingham et al.* (2021) for a discussion of this system.

where we studied angular momentum in a rotating tank of shallow water fluid.

59.3.1 Equations of motion

We studied the angular momentum of this rotating shallow water system in Section 36.8, where we made use of a rotating reference frame and polar coordinates (r, ϑ) (Section 4.22) measured in the rotating frame. Here, r is the radial position from the rotational axis and ϑ is the azimuthal angle measured counter-clockwise from the rotating x-axis. We furthermore derived the acceleration in cylindrical-polar coordinates in Exercise 13.3. Making use of those results allows us to write down the horizontal components to the inviscid velocity equation as well as the thickness equation

$$\mathrm{D}v^r/\mathrm{D}t = -g\,\partial_r\eta + r^{-3}\,(l^z)^2 \tag{59.1a}$$

$$\mathrm{D}l^z/\mathrm{D}t = -g\,\partial_\vartheta\eta \tag{59.1b}$$

$$r\,\partial_t\eta = -\partial_r(h\,r\,v^r) - \partial_\vartheta(h\,v^\vartheta). \tag{59.1c}$$

In these equations, h is the layer thickness and η is the free surface height for the shallow water layer (see Figure 35.1). The radial and azimuthal velocity components are given by

$$v^r = \mathrm{D}r/\mathrm{D}t \quad \text{and} \quad v^\vartheta = r\,\mathrm{D}\vartheta/\mathrm{D}t, \tag{59.2}$$

and the angular momentum per mass computed about the rotation axis (the z-axis) is

$$l^z = \hat{\boldsymbol{z}}\cdot[\boldsymbol{r}\times(\boldsymbol{u}+\boldsymbol{U}_{\text{rigid}})] = r\,(v^\vartheta + r\,\Omega). \tag{59.3}$$

Material evolution of the radial velocity (equation (59.1a)) is affected by the radial pressure gradient plus centrifugal acceleration, whereas the material evolution of angular momentum (equation (59.1b)) is affected by angular gradients in the pressure field as realized by angular gradients in the free surface.

We consider equilibrium states where the radial acceleration vanishes. Such states are said to be in *cyclostrophic balance*, whereby the radial pressure gradient balances the centrifugal acceleration

$$\mathrm{D}v^r/\mathrm{D}t = 0 \Longrightarrow g\,\partial_r\eta = (v^\vartheta + r\,\Omega)^2/r = r^{-3}\,(l^z)^2 \qquad \text{cyclostrophic balance.} \tag{59.4}$$

Is cyclostrophically balanced flow stable? To answer this question we examine the more restricted problem of stability of rotational symmetric flow, and with perturbations also assumed to be rotationally symmetric. Rotational symmetry also means that all flow fields are a function only of the radial direction. As such, angular momentum is materially constant

$$\partial_\vartheta\eta = 0 \Longrightarrow \mathrm{D}l^z/\mathrm{D}t = 0. \tag{59.5}$$

This constraint on the flow plays a fundamental role in the stability analysis.

59.3.2 Elements of angular momentum

Consider a spinning top in a gravitational field, in which conservation of angular momentum (holding in the absence of friction) keeps the top upright. Yet in the presence of friction, the angular momentum is dissipated so that the top eventually falls. There is an analog with a rotating fluid. Namely, we find that a state of zero angular momentum leads to centrifugal instability. To develop this result we study basic properties for angular momentum in the rotating tank.

Rigid-body motion

A fluid in rigid-body motion has $v^\vartheta = 0$ and angular momentum per mass

$$l^z_{\text{rigid-body}} = r^2\,\Omega. \tag{59.6}$$

Evidently, the magnitude of the angular momentum increases as the square of the radial distance. In the following we find it more convenient to use the square of the angular momentum (as it appears in the radial velocity equation (59.1a)), which also increases radially for the rigid-body motion

$$\frac{\mathrm{d}[l^z(r)]^2}{\mathrm{d}r} = 4\,r^3\,\Omega^2 > 0. \tag{59.7}$$

We will find that flow is centrifugally unstable if the square of its angular momentum is a decreasing function of its radial distance. Such unstable configurations adjust through *centrifugal instability* towards a configuration with squared angular momentum that increases radially. The instability is termed "centrifugal" since it is the centrifugal acceleration that "throws outward" the fluid if its squared angular momentum decreases radially, thus bringing the fluid back into a stable state. More precisely, a flow where the angular momentum decreases outward has pressure gradients that cannot balance the centrifugal acceleration from the outward movement of angular momentum conserving fluid parcels.

Zero angular momentum flow

Consider a non-rotating tank with zero flow, so that the angular momentum is zero. In a perfect fluid the angular momentum of each fluid parcel remains zero, even if we start the tank rotating. That is, for a perfect fluid with zero angular momentum, the tank simply rotates but the fluid remains at rest in the inertial reference frame. To generate non-zero angular momentum for the fluid requires friction between the rotating tank and fluid. After sufficient time, friction transfers angular momentum from the tank walls throughout the fluid, thus leading to a steady state flow in rigid-body motion. Upon reaching the steady rigid-body flow, there are no strains in the fluid and thus no viscous stresses to impart friction (Section 25.8).

In a flow with zero angular momentum, the relative angular velocity is given by

$$l^z = 0 \implies v^\vartheta = -r\,\Omega, \tag{59.8}$$

so that the flow is anti-cyclonic (i.e., directed counter to the tank's rotation). Furthermore, the zero angular momentum flow has the relative vorticity

$$l^z = 0 \implies \zeta = \frac{1}{r}\frac{\mathrm{d}(r\,v^\vartheta)}{\mathrm{d}r} = -2\,\Omega. \tag{59.9}$$

That is, the relative vorticity is anti-cyclonic with a Rossby number

$$l^z = 0 \implies \mathrm{Ro} = \zeta/(2\,\Omega) = -1. \tag{59.10}$$

As we show in the following, the $l^z = 0$ flow is the onset point for centrifugal instability. Again, we conceive of this flow as analogous to a rotating top that falls over (goes unstable) when its angular momentum vanishes.

Establishing zero angular momentum flow

It is relatively simple to establish rigid-body motion of a fluid in a tank; all it takes is sufficient time for transients to relax and friction to fully transfer momentum from the tank walls throughout the fluid. For the complement task, consider a rigid-body flow that is subjected to

an irreversible force that brings the fluid to zero angular momentum. The question we ask in our stability analysis is not concerned with details of how such forces arise. Instead, we are interested in what happens to the flow when it reaches zero angular momentum.

59.3.3 Energetic stability analysis

As first introduced by Rayleigh, we consider a thought experiment in which two adjacent equal mass circular fluid rings are swapped, one originating from radial position $r = r_1$ and the other at $r = r_2 = r_1 + \Delta r$ (see Figure 59.2). Furthermore, assume that the radial velocity vanishes so that the kinetic energy of the rings is due only to their rotational motion. If swapping the rings decreases the kinetic energy in the base state, then the released kinetic energy can be used to fuel an instability.[4] In this case we say that the flow is *centrifugally unstable*, with this name used since it is the centrifugal acceleration from the circular parcel trajectory that promotes the instability. In general, any curved flow will be exposed to centrifugal instability if swapping parcels reduces the kinetic energy of the base state while maintaining constant angular momentum.

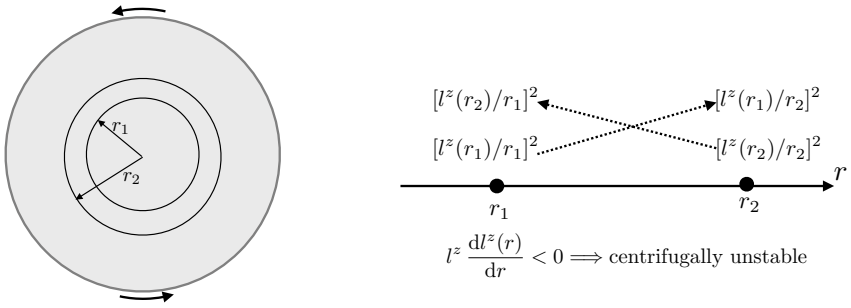

FIGURE 59.2: Illustrating Rayleigh's energetic method for centrifugal instability. The initial configuration defines two rings of fluid at radii r_1 and $r_2 = r_1 + \Delta r$, as shown in the left panel, with the two rings having a combined kinetic energy per mass $2\,E_{\text{init}} = [l^z(r_1)/r_1]^2 + [l^z(r_2)/r_2]^2$. Swapping the two rings while maintaining a constant angular momentum (and assuming nothing else changes) leads to the swapped kinetic energy per mass, $2\,E_{\text{swap}} = [l^z(r_1)/r_2]^2 + [l^z(r_2)/r_1]^2$. If $E_{\text{swap}} - E_{\text{init}} < 0$ then energy is released upon the swap and the rotationally symmetric flow is centrifugally unstable. Energy is released upon swapping fluid rings if the angular momentum condition (59.15) is satisfied: $\mathrm{d}[l^z(r)]^2/\mathrm{d}r < 0$.

With no radial flow, kinetic energy only arises from angular motion so that a ring of mass $\delta m = \rho\,\delta V$ and radius r_1 has kinetic energy

$$E(r_1) = (\delta m/2)\,[v^\vartheta(r_1) + r_1\,\Omega]^2 = (\delta m/2)\,[l^z(r_1)/r_1]^2. \tag{59.11}$$

The initial kinetic energy for the two rings is thus given by the sum

$$E_{\text{init}} = (\delta m/2)\,\big([l^z(r_1)/r_1]^2 + [l^z(r_2)/r_2]^2\big). \tag{59.12}$$

The equilibrium state and the perturbation each maintain rotational symmetry. Hence, when swapping their radial positions, the rings each maintain their respective angular momentum. But by changing radial positions their kinetic energy changes, thus leading to the kinetic energy of the swapped state

$$E_{\text{swap}} = (\delta m/2)\,\big([l^z(r_1)/r_2]^2 + [l^z(r_2)/r_1]^2\big). \tag{59.13}$$

The difference in energy is given by

$$E_{\text{swap}} - E_{\text{init}} = (\delta m/2)\,\big([l^z(r_2)]^2 - [l^z(r_1)]^2\big)\big(r_1^{-2} - r_2^{-2}\big). \tag{59.14}$$

[4] Gravitational potential energy plays no role here, as we are swapping fluid rings at the same vertical position.

Since $r_2 = r_1 + \Delta r > r_1$, we have a release of kinetic energy ($E_{\text{swap}} - E_{\text{init}} < 0$) if the squared angular momentum decreases upon moving outward

$$\frac{\mathrm{d}[l^z(r)]^2}{\mathrm{d}r} = 2\, l^z(r)\, \frac{\mathrm{d}l^z(r)}{\mathrm{d}r} < 0 \implies \text{necessary + sufficient for centrifugally unstable flow.} \tag{59.15}$$

Recall from equation (59.7) that the angular momentum of rigid-body flow is an increasing function of radius. Hence, the instability condition (59.15) signals a distinctively non-rigid-body angular momentum configuration. We can consider a thought experiment in which a stable flow (one where $\mathrm{d}[l^z(r)]^2/\mathrm{d}r > 0$) is somehow forced towards a centrifugally unstable state with $\mathrm{d}[l^z(r)]^2/\mathrm{d}r < 0$. A vanishing angular momentum at a particular radius, $l^z = 0$, is a sufficient condition to ensure $\mathrm{d}[l^z(r)]^2/\mathrm{d}r = 0$ at that radius. Evidently, if the angular momentum of the cyclostrophic flow is reduced toward zero, the fluid will go centrifugally unstable upon reaching just below zero angular momentum.

59.3.4 Instability condition in terms of absolute vorticity

The angular momentum condition (59.15) is the traditional way to write the necessary and sufficient condition for centrifugal instability. However, to anticipate the role of vorticity found in the case of inertial and symmetric instability, we rewrite the stability condition (59.15) in terms of absolute vorticity. For this purpose, introduce the vertical component of the relative vorticity,

$$\zeta = \frac{1}{r}\frac{\mathrm{d}(r\, v^\vartheta)}{\mathrm{d}r}, \tag{59.16}$$

and thus write the angular velocity as the radial integral of the radius weighted vorticity

$$v^\vartheta = \frac{1}{r}\int_0^r r'\, \zeta(r')\, \mathrm{d}r'. \tag{59.17}$$

This result allows us to write the angular momentum (59.3) in terms of the absolute vorticity

$$l^z = \Omega\, r^2 + \int_0^r r'\, \zeta(r')\, \mathrm{d}r' = \int_0^r r'\, (\zeta(r') + 2\,\Omega)\, \mathrm{d}r' = \int_0^r r'\, \zeta_{\mathsf{a}}(r')\, \mathrm{d}r'. \tag{59.18}$$

This equation allows us to write the stability condition (59.15) in the form

$$\frac{\mathrm{d}[l^z(r)]^2}{\mathrm{d}r} = 2\, l^z\, \frac{\mathrm{d}l^z(r)}{\mathrm{d}r} = 2\, r\, \zeta_{\mathsf{a}}(r) \int_0^r r'\, \zeta_{\mathsf{a}}(r')\, \mathrm{d}r' < 0 \implies \text{centrifugally unstable.} \tag{59.19}$$

For $\mathrm{d}[l^z(r)]^2/\mathrm{d}r < 0$ at a particular radius, r, and thus for the cyclostrophic flow to be unstable, requires the absolute vorticity at that radius to have the opposite sign to the integral of the radius weighted absolute vorticity from the origin to r. Since $r \geq 0$, a necessary condition for the instability is for the absolute vorticity to have a sign change somewhere within the region $0 \leq r$.

59.3.5 Parcel stability analysis

As a complement to the energetic stability analysis of Section 59.3.3, we here study the force balance in the radial momentum equation. This analysis shows that an unstable angular momentum profile corresponds to a situation where the outward centrifugal acceleration is stronger than the radially inward pressure gradient acceleration, thus allowing for the fluid parcel to be "thrown" outward.

We again assume rotational symmetry so that the angular momentum is a material invariant, and assume the base state is in cyclostrophic balance. As such, the radial momentum equation

(59.1a) leads to

$$0 = -g\,\partial_r \overline{\eta} + r^{-3}\,(\overline{l^z})^2, \tag{59.20}$$

with the overline denoting the cyclostrophic base state. Subtracting this equilibrium flow from the full momentum equation (59.1a) leads to an equation for radial acceleration of perturbations about the equilibrium state

$$\frac{\mathrm{D}v^r}{\mathrm{D}t} = -g\,\frac{\partial \eta'}{\partial r} + r^{-3}\left[(l^z)^2 - (\overline{l^z})^2\right], \tag{59.21}$$

where

$$\eta' = \eta - \overline{\eta} \tag{59.22}$$

is the perturbation surface height. We focus now on the difference in squared angular momentum, with questions about the perturbation pressure gradient, $-g\,\partial\eta'/\partial r$, falling outside the parcel method of stability analysis.

Probing stability by perturbing the radius of a circular fluid ring

Consider a perturbation realized by moving a constant mass circular fluid ring outward from its initial equilibrium state at radius r to a radius $r + \Delta r$. During expansion of the ring, its angular momentum remains constant due to the rotational symmetry, so that

$$(l^z)^2(r + \Delta r) = (l^z)^2(r) = (\overline{l^z})^2(r), \tag{59.23}$$

where the second equality holds since we are starting the ring from its cyclostrophic initial condition (59.20). To determine the radial acceleration at $r + \Delta r$ appearing on the right hand side of the radial velocity equation (59.21), we compute

$$(l^z)^2(r + \Delta r) - (\overline{l^z})^2(r + \Delta r) = (\overline{l^z})^2(r) - (\overline{l^z})^2(r + \Delta r) \approx -\Delta r\,\frac{\mathrm{d}(\overline{l^z})^2(r)}{\mathrm{d}r}, \tag{59.24}$$

so that the equation (59.21) evaluated at $r + \Delta r$ is

$$\frac{\mathrm{D}v^r}{\mathrm{D}t} = -g\,\frac{\partial \eta'}{\partial r} - \frac{\Delta r}{(r + \Delta r)^3}\,\frac{\mathrm{d}(\overline{l^z})^2(r)}{\mathrm{d}r}. \tag{59.25}$$

We thus see that if the squared angular momentum decreases upon moving the ring to a larger radius, then the second right hand side term in equation (59.25) provides a positive radial acceleration, thus supporting the initial outward perturbation. Ignoring the possibility for the perturbation pressure gradient, $-g\partial\eta'/\partial r$, to counter-act the acceleration, we are left with the same instability condition (59.15) derived using energetic arguments.

Describing the instability mechanism

When the fluid is in cyclostrophic balance, the radial pressure gradient acceleration (which is pointing radially inward) balances the centrifugal acceleration (which is pointing radially outward) as per equation (59.20). When a constant mass fluid ring is perturbed outward, from r to $r + \Delta r$, it carries its angular momentum, $\overline{l^z}(r)$, to the new location. This displaced ring is generally not in cyclostrophic balance with the pressure gradient at the new position. That is, the centrifugal acceleration of the displaced ring does not equal the pressure gradient of the new position

$$\underbrace{(r + \Delta r)^{-3}\,[\overline{l^z}(r)]^2}_{\text{centrifugal of displaced ring}} \quad \neq \quad \underbrace{g\frac{\partial \overline{\eta}(r + \Delta r)}{\partial r}}_{\text{pressure gradient at } r + \Delta r} \tag{59.26}$$

If the centrifugal acceleration of the displaced ring is greater than the local pressure gradient acceleration, then the ring will continue to move outward. That is, the outward centrifugal acceleration at the new location is greater than the inward pressure gradient so that the fluid ring is flung further outward. This process characterizes a centrifugally unstable state, and it occurs if the squared angular momentum decreases when moving radially outward, as per equation (59.15). Conversely, if the local pressure gradient is greater than the centrifugal acceleration of the dispaced ring, then the ring returns to its original radius and exhibits stable centrifugal oscillations.

Centrifugal oscillations

Ignoring the perturbation pressure gradient, and introducing a squared centrifugal angular frequency,

$$\sigma^2(r) \equiv \frac{1}{(r+\Delta r)^3} \frac{\mathrm{d}(\overline{l^z})^2(r)}{\mathrm{d}r}, \tag{59.27}$$

leads to the free oscillator equation for the fluctuation of a fluid ring from its equilibrium radial position

$$\frac{\mathrm{D}^2\Delta r}{\mathrm{D}t^2} + \sigma^2 \Delta r = 0, \tag{59.28}$$

where $u^r = \mathrm{D}(\Delta r)/\mathrm{D}t$ is the radial velocity of a fluid parcel relative to its equilibrium radial position. For stable cases with $\sigma^2 > 0$, the ring exhibits harmonic centrifugal oscillations around the equilibrium radius with period $2\pi/\sigma$. In contrast, for the unstable case with $\sigma^2 < 0$, then Δr grows exponentially.

59.3.6 Stability condition in terms of the surface height

The equilibrium angular momentum and free surface height are related by the cyclostrophic balance (59.20). So rather than focusing on the angular momentum, we can develop an equivalent stability condition in terms of radial derivatives of the free surface height. For this purpose, write the difference in angular momentum

$$(\overline{l^z})^2(r) - (\overline{l^z})^2(r+\Delta r) = g\,[r^3\,\mathrm{d}\overline{\eta}(r)/\mathrm{d}r - (r+\Delta r)^3\,\mathrm{d}\overline{\eta}(r+\Delta r)/\mathrm{d}r], \tag{59.29}$$

and then perform a Taylor series

$$\begin{aligned} F(r+\Delta r) &\equiv (r+\Delta r)^3\,\mathrm{d}\overline{\eta}(r+\Delta r)/\mathrm{d}r && \text{(59.30a)}\\ &\approx F(r) + \Delta r\,\mathrm{d}F(r)/\mathrm{d}r && \text{(59.30b)}\\ &= r^3\,\mathrm{d}\overline{\eta}(r)/\mathrm{d}r + \Delta r\,\mathrm{d}[r^3\,\mathrm{d}\overline{\eta}/\mathrm{d}r]/\mathrm{d}r, && \text{(59.30c)} \end{aligned}$$

which renders

$$(\overline{l^z})^2(r) - (\overline{l^z})^2(r+\Delta r) \approx -g\,\Delta r \frac{\mathrm{d}}{\mathrm{d}r}\left[r^3 \frac{\mathrm{d}\overline{\eta}}{\mathrm{d}r}\right]. \tag{59.31}$$

The radial momentum equation (59.25) thus takes the form

$$\frac{\mathrm{D}v^r}{\mathrm{D}t} = -g\frac{\partial \eta'}{\partial r} - \frac{g\,\Delta r}{(r+\Delta r)^3}\frac{\mathrm{d}}{\mathrm{d}r}\left[r^3\frac{\mathrm{d}\overline{\eta}}{\mathrm{d}r}\right]. \tag{59.32}$$

We are thus led to the instability condition written in terms of the surface height in the cyclostrophically balanced base state

$$\frac{\mathrm{d}}{\mathrm{d}r}\left[r^3\frac{\mathrm{d}\overline{\eta}}{\mathrm{d}r}\right] < 0 \Longrightarrow \text{centrifugally unstable.} \tag{59.33}$$

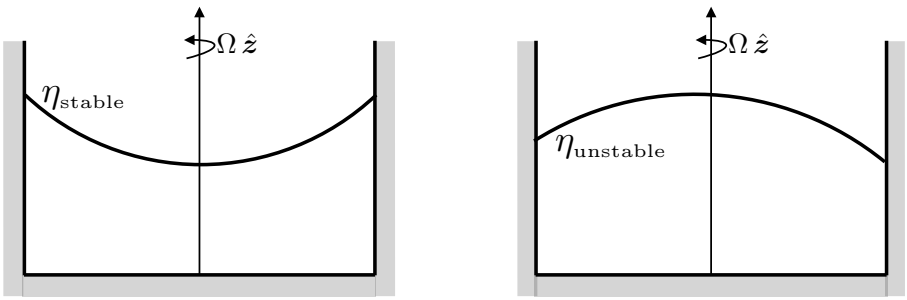

FIGURE 59.3: Example free surface heights for a shallow water layer in a rotating tank. The left panel exhibits a free surface height that is stable to centrifugal instability, whereas the right is unstable, with stability determined by the condition (59.33). The stable configuration approximates the parabolic profile that is realized for a rigid-body flow as in equation (59.35). The unstable profile has its layer thickness decrease with increasing radius, so that the radial pressure gradient acceleration cannot balance the centrifugal acceleration.

A particular example of a centrifugally unstable free surface configuration is the decreasing function

$$\overline{\eta} = \eta_0 - a\, r^b \implies \left[r^3\, \frac{\mathrm{d}\overline{\eta}}{\mathrm{d}r} \right] = -a\, b\, (2+b)\, r^{b+1}, \tag{59.34}$$

with η_0 the free surface height at the origin, b a dimensionless constant, and a having dimensions so that $a\, r^b$ has dimensions of length. Furthermore, we require with $a\, b > 0$, and $b > -2$. Recall that the free surface is parabolic when the fluid is in rigid-body motion, as given by equation (27.103)

$$\overline{\eta} = \eta_0 + \Omega^2\, r^2/(2\, g_{\mathrm{e}}) \implies \left[r^3\, \frac{\mathrm{d}\overline{\eta}}{\mathrm{d}r} \right] = 4\, \Omega^2\, r^3/g_{\mathrm{e}} > 0, \tag{59.35}$$

which is stable.

59.3.7 Comments and further study

Chapter 3 of *Drazin and Reid* (1981) is the canonical reference for centrifugal instability, where they provide a stability analysis including both axisymmetric and non-axisymmetric perturbations. In our treatment, we also made use of the parcel arguments from Section 3.2 of *Markowski and Richardson* (2010). Furthermore, *Markowski and Richardson* (2010) comment on the perturbation pressure gradient in equation (59.25), emphasizing that parcel stability arguments generally ignore changes to the pressure gradient. Stated otherwise, a parcel analysis concerns the equilibrium angular momentum profile and its contribution to movement away from equilibrium. It is not concerned with back reaction from pressure perturbations associated with movement of parcels or fluid rings. A fuller treatment generally requires analysis beyond the parcel framework. Section 11.6 of *Kundu et al.* (2016) presents centrifugal instability in the context of viscous Couette flow, which is the flow of fluid between two rotating co-axial cylinders.

For a laboratory realization of centrifugal instability, see this video from the UCLA spin lab. The laboratory technique spins up a fluid to rigid-body motion in a tank, and then quickly reduces the rotation rate to induce $\mathrm{d}[l^z(r)]^2/\mathrm{d}r < 0$. The instability manifests as roll vorticies aligned along the tank wall, with the character of the vorticies a function of $\mathrm{d}[l^z(r)]^2/\mathrm{d}r$ and other parameters.

59.4 Potential momentum on the f-plane

A front is a region of enhanced lateral gradients in the buoyancy field (baroclinic front) or sea level (shallow water front). These fronts generally have corresponding currents (jets) arising from geostrophic balance (when off-equator). Figure 59.4 illustrates a baroclinic front that

is symmetric in the zonal direction so that the buoyancy field is only a function of latitude, depth, and time, $b = b(y, z, t)$. We likewise assume that all other fields possess zonal symmetry, including pressure and velocity. Fronts can generally be oriented in any direction. Furthermore, there is rotational symmetry on the f-plane so that we can orient the horizontal coordinate axes as desired. In later sections we study the stability of fronts. Here, we establish some basic properties of *potential momentum*, which proves central to the stability analysis.

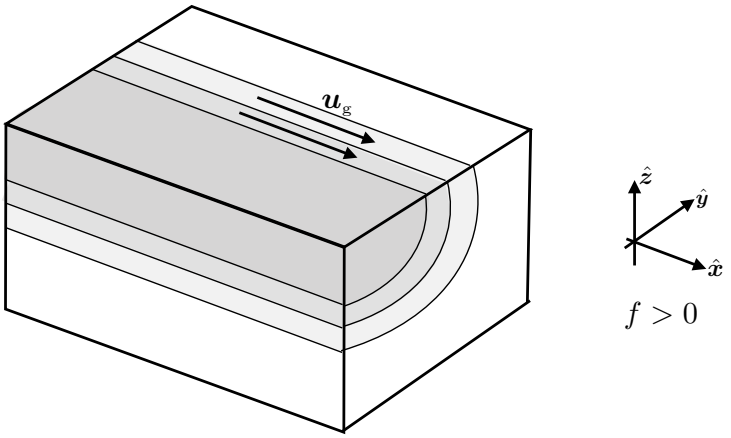

FIGURE 59.4: Example of a zonally symmetric baroclinic frontal region, showing iso-buoyancy surfaces with $b = b(y, z, t)$. With $\partial b/\partial y < 0$ as drawn, the corresponding zonal thermal wind shear, $f\,\partial u_g/\partial z = -\partial b/\partial y > 0$, is eastward for a northern hemisphere front; i.e., stronger eastward flow with increasing height (see Section 31.4.3).

59.4.1 Linear momentum and potential momentum

The horizontal linear momentum per mass for a perfect Boussinesq ocean on an f-plane evolves according to (see Section 29.1.6)

$$\frac{\mathrm{D}\boldsymbol{u}}{\mathrm{D}t} + f\,\hat{\boldsymbol{z}} \times \boldsymbol{u} = -\nabla_h \varphi. \tag{59.36}$$

Since f is a constant, this equation can be written

$$\frac{\mathrm{D}\boldsymbol{M}}{\mathrm{D}t} = -\nabla_h \varphi, \tag{59.37}$$

where we introduced the *potential momentum* per mass

$$\boldsymbol{M} \equiv \boldsymbol{u} + f\,\hat{\boldsymbol{z}} \times \boldsymbol{x} = (u - f\,y)\,\hat{\boldsymbol{x}} + (v + f\,x)\,\hat{\boldsymbol{y}}, \tag{59.38}$$

and noted that $\boldsymbol{v} = \mathrm{D}\boldsymbol{x}/\mathrm{D}t$. Notably, the potential momentum remains materially invariant in directions where the horizontal pressure gradient vanishes. We described the potential momentum for a point particle in Section 14.3, and here make use of it to study the stability of certain f-plane fluid flows.

Materially constant zonal potential momentum

For the zonally aligned buoyancy front illustrated in Figure 59.4, we assume all fields are independent of the zonal direction so that

$$\partial_x \varphi = 0. \tag{59.39}$$

A vanishing zonal pressure gradient means that the zonal potential momentum per mass is a material invariant

$$\mathrm{D}M^x/\mathrm{D}t = 0 \quad \text{where } M^x \equiv u - f\,y. \tag{59.40}$$

This material invariance greatly constrains the flow. For example, consider a fluid parcel at an initial latitude y_0 with zonal velocity u_0. Movement of the parcel to a new latitude leads to the equality

$$u_0 - f y_0 = u_1 - f\,y_1, \tag{59.41}$$

so that the zonal velocity at the new latitude is given by

$$u_1 = u_0 - f(y_0 - y_1). \tag{59.42}$$

Motivating the name potential momentum

Although *absolute momentum* or *geostrophic momentum* are more commonly used in the literature, we prefer the term *potential momentum* as motivated by the same reasoning used for potential temperature (Section 23.3), potential density (Section 30.3.4), and potential vorticity (Section 39.3.2). Namely, the zonal potential momentum identifies that amount of zonal linear momentum per mass (i.e., the velocity) that a parcel would acquire if moved from an arbitrary latitude y_1, to a reference latitude, y_0. More specifically, inverting equation (59.42) we see that

$$u_0 = M^x(y_1) + f y_0. \tag{59.43}$$

Hence, the quantity $M^x(y_1)$ is the extra zonal momentum per mass available at the reference latitude, y_0, upon moving a parcel from y_1 to y_0. We thus see that the potential momentum is a material invariant in the way that potential temperature is for a perfect fluid. Furthermore, as seen in Section 59.5, meridional gradients of M^x measure the *inertial* stability of a flow configuration in a manner directly analogous to how vertical gradients of potential temperature (or buoyancy) measure gravitational stability.

Meridional potential momentum

There are occasions when a front exhibits meridional symmetry, in which case the perfect Boussinesq equations take the form

$$\mathrm{D}u/\mathrm{D}t = fv - \partial_x\varphi \tag{59.44a}$$
$$\mathrm{D}v/\mathrm{D}t = -fu. \tag{59.44b}$$

In this case the meridional potential momentum is materially invariant

$$\mathrm{D}M^y/\mathrm{D}t = 0 \quad \text{where} \quad M^y \equiv v + fx. \tag{59.45}$$

59.4.2 Zonal potential momentum on a β-plane

The f-plane is rotationally invariant about the rotational axis. Correspondingly, we can write the momentum equation in the form (59.37), thus exposing the potential momentum. Material invariance for potential momentum holds along the symmetry direction of an arbitrarily oriented symmetric front.

The β-plane is not rotationally invariant. Rather, it only maintains symmetry along lines of constant latitude (zonal directions). Consequently, only zonally oriented symmetric fronts maintain material invariance of zonal potential momentum. To see this property, write the zonal

momentum equation in the form

$$\partial_t u + v\,\partial_y u + w\,\partial_z u - f\,v = 0, \tag{59.46}$$

where we assumed zonal symmetry ($\partial_x = 0$). Now write the Coriolis parameter in the form

$$\Gamma = f_\circ\, y + \beta\, y^2/2 \Longrightarrow f = \mathrm{d}\Gamma/\mathrm{d}y, \tag{59.47}$$

so that the zonal momentum equation takes the form

$$\partial_t(u - \Gamma) + v\,\partial_y(u - \Gamma) + w\,\partial_z(u - \Gamma) = 0. \tag{59.48}$$

Evidently, $M^x = u - \Gamma$ is materially invariant for this zonally symmetric front.

59.4.3 Further reading

See Section 14.4 for more discussion of potential momentum as it concerns a point particle. The term *absolute momentum* follows the arguments given on page 51 of *Markowski and Richardson* (2010).

59.5 Horizontal inertial instability of geostrophic fronts

We now examine stability of an f-plane geostrophically balanced front for an inviscid Boussinesq fluid. The analysis of centrifugal instability in Section 59.3 is closely followed, with rotational symmetry replaced by along-front symmetry and angular momentum replaced by potential momentum. We consider both the Rayleigh energetic stability analysis and the parcel analysis. Furthermore, the perturbations maintain symmetry in the along-front direction, so perturbations consist of a horizontally displaced row of parcels oriented along the front. Stability to more general perturbations, such as those that are not symmetric along the front, is not addressed here.

The results of our analysis are rotationally invariant since the f-plane is rotationally invariant. Hence, we choose to orient the coordinate system based on convenience whereby the x-axis is the along front axis and the y-axis is across the front (as in Figure 59.4). Furthermore, their relative orientation is chosen in the usual righthand sense, so that $\hat{\boldsymbol{x}} \times \hat{\boldsymbol{y}} = \hat{\boldsymbol{z}}$, where $\hat{\boldsymbol{z}}$ is anti-parallel to gravity.

Although we make use of a continuously stratified Boussinesq fluid, the inertial instability considered in this section is not associated with baroclinicity. Rather, as for the centrifugal case in Section 59.3, it is associated with stability of an equilibrium state to horizontal displacements along geopotential surfaces. In a continuously stratified adiabatic fluid, horizontal displacements generally cross isentropic surfaces and so comprise irreversible perturbations. So long as the associated mixing of momentum is negligible, we can still make use of material invariance of potential momentum. We return to this point when studying isentropic inertial (symmetric) instability in Section 59.6, in which perturbations are along sloped buoyancy surfaces rather than geopotential surfaces.

59.5.1 Equations of motion relative to the geostrophic equilibrium state

The horizontal momentum equation for an inviscid Boussinesq fluid on an f-plane is given by (see Section 29.1)

$$\mathrm{D}\boldsymbol{u}/\mathrm{D}t + f\,\hat{\boldsymbol{z}} \times \boldsymbol{u} = -\nabla_{\!\mathrm{h}}\varphi. \tag{59.49}$$

In the presence of along-front symmetry, an exact solution to the horizontal momentum equation is given by along-front geostrophic flow and zero flow across the front

$$u_{\rm g} = -f^{-1}\,\partial_y\varphi \quad \text{and} \quad v = 0 \quad \text{and} \quad \partial_x\varphi = 0. \tag{59.50}$$

We examine the stability of this exact equilibrium base state[5] to perturbations aligned with the front. To study evolution of the perturbations relative to the base state, subtract the base state solution from the full momentum equation (59.49) to render

$$\mathrm{D}u/\mathrm{D}t = f\,v \tag{59.51a}$$
$$\mathrm{D}v/\mathrm{D}t = f\,(u_{\rm g} - u). \tag{59.51b}$$

We continue to assume along-front symmetry in the perturbation so that there is no along-front pressure gradient ($\partial_x\varphi = 0$) in equation (59.51a). Equation (59.51b) says that across-front accelerations are determined by deviations from geostrophy of the along-front velocity, and equation (59.51a) says that along-front accelerations are determined by the Coriolis acceleration arising from a non-zero across-front velocity.

Following the treatment of potential momentum in Section 14.3, we write the along-front momentum equation (59.51a) as the material time derivative of the along-front potential momentum per mass

$$M^x = u - fy, \tag{59.52}$$

bringing the suite of perturbation equations to

$$\mathrm{D}M^x/\mathrm{D}t = 0 \tag{59.53a}$$
$$\mathrm{D}v/\mathrm{D}t = f(u_{\rm g} - u). \tag{59.53b}$$

Material invariance of the along-front potential momentum plays a fundamental role in the stability analysis, analogous to the role of angular momentum for centrifugal instability in Section 59.3. Finally, we can write the equations in terms of just M^x and v via

$$\mathrm{D}M^x/\mathrm{D}t = 0 \tag{59.54a}$$
$$\mathrm{D}v/\mathrm{D}t = f(M^x_{\rm g} - M^x). \tag{59.54b}$$

59.5.2 Stability analysis based on energetic arguments

We follow the energetic arguments given in Section 59.3.3 for centrifugal instability of cyclostrophic flow. Here, we ask whether the along-front geostrophic flow is stable to a swap of two along-front oriented rows that have the same geopotential. If the swap releases kinetic energy from the base state, then the base state flow is *inertially unstable* to an along-front symmetric perturbation. In that case, perturbations spontaneously initiate inertial instability to affect a return to an inertially stable state.

Instability condition

The kinetic energy per mass for the along-front geostrophic flow is given by

$$E = u_{\rm g}^2/2 = (M^x_{\rm g} + fy)^2/2, \tag{59.55}$$

[5] It is useful to confirm that $u_{\rm g} = -f^{-1}\,\partial_y\varphi$ and $v = 0$ are indeed exact solutions to equation (59.49).

where we replaced the geostrophic velocity with the geostrophic potential momentum through equation (59.52)

$$M^x_{\text{g}} = u_{\text{g}} - f\,y. \tag{59.56}$$

The kinetic energy per mass contained in two equal mass parcels at distinct meridional cross-front positions, $y = y_1$, and

$$y_2 = y_1 + (y_2 - y_1) = y_1 + \Delta y, \tag{59.57}$$

is given by

$$E_{\text{init}} = [M^x_{\text{g}}(y_1) + f y_1]^2/2 + [M^x_{\text{g}}(y_2) + f y_2]^2/2. \tag{59.58}$$

Swapping the parcels and making use of the invariance of potential momentum leads to the kinetic energy in the swapped state

$$E_{\text{swap}} = [M^x_{\text{g}}(y_1) + f\,y_2]^2/2 + [M^x_{\text{g}}(y_2) + f\,y_1]^2/2. \tag{59.59}$$

A bit of algebra leads to the difference in kinetic energy between the two states

$$E_{\text{swap}} - E_{\text{init}} = -f\,(y_2 - y_1)\,[M^x_{\text{g}}(y_2) - M^x_{\text{g}}(y_1)] = -f\,\Delta y\,\Delta M^x_{\text{g}}. \tag{59.60}$$

Now compute a Taylor series of the potential momentum, $M^x_{\text{g}}(y_2)$, relative to the across-front position, $y = y_1$,

$$M^x_{\text{g}}(y_2) \approx M^x_{\text{g}}(y_1) + (y_2 - y_1)\,\frac{\mathrm{d}M^x_{\text{g}}}{\mathrm{d}y}\bigg|_{y=y_1}, \tag{59.61}$$

which then leads to the energy difference

$$\begin{aligned} E_{\text{swap}} - E_{\text{init}} &= -f\,(\Delta y)^2\,\frac{\mathrm{d}M^x_{\text{g}}}{\mathrm{d}y} && \text{(59.62a)}\\ &= -f\,(\Delta y)^2\,(\partial_y u_{\text{g}} - f) && \text{(59.62b)}\\ &= f\,(\Delta y)^2\,(\zeta_{\text{g}} + f), && \text{(59.62c)} \end{aligned}$$

where

$$\zeta_{\text{g}} = -\partial_y u_{\text{g}} \tag{59.63}$$

is the vertical component to the geostrophic relative vorticity for the symmetric base state. Evidently, kinetic energy is released upon swapping the two rows if the following condition is satisfied

$$-f\,\partial_y M^x_{\text{g}} = f\,(\zeta_{\text{g}} + f) < 0 \Longrightarrow \text{inertial instability}. \tag{59.64}$$

The second instability condition says that the base state is unstable if the absolute geostrophic vorticity, $\zeta_{\text{g}} + f$, has an opposite sign to the planetary vorticity. This stability condition has a natural generalization to the case of symmetric instability considered in Sections 59.6 and 59.8.

Interpreting the instability condition

The first instability condition in equation (59.64) arises if the cross-front gradient of the geostrophic potential momentum has the same sign as the Coriolis parameter. To help understand this condition we examine the inertial stability of a base state with zero flow. Zero flow in a rotating reference frame corresponds to rigid-body motion with potential momentum $M^x_{\text{g}} = -fy$. For this base state, the inertial stability condition (59.64) is given by

$$-f\,(\partial M^x_{\text{g}}/\partial y) = f^2 > 0, \tag{59.65}$$

thus signaling the rigid-body flow is inertially stable. By contrast, we infer that an inertially unstable base state is rendered unstable by having an along-front flow that overcomes the stabilizing contribution to potential momentum from planetary rotation. This situation is directly analogous to the centrifugal instability studied in Section 59.3.

Summarizing the conditions for inertial instability

The instability condition (59.64) takes the following form for the northern and southern hemispheres. Again, the x-axis is oriented along the front and y-axis is across the front with $\hat{\boldsymbol{x}} \times \hat{\boldsymbol{y}} = \hat{\boldsymbol{z}}$ and $M^x_{\rm g} = u_{\rm g} - f\, y$

$$\text{northern hemisphere } (f > 0): \qquad \partial_y M^x_{\rm g} > 0 \qquad \zeta_{\rm g} < -|f| \qquad \partial_y u_{\rm g} > +|f| \tag{59.66a}$$

$$\text{southern hemisphere } (f < 0): \qquad \partial_y M^x_{\rm g} < 0 \qquad \zeta_{\rm g} > +|f| \qquad \partial_y u_{\rm g} < -|f|. \tag{59.66b}$$

In both hemispheres, instability arises when the relative geostrophic vorticity is anti-cyclonic and larger in magnitude than the cyclonic vorticity from planetary rotation. Under such conditions, inertial instability allows the flow to readjust toward a state of less extreme relative vorticity, thus returning the flow to a state with absolute vorticity dominated by planetary vorticity. Equivalently, inertial instability arises for flows where $\partial M^x_{\rm g}/\partial y > 0$ in the northern hemisphere and $\partial M^x_{\rm g}/\partial y < 0$ in the southern hemisphere, so that potential momentum of the geostrophic base state increases poleward.

59.5.3 Stability analysis based on parcel arguments

Following the analysis for centrifugal instability in Section 59.3.5, we here consider a parcel stability analysis to provide a force-balance interpretation of the inertial instability. For this purpose, return to the perturbation equations (59.53a) and (59.53b), again with the equilibrium base state of along-front geostrophic balance with zero motion in the across-front direction

$$f\, u_{\rm g} = -\partial_y \varphi. \tag{59.67}$$

We examine the stability of this geostrophic base state with respect to along-front perturbations of fluid parcels. For this purpose, imagine moving a row of fluid parcels from position y to a new position, $y + \Delta y$. As per the usual assumption of a parcel analysis, this move is assumed to have no impact on the surrounding fluid environment, including the pressure field.[6] In general, the displaced row of fluid parcels will not be in geostrophic balance at the new position, thus providing for a non-zero acceleration in the across-front direction. If the acceleration is directed back to the original position, then the base state is stable and displaced parcels exhibit inertial oscillations in the x-y plane. In contrast, the base state is inertially unstable if the net acceleration acts to further the initial displacement. Note that while the fluid parcels are moved meridionally, they will be displaced zonally due to the Coriolis acceleration. However, we focus attention on the meridional motion to determine whether the parcel accelerates further away from its initial latitude or returns. We illustrate facets of the stable and unstable situations in Figures 59.5 and 59.6, with details of these figures explained in the remainder of this section.

Mathematical formulation

Equation (59.53b) for the across-front motion is given by

$$\mathrm{D}v/\mathrm{D}t = f\,(u_{\rm g} - u). \tag{59.68}$$

[6] With this assumption, the pressure field remains in geostrophic balance with the unperturbed background geostrophic flow.

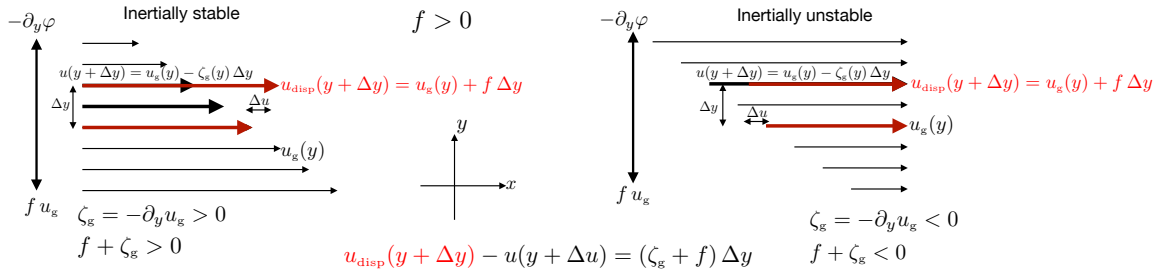

FIGURE 59.5: Schematics of an inertially stable (left panel) and inertially unstable (right panel) geostrophic base flow in the northern hemisphere. One of the red vectors is for the geostrophic velocity, $u_g(y)$, and the second for the velocity at a displaced position $u_{disp}(y+\Delta y)$. The displaced velocity is determined by conservation of zonal potential momentum, $u_{disp}(y+\Delta y) = u_g(y) + f\,\Delta y$, from equation (59.71). In the unperturbed flow, the eastward geostrophic velocity is generated by a northward pressure gradient acceleration that balances a southward Coriolis acceleration. The base state pressure gradient remains unchanged even as the fluid parcels are perturbed, with this assumption basic to the parcel method of stability analysis. At the displaced position we also show the base state velocity at the displaced position, $u(y+\Delta y) = u_g(y) + \partial_y u(y)\,\Delta y = u_g(y) - \zeta_g(y)\,\Delta y$. The difference between the displaced velocity and the base state velocity is $u_{disp}(y+\Delta y) - u(y+\Delta y) = (f+\zeta_g)\,\Delta y$. For the left panels, the flow has positive relative vorticity so that $\zeta_g + f > 0$ and the flow is inertially stable. In this case, the displaced parcel has a southward Coriolis acceleration larger than the local Coriolis, thus returning the row of fluid parcels back towards its initial latitude. For the right panel, the flow has negative relative geostrophic vorticity, and that vorticity is strong enough so that the absolute geostrophic vorticity is negative, $\zeta_g + f < 0$, in which case the flow is inertially unstable. In this case, the displaced parcel has a southward Coriolis acceleration smaller than the local Coriolis. Hence, the northward pressure gradient is strong enough to keep the parcel moving northward, away from its initial position, thus signaling a base state that is inertially unstable.

This equation holds everywhere, in particular at the displaced cross-front position, $y + \Delta y$. At this position, the right hand side has $u(y + \Delta y)$, which is the along-front velocity of the displaced parcel at the new position. Likewise, $u_g(y + \Delta y)$ is the geostrophic velocity at $y + \Delta y$ of the prescribed background flow. According to equation (59.67), the geostrophic velocity, $u_g(y+\Delta y)$, determines a Coriolis acceleration at the displaced position, $y+\Delta y$, with this Coriolis acceleration balanced by the cross-front pressure gradient, also evaluated at $y + \Delta y$.

To determine the sign of the cross-front acceleration in equation (59.68) acting on the displaced parcel at $y + \Delta y$, we make use of the material invariance of along-front potential momentum. This invariance means that each fluid parcel carries its potential momentum from the original position.[7] For example, the potential momentum of a fluid parcel initially at position y has the value given by the geostrophic base state at that latitude

$$M^x(y) = M^x_g(y) = u_g(y) - f\,y. \tag{59.69}$$

Material invariance means that the parcel retains this potential momentum as it moves to the new position, $y + \Delta y$. In turn, invariance of along-front potential momentum allows us to determine the along-front velocity of the parcel at the displaced position in terms of $u_g(y)$ (recall the procedure leading to equation (59.42))

$$\begin{aligned} M^x(y+\Delta y) &= u(y+\Delta y) - f\,(y+\Delta y) && \text{(59.70a)} \\ &= M^x(y) && \text{(59.70b)} \\ &= u_g(y) - f\,y, && \text{(59.70c)} \end{aligned}$$

which leads to

$$u(y+\Delta y) = u_g(y) + f\,\Delta y. \tag{59.71}$$

[7] We offer a cautionary remark about notation. Namely, f is a constant so that $f\,y$ is f times the latitude position y, and likewise for $f\,(y+\Delta y)$. In contrast, the zonal velocity, u, is a function of y, so that $u(y)$ and $u(y+\Delta y)$ represent the zonal velocity evaluated at the latitude positions y and $y+\Delta y$, respectively.

The cross-front acceleration (59.68) at the new latitude position thus takes the form

$$\frac{\mathrm{D}v(y+\Delta y)}{\mathrm{D}t} = f\,[u_{\mathrm{g}}(y+\Delta y) - u(y+\Delta y)] \tag{59.72a}$$

$$= f[u_{\mathrm{g}}(y+\Delta y) - u_{\mathrm{g}}(y) - f\,\Delta y] \tag{59.72b}$$

$$\approx f\Delta y\left[\frac{\partial u_{\mathrm{g}}}{\partial y} - f\right] \tag{59.72c}$$

$$= -f\,\Delta y\,(\zeta_{\mathrm{g}} + f). \tag{59.72d}$$

The initial displacement grows,

$$\frac{1}{\Delta y}\frac{\mathrm{D}v(y+\Delta y)}{\mathrm{D}t} > 0, \tag{59.73}$$

if the following instability condition holds

$$f\,(\zeta_{\mathrm{g}} + f) < 0 \Longrightarrow \text{inertially unstable}, \tag{59.74}$$

which is the same instability condition as found via the energetic arguments in Section 59.5.2.

Oscillations or exponential growth?

Let y be the arbitrary initial meridional position for a fluid parcel, and Δy the meridional position relative to y. The equation of motion (59.72d) can be written in terms of the relative position so that

$$\frac{\mathrm{d}^2\Delta y}{\mathrm{d}t^2} + f\,(\zeta_{\mathrm{g}} + f)\,\Delta y = 0. \tag{59.75}$$

If $f\,(\zeta_{\mathrm{g}} + f) < 0$ then Δy has an exponentially growing (and decaying) solution, thus indicating instability. For the alternative case with $f\,(\zeta_{\mathrm{g}} + f) > 0$ we expect to find inertial-like oscillations.

A quick derivation of the instability condition

The displaced parcel at $y+\Delta y$ has zonal velocity $u(y+\Delta y) = u_{\mathrm{g}}(y) + f\,\Delta y$ according to equation (59.71), which follows from the material conservation of zonal potential momentum. The velocity of the background geostrophic flow at $y+\Delta y$ is given by the Taylor series approximation relative to the flow at y (keeping terms up to first order):

$$u_{\mathrm{g}}(y+\Delta y) \approx u_{\mathrm{g}}(y) + \Delta y\,\partial_y u_{\mathrm{g}}(y) = u_{\mathrm{g}}(y) - \Delta y\,\zeta_{\mathrm{g}}(g). \tag{59.76}$$

The difference between these two zonal velocities is

$$u_{\mathrm{g}}(y+\Delta y) - u(y+\Delta y) = -(f+\zeta_{\mathrm{g}})\,\Delta y, \tag{59.77}$$

which recovers the inertial stability condition derived above.

Summary of the parcel argument

As summarized in Figures 59.5 and 59.6, at the initial location in the base state, a parcel under geostrophic balance has its Coriolis acceleration balanced by its pressure acceleration. However, the displaced parcel generally will not be in geostrophic balance at the new location, in which case its Coriolis acceleration does not balance the local pressure gradient. The parcel approach determines a stability condition based on whether the imbalance leads to an acceleration back towards its initial position (stable inertial oscillations) or further away (inertial instability). For the unstable case, the Coriolis acceleration of the displaced parcel at its new location cannot

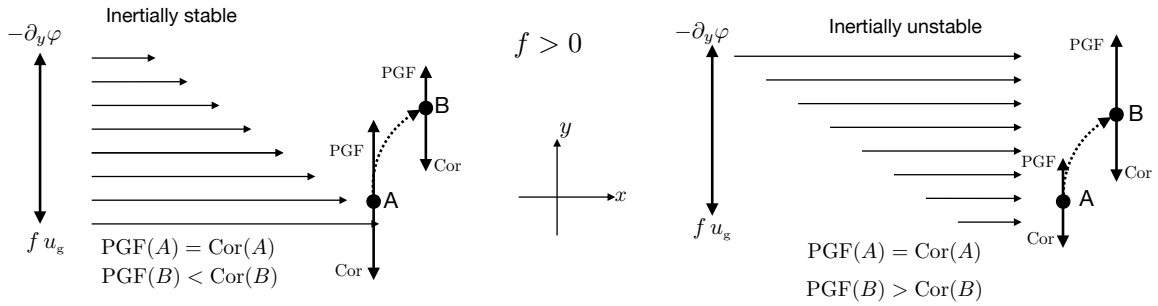

FIGURE 59.6: Further depiction of inertially stable geostrophic flow (left panel) and unstable geostrophic flow (right panel), complementing features presented in Figure 59.5. Here we show a fluid parcel starting at point A and displaced to point B, with the curved motion due to the zonal Coriolis acceleration that acts when the parcel is displaced in the meridional direction ($f > 0$). For the inertially stable case, the pressure gradient acceleration acting on the displaced parcel at point B is weaker than the parcel's Coriolis acceleration, so that the parcel exhibits stable inertial oscillations in the x-y plane. For the inertially ustable case, the pressure gradient acceleration acting on the parcel at point B is stronger than the parcel's Coriolis acceleration, so that the parcel continues to move further away and thus exhibits inertial instability.

match the local pressure gradient, thus causing the parcel to be thrust away from its initial latitude.

Along-front symmetry of both the base state and the perturbation ensures material invariance of along-front potential momentum. This invariance provides an explicit expression for the acceleration felt by the displaced parcel, thus determining a condition on stability of the base state to such symmetric perturbations. The method of analysis is directly analogous to that applied to the rotating tank of fluid in Section 59.3 for centrifugal instability, as well as for a vertical column of fluid in Section 30.4 for gravitational stability. We follow this procedure again in Section 59.6 for studying symmetric instability.

59.6 Symmetric instability and the $f\,Q < 0$ criteria

In this section we examine stability of a geostrophically balanced baroclinic front on an f-plane. We continue to assume the front is gravitationally stable ($N^2 > 0$) and that it exhibits along-front symmetry so that the along-front potential momentum is a material invariant (Figure 59.4). Different from the inertial instability case in Section 59.5, we here assume the fluid to be adiabatic so that Archimedean buoyancy is a second materially invariant property. We investigate stability of a geostrophically balanced along-front flow using the parcel method and make use of buoyancy as the vertical coordinate. We follow up this analysis in Section 59.8 with an Eulerian modal analysis. Both approaches reveal the fundamental importance of potential vorticity as a signature of symmetric instability. More precisely, the product, $f\,Q$, if negative, indicates a symmetrically unstable front.

59.6.1 Equations using buoyancy as the vertical coordinate

Given the adiabatic nature of the fluid, and the role of baroclinicity, we are motivated to use buoyancy as the vertical coordinate for a Boussinesq fluid as detailed in Section 66.2. That is, we consider symmetric displacements of parcels along a constant buoyancy surface. By construction, this displacement is neutral to gravitational instability since it occurs along a constant buoyancy surface. However, a displaced parcel could still find itself in an unstable position depending on the potential momentum of the local environment relative to the buoyancy surfaces. The analysis proceeds just like for the horizontal inertial instability of Section 59.5.3, yet with the displacements here being isentropic (constant buoyancy) rather than horizontal

(constant geopotential). We are thus motivated to refer to the ensuing instability as *isentropic inertial instability*, though note that it is more commonly referred to as *symmetric instability*.

With buoyancy as the vertical coordinate, the horizontal momentum equation is[8]

$$\mathrm{D}\boldsymbol{u}/\mathrm{D}t + f\,\hat{\boldsymbol{z}} \times \boldsymbol{u} = -\nabla_{\mathrm{hb}} M \tag{59.78}$$

where ∇_{hb} is a horizontal gradient computed along constant buoyancy surfaces. Furthermore,

$$M = \varphi - b\,z \tag{59.79}$$

is the Montomery potential that contributes an acceleration via[9]

$$-\nabla_{\mathrm{hb}} M = -\nabla_{\mathrm{hb}} \varphi + b\,\nabla_{\mathrm{hb}} z. \tag{59.80}$$

The first term arises from pressure gradients and the second from geopotential gradients, both computed along constant buoyancy surfaces. In the presence of along-front symmetry, an exact solution to the horizontal momentum equation is given by along-front geostrophic flow and zero cross-front flow

$$u_{\mathrm{g}} = -\frac{1}{f\,\rho_\circ}\left[\frac{\partial M}{\partial y}\right]_b \quad \text{and} \quad v = 0 \quad \text{and} \quad \left[\frac{\partial M}{\partial x}\right]_b = 0. \tag{59.81}$$

We examine stability of this base state to perturbations that are symmetric in the along-front direction. Subtracting the exact equilibrium solution from the full momentum equation (59.49) leads to

$$\mathrm{D}u/\mathrm{D}t = fv \quad \text{and} \quad \mathrm{D}v/\mathrm{D}t = f(u_{\mathrm{g}} - u), \tag{59.82}$$

where we assume along-front symmetry thus allowing us to drop the along-front gradient of the Montgomery potential. Following the treatment in Sections 14.3 and 59.5.1, we write the along-front momentum equation as the material time derivative of the along-front potential momentum per mass, $M^x = u - fy$ (equation (59.52)), thus bringing the perturbation equations to

$$\mathrm{D}M^x/\mathrm{D}t = 0 \quad \text{and} \quad \mathrm{D}v/\mathrm{D}t = f\,(M^x_{\mathrm{g}} - M). \tag{59.83}$$

59.6.2 Parcel stability analysis

We follow the parcel analysis used for inertial instability in Section 59.5.3, starting with an equilibrium base state of along-front geostrophic balance with zero meridional motion and then examine the stability of this state to symmetric perturbations of fluid parcels along a constant buoyancy surface. For this purpose, imagine moving a row of fluid parcels from cross-front position y to position $y + \Delta y$ while maintaining a fixed buoyancy *and* fixed potential momentum. Furthermore, assume the displacement has no impact on the base state, which is the typical assumption of the parcel approach to stabilty analysis. In general, the displaced row of parcels will not be in geostrophic balance at the new position, thus providing for a non-zero cross-front acceleration at that displaced position. The sign of that acceleration determines stability of the flow to the symmetric perturbation.

At the new cross-front position, the meridional acceleration acting on the displaced parcels

[8] In Part XII of this book, we develop the mathematical and physical details for generalized vertical coordinates, such as buoyancy or isopycnal coordinates. In particular, the essential features of the ∇_{hb} gradient operator are provided in Figure 63.4. For purposes of the present chapter, one merely needs to know that ∇_{hb} provides a measure of the property gradients computed along constant buoyancy surfaces, and yet with ∇_{hb} still having only horizontal components: $\nabla_{\mathrm{hb}} = \hat{\boldsymbol{x}}\,(\partial/\partial x)_b + \hat{\boldsymbol{y}}\,(\partial/\partial y)_b$, where the b subscript means that the derivative is computed while holding b constant.

[9] Be careful to distinguish the Montgomery potential, M, in equation (59.79) from the zonal potential momentum, M^x, in equation (59.40).

is given by[10]

$$\frac{\mathrm{D}v(y+\Delta y)}{\mathrm{D}t} = f\,[M^x_{\mathrm{g}}(y+\Delta y) - M^x(y+\Delta y)], \tag{59.84}$$

where $M^x(y+\Delta y)$ is the potential momentum at $y+\Delta y$, and $M^x_{\mathrm{g}}(y+\Delta y)$ is the geostrophic potential momentum at $y+\Delta y$. To determine the sign of the acceleration acting on the displaced parcel, we make use of the material invariance of along-front potential momentum,

$$M^x(y+\Delta y) = M^x(y) = M^x_{\mathrm{g}}(y), \tag{59.85}$$

so that the meridional acceleration is

$$\frac{\mathrm{D}v(y+\Delta y)}{\mathrm{D}t} = f\left[\frac{\partial M^x_{\mathrm{g}}}{\partial y}\right]_b \Delta y. \tag{59.86}$$

Evidently, if $\Delta y > 0$ then the displacement is unstable if

$$f\left[\frac{\partial M^x_{\mathrm{g}}}{\partial y}\right]_b > 0 \Longrightarrow \text{symmetrically unstable geostrophic state.} \tag{59.87}$$

We can write this condition in terms of the absolute geostrophic vorticity by noting that

$$\left[\frac{\partial M^x_{\mathrm{g}}}{\partial y}\right]_b = \left[\frac{\partial u_{\mathrm{g}}}{\partial y}\right]_b - f = -(\widetilde{\zeta}_{\mathrm{g}} + f), \tag{59.88}$$

where $\widetilde{\zeta}_{\mathrm{g}}$ is the relative vorticity of the geostrophic flow computed on buoyancy surfaces (see Section 66.2)

$$\widetilde{\zeta}_{\mathrm{g}} = \left[\frac{\partial v_{\mathrm{g}}}{\partial x}\right]_b - \left[\frac{\partial u_{\mathrm{g}}}{\partial y}\right]_b, \tag{59.89}$$

with $v_{\mathrm{g}} = 0$ for this zonal geostrophic front. Evidently, we have arrived at the alternative expression of a symmetrically unstable geostrophic base flow

$$f\,(f + \widetilde{\zeta}_{\mathrm{g}}) < 0 \Longrightarrow \text{symmetrically unstable geostrophic state.} \tag{59.90}$$

Finally, we can introduce the Boussinesq Ertel potential vorticity in the form[11]

$$Q = (\boldsymbol{\omega} + f\,\hat{\boldsymbol{z}}) \cdot \nabla b = (\widetilde{\zeta} + f)\,N^2, \tag{59.91}$$

with $N^2 = \partial_z b > 0$ the squared buoyancy frequency for gravitationally stable flows. Bringing these results together leads to the equivalent expressions of the necessary and sufficient conditions for a geostrophic base flow to be symmetrically unstable

$$f\left[\frac{\partial M^x_{\mathrm{g}}}{\partial y}\right]_b > 0 \tag{59.92a}$$

$$f\,(\widetilde{\zeta}_{\mathrm{g}} + f) < 0 \tag{59.92b}$$

$$f\,Q_{\mathrm{g}} < 0. \tag{59.92c}$$

[10] We only expose the meridional coordinate dependence in equation (59.84), but note that the velocity and potential momentum are also a function of the vertical position and time.

[11] We derive equation (59.91) when studying potential vorticity in the Boussinesq ocean using buoyancy coordinates; see equation (66.38).

59.6.3 Geometric perspective on the instability condition

The instability condition (59.92b) is a direct translation of the inertial instability condition (59.74), swapping horizontal displacements with displacements along buoyancy surfaces. Likewise, the instability condition (59.92a) is directly analogous to the inertial instability condition (59.64), only here with displacement along a buoyancy surface rather than a geopotential. In the northern hemisphere, if one moves in the $+\hat{\boldsymbol{y}}$ direction on a constant buoyancy surface and encounters increasing values for the potential momentum, then the base state flow is symmetrically unstable. Conversely in the southern hemisphere, if one moves in $-\hat{\boldsymbol{y}}$ direction on a constant buoyancy surface and encounters increasing values for the potential momentum, then the base state flow is symmetrically unstable. We illustrate this situation in Figure 59.7.

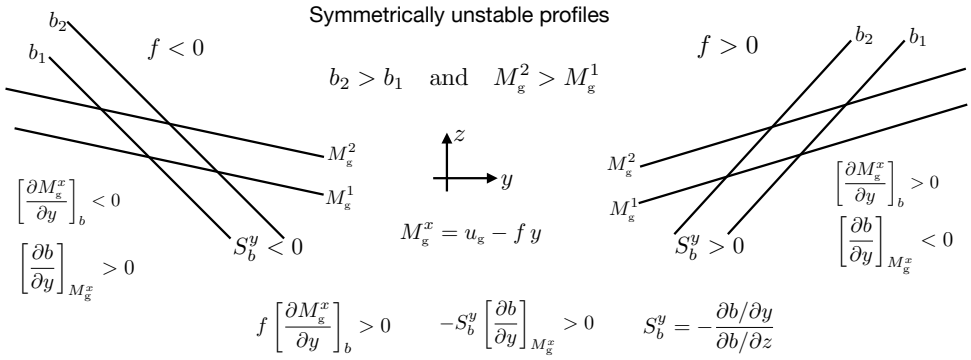

FIGURE 59.7: Example geostrophically balanced flow configurations that are symmetrically unstable; i.e., inertially unstable to a perturbation with symmetry along the front. We show example buoyancy surfaces and potential momentum surfaces for the southern hemisphere (left) and northern hemisphere (right). The instability conditions (59.99a) and (59.99b) are indicated on the respective panels. In both cases, surfaces of constant buoyancy are more steeply sloped than constant potential momentum surfaces. The x coordinate measures distance in the along-front direction and y measures distance in the cross-front direction, oriented so that $\hat{\boldsymbol{x}} \times \hat{\boldsymbol{y}} = \hat{\boldsymbol{z}}$ where $\hat{\boldsymbol{z}}$ is anti-parallel to gravity ($\hat{\boldsymbol{x}}$ is out of the page). A means to quickly judge whether a flow is symmetrically unstable is to note that the *wedge of instability* region between buoyancy and potential momentum surfaces provides a source of available potential energy. Symmetric instability can feed off the potential energy only when buoyancy surfaces are more steeply sloped than potential momentum surfaces.

As another way to write the instability condition (59.92a), make use of the expression (63.78b) to transform the derivative on buoyancy surfaces back to geopotential coordinates

$$\left[\frac{\partial M_{\mathrm{g}}^x}{\partial y}\right]_b = \left[\frac{\partial M_{\mathrm{g}}^x}{\partial y}\right]_z - \frac{\partial b/\partial y}{\partial b/\partial z}\frac{\partial M_{\mathrm{g}}^x}{\partial z} \tag{59.93a}$$

$$= (\partial b/\partial z)^{-1}\left[\frac{\partial M_{\mathrm{g}}^x}{\partial y}\frac{\partial b}{\partial z} - \frac{\partial M_{\mathrm{g}}^x}{\partial z}\frac{\partial b}{\partial y}\right] \tag{59.93b}$$

$$= -N^{-2}\,\hat{\boldsymbol{x}} \cdot (\nabla b \times \nabla M_{\mathrm{g}}^x). \tag{59.93c}$$

Similarly, we have

$$\left[\frac{\partial b}{\partial y}\right]_{M_{\mathrm{g}}^x} = (\partial M_{\mathrm{g}}^x/\partial z)^{-1}\left[\frac{\partial b}{\partial y}\frac{\partial M_{\mathrm{g}}^x}{\partial z} - \frac{\partial b}{\partial z}\frac{\partial M_{\mathrm{g}}^x}{\partial y}\right] \tag{59.94a}$$

$$= (\partial M_{\mathrm{g}}^x/\partial z)^{-1}\,\hat{\boldsymbol{x}} \cdot (\nabla b \times \nabla M_{\mathrm{g}}^x), \tag{59.94b}$$

which then leads to

$$\frac{(\partial b/\partial y)_{M_{\mathrm{g}}^x}}{\partial b/\partial z} = -\frac{(\partial M_{\mathrm{g}}^x/\partial y)_b}{\partial M_{\mathrm{g}}^x/\partial z}. \tag{59.95}$$

Furthermore, with $M^x_{\mathrm{g}} = u_{\mathrm{g}} - f\,y$ we have

$$\partial_z M^x_{\mathrm{g}} = \partial_z u_{\mathrm{g}} = -f^{-1}\,(\partial b/\partial y)_z, \tag{59.96}$$

so that

$$S^y_b\,(\partial b/\partial y)_{M^x_{\mathrm{g}}} = -f\,(\partial M^x_{\mathrm{g}}/\partial y)_b, \tag{59.97}$$

where we introduced the slope of the meridional buoyancy surface

$$S^y_b \equiv -\frac{\partial b/\partial y}{\partial b/\partial z}. \tag{59.98}$$

Use of the identity (59.97) in the instability condition (59.92a) leads to the equivalent expressions of a symmetrically unstable geostrophically balances state

$$f\left[\frac{\partial M^x_{\mathrm{g}}}{\partial y}\right]_b = -S^y_b\left[\frac{\partial b}{\partial y}\right]_{M^x_{\mathrm{g}}} > 0 \quad \Longrightarrow \text{symmetrically unstable} \tag{59.99a}$$

$$f\,N^2\left[\frac{\partial M^x_{\mathrm{g}}}{\partial y}\right]_b = \left[\frac{\partial b}{\partial y}\right]_z\left[\frac{\partial b}{\partial y}\right]_{M^x_{\mathrm{g}}} > 0 \Longrightarrow \text{symmetrically unstable.} \tag{59.99b}$$

Consider a configuration with buoyancy slopes rising to the north, so that the meridional buoyancy slope is positive, $S^y_b > 0$. Equation (59.99a) says that if the buoyancy decreases moving in the $+\hat{\boldsymbol{y}}$ direction while moving along constant potential momentum surfaces, then the flow is symmetrically unstable. Equivalently, equation (59.99b) says that if buoyancy has a meridional derivative of the same sign on both a constant z surface and a constant M^x_{g} surface, then the flow is symmetrically unstable. In Figure 59.7 we depict various properties of symmetrically unstable configurations.

59.7 Symmetric instability and the wedge of instability

We here formulate the stability of a symmetric front using geopotential vertical coordinate equations, thus serving as a complement to the analysis in Section 59.6 based on buoyancy as the vertical coordinate. Furthermore, we here focus on perturbations that lead to an instability if presented with a base flow state that is unstable. More precisely, we consider zonally symmetric perturbations (i.e., a row of fluid parcels) that carry buoyancy and zonal potential momentum from the initial position into a new position. The question is whether the displaced row of fluid parcels feels a net force that sends it back to where it came (stable perturbation), or if the force sends it further away (unstable perturbation). Through this analysis we show that flow configurations with buoyancy and potential momentum surfaces oriented as in Figure 59.7 admit unstable perturbations that probe the *wedge of instability* (see Figure 59.8). The existence of such perturbations is a signature of a symmetrically unstable background flow state.

59.7.1 Formulation of the basic equations

Take the inviscid Boussinesq equation (30.91b) as a starting point, here written as

$$\mathrm{D}M^x/\mathrm{D}t = 0 \quad \text{and} \quad \mathrm{D}v/\mathrm{D}t = f\,(M^x_{\mathrm{g}} - M^x) \quad \text{and} \quad \mathrm{D}w/\mathrm{D}t = -\partial_z\varphi + b. \tag{59.100}$$

The base state is assumed to be in geostrophic and hydrostatic balance, in which

$$\text{base flow state} \Longleftrightarrow \mathrm{D}\boldsymbol{v}/\mathrm{D}t = 0 \quad \text{and} \quad M^x = M^x_{\mathrm{g}} \quad \text{and} \quad \partial_z\varphi = b\,g. \tag{59.101}$$

To examine stability of this base state, displace a row of fluid parcels from its original y-z position, (y_A, z_A), to a new position,

$$y_B = y_A + \Delta y \quad \text{and} \quad z_B = z_A + \Delta z, \tag{59.102}$$

such as depicted in Figure 59.8. Notably, the buoyancy and potential momentum at point (y_B, z_B) are distinct from those at (y_A, z_A). Importantly, the displacement materially preserves the buoyancy and potential momentum of the displaced row of parcels, so that

$$b_{\text{parcel}} = b(A) \quad \text{and} \quad M^x_{\text{parcel}} = M^x(A) = M^x_{\text{g}}(A). \tag{59.103}$$

At the displaced position, the row of parcels finds itself in a local environment where it feels a nonzero acceleration. Does this acceleration act to further the displacement (unstable perturbation) or return the row of parcels to its original position (stable perturbation)?

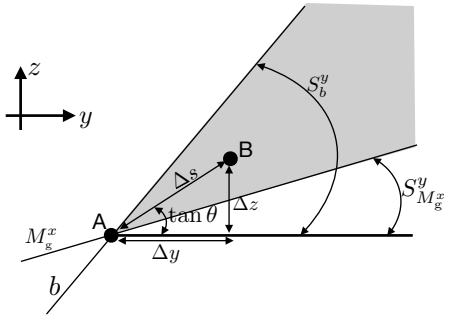

$$\tan\theta = \frac{\Delta z}{\Delta y}$$

$$S^y_b = \left[\frac{\Delta z}{\Delta y}\right]_b = -\frac{\partial b/\partial y}{\partial b/\partial z} = \frac{f\,\partial_z u_g}{N^2}$$

$$S^y_{M^x_g} = \left[\frac{\Delta z}{\Delta y}\right]_{M^x_g} = -\frac{\partial M^x_g/\partial y}{\partial M^x_g/\partial z} = \frac{\zeta_g + f}{\partial_z u_g}$$

FIGURE 59.8: Illustrating the parcel argument for symmetric instability, whereby we displace a zonally ($\hat{\boldsymbol{x}}$ points out of the page) symmetric row of parcels from A to B while retaining their buoyancy, $b(A)$, and potential momentum, $M^x(A) = M^x_{\text{g}}(A)$. We also depict the slope of the displacement, $\tan\theta = \Delta z/\Delta y$, the slope of the buoyancy surface, $S^y_b = (\Delta z/\Delta y)_b = f\,\partial_z u_{\text{g}}/N^2$, and slope of the potential momentum surface, $S^y_{M^x_{\text{g}}} = (\Delta y/\Delta z)_{M^x_{\text{g}}} = (\zeta_{\text{g}} + f)/\partial_z u_{\text{g}}$. When the buoyancy surface is sloped more steeply than the potential momentum surface, then that base state flow is subject to symmetrically unstable perturbations, with the unstable perturbations extending into the gray *wedge of instability*.

59.7.2 Assessing stability of the perturbation

To answer the above stability question, write the acceleration for the parcel displaced from point A to point B in the form

$$\frac{\mathrm{D}\boldsymbol{v}_{\text{parcel}}}{\mathrm{D}t} = f\,[M^x_{\text{g}}(B) - M^x_{\text{parcel}}]\,\hat{\boldsymbol{y}} + [b_{\text{parcel}} - \partial_z\varphi(B)]\,\hat{\boldsymbol{z}} \tag{59.104a}$$

$$= f\,[M^x_{\text{g}}(B) - M^x_{\text{parcel}}]\,\hat{\boldsymbol{y}} + [b_{\text{parcel}} - b(B)]\,\hat{\boldsymbol{z}}, \tag{59.104b}$$

where M^x_{g} and $\partial_z\varphi$ are taken from the base state at point B, and for the second equality we set the base state vertical pressure gradient equal to the buoyancy according to the hydrostatic balance, $\partial_z\varphi(B) = b(B)$. We are interested in whether this displacement leads to an acceleration of the parcel further in the direction of the displacement, beyond point B, in which case the base state is symmetrically unstable, otherwise it is stable.

To determine stability conditions, use material invariance of the potential momentum and buoyancy in the form of equation (59.103), thus leading to the parcel acceleration

$$\frac{\mathrm{D}\boldsymbol{v}_{\text{parcel}}}{\mathrm{D}t} = f\,[M^x_{\text{g}}(B) - M^x_{\text{g}}(A)]\,\hat{\boldsymbol{y}} + [b(A) - b(B)]\,\hat{\boldsymbol{z}}. \tag{59.105}$$

For orientation, let the unit vector in the direction of the displacement be written

$$\hat{\boldsymbol{s}} = \hat{\boldsymbol{y}} \cos\theta + \hat{\boldsymbol{z}} \sin\theta = \hat{\boldsymbol{y}} \, (\Delta y/\Delta s) + \hat{\boldsymbol{z}} \, (\Delta z/\Delta s), \tag{59.106}$$

where θ is the angle of the displacement with respect to the horizontal plane, and

$$\Delta s = \sqrt{(\Delta y)^2 + (\Delta z)^2}, \tag{59.107}$$

is the distance of the displacement (see Figure 59.8). Taking the $\hat{\boldsymbol{s}}$ projection of the parcel acceleration (59.105) leads to

$$\hat{\boldsymbol{s}} \cdot \frac{\mathrm{D}\boldsymbol{v}_{\text{parcel}}}{\mathrm{D}t} = f \, [M^x_{\text{g}}(B) - M^x_{\text{g}}(A)] \cos\theta - [b(B) - b(A)] \sin\theta. \tag{59.108}$$

Now expand the terms on the right hand side in a Taylor series, expressing values at point B in terms of those at point A, so that (keeping terms up to first order)

$$b(B) - b(A) = \partial_y b \, \Delta y + \partial_z b \, \Delta z = \Delta y \, (\partial_y b + \partial_z b \tan\theta) \tag{59.109a}$$

$$M^x_{\text{g}}(B) - M^x_{\text{g}}(A) = \partial_y M^x_{\text{g}} \, \Delta y + \partial_z M^x_{\text{g}} \, \Delta z = \Delta y \, (\partial_y M^x_{\text{g}} + \partial_z M^x_{\text{g}} \tan\theta), \tag{59.109b}$$

with terms on the right hand side evaluated at point A. These expansions bring the equation of motion (59.108) to

$$\hat{\boldsymbol{s}} \cdot \frac{\mathrm{D}\boldsymbol{v}_{\text{parcel}}}{\mathrm{D}t} = f \, \Delta y \, (\partial_y M^x_{\text{g}} + \partial_z M^x_{\text{g}} \tan\theta) \cos\theta - \Delta y \, (\partial_y b + \partial_z b \tan\theta) \sin\theta. \tag{59.110}$$

For a northward and upward perturbation as depicted in Figure 59.8, the symmetric perturbation is unstable if the right hand side of equation (59.110) is positive, which requires

$$f \, (\partial_y M^x_{\text{g}} + \partial_z M^x_{\text{g}} \tan\theta) \cos\theta > (\partial_y b + N^2 \tan\theta) \sin\theta, \tag{59.111}$$

which can be written in terms of the slope of the buoyancy surface, S^y_b, the slope of the potential momentum surface, $S^y_{M^x_{\text{g}}}$, and the slope of the perturbation, $\tan\theta$

$$f \, \partial_z M^x_{\text{g}} \, (\tan\theta - S^y_{M^x_{\text{g}}}) > \partial_z b \, (\tan\theta - S^y_b). \tag{59.112}$$

Finally, we make use of thermal wind

$$f \, \partial_z M^x_{\text{g}} = f \, \partial_z u_{\text{g}} = -\partial_y b, \tag{59.113}$$

so that the inequality (59.112) is

$$S^y_b \, (\tan\theta - S^y_{M^x_{\text{g}}}) > \tan\theta - S^y_b. \tag{59.114}$$

We now assume the following properties of the base state

$$S^y_b > 0 \quad \text{and} \quad S^y_{M^x_{\text{g}}} > 0 \quad \text{and} \quad \tan\theta > 0, \tag{59.115}$$

which correspond to the base state configuration in Figure 59.8. The inequality (59.114) yields the following condition for symmetric instability (as signaled by an acceleration in the direction of the displacement)

$$S^y_{M^x_{\text{g}}} < \tan\theta < S^y_b. \tag{59.116}$$

This slope condition means that a symmetric perturbation that falls within the wedge of instability in Figure 59.8 initiates a symmetric unstability. Conversely, perturbations that fall

outside of the wedge do not initiate a symmetric instability.

59.7.3 Symmetrically unstable while inertially and gravitationally stable

An alternative means to write the parcel acceleration equation (59.110) is given by

$$\hat{\boldsymbol{s}} \cdot \frac{\mathrm{D}\boldsymbol{v}_{\text{parcel}}}{\mathrm{D}t} = \Delta y \cos\theta \, [-f \, (f + \zeta_{\text{g}}) - N^2 \tan^2\theta + 2 \, f \, \partial_z u_{\text{g}} \tan\theta], \tag{59.117}$$

where we used $\partial_y M^x_{\text{g}} = -(f + \zeta_{\text{g}})$ and $\partial_z b = N^2$. The assumptions (59.115) are equivalent to (it is useful to prove this)

$$f \, (f + \zeta_{\text{g}}) > 0 \quad \text{and} \quad N^2 > 0, \tag{59.118}$$

which means the base state flow is stable to horizontal inertial instability and to gravitational instability. We thus find from equation (59.117) that the perturbation is unstable if

$$2 \, f \, \partial_z u_{\text{g}} \tan\theta > f \, (f + \zeta_{\text{g}}) + N^2 \tan^2\theta. \tag{59.119}$$

This instability condition is equivalent to the purely geometric form given by equation (59.116).

59.8 Symmetric instability and linear modal analysis

We now consider symmetric instability following the linear stability analysis of *Hoskins* (1974). This approach recovers the same stability condition as for the parcel method in Section 59.6. However, linear stability analysis offers added insights concerning the central role of Ertel potential vorticity and it provides further details of the instability. The mathematical analysis here also offers useful practice for the study of baroclinic instability in Chapter 62.

59.8.1 Geostrophic base state and the perturbation equations

Our goal is to examine the stability of a zonally symmetric geostrophic front to zonally symmetric perturbations. Whereas the base state for the study of gravity waves has zero baroclinicity, here we consider a geostrophic front with meridional (across-front) baroclinicity. Rather than the buoyancy coordinates used for the parcel stability analusis in Section 59.6.1, we here make use of geopotential vertical coordinates and linearize the Boussinesq ocean equations. The starting point for this development is the f-plane version of the perfect Boussinesq ocean equations from Section 29.1.6

$$\partial_t \boldsymbol{v} + (\boldsymbol{v} \cdot \nabla) \, \boldsymbol{v} + f \, \hat{\boldsymbol{z}} \times \boldsymbol{v} = -\nabla\varphi + b \, \hat{\boldsymbol{z}} \tag{59.120a}$$

$$\partial_t b + \boldsymbol{v} \cdot \nabla b = 0. \tag{59.120b}$$

Equations for the geostrophic base state

The equations describing the zonal geostrophic and hydrostatic base state are given by

$$f \, u_{\text{g}} = -\partial_y \varphi_{\text{g}} \quad \text{zonal flow in geostrophic balance} \tag{59.121a}$$

$$\partial_z \varphi_{\text{g}} = b_{\text{g}} \quad \text{hydrostatic balance} \tag{59.121b}$$

$$f \, \partial_z u_{\text{g}} = -\partial_y b_{\text{g}} \quad \text{thermal wind of zonal flow} \tag{59.121c}$$

$$\zeta_{\text{g}} = -\partial_y u_{\text{g}} \quad \text{relative vorticity.} \tag{59.121d}$$

The pressure field, $\varphi_{\text{g}}(y, z)$, has a meridional derivative that supports the zonal geostrophic flow, $u_{\text{g}}(y, z)$, and which is in hydrostatic balance with the base state buoyancy, $b_{\text{g}}(y, z)$. Combining geostrophy with the hydrostatic balance leads to the thermal wind shear in equation (59.121c).

Due to zonal symmetry, the only contribution to the relative vorticity comes from the meridional shear of the zonal geostrophic flow, $\zeta_{\mathrm{g}} = -\partial_y u_{\mathrm{g}}$. Ertel potential vorticity (Chapter 41) of the base state proves to be central to the stability conditions

$$Q_{\mathrm{g}} = (\omega_{\mathrm{g}} + f\,\hat{\boldsymbol{z}}) \cdot \nabla b_{\mathrm{g}} = N^2\,(f + \zeta_{\mathrm{g}}) - f\,(\partial_z u_{\mathrm{g}})^2, \tag{59.122}$$

where we made use of the thermal wind equation (59.121c) as well as the relative vorticity for the zonal geostrophic background flow

$$\omega_{\mathrm{g}} = \nabla \times \hat{\boldsymbol{x}}\, u_{\mathrm{g}} = \hat{\boldsymbol{y}}\, \partial_z u_{\mathrm{g}} - \hat{\boldsymbol{z}}\, \partial_y u_{\mathrm{g}} = -\hat{\boldsymbol{y}}\, f^{-1} \partial_y b_{\mathrm{g}} + \hat{\boldsymbol{z}}\, \zeta_{\mathrm{g}}. \tag{59.123}$$

Linearized perturbation equations

To develop perturbation equations, we decompose the flow into the geostrophic base state plus a perturbation. The perturbation is time dependent and ageostrophic, and, importantly, is assumed to retain the zonal symmetry of the base state

$$\boldsymbol{v}(y,z,t) = \boldsymbol{v}'(y,z,t) + \hat{\boldsymbol{x}}\, u_{\mathrm{g}}(y,z) \tag{59.124a}$$
$$\varphi(y,z,t) = \varphi'(y,z,t) + \varphi_{\mathrm{g}}(y,z) \tag{59.124b}$$
$$b(y,z,t) = b'(y,z,t) + b_{\mathrm{g}}(y,z). \tag{59.124c}$$

The linearized version of the velocity equation (59.120a) and buoyancy equation (59.120b) take the form

$$\partial_t u' = v'\,(f - \partial_y u_{\mathrm{g}}) - w'\,\partial_z u_{\mathrm{g}} \quad \text{zonal velocity} \tag{59.125a}$$
$$\partial_t v' = -f\,u' - \partial_y \varphi' \quad \text{meridional velocity} \tag{59.125b}$$
$$\partial_t w' = -\partial_z \varphi' + b' \quad \text{vertical velocity} \tag{59.125c}$$
$$\partial_t b' = -(v'\,\partial_y b_{\mathrm{g}} + w'\,\partial_z b_{\mathrm{g}}) \quad \text{buoyancy} \tag{59.125d}$$
$$\partial_y v' + \partial_z w' = 0 \quad \text{continuity.} \tag{59.125e}$$

Observe that the zonal velocity evolves according to the Coriolis acceleration plus the convergence of the advective flux of the base state geostrophic velocity

$$-v'\,\partial_y u_{\mathrm{g}} - w'\,\partial_z u_{\mathrm{g}} = -\nabla \cdot (\boldsymbol{v}'\,u_{\mathrm{g}}). \tag{59.126}$$

Likewise, the buoyancy evolves according to the convergence of the advective flux of the base state buoyancy

$$-(v'\,\partial_y b_{\mathrm{g}} + w'\,\partial_z b_{\mathrm{g}}) = -\nabla \cdot (\boldsymbol{v}'\,b_{\mathrm{g}}). \tag{59.127}$$

In both cases, the advection velocity arises from the non-divergent anomalous flow, $\boldsymbol{v}'$, with zonal symmetry meaning there is no contribution to the flux convergences from the anomalous zonal velocity, u'.

59.8.2 Inertia-vorticity oscillator equations

As in our study of buoyancy oscillations in Section 57.3 and inertia-gravity oscillations in Section 57.8, we here develop forced oscillator equations for the zonal and meridional velocity components. To do so, take a time derivative of the zonal velocity equation (59.125a) and then substitute the meridional velocity equation (59.125b) to find the zonal velocity oscillator equation

$$[\partial_{tt} + f\,(f + \zeta_{\mathrm{g}})]\,u' = -(f + \zeta_{\mathrm{g}})\,\partial_y \varphi' + \partial_z u_{\mathrm{g}}\,(\partial_z \varphi' - b'). \tag{59.128}$$

Similar manipulations lead to the forced oscillator equation for the meridional velocity

$$[\partial_{tt} + f\,(f + \zeta_{\rm g})]\,v' = f\,w'\,\partial_z u_{\rm g} - \partial_{ty}\varphi'. \tag{59.129}$$

The forcing functions on the right hand side of both equations (59.128) and (59.129) are generally nonzero. However, in their absence both the zonal and meridional velocity components satisfy a free oscillator equation with squared natural angular frequency, $f\,(f + \zeta_{\rm g})$. We refer to these as *inertia-vorticity* oscillations given the dual role of the Coriolis and vorticity for determining the oscillations. The motion is oscillatory if $f\,(f + \zeta_{\rm g}) > 0$, whereas it is exponentially growing if $f\,(f + \zeta_{\rm g}) < 0$. This stability condition for the oscillators is consistent with that found for the parcel stability analysis leading to equation (59.92a). To develop more insight into the nature of the instability for $f\,(f + \zeta_{\rm g}) < 0$, we next develop an equation for the overturning streamfunction in the meridional-vertical plane.

59.8.3 Ageostrophic overturning circulation streamfunction

The continuity equation (59.125e) means that the meridional-vertical circulation is non-divergent so that we can introduce a streamfunction for the perturbation flow

$$\boldsymbol{v}' = -\hat{\boldsymbol{x}} \times \nabla\psi \implies v' = \partial_z\psi \quad \text{and} \quad w' = -\partial_y\psi. \tag{59.130}$$

The perturbed fields are ageostrophic and are sometimes referred to as the *ageostrophic secondary circulation*, with this circulation described by the ageostrophic overturning circulation streamfunction, ψ. Based on the oscillator equations (59.128) and (59.129), we anticipate that the overturning circulation is unstable for $f\,(f + \zeta_{\rm g}) < 0$.

Zonal vorticity equation

Taking the z derivative of the meridional velocity equation (59.125b) and the y derivative of the vertical velocity equation (59.125c), and then subtracting, leads to the equation for the zonal component of the vorticity[12]

$$\partial_t(\partial_y w' - \partial_z v') - f\,\partial_z u' = \partial_y b', \tag{59.131}$$

which takes on the form using the overturning streamfunction

$$\partial_t(\partial_{yy} + \partial_{zz})\,\psi = -f\,\partial_z u' - \partial_y b'. \tag{59.132}$$

Further assumptions for the base state flow

To enable the next steps of the derivation, which makes use of a plane wave ansatz in Section 59.8.4, we make use of the following assumptions about the base state:

$$\zeta_{\rm g} = -\partial_y u_{\rm g} \quad \text{constant relative vorticity} \tag{59.133a}$$

$$f\,\partial_z u_{\rm g} = -\partial_y b_{\rm g} \quad \text{constant thermal wind shear} \tag{59.133b}$$

$$N^2 = \partial_z b_{\rm g} \quad \text{constant buoyancy frequency.} \tag{59.133c}$$

These assumptions are restrictive, and yet the resulting instabiliity calculation provides great insights into base state flow configurations that are more general.

[12]The zonal component of the perturbation vorticity is given by $\hat{\boldsymbol{x}} \cdot (\nabla \times \boldsymbol{v}') = \partial_y w' - \partial_z v' = -(\partial_{yy} + \partial_{zz})\psi$.

Eliminating the zonal velocity and the buoyancy

We can eliminate the perturbation zonal velocity, u', and the perturbation buoyancy, b', from the vorticity equation (59.132) by taking another time derivative. Upon doing so we make use of the zonal velocity equation (59.125a) and the buoyancy equation (59.125d), and make use of the assumptions (59.133a)-(59.133c) for the base state:

$$\begin{aligned} -\partial_{tt}(\partial_{yy} + \partial_{zz})\,\psi &= f\,\partial_{zt}u' + \partial_{yt}b' && \text{(59.134a)}\\ &= f\,\partial_z[v'\,(f + \zeta_{\mathrm{g}}) - w'\,\partial_z u_{\mathrm{g}}] - \partial_y(v'\,\partial_y b_{\mathrm{g}} + w'\,\partial_z b_{\mathrm{g}}) && \text{(59.134b)}\\ &= f\,\partial_{zz}\psi\,(f + \zeta_{\mathrm{g}}) - 2\,\partial_{yz}\psi\,\partial_y b_{\mathrm{g}} + \partial_{yy}\psi\,\partial_z b_{\mathrm{g}} && \text{(59.134c)}\\ &= [f\,(f + \zeta_{\mathrm{g}})\,\partial_{zz} + 2\,f\,\partial_z u_{\mathrm{g}}\,\partial_{yz} + N^2\,\partial_{yy}]\psi. && \text{(59.134d)} \end{aligned}$$

Rearrangement leads to the equation for the ageostrophic overturning circulation streamfunction

$$[\partial_{tt}(\partial_{yy} + \partial_{zz}) + f\,(f + \zeta_{\mathrm{g}})\,\partial_{zz} + 2\,f\,\partial_z u_{\mathrm{g}}\,\partial_{yz} + N^2\,\partial_{yy}]\,\psi = 0. \tag{59.135}$$

59.8.4 Dispersion relation for meridional-vertical plane waves

Equation (59.135) is a constant coefficient partial differential equation for the overturning streamfunction. We examine its properties by considering a plane wave ansatz just as for our study of linear waves in Part X of this book. Since the flow is non-divergent, the plane waves are transverse. Furthermore, we continue to assume zonal symmetry with the perturbations, so that the waves have no x dependence. We thus consider waves propagating in the meridional-vertical plane, in which case we take the plane wave ansatz

$$\psi(y, z, t) = \tilde{\psi}\,\mathrm{e}^{\mathrm{i}\,(k_y\,y + k_z\,z - \omega\,t)}, \tag{59.136}$$

with Figure 59.9 depicting the wave geometry. Plugging this ansatz into the streamfunction equation (59.135) leads to the dispersion relation

$$\begin{aligned} \omega^2 &= \frac{f\,(f + \zeta_{\mathrm{g}})\,k_z^2 + 2\,f\,\partial_z u_{\mathrm{g}}\,k_y\,k_z + N^2\,k_y^2}{k_y^2 + k_z^2} && \text{(59.137a)}\\ &= f\,(f + \zeta_{\mathrm{g}})\cos^2\alpha + 2\,f\,\partial_z u_{\mathrm{g}}\sin\alpha\cos\alpha + N^2\sin^2\alpha && \text{(59.137b)}\\ &= \cos^2\alpha\,[f\,(f + \zeta_{\mathrm{g}}) + 2\,f\,\partial_z u_{\mathrm{g}}\tan\alpha + N^2\tan^2\alpha]. && \text{(59.137c)} \end{aligned}$$

Note that the convention for symmetric instability is to use the angle, α, that the particle trajectories make with the vertical, whereas for our study of internal gravity waves (Section 57.5) and inertia-gravity waves (Section 57.9), we used the angle $\gamma = \pi/2 - \alpha$ that the phase velocity makes with the horizontal. Either way, we see that the dispersion relation (59.137c) depends only on the wave direction along with the prescribed rotation and properties of the background flow. This "orientation-only" character of the dispersion relation is also shared by the dispersion relation for internal gravity waves (equation (57.65)) and inertia-gravity waves (equation (57.147)). Indeed, for the case with zero baroclinicity, in which $u_{\mathrm{g}} = 0$, then the dispersion relation (59.137c) reduces to that for inertia-gravity waves.

59.8.5 Stability conditions

The dispersion relation (59.137c) determines the squared angular frequency, ω^2, for a plane wave ansatz. If $\omega^2 > 0$ then there are propagating waves. However, if $\omega^2 < 0$ then the waves can be exponentially growing, in which case we say the flow is unstable. To determine the condition for

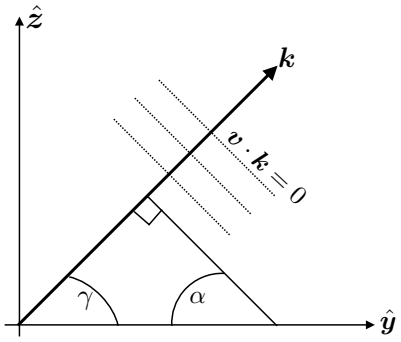

$$\begin{aligned}
&\boldsymbol{k} = \hat{\boldsymbol{y}}\, k_y + \hat{\boldsymbol{z}}\, k_z \\
&\cos\gamma = \sin\alpha = k_y/|\boldsymbol{k}| \\
&\sin\gamma = \cos\alpha = k_z/|\boldsymbol{k}| \\
&\tan\alpha = k_y/k_z \\
&\tan\gamma = k_z/k_y \\
&\alpha = \pi/2 - \gamma
\end{aligned}$$

FIGURE 59.9: Transverse plane wave used to probe the stability of a baroclinic front. The phase vector, $\boldsymbol{k}$, makes an angle γ with the horizontal and α with the vertical.

stability, write the dispersion relation in the form

$$\omega^2 = F(\tan\alpha)\cos^2\alpha, \tag{59.138}$$

where we introduced the quadratic stability function

$$F(\tau) = f\,(f + \zeta_{\mathrm{g}}) + (2\,f\,\partial_z u_{\mathrm{g}})\,\tau + N^2\,\tau^2. \tag{59.139}$$

The question of stability has been reduced to the question of whether there are wave perturbations that realize $F(\tan\alpha) < 0$, in which case $\omega^2 < 0$. To answer this question we write

$$F(\tau) = (\tau - R_+)\,(\tau - R_-), \tag{59.140}$$

with the two roots given by the quadratic formula

$$N^2\,R_\pm = -f\,\partial_z u_{\mathrm{g}} \pm \sqrt{(f\,\partial_z u_{\mathrm{g}})^2 - N^2\,f\,(f + \zeta_{\mathrm{g}})} = -f\,\partial_z u_{\mathrm{g}} \pm \sqrt{-f\,Q_{\mathrm{g}}}, \tag{59.141}$$

where the final equality introduced the base state potential vorticity, Q_{g}, from equation (59.122). Remarkably, local stability has boiled down to the sign of $f\,Q_{\mathrm{g}}$ at any point within the fluid.

Stable case

If $f\,Q_{\mathrm{b}} > 0$, then the two roots, $R_\pm$, are complex conjugates. Yet $\tan\alpha$ is real for all waves with real wavevectors. Hence, if $f\,Q_{\mathrm{g}} > 0$ then there are no waves for which $F(\tan\alpha)$ vanishes, meaning that the stability function has one sign for all waves. To establish the sign, note that for very weak fronts in stably stratified fluids,

$$F(\tau) \approx f^2 + N^2\,\tau^2 > 0, \tag{59.142}$$

which is the case for linear, and stable, inertia-gravity waves. Ramping up the strength of the geostrophic front, while maintaining $f\,Q_{\mathrm{g}} > 0$, ensures that such geostrophic fronts are locally stable.

For the typical case in stratified geophysical fluids, we have $N^2 > f^2$, so that the maximum angular frequency (59.137c) occurs with horizontally propagating waves where $\alpha = \pi/2$ so that

$$\omega^2_{\mathrm{max}} = N^2, \tag{59.143}$$

in which case fluid particles exhibit buoyancy oscillations in the vertical. At the other end of the spectrum, the minimum angular frequency occurs when $\alpha = 0$ so that the wavevector is vertical

and

$$\omega^2_{\text{min}} = f\,(f + \zeta_{\text{g}}), \tag{59.144}$$

which are inertial oscillations in the presence of a nonzero relative vorticity.

Unstable case

If $f\,Q_{\text{g}} < 0$ then the two roots, $R_\pm$, are real

$$R_\pm = \frac{-f\,\partial_z u_{\text{g}} \pm \sqrt{|f\,Q_{\text{g}}|}}{N^2}, \tag{59.145}$$

thus ensuring that there are waves that render $F(\tan\alpha) = 0$. Hence, the stability function changes sign so that waves are unstable if $\omega^2 < 0$. In the unstable case, ω is not an angular frequency but instead it measures the exponential *growth rate* for the unstable wave.

59.8.6 Ertel potential vorticity and local stability

In developing the stability conditions in Section 59.8.5, appearance of the Ertel potential vorticity might not have seemed so remarkable. Namely, it seemingly just provided a useful shorthand for the discriminant of the square root appearing the quadratic formula. In fact, potential vorticity is central to the power of the stability analysis since it provides a direct connection to physical processes required to initiate symmetric instability. Namely, potential vorticity is materially invariant in a perfect fluid (Chapters 41 and 42). Hence, if a fluid starts in a stable state with $f\,Q > 0$, say it starts with zero baroclinicity and with stable stratification so that $f\,Q = f^2\,N^2 > 0$, then it has very restrictive means to evolve into an unstable state with $f\,Q < 0$. One means for inducing $f\,Q < 0$ is to introduce friction, diffusion, boundary processes, and/or other irreversible processes that materially alter Q in such a manner that brings $f\,Q < 0$. Another means is for a perfect fluid parcel to cross the equator so that f changes sign. If the parcel starts from a side of the equator with $f\,Q > 0$, then on the other side it has $f\,Q < 0$ and so it is symmetrically unstable.

As noted by *Thomas et al.* (2013), the instability criteria, $f\,Q < 0$, embodies three instabilities. Namely, for a barotropic fluid, whereby $\nabla_{\text{h}} b = 0$, then the potential vorticity is given by

$$f\,Q = f\,(f + \zeta)\,N^2. \tag{59.146}$$

The $f\,Q > 0$ stability criteria is satisfied with $N^2 > 0$ (gravitational stability; Section 30.6) and $f\,(f + \zeta) > 0$ (horizontal inertial stability; Section 59.5). In the presence of baroclinicity with a symmetric front, the $f\,Q > 0$ stability criteria then reflects symmetric stability of the present section. *Buckingham et al.* (2021) offer a generalization of the stability criteria by allowing for curvature of the front, thus providing a criteria to determine stability with regard to gravitational, centrifugal, horizontal inertial, and symmetric instabilities.

59.8.7 Comments and further study

The bulk of this section is an elaboration of *Hoskins* (1974), which exposed the connection between symmetric instability and Ertel potential vorticity. The study from *Thomas et al.* (2013) provides an example of these ideas for the ocean, offering practical details to map out stability regimes across the spectrum of gravitational, inertial, and symmetric instabilities. *Buckingham et al.* (2021) generalized *Hoskins* (1974) to the allow for a curved front.

59.9 Semi-geostrophy and ageostrophic overturning

We here study the overturning circulation that arises in a symmetric front on an f-plane. This overturning circulation is ageostrophic, and it is sometimes referred to as the *ageostrophic secondary circulation*. *Hoskins* (1975) advanced the study of frontal secondary circulations by rationalizing the equations of *semi-geostrophy*, making use of the *geostrophic momentum approximation*. Semi-geostrophy is a balanced theory (i.e., gravity waves are filtered), just like in the quasi-geostrophic theory of Chapter 45. However, the semi-geostrophic equations allow us to study flows associated with fronts and where the cross-front flows can have relatively small length scales sufficient to reach order unity Rossby numbers. Hence, semi-geostrophic equations are quite useful for studying submesoscale flows surrounding geostrophic fronts and eddies (e.g., see the book chapter by *Thomas et al.* (2008)), as well as the study of atmospheric fronts associated with synoptic scale weather patterns (which motivated *Hoskins* (1975); see also Chapter 9 of *Holton and Hakim* (2013)). In this section we provide just a taste of semi-geostrophy sufficient to derive a diagnostic equation for the ageostrophic secondary overturning circulation.

59.9.1 Hydrostatic and Boussinesq ocean on an f-plane

We develop the semi-geostrophic equations within the perfect fluid hydrostatic Boussinesq ocean equations (see Section 43.7) on an f-plane

$$\frac{\mathrm{D}\boldsymbol{u}}{\mathrm{D}t} + f\,\hat{\boldsymbol{z}} \times \boldsymbol{u} = -\nabla_{\mathrm{h}}\varphi \tag{59.147a}$$

$$\partial_z \varphi = b \tag{59.147b}$$

$$\frac{\mathrm{D}b}{\mathrm{D}t} = 0 \tag{59.147c}$$

$$\nabla \cdot \boldsymbol{v} = \nabla_{\mathrm{h}} \cdot \boldsymbol{u} + \partial_z w = 0. \tag{59.147d}$$

The geostrophic velocity is written in terms of the pressure field

$$\boldsymbol{u}_{\mathrm{g}} = f^{-1}\,\hat{\boldsymbol{z}} \times \nabla_{\mathrm{h}}\varphi \Longrightarrow u_{\mathrm{g}} = -f^{-1}\,\partial_y \varphi \quad \text{and} \quad v_{\mathrm{g}} = f^{-1}\,\partial_x \varphi, \tag{59.148}$$

which is horizontally non-divergent on the f-plane. It is notable that this geostrophic velocity is written in terms of the pressure field, φ, just like in the planetary geostrophic theory of Chapter 44. It also accords with the gauge choice discussed in Section 45.3.9 for quasi-geostrophy.

Inserting the geostrophic velocity (59.148) into the horizontal momentum equation (59.147a) yields the identity

$$\boldsymbol{u} - \boldsymbol{u}_{\mathrm{g}} = \hat{\boldsymbol{z}} \times \mathcal{D}\boldsymbol{u} \Longrightarrow u - u_{\mathrm{g}} = -\mathcal{D}v \quad \text{and} \quad v - v_{\mathrm{g}} = \mathcal{D}u, \tag{59.149}$$

where we introduced the dimensionless material time derivative operator

$$\mathcal{D} = \frac{1}{f}\frac{\mathrm{D}}{\mathrm{D}t}. \tag{59.150}$$

The horizontal ageostrophic flow can thus be written

$$\boldsymbol{u}_{\mathrm{ag}} = \boldsymbol{u} - \boldsymbol{u}_{\mathrm{g}} = \hat{\boldsymbol{z}} \times \mathcal{D}\boldsymbol{u}, \tag{59.151}$$

with one iteration of this equation leading to

$$\boldsymbol{u}_{\mathrm{ag}} = \hat{\boldsymbol{z}} \times \mathcal{D}\boldsymbol{u}_{\mathrm{g}} - \mathcal{D}^2\boldsymbol{u} \Longrightarrow u_{\mathrm{ag}} = -\mathcal{D}(v_{\mathrm{g}} + \mathcal{D}u) \quad \text{and} \quad v_{\mathrm{ag}} = \mathcal{D}(u_{\mathrm{g}} - \mathcal{D}v). \tag{59.152}$$

This identity motivates the *geostrophic momentum approximation* in Section 59.9.3 that ignores the $\mathcal{D}^2\boldsymbol{u}$ term.

59.9.2 Scaling for frontal flows

For f-plane flow, we lose no generality by orienting the front parallel to the $\hat{\boldsymbol{x}}$ direction, so that the across-front flow is in the $\hat{\boldsymbol{y}}$ direction. We write U for the velocity scale of the along-front flow and L_x for the corresponding length scale.[13] Likewise, write V and L_y for the across-front scales, with our interest in flows satisfying the inequalities

$$L_x \gg L_y \quad \text{and} \quad U \gg V \quad \text{with} \quad L_x/L_y = U/V. \tag{59.153}$$

Inserting these scales into horizontal momentum equation (59.147a) yields

$$\frac{U}{T} + \frac{U\,U}{L_x} + \frac{U\,V}{L_y} - f\,V = -\Phi/L_x \tag{59.154a}$$

$$\frac{V}{T} + \frac{V\,U}{L_x} + \frac{V\,V}{L_y} + f\,U = -\Phi/L_y, \tag{59.154b}$$

where Φ is the pressure scale. Now introduce two Rossby numbers according to

$$\mathrm{Ro}_x = \frac{U}{f\,L_x} \quad \text{and} \quad \mathrm{Ro}_y = \frac{V}{f\,L_y}, \tag{59.155}$$

and then divide equation (59.154a) by $f\,V$ and equation (59.154b) by $f\,U$, thus yielding

$$\mathrm{Ro}_x\,\frac{L_x}{T\,V} + \mathrm{Ro}_x\,\frac{U}{V} + \mathrm{Ro}_x\,\frac{L_x}{L_y} - 1 = -\frac{\Phi}{L_x\,f\,V} \tag{59.156a}$$

$$\mathrm{Ro}_y\,\frac{L_y}{T\,U} + \mathrm{Ro}_y\,\frac{V}{U} + \mathrm{Ro}_y\,\frac{L_y}{L_x} + 1 = -\frac{\Phi}{L_y\,f\,U}. \tag{59.156b}$$

Now assume the time scale is advective so that

$$T = L_x/U = L_y/V, \tag{59.157}$$

in which case equations (59.156a) and (59.156b) become

$$\mathrm{Ro}_x\,L_x/L_y + \mathrm{Ro}_x\,U/V + \mathrm{Ro}_x\,L_x/L_y - 1 = -\Phi/(L_x\,f\,V) \tag{59.158a}$$

$$\mathrm{Ro}_y\,L_y/L_x + \mathrm{Ro}_y\,V/U + \mathrm{Ro}_y\,L_y/L_x + 1 = -\Phi/(L_y\,f\,U). \tag{59.158b}$$

Consider the across-front momentum equation (59.158b). Since $L_y/L_x = V/U \ll 1$, and assuming Ro_y is at most order unity, terms in the across-front momentum equation (59.158b) balance only if the along-front flow is geostrophic

$$f\,U = -\Phi/L_y. \tag{59.159}$$

In turn, the along-front flow has a small Rossby number, $\mathrm{Ro}_x \ll 1$. We emphasize that the along-front flow is geostrophic even if $\mathrm{Ro}_y \sim 1$. In contrast, even with $\mathrm{Ro}_x \ll 1$, each term in equation (59.158a) can be order unity since $U/V = L_x/L_y \gg 1$, so that the across-front flow is not geostrophic. That is, $\mathrm{Ro}_y \sim 1$, so that the across-front flow is ageostrophic.

[13] The radius of curvature for the front provides a suitable along-front length scale. Recall we introduced the radius of curvature in decomposing horizontal flows in Chapter 32. Also, the mathematics of the radius of curvature was introduced in Chapter 5.

Semi-geostrophy is designed to study flow along and across geostrophic fronts, with the along front flow geostrophic and across-front flow ageostrophic. Equivalently, semi-geostrophy is designed to study flows with relatively large cross-front shear induced relative vorticity (and small curvature induced relative vorticity), with correspondingly large vertical velocity magnitudes, both of which are signatures of $\mathrm{Ro}_y \sim 1$ flow (see Section 3 of *Hoskins* (1975)).[14]

59.9.3 Geostrophic momentum approximation

The *geostrophic momentum approximation* assumes the horizontal ageostrophic velocity is given by

$$\boldsymbol{u}_{\text{ag}} \approx \hat{\boldsymbol{z}} \times \mathcal{D}\boldsymbol{u}_{\text{g}}, \tag{59.160}$$

which results from truncating equation (59.152) at the leading order. From equation (59.152) we see that the geostrophic momentum approximation holds so long as the horizontal velocity components satisfy the following respective inequalities

$$|u| \gg |\mathcal{D}^2 u| \implies f^2 \gg \left| \frac{1}{u} \frac{\mathrm{D}^2 u}{\mathrm{D}t^2} \right| \tag{59.161a}$$

$$|v| \gg |\mathcal{D}^2 v| \implies f^2 \gg \left| \frac{1}{v} \frac{\mathrm{D}^2 v}{\mathrm{D}t^2} \right|. \tag{59.161b}$$

These inequalities are satisfied if the Lagrangian timescale of variability for the flow (both its magnitude and direction; see Section 3 of *Hoskins* (1975)) is much longer than an inertial period. Rearranging the geostrophic momentum approximation (59.160) leads to

$$\mathcal{D}\boldsymbol{u}_{\text{g}} + \hat{\boldsymbol{z}} \times \boldsymbol{u}_{\text{ag}} = 0, \tag{59.162}$$

which is equivalent to

$$\frac{\mathrm{D}\boldsymbol{u}_{\text{g}}}{\mathrm{D}t} + f\hat{\boldsymbol{z}} \times \boldsymbol{u}_{\text{ag}} = 0, \tag{59.163}$$

Hence, for the geostrophic momentum approximation, the material time evolution of the geostrophic velocity is forced by the Coriolis acceleration arising from the horizontal ageostrophic velocity. Furthermore, the material time derivative for the semi-geostrophic system is given by

$$\frac{\mathrm{D}}{\mathrm{D}t} = \partial_t + \boldsymbol{v} \cdot \nabla = \partial_t + (\boldsymbol{u}_{\text{g}} + \boldsymbol{u}_{\text{ag}}) \cdot \nabla_{\text{h}} + w_{\text{ag}}\, \partial_z, \tag{59.164}$$

with

$$\boldsymbol{v} = (\boldsymbol{u}_{\text{g}} + \boldsymbol{u}_{\text{ag}}) + \hat{\boldsymbol{z}}\, w_{\text{ag}}. \tag{59.165}$$

Note that any vertical flow is ageostrophic, so that it is not really necessary to place the "ag" subscript on w_{ag}. Even so, we do so to remind us that it lives at the same order as the horizontal ageostrophic flow, $\boldsymbol{u}_{\text{ag}}$. Furthermore, note that the key distinction between semi-geostrophy and quasi-geostrophy is the presence of w_{ag} in the material time derivative operator for semi-geostrophy, whereas quasi-geostrophy only makes use of advection by the geostrophic flow (see Section 45.3.9).

The geostrophic momentum approximation is consistent with the frontal scaling given in Section 59.9.2, and so it offers a suitable starting point for the study of frontal dynamics. Even so, to make use of the geostrophic momentum approximation to evolve the geostrophic flow requires further work since the ageostrophic velocity appears as part of the material time derivative operator. This situation is analogous to quasi-geostrophy, whereby evolution of the geostrophic flow arises from ageostrophic processes. To derive a closed equation set, *Hoskins* (1975) developed

[14] In Section 38.5 we decomposed relative vorticity into from cross-flow shear and along-flow curvature.

the semi-geostrophic momentum equations via a coordinate transformation to *geostrophic coordinates*, making use also of material constancy of the buoyancy and potential vorticity.[15] We do not present that formulation here. Instead, we focus on deriving a diagnostic equation for the secondary ageostrophic overturning circulation, with the manipulations reminiscent of those used in Section 59.8 for symmetric instability of a baroclinic front.

59.9.4 Geostrophic evolution of the buoyancy gradient

As a preface to the diagnostic equations for the ageostrophic flow, consider the evolution of the horizontal buoyancy gradient, considering just that evolution arising from geostrophic flow. Recall that for the Boussinesq ocean, the horizontal gradient of buoyancy provides a measure of baroclinicity (Section 40.7.2). Flow processes that increase the magnitude of the buoyancy gradient lead to growth of the thermal wind flow and thus the frontal strength.

Start by considering the buoyancy equation for adiabatic and geostrophic flow

$$(\partial_t + \boldsymbol{u}_{\mathsf{g}} \cdot \nabla_{\mathsf{h}})\, b = 0. \tag{59.166}$$

Separately taking the zonal and meridional derivatives and rearranging leads to

$$(\partial_t + \boldsymbol{u}_{\mathsf{g}} \cdot \nabla_{\mathsf{h}})(\partial_x b) = -\partial_x \boldsymbol{u}_{\mathsf{g}} \cdot \nabla_{\mathsf{h}} b \quad \text{and} \quad (\partial_t + \boldsymbol{u}_{\mathsf{g}} \cdot \nabla_{\mathsf{h}})(\partial_y b) = -\partial_y \boldsymbol{u}_{\mathsf{g}} \cdot \nabla_{\mathsf{h}} b, \tag{59.167}$$

which can be combined to

$$(\partial_t + \boldsymbol{u}_{\mathsf{g}} \cdot \nabla_{\mathsf{h}})(\nabla_{\mathsf{h}} b) = \mathbf{Q}, \tag{59.168}$$

where we introduced the horizontal vector

$$\mathbf{Q} = -(\partial_x \boldsymbol{u}_{\mathsf{g}} \cdot \nabla_{\mathsf{h}} b)\, \hat{\boldsymbol{x}} - (\partial_y \boldsymbol{u}_{\mathsf{g}} \cdot \nabla_{\mathsf{h}} b)\, \hat{\boldsymbol{y}}. \tag{59.169}$$

Correspondingly, geostrophic evolution of the squared buoyancy gradient is

$$(\partial_t + \boldsymbol{u}_{\mathsf{g}} \cdot \nabla_{\mathsf{h}})|\nabla_{\mathsf{h}} b|^2 = 2\, \mathbf{Q} \cdot \nabla_{\mathsf{h}} b. \tag{59.170}$$

Evidently, the buoyancy gradient grows in magnitude if $\mathbf{Q}$ has a positive projection onto the horizontal buoyancy gradient.

59.9.5 Secondary ageostrophic circulation

In Sections 59.5 and 59.6 we focused on the stability of a geostrophically balanced equilibrium with flow along a symmetric front. In addition to the geostrophic flow along the front, there is generally an ageostrophic circulation that circulates in the plane orthogonal to the front. We here derive an equation describing this overturning circulation, and then specialize that equation in Section 59.9.6 to a zonally symmetric front. For this purpose, start from the zonal momentum equation, buoyancy equation, and continuity equation within the semi-geostrophic system

$$\partial_t u_{\mathsf{g}} + (\boldsymbol{u}_{\mathsf{g}} \cdot \nabla_{\mathsf{h}}) u_{\mathsf{g}} + (\boldsymbol{u}_{\mathsf{ag}} \cdot \nabla_{\mathsf{h}}) u_{\mathsf{g}} + w_{\mathsf{ag}}\, \partial_z u_{\mathsf{g}} - f v_{\mathsf{ag}} = 0 \tag{59.171a}$$

$$\partial_t b + \boldsymbol{u}_{\mathsf{g}} \cdot \nabla_{\mathsf{h}} b + \boldsymbol{u}_{\mathsf{ag}} \cdot \nabla_{\mathsf{h}} b + w_{\mathsf{ag}} N^2(z) = 0 \tag{59.171b}$$

$$\partial_x u_{\mathsf{ag}} + \partial_y v_{\mathsf{ag}} + \partial_z w_{\mathsf{ag}} = 0. \tag{59.171c}$$

[15] Some authors reserve the name *semi-geostrophy* for the transformed equations derived by *Hoskins* (1975).

The vertical derivative of the zonal momentum equation (59.171a) leads to

$$\partial_t\partial_z u_{\mathrm{g}} + (\partial_z \boldsymbol{u}_{\mathrm{g}}\cdot\nabla_{\mathrm{h}})u_{\mathrm{g}} + (\boldsymbol{u}_{\mathrm{g}}\cdot\nabla_{\mathrm{h}})\partial_z u_{\mathrm{g}} + (\partial_z \boldsymbol{u}_{\mathrm{ag}}\cdot\nabla_{\mathrm{h}})u_{\mathrm{g}} + (\boldsymbol{u}_{\mathrm{ag}}\cdot\nabla_{\mathrm{h}})\partial_z u_{\mathrm{g}} + \partial_z(w_{\mathrm{ag}}\,\partial_z u_{\mathrm{g}}) - f\,\partial_z v_{\mathrm{ag}} = 0, \quad (59.172)$$

and the meridional derivative of the buoyancy equation (59.171b) yields

$$\partial_t\partial_y b + (\partial_y \boldsymbol{u}_{\mathrm{g}}\cdot\nabla_{\mathrm{h}})b + (\boldsymbol{u}_{\mathrm{g}}\cdot\nabla_{\mathrm{h}})\partial_y b + (\partial_y \boldsymbol{u}_{\mathrm{ag}}\cdot\nabla_{\mathrm{h}})b + (\boldsymbol{u}_{\mathrm{ag}}\cdot\nabla_{\mathrm{h}})\partial_y b + \partial_y w_{\mathrm{ag}}\,N^2 = 0. \quad (59.173)$$

The thermal wind relation,

$$f\,\partial_z \boldsymbol{u}_{\mathrm{g}} = \hat{\boldsymbol{z}}\times\nabla_{\mathrm{h}} b \Longrightarrow \partial_z u_{\mathrm{g}} = -f^{-1}\,\partial_y b \quad \text{and} \quad \partial_z v_{\mathrm{g}} = f^{-1}\,\partial_x b, \quad (59.174)$$

brings equation (59.172) to the form

$$\partial_t(\partial_y b) - f\,(\partial_z \boldsymbol{u}_{\mathrm{g}}\cdot\nabla_{\mathrm{h}})u_{\mathrm{g}} + (\boldsymbol{u}_{\mathrm{g}}\cdot\nabla_{\mathrm{h}})\partial_y b - f\,(\partial_z \boldsymbol{u}_{\mathrm{ag}}\cdot\nabla_{\mathrm{h}})u_{\mathrm{g}} + (\boldsymbol{u}_{\mathrm{ag}}\cdot\nabla_{\mathrm{h}})\partial_y b + \partial_z(w_{\mathrm{ag}}\,\partial_y b) + f^2\partial_z v_{\mathrm{ag}} = 0, \quad (59.175)$$

and equation (59.173) becomes

$$\partial_t(\partial_y b) + (\partial_y \boldsymbol{u}_{\mathrm{g}}\cdot\nabla_{\mathrm{h}})b + (\boldsymbol{u}_{\mathrm{g}}\cdot\nabla_{\mathrm{h}})\partial_y b + (\partial_y \boldsymbol{u}_{\mathrm{ag}}\cdot\nabla_{\mathrm{h}})b + (\boldsymbol{u}_{\mathrm{ag}}\cdot\nabla_{\mathrm{h}})\partial_y b + \partial_y w_{\mathrm{ag}}\,N^2 = 0. \quad (59.176)$$

Subtracting equation (59.176) from equation (59.175) eliminates the time derivative thus revealing the diagnostic relation

$$-f\,(\partial_z \boldsymbol{u}_{\mathrm{g}}\cdot\nabla_{\mathrm{h}})u_{\mathrm{g}} - f\,(\partial_z \boldsymbol{u}_{\mathrm{ag}}\cdot\nabla_{\mathrm{h}})u_{\mathrm{g}} + \partial_z\,(w_{\mathrm{ag}}\,\partial_y b) + f^2\,\partial_z v_{\mathrm{ag}} - (\partial_y \boldsymbol{u}_{\mathrm{g}}\cdot\nabla_{\mathrm{h}})b - (\partial_y \boldsymbol{u}_{\mathrm{ag}}\cdot\nabla_{\mathrm{h}})b - \partial_y w_{\mathrm{ag}}\,N^2 = 0. \quad (59.177)$$

Making use of thermal wind and horizontal non-divergence for the geostrophic velocity allows us to write

$$f(\partial_z \boldsymbol{u}_{\mathrm{g}}\cdot\nabla_{\mathrm{h}})u_{\mathrm{g}} = (\partial_y \boldsymbol{u}_{\mathrm{g}}\cdot\nabla_{\mathrm{h}})b = -\mathrm{Q}^y, \quad (59.178)$$

where Q^y is the meridional component of the geostrophic $\mathbf{Q}$-vector introduced in Section 45.4.1 (see equation (45.67)).[16]

$$\mathbf{Q} \equiv -(\partial_x \boldsymbol{u}_{\mathrm{g}}\cdot\nabla_{\mathrm{h}} b)\,\hat{\boldsymbol{x}} - (\partial_y \boldsymbol{u}_{\mathrm{g}}\cdot\nabla_{\mathrm{h}} b)\,\hat{\boldsymbol{y}}. \quad (59.179)$$

Introduction of Q^y into equation (59.177) yields

$$-f\,(\partial_z \boldsymbol{u}_{\mathrm{ag}}\cdot\nabla_{\mathrm{h}})u_{\mathrm{g}} + \partial_z w_{\mathrm{ag}}\,\partial_y b + w_{\mathrm{ag}}\,\partial_{yz} b + f^2\,\partial_z v_{\mathrm{ag}} - (\partial_y \boldsymbol{u}_{\mathrm{ag}}\cdot\nabla_{\mathrm{h}})b - \partial_y w_{\mathrm{ag}} N^2 = -2\,\mathrm{Q}^y. \quad (59.180)$$

Again making use of thermal wind and $\nabla_{\mathrm{h}}\cdot\boldsymbol{u}_{\mathrm{g}} = 0$ renders

$$-f\,(\partial_z \boldsymbol{u}_{\mathrm{ag}}\cdot\nabla_{\mathrm{h}})u_{\mathrm{g}} - (\partial_y \boldsymbol{u}_{\mathrm{ag}}\cdot\nabla_{\mathrm{h}})b = f\partial_z u_{\mathrm{ag}}\,\partial_y v_{\mathrm{g}} - f\partial_z v_{\mathrm{ag}}\,\partial_y u_{\mathrm{g}} + f\partial_y u_{\mathrm{ag}}\,\partial_z v_{\mathrm{g}} + f\partial_y v_{\mathrm{ag}}\,\partial_z u_{\mathrm{g}}. \quad (59.181)$$

The mixed partial derivative of the buoyancy vanishes

$$\frac{\partial^2 b}{\partial z\partial y} = \frac{\partial}{\partial y}\frac{\partial b}{\partial z} = \frac{\partial N^2(z)}{\partial y} = 0, \quad (59.182)$$

[16] Be careful to distinguish the geostrophic $\mathbf{Q}$-vector from the potential vorticity, Q. In particular, note the upright $\mathbf{Q}$ versus the slanted Q.

which follows since the background vertical stratification is assumed to be independent of the horizontal direction. Bringing these results together into equation (59.180) leads to

$$f\partial_z u_{\text{ag}}\,\partial_y v_{\text{g}} + f\partial_y u_{\text{ag}}\,\partial_z v_{\text{g}} + f\partial_y v_{\text{ag}}\,\partial_z u_{\text{g}} + \partial_z w_{\text{ag}}\,\partial_y b + f\partial_z v_{\text{ag}}\,(f - \partial_y u_{\text{g}}) - \partial_y w_{\text{ag}} N^2 = -2\mathrm{Q}^y, \quad (59.183)$$

with another use of thermal wind yielding

$$f\partial_z u_{\text{ag}}\,\partial_y v_{\text{g}} + f\partial_y u_{\text{ag}}\,\partial_z v_{\text{g}} + f\partial_z u_{\text{g}}\,(\partial_y v_{\text{ag}} - \partial_z w_{\text{ag}}) + f\partial_z v_{\text{ag}}\,(f - \partial_y u_{\text{g}}) - \partial_y w_{\text{ag}} N^2 = -2\mathrm{Q}^y. \quad (59.184)$$

This equation provides a relation for the ageostrophic cross-flow and vertical circulation, $(v_{\text{ag}}, w_{\text{ag}})$, written in terms of the buoyancy field and the geostrophic flow. We next next consider flow surrounding a symmetric front, in which case equation (59.184) becomes a diagnostic equation for the ageostrophic overturning streamfunction.

59.9.6 Ageostrophic overturning circulation for a symmetric front

Equation ((59.184) is now specialized by assuming the zonal velocity is purely geostrophic (as in a zonal geostrophic front) so that

$$u_{\text{ag}} = 0. \quad (59.185)$$

For this flow, the ageostrophic flow in the cross-flow/depth plane is non-divergent

$$\partial_y v_{\text{ag}} + \partial_z w_{\text{ag}} = 0. \quad (59.186)$$

The diagnostic equation (59.184) now takes on the specialized form for a symmetric front

$$-2\,f\,\partial_z u_{\text{g}}\,\partial_z w_{\text{ag}} + f\,(f + \zeta_{\text{g}})\,\partial_z v_{\text{ag}} - \partial_y w_{\text{ag}}\,N^2 = -2\mathrm{Q}^y, \quad (59.187)$$

where

$$\zeta_{\text{g}} = -\partial_y u_{\text{g}} \quad (59.188)$$

is the vertical component of the geostrophic relative vorticity. Introducing an overturning streamfunction for the cross-flow/vertical ageostrophic circulation

$$\boldsymbol{u}_{\text{ag}} = -\hat{\boldsymbol{x}} \times \nabla\psi \Longrightarrow v_{\text{ag}} = \partial_z\psi \quad \text{and} \quad w_{\text{ag}} = -\partial_y\psi, \quad (59.189)$$

and using thermal wind brings equation (59.187) into the form

$$[N^2\,\partial_{yy} - 2\,\partial_y b\,\partial_{yz} + f\,(f + \zeta_{\text{g}})\,\partial_{zz}]\psi = -2\mathrm{Q}^y. \quad (59.190)$$

Equation (59.190) is useful for the study of ageostrophic (Ro $\sim$ 1) dynamics along a front in which there is an ageostrophic overturning circulation in response to geostrophic forcing from Q^y.

59.9.7 Connection to potential vorticity and symmetric instability

The partial differential equation (59.190) can be written

$$\mathcal{K}\psi = -2\,\mathrm{Q}^y, \quad (59.191)$$

where

$$\mathcal{K} = N^2\,\partial_{yy} - 2\,\partial_y b\,\partial_{zy} + f\,(f + \zeta_{\text{g}})\,\partial_{zz} \quad (59.192)$$

is a linear partial differential operator that is a function of the geostrophic flow and the buoyancy. Following the considerations in Section 6.5, we know that this operator is elliptic if the following inequality holds

$$(\partial_y b)^2 - N^2 f (f + \zeta_g) < 0. \tag{59.193}$$

We can relate the ellipticity condition (59.193) to the Ertel potential vorticity for the Boussinesq geostrophic flow. For this purpose, write the geostrophic vorticity as

$$\begin{aligned} \boldsymbol{\omega}_g &= \nabla \times \boldsymbol{u}_g && \text{(59.194a)} \\ &= -\hat{\boldsymbol{x}}\, \partial_z v_g + \hat{\boldsymbol{y}}\, \partial_z u_g + \hat{\boldsymbol{z}}\, \partial_x v_g - \partial_y u_g) && \text{(59.194b)} \\ &= -f^{-1} (\hat{\boldsymbol{x}}\, \partial_x b + \hat{\boldsymbol{y}}\, \partial_y b) + \hat{\boldsymbol{z}}\, (\partial_x v_g - \partial_y u_g). && \text{(59.194c)} \end{aligned}$$

If we assume the front is zonally symmetric, then the relative vorticity in the geostrophic flow takes the form

$$\boldsymbol{\omega}_g^{2d} = -f^{-1}\, \partial_y b\, \hat{\boldsymbol{y}} - \hat{\boldsymbol{z}}\, \partial_y u_g, \tag{59.195}$$

in which case the Ertel potential vorticity (for the Boussinesq geostrophic flow) takes the form

$$\begin{aligned} Q_g^{2d} &= \nabla b \cdot (\boldsymbol{\omega}_g + f\, \hat{\boldsymbol{z}}) && \text{(59.196a)} \\ &= -f^{-1} (\partial_y b)^2 + N^2 (f - \partial_y u_g). && \text{(59.196b)} \\ &= -f^{-1} (\partial_y b)^2 + N^2 (f + \zeta_g). && \text{(59.196c)} \end{aligned}$$

Ellipticity of the PDE (59.190) is thus assured so long as

$$f\, Q_g^{2d} = -(\partial_y b)^2 + N^2 f (f + \zeta_g) > 0. \tag{59.197}$$

The PDE (59.6) transitions to a hyperbolic system when $f\, Q_g^{2d} < 0$, which is the condition for symmetric instability detailed in Section 59.6. Hence, when $f\, Q_g^{2d} > 0$ the front is stable to symmetric instability, with the ageostrophic circulation acting to relax the front. In contrast, when $f\, Q_g^{2d} > 0$ the front is symmetrically unstable.

59.9.8 Further study

Chapter 9 of *Holton and Hakim* (2013) provides a pedagogical discussion of semi-geostrophy and the study of atmospheric fronts.

59.10 Exercises

EXERCISE 59.1: INERTIAL INSTABILITY IN A SHALLOW WATER LAYER
In Section 59.5 we developed the physics of horizontal inertial instability within the continuous Boussinesq equations. Consider the analysis instead within the context of a single layer of shallow water fluid. What are the conditions for inertial instability within the shallow water layer? Are they the same as for the continuous Boussinesq equations? Why?

EXERCISE 59.2: SYMMETRIC INSTABILITY CRITERIA IN TERMS OF BALANCED RICHARDSON NUMBER
Consider the balanced Richardson number, defined for the geostrophic and hydrostatic balanced

flow, along with a corresponding angle

$$\mathrm{Ri}_{\mathrm{b}} = \frac{N^2}{(\partial_z u_{\mathrm{g}})^2} \quad \text{and} \quad \phi_{\mathrm{Ri}_{\mathrm{b}}} \equiv \tan^{-1}(-1/\mathrm{Ri}_{\mathrm{b}}). \tag{59.198}$$

Show that the instability criteria, $f\,Q < 0$, from Section 59.8 can be written in the equivalent form

$$\phi_{\mathrm{Ri}_{\mathrm{b}}} < \phi_{\mathrm{c}} \equiv \tan^{-1}(-(f + \zeta_{\mathrm{g}})/f). \tag{59.199}$$

As shown by *Thomas et al.* (2013), this alternative form of the instability criteria allows for a very effective means to characterize flow regimes conducive to the suite of local instabilities: gravitational, inertial, and symmetric.

EXERCISE 59.3: GROUP VELOCITY FOR SYMMETRIC MERIDIONAL-VERTICAL WAVES
In this exercise we derive some properties for the group velocity of the stable meridional-vertical plane waves discussed in Section 59.8.4.

(a) Derive the group velocity, $\boldsymbol{c}_{\mathrm{g}}$, for the stable meridional-vertical waves whose dispersion relation is given by equation (59.137c).

(b) Compute $\boldsymbol{c}_{\mathrm{g}} \cdot \boldsymbol{k}$, where the wavevector is $\boldsymbol{k} = k_y\,\hat{\boldsymbol{y}} + k_z\,\hat{\boldsymbol{z}}$.

Chapter 60

STABILITY OF FLUID INTERFACES

In this chapter we study the *Rayleigh-Taylor* and *Kelvin-Helmholtz* instabilities as realized along an infinitesimal material fluid interface that separates two homogeneous (constant density) fluid layers of differing densities, and with the two fluids immiscible and inviscid. The gravitational body force is active throughout the fluid layers, and the surface tension is active at the interface between the layers. We do not consider Coriolis or centrifugal acceleration in this chapter (non-rotating reference frame), and the relative vorticity vanishes in both layers. The *normal mode method*, based on Fourier modal analysis, is suited to developing necessary and sufficient conditions for instability.

The physical system is highly idealized in its assumption that the interface between the fluid layers is infinitesimal, and furthermore that the fluids are inviscid and immiscible. Both assumptions accord with our treatment of surface gravity and capillary waves in Chapter 52. Even though quite idealized, the methods and concepts encountered in studying the instabilities are useful in more realistic cases. Furthermore, experimental results support the relevance of the instability conditions found in this chapter.

READER'S GUIDE FOR THIS CHAPTER

This chapter is an extension of the material in Chapter 52, which is concerned with stable linear surface waves on an interface arising from gravity and/or surface tension. The methods of modal instability analysis used in this chapter are also used for a variety of other instabilities elsewhere in this book.

60.1 Governing equations

Formulation of the stability problem in this chapter closely follows that pursued in Chapter 52 for surface gravity waves and capillary waves. In that study we assumed the waves occur on the interface between two regions of constant density, yet with the upper region having zero density, as motivated by waves on the free surface of the ocean underneath the much less massive atmosphere. Here, we allow for the upper region to have a nonzero density. Under certain circumstances, fluctuations on the interface lead to stable linear waves, and we develop the associated dispersion relations. However, a Rayleigh-Taylor instability occurs when the smaller density layer sits below a heavier layer, and with a base state that is at rest. More precisely, an instability occurs when the destabilizing effects from gravity overcome the stabilizing effects from surface tension. In the absence of surface tension, there is always a Rayleigh-Taylor instability when heavy fluid sits above light fluid.

For the Kelvin-Helmholtz instability, we consider the heavy fluid below the light fluid, yet with a base state velocity that differs between the two layers so that there is a velocity shear (more precisely, a velocity jump) at the interface and an associated vorticity singularity. An instability occurs when the destabilizing effects from the velocity shear are sufficiently strong so as to overcome the stabilizing effects from gravity and surface tension. In the absence of both gravity and surface tension, any velocity shear renders an instability of the interface which, as noted on page 485 of *Chandrasekhar* (1961), leads one to conclude that *the Kelvin-Helmholtz instability arises by the crinkling of the interface by the shear that is present; and this crinkling occurs even for the smallest differences in the velocities of the two fluids.* We find in Chapter 61 a modification to this result when considering a finite shear layer rather than the infinitesimal interface considered in the current chapter.

In this section we develop the equations describing motion of an interface separating two homogeneous, inviscid, and immiscible fluids in a non-rotating reference frame and with densities, ρ_1 and ρ_2, and constant zonal velocities, $\hat{\boldsymbol{x}}\, U_1$ and $\hat{\boldsymbol{x}}\, U_2$. (Figure 60.1). We ignore side boundaries by assuming the domain to be horizontally infinite. This is the idealized physical system that is used to study the Rayleigh-Taylor instability and the Kelvin-Hemholtz instability.

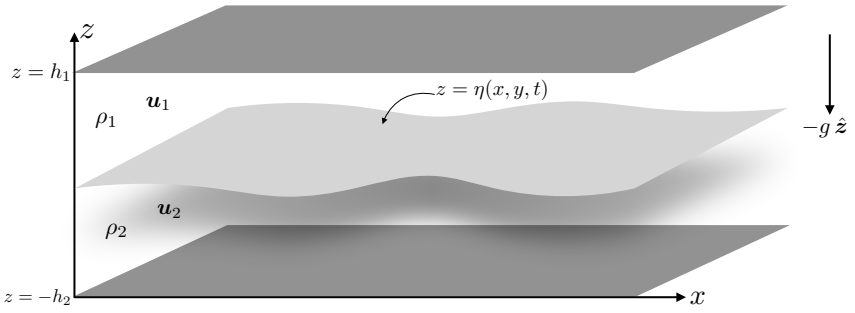

FIGURE 60.1: An infinite box filled with two homogeneous and immiscible fluids with densities, ρ_1 and ρ_2, and horizontal velocities, $\boldsymbol{u}_1$ and $\boldsymbol{u}_2$. The material interface between the layers is located at $z = \eta(x, y, t)$, with $\eta = 0$ when the interface is flat. The fluid region is denoted $\mathcal{R}$, which is infinite in the horizontal directions. For study of the Rayleigh-Taylor instability we assume rigid and flat plates located at $z = -h_2$ and $z = h_1$, whereas for Kelvin-Helmholtz instability we let h_1 and h_2 go to infinity. The interface generally experiences a surface tension due to the density jump.

60.1.1 Equations from potential theory

The fluid in each layer has a constant density and so is incompressible, so that the velocity in each layer is non-divergent, $\nabla \cdot \boldsymbol{v} = 0$. Furthermore, we assume the flow is irrotational ($\nabla \times \boldsymbol{v} = 0$) and so can make use of the potential theory detailed in Section 52.2. In particular, the velocity potential has a time tendency given by Bernoulli's equation of motion (52.16)

$$\partial_t \Psi = \Phi + \mathcal{K} + p/\rho = \mathcal{K} + p_{\mathrm{d}}/\rho, \tag{60.1}$$

where

$$\begin{aligned}
\boldsymbol{v} &= -\nabla\Psi && \text{velocity and velocity potential} && (60.2a)\\
\Phi &= g\,z && \text{geopotential} && (60.2b)\\
\mathcal{K} &= \boldsymbol{v}\cdot\boldsymbol{v}/2 && \text{kinetic energy per mass} && (60.2c)\\
p &= -\rho\,\Phi + p_{\mathrm{d}} && p = \text{pressure and } p_{\mathrm{d}} = \text{dynamic pressure.} && (60.2d)
\end{aligned}$$

The velocity potential, Ψ, satisfies Laplace's equation in the fluid interior and the no-normal flow kinematic boundary condition (Neumann boundary condition) at the rigid top and rigid bottom

$$\begin{aligned}
\nabla^2\Psi &= 0 \quad \boldsymbol{x} \in \mathcal{R} && (60.3a)\\
\hat{\boldsymbol{n}}\cdot\nabla\Psi &= 0 \quad \boldsymbol{x} \in \partial\mathcal{R}. && (60.3b)
\end{aligned}$$

When considering a background zonal velocity, we extract the velocity potential for the static background potential, $\Psi_n^\circ = -U_n\,x$, with $n = 1, 2$ the layer index and with the remaining portion of the velocity potential capturing the perturbation relative to the background. The background velocity potential trivially satisfies Laplace's equation and the no-normal flow boundary condition at the flat and rigid top and bottom boundaries.

60.1.2 Kinematic boundary condition at the interface

Motion of the interface, $z = \eta(x, y, t)$, is determined by boundary conditions evaluated at the interface. The interface is material since the fluid layers are assumed to be immiscible. Focusing first on the lower side, in region 2, the kinematic boundary condition from Section 19.6.2 states that

$$(\boldsymbol{v}_2 - \boldsymbol{v}_\eta)\cdot\hat{\boldsymbol{n}}_2 = 0 \quad \text{at } z = \eta, \tag{60.4}$$

where $\boldsymbol{v}_2$ is the fluid velocity in the lower region, and

$$\hat{\boldsymbol{n}}_2 = \hat{\boldsymbol{n}} = \frac{\nabla(z-\eta)}{|\nabla(z-\eta)|} \quad \text{at } z = \eta, \tag{60.5}$$

is the outward normal direction pointing into the upper layer. The analysis for layer-2 holds equivalantly for layer-1, only with the normal direction pointing from layer-1 down to layer-2. We thus have

$$(\boldsymbol{v}_2 - \boldsymbol{v}_\eta)\cdot\hat{\boldsymbol{n}} = 0 \quad \text{and} \quad (\boldsymbol{v}_\eta - \boldsymbol{v}_1)\cdot\hat{\boldsymbol{n}} = 0 \Longrightarrow (\boldsymbol{v}_2 - \boldsymbol{v}_1)\cdot\hat{\boldsymbol{n}} = 0. \tag{60.6}$$

That is, the normal components to the layer velocities match at the interface. Consequently, the normal derivative of the velocity potential also matches at the interface

$$\hat{\boldsymbol{n}}\cdot(\nabla\Psi_2 - \nabla\Psi_1) = 0 \quad \text{at } z = \eta. \tag{60.7}$$

The velocity of the interface, $\boldsymbol{v}_\eta$, has a normal component given by

$$|\nabla(z-\eta)|\,\boldsymbol{v}_\eta \cdot \hat{\boldsymbol{n}} = \partial_t \eta \quad \text{at } z = \eta, \tag{60.8}$$

so that the kinematic boundary condition (60.4) can be written in the equivalent form

$$(\partial_t + \boldsymbol{u}_1 \cdot \nabla)\,\eta = w_1 \quad \text{and} \quad (\partial_t + \boldsymbol{u}_2 \cdot \nabla)\,\eta = w_2 \quad \text{at } z = \eta. \tag{60.9}$$

Inserting the background velocity and the velocity potential leads to the kinematic boundary conditions at the fluid interface

$$(\partial_t + U_1\,\partial_x - \nabla\Psi_1 \cdot \nabla)\,\eta = -\partial_z \Psi_1 \quad \text{and} \quad (\partial_t + U_2\,\partial_x - \nabla\Psi_2 \cdot \nabla)\,\eta = -\partial_z \Psi_2 \quad \text{at } z = \eta. \tag{60.10}$$

60.1.3 Dynamic boundary condition at the interface

The dynamic boundary condition from Section 25.10 says that the pressure is continuous across the interface so long as we ignore surface tension. For the case with surface tension, the discussion in Section 25.11 reveals a pressure jump across the interface, which here takes the form given by the Young-Laplace formula (25.149),[1]

$$p_2 - p_1 = -\gamma\,\nabla_{\!\mathsf{h}}^2 \eta \quad \text{at } z = \eta. \tag{60.11}$$

In this equation, $\gamma > 0$ is the surface tension (dimensions of force per length = $\mathrm{M\,T^{-2}}$). Evidently, pressure on the concave side of the interface is higher than on the convex side. For example, if the interface extends upward then $p_2 - p_1 > 0$ since the layer-2 fluid is on the concave side and so it has the higher interface pressure. This result also follows since $\nabla_{\!\mathsf{h}}^2 \eta < 0$ for an upward extension of the interface, which leads to a local free surface maximum. The treatment here follows our approach for surface capillary-gravity waves in Section 52.10.1.

60.1.4 Pressures within the two layers

We find it convenient to isolate the hydrostatic pressure within the two layers. For the upper layer we have

$$p_1^{\mathsf{h}} = g\,\rho_1\,(h_1 - z) \quad \text{for } \eta \le z \le h_1, \tag{60.12}$$

where we assumed pressure at $z = h_1$ is zero. Similarly, the hydrostatic pressure in layer two is

$$p_2^{\mathsf{h}} = p_1^{\mathsf{h}}(\eta) + g\,\rho_2\,(\eta - z) = g\,\rho_1\,(h_1 - \eta) + g\,\rho_2\,(\eta - z) \quad \text{for } -h_2 \le z \le 0. \tag{60.13}$$

Note that these hydrostatic pressures match at the interface

$$p_2^{\mathsf{h}}(x, y, z = \eta, t) = p_1^{\mathsf{h}}(x, y, z = \eta, t). \tag{60.14}$$

If there is fluid motion within the layers, then the layer interface is not flat and the pressure is not equal to its resting pressure. In this case we write the pressure as

$$p_1(x, y, z, t) = p_1^{\mathsf{h}}(x, y, z, t) + \delta p_1(x, y, z, t) \tag{60.15a}$$

$$p_2(x, y, z, t) = p_2^{\mathsf{h}}(x, y, z, t) + \delta p_2(x, y, z, t) - \gamma\,\nabla_{\!\mathsf{h}}^2 \eta(x, y, t), \tag{60.15b}$$

[1] We write $\nabla_{\!\mathsf{h}}^2 \eta$ to emphasize that the Laplacian is only acting in the horizontal directions. This notation is not needed when the Laplacian acts on the interface, η, since this field is just a spatial function of the horizontal positions, x, y. However, in equation (60.24) we replace $\partial_t \eta(x, y, t)$ with $-\partial_z \Psi(x, y, z = 0, t)$ as per the linearized kinematic boundary condition (60.20c) with $u_1 = u_2 = 0$. It is this replacement that makes it important to note that the Laplacian is acting just in the horizontal.

where δp_1 and δp_2 are pressures associated with the fluid motion and that vanish when the fluid is at rest. Furthermore, these pressures are continuous at the interface just like the hydrostatic pressures

$$\delta p_1 = \delta p_2 \quad \text{at } z = \eta, \tag{60.16}$$

so that there remains a pressure jump (60.11) in the presence of surface tension

$$p_2 - p_1 = -\gamma \nabla_{\mathrm{h}}^2 \eta \quad \text{at } z = \eta. \tag{60.17}$$

60.1.5 Linearized equations

As for the study of surface gravity waves and capillary waves in Chapter 52, linearization of this system is based on an assumed small slope for the interfaces. Hence, we follow the study of surface waves in Section 52.3 to linearize the Bernoulli equation of motion (60.1). Correspondingly, we linearize the kinematic boundary condition (60.9) and dynamic boundary condition (60.17). In particular, the linearized boundary conditions are evaluated at $z = 0$ rather than at $z = \eta$, in which case the linearized version of p_2^{h} is a function just of z alone.

A new feature here beyond the case of surface waves concerns the presence of a background flow, in which case the kinetic energy contributes at linear order. In particular, the layer-1 Bernoulli equation yields

$$\rho_1 \, \partial_t \Psi_1 = g \, z \, \rho_1 + p_1 + \rho_1 \, [U_1 \, u_1 + (U_1)^2/2]. \tag{60.18}$$

The constant, $\rho_1 \, (U_1)^2/2$, can be eliminated by taking a gauge transformation, as detailed in Section 52.2.3 when studying surface waves. Hence, we drop this term in the following. Writing $u_1 = -\partial_x \Psi_1$ then brings the linearized Bernoulli equation to the form

$$\rho_1 \, (\partial_t + U_1 \, \partial_x) \Psi_1 = g \, z \, \rho_1 + p_1, \tag{60.19}$$

so that the background zonal flow provides a constant advection of the velocity potential. We are thus led to the following linearized layer equations

$$\rho_1 \, (\partial_t + U_1 \, \partial_x) \Psi_1 = g \, z \, \rho_1 + p_1 \quad \text{linearized Bernoulli equation for layer 1} \tag{60.20a}$$
$$\rho_2 \, (\partial_t + U_2 \, \partial_x) \Psi_2 = g \, z \, \rho_2 + p_2 \quad \text{linearized Bernoulli equation for layer 2} \tag{60.20b}$$
$$(\partial_t + U_1 \, \partial_x) \eta = -\partial_z \Psi_1 \quad \text{linearized kinematic b.c. at } z = 0 \tag{60.20c}$$
$$(\partial_t + U_2 \, \partial_x) \eta = -\partial_z \Psi_2 \quad \text{linearized kinematic b.c. at } z = 0 \tag{60.20d}$$
$$\delta p_2 - \delta p_1 = 0 \quad \text{dynamic b.c. at } z = 0 \tag{60.20e}$$
$$p_2 - p_1 = -\gamma \nabla_{\mathrm{h}}^2 \eta \quad \text{dynamic jump b.c. at } z = 0. \tag{60.20f}$$

Taking the difference between the Bernoulli equations in the two layers gives

$$\rho_2 \, (\partial_t + U_2 \, \partial_x) \Psi_2 - \rho_1 \, (\partial_t + U_1 \, \partial_x) \Psi_1 = g \, (\rho_2 \, z_2 - \rho_1 \, z_1) + p_2 - p_1, \tag{60.21}$$

and then evaluating this difference on the interface ($z_1 = z_2 = \eta$) leads to

$$\rho_2 \, (\partial_t + U_2 \, \partial_x) \Psi_2 - \rho_1 \, (\partial_t + U_1 \, \partial_x) \Psi_1 = (g \, \delta\rho - \gamma \nabla_{\mathrm{h}}^2) \, \eta \tag{60.22}$$

where the density difference is written

$$\delta\rho = \rho_2 - \rho_1. \tag{60.23}$$

Note that when multiplied by gravity, we evaluate the interface position at $z = \eta$, whereas other

terms in the linear theory are evaluated at $z = 0$.[2]

60.2 Rayleigh-Taylor instability

For the Rayleigh-Taylor instability analysis, we assume the background flow is at rest so that $U_1 = U_2 = 0$. Hence, we are here examining stability of the rest state to small perturbations of the layer interface.

60.2.1 Boundary value problem and dispersion relation

With zero background flow it is a simple matter to eliminate the free surface from the interface condition (60.22). We do so by taking a time derivative and using the linearized kinematic boundary condition (60.20c) (or equivalently equation (60.20d))

$$\partial_{tt}(\rho_2 \Psi_2 - \rho_1 \Psi_1) = -[g\,\delta\rho - \gamma\,\nabla_h^2]\,\partial_z \Psi \quad \text{at } z = 0, \tag{60.24}$$

where $w_1 = w_2 = -\partial_z \Psi$ at $z = 0$. We are thus led to the boundary value problem

$$\partial_z \Psi_1 = 0 \qquad z = h_1 \tag{60.25a}$$
$$\nabla^2 \Psi_1 = 0 \qquad 0 < z < h_1 \tag{60.25b}$$
$$\partial_{tt}(\rho_2 \Psi_2 - \rho_1 \Psi_1) = -[g\,\delta\rho - \gamma\,\nabla_h^2]\,\partial_z \Psi \qquad z = 0 \tag{60.25c}$$
$$\nabla^2 \Psi_2 = 0 \qquad -h_2 < z < 0 \tag{60.25d}$$
$$\partial_z \Psi_2 = 0 \qquad z = -h_2. \tag{60.25e}$$

Following the approach for surface waves in Section 52.5, we seek a traveling plane wave solution with horizontal wavevector,

$$\boldsymbol{k} = k_x\,\hat{\boldsymbol{x}} + k_y\,\hat{\boldsymbol{y}} \quad \text{and} \quad \hat{\boldsymbol{k}} = \boldsymbol{k}/|\boldsymbol{k}|, \tag{60.26}$$

and a wave ansatz in the form of a cosine modulated by a vertical structure function

$$\Psi(x, y, z, t) = A\,\Gamma(z)\cos(\boldsymbol{k}\cdot\boldsymbol{x} - \omega\,t), \tag{60.27}$$

where A is a real amplitude. The solution to Laplace's equation with Neumann boundary conditions in the two half-domains is given by[3]

$$\Psi_1 = A\,\frac{\cosh[|\boldsymbol{k}|\,(z - h_1)]}{\sinh[-|\boldsymbol{k}|h_1]}\cos(\boldsymbol{k}\cdot\boldsymbol{x} - \omega\,t) \qquad 0 \le z \le h_1 \tag{60.28a}$$
$$\Psi_2 = A\,\frac{\cosh[|\boldsymbol{k}|\,(z + h_2)]}{\sinh[|\boldsymbol{k}|h_2]}\cos(\boldsymbol{k}\cdot\boldsymbol{x} - \omega\,t), \qquad -h_2 \le z \le 0. \tag{60.28b}$$

The dispersion relation is obtained by plugging equations (60.28a)-(60.28b) into the interface

[2] We detailed this treatment of the boundary position when deriving the linear equations for surface waves in Section 52.3.4. The same considerations hold here.

[3] As noted in Section 52.2.2, solutions to Laplace's equation do not support spatial oscillations in all three directions since the sum of the curvature in each direction (i.e., second partial derivatives) must vanish. Correspondingly, the velocity potential supports traveling waves in the horizontal and exponential behavior in the vertical.

condition (60.25e), with the following pieces needed (recall each term is evaluated at $z = 0$)

$$\partial_{tt}(\rho_2 \Psi_2 - \rho_1 \Psi_1) = -\omega^2 A [\rho_2 \coth(|\boldsymbol{k}| h_2) - \rho_1 \coth(-|\boldsymbol{k}| h_1)] \cos(\boldsymbol{k} \cdot \boldsymbol{x} - \omega t) \tag{60.29a}$$

$$\partial_z \Psi_1 = \partial_z \Psi_2 = A |\boldsymbol{k}| \cos(\boldsymbol{k} \cdot \boldsymbol{x} - \omega t) \tag{60.29b}$$

$$(\partial_{xx} + \partial_{yy})\Psi = -|\boldsymbol{k}|^2 \Psi, \tag{60.29c}$$

thus leading to the dispersion relation

$$\omega^2 = \frac{|\boldsymbol{k}| (g \delta\rho + \gamma |\boldsymbol{k}|^2)}{\rho_1 \coth(|\boldsymbol{k}| h_1) + \rho_2 \coth(|\boldsymbol{k}| h_2)}. \tag{60.30}$$

As for the surface waves in Chapter 52, the horizontal wavenumber, $|\boldsymbol{k}|$, determines the vertical scale of the wave. We now examine various cases for stable and unstable waves.

60.2.2 Stable traveling plane waves

When the squared angular frequency (60.30) is positive, $\omega^2 > 0$, then the waves are interface waves related to those studied in Chapter 52.[4] For example, when the waves are so short that they do not feel the rigid boundaries at $z = h_1$ and $z = -h_2$, then we can set $\coth(|\boldsymbol{k}| h_2) \approx 1$ and $\coth(|\boldsymbol{k}| h_1) \approx 1$, in which case the dispersion relation takes on the approximate form

$$\omega^2 \approx \frac{|\boldsymbol{k}| (g \delta\rho + \gamma |\boldsymbol{k}|^2)}{\rho_1 + \rho_2} \quad \text{shortwave limit with } |\boldsymbol{k}| h_1 \gg 1 \text{ and } |\boldsymbol{k}| h_2 \gg 1. \tag{60.31}$$

This limit (when surface tension is set to zero) corresponds to the deep water waves from Section 52.5.5. For the longwave limit, in which case the waves feel the top and bottom boundaries, we set $\coth(|\boldsymbol{k}| h_1) \approx 1/(|\boldsymbol{k}| h_1)$ and $\coth(|\boldsymbol{k}| h_2) \approx 1/(|\boldsymbol{k}| h_2)$ so that

$$\omega^2 \approx \frac{|\boldsymbol{k}|^2 g \delta\rho}{\rho_1/h_1 + \rho_2/h_2} \quad \text{longwave limit with } |\boldsymbol{k}| h_1 \ll 1 \text{ and } |\boldsymbol{k}| h_2 \ll 1. \tag{60.32}$$

Note that we dropped the surface tension term since $|\boldsymbol{k}|$ is very small in the longwave limit. Evidently, since $\omega^2/|\boldsymbol{k}|^2$ is independent of $\boldsymbol{k}$, the longwaves are non-dispersive gravity waves and are thus the analog of non-dispersive shallow water gravity waves studied in Section 55.5. The waves here are affected by a modified value for the gravitational acceleration, which we write as[5]

$$g^r H \equiv \frac{g \delta\rho}{\rho_1/h_1 + \rho_2/h_2} \quad \text{with} \quad H = h_1 + h_2. \tag{60.33}$$

By introducing this *reduced gravity*, g^r, the two-layer shallow water dispersion relation (60.32) takes the form

$$\omega^2 = (g^r H) |\boldsymbol{k}|^2. \tag{60.34}$$

Recall that the dispersion relation for a single shallow water layer (Section 55.5) is given by $\omega^2 = (g H) |\boldsymbol{k}|^2$. We thus see that long gravity waves on an interface between two fluid layers feels a reduced version of the gravitational acceleration, with $g^r \ll g$ when there is a small density difference. In fact, even the case of a single shallow water can be formulated as a two-layer system, with the upper layer having zero density so that the reduced gravity equals to g.

[4] More precisely, if we set $\rho_1 = 0$ as for a vacuum, then the waves are identical to the surface waves from Chapter 52.

[5] The reduced gravity in a shallow water model is defined (e.g., see equation (35.54)) without the layer thicknesses introduced in equation (60.33). A key difference is that in the present section we start with the non-hydrostatic equations and then take the longwave limit, whereas in Section 35.3.2 we only work with the hydrostatic shallow water equations.

60.2.3 Unstable exponentially growing plane waves

The case with $\omega^2 < 0$ leads to unstable wave growth. This case is rendered by $\delta\rho = \rho_2 - \rho_1 < 0$. That is, if there is heavy fluid above light fluid then the system can be unstable, depending on whether the gravitationally unstable stratification can overcome the stabilizing effects from surface tension. We now examine various cases to explore this unstable case, known as the *Rayleigh-Taylor instability.*

The growth rate

To express the temporal structure of the unstable wave, introduce the growth rate

$$\omega^2 = -\sigma^2 \Longrightarrow \omega = \pm \mathrm{i}\,\sigma, \tag{60.35}$$

where $\sigma > 0$ is given by

$$\sigma = \left[\frac{|\boldsymbol{k}| \left(g\,|\delta\rho| - \gamma\,|\boldsymbol{k}|^2 \right)}{\rho_2 \coth(|\boldsymbol{k}|\,h_2) + \rho_1 \coth(|\boldsymbol{k}|\,h_1)} \right]^{1/2} > 0. \tag{60.36}$$

We furthermore express the velocity potential (60.28a) and (60.28b) as the real part of complex exponentials. In particular, write for the top layer

$$\Psi_1 = A\,\Gamma(z)\ \mathrm{Re}[\mathrm{e}^{\mathrm{i}\,(\boldsymbol{k}\cdot\boldsymbol{x} - \omega\,t)}] = A\,\Gamma(z)\,\mathrm{e}^{\pm\sigma\,t}\,\mathrm{Re}[\mathrm{e}^{\mathrm{i}\,\boldsymbol{k}\cdot\boldsymbol{x}}] = A\,\Gamma(z)\,\mathrm{e}^{\pm\sigma\,t}\cos(\boldsymbol{k}\cdot\boldsymbol{x}). \tag{60.37}$$

The solution with the time behavior, $\mathrm{e}^{\sigma\,t}$, is exponentially growing and this is the unstable wave.

All waves are unstable in the absence of surface tension

In the absence of surface tension, the growth rate is given by

$$\sigma = \left[\frac{g\,|\boldsymbol{k}|\,|\delta\rho|}{\rho_2 \coth(|\boldsymbol{k}|\,h_2) + \rho_1 \coth(|\boldsymbol{k}|\,h_1)} \right]^{1/2} \quad \text{if } \gamma = 0. \tag{60.38}$$

Evidently, all waves are unstable, with the smallest waves having the largest growth rate given approximately by

$$\sigma \approx \sqrt{g\,|\boldsymbol{k}|\,|\delta\rho|/(\rho_1 + \rho_2)} \quad \text{with } |\boldsymbol{k}|\,h_2 \gg 1 \text{ and } |\boldsymbol{k}|\,h_1 \gg 1. \tag{60.39}$$

We thus expect to find the smallest scales rapidly going unstable, with the instability halted only after all of the denser fluid occupies the lower layer.

The stabilizing role of surface tension

The growth rate (60.36) vanishes at the critical wavenumber

$$|\boldsymbol{k}|_{\mathrm{c}}^2 = g\,|\delta\rho|/\gamma. \tag{60.40}$$

All waves with wavenumbers larger than $|\boldsymbol{k}|_{\mathrm{c}}$ are stablized by surface tension, in which case the stable linear waves are capillary-gravity waves. We studied the physics of surface tension in Section 25.11, where we noted that it can counteract the effects from gravity when the radius of curvature is sufficiently small. To get a sense for the size of these stable waves, recall our discussion of capillary-gravity waves in Section 52.10. For an air-water interface the surface tension is approximately $\gamma = 0.072$ N m^{-1} $= 0.072$ kg s^{-2}, along with the air density $\rho_1 = 1$ kg m^{-3}, water density of $\rho_2 = 1020$ kg m^{-3}. With these physical constants the critical

wavenumber is given by

$$|\boldsymbol{k}|_{\mathrm{c}} \approx 372 \text{ m}^{-1} \Longrightarrow \Lambda_{\mathrm{c}} = 2\pi/|\boldsymbol{k}|_{\mathrm{c}} \approx 1.7 \text{ cm}. \tag{60.41}$$

Again, waves of wavelength smaller than Λ_{c} are stable.

Maximum growth rate with both surface tension and gravity

We saw above that all waves are unstable without surface tension, with the growth rate increasing as $|\boldsymbol{k}|^{1/2}$ as per equation (60.39). However, surface tension introduces a high wavenumber cutoff so that all waves with $|\boldsymbol{k}| > |\boldsymbol{k}|_{\mathrm{c}}^2$ are stable. Again, such waves are stablized since surface tension dominates over gravity when the radius of curvature is small enough. What is the most unstable wave when there is both surface tension and gravity? One might expect that in the presence of random forcing, this wavenumber will be the one most visibly growing in any particular situation.

To simplify the algebra for computing the most unstable wave, we consider the growth rate (60.36) in the limit that the two rigid boundaries separate to infinity. This limit is not overly constraining since the waves exponentially decay away from the interface, and we expect that the most unstable wavenumber is within an order of magnitude of $|\boldsymbol{k}|_{\mathrm{c}}$. With h_1, h_2 set to infinity the dispersion relation is given by

$$\sigma^2 = \frac{g\,|\delta\rho|\,|\boldsymbol{k}| - \gamma\,|\boldsymbol{k}|^3}{\rho_2 + \rho_1}. \tag{60.42}$$

The wavenumber leading to the maximum growth rate is found by setting $\partial\sigma^2/\partial|\boldsymbol{k}| = 0$, in which case

$$|\boldsymbol{k}|_{\mathrm{max}}^2 = g\,|\delta\rho|/(3\,\gamma) = |\boldsymbol{k}|_{\mathrm{c}}^2/3. \tag{60.43}$$

Using the numbers above for an air-water interface, we see that the wavelength for the most unstable wave is roughly $1.7 \text{ cm} * \sqrt{3} \approx 3$ cm.

60.2.4 Further study

The current section follows the approach from section 2 from *Fetter and Walecka* (2003), whereas chapter X of *Chandrasekhar* (1961) and chapter 2 of *Sutherland* (2010) provide more detailed presentations. The 18 minute mark of this video from Prof. Mollo-Christensen provides a laboratory example of Rayleigh-Taylor instability.

60.3 Kelvin-Helmholtz instability

Kelvin-Helmholtz instability arises when the two fluid layers in Figure 60.1 are moving horizontally relative to each other. In the following we assume the velocities are zonal and written $\hat{\boldsymbol{x}}\,U_1$ and $\hat{\boldsymbol{x}}\,U_2$. Furthermore, we assume the fluids are stably stratified so that $\delta\rho > 0$. Finally, to simplify the analysis, assume the rigid boundaries are moved to infinity so that the only boundary of concern is at the fluid interface.

60.3.1 Velocity potential

The velocity potential satisfying Laplace's equation in the two half spaces is given by

$$\Psi_1 = -U_1\,x + A_1\,\mathrm{e}^{-|\boldsymbol{k}|z}\,\mathrm{e}^{\mathrm{i}\,(\boldsymbol{k}\cdot\boldsymbol{x}-\omega\,t)} \qquad 0 \leq z < \infty \tag{60.44a}$$

$$\Psi_2 = -U_2\,x + A_2\,\mathrm{e}^{|\boldsymbol{k}|z}\,\mathrm{e}^{\mathrm{i}\,(\boldsymbol{k}\cdot\boldsymbol{x}-\omega\,t)} \qquad -\infty < z \leq 0. \tag{60.44b}$$

In contrast to the Rayleigh-Taylor instability, as given by equations (60.28a) and (60.28b), we here use complex exponentials, with the real part of each expression assumed. We also introduced two real amplitudes, A_1 and A_2. Both of these features proves of use in the following analysis. Furthermore, the nonzero background flow makes it less convenient to eliminate the interface height, so that we explicitly consider its wave ansatz in the form

$$\eta = \eta_\circ \, \mathrm{e}^{\mathrm{i}\,(\boldsymbol{k}\cdot\boldsymbol{x} - \omega\, t)}. \tag{60.45}$$

To develop a dispersion relation, we make use of the difference in the Bernoulli equation of motion when evaluated at the interface (equation (60.22)), as well as the kinematic and dynamic boundary conditions (60.20c)-(60.20f).

60.3.2 Dispersion relation from the interface conditions

Evaluating equation (60.22) at $z = 0$ for the waves (60.44a), (60.44b), and (60.45), leads to the following relation between the wave amplitudes

$$\mathrm{i}\,[\rho_2\,(-\omega + k_x\,U_2)\,A_2 - \rho_1\,(-\omega + k_x\,U_1)\,A_1] = (g\,\delta\rho + \gamma|\boldsymbol{k}|^2)\,\eta_\circ \tag{60.46}$$

Likewise, the linearized kinematic boundary conditions (60.20c) and (60.20d) render the relations

$$\mathrm{i}\,(-\omega + k_x\,U_1)\,\eta_\circ = |\boldsymbol{k}|\,A_1 \tag{60.47a}$$

$$\mathrm{i}\,(-\omega + k_x\,U_2)\,\eta_\circ = -|\boldsymbol{k}|\,A_2. \tag{60.47b}$$

Use of equations (60.47a) and (60.47b) in equation (60.46) leads to the dispersion relation

$$\rho_1\,(\omega - k_x\,U_1)^2 + \rho_2\,(\omega - k_x\,U_2)^2 = |\boldsymbol{k}|\,(g\,\delta\rho + \gamma|\boldsymbol{k}|^2). \tag{60.48}$$

We can readily check that this result agrees with that found for the Rayleigh-Taylor instability in equation (60.30). Expanding equation (60.48) and solving the quadratic expression leads to the more conventional form of the dispersion relation

$$\omega = \frac{k_x\,(U_1\,\rho_1 + U_2\,\rho_2)}{\rho_1 + \rho_2} \pm \sqrt{\frac{|\boldsymbol{k}|\,(g\,\delta\rho + \gamma\,|\boldsymbol{k}|^2)}{\rho_1 + \rho_2} - \frac{k_x^2\,\rho_1\,\rho_2\,(U_1 - U_2)^2}{(\rho_1 + \rho_2)^2}}. \tag{60.49}$$

We consider facets of this dispersion relation in the following.

60.3.3 Analysis of the stability condition

The angular frequency is a real number, and the flow is stable, so long as the discriminant in equation (60.49) is positive,

$$\frac{\rho_1\,\rho_2\,(U_1 - U_2)^2}{(\rho_1 + \rho_2)} < \frac{|\boldsymbol{k}|\,(g\,\delta\rho + \gamma\,|\boldsymbol{k}|^2)}{k_x^2} \quad \Longrightarrow \text{stable state}, \tag{60.50}$$

with the perturbations organizing into stable linear capillary-gravity waves modified by the background velocity. To help understand this stability condition, we find it useful to consider a few special cases. To reduce algebra, assume the wavevector is aligned in the $\hat{\boldsymbol{x}}$ direction so that $|\boldsymbol{k}|^2 = k_x^2$. Now write the stability condition (60.50) as a condition on the squared velocity difference, in which case

$$(U_1 - U_2)^2 < \frac{(\rho_1 + \rho_2)}{\rho_1\,\rho_2}\,(g\,\delta\rho/|\boldsymbol{k}| + \gamma\,|\boldsymbol{k}|) \quad \Longrightarrow \text{stable state}. \tag{60.51}$$

This equation says that the waves are stable so long as the squared velocity difference is insufficient to counteract the stabilizing effects from surface tension and gravity. Notice that the gravitational effects are weighted by the density difference, $\delta\rho = \rho_2 - \rho_1$, so that gravity plays no role when the densities are the same. In general, as the wave number increases (wavelength decreases), the effects from gravity acting to stabilize the waves become less important than those from surface tension, whereas the converse situation holds for low wavenumber waves (long wavelength). We illustrate these properties in Figure 60.2.

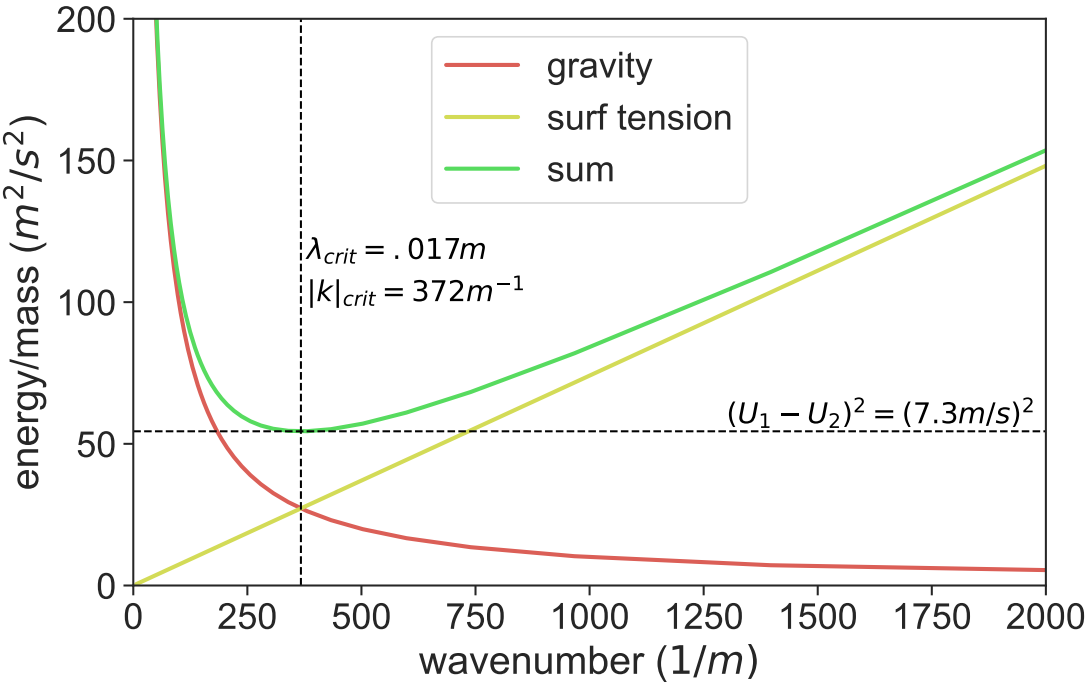

FIGURE 60.2: Stability diagram for Kelvin-Helmholtz instability of the interface between two constant density layers in a gravity field and with surface tension at the interface. The red curve arises from the gravity contribution to equation (60.51); the yellow curve is for the surface tension; and the green curve is the sum. If the squared velocity difference, $(U_1 - U_2)^2$, is above the green line then there are unstable waves whose wavenumbers are between the low and high wavenumber bounds defined by the green line. This figure is generated using the following numbers appropriate for the interface between the atmosphere (region 1) and ocean (region 2): $\rho_1 = 1$ kg m^{-3}, $\rho_2 = 1020$ kg m^{-3}, $g = 9.8$ m s^{-2}, $\gamma = 0.072$ kg s^{-2}. The critical wavenumber from equation (60.52) equals to $|\boldsymbol{k}|_c = \sqrt{g\,\delta\rho/\gamma} = 372$ m^{-1}, which corresponds to a critical wavelength $\lambda_{\text{crit}} = 2\pi/|\boldsymbol{k}|_c = 0.017$ m. As the velocity difference increases from zero, this is the first wave that goes unstable when the velocity difference reaches $U_1 - U_2 = 7.3$ m s^{-1} $= 26$ km hr^{-1}.

Most easily growing wave

The stability condition (60.51) indicates that that waves that are either small enough or large enough are stable, whereas waves of intermediate length are unstable in the presence of sufficient velocity difference (shear) across the interface. To find the wavenumber of the unstable wave that appears with the least amount of shear (e.g., minimum of the green curve in Figure 60.2), we find where the derivative, $\partial/\partial|\boldsymbol{k}|$, of the right hand of equation (60.51) vanishes, which leads to the critical squared wavenumber

$$|\boldsymbol{k}|_c^2 = g\,\delta\rho/\gamma, \tag{60.52}$$

which is the same as found for the Rayleigh-Taylor instability in Section 60.2.3. Evidently, when the wavenumber equals to $|\boldsymbol{k}|_c$, then the stability condition is most easily violated by the smallest squared shear, thus leading to exponential growth for this wave. Plugging in $|\boldsymbol{k}|_c$ to the stability

condition (60.51) leads to

$$(U_1 - U_2)^4_{\text{crit}} < \frac{4\,\gamma\,g\,(\rho_1+\rho_2)^2\,(\rho_2-\rho_1)}{\rho_1^2\,\rho_2^2} \quad \Longrightarrow \text{stable state.} \tag{60.53}$$

This expression shows how surface tension and gravity act together to help maintain stability in the face of a velocity difference. Yet if the velocity difference grows, eventually the inequality swaps sign so that the flow becomes unstable. Furthermore, the wavenumber $|\boldsymbol{k}|_{\text{c}}$ is the first wave to exponentially grow.

The case of vanishing surface tension

If the surface tension vanishes then equation (60.53) says that there are always unstable high wavenumber waves for an arbitrarily small velocity difference. More precisely, we return to the general condition (60.51) with $\gamma = 0$ to find

$$(U_1 - U_2)^2 < \frac{g\,(\rho_1+\rho_2)\,\delta\rho}{|\boldsymbol{k}|\,\rho_1\,\rho_2} \quad \Longrightarrow \text{stable state.} \tag{60.54}$$

Evidently, no matter how small the velocity difference, there are waves with high enough wavenumber that violate this inequality and thus lead to an instability. In Figure 60.2, the case with zero surface tension means that the green and red curves are identical, so that without the effects from surface tension, there is no high wavenumber cutoff for the instability.

The case of vanishing gravity

If we align the layers horizontally rather than vertically, then gravity is no longer able to enhance stability in the face of the velocity difference. Just like in the case with zero surface tension, there are always waves that go unstable in this case. However, the unstable waves here have arbitrarily low wavenumber, so that in the absence of gravity there is no low wavenumber cutoff.

Stability is enhanced when $\rho_1/\rho_2 \ll 1$

If the upper layer has a vanishingly small density relative to the lower layer, then the right hand side of the stability condition (60.51) becomes large. We say that this case is strongly stable since it takes a large velocity difference to produce an instability. A geophysically relevant example is air blowing over water with $\gamma = 0.072$ N m^{-1} $= 0.072$ kg s^{-2}, $\rho_2 = 1020$ kg m^{-3} and air density $\rho_1 = 1$ kg m^{-3}. Equation (60.53) says that the most unstable wave is stimulated with an air-sea velocity difference

$$U_1 - U_2 = 7.3 \text{ m s}^{-1} = 26 \text{ km hr}^{-1}. \tag{60.55}$$

These numbers are used to generate Figure 60.2.

60.3.4 Insights from vorticity

The vorticity vanishes everywhere in the fluid, except at the interface. At the interface the velocity jump leads to a Dirac delta *vortex sheet*. We compute the vorticity of the base state by writing the velocity in terms of Heaviside step functions (equation (7.19))

$$\boldsymbol{v} = \hat{\boldsymbol{x}}\,[U_1\,\mathcal{H}(z) + U_2\,\mathcal{H}(-z)] \tag{60.56}$$

so that the vorticity is given by

$$\hat{\boldsymbol{y}} \cdot \nabla \times \boldsymbol{v} = \partial_z [U_1 \, \mathcal{H}(z) + U_2 \, \mathcal{H}(-z)] = (U_1 - U_2) \, \delta(z), \tag{60.57}$$

with Figure 60.3 providing an illustration. The vortex sheet is a stationary equilibrium state since the flow felt by adjacent vortices exactly cancels. However, as shown in Figure 60.4, the vortex sheet is unstable to small perturbations. Indeed, in the absence of gravity or surface tension then any perturbation is unstable, which is the Kelvin-Helmholtz instability.

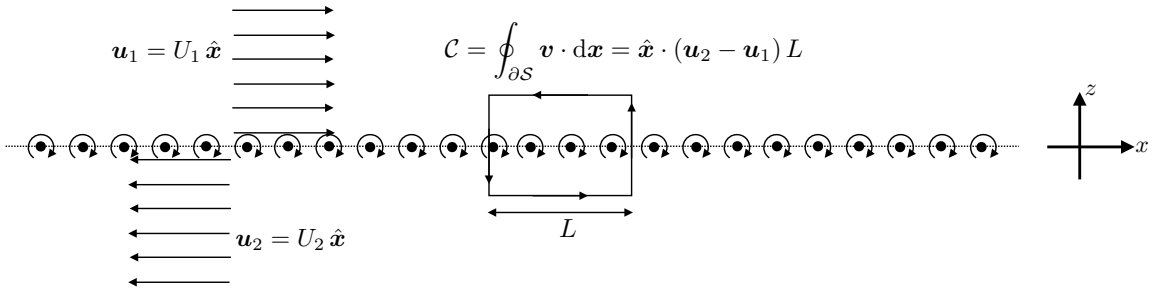

FIGURE 60.3: A vorticity perspective on the Kelvin-Helmholtz instability, whereby the velocity jump leads to a Dirac delta vorticity at the interface and a corresponding circulation for loops that enclose a portion of the sheet. Each circular arrow surrounding a black dot represents a point vortex induced by the velocity jump, with the $z = 0$ plane filled with a continuum of such point vortices. The circulation around the sheet is $\mathcal{C} = \hat{\boldsymbol{x}} \cdot (\boldsymbol{u}_2 - \boldsymbol{u}_1) \, L$, where L is the length of the side parallel to the sheet. This configuration is a stationary equilibrium since the flow felt by adjacent vortices exactly cancels so that they remain fixed. However, it is generally unstable, as shown in Figure 60.4.

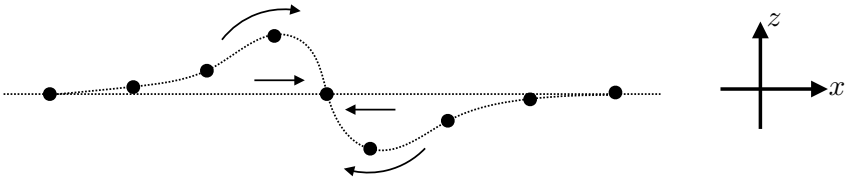

FIGURE 60.4: The equilibrium configuration from Figure 60.3 is unstable to small perturbations, and in the case of zero surface tension and zero gravity any perturbation is unstable. We understand the cause of the instability by observing that if a vortex is displaced away from the sheet, the flow from adjacent vortices and the background flow causes the sheet to roll-up on itself, which is the Kelvin-Helmholtz instability. This figure is a variant of Figure 7.1.3 of *Batchelor* (1967) (who provides full details of the vorticity interpretation of the Kelvin-Helmholtz instability), Figure 1.3 of *Drazin and Reid* (1981), and Figure 3.9 of *McWilliams* (2006).

60.3.5 Insights from Bernoulli's theorem

Figure 60.5 provides a schematic of the pressure forces active next to the interface in the presence of a wavelike perturbation. A wavelike perturbation along the interface gives rise, through Bernoulli's theorem, to pressure anomalies of opposite sign in the regions near to the interface.[6] In particular, consider the case of an interface that enters one of the two regions and so reduces the cross-sectional area for the fluid flow. The flow is incompressible, and so the flow speed increases in this region, with increased speed associated with an anomalously low pressure. The opposite occurs in the other region, where there is an anomalously high pressure. Evidently, the pressure dipoles increase the amplitude of the wavelike perturbation. If the pressure perturbation

[6] At the interface, the pressure has a jump given by the Young-Laplace equation (60.11). We are here interested in the region local to the boundary.

is sufficiently strong to overcome the stabilizing effects from gravity and surface tension, then the perturbation grows and becomes nonlinear, which is the Kelvin-Helmholtz instability.

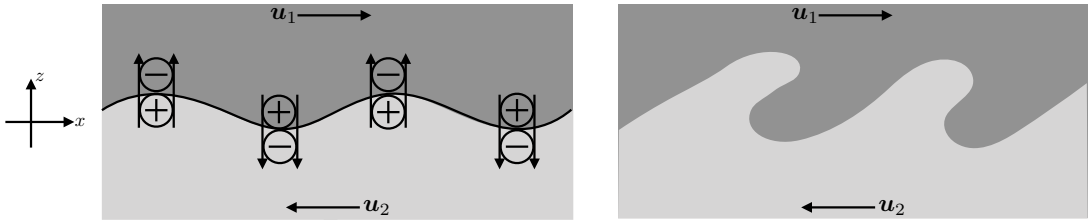

FIGURE 60.5: Schematic of a region near the interface between two uniform density and immiscible fluid regions with nonzero relative motion between the regions. The left panel shows a small wavelike perturbation along the interface that gives rise, through Bernoulli's theorem, to pressure anomalies of opposite signs in the regions on either side of the interface. Evidently, the pressure dipoles increase the amplitude of the wavelike perturbation, thus leading to a positive feedback. If the feedback is sufficiently strong to overcome the stabilizing effects from gravity and surface tension, then it will lead to the Kelvin-Helmholtz instability. The right panel shows the nonlinear stage in which the waves are growing and eventually break.

60.3.6 An energetic perspective on Kelvin-Helmholtz induced mixing

Kinetic energy of the background flow provides the energy source for the Kelvin-Helmholtz instability. Once the instability fully acts, it produces a well mixed state whereby the density and velocity are mixed within a region local to the initial interface. The kinetic energy of the final mixed state is less than the initial state, which we can infer since mixing removes the velocity jump across the interface; i.e., mixing smooths the velocity profile. Conversely, the gravitational potential energy is increased since some of the light fluid from the upper region is mixed with the heavy fluid from the lower region, and vice versa, thus raising the center of mass of the fluid column.[7]

A deductive analysis of the energetics of mixing is outside our scope. Indeed, without information about the pressure forces causing the base flow, we do not have sufficient information to perform an energy budget. However, we can study the energetic effects from mixing by making reasonable assumptions about the final flow profile, and in so doing we can quantitatively support the above inferences about the effects of mixing on kinetic energy and gravitational potential energy. For analytical tractability we assume the mixing region extends over the symmetric range, $-H \leq z \leq H$, with negligible signature of mixing outside of this range. Furthermore, we make use of the Boussinesq ocean from Chapter 29 with density a linear function of temperature and with a reference density ρ_o.

To estimate the thickness, H, of the mixing region, recall the expression (60.54) allows us to compute the low wavenumber cutoff for the case of Kelvin-Helmholtz instability in the absence of surface tension

$$|\boldsymbol{k}|_{\text{low}} = \frac{g\,(\rho_1 + \rho_2)\,\delta\rho}{\rho_1\,\rho_2\,(U_1 - U_2)^2}. \tag{60.58}$$

The unstable waves riding on the interface are exponentially decaying in the direction away from the interface, with their decay scale given by $|\boldsymbol{k}|$. Evidently, unstable Kelvin-Helmholtz waves extend a distance $\sim 1/|\boldsymbol{k}|_{\text{low}}$ away from the interface, thus suggesting that a scale for the associated mixing is given by

$$H \sim \frac{\rho_1\,\rho_2\,(U_1 - U_2)^2}{g\,(\rho_1 + \rho_2)\,\delta\rho} \approx \frac{\rho_o\,(U_1 - U_2)^2}{2\,g\,\delta\rho}, \tag{60.59}$$

[7] We studied this effect of mixing on gravitational potential energy in Section 26.2.6.

where the approximate expression made use of the oceanic Boussinesq approximation.

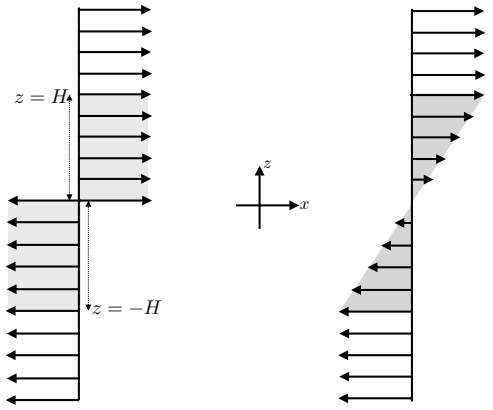

FIGURE 60.6: The initial velocity profile (left panel) for the study of Kelvin-Helmholtz instability, with $U_1 = U_2$. This profile is assumed to evolve to the linear profile (right panel) after mixing. The kinetic energy in the mixed profile is less than the kinetic energy in the initial profile. In turn, mixing raises the center of mass of the fluid so that it increases the gravitational potential energy. It is notable that the final state velocity profile shown here could be unstable to shear instability, as discussed in Chapter 61, in which case the shear instability will further act to homogenize the velocity and density.

The initial density and velocity profiles are given by the jump across the interface at $z = 0$, with the initial velocity and density having a depth integral of

$$\int_{-H}^{H} u \, \mathrm{d}z = H \, (U_1 + U_2) \quad \text{and} \quad \int_{-H}^{H} \rho \, \mathrm{d}z = H \, (\rho_1 + \rho_2). \tag{60.60}$$

We assume the final density and velocity profiles have a depth integral equal to those in the initial state, thus ensuring that zonal momentum and heat are conserved by the mixing. For simplicity, assume the final state profiles are linear, in which case (see Figure 60.6)

$$\overline{\rho}(z) = \rho_2 - (\rho_2 - \rho_1) \, (1 + z/H)/2 = (\rho_1 + \rho_2)/2 - z \, \delta\rho/(2\,H) \qquad \text{for } -H \le z \le H \tag{60.61a}$$

$$\overline{u}(z) = U_2 - (U_2 - U_1) \, (1 + z/H)/2 = (U_1 + U_2)/2 - z \, \delta U/(2\,H) \quad \text{for } -H \le z \le H. \tag{60.61b}$$

The depth integrated kinetic energy and gravitational potential energy per horizontal area

$$K = \frac{\rho_\circ}{2} \int_{-H}^{H} u^2 \, \mathrm{d}z \quad \text{and} \quad P = g \int_{-H}^{H} z \, \rho \, \mathrm{d}z, \tag{60.62}$$

take on the following initial values

$$K_{\text{init}} = \frac{\rho_\circ}{2} \int_{-H}^{H} u^2 \, \mathrm{d}z = H \, \rho_\circ \, (U_1^2 + U_2^2)/2 \tag{60.63a}$$

$$P_{\text{init}} = g \, \rho_2 \int_{-H}^{0} z \, \mathrm{d}z + g \, \rho_1 \int_{0}^{H} z \, \mathrm{d}z = -g \, H^2 \, \delta\rho/2. \tag{60.63b}$$

Use of the linear profiles (60.61a) and (60.61b) render the final mixed state energies

$$K_{\text{final}} = \frac{\rho_\circ}{2} \int_{-H}^{H} u^2 \, \mathrm{d}z = H \, \rho_\circ \left[U_1^2 + U_2^2 + U_1 \, U_2 \right] /3 \tag{60.64a}$$

$$P_{\text{final}} = g \int_{-H}^{H} \overline{\rho} \, z \, \mathrm{d}z = -g \, H^2 \, \delta\rho/6. \tag{60.64b}$$

As anticipated, we find that the kinetic energy is reduced upon mixing whereas the gravitational potential energy increases

$$K_{\text{final}} - K_{\text{init}} = -H\,\rho_\circ\,(U_1 - U_2)^2/6 < 0 \quad \text{and} \quad P_{\text{final}} - P_{\text{init}} = g\,H^2\,\delta\rho/3 > 0. \tag{60.65}$$

The ratio of the change in potential energy to the change in kinetic energy is

$$\frac{P_{\text{final}} - P_{\text{init}}}{K_{\text{final}} - K_{\text{init}}} = -\frac{2\,g}{\rho_\circ}\,\frac{\delta\rho/H}{[(U_1 - U_2)/H]^2}, \tag{60.66}$$

which is the ratio of the density stratification to the squared vertical shear. This ratio is a discrete version of the *gradient Richardson number* as discussed in Section 61.7.5. Indeed, in Section 61.7.5 we consider an energetic argument similar to that given here as applied to the final state linear sheared profile in Figure 60.6, which can be unstable to strataified shear instability if the Richardson number is less than 1/4.

60.3.7 Further study

Chapter XI of *Chandrasekhar* (1961) provides a detailed study of Kelvin-Helmholtz instability, with particular comments in Section 101b on the geophysical relevance of the critical shear. Section 2 of *Fetter and Walecka* (2003) also provides a presentation consistent with that gien here. The first half of this video from Prof. Mollo-Christensen provides laboratory examples of Kelvin-Helmholtz instabilities. This video from Prof. Worster's fluids lab provides a vivid illustration of Kelvin-Helmholtz instability in a two-layer fluid.

Chapter 61

SHEAR INSTABILITY

In this chapter we study *shear instability* as realized in two canonical cases. The first concerns a meridionally sheared zonal flow in a horizontally non-divergent barotropic fluid, with this instability sometimes called *barotropic instability*. We derive integral stability conditions for arbitrary zonal flow profiles, and then study a special flow profile that admits an analytic solution. The analytic study exposes the underlying *wave resonance* mechanism active in shear instability, with this mechanism involving the interaction of *edge waves* that live on the background vorticity field (Section 54.5). We thus interpret shear instability as the constructive interference of two vorticity (edge) waves, where interference supports the mutual exponential growth of both waves that is characteristic of a modal instability.

The second kind of shear instability concerns vertically sheared flows in a gravitationally stratified fluid ($N^2 > 0$) in the absence of planetary rotation ($f = 0$). The stable vertical stratification creates a potential energy barrier that stabilizes the vertically sheared flow relative to the horizontally sheared case without gravity. If the kinetic energy of the vertically sheared flow is large enough, then the potential energy barrier can be overcome to produce a shear instability. Our study of *stratified shear instability* makes use of normal mode stability analysis just like for the barotropic shear flow. The *gradient Richardson number* provides a non-dimensional measure of the potential energy relative to the kinetic energy, with a normal mode instability occuring if the Richardson number is below a critical value. We offer a derivation following *Miles* (1961) revealing that the critical Richardson number is 1/4.

READER'S GUIDE FOR THIS CHAPTER

Surface tension is ignored throughout this chapter, so that we focus on sheared flows of scales larger than the $\approx 10^{-3}$ m characteristic of capillary waves. To study horizontal shear instability, we assume familiarity with the horizontally non-divergent barotropic model from Chapter 38 and the associated wave mechanics in Sections 54.2 and 54.3. We make particular use of edge waves studied in Section 54.5 as part of our wave resonance interpretatation of shear instability. For our study of stratified shear instability, we make use of the perfect Boussinesq fluid from Chapter 29. In linearizing the equations we follow many of the same steps used for the study of internal gravity waves in Chapter 57. The linear partial differential equation appearing in the stability analysis is known as the *Taylor-Goldstein* equation, which is very similar to the *Rayleigh* equation encountered in the barotropic shear instability. Methods and concepts from this chapter are very useful in the study of baroclinic instability in Chapter 62.

Kelvin and Helmholtz studied the interfacial instability described in Chapter 60. Even so, the continuous shear layer instability of the present chapter is also, sometimes, referred to as Kelvin-Helmholtz instability.

61.1 Loose threads

- Discuss Couette flow stability in Section 61.5.1 even though it satisfies the Rayleigh inflection point theorem.

- Look at the pressure field in the waves to offer a force balance interpretation of the instabilties. Also, to help understand why unstable waves tilt into the shear.

61.2 Global versus local instabilities

The wave/modal interpretation of shear instability that we pursue in this chapter contrasts to the variety of symmetric instabilities studied in Chapter 59. In particular, symmetric stablility of a given flow can be deduced by the local necessary and sufficient condition, $f\,Q < 0$, with Q the Ertel potential vorticity. A corresponding mechanistic interpretation follows from parcel arguments. As emphasized by *Cushman-Roisin and Beckers* (2011) (see their Chapter 17), wave instabilities, such as shear instability of this chapter, are not characterized by a local flow property. The reason is that a wave instability arises from the constructive interaction between coherent wave motion, with that interaction a function of boundary conditions and phase relations. Hence, a quantitative understanding of shear instability requires the solution of an eigenvalue problem to determine properties of the interacting waves.

Squire's theorem (*Squire*, 1933) states that for every three-dimensional perturbation to a plane shear flow, there exists a more unstable two-dimensional perturbation.[1] Hence, to characterize the most unstable perturbations, it is sufficient to study shear instability in a two-dimensional flow. Even so, as presented in Chapter 3 of *Smyth and Carpenter* (2019), it can be pedagogically useful to start from the more general three-dimensional case and then show the validity of Squire's theorem.

61.3 Governing barotropic equations

As in the study of edge waves in Section 54.5, we here consider flow of a horizontally non-divergent barotropic fluid in the presence of a prescribed background zonal flow that is a function of latitude

$$\boldsymbol{u}_{\mathrm{b}} = u_{\mathrm{b}}(y)\,\hat{\boldsymbol{x}}. \tag{61.1}$$

This background velocity has zero material acceleration

$$(\partial_t + \boldsymbol{u}_{\mathrm{b}} \cdot \nabla)\boldsymbol{u}_{\mathrm{b}} = 0, \tag{61.2}$$

so that it is in exact geostrophic balance with a background pressure gradient

$$f\,\hat{\boldsymbol{z}} \times \boldsymbol{u}_{\mathrm{b}} = -\nabla\varphi_{\mathrm{b}} \implies f\,u_{\mathrm{b}} = -\partial_y\varphi_{\mathrm{b}}. \tag{61.3}$$

Much of this chapter (e.g., the linearized equations with a modulated wave ansatz in Section 61.4 and the interacting edge waves in Section 61.6) considers the case of a non-rotating reference frame ($f = 0$), in which case the background flow is generated by an unspecified pressure gradient. In other sections we retain planetary rotation in the form of the β plane, such as for the integral stability conditions of Section 61.5. In the remainder of this section we develop the equations describing the velocity and the kinetic energy of fluid flow in the presence of the prescribed zonal background flow, and with details for generation of the background flow left unspecified.

61.3.1 Velocity equation

Writing the velocity and pressure as the sum of a background plus a fluctuation

$$\boldsymbol{u} = \boldsymbol{u}_{\mathrm{b}} + \boldsymbol{u}' \quad \text{and} \quad \varphi = \varphi_{\mathrm{b}} + \varphi', \tag{61.4}$$

[1] See *Drazin and Reid* (2004) or Section 11.8 of *Kundu et al.* (2016) for more details of Squire's theorem. We illustrate Squre's theorem in Section 62.7.3 when studying the growth rate of unstable Eady edge waves.

leads to the material acceleration

$$\frac{\mathrm{D}\boldsymbol{u}}{\mathrm{D}t} = (\partial_t + \boldsymbol{u}\cdot\nabla)\boldsymbol{u} = (\partial_t + \boldsymbol{u}'\cdot\nabla)\boldsymbol{u}' + (\boldsymbol{u}'\cdot\nabla)\boldsymbol{u}_\mathrm{b} + (\boldsymbol{u}_\mathrm{b}\cdot\nabla)\boldsymbol{u}', \tag{61.5}$$

and the corresponding equation of motion

$$(\partial_t + \boldsymbol{u}'\cdot\nabla)\boldsymbol{u}' + (\boldsymbol{u}'\cdot\nabla)\boldsymbol{u}_\mathrm{b} + (\boldsymbol{u}_\mathrm{b}\cdot\nabla)\boldsymbol{u}' + f\,\hat{\boldsymbol{z}}\times\boldsymbol{u}' = -\nabla\varphi', \tag{61.6}$$

which takes on the linearized form with the given background flow (61.1)

$$(\partial_t + u_\mathrm{b}\,\partial_x)\boldsymbol{u}' + \hat{\boldsymbol{x}}\,v'\,\partial_y u_\mathrm{b} + f\,\hat{\boldsymbol{z}}\times\boldsymbol{u}' = -\nabla\varphi'. \tag{61.7}$$

61.3.2 Eddy kinetic energy

As detailed in Section 38.1.2, energetic transfers in the horizontally non-divergent barotropic fluid only involve the kinetic energy since the gravitational potential energy is a constant. Working with the linearized equation of motion (61.7), we find that the kinetic energy per mass contained in the fluctuating flow, $\boldsymbol{u}'\cdot\boldsymbol{u}'/2$, satisfies

$$[\partial_t + u_\mathrm{b}\,\partial_x](\boldsymbol{u}'\cdot\boldsymbol{u}')/2 = -u'\,v'\,\partial_y u_\mathrm{b} - \nabla\cdot(\boldsymbol{u}'\,\varphi). \tag{61.8}$$

We commonly refer to $\boldsymbol{u}'\cdot\boldsymbol{u}'/2$ as the *eddy kinetic energy*. The first term on the right hand side of equation (61.8) arises from fluctuations of the zonal and meridional velocity weighted by the meridional derivative of the background zonal flow. This term is associated with the transfer of kinetic energy from the background flow to the fluctuating flow.[2] The second term is the convergence of the pressure flux that is determined by the fluctuating flow. Taking a zonal average over the domain, and assuming all zonal boundary contributions vanish, leads to

$$\partial_t\overline{\mathcal{K}} = -\overline{u'\,v'}\,\partial_y u_\mathrm{b} - \partial_y(\overline{v'\,\varphi'}), \tag{61.9}$$

where we defined the zonal averaged eddy kinetic energy in the fluctuating fields

$$\overline{\mathcal{K}} = \overline{\boldsymbol{u}'\cdot\boldsymbol{u}'}/2. \tag{61.10}$$

Evidently, equation (61.9) says that the zonal averaged kinetic energy of the fluctuating fields has an Eulerian time derivative determined by the following two terms:

$$-\partial_y(\overline{v'\,\varphi'}) = \text{meridional convergence of pressure flux} \tag{61.11a}$$

$$-\overline{u'\,v'}\,\partial_y u_\mathrm{b} = \text{shear production}. \tag{61.11b}$$

We assume that the pressure convergence term vanishes when integrated over the meridional extent of the domain (e.g., $v' = 0$ along the meridional boundaries), in which case it represents a redistribution or transport that moves eddy kinetic energy around but does not alter its domain integrated value. In contrast, the shear production term is a source/sink that measures the rate that eddy kinetic energy is modified via the zonal correlations between u' and v' and as modulated by the meridional gradient of the background flow. As noted above, this term provides a transfer of kinetic energy between the mean flow and the fluctuating flow. It is expected that this term provides the source of the growing kinetic energy of an unstable wave. Note that its name arises since it is a nonzero production of kinetic energy in the presence of a background shear.

[2] Note that we do not have access to the energy equation for the background flow since it is prescribed and remains static.

We can interpret the shear production term as the meridional flux of zonal momentum contained in the fluctuating field. Evidently, kinetic energy in the fluctuating fields increases if this flux is down the gradient of the background meridional shear

$$\overline{v'\,u'}\,\partial_y u_\mathsf{b} < 0 \quad \text{growing kinetic energy of fluctuations.} \tag{61.12}$$

Such downgradient transport by the growing fluctuations acts in a direction that smooths the meridional shear of the backgound zonal flow.

61.3.3 Pressure equation

Taking the divergence of the linearized velocity equation (61.7), and noting that $\nabla \cdot \boldsymbol{u}' = 0$, leads to the Poisson equation for pressure

$$-\nabla^2 \varphi' = 2\,(\partial_y u_\mathsf{b})\,(\partial_x v') + \beta\,u' - f\,\zeta', \tag{61.13}$$

where we introduced the relative vorticity contained in the fluctuating field (i.e., the eddy vorticity)

$$\zeta' = \partial_x v' - \partial_y u'. \tag{61.14}$$

The analysis of interacting edge waves in Section 61.6 is formulated in a non-rotating reference frame, in which the pressure equation simplifies to

$$-\nabla^2 \varphi' = 2\,(\partial_y u_\mathsf{b})\,(\partial_x v'). \tag{61.15}$$

61.3.4 Meridional velocity equation

The meridional component of the linearized velocity equation (61.7) is given by

$$\partial_t v' + u_\mathsf{b}\,\partial_x v' + f\,u' = -\partial_y \varphi'. \tag{61.16}$$

Setting $f = 0$ and taking the Laplacian leads to

$$\partial_t(\nabla^2 v') + \nabla^2(u_\mathsf{b}\,\partial_x v') = -\partial_y(\nabla^2 \varphi'). \tag{61.17}$$

Use of the pressure equation (61.15) then provides an equation for the meridional velocity

$$(\partial_t + u_\mathsf{b}\,\partial_x)(\nabla^2 v') = (\partial_x v')\,\partial_{yy} u_\mathsf{b}. \tag{61.18}$$

Evidently, the background zonal flow provides an advection of $\nabla^2 v'$ as well as an interaction term on the right hand side.

61.4 Barotropic flow with a modulated wave ansatz

We here study a modulated wave ansatz for a non-rotating reference frame using the linearized flow in the presence of a background state with a meridionally sheared zonal flow. Following the development in Section 54.5, we expect plane traveling waves in the zonal direction, with a meridionally dependent modulation function. This expectation leads to the ansatz for the streamfunction

$$\psi(x, y, t) = \widetilde{\psi}(y)\,\mathrm{e}^{\mathrm{i}\,(k\,x - \omega\,t)}. \tag{61.19}$$

61.4.1 Accounting for the edge wave direction

An edge wave can move in either the positive or negative $\hat{\boldsymbol{x}}$ direction, so that the wavevector is

$$\boldsymbol{k} = |\boldsymbol{k}|\,\hat{\boldsymbol{k}} = |k|\,\hat{\boldsymbol{k}} = \pm|k|\,\hat{\boldsymbol{x}}. \tag{61.20}$$

A convenient means to incorporate the two directions of motion is to write the phase as

$$k\,x - \omega\,t = k\,[x - (\omega/k)\,t] = k\,(x - c\,t), \tag{61.21}$$

where the phase velocity is[3]

$$\boldsymbol{c}_{\mathsf{p}} = (\omega/|k|)\,\hat{\boldsymbol{k}} = (\omega/k)\,\hat{\boldsymbol{x}} = c\,\hat{\boldsymbol{x}}. \tag{61.22}$$

For the geometry of this problem, an edge wave only moves along one-dimension, in which case it is sufficient to refer to $c = \omega/k$ as the phase velocity and $|c| = \omega/|k|$ the phase speed.[4] A real and positive wave velocity, $c > 0$, has $\boldsymbol{k} = k\,\hat{\boldsymbol{x}}$ with $k > 0$, thus indicating a stable edge wave with phase moving in the $+\hat{\boldsymbol{x}}$ direction. Conversely, $c < 0$ has $\boldsymbol{k} = k\,\hat{\boldsymbol{x}} = -|k|\,\hat{\boldsymbol{x}}$ with $k < 0$, thus indicating a stable edge wave with phase moving in the $-\hat{\boldsymbol{x}}$ direction.

61.4.2 Polarization relations

The horizontal velocity components are computed from the streamfunction via

$$\psi = \widetilde{\psi}\,\mathrm{e}^{\mathrm{i}\,k\,(x-c\,t)} \tag{61.23a}$$

$$\boldsymbol{u}' = \hat{\boldsymbol{z}} \times \nabla\psi = \mathrm{e}^{\mathrm{i}\,k\,(x-c\,t)}\,(-\hat{\boldsymbol{x}}\,\partial_y + \hat{\boldsymbol{y}}\,\mathrm{i}\,k)\widetilde{\psi} \tag{61.23b}$$

$$u' = (\mathrm{i}/k)\,\partial_y v' = -\mathrm{e}^{\mathrm{i}\,k\,(x-c\,t)}\,\partial_y\widetilde{\psi} \tag{61.23c}$$

$$v' = \mathrm{i}\,k\,\psi = \mathrm{i}\,k\,\mathrm{e}^{\mathrm{i}\,k\,(x-c\,t)}\,\widetilde{\psi}. \tag{61.23d}$$

As a check we confirm that the horizontal velocity is non-divergent

$$\partial_x u' + \partial_y v' = \mathrm{i}\,k\,\partial_y\widetilde{\psi}\,\mathrm{e}^{\mathrm{i}\,k\,(x-c\,t)}\,(-1+1) = 0. \tag{61.24}$$

To get the pressure perturbation, return to the zonal component of the velocity equation (61.7) (with $f = 0$)

$$(\partial_t + u_{\mathsf{b}}\,\partial_x)u' + v'\,\partial_y u_{\mathsf{b}} = -\partial_x\varphi', \tag{61.25}$$

and make the ansatz

$$\varphi' = \widetilde{\varphi}(y)\,\mathrm{e}^{\mathrm{i}\,k\,(x-c\,t)}. \tag{61.26}$$

Use of this pressure ansatz along with the horizontal velocity equations (61.23c) and (61.23d), yields the pressure amplitude in terms of the streamfunction amplitude

$$\widetilde{\varphi} = [(u_{\mathsf{b}} - c)\,\partial_y - \partial_y u_{\mathsf{b}}]\widetilde{\psi}. \tag{61.27}$$

In summary, the amplitude equations (polarization relations) for the horizontal velocity components and the pressure are given, in terms of the streamfunction, by

$$\psi = \widetilde{\psi}(y)\,\mathrm{e}^{\mathrm{i}\,k\,(x-c\,t)} \tag{61.28a}$$

$$u' = \widetilde{u}(y)\,\mathrm{e}^{\mathrm{i}\,k\,(x-c\,t)} \quad \text{and} \quad v' = \widetilde{v}(y)\,\mathrm{e}^{\mathrm{i}\,k\,(x-c\,t)} \quad \text{and} \quad \varphi' = \widetilde{\varphi}(y)\,\mathrm{e}^{\mathrm{i}\,k\,(x-c\,t)} \tag{61.28b}$$

[3] Remember that for a stable wave, $\omega \geq 0$ in this book (see Section 49.2.3).

[4] Many books refer to c as the phase speed, even though c can be positive or negative. However, as emphasized in Section 49.5.2, the phase speed is the non-negative magnitude of the phase velocity.

$$\widetilde{u} = -\partial_y \widetilde{\psi} \qquad \text{and} \quad \widetilde{v} = \mathrm{i}\, k\, \widetilde{\psi} \qquad \text{and} \quad \widetilde{\varphi} = [(u_\mathrm{b} - c)\, \partial_y - \partial_y u_\mathrm{b}]\widetilde{\psi}. \tag{61.28c}$$

61.4.3 Complex phase velocity

To investigate shear instability, we are interested in flow properties that lead to the phase velocity, c, having an imaginary part, in which case

$$c = c_\mathrm{r} + \mathrm{i}\, c_\mathrm{i} = c_\mathrm{r} + \mathrm{i}\, \sigma/k. \tag{61.29}$$

In this case, it is the real part, c_r, that is the phase velocity whereas c_i measures the decay rate or growth rate for the wave amplitude

$$\psi(x, y, t) = \widetilde{\psi}(y)\, \mathrm{e}^{\mathrm{i}\, k\, (x - c_\mathrm{r}\, t)}\, \mathrm{e}^{k\, c_\mathrm{i}\, t} = \widetilde{\psi}(y)\, \mathrm{e}^{\mathrm{i}\, k\, (x - c_\mathrm{r}\, t)}\, \mathrm{e}^{\sigma\, t}. \tag{61.30}$$

If $c_\mathrm{i} > 0$ then the wave is exponentially unstable with *growth rate*,

$$\sigma = k\, c_\mathrm{i}, \tag{61.31}$$

whereas if $\sigma < 0$ then the wave exponentially decays.

As we see in Section 61.4.4, if c is complex then it appears along with its complex conjugate, so that the exponentially growing mode and the decaying mode appear as a pair. Furthermore, note that the complex conjugate of the streamfunction (61.30) is given by

$$\psi^* = \widetilde{\psi}^*(y)\, \mathrm{e}^{-\mathrm{i}\, k\, (x - c_\mathrm{r}\, t)}\, \mathrm{e}^{\sigma\, t}, \tag{61.32}$$

so that

$$|\psi|^2 = \psi^*\, \psi = |\widetilde{\psi}|^2\, \mathrm{e}^{2\, \sigma\, t}, \tag{61.33}$$

along with the analogs for the horizontal velocity components

$$|u'|^2 = u'\, (u')^* = |\partial_y \widetilde{\psi}|^2\, \mathrm{e}^{2\, \sigma\, t} \quad \text{and} \quad |v'|^2 = v'\, (v')^* = k^2\, |\widetilde{\psi}|^2\, \mathrm{e}^{2\, \sigma\, t}. \tag{61.34}$$

These identities are used when developing the phase averaged kinetic energy budget in Section 61.4.6.

61.4.4 Rayleigh-Kuo equation for the streamfunction

Inserting the modulated wave ansatz (61.19) into the linearized vorticity equation (54.82) leads to the *Rayleigh equation*

$$(u_\mathrm{b} - c)\, (\partial_{yy} - k^2)\, \widetilde{\psi} + \partial_y \zeta_\mathrm{b}\, \widetilde{\psi} = 0. \tag{61.35}$$

Or, in the presence of $\beta \neq 0$ we find the Rayleigh-Kuo equation (54.84)

$$(u_\mathrm{b} - c)\, (\partial_{yy} - k^2)\, \widetilde{\psi} + (\beta + \partial_y \zeta_\mathrm{b})\, \widetilde{\psi} = 0. \tag{61.36}$$

For a study of instabilities, the phase velocity, $c = \omega/k$, and the streamfunction, $\widetilde{\psi}$, are generally complex, whereas all other terms are real. Hence, the complex conjugate of the Rayleigh-Kuo equation (61.36) is given by

$$(u_\mathrm{b} - c^*)\, (\partial_{yy} - k^2)\, \widetilde{\psi}^* + (\beta + \partial_y \zeta_\mathrm{b})\, \widetilde{\psi}^* = 0. \tag{61.37}$$

Evidently, if c satisfies the Rayleigh-Kuo equation (61.36) with streamfunction $\widetilde{\psi}$, then c^* satisfies the complex conjugate equation (61.37) with streamfunction $\widetilde{\psi}^*$. Hence, the phase velocities come in complex conjugate pairs.

61.4.5 Rayleigh-Kuo equation for the meridional displacement

Let $\xi(x,y,t)$ be the meridional component of the fluid particle displacement from its equilibrium position. This particle displacement satisfies the evolution equation

$$v' = (\partial_t + u\,\partial_x)\xi = [\partial_t + (u' + u_\text{b})\,\partial_x]\xi. \tag{61.38}$$

Linearizing for small amplitude displacements leads to

$$v' = (\partial_t + u_\text{b}\,\partial_x)\xi, \tag{61.39}$$

with the usual ansatz,

$$\xi = \widetilde{\xi}(y)\,\mathrm{e}^{\mathrm{i}\,k\,(x-c\,t)}, \tag{61.40}$$

yielding

$$\widetilde{\psi} = (u_\text{b} - c)\,\widetilde{\xi}. \tag{61.41}$$

Evidently, for small amplitude motion, the streamfunction amplitude, $\widetilde{\psi}$, equals to the meridional particle excursion amplitude, $\widetilde{\xi}$, multiplied by the difference between the phase velocity and the background flow, $u_\text{b} - c$.

With the relation (61.41), we can convert the Rayleigh equation (61.35) for the streamfunction into an equation for the meridional particle excursion. For this purpose make use of the derivative

$$\partial_{yy}\widetilde{\psi} = \widetilde{\xi}\,\partial_{yy}u_\text{b} + 2\,\partial_y\widetilde{\xi}\,\partial_y u_\text{b} + (u_\text{b} - c)\,\partial_{yy}\widetilde{\xi}, \tag{61.42}$$

along with a few lines of algebra to derive the Rayleigh-Kuo equation in terms of the meridional excursion

$$\partial_y[(u_\text{b} - c)^2\,\partial_y\widetilde{\xi}] = (u_\text{b} - c)\,[-\beta + k^2\,(u_\text{b} - c)]\,\widetilde{\xi}. \tag{61.43}$$

We make use of equation (61.43) in Section 61.5.3 to derive a condition required for a modal perturbation to initiate an instability.

61.4.6 Phase and zonal averaged eddy kinetic energy equation

In Section 61.3.2 we developed the equation for the kinetic energy of the fluctuating field and took its zonal average to find

$$\partial_t(\overline{u'\,u' + v'\,v'})/2 = -\overline{u'\,v'}\,\partial_y u_\text{b} - \partial_y(\overline{v'\,\varphi'}). \tag{61.44}$$

Following the methods of complex variables and phase averaging as detailed in Section 8.1, use of the polarization relations from Section 61.4.2, and recognition that the phase velocity is generally complex according to equations (61.33) and (61.34), lead to[5]

$$2\,\langle\overline{u'\,u'}\rangle = |\partial_y\widetilde{\psi}|^2\,\mathrm{e}^{2\,\sigma\,t} \tag{61.45a}$$

$$2\,\langle\overline{v'\,v'}\rangle = k^2\,|\widetilde{\psi}|^2\,\mathrm{e}^{2\,\sigma\,t} \tag{61.45b}$$

$$2\,\langle\overline{u'\,v'}\rangle = k\,\mathrm{Re}[\mathrm{i}\,\widetilde{\psi}^*\,\partial_y\widetilde{\psi}]\,\mathrm{e}^{2\,\sigma\,t} = -k\,\mathrm{Im}[\widetilde{\psi}^*\,\partial_y\widetilde{\psi}]\,\mathrm{e}^{2\,\sigma\,t} = k\,\mathrm{Im}[\widetilde{\psi}\,\partial_y\widetilde{\psi}^*]\,\mathrm{e}^{2\,\sigma\,t}, \tag{61.45c}$$

along with the phase average of the meridional velocity and pressure

$$2\,\mathrm{e}^{-2\,\sigma\,t}\,\langle\overline{v'\,\varphi'}\rangle = k\,\mathrm{Re}[\mathrm{i}\,\widetilde{\psi}\,\widetilde{\varphi}^*] \tag{61.46a}$$

$$= -k\,\mathrm{Im}[\widetilde{\psi}\,\widetilde{\varphi}^*] \tag{61.46b}$$

$$= -k\,\mathrm{Im}[(u_\text{b} - c)\,\widetilde{\psi}\,\partial_y\widetilde{\psi}^* - \partial_y u_\text{b}\,|\widetilde{\psi}|^2] \tag{61.46c}$$

[5]Exercise 61.1 derives the identity $\mathrm{Im}\left[\widetilde{\psi}^*\,\partial_y\widetilde{\psi}\right] = -\,\mathrm{Im}\left[\widetilde{\psi}\,\partial_y\widetilde{\psi}^*\right]$ used in equation (61.45c).

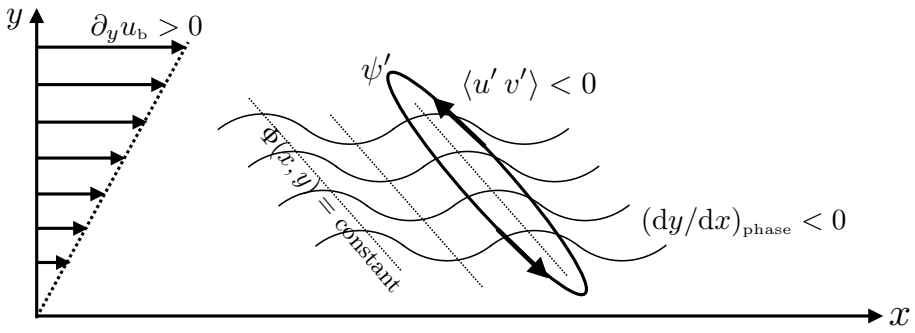

FIGURE 61.1: The lines of constant phase, $\Phi(x, y) = k\, x - \alpha(y)$, for the streamfunction (or the meridional velocity) in an unstable barotropic wave. The wave depicted here has an increasing kinetic energy since the phase lines are tilted into the shear. That is, this orientation of the wave ensures that the barotropic shear production increases the kinetic energy of the wave as per equation (61.56). Namely, since the waves are transverse, fluid particles move on constant phase lines, with the tilt shown here ensuring that $\langle u'\, v' \rangle < 0$. That is, a meridionally positive particle motion corresponds to a zonally negative motion, and vice versa. This behavior is characteristic of unstable waves whose kinetic energy grows by feeding off the unstable background shear state. Observe that if one placed a passive tracer in the flow, or an array of fluid particles, then they would be stretched to align with the shear rather than against the shear. The growing wave, however, is an active flow feature, with the present analysis indicating that energy growth for this feature requires phase lines to tilt into the shear as depicted here.

$$= -k\, \mathrm{Im}[(u_\flat - c)\, \widetilde{\psi}\, \partial_y \widetilde{\psi}^*], \tag{61.46d}$$

where we used $\mathrm{Im}[\partial_y u_\flat\, |\widetilde{\psi}|^2] = 0$ for the final equality. Bringing terms together leads to the phase and zonal averaged eddy kinetic energy budget

$$2\,\sigma \left[|\partial_y \widetilde{\psi}|^2 + k^2\, |\widetilde{\psi}|^2 \right] /2 = \underbrace{-k\, \partial_y u_\flat\, \mathrm{Im}\left[\widetilde{\psi}\, \partial_y \widetilde{\psi}^* \right] /2}_{\text{shear production}} + \underbrace{k\, \partial_y\, \mathrm{Im}\left[(u_\flat - c)\, \widetilde{\psi}\, \partial_y \widetilde{\psi}^* \right] /2}_{\text{KE flux convergence}}, \tag{61.47}$$

where we recognize $\sigma/k = c_\mathrm{i}$ according to equation (61.29).

61.4.7 Phase lines of unstable waves tilt into the shear

As noted in Section 61.3.2, the only way for the globally integrated kinetic energy to grow is through the shear production term, since the globally integrated pressure flux convergence vanishes. A sufficient, though not necessary, condition for global kinetic energy growth is that the shear production is positive at each point within the fluid domain. From equation (61.47) we thus have

$$k\, \partial_y u_\flat\, \mathrm{Im}\left[\widetilde{\psi}^*\, \partial_y \widetilde{\psi} \right] > 0 \Longrightarrow \text{sufficient condition for kinetic energy growth.} \tag{61.48}$$

If the kinetic energy growth arises from shear instability, then equation (61.48) offers a sufficient condition for shear instability.

To develop a geometric view for the energy growth condition (61.48), introduce the phase, $\alpha(y)$, of the streamfunction via

$$\widetilde{\psi}(y) = |\widetilde{\psi}(y)|\, \mathrm{e}^{\mathrm{i}\,\alpha(y)}, \tag{61.49}$$

so that

$$\mathrm{Im}\left[\widetilde{\psi}^*\, \partial_y \widetilde{\psi} \right] = \mathrm{Im}\left[|\widetilde{\psi}|\, \mathrm{e}^{-\mathrm{i}\,\alpha(y)}\, (\partial_y |\widetilde{\psi}| + \mathrm{i}\, |\widetilde{\psi}|\, \partial_y \alpha)\, \mathrm{e}^{\mathrm{i}\,\alpha(y)} \right] = |\widetilde{\psi}|^2\, \partial_y \alpha, \tag{61.50}$$

thus bringing the sufficient condition (61.48) to the form

$$k\, \partial_y u_\flat |\widetilde{\psi}|^2\, \partial_y \alpha > 0 \Longrightarrow \text{sufficient condition for energy growth.} \tag{61.51}$$

Now write the full streamfunction as

$$\psi = \widetilde{\psi}(y)\, \mathrm{e}^{\mathrm{i}\, k\, (x - c\, t)} = |\widetilde{\psi}(y)|\, \mathrm{e}^{\mathrm{i}\, \alpha(y)}\, \mathrm{e}^{\mathrm{i}\, (k\, x - c\, t)} = |\widetilde{\psi}(y)|\, \mathrm{e}^{\mathrm{i}\, (\Phi(x,y) - c\, t)}, \tag{61.52}$$

where we defined the spatial phase function

$$\Phi(x, y) \equiv k\, x + \alpha(y). \tag{61.53}$$

Lines of constant phase are defined by

$$\mathrm{d}\Phi = 0 = k\, \mathrm{d}x + (\partial_y \alpha)\, \mathrm{d}y \implies (\mathrm{d}y/\mathrm{d}x)_{\text{phase}} = -k/\partial_y \alpha, \tag{61.54}$$

so that the instability condition (61.48) can be written

$$k\, \partial_y u_{\mathsf{b}}\, |\widetilde{\psi}|^2\, \partial_y \alpha = -k^2\, |\widetilde{\psi}|^2 \frac{\partial_y u_{\mathsf{b}}}{(\mathrm{d}y/\mathrm{d}x)_{\text{phase}}} > 0 \implies \text{sufficient condition for energy growth.} \tag{61.55}$$

Simplifying this equation leads to the condition for the ratio of the shear and the phase slope

$$\frac{\partial_y u_{\mathsf{b}}}{(\mathrm{d}y/\mathrm{d}x)_{\text{phase}}} < 0 \implies \text{sufficient condition for energy growth.} \tag{61.56}$$

This inequality says that kinetic energy of the wave grows when the wave's phase lines tilt into the background flow shear, such as depicted in Figure 61.1. The tilted phase lines reflect the ability of the wave to extract kinetic energy from the background state. This geometric property offers a visual indicator that the wave is acting on an unstable shear state, thus providing a valuable diagnostic tool for identifying shear instabilities as they are happening.

61.5 Integral conditions necessary for shear instability

In this section we develop integral conditions for stability of an inviscid horizontally sheared fluid on a β plane, with the conditions arrived at by forming spatial integrals of the Rayleigh equation (61.35) and the Rayleigh-Kuo equation (61.36). These integral conditions allow us to determine stability properties even without explicitly solving the detailed instability problem for a particular flow (see Section 61.6 for a solution example). We do so by deriving geometric conditions that are necessary for the flow to be unstable, or conversely that are sufficient to ensure the flow is stable. We also consider conditions needed for a particular perturbation to initiate an instability. Generally, the conditions we derive are necessary though not sufficient to ensure instability. Evidently, even if a flow satisfies the necessary conditions for instability, the flow can still be stable. This situation for the modal instabilities of sheared flows contrasts to the parcel instabilities from Chapter 59, where the instability conditions are both necessary and sufficient.

61.5.1 Rayleigh-Kuo inflection point theorem

Here we establish the *Rayleigh instability criteria*, also known as the *Rayleigh inflection-point criteria*. In the presence of β, it is known as the *Rayleigh-Kuo condition*. To proceed, start from the Rayleigh-Kuo equation (61.36) written as

$$(\partial_{yy} - k^2)\, \widetilde{\psi} + \frac{(\beta - \partial_{yy} u_{\mathsf{b}})\, \widetilde{\psi}}{u_{\mathsf{b}} - c} = 0. \tag{61.57}$$

Multiplying by $\widetilde{\psi}^*$ (complex conjugate of $\widetilde{\psi}$) and integrating over the meridional extent of the domain, $\mathcal{R}$, leads to

$$\int_{\mathcal{R}} [\partial_y(\widetilde{\psi}^* \, \partial_y \widetilde{\psi}) - |\partial_y \widetilde{\psi}|^2 - k^2 \, |\widetilde{\psi}|^2] \, \mathrm{d}y = - \int_{\mathcal{R}} \frac{(\beta - \partial_{yy} u_\mathrm{b}) \, |\widetilde{\psi}|^2}{u_\mathrm{b} - c} \, \mathrm{d}y. \tag{61.58}$$

If the streamfunction or its derivatives vanish on the meridional boundaries (or vanish when bounded away from the region of interest), then the left hand side is a negative real number. Now all terms on the right hand side are real except, possibly, the phase velocity, c. Hence, this equation is self-consistent only if the imaginary part of the right hand side vanishes

$$c_\mathrm{i} \int_{\mathcal{R}} \frac{(\beta - \partial_{yy} u_\mathrm{b}) \, |\widetilde{\psi}|^2}{|u_\mathrm{b} - c|^2} \, \mathrm{d}y = 0. \tag{61.59}$$

This condition can be satisfied in two ways. The first way is if the phase velocity is real, so that $c_\mathrm{i} = 0$ and hence all waves are stable.[6] The second way is if the integral vanishes. For the integral to vanish requires $\beta - \partial_{yy} u_\mathrm{b}$ to change sign somewhere in the domain, since all the other terms in the integral are positive. That is, somewhere in the domain there must be an extrema of the base state's absolute vorticity,

$$\beta - \partial_{yy} u_\mathrm{b} = \partial_y (f + \zeta_\mathrm{b}). \tag{61.60}$$

There are many qualifiers to this result. In particular, for $\beta - \partial_{yy} u_\mathrm{b}$ to change sign in the domain represents a necessary condition for a shear instability, and yet it is not a sufficient condition for instability. Indeed, there are flow profiles that satisfy the inflection point criteria and yet there are still no growing wave modes. Turning the condition around we find that a sufficient condition for stability is that there are no sign changes for $\beta - \partial_{yy} u_\mathrm{b}$. We summarize the result by stating the following theorem.

> RAYLEIGH-KUO INFLECTION POINT THEOREM: Consider an inviscid and homogeneous (constant density) fluid, with flow in an inertial reference frame (no Coriolis) and with a base state of zonal flow with meridional shear. A necessary condition for shear instability is that there exists an inflection point in the base state zonal flow somewhere in the domain; i.e., where $\partial_{yy} u_\mathrm{b} = 0$ and so where the relative vorticity has an extrema, $\partial_y \zeta_\mathrm{b} = -\partial_{yy} u_\mathrm{b} = 0$. For flow on the β-plane, this criteria is generalized to $\partial_y (f + \zeta_\mathrm{b}) = \beta - \partial_{yy} u_\mathrm{b} = 0$, in which case the absolute vorticity must have an extrema in the domain in order to admit an instability. If there is no inflection point, then its absence is sufficient to conclude that the flow is stable to shear instability.

It is notable that $\beta > 0$ always acts to stabilize the flow since its contribution requires a stronger background flow curvature to realize an inflection point. So if β is large enough then it can eliminate the inflection point, $\partial_y (f + \zeta_\mathrm{b}) = \beta - \partial_{yy} u_\mathrm{b} = 0$, from the domain, and in so doing it can stabilize the flow according to the Rayleigh-Kuo theorem. We can understand this stabilizing effect by noting that β supports planetary Rossby waves (Section 54.3), with such waves offering an alternative means to discharge the kinetic energy carried by shear in the base state flow.

61.5.2 Fjørtoft's theorem

Roughly 70 years after *Rayleigh* (1880) introduced the inflection point theorem, and a year after *Kuo* (1949) extended the inflection point theorem to the β-plane, *Fjørtoft* (1950) established

[6] Recall from Section 61.6.1 that if c solves the Rayleigh equation with streamfunction $\widetilde{\psi}$, then c^* also satisfies the equation with streamfunction $\widetilde{\psi}^*$. Hence, for each decaying mode there is a growing mode. So a sufficient condition for instability is to find a wave in which $c_\mathrm{i} \neq 0$.

another necessary condition for instability that is somewhat more constraining than the Rayleigh-Kuo theorem from Section 61.5.1.

To derive Fjørtoft's theorem, return to equation (61.58). Rather than focus on the imaginary part as done for the Rayleigh criteria, consider the real part

$$\int_{\mathcal{R}} \frac{(u_b - c_r)\,(\beta - \partial_{yy} u_b)\,|\widetilde{\psi}|^2}{|u_b - c|^2}\,dy = \int_{\mathcal{R}} [|\partial_y \widetilde{\psi}|^2 + k^2\,|\widetilde{\psi}|^2]\,dy > 0. \tag{61.61}$$

We are interested in profiles that satisfy the Rayleigh criteria for instability, so that the integral (61.59) vanishes, in which case we have

$$\int_{\mathcal{R}} \frac{c_r\,(\beta - \partial_{yy} u_b)\,|\widetilde{\psi}|^2}{|u_b - c|^2}\,dy = 0, \tag{61.62}$$

since c_r is a constant. Hence, equation (61.61) is trivially satisfied with any constant, U_s, inserted into the integral

$$\int_{\mathcal{R}} \frac{(u_b - U_s)\,(\beta - \partial_{yy} u_b)\,|\widetilde{\psi}|^2}{|u_b - c|^2}\,dy > 0. \tag{61.63}$$

A particularly useful constant is the value of the zonal velocity at the inflection point, $y = y_s$, where the absolute vorticity has an extrema $\partial_y(f + \zeta_b) = \beta - \partial_{yy} u_b = 0$. We are thus led to the following theorem.

> FJØRTOFT'S THEOREM: Under the same assumptions as the Rayleigh-Kuo theorem (Section 61.5.1), a necessary condition for shear instability is that $(u_b - U_s)\,(\beta - \partial_{yy} u_b) > 0$ occurs somewhere in the domain in order to satisfy the condition (61.63). Here, the inflection point is determined by $\partial_y(f + \zeta_b) = \beta - \partial_{yy} u_b(y_s) = 0$, with $U_s = u_b(y_s)$ the velocity at the inflection point.

Fjørtoft's theorem is rather subtle in its meaning, in particular it implies that an instability can occur only if the absolute vorticity has its maximum magnitude within the domain interior rather than at the domain boundary. One means to support this conclusion is by considering example zonal velocity profiles in Section 61.5.4.

61.5.3 Critical latitude theorem

The Rayleigh-Kuo condition and Fjørtoft's condition are statements about the geometry of the base flow state. Here we derive a condition necessary for a wave perturbation to support an instability. To do so, consider the Rayleigh-Kuo equation (61.43) written in terms of the meridional displacement

$$\partial_y[(u_b - c)^2\,\partial_y \widetilde{\xi}] = (u_b - c)\,[-\beta + k^2\,(u_b - c)]\,\widetilde{\xi}. \tag{61.64}$$

Following the approach taken for the Rayleigh-Kuo theorem in Section 61.5.1, multiply by $\widetilde{\xi}^*$, integrate over the domain, and assume boundary contributions are zero so that

$$\int_{\mathcal{R}} (|\partial_y \xi|^2 + k^2\,|\xi|^2)\,(u_b - c)^2\,dy = \beta \int_{\mathcal{R}} (u_b - c)\,|\xi|^2\,dy. \tag{61.65}$$

Writing

$$(u_b - c)^2 = (u_b - c_r)^2 - (c_i)^2 - 2\,i\,c_i\,(u_b - c_r), \tag{61.66}$$

leads to the two conditions taken from the real and imaginary parts of equation (61.65)

$$\int_{\mathcal{R}} (|\partial_y \xi|^2 + k^2 |\xi|^2) [(u_{\mathsf{b}} - c_{\mathsf{r}})^2 - (c_{\mathsf{i}})^2] \, \mathrm{d}y = \beta \int_{\mathcal{R}} (u_{\mathsf{b}} - c_{\mathsf{r}}) |\xi|^2 \, \mathrm{d}y \tag{61.67a}$$

$$2 c_{\mathsf{i}} \int_{\mathcal{R}} (|\partial_y \xi|^2 + k^2 |\xi|^2) (u_{\mathsf{b}} - c_{\mathsf{r}}) \, \mathrm{d}y = c_{\mathsf{i}} \beta \int_{\mathcal{R}} |\xi|^2 \, \mathrm{d}y. \tag{61.67b}$$

We are interested in unstable flows, in which case $c_{\mathsf{i}} \neq 0$. So the second condition provides a statement about the value of the real phase velocity relative to the background flow

$$2 \int_{\mathcal{R}} (|\partial_y \xi|^2 + k^2 |\xi|^2) (u_{\mathsf{b}} - c_{\mathsf{r}}) \, \mathrm{d}y = \beta \int_{\mathcal{R}} |\xi|^2 \, \mathrm{d}y \geq 0. \tag{61.68}$$

Since the first portion of the left hand side integral is positive, the integral condition (61.68) can only be met if $u_{\mathsf{b}} - c_{\mathsf{r}}$ is predominantly positive throughout the domain. For the special case of $\beta = 0$, we find the more definitive statement

$$\int_{\mathcal{R}} (|\partial_y \xi|^2 + k^2 |\xi|^2) (u_{\mathsf{b}} - c_{\mathsf{r}}) \, \mathrm{d}y = 0 \quad \text{if } \beta = 0. \tag{61.69}$$

Evidently, when $\beta = 0$ then $u_{\mathsf{b}} - c_{\mathsf{r}}$ must change sign within the domain in order to support an instability. That is, for an instability to exist we must have the real phase velocity of a modal perturbation equal the background velocity at some latitude within the domain. For a wave perturbation to grow requires it to travel with the flow at least at one latitude, where the wave perturbation is stationary relative to the background flow and can thus extract kinetic energy to feed the growing wave. We are thus led to the *critical latitude theorem*.

> Critical latitude theorem: Under the same assumptions as the Rayleigh-Kuo theorem (Section 61.5.1), a modal perturbation to a sheared flow with $\beta = 0$ is able to initiate an instability if its real phase velocity equals to the background flow velocity somewhere in the domain, thus ensuring that the real phase velocity is within the range of the background velocity.

We return to this theorem in Section 61.7.6, where we find that this result also holds for stratified shear instability as represented by Howard's semi-circle theorem.

61.5.4 Stability conditions for sample profiles

We here consider a suite of example velocity profiles and discuss their stability properties as per the Rayleigh inflection point theorem and Fjørtoft's theorem, with consideration given only to the case of $\beta = 0$. We leave the velocity, U, and length L, scales arbitrary, noting that the stability theorems of Rayleigh and Fjørtoft are statements about the flow geometry rather than the scale of the flow.

Parabolic profile is stable

In Figure 61.2 we display a parabolic velocity profile, sometimes referred to as *Poiseuille flow*, which can be considered a highly smoothed version of the point jet studied in Section 54.5. Recall the point jet supports stable edge waves. In the absence of multiple point jets that can interact with one another, we expect the flow to be stable. Hence, extrapolating from the point jet motivates us to guess that the parabolic jet in Figure 61.2 is stable. Indeed, it is stable according to the Rayleigh inflection point theorem simply because there is no inflection point given that the derivative of the vorticity is constant.

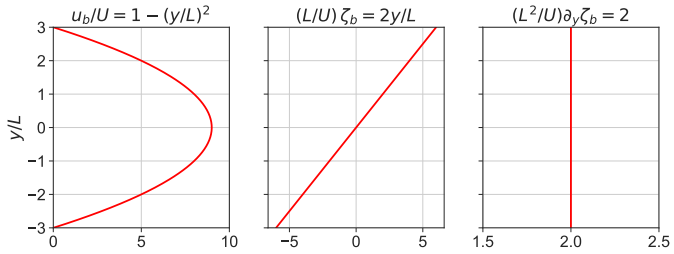

FIGURE 61.2: A parabolic velocity profile (Poiseuille flow) and its derivatives. Left panel: $u_b/U = (y/L)^2$. Middle panel: vorticity, $(L/U)\,\zeta_b = -(L/U)\,\partial_y u_b = -2\,(y/L)$. Right panel: derivative of the vorticity, $(L^2/U)\,\partial_y\zeta_b = -(L^2/U)\,\partial_{yy}u_b = -2$. Rayleigh's inflection point theorem says that this profile is stable since there is no inflection point.

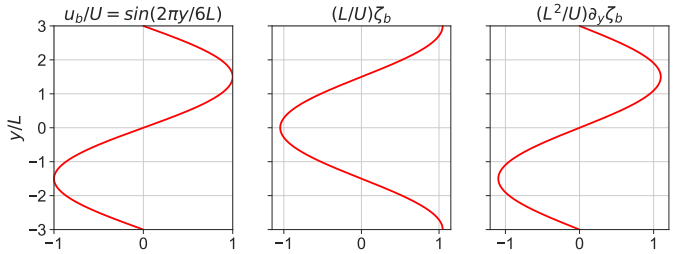

FIGURE 61.3: A sinusoidal velocity profile and its derivatives. Left panel: $u_b/U = \sin(2\pi\, y/6L)$. Middle panel: vorticity, $(L/U)\,\zeta_b = -(L/U)\,\partial_y u_b = -(2\pi/6)\cos(2\pi\, y/6L)$. Right panel: derivative of the vorticity, $(L^2/U)\,\partial_y\zeta_b = -(2\pi/6)^2\,u_b/U$. This velocity profile satisfies both the Rayleigh and Fjørtoft criteria for instability.

Sinusoidal profile is unstable according Rayleigh and Fjørtoft

Figure 61.3 shows a sinusoidal velocity profile. This flow has an inflection point at $y = 0$, and so satisfies the Rayleigh inflection point condition for instability. It also satisfies the Fjørtoft condition for instability, which we see with $U_s = 0$ at the $y = 0$ inflection point so that

$$(u_b - U_s)\,(\beta - \partial_{yy}u_b) = (u_b - 0)\,(0 - \partial_{yy}u_b) = (2\pi\, y/6L)^2\,(u_b)^2 > 0. \tag{61.70}$$

Gaussian jet profile is unstable according to Rayleigh and Fjørtoft

Figure 61.4 shows a Gaussian jet profile. There are two inflections points, $y = \pm L$, so that this profile is unstable according to the Rayleigh inflection point theorem. It is also unstable due to Fjørtoft's theorem since the vorticity extrema are within the domain.

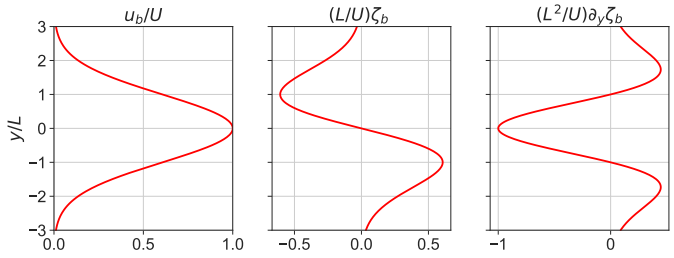

FIGURE 61.4: A Gaussian velocity profile and its derivatives. Left panel: $u_b/U = \mathrm{e}^{-(y/L)^2/2}$. Middle panel: vorticity, $(L/U)\,\zeta_b = -(L/U)\,\partial_y u_b = -(y/L)\,u_b/U$. Right panel: derivative of the vorticity, $(L^2/U)\,\partial_y\zeta_b = -(L^2/U)\,\partial_{yy}u_b = [(y/L)^2 - 1]\,(u_b/U)$. This velocity profile is unstable according to the Rayleigh inflection point theorem, with the two inflection points at $y = \pm L$.

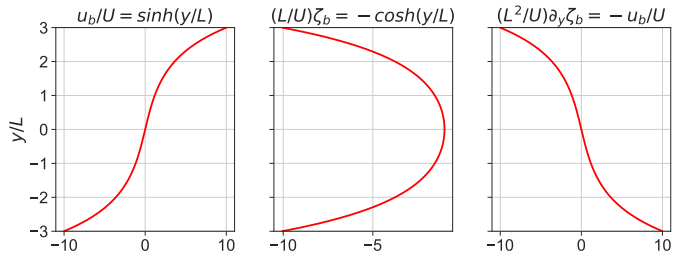

FIGURE 61.5: A sinh velocity profile and its derivatives. Left panel: $u_b/U = \sinh(y/L)$. Middle panel: vorticity, $(L/U)\,\zeta_b = -(L/U)\,\partial_y u_b = -\cosh(y/L)$. Right panel: derivative of the vorticity, $(L^2/U)\,\partial_y\zeta_b = -(L^2/U)\,\partial_{yy}u_b = -\sinh(y/L)$. This velocity profile satisfies the Rayleigh inflection point theorem, suggesting that it is unstable to shear instability. However, Fjørtoft's theorem says that it is stable.

Sinh profile is unstable according to Rayleigh but stable according to Fjørtoft

Consider the sinh velocity profile,

$$u_b = U\sinh(y/L) \tag{61.71a}$$
$$\zeta_b = -\partial_y u_b = -(U/L)\cosh(y/L) \tag{61.71b}$$
$$\partial_y\zeta_b = -\partial_{yy}u_b = -(U/L^2)\sinh(y/L), \tag{61.71c}$$

as shown in Figure 61.5. The velocity vanishes at the $y = 0$ inflection point (where $\partial_y\zeta_b = -\partial_{yy}u_b = 0$), so that $U_s = 0$. Consequently, the velocity profile satisfies Rayleigh's necessary condition for instability. However, for Fjørtoft's theorem we note that

$$(u_b - U_s)\,(\beta - \partial_{yy}u_b) = (u_b - 0)\,(0 - \partial_{yy}u_b) = -(U/L)^2\sinh^2(y/L) < 0. \tag{61.72}$$

Evidently, the flow is stable via the Fjørtoft theorem since $(u_b - U_s)\,(\beta - \partial_{yy}u_b)$ is never positive in the domain. In particular, the vorticity extrema are at the latitudinal bounds of the domain (see middle panel of Figure 61.5), with the extrema increasing in magnitude as the domain is expanded. In Exercise 61.2 we consider $\beta > 0$, where we find that the sinh profile is also stable according to Fjørtoft.

61.6 Interacting edge waves and shear instability

So far in this chapter we developed sufficient conditions for sheared flows to be stable. Conversely, we developed necessary conditions for the sheared flow to be unstable. In this section we study a particular flow configuration and solve the Rayleigh equation to determine the dispersion relation and corresponding instability conditions. This case study exposes the interacting wave mechanism for shear instability. For this purpose, recall from Section 54.5 the theory for edge waves riding on a single jump in the base state vorticity, with salient features given by the following.

- Edge waves propagate along the interface where vorticity experiences a jump, with the waves trapped to this interface due to the exponential decay of the wave in the direction orthogonal to the jump surface.
- The edge wave phase velocity, $\boldsymbol{c}_p$, is built from two contributions: one due to a Doppler shift from the background flow, and the other from the vorticity jump. The vorticity jump contribution is referred to as the intrinsic phase velocity, $\boldsymbol{c}_{\text{phase}}^{\text{intrinsic}}$.
- The intrinsic phase velocity is directed so that the higher relative vorticity is to the right when facing in the direction of the phase velocity. Equivalently, the phase velocity is

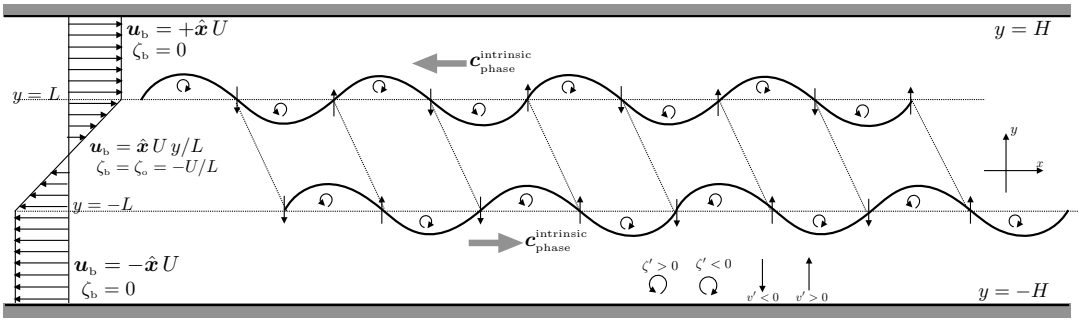

FIGURE 61.6: Depicting the interaction between two edge waves generated by a base flow that is unstable to shear instability. On the left we show the zonal base flow, with velocity kinks at $y = \pm L$. At $y = -L$, the vorticity jumps from zero to the south to a negative value to the north, so that the higher vorticity is to the south. This vorticity jump supports an edge wave with eastward intrinsic phase velocity, $\boldsymbol{c}_{\text{phase}}^{\text{intrinsic}}$. For the $y = L$ kink, the vorticity jumps from negative to zero when moving north. This vorticity configuration has higher vorticity to the north, thus supporting an edge wave with westward intrinsic phase velocity. These phase directions, both of which are contrary to the background flow, allow for Doppler shifting to make each of the edge waves stationary (i.e., zero real phase velocity). The oriented circles denote the anomalous vorticity associated with a particular fluctuation of the respective interfaces. For example, on the southern edge wave, a northward fluctuation brings fluid with higher relative vorticity northward, thus denoted by $\zeta' > 0$ and a counter-clockwise oriented circle. The secondary circulations induced by the anomalous vorticity induce anomalous meridional flows, depicted by the meridional arrows. These meridional flows have maximum amplitude at the wave nodes, pointing upward in front of a wave peak and downward on the back side. Interactions between the waves are mutually constructive with a phase shift whereby the southern wave is shifted to the east of the northern wave (see Figure 61.1); i.e., with the $y = L$ wave shifted ahead of the $y = -L$ wave so that lines of constant phase are slanted into the background shear. With this phase shift, a northward anomalous flow from the southern wave enhances the peak of the northern wave, thus supporting its further growth. A similar enhancement occurs for the opposite wave, thus resulting in mutual amplification of each wave's amplitude. To optimize the growth requires the waves to be *phase locked*, whereby they stay stationary relative to one another, thus allowing the positive feedback to create the exponential wave growth.

directed towards the concave portion of the velocity profile. One can understand this orientation via the conservation of relative vorticity (holding for an inviscid flow in an inertial reference frame), as explained for the point jet in Figure 54.8.

We focus in this section on interactions between two edge waves, with the aim to characterize conditions that support shear instability. For analytical tractability, we focus on the case with zero planetary beta ($\beta = 0$). This assumption serves to clearly expose the underlying *wave resonance* instability mechanism that arises from mutually reinforcing edge wave interactions. Additionally, it is convenient to set $H \to \infty$ so that there are no solid boundaries, thus studying stability of a *free shear layer*.

Figure 61.6 illustrates the wave resonance mechanism, with the figure caption detailing the basic ingredients. In brief, the two edge waves, with oppositvely directed intrinsic phase velocities, are *phase locked* due to Doppler shifting by the background flow. Phase locking means that the interacting waves move with the same phase velocity. Indeed, symmetry of the setup in Figure 61.6 leads to phase locked waves that are stationary, meaning that the real part of the phase velocity vanishes. When the waves are phase locked with a phase shift so that lines of constant phase are slanted into the background shear, then that orientation supports a mutual reinforcement of the opposing wave's amplitude, which is a signature of a modal instability. The goal of this section is to expose mathematical details supporting this figure.

61.6.1 Phase locked streamfunction and Rayleigh equation

Our mathematical task is to derive the streamfunction corresponding to the interacting edge waves supported by the velocity kinks at $y = L$ and $y = -L$ shown in Figure 61.6. Ingredients

for this derivation were developed in Section 54.5 when studying a single edge wave along a single velocity jump. As for that analysis, start with the wave ansatz given by equation (61.30), written here again

$$\psi(x,y,t) = \widetilde{\psi}(y)\, \mathrm{e}^{\mathrm{i}\, k\,(x - c_\mathrm{r}\, t)}\, \mathrm{e}^{k\, c_\mathrm{i}\, t} = \widetilde{\psi}(y)\, \mathrm{e}^{\mathrm{i}\, k\,(x - c_\mathrm{r}\, t)}\, \mathrm{e}^{\sigma\, t}. \tag{61.73}$$

As noted at the start of this section, writing a wave function with a single phase velocity is consistent with a phase locked system of two edge waves. With this wave ansatz we then solve the Rayleigh equation (61.35) (i.e., the vorticity equation) in the fluid region between the kinks, and use kinematic and dynamic boundary conditions to match the streamfunction across the kinks.

With the velocity profile in Figure 61.6, the meridional derivative of the background vorticity, $\partial_y \zeta_\mathrm{b}$, has a Dirac delta at each of the vorticity jumps so that the Rayleigh equation (61.35) is

$$(u_\mathrm{b} - c)\,(\partial_{yy} - k^2)\,\widetilde{\psi} + \zeta_\circ\,[\delta(y+L) - \delta(y-L)]\,\widetilde{\psi} = 0 \quad \text{with} \quad \zeta_\circ = -U/L. \tag{61.74}$$

The solution to this equation outside of the singular vorticity interfaces (at $y = \pm L$) is given by

$$\widetilde{\psi}(y) = \begin{cases} A_1\, \mathrm{e}^{-|k|(y-L)} & y \geq L \\ A_2\, \mathrm{e}^{|k|(y-L)} + A_3\, \mathrm{e}^{-|k|(y+L)} & -L \leq y \leq L \\ A_4\, \mathrm{e}^{+|k|(y+L)} & y \leq -L, \end{cases} \tag{61.75}$$

where $A_{1,2,3,4}$ are constants determined by the kinematic and dynamic boundary conditions applied (in the linear theory) at $y = \pm L$.

61.6.2 Kinematic boundary condition at $y = \pm L$

We derived the kinematic boundary condition in Section 54.5.4, which arises from the material nature of the interface. The velocity is continuous at $y = \pm L$, so that the kinematic boundary condition means that the streamfunction is also continuous at the kinks. Evaluating equation (61.75) at $y = \pm L$ leads to the relations

$$A_1 = A_2 + A_3\, \mathrm{e}^{-2|k|L} \quad \text{and} \quad A_4 = A_3 + A_2\, \mathrm{e}^{-2|k|L}, \tag{61.76}$$

so that

$$\widetilde{\psi}(y) = \begin{cases} A_\mathrm{up}\, \mathrm{e}^{-|k|(y-L)} + A_\mathrm{lo}\, \mathrm{e}^{-|k|(y+L)} & y \geq L \\ A_\mathrm{up}\, \mathrm{e}^{|k|(y-L)} + A_\mathrm{lo}\, \mathrm{e}^{-|k|(y+L)} & -L \leq y \leq L \\ A_\mathrm{up}\, \mathrm{e}^{|k|(y-L)} + A_\mathrm{lo}\, \mathrm{e}^{|k|(y+L)} & y \leq -L, \end{cases} \tag{61.77}$$

which can be written in the more succinct form

$$\widetilde{\psi}(y) = A_\mathrm{up}\, \mathrm{e}^{-|k||y-L|} + A_\mathrm{lo}\, \mathrm{e}^{-|k||y+L|}, \tag{61.78}$$

where we wrote

$$A_\mathrm{up} = A_2 \quad \text{and} \quad A_\mathrm{lo} = A_3. \tag{61.79}$$

The notation (61.79) for the amplitudes correspond to the latitude ($y = L$ or $y = -L$) where their respective exponentials are maximized. Equation (61.78) reveals that the streamfunction is the sum of two functions, each peaked at one of the kinks in the background flow.

The coefficients, A_up and A_lo, are generally complex. However, symmetry of the setup for when the edge waves are phase locked requires their magnitudes to be equal, in which case

$$A_\mathrm{up} = \Gamma\, \mathrm{e}^{\mathrm{i}\,\theta_\mathrm{up}} \quad \text{and} \quad A_\mathrm{lo} = \Gamma\, \mathrm{e}^{\mathrm{i}\,\theta_\mathrm{lo}} \quad \text{with} \quad \Gamma > 0, \tag{61.80}$$

and the corresponding streamfunction

$$\widetilde{\psi}(y) = \Gamma \left[\mathrm{e}^{-|k||y-L|+\mathrm{i}\,\theta_{\mathsf{up}}} + \mathrm{e}^{-|k||y+L|+\mathrm{i}\,\theta_{\mathsf{lo}}} \right]. \tag{61.81}$$

61.6.3 Dynamic boundary condition at $y = L$

As detailed in Section 54.5.5, the dynamic boundary condition is based on continuity of pressure across an interface (ignoring surface tension). Equivalently, it arises from integrating the Rayleigh equation (61.74) across each interface, with the Dirac delta rendering a jump condition. For this purpose, it is convenient to write the Rayleigh equation in the form of equation (54.85)

$$\partial_y[(u_{\mathsf{b}} - c)\,\partial_y\widetilde{\psi} - \widetilde{\psi}\,\partial_y u_{\mathsf{b}}] + [-k^2\,(u_{\mathsf{b}} - c)]\,\widetilde{\psi} = 0. \tag{61.82}$$

Since u_{b} and $\widetilde{\psi}$ are everywhere continuous, integration across $y = L$ yields

$$\lim_{\epsilon\to 0} \int_{L-\epsilon}^{L+\epsilon} \partial_y[(u_{\mathsf{b}} - c)\,\partial_y\widetilde{\psi} - \widetilde{\psi}\,\partial_y u_{\mathsf{b}}]\,\mathrm{d}y = 0, \tag{61.83}$$

which leads to the jump condition

$$\left[(U-c)\,\partial_y\widetilde{\psi} + \widetilde{\psi}\,\zeta_{\mathsf{o}}\right]_{y=L-\epsilon} = \left[(U-c)\,\partial_y\widetilde{\psi}\right]_{y=L+\epsilon}, \tag{61.84}$$

where we noted that there is zero vorticity for $y > L$, and the zonal velocity equals to $+U$ at $y = L$. Note that ϵ is set to zero once evaluating the expressions. Making use of the streamfunction (61.77) and its derivative,

$$\partial_y\widetilde{\psi} = |k| \begin{bmatrix} -A_{\mathsf{up}}\,\mathrm{e}^{-|k|(y-L)} - A_{\mathsf{lo}}\,\mathrm{e}^{-|k|(y+L)} & y \geq L \\ A_{\mathsf{up}}\,\mathrm{e}^{|k|(y-L)} - A_{\mathsf{lo}}\,\mathrm{e}^{-|k|(y+L)} & -L \leq y \leq L \\ A_{\mathsf{up}}\,\mathrm{e}^{|k|(y-L)} + A_{\mathsf{lo}}\,\mathrm{e}^{|k|(y+L)} & y \leq -L, \end{bmatrix} \tag{61.85}$$

brings the $y = L$ jump boundary condition to

$$A_{\mathsf{up}}\,[2\,(U-c)\,|k| + \zeta_{\mathsf{o}}] + A_{\mathsf{lo}}\,\zeta_{\mathsf{o}}\,\mathrm{e}^{-2|k|L} = 0, \tag{61.86}$$

which, with $\zeta_{\mathsf{o}} = -U/L$ (equation (61.74)), can be written as

$$A_{\mathsf{up}}\,[2\,(1-c/U)\,|k|\,L - 1] = A_{\mathsf{lo}}\,\mathrm{e}^{-2|k|L}. \tag{61.87}$$

Solving for the dimensionless phase velocity leads to

$$c/U = 1 - \frac{1}{2\,|k|\,L}\left[1 + \frac{A_{\mathsf{lo}}}{A_{\mathsf{up}}}\,\mathrm{e}^{-2\,|k|\,L}\right] = 1 - \frac{1}{2\,|k|\,L}\left[1 + \mathrm{e}^{-2\,|k|\,L - \mathrm{i}\,\Delta\theta}\right], \tag{61.88}$$

where we introduced the phase for the amplitudes according to equation (61.80) and wrote the phase difference as

$$\Delta\theta = \theta_{\mathsf{up}} - \theta_{\mathsf{lo}}. \tag{61.89}$$

The phase velocity (61.88) is comprised of three terms

$$c = \underbrace{U}_{\text{Doppler}} \underbrace{-\frac{U}{2\,|k|\,L}}_{\text{free wave}} \underbrace{-\frac{U}{2\,|k|\,L}\,\mathrm{e}^{-2\,|k|\,L - \mathrm{i}\,\Delta\theta}}_{\text{interaction}}. \tag{61.90}$$

The first term arises from the Doppler shift via the background flow at the upper interface that

is directed to the east,

$$\boldsymbol{u}_{\mathsf{b}}(y = L) = U\,\hat{\boldsymbol{x}}. \tag{61.91}$$

The second term corresponds to the phase velocity of a free edge wave at the upper interface, with the westward intrinsic phase velocity

$$\boldsymbol{c}_{\text{phase}}^{\text{intrinsic}} = -U/(2\,|k|\,L)\,\hat{\boldsymbol{x}} = \zeta_{\mathsf{o}}/(2\,|k|)\,\hat{\boldsymbol{x}}. \tag{61.92}$$

For high wavenumbers (short wavelengths), the first and second terms dominate, with the phase velocity positive (eastward) as it is dominated by the Doppler term.

The final term in the phase velocity (61.90) arises from interactions between the upper and lower edge waves. The interaction decays both exponentially and algebraically according to $|k|\,L$, meaning that the edge waves have vanishingly small interactions for short wavelength zonal waves. Furthermore, the interaction term is generally a complex number that can be written

$$-\frac{U}{2\,|k|\,L}\,\mathrm{e}^{-2\,|k|\,L - \mathrm{i}\,\Delta\theta} = \frac{U\,\mathrm{e}^{-2\,|k|\,L}}{2\,|k|\,L}\left[-\cos(\Delta\theta) + \mathrm{i}\sin(\Delta\theta)\right] = c_{\mathsf{r}} + \mathrm{i}\,c_{\mathsf{i}}. \tag{61.93}$$

Evidently, the growth rate, $\sigma = c_{\mathsf{i}}\,k$, is positive (meaning the wave grows) if

$$k\sin(\Delta\theta) > 0 \implies \sigma = c_{\mathsf{i}}\,k > 0 \implies \text{growing waves}. \tag{61.94}$$

For $k > 0$ this condition means that the lines of constant phase are slanted into the background shear, just as anticipated by Figures 61.1 and 61.6.

61.6.4 Dynamic boundary condition at $y = -L$

The interface at $y = -L$ has the jump condition

$$\left[(-U - c)\,\partial_y\widetilde{\psi}\right]_{y=-L-\epsilon} = \left[(-U - c)\,\partial_y\widetilde{\psi} + \widetilde{\psi}\,\zeta_{\mathsf{o}}\right]_{y=-L+\epsilon}, \tag{61.95}$$

where the vorticity is zero for $y < -L$ and the zonal velocity is $-U$. Making use of the streamfunction (61.77) and the derivative (61.85) brings the $y = -L$ jump boundary condition to

$$A_{\mathsf{up}}\,\zeta_{\mathsf{o}}\,\mathrm{e}^{-2|k|L} + A_{\mathsf{lo}}\left[2\,(U + c)\,|k| + \zeta_{\mathsf{o}}\right] = 0, \tag{61.96}$$

which can be written as

$$A_{\mathsf{lo}}\left[2\,(1 + c/U)\,|k|\,L - 1\right] = A_{\mathsf{up}}\,\mathrm{e}^{-2|k|L}, \tag{61.97}$$

thus leading to the dimensionless phase velocity

$$c/U = -1 + \frac{1}{2\,|k|\,L}\left[1 + \frac{A_{\mathsf{up}}}{A_{\mathsf{lo}}}\,\mathrm{e}^{-2\,|k|\,L}\right] = -1 + \frac{1}{2\,|k|\,L}\left[1 + \mathrm{e}^{-2\,|k|\,L + \mathrm{i}\,\Delta\theta}\right], \tag{61.98}$$

where we introduced the phase for the amplitudes according to equation (61.80). Just like for the $y = L$ interface, we have the following interpretation for the phase velocity

$$c = \underbrace{-U}_{\text{Doppler}}\ \underbrace{+\frac{U}{2\,|k|\,L}}_{\text{free wave}}\ \underbrace{+\frac{U}{2\,|k|\,L}\,\mathrm{e}^{-2\,|k|\,L + \mathrm{i}\,\Delta\theta}}_{\text{interaction}} = c_{\mathsf{r}} + \mathrm{i}\,c_{\mathsf{i}}. \tag{61.99}$$

At the $y = -L$ interface the background flow is

$$\boldsymbol{u}_{\mathsf{b}}(y = -L) = -U\,\hat{\boldsymbol{x}}, \tag{61.100}$$

so that the Doppler shift is in the opposite direction to that at the upper interface, as is the free edge wave intrinsic phase velocity

$$\boldsymbol{c}_{\text{phase}}^{\text{intrinsic}} = U/(2\,|k|\,L)\,\hat{\boldsymbol{x}} = -\zeta_o/(2\,|k|)\,\hat{\boldsymbol{x}}. \tag{61.101}$$

The interaction term in equation (61.99) shares much with that at the upper interface given by equation (61.90). Namely, both decay exponentially and algebraically according to $|k|\,L$. Furthermore, the interaction term is generally a complex number that can be written

$$\frac{U}{2\,|k|\,L}\,\mathrm{e}^{-2|k|L+\mathrm{i}\,\Delta\theta} = \frac{U\,\mathrm{e}^{-2|k|L}}{2\,|k|\,L}\,\big[\cos(\Delta\theta) + \mathrm{i}\sin(\Delta\theta)\big] = c_r + \mathrm{i}\,c_i. \tag{61.102}$$

Just like for the upper interface, the growth rate, $\sigma = c_i\,k$, is positive (meaning the wave grows) if

$$k\,\Delta\theta > 0 \Longrightarrow \sigma = c_i\,k > 0 \Longrightarrow \text{growing waves}. \tag{61.103}$$

61.6.5 Phase velocity for phase locked edge waves

Application of the dynamical boundary condition at $y = L$ and $y = -L$ resulted in two expressions for the phase velocity as given by equations (61.88) and (61.98). The two phase velocities must be identical for the edge waves to be phase locked, with inspection of the two expressions leading to

$$c_r/U = 0 = \pm\left[-1 + \frac{1}{2\,|k|\,L} + \frac{\mathrm{e}^{-2\,|k|L}\cos\Delta\theta}{2\,|k|\,L}\right] \tag{61.104a}$$

$$c_i/U = \frac{\sin(\Delta\theta)\,\mathrm{e}^{-2|k|L}}{2\,|k|\,L}. \tag{61.104b}$$

That is, the phase velocity for the phase locked edge waves is purely imaginary, so that the edge waves are stationary and have a streamfunction given by

$$\psi(x,y,t) = \widetilde{\psi}(y)\,\mathrm{e}^{\mathrm{i}\,k\,x + k\,c_i\,t} = \widetilde{\psi}(y)\,\mathrm{e}^{\mathrm{i}\,k\,x+\sigma\,t}. \tag{61.105}$$

Growth rate

The phase velocity for the phase locked edge waves has a nonzero imaginary component when there is a nonzero phase shift between the two edge waves. Growth occurs when $k\,c_i = \sigma > 0$, which leads to the sufficient condition for instability

$$k\,\Delta\theta > 0 \Longrightarrow \sigma > 0 \Longrightarrow \text{unstable waves}. \tag{61.106}$$

Vanishing real phase velocity

The vanishing real phase velocity puts a constraint on the zonal wavenumber, in which case

$$2\,|k|\,L = 1 + \mathrm{e}^{-2|k|L}\cos\Delta\theta. \tag{61.107}$$

The maximum wavenumber that can satisfy this constraint is found when there is no phase shift ($\Delta\theta = 0$), in which we define a critical wavenumber

$$(1 - 2\,|k|\,L) = \mathrm{e}^{-2|k|L} \Longrightarrow (|k|\,L)_{\text{crit}} = 0.6329. \tag{61.108}$$

This is a high wavenumber cutoff, meaning that for wavenumbers larger than $(|k|\,L)_{\text{crit}}$ (i.e., relatively short waves), then there is a nonzero real component to the phase velocity. The nonzero real component to the phase velocity means that the two edge waves are in fact not phase locked, and as a result their amplitudes do not grow. Hence, the dimensionless wavenumber (61.108) separates the stable regime (high wavenumbers, $|k|\,L > (|k|\,L)_{\text{crit}}$) from the unstable regime (low wavenumbers, $|k|\,L < (|k|\,L)_{\text{crit}}$).

61.6.6 Dispersion relation and its interpretation

Here we derive the dispersion relation, which captures much of the information already gleaned by studying the phase velocity as well as some complementary perspectives.

Deriving the dispersion relation

Combine the two jump conditions (61.86) and (61.96) into a matrix-vector equation

$$\begin{bmatrix} [2\,(U-c)\,|k| + \zeta_{\text{o}}] & \zeta_{\text{o}}\,\text{e}^{-2|k|L} \\ \zeta_{\text{o}}\,\text{e}^{-2|k|L} & [2\,(U+c)\,|k| + \zeta_{\text{o}}] \end{bmatrix} \begin{bmatrix} A_{\text{up}} \\ A_{\text{lo}} \end{bmatrix} = \begin{bmatrix} 0 \\ 0 \end{bmatrix}. \tag{61.109}$$

Nontrivial solutions to this equation exist if the determinant of the 2×2 matrix vanishes, which then leads to the dispersion relation

$$(c/U)^2 = \frac{1}{(2\,|k|\,L)^2}\left[(1 - 2\,|k|\,L)^2 - \text{e}^{-4|k|L}\right] = \left[1 - \frac{1}{2\,|k|\,L}\right]^2 - \frac{\text{e}^{-4|k|L}}{(2\,|k|\,L)^2}. \tag{61.110}$$

Interpreting the two roots to the dispersion relation

The dispersion relation (61.110) leads to two roots for the phase velocity, $c = \omega/k$, with roots either both real or both imaginary. We already saw in Section 61.6.5 that the real roots must vanish for phase locked edge waves, with a vanishing real phase velocity present when the horizontal wavenumber satisfies $|k|\,L < (|k|\,L)_{\text{crit}}$ from equation (61.108). We interpret the nonzero real roots that arise with $|k|\,L > (|k|\,L)_{\text{crit}}$ as stable and non-phase locked edge waves moving in opposite directions along the velocity kinks at $y = L$ and $y = -L$. For example, in the high wavenumber limit the roots are real and have the approximate value

$$c \approx \pm U\left[1 - \frac{1}{2\,|k|\,L}\right]. \tag{61.111}$$

In this limit, the two edge waves correspond to the isolated edge waves studied in Section 54.5. Evidently, the wavenumber is so large (small wavelength) that the meridional structure of the edge waves rapidly decays in the direction away from their respective interfaces. As a result the two edge waves are effectively free waves since their interaction is negligible and they are not phase locked. As $|k|\,L$ gets smaller, the wavelength gets longer and the meridional extent of the two edge waves broadens. Interactions between the waves thus occurs, with these interactions possible even when the waves are stable. However, phase locking occurs for $|k|\,L < (|k|\,L)_{\text{crit}}$, with such waves unstable.

Critical wavenumber separating the stable and unstable regimes

As seen in equation (61.108), the real part of the phase velocity vanishes when the dimensionless wavenumber satisfies

$$(1 - 2\,|k|\,L)^2 = \text{e}^{-4|k|L} \implies (|k|\,L)_{\text{crit}} = 0.6329. \tag{61.112}$$

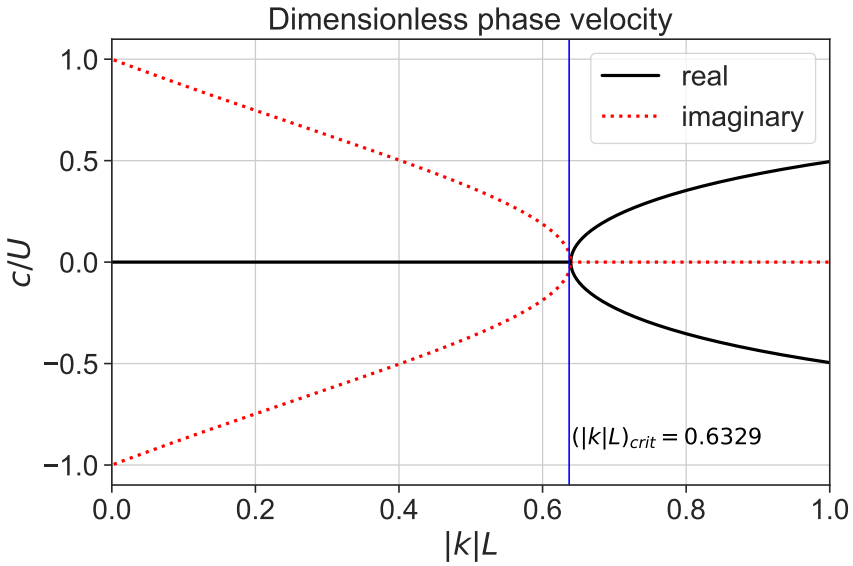

FIGURE 61.7: Dimensionless phase velocity, $c/U = \omega/(k\,U)$, from equation (61.110) derived for the piecewise linear velocity profile shown in Figure 61.6. A nonzero real phase velocity corresponds to stable edge waves that are not phase locked. If there are two edge waves, one on each of the velocity jumps and moving in the opposite directions, then they can interact. If the interaction is weak then it does not support a growing instability. Imaginary phase velocities correspond to phase locked edge waves with zero real phase velocity, so that the waves are stationary and have both an exponentially growing and decaying mode. The dimensionless wavenumber, $|k|_{\rm crit}\,L = 0.6329$, separates the stable (high wavenumber) regime from the unstable (low wavenumber) regime.

That is, for lower dimensionless wavenumbers, the squared phase speed (61.110) becomes negative

$$(c/U)^2 < 0 \Longrightarrow c = \mathrm{i}\,c_{\rm i}, \tag{61.113}$$

in which case the two real roots vanish and, for smaller wavenumbers, become two imaginary roots. One of the imaginary roots is an exponentially decaying mode and the other is the exponentially growing mode. Since the real part of the phase velocity vanishes, the modes are stationary relative to the shear layer, and thus they are either decaying or growing in place.

Fastest growth rate

The growth rate, $\sigma = c_{\rm i}\,k$, is given by

$$(\sigma\,L/U) = \pm\left[\mathrm{e}^{-4|k|L}/4 - (|k|\,L - 1/2)^2\right]^{1/2}, \tag{61.114}$$

which we plot in Figure 61.8. The fastest growth rate is given by

$$\frac{\mathrm{d}(\sigma\,L/U)^2}{\mathrm{d}(|k|L)} = 0 \Longrightarrow (|k|\,L)_{\rm fastest} \approx 0.4 \Longrightarrow \Lambda_{\rm fastest} \approx 2\pi L/0.4 = 5\pi L. \tag{61.115}$$

Evidently, the most unstable mode has a zonal wavelength that is roughly 16 times the meridional width of the shear zone (see Figure 61.6). For this mode the positive dimensionless growth rate is

$$(\sigma\,L/U) \approx 0.2 \Longrightarrow \sigma = 0.2\,U/L. \tag{61.116}$$

The growth rate increases as the horizontal shear, U/L, increases, either by increasing the background flow speed, U, or by decreasing the width of the shear zone.

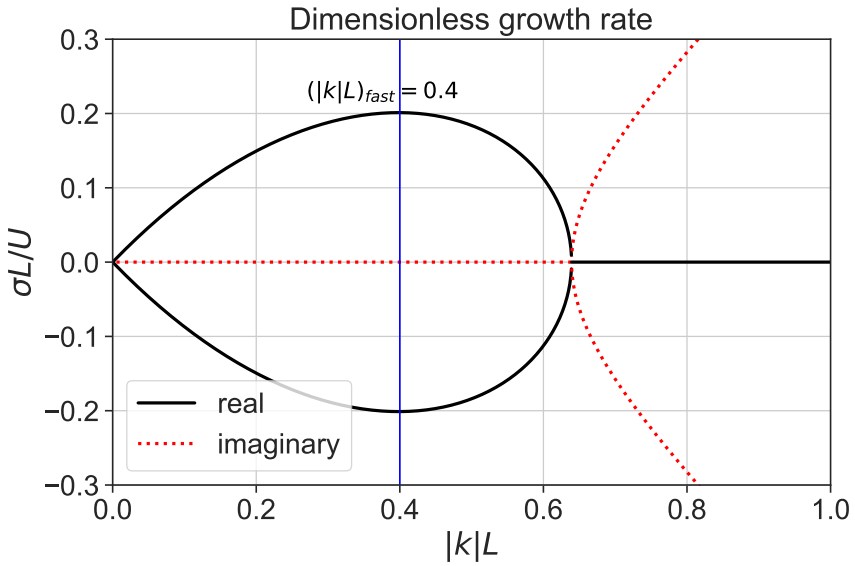

FIGURE 61.8: Dimensionless growth rate, $\sigma\, L/U$, from equation (61.114) derived for the piecewise linear velocity profile shown in Figure 61.6. A real growth rate corresponds to imaginary phase velocity from Figure 61.7, and represents exponentially growing ($\sigma > 0$) and decaying ($\sigma < 0$) modes. The dimensionless wavenumber, $|k|_{\text{crit}}\, L = 0.6329$, separates the stable (higher wavenumber) from unstable (lower wavenumber) regimes.

Phase shift for the fastest growing unstable mode

Making use of equation (61.104b) renders the expression for the phase shift present for phase locked unstable edge waves

$$\sin(\Delta\theta) = \frac{2\,|k|\,L\,\sigma}{k\,U}\,\mathrm{e}^{-2|k|L}. \tag{61.117}$$

Equation (61.116) says that the fastest growing mode has a growth rate of $\sigma\, L/U \approx 0.2$ at the non-dimensional wavenumber $|k|\, L \approx 0.4$ (equation (61.115)), so that

$$\sin(\Delta\theta) = \pm 2\,(\sigma\, L/U)\,\mathrm{e}^{2|k|L} \approx \pm 0.4\,\mathrm{e}^{0.8}. \tag{61.118}$$

For an eastward intrinsic phase velocity, so that $k > 0$, the constraint (61.94) says that the growing wave has $k \sin(\Delta\theta) > 0$, with $\sin(\Delta\theta) = 0.4\,\mathrm{e}^{0.8}$ yielding a phase shift of

$$\Delta\theta \approx 1.3\,\pi/2. \tag{61.119}$$

From Figure 61.6 we infer that the optimal alignment for growth of the two edge waves occurs with a $\pi/2$ phase shift. However, this phase shift requires a larger $|k|\, L$, and a larger $|k|\, L$ reduces the exponential appearing in the interaction between the two edge waves and thus slows the growth rate. Hence, the most unstable wave results from the dual need to optimize the relative phase of the two waves as well as the amplitude of the interaction.

61.6.7 Plotting the $\widetilde{\psi}(y)$ streamfunctions

In Figure 61.9 we plot the streamfunction based on equation (61.78)

$$\widetilde{\psi}(y) = A_{\text{up}}\,\mathrm{e}^{-L|k|\,|y/L-1|} + A_{\text{lo}}\,\mathrm{e}^{-L|k|\,|y/L+1|}, \tag{61.120}$$

for stable waves with $k\, L = 1$ and $k\, L = -1$, and for an unstable wave with $k\, L = 0.4$. There are some subtleties with producing these plots, thus motivating the following presentation of details.

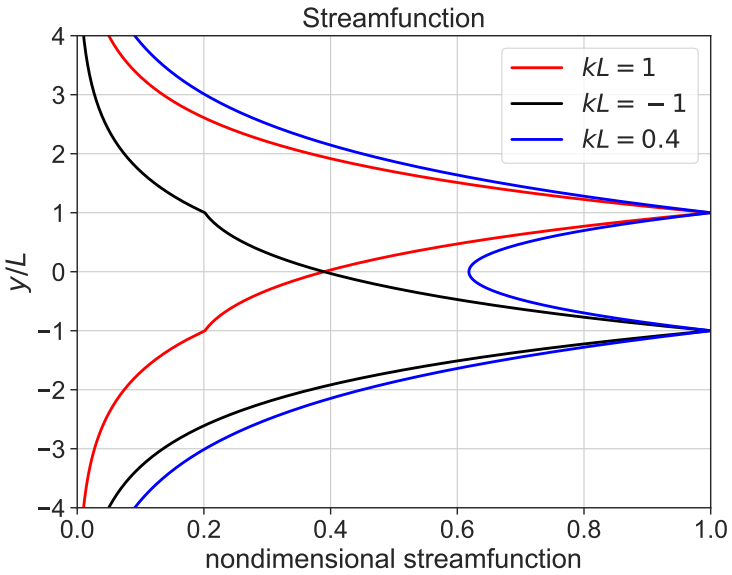

FIGURE 61.9: Streamfunction, $\widetilde{\psi}(y)$, for stable and unstable edge waves on the free shear layer shown in Figure 61.6. Each streamfunction is non-dimensionalized with an amplitude set so that the maximum streamfunction is unity. The black and red streamfunctions are for stable and non-phase locked edge waves maximized at the upper velocity kink (red at $y = L$) and lower kink (black at $y = -L$). The two stable streamfunctions have zero phase shift ($\theta_{\text{lo}} = \theta_{\text{up}} = 0$). The blue streamfunction is for the unstable mode with $|k|L = 0.4$ and with the phase shift $\Delta\theta = 1.3\,\pi/2$, with the streamfunction given by equation (61.127). Details for how to compute these streamfunctions are given in Section 61.6.7.

The stable streamfunction maximized at $y = L$

The stable streamfunctions have zero phase shifts (since they are stable waves) and they have unequal amplitudes, $A_{\text{up}} \neq A_{\text{lo}}$. The $k\,L = -1$ wave is maximized on the $y = L$ velocity kink since this is where the edge wave has a westward intrinsic phase velocity. The dimensionless phase velocity is given by the dispersion relation (61.110) with $k\,L = -1$, which yields (see also equation (61.90))

$$c/U \approx 0.495, \tag{61.121}$$

with the eastward phase velocity arising from dominance of the eastward background flow at $y = L$. That is, the stable edge wave maximized at $y = L$ is swept eastward by the background flow, thus precluding it from being phase locked with the edge wave centered on $y = -L$. The amplitude ratio is computed from equation (61.87)

$$A_{\text{lo}}/A_{\text{up}} = \mathrm{e}^2\,[2\,(1 - c/U) - 1] \approx 0.068, \tag{61.122}$$

with the resulting streamfunction (61.120)

$$\widetilde{\psi}^{(\text{L})}(y) = A_{\text{up}}\left[\mathrm{e}^{-|y/L-1|} + (A_{\text{lo}}/A_{\text{up}})\,\mathrm{e}^{-|y/L+1|}\right]. \tag{61.123}$$

We specify the amplitude, A_{up}, so that the maximum of $\widetilde{\psi}^{(\text{L})}(y)$ is unity as plotted in Figure 61.9.

The stable streamfunction maximized at $y = -L$

The $k\,L = 1$ wave is symmetric with respect to the $k\,L = -1$ wave. Namely, the $k\,L = 1$ wave is maximized on the $y = -L$ velocity kink since this is where the edge wave has a westward intrinsic phase velocity. The dimensionless phase velocity is given by the dispersion relation

(61.110) with $k\,L = 1$, which yields (see also equation (61.99))

$$c/U \approx -0.495, \tag{61.124}$$

with the westward phase velocity due to dominance of the westward background flow at $y = -L$. That is, the stable edge wave maximized at $y = -L$ is swept westward by the background flow, thus precluding it from being phase locked with the edge wave centered on $y = L$. The amplitude ratio is computed from equation (61.97)

$$A_{\text{up}}/A_{\text{lo}} = \mathrm{e}^2\,[2\,(1 + c/U) - 1] \approx 0.068, \tag{61.125}$$

which is numerically equal to the ratio $A_{\text{lo}}/A_{\text{up}}$ in equation (61.122) for the wave maximized at $y = L$. The resulting streamfunction (61.120) is

$$\widetilde{\psi}^{(-\text{L})}(y) = A_{\text{lo}}\left[(A_{\text{up}}/A_{\text{lo}})\,\mathrm{e}^{-|y/L-1|} + \mathrm{e}^{-|y/L+1|}\right]. \tag{61.126}$$

We specify the amplitude, A_{lo}, so that the maximum of $\widetilde{\psi}^{(-\text{L})}(y)$ is unity as plotted in Figure 61.9.

The unstable streamfunction

When the zonal wavenumber gets smaller than $(|k|\,L)_{\text{crit}} = 0.6329$, then the two edge waves become phase locked and stationary (zero real phase velocity), with a phase shift allowing for mutual growth to manifest shear instability. In Figure 61.9 we plot the magnitude of the streamfunction for $|k|\,L = 0.4$ according to equation (61.81)

$$\widetilde{\psi}(y) = \Gamma\,\mathrm{e}^{\mathrm{i}\,\theta_{\text{up}}}\left[\mathrm{e}^{-L|k|\,|y/L-1|} + \mathrm{e}^{-L|k|\,|y/L+1|+\mathrm{i}\,\Delta\theta}\right], \tag{61.127}$$

where the phase shift is given by $\Delta\theta = 1.3\,\pi/2$ as per equation (61.119), and the magnitude is computed by

$$|\widetilde{\psi}| = \sqrt{\widetilde{\psi}\,\widetilde{\psi}^*}. \tag{61.128}$$

61.6.8 Lack of mutual wave growth for stable flows

The wave mechanism for shear instability offers a mechanistic understanding of the integral stability theorems from Section 61.5. For example, the case of Figure 61.6 illustrates how waves can mutually reinforce each other's amplitudes if there is an inflection point in the background flow, thus satisfying the necessary condition for Rayleigh's inflection point theorem. We sketch a profile in Figure 61.10 that has no inflection point, and for which the edge waves have their phase velocities in the same direction. If their relative phases are oriented so that the lower wave enhances the amplitude of the upper wave, as in Figure 61.10, then the upper wave in turn diminishes the amplitude of the lower. This result holds regardless the value for the relative phase. Whereas one wave's amplitude growth is supported by the other wave, that growth comes at the cost of diminishing the amplitude of its partner. We conclude that no matter what the relative phase relations, no mutual wave resonance can occur for the background flow profile of Figure 61.10 so there is no instability.

61.6.9 Further study

The linear sheared velocity profile in an unbounded domain was first analyzed by *Rayleigh* (1894) (volume II, page 393), and it forms the basis for most subsequent treatments, such as *Chandrasekhar* (1961), *Drazin and Reid* (2004), *Vallis* (2017), and *Smyth and Carpenter* (2019).

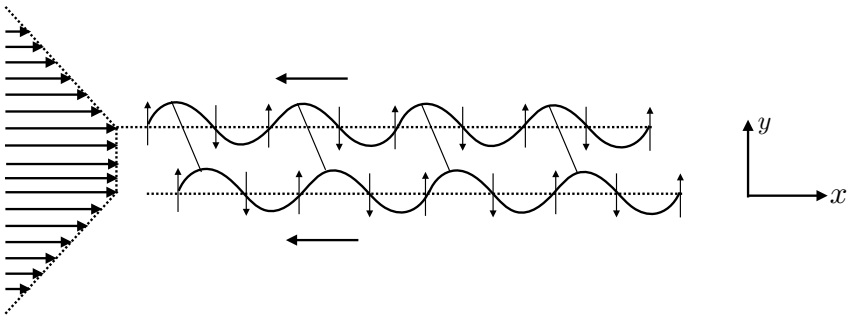

FIGURE 61.10: Two edge waves riding on their respective velocity jumps. There is no inflection point for this velocity profile, so that the velocity profile is stable according to the Rayleigh inflection point theorem from Section 61.5.1. We can mechanistically understand this result by noting the that two edge waves have a phase velocity in the same direction. Consequently, the waves cannot enter into the mutual resonance condition needed to create exponential growth. In this sketch, the secondary circulation from the lower wave enhances the amplitude of the upper wave. However, the upper wave diminishes the amplitude of the lower wave. Any other phase arrangement results in a similar situation whereby the two waves cannot mutually enhance each other's amplitude.

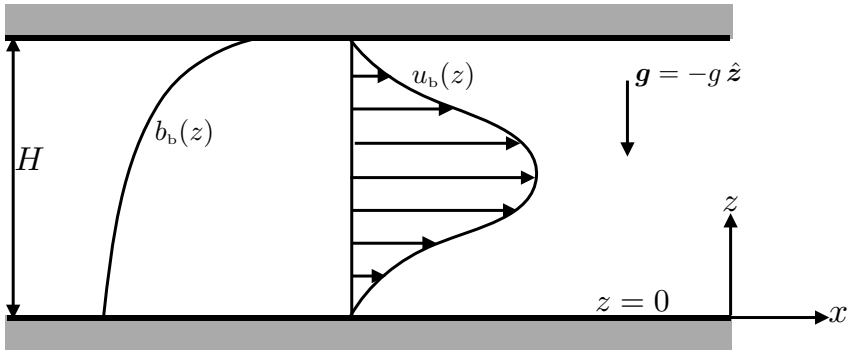

FIGURE 61.11: Schematic of the flow configuration used to examine stratified shear instability. The fluid is contained within a vertically bounded yet horizontally unbounded domain, with no-normal flow at the top and bottom meaning that the vertical flow vanishes at these boundaries, $w(0) = w(H) = 0$. The background flow is zonal with a vertical shear, $u_b(z)\,\hat{\boldsymbol{x}}$. The background buoyancy, $b_b(z)$, is stably stratified with $\mathrm{d}b_b/\mathrm{d}z = N^2(z) > 0$. The analysis in Section 61.7 reveals that the flow is stable if the gradient Richardson number, $\mathrm{Ri} = N^2/(\mathrm{d}u_b/\mathrm{d}z)^2$, is everywhere less than the critical value of 1/4. In contrast, the flow satisfies a necessary (though not sufficient) condition for shear instability if the Richardson number somewhere drops below 1/4.

In particular, the treatment of *Smyth and Carpenter* (2019) offers many insights into the nature of the wave phases and phase speeds, with the presentation in this section emulating much from theirs. This video from Prof. Mollo-Christensen provides a pedagogical introduction to a variety of instabilities.

61.7 Integral conditions for stratified shear stability/instability

In this section we examine the stability of a vertically sheared zonal flow in the presence of gravity and with a gravitationally stable vertical buoyancy stratification. The fluid is contained within a vertically bounded domain yet with no boundaries in the horizontal, with Figure 61.11 providing an illustration of the configuration. Much in this discussion reflects that given for the meridionally sheared zonal flow in Section 61.5, here with the added feature of buoyancy stratification along with a slight increase in algebraic complexity.

61.7.1 Governing equations

We formulate the problem using the inviscid and adiabatic Boussinesq ocean equations in a rotating reference frame as developed in Section 29.1.6, with the governing equations given by

$$\partial_t \boldsymbol{v} + (\boldsymbol{v} \cdot \nabla)\boldsymbol{v} + f\,\hat{\boldsymbol{z}} \times \boldsymbol{v} = -\nabla\varphi + b\,\hat{\boldsymbol{z}} \tag{61.129a}$$

$$(\partial_t + \boldsymbol{v} \cdot \nabla)\, b = 0 \tag{61.129b}$$

$$\nabla \cdot \boldsymbol{v} = 0, \tag{61.129c}$$

where b is the buoyancy, φ is the pressure divided by the Boussinesq reference density, and $\boldsymbol{v}$ is the non-divergent velocity.

The Coriolis acceleration generally plays a minor role in the mechanics of stratified shear instabilities, since the space-time scales are far too small for the Coriolis acceleration to play a noticeable role in the dynamics. We thus set $f = 0$ in this section. In this case,

$$\boldsymbol{v} = u_{\mathrm{b}}(z)\,\hat{\boldsymbol{x}} + v_{\mathrm{b}}(z)\,\hat{\boldsymbol{y}}, \tag{61.130}$$

is an exact solution to the inviscid equations (61.129a)-(61.129c) if the background pressure has a zero horizontal gradient.[7] Evidently, the static and depth dependent horizontal flow (61.130) is an exact solution to the inviscid equations of motion in the absence of a Coriolis acceleration. It represents an unforced (free) mode for inviscid hydrostatic flow with pressure, $\varphi(z)$, and buoyancy $b(z)$, in exact hydrostatic balance.

With zero Coriolis acceleration, it is sufficient to orient the background flow along the $\hat{\boldsymbol{x}}$ axis so that we set $v_{\mathrm{b}} = 0$ in the following. We can further make use of Squire's theorem (Section 61.2) to note that the most unstable perturbation is two-dimensional and in the x-z plane (the plane of the background flow). We thus focus on stability of two-dimensional flows in the form

$$\boldsymbol{v} = [u_{\mathrm{b}}(z) + u'(x,z,t)]\,\hat{\boldsymbol{x}} + w'(x,z,t)\,\hat{\boldsymbol{z}}, \tag{61.131}$$

where $u'\,\hat{\boldsymbol{x}} + w'\,\hat{\boldsymbol{z}}$ is the non-divergent perturbation flow in the x-z plane

$$\partial_x u' + \partial_z w' = 0. \tag{61.132}$$

Given the above flow perturbation, we decompose the buoyancy and pressure fields according to

$$\varphi = \varphi_{\mathrm{b}}(z) + \varphi'(x,z,t) \quad \text{and} \quad b = b_{\mathrm{b}}(z) + b'(x,z,t), \tag{61.133}$$

where

$$\frac{\mathrm{d}\varphi_{\mathrm{b}}}{\mathrm{d}z} = b_{\mathrm{b}} \quad \text{and} \quad \frac{\mathrm{d}b_{\mathrm{b}}}{\mathrm{d}z} = N^2 > 0. \tag{61.134}$$

In this manner, the governing equations (61.129a)-(61.129c) take the form

$$\partial_t u' + (u_{\mathrm{b}} + u')\,\partial_x u' + w'\,\partial_z(u_{\mathrm{b}} + u') = -\partial_x \varphi' \tag{61.135a}$$

$$\partial_t w' + (u_{\mathrm{b}} + u')\,\partial_x w' + w'\,\partial_z w' = -\partial_z \varphi' + b' \tag{61.135b}$$

$$\partial_t b' + (u_{\mathrm{b}} + u')\,\partial_x b' + w'\,\partial_z b' = -w'\,N^2 \tag{61.135c}$$

$$\partial_x u' + \partial_z w' = 0. \tag{61.135d}$$

[7] This point is noted in Section 21 of *Drazin and Reid* (2004).

61.7.2 The linear vorticity equation

To develop an integral condition for stability, linearize the governing equations (61.135a)-(61.135d) (i.e., drop all terms with products of primed fields) to have

$$\partial_t u' + u_{\mathrm{b}}\,\partial_x u' + w'\,\partial_z u_{\mathrm{b}} = -\partial_x \varphi' \tag{61.136a}$$

$$\partial_t w' + u_{\mathrm{b}}\,\partial_x w' = -\partial_z \varphi' + b' \tag{61.136b}$$

$$(\partial_t + u_{\mathrm{b}}\,\partial_x) b' = -w'\,N^2 \tag{61.136c}$$

$$\partial_x u' + \partial_z w' = 0. \tag{61.136d}$$

Taking the z-derivative of the zonal equation (61.136a) and the x-derivative of the vertical equation (61.136b), and then subtracting, eliminates the pressure gradient to render

$$\partial_t(\partial_z u' - \partial_x w') + \partial_z(u_{\mathrm{b}}\,\partial_x u') - u_{\mathrm{b}}\,\partial_{xx} w' + \partial_z(w'\,\partial_z u_{\mathrm{b}}) = -\partial_x b'. \tag{61.137}$$

A bit of rearrangement, and use of the continuity equation (61.136d), yields the linearized vorticity equation

$$(\partial_t + u_{\mathrm{b}}\,\partial_x)(\partial_z u' - \partial_x w') + w'\,\partial_{zz} u_{\mathrm{b}} = -\partial_x b', \tag{61.138}$$

with

$$\partial_z u' - \partial_x w' = \hat{\boldsymbol{y}} \cdot (\nabla \times \boldsymbol{v}') \tag{61.139}$$

the meridional component to the vorticity of the fluctuating flow.

Since the x-z flow is non-divergent (equation (61.136d)), it is convenient to introduce a zonal-depth streamfunction

$$u'\,\hat{\boldsymbol{x}} + w'\,\hat{\boldsymbol{z}} = \hat{\boldsymbol{y}} \times \nabla\psi = \partial_z\psi\,\hat{\boldsymbol{x}} - \partial_x\psi\,\hat{\boldsymbol{z}}, \tag{61.140}$$

in which case the linear vorticity equation (61.138) becomes

$$(\partial_t + u_{\mathrm{b}}\,\partial_x)(\partial_{xx} + \partial_{zz})\psi - \partial_x\psi\,\partial_{zz} u_{\mathrm{b}} = -\partial_x b', \tag{61.141}$$

where the meridional component to the vorticity is given by the Laplacian of the streamfunction

$$\hat{\boldsymbol{y}} \cdot (\nabla \times \boldsymbol{v}') = (\partial_{xx} + \partial_{zz})\psi. \tag{61.142}$$

Likewise, the linear buoyancy equation (61.136c) becomes

$$(\partial_t + u_{\mathrm{b}}\,\partial_x) b' = \partial_x\psi\,N^2. \tag{61.143}$$

Since the fluid is contained by a top and bottom boundary as per Figure 61.11, the no-normal flow condition for the vertical velocity,

$$w' = 0 \quad \text{at } z = 0, H, \tag{61.144}$$

means that the streamfunction is a spatial constant along the top and bottom boundaries

$$\partial_x\psi = 0 \quad \text{at } z = 0, H. \tag{61.145}$$

Without loss of generality we take these constant streamfunction values to be zero, thus rendering the homogeneous Dirichlet boundary conditions

$$\psi = 0 \quad \text{at } z = 0, H. \tag{61.146}$$

61.7.3 Taylor-Goldstein equation

The vorticity equation (61.141) and buoyancy equation (61.143) are two coupled linear partial differential equations with independent variables, (x, z, t), and with z-dependent coefficients via $\mathrm{d}^2 u_\mathsf{b}(z)/\mathrm{d}z^2$ and $N^2(z)$. To study the stability of this flow, we pursue a modal analysis based on the wave ansatz

$$\psi(x, z, t) = \tilde{\psi}(z)\, \mathrm{e}^{\mathrm{i}\, k\, (x - c\, t)} \quad \text{and} \quad b'(x, z, t) = \tilde{b}(z)\, \mathrm{e}^{\mathrm{i}\, k\, (x - c\, t)}, \tag{61.147}$$

which accords with the wave ansatz (61.147) used to study stability of meridionally sheared flows in Section 61.4. In particular, the phase velocity,

$$\boldsymbol{c}_\mathsf{p} = c\, \hat{\boldsymbol{x}} = (\omega/k)\, \hat{\boldsymbol{x}}, \tag{61.148}$$

follows the conventions in Section 61.4.1. Use of the ansatz (61.147) brings the vorticity equation (61.141) and buoyancy equation (61.143) to

$$(-\omega + u_\mathsf{b}\, k)(-k^2 + \partial_{zz})\tilde{\psi} - k\, \tilde{\psi}\, \partial_{zz} u_\mathsf{b} = -k\, \tilde{b} \tag{61.149a}$$

$$(-\omega + u_\mathsf{b}\, k)\tilde{b} = -k\, \tilde{\psi}\, N^2. \tag{61.149b}$$

Substituting the buoyancy equation (61.149b) into the vorticity equation (61.149a) leads to the *Taylor-Goldstein equation* for the streamfunction

$$(u_\mathsf{b} - c)\, \left[\frac{\mathrm{d}^2}{\mathrm{d}z^2} - k^2\right] \tilde{\psi} + \left[\frac{N^2}{u_\mathsf{b} - c} - \frac{\mathrm{d}^2 u_\mathsf{b}}{\mathrm{d}z^2}\right] \tilde{\psi} = 0. \tag{61.150}$$

In the special case of $N^2 = 0$ and with z swapped to y, the Taylor-Goldstein equation reduces to the Rayleigh equation (61.35).

61.7.4 Richardson number and the stability conditions

An inspired transformation of the Taylor-Goldstein equation

To develop conditions for stability/instability, we make the inspired transformation of the streamfunction to

$$\tilde{\psi} = \tilde{\phi}\, \sqrt{u_\mathsf{b} - c} \quad \text{and} \quad \tilde{\phi}(0) = \tilde{\phi}(H) = 0. \tag{61.151}$$

A bit of algebra yields the second derivative

$$(u_\mathsf{b} - c)\, \frac{\mathrm{d}^2 \tilde{\psi}}{\mathrm{d}z^2} = \left[-\frac{1}{4\, (u_\mathsf{b} - c)^{1/2}} \left(\frac{\mathrm{d}u_\mathsf{b}}{\mathrm{d}z}\right)^2 + \frac{(u_\mathsf{b} - c)^{1/2}}{2}\, \frac{\mathrm{d}^2 u_\mathsf{b}}{\mathrm{d}z^2}\right] \tilde{\phi} + (u_\mathsf{b} - c)^{1/2}\, \frac{\mathrm{d}}{\mathrm{d}z}\left[(u_\mathsf{b} - c)\, \frac{\mathrm{d}\tilde{\phi}}{\mathrm{d}z}\right], \tag{61.152}$$

and the consequent transformation of the Taylor-Goldstein equation (61.150)

$$\left[\frac{1}{u_\mathsf{b} - c}\, \left[N^2 - \frac{1}{4}\left(\frac{\mathrm{d}u_\mathsf{b}}{\mathrm{d}z}\right)^2\right] - (u_\mathsf{b} - c)\, k^2 - \frac{1}{2}\, \frac{\mathrm{d}^2 u_\mathsf{b}}{\mathrm{d}z^2}\right] \tilde{\phi} + \frac{\mathrm{d}}{\mathrm{d}z}\left[(u_\mathsf{b} - c)\, \frac{\mathrm{d}\tilde{\phi}}{\mathrm{d}z}\right] = 0. \tag{61.153}$$

This form of the Taylor-Goldstein equation is actually a bit less compact than the original form (61.150). Even so, as we now show, it offers an elegant stability condition in terms of the gradient Richardson number.

Sufficient condition for stability and necessary condition for instability

To develop an integral stability theorem, multiply equation (61.153) by the complex conjugate, $\tilde{\phi}^*$, and integrate over the depth range $0 \le z \le H$. Performing this integral on the derivative term in equation (61.153) leads to

$$\int_0^H \tilde{\phi}^* \frac{\mathrm{d}}{\mathrm{d}z}\left[(u_\mathrm{b}-c)\,\frac{\mathrm{d}\tilde{\phi}}{\mathrm{d}z}\right]\mathrm{d}z = \int_0^H \frac{\mathrm{d}}{\mathrm{d}z}\left[\tilde{\phi}^*\,(u_\mathrm{b}-c)\,\frac{\mathrm{d}\tilde{\phi}}{\mathrm{d}z}\right]\mathrm{d}z - \int_0^H (u_\mathrm{b}-c)\left|\frac{\mathrm{d}\tilde{\phi}}{\mathrm{d}z}\right|^2\mathrm{d}z, \quad (61.154)$$

with the total derivative term vanishing through use of the homogeneous Dirichlet boundary conditions in equation (61.151). Rearrangement thus renders

$$\int_0^H \frac{|\tilde{\phi}|^2}{u_\mathrm{b}-c}\left[N^2 - \frac{1}{4}\left(\frac{\mathrm{d}u_\mathrm{b}}{\mathrm{d}z}\right)^2\right]\mathrm{d}z = \int_0^H (u_\mathrm{b}-c)\left[k^2\,|\tilde{\phi}|^2 + \left|\frac{\mathrm{d}\tilde{\phi}}{\mathrm{d}z}\right|^2\right]\mathrm{d}z + \frac{1}{2}\int_0^H \frac{\mathrm{d}^2 u_\mathrm{b}}{\mathrm{d}z^2}\,|\tilde{\phi}|^2\,\mathrm{d}z. \quad (61.155)$$

This integral condition provides the basis for developing a sufficient condition for stability and, conversely, a necessary condition for instability.

The final term on the right hand side of equation (61.155) is real, so that the imaginary part of this equation is given by

$$c_\mathrm{i}\int_0^H \frac{|\tilde{\phi}|^2\,(\mathrm{d}u_\mathrm{b}/\mathrm{d}z)^2\,(\mathrm{Ri}-1/4)}{|u_\mathrm{b}-c|^2}\,\mathrm{d}z = -c_\mathrm{i}\int_0^H \left[k^2\,|\tilde{\phi}|^2 + \left|\frac{\mathrm{d}\tilde{\phi}}{\mathrm{d}z}\right|^2\right]\mathrm{d}z, \quad (61.156)$$

where we used the identity

$$\frac{1}{u_\mathrm{b}-c} = \frac{u_\mathrm{b}-c^*}{(u_\mathrm{b}-c)\,(u_\mathrm{b}-c^*)} = \frac{u_\mathrm{b}-c_\mathrm{r}+\mathrm{i}\,c_\mathrm{i}}{|u_\mathrm{b}-c|^2}, \quad (61.157)$$

and introduced the *gradient Richardson number* (assuming nonzero vertical shear)

$$\mathrm{Ri} = \frac{N^2}{(\mathrm{d}u_\mathrm{b}/\mathrm{d}z)^2}. \quad (61.158)$$

Evidently, if the Richardson number is greater than the critical value,

$$\mathrm{Ri}_\mathrm{crit} = 1/4, \quad (61.159)$$

throughout the vertical column, then the only way to satisfy equation (61.156) is for $c_\mathrm{i} = 0$, which establishes a sufficient condition for stratified shear stability

$$\mathrm{Ri}(z) > \mathrm{Ri}_\mathrm{crit} = 1/4 \quad \forall\, z \in [0,H] \Longrightarrow \text{sufficient condition for stability.} \quad (61.160)$$

Conversely, a necessary condition for stratified shear instability is for the Richardson number to be less than 1/4 somewhere in the vertical column

$$\mathrm{Ri}(z) < \mathrm{Ri}_\mathrm{crit} = 1/4 \quad \text{for some } z \in [0,H] \Longrightarrow \text{necessary condition for instability.} \quad (61.161)$$

We emphasize that a Richardson number less than the critical value is necessary but not sufficient for stratified shear instability. Although for many purposes it is sufficient, there are examples

where it is not. For example, flows near boundaries generally require a smaller Richardson number to go unstable. Even so, for most geophysical applications, $\mathrm{Ri}_{\mathrm{crit}} = 1/4$ is a very good indicator for stratified shear instability.

Comparison to barotropic shear instability

The gradient Richardson number (61.158) is the ratio of the buoyancy stratification to the vertical shear of the horizontal flow. It is notable that the necessary condition for instability, $\mathrm{Ri} < 1/4$, does not depend on the curvature of the background flow, which contrasts to the case of barotropic shear instability studied in Section 61.5. For stratified shear instability, there is a direct struggle by the vertical shear to overcome the stabilizing effects from the background buoyancy stratification.

61.7.5 Richardson number and mixing energetics

The gradient Richardson number (61.158) provides a measure of the struggle between stabilizing effects from vertical stratification to the destabilizing effects from vertical shear. Here we provide an interpretation of the Richardson number in terms of mixing energetics, with mixing induced by the stratified shear instability. For this purpose we examine the thought experiment illustrated in Figure 61.12, with the analysis emulating that in Section 60.3.6 for mixing induced by Kelvin-Helmholtz instability.

Initial and final states of the thought experiment

Consider a Boussinesq ocean whose initial flow has a linear shear and a linear density profile

$$u_{\mathrm{b}}(z) = U_0 + (z/H)\,\delta U \quad \text{and} \quad \rho_{\mathrm{b}}(z) = \rho_{\circ} - (z/H)\,\delta\rho, \tag{61.162}$$

where U_0 is the velocity at $z = 0$, $\rho_{\circ}$ is the Boussinesq reference density, $\delta\rho > 0$ is a constant that sets the strength of the vertical stratification, and δU is a constant that sets the strength of the vertical shear. The initial Richardson number is assumed to be less than the critical value of 1/4,

$$\mathrm{Ri} = \frac{N^2}{(\partial_z u_{\mathrm{b}})^2} = \frac{g}{\rho_{\circ}} \frac{(\delta\rho/H)}{(\delta U/H)^2} < 1/4, \tag{61.163}$$

thus satisfying the necessary condition for stratified shear instability. For the final state, assume the fluid completely mixes to produce a uniform density and uniform velocity, which are taken to be the vertical average of the initial values

$$\overline{\rho} = U_0 + \delta U/2 \quad \text{and} \quad \overline{\rho} = \rho_{\circ} - \delta\rho/2. \tag{61.164}$$

We might think of this configuration as a tiny region where the shear and density are well approximated with a linear vertical profile, and where shear induced mixing homogenizes the density and velocity.

Change in the potential and kinetic energies per area

The difference in the potential energy (per horizontal area) between the final and initial states is given by

$$P_{\mathsf{final}} - P_{\mathsf{init}} = g \int_0^H z\,[\overline{\rho} - \rho_{\mathrm{b}}(z)]\,\mathrm{d}z = g\,\delta\rho\,H^2/12. \tag{61.165}$$

An increase in potential energy upon mixing is anticipated by the study in Section 60.3.6 of Kelvin-Helmholtz induced mixing, and from the more general examination of potential energy

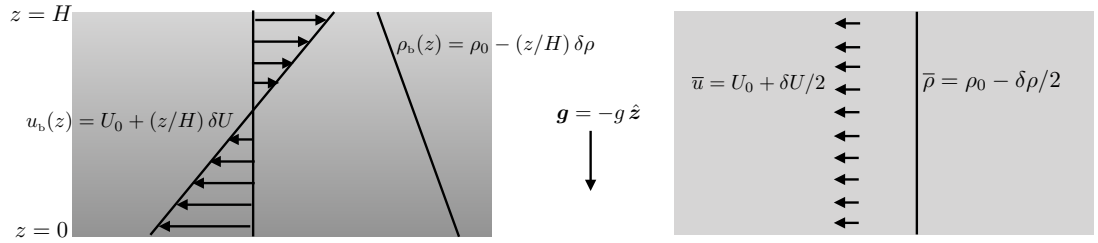

FIGURE 61.12: Left panel: initial conditions for a linearly stratified flow specified by a constant density parameter, $\delta\rho > 0$, that sets the strength of the linear stratification, and a constant shear parameter, δU, that sets the strength of the linear vertical shear. Right panel: a homogenized final state in which the density equals to the average of the initial density, $\overline{\rho} = \rho_0 - \delta\rho/2$, and the velocity equals to the average of the initial velocity, $\overline{u} = U_0 + \delta U/2$. The ratio of the potential energy change to the kinetic energy change is proportional to the gradient Richardson number as given by equation (61.167).

in Section 26.2.6. The basic idea is that vertical mixing raises the center of mass of the fluid, thus increasing the gravitational potential energy.

Where does the energy come from to raise the center of mass? For this thought experiment it must come from the kinetic energy, as that is the only other energy source. We thus anticipate that the kinetic energy decreases upon mixing. Indeed, the change in the kinetic energy (per horizontal area) is given by

$$K_{\text{final}} - K_{\text{init}} = \frac{\rho_0}{2}\int_0^H (\overline{u}^2 - u_b^2)\,\mathrm{d}z = -\frac{\rho_0}{2}\int_0^H (u_b - \overline{u})^2\,\mathrm{d}z = -\rho_0\, H\,(\delta U)^2/24. \tag{61.166}$$

A decrease in kinetic energy follows since the square of a spatially variable velocity is always greater than the square of its spatial average.

Taking the absolute ratio of the change in potential energy to the change in kinetic energy renders

$$\left|\frac{P_{\text{final}} - P_{\text{init}}}{K_{\text{final}} - K_{\text{init}}}\right| = \frac{2\,g}{\rho_0}\,\frac{\delta\rho/H}{(\delta U/H)^2} = 2\,\text{Ri}, \tag{61.167}$$

where the second equality introduced the Richardson number (61.163) of the initial state. Evidently, the Richardson number in this thought experiment is directly proportional to the absolute ratio of the potential energy change upon mixing to the kinetic energy change upon mixing. In Exercise 61.3 we find a similar result for a two-layer system, yet with a different proportionality constant. These two thought experiments support the general connection between the Richardson number and the energy ratio. Namely, the numerator is proportional to the potential energy increase due to mixing (presenting a barrier to mixing), and the denominator is proportional to the kinetic energy available from the shear to overcome the potential energy barrier.

61.7.6 Constraining the phase velocity of unstable waves

The inspired transformation (61.151) is not the only one that can extract useful information about stability from the Taylor-Goldstein equation (61.150). Another transformation, following *Howard* (1961), is motivated by considering the vertical displacement of a fluid particle under small amplitude linear waves, with this approach following that given in Section 61.4.5, where we considered meridional displacements of fluid particles. The particle following approach motivates a transformation of the Taylor-Goldstein equation that then leads to constraints on the real and imaginary part of the phase velocity for unstable waves. That is, we derive conditions that must be satisfied for a wave to grow when placed in an unstable background flow. The development leads to the *critical height theorem* as well as *Howard's semi-circle theorem*, which are generalizations of the critical latitude theorem from Section 61.5.3.

Taylor-Goldstein equation in terms of a fluid particle's vertical displacement

Introduce the field, $\eta(x,z,t)$, which measures the vertical displacement of a fluid particle that has its rest vertical position at z. As such, this field satisfies

$$w' = [\partial_t + (u' + u_\mathsf{b})\,\partial_x]\eta \approx (\partial_t + u_\mathsf{b}\,\partial_x)\eta, \tag{61.168}$$

with the linearization step following from the assumed small displacements. As defined, $\eta(x,z,t)$ is the vertical displacement of a fluid particle that has its rest position at z. Now assume the displacements are generated by small amplitude waves of the form

$$\eta(x,z,t) = \tilde{\eta}(z)\,\mathrm{e}^{\mathrm{i}\,k\,(x-c\,t)}. \tag{61.169}$$

The corresponding wave ansatz for the vertical velocity,

$$w' = -\partial_x\psi = -\mathrm{i}\,k\,\tilde{\psi}(z)\,\mathrm{e}^{\mathrm{i}\,k\,(x-c\,t)}, \tag{61.170}$$

leads to the relation between the streamfunction amplitude and the particle displacement amplitude

$$\tilde{\psi} = -(u_\mathsf{b} - c)\tilde{\eta}. \tag{61.171}$$

The corresponding relation between second derivatives

$$-(u_\mathsf{b} - c)\,\frac{\mathrm{d}^2\tilde{\psi}}{\mathrm{d}z^2} = \frac{\mathrm{d}}{\mathrm{d}z}\left[(u_\mathsf{b} - c)^2\,\frac{\mathrm{d}\tilde{\eta}}{\mathrm{d}z}\right] + \tilde{\eta}\,(u_\mathsf{b} - c)\,\frac{\mathrm{d}^2 u_\mathsf{b}}{\mathrm{d}z^2} \tag{61.172}$$

leads to the Taylor-Goldstein equation (61.150) written in terms of the vertical particle displacement

$$\frac{\mathrm{d}}{\mathrm{d}z}\left[(u_\mathsf{b} - c)^2\,\frac{\mathrm{d}\tilde{\eta}}{\mathrm{d}z}\right] = [-N^2 + k^2\,(u_\mathsf{b} - c)^2]\,\tilde{\eta} \quad \text{with } \tilde{\eta}(0) = \tilde{\eta}(H) = 0. \tag{61.173}$$

Multiplying by $\tilde{\eta}^*$, then integrating over the vertical extent of the domain and using the homogeneous Dirichlet boundary conditions, $\tilde{\eta}(0) = \tilde{\eta}(H) = 0$, leads to the identity

$$\int_0^H N^2\,|\tilde{\eta}|^2\,\mathrm{d}z = \int_0^H \left[k^2\,|\tilde{\eta}|^2 + \left|\frac{\mathrm{d}\tilde{\eta}}{\mathrm{d}z}\right|^2\right](u_\mathsf{b} - c)^2\,\mathrm{d}z. \tag{61.174}$$

The critical height theorem

The imaginary part of the integral condition (61.174) leads to the constraint

$$2\,c_\mathsf{i}\int_0^H \left[k^2\,|\tilde{\eta}|^2 + \left|\frac{\mathrm{d}\tilde{\eta}}{\mathrm{d}z}\right|^2\right](u_\mathsf{b} - c_\mathsf{r})\,\mathrm{d}z = 0, \tag{61.175}$$

where we used

$$(u_\mathsf{b} - c)^2 = (u_\mathsf{b} - c_\mathsf{r})^2 - c_\mathsf{i}^2 - 2\,\mathrm{i}\,c_\mathsf{i}\,(u_\mathsf{b} - c_\mathsf{r}). \tag{61.176}$$

The constraint (61.175) holds in the presence of an instability ($c_\mathsf{i} \neq 0$) only if the real part of the phase velocity lives within the bounds of the background flow

$$u_\mathsf{b}^{\min} < c_\mathsf{r} < u_\mathsf{b}^{\max} \Longrightarrow u_\mathsf{b}(z_{\mathrm{crit}}) = c_\mathsf{r}. \tag{61.177}$$

That is, for a wave to grow in the presence of an unstable background flow, its phase velocity must have a real part within the bounds of the background flow. It follows that there is a vertical

position, $z = z_{\text{crit}}$, where the background flow and the real part of the phase velocity are equal,

$$u_{\text{b}}(z_{\text{crit}}) = c_{\text{r}}. \tag{61.178}$$

This *critical height theorem* is the vertical analog to the critical latitude theorem from Section 61.5.3. Evidently, for a wave to grow, the real part of its phase velocity must match that of the background flow at no less than one vertical position. Otherwise, if c_{r} is outside of the bound (61.177), then the wave simply moves too fast for it to extract energy from the background flow.

Howard's semi-circle theorem

The real part of the integral condition (61.174) leads to the constraint

$$\int_0^H \mathcal{Q}\,[(u_{\text{b}} - c_{\text{r}})^2 - c_{\text{i}}^2]\,\mathrm{d}z \geq 0, \tag{61.179}$$

where we introduced the shorthand for the non-negative quantity

$$\mathcal{Q} = k^2\,|\tilde{\eta}|^2 + \left|\frac{\mathrm{d}\tilde{\eta}}{\mathrm{d}z}\right|^2 \geq 0. \tag{61.180}$$

For the case with $c_{\text{i}} \neq 0$, which means there is an unstable wave, then equation (61.175) implies

$$2\int_0^H \mathcal{Q}\,(u_{\text{b}} - c_{\text{r}})\,\mathrm{d}z = 0. \tag{61.181}$$

We can thus add this term to the constraint (61.179) to render

$$\int_0^H \mathcal{Q}\,[(u_{\text{b}} - c_{\text{r}})^2 - c_{\text{i}}^2]\,\mathrm{d}z = \int_0^H \mathcal{Q}\,[(u_{\text{b}} - c_{\text{r}})^2 - c_{\text{i}}^2 + 2\,c_{\text{r}}\,(u_{\text{b}} - c_{\text{r}})]\,\mathrm{d}z \geq 0, \tag{61.182}$$

which then leads to

$$\int_0^H \mathcal{Q}\,u_{\text{b}}^2\,\mathrm{d}z \geq \int_0^H \mathcal{Q}\,(c_{\text{r}}^2 + c_{\text{i}}^2)\,\mathrm{d}z \Longrightarrow (c_{\text{r}}^2 + c_{\text{i}}^2) \leq \frac{\int_0^H \mathcal{Q}\,u_{\text{b}}^2\,\mathrm{d}z}{\int_0^H \mathcal{Q}\,\mathrm{d}z}. \tag{61.183}$$

This inequality places a constraint on the real and imaginary part of the phase velocity. However, it is not so practical since we need to specify $\mathcal{Q}$ from equation (61.180), which requires information about the wavenumber and particle displacements.

A more useful practical constraint can be derived by starting from the inequality

$$\int_0^H \mathcal{Q}\,(u_{\text{b}} - u_{\text{b}}^{\min})\,(u_{\text{b}} - u_{\text{b}}^{\max})\,\mathrm{d}z = \int_0^H \mathcal{Q}\,[u_{\text{b}}^2 - u_{\text{b}}\,u_{\text{b}}^{\min} - u_{\text{b}}\,u_{\text{b}}^{\max} + u_{\text{b}}^{\min}\,u_{\text{b}}^{\max}]\,\mathrm{d}z \leq 0, \tag{61.184}$$

which follows from the definition of the $u_{\text{b}}^{\min}$ and $u_{\text{b}}^{\max}$, and recalling that $\mathcal{Q} \geq 0$. Making use of equation (61.183) allows us to replace u_{b}^2 with $c_{\text{r}}^2 + c_{\text{i}}^2$ and still maintain the inequality, so that

$$\int_0^H \mathcal{Q}\,[c_{\text{r}}^2 + c_{\text{i}}^2 - u_{\text{b}}\,(u_{\text{b}}^{\min} + u_{\text{b}}^{\max}) + u_{\text{b}}^{\min}\,u_{\text{b}}^{\max}]\,\mathrm{d}z \leq 0, \tag{61.185}$$

and use of the constraint (61.181) then allows us to replace u_{b} with c_{r} to have

$$\int_0^H \mathcal{Q}\,[c_{\text{r}}^2 + c_{\text{i}}^2 - c_{\text{r}}\,(u_{\text{b}}^{\min} + u_{\text{b}}^{\max}) + u_{\text{b}}^{\min}\,u_{\text{b}}^{\max}]\,\mathrm{d}z \leq 0. \tag{61.186}$$

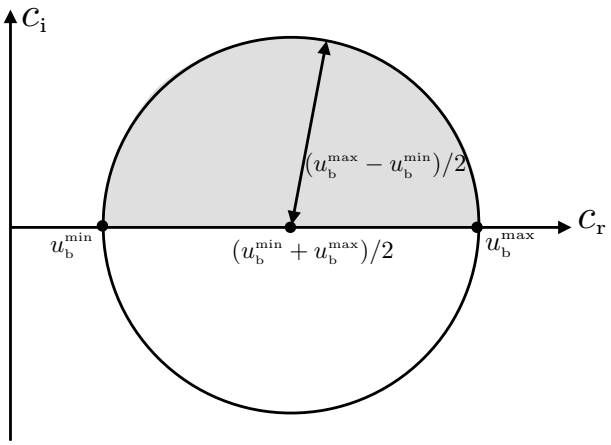

FIGURE 61.13: Illustrating Howard's semi-circle theorem (61.188) in the complex plane defined by the phase velocity. The semi-circle theorem says that growing waves (with $c_\mathrm{i} > 0$) in a sheared flow have their phase velocity within the gray region, with radius $(u_\mathrm{b}^\mathrm{max} - u_\mathrm{b}^\mathrm{min})/2$ and center along the real axis at $c_\mathrm{r} = (u_\mathrm{b}^\mathrm{min} + u_\mathrm{b}^\mathrm{max})/2$.

This constraint is more practical since it only involves the phase velocity and the maximum and minimum values of the background velocity, each of which are independent of z. Evidently, since $\mathcal{Q}$ is positive, we must have

$$c_\mathrm{r}^2 + c_\mathrm{i}^2 - c_\mathrm{r}\,(u_\mathrm{b}^\mathrm{min} + u_\mathrm{b}^\mathrm{max}) + u_\mathrm{b}^\mathrm{min}\,u_\mathrm{b}^\mathrm{max} \leq 0, \tag{61.187}$$

which can be rearranged to

$$[c_\mathrm{r} - (u_\mathrm{b}^\mathrm{min} + u_\mathrm{b}^\mathrm{max})/2]^2 + c_\mathrm{i}^2 \leq [(u_\mathrm{b}^\mathrm{max} - u_\mathrm{b}^\mathrm{min})/2]^2. \tag{61.188}$$

This constraint is depicted in Figure 61.13, where we see that unstable waves (with $c_\mathrm{i} > 0$) have phase velocities that sit within the semi-circle in the upper half of the complex plane whose center is along the real axis with $c_\mathrm{r} = (u_\mathrm{b}^\mathrm{min} + u_\mathrm{b}^\mathrm{max})/2$ and whose radius is $(u_\mathrm{b}^\mathrm{max} - u_\mathrm{b}^\mathrm{min})/2$.

The semi-circle theorem is particularly useful when designing numerical algorithms to find unstable waves. Also note that we derived this theorem starting from the case of a stratified shear layer. However, the same result holds for unstable waves in the presence of a meridionally sheared barotropic flow discussed as earlier in this chapter.

61.7.7 Further study

The $\mathrm{Ri} = 1/4$ stability argument was first presented by *Miles* (1961) and soon thereafter it was extended by *Howard* (1961). Our derivation of Howard's semi-circle theorem (61.188) follows Section 11.7 of *Kundu et al.* (2016).

61.8 A vertically sheared homogeneous fluid with a free surface

In this chapter we studied horizontal sheared flow in a homogeneous fluid, and then rotated the geometry to consider vertically sheared flow in a gravitationally stratified fluid. Here we consider a vertically sheared homogeneous fluid moving over a flat surface at $z = 0$ and with a free surface at $z = \eta$, as depicted in Figure 61.14. Directly translating the analysis of stratified shear instability from Section 61.7 to the present case, we might presume that since the Richardson number vanishes here, then any flow satisfies the necessary condition for vertical shear instability. However, besides having a vanishing buoyancy (since the fluid is homogeneous), the free upper surface further distinguishes this configuration from the vertically stratified shear instability studied in Section 61.7 (where we assumed the flow to occur between two rigid boundaries). The

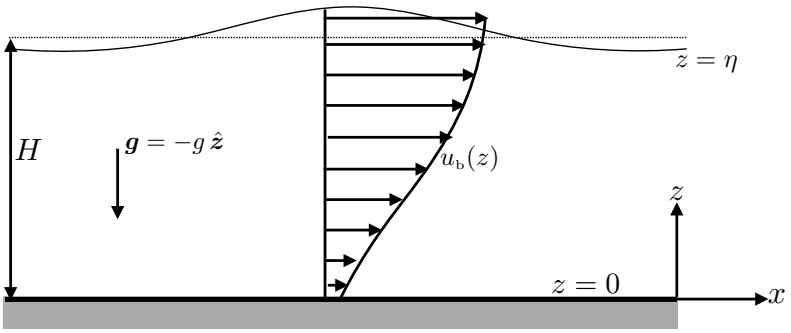

FIGURE 61.14: Schematic of the flow configuration used to examine vertical shear instability in a homogeneous inviscid flow with a free upper surface. The background flow is zonal with a vertical shear, $u_\mathrm{b}(z)\,\hat{\boldsymbol{x}}$. The fluid domain has a rigid lower bound at $z = 0$, where the bottom kinematic boundary condition means that $w(0) = 0$. The upper surface is free at $z = \eta = H + \eta'(x,t)$, so that the linearized upper kinematic boundary condition is $(\partial_t + u_\mathrm{b}\,\partial_x)\,\eta' = w'$, and this boundary condition is evaluated at $z = H$ rather than $z = \eta$.

presence of a free surface removes the ability to make general statements about the stability, thus illustrating the importance of boundary conditions when studying modal instabilities. This section also serves to highlight the role of non-hydrostatic pressure for enabling vertical shear instability.

61.8.1 Linearized governing equations

The linearized governing equations are given by equations (61.136a)-(61.136d) with identically zero buoyancy

$$\partial_t u' + u_\mathrm{b}\,\partial_x u' + w'\,\partial_z u_\mathrm{b} = -\partial_x \varphi' \tag{61.189a}$$
$$\partial_t w' + u_\mathrm{b}\,\partial_x w' = -\partial_z \varphi' \tag{61.189b}$$
$$\partial_x u' + \partial_z w' = 0, \tag{61.189c}$$

along with the bottom kinematic boundary condition and the linearized kinematic free surface boundary condition

$$w' = 0 \quad \text{at } z = 0 \tag{61.190a}$$
$$(\partial_t + u_\mathrm{b}\,\partial_x)\,\eta' = w' \quad \text{at } z = H. \tag{61.190b}$$

Since the x-z flow is non-divergent we can introduce a streamfunction as in equation (61.140)

$$u'\,\hat{\boldsymbol{x}} + w'\,\hat{\boldsymbol{z}} = \hat{\boldsymbol{y}} \times \nabla\psi = \partial_z \psi\,\hat{\boldsymbol{x}} - \partial_x \psi\,\hat{\boldsymbol{z}}, \tag{61.191}$$

which yields the governing equations

$$(\partial_t + u_\mathrm{b}\,\partial_x)\,\partial_z \psi - \partial_x \psi\,\partial_z u_\mathrm{b} = -\partial_x \varphi' \quad \text{for } 0 < z < H \tag{61.192a}$$
$$(\partial_t + u_\mathrm{b}\,\partial_x)\,\partial_x \psi = \partial_z \varphi' \quad \text{for } 0 < z < H \tag{61.192b}$$
$$\psi = 0 \quad \text{at } z = 0 \tag{61.192c}$$
$$(\partial_t + u_\mathrm{b}\,\partial_x)\eta' = -\partial_x \psi \quad \text{at } z = H. \tag{61.192d}$$

61.8.2 Hydrostatic fluctuations are stable

If we assume the fluctuations are hydrostatic then the zonal pressure gradient is given by the zonal derivative of the free surface (as in the case of a hydrostatic shallow water fluid),

$$\partial_x \varphi' = g\, \partial_x \eta', \tag{61.193}$$

so that the zonal velocity equation (61.192a) becomes

$$(\partial_t + u_{\mathrm{b}}\, \partial_x)\, \partial_z \psi - \partial_x \psi\, \partial_z u_{\mathrm{b}} = -g\, \partial_x \eta'. \tag{61.194}$$

Now assume the small amplitude fluctuations of the streamfunction and free surface take the propagating plane wave form

$$\psi(x,z,t) = \widetilde{\psi}(z)\, \mathrm{e}^{\mathrm{i}\, k\,(x-c\,t)} \quad \text{and} \quad \eta'(x,t) = \widetilde{\eta}\, \mathrm{e}^{\mathrm{i}\, k\,(x-c\,t)}. \tag{61.195}$$

For these fluctuations the kinematic boundary conditions (61.192c) and (61.192d) become

$$\widetilde{\psi} = 0 \qquad \text{at } z = 0 \tag{61.196a}$$

$$(u_{\mathrm{b}} - c)\widetilde{\eta} = -\widetilde{\psi} \quad \text{at } z = H. \tag{61.196b}$$

Similarly, the zonal velocity equation (61.194) renders the relations between the amplitude functions

$$(u_{\mathrm{b}} - c)\partial_z \widetilde{\psi} - \widetilde{\psi}\, \partial_z u_{\mathrm{b}} = -g\, \widetilde{\eta} \quad \text{for } 0 < z < H. \tag{61.197}$$

Dividing by $(u_{\mathrm{b}} - c)^2$ brings about

$$\frac{\mathrm{d}}{\mathrm{d}z}\left[\frac{\widetilde{\psi}}{u_{\mathrm{b}} - c}\right] = -\frac{g\, \widetilde{\eta}}{(u_{\mathrm{b}} - c)^2}, \tag{61.198}$$

whose vertical integral renders

$$\left.\frac{\widetilde{\psi}}{u_{\mathrm{b}} - c}\right|_{z=H} - \left.\frac{\widetilde{\psi}}{u_{\mathrm{b}} - c}\right|_{z=0} = -g\, \widetilde{\eta} \int_0^H \frac{\mathrm{d}z}{(u_{\mathrm{b}} - c)^2}, \tag{61.199}$$

where we evaluated the upper integral limit at $z = H$ as per the linear theory. Making use of the kinematic boundary conditions (61.196a) and (61.196b) brings this equation into the form

$$g \int_0^H \frac{\mathrm{d}z}{(u_{\mathrm{b}} - c)^2} = 1. \tag{61.200}$$

This identity can only be satisfied if the phase velocity, c, has zero imaginary part, in which case we conclude that the fluctuations are stable to vertical shear instability. In particular, for u_{b} a constant we recover the case considered in Exercise 55.4 for gravity waves moving on a constant background flow, in which the phase velocity is $c = u_{\mathrm{b}} \pm \sqrt{g\, H} = u_{\mathrm{b}} \pm c_{\mathsf{grav}}$.

We understand why the hydrostatic fluctuations are stable by appealing to the discussion of shallow water dynamics in Section 35.2. In that section we observed that a homogeneous fluid layer with a hydrostatic pressure (i.e., a shallow water fluid layer) renders a horizontal pressure gradient that is depth independent, which in turn leads to a depth independent horizontal velocity. That is, the homogeneous hydrostatic fluid cannot support a vertical shear in the horizontal flow, so that there can be no vertical shear instability. That is, when studying stability of a vertically sheared homogeneous fluid layer, hydrostatic fluctuations are depth independent and so they cannot lead to a vertical shear instability.

61.8.3 Taylor-Goldstein equation

Accepting that unstable fluctuations must involve a non-hydrostatic pressure, we make use of the analysis in Section 61.7.3 for stratified shear instability, in which we formed the linearized vorticity equation and introduced the streamfunction to render the Taylor-Goldstein equation (61.150). Specializing Taylor-Goldstein to the case of zero buoyancy ($N^2 = 0$) yields

$$(u_\mathrm{b} - c)\left[\frac{\mathrm{d}^2}{\mathrm{d}z^2} - k^2\right]\tilde{\psi} = \frac{\mathrm{d}^2 u_\mathrm{b}}{\mathrm{d}z^2}\,\tilde{\psi} \tag{61.201a}$$

$$\widetilde{\psi} = 0 \qquad \text{at } z = 0 \tag{61.201b}$$

$$(u_\mathrm{b} - c)\widetilde{\eta} = -\widetilde{\psi} \qquad \text{at } z = H. \tag{61.201c}$$

In deriving the necessary condition for vertical shear instability in Section 61.7.4, we made use of the assumed rigid top and bottom boundaries to eliminate the two boundary contributions appearing in equation (61.154). Yet with a free surface the $z = H$ boundary contribution no longer vanishes, instead it satisfies the kinematic condition (61.201c).

61.8.4 Necessary conditions for instability

To develop an integral condition, rather than introduce the ansatz (61.151), we work directly with the Taylor-Goldstein equation (61.201a). Since $N^2 = 0$, the manipulations are quite similar to those used to derive the Rayleigh-Kuo inflection point theorem in Section 61.5.1. For this purpose, multiply the Taylor-Goldstein equation (61.151) by $\widetilde{\psi}^*$ and rearrange to yield

$$\frac{\mathrm{d}}{\mathrm{d}z}\left[\widetilde{\psi}^*\,\frac{\mathrm{d}\widetilde{\psi}}{\mathrm{d}z}\right] = \left[k^2 + \frac{1}{u_\mathrm{b} - c}\,\frac{\mathrm{d}^2 u_\mathrm{b}}{\mathrm{d}z^2}\right]|\widetilde{\psi}|^2 + \left|\frac{\mathrm{d}\widetilde{\psi}}{\mathrm{d}z}\right|^2 \tag{61.202}$$

Vertical integration and use of the kinematic boundary conditions leads to

$$\widetilde{\psi}^*\,\frac{\mathrm{d}\widetilde{\psi}}{\mathrm{d}z}\bigg|_{z=H} = \int_0^H \left[k^2\,|\widetilde{\psi}|^2 + \left|\frac{\mathrm{d}\widetilde{\psi}}{\mathrm{d}z}\right|^2\right]\mathrm{d}z + \int_0^H \frac{\mathrm{d}^2 u_\mathrm{b}}{\mathrm{d}z^2}\,\frac{|\widetilde{\psi}|^2}{u_\mathrm{b} - c}\,\mathrm{d}z. \tag{61.203}$$

Taking the imaginary part of this equation and exposing the amplitude and phase for $\widetilde{\psi}$,

$$\widetilde{\psi} = |\widetilde{\psi}(z)|\,\mathrm{e}^{\mathrm{i}\,\alpha(z)}, \tag{61.204}$$

leads to

$$\left[|\widetilde{\psi}|^2\,\frac{\mathrm{d}\alpha}{\mathrm{d}z}\right]_{z=H} = c_\mathrm{i}\int_0^H \frac{\mathrm{d}^2 u_\mathrm{b}}{\mathrm{d}z^2}\,\frac{|\widetilde{\psi}|^2}{|u_\mathrm{b} - c|^2}\,\mathrm{d}z. \tag{61.205}$$

The left hand side vanishes for a rigid upper boundary, in which case we recover the Rayleigh-Kuo inflection point theorem (61.59). But with a free surface there are other situations that support instability since the left hand side is no longer zero. That is, allowing for a free surface opens up further avenues for instabilities. When developing necessary conditions for baroclinic instability in Section 62.8, we also find a fundamental role for boundary processes.

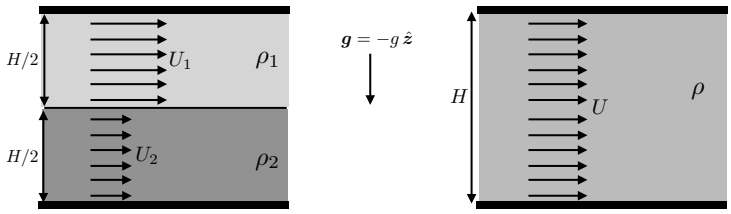

FIGURE 61.15: Initial (left) and final (right) conditions for a two-layer stratified flow that completely mixes its density and velocity. In Exercise 61.3 we work through the energetics of mixing and show that the ratio of the potential energy change to the kinetic energy change is proportional to a discrete version of the gradient Richardson number.

61.9 Exercises

EXERCISE 61.1: COMPLEX CONJUGATE FORMULA
In equations (61.45c) and (61.48) we made use of the identity

$$\mathrm{Im}\left[\widetilde{\psi}^* \, \partial_y \widetilde{\psi}\right] = -\,\mathrm{Im}\left[\widetilde{\psi} \, \partial_y \widetilde{\psi}^*\right]. \tag{61.206}$$

Derive this identity. Hint: make use of equation (61.49) for the streamfunction.

EXERCISE 61.2: FJØRTOFT'S THEOREM WITH SINH PROFILE AND $\beta \neq 0$
Consider the sinh velocity profile from Section 61.5.4. Show that with $\beta \neq 0$ the flow remains stable according to Fjørtoft's theorem.

EXERCISE 61.3: RICHARDSON NUMBER AND ENERGETICS OF MIXING
Rework the energetics from Section 61.7.5, only now with the two-layer stratified shear profile shown in Figure 61.15. In particular, compute the ratio of the potential energy increase to the kinetic energy decrease and show that this ratio is proportional to a discrete version of the gradient Richardson number

$$\frac{P_{\text{final}} - P_{\text{init}}}{K_{\text{init}} - K_{\text{final}}} \propto \mathrm{Ri}. \tag{61.207}$$

Assume a Boussinesq ocean for purposes of computing the kinetic energy. Hint: the solution to this exercise is detailed in Section 14.1 of *Cushman-Roisin and Beckers* (2011).

Chapter 62

QUASI-GEOSTROPHIC WAVES AND BAROCLINIC INSTABILITY

In this chapter we study waves and *baroclinic instability* in a continuously stratified quasi-geostrophic flow within a vertically bounded domain. The vertically bounded domain is more relevant to the ocean, with the atmosphere top boundary more suitably assumed to be at infinity. However, beyond the ocean case, we are motivated to consider the vertically bounded domain since it is assumed for the *Eady model* of baroclinic instability (*Eady*, 1949), which is a particularly elegant example of baroclinic instability. We furthermore find it is convenient to study waves in combination with baroclinic instability since baroclinic instability follows a *wave resonance* mechanism, much like that considered for shear instability in Chapter 61.

The waves we encounter in this chapter include *planetary Rossby waves*, *topographic Rossby waves*, and *Eady edge waves*. Recall that we encountered Rossby waves and edge waves in the horizontally non-divergent barotropic model of Chapter 54, as well as Rossby waves and topographic waves for the shallow water model in Chapter 55. In the present chapter, we work fully within the quasi-geostrophic theory and allow for continuous stratification. In addition to Rossby waves, we here consider a thermal wind background state, in which the quasi-geostrophic flow supports Eady edge waves. As shown here, Eady edge waves rely on the presence of a buoyancy gradient along the top and/or bottom boundaries of the domain. Eady waves are the primary actors in the Eady model of baroclinic instability.

The study of baroclinic instability is motivated by asking whether a thermal wind flow is stable to small amplitude geostrophic perturbations. Under certain circumstances, there are unstable wave modes whose energy grows by feeding off the potential energy of the thermal wind state. The Eady model considers the constructive interference of edge waves that leads to wave resonance. This resonance then drives the mutual growth of the edge waves, which constitutes baroclinic instability. Baroclinic instability dominates the fluctuations of the large-scale (order deformation radius) flows in the middle latitude atmosphere (*synoptic scale*) and the *mesoscale* ocean.

READER'S GUIDE FOR THIS CHAPTER

In this chapter we make use of the governing equations of continuously stratified quasi-geostrophic flow from Chapter 45, as well as the Rossby wave discussions in Chapter 54 (horizontally non-divergent barotropic model) and Section 55.9 (shallow water layer). The wave resonance interpretation of Eady's model of baroclinic instability closely follows that given for shear instability in Chapter 61.

62.1 Loose threads

- Split this chapter into one with the linear waves and placed into Part X, and another chapter focusing on baroclinic instability.
- Vertically propagating Rossby waves with an infinite top
- Continuous modes
- Show some vertical baroclinic modes in Section 62.4.1 for constant N^2 and for an exponential thermocline.
- Polarization relations for Eady waves.

- Group velocity for Eady waves
- Energetics for planetary waves, topographic waves, and Eady waves. Prove that phase averaged energy flux equals to the group velocity times the energy.
- Discuss the neutral wave case with $u_{\mathrm{b}} = c$ and further explore Footnote 10 in Chapter 9 of *Vallis* (2017).
- Offer further elaborations from *Vallis* (2017) and *Cushman-Roisin and Beckers* (2011).
- Eliasen-Palm fluxes and potential vorticity fluxes in Section 62.9.
- Discuss Figures 13.1 and 13.4 of *Gill* (1982).
- Charney model

62.2 Equations of quasi-geostrophy

As developed in Chapter 45, quasi-geostrophy is concerned with the evolution of hydrostatic and nearly geostrophic flow in the presence of a prescribed and gravitationally stable background state that is itself in hydrostatic and geostrophic balance. In this section we summarize salient features of continuously stratified quasi-geostrophy that are useful in the study of quasi-geostrophic waves and baroclinic instability.

62.2.1 Equations in the fluid interior

Within the interior of the fluid domain, the quasi-geostrophic buoyancy equation (45.42), relative vorticity equation (45.47), and potential vorticity equation (45.54), are given by

$$(\partial_t + \boldsymbol{u} \cdot \nabla)\, b = -w\, N^2 \qquad \text{buoyancy equation} \tag{62.1a}$$

$$(\partial_t + \boldsymbol{u} \cdot \nabla)\, \zeta = -\beta\, v + f_{\circ}\, \partial_z w \qquad \text{relative vorticity equation} \tag{62.1b}$$

$$(\partial_t + \boldsymbol{u} \cdot \nabla)\, q = 0, \qquad \text{quasi-geostrophic potential vorticity equation,} \tag{62.1c}$$

in which

$$\psi = p/(\rho_{\circ}\, f_{\circ}) \qquad \text{quasi-geostrophic streamfunction } (p = \text{pressure}) \tag{62.2a}$$

$$\boldsymbol{u} = \hat{\boldsymbol{z}} \times \nabla\psi \qquad \text{non-divergent geostrophic velocity} \tag{62.2b}$$

$$b = f_{\circ}\, \partial_z \psi \qquad \text{buoyancy} \tag{62.2c}$$

$$\zeta = \hat{\boldsymbol{z}} \cdot (\nabla \times \boldsymbol{u}) = \nabla_{\mathrm{h}}^2 \psi \qquad \text{geostrophic relative vorticity} \tag{62.2d}$$

$$q = f_{\circ} + \beta\, y + \zeta + f_{\circ}\, \partial_z (b/N^2) \qquad \text{quasi-geostrophic potential vorticity} \tag{62.2e}$$

$$q = f_{\circ} + \beta\, y + \nabla_{\mathrm{h}}^2 \psi + f_0^2\, \partial_z (\partial_z \psi / N^2) \qquad \text{potential vorticity in terms of streamfunction.} \tag{62.2f}$$

The prescribed time-independent parameters are given by

$$N^2(z) > 0 \qquad \text{background stratification} \tag{62.3a}$$

$$f(y) = f_{\circ} + \beta\, y \qquad \beta\text{-plane Coriolis frequency.} \tag{62.3b}$$

Quasi-geostrophy is based on the following scale assumptions

$$\begin{aligned}
&\mathrm{Ro} = U/f_\circ L \ll 1 && \text{small Rossby number} && (62.4a)\\
&\beta\, L/f_\circ \ll 1 && \beta\text{-plane approximation} && (62.4b)\\
&\mathrm{Bu}(z) = [L_\mathsf{d}(z)/L]^2 = [N(z)\, H/f_\circ]^2\, L^{-2} \sim 1 && \text{order unity Burger number} && (62.4c)\\
&\mathrm{Ri}(z) = \mathrm{Ro}^{-2}\, \mathrm{Bu}(z) \gg 1 && \text{very large Richardson number.} && (62.4d)
\end{aligned}$$

The small Rossby number, Ro, means that the flow is strongly affected by the Coriolis acceleration, which furthermore means it is in near geostrophic balance. This scaling holds for both the background flow, which is prescribed, and perturbations to the background. The order unity Burger number says that the horizontal length scale of the flow, L, is comparable to the deformation radius, L_d, with the deformation radius a function of the vertical scale of motion, H (also the vertical size of the Eady model domain), the f-plane Coriolis parameter, $f_\circ$, and the prescribed background buoyancy frequency, $N(z)$. The large Richardson number, Ri, means that the flow is stable with respect to stratified shear instability (Chapter 61). Note that when writing the potential vorticity, the constant $f_\circ$ can be dropped since it plays no role in the potential vorticity equation.

The evolution of buoyancy (equation (62.1a)) and relative vorticity (equation (62.1b)) are both impacted by the ageostrophic vertical velocity, w. However, we do not need to explicity compute w to evolve the flow within the domain interior. The reason is that we can instead evolve the quasi-geostrophic potential vorticity through equation (62.1c). Thereafter, we solve the Poisson equation (with boundary conditions) for the geostrophic streamfunction

$$\nabla_\mathsf{h}^2 \psi + f_\circ^2\, \partial_z(\partial_z \psi / N^2) = q - (f_\circ + \beta\, y). \tag{62.5}$$

Upon updating the streamfunction we then update the velocity, buoyancy, and relative vorticity. Even though w is unnecessary for updating the flow state, it can be useful for a variety of diagnostic purposes. In Section 45.4.2 we derive a diagnostic equation for this ageostrophic velocity component.

62.2.2 Boundary conditions for vertically bounded domain

For the lateral boundaries, we assume either an infinite horizontal domain with all fields assumed to be finite or vanishing at spatial infinity, or assume doubly periodic domains. In this manner, the lateral boundaries play no fundamental role in the dynamics of concern in this chapter. In contrast, we are concerned with vertically bounded domains in which the top and bottom boundaries are central to the dynamics. To establish the corresponding boundary conditions, we make use of the buoyancy equation (62.1a), given the presence of the vertical velocity. Furthermore, we are concerned with perfect fluid quasi-geostrophy, so consider just the kinematic boundary conditions. The dynamic boundary conditions involve frictional stresses and are not considered here.

The top and bottom boundary conditions for quasi-geostrophy were studied in Sections 45.6 and 45.7. For the upper surface (top) boundary, the vertical velocity is vanishingly small relative to interior vertical motion, thus prompting the rigid lid approximation. Evaluating the buoyancy equation (62.1a) at the rigid lid top boundary means that the boundary buoyancy is materially invariant

$$(\partial_t + \boldsymbol{u} \cdot \nabla_\mathsf{h})\, b = 0 \implies (\partial_t + \boldsymbol{u} \cdot \nabla_\mathsf{h})\, \partial_z \psi = 0 \quad \text{at } z = \overline{\eta}. \tag{62.6}$$

To within the accuracy of quasi-geostrophy, this boundary condition is evaluated at the resting position of the top boundary, $z = \overline{\eta}$, which is typically taken as $\overline{\eta} = 0$.

The analogous boundary condition at the domain bottom, $z = \eta_b(x, y)$, is given by

$$(\partial_t + \boldsymbol{u} \cdot \nabla_h)\, b = -N^2\, \boldsymbol{u} \cdot \nabla \eta_b \quad \text{at } z = \overline{\eta_b}. \tag{62.7}$$

which takes on the following form with the streamfunction

$$(\partial_t + \boldsymbol{u} \cdot \nabla_h)\, (f_o\, \partial_z \psi) = -N^2\, \boldsymbol{u} \cdot \nabla \eta_b \quad \text{at } z = \overline{\eta_b}. \tag{62.8}$$

The bottom boundary condition is evaluated at the horizontally averaged position, $z = \overline{\eta_b}$, since the more precise boundary location, $z = \eta_b(x, y)$, is one order higher in Rossby number and so is dropped from quasi-geostrophic theory. Correspondingly, quasi-geostrophic theory is formally valid only for very gently sloping bottom boundaries. Note that when η_b is a constant, then $\nabla_h \eta_b = 0$, so that the bottom boundary condition reduces to the material invariance of the boundary buoyancy, just like the top boundary condition.

Quasi-geostrophic theory based on studies of just the top and/or bottom boundary conditions is known as *surface quasi-geostrophy* (e.g., *Held et al.* (1995), *Yassin and Griffies* (2022)), where the interior potential vorticity is assumed to be a constant, which can be set to zero without loss of generality. Surface quasi-geostrophy shares mathematically elements with the study of surface gravity waves in Chapter 52. Namely, surface quasi-geostrophy supports edge waves that are exponentially trapped at the boundaries and with a vertical length scale inversely proportional to the horizontal wavelength (i.e., shorter edge waves are more trapped next to the boundary than longer edge waves). As we see later in this chapter, edge waves are central to baroclinic instability as realized in the Eady model.

62.3 Linear fluctuations on a zonal geostrophic background flow

We here formulate equations for a zonal background flow state and the linear fluctuations relative to that flow. The static and prescribed background state is assumed to be in thermal wind balance, and all perturbations to that background state satisfy the scalings of quasi-geostrophy. All background fields have a "b" subscript to remind us that these fields are prescribed.

The linear analysis in this section forms the baseline for subsequent sections that specialize these results. In particular, in Section 62.4 we specialize to the case of zero thermal wind flow with planetary beta, thus considering planetary Rossby waves. In Section 62.5, we set planetary beta to zero but allow for a topographic slope, thus considering topographic Rossby waves. In Section 62.6, we maintain the thermal wind state but assume zero planetary beta and zero topographic beta, thus focusing on the mechanics of *Eady edge waves*, whose existence along either the top or bottom boundary relies on the presence of a horizontal buoyancy gradient along that boundary. In Section 62.7 we study the unstable Eady edge waves arising in the Eady model, thus forming the wave mechanism for baroclinic instability.

62.3.1 Zonal geostrophic background flow

Consider a geostrophic background state described by a streamfunction, $\Psi_b(y, z)$, with a corresponding zonal flow and thermal wind shear

$$u_b(y, z) = -\partial_y \Psi_b \quad \text{and} \quad \partial_z u_b = -\partial_{yz} \Psi_b = -f_o^{-1}\, \partial_y b_b, \tag{62.9}$$

where $b_b(y, z)$ is the prescribed background buoyancy field supporting the background geostrophic flow.

A particular example of buoyancy supporting a geostrophic flow with a constant thermal

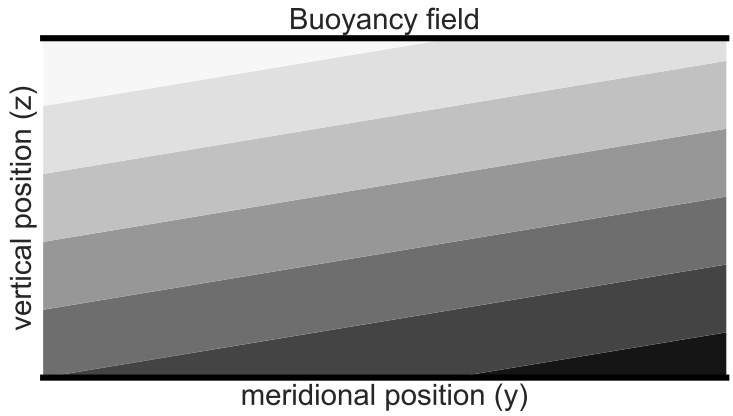

FIGURE 62.1: Example background buoyancy field written as the linear function, $b_b = N^2\,[z - y\,(\mathrm{d}z/\mathrm{d}y)_{b_b}]$, as per equation (62.13). The squared buoyancy frequency is positive, $N^2 = \partial_z b_b > 0$, whereas the northward buoyancy gradient is negative, $\partial_y b_b < 0$. Correspondingly, the buoyancy slope, $(\mathrm{d}z/\mathrm{d}y)_{b_b} = -\partial_y b_b/\partial_z b_b = f_o\,\partial_z u_b/N^2 > 0$, is positive to the north (north is to the right). There are no lateral boundaries, so that the fluid is assumed to be unbounded in the horizontal directions. However, the top and bottom are rigid.

wind shear is given by the sloped and planar buoyancy surfaces

$$b_b = N^2\,z + (\partial_y b_b)\,y = N^2\,z - f_o\,(\partial_z u_b)\,y, \quad \text{with } N^2,\ \partial_y b_b, \text{ and } \partial_z u_b \text{ constants.} \tag{62.10}$$

We consider this special case when studying Eady waves in Section 62.6 and the Eady model of baroclinic instability in Section 62.7. Although very idealized, it provides the core features of Eady waves and baroclinic instability, and it does so in an analytically tractable manner.

The buoyancy (62.10) can be written in a geometric form by introducing the meridional slope of the background buoyancy surfaces. To derive an expression for the slope, note that constant buoyancy surfaces are defined by[1]

$$b_b = \text{constant} \implies \mathrm{d}b_b = 0 = (\partial b_b/\partial y)\,\mathrm{d}y + (\partial b_b/\partial z)\,\mathrm{d}z, \tag{62.11}$$

which means that the slope of constant buoyancy surfaces is given by

$$\left[\frac{\mathrm{d}z}{\mathrm{d}y}\right]_{b_b} = -\frac{\partial_y b_b}{\partial_z b_b} = -\frac{\partial_y b_b}{N^2} = \frac{f_o\,\partial_z u_b}{N^2}, \tag{62.12}$$

so that the buoyancy (62.10) is

$$b_b = N^2\,[z - y\,(\mathrm{d}z/\mathrm{d}y)_{b_b}] \quad \text{with } (\mathrm{d}z/\mathrm{d}y)_{b_b} \text{ a constant slope.} \tag{62.13}$$

Figure 62.1 illustrates such a buoyancy field with a constant and positive meridional slope, $(\mathrm{d}z/\mathrm{d}y)_{b_b} > 0$.

It is common to forget the minus signs appearing in the first and second expressions for the slope in equation (62.12). Examination of Figure 62.1 quickly remedies this mistake. Namely, this figure depicts a buoyancy field that has a positive slope towards the north, $(\mathrm{d}z/\mathrm{d}y)_{b_b} > 0$. This slope arises due to the reduction in buoyancy moving north ($\partial_y b_b < 0$) in the presence of a vertically stable stratification ($\partial_z b_b > 0$).

62.3.2 Background state is an exact quasi-geostrophic solution

We here show that the thermal wind flow (62.9) identically satisfies the quasi-geostrophic equations, thus constituting an exact solution to quasi-geostrophy. For this purpose, introduce

[1] See Section 63.12.2 for mathematical details on the treatment of generalized vertical coordinates.

the quasi-geostrophic potential vorticity for the background flow

$$q_\mathsf{b} = f_\circ + \beta\, y + \zeta_\mathsf{b} + f_\circ^2\, \partial_z(N^{-2}\, \partial_z \Psi_\mathsf{b}) = f_\circ + \beta\, y - \partial_y u_\mathsf{b} + f_\circ^2\, \partial_z(N^{-2}\, \partial_z \Psi_\mathsf{b}), \tag{62.14}$$

where we introduced the relative vorticity of the background zonal geostrophic flow

$$\zeta_\mathsf{b} = -\partial_y u_\mathsf{b}. \tag{62.15}$$

Since q_b is static and a spatial function just of (y, z), it trivially satisfies the potential vorticity equation

$$(\partial_t + u_\mathsf{b}\, \hat{\boldsymbol{x}} \cdot \nabla_\mathsf{h})\, q_\mathsf{b} = u_\mathsf{b}\, \partial_x\, q_\mathsf{b} = 0. \tag{62.16}$$

Likewise, the background buoyancy field, $b_\mathsf{b}(y, z)$, trivially satisfies the top boundary condition (62.6) since

$$(\partial_t + u_\mathsf{b}\, \hat{\boldsymbol{x}} \cdot \nabla_\mathsf{h})\, b_\mathsf{b} = u_\mathsf{b}\, \partial_x\, b_\mathsf{b} = 0 \quad \text{at } z = \overline{\eta}. \tag{62.17}$$

For the bottom boundary condition (62.8) we have

$$(\partial_t + u_\mathsf{b}\, \partial_x)\, b_\mathsf{b} + u_\mathsf{b}\, \partial_x(N^2\, \eta_\mathsf{b}) = 0 \quad \text{at } z = \overline{\eta_\mathsf{b}}, \tag{62.18}$$

which is satisfied if the topography is a function only of latitude, $\eta_\mathsf{b} = \eta_\mathsf{b}(y)$. Hence, the background thermal wind flow, $u_\mathsf{b}(y, z)$, and corresponding buoyancy, $b_\mathsf{b}(y, z)$, are exact solutions to quasi-geostrophy if the bottom is either flat or has a meridional slope.

62.3.3 Fluctuating streamfunction, potential vorticity, and buoyancy

Now consider fluctuations relative to the zonal geostrophic flow, with streamfunction and buoyancy decomposed as

$$\psi(x, y, z, t) = \Psi_\mathsf{b}(y, z) + \psi'(x, y, z, t) \quad \text{and} \quad b(x, y, z, t) = b_\mathsf{b}(y, z) + b'(x, y, z, t). \tag{62.19}$$

The corresponding quasi-geostrophic potential vorticity is decomposed according to

$$q(x, y, z, t) = q_\mathsf{b}(y, z) + q'(x, y, z, t), \tag{62.20}$$

with q_b given by equation (62.14). The fluctuating potential vorticity arises from relative vorticity and stretching

$$q' = \nabla_\mathsf{h}^2 \psi' + f_\circ^2\, \partial_z(N^{-2}\, \partial_z \psi'). \tag{62.21}$$

Substituting these expressions into the quasi-geostrophic potential vorticity equation (62.1c) leads to

$$[\partial_t + (\boldsymbol{u}' + \boldsymbol{u}_\mathsf{b}) \cdot \nabla]\, (q_\mathsf{b} + q') = [\partial_t + (\boldsymbol{u}' + \boldsymbol{u}_\mathsf{b}) \cdot \nabla]\, q' + \boldsymbol{u}' \cdot \nabla q_\mathsf{b} = 0, \tag{62.22}$$

where we set

$$\partial_t q_\mathsf{b} + \boldsymbol{u}_\mathsf{b} \cdot \nabla q_\mathsf{b} = 0, \tag{62.23}$$

since q_b is an exact solution to quasi-geostrophy (Section 62.3.2). Rearranging equation (62.22), and setting $\boldsymbol{u}_\mathsf{b} = u_\mathsf{b}\, \hat{\boldsymbol{x}}$, leads to

$$[\partial_t + (u_\mathsf{b}\, \hat{\boldsymbol{x}} + \boldsymbol{u}') \cdot \nabla_\mathsf{h}]\, q' + v'\, \partial_y q_\mathsf{b} = 0. \tag{62.24}$$

We are concerned in this chapter with linear theory, with the linearized equation for the perturbation potential vorticity given by

$$(\partial_t + u_\mathsf{b}\, \partial_x)\, q' = -v'\, \partial_y q_\mathsf{b} \Longrightarrow (\partial_t + u_\mathsf{b}\, \partial_x)\, [\nabla_\mathsf{h}^2 \psi' + f_\circ^2\, \partial_z(N^{-2}\, \partial_z \psi')] = -\partial_x \psi'\, \partial_y q_\mathsf{b}. \tag{62.25}$$

Evidently, in the linear theory we find that q' is advected by the zonal background flow, u_b, and it has a source determined by the anomalous meridional advection of the background quasi-geostrophic potential vorticity, q_b.

For the buoyancy, $b(x, y, z, t) = b_\mathrm{b}(y, z) + b'(x, y, z, t)$, we linearize the buoyancy equation (62.1a) to find

$$(\partial_t + u_\mathrm{b}\,\partial_x)\,b' = -v'\,\partial_y b_\mathrm{b} - w'\,N^2. \tag{62.26}$$

The right hand side source terms can be written in terms of the slope of the buoyancy surfaces (62.12)

$$(\partial_t + u_\mathrm{b}\,\partial_x)\,b' = -N^2\,[w' - v'\,(\mathrm{d}z/\mathrm{d}y)_{b_\mathrm{b}}]. \tag{62.27}$$

62.3.4 Linearized upper boundary condition

The upper surface boundary condition (62.6) is

$$\partial_t b' + (u_\mathrm{b}\,\partial_x + \boldsymbol{u}'\cdot\nabla_\mathrm{h})(b_\mathrm{b} + b') = 0, \tag{62.28}$$

which linearizes to

$$(\partial_t + u_\mathrm{b}\,\partial_x)\,b' = -v'\,\partial_y b_\mathrm{b} \Longrightarrow (\partial_t + u_\mathrm{b}\,\partial_x)\,\partial_z\psi' = \partial_x\psi'\,\partial_z u_\mathrm{b}. \tag{62.29}$$

As we see in Section 62.6, advection by the zonal geostrophic flow provides a frequency shift to the linear waves, whereas the source, $\partial_x\psi'\,\partial_z u_\mathrm{b}$, supports the propagation of surface trapped edge waves relative to the flow.

62.3.5 Linearized bottom boundary condition

The bottom boundary condition (62.8), with $\eta_\mathrm{b} = \eta_\mathrm{b}(y)$, is given by

$$f_\circ\,(\partial_t + u_\mathrm{b}\,\partial_x + \boldsymbol{u}'\cdot\nabla_\mathrm{h})\,\partial_z\psi' = v'\,(f_\circ\,\partial_z u_\mathrm{b} - N^2\,\partial_y\eta_\mathrm{b}), \tag{62.30}$$

which linearizes to

$$f_\circ\,(\partial_t + u_\mathrm{b}\,\partial_x)\,\partial_z\psi' = \partial_x\psi'\,(f_\circ\,\partial_z u_\mathrm{b} - N^2\,\partial_y\eta_\mathrm{b}). \tag{62.31}$$

The right hand side can be written in a geometric manner by introducing the slope of the background buoyancy as per equation (62.12), so that

$$(\mathrm{d}z/\mathrm{d}y)_{b_\mathrm{b}} = -\partial_y b_\mathrm{b}/\partial_z b_\mathrm{b} = f_\circ\,\partial_z u_\mathrm{b}/N^2. \tag{62.32}$$

The bottom boundary condition (62.31) can thus be written as

$$f_\circ\,(\partial_t + u_\mathrm{b}\,\partial_x)\,\partial_z\psi' = \partial_x\psi'\,N^2\,[(\mathrm{d}z/\mathrm{d}y)_{b_\mathrm{b}} - \partial_y\eta_\mathrm{b}], \tag{62.33}$$

in which the forcing on the right hand side is proportional to the difference between the buoyancy slope and bottom topography slope. When the bottom topography is flat then the bottom boundary condition reduces to the same condition as the top

$$(\partial_t + u_\mathrm{b}\,\partial_x)\,\partial_z\psi' = \partial_x\psi'\,\partial_z u_\mathrm{b}. \tag{62.34}$$

62.4 Vertically bounded planetary Rossby waves

In this section we simplify the background state by assuming zero background flow with flat top and bottom boundaries, yet affected by a nonzero planetary beta. That is, we here study continuously stratified planetary Rossby waves in a vertically bounded domain. We already

encountered planetary Rossby waves in Section 54.3 for the horizontally non-divergent barotropic model, and in Section 55.9 for the shallow water model. The goal here is to extend those earlier discussions to the case of continuous stratification.

62.4.1 Governing linear equations

Again, we assume the background state has a flat bottom with zero background thermal wind flow, so that the background consists solely of planetary beta. Hence, the background potential vorticity equals to the planetary vorticity

$$q_{\mathsf{b}} = f_{\circ} + \beta\, y \Longrightarrow \nabla q_{\mathsf{b}} = \beta\, \hat{\boldsymbol{y}}. \tag{62.35}$$

The linearized potential vorticity equation (62.25) and linearized boundary conditions (62.29) and (62.31), each with zero background flow, are given by

$$\partial_t q' + \beta\, v' = 0 \Longrightarrow \partial_t[\nabla_{\mathsf{h}}^2 \psi' + f_0^2\, \partial_z(N^{-2}\, \partial_z \psi')] + \beta\, \partial_x \psi' = 0 \tag{62.36a}$$

$$\partial_{tz} \psi' = 0 \quad \text{at } z = \overline{\eta} \text{ and } z = \overline{\eta_{\mathsf{b}}}. \tag{62.36b}$$

In the presence of a horizontally homogeneous vertical stratification, $N^2(z) > 0$, we can introduce a wave ansatz consisting of horizontally traveling free plane waves that are modulated by a vertically dependent (generally complex) amplitude

$$\psi'(x,y,z,t) = \widetilde{\psi}(z)\, \mathrm{e}^{\mathrm{i}\,(k_x\, x + k_y\, y - \omega\, t)} \Longrightarrow \boldsymbol{u} = (\hat{\boldsymbol{z}} \times \mathrm{i}\, \boldsymbol{k})\, \widetilde{\psi}(z)\, \mathrm{e}^{\mathrm{i}\,(k_x\, x + k_y\, y - \omega\, t)}. \tag{62.37}$$

As we will see when analytically calculating the vertical structure for constant N^2 in Section 62.4.3, the vertical structure takes the form of vertically standing waves, which accords with our prior experience of waves in a bounded domain (e.g., acoustic waves in a rectangular cavity in Exercise 51.1; surface gravity waves in Section 52.8). Plugging the ansatz (62.37) into the streamfunction equation (62.36a) and boundary condition equation (62.36b) leads to the *Sturm-Liouville* eigenvalue problem[2]

$$\frac{\mathrm{d}}{\mathrm{d}z}\left[\frac{f_{\circ}^2}{N^2}\, \frac{\mathrm{d}\widetilde{\psi}}{\mathrm{d}z}\right] = -\lambda\, \widetilde{\psi} \tag{62.38a}$$

$$\frac{\mathrm{d}\widetilde{\psi}}{\mathrm{d}z} = 0 \quad \text{at } z = \overline{\eta}, \overline{\eta_{\mathsf{b}}} \tag{62.38b}$$

$$\lambda = -(|\boldsymbol{k}|^2 + \beta\, k_x/\omega). \tag{62.38c}$$

We refer to solutions $\widetilde{\psi}$ as *eigenmodes* with λ the corresponding *eigenvalues*. From the Sturm-Liouville theory we know there are a countably infinite number of eigenmodes, with the higher eigenvalues corresponding to modes with more zero crossings.

62.4.2 Barotropic mode and baroclinic modes

Multiplying the eigenvalue equation (62.38a) by $\widetilde{\psi}^*$, integrating over the depth of the fluid, and making use of the Neumann boundary conditions (62.38b), leads to the expression for the eigenvalue in terms of the eigenmodes

$$\lambda = -(|\boldsymbol{k}|^2 + \beta\, k_x/\omega) = \frac{\int_{\overline{\eta_{\mathsf{b}}}}^{\overline{\eta}} |(f_{\circ}/N)\, \mathrm{d}\widetilde{\psi}/\mathrm{d}z|^2\, \mathrm{d}z}{\int_{\overline{\eta_{\mathsf{b}}}}^{\overline{\eta}} |\widetilde{\psi}|^2\, \mathrm{d}z}, \tag{62.39}$$

[2] Sturm-Liouville eigenvalue problems have a well established theory in differential equations and mathematical physics. Chapter 11 of *Boyce and DiPrima* (2009) is a classic reference, now in its 9th edition!

which proves that the eigenvalues are non-negative

$$\lambda \geq 0. \tag{62.40}$$

Barotropic mode

The case with zero eigenvalue, $\lambda = 0$, has a dispersion relation given by

$$\omega = -k_x \, \beta / |\boldsymbol{k}|^2 \quad \text{barotropic mode}, \tag{62.41}$$

and a corresponding depth independent eigenmode ($\mathrm{d}\widetilde{\psi}/\mathrm{d}z = 0$), with this mode referred to as the *barotropic mode*. Notice that the barotropic mode's frequency is unbounded as the wavenumber gets smaller (longer waves). That is, the longer wavelength modes have higher frequency. Also note that the phase velocity (equation (49.26))

$$\boldsymbol{c}_{\mathsf{p}} = (\omega/|\boldsymbol{k}|) \, \hat{\boldsymbol{k}} = (\omega/|\boldsymbol{k}|^2) \, \boldsymbol{k}, \tag{62.42}$$

has a westward component

$$(\boldsymbol{c}_{\mathsf{p}} \cdot \hat{\boldsymbol{x}})^{\text{barotropic}} = (\omega/|\boldsymbol{k}|^2) \, \boldsymbol{k} \cdot \hat{\boldsymbol{x}} = -k_x^2 \, \beta / |\boldsymbol{k}|^2 < 0. \tag{62.43}$$

This westward phase velocity accords with our earlier studies of Rossby waves. Even though this barotropic mode appears in a stratified fluid, its properties are equivalent to that of the Rossby waves appearing in a horizontally non-divergent barotropic model as studied in Section 54.3, further supporting this mode being referred to it as the barotropic mode.

Baroclinic modes

Equation (62.39) shows that all nonzero eigenvalues are positive

$$\lambda = -(|\boldsymbol{k}|^2 + \beta \, k_x/\omega) > 0. \tag{62.44}$$

Furthermore, upon vertically integrating the eigenvalue equation (62.38a) and using the boundary conditions (62.38b) we find that all higher modes have zero depth integral

$$\int_{\overline{\eta_{\mathsf{b}}}}^{\overline{\eta}} \widetilde{\psi} \, \mathrm{d}z = 0. \tag{62.45}$$

We refer to these as *baroclinic modes* since they are depth dependent, with the baroclinic modes having eigenvalues that form a monotonically increasing and countably infinite sequence. Each successive baroclinic mode has one more zero crossing, and thus more vertical structure. We display this behavior in Section 62.4.3 when analytically determing the eigenmodes with a constant N^2.

62.4.3 Planetary Rossby waves with constant N^2

An analytic solution to the eigenvalue problem (62.38a)-(62.38b) for vertically bounded Rossby waves can be found for the case of constant N^2, whereby the eigenmode is given by the cosine function

$$\widetilde{\psi} = \widetilde{\psi}_{\circ} \cos[n \, \pi \, (z - \overline{\eta_{\mathsf{b}}})/H] \quad \text{with } H = \overline{\eta} - \overline{\eta_{\mathsf{b}}}, \tag{62.46}$$

with $\widetilde{\psi}_{\circ}$ a constant real amplitude. The eigenvalues can be found through equation (62.39),

$$\lambda = (n \, \pi / L_{\mathsf{d}})^2 \quad \text{with } n = 0, 1, 2, 3... \text{ and } L_{\mathsf{d}} = N \, H / f_{\circ}, \tag{62.47}$$

which then lead to the dispersion relation for the baroclinic modes

$$\omega = -\frac{\beta\, k_x}{(n\,\pi/L_\mathsf{d})^2 + k_x^2 + k_y^2}. \tag{62.48}$$

Since the angular frequency is non-negative (Section 49.2.3), all planetary Rossby wave modes have a westward, $k_x < 0$, phase propagation, just like we saw for the barotropic planetary wave with $n = 0$. We display this property by writing the zonal component of the phase velocity

$$\boldsymbol{c}_\mathsf{p} \cdot \hat{\boldsymbol{x}} = (\omega/|\boldsymbol{k}|^2)\, k_x = -\frac{\beta\, k_x^2/|\boldsymbol{k}|^2}{(n\,\pi/L_\mathsf{d})^2 + k_x^2 + k_y^2} < 0. \tag{62.49}$$

Observe that a useful way to non-dimensionalize the dispersion relation (62.48) is to write

$$\omega/(\beta\, L_\mathsf{d}) = -\frac{k_x\, L_\mathsf{d}}{(n\,\pi)^2 + (k_x\, L_\mathsf{d})^2 + (k_y\, L_\mathsf{d})^2}, \tag{62.50}$$

with this expression plotted in Figure 62.2 for the $n = 0, 1, 2$ Rossby wave modes with $k_y = 0$.

A packet of Rossby waves with carrier wavevector $\boldsymbol{k}$ moves with the group velocity

$$\boldsymbol{c}_\mathsf{g} = \nabla_{\boldsymbol{k}}\omega = \frac{\beta\,[\hat{\boldsymbol{x}}\,(k_x^2 - k_y^2 - (n\,\pi/L_\mathsf{d})^2) + 2\,k_x\,k_y\,\hat{\boldsymbol{y}}]}{[(n\,\pi/L_\mathsf{d})^2 + k_x^2 + k_y^2]^2}. \tag{62.51}$$

In Section 54.3 we studied Rossby waves in the horizontally non-divergent barotropic model, and then in Section 55.9 we studied Rossby waves in a single shallow water layer. Both of those discussions share much with the present case, in particular the shallow water Rossby waves since they have a finite deformation radius whereas the deformation radius is formally infinite in the barotropic model. Hence, each baroclinic mode found in the continuously stratified case can be understood as a Rossby wave in a single shallow water layer whose deformation radius,

$$L_\mathsf{d} = c_\mathsf{grav}/f_\circ = \sqrt{g\,H}/f_\circ, \tag{62.52}$$

is chosen to fit that of the baroclinic mode. By extension, we can understand the geometry of baroclinic Rossby wave packets, including their reflection from surfaces, by referring to the earlier shallow water discussion.

62.5 Topographic Rossby waves

Now set $\beta = 0$, to eliminate planetary Rossby waves, but maintain a background potential vorticity gradient by allowing the bottom to have a nonzero slope. In so doing we extend the study of topographic Rossby waves from the shallow water in Section 55.4.6 to the continuously stratified case. The resulting linearized potential vorticity equation and boundary conditions are

$$\partial_t q' = 0 \Longrightarrow \partial_t[\nabla_\mathsf{h}^2\psi' + f_0^2\,\partial_z(N^{-2}\,\partial_z\psi')] = 0 \tag{62.53a}$$

$$\partial_{tz}\psi' = 0 \quad \text{at } z = \overline{\eta}. \tag{62.53b}$$

$$f_\circ\,\partial_{tz}\psi' + N^2\,\hat{\boldsymbol{z}}\cdot(\nabla\psi'\times\nabla\eta_\mathsf{b}) = 0 \quad \text{at } z = \overline{\eta_\mathsf{b}}. \tag{62.53c}$$

To study plane waves in the horizontal, assume the special case of a gentle and constant linear slope, $\partial_y\eta_\mathsf{b}$, in the meridional direction so that

$$\eta_\mathsf{b} = \eta_\text{const} + y\,\partial_y\eta_\mathsf{b} \quad \text{with } |\partial_y\eta_\mathsf{b}| \ll 1, \tag{62.54}$$

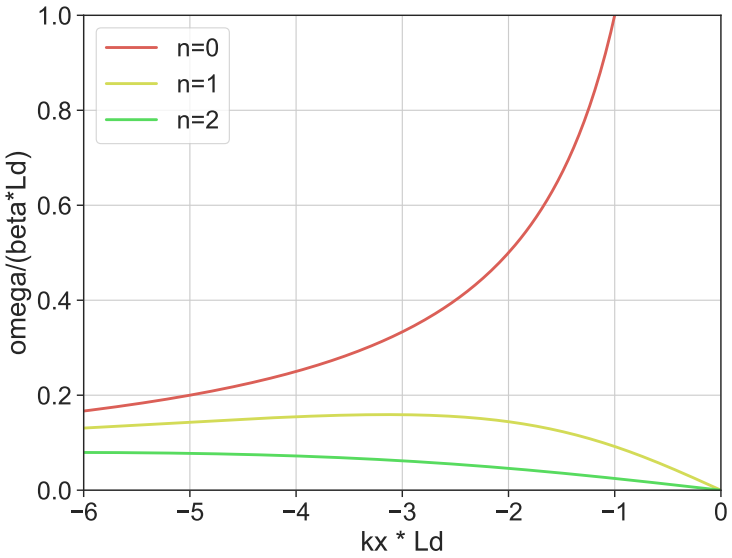

FIGURE 62.2: Dispersion relation for planetary Rossby waves according to equation (62.50), $\omega/(\beta\, L_\mathrm{d}) = -k_x\, L_\mathrm{d}/[(n\,\pi)^2 + (k_x\, L_\mathrm{d})^2 + (k_y\, L_\mathrm{d})^2]$, showing the $n = 0$ barotropic mode and $n = 1, 2$ baroclinic modes, each with $k_y = 0$. A positive angular frequency is realized with $k_x < 0$, so that the phase propagates to the west. The frequency for the barotropic mode is unbounded approaching the origin, so that long barotropic Rossby waves are high frequency waves. Both the barotropic and baroclinic wave modes have a vanishing frequency as the waves become shorter ($|\boldsymbol{k}| \to \infty$).

in which case the bottom boundary condition (62.53c) becomes

$$f_\circ\, \partial_{tz}\psi' + N^2\, \partial_y \eta_\mathrm{b}\, \partial_x \psi' = 0 \quad \text{at } z = \overline{\eta_\mathrm{b}}. \tag{62.55}$$

62.5.1 Eigenvalue problem for $\widetilde{\psi}$

Taking the linear bottom slope (62.54) allows us to consider the same wave ansatz (62.37) as used for planetary Rossby waves in Section 62.4.1, which then converts equations (62.53a), (62.53b), and (62.55) into the eigenvalue problem

$$\omega \frac{\mathrm{d}}{\mathrm{d}z}\left[\frac{f_\circ^2}{N^2}\frac{\mathrm{d}\widetilde{\psi}}{\mathrm{d}z}\right] = \omega\, |\boldsymbol{k}|^2\, \widetilde{\psi} \qquad \overline{\eta_\mathrm{b}} < z < \overline{\eta} \tag{62.56a}$$

$$\omega \frac{\mathrm{d}\widetilde{\psi}}{\mathrm{d}z} = 0 \qquad \text{at } z = \overline{\eta}, \tag{62.56b}$$

$$f_\circ\, \omega \frac{\mathrm{d}\widetilde{\psi}}{\mathrm{d}z} = N^2\, \partial_y \eta_\mathrm{b}\, k_x\, \widetilde{\psi} \quad \text{at } z = \overline{\eta_\mathrm{b}}. \tag{62.56c}$$

The differential equation (62.56a) and surface boundary condition (62.56b) can be satisfied with a zero frequency wave, $\omega = 0$, in which case there is no propagating wave. However, the bottom boundary condition (62.56c) cannot be satisfied with $\omega = 0$ in the presence of a nonzero bottom slope and nonzero Coriolis frequency. Evidently, the Coriolis frequency plays a fundamental role in supporting a propagating topographic Rossby waves in the presence of a sloping bottom.

Cancelling the angular frequency in equation (62.56a) (since $\omega \neq 0$ for topographic waves), then multiplying by $\widetilde{\psi}^*$ and integrating over the depth of the domain leads to

$$\int_{\overline{\eta_\mathrm{b}}}^{\overline{\eta}} \frac{\mathrm{d}}{\mathrm{d}z}\left[\widetilde{\psi}^*\, \frac{f_\circ^2}{N^2}\frac{\mathrm{d}\widetilde{\psi}}{\mathrm{d}z}\right] \mathrm{d}z = \int_{\overline{\eta_\mathrm{b}}}^{\overline{\eta}} \left[|\boldsymbol{k}|^2\, |\widetilde{\psi}|^2 + \frac{f_\circ^2}{N^2}\left|\frac{\mathrm{d}\widetilde{\psi}}{\mathrm{d}z}\right|^2\right] \mathrm{d}z. \tag{62.57}$$

Use of the surface boundary condition (62.56b) and bottom boundary condition (62.56c) render

$$f_o \, \partial_y \eta_b \, k_x = -\frac{\omega}{|\widetilde{\psi}(\overline{\eta_b})|^2} \int_{\overline{\eta_b}}^{\overline{\eta}} \left[|\boldsymbol{k}|^2 \, |\widetilde{\psi}|^2 + \frac{f_o^2}{N^2} \left| \frac{d\widetilde{\psi}}{dz} \right|^2 \right] dz. \tag{62.58}$$

The right hand side is a negative number (recall $\omega > 0$), which then orients the zonal component to the phase velocity according to the sign of $f_o \, \partial_y \eta_b$. For example, in the northern hemisphere with a bottom slope rising to the north, so that $f_o \, \partial_y \eta_b > 0$, then $k_x < 0$, which means that the zonal phase velocity is to the west. Likewise, for the southern hemisphere, a bottom slope that is rising to the south has $f_o \, \partial_y \eta_b > 0$, which also yields $k_x < 0$.

62.5.2 Topographic Rossby waves with constant N^2

Following our approach for planetary Rossby waves in Section 62.4.3, assume the buoyancy frequency is constant so that the eigenvalue problem (62.56a)-(62.56c) reduces to

$$\frac{d^2\widetilde{\psi}}{dz^2} = k_R^2 \, \widetilde{\psi} \qquad \overline{\eta_b} < z < \overline{\eta} \tag{62.59a}$$

$$f_o \, \omega \, \frac{d\widetilde{\psi}}{dz} = N^2 \, \partial_y \eta_b \, k_x \, \widetilde{\psi} \quad \text{at } z = \overline{\eta_b} \tag{62.59b}$$

$$\omega \, \frac{d\widetilde{\psi}}{dz} = 0 \qquad \text{at } z = \overline{\eta}, \tag{62.59c}$$

where we introduced the inverse *Rossby height*

$$k_R = |\boldsymbol{k}| \, N / f_o = |\boldsymbol{k}| \, L_d / H \quad \text{with } L_d = N \, H / f_o. \tag{62.60}$$

As we see below, k_R^{-1} defines an exponential scale height over which the wave decays moving away from the bottom boundary.

Bottom trapped streamfunction

To further simplify the analysis, assume the upper boundary, at $z = \overline{\eta}$, is far enough away that it can be ignored. In this case the streamfunction takes on the bottom trapped form

$$\widetilde{\psi} = \widetilde{\psi}_o \, e^{-k_R \, (z - \overline{\eta_b})}. \tag{62.61}$$

To determine what is "far enough away", evaluate the streamfunction at $z = \overline{\eta}$, whereby

$$\widetilde{\psi}(z = \overline{\eta}) = \widetilde{\psi}_o \, e^{-k_R \, H} = \widetilde{\psi}_o \, e^{-|\boldsymbol{k}| \, L_d}. \tag{62.62}$$

This streamfunction is exponentially small for wavenumbers satisfying

$$|\boldsymbol{k}| \gg L_d^{-1}. \tag{62.63}$$

That is, the topographic Rossby waves do not feel the upper boundary if their horizontal wavelength is small compared to the deformation radius

$$\Lambda \ll 2\pi \, L_d. \tag{62.64}$$

Dispersion relation

Inserting the streamfunction (62.61) into the bottom boundary condition (62.59b) leads to the dispersion relation

$$\omega = -N\, \partial_y \eta_{\mathsf{b}}\, k_x / |\boldsymbol{k}|. \tag{62.65}$$

Since the angular frequency is positive, the wave vector is constrained so that $\partial_y \eta_{\mathsf{b}}\, k_x < 0$. That is, if the bottom slope is rising to the north ($\partial_y \eta_{\mathsf{b}} > 0$) then the phase velocity has a westward component ($k_x < 0$), whereas a slope rising to the south ($\partial_y \eta_{\mathsf{b}} < 0$) has an eastward phase velocity ($k_x > 0$). We can also see this orientation by looking at the zonal component to the phase velocity

$$\boldsymbol{c}_{\mathsf{p}} \cdot \hat{\boldsymbol{x}} = (\omega/|\boldsymbol{k}|^2)\, k_x = -N\, \partial_y \eta_{\mathsf{b}}\, k_x^2 / |\boldsymbol{k}|^3, \tag{62.66}$$

with the sign of $\partial_y \eta_{\mathsf{b}}$ determining the orientation of the zonal phase velocity.

Evidently, the topographic slope acts as a background potential vorticity gradient just like planetary beta. To further this correspondence, define *topographic beta*

$$\beta_{\text{topo}} = f_{\mathsf{o}}\, \partial_y \eta_{\mathsf{b}} / H, \tag{62.67}$$

so that the dispersion relation (62.65) takes on the form

$$\omega = -\frac{\beta_{\text{topo}}\, k_x\, L_{\mathsf{d}}}{|\boldsymbol{k}|}, \tag{62.68}$$

which shares features with the planetary Rossby wave from Section 62.4.1. However, in contrast to planetary beta, the topographic beta can be either sign.

62.6 Non-interacting Eady waves

The geometric expression for the bottom boundary condition (62.33) suggests that sloping buoyancy surfaces support waves in a manner akin to sloping bottom topography. Whereas a sloping bottom in the presence of flat buoyancy surfaces supports topographic Rossby waves, a sloping buoyancy surface in the presence of a flat bottom or rigid lid top supports *Eady waves*. More precisely, a nonzero gradient of boundary buoyancy supports Eady edge waves.

62.6.1 Assumptions for Eady waves

We make the following assumptions to support an analytic derivation of the dispersion relation for Eady waves.

- Disable planetary Rossby waves by setting $\beta = 0$.
- Disable topographic Rossby waves by setting $\nabla \eta_{\mathsf{b}} = 0$.
- The flow occurs between a flat bottom at $z = \overline{\eta_{\mathsf{b}}} = 0$ and flat top at $z = \overline{\eta} = H$.
- A linear thermal wind front is supported by the buoyancy in equation (62.10), in which N^2, $\partial_y b_{\mathsf{b}}$, and $\partial_z u_{\mathsf{b}}$ are constants, thus implying that the buoyancy slope, $(\mathrm{d}z/\mathrm{d}y)_{b_{\mathsf{b}}}$, is also a constant;
- The background zonal geostrophic flow is a linear function of vertical position so that

$$u_{\mathsf{b}} = u_{\mathsf{b}}(z) = U_0 + \partial_z u_{\mathsf{b}}\, (z - \overline{\eta_{\mathsf{b}}}), \tag{62.69}$$

  where

$$\partial_z u_{\mathsf{b}} = \text{constant}. \tag{62.70}$$

In turn, the corresponding geostrophic streamfunction is

$$\Psi_\mathsf{b} = -y\,[U_0 + \partial_z u_\mathsf{b}\,(z - \overline{\eta_\mathsf{b}})]. \tag{62.71}$$

- With these assumptions the background potential vorticity (62.14) is a constant throughout the fluid interior

$$q_\mathsf{b} = f_\circ \Longrightarrow \nabla q_\mathsf{b} = 0, \tag{62.72}$$

and thus it plays no dynamical role.

Each of the above assumptions is rather restrictive. Indeed, the use of a top boundary is not very relevant to the atmosphere. However, these assumptions offer a streamlined means to analytically reveal the core physics of Eady waves, and in turn the interaction of such waves to produce baroclinic instability (Section 62.7). It is for this reason that the Eady model has proven so compelling pedagogically.

62.6.2 Streamfunction equation

The linearized potential vorticity equation (62.25) and corresponding boundary conditions (62.29) and (62.33) take on the form

$$[\partial_t + u_\mathsf{b}(z)\,\partial_x]\,q' = 0 \qquad \overline{\eta_\mathsf{b}} < z < \overline{\eta} \tag{62.73a}$$

$$[\partial_t + u_\mathsf{b}(\overline{\eta})\,\partial_x]\,\partial_z\psi' = \partial_x\psi'\,\partial_z u_\mathsf{b} \quad z = \overline{\eta} \tag{62.73b}$$

$$(\partial_t + u_\mathsf{b}(\overline{\eta_\mathsf{b}})\,\partial_x)\,\partial_z\psi' = \partial_x\psi'\,\partial_z u_\mathsf{b} \quad z = \overline{\eta_\mathsf{b}}, \tag{62.73c}$$

with the bottom boundary condition resulting from the meridional gradient of the background buoyancy, or equivalently the zonal thermal wind shear

$$N^2\,(\mathrm{d}z/\mathrm{d}y)_{b_\mathsf{b}} = -\partial_y b_\mathsf{b} = f_\circ\,\partial_z u_\mathsf{b}. \tag{62.74}$$

The simplifying assumptions from Section 62.6.1 have led to a linear boundary value problem in which the only spatial dependence is in the vertical. Hence, we can consider the familiar wave ansatz (62.37) for the streamfunction, in which fluctuations are organized into horizontally propagating free plane waves that are modulated by a vertically dependent amplitude function

$$\psi'(x, y, z, t) = \widetilde{\psi}(z)\,\mathrm{e}^{\mathrm{i}\,(k_x\,x + k_y\,y - \omega\,t)}. \tag{62.75}$$

With this ansatz we find the fluctuating potential vorticity (62.21) is given by

$$q' = (f_\circ/N)^2\,(\partial_{zz} - k_\mathsf{R}^2)\,\psi', \tag{62.76}$$

and the linear potential vorticity equation (62.73a) is

$$(-\omega + u_\mathsf{b}\,k_x)\,(\partial_{zz} - k_\mathsf{R}^2)\,\widetilde{\psi} = 0, \tag{62.77}$$

where

$$k_\mathsf{R} = |\boldsymbol{k}|\,N/f_\circ = |\boldsymbol{k}|\,L_\mathsf{d}/H \tag{62.78}$$

is the inverse Rossby height originally introduced for topographic waves in equation (62.60).

Throughout the analysis we assume the angular frequency satisfies

$$\omega \neq u_\mathsf{b}\,k_x, \tag{62.79}$$

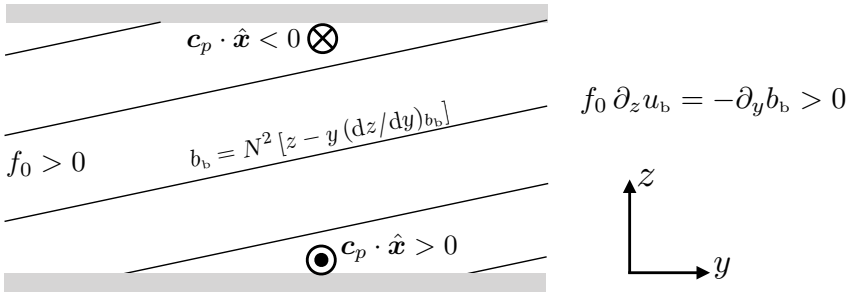

FIGURE 62.3: Depicting the orientation for the intrinsic phase velocity of Eady edge waves for a northern hemisphere thermal wind balanced base state with buoyancy decreasing northward. Relative to the local background flow, the upper boundary has westward propagating Eady waves whereas the Eady waves are eastward at the lower boundary (see Section 62.6.5).

which then means that the streamfunction equation (62.77) reduces to

$$\frac{\mathrm{d}^2 \widetilde{\psi}}{\mathrm{d}z^2} = k_\mathsf{R}^2 \, \widetilde{\psi}, \tag{62.80}$$

which is the same equation as satisfied by the topographic Rossby wave (62.59a). As seen below, the angular frequency assumption (62.79) indeed holds for Eady waves.

62.6.3 Bottom trapped Eady waves

As in our discussion of topographic Rossby waves in Section 62.5, assume here that the upper boundary is far from the lower boundary, with "far" determined by a horizontal wavenumber satisfying equation (62.63), i.e.,

$$|\boldsymbol{k}| \gg L_\mathsf{d}^{-1}. \tag{62.81}$$

In this case, the bottom trapped streamfunction solution to equation (62.80) is given by

$$\widetilde{\psi} = \widetilde{\psi}_\mathrm{bot} \, \mathrm{e}^{-k_\mathsf{R} \, (z - \overline{\eta_\mathsf{b}})}, \tag{62.82}$$

which is, as expected, the same as for the topographic Rossby wave (62.61). Even though they have the same form for their streamfunctions, the Eady wave dispersion relation differs from that of the topographic Rossby wave. Here, we derive the dispersion relation through use of the bottom boundary condition (62.73c), which takes the form

$$(-\omega + u_\mathsf{b}(\overline{\eta_\mathsf{b}}) \, k_x)(-k_\mathsf{R}) = k_x \, \partial_z u_\mathsf{b}, \tag{62.83}$$

thus leading to the dispersion relation

$$\omega_\mathrm{bot} = k_x \, u_\mathsf{b}(\overline{\eta_\mathsf{b}}) + (k_x / k_\mathsf{R}) \, \partial_z u_\mathsf{b}. \tag{62.84}$$

The vertical shear portion of the right hand side can be written in the following equivalent forms (again, each evaluated at $z = \overline{\eta_\mathsf{b}}$)

$$\frac{f_\circ \, \partial_z u_\mathsf{b}}{N} = \frac{H}{L_\mathsf{d}} \frac{\partial u_\mathsf{b}}{\partial z} = -N^{-1} \, \partial_y b_\mathsf{b} = N \, (\mathrm{d}z/\mathrm{d}y)_{b_\mathsf{b}}, \tag{62.85}$$

where the final equality introduced the meridional buoyancy slope (62.12). We are thus led to the dispersion relation for the bottom trapped edge waves

$$\omega_{\rm bot} = k_x \left[u_{\rm b} + k_{\rm R}^{-1} \, \partial_z u_{\rm b} \right]_{z=\overline{\eta_{\rm b}}} = k_x \left[u_{\rm b} + \frac{N}{|\boldsymbol{k}|} \left(\frac{{\rm d}z}{{\rm d}y} \right)_{b_{\rm b}} \right]_{z=\overline{\eta_{\rm b}}} . \tag{62.86}$$

The $k_x \, u_{\rm b}(\overline{\eta_{\rm b}})$ term provides a Doppler shifted frequency due to motion of the background zonal flow at the bottom. The next term arises from thermal wind shear in the presence of rotation and stratification, with the zonal thermal wind shear reliant on the meridionally sloped buoyancy surfaces that intersect the bottom.

62.6.4 Upper surface trapped Eady waves

Proceeding just like for the bottom, we now focus on the upper (top) boundary and assume the bottom boundary is far away. In this case the upper surface trapped streamfunction is given by

$$\widetilde{\psi} = \psi_{\rm top} \, {\rm e}^{k_{\rm R} \, (z - \overline{\eta})}, \tag{62.87}$$

which, when used in the upper boundary condition (62.29), leads to the dispersion relation

$$\omega_{\rm top} - k_x \, u_{\rm b}(\overline{\eta}) = -(k_x / k_{\rm R}) \, \partial_z u_{\rm b}. \tag{62.88}$$

This relation can be written just like equation (62.86) for the bottom boundary condition, only with a swapped sign on the buoyancy slope term

$$\omega_{\rm top} = k_x \left[u_{\rm b} - k_{\rm R}^{-1} \, \partial_z u_{\rm b} \right]_{z=\overline{\eta}} = k_x \left[u_{\rm b} - \frac{N}{|\boldsymbol{k}|} \left(\frac{{\rm d}z}{{\rm d}y} \right)_{b_{\rm b}} \right]_{z=\overline{\eta}} . \tag{62.89}$$

As for the bottom trapped Eady waves, the term $k_x \, u_{\rm b}(\overline{\eta})$ is a Doppler shift in the frequency arising from the zonal velocity at the upper boundary that couples to the zonal component of the phase velocity. The other term arises from the thermal wind shear coupled to rotation and stratification, which itself relies on the slope of the buoyancy surfaces that intersect the upper boundary.

62.6.5 Comparing the top and bottom dispersion relations

It is useful to compare the dispersion relations (62.86) and (62.89), rewritten here as the $\hat{\boldsymbol{x}}$ component of the phase velocity

$$\boldsymbol{c}_{\rm p} \cdot \hat{\boldsymbol{x}} = (\omega / |\boldsymbol{k}|^2) \, k_x, \tag{62.90}$$

which are given by

$$(\boldsymbol{c}_{\rm p} \cdot \hat{\boldsymbol{x}})_{\rm bot} = \frac{k_x^2}{|\boldsymbol{k}|^2} \left[u_{\rm b} + \frac{H \, \partial_z u_{\rm b}}{L_{\rm d} \, |\boldsymbol{k}|} \right]_{z=\overline{\eta_{\rm b}}} = \frac{k_x^2}{|\boldsymbol{k}|^2} \left[u_{\rm b} + \frac{N}{|\boldsymbol{k}|} \left(\frac{{\rm d}z}{{\rm d}y} \right)_{b_{\rm b}} \right]_{z=\overline{\eta_{\rm b}}} \tag{62.91a}$$

$$(\boldsymbol{c}_{\rm p} \cdot \hat{\boldsymbol{x}})_{\rm top} = \frac{k_x^2}{|\boldsymbol{k}|^2} \left[u_{\rm b} - \frac{H \, \partial_z u_{\rm b}}{L_{\rm d} \, |\boldsymbol{k}|} \right]_{z=\overline{\eta}} = \frac{k_x^2}{|\boldsymbol{k}|^2} \left[u_{\rm b} - \frac{N}{|\boldsymbol{k}|} \left(\frac{{\rm d}z}{{\rm d}y} \right)_{b_{\rm b}} \right]_{z=\overline{\eta}} . \tag{62.91b}$$

The first difference between these expressions arises from the differences in the background zonal flow at $z = \overline{\eta_{\rm b}}$ versus $z = \overline{\eta}$. Assuming $\partial_z u_{\rm b} > 0$, the background flow at the top has a larger eastward value than the background flow at the bottom, as given by

$$u_{\rm b}(\overline{\eta}) = u_{\rm b}(\overline{\eta_{\rm b}}) + (\overline{\eta} - \overline{\eta_{\rm b}}) \, \partial_z u_{\rm b} = u_{\rm b}(\overline{\eta_{\rm b}}) + H \, \partial_z u_{\rm b}. \tag{62.92}$$

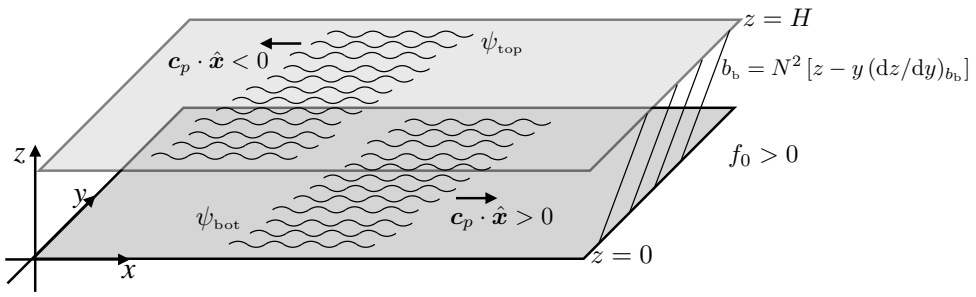

FIGURE 62.4: A perspective view of the intrinsic phase velocity of Eady edge waves for a northern hemisphere thermal wind balanced base state with buoyancy increasing northward. The upper boundary has westward propagating Eady waves whereas the Eady waves are eastward at the lower boundary. The top and bottom boundaries are flat, and so we write $z = \overline{\eta} = H$ for the upper boundary and $z = \overline{\eta_{\rm b}} = 0$ for the lower boundary.

The second difference between the bottom dispersion relation (62.91a) and top dispersion relation (62.91b) arises from the swapped signs for the buoyancy slope term. This term represents the *intrinsic frequency* for the two edge waves (i.e., the frequency seen by an observer moving with the background flow)

$$\omega^{\rm intrinsic}_{\rm bot} = \frac{N\,k_x^{\rm bot}}{|\boldsymbol{k}|}\left(\frac{{\rm d}z}{{\rm d}y}\right)_{b_{\rm b}} \quad \text{and} \quad \omega^{\rm intrinsic}_{\rm top} = -\frac{N\,k_x^{\rm top}}{|\boldsymbol{k}|}\left(\frac{{\rm d}z}{{\rm d}y}\right)_{b_{\rm b}}. \tag{62.93}$$

For surfaces of constant buoyancy that slope upward to the north, $({\rm d}z/{\rm d}y)_{b_{\rm b}} > 0$, the intrinsic frequency for the bottom wave is positive if the phase velocity is eastward relative to the background flow ($k_x^{\rm bot} > 0$), whereas a positive frequency for the top wave requires a westward phase velocity ($k_x^{\rm top} < 0$). We also see this orientation by writing the intrinsic components to the zonal phase velocities

$$(\boldsymbol{c}_{\rm p} \cdot \hat{\boldsymbol{x}})^{\rm intrinsic}_{\rm bot} = \frac{N\,k_x^2}{|\boldsymbol{k}|^2}\left(\frac{{\rm d}z}{{\rm d}y}\right)_{b_{\rm b}} > 0 \quad \text{and} \quad (\boldsymbol{c}_{\rm p} \cdot \hat{\boldsymbol{x}})^{\rm intrinsic}_{\rm top} = -\frac{N\,k_x^2}{|\boldsymbol{k}|^2}\left(\frac{{\rm d}z}{{\rm d}y}\right)_{b_{\rm b}} < 0. \tag{62.94}$$

The zonal component to the phase velocity in equations (62.91a) and (62.91b) are equal for that wavevector whose magnitude satisfies

$$L_{\rm d}\,|\boldsymbol{k}| = 2, \tag{62.95}$$

in which case

$$(\boldsymbol{c}_{\rm p} \cdot \hat{\boldsymbol{x}})_{\rm top} = (k_x^2/|\boldsymbol{k}|^2)\,[u_{\rm b}(\overline{\eta}) - (H/2)\,\partial_z u_{\rm b}] = (k_x^2/|\boldsymbol{k}|^2)\,[u_{\rm b}(\overline{\eta_{\rm b}}) + (H/2)\,\partial_z u_{\rm b}] = (\boldsymbol{c}_{\rm p} \cdot \hat{\boldsymbol{x}})_{\rm bot}. \tag{62.96}$$

Evidently, waves with $L_{\rm d}\,|\boldsymbol{k}| = 2$ have the opportunity to phase lock and thus to interact. This possibility motivates the work in Section 62.7 whereby we include interactions in the formulation.

62.6.6 Meridional and vertical motion within an Eady wave

To help understand fluid particle motion in a stable Eady wave, we compute the meridional velocity, v', and vertical velocity, w', for a wave moving along the bottom boundary, with a similar calculation holding along the top. Recall that since the flow is quasi-geostrophic that the vertical velocity is much smaller than the horizontal. Even so, it is nonzero and we can compute it for the Eady wave, thus revealing motion in the meridional-depth plane. For this calculation we use the streamfunction for a bottom trapped Eady wave

$$\psi'(x, y, z, t) = \widetilde{\psi}_{\rm o}\, {\rm e}^{-k_{\rm R}\,(z - \overline{\eta_{\rm b}})}\, {\rm e}^{{\rm i}\,(\boldsymbol{k}\cdot\boldsymbol{x} - \omega_{\rm bot}\,t)}, \tag{62.97}$$

with ω_{bot} given by the dispersion relation (62.86).

The meridional velocity of fluid particles within the bottom Eady wave is given by

$$v' = \partial_x \psi' = \mathrm{i}\, k_x\, \widetilde{\psi}_{\mathsf{o}}\, \mathrm{e}^{-k_{\mathsf{R}}\,(z-\overline{\eta_{\mathsf{b}}})}\, \mathrm{e}^{\mathrm{i}\,(\boldsymbol{k}\cdot\boldsymbol{x}-\omega_{\text{bot}}\,t)}, \tag{62.98}$$

whose real part is

$$v' = -k_x\, \widetilde{\psi}_{\mathsf{o}}\, \mathrm{e}^{-k_{\mathsf{R}}\,(z-\overline{\eta_{\mathsf{b}}})} \sin(\boldsymbol{k}\cdot\boldsymbol{x} - \omega_{\text{bot}}\,t). \tag{62.99}$$

A similar calculation leads to the zonal velocity within the wave

$$u' = k_y\, \widetilde{\psi}_{\mathsf{o}}\, \mathrm{e}^{-k_{\mathsf{R}}\,(z-\overline{\eta_{\mathsf{b}}})} \sin(\boldsymbol{k}\cdot\boldsymbol{x} - \omega_{\text{bot}}\,t). \tag{62.100}$$

Calculating the vertical velocity takes a bit more work, for which we make use of the linearized buoyancy equation (62.26) so that

$$w'\, N^2 = -(\partial_t + u_{\mathsf{b}}\,\partial_x) b' - v'\,\partial_y b_{\mathsf{b}}. \tag{62.101}$$

The first term is given by

$$-(\partial_t + u_{\mathsf{b}}\,\partial_x) b' = \mathrm{i}\, k_{\mathsf{R}}\, f_{\mathsf{o}}\, (-\omega_{\text{bot}} + k_x\, u_{\mathsf{b}})\, \psi', \tag{62.102}$$

whose real part is

$$-(\partial_t + u_{\mathsf{b}}\,\partial_x) b' = k_{\mathsf{R}}\, f_{\mathsf{o}}\, (\omega_{\text{bot}} - k_x\, u_{\mathsf{b}})\, \widetilde{\psi}_{\mathsf{o}}\, \mathrm{e}^{-k_{\mathsf{R}}\,(z-\overline{\eta_{\mathsf{b}}})} \sin(\boldsymbol{k}\cdot\boldsymbol{x} - \omega_{\text{bot}}\,t), \tag{62.103}$$

and the meridional velocity term is

$$-v'\,\partial_y b_{\mathsf{b}} = k_x\,\partial_y b_{\mathsf{b}}\, \widetilde{\psi}_{\mathsf{o}}\, \mathrm{e}^{-k_{\mathsf{R}}\,(z-\overline{\eta_{\mathsf{b}}})} \sin(\boldsymbol{k}\cdot\boldsymbol{x} - \omega_{\text{bot}}\,t), \tag{62.104}$$

so that

$$w'\, N^2 = \widetilde{\psi}_{\mathsf{o}}\, \mathrm{e}^{-k_{\mathsf{R}}\,(z-\overline{\eta_{\mathsf{b}}})} \sin(\boldsymbol{k}\cdot\boldsymbol{x} - \omega_{\text{bot}}\,t)[k_x\,\partial_y b_{\mathsf{b}} + k_{\mathsf{R}}\, f_{\mathsf{o}}\, (\omega_{\text{bot}} - k_x\, u_{\mathsf{b}})]. \tag{62.105}$$

Making use of the dispersion relation (62.86) for the bottom trapped Eady edge waves leads to

$$\begin{aligned} k_x\,\partial_y b_{\mathsf{b}} + k_{\mathsf{R}}\, f_{\mathsf{o}}\, (\omega_{\text{bot}} - k_x\, u_{\mathsf{b}}) &= k_x\,\partial_y b_{\mathsf{b}} + k_{\mathsf{R}}\, f_{\mathsf{o}}\, k_x\, (k_{\mathsf{R}}^{-1} - z)\,\partial_z u_{\mathsf{b}} && \text{(62.106a)} \\ &= k_{\mathsf{R}}\, k_x\, z\,\partial_y b_{\mathsf{b}}, && \text{(62.106b)} \end{aligned}$$

so that the vertical velocity component is

$$w' = -k_{\mathsf{R}}\, k_x\, z\, (\mathrm{d}z/\mathrm{d}y)_{b_{\mathsf{b}}}\, \widetilde{\psi}_{\mathsf{o}}\, \mathrm{e}^{-k_{\mathsf{R}}\,(z-\overline{\eta_{\mathsf{b}}})} \sin(\boldsymbol{k}\cdot\boldsymbol{x} - \omega_{\text{bot}}\,t) \tag{62.107}$$

and its ratio with the meridional velocity is

$$w'/v' = z\, k_{\mathsf{R}}\, (\mathrm{d}z/\mathrm{d}y)_{b_{\mathsf{b}}} = z\, |\boldsymbol{k}|\, (N/f_{\mathsf{o}})\, (\mathrm{d}z/\mathrm{d}y)_{b_{\mathsf{b}}}. \tag{62.108}$$

For vertical positions less than the Rossby height, k_{R}^{-1}, the fluid particle motion is more horizontal than the buoyancy slope, whereas the motion is more vertical than the slope for positions higher than k_{R}^{-1}. Also note that the amplitude of the motion exponentially decays moving away from the bottom boundary with an efolding height k_{R}^{-1} Figure 62.5 provides a schematic of this motion.

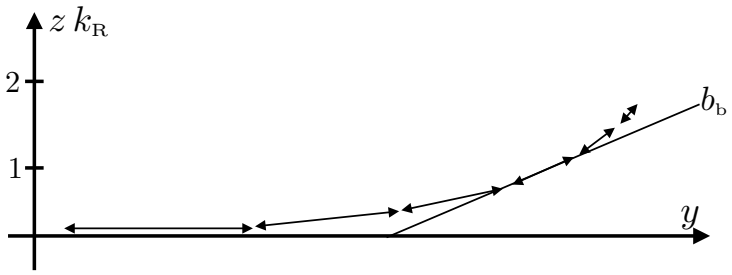

FIGURE 62.5: A meridional-vertical view of fluid particle velocity within a stable bottom trapped Eady wave, as given by equation (62.108). The particle velocity is parallel to the bottom when at $z = \overline{\eta_{\mathrm{b}}} = 0$, and parallel to the buoyancy surface at vertical position $z\,k_{\mathrm{R}} = 1$, and further steepens when moving higher in the column. The amplitude of the oscillatory motion exponentially decays away from the bottom with an e-folding scale given by the Rossby height, k_{R}^{-1}. This figure is adapted from Figure 13.1(e) in *Gill* (1982).

62.6.7 Further study

The treatment in this section is compatible with Section 13.2 of *Gill* (1982), Chapter 19 of *Pedlosky* (2003) and Section 8.7 of *Smyth and Carpenter* (2019).

62.7 Interacting Eady waves and baroclinic instability

The analysis from Section 62.6 revealed the presence of Eady edge waves that are exponentially trapped next to the rigid top and bottom boundaries, with the wave supported by the thermal wind shear intersecting the boundaries. Furthermore, the zonal component to the phase velocity of the two waves is equal (equation (62.6.5)) for a horizontal wavenumber

$$\omega_{\mathrm{top}} = \omega_{\mathrm{bot}} \implies |\boldsymbol{k}| = 2\,L_{\mathrm{d}}^{-1}. \tag{62.109}$$

For this wave, and for longer waves (smaller wavenumbers), we cannot ignore wave interactions. Under specific circumstances detailed in this section, the waves constructively interact to support mutual exponential growth, thus signaling *baroclinic instability*. The treatment is directly analogous to our study in Section 61.6 of interacting vortex edge waves in a horizontally sheared fluid.

62.7.1 Streamfunction solution

As before, we take the streamfunction ansatz (62.75), which builds in an assumption that the Eady waves at the two boundaries move with the same phase velocity to thus allow them to interact. We are thus led to the differential equation (62.80) and boundary conditions (62.73c) and (62.83)

$$\mathrm{d}^2\widetilde{\psi}/\mathrm{d}z^2 = k_{\mathrm{R}}^2\,\widetilde{\psi} \qquad 0 < z < H \tag{62.110a}$$

$$[-\omega + u_{\mathrm{b}}(H)\,k_x]\,\partial_z\widetilde{\psi} = k_x\,\partial_z u_{\mathrm{b}}\,\widetilde{\psi} \qquad z = H \tag{62.110b}$$

$$[-\omega + u_{\mathrm{b}}(0)\,k_x]\,\partial_z\widetilde{\psi} = k_x\,\partial_z u_{\mathrm{b}}\,\widetilde{\psi} \qquad z = 0, \tag{62.110c}$$

where we made use of the inverse Rossby height (62.60)

$$k_{\mathrm{R}} = |\boldsymbol{k}|\,N/f_{\mathrm{o}} = |\boldsymbol{k}|\,L_{\mathrm{d}}/H \quad \text{with } L_{\mathrm{d}} = N\,H/f_{\mathrm{o}}. \tag{62.111}$$

Additionally, we set

$$\overline{\eta} = H \quad \text{and} \quad \overline{\eta_{\mathrm{b}}} = 0, \tag{62.112}$$

to help reduce notational clutter (see Figure 62.4).

Solution to the boundary value problem

The solution to the differential equation (62.110a) is given by the hyperbolic functions

$$\widetilde{\psi} = C_1 \cosh(k_\mathsf{R}\, z) + C_2 \sinh(k_\mathsf{R}\, z), \tag{62.113}$$

where the coefficients C_1 and C_2, are specified from the boundary conditions. Making use of the upper surface boundary condition (62.110b) and bottom boundary condition (62.110c) leads to the coupled linear equations

$$(-\tilde{c} + H\,\partial_z u_\mathsf{b})\, k_\mathsf{R}\, [C_1 \sinh(k_\mathsf{R}\, H) + C_2 \cosh(k_\mathsf{R}\, H)] = \partial_z u_\mathsf{b}\, [C_1 \cosh(k_\mathsf{R}\, H) + C_2 \sinh(k_\mathsf{R}\, H)] \tag{62.114a}$$

$$-\tilde{c}\, k_\mathsf{R}\, C_2 = C_1\, \partial_z u_\mathsf{b}, \tag{62.114b}$$

where we introduced the shorthand

$$\tilde{c} \equiv \omega/k_x - u_\mathsf{b}(0), \tag{62.115}$$

and noted that the constant thermal wind shear means that

$$u_\mathsf{b}(H) = u_\mathsf{b}(0) + H\,\partial_z u_\mathsf{b}. \tag{62.116}$$

62.7.2 Dispersion relation

Equations (62.114a) and (62.114b) are two homogeneous linear equations for the two unknowns, C_1 and C_2. A nontrivial solution exists if the determinant of the 2×2 coefficient matrix vanishes. This condition leads to the quadratic equation for $\tilde{c}$

$$\tilde{c}^2 - \tilde{c}\, H\, \partial_z u_\mathsf{b} + (\partial_z u_\mathsf{b}/k_\mathsf{R})^2\, (H\, k_\mathsf{R} \coth(k_\mathsf{R}\, H) - 1) = 0, \tag{62.117}$$

which has two roots given by the quadratic formula

$$\tilde{c} = \frac{H\,\partial_z u_\mathsf{b}}{2} \pm \frac{\partial_z u_\mathsf{b}}{k_\mathsf{R}} \left[\frac{(k_\mathsf{R}\, H)^2}{4} - k_\mathsf{R}\, H \coth(k_\mathsf{R}\, H) + 1 \right]^{1/2}. \tag{62.118}$$

A further simplification arises from use of the identity

$$2 \coth x = \tanh(x/2) + \coth(x/2), \tag{62.119}$$

in which case we have the roots

$$\omega/k_x = u_\mathsf{b}(z=0) + \frac{H\,\partial_z u_\mathsf{b}}{2} \pm \frac{\partial_z u_\mathsf{b}}{k_\mathsf{R}} \left[\left(\frac{k_\mathsf{R}\, H}{2} - \coth(k_\mathsf{R}\, H/2) \right) \left(\frac{k_\mathsf{R}\, H}{2} - \tanh(k_\mathsf{R}\, H/2) \right) \right]^{1/2}. \tag{62.120}$$

Since

$$x \geq \tanh x, \tag{62.121}$$

the only way to realize a negative discriminant is for

$$k_\mathsf{R}\, H \leq 2 \coth(k_\mathsf{R}\, H/2). \tag{62.122}$$

A graphical solution to the equality finds the critical nondimensional wavenumber

$$k_{\mathsf{R}}\, H = |\boldsymbol{k}|\, L_{\mathsf{d}} \approx 2.399. \tag{62.123}$$

Longer waves that satisfy the inequality are baroclinically unstable

$$k_{\mathsf{R}}\, H = |\boldsymbol{k}|\, L_{\mathsf{d}} < 2.399 \Longrightarrow \text{unstable} \tag{62.124}$$

Note how $|\boldsymbol{k}|\, L_{\mathsf{d}} \approx 2.399$ is rather close to the $|\boldsymbol{k}|\, L_{\mathsf{d}} = 2$ value from equation (62.109), computed by setting the frequencies equal for two non-interacting Eady edge waves.

62.7.3 Growth rate

For unstable waves, the growth rate is given by the imaginary part of the angular frequency

$$\sigma = \frac{|k_x\, \partial_z u_{\mathsf{b}}|}{k_{\mathsf{R}}} \left[\left| \frac{k_{\mathsf{R}}\, H}{2} - \coth(k_{\mathsf{R}}\, H/2) \right| \left| \frac{k_{\mathsf{R}}\, H}{2} - \tanh(k_{\mathsf{R}}\, H/2) \right| \right]^{1/2}. \tag{62.125}$$

Due to the k_x factor in the front, we see that for any given horizontal wavenumber,

$$|\boldsymbol{k}| = \sqrt{k_x^2 + k_y^2}, \tag{62.126}$$

the growth rate is maximized for waves with a zonal phase velocity, in which case

$$|\boldsymbol{k}| = |k_x|. \tag{62.127}$$

That is, the most unstable waves whose phase velocity is aligned with the background flow[3]

$$\sigma(\boldsymbol{k} = \hat{\boldsymbol{x}}\, k_x) = \frac{H\, |\partial_z u_{\mathsf{b}}|}{L_{\mathsf{d}}} \left[\left| \frac{|\boldsymbol{k}|\, L_{\mathsf{d}}}{2} - \coth(|\boldsymbol{k}|\, L_{\mathsf{d}}/2) \right| \left(\frac{|\boldsymbol{k}|\, L_{\mathsf{d}}}{2} - \tanh(|\boldsymbol{k}|\, L_{\mathsf{d}}/2) \right) \right]^{1/2}. \tag{62.128}$$

Since the horizontal flow is non-divergent, Eady waves are horizontally transverse so that fluid particle movement is perpendicular to the phase velocity. With a zonal phase velocity, fluid particles move in the meridional direction.

Maximum growth rate

To determine the maximum growth rate we compute the wavenumber, $|\boldsymbol{k}| = |k_x|$, that satisfies

$$\frac{\mathrm{d}\sigma^2}{\mathrm{d}k_x} = 0, \tag{62.129}$$

which yields

$$|\boldsymbol{k}|_{\max} = |k_x|_{\max} \approx 1.6/L_{\mathsf{d}} \Longrightarrow \Lambda_{\max} \approx (2\pi/1.6)\, L_{\mathsf{d}} \approx 3.9\, L_{\mathsf{d}}. \tag{62.130}$$

Evidently, the fastest growing Eady waves are purely zonal and have wavelength about four times the deformation radius. It is this connection to the deformation radius that directly connects these unstable Eady waves to synoptic eddies in the atmosphere and mesoscale eddies in the ocean.

[3] This is a version of Squires theorem described at the start of Chapter 61.

Eady growth rate

The growth rate (62.128) is the product of an inverse time scale, T_{Eady}^{-1}, and a non-dimensional function, where the Eady time scale is given by

$$T_{\text{Eady}} = \frac{L_{\text{d}}}{H\,\partial_z u_{\text{b}}} = \frac{1}{f_{\circ}}\,\frac{N}{\partial_z u_{\text{b}}} = \frac{\sqrt{\text{Ri}}}{f_{\circ}} = [N\,|(\text{d}z/\text{d}y)_{b_{\text{b}}}|]^{-1}. \tag{62.131}$$

We here introduced the *balanced Richardson number* from Section 43.7.5

$$\text{Ri} = N^2/(\partial_z u_{\text{b}})^2 = f_{\circ}^2\,[N\,(\text{d}z/\text{d}y)_{b_{\text{b}}}]^{-2}. \tag{62.132}$$

For quasi-geostrophic flows, the balanced Richardson number is normally quite large. Evaluating the growth rate expression (62.128) with the fastest growing wave (62.130) renders

$$\sigma_{\max} = 0.31\,T_{\text{Eady}}^{-1} = 0.31\,|\partial_z u_{\text{b}}\,(f_{\circ}/N)| = 0.31\,\frac{|f_{\circ}|}{\sqrt{\text{Ri}}}. \tag{62.133}$$

This maximum growth rate is sometimes generically called *the Eady growth rate*. For a background state with $\text{Ri} = 100$ and $f_{\circ} = 10^{-4}$ s^{-1}, we find the growth rate of the most unstable Eady wave

$$\sigma_{\max} \approx (3.7 \text{ days})^{-1}, \tag{62.134}$$

which accords with the growth rate of middle latitude atmospheric cyclones. For the ocean, the Eady growth rate is roughly ten times slower than the atmosphere (e.g., see Figure 1 in *Treguier et al.* (1997)).

62.7.4 Further study

Our presentation of the Eady model is consistent with that found in *Pedlosky* (2003) and *Vallis* (2017). Although maths and pictures are revealing, it is also useful to observe laboratory rotating tank experiments to further ones understanding of the Eady model and baroclinic instability.

62.8 Necessary conditions for instability

In Section 61.5 we established the Rayleigh-Kuo inflection point theorem as well as Fjørtoft's theorem, each establishing necessary conditions for shear instability. Here we pursue a similar approach for baroclinic instability of a zonal background flow

$$u_{\text{b}} = u_{\text{b}}(y, z), \tag{62.135}$$

and maintain nonzero planetary β so that

$$f = f_{\circ} + \beta\, y. \tag{62.136}$$

The analysis of non-zonal flows greatly adds to the technical overhead, largely since the flow is no longer perpendicular to the planetary vorticity gradient. We thus restrict attention to zonal background flows.

As for the shear instability case, the necessary conditions for instability identifies cases whereby instabilities are possible. However, the integral conditions are not sufficient conditions. Hence, detailed calculations are required to determine if the flow is indeed unstable even if it satisfies the necessary conditions. Both the derivation of the necessary conditions, and their form, offer insights into the mechanics of baroclinic instability.

62.8.1 Summary of the governing linear equations

From Section 62.3.3, we have the governing linear equation (62.25) for the geostrophic streamfunction and the boundary conditions (62.29) and (62.33)

$$(\partial_t + u_\mathsf{b}\,\partial_x)\,[\nabla_\mathsf{h}^2\psi' + f_\circ^2\,\partial_z(N^{-2}\,\partial_z\psi')] = -\partial_x\psi'\,\partial_y q_\mathsf{b} \qquad \overline{\eta_\mathsf{b}} < z < \overline{\eta} \tag{62.137a}$$

$$(\partial_t + u_\mathsf{b}\,\partial_x)\,\partial_z\psi' = \partial_x\psi'\,\partial_z u_\mathsf{b} \qquad z = \overline{\eta} \tag{62.137b}$$

$$f_\circ\,(\partial_t + u_\mathsf{b}\,\partial_x)\,\partial_z\psi' = \partial_x\psi'\,N^2\,[(\mathrm{d}z/\mathrm{d}y)_{b_\mathsf{b}} - \partial_y\eta_\mathsf{b}] \qquad z = \overline{\eta_\mathsf{b}}, \tag{62.137c}$$

where the meridional derivative of the background potential vorticity is given by equation (62.14)

$$\partial_y q_\mathsf{b} = \partial_y[f_\circ + \beta\,y - \partial_y u_\mathsf{b} + f_\circ^2\,\partial_z(N^{-2}\,\partial_z\Psi_\mathsf{b})] = \beta - \partial_{yy}u_\mathsf{b} + f_\circ^2\,\partial_{yz}(N^{-2}\,\partial_z\Psi_\mathsf{b}). \tag{62.138}$$

The background flow is a function of (y,z), which means it only supports freely propagating plane waves in the zonal direction. We thus consider the following wave ansatz for the streamfunction

$$\psi'(x,y,z,t) = \widetilde{\psi}(y,z)\,\mathrm{e}^{\mathrm{i}\,(k_x\,x - \omega\,t)}. \tag{62.139}$$

Use of this ansatz in the boundary value problem (62.137a)-(62.137c) yields

$$(u_\mathsf{b} - c)\,[(\partial_{yy} - k_x^2)\,\widetilde{\psi} + f_\circ^2\,\partial_z(N^{-2}\,\partial_z\widetilde{\psi})] = -\widetilde{\psi}\,\partial_y q_\mathsf{b} \qquad \overline{\eta_\mathsf{b}} < z < \overline{\eta} \tag{62.140a}$$

$$(u_\mathsf{b} - c)\,\partial_z\widetilde{\psi} = \widetilde{\psi}\,\partial_z u_\mathsf{b} \qquad z = \overline{\eta} \tag{62.140b}$$

$$f_\circ\,(u_\mathsf{b} - c)\,\partial_z\widetilde{\psi} = N^2\,\widetilde{\psi}\,[(\mathrm{d}z/\mathrm{d}y)_{b_\mathsf{b}} - \partial_y\eta_\mathsf{b}] \qquad z = \overline{\eta_\mathsf{b}}, \tag{62.140c}$$

where the zonal phase velocity is written

$$\boldsymbol{c}_\mathsf{p} = (\omega/|\boldsymbol{k}|)\,\hat{\boldsymbol{k}} = (\omega/k_x)\,\hat{\boldsymbol{x}} = c\,\hat{\boldsymbol{x}}. \tag{62.141}$$

Note that the phase velocity, c, is generally complex, which means that the streamfunction, $\widetilde{\psi}$, is also complex. Just like for the horizontal shear case in Section 61.6, if c and $\widetilde{\psi}$ satisfy the boundary value problem (62.140a)-(62.140c), then so do their complex conjugates, c^* and $\widetilde{\psi}^*$.

62.8.2 Steps for deriving the necessary conditions

To develop a necessary condition for instability, multiply the differential equation (62.140a) by $\widetilde{\psi}^*$ and integrate over the full domain

$$\int \left[\widetilde{\psi}^*\,(\partial_{yy} - k_x^2)\,\widetilde{\psi} + \widetilde{\psi}^*\,f_\circ^2\,\partial_z(N^{-2}\,\partial_z\widetilde{\psi}) + \frac{|\widetilde{\psi}|^2\,\partial_y q_\mathsf{b}}{U - c}\right]\mathrm{d}y\,\mathrm{d}z = 0. \tag{62.142}$$

Meridional derivative term

Consider the meridional derivative term, in which we have

$$\int \widetilde{\psi}^*\,\partial_{yy}\widetilde{\psi}\,\mathrm{d}y = \int [\partial_y(\widetilde{\psi}^*\,\partial_y\widetilde{\psi}) - |\partial_y\widetilde{\psi}|^2]\,\mathrm{d}y. \tag{62.143}$$

Assuming either meridionally periodic conditions, or fields that decay at infinity, allows us to drop the total derivative term to have

$$\int \widetilde{\psi}^*\,\partial_{yy}\widetilde{\psi}\,\mathrm{d}y = -\int |\partial_y\widetilde{\psi}|^2\,\mathrm{d}y. \tag{62.144}$$

Vertical derivative term

For the vertical derivative term we have

$$\int \widetilde{\psi}^* \, \partial_z (N^{-2} \, \partial_z \widetilde{\psi}) \, \mathrm{d}z = \int [\partial_z (\widetilde{\psi}^* \, N^{-2} \, \partial_z \widetilde{\psi}) - N^{-2} \, |\partial_z \widetilde{\psi}|^2] \, \mathrm{d}z. \tag{62.145}$$

The boundary conditions (62.140b) and (62.140c) lead to

$$[\widetilde{\psi}^* \, N^{-2} \, \partial_z \widetilde{\psi}]_{z=\overline{\eta}} = \left[\frac{|\widetilde{\psi}|^2 \, \partial_z u_\mathrm{b}}{N^2 \, (u_\mathrm{b} - c)} \right]_{z=\overline{\eta}} \tag{62.146a}$$

$$[\widetilde{\psi}^* \, N^{-2} \, \partial_z \widetilde{\psi}]_{z=\overline{\eta_\mathrm{b}}} = \left[\frac{|\widetilde{\psi}|^2 \, [(\mathrm{d}z/\mathrm{d}y)_{b_\mathrm{b}} - \partial_y \eta_\mathrm{b}]}{f_\circ \, (u_\mathrm{b} - c)} \right]_{z=\overline{\eta_\mathrm{b}}} \tag{62.146b}$$

It is important to note that these boundary terms are generally nonzero, and so they play a role in determining the necessary conditions for instability.

62.8.3 Necessary conditions based on the imaginary part

The various pieces bring the integral (62.142) into the form

$$\begin{aligned} &\int \left[k_x^2 \, |\widetilde{\psi}|^2 + |\partial_y \widetilde{\psi}|^2 + (f_\circ/N)^2 \, |\partial_z \widetilde{\psi}|^2 \right] \mathrm{d}y \, \mathrm{d}z \\ &\quad = \int \frac{|\widetilde{\psi}|^2 \, \partial_y q_\mathrm{b}}{u_\mathrm{b} - c} \, \mathrm{d}y \, \mathrm{d}z + \int_{z=\overline{\eta}} \frac{f_\circ^2 \, |\widetilde{\psi}|^2 \, \partial_z u_\mathrm{b}}{N^2 \, (u_\mathrm{b} - c)} \, \mathrm{d}y - \int_{z=\overline{\eta_\mathrm{b}}} \frac{f_\circ \, |\widetilde{\psi}|^2 \, [(\mathrm{d}z/\mathrm{d}y)_{b_\mathrm{b}} - \partial_y \eta_\mathrm{b}]}{(u_\mathrm{b} - c)} \, \mathrm{d}y. \end{aligned} \tag{62.147}$$

The left hand side is a real and non-negative number. For consistency, the imaginary part of the right hand side must vanish. Making use of the identity

$$\frac{1}{u_\mathrm{b} - c} = \frac{u_\mathrm{b} - c_\mathrm{r} - \mathrm{i} \, c_\mathrm{i}}{|u_\mathrm{b} - c|^2} \tag{62.148}$$

leads to the constraint

$$c_\mathrm{i} \left[\int \frac{|\widetilde{\psi}|^2 \, \partial_y q_\mathrm{b}}{|u_\mathrm{b} - c|^2} \, \mathrm{d}y \, \mathrm{d}z + \int_{z=\overline{\eta}} \frac{f_\circ^2 \, |\widetilde{\psi}|^2 \, \partial_z u_\mathrm{b}}{N^2 \, |u_\mathrm{b} - c|^2} \, \mathrm{d}y - \int_{z=\overline{\eta_\mathrm{b}}} \frac{f_\circ \, |\widetilde{\psi}|^2 \, [(\mathrm{d}z/\mathrm{d}y)_{b_\mathrm{b}} - \partial_y \eta_\mathrm{b}]}{|u_\mathrm{b} - c|^2} \, \mathrm{d}y \right] = 0. \tag{62.149}$$

An instability exists only if $c_\mathrm{i} \neq 0$. We thus see that if the sum of the integrals does not vanish, then there can be no instability. That is, a sufficient condition for baroclinic stability of a zonal geostrophic flow, $u_\mathrm{b}(y, z)$, is that the sum of the integrals is nonzero. Conversely, a necessary condition for baroclinic instability of the zonal flow is that the sum of the three integrals in equation (62.149) vanishes. This necessary condition is known as the *Charney-Stern-Pedlosky* condition (*Charney and Stern*, 1962; *Pedlosky*, 1964).

In summary, the necessary conditions for instability are that the following three functions must not have the same sign everywhere

$$\partial_y q_\mathrm{b} \quad \text{must change sign within } \overline{\eta_\mathrm{b}} < z < \overline{\eta} \tag{62.150a}$$

$$f_\circ \, \partial_y u_\mathrm{b} = -\partial_y b_\mathrm{b} \quad \text{must change sign along } z = \overline{\eta} \tag{62.150b}$$

$$(\mathrm{d}z/\mathrm{d}y)_{b_\mathrm{b}} - \partial_y \eta_\mathrm{b} \quad \text{must change sign along } z = \overline{\eta_\mathrm{b}}. \tag{62.150c}$$

Conversely, if each of these conditions fails, then that is sufficient to conclude that the flow is stable to baroclinic instability.

62.8.4 Necessary conditions based on the real part

Following from Fjørtoft's theorem for shear instability in Section 61.5.2, consider the real part of equation (62.147), which says

$$\Gamma = \int \frac{(u_\mathrm{b} - c_\mathrm{r})\,|\widetilde{\psi}|^2\,\partial_y q_\mathrm{b}}{|u_\mathrm{b} - c|^2}\,\mathrm{d}y\,\mathrm{d}z + \int_{z=\overline{\eta}} \frac{(u_\mathrm{b} - c_\mathrm{r})\,f_\circ^2\,|\widetilde{\psi}|^2\,\partial_z u_\mathrm{b}}{N^2\,|u_\mathrm{b} - c|^2}\,\mathrm{d}y - \int_{z=\overline{\eta_\mathrm{b}}} \frac{(u_\mathrm{b} - c_\mathrm{r})\,f_\circ\,|\widetilde{\psi}|^2\,[(\mathrm{d}z/\mathrm{d}y)_{b_\mathrm{b}} - \partial_y \eta_\mathrm{b}]}{|u_\mathrm{b} - c|^2}\,\mathrm{d}y, \quad (62.151)$$

where we introduced the non-negative number

$$\Gamma = \int \left[k_x^2\,|\widetilde{\psi}|^2 + |\partial_y \widetilde{\psi}|^2 + (f_\circ/N)^2\,|\partial_z \widetilde{\psi}|^2\right]\mathrm{d}y\,\mathrm{d}z \geq 0. \quad (62.152)$$

Given that the condition (62.149) is maintained (with $c_\mathrm{i} \neq 0$), then we can replace c_r in equation (62.151) with an arbitrary constant, referred to as U_s in Fjørtoft's theorem from Section 61.5.2. We conclude that a sufficient condition for stability is if there is any constant, U_s, whereby all of the following conditions hold

$$(u_\mathrm{b} - c_\mathrm{r})\,\partial_y q_\mathrm{b} < 0 \qquad \overline{\eta_\mathrm{b}} < z < \overline{\eta} \quad (62.153a)$$

$$(u_\mathrm{b} - U_s)\,\partial_z u_\mathrm{b} < 0 \qquad z = \overline{\eta} \quad (62.153b)$$

$$-(u_\mathrm{b} - U_s)\,[(\mathrm{d}z/\mathrm{d}y)_{b_\mathrm{b}} - \partial_y \eta_\mathrm{b}] < 0 \qquad z = \overline{\eta_\mathrm{b}}. \quad (62.153c)$$

62.8.5 Necessary condition for instability of the Eady model

To help understand features of the necessary condition (62.149), and the summary statements (62.150a)–(62.150c), we consider some special cases, starting with the Eady model from Sections 62.6 and 62.7. In this case, there is a constant interior potential vorticity of the background state, so that $\partial_y q_\mathrm{b} = 0$. Hence, the necessary condition for instability (62.149) reduces to a condition on the boundary integrals

$$\int_{z=\overline{\eta}} \frac{|\widetilde{\psi}|^2\,\partial_z u_\mathrm{b}}{N^2\,|u_\mathrm{b} - c|^2}\,\mathrm{d}y = \int_{z=\overline{\eta_\mathrm{b}}} \frac{|\widetilde{\psi}|^2\,\partial_z u_\mathrm{b}}{N^2\,|u_\mathrm{b} - c|^2}\,\mathrm{d}y, \quad (62.154)$$

where we set $\partial_y \eta_\mathrm{b} = 0$ as per the Eady model, and the buoyancy slope is

$$(\mathrm{d}z/\mathrm{d}y)_{b_\mathrm{b}} = -\partial_y b_\mathrm{b}/\partial_z b_\mathrm{b} = f_\circ\,\partial_z u_\mathrm{b}/N^2. \quad (62.155)$$

Furthermore, N^2 and $\partial_z u_\mathrm{b}$ are constants in the Eady model, and the zonal flow is a function only of vertical, $u_\mathrm{b}(z)$, so that the necessary condition for instability (62.154) reduces to

$$\left[\frac{|\widetilde{\psi}|^2}{|u_\mathrm{b} - c|^2}\right]_{z=\overline{\eta}} = \left[\frac{|\widetilde{\psi}|^2}{|u_\mathrm{b} - c|^2}\right]_{z=\overline{\eta_\mathrm{b}}}. \quad (62.156)$$

For this condition to hold requires the streamfunction to be nonzero at both boundaries. We are ensured that the streamfunction is not exponentially small at the boundaries when the edge waves have small enough wavenumber that the waves can overlap and have a nontrivial presence at both boundaries

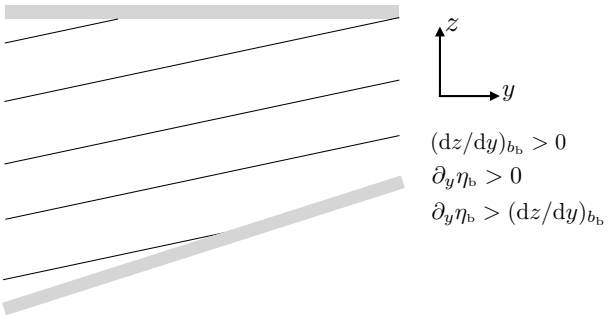

FIGURE 62.6: The Eady model with constant sloping buoyancy surfaces and with a bottom slope that is steeper than the buoyancy surfaces. This flow state is baroclinically stable according to equation (62.157) since the slope of the topography is steeper than the buoyancy surface.

62.8.6 Effects from adding a bottom slope to the Eady model

Consider the Eady model but with a sloping bottom, in which case the necessary condition for instability, equation (62.149), becomes

$$\int_{z=\overline{\eta}} \frac{|\widetilde{\psi}|^2 \, (\mathrm{d}z/\mathrm{d}y)_{b_\mathrm{b}}}{|u_\mathrm{b} - c|^2} \, \mathrm{d}y = \int_{z=\overline{\eta_\mathrm{b}}} \frac{|\widetilde{\psi}|^2 \, [(\mathrm{d}z/\mathrm{d}y)_{b_\mathrm{b}} - \partial_y \eta_\mathrm{b}]}{|u_\mathrm{b} - c|^2} \, \mathrm{d}y. \tag{62.157}$$

For the Eady model the buoyancy slope is constant, and let us assume it is positive. If the bottom topography slope has the same sign as the buoyancy slope, but is larger in magnitude, then the right hand side of equation (62.157) is negative whereas the left hand side is positive. We reach a contradiction, which means this necessary condition for instability cannot be satisfied. Evidently, the flow is baroclinically stable if the bottom slope is steeper than the buoyancy slope. We depict this situation in Figure 62.6.

62.8.7 Flat bottom with constant buoyancy along the two boundaries

The Eady model has horizontally varying buoyancy along the top and bottom boundaries, and stability of the Eady waves is determined by the boundary buoyancy. But what if there is a constant buoyancy along the two boundaries (so $(\mathrm{d}z/\mathrm{d}y)_{b_\mathrm{b}} = 0$) and with the bottom boundary flat ($\partial_y \eta_\mathrm{b} = 0$)? In this case there are no topographic waves nor Eady waves along the boundaries, and both boundary integrals in the necessary condition (62.149) vanish. The necessary condition for instability (62.149) reduces to

$$\int \frac{|\widetilde{\psi}|^2 \, \partial_y q_\mathrm{b}}{|u_\mathrm{b} - c|^2} \, \mathrm{d}y \, \mathrm{d}z = 0. \tag{62.158}$$

We thus find that in the absence of boundary contributions, the necessary condition for baroclinic instability holds so long as the meridional derivative of the background potential vorticity changes sign somewhere in the domain. This condition is reminiscent of the Rayleigh-Kuo inflection point theorem for horizontal shear instability (Section 61.5).

62.9 Energetics of small amplitude fluctuations

In this section we offer another means to help understand the mechanics of quasi-geostrophic waves and baroclinic instability, as well as conditions required for a fluctuation to grow. Elements of this section are shared with Section 62.8, yet here we focus on the mechanical energy budget of the fluctuating fields. As with Section 62.8, the results here are more general than those found

for the Eady model in Section 62.7, since we allow for the general linear theory from Sections 62.3 and 62.8.

Recall the energetics of quasi-geostrophy as studied in Section 45.9, where we identify the mechanical energy per mass of the fluctuations

$$E = [\nabla_h \psi' \cdot \nabla_h \psi' + (f_o \, \partial_z \psi' / N)^2]/2, \tag{62.159}$$

which is the sum of the kinetic energy per mass

$$\nabla_h \psi' \cdot \nabla_h \psi' / 2 = \boldsymbol{u}' \cdot \boldsymbol{u}' / 2, \tag{62.160}$$

plus the available potential energy per mass

$$(f_o \, \partial_z \psi' / N)^2 / 2 = (b'/N)^2 / 2. \tag{62.161}$$

To derive the energy budget equation, we follow the standard procedure in quasi-geostrophy by multiplying the potential vorticity equation (62.25) by ψ'

$$\psi' \, (\partial_t + u_b \, \partial_x) \, [\nabla_h^2 \psi' + f_o^2 \, \partial_z (N^{-2} \, \partial_z \psi')] = -\psi' \, \partial_x \psi' \, \partial_y q_b. \tag{62.162}$$

We now move derivatives around, with the manipulations relatively straightforward with $u_b = 0$, but somewhat more tedious with $u_b \neq 0$.

62.9.1 Time derivative terms

The time derivative can be written

$$\begin{aligned} \psi' \, \partial_t (\nabla_h^2 \psi') &= \psi' \, \nabla_h \cdot \nabla_h (\partial_t \psi') && \text{(62.163a)} \\ &= \nabla_h \cdot [\psi' \, \nabla_h (\partial_t \psi')] - \nabla_h \psi' \cdot \nabla_h (\partial_t \psi') && \text{(62.163b)} \\ &= \nabla_h \cdot [\psi' \, \nabla_h (\partial_t \psi')] - \partial_t (\nabla_h \psi' \cdot \nabla_h \psi')/2, && \text{(62.163c)} \end{aligned}$$

along with

$$\begin{aligned} \psi' \, \partial_t \partial_z [(f_o^2/N^2) \, \partial_z \psi'] &= \psi' \, \partial_z [(f_o^2/N^2) \, \partial_{zt} \psi'] && \text{(62.164a)} \\ &= \partial_z [\psi' \, (f_o^2/N^2) \, \partial_{zt} \psi'] - \partial_z \psi' \, (f_o^2/N^2) \, \partial_{zt} \psi' && \text{(62.164b)} \\ &= \partial_z [\psi' \, (f_o^2/N^2) \, \partial_{zt} \psi'] - \partial_t (f_o \, \partial_z \psi' / N)^2 / 2, && \text{(62.164c)} \end{aligned}$$

which yields

$$\psi' \, \partial_t [\nabla_h^2 \psi' + f_o^2 \, \partial_z (N^{-2} \, \partial_z \psi')] = -\partial_t E + \nabla_h \cdot [\psi' \, \nabla_h (\partial_t \psi')] + \partial_z [\psi' \, (f_o^2/N^2) \, \partial_{zt} \psi']. \tag{62.165}$$

62.9.2 Advection by the background zonal flow

To account for advection by the zonal background geostrophic flow, it is important to remember that $u_b = u_b(y, z)$, so that

$$\begin{aligned} \psi' \, u_b \, \partial_x (\nabla_h^2 \psi') &= \psi' \, u_b \, \nabla_h \cdot \nabla_h (\partial_x \psi') && \text{(62.166a)} \\ &= \nabla_h \cdot [\psi' \, u_b \, \nabla_h (\partial_x \psi')] - \nabla_h (\psi' \, u_b) \cdot \nabla_h (\partial_x \psi') && \text{(62.166b)} \\ &= \nabla_h \cdot [\psi' \, u_b \, \nabla_h (\partial_x \psi')] - \psi' \, \nabla_h u_b \cdot \nabla_h (\partial_x \psi') - u_b \, \nabla_h \psi' \cdot \nabla_h (\partial_x \psi') && \text{(62.166c)} \\ &= \nabla_h \cdot [\psi' \, u_b \, \nabla_h (\partial_x \psi')] - \psi' \, \partial_y u_b \, \partial_{xy} \psi' - u_b \, \partial_x (\nabla_h \psi' \cdot \nabla_h \psi')/2. && \text{(62.166d)} \end{aligned}$$

One further step is key, whereby we write

$$\psi' \, \partial_y u_\mathsf{b} \, \partial_{xy} \psi' = \partial_x (\psi' \, \partial_y u_\mathsf{b} \, \partial_y \psi') - \partial_x \psi' \, \partial_y u_\mathsf{b} \, \partial_y \psi', \tag{62.167}$$

so that

$$\psi' \, u_\mathsf{b} \, \partial_x (\nabla_\mathsf{h}^2 \psi') = \nabla_\mathsf{h} \cdot [\psi' \, u_\mathsf{b} \, \nabla_\mathsf{h} (\partial_x \psi')] - \partial_x (\psi' \, \partial_y u_\mathsf{b} \, \partial_y \psi') + \partial_x \psi' \, \partial_y u_\mathsf{b} \, \partial_y \psi' \\ - u_\mathsf{b} \, \partial_x (\nabla_\mathsf{h} \psi' \cdot \nabla_\mathsf{h} \psi')/2. \tag{62.168}$$

A similar set of steps for the stretching term (temporarily dropping the constant f_o^2 for brevity) leads to

$$\psi' \, u_\mathsf{b} \, \partial_x \partial_z (N^{-2} \, \partial_z \psi') = \psi' \, u_\mathsf{b} \, \partial_z (N^{-2} \, \partial_{xz} \psi') \tag{62.169a}$$
$$= \partial_z [\psi' \, u_\mathsf{b} \, N^{-2} \, \partial_{xz} \psi'] - \partial_z (\psi' \, u_\mathsf{b}) \, N^{-2} \, \partial_{xz} \psi' \tag{62.169b}$$
$$= \partial_z [\psi' \, u_\mathsf{b} \, N^{-2} \, \partial_{xz} \psi'] - \psi' \, \partial_z u_\mathsf{b} \, N^{-2} \, \partial_{xz} \psi' - u_\mathsf{b} \, \partial_z \psi' \, N^{-2} \, \partial_{xz} \psi' \tag{62.169c}$$
$$= \partial_z [\psi' \, u_\mathsf{b} \, N^{-2} \, \partial_{xz} \psi'] - \psi' \, \partial_z u_\mathsf{b} \, N^{-2} \, \partial_{xz} \psi' - u_\mathsf{b} \, \partial_x (\partial_z \psi'/N)^2/2. \tag{62.169d}$$

As for the relative vorticity terms, write

$$\psi' \, \partial_z u_\mathsf{b} \, N^{-2} \, \partial_{xz} \psi' = \partial_x (\psi' \, \partial_z u_\mathsf{b} \, N^{-2} \, \partial_z \psi') - \partial_x \psi' \, \partial_z u_\mathsf{b} \, N^{-2} \, \partial_z \psi', \tag{62.170}$$

which then leads to

$$\psi' \, u_\mathsf{b} \, \partial_{xz} (f_\mathsf{o}^2 \, N^{-2} \, \partial_z \psi') = \partial_z (\psi' \, u_\mathsf{b} \, f_\mathsf{o}^2 \, N^{-2} \, \partial_{xz} \psi') - \partial_x (\psi' \, \partial_z u_\mathsf{b} \, f_\mathsf{o}^2 \, N^{-2} \, \partial_z \psi') \\ + \partial_x \psi' \, \partial_z u_\mathsf{b} \, f_\mathsf{o}^2 \, N^{-2} \, \partial_z \psi' - u_\mathsf{b} \, \partial_x (f_\mathsf{o} \, \partial_z \psi'/N)^2/2. \tag{62.171}$$

62.9.3 Summary of the energy equation

Bringing terms together gives

$$0 = \psi' \, (\partial_t + u_\mathsf{b} \, \partial_x) \, [\nabla_\mathsf{h}^2 \psi' + f_\mathsf{o}^2 \, \partial_z (N^{-2} \, \partial_z \psi')] + \psi' \, \partial_x \psi' \, \partial_y q_\mathsf{b} \\ = -(\partial_t + u_\mathsf{b} \, \partial_x) E - \nabla_\mathsf{h} \cdot \boldsymbol{F}^\mathsf{h} - \partial_z F^z + \partial_x \psi' \, \partial_y u_\mathsf{b} \, \partial_y \psi' + \partial_x \psi' \, \partial_z u_\mathsf{b} \, f_\mathsf{o}^2 \, N^{-2} \, \partial_z \psi', \tag{62.172}$$

where we introduced the horizontal and vertical components to the energy flux vector

$$\boldsymbol{F}^\mathsf{h} = -\psi' \, (\partial_t + u_\mathsf{b} \, \partial_x) \nabla_\mathsf{h} \psi' + \hat{\boldsymbol{x}} \, \psi' \, (-\psi' \, \partial_y q_\mathsf{b}/2 + \partial_y u_\mathsf{b} \, \partial_y \psi' + \partial_z u_\mathsf{b} \, f_\mathsf{o}^2 \, N^{-2} \, \partial_z \psi') \tag{62.173a}$$
$$F^z = -\psi' \, f_\mathsf{o}^2 \, N^{-2} \, (\partial_t + u_\mathsf{b} \, \partial_x) \partial_z \psi' = -\psi' \, f_\mathsf{o} \, N^{-2} \, (\partial_t + u_\mathsf{b} \, \partial_x) b', \tag{62.173b}$$

which gives the energy equation

$$(\partial_t + u_\mathsf{b} \, \partial_x) E = -\nabla_\mathsf{h} \cdot \boldsymbol{F}^\mathsf{h} - \partial_z F^z + \partial_x \psi' \, \partial_y u_\mathsf{b} \, \partial_y \psi' + \partial_x \psi' \, \partial_z u_\mathsf{b} \, f_\mathsf{o}^2 \, N^{-2} \, \partial_z \psi'. \tag{62.174}$$

Since u_b is independent of x, one may choose to place the zonal advection term inside of the horizontal flux by noting that

$$u_\mathsf{b} \, \partial_x E = \partial_x (u_\mathsf{b} \, E), \tag{62.175}$$

so that

$$\partial_t E = -\nabla_\mathsf{h} \cdot (E \, u_\mathsf{b} \, \hat{\boldsymbol{x}} + \boldsymbol{F}^\mathsf{h}) - \partial_z F^z + \partial_x \psi' \, \partial_y u_\mathsf{b} \, \partial_y \psi' + \partial_x \psi' \, \partial_z u_\mathsf{b} \, f_\mathsf{o}^2 \, N^{-2} \, \partial_z \psi'. \tag{62.176}$$

62.9.4 Horizontal and thermal wind shear production

Equation (62.176) indicates that time changes to the mechanical energy contained in the small amplitude fluctuations is driven by the convergence of an energy flux, plus two source terms arising from shears in the background zonal geostrophic flow. The flux convergence acts to move energy around, and its domain integral provides possible sources for energy at the boundaries. We do not study this term in this section since it is quite dependent on assumptions about the boundaries, though we comment on this limitation in the analysis in Section 62.9.7.

Instead, we focus here on the two source terms in equation (62.176). The source arising from horizontal shear can be written

$$\partial_x \psi' \, \partial_y u_{\mathrm{b}} \, \partial_y \psi' = -v' \, u' \, \partial_y u_{\mathrm{b}}, \tag{62.177}$$

and the source arising from vertical shear is

$$\partial_x \psi' \, \partial_z u_{\mathrm{b}} \, f_{\mathrm{o}}^2 \, N^{-2} \, \partial_z \psi' = v' \, b' \, (f_{\mathrm{o}} \, \partial_z u_{\mathrm{b}} / N^2) = v' \, b' \, (\mathrm{d}z/\mathrm{d}y)_{b_{\mathrm{b}}}, \tag{62.178}$$

where the final step introduced the slope of the background buoyancy surface according to equation (62.12).

Horizontal shear production and thermal wind shear production

As in the study of horizonal shear instability in Section 61.4.6, we identify

$$-v' \, u' \, \partial_y u_{\mathrm{b}} = \text{horizontal shear production}. \tag{62.179}$$

This shear production term is generally rather small for geostrophic flows in comparison to the ageostrophic flows considered in Chapter 61. In analogy, we introduce

$$v' \, b' \, (\mathrm{d}z/\mathrm{d}y)_{b_{\mathrm{b}}} = -v' \, b' \, \partial_y b_{\mathrm{b}} / N^2 = \text{thermal wind shear production}. \tag{62.180}$$

The thermal wind shear production is fundamentally distinct from horizontal shear production. The reason is that $v' \, b' \, (\mathrm{d}z/\mathrm{d}y)_{b_{\mathrm{b}}}$ arises from the potential energy in the background state that supports the thermal wind shear, rather than from the background kinetic energy that supports horizontal (or vertical) shear production described in Section 61.4.6. For quasi-geostrophic flows, kinetic energy sourced shear production is generally far smaller than potential energy sourced thermal wind shear production.

62.9.5 Meridional and vertical eddy buoyancy fluxes

As shown in the following, fluctuations that increase their energy through making use of the prescribed background potential energy have a tendency to flux buoyancy down the meridional gradient and upward. These two effects act in a manner that increases the total quasi-geostrophic mechanical energy (sum of kinetic plus available potential) of the fluctuations, while feeding off the available potential energy of the background flow.

Meridionally downgradient flux of buoyancy increases mechanical energy of the fluctuations

Mechanical energy of the fluctuations increases through the thermal wind shear production (62.180) if the meridional *eddy buoyancy flux* is down the meridional gradient of the background buoyancy

$$v' \, b' \, \partial_y b_{\mathrm{b}} = -v' \, b' \, f_{\mathrm{o}} \, \partial_z u_{\mathrm{b}} < 0 \quad \text{mechanical energy of fluctuations increases}. \tag{62.181}$$

In practice, this downgradient behavior occurs over a space and/or time and/or ensemble average, in which we use an overbar as a generic average so that

$$\overline{v'\,b'}\,\partial_y b_{\mathsf{b}} = -\overline{v'\,b'}\,f_{\mathsf{o}}\,\partial_z u_{\mathsf{b}} < 0 \quad \text{averaged mechanical energy of fluctuations increases.} \tag{62.182}$$

This downgradient meridional buoyancy flux leads to a poleward heat transport for flows where temperature dominates buoyancy. Furthermore, the poleward heat transport extracts potential energy from the background flow since it acts in a direction that flattens the background buoyancy surfaces. Such fluctuations increase their energy at the expense of the available potential energy of the background state.

Fluid particle motion leading to an increase in available potential energy of the fluctuations

Available potential energy contained in the fluctuations evolves according to

$$\begin{aligned}
(\partial_t + u_{\mathsf{b}}\,\partial_x)[(f_{\mathsf{o}}\,\partial_z\psi'/N)^2/2] &= (\partial_t + u_{\mathsf{b}}\,\partial_x)(b'/N)^2/2 && \text{(62.183a)}\\
&= (b'/N^2)\,(\partial_t + u_{\mathsf{b}}\,\partial_x)b' && \text{(62.183b)}\\
&= -b'\,[w' - v'\,(\mathrm{d}z/\mathrm{d}y)_{b_{\mathsf{b}}}] && \text{(62.183c)}\\
&= -b'\,(w' + v'\,\partial_y b_{\mathsf{b}}/N^2), && \text{(62.183d)}
\end{aligned}$$

where we used the linear buoyancy equation (62.27) for the penultimate step. The available potential energy of the fluctuations increases if

$$b'\,[w' - v'\,(\mathrm{d}z/\mathrm{d}y)_{b_{\mathsf{b}}}] = b'\,(w' + v'\,\partial_y b_{\mathsf{b}}/N^2) < 0 \quad \text{APE of the fluctuations increases.} \tag{62.184}$$

An increasing available potential energy in the fluctuations is expected for a growing disturbance, in which fluctuating buoyancy surfaces have growing amplitudes. The condition (62.184) takes on a geometric expression by cancelling the buoyancy fluctuation and writing

$$w'/v' < (\mathrm{d}z/\mathrm{d}y)_{b_{\mathsf{b}}} \implies \quad \text{APE of the fluctuations increases,} \tag{62.185}$$

whereas the fluctuations maintain a fixed available potential energy if the meridional and vertical velocity components align with the background buoyancy surfaces

$$w'/v' = (\mathrm{d}z/\mathrm{d}y)_{b_{\mathsf{b}}}] \implies \text{APE of the fluctuations remains constant.} \tag{62.186}$$

We have more to say on these geometric conditions in Section 62.9.7.

Kinetic energy of the fluctuations

Substituting the available potential energy equation (62.183d) into the mechanical energy equation (62.174) leads to the equation for the kinetic energy of the fluctuations

$$(\partial_t + u_{\mathsf{b}}\,\partial_x)(\boldsymbol{u}'\cdot\boldsymbol{u}'/2) = -\nabla_{\mathsf{h}}\cdot\boldsymbol{F}^{\mathsf{h}} - \partial_z F^z - v'\,u'\,\partial_y u_{\mathsf{b}} + w'\,b'. \tag{62.187}$$

Growth in the kinetic energy of the fluctuations arises if positive buoyancy anomalies are fluxed upward,

$$w'\,b' > 0 \quad \text{kinetic energy of the fluctuations increases.} \tag{62.188}$$

This flux lowers the center of mass for the fluid and so decreases the potential energy.

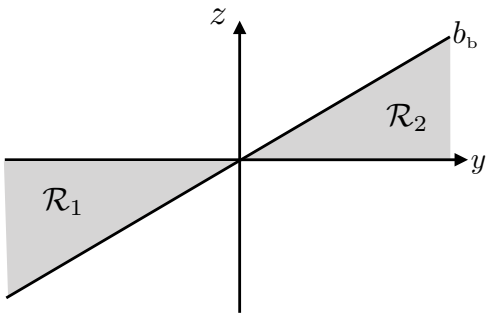

FIGURE 62.7: Depicting the wedge of instability for baroclinic instability. The background buoyancy is oriented with $\partial_y b_\mathrm{b} < 0$, so that less buoyant fluid sits to the north (to the right), as well as $\partial_z b_\mathrm{b} > 0$, so that the fluid is stably stratified in the vertical. A buoyancy fluctuation, b', in region $\mathcal{R}_1$ is more buoyant than b_b, so that $b' > 0$, whereas in region $\mathcal{R}_2$ we find $b' < 0$ relative to b_b. Hence, motion of fluid within a fluctuation that moves from region $\mathcal{R}_1$ to region $\mathcal{R}_2$ represents motion of relatively buoyant fluid ($b' > 0$) upward ($w' > 0$). This motion thus has $w'\,b' > 0$, which leads to an increase in kinetic energy of the fluctuation (equation (62.188)). This same motion also carries $v'\,b' > 0$ so that $v'\,b'\,\partial_y b_\mathrm{b} < 0$, meaning that the mechanical energy of the fluctuation increases (equation (62.181)). Finally, this motion ensures that $w'\,b' \le v'\,b'\,(\mathrm{d}z/\mathrm{d}y)_{b_\mathrm{b}}$, so that the available potential energy of the fluctuation increases (equation (62.189)). Motion from region $\mathcal{R}_2$ to region $\mathcal{R}_1$ reverses all signs of the perturbations, so that their products remain the same, thus ensuring that energies increase for fluctuations moving from $\mathcal{R}_2$ to region $\mathcal{R}_1$.

Summary of the inequalities

We summarize the considerations thus far by noting that the mechanical energy, kinetic energy, and available potential energy of the fluctuating field increases for fluid particle displacements that are sloped between the horizontal plane and the constant buoyancy surface passing through the origin as in the *wedge of instability* in Figure 62.7

$$w'/v' \le (\mathrm{d}z/\mathrm{d}y)_{b_\mathrm{b}} \Longrightarrow N^2\,w'\,b' < -v'\,b'\,\partial_y b_\mathrm{b}. \tag{62.189}$$

Recall that $w'\,b' > 0$ means that kinetic energy in the fluctuating fields increases (equation (62.188)), and $v'\,b'\,\partial_y b_\mathrm{b} < 0$ means that the mechanical energy increases (equation (62.181)). Inequality (62.189) thus ensures that available potential energy for the fluctuations also increases.

62.9.6 Tilting phase lines of unstable baroclinic waves

In Section 61.4.7 we showed that phase lines of unstable barotropic waves tilt into the meridional shear of the zonal flow, with this orientation allowing the wave perturbations to grow by extracting kinetic energy from the background shear. Here we pursue a similar argument to reveal that unstable baroclinic waves tilt into the vertical shear of the zonal flow, with this orientation allowing the waves to extract potential energy from the background thermal wind flow.

Start with the phase average of the inequality (62.182) that provides a sufficient condition for wave fluctuations to increase their mechanical energy

$$\langle v'\,b' \rangle\, f_\circ\, \partial_z u_\mathrm{b} > 0 \quad \text{mechanical energy of fluctuations increases.} \tag{62.190}$$

Writing the streamfunction in the form

$$\psi'(x,y,z,t) = \tilde{\psi}(z)\, \mathrm{e}^{\mathrm{i}\,(k_x\,x + k_y\,y - \omega_\mathrm{r}\,t) + \omega_\mathrm{i}\,t} = |\tilde{\psi}(z)|\, \mathrm{e}^{\mathrm{i}\,(k_x\,x + k_y\,y + \alpha(z) - \omega_\mathrm{r}\,t) + \omega_\mathrm{i}\,t}, \tag{62.191}$$

leads to

$$v' = \partial_x \psi' = \mathrm{i}\,k_x\,|\tilde{\psi}|\, \mathrm{e}^{\mathrm{i}\,(k_x x + k_y y + \alpha - \omega_r t) + \omega_i t} \tag{62.192a}$$

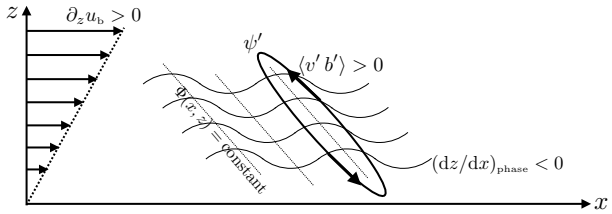

FIGURE 62.8: The lines of constant phase, $\Phi(x,z) = k\,x - \alpha(z)$, for the streamfunction (or the meridional velocity) in a northern hemisphere ($f_\circ > 0$) baroclinic wave. The wave depicted here has an increasing mechanical energy since the phase lines are tilted into the vertical shear of the zonal background flow, thus allowing for thermal wind shear production to increase the mechanical energy as per equation (62.197). This figure is directly analogous to the case of barotropic shear production as given by Figure 61.1.

$$b' = f_\circ\, \partial_z \psi' = f_\circ\, [\partial_z |\tilde{\psi}| + \mathrm{i}\, |\tilde{\psi}|\, \partial_z \alpha]\, \mathrm{e}^{\mathrm{i}\,(k_x x + k_y y + \alpha - \omega_\mathsf{r} t) + \omega_\mathsf{i} t}, \tag{62.192b}$$

and with the phase averaging identity (8.17e) yielding

$$\langle v'\, b' \rangle = (1/2)\ \mathrm{Re}[v'\, b^*] = (1/2)\, k_x\, f_\circ\, |\tilde{\psi}|^2\, \mathrm{e}^{2\omega_\mathsf{i} t}\, \partial_z \alpha. \tag{62.193}$$

We focus on phase lines in the x-z plane (so that $k_y = 0$), as that is the plane of the zonal flow with a vertical shear and so it is the plane of the most unstable wave as per *Squire's theorem*. We thus consider the spatial phase function

$$\Phi(x,z) \equiv k_x\, x + \alpha(z), \tag{62.194}$$

whose constant surfaces are defined by

$$\mathrm{d}\Phi = 0 = k_x\, \mathrm{d}x + (\partial_z \alpha)\, \mathrm{d}z \Longrightarrow (\mathrm{d}z/\mathrm{d}x)_{\text{phase}} = -k_x/\partial_z \alpha, \tag{62.195}$$

so that the instability condition (62.190) takes the form

$$(1/2)\, k_x^2\, f_\circ^2\, |\tilde{\psi}|^2\, \mathrm{e}^{2\omega_\mathsf{i} t}\, \frac{\partial_z u_\mathsf{b}}{(\mathrm{d}z/\mathrm{d}x)_{\text{phase}}} < 0 \Longrightarrow \text{sufficient condition for energy growth.} \tag{62.196}$$

Simplifying this equation leads to the condition for the ratio of the vertical shear to the phase slope

$$\frac{\partial_z u_\mathsf{b}}{(\mathrm{d}z/\mathrm{d}x)_{\text{phase}}} < 0 \Longrightarrow \text{sufficient condition for energy growth.} \tag{62.197}$$

This inequality says that mechanical energy of the wave grows when the wave's phase lines tilt into the background vertical shear, such as depicted in Figure 62.8. This condition is directly analogous to equation (61.56) and Figure 61.1, which hold for unstable barotropic waves on a meridional sheared zonal flow. Here, the tilt of the phase lines reflects the ability of the wave to extract potential energy from the background state, thus leading to growth of energy for the unstable wave. The geometric property (62.197) offers a visual indicator that the wave is acting on a baroclinically unstable background state, thus providing a valuable diagnostic tool for identifying when baroclinic instability is happening.

62.9.7 Caveats for extending the wedge of instability to parcels

Inequality (62.189) refers to the orientation of fluid particles affected by small amplitude wave fluctuations that lead to baroclinic instability, as illustrated in Figure 62.7. Even so, this figure is the basis for a parcel argument that goes beyond that of a small amplitude wave argument, with the parcel argument presented in many texts, such as Section 7.6 of *Pedlosky* (1987), Lecture 20 of *Pedlosky* (2003), Section 13.15 of *Kundu et al.* (2016), and Section 9.4.1 of *Vallis* (2017), and

originating from *Eady* (1949). Here we offer some caveats about this argument.

Baroclinic instability versus symmetric instability

The parcel arguments associated with the wedge of instability do not represent necessary conditions for baroclinic instability, and so they are no substitute for the integral statements in Section 62.8. This situation contrasts to parcel arguments considered for symmetric instability, where the necessary and sufficient condition for symmetric instability is summarized by its wedge of instability shown in Figure 59.8.

Furthermore, the parcel argument used for symmetric instability is based on a force balance, and so it incorporates accelerations from both buoyancy and Coriolis to account for the vertical and horizontal motion of the parcels. In contrast, the wedge of instability in Figure 62.7 is based on energetic arguments for baroclinic instability, with Coriolis acceleration absent from such arguments.

Baroclinic instability is a wave instability not a local instability

As explored in our study of the Eady model in Section 62.7, baroclinic instability mechanistically occurs through wave resonance. The realization of wave resonance relies on boundary conditions and phase locking of waves so that they can mutually reinforce one another. This mechanism is directly analogous to that considered for horizontal shear instability in Chapter 61.

In contrast, parcel arguments, such as used for symmetric instability, do not know about boundary conditions or phase locking. Instead, they are only concerned with local environmental conditions. Consider the following case in point for limitions of parcel arguments for baroclinic instability. Namely, observe that the wedge of instability does do not distinguish between flat bottom boundary or sloping bottom boundary. However, in Section 62.8.6 we found that the Eady model is stable in the presence of a bottom slope that is steeper than the buoyancy surfaces (Figure 62.6).

Additional points

Focusing specifically on the arguments leading up to inequality (62.189), note that these arguments have ignored all contributions from the convergence of energy fluxes that appear in the energy equation (62.174). These fluxes, particularly at domain boundaries, provide further influences on the domain integrated energetics and hence on stability of the flow (e.g., boundary terms are critical for the necessary instability conditions in Section 62.8). Additional caveats are raised by *Heifetz et al.* (1998) related to the problems with ignoring pressure fluctuations acting on the fluid particles. These caveats are analogous to those raised in Section 30.11 when studying effective buoyancy.

62.9.8 Further reading

Chapter 17 of *Cushman-Roisin and Beckers* (2011) offers qualifiers similar to those raised in Section 62.9.7 regarding the conceptual limitations of using parcel arguments for describing the mechanism of instabilities occuring via wave resonance.

Part XII

Generalized vertical coordinates

Generalized vertical coordinates (GVCs) offer a mathematical framework for describing fluid mechanics according to monotonically stacked surfaces that are a general function of space and time. For studying stratified fluid mechanics, the most common generalized vertical coordinate is based on Archimedean buoyancy or specific entropy. Generalized vertical coordinates appear in many guises throughout geophysical fluid mechanics, and they were introduced by *Starr* (1945) for atmospheric modeling and *Bleck* (1978) for ocean modeling. There is a growing use of GVC-based numerical ocean (e.g., *Griffies et al.* (2020)) and atmospheric models. This usage prompts the need to master their use for analysis, model formulation, and theory, thus providing motivation for this part of the book.

Time dependence of generalized vertical coordinates means that observers situated on a fixed generalized vertical coordinate surface are non-inertial, in a manner akin to the Lagrangian reference frame. Generalized vertical coordinates are also non-orthogonal, which contrasts to the static and locally orthogonal coordinates described in Sections 4.21, 4.22, and 4.23 (e.g., Cartesian, cylindrical, spherical). Both time dependence and non-orthogonality offer advantages for describing certain features of geophysical fluid motion. Yet there is a price to pay due to the added mathematical complexity that requires care beyond that needed with the coordinates in Chapter **??**.

The key reason we fravor a locally non-orthogonal coordinate set is that gravity plays a dominant role in orienting geophysical fluid motion. Hence, it is strategically useful to decompose the equations of motion so that lateral motions are perpendicular to gravity, just like with geopotential vertical coordinates. That is, we orient horizontal motions the same regardless whether we use geopotential coordinates or generalized vertical coordinates, since doing so removes the vertical pressure force from the horizontal equations of motion. If we were to instead locally rotate the components of the velocity vector to be parallel and perpendicular to the surface of constant generalized vertical coordinate, as per a locally orthogonal coordinate description, then that representation would introduce a portion of the vertical pressure gradient into the equations for lateral motion. Having the vertical pressure gradient appear in each of the three components to the equations of motion makes it very difficult to isolate the hydrostatic pressure force. In turn, it makes it difficult to describe nearly all of the basic features of geophysical flows, such as the geostrophic and hydrostatic balances.[4]

In this part of the book we develop the mathematics of generalized vertical coordinates, and then build up the kinematics and dynamics of stratified fluid mechanics using these coordinates. These chapters are written in the style of a monograph, with equations derived in detail and concepts explored. Here is a brief summary of these chapters.

- MATHEMATICAL FOUNDATIONS: Chapter 63 establishes the mathematics of generalized vertical coordinates. As noted already, their time dependence and their non-orthogonality present some complexity in both concept and detail. Even so, with practice, generalized vertical coordinates can become a versatile member of our theoretical and numerical toolkit.

- Chapters 64 and 65 describe elements of fluid kinematics and dynamics using generalized vertical coordinates.

- Chapter 66 formulates the hydrostatic Boussinesq equations using buoyancy as the vertical coordinate. This chapter specializes elements from the previous chapters, and in so doing provides a mathematical and physical basis for *isopycnal* models of the ocean and isentropic models of the atmosphere.

- Chapter 67 provides further insights into eddy and mean flow decomposition as viewed through the lens of thickness weighted averaging (TWA) for the shallow water model.

[4] The one case where locally orthogonal coordinate are useful concerns the tracer diffusion operator within the ocean interior, as discussed in Section 71.4.

We position this chapter in this part of this book since it makes use of the layered perspective of generalized vertical coordinates, particularly isopycnal coordinates. Indeed, the adiabatic stacked shallow water model is a discrete realization of the perfect fluid isopycnal equations. The TWA formalism of the shallow water equations offers a technically less difficult rendition of the formalism when applied to the continuously stratified isopycnal coordinates.

Chapter 63

Mathematical foundations

In this chapter we present the mathematics of generalized vertical coordinates (GVC), with Figure 63.1 offering a schematic of how these coordinates monotonically partition the vertical direction. Such coordinates are of particular use for stratified fluid mechanics, where it is often convenient to make use of a vertical coordinate distinct from, but uniquely related to, the geopotential vertical coordinate.

CHAPTER GUIDE

We make use of the general tensor analysis detailed in Chapter 4. We mostly consider just the spatial tensors in this chapter, consistent with the Newtonian perspective whereby time is universal. However, since the vertical coordinate is a function of time, we follow the space-time perspective from Section 4.9 for transforming the partial derivative operator. Chapters directly relying on the material from this chapter include the fluid kinematics discussed in Chapter 64, the general vertical coordinate dynamics discussed in Chapter 65, and the tracer equation diffusion and stirring operators discussed in Chapter 71.

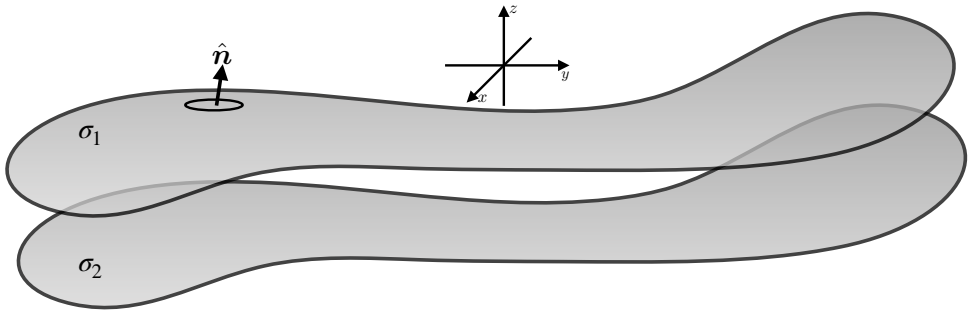

FIGURE 63.1: This stylized schematic illustrates the geometry of two surfaces of constant generalized vertical coordinate $\sigma(x, y, z, t) = \sigma_1$ and $\sigma(x, y, z, t) = \sigma_2$, here showing patches on two such surfaces. The surfaces are generally undulating in space and time yet are assumed to monotonically layer the fluid. Monotonic layering means that the surface normal, $\hat{\boldsymbol{n}}$, always has a non-zero projection onto the vertical: $\hat{\boldsymbol{n}} \cdot \hat{\boldsymbol{z}} \neq 0$. That is, the surfaces never become vertical nor do they overturn. It also means that there is a 1-to-1 invertible relation between σ and geopotential, so that specifying $(x, y, \sigma(x, y, z, t))$ is sufficient to yield a unique z.

63.1 Relating Cartesian and GVCs

We make use of the symbol σ for a generalalized vertical coordinate. This coordinate is *not* orthogonal to the horizontal spatial coordinates x, y. This is a central property of GVCs that influences nearly all aspects of their calculus. To help develop the mathematics for transforming between Cartesian coordinates and GVCs, it is important to distinguish the two coordinate systems. For that purpose we write the time coordinate and spatial Cartesian coordinates according to

$$\xi^\alpha = (\xi^0, \xi^a) = (\xi^0, \xi^1, \xi^2, \xi^3) = (t, x, y, z) \text{ with } \alpha = 0, 1, 2, 3, \text{ and } a = 1, 2, 3. \tag{63.1}$$

As defined, the tensor label a runs over the spatial coordinates $1, 2, 3$ whereas α also includes the time coordinate with $\alpha = 0$. The corresponding generalized vertical coordinates are denoted with an overbar

$$\xi^{\overline{\alpha}} = (\xi^{\overline{0}}, \xi^{\overline{1}}, \xi^{\overline{2}}, \xi^{\overline{3}}) = (\overline{t}, \overline{x}, \overline{y}, \sigma). \tag{63.2}$$

The 1-to-1 coordinate transformation between Cartesian and GVC coordinates is written

$$\xi^{\overline{0}} = \xi^0 \Longleftrightarrow \overline{t} = t \tag{63.3a}$$

$$\xi^{\overline{1}} = \xi^1 \Longleftrightarrow \overline{x} = x \tag{63.3b}$$

$$\xi^{\overline{2}} = \xi^2 \Longleftrightarrow \overline{y} = y \tag{63.3c}$$

$$\xi^{\overline{3}} = \sigma(x, y, z, t), \tag{63.3d}$$

with the final relation expressing the generalized vertical coordinate as a function of space and time. We ordered the appearance of independent variables in σ with time in the last position, which is the conventional ordering in this book for functions of space and time even though the zeroth coordinate is time.

The coordinate transformation is invertible so that we can write

$$\xi^0 = \xi^{\overline{0}} \tag{63.4a}$$

$$\xi^1 = \xi^{\overline{1}} \tag{63.4b}$$

$$\xi^2 = \xi^{\overline{2}} \tag{63.4c}$$

$$\xi^3 = \xi^3(\overline{x}, \overline{y}, \sigma, \overline{t}) = \xi^3(x, y, \sigma, t). \tag{63.4d}$$

The relation

$$\xi^3 = \xi^3(\xi^{\overline{a}}) = \xi^3(x, t, \sigma, t) \tag{63.5}$$

provides the vertical position of a given σ surface. Since $\xi^3 = z$ one commonly writes

$$z = z(x, y, \sigma, t). \tag{63.6}$$

However, this expression is prone to confusion since the meaning of z is overloaded.[1] Namely, one meaning ascribes z to a particular value of the vertical position; i.e., $z = -100$ m. The other meaning, as on the right hand side, is for z as the vertical coordinate function of a particular σ surface, with this value a function of space, time, and σ. Learning to distinguish when z refers to a particular vertical position or as a coordinate function takes some practice, and those who routinely work with generalized vertical coordinates typically find no problem with the overloaded meanings. Indeed, after reading this chapter we should be able to hold the two meanings in our mind without confusion. As a reminder, we commonly write the vertical coordinate function as

$$z = \eta(x, y, \sigma, t), \tag{63.7}$$

where η is used throughtout this book to represent the vertical position of a surface, such as the ocean free surface, solid-earth topography, or a generalized vertical coordinate surface. Hence, for example, the vertical position of a pressure surface of chosen value p is given by the functional relation

$$\xi^3 = z = \eta(\overline{x}, \overline{y}, p, \overline{t}) = \eta(x, y, p, t). \tag{63.8}$$

We make use of the η nomenclature where it seems useful but gradually sprinkle in more use of the $z(x, y, \sigma, t)$ notation since it is proves to be natural for many of the formulations.

63.2 Example generalized vertical coordinates

Before further diving into the mathematics, we here offer some examples of generalized vertical coordinates commonly used to study geophysical fluid flows.

63.2.1 Pressure coordinates

Hydrostatic compressible fluids, such as the large-scale atmosphere, pressure is a convenient choice as vertical since it absorbs the appearance of density in many formula such as mass

[1] We use the term *overloaded* as in computer science where a symbol has more than one meaning or usage.

continuity as discussed in Section 64.9.2 and the geostrophic balance given by equation (31.1a). Hence, a natural expression of the compressible hydrostatic equations of motion make use of pressure rather than geopotential for the vertical coordinate, in which case $\sigma = p(x, y, z, t)$.

63.2.2 Terrain following coordinates

When allowing for a time dependent ocean free surface, the terrain following coordinate in oceanography is given by

$$\sigma = \frac{z - \eta_{\text{surf}}}{-\eta_{\text{b}} + \eta_{\text{surf}}} \qquad \text{terrain following ocean coordinate,} \tag{63.9}$$

where $z = \eta_{\text{surf}}(x, y, t)$ is the vertical position of the ocean surface. The terrain following coordinate is non-dimensional and extends from $\sigma = 0$ at the ocean surface and $\sigma = -1$ at the ocean bottom (where $z = \eta_{\text{b}}(x, y)$). For rigid lid ocean models with $\eta_{\text{surf}} = 0$, the terrain following coordinate becomes time independent

$$\sigma = -\frac{z}{\eta_{\text{b}}} \qquad \text{terrain following rigid lid ocean.} \tag{63.10}$$

Finally, for a compressible ocean, it is more convenient to use pressure to define the terrain following coordinate so that

$$\sigma = \frac{p - p_{\text{a}}}{p_{\text{b}} - p_{\text{a}}} \qquad \text{terrain following atmosphere coordinate.} \tag{63.11}$$

In this equation, p_{a} is the pressure applied at the ocean surface and p_{b} is the pressure at the ocean bottom. For an atmosphere model we might set p_{a} as the top of the atmosphere pressure, which is typically assumed to be zero as in *Phillips* (1957).

63.2.3 Bottom slope oriented coordinates

Peterson and Callies (2022) consider an alternative to the traditional terrain following coordinates from Section 63.2.2, here defining a bottom slope oriented coordinate (recall $\eta_{\text{b}} = \eta_{\text{b}}(x, y)$)

$$\sigma = z - \boldsymbol{x} \cdot \nabla \eta_{\text{b}} = z - x\, \partial \eta_{\text{b}}/\partial x - y\, \partial \eta_{\text{b}}/\partial y, \tag{63.12}$$

with $\nabla \eta_{\text{b}}$ the slope of the bottom topography.

63.2.4 Isopycnal or buoyancy coordinates

Buoyancy surfaces are material when there is no mixing. Hence, for the study of perfect fluid mechanics it is quite convenient to use the Archimedian buoyancy, b, as the vertical coordinate, $\sigma = b(x, y, z, t)$. Equivalently, one may choose the potential density as the vertical coordinate. We have more to say about such vertical coordinates in Chapter 66 when developing the equations for isopycnal ocean models.

63.3 Spatial basis vectors

Making use of the tensor formalism from Chapter 4, consider the transformation of the Cartesian basis vectors into their corresponding GVC representation. This transformation takes is given by

$$\boldsymbol{e}_{\overline{a}} = \Lambda^{a}{}_{\overline{a}}\, \boldsymbol{e}_{a}, \tag{63.13}$$

where the transformation matrix is

$$\Lambda^{a}{}_{\overline{a}} = \begin{bmatrix} \partial x/\partial\overline{x} & \partial x/\partial\overline{y} & \partial x/\partial\sigma \\ \partial y/\partial\overline{x} & \partial y/\partial\overline{y} & \partial y/\partial\sigma \\ \partial z/\partial\overline{x} & \partial z/\partial\overline{y} & \partial z/\partial\sigma \end{bmatrix} = \begin{bmatrix} 1 & 0 & 0 \\ 0 & 1 & 0 \\ \partial\eta/\partial\overline{x} & \partial\eta/\partial\overline{y} & \partial\eta/\partial\sigma \end{bmatrix}, \tag{63.14}$$

where the second equality used our preferred notation $z = \eta(x, y, \sigma, t)$ for the vertical position of a σ surface. The diagonal unit values for the space-space components arise since a horizontal position in Cartesian and GVCs is the same and the horizontal directions are orthogonal. Likewise, the time coordinate does not change when changing $\overline{x}$, $\overline{y}$, or σ. Additionally, $\partial x/\partial\sigma = \partial y/\partial\sigma = 0$ since the horizontal position remains unchanged when moving across a GVC surface. In contrast, a non-zero value for $\partial\eta/\partial\overline{x}$ and $\partial\eta/\partial\overline{y}$ arise since we generally change vertical position when moving horizontally along a sloped σ surface. Finally, the element $\partial\eta/\partial\sigma$ is nonzero due to vertical stratification of the fluid when represented using general vertical coordinates.

63.3.1 More on the transformation matrix

To further detail how to produce elements of the transformation matrix (63.14), it is crucial to ensure that the proper variables are held fixed when performing the partial derivatives. For example, consider the top row where we compute

$$\Lambda^{1}{}_{\overline{a}} = \begin{bmatrix} [\partial x/\partial\overline{x}]_{\overline{y},\sigma} & [\partial x/\partial\overline{y}]_{\overline{x},\sigma} & [\partial x/\partial\sigma]_{\overline{x},\overline{y}} \end{bmatrix} \tag{63.15}$$

Since $x = \overline{x}$, all elements vanish except for the first. Namely, $[\partial x/\partial\overline{y}]_{\overline{x},\sigma} = 0$ since x cannot change when $\overline{x}$ is fixed. The same idea leads to the results for y derivatives.

63.3.2 Expressions for the basis vectors

Use of the transformation matrix (63.14) renders the spatial components of the GVC basis vectors

$$\boldsymbol{e}_{\overline{1}} = \hat{\boldsymbol{x}} + \hat{\boldsymbol{z}}\,(\partial\eta/\partial\overline{x}) \tag{63.16a}$$
$$\boldsymbol{e}_{\overline{2}} = \hat{\boldsymbol{y}} + \hat{\boldsymbol{z}}\,(\partial\eta/\partial\overline{y}) \tag{63.16b}$$
$$\boldsymbol{e}_{\overline{3}} = \hat{\boldsymbol{z}}\,(\partial\eta/\partial\sigma). \tag{63.16c}$$

The basis vectors $\boldsymbol{e}_{\overline{1}}$ and $\boldsymbol{e}_{\overline{2}}$ have a vertical component due to sloping GVC surfaces. These basis vectors lie within the tangent plane of the GVC surface. The basis vector $\boldsymbol{e}_{\overline{3}}$ is purely vertical and has a non-unit magnitude due to the inverse vertical stratification, $\partial\eta/\partial\sigma$. The left panel of Figure 63.2 illustrates the basis vectors.

As an example, consider the rigid lid terrain following vertical coordinate (63.10), where $\sigma = -z/\eta_{\text{b}}$. In this case, the vertical position of a generalized vertical surface is given by $\eta = -\sigma\,\eta_{\text{b}}$ so that the basis vectors are

$$\boldsymbol{e}_{\overline{1}} = \hat{\boldsymbol{x}} - \hat{\boldsymbol{z}}\,\sigma\,(\partial\eta_{\text{b}}/\partial\overline{x}) \quad \text{and} \quad \boldsymbol{e}_{\overline{2}} = \hat{\boldsymbol{y}} - \hat{\boldsymbol{z}}\,\sigma\,(\partial\eta_{\text{b}}/\partial\overline{y}) \quad \text{and} \quad \boldsymbol{e}_{\overline{3}} = -\hat{\boldsymbol{z}}\,\eta_{\text{b}}. \tag{63.17}$$

Similarly, the bottom slope oriented coordinate (63.12), with $\sigma = z - \boldsymbol{x}\cdot\nabla\eta_{\text{b}}$ so that $\eta = \sigma + \boldsymbol{x}\cdot\nabla\eta_{\text{b}}$, has the corresponding basis vectors

$$\boldsymbol{e}_{\overline{1}} = \hat{\boldsymbol{x}} + \hat{\boldsymbol{z}}\,(\partial\eta_{\text{b}}/\partial\overline{x}) \quad \text{and} \quad \boldsymbol{e}_{\overline{2}} = \hat{\boldsymbol{y}} + \hat{\boldsymbol{z}}\,(\partial\eta_{\text{b}}/\partial\overline{y}) \quad \text{and} \quad \boldsymbol{e}_{\overline{3}} = \hat{\boldsymbol{z}}. \tag{63.18}$$

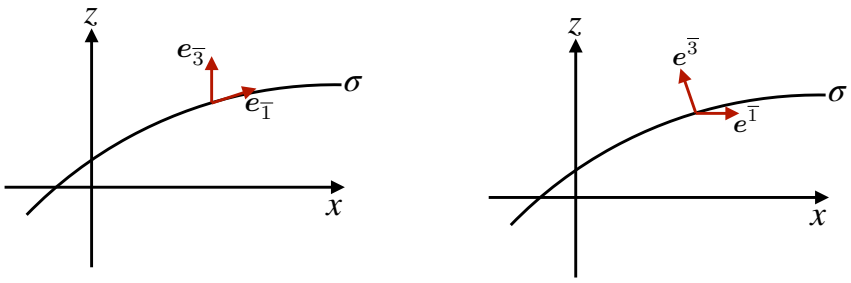

FIGURE 63.2: Illustrating the basis vectors (left panel) and basis one-forms (right panel) for generalized vertical coordinates. The $\boldsymbol{e}_{\overline{3}}$ basis vector is vertical whereas $\boldsymbol{e}_{\overline{1}}$ and $\boldsymbol{e}_{\overline{2}}$ lie within the tangent plane to the σ surface. As a complement, the basis one-form $\boldsymbol{e}^{\overline{3}}$ is normal to the σ surface whereas the basis one-forms $\boldsymbol{e}^{\overline{1}}$ and $\boldsymbol{e}^{\overline{2}}$ are horizontal.

63.4 Basis one-forms

The basis one-forms are obtained by transforming from Cartesian into GVCs through use of the inverse transformation

$$\boldsymbol{e}^{\overline{a}} = \Lambda^{\overline{a}}{}_{a}\, \boldsymbol{e}^{a}, \tag{63.19}$$

where the inverse transformation matrix takes the form

$$\Lambda^{\overline{a}}{}_{a} = \begin{bmatrix} \partial\overline{x}/\partial x & \partial\overline{x}/\partial y & \partial\overline{x}/\partial z \\ \partial\overline{y}/\partial x & \partial\overline{y}/\partial y & \partial\overline{y}/\partial z \\ \partial\sigma/\partial x & \partial\sigma/\partial y & \partial\sigma/\partial z \end{bmatrix} = \begin{bmatrix} 1 & 0 & 0 \\ 0 & 1 & 0 \\ \partial\sigma/\partial x & \partial\sigma/\partial y & \partial\sigma/\partial z \end{bmatrix}. \tag{63.20}$$

As for the transformation matrix (63.14), the unit diagonal values arise since a horizontal position in Cartesian and GVCs is the same and the horizontal directions are orthogonal. Likewise, $\partial\overline{x}/\partial z = \partial\overline{y}/\partial z = 0$ since the horizontal position on a GVC surface remains unchanged when moving across a depth surface. The nonzero values for $\partial\sigma/\partial x$, $\partial\sigma/\partial y$, and $\partial\sigma/\partial z$, arise in the presence of horizontal and vertical stratification of the generalized vertical coordinate.

63.4.1 More on the inverse transformation matrix

When computing elements of the inverse transformation matrix (63.20), it is crucial to ensure that the proper variables are held fixed. For example, consider the top row where we compute

$$\Lambda^{\overline{1}}{}_{a} = \begin{bmatrix} [\partial\overline{x}/\partial x]_{y,z} & [\partial\overline{x}/\partial y]_{x,z} & [\partial\overline{x}/\partial z]_{x,y} \end{bmatrix}. \tag{63.21}$$

Just as for the transformation matrix (63.15), since $x = \overline{x}$, all but the first element vanish in equation (63.21). Namely, $[\partial\overline{x}/\partial y]_{x,z} = 0$ since the $\overline{x}$ cannot change when x is fixed. The same idea holds for the $\overline{y}$ row.

63.4.2 GVC basis one-forms

Use of the inverse transformation matrix (63.20) renders the spatial components of the GVC basis one-forms

$$\boldsymbol{e}^{\overline{1}} = \hat{\boldsymbol{x}} \tag{63.22a}$$

$$\boldsymbol{e}^{\overline{2}} = \hat{\boldsymbol{y}} \tag{63.22b}$$

$$\boldsymbol{e}^{\overline{3}} = \boldsymbol{e}^{a}\, \partial_a \sigma = \hat{\boldsymbol{x}}\, (\partial\sigma/\partial x) + \hat{\boldsymbol{y}}\, (\partial\sigma/\partial y) + \hat{\boldsymbol{z}}\, (\partial\sigma/\partial z) = \nabla\sigma. \tag{63.22c}$$

The left panel of Figure 63.2 illustrates the basis one-forms.

As an example, consider again the rigid lid terrain following coordinate (63.10), $\sigma = -z/\eta_\mathrm{b}$, in which case

$$\boldsymbol{e}^{\overline{3}} = \nabla\sigma = -(1/\eta_\mathrm{b})\,[\hat{\boldsymbol{z}} - (z/\eta_\mathrm{b})\,\nabla\eta_\mathrm{b}]. \tag{63.23}$$

Similarly, the bottom slope oriented coordinate (63.12), with $\sigma = z - \boldsymbol{x}\cdot\nabla\eta_\mathrm{b}$, has

$$\boldsymbol{e}^{\overline{3}} = \hat{\boldsymbol{z}} - \nabla\eta_\mathrm{b} - \hat{\boldsymbol{x}}\,(\boldsymbol{x}\cdot\partial_x\nabla\eta_\mathrm{b}) - \hat{\boldsymbol{y}}\,(\boldsymbol{x}\cdot\partial_y\nabla\eta_\mathrm{b}) = \hat{\boldsymbol{z}} - \nabla\eta_\mathrm{b} - (\boldsymbol{x}\cdot\nabla)\,\nabla\eta_\mathrm{b}. \tag{63.24}$$

In the case where the bottom slope is constant in both directions then this result simplifies to

$$\boldsymbol{e}^{\overline{3}} = \hat{\boldsymbol{z}} - \nabla\eta_\mathrm{b}. \tag{63.25}$$

63.4.3 Verifying the bi-orthogonality relation

The basis one-forms satisfy the bi-orthogonality relation (4.25) with the basis vectors

$$\boldsymbol{e}^{\overline{a}}\cdot\boldsymbol{e}_{\overline{b}} = \delta^{\overline{a}}_{\overline{b}}. \tag{63.26}$$

This identity is trivial to verify for all $\overline{a} = 1, 2, 3$.

63.5 Triple product identities

We find various occasions to make use of a suite of triple product identities that hold for GVCs. For this purpose we write σ as a composite function as in Section 4.9.3

$$\sigma = \sigma(x, y, z, t) = \sigma[x, y, z(\overline{t}, \overline{x}, \overline{y}, \sigma), t], \tag{63.27}$$

with $\eta(\overline{x}, \overline{y}, \sigma, \overline{t})$ written as $z(\overline{x}, \overline{y}, \sigma, \overline{t})$ as it here eases the manipulations. Use of the chain rule leads to the space-time differential increment

$$\mathrm{d}\sigma = \mathrm{d}t\left[\frac{\partial\sigma}{\partial t}\right]_{x,y,z} + \mathrm{d}x\left[\frac{\partial\sigma}{\partial x}\right]_{t,y,z} + \mathrm{d}y\left[\frac{\partial\sigma}{\partial y}\right]_{t,x,z} + \mathrm{d}z\left[\frac{\partial\sigma}{\partial z}\right]_{t,x,y}. \tag{63.28}$$

Likewise, writing $z = z[\overline{t}, \overline{x}, \overline{y}, \sigma]$ leads to the space-time differential increment $\mathrm{d}z$

$$\mathrm{d}z = \mathrm{d}\overline{t}\left[\frac{\partial z}{\partial \overline{t}}\right]_{\overline{x},\overline{y},\sigma} + \mathrm{d}\overline{x}\left[\frac{\partial z}{\partial \overline{x}}\right]_{\overline{t},\overline{y},\sigma} + \mathrm{d}\overline{y}\left[\frac{\partial z}{\partial \overline{y}}\right]_{\overline{t},\overline{x},\sigma} + \mathrm{d}\sigma\left[\frac{\partial z}{\partial \sigma}\right]_{\overline{t},\overline{x},\overline{y}}. \tag{63.29}$$

We note the identities

$$\left[\frac{\partial\sigma}{\partial z}\right]_{t,x,y}\left[\frac{\partial z}{\partial\sigma}\right]_{\overline{t},\overline{x},\overline{y}} = 1 \qquad \mathrm{d}\overline{t} = \mathrm{d}t \qquad \mathrm{d}\overline{x} = \mathrm{d}x \qquad \mathrm{d}\overline{y} = \mathrm{d}y, \tag{63.30}$$

which follow since $t = \overline{t}$, $x = \overline{x}$, and $y = \overline{y}$. Substituting equation (63.29) into equation (63.28) and making use of the identities (63.30) yields

$$\begin{aligned} 0 = \mathrm{d}t &\left[\left[\frac{\partial\sigma}{\partial t}\right]_{x,y,z} + \left[\frac{\partial\sigma}{\partial z}\right]_{t,x,y}\left[\frac{\partial z}{\partial \overline{t}}\right]_{\overline{x},\overline{y},\sigma}\right] \\ + \mathrm{d}x &\left[\left[\frac{\partial\sigma}{\partial x}\right]_{t,y,z} + \left[\frac{\partial\sigma}{\partial z}\right]_{t,x,y}\left[\frac{\partial z}{\partial \overline{x}}\right]_{\overline{t},\overline{y},\sigma}\right] + \mathrm{d}y\left[\left[\frac{\partial\sigma}{\partial y}\right]_{t,x,z} + \left[\frac{\partial\sigma}{\partial z}\right]_{t,x,y}\left[\frac{\partial z}{\partial \overline{y}}\right]_{\overline{t},\overline{x},\sigma}\right]. \end{aligned} \tag{63.31}$$

For this equation to hold with general increments $\mathrm{d}t$, $\mathrm{d}x$, and $\mathrm{d}y$ requires that each bracketed term vanish, which in turn leads to the following set of triple product identities[2]

$$\left[\frac{\partial\sigma}{\partial z}\right]_{t,x,y}\left[\frac{\partial z}{\partial\overline{t}}\right]_{\overline{x},\overline{y},\sigma} = -\left[\frac{\partial\sigma}{\partial t}\right]_{x,y,z} \tag{63.32a}$$

$$\left[\frac{\partial\sigma}{\partial z}\right]_{t,x,y}\left[\frac{\partial z}{\partial\overline{x}}\right]_{\overline{t},\overline{y},\sigma} = -\left[\frac{\partial\sigma}{\partial x}\right]_{t,y,z} \tag{63.32b}$$

$$\left[\frac{\partial\sigma}{\partial z}\right]_{t,x,y}\left[\frac{\partial z}{\partial\overline{y}}\right]_{\overline{t},\overline{x},\sigma} = -\left[\frac{\partial\sigma}{\partial y}\right]_{t,x,z}. \tag{63.32c}$$

If the vertical stratification, $\partial\sigma/\partial z$, is non-zero, the triple product identities are equivalent to

$$\left[\frac{\partial z}{\partial\overline{t}}\right]_{\overline{x},\overline{y},\sigma} = -\frac{[\partial\sigma/\partial t]_{x,y,z}}{[\partial\sigma/\partial z]_{t,x,y}} = -\left[\frac{\partial\sigma}{\partial t}\right]_{x,y,z}\left[\frac{\partial z}{\partial\sigma}\right]_{t,x,y} \tag{63.33a}$$

$$\left[\frac{\partial z}{\partial\overline{x}}\right]_{\overline{t},\overline{y},\sigma} = -\frac{[\partial\sigma/\partial x]_{t,y,z}}{[\partial\sigma/\partial z]_{t,x,y}} = -\left[\frac{\partial\sigma}{\partial x}\right]_{t,y,z}\left[\frac{\partial z}{\partial\sigma}\right]_{t,x,y} \tag{63.33b}$$

$$\left[\frac{\partial z}{\partial\overline{y}}\right]_{\overline{t},\overline{x},\sigma} = -\frac{[\partial\sigma/\partial y]_{t,x,z}}{[\partial\sigma/\partial z]_{t,x,y}} = -\left[\frac{\partial\sigma}{\partial y}\right]_{t,x,z}\left[\frac{\partial z}{\partial\sigma}\right]_{t,x,y}. \tag{63.33c}$$

Since $t=\overline{t}$, $x=\overline{x}$, and $y=\overline{y}$ we can write these identities in the more succinct form

$$\left[\frac{\partial z}{\partial\overline{t}}\right]_{\sigma} = \left[\frac{\partial\eta}{\partial\overline{t}}\right]_{\sigma} = -\frac{[\partial\sigma/\partial t]_z}{[\partial\sigma/\partial z]} \tag{63.34a}$$

$$\left[\frac{\partial z}{\partial\overline{x}}\right]_{\sigma} = \left[\frac{\partial\eta}{\partial\overline{x}}\right]_{\sigma} = -\frac{[\partial\sigma/\partial x]_z}{[\partial\sigma/\partial z]} \tag{63.34b}$$

$$\left[\frac{\partial z}{\partial\overline{y}}\right]_{\sigma} = \left[\frac{\partial\eta}{\partial\overline{y}}\right]_{\sigma} = -\frac{[\partial\sigma/\partial y]_z}{[\partial\sigma/\partial z]}, \tag{63.34c}$$

where we reintroduced the notation $\eta(x,y,\sigma,t)=z(x,y,\sigma,t)$. These identities are quite useful for manipulating equations involving GVCs. In particular, equations (63.34b) and (63.34c) provide alternate expressions for the slope of σ isosurfaces relative to the horizontal plane (see Section 63.12).

63.6 Position vector

We are familiar with locating a point in space using Cartesian coordinates as in Figure 1.1. What about specifying the position using GVCs? We can do so by making use of the basis vectors (63.16a)-(63.16c) so that the position of an arbitrary point in space is given by

$$\mathscr{P} = \xi^{\overline{a}}\,\boldsymbol{e}_{\overline{a}} \tag{63.35a}$$

$$= \overline{x}\,[\hat{\boldsymbol{x}} + (\partial\eta/\partial\overline{x})\,\hat{\boldsymbol{z}}] + \overline{y}\,[\hat{\boldsymbol{y}} + (\partial\eta/\partial\overline{y})\,\hat{\boldsymbol{z}}] + \sigma\,(\partial\eta/\partial\sigma)\,\hat{\boldsymbol{z}} \tag{63.35b}$$

$$= \hat{\boldsymbol{x}}\,\overline{x} + \hat{\boldsymbol{y}}\,\overline{y} + \hat{\boldsymbol{z}}\,[\overline{x}\,(\partial\eta/\partial\overline{x}) + \overline{y}\,(\partial\eta/\partial\overline{y}) + \sigma\,(\partial\eta/\partial\sigma)] \tag{63.35c}$$

$$= \hat{\boldsymbol{x}}\,\overline{x} + \hat{\boldsymbol{y}}\,\overline{y} + \hat{\boldsymbol{z}}\,\xi^{\overline{a}}\,\partial_{\overline{a}}\eta. \tag{63.35d}$$

We identify the following properties as a means to help understand these expressions, with Figure 63.3 offering a schematic.

[2] These identities are directly analogous to the Maxwell relations from thermodynamics, with an introduction in Section 22.8 and full details in the book by *Callen* (1985).

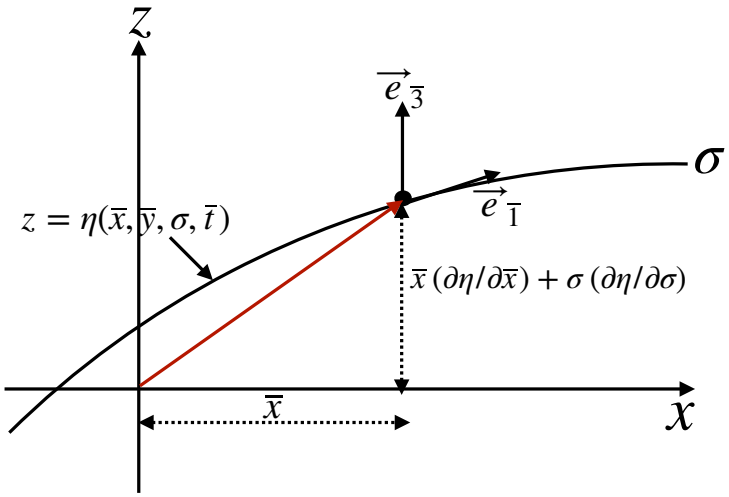

FIGURE 63.3: The position of a point in space as represented using GVCs following equation (63.36a). For this example, $\overline{y} = 0$ so that the horizontal position is determined by the coordinate $\overline{x} = x$, whereas the vertical postion is determined by $\overline{x}\,(\partial z/\partial\overline{x}) + \sigma\,(\partial z/\partial\sigma) = \overline{x}\,(\partial\eta/\partial\overline{x}) + \sigma\,(\partial\eta/\partial\sigma)$.

- The expression (63.35b) has horizontal positions $\overline{x}$ and $\overline{y}$ multiplying the basis vectors $\boldsymbol{e}_{\overline{x}}$ and $\boldsymbol{e}_{\overline{y}}$, with these vectors oriented parallel to a surface of constant GVC as in Figure 63.3. Likewise, the third term, $\sigma\,(\partial\eta/\partial\sigma)\,\hat{\boldsymbol{z}}$, positions the point vertically according to the value of the GVC and its inverse stratification.

- Consider the case of $\overline{y} = 0$ so that

$$\begin{aligned} \mathscr{P} &= \overline{x}\,\hat{\boldsymbol{x}} + \hat{\boldsymbol{z}}\,[\overline{x}\,(\partial\eta/\partial\overline{x}) + \sigma\,(\partial\eta/\partial\sigma)] && \text{(63.36a)} \\ &= \overline{x}\,\hat{\boldsymbol{x}} + \hat{\boldsymbol{z}}\,(\partial\eta/\partial\sigma)\,[\overline{x}\,(\partial\sigma/\partial z)_x(\partial\eta/\partial\overline{x})_\sigma + \sigma] && \text{(63.36b)} \\ &= \overline{x}\,\hat{\boldsymbol{x}} + \hat{\boldsymbol{z}}\,(\partial\eta/\partial\sigma)\,[-\overline{x}\,(\partial\sigma/\partial x)_z + \sigma], && \text{(63.36c)} \end{aligned}$$

  where we used the triple product identity (63.34b) for the final equality. Consequently, a horizontal position vector is realized using GVC coordinates with $\sigma = \overline{x}\,(\partial\sigma/\partial x)$. That is, a horizontal position vector crosses surfaces of constant GVC when the GVC surface has a nonzero horizontal slope.

- The projection of the position vector onto the basis one-forms leads to

$$\mathscr{P} \cdot \boldsymbol{e}^{\overline{b}} = \xi^{\overline{a}}\,\boldsymbol{e}_{\overline{a}} \cdot \boldsymbol{e}^{\overline{b}} = \xi^{\overline{b}}. \tag{63.37}$$

  This result follows from the orthogonality relation (4.25). So the projection of the position vector onto a basis one-form picks out the corresponding coordinate value.

- Equation (63.7) provides the spatial dependence for the vertical position of the surface of constant GVC

$$z = z(\xi^{\overline{a}}) = \eta(\xi^{\overline{a}}). \tag{63.38}$$

  At any particular time instance we can perform a Taylor series about a reference geopotential $z_0 = \eta_0$, so that

$$\eta(\xi^{\overline{a}}) \approx \eta_0 + \xi^{\overline{a}}\,\partial_{\overline{a}}\eta. \tag{63.39}$$

  We can thus write the position (63.35d) in the form

$$\mathscr{P} = \hat{\boldsymbol{x}}\,\overline{x} + \hat{\boldsymbol{y}}\,\overline{y} + \hat{\boldsymbol{z}}\,[\eta - \eta_0]. \tag{63.40}$$

  Taking the reference geopotential as $\eta_0 = 0$ recovers the Cartesian expression. Since the

position vector is a geometric object, it is reassuring that the GVC representation is the same as the Cartesian representation; it is merely a reorganization of the basis vectors and corresponding coordinates.

63.7 Transforming components of a vector

Consider a vector field $\vec{F}$ with Cartesian representation

$$\vec{F} = \boldsymbol{F} = F^a \, \boldsymbol{e}_a = F^x \, \hat{\boldsymbol{x}} + F^y \, \hat{\boldsymbol{y}} + F^z \, \hat{\boldsymbol{z}}. \tag{63.41}$$

The corresponding GVC components are related through the transformation matrix

$$F^{\overline{a}} = \Lambda^{\overline{a}}{}_a \, F^a. \tag{63.42}$$

Making use of the transformation matrix (63.20) yields the relations between GVC components and Cartesian components

$$F^{\overline{1}} = F^1 \quad \text{and} \quad F^{\overline{2}} = F^2 \quad \text{and} \quad F^{\overline{3}} = \nabla\sigma \cdot \boldsymbol{F}, \tag{63.43}$$

where we wrote

$$\nabla\sigma \cdot \boldsymbol{F} = (\partial\sigma/\partial x) \, F^1 + (\partial\sigma/\partial y) \, F^2 + (\partial\sigma/\partial z) \, F^3. \tag{63.44}$$

The vector field thus can be represented in GVC coordinates as

$$\vec{F} = F^{\overline{a}} \, \boldsymbol{e}_{\overline{a}} = F^1 \, \boldsymbol{e}_{\overline{1}} + F^2 \, \boldsymbol{e}_{\overline{2}} + (\nabla\sigma \cdot \boldsymbol{F}) \, \boldsymbol{e}_{\overline{3}}. \tag{63.45}$$

Similarly, the covariant components transform as $F_{\overline{a}} = \Lambda^a{}_{\overline{a}} \, F_a$, where use of the inverse transformation matrix (63.20) renders

$$F_{\overline{1}} = F_1 + (\partial z/\partial\overline{x}) \, F_3 = F_1 + (\partial\eta/\partial\overline{x}) \, F_3 \tag{63.46a}$$
$$F_{\overline{2}} = F_2 + (\partial z/\partial\overline{y}) \, F_3 = F_2 + (\partial\eta/\partial\overline{y}) \, F_3 \tag{63.46b}$$
$$F_{\overline{3}} = (\partial z/\partial\sigma) \, F_3 = (\partial\eta/\partial\sigma) \, F_3, \tag{63.46c}$$

and the expression for the vector field

$$\vec{F} = F_{\overline{a}} \, \boldsymbol{e}^{\overline{a}} = [F_1 + (\partial\eta/\partial\overline{x}) \, F_3] \, \boldsymbol{e}^{\overline{1}} + [F_2 + (\partial\eta/\partial\overline{y}) \, F_3] \, \boldsymbol{e}^{\overline{2}} + (\partial\eta/\partial\sigma) \, F_3 \, \boldsymbol{e}^{\overline{3}}. \tag{63.47}$$

Recall also that for Cartesian coordinates the contravarient and covariant components to a vector are identical: $F^a = F_a$.

63.8 Velocity

As an example of the results from Section 63.7, we here represent the velocity vector, considering both covariant and contravariant representations. As for the position vector detailed in Section 63.6, we are assured that both representations lead to the same velocity vector since the velocity is an objective geometric object (i.e., an arrow with a magnitude). In Section 63.8.4 we verify that the transformation formalism indeed respects this equivalance, with the GVC representations equivalent to the Cartesian representation

$$\vec{v} = u \, \hat{\boldsymbol{x}} + v \, \hat{\boldsymbol{y}} + w \, \hat{\boldsymbol{z}}. \tag{63.48}$$

63.8.1 Contravariant components

Following Section 63.7, we have the contravariant velocity components

$$v^{\overline{1}} = u \qquad \text{and} \qquad v^{\overline{2}} = v \qquad \text{and} \qquad v^{\overline{3}} = \boldsymbol{v} \cdot \nabla\sigma. \tag{63.49}$$

Use of the basis vectors (63.16a)-(63.16c) then leads to

$$\begin{aligned} \vec{v} &= v^{\overline{a}}\, \boldsymbol{e}_{\overline{a}} && \text{(63.50a)} \\ &= u\, \boldsymbol{e}_{\overline{x}} + v\, \boldsymbol{e}_{\overline{y}} + (\boldsymbol{v} \cdot \nabla\sigma)\, \boldsymbol{e}_{\sigma} && \text{(63.50b)} \\ &= u\, [\hat{\boldsymbol{x}} + (\partial\eta/\partial\overline{x})\, \hat{\boldsymbol{z}}] + v\, [\hat{\boldsymbol{y}} + (\partial\eta/\partial\overline{y})\, \hat{\boldsymbol{z}}] + (\boldsymbol{v} \cdot \nabla\sigma)\, (\partial\eta/\partial\sigma)\, \hat{\boldsymbol{z}}. && \text{(63.50c)} \end{aligned}$$

63.8.2 Covariant components

The covariant velocity components are given by

$$v_{\overline{1}} = u + (\partial\eta/\partial\overline{x})\, w \qquad \text{and} \qquad v_{\overline{2}} = v + (\partial\eta/\partial\overline{y})\, w \qquad \text{and} \qquad v_{\overline{3}} = (\partial\eta/\partial\sigma)\, w. \tag{63.51}$$

The one-form basis (63.22a)–(63.22c) thus leads to the velocity vector

$$\vec{v} = v_{\overline{a}}\, \tilde{e}^{\overline{a}} = [u + (\partial\eta/\partial\overline{x})\, w]\, \hat{\boldsymbol{x}} + [v + (\partial\eta/\partial\overline{y})\, w]\, \hat{\boldsymbol{y}} + w\, (\partial\eta/\partial\sigma)\, \nabla\sigma. \tag{63.52}$$

63.8.3 Introducing the material time derivative

The material evolution for the generalized vertical coordinate can be written

$$\frac{\mathrm{D}\sigma}{\mathrm{D}t} = \frac{\partial\sigma}{\partial t} + \boldsymbol{v} \cdot \nabla\sigma = \dot{\sigma}, \tag{63.53}$$

with $\dot{\sigma}$ symbolizing any process contributing to motion across σ isosurfaces (as fully explained in Section 64.3). Using the expression (63.53) in the velocity vector expression (63.50c) leads to

$$\begin{aligned} \vec{v} &= u\, [\hat{\boldsymbol{x}} + (\partial\eta/\partial\overline{x})\, \hat{\boldsymbol{z}}] + v\, [\hat{\boldsymbol{y}} + (\partial\eta/\partial\overline{y})\, \hat{\boldsymbol{z}}] + (\boldsymbol{v} \cdot \nabla\sigma)\, (\partial\eta/\partial\sigma)\, \hat{\boldsymbol{z}}. && \text{(63.54a)} \\ &= u\, [\hat{\boldsymbol{x}} + (\partial\eta/\partial\overline{x})\, \hat{\boldsymbol{z}}] + v\, [\hat{\boldsymbol{y}} + (\partial\eta/\partial\overline{y})\, \hat{\boldsymbol{z}}] + (\dot{\sigma} - \partial\sigma/\partial t)\, (\partial\eta/\partial\sigma)\, \hat{\boldsymbol{z}} && \text{(63.54b)} \\ &= u\, \hat{\boldsymbol{x}} + v\, \hat{\boldsymbol{y}} + [\partial\eta/\partial\overline{t} + \boldsymbol{u} \cdot \nabla_{\!\varpi} z + (\partial\eta/\partial\sigma)\dot{\sigma}]\, \hat{\boldsymbol{z}}, && \text{(63.54c)} \end{aligned}$$

where the final equality made use of the triple product (63.33a): $(\partial\sigma/\partial t)\, (\partial\eta/\partial\sigma) = -\partial\eta/\partial\overline{t}$. In the steady state and in the absence of material changes to σ, the three dimensional flow lies within a surface of constant σ, whereby $\boldsymbol{v} \cdot \nabla\sigma = 0$ and

$$\vec{v} = u\, [\hat{\boldsymbol{x}} + (\partial\eta/\partial\overline{x})\, \hat{\boldsymbol{z}}] + v\, [\hat{\boldsymbol{y}} + (\partial\eta/\partial\overline{y})\, \hat{\boldsymbol{z}}] \qquad \text{if } \partial_t\sigma = 0 \text{ and } \dot{\sigma} = 0. \tag{63.55}$$

However, in general there are transient fluctuations and material changes to σ so that $\boldsymbol{v} \cdot \nabla\sigma \neq 0$.

63.8.4 Equivalence to the Cartesian velocity representation

Use of the triple product identities (63.34b)-(63.34c) allows us to manipulate both expressions (63.50c) and (63.52) to recover the Cartesian expression

$$\vec{v} = u\, \hat{\boldsymbol{x}} + v\, \hat{\boldsymbol{y}} + w\, \hat{\boldsymbol{z}}. \tag{63.56}$$

Another way to see this identity is to note that in equation (63.54c), the vertical component is an expression for the material time derivative of the vertical position

$$w = \frac{\mathrm{D}z}{\mathrm{D}t} = \frac{\partial \eta}{\partial \overline{t}} + \boldsymbol{u} \cdot \nabla_{\!\!\varpi} \eta + \frac{\partial \eta}{\partial \sigma} \, \dot{\sigma}. \tag{63.57}$$

We derive this identity in Section 64.4 where we discuss further kinematic results using GVCs.

63.9 Metric tensor

Recall from Section 4.1 that we make use of a metric tensor to measure the distance between two points in space. The GVC representation of the metric tensor is given by

$$g_{\overline{a}\overline{b}} = \boldsymbol{e}_{\overline{a}} \cdot \boldsymbol{e}_{\overline{b}} = \begin{bmatrix} 1 + (\partial z/\partial \overline{x})^2 & (\partial z/\partial \overline{x}) \, (\partial z/\partial \overline{y}) & (\partial z/\partial \overline{x}) \, (\partial z/\partial \sigma) \\ (\partial z/\partial \overline{x}) \, (\partial z/\partial \overline{y}) & 1 + (\partial z/\partial \overline{y})^2 & (\partial z/\partial \overline{y}) \, (\partial z/\partial \sigma) \\ (\partial z/\partial \overline{x}) \, (\partial z/\partial \sigma) & (\partial z/\partial \overline{y}) \, (\partial z/\partial \sigma) & (\partial z/\partial \sigma)^2 \end{bmatrix}, \tag{63.58}$$

with the triple product identities (63.34b) and (63.34c) bringing the metric into the form

$$g_{\overline{a}\overline{b}} = \begin{bmatrix} 1 + [(\partial \sigma/\partial x) \, (\partial z/\partial \sigma)]^2 & (\partial \sigma/\partial x) \, (\partial \sigma/\partial y) \, (\partial z/\partial \sigma)^2 & -(\partial \sigma/\partial x) \, (\partial z/\partial \sigma)^2 \\ (\partial \sigma/\partial x) \, (\partial \sigma/\partial y) \, (\partial z/\partial \sigma)^2 & 1 + [(\partial \sigma/\partial y) \, (\partial z/\partial \sigma)]^2 & -(\partial \sigma/\partial y) \, (\partial z/\partial \sigma)^2 \\ -(\partial \sigma/\partial x) \, (\partial z/\partial \sigma)^2 & -(\partial \sigma/\partial y) \, (\partial z/\partial \sigma)^2 & (\partial z/\partial \sigma)^2 \end{bmatrix}. \tag{63.59}$$

The representation of the inverse metric tensor is given by the somewhat simpler expression

$$g^{\overline{a}\overline{b}} = \boldsymbol{e}^{\overline{a}} \cdot \boldsymbol{e}^{\overline{b}} = \begin{bmatrix} 1 & 0 & \partial \sigma/\partial x \\ 0 & 1 & \partial \sigma/\partial y \\ \partial \sigma/\partial x & \partial \sigma/\partial y & |\nabla \sigma|^2 \end{bmatrix}. \tag{63.60}$$

Proof that $g^{\overline{a}\overline{b}} \, g_{\overline{b}\overline{c}} = \delta^{\overline{a}}_{\overline{c}}$ requires use of the triple product identities (63.34b) and (63.34c). Note that an additional means to derive the metric tensor (63.58) is given by writing the squared line element as[3]

$$\mathrm{d}s^2 = \mathrm{d}x^2 + \mathrm{d}y^2 + \mathrm{d}z^2 \tag{63.61a}$$

$$= \mathrm{d}x^2 + \mathrm{d}y^2 + [(\partial z/\partial \overline{x}) \, \mathrm{d}x + (\partial z/\partial \overline{y}) \, \mathrm{d}y + (\partial z/\partial \sigma) \, \mathrm{d}\sigma]^2, \tag{63.61b}$$

from which the metric tensor (63.58) is revealed upon expanding the quadratic term and then rearranging.

63.9.1 Jacobian of transformation

The determinant of the GVC representation of the metric tensor (63.58) is

$$\det(g_{\overline{a}\overline{b}}) = (\partial z/\partial \sigma)^2 = (\partial \eta/\partial \sigma)^2 \tag{63.62}$$

so that the Jacobian of transformation (Section 4.5) is the specific thickness

$$\frac{\partial(x, y, z)}{\partial(\overline{x}, \overline{y}, \sigma)} = \frac{\partial z}{\partial \sigma} = \frac{\partial \eta}{\partial \sigma}. \tag{63.63}$$

[3]The traditional notation in physics writes the squared line element as $\mathrm{d}s^2 = (\mathrm{d}s)^2$. Likewise, $\mathrm{d}x^2 = (\mathrm{d}x)^2$, etc.

The coordinate transformation from Cartesian to generalized vertical is invertible only so long as the Jabobian remains nonzero and single-signed, meaning the fluid retains a monotonic vertical stratification of GVC surfaces. The invertible relation between z and σ means that each point in the vertical can be uniquely specified by either of the two vertical coordinates, z or σ. For example, the Jacobian for pressure as the generalized vertical coordinate in a hydrostatic fluid is given by[4]

$$\frac{\partial z}{\partial \sigma} = \frac{\partial z}{\partial p} = -\frac{1}{\rho g}, \tag{63.64}$$

which is indeed single-signed since the mass density is always positive.

63.9.2 Covariant and contravariant representations

The metric tensor allows us to convert between the covariant and contravariant representations of a vector via the identity (Section 4.2.3)

$$F_{\overline{a}} = g_{\overline{a}\overline{b}} F^{\overline{b}}. \tag{63.65}$$

We use triple product identities (63.34b)-(63.34c) to verify that this relation agrees with the transformation matrix approach detailed in Section 63.7. For example,

$$\begin{aligned}
F_{\overline{1}} &= g_{\overline{1}\overline{b}} F^{\overline{b}} && \text{(63.66a)}\\
&= [1 + (\partial\eta/\partial\overline{x})^2] F^{\overline{1}} + (\partial\eta/\partial\overline{x})(\partial\eta/\partial\overline{y}) F^{\overline{2}} + (\partial\eta/\partial\overline{x})(\partial\eta/\partial\sigma) F^{\sigma} && \text{(63.66b)}\\
&= [1 + (\partial\eta/\partial\overline{x})^2] F^{1} + (\partial\eta/\partial\overline{x})(\partial\eta/\partial\overline{y}) F^{2} + (\partial\eta/\partial\overline{x})(\partial\eta/\partial\sigma) \nabla\sigma \cdot \boldsymbol{F} && \text{(63.66c)}\\
&= F^1 + (\partial\eta/\partial\overline{x}) F^3 && \text{(63.66d)}\\
&= F_1 + (\partial\eta/\partial\overline{x}) F_3, && \text{(63.66e)}
\end{aligned}$$

where the final equality holds since $F^1 = F_1$ and $F^3 = F_3$ for Cartesian tensor components.

63.10 Volume element and the Levi-Civita tensor

The square root of the determinant of the metric tensor (63.58) is

$$\sqrt{\det(g_{\overline{a}\overline{b}})} = \partial z/\partial\sigma = \partial\eta/\partial\sigma \tag{63.67}$$

so that the volume element (Section 4.5) is

$$\mathrm{d}V = (\partial z/\partial\sigma)\,\mathrm{d}x\,\mathrm{d}y\,\mathrm{d}\sigma. \tag{63.68}$$

The covariant Levi-Civita tensor (Section 4.7) has the GVC representations

$$\varepsilon_{\overline{a}\overline{b}\overline{c}} = (\partial z/\partial\sigma)\,\epsilon_{\overline{a}\overline{b}\overline{c}} \qquad \varepsilon^{\overline{a}\overline{b}\overline{c}} = (\partial z/\partial\sigma)^{-1}\,\epsilon^{\overline{a}\overline{b}\overline{c}} \tag{63.69}$$

where ϵ is the permutation symbol introduced in Section 1.7.1 with its components independent of coordinate representation.

[4] We derive the hydrostatic balance in Section 27.2.

63.11 Vector cross product of basis vectors

We now verify the relation (4.87) for the cross product of two basis vectors using GVCs

$$\boldsymbol{e}_{\overline{a}} \times \boldsymbol{e}_{\overline{b}} = \varepsilon_{\overline{a}\overline{b}\overline{c}}\, \boldsymbol{e}^{\overline{c}} \implies \boldsymbol{e}_{\overline{a}} \times \boldsymbol{e}_{\overline{b}} = (\partial z/\partial\sigma)\epsilon_{\overline{a}\overline{b}\overline{c}}\, \boldsymbol{e}^{\overline{c}}. \tag{63.70}$$

Making use of the basis vectors from Section 63.3 and the basis one-forms from Section 63.4 renders

$$\boldsymbol{e}_{\overline{x}} \times \boldsymbol{e}_{\overline{y}} = \hat{\boldsymbol{z}} - \hat{\boldsymbol{x}}\,(\partial\eta/\partial\overline{x}) - \hat{\boldsymbol{y}}\,(\partial\eta/\partial\overline{y}) = (\partial z/\partial\sigma)\,\nabla\sigma = \varepsilon_{\overline{x}\overline{y}\sigma}\,\boldsymbol{e}^{\sigma} \tag{63.71a}$$

$$\boldsymbol{e}_{\overline{y}} \times \boldsymbol{e}_{\sigma} = \hat{\boldsymbol{x}}\,(\partial z/\partial\sigma) = \varepsilon_{\overline{y}\sigma\overline{x}}\,\boldsymbol{e}^{\overline{x}} \tag{63.71b}$$

$$\boldsymbol{e}_{\sigma} \times \boldsymbol{e}_{\overline{x}} = \hat{\boldsymbol{y}}\,(\partial z/\partial\sigma) = \varepsilon_{\sigma\overline{x}\overline{y}}\,\boldsymbol{e}^{\overline{y}}. \tag{63.71c}$$

63.12 Partial derivative operators

We here consider the partial derivative operators and their transformation between coordinate systems. These identities are used throughout GVC calculus. Given the importance of these expressions, we offer two derivations. Notably, the geometric derivation in Section 63.12.2 requires minimal use of the previous tensor formalism.

63.12.1 Analytical derivation

The partial derivative operators in GVCs are computed via $\partial_{\overline{a}} = \Lambda^{a}{}_{\overline{a}}\,\partial_a$. Including also the time component leads to the relations

$$\partial_{\overline{t}} = \partial_t + (\partial z/\partial\overline{t})\,\partial_z = \partial_t + (\partial\eta/\partial\overline{t})\,\partial_z \tag{63.72a}$$

$$\partial_{\overline{x}} = \partial_x + (\partial z/\partial\overline{x})\,\partial_z = \partial_x + (\partial\eta/\partial\overline{x})\,\partial_z \tag{63.72b}$$

$$\partial_{\overline{y}} = \partial_y + (\partial z/\partial\overline{y})\,\partial_z = \partial_y + (\partial\eta/\partial\overline{y})\,\partial_z \tag{63.72c}$$

$$\partial_{\sigma} = (\partial z/\partial\sigma)\,\partial_z = (\partial\eta/\partial\sigma)\,\partial_z. \tag{63.72d}$$

We can make use of the triple product identities (63.34b) and (63.34c) to express the slope of a constant GVC surface in the equivalent manners

$$\boldsymbol{S} = \nabla_{\!\!\text{h}\sigma}\eta = \nabla_{\!\!\text{h}\sigma} z = -(\partial\sigma/\partial z)^{-1}\,\nabla_{\!\!\text{h}}\sigma \tag{63.73}$$

where we introduced the standard shorthand notation

$$\nabla_{\!\!\text{h}\sigma} = \hat{\boldsymbol{x}}\,\partial/\partial\overline{x} + \hat{\boldsymbol{y}}\,\partial/\partial\overline{y} \qquad \text{and} \qquad \nabla_{\!\!\text{h}} = \hat{\boldsymbol{x}}\,\partial/\partial x + \hat{\boldsymbol{y}}\,\partial/\partial y. \tag{63.74}$$

It is common to transform between the horizontal gradient operators, in which case we write

$$\nabla_{\!\!\text{h}\sigma} = \nabla_{\!\!\text{h}} + (\nabla_{\!\!\text{h}\sigma} z)\,\partial_z \equiv \nabla_{\!\!\text{h}} + \boldsymbol{S}\,\partial_z. \tag{63.75}$$

We emphasize that $\nabla_{\!\!\text{h}\sigma}$ is merely a shorthand for the two partial derivative operators and that it only has components in the horizontal directions. Furthermore, the σ subscript is not a tensor index.

63.12.2 Geometrical derivation

We provide a geometric derivation for the lateral derivative operator that complements the previous analytical derivation. This operator is computed by taking the difference of a function along surfaces of constant generalized vertical coordinate, but with the lateral distance computed

in the horizontal direction as show in Figure 63.4. This feature of the horizontal derivative operator is a key aspect of the GVCs' non-orthogonality.

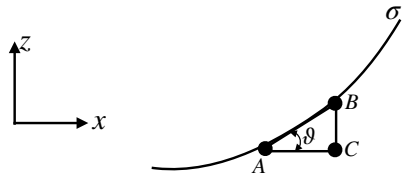

$$\left[\frac{\partial \psi}{\partial x}\right]_\sigma \approx \frac{\psi(B)-\psi(A)}{x(C)-x(A)}$$

FIGURE 63.4: A surface of constant generalized vertical coordinate, σ, along with a local tangent plane with a slope $\tan\vartheta$ with respect to the horizontal plane. This figure illustrates the identities (63.77a)-(63.77d), with these identities relating a lateral derivative taken along the GVC surface to horizontal and vertical derivatives taken along orthogonal Cartesian axes.

Consider the geometry shown in Figure 63.4, which shows a generalized vertical coordinate surface (constant σ surface) along with a sample tangent plane with a slope

$$S^x = \frac{\text{rise}}{\text{run}} = \tan\vartheta = \frac{z(B)-z(C)}{x(C)-x(A)} \approx \left[\frac{\partial z}{\partial x}\right]_\sigma = -\frac{(\partial\sigma/\partial x)_z}{(\partial\sigma/\partial z)} \tag{63.76}$$

relative to the horizontal. We readily verify the following identities based on finite difference operations for an arbitrary function

$$\left[\frac{\partial \psi}{\partial x}\right]_\sigma \approx \frac{\psi(B)-\psi(A)}{x(C)-x(A)} \tag{63.77a}$$

$$= \frac{\psi(C)-\psi(A)}{x(C)-x(A)} + \frac{\psi(B)-\psi(C)}{x(C)-x(A)} \tag{63.77b}$$

$$= \frac{\psi(C)-\psi(A)}{x(C)-x(A)} + \left[\frac{z(B)-z(C)}{x(C)-x(A)}\right]\frac{\psi(B)-\psi(C)}{z(B)-z(C)} \tag{63.77c}$$

$$= \left[\frac{\partial \psi}{\partial x}\right]_z + S^x \left[\frac{\partial \psi}{\partial z}\right]_x. \tag{63.77d}$$

Taking the continuum limit then leads to the relations between horizontal derivatives computed on constant σ surfaces to those computed on constant z surfaces

$$\left[\frac{\partial}{\partial x}\right]_\sigma = \left[\frac{\partial}{\partial x}\right]_z + \left[\frac{\partial z}{\partial x}\right]_\sigma \frac{\partial}{\partial z} = \left[\frac{\partial}{\partial x}\right]_z + \left[\frac{\partial \eta}{\partial x}\right]_\sigma \frac{\partial}{\partial z} \tag{63.78a}$$

$$\left[\frac{\partial}{\partial y}\right]_\sigma = \left[\frac{\partial}{\partial y}\right]_z + \left[\frac{\partial z}{\partial y}\right]_\sigma \frac{\partial}{\partial z} = \left[\frac{\partial}{\partial y}\right]_z + \left[\frac{\partial \eta}{\partial y}\right]_\sigma \frac{\partial}{\partial z}, \tag{63.78b}$$

which can be written in the shorthand vector notation

$$\nabla_{\!\sigma} = \hat{\boldsymbol{x}}\left[\frac{\partial}{\partial x}\right]_\sigma + \hat{\boldsymbol{y}}\left[\frac{\partial}{\partial y}\right]_\sigma = \nabla_{\!\mathrm{h}} + (\nabla_{\!\sigma} z)\,\partial_z = \nabla_{\!\mathrm{h}} + (\nabla_{\!\sigma}\eta)\,\partial_z. \tag{63.79}$$

63.12.3 The gradient as a tensor operator

The gradient is given by the equivalent expressions

$$\nabla = \boldsymbol{e}^a\,\partial_a = \boldsymbol{e}^{\overline{a}}\,\partial_{\overline{a}}. \tag{63.80}$$

The gradient has the following Cartesian coordinate expression

$$\nabla = \hat{\boldsymbol{x}}\,\partial_x + \hat{\boldsymbol{y}}\,\partial_y + \hat{\boldsymbol{z}}\,\partial_z, \tag{63.81}$$

and the equivalent generalized vertical coordinate expression

$$\nabla = \hat{\boldsymbol{x}}\,\partial_{\overline{x}} + \hat{\boldsymbol{y}}\,\partial_{\overline{y}} + (\nabla\sigma)\,\partial_\sigma. \tag{63.82}$$

As a check on the equality between equations (63.81) and (63.82), make use of equations (63.72b)-(63.72d) for the partial derivatives and equations (63.22a)-(63.22c) for the one-form basis so that

$$\hat{\boldsymbol{x}}\,\partial_{\overline{x}} + \hat{\boldsymbol{y}}\,\partial_{\overline{y}} + (\nabla\sigma)\,\partial_\sigma = \hat{\boldsymbol{x}}\,[\partial_x + (\partial_{\overline{x}} z)\,\partial_z] + \hat{\boldsymbol{y}}\,[\partial_y + (\partial_{\overline{y}} z)\,\partial_z] + (\nabla\sigma)\,(\partial z/\partial\sigma)\,\partial_z. \tag{63.83}$$

Next use the triple product identities (63.34b) and (63.34c) to have

$$\partial_{\overline{x}} z + (\partial\sigma/\partial x)\,(\partial z/\partial\sigma) = 0 \tag{63.84a}$$
$$\partial_{\overline{y}} z + (\partial\sigma/\partial y)\,(\partial z/\partial\sigma) = 0, \tag{63.84b}$$

in which case

$$\hat{\boldsymbol{x}}\,[\partial_x + (\partial_{\overline{x}} z)\,\partial_z] + \hat{\boldsymbol{y}}\,[\partial_y + (\partial_{\overline{y}} z)\,\partial_z] + (\nabla\sigma)\,(\partial z/\partial\sigma)\,\partial_z = \hat{\boldsymbol{x}}\,\partial_x + \hat{\boldsymbol{y}}\,\partial_y + \hat{\boldsymbol{z}}\,\partial_z. \tag{63.85}$$

63.13 Material time derivative

Making use of the relations for the partial derivative operators in Section 63.12 allows us to write the material time derivative in the following equivalent forms

$$\frac{\mathrm{D}}{\mathrm{D}t} = \left[\frac{\partial}{\partial t}\right]_z + \boldsymbol{u}\cdot\nabla_{\!\mathrm{h}} + w\,\frac{\partial}{\partial z} \tag{63.86a}$$
$$= \left[\frac{\partial}{\partial t}\right]_\sigma - (\partial\eta/\partial\overline{t})\,\partial_z + \boldsymbol{u}\cdot[\nabla_{\!\mathrm{h}\sigma} - (\nabla_{\!\mathrm{h}\sigma}\eta)\,\partial_z] + w\,\partial/\partial z \tag{63.86b}$$
$$= \left[\frac{\partial}{\partial t}\right]_\sigma + \boldsymbol{u}\cdot\nabla_{\!\mathrm{h}\sigma} + \left[w - \boldsymbol{u}\cdot\nabla_{\!\mathrm{h}\sigma}\eta - \partial\eta/\partial\overline{t}\right](\partial\sigma/\partial z)\,\partial/\partial\sigma \tag{63.86c}$$
$$= \left[\frac{\partial}{\partial t}\right]_\sigma + \boldsymbol{u}\cdot\nabla_{\!\mathrm{h}\sigma} + \frac{\mathrm{D}\sigma}{\mathrm{D}t}\,\frac{\partial}{\partial\sigma} \tag{63.86d}$$
$$= \left[\frac{\partial}{\partial t}\right]_\sigma + \boldsymbol{u}\cdot\nabla_{\!\mathrm{h}\sigma} + \frac{\partial z}{\partial\sigma}\,\frac{\mathrm{D}\sigma}{\mathrm{D}t}\,\frac{\partial}{\partial z}. \tag{63.86e}$$

The equality (63.86d) made use of the identity (63.57), which is itself derived in Section 64.4 where we discuss further kinematic results using GVCs. Besides differences in the spatial operators, it is important to note that the time derivative operators are computed on constant geopotential and constant GVC surfaces, respectively. However, the horizontal velocity component is the *same* for both forms of the material time derivative

$$(u, v) = \frac{\mathrm{D}(x, y)}{\mathrm{D}t}. \tag{63.87}$$

63.14 Divergence of a vector and the divergence theorem

Making use of the general expression (4.15) for the covariant divergence of a vector renders the GVC expression

$$\nabla_{\overline{a}}\, F^{\overline{a}} = [\det(g_{\overline{a}\overline{b}})]^{-1/2}\,\partial_{\overline{a}}\left[[\det(g_{\overline{a}\overline{b}})]^{1/2}\, F^{\overline{a}}\right] = (\partial z/\partial\sigma)^{-1}\partial_{\overline{a}}\,[(\partial z/\partial\sigma)\, F^{\overline{a}}]. \tag{63.88}$$

Recall that the GVC vector components, $F^{\overline{a}}$, are related to the Cartesian components in equation (63.43), and the GVC components of the partial derivative operator, $\partial_{\overline{a}}$, are related to the Cartesian operator in equation (63.74).

When making use of the divergence theorem (Section 4.19), we require the product of the volume element and the covariant divergence. For GVCs this product takes on the form

$$(\nabla_{\overline{a}} F^{\overline{a}}) \, \mathrm{d}V = \partial_{\overline{a}} \left[(\partial z / \partial \sigma) \, F^{\overline{a}} \right] \mathrm{d}\overline{x} \, \mathrm{d}\overline{y} \, \mathrm{d}\sigma, \tag{63.89}$$

which reduces to a boundary integral when integrating over a volume.

63.15 The diffusion operator

As an explicit example of the covariant divergence operator (63.88), we here consider the diffusion operator discussed in Chapter 69. The derivation here recovers much of what we just discussed in Section 63.14, yet we make use of a bit less tensor formalism though at the cost of more algebra.

63.15.1 Continuous expression

The diffusion operator is the convergence of the diffusive flux

$$\mathcal{R} = -\nabla \cdot \mathbf{J}, \tag{63.90}$$

where $\mathbf{J}$ is the tracer flux vector. Let us convert the pieces of this operator from Cartesian coordinates into generalized vertical coordinate, making use of the transformation of partial derivative operators given in Section 63.12. Also, we make use of the shorthand $z(x, y, \sigma, t)$ rather than $\eta(x, y, \sigma, t)$

$$\begin{aligned}
-\mathcal{R} &= \nabla \cdot \boldsymbol{J} && \text{(63.91a)} \\
&= \nabla_{\!\mathrm{h}} \cdot \boldsymbol{J}^{\mathrm{h}} + \partial_z J^z && \text{(63.91b)} \\
&= (\nabla_{\!\mathrm{h}\sigma} - \nabla_{\!\mathrm{h}\sigma} z \, \partial_z) \cdot \boldsymbol{J}^{\mathrm{h}} + (\sigma_z) \, \partial_\sigma J^z && \text{(63.91c)} \\
&= \sigma_z \left[z_\sigma \, \nabla_{\!\mathrm{h}\sigma} \cdot \boldsymbol{J}^{\mathrm{h}} + (\hat{\boldsymbol{z}} \, \partial_\sigma - \nabla_{\!\mathrm{h}\sigma} z \, \partial_\sigma) \cdot \boldsymbol{J} \right] && \text{(63.91d)} \\
&= \sigma_z \left[\nabla_{\!\mathrm{h}\sigma} \cdot (z_\sigma \, \boldsymbol{J}^{\mathrm{h}}) - \boldsymbol{J}^{\mathrm{h}} \cdot \nabla_{\!\mathrm{h}\sigma} (z_\sigma) + \partial_\sigma J^z - \partial_\sigma \left(\nabla_{\!\mathrm{h}\sigma} z \cdot \boldsymbol{J} \right) + \boldsymbol{J} \cdot \partial_\sigma \left(\nabla_{\!\mathrm{h}\sigma} z \right) \right] && \text{(63.91e)} \\
&= \sigma_z \left[\nabla_{\!\mathrm{h}\sigma} \cdot (z_\sigma \, \boldsymbol{J}^{\mathrm{h}}) + \partial_\sigma J^z - \partial_\sigma \left(\nabla_{\!\mathrm{h}\sigma} z \cdot \boldsymbol{J}^{\mathrm{h}} \right) \right] && \text{(63.91f)} \\
&= \sigma_z \left(\nabla_{\!\mathrm{h}\sigma} \cdot (\partial_\sigma z \, \boldsymbol{J}^{\mathrm{h}}) + \partial_\sigma \left[(\hat{\boldsymbol{z}} - \nabla_{\!\mathrm{h}\sigma} z) \cdot \boldsymbol{J} \right] \right) && \text{(63.91g)} \\
&= \sigma_z \left[\nabla_{\!\mathrm{h}\sigma} \cdot (z_\sigma \, \boldsymbol{J}^{\mathrm{h}}) + \partial_\sigma \left(z_\sigma \, \nabla\sigma \cdot \boldsymbol{J} \right) \right], && \text{(63.91h)}
\end{aligned}$$

where we used

$$z_\sigma \nabla \sigma = \hat{\boldsymbol{z}} - \nabla_{\!\mathrm{h}\sigma} z \tag{63.92}$$

to reach the final equality, and made use of the shorthand

$$z_\sigma = \partial z / \partial \sigma \qquad \text{and} \qquad \sigma_z = \partial \sigma / \partial z = (z_\sigma)^{-1}. \tag{63.93}$$

The coordinate transformations in Section 63.7 for vector components reveal that the expression (63.91h) is identical to equation (63.88) derived using formal tensor methods. Likewise, multiplying by the volume element

$$\mathrm{d}V = \mathrm{d}x \, \mathrm{d}y \, \mathrm{d}z = \mathrm{d}x \, \mathrm{d}y \, z_\sigma \, \mathrm{d}\sigma, \tag{63.94}$$

leads to

$$-\mathcal{R}\,\mathrm{d}V = [\nabla_{h\sigma}\cdot(z_\sigma\,\boldsymbol{J}^{h}) + \partial_\sigma\,(z_\sigma\,\nabla\sigma\cdot\boldsymbol{J})]\,\mathrm{d}x\,\mathrm{d}y\,\mathrm{d}\sigma, \tag{63.95}$$

which is identical to the expression (63.89).

63.15.2 Layer thickness weighted diffusion operator

Consider a prescribed increment, $\delta\sigma$, separating two σ isosurfaces. This increment commutes with the horizontal operator $\nabla_{h\sigma}$, acting within the layer. We can thus formally consider the following layer-integrated or thickness weighted form of the diffusion operator

$$-\mathcal{R}\,\delta V = [\nabla_{h\sigma}\cdot(\delta\sigma\,z_\sigma\,\boldsymbol{J}^{h}) + \delta\sigma\,\partial_\sigma\,(z_\sigma\,\nabla\sigma\cdot\boldsymbol{J})]\,\delta x\,\delta y \tag{63.96a}$$

$$= \frac{1}{\delta z}\,[\nabla_{h\sigma}\cdot(\delta\sigma\,z_\sigma\,\boldsymbol{J}^{h}) + \delta\sigma\,\partial_\sigma\,(z_\sigma\,\nabla\sigma\cdot\boldsymbol{J})]\,\delta x\,\delta y\,\delta z \tag{63.96b}$$

$$= \frac{1}{h}\,[\nabla_{h\sigma}\cdot(h\,\boldsymbol{J}^{h}) + \Delta_\sigma(z_\sigma\,\nabla\sigma\cdot\boldsymbol{J})]\,\delta x\,\delta y\,h, \tag{63.96c}$$

where we introduced the infinitesimal layer thickness

$$h = z_\sigma\,\delta\sigma \tag{63.97}$$

and the non-dimensional differential operator

$$\Delta_\sigma \equiv \delta\sigma\,\frac{\partial}{\partial\sigma}. \tag{63.98}$$

Cancelling the volume element on both sides leads to the diffusion operator

$$\mathcal{R} = -\frac{1}{h}\,[\nabla_{h\sigma}\cdot(h\,\boldsymbol{J}^{h}) + \Delta_\sigma(z_\sigma\,\nabla\sigma\cdot\boldsymbol{J})]\,. \tag{63.99}$$

This form is commonly found in the numerical modeling literature when considering generalized vertical coordinate models.

We make the following comments concerning the diffusion operator in equation (63.99).

- Our introduction of the layer thickness $h = z_\sigma\,\delta\sigma$ is treated a bit more formally in Sections 64.9 and 64.10 by considering a vertical integral over a coordinate layer. Even so, the resulting diffusion operator is the same as that derived here.

- The thickness weighted flux, $h\,\boldsymbol{J}^{h}$, is oriented within the horizontal plane. However, its contribution to the diffusion operator is computed by taking its convergence using the operator $\nabla_{h\sigma}$ rather than the horizontal operator ∇_{h}. This distinction is fundamental to how operators, such as advection and diffusion, appear using generalized vertical coordinates.

- The flux $z_\sigma\nabla\sigma\cdot\boldsymbol{J}$ is commonly referred to as the dia-surface subgrid scale flux.

- For the special case of a diffusive flux with zero component parallel to $\nabla\sigma$, the diffusion operator reduces to

$$\mathcal{R} = -\frac{1}{h}\,[\nabla_{h\sigma}\cdot(h\,\boldsymbol{J}^{h})] \qquad \text{if } \nabla\sigma\cdot\boldsymbol{J} = 0. \tag{63.100}$$

  The neutral diffusion operator of Section 71.4.4 is an example of such an operator, with σ in that case given by the locally referenced potential density.

63.16 Vorticity

As detailed in Chapter 40, vorticity is the curl of the velocity

$$\vec{\omega} = \text{curl}(\vec{v}), \tag{63.101}$$

where the curl has components (Section 4.18)

$$\text{curl}(\vec{v}) = \boldsymbol{e}_{\overline{a}}\, \varepsilon^{\overline{a}\overline{b}\overline{c}} \partial_{\overline{b}} v_{\overline{c}}. \tag{63.102}$$

63.16.1 The components

We identify the contravariant components of the vorticity via

$$\omega^{\overline{a}} = \varepsilon^{\overline{a}\overline{b}\overline{c}} \partial_{\overline{b}} v_{\overline{c}} = (\partial z/\partial\sigma)^{-1}\, \epsilon^{\overline{a}\overline{b}\overline{c}}\, \partial_{\overline{b}} v_{\overline{c}} \tag{63.103}$$

where we made use of equation (63.69) to introduce the permutation symbol. Expanding the components leads to

$$\omega^{\overline{1}} = (\partial\sigma/\partial z)\, (\partial_{\overline{2}}\, v_{\overline{3}} - \partial_{\overline{3}}\, v_{\overline{2}}) \tag{63.104a}$$

$$\omega^{\overline{2}} = (\partial\sigma/\partial z)\, (\partial_{\overline{3}}\, v_{\overline{1}} - \partial_{\overline{1}}\, v_{\overline{3}}) \tag{63.104b}$$

$$\omega^{\overline{3}} = \omega^{\sigma} = (\partial\sigma/\partial z)\, (\partial_{\overline{1}}\, v_{\overline{2}} - \partial_{\overline{2}}\, v_{\overline{1}}). \tag{63.104c}$$

63.16.2 Transforming from Cartesian coordinates

The above approach works solely with the GVC coordinates. An alternative approach connects the GVC vorticity components and the Cartesian vorticity components. For that purpose we use the transformation matrix via

$$\omega^{\overline{a}} = \Lambda^{\overline{a}}{}_{a}\, \omega^{a}, \tag{63.105}$$

where ω^a are the Cartesian components

$$\boldsymbol{\omega} = \hat{\boldsymbol{x}} \left(\frac{\partial w}{\partial y} - \frac{\partial v}{\partial z} \right) + \hat{\boldsymbol{y}} \left(\frac{\partial u}{\partial z} - \frac{\partial w}{\partial x} \right) + \hat{\boldsymbol{z}} \left(\frac{\partial v}{\partial x} - \frac{\partial u}{\partial y} \right). \tag{63.106}$$

Making use of the transformation matrix $\Lambda^{\overline{a}}{}_{a}$ from equation (63.20) yields (as in Section 63.7)

$$\omega^{\overline{x}} = \omega^{x} = \frac{\partial w}{\partial y} - \frac{\partial v}{\partial z} \qquad \text{and} \qquad \omega^{\overline{y}} = \omega^{y} = \frac{\partial u}{\partial z} - \frac{\partial w}{\partial x} \qquad \text{and} \qquad \omega^{\sigma} = \boldsymbol{\omega} \cdot \nabla\sigma. \tag{63.107}$$

Note that for isopycnal coordinates in a Boussinesq fluid, ω^σ equals to the potential vorticity when the vorticity is the absolute vorticity (Section 66.3). That is, the potential vorticity is the isopycnal component of the absolute vorticity.

63.17 Velocity circulation

The velocity circulation (Section 37.4) is given by the closed oriented path integral of the velocity projected into the direction of the path

$$\mathcal{C} \equiv \oint_{\partial S} \boldsymbol{v} \cdot \mathrm{d}\boldsymbol{x} \tag{63.108}$$

where $\mathrm{d}\boldsymbol{x}$ is the vector line element along the path and $\partial\mathcal{S}$ is the closed path defining the boundary to a two-dimensional surface $\mathcal{S}$. Stokes' Theorem from Section 2.6 leads to the identity

$$\mathcal{C} = \oint_{\partial\mathcal{S}} \boldsymbol{v} \cdot \mathrm{d}\boldsymbol{x} = \int_{\mathcal{S}} (\nabla \times \boldsymbol{v}) \cdot \hat{\boldsymbol{n}} \, \mathrm{d}\mathcal{S} = \int_{\mathcal{S}} \boldsymbol{\omega} \cdot \hat{\boldsymbol{n}} \, \mathrm{d}\mathcal{S}, \tag{63.109}$$

where $\hat{\boldsymbol{n}}$ is the outward normal vector orienting the area element $\mathrm{d}\mathcal{S}$ according to the right-hand rule applied to the bounding circuit. These results are all written in a generally covariant manner (Section 3.1) so that they hold for an arbitrary coordinate representation.

As a particular case, consider the circulation around a closed path on a constant σ surface, in which

$$\hat{\boldsymbol{n}} = \frac{\nabla\sigma}{|\nabla\sigma|} \tag{63.110}$$

is the outward normal and

$$\boldsymbol{\omega} \cdot \hat{\boldsymbol{n}} = \frac{\omega^\sigma}{|\nabla\sigma|} \tag{63.111}$$

where $\omega^\sigma = \boldsymbol{\omega} \cdot \nabla\sigma$ (equation (63.107)). So long as the vertical stratification remains non-zero ($\partial\sigma/\partial z \neq 0$) we can write the area factor in the form

$$\frac{\mathrm{d}\mathcal{S}}{|\nabla\sigma|} = \frac{\mathrm{d}\mathcal{S}}{\sqrt{(\partial\sigma/\partial x)^2 + (\partial\sigma/\partial y)^2 + (\partial\sigma/\partial z)^2}} \tag{63.112a}$$

$$= \frac{\mathrm{d}\mathcal{S}}{|\partial\sigma/\partial z| \, \sqrt{[(\partial\sigma/\partial x)/(\partial\sigma/\partial z)]^2 + [(\partial\sigma/\partial y)/(\partial\sigma/\partial z)]^2 + 1}} \tag{63.112b}$$

$$= \frac{\mathrm{d}\mathcal{S}}{|\partial\sigma/\partial z| \sqrt{1 + \tan^2\vartheta}} \tag{63.112c}$$

$$= \left| \frac{\partial z}{\partial \sigma} \right| |\cos\vartheta| \, \mathrm{d}\mathcal{S} \tag{63.112d}$$

$$= \left| \frac{\partial z}{\partial \sigma} \right| \mathrm{d}A. \tag{63.112e}$$

The equality (63.112c) introduces the angle, ϑ, between the boundary surface and the horizontal plane as in Figure 63.4. The squared slope of this surface given by

$$\tan^2\vartheta = \frac{\nabla_{\!\mathrm{h}}\sigma \cdot \nabla_{\!\mathrm{h}}\sigma}{(\partial\sigma/\partial z)^2} = \nabla_{\!\mathrm{h}\sigma} z \cdot \nabla_{\!\mathrm{h}\sigma} z. \tag{63.113}$$

The equality (63.112d) made use of a trigonometric identity, and the equality (63.112e) introduced the horizontal projection of the area,

$$\mathrm{d}A = |\cos\vartheta| \, \mathrm{d}\mathcal{S}. \tag{63.114}$$

Bringing these results together leads to the expression for circulation around a closed loop on a constant σ surface

$$\mathcal{C}_{\sigma-\text{surface}} = \int_{\mathcal{S}} (\boldsymbol{\omega} \cdot \nabla\sigma) \, |\partial z/\partial\sigma| \, \mathrm{d}A. \tag{63.115}$$

Chapter 64

KINEMATIC EQUATIONS

In providing a mechanistic description of budgets within the ocean or atmosphere, it is often useful to measure the material or momentum transfer through a surface. This transport is termed the *dia-surface transport*. Our discussion in this chapter unifies ideas developed for kinematic boundary conditions in Section 19.6 with transport across an arbitrary surface in the fluid interior. We do so by making use of the generalized vertical coordinates (GVCs) from Chapter 63. We make use of the dia-surface transport formulation to express the material time derivative operator using GVCs. This form for the material time derivative allows us to decompose the vertical velocity into motion relative to a moving GVC surface. In turn, we are afforded a means to reinterpret the velocity vector and corresponding particle trajectories. GVC kinematics also provides a means to express the subduction of fluid into the ocean interior beneath the mixed layer base. We close the chapter with derivations of the GVC version of mass continuity and the tracer equation. We also introduce the layer integrated version of the continuity and tracer equations, with the layer integrated equations appropriate for discrete numerical fluid models.

CHAPTER GUIDE

We introduced mathematical properties of generalized vertical coordinates in Chapter 63, including the calculus using these non-orthogonal coordinates. It is essential to have a working knowledge of that material to understand the present chapter. Later in Chapter 65 we detail the dynamical equations using GVCs, with material in that chapter relying on the kinematics presented here. Following the treatment in Chapter 63, we here use the symbol σ to denote a generalized vertical coordinate, where σ has functional dependence $\sigma(x, y, z, t)$.

64.1 Example generalized vertical coordinates

We here consider some generalized vertical coordinates that will prove of use for our discussion in this chapter, with Figure 64.1 illustrating the examples.

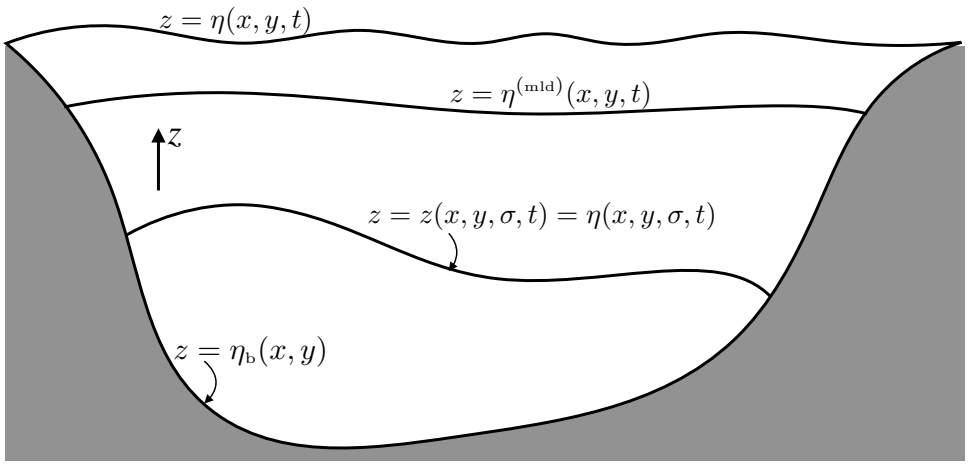

FIGURE 64.1: Example surface upon which a generalized vertical coordinate, $\sigma(x, y, z, t)$, is constant. The ocean free surface can be represented mathematically by $\sigma(x, y, z, t) = z - \eta(x, y, t) = 0$; the ocean mixed layer base by $\sigma(x, y, z, t) = z - \eta^{\mathrm{mld}}(x, y, t) = 0$; and the solid earth bottom $\sigma(x, y, z) = z - \eta_{\mathrm{b}}(x, y) = 0$. Likewise, the vertical position of an interior generalized vertical coordinate surface can be written $z - \eta(x, y, \sigma, t) = \text{constant}$, where $\eta(x, y, \sigma, t)$ is a function of horizontal position and time for the surface defined by a particular σ value.

64.1.1 Ocean free surface

The first surface is the ocean free surface, whose kinematic boundary conditions were derived in Section 19.6.3. Here, water and tracer penetrate this surface through precipitation, evaporation, river runoff (when applied as an upper ocean boundary condition), and sea ice melt. Momentum exchange arises from stresses between the ocean and atmosphere or ice. The ocean free surface

can be represented mathematically by the identity

$$\sigma(x, y, z, t) = z - \eta(x, y, t) = 0 \qquad \text{ocean free surface.} \tag{64.1}$$

This identity holds so long as we assume the surface height η is smooth and contains no overturns at the scales of interest. That is, we assume breaking surface waves are filtered from the description.

64.1.2 Solid earth boundary

We may describe the solid Earth lower boundary mathematically by using the time independent expression

$$\sigma(x, y, z) = z + H(x, y) = z - \eta_{\mathsf{b}}(x, y) = 0 \qquad \text{ocean bottom,} \tag{64.2}$$

where we introduce the two common symbols used for the bottom, $\eta_{\mathsf{b}} = -H$. We generally prefer η_{b} since H is used elsewhere in this book for vertical scale. As detailed in Section 19.6.1, we typically assume that there is no fluid mass transport through the solid Earth. However, in the case of geothermal heating, we may consider an exchange of heat between the ocean and the solid Earth. Momentum exchange through the action of stresses occur between the solid Earth and ocean fluid.

64.1.3 Ocean mixed layer base

Let

$$\sigma = z - \eta^{\mathsf{mld}}(x, y, t) = 0 \tag{64.3}$$

represent the vertical position of the ocean mixed layer base. The corresponding normal vector is given by

$$\hat{\boldsymbol{n}}^{(\mathrm{mld})} = \frac{\nabla\,(z - \eta^{\mathsf{mld}})}{|\nabla\,(z - \eta^{\mathsf{mld}})|} = \frac{\nabla\,(\hat{\boldsymbol{z}} - \nabla\eta^{\mathsf{mld}})}{\sqrt{1 + |\nabla\eta^{\mathsf{mld}}|^2}}. \tag{64.4}$$

This example is relevant for the study of ocean ventilation, whereby we are interested in measuring the transport of fluid that enters the ocean interior across the mixed layer base (see Section 64.7).

64.1.4 Interior generalized vertical coordinate surfaces

Within the ocean interior, transport across surfaces of constant generalized vertical coordinate $\sigma = \sigma(x, y, z, t)$ constitutes the dia-surface transport affecting budgets of mass, tracer, and momentum within layers bounded by two generalized vertical coordinate surfaces. A canonical example is provided by isopycnal layers formed by surfaces of constant potential density (or equivalently constant buoyancy surfaces) as used in isopycnal ocean models as well as theoretical descriptions of adiabatic ocean dynamics. The vertical position of this surface is written in one of two equivalent manners

$$z = z(x, y, \sigma, t) = \eta(x, y, \sigma, t). \tag{64.5}$$

The first expression exposes the functional dependence of the vertical position of the σ surface at a horizontal position and time. In Section 63.1 we discussed the potential for confusion between writing z as a particular vertical position versus a function, thus motivating $z = \eta(x, y, \sigma, t)$. However, by now we should have sufficient experience with generalized vertical coordinates so that we can well distinguish when z refers to a particular vertical position versus $z(x, y, \sigma, t)$ as a coordinate function. For this reason we only infrequently use the nomenclature $z = \eta(x, y, \sigma, t)$ in this chapter.

64.2 Specific thickness

As mentioned in Section 63.9.1, a surface of constant generalized vertical coordinate can be successfully used to partition the vertical so long as the transformation between the generalized vertical coordinate and the geopotential coordinate is invertible. The Jacobian of transformation is given by

$$\frac{\partial z}{\partial \sigma} = z_\sigma, \tag{64.6}$$

which must be single signed for suitable generalized vertical coordinates. This constraint means that we do not allow the surfaces to overturn, which is the same assumption made about the ocean surface, $z = \eta(x, y, t)$, and solid earth bottom, $z = \eta_{\mathrm{b}}(x, y)$. This restriction places a limitation on the ability of certain GVC models (e.g., isopycnal models) to describe non-hydrostatic processes, such as the overturning common in Kelvin-Helmholtz billows and gravitational convection. Note that for both the solid earth bottom and ocean free surface

$$\frac{\partial z}{\partial \sigma} = 1 \qquad \text{ocean free surface and fluid/solid interface.} \tag{64.7}$$

Furthermore, this relation also holds, trivially, for geopotential coordinates in which $\sigma = z$.

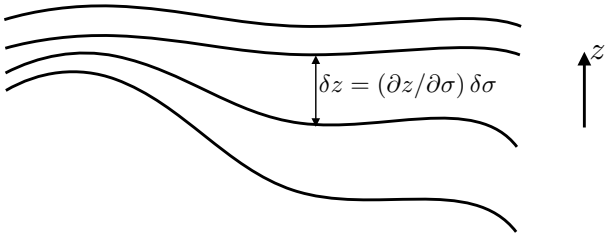

FIGURE 64.2: Illustrating the thickness between surfaces of constant generalized vertical coordinates, $\delta z = (\partial z/\partial \sigma)\, \delta \sigma$. In regions with larger magnitude for the specific thickness, $\partial z/\partial \sigma$, or equivalently smaller vertical stratification of the σ surfaces, $\partial \sigma/\partial z$, the layer thicknesses are further apart. The converse holds where $\partial z/\partial \sigma$ is small (equivalently $\partial \sigma/\partial z$ is large).

We refer to the Jacobian z_σ as the *specific thickness* and sometimes find it useful to write it as

$$\hbar = z_\sigma = \frac{\partial z}{\partial \sigma}. \tag{64.8}$$

This name is motivated by noting that the vertical thickness of an infinitesimal layer of coordinate thickness $\delta\sigma$ is given by

$$\delta z = \frac{\partial z}{\partial \sigma}\, \delta \sigma = \hbar\, \delta \sigma, \tag{64.9}$$

with Figure 64.2 providing an example with finitely thick layers. For example, if $\sigma = b(x, y, z, t)$ (buoyancy or potential density as in isopycnal models), then the thickness of a buoyancy layer is given by

$$\delta z = \frac{\partial z}{\partial \sigma}\, \delta b = N^{-2}\, \delta b, \tag{64.10}$$

with

$$N^2 = \frac{\partial b}{\partial z} \tag{64.11}$$

the squared buoyancy frequency (Section 30.6) in a Boussinesq fluid (Chapter 29). For a hydrostatic fluid using pressure as the vertical coordinate, the thickness of a pressure layer is

$$\delta z = \frac{\partial z}{\partial p}\, \delta p = -\frac{1}{\rho\, g}\, \delta p \tag{64.12}$$

where we used the hydrostatic relation (Section 27.2)

$$\frac{\partial p}{\partial z} = -\rho\, g \tag{64.13}$$

with g the constant acceleration due to effective gravity. Note that we assume the layer thickness is positive, $\delta z > 0$. For this purpose, with hydrostatic pressure we might choose to consider negative pressure increments, $\delta p < 0$, as this corresponds to vertically upward movement in a fluid column.

64.3 The dia-surface transport

In this section we develop the concept of dia-surface transport and derive its expression in terms of the material time derivative of the GVC surface.

64.3.1 Flow normal to the GVC surface

At an arbitrary point on a surface of constant generalized vertical coordinate (see Figure 64.3), the rate at which fluid moves in the direction normal to the surface is given by

$$\text{RATE OF FLUID FLOW IN DIRECTION } \hat{\boldsymbol{n}} = \boldsymbol{v} \cdot \hat{\boldsymbol{n}}, \tag{64.14}$$

where

$$\hat{\boldsymbol{n}} = \frac{\nabla \sigma}{|\nabla \sigma|}, \tag{64.15}$$

is the surface unit normal. Two examples are useful to ground this expression in common experience. For the ocean free surface, $\sigma = z - \eta(x, y, t) = 0$, the unit normal takes the form

$$\hat{\boldsymbol{n}} = \frac{\nabla\,(z - \eta)}{|\nabla\,(z - \eta)|} = \frac{\hat{\boldsymbol{z}} - \nabla \eta}{\sqrt{1 + |\nabla \eta|^2}}, \tag{64.16}$$

whereas at the solid Earth bottom, $\sigma = z - \eta_{\mathrm{b}}(x, y) = 0$,

$$\hat{\boldsymbol{n}} = -\frac{\nabla\,(z - \eta_{\mathrm{b}})}{|\nabla\,(z - \eta_{\mathrm{b}})|} = -\frac{\hat{\boldsymbol{z}} - \nabla \eta_{\mathrm{b}}}{\sqrt{1 + |\nabla \eta_{\mathrm{b}}|^2}}. \tag{64.17}$$

Introducing the material time derivative

$$\frac{\mathrm{D}\sigma}{\mathrm{D}t} = \frac{\partial \sigma}{\partial t} + \boldsymbol{v} \cdot \nabla \sigma \tag{64.18}$$

to equation (64.14) leads to the identity

$$\boldsymbol{v} \cdot \hat{\boldsymbol{n}} = \frac{1}{|\nabla \sigma|} \left[\frac{\mathrm{D}\sigma}{\mathrm{D}t} - \frac{\partial \sigma}{\partial t} \right]. \tag{64.19}$$

Hence, the component to the velocity of a fluid particle that is normal to a GVC surface is proportional to the difference between the material time derivative of the surface coordinate and its partial time derivative.

64.3.2 Accounting for movement of the surface

A generalized vertical coordinate surface is generally moving. So to diagnose the net transport of fluid penetrating the surface requires us to subtract the velocity of the surface, $\boldsymbol{v}^{(\sigma)}$, from the

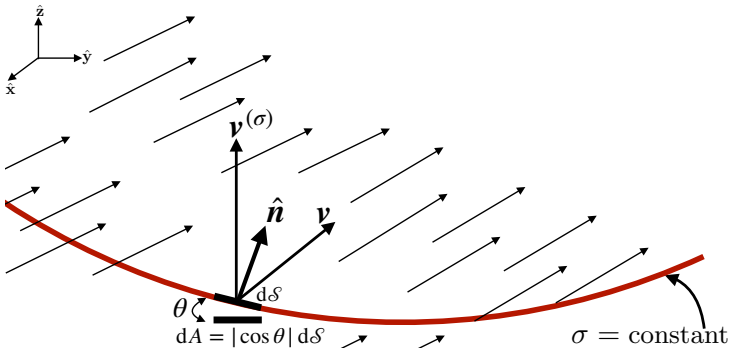

FIGURE 64.3: A surface of constant generalized vertical coordinate, $\sigma = \text{constant}$, within a fluid. The normal direction, $\hat{\boldsymbol{n}} = \nabla\sigma/|\nabla\sigma|$, points in the direction of increasing σ. We show an example velocity vector for a fluid particle, $\boldsymbol{v}$, at a point on the surface as well as the velocity, $\boldsymbol{v}^{(\sigma)}$, of a point that lives on the surface. Note that kinematics is only concerned with the normal component to the surface velocity, $\boldsymbol{v}^{(\sigma)} \cdot \hat{\boldsymbol{n}}$, as per equation (64.25). We require dynamical information to obtain information about the tangential component of $\boldsymbol{v}^{(\sigma)}$, but such information is not required for this chapter. Following equation (64.30), the horizontal projection of the surface area element is given by $\mathrm{d}A = |\cos\vartheta|\,\mathrm{d}\mathcal{S}$, where ϑ is the angle between the surface and the horizontal and $\mathrm{d}A = \mathrm{d}x\,\mathrm{d}y$.

velocity of a fluid particle. We are thus led to

$$\text{RATE THAT FLUID CROSSES A MOVING GVC SURFACE} = \hat{\boldsymbol{n}} \cdot (\boldsymbol{v} - \boldsymbol{v}^{(\sigma)}). \tag{64.20}$$

We next develop a kinematic property of the surface velocity, or more precisely the normal component to that velocity. For that purpose, consider an infinitesimal increment in both space and time under which σ undergoes an infinitesimal change

$$\delta\sigma = \delta\boldsymbol{x} \cdot \nabla\sigma + \delta t\, \partial_t \sigma. \tag{64.21}$$

Now restrict attention to a point fixed on a constant σ surface, in which

$$\delta\sigma = \delta\boldsymbol{x}^{(\sigma)} \cdot \nabla\sigma + \delta t\, \partial_t \sigma = 0, \tag{64.22}$$

where $\delta\boldsymbol{x}^{(\sigma)}$ is a differential increment following the moving surface. We define the velocity of that point as

$$\boldsymbol{v}^{(\sigma)} = \frac{\delta\boldsymbol{x}^{(\sigma)}}{\delta t}, \tag{64.23}$$

in which case equation (64.22) implies that at each point within the fluid,

$$\frac{\partial\sigma}{\partial t} + \boldsymbol{v}^{(\sigma)} \cdot \nabla\sigma = 0. \tag{64.24}$$

We can likewise write this equation as one for the normal component of the surface velocity

$$\boldsymbol{v}^{(\sigma)} \cdot \hat{\boldsymbol{n}} = -\frac{1}{|\nabla\sigma|}\,\frac{\partial\sigma}{\partial t}. \tag{64.25}$$

Hence, we reach the sensible result that the normal component to the velocity of the surface vanishes when the surface is static.

64.3.3 We only care about divergent surface motion

For the kinematics of fluid motion relative to a surface of constant generalized vertical coordinates, we are only concerned with the normal component to the surface velocity, $\boldsymbol{v}^{(\sigma)} \cdot \hat{\boldsymbol{n}}$. That is, we are only concerned with divergent motion of the surface, defined as motion parallel to the surface normal direction, $\hat{\boldsymbol{n}}$. We have no concern for rotational or tangential motion, which is motion perpendicular to $\hat{\boldsymbol{n}}$. Even so, some authors, by fiat, choose to set to zero the tangential component of the surface motion. In fact, specification of the tangential surface velocity component is generally not available without extra information about the surface motion, nor is its specification necessary for developing kinematic properties of fluid motion relative to arbitrary generalized vertical coordinate surfaces. Hence, we make no statement about tangential motion of the surface.

64.3.4 Cross GVC transport in terms of GVC material evolution

Using expression (64.25) in equation (64.20) leads to the net flux of fluid crossing the GVC surface

$$\hat{\boldsymbol{n}} \cdot (\boldsymbol{v} - \boldsymbol{v}^{(\sigma)}) = \frac{1}{|\nabla\sigma|} \frac{\mathrm{D}\sigma}{\mathrm{D}t}. \tag{64.26}$$

The material time derivative of the GVC surface thus vanishes if no fluid crosses the surface. Notably, this result holds for motion of the fluid as defined by the barycentric velocity, $\boldsymbol{v}$, of Section 20.1.2. For multi-component fluids, $\dot{\sigma} = 0$ can still, in principle, be associed with trace matter exchange across the surface via diffusion so long as the net matter crossing the surface is zero. But this situation is rather fine tuned and thus unlikely. Additionally, matter diffusion also occurs with heat diffusion, in which case $\dot{\sigma} = 0$ only occurs in the absence of both matter and heat diffusion, which then means that σ is a material surface.

64.3.5 Defining the dia-surface transport

The area normalizing the volume flux in equation (64.26) is the area $\mathrm{d}\mathcal{S}$ of an infinitesimal patch on the surface of constant generalized vertical coordinate with outward unit normal $\hat{\boldsymbol{n}}$. We now follow the trigonometry discussed in Section 63.17 to introduce the horizontal projection of this area, $\mathrm{d}A$, which is more convenient to work with for many purposes. So long as the vertical stratification remains non-zero ($\partial\sigma/\partial z \neq 0$) we can write the area factor in the form

$$\begin{aligned}
\frac{\mathrm{d}\mathcal{S}}{|\nabla\sigma|} &= \frac{\mathrm{d}\mathcal{S}}{\sqrt{(\partial\sigma/\partial x)^2 + (\partial\sigma/\partial y)^2 + (\partial\sigma/\partial z)^2}} && \text{(64.27a)} \\
&= \frac{\mathrm{d}\mathcal{S}}{|\partial\sigma/\partial z| \sqrt{[(\partial\sigma/\partial x)/(\partial\sigma/\partial z)]^2 + [(\partial\sigma/\partial y)/(\partial\sigma/\partial z)]^2 + 1}} && \text{(64.27b)} \\
&= \frac{\mathrm{d}\mathcal{S}}{|\partial\sigma/\partial z| \sqrt{1 + \tan^2\vartheta}} && \text{(64.27c)} \\
&= \left|\frac{\partial z}{\partial\sigma}\right| |\cos\vartheta| \, \mathrm{d}\mathcal{S} && \text{(64.27d)} \\
&= \left|\frac{\partial z}{\partial\sigma}\right| \mathrm{d}A. && \text{(64.27e)}
\end{aligned}$$

The equality (64.27c) introduced the angle, ϑ, between the boundary surface and the horizontal plane. The squared slope of this surface given by (see Section 63.12)

$$\tan^2\vartheta = \frac{\nabla_{\!\mathrm{h}}\sigma \cdot \nabla_{\!\mathrm{h}}\sigma}{(\partial\sigma/\partial z)^2} = \nabla_{\!\mathrm{h}\sigma} z \cdot \nabla_{\!\mathrm{h}\sigma} z. \tag{64.28}$$

The equality (64.27d) made use of a trigonometric identity so that

$$|\cos\vartheta|^{-1} = |z_\sigma \, \nabla\sigma|. \tag{64.29}$$

Furthermore, the equality (64.27e) introduced the horizontal projection of the area,

$$\mathrm{d}A = |\cos\vartheta| \, \mathrm{d}\mathcal{S}. \tag{64.30}$$

We now introduce the *dia-surface velocity component* for the GVC coordinate

$$w^{(\dot\sigma)} = \frac{\partial z}{\partial \sigma} \frac{\mathrm{D}\sigma}{\mathrm{D}t} = z_\sigma \, \dot\sigma, \tag{64.31}$$

which measures the volume of fluid passing through the surface, per unit horizontal area, per unit time

$$w^{(\dot\sigma)} \equiv \hat{\boldsymbol{n}} \cdot (\boldsymbol{v} - \boldsymbol{v}^{(\sigma)}) \, \frac{\mathrm{d}\mathcal{S}}{\mathrm{d}A} \tag{64.32}$$

$$= \frac{\text{(VOLUME/TIME) FLUID THROUGH SURFACE}}{\text{HORIZONTAL AREA OF SURFACE}}, \tag{64.33}$$

so that

$$w^{(\dot\sigma)} \, \mathrm{d}A \equiv \hat{\boldsymbol{n}} \cdot (\boldsymbol{v} - \boldsymbol{v}^{(\sigma)}) \, \mathrm{d}\mathcal{S}. \tag{64.34}$$

The velocity component $w^{(\dot\sigma)}$ is referred to as the dia-surface velocity component since it measures flow rate of fluid through the surface. We can think of $w^{(\dot\sigma)}$ as the "vertical" velocity which, when multiplied by the horizontal area element, measures the transport of fluid that crosses the surface in the normal direction.

64.3.6 Expressions for the dia-surface velocity component

Making use of various identities derived above, as well as the transformation of partial derivative operators in Section 63.12, allows us to write the dia-surface velocity component in the following equivalent forms

$$w^{(\dot\sigma)} = \frac{\partial z}{\partial \sigma} \frac{\mathrm{D}\sigma}{\mathrm{D}t} \tag{64.35a}$$

$$= \frac{\partial z}{\partial \sigma} |\nabla\sigma| \, \hat{\boldsymbol{n}} \cdot (\boldsymbol{v} - \boldsymbol{v}^{(\sigma)}) \tag{64.35b}$$

$$= \frac{\partial z}{\partial \sigma} \nabla\sigma \cdot \boldsymbol{v} - \frac{\partial z}{\partial \sigma} |\nabla\sigma| \, \hat{\boldsymbol{n}} \cdot (\boldsymbol{v} - \boldsymbol{v}^{(\sigma)}) \tag{64.35c}$$

$$= (\hat{\boldsymbol{z}} - \nabla_{\!\mathrm{h}\sigma} z) \cdot \boldsymbol{v} + \frac{\partial z}{\partial \sigma} \frac{\partial \sigma}{\partial t} \tag{64.35d}$$

$$= (\hat{\boldsymbol{z}} - \nabla_{\!\mathrm{h}\sigma} z) \cdot \boldsymbol{v} - \frac{\partial z}{\partial t} \tag{64.35e}$$

$$= w - (\partial_t + \boldsymbol{u} \cdot \nabla_{\!\mathrm{h}\sigma}) z, \tag{64.35f}$$

where $\partial z/\partial t = (\partial z/\partial t)_\sigma$ is the time derivative for the depth of the σ surface. We also made use of the identity (see equations (63.34b) and (63.34c))

$$\nabla_{\!\mathrm{h}\sigma} z = -z_\sigma \, \nabla_{\!\mathrm{h}}\sigma \tag{64.36}$$

to express the slope of the σ surface as projected onto the horizontal direction plane, as well as the corresponding identity (63.34a) for the time derivative

$$\left[\frac{\partial z}{\partial t}\right]_{\sigma} = -\frac{[\partial\sigma/\partial t]_z}{[\partial\sigma/\partial z]}. \tag{64.37}$$

The form given by equation (64.35f) directly relates the vertical component to the fluid particle velocity to the dia-surface velocity component

$$w = \frac{\mathrm{D}z}{\mathrm{D}t} \longleftrightarrow w^{(\dot\sigma)} = \frac{\partial z}{\partial\sigma}\frac{\mathrm{D}\sigma}{\mathrm{D}t} = w - (\partial_t + \boldsymbol{u}\cdot\nabla_{h\sigma})z. \tag{64.38}$$

When the GVC surface is static, so that it occupies a constant vertical position $\partial z/\partial t = 0$, then the dia-surface velocity component reduces to

$$w^{(\dot\sigma)} = w - \boldsymbol{u}\cdot\nabla_{h\sigma} z \qquad \text{static surface,} \tag{64.39}$$

whereas if the GVC surface is flat, then the dia-surface velocity component measures the flux of fluid moving vertically relative to the motion of the GVC surface. Finally, if the surface is flat and static, the dia-surface velocity component becomes the vertical velocity component

$$w^{(\dot\sigma)} = w = \frac{\mathrm{D}z}{\mathrm{D}t} \qquad \text{GVC surface static and flat,} \tag{64.40}$$

which is the case for the geopotential vertical coordinate. This relation reveals the kinematic distinction between w and $w^{(\dot\sigma)}$, with the two differing in the presence of GVC transients and horizontal velocities that project onto a non-horizontal GVC surface. Equation (64.35f) thus offers a useful means to distinguish w from $w^{(\dot\sigma)}$.

64.3.7 An alternative definition of dia-surface velocity component

In some literature presentations, the dia-surface velocity component is taken to be

$$w^{\text{dia}} = \hat{\boldsymbol{n}}\cdot(\boldsymbol{v} - \boldsymbol{v}^{(\sigma)}) = \frac{1}{|\nabla\sigma|}\frac{\mathrm{D}\sigma}{\mathrm{D}t}. \tag{64.41}$$

For example, *Groeskamp et al.* (2019) prefer this definition for watermass analysis. As seen in Chapter 73, the reason to prefer expression (64.41) for watermass analysis is that we do not wish to assume vertically stable stratification for surfaces of constant σ. Dropping that assumption allows us to consider transformation between arbitrarily oriented elements of seawater, even those that are gravitationally unstable.

64.3.8 Area integrated dia-surface transport for non-divergent flows

We close this section by further emphasizing the distinction in time dependent flows between dia-surface transport and flow normal to a surface. For this purpose consider a non-divergent flow whereby $\nabla\cdot\boldsymbol{v} = 0$. Non-divergence means that for any closed surface within the fluid interior, the following identity holds via the divergence theorem

$$0 = \int_{\mathscr{R}} \nabla\cdot\boldsymbol{v}\,\mathrm{d}V = \oint_{\partial\mathscr{R}} \hat{\boldsymbol{n}}\cdot\boldsymbol{v}\,\mathrm{d}\mathcal{S}. \tag{64.42}$$

Notably, only in the case of a static surface do we conclude there is no net flow across the surface (see Exercise 21.6). For surfaces that move, there is generally a nonzero net dia-surface transport. We clarify this rather puzzling statement in the following.

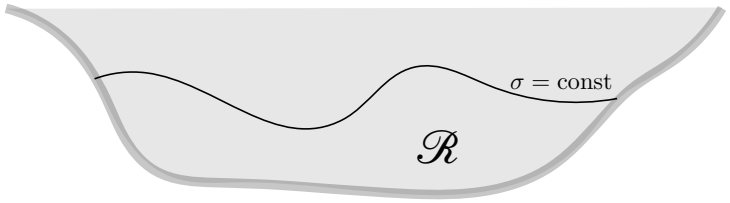

FIGURE 64.4: A constant GVC surface, $\sigma =$ constant, within an ocean basin that intersects the bottom. The region $\mathscr{R}$ is bounded above by the σ surface and below by the solid-earth. Along the constant σ surface a non-divergent flow satisfies $\int_{\sigma=\text{const}} \hat{\boldsymbol{n}} \cdot \boldsymbol{v} \, \mathrm{d}\mathcal{S} = 0$.

As a specific example, consider a fluid region such as shown in Figure 64.4, which is bounded by the solid-earth bottom and a constant GVC surface. Since the solid-earth bottom is static and there is no-normal flow through the bottom, the identity (64.42) means that the area integrated flow normal to the GVC vanishes

$$\int_{\sigma=\text{const}} \hat{\boldsymbol{n}} \cdot \boldsymbol{v} \, \mathrm{d}\mathcal{S} = 0. \tag{64.43}$$

But what does this identity imply about the area integrated dia-surface velocity? For the case of a geopotential vertical coordinate, $\sigma = z$, it means that the area integrated vertical velocity vanishes across any geopotential surface below the ocean free surface, $\int_{z=\text{const}} w \, \mathrm{d}A = 0$ (see Exercise 21.6). What about other GVCs?

To address this question consider the general result

$$\int_{\sigma=\text{const}} \hat{\boldsymbol{n}} \cdot (\boldsymbol{v} - \boldsymbol{v}^{(\sigma)}) \, \mathrm{d}\mathcal{S} = \int_{\sigma=\text{const}} w^{\text{dia}} \, \mathrm{d}\mathcal{S} = \int_{\sigma=\text{const}} w^{(\dot\sigma)} \, \mathrm{d}A, \tag{64.44}$$

where again $\mathrm{d}A = \mathrm{d}x \, \mathrm{d}y$. Now make use of the property (64.43) for non-divergent flows as well as the identity (64.25) to render

$$\begin{aligned}
\int_{\sigma=\text{const}} w^{(\dot\sigma)} \, \mathrm{d}A &= 0 - \int_{\sigma=\text{const}} \hat{\boldsymbol{n}} \cdot \boldsymbol{v}^{(\sigma)} \, \mathrm{d}\mathcal{S} && \text{(64.45a)} \\
&= \int_{\sigma=\text{const}} \frac{\partial\sigma/\partial t}{|\nabla\sigma|} \, \mathrm{d}\mathcal{S} && \text{(64.45b)} \\
&= \int_{\sigma=\text{const}} \frac{\partial\sigma}{\partial t} \left| \frac{\partial z}{\partial\sigma} \right| \mathrm{d}A && \text{(64.45c)} \\
&= -\int_{\sigma=\text{const}} \left[\frac{\partial z}{\partial t} \right]_\sigma \mathrm{d}A. && \text{(64.45d)}
\end{aligned}$$

The final equality holds if $\partial z/\partial\sigma > 0$, whereas we swap signs when the vertical stratification is $\partial z/\partial\sigma < 0$. We can go one further step by noting that the time derivative is computed with σ constant, as is the horizontal area integral. Hence, we can pull the time derivative outside the integral to render

$$\int_{\sigma=\text{const}} w^{(\dot\sigma)} \, \mathrm{d}A = -\left[\frac{\partial}{\partial t} \right]_\sigma \int_{\sigma=\text{const}} z \, \mathrm{d}A. \tag{64.46}$$

This identity means that for a non-divergent flow, the integrated dia-surface transport across the GVC surface equals to minus the time tendency for the area integrated vertical position of that surface. Hence, there is an area integrated dia-surface transport across the GVC surface so long as there is a volume change for the region beneath the surface.

For the case of an isopycnal surface in an adiabatic fluid, there is no change in the volume beneath any interior isopycnal since no flow crosses the isopycnal, in which case we recover the

expected result $\int_{\sigma=\text{const}} w^{(\dot{\sigma})}\,\mathrm{d}A = 0$. However, this result does not hold for other coordinates, such as the rescaled vertical coordinate, $\sigma = z^*$ defined by equation (64.112). In this case

$$z^* = H\,\frac{z-\eta}{H+\eta} \tag{64.47a}$$

$$\frac{\partial z}{\partial z^*} = 1 + H/\eta > 0 \tag{64.47b}$$

$$\left[\frac{\partial z}{\partial t}\right]_{z^*} = \frac{\partial \eta}{\partial t}\,(1 + z^*/H), \tag{64.47c}$$

so that

$$\int_{z^*=\text{const}} w^{(\dot{z^*})}\,\mathrm{d}A = \int_{z^*=\text{const}} (\partial\eta/\partial t)\,(1 + z^*/H)\,\mathrm{d}A, \tag{64.48}$$

which is generally nonzero. For example, consider a flat bottom so that

$$\int_{z^*=\text{const}} w^{(\dot{z^*})}\,\mathrm{d}A = (1 + z^*/H)\int_{z^*=\text{const}} (\partial\eta/\partial t)\,\mathrm{d}A = (1 + z^*/H)\int_{z^*=\text{const}} (Q_\text{m}/\rho_\text{o})\,\mathrm{d}A, \tag{64.49}$$

where Q_m is the surface mass flux and we made use of the free surface equation (21.81) holding for a non-divergent flow. In this case the area integrated dia-surface transport across a z^* surface is proportional to the area integrated surface mass flux.

64.4 Material time derivative

The expression (64.31) for $w^{(\dot{\sigma})}$ brings the material time derivative operator into the following equivalent forms

$$\frac{\mathrm{D}}{\mathrm{D}t} = \left[\frac{\partial}{\partial t}\right]_z + \boldsymbol{u}\cdot\nabla_\text{h} + w\,\frac{\partial}{\partial z} \tag{64.50a}$$

$$= \left[\frac{\partial}{\partial t}\right]_\sigma + \boldsymbol{u}\cdot\nabla_{\text{h}\sigma} + \frac{\mathrm{D}\sigma}{\mathrm{D}t}\,\frac{\partial}{\partial \sigma} \tag{64.50b}$$

$$= \left[\frac{\partial}{\partial t}\right]_\sigma + \boldsymbol{u}\cdot\nabla_{\text{h}\sigma} + w^{(\dot{\sigma})}\,\frac{\partial}{\partial z}. \tag{64.50c}$$

Note that the chain-rule means that

$$\frac{\partial}{\partial \sigma} = \frac{\partial z}{\partial \sigma}\,\frac{\partial}{\partial z}, \tag{64.51}$$

thus providing a relationship between the two vertical coordinate partial derivatives. Furthermore, recall that subscripts in the above derivative operators denote variables held fixed when taking the partial derivatives.

We highlight the special case of no fluid particles crossing the generalized coordinate surface. This sitution occurs in the case of adiabatic flows with σ equal to the buoyancy or isopycnal coordinate. For adiabatic flow, the material time derivative in equation (64.50c) only has a horizontal two-dimensional advective component, $\boldsymbol{u}\cdot\nabla_{\text{h}\sigma}$. This result should not be interpreted to mean that the fluid particle velocity in an adiabatic flow is strictly horizontal. Indeed, it generally is not, as the form given by equation (64.50a) makes clear. Rather, it means that the advective transport of fluid properties occurs along surfaces of constant buoyancy, and such transport is measured by the convergence of horizontal advective fluxes as measured along these constant buoyancy surfaces.

64.5 Vertical velocity and dia-surface velocity

Making use of the material time derivative operator (64.50c) affords us an opportunity to emphasize both the differences and similarities between the vertical velocity component and the dia-surface velocity component. Namely, the vertical velocity component takes on the equivalent forms

$$w = \frac{\mathrm{D}z}{\mathrm{D}t} = \left[\frac{\partial z}{\partial t}\right]_\sigma + \boldsymbol{u} \cdot \nabla_{\!\!\mathrm{h}\sigma} z + w^{(\dot\sigma)} = \frac{\partial z}{\partial \sigma}\left[-\frac{\partial \sigma}{\partial t} - \boldsymbol{u} \cdot \nabla_{\!\!\mathrm{h}} \sigma + \frac{\mathrm{D}\sigma}{\mathrm{D}t}\right], \tag{64.52}$$

and the corresponding expressions for the dia-surface velocity component are given by

$$w^{(\dot\sigma)} = \frac{\partial z}{\partial \sigma}\frac{\mathrm{D}\sigma}{\mathrm{D}t} = \frac{\partial z}{\partial \sigma}\left[\frac{\partial \sigma}{\partial t} + \boldsymbol{u} \cdot \nabla_{\!\!\mathrm{h}} \sigma + w \frac{\partial \sigma}{\partial z}\right] = -\left[\frac{\partial z}{\partial t}\right]_\sigma - \boldsymbol{u} \cdot \nabla_{\!\!\mathrm{h}\sigma} z + w. \tag{64.53}$$

Whereas the vertical velocity component, w, measures the transport crossing z surfaces, which are static and horizontal, the dia-surface velocity component, $w^{(\dot\sigma)}$, measures the transport crossing σ surfaces, which are generally moving and sloped. It is notable that the area normalization used in equation (64.33) for the dia-surface velocity component means that it appears only in the expression for the vertical velocity. However, as we will see in the following, the appearance of $w^{(\dot\sigma)}$ in the w equation does not necessarily mean that $w^{(\dot\sigma)}$ corresponds to vertical particle motion. Instead, when it arises from mixing, $w^{(\dot\sigma)}$ can lead to vertical motion of the σ surface while maintaining a fixed position for the fluid particle.

64.5.1 Decomposing the vertical velocity

The expression

$$w = \left[\frac{\partial z}{\partial t}\right]_\sigma + \boldsymbol{u} \cdot \nabla_{\!\!\mathrm{h}\sigma} z + w^{(\dot\sigma)} \tag{64.54}$$

decomposes the vertical velocity of a fluid particle into (i) changes to the vertical position of the σ-surface at a particular horizontal point, (ii) lateral particle motion projected onto a sloped σ-surface, (iii) motion that crosses a σ-surface. Importantly, the three terms are coupled. For example, consider the case of σ defined by isopycnals, in which case irreversible mixing ($w^{(\dot\sigma)} \neq 0$) changes the configuration of σ surfaces by changing both their height, $(\partial z/\partial t)_\sigma$, and slope $\nabla_{\!\!\mathrm{h}\sigma} z$.

64.5.2 Another form of the vertical velocity decomposition

Consider the velocity for a point on the surface, $\boldsymbol{v}^{(\sigma)}$, which satisfies (Section 64.3.2)

$$\frac{\partial \sigma}{\partial t} + \boldsymbol{v}^{(\sigma)} \cdot \nabla \sigma = 0. \tag{64.55}$$

Making use of the triple product identities from Section 63.5

$$\frac{\partial z}{\partial \sigma}\nabla\sigma = -\nabla_{\!\!\mathrm{h}\sigma} z + \hat{\boldsymbol{z}} \qquad \text{and} \qquad \frac{\partial z}{\partial \sigma}\left[\frac{\partial \sigma}{\partial t}\right]_z = -\left[\frac{\partial z}{\partial t}\right]_\sigma \tag{64.56}$$

brings equation (64.55) into the form

$$\left[\frac{\partial z}{\partial t}\right]_\sigma = (\hat{\boldsymbol{z}} - \nabla_{\!\!\mathrm{h}\sigma} z) \cdot \boldsymbol{v}^{(\sigma)} \Longrightarrow \hat{\boldsymbol{z}} \cdot \boldsymbol{v}^{(\sigma)} = \left[\frac{\partial z}{\partial t}\right]_\sigma + \boldsymbol{u}^{(\sigma)} \cdot \nabla_{\!\!\mathrm{h}\sigma} z, \tag{64.57}$$

where $\boldsymbol{u}^{(\sigma)}$ is the horizontal component to the surface velocity $\boldsymbol{v}^{(\sigma)}$. This equation shows that the vertical component to the σ-surface velocity is given by the sum of the changes to the vertical position of the surface plus the projection of the horizontal motion of the surface onto the slope

of the surface. Additionally, even if the σ-surface has no component of velocity in the vertical, the depth of the σ-surface measured at a horizontal point generally changes if the surface is sloped and moves horizontally pass that point

$$\left[\frac{\partial z}{\partial t}\right]_\sigma = -\boldsymbol{u}^{(\sigma)} \cdot \nabla_{\!\!\text{h}\sigma} z \qquad \text{if } \hat{\boldsymbol{z}} \cdot \boldsymbol{v}^{(\sigma)} = 0. \tag{64.58}$$

Returning to the general result (64.57) allows us to write

$$\left[\frac{\partial z}{\partial t}\right]_\sigma + \boldsymbol{u} \cdot \nabla_{\!\!\text{h}\sigma} z = \hat{\boldsymbol{z}} \cdot \boldsymbol{v}^{(\sigma)} + (\boldsymbol{u} - \boldsymbol{u}^{(\sigma)}) \cdot \nabla_{\!\!\text{h}\sigma} z. \tag{64.59}$$

Furthermore, return to the fundamental definition of the dia-surface velocity component detailed in Section 64.3, in which we showed that

$$w^{(\dot\sigma)} = \frac{\partial z}{\partial \sigma} \frac{\mathrm{D}\sigma}{\mathrm{D}t} = \frac{\partial z}{\partial \sigma} \nabla\sigma \cdot (\boldsymbol{v} - \boldsymbol{v}^{(\sigma)}) = (-\nabla_{\!\!\text{h}\sigma} z + \hat{\boldsymbol{z}}) \cdot (\boldsymbol{v} - \boldsymbol{v}^{(\sigma)}). \tag{64.60}$$

This expression, along with equation (64.59), leads to the rather elaborate decomposition of the vertical velocity component according to motion of a generalized vertical coordinate surface

$$w = \underbrace{\left[\hat{\boldsymbol{z}} \cdot \boldsymbol{v}^{(\sigma)} + (\boldsymbol{u} - \boldsymbol{u}^{(\sigma)}) \cdot \nabla_{\!\!\text{h}\sigma} z\right]}_{(\partial_t + \boldsymbol{u} \cdot \nabla_{\!\!\text{h}\sigma}) z} + \underbrace{\left[\hat{\boldsymbol{z}} \cdot \boldsymbol{v} - \hat{\boldsymbol{z}} \cdot \boldsymbol{v}^{(\sigma)} - (\boldsymbol{u} - \boldsymbol{u}^{(\sigma)}) \cdot \nabla_{\!\!\text{h}\sigma} z\right]}_{w^{(\dot\sigma)}}. \tag{64.61}$$

Terms in the first bracket compute vertical particle motion relative to the σ-surface. The dia-surface contribution from the second bracket removes the contribution from σ-surface motion to leave just the vertical motion of the particle. All terms on the right hand side cancel, except for $\hat{\boldsymbol{z}} \cdot \boldsymbol{v} = w$, thus trivially revealing $w = w$. The decomposition of w is rather pedantic when viewed in the unpacked form of equation (64.61). Even so, let us consider some special cases to offer further interpretation.

- NO HORIZONTAL CONTRIBUTION: Consider the case where the horizontal velocity of a fluid particle matches that of the σ-surface: $\boldsymbol{u} = \boldsymbol{u}^{(\sigma)}$. Alternatively, consider the case with flat σ-surfaces so that $\nabla_{\!\!\text{h}\sigma} z = 0$. In either case the vertical velocity is given by

$$w = \underbrace{\left[\hat{\boldsymbol{z}} \cdot \boldsymbol{v}^{(\sigma)}\right]}_{(\partial_t + \boldsymbol{u} \cdot \nabla_{\!\!\text{h}\sigma}) z} + \underbrace{\left[\hat{\boldsymbol{z}} \cdot (\boldsymbol{v} - \boldsymbol{v}^{(\sigma)})\right]}_{w^{(\dot\sigma)}}. \tag{64.62}$$

  The first contribution is from vertical motion of the σ-surface. The second contribution adjusts for the vertical motion of the particle relative to the σ-surface, leaving behind just the vertical motion of the particle. This rather trivial case exemplifies the contributions from the two pieces of the vertical velocity.

- ZERO VERTICAL PARTICLE MOTION: Consider the case where $w = 0$ so that

$$\begin{aligned} w &= 0 && \text{(64.63a)} \\ &= \left[\frac{\partial z}{\partial t}\right]_\sigma + \boldsymbol{u} \cdot \nabla_{\!\!\text{h}\sigma} z + w^{(\dot\sigma)} && \text{(64.63b)} \\ &= \underbrace{\left[\hat{\boldsymbol{z}} \cdot \boldsymbol{v}^{(\sigma)} + (\boldsymbol{u} - \boldsymbol{u}^{(\sigma)}) \cdot \nabla_{\!\!\text{h}\sigma} z\right]}_{(\partial_t + \boldsymbol{u} \cdot \nabla_{\!\!\text{h}\sigma}) z} + \underbrace{\left[-\hat{\boldsymbol{z}} \cdot \boldsymbol{v}^{(\sigma)} - (\boldsymbol{u} - \boldsymbol{u}^{(\sigma)}) \cdot \nabla_{\!\!\text{h}\sigma} z\right]}_{w^{(\dot\sigma)}}. && \text{(64.63c)} \end{aligned}$$

  The final expression is trivial since each term in one bracket identically cancels terms in

the other bracket. The penultimate expression reveals the balance between dia-surface transport and motion relative to the σ surface

$$-w^{(\dot\sigma)} = \left[\frac{\partial z}{\partial t}\right]_\sigma + \boldsymbol{u}\cdot\nabla_\sigma z \qquad \text{if } \; w = 0. \tag{64.64}$$

A particularly simple realization of this balance holds for σ given by isopycnals and where the isosurfaces are horizontal. In the presence of uniform mixing, the flat isopycnals stay flat and there is correspondingly no vertical motion of fluid particles even as the vertical stratification is modified. In contrast, the vertical position of an isopycnal surface changes according to the dia-surface velocity component $(\partial z/\partial t)_\sigma = -w^{(\dot\sigma)} \neq 0$. This case illustrates that $w^{(\dot\sigma)} \neq 0$ can still occur even when there is zero fluid particle motion since $w^{(\dot\sigma)} \neq 0$ can arise from motion of a σ-surface alone.

64.6 The velocity vector and fluid particle trajectories

Recall from Section 64.5 the alternative forms for the vertical velocity component given by equation (64.52). We focus on the form

$$w = \left[\frac{\partial z}{\partial t}\right]_\sigma + \boldsymbol{u}\cdot\nabla_\sigma z + w^{(\dot\sigma)} \tag{64.65}$$

so that the velocity vector is written[1]

$$\boldsymbol{v} = u\,\hat{\boldsymbol{x}} + v\,\hat{\boldsymbol{y}} + w\,\hat{\boldsymbol{z}} \tag{64.66a}$$

$$= u\,\hat{\boldsymbol{x}} + v\,\hat{\boldsymbol{y}} + \left[(\partial z/\partial t)_\sigma + \boldsymbol{u}\cdot\nabla_\sigma z + w^{(\dot\sigma)}\right]\hat{\boldsymbol{z}} \tag{64.66b}$$

$$= u\,[\hat{\boldsymbol{x}} + \hat{\boldsymbol{z}}\,(\partial z/\partial x)_\sigma] + v\,[\hat{\boldsymbol{y}} + \hat{\boldsymbol{z}}\,(\partial z/\partial y)_\sigma] + \left[(\partial z/\partial t)_\sigma + w^{(\dot\sigma)}\right]\hat{\boldsymbol{z}}. \tag{64.66c}$$

To help further understand these velocity expressions we consider the following three cases, each of which are illustrated in Figure 64.5.

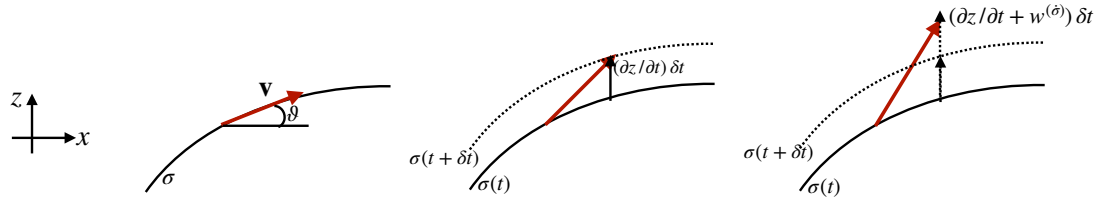

FIGURE 64.5: This schematic shows the various contributions to the fluid particle velocity (red vector) when written relative to motion of a particular generalized vertical coordinate surface. The fluid particle sits at the tail of the velocity vector at time t and at the head at time $t+\delta t$. The left panel is for the case of a static and material σ-surface so that the particle remains on the σ-surface and has a velocity vector given by equation (64.68). The slope of the σ-surface in the $\hat{\boldsymbol{x}}$-direction is given by $\tan\vartheta = (\partial z/\partial x)_\sigma$. The middle panel is for a non-steady material σ-surface whereby the velocity of a particle takes on the form (64.69), with the particle remaining on the moving σ-surface. The right panel shows the case of a non-steady and non-material σ-surface with velocity (64.70). In this final case the particle position departs from the original σ-surface due to the nonzero dia-surface velocity component, $w^{(\dot\sigma)} \neq 0$. However, it is not known *a priori* whether this departure is due to particle motion or motion of the surface. Notably, the horizontal position of the particle remains identical for each of the three cases. It is only the vertical position that is modified according to the slope of the σ-surface (left panel), motion of the σ-surface (middle panel), and motion crossing the σ-surface (right panel).

[1] As discussed in Section 63.7, we can connect these expressions to the contravariant representation of the velocity vector using GVCs.

- STEADY AND MATERIAL σ-SURFACE: The velocity vector is aligned with the instantaneous σ-surface ($\boldsymbol{v} \cdot \nabla\sigma = 0$) when the σ-surface is steady ($\partial\sigma/\partial t = 0$) and material ($\mathrm{D}\sigma/\mathrm{D}t = 0$). Hence, we can diagnose the vertical velocity component in terms of the horizontal via

$$w\,\partial\sigma/\partial z = -\boldsymbol{u} \cdot \nabla_{\mathsf{h}}\sigma \Longrightarrow w = \boldsymbol{u} \cdot \nabla_{\mathsf{h}\sigma} z, \tag{64.67}$$

  where we used the triple product identities (63.34b) and (63.34c) for the final equality. The velocity vector thus takes on the form

$$\boldsymbol{v} = u\,[\hat{\boldsymbol{x}} + \hat{\boldsymbol{z}}\,(\partial z/\partial x)_\sigma] + v\,[\hat{\boldsymbol{y}} + \hat{\boldsymbol{z}}\,(\partial z/\partial y)_\sigma] \qquad \partial\sigma/\partial t = 0 \text{ and } \mathrm{D}\sigma/\mathrm{D}t = 0. \tag{64.68}$$

  In this case, the velocity vector is determined only by the horizontal velocity plus the slope of the σ surface.

- NON-STEADY AND MATERIAL σ-SURFACE: Next consider material σ surfaces ($\mathrm{D}\sigma/\mathrm{D}t = 0$) that move ($\partial_t\sigma \neq 0$), in which case the velocity vector is

$$\boldsymbol{v} = u\,[\hat{\boldsymbol{x}} + \hat{\boldsymbol{z}}\,(\partial z/\partial x)_\sigma] + v\,[\hat{\boldsymbol{y}} + \hat{\boldsymbol{z}}\,(\partial z/\partial y)_\sigma] + (\partial z/\partial t)_\sigma\,\hat{\boldsymbol{z}} \qquad \mathrm{D}\sigma/\mathrm{D}t = 0. \tag{64.69}$$

  To remain on the moving surface, the fluid particle must move vertically by the extra amount $(\partial z/\partial t)_\sigma\,\delta t\,\hat{\boldsymbol{z}}$ relative to the case of a static σ-surface.

- NON-STEADY AND NON-MATERIAL σ-SURFACE: The general case with a non-material and non-steady σ also requires the dia-surface velocity component, $w^{(\dot\sigma)}$, which is diagnosed based on the material time derivative of σ and the inverse stratification, $w^{(\dot\sigma)} = (\partial z/\partial\sigma)\,\mathrm{D}\sigma/\mathrm{D}t$:

$$\boldsymbol{v} = u\,[\hat{\boldsymbol{x}} + \hat{\boldsymbol{z}}\,(\partial z/\partial x)_\sigma] + v\,[\hat{\boldsymbol{y}} + \hat{\boldsymbol{z}}\,(\partial z/\partial y)_\sigma] + \left[(\partial z/\partial t)_\sigma + w^{(\dot\sigma)}\right]\hat{\boldsymbol{z}}. \tag{64.70}$$

  The contribution $w^{(\dot\sigma)}$ measures the vertical motion of the particle relative to the moving σ-surface. Hence, the sum, $(\partial z/\partial t)_\sigma + w^{(\dot\sigma)}$, measures the vertical motion of the particle relative to a fixed origin. As emphasized in Section 64.5, a non-zero $w^{(\dot\sigma)}$ arises from motion of the fluid particle relative to the σ-surface, and this relative motion does not necessarily mean that the particle moves; e.g., recall the example discussed in Section 64.5.2 with a static particle and moving σ-surface.

64.7 Subduction across the mixed layer base

Consider the generalized vertical coordinate defined according to the mixed layer base as in equation (64.3). The dia-surface mass transport across this surface leads us to define the subduction

$$-\mathcal{S}^{(\text{subduction})} \equiv \rho\,\mathrm{d}A\left[\frac{\mathrm{D}(z - \eta^{\mathsf{mld}})}{\mathrm{D}t}\right] \qquad \text{at } z = \eta^{\mathsf{mld}}(x, y, t), \tag{64.71}$$

where the mass transport $\mathcal{S}^{(\text{subduction})}$ (dimensions of mass per time) is positive for fluid moving downward beneath the mixed layer base into the pycnocline (subduction) and negative for water moving into the mixed layer (obduction). The area element $\mathrm{d}A$ is the horizontal projection of the area on the mixed layer base. Expanding the material time derivative leads to

$$-\left[\frac{\mathcal{S}^{(\text{subduction})}}{\rho\,\mathrm{d}A}\right] = w - [\partial_t + \boldsymbol{u} \cdot \nabla]\,\eta^{\mathsf{mld}} \qquad \text{at } z = \eta^{\mathsf{mld}}(x, y, t), \tag{64.72}$$

where again we define

$$\mathcal{S}^{(\text{subduction})} > 0 \qquad \text{subduction} \tag{64.73}$$

$$\mathcal{S}^{(\text{subduction})} < 0 \qquad \text{obduction.} \tag{64.74}$$

We illustrate this definition in Figure 64.6, and note that this definition is consistent with that introduced by *Cushman-Roisin* (1987).

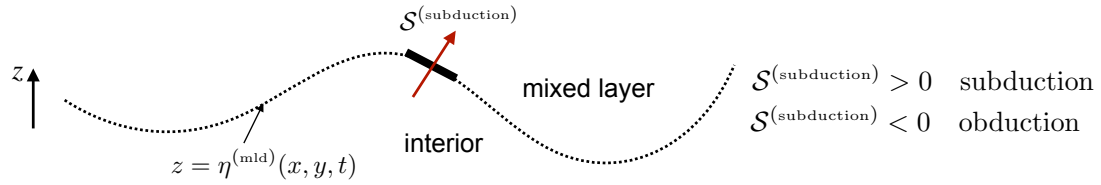

FIGURE 64.6: Illustrating the subduction rate as defined by equation (64.72), which measures the mass transport acrros the base of the ocean mixed layer. When water enters the ocean interior, $\mathcal{S}^{(\text{subduction})} > 0$, and we say that water subducts from the mixed layer to the ocean interior. Conversely, when water enters the mixed layer from below, $\mathcal{S}^{(\text{subduction})} < 0$ and we say that water is obducted from the interior to the mixed layer.

64.8 Mass continuity

We here derive the Eulerian expression for mass continuity (19.6) using generalized vertical coordinates. We then specialize to non-divergent flows, in which mass conservation is converted to volume conservation. To start, recall that mass conservation for a fluid element states that

$$\rho \, \delta V = \rho \, \delta x \, \delta y \, \delta z = \rho \, \delta x \, \delta y \, z_\sigma \, \delta\sigma \tag{64.75}$$

is constant following a fluid element.[2] To develop the Eulerian expressions we first consider the case of Cartesian coordinates.

64.8.1 Cartesian coordinates

Consider the expression

$$\frac{1}{\rho \, \delta V} \frac{\mathrm{D}(\rho \, \delta V)}{\mathrm{D}t} = \frac{1}{\rho} \frac{\mathrm{D}\rho}{\mathrm{D}t} + \frac{1}{\delta V} \frac{\mathrm{D}(\delta V)}{\mathrm{D}t}. \tag{64.76}$$

Now make use of Cartesian coordinates to write the volume

$$\frac{1}{\delta V} \frac{\mathrm{D}(\delta V)}{\mathrm{D}t} = \frac{1}{\delta x \, \delta y \, \delta z} \frac{\mathrm{D}(\delta x \, \delta y \, \delta z)}{\mathrm{D}t} \tag{64.77a}$$

$$= \frac{1}{\delta x} \frac{\mathrm{D}(\delta x)}{\mathrm{D}t} + \frac{1}{\delta y} \frac{\mathrm{D}(\delta y)}{\mathrm{D}t} + \frac{1}{\delta z} \frac{\mathrm{D}(\delta z)}{\mathrm{D}t} \tag{64.77b}$$

$$= \frac{\delta u}{\delta x} + \frac{\delta v}{\delta y} + \frac{\delta w}{\delta z} \tag{64.77c}$$

$$= \nabla \cdot \boldsymbol{v}. \tag{64.77d}$$

Setting $\mathrm{D}(\rho \, \delta V)/\mathrm{D}t = 0$ leads to the familiar expression for the continuity equation

$$\frac{\mathrm{D}\rho}{\mathrm{D}t} = -\rho \, \nabla \cdot \boldsymbol{v}. \tag{64.78}$$

[2] Recall that we write δ as an infinitesimal increment following a fluid element.

64.8.2 Generalized vertical coordinates

We follow the above procedure but now with generalized vertical coordinates so that

$$\frac{1}{\delta V}\frac{\mathrm{D}\,(\delta V)}{\mathrm{D}t} = \frac{1}{\delta x\,\delta y\,z_\sigma\,\delta\sigma}\frac{\mathrm{D}(\delta x\,\delta y\,z_\sigma\,\delta\sigma)}{\mathrm{D}t} \tag{64.79a}$$

$$= \frac{1}{\delta x}\frac{\mathrm{D}(\delta x)}{\mathrm{D}t} + \frac{1}{\delta y}\frac{\mathrm{D}(\delta y)}{\mathrm{D}t} + \frac{1}{z_\sigma}\frac{\mathrm{D}(z_\sigma)}{\mathrm{D}t} + \frac{1}{\delta\sigma}\frac{\mathrm{D}(\delta\sigma)}{\mathrm{D}t} \tag{64.79b}$$

$$= \frac{\delta u}{\delta x} + \frac{\delta v}{\delta y} + \frac{1}{z_\sigma}\frac{\mathrm{D}(z_\sigma)}{\mathrm{D}t} + \frac{\delta(\dot\sigma)}{\delta\sigma} \tag{64.79c}$$

$$= \nabla_{\!\mathrm{h}\sigma}\cdot\boldsymbol{u} + \frac{1}{z_\sigma}\frac{\mathrm{D}(z_\sigma)}{\mathrm{D}t} + \frac{\partial\dot\sigma}{\partial\sigma} \tag{64.79d}$$

where we introduced the shorthand $\dot\sigma = \mathrm{D}\sigma/\mathrm{D}t$. Note that we set

$$\frac{\delta u}{\delta x} + \frac{\delta v}{\delta y} = \nabla_{\!\mathrm{h}\sigma}\cdot\boldsymbol{u} \tag{64.80}$$

since we are working with generalized vertical coordinates so that we consider infinitesimal displacements occurring on constant σ surfaces. We are thus led to

$$\frac{1}{\rho\,\delta V}\frac{\mathrm{D}(\rho\,\delta V)}{\mathrm{D}t} = \nabla_{\!\mathrm{h}\sigma}\cdot\boldsymbol{u} + \frac{1}{z_\sigma}\frac{\mathrm{D}z_\sigma}{\mathrm{D}t} + \frac{\partial\dot\sigma}{\partial\sigma} + \frac{1}{\rho}\frac{\mathrm{D}\rho}{\mathrm{D}t} = 0. \tag{64.81}$$

Now use the material time derivative in the form (64.50b) to derive the Eulerian expression of mass conservation

$$\frac{\partial(\rho\,z_\sigma)}{\partial t} + \nabla_{\!\mathrm{h}\sigma}\cdot(\rho\,z_\sigma\boldsymbol{u}) + \frac{\partial(\rho\,z_\sigma\,\dot\sigma)}{\partial\sigma} = 0, \tag{64.82}$$

where the time derivative is computed holding σ fixed. We can furthermore introduce the dia-surface velocity component

$$w^{(\dot\sigma)} = z_\sigma\,\dot\sigma \tag{64.83}$$

so that mass continuity takes the form

$$\frac{\partial(\rho\,z_\sigma)}{\partial t} + \nabla_{\!\mathrm{h}\sigma}\cdot(\rho\,z_\sigma\boldsymbol{u}) + \frac{\partial(\rho\,w^{(\dot\sigma)})}{\partial\sigma} = 0. \tag{64.84}$$

Alternatively, we can reintroduce the material time derivative operator to write the mass continuity equation (64.82) in the form

$$\frac{1}{\rho\,z_\sigma}\frac{\mathrm{D}(\rho\,z_\sigma)}{\mathrm{D}t} = -(\nabla_{\!\mathrm{h}\sigma}\cdot\boldsymbol{u} + \partial\dot\sigma/\partial\sigma), \tag{64.85}$$

where we used equation (64.50b) to write

$$\frac{\mathrm{D}}{\mathrm{D}t} = \left[\frac{\partial}{\partial t}\right]_\sigma + \boldsymbol{u}\cdot\nabla_{\!\mathrm{h}\sigma} + \dot\sigma\,\frac{\partial}{\partial\sigma}. \tag{64.86}$$

64.9 Layer integrated mass continuity

The formulation thus far has been continuous, with the only assumption made that the specific thickness, $\hbar = \partial z/\partial\sigma$, is single signed. We here consider a discrete increment in the generalized vertical coordinate,

$$\sigma - \delta\sigma/2 \le \sigma' \le \sigma + \delta\sigma/2, \tag{64.87}$$

and formulate the mass budget over this layer whose thickness is given by

$$h \equiv \int_{z(\sigma-\delta\sigma/2)}^{z(\sigma+\delta\sigma/2)} \mathrm{d}z = \int_{\sigma-\delta\sigma/2}^{\sigma+\delta\sigma/2} \frac{\partial z}{\partial \sigma}\, \mathrm{d}\sigma, \tag{64.88}$$

and whose mass per horizontal area is

$$\delta m = \int_{z(\sigma-\delta\sigma/2)}^{z(\sigma+\delta\sigma/2)} \rho\, \mathrm{d}z = \int_{\sigma-\delta\sigma/2}^{\sigma+\delta\sigma/2} \rho\, z_\sigma\, \mathrm{d}\sigma = \overline{\rho}\, h, \tag{64.89}$$

where $\overline{\rho}$ is the layer averaged density. Note that for Boussinesq fluids the mass per area equals to the layer thickness times the reference density

$$\delta m = \rho_o\, h \qquad \text{Boussinesq.} \tag{64.90}$$

As defined by equation (64.88) and illustrated in Figure 64.2, the thickness of a layer is relatively large in regions where $\partial\sigma/\partial z$ is small; i.e., in regions where σ is weakly stratified in the vertical. Conversely, the layer thickness is relatively small where the vertical stratification is large. Furthermore, if the specific thickness is negative, then the layer thickness remains positive by choosing $\delta\sigma < 0$. For example, in a stably stratified fluid with σ given by potential density, $\partial\sigma/\partial z = -(g/\rho_o)\, N^2 < 0$ so that we take $\delta\sigma < 0$ to move vertically upward in the water column to regions of lower potential density. The same situation holds when σ is the hydrostatic pressure in which $\partial p/\partial z = -\rho\, g$ (Section 64.9.2).

The formulation in this section, and its companion for tracers in Section 64.10, holds across all generalized vertical coordinates, even incorporating the trivial case of geopotential coordinates ($\sigma = z$) whereby the specific thickness is unity. Application of the resulting layer integrated kinematics include the development of discrete equations for numerical layered models (see *Griffies et al.* (2020) for a review), as well as the shallow water models discussed in Part VI of this book.

64.9.1 Compressible fluids

Performing a layer integral of the specific thickness equation (64.84) renders

$$\int_{\sigma-\delta\sigma/2}^{\sigma+\delta\sigma/2} \left[\frac{\partial(\rho\, z_\sigma)}{\partial t} + \nabla_{h\sigma} \cdot (\rho\, z_\sigma \boldsymbol{u}) + \frac{\partial(\rho\, w^{(\dot\sigma)})}{\partial \sigma} \right] \mathrm{d}\sigma = 0. \tag{64.91}$$

The dia-surface term integrates to a finite difference across the layer

$$\int_{\sigma-\delta\sigma/2}^{\sigma+\delta\sigma/2} \left[\frac{\partial(\rho\, z_\sigma)}{\partial t} + \nabla_{h\sigma} \cdot (\rho\, z_\sigma \boldsymbol{u}) \right] = -\Delta_\sigma(\rho\, w^{(\dot\sigma)}), \tag{64.92}$$

where we introduced the dimensionless finite difference operator for properties defined at the layer interface

$$\Delta_\sigma(A) = A(\sigma + \delta\sigma/2) - A(\sigma - \delta\sigma/2). \tag{64.93}$$

The time derivative and horizontal space derivative commute with the layer integral, since the limits are specified fixed values for the layer increment, $\delta\sigma$, and the derivatives are computed with σ fixed. Hence, layer mass continuity takes the form

$$\left[\frac{\partial}{\partial t}\right]_\sigma \int_{\sigma-\delta\sigma/2}^{\sigma+\delta\sigma/2} \rho\, z_\sigma\, \mathrm{d}\sigma + \nabla_{h\sigma} \cdot \int_{\sigma-\delta\sigma/2}^{\sigma+\delta\sigma/2} \rho\, \boldsymbol{u}\, z_\sigma\, \mathrm{d}\sigma = -\Delta_\sigma(\rho\, w^{(\dot\sigma)}). \tag{64.94}$$

The first term involves the layer averaged density times the layer thickness as per equation (64.89). The second term involves the layer averaged density-weighted velocity, which is the layer averaged horizontal mass flux

$$\int_{\sigma-\delta\sigma/2}^{\sigma+\delta\sigma/2} \rho\, \boldsymbol{u}\, z_\sigma \,\mathrm{d}\sigma = h\, \overline{\rho\, \boldsymbol{u}}. \tag{64.95}$$

We are thus led to the layer integrated continuity equation

$$\left[\frac{\partial (h\, \overline{\rho})}{\partial t}\right]_\sigma + \nabla_{h\sigma} \cdot (h\, \overline{\rho\, \boldsymbol{u}}) + \Delta_\sigma(\rho\, w^{(\dot{\sigma})}) = 0. \tag{64.96}$$

When evolving the fields in a discrete numerical model, we have information only about layer averaged fields. So how do we estimate the depth average of the horizontal advective flux, $\overline{\rho\, \boldsymbol{u}}$, appearing in equation (64.96)? One method interprets all fields as their layer averaged values so that $\overline{\rho\, \boldsymbol{u}} = \overline{\rho}\, \overline{\boldsymbol{u}}$, thus considering uncomputed sub-layer correlations $\overline{\rho'\, \boldsymbol{u}'}$ as part of the truncation error. Alternately, we note that compressible hydrostatic flows can be described by a pressure-based vertical coordinate in which case the layer mass per horizontal area is proportional to a prescribed increment in pressure

$$\delta m = \int_{\sigma-\delta\sigma/2}^{\sigma+\delta\sigma/2} \rho\, z_\sigma \,\mathrm{d}\sigma = \overline{\rho}\, h = -g^{-1}\, \delta p. \tag{64.97}$$

Correspondingly, the layer integrated horizontal mass flux equals to the mass increment times the pressure-layer averaged velocity

$$\int_{\sigma-\delta\sigma/2}^{\sigma+\delta\sigma/2} \rho\, \boldsymbol{u}\, z_\sigma \,\mathrm{d}\sigma = -g^{-1} \int_{p-\delta p/2}^{p+\delta p/2} \boldsymbol{u} \,\mathrm{d}p = -g^{-1}\, \overline{\boldsymbol{u}}\, \delta p = h\, \overline{\rho}\, \overline{\boldsymbol{u}}. \tag{64.98}$$

With either of the above two methods, we are led to the same layer integrated continuity equation, which we write in the generic form that drops overbars

$$\left[\frac{\partial (h\, \rho)}{\partial t}\right]_\sigma + \nabla_{h\sigma} \cdot (h\, \rho\, \boldsymbol{u}) + \Delta_\sigma\, (\rho\, w^{(\dot{\sigma})}) = 0. \tag{64.99}$$

We illustrate contributions to this layer mass budget in Figure 64.7.

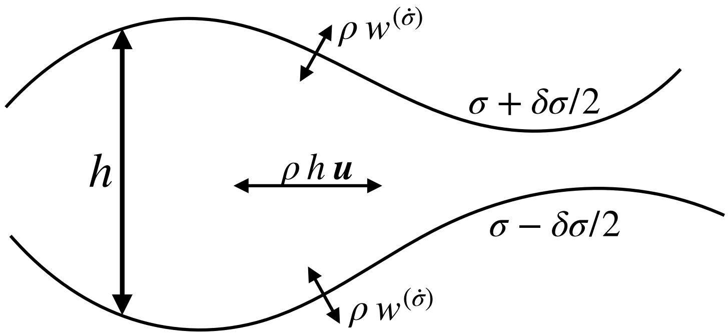

FIGURE 64.7: Illustrating the terms contributing to changes in layer mass according to the layer integrated continuity equation (64.99). The discrete layer is shown here with bounding interfaces at $\sigma - \delta\sigma/2$ and $\sigma + \delta\sigma/2$. Within a layer there is a horizontal redistribution due to horizontal advective transport. Additionally, matter can cross the layer due to dia-surface transport via $w^{(\dot{\sigma})}$.

64.9.2 Mass continuity using pressure coordinates

Let us here consider in some detail the special case of pressure coordinates in a hydrostatic fluid, and thus derive mass continuity using these coordinates.

Method I

The thickness of a hydrostatic pressure layer (equation (64.88)) takes on the following form

$$h = \int_{p-\delta p/2}^{p+\delta p/2} \frac{\partial z}{\partial p}\, \mathrm{d}p = -\int_{p-\delta p/2}^{p+\delta p/2} \frac{\mathrm{d}p}{\rho\, g}, \tag{64.100}$$

so that its mass per unit area is

$$\int_{p-\delta p/2}^{p+\delta p/2} \rho\, \frac{\partial z}{\partial p}\, \mathrm{d}p = -\delta p/g. \tag{64.101}$$

The mass continuity equation (64.99) thus becomes

$$\frac{\partial(\delta p)}{\partial t} + \nabla_{\mathsf{hp}} \cdot (\boldsymbol{u}\, \delta p) + \Delta_p\, (\dot{p}) = 0. \tag{64.102}$$

The partial time derivative vanishes since it is computed by holding pressure fixed so that the pressure increment has a zero time tendency

$$\left[\frac{\partial(\delta p)}{\partial t}\right]_p = 0. \tag{64.103}$$

Likewise, $\nabla_{\mathsf{hp}}\, (\delta p) = 0$. Thus, we can divide by δp to render the continuity equation

$$\nabla_{\mathsf{hp}} \cdot \boldsymbol{u} + \frac{\partial \dot{p}}{\partial p} = 0 \qquad \text{compressible hydrostatic.} \tag{64.104}$$

This equation is isomorphic to the continuity equation for non-divergent flows written using geopotential coordinates

$$\nabla_{\mathsf{h}} \cdot \boldsymbol{u} + \frac{\partial \dot{z}}{\partial z} = \nabla_{\mathsf{h}} \cdot \boldsymbol{u} + \frac{\partial w}{\partial z} 0 \qquad \text{non-divergent flow,} \tag{64.105}$$

where $w = \dot{z}$ is the vertical component to the velocity vector. For both pressure coordinates, describing non-Boussinesq fluids, and depth coordinates, describing Boussinesq fluids, the continuity equation is a diagnostic relation (i.e., no time derivatives) rather than prognostic (i.e., containing time derivatives).

Method II

For the second method we make use of the approach detailed in Section 64.8.2, which starts from

$$\frac{\mathrm{D}(\rho\, \delta V)}{\mathrm{D}t} = 0. \tag{64.106}$$

In pressure coordinates the volume of the fluid element takes the form

$$\delta V = \delta x\, \delta y\, \delta z = \delta x\, \delta y \left[\frac{\partial z}{\partial p}\right] \delta p = -(\rho\, g)^{-1}\, \delta x\, \delta y\, \delta p. \tag{64.107}$$

Consequently,

$$0 = \frac{\mathrm{D}(\rho\,\delta V)}{\mathrm{D}t} = g^{-1}\left(\frac{\mathrm{D}\left(\delta x\,\delta y\,\delta p\right)}{\mathrm{D}t}\right), \tag{64.108}$$

so that

$$0 = \frac{1}{\delta x\,\delta y\,\delta p}\left(\frac{\mathrm{D}\left(\delta x\,\delta y\,\delta p\right)}{\mathrm{D}t}\right) = \nabla_{\mathsf{hp}}\cdot\boldsymbol{u} + \frac{\partial\dot{p}}{\partial p}. \tag{64.109}$$

The second step made use of the isomorphism between this result and that for equation (18.140) that holds for a geopotential vertical coordinate.

64.9.3 Non-divergent flow

Specializing to a non-divergent flow where fluid elements conserve their volume (see Chapters 21 and 29) yields the layer thickness equation

$$\frac{\partial h}{\partial t} + \nabla_{\mathsf{h}\sigma}\cdot(h\,\boldsymbol{u}) + \Delta_\sigma w^{(\dot{\sigma})} = 0. \tag{64.110}$$

Further specializing to the case of zero dia-surface transport leads to

$$\frac{\partial h}{\partial t} + \nabla_{\mathsf{h}\sigma}\cdot(h\,\boldsymbol{u}) = 0 \qquad \text{no dia-surface transport.} \tag{64.111}$$

This case is commonly studied for adiabatic fluids using isopycnal coordinates, in which isopycnal surfaces are material (Section 66.2).

64.9.4 Rescaled geopotential coordinates

The rescaled geopotential coordinate

$$z^* = \frac{H\,(z-\eta)}{H+\eta} = \frac{\eta_{\mathsf{b}}\,(z-\eta)}{\eta_{\mathsf{b}}-\eta} \quad \text{and} \quad \eta_{\mathsf{b}}(x,y) \le z^* \le 0, \tag{64.112}$$

is commonly used in Boussinesq ocean models, where $z=\eta(x,y,t)$ is the ocean free surface and $z=\eta_{\mathsf{b}}(x,y)=-H(x,y)$ is the ocean bottom. The thickness of a coordinate layer is given by

$$h = \mathrm{d}z = \frac{\partial z}{\partial z^*}\,\mathrm{d}z^* = (1+\eta/H)\,\mathrm{d}z^* = (1-\eta/\eta_{\mathsf{b}})\,\mathrm{d}z^*. \tag{64.113}$$

The depth integrated column thickness and depth integrated coordinate thickness are given by

$$\int_{\eta_{\mathsf{b}}}^{\eta}\mathrm{d}z = \eta-\eta_{\mathsf{b}} = \eta+H \qquad \text{and} \qquad \int_{z^*(\eta_{\mathsf{b}})}^{z^*(\eta)}\mathrm{d}z^* = -\eta_{\mathsf{b}} = H. \tag{64.114}$$

Correspondingly, the depth integrated thickness equation is given by the depth integrated volume budget derived in Section 21.8

$$\frac{\partial\eta}{\partial t} + \nabla\cdot\boldsymbol{U} + [w^{(\dot{\sigma})}_{z^*=0} - w^{(\dot{\sigma})}_{z^*=\eta_{\mathsf{b}}}] = 0. \tag{64.115}$$

We assume no volume flow through the ocean bottom so that $w^{(\dot{\sigma})}_{z^*=\eta_{\mathsf{b}}}=0$, whereas

$$-\rho_{\mathsf{o}}\,w^{(\dot{\sigma})}_{z^*=0} = Q_{\mathrm{m}} \tag{64.116}$$

is the mass flux crossing the ocean free surface (Section 19.6.3).

64.10 Layer integrated tracer equation

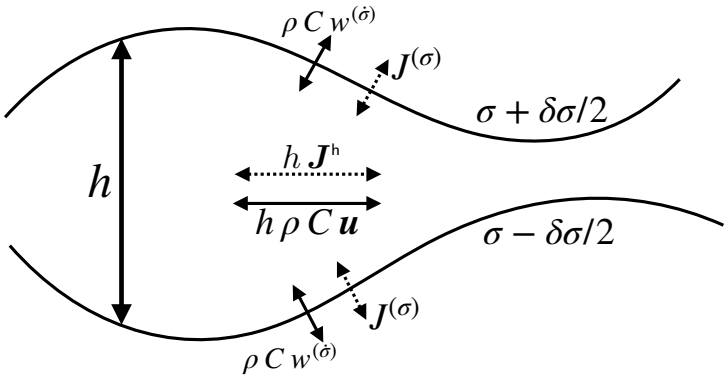

FIGURE 64.8: Illustrating the terms contributing to changes in layer tracer content according to the layer integrated tracer equation (64.121). The layer is shown here with bounding interfaces at $\sigma - \delta\sigma/2$ and $\sigma + \delta\sigma/2$. Within a layer there is a redistribution of tracer due to horizontal advective and subgrid scale tracer fluxes. Additionally, matter can cross the layer due to dia-surface transport via $\rho\, C\, w^{(\dot\sigma)}$ and subgrid tracer transport $J^{(\sigma)}$.

The tracer equation from Section 20.1.3 is given by

$$\rho\, \frac{\mathrm{D}C}{\mathrm{D}t} = -\nabla \cdot \boldsymbol{J}, \tag{64.117}$$

where $\boldsymbol{J}$ is a subgrid scale flux. Now introduce the material time derivative operator in the form (64.50b) to have

$$\rho \left[\frac{\partial C}{\partial t} + \boldsymbol{u} \cdot \nabla_{\!\mathrm{h}\sigma} C + \dot\sigma\, \partial_\sigma C \right] = -\nabla \cdot \boldsymbol{J}, \tag{64.118}$$

Multiplying by the specific thickness and making use of the mass conservation equation (64.84) renders the flux-form Eulerian equation

$$\frac{\partial(z_\sigma\, \rho\, C)}{\partial t} + \nabla_{\!\mathrm{h}\sigma} \cdot (z_\sigma\, \rho\, C\, \boldsymbol{u}) + \frac{\partial(\rho\, C\, w^{(\dot\sigma)})}{\partial \sigma} = -\left[\nabla_{\!\mathrm{h}\sigma} \cdot (z_\sigma\, \boldsymbol{J}^{\mathrm{h}}) + \frac{\partial(z_\sigma\, \nabla\sigma \cdot \boldsymbol{J})}{\partial \sigma} \right], \tag{64.119}$$

where we made use of expression (63.99) for the subgrid scale operator. Now perform a layer integral as detailed in Section 64.9 and use the layer mass continuity equation (64.99) to yield the layer integrated tracer equation

$$\frac{\partial(h\, \rho\, C)}{\partial t} + \nabla_{\!\mathrm{h}\sigma} \cdot (h\, \rho\, C\, \boldsymbol{u}) + \Delta_\sigma(\rho\, C\, w^{(\dot\sigma)}) = -\left[\nabla_{\!\mathrm{h}\sigma} \cdot (h\, \boldsymbol{J}^{\mathrm{h}}) + \Delta_\sigma(z_\sigma\, \nabla\sigma \cdot \boldsymbol{J}) \right]. \tag{64.120}$$

Alternatively, we can bring all terms to the left hand side to yield

$$\frac{\partial(h\, \rho\, C)}{\partial t} + \nabla_{\!\mathrm{h}\sigma} \cdot (h\, \rho\, C\, \boldsymbol{u} + h\, \boldsymbol{J}^{\mathrm{h}}) + \Delta_\sigma(\rho\, C\, w^{(\dot\sigma)} + J^{(\sigma)}) = 0 \tag{64.121}$$

where we wrote

$$J^{(\sigma)} = z_\sigma\, \nabla\sigma \cdot \boldsymbol{J}. \tag{64.122}$$

We illustrate contributions to the layer tracer budget (64.121) in Figure 64.8. Note that we interpret these layer integrated fields and fluxes as per the discussion in Section 64.9.1.

64.11 Overturning circulation in the meridional-σ plane

In Section 21.7 we studied the meridional-depth streamfunction, where we showed that equation (21.73), or the equivalent form (21.78), are streamfunctions for the meridional-depth circulation. Here we introduce a streamfunction defined according to generalized vertical coordinate, $\sigma(x, y, z, t)$. This generalization is useful for studying the zonally integrated circulation partitioned according to σ surfaces rather than z surfaces, in particular when σ is potential density or entropy surface. We make use of Figure 64.9 for the derivation.

As noted in Section 21.7, we can make use of the Boussinesq fluid, where the flow field is non-divergent. Alternatively, we make use of a non-Boussinesq fluid when the flow is steady. As shown in this section, we are afforded a meridional-σ streamfunction only when σ is time independent.

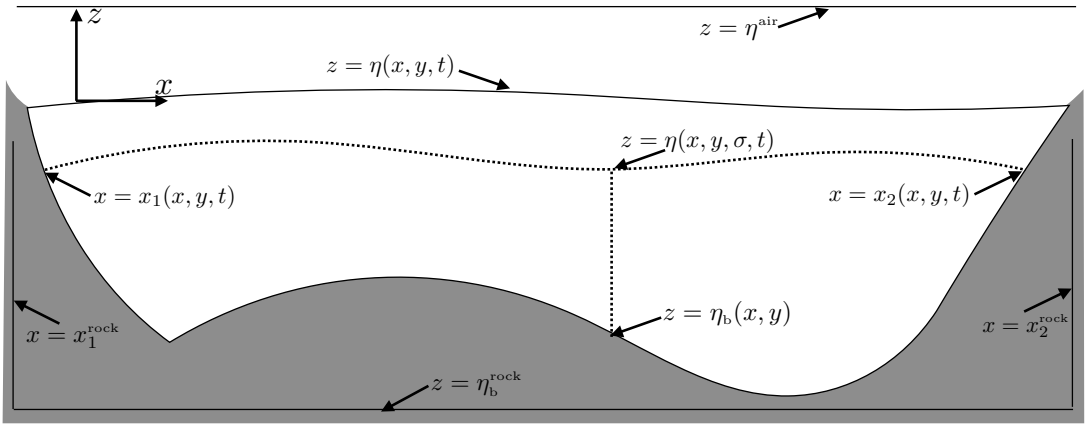

FIGURE 64.9: Geometry for computing the meridional streamfunction, here generalizing the meridional-depth streamfunction geometry in Figure 21.5 to meridional-σ. The zonal boundaries are written $x = x_1(y, z, t)$ and $x = x_2(y, z, t)$, which are generally functions of latitude and vertical position as well as time. The bottom is written as $z = \eta_{\text{b}}(x, y)$ and the vertical position of an arbitrary surface is written $z = \eta(x, y, \sigma, t)$, where we assume this surface is monotonic in the vertical. Note that for shorthand, we often find it convenient to write $z = \eta_\sigma(x, y, t)$, particularly when suppressing the dependencies on horizontal position and time. We also display the constant zonal positions, $x_{1,2}^{\text{rock}}$, which are fully within the rock, as well as the bottom position, $\eta_{\text{b}}^{\text{rock}}$, which is also within the rock.

64.11.1 Overturning streamfunction

Start from equation (21.78) for the meridional-depth streamfunction, here generalized to

$$\Psi(y, \sigma, t) = -\int_{x_1^{\text{rock}}}^{x_2^{\text{rock}}} \left[\int_{\eta_{\text{b}}(x', y)}^{z=\eta(x', y, \sigma, t)} v(x', y, z', t)\, \mathrm{d}z' \right] \mathrm{d}x'. \tag{64.123}$$

As defined, $\Psi(y, \sigma, t)$ makes use of $z = \eta(x', y, \sigma, t)$ for the upper bound on the vertical integral, where $\eta(x', y, \sigma, t)$ is the vertical position of a generalized vertical coordinate surface with value σ, such as depicted in Figure 64.9. In this manner, $\Psi(y, \sigma, t)$, is a function of latitude, σ, and time. Our job in the next subsection is to prove that $\Psi(y, \sigma, t)$ indeed serves as a streamfunction for the zonally integrated flow, with the zonal integral along constant σ surfaces rather than constant z surfaces.

64.11.2 Proving that $\Psi(y, \sigma, t)$ is a streamfunction

To prove that $\Psi(y, \sigma, t)$ is indeed a streamfunction, we proceed much like in Section 21.7.3 for the meridional-depth streamfunction, $\Psi(y, z, t)$, with the key new piece in the derivation

concerning the space-time dependence of the $z = \eta(x, y, \sigma, t)$ surface. The vertical derivative of the streamfunction is given by

$$\frac{\partial \Psi}{\partial z} = -\frac{\partial}{\partial z} \int_{x_1^{\text{rock}}}^{x_2^{\text{rock}}} \left[\int_{\eta_{\mathsf{b}}(x',y)}^{z=\eta(x',y,\sigma,t)} v(x', y, z', t)\, \mathrm{d}z' \right] \mathrm{d}x' \tag{64.124a}$$

$$= -\int_{x_1^{\text{rock}}}^{x_2^{\text{rock}}} \left[\frac{\partial}{\partial z} \int_{\eta_{\mathsf{b}}(x',y)}^{z=\eta(x',y,\sigma,t)} v(x', y, z', t)\, \mathrm{d}z' \right] \mathrm{d}x' \tag{64.124b}$$

$$= -\int_{x_1^{\text{rock}}}^{x_2^{\text{rock}}} v(x', y, z = \eta(x', y, \sigma, t))\, \mathrm{d}x' \tag{64.124c}$$

$$= -V(y, \sigma, t). \tag{64.124d}$$

In these steps we used used Leibniz's rule and noted that only the upper integration limit is a function of z. Furthermore, the upper limit on the vertical integral is evaluated at the vertical position of the σ surface. Hence, the zonal integral is defined while keeping the vertical position on the σ surface rather than on a constant geopotential surface.

For the meridional derivative we have

$$\frac{\partial \Psi}{\partial y} = -\int_{x_1^{\text{rock}}}^{x_2^{\text{rock}}} \left[\frac{\partial}{\partial y} \int_{\eta_{\mathsf{b}}(x',y)}^{z=\eta(x',y,\sigma,t)} v(x', y, z', t)\, \mathrm{d}z' \right] \mathrm{d}x'. \tag{64.125}$$

Focusing on the vertical integral yields (dropping various coordinate dependencies when not essential)

$$\frac{\partial}{\partial y} \int_{\eta_{\mathsf{b}}(x',y)}^{z=\eta(x',y,\sigma)} v(x', y, z')\, \mathrm{d}z' = v(\eta_\sigma)\, \partial_y \eta_\sigma - v(\eta_{\mathsf{b}})\, \partial_y \eta_{\mathsf{b}} + \int_{\eta_{\mathsf{b}}(x',y)}^{z=\eta(x',y,\sigma)} \partial_y v(x', y, z')\, \mathrm{d}z'. \tag{64.126}$$

Focus again on the vertical integral and make use of the non-divergence condition to yield

$$\int_{\eta_{\mathsf{b}}(x',y)}^{z=\eta(x',y,\sigma)} \partial_y v(x', y, z')\, \mathrm{d}z' = -\int_{\eta_{\mathsf{b}}(x',y)}^{z=\eta(x',y,\sigma)} [\partial_{x'} u(x', y, z') + \partial_{z'} w(x', y, z')]\, \mathrm{d}z'. \tag{64.127}$$

Leibniz's rule on the $\partial_{x'} u(x', y, z')$ term then brings us to

$$\frac{\partial}{\partial y} \int_{\eta_{\mathsf{b}}(x',y)}^{z=\eta(x',y,\sigma)} v(x', y, z')\, \mathrm{d}z' = -[w(\eta_\sigma) - \boldsymbol{u}(\eta_\sigma) \cdot \nabla \eta_\sigma] + [w(\eta_{\mathsf{b}}) - \boldsymbol{u}(\eta_{\mathsf{b}}) \cdot \nabla \eta_{\mathsf{b}}] - \frac{\partial}{\partial x} \int_{\eta_{\mathsf{b}}(x',y)}^{z=\eta(x',y,\sigma)} u(x', y, z')\, \mathrm{d}z'. \tag{64.128}$$

Recall that $w(\eta_{\mathsf{b}}) - \boldsymbol{u}(\eta_{\mathsf{b}}) \cdot \nabla \eta_{\mathsf{b}} = 0$ from the bottom kinematic boundary condition (19.56). Furthermore, from equation (64.35f) for the dia-surface velocity, we have

$$w(\eta_\sigma) - \boldsymbol{u}(\eta_\sigma) \cdot \nabla \eta_\sigma = w^{(\dot\sigma)} + \partial_t \eta_\sigma. \tag{64.129}$$

Bringing these results together then renders

$$\frac{\partial \Psi}{\partial y} = \int_{x_1^{\text{rock}}}^{x_2^{\text{rock}}} [w^{(\dot\sigma)}(x', y, z = \eta_\sigma) + \partial_t \eta_\sigma]\, \mathrm{d}x', \tag{64.130}$$

where we set

$$u(x_1^{\text{rock}}) = u(x_2^{\text{rock}}) = 0. \tag{64.131}$$

We conclude that $\Psi(y, \sigma, t)$ is a streamfunction for the special case where σ is time independent, in which case

$$\frac{\partial \Psi}{\partial y} = \int_{x_1^{\text{rock}}}^{x_2^{\text{rock}}} w^{(\dot{\sigma})}(x', y, z = \eta_\sigma) \, \mathrm{d}x' = W^{(\dot{\sigma})}(y, \sigma, t). \tag{64.132}$$

We can understand the need for time independence since that ensures that the flow underneath the σ surface is non-divergent, much like the case for a shallow water model in steady state (see Chapter 35). In the literature, one can find $\Psi(y, \sigma, t)$ referred to as a streamfunction even when the flow has time dependence, in which case extra caution is needed if inferring the associated flow patterns.

Chapter 65

Dynamical equations

In this chapter we derive the dynamical equations for momentum, vorticity, and potential vorticity using generalized vertical coordinates. These equations provide the foundations for many numerical models of the atmosphere and ocean. Besides being essential for developing methods for numerical simulations, understanding the physical and mathematical basis of these equations supports the analysis of simulations.

READER'S GUIDE TO THIS CHAPTER

We assume a working knowledge of the mathematics of generalized vertical coordinates as detailed in Chapter 63 and the corresponding kinematics in Chapter 64. We make particular use of the layer integrated notions introduced for mass continuity and the tracer equations in Sections 64.9 and 64.10. We also make use of the dynamical equations derived in Chapter 24. For most purposes in this chapter we find Cartesian horizontal coordinates sufficient. However, we note some places where spherical coordinates warrant special consideration.

65.1 Equations of motion

We here derive the equations of motion based on generalized vertical coordinates. The scalar equations were already discussed in Sections 64.8, 64.9, and 64.10, so our main focus concerns the momentum equation.

65.1.1 Notation

For much of this chapter we focus on the continuous formulation of the generalized vertical coordinates. Following the discussion in Section 64.2, we encounter the specific thickness throughout the equations

$$\hbar = \frac{\partial z}{\partial \sigma} = z_\sigma. \tag{65.1}$$

Using this notation we write the dia-surface transport velocity as

$$w^{(\dot\sigma)} = \frac{\partial z}{\partial \sigma}\,\dot\sigma = \hbar\,\dot\sigma, \tag{65.2}$$

and the dia-surface advection operator is

$$w^{(\dot\sigma)}\,\partial_z = \dot\sigma\,\partial_\sigma. \tag{65.3}$$

65.1.2 Mass and tracer equations

The mass and tracer equations were derived in Sections 64.8, 64.9, and 64.10, with their continuous vertical coordinate formulation given by

$$\frac{\partial(\rho\,\hbar)}{\partial t} + \nabla_{h\sigma}\cdot(\rho\,\hbar\,\boldsymbol{u}) + \partial_\sigma(\rho\,\hbar\,\dot\sigma) = 0 \tag{65.4a}$$

$$\frac{\partial(\hbar\,\rho\,C)}{\partial t} + \nabla_{h\sigma}\cdot(\hbar\,\rho\,C\,\boldsymbol{u} + \hbar\,\boldsymbol{J}^{\mathrm{h}}) + \partial_\sigma(\rho\,\hbar\,\dot\sigma\,C + \hbar\,\nabla\sigma\cdot\boldsymbol{J}) = 0. \tag{65.4b}$$

Compatibility is maintained between the mass continuity equation (65.4a) and the tracer equation (65.4b) so long as the tracer equation reduces to the mass equation upon setting the tracer concentration to a spatial constant. Hence, for compatibility we must have the subgrid fluxes, $\boldsymbol{J}$, vanish when the tracer is a spatial constant. For example, diffusive fluxes, which are proportional to the tracer gradient, respect this constraint. These properties originate from our discussion of mass budgets and the barycentric velocity in Section 20.1.

65.1.3 Momentum equation

From Section 26.13, the horizontal and vertical components to the momentum equation are

$$\rho\,\frac{\mathrm{D}\boldsymbol{u}}{\mathrm{D}t} + 2\,\rho\,\boldsymbol{\Omega}\times\boldsymbol{u} = -\rho\,\nabla_{\!h}\Phi - \nabla_{\!h}p + \rho\boldsymbol{F}^{\mathrm{h}} \tag{65.5a}$$

$$\rho\,\frac{\mathrm{D}w}{\mathrm{D}t} = -\rho\,\frac{\partial\Phi}{\partial z} - \frac{\partial p}{\partial z} + \rho F^z. \tag{65.5b}$$

The simple form of the geopotential sets $\Phi = g\,z$ (Section 13.10), so that the horizontal gradient of the geopotential vanishes

$$\Phi = g\,z \implies \nabla_{\!h}\Phi = 0. \tag{65.6}$$

However, this gradient is nonzero in the presence of astronomical tide forcing, such as discussed in Chapter 34.

Horizontal momentum equation

We transform the horizontal derivatives from geopotential coordinates to generalized vertical coordinates according to (see equation (63.75))

$$\nabla_{\!h} = \nabla_{h\sigma} - (\nabla_{h\sigma} z)\,\partial_z \tag{65.7}$$

thus leading to the horizontal momentum equation

$$\rho \frac{\mathrm{D}\boldsymbol{u}}{\mathrm{D}t} + 2\,\rho\,\boldsymbol{\Omega} \times \boldsymbol{u} = -\rho\,[\nabla_{\!\mathrm{h}\sigma} - (\nabla_{\!\mathrm{h}\sigma} z)\,\partial_z]\,\Phi - [\nabla_{\!\mathrm{h}\sigma} - (\nabla_{\!\mathrm{h}\sigma} z)\,\partial_z]\,p + \rho \boldsymbol{F}^{\mathrm{h}}. \tag{65.8}$$

In Section 65.1.6 we present some special cases for this equation that simplify the pressure and geopotential terms.

Vertical momentum equation

The vertical momentum equation is transformed into

$$\rho \frac{\mathrm{D}w}{\mathrm{D}t} = -\frac{\partial \sigma}{\partial z}\left[\rho \frac{\partial \Phi}{\partial \sigma} + \frac{\partial p}{\partial \sigma}\right] + \rho\, F^z, \tag{65.9}$$

with the hydrostatic form given by

$$\frac{\partial p}{\partial \sigma} = -\rho \frac{\partial \Phi}{\partial \sigma}. \tag{65.10}$$

65.1.4 Flux-form horizontal momentum equation

Using Cartesian horizontal coordinates and generalized vertical coordinates, the horizontal momentum equation includes a contribution from the acceleration that has a form similar to that for a tracer (Section 64.10)

$$\hbar\,\rho \frac{\mathrm{D}u}{\mathrm{D}t} = \left[\frac{\partial(\hbar\,\rho\,u)}{\partial t}\right]_\sigma + \nabla_{\!\mathrm{h}\sigma} \cdot (\hbar\,\rho\,u\,\boldsymbol{u}) + \partial_\sigma(\hbar\,\rho\,u\,\dot{\sigma}) \tag{65.11a}$$

$$\hbar\,\rho \frac{\mathrm{D}v}{\mathrm{D}t} = \left[\frac{\partial(\hbar\,\rho\,v)}{\partial t}\right]_\sigma + \nabla_{\!\mathrm{h}\sigma} \cdot (\hbar\,\rho\,v\,\boldsymbol{u}) + \partial_\sigma(\hbar\,\rho\,v\,\dot{\sigma}). \tag{65.11b}$$

We provide a σ subscript on the time derivative operator to signal that this derivative is taken with σ held fixed. With spherical coordinates there are additional metric terms appearing on the right hand side, as detailed in Section 24.3. In particular, there is a metric term that contains the vertical velocity component, $w = \mathrm{D}z/\mathrm{D}t$. The appearance of w is awkward since the vertical velocity is not naturally computed using generalized vertical coordinates. This limitation is overcome through use of the vector-invariant velocity equation derived in Section 65.1.5.

65.1.5 Vector-invariant horizontal momentum equation

As noted in Section 24.4, the *vector-invariant* form of the velocity equation eliminates the metric terms that appear in the non-Cartesian flux-form equations. The vector-invariant form is also suited for deriving the vorticity equation (see Section 65.3). Here, we start with the material time derivative in the form (64.50c) appropriate for generalized vertical coordinates, in which case the horizontal acceleration is given by

$$\frac{\mathrm{D}\boldsymbol{u}}{\mathrm{D}t} = \left[\frac{\partial \boldsymbol{u}}{\partial t}\right]_\sigma + (\boldsymbol{u} \cdot \nabla_{\!\mathrm{h}\sigma})\,\boldsymbol{u} + (\dot{\sigma}\,\partial_\sigma)\,\boldsymbol{u}. \tag{65.12}$$

Now make use of the vector identity (see Section 2.3.4)

$$(\boldsymbol{u} \cdot \nabla_{\!\mathrm{h}\sigma})\,\boldsymbol{u} = \nabla_{\!\mathrm{h}\sigma} K + (\nabla_{\!\mathrm{h}\sigma} \times \boldsymbol{u}) \times \boldsymbol{u}, \tag{65.13}$$

where

$$K = \boldsymbol{u} \cdot \boldsymbol{u}/2 \tag{65.14}$$

is the kinetic energy per mass of the horizontal flow. Introducing the generalized vertical coordinate version of the relative vorticity (see Section 66.3.1)

$$\widetilde{\zeta} \equiv \hat{\boldsymbol{z}} \cdot (\nabla_{\!\mathrm{h}\sigma} \times \boldsymbol{u}) = \left[\frac{\partial v}{\partial x}\right]_{\sigma} - \left[\frac{\partial u}{\partial y}\right]_{\sigma} \tag{65.15}$$

renders

$$\frac{\mathrm{D}\boldsymbol{u}}{\mathrm{D}t} = \left[\frac{\partial \boldsymbol{u}}{\partial t}\right]_{\sigma} + \nabla_{\!\mathrm{h}\sigma}\, K + \widetilde{\zeta}\, \hat{\boldsymbol{z}} \times \boldsymbol{u} + \dot{\sigma}\, \partial_{\sigma}\, \boldsymbol{u}, \tag{65.16}$$

so that the horizontal momentum equation takes the form

$$\left[\frac{\partial \boldsymbol{u}}{\partial t}\right]_{\sigma} + \dot{\sigma}\, \frac{\partial \boldsymbol{u}}{\partial \sigma} + (2\,\boldsymbol{\Omega} + \hat{\boldsymbol{z}}\, \widetilde{\zeta}) \times \boldsymbol{u} = -\nabla_{\!\mathrm{h}\sigma} K - \nabla_{\!\mathrm{h}} \Phi - (1/\rho)\, \nabla_{\!\mathrm{h}} p + \boldsymbol{F}^{\mathrm{h}}, \tag{65.17}$$

where again $\nabla_{\!\mathrm{h}} = \nabla_{\!\mathrm{h}\sigma} - (\nabla_{\!\mathrm{h}\sigma} z)\, \partial_z$ as per equation (65.7). This equation is form-invariant regardless the horizontal coordinates, thus motivating the name *vector-invariant*.[1]

65.1.6 Hydrostatic balance with constant gravitational acceleration

There are many special cases that simplify various terms in the momentum equation. For example, when considering a geopotential in the form $\Phi = g\, z$ (Section 13.10) with g assumed to be a constant effective gravitational acceleration, then the horizontal momentum equation (65.8) becomes

$$\rho\, \frac{\mathrm{D}\boldsymbol{u}}{\mathrm{D}t} + 2\, \rho\, \boldsymbol{\Omega} \times \boldsymbol{u} = -[\nabla_{\!\mathrm{h}\sigma} - (\nabla_{\!\mathrm{h}\sigma} z)\, \partial_z]\, p + \rho \boldsymbol{F}^{\mathrm{h}}. \tag{65.18}$$

Furthermore, assuming an approximate hydrostatic balance (and corresponding simplification of the Coriolis acceleration as per Section 27.1.3) allows us to write $\partial p/\partial z = -g\, \rho$ so that

$$\rho\, \frac{\mathrm{D}\boldsymbol{u}}{\mathrm{D}t} + \rho\, f\, \hat{\boldsymbol{z}} \times \boldsymbol{u} = -[\nabla_{\!\mathrm{h}\sigma} p + \rho\, \nabla_{\!\mathrm{h}\sigma} \Phi] + \rho \boldsymbol{F}^{\mathrm{h}}, \tag{65.19}$$

which also takes on the vector-invariant form

$$\left[\frac{\partial \boldsymbol{u}}{\partial t}\right]_{\sigma} + \dot{\sigma}\, \frac{\partial \boldsymbol{u}}{\partial \sigma} + (f + \widetilde{\zeta})\, \hat{\boldsymbol{z}}\, \times \boldsymbol{u} = -\nabla_{\!\mathrm{h}\sigma}(K + \Phi) - (1/\rho)\, \nabla_{\!\mathrm{h}\sigma} p + \boldsymbol{F}^{\mathrm{h}}. \tag{65.20}$$

This form is commonly used for hydrostatic models of the ocean and atmosphere, such as discussed in *Griffies et al.* (2020).

65.2 Concerning the pressure force

As seen in Section 25.2.3, the pressure force acting on a fluid region is given by the integral

$$\boldsymbol{F}^{\mathrm{press}} = -\oint_{\partial \mathcal{R}} p\, \hat{\boldsymbol{n}}\, \mathrm{d}\mathcal{S} = -\int_{\mathcal{R}} \nabla p\, \mathrm{d}V, \tag{65.21}$$

where the second equality follows from Gauss's divergence theorem applied to a scalar field (Section 2.7.2). We refer to the right-most expression as the pressure gradient body force, and this expression is the basis for the discussion in Sections 65.1.6 and 65.2.1. In this formulation, the pressure force at a point is oriented down the pressure gradient, so that the net pressure force acting on a region is the volume integral of pressure gradient.

[1] See Section 4.4.4 of *Griffies* (2004) for a detailed derivation using arbitrary horizontal coordinates.

The middle expression in equation (65.21) formulates the pressure force as the area integrated pressure contact force acting on the region boundaries. In this form, the pressure acting on a region is computed as the integral of pressure over the area bounding the region, with the orientation determined by the inward normal at each point on the boundary. Much of this section is concerned with the contact force expression as a basis for computing the pressure force acting on a finite region as shown in Figure 65.2. The contact force perspective was taken by *Lin* (1997) and *Adcroft et al.* (2008) in their finite volume approach to computing the pressure force acting on a numerical model grid cell.

65.2.1 Computing the horizontal pressure gradient

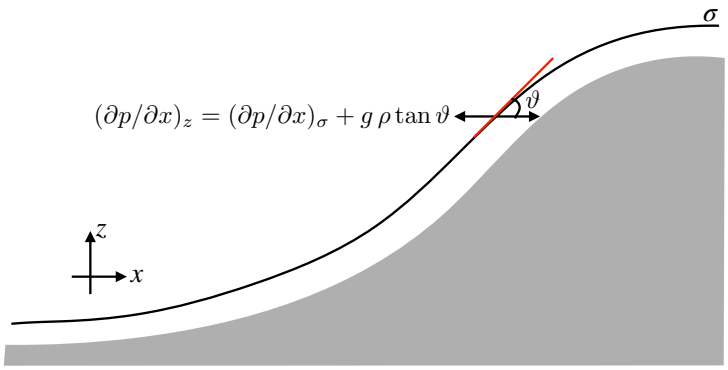

FIGURE 65.1: Illustrating how the horizontal pressure gradient is decomposed into two terms, one aligned with the surface of constant σ, and another associated with the slope of the σ-surface relative to the horizontal, $\tan\vartheta = (\partial z/\partial x)_\sigma$. We here consider the decomposition using terrain following vertical coordinates, where the vertical coordinate is aligned according to the solid-earth bottom (shaded region). Specifically, for terrain following Boussinesq ocean models we set $\sigma = (z-\eta)/(-\eta_b+\eta)$, where $z = \eta(x,y,t)$ is the ocean free surface and $z = \eta_b(x,y)$ is the ocean bottom topography. Terrain-following atmospheric models have a similar definition, often using pressure rather than geopotential so that $\sigma = (p - p_a)/(p_b - p_a)$, where p is the pressure, $p_a = p_a(x,y,t)$ is the pressure applied at the top of the atmosphere (typically assumed to be zero), and $p_b = p_b(x,y,t)$ is the pressure at the bottom of the atmosphere.

The horizontal pressure gradient is aligned perpendicular to the local gravitational direction. It is generally among the dominant horizontal forces acting on a fluid element. Hence, its accurate representation in numerical models is crucial for the physical integrity of a simulation. Unfortunately, decomposition of the horizontal pressure gradient into two terms according to the transformation (65.7) can lead to numerical difficulties. For example, with a simple geopotential and a hydrostatic fluid, equation (65.19) shows that the horizontal pressure gradient takes the form

$$\nabla_h p = \nabla_{h\sigma} p + \rho\, \nabla_{h\sigma} \Phi = \nabla_{h\sigma} p + g\, \rho\, \nabla_{h\sigma} z, \tag{65.22}$$

with this decomposition illustrated in Figure 65.1 for the case of terrain following vertical coordinates. Numerical difficulties occur when the two terms on the right hand side have comparable magnitude but distinct signs. We are thus confronted with computing the small difference between two large numbers, and that situation generally exposes a numerical simulation to nontrivial truncation errors. Unfortunately, these errors can corrupt the integrity of the computed pressure forces and in turn contribute to spurious flow. An overview of this issue for ocean models is given by *Haney* (1991), *Mellor et al.* (1998), *Griffies et al.* (2000), with advances offered by *Lin* (1997), *Shchepetkin and McWilliams* (2002), and *Adcroft et al.* (2008). In the remainder of this section, we outline a finite volume method for computing the pressure force as proposed by *Lin* (1997) for atmosphere models and *Adcroft et al.* (2008) for ocean models. This approach starts from the middle expression in equation (65.21) for the pressure force; i.e., it

formulates the pressure force as the area integral of the pressure contact force rather than the volume integral of the pressure gradient force.

65.2.2 Integrated pressure force on the cell faces

The inward normal on the grid cell vertical side boundaries points in the horizontal direction. For example, on the left side of Figure 65.2 the pressure force acts in the positive $\hat{\boldsymbol{y}}$ direction

$$\boldsymbol{F}^{\text{press}}_{\text{left}} = \hat{\boldsymbol{y}} \int_{\text{left}} p \, \mathrm{d}x \, \mathrm{d}z \tag{65.23}$$

whereas pressure on the right wall acts in the opposite direction

$$\boldsymbol{F}^{\text{press}}_{\text{right}} = -\hat{\boldsymbol{y}} \int_{\text{right}} p \, \mathrm{d}x \, \mathrm{d}z. \tag{65.24}$$

Similar expressions appear for the front and back vertical boundaries acting in the $\hat{\boldsymbol{x}}$ direction.

Since the top and bottom boundaries of the grid cell are sloped, there is a pressure force acting on this surface directed in both the horizontal and vertical directions. To unpack the form of this force, write the vertical position of a point on the top interface as $z = \eta(x, y, t)$ so that the outward normal is given by

$$\hat{\boldsymbol{n}} = \frac{\nabla(z - \eta)}{|\nabla(z - \eta)|} = \frac{\hat{\boldsymbol{z}} - \nabla\eta}{\sqrt{1 + |\nabla\eta|^2}}. \tag{65.25}$$

Following our discussion of dia-surface transport in Section 64.3.5, we know that the product of the normal direction and the area element can be written

$$\hat{\boldsymbol{n}} \, \mathrm{d}\mathcal{S} = (\hat{\boldsymbol{z}} - \nabla\eta) \, \mathrm{d}A, \tag{65.26}$$

where $\mathrm{d}A = \mathrm{d}x \, \mathrm{d}y$ is the horizontal projection of the area element (see Figure 64.3). Hence, the net pressure force acting on the top face is given by

$$\boldsymbol{F}^{\text{press}}_{\text{top}} = -\hat{\boldsymbol{z}} \int_{\text{top}} p \, \mathrm{d}x \, \mathrm{d}y + \hat{\boldsymbol{x}} \int_{\text{top}} p \, (\partial z/\partial x)_\sigma \, \mathrm{d}x \, \mathrm{d}y + \hat{\boldsymbol{y}} \int_{\text{top}} p \, (\partial z/\partial y)_\sigma \, \mathrm{d}x \, \mathrm{d}y, \tag{65.27}$$

where we set $z = \eta$ in the second and third terms and placed a σ subscript to emphasize that the horizontal derivative is taken with σ held constant. Notice that the pressure acts in the positive horizontal direction if the top surface slopes upward (surface shoaling) when moving in either of the two horizontal directions. Pressure acting on the bottom face has the same appearance yet with opposite signs

$$\boldsymbol{F}^{\text{press}}_{\text{bott}} = \hat{\boldsymbol{z}} \int_{\text{bott}} p \, \mathrm{d}x \, \mathrm{d}y - \hat{\boldsymbol{x}} \int_{\text{bott}} p \, (\partial z/\partial x)_\sigma \, \mathrm{d}x \, \mathrm{d}y - \hat{\boldsymbol{y}} \int_{\text{bott}} p \, (\partial z/\partial y)_\sigma \, \mathrm{d}x \, \mathrm{d}y. \tag{65.28}$$

The pressure acts in the positive horizontal direction if the bottom surface slopes downward (surface deepens) when moving in either of the two horizontal directions. As discussed in Section 25.2.3, the horizontal pressure acting on a sloped surface is known as *form stress*. Here the sloped surface is defined by a constant generalized vertical coordinate.

65.2.3 Net vertical pressure force

Bringing the pieces together leads to the net vertical pressure force acting on the grid cell

$$\boldsymbol{F}^{\text{press}}_{\text{vertical}} = -\hat{\boldsymbol{z}} \left[\int_{\text{top}} p \, \mathrm{d}x \, \mathrm{d}y - \int_{\text{bott}} p \, \mathrm{d}x \, \mathrm{d}y \right]. \tag{65.29}$$

If the fluid is in hydrostatic balance, then this vertical force is given by the weight of fluid within the cell

$$\boldsymbol{F}^{\text{press}}_{\text{vertical}} = \hat{\boldsymbol{z}} \, M g, \tag{65.30}$$

where M is the mass of fluid in the grid cell. The net vertical hydrostatic pressure force acts vertically upward since hydrostatic pressure at the cell bottom is greater than at the cell top.

65.2.4 Net horizontal pressure force

The net meridional pressure force is given by the forces acting on the sides as well as those acting on the sloped top and bottom boundaries

$$\boldsymbol{F}^{\text{press}}_{\text{merid}} = \left[\int_{\text{left}} p \, \mathrm{d}x \, \mathrm{d}z - \int_{\text{right}} p \, \mathrm{d}x \, \mathrm{d}z \right] + \left[\int_{\text{top}} p \, (\partial z / \partial y)_\sigma \, \mathrm{d}x \, \mathrm{d}y - \int_{\text{bott}} p \, (\partial z / \partial y)_\sigma \, \mathrm{d}x \, \mathrm{d}y \right]. \tag{65.31}$$

We can write this expression in a more compact form by orienting our integration in a counter-clockwise manner around the cell boundaries, and making use of the identity $(\partial z / \partial y)_\sigma \, \mathrm{d}y = \mathrm{d}z$ on the top and bottom faces, so that

$$\boldsymbol{F}^{\text{press}}_{\text{merid}} = -\oint p \, \mathrm{d}x \, \mathrm{d}z. \tag{65.32}$$

For some purposes it is more convenient to work with the geopotential, $\Phi = g \, z$, than the pressure. In this case we can write the meridional pressure force as

$$\boldsymbol{F}^{\text{press}}_{\text{merid}} = -\oint p \, \mathrm{d}x \, \mathrm{d}z = -\oint \mathrm{d}x \, [\mathrm{d}(p \, z) - z \, \mathrm{d}p] = g^{-1} \oint \Phi \, \mathrm{d}x \, \mathrm{d}p, \tag{65.33}$$

where $\oint \mathrm{d}x \, \mathrm{d}(p \, z) = 0$. This form is useful with compressible / non-Boussinesq models, in which pressure is a natural vertical coordinate (e.g., see the caption to Figure 65.1).

65.2.5 Comments

A numerical realization of the integrated contact pressure force requires a representation of pressure along the boundaries of the grid cell. A variety of methods are available with differing accuracies. *Adcroft et al.* (2008) are notable in proposing an analytic form that allows for an exact integration along the cell faces in special cases, and a highly accurate numerical integration in other cases. In general, this method for computing pressure forces is highly suited to generalized vertical coordinate grid cells, which was the motivation offered by *Lin* (1997) in the context of terrain following atmospheric models.

65.3 Hydrostatic vorticity and potential vorticity

Generalized vertical coordinates are most commonly used to study hydrostatic fluids. We are thus motivated to develop the evolution equation for the vertical component of vorticity, $\widetilde{\zeta}$, in a hydrostatic fluid as written using generalized vertical coordinates. By extension, we derive the budget equation for the corresponding potential vorticity.

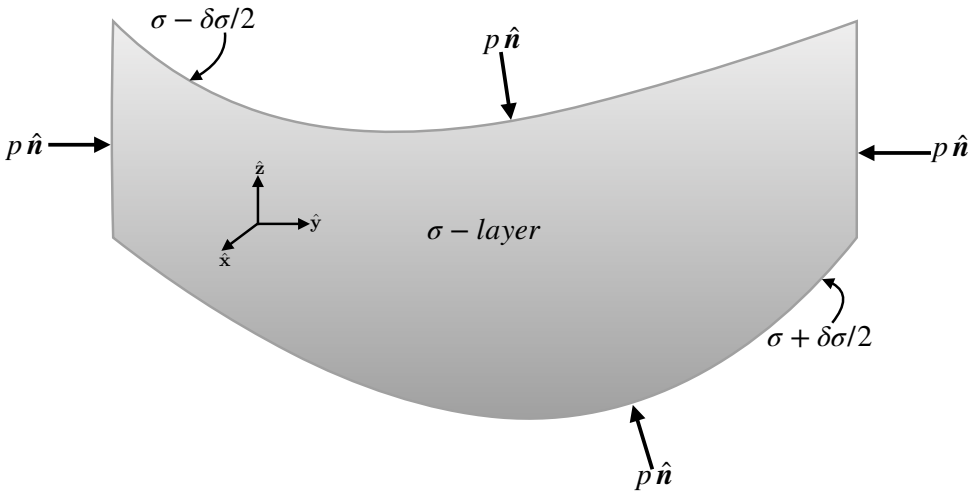

FIGURE 65.2: Schematic of pressure forces acting on the boundaries of a finite region such as a discrete model grid cell. In generalized vertical coordinate models, the side faces are vertical, so that pressure acts only in the horizontal directions. The top and bottom faces are defined by surfaces of constant generalized vertical coordinates with depth $\sigma(x, y, z, t) =$ constant. We assume that these surfaces have an outward normal that has a nonzero projection into the vertical so that we can write the depth of a point on these surfaces as $z = \eta(x, y, t)$. Because of the slope of the top and bottom surfaces, pressure has both a horizontal and vertical component when acting on these surfaces. The net pressure acting on the grid cell is given by the area integral of the pressures around the grid cell boundary.

65.3.1 Basic manipulations

Recall the the vector-invariant velocity equation given by equation (65.20)

$$\left[\frac{\partial \boldsymbol{u}}{\partial t}\right]_\sigma + \dot\sigma\,\frac{\partial \boldsymbol{u}}{\partial \sigma} + \widetilde{\zeta}_\mathsf{a}\,\hat{\boldsymbol{z}}\times\boldsymbol{u} = -\nabla_{h\sigma}(K+\Phi) - (1/\rho)\,\nabla_{h\sigma} p + \boldsymbol{F}^\mathrm{h}, \tag{65.34}$$

where $\widetilde{\zeta}_\mathsf{a} = \widetilde{\zeta} + f$ is the absolute vorticity. Taking the curl of this equation and projecting onto the vertical direction leads to

$$\frac{\mathrm{D}\widetilde{\zeta}_\mathsf{a}}{\mathrm{D}t} = -\widetilde{\zeta}_\mathsf{a}\,\nabla_{h\sigma}\cdot\boldsymbol{u} + \frac{\hat{\boldsymbol{z}}\cdot(\nabla_{h\sigma}\rho\times\nabla_{h\sigma}p)}{\rho^2} + \hat{\boldsymbol{z}}\cdot\left[\frac{\partial \boldsymbol{u}}{\partial\sigma}\times\nabla_{h\sigma}\dot\sigma + \nabla_{h\sigma}\times\boldsymbol{F}^\mathrm{h}\right] \tag{65.35}$$

where we noted that the planetary vorticity, f, is independent of time and vertical position.

Making use of the mass conservation equation

Mass conservation in the form of equation (64.85)

$$\frac{1}{\rho\hbar}\,\frac{\mathrm{D}(\rho\hbar)}{\mathrm{D}t} = -(\nabla_{h\sigma}\cdot\boldsymbol{u} + \partial\dot\sigma/\partial\sigma), \tag{65.36}$$

renders

$$\rho\hbar\,\frac{\mathrm{D}}{\mathrm{D}t}\left[\frac{\widetilde{\zeta}_\mathsf{a}}{\rho\hbar}\right] = \frac{\hat{\boldsymbol{z}}\cdot(\nabla_{h\sigma}\rho\times\nabla_{h\sigma}p)}{\rho^2} + \widetilde{\zeta}_\mathsf{a}\,\frac{\partial\dot\sigma}{\partial\sigma} + \hat{\boldsymbol{z}}\cdot\left[\frac{\partial \boldsymbol{u}}{\partial\sigma}\times\nabla_{h\sigma}\dot\sigma + \nabla_{h\sigma}\times\boldsymbol{F}^\mathrm{h}\right]. \tag{65.37}$$

Massaging the $\dot{\sigma}$ terms

The terms containing $\dot{\sigma}$ can be written in the form

$$\widetilde{\zeta}_{\mathrm{a}}\,\partial_\sigma\dot{\sigma} + \hat{\boldsymbol{z}}\cdot(\partial_\sigma\boldsymbol{u}\times\nabla_{\!\mathrm{h}\sigma}\dot{\sigma}) = \widetilde{\zeta}_{\mathrm{a}}\,\partial_\sigma\dot{\sigma} + \hat{\boldsymbol{z}}\cdot[-\nabla_{\!\mathrm{h}\sigma}\times(\dot{\sigma}\,\partial_\sigma\boldsymbol{u}) + \dot{\sigma}\,\nabla_{\!\mathrm{h}\sigma}\times\partial_\sigma\boldsymbol{u}] \tag{65.38a}$$

$$= \widetilde{\zeta}_{\mathrm{a}}\,\partial_\sigma\dot{\sigma} + \dot{\sigma}\,\partial_\sigma\widetilde{\zeta}_{\mathrm{a}} - \hat{\boldsymbol{z}}\cdot[\nabla_{\!\mathrm{h}\sigma}\times(\dot{\sigma}\,\partial_\sigma\boldsymbol{u})] \tag{65.38b}$$

$$= \partial_\sigma(\dot{\sigma}\,\widetilde{\zeta}_{\mathrm{a}}) - \hat{\boldsymbol{z}}\cdot[\nabla_{\!\mathrm{h}\sigma}\times(\dot{\sigma}\,\partial_\sigma\boldsymbol{u})]\,. \tag{65.38c}$$

65.3.2 Vorticity and potential vorticity equation

The above results allow us to write equation (65.37) in the form

$$\rho\,\hbar\,\frac{\mathrm{D}Q}{\mathrm{D}t} = \frac{\hat{\boldsymbol{z}}\cdot(\nabla_{\!\mathrm{h}\sigma}\rho\times\nabla_{\!\mathrm{h}\sigma}p)}{\rho^2} + \partial_\sigma(\dot{\sigma}\,\widetilde{\zeta}_{\mathrm{a}}) + \nabla_{\!\mathrm{h}\sigma}\cdot[\hat{\boldsymbol{z}}\times\dot{\sigma}\,\partial_\sigma\boldsymbol{u} - \hat{\boldsymbol{z}}\times\boldsymbol{F}^{\mathrm{h}}]\,, \tag{65.39}$$

where we introduced the potential vorticity defined according to the generalized vertical coordinates

$$Q = \frac{\widetilde{\zeta}_{\mathrm{a}}}{\rho\,\hbar}. \tag{65.40}$$

The potential vorticity equation (65.39) has a generally nonzero baroclinicity contribution (see Section 40.4 for more on baroclinicity)

$$\frac{\hat{\boldsymbol{z}}\cdot(\nabla_{\!\mathrm{h}\sigma}\rho\times\nabla_{\!\mathrm{h}\sigma}p)}{\rho^2}, \tag{65.41}$$

so that the potential vorticity (65.40) is generally not materially invariant even if $\dot{\sigma}=0$. Finally, note that it is sometimes convenient to make use of the potential vorticity (65.40) in the horizontal velocity equation (65.34) so that

$$\left[\frac{\partial\boldsymbol{u}}{\partial t}\right]_\sigma + \dot{\sigma}\,\frac{\partial\boldsymbol{u}}{\partial\sigma} + (\hbar\,\rho\,Q)\,\hat{\boldsymbol{z}}\times\boldsymbol{u} = -\nabla_{\!\mathrm{h}\sigma}(K+\Phi) - (1/\rho)\,\nabla_{\!\mathrm{h}\sigma}p + \boldsymbol{F}^{\mathrm{h}}. \tag{65.42}$$

Pressure coordinates

The baroclinicity (65.41) vanishes when choosing $\sigma = p$. We already noted this property in the discussion of baroclinicity in Section 40.4. As noted there, pressure does not render a useful potential vorticity since $\dot{\sigma} = \dot{p}$ does not generally vanish for a perfect fluid. Namely, a nonzero $\dot{p}$ merely signals vertical motion, so that $\dot{p}\neq 0$ for both real and perfect fluids. Hence, even though the baroclinicity vanishes by choosing $\sigma = p$, the $\partial_\sigma(\dot{\sigma}\,\widetilde{\zeta}_{\mathrm{a}})$ term does not.

Flux-form potential vorticity budget

Just like we did in Section 65.1.4 for the velocity equation, we can make use of the thickness equation (65.4a) to bring the material time derivative in equation (65.39) into the form

$$\rho\,\hbar\,\frac{\mathrm{D}Q}{\mathrm{D}t} = \rho\,\hbar\,(\partial_t + \boldsymbol{u}\cdot\nabla_{\!\mathrm{h}\sigma} + \dot{\sigma}\partial_\sigma)\,Q + Q\,[\partial_t(\rho\,\hbar) + \nabla_{\!\mathrm{h}\sigma}\cdot(\rho\,\hbar\,\boldsymbol{u}) + \partial_\sigma(\rho\,\hbar\,\dot{\sigma})] \tag{65.43a}$$

$$= \partial_t(\rho\,\hbar\,Q) + \nabla_{\!\mathrm{h}\sigma}\cdot(\rho\,\hbar\,\boldsymbol{u}\,Q) + \partial_\sigma(\rho\,\hbar\,\dot{\sigma}\,Q). \tag{65.43b}$$

Since $\widetilde{\zeta}_{\mathrm{a}} = \hbar\,\rho\,Q$, we see that the term

$$\partial_\sigma(\rho\,\hbar\,\dot{\sigma}\,Q) = \partial_\sigma(\dot{\sigma}\,\widetilde{\zeta}_{\mathrm{a}}), \tag{65.44}$$

also appears on the right hand side of equation (65.39). Hence, it cancels from the flux form potential vorticity equation

$$\left[\frac{\partial(\rho\,\hbar\,Q)}{\partial t}\right]_\sigma = \frac{\hat{\boldsymbol{z}}\cdot(\nabla_\sigma\rho\times\nabla_\sigma p)}{\rho^2} - \nabla_\sigma\cdot\left[\rho\,\hbar\,\boldsymbol{u}\,Q + \hat{\boldsymbol{z}}\times\dot\sigma\,\partial_\sigma\boldsymbol{u} + \hat{\boldsymbol{z}}\times\boldsymbol{F}^{\text{h}}\right], \tag{65.45}$$

which is equivalent to the absolute vorticity equation

$$\left[\frac{\partial\widetilde{\zeta}_{\text{a}}}{\partial t}\right]_\sigma = \frac{\hat{\boldsymbol{z}}\cdot(\nabla_\sigma\rho\times\nabla_\sigma p)}{\rho^2} - \nabla_\sigma\cdot\left[\boldsymbol{u}\,\widetilde{\zeta}_{\text{a}} + \hat{\boldsymbol{z}}\times\dot\sigma\,\partial_\sigma\boldsymbol{u} + \hat{\boldsymbol{z}}\times\boldsymbol{F}^{\text{h}}\right]. \tag{65.46}$$

As a check, note that setting $\sigma = z$ so that $\hbar = 1$ reduces the vorticity equation (65.46) to the vertical component of the vorticity equation (40.42).

65.3.3 Boussinesq ocean

Recall the discussion of the Boussinesq ocean vorticity budget in Section 40.7, where we noted that the vertical component to the absolute vorticity is unaffected by baroclinicity. This property holds in the present context, as seen by returning to the vector-invariant velocity equation (65.34) and setting the factor $1/\rho$ multiplying the pressure gradient to $1/\rho_{\text{o}}$ as part of the Boussinesq ocean

$$(1/\rho)\,\nabla_\sigma p \longrightarrow (1/\rho_{\text{o}})\,\nabla_\sigma p, \tag{65.47}$$

in which ρ_{o} is a constant. In this case the $\nabla_\sigma\times$ operation annihilates pressure and we are left with no vertical component to the baroclinicity. We are thus led to define the Boussinesq potential vorticity

$$Q = \frac{\widetilde{\zeta}_{\text{a}}}{\hbar} \tag{65.48}$$

which satisfies the material and flux-form evolution equations

$$\hbar\,\frac{\mathrm{D}Q}{\mathrm{D}t} = \partial_\sigma(\dot\sigma\,\hbar\,Q) + \nabla_\sigma\cdot[\hat{\boldsymbol{z}}\times\dot\sigma\,\partial_\sigma\boldsymbol{u} - \hat{\boldsymbol{z}}\times\boldsymbol{F}^{\text{h}}] \tag{65.49}$$

$$\left[\frac{\partial(\hbar\,Q)}{\partial t}\right]_\sigma = -\nabla_\sigma\cdot\left[\hbar\,\boldsymbol{u}\,Q + \hat{\boldsymbol{z}}\times\dot\sigma\,\partial_\sigma\boldsymbol{u} + \hat{\boldsymbol{z}}\times\boldsymbol{F}^{\text{h}}\right]. \tag{65.50}$$

We again emphasize that $\dot\sigma$ is generally non-zero, even for a perfect fluid, so that potential vorticity as defined via σ is not generally a material constant for a perfect fluid. It is only when $\dot\sigma = 0$ for a perfect fluid (e.g., σ is buoyancy or specific entropy) that we recover the desirable perfect fluid properties of potential vorticity. We develop the theory for this case in Sections 66.3 and 66.4.

65.4 Exercises

EXERCISE 65.1: CHECKING THE VORTICITY EQUATION
Verify that for $2\,\boldsymbol{\Omega} = f\,\hat{\boldsymbol{z}}$ the choice $\sigma = z$ reduces the vorticity equation (65.46) to the vertical component of the vorticity equation (40.42).

Chapter 66

ISOPYCNAL PRIMITIVE EQUATIONS

For stably stratified fluids, buoyancy is a particularly useful generalized vertical coordinate. Most notably, physical processes away from turbulent boundary layers are oriented according to buoyancy surfaces, and horizontal buoyancy gradients give rise to thermal wind shears in a geostrophically balanced flow. For this reason buoyancy (or entropy) plays a key role in theoretical and numerical models of ocean and atmospheric circulation.

In this chapter we study the hydrostatic Boussinesq equations using buoyancy as the vertical coordinate. The resulting primitive equation set forms the basis for *isopycnal* models of the ocean or isentropic models of the atmosphere. We pay particular attention to the needs of vertically integrating the equations over discrete layers, as required to develop discrete numerical models. In the adiabatic limit, the isopycnal equations reduce to the stacked shallow water equations. After deriving the primitive equations using isopycnal coordinates, we derive the corresponding vorticity and potential vorticity equations. Throughout this chapter we expose details for the practitioner interested in the mathematical formalism for the purpose of analyzing ocean momentum, vorticity and potential vorticity budgets using isopycnal models.

READER'S GUIDE FOR THIS CHAPTER

We assume an understanding of the generalized vertical coordinate mathematics in Chapter 63, kinematics in Chapter 64, and dynamics in Chapter 65. Furthermore, we are concerned with details of vorticity and PV budgets in isopycnal coordinates, with the presentation building from our study of vorticity and potential vorticity in generalized vertical coordinates from Chapter 65.

66.1 Loose threads

When defining PV using h versus $\hbar$, it is best to use different symbols to avoid confusion.

66.2 Layered isopycnal primitive equations

Rather than specializing the generalized vertical coordinate equations provided in Section 65.1, we find it pedagogical to start from the equations written using the geopotential vertical coordinate (see Section 29.1.6)

$$\frac{\mathrm{D}\boldsymbol{u}}{\mathrm{D}t} + f\,\hat{\boldsymbol{z}} \times \boldsymbol{u} = -\nabla_{\mathrm{h}}\varphi + \boldsymbol{F} \qquad \text{horizontal momentum} \tag{66.1a}$$

$$\frac{\partial \varphi}{\partial z} = b \qquad \text{hydrostatic} \tag{66.1b}$$

$$\nabla_{\mathrm{h}} \cdot \boldsymbol{u} + \frac{\partial w}{\partial z} = 0 \qquad \text{continuity} \tag{66.1c}$$

$$\frac{\mathrm{D}b}{\mathrm{D}t} = \dot{b} \qquad \text{thermodynamics} \tag{66.1d}$$

$$\frac{\mathrm{D}C}{\mathrm{D}t} = \dot{C} \qquad \text{tracers,} \tag{66.1e}$$

where $\boldsymbol{v} = (\boldsymbol{u}, w)$ is the velocity field, $\boldsymbol{u}$ is its horizontal component, φ is the dynamic pressure, b is the buoyancy, and C is an arbitrary tracer concentration. A discrete realization of the isopycnal layer-integrated form of these equations is depicted in Figure 66.1, with the remainder of this section detailing the formulation using isopycnal coordinates for the vertical.

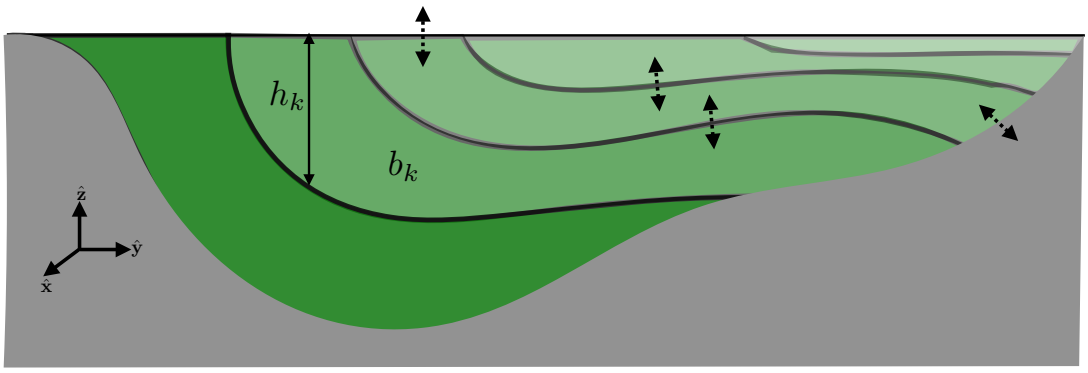

FIGURE 66.1: Schematic of an isopycnal model, formulated as stacked shallow water layers (green layers) that generally allow for the transfer of matter and energy across the layer interfaces as well as across the ocean surface and ocean bottom (as depicted by the double-headed dashed arrows). The dark gray region is land. Discrete layer thicknesses are denoted h_k with corresponding layer buoyancy, b_k.

66.2.1 Montgomery potential and the pressure force

We here consider the horizontal pressure force appearing in isopycnal models, in which we uncover the importance of the Montgomery potential.

Horizontal pressure gradient force

Throughout this chapter we make use of the horizontal derivatives on constant buoyancy surfaces (derived in Section 63.12), written here in the form

$$\nabla_{hb} = \hat{\boldsymbol{x}} \left[\frac{\partial}{\partial x} \right]_b + \hat{\boldsymbol{y}} \left[\frac{\partial}{\partial y} \right]_b . \tag{66.2}$$

Following the discussion in Section 65.1.3, the horizontal pressure thus gradient transforms as

$$\nabla_h \varphi = \nabla_{hb} \varphi - \frac{\partial \varphi}{\partial z} \nabla_{hb} z \tag{66.3a}$$

$$= \nabla_{hb} \varphi - b \nabla_{hb} z \tag{66.3b}$$

$$= \nabla_{hb} (\varphi - b\, z) \tag{66.3c}$$

$$= \nabla_{hb} M, \tag{66.3d}$$

where

$$M = \varphi - b\, z \tag{66.4}$$

defines the Montgomery potential. As the contribution to the horizontal pressure force, the Montgomery potential is the geostrophic streamfunction in buoyancy coordinates (see Section 66.2.4).

The horizontal pressure gradient force for numerical models

It is notable that the horizontal pressure gradient force is determined by the horizontal isopycnal gradient of a single term, the Montgomery potential. Furthermore, as shown below, the Montgomery potential satisfies the buoyancy coordinate form of the hydrostatic balance. Hence, numerical isopycnal models do not suffer from problems with computing the horizontal pressure gradient that can occur with other generalized vertical coordinate models, such as terrain-following models (see Figure 65.1).

Equation (66.3c) is the key step in the formulation, whereby we made use of $\nabla_{hb} b = 0$. This step is available only under certain cases that utilize an idealized equation of state for seawater. In more realistic cases, the buoyancy determining the hydrostatic pressure (i.e., the *mass buoyancy*) is defined locally whereas the generalized vertical coordinate must be defined globally. As a result, there are two terms contributing to the pressure gradient in a manner similar to terrain-following models. *Sun et al.* (1999) and *Hallberg* (2005) discuss this issue in the context of numerical ocean modeling. For present purposes we ignore this detail and continue to assume a simplified equation of state so that $\nabla_{hb} b = 0$.

Hydrostatic balance

Supporting our use of the Montgomery potential as a pressure field, the hydrostatic balance takes the form

$$\frac{\partial M}{\partial b} = \frac{\partial \varphi}{\partial b} - b \frac{\partial z}{\partial b} - z = \frac{\partial \varphi}{\partial z} \frac{\partial z}{\partial b} - b \frac{\partial z}{\partial b} - z = -z, \tag{66.5}$$

where we made use of the hydrostatic balance $\partial \varphi / \partial z = b$ (equation (66.1b)). This result means that M is the buoyancy coordinate version of pressure.

66.2.2 Material time derivative

As seen in Section 64.4, there are two equivalent forms for the material time derivative

$$\frac{\mathrm{D}}{\mathrm{D}t} = \left[\frac{\partial}{\partial t}\right]_z + \boldsymbol{u}\cdot\nabla_{\mathsf{h}} + w\,\frac{\partial}{\partial z} \qquad \text{geopotential form} \tag{66.6a}$$

$$= \left[\frac{\partial}{\partial t}\right]_b + \boldsymbol{u}\cdot\nabla_{\mathsf{hb}} + w^{(\dot{b})}\,\frac{\partial}{\partial z} \qquad \text{isopycnal form,} \tag{66.6b}$$

where

$$w^{(\dot{b})} = \frac{\partial z}{\partial b}\,\frac{\mathrm{D}b}{\mathrm{D}t} \tag{66.7}$$

is the diapycnal velocity component that measures the rate of flow crossing buoyancy surfaces (Section 64.3). Besides differences in the spatial operators, it is important to note that the time derivative operators in equations (66.6a) and (66.6b) are computed on constant geopotential and constant buoyancy surfaces, respectively. However, the horizontal velocity component is the *same* for both forms of the material time derivative

$$\boldsymbol{u} = \hat{\boldsymbol{x}}\,u + \hat{\boldsymbol{y}}\,v = (\mathrm{D}/\mathrm{D}t)\,(\hat{\boldsymbol{x}}\,x + \hat{\boldsymbol{y}}\,y). \tag{66.8}$$

66.2.3 Layer thickness and specific thickness

The continuity equation, $\nabla_{\mathsf{h}}\cdot\boldsymbol{u} + \partial_z w = 0$, is an expression of volume conservation. We already derived the generalized vertical coordinate version of this equation in Section 64.9.3, and thus quote the isopycnal layer thickness result here

$$\left[\frac{\partial h}{\partial t}\right]_b + \nabla_{\mathsf{hb}}\cdot(h\,\boldsymbol{u}) + \Delta_b\,w^{(\dot{b})} = 0. \tag{66.9}$$

The field h measures the isopycnal layer thickness (dimensions of length) and is given by the vertical integral over a layer

$$h = \int_{z(b-\delta b/2)}^{z(b+\delta b/2)} \mathrm{d}z = \int_{b-\delta b/2}^{b+\delta b/2} \frac{\partial z}{\partial b}\,\mathrm{d}b = \int_{b-\delta b/2}^{b+\delta b/2} \hbar\,\mathrm{d}b = \int_{b-\delta b/2}^{b+\delta b/2} N^{-2}\,\mathrm{d}b = \overline{\hbar}\,\mathrm{d}b. \tag{66.10}$$

The specific thickness, $\hbar$, equals to the inverse squared buoyancy frequency

$$\hbar = \frac{\partial z}{\partial b} = N^{-2}, \tag{66.11}$$

and its layer averaged value is

$$\overline{\hbar} = h/\delta b. \tag{66.12}$$

Furthermore, the dia-surface transport velocity is given by

$$w^{(\dot{b})} = \hbar\,\dot{b}. \tag{66.13}$$

Its difference across layer interfaces

$$\Delta_b\,w^{(\dot{b})} = \int_{b-\delta b/2}^{b+\delta b/2} \frac{\partial w^{(\dot{b})}}{\partial b}\,\mathrm{d}b = w^{(\dot{b})}(b+\delta b/2) - w^{(\dot{b})}(b-\delta b/2) \tag{66.14}$$

measures the amount of fluid that diverges from the layer through cross-layer transport.

In the limit that $\delta b \to 0$, we find that the non-dimensional vertical difference operator can

be written in one of the following equivalant manners

$$\lim_{\delta b \to 0} \Delta_b = \delta b \frac{\partial}{\partial b} = \delta b \frac{\partial z}{\partial b} \frac{\partial}{\partial z} = \delta z \frac{\partial}{\partial z} = h \frac{\partial}{\partial z}. \tag{66.15}$$

The relations are useful in moving between discrete and continuous formulations of the isopycnal equations.

Specific thickness equation

Inserting $h = \overline{\hbar}\, \delta b$ into the thickness equation (66.9) leads to

$$\left[\frac{\partial \overline{\hbar}}{\partial t}\right]_b + \nabla_{\mathsf{hb}} \cdot (\overline{\hbar}\, \boldsymbol{u}) + \partial_b\, w^{(\dot{b})} = 0, \tag{66.16}$$

where we pulled the buoyancy increment, δb, outside of the time and horizontal derivative operators since δb is a fixed number for a chosen layer. We also used the identity (66.15) relating the difference operator to a differential operator

$$\delta b\, \partial_b = \Delta_b. \tag{66.17}$$

For a vertically continuous treatment, equation (66.16) can be written with $\hbar$ rather than the discrete layer averaged value

$$\left[\frac{\partial \hbar}{\partial t}\right]_b + \nabla_{\mathsf{hb}} \cdot (\hbar\, \boldsymbol{u}) + \partial_b\, w^{(\dot{b})} = 0. \tag{66.18}$$

It is generally more convenient to use the specific thickness when working with the vertically continuous equations, whereas the finite layer thickness, h, is more suitable for the layer integrated equations.

Adiabatic limit

When $w^{(\dot{b})} \neq 0$, the three terms in the thickness equation (66.9) or the specific thickness equation (66.16) are coupled. We discussed this coupling in Section 64.5 as part of our broader study of the vertical velocity and the dia-surface velocity. When considering perfect fluids, we can set $w^{(\dot{b})} = \hbar\, \dot{b} = 0$ since the fluid has no mixing. In this case the layer thickness is altered only through horizontal rearrangements of volume within a layer according to the adiabatic thickness equation

$$\left[\frac{\partial h}{\partial t}\right]_b + \nabla_{\mathsf{hb}} \cdot (h\, \boldsymbol{u}) = 0. \tag{66.19}$$

As further discussed in Section 66.2.7, the adiabatic limit brings the discrete isopycnal model into accord with the immiscible stacked shallow water models discussed in Part VI of this book.

66.2.4 Ocean equations

Bringing the pieces together leads to the isopycnal version of the hydrostatic Boussinesq equations, which are the basis for numerical isopycnal ocean models

$$\left[\frac{\partial \boldsymbol{u}}{\partial t}\right]_b + (\boldsymbol{u} \cdot \nabla_{\mathsf{hb}})\, \boldsymbol{u} + (w^{(\dot{b})}\, \partial_z)\, \boldsymbol{u} + f\, \hat{\boldsymbol{z}} \times \boldsymbol{u} = -\nabla_{\mathsf{hb}}\, M + \boldsymbol{F}^h \tag{66.20a}$$

$$\frac{\partial M}{\partial b} = -z \tag{66.20b}$$

$$\left[\frac{\partial h}{\partial t}\right]_b + \nabla_{\mathsf{hb}} \cdot (h\,\boldsymbol{u}) + \Delta_b w^{(\dot{b})} = 0 \tag{66.20c}$$

$$\left[\frac{\partial (h\,C)}{\partial t}\right]_b + \nabla_{\mathsf{hb}} \cdot (h\,C\,\boldsymbol{u} + h\,\boldsymbol{J}^h) + \Delta_b(C\,w^{(\dot{b})} + J^{(b)}) = 0, \tag{66.20d}$$

where the tracer equation includes possible subgrid scale flux contributions as well as advective transport. Notice how the advective transport is two-dimensional in the adiabatic case with $\dot{b} = 0$, in which case layer-integrated scalar properties, such as volume and tracer content, are constant within buoyancy layers. Also note that geostrophic balance in the horizontal momentum equation (66.20a) gives

$$f\,\hat{\boldsymbol{z}} \times \boldsymbol{u}_{\mathsf{g}} = -\nabla_{\mathsf{hb}}\,M \implies f\,u_{\mathsf{g}} = -\left[\frac{\partial M}{\partial y}\right]_b \qquad \text{and} \qquad f\,v_{\mathsf{g}} = \left[\frac{\partial M}{\partial x}\right]_b . \tag{66.21}$$

Hence, the Montgomery potential is the streamfunction for geostrophic flow as represented using buoyancy coordinates.

66.2.5 Thickness weighted velocity equation

As in our discusion of the stacked shallow water system in Section 36.3, we can write the velocity equation (66.20a) in its thickness weighted form, with this form suited to studying momentum balances and pressure form stresses. The manipulations are directly analogous to the shallow water case in Section 36.3, whereby we multiply equation (66.20a) by the thickness, h, and multiply the thickness equation (66.20c) by the horizontal velocity, $\boldsymbol{u}$, and then summing to find

$$\left[\frac{\partial (h\,\boldsymbol{u})}{\partial t}\right]_b + \nabla_{\mathsf{hb}} \cdot (h\,\boldsymbol{u} \otimes \boldsymbol{u}) + \Delta_b(w^{(\dot{b})}\,\boldsymbol{u}) + f\,\hat{\boldsymbol{z}} \times (h\,\boldsymbol{u}) = -h\,\nabla_{\mathsf{hb}}\,M + h\,\boldsymbol{F}^h. \tag{66.22}$$

For the diapycnal transfer term, we made use of the identity

$$\lim_{\delta b \to 0} \Delta_b = h\,\partial_z \tag{66.23}$$

from equation (66.15).

66.2.6 Vector-invariant horizontal momentum equation

It is common for isopycnal models to make use of the vector-invariant form of the momentum equation derived in Section 65.1.5. Introducing the isopycnal version of the relative vorticity

$$\hat{\boldsymbol{z}}\,\widetilde{\zeta} \equiv \nabla_{\mathsf{hb}} \times \boldsymbol{u} = \left[\frac{\partial v}{\partial x}\right]_b - \left[\frac{\partial u}{\partial y}\right]_b \tag{66.24}$$

renders the vector-invariant horizontal momentum equation

$$\left[\frac{\partial \boldsymbol{u}}{\partial t}\right]_b + w^{(\dot{b})}\,\partial_z \boldsymbol{u} + \widetilde{\zeta}_{\mathsf{a}}\,\hat{\boldsymbol{z}} \times \boldsymbol{u} = -\nabla_{\mathsf{hb}}\mathcal{B} + \boldsymbol{F}^h, \tag{66.25}$$

where

$$\mathcal{B} = M + \boldsymbol{u} \cdot \boldsymbol{u}/2 = \varphi - b\,z + \boldsymbol{u} \cdot \boldsymbol{u}/2 \tag{66.26}$$

is the Bernoulli potential for a hydrostatic Boussinesq fluid (see Section 26.9.3), and

$$\widetilde{\zeta}_{\mathsf{a}} = \widetilde{\zeta} + f \tag{66.27}$$

is the vertical component to the absolute vorticity using isopycnal coordinates. Note that we can further introduce the isopycnal potential vorticity (Section 66.3.2)

$$h\,Q = \widetilde{\zeta}_{\mathsf{a}} \tag{66.28}$$

to bring the momentum equation to the form

$$\left[\frac{\partial \boldsymbol{u}}{\partial t}\right]_b + w^{(\dot{b})}\,\partial_z \boldsymbol{u} + Q\,\hat{\boldsymbol{z}} \times (h\,\boldsymbol{u}) = -\nabla_{\mathsf{hb}}\mathcal{B} + \boldsymbol{F}^h. \tag{66.29}$$

This form is commonly used as the starting point for certain theoretical analyses, particularly when considering the adiabatic limit in which $w^{(\dot{b})} = 0$.

66.2.7 Connection to the stacked shallow water equations

We can make use of the material time derivative operator (66.6b) to write the material form of the adiabatic and inviscid equations (66.20a)-(66.20c)

$$\frac{\mathrm{D}\boldsymbol{u}}{\mathrm{D}t} + f\,\hat{\boldsymbol{z}} \times \boldsymbol{u} = -\nabla_{\mathsf{hb}}\,M \tag{66.30a}$$

$$\frac{\partial M}{\partial b} = -z \tag{66.30b}$$

$$\frac{\mathrm{D}h}{\mathrm{D}t} + h\,\nabla_{\mathsf{hb}} \cdot \boldsymbol{u} = 0. \tag{66.30c}$$

These isopycnal momentum and thickness equations are isomorphic to those for a single layer of adiabatic shallow water fluid (see Section 35.2). This isomorphism allows us to derive the vorticity and potential vorticity equations in Section 66.3, making use of the shallow water manipulations from Section 39.3.

66.2.8 Diapycnal transfer

At ocean boundaries, the diapycnal term, $w^{(\dot{b})}$, acccounts for the transfer of matter across the ocean boundaries via precipitation, evaporation, ice melt/form, and river runoff. Notably, this matter transfer also generally gives rise to a transfer of trace matter (tracers), heat (evaporation and precipitation carry a heat content), and momentum (precipitation generally has nonzero momentum). In the ocean interior, $w^{(\dot{b})}$ affects the transfer of volume, tracer, and momentum between layers as induced by irreversible processes such as mixing.

66.2.9 Momentum transfer

Pressure form stress mechanically couples isopycnal layers even in the absence of diapycnal matter transfer. We discussed the physics of form stress for the shallow water system in Section 36.4 and more generally in Section 28.1. Furthermore, there are a suite of unresolved processes giving rise to lateral and vertical stresses. Typical ocean model treatments incorporate a turbulent friction in the ocean interior, with lateral stresses acting within a layer and diapycnal stresses acting across isopycnal layer interfaces. A bottom drag is typically applied at the ocean bottom and a turbulent stress applied at the ocean surface. Details for the boundary stresses involve the physics of boundary layer turbulence, which is a topic outside of our scope.

66.2.10 Allowing for layers to vanish and reappear

Isopycnal layers have a transient existence at any particular horizontal position since a layer can incrop at the ocean bottom and outcrop at the ocean surface (see Figure 66.1). The seasonal

cycle of warming and cooling is a canonical example of layer outcropping at the surface ocean. A formulational expedient to handle vanishing layers is to assume that all layers exist everywhere horizontally across the ocean domain, but to allow for zero layer thickness where a layer has zero volume. We made use of this approach when discussing available potential energy in Section 29.9. To admit this feature in a discrete model requires a careful realization of L'Hôpital's rule of differential calculus, thus ensuring the discrete model conserves properties in the presence of layers that can appear and disappear at any particular point in the domain.

66.3 Perfect fluid PV using isopycnal coordinates

In Section 41.5, we showed that the absolute vorticity in a Boussinesq hydrostatic fluid with a simplified seawater equation of state (Section 42.3), when projected into the direction normal to constant buoyancy surface, $\boldsymbol{\omega}_a \cdot \nabla b$, is not affected by baroclinicity; i.e., that projection annihilates the baroclinicity vector. From that property we conclude that $\boldsymbol{\omega}_a \cdot \nabla b$ is the potential vorticity for the Boussinesq hydrostatic fluid.

For a Boussinesq hydrostatic fluid, isopycnal coordinates build in the above feature of buoyancy surfaces. Indeed, as shown in Section 65.3.3, the vertical component to baroclinicity vanishes for any generalized vertical coordinate representation of a Boussinesq fluid. Hence, buoyancy coordinates are not special from this perspective. Instead, they are special since in the case of a perfect fluid, the buoyancy based potential vorticity is materially invariant. Deriving this result is one purpose of this section. Note that in Section 65.3, we derived the potential vorticity equation for a hydrostatic fluid represented with generalized vertical coordinates. We could merely specialize that result to the current case. However, we prefer to here work through the maths to help further our experience performing certain of the key manipulations arising with vorticity in rotating and stratified fluids. Hence, consider this section, as well as Section 66.4, to be extended worked exercises.

66.3.1 Derivation of the vorticity equation

Acting with the vertical projection of the curl, $\hat{\boldsymbol{z}} \cdot (\nabla_{hb} \times)$, onto the adiabatic and inviscid form of the vector-invariant velocity equation (66.25) leads to the isopycnal vorticity equation

$$\left[\frac{\partial \widetilde{\zeta}_a}{\partial t}\right]_b + (\boldsymbol{u} \cdot \nabla_{hb})\, \widetilde{\zeta}_a = -\widetilde{\zeta}_a\, \nabla_{hb} \cdot \boldsymbol{u} \tag{66.31}$$

where

$$\widetilde{\zeta}_a = f + \hat{\boldsymbol{z}} \cdot (\nabla_{hb} \times \boldsymbol{u}) = f + \widetilde{\zeta} \tag{66.32}$$

is the absolute vorticity, written as the planetary vorticity plus the isopycnal relative vorticity. The left hand side of equation (66.31) is the material time derivative of absolute vorticity (see equation (66.6b)), so that we can write

$$\frac{\mathrm{D}\widetilde{\zeta}_a}{\mathrm{D}t} = -\widetilde{\zeta}_a\, \nabla_{hb} \cdot \boldsymbol{u}. \tag{66.33}$$

As advertised above, there is no baroclinicity vector on the right hand side of this vorticity equation. Again, that property results from our choice to use isopycnal coordinates.

66.3.2 Derivation of the potential vorticity equation

We now make use of the thickness equation derived in Section 66.2.3, here realized in its material form to eliminate the convergence $\nabla_{hb} \cdot \boldsymbol{u}$ on the right hand side of equation (66.33), thus leading

to

$$\frac{\mathrm{D}\widetilde{\zeta}_{\mathsf{a}}}{\mathrm{D}t} - \frac{\widetilde{\zeta}_{\mathsf{a}}}{h}\frac{\mathrm{D}h}{\mathrm{D}t} = 0. \tag{66.34}$$

Introducing the isopycnal potential vorticity

$$Q = \frac{\widetilde{\zeta}_{\mathsf{a}}}{h} = \frac{f + \widetilde{\zeta}}{h} \tag{66.35}$$

leads to

$$\frac{\mathrm{D}Q}{\mathrm{D}t} = 0. \tag{66.36}$$

Expanding the material time derivative into its components according to equation (66.6b), and making use of the adiabatic form of the thickness equation leads to the flux-form equation

$$\left[\frac{\partial (h\,Q)}{\partial t}\right]_b + \nabla_{\mathsf{hb}} \cdot (h\,Q\,\boldsymbol{u}) = 0. \tag{66.37}$$

As noted in Section 66.2.3, when formulating the vertically continuous equations rather than finite thickness layered equations, it is more convenient to make use of the specific thickness, $\hbar$, rather than the layer thickness, h. In this case we are motivated to define the potential vorticity as

$$Q = \frac{\widetilde{\zeta}_{\mathsf{a}}}{\hbar} = \frac{f + \widetilde{\zeta}}{\hbar} = (f + \widetilde{\zeta})\, N^2. \tag{66.38}$$

The corresponding PV equation is identical to equation (66.37), only now with h replaced by $\hbar$.

66.3.3 Coordinate transforming vorticity and potential vorticity

As just shown, PV for a hydrostatic Boussinesq fluid can be written in the relatively simple form of a shallow water PV when choosing isopycnal coordinates. Here is a direct transformation from Cartesian to isopyncal coordinates that also reveals this form

$$(\boldsymbol{\omega}^{\mathrm{hy}} + f\,\hat{\boldsymbol{z}}) \cdot \nabla b = -\frac{\partial v}{\partial z}\frac{\partial b}{\partial x} + \frac{\partial u}{\partial z}\frac{\partial b}{\partial y} + \left(\frac{\partial v}{\partial x} - \frac{\partial u}{\partial y} + f\right)\frac{\partial b}{\partial z} \tag{66.39a}$$

$$= \frac{\partial b}{\partial z}\left[f + \left(\frac{\partial v}{\partial x} - \frac{\partial v}{\partial z}\frac{\partial b/\partial x}{\partial b/\partial z}\right) - \left(\frac{\partial u}{\partial y} - \frac{\partial u}{\partial z}\frac{\partial b/\partial y}{\partial b/\partial z}\right)\right] \tag{66.39b}$$

$$= \frac{\partial b}{\partial z}\left[f + \left(\frac{\partial v}{\partial x}\right)_b - \left(\frac{\partial u}{\partial y}\right)_b\right] \tag{66.39c}$$

$$= \frac{f + (\partial v/\partial x)_b - (\partial u/\partial y)_b}{\partial z/\partial b} \tag{66.39d}$$

$$= \frac{f + \widetilde{\zeta}}{\hbar} \tag{66.39e}$$

$$= Q. \tag{66.39f}$$

66.4 Isopycnal coordinate PV with irreversible processes

In Section 66.3, we considered the PV equation for an adiabatic, inviscid, hydrostatic, Boussinesq fluid using isopycnal vertical coordinates. We here extend to the case of friction in the momentum equation and diabatic heating in the buoyancy equation. We consider two ways to derive the governing equations. One is to convert the non-hydrostatic PV equation in Exercise 41.2 to isopycnal coordinates, after making the hydrostatic approximation. The second is to start from the equations of motion in isopycnal coordinates and derive the vorticity equation and then the

PV equation. We make use of the vertically continuous equations, thus warranting our use of specific thickness, $\hbar$, rather than layer thickness, h (see Section 66.2.3).

Note that much of this section is a specialization of the more general considerations of Section 65.3. Nonetheless, we here revisit some of the earlier derivations as a means to bolster our mathematical manipulation muscle.

66.4.1 Derivation method I

As derived earlier in this chapter, the equations of motion with diabatic heating and friction, written using isopycnal (or buoyancy) vertical coordinates, take the form

$$\left[\frac{\partial \boldsymbol{u}}{\partial t}\right]_b + (\boldsymbol{u}\cdot\nabla_{\mathsf{hb}})\,\boldsymbol{u} + \dot{b}\,\frac{\partial \boldsymbol{u}}{\partial b} + \boldsymbol{f}\times\boldsymbol{u} = -\nabla_{\mathsf{hb}}\,M + \boldsymbol{F} \tag{66.40a}$$

$$\frac{\partial M}{\partial b} = -z \tag{66.40b}$$

$$\left[\frac{\partial \hbar}{\partial t}\right]_b + \nabla_{\mathsf{hb}}\cdot(\hbar\,\boldsymbol{u}) = -\frac{\partial(\hbar\,\dot{b})}{\partial b} \tag{66.40c}$$

$$\frac{\mathrm{D}\,b}{\mathrm{D}t} = \dot{b}. \tag{66.40d}$$

Note that in this section choose to write the dia-surface transport operator in the form

$$w^{(\dot{b})}\,\partial_z = \dot{b}\,\partial_b. \tag{66.41}$$

We can make use of the material time derivative operator (66.6b) to write the material form of the equations

$$\frac{\mathrm{D}\boldsymbol{u}}{\mathrm{D}t} + \boldsymbol{f}\times\boldsymbol{u} = -\nabla_{\mathsf{hb}}\,M + \boldsymbol{F} \tag{66.42a}$$

$$\frac{\partial M}{\partial b} = -z \tag{66.42b}$$

$$\frac{\mathrm{D}\hbar}{\mathrm{D}t} + \hbar\,\nabla_{\mathsf{hb}}\cdot\boldsymbol{u} = -\hbar\,\frac{\partial \dot{b}}{\partial b}. \tag{66.42c}$$

Curl of the velocity equation

We start taking the curl, $\nabla_{\mathsf{hb}}\times$, of the velocity equation (66.40a), thus leading to the isopycnal vorticity equation

$$\left[\frac{\partial \widetilde{\zeta}_{\mathsf{a}}}{\partial t}\right]_b + (\boldsymbol{u}\cdot\nabla_{\mathsf{hb}})\,\widetilde{\zeta}_{\mathsf{a}} + \dot{b}\left[\frac{\partial \widetilde{\zeta}_{\mathsf{a}}}{\partial b}\right] = -\widetilde{\zeta}_{\mathsf{a}}\,\nabla_{\mathsf{hb}}\cdot\boldsymbol{u} + \hat{\boldsymbol{z}}\cdot\left[\frac{\partial \boldsymbol{u}}{\partial b}\times\nabla_{\mathsf{hb}}\dot{b} + \nabla_{\mathsf{hb}}\times\boldsymbol{F}\right]. \tag{66.43}$$

The left hand side of equation (66.43) is the material time derivative of absolute vorticity (see equation (66.6b)), so that

$$\frac{\mathrm{D}\widetilde{\zeta}_{\mathsf{a}}}{\mathrm{D}t} = -\widetilde{\zeta}_{\mathsf{a}}\,\nabla_{\mathsf{hb}}\cdot\boldsymbol{u} + \hat{\boldsymbol{z}}\cdot\left[\frac{\partial \boldsymbol{u}}{\partial b}\times\nabla_{\mathsf{hb}}\dot{b} + \nabla_{\mathsf{hb}}\times\boldsymbol{F}\right]. \tag{66.44}$$

Now make use of the thickness equation in the material form (66.42c) to eliminate the convergence $\nabla_{\mathsf{hb}}\cdot\boldsymbol{u}$ on the right hand side, thus leading to

$$\frac{\mathrm{D}\widetilde{\zeta}_{\mathsf{a}}}{\mathrm{D}t} - \frac{\widetilde{\zeta}_{\mathsf{a}}}{\hbar}\left[\frac{\mathrm{D}\hbar}{\mathrm{D}t} - \hbar\,\frac{\partial \dot{b}}{\partial b}\right] = \hat{\boldsymbol{z}}\cdot\left[\frac{\partial \boldsymbol{u}}{\partial b}\times\nabla_{\mathsf{hb}}\dot{b} + \nabla_{\mathsf{hb}}\times\boldsymbol{F}\right]. \tag{66.45}$$

Introducing the isopycnal potential vorticity

$$Q = \frac{\widetilde{\zeta}_{\mathsf{a}}}{\hbar} = \frac{\widetilde{\zeta} + f}{\hbar} \tag{66.46}$$

leads to

$$\hbar \, \frac{\mathrm{D}Q}{\mathrm{D}t} = \zeta_a \, \frac{\partial \dot{b}}{\partial b} + \hat{\boldsymbol{z}} \cdot \left[\frac{\partial \boldsymbol{u}}{\partial b} \times \nabla_{\mathsf{hb}} \dot{b} + \nabla_{\mathsf{hb}} \times \boldsymbol{F} \right]. \tag{66.47}$$

Massaging the diabatic terms

The diabatic terms can be written

$$\zeta_a \, \frac{\partial \dot{b}}{\partial b} + \hat{\boldsymbol{z}} \cdot \left[\frac{\partial \boldsymbol{u}}{\partial b} \times \nabla_{\mathsf{hb}} \dot{b} \right] = \zeta_a \, \frac{\partial \dot{b}}{\partial b} + \dot{b} \, \frac{\partial \widetilde{\zeta}}{\partial b} - \hat{\boldsymbol{z}} \cdot \left[\nabla_{\mathsf{hb}} \times \dot{b} \frac{\partial \boldsymbol{u}}{\partial b} \right] \tag{66.48a}$$

$$= \zeta_a \, \frac{\partial \dot{b}}{\partial b} + \dot{b} \, \frac{\partial \widetilde{\zeta}_{\mathsf{a}}}{\partial b} - \hat{\boldsymbol{z}} \cdot \left[\nabla_{\mathsf{hb}} \times \dot{b} \frac{\partial \boldsymbol{u}}{\partial b} \right] \tag{66.48b}$$

$$= \frac{\partial (\widetilde{\zeta}_{\mathsf{a}} \, \dot{b})}{\partial b} - \hat{\boldsymbol{z}} \cdot \left[\nabla_{\mathsf{hb}} \times \dot{b} \frac{\partial \boldsymbol{u}}{\partial b} \right] \tag{66.48c}$$

$$= \frac{\partial (\widetilde{\zeta}_{\mathsf{a}} \, \dot{b})}{\partial b} + \nabla_{\mathsf{hb}} \cdot \left[\hat{\boldsymbol{z}} \times \dot{b} \frac{\partial \boldsymbol{u}}{\partial b} \right], \tag{66.48d}$$

where the second equality follows since the Coriolis parameter is independent of the buoyancy.

The PV equation

The PV equation takes the material form

$$\hbar \left[\frac{\mathrm{D}Q}{\mathrm{D}t} \right] = \frac{\partial (\widetilde{\zeta}_{\mathsf{a}} \, \dot{b})}{\partial b} + \nabla_{\mathsf{hb}} \cdot \left[\hat{\boldsymbol{z}} \times \dot{b} \frac{\partial \boldsymbol{u}}{\partial b} - \hat{\boldsymbol{z}} \times \boldsymbol{F} \right]. \tag{66.49}$$

Expanding the material time derivative into its components (66.6b), and making use of the thickness equation (66.40c), leads to the flux-form equation

$$\left[\frac{\partial (\hbar \, Q)}{\partial t} \right]_b + \nabla_{\mathsf{hb}} \cdot (\hbar \, Q \, \boldsymbol{u}) + \frac{\partial (\hbar \, Q \, \dot{b})}{\partial b} = \frac{\partial (\widetilde{\zeta}_{\mathsf{a}} \, \dot{b})}{\partial b} + \nabla_{\mathsf{hb}} \cdot \left[\hat{\boldsymbol{z}} \times \dot{b} \frac{\partial \boldsymbol{u}}{\partial b} - \hat{\boldsymbol{z}} \times \boldsymbol{F} \right]. \tag{66.50}$$

Since $\hbar \, Q = \widetilde{\zeta}_{\mathsf{a}}$, the ∂_b terms cancel, thus leaving the flux-form PV equation

$$\left[\frac{\partial (\hbar \, Q)}{\partial t} \right]_b = -\nabla_{\mathsf{hb}} \cdot \left[\hbar \, Q \, \boldsymbol{u} - \hat{\boldsymbol{z}} \times \dot{b} \frac{\partial \boldsymbol{u}}{\partial b} + \hat{\boldsymbol{z}} \times \boldsymbol{F} \right]. \tag{66.51}$$

66.4.2 Derivation method II

The alternative method to derive the PV equation in isopycnal coordinates is to start from the hydrostatic Boussinesq PV equation in geopotential vertical coordinates, and directly transform to isopycnal coordinates. For this purpose we start from the discussion in Section 41.5.2 to write the material evolution of PV for a hydrostatic and Boussinesq fluid

$$\frac{\mathrm{D}Q}{\mathrm{D}t} = \nabla \cdot \left[(f \, \hat{\boldsymbol{z}} + \boldsymbol{\omega}_{\mathrm{hy}}) \, \dot{b} + b \, \nabla \times \boldsymbol{F} \right], \tag{66.52}$$

where

$$Q = \boldsymbol{\omega}_{\text{a}}^{\text{hy}} \cdot \nabla b = \boldsymbol{\omega}^{\text{hy}} \cdot \nabla b + f \, \frac{\partial b}{\partial z} \qquad \text{and} \qquad \boldsymbol{\omega}_{\text{hy}} = -\hat{\boldsymbol{x}} \frac{\partial v}{\partial z} + \hat{\boldsymbol{y}} \frac{\partial u}{\partial z} + \hat{\boldsymbol{z}} \left[\frac{\partial v}{\partial x} - \frac{\partial u}{\partial y} \right]. \tag{66.53}$$

The simplest term in equation (66.52) to transform to isopycnal coordinates is the curl of the horizontal friction vector

$$\hat{\boldsymbol{z}} \cdot (\nabla \times \boldsymbol{F}) = \hat{\boldsymbol{z}} \cdot \nabla \times (F^x, F^y, 0), \tag{66.54}$$

which takes the form

$$\hat{\boldsymbol{z}} \cdot (\nabla \times \boldsymbol{F}) = \hbar^{-1} \, \hat{\boldsymbol{z}} \cdot (\nabla_{\text{hb}} \times \boldsymbol{F}) = -\hbar^{-1} \, \nabla_{\text{hb}} \cdot (\hat{\boldsymbol{z}} \times \boldsymbol{F}). \tag{66.55}$$

The diabatic term requires some more work. Since the vorticity has zero divergence, the diabatic term can be written as

$$\nabla \cdot \left[(f \, \hat{\boldsymbol{z}} + \boldsymbol{\omega}_{\text{hy}}) \, \dot{b} \right] = (f \, \hat{\boldsymbol{z}} + \boldsymbol{\omega}_{\text{hy}}) \cdot \nabla \dot{b} \tag{66.56a}$$

$$= f \, \frac{\partial \dot{b}}{\partial z} - \frac{\partial v}{\partial z} \frac{\partial \dot{b}}{\partial x} + \frac{\partial u}{\partial z} \frac{\partial \dot{b}}{\partial y} + \left[\frac{\partial v}{\partial x} - \frac{\partial u}{\partial y} \right] \frac{\partial \dot{b}}{\partial z}. \tag{66.56b}$$

We now introduce horizontal derivatives on isopycnal surfaces according to the following relation (see Section 63.12.2)

$$\nabla_{\text{h}} = \nabla_{\text{hb}} + \nabla_{\text{h}} b \left[\frac{\partial z}{\partial b} \right] \frac{\partial}{\partial z} \tag{66.57}$$

Doing so leads to

$$\begin{aligned}
\nabla \cdot \left[(f \, \hat{\boldsymbol{z}} + \boldsymbol{\omega}_{\text{hy}}) \, \dot{b} \right] &= f \, \frac{\partial \dot{b}}{\partial z} - \frac{\partial v}{\partial z} \frac{\partial \dot{b}}{\partial x} + \frac{\partial u}{\partial z} \frac{\partial \dot{b}}{\partial y} + \left[\frac{\partial v}{\partial x} - \frac{\partial u}{\partial y} \right] \frac{\partial \dot{b}}{\partial z} \\
&= f \, \frac{\partial \dot{b}}{\partial z} - \frac{\partial v}{\partial z} \left(\left[\frac{\partial \dot{b}}{\partial x} \right]_b + \left[\frac{\partial b}{\partial x} \right]_z \frac{\partial z}{\partial b} \frac{\partial \dot{b}}{\partial z} \right) + \frac{\partial u}{\partial z} \left(\left[\frac{\partial \dot{b}}{\partial y} \right]_b + \left[\frac{\partial b}{\partial y} \right]_z \frac{\partial z}{\partial b} \frac{\partial \dot{b}}{\partial z} \right) \\
&\quad + \frac{\partial \dot{b}}{\partial z} \left(\left[\frac{\partial v}{\partial x} \right]_b + \left[\frac{\partial b}{\partial x} \right]_z \frac{\partial z}{\partial b} \frac{\partial v}{\partial z} \right) - \frac{\partial \dot{b}}{\partial z} \left(\left[\frac{\partial u}{\partial y} \right]_b + \left[\frac{\partial b}{\partial y} \right]_z \frac{\partial z}{\partial b} \frac{\partial u}{\partial z} \right) \\
&= f \, \frac{\partial \dot{b}}{\partial z} - \frac{\partial v}{\partial z} \left[\frac{\partial \dot{b}}{\partial x} \right]_b + \frac{\partial u}{\partial z} \left[\frac{\partial \dot{b}}{\partial y} \right]_b + \widetilde{\zeta} \left[\frac{\partial \dot{b}}{\partial z} \right] \\
&= \frac{\partial b}{\partial z} \left(\widetilde{\zeta}_{\text{a}} \left[\frac{\partial \dot{b}}{\partial b} \right] - \frac{\partial v}{\partial b} \left[\frac{\partial \dot{b}}{\partial x} \right]_b + \frac{\partial u}{\partial b} \left[\frac{\partial \dot{b}}{\partial y} \right]_b \right) \\
&= \hbar^{-1} \left(\widetilde{\zeta}_{\text{a}} \left[\frac{\partial \dot{b}}{\partial b} \right] + \hat{\boldsymbol{z}} \cdot \left[\frac{\partial \boldsymbol{u}}{\partial b} \times \nabla_{\text{hb}} \dot{b} \right] \right) \\
&= \hbar^{-1} \left(\widetilde{\zeta}_{\text{a}} \left[\frac{\partial \dot{b}}{\partial b} \right] + \dot{b} \left[\frac{\partial \widetilde{\zeta}_{\text{a}}}{\partial b} \right] + \nabla_{\text{hb}} \cdot \left[\hat{\boldsymbol{z}} \times \dot{b} \, \frac{\partial \boldsymbol{u}}{\partial b} \right] \right) \\
&= \hbar^{-1} \left(\frac{\partial (\dot{b} \, \widetilde{\zeta}_{\text{a}})}{\partial b} + \nabla_{\text{hb}} \cdot \left[\hat{\boldsymbol{z}} \times \dot{b} \, \frac{\partial \boldsymbol{u}}{\partial b} \right] \right).
\end{aligned} \tag{66.58}$$

To reach the penultimate step we noted that $\partial f / \partial b = 0$ so that we could form the derivative of the absolute vorticity. Bringing the pieces together leads to the PV equation (66.49) derived starting from the isopycnal version of the equations of motion.

66.4.3 Comments

The flux-form PV equation (66.51) manifests the impermeability theorem of Chapter 42 since the right hand side is the isopycnal convergence of a flux.

Chapter 67

SHALLOW WATER THICKNESS WEIGHTED AVERAGING

There are a variety of mathematical formalisms used to frame the study of how linear waves, nonlinear waves, eddies, and fully developed turbulence interact with a mean flow. A distinctly geophysical element enters these studies through the primary role of vertical stratification arising from gravitation, with stratification particularly important for large scales flows where motions are approximately hydrostatic. A further specialization to the oceanographic context arises since there are few regions where zonal averages apply, which contrasts to the atmospheric case.[1] The *thickness weighted averaging* (TWA) method has emerged as a useful formalism for stratified flows, with particular use for studies of geostrophic eddies and their parameterization. In this chapter, we develop the TWA equations for the adiabatic stacked shallow water model. Our focus concerns the derivation of the TWA equations as well as their physical interpretation.

As noted in the introduction to Part VI of this book, the adiabatic stacked shallow water model exposes key facets of stratified geophysical flows without requiring the mathematics of generalized vertical coordinates developed in Chapters 63, 64, 65, and 66. The core simplification arises by assuming that horizontal motion has no vertical dependence within each shallow water layer, which then means that vertical motion as well as the hydrostatic pressure are linear functions of vertical position within each layer. That is, the shallow water fluid moves as extensible vertical columns (Section 35.2.8). It follows that horizontal pressure gradients do not need to be projected along the slope of the layer since they are vertically constant within a layer. In contrast, this projection is needed for a continuously stratified fluid described by generalized vertical coordinates, as illustrated in Figure 63.4. Hence, the shallow water equations for momentum, thickness, and tracers retain their use of Cartesian coordinates even though the layer interfaces undulate and are thus not generally horizontal. This mathematical feature of shallow water fluids aids in our pedagogical development of the TWA method.

Young (2012) offers an elegant application of the TWA to the continuously stratified Boussinesq hydrostatic fluid, with this paper the culmination of many years of prior work (see *Young* (2012) for citations). Penetrating the TWA approach for continuously stratified fluids requires an understanding of generalized vertical coordinates and the attendant tensor analysis such as that developed in Chapters 63, 64, 65, and 66. In the present chapter, we focus on the TWA equations for the adiabatic shallow water model. Doing so minimizes the mathematical requirements while exposing the key physical concepts. It also offers a useful baseline for those using stacked shallow water models for studies of adiabatic waves and geostrophic turbulence. Digesting the material in this chapter, and then coupling to skills in generalized vertical coordinate tensor analysis, prepares one for penetrating *Young* (2012). Afterward, the mathematically inclined reader may study the work of *Maddison and Marshall* (2013), who provide a somewhat more general mathematical framework for thickness weighted averaging.

[1] The Southern Ocean is a notable ocean exception, as discussed in Sections 28.5 and 36.7.

READER'S GUIDE FOR THIS CHAPTER

In this chapter we assume a working knowledge of the shallow water model presented in Chapters 35, 36, and 39, with particular attention given to the pressure force as realized both as a contact force and a body force (see Chapter 28 and Section 36.4). The TWA equations offer a useful framework for eddy parameterizations, with parameterizations for the tracer equation discussed in Chapters 70 and 71. Parameterizations for both the tracer equation and the momentum equation remain a topic of ongoing research, particularly in the oceanography literature.

67.1 Loose threads

- Build more into the bolus discussion in Section 67.3 as per Section 4.5 of *McWilliams* (2006).
- More discussion of Taylor-Bretherton relation (67.92).
- Write the EP fluxes for quasi-geostrophic shallow water Rossby waves.
- Write the EP fluxes for 2d non-divergent Rossby waves.
- Formulate the TWA energy equations as in Loose et al.

- Is there a gauge that offers good options for parameterization?

67.2 The unaveraged thickness weighted equations

The thickness weighted averaging formalism starts from flux-form evolution equations rather than advective form equations. Applying this approach to the shallow water model means that we focus on the thickness equation (35.79a), the thickess weighted tracer equation (35.79b), and the thickness weighted velocity equation (36.45) (also called the momentum equation)

$$\frac{\partial h_{\mathsf{k}}}{\partial t} + \nabla \cdot (h_{\mathsf{k}} \, \boldsymbol{u}_{\mathsf{k}}) = 0 \tag{67.1a}$$

$$\frac{\partial (h_{\mathsf{k}} \, C)}{\partial t} + \nabla \cdot (h_{\mathsf{k}} \, \boldsymbol{u}_{\mathsf{k}} \, C) = 0 \tag{67.1b}$$

$$\frac{\partial (h_{\mathsf{k}} \, \boldsymbol{u}_{\mathsf{k}})}{\partial t} + \nabla \cdot [h_{\mathsf{k}} \, \boldsymbol{u}_{\mathsf{k}} \otimes \boldsymbol{u}_{\mathsf{k}}] + f \, \hat{\boldsymbol{z}} \times (h_{\mathsf{k}} \, \boldsymbol{u}_{\mathsf{k}}) = -(h_{\mathsf{k}}/\rho_{\mathsf{ref}}) \, \nabla p_{\mathsf{k}}. \tag{67.1c}$$

The density, ρ_{ref}, appearing in the momentum equation (67.1c) is the Boussinesq reference density, pften chosen as the density of the uppermost layer,

$$\rho_{\mathsf{ref}} = \rho_1. \tag{67.2}$$

The thickness and tracer equations do not couple to other layers, and as such we can drop the layer index, $\mathsf{k} = 1, N$, when analyzing these equations. For the momentum equation, we expose the interface indices, $\mathsf{k} \pm 1/2$, when considering pressure form stresses.

For this chapter, it proves useful to move seamlessly between the thickness weighted pressure gradient body force and its equivalent contact force version studied in Section 36.4. The contact force version of the momentum equation reveals the pressure form stresses acting on the upper and lower interfaces of a shallow water layer. It also brings stresses (kinetic stresses and pressure stresses) together into the divergence of a momentum flux. As such, this formulation follows that of Cauchy as discussed in Section 24.2.3. The eddy correlation portion of the momentum flux is known as the *Eliassen-Palm* flux.[2]

When the dust settles, the TWA equations are isomorphic to the unaveraged equations (67.1a)-(67.1c), yet with the addition of momentum flux convergences to the right hand sides that arise from subgrid correlations (i.e., convergence of the Eliassen-Palm flux). The momentum eddy fluxes are connected to the potential vorticity fluxes, with the connection known as the *Taylor-Bretherton identity*. The isomorphism provides some motivation to favor the TWA approach since properties of the unaveraged equations are directly reflected in the TWA equations. It also provides a suitable framework for parameterizing the subgrid correlations within the context of flux-form conservation laws. Even so, any formalism for an eddy and mean decomposition is subjective since the mean flow and eddying fluctuations are defined by the analyst not by the physics. Hence, arguments concerning what is a preferable framework are subject to the needs of the analyst and have no physically objective foundation.

67.3 Thickness transport by the bolus velocity

Prior to diving into the formalism of thickness weighted averaging, we study the eddy-induced volume transport (more precisely, thickness transport) realized by linear waves within a layer of shallow water fluid. This discussion provides a specific example of the thickness transport

[2] See *Bühler* (2014b) for a historical perspective on the Eliassen-Palm flux, which was introduced by *Eliassen and Palm* (1960) in their study of stationary mountain waves.

by the *bolus velocity*, with further discussion offered in Sections 67.5.1 and 70.4.5. Much of our intuition for bolus transport is based on the following relatively simple example of Stokes drift.[3]

Part of the motivation for TWA is that we do not need to compute the bolus velocity. Even so, understanding the basic physics of the bolus velocity renders useful insights into how eddies, even eddies as simple as linear waves, can provide a rectified transport of properties. We also comment on this point in Section 36.4.

67.3.1 Rectified effects

Rectification is the conversion of a fluctuating motion into motion in a particular direction. For example, the transformation of an alternating electrical current into a direct electrical current occurs through a rectifier. More generally, rectification arises from the breaking of a symmetry typically through a nonlinear mechanism. The primary example in fluid mechanics is the Stokes drift discussed in Section 52.11 as well as the current section. Stokes drift arises when linear waves have an amplitude that is a function of space, with this spatial dependence giving rise to net particle transport (the Stokes drift) in a preferred direction. Another example concerns the turbulent Stokes drift arising from nonlinear geostrophic waves and eddies in the ocean and atmosphere that lead to a net transport of buoyancy. In Section 36.7 we discuss the meridional transport of buoyancy by eddies in a channel, which is the canonical geophysical example of eddy induced transport.

67.3.2 An undulating fluid layer

Figure 67.1 shows a layer of constant density shallow water fluid within an adiabatic stacked shallow water model. Since the layers are immiscible, the total volume of fluid within this layer remains constant. In its unperturbed state with flat layer interfaces, the meridional velocity in the fluid layer is zero and the thickness is a constant, h_o. When perturbed, the thickness is written

$$h(y,t) = h_o + h'(y,t), \tag{67.3}$$

where we assume the perturbation only depends on (y,t) for simplicity. The layer thickness changes in time according to the convergence of the advective transport of thickness as found by the thickness equation (67.1a)

$$\frac{\partial h}{\partial t} = -\nabla \cdot (h\,\mathbf{u}), \tag{67.4}$$

where the convergence is computed within the layer and we drop the κ layer index for brevity. As seen by Figure 67.1, undulations of the layer thickness at a point arise from the convergence of thickness advected to that point. Further assuming that there is no zonal dependence ($\partial_x = 0$) leads to the one-dimensional thickness equation

$$\frac{\partial h}{\partial t} = -\frac{\partial (h\,v)}{\partial y}. \tag{67.5}$$

67.3.3 Stokes drift

Consider a linear wave perturbation in the meridional velocity that propagates in the meridional direction

$$v'(y,t) = v_o \sin(\kappa\, y - \omega\, t), \tag{67.6}$$

where κ is a constant wave number and ω is a constant frequency. This longitudinal wave is depicted in Figure 67.1. We now follow the general formalism developed in Section 52.11 (or

[3] This example is based Section 2 of *Lee et al.* (1997).

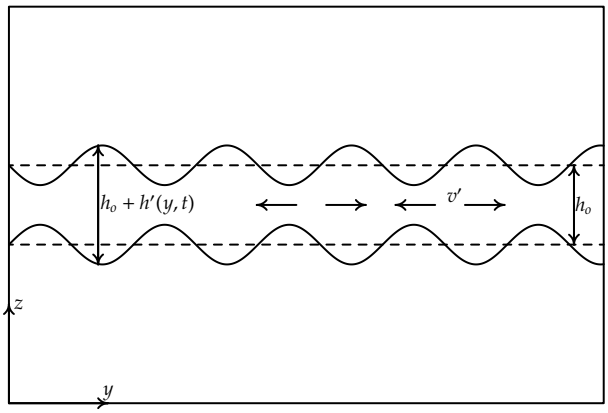

FIGURE 67.1: Shown here is a single layer of constant density fluid, with resting thickness $h = h_o$ and instantanous thickness $h = h_o + h'(y,t)$. Associated with the undulations in thickness are fluctuations in the meridional velocity $v' = v_o \sin(k\,y - \omega\,t)$, depicted here by the alternating vectors within the layer. Vertical-meridional axes are shown in the lower left corner for orientation. We are not concerned with boundaries in the meridional direction.

equivalently in Section 70.2.4) to determine the Stokes drift associated with this wave.

We are only concerned with the meridional component of the velocity, so the fluid particle trajectory equation is given by

$$\frac{\mathrm{d}Y}{\mathrm{d}t} = v_o \sin(\kappa\, Y - \omega\, t), \tag{67.7}$$

where $Y = Y(Y_o, t)$ is the meridional trajectory with initial postion Y_o. Following equation (52.194) we can write the difference between the velocity following a fluid particle (the Lagrangian velocity for the moving fluid particle) from the velocity at the initial particle point (the Eulerian velocity at the initial point of the trajectory)

$$\frac{\mathrm{d}Y}{\mathrm{d}t} - v(y,t) = v_o^2\, \kappa \cos(\kappa y - \omega t) \int_0^t \sin(\kappa y - \omega t')\, \mathrm{d}t' \tag{67.8a}$$

$$= \frac{v_o^2\, \kappa}{\omega} \left[\cos^2(\kappa y - \omega t) - \cos(\kappa y - \omega t)\cos(\kappa y)\right]. \tag{67.8b}$$

Time averaging over a single wave period,

$$T = 2\pi/\omega \tag{67.9}$$

leads to the Stokes drift as per the general expression in equation (52.196)

$$V_{\text{Stokes}} = \frac{v_o^2\, \kappa}{2\omega}. \tag{67.10}$$

Introducing the phase speed for the monochromatic wave,

$$c = \omega/\kappa \tag{67.11}$$

allows us to write the Stokes drift as

$$V_{\text{Stokes}} = \frac{v_o^2}{2\, c}. \tag{67.12}$$

Notice how the Stokes drift becomes small when the phase speed is large. The reason is that for this case, the fluid particles have only a short time to feel each wave, and thus can only experience a relatively small amount of drift. Correspondingly, there is only a small difference between the Eulerian and Lagrangian velocities. The converse holds for slow phase speeds, where

Eulerian and Lagrangian velocities have a relatively large difference.[4]

67.3.4 Linearized thickness perturbations

The velocity and thickness are written in terms of their rest state plus a perturbation due to the wave

$$h = h_o + h' \quad \text{and} \quad v = v', \tag{67.13}$$

where the velocity vanishes when the wave is absent. The thickness equation (67.5) thus takes the form

$$\frac{\partial h'}{\partial t} + h_o \frac{\partial v'}{\partial y} + v' \frac{\partial h'}{\partial y} = 0. \tag{67.14}$$

Linearizing this equation, and using the wave perturbation (67.6), leads to

$$\frac{\partial h'}{\partial t} + h_o \, v_o \, \kappa \cos(\kappa y - \omega t) = 0. \tag{67.15}$$

Time integrating this equation, and making use of the velocity perturbation in the form of equation (67.6), renders the thickness perturbation

$$h' = h_o \, v'/c. \tag{67.16}$$

Hence, to leading order, the thickness perturbation is directly proportional to and in phase with the velocity perturbation.

67.3.5 Correlation between thickness and velocity

Over a single wave period, $T = 2\pi/\omega$, the temporal correlation between the linear thickness perturbation and velocity perturbation is given by

$$\begin{aligned}
\overline{h' \, v'} &= \frac{1}{T} \int_0^T h' \, v' \, \mathrm{d}t && \text{(67.17a)} \\
&= \frac{h_o}{c\,T} \int_0^T v' \, v' \, \mathrm{d}t && \text{(67.17b)} \\
&= \frac{v_o^2 \, h_o}{c\,T} \int_0^T \sin^2(\kappa y - \omega t) \, \mathrm{d}t && \text{(67.17c)} \\
&= \frac{v_o^2 \, h_o}{2\,c} && \text{(67.17d)} \\
&= h_o \, V_{\text{Stokes}}, && \text{(67.17e)}
\end{aligned}$$

where we introduced the Stokes drift (67.12) to reach the final equality. A nonzero correlation $\overline{h' \, v'}$ means that the thickness has a nonzero tendency when averaged over a wave period.

The nonzero correlation in equation (67.17e) induces a thickness transport from the one-dimensional linear longitudinal waves. This transport arises from the Stokes drift induced by the waves; without Stokes drift there is no eddy thickness transport. This behavior exemplifies the case for more general waves and nonlinear eddies moving through fluid layers. For the general case, a nonzero bolus velocity (Section 67.5.1), as determined by velocity-thickness correlations, induces an eddy thickness transport. We see that for the one-dimensional linear longitudinal wave example, the bolus velocity is the Stokes velocity, thus prompting certain authors to make the equality in general.

[4] If we were to consider a formal asymptotic expansion, then the case of relatively slow phase speeds would require us to keep more terms in the expansion than those carried here.

67.3.6 Do we need the bolus velocity?

The bolus transport is of fundamental importance for how we think about eddy induced Stokes transport from shallow water waves. More general fluctuations, such as those from turbulent geostrophic eddies, require a parameterization to determine the thickness transport. We consider such in Section 31.7 when studying geostrophic eddies in a zonally reentrant channel. As we see in the remainder of the current chapter, the allure of the thickness weighted averaging formalism is that it dispenses with the need to parameterize the bolus velocity. Instead, the TWA equations absorb the bolus transport into the residual mean advection operator. Operationally, the TWA exposes the eddy correlation terms only in the momentum equation, leaving the TWA thickness and TWA tracer equations in a form directly parallel to the unaveraged equations.

67.4 Averaging operators

There are many averaging operators used in fluid mechanics, such as the wave average from Section 67.3, which is useful when the flow is dominantly linear waves; a long time average (formally an infinitely long time average), which is commonly used for climate studies; a space average, which is appropriate when the spatial sampling is coarse; general space filters or kernels, which are commonly used in large eddy simulations; and ensemble averages, which are generally assumed in traditional studies of turbulence. In the following, we denote the averaging or mean operator by an overbar

$$\text{average}(\Phi) = \overline{\Phi}, \tag{67.18}$$

where Φ is any field such as velocity, thickness, or tracer concentration. Deviations (also called fluctations) from the mean are denoted by a prime so that the full field is decomposed into a mean and eddy term according to

$$\Phi = \overline{\Phi} + \Phi'. \tag{67.19}$$

Since the equations of fluid mechanics are nonlinear, this decomposition into eddy and mean leads to nonlinear eddy correlation terms, which are the source of both the richness and complexity of eddying fluid flows.

67.4.1 Reynolds average

A *Reynolds average* is an operator that annihilates its corresponding fluctuating quantity, which then means that the average of an average is the identity operator

$$\overline{\Phi'} = 0 \Longleftrightarrow \overline{\overline{\Phi}} = \overline{\Phi}, \tag{67.20}$$

which in turn means that

$$\overline{\Phi}\,\overline{\Psi} = \overline{(\overline{\Phi} + \Phi')}\,\overline{\Psi} = \overline{\Phi}\,\overline{\Psi}. \tag{67.21}$$

Reynolds averages are commonly used when deriving mean field equations. Even so, the assumptions of Reyynolds averaging operators are not satisfied by many operators in practice. Extra technical issues arise when averaging operators do not satisfy the properties of a Reynolds average, with these issues beyond our aims in the present chapter. Hence, in this chapter we retain the Reynolds average assumption (67.20) for the averaging operator.

67.4.2 Ensemble average

A further assumption we make is that the average operator commutes with space and time derivatives as well as integrals. This assumption does not strictly hold if the operator is a space and/or time average operator, at least not without a bit of work. However, this assumption holds

for ensemble averages. An *ensemble average* is computed over an infinite number of realizations of the fluid flow, with approximations to this average afforded by finite sized ensembles.

Ensemble averages are typically assumed in traditional fluid turbulence studies. However, they are not always very practical nor are they the obvious choice when targeting a frameowork for parameterization. Even so, we prefer ensemble averages for this chapter in order to dispense with concerns about commutation of the averaging operator with derivative and integral operators. We also make use of ensemble averaging for our discussion of tracer kinematics in Chapter 70.

67.4.3 Thickness weighted average

The thickness weighted average of a field is defined as the ensemble average of the thickness weighted field, and then divided by the averaged thickness:

$$\widehat{\Phi} \equiv \frac{\overline{h\,\Phi}}{\overline{h}} \Longleftrightarrow \overline{h}\,\widehat{\Phi} = \overline{h\,\Phi}, \tag{67.22}$$

with widehats adorning a thickness weighted average. Deviations from the thickness weighted average are denoted with two primes so that the unaveraged field is decomposed into its average plus fluctuation

$$\Phi = \widehat{\Phi} + \Phi''. \tag{67.23}$$

Since the overline average from Section 67.4.1 satisfies the Reynolds averaging assumption, so too does the thickness weighted average

$$\Phi = \widehat{\Phi} + \Phi'' \Longrightarrow \widehat{\Phi''} = \frac{\overline{h\,\Phi''}}{\overline{h}} = 0. \tag{67.24}$$

We are thus able to derive the following related identities

$$\Phi\,\Psi = (\widehat{\Phi} + \Phi'')\,(\widehat{\Phi} + \Phi'') \Longrightarrow \widehat{\Phi\,\Psi} = \widehat{\Phi}\,\widehat{\Psi} + \widehat{\Phi''\,\Psi''} \Longrightarrow \overline{h\,\Phi\,\Psi} = \overline{h}\,\widehat{\Phi}\,\widehat{\Psi}. \tag{67.25}$$

We sometimes need to consider mixed averages and primes, such as for

$$\overline{\overline{h}\,\widehat{\Phi}} = \overline{h\,\Phi} = \overline{h}\,\widehat{\Phi}, \tag{67.26}$$

in which case[5]

$$\overline{h}\,\overline{\Phi''} = \overline{h}(\overline{\Phi} - \widehat{\Phi}) = \overline{h}\,\overline{\Phi} - \overline{h'\,\Phi'} \neq 0. \tag{67.27}$$

Hence, the ensemble average of a fluctuation, Φ'' (which is computed relative to the thickness weighted mean), is generally nonzero. Furthermore, we sometimes find it useful to write the ensemble mean correlation between thickness and a field according to

$$\overline{h}\,\widehat{\Phi'} = \overline{h\,\Phi'} = \overline{h'\,\Phi'}, \tag{67.28}$$

with the second equality following since

$$\overline{\overline{h}\,\Phi'} = \overline{h}\,\overline{\Phi'} = 0. \tag{67.29}$$

The identity (67.28) allows us to write equation (67.27) as

$$\overline{h}\,\overline{\Phi''} = \overline{h}\,(\overline{\Phi} - \widehat{\Phi'}). \tag{67.30}$$

[5]Footnote #4 in *Young* (2012) is missing the $\overline{h}\,\overline{\Phi}$ term appearing in equation (67.27).

A similar identity holds according to the following manipulations

$$\overline{h' \Phi'} = \overline{h \Phi'} = \overline{h (\Phi - \overline{\Phi})} = \overline{h \Phi} - \overline{h} \, \overline{\Phi} = \overline{h} (\widehat{\Phi} - \overline{\Phi}), \tag{67.31}$$

so that

$$\widehat{\Phi}' = \widehat{\Phi} - \overline{\Phi} = \frac{\overline{h' \Phi'}}{\overline{h}}. \tag{67.32}$$

Derivative operators *do not* commute with the thickness weighted average, so that, for example,

$$\partial_x \widehat{u} \neq \widehat{\partial_x u}. \tag{67.33}$$

Hence, when deriving differential equations for thickness weighted fields, we first derive equations for the unaveraged thickness weighted quantities, and only thereafter do we apply the ensemble mean operator.

67.4.4 Comments

For the most part, we follow the notation of *Young* (2012). Nonetheless, we caution that notational clutter and variations on conventions can present a nontrivial barrier to penetrating the TWA literature. Indeed, for our purposes with the stacked shallow water model, there is one additional piece of notation concerning the discrete layer indices. Fortunately, much of the discrete layer notation can be streamlined by exposing just the half-integer indices for fields situated at layer interfaces, along with the layer density.

67.5 Thickness equation and tracer equation

In this section we derive the TWA versions of the thickness equation (67.1a) and the tracer equation (67.1b). The derivations involve straightforward applications of the TWA averaging properties (67.24) and (67.25).

67.5.1 TWA thickness equation

Taking the ensemble average of the thickness equation (67.1a) renders

$$\partial_t \overline{h} + \nabla \cdot \overline{h \, \boldsymbol{u}} = 0, \tag{67.34}$$

where we dropped the layer index, κ, to reduce notation. Introducing the thickness weighted average according to equation (67.22) brings the thickness equation to the form

$$\partial_t \overline{h} + \nabla \cdot (\overline{h} \, \widehat{\boldsymbol{u}}) = 0. \tag{67.35}$$

Consequently, the mean layer thickness, $\overline{h}$, evolves at a point in space according to the convergence of the thickness flux, $-\nabla \cdot (\overline{h} \, \widehat{\boldsymbol{u}})$, with the flux determined by the thickness weighted velocity, $\widehat{\boldsymbol{u}}$.

We find it useful to introduce the material time derivative operator defined with the thickness weighted velocity

$$\frac{\mathrm{D}^\sharp}{\mathrm{D}t} = \frac{\partial}{\partial t} + \widehat{\boldsymbol{u}} \cdot \nabla = \frac{\partial}{\partial t} + \widehat{u} \, \partial_x + \widehat{v} \, \partial_y, \tag{67.36}$$

so that the flux-form thickness equation (67.35) can be written in the material time derivative or advective form

$$\frac{\mathrm{D}^\sharp \overline{h}}{\mathrm{D}t} = -\overline{h} \, \nabla \cdot \widehat{\boldsymbol{u}}. \tag{67.37}$$

The $\mathrm{D}^\sharp/\mathrm{D}t$ notation is based on that used by *Young* (2012). The alternative $\widehat{\mathrm{D}}/\mathrm{D}t$ is less suitable since $\overline{h\,(\mathrm{D}/\mathrm{D}t)} \neq \overline{(\mathrm{D}/\mathrm{D}t)\,h}$. In brief, an object adorned with a sharp symbol is consistent with thickness weighted averaging but is itself not the direct result of a thickness weighted average. In the following, we find it useful to also introduce the vertical velocity, $w^\sharp$, in equation (67.43), and the potential vorticity, $\Pi^\sharp$, in equation (67.91).

The isomorphism between the TWA thickness equation (67.35) with the unaveraged thickness equation (67.1a) illustrates a distinct advantage of using the thickness weighted velocity, $\widehat{\boldsymbol{u}}$. Even so, for some purposes it is useful to unpack the thickness weighted velocity into its two components

$$\widehat{\boldsymbol{u}} = \overline{u} + \frac{\overline{h'\,\boldsymbol{u}'}}{\overline{h}} \equiv \overline{u} + \boldsymbol{u}^{\text{bolus}}, \tag{67.38}$$

where we defined the bolus velocity via

$$\overline{h}\,\boldsymbol{u}^{\text{bolus}} = \overline{h'\,\boldsymbol{u}'} = \overline{h}\,\widehat{\boldsymbol{u}'}, \tag{67.39}$$

where the second equality follows from the identity (67.28).

We discussed the bolus velocity in Section 67.3 and see it again in Section 70.4.5 when developing the ensemble mean tracer equation in isopycnal coordinates. However, as per our discussion in Section 67.3.6, we do not need to know the bolus velocity if we write the averaged tracer and momentum equations in terms of the thickness weighted velocity, $\widehat{\boldsymbol{u}}$.

67.5.2 Tracer equation

Taking the ensemble average of the tracer concentration equation (67.1b) for a shallow water fluid layer renders

$$\partial_t(\overline{h\,C}) + \nabla \cdot \overline{h\,C\,\boldsymbol{u}} = 0. \tag{67.40}$$

Making use of the thickness weighted averages from Section 67.4.3 allows us to write

$$\overline{h\,C} = \overline{h}\,\widehat{C} \quad \text{and} \quad \overline{h\,C\,\boldsymbol{u}} = \overline{h}\,(\widehat{C}\,\widehat{\boldsymbol{u}} + \widehat{C''\,\boldsymbol{u}''}), \tag{67.41}$$

thus yielding the TWA tracer equation

$$\partial_t(\overline{h}\,\widehat{C}) + \nabla \cdot (\overline{h}\,\widehat{C}\,\widehat{\boldsymbol{u}}) = -\nabla \cdot (\overline{h}\,\widehat{C''\,\boldsymbol{u}''}). \tag{67.42}$$

The right hand side is the convergence of the thickness weighted eddy tracer flux. As seen in Section 70.5, the isopycnal form of the tracer equation is identical to that given here for a shallow water layer. In that discussion we present methods commonly used to parameterize the eddy flux convergence.

67.5.3 Vertical velocity

We generally have no need for the vertical velocity when working with the adiabatic stacked shallow water model. Nonetheless, it is interesting to define a vertical velocity component, $w^\sharp$, satisfying the continuity equation

$$\nabla_{\mathsf{h}} \cdot \widehat{\boldsymbol{u}} + \partial_z w^\sharp = 0. \tag{67.43}$$

As for the unaveraged vertical velocity component discussed in Section 35.2.8, $w^\sharp$ is a linear function of z within the ensemble mean shallow water layers (see equation (35.39)). Note that $w^\sharp$ is not a thickness weighted velocity. Rather, it is the vertical velocity that is compatible, through the continuity equation, with the thickness weighted horizontal velocity. A vertical velocity is needed for the continuously stratified Boussinesq fluid, and it is defined as done here

for the shallow water.[6]

67.6 Horizontal momentum equation

Taking the ensemble mean of the horizontal momentum equation (67.1c) renders

$$\partial_t(\overline{h\,\boldsymbol{u}}) + \nabla\cdot[\overline{h\,\boldsymbol{u}\otimes\boldsymbol{u}}] + f\,\hat{\boldsymbol{z}}\times(\overline{h\,\boldsymbol{u}}) = -\overline{h\,\nabla p}/\rho_{\text{ref}}, \tag{67.44}$$

where we dropped the layer interface lable, k, for brevity. Again, we make use of the thickness weighted averages from Section 67.4.3 to write

$$\overline{h\,\boldsymbol{u}} = \overline{h}\,\widehat{\boldsymbol{u}} \tag{67.45a}$$

$$\overline{h\,\boldsymbol{u}\otimes\boldsymbol{u}} = \overline{h}\,(\widehat{\boldsymbol{u}}\otimes\widehat{\boldsymbol{u}} + \widehat{\boldsymbol{u}''\otimes\boldsymbol{u}''}), \tag{67.45b}$$

so that equation (67.44) becomes

$$\partial_t(\overline{h}\,\widehat{\boldsymbol{u}}) + \nabla\cdot[\overline{h}\,\widehat{\boldsymbol{u}}\otimes\widehat{\boldsymbol{u}}] + f\,\hat{\boldsymbol{z}}\times(\overline{h}\,\widehat{\boldsymbol{u}}) = -\nabla\cdot[\overline{h}\,\widehat{\boldsymbol{u}''\otimes\boldsymbol{u}''}] - \overline{h\,\nabla p}/\rho_{\text{ref}}. \tag{67.46}$$

The first term on the right hand side is similar to the eddy tracer flux convergence appearing in the TWA tracer equation (67.42). In contrast, the thickness weighted pressure gradient is fundamentally distinct from anything appearing in the tracer equation. Much in the remainder of this section is devoted to developing a physical and mathematical understanding of $\overline{h\,\nabla p}$.

67.6.1 Kinetic stress and Reynolds stress

Following our discussion in Section 25.6, we introduce the shallow water kinetic stress tensor

$$\mathbb{T}^{\text{sw kinetic}} = -\rho_{\text{ref}}\,\boldsymbol{u}\otimes\boldsymbol{u}. \tag{67.47}$$

The kinetic stress arises from motion of the fluid, with its divergence, $\nabla\cdot(h\,\mathbb{T}^{\text{kinetic}})$, contributing to changes in the momentum of a shallow water fluid column. Decomposing the velocity into the TWA velocity and fluctuation leads to the ensemble mean of the thickness weighted kinetic stress

$$\overline{h\,\mathbb{T}^{\text{kinetic}}(\boldsymbol{u})} = -\rho_{\text{ref}}\,\overline{h\,\boldsymbol{u}\otimes\boldsymbol{u}} \tag{67.48a}$$

$$= -\rho_{\text{ref}}\,\overline{h}\,[\widehat{\boldsymbol{u}}\otimes\widehat{\boldsymbol{u}} + \widehat{\boldsymbol{u}''\otimes\boldsymbol{u}''}] \tag{67.48b}$$

$$= \overline{h}\,\mathbb{T}^{\text{kinetic}}(\widehat{\boldsymbol{u}}) + \overline{h}\,\mathbb{T}^{\text{Reynolds}}, \tag{67.48c}$$

where the eddy correlation is known as the *Reynolds stress*. The divergence of the thickness weighted Reynolds stress provides a rectified effect onto the mean flow due to nonzero eddy correlations.

67.6.2 Thickness and pressure gradient correlation

The ensemble mean of the thickness weighted pressure gradient can be written

$$\overline{h_{\text{k}}\,\nabla p_{\text{k}}} = \overline{h}_{\text{k}}\,\widehat{\nabla p_{\text{k}}} \qquad \text{equation (67.22) defining the TWA} \tag{67.49a}$$

$$= \overline{h}_{\text{k}}\,\nabla\overline{p}_{\text{k}} + \overline{h'_{\text{k}}\,\nabla p'_{\text{k}}} \qquad \text{expanding the ensemble mean} \tag{67.49b}$$

$$= \overline{h}_{\text{k}}\,(\nabla\overline{p}_{\text{k}} + \widehat{\nabla p'_{\text{k}}}) \qquad \text{equation (67.28).} \tag{67.49c}$$

[6] See equation (73) in *Young* (2012).

The eddy term is the correlation between layer thickness fluctuations and horizontal pressure gradient fluctuations

$$\overline{h}_{\mathsf{k}} \, \widehat{\nabla p'_{\mathsf{k}}} = \overline{h'_{\mathsf{k}} \, \nabla p'_{\mathsf{k}}}, \tag{67.50}$$

which can be written in terms of the eddy geostrophic velocity

$$\overline{h}_{\mathsf{k}} \, \widehat{\nabla p'_{\mathsf{k}}} = -\rho_{\mathsf{ref}} \, f \, \hat{\boldsymbol{z}} \times \overline{h'_{\mathsf{k}} \, \boldsymbol{u}'_{\mathsf{k,g}}} = -\rho_{\mathsf{ref}} \, f \, \hat{\boldsymbol{z}} \times \overline{h}_{\mathsf{k}} \, \widehat{\boldsymbol{u}'_{\mathsf{k,g}}}. \tag{67.51}$$

For geostrophic flows, the bolus velocity (67.39) equals to $\widehat{\boldsymbol{u}'_{\mathsf{k,g}}}$, in which case we write

$$\overline{h}_{\mathsf{k}} \, \widehat{\nabla p'_{\mathsf{k}}} = -\rho_{\mathsf{ref}} \, f \, \hat{\boldsymbol{z}} \times \overline{h}_{\mathsf{k}} \, \boldsymbol{u}^{\mathrm{bolus}}_{\mathsf{k}}. \tag{67.52}$$

67.6.3 Unpacking the thickness and pressure gradient correlation

We here unpack the correlation between eddy thickness and eddy pressure gradient as given by $\overline{h}_{\mathsf{k}} \, \widehat{\nabla p'_{\mathsf{k}}} = \overline{h'_{\mathsf{k}} \, \nabla p'_{\mathsf{k}}}$ in equation (67.50). We do so by writing the pressure as a contact force rather than a body force. Doing so exposes the eddy interfacial form stresses that provide a vertical transfer of horizontal momentum. In addition, there is a term arising from the gradient in the layer depth integrated pressure or, alternatively, the layer potential energy. To proceed we rely on the development given in Section 36.4.9, in which we exposed two equivalent expressions for the contact pressure.

As part of the following derivation we make use of relations for pressure within a layer and at an interface

$$p_{\mathsf{k}}(z) = p_{\mathsf{k}-1/2} + g \, \rho_{\mathsf{k}} \, (\eta_{\mathsf{k}-1/2} - z) \tag{67.53a}$$

$$p_{\mathsf{k}+1/2} - p_{\mathsf{k}-1/2} = g \, \rho_{\mathsf{k}} \, h_{\mathsf{k}} = -g \, \rho_{\mathsf{k}} \, (\eta_{\mathsf{k}+1/2} - \eta_{\mathsf{k}-1/2}) \tag{67.53b}$$

$$p_{1/2} = p_{\mathsf{a}}, \tag{67.53c}$$

with p_{a} the applied (or atmospheric) pressure at the ocean surface. We emphasize that the layer pressure, $p_{\mathsf{k}}(z)$, is a linear function of vertical position within the layer so that its horizontal gradient, $\nabla_{\mathsf{h}} p_{\mathsf{k}}$, is depth independent.

Interfacial form stress plus gradient of layer depth integrated pressure

The first expression for thickness weighted pressure gradient is given by

$$-h_{\mathsf{k}} \nabla p_{\mathsf{k}} = -\nabla P_{\mathsf{k}} + \boldsymbol{F}^{\mathrm{form}}_{\mathsf{k}}. \tag{67.54}$$

In this equation we introduced the pressure vertically integrated over layer-k

$$P_{\mathsf{k}} = \int_{\eta_{\mathsf{k}+1/2}}^{\eta_{\mathsf{k}-1/2}} p_{\mathsf{k}}(z) \, \mathrm{d}z = h_{\mathsf{k}} \, (g \, \rho_{\mathsf{k}} \, h_{\mathsf{k}}/2 + p_{\mathsf{k}-1/2}), \tag{67.55}$$

with its negative gradient

$$-\nabla P_{\mathsf{k}} = -\nabla \left[h_{\mathsf{k}} \, (p_{\mathsf{k}-1/2} + g \, \rho_{\mathsf{k}} \, h_{\mathsf{k}}/2) \right] \tag{67.56a}$$

$$= -\nabla \left[h_{\mathsf{k}} \, (p_{\mathsf{k}+1/2} - g \, \rho_{\mathsf{k}} \, h_{\mathsf{k}}/2) \right] \tag{67.56b}$$

$$= -[h_{\mathsf{k}} \nabla p_{\mathsf{k}+1/2} + p_{\mathsf{k}-1/2} \nabla h_{\mathsf{k}}] \tag{67.56c}$$

leading to a horizontal acceleration from imbalances in the contact pressure acting along the vertical sides of a shallow water column. The second stress in equation (67.54) is the pressure

form stress acting on the upper and lower layer interfaces

$$\boldsymbol{F}_{\mathsf{k}}^{\text{form}} = p_{\mathsf{k}-1/2}\nabla\eta_{\mathsf{k}-1/2} - p_{\mathsf{k}+1/2}\nabla\eta_{\mathsf{k}+1/2} \equiv \delta_{\mathsf{k}}(p_{\mathsf{k}-1/2}\nabla\eta_{\mathsf{k}-1/2}), \tag{67.57}$$

where

$$\delta_{\mathsf{k}}\Phi_{\mathsf{k}-1/2} = \Phi_{\mathsf{k}-1/2} - \Phi_{\mathsf{k}+1/2} = -(\Phi_{\mathsf{k}+1/2} - \Phi_{\mathsf{k}-1/2}) \tag{67.58}$$

is a difference operator acting on interface properties. The use of a backward difference operator is motivated since k increases down whereas $\hat{\boldsymbol{z}}$ points up. Additionally, we define the difference operator to only act on fields defined at the layer interface, with layer fields commuting with this operator so that, for example,

$$\delta_{\mathsf{k}}(h_{\mathsf{k}}\,\eta_{\mathsf{k}-1/2}) = h_{\mathsf{k}}\,\delta_{\mathsf{k}}(\eta_{\mathsf{k}-1/2}). \tag{67.59}$$

This convention helps produce a tidy form of the Eliassen-Palm flux in Sections 67.6.4 and 67.6.5.

Making use of the depth integrated pressure and form stress as given by equation (67.54) allows us to write the ensemble mean thickness weighted pressure gradient as

$$-\overline{h_{\mathsf{k}}\,\nabla p_{\mathsf{k}}} = -\nabla\overline{P_{\mathsf{k}}} + \delta_{\mathsf{k}}[\overline{p_{\mathsf{k}-1/2}\nabla\eta_{\mathsf{k}-1/2}}]. \tag{67.60}$$

Following equation (67.56a), we write the ensemble mean for the layer integrated pressure as

$$-\nabla\overline{P_{\mathsf{k}}} = -\nabla[\overline{h_{\mathsf{k}}}\,(\overline{p_{\mathsf{k}-1/2}} + g\,\rho_{\mathsf{k}}\,\overline{h_{\mathsf{k}}}/2)] - \nabla[\overline{h'_{\mathsf{k}}\,(p'_{\mathsf{k}-1/2} + g\,\rho_{\mathsf{k}}\,h'_{\mathsf{k}}/2)}] \tag{67.61}$$

and the vertical divergence of the form stress is

$$\overline{\boldsymbol{F}_{\mathsf{k}}^{\text{form}}} = \delta_{\mathsf{k}}[\overline{p_{\mathsf{k}-1/2}\,\nabla\eta_{\mathsf{k}-1/2}}] = \delta_{\mathsf{k}}\left[\overline{p_{\mathsf{k}-1/2}}\,\overline{\nabla\eta_{\mathsf{k}-1/2}} + \overline{p'_{\mathsf{k}-1/2}\,\nabla\eta'_{\mathsf{k}-1/2}}\right]. \tag{67.62}$$

We are thus led to the following decomposition of the eddy contribution to the thickness weighted pressure gradient

$$-\overline{h'_{\mathsf{k}}\,\nabla p'_{\mathsf{k}}} = -\nabla[\overline{h'_{\mathsf{k}}\,(p'_{\mathsf{k}-1/2} + g\,\rho_{\mathsf{k}}\,h'_{\mathsf{k}}/2)}] + \delta_{\mathsf{k}}\left[\overline{p'_{\mathsf{k}-1/2}\,\nabla\eta'_{\mathsf{k}-1/2}}\right]. \tag{67.63}$$

For orientation, in Figure 67.2 we illustrate the deviations of the interface positions relative to the ensemble mean.

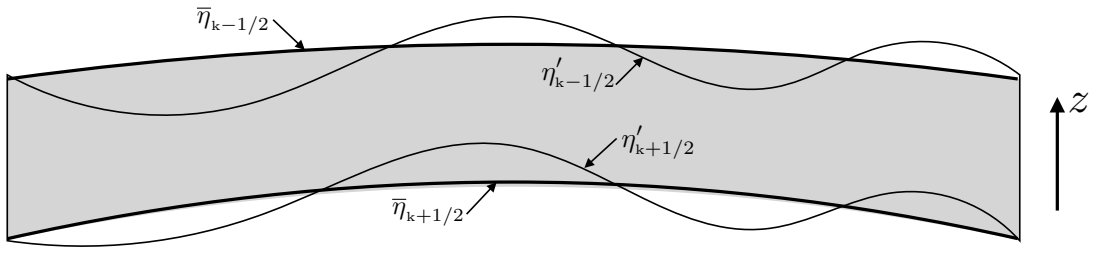

FIGURE 67.2: Schematic of the interface positions for a shallow water layer. The ensemble mean layer interfaces have vertical positions given by $z = \overline{\eta}_{\mathsf{k}\pm1/2}$, whereas the fluctuating interfaces are located at $z = \overline{\eta}_{\mathsf{k}\pm1/2} + \eta'_{\mathsf{k}\pm1/2}$. As depicted here, the ensemble mean interface positions are not generally horizontal.

Dual interfacial pressure form stress plus gradient of layer potential energy

An alternative formulation uses the dual form stress and potential energy, in which case we write the thickness weighted horizontal pressure gradient as

$$-h_{\mathsf{k}}\nabla p_{\mathsf{k}} = -\nabla\mathscr{P}_{\mathsf{k}} + \boldsymbol{F}_{\mathsf{k}}^{\text{dual}}. \tag{67.64}$$

In this equation we introduced the layer gravitational potential energy per area

$$\mathscr{P}_{\mathsf{k}} = g\,\rho_{\mathsf{k}}\int_{\eta_{\mathsf{k}+1/2}}^{\eta_{\mathsf{k}-1/2}} z\,\mathrm{d}z = (g\,\rho_{\mathsf{k}}/2)\,(\eta_{\mathsf{k}-1/2}^2 - \eta_{\mathsf{k}+1/2}^2) = (g\,\rho_{\mathsf{k}}/2)\,\delta_{\mathsf{k}}(\eta_{\mathsf{k}-1/2}^2), \tag{67.65}$$

and the *dual pressure form stress* (see Section 36.4.8),

$$\boldsymbol{F}_{\mathsf{k}}^{\text{dual}} = -\delta_{\mathsf{k}}(\eta_{\mathsf{k}-1/2}\nabla p_{\mathsf{k}-1/2}) = \boldsymbol{F}_{\mathsf{k}}^{\text{form}} - \nabla[\delta_{\mathsf{k}}(\eta_{\mathsf{k}-1/2}\,p_{\mathsf{k}-1/2})]. \tag{67.66}$$

Since they differ by a gradient, the form stress and dual form stress have identical curls and so they contribute the same interfacial pressure torque as part of the layer vorticity evolution

$$-\nabla\times(h_{\mathsf{k}}\nabla p_{\mathsf{k}}) = \nabla\times\boldsymbol{F}_{\mathsf{k}}^{\text{dual}} = \nabla\times\boldsymbol{F}_{\mathsf{k}}^{\text{form}}. \tag{67.67}$$

Making use of the potential energy and dual form stress as given by equation (67.64) allows us to write the ensemble mean thickness weighted pressure gradient as

$$-\overline{h_{\mathsf{k}}\,\nabla p_{\mathsf{k}}} = -\nabla\overline{\mathscr{P}_{\mathsf{k}}} - \delta_{\mathsf{k}}[\overline{\eta_{\mathsf{k}-1/2}\,\nabla p_{\mathsf{k}-1/2}}] \tag{67.68}$$

where minus the potential energy gradient is decomposed as

$$-\nabla\overline{\mathscr{P}_{\mathsf{k}}} = -(g\,\rho_{\mathsf{k}}/2)\,\delta_{\mathsf{k}}\left[\nabla(\overline{\eta_{\mathsf{k}-1/2}})^2 + \nabla\overline{(\eta'_{\mathsf{k}-1/2})^2}\right] \tag{67.69}$$

and the vertical convergence of the dual form stress is

$$-\delta_{\mathsf{k}}[\overline{\eta_{\mathsf{k}-1/2}\,\nabla p_{\mathsf{k}-1/2}}] = -\delta_{\mathsf{k}}\left[\overline{\eta_{\mathsf{k}-1/2}}\,\overline{\nabla p_{\mathsf{k}-1/2}} + \overline{\eta'_{\mathsf{k}-1/2}\,\nabla p'_{\mathsf{k}-1/2}}\right]. \tag{67.70}$$

We are thus led to decompose the thickness weighted pressure gradient correlation as

$$-\overline{h'_{\mathsf{k}}\,\nabla p'_{\mathsf{k}}} = -(g\,\rho_{\mathsf{k}}/2)\,\nabla[\delta_{\mathsf{k}}\overline{(\eta'_{\mathsf{k}-1/2})^2}] - \delta_{\mathsf{k}}[\overline{\eta'_{\mathsf{k}-1/2}\nabla p'_{\mathsf{k}-1/2}}]. \tag{67.71}$$

Again, the first term on the right hand side arises from the eddy potential energy and the second term from the dual eddy form stress.

67.6.4 Zonal and meridional Eliassen-Palm fluxes: Version I

Making use of the thickness and pressure gradient correlation in the form of equation (67.63) (the version with the form stress) leads to the thickness weighted momentum equation

$$\begin{aligned}\partial_t(\overline{h}\,\widehat{\boldsymbol{u}}) + \nabla\cdot(\overline{h}\,\widehat{\boldsymbol{u}}\otimes\widehat{\boldsymbol{u}}) + f\,\hat{\boldsymbol{z}}\times\overline{h}\,\widehat{\boldsymbol{u}} + \overline{h}\,\nabla\overline{p}/\rho_{\text{ref}}&\\ = -\nabla\cdot(\overline{h}\,\widehat{\boldsymbol{u}''\otimes\boldsymbol{u}''}) - \rho_{\text{ref}}^{-1}\,\nabla[\overline{h'_{\mathsf{k}}\,(p'_{\mathsf{k}-1/2} + g\,\rho_{\mathsf{k}}\,h'_{\mathsf{k}}/2)}] + \rho_{\text{ref}}^{-1}\,\delta_{\mathsf{k}}\overline{(p'\,\nabla\eta')_{\mathsf{k}-1/2}},&\end{aligned} \tag{67.72}$$

where we only exposed the interface indices to reduce notational clutter, and where we introduced the shorthand for the eddy form stress at the $\mathsf{k}-1/2$ interface

$$(p'\,\nabla\eta')_{\mathsf{k}-1/2} = p'_{\mathsf{k}-1/2}\,\nabla\eta'_{\mathsf{k}-1/2}. \tag{67.73}$$

The subgrid scale correlations on the right hand side of equation (67.72) can be organized into the divergence of two tensors

$$\begin{aligned}
&\nabla \cdot (\overline{h}\, \widehat{\boldsymbol{u}'' \otimes \boldsymbol{u}''}) + \rho_{\mathsf{ref}}^{-1}\, \nabla[\overline{h'_{\mathsf{k}}\,(p'_{\mathsf{k}-1/2} + g\,\rho_{\mathsf{k}}\,h'_{\mathsf{k}}/2)}] - (\overline{h}\,\rho_{\mathsf{ref}})^{-1}\,\delta_{\mathsf{k}}\left[\overline{h}\,\overline{(p'\,\nabla\eta')_{\mathsf{k}-1/2}}\right] \\
&= \begin{bmatrix} \partial_x & \partial_y & (1/\overline{h})\,\delta_{\mathsf{k}} \end{bmatrix} \begin{bmatrix} \overline{h}\,\widehat{u''\,u''} & \overline{h}\,\widehat{u''\,v''} & 0 \\ \overline{h}\,\widehat{u''\,v''} & \overline{h}\,\widehat{v''\,v''} & 0 \\ 0 & 0 & 0 \end{bmatrix} \\
&+ \rho_{\mathsf{ref}}^{-1} \begin{bmatrix} \partial_x & \partial_y & (1/\overline{h})\,\delta_{\mathsf{k}} \end{bmatrix} \begin{bmatrix} \overline{h'_{\mathsf{k}}\,(p'_{\mathsf{k}-1/2} + g\,\rho_{\mathsf{k}}\,h'_{\mathsf{k}}/2)} & 0 & 0 \\ 0 & \overline{h'_{\mathsf{k}}\,(p'_{\mathsf{k}-1/2} + g\,\rho_{\mathsf{k}}\,h'_{\mathsf{k}}/2)} & 0 \\ -\overline{h}\,\overline{(p'\,\partial_x\eta')_{k-1/2}} & -\overline{h}\,\overline{(p'\,\partial_y\eta')_{k-1/2}} & 0 \end{bmatrix},
\end{aligned} \tag{67.74}$$

where we recall from equation (67.59) that the vertical difference operator, δ_{k}, only acts on layer interface fields so that $\overline{h}_{\mathsf{k}}$ commutes with δ_{k}. The first tensor in equation (67.74) arises from Reynolds stresses and the second tensor arises from eddy pressures, including the eddy form stress in the third row.

When combined, the columns of the tensors appearing in equation (67.74) are the thickness weighted shallow water *Eliassen-Palm fluxes* for the zonal (column 1) and meridional (column 2) momentum equation

$$\boldsymbol{E}^{(\mathrm{uEP})} = \left[\overline{h}\,\widehat{u''\,u''} + \rho_{\mathsf{ref}}^{-1}\,\overline{h'_{\mathsf{k}}\,(p'_{\mathsf{k}-1/2} + g\,\rho_{\mathsf{k}}\,h'_{\mathsf{k}}/2)}\right]\hat{\boldsymbol{x}} + \overline{h}\,\widehat{u''\,v''}\,\hat{\boldsymbol{y}} - (\overline{h}/\rho_{\mathsf{ref}})\,\overline{(p'\,\partial_x\eta')_{k-1/2}}\,\hat{\boldsymbol{z}} \tag{67.75a}$$

$$\boldsymbol{E}^{(\mathrm{vEP})} = \overline{h}\,\widehat{u''\,v''}\,\hat{\boldsymbol{x}} + \left[\overline{h}\,\widehat{v''\,v''} + \rho_{\mathsf{ref}}^{-1}\,\overline{h'_{\mathsf{k}}\,(p'_{\mathsf{k}-1/2} + g\,\rho_{\mathsf{k}}\,h'_{\mathsf{k}}/2)}\right]\hat{\boldsymbol{y}} - (\overline{h}/\rho_{\mathsf{ref}})\,\overline{(p'\,\partial_y\eta')_{k-1/2}}\,\hat{\boldsymbol{z}}. \tag{67.75b}$$

The Eliassen-Palm flux has physical dimensions of thickness times squared velocity. We encountered the unaveraged version of the Eliassen-Palm flux in Sections 36.3.3 and 36.4.9 when studying the shallow water momentum equation. *Maddison and Marshall* (2013) included the third column of zeros in equation (67.74) to emphasize that the Eliassen-Palm fluxes are the first and second columns to the *Eliassen-Palm flux tensor*. They illustrated the utility of this perspective by considering gauge transformations that result in non-zero elements in the third column.

The Eliassen-Palm fluxes are second order in eddy amplitude; i.e., they are quadratic in eddy fluctuations. Furthermore, they bring together the Reynolds stress and eddy pressure terms, including the eddy form stress. The convergence of the Eliassen-Palm fluxes provides an eddy rectified acceleration on the thickness weighted velocity. To explicitly see this forcing, write the components to the mean field momentum equation (67.72) as[7]

$$\partial_t(\overline{h}\,\widehat{u}) + \nabla \cdot (\overline{h}\,\widehat{\boldsymbol{u}}\,\widehat{u}) - f\,\overline{h}\,\widehat{v} + \overline{h}\,\partial_x\overline{p}/\rho = -(\nabla_{\mathsf{h}} + \hat{\boldsymbol{z}}\,\overline{h}^{-1}\delta_{\mathsf{k}}) \cdot \boldsymbol{E}^{(\mathrm{uEP})} \tag{67.76a}$$

$$\partial_t(\overline{h}\,\widehat{v}) + \nabla \cdot (\overline{h}\,\widehat{\boldsymbol{u}}\,\widehat{v}) + f\,\overline{h}\,\widehat{u} + \overline{h}\,\partial_y\overline{p}/\rho = -(\nabla_{\mathsf{h}} + \hat{\boldsymbol{z}}\,\overline{h}^{-1}\delta_{\mathsf{k}}) \cdot \boldsymbol{E}^{(\mathrm{vEP})}. \tag{67.76b}$$

Equations (67.76a) and (67.76b) are isomorphic to the unaveraged horizontal momentum equation (67.1c), yet with the addition of the convergence of the Eliassen-Palm flux on the right hand side that encapsulates rectified effects from eddies. They can be written using the material time

[7] Recall from equation (67.59) that the operator δ_{k} only acts on interface fields, so that $\overline{h}^{-1}\,\delta_{\mathsf{k}}(\overline{h}) = \delta_{\mathsf{k}}$. This convention allows us to combine the horizontal components to the Eliassen-Palm flux with the vertical component, as written in equations (67.80a) and (67.80b).

derivative (67.36)

$$\frac{\mathrm{D}^\sharp \widehat{u}}{\mathrm{D}t} - f\,\widehat{v} + \partial_x \overline{p}/\rho = -\overline{h}^{-1}\,(\nabla_\mathsf{h} + \hat{\boldsymbol{z}}\,\overline{h}^{-1}\delta_\mathsf{k})\cdot \boldsymbol{E}^{(\mathrm{uEP})} \tag{67.77a}$$

$$\frac{\mathrm{D}^\sharp \widehat{v}}{\mathrm{D}t} + f\,\widehat{u} + \partial_y \overline{p}/\rho = -\overline{h}^{-1}\,(\nabla_\mathsf{h} + \hat{\boldsymbol{z}}\,\overline{h}^{-1}\delta_\mathsf{k})\cdot \boldsymbol{E}^{(\mathrm{vEP})}. \tag{67.77b}$$

We emphasize that these equations only make use of the thickness weighted velocity, $\widehat{\boldsymbol{u}}$, as do the averaged thickness equation (67.35) and averaged tracer equation (67.42). We advertised this point near the start of this chapter, noting that it facilitates the practical use of the TWA equations for numerical simulations. We further this correspondence in Section 67.7 by showing that the vorticity and potential vorticity equations also make use of $\widehat{\boldsymbol{u}}$.

67.6.5 Zonal and meridional Eliassen-Palm fluxes: Version II

We here follow the development in Section 67.6.4, only now making use of the thickness and pressure gradient correlation in the form of equation (67.71) (the version with the dual form stress). Our presentation is terse since there are few differences from Section 67.6.4. We start from the thickness weighted momentum equation

$$\begin{aligned}\partial_t(\overline{h}\,\widehat{\boldsymbol{u}}) + \nabla\cdot(\overline{h}\,\widehat{\boldsymbol{u}}\otimes\widehat{\boldsymbol{u}}) + f\,\hat{\boldsymbol{z}}\times\overline{h}\,\widehat{\boldsymbol{u}} + \overline{h}\,\nabla\overline{p}/\rho \\ = -\nabla\cdot(\overline{h}\,\widehat{\boldsymbol{u}''\otimes\boldsymbol{u}''}) - (g\,\rho_\mathsf{k}/2\rho_\mathsf{ref})\,\nabla[\delta_\mathsf{k}\overline{(\eta'_{\mathsf{k}-1/2})^2}] - \delta_\mathsf{k}[\overline{(\eta'\,\nabla p')_{\mathsf{k}-1/2}}/\rho_\mathsf{ref}].\end{aligned} \tag{67.78}$$

The subgrid scale correlations on the right hand side can be organized into the divergence of two tensors

$$\begin{aligned}&\nabla\cdot(\overline{h}\,\widehat{\boldsymbol{u}''\otimes\boldsymbol{u}''}) + (g\,\rho_\mathsf{k}/2\rho_\mathsf{ref})\,\nabla[\delta_\mathsf{k}\overline{(\eta'_{\mathsf{k}-1/2})^2}] + \delta_\mathsf{k}[\overline{(\eta'\,\nabla p')_{\mathsf{k}-1/2}}/\rho_\mathsf{ref}] \\ &= \begin{bmatrix}\partial_x & \partial_y & \overline{h}^{-1}\,\delta_\mathsf{k}\end{bmatrix}\begin{bmatrix}\overline{h}\,\widehat{u''u''} & \overline{h}\,\widehat{u''v''} & 0\\ \overline{h}\,\widehat{u''v''} & \overline{h}\,\widehat{v''v''} & 0\\ 0 & 0 & 0\end{bmatrix} \\ &+ \begin{bmatrix}\partial_x & \partial_y & \overline{h}^{-1}\,\delta_\mathsf{k}\end{bmatrix}\begin{bmatrix}(g\,\rho_\mathsf{k}/2\,\rho_\mathsf{ref})\,[\delta_\mathsf{k}\overline{(\eta'_{\mathsf{k}-1/2})^2}] & 0 & 0\\ 0 & (g\,\rho_\mathsf{k}/2\,\rho_\mathsf{ref})\,[\delta_\mathsf{k}\overline{(\eta'_{\mathsf{k}-1/2})^2}] & 0\\ (\overline{h}/\rho_\mathsf{ref})\,\overline{(\eta'\,\partial_x p')_{k-1/2}} & (\overline{h}/\rho_\mathsf{ref})\,\overline{(\eta'\,\partial_y p')_{k-1/2}} & 0\end{bmatrix}.\end{aligned} \tag{67.79}$$

The first tensor arises from Reynolds stresses and the second arises from eddy potential energy and dual eddy form stresses. When combined, the columns are the thickness weighted *Eliassen-Palm fluxes* for the zonal (column 1) and meridional (column 2), here making use of the dual form stress

$$\boldsymbol{E}^{(\mathrm{uEP})}_{\mathrm{dual}} = \Big[\overline{h}\,\widehat{u''u''} + (g\,\rho_\mathsf{k}/2\rho_\mathsf{ref})\,[\delta_\mathsf{k}\overline{(\eta'_{\mathsf{k}-1/2})^2}]\Big]\,\hat{\boldsymbol{x}} + \overline{h}\,\widehat{u''v''}\,\hat{\boldsymbol{y}} + \overline{h}\,\overline{(\eta'\,\partial_x p')_{k-1/2}}/\rho_\mathsf{ref})\,\hat{\boldsymbol{z}} \tag{67.80a}$$

$$\boldsymbol{E}^{(\mathrm{vEP})}_{\mathrm{dual}} = \overline{h}\,\widehat{u''v''}\,\hat{\boldsymbol{x}} + \Big[\overline{h}\,\widehat{v''v''} + (g\,\rho_\mathsf{k}/2\rho_\mathsf{ref})\,[\delta_\mathsf{k}\overline{(\eta'_{\mathsf{k}-1/2})^2}]\Big]\,\hat{\boldsymbol{y}} + \overline{h}\,\overline{(\eta'\,\partial_y p')_{k-1/2}}/\rho_\mathsf{ref})\,\hat{\boldsymbol{z}}. \tag{67.80b}$$

The convergence of the Eliassen-Palm fluxes provides an eddy rectified acceleration on the thickness weighted velocity

$$\partial_t(\overline{h}\,\widehat{u}) + \nabla\cdot(\overline{h}\,\widehat{\boldsymbol{u}}\,\widehat{u}) - f\,\overline{h}\,\widehat{v} + \overline{h}\,\partial_x\overline{p}/\rho = -(\nabla_\mathsf{h} + \hat{\boldsymbol{z}}\,\overline{h}^{-1}\delta_\mathsf{k})\cdot\boldsymbol{E}^{(\mathrm{uEP})}_{\mathrm{dual}} \tag{67.81a}$$

$$\partial_t(\overline{h}\,\widehat{v}) + \nabla\cdot(\overline{h}\,\widehat{\boldsymbol{u}}\,\widehat{v}) + f\,\overline{h}\,\widehat{u} + \overline{h}\,\partial_y\overline{p}/\rho = -(\nabla_\mathsf{h} + \hat{\boldsymbol{z}}\,\overline{h}^{-1}\delta_\mathsf{k})\cdot\boldsymbol{E}^{(\mathrm{vEP})}_{\mathrm{dual}}. \tag{67.81b}$$

67.6.6 Interfacial stresses from geostrophic eddies

In Section 31.7 we studied the rectified effects from geostrophic eddies in a zonally re-entrant channel for a continuously stratified fluid. In that analysis we found that the zonal mean of isopycnal eddy form stresses are equivalent to the meridional eddy flux of buoyancy. We here consider similar questions within the context of the TWA shallow water fluid, here focusing on the interfacial transfer of momentum due to eddy dual form stresses as given by the vertical vectors

$$\rho_{\text{ref}} \left[\boldsymbol{E}^{(\text{uEP})}_{\text{dual}} \right]_{\text{interface}} = \hat{\boldsymbol{z}}\, \overline{h}\, \overline{(\eta' \partial_x p')_{k-1/2}} \tag{67.82a}$$

$$\rho_{\text{ref}} \left[\boldsymbol{E}^{(\text{vEP})}_{\text{dual}} \right]_{\text{interface}} = \hat{\boldsymbol{z}}\, \overline{h}\, \overline{(\eta' \partial_y p')_{k-1/2}}. \tag{67.82b}$$

Let us now write the interface pressure gradient fluctuation as

$$\nabla p_{\text{k}-1/2} = \nabla p_{\text{k}} - g\, \rho_{\text{k}}\, \nabla \eta_{\text{k}-1/2} \tag{67.83}$$

so that

$$\overline{(\eta' \nabla p')_{k-1/2}} = \overline{\eta'_{k-1/2}\, \nabla p'_{\text{k}}} + g\, \rho_{\text{k}}\, \overline{(\eta' \nabla \eta')_{\text{k}-1/2}}. \tag{67.84}$$

As for the analysis in Section 31.7, we assume the fluctuations are geostrophic so that we can introduce the layer geostrophic velocity corresponding to the gradient of the layer pressure fluctuations

$$\partial_x p'_{\text{k}} = f\, \rho_{\text{ref}}\, v'_{\text{k}} \quad \text{and} \quad \partial_y p'_{\text{k}} = -f\, \rho_{\text{ref}}\, u'_{\text{k}}, \tag{67.85}$$

in which case the dual form stress portion of the Eliassen-Palm fluxes take the form

$$\rho_{\text{ref}} \left[\boldsymbol{E}^{(\text{uEP})}_{\text{dual}} \right]_{\text{interface}} = \hat{\boldsymbol{z}}\, \overline{h} \left[f\, \rho_{\text{ref}}\, \overline{\eta'_{k-1/2}\, v'_{\text{k}}} + g\, \rho_{\text{k}}\, \overline{(\eta' \partial_x \eta')_{\text{k}-1/2}} \right] \tag{67.86a}$$

$$\rho_{\text{ref}} \left[\boldsymbol{E}^{(\text{vEP})}_{\text{dual}} \right]_{\text{interface}} = \hat{\boldsymbol{z}}\, \overline{h} \left[-f\, \rho_{\text{ref}}\, \overline{\eta'_{k-1/2}\, u'_{\text{k}}} + g\, \rho_{\text{k}}\, \overline{(\eta' \partial_y \eta')_{\text{k}-1/2}} \right]. \tag{67.86b}$$

The $\overline{\eta'_{\text{k}-1/2}\, \boldsymbol{u}'_{\text{k}}}$ term is an eddy transport of the area between $z = \overline{\eta}_{\text{k}-1/2}$ and $z = \eta'_{\text{k}-1/2}$ (see Figure 67.2). We studied the same transport for the continuously stratified fluid in Section 31.7. In that discussion, we found that the interface fluctuations, η', can be related to the buoyancy fluctuations, b', in which case $\overline{\eta'_{\text{k}-1/2}\, \boldsymbol{u}'_{k}}$ is proportional to the eddy buoyancy flux for the layer.

67.6.7 Comments

Greatbatch and Lamb (1990) and *Greatbatch* (1998) pursue a similar analysis for the purpose of framing the mesoscale eddy parameterization problem. They focus on the interfacial form stress contribution since, for geostrophic eddies, it dominates over the other terms in the Eliassen-Palm fluxes (67.80a) and (67.80b).

67.7 Vorticity and potential vorticity

We follow the procedure from Chapter 39 to derive the vorticity and potential vorticity for the thickness weighted shallow water equations. In the process, we connect the eddy flux of potential vorticity to the Eliassen-Palm fluxes (67.75a) and (67.75b). Note that the same manipulations also hold for the dual Eliassen-Palm fluxes (67.80a) and (67.80b).

67.7.1 Derivation

Use the vector identities from Sections 35.5 and 39.1 to bring the material evolution equations (67.77a) and (67.77b) into their equivalent vector invariant forms[8]

$$\partial_t \widehat{u} - (f + \widehat{\zeta})\, \widehat{v} = -\partial_x(\overline{p}/\rho + \widehat{\boldsymbol{u}} \cdot \widehat{\boldsymbol{u}}/2) - \overline{h}^{-1}\, (\nabla_{\mathrm{h}} + \hat{\boldsymbol{z}}\, \overline{h}^{-1} \delta_{\mathrm{k}}) \cdot \boldsymbol{E}^{(\mathrm{uEP})} \tag{67.87a}$$

$$\partial_t \widehat{v} + (f + \widehat{\zeta})\, \widehat{u} = -\partial_y(\overline{p}/\rho + \widehat{\boldsymbol{u}} \cdot \widehat{\boldsymbol{u}}/2) - \overline{h}^{-1}\, (\nabla_{\mathrm{h}} + \hat{\boldsymbol{z}}\, \overline{h}^{-1} \delta_{\mathrm{k}}) \cdot \boldsymbol{E}^{(\mathrm{vEP})}, \tag{67.87b}$$

where we introduced the relative vorticity of the thickness weighted horizontal velocity

$$\widehat{\zeta} = \partial_x \widehat{v} - \partial_y \widehat{u}. \tag{67.88}$$

Taking ∂_x of the meridional equation (67.87b) and subtracting ∂_y of the zonal equation (67.87a) renders the evolution equation for absolute vorticity, $\widehat{\zeta}_{\mathrm{a}} = \widehat{\zeta} + f$,

$$\frac{\mathrm{D}^\sharp \widehat{\zeta}_{\mathrm{a}}}{\mathrm{D}t} + \widehat{\zeta}_{\mathrm{a}}\, \nabla \cdot \widehat{\boldsymbol{u}} = \partial_y[\overline{h}^{-1}\, (\nabla_{\mathrm{h}} + \hat{\boldsymbol{z}}\, \overline{h}^{-1} \delta_{\mathrm{k}}) \cdot \boldsymbol{E}^{(\mathrm{uEP})}] - \partial_x[\overline{h}^{-1}\, (\nabla_{\mathrm{h}} + \hat{\boldsymbol{z}}\, \overline{h}^{-1} \delta_{\mathrm{k}}) \cdot \boldsymbol{E}^{(\mathrm{vEP})}]. \tag{67.89}$$

Making use of the thickness equation (67.37) to replace $\nabla \cdot \widehat{\boldsymbol{u}}$ leads to the potential vorticity equation

$$\overline{h}\, \frac{\mathrm{D}^\sharp \Pi^\sharp}{\mathrm{D}t} = -\nabla \cdot \boldsymbol{F}^\sharp \tag{67.90}$$

where

$$\Pi^\sharp = \frac{f + \partial_x \widehat{v} - \partial_y \widehat{u}}{\overline{h}} = \frac{f + \widehat{\zeta}}{\overline{h}} \tag{67.91}$$

is the potential vorticity defined with the thickness weighted velocity and ensemble mean thickness. The corresponding eddy potential vorticity flux is a horizontal vector and given in terms of the divergence of the Eliassen-Palm fluxes

$$\boldsymbol{F}^\sharp = \hat{\boldsymbol{x}}\, [\overline{h}^{-1}\, (\nabla_{\mathrm{h}} + \hat{\boldsymbol{z}}\, \overline{h}^{-1} \delta_{\mathrm{k}}) \cdot \boldsymbol{E}^{(\mathrm{vEP})}] - \hat{\boldsymbol{y}}\, [\overline{h}^{-1}\, (\nabla_{\mathrm{h}} + \hat{\boldsymbol{z}}\, \overline{h}^{-1} \delta_{\mathrm{k}}) \cdot \boldsymbol{E}^{(\mathrm{uEP})}] + \hat{\boldsymbol{z}} \times \nabla \Upsilon, \tag{67.92}$$

where Υ is an arbitrary gauge function.[9] This equation connects the potential vorticity flux to the Eliassen-Palm fluxes and it is known as the *Taylor-Bretherton identity*. Remarkably, the potential vorticity flux also provides the eddy forcing to the thickness weighted velocity equation

$$\partial_t \widehat{\boldsymbol{u}} + (f + \widehat{\zeta})\, \hat{\boldsymbol{z}} \times \widehat{\boldsymbol{u}} + \nabla(\overline{p}/\rho + \widehat{\boldsymbol{u}} \cdot \widehat{\boldsymbol{u}}/2) = -\hat{\boldsymbol{z}} \times (\boldsymbol{F}^\sharp - \hat{\boldsymbol{z}} \times \nabla \Upsilon), \tag{67.93}$$

which can also be written

$$\partial_t \widehat{\boldsymbol{u}} + \hat{\boldsymbol{z}} \times (\overline{h}\, \widehat{\boldsymbol{u}}\, \Pi^\sharp + \boldsymbol{F}^\sharp - \hat{\boldsymbol{z}} \times \nabla \Upsilon) + \nabla(\overline{p}/\rho + \widehat{\boldsymbol{u}} \cdot \widehat{\boldsymbol{u}}/2) = 0, \tag{67.94}$$

where $\overline{h}\, \widehat{\boldsymbol{u}}\, \Pi^\sharp + \boldsymbol{F}^\sharp - \hat{\boldsymbol{z}} \times \nabla \Upsilon$ is the net (mean plus eddy plus gauge) potential vorticity flux.

67.7.2 Concerning the mean field potential vorticity

We emphasize that the mean field potential vorticity arising from our development is $\Pi^\sharp$, which is defined by equation (67.91) using the thickness weighted velocity, $\widehat{\boldsymbol{u}}$ for the relative vorticity.

[8] In Section D.6 of *Griffies et al.* (2020), the authors state "In contrast to the flux-form momentum equation, the vector-invariant velocity equation does not admit a finite volume formulation." That statement is incorrect, with equations (67.87a) and (67.87b) the finite volume vector-invariant velocity equation.

[9] Equation (129) in *Young* (2012) should have a gauge function on its right hand side, which follows from his footnote #3. We provide an example of the need for a gauge function in Section 67.8.

This potential vorticity is distinct from the thickness weighted average potential vorticity

$$\widehat{\Pi} = \frac{\overline{\Pi\, h}}{\overline{h}} = \frac{f + \overline{\zeta}}{\overline{h}} = \frac{f + \partial_x \overline{v} - \partial_y \overline{u}}{\overline{h}}, \tag{67.95}$$

which is the mean field potential vorticity considered by *Greatbatch* (1998) and *Peterson and Greatbatch* (2001). The two forms of potential vorticity differ by the potential vorticity of the bolus velocity

$$\Pi^\sharp - \widehat{\Pi} = \frac{(f + \widehat{\zeta}) - (f + \overline{\zeta})}{\overline{h}} = \frac{\hat{\boldsymbol{z}} \cdot [\nabla \times (\widehat{\boldsymbol{u}} - \overline{\boldsymbol{u}})]}{\overline{h}} = \frac{\hat{\boldsymbol{z}} \cdot (\nabla \times \widehat{\boldsymbol{u}'})}{\overline{h}} = \frac{\hat{\boldsymbol{z}} \cdot (\nabla \times \boldsymbol{u}^{\text{bolus}})}{\overline{h}}, \tag{67.96}$$

where the penultimate equality made use of equation (67.32) for $\widehat{\boldsymbol{u}'}$, and the final equality introduced the bolus velocity according to equation (67.39). Use of $\Pi^\sharp$ allows us to develop a potential vorticity conservation statement solely in terms of $\widehat{\boldsymbol{u}}$, whereas the use of $\widehat{\Pi}$ by *Greatbatch* (1998) and *Peterson and Greatbatch* (2001) requires both $\overline{\boldsymbol{u}}$ and $\widehat{\boldsymbol{u}}$.

67.7.3 Comments

As in *Young* (2012), and as advertised at the start of this chapter, we have developed the equations for the thickness weighted averaged shallow water solely in terms of the thickness weighted velocity, $\widehat{\boldsymbol{u}}$. This development includes the thickness equation (67.35), the tracer equation (67.42), the velocity equation (67.46) and the potential vorticity equation (67.90). There is no need for the ensemble mean velocity, $\overline{\boldsymbol{u}}$, and thus no need to parameterize the bolus velocity.

67.8 Vorticity fluxes for non-divergent barotropic flow

In Chapter 38 we studied the mechanics of a two dimensional fluid whose horizontal flow is non-divergent. As for the shallow water, the fluid moves as columns. However, since the horizontal flow is non-divergent, each column is rigid and so there is no stretching or squashing of columns. Correspondingly, there are no form stresses acting on these columns. We specialize the shallow water analysis in this section to rigid columnar motion as a means to verify that the Reynolds stresses appearing in the Eliassen-Palm flux formulation correspond to that arising in the non-divergent barotropic model.

For rigid fluid columns, the thickness weighted average reduces to just the ensemble mean since all layer thicknesses are fixed. Correspondingly, there are no form stresses acting at the layer interfaces since interfaces are horizontal. Hence, the Eliassen-Palm fluxes (67.75a) and (67.75b) reduce to just their Reynold stress contributions

$$h^{-1}\, \boldsymbol{E}^{(\text{uEP})} = \overline{u'\, u'}\, \hat{\boldsymbol{x}} + \overline{u'\, v'}\, \hat{\boldsymbol{y}} \tag{67.97a}$$

$$h^{-1}\, \boldsymbol{E}^{(\text{vEP})} = \overline{u'\, v'}\, \hat{\boldsymbol{x}} + \overline{v'\, v'}\, \hat{\boldsymbol{y}}. \tag{67.97b}$$

The corresponding eddy potential vorticity flux (67.92), absent the gauge term, is

$$\boldsymbol{F}^\sharp = \hat{\boldsymbol{x}}\, \nabla \cdot [\overline{u'\, v'}\, \hat{\boldsymbol{x}} + \overline{v'\, v'}\, \hat{\boldsymbol{y}}] - \hat{\boldsymbol{y}}\, \nabla \cdot [\overline{u'\, u'}\, \hat{\boldsymbol{x}} + \overline{u'\, v'}\, \hat{\boldsymbol{y}}] \tag{67.98a}$$

$$= \hat{\boldsymbol{x}}\, [\partial_x(\overline{u'\, v'}) + \partial_y(\overline{v'\, v'})] - \hat{\boldsymbol{y}}\, [\partial_x(\overline{u'\, u'}) + \partial_y(\overline{u'\, v'})]. \tag{67.98b}$$

Does the eddy potential vorticity flux (67.98b) agree, to within a gauge function, with the eddy flux resulting from a direct decomposition into eddy and mean within a two dimensional non-divergent model? To address this question, recall that the advective flux of potential vorticity

for the two dimensional non-divergent flow is given by equation (38.52)

$$\boldsymbol{u}\, q = \boldsymbol{u}\, f + \nabla \cdot (\hat{\boldsymbol{z}} \times \mathcal{E}), \tag{67.99}$$

where $\mathcal{E}$ is the trace-free anisotropic portion of the kinetic stress tensor

$$\mathcal{E} = \begin{bmatrix} -(u^2 - v^2)/2 & -u\, v \\ -u\, v & (u^2 - v^2)/2 \end{bmatrix}. \tag{67.100}$$

The mean of the potential vorticity flux is (67.99) is given by

$$\overline{\boldsymbol{u}\, q} = \overline{\boldsymbol{u}}\, \overline{q} + \overline{\boldsymbol{u}'\, q'}, \tag{67.101}$$

where the flux computed from the mean fields is

$$\overline{\boldsymbol{u}}\, \overline{q} = \overline{\boldsymbol{u}}\, (f + \overline{\zeta}), \tag{67.102}$$

whereas the eddy potential vorticity flux is

$$\begin{aligned}
\overline{\boldsymbol{u}'\, q'} &= \nabla \cdot [\hat{\boldsymbol{z}} \times \overline{\mathcal{E}(\boldsymbol{u}')}] && \text{(67.103a)} \\
&= \hat{\boldsymbol{x}}\, [\partial_x(\overline{u'\, v'}) + \partial_y(\overline{v'\, v' - u'\, u'})/2] + \hat{\boldsymbol{y}}\, [\partial_x(\overline{v'\, v' - u'\, u'})/2 - \partial_y(\overline{u'\, v'})] && \text{(67.103b)} \\
&= \hat{\boldsymbol{x}}\, [\partial_x(\overline{u'\, v'}) + \partial_y(\overline{v'\, v'})] - \hat{\boldsymbol{y}}\, [\partial_x(\overline{u'\, u'}) + \partial_y(\overline{u'\, v'})] + (\hat{\boldsymbol{x}}\, \partial_y - \hat{\boldsymbol{y}}\, \partial_x)\, \overline{\boldsymbol{u}' \cdot \boldsymbol{u}'}/2 && \text{(67.103c)} \\
&= \boldsymbol{F}^\sharp - \hat{\boldsymbol{z}} \times \nabla(\overline{\boldsymbol{u}' \cdot \boldsymbol{u}'})/2. && \text{(67.103d)}
\end{aligned}$$

Hence, $\overline{\boldsymbol{u}'\, q'}$ agrees with $\boldsymbol{F}^\sharp$ in equation (67.98b) to within a gauge function given by the rotated gradient of the eddy kinetic energy, so that their divergences are equal

$$\nabla \cdot \boldsymbol{F}^\sharp = \nabla \cdot \overline{\boldsymbol{u}'\, q'}. \tag{67.104}$$

That is, when diagnosing contributions to the potential vorticity flux, the gauge term, $-\hat{\boldsymbol{z}} \times \nabla(\overline{\boldsymbol{u}' \cdot \boldsymbol{u}'})/2$, plays no role in forcing potential vorticity.

Part XIII

Scalar fields

In this part of the book, we study the physics and maths of passive tracers, *conservative tracers*,[10] as well as density and Archimedean buoyancy. Tensorially, these fields are scalars and so they provide a number (e.g., temperature, humidity, mass density) throughout the continuum fluid. This study of *scalar mechanics* complements that of momentum, vorticity, and energy considered in other parts of this book, with each scalar offering information about the mechanics of fluid motion. Much of the material is relevant to both the atmosphere and ocean, though specialized topics are motivated from ocean applications.

Although the physics and maths of scalar fields is simpler than that describing momentum, vorticity, and energy, there is a remarkable richness to the study. We only touch upon a few of the many topics, aiming to provide a theoretical platform for further study by the interested reader. Here is a synopsis of the chapters in this part of the book.

- In Chapter 68 we focus on tracer diffusion in the absence of advection. The diffusion equation is the canonical parabolic partial differential equation, and we studied a variety of its mathematical properties in Chapters 6 and 9. Indeed, there is a long and rich history of research into diffusive (or conductive) processes across science and engineering, with books such as *Crank* (1956) and *Carslaw and Jaeger* (1959) offering a wealth of theoretical results and mathematical methods. Our focus in Chapter 68 is somewhat more physical than our earlier presentations of diffusion, though with much of the physics revealed via deriving mathematical properties of the diffusion equation.

- In Chapter 69 we consider advection along with diffusion in affecting the evolution of tracer concentration. Advection results through viewing evolution from within the Eulerian reference frame. When acting alone on a conservative tracer, advection affects a reversible stirring of tracer concentration that can increase tracer gradients. When diffusion is included along with advection, reversibility is lost and tracer gradients increase or decrease depending on the relative dominance of advection or diffusion.

- In Chapter 70 we introduce notions of wave-mean flow interactions that give rise to eddy-induced advection (or skew diffusion) as well as diffusion. This chapter, which mostly focuses on kinematic properties and is restricted to tracers, makes use of both geopotential coordinates as well as isopycnal coordinate equations from Chapter 66. Doing so provides examples of the dual roles these two vertical coordinate choices fill for describing turbulent geophysical flows.

- In Chapter 71 we study elements of tracer parameterizations used for coarse resolution models of the ocean circulation. We particularly focus on a variety of mathematical properties of the parameterizations, and unpack the physics embodied within the mathematics. This chapter exposes a handful of questions at the leading edge of research, with that material among the less mature found in this book.

- In Chapter 72 we consider ocean density and the budget for global sea level. This study requires us to dive into the niceties of the enthalpy (heat), salt, and mass budgets for the ocean. These budgets are central to climate science through the ocean's role as the dominant sink of anthropogenically induced increase in planetary enthalpy, and with that increase affecting a rise in sea level.

- In Chapter 73 we present fundamental elements to the theory of water mass transformation analysis. This analysis offers a view on ocean circulation mechanics that complements those available from Eulerian and Lagrangian approaches. Many of the methods of ocean water

[10] Conservative tracers evolve only via the convergence of advective and diffusive fluxes within the fluid interior, along with boundary conditions. That is, conservative tracers have no interior sources or sinks. Hence, the net content of a conservatice tracer over any finite volume domain is affected only through transport across boundaries.

mass analysis are relevant to atmospheric analyses as well, though this chapter is written from an oceanographic perspective. Furthermore, this chapter is arguably the toughest in this part of the book, with progress in understanding water mass transformation theory sometimes taking years to ponder the concepts and apply the methods.

Chapter 68

TRACER DIFFUSION

In this chapter we study tracer diffusion in geophysical fluids. Diffusion affects an irreversible exchange of propertes between fluid elements, thus offering a conceptual and mathematical depiction of how such properties are mixed at the microscale through chaotic molecular motions. Furthermore, diffusion forms the null hypothesis for how turbulent eddying flows disperse and mix tracers at scales larger than the microscale. Diffusion is thus central to how environmental and geophysical fluid flows act to transport matter and thermodynamic properties, thus motivating an exploration into a variety of physical and mathematical aspects of tracer diffusion.

CHAPTER GUIDE

We presume an understanding of the tracer equation as studied in Chapter 20. We considered mathematical elements of the diffusion equation in Chapter 6 as part of our study of parabolic partial differential equations. We also considered the diffusion equation when studying Green's function solutions for passive tracers in Chapter 9. Those presentations are very useful for the present chapter, though not essential.

In Section 69.2, we summarize some tensor analysis tools for use in studying tracer diffusion, with that material drawing upon the tensor analysis material in Chapters 1-4. We work in the context of a non-Boussinesq fluid, with results for the Boussinesq ocean of Chapter 29 found merely by setting the density factor, ρ, to the Boussinesq reference density, ρ_o. Chapter 69 is a direct descendant of the current chapter, where we study the combined effects of advection and diffusion.

68.1 Loose threads

- Add a new section working through some of the classic BVPs for diffusion, such as those in *Csanady* (1973). Also add some of these to the exercises.

68.2 Mathematical preliminaries

As derived in Section 20.1, the equation for a *conservative tracer*[1] takes on the form

$$\rho \frac{\mathrm{DC}}{\mathrm{D}t} = -\nabla \cdot \mathbf{J}, \tag{68.1}$$

where C is the tracer concentration scalar, and $\mathbf{J}$ is a tracer flux vector that embodies molecular diffusion as well as subgrid scale advection and subgrid scale diffusion (Chapter 71). Advective transport from the resolved flow, $\mathbf{v}$, appears when transforming to an Eulerian or laboratory reference frame, in which case the tracer equation takes on the equivalent forms

$$\rho \frac{\mathrm{DC}}{\mathrm{D}t} = -\nabla \cdot \mathbf{J} \iff \partial_t(\rho\,\mathrm{C}) + \nabla \cdot (\mathbf{v}\,\rho\,\mathrm{C} + \mathbf{J}) = 0, \tag{68.2}$$

with $\mathbf{v}\,\rho\,\mathrm{C}$ the advective flux. In this chapter we assume $\mathbf{J}$ arises just from diffusion, and we furthermore ignore any flow (i.e., $\mathbf{v} = 0$) so that advection is absent.

68.2.1 Concerning the upright versus slanted notation

The two forms of the tracer in equation (68.2) are written as a tensor equation, prompting the upright C, $\mathbf{v}$, and $\mathbf{J}$, which follows the notation convention of Section 1.2.2. Hence, these equations are valid in any coordinate system. When represented in a particular coordinate system, such as Cartesian, then we write the slanted C, $\boldsymbol{v}$, and $\boldsymbol{J}$, which are particular coordinate representations of the fields C, $\mathbf{v}$, and $\mathbf{J}$.

The upright versus slanted notation is fundamental conceptually, since it is important to appreciate that tensors are geometric objects that are not subject to the whims of a particular coordinate choice. Correspondingly, physically robust differential and integral equations are coordinate invariant. Even so, the upright-slanted notation can be softly adhered to without much cause for concern, so long as we are careful to write the coordinate equations using rules of tensor analysis. In that case, the coordinate equations are unaltered in form when changing coordinates; i.e., they are tensor equations. Developing a practical and conceptual understanding of what careful means in this context requires the tensor analysis material presented in Chapters

[1] Conservative tracers evolve without sources or sinks, and so their material time evolution is only affected by the convergence of a flux.

1 through 4. In the remainder of this section, we summarize salient points from those chapters that are of particular use in the study of tracer diffusion.

68.2.2 Metric tensor allows us to measure distance

The metric tensor, $\mathbb{g}$, is a symmetric and positive-definite (i.e., all eigenvalues are positive) second order tensor that is used to measure the distance between points in space. The *Kronecker tensor* (unit tensor) is the representation of the metric tensor for Euclidean space when using Cartesian coordinates. In this case, $\mathbb{g}_{mn} = \delta_{mn}$, where δ_{mn} is unity when $m = n$ and zero otherwise. In this book, we are only concerned with fluid motion through a background Euclidean space. Even so, we find many occasions to use non-Cartesian coordinates and/or to consider flow constrained to non-Euclidean surfaces that are embedded in Euclidean space (e.g., a spherical planet or an isopycnal surface). Example non-Cartesian coordinates of use for geophysical fluids include spherical coordinates (Section 4.23), cylindrical-polar coordinates (Section 4.22), generalized vertical coordinates (Part XII), and Lagrangian coordinates (Chapter 18). For these cases, and others, a coordinate representation of the metric tensor is distinct from the Kronecker tensor.

We often have need to work with the inverse metric tensor, $\mathbb{g}^{-1}$, which we know exists since the metric is a symmetric and positive-definite tensor. To reduce notational clutter, we write $\mathbb{g}^{mn}$ for the coordinate representation of the inverse metric, rather than the more clunky $(\mathbb{g}^{-1})^{mn}$. By definition of the inverse metric, we have the following identity holding for any coordinate choice

$$\delta^m{}_n = \mathbb{g}^{mp}\, \mathbb{g}_{pn}, \tag{68.3}$$

where $\delta^m{}_n$ is an expression of the identity tensor, which is coordinate invariant.[2] Notably, for Cartesian tensors, where $\mathbb{g}_{mn} = \delta_{mn}$, the identity (68.3) reduces to the identity across Kronecker tensor representations

$$\delta^m{}_n = \delta^{mp}\, \delta_{pn}. \tag{68.4}$$

Since $\delta^{mn} = \delta_{mn}$ (inverse of the Kronecker tensor is the tensor itself), equation (68.4) means that

$$\delta^{mn} = \delta_{mn} = \delta^m{}_n. \tag{68.5}$$

Identities (68.4) and (68.5) are indicative of the relative simplicity of Cartesian tensor analysis, in which there is no distinction between index placement so that there is no quantitative need to keep track of upstairs versus downstairs indices. Yet there is a distinction for general tensors, and so we must be careful to use the metric tensor to raise and lower indices, as now discussed.

68.2.3 Raising and lowering tensor indices via the metric tensor

Besides measuring distance between points in space, the metric tensor provides the operational means to raise and lower indices that appear on the representations of tensors (see Section 4.2.3 for details). For example, consider the second order diffusion tensor, $\mathbf{K}$, with a particular coordinate representation for $K^m{}_n$. The $K^m{}_n$ representation is sometimes referred to as the $(1,1)$ *natural* representation, and it is related to its totally contravariant $(2,0)$ *sharp* representation, K^{mn}, through contraction with the metric tensor,[3]

$$K^m{}_n = \mathbb{g}_{pn}\, K^{mp}. \tag{68.6}$$

[2] Coordinate invariant means that the Kronecker tensor has the same numerical values for all coordinates. Namely, it is unity when its two indices are the same and zero when the indices differ.

[3] In Section 1.6.1 we introduced the musical nomenclature sometimes used for the representations of second order tensors. The *natural* representation of a second order tensor occurs with one tensor index upstairs and the other downstairs. The natural representation is sometimes denoted by $(1,1)$, to indicate the number of indices up and down. The *sharp* or $(2,0)$ representation is when the tensor is represented with both indices upstairs. Finally, the *flat* or $(0,2)$ representation is where both indices are downstairs.

It follows that to relate the *flat* or $(0,2)$ representation to the sharp representation requires two contractions with the metric tensor,

$$K_{mn} = \mathfrak{g}_{mq}\, \mathfrak{g}_{pn}\, K^{qp}. \tag{68.7}$$

Note that since the metric is symmetric, $\mathfrak{g}_{mn} = \mathfrak{g}_{nm}$, there is no need to be concerned with the ordering of its indices.

68.2.4 Divergence of a vector and the divergence theorem

As seen from the tracer equation (68.2), the convergence of the tracer flux drives the time evolution of conservative tracers. It is thus important to know how the divergence is expressed as a tensor equation. In Section 4.15 we derived the coordinate invariant expression (4.134) for the divergence of a vector

$$\nabla \cdot \mathbf{J} = \nabla_m\, J^m = \frac{1}{\sqrt{\det(\mathfrak{g}_{mn})}}\, \partial_m\, [\sqrt{\det(\mathfrak{g}_{mn})}\; J^m], \tag{68.8}$$

where ∇_m are components to the *covariant derivative*. Equation (68.10) is a convenient result since it only requires partial derivatives in the chosen coordinate system, with all the coordinate dependent properties summarized by the square root of the metric determinant, $\sqrt{\det(\mathfrak{g}_{mn})}$. Since $\sqrt{\det(\mathfrak{g}_{mn})}$ appears in many places within this chapter, we find it useful to introduce the shorthand

$$g \equiv \sqrt{\det(\mathfrak{g}_{mn})}, \tag{68.9}$$

in which the covariant divergence (68.10) is written in the more tidy manner

$$\nabla \cdot \mathbf{J} = g^{-1}\, \partial_m\, (g\, J^m). \tag{68.10}$$

For Cartesian coordinates, $g = \sqrt{\det(\mathfrak{g}_{mn})} = 1$, in which case the divergence in equation (68.10) reduces to its familiar Cartesian form (Section 4.21.3). Yet other coordinates have a nonzero g, which accounts for the squeezing and expansion of the coordinate surfaces that affect the divergence. For example coordinate expressions of the divergence, see Section 4.23.8 for spherical coordinates, Section 4.22.10 for cylindrical-polar coordinates, and Sections 63.14 and 63.15 for generalized vertical coordinates.

The $1/g$ factor appearing in the covariant divergence (68.10) is convenient since it cancels the same factor appearing in the invariant volume element (4.60). This cancellation greatly simplifies the divergence theorem as presented in Section 4.19 and given by equation (4.148)

$$\int_{\mathcal{R}} \nabla \cdot \mathbf{J}\, \mathrm{d}V = \int_{\mathcal{R}} \nabla_m\, J^m\, \mathrm{d}V = \int_{\mathcal{R}} \partial_m (g\, J^m)\, \mathrm{d}^3\xi = \oint_{\partial\mathcal{R}} J^m\, \hat{n}_m\, \mathrm{d}\mathcal{S}, \tag{68.11}$$

where $\hat{\boldsymbol{n}}$ is the outward normal, and $\mathrm{d}^3\xi = \mathrm{d}\xi^1\, \mathrm{d}\xi^2\, \mathrm{d}\xi^3$ is the coordinate volume element.

68.2.5 Example tracer fluxes

We here briefly consider example tracer fluxes that are studied later in this chapter or in Chapter 69. We start from their form written in Cartesian coordinates and then transform to general coordinates.

Advective tracer flux

The advective tracer flux has Cartesian coordinates, denoted by ξ^m, written as

$$J^m = \rho\, v^m\, C, \tag{68.12}$$

where ρ, C, and v^m are functions that represent the density, tracer concentration, and velocity using Cartesian coordinates as independent variables. To transform the advective tracer flux to another set of coordinates, $\xi^{\overline{m}}$, requires the transformation matrix as detailed in Section 4.1.4, where

$$J^{\overline{m}} = \overline{\rho}\,\overline{C}\,\Lambda^{\overline{m}}{}_m\, v^m = \overline{\rho}\,\overline{C}\, v^{\overline{m}}. \tag{68.13}$$

In this equation we wrote $\overline{\rho}$, $\overline{C}$, and $v^{\overline{m}}$ for the functions representing the density, tracer concentration, and velocity with $\xi^{\overline{m}}$ as the independent variables. Furthermore, the transformation matrix, $\Lambda^{\overline{m}}{}_m$, is built from the partial derivatives of the two sets of coordinates

$$\Lambda^{\overline{m}}{}_m = \partial \xi^{\overline{m}} / \partial \xi^m. \tag{68.14}$$

For nomenclature brevity in the following, we do not write $\overline{\rho}$ and $\overline{C}$, thus relying on the functional dependence implicit in the coordinate choice.

Isotropic diffusive tracer flux and the Laplace-Beltrami operator

The isotropic diffusive tracer flux has the following representation using Cartesian coordinates

$$J^m = -\rho\,\kappa\,\delta^{mn}\,\partial_n C, \tag{68.15}$$

with $\kappa > 0$ the diffusivity scalar. We generalize the isotropic diffusive flux to arbitrary coordinates, $\xi^{\overline{m}}$, by introducing the inverse metric tensor represented using the $\xi^{\overline{m}}$ coordinates[4]

$$J^{\overline{m}} = -\rho\,\kappa\,\mathbb{g}^{\overline{mn}}\,\partial_{\overline{n}} C. \tag{68.16}$$

Making use of equation (68.10) leads to the flux convergence

$$-\nabla \cdot \mathbf{J} = g^{-1}\,\partial_{\overline{m}}\,(\rho\,\kappa\, g\, \mathbb{g}^{\overline{mn}}\,\partial_{\overline{n}} C). \tag{68.17}$$

If the product, $\rho\,\kappa$, is a constant in space then the resulting flux convergence exposes the *Laplace-Beltrami operator* acting on the tracer concentration

$$-\nabla \cdot \mathbf{J} = \rho\,\kappa\, \underbrace{g^{-1}\,\partial_{\overline{m}}\,(g\,\mathbb{g}^{\overline{mn}}\,\partial_{\overline{n}} C)}_{\text{Laplace-Beltrami acting on C}} \equiv \rho\,\kappa\,\overline{\nabla}^2 C. \tag{68.18}$$

Diffusive tracer flux with an anisotropic diffusion tensor

With a general diffusion tensor (whose form is discussed more in later sections), the Cartesian expression for the diffusive flux is given by

$$J^m = -\rho\, K^{mn}\,\partial_n C. \tag{68.19}$$

The tracer flux has a corresponding expression using arbitrary coordinates

$$J^{\overline{m}} = -\rho\, K^{\overline{mn}}\,\partial_{\overline{n}} C, \tag{68.20}$$

[4]The covariant derivative acting on a scalar field is just the partial derivative. So we could just as well have written $J^{\overline{m}} = -\rho\,\mathbb{g}^{\overline{mn}}\,\nabla_{\overline{n}} C$ for equation (68.16).

which is identical in form to the Cartesian expression (68.19). We make use of the transformation matrix and its inverse to write

$$\partial_{\overline{n}} = \partial_n \, \Lambda^n{}_{\overline{n}} \quad \text{and} \quad K^{\overline{m}\overline{n}} = \Lambda^{\overline{m}}{}_m \, \Lambda^{\overline{n}}{}_n \, K^{mn}. \tag{68.21}$$

Note that we actually only need to perform a single transformation since the contraction between the diffusion tensor and the derivative of the tracer concentration is coordinate invariant

$$J^{\overline{m}} = -\rho \, K^{\overline{m}\overline{n}} \, \partial_{\overline{n}} C = -\rho \, K^{\overline{m}n} \, \partial_n C = -\rho \, \Lambda^{\overline{m}}{}_m \, K^{mn} \, \partial_n C = \Lambda^{\overline{m}}{}_m \, J^m. \tag{68.22}$$

68.2.6 Comments about the tensor tools

Most of this chapter is unconcerned with the niceties of general tensor analysis. Part of the reason is that Cartesian coordinates are sufficient to exemplify the key maths and physics ideas. Even so, we are mindful to use rudimentary tensor notation, thus allowing for the equations derived with Cartesian coordinates to be valid tensor equations that hold for all coordinates. Given the growing suite of coordinates used in geophysical fluid studies, this extra bit of formalism has a nontrivial payoff.

68.3 Basic physics of tracer diffusion

The continuum approximation from Chapter 16 proposes that a macroscopic description of fluid motion does not require direct information about the motion of individual molecules. Nonetheless, random molecular motion and properties of the constituent molecules impact on fluid motion through the process of *molecular diffusion* of matter. Analogously, the random motion of fluid elements within a turbulent fluid give rise to *turbulent diffusive* transport.[5] In this section we explore the basic physical nature of molecular and turbulent diffusion.

68.3.1 Diffusion of matter by random molecular motions

Consider a fluid comprised of a single matter constituent, such as a lake of pure H_2O. As discussed in Section 17.2, for a macroscopic description of this single-component fluid, a constant mass fluid element is identical to a constant mass material fluid parcel. That is, there is no mixing of matter since there is just a single matter component. Now place a dye tracer (Section 20.1.5) into a corner of the lake so that the lake is comprised of two material components (H_2O and dye). Even in the absence of ambient macroscopic fluid motion, the random motion of water and dye molecules produces an exchange of matter constituents between fluid elements. Consequently, the dye spreads outward from its initial position; i.e., it *diffuses* into the surrounding water.

We introduced the notion of matter exchange between fluid elements when discussing the tracer equation in Section 20.1. In the present context, matter exchange occurs through the random motion of molecules acting in the presence of a matter concentration gradient. Even though the continuum approximation has removed all explicit concern for details of molecular motion, we confront the underlying molecular nature of matter since molecular motions have a measurable impact on macroscopic fluid properties. This transport of matter by random molecular motions is known as *molecular diffusion*. A statistical description of molecular diffusion is available for certain ideal-like gases, using methods from kinetic theory. *Einstein* (1905) advanced the theory by studying *Brownian motion*, in which a relatively large particle (e.g., dust) is transported by the random motion of molecules within the fluid. As noted on page 4 of *Csanady* (1973), results from both kinetic theory of gases and Brownian motion suggest

[5] For our purposes, turbulence is characterized by a quasi-random fluid flow that acts on fluid elements and their properties.

that the distance over which a typical mixing "event" occurs is small relative to the macroscopic scales of motion of concern for continuum mechanics. Consequently, we are justified in using the diffusive flux expression (68.23) arising from Fick's law as considered in Section 68.3.3.

68.3.2 Diffusion of matter by random turbulent motions

Diffusion of matter is a familiar process. For example, the odor from an open perfume bottle spreads throughout a room, even in the absence of macroscopic motion of air in the room. When the ambient macroscopic motion is zero (which is rare indeed), spread of the perfume arises solely from random molecular motions whose properties depend on details of the molecules (e.g., their size, speed, inter-molecular forces). The time scale for molecular diffusion is generally much longer than the analogous *turbulent diffusion* that results if there is random motion in the macroscopic fluid, such as occurs by placing a fan next to the perfume bottle.

It is common for environmental and geophysical fluid systems to exhibit some form of turbulent motion. In these systems, the transport of matter by macroscopic turbulent motion is much more efficient than from molecular motion. In the case of turbulent transport, we can generally ignore molecular diffusion since efficiency of the turbulent diffusive transport is far greater than that from molecular diffusion. *Taylor* (1921) described the statistical properties of turbulent diffusion, and many of his insights form the basis for theories of how turbulent motion impacts on matter concentrations. In Taylor's theory, turbulent diffusion is not concerned with molecular properties of the fluid. Rather, the properties of turbulent diffusion (e.g., its efficiency) depend on the nature of the turbulent motion of fluid elements. In this way, turbulent diffusion sits within the realm of continuum mechanics, whereas molecular diffusion is a subject for kinetic theory and statistical mechanics. Each type of turbulent motion gives rise to a distinct form of turbulent diffusion. For example, turbulent diffusion associated with a turbulent field of internal gravity waves is distinct from turbulent diffusion from geostrophic eddies.

68.3.3 Fick's law for matter diffusion

Consider a fluid with a non-uniform tracer concentration such as that drawn for a one-dimensional case in Figure 68.1. Random motion, due either to molecular motion or turbulent fluctuations, will transfer tracer across an arbitrary point, line, or plane. Random motion preferentially moves tracer from regions of high concentration to regions of low concentration, thus smoothing gradients.

To a good approximation, the mass flux (mass per time per cross-sectional area) of a material tracer is linearly proportional to the concentration gradient, and thus can be written in the form

$$\boldsymbol{J} = -\kappa_{\mathrm{c}}\, \rho\, \nabla C. \tag{68.23}$$

In this equation, we introduced the positive proportionality factor, $\kappa_{\mathrm{c}} > 0$, known as the *kinematic diffusivity*, whereas the product $\kappa_{\mathrm{c}}\, \rho$ is known as the *dynamic diffusivity*:

$$\kappa_{\mathrm{c}} \qquad \text{kinematic diffusivity with SI units m s}^{-2} \tag{68.24}$$

$$\rho\, \kappa_{\mathrm{c}} \qquad \text{dynamic diffusivity with SI units kg m}^{-2}\ \text{s}^{-2}. \tag{68.25}$$

The kinematic diffusivity has dimensions of squared length per time and it sets the efficiency or strength of the diffusion. The diffusive flux (68.23) is known as *Fick's law* of matter diffusion, and it is commonly used in geophysical fluid mechanics to represent the mixing of matter through diffusion. The minus sign in the diffusive flux arises since the flux is directed down the concentration gradient. When considering molecular diffusion, we distinguish diffusivities according to their respective tracers since they generally differ, whereas turbulent diffusivities are commonly assumed to be independent of tracer, in which case we write the generic, κ.

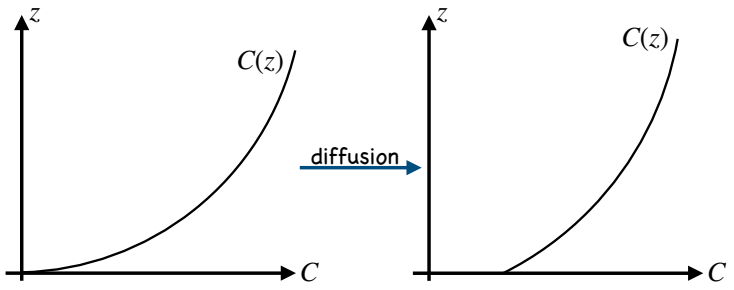

FIGURE 68.1: A graph illustrating a material tracer concentration, C as a function of the space coordinate z, with the left panel showing the concentration at an earlier time than the right panel. Across any arbitrary point, matter is transported through random motions, with this transport generally reducing the magnitude of the concentration gradient. This reduction of concentration gradient is a direct result of the downgradient (i.e., down the concentration gradient) orientation of the diffusive transport. For example, where the concentration is relatively high, random motion mixes this high concentration with adjacent lower concentration, thus acting to lower the concentration in the originally high concentration region and raise the concentration in the originally low concentration region. In this particlar example, $\partial C/\partial z > 0$, so that random fluid motions (either molecular or turbulent) lead to a diffusive flux directed in the $-\hat{\boldsymbol{z}}$ direction; i.e., downward. This downward flux brings high concentration fluid into the lower/deeper regions and low concentration fluid into higher/shallower regions. The concentration is vertically uniform if allowed to equilibrate under the action of diffusion.

The kinematic diffusivity has physical dimensions equal to the product of a length and a speed. For molecular diffusion, the kinematic diffusivity is proportional to the mean free path, $L_{\rm mfp}$ (see Section 16.3.3), and the root-mean-square molecular speed, $v_{\rm rms}$ (see Section 16.3.4). Each of these properties is a function of the molecules comprising the matter. For air, the mean free path is roughly 2×10^{-7} m and the root-mean-square speed is 500 m s^{-1}, so that $L_{\rm mfp}\, v_{\rm rms} \approx 10^{-4}$m^2 s^{-1}. The precise value for the molecular diffusivity depends on the molecular properties of the matter diffusing through the fluid; e.g., molecular size and speed.

For turbulent diffusion, Prandtl suggested that the characteristic length and velocity scales are determined by properties of the turbulent flow, not by the molecular properties of the fluid or the tracer. The turbulent length scale (also called the *mixing length*) is generally much larger than the molecular mean free path, whereas the turbulent velocity scale is much smaller than molecular speeds. Determination of turbulent length and velocity scales is subject to large uncertainties and variations given the multiple regimes of turbulence exhibited by geophysical flows. As a result, tracer transport by turbulent flows has remained a topic of much research since the early 20th century.

In regions where the diffusive flux is not a constant, there is generally a net transport of matter that leads to the reduction of the tracer concentration gradient as determined by the convergence of the diffusive flux

$$\rho \frac{\mathrm{D}C}{\mathrm{D}t} = -\nabla \cdot \boldsymbol{J} = \nabla \cdot (\kappa_{\rm c}\, \rho\, \nabla C). \tag{68.26}$$

That is, the concentration increases in regions where the diffusive flux, $\boldsymbol{J}$, converges, and decreases where the flux diverges. Expanding the divergence operator leads to

$$\rho \frac{\mathrm{D}C}{\mathrm{D}t} = \nabla(\kappa_{\rm c}\, \rho) \cdot \nabla C + \kappa_{\rm c}\, \rho\, \nabla^2 C. \tag{68.27}$$

The first term is nonzero in regions where the dynamic diffusivity, $\kappa_{\rm c}\, \rho$, spatially varies. This term vanishes for molecular diffusion, in which case the diffusivity is a spatial constant. However, for turbulent diffusion this term can be quite important given the potential for strong flow dependence to the diffusivity. Indeed, there are cases in which this spatial dependence can enhance tracer gradients, overcoming the effects from the curvature term. We consider an example in Exercise 68.5 known as the *Phillip's layering instability.*

The second term in the diffusion equation (68.27) is proportional to the Laplacian of the tracer concentration, which provides a measure of the curvature in the tracer field. Hence, this term vanishes when the tracer concentration is a constant or a linear function of space, whereas it is nonzero for tracers having less trivial spatial structure. As discussed in Section 68.3.6, this term provides a scale selectivity to the diffusion operator, thus resulting in a preferential dampening of small scale features relative to large scale features.

68.3.4 Fourier's law for heat diffusion

In the same way that matter concentration gradients lead to diffusion by random motions, temperature gradients lead to diffusion of heat. The corresponding phenomenological relation is known as *Fourier's law*, with the diffusive flux given by

$$\boldsymbol{J} = -\kappa_{\mathrm{T}}\, \rho\, \nabla T, \tag{68.28}$$

where $\kappa_{\mathrm{T}} > 0$ is the temperature kinematic diffusivity. As for the matter diffusivity, the molecular thermal diffusivity can be expressed in terms of fundamental properties of the fluid, and it is different from the matter diffusivity. In general, molecular processes diffuse matter slower than heat, so that the matter molecular diffusivity is smaller than the heat molecular diffusivity. The reason for the difference is that matter diffusion requires the movement of matter (molecules), whereas heat diffusion occurs through the exchange of thermal energy between molecules, and that exchange does not require the motion of matter. For turbulent transport, however, the turbulent thermal diffusivity is roughly the same as the turbulent matter diffusivity. The reason is that the turbulent diffusion of both matter and heat are mediated by the same turbulent fluctuations of fluid elements.

68.3.5 Newtonian frictional stress and momentum diffusion

In the same way that matter and temperature gradients lead to diffusion by random molecular and turbulent motions, the momentum of fluid elements is exchanged through diffusion in the presence of viscosity. The corresponding phenomenological relation is known as *Newton's law* of viscous friction. As momentum is a vector, a general treatment of momentum transport through irreversible viscous processes involves a second order stress tensor and a fourth order viscosity tensor. For the specific case shown in Figure 68.2, with shear (i.e., nonzero velocity gradient) in a single direction, Newtonian frictional stress takes the form

$$\tau = \rho\, \mu\, \partial_z u, \tag{68.29}$$

where $\mu > 0$ is the kinematic viscosity. Note the absence of a minus sign, in contrast to diffusive fluxes of scalars. The sign difference arises since it is the divergence of the stress tensor that leads to contact forces on the fluid, whereas it is the convergence of diffusive fluxes that leads to diffusion of matter and heat. We consider these general properties of the stress tensor when exploring the fluid dynamical equations in Chapter 24 and further study the physical nature of stress in Chapter 25.

For geophysical fluid mechanics, we are most generally interested in the molecular viscosity of water and air. Quite generally, the dynamic viscosity of water ($\rho\, \mu$) is about 10^2 times larger than that for air. But since the density of water is about 10^3 times larger than air, the kinematic viscosity of air is roughly 10 times greater than that of water.

The molecular kinematic viscosity can be expressed in terms of fundamental properties of the fluid, and it is different from the molecular matter diffusivity and molecular thermal diffusivity. For some turbulent processes, the turbulent viscosity, μ, is proportional to the turbulent diffusivity, κ, of scalar fields (e.g., temperature, salinity, humidity). In general, the

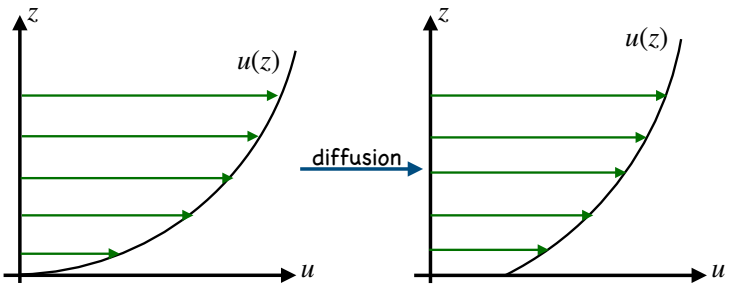

FIGURE 68.2: A graph illustrating the zonal velocity, u, as a function of the space coordinate z, with the left panel showing the velocity at an earlier time than the right panel. Across any arbitrary point, transport of momentum through random motions generally reduces the magnitude of the velocity gradient; i.e., the diffusive transport leads to a viscous stress that acts to reduce the velocity shear.

non-dimensional ratio of the viscosity to the diffusivity is known as the *Prandtl number*

$$\mathrm{Pr} = \mu/\kappa. \tag{68.30}$$

Theories for the turbulent Prandtl number are largely empirical, with first principles arguments elusive.

68.3.6 The scale selectivity of Laplacian diffusion

Let us focus on the Laplacian term appearing in the tracer equation (68.27) to establish some properties characteristic of Laplacian diffusion. Start by considering a tracer concentration whose spatial structure is given by two Fourier modes,

$$C(\boldsymbol{x}) = c_{\boldsymbol{p}} \sin(\boldsymbol{p}\cdot\boldsymbol{x}) + c_{\boldsymbol{q}} \sin(\boldsymbol{q}\cdot\boldsymbol{x}), \tag{68.31}$$

where $\boldsymbol{p}$ and $\boldsymbol{q}$ are specified wavevectors and $c_{\boldsymbol{p}}$, $c_{\boldsymbol{q}}$ are their corresponding amplitudes. In this case the Laplacian of the tracer is given by

$$\nabla^2 C = -[|\boldsymbol{p}|^2 c_{\boldsymbol{p}} \sin(\boldsymbol{p}\cdot\boldsymbol{x}) + |\boldsymbol{q}|^2 c_{\boldsymbol{q}} \sin(\boldsymbol{q}\cdot\boldsymbol{x})]. \tag{68.32}$$

Consequently, the Laplacian diffusion operator acts preferentially on waves of smaller wavelength (and larger wavenumber). For example, assume $|\boldsymbol{p}| \ll |\boldsymbol{q}|$, in which case the $\boldsymbol{q}$-mode is more rapidly damped towards zero than the $\boldsymbol{p}$-mode.[6] For this reason we say that Laplacian diffusion is *scale selective*. Note that zero is the wave averaged concentration for each Fourier mode. We thus see that diffusion acts to dampen each mode towards is average. Scale selectivity results geometrically from a property of the Laplacian operator as a measure of curvature. Tracer features with large curvature have a larger magnitude for their Laplacian, and as such they are damped more rapidly than tracer features with relatively small curvature.[7]

As a second means to understand properties of Laplacian diffusion, consider a Taylor series for the tracer concentration computed relative to an arbitrarily chosen origin,

$$C(\boldsymbol{x}) = C(0) + x^m \, \partial_m C|_{\boldsymbol{x}=0} + (1/2)\, x^m \, x^n \, \partial_n \partial_m C|_{\boldsymbol{x}=0} + \ldots \tag{68.33}$$

Now compute the average of this tracer concentration over a cube centered at the origin with

[6] Figure 8.2 illustrates this idea in the context of Fourier analysis.
[7] Recall our discussion of curvature in Chapter 5.

sides L and volume L^3, and furthermore make use of the identities

$$\int_{-L/2}^{L/2}\int_{-L/2}^{L/2}\int_{-L/2}^{L/2} x^m \,\mathrm{d}x\,\mathrm{d}y\,\mathrm{d}z = 0 \tag{68.34a}$$

$$\int_{-L/2}^{L/2}\int_{-L/2}^{L/2}\int_{-L/2}^{L/2} x^m\, x^n \,\mathrm{d}x\,\mathrm{d}y\,\mathrm{d}z = \delta^{mn}\,(L^5/12). \tag{68.34b}$$

We thus find that the volume averaged tracer concentration, $\langle C\rangle$, deviates from the concentration at the origin by a term proportional to the Laplacian of the concentration evaluated at the origin

$$\langle C\rangle - C(0) = (L^2/24)\,\nabla^2 C\big|_{\boldsymbol{x}=0} \implies \partial_t C\big|_{\boldsymbol{x}=0} = (24\,\kappa_{\mathrm{c}}\,\rho/L^2)\,[\langle C\rangle - C(0)], \tag{68.35}$$

where we made use of the Laplacian portion of the diffusion equation (68.27) for the second expression. Evidently, Laplacian diffusion provides a tendency to bring the tracer concentration at a point towards the average tracer concentration in a region surrounding that point. For example, consider the case where the averaged tracer concentration has no time dependence, as occurs in a region with zero boundary fluxes of tracer. If we are at a point in the region where the concentration is less than the average concentration, $C < \langle C\rangle$, then diffusion provides a positive tendency to increase C towards $\langle C\rangle$, and vice versa if $C > \langle C\rangle$. These results offer another expression of what we found in studying Laplacian diffusion on Fourier modes. In that case, the Laplacian operator, as revealed through equation (68.32), damps each mode towards its average, which is zero.

68.3.7 A Gaussian tracer concentration generated by a Dirac source

Consider a one-dimensional tracer concentration in an unbounded domain whose initial ($t = 0$) value vanishes everywhere except at the origin, where it is given by a Dirac delta

$$C(x, t = 0) = Q\,\delta(x), \tag{68.36}$$

where $\delta(x)$ is the Dirac delta studied in Chapter 7. The Dirac delta has dimensions of inverse length, so that the constant, Q, has dimensions of $[C]\ L$. Integrating over any region containing the origin reveals that Q is the domain integrated tracer concentration at the initial time,

$$\int_{-\infty}^{\infty} C(x, t = 0)\,\mathrm{d}x = Q. \tag{68.37}$$

We are ensured that this integral holds for all time if the domain has no boundary fluxes of tracer nor any interior tracer sources.

Assume now that the tracer concentration evolves according to the one-dimensional (one space dimension) diffusion equation with a constant diffusivity, κ, and in a fluid with a constant density. In the absence of spatial boundaries (i.e., diffusion occurs on the real line, $\mathbb{R}^1$), the concentration is proportional to the causal free space Green's function given by the Gaussian function (9.136)

$$C(x, t) = \frac{Q}{(4\,\pi\,\kappa\,t)^{1/2}}\mathrm{e}^{-x^2/(4\,\kappa\,t)}, \tag{68.38}$$

which indeed satisfies (for any time, t)

$$Q = \int_{-\infty}^{\infty} C(x, t)\,\mathrm{d}x, \tag{68.39}$$

as required by tracer conservation for the infinite domain. We illustrate the Gaussian tracer

concentration (68.38) in Figure 68.3. The variance of the tracer distribution is given by

$$Q^{-1} \int_{-\infty}^{\infty} C\, x^2 \, \mathrm{d}x = 2\,\kappa\, t, \tag{68.40}$$

so that the standard deviation grows according to $\sqrt{2\,\kappa\, t}$.

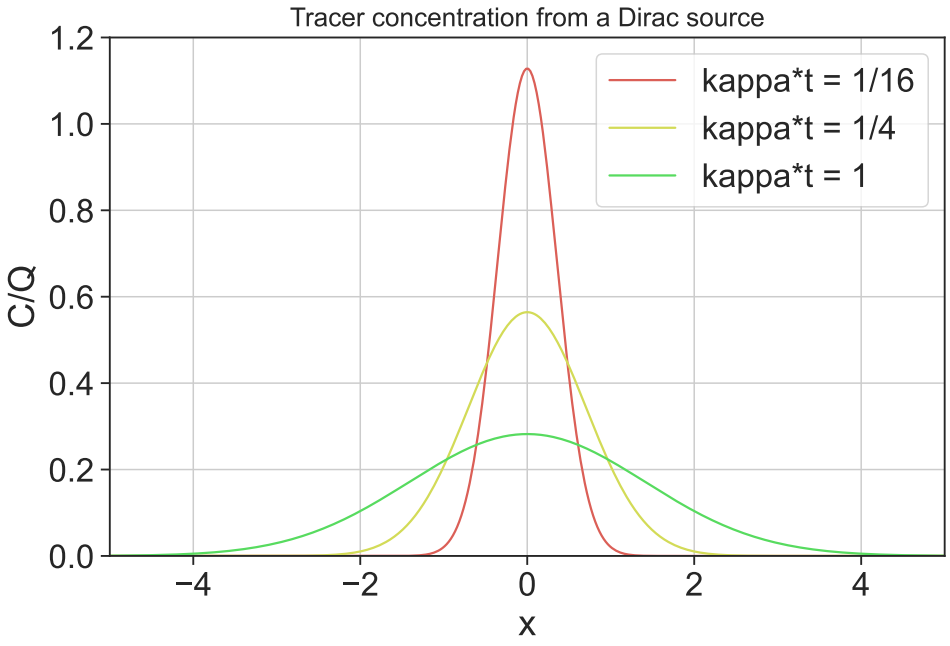

FIGURE 68.3: Illustrating the tracer concentration resulting from a Dirac source at the origin, as given by the Gaussian Green's function (68.38) for three values of $\kappa\, t$. According to equation (68.40), the standard deviation is given by $\sqrt{2\,\kappa\, t}$, with the standard deviation measuring the spread of the distribution.

68.3.8 Further study

The treatment given in this section is consistent with that from Section 1.5 of *Kundu et al.* (2016) and Chapter 1 of *Csanady* (1973). Molecular diffusion for ideal gases is examined in books that consider the kinetic theory of gases, such as *Reif* (1965) and *Huang* (1987). Treatments of Brownian motion in the context of turbulent diffusion can be found in *Csanady* (1973), who focuses on turbulent diffusion in the environment (e.g., for the study of pollution dispersal), and in Chapter 13 of *Vallis* (2017), who focuses on geophysical flows.

68.4 Further properties of tracer diffusion

We considered mathematical properties of the diffusion equation in Chapter 6 as part of our study of parabolic partial differential equations. We also examined the diffusion equation as part of our analysis of Green's function solutions for passive tracers in Chapter 9. Here, we explore further mathematical properties of diffusion motivated in part by the discussion in Section 68.3. In particular, we here allow for distinct behavior of the diffusive fluxes in the different directions. Such distinctions are relevant especially for the turbulent diffusivity arising in stratified fluids, where turbulent mixing across stratification surfaces is suppressed relative to turbulent mixing parallel to these surfaces (see Section 30.4). For this purpose we make use of the second order positive definite and symmetric *diffusion tensor*, $\mathbf{K} = \mathbf{K}^{\mathrm{T}}$, with the resulting downgradient

diffusive tracer flux given by

$$J^m = -\rho\, K^{mn}\, \partial_n C. \tag{68.41}$$

68.4.1 Sample diffusion tensors

For the case of molecular diffusion considered in equation (68.23), the diffusion tensor is generally assumed to be isotropic.[8] Written in Cartesian coordinates, the isotropic diffusion tensor takes the form

$$K^{mn} = \kappa\, \delta^{mn}, \tag{68.42}$$

whereas with general coordinates it is

$$K^{\overline{mn}} = \kappa\, \mathbb{g}^{\overline{mn}}. \tag{68.43}$$

It is notable that the natural or $(1,1)$ form for the diffusion tensor is numerically identical across coordinates, in that

$$K^m{}_p = \kappa\, \delta^m{}_p \quad \text{and} \quad K^{\overline{m}}{}_{\overline{p}} = \kappa\, \mathbb{g}_{\overline{np}}\, \mathbb{g}^{\overline{mn}} = \kappa\, \delta^{\overline{m}}{}_{\overline{p}}, \tag{68.44}$$

where we made use of the identity (68.3) satisfied by the metric and its inverse.

To parameterize flows that are turbulent and larger than the microscale (e.g., ocean mesoscale turbulence), it is common to rotate the diffusive fluxes to be along surfaces of constant scalar field, $\gamma(\boldsymbol{x}, t)$, in which case the diffusion tensor is

$$K^{mn} = \kappa\, (\delta^{mn} - \hat{\gamma}^m\, \hat{\gamma}^n), \tag{68.45}$$

where

$$\hat{\boldsymbol{\gamma}}_n = \frac{\partial_n \gamma}{|\nabla \gamma|} \tag{68.46}$$

is the surface normal direction. The general coordinate representation of this anisotropic diffusion tensor is

$$K^{\overline{mn}} = \kappa\, (\mathbb{g}^{\overline{mn}} - \hat{\gamma}^{\overline{m}}\, \hat{\gamma}^{\overline{n}}). \tag{68.47}$$

One choice for the orientation direction is to set $\hat{\gamma} = \hat{\boldsymbol{z}}$, in which case the diffusion tensor orients the tracer fluxes along surfaces of constant geopotential to thus realize *horizontal diffusion*. Another choice, motivated from the physics of ocean mesoscale eddy transport, sets γ equal to a measure of the local buoyancy. In this case we have the *neutral diffusion* process studied in Section 71.4.

68.4.2 Diffusion of tracer concentration powers

We here establish how diffusion affects the evolution of powers of the tracer concentration. For that purpose, consider the material evolution of C^Γ, where $\Gamma \geq 1$

$$\rho\, \frac{\mathrm{D}C^\Gamma}{\mathrm{D}t} = \Gamma\, C^{\Gamma-1}\, \rho\, \frac{\mathrm{D}C}{\mathrm{D}t} = -\Gamma\, C^{\Gamma-1}\, \nabla \cdot \boldsymbol{J}. \tag{68.48}$$

Making use of equation (68.10) for the covariant divergence leads to

$$\Gamma\, C^{\Gamma-1}\, \nabla \cdot \boldsymbol{J} = g^{-1}\, \Gamma\, C^{\Gamma-1}\, \partial_m (g\, J^m) \tag{68.49a}$$

$$= g^{-1}\, \partial_m (\Gamma\, C^{\Gamma-1}\, g\, J^m) - \Gamma\, (\Gamma - 1)\, C^{\Gamma-2}\, J^m\, \partial_m C. \tag{68.49b}$$

[8] We discussed isotropic tensors in Section 1.11.

Notice that

$$g^{-1}\,\partial_m(\Gamma\,C^{\Gamma-1}\,g\,J^m) = -g^{-1}\,\partial_m(\Gamma\,C^{\Gamma-1}\,g\,\rho\,K^{mn}\,\partial_n C) \tag{68.50a}$$
$$= -g^{-1}\,\partial_m(g\,\rho\,K^{mn}\,\partial_n C^{\Gamma}) \tag{68.50b}$$
$$= \nabla\cdot\boldsymbol{J}(C^{\Gamma}), \tag{68.50c}$$

which leads to the evolution equation

$$\rho\,\frac{\mathrm{D}C^{\Gamma}}{\mathrm{D}t} = -\nabla\cdot\boldsymbol{J}(C^{\Gamma}) + \Gamma\,(\Gamma-1)\,C^{\Gamma-2}\,\boldsymbol{J}\cdot\nabla C. \tag{68.51}$$

The first term in equation (68.51) is the convergence of the diffusive flux defined in terms of C^{Γ}. This term acts to diffuse C^{Γ} just like diffusion acts on C. The second term in equation (68.51) is negative since the diffusion tensor is symmetric and positive-definite so that

$$\boldsymbol{J}\cdot\nabla C = -\rho\,K^{mn}\,\partial_m C\,\partial_n C < 0. \tag{68.52}$$

That is, the diffusive flux, by construction, is oriented down the tracer concentration gradient. Consequently, the second term in equation (68.51) always acts to reduce the magnitude of C^{Γ} towards zero.

68.4.3 Moments of tracer concentration

Next we consider the evolution of domain integrated tracer concentration and its powers. To focus on impacts just from diffusion, we assume the boundaries are insulating (i.e., zero normal boundary flux) so that $\boldsymbol{J}\cdot\hat{\boldsymbol{n}} = 0$ with $\hat{\boldsymbol{n}}$ the outward normal at the boundary. We also assume the total fluid mass in the domain remains fixed

$$M = \int \rho\,\mathrm{d}V \quad \text{with} \quad \frac{\mathrm{d}M}{\mathrm{d}t} = 0. \tag{68.53}$$

We can thus treat the domain as material given that there is no exchange of mass or tracer across the boundaries. These assumptions allow us to focus just on the effects from tracer diffusion.

Domain average tracer concentration

The domain averaged tracer concentration is defined by

$$\overline{C} = \frac{\int C\,\rho\,\mathrm{d}V}{M}, \tag{68.54}$$

and it follows that its time derivative vanishes since

$$M\,\frac{\mathrm{d}\overline{C}}{\mathrm{d}t} = \frac{\mathrm{d}}{\mathrm{d}t}\int C\,\rho\,\mathrm{d}V = \int \frac{\mathrm{D}C}{\mathrm{D}t}\,\rho\,\mathrm{d}V = -\int \nabla\cdot\boldsymbol{J}\,\mathrm{d}V = -\oint \boldsymbol{J}\cdot\hat{\boldsymbol{n}}\,\mathrm{d}\mathcal{S} = 0, \tag{68.55}$$

where $\boldsymbol{J}\cdot\hat{\boldsymbol{n}} = 0$ since we are assuming an insulating boundary. Also note that we brought the time derivative inside the integral as a material derivative since the region is itself material, thus allowing us to make use of Reynold's transport theorem from Section 20.2.6. The result (68.55) follows since there is no change in the total mass of fluid nor is there any exchange of tracer across the boundaries. Hence, the domain averaged tracer concentration remains fixed in time.

Tracer variance within the domain

The variance of the tracer concentration is defined by

$$\text{var}(C) \equiv \frac{\int (C - \overline{C})^2 \, \rho \, \mathrm{d}V}{M} = \overline{C^2} - \overline{C}^2 \geq 0. \tag{68.56}$$

The tracer variance measures the deviation of the tracer concentration relative to the domain averaged concentration. Since the domain average remains fixed in time, the time change of the variance is given by

$$\frac{\mathrm{d}[\text{var}(C)]}{\mathrm{d}t} = \frac{\mathrm{d}\overline{C^2}}{\mathrm{d}t}. \tag{68.57}$$

Thus, it is common to refer to $\overline{C^2}$ as the tracer variance, though strictly speaking only time derivatives of $\overline{C^2}$ and $\text{var}(C)$ are equal as per equation (68.57). Performing the time derivative, and again noting that the domain is material thus allowing us to use Reynolds transport theorem, renders

$$M \frac{\mathrm{d}\overline{C^2}}{\mathrm{d}t} = \frac{\mathrm{d}}{\mathrm{d}t} \int C^2 \, \rho \, \mathrm{d}V = 2 \int C \frac{\mathrm{D}C}{\mathrm{D}t} \, \rho \, \mathrm{d}V = -2 \int C \, \nabla \cdot \boldsymbol{J} \, \mathrm{d}V = 2 \int \nabla C \cdot \boldsymbol{J} \, \mathrm{d}V. \tag{68.58}$$

The final equality again made use of the insulating boundary condition, $\boldsymbol{J} \cdot \hat{\boldsymbol{n}} = 0$. The time change in the tracer variance is thus determined by the integral of the projection of the tracer flux onto the tracer gradient. We already saw from equation (68.52) that diffusive fluxes are oriented down the tracer gradient. Consequently, diffusion of the tracer concentration results in a reduction in tracer variance

$$\frac{\mathrm{d}[\text{var}(C)]}{\mathrm{d}t} = \frac{\mathrm{d}\overline{C^2}}{\mathrm{d}t} \leq 0. \tag{68.59}$$

This result further supports our common experience where diffusion removes differences (i.e., gradients) within the tracer field.

Diffusion of arbitrary tracer moments

Proceeding as before, and dropping boundary contributions since the domain is material and insulating, the identity (68.51) shows that the time derivative of an arbitrary tracer moment is given by

$$\frac{\mathrm{d}\overline{C^\Gamma}}{\mathrm{d}t} = \Gamma \left(\Gamma - 1 \right) \int C^{\Gamma - 2} \, \nabla C \cdot \boldsymbol{J} \, \mathrm{d}V \leq 0. \tag{68.60}$$

For $\Gamma = 0$ we have an expression of mass conservation for the domain, whereas $\Gamma = 1$ is an expression of tracer conservation. The case of $\Gamma = 2$ yields the tracer variance result (68.59). The result for higher powers also holds. Hence, we conclude that the downgradient orientation of diffusive tracer fluxes acts to dissipate all powers of tracer concentration when integrated globally; i.e., all tracer moments are dissipated by diffusion.

68.5 Connecting tracer dissipation to the diffusion operator

We here take an excursion into linear operator theory. In particular, we make a connection between the diffusion operator with natural boundary conditions (defined below) and the functional derivative of the global tracer dissipation functional. This connection holds so long as the diffusion operator is self-adjoint and linear, as it is when diffusing passive tracers and

with natural boundary conditions.[9] The connection between a linear self-adjoint operator and a functional is developed in such books as *Courant and Hilbert* (1953, 1962). In the simplest case, the Laplacian of the tracer, $\nabla^2 C$, is equal to the functional derivative,

$$\nabla^2 C = \frac{\delta \mathcal{F}}{\delta C}, \tag{68.61}$$

where[10]

$$\mathcal{F} \equiv -\frac{1}{2} \int |\nabla C|^2 \, \rho \, \mathrm{d}^3 x \tag{68.62}$$

is the associated functional. In the following, we prove this result for a general diffusion tensor acting on an arbitrary tracer concentration, C, with the proof holding so long as the diffusion tensor is not a function of the tracer concentration. Besides offering an interesting theoretical tidbit, this result provides a suitable framework for developing numerical methods for discretizing the diffusion operator, with examples provided by *Griffies et al.* (1998) and Chapter 16 of *Griffies* (2004).

68.5.1 Fréchet derivative of the diffusion dissipation functional

Define the *diffusion dissipation functional*

$$\mathcal{F} = \int \mathcal{L} \, \mathrm{d}^3 x, \tag{68.63}$$

where the integrand is the negative semi-definite quadratic form

$$2 \, \mathcal{L} = \boldsymbol{J} \cdot \nabla C = -\rho \, K^{mn} \, \partial_m C \, \partial_n C \leq 0. \tag{68.64}$$

The goal is to relate the diffusion operator, given by the convergence of the diffusion flux, $-\nabla \cdot \boldsymbol{J}$, to the functional derivative of $\mathcal{F}$, with the derivative taken with respect to the tracer concentration, C. We compute the functional derivative using variational calculus technology detailed in Chapters 10, 46, and 47, mostly in relation to Hamilton's principle for non-dissipative dynamical systems.

For that purpose, consider a functional variation to the tracer concentration, δC, and insert it into the dissipation functional

$$\delta \mathcal{F} = \int \left[\delta C \, \frac{\delta \mathcal{L}}{\delta C} + \delta(\partial_m C) \, \frac{\delta \mathcal{L}}{\delta(\partial_m C)} \right] \mathrm{d}^3 x. \tag{68.65}$$

As discussed in Chapter 46, functional variations are perturbations to the form of the function, in which case

$$C \to C + \delta C \qquad \text{with} \qquad |\delta C| \ll |C|. \tag{68.66}$$

Notably, δC is itself a function of space and time, $\delta C(\boldsymbol{x}, t)$, but it is assumed to have much smaller magnitude than the concentration, $C(\boldsymbol{x}, t)$. Additionally, the functional variation, δC, has no affect on the space-time points so that the variational operator, δ, commutes with space and time derivatives and integrals. Integration by parts on the second term in equation (68.65) leads to

$$\delta \mathcal{F} = \int \left[\delta C \, \frac{\delta \mathcal{L}}{\delta C} + \partial_m \left(\delta C \, \frac{\delta \mathcal{L}}{\delta(\partial_m C)} \right) - \delta C \, \partial_m \left(\frac{\delta \mathcal{L}}{\delta(\partial_m C)} \right) \right] \mathrm{d}^3 x. \tag{68.67}$$

[9] We discussed the self-adjoint nature of the diffusion operator in Section 9.3.6 when developing the Green's function for the diffusion equation.

[10] In this section we write the integration volume element as $\mathrm{d}^3 x = \mathrm{d}V$. Motivation for this notation will become apparent at the point of equation (68.70).

The middle term is a total derivative that integrates to a boundary contribution and the associated *natural boundary condition*

$$\hat{\boldsymbol{n}} \cdot \frac{\delta \mathscr{L}}{\delta \nabla C} = \hat{\boldsymbol{n}} \cdot \boldsymbol{J} = \text{boundary flux}, \tag{68.68}$$

with $\hat{\boldsymbol{n}}$ the boundary outward normal. This natural boundary condition is the *Neumann boundary condition* from Chapter 9.

To focus on the connection between the diffusion operator and the diffusion dissipation functional, we ignore boundary fluxes so that the functional variation is given by

$$\delta \mathscr{F} = \int \delta C \left[\frac{\delta \mathscr{L}}{\delta C} - \partial_m \left(\frac{\delta \mathscr{L}}{\delta (\partial_m C)} \right) \right] \mathrm{d}^3 x. \tag{68.69}$$

Consequently, the functional derivative (also known as the *Fréchet derivative*) is given by

$$(\mathrm{d}^3 y)^{-1} \frac{\delta \mathscr{F}}{\delta C(\boldsymbol{y})} = \frac{\delta \mathscr{L}}{\delta C} - \partial_m \left[\frac{\delta \mathscr{L}}{\delta (\partial_m C)} \right], \tag{68.70}$$

where $\mathrm{d}^3 y$ is the volume element at the field point, $\boldsymbol{y}$. To reach the last step required the identity

$$\frac{\delta C(\boldsymbol{x})}{\delta C(\boldsymbol{y})} = \mathrm{d}^3 y \, \delta(\boldsymbol{x} - \boldsymbol{y}), \tag{68.71}$$

where $\delta(\boldsymbol{x} - \boldsymbol{y})$ is the *Dirac delta*[11] satisfying

$$\int \delta(\boldsymbol{x} - \boldsymbol{y}) \, \mathrm{d}^3 y = 1, \tag{68.72}$$

so long as the integration domain includes the singular point $\boldsymbol{x} = \boldsymbol{y}$. Note that the Dirac delta has dimensions of inverse volume, which necessitates the appearance of the volume factor, $\mathrm{d}^3 y$, on the right hand side of equation (68.71).[12]

68.5.2 Connection to the diffusion operator

Reintroducing the specific form of the diffusion integrand $2\,\mathscr{L} = -\rho\, K^{mn}\, \partial_m C\, \partial_n C$ leads to

$$\frac{\delta \mathscr{F}}{\delta C(\boldsymbol{y})} = -\partial_m \left[\frac{\delta \mathscr{L}}{\delta (\partial_m C)} \right] \mathrm{d}^3 y = \partial_m (\rho\, K^{mn}\, \partial_n C)\, \mathrm{d}\boldsymbol{y}. \tag{68.73}$$

The second equality identifies the diffusion operator, thus revealing the connection between the dissipation functional, the diffusion fluxes, and the diffusion operator

$$\frac{\delta \mathscr{F}}{\delta C(\boldsymbol{y})} = -(\nabla \cdot \boldsymbol{J})\, \mathrm{d}^3 y. \tag{68.74}$$

68.5.3 Why we need to assume K^{mn} is independent of C

There are many geophysical applications in which the diffusion tensor is a function of the tracer concentration, in which case the diffusion equation is no longer a linear differential equation. For

[11] We study the Dirac delta in Chapter 7. Additionally, note the unfortunate, though nearly universal, double meaning for the δ symbol: one referring to the variation operator and one referring to the Dirac delta.

[12] Many treatments of functional derivatives in mathematics texts ignore the volume factor, $\mathrm{d}^3 y$, in equation (68.71). Yet for physical applications it is necessary to maintain dimensional consistency, with the volume factor required for that reason. The volume factor also appears when using functional methods to derive numerical discretizations, with examples provided by *Griffies et al.* (1998), *Griffies and Hallberg* (2000), and *Griffies* (2004).

example, the neutral diffusion of Section 71.4 makes use of a diffusion tensor that is a function of temperature and salinity gradients. In this case the functional derivative in terms of temperature or salinity appearing in equation (68.73) becomes

$$2 \frac{\delta \mathcal{L}}{\delta(\partial_m C)} = -2 \rho K^{mn} \partial_n C - \rho \partial_m C \partial_n C \frac{\delta K^{mn}}{\delta(\partial_m C)}. \tag{68.75}$$

The specific form of the term $\delta K^{mn}/\delta(\partial_m C)$ depends on details of the diffusion tensor. Hence, the general results derived above for the linear diffusion equation no longer hold for this nonlinear diffusion equation. We have more to say about nonlinear advection-diffusion in Section 69.7.

68.5.4 Relation to Hamilton's principle

Recall our application of a functional derivative within the context of Hamilton's principle, which we studied in Chapters 46 and 47 for non-dissipative continuum systems. For those systems, the Euler-Lagrange equations of motion result from setting the functional derivative of the action to zero, which is the mathematical statement of Hamilton's principle. In contrast, we here showed that the functional derivative of the tracer dissipation equals to the diffusion operator. In fact, the construction in this section suggests that linear self-adjoint operators, such as generalized Laplacian operators, can generally be expressed as the functional derivative of its corresponding functional. Chapters 16 and 19 of *Griffies* (2004) provide further examples, with applications to numerical methods. Further mathematical details can be found in such books as *Courant and Hilbert* (1953, 1962).

68.6 Exercises

EXERCISE 68.1: VERTICAL DIFFUSION OF TEMPERATURE IN THE OCEAN (*Vallis*, 2017)
There is a natural time scale associated with diffusive transport. This time scale can be found from scaling the diffusion equation, which reveals that it takes the form

$$\tau_{\text{diffusion}} = \Delta^2/\kappa, \tag{68.76}$$

where Δ is the length scale and κ is the kinematic diffusivity (dimensions of squared length per time). We now make use of this time scale to consider the diffusion of temperature in the ocean, with diffusion due solely to molecular processes.

Using the observed value of molecular diffusivity of temperature in water (look it up), estimate the time for a temperature anomaly to mix from the top of the ocean to the bottom, assuming vertical diffusion through the molecular diffusivity is the only means for mixing. This time scale follows from the one-dimensional diffusion equation and is determined by the diffusivity and the depth of the ocean. Comment on whether you think the real ocean has reached equilibrium after the last ice age (which ended about 12Kyr ago).

EXERCISE 68.2: ANALYTICAL SOLUTION TO ONE-DIMENSIONAL DIFFUSION EQUATION
Consider a one-dimensional diffusion equation

$$\partial_t C = \kappa \partial_{zz} C, \tag{68.77}$$

where C is a tracer concentration (e.g., temperature or salinity), κ is a constant kinematic diffusivity, and z is the vertical coordinate. Assume the domain has fixed boundaries at $z = 0$ and $z = H$.

(a) Assume there is a zero flux of tracer at the two boundaries. Mathematically express this no-flux boundary condition.

(b) Assume that the initial tracer concentration is confined to an area near the center of the domain. Use dimensional analysis to estimate the time scale for the concentration to homogenize throughout the domain.

(c) Consider the initial-boundary value problem

$$\partial_t C = \kappa \partial_{zz} C, \tag{68.78a}$$

$$\text{no-flux boundary condition from part (b)} \tag{68.78b}$$

$$C(z, t = 0) = C_0 \cos(kz), \tag{68.78c}$$

where C_0 is a constant. What values for the wave-number, k, satisfy the no-flux boundary condition?

(d) Solve the diffusion equation analytically for the given initial condition. Hint: consult your favorite partial differential equation book to learn how to solve this linear 1+1 dimensional diffusion equation.

(e) Explain how the analytical answer you obtained is consistent with the dimensional analysis answer from part (b).

EXERCISE 68.3: DISSIPATIVE PROPERTIES OF DIFFUSION

This exercise explores the dissipative property of diffusion when acting on a tracer extrema.

(a) ONE-DIMENSIONAL DIFFUSION

Consider the diffusion equation in one spatial dimension, and assume a Boussinesq ocean in which case the density factors are all constant and so can be dropped

$$\partial_t C = \partial_z(\kappa\, \partial_z C) = \partial_z \kappa\, \partial_z C + \kappa\, \partial_{zz} C, \tag{68.79}$$

where $\kappa(z, t)$ is an *eddy diffusivity* (also *turbulent diffusivity*). The eddy diffusivity is assumed to be a function of (z, t), with the spatial dependence determined by the flow. Show that a tracer extrema, C^*, evolves under diffusion according to

$$\partial_t C^* = \kappa\, \partial_{zz} C^*. \tag{68.80}$$

So what does diffusion do to a local maxima (e.g., a local hot region) in the tracer field? What about a minima (e.g., a local cold region)? To answer this question, discuss the mathematical equation satisfied by the tracer extrema.

(b) THREE-DIMENSIONAL DIFFUSION

Generalize the above one dimensional result to three dimensions, whereby the diffusivity κ becomes a symmetric positive-definite diffusion *tensor*, in which case

$$\partial_t C = \partial_m(K^{mn}\, \partial_n C). \tag{68.81}$$

Now consider an extrema in the tracer field, which is defined by

$$\partial_n C^* = 0 \qquad \forall\ n = 1, 2, 3. \tag{68.82}$$

Prove that three dimensional diffusion acts to *dissipate* an extrema. Hint: recall some linear algebra properties of a symmetric positive-definite matrix. In particular, note that a symmetric positive-definite matrix has positive eigenvalues.

EXERCISE 68.4: DIFFUSION INCREASES INFORMATION ENTROPY OF A TRACER CONCENTRATION
Diffusion is an irreversible process. Here we illustrate this property by considering the *information entropy* associated with a non-negative tracer concentration[13]

$$\mathcal{S}_C \equiv -\int (C \ln C)\, \rho \, \mathrm{d}V. \tag{68.83}$$

Show that

$$\frac{\mathrm{d}\mathcal{S}_C}{\mathrm{d}t} \geq 0 \tag{68.84}$$

over a material region with $C > 0$ and diffusion downgradient, $\boldsymbol{J} \cdot \nabla C < 0$. That is, diffusion always increases the information entropy. Hint: follow the discussion of tracer moments in Section 68.4.3.

EXERCISE 68.5: PHILLIPS LAYERING INSTABILITY
This exercise is based on the discussion in Section 12.2 of *Smyth and Carpenter* (2019), in which we consider an oceanographically relevant example of a turbulent diffusivity that is a function of vertical buoyancy stratification. Under certain circumstances, the flow dependent diffusivity can enhance, rather than reduce, vertical gradients in the buoyancy, with the associated *Phillips layering instability* leading to layering. We here only work through the basic mathematical formulation, leaving the interested reader to consult *Smyth and Carpenter* (2019) for more details.

Consider a buoyancy field that is a function of vertical position and time, $b(z, t)$, and let the squared buoyancy frequency be given by the vertical derivative of the buoyancy

$$N^2 = \partial_z b. \tag{68.85}$$

If buoyancy is affected only by vertical diffusion, then its evolution equation is the one-dimensional vertical diffusion equation

$$\partial_t b = \partial_z(\kappa N^2), \tag{68.86}$$

where $\kappa > 0$ is the vertical diffusivity for buoyancy. Correspondingly, a vertical derivative of the buoyancy equation leads to the evolution equation for the squared buoyancy frequency

$$\partial_t N^2 = \partial_{zz}(\kappa N^2). \tag{68.87}$$

Assume the diffusivity has the following functional dependence

$$\kappa = \kappa(N^2), \tag{68.88}$$

so that it is a function of the squared buoyancy frequency. A physically relevant choice has the diffusivity get smaller as the stratification increases, so that

$$\frac{\mathrm{d}\kappa}{\mathrm{d}N^2} < 0. \tag{68.89}$$

Now consider the case of a squared buoyancy frequency that is a small deviation relative to a constant background value

$$N^2(z, t) = N_0^2 + \epsilon N_1^2(z, t), \tag{68.90}$$

where ϵ is a small non-dimensional number. Derive the condition whereby, to first order in ϵ, we have N_1^2 growing in the presence of downgradient diffusion rather than decaying. That is, what is the condition satisfied by $\mathrm{d}\kappa/\mathrm{d}N^2$, N_0^2, and κ that renders an unstable diffusion equation,

[13] Information entropy is used in statistical physics as a measure of the order/disorder of a probability distribution. We here apply these notions to measure the information entropy of a tracer concentration.

whereby $\kappa > 0$ leads to an increase in N^2 rather than a decrease?

Chapter 69

Tracer advection and diffusion

In this chapter we study tracer advection and diffusion, building on the study of tracer diffusion in Chapter 68. We focus on the particular case of *conservative tracers*, which are tracers whose evolution is only affected by advection and diffusion within the fluid interior, along with boundary conditions. The adjective "conservative" refers to the property that such tracers evolve only through the convergence of a tracer flux vector, and so the net tracer content is altered only through transport across boundaries. That is, conservative tracers have no interior sources or sinks, thus making their budgets simpler than tracers, such as chemical and biogeochemical treacers, that are also affected by sources and sinks.

Example geophysical tracers that are nearly conservative include salinity in the ocean and humidity in the atmosphere. Both of these tracers are *material tracers*, in that they measure the mass of a matter substance within a fluid element, per mass of the fluid element. Hence, these material tracers are non-dimensional scalar fields whose concentrations range from zero to unity. We derived their budget equations in Chapter 20. Conservative Temperature, Θ, as defined in Section 26.11, is a nearly conservative thermodynamical tracer that provides a measure of the relative heat content in a fluid element. Conservative Temperature is typically measured in K in the atmosphere and $^\circ C$ in the ocean. Finally, there are many applications of idealized or theoretical *passive tracers* whose impacts on the flow are assumed to vanish (Section 20.1.5). Passive tracers are versatile theoretical tools for probing aspects of the flow, including pathways and time scales.

CHAPTER GUIDE

This chapter follows directly from our study of tracer diffusion in Chapter 68. We make use of the tracer equation and associated properties (including boundary conditions) studied in Chapter 20, with results relevant for tracer transport in both the atmosphere and ocean. Results for the Boussinesq ocean of Chapter 29 are found merely by setting the density factor, ρ, to the Boussinesq reference density, ρ_o, where it appears in the budget equations of this chapter. The discussion of Green's functions in Section 69.9 assumes familiarity with the Green's function material detailed in Chapter 9. The review paper from *Haine et al.* (2025) offers example applications of passive tracers facilitated by the Green's function method, with Section 69.9 serving as an extended introduction to *Haine et al.* (2025). We generally assume Cartesian coordinates in this chapter. Even so, the equations are written in a tensorially consistent manner to allow them to be valid for arbitrary coordinates.

69.1 Loose threads

- Schematic for the boundary propagator.

69.2 Introduction to advection and diffusion

In this chapter we consider the equation describing the evolution of *conservative tracers*

$$\rho \frac{\mathrm{D}C}{\mathrm{D}t} = -\nabla \cdot \mathbf{J} \iff \partial_t(\rho\, C) + \nabla \cdot (\mathbf{v}\, \rho\, C + \mathbf{J}) = 0, \tag{69.1}$$

where the flow is nonzero, $\mathbf{v} \neq 0$, so that advection contributes to the tracer evolution in addition to subgrid scale fluxes, such as diffusion, captured by the tracer flux $\mathbf{J}$. For the first part of this chapter, we focus on the effects from advection alone, in which $\mathbf{J} = 0$. In this case, the advective

tracer flux renders a reversible stirring and stretching of fluid elements. This stirring, particularly in the presence of turbulent flows, can increase the magnitude of tracer concentration gradients (see Section 69.4.2), and it does so while maintaining, for each fluid element, a fixed mass for all matter constituents and fixed specific entropy.[1]

When diffusion is enabled, as seen in Chapter 68, the fluid experiences an irreversible exchange, or mixing, of properties between fluid elements. Correspondingly, diffusion reduces the magnitude of property gradients between fluid elements. When acting together, advection is no longer a pure stirring and diffusion is no longer a pure mixing. Indeed, in the steady state, advection and diffusion exactly balance. *Eckart* (1948) articulated what has become the standard conceptual paradigm for stirring and mixing in geophysical fluids, with elements of that paradigm reflected in this chapter.

69.3 Perfect fluid tracer advection

A *perfect* fluid is comprised of material fluid elements whose matter content and thermodynamic properties remain fixed. From the discussion of molecular diffusion in Section 68.3, we know that a perfect fluid can at most consist of a single matter constituent and uniform thermodynamic properties. The reason is that in the presence of multiple constituents with non-uniform concentrations, molecular motions irreversibly exchange matter and thermodynamic properties (e.g., temperature, specific entropy) among fluid elements. This exchange, or mixing, breaks the assumption of a perfect fluid. Nonetheless, we find many occasions to ignore molecular diffusion when focusing on macroscopic motions of the continuum fluid. Such is the case when considering the advection equation in the absence of mixing.

69.3.1 The advection equation

In the absence of mixing or other irreversible processes, the matter content of a fluid element remains fixed as the element moves within the fluid environment. Since the total mass of the element is also constant, then the tracer concentration remains constant and thus satisfies the reversible (source-free) *advection equation*

$$\frac{\mathrm{D}C}{\mathrm{D}t} = (\partial_t + \boldsymbol{v} \cdot \nabla)C = 0. \tag{69.2}$$

The first equality relates the material time derivative to the Eulerian time derivative plus advective transport (see Section 17.4), with $\boldsymbol{v}$ the *barycentric velocity* of a fluid element (Section 20.1.2). We can convert the *material* form of the advection equation (69.2) into its flux-form by combining with the mass continuity equation (19.6)

$$\partial_t \rho + \nabla \cdot (\rho \, \boldsymbol{v}) = 0, \tag{69.3}$$

which yields

$$\partial_t (\rho \, C) + \nabla \cdot (\rho \, C \, \boldsymbol{v}) = 0. \tag{69.4}$$

Again, the material form of the advection equation is the trivial statement that tracer concentration remains constant on a fluid element in the absence of sources or mixing. Hence, a general solution to the advection equation is given by

$$C(\boldsymbol{x}, t) = C[\boldsymbol{X}(0)], \tag{69.5}$$

[1] Recall from Chapter 22 that specific entropy remains materially constant on fluid elements in the absence of mixing or diabatic sources.

where $\boldsymbol{X}(0)$ is the initial position of a fluid element that is at the position $\boldsymbol{x}$ at time t. If we know the trajectories for all fluid elements and their initial tracer concentration, then we know the tracer concentration for all space and time. For those cases where trajectories are unknown, it is useful to make use of the Eulerian form of the advection equation in order to deduce the evolution of tracer concentration.

69.3.2 Eulerian time tendencies from advection

At a point in the fluid, the advection equation (69.2) leads to the Eulerian time tendency for tracer concentration

$$\partial_t C = -\boldsymbol{v} \cdot \nabla C. \tag{69.6}$$

Geometrically, the tendency arises from the projection of the fluid velocity onto the normal to concentration iso-surfaces. The concentration remains fixed in time (steady) at points where the velocity is parallel to concentration iso-surfaces. From the flux-form advection equation (69.4), the density-weighted tracer concentration (the tracer mass per volume) has an Eulerian time tendency given by the convergence of the advective flux

$$\partial_t(\rho\, C) = -\nabla \cdot (\rho\, C\, \boldsymbol{v}). \tag{69.7}$$

The tendency vanishes at a point if there is no convergence of tracer mass towards the point.

69.3.3 Impermeability property of tracer isosurfaces

We now offer a geometric interpretation of the advection equation

$$(\partial_t + \boldsymbol{v} \cdot \nabla) C = 0, \tag{69.8}$$

following the discussion of dia-surface transport in Section 64.3. For this purpose, introduce the unit normal on a tracer isosurface

$$\hat{\boldsymbol{n}} = \frac{\nabla C}{|\nabla C|} \tag{69.9}$$

and the normal projection for the velocity of a point on that surface

$$\boldsymbol{v}^{(\mathsf{C})} \cdot \hat{\boldsymbol{n}} = -\frac{\partial_t C}{|\nabla C|}. \tag{69.10}$$

The advection equation (69.8) thus can be written as an impermeability condition for a tracer isosurface

$$\rho\, (\boldsymbol{v} - \boldsymbol{v}^{(\mathsf{C})}) \cdot \hat{\boldsymbol{n}} = 0 \qquad \text{on } C \text{ isosurfaces.} \tag{69.11}$$

We encountered this condition in Section 19.6.2 when studying the kinematics of a moving material surface. Hence, in the absence of mixing, tracer isosurfaces are indeed material surfaces since they allow no fluid elements, moving with the fluid velocity $\boldsymbol{v}$, to cross them. This is an important kinematic result that is extended in Section 69.6.5 to include effects from an eddy induced velocity.

69.4 Some mathematical properties of tracer advection

We now explore various mathematical properties of the advection equation. For that purpose, recall the mass continuity equation (69.3) and flux-form tracer advection equation (69.7)

$$\partial_t \rho + \nabla \cdot (\rho\, \boldsymbol{v}) = 0 \tag{69.12a}$$

$$\partial_t(\rho\, C) + \nabla\cdot(\rho\, C\, \boldsymbol{v}) = 0. \tag{69.12b}$$

These equations are manifestly compatible in that the tracer equation (69.12b) reduces to the continuity equation (69.12a) if the tracer concentration is spatially uniform (see Section 20.1.4 for more discussion of compatibility).

69.4.1 Material constancy of C^Γ

A trivial consequence of the material constancy of tracer concentration is that C^Γ is also materially constant, for Γ an arbitrary number. We show this property mathematically by noting that the chain rule holds for a material time derivative, so that

$$\frac{\mathrm{D}C^\Gamma}{\mathrm{D}t} = \Gamma\, C^{\Gamma-1}\frac{\mathrm{D}C}{\mathrm{D}t} = 0. \tag{69.13}$$

Likewise, making use of the Eulerian form yields

$$\partial_t C^\Gamma + \boldsymbol{v}\cdot\nabla C^\Gamma = \Gamma\, C^{\Gamma-1}\,[\partial_t C + \boldsymbol{v}\cdot\nabla C] = 0. \tag{69.14}$$

We conclude that advection, in the absence of diffusion, serves to reversibly transport the tracer concentration without altering any of its powers. Correspondingly, all tracer moments are untouched by advection, which contrasts to the case of diffusion considered in Section 68.4.3.

69.4.2 Evolution of squared tracer gradient

As noted at the start of Section 69.2, some flows can enhance the magnitude of the tracer concentration gradient, $|\nabla C|^2 = \partial_m C\, \delta^{mn}\, \partial_n C$. The kinematics of that process begin with the following equation for the evolution of the squared gradient

$$\begin{aligned}
(1/2)\,\partial_t(\partial_m C\,\delta^{mn}\,\partial_n C) &= \partial_m C\,\delta^{mn}\,\partial_n\partial_t C && \text{(69.15a)}\\
&= -\partial_m C\,\delta^{mn}\,\partial_n(v^k\,\partial_k C) && \text{(69.15b)}\\
&= -\partial_m C\,\delta^{mn}\,(v^k\,\partial_k\,\partial_n C + \partial_n v^k\,\partial_k C) && \text{(69.15c)}\\
&= -(1/2)\,v^k\,\partial_k\,(\partial_m C\,\delta^{mn}\,\partial_n C) - \partial_m C\,\delta^{mn}\,G^k{}_n\,\partial_k C && \text{(69.15d)}\\
&= -(1/2)\,(\boldsymbol{v}\cdot\nabla)|\nabla C|^2 - \partial_m C\,\delta^{mn}\,S^k{}_n\,\partial_k C && \text{(69.15e)}\\
&= -(1/2)\,(\boldsymbol{v}\cdot\nabla)|\nabla C|^2 - \nabla C\cdot\boldsymbol{S}\cdot\nabla C. && \text{(69.15f)}
\end{aligned}$$

The second equality made use of the advection equation, $\partial_t C = -v^k\,\partial_k C$, and then we introduced the velocity gradient tensor, $\boldsymbol{G}$, from equation (18.86), and its symmetric component, the strain rate tensor, $\boldsymbol{S}$, from equation (18.90a)

$$G^m{}_n = \partial_n v^m \quad\text{and}\quad S^m{}_n = (G^m{}_n + G_n{}^m)/2. \tag{69.16}$$

We are thus led to the material evolution equation

$$\frac{1}{2}\frac{\mathrm{D}|\nabla C|^2}{\mathrm{D}t} = -\nabla C\cdot\boldsymbol{S}\cdot\nabla C. \tag{69.17}$$

The strain rate tensor is symmetric and yet it is not positive-definite. Hence, we can have either growth or decay of the squared tracer gradient depending on details of the velocity gradient and tracer gradient.

69.4.3 Eddy-induced and residual mean

The mass density time tendency

$$\partial_t \rho = -\nabla \cdot (\boldsymbol{v}\, \rho) \tag{69.18}$$

remains unchanged if the advective mass flux, $\rho\, \boldsymbol{v}$ (dimensions of mass per time per area), is modified by the addition of a total curl

$$\rho\, \boldsymbol{v} \to \rho\, \boldsymbol{v}^\dagger = \rho\, \boldsymbol{v} + \nabla \times (\rho\, \boldsymbol{\Psi}^*). \tag{69.19}$$

As in Section 21.5.1, the arbitrariness manifest in equation (69.19) is known as a *gauge symmetry*. The additional mass flux, $\nabla \times (\rho\, \boldsymbol{\Psi}^*)$, leads to no accumulation of mass at a point since it has zero divergence. In the case of a Boussinesq ocean with ρ set to a constant $\rho_\circ$, the divergent-free velocity $\nabla \times \boldsymbol{\Psi}^*$ leads to zero accumulation of volume at a point.

The non-divergent mass flux

$$\rho\, \boldsymbol{v}^* \equiv \nabla \times (\rho\, \boldsymbol{\Psi}^*) \tag{69.20}$$

often arises when we decompose the mass flux into a mean and non-divergent eddy fluctuations. In that context, we make use of the following terminology:

$$\begin{aligned}
\boldsymbol{v} &= \text{Eulerian mean velocity} && \text{(69.21a)}\\
\rho\, \boldsymbol{v} &= \text{Eulerian mean mass flux} && \text{(69.21b)}\\
\boldsymbol{v}^* &= \text{eddy-induced velocity} && \text{(69.21c)}\\
\rho\, \boldsymbol{\Psi}^* &= \text{eddy-induced mass streamfunction} && \text{(69.21d)}\\
\rho\, \boldsymbol{v}^* &= \nabla \times (\rho\, \boldsymbol{\Psi}^*) = \text{eddy-induced mass flux} && \text{(69.21e)}\\
\boldsymbol{v}^\dagger &= \boldsymbol{v} + \boldsymbol{v}^* = \text{residual mean velocity} && \text{(69.21f)}\\
\rho\, \boldsymbol{v}^\dagger &= \rho\, (\boldsymbol{v} + \boldsymbol{v}^*) = \text{residual mean mass flux.} && \text{(69.21g)}
\end{aligned}$$

The name "residual mean" is motivated since the sum $\boldsymbol{v} + \boldsymbol{v}^*$ is often smaller than either term individually. That is, the eddy contribution often compensates for the mean, with sum of the mean and eddy representing a residual. We study particular forms of the eddy induced velocity in Chapter 71.

69.4.4 Advective tracer fluxes and skew tracer fluxes

Following from the previous discussion, we consider the advection equation with the advective tracer transport determined by the residual mean velocity

$$\partial_t(\rho\, C) + \nabla \cdot (\rho\, C\, \boldsymbol{v}^\dagger) = 0. \tag{69.22}$$

Given the form (69.20) for the eddy mass flux $\rho\, \boldsymbol{v}^*$, we can write the *advective tracer flux* as

$$\begin{aligned}
\rho\, C\, \boldsymbol{v}^\dagger &= C\, (\rho\, \boldsymbol{v} + \rho\, \boldsymbol{v}^*) && \text{(69.23a)}\\
&= C\, \rho\, \boldsymbol{v} + C\, \nabla \times (\rho\, \boldsymbol{\Psi}^*) && \text{(69.23b)}\\
&= C\, \rho\, \boldsymbol{v} + \nabla \times (C\, \rho\, \boldsymbol{\Psi}^*) - \nabla C \times \rho\, \boldsymbol{\Psi}^*. && \text{(69.23c)}
\end{aligned}$$

It is the divergence of the tracer flux that determines the time tendency, in which case the total curl plays no role

$$\begin{aligned}
\nabla \cdot (\rho\, C\, \boldsymbol{v}^\dagger) &= \nabla \cdot (\rho\, C\, \boldsymbol{v} + \rho\, C\, \boldsymbol{v}^*) && \text{(69.24a)}\\
&= \nabla \cdot (\rho\, C\, \boldsymbol{v} - \nabla C \times \rho\, \boldsymbol{\Psi}^*). && \text{(69.24b)}
\end{aligned}$$

That is, the divergence of the advective tracer flux equals to the divergence of the *skew tracer flux*

$$\underbrace{\nabla \cdot (\rho\, C\, \boldsymbol{v}^*)}_{\text{advective flux divergence}} = \underbrace{\nabla \cdot (-\nabla C \times \rho\, \boldsymbol{\Psi}^*)}_{\text{skew flux divergence}} \tag{69.25}$$

since the advective flux and skew flux differ by a rotational flux

$$\boldsymbol{J}^{\text{adv}} = \boldsymbol{J}^{\text{skew}} + \boldsymbol{J}^{\text{rot}} \tag{69.26}$$

where

$$\boldsymbol{J}^{\text{adv}} = C\, \rho\, \boldsymbol{v}^* \quad \text{and} \quad \boldsymbol{J}^{\text{skew}} = -\nabla C \times \rho\, \boldsymbol{\Psi}^* \quad \text{and} \quad \boldsymbol{J}^{\text{rot}} = \nabla \times (\rho\, C\, \boldsymbol{\Psi}^*). \tag{69.27}$$

Notably, the skew tracer flux is neither upgradient nor downgradient. Rather, it is oriented parallel to iso-surfaces of tracer concentration

$$\nabla C \cdot \boldsymbol{J}^{\text{skew}} = \nabla C \cdot (-\nabla C \times \rho\, \boldsymbol{\Psi}^*) = 0. \tag{69.28}$$

This orientation serves as motivation for the name *skew*, with Figure 69.1 providing a schematic of these tracer fluxes.

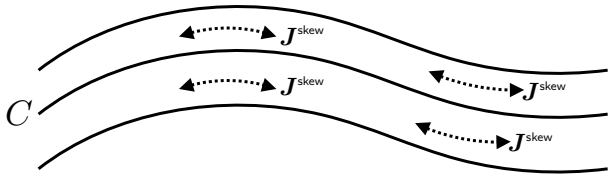

FIGURE 69.1: Skew fluxes (dashed lines with arrows) for a tracer C are oriented parallel to lines of constant tracer concentration (tracer isolines are the solid lines). Even though the skew fluxes are aligned with tracer contours, these fluxes generally affect a time change to the tracer concentration through their convergence.

69.4.5 Skew diffusion

Introducing tensor labels brings the skew tracer flux into the form

$$\begin{aligned} (J^{\text{skew}})^m &= -(\nabla C \times \rho\, \boldsymbol{\Psi}^*)^m && \text{(69.29a)} \\ &= -\epsilon^{mnp}\, \partial_n C\, \rho\, \Psi^*_p && \text{(69.29b)} \\ &= -\rho\, A^{mn}\, \partial_n C, && \text{(69.29c)} \end{aligned}$$

where we defined the anti-symmetric *skew diffusion* tensor

$$A^{mn} = \epsilon^{mnp}\, \Psi^*_p \Longrightarrow \boldsymbol{A} = \begin{bmatrix} 0 & \Psi^*_3 & -\Psi^*_2 \\ -\Psi^*_3 & 0 & \Psi^*_1 \\ \Psi^*_2 & -\Psi^*_1 & 0 \end{bmatrix}. \tag{69.30}$$

Evidently, advection by a non-divergent mass flux is equivalent to skew-diffusion through the action of an anti-symmetric tensor.

Although leading to the same stirring operator, skew and advective fluxes possess the following complementary properties.

- DERIVATIVE OPERATOR: The skew flux is proportional to the vector streamfunction and the gradient of the tracer, whereas the advective flux is related to the curl of the streamfunction and the value of the tracer concentration. In effect, the fluxes swap their placement of the

derivative operator. Correspondingly, the advective flux vanishes if the velocity vanishes, whereas the skew flux vanishes of the tracer gradient vanishes (just as for a diffusive flux).

- FLUX ORIENTATION: The orientation of the advective flux is determined by the velocity field, which is oriented according to trajectories of fluid particles. This orientation is the same regardless of the tracer. In contrast, a skew tracer flux is directed along lines of constant tracer; i.e., it is neither upgradient nor downgradient. Hence, orientation of the skew flux is directly tied to the tracer field, with each tracer yielding a generally distinct flux orientation. The very distinct orientations of the advective and skew fluxes can be the origin of confusion. We explore many features of these geometric distinctions in Section 70.3 in studying eddy induced tracer fluxes.

- MATERIAL FLUX: Fluid elements carry a particular amount of trace matter so that an advective flux of a material tracer measures the passage of matter across an area per unit time (dimensions of mass per area per time). In contrast, a skew flux is not interpreted as the passage of matter across an area per time. This distinction is particularly important when interpreting boundary conditions discussed in Section 69.5.3.

In Section 69.5 we pursue the above points to further reveal the dual relation between advective fluxes and skew fluxes.

69.4.6 A comment about skew fluxes and Lagrangian kinematics

The advective tracer flux and skew tracer flux are very distinct vectors and we further explore the distinction in Sections 69.5 and 70.3. As detailed in each of those sections, it is a matter of convenience how one chooses to formulate the Eulerian tracer equation since the advective flux and skew flux lead to the same tracer evolution. Furthermore, the choice to formulate the tracer equation in terms of a skew flux in no way eliminates the Lagrangian perspective. That is, fluid particles, or fluid elements, still move through the fluid and transport tracer as part of this motion. The Lagrangian formulation of tracer evolution is naturally connected, via a transformation of reference frames, to the Eulerian advection equation. Even so, we do not eliminate fluid particle motion when choosing to work with skew tracer fluxes. Instead, we merely choose to formulate the tracer equation in terms of the vector streamfunction rather than the velocity. This choice is typically based on mathematical and/or physical convenience.

69.4.7 Further reading

The uses of residual-mean transport are many and varied in the ocean and atmospheric literature. *Vallis* (2017) offers a thorough and pedagogical treatment. Skew diffusion is treated in *Moffatt* (1983), in which he raises the connection to fluids with rotation and/or magnetic fields. *Middleton and Loder* (1989) applied these ideas to ocean gravity waves, tides, and Rossby waves. *Griffies* (1998) applied these ideas to the methods used for parameterizing tracer transport from ocean mesoscale eddies.

69.5 Advection and skewsion

We introduced skew diffusion in Section 69.4.5 and will again encounter it in Chapterd 70 and 71. Following the terminology of Section 9.2 of *Griffies* (2004), we refer to *skewsion* as any process that leads to tracer transport via skew fluxes, with skew diffusion a particular example. There are occasions where it is conceptually and operationally more convenient to use advective fluxes, such as when considering the transport of tracers by the flow field explicitly resolved by a numerical simulation. In contrast, skew fluxes are sometimes more convenient for certain subgrid

scale eddy parameterizations, such as the one discussed in Section 71.1. We here consider facets of advection and skewsion for those interested in diving deeper into the mathematical physics.

69.5.1 Choosing a gauge

Consider an arbitrary divergent-free mass transport

$$\nabla \cdot (\rho \boldsymbol{v}^*) = 0, \tag{69.31}$$

where the divergent-free constraint is satisfied by introducing a vector streamfunction

$$\rho \boldsymbol{v}^* = \nabla \times (\rho \boldsymbol{\Psi}^*). \tag{69.32}$$

The streamfunction is arbitrary up to a gauge transformation

$$\rho \boldsymbol{\Psi}' = \rho \boldsymbol{\Psi}^* + \nabla(\rho \Lambda), \tag{69.33}$$

where Λ is a gauge function.

Changes to the skew flux under a gauge transformation

Although the velocity is invariant up to an arbitrary gauge function, the skew flux, $\boldsymbol{J}^{\text{skew}} = -\nabla C \times \rho \boldsymbol{\Psi}^*$, changes. Nonetheless, the divergence of the skew flux is invariant, as we see by noting that

$$\nabla C \times [\rho \boldsymbol{\Psi}^* + \nabla(\rho\Lambda)] = \nabla C \times (\rho \boldsymbol{\Psi}^*) + \nabla \times [C \nabla(\rho\Lambda)]. \tag{69.34}$$

and since $\nabla \cdot \nabla \times [C \nabla(\rho\Lambda)] = 0$, the flux divergence, $\nabla \cdot \boldsymbol{J}^{\text{skew}}$, remains unchanged.

Coulomb gauge

We have some freedom in specifying the gauge function. One choice is to set $\Lambda = 0$. However, there are occasions in which it is useful to set the gauge function in a manner to cancel unwanted terms. The *Coulomb gauge* is commonly used in electrostatics (e.g., *Jackson* (1975)), which is defined by setting

$$\nabla \cdot (\rho \boldsymbol{\Psi}^*) = 0 \qquad \text{Coulomb gauge.} \tag{69.35}$$

Making use of the curl identity (2.42c) leads to the Poisson equation for the vector potential

$$\nabla^2(\rho\boldsymbol{\Psi}^*) = -\nabla \times (\rho \boldsymbol{v}^*). \tag{69.36}$$

In the absence of boundaries, this equation has a *Coulomb-Ampere solution* comprised of the convolution of the source with the free-space Green's function[2]

$$\rho(\boldsymbol{x}, t)\, \boldsymbol{\Psi}^*(\boldsymbol{x}, t) = \int \frac{\nabla \times [\rho(\boldsymbol{x}', t)\, \boldsymbol{v}^*(\boldsymbol{x}', t)]}{4\pi\, |\boldsymbol{x} - \boldsymbol{x}'|}\, \mathrm{d}V', \tag{69.37}$$

where $\mathrm{d}V'$ is the volume element for integration over the test points, $\boldsymbol{x}'$. We know of no geophysical fluid application making use of the Coulomb gauge.

69.5.2 Vertical gauge

As introduced in Section 21.5.5, a gauge commonly used for eddy parameterizations (Section 71.1) sets to zero one of the three components of the vector streamfunction. This gauge choice

[2] See Section 9.3 for a discussion of Green's function methods for elliptic operators.

is available since there are only two independent functional degrees of freedom available from a divergence-free mass transport field. A common choice is the *vertical gauge* in which

$$\Psi_3^* = 0 \qquad \text{vertical gauge.} \tag{69.38}$$

To further specify the vertical gauge we invert the relations

$$\rho\, u^* = -\partial_z(\rho \Psi_2^*) \quad \text{and} \quad \rho\, v^* = \partial_z\,(\rho \Psi_1^*) \quad \text{and} \quad \rho\, w^* = \partial_x\,(\rho \Psi_2^*) - \partial_y(\rho \Psi_1^*) \tag{69.39}$$

to render the vector streamfunction

$$\rho\, \boldsymbol{\Psi}^* = \hat{\boldsymbol{z}} \times \int_{-H}^{z} \rho\, \boldsymbol{u}^*\, \mathrm{d}z' = \hat{\boldsymbol{z}} \times \underline{\boldsymbol{U}}^{(*\rho)} \tag{69.40}$$

where

$$\underline{\boldsymbol{U}}^{(*\rho)}(z) = \int_{-H}^{z} \rho\, \boldsymbol{u}^*\, \mathrm{d}z' \tag{69.41}$$

is the horizontal mass transport associated with $\boldsymbol{u}^*$ passing between the bottom and a depth $z \geq -H$. The anti-symmetric stirring tensor for the vertical gauge is given by

$$\rho\, A^{mn} = \begin{pmatrix} 0 & 0 & \underline{U}^{(*\rho)} \\ 0 & 0 & \underline{V}^{(*\rho)} \\ -\underline{U}^{(*\rho)} & -\underline{V}^{(*\rho)} & 0 \end{pmatrix}, \tag{69.42}$$

and the corresponding skew, rotational, and advective fluxes are

$$\boldsymbol{J}^{\text{skew}} = -\underline{\boldsymbol{U}}^{(*\rho)}\, \partial_z C + \hat{\boldsymbol{z}}\, \underline{\boldsymbol{U}}^{(*\rho)} \cdot \nabla_{\!\text{h}} C \tag{69.43a}$$

$$\boldsymbol{J}^{\text{rot}} = \partial_z(C\, \underline{\boldsymbol{U}}^{(*\rho)}) - \hat{\boldsymbol{z}}\, \nabla_{\!\text{h}} \cdot (C\, \underline{\boldsymbol{U}}^{(*\rho)}) \tag{69.43b}$$

$$\boldsymbol{J}^{\text{adv}} = C\, (\partial_z \underline{\boldsymbol{U}}^{(*\rho)}) - \hat{\boldsymbol{z}}\, C\, \nabla_{\!\text{h}} \cdot \underline{\boldsymbol{U}}^{(*\rho)}. \tag{69.43c}$$

Note that the identity $\boldsymbol{J}^{\text{adv}} = \boldsymbol{J}^{\text{skew}} + \boldsymbol{J}^{\text{rot}}$ is maintained by these expressions. The horizontal components to the skew flux vanish when the tracer is uniform in the vertical, and the vertical skew flux vanishes with a horizontally uniform tracer field. These properties manifest the skewed nature of the fluxes.

69.5.3 Boundary conditions

We assume that all external domain boundaries are material in regards to the velocity $\boldsymbol{v}^*$. Furthermore, even for moving domain boundaries, we assume that the suite of kinematic boundary conditions is based on the barycentric velocity $\boldsymbol{v}$ (see Section 19.6), so that $\boldsymbol{v}^*$ satisfies the no-normal flow condition even on moving boundaries

$$\hat{\boldsymbol{n}} \cdot \boldsymbol{v}^* = 0 \qquad \text{external domain boundaries.} \tag{69.44}$$

As we discuss in Section 69.6.1, this boundary condition is required for the eddy-induced velocity to have zero impact on the total mass of an arbitrary tracer within the full fluid domain.

Correspondingly, the advective tracer flux also satisfies a no-normal boundary condition on all external boundaries

$$\hat{\boldsymbol{n}} \cdot \boldsymbol{J}^{\text{adv}} = \hat{\boldsymbol{n}} \cdot \boldsymbol{v}^* \rho\, C = 0. \tag{69.45}$$

The corresponding boundary condition for the skew flux is found by inserting the relation (69.26)

into the advective flux boundary condition (69.45) to render

$$\hat{\boldsymbol{n}} \cdot \boldsymbol{J}^{\text{adv}} = \hat{\boldsymbol{n}} \cdot [\boldsymbol{J}^{\text{skew}} + \boldsymbol{J}^{\text{rot}}] = 0. \tag{69.46}$$

Hence, the skew flux generally has a non-zero normal component at the solid boundaries as determined by the rotational flux

$$\hat{\boldsymbol{n}} \cdot \boldsymbol{J}^{\text{skew}} = -\hat{\boldsymbol{n}} \cdot \boldsymbol{J}^{\text{rot}}. \tag{69.47}$$

Even so, there might be occasions in which $\hat{\boldsymbol{n}} \cdot \boldsymbol{J}^{\text{skew}} = 0$, which is ensured so long as

$$(-\nabla C \times \rho \boldsymbol{\Psi}^*) \cdot \hat{\boldsymbol{n}} = -(\rho\, \boldsymbol{\Psi}^* \times \hat{\boldsymbol{n}}) \cdot \nabla C = 0. \tag{69.48}$$

A sufficient condition is to have $\boldsymbol{\Psi}^* \times \hat{\boldsymbol{n}} = 0$, in which case the vector streamfunction is parallel to the boundary normal. An alternative sufficient condition is to have the streamfunction vanish at the boundary. Further details for boundary conditions depend on physical properties of the velocity $\boldsymbol{v}^*$. We discuss one example in Section 71.1 as prescribed by the *Gent et al.* (1995) mesoscale eddy parameterization.

69.6 Finite volume budgets with eddy velocities

In this section we examine how an eddy induced velocity modifies the budgets for fluid mass and tracer mass in finite domains. The discussion is nuanced, and yet it is relevant to those aiming to diagnose tracer budgets computed over finite regions. We start by writing the local/differential mass and tracer budgets in the form

$$\partial_t \rho + \nabla \cdot (\rho\, \boldsymbol{v}^\dagger) = 0 \tag{69.49a}$$

$$\partial_t (\rho\, C) + \nabla \cdot (\rho\, \boldsymbol{v}^\dagger\, C + \boldsymbol{J}^{\text{diff}}) = 0, \tag{69.49b}$$

where (see Section 69.5)

$$\boldsymbol{v}^\dagger = \boldsymbol{v} + \boldsymbol{v}^* \quad \text{and} \quad \nabla \cdot (\rho\, \boldsymbol{v}^*) = 0, \tag{69.50}$$

and where $\boldsymbol{J}^{\text{diff}}$ is a subgrid scale flux encompassing all processes, such as diffusion and boundary conditions, that are not represented by an eddy-induced advection. Given that $\nabla \cdot (\rho\, \boldsymbol{v}^*) = 0$, the mass budget (69.49a) can we written in the equivalent manners

$$\partial_t \rho + \nabla \cdot (\rho\, \boldsymbol{v}^\dagger) = \partial_t \rho + \nabla \cdot (\rho\, \boldsymbol{v}) = 0. \tag{69.51}$$

That is, the eddy-induced velocity does not lead to any local sources of fluid mass. This property is very important for the budget analysis in this section.

As shown in the following, the finite volume budgets for fluid mass and tracer mass also make use of the residual mean velocity, $\boldsymbol{v}^\dagger$. That result is not surprising, since the finite volume budgets are consistent with the differential budgets (69.49a) and (69.49b). Nonetheless, it is useful to expose the details as they appear in many budget analysis applications, such as the water mass and tracer mass analysis of Chapter 73. We furthermore explore how the budgets for tracer mass appear when formulated using advective fluxes versus skew fluxes. As we show, the finite volume budgets are consistent across the variety of formulations only if the eddy velocity and eddy vector streamfunction satisfy boundary conditions detailed in Section 69.5.3.

69.6.1 Advective formulation

Making use of the tracer equation (69.49b) in the Leibniz-Reynolds transport theorem (20.49) renders the finite volume tracer mass budget for an arbitrary domain, $\mathcal{R}$

$$\frac{\mathrm{d}}{\mathrm{d}t}\left[\int_{\mathcal{R}} \rho\, C\, \mathrm{d}V\right] = -\oint_{\partial\mathcal{R}} \left[\rho\, C\, (\boldsymbol{v}^{\dagger} - \boldsymbol{v}^{(\mathrm{b})}) + \boldsymbol{J}^{\mathrm{diff}}\right] \cdot \hat{\boldsymbol{n}}\, \mathrm{d}\mathcal{S}, \tag{69.52}$$

where $\boldsymbol{v}^{(\mathrm{b})}$ is the velocity of a point on the domain boundary. Appearance of the residual mean velocity, $\boldsymbol{v}^{\dagger}$, in the finite volume budget (69.52) follows from its appearance in the local tracer budget (69.49b). We thus see that the eddy-induced velocity impacts on the tracer mass budget for an arbitrary domain. However, its impacts disappear when integrating over a closed or periodic fluid domain so long as

$$\boldsymbol{v}^{*} \cdot \hat{\boldsymbol{n}} = 0 \qquad \text{on all boundaries.} \tag{69.53}$$

We already encountered this boundary condition in Section 69.5.3. It holds on all boundaries, including those such as the ocean free surface that are time dependent and/or permeable. It is required if we assume the eddy-induced velocity does not modify the mass of any tracer in the full fluid domain. That assumption is generally made for eddy-induced velocities such as those associated with mesoscale and submesoscale eddies in the ocean (see Section 71.3).

Setting the tracer concentration to a constant in equation (69.52) leads to the fluid mass budget

$$\frac{\mathrm{d}}{\mathrm{d}t}\left[\int_{\mathcal{R}} \rho\, \mathrm{d}V\right] = -\oint_{\partial\mathcal{R}} \rho\, (\boldsymbol{v}^{\dagger} - \boldsymbol{v}^{(\mathrm{b})}) \cdot \hat{\boldsymbol{n}}\, \mathrm{d}\mathcal{S}, \tag{69.54}$$

where we set the diffusive tracer flux, $\boldsymbol{J}^{\mathrm{diff}}$, to zero since there is no diffusion of fluid mass between fluid elements (Section 20.1). As for the differential expression (69.49a), the mass budget for any domain is not changed by the eddy-induced velocity since

$$\nabla \cdot (\rho\, \boldsymbol{v}^{*}) = 0 \Longrightarrow \oint_{\partial\mathcal{R}} \rho\, \boldsymbol{v}^{*} \cdot \hat{\boldsymbol{n}}\, \mathrm{d}\mathcal{S} = 0, \tag{69.55}$$

so that the mass budget is given by

$$\frac{\mathrm{d}}{\mathrm{d}t}\left[\int_{\mathcal{R}} \rho\, \mathrm{d}V\right] = -\oint_{\partial\mathcal{R}} \left[\rho\, (\boldsymbol{v}^{\dagger} - \boldsymbol{v}^{(\mathrm{b})})\right] \cdot \hat{\boldsymbol{n}}\, \mathrm{d}\mathcal{S} = -\oint_{\partial\mathcal{R}} \left[\rho\, (\boldsymbol{v} - \boldsymbol{v}^{(\mathrm{b})})\right] \cdot \hat{\boldsymbol{n}}\, \mathrm{d}\mathcal{S} \tag{69.56}$$

Hence, the eddy velocity contribution to the mass budget for any finite region vanishes, which is expected since it provides no net mass source to a region. Furthermore, one may choose to diagnose the right hand side of the mass budget in either the residual mean or Eulerian mean form. The choice is based on convenience, such as whether one has easier access to the residual mean velocity or the Eulerian mean velocity. Although the patterns of the fluxes across any particular boundary differs if $\boldsymbol{v}^{*} \neq 0$, the accumulation of mass within the region is identical for the two formulations.

69.6.2 Skew flux formulation

Now consider the complement perspective afforded by the skew flux formulation from Section 69.5. Here we decompose the advective tracer flux according to

$$C\, \rho\, \boldsymbol{v}^{\dagger} = C\, \rho\, \boldsymbol{v} - \nabla C \times \rho\, \boldsymbol{\Psi}^{*} + \nabla \times (C\, \rho\, \boldsymbol{\Psi}^{*}) = C\, \rho\, \boldsymbol{v} + \boldsymbol{J}^{\mathrm{skew}} + \nabla \times (C\, \rho\, \boldsymbol{\Psi}^{*}), \tag{69.57}$$

where we introduced the skew tracer flux arising from the eddy-induced streamfunction

$$\boldsymbol{J}^{\text{skew}} = -\nabla C \times (\rho\, \boldsymbol{\Psi}^*). \tag{69.58}$$

The differential budget for tracer is thus given by

$$\partial_t(\rho\, C) + \nabla \cdot [\rho\, C\, \boldsymbol{v} + \boldsymbol{J}^{\text{skew}} + \boldsymbol{J}^{\text{diff}}] = 0, \tag{69.59}$$

where the rotational term, $\nabla \times (C\, \rho\, \boldsymbol{\Psi}^*)$, has zero divergence and so does not affect the tracer budget. The corresponding finite volume tracer mass budget is

$$\frac{\mathrm{d}}{\mathrm{d}t}\left[\int_{\mathscr{R}} \rho\, C\, \mathrm{d}V\right] = -\oint_{\partial\mathscr{R}} \left[\rho\, C\, (\boldsymbol{v} - \boldsymbol{v}^{(\mathsf{b})}) - \nabla C \times (\rho\, \boldsymbol{\Psi}^*) + \boldsymbol{J}^{\text{diff}}\right] \cdot \hat{\boldsymbol{n}}\, \mathrm{d}\mathcal{S}. \tag{69.60}$$

In this form, the contribution from the eddy induced transport is now included inside the skew tracer flux rather than in the residual mean advective tracer flux. Setting C to a constant reveals the mass budget as in the second form of equation (69.56).

69.6.3 Domain with a tracer boundary

We now apply the previous general budget discussion to a specific domain that anticipates the more complete budget analysis provided in Section 73.10 as part of our study of water mass analysis. Here, we consider the fluid mass and tracer mass within an ocean region with at least one of its bounds determined by an isosurface of constant tracer concentration, as in Figure 69.2.

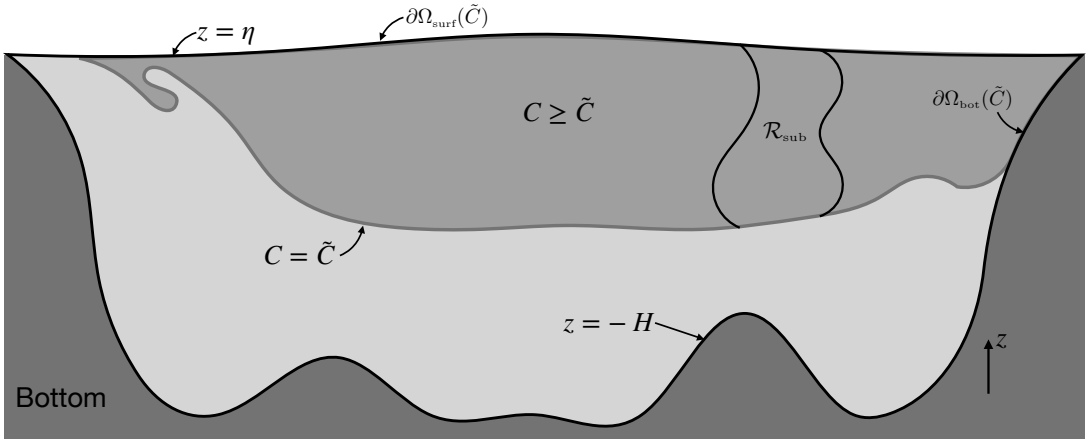

FIGURE 69.2: An ocean region with one of its boundaries set by a surface of constant tracer, $C = \tilde{C}$. Note that the region need not be monotonically stratified in the tracer concentration, nor does it need to be simply connected. The region is bounded at the top by $\partial\Omega_{\text{surf}}(\tilde{C})$, with the geometry of this surface depending on $\tilde{C}$. The bottom boundary is set by the tracer surface, $C = \tilde{C}$, as well as the solid-earth bottom, $\partial\Omega_{\text{bot}}(\tilde{C})$. The region can generally be multiply connected. A subregion, $\mathcal{R}_{\text{sub}}$, is also considered where its sides extend from the free surface to the tracer isosurface, and they are assumed to be fully within the fluid domain. We develop the tracer and fluid mass budgets for region $\mathcal{R}_{\text{sub}}$ in Section 69.6.4, whereas the budget in the full region $C \geq \tilde{C}$ is considered in Section 69.6.3.

Advective formulation

The tracer mass budget written using the advective formulation (69.52) is given by

$$\frac{\mathrm{d}}{\mathrm{d}t}\left[\int_{\mathscr{R}} \rho\, C\, \mathrm{d}V\right] = \int_{\partial\Omega_{\text{surf}}(\tilde{C})} Q_{\mathsf{m}}\, C\, \mathrm{d}A - \tilde{C} \int_{C=\tilde{C}} \rho\, (\boldsymbol{v}^{\dagger} - \boldsymbol{v}^{(\mathsf{b})}) \cdot \hat{\boldsymbol{n}}\, \mathrm{d}\mathcal{S} - \oint_{\partial\mathscr{R}} \boldsymbol{J}^{\text{diff}} \cdot \hat{\boldsymbol{n}}\, \mathrm{d}\mathcal{S}. \tag{69.61}$$

For the first right hand side term we made use of the surface kinematic boundary condition (19.88c), with $Q_\mathsf{m}\,\mathrm{d}A$ the mass per time crossing the surface interface and where $\mathrm{d}A$ is the horizontal projection of the interface area element, $\mathrm{d}\mathcal{S}$. We also made use of the exterior boundary condition (69.53) for the eddy-induced velocity. For the second term we pulled the tracer concentration outside of the boundary integral over the $C = \tilde{C}$ interface, since the concentration is fixed at $\tilde{C}$ on this interface.

The mass budget for this region, also formulated using advective fluxes, is given by

$$\frac{\mathrm{d}}{\mathrm{d}t}\left[\int_{\mathcal{R}} \rho\,\mathrm{d}V\right] = \int_{\partial\Omega_{\mathrm{surf}}(\tilde{C})} Q_\mathsf{m}\,\mathrm{d}A - \int_{C=\tilde{C}} \rho\,(\boldsymbol{v}^\dagger - \boldsymbol{v}^{(\mathsf{b})})\cdot\hat{\boldsymbol{n}}\,\mathrm{d}\mathcal{S}. \tag{69.62}$$

Combining this budget with the tracer mass budget allows us to write

$$\frac{\mathrm{d}}{\mathrm{d}t}\left[M_C - \tilde{C}\,M\right] = \int_{\partial\Omega_{\mathrm{surf}}(\tilde{C})} Q_\mathsf{m}\,(C-\tilde{C})\,\mathrm{d}A - \oint_{\partial\mathcal{R}} \boldsymbol{J}^{\mathsf{diff}}\cdot\hat{\boldsymbol{n}}\,\mathrm{d}\mathcal{S}, \tag{69.63}$$

where we introduced the shorthand for the tracer mass and fluid mass in the region

$$M_C = \int_{\mathcal{R}} C\,\rho\,\mathrm{d}V \qquad \text{and} \qquad M = \int_{\mathcal{R}} \rho\,\mathrm{d}V. \tag{69.64}$$

In Section 73.10.2 we motivate the name *internal tracer mass* for the quantity $M_C - \tilde{C}\,M$.

Skew flux formulation

The tracer mass budget formulated using skew tracer fluxes is generally given by equation (69.60). It takes on the following form for the domain in Figure 69.2

$$\begin{aligned}\frac{\mathrm{d}}{\mathrm{d}t}\left[\int_{\mathcal{R}} \rho\,C\,\mathrm{d}V\right] = \int_{\partial\Omega_{\mathrm{surf}}(\tilde{C})} Q_\mathsf{m}\,C\,\mathrm{d}A - \tilde{C}\int_{C=\tilde{C}} \rho\,(\boldsymbol{v}-\boldsymbol{v}^{(\mathsf{b})})\cdot\hat{\boldsymbol{n}}\,\mathrm{d}\mathcal{S} \\ - \oint_{\partial\mathcal{R}} [-\nabla C\times(\rho\,\boldsymbol{\Psi}^*) + \boldsymbol{J}^{\mathsf{diff}}]\cdot\hat{\boldsymbol{n}}\,\mathrm{d}\mathcal{S},\end{aligned} \tag{69.65}$$

and the corresponding budget for the fluid mass is

$$\frac{\mathrm{d}}{\mathrm{d}t}\left[\int_{\mathcal{R}} \rho\,\mathrm{d}V\right] = \int_{\partial\Omega_{\mathrm{surf}}(\tilde{C})} Q_\mathsf{m}\,\mathrm{d}A - \int_{C=\tilde{C}} \rho\,(\boldsymbol{v}-\boldsymbol{v}^{(\mathsf{b})})\cdot\hat{\boldsymbol{n}}\,\mathrm{d}\mathcal{S}. \tag{69.66}$$

As for the advective formulation, we combine the fluid mass budget equation (69.66) with the tracer mass equation (69.65) to render a budget equation for the internal mass content

$$\frac{\mathrm{d}}{\mathrm{d}t}\left[M_C - \tilde{C}\,M\right] = \int_{\partial\Omega_{\mathrm{surf}}(\tilde{C})} Q_\mathsf{m}\,(C-\tilde{C})\,\mathrm{d}A - \oint_{\partial\mathcal{R}} \boldsymbol{J}^{\mathsf{diff}}\cdot\hat{\boldsymbol{n}}\,\mathrm{d}\mathcal{S}, \tag{69.67}$$

which is identical to the advective formulation given by equation (69.63).

Proving the budgets based on the two formulations are equivalent

The two tracer budgets, (69.61) and (69.65), must be the same since they measure changes to the tracer mass within the same region. Likewise, the two mass budgets, (69.62) and (69.66), must be the same, as are the two internal tracer mass budgets (69.63) and (69.67). We here expose the manipulations required to verify these equalities.

To prove the $C = \tilde{C}$ terms in the tracer budget equations (69.61) and (69.65) are the same,

consider the identity (69.55) applied to the region under consideration

$$0 = \oint_{\partial\mathcal{R}} \rho\, \boldsymbol{v}^* \cdot \hat{\boldsymbol{n}}\, \mathrm{d}\mathcal{S} = \int_{\partial\Omega_{\mathrm{surf}}(\tilde{C})} \rho\, \boldsymbol{v}^* \cdot \hat{\boldsymbol{n}}\, \mathrm{d}\mathcal{S} + \int_{\partial\Omega_{\mathrm{bot}}(\tilde{C})} \rho\, \boldsymbol{v}^* \cdot \hat{\boldsymbol{n}}\, \mathrm{d}\mathcal{S} + \int_{C=\tilde{C}} \rho\, \boldsymbol{v}^* \cdot \hat{\boldsymbol{n}}\, \mathrm{d}\mathcal{S}. \quad (69.68)$$

The surface and bottom boundary terms vanish due to the external boundary condition (69.53); namely, $\boldsymbol{v}^* \cdot \hat{\boldsymbol{n}} = 0$ for each point along an external fluid boundary. We are thus led to conclude that

$$\int_{C=\tilde{C}} \rho\, \boldsymbol{v}^* \cdot \hat{\boldsymbol{n}}\, \mathrm{d}\mathcal{S} = 0. \quad (69.69)$$

This boundary integral means that there is no net accumulation of mass in the region due to action of the eddy velocity. Notably, we generally have $\boldsymbol{v}^* \cdot \hat{\boldsymbol{n}} \neq 0$ at any particular point on the $C = \tilde{C}$ surface, yet its integral over the $C = \tilde{C}$ interface vanishes. Given the boundary integral (69.69) we are led to conclude

$$\int_{C=\tilde{C}} \rho\, (\boldsymbol{v}^\dagger - \boldsymbol{v}^{(\mathsf{b})}) \cdot \hat{\boldsymbol{n}}\, \mathrm{d}\mathcal{S} = \int_{C=\tilde{C}} \rho\, (\boldsymbol{v} - \boldsymbol{v}^{(\mathsf{b})}) \cdot \hat{\boldsymbol{n}}\, \mathrm{d}\mathcal{S}. \quad (69.70)$$

This identity proves that the two mass budgets (69.62) and (69.66) are indeed measuring changes to the same fluid mass, even though one computes the domain boundary fluxes based on the residual mean velocity, $\boldsymbol{v}^\dagger$, whereas the other uses the Eulerian mean, $\boldsymbol{v}$.

Next we need to show that the skew flux term vanishes when integrated around the domain boundary. For the $C = \tilde{C}$ boundary we have

$$\int_{C=\tilde{C}} [\nabla C \times (\rho\, \boldsymbol{\Psi}^*)] \cdot \hat{\boldsymbol{n}}\, \mathrm{d}\mathcal{S} = 0, \quad (69.71)$$

which follows since $\hat{\boldsymbol{n}}$ is parallel to ∇C along this boundary. For the external boundaries, equality of the tracer mass budgets (69.61) and (69.65) is satisfied for an arbitrary tracer concentration if one of the boundary conditions discussed in Section (69.5.3) is maintained; i.e., if $\boldsymbol{\Psi}^*$ vanishes on an external boundary or if it is parallel to the boundary normal direction ($\hat{\boldsymbol{n}} \times \boldsymbol{\Psi}^* = 0$). Maintenance of either of these two boundary conditions allows us to conclude that the two budgets (69.61) and (69.65) are indeed identical.

69.6.4 Budget for a region with interior sides

Consider the subregion, $\mathcal{R}_{\mathrm{sub}}$, shown in Figure 69.2. This region is bounded above by the free surface and below by the tracer isosurface, $C = \tilde{C}$, just like the region $\mathcal{R}$ encountered in Section 69.6.3. Additionally, region $\mathcal{R}_{\mathrm{sub}}$ is bounded along its sides by surfaces assumed to be within the fluid interior. For much of this discussion we allow the sides to have an arbitrary shape and to move. Towards the end of this section we specialize to the case of static sides, such as relevant for a vertical section through the fluid and/or a numerical model grid cell.

Fluid mass budget

The fluid mass budget for the region, $\mathcal{R}_{\mathrm{sub}}$, can be formulated using either the residual mean velocity or the Eulerian mean velocity

$$\frac{\mathrm{d}}{\mathrm{d}t}\left[\int_{\mathcal{R}_{\mathrm{sub}}} \rho\, \mathrm{d}V\right] = \int_{\partial\Omega_{\mathrm{surf}}(\tilde{C})} Q_{\mathsf{m}}\, \mathrm{d}A - \int_{C=\tilde{C}} \rho\, (\boldsymbol{v}^\dagger - \boldsymbol{v}^{(\mathsf{b})}) \cdot \hat{\boldsymbol{n}}\, \mathrm{d}\mathcal{S} - \int_{\mathrm{sides}} \rho\, (\boldsymbol{v}^\dagger - \boldsymbol{v}^{(\mathsf{b})}) \cdot \hat{\boldsymbol{n}}\, \mathrm{d}\mathcal{S} \quad (69.72a)$$

$$\frac{\mathrm{d}}{\mathrm{d}t}\left[\int_{\mathcal{R}_{\text{sub}}} \rho \,\mathrm{d}V\right] = \int_{\partial\Omega_{\text{surf}}(\tilde{C})} Q_{\mathsf{m}} \,\mathrm{d}A - \int_{C=\tilde{C}} \rho\,(\boldsymbol{v} - \boldsymbol{v}^{(\mathrm{b})}) \cdot \hat{\boldsymbol{n}} \,\mathrm{d}\mathcal{S} - \int_{\text{sides}} \rho\,(\boldsymbol{v} - \boldsymbol{v}^{(\mathrm{b})}) \cdot \hat{\boldsymbol{n}} \,\mathrm{d}\mathcal{S}. \tag{69.72b}$$

The two budgets are identical since the eddy velocity satisfies $\oint \rho\, \boldsymbol{v}^* \cdot \hat{\boldsymbol{n}} \,\mathrm{d}\mathcal{S} = 0$ for any domain, as well as $\boldsymbol{v}^* \cdot \hat{\boldsymbol{n}} = 0$ along any external domain boundary. Hence, as already noted in Section 69.6.1, the eddy velocity contribution to the right hand side of equation (69.72a) vanishes; it provides no net mass source to any region. We next show the same equality holds for the tracer mass budgets, with that equality requiring a bit more effort.

Tracer mass budget

The advective flux formulation of the tracer mass budget is given by

$$\frac{\mathrm{d}}{\mathrm{d}t}\left[\int_{\mathcal{R}_{\text{sub}}} \rho\, C \,\mathrm{d}V\right] = \int_{\partial\Omega_{\text{surf}}(\tilde{C})} Q_{\mathsf{m}}\, C \,\mathrm{d}A - \tilde{C} \int_{C=\tilde{C}} \rho\,(\boldsymbol{v}^{\dagger} - \boldsymbol{v}^{(\mathrm{b})}) \cdot \hat{\boldsymbol{n}} \,\mathrm{d}\mathcal{S} - \oint_{\partial\mathcal{R}_{\text{sub}}} \boldsymbol{J}^{\mathsf{diff}} \cdot \hat{\boldsymbol{n}} \,\mathrm{d}\mathcal{S} - \int_{\text{sides}} C\,\rho\,(\boldsymbol{v}^{\dagger} - \boldsymbol{v}^{(\mathrm{b})}) \cdot \hat{\boldsymbol{n}} \,\mathrm{d}\mathcal{S}, \tag{69.73}$$

and the corresponding skew flux formulation is

$$\frac{\mathrm{d}}{\mathrm{d}t}\left[\int_{\mathcal{R}_{\text{sub}}} \rho\, C \,\mathrm{d}V\right] = \int_{\partial\Omega_{\text{surf}}(\tilde{C})} Q_{\mathsf{m}}\, C \,\mathrm{d}A - \tilde{C} \int_{C=\tilde{C}} \rho\,(\boldsymbol{v} - \boldsymbol{v}^{(\mathrm{b})}) \cdot \hat{\boldsymbol{n}} \,\mathrm{d}\mathcal{S} - \oint_{\partial\mathcal{R}_{\text{sub}}} \boldsymbol{J}^{\mathsf{diff}} \cdot \hat{\boldsymbol{n}} \,\mathrm{d}\mathcal{S} - \int_{\text{sides}} C\,\rho\,(\boldsymbol{v} - \boldsymbol{v}^{(\mathrm{b})}) \cdot \hat{\boldsymbol{n}} \,\mathrm{d}\mathcal{S} - \int_{\text{sides}} [-\nabla C \times (\rho\, \boldsymbol{\Psi}^*)] \cdot \hat{\boldsymbol{n}} \,\mathrm{d}\mathcal{S}. \tag{69.74}$$

As for the discussion in Section 69.6.3, we introduce the internal tracer mass and make use of the fluid mass budgets (69.72a) and (69.72b) to write the advective form of the internal mass budget

$$\frac{\mathrm{d}}{\mathrm{d}t}\left[M_C - \tilde{C}\, M\right] = \int_{\partial\Omega_{\text{surf}}(\tilde{C})} Q_{\mathsf{m}}\,(C - \tilde{C}) \,\mathrm{d}A - \oint_{\partial\mathcal{R}} \boldsymbol{J}^{\mathsf{diff}} \cdot \hat{\boldsymbol{n}} \,\mathrm{d}\mathcal{S} - \int_{\text{sides}} (C - \tilde{C})\,\rho\,(\boldsymbol{v}^{\dagger} - \boldsymbol{v}^{(\mathrm{b})}) \cdot \hat{\boldsymbol{n}} \,\mathrm{d}\mathcal{S}, \tag{69.75}$$

and the corresponding skew flux form of the same budget

$$\frac{\mathrm{d}}{\mathrm{d}t}\left[M_C - \tilde{C}\, M\right] = \int_{\partial\Omega_{\text{surf}}(\tilde{C})} Q_{\mathsf{m}}\,(C - \tilde{C}) \,\mathrm{d}A - \oint_{\partial\mathcal{R}} \boldsymbol{J}^{\mathsf{diff}} \cdot \hat{\boldsymbol{n}} \,\mathrm{d}\mathcal{S} - \int_{\text{sides}} (C - \tilde{C})\,\rho\,(\boldsymbol{v} - \boldsymbol{v}^{(\mathrm{b})}) \cdot \hat{\boldsymbol{n}} \,\mathrm{d}\mathcal{S} - \int_{\text{sides}} [-\nabla C \times (\rho\, \boldsymbol{\Psi}^*)] \cdot \hat{\boldsymbol{n}} \,\mathrm{d}\mathcal{S}. \tag{69.76}$$

We now examine the right hand side of the budgets (69.75) and (69.76) to show they are indeed measuring the same tracer mass budget. For that purpose, consider the skew flux integral in equation (69.76) and note that the integrand vanishes on both the top of the domain, at $z = \eta$, and bottom at $C = \tilde{C}$, thus allowing us to write

$$-\int_{\text{sides}} [-\nabla C \times (\rho\, \boldsymbol{\Psi}^*)] \cdot \hat{\boldsymbol{n}} \,\mathrm{d}\mathcal{S} = -\oint_{\partial\mathcal{R}_{\text{sub}}} [-\nabla C \times (\rho\, \boldsymbol{\Psi}^*)] \cdot \hat{\boldsymbol{n}} \,\mathrm{d}\mathcal{S}, \tag{69.77}$$

where the right hand side is an integral around the full domain boundaries. Now reintroduce

the eddy induced velocity and rotational flux to have

$$-\oint_{\partial\mathcal{R}_{\text{sub}}} [-\nabla C \times (\rho\,\boldsymbol{\Psi}^*)] \cdot \hat{\boldsymbol{n}}\,\mathrm{d}\mathcal{S} = -\oint_{\partial\mathcal{R}_{\text{sub}}} [C\,\rho\,\boldsymbol{v}^* - \nabla \times (C\,\rho\,\boldsymbol{\Psi}^*)] \cdot \hat{\boldsymbol{n}}\,\mathrm{d}\mathcal{S}. \tag{69.78}$$

The rotational flux has zero divergence, so that Gauss's divergence theorem means that the rotational flux vanishes when integrated along the domain boundaries

$$\oint_{\partial\mathcal{R}_{\text{sub}}} \nabla \times (C\,\rho\,\boldsymbol{\Psi}^*) \cdot \hat{\boldsymbol{n}}\,\mathrm{d}\mathcal{S} = 0. \tag{69.79}$$

The eddy advection term in equation (69.78) vanishes on the top boundary at $z = \eta$ due to the boundary condition $\boldsymbol{v}^* \cdot \hat{\boldsymbol{n}} = 0$, thus yielding

$$\oint_{\partial\mathcal{R}_{\text{sub}}} C\,\rho\,\boldsymbol{v}^* \cdot \hat{\boldsymbol{n}}\,\mathrm{d}\mathcal{S} = \int_{\text{sides}} C\,\rho\,\boldsymbol{v}^* \cdot \hat{\boldsymbol{n}}\,\mathrm{d}\mathcal{S} + \int_{C=\tilde{C}} C\,\rho\,\boldsymbol{v}^* \cdot \hat{\boldsymbol{n}}\,\mathrm{d}\mathcal{S} \tag{69.80a}$$

$$= \int_{\text{sides}} C\,\rho\,\boldsymbol{v}^* \cdot \hat{\boldsymbol{n}}\,\mathrm{d}\mathcal{S} + \tilde{C} \int_{C=\tilde{C}} \rho\,\boldsymbol{v}^* \cdot \hat{\boldsymbol{n}}\,\mathrm{d}\mathcal{S}. \tag{69.80b}$$

Again make use of the property $\nabla \cdot (\rho\,\boldsymbol{v}^*) = 0$ and $\hat{\boldsymbol{n}} \cdot \boldsymbol{v}^* = 0$ at $z = \eta$ to write

$$0 = \oint_{\partial\mathcal{R}_{\text{sub}}} \rho\,\boldsymbol{v}^* \cdot \hat{\boldsymbol{n}}\,\mathrm{d}\mathcal{S} = \oint_{\text{sides}} \rho\,\boldsymbol{v}^* \cdot \hat{\boldsymbol{n}}\,\mathrm{d}\mathcal{S} + \oint_{C=\tilde{C}} \rho\,\boldsymbol{v}^* \cdot \hat{\boldsymbol{n}}\,\mathrm{d}\mathcal{S}, \tag{69.81}$$

which gives us

$$-\int_{\text{sides}} [-\nabla C \times (\rho\,\boldsymbol{\Psi}^*)] \cdot \hat{\boldsymbol{n}}\,\mathrm{d}\mathcal{S} = -\oint_{\partial\mathcal{R}_{\text{sub}}} C\,\rho\,\boldsymbol{v}^* \cdot \hat{\boldsymbol{n}}\,\mathrm{d}\mathcal{S} = -\int_{\text{sides}} (C - \tilde{C})\,\rho\,\boldsymbol{v}^* \cdot \hat{\boldsymbol{n}}\,\mathrm{d}\mathcal{S}. \tag{69.82}$$

Making use of this result in the skew flux formulated budget equation (69.76) brings it to the advective flux form found in equation (69.75).

We are thus led to conclude that the right hand side to equation (69.76) does indeed equal to the right hand side of equation (69.75). So although the formulation of the boundary flux contributions is rather distinct between the advective flux and skew flux formulations, the resulting tracer mass budget is the same. The choice for how to formulate the budget is thus a matter of convenience.

69.6.5 Budget for a stirred fluid in a region with interior sides

Although contained within the formalism developed in Section 69.6.4, it is revealing to specialize those budgets to the case of zero mixing, in which $\boldsymbol{J}^{\text{diff}} = 0$, and there is zero boundary mass flux, $Q_{\mathsf{m}} = 0$. In this case the fluid is reversibly stirred. Examining the finite region budgets for this pure stirring case allows us to further reveal the complementary treatments available from advection versus skewsion.

Summary of the differential stirring formalism

As explored in this chapter, an Eulerian description of tracer stirring can arise from either advection or skewsion. In the presence of an eddy induced velocity we here consider two representations of tracer stirring, with the first being advection by the residual mean velocity, $\boldsymbol{v}^\dagger$

$$\rho\,\frac{\mathrm{D}^\dagger C}{\mathrm{D}t} = \partial_t(\rho\,C) + \nabla \cdot (\rho\,\boldsymbol{v}^\dagger\,C) = 0. \tag{69.83}$$

This formulation makes it clear that surfaces of constant C are material as defined by the residual mean velocity rather than by the Eulerian mean, $\boldsymbol{v}$. That is, tracer isosurfaces satisfy the residual mean impermeability condition

$$\rho\,(\boldsymbol{v}^\dagger - \boldsymbol{v}^{(\mathrm{b})}) \cdot \hat{\boldsymbol{n}} = 0 \qquad \text{on } C \text{ isosurfaces,} \tag{69.84}$$

with

$$\hat{\boldsymbol{n}} = \frac{\nabla C}{|\nabla C|} \qquad \text{and} \qquad \boldsymbol{v}^{(\mathrm{b})} \cdot \hat{\boldsymbol{n}} = -\frac{\partial_t C}{|\nabla C|}. \tag{69.85}$$

The impermeability condition (69.84) offers a geometric interpretation of the tracer equation (69.83) following from the discussion of dia-surface transport in Section 64.3. Correspondingly, Lagrangian fluid particles moving with the residual mean velocity do not cross tracer isosurfaces even if those isosurfaces move. Furthermore, we observe that the eddy induced velocity has a nonzero projection across tracer isosurfaces

$$(\boldsymbol{v}^\dagger - \boldsymbol{v}^{(\mathrm{b})}) \cdot \hat{\boldsymbol{n}} = 0 \Longrightarrow (\boldsymbol{v} - \boldsymbol{v}^{(\mathrm{b})}) \cdot \hat{\boldsymbol{n}} = -\boldsymbol{v}^* \cdot \hat{\boldsymbol{n}} \qquad \text{on } C \text{ isosurfaces.} \tag{69.86}$$

This property of the eddy induced velocity was emphasized by *McDougall and McIntosh* (2001). It reveals that in the absence of mixing, eddy motion crossing tracer isosurfaces is exactly balanced by Eulerian motion plus surface motion, thus leaving a net zero residual mean transfer of matter across the surface. Equation (69.86) is a key kinematic property used for interpreting features of the finite volume budgets detailed below.

Our second means to represent tracer stirring makes use of advection by the Eulerian mean velocity plus skewsion by the eddy induced streamfunction

$$\rho \frac{\mathrm{D}C}{\mathrm{D}t} + \nabla \cdot [-\nabla C \times (\rho\, \boldsymbol{\Psi}^*)] = \partial_t(\rho\, C) + \nabla \cdot [\rho\, \boldsymbol{v}\, C - \nabla C \times (\rho\, \boldsymbol{\Psi}^*)] = 0. \tag{69.87}$$

In terms of the eddy streamfunction, $\rho\, \boldsymbol{\Psi}^*$, the impermeability condition (69.84) takes on the form

$$\left[\rho\, \boldsymbol{v} + \nabla \times (\rho\, \boldsymbol{\Psi}^*) - \rho\, \boldsymbol{v}^{(\mathrm{b})}\right] \cdot \hat{\boldsymbol{n}} = 0 \qquad \text{on } C \text{ isosurfaces.} \tag{69.88}$$

Budgets via residual mean advection

The mass budget formulated in terms of residual mean advection, and the corresponding residual mean advective flux formulation of the tracer mass budget, are given by

$$\frac{\mathrm{d}}{\mathrm{d}t}\left[\int_{\mathcal{R}_{\mathrm{sub}}} \rho\, \mathrm{d}V\right] = -\int_{C=\tilde{C}} \rho\,(\boldsymbol{v}^\dagger - \boldsymbol{v}^{(\mathrm{b})}) \cdot \hat{\boldsymbol{n}}\, \mathrm{d}\mathcal{S} - \int_{\mathrm{sides}} \rho\,(\boldsymbol{v}^\dagger - \boldsymbol{v}^{(\mathrm{b})}) \cdot \hat{\boldsymbol{n}}\, \mathrm{d}\mathcal{S} \tag{69.89a}$$

$$\frac{\mathrm{d}}{\mathrm{d}t}\left[\int_{\mathcal{R}_{\mathrm{sub}}} \rho\, C\, \mathrm{d}V\right] = -\tilde{C}\int_{C=\tilde{C}} \rho\,(\boldsymbol{v}^\dagger - \boldsymbol{v}^{(\mathrm{b})}) \cdot \hat{\boldsymbol{n}}\, \mathrm{d}\mathcal{S} - \int_{\mathrm{sides}} C\,\rho\,(\boldsymbol{v}^\dagger - \boldsymbol{v}^{(\mathrm{b})}) \cdot \hat{\boldsymbol{n}}\, \mathrm{d}\mathcal{S}. \tag{69.89b}$$

The residual mean impermeability condition (69.84) for the $C = \tilde{C}$ surface renders a simplification to the flud mass and tracer mass budgets

$$\frac{\mathrm{d}}{\mathrm{d}t}\left[\int_{\mathcal{R}_{\mathrm{sub}}} \rho\, \mathrm{d}V\right] = -\int_{\mathrm{sides}} \rho\,(\boldsymbol{v}^\dagger - \boldsymbol{v}^{(\mathrm{b})}) \cdot \hat{\boldsymbol{n}}\, \mathrm{d}\mathcal{S} \tag{69.90a}$$

$$\frac{\mathrm{d}}{\mathrm{d}t}\left[\int_{\mathcal{R}_{\mathrm{sub}}} \rho\, C\, \mathrm{d}V\right] = -\int_{\mathrm{sides}} C\,\rho\,(\boldsymbol{v}^\dagger - \boldsymbol{v}^{(\mathrm{b})}) \cdot \hat{\boldsymbol{n}}\, \mathrm{d}\mathcal{S}. \tag{69.90b}$$

Hence, in the residual mean formulation, the only fluxes that affect changes to the mass budgets are those that cross the side faces of the region.

Budgets via Eulerian mean advection plus eddy skewsion

The mass budget formulated in terms of Eulerian mean advection, and the corresponding tracer mass budget using eddy skewsion, are given by

$$\frac{\mathrm{d}}{\mathrm{d}t}\left[\int_{\mathcal{R}_{\text{sub}}} \rho \,\mathrm{d}V\right] = -\int_{C=\tilde{C}} \rho\,(\boldsymbol{v}-\boldsymbol{v}^{(\mathrm{b})})\cdot\hat{\boldsymbol{n}}\,\mathrm{d}\mathcal{S} - \int_{\text{sides}} \rho\,(\boldsymbol{v}-\boldsymbol{v}^{(\mathrm{b})})\cdot\hat{\boldsymbol{n}}\,\mathrm{d}\mathcal{S} \tag{69.91a}$$

$$\begin{aligned}\frac{\mathrm{d}}{\mathrm{d}t}\left[\int_{\mathcal{R}_{\text{sub}}} \rho\, C \,\mathrm{d}V\right] &= -\tilde{C}\int_{C=\tilde{C}} \rho\,(\boldsymbol{v}-\boldsymbol{v}^{(\mathrm{b})})\cdot\hat{\boldsymbol{n}}\,\mathrm{d}\mathcal{S} - \int_{\text{sides}} C\,\rho\,(\boldsymbol{v}-\boldsymbol{v}^{(\mathrm{b})})\cdot\hat{\boldsymbol{n}}\,\mathrm{d}\mathcal{S} \\ &\quad - \int_{\text{sides}} [-\nabla C \times (\rho\,\boldsymbol{\Psi}^{*})]\cdot\hat{\boldsymbol{n}}\,\mathrm{d}\mathcal{S}.\end{aligned} \tag{69.91b}$$

We already saw in Section 69.6.4 how to bring the right hand side terms into the form realized by the residual mean advective approach. So there is no question concerning the equivalance of the advective and skew flux formulations for the tracer mass budget. Nonetheless, what is here clearly emphasized is that the skew flux approach requires us to account for Eulerian advective transport across the $C = \tilde{C}$ isosurface, whereas for the advective flux approach the only flux in equation (69.90b) is that crossing the region side boundaries. Even so, as stated earlier, an Eulerian mean transport of tracer across the $C = \tilde{C}$ isosurface *does not* correspond to material transport across this surface. The reason is that material transport is determined by the residual mean velocity, $\boldsymbol{v}^{\dagger}$, as per the residual mean impermeability conditions 69.86 and 69.88. So even though there is a contribution to the skew flux formulated budget from Eulerian transport across the $C = \tilde{C}$ material surface, there remains zero net material crossing that surface.

Zero Eulerian mean advection and static side walls

One further specialization serves to clearly emphasize the complementary nature of the advective and skew flux approaches. Here, we assume the sides of the region are static and the Eulerian mean velocity vanishes. With a zero Eulerian velocity, the residual mean impermeability condition (69.86) means that on the $C = \tilde{C}$ isosurface, the normal component of the eddy velocity is balanced by the boundary velocity as per the impermeability condition (69.92):

$$(\boldsymbol{v}^{*}-\boldsymbol{v}^{(\mathrm{b})})\cdot\hat{\boldsymbol{n}} = 0 \qquad \text{on } C \text{ isosurfaces and with } \boldsymbol{v}=0. \tag{69.92}$$

When formulated using the residual mean advection, the fluid mass budget (69.90a) and tracer mass budget (69.90b) reduce in this case to

$$\frac{\mathrm{d}}{\mathrm{d}t}\left[\int_{\mathcal{R}_{\text{sub}}} \rho \,\mathrm{d}V\right] = -\int_{\text{sides}} \rho\,\boldsymbol{v}^{*}\cdot\hat{\boldsymbol{n}}\,\mathrm{d}\mathcal{S} \tag{69.93a}$$

$$\frac{\mathrm{d}}{\mathrm{d}t}\left[\int_{\mathcal{R}_{\text{sub}}} \rho\, C \,\mathrm{d}V\right] = -\int_{\text{sides}} C\,\rho\,\boldsymbol{v}^{*}\cdot\hat{\boldsymbol{n}}\,\mathrm{d}\mathcal{S}, \tag{69.93b}$$

so that these budgets are only affected by eddy advection across the side boundaries. The corresponding mass budget written in terms of Eulerian mean advection, (69.91a), and tracer mass budget written in terms of skew fluxes, (69.91b), are given by

$$\frac{\mathrm{d}}{\mathrm{d}t}\left[\int_{\mathcal{R}_{\text{sub}}} \rho \,\mathrm{d}V\right] = +\int_{C=\tilde{C}} \rho\,\boldsymbol{v}^{(\mathrm{b})}\cdot\hat{\boldsymbol{n}}\,\mathrm{d}\mathcal{S} \tag{69.94a}$$

$$\frac{\mathrm{d}}{\mathrm{d}t}\left[\int_{\mathcal{R}_{\text{sub}}} \rho\, C \,\mathrm{d}V\right] = +\tilde{C}\int_{C=\tilde{C}} \rho\,\boldsymbol{v}^{(\mathrm{b})}\cdot\hat{\boldsymbol{n}}\,\mathrm{d}\mathcal{S} - \int_{\text{sides}} [-\nabla C \times (\rho\,\boldsymbol{\Psi}^{*})]\cdot\hat{\boldsymbol{n}}\,\mathrm{d}\mathcal{S}. \tag{69.94b}$$

For the mass budget, (69.94a), there are no contributions to the side walls since they are static

and the Eulerian advection is assumed to vanish. The only contribution comes from the eddy term acting on the $C = \tilde{C}$ isosurface where $\boldsymbol{v}^{(b)} \cdot \hat{\boldsymbol{n}} = \boldsymbol{v}^{*} \cdot \hat{\boldsymbol{n}}$. For the tracer mass budget, (69.94b), we also have the eddy contribution on the $C = \tilde{C}$ isosurface, plus skew fluxes that penetrate the side walls.

The right hand sides to the fluid mass budgets (69.93a) and (69.94a), and tracer mass budgets (69.93b) and (69.94b), are remarkably distinct. Even so, they both measure the same budgets. Furthermore, in both cases the $C = \tilde{C}$ boundary is a material boundary as defined by the residual mean velocity.

69.7 Active tracers and dia-surface flow

An *active tracer* impacts the fluid flow, with Conservative Temperature and salinity the canonical examples for the ocean. Active tracers directly impact the buoyancy, which in turn affects pressure and velocity. Hence, the advection-diffusion equation for active tracers is nonlinear since the velocity field is dependent on active tracers. We here write the advection-diffusion equation in terms of the residual mean velocity using Conservative Temperature as an example active tracer

$$\rho \frac{\mathrm{D}^{\dagger}\Theta}{\mathrm{D}t} = \rho \, (\partial_t + \boldsymbol{v}^{\dagger} \cdot \nabla)\Theta = -\nabla \cdot \boldsymbol{J}^{\mathrm{diff}}(\Theta). \tag{69.95}$$

Further nonlinearities arise when the subgrid scale diffusion tensor is itself a function of the buoyancy, as discussed at the end of Section 68.5, and/or when the parameterized eddy-induced velocity is a function of the buoyancy, as discussed in Section 71.3.

69.7.1 Adiabatic flow

Conservative Temperature is materially invariant in an adiabatic flow, so that advected by the residual mean velocity we have

$$\frac{\mathrm{D}^{\dagger}\Theta}{\mathrm{D}t} = (\partial_t + \boldsymbol{v}^{\dagger} \cdot \nabla)\Theta = 0 \qquad \text{adiabatic.} \tag{69.96}$$

Furthermore, following the kinematics of Section 19.6.2, the adiabatic residual mean flow field does not penetrate surfaces of constant Conservative Temperature (Θ-isosurfaces are impermeable) since

$$\boldsymbol{v}^{\dagger} \cdot \nabla\Theta = -\partial_t \Theta. \tag{69.97}$$

In this case we say that residual mean advection reversibly stirs the Conservative Temperature field. This property of the residual mean velocity was also considered in the discussion of pure stirring in Section 69.6.4.

69.7.2 Diabatic processes generating dia-Θ transport

Conservative Temperature is not materially invariant in the presence of diabatic processes, such as mixing typically parameterized by diffusion. Correspondingly, the residual mean velocity picks up a component, w^{dia}, that crosses the moving Conservative Temperature surface, thus making Θ surfaces permeable to fluid flow. In turn, advective transport in the presence of mixing is not reversible. We follow the kinematics from Section 64.3 to render the expression (64.26) for w^{dia}, which we here write as

$$w^{\mathrm{dia}} \equiv \hat{\boldsymbol{n}} \cdot (\boldsymbol{v}^{\dagger} - \boldsymbol{v}^{(\Theta)}) = \frac{1}{|\nabla\Theta|} \frac{\mathrm{D}^{\dagger}\Theta}{\mathrm{D}t} \tag{69.98}$$

where

$$\hat{\boldsymbol{n}} = \frac{\nabla\Theta}{|\nabla\Theta|} \qquad \text{and} \qquad \boldsymbol{v}^{(\Theta)} \cdot \nabla\Theta = -\partial_t \Theta. \tag{69.99}$$

Rearrangement of equation (69.98) renders the kinematic identity

$$\frac{\mathrm{D}^{\dagger}\Theta}{\mathrm{D}t} = \partial_t\Theta + \boldsymbol{v}^{\dagger}\cdot\nabla\Theta = w^{\mathsf{dia}}\,|\nabla\Theta|. \tag{69.100}$$

With nonzero w^{dia}, we no longer have residual mean advection preserving properties along fluid element trajectories. There can be many physical processes contributing to a nonzero w^{dia}, such as from the following examples.

Diffusion with no fluid motion

Diffusion is the canonical example of a diabatic process (Section 68.3), with molecular diffusion leading to

$$\rho\,\frac{\mathrm{D}^{\dagger}\Theta}{\mathrm{D}t} = \nabla\cdot(\kappa\,\rho\,\nabla\Theta), \tag{69.101}$$

with $\kappa > 0$ the scalar kinematic diffusivity and the product, $\kappa\,\rho$, the dynamic diffusivity. Following the definition (69.98), we see that diffusion drives the following diabatic transport velocity

$$\rho\,w^{\mathsf{dia}} = \frac{\nabla\cdot(\kappa\,\rho\,\nabla\Theta)}{|\nabla\Theta|}. \tag{69.102}$$

Consider a horizontally homogeneous Conservative Temperature field. If buoyancy is alone determined by Θ, then there is no fluid motion since buoyancy surfaces are flat (and we assume the eddy-induced motion is also zero). Yet in the presence of vertical diffusion and vertical stratification there is a diabatic transport since

$$\rho\,w^{\mathsf{dia}} = \frac{\partial_z(\kappa\,\rho\,\partial_z\Theta)}{|\partial_z\Theta|} \neq 0. \tag{69.103}$$

In the absence of fluid flow, the dia-surface transport is determined solely by movement of the Θ surfaces. Correspondingly, Θ evolution is determined only by vertical diffusion since with $\boldsymbol{v}^{\dagger} = 0$ we have

$$\partial_t\Theta = \rho^{-1}\,\partial_z(\kappa\,\rho\,\partial_z\Theta) = w^{\mathsf{dia}}\,|\partial_z\Theta|. \tag{69.104}$$

Steady state advective-diabatic balance

A steady state Conservative Temperature field in the presence of diabatic processes is realized when there is an exact balance between advective transport and dia-surface transport enabled by diffusion

$$\rho\,\boldsymbol{v}^{\dagger}\cdot\nabla\Theta = \rho\,w^{\mathsf{dia}}\,|\nabla\Theta| = \nabla\cdot(\kappa\,\rho\,\nabla\Theta). \qquad \text{steady state.} \tag{69.105}$$

That is, maintaining static Θ-surfaces ($\partial_t\Theta = 0$) requires the residual mean advective transport to cross Θ surfaces (left hand side) by an amount that exactly balances diabatic processes such as diffusion (right hand side). This example illustrates that in the presence of mixing, advection is no longer an adiabatic stirring process. Indeed, in the steady state, advection exactly balances diffusion.

69.8 Tracer homogenization inside closed tracer contours

In this section we prove a far reaching theorem involving the steady advective-diffusive balance that holds within closed tracer contours. For this purpose, consider the equation for a conservative tracer

$$\partial_t(\rho\,C) + \nabla\cdot(\rho\,\boldsymbol{v}\,C) = -\nabla\cdot\boldsymbol{J} \tag{69.106}$$

where

$$\boldsymbol{J} = -\rho \boldsymbol{K} \cdot \nabla C \tag{69.107}$$

is a downgradient diffusive flux with $\boldsymbol{K}$ a symmetric positive-definite diffusion tensor. In the steady state, the divergence of the advective tracer flux balances the convergence of the diffusive flux

$$\nabla \cdot (\rho \boldsymbol{v} C) = -\nabla \cdot \boldsymbol{J}. \tag{69.108}$$

Now specialize to a two-dimensional steady state flow in a region enclosed by a constant tracer contour. We here prove that the tracer concentration is homogeneous (i.e., a spatially constant) within the contour of constant C, as shown in Figure 69.3. Evidently, in the steady state, diffusion removes all tracer variations within closed tracer contours; i.e., there are no tracer extrema within a closed tracer contour.

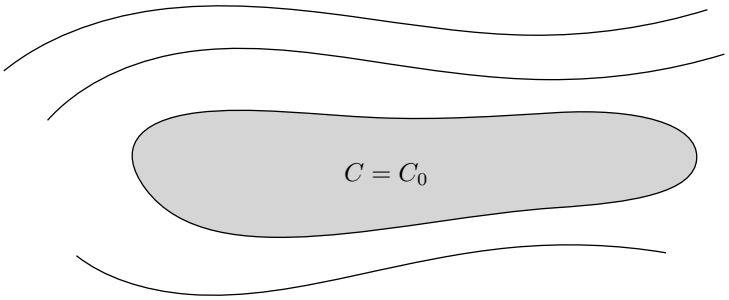

FIGURE 69.3: In a steady flow, the tracer concentration within a region bounded by a constant tracer contour is uniform, with diffusion providing the mechanism for homogenizing the tracer. Evidently, diffusion expells all variations in tracer concentration from the region. In this figure, the concentration within the closed region has constant value $C = C_0$.

69.8.1 Proof of the theorem

The following proof follows that given in Section 3.2 of *Rhines and Young* (1982) and Section 13.5 of *Vallis* (2017) for a horizontally non-divergent flow as per a Boussinesq ocean. Here, we show the result also holds for a steady state divergent flow, as per a non-Boussinesq fluid. The proof is based on a *reductio ad absurdum* argument, whereby we first assume the tracer is not homogeneous within a closed tracer contour, and then show that this assumption leads to an inconsistency and so is wrong. Notably, if the tracer concentration is not homogeneous within a contour, then there is an extrema within that contour.

To start the proof, integrate the left hand side of the steady state advection-diffusion equation (69.108) around an arbitrary simply connected surface and make use of the divergence theorem

$$\int_{\mathcal{S}} \nabla \cdot (\rho \boldsymbol{u} C) \, \mathrm{d}\mathcal{S} = \oint_{\partial \mathcal{S}} \rho \boldsymbol{u} C \cdot \hat{\boldsymbol{n}} \, \mathrm{d}l, \tag{69.109}$$

where $\hat{\boldsymbol{n}}$ is the outward normal along the area's boundary, $\partial \mathcal{S}$, and $\mathrm{d}l$ is the line element around the boundary. Now specify the surface under consideration to be bounded by a constant contour with $C = C_0$. We can thus remove the tracer concentration from the contour integral to have

$$\oint_{\partial \mathcal{S}} \rho \boldsymbol{u} C \cdot \hat{\boldsymbol{n}} \, \mathrm{d}l = C_0 \oint_{\partial \mathcal{S}} \rho \boldsymbol{u} \cdot \hat{\boldsymbol{n}} \, \mathrm{d}l = C_0 \int_{\mathcal{S}} \nabla \cdot (\rho \boldsymbol{u}) \, \mathrm{d}\mathcal{S}, \tag{69.110}$$

where the second equality follows from the divergence theorem. For a steady state flow, mass continuity means that density at a point is time independent, so that the density-weighted velocity has zero divergence

$$\nabla \cdot (\rho \boldsymbol{u}) = 0. \tag{69.111}$$

Consequently, when integrated over a closed tracer contour we have the identity

$$\int_{\mathcal{S}} \nabla \cdot (\rho \, \boldsymbol{u} \, C) \, \mathrm{d}\mathcal{S} = C_0 \int_{\mathcal{S}} \nabla \cdot (\rho \, \boldsymbol{u}) \, \mathrm{d}\mathcal{S} = 0 \qquad \text{with } \mathcal{S} \text{ enclosed by a closed } C \text{ contour.} \tag{69.112}$$

Returning to the steady state advection-diffusion equation (69.108), the identity (69.112) then implies the analogous result for the diffusive flux

$$\int_{\mathcal{S}} \nabla \cdot \boldsymbol{J} \, \mathrm{d}\mathcal{S} = 0 \qquad \text{with } \mathcal{S} \text{ enclosed by a closed } C \text{ contour.} \tag{69.113}$$

We now show that the identity (69.113) holds only if the tracer is homogeneous inside the closed contour; i.e., there are no extrema within a closed contour.

Appealing to a nonzero flux in the presence of an extrema

Consider the right hand side of the steady state advection-diffusion equation (69.108) and integrate it over a closed region

$$-\int_{\mathcal{S}} \nabla \cdot \boldsymbol{J} \, \mathrm{d}\mathcal{S} = -\oint_{\partial\mathcal{S}} \boldsymbol{J} \cdot \hat{\boldsymbol{n}} \, \mathrm{d}l = \oint_{\partial\mathcal{S}} (\boldsymbol{K} \cdot \nabla C) \cdot \hat{\boldsymbol{n}} \, \rho \, \mathrm{d}l. \tag{69.114}$$

If the contour surrounds an extremum of the tracer concentration, then a downgradient diffusive flux is nonzero and has a nonzero projection in the outward normal direction.[3] Hence, the integral is nonzero, which then contradicts equation (69.113). Consistency thus implies that the diffusive flux vanishes, which means the tracer contour does not surround an extrema. That is, the tracer concentration is homogeneous inside the closed tracer contour.

Introducing an expression for the outward normal

If the tracer is not homogeneous, so that $\nabla C \neq 0$, then we can introduce the normal direction,

$$\hat{\boldsymbol{n}} = \frac{\nabla C}{|\nabla C|}, \tag{69.115}$$

which is directed orthogonal to a constant tracer contour. Using this expression for the normal direction within the tracer flux integral leads to

$$-\int_{\mathcal{S}} \nabla \cdot \boldsymbol{J} \, \mathrm{d}\mathcal{S} = \oint_{\partial\mathcal{S}} \nabla C \cdot \boldsymbol{K} \cdot \nabla C \, \frac{\rho \, \mathrm{d}l}{|\nabla C|}. \tag{69.116}$$

The diffusion tensor is a symmetric positive-definite second order tensor, so that the quadratic form in the integral is positive,

$$\nabla C \cdot \boldsymbol{K} \cdot \nabla C = K^{mn} \, \partial_m C \, \partial_n C > 0. \tag{69.117}$$

Furthermore, the line element, $\mathrm{d}l$, is positive, and so are ρ and $|\nabla C|$. Consequently, the integral around a closed tracer contour, where the normal to that contour is given by equation (69.115), is positive

$$-\int_{\mathcal{S}} \nabla \cdot \boldsymbol{J} \, \mathrm{d}\mathcal{S} = \int_{\partial\mathcal{S}} \partial_m C \, K^{mn} \, \partial_n C \, \mathrm{d}\mathrm{d}l > 0 \qquad \text{if } \hat{\boldsymbol{n}} = \nabla C / |\nabla C|. \tag{69.118}$$

[3] For example, consider a circular tracer contour surrounding a circular maximum, and assume isotropic diffusion. In this case the diffusive flux is radial so that it has a nonzero projection onto the outward normal.

However, this inequality contradicts the zero result (69.113). The zero result (69.113) is based only on the steady state assumption, whereas the inequality (69.118) is a direct result of assuming the tracer is inhomogeneous. Dropping the tracer inhomogeneity assumption is the only way to recover consistency.

69.8.2 Comments

Both of the above approaches led us to conclude that the tracer has zero gradient within the interior of a closed constant C contour; i.e., the steady state tracer concentration is homogeneous within a closed tracer contour. Given enough time to reach a steady state, diffusion, no matter how weak, expells all steady state tracer gradients from within regions bounded by closed tracer contours. This result can be extended to three dimensions, in which case steady state tracers are homogenous within closed volumes bounded by a constant tracer concentration. However, such bubble-like regions are less common for geophysical flows. In contrast, they are commonly found in quasi-two dimensional flows, including flows on constant isopycnals. So the theorem is more readily applied to two dimensional (or quasi two dimensional) flows. We offer another proof of the tracer homogenization result in Section 73.10.1 as part of our study of tracer mass analysis.

Furthermore, we assumed that the tracer equation included just a symmetric diffusion tensor, $\boldsymbol{K}$, in defining the subgrid flux (69.107). However, the theorem also holds if there is an additional anti-symmetric tensor, $\boldsymbol{A}$, added to $\boldsymbol{K}$. The reason is that an anti-symmetric tensor vanishes from the quadratic form (69.117)

$$\nabla C \cdot \boldsymbol{A} \cdot \nabla C = A^{mn}\, \partial_m C\, \partial_n C = 0. \tag{69.119}$$

That is, the tracer skew flux, $\boldsymbol{J}^{\text{skew}} = -\boldsymbol{A} \cdot \nabla C$, does not cross tracer isolines: $\nabla C \cdot \boldsymbol{J} = 0$, which we already found when studying skew fluxes in Section 69.5.

69.8.3 Further study

A powerful application of this theorem appears when the tracer, C, is a dynamically active tracer, such as vorticity or quasi-geostrophic potential vorticity (Chapter 45). The case of vorticity was discussed by *Batchelor* (1956), with *Rhines and Young* (1982) extending that work to the case of quasi-geostrophic potential vorticity. For the quasi-geostrophic case, contours of constant potential vorticity are known as *geostrophic contours*. *Rhines and Young* (1982) used the homogenization theorem to develop a theory of ocean circulation. They did so by considering potential vorticity homogenization by the mesoscale eddies that are active in regions of closed geostrophic contours, such as in mid-latitude ocean gyres.

69.9 Green's function method for passive tracers

Passive tracers (Section 20.1.5) have no impact on the flow field, so that they do not impact the fluid density nor the diffusion tensor. Hence, passive tracer patterns serve to "trace" the effects from advective and diffusive transport without affecting the transport velocity or diffusion tensor. Correspondingly, the passive tracer advection-diffusion equation is a linear partial differential equation. With some qualifications identified below, we can make use of the Green's function methods from Chapter 9 when studying solutions to the passive tracer equation. This section offers a supplement to the review paper from *Haine et al.* (2025) who synthesize the variety of Green's function methods of use for studying geophysical fluids. Although our formulation is largely based on ocean applications, the Green's function method for the advection-diffusion equation is also applicable to the atmosphere.

69.9.1 Concerning time dependent domain boundaries

The ocean free surface is time dependent, so that the domain, $\mathcal{R}$, is itself time dependent. Mathematically, this time dependence means that time and space integrations do not commute. In particular, space integration is generally written in the form

$$\int_{\mathcal{R}} \mathrm{d}V = \iint \left[\int_{\eta_b}^{\eta} \mathrm{d}z \right] \mathrm{d}x \, \mathrm{d}y, \tag{69.120}$$

where $z = \eta_b(x, y)$ is the static bottom and $z = \eta(x, y, t)$ is the time dependent free surface. We must, in turn, first compute the space integration over the full domain and then do the time time integration when deriving the reciprocity relation and the Green's function solution.

The free surface undulations make the vertical extent of the domain time dependent. Additionally, in an ocean with sloping sidewalls, the horizontal domain boundaries are also time dependent as the ocean moves up and down the sloping sides. However, allowing for the horizontal domain extent to fluctuate does not introduce any fundamentally new kinematics in our analysis. The reason is that when integrating to the lateral domain boundaries, all terms vanish since the water depth vanishes at the edge of the sloping beaches. We saw this kinematic result in Section 28.5 when integrating the angular momentum budget in a channel with sloping sidewalls.

Therefore, we assume the horizontal extent of the domain to be static in order to slightly ease the analysis. We do so by imagining a few meter high vertical seawall placed around the ocean domain edges, and by assuming a minimum depth so that there is nonzero water everywhere in the domain. These assumptions are common in ocean modeling, except in models allowing for wetting and drying of land/ocean cells. So in conclusion, we limit our analysis to time dependence of the vertical extent of the domain, with the horizontal extent static. Such limitation can be removed without much difficulty but doing so adds nothing new fundamentally.

69.9.2 Passive tracer boundary conditions

In this section, we are concerned with the evolution of a smooth passive tracer concentration, C, which is the dimensionless ratio of the tracer mass to seawater mass. Boundary conditions play a key role in the evolution. We here discuss the boundary conditions placed on the passive tracer along the ocean bottom, at $z = \eta_b(x, y)$, and the free surface, at $z = \eta(x, y, t)$.

Ocean bottom

At the static ocean bottom we generically consider a no-flux condition for the diffusive flux

$$\boldsymbol{J} \cdot \hat{\boldsymbol{n}} = -\rho \, \boldsymbol{K} \cdot \nabla C \cdot \hat{\boldsymbol{n}} = 0 \quad \text{at } z = \eta_b. \tag{69.121}$$

The no-flux condition, along with the kinematic no-normal flow condition, $\boldsymbol{v} \cdot \hat{\boldsymbol{n}} = 0$, means that there is zero tracer flux through the bottom.

Ocean free surface

At the ocean free surface we use results from Section 19.6.3, which developed the boundary conditions for mass flux $\mathcal{Q}_m$ (mass per time per area) across a permeable free surface, as well as Section 20.4, which developed the analogous boundary conditions for tracers. In particular, equation (20.84) provides an expression for the net mass flux of tracer crossing the free surface,

$\mathcal{Q}_C$, written as the sum of an advective flux plus a non-advective flux

$$\mathcal{Q}_C = C\,\mathcal{Q}_m - \boldsymbol{J}\cdot\hat{\boldsymbol{n}} = \underbrace{C\,\mathcal{Q}_m}_{\text{advective}} + \underbrace{\rho\,\boldsymbol{K}\cdot\nabla C\cdot\hat{\boldsymbol{n}}}_{\text{diffusive}} \quad \text{for } \boldsymbol{x}\in\partial\mathcal{R}_{\text{surface}}, \tag{69.122}$$

where C is the concentration at $z=\eta$, and we assumed the non-advective flux is given by a diffusive flux. We consider the following prescribed boundary conditions.

- ROBIN CONDITIONS: Prescribing the boundary tracer mass flux, $\mathcal{Q}_C$, leads to a Robin or mixed boundary condition

$$\mathcal{Q}_C = \text{prescribed} = C\,\mathcal{Q}_m + \rho\,\boldsymbol{K}\cdot\nabla C\cdot\hat{\boldsymbol{n}} \quad \text{for } \boldsymbol{x}\in\partial\mathcal{R}_{\text{surface}}. \tag{69.123}$$

  This boundary condition is relevant for enthalpy and salt, with full discussion given in Section 72.5. However, the Robin condition is rarely used for passive tracers along the ocean surface and so it is not further considered in this section.

- NEUMANN CONDITIONS: Prescribing the diffusive flux leads to the Neumann boundary condition

$$\rho\,\boldsymbol{K}\cdot\nabla C\cdot\hat{\boldsymbol{n}} = \text{prescribed} \equiv \Sigma(\boldsymbol{x},t) \quad \text{for } \boldsymbol{x}\in\partial\mathcal{R}_{\text{surface}}. \tag{69.124}$$

  This surface ocean boundary condition is also rarely used for passive tracers, though we do examine it within the following.

- DIRICHLET CONDITIONS: Prescribing the value of the tracer concentration at the boundary leads to the Dirichlet boundary condition

$$C = \text{prescribed} \equiv \sigma(\boldsymbol{x},t) \quad \text{for } \boldsymbol{x}\in\partial\mathcal{R}_{\text{surface}}. \tag{69.125}$$

  This boundary condition is the most commonly used condition for passive tracers, and thus it is our favored choice in the following. Note that both the Neumann and Dirichlet conditions generally involve a net transport of tracer, $\mathcal{Q}_C \neq 0$, across the ocean boundary.

As shown in Section 69.9.5, the Neumann boundary condition in the presence of a surface mass flux is problematic due to the associated non-closed reciprocity relation satisfied by the Green's function and its adjoint. The absence of a suitable reciprocity relation makes it difficult to use the Green's function method, since one would need to solve for both the Green's function and its adjoint. In contrast, the Dirichlet condition allows for a simple reciprocity relation, identical to that for the diffusion equation (Section 9.5.7), thus making the Green's function method for the advection-diffusion equation with a Dirichlet condition suitable even in the presence of a surface mass flux (see page 2450 of *Larson* (1999) for a similar point).

69.9.3 Advection-diffusion initial-boundary value problem

We study the initial-boundary value problem for a smooth passive tracer concentration, C, which is the dimensionless ratio of the tracer mass to seawater mass. The tracer is affected by advection and diffusion on a spatial domain, $\mathcal{R}$, in the presence of a tracer source, $\rho\,\Lambda$ (with dimensions of tracer mass per volume per time), with initial data available for the density and tracer concentration at time $t = t_{\text{init}}$. The initial-boundary value problem in the presence of Neumann or Dirichlet boundary conditions is given by

$$\partial_t(\rho\,C) + \nabla\cdot(\rho\,\boldsymbol{v}^\dagger\,C - \rho\,\boldsymbol{K}\cdot\nabla C) = \rho\,\Lambda \qquad \boldsymbol{x}\in\mathcal{R}, t\geq t_{\text{init}} \tag{69.126a}$$

$$\rho\,C = \rho\,I \qquad \boldsymbol{x}\in\mathcal{R}, t = t_{\text{init}} \tag{69.126b}$$

$$\hat{\boldsymbol{n}}\cdot\rho\,\boldsymbol{K}\cdot\nabla C = \rho\,\Sigma \quad \text{or} \quad \rho\,C = \rho\,\sigma \qquad \boldsymbol{x}\in\partial\mathcal{R}, t\geq t_{\text{init}}. \tag{69.126c}$$

The prescribed initial condition data for the tracer concentration at time $t = t_{\text{init}}$ is given by $I(\boldsymbol{x})$, and the initial density is also prescribed at this time, $\rho(\boldsymbol{x}, t_{\text{init}})$. We consider two options for the boundary condition at $\boldsymbol{x} \in \partial\mathcal{R}$: (i) the Neumann boundary condition with a prescribed flux, $\hat{\boldsymbol{n}} \cdot \rho \boldsymbol{K} \cdot \nabla C = \rho \Sigma$, or the (ii) Dirichlet boundary condition with a prescribed value, $\rho C = \rho \sigma$. Furthermore, we assume the flow field, $\boldsymbol{v}(\boldsymbol{x}, t)$, the eddy-induced velocity, $\boldsymbol{v}^*(\boldsymbol{x}, t)$, the seawater density, $\rho(\boldsymbol{x}, t)$, and the diffusivity tensor, $\boldsymbol{K}(\boldsymbol{x}, t)$, are known functions of space-time that are determined by solving for the dynamics, kinematics, thermodynamics, and active tracers. Finally, we assume the tracer concentration source, $\Lambda(\boldsymbol{x}, t)$, does not itself depend on the tracer concentration, C, thus ensuring linearity of the partial differential equation (69.126a).

69.9.4 The Green's function and its adjoint

Green's function problem

The Green's function corresponding to the passive tracer advection-diffusion equations (69.126a)-(69.126c) satisfies the following causal boundary value problem

$$\partial_t[\rho\, G(\boldsymbol{x}, t|\boldsymbol{x}_0, t_0)] + \nabla_{\boldsymbol{x}} \cdot [\rho\, \boldsymbol{v}^\dagger\, G(\boldsymbol{x}, t|\boldsymbol{x}_0, t_0) - \rho\, \boldsymbol{K} \cdot \nabla_{\boldsymbol{x}} G(\boldsymbol{x}, t|\boldsymbol{x}_0, t_0)] = \delta(\boldsymbol{x} - \boldsymbol{x}_0)\, \delta(t - t_0) \tag{69.127a}$$

$$G(\boldsymbol{x}, t < t_0|\boldsymbol{x}_0, t_0) = 0 \tag{69.127b}$$

$$\hat{\boldsymbol{n}}_{\boldsymbol{x}} \cdot \boldsymbol{K} \cdot \nabla_{\boldsymbol{x}} G(\boldsymbol{x} \in \partial\mathcal{R}, t|\boldsymbol{x}_0, t_0) = 0 \;\text{ or }\; G(\boldsymbol{x} \in \partial\mathcal{R}, t|\boldsymbol{x}_0, t_0) = 0. \tag{69.127c}$$

The space-time point, $(\boldsymbol{x}_0, t_0)$, is where the Dirac delta source is located, which is within the spatial domain, $\mathcal{R}$, and it fires at a time after the initial time

$$\boldsymbol{x}_0 \in \mathcal{R} \quad \text{and} \quad t_0 \geq t_{\text{init}}. \tag{69.128}$$

The Green's function satisfies homogeneous boundary conditions that correspond to the boundary conditions satisfied by the passive tracer concentration in equation (69.126c). That is, if the passive tracer satisfies a Dirichlet boundary condition, then the Green's function satisfies a homogeneous Dirichlet condition, and likewise for Neumann boundary conditions. Finally, since the Dirac delta source, $\delta(\boldsymbol{x} - \boldsymbol{x}_0)\, \delta(t - t_0)$, has dimensions of inverse volume times inverse time, the Green's function has dimensions of inverse mass. We physically interpret the Green's function as the tracer concentration resulting from an impulsive tracer concentration source, divided by the mass of tracer injected by the source.

Adjoint Green's function problem

The adjoint Green's function, $G^\ddagger$, satisfies the adjoint problem[4]

$$-\partial_t[\rho\, G^\ddagger(\boldsymbol{x}, t|\boldsymbol{x}_0, t_0)] + \nabla_{\boldsymbol{x}} \cdot [-\rho\, \boldsymbol{v}^\dagger\, G^\ddagger(\boldsymbol{x}, t|\boldsymbol{x}_0, t_0) - \rho\, \boldsymbol{K} \cdot \nabla_{\boldsymbol{x}} G^\ddagger(\boldsymbol{x}, t|\boldsymbol{x}_0, t_0)] = \delta(\boldsymbol{x} - \boldsymbol{x}_0)\, \delta(t - t_0) \tag{69.129a}$$

$$G^\ddagger(\boldsymbol{x}, t > t_0|\boldsymbol{x}_0, t_0) = 0 \tag{69.129b}$$

$$\hat{\boldsymbol{n}}_{\boldsymbol{x}} \cdot \boldsymbol{K} \cdot \nabla_{\boldsymbol{x}} G^\ddagger(\boldsymbol{x} \in \partial\mathcal{R}, t|\boldsymbol{x}_0, t_0) = 0 \;\text{ or }\; G^\ddagger(\boldsymbol{x} \in \partial\mathcal{R}, t|\boldsymbol{x}_0, t_0) = 0. \tag{69.129c}$$

Note the sign change on both the time derivative, as for the diffusion equation in Section 9.5.6, as well as the advection term. The sign change on advection is expected since with time running backwards, so too does the velocity of a fluid particle. Hence, the adjoint advection-diffusion equation is a backwards in time advection-diffusion equation.

[4] Note the use of the double dagger, ‡, for the adjoint Green's function, $G^\ddagger$, versus the single dagger, †, for the residual velocity, $\boldsymbol{v}^\dagger$.

69.9.5 Reciprocity relation

We here derive the reciprocity relation satisfied by the Green's function, G, and its adjoint, $G^\ddagger$. The derivation follows that in Section 9.3.6 for the Poisson equation and Section 9.5.7 for the diffusion equation. A new feature here arises from the advection operator, and another arises from allowing the domain boundary to be time dependent as occurs at the ocean free surface. We will see that the reciprocity relation for Neumann boundary conditions (69.127c) and (69.129c) does not "close" when there is mass transport across the ocean free surface (see equation (69.144) below). In contrast, the reciprocity relation closes with Dirichlet boundary conditions, taking the same form as for the diffusion equation in equation (9.156). We have more to say on this distinct behavior after its derivation.

Notation and setup

Consider the Green's function partial differential equation (69.127a) with a Dirac delta source, $\delta(\boldsymbol{x} - \boldsymbol{x}_1)\,\delta(t - t_1)$, along with the adjoint Green's function equation (69.129a) with a Dirac delta source, $\delta(\boldsymbol{x} - \boldsymbol{x}_2)\,\delta(t - t_2)$, where both sources are within the spatial domain and both occur later than the initial time:

$$\boldsymbol{x}_1, \boldsymbol{x}_2 \in \mathcal{R} \quad \text{and} \quad t_{\text{init}} < t_1, t_2. \tag{69.130}$$

We follow the approach in Section 9.5.7 for the diffusion equation by introducing the arbitrarily large time, T, such that $-T < t_1, t_2 < T$. As for the diffusion equation, causality conditions ensure that T drops out from the final expression for the tracer concentration. Additionally, to help ease notational clutter, we make use of the following shorthand where convenient

$$G(\boldsymbol{x}, t|\boldsymbol{x}_1, t_1) = G(1) \quad \text{and} \quad G^\ddagger(\boldsymbol{x}, t|\boldsymbol{x}_2, t_2) = G^\ddagger(2). \tag{69.131}$$

Cross-multiplication

Multiply the Green's function equation (69.127a) by $G^\ddagger(2)$ and the adjoint equation (69.129a) by $G(1)$ to find

$$G^\ddagger(2)\left(\partial_t[\rho\, G(1)] + \nabla_{\boldsymbol{x}} \cdot [\rho\, \boldsymbol{v}^\dagger\, G(1) - \rho\, \boldsymbol{K} \cdot \nabla_x G(1)]\right) = G^\ddagger(2)\,\delta(\boldsymbol{x} - \boldsymbol{x}_1)\,\delta(t - t_1) \tag{69.132a}$$

$$G(1)\left(-\partial_t[\rho\, G^\ddagger(2)] + \nabla_{\boldsymbol{x}} \cdot [-\rho\, \boldsymbol{v}^\dagger\, G^\ddagger(2) - \rho\, \boldsymbol{K} \cdot \nabla_{\boldsymbol{x}} G^\ddagger(2)]\right) = G(1)\,\delta(\boldsymbol{x} - \boldsymbol{x}_2)\,\delta(t - t_2). \tag{69.132b}$$

In the following, we work from the left hand side of equation (69.132a) and bring the differential operators from $G(1)$ onto $G^\ddagger(2)$. The result of this movement will be equation (69.132b) plus some extra terms whose form depends on the causality condition and boundary conditions. Integration over space and time will then render the reciprocity relation.

Self-adjointness of the generalized Laplacian operator

The generalized Laplacian operator term on the left hand side of equation (69.132a) can be written

$$\begin{aligned} &- G^\ddagger(2)\,\nabla_{\boldsymbol{x}} \cdot [\rho\, \boldsymbol{K} \cdot \nabla_{\boldsymbol{x}} G(1)] \\ &= \nabla_{\boldsymbol{x}} \cdot [-G^\ddagger(2)\,\rho\, \boldsymbol{K} \cdot \nabla_{\boldsymbol{x}} G(1) + G(1)\,\rho\, \boldsymbol{K} \cdot \nabla_{\boldsymbol{x}} G^\ddagger(2)] - G(1)\,\nabla_{\boldsymbol{x}} \cdot [\rho\, \boldsymbol{K} \cdot \nabla_{\boldsymbol{x}} G^\ddagger(2)]. \end{aligned} \tag{69.133}$$

A spatial integration of this equation over the region $\mathcal{R}$, and use of the homogeneous boundary conditions in equations (69.126c) or (69.129c) eliminates the divergence term to reveal

$$\int_{\mathcal{R}} G^{\ddagger}(\boldsymbol{x},t|\boldsymbol{x}_2,t_2)\,\nabla_{\boldsymbol{x}}\cdot[\rho\,\boldsymbol{K}\cdot\nabla_{\boldsymbol{x}}G(\boldsymbol{x},t|\boldsymbol{x}_1,t_1)]\,\mathrm{d}V = \int_{\mathcal{R}} G(\boldsymbol{x},t|\boldsymbol{x}_1,t_1)\,\nabla_{\boldsymbol{x}}\cdot[\rho\,\boldsymbol{K}\cdot\nabla_{\boldsymbol{x}}G^{\ddagger}(\boldsymbol{x},t|\boldsymbol{x}_2,t_2)]\,\mathrm{d}V. \quad (69.134)$$

This equality proves that the generalized Laplacian operator with a symmetric diffusion tensor is self-adjoint, which is a result already encountered in Section 9.5.7 when discussing the diffusion equation. This result holds for either Neumann or Dirichlet boundary conditions.

Time derivative plus advection

Next write the time derivative and advection portion of equation (69.132a) as

$$\begin{aligned}
&G^{\ddagger}(2)\left(\partial_t[\rho\,G(1)]+\nabla_{\boldsymbol{x}}\cdot[\rho\,\boldsymbol{v}^{\dagger}\,G(1)]\right)\\
&=\partial_t[G^{\ddagger}(2)\,\rho\,G(1)]+\nabla_{\boldsymbol{x}}\cdot[G^{\ddagger}(2)\,\rho\,\boldsymbol{v}^{\dagger}\,G(1)]-G(1)\,\rho\left[\partial_t G^{\ddagger}(2)+\boldsymbol{v}^{\dagger}\cdot\nabla_{\boldsymbol{x}}G^{\ddagger}(2)\right]\\
&=\partial_t[G^{\ddagger}(2)\,\rho\,G(1)]+\nabla_{\boldsymbol{x}}\cdot[G^{\ddagger}(2)\,\rho\,\boldsymbol{v}^{\dagger}\,G(1)]-G(1)\left(\partial_t(\rho\,G^{\ddagger}(2))+\nabla\cdot[\rho\,\boldsymbol{v}^{\dagger}G^{\ddagger}(2)]\right), \quad (69.135)
\end{aligned}$$

where we used the mass continuity equation (19.6) for the final equality. Rearrangment thus leads to

$$G^{\ddagger}(2)\left(\partial_t[\rho\,G(1)]+\nabla_{\boldsymbol{x}}\cdot[\rho\,\boldsymbol{v}^{\dagger}\,G(1)]\right)-G(1)\left(-\partial_t[\rho\,G^{\ddagger}(2)]-\nabla\cdot[\rho\,\boldsymbol{v}^{\dagger}G^{\ddagger}(2)]\right) = \partial_t[G^{\ddagger}(2)\,\rho\,G(1)]+\nabla_{\boldsymbol{x}}\cdot[G^{\ddagger}(2)\,\rho\,\boldsymbol{v}^{\dagger}\,G(1)]. \quad (69.136)$$

Space integration

Now integrate equations (69.132a) and (69.132b) over the spatial domain, $\mathcal{R}$, subtract these two equations, and make use of the results (69.134) and (69.136) to reveal

$$G^{\ddagger}(\boldsymbol{x}_1,t|\boldsymbol{x}_2,t_2)\,\delta(t-t_1)-G(\boldsymbol{x}_2,t|\boldsymbol{x}_1,t_1)\,\delta(t-t_2) = \int_{\mathcal{R}}\left[\partial_t[G^{\ddagger}(2)\,\rho\,G(1)]+\nabla_{\boldsymbol{x}}\cdot[G^{\ddagger}(2)\,\rho\,\boldsymbol{v}^{\dagger}\,G(1)]\right]\mathrm{d}V. \quad (69.137)$$

The divergence term on the right hand side takes the form

$$\int_{\mathcal{R}}\nabla_{\boldsymbol{x}}\cdot[G^{\ddagger}(2)\,\rho\,\boldsymbol{v}^{\dagger}\,G(1)]\,\mathrm{d}V = \oint_{\partial\mathcal{R}} G^{\ddagger}(2)\,G(1)\,\rho\,\boldsymbol{v}^{\dagger}\cdot\hat{\boldsymbol{n}}_{\boldsymbol{x}}\,\mathrm{d}\mathcal{S} \qquad \text{divergence theorem} \quad (69.138a)$$

$$= \oint_{\partial\mathcal{R}} G^{\ddagger}(2)\,G(1)\,\rho\,\boldsymbol{v}\cdot\hat{\boldsymbol{n}}_{\boldsymbol{x}}\,\mathrm{d}\mathcal{S} \qquad \hat{\boldsymbol{n}}\cdot\boldsymbol{v}^{*}=0 \quad (69.138b)$$

$$= \int_{z=\eta} G^{\ddagger}(2)\,G(1)\,\rho\,\boldsymbol{v}\cdot\hat{\boldsymbol{n}}_{\boldsymbol{x}}\,\mathrm{d}\mathcal{S} \qquad \boldsymbol{v}\cdot\hat{\boldsymbol{n}}=0 \text{ for } z=\eta_{\mathrm{b}} \quad (69.138c)$$

$$= \int_{z=\eta} G^{\ddagger}(2)\,G(1)\,\rho\,\boldsymbol{v}\cdot\nabla(z-\eta)\,\mathrm{d}A \qquad \text{equation (19.91)} \quad (69.138d)$$

$$= \int_{z=\eta} G^\ddagger(2)\, G(1)\, \rho\, (w - \boldsymbol{u} \cdot \nabla \eta)\, \mathrm{d}A. \tag{69.138e}$$

The time derivative term takes the form

$$\int_{\mathscr{R}} \partial_t [G^\ddagger(2)\, G(1)\, \rho]\, \mathrm{d}V = \frac{\partial}{\partial t} \left[\int_{\mathscr{R}} G^\ddagger(2)\, G(1)\, \rho\, \mathrm{d}V \right] - \int_{z=\eta} \left[G^\ddagger(2)\, G(1)\, \rho\, \partial_t \eta \right] \mathrm{d}A, \tag{69.139}$$

where we made use of Leibniz's rule to bring the time derivative across the integral sign and made note of the time dependent free surface, $z = \eta(x, y, t)$. Combining equations (69.139) and (69.138e) leads to

$$G^\ddagger(\boldsymbol{x}_1, t | \boldsymbol{x}_2, t_2)\, \delta(t - t_1) - G(\boldsymbol{x}_2, t | \boldsymbol{x}_1, t_1)\, \delta(t - t_2) \tag{69.140a}$$

$$= \frac{\partial}{\partial t} \left[\int_{\mathscr{R}} G^\ddagger(2)\, G(1)\, \rho\, \mathrm{d}V \right] + \int_{z=\eta} G^\ddagger(2)\, G(1)\, [\rho\, (w - \boldsymbol{u} \cdot \nabla \eta - \partial_t \eta)]\, \mathrm{d}A \tag{69.140b}$$

$$= \frac{\partial}{\partial t} \left[\int_{\mathscr{R}} G^\ddagger(2)\, G(1)\, \rho\, \mathrm{d}V \right] - \int_{z=\eta} G^\ddagger(2)\, G(1)\, Q_{\mathsf{m}}\, \mathrm{d}A, \tag{69.140c}$$

where the final equality follows from the surface ocean kinematic boundary condition (19.94), with Q_{m} the mass per time per horizontal area crossing the ocean surface.

Time integration

We are now ready to integrate equation (69.140c) over time, with its left hand side leading to

$$\int_{-T}^{T} \left[G^\ddagger(\boldsymbol{x}_1, t | \boldsymbol{x}_2, t_2)\, \delta(t - t_1) - G(\boldsymbol{x}_2, t | \boldsymbol{x}_1, t_1)\, \delta(t - t_2) \right] \mathrm{d}t$$

$$= G^\ddagger(\boldsymbol{x}_1, t_1 | \boldsymbol{x}_2, t_2) - G(\boldsymbol{x}_2, t_2 | \boldsymbol{x}_1, t_1), \tag{69.141}$$

which used the sifting property (7.69). There are two terms that appear when time integrating the time derivative on the right hand side of equation (69.140c), with each term vanishing due to the causality conditions (69.127b) and (69.129b)

$$\int_{\mathscr{R}} G^\ddagger(\boldsymbol{x}, t = T | \boldsymbol{x}_2, t_2)\, G(\boldsymbol{x}, t = T | \boldsymbol{x}_1, t_1)\, \rho\, \mathrm{d}V = 0 \quad \Longleftarrow G^\ddagger(\boldsymbol{x}, t = T | \boldsymbol{x}_2, t_2) = 0 \tag{69.142}$$

$$\int_{\mathscr{R}} G^\ddagger(\boldsymbol{x}, t = t_{\text{init}} | \boldsymbol{x}_2, t_2)\, G(\boldsymbol{x}, t = t_{\text{init}} | \boldsymbol{x}_1, t_1)\, \rho\, \mathrm{d}V = 0 \quad \Longleftarrow G(\boldsymbol{x}, t = t_{\text{init}} | \boldsymbol{x}_1, t_1) = 0. \tag{69.143}$$

We are thus left with

$$G^\ddagger(\boldsymbol{x}_1, t_1 | \boldsymbol{x}_2, t_2) - G(\boldsymbol{x}_2, t_2 | \boldsymbol{x}_1, t_1)$$

$$= - \int_{t_{\text{init}}}^{t_1} \left[\int_{z=\eta} G^\ddagger(\boldsymbol{x}, t | \boldsymbol{x}_2, t_2)\, G(\boldsymbol{x}_1, t_1 | \boldsymbol{x}, t)\, Q_{\mathsf{m}}\, \mathrm{d}A \right] \mathrm{d}t, \tag{69.144}$$

which we refer to as a *non-closed reciprocity relation* between G and $G^\ddagger$. Note that the time limits on the integral follow from causality on the Green's function and its adjoint.

Closed form reciprocity in special cases

There are two cases in which the relation (69.144) leads to a closed reciprocity relation:

- Zero mass flux across surface: $Q_{\mathsf{m}} = 0$.

- Homogeneous Dirichlet boundary conditions, in which case $G^\ddagger(\boldsymbol{x} \in \partial\mathcal{R}, t|\boldsymbol{x}_0, t_0) = G(\boldsymbol{x} \in \partial\mathcal{R}, t|\boldsymbol{x}_0, t_0) = 0$.

In either case we are led to

$$G^\ddagger(\boldsymbol{x}_1, t_1|\boldsymbol{x}_2, t_2) = G(\boldsymbol{x}_2, t_2|\boldsymbol{x}_1, t_1), \tag{69.145}$$

which is the same reciprocity (9.156) satisfied for the diffusion equation Green's functions.

The more nuanced reciprocity for the advection-diffusion equation arises from the advective mass flux at the ocean free surface boundary. The mass flux couples the ocean with its surrounding media (e.g., the atmosphere, rivers, or cryosphere), and in so doing precludes a general closed reciprocity relation. However, the Dirichlet boundary condition closes the surface boundary through the homogeneous Green's function boundary conditions. Most applications of Green's function methods for passive ocean tracers make use of Dirichlet boundary conditions, in which case we are afforded a closed reciprocity relation even with a free surface open to mass transport.

69.9.6 Composition property

We here follow the analysis of Section 9.5.8 to derive the composition property of the Green's function for the advection-diffusion equation. For this purpose, return to the cross-multiplication equations (69.132a) and (69.132b) used to derive reciprocity, here written as

$$G^\ddagger(2)\left(\partial_t[\rho\, G(1)] + \nabla_{\boldsymbol{x}} \cdot [\rho\, \boldsymbol{v}^\dagger\, G(1) - \rho\, \boldsymbol{K} \cdot \nabla_x G(1)]\right) = G^\ddagger(2)\, \delta(\boldsymbol{x} - \boldsymbol{x}_1)\, \delta(t - t_1) \tag{69.146a}$$

$$G(1)\left(\partial_t[\rho\, G^\ddagger(2)] + \nabla_{\boldsymbol{x}} \cdot [\rho\, \boldsymbol{v}^\dagger\, G^\ddagger(2) + \rho\, \boldsymbol{K} \cdot \nabla_{\boldsymbol{x}} G^\ddagger(2)]\right) = -G(1)\, \delta(\boldsymbol{x} - \boldsymbol{x}_2)\, \delta(t - t_2). \tag{69.146b}$$

Adding these two equations and use of mass continuity (19.6) brings the left hand side to

$$\text{LHS} = \partial_t[\rho\, G(1)\, G^\ddagger(2)] + \nabla_{\boldsymbol{x}} \cdot [\rho\, \boldsymbol{v}^\dagger\, G(1)\, G^\ddagger(2) + \rho\, G(1)\, \boldsymbol{K} \cdot \nabla_{\boldsymbol{x}} G^\ddagger(2) - \rho\, G^\ddagger(2)\, \boldsymbol{K} \cdot \nabla_{\boldsymbol{x}} G(1)]. \tag{69.147}$$

Integration over the domain $\mathcal{R}$ eliminates the diffusion terms for both the Dirichlet and Neumann boundary conditions. For the time derivative term we use Leibniz's rule to write

$$\int_{\mathcal{R}} \partial_t[\rho\, G(1)\, G^\ddagger(2)]\, \mathrm{d}V = \frac{\mathrm{d}}{\mathrm{d}t} \int_{\mathcal{R}} \rho\, G(1)\, G^\ddagger(2)\, \mathrm{d}V - \int_{z=\eta} \rho\, G(1)\, G^\ddagger(2)\, \partial_t \eta\, \mathrm{d}A. \tag{69.148a}$$

For the advection term we follow the manipulations used for equation (69.138e) to derive

$$\int_{\mathcal{R}} \nabla_{\boldsymbol{x}} \cdot [\rho\, \boldsymbol{v}^\dagger\, G(1)\, G^\ddagger(2)]\, \mathrm{d}V = \int_{z=\eta} \rho\, G(1)\, G^\ddagger(2)\, \boldsymbol{v}^\dagger \cdot \hat{\boldsymbol{n}}\, \mathrm{d}\mathcal{S} \tag{69.149a}$$

$$= \int_{z=\eta} \rho\, G(1)\, G^\ddagger(2)\, (w - \boldsymbol{u} \cdot \nabla\eta)\, \mathrm{d}A \tag{69.149b}$$

$$= \int_{z=\eta} G(1)\, G^\ddagger(2)\, (\rho\, \partial_t \eta - Q_{\mathsf{m}})\, \mathrm{d}A. \tag{69.149c}$$

Bringing the pieces together and expanding the arguments leads to

$$\frac{\mathrm{d}}{\mathrm{d}t} \int_{\mathcal{R}} \rho(\boldsymbol{x}, t)\, G(\boldsymbol{x}, t|\boldsymbol{x}_1, t_1)\, G^\ddagger(\boldsymbol{x}, t|\boldsymbol{x}_2, t_2)\, \mathrm{d}V = G^\ddagger(\boldsymbol{x}_1, t|\boldsymbol{x}_2, t_2)\, \delta(t - t_1) - G(\boldsymbol{x}_2, t|\boldsymbol{x}_1, t_1)\, \delta(t - t_2) - \int_{z=\eta} G(\boldsymbol{x}, t|\boldsymbol{x}_1, t_1)\, G^\ddagger(\boldsymbol{x}, t|\boldsymbol{x}_2, t_2)\, Q_{\mathsf{m}}(\boldsymbol{x}, t)\, \mathrm{d}A. \tag{69.150}$$

As for the derivation of reciprocity in Section 69.9.5, we here assume either $Q_m = 0$ or a homogeneous Dirichlet boundary condition so that

$$\frac{\mathrm{d}}{\mathrm{d}t}\int_{\mathcal{R}} \rho(\boldsymbol{x},t)\, G(\boldsymbol{x},t|\boldsymbol{x}_1,t_1)\, G^\ddagger(\boldsymbol{x},t|\boldsymbol{x}_2,t_2)\,\mathrm{d}V = G^\ddagger(\boldsymbol{x}_1,t|\boldsymbol{x}_2,t_2)\,\delta(t-t_1) - G(\boldsymbol{x}_2,t|\boldsymbol{x}_1,t_1)\,\delta(t-t_2). \quad (69.151)$$

This equation is directly analogous to equation (9.165) satisfied by the diffusion equation Green's function. Following from that analysis, and making use of reciprocity (69.145), we find the composition property for the advection-diffusion equation

$$G(\boldsymbol{x}_2,t_2|\boldsymbol{x}_1,t_1) = \int_{\mathcal{R}} \rho(\boldsymbol{x},\tau)\, G(\boldsymbol{x}_2,t_2|\boldsymbol{x},\tau)\, G(\boldsymbol{x},\tau|\boldsymbol{x}_1,t_1)\,\mathrm{d}V \quad \text{if } t_1 < \tau < t_2. \quad (69.152)$$

The left hand side of this equation is the response from a Dirac source that is advected-diffused from $(\boldsymbol{x}_1,t_1)$ and measured at the space-time point $(\boldsymbol{x}_2,t_2)$. The right hand side is the composition of a Green's function feeling the source at $(\boldsymbol{x}_1,t_1)$ but now sampled at an intermediate space-time position, $(\boldsymbol{x},\tau)$, and then further advective-diffused to $(\boldsymbol{x}_2,t_2)$, with integration over all possible intermediate positions $\boldsymbol{x}$. The intermediate sampling can occur at an arbitrary intermediate time τ, so long as $t_1 < \tau < t_2$. The composition property (69.152) allows us to conceive of a long-time interval Green's function as the composition of an arbitrary number of shorter time interval Green's functions.

69.9.7 Integral expression for the tracer concentration

We are now ready to express the passive tracer concentration, C, as a suite of integrals involving the Green's function and the known boundary and initial conditions as well as the known source function. The process for deriving this expression is identical to that used in Section 69.9.5 for reciprocity, with the following steps offered for completeness.

Derivation setup

The initial-boundary value problem for the passive tracer is given by

$$\partial_t(\rho C) + \nabla\cdot(\rho\,\boldsymbol{v}^\dagger\, C - \rho\,\boldsymbol{K}\cdot\nabla C) = \rho\,\Lambda \qquad \boldsymbol{x}\in\mathcal{R}, t\geq t_{\text{init}} \quad (69.153a)$$

$$\rho\, C = \rho\, I \qquad \boldsymbol{x}\in\mathcal{R}, t = t_{\text{init}} \quad (69.153b)$$

$$\rho\, C = \rho\,\sigma \qquad \boldsymbol{x}\in\partial\mathcal{R}, t\geq t_{\text{init}} \quad (69.153c)$$

where we only consider the Dirichlet boundary condition to ensure a closed reciprocity relation in the presence of surface mass fluxes (Section 69.9.5). The corresponding adjoint Green's function satisfies

$$-\partial_t[\rho\, G^\ddagger(\boldsymbol{x},t|\boldsymbol{x}_0,t_0)] + \nabla_{\boldsymbol{x}}\cdot[-\rho\,\boldsymbol{v}^\dagger\, G^\ddagger(\boldsymbol{x},t|\boldsymbol{x}_0,t_0) - \rho\,\boldsymbol{K}\cdot\nabla_{\boldsymbol{x}} G^\ddagger(\boldsymbol{x},t|\boldsymbol{x}_0,t_0)] = \delta(\boldsymbol{x}-\boldsymbol{x}_0)\,\delta(t-t_0) \quad (69.154a)$$

$$G^\ddagger(\boldsymbol{x},t>t_0|\boldsymbol{x}_0,t_0) = 0 \quad (69.154b)$$

$$G^\ddagger(\boldsymbol{x}\in\partial\mathcal{R},t|\boldsymbol{x}_0,t_0) = 0, \quad (69.154c)$$

with the reciprocity condition (69.145) holding since we chose Dirichlet boundary conditions. Multiplying the adjoint Green's function equation (69.154a) by $C(\boldsymbol{x},t)$ and performing manipulations just like those for reciprocity leads to

$$-\partial_t(\rho\, C\, G^\ddagger) + \nabla_{\boldsymbol{x}}\cdot\Big[G^\ddagger\,\rho\,\boldsymbol{K}\cdot\nabla C - C\,\rho\,\boldsymbol{K}(\boldsymbol{x},t)\cdot\nabla_{\boldsymbol{x}} G^\ddagger - C\,\rho\,\boldsymbol{v}^\dagger\, G^\ddagger\Big] + G^\ddagger\,\rho\,\Lambda$$

$$= C(\boldsymbol{x}, t)\, \delta(\boldsymbol{x} - \boldsymbol{x}_0)\, \delta(t - t_0). \quad (69.155)$$

With the homogeneous Dirichlet conditions satisfied by $G^\ddagger$ on the spatial boundaries, a space and time integration over $(\boldsymbol{x}, t)$ leads to

$$\begin{aligned} C(\boldsymbol{x}_0, t_0) = &\int_{\mathscr{R}} G^\ddagger(\boldsymbol{x}, t_{\text{init}} | \boldsymbol{x}_0, t_0)\, \rho(\boldsymbol{x}, t_{\text{init}})\, I(\boldsymbol{x})\, \mathrm{d}V \\ &+ \int_{t_{\text{init}}}^{t_0} \left[\int_{\mathscr{R}} G^\ddagger(\boldsymbol{x}, t | \boldsymbol{x}_0, t_0)\, \rho(\boldsymbol{x}, t)\, \Lambda(\boldsymbol{x}, t)\, \mathrm{d}V \right] \mathrm{d}t \\ &- \int_{t_{\text{init}}}^{t_0} \left[\oint_{\partial\mathscr{R}} \sigma(\boldsymbol{x}, t)\, \rho(\boldsymbol{x}, t)\, \boldsymbol{K}(\boldsymbol{x}, t) \cdot \nabla_{\boldsymbol{x}} G^\ddagger(\boldsymbol{x}, t | \boldsymbol{x}_0, t_0) \cdot \hat{\boldsymbol{n}}_{\boldsymbol{x}}\, \mathrm{d}\mathcal{S} \right] \mathrm{d}t. \quad (69.156) \end{aligned}$$

Use of the reciprocity relation (69.145) allows us to write this equation in terms of the Green's function rather than the adjoint Green's function

$$\begin{aligned} C(\boldsymbol{x}_0, t_0) = &\int_{\mathscr{R}} G(\boldsymbol{x}_0, t_0 | \boldsymbol{x}, t_{\text{init}})\, \rho(\boldsymbol{x}, t_{\text{init}})\, I(\boldsymbol{x})\, \mathrm{d}V \\ &+ \int_{t_{\text{init}}}^{t_0} \left[\int_{\mathscr{R}} G(\boldsymbol{x}_0, t_0 | \boldsymbol{x}, t)\, \rho(\boldsymbol{x}, t)\, \Lambda(\boldsymbol{x}, t)\, \mathrm{d}V \right] \mathrm{d}t \\ &- \int_{t_{\text{init}}}^{t_0} \left[\oint_{\partial\mathscr{R}} \sigma(\boldsymbol{x}, t)\, \rho(\boldsymbol{x}, t)\, \boldsymbol{K}(\boldsymbol{x}, t) \cdot \nabla_{\boldsymbol{x}} G(\boldsymbol{x}_0, t_0 | \boldsymbol{x}, t) \cdot \hat{\boldsymbol{n}}_{\boldsymbol{x}}\, \mathrm{d}\mathcal{S} \right] \mathrm{d}t. \quad (69.157) \end{aligned}$$

Finally, swapping labels $(\boldsymbol{x}_0, t_0) \leftrightarrow (\boldsymbol{x}, t)$ renders

$$\begin{aligned} C(\boldsymbol{x}, t) = &\int_{\mathscr{R}} G(\boldsymbol{x}, t | \boldsymbol{x}_0, t_{\text{init}})\, \rho(\boldsymbol{x}_0, t_{\text{init}})\, I(\boldsymbol{x}_0)\, \mathrm{d}V_0 \\ &+ \int_{t_{\text{init}}}^{t} \left[\int_{\mathscr{R}} G(\boldsymbol{x}, t | \boldsymbol{x}_0, t_0)\, \rho(\boldsymbol{x}_0, t_0)\, \Lambda(\boldsymbol{x}_0, t_0)\, \mathrm{d}V_0 \right] \mathrm{d}t_0 \\ &- \int_{t_{\text{init}}}^{t} \left[\oint_{\partial\mathscr{R}} \sigma(\boldsymbol{x}_0, t_0)\, \rho(\boldsymbol{x}_0, t_0)\, \boldsymbol{K}(\boldsymbol{x}_0, t_0) \cdot \nabla_{\boldsymbol{x}_0} G(\boldsymbol{x}, t | \boldsymbol{x}_0, t_0) \cdot \hat{\boldsymbol{n}}_{\boldsymbol{x}_0}\, \mathrm{d}\mathcal{S}_0 \right] \mathrm{d}t_0. \quad (69.158) \end{aligned}$$

This solution manifests causality since the tracer concentration at time t is a function only of processes occuring from t_{init} up to time t.

69.9.8 Properties of the tracer concentration

The integral solution (69.158) is of the same form as equation (9.176) for the diffusion equation. Properties of this solution, and corresponding properties of the Green's function, follow from those satisfied by the diffusion equation as detailed in Section 9.5. We here summarize these properties for completeness.

The role of advection and diffusion at boundaries

Explicit contributions from the advective flux are absent from the solution (69.158). Namely, there are no advective flux contributions at the surface boundary due to the homogeneous Dirichlet boundary conditions imposed on the Green's function. For the ocean bottom, material and rigid no-flux conditions mean that $\boldsymbol{v} \cdot \hat{\boldsymbol{n}} = 0$ at the bottom. The presence of advection arises only through its effect on the Green's function, which is affected by both advection and diffusion.

Furthermore, notice how in the absence of diffusion (i.e., $\boldsymbol{K} = 0$) the Dirichlet boundary data is unable to penetrate into the ocean interior since the surface boundary integral vanishes from equation (69.158). In effect, the surface boundary becomes a material surface when there

is no diffusion. That is, diffusive mixing is needed for boundary data to move into the interior. This role for diffusion was also identified when studying the surface flux condition for salt and freshwater in Section 72.5 (see also *Nurser and Griffies* (2019)).

Initial conditions

When sampling the tracer concentration at the initial time, $t \to t_{\text{init}}$, all the time integrals vanish from the solution (69.158), thus leaving

$$\lim_{t \to t_{\text{init}}} C(\boldsymbol{x}, t) = \lim_{t \to t_{\text{init}}} \int_{\mathscr{R}} G(\boldsymbol{x}, t | \boldsymbol{x}_0, t_{\text{init}})\, \rho(\boldsymbol{x}_0, t_{\text{init}})\, I(\boldsymbol{x}_0)\, \mathrm{d}V_0. \tag{69.159}$$

Self-consistency implies that the Green's function satisfies

$$\lim_{t \to t_{\text{init}}} G(\boldsymbol{x}, t | \boldsymbol{x}_0, t_{\text{init}})\, \rho(\boldsymbol{x}_0, t_{\text{init}}) = \delta(\boldsymbol{x} - \boldsymbol{x}_0) \quad \text{with } \boldsymbol{x}, \boldsymbol{x}_0 \in \mathscr{R}, \tag{69.160}$$

so that

$$\lim_{t \to t_{\text{init}}} \int_{\mathscr{R}} \rho(\boldsymbol{x}, t_{\text{init}})\, G(\boldsymbol{x}, t | \boldsymbol{x}_0, t_{\text{init}})\, I(\boldsymbol{x}_0)\, \mathrm{d}V_0 = \int_{\mathscr{R}} \delta(\boldsymbol{x} - \boldsymbol{x}_0)\, I(\boldsymbol{x}_0)\, \mathrm{d}V_0 = I(\boldsymbol{x}). \tag{69.161}$$

Dirichlet boundary conditions

Evaluating the Dirichlet solution (69.158) on a spatial boundary, $\boldsymbol{x} \in \partial\mathscr{R}$, eliminates both the volume integrals given that the Green's function satisfies homogeneous Dirichlet boundary conditions. The tracer concentration (69.158) thus takes the form

$$C(\boldsymbol{x}, t) = -\int_{t_{\text{init}}}^{t} \left[\oint_{\partial\mathscr{R}} \sigma(\boldsymbol{x}_0, t_0)\, \rho(\boldsymbol{x}_0, t_0)\, \boldsymbol{K}(\boldsymbol{x}_0, t_0) \cdot \nabla_{\boldsymbol{x}_0} G(\boldsymbol{x}, t | \boldsymbol{x}_0, t_0) \cdot \hat{\boldsymbol{n}}_{\boldsymbol{x}_0}\, \mathrm{d}\mathcal{S}_0 \right] \mathrm{d}t_0 \quad \text{with } \boldsymbol{x} \in \partial\mathscr{R}. \tag{69.162}$$

Self-consistency with the Dirichlet boundary condition (69.126c) implies that the Green's function, when both spatial points are evaluated on the boundary, satisfies

$$\rho(\boldsymbol{x}_0, t_0)\, \boldsymbol{K}(\boldsymbol{x}_0, t_0) \cdot \nabla_{\boldsymbol{x}_0} G(\boldsymbol{x}, t | \boldsymbol{x}_0, t_0) \cdot \hat{\boldsymbol{n}}_{\boldsymbol{x}_0} = -\delta(t - t_0)\, \delta^{(2)}(\boldsymbol{x} - \boldsymbol{x}_0) \quad \text{with } \boldsymbol{x}, \boldsymbol{x}_0 \in \partial\mathscr{R}, \tag{69.163}$$

so that

$$C(\boldsymbol{x}, t) = \int_{t_{\text{init}}}^{t} \left[\oint_{\partial\mathscr{R}} \sigma(\boldsymbol{x}_0, t_0)\, \delta(t - t_0)\, \delta^{(2)}(\boldsymbol{x} - \boldsymbol{x}_0) \mathrm{d}\mathcal{S}_0 \right] \mathrm{d}t_0 = \sigma(\boldsymbol{x}, t) \quad \text{with } \boldsymbol{x} \in \partial\mathscr{R}. \tag{69.164}$$

69.9.9 Boundary propagator

Defining the boundary propagator

As for the diffusion equation in Section 9.5.13, we here introduce the boundary propagator for the advection-diffusion equation with Dirichlet boundary conditions. For this purpose, consider the special case of a passive tracer with zero interior source and with zero initial condition, thus satisfying the initial-boundary value problem

$$\partial_t(\rho\, C) + \nabla \cdot (\rho\, \boldsymbol{v}^{\dagger}\, C - \rho\, \boldsymbol{K} \cdot \nabla C) = 0 \qquad \boldsymbol{x} \in \mathscr{R}, t \geq t_{\text{init}} \tag{69.165a}$$

$$\rho\, C = 0 \qquad \boldsymbol{x} \in \mathscr{R}, t = t_{\text{init}} \tag{69.165b}$$

$$\rho\, C = \rho\, \sigma \qquad \boldsymbol{x} \in \partial\mathscr{R}, t \geq t_{\text{init}}, \tag{69.165c}$$

which leads to the simplification of the Green's function solution (69.158)

$$C(\boldsymbol{x},t) = -\int_{t_{\text{init}}}^{t} \left[\oint_{\partial\mathcal{R}} \sigma(\boldsymbol{x}_0,t_0)\, \rho(\boldsymbol{x}_0,t_0)\, \boldsymbol{K}(\boldsymbol{x}_0,t_0) \cdot \nabla_{\boldsymbol{x}_0} G(\boldsymbol{x},t|\boldsymbol{x}_0,t_0) \cdot \hat{\boldsymbol{n}}_{\boldsymbol{x}_0}\, \mathrm{d}\mathcal{S}_0 \right] \mathrm{d}t_0. \quad (69.166)$$

The tracer concentration at a point in space-time is determined by the history of the advection and diffusion that transfers boundary information to this point. To manifest this cause-effect relation, it is useful to define the boundary propagator just as for the diffusion equation

$$G^{\text{bp}}(\boldsymbol{x},t|\boldsymbol{x}_0,t_0) \equiv -\rho(\boldsymbol{x}_0,t_0)\, \boldsymbol{K}(\boldsymbol{x}_0,t_0) \cdot \nabla_{\boldsymbol{x}_0} G(\boldsymbol{x},t|\boldsymbol{x}_0,t_0) \cdot \hat{\boldsymbol{n}}_{\boldsymbol{x}_0} \quad \text{with } \boldsymbol{x}_0 \in \partial\mathcal{R}, \quad (69.167)$$

with G^{bp} having dimensions $\mathrm{L}^{-2}\ \mathrm{T}^{-1}$. The boundary propagator thus brings the tracer concentration (69.166) into the rather tidy form

$$C(\boldsymbol{x},t) = \int_{t_{\text{init}}}^{t} \left[\oint_{\partial\mathcal{R}} \sigma(\boldsymbol{x}_0,t_0)\, G^{\text{bp}}(\boldsymbol{x},t|\boldsymbol{x}_0,t_0)\, \mathrm{d}\mathcal{S}_0 \right] \mathrm{d}t_0. \quad (69.168)$$

Inhomogeneous Dirichlet at the surface and homogeneous Neumann at the bottom

In applications of passive tracers to study ocean circulation, it is common to apply inhomogeneous Dirichlet boundary conditions just at the ocean surface, and homogeneous Neumann boundary conditions (no-flux) at the ocean bottom

$$\partial_t(\rho\, C) + \nabla \cdot (\rho\, \boldsymbol{v}^{\dagger}\, C - \rho\, \boldsymbol{K} \cdot \nabla C) = 0 \qquad \boldsymbol{x} \in \mathcal{R}, t \geq t_{\text{init}} \quad (69.169a)$$

$$C = 0 \qquad \boldsymbol{x} \in \mathcal{R}, t = t_{\text{init}} \quad (69.169b)$$

$$\rho\, C = \rho\, \sigma \qquad \boldsymbol{x} \in \partial\mathcal{R}_{\text{surface}}, t \geq t_{\text{init}} \quad (69.169c)$$

$$\hat{\boldsymbol{n}}_{\boldsymbol{x}} \cdot \boldsymbol{K} \cdot \nabla_{\boldsymbol{x}} C = 0 \qquad \boldsymbol{x} \in \partial\mathcal{R}_{\text{bottom}}, t \geq t_{\text{init}}. \quad (69.169d)$$

Note that since $\hat{\boldsymbol{n}} \cdot \boldsymbol{v} = 0$ at the solid earth ocean bottom, kinematics imposes no advective flux through the bottom, $\hat{\boldsymbol{n}} \cdot \boldsymbol{v}\, C = 0$. Since the bottom boundary conditions are homogeneous, the solution (69.166) also holds for the initial-boundary value problem (69.169a)-(69.169d). The key distinction, however, is that the Green's function now satisfies the following boundary value problem

$$\partial_t[\rho\, G(\boldsymbol{x},t|\boldsymbol{x}_0,t_0)] + \nabla_{\boldsymbol{x}} \cdot [\rho\, \boldsymbol{v}^{\dagger}\, G(\boldsymbol{x},t|\boldsymbol{x}_0,t_0) - \rho\, \boldsymbol{K} \cdot \nabla_{\boldsymbol{x}} G(\boldsymbol{x},t|\boldsymbol{x}_0,t_0)] = \delta(\boldsymbol{x}-\boldsymbol{x}_0)\, \delta(t-t_0) \quad (69.170a)$$

$$G(\boldsymbol{x},t<t_0|\boldsymbol{x}_0,t_0) = 0 \quad (69.170b)$$

$$G(\boldsymbol{x},t|\boldsymbol{x}_0,t_0) = 0 \quad \boldsymbol{x} \in \partial\mathcal{R}_{\text{surface}} \quad (69.170c)$$

$$\hat{\boldsymbol{n}}_{\boldsymbol{x}} \cdot \boldsymbol{K} \cdot \nabla_{\boldsymbol{x}} G(\boldsymbol{x},t|\boldsymbol{x}_0,t_0) = 0 \quad \boldsymbol{x} \in \partial\mathcal{R}_{\text{bottom}}. \quad (69.170d)$$

Boundary value problem for the boundary propagator

Following the more detailed presentation in Section 9.5.13 for the diffusion equation, we are led to the following boundary value problem satisfied by the boundary propagator

$$\partial_t[\rho\, G^{\text{bp}}(\boldsymbol{x},t|\boldsymbol{x}_0,t_0)] + \nabla_{\boldsymbol{x}} \cdot [\rho\, \boldsymbol{v}^{\dagger}\, G^{\text{bp}}(\boldsymbol{x},t|\boldsymbol{x}_0,t_0) - \rho\, \boldsymbol{K} \cdot \nabla_{\boldsymbol{x}} G^{\text{bp}}(\boldsymbol{x},t|\boldsymbol{x}_0,t_0)] = 0, \quad \boldsymbol{x} \in \mathcal{R} \quad (69.171a)$$

$$G^{\text{bp}}(\boldsymbol{x},t|\boldsymbol{x}_0,t_0) = 0, \quad \boldsymbol{x} \notin \partial\mathcal{R}, t \leq t_0 \quad (69.171b)$$

$$G^{\text{bp}}(\boldsymbol{x},t|\boldsymbol{x}_0,t_0) = \delta(t-t_0)\, \delta^{(2)}(\boldsymbol{x}-\boldsymbol{x}_0), \quad \boldsymbol{x},\boldsymbol{x}_0 \in \partial\mathcal{R}. \quad (69.171c)$$

The boundary propagator acts as the mediator between boundary data, σ, and interior points, with the transfer of information realized through both advection and diffusion. A focus on the boundary propagator rather than the Green's function allows us to dispense with the need to compute the normal gradient of the Green's function at the boundary, with that calculation rather awkward in practice. Also recall our discussion in Section 9.7.5, where we argued that the

boundary propagator can be considered the impulse response function for spatially distributed sources. Here, the mediation of the Dirac boundary sources is performed by advection plus diffusion, whereas in Section 9.7 we only considered linear damping and diffusion.

Normalization of the boundary propagator

As seen in Sections 68.3 and 68.4, diffusion acts to smooth all structure in the tracer field. Hence, if the boundary data is a uniform constant, $\sigma = \sigma_{\text{const}}$, then given sufficient time the tracer concentration will equal to this constant, $C = \sigma_{\text{const}}$. This steady state result is independent of details for the velocity field and for the diffusivity tensor, with details of advection and the diffusivity acting only to modify the time scale for the equilibration. Assuming we wait long enough, or equivalently that the initial condition occurs infinitely far in the past, then the tracer concentration solution (69.168) leads to the normalization of the boundary propagator

$$\lim_{t_{\text{init}} \to -\infty} \int_{t_{\text{init}}}^{t} \left[\oint_{\partial \mathcal{R}} G^{\text{bp}}(\boldsymbol{x}, t | \boldsymbol{x}_0, t_0) \, \mathrm{d}\mathcal{S}_0 \right] \mathrm{d}t_0 = 1 \quad \text{for } \boldsymbol{x} \in \mathcal{R}. \tag{69.172}$$

This normalization holds for all field points, $\boldsymbol{x}$, within the region. Even though this condition was derived by assuming the special case of constant boundary data, it holds in general since the Green's function, and by extension the boundary propagator, are independent of the boundary data prescribed for the tracer concentration.

69.9.10 Comments

The Green's function method is a powerful and elegant means to study passive ocean tracers, with *Haine et al.* (2025) reviewing the theory and practice. However, the method is also technically challenging for realistic applications, in part due to doubling of the space-time dimensions to hold the Green's function, $G(\boldsymbol{x}, t | \boldsymbol{x}_0, t_0)$, in memory. As a result, realistic applications make approximations to reduce the dimensionality, such as to assume steady state or to focus only on boundary propagators. Hence, there has yet to be a calculation of the full Green's function for a realistic ocean, with that calculation awaiting bigger computers and/or novel methods to side-step the nontrivial memory requirements.

69.10 Exercises

EXERCISE 69.1: ONE-DIMENSIONAL ADVECTION
Consider the advection equation in one space dimension without boundaries

$$(\partial_t + u \, \partial_x) \, C = 0 \tag{69.173a}$$
$$C(x, z, t = 0) = C_0 \, \cos(k \, x) \tag{69.173b}$$
$$u(z, t) = \alpha \, z \cos(\omega \, t). \tag{69.173c}$$

The specified zonal velocity is non-divergent, oscillatory in time, and vertically sheared

$$\partial_z u = \alpha \cos(\omega \, t), \tag{69.174}$$

with ω the angular frequency of the temporal oscillations. What is the tracer concentration at times $t > 0$? Hint: make use of the exact solution given by equation (69.5).

EXERCISE 69.2: SKEW FLUX FOR OCEAN MESOSCALE EDDIES
Consider a middle-latitude mesoscale ocean eddy respecting geostrophic balance (see Section 31.4) on an f-plane (constant Coriolis parameter) and incompressibility. In this case, the horizontal eddy-induced velocity at the ocean surface is non-divergent

$$\boldsymbol{u}^* = \nabla \times \hat{\boldsymbol{z}}\, \psi. \tag{69.175}$$

In this equation, the geostrophic streamfunction is given by

$$\psi = -\hat{\boldsymbol{z}}\, g\, \eta / f, \tag{69.176}$$

with f the Coriolis parameter, g the gravitational acceleration, and η the sea level undulation associated with the eddy. Since the fluid is incompressible, the mass transport equals to the volume transport times a constant reference density, ρ_o.

(a) Determine the skew diffusion tensor (69.30).

(b) Determine the skew tracer flux (69.43a).

EXERCISE 69.3: INTEGRATION BETWEEN TWO CLOSED TRACER CONTOURS
This exercise introduces some ideas of use for determining processes affecting the transport of matter across a tracer contour. Note that in general, the tracer concentration is a function of time. However, the present suite of questions concerns the instantaneous geometry of the tracer field, so that time dependence is not considered.

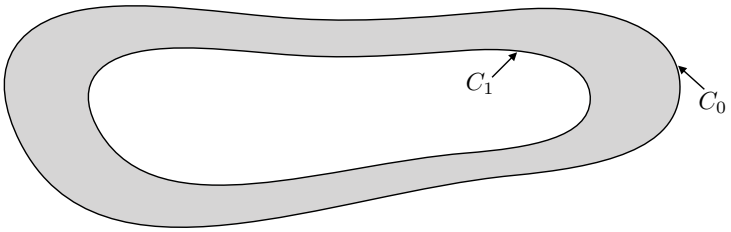

FIGURE 69.4: Illustrating the area contained between two closed tracer contours, $C_0 \leq C(x, y, t) \leq C_1$. Exercise 69.3 develops some mathematical expressions for integration within this area, with the resulting expressions of use for the analyses of tracer transport.

(a) Consider a closed two-dimensional region bounded by two contours of tracer concentration, $C_0 \leq C(x, y, t) \leq C_1$, such as shown in Figure 69.4. Derive the following expression for the area enclosed by the two contours

$$\mathcal{A} = \int_{C_0}^{C_1} \mathrm{d}C \oint \frac{\mathrm{d}l}{|\nabla C|}. \tag{69.177}$$

In this expression, $\mathrm{d}l$ is the line element for a path taken in a counter-clockwise direction along a contour of constant C. We also assume the tracer concentration is not uniform in the region of interest so that $\nabla C \neq 0$.

(b) As a corollary, show that for

$$\mathcal{A}(C) = \int_{C_0}^{C} \mathrm{d}C' \oint \frac{\mathrm{d}l}{|\nabla C'|} \tag{69.178}$$

we have the identity

$$\frac{\partial \mathcal{A}(C)}{\partial C} = \oint \frac{\mathrm{d}l}{|\nabla C|}. \tag{69.179}$$

In words, this result means that the area between two tracer contours has a partial derivative, with respect to the tracer contour, equal to the line integral on the right hand side. The area per C is smaller in regions where the tracer gradient is larger; i.e., there is less area "concentration" in regions of strong tracer gradient.

(c) Use the above two results to prove the following form of the Fundamental Theorem of Calculus

$$\frac{\partial}{\partial C}\left[\int \Phi(\boldsymbol{x})\,\mathrm{d}\mathcal{A}\right] = \frac{\partial}{\partial C}\left[\int_{C_0}^{C} \mathrm{d}C' \oint \frac{\Phi\,\mathrm{d}l}{|\nabla C'|}\right] = \oint \frac{\Phi\,\mathrm{d}l}{|\nabla C|}, \tag{69.180}$$

with Φ an arbitrary function. This is a remarkable identity with many useful applications such as those discussed in *Marshall et al.* (2006).

EXERCISE 69.4: EVOLUTION OF TRACER CENTER OF MASS IN A STATIC DOMAIN

The exercise introduces us to how the tracer center of mass evolves within a Boussinesq ocean. We define the tracer center of mass as

$$\langle \boldsymbol{x} \rangle^{C} = \frac{\int \boldsymbol{x}\, C\,\mathrm{d}V}{\int C\,\mathrm{d}V}, \tag{69.181}$$

with C the tracer concentration, $\boldsymbol{x}$ the coordinate of a point in the fluid, and integration is over the full fluid domain. For example, with a spherically symmetric tracer cloud, the center of mass position is at the sphere's center. The center of mass position is not necessarily where the largest tracer concentration sits, in the same way that the center of mass of a massive object is not necessarily where the object is most dense. For example, a hollow spherical shell has its center of mass at the center of the sphere, even though there is no mass there.

For this exercise, assume the fluid is within a domain whose static boundaries are either material (no normal component to the boundary flux) or periodic. Hence, the total fluid volume and total tracer content remain constant

$$\mathcal{V} = \int \mathrm{d}V \qquad \text{and} \qquad \mathcal{C} = \int C\,\mathrm{d}V. \tag{69.182}$$

Furthermore, when computing the time derivative acting on the integral, make use of the kinematic results from Section 20.2.3, in which for any integrand φ

$$\frac{\mathrm{d}}{\mathrm{d}t}\int \varphi\,\mathrm{d}V = \int \partial_t \varphi\,\mathrm{d}V, \tag{69.183}$$

which follows since the region boundaries are assumed to be static. Equivalently, since the region under consideration is material (no matter crosses the boundaries), we can make use of Reynold's transport theorem from Section 20.2.4 to write

$$\frac{\mathrm{d}}{\mathrm{d}t}\int \varphi\,\mathrm{d}V = \int \frac{\mathrm{D}\varphi}{\mathrm{D}t}\,\mathrm{d}V. \tag{69.184}$$

(a) Consider a tracer concentration whose tendency at a point in space is affected only by advection

$$\frac{\mathrm{D}C}{\mathrm{D}t} = 0 \Longrightarrow \partial_t C + \nabla\cdot(\boldsymbol{v}\,C) = 0, \tag{69.185}$$

with $\boldsymbol{v}$ a non-divergent velocity, $\nabla\cdot\boldsymbol{v} = 0$. Show that the tracer center of mass position evolves according to the tracer center of mass velocity

$$\frac{\mathrm{d}\langle \boldsymbol{x}\rangle^{C}}{\mathrm{d}t} = \langle \boldsymbol{v}\rangle^{C}, \tag{69.186}$$

where the tracer center of mass velocity is given by

$$\langle \boldsymbol{v} \rangle^C = \frac{\int \boldsymbol{v}\, C \,\mathrm{d}V}{\int C \,\mathrm{d}V} = \frac{1}{\mathcal{C}} \int \boldsymbol{v}\, C \,\mathrm{d}V. \tag{69.187}$$

(b) Consider a tracer concentration whose tendency at a point in space affected only by diffusion

$$\partial_t C = \nabla \cdot (K \cdot \nabla C)\,, \tag{69.188}$$

where $K = K(\boldsymbol{x}, t) > 0$ is a kinematic diffusivity (physical dimensions of squared length per time), and which is assumed to vanish at the domain boundaries. Show that the tracer center of mass drifts up the diffusivity gradient

$$\frac{\mathrm{d}\langle \boldsymbol{x} \rangle^C}{\mathrm{d}t} = \langle \nabla K \rangle^C. \tag{69.189}$$

Hint: use the product rule and drop boundary terms.

(c) Consider an initial tracer concentration that is a function only of latitude,

$$C(x, y, z, t = 0) = C_0(y), \tag{69.190}$$

and assume a smooth spherical domain. Assume the diffusivity, K, is a turbulent diffusivity proportional to the eddy kinetic energy of the flow, so that large diffusivity occurs in regions with large eddy activity; i.e., there is a lot of turbulent mixing where turbulence is active. Introduce an stirring from the eddies that breaks the zonal symmetry. Qualitatively discuss the process whereby this turbulent diffusive mixing causes the tracer center of mass to drift towards the turbulent region.

(d) Generalize the result from part (b) to the case of the diffusion equation

$$\partial_t C = \nabla \cdot (\boldsymbol{K} \cdot \nabla C) = \partial_p (K^{pq}\, \partial_q C), \tag{69.191}$$

where $\boldsymbol{K}$ is a second order symmetric diffusion tensor.

EXERCISE 69.5: EVOLUTION OF TRACER CENTER OF MASS IN MOVING REGION

Consider a finite region of fluid with fixed mass that is moving with the fluid velocity field, $\mathcal{R}(\boldsymbol{v})$. The fluid is assumed to have a tracer whose concentration is affected by an irreversible process so that

$$\frac{\mathrm{D}C}{\mathrm{D}t} = \dot{C} \neq 0. \tag{69.192}$$

For example, $\dot{C}$ may represent a diffusive process, in which case the tracer content within the region changes due to diffusion of tracer across the region boundary.

Determine the evolution equation for the tracer center of mass position

$$\langle \boldsymbol{x} \rangle^C = \frac{\int_{\mathcal{R}(\boldsymbol{v})} \boldsymbol{x}\, C\, \rho \,\mathrm{d}V}{\int_{\mathcal{R}(\boldsymbol{v})} C\, \rho \,\mathrm{d}V}. \tag{69.193}$$

Hint: the region under consideration is moving with the fluid and has constant mass. Although the region boundaries are not material, we can make use of Reynold's transport theorem from Section 20.2.6 since the region has a constant mass. Consequently, we can set

$$\frac{\mathrm{d}}{\mathrm{d}t} \int_{\mathcal{R}(\boldsymbol{v})} \psi\, \rho \,\mathrm{d}V = \int_{\mathcal{R}(\boldsymbol{v})} \frac{\mathrm{D}\psi}{\mathrm{D}t}\, \rho \,\mathrm{d}V. \tag{69.194}$$

EXERCISE 69.6: STEADY TWO DIMENSIONAL ADVECTION-DIFFUSION

Consider the steady state advection-diffusion equation for a scalar field, Q, in a two dimensional non-divergent flow

$$\nabla \cdot (\boldsymbol{u}\, Q) = \nabla \cdot (\boldsymbol{K} \cdot \nabla Q) \quad \text{with} \quad \boldsymbol{u} = \hat{\boldsymbol{z}} \times \nabla \psi, \tag{69.195}$$

and $\boldsymbol{K}$ a diffusion tensor. Show that when evaluated along a contour of constant Q we can write

$$-(\hat{\boldsymbol{n}} \cdot \nabla Q)\, (\hat{\boldsymbol{t}} \cdot \nabla \psi) = \nabla \cdot (\boldsymbol{K} \cdot \nabla Q) \tag{69.196}$$

where $\hat{\boldsymbol{t}}$ is the unit tangent along the contour and $\hat{\boldsymbol{n}}$ is a unit vector pointing to the left of the tangent (e.g., see Figure 5.6). Assuming $\hat{\boldsymbol{n}} \cdot \nabla Q \neq 0$, this equation takes on the form

$$\hat{\boldsymbol{t}} \cdot \nabla \psi = -\frac{\nabla \cdot (\boldsymbol{K} \cdot \nabla Q)}{(\hat{\boldsymbol{n}} \cdot \nabla Q)}, \tag{69.197}$$

which provides a means to integrate the streamfunction, ψ, along contours of constant Q.

If Q is the quasi-geostrophic potential vorticity (Chapter 45), then contours of constant Q are known as *geostrophic contours*. Within this context, *Rhines and Holland* (1979) made use of the identity (69.197) in their study of ocean circulation in the presence of eddy diffusion of potential vorticity.

Hint: write the advection operator as a Jacobian and make use of Exercise 5.1.

EXERCISE 69.7: DISTRIBUTION OF ONE TRACER WITH RESPECT TO ANOTHER

Consider two tracers, ψ and B, that satisfy the advection-diffusion equation with the same diffusion tensor

$$\rho \frac{\mathrm{D}\psi}{\mathrm{D}t} = \nabla \cdot (\rho\, \boldsymbol{K} \cdot \nabla \psi) \tag{69.198a}$$

$$\rho \frac{\mathrm{D}B}{\mathrm{D}t} = \nabla \cdot (\rho\, \boldsymbol{K} \cdot \nabla B). \tag{69.198b}$$

Having access to two tracers allows us to diagnose certain properties of the flow, both in geographical/depth space as well as in the space defined by the tracers. We here study how the tracer B is distributed within layers defined by ψ, and how that distribution evolves in time. These considerations are partly motivated by the work of *Ruan and Ferrari* (2021), who assumed B to be buoyancy (with a linear equation of state). Whereas *Ruan and Ferrari* (2021) assumed a Boussinesq ocean with a constant scalar diffusivity, here we generalize to the non-Boussinesq case with a flow-dependent diffusion tensor, $\boldsymbol{K}$, which is a symmetric and positive-definite second order tensor.

(a) Derive the following identity

$$\rho \frac{\mathrm{D}(\psi\, B^{\Gamma})}{\mathrm{D}t} = \nabla \cdot (B^{\Gamma}\, \rho\, \boldsymbol{K} \cdot \nabla \psi - \psi\, \rho\, \boldsymbol{K} \cdot \nabla B^{\Gamma}) + \Gamma\, \psi\, \nabla B^{\Gamma-1} \cdot \rho\, \boldsymbol{K} \cdot \nabla B + 2\, \Gamma\, \psi\, B^{\Gamma-1}\, \rho\, \dot{B}, \tag{69.199}$$

where B^{Γ} is B raised to the integer power Γ, and where we made use of the shorthand

$$\dot{B} = \frac{\mathrm{D}B}{\mathrm{D}t}. \tag{69.200}$$

Show all relevant steps in the derivation of equation (69.199). Hint: as an optional warm-up, derive the special case with $\Gamma = 1$

$$\rho \frac{\mathrm{D}(\psi\, B)}{\mathrm{D}t} = \nabla \cdot (B\, \rho\, \boldsymbol{K} \cdot \nabla \psi - \psi\, \rho\, \boldsymbol{K} \cdot \nabla B) + 2\, \psi\, \rho\, \dot{B} \tag{69.201}$$

and then the case with $\Gamma = 2$

$$\rho \frac{\mathrm{D}(\psi B^2)}{\mathrm{D}t} = \nabla \cdot (B^2 \rho \boldsymbol{K} \cdot \nabla \psi - \psi \rho \boldsymbol{K} \cdot \nabla B^2) + 2 \psi \nabla B \cdot \rho \boldsymbol{K} \cdot \nabla B + 4 \psi B \rho \dot{B}. \quad (69.202)$$

(b) Introduce the ψ-weighted mean of an arbitrary field, Γ, according to

$$\overline{\Gamma} \equiv \frac{\int_{\mathscr{R}} \Gamma \psi \rho \, \mathrm{d}V}{\int_{\mathscr{R}} \psi \rho \, \mathrm{d}V}. \quad (69.203)$$

Furthermore, assume all boundaries to the domain are material, which means that the domain matter content is fixed in time

$$\frac{\mathrm{d}}{\mathrm{d}t} \int_{\mathscr{R}} \rho \, \mathrm{d}V = 0 \qquad \text{and} \qquad \frac{\mathrm{d}}{\mathrm{d}t} \int_{\mathscr{R}} \psi \rho \, \mathrm{d}V = 0 \qquad \text{and} \qquad \frac{\mathrm{d}}{\mathrm{d}t} \int_{\mathscr{R}} B \rho \, \mathrm{d}V = 0. \quad (69.204)$$

Make use of equation (69.201) to derive the following identity

$$\frac{\mathrm{d}\overline{B}}{\mathrm{d}t} = 2 \overline{\dot{B}}, \quad (69.205)$$

and offer some discussion.

EXERCISE 69.8: EVOLUTION OF TRACER MOMENTS

In Section 68.4.3 we studied how tracer diffusion affects tracer moments. Here we consider the combined effects of advection and diffusion. We assume the boundaries are insulating (i.e., zero normal boundary flux of tracer) so that $\boldsymbol{J} \cdot \hat{\boldsymbol{n}} = 0$ with $\hat{\boldsymbol{n}}$ the outward normal at the boundary. We also assume there is no matter crossing the boundary, so that $(\boldsymbol{v} - \boldsymbol{v}^{(\mathrm{b})}) \cdot \hat{\boldsymbol{n}} = 0$, where $\boldsymbol{v}^{(\mathrm{b})}$ is the velocity of a point stuck to the boundary. Correspondingly, the total fluid mass in the domain remains fixed

$$M = \int \rho \, \mathrm{d}V \quad \text{with} \quad \frac{\mathrm{d}M}{\mathrm{d}t} = 0, \quad (69.206)$$

so that the domain is material since we assume no exchange of mass or tracer across the boundaries. These assumptions allow us to focus on the effects from tracer diffusion and advection within the domain interior.

(a) DOMAIN AVERAGED TRACER CONCENTRATION: The domain averaged tracer concentration is defined by

$$\overline{C} = \frac{\int_{\mathscr{R}} C \rho \, \mathrm{d}V}{M}. \quad (69.207)$$

Show that its time derivative vanishes.

(b) TRACER VARIANCE WITHIN THE DOMAIN: The variance of the tracer concentration is defined by

$$\mathrm{var}(C) \equiv \frac{\int_{\mathscr{R}} (C - \overline{C})^2 \rho \, \mathrm{d}V}{M} = \overline{C^2} - \overline{C}^2 \geq 0. \quad (69.208)$$

The tracer variance measures the deviation of the tracer concentration relative to the domain averaged concentration. Since the domain average tracer concentration remains fixed in time, the time change of the variance is given by

$$\frac{\mathrm{d}[\mathrm{var}(C)]}{\mathrm{d}t} = \frac{\mathrm{d}\overline{C^2}}{\mathrm{d}t}. \quad (69.209)$$

Thus, it is common to refer to $\overline{C^2}$ as the tracer variance, though strictly speaking only

time derivatives of $\overline{C^2}$ and $\text{var}(C)$ are equal as per equation (69.209). Show that

$$\frac{\text{d}[\text{var}(C)]}{\text{d}t} = \frac{\text{d}\overline{C^2}}{\text{d}t} \leq 0, \tag{69.210}$$

with this inequality determined solely by diffusion, whereas advection has no impact on the variance.

(c) DIFFUSION OF ARBITRARY TRACER MOMENTS: Prove that

$$\frac{\text{d}\overline{C^\Gamma}}{\text{d}t} = \Gamma\,(\Gamma - 1) \int C^{\Gamma-2}\, \nabla C \cdot \boldsymbol{J}\, \text{d}V \leq 0. \tag{69.211}$$

For $\Gamma = 0$ we have an expression of mass conservation for the domain, whereas $\Gamma = 1$ is an expression of tracer conservation. The case of $\Gamma = 2$ yields the tracer variance result (69.210).

Hint: This exercise reveals that tracer moments evolve solely through the effects of diffusion, whereas advection does not touch the tracer moments. The goal of this exercise is to emphasize these results by working through the details, which are largely identical to those presented in Section 68.4.3 when studying diffusion alone.

Chapter 70

EDDY AND MEAN TRACER KINEMATICS

Geophysical fluid flows exhibit multiple scales in both space and time. In the analysis of these flows, it is useful to seek a description that decomposes fluid properties into a mean component and a fluctuation relative to the mean. We perform an eddy-mean decomposition when interest concerns the mean field and impacts on the mean by the fluctuating instantaneous flow, with such impacts often termed *rectified* effects. The mean field can be defined in many fashions with subjective choices based on particulars of the flow and the analysis goals. The definition for the mean in turn affects what we refer to as the fluctuation. Quite generally, fluctuations take the form of transient linear waves, nonlinear and/or breaking waves, coherent structures, and/or a chaotic/turbulent soup of eddying features. In this chapter we develop a kinematic framework originally motivated by the analysis of scalar transport induced by small amplitude wave-like eddying features. This framework can also be used for turbulent processes and their parameterizations (e.g., Chapter 71).

We consider two kinematic methods to decompose the flow into a mean and eddy, with elements of these methods pervasive in the geophysical fluids literature. The first method is the *generalized Lagrangian mean (GLM)*, which is a hybrid Eulerian/Lagrangian method that introduces an Eulerian disturbance field to measure the position of a fluid particle relative to its mean position (*Andrews and McIntyre*, 1978a,b; *Bühler*, 2014a; *Gilbert and Vanneste*, 2025). We only access a small portion of the GLM framework, used here to help unpack the kinematics of eddy tracer fluxes following from *Middleton and Loder* (1989). A more thorough treatment that considers the momentum and vorticity equations is outside the scope for this chapter.

The second kinematic method makes use of isopycnal vertical coordinates. The isopycnal approach is quasi-Lagrangian since it fixes the horizontal position (Eulerian) yet allows the vertical to follow an adiabatic fluid parcel (Lagrangian). Furthermore, we show that the isopycnal description is a special case of the GLM, where the GLM displacement field is restricted to the vertical direction. The isopycnal approach is frequently used to describe how ocean mesoscale eddies affect stratification and tracer transport in stably stratified flows. Our presentation follows the methods developed by *McDougall and McIntosh* (2001) and summarized in Chapter 9 of *Griffies* (2004). A directly related approach is considered in Chapter 67 for the stacked shallow water equations, in which we develop the thickness weighted tracer, momentum, and vorticity budgets (see also *Young* (2012) and *Jansen et al.* (2024)).

CHAPTER GUIDE

This chapter relies on an understanding of the tracer equation as derived in Section 20.1 and the maths and physics of the advection-diffusion equation explored in Chapter 69. We focus on non-divergent flows with kinematics presented in Chapter 21 and as applicable to the Boussinesq ocean studied in Chapter 29. Generalizations to non-Boussinesq flows are straightforward, with examples provided by *Griffies and Greatbatch* (2012). The kinematics of isopycnal fluid layers in a perfect fluid (Sections 70.4 and 70.5) are posed using the isopycnal vertical coordinates detailed in Chapter 63 and further pursued in Chapter 65. This discussion is served by experience with the shallow water thickness weighted averaging from Chapter 67.

Throughout this chapter we assume Cartesian tensors in the horizontal directions, which simplifies the necessary mathematical tools. This assumption is sufficient for the isopycnal averaging in Sections 70.4 and 70.5. Indeed, this assumption is sufficient for any generalized vertical coordinate discussed in Part XII of this book. However, to extend the full GLM theory to arbitrary horizontal coordinates requires more sophisticated mathematical tools, such as those reviewed by *Gilbert and Vanneste* (2025).

70.1 Reynolds decomposition

At any point in space and time, we can perform an *Eulerian average* operation to decompose a field into a mean, $\overline{\Psi}(\boldsymbol{x}, t)$, and a departure from the mean, $\Psi'(\boldsymbol{x}, t)$

$$\Psi(\boldsymbol{x}, t) = \overline{\Psi}(\boldsymbol{x}, t) + \Psi'(\boldsymbol{x}, t). \tag{70.1}$$

The departure from the mean is generally termed the "eddy" or the "fluctuation". The following offers a non-exhaustive list of mean operators computed at a fixed point in space (i.e., Eulerian mean operators).

- TIME MEAN: If the mean operator is based on a long time average, then the mean fields are assumed to be time independent: $\overline{\Psi}(\boldsymbol{x}, t) = \overline{\Psi}(\boldsymbol{x})$. This is a common operator when interest is focused on the long term mean fluid properties. Additionally, it is often the mean operator of choice with realistic climate modeling.
- PHASE AVERAGE: Rather than a time mean, we may choose to average over the phase (or period) of a wave. This choice is particularly relevant when the fluctuating field involves quasi-linear waves such as studied in Part X of this book.
- ZONAL MEAN: If the mean operator is based on an average along a particular coordinate direction (e.g., zonal average), then the mean field is independent of the "averaged out" direction.
- COARSE GRAINING: If the mean operator is based on an average over a spatial and temporal region, such as the mesoscale, then such coarse-graining averages out smaller scales. A systematic means for doing so is detailed in *Buzzicotti et al.* (2023).
- ENSEMBLE AVERAGE: Rather than a space or time mean operation, we may consider the mean or average computed over an ensemble of many flow realizations. For many purposes this is the most analytically convenient mean operator, though it is often difficult to realize in practice.

If a mean operator satisfies the following properties then it is said to provide a *Reynolds decomposition*

$$\overline{\Psi'} = 0 \tag{70.2a}$$

$$\overline{\overline{\Psi}} = \overline{\Psi} \tag{70.2b}$$

$$\overline{A\,\overline{\Psi}} = A\,\overline{\Psi} \qquad \text{for } A \text{ a constant.} \tag{70.2c}$$

Equation (70.2a) says that the mean of an eddy fluctuation vanishes. The equality (70.2b) says that the mean of a mean field returns the mean field. The final equality, (70.2c), says that a constant commutes with the mean operator. Notably, some or all of these properties are not satisfied by certain operators used for eddy-mean decompositions. However, in the following we assume they are satisfied.

A Reynolds average acting on a linear equation means that both the mean and fluctuating quantity satisfy the linear equation. In particular, consider the non-divergence condition for a Boussinesq ocean flow, $\nabla \cdot \boldsymbol{v} = 0$. Taking the mean of this equation renders

$$\nabla \cdot \boldsymbol{v} = 0 \Longrightarrow \nabla \cdot \overline{\boldsymbol{v}} = 0, \tag{70.3}$$

so that the mean velocity is non-divergent. So since both the full velocity and mean velocity are non-divergent, then so is the fluctuating velocity

$$\nabla \cdot (\overline{\boldsymbol{v}} + \boldsymbol{v}') = \nabla \cdot \boldsymbol{v}' = 0. \tag{70.4}$$

70.2 GLM kinematics for scalar fields

We here consider basic elements of generalized Lagrangian mean (GLM) theory. GLM is a hybrid between Lagrangian and Eulerian descriptions of fluid motions, so that it might be more appropriate to refer to it as the "hybrid Lagrangian-Eulerian mean theory". The GLM and the Eulerian mean for a fluid property are generally distinct, with their difference referred to as the *Stokes mean*

$$\text{generalized Lagrangian mean} = \text{Eulerian mean} + \text{Stokes mean}. \tag{70.5}$$

This name is motivated from the *Stokes drift* introduced in Section 52.11, which is the difference between the Lagrangian and Eulerian means. Note that the literature sometimes refers to the Stokes mean as the "Stokes correction". We avoid that terminology in order to avoid the spurious notion that one type of mean operator is more correct than the other. Instead, a mean operator is subjectively chosen based on its suitability to a particular question.

70.2.1 Motivation

Consider a materially constant scalar field

$$\frac{\mathrm{D}\Psi}{\mathrm{D}t} = \frac{\partial \Psi}{\partial t} + \boldsymbol{v} \cdot \nabla \Psi = 0. \tag{70.6}$$

The scalar, Ψ, is constant following fluid particles whose trajectories are integral curves of the fluid velocity, $\boldsymbol{v}$. The goal is to develop a mean operator that averages over fluctuations in the trajectories while preserving the material constancy nature of the instantaneous equation. This goal is not trivial.

Eulerian mean

An Eulerian mean operator considered in Section 70.1 leads to the mean field equation, here written either in advective form or flux form

$$\frac{\partial \overline{\Psi}}{\partial t} + \overline{\boldsymbol{v}} \cdot \nabla \overline{\Psi} = -\overline{\boldsymbol{v}' \cdot \nabla \Psi'} \qquad \text{advective form} \tag{70.7a}$$

$$\frac{\partial \overline{\Psi}}{\partial t} + \nabla \cdot (\overline{\boldsymbol{v}}\, \overline{\Psi}) = -\nabla \cdot (\overline{\boldsymbol{v}'\, \Psi'}) \qquad \text{flux form}. \tag{70.7b}$$

The equations are equivalent since both the Eulerian mean velocity and the fluctuating velocity are non-divergent, as shown in Section 70.1. Whereas Ψ is materially constant when following the instantaneous flow field, $\boldsymbol{v}$, the Eulerian mean, $\overline{\Psi}$, is not materially constant when following the Eulerian mean velocity, $\overline{\boldsymbol{v}}$, due to the source term, $-\overline{\boldsymbol{v}' \cdot \nabla \Psi'}$, provided by the eddy correlation. Furthermore, when given information only about the mean fields, then we must develop a closure for the unresolved correlation. Accurate and physically motivatived closures are not simple to derive.

Lagrangian mean

An alternative approach is to remain in the Lagrangian frame, where we work with the scalar property evaluated along a fluid particle trajectory as in Section 18.3.3[1]

$$\Psi^{\mathrm{L}}(\boldsymbol{a}, T) = \text{property } \Psi \text{ following the fluid particle trajectory } \boldsymbol{X}(\boldsymbol{a}, T), \tag{70.8}$$

where $\boldsymbol{a}$ is the material label coordinate, and T is the time measured in the co-moving fluid particle frame. Since we are not considering relativistic motions, $T = t$, and yet it is useful to make the distinction for purposes of time derivatives. As such, the material constancy equation (70.6) becomes

$$\frac{\partial \Psi^{\mathrm{L}}(\boldsymbol{a}, T)}{\partial T} = 0. \tag{70.9}$$

Consider a mean operator computed as an average over a region of material space. For example, if $\boldsymbol{a}$ is the initial fluid particle position, then an average coordinate, $\overline{\boldsymbol{a}}$, and corresponding averaged field, $\overline{\Psi}^{\mathrm{L}}$, render a coarse-graining over the initial positions. Since each member of the Lagrangian average satisfies equation (70.9), so too does the Lagrangian mean

$$\frac{\partial \overline{\Psi}^{\mathrm{L}}(\overline{\boldsymbol{a}}, T)}{\partial T} = 0. \tag{70.10}$$

Although this equation retains the simplicity of the unaveraged version, it still requires information about trajectories. Trajectories are computed based on the flow map (i.e., the velocity field), with trajectories not always convenient when describing chaotic or turbulent fluids. GLM offers an alternative that aims to meld elements of the Eulerian (e.g., computability) to the Lagrangian (e.g., material constancy).

Generalized Lagrangian mean

The GLM approach produces a field that remains constant following the GLM velocity

$$\frac{\partial \overline{\Psi}^{(\mathrm{GLM})}}{\partial t} + \overline{\boldsymbol{v}}^{(\mathrm{GLM})} \cdot \nabla \overline{\Psi}^{(\mathrm{GLM})} = 0. \tag{70.11}$$

Hence, GLM maintains the desirable properties of the Lagrangian mean. However, it does so using Eulerian methods that prove to be more practical for many cases. Notably, even if the Eulerian velocity is non-divergent, as for a Boussinesq ocean, the GLM velocity is divergent. Although we do not derive the GLM equation (70.11), in the following we motivate the GLM average from the analysis of small amplitude eddying motions.

70.2.2 Length scales and the small parameter

We consider two length scales associated with an eddy or wave fluctuation. One characterizes the size of the eddy whose length scale we write as λ. If the eddy is a monochromatic wave, then λ is its wave length. The other length scale characterizes the size of particle displacements, $|\boldsymbol{\xi}|$. In the following, we assume the particle displacements are small relative to λ

$$|\boldsymbol{\xi}| \ll \lambda \qquad \text{small amplitude waves.} \tag{70.12}$$

[1]We here use the notation $\boldsymbol{X}(\boldsymbol{a}, T)$ for the trajectory of fluid particles, whereas in Chapter 18 we generally used the motion field, $\boldsymbol{\varphi}(\boldsymbol{a}, T)$. As discussed in Section 18.2.1, the two are the same when fixing a particular particle label, $\boldsymbol{a}$.

We thus introduce the small non-dimensional ratio of length scales for the following analysis

$$\alpha = |\boldsymbol{\xi}|/\lambda \ll 1. \tag{70.13}$$

70.2.3 Decomposing the particle trajectory

Recall the discussion of fluid particle trajectories given in Chapter 17. In this description, the trajectory of a particle is determined by integrating the relation between the particle trajectory and the particle velocity

$$\left[\frac{\partial \boldsymbol{X}(\boldsymbol{a},T)}{\partial T}\right]_{\boldsymbol{a}} = \boldsymbol{v}[\boldsymbol{X}(\boldsymbol{a},T)] \Longrightarrow \boldsymbol{X}(\boldsymbol{a},T) = \boldsymbol{X}(\boldsymbol{a},0) + \int_0^T \boldsymbol{v}[\boldsymbol{X}(\boldsymbol{a},T')]\,\mathrm{d}T', \tag{70.14}$$

so that the trajectory measures the position of a particle relative to a chosen origin. The material coordinate, $\boldsymbol{a}$, distinguishes the continuum of fluid particles, thus making the trajectory a field in material space-time.

The GLM develops a hybrid Eulerian-Lagrangian method and it is motivated by linear or quasi-linear disturbances. Keeping this motivation in mind, we consider each point in space, $\boldsymbol{x}$, to be the mean position of a unique fluid particle. In turn, we introduce an Eulerian field, $\boldsymbol{\xi}(\boldsymbol{x},t)$, that measures the position of a fluid particle relative to its mean position.[2] Correspondingly, the Eulerian mean of the disturbance field vanishes

$$\overline{\boldsymbol{\xi}(\boldsymbol{x},t)} = 0. \tag{70.15}$$

Note that the Eulerian mean operator can be any of the operators (or others) satisfying the Reynold's decomposition property discussed in Section 70.1

Specification of $\boldsymbol{\xi}(\boldsymbol{x},t)$ for large amplitude disturbances (i.e., nonlinear waves) requires the full machinery of GLM, which is beyond our scope. Instead, to expose the rudiments we here assume small amplitude disturbances such as shown in Figure 70.1, for which the particle displacement amplitude is much smaller than the wavelength of the disturbance as given by the inequality (70.13). In this case the disturbance field is constructed by time integration of the eddy velocity field

$$\left[\frac{\partial \boldsymbol{\xi}(\boldsymbol{x},t)}{\partial t}\right]_{\boldsymbol{x}} = \boldsymbol{v}'(\boldsymbol{x},t) \Longrightarrow \boldsymbol{\xi}(\boldsymbol{x},t) = \int^t \boldsymbol{v}'(\boldsymbol{x},t')\,\mathrm{d}t'. \tag{70.16}$$

With this specification for the disturbance field, we see that if the eddy velocity is non-divergent then so is the disturbance field

$$\nabla\cdot\boldsymbol{v}' = 0 \Longrightarrow \nabla\cdot\boldsymbol{\xi} = 0. \tag{70.17}$$

The definition (70.16) for the disturbance field, $\boldsymbol{\xi}(\boldsymbol{x},t)$, is directly analogous to the particle trajectory position, $\boldsymbol{X}(\boldsymbol{a},T)$, given by equation (70.14). However, there are important distinctions. Namely, the disturbance, $\boldsymbol{\xi}(\boldsymbol{x},t)$, is an Eulerian field that measures the position of a fluid particle relative to its mean position, with each Eulerian position, $\boldsymbol{x}$, corresponding to the mean position for a distinct fluid particle. In contrast, the particle position, $\boldsymbol{X}(\boldsymbol{a},T)$, is a Lagrangian field that is attached to each fluid particle and measures the position of that particle relative to a chosen origin.

[2] We introduced a one-dimensional disturbance field in Section 51.3 when taking a Lagrangian perspective to derive the equations for acoustic waves. Hence, the GLM disturbance field, $\boldsymbol{\xi}(\boldsymbol{x},t)$, provides a three-dimensional generalization of that approach.

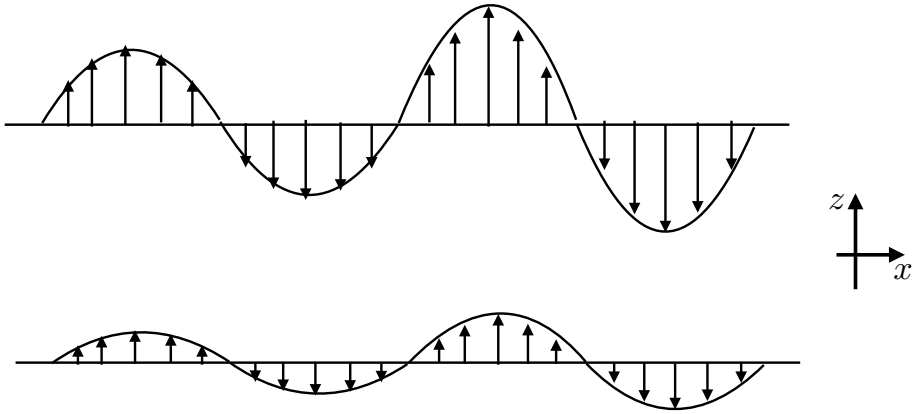

FIGURE 70.1: Illustrating the displacement of fluid particles at two selective vertical positions due to a linear transverse wave disturbance. The particle positions, $\boldsymbol{x}^{(\xi)}(\boldsymbol{x},t) = \boldsymbol{x} + \boldsymbol{\xi}(\boldsymbol{x},t)$, here have a disturbance field of the form $\boldsymbol{\xi}(\boldsymbol{x},t) = \hat{\boldsymbol{z}}\,\xi_0(x,z)\sin(k\,x - \omega\,t)$, with $\xi_0(x,z)$ a spatially dependent wave amplitude, $\lambda = 2\pi/k$ the wavelength, $\boldsymbol{k} = \hat{\boldsymbol{x}}\,k$ the wavevector, $\omega = c\,k$ the angular frequency, and c the phase speed. Small amplitude waves satisfy $|\xi_0| \ll \lambda$. Note that this wave does not produce a Stokes drift since particle displacements are perpendicular to the wavevector: $\boldsymbol{\xi} \cdot \boldsymbol{k} = 0$ (see Section 70.2.5), whereas Stokes drift requires particle motion to have a nonzero component in the wave direction (see Figures 52.4 and 52.9). Even so, it does generally produced a Stokes mean for an arbitrary field Ψ (Section 70.2.4).

70.2.4 GLM and the Stokes mean

The mean of a fluid property, Ψ, is a function of how the property is sampled when computing the mean. For example, the mean sampled on a fluctuating fluid particle differs from the mean sampled at the particle's mean position. Mathematically, this distinction implies that

$$\underbrace{\overline{\Psi(\boldsymbol{x} + \boldsymbol{\xi}(\boldsymbol{x},t))}}_{\text{GLM}} \neq \underbrace{\overline{\Psi(\boldsymbol{x},t)}}_{\text{Eulerian}}, \tag{70.18}$$

where it is common to make use of the shorthand

$$\boldsymbol{x}^{(\xi)}(\boldsymbol{x},t) \equiv \boldsymbol{x} + \boldsymbol{\xi}(\boldsymbol{x},t) \tag{70.19}$$

for the instantaneous position of the fluid particle. The average,

$$\overline{\Psi}^{(\text{GLM})}(\boldsymbol{x},t) \equiv \overline{\Psi(\boldsymbol{x} + \boldsymbol{\xi}(\boldsymbol{x},t),t)} = \overline{\Psi(\boldsymbol{x}^{(\xi)},t)}, \tag{70.20}$$

defines the generalized Lagrangian mean for the fluid property, Ψ. That is, the GLM is computed by evaluating the property, Ψ, at the position of a fluid particle, $\boldsymbol{x}^{(\xi)}(\boldsymbol{x},t) = \boldsymbol{x} + \boldsymbol{\xi}(\boldsymbol{x},t)$, and then performing an Eulerian average. We emphasize that $\boldsymbol{x}$ is both an arbitrary Eulerian field point *and* the mean position of a fluid particle, $\overline{\boldsymbol{x}^{(\xi)}} = \boldsymbol{x}$. In contrast, the Eulerian mean is determined by evaluating Ψ at a fixed Eulerian point in space

$$\overline{\Psi}^{(\text{E})}(\boldsymbol{x},t) \equiv \overline{\Psi(\boldsymbol{x},t)}, \tag{70.21}$$

where there is no consideration of instantaneous particle positions. Given this identity, we sometimes drop the (E) superscript on the Eulerian mean to reduce clutter.

Following our discussion at the start of Section 70.2, we define the Stokes mean as the difference between the GLM and Eulerian mean

$$\overline{\Psi}^{(\text{S})}(\boldsymbol{x},t) = \overline{\Psi}^{(\text{GLM})}(\boldsymbol{x},t) - \overline{\Psi}(\boldsymbol{x},t). \tag{70.22}$$

The Stokes mean arises from inhomogenities in Ψ, which in turn lead to differences in its mean

depending on how that field is sampled, whether sampled on a fluid particle, $\boldsymbol{x}^{(\xi)}(\boldsymbol{x},t)$, or sampled at the mean position of the fluid particle, $\boldsymbol{x}$.

We mathematically expose the origin of the Stokes mean by performing a Taylor series expansion around the mean particle position

$$\Psi(\boldsymbol{x}+\boldsymbol{\xi},t) = \Psi(\boldsymbol{x},t) + \boldsymbol{\xi}\cdot\nabla\Psi(\boldsymbol{x},t) + \frac{1}{2}\,\xi^m\,\xi^n\partial_m\partial_n\Psi(\boldsymbol{x},t) + \mathcal{O}(\alpha^3). \tag{70.23}$$

The non-dimensional ratio, $\alpha = |\boldsymbol{\xi}|/\lambda \ll 1$, was introduced in equation (70.13). It measures the ratio of the amplitude for particle displacements to the wavelength, λ, of fluctuations in the field Ψ. Taking the mean of equation (70.23) then leads to an expression for the Stokes mean

$$\overline{\Psi}^{(\mathrm{S})}(\boldsymbol{x},t) = \overline{\Psi}^{(\mathrm{GLM})}(\boldsymbol{x},t) - \overline{\Psi}(\boldsymbol{x},t) \tag{70.24a}$$

$$= \overline{\boldsymbol{\xi}\cdot\nabla\Psi} + \frac{1}{2}\,\overline{\xi^m\,\xi^n\partial_m\partial_n\Psi} + \mathcal{O}(\alpha^3). \tag{70.24b}$$

$$= \overline{\boldsymbol{\xi}\cdot\nabla\Psi'} + \frac{1}{2}\,\overline{\xi^m\,\xi^n}\,\partial_m\partial_n\overline{\Psi} + \mathcal{O}(\alpha^3), \tag{70.24c}$$

where we introduced the Eulerian fluctuation,

$$\Psi'(\boldsymbol{x},t) = \Psi(\boldsymbol{x},t) - \overline{\Psi}(\boldsymbol{x},t), \tag{70.25}$$

and all terms on the right hand side of equation (70.24c) are evaluated at $(\boldsymbol{x},t)$. Observe that the Stokes mean (70.24c) is nonzero only starting at $\mathcal{O}(\alpha^2)$. When Ψ represents the velocity field, we refer to the Stokes mean as the *Stokes drift* (Section 52.11), in which

$$\boldsymbol{v}^{(\mathrm{S})} = \overline{(\boldsymbol{\xi}\cdot\nabla)\,\boldsymbol{v}'} + \frac{1}{2}\,\overline{\xi^m\,\xi^n}\,\partial_m\partial_n\overline{\boldsymbol{v}} + \mathcal{O}(\alpha^3). \tag{70.26}$$

70.2.5 An example wave

We exemplify the previous discussion by considering the small amplitude wave

$$\boldsymbol{\xi} = -\omega^{-1}\,\boldsymbol{U}(\boldsymbol{x})\sin(\boldsymbol{k}\cdot\boldsymbol{x}-\omega\,t) \tag{70.27a}$$

$$\boldsymbol{v}' = \partial_t\boldsymbol{\xi} = \boldsymbol{U}(\boldsymbol{x})\cos(\boldsymbol{k}\cdot\boldsymbol{x}-\omega\,t) \tag{70.27b}$$

$$\nabla v'^p = \nabla U^p\cos(\boldsymbol{k}\cdot\boldsymbol{x}-\omega\,t) - \boldsymbol{k}\,U^p\sin(\boldsymbol{k}\cdot\boldsymbol{x}-\omega\,t) \tag{70.27c}$$

$$\nabla\cdot\boldsymbol{v}' = (\nabla\cdot\boldsymbol{U})\cos(\boldsymbol{k}\cdot\boldsymbol{x}-\omega\,t) - \boldsymbol{k}\cdot\boldsymbol{U}\sin(\boldsymbol{k}\cdot\boldsymbol{x}-\omega\,t), \tag{70.27d}$$

where $\boldsymbol{U}$ is the velocity amplitude that is generally a function of space, $\boldsymbol{k}$ is the wavevector, and $2\,\pi/\omega$ is the wave period. The wave renders an oscillatory motion to fluid particles, with the disturbance field specifying the instantaneous position of fluid particles whose mean position is $\boldsymbol{x}$. The disturbance field and velocity field both have a zero mean when time integrated over a wave period

$$\frac{1}{2\,\pi/\omega}\int_0^{2\,\pi/\omega}\boldsymbol{\xi}(\boldsymbol{x},t)\,\mathrm{d}t = 0 \tag{70.28a}$$

$$\frac{1}{2\,\pi/\omega}\int_0^{2\,\pi/\omega}\boldsymbol{v}'(\boldsymbol{x},t)\,\mathrm{d}t = 0. \tag{70.28b}$$

To maintain a non-divergent eddy velocity at arbitrary times requires

$$\nabla\cdot\boldsymbol{v}' = 0 \Longrightarrow \nabla\cdot\boldsymbol{U} = \boldsymbol{U}\cdot\boldsymbol{k} = 0. \tag{70.29}$$

As studied in Part X of this book, $\boldsymbol{U} \cdot \boldsymbol{k} = 0$ means that the wave is transverse, so that particle displacements arising from the wave are orthogonal to the wavevector (e.g., Figure 70.1)

Stokes drift

Specializing to the velocity field (70.27b), substituting into the Stokes drift expression (70.26), and making use of an average over a wave period yields

$$\overline{(\boldsymbol{\xi} \cdot \nabla) v'^p} = \frac{U^p \, \boldsymbol{U} \cdot \boldsymbol{k}}{2\,\omega} \quad \text{and} \quad \overline{\boldsymbol{v}} = 0. \tag{70.30}$$

The second equality holds since the velocity at a point arises just from the wave field, which has a zero Eulerian mean. Hence, to $\mathcal{O}(\alpha^2)$, the Stokes drift velocity associated with the GLM is given by

$$\boldsymbol{v}^{(\mathrm{S})} = \frac{\boldsymbol{U}\,(\boldsymbol{U} \cdot \boldsymbol{k})}{2\,\omega} + \mathcal{O}(\alpha^2). \tag{70.31}$$

The Stokes drift vanishes at this order of accuracy for transverse waves since $\boldsymbol{U} \cdot \boldsymbol{k} = 0$.

As a check on the formalism, consider a one-dimensional longitudinal wave, in which the Stokes drift is given by

$$\overline{v}^{(\mathrm{S})} = \frac{U^2}{2\,c} + \mathcal{O}(\alpha^2), \tag{70.32}$$

where $c = \omega/k$ is the wave speed. This result agrees with that derived using Lagrangian trajectories in Section 52.11 (see Exercise 52.7). Use of the GLM displacement field offers a somewhat more streamlined method for computing Stokes drift.

Stokes mean for an arbitrary field

The Stokes mean for an arbitrary field is given by

$$\overline{\Psi}^{(\mathrm{S})}(\boldsymbol{x}, t) = -\omega^{-1}\, \boldsymbol{U} \cdot \overline{\nabla \Psi' \sin(\boldsymbol{k} \cdot \boldsymbol{x} - \omega t)} + \mathcal{O}(\alpha^2) \tag{70.33a}$$

$$= -\omega^{-1}\, \overline{\nabla \cdot (\boldsymbol{U}\, \Psi') \sin(\boldsymbol{k} \cdot \boldsymbol{x} - \omega t)} + \mathcal{O}(\alpha^2), \tag{70.33b}$$

where the second equality made use of the non-divergent nature of the wave field (70.29). To second order in wave amplitude, the Stokes mean is determined by the projection of the gradient of the Eulerian fluctuation, $\nabla \Psi'$, onto the wave amplitude, $\boldsymbol{U}$. For example, consider a transverse wave such as that shown in Figure 70.1. Even though the Stokes drift vanishes to order $\mathcal{O}(\alpha^2)$, the Stokes mean, $\overline{\Psi}^{(\mathrm{S})}(\boldsymbol{x}, t)$, can be nonzero so long as there is a nonzero vertical gradient in the Eulerian fluctuation.

70.2.6 GLM with a materially constant scalar

Consider a materially constant scalar field, such as a tracer concentration in the absence of mixing and sources

$$\frac{\mathrm{D}C}{\mathrm{D}t} = 0. \tag{70.34}$$

How the GLM for C is related to the instantaneous C

The GLM for C equals to the value of C on a fluid particle

$$\overline{C(\boldsymbol{x} + \boldsymbol{\xi}, t)} = \overline{C}^{(\mathrm{GLM})}(\boldsymbol{x}, t) = C(\boldsymbol{x} + \boldsymbol{\xi}, t). \tag{70.35}$$

This is a subtle identity that packs in a lot of information. It says that when evaluated at the mean fluid particle position, $\boldsymbol{x}$, the GLM tracer concentration, $\overline{C}^{(\mathrm{GLM})}(\boldsymbol{x}, t)$, equals to the concentration evaluated on a fluid particle, $C(\boldsymbol{x} + \boldsymbol{\xi}, t)$. One way to understand this identity is to assume the averaging operator is an ensemble mean, so that the GLM is an ensemble mean following fluid particles. Since C is constant on fluid particles, each ensemble member has the same value for C, in which case the GLM for C clearly equals the value of C for each ensemble member. We make particular use of the identity (70.35) when considering isopycnal kinematics in Sections 70.4 and 70.5.

Relating the particle disturbance field to Eulerian properties of C

There is a frequently used consequence of the identity (70.35) involving the Eulerian fluctuation

$$C'(\boldsymbol{x}, t) = C(\boldsymbol{x}, t) - \overline{C}(\boldsymbol{x}, t) \tag{70.36}$$

and the Eulerian mean

$$C^{(\mathrm{E})}(\boldsymbol{x}, t) = \overline{C}(\boldsymbol{x}, t). \tag{70.37}$$

To derive it, recall the Taylor series expansion (70.23) truncated here to first order accuracy

$$C(\boldsymbol{x} + \boldsymbol{\xi}, t) = C(\boldsymbol{x}, t) + \boldsymbol{\xi} \cdot \nabla \overline{C}(\boldsymbol{x}, t) + \mathcal{O}(\alpha^2). \tag{70.38}$$

Taking the Eulerian mean of both sides renders

$$\overline{C(\boldsymbol{x} + \boldsymbol{\xi}, t)} = \overline{C}(\boldsymbol{x}, t) + \mathcal{O}(\alpha^2), \tag{70.39}$$

which follows since $\overline{\xi^p} = 0$ for each component of the displacement field. The identity (70.39) says that the GLM equals to the Eulerian mean to order $\mathcal{O}(\alpha^2)$, which is a result consistent with the Stokes mean being an order $\mathcal{O}(\alpha^2)$ quantity as revealed by equation (70.24c). From equation (70.35) we know that $C(\boldsymbol{x} + \boldsymbol{\xi}, t) = \overline{C(\boldsymbol{x} + \boldsymbol{\xi}, t)}$, so that we can subtract equations (70.38) and (70.39) to find

$$C'(\boldsymbol{x}, t) = -\boldsymbol{\xi} \cdot \nabla \overline{C}(\boldsymbol{x}, t) + \mathcal{O}(\alpha^2). \tag{70.40}$$

Hence, to first order accuracy, the Eulerian fluctuation equals to minus the disturbance field projected onto the gradient of the mean field; i.e., the Eulerian fluctuation in the tracer is first order in the disturbance. We make use of this result when discussing the kinematics of eddy tracer fluxes in Section 70.3. Furthermore, for the isopycnal kinematics in Sections 70.4 and 70.5, we focus on vertical particle displacements, $\boldsymbol{\xi} = \xi\, \hat{\boldsymbol{z}}$, in which case the Eulerian fluctuation is given by

$$C'(z, t) = -\xi\, \partial_z \overline{C}(z, t) + \mathcal{O}(\alpha^2). \tag{70.41}$$

70.2.7 Further study

GLM was introduced in the seminal papers by *Andrews and McIntyre* (1978a,b). These papers offer a wealth of intellectual rewards after much study. GLM is also detailed in the monograph on waves and mean flows by *Bühler* (2014a). *Gilbert and Vanneste* (2025) provide an elegant and powerful mathematical framework for GLM that allows for its use for arbitrary manifolds.

70.3 Kinematics of eddy tracer fluxes

As introduced in Section 70.2.1, consider the Eulerian eddy-mean decomposition for a materially constant tracer in an non-divergent flow. The advection equation for this tracer is given by

$$\partial_t C + \nabla \cdot (\boldsymbol{v}\, C) = 0, \tag{70.42}$$

and its Eulerian mean is

$$\partial_t \overline{C} + \nabla \cdot (\overline{\boldsymbol{v}}\, \overline{C}) = -\nabla \cdot (\overline{\boldsymbol{v}'\, C'}). \tag{70.43}$$

The eddy advective flux, $\boldsymbol{v}'\, C'$, is the product of the eddy velocity and eddy tracer concentration. Its mean provides the correlation or mean eddy flux, $\overline{\boldsymbol{v}'\, C'}$. The convergence of this mean eddy flux provides a source to the advection equation for the Eulerian mean tracer concentration.

In this section we make use of the particle disturbance field of Section 70.2 to unpack the kinematics of eddy tracer fluxes induced by small amplitude waves. As we see, the particle disturbance field is a useful conceptual tool to frame the kinematics of tracer eddy fluxes.

70.3.1 Particle displacements and eddy tracer fluxes

Following Section 70.2, we here introduce a particle disturbance vector corresponding to small amplitude eddy fluctuations

$$\partial_t \boldsymbol{\xi}(\boldsymbol{x}, t) = \boldsymbol{v}'(\boldsymbol{x}, t) + \mathcal{O}(\alpha^2) \tag{70.44a}$$

$$\overline{\boldsymbol{\xi}} = 0. \tag{70.44b}$$

Correspondingly, each spatial point, $\boldsymbol{x}$, is the mean position of a fluid particle whose instantaneous position is $\boldsymbol{x} + \boldsymbol{\xi}(\boldsymbol{x}, t)$. Following the results from Section 70.2.6, to leading order we can write the Eulerian fluctuation in terms of the particle displacement (equation (70.40))

$$C'(\boldsymbol{x}, t) = -\boldsymbol{\xi} \cdot \nabla \overline{C}(\boldsymbol{x}, t) + \mathcal{O}(\alpha^2). \tag{70.45}$$

Notice that if the particle displacement is oriented along a mean tracer iso-surface, then $\boldsymbol{\xi} \cdot \nabla \overline{C}(\boldsymbol{x}, t) = 0$ and there is no tracer fluctuation, $C' = 0$, to order $\mathcal{O}(\alpha^2)$. More general eddy motions lead to a nonzero tracer fluctuation with the eddy tracer flux taking on the form

$$\boldsymbol{v}'\, C' = -\partial_t \boldsymbol{\xi}\, (\boldsymbol{\xi} \cdot \nabla) \overline{C} + \mathcal{O}(\alpha^2). \tag{70.46}$$

We unpack this expression for the purpose of characterizing kinematic properties of the eddy tracer flux.

70.3.2 Decomposing into symmetric and skew symmetric fluxes

From equation (70.46), the m'th component of the eddy tracer flux is given by

$$v'^m\, C' = -\left[(\partial_t\, \xi^m)\, \xi^n\right] \partial_n \overline{C}. \tag{70.47}$$

To explore the kinematic properties of the tracer flux (70.47), decompose the second order tensor, $(\partial_t\, \xi^m)\, \xi^n$, into its symmetric and anti-symmetric components[3]

$$2\, (\partial_t\, \xi^m)\, \xi^n = [(\partial_t\, \xi^m)\, \xi^n + (\partial_t\, \xi^n)\, \xi^m] + [(\partial_t\, \xi^m)\, \xi^n - (\partial_t\, \xi^n)\, \xi^m] \tag{70.48a}$$

$$= \partial_t (\xi^m\, \xi^n) + [(\partial_t\, \xi^m)\, \xi^n - (\partial_t\, \xi^n)\, \xi^m]\,. \tag{70.48b}$$

[3] See Section 18.8 for a similar decomposition of the velocity gradient tensor.

Introducing the symmetric and anti-symmetric correlation tensors

$$2\,K^{mn} \equiv \overline{\partial_t\,(\xi^m\,\xi^n)} \tag{70.49a}$$

$$2\,A^{mn} \equiv \overline{(\partial_t\,\xi^m)\,\xi^n} - \overline{(\partial_t\,\xi^n)\,\xi^m} \tag{70.49b}$$

allows us to write the mean eddy tracer flux

$$\overline{v'^m\,C'} = -(K^{mn} + A^{mn})\,\partial_n \overline{C} \tag{70.50}$$

and the mean field tracer equation (70.43)

$$\partial_t \overline{C} + \nabla \cdot (\overline{\boldsymbol{v}}\,\overline{C}) = \nabla \cdot \left[(\boldsymbol{K} + \boldsymbol{A}) \cdot \nabla \overline{C}\right]. \tag{70.51}$$

The right hand side of this equation equals to the convergence of the symmetric and skew-symmetric tracer fluxes

$$\nabla \cdot \left[(\boldsymbol{K} + \boldsymbol{A}) \cdot \nabla \overline{C}\right] = -\nabla \cdot (\boldsymbol{F}^{\text{sym}} + \boldsymbol{F}^{\text{skew}}), \tag{70.52}$$

where

$$\boldsymbol{F}^{\text{sym}} = -\boldsymbol{K} \cdot \nabla \overline{C} \tag{70.53a}$$

$$\boldsymbol{F}^{\text{skew}} = -\boldsymbol{A} \cdot \nabla \overline{C} \tag{70.53b}$$

$$\overline{\boldsymbol{v}'\,C'} = \boldsymbol{F}^{\text{sym}} + \boldsymbol{F}^{\text{skew}}. \tag{70.53c}$$

70.3.3 The symmetric tracer flux

In terms of particle displacements, the symmetric flux (70.53a) is given by

$$(F^{\text{sym}})^m = -K^{mn}\,\partial_n \overline{C} = -\frac{1}{2}\,\overline{\partial_t(\xi^m\,\xi^n)}\,\partial_n \overline{C}. \tag{70.54}$$

The symmetric tensor, $\boldsymbol{K}$, vanishes when the average is over the period of a periodic wave, in which the particle displacements undergo reversible periodic excursions (see Section 70.3.9). For waves that decay in amplitude over the averaging period, particle displacements decrease in magnitude thus leading to an upgradient symmetric flux. In contrast, particle displacements increase in magnitude for waves that grow over the averaging period, in which case the flux is downgradient, just as for diffusion. Furthermore, growing nonlinear waves generally break and then develop into turbulence, with turbulence leading to further particle separation and dispersive tracer mixing. Dispersive mixing from turbulent motions is generally parameterized by downgradient diffusion, and we have more to say about diffusive parameterizations of lateral dispersion in Section 71.4.

70.3.4 The skew, advective, and rotational tracer fluxes

Following our discussion in Section 69.5, we write the skew flux as

$$(F^{\text{skew}})^m = -A^{mn}\,\partial_n \overline{C} = -\epsilon^{mnp}\,\Psi_p\,\partial_n \overline{C} = -\left(\nabla \overline{C} \times \boldsymbol{\Psi}\right)^m, \tag{70.55}$$

where we introduced the vector streamfunction (dimensions squared length per time)[4]

$$\boldsymbol{\Psi} = \frac{1}{2}\,\overline{\partial_t \boldsymbol{\xi} \times \boldsymbol{\xi}} = \frac{1}{2}\,\overline{\boldsymbol{v}' \times \boldsymbol{\xi}}. \tag{70.56}$$

[4] *Middleton and Loder* (1989) and *Garrett* (2006) introduce a skew-diffusivity, $\boldsymbol{D}$, which is opposite in sign to the vector streamfunction: $\boldsymbol{\Psi} = -\boldsymbol{D}$.

The vector streamfunction is half the angular momentum per mass of a fluid particle undergoing eddying motion, with the angular momentum computed relative to the mean particle position. The vector streamfunction is nonzero only if the eddy has a preferred sense of rotation, in which case the wave field is said to be *polarized*. That is, polarization results if the fluctuating velocity, $\boldsymbol{v}'$, is correlated to a fluid particle displacement, $\boldsymbol{\xi}$, in an orthogonal direction, thus giving rise to a nonzero angular momentum.

The skew flux can be written

$$\begin{aligned} \boldsymbol{F}^{\text{skew}} &= -\nabla \overline{C} \times \boldsymbol{\Psi} && \text{(70.57a)} \\ &= (\nabla \times \boldsymbol{\Psi})\, \overline{C} - \nabla \times (\overline{C}\, \boldsymbol{\Psi}) && \text{(70.57b)} \\ &= \boldsymbol{U}^{\text{A}}\, \overline{C} - \nabla \times (\overline{C}\, \boldsymbol{\Psi}) && \text{(70.57c)} \\ &= \boldsymbol{F}^{\text{adv}} - \boldsymbol{F}^{\text{rot}}, && \text{(70.57d)} \end{aligned}$$

so that the skew flux equals to an advective flux minus a rotational flux. We here introduced the non-divergent velocity

$$\boldsymbol{U}^{\text{A}} = \nabla \times \boldsymbol{\Psi} \tag{70.58}$$

and the non-divergent rotational flux

$$\boldsymbol{F}^{\text{rot}} = \nabla \times (\overline{C}\, \boldsymbol{\Psi}). \tag{70.59}$$

Since $\nabla \cdot \boldsymbol{F}^{\text{rot}} = 0$, we see that the divergence of the skew flux equals to the divergence of the advective flux

$$\nabla \cdot \boldsymbol{F}^{\text{skew}} = \nabla \cdot (\boldsymbol{F}^{\text{adv}} - \boldsymbol{F}^{\text{rot}}) = \nabla \cdot \boldsymbol{F}^{\text{adv}}. \tag{70.60}$$

Consequently, the rotational flux, $\boldsymbol{F}^{\text{rot}}$, has no impact on evolution of the mean tracer concentration.

70.3.5 What does a point measurement estimate?

From equation (70.53c), we see that a point measurement of the correlation, $\overline{\boldsymbol{v}'\, C'}$, provides an estimate of the symmetric tracer flux plus the skew tracer flux

$$\overline{\boldsymbol{v}'\, C'} = \boldsymbol{F}^{\text{sym}} + \boldsymbol{F}^{\text{skew}} = -(\boldsymbol{K} + \boldsymbol{A}) \cdot \nabla \overline{C}. \tag{70.61}$$

Furthermore, for a periodic wave field, where the symmetric tensor vanishes, the correlation, $\overline{\boldsymbol{v}'\, C'}$, provides a direct estimate of the skew flux, $-\nabla \overline{C} \times \boldsymbol{\Psi}$. This latter result might seem puzzling on first encounter, since one could imagine $\overline{\boldsymbol{v}'\, C'}$ instead provides an estimate for the advective flux, $\overline{C}\, \boldsymbol{U}^{\text{A}}$. But that presumption is wrong, as indicated by the decomposition (70.61). We emphasize this point by summarizing the various relations

$$\begin{aligned} \overline{\boldsymbol{v}'\, C'} &= \boldsymbol{F}^{\text{sym}} + \boldsymbol{F}^{\text{skew}} && \text{(70.62a)} \\ &= -\boldsymbol{K} \cdot \nabla \overline{C} - \nabla \overline{C} \times \boldsymbol{\Psi} && \text{(70.62b)} \\ &= -\boldsymbol{K} \cdot \nabla \overline{C} - \nabla \times (\overline{C}\, \boldsymbol{\Psi}) + \overline{C}\, \nabla \times \boldsymbol{\Psi} && \text{(70.62c)} \\ &= \boldsymbol{F}^{\text{sym}} - \boldsymbol{F}^{\text{rot}} + \boldsymbol{F}^{\text{adv}}. && \text{(70.62d)} \end{aligned}$$

The rotational flux is generally nontrivial for polarized waves or turbulent eddies. Hence, the rotational flux provides a sizable contribution to any measurement of $\overline{\boldsymbol{v}'\, C'}$ either from a field measurement or numerical simulation. Hence, for some purposes it can be more convenient to work directly with the skew flux rather than the advective flux.

70.3.6 Area integrated tracer flux

We further our understanding of the rotational contribution by considering the mean of the tracer flux integrated over a static area $\mathcal{S}$

$$\mathcal{T} = \overline{\int_{\mathcal{S}} \boldsymbol{v}\, C \cdot \hat{\boldsymbol{n}}\, \mathrm{d}\mathcal{S}} = \int_{\mathcal{S}} \overline{\boldsymbol{v}\, C} \cdot \hat{\boldsymbol{n}}\, \mathrm{d}\mathcal{S} = \int_{\mathcal{S}} [\overline{\boldsymbol{v}}\, \overline{C} + \overline{\boldsymbol{v}'\, C'}] \cdot \hat{\boldsymbol{n}}\, \mathrm{d}\mathcal{S}. \tag{70.63}$$

Introducing the diffusive, advective, and rotational flux as in equation (70.62d) renders

$$\mathcal{T} = \int_{\mathcal{S}} [\overline{\boldsymbol{v}}\, \overline{C} + \boldsymbol{U}^{\mathsf{A}}\, \overline{C} - \nabla \times (\overline{C}\, \boldsymbol{\Psi}) - \boldsymbol{K} \cdot \nabla \overline{C}] \cdot \hat{\boldsymbol{n}}\, \mathrm{d}\mathcal{S}. \tag{70.64}$$

Use of Stokes' Theorem transforms the rotational term to a line integral around the boundary of the area

$$\mathcal{T} = \int_{\mathcal{S}} [\overline{\boldsymbol{v}}\, \overline{C} + \boldsymbol{U}^{\mathsf{A}}\, \overline{C} - \boldsymbol{K} \cdot \nabla \overline{C}] \cdot \hat{\boldsymbol{n}}\, \mathrm{d}S - \oint_{\partial \mathcal{S}} \overline{C}\, \boldsymbol{\Psi} \cdot \mathrm{d}\boldsymbol{l}. \tag{70.65}$$

Following Section 2b of *Middleton and Loder* (1989), we interpret the boundary term as a Stokes contribution associated with the correlation of particle motion and perturbation velocity along the boundary

$$\oint_{\partial \mathcal{S}} \overline{C}\, \boldsymbol{\Psi} \cdot \mathrm{d}\boldsymbol{l} = \frac{1}{2} \oint_{\partial \mathcal{S}} \overline{C}\, (\overline{\boldsymbol{v}' \times \boldsymbol{\xi}}) \cdot \mathrm{d}\boldsymbol{l}. \tag{70.66}$$

We further this interpretation when considering the transport beneath a fluctuating isopycnal surface in Section 70.5.4.

70.3.7 Massaging the mean field tracer equation

We here write the mean tracer equation (70.51) in various forms that can be found throughout the literature. For this purpose, write the right hand side of equation (70.51) in the form

$$\nabla \cdot \left[(\boldsymbol{K} + \boldsymbol{A}) \cdot \nabla \overline{C} \right] = \partial_m \left[(K^{mn} + A^{mn})\, \partial_n \overline{C} \right] \tag{70.67a}$$

$$= \partial_m \left(K^{mn} + A^{mn} \right) \partial_n \overline{C} + (K^{mn} + A^{mn})\, \partial_m \partial_n \overline{C} \tag{70.67b}$$

$$= \partial_m \left(K^{mn} + A^{mn} \right) \partial_n \overline{C} + K^{mn}\, \partial_m \partial_n \overline{C}. \tag{70.67c}$$

The final equality follows from the identity

$$A^{mn}\, \partial_m \partial_n \overline{C} = 0, \tag{70.68}$$

which results from the contraction of the anti-symmetric tensor, A^{mn}, with the symmetric derivative operator $\partial_m \partial_n$. The second term, $K^{mn}\, \partial_m \partial_n \overline{C}$, is a diffusion operator *if* the symmetric tensor $\boldsymbol{K}$ is also positive-definite. The first term in equation (70.67c) can be interpreted as an advection operator through the action of a non-divergent plus a divergent advection velocity

$$\partial_m \left(K^{mn} + A^{mn} \right) \partial_n \overline{C} \equiv -(\boldsymbol{U}^{\mathsf{K}} + \boldsymbol{U}^{\mathsf{A}}) \cdot \nabla \overline{C}, \tag{70.69}$$

where we defined[5]

$$\boldsymbol{U}^{\mathsf{K}} \equiv -\nabla \cdot \boldsymbol{K} \Longrightarrow \nabla \cdot \boldsymbol{U}^{\mathsf{K}} = -\partial_n \partial_m K^{mn} \neq 0 \tag{70.70a}$$

$$\boldsymbol{U}^{\mathsf{A}} \equiv -\nabla \cdot \boldsymbol{A} \Longrightarrow \nabla \cdot \boldsymbol{U}^{\mathsf{A}} = -\partial_n \partial_m A^{mn} = 0. \tag{70.70b}$$

Bringing the above results together allows us to write the mean field tracer equation (70.51)

[5] Note that *Middleton and Loder* (1989) define $\boldsymbol{U}^{\mathsf{K}} = \nabla \cdot \boldsymbol{K}$, which is the opposite sign to that used here in equation (70.70a), whereas they define $\boldsymbol{U}^{\Psi} = -\nabla \cdot \boldsymbol{A}$ as in equation (70.70b).

in the following equivalent forms

$$\partial_t \overline{C} + (\overline{\boldsymbol{v}} + \boldsymbol{U}^{\mathsf{A}} + \boldsymbol{U}^{\mathsf{K}}) \cdot \nabla \overline{C} = K^{mn}\, \partial_m \partial_n \overline{C} \qquad \text{advective form} \tag{70.71a}$$

$$\partial_t \overline{C} + \nabla \cdot [(\overline{\boldsymbol{v}} + \boldsymbol{U}^{\mathsf{A}})\, \overline{C}] = \nabla \cdot (\boldsymbol{K} \cdot \nabla \overline{C}) \qquad \text{flux form} \tag{70.71b}$$

$$\partial_t \overline{C} + \nabla \cdot [(\overline{\boldsymbol{v}} + \boldsymbol{U}^{\mathsf{A}})\, \overline{C} + \boldsymbol{F}^{\mathsf{sym}}] = 0, \qquad \text{alternate flux form} \tag{70.71c}$$

where we made use of the identities

$$\nabla \cdot \overline{\boldsymbol{v}} = 0 \quad \text{and} \quad \nabla \cdot \boldsymbol{U}^{\mathsf{A}} = 0 \quad \text{and} \quad \nabla \cdot \boldsymbol{U}^{\mathsf{K}} \neq 0. \tag{70.72}$$

70.3.8 Connection to Stokes drift

From equation (70.26) we have the leading order expression for the Stokes drift

$$\boldsymbol{v}^{(\mathsf{S})} = \overline{\xi^n\, \partial_n\, \partial_t\, \boldsymbol{\xi}} + \mathcal{O}(\alpha^2). \tag{70.73}$$

As noted in equation (70.17), with $\partial_t \boldsymbol{\xi} = \boldsymbol{v}'$ and with $\nabla \cdot \boldsymbol{v}' = 0$, the corresponding particle displacements are non-divergent, $\nabla \cdot \boldsymbol{v}' = 0 \Rightarrow \nabla \cdot \boldsymbol{\xi} = 0$. Consequently, to second order accuracy, the Stokes drift velocity can be written

$$(v^{(\mathsf{S})})^p = \overline{\xi^n\, \partial_n\, \partial_t\, \xi^p} \tag{70.74a}$$

$$= \partial_n\, [\overline{(\partial_t\, \xi^p)\, \xi^n}] \tag{70.74b}$$

$$= \partial_n\, (K^{pn} + A^{pn}) \tag{70.74c}$$

$$= \partial_n\, (K^{np} - A^{np}) \tag{70.74d}$$

$$= -(U^{\mathsf{K}})^p + (U^{\mathsf{A}})^p. \tag{70.74e}$$

For the case of periodic fluid particle motion, the Stokes drift velocity equals to the non-divergent skew velocity

$$\boldsymbol{v}^{(\mathsf{S})} = \boldsymbol{U}^{\mathsf{A}} \Longrightarrow \nabla \cdot \boldsymbol{v}^{(\mathsf{S})} = 0 \qquad \text{periodic motion.} \tag{70.75}$$

More generally, for non-periodic motion, the divergent velocity is non-zero so that the Stokes velocity is also divergent

$$\boldsymbol{v}^{(\mathsf{S})} = \boldsymbol{U}^{\mathsf{A}} - \boldsymbol{U}^{\mathsf{K}} \Longrightarrow \nabla \cdot \boldsymbol{v}^{(\mathsf{S})} = -\nabla \cdot \boldsymbol{U}^{\mathsf{K}} \neq 0 \qquad \text{non-periodic motion.} \tag{70.76}$$

70.3.9 A polarized periodic example

We illustrate some of the previous analysis by considering a particle displacement vector comprised of periodic and polarized motion in the horizontal plane

$$\boldsymbol{\xi}(\boldsymbol{x}, t) = \Gamma\, [\hat{\boldsymbol{x}}\, \cos(\omega\, t) + \hat{\boldsymbol{y}}\, \sin(\omega\, t)] \tag{70.77a}$$

$$\partial_t \boldsymbol{\xi}(\boldsymbol{x}, t) = \omega\, \Gamma\, [-\hat{\boldsymbol{x}}\, \sin(\omega\, t) + \hat{\boldsymbol{y}}\, \cos(\omega\, t)], \tag{70.77b}$$

where $\Gamma > 0$ a time-independent amplitude and $2\pi/\omega > 0$ is the period. The fluid particles exhibit counter-clockwise circular and periodic motion in the horizontal plane with squared radius

$$\boldsymbol{\xi} \cdot \boldsymbol{\xi} = \Gamma^2. \tag{70.78}$$

Define the mean operator be a phase average

$$\overline{\phi} = \frac{1}{2\pi/\omega} \int_0^{2\pi/\omega} \phi(t)\, \mathrm{d}t, \tag{70.79}$$

which is a suitable averaging operator for examining the impacts of oscillatory motion on mean fields. For a spatially constant amplitude, we find below that the mean tracer concentration, $\overline{C}$, remains unchanged. The absence of a rectified change to $\overline{C}$ reflects the assumed periodic nature of the fluid particle motion.

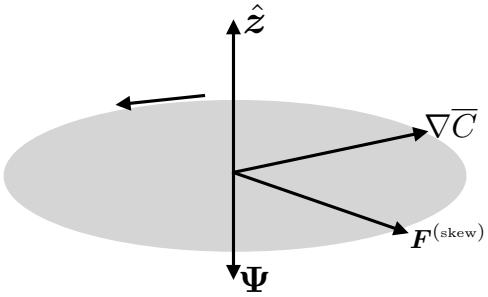

FIGURE 70.2: Sketch of the skew tracer flux associated with the polarized displacement vector (70.77a). The fluid particles are moving in the horizontal plane along a circle with a constant radius, Γ. The vector streamfunction (70.82) points in the negative $\hat{\boldsymbol{z}}$ direction. The mean concentration gradient, $\nabla\overline{C}$, generally points outside of the horizontal plane. However, it is only the horizontal components that contribute since the displacement vector is in the horizontal plane, thus resulting in a horizontal skew tracer flux. The advective velocity vanishes since the amplitude, Γ, is assumed to be spatially constant. Hence, the skew flux is purely rotational, which means there is no rectified effects on the mean tracer concentration.

Symmetric mixing tensor

In the presence of the oscillatory particle displacement (70.77a), the symmetric mixing tensor (70.49a) is given by

$$2\,K^{mn} = \frac{\Gamma^2}{2\pi/\omega}\int_0^{2\pi/\omega} \mathrm{d}t\,\frac{\partial}{\partial t}\begin{bmatrix} \cos^2(\omega\,t) & \cos(\omega\,t)\,\sin(\omega\,t) \\ \cos(\omega\,t)\,\sin(\omega\,t) & \sin^2(\omega\,t)\end{bmatrix} = 0, \tag{70.80}$$

which vanishes identically since the particles exhibit periodic motion.

Skew symmetric stirring tensor

The skew-symmetric tensor (70.49b) has non-zero components due to the polarization

$$2\,A^{12} = -A^{21} = \overline{(\partial_t\,\xi^1)\,\xi^2} - \overline{(\partial_t\,\xi^2)\,\xi^1} = -\Gamma^2\,\omega\,\overline{\sin^2(\omega\,t) + \cos^2(\omega\ ,t)} = -\Gamma^2\,\omega. \tag{70.81}$$

The corresponding vector streamfunction (70.56) is vertical

$$\boldsymbol{\Psi} = -\frac{\Gamma^2\,\omega}{2}\,\hat{\boldsymbol{z}}, \tag{70.82}$$

and the skew flux is horizontal

$$\boldsymbol{F}^{\text{skew}} = -\frac{\Gamma^2\,\omega}{2}\,(\hat{\boldsymbol{z}}\times\nabla\overline{C}). \tag{70.83}$$

Finally, the advective velocity is given by

$$\nabla\times\boldsymbol{\Psi} = -\omega\,\Gamma\,\nabla\Gamma\times\hat{\boldsymbol{z}}. \tag{70.84}$$

The advective velocity vanishes when the wave amplitude, Γ, is a constant, in which case the advective tracer flux is zero although the skew flux is non-zero. Indeed, with a constant wave amplitude, the skew tracer flux has a zero divergence so that it is a purely rotational flux. Hence,

for a constant wave amplitude, neither the skew flux nor the advective flux affect the evolution of $\overline{C}$. Figure 70.2 offers a schematic of the skew flux induced by the periodic rotating particle motion in the horizontal plane.

70.3.10 Further study

Much of this section follows *Plumb* (1979), *Middleton and Loder* (1989), and *Garrett* (2006), each of whom considered elements of tracer dispersion by waves and nonlinear eddies. *Middleton and Loder* (1989) work through a few oceanographically motivated examples that offer further understanding of skew fluxes. Additional treatments can be found in the review article of *Moffatt* (1983), who considers flow in a rotating reference frame as well as magneto-hydrodynamic flows.

70.4 Kinematics of volume transport in isopycnal layers

In this section we consider the reversible stirring of fluid parcels by turbulent flow in a perfect (i.e., no mixing or sources) stratified Boussinesq fluid. As the fluid parcels are stirred, they preserve their volume while changing their shape and stretching into finer scale features. Stirring by ocean mesoscale/baroclinic eddies offers the canonical example of such stirring. Eventually, small-scale processes, such as those summarized in Section 71.1.1, irreversibly mix properties. We are here focused just on the stirring part of this process.

Over space and time scales larger than the mesoscale, the stirring by ocean mesoscale eddies can be considered chaotic, which in turn motivates a stochastic perspective in which an ensemble of eddies is considered. The goal is to describe the ensemble mean properties of the perfect fluid, with a focus in this section on the kinematics of parcel rearrangement. Hence, eddy correlations in the present section appear between the thickness of a fluid layer and the velocity. We introduce tracers in Section 70.5, at which point we also consider eddy correlations between velocity and tracer as in Section 70.3.

The material in this section is rather detailed. However, its mastery comes readily by keeping in mind the more general (and somewhat simpler) presentation of GLM offered in Section 70.2. We are motivated to provide full details in this section since the kinematics of isopycnal ensembles appears throughout the study of wave-mean flow interactions in adiabatic geophysical fluid mechanics, such as in the study of ocean mesoscale eddies.

70.4.1 Isopycnal mean

Each fluid parcel in a stably stratified perfect Boussinesq ocean preserves its potential density. We are interested in following the vertical motion of potential density layer interfaces as waves and turbulent processes transport layer thickness from one region to another. In contrast, we are not concerned with following the lateral position of a fluid parcel within a layer. Here we introduce the isopycnal mean, which is based on describing ensembles of perfect fluid parcels using isopycnal coordinates. In Sections 70.4.2 and 70.4.3, we relate this isopycnal approach to the GLM restricted to the vertical direction.

Defining the isopycnal ensemble

An overbar with a potential density label, $\overline{(\,)}^{(\varrho)}$, denotes a mean over an ensemble of fluid parcels, each having the same potential density, ϱ, the same horizontal position, (x, y), and the same time, t. Isopycnals undulate in space and time, which means that each ensemble member has a vertical position that is generally distinct from the ensemble mean vertical position, z. Furthermore, when the context is clear, it is useful to drop the dependence on (x, y, t) to highlight the dependence on potential density and/or the vertical position.

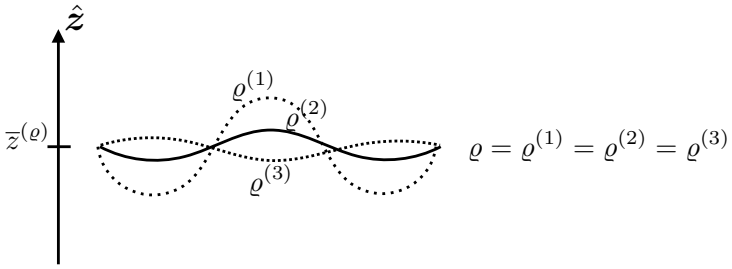

FIGURE 70.3: Schematic of the ensemble mean vertical position, $\overline{z}^{\varrho}(x, y, \varrho, t)$, for a particular potential density surface ϱ, here illustrated with a three member ensemble whose potential density is ϱ. In general, different members of an isopycnal ensemble live on different geopotentials. Therefore, when considering ensemble members with the same potential density, the ensemble mean vertical position is the average over the different members. For the case of a three member ensemble, as shown here, the averaged vertical position is $3\,\overline{z}^{\varrho}(x, y, \varrho, t) = z^{(1)}(x, y, \varrho, t) + z^{(2)}(x, y, \varrho, t) + z^{(3)}(x, y, \varrho, t)$.

Isopycnal ensemble mean

The isopycnal ensemble mean makes use of potential density as a vertical coordinate (Chapters 63 and 65), with the mean field denoted by

$$\overline{\Psi}^{(\varrho)}(x, y, \varrho, t) \equiv \text{ensemble mean using isopycnal vertical coordinates.} \tag{70.85}$$

This average is straightforward to compute when using isopycnal coordinates, thus producing an isopycnal mean that is a function of the potential density, ϱ. Figure 70.3 depicts this average.

70.4.2 Modified mean is the vertical GLM

As a complement to the isopycnal approach in Section 70.4.1, we here introduce the vertical GLM following isopycnals, which is also known as the *modified mean*.

The vertical GLM following isopycnal surfaces

The discussion in Section 70.2 considered a three dimensional particle displacement vector $\boldsymbol{\xi}(\boldsymbol{x}, t)$. In contrast, we are here interested just in the vertical displacement of an isopycnal layer interface

$$\boldsymbol{\xi}(x, y, \varrho, t) = \hat{\boldsymbol{z}}\, \xi(x, y, \varrho, t). \tag{70.86}$$

The displacement field, $\xi(x, y, \varrho, t)$, measures the vertical position of a potential density interface, ϱ, relative to its ensemble mean vertical position. For any particular ensemble member with potential density, ϱ, we write its vertical position as (dropping x, y, t dependence for brevity)

$$z(\varrho) = \overline{z}^{(\varrho)} + \xi(\varrho), \tag{70.87}$$

where

$$\overline{z}^{(\varrho)} = \overline{z(\varrho)}^{(\varrho)} \tag{70.88}$$

is the vertical position for the isopycnal ensemble mean, and the displacement field has a zero ensemble mean

$$\overline{\xi(\varrho)}^{(\varrho)} = 0. \tag{70.89}$$

Given the above definitions for the vertical position, we define the *vertical GLM* for an arbitrary function

$$\widetilde{\Psi}(x, y, \overline{z}^{(\varrho)}, t) \equiv \overline{\Psi(x, y, \overline{z}^{(\varrho)} + \xi(x, y, \varrho, t), t)}^{(\varrho)}. \tag{70.90}$$

As defined, the vertical GLM, $\widetilde{\Psi}$, is a function of the ensemble mean vertical position, $\overline{z}^{(\varrho)}$ (left hand side), and it is determined by an ensemble mean of Ψ sampled at the vertical position of each ensemble member, $\overline{z}^{(\varrho)} + \xi(\varrho)$. *McDougall and McIntosh* (2001) refer to the vertical GLM defined by equation (70.90) as the *modified mean*.

Relating the modified mean to the isopycnal mean

Following the general result (70.35), we know that the modified mean potential density, $\widetilde{\varrho}(x, y, \overline{z}^{(\varrho)}, t)$, equals to the potential density of each ensemble member so that

$$\widetilde{\varrho}(x, y, \overline{z}^{(\varrho)}, t) = \varrho(x, y, \overline{z}^{(\varrho)} + \xi(x, y, \varrho, t), t). \tag{70.91}$$

This relation means that the modified mean potential density is the functional inverse of the isopycnal ensemble mean vertical position. Consequently, the isopycnal ensemble mean of a function, $\overline{\Psi}^{(\varrho)}$ (equation (70.85)), when evaluated at the modified mean potential density, $\widetilde{\varrho}$, equals to the modified mean $\widetilde{\Psi}$ when evaluated at the vertical position of the mean density

$$\overline{\Psi}^{(\varrho)}(x, y, \widetilde{\varrho}, t) = \widetilde{\Psi}(x, y, \overline{z}^{(\varrho)}, t). \tag{70.92}$$

This is a very important identity that will be used in the following.

70.4.3 Transformed residual mean (TRM)

When working with isopycnal layers, it is very useful to use specific thickness weighting to account for the net amount of material within a layer, or to measure the net transport in the layer.[6] For this purpose we make use of the *specific thickness* from Section 64.2 as given by[7]

$$\hbar = \partial z / \partial \varrho = 1 / (\partial \varrho / \partial z), \tag{70.93}$$

and thus make use of thickness weighted fields, $\hbar\, \Psi$, and the corresponding thickness weighted isopycnal ensemble mean

$$\widehat{\Psi}(\varrho) = \frac{\overline{\hbar\, \Psi}^{(\varrho)}}{\overline{\hbar}^{(\varrho)}}. \tag{70.94}$$

The identity (70.91) then renders

$$\overline{\Psi}^{\#}(x, y, \overline{z}^{(\varrho)}, t) \equiv \widehat{\Psi}(x, y, \widetilde{\varrho}, t), \tag{70.95}$$

where $\overline{\Psi}^{\#}$ is the *transformed residual mean* (TRM) evaluated at the isopycnal ensemble mean vertical position. This is yet another important identity that will be used in the following.

Depth integrated TRM transport

The horizontal TRM velocity is a particularly key TRM field

$$\widehat{\boldsymbol{u}}(x, y, \widetilde{\varrho}, t) = \overline{\boldsymbol{u}}^{\#}(x, y, \overline{z}^{(\varrho)}, t). \tag{70.96}$$

[6] We pursue a vertical discrete version of this *thickness weighted averaging* approach for the stacked shallow water model in Chapter 67.

[7] As discussed in Section 63.9.1, specific thickness is the Jacobian of transformation between geopotential coordinates, (x, y, z, t), and isopycnal coordinates, (x, y, ϱ, t). For stably stratified ideal fluids, $\hbar$ is one-signed, hence making the coordinate transformation well defined. It is also related to the buoyancy frequency through (Section 30.6.1) $N^2 = -(g/\rho_o)\,(\partial \varrho / \partial z) = -g/(\rho_o\, \hbar)$.

Following the discussion of the vertical gauge in Section 69.5.1 (see in particular equation (69.41)), we are led to define the depth integrated TRM transport

$$\overline{\boldsymbol{U}}^{\#}(\overline{z}^{(\varrho)}) = \int_{-H}^{\overline{z}^{(\varrho)}} \overline{\boldsymbol{u}}^{\#}(z)\,\mathrm{d}z = \int_{\varrho(-H)}^{\widetilde{\varrho}(\overline{z}^{(\varrho)})} \widehat{\boldsymbol{u}}(\gamma)\,\overline{h}^{(\gamma)}\,\mathrm{d}\gamma, \tag{70.97}$$

with the second equality following from a change of coordinates from geopotential to isopycnal. We can go further with this expression by writing

$$\begin{aligned}
\overline{\boldsymbol{U}}^{\#}(\overline{z}^{(\varrho)}) &= \int_{\varrho(-H)}^{\widetilde{\varrho}(\overline{z}^{(\varrho)})} \widehat{\boldsymbol{u}}(\gamma)\,\overline{h}^{(\gamma)}\,\mathrm{d}\gamma && \text{from equation (70.97)} && \text{(70.98a)}\\
&= \int_{\varrho(-H)}^{\widetilde{\varrho}(\overline{z}^{(\varrho)})} \overline{\boldsymbol{u}\,h}^{(\gamma)}\,\mathrm{d}\gamma && \text{from equation (70.94)} && \text{(70.98b)}\\
&= \int_{\varrho(-H)}^{\varrho(\overline{z}^{(\varrho)}+\xi)} \overline{\boldsymbol{u}\,h}^{(\gamma)}\,\mathrm{d}\gamma && \text{from equation (70.91).} && \text{(70.98c)}
\end{aligned}$$

The final equality makes it clear that the TRM transport, $\overline{\boldsymbol{U}}^{\#}(\overline{z}^{(\varrho)})$, is the ensemble mean volume transport for fluid denser than $\varrho(\overline{z}^{(\varrho)}+\xi) = \widetilde{\varrho}(\overline{z}^{(\varrho)})$. This transport can also be written using geopotential coordinates

$$\overline{\boldsymbol{U}}^{\#}(\overline{z}^{(\varrho)}) = \overline{\int_{-H}^{\overline{z}^{(\varrho)}+\xi} \boldsymbol{u}\,\mathrm{d}z}. \tag{70.99}$$

The transport from each ensemble member is determined by integrating from the bottom to the vertical position, $\overline{z}^{(\varrho)}+\xi$, and then the TRM transport is determined by computing the ensemble mean for this transport.

Quasi-Stokes transport

The TRM transport (70.99) can be decomposed into an Eulerian mean plus the correlation of a fluctuation

$$\overline{\boldsymbol{U}}^{\#}(\overline{z}^{(\varrho)}) \equiv \overline{\boldsymbol{U}}(\overline{z}^{(\varrho)}) + \overline{\boldsymbol{U}}^{\mathsf{qs}}(\overline{z}^{(\varrho)}). \tag{70.100}$$

The first term,

$$\overline{\boldsymbol{U}}(\overline{z}^{(\varrho)}) = \int_{-H}^{\overline{z}^{(\varrho)}} \boldsymbol{u}\,\mathrm{d}z \tag{70.101}$$

is the ensemble mean transport between the bottom and the ensemble mean vertical position, $\overline{z}^{(\varrho)}$. We interpret this transport as an Eulerian mean since the depth ranges are fixed. In contrast, the *quasi-Stokes* transport

$$\overline{\boldsymbol{U}}^{\mathsf{qs}}(\overline{z}^{(\varrho)}) \equiv \overline{\int_{\overline{z}^{(\varrho)}}^{\overline{z}^{(\varrho)}+\xi} \boldsymbol{u}\,\mathrm{d}z} \tag{70.102}$$

measures the ensemble mean transport between the mean vertical position of an isopycnal, $\overline{z}^{(\varrho)}$, and that of each ensemble member, $\overline{z}^{(\varrho)} + \xi(\varrho)$. We refer to transport as "quasi-Stokes" given that it is the difference between an isopycnal (i.e., quasi-Lagrangian) mean and an Eulerian mean (see Section 70.2)

$$\overline{\boldsymbol{U}}^{\mathsf{qs}} = \overline{\boldsymbol{U}}^{\#} - \overline{\boldsymbol{U}}. \tag{70.103}$$

As for the traditional Stokes drift discussed in Sections 52.11, and 70.2.5, which arises from a correlation between larger velocity when a wave crest is present, so too does the quasi-Stokes transport arise from a correlation between a larger velocity and a larger undulation in isopycnal thickness.

Three-component TRM velocity

Following from the vertical gauge expression (69.40), we introduce the TRM vector streamfunction

$$\overline{\boldsymbol{\Psi}}^{\#} = \overline{\boldsymbol{U}}^{\#} \times \hat{\boldsymbol{z}}, \tag{70.104}$$

and the corresponding three-dimensional non-divergent TRM velocity

$$\overline{\boldsymbol{v}}^{\#} = \nabla \times \overline{\boldsymbol{\Psi}}^{\#}. \tag{70.105}$$

The vertical component,

$$\overline{w}^{\#} = \hat{\boldsymbol{z}} \cdot (\nabla \times \overline{\boldsymbol{\Psi}}^{\#}), \tag{70.106}$$

has no corresponding component in an isopycnal description, which only requires the horizontal thickness weighted transport, $\widehat{\boldsymbol{u}}$. However, the TRM vector streamfunction only requires the horizontal TRM transport, $\overline{\boldsymbol{U}}^{\#}$, so the two descriptions in effect make use of the same number of degrees of freedom.

70.4.4 Volume conservation and the thickness equation

Consider two perspectives on volume conservation: one based on isopycnal coordinates and the other based on geopotential coordinates.

Isopycnal coordinates

In isopycnal vertical coordinates, the volume of a fluid element is written

$$\delta V = \delta x \, \delta y \, \delta z = \delta x \, \delta y \, \delta \varrho \, \hbar, \tag{70.107}$$

where we introduced the specific thickness, $\hbar$, from equation (70.93). Geometrically, the product $|\hbar \, \delta \varrho|$ represents the vertical distance, or *thickness*, between two infinitesimally close density interfaces, ϱ and $\varrho + \delta \varrho$ (see Figure 64.2). Material conservation of both volume and potential density implies conservation of the product of specific thickness and horizontal area, $\delta x \, \delta y \, \hbar$, which leads to the thickness equation (Section 66.2.3)

$$\frac{\partial \hbar}{\partial t} + \nabla_{\varrho} \cdot (\hbar \, \boldsymbol{u}) = 0, \tag{70.108}$$

with $\boldsymbol{u}$ the horizontal velocity field, the time derivative is computed with ϱ held fixed, and

$$\nabla_{\varrho} = \nabla_{\hbar} + \boldsymbol{S} \, \partial_z \tag{70.109}$$

is the horizontal derivative operator with ϱ held fixed, and

$$\boldsymbol{S} = \nabla_{\varrho} z \tag{70.110}$$

is the horizontal slope of the potential density surface.

Geopotential coordinates

An Eulerian z-coordinate description of volume stirring within isopycnal layers is rendered via a combination of volume conservation, $\nabla \cdot \boldsymbol{v} = 0$, and material conservation of potential density, $\mathrm{D}\varrho/\mathrm{D}t = 0$. When written as skewsion rather than advection, the natural gauge is the vertical gauge introduced in Section 69.5.1, since this gauge only requires the same horizontal velocity field, $\boldsymbol{u}$, used with the isopycnal coordinate description. This gauge has an associated potential density skew flux, $\boldsymbol{F}^{\text{skew}} = -\nabla\varrho \times \boldsymbol{\Psi}$, which leads to the evolution

$$\partial_t \varrho = \nabla \cdot (\nabla\varrho \times \boldsymbol{\Psi}), \tag{70.111}$$

where all derivatives are here taken with fixed Eulerian (geopotential) coordinates, (x, y, z), and the ∇ operator is three-dimensional.

70.4.5 Ensemble mean kinematics in isopycnal coordinates

Consider an ensemble of stably stratified (so that the layer specific thickness, $\hbar$, is single-signed and nonvanishing) perfect Boussinesq fluid parcels with the same infinitesimal volume, $\delta V = \delta x\, \delta y\, \delta z = \delta x\, \delta y\, \hbar\, \delta\varrho$, and same potential density, ϱ. Lacking any other marker, such as a tracer concentration, the ensemble members are distinguished from one another by values of their horizontal area, $\delta A = \delta x\, \delta y$, and their specific thickness, $\hbar$, that is, their geometric attributes. The ensemble members are assumed to be stirred by different stochastic realizations of the fluid flow. Since each flow realization alters the geometric properties of the parcels, a mean field description focuses on the mean of these geometric properties.

In isopycnal coordinates, (x, y, ϱ, t), the thickness equation (70.108) is satisfied by each ensemble member

$$\partial_t \hbar + \nabla_{\!\varrho} \cdot (\hbar\, \boldsymbol{u}) = 0. \tag{70.112}$$

The ensemble mean computed over these fluid parcels, each with potential density ϱ, satisfies

$$\partial_t\, \overline{\hbar}^{(\varrho)} + \nabla_{\!\varrho} \cdot \left(\overline{\hbar}^{(\varrho)}\, \overline{\boldsymbol{u}}^{(\varrho)} + \overline{\hbar'\, \boldsymbol{u}'}^{(\varrho)} \right) = 0, \tag{70.113}$$

where primed variables represent deviations from the isopycnal mean. It follows that the mean specific thickness, $\overline{\hbar}^{(\varrho)}$, of parcels with potential density, ϱ, satisfies the conservation equation

$$\partial_t\, \overline{\hbar}^{(\varrho)} + \nabla_{\!\varrho} \cdot (\overline{\hbar}^{(\varrho)}\, \widehat{\boldsymbol{u}}) = 0. \tag{70.114}$$

In this equation we introduced the thickness weighted isopycnal ensemble mean horizontal velocity

$$\widehat{\boldsymbol{u}} = \frac{\overline{\hbar\, \boldsymbol{u}}^{(\varrho)}}{\overline{\hbar}^{(\varrho)}} = \overline{\boldsymbol{u}}^{(\varrho)} + \frac{\overline{\hbar'\, \boldsymbol{u}'}^{(\varrho)}}{\overline{\hbar}^{(\varrho)}} \equiv \overline{\boldsymbol{u}}^{(\varrho)} + \boldsymbol{u}^{\text{bolus}}, \tag{70.115}$$

along with the isopycnal ensemble mean horizontal velocity, $\overline{\boldsymbol{u}}^{(\varrho)}$, and the horizontal *bolus velocity*, $\boldsymbol{u}^{\text{bolus}}$, originally introduced by *Rhines* (1982). The bolus velocity for an isopycnal layer corresponds to the transport

$$\overline{\hbar}^{(\varrho)}\, \boldsymbol{u}^{\text{bolus}} = \overline{\hbar}^{(\varrho)}\, (\widehat{\boldsymbol{u}} - \overline{\boldsymbol{u}}^{(\varrho)}) = \overline{\hbar'\, \boldsymbol{u}'}^{(\varrho)}, \tag{70.116}$$

which arises from the along-isopycnal correlations between specific thickness and horizontal velocity.

Quite conveniently, the mean conservation equation (70.114) takes the *same* mathematical form as the conservation equation (70.112) satisfied by each ensemble member. The key difference is that the isopycnal ensemble mean thickness, $\overline{\hbar}^{(\varrho)}$, is stirred by the thickness weighted isopycnal

ensemble mean horizontal velocity, $\widehat{\boldsymbol{u}}$, whereas the thickness of each ensemble member is stirred by a randomly different realization of the horizontal velocity, $\boldsymbol{u}$. The simplicity of the mean field description (70.114) is afforded by use of the Lagrangian vertical coordinate, ϱ.

70.4.6 Ensemble mean kinematics in geopotential coordinates

Now consider a geopotential coordinate description of the isopycnal ensemble. For this purpose, we interpret a vertical position, z, as the ensemble mean vertical position, $\overline{z}^{(\varrho)}$. Consequently, mean fields defined at the fixed vertical position correspond to either modified mean fields when not thickness weighted (equation (70.90)), or TRM fields when thickness weighted (equation (70.95)).

Evolution of modified mean density

Following the skewsion formulation from Section 69.5, at the ensemble mean vertical position, $z = \overline{z}^{\rho}$, the streamfunction $\overline{\boldsymbol{\Psi}}^{\#}$ defines an effective skew flux of the modified mean potential density given by

$$\overline{\boldsymbol{F}}^{\#} = -\nabla\widetilde{\varrho} \times \overline{\boldsymbol{\Psi}}^{\#}. \tag{70.117}$$

Using the identity $\overline{\boldsymbol{\Psi}}^{\#} = \overline{\boldsymbol{U}}^{\#} \times \hat{\boldsymbol{z}}$, we can write this skew flux as

$$\overline{\boldsymbol{F}}^{\#} = -\overline{\boldsymbol{U}}^{\#}\, \partial_z \widetilde{\varrho} + \hat{\boldsymbol{z}}\, \overline{\boldsymbol{U}}^{\#} \cdot \nabla_{\mathrm{h}} \widetilde{\varrho} \tag{70.118a}$$

$$= -(\overline{\boldsymbol{U}}^{\#} + \hat{\boldsymbol{z}}\, \boldsymbol{S} \cdot \overline{\boldsymbol{U}}^{\#})\, \partial_z \widetilde{\varrho}, \tag{70.118b}$$

where

$$\boldsymbol{S} = -\frac{\nabla_{\mathrm{h}} \widetilde{\varrho}}{\partial_z \widetilde{\varrho}} \tag{70.119}$$

is the slope of the modified mean density field originally introduced via equation (70.110), and $\nabla_{\mathrm{h}} = (\partial_x, \partial_y, 0)$ is the horizontal gradient operator taken with constant geopotential, $z = \overline{z}^{(\varrho)}$. The convergence of the effective skew flux leads to a stirring of the modified mean density $\widetilde{\varrho}$ at the mean vertical position, $z = \overline{z}^{(\varrho)}$,

$$\partial_t \widetilde{\varrho} = \nabla \cdot (\nabla\widetilde{\varrho} \times \overline{\boldsymbol{\Psi}}^{\#}). \tag{70.120}$$

This equation represents a geopotential coordinate specification of the evolution of the modified mean density due to stirring by the mean eddies. It corresponds directly to the evolution equation (70.111) satisfied at vertical position, z, by a single member of the ensemble.

70.4.7 Approximate ensemble mean kinematics in geopotential coordinates

Equation (70.120) represents an exact z-coordinate description of the stirring of modified mean potential density. However, when working in geopotential coordinates, all that is available is Eulerian information. Hence, the Lagrangian information used to realize this exact description must be approximated.

Estimating the quasi-Stokes transport

The approximation requires an estimate of the quasi-Stokes transport, $\overline{\boldsymbol{U}}^{\mathrm{qs}}$, defined by equation (70.102). We addressed a similar estimation in Section 70.2.4 when discussing the Stokes mean.

Here, we expand the TRM transport in a Taylor series about the vertical position, $z = \overline{z}^{(\varrho)}$

$$\overline{\boldsymbol{U}}^{\#}(z) = \overline{\int_{-H}^{z+\xi} \boldsymbol{u}(s)\, \mathrm{d}s} \tag{70.121a}$$

$$= \overline{\boldsymbol{U}}(z) + \overline{\boldsymbol{u}\,\xi}^{(z)} + \frac{1}{2}\,\overline{\partial_z \boldsymbol{u}\,\xi\,\xi}^{(z)} + \mathcal{O}(\alpha^3), \tag{70.121b}$$

where neglected terms are third order in deviation quantities. Note that all ensemble means are taken at fixed vertical position, which accords with taking a Taylor series about the ensemble mean vertical position, $z = \overline{z}^{(\varrho)}$.

The ensemble means in equation (70.121b) are interpreted as follows. The first term is the Eulerian mean horizontal transport passing beneath the ensemble mean vertical position, $z = \overline{z}^{(\varrho)}$. The second term, $\overline{\boldsymbol{u}\,\xi}$, is the horizontal velocity evaluated at the ensemble mean vertical position and multiplied by the deviation, ξ, of the potential density surface from its mean vertical position, all averaged at fixed vertical position. An Eulerian split of the horizontal velocity, $\boldsymbol{u}$, into its Eulerian mean, $\overline{\boldsymbol{u}}^{(z)}$, and deviation, $\boldsymbol{u}'$, leads to the correlation

$$\overline{\boldsymbol{u}\,\xi}^{(z)} = \overline{\boldsymbol{u}'\,\xi}^{(z)}. \tag{70.122}$$

For the second order term, similar considerations lead to

$$\overline{\partial_z \boldsymbol{u}\,\xi\,\xi}^{(z)} \approx \partial_z \overline{\boldsymbol{u}}^{(z)}\, \overline{\xi\,\xi}^{(z)}, \tag{70.123}$$

where neglected terms are third order and higher. Combining these relations leads to the second order accurate expression

$$\overline{\boldsymbol{U}}^{\#} \approx \overline{\boldsymbol{U}} + \overline{\boldsymbol{u}'\,\xi}^{(z)} + \frac{1}{2}\,\overline{\xi\,\xi}^{(z)}\, \partial_z \overline{\boldsymbol{u}}^{(z)}. \tag{70.124}$$

The disturbance field

Following the discussion in Section 70.2.6, we here determine the disturbance field, ξ, in terms of fields at constant vertical position. For this purpose, use the identity (70.91) to give

$$\widetilde{\varrho}(z) = \varrho(z+\xi) \tag{70.125a}$$

$$= \varrho(z) + \partial_z \varrho(z)\, \xi + \frac{1}{2}\, \partial_{zz} \varrho(z)\, \xi^2 + \mathcal{O}(\alpha^3). \tag{70.125b}$$

Subtracting the Eulerian mean of equation (70.125b) from the unaveraged equation (70.125b), and noting that $\widetilde{\varrho}$ is already a mean field, leads to the second order accurate expression for the deviation

$$\xi = -\varrho'(z)/\partial_z \overline{\varrho}^{(z)} + \mathcal{O}(\alpha^2), \tag{70.126}$$

where

$$\varrho(z) = \overline{\varrho}^{(z)} + \varrho'(z). \tag{70.127}$$

To within the same order, the deviation can be written

$$\xi = -\varrho'(z)/\partial_z \widetilde{\varrho}(z) + \mathcal{O}(\alpha^2). \tag{70.128}$$

Approximate quasi-Stokes transport

Substituting the deviation (70.128) into the approximate expression (70.121b) for the TRM transport yields an approximate expression for the quasi-Stokes transport

$$\overline{\boldsymbol{U}}^{\text{qs}} = -\frac{\overline{\boldsymbol{u}'\,\varrho'}^{(z)}}{\partial_z \widetilde{\varrho}} + \frac{\overline{\phi}^{(z)}\,\partial_z \overline{\boldsymbol{u}}^{(z)}}{(\partial_z \widetilde{\varrho})^2} + \mathcal{O}(\alpha^3), \tag{70.129}$$

where

$$\overline{\phi}^{(z)} = \frac{1}{2}\,\overline{\varrho'\,\varrho'}^{(z)} \tag{70.130}$$

is the mean potential density variance. *McDougall and McIntosh* (2001) noted that the *Gent et al.* (1995) scheme offers a parameterization of the two correlations on the right hand side of equation (70.129). We have more to say regarding this parameterization in Section 71.1.

Substituting the deviation (70.128) into the approximate expression (70.125b) yields, to within terms of third order, the relation

$$\widetilde{\varrho} = \overline{\varrho}^{(z)} - \partial_z \left[\frac{\overline{\phi}^{(z)}}{\partial_z \overline{\varrho}^{(z)}} \right] + \mathcal{O}(\alpha^3). \tag{70.131}$$

As for the Stokes transport, the modified mean density and Eulerian mean density, when evaluated at the same vertical position, differ by terms that are second order in eddy amplitude.

70.4.8 Further study

This section is largely based on approaches used by *DeSzoeke and Bennett* (1993), *McIntosh and McDougall* (1996), *Kushner and Held* (1999), and *McDougall and McIntosh* (2001) as summarized in Section 9.3 of *Griffies* (2004). Many other papers have applied this formalism to a variety of analyses, with examples including *Nurser and Lee* (2004a), *Nurser and Lee* (2004b), *Young* (2012), *Wolfe* (2014), and *Jansen et al.* (2024).

70.5 Mean tracer equation

We now include a tracer field to the ideal Boussinesq fluid element and determine a mean field description for the tracer. The transport of tracer by eddies has both a reversible stirring component and an irreversible mixing component. The stirring arises from both the thickness correlation to velocity as well as the velocity correlated with tracer.

70.5.1 Thickness weighted average[8]

In equation (70.115) we introduced a specific thickness weighted average (or mean) operator, which is quite useful when considering the mean tracer equation. In general, for any field, Ψ, associated with a potential density layer, ϱ, we define the decomposition into thickness weighted average and deviation

$$\Psi(\varrho) = \widehat{\Psi}(\varrho) + \Psi''(\varrho) \tag{70.132a}$$

$$= \frac{\overline{h\,\Psi}^{(\varrho)}}{\overline{h}^{(\varrho)}} + \Psi''. \tag{70.132b}$$

[8]We also considered thickness weighted averaging for the shallow water equations in Chapter 67. The same identities hold here for the continuously stratified fluid.

It follows by definition that the thickness weighted average of Ψ'' vanishes,

$$\overline{\hbar\, \Psi''}^{(\varrho)} = 0. \tag{70.133}$$

70.5.2 Isopycnal mean thickness weighted tracer equation

When attaching a tracer to fluid elements, each member of the ensemble satisfies the isopycnal tracer equation

$$\partial_t C + \boldsymbol{u} \cdot \nabla_{\!\varrho} C = 0. \tag{70.134}$$

Combining the tracer and thickness equations leads to the thickness weighted tracer equation

$$\partial_t(\hbar\, C) + \nabla_{\!\varrho} \cdot (\hbar\, \boldsymbol{u}\, C) = 0. \tag{70.135}$$

Hence, in isopycnal coordinates and in the absence of irreversible processes, the evolution of thickness weighted tracer occurs via the isopycnally oriented convergence of the two-dimensional thickness weighted horizontal advective flux, $\hbar\, \boldsymbol{u}\, C$.

To address the problem of describing the ensemble mean tracer equation in isopycnal coordinates, decompose the tracer and velocity field into their thickness weighted average and deviation

$$\partial_t[\hbar\, (\widehat{C} + C'')] + \nabla_{\!\varrho} \cdot [\hbar\, (\widehat{\boldsymbol{u}} + \boldsymbol{u}'')\, (\widehat{C} + C'')] = 0. \tag{70.136}$$

Taking an ensemble average over fluid elements with the same potential density, and using equation (70.133), yield the mean thickness weighted tracer equation

$$\partial_t(\overline{h}^{(\varrho)}\, \widehat{C}) + \nabla_{\!\varrho} \cdot (\overline{h}^{(\varrho)}\, \widehat{C}\, \widehat{\boldsymbol{u}}) = -\nabla_{\!\varrho} \cdot (\overline{h\, C''\, \boldsymbol{u}''}^{(\varrho)}). \tag{70.137}$$

Now introduce the correlation,

$$\overline{\hbar\, C''\, \boldsymbol{u}''}^{(\varrho)} = \overline{\hbar}^{(\varrho)}\, \widehat{C''\, \boldsymbol{u}''}, \tag{70.138}$$

(see equation (70.132b)), and recall that the mean thickness $\overline{\hbar}^{(\varrho)}$ satisfies the mean thickness equation (70.114). These two points lead to the evolution equation for the mean thickness weighted tracer concentration

$$(\partial_t + \widehat{\boldsymbol{u}} \cdot \nabla_{\!\varrho})\, \widehat{C} = -\frac{1}{\overline{\hbar}^{(\varrho)}}\, \nabla_{\!\varrho} \cdot (\overline{\hbar}^{(\varrho)}\, \widehat{C''\, \boldsymbol{u}''}). \tag{70.139}$$

70.5.3 Subgrid scale tracer transport tensor

The correlation between tracer and velocity found on the right-hand side of the mean thickness weighted tracer equation (70.139) is typically written in terms of a subgrid scale tracer transport tensor

$$\widehat{C''\, \boldsymbol{u}''} = -\mathbb{J} \cdot \nabla_{\!\varrho} \widehat{C}. \tag{70.140}$$

This definition leads to the evolution equation

$$(\partial_t + \widehat{\boldsymbol{u}} \cdot \nabla_{\!\varrho})\, \widehat{C} = \frac{1}{\overline{h}^{(\varrho)}}\, \nabla_{\!\varrho} \cdot (\overline{h}^{(\varrho)}\, \mathbb{J} \cdot \nabla_{\!\varrho} \widehat{C}). \tag{70.141}$$

The subgrid scale operator on the right hand side has the same general form as the diffusion operator written in isopycnal coordinates as derived in Section 63.15. However, in addition to symmetric diffusion processes, this operator includes skewed fluxes that lead to skew diffusion as discussed in Section 70.3.2. Whereas the diffusive aspect is commonly parameterized as dianeutral diffusion and neutral diffusion (Section 71.1), there is no parameterization for the

skewed correlations for use in ocean models. We comment further on this situation in Section 71.3.9.

70.5.4 Mean tracer transport beneath a density surface

It is useful to further elucidate the relevance of mean thickness weighted fields. For this purpose, consider the mean horizontal tracer transport occurring beneath a particular potential density surface $\varrho = \widetilde{\varrho}$,

$$\overline{\boldsymbol{C}}^{\#}(\overline{z}^{(\varrho)}) = \overline{\int_{-H}^{\overline{z}^{\varrho}+\xi} C\,\boldsymbol{u}\,\mathrm{d}z}. \tag{70.142}$$

Setting tracer concentration to unity recovers the expression (70.99) for the TRM transport. Changing coordinates and making use of the subgrid scale tracer tensor renders

$$\begin{aligned}
\overline{\boldsymbol{C}}^{\#}(\overline{z}^{(\varrho)}) &= \int_{\varrho(-H)}^{\widetilde{\varrho}(\overline{z}^{(\varrho)})} \overline{C\,\boldsymbol{u}\,h}^{(\varrho)}\,\mathrm{d}\varrho && (70.143a)\\
&= \int_{\varrho(-H)}^{\widetilde{\varrho}(\overline{z}^{(\varrho)})} (\widehat{C}\,\widehat{\boldsymbol{u}} + \widehat{C''\,\boldsymbol{u}''})\,\overline{h}^{(\varrho)}\,\mathrm{d}\varrho && (70.143b)\\
&= \int_{\varrho(-H)}^{\widetilde{\varrho}(\overline{z}^{(\varrho)})} (\widehat{C}\,\widehat{\boldsymbol{u}} - \mathbb{J}\cdot\nabla_{\!\!\varrho}\widehat{C})\,\overline{h}^{(\varrho)}\,\mathrm{d}\varrho && (70.143c)\\
&= \int_{-H}^{\overline{z}^{(\varrho)}} (\widehat{C}\,\widehat{\boldsymbol{u}} - \mathbb{J}\cdot\nabla_{\!\!\varrho}\widehat{C})\,\mathrm{d}z. && (70.143d)
\end{aligned}$$

Hence, the mean thickness weighted fields naturally appear when considering such physically interesting quantities as the mean horizontal transport of a tracer beneath the modified mean potential density surface.

70.5.5 Summary of the tracer parameterization problem

Traditionally, the isopycnal parameterization problem for the evolution of the mean thickness weighted tracer requires a parameterization of the bolus velocity $\boldsymbol{u}^{\text{bolus}}$, which again is related to the thickness weighted horizontal velocity via

$$\widehat{\boldsymbol{u}}((\varrho)) = \frac{\overline{h\,\boldsymbol{u}}^{(\varrho)}}{\overline{h}^{(\varrho)}} = \overline{\boldsymbol{u}}^{(\varrho)} + \frac{\overline{h'\,\boldsymbol{u}'}^{(\varrho)}}{\overline{h}^{(\varrho)}} = \overline{\boldsymbol{u}}^{(\varrho)} + \boldsymbol{u}^{\text{bolus}}. \tag{70.144}$$

In addition to the bolus velocity, it is necessary to parameterize the subgrid scale tracer transport tensor

$$\widehat{C''\,\boldsymbol{u}''} = -\mathbb{J}\cdot\nabla_{\!\!\varrho}\widehat{C}, \tag{70.145}$$

which generally has symmetric (diffusive) and antisymmetric (stirring) components (Section 70.3).

For a geopotential coordinate description, equation (70.95) is used to relate thickness weighted mean fields, defined as a function of ϱ, and TRM fields, defined as a function of the mean vertical position of ϱ, to write for the tracer field

$$\widehat{C}(x, y, \widetilde{\varrho}, t) = \overline{C}^{\#}(x, y, \overline{z}^{(\varrho)}, t). \tag{70.146}$$

Equation (70.146), and the developed formalism, leads to the mean field tracer equation in geopotential coordinates

$$\partial_t \overline{C}^{\#} = \nabla\cdot(\nabla\overline{C}^{\#} \times \overline{\boldsymbol{\Psi}}^{\#}) + R(\overline{C}^{\#}), \tag{70.147}$$

where $R(\overline{C}^{\#})$ is the geopotential coordinate form of the mixing/stirring operator on the right-hand side of equation (70.141). Details for the transformation of the mixing/stirring opertor from isopycnal to geopotential coordinates are provided in Section 63.15.

70.5.6 Comments

Much in this section follows from *Smith* (1999), *McDougall and McIntosh* (2001), *Young* (2012), and *Jansen et al.* (2024), each of which focused on the hydrostatic primitive equations assuming a vertically stable buoyancy stratification. The paper by *Young* (2012) is the first to formulate the ensemble mean primitive equations (continuity, tracer, momentum, vorticity, and energy equations) in a form where only the thickness weighted (residual mean) velocity appears. Hence, the formulation of *Young* (2012) eliminates the need to parameterize the bolus velocity or the quasi-Stokes transport since neither appear as separately identified terms. The paper by *Jansen et al.* (2024) further pursues the ideas from *Young* (2012) within the context of generalized vertical coordinate ocean models (see Part XII of this book), and they identify some inconsistencies in how certain ocean models are implementing the eddy parameterizations. The topic of formulating the equations of motion remains an active topic of research for purposes of facilitating subgrid scale closure.

Chapter 71

ELEMENTS OF PARAMETERIZED OCEAN TRACER TRANSPORT

In the presence of turbulent flows, tracer variance directly cascades to the small scales. This *downscale cascade* is facilitated by reversible stirring from balanced and unbalanced fluctuations (e.g., mesoscale eddies, submesoscale eddies, breaking gravity and lee waves, turbulent boundary layer processes). The cascade to progressively smaller scales eventually reaches the *Batchelor scale* (order millimetres; e.g., Section 11.5.1 of *Vallis* (2017)). At this scale, tracer gradients are sufficiently large in magnitude that molecular diffusion can readily act to dissipate tracer variance through irreversible diffusive mixing. Tracer transport at scales larger than the Batchelor scale is dominated by nearly reversible stirring, whereas transport at and below the Batchelor scale is dominated by irreversible mixing from molecular diffusion. This phenomenology provides a constraint on the form of the tracer equation to be used for coarse grained numerical models, where the model grid scale is generally much larger than the Batchelor scale.

In this chapter, we study certain of the mathematical and physical properties of parameterized advective and diffusive tracer transport. In general, such parameterizations aim to encapsulate key aspects of physical processes too small to observe and/or to simulate. This *subgrid scale parameterization problem* is far broader and deeper than available from a single chapter. We focus mostly on subgrid scale tracer advection and diffusion operators arising from mesoscale eddy motions, yet even this limited focus involves far more than can be covered here. In particular, we do not discuss theories for how the eddy diffusivities are computed, which generally require studies of the momentum, energy, and vorticity budgets that are not considered here. Furthermore, we only consider parameterizations of the subgrid scale tracer flux, whose convergence provides a subgrid tendency for the coarse-grained tracer equation. Focusing on fluxes supports locality and conservation for the coarse-grained tracer equation, with these properties also shared by the uncoarsened tracer equation.

CHAPTER GUIDE

We studied the physics of tracer diffusion in Chapter 68 and then advection-diffusion in Chapter 69. We also studied the kinematics of tracer transport in Chapter 70. The present chapter relies on that material, with a focus on the maths and physics of advective-diffusive parameterizations of tracer transport. We also make use of neutral directions as detailed in Section 30.5. Mathematically, we rely on Cartesian tensor analysis from Chapters 1 and 2.

The reader is cautioned that the notation in this chapter is somewhat tedious, which arises from the many variants of tracer fluxes considered. Furthermore, there are a variety of unanswered questions about the suitability of certain parameterizations for ocean circulation models, particularly the anisotropic neutral diffusion discussed in Section 71.5 and the anisotropic Gent-McWilliams stirring in Section 71.6. These sections are written in the hope that they offer a framework for numerically implementing and testing these schemes in models.

71.1 Summarizing tracer transport parameterizations

In this section we offer an outline of the tracer transport parameterizations, starting from the small scales and moving to the mesoscale. We mostly focus on ocean applications, though similar arguments hold for the atmosphere as well.

71.1.1 A synopsis of ocean mixing processes

Irreversible mixing in the ocean takes place at the millimeter scale through the action of chaotic molecular motions that act to dissipate property gradients. This mixing is generally represented by downgradient molecular diffusion. The molecular diffusivity of matter (e.g., salt) in seawater is roughly 10^{-9} m^2 s^{-1}, whereas the molecular thermal diffusivity is roughly 100 times larger (it is easier to diffuse enthalpy (heat) than matter, *Gill*, 1982). Reversible stirring by turbulent eddies greatly increases the magnitude of property gradients upon which *molecular diffusion* acts (*Eckart*, 1948; *Nakamura*, 2001; *Müller and Garrett*, 2002), thereby increasing the total amount of irreversible mixing. Motivated by molecular diffusion and *Brownian motion* *Einstein* (1905), and following the pioneering work of *Taylor* (1921), it is common to parameterize mixing induced by turbulent eddy stirring as a diffusive closure with an eddy diffusivity that is far larger than molecular values. Furthermore, the eddy diffusivities are generally the same for all tracers since eddies generally act the same regardless the tracer. Double diffusive processes is the notable counter-example to this equivalence *Schmitt* (1994).

Mixing induced by eddies of length scale $\mathcal{O}(\text{centimeters} - \text{metres})$ is associated with *fine scale mixing* processes such as gravitational instability, shear instability and breaking internal gravity waves (*MacKinnon et al.*, 2013), as well as a suite of boundary layer processes (*Large et al.*, 1994). This mixing is commonly parameterized by a flow dependent isotropic eddy diffusivity. The magnitude of the eddy diffusivity is typically $\mathcal{O}(10^{-3} - 10^{-2}$ m^2 s$^{-1})$ in boundary layers, and $\mathcal{O}(10^{-5}$ m^2 s$^{-1})$ in the quiescent ocean interior (*Polzin et al.*, 1997; *Whalen et al.*, 2012; *Waterhouse et al.*, 2014).

Mesoscale eddies, with size $\mathcal{O}(10 - 100)$ km, preferentially stir tracers along neutral directions (*McDougall*, 1987a,b; *McDougall et al.*, 2014). The mesoscale eddy stirring in turn induces a mixing that is parametrized by downgradient diffusion along neutral directions (Section 71.4). When feeling the geometric constraints of the surface boundary, mesoscale stirring leads to horizontal oriented mixing across outcropped density surfaces (*Treguier et al.*, 1997; *Ferrari et al.*, 2008; *Danabasoglu et al.*, 2008). This mixing is parameterized by downgradient horizontal diffusion. The neutral and horizontal eddy diffusivities associated with mesoscale processes are typically $\mathcal{O}(10^2 - 10^3$ m^2 s$^{-1})$ in the ocean interior and can rise to $\mathcal{O}(10^4$ m^2 s$^{-1})$ in the ocean surface layer (*Abernathey et al.*, 2013; *Klocker and Abernathey*, 2014; *Cole et al.*, 2015).

71.1.2 A rough comparison

What process is more important for setting tracer distributions: neutral diffusion induced by mesoscale eddies or small scale isotropic diffusion induced by breaking gravity waves? Since the neutral diffusivity arises from mesoscale eddy stirring, it is many orders of magnitude larger than the isotropic diffusivity arising from fine scale mixing. However, these two eddy diffusivities act on very different tracer gradients, in which case the net effects on tracer distributions could be more comparable.

To help answer the question, consider a scaling with a constant neutral diffusivity and a constant isotropic diffusivity. Furthermore, assume Cartesian orientation of the diffusion operators (i.e., zero neutral slope) and assume the isotropic diffusion is dominated by vertical diffusion (see Section 71.2). We are thus comparing the following two diffusion processes

$$\text{horizontal diffusion} = \kappa_{\text{horz}} \nabla_h^2 C \quad \text{and} \quad \text{vertical diffusion} = \kappa_{\text{vert}} \, \partial_{zz} C. \tag{71.1}$$

Now introduce a vertical length scale, H, and horizontal scale, L, over which the tracer concentration changes by the same amount δC. Doing so leads to the scaled diffusion operators

$$\text{horizontal diffusion} \sim (\kappa_{\text{horz}}/L^2) \, \delta C \quad \text{and} \quad \text{vertical diffusion} \sim (\kappa_{\text{vert}}/H^2) \, \delta C. \tag{71.2}$$

These operators have the same scale when

$$\kappa_{\text{vert}} = (H/L)^2 \, \kappa_{\text{horz}}. \tag{71.3}$$

Choosing $L = 10^5$ m and $H = 10^1$ m leads to

$$\kappa_{\text{vert}} = 10^{-8} \, \kappa_{\text{horz}}. \tag{71.4}$$

Furthermore, if $\kappa_{\text{horz}} = 10^3$ m^2 s^{-1}, then the two operators provide a similar contribution to tracer evolution if $\kappa_{\text{vert}} = 10^{-5}$ m^2 s^{-1}. This is a rather small diffusivity that is generally thought to be on the order of that afforded by the background of breaking gravity waves in the ocean interior (*MacKinnon et al.*, 2013). This scaling is crude since the length scales are dependent on details of the flow regime, as are the eddy diffusivities. Even so, it suggests that the two diffusive processes can indeed contribute to tracer distributions by a similar amount.

71.1.3 Diffusive parameterization of fine scale mixing

Ignoring the cross-diffusion processes introduced in Section 26.10 (see also *IOC et al.* (2010), Section 2.5 of *Olbers et al.* (2012), and *Graham and McDougall* (2013)), the molecular diffusion of Θ and S lead to the material evolution equations

$$\rho \frac{\mathrm{D}\Theta}{\mathrm{D}t} = \nabla \cdot (\rho \, \kappa_\Theta \, \nabla \Theta) \tag{71.5a}$$

$$\rho \frac{\mathrm{D}S}{\mathrm{D}t} = \nabla \cdot (\rho \, \kappa_S \, \nabla S), \tag{71.5b}$$

where $\kappa_\Theta > 0$ and $\kappa_S > 0$ are the molecular kinematic diffusivities for Conservative Temperature, Θ, and salinity, S, respectively. For a measured scale, Δ, larger than the scale where gravity waves break and dissipate kinetic energy (i.e., tens to hundreds of metres), diffusion is commonly used to parameterize the associated irreversible tracer mixing (e.g., *MacKinnon et al.*, 2013). Diffusion is also used to parameterize mixing from other small scale processes, such as turbulent boundary layer processes, double-diffusion, and breaking leewaves. As discussed in Section 4 of *McDougall et al.* (2014), small scale mixing generally takes place in an isotropic manner. Its parameterization thus appears just as for isotropic molecular diffusion given by equation (71.5b), yet with a far larger eddy diffusivity $\kappa_{\text{fine}} \gg \kappa_\Theta, \kappa_S$ that is a function of the flow

$$\rho \frac{\mathrm{D}\Theta}{\mathrm{D}t} = \nabla \cdot (\rho \, \kappa_{\text{fine}} \, \nabla \Theta) \tag{71.6a}$$

$$\rho \frac{\mathrm{D}S}{\mathrm{D}t} = \nabla \cdot (\rho \, \kappa_{\text{fine}} \, \nabla S). \tag{71.6b}$$

The same eddy diffusivity is used for both Θ and S. This assumption follows the general approach for turbulent transport parameterizations (e.g, *Vallis*, 2017), whereby eddies are assumed to act in the same manner on any conserved scalar tracer.

71.1.4 Advective-diffusive parameterization of eddy-induced transport

Stirring from turbulent scales smaller than the grid scale is commonly parameterized by an eddy-induced stirring velocity, $\boldsymbol{v}^*$. For ocean mesoscale eddies, such parameterized stirring generally follows a variant of *Gent and McWilliams* (1990) and *Gent et al.* (1995), with this stirring quite important for setting large-scale ocean tracer distributions. In addition, mixing is promoted by the direct cascade from stirring. This mixing is parameterized by a diffusion operator distinct from that used for the small scale mixing discussed in Section 71.1.3.

Consider a second order subgrid scale eddy transport tensor, $\boldsymbol{E}$, meant to parameterize both subgrid scale eddy stirring and eddy mixing. With this tensor, the evolution of salinity and Conservative Temperature takes the form

$$\rho \frac{\mathrm{D}S}{\mathrm{D}t} = \nabla \cdot (\rho \boldsymbol{E} \cdot \nabla S) \tag{71.7a}$$

$$\rho \frac{\mathrm{D}\Theta}{\mathrm{D}t} = \nabla \cdot (\rho \boldsymbol{E} \cdot \nabla \Theta). \tag{71.7b}$$

As for the fine scale diffusion equations (71.6a) and (71.6b), we here use the same transport tensor for both S and Θ as eddies are assumed to act in the same manner on any conserved scalar tracer. As presented in Chapter 69, we decompose the second order transport tensor into the sum of its symmetric and anti-symmetric components

$$\boldsymbol{E} = \boldsymbol{K} + \boldsymbol{A}. \tag{71.8}$$

When the symmetric tensor, $\boldsymbol{K}$, is positive-definite, it gives rise to downgradient diffusion, whereas the anti-symmetric tensor, $\boldsymbol{A}$, gives rise to skew-diffusion or eddy-induced advection.

71.1.5 Mathematical elements of eddy-induced stirring

As detailed in Sections 69.3, 69.4, and 70.3, the anti-symmetric tensor, $\boldsymbol{A}$, contributes to the parameterized transport according to

$$\nabla \cdot (\rho \boldsymbol{A} \cdot \nabla S) = \partial_m (\rho A^{mn} \partial_n S) \tag{71.9a}$$

$$= \partial_m (\rho A^{mn}) \partial_n S + \rho A^{mn} \partial_m \partial_n S \tag{71.9b}$$

$$= -\rho v^{*n} \partial_n S, \tag{71.9c}$$

where A^{mn} are the components to the anti-symmetric transport tensor $\boldsymbol{A}$. Additionally, we noted that

$$\rho A^{mn} \partial_m \partial_n S = 0 \tag{71.10}$$

since A^{mn} is anti-symmetric on the indices m, n whereas $\partial_m \partial_n S$ is symmetric (see Exercise 1.2). Finally, we introduced a density-weighted *eddy-induced velocity*

$$\rho v^{*n} = -\partial_m (\rho A^{mn}) \Longleftrightarrow \rho \boldsymbol{v}^* = -\nabla \cdot (\rho \boldsymbol{A}). \tag{71.11}$$

Importantly, $\rho \boldsymbol{v}^*$ has a zero divergence, again due to anti-symmetry of A^{mn}

$$\nabla \cdot (\rho \boldsymbol{v}^*) = \partial_n (\rho v^{*n}) = -\partial_n \partial_m (\rho A^{mn}) = 0. \tag{71.12}$$

A zero-divergence for $\rho \boldsymbol{v}^*$ means that it contributes no mass sources or sinks to the fluid.[1]

Transport from the anti-symmetric tensor thus provides a means to stir tracers due to unresolved eddy processes. The mathematical form of the stirring can be either through skew-diffusion or through advection (see Section 69.4). Choosing to make use of the advection form allows us to combine the contribution from the anti-symmetric transport tensor with the resolved advection operator, thus resulting in a *residual mean* material transport equation

$$\rho \frac{\mathrm{D}^\dagger S}{\mathrm{D}t} = \nabla \cdot (\rho \boldsymbol{K} \cdot \nabla S) \tag{71.13a}$$

$$\rho \frac{\mathrm{D}^\dagger \Theta}{\mathrm{D}t} = \nabla \cdot (\rho \boldsymbol{K} \cdot \nabla \Theta), \tag{71.13b}$$

where the residual mean material time derivative is given by

$$\frac{\mathrm{D}^\dagger}{\mathrm{D}t} = \frac{\partial}{\partial t} + \boldsymbol{v}^\dagger \cdot \nabla \tag{71.14}$$

and the *residual mean velocity* is

$$\boldsymbol{v}^\dagger = \boldsymbol{v} + \boldsymbol{v}^*. \tag{71.15}$$

71.1.6 Dianeutral unit vector and the neutral slope

When considering closures for subgrid mixing and stirring arising from mesoscale motions, we orient the parameterized processes according to buoyancy as that reflects the physics of mesoscale motions.[2] We thus follow the discussion in Section 30.5 by working with locally referenced Archimedean buoyancy to determine neutral directions. In particular, at each point in the fluid we orient stirring and mixing through use of the dianeutral unit vector (Section 30.5.3)

$$\hat{\boldsymbol{\gamma}} = \frac{-\alpha \nabla \Theta + \beta \nabla S}{|-\alpha \nabla \Theta + \beta \nabla S|} \quad \text{and} \quad \hat{\boldsymbol{\gamma}} = \hat{\boldsymbol{x}}\, \hat{\gamma}_x + \hat{\boldsymbol{y}}\, \hat{\gamma}_y + \hat{\boldsymbol{z}}\, \hat{\gamma}_z \quad \text{and} \quad \hat{\boldsymbol{\gamma}} \cdot \hat{\boldsymbol{\gamma}} = \hat{\gamma}_x^2 + \hat{\gamma}_y^2 + \hat{\gamma}_z^2 = 1, \tag{71.16}$$

with $\hat{\boldsymbol{\gamma}}$ pointing perpendicular to the neutral tangent plane in a direction towards larger density.[3] Furthermore, when the fluid is stably stratified in the vertical, which is common for the mesoscale and larger, then the squared buoyancy frequency is positive (Section 30.4)

$$N^2 = -g\,(-\alpha\, \partial_z \Theta + \beta\, \partial_z S) > 0. \tag{71.17}$$

We can thus introduce the slope of the neutral tangent plane relative to the (x, y) horizontal plane

$$\boldsymbol{S} = -\left[\frac{-\alpha\, \nabla_{\mathrm{h}} \Theta + \beta\, \nabla_{\mathrm{h}} S}{-\alpha\, \partial_z \Theta + \beta\, \partial_z S}\right] = \frac{g\,(-\alpha\, \nabla_{\mathrm{h}} \Theta + \beta\, \nabla_{\mathrm{h}} S)}{N^2} = \hat{\boldsymbol{x}}\, S_x + \hat{\boldsymbol{y}}\, S_y. \tag{71.18}$$

For such stably stratified fluids, the dianeutral direction can be written in terms of the neutral slope

$$\hat{\boldsymbol{\gamma}} = \frac{\boldsymbol{S} - \hat{\boldsymbol{z}}}{(1 + \boldsymbol{S}^2)^{1/2}}. \tag{71.19}$$

[1] For a Boussinesq fluid, the density factor is replaced by the constant reference density, ρ_o, so that $\nabla \cdot \boldsymbol{v}^* = 0$ in the Boussinesq fluid. See section 7 of *Griffies and Greatbatch* (2012) for more details of the Boussinesq and non-Boussinesq forms for the parameterized eddy-induced transport.

[2] We offer further discussion of this point at the start of Section 71.4.

[3] Equation (4) in *McDougall et al.* (2014) makes use of the opposite convention so that their dianeutral direction points towards decreasing density. We instead follow the water mass transformation convention as in equation (73.38), so that $\hat{\boldsymbol{\gamma}}$ points in the direction of increasing density.

In this form we see that the dianeutral direction is vertically downward when the slopes vanish (i.e., horizontal neutral directions), which accords with this direction generally pointing toward increasing density.

71.2 Expressions of small scale diffusion

We here follow Section 4 from *McDougall et al.* (2014) to highlight distinctions between isotropic diffusion, dianeutral diffusion,[4] and vertical diffusion. Although commonly considered interchangeable in the literature as parameterizations of small scale mixing, there are conceptual distinctions that we identify here. Note that the distinctions between these three diffusions are quantitatively small when neutral slopes are modest and when $\kappa_{\text{ntr}} \gg \kappa_{\text{fine}}$.

71.2.1 Isotropic diffusion

As discussed in Section 71.1.3, we generally parameterize fine scale mixing processes via an isotropic diffusion process using a diffusivity $\kappa_{\text{fine}} > 0$, diffusion tensor

$$\boldsymbol{K}^{\text{iso}} = \kappa_{\text{fine}} \begin{bmatrix} 1 & 0 & 0 \\ 0 & 1 & 0 \\ 0 & 0 & 1 \end{bmatrix}, \tag{71.20}$$

and corresponding diffusion flux

$$\boldsymbol{J}^{\text{iso}} = -\rho\, \boldsymbol{K}^{\text{iso}} \cdot \nabla C. \tag{71.21}$$

As illustrated in Figure 71.1, under the effects from isotropic diffusion, a region of tracer is diffused the same in all three directions so that, for example, a spherical tracer distribution remains spherical.

71.2.2 Vertical diffusion

Because vertical density gradients are generally much larger than lateral gradients, it is common to approximate the small scale isotropic diffusion tensor with a vertical diffusion tensor

$$\boldsymbol{K}^{\text{vert}} = \kappa_{\text{fine}} \begin{bmatrix} 0 & 0 & 0 \\ 0 & 0 & 0 \\ 0 & 0 & 1 \end{bmatrix}, \tag{71.22}$$

with a corresponding vertical diffusive flux

$$\boldsymbol{J}^{\text{vert}} = -\rho\, \kappa_{\text{fine}}\, (\nabla C \cdot \hat{\boldsymbol{z}})\, \hat{\boldsymbol{z}} = -\rho\, \boldsymbol{K}^{\text{iso}} \cdot \nabla C = -\rho\, \kappa_{\text{fine}}\, \partial_z C\, \hat{\boldsymbol{z}}. \tag{71.23}$$

In this manner, vertical mixing of a tracer patch occurs only in the vertical direction (see Figure 71.1).

71.2.3 Dianeutral diffusion

Dianeutral diffusion orients tracer fluxes according to the dianeutral direction (71.16)

$$\boldsymbol{J}^{\text{dia}} = -\rho\, \kappa_{\text{fine}}\, (\nabla C \cdot \hat{\boldsymbol{\gamma}})\, \hat{\boldsymbol{\gamma}} = -\rho\, \boldsymbol{K}^{\text{dia}} \cdot \nabla C, \tag{71.24}$$

[4] Dianeutral diffusion is commonly also referred to as *diapycnal diffusion*, with diapycnal diffusion referring to diffusion across constant potential density surfaces. We distinguish dianeutral from diapycnal in this chapter since neutral directions are defined by locally referenced potential density, and as such neutral directions generally differ from isopycnals. Further discussion is provided in Section 30.5 as well as *McDougall* (1987a).

where the dianeutral diffusion tensor is given by

$$\boldsymbol{K}^{\text{dia}} = \kappa_{\text{fine}} \begin{bmatrix} \hat{\gamma}_x^2 & \hat{\gamma}_x \hat{\gamma}_y & \hat{\gamma}_x \hat{\gamma}_z \\ \hat{\gamma}_x \hat{\gamma}_y & \hat{\gamma}_y^2 & \hat{\gamma}_y \hat{\gamma}_z \\ \hat{\gamma}_x \hat{\gamma}_z & \hat{\gamma}_y \hat{\gamma}_z & \hat{\gamma}_z^2 \end{bmatrix} . \tag{71.25}$$

Assuming a vertically stable stratification, we can make use of the relation (71.19) to write $\hat{\boldsymbol{\gamma}}$ in terms of the slope, $\boldsymbol{S}$, thus rendering

$$(\nabla C \cdot \hat{\boldsymbol{\gamma}})\, \hat{\boldsymbol{\gamma}} = \frac{(\boldsymbol{S} - \hat{\boldsymbol{z}}) \cdot \nabla C}{1 + \boldsymbol{S}^2} (\boldsymbol{S} - \hat{\boldsymbol{z}}) = \frac{1}{1 + \boldsymbol{S}^2} \begin{bmatrix} S_x^2 & S_x S_y & -S_x \\ S_x S_y & S_y^2 & -S_y \\ -S_x & -S_y & 1 \end{bmatrix} \begin{bmatrix} \partial_x C \\ \partial_y C \\ \partial_z C \end{bmatrix} , \tag{71.26}$$

so that the dianeutral diffusion tensor now takes on the form

$$\boldsymbol{K}^{\text{dia}} = \frac{\kappa_{\text{fine}}}{1 + \boldsymbol{S}^2} \begin{bmatrix} S_x^2 & S_x S_y & -S_x \\ S_x S_y & S_y^2 & -S_y \\ -S_x & -S_y & 1 \end{bmatrix} . \tag{71.27}$$

As illustrated in Figure 71.1, dianeutral diffusion elongates a tracer patch in the direction normal to the neutral tangent plane.

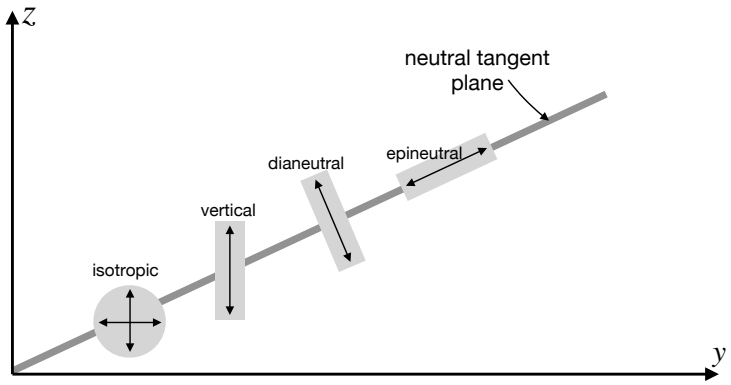

FIGURE 71.1: Illustrating the effects from various forms of diffusion on a tracer patch. When diffused with an isotropic diffusion tensor (equation (71.20)), a spherical patch remains spherical. When diffused with a vertical diffusion tensor (equation (71.22)), a tracer patch elongates in the vertical direction. When diffused with a dianeutral diffusion tensor (equation (71.27)), a tracer patch elongates in the direction normal to the slanted neutral tangent plane. Finally, when diffused with a neutral diffusion tensor, such as the Redi tensor (71.74) or the small slope tensor (71.75), a tracer patch elongates along the neutral tangent plane; i.e., in the *epineutral* direction. This figure is adapted from Figure 4 of *McDougall et al.* (2014).

71.3 Gent-McWilliams eddy-induced advection

As mentioned in Section 70.5.3, there are two processes that contribute to eddy-induced advection/stirring. One involves the correlations between eddy fluctuations in the velocity and tracer fields. In Section 70.3, we considered the kinematics of correlations induced by small amplitude eddying motions, where we found that the eddy-induced motion of fluid particles leads to both a symmetric (mixing) and anti-symmetric (stirring) dispersion of tracer concentrations. There is currently no method proposed for parameterizing this form of eddy-induced stirring when it arises from subgrid scale processes, thus leaving unanswered its importance to large-scale tracer distributions.

The second process leading to eddy-induced stirring arises from correlations between fluctuations in isopycnal layer thickness and horizontal velocity. As detailed in Section 70.4, this

second effect leads to a movement of volume between isopycnal layers, or equivalently we can conceive of it as the quasi-Stokes transport of volume arising from transient eddy motion. This eddy-induced volume transport affects an eddy-induced tracer transport within isopycnal layers. Transient mesoscale eddies are the canonical dynanical process leading to this form of transport. For simulations that do not resolve transient mesoscale eddies, we commonly parameterize the subgrid scale stirring through variants of the *Gent et al.* (1995) scheme. Mathematical elements of this scheme are detailed in this section.

Most presentations of the *Gent et al.* (1995) scheme assume a Boussinesq fluid, though with Section 7 of *Griffies and Greatbatch* (2012) an exception. We here present the non-Boussinesq form, though in places make the Boussinesq approximation since doing so simplifies the presentation without losing anything fundamental.[5]

71.3.1 Details of the parameterization

Gent et al. (1995) parameterize the three-dimensional non-divergent eddy-induced mass flux (recall Section 69.4.3) according to

$$\rho \boldsymbol{v}^* = \nabla \times (\rho \boldsymbol{\Psi}^*) \quad \text{with} \quad \boldsymbol{\Psi}^* = \hat{\boldsymbol{z}} \times \kappa_{\text{gm}} \boldsymbol{S}, \tag{71.28}$$

where $\boldsymbol{S}$ is the neutral slope given by equation (71.18), and $\kappa_{\text{gm}} > 0$ is a kinematic eddy diffusivity with dimensions of velocity times a length. Performing the curl on the streamfunction leads to the horizontal and vertical components to the eddy-induced mass flux

$$\rho \boldsymbol{u}^* = -\partial_z (\kappa_{\text{gm}} \rho \boldsymbol{S}) \quad \text{and} \quad \rho w^* = \nabla_{\text{h}} \cdot (\kappa_{\text{gm}} \rho \boldsymbol{S}), \tag{71.29}$$

along with the skew diffusive tensor

$$A^{\text{gm}} = \kappa_{\text{gm}} \begin{bmatrix} 0 & 0 & -S_x \\ 0 & 0 & -S_y \\ S_x & S_y & 0 \end{bmatrix}. \tag{71.30}$$

Following the discussion in Section 69.4.4, we can identify the advective tracer flux, skew tracer flux, and rotational tracer flux corresponding to the Gent-McWilliams parameterization

$$\boldsymbol{J}^{\text{adv}} = \boldsymbol{J}^{\text{skew}} + \boldsymbol{J}^{\text{rot}} \tag{71.31}$$

where

$$\boldsymbol{J}^{\text{adv}} = C \rho \boldsymbol{v}^* = C \rho [-\partial_z (\kappa_{\text{gm}} \rho \boldsymbol{S}) + \hat{\boldsymbol{z}} \nabla_{\text{h}} \cdot (\kappa_{\text{gm}} \rho \boldsymbol{S})] \tag{71.32a}$$

$$\boldsymbol{J}^{\text{skew}} = -\nabla C \times \rho \boldsymbol{\Psi}^* = \rho \kappa_{\text{gm}} [\boldsymbol{S} \partial_z C - \hat{\boldsymbol{z}} (\boldsymbol{S} \cdot \nabla C)] \tag{71.32b}$$

$$\boldsymbol{J}^{\text{rot}} = \nabla \times (\rho C \boldsymbol{\Psi}^*). \tag{71.32c}$$

71.3.2 Effects on buoyancy

We now consider a Boussinesq fluid with a linear equation of state in order to focus on the impact of the Gent-McWilliams parameterization on buoyancy, which we measure with potential density, ϱ. In this case the parameterized skew flux of potential density due to the quasi-Stokes transport is given by

$$\rho_{\text{o}}^{-1} \boldsymbol{J}^{\text{skew}} = -\kappa_{\text{gm}} [\nabla_{\text{h}} \varrho - \hat{\boldsymbol{z}} \boldsymbol{S}^2 \partial_z \varrho] = -\kappa_{\text{gm}} [\nabla_{\text{h}} \varrho + \hat{\boldsymbol{z}} (\rho_{\text{o}}/g) (\boldsymbol{S} N)^2], \tag{71.33}$$

[5] In brief, for a Boussinesq fluid, the *in situ* density factor found throughout this section is set to the constant Boussinesq reference density, ρ_{o}.

with the squared neutral slope and squared buoyancy frequency written

$$\boldsymbol{S}^2 = \boldsymbol{S} \cdot \boldsymbol{S} \quad \text{and} \quad N^2 = -\frac{g}{\rho_o} \frac{\partial \varrho}{\partial z}. \tag{71.34}$$

The parameterization yields a horizontal downgradient diffusive flux of potential density along with a vertical upgradient diffusive flux. As illustrated by Figure 71.2, so long as the stratification is stable ($N^2 > 0$), which is assumed by the parameterization, the vertical component to the potential density skew flux is vertically downward, which corresponds to a vertically upward buoyancy skew flux. As we see in Section 71.3.3, this orientation ensures that the parameterization reduces available potential energy. Additionally, *Gent et al.* (1995) prescribe a diffusivity that vanishes at the ocean surface and ocean bottom. *McIntosh and McDougall* (1996) and *McDougall and McIntosh* (2001) present more discussion of the boundary conditions, which can be understood by considering the exact form of the quasi-Stokes transport defined by equation (70.102). Furthermore, we consider a boundary value problem approach in Section 71.3.8 that also pays particular attention to the boundary conditions.

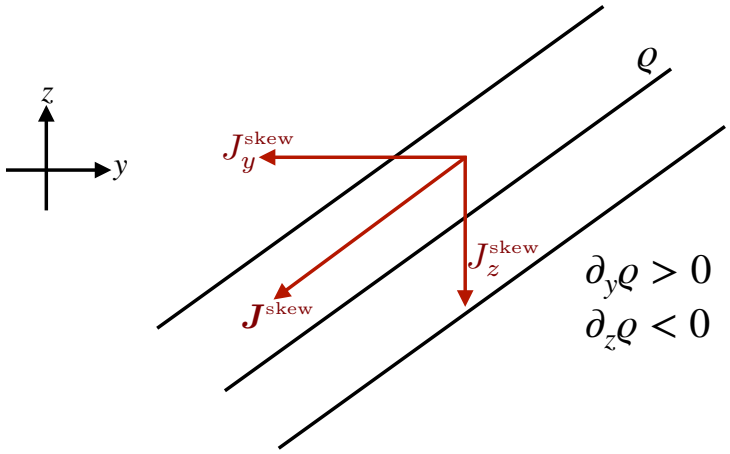

FIGURE 71.2: Orientation of the skew flux of potential density, ϱ, arising from the *Gent et al.* (1995) parameterization and as described by *Griffies* (1998). The sloped black lines are constant ϱ isosurfaces (isopycnals). The horizontal skew flux of potential density is downgradient (directed from high density to low density), whereas the vertical skew flux component is upgradient (directed from low density to high density). The net effect is a skew flux that is oriented parallel to isopycnals.

Figure 71.3 brings elements of the parameterization together by illustrating the *Gent-McWilliams effect* for a meridional potential density front in the southern hemisphere. The mean geostrophic thermal wind flow is eastward, as in the Antarctic Circumpolar Current, whereas a parameterized *secondary circulation* acts to weaken the front, with the secondary circulation proportional to the strength of the front as measured by the isopycnal slope. That is, the parameterization assumes that the mean effects from geostrophic eddies, whose kinetic energy is supported by the potential energy in the front, lead to a weakening of the potential density slope so that the front relaxes toward the horizontal.

71.3.3 Local adiabatic dissipation of available potential energy

We here consider the effects from the *Gent et al.* (1995) scheme on the available potential energy, continuing to assume a Boussinesq fluid with a linear equation of state. We express the behavior using both skew fluxes and advective fluxes. Since we are assuming the parameterization is adiabatic, the change in potential energy is identical to the change in available potential energy.

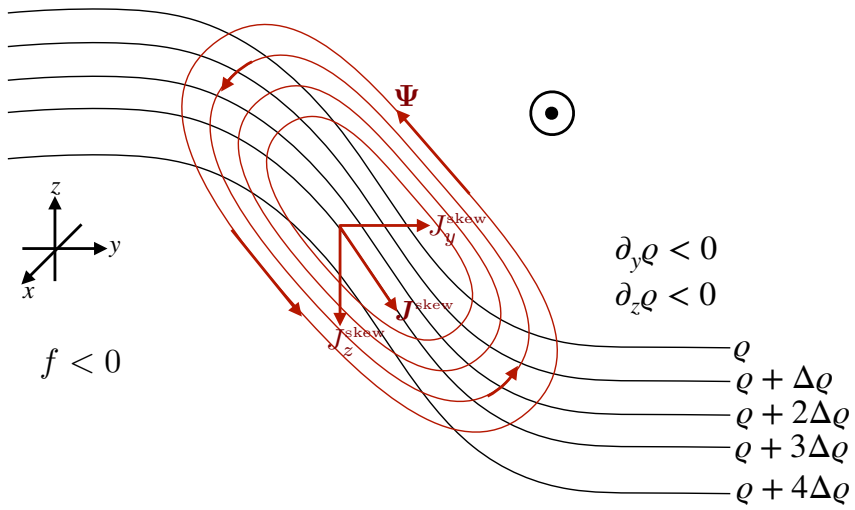

FIGURE 71.3: The Gent-McWilliams effect for a meridional potential density front in the Southern Hemisphere, where dense water rises to the south so that $\partial_y \varrho < 0$. The mean geostrophic thermal wind flow is eastward (out of the page), as in the Antarctic Circumpolar Current. With a stable stratification, whereby $\partial_z \varrho < 0$, the Gent-McWilliams streamfuction given by equation (71.28) leads to a counter-clockwise circulation (red isolines). The dual perspective offered by the Gent-McWilliams skew flux for potential density, given by equation (71.33), reveals a northward (downgradient) meridional skew flux component along with a downward (upgradient) vertical component (red vectors). The result from either the streamfunction perspective or the skew flux perspective is a potential density tendency that relaxes the front towards the horizontal so to reduce the isopycnal slope.

Skew flux approach

Let us approach the parameterization problem from the perspective of satisfying two general properties: (I) the subgrid scale operator adiabatically stirs while maintaining the same amount of fluid within isopycnal layers, (II) the subgrid operator locally dissipates potential energy through an abiabatic rearrangement of the potential density surfaces, with the dissipation vanishing when there is zero baroclinicity. That is, the scheme dissipates available potential energy. What is the form of the stirring operator implied by these two assumptions?

Adiabatic stirring of potential density can be realized via the convergence of a skew flux oriented parallel to potential density surfaces

$$\rho_o^{-1} \boldsymbol{J}^{\text{skew}} = -\nabla \varrho \times \boldsymbol{\Psi}^*, \tag{71.35}$$

where at this point we have yet to specify $\boldsymbol{\Psi}^*$. To see what the local dissipation of available potential energy imposes, consider the gravitational potential energy

$$P = g \int \varrho \, z \, \mathrm{d}V, \tag{71.36}$$

where, again, we assume the *in situ* density equals to the potential density as per a linear equation of state (Section 30.3.5). Assuming all boundaries are material and static allows us to focus on the time tendency of potential energy associated with the unknown flux

$$\frac{\mathrm{d}P}{\mathrm{d}t} = g \int z \, \frac{\partial \varrho}{\partial t} \, \mathrm{d}V = -\frac{g}{\rho_o} \int (z \, \nabla \cdot \boldsymbol{J}^{\text{skew}}) \, \mathrm{d}V = -\frac{g}{\rho_o} \int (z \, \partial_z J^z) \, \mathrm{d}V = \frac{g}{\rho_o} \int J^z \, \mathrm{d}V, \tag{71.37}$$

where J^z is the vertical flux component. We drop boundary effects by assuming the subgrid scale flux vanishes on all boundaries. To provide a *local* available potential energy sink requires

$$J^z \leq 0, \tag{71.38}$$

where zero occurs when the isopycnals are flat. It is sufficient to construct the vertical flux component using only the potential density field itself. For a stably stratified fluid in which $\partial_z \varrho < 0$, the following form provides a local available potential energy sink

$$\rho_o^{-1} J^z = \kappa_{gm} \boldsymbol{S}^2 \partial_z \varrho = -(\kappa_{gm} \rho_o / g) (\boldsymbol{S} N)^2 \leq 0. \tag{71.39}$$

The corresponding horizontal flux is given by a downgradient diffusive flux

$$\boldsymbol{J}^h = -\rho_o \kappa_{gm} \nabla_h \varrho. \tag{71.40}$$

We have thus recovered the skew flux (71.33) as proposed by *Gent et al.* (1995). Note that *Aiki et al.* (2004) proceed in a similar manner yet do not assume locality of the available potential energy sink, thus deriving a more general subgrid scale operator.

Advective flux approach

The impacts on potential energy should be the same when representing the parameterization as an advective flux. To verify this result, return to equation (71.37) and make use of the vertical component of the advective flux rather than the skew flux

$$\frac{dP}{dt} = g \int \varrho \, w^* \, dV \tag{71.41a}$$

$$= g \int \varrho \, \nabla_h \cdot (\kappa_{gm} \boldsymbol{S}) \, dV \tag{71.41b}$$

$$= g \int \nabla_h \cdot (\varrho \, \kappa_{gm} \boldsymbol{S}) \, dV - g \int \nabla_h \varrho \cdot \kappa_{gm} \boldsymbol{S} \, dV \tag{71.41c}$$

$$= -\rho_o \int \kappa_{gm} (\boldsymbol{S} N)^2 \, dV, \tag{71.41d}$$

which is the same result as for the skew flux.

71.3.4 Meridional overturning mass transport

It is often of interest to compute the mass transport across a portion of the ocean. In particular, meridional-depth or meridional-potential density streamfunctions allow one to visualize and quantify the zonally integrated transport occurring in a closed basin or over the full globe. The quasi-Stokes transport provides a transport in addition to that from the resolved scale Eulerian mean transport, and the parameterization of *Gent et al.* (1995) leads to a straightforward computation of the quasi-Stokes contribution. For this purpose, write the net meridional mass transport of fluid across a basin and passing beneath a particular depth in the form (the minus sign is conventional)

$$\mathcal{T}(y,z,t) = -\int dx \int_{-H}^{z} \rho \, (v + v^*) \, dz \tag{71.42a}$$

$$= -\int dx \int_{-H}^{z} \rho \, v \, dz + \int dx \int_{-H}^{z} \partial_z (\kappa_{gm} \rho \, S_y) \, dz \tag{71.42b}$$

$$= -\int dx \int_{-H}^{z} \rho \, v \, dz + \int \kappa_{gm} \rho \, S_y \, dx \tag{71.42c}$$

$$\equiv \mathcal{T}^{\text{eulerian}}(y,z,t) + \mathcal{T}^{\text{gm}}(y,z,t). \tag{71.42d}$$

For the penultimate step we set the parameterized quasi-Stokes transport to zero at the ocean bottom. We thus see that the parameterized quasi-Stokes transport adds a contribution that

scales linearly with basin size, isopyncal slope, and diffusivity,

$$\mathcal{T}^{\text{qs}} \sim \rho_o \, L \, |\boldsymbol{S}| \, \kappa_{\text{gm}}. \tag{71.43}$$

As an example, let $\rho = 1035$ kg m^{-3}, $\kappa_{\text{gm}} = 10^3$ m^2 s^{-1}, $|\boldsymbol{S}| = 10^{-3}$, and $L = 10^7$ m, which yields $\mathcal{T}^{\text{qs}} \approx 10 \times 10^9$ kg s^{-1}. This additional transport is a nontrivial addition to that from the resolved scale velocity field.

71.3.5 Connection to form stress

We now connect the *Gent et al.* (1995) closure, normally implemented in the tracer equation, to vertical transfer of momentum through form stress. For this purpose, recall the general discussion of form stress in Section 28.1 and the more detailed discussions in Sections 31.7 and 36.4. In those discussions, we identify form stress as the horizontal pressure force acting on a sloped surface, with our present concern with surfaces of constant isopycnals as discussed in Sections 31.7 and 36.4.

Young (2012) provides a general means for making the connection between *Gent et al.* (1995) and form stress for a continuously stratified fluid. *Loose et al.* (2023) and *Jansen et al.* (2024) provide further theoretical and numerical analysis of this approach. For our more schematic purposes, we follow the treatment in *Greatbatch and Lamb* (1990), *Gent et al.* (1995) (their Section 4), *Ferreira and Marshall* (2006) (their Section 2), and *Zhao and Vallis* (2008) (their Section 2.2). For this purpose, assume the fluid is in Boussinesq planetary geostrophic balance (detailed in Section 31.5) whereby the horizontal momentum satisfies

$$\rho_o \, f \, (\hat{\boldsymbol{z}} \times \boldsymbol{u}) = -\nabla_h p + \partial_z \boldsymbol{\tau}, \tag{71.44}$$

with $\boldsymbol{\tau}$ a horizontal subgrid scale stress vector. The Coriolis acceleration balances the acceleration from horizontal pressure gradients plus a vertical transfer of horizontal stress. The horizontal stress term is generally quite small in the ocean interior, where the flow is in geostrophic balance, whereas it is large at the ocean surface where it arises from turbulent air-sea interactions; i.e., wind stress. Furthermore, it can be large at the bottom through turbulent bottom stresses.

To make the connection between *Gent et al.* (1995) and the vertical transfer of horizontal form stress, add $\rho_o \, f \, (\hat{\boldsymbol{z}} \times \boldsymbol{u}^*)$ to both sides of equation (71.44) to obtain

$$\rho_o \, f \, (\hat{\boldsymbol{z}} \times \boldsymbol{u}^\dagger) = -\nabla_h p + \partial_z \boldsymbol{\tau} + \rho_o \, f \, (\hat{\boldsymbol{z}} \times \boldsymbol{u}^*), \tag{71.45}$$

where $\boldsymbol{u}^\dagger = \boldsymbol{u} + \boldsymbol{u}^*$ is the horizontal residual mean velocity. This equation says that the Coriolis acceleration from the horizontal residual mean velocity balances pressure gradients, the vertical divergence of the horizontal frictional stresses, plus the Coriolis acceleration from the eddy-induced velocity. We further unpack the eddy Coriolis acceleration by noting that the planetary geostrophic velocity satisfies the thermal wind relation in the ocean interior (Section 31.6), whereby

$$f \, \partial_z \boldsymbol{u} = -(g/\rho_o) \, \hat{\boldsymbol{z}} \times \nabla \rho = -\hat{\boldsymbol{z}} \times N^2 \boldsymbol{S}. \tag{71.46}$$

We can thus write the Coriolis acceleration from the eddy-induced velocity as

$$f \, (\hat{\boldsymbol{z}} \times \boldsymbol{u}^*) = -f \, [\hat{\boldsymbol{z}} \times \partial_z (\kappa_{\text{gm}} \, \boldsymbol{S})] \tag{71.47a}$$

$$= -\partial_z \, [\hat{\boldsymbol{z}} \times (f \, \kappa_{\text{gm}} \, \boldsymbol{S})] \tag{71.47b}$$

$$= \frac{\partial}{\partial z} \left[\frac{\kappa_{\text{gm}} \, f^2}{N^2} \, \frac{\partial \boldsymbol{u}}{\partial z} \right] \tag{71.47c}$$

$$= \partial_z (\nu_e \, \partial_z \boldsymbol{u}), \tag{71.47d}$$

where the final equality introduced an eddy-induced vertical viscosity

$$\nu_{\mathsf{e}} \equiv \kappa_{\mathsf{gm}} \, (f^2/N^2). \tag{71.48}$$

Making use of this result in the planetary geostrophic equation (71.45) thus leads to

$$\rho_{\mathsf{o}} \, f \, (\hat{\boldsymbol{z}} \times \boldsymbol{u}^{\dagger}) = -\nabla_{\mathsf{h}} p + \partial_z (\boldsymbol{\tau} + \boldsymbol{\tau}_{\mathsf{e}}), \tag{71.49}$$

where

$$\rho_{\mathsf{o}}^{-1} \, \boldsymbol{\tau}_{\mathsf{e}} = \nu_{\mathsf{e}} \, \partial_z \boldsymbol{u} \tag{71.50}$$

defines a horizontal mesoscale eddy stress arising from the thermal wind shears. Equation (71.49) says that the Coriolis acceleration from the horizontal residual mean velocity is in balance with the horizontal pressure gradient plus the vertical transfer of horizontal shears arising from both friction/wind/bottom drag *plus* a contribution from parameterized mesoscale eddies.

We conclude that the *Gent et al.* (1995) parameterization appears in the planetary geostrophic residual mean momentum equation as a vertical transport of horizontal stress determined by a viscosity $\nu_{\mathsf{e}} = \kappa_{\mathsf{gm}} \, (f/N)^2$. Notably, this vertical eddy transfer occurs in the absence of irreversible mixing. We thus interpret it as a parameterization of the vertical transfer of pressure form stress via mesoscale eddies that act between isopycnal layers. That is, the *Gent et al.* (1995) scheme offers a means to parameterize vertical transfer of horizontal form stress arising from undulating mesoscale eddies in the ocean interior. This interpretation is more thoroughly discussed in Section 31.7 (see also *Greatbatch and Lamb* (1990) and *Loose et al.* (2023)).

71.3.6 Connection to isopycnal thickness diffusion

Recall the ensemble mean thickness equation (70.114) for a Boussinesq fluid was derived in Section 70.4.5

$$\partial_t \hbar + \nabla_{\varrho} \cdot (\hbar \, \widehat{\boldsymbol{u}}) = 0, \tag{71.51}$$

where

$$\widehat{\boldsymbol{u}} = \boldsymbol{u} + \boldsymbol{u}^{\mathrm{bolus}} \tag{71.52}$$

is the thickness weighted transport velocity affecting evolution of the ensemble mean thickness $\hbar$. Note that for brevity we here drop the nomenclature $(\ )^{(\varrho)}$ used in Section 70.4.5.

Isopycnal correlations of horizontal velocity and layer thickness define the bolus velocity via

$$\hbar \, \boldsymbol{u}^{\mathsf{bolus}} = \overline{\hbar' \, \boldsymbol{u}'} \tag{71.53}$$

Now consider a downgradient diffusive closure for this correlation

$$\hbar \, \boldsymbol{u}^{\mathsf{bolus}} = \overline{\hbar' \, \boldsymbol{u}'}^{(\varrho)} = -\boldsymbol{K}^{\mathsf{thick}} \cdot \nabla_{\varrho} h, \tag{71.54}$$

with $\boldsymbol{K}^{\mathsf{thick}}$ a symmetric and positive-definite 2×2 diffusion tensor. The mean thickness equation thus takes the form of an advection-diffusion equation in isopycnal coordinates

$$\partial_t \hbar + \nabla_{\varrho} \cdot (\hbar \, \boldsymbol{u}) = \nabla_{\varrho} \cdot (\boldsymbol{K}^{\mathsf{thick}} \cdot \nabla_{\varrho} \hbar). \tag{71.55}$$

We note one special property of the closure (71.54) revealed when considering discrete shallow water layers and assuming the thickness diffusion tensor is depth independent. Vertically summing the eddy transport from the ocean bottom up to a particular layer yields

$$\sum_{n=k_{\mathrm{b}}}^{n=k} \overline{\hbar_n' \, \boldsymbol{u}_n'}^{(\varrho)} = -\sum_{n=k_{\mathrm{b}}}^{n=k} \boldsymbol{K}^{\mathsf{thick}} \cdot \nabla_{\varrho} h_n = -\boldsymbol{K}^{\mathsf{thick}} \cdot \sum_{n=k_{\mathrm{b}}}^{n=k} \nabla_{\varrho} h_n = -\boldsymbol{K}^{\mathsf{thick}} \cdot \nabla_{\varrho} \eta_{k-1/2}, \tag{71.56}$$

where $\eta_{k-1/2}$ is the upper interface of layer k (see Figure 35.6), and where $k_{\rm b}$ is the index for the layer at the ocean bottom. In this case we see that the eddy transport below an isopycnal interface is directly proportional to the slope of that interface.

71.3.7 Connection to Gent-McWilliams parameterization

To make a direct connection between the thickness diffusion closure (71.54) and the *Gent et al.* (1995) closure discussed in Section 71.3.1, note that the specific thickness is the inverse of the vertical derivative of the potential density

$$\hbar = (\partial_z \varrho)^{-1}. \tag{71.57}$$

Correspondingly, using the relation between derivative operators, $\nabla_{\hbar\varrho} = \nabla_{\rm h} + \boldsymbol{S}\,\partial_z$, gives

$$\begin{aligned}
\hbar^{-1}\,\nabla_{\hbar\varrho}\hbar &= -\hbar\,\nabla_{\hbar\varrho}(1/\hbar) && \text{product rule identity} && (71.58a)\\
&= -(\partial_z\varrho)^{-1}\,(\nabla_{\rm h} + \boldsymbol{S}\,\partial_z)\,\partial_z\varrho && \hbar = \partial z/\partial\varrho \text{ and } \nabla_{\hbar\varrho} = \nabla_{\rm h} + \boldsymbol{S}\,\partial_z && (71.58b)\\
&= -\frac{\partial_z(\nabla_{\rm h}\varrho)}{\partial_z\varrho} + \frac{\partial_{zz}\varrho\,\nabla_{\rm h}\varrho}{(\partial_z\varrho)^2} && \text{rearrangement} && (71.58c)\\
&= -\partial_z[\nabla_{\rm h}\varrho/(\partial_z\varrho)] && \text{product rule identity} && (71.58d)\\
&= \partial_z \boldsymbol{S} && \text{isopycnal slope } \boldsymbol{S} = -\nabla_{\rm h}\varrho/(\partial_z\varrho). && (71.58e)
\end{aligned}$$

Consequently, the bolus velocity takes the form

$$\boldsymbol{u}^{\rm bolus} = -\hbar^{-1}\,\boldsymbol{K}^{\rm thick}\cdot\nabla_{\hbar\varrho}\hbar = -\boldsymbol{K}^{\rm thick}\cdot\partial_z\boldsymbol{S}. \tag{71.59}$$

The special case of depth independent diffusivity

For the special case of $\boldsymbol{K}^{\rm thick}$ that is independent of depth and proportional to the 2×2 identity matrix, we recover the identity

$$\boldsymbol{u}^{\rm bolus} = -\partial_z(\kappa_{\rm gm}\,\boldsymbol{S}) = \boldsymbol{u}^*, \tag{71.60}$$

where the horizontal component of the *Gent et al.* (1995) velocity, $\boldsymbol{u}^*$, was identified from equation (71.29). Again, this identity holds only for the special case of a vertically independent diffusivity tensor proportional to the identity.

Further caveats

The relevance of a depth-independent diffusivity has been questioned by many authors, such as *Killworth* (1997), *Treguier et al.* (1997), *Smith and Vallis* (2002), *Smith and Marshall* (2009), and *Abernathey et al.* (2013). We conclude from these studies that a depth independent diffusivity is not the best choice for the *Gent et al.* (1995) parameterization, in which case where one places the vertical derivative is crucial.

The relation between thickness diffusion with the *Gent et al.* (1995) parameterization further breaks down near boundaries. The reason is that the eddy diffusivity vanishes next to boundaries and thus has a depth-dependence. Additionally, as noted by *Holloway* (1997) and *Griffies et al.* (2000), thickness diffusion next to solid earth boundaries leads to an increase in potential energy, with isopycnals creeping up the topographic slope. Such unphysical behavior motivates isopycnal modelers instead to use *interfacial height* diffusion to dissipate noise in the thickness field.

71.3.8 A parameterization based on a boundary value problem

There have been variants of the *Gent et al.* (1995) scheme proposed in the literature, such as those of *Aiki et al.* (2004) and *Ferrari et al.* (2010). As for the *Gent et al.* (1995) scheme, these alternatives dissipate available potential energy without mixing between isopycnal classes. We here briefly discuss the scheme of *Ferrari et al.* (2010), which is used by a variety of ocean climate models largely since it contains a natural means to numerically regularize the eddy-induced streamfunction in regions of weak vertical stratification. These considerations are relevant especially in ocean climate models, where weak or zero vertical stratification is inevitable and so it is necessary to handle such regimes.

For the *Ferrari et al.* (2010) scheme we write the parameterized eddy streamfunction as

$$\boldsymbol{\Psi}^* = \hat{\boldsymbol{z}} \times \boldsymbol{\Upsilon} \Longrightarrow \boldsymbol{u}^* = -\partial_z \boldsymbol{\Upsilon} \quad \text{and} \quad w^* = \nabla_h \cdot \boldsymbol{\Upsilon}, \tag{71.61}$$

with $\boldsymbol{\Upsilon}$ determined by solving the following vertical boundary value problem at each horizontal position[6]

$$(c^2\, \partial_{zz} - N^2)\boldsymbol{\Upsilon} = -N^2\, \boldsymbol{\Upsilon}^{\text{gm}} \quad \text{and} \quad \boldsymbol{\Upsilon}(\eta_b) = \boldsymbol{\Upsilon}(\eta) = 0, \tag{71.62}$$

where (see equation (71.28))

$$\boldsymbol{\Upsilon}^{\text{gm}} = \kappa_{\text{gm}}\, \boldsymbol{S} \quad \text{and} \quad N^2\, \boldsymbol{S} = (g/\rho_o)\, \nabla_h \varrho. \tag{71.63}$$

We recover the *Gent et al.* (1995) scheme when setting the squared speed to zero, $c^2 = 0$, in which case $\boldsymbol{\Upsilon} = \boldsymbol{\Upsilon}^{\text{gm}}$. For $c^2 > 0$, the second order differential operator ensures that $\boldsymbol{\Upsilon}$ smoothly and continuously transitions through regions where the vertical stratification is weak (N^2 is small), and hence where $|\boldsymbol{S}|$ is large. In contrast, the standard regularization approaches, with $c^2 = 0$, are somewhat more *ad hoc* (e.g., see Chapter 15 of *Griffies* (2004)) or very tedious (e.g., *Ferrari et al.* (2008)).

Following the discussion in Section 71.3.3, we deduce the impacts on potential energy (assuming a linear equation of state) via equation (71.37), where we make use of the vertical component of the potential density skew flux

$$\frac{1}{g}\frac{\mathrm{d}P}{\mathrm{d}t} = \frac{1}{\rho_o}\int J^z \,\mathrm{d}V = -\int \hat{\boldsymbol{z}} \cdot (\nabla\varrho \times \boldsymbol{\Psi}^*)\,\mathrm{d}V = -\int \nabla_h \varrho \cdot \boldsymbol{\Upsilon}\,\mathrm{d}V = -\frac{\rho_o}{g}\int N^2\, \boldsymbol{S}\cdot\boldsymbol{\Upsilon}\,\mathrm{d}V. \tag{71.64}$$

The governing differential equation (71.62) leads to

$$\boldsymbol{\Upsilon} \cdot (c^2\, \partial_{zz} - N^2)\boldsymbol{\Upsilon} = -(g/\rho_o)\, \kappa_{\text{gm}}\, \boldsymbol{\Upsilon} \cdot \nabla_h \varrho, \tag{71.65}$$

which rearranges to

$$(g/\rho_o)\, \kappa_{\text{gm}}\, \boldsymbol{\Upsilon} \cdot \nabla_h \varrho = -c^2\, \partial_z(\boldsymbol{\Upsilon} \cdot \partial_z \boldsymbol{\Upsilon}) + c^2\, (\partial_z \boldsymbol{\Upsilon} \cdot \partial_z \boldsymbol{\Upsilon}) + N^2\, \boldsymbol{\Upsilon} \cdot \boldsymbol{\Upsilon}. \tag{71.66}$$

Integrating over a vertical column and making use of the homogeneous Dirichlet boundary conditions from equation (71.62) leads to

$$\frac{g}{\rho_o}\int \kappa_{\text{gm}}\, \boldsymbol{\Upsilon} \cdot \nabla_h \varrho \,\mathrm{d}z = \int (c^2\, \partial_z \boldsymbol{\Upsilon} \cdot \partial_z \boldsymbol{\Upsilon} + N^2\, \boldsymbol{\Upsilon} \cdot \boldsymbol{\Upsilon})\,\mathrm{d}z \geq 0. \tag{71.67}$$

This inequality means that the potential energy of a vertical column is dissipated. However, locally at any point in the column the potential energy might increase due to the sign-indefinite term, $-c^2\, \partial_z(\boldsymbol{\Upsilon} \cdot \partial_z \boldsymbol{\Upsilon})$. Notably, there is no *a priori* reason that mesoscale eddies dissipate potential energy at every point in space. Furthermore, numerical experiments documented

[6] Note that *Ferrari et al.* (2010) used the opposite sign convention on $\boldsymbol{\Upsilon}$ from that used here.

in *Ferrari et al.* (2010) suggest that local potential energy dissipation is not necessary for a numerically stable operator. We conclude that this approach offers a suitable method for ocean climate simulations.

71.3.9 Comments

As noted in Section 70.5.3, there is presently no parameterization of subgrid scale stirring along neutral directions arising from the correlations between tracer and velocity fluctuations. Rather, the only parameterized subgrid scale stirring is associated with quasi-Stokes transport, with *Gent et al.* (1995) providing the canonical approach as summarized in this section. To parameterize the skew fluxes arising from tracer-velocity correlations requires one to study the polarization of the eddies giving rise to these skew fluxes, as per the discussion in Section 70.3.2 and *Middleton and Loder* (1989).

71.4 Neutral diffusion

Neutral diffusion, also referred to as *epineutral diffusion*, parameterizes the mixing induced by mesoscale eddy transport. The parameterization assumes that the neutral diffusive flux of a tracer is oriented along a neutral direction or a *neutral tangent plane*. The neutral diffusive tracer flux, $\boldsymbol{J}$, for an arbitrary tracer, C, is perpendicular to the dianeutral unit vector

$$\boldsymbol{J} \cdot \hat{\boldsymbol{\gamma}} = 0 \implies \boldsymbol{J} \cdot (-\alpha \nabla \Theta + \beta \nabla S) = 0, \tag{71.68}$$

where $\hat{\boldsymbol{\gamma}}$ is defined by equation (71.16).

71.4.1 Motivation for neutral diffusion

Pioneering models of the ocean circulation, such as *Cox and Bryan* (1984), were formulated with the tracer mixing tensor oriented according to the horizontal and vertical directions. These simulations exhibited problems near strong density fronts, such as those found in western boundary currents. In such regions, the horizontally oriented diffusion spuriously fluxed temperature and salinity across isopyncnals, thus degrading the strength of the front and leading to, among other problems, unphysically weak meridional heat transport (*Böning et al.*, 1995). In earlier work based on tracer measurements, *Montgomery* (1938), *Veronis* (1975), and *Rooth* (1982) suggested that ocean properties were preferentially homogenized along local potential density surfaces rather than geopotential surfaces. Such measurements motivated *Solomon* (1971) and *Redi* (1982) to propose rotating the tracer mixing tensor according to neutral directions.

We offer further indirect evidence that mesoscale eddy induced diffusion is preferentially aligned along neutral directions. For that purpose, consider a diffusive flux that is not aligned with neutral directions. In this case, diffusive mixing can cause tracer distributions to cross neutral directions, thus adding to the mixing that is already parameterized from small scale mixing processes from Section 71.2. As discussed in Section 14.1.5 of *Griffies* (2004) as well as Section 1 of *McDougall et al.* (2014), the extra mixing induced by this non-neutral orientation of the mesoscale induced diffusive fluxes is proportional to the squared slope between the proposed new direction and the neutral tangent plane. Estimates based on field measurements for interior ocean mixing constrain the magnitude of the miss-alignment to be less than 10^{-4}. This number is very small, indeed it is zero within error bars of field measurements. Although the measurements are sparse, they do support the use of mesoscale eddy induced diffusive fluxes that are oriented according to neutral directions. We thus make use of this constraint in designing the diffusion tensor in the remainder of this section.

71.4.2 Redi neutral diffusion

One diffusive flux satisfying the property (71.68) is given by

$$\boldsymbol{J}^{\text{redi}} = -\rho\,\kappa_{\text{ntr}}\,[\nabla C - \hat{\boldsymbol{\gamma}}\,(\hat{\boldsymbol{\gamma}}\cdot\nabla C)], \tag{71.69}$$

where $\kappa_{\text{ntr}} > 0$ is the eddy neutral diffusivity (dimensions of squared length per time). In Figure 71.4 we illustrate the diffusive flux arising for a particular configuration of the neutral directions and the tracer concentration.

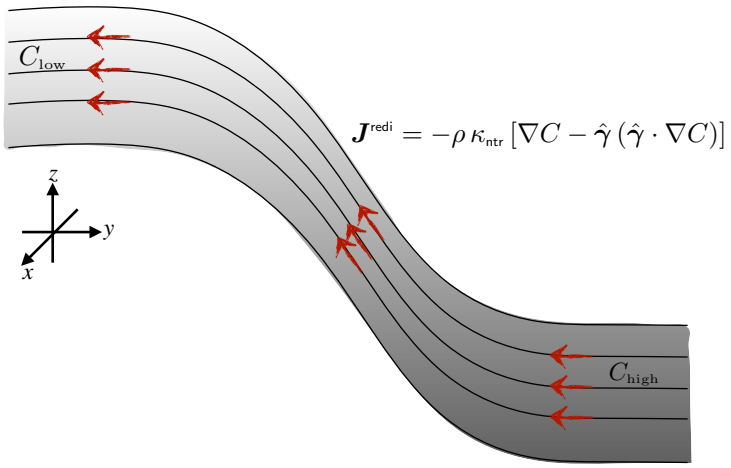

FIGURE 71.4: Schematic of the Redi neutral diffusion flux, $\boldsymbol{J}^{\text{redi}} = -\rho\,\kappa_{\text{ntr}}\,[\nabla C - \hat{\boldsymbol{\gamma}}\,(\hat{\boldsymbol{\gamma}}\cdot\nabla C)]$, from equation (71.69). The sloping lines represent surfaces whose local tangent is in the neutral direction, so that the tracer flux is aligned parallel to the surfaces. We here depict the case with higher tracer concentration on the right side so that the downgradient neutral diffusive flux is to the left and upward.

We confirm that $\boldsymbol{J}^{\text{redi}}$ is oriented down the tracer gradient by noting that

$$\boldsymbol{J}^{\text{redi}}\cdot\nabla C = -\rho\,\kappa_{\text{ntr}}\left[|\nabla C|^2 - (\hat{\boldsymbol{\gamma}}\cdot\nabla C)^2\right] \leq 0. \tag{71.70}$$

We can write the neutral diffusive flux (71.69) in the downgradient flux-gradient relation

$$\boldsymbol{J}^{\text{redi}} = -\rho\,\boldsymbol{K}^{\text{redi}}\cdot\nabla C, \tag{71.71}$$

with the neutral diffusion tensor, $\boldsymbol{K}^{\text{redi}}$, given by

$$\boldsymbol{K}^{\text{redi}} = \kappa_{\text{ntr}}\begin{bmatrix} 1-\hat{\gamma}_x^2 & -\hat{\gamma}_x\,\hat{\gamma}_y & -\hat{\gamma}_x\,\hat{\gamma}_z \\ -\hat{\gamma}_x\,\hat{\gamma}_y & 1-\hat{\gamma}_y^2 & -\hat{\gamma}_y\,\hat{\gamma}_z \\ -\hat{\gamma}_x\,\hat{\gamma}_z & -\hat{\gamma}_y\,\hat{\gamma}_z & 1-\hat{\gamma}_x^2 \end{bmatrix} \Longrightarrow (K^{\text{redi}})^{mn} = \kappa_{\text{ntr}}\,(\delta^{mn} - \hat{\gamma}^m\,\hat{\gamma}^n). \tag{71.72}$$

The corresponding neutral diffusion operator is given by the three-dimensional flux convergence

$$\mathcal{R}^{\text{redi}} = -\nabla\cdot\boldsymbol{J}^{\text{redi}} = \nabla\cdot(\rho\,\boldsymbol{K}^{\text{redi}}\cdot\nabla C). \tag{71.73}$$

When the neutral surfaces are stably stratified in the vertical, so that their slopes are bounded, then the diffusion tensor takes the following form originally suggested by *Redi* (1982), which is written in terms of the neutral slope

$$\boldsymbol{K}^{\text{redi}} = \frac{\kappa_{\text{ntr}}}{1+\boldsymbol{S}^2}\begin{bmatrix} 1+S_y^2 & -S_xS_y & S_x \\ -S_xS_y & 1+S_x^2 & S_y \\ S_x & S_y & \boldsymbol{S}^2 \end{bmatrix}. \tag{71.74}$$

71.4.3 Small slope neutral diffusion

Another form of the neutral diffusion flux is based on assuming a small magnitude for the slope of the neutral tangent plane relative to the horizontal, which is the case for most of the ocean interior even in frontal regions. With this approximation, the small slope neutral diffusion tensor takes the form

$$\boldsymbol{K}^{\text{small}} = \kappa_{\text{ntr}} \begin{bmatrix} 1 & 0 & S_x \\ 0 & 1 & S_y \\ S_x & S_y & \boldsymbol{S}^2 \end{bmatrix}. \tag{71.75}$$

The corresponding small slope neutral diffusive flux is

$$\boldsymbol{J}^{\text{small}} = -\rho\, \kappa_{\text{ntr}} \left[\nabla_{\text{h}\gamma} + \hat{\boldsymbol{z}}\, (\boldsymbol{S} \cdot \nabla_{\text{h}\gamma})\right] C \tag{71.76}$$

where

$$\nabla_{\text{h}\gamma} = \nabla_{\text{h}} + \boldsymbol{S}\, \partial_z \tag{71.77}$$

is the horizontal derivative operator computed on the neutral tangent plane (see equation (63.75)). To show that $\boldsymbol{J}^{\text{small}} \cdot \hat{\boldsymbol{\gamma}} = 0$, we make use of the identity (71.19) so that

$$\boldsymbol{J}^{\text{small}} \cdot \hat{\boldsymbol{\gamma}} = \frac{\boldsymbol{J}^{\text{small}} \cdot \boldsymbol{S} - \boldsymbol{J}^{\text{small}} \cdot \boldsymbol{S}}{(1 + \boldsymbol{S}^2)^{1/2}} = 0. \tag{71.78}$$

Furthermore, we confirm that $\boldsymbol{J}^{\text{small}}$ is oriented down the tracer gradient by noting that

$$\begin{aligned}
\boldsymbol{J}^{\text{small}} \cdot \nabla C &= -\rho\, \kappa_{\text{ntr}} \left[\nabla_{\text{h}\gamma} C \cdot \nabla_{\text{h}} C + (\boldsymbol{S} \cdot \nabla_{\text{h}\gamma} C)\, \partial_z C\right] && \text{(71.79a)} \\
&= -\rho\, \kappa_{\text{ntr}} \left[|\nabla_{\text{h}} C|^2 + 2\, (\boldsymbol{S} \cdot \nabla_{\text{h}} C)\, \partial_z C + |\boldsymbol{S}\, \partial_z C|^2\right] && \text{(71.79b)} \\
&= -\rho\, \kappa_{\text{ntr}} \left|\nabla_{\text{h}} C + \boldsymbol{S}\, \partial_z C\right|^2 && \text{(71.79c)} \\
&= -\rho\, \kappa_{\text{ntr}} \left|\nabla_{\text{h}\gamma} C\right|^2 && \text{(71.79d)} \\
&\le 0. && \text{(71.79e)}
\end{aligned}$$

The small slope approximation was proposed by *Cox* (1987). However, his form for the small slope neutral diffusion flux was incorrect as it did not satisfy $\boldsymbol{J}^{\text{small}} \cdot \hat{\boldsymbol{\gamma}} = 0$. The corrected form given by equation (71.76) was first written by *Gent and McWilliams* (1990). The resulting small slope neutral diffusion operator is commonly used in ocean climate models (*Griffies et al.*, 1998; *Lemarié et al.*, 2012), which results from computing the three-dimensional convergence

$$\mathcal{R}^{\text{small}} = -\nabla \cdot \boldsymbol{J}^{\text{small}} = \nabla_{\text{h}} \cdot (\rho\, \kappa_{\text{ntr}}\, \nabla_{\text{h}\gamma} C) + \partial_z (\rho\, \kappa_{\text{ntr}}\, \boldsymbol{S} \cdot \nabla_{\text{h}\gamma} C). \tag{71.80}$$

71.4.4 Neutral tangent plane neutral diffusion

A third method to compute neutral diffusion is motivated by the form of isopycnal diffusion in isopycnal layered models. Rather than isopycnal layers, we work with layers determined locally by neutral tangent planes. The neutral tangent frame makes use of projected non-orthogonal generalized vertical coordinates detailed in Chapter 63.

Following the derivations given in Section 63.15, the neutral diffusive flux in the neutral tangent frame is given by the horizontal flux

$$\boldsymbol{J}^{\text{ntp}} = -\rho\, \kappa_{\text{ntr}}\, \nabla_{\text{h}\gamma} C. \tag{71.81}$$

This flux is oriented down the tracer gradient as oriented along neutral directions

$$\boldsymbol{J}^{\text{ntp}} \cdot \nabla_{\text{h}\gamma} C = -\rho\, \kappa_{\text{ntr}} \left|\nabla_{\text{h}\gamma} C\right|^2, \tag{71.82}$$

which is the same as equation (71.79d) for the small slope fluxes. However, as a purely horizontal flux, $\boldsymbol{J}^{\text{ntp}}$ is not oriented along neutral directions

$$\boldsymbol{J}^{\text{ntp}} \cdot \hat{\boldsymbol{\gamma}} \neq 0. \tag{71.83}$$

Nevertheless, rather than computing the neutral diffusion operator as a horizontal convergence of this flux, the neutral tangent plane diffusion operator is computed by taking the convergence of $\boldsymbol{J}^{\text{ntp}}$ along the neutral tangent plane as per equation (63.100)

$$\mathcal{R}^{\text{ntp}} = -\frac{1}{h^\gamma} \left[\nabla_{h\gamma} \cdot (h^\gamma \, \boldsymbol{J}^{\text{ntp}}) \right] = \frac{1}{h^\gamma} \left[\nabla_{h\gamma} \cdot (h^\gamma \, \rho \, \kappa_{\text{ntr}} \, \nabla_{h\gamma} C) \right], \tag{71.84}$$

where

$$h^\gamma = \frac{\partial z}{\partial \gamma} \, \mathrm{d}\gamma = - \left[\frac{g}{\rho_o \, N^2} \right] \mathrm{d}\gamma \tag{71.85}$$

measures the thickness of a layer defined by two neutral tangent planes (see equation (63.97)).

As detailed in Section 63.15, $\mathcal{R}^{\text{ntp}}$ is identical to the small slope neutral diffusion operator (71.80)

$$\mathcal{R}^{\text{ntp}} = \mathcal{R}^{\text{small}}. \tag{71.86}$$

In principle, it is a matter of convenience which form of the operator one uses. However, there are certain issues to consider when implementing these operators in a numerical model. Notably, a discrete realization of $\mathcal{R}^{\text{ntp}}$ allows for a diagonal downgradient implementation of neutral diffusion, just as isopycnal diffusion in an isopycnal ocean model. In contrast, a discrete realization of either $\mathcal{R}^{\text{redi}}$ or $\mathcal{R}^{\text{small}}$ cannot guarantee downgradient fluxes due to the off-diagonal nature of its neutral diffusive flux components (*Griffies et al.* (1998), *Beckers et al.* (1998), *Gnanadesikan* (1999), *Beckers et al.* (2000) *Lemarié et al.* (2012), *Shao et al.* (2020)). As a result, discrete realizations of $\mathcal{R}^{\text{redi}}$ or $\mathcal{R}^{\text{small}}$ can produce extrema, which are distinctly not properties of diffusion in the continuum (see Exercise 68.3). Hence, even though the continuum identity holds $\mathcal{R}^{\text{ntp}} = \mathcal{R}^{\text{small}}$, there are important differences that arise upon realizing these operators on a discrete lattice. *Shao et al.* (2020) provide further discussion of these points as part of their numerical realization of neutral diffusion.

71.4.5 Neutrality condition

Given the expression (71.16) for the dianeutral unit vector, $\hat{\boldsymbol{\gamma}}$, it is straightforward to show that the neutral diffusive flux for Conservative Temperature and salinity satisfy the constraints

$$\nabla\Theta \cdot [-\alpha \, \boldsymbol{J}(\Theta) + \beta \, \boldsymbol{J}(S)] = 0 \quad \text{and} \quad \nabla S \cdot [-\alpha \, \boldsymbol{J}(\Theta) + \beta \, \boldsymbol{J}(S)] = 0. \tag{71.87}$$

These constraints are generally satisfied if the diffusive fluxes satisfy the balance

$$\alpha \, \boldsymbol{J}(\Theta) = \beta \, \boldsymbol{J}(S) \Longrightarrow \boldsymbol{K} \cdot \hat{\boldsymbol{\gamma}} = 0. \tag{71.88}$$

We refer to this balance as the *neutrality condition*. It reflects the vanishing of the neutral diffusive flux of locally referenced potential density. It is maintained by the diffusive flux (71.69) of *Redi* (1982), the small slope flux (71.76) of *Gent and McWilliams* (1990), and the neutral tangent frame neutral diffusive flux (71.81). However, it is not maintained by the small slope fluxes from *Cox* (1987). Furthermore, *Griffies et al.* (1998) argued for the importance of maintaining this balance to avoid a nonlinear instability plaguing certain numerical realizations of neutral diffusion such as that from *Cox* (1987).

71.4.6 Symmetry condition

Since the neutral diffusion tensor is symmetric (as are all diffusion tensors), we have

$$\begin{aligned} \boldsymbol{J}(\Theta) \cdot \nabla S &= -\kappa_{\text{ntr}}\, \rho\, K^{mn} \partial_n \Theta\, \partial_m S && \text{(71.89a)} \\ &= -\kappa_{\text{ntr}}\, \rho\, K^{nm}\, \partial_n S\, \partial_m \Theta && \text{(71.89b)} \\ &= -\kappa_{\text{ntr}}\, \rho\, K^{nm}\, \partial_n S\, \partial_m \Theta && \text{(71.89c)} \\ &= \boldsymbol{J}(S) \cdot \nabla \Theta. && \text{(71.89d)} \end{aligned}$$

This symmetry condition holds for for any of the diffusion tensors introduced in this chapter. It is particularly useful in our discussion of cabbeling and thermobaricity in Section 72.3.

71.4.7 GM skewsion plus small slope neutral diffusion

A parameterization of mesoscale eddy stirring and mixing often appears in geopotential coordinate ocean models in the form of GM skewsion (Section 71.3.1) and small slope neutral diffusion (Section 71.4.3). The combined tracer flux takes the form

$$\rho^{-1}\, \boldsymbol{J} = -\kappa_{\text{ntr}}\, \nabla_{\text{h}} C - (\kappa_{\text{ntr}} - \kappa_{\text{gm}})\, \boldsymbol{S}\, \partial_z C - \hat{\boldsymbol{z}}\, [(\kappa_{\text{ntr}} + \kappa_{\text{gm}})\, \boldsymbol{S} \cdot \nabla_{\text{h}} C + \kappa_{\text{ntr}}\, \boldsymbol{S}^2\, \partial_z C], \tag{71.90}$$

which can be written in terms of a subgrid scale transport tensor

$$\rho^{-1} \begin{bmatrix} J^x \\ J^y \\ J^z \end{bmatrix} = - \begin{bmatrix} \kappa_{\text{ntr}} & 0 & (\kappa_{\text{ntr}} - \kappa_{\text{gm}})\, S_x \\ 0 & \kappa_{\text{ntr}} & (\kappa_{\text{ntr}} - \kappa_{\text{gm}})\, S_y \\ (\kappa_{\text{ntr}} + \kappa_{\text{gm}})\, S_x & (\kappa_{\text{ntr}} + \kappa_{\text{gm}})\, S_y & \kappa_{\text{ntr}}\, \boldsymbol{S}^2 \end{bmatrix} \begin{bmatrix} \partial_x C \\ \partial_y C \\ \partial_z C \end{bmatrix}. \tag{71.91}$$

In the 1990s and throughout much of the 2000s, it was common to assume that $\kappa_{\text{ntr}} = \kappa_{\text{gm}}$, in which case the combined mixing tensor is

$$\boldsymbol{K}^{\text{small}} + A^{\text{gm}} = \kappa_{\text{ntr}} \begin{bmatrix} 1 & 0 & 0 \\ 0 & 1 & 0 \\ 2\, S_x & 2\, S_y & \boldsymbol{S}^2 \end{bmatrix} \quad \text{if } \kappa_{\text{ntr}} = \kappa_{\text{gm}}, \tag{71.92}$$

so that the subgrid scale flux simplifies to

$$\rho^{-1}\, \boldsymbol{J} = -\kappa_{\text{ntr}} \nabla_{\text{h}} C - \hat{\boldsymbol{z}}\, \kappa_{\text{ntr}}\, (2\, \boldsymbol{S} \cdot \nabla_{\text{h}} C + \boldsymbol{S}^2\, \partial_z C) \quad \text{if } \kappa_{\text{ntr}} = \kappa_{\text{gm}}. \tag{71.93}$$

Notably, the 2×2 horizontal mixing tensor is diagonal. Hence, the horizontal tracer flux is the same as that which arises from downgradient horizontal tracer diffusion. The simplicity of the horizontal flux component was alluring to modelers. It was furthermore argued by *Dukowicz and Smith* (1997) to be a fundamental property of mesoscale turbulence. However, as emphasized through the works of *Treguier et al.* (1997), *Ferrari et al.* (2008), *Danabasoglu et al.* (2008), and *Ferrari et al.* (2010), the boundary conditions for neutral diffusion and GM skewsion are distinct, thus breaking their symmetry. Furthermore, studies such as *Smith and Marshall* (2009) and *Abernathey et al.* (2013) clearly point to the distinct vertical structure for the two diffusivities. Such distinctions are expected since the skew diffusivity and neutral diffusivity parameterize physically distinct processes: one parameterizes the quasi-Stokes transport, associated with velocity and layer thickness correlations, whereas the other parameterizes downgradient diffusion along neutral directions, associated with velocity and tracer correlations.

71.4.8 Generalized vertical coordinates

Thus far we have considered neutral diffusion as realized in geopotential coordinates or using neutral tangent plane coordinates. Here, we detail the steps needed to realize neutral diffusion using the generalized vertical coordinates (GVCs) detailed in Chapters 63 and 64. This formulation is relevant for the now common use of generalized vertical coordinates for ocean modeling as reviewed by *Griffies et al.* (2020).

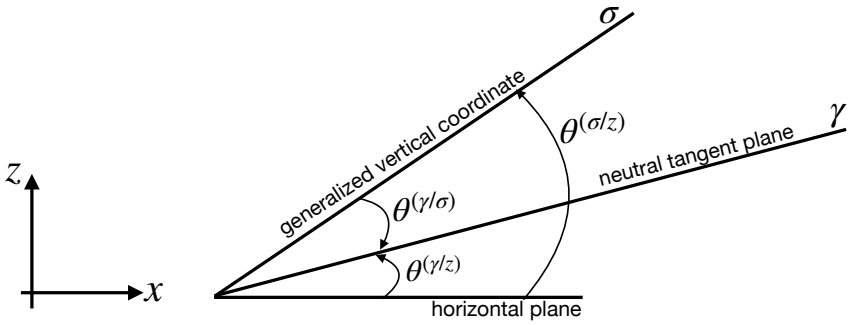

FIGURE 71.5: Slopes of a neutral tangent plane (denoted by γ) relative to both the horizontal plane, $\tan\theta^{(\gamma/z)}$, and relative to a generalized vertical coordinate isoline, $\tan\theta^{(\gamma/\sigma)}$, where σ is a generalized vertical coordinate. We assume positive angles as measure counter-clockwise relative to the horizontal and relative to the σ-isoline, respectively. Hence, for this example, $\theta^{(\gamma/z)} > 0$ yet $\theta^{(\gamma/\sigma)} < 0$. When extending to the two horizontal directions, the slopes generally satisfy $\boldsymbol{S}^{(\sigma/z)} = \boldsymbol{S}^{(\gamma/z)} - \boldsymbol{S}^{(\gamma/\sigma)}$, where $|\boldsymbol{S}^{(\gamma/z)}| = |\tan\theta^{(\gamma/z)}|$ and $|\boldsymbol{S}^{(\gamma/\sigma)}| = |\tan\theta^{(\gamma/\sigma)}|$. Note that this relation between slope vectors also holds for arbitrary orientations of the σ isolines and neutral tangent planes.

Start by recalling the expression (63.99) for a general diffusion operator written in terms of the generalized vertical coordinate, $\sigma = \sigma(x, y, z, t)$

$$\mathcal{R} = -\frac{1}{h^\sigma}\left[\nabla_{h\sigma} \cdot (h^\sigma \, \boldsymbol{J}^h) + \delta_\sigma(z_\sigma \, \nabla\sigma \cdot \boldsymbol{J})\right], \tag{71.94}$$

where $\delta_\sigma \equiv \mathrm{d}\sigma \, \partial_\sigma$ is the dimensionless derivative operator, and the thickness of a σ-layer is

$$h^\sigma = \mathrm{d}z = z_\sigma \, \mathrm{d}\sigma = \frac{\partial z}{\partial \sigma}\, \mathrm{d}\sigma. \tag{71.95}$$

Now assume the flux, $\boldsymbol{J}$, is given by equation (71.76) for small slope neutral diffusion. Transforming to generalized vertical coordinates leads to the horizontal flux component

$$\begin{aligned}
\boldsymbol{J}^{h\text{small}} &= -\rho \, \kappa_{\text{ntr}} \, \nabla_{h\gamma} C && \text{(71.96a)}\\
&= -\rho \, \kappa_{\text{ntr}} \left[\nabla_h + (\nabla_{h\gamma} z)\, \partial_z\right] C && \text{(71.96b)}\\
&= -\rho \, \kappa_{\text{ntr}} \left[\nabla_{h\sigma} + (-\nabla_{h\sigma} z + \nabla_{h\gamma} z)\, \partial_z\right] C && \text{(71.96c)}\\
&= -\rho \, \kappa_{\text{ntr}} \left[\nabla_{h\sigma} + (-\boldsymbol{S}^{(\sigma/z)} + \boldsymbol{S}^{(\gamma/z)})\, \partial_z\right] C && \text{(71.96d)}\\
&= -\rho \, \kappa_{\text{ntr}} \left(\nabla_{h\sigma} + \boldsymbol{S}^{(\gamma/\sigma)}\, \partial_z\right) C, && \text{(71.96e)}
\end{aligned}$$

where the neutral slopes as shown in Figure 71.5 satisfy the identity

$$\boldsymbol{S}^{(\sigma/z)} = \boldsymbol{S}^{(\gamma/z)} - \boldsymbol{S}^{(\gamma/\sigma)}. \tag{71.97}$$

Furthermore, we made use of the identity (63.75) relating the partial derivative operators

$$\nabla_{h\gamma} = \nabla_h + (\nabla_{h\gamma} z)\, \partial_z \quad \text{and} \quad \nabla_h = \nabla_{h\sigma} - (\nabla_{h\sigma} z)\, \partial_z. \tag{71.98}$$

The horizontal flux (71.96e) has the same form as when written using geopotential coordinates,

only now with the derivative operator $\nabla_{h\sigma}$ and the slope $\boldsymbol{S}^{(\gamma/\sigma)}$. Correspondingly, the vertical flux component

$$\boldsymbol{J}^{z\text{small}} = \boldsymbol{J}^{h\text{small}} \cdot \boldsymbol{S}^{(\gamma/z)} \tag{71.99}$$

takes the form

$$z_\sigma \, \nabla\sigma \cdot \boldsymbol{J}^{\text{small}} = -\boldsymbol{S}^{(\sigma/z)} \cdot \boldsymbol{J}^{h\text{small}} + \boldsymbol{J}^{z\text{small}} = \boldsymbol{J}^{h\text{small}} \cdot \boldsymbol{S}^{(\gamma/\sigma)}, \tag{71.100}$$

which in turn yields the diffusion operator (71.94)

$$\mathcal{R} = -\frac{1}{h^\sigma} \left[\nabla_{h\sigma} \cdot (h^\sigma \, \boldsymbol{J}^{h\text{small}}) + \delta_\sigma (\boldsymbol{J}^{h\text{small}} \cdot \boldsymbol{S}^{(\gamma/\sigma)}) \right]. \tag{71.101}$$

In the special case when σ is parallel to the neutral direction so that $\boldsymbol{S}^{(\gamma/\sigma)} = 0$, the diffusion operator (71.101) reduces to the neutral tangent plane version given by equation (71.84).

71.5 Anisotropic neutral diffusion

The neutral diffusion discussed in Section 71.4 is based on isotropic diffusion in the neutral tangent plane. That assumption has been questioned by *Smith and Gent* (2004) and *Fox-Kemper et al.* (2013). We here develop some of the formalism appropriate for studying anisotropic neutral diffusion.

71.5.1 Orthonormal triad of basis vectors

We make use of the following orthonormal unit vectors[7] as depicted in Figure 71.6

$$\hat{\boldsymbol{e}}_{\overline{1}} = \frac{\hat{\boldsymbol{d}} \times \hat{\boldsymbol{\gamma}}}{|\hat{\boldsymbol{d}} \times \hat{\boldsymbol{\gamma}}|} \tag{71.102a}$$

$$\hat{\boldsymbol{e}}_{\overline{2}} = \frac{\hat{\boldsymbol{\gamma}} \times (\hat{\boldsymbol{d}} \times \hat{\boldsymbol{\gamma}})}{|\hat{\boldsymbol{d}} \times \hat{\boldsymbol{\gamma}}|} = \frac{\hat{\boldsymbol{d}} - (\hat{\boldsymbol{\gamma}} \cdot \hat{\boldsymbol{d}}) \, \hat{\boldsymbol{\gamma}}}{|\hat{\boldsymbol{d}} \times \hat{\boldsymbol{\gamma}}|} \tag{71.102b}$$

$$\hat{\boldsymbol{e}}_{\overline{3}} = \hat{\boldsymbol{\gamma}} \tag{71.102c}$$

where

$$\hat{\boldsymbol{d}} = \hat{\boldsymbol{x}} \, \hat{d}_x + \hat{\boldsymbol{y}} \, \hat{d}_y + \hat{\boldsymbol{z}} \, \hat{d}_z \tag{71.103}$$

is an arbitrary unit vector that is not parallel to $\hat{\boldsymbol{\gamma}}$. The three unit vectors $(\hat{\boldsymbol{e}}_{\overline{1}}, \hat{\boldsymbol{e}}_{\overline{2}}, \hat{\boldsymbol{e}}_{\overline{3}})$ form an orthonormal triad at each point in the fluid so that

$$\hat{\boldsymbol{e}}_{\overline{1}} = \hat{\boldsymbol{e}}_{\overline{2}} \times \hat{\boldsymbol{e}}_{\overline{3}} \quad \text{and} \quad \hat{\boldsymbol{e}}_{\overline{2}} = \hat{\boldsymbol{e}}_{\overline{3}} \times \hat{\boldsymbol{e}}_{\overline{1}} \quad \text{and} \quad \hat{\boldsymbol{e}}_{\overline{3}} = \hat{\boldsymbol{e}}_{\overline{1}} \times \hat{\boldsymbol{e}}_{\overline{2}}. \tag{71.104}$$

These vectors are oriented by the arbitrary direction, $\hat{\boldsymbol{d}}$, and the dianeutral direction, $\hat{\boldsymbol{\gamma}}$. We verify that $\hat{\boldsymbol{e}}_{\overline{2}}$ has unit magnitude by noting that

$$|\hat{\boldsymbol{d}} \times \hat{\boldsymbol{\gamma}}|^2 = |\hat{\boldsymbol{\gamma}} \times (\hat{\boldsymbol{d}} \times \hat{\boldsymbol{\gamma}})|^2 = 1 - (\hat{\boldsymbol{d}} \cdot \hat{\boldsymbol{\gamma}})^2. \tag{71.105}$$

It is also useful to verify that $\hat{\boldsymbol{e}}_{\overline{3}} = \hat{\boldsymbol{e}}_{\overline{1}} \times \hat{\boldsymbol{e}}_{\overline{2}}$ through the following vector identity (see equation (1.71g))

$$(\hat{\boldsymbol{d}} \times \hat{\boldsymbol{\gamma}}) \times [\hat{\boldsymbol{\gamma}} \times (\hat{\boldsymbol{d}} \times \hat{\boldsymbol{\gamma}})] = \hat{\boldsymbol{\gamma}} \, |\hat{\boldsymbol{d}} \times \hat{\boldsymbol{\gamma}}|^2. \tag{71.106}$$

[7] The basis vectors (71.102a)-(71.102c) are more suitable for present purposes than the analogous basis vectors defined by equations (14.4)-(14.6) in *Griffies* (2004). In particular, the basis (71.102a)-(71.102c) has a sensible limit when the neutral slopes are horizontal, in which $\hat{\boldsymbol{\gamma}} = -\hat{\boldsymbol{z}}$.

The unit vectors $\hat{\boldsymbol{e}}_{\overline{1}}$ and $\hat{\boldsymbol{e}}_{\overline{2}}$ are both within the neutral tangent plane since they are both orthogonal to $\hat{\boldsymbol{\gamma}}$.

The unit vector $\hat{\boldsymbol{e}}_{\overline{1}}$ is orthogonal to $\hat{\boldsymbol{d}}$ whereas $\hat{\boldsymbol{e}}_{\overline{2}}$ is parallel to $\hat{\boldsymbol{d}}$ if $\hat{\boldsymbol{d}} \cdot \hat{\boldsymbol{\gamma}} = 0$. For example, *Smith and Gent* (2004) proposed setting $\hat{\boldsymbol{d}}$ to be a horizontal vector set according to the local horizontal flow direction, in which case

$$\hat{\boldsymbol{d}} = \frac{u\,\hat{\boldsymbol{x}} + v\,\hat{\boldsymbol{y}}}{(u^2 + v^2)^{1/2}}. \tag{71.107}$$

With $\hat{\boldsymbol{\gamma}}$ nearly vertical for much of the ocean interior, then $\hat{\boldsymbol{e}}_{\overline{2}}$ becomes nearly aligned with $\hat{\boldsymbol{d}}$. For these reasons we refer to $\hat{\boldsymbol{e}}_{\overline{1}}$ as the across-$\hat{\boldsymbol{d}}$ direction and $\hat{\boldsymbol{e}}_{\overline{2}}$ as the along-$\hat{\boldsymbol{d}}$ direction.

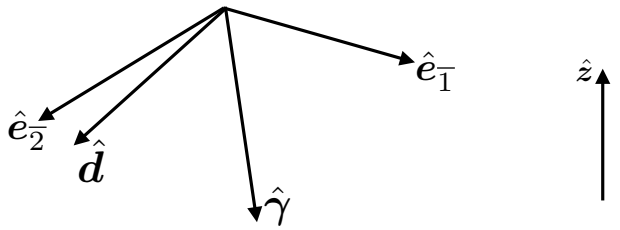

FIGURE 71.6: Depicting the orthonormal triad of basis vectors given by equations (71.102a)-(71.102c). Our convention is such that $\hat{\boldsymbol{\gamma}}$ typically points downward toward increasing density. The unit vector $\hat{\boldsymbol{d}}$ is arbitrary so long as it is not parallel to the dianeutral unit vector, $\hat{\boldsymbol{\gamma}}$. It is horizontal when making use of the *Smith and Gent* (2004) proposal whereby $\hat{\boldsymbol{d}} = \boldsymbol{u}/|\boldsymbol{u}|$, with $\boldsymbol{u} = \hat{\boldsymbol{x}}\,u + \hat{\boldsymbol{y}}\,v$ the horizontal velocity vector. Since $\hat{\boldsymbol{e}}_{\overline{1}}$ is orthogonal to $\hat{\boldsymbol{d}}$, we refer to $\hat{\boldsymbol{e}}_{\overline{1}}$ as the cross-$\hat{\boldsymbol{d}}$ basis vector. Likewise, since $\hat{\boldsymbol{e}}_{\overline{2}}$ is nearly parallel to $\hat{\boldsymbol{d}}$, especially when $\hat{\boldsymbol{d}}$ is close to horizontal and $\hat{\boldsymbol{\gamma}}$ is close to vertical (e.g., Section 71.5.4), then $\hat{\boldsymbol{e}}_{\overline{2}}$ is referred to as the along-$\hat{\boldsymbol{d}}$ basis vector.

71.5.2 Anisotropic neutral diffusion tensor

We consider anisotropy according to the unit vectors $\hat{\boldsymbol{e}}_{\overline{1}}$ and $\hat{\boldsymbol{e}}_{\overline{2}}$. Hence, the diffusion tensor as represented using the locally orthogonal triad $(\hat{\boldsymbol{e}}_{\overline{1}}, \hat{\boldsymbol{e}}_{\overline{2}}, \hat{\boldsymbol{e}}_{\overline{3}})$ is given by

$$\overline{\boldsymbol{K}^{\text{aniso}}} = \begin{bmatrix} \kappa_{\text{cross}} & 0 & 0 \\ 0 & \kappa_{\text{along}} & 0 \\ 0 & 0 & 0 \end{bmatrix}, \tag{71.108}$$

where $\kappa_{\text{cross}} > 0$ and $\kappa_{\text{along}} > 0$ are the generally distinct neutral diffusivities. This tensor takes on the component form

$$(\boldsymbol{K}^{\text{aniso}})^{\overline{mn}} = \kappa_{\text{cross}}\, \hat{e}_{\overline{1}}^{\overline{m}}\, \hat{e}_{\overline{1}}^{\overline{n}} + \kappa_{\text{along}}\, \hat{e}_{\overline{2}}^{\overline{m}}\, \hat{e}_{\overline{2}}^{\overline{n}} \tag{71.109a}$$

$$= \kappa_{\text{cross}}\, (\delta^{\overline{mn}} - \hat{e}_{\overline{2}}^{\overline{m}}\, \hat{e}_{\overline{2}}^{\overline{n}} - \hat{e}_{\overline{3}}^{\overline{m}}\, \hat{e}_{\overline{3}}^{\overline{n}}) + \kappa_{\text{along}}\, (\delta^{\overline{mn}} - \hat{e}_{\overline{1}}^{\overline{m}}\, \hat{e}_{\overline{1}}^{\overline{n}} - \hat{e}_{\overline{3}}^{\overline{m}}\, \hat{e}_{\overline{3}}^{\overline{n}}), \tag{71.109b}$$

where the second expression made use of the following decomposition of the unit tensor in terms of the orthonormal basis vectors

$$\delta^{\overline{mn}} = \hat{e}_{\overline{1}}^{\overline{m}}\, \hat{e}_{\overline{1}}^{\overline{n}} + \hat{e}_{\overline{2}}^{\overline{m}}\, \hat{e}_{\overline{2}}^{\overline{n}} + \hat{e}_{\overline{3}}^{\overline{m}}\, \hat{e}_{\overline{3}}^{\overline{n}}. \tag{71.110}$$

Note that $(\boldsymbol{K}^{\text{aniso}})^{\overline{mn}}$ is invariant under $\hat{\boldsymbol{d}} \to -\hat{\boldsymbol{d}}$. Likewise, it is invariant under a change in the sign of $\hat{\boldsymbol{\gamma}}$. Furthermore, note that we recover the isotropic Redi diffusion tensor (71.72) by setting $\kappa_{\text{cross}} = \kappa_{\text{along}} = \kappa_{\text{ntr}}$ and in which case

$$(K^{\text{aniso}})^{\overline{mn}} = 2\,\kappa_{\text{ntr}}\, (\delta^{\overline{mn}} - \hat{e}_{\overline{3}}^{\overline{m}}\, \hat{e}_{\overline{3}}^{\overline{n}}) - \kappa_{\text{ntr}}\, (\hat{e}_{\overline{1}}^{\overline{m}}\, \hat{e}_{\overline{1}}^{\overline{n}} + \hat{e}_{\overline{2}}^{\overline{m}}\, \hat{e}_{\overline{2}}^{\overline{n}}) \tag{71.111a}$$

$$= \kappa_{\text{ntr}}\, (\delta^{\overline{mn}} - \hat{e}_{\overline{3}}^{\overline{m}}\, \hat{e}_{\overline{3}}^{\overline{n}}) \tag{71.111b}$$

$$= (K^{\text{redi}})^{\overline{mn}} \tag{71.111c}$$

To render a geopotential-Cartesian representation of the anisotropic diffusion tensor, we can make use of the transformation methods for Cartesian tensors developed in Section 1.10. We do so by transforming from the locally orthogonal neutral plane coordinate system, defined by the orthonormal triad (71.102a)-(71.102c), to the geopotential-Cartesian coordinate system, defined by the Cartesian triad

$$\hat{\boldsymbol{e}}_1 = \hat{\boldsymbol{x}} \quad \text{and} \quad \hat{\boldsymbol{e}}_2 = \hat{\boldsymbol{y}} \quad \text{and} \quad \hat{\boldsymbol{e}}_3 = \hat{\boldsymbol{z}}. \tag{71.112}$$

Since we are working with Cartesian tensors, this transformation is a local rotation matrix, $\mathcal{R}$, so that[8]

$$(K^{\text{aniso}})^{mn} = \mathcal{R}^m{}_{\overline{m}} \mathcal{R}^n{}_{\overline{n}} (K^{\text{aniso}})^{\overline{mn}} \Longrightarrow \boldsymbol{K}^{\text{aniso}} = \mathcal{R}\, \overline{\boldsymbol{K}^{\text{aniso}}}\, \mathcal{R}^T, \tag{71.113}$$

where the second equality made use of matrix notation with $\mathcal{R}^T$ the transpose, and where the elements to the rotation matrix are given by the direction cosines following equation (1.87)

$$\mathcal{R} = \begin{bmatrix} \hat{\boldsymbol{e}}^1 \cdot \hat{\boldsymbol{e}}_{\overline{1}} & \hat{\boldsymbol{e}}^1 \cdot \hat{\boldsymbol{e}}_{\overline{2}} & \hat{\boldsymbol{e}}^1 \cdot \hat{\boldsymbol{e}}_{\overline{3}} \\ \hat{\boldsymbol{e}}^2 \cdot \hat{\boldsymbol{e}}_{\overline{1}} & \hat{\boldsymbol{e}}^2 \cdot \hat{\boldsymbol{e}}_{\overline{2}} & \hat{\boldsymbol{e}}^2 \cdot \hat{\boldsymbol{e}}_{\overline{3}} \\ \hat{\boldsymbol{e}}^3 \cdot \hat{\boldsymbol{e}}_{\overline{1}} & \hat{\boldsymbol{e}}^3 \cdot \hat{\boldsymbol{e}}_{\overline{2}} & \hat{\boldsymbol{e}}^3 \cdot \hat{\boldsymbol{e}}_{\overline{3}} \end{bmatrix} = \begin{bmatrix} \hat{\boldsymbol{x}} \cdot \hat{\boldsymbol{e}}_{\overline{1}} & \hat{\boldsymbol{x}} \cdot \hat{\boldsymbol{e}}_{\overline{2}} & \hat{\boldsymbol{x}} \cdot \hat{\boldsymbol{e}}_{\overline{3}} \\ \hat{\boldsymbol{y}} \cdot \hat{\boldsymbol{e}}_{\overline{1}} & \hat{\boldsymbol{y}} \cdot \hat{\boldsymbol{e}}_{\overline{2}} & \hat{\boldsymbol{y}} \cdot \hat{\boldsymbol{e}}_{\overline{3}} \\ \hat{\boldsymbol{z}} \cdot \hat{\boldsymbol{e}}_{\overline{1}} & \hat{\boldsymbol{z}} \cdot \hat{\boldsymbol{e}}_{\overline{2}} & \hat{\boldsymbol{z}} \cdot \hat{\boldsymbol{e}}_{\overline{3}} \end{bmatrix}. \tag{71.114}$$

The machinery outlined here for the transformation is straightforward but tedious (i.e., two matrix multiplies). A more streamlined approach, also used for determining the Cartesian components to the Redi tensor (71.74), is to simply express $(\hat{\boldsymbol{e}}_{\overline{1}}, \hat{\boldsymbol{e}}_{\overline{2}}, \hat{\boldsymbol{e}}_{\overline{3}})$ using geopotential-Cartesian coordinates and then plug directly into equation (71.109b).

71.5.3 Properties of the anisotropic neutral diffusive fluxes

We here verify some standard properties for the anisotropic neutral diffusive flux for tracers

$$\boldsymbol{J}^{\text{aniso}} = -\rho\, \boldsymbol{K}^{\text{aniso}} \cdot \nabla C. \tag{71.115}$$

Downgradient orientation within the neutral tangent plane

By construction, the flux is downgradient along the two orthogonal directions, $\hat{\boldsymbol{e}}_{\overline{1}}$ and $\hat{\boldsymbol{e}}_{\overline{2}}$,

$$\boldsymbol{J}^{\text{aniso}} = -\rho\, \kappa_{\text{cross}}\, \hat{\boldsymbol{e}}_{\overline{1}} (\hat{\boldsymbol{e}}_{\overline{1}} \cdot \nabla C) - \rho\, \kappa_{\text{along}}\, \hat{\boldsymbol{e}}_{\overline{2}} (\hat{\boldsymbol{e}}_{\overline{2}} \cdot \nabla C). \tag{71.116}$$

Furthermore, the flux is within the neutral tangent plane

$$\boldsymbol{J}^{\text{aniso}} \cdot \hat{\boldsymbol{\gamma}} = 0 \tag{71.117}$$

due to orthogonality between the basis vectors

$$\hat{\boldsymbol{e}}_{\overline{1}} \cdot \hat{\boldsymbol{\gamma}} = \hat{\boldsymbol{e}}_{\overline{2}} \cdot \hat{\boldsymbol{\gamma}} = 0. \tag{71.118}$$

Neutrality condition

The neutrality condition (71.88) follows since

$$(-\alpha\, \nabla\Theta + \beta\, \nabla S) \cdot \hat{\boldsymbol{e}}_{\overline{1}} = (-\alpha\, \nabla\Theta + \beta\, \nabla S) \cdot \hat{\boldsymbol{e}}_{\overline{2}} = 0, \tag{71.119}$$

[8] Since we are dealing with Cartesian tensors there is no distinction between raised or lowered tensor indices in equation (71.113). We choose to follow the convention of general tensors in Chapters 3 and 4 simply to help organize elements of the tensor.

so that

$$\alpha\, \boldsymbol{J}^{\text{aniso}}(\Theta) = \beta\, \boldsymbol{J}^{\text{aniso}}(S). \tag{71.120}$$

71.5.4 Small slope anisotropic neutral diffusion

We now consider the special case in which the orientation direction, $\hat{\boldsymbol{d}}$, is strictly horizontal and normalized so that

$$\hat{\boldsymbol{d}} \cdot \hat{\boldsymbol{d}} = \hat{d}_x^2 + \hat{d}_y^2 = 1. \tag{71.121}$$

Additionally, we assume the neutral slope is small so that the neutral directions are nearly horizontal. In this case the basis vectors (71.102a)-(71.102c) take on the following form valid to $\mathcal{O}(|\boldsymbol{S}|)$

$$\hat{\boldsymbol{e}}_{\overline{1}_{\text{small}}} = \hat{\boldsymbol{d}} \times (\boldsymbol{S} - \hat{\boldsymbol{z}}) \tag{71.122a}$$

$$\hat{\boldsymbol{e}}_{\overline{2}} = \hat{\boldsymbol{d}} + \hat{\boldsymbol{z}}\, (\hat{\boldsymbol{d}} \cdot \boldsymbol{S}) \tag{71.122b}$$

$$\hat{\boldsymbol{e}}_{\overline{3}_{\text{small}}} = \boldsymbol{S} - \hat{\boldsymbol{z}}. \tag{71.122c}$$

Note that $\hat{\boldsymbol{e}}_{\overline{3}_{\text{small}}}$ is orthogonal to $\hat{\boldsymbol{e}}_{\overline{1}_{\text{small}}}$ and $\hat{\boldsymbol{e}}_{\overline{2}_{\text{small}}}$, however $\hat{\boldsymbol{e}}_{\overline{1}_{\text{small}}} \cdot \hat{\boldsymbol{e}}_{\overline{2}_{\text{small}}}$ is $\mathcal{O}(\boldsymbol{S} \cdot \boldsymbol{S})$. Likewise, each of these vectors is normalized only to $\mathcal{O}(\boldsymbol{S} \cdot \boldsymbol{S})$.

Making use of the small slope basis vectors in the anisotropic diffusion tensor (71.109a), and expressing them in geopotential-Cartesian coordinates leads to the small slope anisotropic neutral diffusion tensor[9]

$$\boldsymbol{K}^{\text{smallaniso}} = \kappa_{\text{cross}} \begin{bmatrix} 1 & 0 & S_x \\ 0 & 1 & S_y \\ S_x & S_y & \boldsymbol{S} \cdot \boldsymbol{S} \end{bmatrix} + \Delta\kappa_{\text{ntr}} \begin{bmatrix} \hat{d}_x^2 & \hat{d}_x\, \hat{d}_y & (\hat{\boldsymbol{d}} \cdot \boldsymbol{S})\, \hat{d}_x \\ \hat{d}_x\, \hat{d}_y & \hat{d}_y^2 & (\hat{\boldsymbol{d}} \cdot \boldsymbol{S})\, \hat{d}_y \\ (\hat{\boldsymbol{d}} \cdot \boldsymbol{S})\, \hat{d}_x & (\hat{\boldsymbol{d}} \cdot \boldsymbol{S})\, \hat{d}_y & (\hat{\boldsymbol{d}} \cdot \boldsymbol{S})^2 \end{bmatrix}, \tag{71.123}$$

where

$$\Delta\kappa_{\text{ntr}} = \kappa_{\text{along}} - \kappa_{\text{cross}}. \tag{71.124}$$

As for the unapproximated anisotropic neutral diffusion tensor (71.109a), its small slope version, $\overline{\boldsymbol{K}}_{\text{small aniso}}$, is invariant if we swap the direction $\hat{\boldsymbol{d}} \to -\hat{\boldsymbol{d}}$. Furthermore, in the form (71.123) we trivially see that $\overline{\boldsymbol{K}}^{\text{smallaniso}} = \overline{\boldsymbol{K}}^{\text{small}}$ (equation (71.75)) in the isotropic limit where $\kappa_{\text{cross}} = \kappa_{\text{along}} = \kappa_{\text{ntr}}$.

The anisotropic small slope neutral diffusive flux is given by

$$\boldsymbol{J}^{h\text{smallaniso}} = -\rho\, \boldsymbol{K}^{\text{smallaniso}} \cdot \nabla C, \tag{71.125}$$

with horizontal and vertical components

$$\boldsymbol{J}^{h\text{smallaniso}} = -\rho\, \kappa_{\text{cross}} \nabla_{\!\gamma} C - \rho\, \Delta\kappa_{\text{ntr}}\, \hat{\boldsymbol{d}}\, (\hat{\boldsymbol{d}} \cdot \nabla_{\!\gamma}) C \tag{71.126a}$$

$$J^{z\text{smallaniso}} = \boldsymbol{S} \cdot \boldsymbol{J}^{h\text{smallaniso}}, \tag{71.126b}$$

where $\nabla_{\!\gamma} = \nabla_{\!\text{h}} + \boldsymbol{S}\, \partial_z$ is the horizontal operator as per equation (71.77). By making use of the expression (71.19), $\hat{\boldsymbol{\gamma}} = (\boldsymbol{S} - \hat{\boldsymbol{z}})\, (1 + \boldsymbol{S}^2)^{-1/2}$, we readily find that

$$\boldsymbol{J}^{h\text{smallaniso}} \cdot \hat{\boldsymbol{\gamma}} = 0. \tag{71.127}$$

Similarly, we can verify that the neutrality condition (Section 71.4.5) is maintained

$$\boldsymbol{K}^{\text{smallaniso}} \cdot \hat{\boldsymbol{\gamma}} = 0 \Longrightarrow \alpha\, \boldsymbol{J}^{h\text{smallaniso}}(\Theta) = \beta\, \boldsymbol{J}^{h\text{smallaniso}}(S). \tag{71.128}$$

[9] Equation (71.123) agrees with equations (10) and (14) from *Smith and Gent* (2004).

Finally, as per the discussion in Section 71.4.4, we can evaluate the small slope anisotropic neutral diffusion operator by following the non-orthogonal neutral tangent approach rather than the three-dimensional Cartesian approach. It is the non-orthogonal neutral tangent approach that is appropriate for vertical Lagrangian ocean models such as detailed in *Griffies et al.* (2020) and *Shao et al.* (2020).

71.6 Anisotropic Gent-McWilliams stirring

In addition to proposing the use of a small slope anisotropic neutral diffusion tensor (equation (71.123)), *Smith and Gent* (2004) proposed a complementary anisotropic version of the Gent-McWilliams stirring. We here detail the parameterization, again assuming the orientation direction, $\hat{\boldsymbol{d}}$, is horizontal

$$\hat{\boldsymbol{d}} = \hat{\boldsymbol{x}}\, \hat{d}_x + \hat{\boldsymbol{y}}\, \hat{d}_y, \tag{71.129}$$

just as assumed when discussing the anisotropic small slope neutral diffusion operator in Section 71.5.4.

71.6.1 Streamfunction and anti-symmetric tensor

The parameterized eddy-induced streamfunction is generalized from that in equation (71.28) to read

$$\boldsymbol{\Psi}^* = \hat{\boldsymbol{z}} \times \kappa_{\text{gmcross}}\, \boldsymbol{S} + \hat{\boldsymbol{z}} \times (\kappa_{\text{gmcross}} - \kappa_{\text{gmalong}})\, (\hat{\boldsymbol{d}} \cdot \boldsymbol{S})\, \hat{\boldsymbol{d}}, \tag{71.130}$$

and the corresponding anti-symmetric stirring tensor is

$$A^{\text{gmaniso}} = \kappa_{\text{gmcross}} \begin{bmatrix} 0 & 0 & -S_x \\ 0 & 0 & -S_y \\ S_x & S_y & 0 \end{bmatrix} + \Delta\kappa_{\text{gm}}\, (\hat{\boldsymbol{d}} \cdot \boldsymbol{S}) \begin{bmatrix} 0 & 0 & -\hat{d}_x \\ 0 & 0 & -\hat{d}_y \\ \hat{d}_x & \hat{d}_y & 0 \end{bmatrix}, \tag{71.131}$$

where

$$\Delta\kappa_{\text{gm}} = \kappa_{\text{gmalong}} - \kappa_{\text{gmcross}}. \tag{71.132}$$

As for the small slope anisotropic neutral diffusion tensor (71.123), we write the skew tensor A^{gmaniso} in equation (71.131) in a form that manifestly reduces to the isotropic Gent-McWilliams stirring tensor A^{gm} when $\kappa_{\text{gmalong}} = \kappa_{\text{gmcross}} = \kappa_{\text{gm}}$.

71.6.2 Anisotropic Gent-McWilliams skew tracer flux

The anisotropic Gent-McWilliams skew tracer flux is

$$\boldsymbol{J}_{\text{gm-aniso}} = -\rho\, A^{\text{gmaniso}} \cdot \nabla C \tag{71.133a}$$

$$= \rho\, \kappa_{\text{gmcross}}\, [\boldsymbol{S}\, \partial_z C - \hat{\boldsymbol{z}}\, (\boldsymbol{S} \cdot \nabla_{\text{h}} C)] + \rho\, \Delta\kappa_{\text{gm}}\, (\hat{\boldsymbol{d}} \cdot \boldsymbol{S})\, [\hat{\boldsymbol{d}}\, \partial_z C - \hat{\boldsymbol{z}}\, (\hat{\boldsymbol{d}} \cdot \nabla_{\text{h}} C)]. \tag{71.133b}$$

When acting on locally referenced potential density, $C = \gamma$, the flux reduces to

$$\boldsymbol{J}_{\text{gm-aniso}} = \rho\, \kappa_{\text{gmcross}}\, [-\nabla_{\text{h}}\gamma + \hat{\boldsymbol{z}}\, \boldsymbol{S}^2\, \partial_z \gamma] + \rho\, \Delta\kappa_{\text{gm}}\, (\boldsymbol{d} \cdot \boldsymbol{S})\, [\hat{\boldsymbol{d}} + \hat{\boldsymbol{z}}\, (\hat{\boldsymbol{d}} \cdot \boldsymbol{S})]\, \partial_z \gamma. \tag{71.134}$$

As discussed in Section 71.3.3, a negative vertical component to the potential density skew flux ensures that the available potential energy is dissipated,

$$\hat{\boldsymbol{z}} \cdot \boldsymbol{J}_{\text{gm-aniso}} = \rho\, [\kappa_{\text{gmcross}}\, \boldsymbol{S}^2 + \Delta\kappa_{\text{gm}}\, (\boldsymbol{d} \cdot \boldsymbol{S})^2]\, \partial_z \gamma < 0 \Longrightarrow \text{APE dissipated}. \tag{71.135}$$

Stably stratified water means that $\partial_z \gamma < 0$, in which case $\hat{\boldsymbol{z}} \cdot \boldsymbol{J}_{\text{gm-aniso}} < 0$ since

$$\kappa_{\text{gmcross}}\, \boldsymbol{S}^2 + \Delta\kappa_{\text{gm}}\, (\boldsymbol{d} \cdot \boldsymbol{S})^2 = \kappa_{\text{gmcross}}\, [\boldsymbol{S}^2 - (\hat{\boldsymbol{d}} \cdot \boldsymbol{S})^2] + \kappa_{\text{gmalong}}\, (\hat{\boldsymbol{d}} \cdot \boldsymbol{S})^2 > 0. \tag{71.136}$$

71.6.3 Anisotropic GM skewsion plus small slope neutral diffusion

As noted in Section 71.4.7, there are strong reasons to keep the Gent-McWilliams skew flux parameterization distinct from the neutral diffusion parameterization. The central practical reason for the distinction concerns their different treatment of boundary conditions and generally distinct diffusivities. Even so, we here briefly comment on the special case where we ignore these distinctions and set the skew flux diffusivities equal to the neutral diffusivities

$$\kappa_{\text{gmcross}} = \kappa_{\text{cross}} \quad \text{and} \quad \kappa_{\text{gmalong}} = \kappa_{\text{along}}. \tag{71.137}$$

This is the approach assumed by *Smith and Gent* (2004). With the small slope approximation to neutral diffusion, we find the combined anisotropic mixing tensor becomes

$$\boldsymbol{K}^{\text{smallaniso}} + A^{\text{gmaniso}} = \kappa_{\text{cross}} \begin{bmatrix} 1 & 0 & 0 \\ 0 & 1 & 0 \\ 2\,S_x & 2\,S_y & \boldsymbol{S} \cdot \boldsymbol{S} \end{bmatrix} + \Delta\kappa \begin{bmatrix} \hat{d}_x^2 & \hat{d}_x\,\hat{d}_y & 0 \\ \hat{d}_x\,\hat{d}_y & \hat{d}_y^2 & 0 \\ 2\,(\hat{\boldsymbol{d}} \cdot \boldsymbol{S})\,\hat{d}_x & 2\,(\hat{\boldsymbol{d}} \cdot \boldsymbol{S})\,\hat{d}_y & (\hat{\boldsymbol{d}} \cdot \boldsymbol{S})^2 \end{bmatrix}. \tag{71.138}$$

The vanishing right hand column terms simplifies the horizontal tracer fluxes computed from this tensor. However, again, this formulation lacks is inconsistent with theory that supports the distinct treatments of the skew flux and neutral flux.

71.6.4 A parameterization based on a boundary value problem

We now follow the approach from Section 71.3.8 to develop a boundary value problem version of the anisotropic Gent-McWilliams stirring. For this purpose we consider the vertical boundary value problem

$$(c^2\, \partial_{zz} - N^2)\, \boldsymbol{\Upsilon} = -N^2\, \boldsymbol{\Upsilon}^{\text{gmaniso}} \quad \text{and} \quad \boldsymbol{\Upsilon}(\eta_{\text{b}}) = \boldsymbol{\Upsilon}(\eta) = 0, \tag{71.139}$$

where (see equation (71.130))

$$\boldsymbol{\Upsilon}^{\text{gmaniso}} = \kappa_{\text{gmcross}}\, \boldsymbol{S} + \hat{\boldsymbol{z}} \times \Delta\kappa_{\text{gm}}\, (\hat{\boldsymbol{d}} \cdot \boldsymbol{S})\, \hat{\boldsymbol{d}}. \tag{71.140}$$

As in Section 71.3.8, we deduce the impacts on potential energy (assuming a linear equation of state) via the vertical component of the potential density skew flux,

$$\frac{1}{g}\frac{\mathrm{d}P}{\mathrm{d}t} = \frac{1}{\rho_{\text{o}}} \int J^z\, \mathrm{d}V = -\int \nabla_{\text{h}} \varrho \cdot \boldsymbol{\Upsilon}\, \mathrm{d}V. \tag{71.141}$$

The governing differential equation (71.139) leads to

$$\boldsymbol{\Upsilon} \cdot (c^2\, \partial_{zz} - N^2)\, \boldsymbol{\Upsilon} = -N^2\, \boldsymbol{\Upsilon} \cdot \boldsymbol{\Upsilon}^{\text{gmaniso}} \tag{71.142}$$

which rearranges to

$$N^2\, \boldsymbol{\Upsilon} \cdot \boldsymbol{\Upsilon}^{\text{gmaniso}} = -c^2\, \partial_z(\boldsymbol{\Upsilon} \cdot \partial_z \boldsymbol{\Upsilon}) + c^2\, \partial_z \boldsymbol{\Upsilon} \cdot \partial_z \boldsymbol{\Upsilon} + N^2\, \boldsymbol{\Upsilon} \cdot \boldsymbol{\Upsilon}. \tag{71.143}$$

Integrating over a vertical column and making use of the homogeneous Dirichlet boundary conditions in equation (71.139) leads to

$$\frac{g}{\rho_\circ}\int \boldsymbol{\Upsilon}\cdot\nabla_{\!\mathsf{h}}\varrho\,\mathrm{d}z = -\int N^2\,\Delta\kappa_{\mathsf{gm}}(\hat{\boldsymbol{d}}\cdot\boldsymbol{S})\,(\hat{\boldsymbol{d}}\cdot\boldsymbol{\Upsilon})\,\mathrm{d}z + \int\left[c^2\,\partial_z\boldsymbol{\Upsilon}\cdot\partial_z\boldsymbol{\Upsilon} + N^2\,\boldsymbol{\Upsilon}\cdot\boldsymbol{\Upsilon}\right]\mathrm{d}z, \quad (71.144)$$

which can be rearranged into the equivalent form

$$\begin{aligned}&\frac{g}{\rho_\circ}\int \boldsymbol{\Upsilon}\cdot\nabla_{\!\mathsf{h}}\varrho\,\mathrm{d}z\\ &= \underbrace{\int\left[c^2\,\partial_z\boldsymbol{\Upsilon}\cdot\partial_z\boldsymbol{\Upsilon} + N^2\,(\boldsymbol{\Upsilon}\cdot\boldsymbol{\Upsilon} - (\hat{\boldsymbol{d}}\cdot\boldsymbol{\Upsilon})^2)\right]\mathrm{d}z}_{\text{positive semi-definite}} + \underbrace{\int N^2\,(\hat{\boldsymbol{d}}\cdot\boldsymbol{\Upsilon})\,\hat{\boldsymbol{d}}\cdot(\boldsymbol{\Upsilon}-\boldsymbol{S}\,\Delta\kappa_{\mathsf{gm}})\,\mathrm{d}z.}_{\text{sign indefinite}} \quad (71.145)\end{aligned}$$

The first term on the right hand side is positive semi-indefinite whereas the second term is sign indefinite. If the second term is positive, or smaller in magnitude than the first term, then the parameterization provides a column integrated sink of potential energy. Otherwise, potential energy for the column can increase. There are no existing numerical implementations of this scheme to determine its suitability for realistic ocean climate simulations.

Chapter 72

Ocean density and sea level

Conservative temperature, Θ, is the preferred means to measure the transport of enthalpy in the ocean (Section 26.11), and salinity, S, measures the concentration of dissolved salt matter. These two scalar fields are referred to as *active* tracers as they both impact density and in turn affect pressure and ocean currents. In this chapter we study how the evolution of Θ and S affects density as well as buoyancy. As part of this study, we examine how to compute air-sea bouyancy fluxes.

Θ and S are conservative tracers so that the net changes in potential enthalpy and salt over the global ocean domain arise from net imbalances in their boundary fluxes. Likewise, ocean mass is a conserved field, with global mass changes arising from imbalances in boundary mass fluxes such as those occuring from increases in land ice melt. However, ocean volume, and hence ocean density and buoyancy, are not conserved fields. Consequently, ocean volume can change even if there is no net volume transferred to the ocean. These points have direct impact on how global mean sea level is affected by ocean processes such as mixing and heating, with the rudiments presented in this chapter.

CHAPTER GUIDE

Basic notions of thermodynamics, such as Section 26.11, motivate the use of Conservative Temperature, Θ, as a measure of ocean enthalpy transfer, rather than *in situ* temperature or potential temperature. We also make use of the ideas of parameterized turbulent mixing discussed in Chapters 68 and 71 when formulating the budget equations for Θ and S. We use Cartesian tensors to reduce the mathematical overhead. Also note that we use subscripts on specific volume, ν, and density, ρ, for partial derivatives with respect to Θ and S. This is the only chapter in this book that makes use of subscript notation for partial derivatives, and we only use it for thermodynamic derivatives.

72.1 Loose threads

- Schematics for cabbeling and thermobarocity.

72.2 Material evolution of *in situ* density

Changes to the *in situ* density of seawater affects pressure forces in the ocean as well as the volume occupied by the ocean fluid (i.e., sea level). As discussed in Section 30.3.2, we write the seawater equation of state for density as a function of salinity, S, and Conservative Temperature, Θ, where Conservative Temperature is the potential enthalpy divided by a constant heat capacity (see Section 26.11.3 and *McDougall* (2003); *IOC et al.* (2010)). We thus make use of the empirical relation for the seawater density in the functional form

$$\rho = \rho(S, \Theta, p), \tag{72.1}$$

where S is the salinity rather than the salt concentration ($S = 1000\,\mathsf{S}$).

We formulate the material evolution of density as weighted by the specific volume[1]

$$\nu = \rho^{-1}, \tag{72.2}$$

so that we study

$$\frac{\mathrm{D} \ln \rho}{\mathrm{D}t} = \frac{\partial \ln \rho}{\partial \Theta} \frac{\mathrm{D}\Theta}{\mathrm{D}t} + \frac{\partial \ln \rho}{\partial S} \frac{\mathrm{D}S}{\mathrm{D}t} + \frac{\partial \ln \rho}{\partial p} \frac{\mathrm{D}p}{\mathrm{D}t} \tag{72.3a}$$

$$= -\alpha \frac{\mathrm{D}\Theta}{\mathrm{D}t} + \beta \frac{\mathrm{D}S}{\mathrm{D}t} + \frac{\dot{p}}{\rho\, c_{\mathrm{s}}^2}. \tag{72.3b}$$

[1] In other chapters we write the specific volume as $\nu_{\mathrm{s}} = 1/\rho$ to distinguish it from ν that is used for kinematic viscosity. However, in this chapter we write $\nu = 1/\rho$ to enable a shorthand for partial derivatives as defined by equation (72.8). We have no use kinematic viscosity in this chapter.

In this equation we introduced the thermal expansion coefficient, the haline contraction coefficient, the squared speed of sound, and the vertical pseudo-velocity in pressure

$$\alpha = -\left[\frac{\partial \ln \rho}{\partial \Theta}\right]_{p,S} \qquad \beta = \left[\frac{\partial \ln \rho}{\partial S}\right]_{p,\Theta} \qquad c_s^2 = \left[\frac{\partial p}{\partial \rho}\right]_{S,\Theta} \qquad \dot{p} = \frac{\mathrm{D}p}{\mathrm{D}t}. \tag{72.4}$$

For the the remainder of this section we unpack the processes contributing to the density material time evolution appearing in equation (72.3).

72.2.1 Material changes to pressure

To garner some exposure to the physics of $\dot{p}$ as it appears in equation (72.3), we consider the special case of a hydrostatic fluid, where the volume per time per horizontal area of fluid crossing a surface of constant hydrostatic pressure is given by (see Section 64.3.6)

$$w^{(\mathrm{p})} = \frac{\partial z}{\partial p}\frac{\mathrm{D}p}{\mathrm{D}t} = -(\rho\, g)^{-1}\, \dot{p}. \tag{72.5}$$

The transport measured by $w^{(\mathrm{p})}$ is the pressure-coordinate analog of the vertical velocity component, $w = \mathrm{D}z/\mathrm{D}t$, that arises in a geopotential coordinate representation of the vertical. That is, fluid moving into regions of increasing hydrostatic pressure ($\dot{p} > 0$) represents downward movement of fluid, with $w^{(\mathrm{p})} < 0$ in this case. Conversely, motion into decreasing hydrostatic pressure represents upward motion, with $w^{(\mathrm{p})} > 0$. This vertical movement generally occurs in the presence of waves, currents, and mixing; i.e., both reversible and irreversible processes give rise to vertical motion.

72.2.2 Material changes to Θ and S

We now focus on the salinity and temperature contributions to the evolution of *in situ* density. To do so, assume that the material evolution of Θ and S are given by the convergence of a subgrid scale flux

$$\rho \frac{\mathrm{D}\Theta}{\mathrm{D}t} = -\nabla \cdot \boldsymbol{J}^{(\Theta)} \tag{72.6a}$$

$$\rho \frac{\mathrm{D}S}{\mathrm{D}t} = -\nabla \cdot \boldsymbol{J}^{(\mathrm{S})}. \tag{72.6b}$$

The Conservative Temperature equation (72.6a) was derived in Section 26.11, whereas the Absolute Salinity equation (72.6b) follows from our derivation of the tracer equation in Section 20.1.[2]

72.2.3 General expression for density changes

The expressions (72.6a) and (72.6b) for material changes in Θ and S then lead to

$$-\alpha \frac{\mathrm{D}\Theta}{\mathrm{D}t} + \beta \frac{\mathrm{D}S}{\mathrm{D}t} = \nu_\Theta \nabla \cdot \boldsymbol{J}^{(\Theta)} + \nu_S \nabla \cdot \boldsymbol{J}^{(\mathrm{S})} \tag{72.7a}$$

$$= \nabla \cdot [\nu_\Theta \boldsymbol{J}^{(\Theta)} + \nu_S \boldsymbol{J}^{(\mathrm{S})}] - \left[\boldsymbol{J}^{(\Theta)} \cdot \nabla \nu_\Theta + \boldsymbol{J}^{(\mathrm{S})} \cdot \nabla \nu_S\right] \tag{72.7b}$$

[2] We here ignore remineralization processes that can contribute to a source term in the salinity equation (72.6b). Such source terms are discussed in *IOC et al.* (2010).

where again $\nu = \rho^{-1}$ is the specific volume and its partial derivatives are written

$$\nu_\Theta = \frac{\partial \nu}{\partial \Theta} = \frac{\alpha}{\rho} \qquad \text{and} \qquad \nu_S = \frac{\partial \nu}{\partial S} = -\frac{\beta}{\rho}. \tag{72.8}$$

Bringing the above results together leads to the density equation

$$\frac{\mathrm{D} \ln \rho}{\mathrm{D}t} - \frac{\dot{p}}{\rho \, c_{\mathrm{s}}^2} = \nabla \cdot [\nu_\Theta \, \boldsymbol{J}^{(\Theta)} + \nu_S \, \boldsymbol{J}^{(S)}] - \left[\boldsymbol{J}^{(\Theta)} \cdot \nabla \nu_\Theta + \boldsymbol{J}^{(S)} \cdot \nabla \nu_S\right], \tag{72.9}$$

which has the equivalent form

$$\frac{\mathrm{D} \rho}{\mathrm{D}t} - \frac{\dot{p}}{c_{\mathrm{s}}^2} = \nabla \cdot [\alpha \, \boldsymbol{J}^{(\Theta)} - \beta \, \boldsymbol{J}^{(S)}] - \left[\boldsymbol{J}^{(\Theta)} \cdot \nabla \alpha - \boldsymbol{J}^{(S)} \cdot \nabla \beta\right]. \tag{72.10}$$

We brought the source term from motion across pressure surfaces (Section 72.2.1) onto the left hand side, as this term appears in the absence of subgrid processes. The first term on the right hand side represents the divergence of a buoyancy flux due to subgrid scale fluxes of Conservative Temperature and salinity. In turn, density increases in regions where the buoyancy flux diverges (e.g., Θ reducing and S increasing). These fluxes arise from a variety of mixing processes, some of which are surveyed in Section 71.1.1. The second term on the right hand side of equations (72.9) and (72.10) relates to properties of the locally referenced potential density surface. We study this source term in Section 72.3 as it appears from the neutral diffusion process. Further effects arise from unresolved eddy-induced stirring, with that process contributing to the material time derivative operator to render a residual mean velocity (Section 71.1.4).

72.2.4 Unpacking the subgrid contributions

Recall from Section 71.1 that the subgrid scale fluxes are generally written in terms of a second order eddy transport tensor, $\boldsymbol{E}$, so that

$$\boldsymbol{J}^{(\Theta)} = -\rho \, \boldsymbol{E} \cdot \nabla \Theta \quad \text{and} \quad \boldsymbol{J}^{(S)} = -\rho \, \boldsymbol{E} \cdot \nabla S. \tag{72.11}$$

Furthermore, $\boldsymbol{E}$ is typically decomposed as in equation (71.8) into a symmetric downgradient diffusion tensor, $\boldsymbol{K}$, and an anti-symmetric skew diffusion (or stirring) tensor, $\boldsymbol{A}$,

$$\boldsymbol{E} = \boldsymbol{K} + \boldsymbol{A}. \tag{72.12}$$

We decompose the contributions to density according to these subgrid tensors using the following manipulations

$$\begin{aligned} \frac{\mathrm{D} \rho}{\mathrm{D}t} - \frac{\dot{p}}{c_{\mathrm{s}}^2} &= \alpha \, \nabla \cdot \boldsymbol{J}^{(\Theta)} - \beta \nabla \cdot \boldsymbol{J}^{(S)} && \text{(72.13a)} \\ &= -\alpha \, \nabla \cdot (\rho \, \boldsymbol{E} \cdot \nabla \Theta) + \beta \, \nabla \cdot (\rho \, \boldsymbol{E} \cdot \nabla S). && \text{(72.13b)} \end{aligned}$$

Expanding the Θ term leads to

$$\begin{aligned} \alpha \, \nabla \cdot \boldsymbol{J}^{(\Theta)} &= -\alpha \, \nabla \cdot (\rho \, \boldsymbol{E} \cdot \nabla \Theta) && \text{(72.14a)} \\ &= -\alpha \, \nabla \cdot (\rho \, \boldsymbol{A} \cdot \nabla \Theta) - \alpha \, \nabla \cdot (\rho \, \boldsymbol{K} \cdot \nabla \Theta) && \text{(72.14b)} \\ &= -\alpha \, \nabla \cdot (\rho \, \boldsymbol{A}) \cdot \nabla \Theta - \alpha \, \nabla \cdot (\rho \, \boldsymbol{K} \cdot \nabla \Theta), && \text{(72.14c)} \\ &= -\alpha \, \boldsymbol{v}^* \cdot \nabla \Theta - \alpha \, \nabla \cdot (\rho \, \boldsymbol{K} \cdot \nabla \Theta). && \text{(72.14d)} \end{aligned}$$

To reach this result we made use of the identities

$$\begin{aligned}
\nabla \cdot (\rho \, \boldsymbol{A} \cdot \nabla \Theta) &= \partial_m (\rho \, A^{mn} \, \partial_n \Theta) && \text{expose tensor indices} && (72.15a)\\
&= \partial_m (\rho \, A^{mn}) \, \partial_n \Theta + \rho \, A^{mn} \, \partial_m \partial_n \Theta && \text{product rule} && (72.15b)\\
&= \partial_m (\rho \, A^{mn}) \, \partial_n \Theta && A^{mn} \, \partial_m \partial_n \Theta = 0 && (72.15c)\\
&= -\rho \, \boldsymbol{v}^* \cdot \nabla \Theta && \partial_m (\rho \, A^{mn}) = -\rho \, v^{*n}. && (72.15d)
\end{aligned}$$

In the final equality we introduced the density weighted eddy-induced velocity, $\rho \, \boldsymbol{v}^*$, defined by equation (71.11). The same manipulations for the salinity term lead to

$$\frac{\mathrm{D}\rho}{\mathrm{D}t} - \frac{\dot{p}}{c_s^2} + \rho \boldsymbol{v}^* \cdot (-\alpha \nabla \Theta + \beta \nabla S) = -\alpha \nabla \cdot (\rho \, \boldsymbol{K} \cdot \nabla \Theta) + \beta \nabla \cdot (\rho \, \boldsymbol{K} \cdot \nabla S). \tag{72.16}$$

We can write this expression in terms of the residual mean material time operator

$$\frac{\mathrm{D}^\dagger}{\mathrm{D}t} = \partial_t + \boldsymbol{v}^\dagger \cdot \nabla = \frac{\mathrm{D}}{\mathrm{D}t} + \boldsymbol{v}^* \cdot \nabla \tag{72.17}$$

through adding and subtracting $c_s^{-2} \, \boldsymbol{v}^* \cdot \nabla p$

$$\rho \, \boldsymbol{v}^* \cdot (-\alpha \nabla \Theta + \beta \nabla S) = \boldsymbol{v}^* \cdot (-\rho \, \alpha \nabla \Theta + \rho \, \beta \nabla S + c_s^{-2} \, \nabla p) - c_s^{-2} \, \boldsymbol{v}^* \cdot \nabla p = \boldsymbol{v}^* \cdot (\nabla \rho - c_s^{-2} \, \nabla p), \tag{72.18}$$

which then leads to

$$\frac{\mathrm{D}\rho}{\mathrm{D}t} - \frac{\dot{p}}{c_s^2} + \rho \boldsymbol{v}^* \cdot (-\alpha \nabla \Theta + \beta \nabla S) = \frac{\mathrm{D}^\dagger \rho}{\mathrm{D}t} - \frac{1}{c_s^2} \frac{\mathrm{D}^\dagger p}{\mathrm{D}t}, \tag{72.19}$$

so that

$$\frac{\mathrm{D}^\dagger \rho}{\mathrm{D}t} - \frac{1}{c_s^2} \frac{\mathrm{D}^\dagger p}{\mathrm{D}t} = -\alpha \nabla \cdot (\rho \, \boldsymbol{K} \cdot \nabla \Theta) + \beta \nabla \cdot (\rho \, \boldsymbol{K} \cdot \nabla S). \tag{72.20}$$

Transport from the symmetric tensor, $\boldsymbol{K}$, corresponds to diffusion so long as the tensor is positive definite. The diffusion operator in the residual mean evolution equation (72.20) can be written

$$\begin{aligned}
&-\alpha \nabla \cdot (\rho \, \boldsymbol{K} \cdot \nabla \Theta) + \beta \nabla \cdot (\rho \, \boldsymbol{K} \cdot \nabla S)\\
&\qquad = \nabla \cdot [\rho \, \boldsymbol{K} \cdot (-\alpha \nabla \Theta + \beta \nabla S)] + \rho \, \nabla \alpha \cdot \boldsymbol{K} \cdot \nabla \Theta - \rho \, \nabla \beta \cdot \boldsymbol{K} \cdot \nabla S, \qquad (72.21)
\end{aligned}$$

so that the *in situ* density evolves according to

$$\frac{\mathrm{D}^\dagger \rho}{\mathrm{D}t} - \frac{1}{c_s^2} \frac{\mathrm{D}^\dagger p}{\mathrm{D}t} = \underbrace{-\nabla \cdot [\rho \, \boldsymbol{K} \cdot (\alpha \nabla \Theta - \beta \nabla S)]}_{\text{conservative processes}} + \underbrace{\rho \, \nabla \alpha \cdot \boldsymbol{K} \cdot \nabla \Theta - \rho \, \nabla \beta \cdot \boldsymbol{K} \cdot \nabla S.}_{\text{sources from nonlinear EOS processes}} \tag{72.22}$$

We now discuss the physical processes associated with the right hand side terms.

- LINEAR EQUATION OF STATE: A linear equation of state has $\nabla \alpha = \nabla \beta = 0$ and is independent of pressure, so that the evolution equation (72.22) takes the form

  $$\frac{\mathrm{D}^\dagger \rho}{\mathrm{D}t} = -\nabla \cdot [\rho \, \boldsymbol{K} \cdot (\alpha \nabla \Theta - \beta \nabla S)] \, . \tag{72.23}$$

  Under the residual mean transport with a linear equation of state, density remains materially constant in the absence of any diffusion.

- NONLINEAR EQUATION OF STATE: A nonlinear equation of state is characterized by spatially

dependent thermal expansion and haline contraction coefficients. Mixing of Θ and S in the presence of a nonlinear equation of state generally gives rise to material evolution of *in situ* density through *cabbeling* and *thermobaricity* (*McDougall*, 1987b). We offer a summary of these processes in Section 72.3.

- NEUTRAL DIFFUSION:

  Neutral diffusion from Section 71.4 maintains a density-compensated diffusive flux of Θ and S so that

  $$\boldsymbol{K}^{\text{neutral}} \cdot (\alpha \nabla\Theta - \beta \nabla S) = 0. \tag{72.24}$$

  Hence, neutral diffusion leaves *in situ* density changed only via the nonlinear equation of state processes.

- ISOTROPIC SMALL SCALE DIFFUSION:

  As discussed in Section 71.1.3, it is common to parameterize fine scale mixing processes using an isotropic diffusivity so that the diffusion tensor is given by

  $$\boldsymbol{K}^{\text{iso}} = \kappa \, \mathbb{I}, \tag{72.25}$$

  where $\mathbb{I}$ is the unit tensor and $\kappa > 0$ is the isotropic eddy diffusivity.

72.2.5 Synthesis of the density equation

In summary, the material time evolution equation for *in situ* density in the presence of subgrid scale processes takes the form

$$\frac{\mathrm{D}\rho}{\mathrm{D}t} = \underbrace{\frac{1}{c_s^2}\frac{\mathrm{D}p}{\mathrm{D}t}}_{\text{compressibility}} \underbrace{- \boldsymbol{v}^* \cdot (-\alpha\nabla\Theta + \beta\nabla S)}_{\text{eddy-induced advection}} \underbrace{- \nabla \cdot [\rho\, \kappa\, (-\alpha\, \nabla\Theta + \beta\, \nabla S)]}_{\text{small scale diffusive mixing}} + \underbrace{\rho\, \nabla\alpha \cdot \boldsymbol{K} \cdot \nabla\Theta - \rho\, \nabla\beta \cdot \boldsymbol{K} \cdot \nabla S.}_{\text{nonlinear EOS processes from eddy mixing}} \tag{72.26}$$

We thus have the following physical processes contributing to the evolution of *in situ* density.

- ADIABATIC COMPRESSION: Material changes to pressure in the presence of a finite sound speed lead to changes in the fluid density.

- SMALL SCALE MIXING: Small scale mixing is parameterized by an isotropic diffusivity, κ. This diffusivity is the same for all tracers, with the exception of double-diffusive processes whereby material tracers (e.g., salinity, nutrients) have a diffusivity distinct from temperature (*Schmitt*, 1994). Given the dominance of vertical stratification over the horizontal, it is common to approximate the isotropic diffusion operator with a vertical diffusion operator (but see Section 4 of *McDougall et al.* (2014) for caveats).

- EDDY-INDUCED STIRRING: For subgrid scale stirring, such as from mesoscale (and sub-mesocale) eddies, we introduce a parameterized eddy-induced advection operator. When combined with the resolved advection, we are led to a residual mean material time derivative, $\mathrm{D}^\dagger/\mathrm{D}t$.

- EDDY-INDUCED DIFFUSION: Subgrid scale eddy-induced stirring leads to a direct cascade of Θ and S variance to the small scales. Mixing arising from this cascade is parameterized by neutral diffusion, whereby the diffusive fluxes of Θ and S are density compensated according to the constraint (72.24).

- NONLINEAR EOS PROCESSES: Mixing of Θ and S in the presence of a nonlinear equation of state means that *in situ* density evolves due to cabbeling and thermobaricity (Section 72.3). The dominant contributions to these processes arise from eddy induced mixing (i.e., neutral diffusion) (*McDougall*, 1987b), though small scale mixing also has a contribution.

72.3 Cabbeling and thermobaricity

We now return to the density equation (72.10)

$$\frac{\mathrm{D} \ln \rho}{\mathrm{D}t} - \frac{\dot{p}}{\rho \, c_s^2} = \nabla \cdot [\nu_\Theta \, \boldsymbol{J}^{(\Theta)} + \nu_S \, \boldsymbol{J}^{(S)}] - \left(\boldsymbol{J}^{(\Theta)} \cdot \nabla \nu_\Theta + \boldsymbol{J}^{(S)} \cdot \nabla \nu_S \right), \tag{72.27}$$

and here focus on Θ and S fluxes arising just from the neutral diffusion process described in Section 71.4. The neutrality condition (71.88) is a fundamental property of neutral diffusion, and it takes the following form in terms of specific volume

$$\nu_\Theta \, \boldsymbol{J}^{(\Theta)} + \nu_S \, \boldsymbol{J}^{(S)} = 0. \tag{72.28}$$

Consequently, neutral diffusion affects density evolution only through the source term

$$\left[\frac{\mathrm{D} \ln \rho}{\mathrm{D}t} \right]_{\text{ntrl diff}} = -\boldsymbol{J}^{(\Theta)} \cdot \nabla \nu_\Theta - \boldsymbol{J}^{(S)} \cdot \nabla \nu_S. \tag{72.29}$$

In the remainder of this section we manipulate the source term in this expression with the goal to identify the variety of physical processes associated with neutral diffusion in the presence of a nonlinear equation of state.

72.3.1 Basic manipulations

As a first step, eliminate the salt flux by using the neutrality condition (72.28)

$$\boldsymbol{J}^{(\Theta)} \cdot \nabla \nu_\Theta + \boldsymbol{J}^{(S)} \cdot \nabla \nu_S = \boldsymbol{J}^{(\Theta)} \cdot [\nu_S \, \nabla \nu_\Theta - \nu_\Theta \, \nabla \nu_S] / \nu_S. \tag{72.30}$$

Next, expand the gradients of the specific volume to write

$$\nabla \nu_\Theta = \nu_{\Theta\Theta} \, \nabla \Theta + \nu_{\Theta S} \, \nabla S + \nu_{\Theta p} \, \nabla p \quad \text{and} \quad \nabla \nu_S = \nu_{SS} \, \nabla S + \nu_{\Theta S} \, \nabla \Theta + \nu_{Sp} \, \nabla p, \tag{72.31}$$

so that

$$\begin{aligned} \nu_S \, \nabla \nu_\Theta - \nu_\Theta \, \nabla \nu_S = \nabla \Theta \, (\nu_S \, \nu_{\Theta\Theta} - \nu_\Theta \, \nu_{\Theta S}) \\ + \nabla S \, (\nu_S \, \nu_{\Theta S} - \nu_\Theta \, \nu_{SS}) + \nabla p \, (\nu_S \, \nu_{\Theta p} - \nu_\Theta \, \nu_{Sp}). \end{aligned} \tag{72.32}$$

We again make use of the neutrality condition (72.28), as well as the symmetry condition (71.89d) to write

$$\boldsymbol{J}^{(\Theta)} \cdot \nabla S \, (\nu_S \, \nu_{\Theta S} - \nu_\Theta \, \nu_{SS}) = -\boldsymbol{J}^{(\Theta)} \cdot \nabla \Theta \left[\nu_\Theta \, \nu_{\Theta S} - \nu_{SS} \frac{(\nu_\Theta)^2}{\nu_S} \right]. \tag{72.33}$$

Bringing these results together leads to

$$\begin{aligned} \boldsymbol{J}^{(\Theta)} \cdot \nabla \nu_\Theta + \boldsymbol{J}^{(S)} \cdot \nabla \nu_S = \boldsymbol{J}^{(\Theta)} \cdot \nabla p \, (\nu_{\Theta p} - \nu_{pS} \, \nu_\Theta / \nu_S) \\ + \boldsymbol{J}^{(\Theta)} \cdot \nabla \Theta \, [\nu_{\Theta\Theta} - 2 \, \nu_{\Theta S} \, \nu_\Theta / \nu_S + \nu_{SS} \, (\nu_\Theta / \nu_S)^2], \end{aligned} \tag{72.34}$$

which can be written in terms of density partial derivatives as

$$\boldsymbol{J}^{(\Theta)} \cdot \nabla \nu_\Theta + \boldsymbol{J}^{(S)} \cdot \nabla \nu_S = -\rho^{-2}\, \boldsymbol{J}^{(\Theta)} \cdot \nabla p\, (\rho_{\Theta p} - \rho_{pS}\, \rho_\Theta / \rho_S) \\ - \rho^{-2}\, \boldsymbol{J}^{(\Theta)} \cdot \nabla \Theta\, [\rho_{\Theta\Theta} - 2\, \rho_{\Theta S}\, \rho_\Theta / \rho_S + \rho_{SS}\, (\rho_\Theta / \rho_S)^2]. \quad (72.35)$$

72.3.2 A tidy form

We next write the bracket terms appearing in equation (72.35) in forms consistent with those written by *McDougall* (1987b). For that purpose, introduce the *thermobaricity* parameter (dimensions of inverse temperature times inverse pressure) whose form is given by

$$\mathcal{T} = \beta\, \partial_p \left[\frac{\alpha}{\beta}\right] \quad (72.36a)$$
$$= \frac{\partial \alpha}{\partial p} - \frac{\alpha}{\beta}\, \frac{\partial \beta}{\partial p} \quad (72.36b)$$
$$= \rho\, \nu_S\, \partial_p (\nu_\Theta / \nu_S) \quad (72.36c)$$
$$= -\rho^{-1}\, \rho_S\, \partial_p (\rho_\Theta / \rho_S) \quad (72.36d)$$
$$= -\rho^{-1}\, (\rho_{\Theta p} - \rho_{pS}\, \rho_\Theta / \rho_S), \quad (72.36e)$$

and the *cabbeling* parameter (dimensions of squared inverse temperature)

$$\mathcal{C} = \frac{\partial \alpha}{\partial \Theta} + 2 \frac{\alpha}{\beta} \frac{\partial \alpha}{\partial S} - \left(\frac{\alpha}{\beta}\right)^2 \frac{\partial \beta}{\partial S} \quad (72.37a)$$
$$= -\rho^{-1}\, [\rho_{\Theta\Theta} - 2\, \rho_{\Theta S}\, (\rho_\Theta / \rho_S) + \rho_{SS}\, (\rho_\Theta / \rho_S)^2] \quad (72.37b)$$
$$= \rho\, [\nu_{\Theta\Theta} - 2\, \nu_{\Theta S}\, (\nu_\Theta / \nu_S) + \nu_{SS}\, (\nu_\Theta / \nu_S)^2] \quad (72.37c)$$

to render the very compact result

$$\boldsymbol{J}^{(\Theta)} \cdot \nabla \nu_\Theta + \boldsymbol{J}^{(S)} \cdot \nabla \nu_S = \rho^{-1}\, \boldsymbol{J}^{(\Theta)} \cdot (\mathcal{T}\, \nabla p + \mathcal{C}\, \nabla \Theta) \quad (72.38)$$

which in turn yields the material evolution of *in situ* density due to neutral diffusion

$$\left[\frac{\mathrm{D}\rho}{\mathrm{D}t}\right]_{\text{ntrl diff}} = -\boldsymbol{J}^{(\Theta)} \cdot (\mathcal{T}\, \nabla p + \mathcal{C}\, \nabla \Theta). \quad (72.39)$$

72.3.3 Cabbeling

Consider the mixing of two seawater elements. Let the fluid elements separately have distinct Conservative Temperature and/or salinity, but equal locally referenced potential density. For a linear equation of state, whereby density is a linear function of Θ and S, then the resulting mixed fluid element has the same density as the unmixed separate elements. However, for a nonlinear equation of state, the mixed element generally has a different density. Furthermore, a property of seawater is that the density of the mixed element is greater than the unmixed elements. This densification upon mixing is a physical process known as *cabbeling* (*McDougall*, 1987b).

The sign definite nature of cabbeling (i.e., cabbeling always results in denser fluid elements after mixing) is a direct result of the geometry of the locally referenced potential density surface when viewed in Conservative Temperature and salinity space. This property in turn manifests

with the following inequality for the cabbeling parameter

$$\mathcal{C} = \frac{\partial \alpha}{\partial \Theta} + 2 \frac{\alpha}{\beta} \frac{\partial \alpha}{\partial S} - \left[\frac{\alpha}{\beta}\right]^2 \frac{\partial \beta}{\partial S} \geq 0. \tag{72.40}$$

Given the downgradient nature of the neutral diffusive fluxes, we have

$$\text{cabbeling} \equiv -\mathcal{C}\, \boldsymbol{J}^{(\Theta)} \cdot \nabla \Theta \geq 0, \tag{72.41}$$

thus providing a mathematical expression for the cabbeling source (with dimensions of density per time). That is, cabbeling results in a positive material evolution of density; i.e., density increases due to cabbeling. An increase in the density within a column of fluid results in the reduction of the sea level due to compression of the column.

72.3.4 Thermobaricity

The thermobaricity parameter

$$\mathcal{T} = \beta\, \partial_p(\alpha/\beta) \tag{72.42}$$

is nonzero due to pressure dependence of the ratio of the thermal expansion coefficient to the haline contraction coefficient. As both thermal and haline effects are present, the parameter $\mathcal{T}$ is more precisely split into two terms

$$\begin{aligned} \mathcal{T} &= \frac{\partial \alpha}{\partial p} - \frac{\alpha}{\beta} \frac{\partial \beta}{\partial p} \\ &= -\frac{\rho_{\Theta p}}{\rho} + \frac{\rho_\Theta}{\rho_S} \frac{\rho_{pS}}{\rho}. \end{aligned} \tag{72.43}$$

Thermobaricity is the common name for the sum, since pressure variations in the thermal expansion coefficient dominate those of the haline contraction coefficient. The thermal expansion coefficient generally increases as pressure increases, thus making the thermobaric parameter positive.

Since the neutral gradient of Θ need not be oriented in a special manner relative to the neutral gradient of pressure, there is no sign-definite nature to the thermobaricity source term (with units of density per time)

$$\text{thermobaricity} \equiv -\mathcal{T}\, \boldsymbol{J}^{(\Theta)} \cdot \nabla p \tag{72.44}$$

appearing in equation (72.38). Thus, thermobaricity can either increase or decrease density, depending on details of the density and fluxes. However, as noted by *McDougall and You* (1990), thermobaricity typically increases density in much of the World Ocean.

72.3.5 Comments

Griffies and Greatbatch (2012) discuss the impacts on global mean sea level from thermobaricity and cabbeling as diagnosed from an ocean model. Given that cabbeling always densifies and thermobaricity is also dominated by densification, these processes lead to a general reduction in global mean sea level. *Klocker and McDougall* (2010a), *Groeskamp et al.* (2016), and *Groeskamp et al.* (2019) diagnose cabbeling and thermobaricity from observational based measurements, with *Groeskamp et al.* (2019) also offering a more robust numerical method for performing that diagnostic calculation.

Cabbeling and thermobaricity lead to watermass transformation and associated transport of water across neutral directions. However, these processes are distinct from other mixing processes such as breaking gravity waves (Section 71.1). Namely, cabbeling and thermobarocity

arise from the transport of Θ and S by mesoscale eddies along neutral directions, which in turn is parameterized via neutral diffusion of these two active tracers. Transient mesoscale eddies impart a downscale cascade of tracer variance that is ultimately halted by irreversible molecular mixing, or microscale processes active before reaching the molecular level. This mixing is the ultimate cause for cabbeling and thermobaricity, with the overall strength of the cabbeling and thermobaricity determined by the strength of the mesoscale transport.

72.4 Salt and freshwater budgets

We specialize the kinematics of material tracers given in Section 20.4, here focusing on seawater, which we treat as a two component fluid comprised of salt and freshwater concentrations. We extend this discussion in Section 72.6 by studying the role of surface boundary salt, enthalpy, and water transports on changes in ocean buoyancy.

72.4.1 Salt and freshwater

Seawater is comprised of two material tracers: freshwater plus a suite of dissolved trace "salts". The ratio of salts is roughly constant over the World Ocean. We are thus able to make use of a single effective mass concentration known as the *salt concentration*[3]

$$\mathsf{S} = \frac{\text{mass of salt}}{\text{mass of seawater}} = \frac{\text{mass of salt}}{\text{mass of freshwater} + \text{mass of salt}} \tag{72.45}$$

to specify the amount of salt within an element of seawater. In practice oceanographers choose to work with the *salinity*,[4]

$$S = 1000\,\mathsf{S}, \tag{72.46}$$

which converts from typical salt concentrations of $\mathsf{S} = 0.035$ to a salinity of $S = 35$. The complement to salt concentration is the freshwater concentration or mass fraction for an element of seawater

$$\mathsf{F} = \frac{\text{mass of freshwater}}{\text{mass of seawater}} = \frac{\text{mass of freshwater}}{\text{mass of freshwater} + \text{mass of salt}} = 1 - \mathsf{S}. \tag{72.47}$$

Other trace matter occurs at very low concentrations so as to make seawater, in effect, a two-component fluid consisting of freshwater plus dissolved salt.[5] We here derive the mass budget for salt and freshwater as well as the associated kinematic boundary conditions.

72.4.2 Mass budgets

Following our discussion of the tracer equation in Section 20.1, the mass budget equations for an element of seawater take the form

$$\frac{\partial \rho}{\partial t} + \nabla \cdot (\rho\, \boldsymbol{v}) = 0 \qquad \text{seawater} \tag{72.48}$$

$$\frac{\partial (\rho\, \mathsf{S})}{\partial t} + \nabla \cdot (\rho\, \boldsymbol{v}\, \mathsf{S} + \boldsymbol{J}^{(\mathsf{S})}) = 0 \qquad \text{salt} \tag{72.49}$$

[3] We use the salt concentration, S, in this section to avoid 1/1000 factors needed if working with salinity, $S = 1000\,\mathsf{S}$.

[4] More precisely, the salinity, S, as defined by equation (72.46) is the *Absolute Salinity*. Absolute Salinity is distinct from the *practical salinity* determined by conductivity measurements. *IOC et al.* (2010) provides a full accounting of the theory and practice of ocean salinity.

[5] See *IOC et al.* (2010) for more discussion of the variations of salt concentration ratios over the ocean, as well as the impacts from biogeochemical tracers.

$$\frac{\partial(\rho \mathsf{F})}{\partial t} + \nabla \cdot (\rho \boldsymbol{v} \mathsf{F} + \boldsymbol{J}^{(\mathsf{F})}) = 0 \qquad \text{freshwater.} \tag{72.50}$$

Equation (72.48) is the mass budget for seawater and equation (72.49) is the mass budget for salt. The freshwater budget (72.50) is derived by subtracting the salt budget (72.49) from the seawater mass budget (72.48). Hence, only two of the three mass budget equations (72.48)-(72.50) are independent.

We make use of the barycentric velocity in the above conservation laws, where the barycentric velocity for the ocean is given by

$$\boldsymbol{v} = \mathsf{S}\, \boldsymbol{v}^{(\mathsf{S})} + \mathsf{F}\, \boldsymbol{v}^{(\mathsf{F})}. \tag{72.51}$$

The velocities $\boldsymbol{v}^{(\mathsf{S})}$ and $\boldsymbol{v}^{(\mathsf{F})}$ are, respectively, the molecular center of mass velocities for salt and freshwater within a fluid element, in which case

$$\frac{\partial \mathsf{S}}{\partial t} + \boldsymbol{v}^{(\mathsf{S})} \cdot \nabla \mathsf{S} = 0 \qquad \text{and} \qquad \frac{\partial \mathsf{F}}{\partial t} + \boldsymbol{v}^{(\mathsf{F})} \cdot \nabla \mathsf{F} = 0. \tag{72.52}$$

Furthermore, the fluxes $\boldsymbol{J}^{(\mathsf{S})}$ and $\boldsymbol{J}^{(\mathsf{F})}$ arise from the difference between the salt and freshwater velocities from the barycentric velocity

$$\boldsymbol{J}^{(\mathsf{S})} = \rho \mathsf{S} \, (\boldsymbol{v}^{(\mathsf{S})} - \boldsymbol{v}) \qquad \text{and} \qquad \boldsymbol{J}^{(\mathsf{F})} = \rho \mathsf{F} \, (\boldsymbol{v}^{(\mathsf{F})} - \boldsymbol{v}). \tag{72.53}$$

These fluxes are often parameterized by downgradient diffusive fluxes

$$\boldsymbol{J}^{(\mathsf{S})} = -\rho \boldsymbol{K} \cdot \nabla \mathsf{S} \qquad \text{and} \qquad \boldsymbol{J}^{(\mathsf{F})} = -\rho \boldsymbol{K} \cdot \nabla \mathsf{F}, \tag{72.54}$$

where $\boldsymbol{K}$ is the kinematic diffusivity tensor for salt in seawater, which is a positive definite symmetric tensor. We use the same diffusivity tensor for salt and freshwater since the diffusion of one is balanced by the other. When concerned with molecular processes, the diffusivity tensor is isotropic with diffusivities set by the molecular value of 10^{-9} m^2 s^{-1}. However, as discussed in Section 71.1, the eddy diffusivity is far larger than the molecular diffusivity in the presence of turbulent eddy processes, which also introduces anisotropies to the diffusion tensor.

The advective flux of seawater is comprised of a salt flux plus a freshwater flux

$$\rho \boldsymbol{v} = \rho \mathsf{S}\, \boldsymbol{v}^{(\mathsf{S})} + \rho \mathsf{F}\, \boldsymbol{v}^{(\mathsf{F})}. \tag{72.55}$$

Conversely, the salt flux and freshwater flux can be represented as a *non-advective flux* plus an advective flux where advection is defined by the barycentric velocity

$$\rho \mathsf{S}\, \boldsymbol{v}^{(\mathsf{S})} = \rho \mathsf{S} \, (\boldsymbol{v}^{(\mathsf{S})} - \boldsymbol{v}) + \rho \mathsf{S}\, \boldsymbol{v} = \boldsymbol{J}^{(\mathsf{S})} + \rho \mathsf{S}\, \boldsymbol{v} \tag{72.56a}$$

$$\rho \mathsf{F}\, \boldsymbol{v}^{(\mathsf{F})} = \rho \mathsf{F} \, (\boldsymbol{v}^{(\mathsf{F})} - \boldsymbol{v}) + \rho \mathsf{F}\, \boldsymbol{v} = \boldsymbol{J}^{(\mathsf{F})} + \rho \mathsf{F}\, \boldsymbol{v}. \tag{72.56b}$$

The non-advective fluxes, $\boldsymbol{J}^{(\mathsf{S})}$ and $\boldsymbol{J}^{(\mathsf{F})}$, lead to an exchange of mass with zero net movement of mass. In contrast, the advective flux moves mass as determined by the barycentric velocity. Furthermore, note that the center of mass velocities, $\boldsymbol{v}^{(\mathsf{S})}$ and $\boldsymbol{v}^{(\mathsf{F})}$, offer a conceptual framework of use to formulate the kinematic boundary conditions. Even so, they offer no new information beyond that contained in the fluxes $\boldsymbol{J}^{(\mathsf{S})}$ and $\boldsymbol{J}^{(\mathsf{F})}$.

72.5 Surface boundary conditions for S and Θ

In this section we summarize the surface boundary conditions holding for the salinity and Conservative Temperature equations. This treatment complements that given in Section 20.4.3.

72.5.1 Salt and freshwater

In deriving the boundary condition (20.83) in Section 19.6.3, we made use of the barycentric velocity, $\boldsymbol{v}$, for an element of seawater. We can garner further kinematic insights into the two-component ocean system by decomposing the total mass flux into contributions from salt and freshwater

$$\mathcal{Q}_{\mathsf{m}} = \mathcal{Q}_{\mathsf{S}} + \mathcal{Q}_{\mathsf{F}}, \tag{72.57}$$

and by introducing the center of mass velocities for salt and freshwater according to

$$\begin{aligned}
-\mathcal{Q}_{\mathsf{m}} &= \rho\,(\boldsymbol{v} - \boldsymbol{v}^{(\eta)}) \cdot \hat{\boldsymbol{n}} && \text{(72.58a)}\\
&= \rho\,[\mathsf{S}\,\boldsymbol{v}^{(\mathsf{S})} + \mathsf{F}\,\boldsymbol{v}^{(\mathsf{F})} - \boldsymbol{v}^{(\eta)}] \cdot \hat{\boldsymbol{n}} && \text{(72.58b)}\\
&= \rho\,[\mathsf{S}\,(\boldsymbol{v}^{(\mathsf{S})} - \boldsymbol{v}^{(\eta)} + \boldsymbol{v}^{(\eta)}) + \mathsf{F}\,\boldsymbol{v}^{(\mathsf{F})} - \boldsymbol{v}^{(\eta)}] \cdot \hat{\boldsymbol{n}} && \text{(72.58c)}\\
&= \mathsf{S}\,\rho\,(\boldsymbol{v}^{(\mathsf{S})} - \boldsymbol{v}^{(\eta)}) \cdot \hat{\boldsymbol{n}} + (1-\mathsf{S})\,\rho\,(\boldsymbol{v}^{(\mathsf{F})} - \boldsymbol{v}^{(\eta)}) \cdot \hat{\boldsymbol{n}} && \text{(72.58d)}\\
&= \mathsf{S}\,\rho\,(\boldsymbol{v}^{(\mathsf{S})} - \boldsymbol{v}^{(\eta)}) \cdot \hat{\boldsymbol{n}} + \mathsf{F}\,\rho\,(\boldsymbol{v}^{(\mathsf{F})} - \boldsymbol{v}^{(\eta)}) \cdot \hat{\boldsymbol{n}} && \text{(72.58e)}\\
&\equiv -(\mathcal{Q}_{\mathsf{S}} + \mathcal{Q}_{\mathsf{F}}), && \text{(72.58f)}
\end{aligned}$$

where we wrote

$$\begin{aligned}
\mathsf{S}\,\rho\,(\boldsymbol{v}^{(\mathsf{S})} - \boldsymbol{v}^{(\eta)}) \cdot \hat{\boldsymbol{n}} &= -\mathcal{Q}_{\mathsf{S}} && \text{(72.59a)}\\
\mathsf{F}\,\rho\,(\boldsymbol{v}^{(\mathsf{F})} - \boldsymbol{v}^{(\eta)}) \cdot \hat{\boldsymbol{n}} &= -\mathcal{Q}_{\mathsf{F}}. && \text{(72.59b)}
\end{aligned}$$

In these equations, we introduced the velocity, $\boldsymbol{v}^{(\eta)}$, of a point fixed to the free surface. We only need the projection of this velocity in the outward normal direction, which is written by equation (19.92)

$$\boldsymbol{v}^{(\eta)} \cdot \hat{\boldsymbol{n}} = \frac{\partial\eta/\partial t}{|\nabla(z-\eta)|} = \frac{\partial\eta/\partial t}{\sqrt{1+|\nabla\eta|^2}} \Longrightarrow \boldsymbol{v}^{(\eta)} \cdot \hat{\boldsymbol{n}}\, \mathrm{d}\mathcal{S} = \partial_t \eta\, \mathrm{d}A, \tag{72.60}$$

where $\mathrm{d}\mathcal{S}$ is the area element on the free surface and $\mathrm{d}A$ is its horizontal projection. Note that in many regions, the ocean surface is impermeable to salt, in which case the ocean surface acts as a material surface in terms of the salt velocity

$$\rho\,(\boldsymbol{v}^{(\mathsf{S})} - \boldsymbol{v}^{(\eta)}) \cdot \hat{\boldsymbol{n}} = 0 \qquad \text{zero surface salt flux.} \tag{72.61}$$

The key exception to this boundary condition concerns sea ice, whereby salt is exchanged between liquid seawater and sea ice upon the melting or freezing of ice.

For most applications, it is preferable to make use of equation (72.56a) to eliminate the salt velocity $\boldsymbol{v}^{(\mathsf{S})}$ in favor of the non-advective flux $\boldsymbol{J}^{(\mathsf{S})} = \rho\,\mathsf{S}\,(\boldsymbol{v}^{(\mathsf{S})} - \boldsymbol{v})$, in which case the kinematic boundary condition (72.59a) takes the form

$$-\mathcal{Q}_{\mathsf{S}} = \mathsf{S}\,\rho\,(\boldsymbol{v}^{(\mathsf{S})} - \boldsymbol{v}^{(\eta)}) \cdot \hat{\boldsymbol{n}} = \mathsf{S}\,\rho\,(\boldsymbol{v}^{(\mathsf{S})} - \boldsymbol{v} + \boldsymbol{v} - \boldsymbol{v}^{(\eta)}) \cdot \hat{\boldsymbol{n}} = \boldsymbol{J}^{(\mathsf{S})} \cdot \hat{\boldsymbol{n}} - \mathsf{S}\,\mathcal{Q}_{\mathsf{m}}. \tag{72.62}$$

Turning this equation around leads to the non-advective flux

$$\boldsymbol{J}^{(\mathsf{S})} \cdot \hat{\boldsymbol{n}} = \mathsf{S}\,\mathcal{Q}_{\mathsf{m}} - \mathcal{Q}_{\mathsf{S}} = \mathsf{S}\,\mathcal{Q}_{\mathsf{F}} - \mathsf{F}\,\mathcal{Q}_{\mathsf{S}}, \tag{72.63}$$

which relates the mass transport crossing the ocean surface at $z = \eta$ (right hand side) to the non-advective salt transport on the ocean side of the surface boundary (left hand side). A form of this equation was also given by equation (20.85). To support intuition and to check signs, consider the case with $\mathcal{Q}_{\mathsf{S}} = 0$ so that $\boldsymbol{J}^{(\mathsf{S})} \cdot \hat{\boldsymbol{n}} = \mathsf{S}\,\mathcal{Q}_{\mathsf{F}}$. This expression means there is an upward non-advective flux of salt ($\boldsymbol{J}^{(\mathsf{S})} \cdot \hat{\boldsymbol{n}} > 0$) on the ocean side of the $z = \eta$ boundary in the presence of an input of freshwater through the ocean surface ($\mathsf{S}\,\mathcal{Q}_{\mathsf{F}} > 0$). For the converse, let $\mathcal{Q}_{\mathsf{F}} = 0$ so

that $\boldsymbol{J}^{(\mathsf{S})} \cdot \hat{\boldsymbol{n}} = -\mathsf{F}\, \mathcal{Q}_{\mathsf{S}}$. Now, there is a downward non-advective flux of salt ($\boldsymbol{J}^{(\mathsf{S})} \cdot \hat{\boldsymbol{n}} < 0$) on the ocean side of the $z = \eta$ boundary in the presence of salt input through the ocean surface ($\mathsf{F}\, \mathcal{Q}_{\mathsf{S}} > 0$).

72.5.2 The non-advective salt flux boundary condition

The above properties of boundary mass transfer result from the kinematic property of a fluid element whose mass is constant, and so the transfer of freshwater across the boundary of a fluid element is compensated by an opposite transfer of salt. The ocean boundary interface acts as a boundary for the fluid elements adjacent to the surface. Hence, to move mass across the $z = \eta$ interface requires mass to be replenished to the surface fluid elements.

Diffusive closure for the non-advective flux

Consider an ocean without any mixing, such as for a perfect fluid. In this case, mass arriving to the ocean surface from $\mathcal{Q}_{\mathsf{m}} > 0$ will not be incorporated into the ambient ocean fluid, but instead will form a separate unmixed surface lens. When mass is exchanged across the ocean surface, mixing is required to incorporate the mass into the ambient ocean fluid. To determine the level of mixing, assume that $\boldsymbol{J}^{(\mathsf{S})}$ takes the form of a diffusive flux (72.54) so that the boundary condition (72.63) becomes

$$\boldsymbol{J}^{(\mathsf{S})} \cdot \hat{\boldsymbol{n}} = -\rho\, [\boldsymbol{K} \cdot \nabla \mathsf{S}] \cdot \hat{\boldsymbol{n}} = \mathsf{S}\, \mathcal{Q}_{\mathsf{m}} - \mathcal{Q}_{\mathsf{S}} = \mathsf{S}\, \mathcal{Q}_{\mathsf{F}} - F\, \mathcal{Q}_{\mathsf{S}}. \tag{72.64}$$

This equation sets the level of diffusion on the ocean side of the surface boundary that is needed to generate the non-advective transport. The diffusive mixing of salt and freshwater mediate the transfer of mass across the ocean surface so to incorporate that mass into the ambient ocean fluid. For example, freshwater added to the ocean ($\mathcal{Q}_{\mathsf{F}} > 0$) diffuses downward as salt diffuses upward toward the surface.

Salt dissolved within the mass transport

In the case when salt is transported across the ocean boundary, as occurs with sea ice melting and formation, it does so largely dissolved in the water that is transported. There can also be a non-advective transport, such as via parameterized turbulent fluxes, so that the net salt flux is given by

$$\mathcal{Q}_{\mathsf{S}} = S_{\mathsf{m}}\, \mathcal{Q}_{\mathsf{m}} + \mathcal{Q}_{\mathsf{S}}^{\text{non-adv}}. \tag{72.65}$$

If there are more sources of this transfer then a relation such as this holds for each process. We are thus led to the net salt flux

$$\mathcal{Q}_{\mathsf{S}} = -[\rho\, \mathsf{S}\, (\boldsymbol{v} - \boldsymbol{v}^{(\eta)}) + \boldsymbol{J}^{(\mathsf{S})}] \cdot \hat{\boldsymbol{n}} = \mathsf{S}\, \mathcal{Q}_{\mathsf{m}} - \boldsymbol{J}^{(\mathsf{S})} \cdot \hat{\boldsymbol{n}} = S_{\mathsf{m}}\, \mathcal{Q}_{\mathsf{m}} + \mathcal{Q}_{\mathsf{S}}^{\text{non-adv}}. \tag{72.66}$$

which leads to the non-advective salt flux on the ocean side of the boundary

$$-\boldsymbol{J}^{(\mathsf{S})} \cdot \hat{\boldsymbol{n}} = \mathcal{Q}_{\mathsf{S}}^{\text{non-adv}} + (S_{\mathsf{m}} - \mathsf{S})\, \mathcal{Q}_{\mathsf{m}}. \tag{72.67}$$

Figure 72.1 provides a schematic summary of the salt flux boundary condition. Furthermore, note that this boundary condition is consistent with that derived in Section 20.4.3 for a general tracer, in particular with equation (20.82).

Treatment in observational analyses and numerical models

In ocean climate modeling applications, the salt mass flux, $\mathcal{Q}_{\mathsf{S}}$, typically does not affect the kinematic boundary conditions. This approximation is reasonable given that the dominant

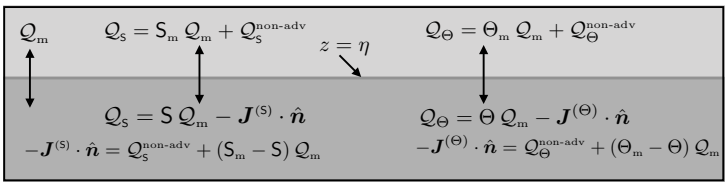

FIGURE 72.1: A schematic of an infinitesimal region of the ocean surface boundary at $z = \eta(x, y, t)$, with $z < \eta$ the ocean. $\mathcal{Q}_m\, dS = Q_m\, dA$ is the mass transport (mass per time) that crosses the interface and carries a tracer concentration. We depict the case for salt concentration, S, and Conservative Temperature, Θ, and the expressions for their net boundary fluxes. These boundary conditions are derived in Section 72.5.2 for salinity and Section 72.5.3 for Conservative Temperature.

contributor to the mass flux, $\mathcal{Q}_m$, is the freshwater. Even so, there remains a net salt transported across the ocean surface in the presence of sea ice melt and formation. The above boundary conditions, in particular equations (72.66) and (72.67), remain unchanged. Furthermore, it is necessary to specify the boundary tracer concentration, $S(z = \eta)$. For salt, this value is typically set equal to that within the ocean model surface grid cell. This choice is also common for observation-based studies.

72.5.3 Conservative Temperature boundary condition

Conservative Temperature, potential temperature, potential vorticity, and passive tracers each satisfy the tracer equation (72.49), with distinct tracer flux vectors $\boldsymbol{J}$. However, they are not material tracers and so the kinematic constraints holding for salt do not hold for these other tracers. We describe the thermodynamic properties of Conservative Temperature in Section 26.11 and the processes affecting its boundary fluxes in Section 72.6. Here we begin our treatment of this tracer by outlining its surface boundary condition.

As per the general discussion in Section 20.4.3, the net surface boundary flux of Conservative Temperature is written

$$\mathcal{Q}_\Theta = \Theta_m\,\mathcal{Q}_m + \mathcal{Q}_\Theta^{\text{non-adv}} = -[\rho\,\Theta\,(\boldsymbol{v} - \boldsymbol{v}^{(\eta)}) + \boldsymbol{J}^{(\Theta)}] \cdot \hat{\boldsymbol{n}} = \Theta\,\mathcal{Q}_m - \boldsymbol{J}^{(\Theta)} \cdot \hat{\boldsymbol{n}}. \tag{72.68}$$

In this equation, $\mathcal{Q}_\Theta^{\text{non-adv}}$ arises from the non-advective enthalpy fluxes outside the ocean domain that impact on the upper ocean interface, such as from radiant and turbulent fluxes, whereas Θ_m is the Conservative Temperature of the boundary mass flux. Rearrangement leads to the net expression for the non-advective flux on the ocean side of the upper ocean boundary

$$-\boldsymbol{J}^{(\Theta)} \cdot \hat{\boldsymbol{n}} = \mathcal{Q}_\Theta^{\text{non-adv}} + (\Theta_m - \Theta)\,\mathcal{Q}_m, \tag{72.69}$$

where $\Theta = \Theta(z = \eta)$ is the Conservative Temperature at the surface interface. A common assumption made for models and observational studies is to set $\Theta_m - \Theta(z = \eta) = 0$, in which case

$$-\boldsymbol{J}^{(\Theta)} \cdot \hat{\boldsymbol{n}} = \mathcal{Q}_\Theta^{\text{non-adv}} \quad \text{if} \quad \Theta_m = \Theta(z = \eta). \tag{72.70}$$

Figure 72.1 provides a schematic summary of the Θ flux boundary condition.

72.5.4 Comments and further reading

We make use of many results from this section when discussing surface ocean buoyancy fluxes in Section 72.6 and water mass transformation in Section 73.6. Furthermore, *Nurser and Griffies* (2019) offer further discussion of the kinematic boundary condition for salt and freshwater, with that paper motivated by questions related to water mass transformation considered in Section 73.6.

72.6 Surface boundary fluxes of buoyancy

As introduced in Chapter 30, buoyancy measures the gravitational acceleration of a fluid element relative to that of the fluid environment surrounding the element. A reduction in density for the fluid element is associated with an increase in buoyancy; that is, the fluid element becomes more *buoyant*. Changes in buoyancy arise through changes in density associated with temperature and salinity changes, with buoyancy changes computed relative to a fixed pressure level. In this way, buoyancy changes are directly related to processes that impact locally referenced potential density through changes in the temperature and salinity of a fluid element.

In this section we derive the equation describing the changes in ocean buoyancy due to enthalpy (commonly referred to as "heat"), salt, and water fluxes crossing the ocean surface boundary. For this purpose, we expose certain of the issues associated with coupling numerical models of the ocean, atmosphere, and land. A detailed treatment of boundary layer physics is well outside of our scope. We thus take a phenomenological perspective, developing budget equations but not diving into details of the turbulent exchange of matter and enthalpy across the ocean surface boundary. Similar, though simpler, considerations holds for the ocean bottom boundary, with this an insulating and material boundary except in regions of geothermal fluxes.

72.6.1 Outlining the surface boundary fluxes of enthalpy and salt

Broadly, the surface boundary fluxes are associated with the following physical processes.

- Turbulent processes transfer enthalpy through latent and sensible heating.
- Longwave radiation cools the upper ocean, with this radiation affected by the upper ocean skin temperature.
- Penetrative shortwave radiation is absorbed in seawater and so increases buoyancy in regions where the thermal expansion coefficient is positive.[6]
- All of the above processes are referred to as *non-advective* transports in that they are not associated with a net mass transport across the ocean surface. In contrast, advective processes transfer enthalpy and salt across the ocean surface through the transfer of mass.
- Salt is transferred between the liquid ocean and sea ice when sea ice melts and forms. This transfer is proportional to the water mass flux and the difference in salinity between the liquid ocean and solid sea ice. There may be additional turbulent salt fluxes as well, but there is a negligible transfer of salt associated with precipitation, evaporation, or river runoff.

72.6.2 Evolution from surface boundary fluxes

We now develop finite volume budget equations for potential enthalpy (via Conservative Temperature, Θ), salt, and seawater mass for a grid cell region next to the ocean surface, with a focus on contributions due to surface boundary fluxes. For that purpose, introduce the following quantities for a grid cell,

$$M = \int_{\text{cell}} \rho \, \mathrm{d}V = \langle \rho \rangle \, V \qquad V = \int_{\text{cell}} \mathrm{d}V = A \, \overline{h} \qquad A = \int_{\text{cell}} \mathrm{d}A \tag{72.71a}$$

$$\overline{h} \, A = \int_{\text{cell}} \left[\int_{\text{cell}} \mathrm{d}z \right] \mathrm{d}A \qquad \langle C \rangle \, M = \int_{\text{cell}} C \, \rho \, \mathrm{d}V, \tag{72.71b}$$

[6] The Baltic Sea is an outlier in the World Ocean, whose fresh and cold waters often realize a negative thermal expansion so that heating can increase density rather than reduce it.

so that $\langle \rho \rangle$ is the cell averaged density, $\langle C \rangle$ is the cell averaged tracer concentration, $\overline{h}$ is the cell area averaged thickness, V is the cell volume, and A is the cell horizontal area. These definitions allow us to write

$$\frac{\mathrm{d}}{\mathrm{d}t}\left[\int_{\text{cell}} \rho\, C\, \mathrm{d}V\right] = \frac{\mathrm{d}}{\mathrm{d}t}\left[\langle C \rangle\, M\right] = A\, \frac{\mathrm{d}}{\mathrm{d}t}\left[\overline{h}\, \langle C \rangle\, \langle \rho \rangle\right], \tag{72.72}$$

where the horizontal area of a cell is assumed to be constant in time and that the cell is bounded by vertical side walls. The surface boundary fluxes have similar grid cell area averages.

Focusing just on contributions from surface boundary transport leads to the budget equations

$$\partial_t(\rho\, h\, \Theta) = Q_{\mathsf{m}}\, \Theta_{\mathsf{m}} + Q_{\Theta}^{\text{non-adv}} \tag{72.73a}$$

$$\partial_t\,(\rho\, h\, S) = Q_{\mathsf{m}}\, S_{\mathsf{m}} + Q_{\mathsf{S}}^{\text{non-adv}} \tag{72.73b}$$

$$\partial_t\,(\rho\, h) = Q_{\mathsf{m}}, \tag{72.73c}$$

where we used a partial time derivative since we are holding the horizontal position fixed. Furthermore, we reduced notational clutter by dropping the angle brackets for volume average and the horizontal overline for area average. For a three-dimensional budget, the right hand side to these equations is combined with fluxes crossing interior cell boundaries. Finally, we wrote the fluxes as

$$Q_{\mathsf{m}}\, A = \mathcal{Q}_{\mathsf{m}}\, \mathcal{S} \quad \text{and} \quad Q_{\Theta}^{\text{non-adv}}\, A = \mathcal{Q}_{\Theta}^{\text{non-adv}}\, \mathcal{S} \quad \text{and} \quad Q_{\mathsf{S}}^{\text{non-adv}}\, A = \mathcal{Q}_{\mathsf{S}}^{\text{non-adv}}\, \mathcal{S}, \tag{72.74}$$

where $\mathcal{S}$ is the area on the free surface and A is the corresponding horizontal area of the grid cell.[7]

72.6.3 Buoyancy tendency from surface fluxes

For many purposes, it is of interest to quantify the impacts on ocean buoyancy arising from surface boundary fluxes. For that purpose, we here develop the budget for buoyancy in a surface model grid cell region, focusing on surface flux contributions.

Buoyancy has a local time tendency given by

$$-\frac{\rho_o}{g}\, \frac{\partial b}{\partial t} = \rho_\Theta\, \frac{\partial \Theta}{\partial t} + \rho_S\, \frac{\partial S}{\partial t}, \tag{72.75}$$

where we introduced the shorthand

$$\rho_\Theta = \left[\frac{\partial \rho}{\partial \Theta}\right]_{S,p} \qquad \text{and} \qquad \rho_S = \left[\frac{\partial \rho}{\partial S}\right]_{\Theta,p} \tag{72.76}$$

for the partial derivatives of density with respect to Conservative Temperature and salinity, respectively, each with pressure held constant. We wish to form an evolution equation for buoyancy at the ocean surface grid cell just due to the effects of surface forcing. For this purpose, multiply the temperature equation (72.73a) by ρ_Θ and add to the salinity equation (72.73b) multiplied by ρ_S

$$\rho_\Theta\left[\frac{\partial(\rho\, h\, \Theta)}{\partial t}\right] + \rho_S\left[\frac{\partial(\rho\, h\, S)}{\partial t}\right] = Q_{\mathsf{m}}\,(\rho_\Theta\, \Theta_{\mathsf{m}} + \rho_S\, S_{\mathsf{m}}) + \rho_\Theta\, Q_{\Theta}^{\text{non-adv}} + \rho_S\, Q_{\mathsf{S}}^{\text{non-adv}}. \tag{72.77}$$

Now use the mass budget (72.73c) and introduce the buoyancy tendency according to equation

[7] The surface area, $\mathcal{S}$, along the $z = \eta$ boundary is not generally horizontal and it is not generally constant in time. Yet its horizontal projection, A, is time independent since we fix the horizontal positions for the vertical cell walls.

(72.75) to render an expression for the time tendency of the surface ocean buoyancy

$$-(\rho_o/g)\,\rho\,h\left[\frac{\partial b}{\partial t}\right]^{\text{surface}} = Q_m\left[\rho_\Theta\,(\Theta_m-\Theta)+\rho_S\,(S_m-S)\right]+\rho_\Theta\,Q_\Theta^{\text{non-adv}}+\rho_S\,Q_S^{\text{non-adv}}. \tag{72.78}$$

Introducing the thermal expansion and saline contraction coefficients

$$\alpha = -\frac{1}{\rho}\left[\frac{\partial \rho}{\partial \Theta}\right]_{S,p} \qquad \text{and} \qquad \beta = \frac{1}{\rho}\left[\frac{\partial \rho}{\partial S}\right]_{\Theta,p} \tag{72.79}$$

yields

$$\left[\frac{\partial b}{\partial t}\right]^{\text{surface}} = \frac{g}{\rho_o\,h}\left(Q_m\left[\alpha\,(\Theta_m-\Theta)-\beta\,(S_m-S)\right]+\alpha\,Q_\Theta^{\text{non-adv}}-\beta\,Q_S^{\text{non-adv}}\right) \tag{72.80a}$$

$$= \frac{g}{\rho_o\,h}\left(\alpha\left[Q_m\,(\Theta_m-\Theta)+Q_\Theta^{\text{non-adv}}\right]-\beta\left[Q_m\,(S_m-S)+Q_S^{\text{non-adv}}\right]\right). \tag{72.80b}$$

In regions where the thermal expansion coefficient is positive ($\alpha > 0$), adding a boundary mass ($Q_m > 0$) that has $\Theta_m > \Theta$ increases the buoyancy of the surface ocean; i.e., adding relatively warm water increases surface ocean buoyancy. Likewise, where the haline contraction coefficient is positive ($\beta > 0$), adding boundary mass with $S_m < S$ increases buoyancy of the surface ocean; i.e., adding relatively freshwater increases surface ocean buoyancy. The same behavior holds for the turbulent fluxes, where $Q_\Theta^{\text{non-adv}} > 0$ (adding turbulent thermal energy to the ocean) increases surface ocean buoyancy whereas $Q_S^{\text{non-adv}} > 0$ (adding salt to the ocean) decreases buoyancy. Finally, note that in some contexts it is useful to take the limit as the thickness, h, becomes vanishingly small and to introduce a Dirac delta (see Chapter 7) and thus write[8]

$$\left[\frac{\partial b}{\partial t}\right]^{\text{surface}} = \frac{g\,\delta(z-\eta)}{\rho_o}\left(Q_m\left[\alpha\,(\Theta_m-\Theta)-\beta\,(S_m-S)\right]+\alpha\,Q_\Theta^{\text{non-adv}}-\beta\,Q_S^{\text{non-adv}}\right) \tag{72.81a}$$

$$= \frac{g\,\delta(z-\eta)}{\rho_o}\left(\alpha\left[Q_m\,(\Theta_m-\Theta)+Q_\Theta^{\text{non-adv}}\right]-\beta\left[Q_m\,(S_m-S)+Q_S^{\text{non-adv}}\right]\right). \tag{72.81b}$$

This form is of use when organizing processes according to interior processes and surface boundary processes, such as when considering water mass transformation analysis in Section 73.8. Also note that we encountered a similar approach when discussing potential vorticity in Section 45.7 when introducing the Dirac delta sheet formulation of the potential vorticity boundary condition. We are afforded the ability to formulate the boundary condition in this manner, so long as the boundary condition is of the Neumann type, with general considerations detailed in Section 9.4.8.

72.6.4 Comments

The buoyancy flux expression (72.80b) is of use for boundary layer parameterizations, such as the KPP scheme of *Large et al.* (1994) and *Van Roekel et al.* (2018). It is furthermore used when studying water mass transformations as reviewed by *Groeskamp et al.* (2019) and summarized in Chapter 73.

[8] From Chapter 7, we know that the Dirac delta, $\delta(z-\eta)$, has dimensions of inverse length, so that equation (72.81b) is dimensionally consistent.

72.7 Global mean sea level

In this section we consider some basic features of global mean sea level by making use of the mass budget of liquid seawater. This analysis highlights the distinction between the mass budget and the volume (sea level) budget. In particular, mass satisfies a conserved budget, so that the total ocean mass is affected only through boundary fluxes. In contrast, volume, just like buoyancy, has interior sources and sinks so that the ocean volume can change even if there are no boundary fluxes of volume.

72.7.1 Definitions and assumptions

Seawater mass is a conserved quantity so that the total liquid seawater mass, $\mathcal{M}$, changes only via boundary mass fluxes

$$\frac{d\mathcal{M}}{dt} = \mathcal{A}\, \overline{Q_m}, \tag{72.82}$$

where $\mathcal{A}$ is the ocean surface area, $\overline{Q_m}$ is the area averaged surface mass flux, and we assume there is no mass entering through the ocean bottom. The global volume of liquid seawater

$$\mathcal{V} = \mathcal{M}/\langle \rho \rangle \tag{72.83}$$

changes due to mass changes *and* changes to the global mean density, $\langle \rho \rangle$. Throughout this section we assume the surface area is constant in time, thus neglecting the relatively small changes associated with volume changes along sloping beaches. We also assume a temporally constant area averaged ocean bottom depth, $\overline{H}$. These two assumptions mean that changes in ocean volume arise just from changes in global mean sea level, $\overline{\eta}$. Since around the year 2000, measurements estimate that global area mean sea level has increased at a rate of

$$\left[\frac{d\overline{\eta}}{dt}\right]_{\text{observed}} \approx 3 \text{ mm yr}^{-1}, \tag{72.84}$$

and that this rate is increasing (positive sea level acceleration). As part of the analysis in this section we make use of the following phenomenological numbers and make a few assumptions to facilitate calculations.

- global seawater volume $\mathcal{V} \approx 1.3 \times 10^{18}$ m^3
- global ocean surface area $\mathcal{A} \approx 3.6 \times 10^{14}$ m^2
- global ocean mean density $\langle \rho \rangle \approx 1035$ kg m^{-3}
- specific heat capacity for seawater $c_p \approx 3992$ J kg^{-1}K^{-1}
- Ignore mass fluxes transported through the sea floor, which are small relative to surface mass fluxes.
- Ignore salinity and pressure effects on density, so that changes in global mean density arise just from changes in global mean Conservative Temperature.
- Assume a constant thermal expansion coefficient

$$\alpha = -\frac{1}{\rho}\left[\frac{\partial \rho}{\partial \Theta}\right]_{S,p} \approx 2 \times 10^{-4} \text{ K}^{-1}. \tag{72.85}$$

  This is not a great approximation, since the thermal expansion coefficient ranges over the ocean by a factor of 10. Nonetheless, for this section it is sufficient for deducing rough

numbers that are consistent with errors in measurements for global boundary enthalpy and mass fluxes.

72.7.2 Budget for global mean sea level

Expression (72.83) for ocean volume leads to its time derivative

$$\frac{\mathrm{d}\mathcal{V}}{\mathrm{d}t} = \frac{1}{\langle\rho\rangle}\frac{\mathrm{d}\mathcal{M}}{\mathrm{d}t} - \frac{\mathcal{M}}{\langle\rho\rangle^2}\frac{\mathrm{d}\langle\rho\rangle}{\mathrm{d}t} \tag{72.86a}$$

$$= \frac{\mathcal{A}\,\overline{Q_{\mathsf{m}}}}{\langle\rho\rangle} - \frac{\mathcal{V}}{\langle\rho\rangle}\frac{\mathrm{d}\langle\rho\rangle}{\mathrm{d}t}, \tag{72.86b}$$

where we used equation (72.82) to express mass changes in terms of the surface mass flux. Additionally, the ocean volume is given by

$$\mathcal{V} = \int \mathrm{d}A \int_{-H}^{\eta} \mathrm{d}z = \mathcal{A}\,(\overline{H} + \overline{\eta}), \tag{72.87}$$

so that its time changes arise from changes in the global mean sea level

$$\frac{\mathrm{d}\mathcal{V}}{\mathrm{d}t} = \mathcal{A}\,\frac{\mathrm{d}\overline{\eta}}{\mathrm{d}t}. \tag{72.88}$$

Combining the two volume equations (72.86b) and (72.88) yields the budget equation for global mean sea level

$$\frac{\mathrm{d}\overline{\eta}}{\mathrm{d}t} = \frac{\overline{Q_{\mathsf{m}}}}{\langle\rho\rangle} - \frac{\mathcal{V}}{\mathcal{A}\,\langle\rho\rangle}\frac{\mathrm{d}\langle\rho\rangle}{\mathrm{d}t}. \tag{72.89}$$

The first term arises from changes in ocean mass (increasing total mass increases sea level) whereas the second term arises from changes in global mean seawater density (increasing the mean density decreases sea level).

72.7.3 Changes due to mass input

To ground these formula in phenomenology, assume that a surface mass flux gives one-half of the observed sea level rise

$$\frac{1}{2}\left[\frac{\mathrm{d}\overline{\eta}}{\mathrm{d}t}\right]_{\text{observed}} = \frac{\overline{Q_{\mathsf{m}}}}{\langle\rho\rangle}. \tag{72.90}$$

This distribution of measured sea level is roughly correct. With $\langle\rho\rangle = 1035$ kg m^{-3} and $\mathrm{d}\overline{\eta}/\mathrm{d}t \approx 3$ mm yr^{-1}, we need an area averaged mass flux across the ocean surface

$$\overline{Q_{\mathsf{m}}} \approx 5 \times 10^{-8} \text{ kg m}^{-2}\text{ s}^{-1}. \tag{72.91}$$

Integrated over the global ocean area, this flux leads to a mass transport of

$$\mathcal{T} = \mathcal{A}\,\overline{Q_{\mathsf{m}}} \approx 1.8 \times 10^{7} \text{ kg s}^{-1} \approx 0.015 \times \mathcal{T}^{\mathsf{river}}. \tag{72.92}$$

That is, global mean sea level rises at a rate of 1.5 mm yr^{-1} if there is a net additional mass added to the ocean equal to roughly 1.5% of the net river water entering the ocean, $\mathcal{T}^{\mathsf{river}}$. This additional net mass is largely coming from the melting of land-ice in the form of mountain glaciers and ice sheets.

72.7.4 Steric changes due to changes in density

Steric effects generally refer to properties of a substance associated with the space occupied by atoms. In the sea level context, steric effects refer to changes in sea level associated with density changes, with changes in density associated with changes in the volume occupied by seawater molecules. Changes in global mean sea level arising from changes in the global mean density are called *global steric sea level changes*. From the sea level budget equation (72.89) we know that steric changes are written mathematically as

$$\left[\frac{d\overline{\eta}}{dt}\right]_{\text{steric}} \equiv -\frac{\mathcal{V}}{\mathcal{A}\,\langle\rho\rangle}\,\frac{d\langle\rho\rangle}{dt}. \tag{72.93}$$

Global mean density changes in time primarily from changes in global mean Conservative Temperature. If we assume the ocean thermal expansion is constant, then

$$\frac{1}{\langle\rho\rangle}\frac{d\langle\rho\rangle}{dt} = -\alpha\frac{d\langle\Theta\rangle}{dt}, \tag{72.94}$$

so that steric sea level changes are primarily driven by *thermosteric* effects

$$\left[\frac{d\overline{\eta}}{dt}\right]_{\text{thermosteric}} \equiv \frac{\alpha\,\mathcal{V}}{\mathcal{A}}\,\frac{d\langle\Theta\rangle}{dt}, \tag{72.95}$$

with increasing water temperature, in the presence of $\alpha > 0$, leading to higher sea levels. With $\alpha \approx 2 \times 10^{-4}$ K^{-1} and $d\overline{\eta}/dt \approx 1.5$ mm yr^{-1}, we have

$$\frac{d\langle\Theta\rangle}{dt} \approx 0.2 \text{ K century}^{-1}. \tag{72.96}$$

That is, a global thermosteric sea level rise of 1.5 mm yr^{-1} corresponds to a rate of increase in the global volume mean ocean temperature of roughly 0.2 K century^{-1}.

72.7.5 Enthalpy flux imbalances giving rise to thermosteric sea level

A global mean ocean temperature change can arise from an area averaged surface ocean enthalpy flux

$$\overline{Q_{\text{H}}} \approx \langle\rho\rangle\, c_{\text{p}}\, \overline{H}\, \frac{d\langle\Theta\rangle}{dt}, \tag{72.97}$$

with numbers leading to

$$\overline{Q_{\text{H}}} \approx 1 \text{ W m}^{-2}. \tag{72.98}$$

That is, a surface ocean enthalpy flux of roughly 1 W m^{-2} (ocean area normalized) gives rise to a global mean thermosteric sea level rise of roughly 1.5 mm yr^{-1}.

An enthalpy flux of 1 W m^{-2} is small compared to, say, that crossing the surface of a typical light bulb. However, 1 W m^{-2} is comparable to that accumulating within the earth system due to increases in greenhouse gases (*Otto et al.*, 2013). That is, 1 W m^{-2} averaged over the global ocean, or 0.7 W m^{-2} averaged over the surface area of the planet,[9] is roughly the net heating associated with anthropogenic climate change. Such seemingly small increases in surface heating represent a nontrivial increase in the earth's energy budget that are leading to the observed climate changes and sea level rise.

As specific means to gauge the magnitude of 1 W m^{-2} distributed over the ocean surface area, $\mathcal{A}$, let us compare it to the enthalpy flux due to blasting one atomic bomb per second

[9] The ocean covers roughly 70% of the earth surface. This factor is commonly forgotten when quoting heat flux numbers, so it is important to note whether the number refers to global area normalized or ocean area normalized.

($\Delta t = 1$ s) and uniformly distributing the bomb's released energy, $\mathcal{E}_{\text{bomb}}$, over the ocean surface area every second. Estimates render $\mathcal{E}_{\text{bomb}} \approx 6.3 \times 10^{13}$ J, so that distributing this energy over the ocean area, and doing so each second, corresponds to a surface ocean enthalpy flux of

$$\mathcal{Q}^{\text{bomb}} = \frac{\mathcal{E}_{\text{bomb}}}{\mathcal{A}\, \Delta t} \approx 0.17 \text{ W m}^{-2}. \tag{72.99}$$

Hence, an enthalpy flux of 1 W m^{-2} due to anthropogenic climate warming corresponds to $1/0.17 \approx 6$ atomic bomb blasts per second. This way of framing the net heating of the ocean due to anthropogenic climate change dramatically illustrates the magnitude of the global warming problem.[10]

72.7.6 Global sea level in a Boussinesq ocean

The sea level for a Boussinesq ocean evolves according to the kinematic free surface equation (21.81)

$$\partial_t \eta^{\text{bouss}} = -\nabla \cdot \boldsymbol{U} + Q_{\text{m}}/\rho_{\circ}, \tag{72.100}$$

where

$$\boldsymbol{U} = \int_{-H}^{\eta} \boldsymbol{u}\, \mathrm{d}z \tag{72.101}$$

is the depth integrated horizontal velocity and $\rho_{\circ}$ is the Boussinesq reference density. This equation results from ignoring all changes to density, except for those related to the buoyancy force appearing in the momentum equations. Integrating the sea surface height equation (72.100) over the surface area of the global ocean reveals that the global mean Boussinesq sea level evolves according to

$$\frac{\mathrm{d}\overline{\eta^{\text{bouss}}}}{\mathrm{d}t} = \frac{\overline{Q_{\text{m}}}}{\rho_{\circ}}. \tag{72.102}$$

Hence, $\overline{\eta^{\text{bouss}}}$ changes only so long as there are boundary mass fluxes. In contrast to the real ocean, the sea level computed from a Boussinesq ocean is unaffected by a surface enthalpy flux, $\overline{Q_{\text{H}}} \neq 0$. This result in turn means that we cannot use the prognostic sea surface height, η^{bouss}, level from a Boussinesq ocean model to compute changes the global mean sea level. Instead, corrections are required, as first identified by *Greatbatch* (1994) and further detailed in Appendix D of *Griffies and Greatbatch* (2012).

72.7.7 Why global halosteric sea level changes are negligible

When freshwater enters the ocean, such as from melting continental ice sheets, it adds to the ocean mass and in turn increases global mean sea level. This change is referred to as *barystatic sea level change* according to the sea level terminology paper from *Gregory et al.* (2019). Although ocean salinity changes upon changing the freshwater content, the net effect on global mean sea level is almost entirely barystatic since the global halosteric effect is negligible. We can understand why the global halosteric effect is so tiny by recognizing that freshwater entering the ocean sees its salinity increase whilst the ambient seawater is itself freshened. These compensating salinity changes (which are often mistakenly ignored) have corresponding compensating sea level changes, thus bringing the global halosteric effect to near zero.

We here summarize the two-bucket thought experiment from Appendix B of *Gregory et al.* (2019). In this experiment, one bucket holds freshwater and the other holds seawater, with the Conservative Temperature and pressures assumed to be identical for the two buckets. By

[10] Importantly, for the global warming problem it is not that industrialization is directly adding 1 W m^{-2} to the planet. Rather, increases in the concentration of greenhouse gases, caused by the burning of fossil fuels, increases the amount of solar radiation that remains within the atmosphere rather than being radiated to space.

working through this example we expose the rather tiny effects on global mean sea level arising from halosteric effects.

Formulating the change in volume

Consider two buckets containing seawater with mass M_n, volume V_n, density $\rho_n = M_n/V_n$, and salinity S_n, where $n = 1, 2$ labels the two buckets. Now fully mix the water in the two buckets, whereby the total mass, M, of seawater remains constant, as does the total mass of salt

$$M = M_1 + M_2 \quad \text{and} \quad M\,S = M_1\,S_1 + M_2\,S_2, \tag{72.103}$$

where S is the salinity of the homogenized fluid so that $M\,S$ is the total mass of salt in the combined system. Now place a mass M_1 of the homogenized fluid back in the first bucket, and a mass M_2 into the second bucket. Our goal is to compute the change in seawater volume

$$\delta V = \delta V_1 + \delta V_2. \tag{72.104}$$

In determining this volume change, we ignore pressure changes as well as changes in enthalpy associated with the heat of mixing. So the only change in volume arises from changes in the salinity.

Since the mass of each bucket remains the same before and after homogenization, then the density of seawater in each bucket changes only due to the volume changes

$$\delta\rho_n = \delta(M_n/V_n) = -(M_n/V_n^2)\,\delta V_n \Longrightarrow \delta\rho_n/\rho_n = -\delta V_n/V_n. \tag{72.105}$$

That is, the relative change in density equals to minus the relative change in volume. Now the density changes arise just from salinity changes, in which

$$\delta\rho_n/\rho_n = \beta_n\,\delta S_n, \tag{72.106}$$

where β_n is the haline contraction coefficient that measures changes in density when fixing pressure and Conservative Temperature. We are thus led to the volume change

$$\delta V = -(V_1\,\delta\rho_1/\rho_1 + V_2\,\delta\rho_2/\rho_2) = -(V_1\,\beta_1\,\delta S_1 + V_2\,\beta_2\,\delta S_2). \tag{72.107}$$

We can simplify this expression by making use of salt conservation in equation (72.103), thus constraining salinity changes according to

$$M_1\,\delta S_1 + M_2\,\delta S_2 = 0 \Longrightarrow \delta S_2 = -(M_1/M_2)\,\delta S_1, \tag{72.108}$$

in which case the volume change takes on the form

$$\delta V = -V_1\,\delta S_1\,(\beta_1 - \beta_2\,\rho_1/\rho_2). \tag{72.109}$$

The haline contraction coefficient changes only by a few percent globally (see *Roquet et al.* (2015) or Figure 1 in *Griffies et al.* (2014)), in which case we set $\beta_1 = \beta_2 = \beta$. Furthermore, to connect to sea level changes we assume the horizontal cross-sectional area of the two buckets is the same, so that the water column thickness differs between the two buckets by the amount

$$\delta h = -h_1\,\beta\,\delta S_1\,(1 - \rho_1/\rho_2). \tag{72.110}$$

Oceanographic numbers

We can compute the relative change in thickness using equation (72.110) and plugging in some numbers. Namely, we assume the first bucket is initially filled with freshwater ($S_1 = 0$) whereas the second bucket is initially filled with ambient seawater, with $S_2 = 35$ ppt a representative value. Homogenization of the two buckets then raises salinity in the first bucket and lowers it for the second. Assume the first bucket has its salinity raised to by $\delta S_1 = S/2$, let the density ratio be $\rho_1/\rho_2 = 1000/1028$, and haline contraction coefficient be $\beta = 0.8 \times 10^{-3}$. These values then yield a thickness change

$$\delta h/h_1 = -3.8 \times 10^{-4}. \tag{72.111}$$

Hence, for every meter of fresh water added to the ocean surface, the halosteric effect contributes a 0.38 mm contraction of the water thickness. That is, the total volume of homogenized water equals to the sum of the volume initially in the two separate buckets to within better than 0.04%. We conclude that the volume change is almost entirely barystatic, so that the global halosteric effect is entirely negligible when considering global sea level changes.

It is important to emphasize that this bucket thought experiment only concerns global sea level. In contrast, regional halosteric effects can be important for studies of sea level patterns, and as such they are the topic of many studies such as *Griffies et al.* (2014).

Comments on global thermosteric sea level changes

The above derivation for the global halosteric changes can be directly transferred to the case of mixing two buckets whose water has different Conservative Temperatures but identical pressure and salinity. Conservation of salt is here replaced by conservation of potential enthalpy, so that the relative thickness change is given by

$$\delta h/h_1 = \alpha\, \delta\Theta_1\, (1 - \rho_1/\rho_2), \tag{72.112}$$

where α is the thermal expansion coefficient. Taking $\alpha \approx 2 \times 10^{-4}$ K^{-1}, we find that δh from thermal effects are on the same order as those from haline effects given by equation (72.110). That is, the contributions to the column thickness are dominated by the barystatic (mass) effects.

However, there is a key distinction between thermal and haline contributions to sea level. Namely, thermal properties are also affected by boundary radiant and turbulent enthalpy fluxes that are not necessarily associated with boundary mass fluxes. These extra effects of boundary heating were studied in Section 72.7.5, where we identified the key role for ocean warming on global thermosteric sea level changes. Such changes are certainly not negligible, comparing to the observed global barystatic contributions.

72.7.8 Further study

The discussion of steric and thermosteric sea level changes are further explored in *Griffies and Greatbatch* (2012) and *Griffies et al.* (2014). The global halosteric discussion is based on Appendix B of the sea level terminology paper from *Gregory et al.* (2019). The *Gregory et al.* (2019) paper is also notable for providing a conceptual rationalization of the often confusing terminology used in sea level studies.

Chapter 73

WATER MASS TRANSFORMATION THEORY

A *water mass* refers to a region of seawater characterized by a suite of quasi-homogeneous properties used to distinguish this water from other water masses. Water masses are typically formed through surface boundary processes. As these waters enter the ocean interior they are advected over basin scales while they are also eroded or *transformed* by irreversible mixing processes. Water masses offer a conceptual means to partition or bin the ocean into distinct classes whose origin, movement, and transformation can be measured, modeled, and studied. Scalar properties generally used to classify water masses are simpler to measure than vector properties such as velocity and vorticity. Hence, a water mass perspective offers the means to infer ocean circulation within water mass space without directly measuring vector fields.

In this chapter we develop the mathematical and physical basis for *water mass transformation* theory, which considers the budgets for seawater mass and tracer mass within layers or classes defined by properties such as buoyancy, Conservative Temperature, salinity, or biogeochemical tracers. The budgets can become rather complex in appearance, given the variety of domains considered in the analysis. To reduce confusion, just remember that these equations are no more than fancy scalar budgets equations. It is through these variants of the scalar budgets, and through examining the processes affecting the budgets, that water mass transformation theory offers a novel lens for describing and understanding facets of geophysical fluid mechanics. Indeed, this lens is distinct from the Eulerian and Lagrangian kinematics considered elsewhere in this book, and it has found great use throughout oceanography and atmospheric sciences, in particular for questions where irreversible transformation is central to the story.

Readers of this chapter may appreciate the following paraphrase from A. Sommerfeld's quote. We gave it at the start of the thermodynamics part of this book (Part IV), and it seems appropriate for the study of water mass transformation.

> Water mass analysis appears somewhat mysterious and puzzling on first encounter. On second encounter things start to fall into place, except perhaps for a few pesky math niceties. On third encounter, when deciding to do calculations, one returns to that unsettled feeling of the first encounter. However, by now, familiarity with the words and maths means that the mystery presents no practical bother. One simply turns the crank without thinking too much about the underlying foundations.

In hopes of partially dispelling the mystery, and maintaining an appreciation for the fundamental processes, we here couple the mathematical equations with schematics, conceptual descriptions, and thought experiments. To do so, we work through a number of budget analysis questions with the aim to ground the theory with examples motivated from the growing literature.

CHAPTER GUIDE

Readers of this chapter should be familiar with the vector calculus encountered in Chapter 2; mass budget kinematics from Chapter 19; tracer budget kinematics from Chapter 20; elements of the generalized vertical coordinates from Chapters 63 and 64; and nearly all of the material presented earlier in this part of the book, including the mathematics and physics of advection and diffusion in Chapters 68, 69, features of parameterized tracer transport and mixing studied in Chapter 71, and buoyancy budgets in Chapter 72, including boundary conditions. Mastery of water mass transformation theory can require years of pondering the fundamentals in the pursuit of applications.

73.1 Conceptual framework

Water mass analysis is a mathematical formalism supporting the study of budgets for seawater mass and tracer mass within layers or classes defined by properties such as Archimedean buoyancy (Chapter 30; shortened to "buoyancy" here), Conservative Temperature, salinity, or biogeochemical tracers. *Water mass transformation theory* is concerned with processes affecting the evolution of fluid within layers and in the characterization of circulation inferred from this evolution. The theory is very useful for oceanography since it is common to describe seawater geography in terms of characteristic water properties, with the evolution of those water masses of primary interest to physical and biogeochemical oceanography.[1]

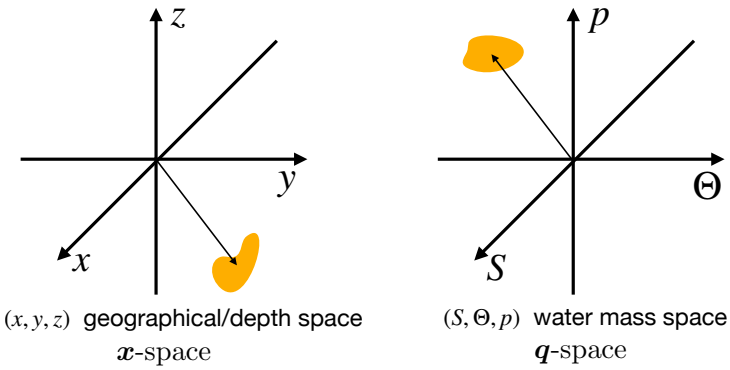

FIGURE 73.1: Left panel: a fluid element is positioned in geographical/depth $\boldsymbol{x}$-space according to its horizontal (x, y) (longitude, latitude) position and its vertical geopotential, z. Right panel: the same fluid element is positioned in a particular water mass configuration space ($\boldsymbol{q}$-space, here defined by $\boldsymbol{q} = (S, \Theta, p)$ with salinity, S, Conservative Temperature, Θ, and pressure, p. Mapping between the two spaces is generally not 1-to-1. Namely, a point in $\boldsymbol{q}$-space can be occupied by more than one point in $\boldsymbol{x}$-space. The reason is that more than a single point in $\boldsymbol{x}$-space can have the same values for (S, Θ, p). Although the coordinate axes in $\boldsymbol{q}$-space are depicted here as mutually orthogonal, there is no objective means to determine angles in $\boldsymbol{q}$-space since it contains no metric. Rather, $\boldsymbol{q}$-space, just like thermodynamic state space (Section 22.1.4), forms a *differentiable manifold* that has no metric.

73.1.1 The novel lens of water mass configuration space

Water mass configuration space (denoted $\boldsymbol{q}$-space) is the space we work within to study water mass transformations. This space has some or all of its coordinates set by properties other than geographic/depth coordinates.[2] For example, in Figure 73.1 we present the three-dimensional $\boldsymbol{q}$-space given by $\boldsymbol{q} = (S, \Theta, p)$, where the position (or bin) for a fluid element is determined by its Conservative Temperature, Θ, salinity, S, and pressure, p. Operationally, we fill $\boldsymbol{q}$-space by forming histograms that result in a $\boldsymbol{q}$-space distribution of seawater properties. For example, a one-dimensional $\boldsymbol{q}$-space results from binning the ocean according to potential density, whereas

[1] Water masses often originate through extremely large buoyancy fluxes at the high latitudes that form waters such as the Antarctic Bottom Water (AABW) and North Atlantic Deep Water (NADW). *Talley et al.* (2011) provides a great place to embark on a study ocean water mass phenomenology.

[2] We prefer the term "configuration space" over the alternative "phase space", since phase space in Hamiltonian dynamics specifically refers to position and momentum coordinates (see Chapter 12). In contrast, configuration space, as used in our discussion of water masses, can be determined by most any property or geographic position.

retaining latitudinal information along with potential density renders a two-dimensional $\boldsymbol{q}$-space. Typically $\boldsymbol{q}$-space has three or fewer dimensions, given the three dimensionality of $\boldsymbol{x}$-space. There no implied constraint that any of the $\boldsymbol{q}$-space coordinates are monotonic with respect to $\boldsymbol{x}$-space. Indeed, there is no presumption that points in $\boldsymbol{q}$-space maintain a 1-to-1 relation to points in $\boldsymbol{x}$-space. For example, many points in $\boldsymbol{x}$-space may fall into a single point (or bin) within $\boldsymbol{q}$-space.

The lack of 1-to-1 mapping between water mass configuration space and geographic/depth space is a fundamental kinematic distinction from the 1-to-1 relation that holds between the Eulerian and Lagrangian descriptions of fluid motion (see Chapter 17). The lack of a 1-to-1 relation can be frustrating since circulation viewed in $\boldsymbol{q}$-space generally has incomplete $\boldsymbol{x}$-space information, whereas oceanographers wish to know where on the planet something is happening.[3] Even so, abandoning the 1-to-1 relation can be liberating since working within $\boldsymbol{q}$-space offers a framework to infer $\boldsymbol{q}$-space circulation even without measuring velocity of the fluid in geographical space. Correspondingly, ocean circulation when viewed through a water mass lens can offer understanding that complements traditional Eulerian or Lagrangian views.

Water mass configuration space generally has no metric, particularly when none of the chosen coordinates are geographical (latitude or longitude) or depth.[4] Hence, there is generally no notion of distance or angles between points in water mass configuration space. For example, what does it mean to be orthogonal in temperature-salinity space or when studying the density-binned distribution of seawater? The absence of a metric is something we have already seen when studying thermodynamic configuration space in Chapter 22 (see in particular Section 22.1.4). Mathematically, we say that both thermodynamic configuration space and water mass configuration space are *differentiable manifolds*. Even so, one commonly sees a point in thermodynamic space depicted on a diagram with orthogonal axes (e.g., pressure-volume diagrams), or a position in water mass configuration space similarly depicted with orthogonal axes as in Figure 73.1. Yet this depiction is arbitrary since there is no geometric structure afforded to such spaces since there is no metric tensor, which in turn means we cannot determine angles or orthogonality. Depictions with orthogonal axes merely satisfy a subjective desire for geometric structure when in fact there is none afforded to the manifold.[5]

73.1.2 Transformation and formation

Water moves through water mass configuration space as it is modified or *transformed* by boundary and interior ocean processes that cause water to cross surfaces defined by the chosen water mass property.[6] Stated differently, a transformation process leads to material changes in the property of a fluid element, with sources of transformation arising from mixing, solar radiation, and chemical reactions. The convergence (i.e., the local imbalance) of such transformation processes leads to the *formation* and destruction of water mass classes. As water moves through water mass configuration space we are afforded a distinct view of ocean circulation that has both direct and indirect connections to circulation in geographical/depth space. Notably, and quite trivially, we measure zero motion along a coordinate axis in water mass configuration space when the property defining that axis remains materially unchanged. For example, adiabatic and isohaline processes such as linear waves can render nontrivial motion in geographical/depth space whereas they lead to no motion in (S, Θ) space.

[3] Auxiliary methods such as the water tagging method of *Groeskamp et al.* (2014) can be used to recover some geographical information.

[4] See Section 4.1 for a discussion of the metric tensor needed to measure distance.

[5] Differential forms provide a suitable formalism for conducting calculus on a differential manifold sans a metric as detailed by *Nurser et al.* (2022). This topic is, however, outside the scope of this book.

[6] In many parts of this book the word "transformation" refers to coordinate transformations. Here, "transformation" refers to a process acting to change a seawater property; i.e., to change one or more of the $\boldsymbol{q}$-space coordinates.

If one is interested in processes that do not give rise to material changes in a fluid property, then the corresponding water mass configuration space generally offers a rather bland kinematic perspective. Furthermore, given the possible non-local $\boldsymbol{x}$-space aspects of water mass configuration space, it provides an unnatural venue to study forces and stresses acting between spatially adjacent fluid elements. Hence, the study of momentum and vorticity dynamics is better handled via Eulerian or Lagrangian kinematics. Where water mass configuration space shines is by revealing the dynamics associated with processes that affect material changes to those properties defining the water mass classes. For example, a water mass perspective has found use in framing key questions of primary interest in the Anthropocene, such as ocean buoyancy and its transformation through interior and boundary mixing, ocean heat uptake and transport, the hydrological cycle, steric sea level rise, and irreversible changes to biogeochemical properties (see *Groeskamp et al.* (2019) for a review with many references).

73.2 Buoyancy transformation and formation

Archimedean buoyancy is a common property used to distribute seawater, with Archimedean buoyancy commonly approximated by potential density (Chapter 30). In this section we introduce the notions of *transformation* and *formation* when partitioning the ocean according to density (γ) classes that locally measure buoyancy.[7] The ideas presented here extend to any scalar property used to bin the ocean fluid.

Quantitatively, the transformation of seawater refers to a measure of the mass per time of water that moves across an isosurface of one of the $\boldsymbol{q}$-space coordinates. Alternatively, a transformation refers to the movement from one $\boldsymbol{q}$-space bin to another bin within the $\boldsymbol{q}$-space distribution. For a $\boldsymbol{q}$-space containing density as one of its coordinates, we say that the transformation is positive if water moves to larger density and negative if it enters a lighter density layer. Indeed, one generally says that movement to a larger value for the water mass property refers to a positive transformation whereas the opposite motion is a negative transformation. Water mass *formation* refers to the difference in transformation across the surfaces bounding a layer, so that formation measures the change in mass of the layer. Evidently, formation is the $\boldsymbol{q}$-space convergence of transformation.

Both transformation and formation have dimensions of mass per time (or volume per time when considering Boussinesq oceans; Chapter 29) and are typically measured in Sverdrup units:

$$1 \text{ Sv} = 10^6 \text{ m}^3 \text{ s}^{-1} \qquad \text{volume-Sverdrup} \tag{73.1a}$$

$$1 \text{ Sv} = 10^9 \text{ kg s}^{-1} \qquad \text{mass-Sverdrup.} \tag{73.1b}$$

The mass-Sverdrup can be routinely used for Boussinesq fluids merely by multiplying the volume-Sverdrup by the constant Boussinesq reference density, ρ_o.

73.2.1 A three-layer thought experiment

To illustrate the concepts of transformation and formation, bin the World Ocean into density classes so that $\boldsymbol{q}$-space is just one dimensional. We thus lose all information about latitude, longitude, and depth, retaining only the information provided by γ-classes. Furthermore, partition the World Ocean into just three density layers (also called classes or bins) that are

[7] Many researchers make use of the *neutral density* coordinate defined by *Jackett and McDougall* (1997).

bounded by four density interfaces:

$$\text{light density layer} = [\gamma - \delta\gamma/2, \gamma + \delta\gamma/2] \tag{73.2a}$$
$$\text{middle density layer} = [\gamma + \delta\gamma/2, \gamma + 3\,\delta\gamma/2] \tag{73.2b}$$
$$\text{heavy density layer} = [\gamma + 3\,\delta\gamma/2, \gamma + 5\,\delta\gamma/2], \tag{73.2c}$$

where $\delta\gamma > 0$ is the size of the density bins. Figure 73.2 depicts a sample mass distribution; i.e., the mass census for seawater binned into these three density layers.[8] Now consider a physical, chemical, or biological process that results in water leaving the middle density layer and entering both the light layer and the heavy layer.[9] Let $G(\sigma)$ measure the mass per time that water crosses the density interface $\gamma = \sigma$; i.e., $G(\sigma)$ is the transformation. This particular thought experiment has the following transformations across the various layer interfaces

$$G(\sigma) = \begin{cases} 0 & \sigma = \gamma - \delta\gamma/2 \quad \text{closed boundary} \\ < 0 & \sigma = \gamma + \delta\gamma/2 \quad \text{mass moves to light density from middle density} \\ > 0 & \sigma = \gamma + 3\,\delta\gamma/2 \quad \text{mass moves from middle density to heavy density} \\ 0 & \sigma = \gamma + 5\,\delta\gamma/2 \quad \text{closed boundary.} \end{cases} \tag{73.3}$$

The difference in the transformation across the interface boundaries of a particular layer determines the formation/destruction of water in that layer. Here, the convergence of water into the light and heavy layers means that there is a positive formation of water in these two density layers. In contrast, the divergence of water from the middle density layer means there is a negative formation or a destruction of some of its water. We write these layer formations mathematically as follows

$$\text{light-formation} = -[G(\gamma + \delta\gamma/2) - G(\gamma - \delta\gamma/2)] > 0 \tag{73.4a}$$
$$\text{middle-formation} = -[G(\gamma + 3\,\delta\gamma/2) - G(\gamma + \delta\gamma/2)] < 0 \tag{73.4b}$$
$$\text{heavy-formation} = -[G(\gamma + 5\,\delta\gamma/2) - G(\gamma + 3\,\delta\gamma/2)] > 0. \tag{73.4c}$$

The minus sign out front emphasizes that the formation is the layer integrated *convergence* of the transformation.

73.2.2 How processes lead to transformations

The central focus of water mass transformation analysis is the movement of water between layers or classes, with this movement modifying the water mass distribution within the chosen water mass configuration space. Here we outline a few of the processes that affect this movement within water mass space, again focusing on buoyancy yet with an easy generalization to any other property that defines the water mass. Notably, we are not concerned with whether the fluid element moves in $\boldsymbol{x}$-space, the boundary moves, or both, since it is only the relative motion that changes the water mass distribution in $\boldsymbol{q}$-space. Indeed, we cannot determine motion of the fluid element in $\boldsymbol{x}$-space without direct information about the velocity. We return to this notion when providing a mathematical expression for these ideas in Section 73.4.1.

[8] A realistic ocean experiences boundary forcing that makes the maximum and minimum density a function of time. It is thus common to fix the lower density limit to be well below the lightest water in the ocean and the upper density limit well above the maximum density, thus ensuring that all seawater is contained by the chosen binning. We introduce such "infinity" bounds in Section 73.3.3.

[9] Since the layer is the result of binning over the World Ocean, there can be some regions within a bin that experience processes that decrease the density, whereas other regions where density increases. In this manner, some water within the bin moves to a denser bin whereas other water moves to a lighter bin.

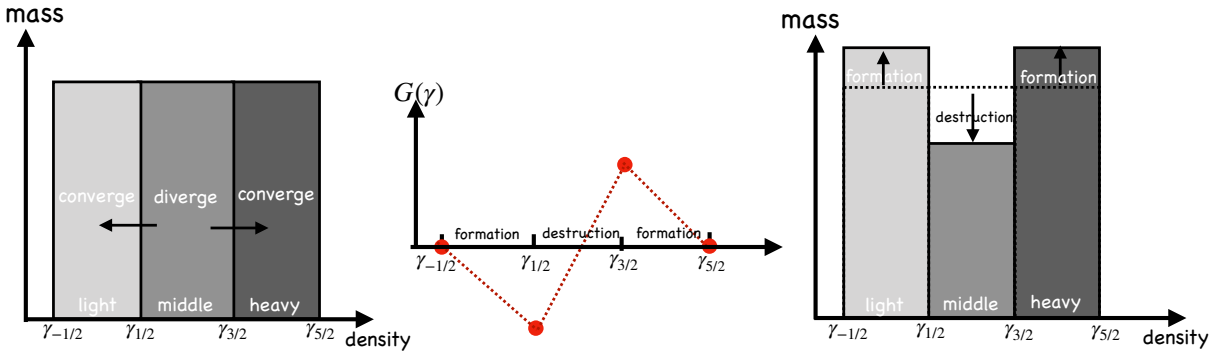

FIGURE 73.2: A sample mass distribution of the ocean binned into three density layers (light, middle, heavy) bounded by four density interfaces: $\gamma_{n/2} = \gamma + n\,\delta\gamma/2$ for $n = -1, 1, 3, 5$. The left panel depicts an ocean state with equal mass in each layer. Some process is then imagined to cause water to diverge from the middle layer and converge to the light and heavy layers. The right panel shows the mass distribution after the water has moved, so that the middle layer has experienced a negative *formation* (i.e., net loss of mass) whereas the light and heavy layers have experienced a positive *formation* (i.e., net mass gain). The middle panel depicts the *transformation*, G, which measures the mass per time moving across the layer boundaries. By convention, $G > 0$ for water moving into a heavier density layer and $G < 0$ for water entering a lighter density layer. The addition of more layers refines the picture (e.g., by smoothing the plot of G) but it does not modify the basic ideas illustrated in this thought experiment.

Interior transformation from mixing

Mixing moves water across layer boundaries in $\boldsymbol{q}$-space, with $\boldsymbol{q}$-space coordinates/properties materially modified in the presence of mixing (so long as there are spatial gradients in the property). For example, recall our discussion in Chapter 20 where as saw that mixing causes tracers to move between fluid elements even as mixing does not alter the net mass of fluid elements (see the discussion of barycentric velocity in Section 20.1.2). Hence, in the presence of mixing, seawater fluid elements retain a fixed mass, and yet the mass is redistributed among layers defined by property isosurfaces since the isosurfaces move in the presence of mixing.

Surface mass fluxes

Rain and evaporation alter the mass of the ocean. In turn, the layers where rain and evaporation occur; i.e., layers that outcrop, have their mass altered through the surface mass fluxes. Additionally, if the buoyancy of the mass flux differs from that of the ocean layer that it enters/leaves, then the buoyancy of the ocean layer is modified upon mixing the ambient seawater with the water entering the ocean.

Surface and bottom boundary transformation

Buoyancy surfaces that outcrop at the ocean surface or incrop at the ocean bottom are exposed to boundary fluxes that generally modify the buoyancy of the fluid within a layer. This modification causes the layer boundaries to move so that the mass distributed within the layers can be modified if the mass moves with a velocity distinct from the buoyancy surface. A particularly striking example occurs in the upper ocean boundary layer where surface forcing leads to the seasonal migration of density outcrops. The associated lateral movement of density layers causes water to entrain and detrain from a layer since the layer boundaries generally have a velocity distinct from fluid elements. In so doing, the seasonal cycle of surface buoyancy forcing can inflate or deflate a buoyancy layer by moving the layer boundaries so that the layer entrains or detrains mass.

Penetrative shortwave radiation provides another means to modify water masses, with penetrative radiation a function of the optical properties of the fluid. This radiation provides a

source of heating that can penetrate into the upper few tens of meters in the ocean, and can impact on the temperature and density structure of the ocean layers affected by radiation.

Finally, layers that intersect the ocean bottom are exposed to geothermal heating as well as enhanced mixing from bottom boundary layer mixing. Each of these processes affects a transformation of the buoyancy, thus modifying the buoyancy layer interfaces and mass distribution within the layers.

Interior sources and sinks

When studying water masses defined by biogeochemical tracers (e.g., carbon, oxygen, nutrients), there are a variety of chemical reactions and biological processes that act to modify these properties. These processes generally cannot be represented mathematically as the convergence of a flux. They are thus sometimes referred to as "non-conservative" processes (see Section 26.12) and written as a source/sink term.

73.3 Mathematical framework

In this section we develop a suite of mathematical tools of use to quantify the conceptual ideas presented in Sections 73.1 and 73.2. In particular, we develop a formalism for integrating properties within a region bounded by isosurfaces of a scalar field, $\lambda = \lambda(\boldsymbol{x}, t)$. The formulation is given from both a geometric perspective afforded by $\boldsymbol{x}$-space, and a complementary distributional perspective afforded by binning seawater mass according to λ-classes that define a one-dimensional $\boldsymbol{q}$-space. As in our study of Eulerian and Lagrangian kinematics elsewhere in this book, it is here useful to be adept at both the $\boldsymbol{x}$-space perspective and the distributional $\boldsymbol{q}$-space perspective.

In Section 73.2 we considered λ to be the buoyancy field, $\lambda = \gamma$, whereas here we assume it is a generic scalar field, $\lambda(\boldsymbol{x}, t)$. In contrast to the case of a generalized vertical coordinate (Chapters 63 and 64), we make no assumption regarding the stratification of λ. Rather, λ-isosurfaces are free to overturn or even to be situated in spatially disconnected regions. This freedom is motivated by the behavior of most oceanographic scalar properties, which commonly exhibit vertically unstratified or negatively stratified profiles, particularly within boundary layers. This degree of freedom comes at the cost of losing the 1-to-1 relation between $\boldsymbol{x}$-space and $\boldsymbol{q}$-space, as mentioned in Section 73.1.1.

73.3.1 Seawater mass in an infinitesimal cylinder

Consider the calculation of seawater mass within an infinitesimal λ-layer bounded by two isosurfaces, $[\lambda - \delta\lambda/2, \lambda + \delta\lambda/2]$, as in Figure 73.3. The mass within a tiny cylinder extending from one interface to the other is given by the seawater density, ρ, multiplied by the volume of the cylinder,[10]

$$\delta M = \rho \, \delta V = \rho \, \delta h \, \delta \mathcal{S}, \tag{73.5}$$

where $\delta\mathcal{S}$ is the cross-sectional area element and δh is the layer thickness. The geometric thickness, δh, is related to the differential λ-increment separating the two interfaces according to

$$\delta\lambda = \nabla\lambda \cdot \delta\boldsymbol{x} = |\nabla\lambda| \, \hat{\boldsymbol{n}} \cdot \delta\boldsymbol{x} = |\nabla\lambda| \, \delta h \qquad \text{with} \qquad \hat{\boldsymbol{n}} = \nabla\lambda \, |\nabla\lambda|^{-1}, \tag{73.6}$$

[10]Recall our notational convention is as follows: δ refers to an infinitesimal increment of a property measured within the fluid whereas d is a differential increment used for computing integrals. We made use of the same geometric analysis in Section 41.1.2 when studying potential vorticity.

where $\delta\boldsymbol{x}$ is a position vector connecting points on the two interfaces. We thus see that the layer thickness is given by

$$\delta h = \frac{\delta\lambda}{|\nabla\lambda|}, \tag{73.7}$$

which connects a geometric property of the layer, δh, to the λ-increment, $\delta\lambda > 0$. For a given λ-increment, the layer thickness is smaller with more tightly packed λ-isosurfaces as reflected by a larger $|\nabla\lambda|$. Furthermore, the geometric thickness is oriented according to the normal direction, $\hat{\boldsymbol{n}}$, so that δh measures the distance between the λ-interfaces in the direction of the normal direction. It follows that the seawater mass within the cylinder is given by

$$\delta M = \rho\,\delta V = \rho\,\delta h\,\delta\mathcal{S} = \frac{\rho\,\delta\lambda\,\delta\mathcal{S}}{|\nabla\lambda|}. \tag{73.8}$$

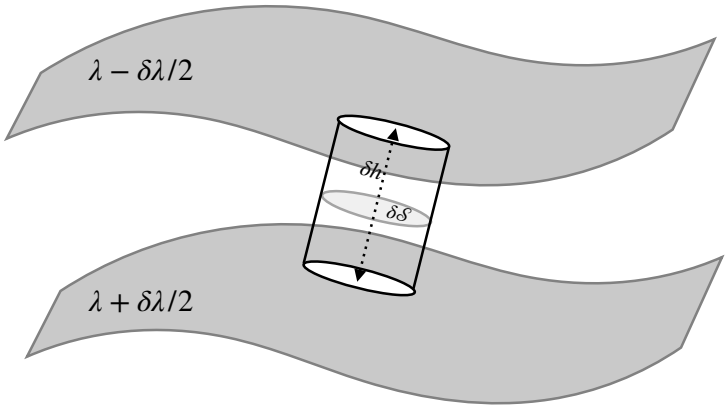

FIGURE 73.3: This schematic shows an infinitesimally thin λ-layer bounded by two interfaces $[\lambda - \delta\lambda/2, \lambda + \delta\lambda/2]$, with the λ-increment $\delta\lambda > 0$. The cylinder region extends between the two iso-surfaces and it has thickness $\delta h = \delta\lambda/|\nabla\lambda|$ and cross-sectional area $\delta\mathcal{S}$. The cylinder is oriented according to the normal direction, $\hat{\boldsymbol{n}} = |\nabla\lambda|^{-1}\,\nabla\lambda$. We assume $|\nabla\lambda| \neq 0$, as required to define a normal direction. Indeed, if $\nabla\lambda = 0$ then we could not perform a binning according to λ classes, so the $|\nabla\lambda| \neq 0$ assumption is basic to the use of the scalar field, λ, for water mass analysis.

73.3.2 Seawater mass within a finite region

Making use of the infinitesimal cylinder mass (73.8) allows us to write the mass of seawater within the λ-region $\lambda_1 \leq \lambda \leq \lambda_2$

$$M(\lambda_1, \lambda_2) \equiv \int_{\Omega(\lambda_1 \leq \lambda \leq \lambda_2)} \mathrm{d}M = \int_{\lambda_1}^{\lambda_2} \left[\int_{\partial\Omega(\lambda)} \frac{\rho\,\mathrm{d}\mathcal{S}}{|\nabla\lambda|} \right] \mathrm{d}\lambda. \tag{73.9}$$

In this equation, $\Omega(\lambda_1 \leq \lambda \leq \lambda_2)$ is the region in space bounded by the λ_1-interface and λ_2-interface, and $\partial\Omega(\lambda)$ is the surface defined by a λ-isosurface. The $\partial\Omega(\lambda)$ integral is taken over the area of the λ-isosurface, which is then integrated over the range, $\lambda_1 \leq \lambda \leq \lambda_2$, to thus accumulate the layer mass.

73.3.3 Seawater mass distribution/density function

The region bounded by the layer interfaces can have any shape in space and can even be spatially disconnected. This complexity motivates us to introduce the *mass distribution* function by

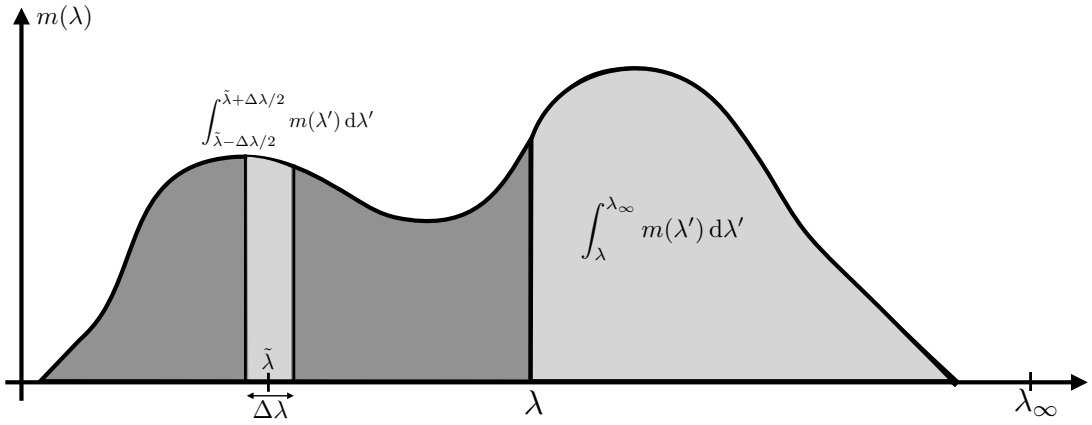

FIGURE 73.4: An example mass distribution function, $m(\lambda) = \mathrm{d}M/\mathrm{d}\lambda$, which measures the mass of seawater per λ-increment. Integration over a finite λ-region measures the seawater mass within that region. For example, the mass within a $\Delta\lambda$-layer is given by $M(\widetilde{\lambda} - \Delta\lambda/2, \widetilde{\lambda} + \Delta\lambda/2) = \int_{\widetilde{\lambda}-\Delta\lambda/2}^{\widetilde{\lambda}+\Delta\lambda/2} m(\lambda')\,\mathrm{d}\lambda'$ whereas the mass within the λ_∞-region is $M(\lambda, \lambda_\infty) = \int_{\lambda}^{\lambda_\infty} m(\lambda')\,\mathrm{d}\lambda'$, where we assume that λ_∞ is an arbitrary fixed value that is larger than any λ realized within the ocean.

integrating the mass over the surface, $\partial\Omega(\lambda)$

$$m(\lambda) \equiv \frac{\mathrm{d}M}{\mathrm{d}\lambda} = \int_{\partial\Omega(\lambda)} \frac{\rho\,\mathrm{d}\mathcal{S}}{|\nabla\lambda|}. \tag{73.10}$$

A mass distribution function is quite useful when the distribution is highly non-local in geographic/depth space. It is also effective when using multiple water mass coordinates such as Θ and S as discussed in *Nurser et al.* (2022). These points motivate leaving the $\boldsymbol{x}$-space perspective altogehter to simply define the mass distribution function so that

$$\mathrm{d}M = m(\lambda)\,\mathrm{d}\lambda = \text{fluid mass within the infinitesimal } \lambda\text{-layer } [\lambda - \mathrm{d}\lambda/2, \lambda + \mathrm{d}\lambda/2], \tag{73.11}$$

with an illustration given by Figure 73.4. The mass distribution function is the mass density within λ space; i.e., the mass per λ. Knowledge of the mass distribution function allows us to compute the seawater mass within a finite region, as in equation (73.9), according to

$$M(\lambda_1, \lambda_2) \equiv \int_{\Omega(\lambda_1 \le \lambda \le \lambda_2)} \mathrm{d}M = \int_{\lambda_1}^{\lambda_2} m(\lambda)\,\mathrm{d}\lambda. \tag{73.12}$$

73.3.4 Example regions

To help ground the previous expressions for mass, consider some example regions commonly considered in water mass analysis.

$\Delta\lambda$-layer defined by $[\lambda_1, \lambda_2] = [\lambda - \Delta\lambda/2, \lambda + \Delta\lambda/2]$

A $\Delta\lambda$-layer is defined with the bounding interface values

$$\lambda_1 = \lambda - \Delta\lambda/2 \ \text{ and } \ \lambda_2 = \lambda + \Delta\lambda/2, \tag{73.13}$$

for some finite difference increment $\Delta\lambda > 0$. In this case the layer mass is

$$M(\lambda - \Delta\lambda/2, \lambda + \Delta\lambda/2) = \int_{\lambda-\Delta\lambda/2}^{\lambda+\Delta\lambda/2} \left[\int_{\partial\Omega(\lambda')} \frac{\rho\,\mathrm{d}\mathcal{S}}{|\nabla\lambda'|} \right] \mathrm{d}\lambda' = \int_{\lambda-\Delta\lambda/2}^{\lambda+\Delta\lambda/2} m(\lambda')\,\mathrm{d}\lambda'. \tag{73.14}$$

Characterizing ocean properties according to their value of λ is generally performed by decomposing the ocean into $\Delta\lambda$-bins and forming histograms to estimate the continuous distribution.

λ_∞-region defined by $[\lambda_1, \lambda_2] = [\lambda, \lambda_\infty]$

A λ_∞-region is defined with

$$\lambda_1 = \lambda \text{ and } \lambda_2 = \lambda_\infty, \tag{73.15}$$

where λ_∞ is an arbitrary fixed constant that is larger than any value of λ realized in the ocean. The region mass is thus given by

$$M(\lambda, \lambda_\infty) = \int_{\Omega(\lambda \le \lambda_\infty)} \mathrm{d}M = \int_\lambda^{\lambda_\infty} \left[\int_{\partial\Omega(\lambda')} \frac{\rho \, \mathrm{d}\mathcal{S}}{|\nabla\lambda'|} \right] \mathrm{d}\lambda' = \int_\lambda^{\lambda_\infty} m(\lambda') \, \mathrm{d}\lambda'. \tag{73.16}$$

An example λ_∞-region is shown in Figure 73.5. The λ_∞-region as so defined provides an expression for the differential mass increment

$$M(\lambda, \lambda_\infty) = \int_\lambda^{\lambda_\infty} m(\lambda') \, \mathrm{d}\lambda' \Longrightarrow \mathrm{d}M(\lambda, \lambda_\infty) = -m(\lambda) \, \mathrm{d}\lambda, \tag{73.17}$$

which follows since λ_∞ is a constant.

The value of the fixed constant, λ_∞, is arbitrarily large, indeed it could be infinite. We can set it to an arbitrarily large constant value since there is no contribution to the integral from regions with λ' outside the range realized within the ocean, merely since there is no ocean mass in that region. As an example, let $\lambda = \Theta$, the Conservative Temperature, in which the region $\Theta \le \Theta_\infty$ encompasses the ocean region where the Conservative Temperature is larger (warmer) than Θ.

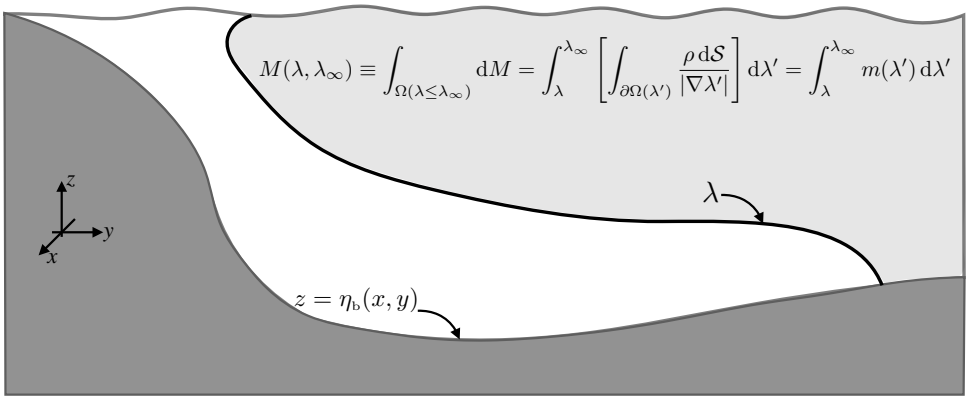

FIGURE 73.5: Depicting the mass of fluid within a λ_∞-region, where $\lambda \le \lambda_\infty$ with λ_∞ is an arbitrary constant that is larger than any value of λ in the ocean domain. This figure is oriented for the southern hemisphere with Antarctica on the left. An example of such a region is for $\lambda = \Theta$, whereby warmer waters are typically shallower and towards the equator.

$\lambda_{-\infty}$-region defined by $[\lambda_1, \lambda_2] = [\lambda_{-\infty}, \lambda]$

A $\lambda_{-\infty}$-region is defined with

$$\lambda_1 = \lambda_{-\infty} \text{ and } \lambda = \lambda, \tag{73.18}$$

where $\lambda_{-\infty}$ is an arbitrary constant that is smaller than any value of λ realized in the ocean. The region mass is thus given by

$$M(\lambda_{-\infty},\lambda) \equiv \int_{\Omega(\lambda_{-\infty}\le\lambda)} \mathrm{d}M = \int_{\lambda_{-\infty}}^{\lambda} \left[\int_{\partial\Omega(\lambda')} \frac{\rho\,\mathrm{d}\mathcal{S}}{|\nabla\lambda'|}\right] \mathrm{d}\lambda' = \int_{\lambda_{-\infty}}^{\lambda} m(\lambda')\,\mathrm{d}\lambda'. \tag{73.19}$$

This mass is the complement of that contained in the λ_∞-region. The $\lambda_{-\infty}$-region mass implies a corresponding differential mass increment via

$$M(\lambda_{-\infty},\lambda) = \int_{\lambda_{-\infty}}^{\lambda} m(\lambda')\,\mathrm{d}\lambda' \Longrightarrow \mathrm{d}M(\lambda_{-\infty},\lambda) = m(\lambda)\,\mathrm{d}\lambda. \tag{73.20}$$

$\lambda_{\pm\infty}$-region defined by $[\lambda_1,\lambda_2] = [\lambda_{-\infty},\lambda_\infty]$

The full ocean is contained in the $\lambda_{\pm\infty}$-region

$$\lambda_1 = \lambda_{-\infty} \;\text{ and }\; \lambda_2 = \lambda_\infty, \tag{73.21}$$

so that the full ocean mass is written

$$M(\lambda_{-\infty},\lambda_\infty) = \int_{\Omega(\lambda_{-\infty}\le\lambda\le\lambda_\infty)} \mathrm{d}M = \int_{\lambda_{-\infty}}^{\lambda_\infty} \left[\int_{\partial\Omega(\lambda)} \frac{\rho\,\mathrm{d}\mathcal{S}}{|\nabla\lambda|}\right] \mathrm{d}\lambda = \int_{\lambda_{-\infty}}^{\lambda_\infty} m(\lambda')\,\mathrm{d}\lambda'. \tag{73.22}$$

Difference of mass between two λ_∞-regions

The difference in mass between two λ_∞-regions is given by

$$M(\lambda_1,\lambda_\infty) - M(\lambda_2,\lambda_\infty) = \int_{\lambda_1}^{\lambda_\infty} \left[\int_{\partial\Omega(\lambda)} \frac{\rho\,\mathrm{d}\mathcal{S}}{|\nabla\lambda|}\right] \mathrm{d}\lambda - \int_{\lambda_2}^{\lambda_\infty} \left[\int_{\partial\Omega(\lambda)} \frac{\rho\,\mathrm{d}\mathcal{S}}{|\nabla\lambda|}\right] \mathrm{d}\lambda. \tag{73.23}$$

The arbitrary constant, λ_∞, drops out when taking the difference so that we are left with the mass within the intersection of the two regions

$$M(\lambda_1,\lambda_2) = M(\lambda_1,\lambda_\infty) - M(\lambda_2,\lambda_\infty) = \int_{\lambda_1}^{\lambda_2} \left[\int_{\partial\Omega(\lambda)} \frac{\rho\,\mathrm{d}\mathcal{S}}{|\nabla\lambda|}\right] \mathrm{d}\lambda = \int_{\lambda_1}^{\lambda_2} m(\lambda')\,\mathrm{d}\lambda'. \tag{73.24}$$

73.3.5 Integrals of arbitrary functions

We can extend the above formalism to integrals of an arbitrary function, $\mathcal{F}(\boldsymbol{x},t)$, over a region defined by $\lambda_{1,2}$-interfaces

$$\mathcal{G}_{\mathcal{F}}(\lambda_1,\lambda_2) \equiv \int_{\Omega(\lambda_1\le\lambda\le\lambda_2)} \mathcal{F}\,\mathrm{d}M = \int_{\lambda_1}^{\lambda_2} \left[\int_{\partial\Omega(\lambda)} \frac{\mathcal{F}\,\rho\,\mathrm{d}\mathcal{S}}{|\nabla\lambda|}\right] \mathrm{d}\lambda. \tag{73.25}$$

Performing the area integral amounts to binning the function according to λ-increments, in which case we define the distribution function

$$m_{\mathcal{F}}(\lambda) = \int_{\partial\Omega(\lambda)} \frac{\mathcal{F}\,\rho\,\mathrm{d}\mathcal{S}}{|\nabla\lambda|}, \tag{73.26}$$

so that an integral over the distribution is given by

$$\mathcal{I}_{\mathcal{F}}(\lambda_1, \lambda_2) = \int_{\lambda_1}^{\lambda_2} m_{\mathcal{F}}(\lambda)\, \mathrm{d}\lambda. \tag{73.27}$$

In particular, consider the integral over a λ_∞-region

$$\mathcal{I}_{\mathcal{F}}(\lambda, \lambda_\infty) = \int_{\lambda}^{\lambda_\infty} \left[\int_{\partial\Omega(\lambda')} \frac{\mathcal{F}\, \rho\, \mathrm{d}\mathcal{S}}{|\nabla\lambda'|} \right] \mathrm{d}\lambda' = \int_{\lambda}^{\lambda_\infty} m_{\mathcal{F}}(\lambda')\, \mathrm{d}\lambda', \tag{73.28}$$

which has the derivative

$$\frac{\partial \mathcal{I}_{\mathcal{F}}(\lambda, \lambda_\infty)}{\partial \lambda} = -\int_{\partial\Omega(\lambda)} \frac{\mathcal{F}\, \rho\, \mathrm{d}\mathcal{S}}{|\nabla\lambda|} = -m_{\mathcal{F}}(\lambda), \tag{73.29}$$

as follows from the fundamental theorem of calculus. Note how the derivative removes the reference value, λ_∞. Analogously, the integral over a $\lambda_{-\infty}$-region has the derivative

$$\frac{\partial \mathcal{I}_{\mathcal{F}}(\lambda_{-\infty}, \lambda)}{\partial \lambda} = \int_{\partial\Omega(\lambda)} \frac{\mathcal{F}\, \rho\, \mathrm{d}\mathcal{S}}{|\nabla\lambda|} = m_{\mathcal{F}}(\lambda). \tag{73.30}$$

73.3.6 Moments of λ

Setting $\mathcal{F} = \lambda$ in the integral (73.25) renders

$$\Lambda(\lambda_1, \lambda_2) \equiv \int_{\Omega(\lambda_1 \le \lambda \le \lambda_2)} \lambda\, \mathrm{d}M = \int_{\Omega(\lambda_1 \le \lambda \le \lambda_2)} \lambda\, \rho\, \mathrm{d}V = \int_{\lambda_1}^{\lambda_2} \left[\int_{\partial\Omega(\lambda)} \frac{\lambda\, \rho\, \mathrm{d}\mathcal{S}}{|\nabla\lambda|} \right] \mathrm{d}\lambda. \tag{73.31}$$

If λ is a tracer concentration (tracer mass per seawater mass), then $\Lambda(\lambda_1, \lambda_2)$ is the mass of tracer within the layer. Observe that λ can be pulled outside of the surface integral in equation (73.31) since λ is constant along $\partial\Omega(\lambda)$, thus rendering

$$\Lambda(\lambda_1, \lambda_2) = \int_{\lambda_1}^{\lambda_2} \left[\int_{\partial\Omega(\lambda)} \frac{\rho\, \mathrm{d}\mathcal{S}}{|\nabla\lambda|} \right] \lambda\, \mathrm{d}\lambda = \int_{\lambda_1}^{\lambda_2} m(\lambda)\, \lambda\, \mathrm{d}\lambda. \tag{73.32}$$

We can likewise define any higher powers as

$$\Lambda^{(n)}(\lambda_1, \lambda_2) \equiv \int_{\lambda_1}^{\lambda_2} \left[\int_{\partial\Omega(\lambda)} \frac{\rho\, \mathrm{d}\mathcal{S}}{|\nabla\lambda|} \right] \lambda^n\, \mathrm{d}\lambda = \int_{\lambda_1}^{\lambda_2} m(\lambda)\, \lambda^n\, \mathrm{d}\lambda = M(\lambda_1, \lambda_2)\, \langle \lambda^n \rangle. \tag{73.33}$$

The final equality introduced the mean value for the power

$$\langle \lambda^n \rangle = \frac{\int_{\lambda_1}^{\lambda_2} m(\lambda)\, \lambda^n\, \mathrm{d}\lambda}{\int_{\lambda_1}^{\lambda_2} m(\lambda)\, \mathrm{d}\lambda} \tag{73.34}$$

as defined over the $[\lambda_1, \lambda_2]$ region. We refer to $\langle \lambda^n \rangle$ as the n-moment of λ, with $n = 1$ yielding the mean.

73.3.7 Internal and external λ-moments

Now specify the region $[\lambda_1, \lambda_2] = [\widetilde{\lambda}, \lambda_\infty]$ for the moment equation (73.33). Making use of the differential mass increment, $\mathrm{d}M(\lambda, \lambda_\infty) = -m(\lambda)\, \mathrm{d}\lambda$ as in equation (73.17) allows us to integrate

the moment equation by parts

$$\Lambda^{(n)}(\widetilde{\lambda}, \lambda_\infty) = \int_{\widetilde{\lambda}}^{\lambda_\infty} \lambda^n \, m(\lambda) \, \mathrm{d}\lambda \tag{73.35a}$$

$$= -\int_{\widetilde{\lambda}}^{\lambda_\infty} \lambda^n \, \mathrm{d}M \tag{73.35b}$$

$$= \int_{\widetilde{\lambda}}^{\lambda_\infty} \left[-\mathrm{d}(\lambda^n \, M) + n \, M \, \lambda^{n-1} \, \mathrm{d}\lambda \right] \tag{73.35c}$$

$$= -\lambda_\infty^n \, M(\lambda_\infty, \lambda_\infty) + \lambda^n \, M(\widetilde{\lambda}, \lambda_\infty) + n \int_{\lambda}^{\lambda_\infty} M(\lambda, \lambda_\infty) \, \lambda^{n-1} \, \mathrm{d}\lambda \tag{73.35d}$$

$$= \lambda^n \, M(\widetilde{\lambda}, \lambda_\infty) + n \int_{\lambda}^{\lambda_\infty} M(\lambda, \lambda_\infty) \, \lambda^{n-1} \, \mathrm{d}\lambda, \tag{73.35e}$$

where the final equality follows since $M(\lambda_\infty, \lambda_\infty) = 0$. Making use of equation (73.33) thus leads to

$$M(\widetilde{\lambda}, \lambda_\infty) \, \langle \lambda^n \rangle = \underbrace{M(\widetilde{\lambda}, \lambda_\infty) \, \widetilde{\lambda}^n}_{\text{external moment}} + \underbrace{n \int_{\widetilde{\lambda}}^{\lambda_\infty} M(\lambda, \lambda_\infty) \, \lambda^{n-1} \, \mathrm{d}\lambda}_{\text{internal moment}}. \tag{73.36}$$

We refer to the rightmost term as the *internal moment* since it is an integral over the region, whereas $M(\widetilde{\lambda}, \lambda_\infty) \, \widetilde{\lambda}^n$ is the *external moment*, which is the region mass times the boundary value, $\widetilde{\lambda}^n$. We choose the moniker "external" since the external moment increases in direct proportion to the mass crossing the ocean layer boundaries, including the external boundaries. In Section 73.6 we develop a budget for the $n = 1$ moment, in which the internal moment from equation (73.36) takes the form

$$M(\widetilde{\lambda}, \lambda_\infty) \, [\langle \lambda \rangle - \widetilde{\lambda}] = \int_{\widetilde{\lambda}}^{\lambda_\infty} M(\lambda, \lambda_\infty) \, \mathrm{d}\lambda. \tag{73.37}$$

We return to the notion of internal and external moments in Section 73.10.2.

73.3.8 Further study

The formulation given here in terms of mass distribution functions follows that of *Walin* (1977) and *Walin* (1982). In these two papers, Walin pioneered the formalism of water mass analysis, which is sometimes referred to as *Walin analysis* in his honor. The concept of internal and external tracer moments follows the internal and external heat introduced by *Holmes et al.* (2019).

73.4 Water mass transformation across a λ-surface

We here develop the formalism to quantify transport of seawater crossing an interior λ-interface. This transport is referred to as the *water mass transformation* and is written as $G(\lambda)$. Figure 73.6 illustrates how this transformation appears in a mass budget for a $\Delta\lambda$-layer, with details provided in this section. We assume that λ satisfies a tracer equation as discussed in Section 73.4.3.

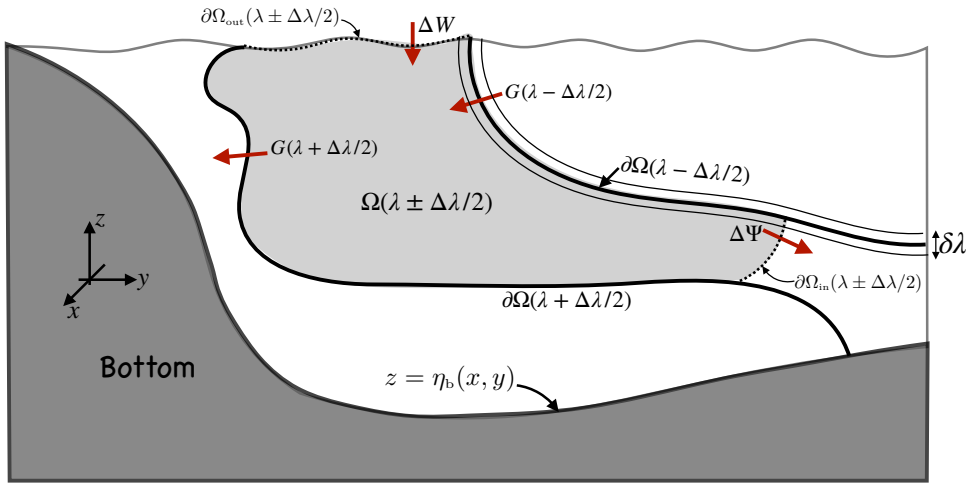

FIGURE 73.6: A layer of seawater with scalar property λ within the range $[\lambda - \Delta\lambda/2, \lambda + \Delta\lambda/2]$ and defined over a geographical domain $\Omega(\lambda \pm \Delta\lambda/2)$. In this example, λ increases to the south, towards Antarctica, with $\lambda = \gamma$ (density) an example (Section 73.2). The net seawater mass transport crossing the layer interfaces, $\partial\Omega(\lambda \pm \Delta\lambda/2)$, is $G(\lambda \pm \Delta\lambda/2)$, with $G > 0$ for water moving to regions of larger λ. The seawater mass crossing the layer through the geographical bounds, $\partial\Omega_{\text{in}}(\lambda \pm \Delta\lambda/2)$, is written $\Delta\Psi(\lambda \pm \Delta\lambda/2)$, with $\Delta\Psi(\lambda \pm \Delta\lambda/2) > 0$ for water leaving $\Omega(\lambda \pm \Delta\lambda/2)$. The boundary $\partial\Omega_{\text{in}}(\lambda \pm \Delta\lambda/2)$ is absent when the domain extends across a basin or the global ocean (e.g., see Figure 73.8). The mass crossing the sea surface, $\partial\Omega_{\text{out}}(\lambda \pm \Delta\lambda/2)$, through rain, evaporation, melt, or rivers is written $\Delta W(\lambda \pm \Delta\lambda/2)$, with $\Delta W(\lambda \pm \Delta\lambda/2) > 0$ for mass entering $\Omega(\lambda \pm \Delta\lambda/2)$. A layer interface can have an arbitrary stratification, such as the vertically non-monotonic profile depicted here for the $\lambda + \Delta\lambda/2$ interface. Additionally, the domain $\Omega(\lambda \pm \Delta\lambda/2)$ can generally be disconnected. The net domain boundaries are written $\partial\Omega_{\text{in}}(\lambda \pm \Delta\lambda/2) + \partial\Omega_{\text{out}}(\lambda \pm \Delta\lambda/2) + \partial\Omega(\lambda + \Delta\lambda/2) + \partial\Omega(\lambda - \Delta\lambda/2)$. The $\delta\lambda$ layer surrounding the $\partial\Omega(\lambda - \Delta\lambda/2)$ interface arises as part of the method detailed in Section 73.4.2 for computing G according to the λ-derivative of an integral over the $\delta\lambda$ layer.

73.4.1 Dia-surface flux and interior transformation

The object that measures the local water mass transformation is the dia-surface flux detailed in Section 64.3.7. This flux is given by

$$w^{\text{dia}} = \hat{\boldsymbol{n}} \cdot (\boldsymbol{v} - \boldsymbol{v}^{(\lambda)}) = \frac{\dot{\lambda}}{|\nabla\lambda|} \quad \text{with} \quad \hat{\boldsymbol{n}} = \frac{\nabla\lambda}{|\nabla\lambda|} \quad \text{and} \quad \dot{\lambda} = \frac{\mathrm{D}\lambda}{\mathrm{D}t}, \tag{73.38}$$

and with $w^{\text{dia}} > 0$ for water moving to regions of larger λ. It is computed as the projection of the relative velocity, $(\boldsymbol{v} - \boldsymbol{v}^{(\lambda)})$, onto the direction normal to the surface, with the relative velocity being the difference between the fluid particle velocity, $\boldsymbol{v}$, and the velocity of a point on the λ-interface, $\boldsymbol{v}^{(\lambda)}$. The velocity of a point on the surface satisfies the following kinematic constraint[11]

$$(\partial_t + \boldsymbol{v}^{(\lambda)} \cdot \nabla)\, \lambda = 0. \tag{73.39}$$

This constraint is based on assuming $\boldsymbol{v}^{(\lambda)}$ measures the velocity of a point fixed to the λ-surface. Evidently, the dia-surface flux, w^{dia}, locally measures the flux of seawater (volume per area per time) that penetrates a λ-interface in the direction of increasing λ.

The interior water mass transformation, $G(\lambda)$, is the area integral of $\rho\, w^{\text{dia}}$ over the full extent of the λ-surface

$$G(\lambda) \equiv \int_{\partial\Omega(\lambda)} \rho\, w^{\text{dia}}\, \mathrm{d}\mathcal{S} = \int_{\partial\Omega(\lambda)} \rho\, \hat{\boldsymbol{n}} \cdot (\boldsymbol{v} - \boldsymbol{v}^{(\lambda)})\, \mathrm{d}\mathcal{S} = \int_{\partial\Omega(\lambda)} \frac{\rho\, \dot{\lambda}}{|\nabla\lambda|}\, \mathrm{d}\mathcal{S}, \tag{73.40}$$

[11] We encountered the relation (73.39) in Section 19.6.2 when deriving the kinematic boundary condition for a moving surface.

where $\partial\Omega(\lambda)$ is the surface occupied by the λ-interface (see Figure 73.6). Furthermore, the dimensions of $G(\lambda)$ are mass per time

$$G(\lambda) \quad [\equiv] \quad \mathrm{M\ T}^{-1}, \tag{73.41}$$

thus measuring the mass per time crossing the λ-interface.

Based on the definition (73.40), we see that interior water mass transformation across a λ-interface occurs when there is a material change, $\dot{\lambda} \neq 0$, in the property defining the interface. Interior material changes arise from mixing, which generally causes irreversible changes to λ, thus driving seawater across the moving λ-interfaces. Material changes can also arise from sources and sinks, as when considering buoyancy surfaces in the presence of a nonlinear equation of state (Chapter 72). Sources and sinks are also commonly encountered by biogeochemical tracers.

73.4.2 Transformation as the derivative of an integral

Following the discussion from Section 73.3.5, we set $\mathscr{F} = \dot{\lambda}$ and consider the mass integral

$$\mathscr{I}_{\dot{\lambda}}(\lambda, \lambda_\infty) = \int_{\Omega(\lambda \leq \lambda_\infty)} \dot{\lambda}' \, \mathrm{d}M = \int_\lambda^{\lambda_\infty} \left[\int_{\partial\Omega(\lambda')} \frac{\rho \, \dot{\lambda}'}{|\nabla \lambda'|} \, \mathrm{d}\mathcal{S} \right] \mathrm{d}\lambda' = \int_\lambda^{\lambda_\infty} G(\lambda') \, \mathrm{d}\lambda'. \tag{73.42}$$

The fundamental theorem of calculus leads to the expression of the water mass transformation as the derivative

$$G(\lambda) = -\frac{\partial \mathscr{I}_{\dot{\lambda}}(\lambda, \lambda_\infty)}{\partial \lambda} \qquad \text{fund. thm of calculus} \tag{73.43a}$$

$$= -\lim_{\delta\lambda \to 0} \frac{1}{\delta\lambda} \left[\int_{\lambda+\delta\lambda/2}^{\lambda_\infty} G(\lambda') \mathrm{d}\lambda' - \int_{\lambda-\delta\lambda/2}^{\lambda_\infty} G(\lambda') \mathrm{d}\lambda' \right] \qquad \text{definition of derivative} \tag{73.43b}$$

$$= \lim_{\delta\lambda \to 0} \frac{1}{\delta\lambda} \int_{\lambda-\delta\lambda/2}^{\lambda+\delta\lambda/2} G(\lambda') \mathrm{d}\lambda' \qquad \text{combine integral limits} \tag{73.43c}$$

$$= \lim_{\delta\lambda \to 0} \frac{1}{\delta\lambda} \int_{\Omega(\lambda \pm \delta\lambda/2)} \dot{\lambda}' \, \mathrm{d}M \qquad \text{equation (73.42)} \tag{73.43d}$$

$$= \lim_{\delta\lambda \to 0} \frac{1}{\delta\lambda} \int_{\Omega(\lambda \pm \delta\lambda/2)} \dot{\lambda}' \, \rho \, \mathrm{d}V \qquad \mathrm{d}M = \rho \, \mathrm{d}V. \tag{73.43e}$$

Evidently, the calculation of interior water mass transformation requires information about the material time change, $\dot{\lambda}$, a weighting of the time changes according to the mass, $\mathrm{d}M = \rho \, \mathrm{d}V$, and a binning of $\rho \, \dot{\lambda} \, \mathrm{d}V$ according to λ-classes. Note that in the final equality, equation (73.43e), the limit $\delta\lambda \to 0$ might appear to lead to a singularity. However, as seen by the form in equation (73.43c), the integration region volume also gets smaller as $\delta\lambda \to 0$ so that the limit is well defined.

73.4.3 Kinematic and process methods of transformation

There are complementary methods to view interior water mass transformation: the *process method* and the *kinematic method*. The two methods are mathematically identical and so they offer two means to compute the same transformation. The kinematic method tells us *how* transformation happens whereas the process method tells us *why*. We here detail these two methods.

Kinematic method

The kinematic method focuses on the kinematic means for realizing dia-surface transport, thus providing information concerning how interior transformation occurs. It does so by binning processes contributing to the right hand side of

$$\rho \dot{\lambda} = \partial_t(\rho \lambda) + \nabla \cdot (\rho \lambda \boldsymbol{v}), \tag{73.44}$$

which arises from the local time tendency plus advection, so that

$$G(\lambda) = \lim_{\delta\lambda \to 0} \frac{1}{\delta\lambda} \int_{\Omega(\lambda \pm \delta\lambda/2)} [\partial_t(\rho \lambda) + \nabla \cdot (\rho \lambda \boldsymbol{v})] \, \mathrm{d}V. \tag{73.45}$$

This method is operationally simpler than the process method since there are fewer terms to bin. However, it does not provide information about why there is transformation, with that information requiring us to bin tendencies arising from individual processes.

Process method

The *process method* focuses on physical processes leading to movement of fluid across the λ-interface, thus providing information concerning *why* interior transformation occurs. It does so by binning processes contributing to the right hand side of the tracer equation

$$\rho \dot{\lambda} = -\nabla \cdot \boldsymbol{J} + \rho \dot{\Upsilon}, \tag{73.46}$$

where $\boldsymbol{J}$ is a flux arising from non-advective processes such as diffusion, and $\dot{\Upsilon}$ is a source/sink term (dimensions of λ per time) that cannot be written as the convergence of a flux. The tracer equation (73.46) inserted into the transformation equation (73.43e) leads to

$$G(\lambda) = \lim_{\delta\lambda \to 0} \frac{1}{\delta\lambda} \int_{\Omega(\lambda \pm \delta\lambda/2)} (-\nabla \cdot \boldsymbol{J} + \rho \dot{\Upsilon}) \, \mathrm{d}V \tag{73.47a}$$

$$= \lim_{\delta\lambda \to 0} \frac{1}{\delta\lambda} \oint_{\partial\Omega(\lambda \pm \delta\lambda/2)} (-\boldsymbol{J} \cdot \hat{\boldsymbol{n}}) \, \mathrm{d}\mathcal{S} + \lim_{\delta\lambda \to 0} \frac{1}{\delta\lambda} \int_{\Omega(\lambda \pm \delta\lambda/2)} \rho \dot{\Upsilon} \, \mathrm{d}V, \tag{73.47b}$$

The second equality made use of the divergence theorem to convert the volume integral into a surface integral. For the tracer sources, we assume they do not modify the seawater mass at a point so that there is no source in the seawater mass equation.

For many purposes it is useful to decompose the non-advective flux divergence into contributions from interior processes, such as ocean mixing, and boundary fluxes

$$\nabla \cdot \boldsymbol{J} = \nabla \cdot (\boldsymbol{J}^{\mathsf{int}} + \boldsymbol{J}^{\mathsf{out}} + \boldsymbol{J}^{\mathsf{bot}}). \tag{73.48}$$

By definition,

$$\boldsymbol{J}^{\mathsf{int}} \cdot \hat{\boldsymbol{n}} = 0 \quad \text{on } \partial\Omega_{\mathsf{out}}(\lambda \pm \delta\lambda/2) \text{ and } \partial\Omega_{\mathsf{bot}}(\lambda \pm \delta\lambda/2), \tag{73.49}$$

whereas $\boldsymbol{J}^{\mathsf{int}} \cdot \hat{\boldsymbol{n}}$ is generally nonzero on interior layer boundaries. In contrast, the boundary fluxes, $\boldsymbol{J}^{\mathsf{out}} \cdot \hat{\boldsymbol{n}}$ and $\boldsymbol{J}^{\mathsf{bot}} \cdot \hat{\boldsymbol{n}}$, are identically zero everywhere except on their respective boundaries. Correspondingly, it is convenient to bin the volume weighted convergence, $-\nabla \cdot \boldsymbol{J}^{\mathsf{int}} \, \mathrm{d}V$, according to λ-classes, and to likewise bin the area weighted boundary fluxes, $\boldsymbol{J}^{\mathsf{out}} \cdot \hat{\boldsymbol{n}} \, \mathrm{d}\mathcal{S}$ and $\boldsymbol{J}^{\mathsf{bot}} \cdot \hat{\boldsymbol{n}} \, \mathrm{d}\mathcal{S}$. In this way we write the non-advective contribution to water mass transformation in the form

$$G(\lambda)_{\text{non-adv}} = \underbrace{- \lim_{\delta\lambda \to 0} \frac{1}{\delta\lambda} \int_{\Omega(\lambda \pm \delta\lambda/2)} \nabla \cdot \boldsymbol{J}^{\mathsf{int}} \, \mathrm{d}V}_{\text{interior transformation = volume integral of convergence}}$$

$$\underbrace{-\lim_{\delta\lambda\to 0}\frac{1}{\delta\lambda}\int_{\partial\Omega_{\text{out}}(\lambda\pm\delta\lambda/2)}\boldsymbol{J}^{\text{out}}\cdot\hat{\boldsymbol{n}}\,\mathrm{d}\mathcal{S}}_{\text{surface transformation = area integral of surface boundary fluxes}}$$
$$\underbrace{-\lim_{\delta\lambda\to 0}\frac{1}{\delta\lambda}\int_{\partial\Omega_{\text{bot}}(\lambda\pm\delta\lambda/2)}\boldsymbol{J}^{\text{bot}}\cdot\hat{\boldsymbol{n}}\,\mathrm{d}\mathcal{S}}_{\text{bottom transformation = area integral of bottom boundary fluxes}}. \tag{73.50}$$

Again, this expression decomposes the contribution from interior processes, here represented as the volume integral of the interior flux convergence, from the surface and bottom contributions, here represented as the area integral of the boundary fluxes. This decomposition is further examined in Section 73.7 where we focus on the surface contribution to water mass transformation.

Since the boundary fluxes are, by definition, zero except on the boundaries, their divergence can be written in terms of a Dirac delta distribution[12]

$$\nabla\cdot[\boldsymbol{J}^{\text{out}}+\boldsymbol{J}^{\text{bot}}]=\boldsymbol{J}^{\text{out}}\cdot\hat{\boldsymbol{n}}\,\delta(z-\eta)+\boldsymbol{J}^{\text{bot}}\cdot\hat{\boldsymbol{n}}\,\delta(z-\eta_{\text{b}}). \tag{73.51}$$

Although this equation is more physically formal than mathematically rigorous, its use in the transformation equation (73.47a) correctly leads to the expression (73.50). Consequently, equation (73.51) proves to be a useful shorthand that is commonly used in the literature (e.g., *Groeskamp et al.* (2019)).[13]

Comments

As we saw, equality of the process method and kinematic method follows simply because the two provide equivalent expressions for the material time derivative. However, in the analysis of numerical model output, it can be nontrivial to realize this equivalance due to the extreme care required to diagnose the terms appearing in the scalar budget equation. See *Drake et al.* (2025) for a thorough discussion of the details as required for the MOM6 finite volume numerical ocean model.

73.4.4 Some details concerning interior transformation

We here consider some details of the water mass transformation arising just from interior processes such as diffusion.

A global integrated constraint on $G(\lambda)_{int}$

Consider the integrated water mass transformation given by equation (73.42), only now integrate over the full ocean domain

$$\mathcal{G}_{\dot{\lambda}}(\lambda_{-\infty},\lambda_{\infty})=\int_{\lambda_{-\infty}}^{\lambda_{\infty}}G(\lambda')\,\mathrm{d}\lambda'=\int_{\Omega(\lambda_{-\infty},\lambda_{\infty})}\rho\,\dot{\lambda}'\,\mathrm{d}V. \tag{73.52}$$

[12] We detail properties of the Dirac delta distribution in Chapter 7. It has dimensions equal to the inverse the dimensions of its argument (Section 7.3). For example, when the argument has dimensions of length then the Dirac delta has dimensions of inverse length. We thus see that equation (73.51) is dimensionally consistent.

[13] As detailed in Section 9.4.8, we are afforded the ability to introduce Dirac deltas into the boundary conditions (73.51) since the boundary conditions are Neumann (flux) conditions. A similar method was used for quasi-geostrophic potential vorticity in Section 45.7 and for the surface buoyancy fluxes in Section 72.6.3.

This integral vanishes for water mass transformations arising from conservative interior processes (i.e., those processes determined by the convergence of a flux)

$$[\mathcal{I}_{\dot\lambda}(\lambda_{-\infty}, \lambda_\infty)]_{\text{int}} = \int_{\lambda_{-\infty}}^{\lambda_\infty} G(\lambda')_{\text{int}} \, \mathrm{d}\lambda' \tag{73.53a}$$

$$= -\int_{\Omega(\lambda_{-\infty}, \lambda_\infty)} \nabla \cdot \boldsymbol{J}^{\text{int}} \, \mathrm{d}V \tag{73.53b}$$

$$= -\oint_{\partial\Omega(\lambda_{-\infty}, \lambda_\infty)} \boldsymbol{J}^{\text{int}} \cdot \hat{\boldsymbol{n}} \, \mathrm{d}\mathcal{S} \tag{73.53c}$$

$$= 0, \tag{73.53d}$$

which follows since $\boldsymbol{J}^{\text{int}} \cdot \hat{\boldsymbol{n}} = 0$ on the ocean boundaries. Hence, there can be no net water mass transformation across a λ surface arising from conservative interior processes

$$\int_{\lambda_{-\infty}}^{\lambda_\infty} G(\lambda')_{\text{int}} \, \mathrm{d}\lambda' = 0. \tag{73.54}$$

Instead, conservative interior processes only lead to rearrangement of water within the λ-bins. This result follows since these interior processes conserve the total content of λ within the global domain. Equation (73.54) provides a constraint that should be verified by any numerical realization of water mass transformation.

Interior transformation across constant λ surfaces

We now focus on the transformation occuring along surfaces of constant λ (Figure 73.7) so that

$$G(\lambda)_{\text{int}} = -\lim_{\delta\lambda \to 0} \frac{1}{\delta\lambda} \int_{\Omega(\lambda \pm \delta\lambda/2)} \nabla \cdot \boldsymbol{J}^{\text{int}} \, \mathrm{d}V \tag{73.55a}$$

$$= -\lim_{\delta\lambda \to 0} \frac{1}{\delta\lambda} \left[\int_{\Omega(\lambda + \delta\lambda/2)} \hat{\boldsymbol{n}} \cdot \boldsymbol{J}^{\text{int}} \, \mathrm{d}\mathcal{S} - \int_{\Omega(\lambda - \delta\lambda/2)} \hat{\boldsymbol{n}} \cdot \boldsymbol{J}^{\text{int}} \, \mathrm{d}\mathcal{S} \right]. \tag{73.55b}$$

Transformation occurs if there is an imbalance between the diffusive transport across the two bounding surfaces, $\Omega(\lambda + \delta\lambda/2)$ and $\Omega(\lambda - \delta\lambda/2)$. As a special case, assume the ocean surface is a constant λ surface with $\lambda = \lambda_{\text{top}}$. Along this surface we have $\hat{\boldsymbol{n}} \cdot \boldsymbol{J}^{\text{int}} = 0$, so that the transformation at $\lambda_{\text{top}} - \delta\lambda/2$ has a contribution just from the flux crossing the $\Omega(\lambda_{\text{top}} - \delta\lambda)$ surface

$$\lim_{\delta\lambda \to 0} G(\lambda_{\text{top}} - \delta\lambda/2)_{\text{int}} = \lim_{\delta\lambda \to 0} \frac{1}{\delta\lambda} \int_{\Omega(\lambda_{\text{top}} - \delta\lambda)} \hat{\boldsymbol{n}} \cdot \boldsymbol{J}^{\text{int}} \, \mathrm{d}\mathcal{S}. \tag{73.56}$$

Likewise, along the top surface we have

$$G(\lambda_{\text{top}})_{\text{int}} = \lim_{\delta\lambda \to 0} \frac{1}{\delta\lambda} \int_{\Omega(\lambda_{\text{top}} - \delta\lambda/2)} \hat{\boldsymbol{n}} \cdot \boldsymbol{J}^{\text{int}} \, \mathrm{d}\mathcal{S}, \tag{73.57}$$

where we set $\hat{\boldsymbol{n}} \cdot \boldsymbol{J}^{\text{int}} = 0$ for the surface $\Omega(\lambda_{\text{top}} + \delta\lambda/2)$, since this surface exists outside of the ocean.

The results (73.56) and (73.57) make it appear that $G(\lambda_{\text{top}} - \delta\lambda/2)_{\text{int}}$ and $G(\lambda_{\text{top}})_{\text{int}}$ are unbounded as $\delta\lambda \to 0$, so long as there is a nonzero diffusive transport through $\Omega(\lambda_{\text{top}} - \delta\lambda)$ or $\Omega(\lambda_{\text{top}} - \delta\lambda/2)$. However, this unbounded water mass transformation is not realized since the diffusive flux gets smaller in magnitude when approaching the ocean surface, and it does so in

order to satisfy the no-flux surface boundary condition (73.49) satisfied by interior processes[14]

$$\hat{\boldsymbol{n}} \cdot \boldsymbol{J}^{\text{int}} = 0 \quad \text{at } z = \eta. \tag{73.58}$$

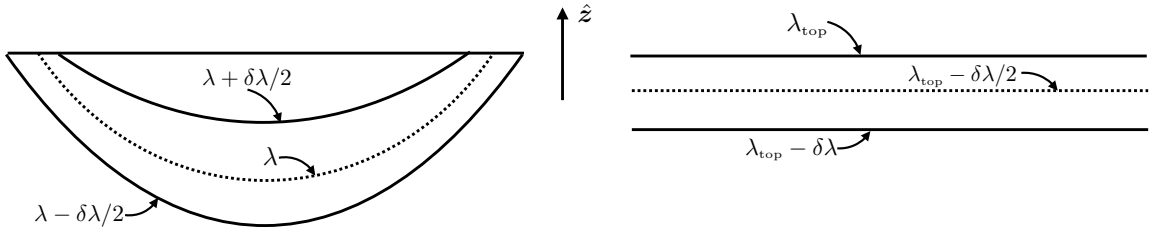

FIGURE 73.7: Example λ surfaces for studying interior transformation due to diffusion. The left panel shows λ surfaces that outcrop to the ocean surface, with the dotted surface the chosen λ surface across which we compute the water mass transformation. The right panel assumes the λ surfaces are flat and with $\lambda = \lambda_{\text{top}}$ the value along the ocean surface.

To further our understanding of the transformation in the region near the ocean surface, let the λ surfaces be flat near the ocean surface so that $\hat{\boldsymbol{n}} = -\hat{\boldsymbol{z}}$ along $\Omega(\lambda_{\text{top}} - \delta\lambda)$. Setting the diffusive flux to

$$\boldsymbol{J} = -\rho_o \, \kappa \, \nabla\lambda \tag{73.59}$$

as per a Boussinesq fluid with reference density ρ_o and diffusivity $\kappa > 0$, leads to the transformation

$$G(\lambda_{\text{top}} - \delta\lambda/2)_{\text{int}} = \frac{1}{\delta\lambda} \int_{\Omega(\lambda_{\text{top}} - \delta\lambda)} (\rho_o \, \kappa \, \partial_z \lambda) \, \mathrm{d}\mathcal{S}. \tag{73.60}$$

With $\kappa \, \partial_z \lambda > 0$, the transformation is positive, $G(\lambda_{\text{top}} - \delta\lambda/2)_{\text{int}} > 0$, so that water is entrained into the layer bounded by $\lambda_{\text{top}} - \delta\lambda$ and λ_{top}. Note that in the absence of boundary fluxes, the value of λ_{top} is reduced due to diffusive mixing with interior waters since these waters have lower values of λ. Furthermore, as the surface is approached, $\partial_z \lambda$ reduces in magnitude to satisfy the no-flux condition, $\kappa \, \partial_z \lambda = 0$, at the ocean surface. In this manner, the transformation remains bounded even as $\delta\lambda \to 0$.

73.5 Budget for seawater mass in a $\Delta\lambda$-layer

In this section we construct the seawater mass budget for a $\Delta\lambda$-layer, making reference to Figure 73.6 for the notation. As a shorthand, we write the layer mass as

$$\Delta M(\lambda \pm \Delta\lambda/2) \equiv M(\lambda - \Delta\lambda/2, \lambda + \Delta\lambda/2), \tag{73.61}$$

along with a similar notation for other contributions to the layer mass budget.

73.5.1 Transport crossing interior open boundaries

As depicted in Figure 73.6, the layer region has an open boundary that is within the interior of the ocean. The mass transport leaving the layer through this interior open boundary is written

$$\Delta\Psi(\lambda \pm \Delta\lambda/2) = \int_{\partial\Omega_{\text{in}}(\lambda \pm \Delta\lambda/2)} \rho \, (\boldsymbol{v} - \boldsymbol{v}^{(\text{b})}) \cdot \hat{\boldsymbol{n}} \, \mathrm{d}\mathcal{S}, \tag{73.62}$$

[14] As discussed in Sections 20.4.3, 72.5, and 73.8.3, when water is transported across the ocean surface the diffusive flux picks up a nonzero boundary contribution. That contribution is assumed to be part of the surface transformation in equation (73.50) so that the interior diffusive flux still satisfies the no-flux boundary condition (73.58). *Nurser and Griffies* (2019) discuss these points for salinity.

where $\boldsymbol{v}^{(\mathsf{b})}$ is the velocity for a point on the boundary and $\hat{\boldsymbol{n}}$ is the outward normal along the boundary. Introducing the mass distribution for this transport renders the equivalent expression

$$\Delta\Psi(\lambda \pm \Delta\lambda/2) = \int_{\lambda-\Delta\lambda/2}^{\lambda+\Delta\lambda/2} \dot{m}_{\Psi}(\lambda')\,\mathrm{d}\lambda', \tag{73.63}$$

where we introduced

$$\dot{m}_{\Psi}(\lambda)\,\mathrm{d}\lambda = \text{mass per time of } \lambda\text{-stuff crossing } \partial\Omega_{\mathsf{in}} \text{ within } [\lambda - \mathrm{d}\lambda/2, \lambda + \mathrm{d}\lambda/2]. \tag{73.64}$$

We make particular use of $\dot{m}_{\Psi}$ in Section 73.6 when studying the λ-budget in a $\Delta\lambda$-layer. One common example for an open interior boundary is when choosing a particular latitude, in which case $\boldsymbol{v}^{(\mathsf{b})} = 0$ and $\hat{\boldsymbol{n}} = \hat{\boldsymbol{y}}$ so that

$$\Delta\Psi(\lambda \pm \Delta\lambda/2) = \int_{\partial\Omega_{\mathsf{in}}(\lambda\pm\Delta\lambda/2)} \rho\, v\, \mathrm{d}x\, \mathrm{d}z. \tag{73.65}$$

In this case, $\partial\Omega_{\mathsf{in}}(\lambda\pm\Delta\lambda/2)$ specifies the depth and longitude range for the layer at its intersection along the constant latitude boundary.

73.5.2 Mass transport crossing the ocean surface

The mass transport crossing the ocean free surface is written

$$\Delta W(\lambda \pm \Delta\lambda/2) = -\int_{\partial\Omega_{\mathsf{out}}(\lambda\pm\Delta\lambda/2)} \rho\,(\boldsymbol{v} - \boldsymbol{v}^{(\eta)}) \cdot \hat{\boldsymbol{n}}\,\mathrm{d}\mathcal{S} = \int_{\partial\Omega_{\mathsf{out}}(\lambda\pm\Delta\lambda/2)} \mathcal{Q}_{\mathsf{m}}\,\mathrm{d}\mathcal{S}, \tag{73.66}$$

where we made use of the surface kinematic boundary condition (19.78) to write

$$\rho\,(\boldsymbol{v} - \boldsymbol{v}^{(\mathsf{b})}) \cdot \hat{\boldsymbol{n}} \equiv -\mathcal{Q}_{\mathsf{m}}, \tag{73.67}$$

where $\mathcal{Q}_{\mathsf{m}}\,\mathrm{d}\mathcal{S}$ is the mass transport of water crossing the free surface ($\mathcal{Q}_{\mathsf{m}} > 0$ for water entering the ocean). Introducing the mass distribution leads to the equivalent expression

$$\Delta W(\lambda \pm \Delta\lambda/2) = \int_{\lambda-\Delta\lambda/2}^{\lambda+\Delta\lambda/2} \dot{m}_{\mathsf{W}}(\lambda')\,\mathrm{d}\lambda', \tag{73.68}$$

where

$$\dot{m}_{\mathsf{W}}(\lambda)\,\mathrm{d}\lambda = \text{mass per time of } \lambda\text{-stuff crossing } \partial\Omega_{\mathsf{out}} \text{ within } [\lambda - \mathrm{d}\lambda/2, \lambda + \mathrm{d}\lambda/2]. \tag{73.69}$$

We make particular use of $\dot{m}_{\mathsf{W}}$ in Section 73.6 when studying the λ-budget in a $\Delta\lambda$-layer.

73.5.3 Mass budget

Bringing the above pieces together leads to the layer mass budget

$$\frac{\mathrm{d}\Delta M}{\mathrm{d}t} = -\Delta\Psi + \Delta W - [G(\lambda + \Delta\lambda/2) - G(\lambda - \Delta\lambda/2)], \tag{73.70}$$

where for brevity we dropped $\lambda \pm \Delta\lambda/2$ arguments for ΔM, $\Delta\Psi$, and ΔW. It is common to define the layer mass *formation* as the mass accumulation within the layer

$$\underbrace{\frac{\mathrm{d}\Delta M}{\mathrm{d}t} + \Delta\Psi}_{\text{storage + outflow}} = \underbrace{\Delta W - [G(\lambda + \Delta\lambda/2) - G(\lambda - \Delta\lambda/2)]}_{\text{formation into layer } \Omega_{(\lambda \pm \Delta\lambda/2)}}. \tag{73.71}$$

This equality defines water mass formation as the time change for the mass within the layer (sometimes referred to as the *storage term*), plus the net mass leaving the interior open boundary. Formation into a layer occurs if there is mass converging through transformation across interior layer interfaces, plus mass entering through the surface boundary outcrop region.

We arrive at a differential equation for the mass budget (73.71) by dividing through by the layer increment, $\Delta\lambda$, and taking the limit as this increment tends to zero

$$\frac{\partial}{\partial\lambda}\left[\frac{\mathrm{d}M}{\mathrm{d}t} + \Psi - W + G\right] = 0. \tag{73.72}$$

Integrating from a reference value $\lambda_{-\infty}$ to λ leads to

$$\int_{\lambda_{-\infty}}^{\lambda} \frac{\partial\Psi}{\partial\lambda}\,\mathrm{d}\lambda = \int_{\lambda_{-\infty}}^{\lambda} \frac{\partial}{\partial\lambda}\left[-\frac{\mathrm{d}M}{\mathrm{d}t} + W - G\right]\mathrm{d}\lambda \Longrightarrow \Psi = -\frac{\mathrm{d}M}{\mathrm{d}t} + W - G. \tag{73.73}$$

We dropped the contribution from the constant reference value, $\lambda_{-\infty}$, since it sits outside of the ocean domain. The differential water mass equation (73.73) is a continuous version of the discrete equation (73.71). We wrote this equation as an expression for Ψ given that an accumulation from the bottom up leads to a transport streamfunction in the steady state, as we discuss in Section 73.7.1.

73.6 Budget for λ mass in a λ_∞-region

We build from our understanding of the seawater mass budget in Section 73.5 to develop a budget for the mass of λ within the λ_∞-region of Section 73.3.4 and as illustrated in Figure 73.8. Part of our aim is to further develop the formalism while also offering added insights into the causes for water mass transformation, $G(\lambda)$.

We here choose to be specific by considering λ to be an intensive property such as a material tracer concentration, in which case $\lambda\,\rho\,\mathrm{d}V$ has dimensions of tracer mass.[15] For non-material scalar fields, such as Conservative Temperature or buoyancy, the dimensions are modified accordingly.

73.6.1 Processes affecting the mass of λ-stuff

Our starting point is the Leibniz-Reynolds budget for a scalar field derived in Section 20.2.4, here including the possibility of scalar sources

$$\frac{\mathrm{d}}{\mathrm{d}t}\left[\int_{\Omega(\lambda\le\lambda_\infty)} \rho\,\lambda\,\mathrm{d}V\right] = \int_{\Omega(\lambda\le\lambda_\infty)} \rho\,\dot{\Upsilon}\,\mathrm{d}V - \int_{\partial\Omega(\lambda\le\lambda_\infty)} \left[\rho\,\lambda\,(\boldsymbol{v} - \boldsymbol{v}^{(\mathrm{b})}) + \boldsymbol{J}\right]\cdot\hat{\boldsymbol{n}}\,\mathrm{d}\mathcal{S}. \tag{73.74}$$

The right hand side of this budget equation can be decomposed into the following processes illustrated in Figure 73.8.

[15] See Section 20.2.1 for more on intensive and extensive fluid properties.

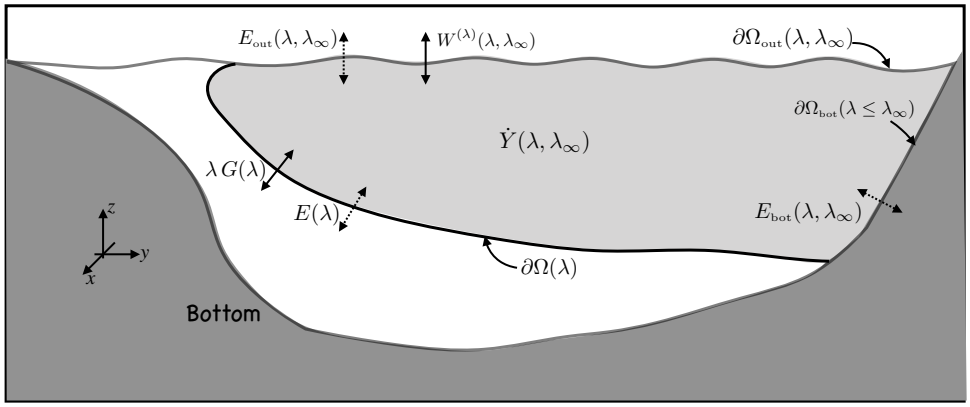

FIGURE 73.8: A λ_∞-region for studying the λ budget, with the region bounded by the solid-earth bottom, $\partial\Omega_{\text{bot}}(\lambda \le \lambda_\infty)$, the ocean surface boundary, $\partial\Omega_{\text{out}}(\lambda, \lambda_\infty)$, and the λ-interface, $\partial\Omega(\lambda)$. Hence, in contrast to the $\Delta\lambda$-region shown in Figure 73.6, the λ_∞-region has no interior open boundary. Along the surface boundary, the λ budget is affected by the non-advective transport, $E_{\text{out}}(\lambda, \lambda_\infty)$, arising from processes such as diffusion, plus advective transport, $W^{(\lambda)}(\lambda, \lambda_\infty)$, arising from mass transported across the surface that can carry a non-zero amount of λ. Along the bottom boundary, the λ budget is affected by non-advective transport, $E_{\text{bot}}(\lambda, \lambda_\infty)$, arising from processes such as geothermal heating. There is no corresponding advective transport along the bottom since we assume there is no mass crossing the ocean bottom. Along the interior boundary, $\partial\Omega(\lambda)$, the budget is affected by non-advective transport, $E(\lambda)$, arising from diffusion, as well as advective transport through $\lambda\, G(\lambda)$, with $G(\lambda)$ the interior water mass transformation from Section 73.4. Finally, there is the possibility for an interior volume source, $\dot{Y}(\lambda \le \lambda_\infty)$, particularly for buoyancy in the presence of a nonlinear equation of state, and for biogeochemical tracers.

Non-conservative sources and sinks

As noted in Section 73.4.3, the source term, $\rho\, \dot{\Upsilon}$, accounts for processes that cannot be represented as the convergence of a flux. We write its region integrated contribution using the shorthand

$$\dot{Y}(\lambda, \lambda_\infty) \equiv \int_{\Omega(\lambda \le \lambda_\infty)} \rho\, \dot{\Upsilon}\, \mathrm{d}V \equiv \int_{\lambda}^{\lambda_\infty} \dot{m}_{\Upsilon}(\lambda')\, \mathrm{d}\lambda'. \tag{73.75}$$

The final equality introduced the distribution function for the source, in which

$$\dot{m}_{\Upsilon}(\lambda)\, \mathrm{d}\lambda = \text{mass per time of } \lambda\text{-stuff created within } [\lambda - \mathrm{d}\lambda/2, \lambda + \mathrm{d}\lambda/2]. \tag{73.76}$$

Transport from non-advective processes

The contribution from boundary area integrated non-advective fluxes appears in the term

$$-\int_{\partial\Omega(\lambda \le \lambda_\infty)} \boldsymbol{J} \cdot \hat{\boldsymbol{n}}\, \mathrm{d}\mathcal{S} = -\int_{\partial\Omega_{\text{out}}(\lambda \le \lambda_\infty)} \boldsymbol{J} \cdot \hat{\boldsymbol{n}}\, \mathrm{d}\mathcal{S} - \int_{\partial\Omega_{\text{bot}}(\lambda \le \lambda_\infty)} \boldsymbol{J} \cdot \hat{\boldsymbol{n}}\, \mathrm{d}\mathcal{S} - \int_{\partial\Omega(\lambda)} \boldsymbol{J} \cdot \hat{\boldsymbol{n}}\, \mathrm{d}\mathcal{S}. \tag{73.77}$$

Recall the minus signs arise since a non-advective flux increases the λ content of the region if the flux is oriented into the region, whereas $\hat{\boldsymbol{n}}$ is the region outward normal. The surface, $\partial\Omega_{\text{out}}(\lambda \le \lambda_\infty)$, extends along the upper ocean boundary and supports non-advective surface boundary fluxes. Likewise, the boundary, $\partial\Omega_{\text{bot}}(\lambda \le \lambda_\infty)$, intersects the ocean bottom and generally experiences bottom boundary fluxes such as geothermal heating. Finally, the surface, $\partial\Omega(\lambda)$, has non-advective fluxes that cross the λ-interface, with diffusive fluxes the canonical example. The boundary area integrated non-advective fluxes give rise to non-advective transports, with dimensions of mass of λ-stuff per time, and they are written using the shorthand

$$-\int_{\partial\Omega(\lambda \le \lambda_\infty)} \boldsymbol{J} \cdot \hat{\boldsymbol{n}}\, \mathrm{d}\mathcal{S} = E_{\text{out}}(\lambda, \lambda_\infty) + E_{\text{bot}}(\lambda, \lambda_\infty) + E(\lambda), \tag{73.78}$$

with a term having a positive value if it increases the λ mass of the region. We furthermore find it useful to introduce the distribution functions according to

$$E_{\text{out}}(\lambda, \lambda_\infty) + E_{\text{bot}}(\lambda, \lambda_\infty) = \int_\lambda^{\lambda_\infty} \left[\dot{m}_{\mathsf{E}}^{\text{out}}(\lambda') + \dot{m}_{\mathsf{E}}^{\text{bot}}(\lambda') \right] \mathrm{d}\lambda', \tag{73.79}$$

where

$$\dot{m}_{\mathsf{E}}^{\text{out}}(\lambda)\, \mathrm{d}\lambda = \text{mass per time of } \lambda\text{-stuff from } \partial\Omega_{\text{out}} \text{ transport in } [\lambda - \mathrm{d}\lambda/2, \lambda + \mathrm{d}\lambda/2] \tag{73.80a}$$

$$\dot{m}_{\mathsf{E}}^{\text{bot}}(\lambda)\, \mathrm{d}\lambda = \text{mass per time of } \lambda\text{-stuff from } \partial\Omega_{\text{bot}} \text{ transport in } [\lambda - \mathrm{d}\lambda/2, \lambda + \mathrm{d}\lambda/2]. \tag{73.80b}$$

λ transported with interior boundary mass fluxes

We next consider the contribution to the budget equation (73.74) arising from the transport of λ with mass that crosses the interior boundary, $\partial\Omega(\lambda)$, whereby

$$-\int_{\partial\Omega(\lambda)} \rho\, \lambda\, (\boldsymbol{v} - \boldsymbol{v}^{(\lambda)}) \cdot \hat{\boldsymbol{n}}\, \mathrm{d}\mathcal{S} = -\lambda \int_{\partial\Omega(\lambda)} \rho\, (\boldsymbol{v} - \boldsymbol{v}^{(\lambda)}) \cdot \hat{\boldsymbol{n}}\, \mathrm{d}\mathcal{S} = \lambda\, G(\lambda), \tag{73.81}$$

To reach this result we noted that λ can be pulled outside of the $\partial\Omega(\lambda)$ integral since it is constant along this surface, thus allowing for the introduction of the water mass transformation, $G(\lambda)$, given by equation (73.40).

Surface boundary mass fluxes

The final term contributing to the right hand side of the λ budget equation (73.74) arises from the surface mass transport along the boundary, $\partial\Omega_{\text{out}}(\lambda \leq \lambda_\infty)$,

$$-\int_{\partial\Omega(\lambda \leq \lambda_\infty)} \rho\, \lambda\, (\boldsymbol{v} - \boldsymbol{v}^{(\text{b})}) \cdot \hat{\boldsymbol{n}}\, \mathrm{d}\mathcal{S} = \int_{\partial\Omega_{\text{out}}(\lambda \leq \lambda_\infty)} \lambda\, \mathcal{Q}_{\mathsf{m}}\, \mathrm{d}\mathcal{S} \equiv W^{(\lambda)}(\lambda, \lambda_\infty). \tag{73.82}$$

To reach the first equality we followed the steps in Section 73.5.2 by using the kinematic boundary condition (19.78) to introduce the surface mass transport, $\mathcal{Q}_{\mathsf{m}}\, \mathrm{d}\mathcal{S}$. The final equality introduced a shorthand that corresponds to the $W(\lambda, \lambda_\infty)$ from Section 73.5.2. In the following, we find it useful to introduce the mass distribution function, $\dot{m}_{\mathsf{W}}(\lambda)$, from equation (73.69), thus rendering

$$W(\lambda, \lambda_\infty) = \int_\lambda^{\lambda_\infty} \dot{m}_{\mathsf{W}}(\lambda')\, \mathrm{d}\lambda' \qquad \text{and} \qquad W^{(\lambda)}(\lambda, \lambda_\infty) = \int_\lambda^{\lambda_\infty} \lambda\, \dot{m}_{\mathsf{W}}(\lambda')\, \mathrm{d}\lambda'. \tag{73.83}$$

Following the discussion in Sections 72.5.2, we have not assumed a relation between λ along the interface, $\partial\Omega_{\text{out}}(\lambda \leq \lambda_\infty)$, and the concentration, λ_{m}, contained in the entering mass. We prefer to keep the discussion general for now, providing a relation only when necessary.

73.6.2 Summary of the λ budget

Bringing terms together leads to the expanded version of the mass budget (73.74) for λ-stuff, now written as

$$\frac{\mathrm{d}}{\mathrm{d}t} \left[\int_{\Omega(\lambda \leq \lambda_\infty)} \rho\, \lambda\, \mathrm{d}V \right] = \dot{Y}(\lambda, \lambda_\infty) + E_{\text{out}}(\lambda, \lambda_\infty) + E_{\text{bot}}(\lambda, \lambda_\infty) + E(\lambda) + W^{(\lambda)}(\lambda, \lambda_\infty) + \lambda\, G(\lambda), \tag{73.84}$$

which has the equivalent expression in terms of distribution functions

$$\frac{\mathrm{d}}{\mathrm{d}t}\int_\lambda^{\lambda_\infty} \lambda'\, m(\lambda')\,\mathrm{d}\lambda' = \int_\lambda^{\lambda_\infty} \big[\dot m_{\mathsf{Y}}(\lambda') + \dot m_{\mathsf{E}}^{\mathsf{out}}(\lambda') + \dot m_{\mathsf{E}}^{\mathsf{bot}}(\lambda') + \lambda\, \dot m_{\mathsf{W}}(\lambda')\big]\,\mathrm{d}\lambda' + E(\lambda) + \lambda\, G(\lambda). \tag{73.85}$$

Setting λ to a global constant and assuming there are no seawater mass sources leads to the seawater mass budget for the λ_∞-region

$$\frac{\mathrm{d}}{\mathrm{d}t}\left[\int_{\Omega(\lambda\le\lambda_\infty)} \rho\,\mathrm{d}V\right] = W(\lambda,\lambda_\infty) + G(\lambda), \tag{73.86}$$

which takes on the following form in terms of distributions

$$\frac{\mathrm{d}}{\mathrm{d}t}\int_\lambda^{\lambda_\infty} m(\lambda')\,\mathrm{d}\lambda' = \int_\lambda^{\lambda_\infty} \dot m_{\mathsf{W}}(\lambda')\,\mathrm{d}\lambda' + G(\lambda). \tag{73.87}$$

73.6.3 Processes leading to water mass transformation

We now massage the budget equations to explicitly identify terms leading to water mass transformation, $G(\lambda)$. For that purpose, make use of the moment equation (73.37) to write

$$\int_{\Omega(\lambda\le\lambda_\infty)} \rho\,\lambda\,\mathrm{d}V = M(\lambda,\lambda_\infty)\,\langle\lambda\rangle = M(\lambda,\lambda_\infty)\,\lambda + \int_\lambda^{\lambda_\infty} M(\lambda',\lambda_\infty)\,\mathrm{d}\lambda', \tag{73.88}$$

which then leads to

$$\frac{\mathrm{d}[M(\lambda,\lambda_\infty)\,\langle\lambda\rangle]}{\mathrm{d}t} = \lambda\,\frac{\mathrm{d}M(\lambda,\lambda_\infty)}{\mathrm{d}t} + \int_\lambda^{\lambda_\infty} \frac{\mathrm{d}M(\lambda',\lambda_\infty)}{\mathrm{d}t}\,\mathrm{d}\lambda'. \tag{73.89}$$

Integrated water mass transformation over the λ_∞-region

Use of the λ budget equation (73.84) for the left hand side of equation (73.89), and the mass budget equation (73.86) for the right hand side, yields

$$\begin{aligned}\dot Y(\lambda,\lambda_\infty) + E_{\mathsf{out}}(\lambda,\lambda_\infty) + E_{\mathsf{bot}}(\lambda,\lambda_\infty) + E(\lambda) + W^{(\lambda)}(\lambda,\lambda_\infty) + \lambda\, G(\lambda) \\ = \lambda\,[W(\lambda,\lambda_\infty) + G(\lambda)] + \int_\lambda^{\lambda_\infty} [W(\lambda',\lambda_\infty) + G(\lambda')]\,\mathrm{d}\lambda'.\end{aligned} \tag{73.90}$$

Observe that the $\lambda\, G(\lambda)$ term cancels on both sides of this equation. The three contributions from the surface boundary mass fluxes also cancel, as revealed through the following identity

$$W^{(\lambda)}(\lambda,\lambda_\infty) - \lambda\, W(\lambda,\lambda_\infty) = \int_\lambda^{\lambda_\infty} (\lambda'-\lambda)\,\dot m_{\mathsf{W}}(\lambda')\,\mathrm{d}\lambda' \tag{73.91a}$$

$$= \int_\lambda^{\lambda_\infty} \left[\int_{\lambda'}^{\lambda_\infty} \dot m_{\mathsf{W}}(\lambda'')\,\mathrm{d}\lambda''\right]\mathrm{d}\lambda' \tag{73.91b}$$

$$= \int_\lambda^{\lambda_\infty} W(\lambda',\lambda_\infty)\,\mathrm{d}\lambda', \tag{73.91c}$$

where the second equality follows from the double integral formula (6.107). To understand the physical reason we see no water mass transformation from surface mass fluxes, recall the discussion in Section 72.5.2. Namely, mixing and internal sources provide the only means for irreversible changes to water masses and thus to water mass transformation. In contrast, boundary mass transport contributes to transformation only if the mass participates in mixing.

That is, the mass associated with boundary mass transport is incorporated into the ocean (or leaves the ocean) only in the presence of mixing. It is thus reassuring that the formalism leads to this same conclusion. Furthermore, this result is consistent with the expression (73.47b), whereby the water mass transformation is, again, determined solely in terms of the non-advective fluxes at the region boundaries plus the interior source term.

Cancelling the mass transport terms thus leads to the integrated water mass transformation

$$\int_{\lambda}^{\lambda_\infty} G(\lambda')\, \mathrm{d}\lambda' = \dot{Y}(\lambda, \lambda_\infty) + E_{\text{out}}(\lambda, \lambda_\infty) + E_{\text{bot}}(\lambda, \lambda_\infty) + E(\lambda). \tag{73.92}$$

Each term in this equation has dimensions mass of λ-stuff per time. This equation is an integrated version of the expression (73.47b) for the water mass transformation, here having exposed the processes contributing to transformation over the range $\lambda \leq \lambda_\infty$. Evidently, the accumulated effects from sources within the interior, plus non-advective fluxes along the surface and interior boundaries, lead to an integrated interior water mass transformation.

Water mass transformation across the λ-interface

We derive an expression for the water mass transformation across the λ-interface by taking $\partial/\partial\lambda$ of equation (73.92) to reveal

$$G(\lambda) = -\frac{\partial}{\partial \lambda} \left[\dot{Y}(\lambda, \lambda_\infty) + E_{\text{out}}(\lambda, \lambda_\infty) + E_{\text{bot}}(\lambda, \lambda_\infty) + E(\lambda) \right], \tag{73.93}$$

thus revealing that the water mass transformation across a λ-surface is the λ-convergence of the mixing processes plus the interior sources. This equation takes on the following distributional form

$$G(\lambda) = \dot{m}_{\mathsf{Y}}(\lambda) + \dot{m}_{\mathsf{E}}^{\text{bot}}(\lambda) + \dot{m}_{\mathsf{E}}^{\text{out}}(\lambda) - \frac{\partial E(\lambda)}{\partial \lambda}. \tag{73.94}$$

73.7 Surface water mass transformation

We have articulated all the terms needed to form the $\Delta\lambda$-layer mass budget according to Figure 73.6 as well as the λ_∞-region mass budget according to Figure 73.8. In this section we focus on contributions to transformation from surface processes in the transformation equation (73.94)

$$G_{\text{out}}(\lambda) \equiv -\frac{\partial E_{\text{out}}(\lambda, \lambda_\infty)}{\partial \lambda} = \dot{m}_{\mathsf{E}}^{\text{out}}(\lambda) = -\lim_{\delta\lambda \to 0} \frac{1}{\delta\lambda} \int_{\partial\Omega_{\text{out}}(\lambda \pm \delta\lambda/2)} \boldsymbol{J} \cdot \hat{\boldsymbol{n}}\, \mathrm{d}\mathcal{S}, \tag{73.95}$$

where the final equality made use of equation (73.47b). Such *surface transformation* forms the focus of many studies of water mass transformation because it only requires surface boundary information, which is generally more accessible than information from interior ocean mixing processes or bottom geothermal processes. Furthermore, much of the transformation of water occurs in surface regions since this region is home to large contributions from surface boundary fluxes and associated ocean mixing. The basic equation we use is the non-advective flux equation (20.85), rewritten here for the scalar field λ

$$-\boldsymbol{J} \cdot \hat{\boldsymbol{n}} = \mathcal{Q}_\lambda - \lambda\, \mathcal{Q}_{\text{m}} = \mathcal{Q}_\lambda^{\text{non-adv}} + (\lambda_{\text{m}} - \lambda)\, \mathcal{Q}_{\text{m}}. \tag{73.96}$$

73.7.1 Circulation driven by surface transformation

The layer mass budget (73.71) and its continuous expression (73.73) provide the basis for inferences about circulation and transformation. As an illustration, consider the continuous

expression (73.73) and integrate from a reference value, $\lambda_{-\infty}$, up to λ

$$\int_{\lambda_{-\infty}}^{\lambda} \Psi \, d\lambda' = \int_{\lambda_{-\infty}}^{\lambda} \left[-\frac{\partial M}{\partial t} + W - G \right] d\lambda'. \tag{73.97}$$

The left hand side is an expression for the circulation in λ-space at the specified interior open boundary. The right hand side means that a nonzero circulation is driven by mass through the ocean surface, convergence of mass transformed across the λ-interfaces, and/or time changes to the mass within the domain. Correspondingly, in the absence of surface boundary mass fluxes, a steady circulation is driven just by water mass transformation

$$\int_{\lambda_{-\infty}}^{\lambda} \Psi \, d\lambda' = - \int_{\lambda_{-\infty}}^{\lambda} G \, d\lambda'. \tag{73.98}$$

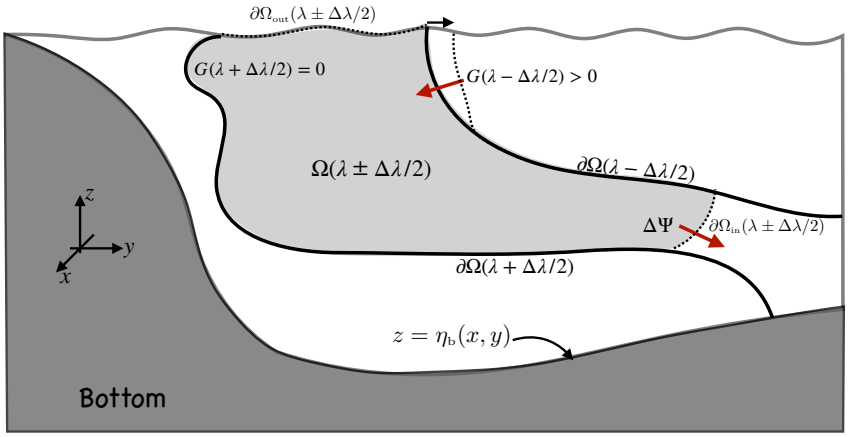

FIGURE 73.9: An example of surface transformation driven circulation oriented according to the Southern Ocean with Antarctica to the left. Here we depict a layer that is exposed to some form of air-sea interaction that causes the interface with $\lambda - \Delta\lambda/2$ to move meridionally. For example, if $\lambda = \gamma$ (neutral density or potential density), then an air-sea buoyancy flux generally causes γ outcrops to move laterally. Movement of the near-surface portion of the $\partial\Omega(\lambda - \Delta\lambda/2)$ interface causes seawater to entrain into the layer and thus contribute to the surface water mass transformation, $G(\lambda - \Delta\lambda/2) > 0$ (red arrow near the surface directed to the south). In turn, the boundary, $\partial\Omega_{\rm in}(\lambda \pm \Delta\lambda/2)$, expands as the near-surface portion of the interface, $\partial\Omega(\lambda - \Delta\lambda/2)$, moves to the north as a result of the entrained new water (black arrow moving to the north). If there is a net convergence of water mass into the layer (as determined by the net mass crossing both layer interfaces $\partial\Omega(\lambda + \Delta\lambda/2)$ and $\partial\Omega(\lambda - \Delta\lambda/2)$), then mass accumulates within the layer $[\lambda - \Delta\lambda/2, \lambda + \Delta\lambda/2]$. There is a steady state mass budget for the layers (i.e., layer mass is constant) only if the same amount of mass that converges into the layer via surface or interior water mass transformation leaves the layer through circulation, Ψ, at the boundary $\partial\Omega_{\rm in}(\lambda \pm \Delta\lambda/2)$.

We depict an example in Figure 73.9 where the surface outcrop of the layer is exposed to air-sea interactions that lead to a meridional movement of the interface $\lambda - \Delta\lambda/2$. This movement laterally entrains mass into the layer. If there is a net convergence of mass into the layer, then the layer mass increases. A steady state mass budget for the layer is reached if the amount of mass entrained through surface transformation is reflected in the same mass leaving through the circulation at the open boundary, $\partial\Omega_{\rm in}(\lambda \pm \Delta\lambda/2)$. We depict another case in Figure 73.10, here focusing on how a meridional gradient in the surface buoyancy loss causes entrainment into buoyancy layers.

These and other statements related to the water mass budget are rather routine mathematically. Yet since the mass budget is formulated over layers, the mass budget offers the means to make very general statements about the circulation even without a direct measurement of the flow. This is a key power of water mass transformation theory.

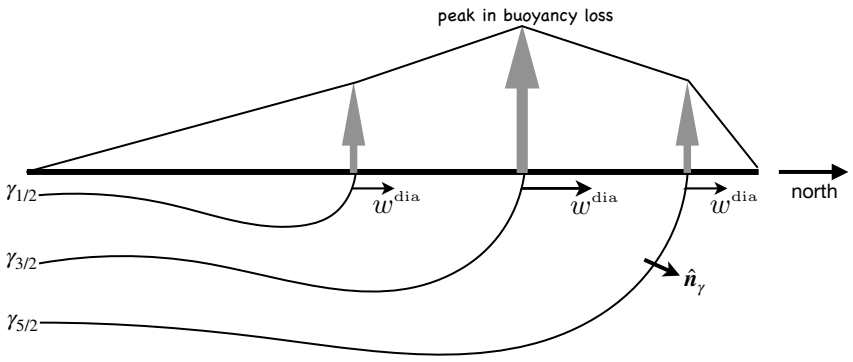

FIGURE 73.10: An example of surface water mass transformation, here illustrating the effects of transformation due to a meridional gradient in the surface buoyancy loss (we here assume that λ is buoyancy as measured by the neutral density, γ). The example is oriented for the northern hemisphere with increasing latitudes to the north/right. Buoyancy loss is denoted by the thick vertical arrows indicating the removal of buoyancy from the ocean, thus causing surface water to loose buoyancy and thus get more dense. The surface buoyancy loss causes γ interfaces to migrate to the south (denser water moves southward)), which in turn causes dianeutral mass flux to move from lighter layers to denser layers (black vectors pointed to the north, w^{dia}). With a peak in the buoyancy loss at a particular latitude, more entrainment is driven into the layer to the north of the peak (water converges to the layer $\gamma_{3/2} \leq \gamma \leq \gamma_{5/2}$) and less entrainment into the layer to the south (water diverges from the layer $\gamma_{1/2} \leq \gamma \leq \gamma_{3/2}$).

73.7.2 Further study

Much of the formalism in this section follows that reviewed by *Groeskamp et al.* (2019). This paper offers specific examples of water mass transformation analysis as well as citations to numerous research papers.

73.8 Buoyancy water mass transformation

In Section 73.2 we considered the transformation of water masses as defined by buoyancy classes, with $\lambda = \gamma$ where γ is a field whose isosurfaces approximate constant buoyancy directions; i.e., the neutral directions from Section 30.5. We here fill in further details for such buoyancy water mass analysis.

73.8.1 Material time changes to S and Θ

The material time derivative of γ can be written as the sum of contributions from salinity and Conservative Temperature

$$\rho \dot{\gamma} = \frac{\partial \gamma}{\partial S} \rho \dot{S} + \frac{\partial \gamma}{\partial \Theta} \rho \dot{\Theta}. \tag{73.99}$$

Following the decomposition of the water mass transformation in Section 73.4.3, for a general tracer, we here write the material time derivatives in the form

$$\rho \dot{S} = -\nabla \cdot \boldsymbol{J}^{(S)}_{\text{int}} - \boldsymbol{J}^{(S)}_{\text{out}} \cdot \hat{\boldsymbol{n}}\, \delta(z-\eta) - \boldsymbol{J}^{(S)}_{\text{bot}} \cdot \hat{\boldsymbol{n}}\, \delta(z-\eta_{\text{b}}) \tag{73.100a}$$

$$\rho \dot{\Theta} = -\nabla \cdot \boldsymbol{J}^{(\Theta)}_{\text{int}} - \boldsymbol{J}^{(\Theta)}_{\text{out}} \cdot \hat{\boldsymbol{n}}\, \delta(z-\eta) - \boldsymbol{J}^{(\Theta)}_{\text{bot}} \cdot \hat{\boldsymbol{n}}\, \delta(z-\eta_{\text{b}}), \tag{73.100b}$$

where we assumed there are no interior sources of S or Θ. The surface and bottom boundary contributions are weighted by Dirac delta distributions and projected into the normal direction along the two respective boundary surfaces. Following from the decomposition of water mass transformation given by equation (73.50), we are thus led to the following form for buoyancy

transformation

$$G(\gamma) = \underbrace{-\lim_{\delta\gamma\to 0}\frac{1}{\delta\gamma}\int_{\Omega(\gamma\pm\delta\gamma/2)}\left(\frac{\partial\gamma}{\partial S}\,\nabla\cdot\boldsymbol{J}^{(S)}_{\text{int}} + \frac{\partial\gamma}{\partial\Theta}\,\nabla\cdot\boldsymbol{J}^{(\Theta)}_{\text{int}}\right)\mathrm{d}V}_{\text{interior buoyancy transformation = volume integral of convergence}}$$
$$\underbrace{-\lim_{\delta\gamma\to 0}\frac{1}{\delta\gamma}\int_{\partial\Omega_{\mathsf{out}}(\gamma\pm\delta\gamma/2)}\left(\frac{\partial\gamma}{\partial S}\,\boldsymbol{J}^{(S)}_{\text{out}} + \frac{\partial\gamma}{\partial\Theta}\,\boldsymbol{J}^{(\Theta)}_{\text{out}}\right)\cdot\hat{\boldsymbol{n}}\,\mathrm{d}\mathcal{S}}_{\text{surface buoyancy transformation = area integral of surface boundary fluxes}}$$
$$\underbrace{-\lim_{\delta\gamma\to 0}\frac{1}{\delta\gamma}\int_{\partial\Omega_{\mathsf{bot}}(\gamma\pm\delta\gamma/2)}\left(\frac{\partial\gamma}{\partial S}\,\boldsymbol{J}^{(S)}_{\text{bot}} + \frac{\partial\gamma}{\partial\Theta}\,\boldsymbol{J}^{(\Theta)}_{\text{bot}}\right)\cdot\hat{\boldsymbol{n}}\,\mathrm{d}\mathcal{S}}_{\text{bottom buoyancy transformation = area integral of bottom boundary fluxes}}. \tag{73.101}$$

This expression is explored in the remainder of this section.

73.8.2 Interior buoyancy water mass transformation

Contributions from cabbeling, thermobaricity, and halobaricity (Section 72.3) arise from the interior transformation appearing in equation (73.101). Furthermore, in the special case of a linear equation of state, whereby $\nabla(\partial\gamma/\partial\Theta) = 0$ and $\nabla(\partial\gamma/\partial S) = 0$, then equation (73.54) means that the global integral of the interior transformation vanishes

$$\int_{\gamma_{-\infty}}^{\gamma_\infty} G_{\text{int}}(\gamma)\,\mathrm{d}\gamma = \int_{\mathscr{R}}\left(\frac{\partial\gamma}{\partial S}\,\nabla\cdot\boldsymbol{J}^{(S)}_{\text{int}} + \frac{\partial\gamma}{\partial\Theta}\,\nabla\cdot\boldsymbol{J}^{(\Theta)}_{\text{int}}\right)\mathrm{d}V = 0 \quad \text{linear equation of state,} \tag{73.102}$$

where $\mathscr{R}$ is the global ocean domain. By inference, we conclude that any nonzero result for this integral is a global measure of the effects from the nonlinear equation of state

$$\text{contribution from nonlinear equation of state} = \int_{\gamma_{-\infty}}^{\gamma_\infty} G_{\text{int}}(\gamma)\,\mathrm{d}\gamma. \tag{73.103}$$

73.8.3 Surface non-advective flux for S and Θ

We review a few of the distinct characteristics of surface non-advective fluxes of S and Θ as detailed in Section 72.5.2, here working with salinity, S, rather than salt concentration, $\mathsf{S} = S/1000$.

Non-advective salt flux

The non-advective surface boundary flux for salt is given by equation (72.67), here written as

$$-\boldsymbol{J}^{(\mathsf{S})}\cdot\hat{\boldsymbol{n}} = \mathcal{Q}_{\mathsf{S}}^{\text{non-adv}} + (S_{\mathsf{m}} - S)\,\mathcal{Q}_{\mathsf{m}}, \tag{73.104}$$

where $\mathcal{Q}_{\mathsf{S}}^{\text{non-adv}}$ is a non-advective salt flux, such as might arise from parameterized turbulent transfer. For the salt concentration of water crossing the ocean surface, we generally take $S_{\mathsf{m}} = 0$ for precipitation, evaporation, and river runoff, whereas $S_{\mathsf{m}} \neq 0$ for ice melt and formation. Furthermore, the boundary term, $S = S(z = \eta)$, is commonly approximated by the bulk salt concentration in the upper ocean.

Non-advective flux for Conservative Temperature

For Conservative Temperature we follow the discussion in Section 72.5.3, whereby the non-advective flux is given by equation

$$-\boldsymbol{J}^{(\Theta)} \cdot \hat{\boldsymbol{n}} = \mathcal{Q}_{\Theta}^{\text{non-adv}} + (\Theta_{\mathsf{m}} - \Theta)\, \mathcal{Q}_{\mathsf{m}}. \tag{73.105}$$

It is common to approximate the difference $\Theta_{\mathsf{m}} - \Theta(z = \eta) = 0$, in which case the non-advective flux is just due to turbulent and radiative heat fluxes

$$-\boldsymbol{J}^{(\Theta)} \cdot \hat{\boldsymbol{n}} = \mathcal{Q}_{\Theta}^{\text{non-adv}} \text{ if } \Theta_{\mathsf{m}} - \Theta(z = \eta) = 0. \tag{73.106}$$

73.8.4 Surface buoyancy water mass transformation

To touch base with the commonly employed surface buoyancy transformation, insert the surface fluxes into equation (73.101) as per Section 73.8.3 to write

$$G(\gamma)^{\text{surface}} = \lim_{\delta\gamma \to 0} \frac{1}{\delta\gamma} \int_{\partial\Omega_{\text{out}}(\gamma \pm \delta\gamma/2)} \big(\gamma\, \beta\, [\mathcal{Q}_S^{\text{non-adv}} + (S_{\mathsf{m}} - S)\, \mathcal{Q}_{\mathsf{m}}] - \gamma\, \alpha\, [\mathcal{Q}_{\Theta}^{\text{non-adv}} + (\Theta_{\mathsf{m}} - \Theta)\, \mathcal{Q}_{\mathsf{m}}]\big) \mathrm{d}\mathcal{S}, \tag{73.107}$$

where we introduced the thermal expansion and saline contraction coefficients, here defined according to[16]

$$\alpha = -\frac{1}{\gamma} \frac{\partial \gamma}{\partial \Theta} \qquad \text{and} \qquad \beta = \frac{1}{\gamma} \frac{\partial \gamma}{\partial S}. \tag{73.108}$$

Recall that $G(\gamma) > 0$ occurs when water is transformed into regions with larger γ. For example, net surface cooling in the presence of a positive thermal expansion coefficient ($\alpha > 0$) leads to $\mathcal{Q}_{\Theta}^{\text{non-adv}} + (\Theta_{\mathsf{m}} - \Theta)\, \mathcal{Q}_{\mathsf{m}} < 0$. Such cooling then leads to a positive contribution to $G(\gamma)_{\text{surface}}$ as water is transformed from light to heavy γ-classes. Likewise, a positive net salt transport into the upper ocean, $\mathcal{Q}_S^{\text{non-adv}} + (S_{\mathsf{m}} - S)\, \mathcal{Q}_{\mathsf{m}} > 0$, leads to a positive contribution to $G(\gamma)_{\text{surface}}$.

The integrand to equation (73.107) corresponds to minus the surface buoyancy flux derived in Section 72.6.3. The only difference is that we here make use of the surface element, $\mathrm{d}\mathcal{S}$, and the corresponding fluxes $\mathcal{Q}_{\Theta}^{\text{non-adv}}$, $\mathcal{Q}_S^{\text{non-adv}}$, and $\mathcal{Q}_{\mathsf{m}}$. However, if the ocean surface has no overturns, we can write its vertical position as $z = \eta(x, y, t)$ and can also define the horizontal projection of the area element as (see equation (5.33))

$$\mathrm{d}\mathcal{S} = \sqrt{1 + |\nabla \eta|^2}\, \mathrm{d}A. \tag{73.109}$$

In this case we can introduce the fluxes $Q_{\Theta}^{\text{non-adv}}$, $Q_{\mathsf{S}}^{\text{non-adv}}$, and Q_{m} used in Section 72.6.3 via

$$\mathcal{Q}_{\Theta}^{\text{non-adv}}\, \mathrm{d}\mathcal{S} = Q_{\Theta}^{\text{non-adv}}\, \mathrm{d}A \tag{73.110a}$$

$$\mathcal{Q}_S^{\text{non-adv}}\, \mathrm{d}\mathcal{S} = Q_{\mathsf{S}}^{\text{non-adv}}\, \mathrm{d}A \tag{73.110b}$$

$$\mathcal{Q}_{\mathsf{m}}\, \mathrm{d}\mathcal{S} = Q_{\mathsf{m}}\, \mathrm{d}A, \tag{73.110c}$$

to render

$$G(\gamma)^{\text{surface}} = \lim_{\delta\gamma \to 0} \frac{1}{\delta\gamma} \int_{\partial\Omega_{\text{out}}(\gamma \pm \delta\gamma/2)} \big(\gamma\, \beta\, [Q_{\mathsf{S}}^{\text{non-adv}} + (S_{\mathsf{m}} - S)\, Q_{\mathsf{m}}] - \gamma\, \alpha\, [Q_{\Theta}^{\text{non-adv}} + (\Theta_{\mathsf{m}} - \Theta)\, Q_{\mathsf{m}}]\big) \mathrm{d}A. \tag{73.111}$$

[16] In practice, it is common to replace the factor of γ^{-1} with ρ_o^{-1} on the right hand side of equation (73.108), with ρ_o the constant Boussinesq reference density from Chapter 29.

Integrating the surface transformation (73.111) over all γ-classes leads to the identity[17]

$$\int_{\gamma_{-\infty}}^{\gamma_\infty} G(\gamma)^{\text{surface}}\, \mathrm{d}\gamma = \int_{z=\eta} \big(\gamma\, \beta\, [Q_{\mathsf{S}}^{\text{non-adv}} + (S_{\mathsf{m}} - S)\, Q_{\mathsf{m}}] - \gamma\, \alpha\, [Q_{\Theta}^{\text{non-adv}} + (\Theta_{\mathsf{m}} - \Theta)\, Q_{\mathsf{m}}]\big) \mathrm{d}A. \quad (73.112)$$

This equality means that the diagnosed surface transformation, $G(\gamma)^{\text{surface}}$, which is obtained by binning surface fluxes into γ-classes, must properly add up to the area integrated surface fluxes as weighted by the surface value of γ. This equality can be a useful check on the integrity of numerical binning code used to diagnose surface water mass transformation.

73.9 Tracer mass analysis

In Sections 73.5 and 73.6 we developed the budgets for λ within layers defined λ. Here we extend that analysis to develop budgets for a tracer concentration, C, localized in a region within a layer of buoyancy, γ, as depicted in Figure 73.11. The upper panels to this figure illustrate a tracer patch in geographic/depth $\boldsymbol{x}$-space along with isolines of buoyancy, whereas the lower panels show the tracer distribution (histogram) binned within the buoyancy classes ($\boldsymbol{q}$-space). If the tracer is mixed within a layer, such as via the neutral diffusion process of Section 71.4, then the tracer patch is spread laterally within the buoyancy layer and yet the distribution (lower panel) is unchanged. In contrast, if the tracer is mixed across layer interfaces then the tracer distribution is spread within buoyancy space.

Another means to alter the tracer distribution is to modify the buoyancy field. This situation is especially common for tracer near the surface, where boundary buoyancy forcing can act to move the layers thus causing tracer to move between layers even if the tracer patch is stationary in $\boldsymbol{x}$-space. That is, if the tracer moves at a velocity distinct from the buoyancy surfaces, then its distribution within buoyancy classes will change.

73.9.1 General form of the mass budget

As depicted in Figure 73.11 for buoyancy layers, and Figure 73.12 for generic layers, there are two general processes whereby a tracer distribution within layers can be modified: (i) the tracer can mix between layers and (ii) the layers can move relative to the tracer. These ideas transcend buoyancy and thus can be applied to any scalar field, λ, used to classify water masses. We quantify these two processes by writing the time change of tracer content within a λ-layer, which is arrived at by applying the Leibniz-Reynolds transport theorem from Section 20.2.4 to a λ-layer

$$\frac{\mathrm{d}}{\mathrm{d}t} \Delta M_{\mathsf{C}}(\lambda \pm \Delta\lambda/2) = \int_{\Omega(\lambda \pm \Delta\lambda/2)} \rho\, \dot{C}\, \mathrm{d}V - \oint_{\partial\Omega(\lambda \pm \Delta\lambda/2)} \rho\, C\, (\boldsymbol{v} - \boldsymbol{v}^{(\mathrm{b})}) \cdot \hat{\boldsymbol{n}}\, \mathrm{d}\mathcal{S}, \quad (73.113)$$

where

$$\Delta M_{\mathsf{C}}(\lambda \pm \Delta\lambda/2) = \int_{\Omega(\lambda \pm \Delta\lambda/2)} \rho\, C\, \mathrm{d}V \quad (73.114)$$

is the mass of tracer within the layer. The volume integral on the right hand side of equation (73.113) arises from material time changes to the tracer within the layer, whereas the surface integral arises from dia-surface transport across the layer boundary.

[17] The density bound $\gamma_{-\infty}$ is a constant that is lower than any γ realized in the global domain, whereas γ_∞ is a constant that is larger than any realized γ.

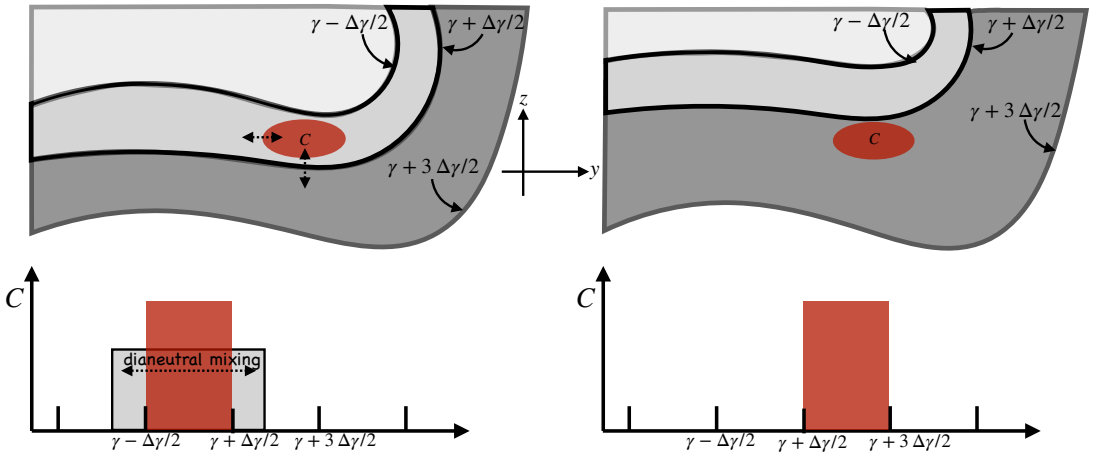

FIGURE 73.11: Depicting a tracer patch within the buoyancy layer bounded by the interface values $[\gamma - \Delta\gamma/2, \gamma + \Delta\gamma/2]$ (left panel) and $[\gamma + \Delta\gamma/2, \gamma + 3\,\Delta\gamma/2]$ (right panel). The upper panels show the tracer and buoyancy in geographic/depth $\boldsymbol{x}$-space whereas the bottom panels show the tracer distribution (histogram) binned according to buoyancy ($\boldsymbol{q}$-space). There are two general means to modify the distribution of tracer within the buoyancy classes. The first occurs via dianeutral mixing that spreads the tracer distribution to other buoyancy layers as depicted by the vertical arrow in the upper left panel and the horizontal arrows in the lower left panel. The lateral arrow in the upper left panel depicts neutral diffusion, which laterally spreads the tracer within a layer but does not alter the distribution across layers (see Section 71.4). The second means to alter the distribution occurs when the buoyancy surfaces move relative to the tracer. This scenario is depicted in the lower right panel whereby the tracer patch originally in buoyancy layer $[\gamma - \Delta\gamma/2, \gamma + \Delta\gamma/2]$ now finds itself in the layer $[\gamma + \Delta\gamma/2, \gamma + 3\,\Delta\gamma/2]$. This depiction is not realistic, since motion of interior buoyancy surfaces generally occurs along with mixing of tracer patches. Nonetheless, this example emphasizes that motion of the buoyancy surfaces need not precisely coincide with motion of the tracer patch.

73.9.2 Tracer processes

We determine the material time changes for a conservative tracer according to the convergence of a flux

$$\rho\, \dot{C} = \rho\, \frac{\mathrm{D}C}{\mathrm{D}t} = -\nabla \cdot \boldsymbol{J}. \tag{73.115}$$

Many biogeochemical tracers have additional source terms beyond the flux convergence considered here. As in Section 73.4.3, sources can be readily incorporated into the following by adding a source tendency term that acts throughout a layer and not just at the layer boundaries.

The divergence theorem converts the convergence, $-\nabla \cdot \boldsymbol{J}$, into the area integral of fluxes over the layer boundaries, including interior layer interfaces as well as intersections with the surface and bottom boundaries. For the interior interfaces it is typically simpler diagnostically to bin the volume integrated material time changes within the λ-classes. In contrast, the surface and bottom boundary contributions are fed into the budget via Neumann boundary conditions applied to the flux $\boldsymbol{J}$

$$\boldsymbol{J} \cdot \hat{\boldsymbol{n}}\, \mathrm{d}\mathcal{S} = \text{boundary tracer transport}. \tag{73.116}$$

Note that when there is an advective/skew diffusive component to the subgrid scale flux (Chapters 70 and 71), then it adds to the resolved advective component to render a residual mean material time operator

$$\rho\, \frac{\mathrm{D}^{\dagger} C}{\mathrm{D}t} = -\nabla \cdot \boldsymbol{J}^{\text{non-adv}}, \tag{73.117}$$

where

$$\frac{\mathrm{D}^{\dagger}}{\mathrm{D}t} = \frac{\partial}{\partial t} + (\boldsymbol{v} + \boldsymbol{v}^{*}) \cdot \nabla, \tag{73.118}$$

with $\boldsymbol{v}^{*}$ an eddy-induced velocity (see Section 71.1). For the purposes of water mass transforma-

tion analysis, we write

$$\dot{C} = \frac{\mathrm{D}^{\dagger} C}{\mathrm{D}t}, \tag{73.119}$$

thus incorporating the eddy-induced stirring into the kinematic expression for the material time derivative.

There are many interior and boundary proceses that contribute to $\dot{C}$ within a layer. Write the following as a general expression for these contributions to the layer budget

$$\Delta E_{\mathsf{C}}(\lambda \pm \Delta\lambda/2) = \int_{\Omega(\lambda \pm \Delta\lambda/2)} \rho\, \dot{C}\, \mathrm{d}V = -\int_{\Omega(\lambda \pm \Delta\lambda/2)} \nabla \cdot \boldsymbol{J}\, \mathrm{d}V \tag{73.120}$$

which is sometimes usefully decomposed into interior and surface boundary processes

$$\Delta E^{\mathsf{int}}_{\mathsf{C}}(\lambda \pm \Delta\lambda/2) = \int_{\Omega(\lambda \pm \Delta\lambda/2)} \rho\, \dot{C}^{\mathsf{int}}\, \mathrm{d}V \tag{73.121a}$$

$$\Delta E^{\mathsf{out}}_{\mathsf{C}}(\lambda \pm \Delta\lambda/2) = -\int_{\partial\Omega_{\mathsf{out}}(\lambda \pm \Delta\lambda/2)} \boldsymbol{J} \cdot \hat{\boldsymbol{n}}\, \mathrm{d}\mathcal{S}. \tag{73.121b}$$

If the region boundary intersects the ocean bottom along $\partial\Omega_{\mathsf{bot}}(\lambda \pm \Delta\lambda/2)$, then there is an additional bottom boundary contribution in the form

$$\Delta E^{\mathsf{bot}}_{\mathsf{C}}(\lambda \pm \Delta\lambda/2) = -\int_{\partial\Omega_{\mathsf{bot}}(\lambda \pm \Delta\lambda/2)} \boldsymbol{J} \cdot \hat{\boldsymbol{n}}\, \mathrm{d}\mathcal{S}. \tag{73.122}$$

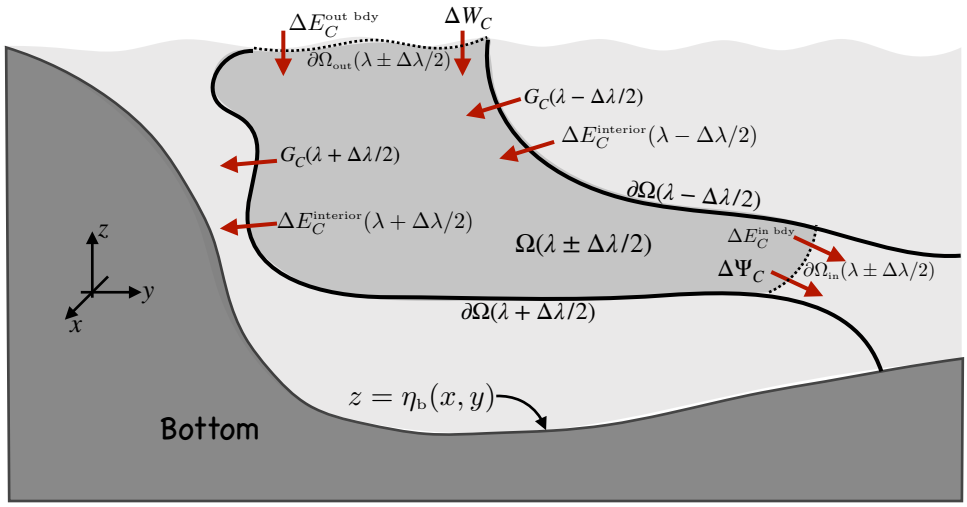

FIGURE 73.12: As for the schematic of a layer seawater mass budget depicted in Figure 73.6, we here illustrate the tracer budget within a layer of seawater with scalar property λ within the range $[\lambda - \Delta\lambda/2, \lambda + \Delta\lambda/2]$ and defined over a geographical/depth domain $\partial\Omega_{\mathsf{in}}(\lambda \pm \Delta\lambda/2) + \partial\Omega_{\mathsf{out}}(\lambda \pm \Delta\lambda/2) + \partial\Omega(\lambda + \Delta\lambda/2) + \partial\Omega(\lambda - \Delta\lambda/2)$. The budget for a tracer, C, over this layer is affected by the transport of tracer substance across the variety of layer boundaries. Transport processes include those determined by mixing and/or radiation across interior and surface boundaries, ΔE_{C} (equation (73.121b)). This term has no associated transfer of seawater mass and thus is absent from the water mass budget in Figure 73.6. Tracer budgets are also affected by processes that move seawater mass across layer boundaries: water mass transformation processes giving rise to $G_{\mathsf{C}}(\lambda \pm \Delta\lambda/2)$ (equation (73.123)); transport across the surface domain boundary, ΔW_{C}, arising from precipitation, evaporation, runoff, and melt (equation (73.124)); and transport within the circulation crossing an interior domain boundary, $\Delta\Psi_{\mathsf{C}}$ (equation (73.125)).

73.9.3 Transport across an interior layer interface

The surface integral in the budget (73.113) involves transport across the layer interfaces, with this transport requiring motion of the interface relative to a fluid particle. The same formalism introduced earlier can be used to compute this transport. That is, we can generalize the transformation equation (73.43e) to write

$$G_{\mathsf{C}}(\lambda) = \int_{\partial\Omega(\lambda)} \rho\, C\, (\boldsymbol{v} - \boldsymbol{v}^{(\mathrm{b})}) \cdot \hat{\boldsymbol{n}}\, \mathrm{d}\mathcal{S} = \frac{\partial}{\partial\lambda} \int_{\Omega(\lambda_0 \leq \lambda)} \rho\, \dot{\lambda}\, C\, \mathrm{d}V. \tag{73.123}$$

As a check, note that for the special case where the tracer concentration is a constant along the layer interface, then $G_{\mathsf{C}}(\lambda) = C\, G(\lambda)$. We consider this special case in Section 73.10 when studying budgets over regions bounded by a tracer isosurface.

73.9.4 Transport across interior and surface boundaries

We now consider the impact on layer tracer mass budgets due to boundary transport. The budget contribution from mass fluxes crossing the ocean surface boundary is determined by making use of the surface kinematic boundary condition (20.84)

$$\Delta W_{\mathsf{C}} = \int_{\partial\Omega_{\mathsf{out}}(\lambda \pm \Delta\lambda/2)} \rho\, C\, (\boldsymbol{v} - \boldsymbol{v}^{(\mathrm{b})}) \cdot \hat{\boldsymbol{n}}\, \mathrm{d}\mathcal{S} = \int_{\partial\Omega_{\mathsf{out}}(\lambda \pm \Delta\lambda/2)} Q_{\mathsf{m}}\, C_{\mathrm{m}}\, \mathrm{d}A, \tag{73.124}$$

where C_{m} is the tracer concentration within the mass transported across the boundary.[18] As a check, note that in the special case of a constant tracer concentration in the mass transported across the boundary, then $\Delta W_{\mathsf{C}} = C_{\mathrm{m}}\, \Delta W$, where ΔW is the water mass transported across the ocean free surface as given by equation (73.66).

For the interior open boundary the contribution is written in the generic manner

$$\Delta \Psi_{\mathsf{C}} = \int_{\partial\Omega_{\mathsf{in}}(\lambda \pm \Delta\lambda/2)} C\, \rho\, (\boldsymbol{v} - \boldsymbol{v}^{(\mathrm{b})}) \cdot \hat{\boldsymbol{n}}\, \mathrm{d}\mathcal{S}. \tag{73.125}$$

Again, in the special case where the tracer concentration is a constant, C_{b}, along the interior boundary, then $\Delta \Psi_{\mathsf{C}} = C_{\mathrm{b}}\, \Delta \Psi$, where $\Delta \Psi$ is the seawater mass transport given by equation (73.62).

73.9.5 The layer tracer budget

Bringing all terms together leads to the layer tracer mass budget

$$\frac{\mathrm{d}\Delta M_{\mathsf{C}}}{\mathrm{d}t} + \Delta \Psi_{\mathsf{C}} = \Delta E_{\mathsf{C}} + \Delta W_{\mathsf{C}} - [G_{\mathsf{C}}(\lambda + \Delta\lambda/2) - G_{\mathsf{C}}(\lambda - \Delta\lambda/2)], \tag{73.126}$$

which is directly analogous to the seawater layer mass budget (73.70), with the added term ΔE_{C} arising from material tracer changes. As for the seawater mass budget discussed in Section 73.5.3, the layer tracer budget (73.126) provides the framework for rather general inferences about tracer transport within λ-classes.

73.9.6 Further study

Much in this section follows the treatment given by *Groeskamp et al.* (2019). This paper offers specific examples of tracer mass analysis, which is an area seeing many new applications within

[18] Note that equation (26) in *Groeskamp et al.* (2019) incorrectly writes the integrand in equation (73.124) as $Q_{\mathrm{m}}\, (C_{\mathrm{m}} - C)$.

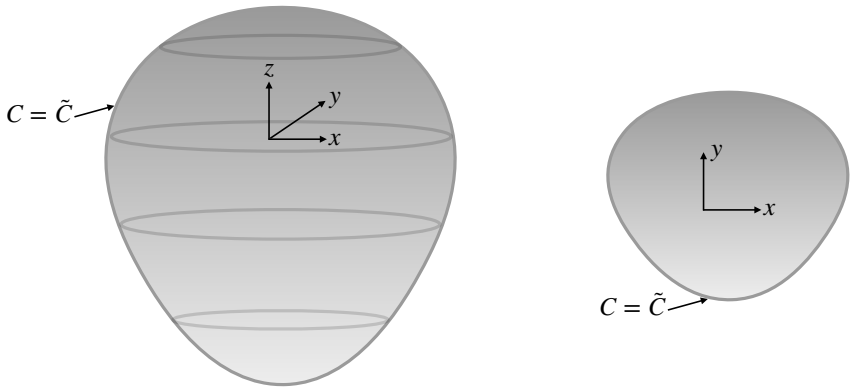

FIGURE 73.13: Left panel: a closed three-dimensional region, $\widetilde{\mathcal{R}}$, with its boundary, $\partial\widetilde{\mathcal{R}}$, defined by a surface of constant tracer concentration, $C = \widetilde{C}$. Right panel: the analog closed two-dimensional region with its boundary defined by a contour of constant tracer concentration, $C = \widetilde{C}$.

the research communities.

73.10 Regions bounded by a tracer contour/surface

In Section 73.9 we developed equations for a layer tracer budget where the scalar field, λ, that defines the layer is generally distinct from the tracer, C, whose budget we are studying. In this section we specialize to the case where we set $\lambda = C$ so that the region boundaries are determined by the tracer whose budget is under study. These budgets were introduced in Sections 73.5 and 73.6, and here we derive some rather useful simplifications that arise as a result of setting $\lambda = C$.

As in Section 73.9, our starting point is the Leibniz-Reynolds budgets from Section 20.2.4 for seawater mass and tracer mass computed over an arbitrary region, $\mathcal{R}$

$$\frac{\mathrm{d}}{\mathrm{d}t}\left[\int_{\mathcal{R}} \rho\, C\, \mathrm{d}V\right] = -\int_{\partial\mathcal{R}} \left[\rho\, C\, (\boldsymbol{v} - \boldsymbol{v}^{(\mathrm{b})}) + \boldsymbol{J}\right] \cdot \hat{\boldsymbol{n}}\, \mathrm{d}\mathcal{S} \tag{73.127a}$$

$$\frac{\mathrm{d}}{\mathrm{d}t}\left[\int_{\mathcal{R}} \rho\, \mathrm{d}V\right] = -\int_{\partial\mathcal{R}} \left[\rho\, (\boldsymbol{v} - \boldsymbol{v}^{(\mathrm{b})})\right] \cdot \hat{\boldsymbol{n}}\, \mathrm{d}\mathcal{S}. \tag{73.127b}$$

The region $\mathcal{R}$ is rather arbitrary, and can in general be disconnected. Throughout this section we make use of the following shorthand notation for region-integrated quantities

$$M = \int_{\mathcal{R}} \rho\, \mathrm{d}V \qquad \text{region seawater mass} \tag{73.128a}$$

$$M_{\mathsf{C}} = \int_{\mathcal{R}} C\, \rho\, \mathrm{d}V \qquad \text{region tracer mass} \tag{73.128b}$$

$$\langle C \rangle = \frac{1}{M}\int_{\mathcal{R}} C\, \rho\, \mathrm{d}V = \frac{M_{\mathsf{C}}}{M} \qquad \text{region averaged tracer concentration.} \tag{73.128c}$$

73.10.1 Closed region bounded by a tracer surface/contour

Consider a closed region, $\widetilde{R}$, bounded by a surface of constant tracer concentration, $C = \widetilde{C}$, such as depicted in Figure 73.13. The tracer budget (73.127a) for this region is given by

$$\frac{\mathrm{d}(M\, \langle C \rangle)}{\mathrm{d}t} = -\widetilde{C} \int_{\partial\widetilde{\mathcal{R}}} \rho\, (\boldsymbol{v} - \boldsymbol{v}^{(\mathrm{b})}) \cdot \hat{\boldsymbol{n}}\, \mathrm{d}\mathcal{S} - \int_{\partial\widetilde{\mathcal{R}}} \boldsymbol{J} \cdot \hat{\boldsymbol{n}}\, \mathrm{d}\mathcal{S} \tag{73.129}$$

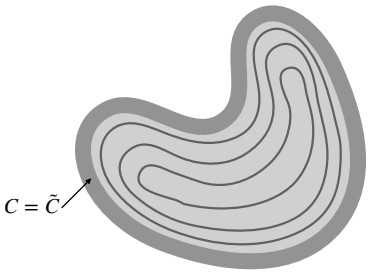

FIGURE 73.14: A two-dimensional region bounded by a finite-thick shell with constant tracer concentration, $C = \widetilde{C}$. Inside the shell region the tracer concentration is not uniform.

where we pulled the tracer concentration outside of the surface integral since, by construction, it is constant on the boundary, $\partial\widetilde{\mathcal{R}}$. Use of the mass budget (73.127b) then leads to the rather tidy result

$$\frac{\mathrm{d}[M\,(\langle C\rangle - \widetilde{C})]}{\mathrm{d}t} = -\int_{\partial\widetilde{\mathcal{R}}} \boldsymbol{J}\cdot\hat{\boldsymbol{n}}\,\mathrm{d}\mathcal{S}. \tag{73.130}$$

The left hand side is the time change of the mass-weighted difference between the region averaged tracer concentration, $\langle C\rangle$, and the value of the tracer concentration defining the region boundary, $\widetilde{C}$. These time changes are driven by a nonzero diffusive tracer transport bringing tracer mass across the region boundary. A nonzero diffusive flux on the region boundary arises only when there is a gradient of tracer concentration across that boundary. In the special case of a zero net diffusive tracer transport across the region boundary, the budget equation (73.130) reaches a steady state whereby

$$\frac{\mathrm{d}}{\mathrm{d}t}\left[M\,(\langle C\rangle - \widetilde{C})\right] = 0 \Longleftrightarrow \int_{\partial\widetilde{\mathcal{R}}} \boldsymbol{J}\cdot\hat{\boldsymbol{n}}\,\mathrm{d}\mathcal{S} = 0. \tag{73.131}$$

A three-dimensional region bounded by a constant tracer concentration is not commonly encountered in large-scale ocean and atmospheric fluids. In contrast, we often encounter quasi-two-dimensional regions as depicted in Figure 73.14, in which one may find two-dimensional regions bounded by a closed contour of constant tracer concentration. For example, in many parts of the ocean and atmosphere transport occurs predominantly along two-dimensional surfaces defined by a constant buoyancy. We may thus find closed contours of tracer concentrations along constant buoyancy surfaces.

To help illustrate a necessary condition to reach a steady state, consider the particular example depicted in Figure 73.14. In this figure, the tracer contour defining the region boundary is a thick shell defined by a uniform concentration $C = \widetilde{C}$. The diffusive flux vanishes at each point within the boundary shell since the tracer concentration is uniform. Hence, the steady budget (73.131) leads to

$$(\langle C\rangle - \widetilde{C})\,\frac{\mathrm{d}M}{\mathrm{d}t} + M\,\frac{\mathrm{d}\langle C\rangle}{\mathrm{d}t} = 0. \tag{73.132}$$

If the total seawater mass within the region is constant, then the averaged tracer concentration is also constant, so that both terms in this steady budget vanish individually. Even so, this configuration does not reach a steady state at each point throughout the domain interior. The reason is that diffusion in the interior causes tracer to move from regions of high concentration to low concentration. Consequently, at any particular point within the domain there is an evolving tracer concentration. The only way for each point to reach a steady state within a region bounded by a tracer contour is for the tracer concentration to be a uniform constant throughout the region interior

$$C = \widetilde{C} \qquad \text{steady state tracer throughout a closed tracer region.} \tag{73.133}$$

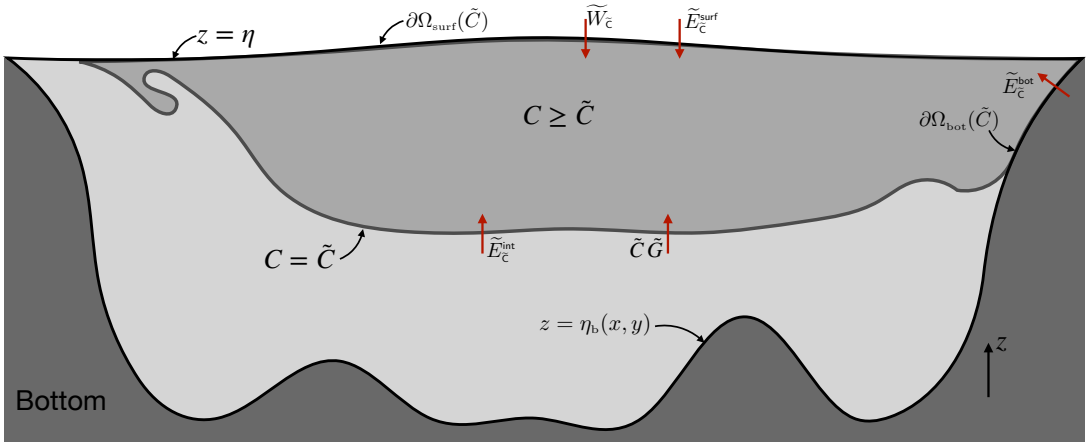

FIGURE 73.15: An ocean region where the tracer concentration is greater than a nominal value, $C \geq \widetilde{C}$. A specific example is with $C = \Theta$, the Conservative Temperature, in which we are concerned with the ocean with temperature greater than $\widetilde{\Theta}$. Here we depict a case where the tracer concentration generally increases upward (as with $C = \Theta$), and yet with vertical stratification not everywhere monotonic, such as for $C = \Theta$ in the high latitudes where salinity effects on density stratification become dominant. Transport processes affecting the budget of C within this region arise from mixing at the interior boundary and surface boundary, $\widetilde{E}^{\text{int}}_{\widetilde{C}}$ and $\widetilde{E}^{\text{surf}}_{\widetilde{C}}$, advection at the surface, $\widetilde{W}_{\widetilde{C}}$, and the tracer weighted water mass transformation across the interior layer boundary, $\widetilde{C}\,\widetilde{G}$. Arrows are oriented in which a positive value for the corresponding term adds tracer to the region.

Diffusion thus expells tracer gradients from steady state regions bounded by closed tracer contours, thus leaving a homogenous interior. We proved this same result from a different perspective in Section 69.8. It is satisfying to see this result follow from the present formalism based on Leibniz-Reynolds.

73.10.2 Region with $C \geq \widetilde{C}$

As a second example of the formalism, consider the tracer budget for a region where the tracer concentration is greater than or equal to a particular tracer value, such as depicted in Figure 73.15. In contrast to the domain in Figure 73.12, here there is no inner boundary. To develop the seawater mass budget and the tracer substance budget, we introduce the seawater mass and tracer mass for the region with $C \geq \widetilde{C}$

$$\widetilde{M} = \int_{C \geq \widetilde{C}} \rho \, dV \tag{73.134a}$$

$$\widetilde{M}_{\widetilde{C}} = \int_{C \geq \widetilde{C}} C \, \rho \, dV = \widetilde{M} \, \langle C \rangle; \tag{73.134b}$$

the terms arising from water mass transformation across the $\widetilde{C}$ interface

$$\widetilde{G} = -\int_{C=\widetilde{C}} \rho \, (\boldsymbol{v} - \boldsymbol{v}^{(b)}) \cdot \hat{\boldsymbol{n}} \, d\mathcal{S} = -\int_{C=\widetilde{C}} \rho \, w^{\text{dia}} \, d\mathcal{S} \tag{73.135a}$$

$$\widetilde{G}_{\widetilde{C}} = -\int_{C=\widetilde{C}} C \, \rho \, (\boldsymbol{v} - \boldsymbol{v}^{(b)}) \cdot \hat{\boldsymbol{n}} \, d\mathcal{S} = -\int_{C=\widetilde{C}} C \, \rho \, w^{\text{dia}} \, d\mathcal{S}; \tag{73.135b}$$

terms arising from ocean surface boundary mass transport

$$\widetilde{W} = -\int_{\partial\Omega_{\text{surf}}(\widetilde{C})} \rho \, (\boldsymbol{v} - \boldsymbol{v}^{(b)}) \cdot \hat{\boldsymbol{n}} \, d\mathcal{S} = \int_{\partial\Omega_{\text{surf}}(\widetilde{C})} Q_m \, dA \tag{73.136a}$$

$$\widetilde{W}_{\widetilde{C}} = -\int_{\partial\Omega_{\text{surf}}(\widetilde{C})} C \, \rho \, (\boldsymbol{v} - \boldsymbol{v}^{(b)}) \cdot \hat{\boldsymbol{n}} \, d\mathcal{S} = \int_{\partial\Omega_{\text{surf}}(\widetilde{C})} C \, Q_m \, dA; \tag{73.136b}$$

and finally, terms arising from subgrid scale transport across the $\widetilde{C}$ interface, ocean surface, and ocean bottom

$$\widetilde{E}^{\text{int}}_{\widetilde{\mathsf{C}}} = -\int_{C=\widetilde{C}} \boldsymbol{J} \cdot \hat{\boldsymbol{n}} \, \mathrm{d}\mathcal{S} \tag{73.137a}$$

$$\widetilde{E}^{\text{surf}}_{\widetilde{\mathsf{C}}} = -\int_{\partial\Omega_{\text{surf}}(\widetilde{C})} \boldsymbol{J} \cdot \hat{\boldsymbol{n}} \, \mathrm{d}\mathcal{S} \tag{73.137b}$$

$$\widetilde{E}^{\text{bot}}_{\widetilde{\mathsf{C}}} = -\int_{\partial\Omega_{\text{bot}}(\widetilde{C})} \boldsymbol{J} \cdot \hat{\boldsymbol{n}} \, \mathrm{d}\mathcal{S}. \tag{73.137c}$$

Recall that $\hat{\boldsymbol{n}}$ is the *outward* normal on a boundary so that positive values for the above transports increase the tracer mass within the region. For equations (73.135a) and (73.135b), we introduced the dia-surface transport velocity according to equation (73.38) for flow across the $C = \widetilde{C}$ layer interface. Likewise, for equations (73.136a) and (73.136b) we made use of the surface kinematic boundary condition (19.88c)

$$\rho \, (\boldsymbol{v} - \boldsymbol{v}^{(s)}) \cdot \hat{\boldsymbol{n}} \, \mathrm{d}\mathcal{S} = -Q_{\mathsf{m}} \, \mathrm{d}A, \tag{73.138}$$

where Q_{m} is the mass transport across the free surface, with $Q_{\mathsf{m}} > 0$ adding mass to the ocean, and $\mathrm{d}A$ is the horizontal projection of the surface area element. By inspection of Figure 73.15, the seawater mass and tracer mass budgets for this region are given by

$$\frac{\mathrm{d}\widetilde{M}}{\mathrm{d}t} = \widetilde{G} + \widetilde{W} \tag{73.139a}$$

$$\frac{\mathrm{d}[\widetilde{M} \, \langle C \rangle]}{\mathrm{d}t} = \widetilde{C} \, \widetilde{G} + \widetilde{W}_{\widetilde{\mathsf{C}}} + \widetilde{E}^{\text{surf}}_{\widetilde{\mathsf{C}}} + \widetilde{E}^{\text{bot}}_{\widetilde{\mathsf{C}}} + \widetilde{E}^{\text{int}}_{\widetilde{\mathsf{C}}}, \tag{73.139b}$$

where we assumed that no mass crosses through the solid earth. Furthermore, along the $\widetilde{C}$-boundary we pulled the tracer concentration outside of the surface integral to write $\widetilde{G}_{\widetilde{\mathsf{C}}} = \widetilde{C} \, \widetilde{G}$.

Just as we did in Section 73.10.1, the tracer budget (73.139b) can be simplified by making use of the seawater mass budget (73.139a) to eliminate the water mass transformation contribution $\widetilde{G}$, thus rendering

$$\frac{\mathrm{d}\widetilde{M}_{\mathsf{I}\widetilde{\mathsf{C}}}}{\mathrm{d}t} = [\widetilde{W}_{\widetilde{\mathsf{C}}} - \widetilde{W} \, \widetilde{C}] + \widetilde{E}^{\text{surf}}_{\widetilde{\mathsf{C}}} + \widetilde{E}^{\text{bot}}_{\widetilde{\mathsf{C}}} + \widetilde{E}^{\text{int}}_{\widetilde{\mathsf{C}}}. \tag{73.140}$$

In this equation we introduced the *internal tracer mass* according to

$$\widetilde{M}_{\mathsf{I}\widetilde{\mathsf{C}}} \equiv \widetilde{M} \, (\langle C \rangle - \widetilde{C}) = \int_{C \geq \widetilde{C}} (C - \widetilde{C}) \, \rho \, \mathrm{d}V. \tag{73.141}$$

For completeness we express the internal tracer mass budget (73.140) in its integral form

$$\frac{\mathrm{d}\widetilde{M}_{\mathsf{I}\widetilde{\mathsf{C}}}}{\mathrm{d}t} = \int_{\partial\Omega_{\text{out}}} \left[Q_{\mathsf{m}} \, (C - \widetilde{C}) \, \mathrm{d}A - \boldsymbol{J} \cdot \hat{\boldsymbol{n}} \, \mathrm{d}\mathcal{S} \right] - \int_{\partial\Omega_{\text{bot}}} \boldsymbol{J} \cdot \hat{\boldsymbol{n}} \, \mathrm{d}\mathcal{S} - \int_{C=\widetilde{C}} \boldsymbol{J} \cdot \hat{\boldsymbol{n}} \, \mathrm{d}\mathcal{S}. \tag{73.142}$$

73.10.3 Comments and further study

Elimination of the water mass transformation, $\widetilde{G}$, from the internal tracer mass budget equations (73.140) and (73.142) offers a practical advantage since $\widetilde{G}$ can be rather noisy in applications. Furthermore, for some applications (e.g., see *Holmes et al.* (2019)) it is sufficient to consider the simpler budget (73.140) for internal tracer mass, rather than the budget (73.139b) for the total tracer mass.

Part XIV

End matter

Appendix A

Glossary of concepts and terms

elements pillar The elements pillar of geophysical fluid mechanics comprises the physical and mathematical formulation of conceptual models used to garner insight into rotating and stratified fluid motion. This pillar is concerned with setting the stage by deductively and descriptively exposing how physical concepts are mathematically expressed to describe geophysical fluid flows. x

emergent phenomena pillar The emergent phenomena pillar of geophysical fluid mechanics studies solutions to equations that describe phenomena, such as waves, instabilities, turbulence, and general circulation, all of which emerge from the fundamental equations based on first principles. These phenomena can emerge in manners that are far from simple to understand deductively, particularly when considering nonlinear behavior such as turbulence. xi

geophysical fluid mechanics A branch of theoretical physics concerned with natural fluid motion on a rotating and gravitating body such as a planet or star, making use of concepts and methods from classical continuum mechanics and thermodynamics. ix

hydrodynamics A branch of fluid mechanics concerned with the flow of a homogeneous (constant density) incompressible fluid. ix

internal gravity waves An internal gravity wave is a transverse wave that is comprised of fluid particles undergoing a simple harmonic oscillation within a continuously and stably stratified buoyancy field. The angular frequency of the oscillation is determined by the buoyancy stratification and the sine of the angle the wave's group velocity makes with respect to the vertical (equivalently, the cosine of the angle the wave's phase velocity makes with horizontal). 1601

irreversible process A physical process that results in the increase of entropy. Processes that increase the entropy of a fluid particle include the mixing of momentum such as through viscous friction; the mixing of matter such as through the diffusion of constituents in a multi-component fluid; and the mixing of enthalpy (diffusion of heat) in a fluid with variable temperature. ix

perfect fluid A fluid that flows in the absence of irreversible processes so that the motion is reversible and the specific ntropy remains constant following a fluid particle. Some authors use the term *ideal fluid*, but we eschew that term to avoid confusion with *ideal gas*. ix

real fluid A fluid whose flow is affected by irreversible processes arising from momentum mixing (nonzero viscous friction); enthalpy mixing (nonzero diffusivity for temperature); matter mixing (nonzero diffusivity of matter constituents); and through sources such as radiation and chemical reactions. The specific entropy increases following a fluid particle moving in a real fluid. ix

specular reflection Wave packets, in the geometrical optics approximation, exhibit specular reflection if the angle the incident wave packet makes with the reflecting surface is preserved upon reflection. Rossby waves, electromagnetic waves, and acoustic waves exhibit specular reflection, whereas internal gravity waves and inertial waves exhibit non-specular reflection. 1624

Appendix B

List of Acronyms

GFM geophysical fluid mechanics ix

Appendix C

List of Symbols

Many symbols encountered in this book are defined local to their usage and are not used far outside of that location. Many other symbols appear in a variety of places and are included in the tables given below. Additionally, we generally aim to respect the following conventions.

- Many symbols are adorned with extra labels. One usage exposes tensor indices, with tensor indices written using the slanted math font, such as F^i for the component i of the vector $\mathbf{F}$. Another usage expresses part of the name for the symbol, with the label written with the upright sans serif. Examples include the "b" in η_{b} for the position of the bottom solid boundary of a fluid domain, and the "b" in ∇_{h} for the horizontal gradient operator.
- We strive for unique symbols to represent distinct mathematical and/or physical objects. Yet that goal must confront the multitude of mathematical expressions appearing in this book. We have chosen, on rare occasions, to allow some symbols to carry multiple meanings. In such cases we emphasize the particular meaning of the symbol to help avoid confusion with its alternative meaning.

NON-DIMENSIONAL NUMBERS

SYMBOL	NAME	MEANING
Bu	Burger	Bu = (deformation radius/horizontal length scale of flow)^2 = $(L_{\mathsf{d}}/L)^2$
Db	Deborah	Db = relaxation time/observation time
Ek	Ekman	Ek = vertical frictional acceleration/planetary Coriolis acceleration
Fr	Froude	Fr = fluid particle speed/fluid wave speed = U/c
Ge	Geostrophic	Ge = horizontal accelerations from Coriolis/pressure acceleration = $f\,U\,L\,\rho_{\mathsf{o}}/p$
Kn	Knudsen	Kn = molecular mean free path/macroscopic length scale
Ma	Mach	Ma = fluid particle speed/sound wave speed = U/c_{s}
Re	Reynolds	Re = inertial acceleration/frictional acceleration = $U\,L/\nu$
Ri	Richardson	Ri = squared buoyancy frequency/squared vertical shear
Ro	Rossby	Ro = horizontal inertial acceleration/planetary Coriolis acceleration = $U/(f\,L)$

SYMBOL	MEANING
$\mathcal{A}$	wave action
$A^{\mathrm{L}}(\boldsymbol{a}, T)$	Lagrangian representation of a fluid property as a function of material coordinates and time
$\boldsymbol{a}$	coordinate position for a fluid particle using arbitrary material/Lagrangian coordinates
$\mathbf{A}, \boldsymbol{A}$	second order skew symmetric tensor with elements satisfying $A^{mn} = -A^{nm}$
A^{v}	Avogadro's number: $A^{\mathrm{v}} = 6.0222 \times 10^{23}$ mole^{-1}
$\mathbf{B}$	baroclinicity vector: $\mathbf{B} = \nabla\rho \times (-\rho^{-1}\nabla p) = (\nabla\rho \times \nabla p)/\rho^2$
$\mathcal{B}$	base (or reference) manifold for describing the space of continuum matter
b	Archimidean buoyancy with $b > 0$ for relatively light fluid: $b = -g\,(\rho - \rho_{\mathrm{b}})/\rho_{\mathrm{b}}$
C	tracer concentration = mass of tracer per mass of fluid = tracer mass fraction
C_{d}	dimensionless bottom drag coefficient: $C_{\mathrm{d}} > 0$
$\mathcal{C}$	circulation of velocity around the boundary of a surface $\mathcal{C} \equiv \oint_{\partial S} \boldsymbol{v} \cdot \mathrm{d}\boldsymbol{r}$
c_{grav}	shallow water gravity wave speed: $c_{\mathrm{grav}} = \sqrt{g\,H}$
$\boldsymbol{c}_{\mathrm{g}}$	wave group velocity, given by wavevector gradient of dispersion relation: $\boldsymbol{c}_{\mathrm{g}} = \nabla_{\boldsymbol{k}}\varpi(\boldsymbol{k})$
$\boldsymbol{c}_{\mathrm{p}}$	wave phase velocity: $\boldsymbol{c}_{\mathrm{p}} = C_{\mathrm{p}}\,\hat{\boldsymbol{k}}$
C_{p}	wave phase speed
c_{s}	sound speed: $c_{\mathrm{s}}^{-2} = [\partial\rho/\partial p]_{\Theta,S}$
c_{p}	heat capacity at constant pressure: $c_{\mathrm{p}} = [\partial\mathcal{H}/\partial T]_{p,C}$
$\mathbf{E}, \boldsymbol{E}$	second order eddy transport tensor for tracers, and with elements E^{mn}
$\mathbb{E}^1, \mathbb{E}^2, \mathbb{E}^3$	one (line), two (plane), and three dimensional Euclidean space
$\mathcal{E}$	total energy per mass of a fluid element = sum of internal plus mechanical energies
$\boldsymbol{e}_a$	basis vectors for a chosen coordinate system, with index $a = 1, 2, 3$ for 3-dimensional space
$\boldsymbol{e}^a$	basis one-forms for a chosen coordinate system, with index $a = 1, 2, 3$ for 3-dimensional space
f	Coriolis parameter, also the planetary vorticity: $f = 2\,\Omega\,\sin\phi$
$f_{\circ}$	Coriolis parameter at a particular latitude: $f_{\circ} = 2\,\Omega\,\sin\phi_0$
$\mathbf{F}$	frictional acceleration vector
$F^i{}_I$	deformation matrix, which transforms between $\boldsymbol{x}$-space (Eulerian) and $\boldsymbol{a}$-space (Lagrangian)
$G = G^{\mathrm{grv}}$	Newton's gravitational constant: $G = 6.674 \times 10^{-11}$ N m^2 kg^{-2} $= 6.674 \times 10^{-11}$ m^3 kg^{-1} s^{-2}
$G(\boldsymbol{x}\vert\boldsymbol{x}_0)$	Green's function with $\boldsymbol{x}$ the observation point (or field point) and $\boldsymbol{x}_0$ the source point
$\widetilde{G}(\boldsymbol{x}\vert\boldsymbol{x}_0)$	modified Green's function for Laplace's operator with Neumann boundary conditions
$G^{\ddagger}(\boldsymbol{x}\vert\boldsymbol{x}_0)$	adjoint Green's function for non-self adjoint operators such as the diffusion operator
$\mathcal{G}(\boldsymbol{x}\vert\boldsymbol{x}_0)$	free space Green's function; i.e., the Green's function without boundaries
$\mathbf{G}$	velocity gradient tensor with elements $G^i{}_j$
$\mathcal{G}$	Gibbs potential per mass of a fluid element
g_{e}	gravitational acceleration from central gravity due to just the mass of the planet
g	effective gravitational acceleration from central gravity + planetary centrifugal: $g \approx 9.8$ m s^{-2}
g^{r}	reduced gravity defined between to shallow water layers: $g^{\mathrm{r}}_{\mathrm{k}+1/2} = g\,(\rho_{\mathrm{k}+1} - \rho_{\mathrm{k}})/\rho_{\mathrm{ref}} \ll g$

SYMBOL	MEANING
$\mathcal{g}$	metric tensor (symmetric positive definite second order tensor) with components $\mathcal{g}_{ab}$
g	square root of the metric tensor determinant: $g = \sqrt{\det(\mathcal{g}_{mn})}$
g^{E}	square root of the metric tensor determinant using Eulerian coordinates: $g^{\mathsf{E}} = \sqrt{\det(\mathcal{g}(\boldsymbol{x})}$
g^{L}	square root of the metric tensor determinant using Lagrangian coordinates: $g^{\mathsf{L}} = \sqrt{\det(\mathcal{g}(\boldsymbol{a}, T)}$
h_{k}	layer thickness for a shallow water fluid: $h_{\mathsf{k}} = \eta_{\mathsf{k}-1/2} - \eta_{\mathsf{k}+1/2} = \delta_{\mathsf{k}}\eta_{\mathsf{k}-1/2}$
h	layer thickness for a continuously stratified fluid: $h = \overline{\hbar}\,\delta\sigma$
$\hbar$	specific thickness for a generalized vertical coordinate: $\hbar = \partial z/\partial\sigma = 1/(\partial\sigma/\partial z)$
$\mathscr{H}(x)$	Heaviside step function: $\mathscr{H}(x) = 0$ for $x < 0$ whereas $\mathscr{H}(x) = 1$ for $x > 0$
H	vertical length scale of the flow under consideration
H	sometimes used as depth of the ocean bottom: $z = -H(x, y) = \eta_{\mathsf{b}}(x, y)$
H	Hamiltonian energy function
$\mathscr{H}$	Hamiltonian density used in field theory; dimensions energy per volume (when in 3d space)
$\mathcal{H}$	enthalpy per mass of a fluid element
$\mathbf{I}$	unit tensor or Kronecker tensor: $\mathbf{I} = \delta^{ab}\,\boldsymbol{e}_a \otimes \boldsymbol{e}_b = \delta^a{}_b\,\boldsymbol{e}_a \otimes \boldsymbol{e}^b = \delta_a{}^b\,\boldsymbol{e}^a \otimes \boldsymbol{e}_b = \delta_{ab}\,\boldsymbol{e}^a \otimes \boldsymbol{e}^b$
$\mathcal{I}$	internal energy per mass of a fluid element
i	$\mathrm{i} = \sqrt{-1}$ used for imaginary numbers
i, j, k	tensor indices/labels for Eulerian coordinates
I, J, K	tensor indices/labels for Lagrangian coordinates
$\mathrm{Im}[\,]$	imaginary part of a complex number; e.g., $\mathrm{Im}[e^{-\mathrm{i}\,\omega\,t}] = -\sin(\omega\,t)$
$\mathbf{J}$	tracer flux; for material tracers the dimensions are mass per time per area
$\boldsymbol{k}$	wavevector (dimensions inverse length) for a wave of wavelength $\Lambda = 2\pi/\lvert\boldsymbol{k}\rvert$
$\hat{\boldsymbol{k}}$	unit vector in the direction of a wave: $\boldsymbol{k} = \hat{\boldsymbol{k}}\,\lvert\boldsymbol{k}\rvert$ (as distinct from the vertical unit vector, $\hat{\boldsymbol{z}}$)
$\lvert\boldsymbol{k}\rvert$	wavenumber: $\lvert\boldsymbol{k}\rvert = 2\pi/\Lambda$
K	kinetic energy for a particle of mass m: $K = m\,\boldsymbol{V}\cdot\boldsymbol{V}/2$
K	kinetic energy for a system of N particles, $\sum_{n=1}^{N} m^n\,\boldsymbol{V}^n\cdot\boldsymbol{V}^n$
$\mathcal{K}$	kinetic energy per mass of a fluid element arising from macroscopic motion: $\mathcal{K} = \boldsymbol{v}\cdot\boldsymbol{v}/2$
$\mathcal{K}^{\mathrm{hyd}}$	kinetic energy per mass for an approximate hydrostatic flow: $\mathcal{K}^{\mathrm{hyd}} = \boldsymbol{u}\cdot\boldsymbol{u}/2$
$\mathcal{K}^{\mathrm{sw}}$	kinetic energy per horizontal area for a shallow water layer: $\mathcal{K}^{\mathrm{sw}} = \rho\,h\,\boldsymbol{u}\cdot\boldsymbol{u}/2$
$\mathbf{K}, \boldsymbol{K}$	positive and symmetric second order tensor parameterizing diffusive mixing
k	integer index to label a layer in a shallow water model with $\mathsf{k} = 1, N$ layers ($\mathsf{k} = 1$ is top layer)
k_{B}	Boltzmann constant: $k_{\mathrm{B}} = 1.3806 \times 10^{-23}$ m^2 kg s^{-2} K^{-1}
k_{R}	Rossby height/depth: $k_{\mathsf{R}} = \lvert\boldsymbol{k}\rvert\,N/f_0$ with horizontal wavenumber $\lvert\boldsymbol{k}\rvert = \sqrt{k_x^2 + k_y^2}$
L	Lagrangian used in Lagrangian mechanics: kinetic minus potential energies: $L = K - P$
L	length scale for a particular physical feature and commonly used in scale analysis

SYMBOL	MEANING
$\mathcal{L}$	Lagrangian density used in field theory; dimensions energy per volume (when in 3d space)
L_{d}	deformation radius: (a) shallow water $L_{\mathsf{d}} = \sqrt{g\,H}/f$; (b) continuous internal $L_{\mathsf{d}} = H\,N/f$
$\mathcal{M}$	mechanical energy per mass of a fluid element arising from macroscopic motion
$\mathcal{M}^{\mathrm{sw}}$	mechanical energy per area of a shallow water fluid column: $\mathcal{M}^{\mathrm{sw}} = \mathcal{K}^{\mathrm{sw}} + \mathcal{P}^{\mathrm{sw}}$
$\mathbf{M}$	moment of inertia tensor
$\mathbf{M}$	potential momentum vector: $\mathbf{M} = \mathbf{u} + 2\,\mathbf{\Omega} \times \mathbf{X}$
M	Montgomergy potential for continuously stratified fluid $M = \varphi - b\,z$
$M_{\mathsf{k}}^{\mathrm{dyn}}$	Montgomergy potential for a shallow water layer: $M_{\mathsf{k}}^{\mathrm{dyn}} = \sum_{\mathsf{j}=0}^{\mathsf{k}-1} g^{\mathsf{r}}_{\mathsf{j}+1/2}\,\eta_{\mathsf{j}+1/2}$
M^{air}	mass per mole of air: $M^{\mathsf{air}} = 28.8 \times 10^{-3}$ kg mole^{-1}
N	buoyancy frequency
$\mathcal{O}$	order of magnitude
P	potential energy of a physical system, with corresponding force $\boldsymbol{F} = -\nabla P$
$\mathcal{P}_{\mathsf{k}}^{\mathrm{sw}}$	potential energy per horizontal area for a shallow water fluid: $\mathcal{P}_{\mathsf{k}}^{\mathrm{sw}} = g\,\rho_{\mathsf{k}} \int_{\eta_{\mathsf{k}+1/2}}^{\eta_{\mathsf{k}-1/2}} z\,\mathrm{d}z$
$\mathcal{P}$	phase of a wave
$\mathcal{P}_\sigma$	generalized momentum for discrete particle system: $\mathcal{P}_\sigma = \partial L/\partial\dot{\xi}^\sigma$
$\mathcal{P}$	generalized momentum density for continuous media: $\mathcal{P} = \partial\mathcal{L}/\partial(\partial_t\psi)$
$\mathbf{P}$	linear momentum of a physical system
p	pressure at a point in the fluid
p_{a}	pressure applied to the ocean surface from the atmosphere or cryosphere
p_{b}	pressure at the bottom of a fluid column, at the fluid-solid earth interface
p_{slp}	sea level pressure with an area average, $\langle p_{\mathrm{slp}} \rangle = 101.325 \times 10^3$ N m^{-2}
$p_{\mathsf{k}-1/2}$	hydrostatic pressure at the layer interface with vertical position $z = \eta_{\mathsf{k}-1/2}$
$p_{\mathsf{k}}^{\mathrm{dyn}}$	dynamic pressure in a shallow water layer: $p_{\mathsf{k}}^{\mathrm{dyn}} = \rho_{\mathsf{ref}} \sum_{\mathsf{j}=0}^{\mathsf{k}-1} g^{\mathsf{r}}_{\mathsf{j}+1/2}\,\eta_{\mathsf{j}+1/2}$
P_{k}	pressure integrated over a shallow water layer: $P_{\mathsf{k}} \equiv \int_{\eta_{\mathsf{k}+1/2}}^{\eta_{\mathsf{k}-1/2}} p_{\mathsf{k}}(z)\,\mathrm{d}z = h_{\mathsf{k}}\,(g\,\rho_{\mathsf{k}}\,h_{\mathsf{k}}/2 + p_{\mathsf{k}-1/2})$
Q	potential vorticity for continuously stratified (Ertel PV) or shallow water (Rossby PV)
q	quasi-geostrophic potential vorticity either for a continuous fluid or shallow water fluid
Q_{m}	mass flux (mass per horizontal area per time) across ocean surface: $Q_{\mathsf{m}} > 0$ enters ocean
$\mathcal{Q}_{\mathsf{m}}$	mass flux (mass per surface area per time) across ocean surface: $\mathcal{Q}_{\mathsf{m}}\,\mathrm{d}\mathcal{S} = Q_{\mathsf{m}}\,\mathrm{d}A$
Q_{C}	turbulent tracer flux (tracer per horiz area per time) across ocean surface: $Q_{\mathsf{C}} > 0$ enters ocean
$\mathcal{Q}_{\mathsf{C}}$	turbulent tracer flux (tracer per surface area per time) across ocean surface: $QCcal\,\mathrm{d}\mathcal{S} = Q_{\mathsf{C}}\,\mathrm{d}A$
r	radial distance of a point relative to an origin
$\mathbf{R}$	rotation tensor: $2\,R_{mn} = \partial_n v_m - \partial_m v_n = -2\,R_{nm}$
$\mathbb{R}^1$	real number line
$\mathbb{R}^2$	two-dimensional space of real numbers
$\mathbb{R}^3$	three-dimensional space of real numbers
R	radius of a sphere

SYMBOL	MEANING
R_{e}	radius of sphere whose volume approximates that of the earth: $R_{\mathsf{e}} = 6.371 \times 10^6$ m
R^{g}	universal gas constant: $R^{\mathsf{g}} = 8.314$ J mole^{-1} K^{-1} $= 8.314$ kg m^2 s^{-2} mole^{-1} K^{-1}
R^{air}	specific gas constant for air: $R^{\mathsf{air}} = R^{\mathsf{g}}/M^{\mathsf{air}} = 2.938 \times 10^2$ m^2 s^{-2} K^{-1}
$\mathcal{R}$	arbitrary region or manifold
$\mathcal{R}^a{}_b$	orthogonal rotation matrix
Re[ ]	real part of a complex number; e.g., $\mathrm{Re}[e^{-\mathrm{i}\,\omega\,t}] = \cos(\omega\,t)$
$\mathcal{S}$	spatial manifold
$\mathcal{S}$	entropy per mass of a fluid element
$\mathcal{S} = \mathcal{S}^{\mathrm{act}}$	action: time integral of the Lagrangian: $\mathcal{S} = \int_{t_A}^{t_B} L\,\mathrm{d}t$
$\mathbf{S}$	strain rate tensor: $2\,S_{mn} = \partial_n v_m + \partial_m v_n$
$\mathbf{S}^{\mathrm{dev}}$	deviatoric strain rate tensor: $S^{\mathrm{dev}}_{mn} = S_{mn} - \delta_{mn}\,S_{qq}/3$
S	salt concentration = mass of salt in a fluid element per mass of seawater
S	Absolute Salinity, generically referred to as salinity: $S = 1000\,\mathsf{S}$
s	expression for a generic surface: $s = s(x, y, z, t)$.
s	arc-length along a curve $\boldsymbol{x}(s)$ with infinitesimal increment $\mathrm{d}s = \sqrt{\mathrm{d}\boldsymbol{x} \cdot \mathrm{d}\boldsymbol{x}}$
$\hat{\boldsymbol{s}}$	unit tangent to a curve, also written as $\hat{\boldsymbol{s}} = \hat{\boldsymbol{t}}$ (see below)
sgn	sign function related to Heaviside step function via $\mathrm{sgn}(x) = 2\,\mathcal{H}(x) - 1$
T	absolute thermodynamic *in situ* temperature (Kelvin if in a thermodynamic equation)
T	time scale for a particular physical process and commonly used in scale analysis
T	time (universal Newtonian time) measured in the Lagrangian reference frame
t	time (universal Newtonian time) measured in the Eulerian reference frame
τ	general symbol for time as considered in the tensor analysis chapters
$\mathbf{T}$	stress tensor with natural elements $T^m n$
$\mathbf{T}^{\mathrm{kinetic}}$	kinetic stress tensor: $\mathbf{T}^{\mathrm{kinetic}} = -\rho\,\mathbf{v} \otimes \mathbf{v}$
$\mathbf{T}^{\mathrm{sw\ kinetic}}$	kinetic stress tensor for shallow water fluid: $\mathbf{T}^{\mathrm{sw\ kinetic}} = -\rho\,\mathbf{u} \otimes \mathbf{u}$
$\hat{\boldsymbol{t}}$	unit tangent to a curve: $\hat{\boldsymbol{t}} = \mathrm{d}\boldsymbol{x}/\mathrm{d}s$, where s is the arc-length so that $\mathrm{d}s = \sqrt{\mathrm{d}\boldsymbol{x} \cdot \mathrm{d}\boldsymbol{x}}$
$\mathbf{u}$	horizontal velocity of a fluid particle, with Cartesian representation: $\boldsymbol{u} = \hat{\boldsymbol{x}}\,u + \hat{\boldsymbol{y}}\,v$
U	horizontal velocity scale of the flow under consideration
$\mathbf{U}$	depth integrated horizontal velocity: $\mathbf{U} = \int_{\eta_{\mathrm{b}}}^{\eta} \mathbf{u}\,\mathrm{d}z$
$\mathbf{v}$	velocity of a fluid particle: $\mathbf{v} = \mathrm{D}\mathbf{x}/\mathrm{D}t$, with Cartesian components $\boldsymbol{v} = \hat{\boldsymbol{x}}\,u + \hat{\boldsymbol{y}}\,v + \hat{\boldsymbol{z}}\,w$
$\mathbf{v}^*$	eddy-induced velocity
$\mathbf{v}^\dagger$	residual velocity of a fluid particle: $\mathbf{v}^\dagger = \mathbf{v} + \mathbf{v}^*$
$\mathbf{v}^{(b)}$	velocity of a point on a region boundary
$\boldsymbol{v}^{\mathrm{L}}(\boldsymbol{a}, T)$	Lagrangian velocity of a fluid particle so that $\boldsymbol{v}^{\mathrm{L}}(\boldsymbol{a}, T) = \boldsymbol{v}[\boldsymbol{x} = \boldsymbol{\varphi}(\boldsymbol{a}, T), t = T]$
$\mathbf{v}_{\mathrm{I}}$	velocity of a fluid particle measured in the inertial/absolute reference frame: $\mathbf{v}_{\mathrm{I}} = \mathbf{v} + \boldsymbol{\Omega} \times \mathbf{x}$
W	vertical velocity scale of the flow under consideration
w	vertical component to the velocity: $w = \mathrm{D}z/\mathrm{D}t$
w^{dia}	dia-surface flux = volume per *horizontal area* per time crossing a σ-surface: $w^{\mathrm{dia}} = (1/\lvert\nabla\sigma\rvert)\,\dot{\sigma}$
$w^{(\dot{\sigma})}$	dia-surface velocity = volume per *horizontal area* per time crossing σ-surface: $w^{(\dot{\sigma})} = \dot{\sigma}\,\partial z/\partial\sigma$

LATIN SYMBOLS AND THEIR MEANING

SYMBOL	MEANING
(x, y, z)	triplet of Cartesian coordinates
$\mathbf{x}$	spatial position
$\boldsymbol{x}$	spatial position represented by either general coordinates or Cartesian coordinates
$\mathring{\mathbf{x}}$	initial position for a fluid particle using arbitrary coordinates
$(\hat{\boldsymbol{x}}, \hat{\boldsymbol{y}}, \hat{\boldsymbol{z}})$	triplet of Cartesian unit vectors oriented in a righthand sense
$\mathbf{X}(t)$	position for a point particle defining a trajectory through space-time
$\boldsymbol{X}(\boldsymbol{a}, T)$	position of a material fluid particle expressed using material coordinates
z_σ	specific thickness for a generalized vertical coordinate: $z_\sigma = \partial z / \partial \sigma = \hbar$

GREEK SYMBOLS AND THEIR MEANING

SYMBOL	MEANING
α	thermal expansion: $\alpha = -\rho^{-1}\,\partial\rho/\partial\theta$ or $\alpha = -\rho^{-1}\,\partial\rho/\partial\Theta$ or $\alpha = -\rho^{-1}\,\partial\rho/\partial T$
α_T	thermal expansion in terms of *in situ* temp: $\alpha = -\rho^{-1}\,\partial\rho/\partial T$
$\alpha^{(\Theta)}$	thermal expansion in terms of Conservative Temperature: $\alpha^{(\Theta)} = -\rho^{-1}\,\partial\rho/\partial\Theta$
α_{aspect}	aspect ratio; ratio of vertical to horizonal scales of the flow: $\alpha_{\text{aspect}} = H/L$
$\beta, \beta^{(\text{S})}$	saline contraction coefficient: $\beta = \beta^{(\text{S})} = \rho^{-1}\,\partial\rho/\partial S$
β	meridional derivative of planetary vorticity: $\beta = \partial_y f$
$\hat{\boldsymbol{\gamma}}$	dianeutral unit direction perpendicular to the neutral tangent plane
δ_{ab}	components to the Kronecker tensor in Cartesian coordinates
δ^a_b	components to the Kronecker tensor in general coordinates
ϵ	kinetic energy dissipation from viscosity (energy per time per mass)
ϵ_{ab}	components to the permutation symbol in two space dimensions
ϵ_{abc}	components to the permutation symbol in three space dimensions
ε_{abc}	components to the Levi-Civita symbol in three space dimensions: $\varepsilon_{abc} = \sqrt{\det(\mathbb{g}_{ab})}\,\epsilon_{abc}$
ζ	vertical component to the relative vorticity; e.g., $\zeta = \partial_x v - \partial_y u$
ζ_{a}	vertical component to the absolute vorticity; e.g., $\zeta_{\mathsf{a}} = f + \zeta$
η	vertical position of the free upper surface of a fluid domain: $z = \eta(x, y, t)$
$\eta_{\mathsf{k}-1/2}$	vertical position of the top interface of the shallow water layer k
$\eta_{\mathsf{k}+1/2}$	vertical position of the lower interface of the shallow water layer k
$\eta_{\mathsf{b}} = -H$	vertical position of static solid-earth boundary: $z = \eta_{\mathsf{b}}(x, y) = -H(x, y)$
θ	potential temperature
Θ	Conservative Temperature
κ	molecular kinematic diffusivity
κ_T	molecular diffusivity for *in situ* temperature in water: $\kappa_T = 1.4 \times 10^{-7}\ \text{m}^2\ \text{s}^{-1}$
κ_S	molecular diffusivity for salt in water: $\kappa_S = 1.5 \times 10^{-9}\ \text{m}^2\ \text{s}^{-1}$
κ_{eddy}	kinematic eddy diffusivity: $\kappa_{\text{eddy}} \gg \kappa$
Λ	wavelength of a wave: $\Lambda = 2\,\pi/\lvert\boldsymbol{k}\rvert$, where $\boldsymbol{k}$ is the wavevector and $\lvert\boldsymbol{k}\rvert$ the wavenumber.
$\lambda\!\!\!^{-}$	reduced wavelength of a wave: $\lambda\!\!\!^{-} = \Lambda/(2\pi) = 1/\lvert\boldsymbol{k}\rvert$.
λ	longitude on the sphere: $0 \le \lambda \le 2\pi$
μ_n	chemical potential for constituent n within a fluid (energy per mass)
$\tilde{\mu}_n$	chemical potential for constituent n within a fluid (energy per mole number)
μ	relative chemical potential for a binary fluid
μ	chemical potential for seawater: $\mu = \mu_{\text{salt}} - \mu_{\text{water}}$
μ_{vsc}	dynamic viscosity $= \rho\,\nu$
ν_{s}	specific volume: $\nu_{\text{s}} = \rho^{-1}$
ν	molecular kinematic viscosity
ν_{air}	molecular kinematic viscosity of air: $\nu_{\text{air}} \approx 1.3 \times 10^{-5}\ \text{m}^2\ \text{s}^{-1}$
ν_{water}	molecular kinematic viscosity of fresh water: $\nu_{\text{water}} \approx 10^{-6}\ \text{m}^2\ \text{s}^{-1}$
ν_{eddy}	eddy viscosity: $\nu_{\text{eddy}} \gg \nu$
ξ^a	a'th component to a generalized coordinate
Π	Exner function
Π	Boussinesq dynamic enthalpy

GREEK SYMBOLS AND THEIR MEANING

SYMBOL	MEANING
ρ	Eulerian *in situ* density (mass per volume) of a fluid element: $\rho = \rho(\boldsymbol{x}, t)$
ρ^{L}	mass density following a fluid particle trajectory (Lagrangian mass density): $\rho^{\text{L}} = \rho^{\text{L}}(\boldsymbol{a}, T)$
$\mathring{\rho}^{\text{L}}$	initial mass density in Lagrangian space-time: $\mathring{\rho}^{\text{L}} = \rho^{\text{L}}(\boldsymbol{a}, T = t_0)$
ρ_{o}	constant reference density used for the Boussinesq ocean
ρ_{ref}	constant reference density used for the shallow water fluid
ϱ	potential density referenced to a specified pressure
σ	generalized vertical coordinate surface with $\sigma(x, y, z, t) =$ constant
$\boldsymbol{\tau}$	stress vector such as from winds or bottom stresses acting on the ocean
$\mathbb{T}$	frictional stress tensor
φ	pressure divided by the Boussinesq reference density: $\varphi = p/\rho_{\text{o}}$
φ	sometimes used as the variable for parameteriing a curve
ϕ	latitude on the sphere: $-\pi/2 \leq \phi \leq \phi/2$
Φ_{e}	gravitational potential from a spherical and homogeneous earth
Φ	geopotential from central gravity plus planetary centrifugal; also, potential energy per mass
$\boldsymbol{\Phi}$	inverse flow map that generates an inverse mapping of the fluid continuum: $\boldsymbol{a} = \boldsymbol{\Phi}(\boldsymbol{x}, t)$
$\boldsymbol{\varphi}$	motion field that maps the fluid continuum as time evolves: $\boldsymbol{x} = \boldsymbol{\varphi}(\boldsymbol{a}, T)$
ψ	streamfunction for two-dimensional non-divergent flow: $\boldsymbol{u} = \hat{\boldsymbol{z}} \times \nabla\psi$
$\boldsymbol{\Psi}$	vector streamfunction for three-dimensional non-divergent flow: $\boldsymbol{v} = \nabla \times \boldsymbol{\Psi}$
$\boldsymbol{\omega}$	relative vorticity: $\boldsymbol{\omega} = \nabla \times \boldsymbol{v}$
ω	angular frequency for a wave so that the wave period is $2\pi/\lvert\omega\rvert$
ϖ	dispersion relation for linear waves, relating angular frequency to the wavevector: $\omega = \varpi(\boldsymbol{k})$
$\boldsymbol{\Omega}$	angular velocity for a rotating reference frame
$\boldsymbol{\Omega}$	earth's angular velocity oriented through the north pole: $\lvert\boldsymbol{\Omega}\rvert = 7.2921 \times 10^{-5}\ \text{s}^{-1}$

SYMBOL	MEANING
$[\equiv]$	"has dimensions" for use in referring to the physical dimensions
$\times$	vector cross product
∇	gradient operator
∇_h	horizontal gradient operator on constant z surface: $\nabla_\mathrm{h} = \hat{\boldsymbol{x}}\,(\partial/\partial x)_z + \hat{\boldsymbol{y}}\,(\partial/\partial y)_z = \hat{\boldsymbol{x}}\,\partial_x + \hat{\boldsymbol{y}}\,\partial_y$
$\nabla\cdot$	covariant divergence operator that acts on a vector to produce a scalar
$\nabla\times$	curl operator
$\nabla_{\mathrm{h}\sigma}$	horizontal gradient on constant σ-surface: $\nabla_{\mathrm{h}\sigma} = \hat{\boldsymbol{x}}\,(\partial/\partial x)_\sigma + \hat{\boldsymbol{y}}\,(\partial/\partial y)_\sigma$
$\partial/\partial\sigma$	vertical partial derivative with general vertical coordinate: $\partial_\sigma = \partial/\partial\sigma = \partial/\partial\sigma = (\partial z/\partial\sigma)\,\partial/\partial z$
$\partial/\partial t$	Eulerian time derivative acting at a fixed spatial position, $\boldsymbol{x}$, also written as ∂_t
$[\partial/\partial t]_\sigma$	time derivative computed on constant σ-surface
$\mathrm{D}/\mathrm{D}t$	material, Lagrangian, or substantial time derivative following a fluid particle
$\mathrm{D}_\mathrm{r}/\mathrm{D}t$	time derivative following a ray (integral lines of the group velocity): $\mathrm{D}_\mathrm{r}/\mathrm{D}t = \partial/\partial t + \boldsymbol{c}_\mathrm{g}\cdot\nabla$
$\mathrm{D}_\mathrm{g}/\mathrm{D}t$	time derivative following the horizontal geostrophic flow $\mathrm{D}_\mathrm{g}/\mathrm{D}t = \partial/\partial t + \boldsymbol{u}_\mathrm{g}\cdot\nabla_\mathrm{h}$
đ	inexact differential operator commonly found in thermodynamics
δ	virtual displacement (also the variation) for Lagrangian mechanics and Hamilton's principle
δ	differential increment that signals an object following the fluid flow
$\delta(x)$	one-dimensional Dirac delta with dimensions of inverse length
$\delta^{(2)}(\boldsymbol{x})$	two-dimensional Dirac delta with dimensions of inverse area
$\delta(\boldsymbol{x})$	three-dimensional Dirac delta with dimensions of inverse volume
$\delta(t)$	temporal Dirac delta with dimensions of inverse time
Δ	finite difference increment in space: $\Delta_x, \Delta_y, \Delta_z, \Delta_\sigma$
$\mathrm{d}A$	infinitesimal horizontal area element: $\mathrm{d}A = \mathrm{d}x\,\mathrm{d}y$
d^3a	infinitesimal region of material space: $\mathrm{d}^3a = \mathrm{d}a\,\mathrm{d}b\,\mathrm{d}c$
$\mathrm{d}\mathcal{S}$	infinitesimal area element on a surface
$\mathrm{d}V$	infinitesimal volume element, sometimes written $\mathrm{d}V = \mathrm{d}\boldsymbol{x}$
$\mathrm{d}\boldsymbol{x}$	infinitesimal volume element, with Cartesian expression $\mathrm{d}\boldsymbol{x} = \mathrm{d}V = \mathrm{d}x\,\mathrm{d}y\,\mathrm{d}z$
δV	infinitesimal volume for a region moving with the fluid (Lagrangian region)
$\int_\mathcal{R}\mathrm{d}V$	volume integral over an arbitrary region, $\mathcal{R}$
$\int_{\mathcal{R}(\boldsymbol{v})}\mathrm{d}V$	volume integral over a region following the fluid flow (Lagrangian integral)
$\int_\mathcal{S}\mathrm{d}\mathcal{S}$	surface integral over an arbitrary surface $\mathcal{S}$
$\oint_{\partial\mathcal{R}}\mathrm{d}\mathcal{S}$	surface integral over a closed surface $\partial\mathcal{R}$ that bounds the volume $\mathcal{R}$
$\oint\mathrm{d}\ell$	closed line integral over a periodic domain
$\oint_{\partial\mathcal{S}}\mathrm{d}\ell$	counter-clockwise closed line integral over the boundary of a surface, $\partial\mathcal{S}$
$\sim$	"similar to" or "scales as"
$\approx$	approximately equal to
$\dot{\Psi}$	time derivative following a trajectory; for fluid particle trajectories then, $\dot{\Psi} = \mathrm{D}\Psi/\mathrm{D}t$

Bibliography

Abernathey, R., D. Ferreira, and A. Klocker, Diagnostics of isopycnal mixing in a circumpolar channel, *Ocean Modelling*, *72*(0), 1 – 16, doi:10.1016/j.ocemod.2013.07.004, 2013. 1989, 2001, 2007

Acheson, D., *Elementary Fluid Dynamics*, Oxford Applied Mathematics and Computing Science Series, Oxford, Oxford, 1990. 43, 696, 1036, 1369

Adcock, S., and D. P. Marshall, Interactions between geostrophic eddies and the mean circulation over large-scale bottom topography, *Journal of Physical Oceanography*, *30*, 3223–3238, 2000. 1119

Adcroft, A., R. Hallberg, and M. Harrison, A finite volume discretization of the pressure gradient force using analytic integration, *Ocean Modelling*, *22*, 106–113, doi:10.1016/j.ocemod.2008.02.001, 2008. 1851, 1853

Adcroft, A., W. Anderson, C. Blanton, M. Bushuk, C. O. Dufour, J. P. Dunne, S. M. Griffies, R. W. Hallberg, M. J. Harrison, I. Held, M. Jansen, J. John, J. P. Krasting, A. Langenhorst, S. Legg, Z. Liang, C. McHugh, B. G. Reichl, A. Radhakrishnan, T. Rosati, B. Samuels, A. Shao, R. J. Stouffer, M. Winton, A. T. Wittenberg, B. Xiang, N. Zadeh, and R. Zhang, The GFDL global ocean and sea ice model OM4.0: Model description and simulation features, *Journal of Advances in Modeling Earth Systems*, *11*, 3167–3211, doi:10.1029/2019MS001726, 2019. 971

Aiki, H., T. Jacobson, and T. Yamagata, Parameterizing ocean eddy transports from surface to bottom, *Journal of Geophysical Research*, *31*, L19 302, doi:10.1029/2004GL020703, 2004. 1998, 2002

Anderson, J., Ludwig Prandtl's boundary layer, *Physics Today*, *58*, 42–48, doi:10.1063/1.2169443, 2005. 658, 660

Anderson, P. W., More is different, *Science*, *177*, 393–396, doi:10.1126/science.177.4047.39, 1972. xi

Andresen, B., R. Berry, R. Gilmore, E. Ihrig, and P. Salamon, Thermodynamic geometry and the metrics of Weinhold and Gilmore, *Physical Review A*, *37*(3), 845–848, doi:10.1103/PhysRevA.37.845, 1988. 558

Andrews, D., and M. McIntyre, An exact theory of nonlinear waves on a Lagrangian-mean flow, *Journal of Fluid Mechanics*, *89*, 609–646, doi:10.1017/S0022112078002773, 1978a. 1959, 1968

Andrews, D. G., A finite-amplitude Eliassen-Palm theorem in isentropic coordinates, *Journal of Atmospheric Sciences*, *40*, 1877–1883, doi:10.1175/1520-0469(1983)040⟨1877:AFAEPT⟩2.0.CO;2, 1983. 808

Andrews, D. G., and M. E. McIntyre, On wave action and its relatives, *Journal of Fluid Mechanics*, *89*, 647–664, doi:10.1017/S0022112078002785, 1978b. 1405, 1959, 1968

Andrews, D. G., J. R. Holton, and C. B. Leovy, *Middle Atmosphere Dynamics*, Academic Press, 1987. 546

Anstey, J., and L. Zanna, A deformation-based parametrization of ocean mesoscale eddy Reynolds stresses, *Ocean Modelling*, *112*, 99–111, 2017. 653

Apel, J. R., *Principles of Ocean Physics*, *International Geophysics Series*, vol. 38, Academic Press, London, 1987. 333, 901, 925

Arakawa, A., and V. R. Lamb, The UCLA general circulation model, in *Methods in Computational Physics: General Circulation Models of the Atmosphere*, vol. 17, edited by J. Chang, pp. 174–265, Academic Press, 1977. 1045

Arbic, B., S. T. Garner, R. W. Hallberg, and H. L. Simmons, The accuracy of surface elevations in forward global barotropic and baroclinic tide models, *Deep Sea Research*, *51*, 3069—3101, 2004. 926

Aris, R., *Vectors, Tensors and the Basic Equations of Fluid Mechanics*, Dover Publishing, New York, 1962. 7, 75, 442, 444, 448, 452, 469, 479, 507, 515, 614, 625, 635, 645, 646, 653

Atkins, P., and J. de Paula, *Atkin's Physical Chemistry*, 8th ed., 1053 pp., W.H. Freeman and Co., 2006. 568, 572

Badin, G., and F. Crisciani, *Variational formulation of fluid and geophysical fluid dynamics*, Springer International Publishing, Switzerland, 218 pages, 2018. xiii, 435, 1337

Barthel, A., A. Hogg, S. Waterman, and S. Keating, Jet-topography interactions affect energy pathways to the deep Southern Ocean, *Journal of Physical Oceanography*, *47*(1799–1816), doi:10.1175/JPO-D-16-0220.1, 2017. 993

Barton, K. N., N. Pal, S. R. Brus, M. R. Petersen, B. K. Arbic, D. Engwirda, A. F. Roberts, J. J. Westerink, D. Wirasaet, and M. Schindelegger, Global barotropic tide modeling using inline self-attraction and loading in MPAS-Ocean, *Journal of Advances in Modeling Earth Systems (JAMES)*, *14*, doi:10.1029/2022MS003207, 2022. 935

Basdevant, J.-L., *Variational Princeiples in Physics*, Springer Press, 2007. 249

Batchelor, G. K., On steady laminar flow with closed streamlines at large Reynolds number, *Journal of Fluid Mechanics*, *1*, 177–190, doi:10.1017/S0022112056000123, 1956. 1940

Batchelor, G. K., *An Introduction to Fluid Dynamics*, Cambridge University Press, Cambridge, England, 1967. 406, 412, 491, 635, 659, 660, 666, 687, 1719

Becker, E., Frictional heating in global climate models, *Monthly Weather Review*, *131*, 508–520, doi:10.1175/1520-0493(2003)131⟨0508:FHIGCM⟩2.0.CO;2, 2003. 689

Becker, J. M., Effect of a western continental slope on the wind-driven circulation, *Journal of Physical Oceanography*, *29*, 512–518, doi:10.1175/1520-0485(1999)029⟨0512:EOAWCS⟩2.0.CO;2, 1999. 1112

Becker, J. M., and R. Salmon, Eddy formation on a continental slope, *Journal of Marine Research*, *55*, 181–200, 1997. 1109, 1112

Beckers, J.-M., H. Burchard, J.-M. Campin, E. Deleersnijder, and P. P. Mathieu, Another reason why simple discretizations of rotated diffusion operators cause problems in ocean models: Comments on isoneutral diffusion in a z-coordinate ocean model, *Journal of Physical Oceanography*, *28*, 1552–1559, doi:10.1175/1520-0485(1998)028⟨1552:ARWSDO⟩2.0.CO;2, 1998. 2006

Beckers, J.-M., H. Burchard, E. Deleersnijder, and P. P. Mathieu, Numerical discretization of rotated diffusion operators in ocean models, *Monthly Weather Review*, *128*, 2711–2733, doi:10.1175/1520-0493(2000)128⟨2711:NDORDO⟩2.0.CO;2, 2000. 2006

Belmadani, A., N. A. Maximenko, J. P. McCreary, R. Furue, O. V. Melnichenko, N. Schneider, and E. D. Lorenzo, Linear wind-forced beta plumes with application to the Hawaiian Lee Countercurrent, *Journal of Physical Oceanography*, *43*, 2071–2094, doi:10.1175/JPO-D-12-0194.1, 2013. 1075

Bender, C., and S. Orszag, *Advanced Mathematical Methods for Scientists and Engineers*, McGraw-Hill Book Company, New York, 593 pp, 1978. 1446

Bennett, A., The geometry of neutral paths, *Journal of Physical Oceanography*, *49*, 3037–3044, doi:10.1175/JPO-D-19-0047.1, 2019. 840

Benthuysen, J., and L. N. Thomas, Friction and diapycnal mixing at a slope: Boundary control of potential vorticity, *Journal of Physical Oceanography*, *42*, 1509–1523, doi:10.1175/JPO-D-11-0130.1, 2012. 1222

Beyer, W., *Standard Mathematical Tables*, 24th Edition, CRC Press, 1973. 1392

Bhatia, H., G. Norgard, V. Pascucci, and P.-T. Bermer, The Helmholtz-Hodge decomposition–a survey, *IEEE Transactions on Visualization and Computer Graphics*, *19*, 1386–1404, doi:10.1109/TVCG.2012.316, 2013. 239, 240

Bingham, R. J., and C. Hughes, Local diagnostics to estimate density-induced sea level variations over topography and along coastlines, *Journal of Geophysical Research*, *117*, doi:10.1029/2011JC007276, 2012. 734, 736

Bishop, S., R. Small, and F. Bryan, The global sink of available potential energy by mesoscale air-sea interaction, *Journal of Advances in Modeling Earth Systems*, *in review*, 2020. 813

Bladwell, C., R. M. Holmes, J. D. Zika, and S. M. Griffies, The hat average: Improved time-averaging for budget analyses in climate models, *Journal of Advances in Modeling Earth Systems*, *in prep*, 2022. 143

Bleck, R., Finite difference equations in generalized vertical coordinates. Part I: Total energy conservation, *Contributions to Atmospheric Physics*, *51*, 360–372, 1978. 1798

Bohm, D., *Quantum Theory*, Dover Publications, Inc., New York, 646 pp, 1951. 1393, 1399

Böning, C. W., W. R. Holland, F. O. Bryan, G. Danabasoglu, and J. C. McWilliams, An overlooked problem in model simulations of the thermohaline circulation and heat transport in the Atlantic Ocean, *Journal of Physical Oceanography*, *8*, 515–523, 1995. 2003

Boyce, W. E., and R. C. DiPrima, *Elementary Differential Equations and Boundary Value Problems*, 9th ed., Wiley Publications, 2009. 1771

Bretherton, C., and C. Schär, Flux of potential vorticity substance: a simple derivation and uniqueness property, *Journal of the Atmospheric Sciences*, *50*, 1834–1836, doi:10.1175/1520-0469(1993)050⟨1834:FOPVSA⟩2.0.CO;2, 1993. 1208, 1210

Bretherton, F. P., Critical layer instability in baroclinic flows, *Quarterly Journal of the Royal Meteorological Society*, *92*, 325–334, 1966. 211, 808, 1300

Bretherton, F. P., The general linearized theory of wave propagation, in *Mathematical Problems in the Geophysical Sciences*, edited by W. H. Reid, pp. 61–102, American Mathematical Society, 1971. 1369, 1372, 1405, 1416, 1417

Bretherton, F. P., and C. J. R. Garrett, Wavetrains in inhomogeneous moving media, *Proceedings of the Royal Society A*, *302*, 529–554, doi:10.1098/rspa.1968.0034, 1969. 1405, 1416

Brown, E., *Waves, tides, and shallow-water processes*, 227 pp., The Open University, Milton Keys, UK, 1999. 925, 1488

Bryan, K., A numerical investigation of a nonlinear model of a wind-driven ocean, *Journal of Atmospheric Sciences*, *20*, 594–606, doi:10.1175/1520-0469(1963)020⟨0594:ANIOAN⟩2.0.CO;2, 1963. 1112

Bryan, K., A numerical method for the study of the circulation of the world ocean, *Journal of Computational Physics*, *4*, 347–376, doi:10.1016/0021-9991(69)90004-7, 1969. 1067, 1279

Buckingham, C., J. Gula, and X. Carton, The role of curvature in modifying frontal instabilities. Part I: Review of theory and presentation of a nondimensional instability criterion, *Journal of Physical Oceanography*, *51*, 299–315, doi:10.1175/JPO-D-19-0265.1, 2021. 1669, 1697

Bühler, O., *Waves and mean flows*, 2nd ed., Cambridge University Press, Cambridge, UK, doi:10.1017/CBO9781107478701, 2014a. 59, 1414, 1494, 1501, 1959, 1968

Bühler, O., A gentle stroll through EP flux theory, *European Journal of Mechanics B*, *47*, 12–15, doi:10.1016/j.euromechflu.2014.01.010, 2014b. 1873

Bühler, O., J. Callies, and R. Ferrari, Wave–vortex decomposition of one-dimensional ship-track data, *Journal of Fluid Mechanics*, *756*, 1007–1026, doi:10.1017/jfm.2014.488, 2014. 814

Buijsman, M. C., B. K. A. an Samuel M. Kelly, and A. F. Waterhouse, Internal gravity waves, in *Encyclopedia of Ocean Sciences*, *Reference Module in Earth Systems and Environmental Sciences*, vol. 3, pp. 622–632, Elsevier, doi:10.1016/B978-0-12-409548-9.04160-9, 2019. 1627, 1639

Butt, T., P. Russell, and R. Grigg, *Surf Science - An Introduction To Waves For Surfing*, University of Hawaii Press, 2004. 1374

Buzzicotti, M., B. A. Storer, H. Khatri, S. M. Griffies, and H. Aluie, Spatio-temporal coarse-graining decomposition of the global ocean geostrophic kinetic energy, *Journal of Advances in Modeling Earth Systems*, *15*, doi:10.1029/2023MS003693, 2023. 1961

Caldwell, D., Thermal and Fickian diffusion of sodium chloride in a solution of oceanic concentration, *Deep-Sea Research*, *20*, 1029–1039, doi:10.1016/0011-7471(73)90073-9, 1973. 701

Caldwell, D., and S. Eide, Soret coefficient and isothermal diffusivity of aqueous solutions of five principal salt constituents of seawater, *Deep-Sea Research*, *28A*, 1605–1618, doi:10.1016/0198-0149(81)90100-X, 1981. 701

Callen, H. B., *Thermodynamics and an Introduction to Thermostatics*, John Wiley and Sons, New York, 493 + xvi pp, 1985. 555, 558, 559, 560, 689, 700, 702, 1808

Callies, J., and R. Ferrari, Dynamics of an abyssal circulation driven by bottom-intensified mixing on slopes, *Journal of Physical Oceanography*, *48*, 1257–1282, doi:10.1175/JPO-D-17-0125.1, 2018. 1204

Cane, M., V. Kamenkovich, and A. Krupitsky, On the utility and disutility of JEBAR, *Journal of Physical Oceanography*, *28*, 519–526, doi:10.1175/1520-0485(1998)028⟨0519:OTUADO⟩2.0.CO;2, 1998. 1281

Carnevale, G., R. Kloosterziel, and G. van Heijst, Propagation of barotropic vorticies over topography in a rotating tank, *Journal of Fluid Mechanics*, *233*, 119–139, doi:10.1017/S0022112091000411, 1991. 1072

Carslaw, H. S., and J. C. Jaeger, *Conduction of Heat in Solids*, Oxford University Press, 1959. 1892

Cauchy, A.-L., *Résumé des leçons données à l'école royale polytechnique sur le calcul infinitésimal*, Imprimerie royale, 1823. 146

Chaikin, P. M., and T. C. Lubensky, *Principles of Condensed Matter Physics*, Cambridge University Press, Cambridge, United Kingdom, 1995. 113

Chandrasekhar, S., *Hydrodynamic and Hydromagnetic Stability*, Dover Publications, New York, 654 pp, 1961. 776, 1708, 1715, 1722, 1747

Chang, E. K. M., and C. L. P. Wolfe, The horizontal components of the real gravity are not relevant to ocean dynamics, *Scientific Reports*, *12*, doi:10.1038/s41598-022-09967-3, 2022. 344

Chang, E. K. M., C. L. P. Wolfe, A. L. Stewart, and J. C. McWilliams, Comments on "horizontal gravity disturbance vector in atmospheric dynamics" by peter c. chu, *Dynamics of Atmospheres and Oceans*, *103*, doi:10.1016/j.dynatmoce.2023.101382, 2023. 344

Charney, J., R. Fjörtjoft, and J. von Neumann, Numerical integration of the barotropic vorticty equation, *Tellus*, *2*, 237–254, doi:10.3402/tellusa.v2i4.8607, 1950. 1050, 1061

Charney, J. G., and M. E. Stern, On the stability of internal baroclinic jets in a rotating atmosphere, *Journal of the Atmospheric Sciences*, *19*, 159–172, doi:10.1175/1520-0469(1962)019⟨0159:OTSOIB⟩2.0.CO;2, 1962. 1787

Chatwin, P. C., The vorticity equation as an angular momentum equation, *Mathematical Proceedings of the Cambridge Philosophical Society*, *74*, 365–367, doi:10.1017/S0305004100048131, 1973. 1043

Cohen-Tannoudji, C., B. Diu, and F. Laloë, *Quantum Mechanics: Volumes One and Two*, John Wiley and Sons, New York, 1524 pp, 1977. 163, 1396, 1397, 1399, 1403

Cole, S. T., C. Wortham, E. Kunze, and W. B. Owens, Eddy stirring and horizontal diffusivity from argo float observations: Geographic and depth variability, *Geophysical Research Letters*, *42*(10), 3989–3997, doi:10.1002/2015GL063827, 2015GL063827, 2015. 1989

Courant, R., and D. Hilbert, *Methods of Mathematical Physics Volume I*, Wiley-Interscience, New York, 1953. 1910, 1912

Courant, R., and D. Hilbert, *Methods of Mathematical Physics Volume II: Partial Differential Equations*, Wiley-Interscience, 1962. 1910, 1912

Cox, M., and K. Bryan, A numerical model of the ventilated thermocline, *Journal of Physical Oceanography*, *14*, 674–687, 1984. 2003

Cox, M. D., Isopycnal diffusion in a z-coordinate ocean model, *Ocean Modelling*, *74*, 1–5, 1987. 2005, 2006

Crank, J., *The Mathematics of Diffusion*, Oxford University Press, 1956. 1892

Crocco, L., Eine neue stromfunktion fur die erforschung der bewegung der gas emit rotation, *Zamm-zeitschrift Fur Angewandte Mathematik Und Mechanik*, *17*, 1, doi:10.1002/ZAMM.19370170103, 1937. 713

Csanady, G. T., *Turbulent Diffusion in the Environment*, D. Reidel Publishing Company, 1973. 1896, 1900, 1906

Csanady, G. T., The pressure field along the western margins of the North Atlantic, *Journal of Geophysical Research*, *84*, 4905–4915, doi:10.1029/JC084iC08p04905, 1979. 734, 736

Cushman-Roisin, B., Subduction, in *Dynamics of the oceanic surface mixed-layer*, pp. 181–196, Hawaii Institude of Geophysical Special Publications, 1987. 1836

Cushman-Roisin, B., and J.-M. Beckers, *Introduction to Geophysical Fluid Dynamics*, Academic-Press, Amsterdam, 828, 2011. xxxiv, xxxv, 900, 901, 951, 959, 1488, 1599, 1601, 1614, 1639, 1668, 1725, 1761, 1765, 1796

Dahlen, F. A., and J. Tromp, *Theoretical Global Seismology*, Princeton University Press, Princeton USA, 1998. xvi, 886

Dahler, J., and L. Scriven, The angular momentum of continua, *Nature*, *4797*, 36–37, 1961. 635

Danabasoglu, G., R. Ferrari, and J. McWilliams, Sensitivity of an ocean general circulation model to a parameterization of near-surface eddy fluxes, *Journal of Climate*, *21*, 1192–1208, doi:10.1175/2007JCLI1508.1, 2008. 1989, 2007

Davidson, P., *Turbulence: an introduction for scientists and engineers*, Oxford University Press, Oxford, UK, 2015. 1043, 1503

Davies-Jones, R., Comments on "A Generalization of Bernoulli's Theorem", *Journal of the Atmospheric Sciences*, *60*, 2039–2041, doi:10.1175/1520-0469(2003)060⟨2039:COAGOB⟩2.0.CO;2, 2003a. 1208

Davies-Jones, R., An expression for effective buoyancy in surroundings with horizontal density gradients, *Journal of the Atmospheric Sciences*, *60*, 2922–2925, doi:10.1175/1520-0469(2003)060,2922:AEFEBI.2.0.CO;2, 2003b. 856

Davis, R. E., Diapycnal mixing in the ocean: equations for large-scale budgets, *Journal of Physical Oceanography*, *24*, 777–800, doi:10.1175/1520-0485(1994)024⟨0777:DMITOE⟩2.0.CO;2, 1994. 687

DeGroot, S. R., and P. Mazur, *Non-Equilibrium Thermodynamics*, Dover Publications, New York, 510 pp, 1984. 507, 515, 681, 687, 689

Denaro, F., On the application of the Helmholtz-Hodge decomposition in projection methods for incompressible flows with general boundary conditions, *International Journal of Numerical Methods in Fluids*, *43*, 43–69, doi:10.1002/fld.598, 2003. 239, 240

Dennery, P., and A. Krzywicki, *Mathematics for Physicists*, Harper & Row, 1967. 192, 231

DeSzoeke, R. A., and A. F. Bennett, Microstructure fluxes across density surfaces, *Journal of Physical Oceanography*, *23*, 2254–2264, 1993. 1983

Doering, C., and J. Gibbon, *Applied analysis of the Navier-Stokes equations*, Cambridge University Press, Cambridge, UK, 217 pp, 1995. 629, 649

Döös, K., and D. J. Webb, The Deacon cell and the other meridional cells in the Southern Ocean, *Journal of Physical Oceanography*, *24*, 429–442, doi:10.1175/1520-0485(1994)024⟨0429:TDCATO⟩2.0.CO;2, 1994. 546

Doswell, C., and P. Markowski, Is bouyancy a relative quantity?, *Monthly Weather Review*, *132*, 853–863, doi:10.1175/1520-0493(2004)132⟨0853:IBARQ⟩2.0.CO;2, 2004. 856

Drake, H. F., S. Bailey, R. Dussin, S. M. Griffies, J. Krasting, G. MacGilchrist, G. Stanley, J.-E. Tesdal, and J. D. Zika, Water mass transformation budgets in finite-volume generalized vertical coordinate ocean models, *Journal of Advances in Modeling Earth Systems (JAMES)*, *17*, doi:10.1029/2024MS004383, 2025. 2058

Drazin, P., and R. Johnson, *Solitons: an introduction*, Cambridge University Press, Cambridge, UK, 226 pp, 1989. 1484

Drazin, P., and W. Reid, *Hydrodynamic stability*, Cambridge University Press, Cambridge, UK, 527 pp, 1981. 1669, 1676, 1719

Drazin, P., and W. Reid, *Hydrodynamic stability*, 2nd ed., Cambridge University Press, Cambridge, UK, 605 pp, 2004. 1662, 1725, 1747, 1749

Drijfhout, S. S., D. P. Marshall, and H. A. Dijkstra, Conceptual models of the wind-driven and thermohaline circulation, in *Ocean Circulation and Climate, 2nd Edition: A 21st Century Perspective*, *International Geophysics Series*, vol. 103, edited by G. Siedler, S. M. Griffies, J. Gould, and J. Church, pp. 257–282, Academic Press, 2013. 1281

Duchateau, P., and D. Zachmann, *Partial differential equations*, Schaum's Outline Series in Mathematics, McGraw-Hill, New York, 1986. 125, 198, 207, 228, 231

Dukowicz, J. K., and R. D. Smith, Stochastic theory of compressible turbulent fluid transport, *Physics of Fluids*, *9*, 3523–3529, doi:10.1063/1.869460, 1997. 2007

Durran, D. R., Is the coriolis force really responsible for the inertial oscillation?, *Bulletin of the American Meteorological Society*, *74*, 2179–2184, doi:10.1175/1520-0477(1993)074⟨2179:ITCFRR⟩2.0.CO;2, 1993. 618

Dyke, M. V., *Perturbation methods in fluid mechanics*, 1st ed., The Parabolic Press, Stanford, California, USA, 271, 1975. 660

Eady, E., Long waves and cyclone waves, *Tellus*, *1*, 33–52, doi:10.1111/j.2153-3490.1949.tb01265.x, 1949. 1763, 1796

Early, J. J., The forces of inertial oscillations, *Quarterly Journal of the Royal Meteorological Society*, *138*, 1914, doi:10.1002/qj.1917, 2012. 341, 355, 394

Ebeling, W., and R. Feistel, *Physics of Self-Organization and Evolution*, John Wiley & Sons, 2011. 555, 561

Eckart, C., An analysis of the stirring and mixing processes in incompressible fluids, *Journal of Marine Research*, *7*, 265–275, 1948. 1919, 1989

Einstein, A., Über die von der molekularkinetischen theorie der wärme geforderte bewegung von in ruhenden flüssigkeiten suspendierten teilchen, *Annalen der Physik (in German)*, *322*, 549–560, 1905. 1900, 1989

Einstein, A., *Autobiographical Notes*, Open Court, 1949. 554

Eliassen, A., and E. Palm, On the transfer of energy in stationary mountain waves, *Geofysiske Publikasjoner*, *22*(1–23), 1960. 1873

Ertel, H., Ein neuer hydrodynamicscher Wirbelsatz, *Meteorol. Z. (Braunschweig)*, *59*, 271–281, 1942. 1179, 1182

Falkovich, G., *Fluid Mechanics: A short course for physicists*, Cambridge University Press, 167pp, 2011. 666

Farrell, W., and J. Clark, On postglacial sea level, *Geophysical Journal of the Royal Astronomical Society*, *46*, 646–667, 1976. 925

Favre, A., Équations des gaz turbulents compressibles. Parts I and II., *Journel de Méchanic*, *4*, 361–421, 1965. 514

Feistel, R., Equilibrium thermodynamics of seawater revisited, *Progress in Oceanography*, *31*, 101–179, 1993. 578

Ferrari, R., J. C. McWilliams, V. M. Canuto, and M. Dubovikov, Parameterization of eddy fluxes near oceanic boundaries, *Journal of Climate*, *21*, 2770–2789, doi:10.1175/2007JCLI1510.1, 2008. 1989, 2002, 2007

Ferrari, R., S. M. Griffies, A. J. G. Nurser, and G. K. Vallis, A boundary-value problem for the parameterized mesoscale eddy transport, *Ocean Modelling*, *32*, 143–156, doi:10.1016/j.ocemod.2010.01.004, 2010. 2002, 2003, 2007

Ferreira, D., and J. Marshall, Formulation and implementation of a residual-mean ocean circulation model, *Ocean Modelling*, *13*, 86–107, 2006. 1999

Fetter, A. L., and J. D. Walecka, *Theoretical Mechanics of Particles and Continua*, Dover Publications, Mineola, New York, 570 pp, 2003. 185, 194, 195, 234, 264, 284, 285, 289, 299, 314, 388, 402, 666, 1314, 1316, 1318, 1320, 1323, 1396, 1397, 1399, 1403, 1425, 1442, 1445, 1453, 1456, 1468, 1473, 1484, 1491, 1494, 1715, 1722

Feynman, R. P., R. B. Leighton, and M. L. Sands, *The Feynman lectures on physics*, Addison-Wesley Publishing Company, Reading, Mass, 1963. 689, 706, 1430

Fjørtoft, R., An application of integral theorems in deriving criteria for laminar flows and for the baroclinic circular vortex, *Geophysics Publications*, *17*, 1–52, 1950. 1733

Fofonoff, N. P., Steady flow in a frictionless homogeneous ocean, *Journal of Marine Research*, *13*, 254–262, 1954. 1112

Fox-Kemper, B., R. Lumpkin, and F. Bryan, Lateral transport in the ocean interior, in *Ocean Circulation and Climate, 2nd Edition: A 21st Century Perspective*, *International Geophysics Series*, vol. 103, edited by G. Siedler, S. M. Griffies, J. Gould, and J. Church, pp. 185–209, Academic Press, 2013. 2009

Frankel, T., *The Geometry of Physics: An Introduction*, Cambridge University Press, 694, 2004. 2, 15, 63

Frankel, T., *The Geometry of Physics: An Introduction*, Cambridge University Press, 686pp, 2012. 75, 239, 240

French, A. P., *Newtonian Mechanics*, 743 pp., W.W. Norton and Company, New York, 1971. 264, 274

Frisch, U., *Turbulence, the Legacy of A.N. Kolmogorov*, Cambridge University Press, 1995. 435

Frisch, U., and B. Villone, Cauchy's almost forgotten Lagrangian formulation of the Euler equation for 3D incompressible flow, *European Physical Journal*, *39*, 325–351, doi:10.1140/epjh/e2014-50016-6, 2014. 462

Gardiner, C. W., *Handbook of stochastic methods for physics, chemstry and the natural sciences*, 2nd ed., 442 pp., Springer-Verlag, Berlin, Heidelberg, New York, 1985. 219

Garrett, C., Turbulent dispersion in the ocean, *Progress in Oceanography*, *70*, 113–125, 2006. 1970, 1975

Garrett, C., P. MacCready, and P. Rhines, Boundary mixing and arrested ekman layers: Rotating stratified flow near a sloping boundary, *Annual Review of Fluid Mechanics*, *25*, 291–323, doi:10.1146/annurev.fl.25.010193.001451, 1993. 921, 922

Gasiorowicz, S., *Quantam Physics*, Wiley International, Hoboken, NJ, USA, 1974. 149, 163, 1393, 1399, 1403, 1404

Gavriel, N., and Y. Kaspi, The number and location of Jupiter's circumpolar cyclones explained by vorticity dynamics, *Nature Geoscience*, *14*, 559–563, doi:10.1038/s41561-021-00781-6, 2021. 1072

Gent, P., The energetically consistent shallow-water equations, *Journal of the Atmospheric Sciences*, *50*, 1323–1325, doi:10.1175/1520-0469(1993)050⟨1323:TECSWE⟩2.0.CO;2, 1993. 800, 968, 970

Gent, P. R., and J. C. McWilliams, Isopycnal mixing in ocean circulation models, *Journal of Physical Oceanography*, *20*, 150–155, doi:10.1175/1520-0485(1990)020⟨0150:IMIOCM⟩2.0.CO;2, 1990. 881, 882, 965, 1991, 2005, 2006

Gent, P. R., J. Willebrand, T. J. McDougall, and J. C. McWilliams, Parameterizing eddy-induced tracer transports in ocean circulation models, *Journal of Physical Oceanography*, *25*, 463–474, doi:10.1175/1520-0485(1995)025⟨0463:PEITTI⟩2.0.CO;2, 1995. 818, 965, 1927, 1983, 1991, 1995, 1996, 1998, 1999, 2000, 2001, 2002, 2003

Gibbs, J. W., *Elements of Vector Analysis*, Tuttle, Morehouse & Taylor, New Haven, USA, 1884. 55

Gilbert, A. D., and J. Vanneste, Geometric approaches to Lagrangian averaging, *Annual Review of Fluid Mechanics*, *57*, 117–140, doi:10.1146/annurev-fluid-030524-095913, 2025. 1959, 1960, 1968

Gill, A., *Atmosphere-Ocean Dynamics*, *International Geophysics Series*, vol. 30, Academic Press, London, 662 + xv pp, 1982. 341, 343, 344, 394, 407, 574, 655, 834, 870, 891, 895, 901, 926, 1601, 1602, 1765, 1782, 1989

Gnanadesikan, A., A global model of silicon cycling: Sensitivity to eddy parameterization and dissolution, *Global Biogeochemical Cycles*, *13*, 199–220, 1999. 2006

Gnanadesikan, A., and R. Weller, Structure and instability of the ekman spiral in the presence of surface gravity waves, *Journal of Physical Oceanography*, *25*, 3148–3171, doi:10.1175/1520-0485(1995)025⟨3148:SAIOTE⟩2.0.CO;2, 1995. 920

Godfrey, J., A Sverdrup model of the depth-integrated flow for the World Ocean allowing for island circulations, *Geophysical and Astrophysical Fluid Dynamics*, *45*, 89–112, doi:10.1080/03091928908208894, 1989. 1115, 1116, 1117

Goldstein, H., *Classical Mechanics*, Addison-Wesley Publishing, Reading, MA, 1980. 249, 259, 264, 273, 285, 384, 1316, 1321, 1410

Graham, F., and T. McDougall, Quantifying the nonconservative production of Conservative Temperature, potential temperature, and entropy, *Journal of Physical Oceanography*, *43*, 838–862, doi:10.1175/JPO-D-11-0188.1, 2013. 702, 705, 1990

Gray, A., and S. Riser, A global analysis of Sverdrup balance using absolute geostrophic velocities from Argo, *Journal of Physical Oceanography*, *44*, 1213–1229, doi:10.1175/JPO-D-12-0206.1, 2014. 1275

Greatbatch, R. J., A note on the representation of steric sea level in models that conserve volume rather than mass, *Journal of Geophysical Research*, *99*, 12,767–12,771, doi:10.1029/94JC00847, 1994. 548, 2037

Greatbatch, R. J., Exploring the relationship between eddy-induced transport velocity, vertical momentum transfer, and the isopycnal flux of potential vorticity, *Journal of Physical Oceanography*, *28*, 422–432, doi:10.1175/1520-0485(1998)028⟨0422:ETRBEI⟩2.0.CO;2, 1998. 1887, 1889

Greatbatch, R. J., and K. G. Lamb, On parameterizing vertical mixing of momentum in non-eddy resolving ocean models, *Journal of Physical Oceanography*, *20*, 1634–1637, doi:10.1175/1520-0485(1990)020⟨1634:OPVMOM⟩2.0.CO;2, 1990. 1887, 1999, 2000

Greenspan, H. P., *The Theory of Rotating Fluids*, Cambridge University Press, Cambridge, UK, 1969. 870

Gregg, M. C., Entropy generation in the ocean by small-scale mixing, *Journal of Physical Oceanography*, *14*, 688–711, 1984. 687

Gregory, J., Vertical heat transports in the ocean and their effect on time-dependent climate change, *Climate Dynamics*, *15*, 501–515, doi:10.1007/s003820000059, 2000. 790

Gregory, J., S. M. Griffies, C. Hughes, J. Lowe, J. Church, I. Fukimori, N. Gomez, R. Kopp, F. Landerer, R. Ponte, D. Stammer, M. Tamisiea, and R. van den Wal, Concepts and terminology for sea level–mean, variability and change, both local and global, *Surveys in Geophysics*, *40*, 1251–1289, doi:10.1007/s10712-019-09555-7, 2019. 344, 926, 2037, 2039

Griffies, S., and R. Hallberg, Biharmonic friction with a Smagorinsky-like viscosity for use in large-scale eddy-permitting ocean models, *Monthly Weather Review*, *128*, 2935–2946, doi:10.1175/1520-0493(2000)128⟨2935:BFWASL⟩2.0.CO;2, 2000. 678, 969, 1911

Griffies, S., A. Adcroft, and R. Hallberg, A primer on the vertical lagrangian-remap method in ocean models based on finite volume generalized vertical coordinates, *Journal of Advances in Modeling Earth Systems*, *12*, doi:10.1029/2019MS001954, 2020. 421, 521, 951, 962, 1155, 1798, 1838, 1850, 1888, 2008, 2013

Griffies, S. M., The Gent-McWilliams skew-flux, *Journal of Physical Oceanography*, *28*, 831–841, doi:10.1175/1520-0485(1998)028⟨0831:TGMSF⟩2.0.CO;2, 1998. 1924, 1996

Griffies, S. M., *Fundamentals of Ocean Climate Models*, Princeton University Press, Princeton, USA, 518+xxxiv pages, 2004. 45, 75, 97, 111, 514, 615, 645, 646, 647, 653, 654, 678, 969, 1067, 1850, 1910, 1911, 1912, 1924, 1959, 1983, 2002, 2003, 2009

Griffies, S. M., and A. J. Adcroft, Formulating the equations for ocean models, in *Ocean Modeling in an Eddying Regime*, *Geophysical Monograph*, vol. 177, edited by M. Hecht and H. Hasumi, pp. 281–317, American Geophysical Union, 2008. 777

Griffies, S. M., and R. J. Greatbatch, Physical processes that impact the evolution of global mean sea level in ocean climate models, *Ocean Modelling*, *51*, 37–72, doi:10.1016/j.ocemod.2012.04.003, 2012. 501, 548, 943, 1960, 1992, 1995, 2025, 2037, 2039

Griffies, S. M., A. Gnanadesikan, R. C. Pacanowski, V. Larichev, J. K. Dukowicz, and R. D. Smith, Isoneutral diffusion in a z-coordinate ocean model, *Journal of Physical Oceanography*, *28*, 805–830, doi:10.1175/1520-0485(1998)028⟨0805:IDIAZC⟩2.0.CO;2, 1998. 1910, 1911, 2005, 2006

Griffies, S. M., C. W. Böning, F. O. Bryan, E. P. Chassignet, R. Gerdes, H. Hasumi, A. Hirst, A.-M. Treguier, and D. Webb, Developments in ocean climate modelling, *Ocean Modelling*, *2*, 123–192, doi:10.1016/S1463-5003(00)00014-7, 2000. 1851, 2001

Griffies, S. M., J. Yin, P. J. Durack, P. Goddard, S. Bates, E. Behrens, M. Bentsen, D. Bi, A. Biastoch, C. W. Böning, A. Bozec, C. Cassou, E. Chassignet, G. Danabasoglu, S. Danilov, C. Domingues, H. Drange, R. Farneti, E. Fernandez, R. J. Greatbatch, D. M. Holland, M. Ilicak, J. Lu, S. J. Marsland, A. Mishra, W. G. Large, K. Lorbacher, A. G. Nurser, D. Salas y Mélia, J. B. Palter, B. L. Samuels, J. Schröter, F. U. Schwarzkopf, D. Sidorenko, A.-M. Treguier, Y. Tseng, H. Tsujino, P. Uotila, S. Valcke, A. Voldoire, Q. Wang, M. Winton, and Z. Zhang, An assessment of global and regional sea level for years 1993-2007 in a suite of interannual CORE-II simulations, *Ocean Modelling*, *78*, 35–89, doi:10.1016/j.ocemod.2014.03.004, 2014. 726, 954, 2038, 2039

Griffiths, D. J., *Introduction to Electrodynamics*, Prentice-Hall, Englewood Cliffs, New Jersey, USA, 479 pp, 1981. 1060

Groeskamp, S., J. Zika, T. McDougall, B. Sloyan, and F. Laliberté, The representation of ocean circulation and variability in thermodynamic coordinates, *Journal of Physical Oceanography*, *44*, 1735–1750, doi:10.1175/JPO-D-13-0213.1, 2014. 2044

Groeskamp, S., R. P. Abernathey, and A. Klocker, Water mass transformation by cabbeling and thermobaricity, *Geophysical Research Letters*, doi:10.1002/2016GL070860, 2016. 2025

Groeskamp, S., S. M. Griffies, D. Iudicone, R. Marsh, A. G. Nurser, and J. D. Zika, The water mass transformation framework for ocean physics and biogeochemistry, *Annual Review of Marine Science*, *11*, 1–35, doi:10.1146/annurev-marine-010318-095421, 2019. 1829, 2025, 2033, 2045, 2058, 2068, 2074

Guggenheim, E. A., *Thermodynamics: An Advanced Treatment for Chemists and Physicists*, 5th ed., North-Holland, Amsterdam, 390, 1967. 572, 585

Gula, J., M. Molemaker, and J. McWilliams, Gulf Stream dynamics along the southeastern U.S. seaboard, *Journal of Physical Oceanography*, *45*, 690–715, doi:10.1175/JPO-D-14-0154.1, 2015. 747, 1166, 1177

Haidvogel, D. B., and P. B. Rhines, Waves and circulation driven by oscillatory winds in an idealized ocean basin, *Geophysical and Astrophysical Fluid Dynamics*, *25*, 1–63, doi:10.1080/03091928308221747, 1983. 1522

Haine, T. W. N., and A. Fuller, Boundary β-plumes and their vorticity budgets, *Quarterly Journal of the Royal Meteorological Society*, *142*, 2758–2767, doi:DOI:10.1002/qj.2866, 2016. 1076

Haine, T. W. N., S. M. Griffies, G. Gebbie, and W. Jiang, A review of Green's function methods for tracer timescales and pathways in ocean models, *Journal of Advances in Modeling Earth Systems (JAMES), in revision*, 2025. 135, 512, 1917, 1940, 1952

Hallberg, R., A thermobaric instability in Lagrangian vertical coordinate ocean models, *Ocean Modelling*, *8*, 227–300, 2005. 1859

Hallberg, R., and P. Rhines, Buoyancy-driven circulation in a ocean basin with isopycnals intersectin the sloping boundary, *Journal of Physical Oceanography*, *26*, 913–940, 1996. 1163, 1167, 1222

Haltiner, G. T., and R. T. Williams, *Numerical Prediction and Dynamic Meteorology*, John Wiley and Sons, New York, USA, 1980. 1061

Haney, R. L., On the pressure gradient force over steep topography in sigma-coordinate ocean models, *Journal of Physical Oceanography*, *21*, 610–619, 1991. 1851

Hasselmann, K., Stochastic climate models. Part I: Theory, *Tellus*, *28*, 473–485, 1976. 234

Hasselmann, K., R. Sausen, E. Maier-Reimer, and R. Voss, On the cold start problem in transient simulations with coupled atmosphere-ocean models, *Climate Dynamics*, *9*, 53–61, doi:10.1007/BF00210008, 1993. 239

Hayes, W. D., Conservation of action and modal wave action, *Proceedings of the Royal Society of London. Series A Mathematical and Physical Sciences*, *320*, 187–206, doi:www.jstor.org/stable/77799, 1970. 1328

Haynes, P. H., and M. E. McIntyre, On the evolution of vorticity and potential vorticity in the presence of diabatic heating and frictional or other forces, *Journal of Atmospheric Sciences*, *44*, 828–841, 1987. 1205, 1207, 1208

Haynes, P. H., and M. E. McIntyre, On the conservation and impermeability theorems for potential vorticity, *Journal of Atmospheric Sciences*, *47*, 2021–2031, 1990. 1208

Heifetz, E., P. Alpert, and A. da Silva, On the parcel method and the baroclinic wedge of instability, *Journal of Atmospheric Sciences*, *55*, 788–795, doi:10.1175/1520-0469(1998)055⟨0788:OTPMAT⟩2.0.CO;2, 1998. 1796

Held, I., R. Pierrehumbert, S. Garner, and K. L. Swanson, Surface quasi-geostrophic dynamics, *Journal of Fluid Mechanics*, *282*, 1–20, doi:10.1017/S0022112095000012, 1995. 1300, 1473, 1767

Helland-Hansen, B., The Sognefjord section: Oceanographic observations in the northernmost part of the North Sea and southern part of the Norwegian Sea, *James Johnstone Memorial Volume*, 1934. 734

Helmholtz, H., On integrals of the hydrodynamical equations, which express vortex-motion, *The London, Edinburgh, and Dublin Philosophical Magazine and Journal of Science*, *33*, 485–512, doi:10.1080/14786446708639824, 1867. 239, 240

Hesselberg, T., Die Gesetze der ausgeglichenen atmosphaerischen Bewegungen, *Beiträgeder Physik der freien Atmosphere*, *12*, 141–160, 1926. 514

Hildebrand, F., *Advanced Calculus for Applications*, Prentice-Hall Publishers, Englewood Cliffs, New Jersey, 1976. 125, 128, 137, 163, 168, 207

Holland, G. J., Tropical cyclone motion: environmental interaction plus a beta effect, *Journal of the Atmospheric Sciences*, *40*, 328–342, doi:10.1175/1520-0469(1983)040⟨0328:TCMEIP⟩2.0.CO;2, 1983. 1072

Holloway, G., Eddy transport of thickness and momentum in layer and level models, *Journal of Physical Oceanography*, *27*, 1153–1157, 1997. 2001

Holloway, G., and P. Rhines, Angular momenta of modeled ocean gyres, *Journal of Geophysical Research*, *27*, 843–846, doi:10.1029/90JC02256, 1991. 1080

Holmes, R. M., J. Zika, and M. H. England, Diathermal heat transport in a global ocean model, *Journal of Physical Oceanography*, *49*, 141–161, doi:10.1175/JPO-D-18-0098.1, 2019. 2054, 2078

Holton, J. R., and G. J. Hakim, *An Introduction to Dynamic Meteorology*, 5th ed., Academic Press, Waltham, Mass, USA, 532 pp, 2013. 600, 623, 624, 760, 766, 891, 895, 897, 899, 900, 1069, 1099, 1150, 1173, 1246, 1247, 1250, 1292, 1293, 1668, 1669, 1698, 1704

Holzer, M., The path density of interhemispheric surface-to-surface transport.Part I: Development of the diagnostic and illustration with an analytic model, *Journal of Atmospheric Sciences*, *66*(8), 2159–2171, doi:10.1175/2009jas2894.1, 2009. 219

Hoskins, B., The role of potential vorticity in symmetric stability and instability, *Quarterly Journal of the Royal Meteorological Society*, *100*, 480–482, 1974. 1692, 1697

Hoskins, B., The geostrophic momentum approximation and the semi-geostrophic equations, *Journal of Atmospheric Sciences*, *32*, 233–242, 1975. 1247, 1293, 1667, 1698, 1700, 1701

Hoskins, B., Towards a PV-θ view of the general circulation, *Tellus*, *43AB*, 27–35, 1991. 1179, 1185, 1224

Hoskins, B., I. Draghici, and H. Davies, A new look at the ω equation, *Quarterly Journal of the Royal Meteorological Society*, *104*, 31–38, 1978. 1294

Hoskins, B., I. James, and G. White, The shape, propagation, and mean flow interaction of large-scale weather systems, *Journal of the Atmospheric Sciences*, *40*, 1595–1612, doi:10.1175/1520-0469(1983)040⟨1595:TSPAMF⟩2.0.CO;2, 1983. 1055

Hoskins, B. J., and I. N. James, *Fluid Dynamics of the Midlatitude Atmosphere*, Wiley Blackwell, Chichester, UK, 2014. 477, 478

Howard, L. N., Note on a paper of John W. Miles, *Journal of Fluid Mechanics*, *10*, 509–512, doi:10.1017/S0022112061000317, 1961. 1754, 1757

Huang, K., *Statistical Mechanics*, John Wiley and Sons, New York, 493 pp, 1987. 404, 412, 681, 1906

Huang, R. X., and R. W. Schmitt, Goldsbrough-Stommel circulation of the World Oceans, *Journal of Physical Oceanography*, *23*, 1277–1284, 1993. 1272

Hughes, C. W., A theoretical reason to expect inviscid western boundary currents in realistic oceans, *Ocean Modelling*, *2*, 73–83, doi:10.1016/S1463-5003(00)00011-1, 2000. 765, 766, 1109, 1112, 1138

Hughes, C. W., and B. de Cueves, Why western boundary currents in realistic oceans are inviscid: A link between form stress and bottom pressure torques, *Journal of Physical Oceanography*, *31*, 2871–2885, 2001. 765, 766, 1012, 1109, 1112, 1163, 1167

Hughes, C. W., I. Fukumori, S. M. Griffies, J. M. Huthnance, S. Minobe, P. Spence, K. R. Thompson, and A. Wise, Sea level and the role of coastal trapped waves in mediating the influence of the open ocean on the coast, *Surveys in Geophysics*, *40*, 1467–1492, doi:10.1007/s10712-019-09535-x, 2019. 1119

IOC, SCOR, and IAPSO, *The international thermodynamic equation of seawater-2010: calculation and use of thermodynamic properties*, Intergovernmental Oceanographic Commission, Manuals and Guides No. 56, UNESCO, doi:10.25607/OBP-1338, 196pp, 2010. 578, 592, 689, 702, 705, 708, 825, 826, 827, 829, 1990, 2018, 2019, 2026

Jackett, D. R., and T. J. McDougall, A neutral density variable for the world's oceans, *Journal of Physical Oceanography*, *27*, 237–263, 1997. 2045

Jackson, J. D., *Classical Electrodynamics*, John Wiley and Sons, New York, USA, 848 pp, 1975. 149, 207, 240, 863, 1060, 1925

Jackson, L., C. Hughes, and R. Williams, Topographic control of basin and channel flows: the role of bottom pressure torques and friction, *Journal of Physical Oceanography*, *36*, 1786–1805, doi:10.1175/JPO2936.1, 2006. 1109, 1167

Jansen, M., A. Adcroft, S. M. Griffies, and I. Grooms, The averaged hydrostatic Boussinesq equations in generalized vertical coordinates, *Journal of Advances in Modeling Earth Systems (JAMES)*, *16*, doi:10.1029/2024MS004506, 2024. 971, 972, 1959, 1983, 1986, 1999

Jeevanjee, N., and D. Romps, Effective buoyancy, inertial pressure, and the mechanical generation of boundary layer mass flux by cold pools, *Journal of Atmospheric Sciences*, *72*, 3199–3213, doi:10.1175/JAS-D-14-0349.1, 2015a. 856, 857, 1067

Jeevanjee, N., and D. Romps, Effective buoyancy at the surface and aloft, *Quarterly Journal of the Royal Meteorological Soceity*, *142*, 811–820, doi:10.1002/qj.2683, 2015b. 850, 856

Jezierski, J., and J. Kijowski, Thermo-hydrodynamics as a field theory, in *Nonequilibrium Theory and Extremum Principles*, *Advances in Thermodynamics*, vol. 3, edited by S. Sieniutycz and P. Salaman, pp. 282–317, Taylor & Francis, 1990. 1337, 1342

Johnson, R. S., *A Modern Introduction fo the Mathematical Theory of Water Waves*, Cambridge Texts in Applied Mathematics, 1997. 444, 445, 548, 624, 1487

José, J. V., and E. J. Saletan, *Classical Dynamics: A Contemporary Approach*, Cambridge Press, 670 pp., 1998. 285, 286, 384, 1316, 1320, 1330, 1406

Kamenkovich, V., *Fundamentals of Ocean Dynamics*, Elsevier Scientific Publishin Company, Amsterdam, 249 pp, 1977. 574, 585, 588, 589, 691

Karoly, D. J., P. C. McIntosh, P. Berrisford, T. J. McDougall, and A. C. Hirst, Similarities of the Deacon cell in the Southern Ocean and Ferrel cells in the atmosphere, *Quarterly Journal of the Royal Meteorological Society*, *123*, 519–526, doi:10.1002/qj.49712353813, 1997. 546

Kellogg, O. D., *Foundations of Potential Theory*, Dover Publications, New York, 1953. 207

Killworth, P. D., On the parameterization of eddy transfer Part I: Theory, *Journal of Marine Research*, *55*, 1171–1197, 1997. 2001

Kiss, A. E., Potential vorticity crises, adverse pressure gradients, and western boundary separation, *Journal of Marine Research*, *60*, 779–803, 2002. 1112

Kiss, A. E., Potential vorticity dynamics in a domain with closed geostrophic contours. I: steady linear flows, *Journal of Marine Research*, *62*, 461–489, 2004. 1112

Klinger, B., and T. Haine, *Ocean Circulation in Three Dimensions*, Cambridge University Press, 466, 2019. 696, 1117

Klocker, A., and R. Abernathey, Global patterns of mesoscale eddy properties and diffusivities, *Journal of Physical Oceanography*, *44*, 1030–1046, 2014. 1989

Klocker, A., and T. J. McDougall, Influence of the nonlinear equation of state on global estimates of dianeutral advection and diffusion, *Journal of Physical Oceanography*, *40*, 1690–1709, doi:10.1175/2010JPO4303.1, 2010a. 840, 2025

Klocker, A., and T. J. McDougall, Quantifying the consequences of the ill-defined nature of neutral surfaces, *Journal of Physical Oceanography*, *40*, 1866—1880, doi:10.1175/2009JPO4212.1, 2010b. 840

Kooloth, P., L. Smith, and S. Stechmann, Conservation laws for potential vorticity in a salty ocean or cloudy atmosphere, *Geophysical Research Letters*, *49*, doi:10.1029/2022GL100009, 2022. 1133, 1198

Kopp, R. E., J. X. Mitrovica, S. M. Griffies, J. Yin, C. C. Hay, and R. J. Stouffer, The impact of Greenland melt on regional sea level: a preliminary comparison of dynamic and static equilibrium effects, *Climatic Change Letters*, *103*, 619–625, doi:10.1007/s10584-010-9935-1, 2010. 925

Kraichnan, R. H., and D. Montgomery, Two-dimensional turbulence, *Reports on Progress in Physics*, *43*, 547–619, 1980. 1061

Kreuzer, H. J., *Nonequilibrium thermodynamics and its statistical foundations*, 438 pp., Oxford Science Publications, New York, 1981. 507, 515

Kundu, P., I. Cohen, and D. Dowling, *Fluid Mechanics*, Academic Press, 921 + xxiv pp, 2016. xxxv, 412, 431, 444, 616, 629, 644, 645, 646, 653, 660, 666, 1425, 1438, 1601, 1639, 1676, 1725, 1757, 1795, 1906

Kuo, H. L., Dynamic stability of two-dimensional nondivergent flow in a barotropic atmosphere, *Journal of the Meteorology*, *6*, 105–122, doi:10.1175/1520-0469(1949)006⟨0105:DIOTDN⟩2.0.CO;2, 1949. 1733

Kushner, P. J., and I. M. Held, Potential vorticity thickness fluxes and wave-mean flow interaction, *Journal of Atmospheric Sciences*, *56*, 948–958, 1999. 1983

Lamb, H., *Hydrodynamics*, 6th ed., Cambridge University Press, 1993. 1466

Landau, L. D., and E. M. Lifshitz, *Mechanics*, Pergamon Press, Oxford, UK, 170 pp, 1976. 285, 286, 300, 307, 314, 351, 384, 1406

Landau, L. D., and E. M. Lifshitz, *Statistical Physics: Part 1*, Pergamon Press, Oxford, UK, 544 pp, 1980. 555, 585, 589, 670, 690, 691

Landau, L. D., and E. M. Lifshitz, *Fluid Mechanics*, Pergamon Press, Oxford, UK, 539 pp, 1987. 576, 666, 681, 683, 687, 689, 692, 1425

Large, W., J. McWilliams, and S. Doney, Oceanic vertical mixing: a review and a model with a nonlocal boundary layer parameterization, *Reviews of Geophysics*, *32*, 363–403, doi:10.1029/94RG01872, 1994. 1989, 2033

Larson, V. E., The relationship between the transilient matrix and the Green's function for the advection-diffusion equation, *Journal of Atmospheric Sciences*, *56*(14), 2447–2453, doi:10.1175/1520-0469(1999)056⟨2447:trbttm⟩2.0.co;2, 1999. 219, 1942

Lauritzen, P., N. Kevlahan, T. Toniazzo, C. Eldred, T. Dubos, A. Gassmann, V. Larson, C. Jablonowski, O. Guba, B. Shipway, B. Harrop, F. Lemarie, R. Tailleux, A. Herrington, W. Large, P. Rasch, A. Donahue, H. Wan, A. Conley, and J. Bacmeister, Reconciling and improving formulations for thermodynamics and conservation principles in Earth System Models (ESMs), *Journal of Advances in Modeling Earth Systems*, doi:10.1029/2022MS003117, 2022. 706

LeCorre, M., J. Gula, and A.-M. Treguier, Barotropic vorticity balance of the North Atlantic subpolar gyre in an eddy-resolving model, *Ocean Science*, *16*, 451–468, doi:10.5194/os-16-451-2020, 2020. 1166, 1167

Lee, M.-M., D. Marshall, and R. Williams, On the eddy transfer of tracers: advective or diffusive?, *Journal of Marine Research*, *55*, 483–505, 1997. 1874

Lemarié, F., L. Debreu, A. F. Shchepetkin, and J. C. McWilliams, On the stability and accuracy of the harmonic and biharmonic isoneutral mixing operators in ocean models, *Ocean Modelling*, *52-53*, 9–35, doi:10.1016/j.ocemod.2012.04.007, 2012. 2005, 2006

Lighthill, J., *Waves in Fluids*, Cambridge University Press, Cambridge, UK, 504 pp, 1978. 1403, 1405, 1430, 1445, 1482, 1503, 1601, 1639

Lilly, J., Kinematics of a fluid ellipse in a linear flow, *Fluids*, *3*(16), doi:10.3390/fluids3010016, 2018. 478

Lilly, J. M., J. Feske, B. Fox-Kemper, and J. J. Early, Integral theorems for the gradient of a vector field, with a fluid dynamical application, *Proceedings of the Royal Society, A*, *480*, doi:10.1098/rspa.2023.0550, 2024. 55

Lin, S. J., A finite volume integration method for computing pressure gradient force in general vertical coordinates, *Quarterly Journal of the Royal Meteorological Society*, *123*, 1749–1762, doi:10.1002/qj.49712354214, 1997. 1851, 1853

Longuet-Higgins, H. C., Planetary waves on a rotating sphere, *Proceedings of the Royal Society of London A*, *279*, 446–473, doi:10.1098/rspa.1964.0116, 1964. 1533, 1535, 1539

Loose, N., S. Bachman, I. Grooms, and M. Jansen, Diagnosing scale-dependent energy cycles in a high-resolution isopycnal ocean model, *Journal of Physical Oceanography*, doi:10.1175/JPO-D-22-0083.1, 2022. 1005

Loose, N., G. M. Marques, A. Adcroft, S. Bachman, S. M. Griffies, I. Grooms, R. W. Hallberg, and M. Jansen, Comparing two parameterizations for the restratification effect of mesoscale eddies in an isopycnal ocean model, *Journal of Advances in Modeling Earth Systems (JAMES)*, *15*, doi:10.1029/2022MS003518, 2023. 751, 1999, 2000

Lorenz, E. N., Available potential energy and the maintenance of the general circulation, *Tellus*, *7*, 157–167, 1955. 807, 808

Lovelock, D., and H. Rund, *Tensors, Differential Forms, and Variational Principles*, 366 pp., Dover Publications, New York, 1989. 7

Luke, J. C., A variational principle for a fluid with a free surface, *Journal of Fluid Mechanics*, *27*, 395–397, doi:10.1017/S0022112067000412, 1967. 1468, 1469, 1471

MacCready, P., and P. Rhines, Buoyant inhibition of ekman transport on a slope and its effect on stratified spin-up, *Journal of Fluid Mechanics*, *223*, 631–661, doi:10.1017/S0022112091001581, 1991. 921, 922

MacCready, P., and P. Rhines, Slippery bottom boundary layers on a slope, *Journal of Physical Oceanography*, *23*, 5–22, doi:10.1175/1520-0485(1993)023⟨0005:SBBLOA⟩2.0.CO;2, 1993. 921, 922, 1254

MacKinnon, J., Louis St. Laurent, and A. C. Naveira Garabato, Diapycnal mixing processes in the ocean interior, in *Ocean Circulation and Climate, 2nd Edition: A 21st century perspective*, *International Geophysics Series*, vol. 103, edited by G. Siedler, S. M. Griffies, J. Gould, and J. Church, pp. 159–183, Academic Press, doi:10.1016/B978-0-12-391851-2.00007-6, 2013. 678, 1627, 1989, 1990

MacKinnon, J., Z. Zhao, C. Whalen, A. Waterhouse, D. Trossman, O. Sun, L. S. Laurent, H. Simmons, K. Polzin, R. Pinkel, A. Pickering, N. Norton, J. Nash, R. Musgrave, L. Merchant, A. Melet, B. Mater, S. Legg, W. Large, E. Kunze, J. Klymak, M. Jochum, S. Jayne, R. Hallberg, S. M. Griffies, P. Gent, S. Diggs, G. Danabasoglu, E. Chassignet, M. Buijsman, F. Bryan, B. Briegleb, A. Barna, B. Arbic, J. Ansong, and M. Alford, Climate process team on internal-wave driven ocean mixing, *Bulletin of the American Meteorological Society*, pp. 2429–2454, doi:10.1175/BAMS-D-16-0030.1, 2017. 1627

Maddison, J., and D. Marshall, The Eliassen-Palm flux tensor, *Journal of Fluid Mechanics*, *729*, 69–102, doi:10.1017/jfm.2013.259, 2013. 984, 993, 1304, 1871, 1885

Malvern, L. E., *Introduction to the Mechanics of a Continuous Media*, Prentice-Hall, Englewoodo Cliffs, USA, 713pp, 1969. 416, 448, 454, 459, 635

Marion, J. B., and S. T. Thornton, *Classical Dynamics of Particles and Systems*, Harcourt Brace Jovanovich, San Diego, USA, 602 pp, 1988. xi, 249, 256, 257, 263, 264, 274, 280, 285, 307, 388, 399, 1087, 1410

Markowski, P., and Y. Richardson, *Mesoscale Meteorology in Midlatitudes*, Wiley-Blackwell Publishers, Oxford, UK, 2010. 353, 786, 856, 1173, 1669, 1676, 1679

Marshall, D., Vertical fluxes of potential vorticity and the structure of the thermocline, *Journal of Physical Oceanography*, *30*, 3102–3112, 2000. 1196, 1210

Marshall, D. P., and H. R. Pillar, Momentum balance of the wind-driven and meridional overturning circulation, *Journal of Physical Oceanography*, *41*, 960–978, doi:10.1175/2011JPO4528.1, 2011. 788

Marshall, D. P., J. Maddison, and P. Berlov, A framework for parameterizing eddy potential vorticity fluxes, *Journal of Physical Oceanography*, *42*, 539–557, doi:10.1175/JPO-D-11-048.1, 2012. 1119

Marshall, J., and R. A. Plumb, *Atmosphere, Ocean, and Climate Dynamics*, 1st ed., Academic Press, Amsterdam, 319pp, 2008. 623, 739, 870, 901, 907, 1016

Marshall, J., D. Jamous, and J. Nilsson, Entry, flux, and exit of potential vorticity in ocean circulation, *Journal of Physical Oceanography*, *31*, 777–789, doi:10.1175/1520-0485(2001)031⟨0777:EFAEOP⟩2.0.CO;2, 2001. 1196, 1208, 1209, 1210, 1221

Marshall, J., K. Armour, J. Scott, Y. Kostov, U. Hausmann, D. Ferreira, T. Shepherd, and C. Bitz, The ocean's role in polar climate change: asymmetric Arctic and Antarctic responses

to greenhouse gas and ozone forcing, *Philosophical Transactions of the the Royal Society A*, *A372*, doi:10.1098/rsta.2013.0040, 2014. 239

Marshall, J. C., E. Shuckburgh, H. Jones, and C. Hill, Estimates and implications of surface eddy diffusivity in the Southern Ocean derived from tracer transport, *Journal of Physical Oceanography*, *36*, 1806–1821, 2006. 1954

Maxwell, J., *Theory of Heat*, 3rd ed., Longmans, Green, and Company, London, 313, 1872. 554, 599

McCabe, R., P. MacCready, and G. Pawlak, Form drag due to flow separation at a headland, *Journal of Physical Oceanography*, *36*, 2136–2152, doi:10.1175/JPO2966.1, 2006. 750

McDougall, T., R. Feistel, and R. Pawlowicz, Thermodynaics of seawater, in *Ocean Circulation and Climate, 2nd Edition: A 21st Century Perspective*, *International Geophysics Series*, vol. 103, edited by G. Siedler, S. M. Griffies, J. Gould, and J. Church, pp. 141–158, Academic Press, 2013. 829

McDougall, T. J., Double-diffusive convection caused by coupled molecular diffusion, *Journal of Fluid Mechanics*, *126*, 379–397, doi:10.1017/S0022112083000221, 1983. 702

McDougall, T. J., Neutral surfaces, *Journal of Physical Oceanography*, *17*, 1950–1967, doi:10.1175/1520-0485(1987)017⟨1950:NS⟩2.0.CO;2, 1987a. 830, 834, 1989, 1993

McDougall, T. J., Thermobaricity, cabbeling, and water-mass conversion, *Journal of Geophysical Research*, *92*, 5448–5464, doi:10.1029/JC092iC05p05448, 1987b. 830, 834, 1989, 2022, 2023, 2024

McDougall, T. J., The vertical motion of submesoscale coherent vortices across neutral surfaces, *Journal of Physical Oceanography*, *17*, 2334–2342, 1987c. 844

McDougall, T. J., Potential enthalpy: a conservative oceanic variable for evaluating heat content and heat fluxes, *Journal of Physical Oceanography*, *33*, 945–963, doi:10.1175/1520-0485(2003)033⟨0945:PEACOV⟩2.0.CO;2, 2003. 592, 704, 705, 826, 2018

McDougall, T. J., and R. Feistel, What causes the adiabatic lapse rate, *Deep-Sea Research*, *50*, 1523–1535, 2003. 591

McDougall, T. J., and D. R. Jackett, On the helical nature of neutral trajectories in the ocean, *Progress in Oceanography*, *20*, 153–183, 1988. 838, 840

McDougall, T. J., and P. C. McIntosh, The temporal-residual-mean velocity. Part II: isopycnal interpretation and the tracer and momentum equations, *Journal of Physical Oceanography*, *31*, 1222–1246, doi:10.1175/1520-0485(2001)031⟨1222:TTRMVP⟩2.0.CO;2, 2001. 1934, 1959, 1977, 1983, 1986, 1996

McDougall, T. J., and J. Turner, The role of cross-diffusion on finger double-diffusive convection, *Nature*, *299*, 812–814, doi:10.1038/299812a0, 1982. 701

McDougall, T. J., and Y. You, Implications of the nonlinear equation of state for upwelling in the ocean interior, *Journal of Geophysical Research*, *95*, 13,263—-13,276, 1990. 2025

McDougall, T. J., S. Groeskamp, and S. M. Griffies, On geometric aspects of interior ocean mixing, *Journal of Physical Oceanography*, *44*, 2164–2175, doi:10.1175/JPO-D-13-0270.1, 2014. 833, 834, 1989, 1990, 1992, 1993, 1994, 2003, 2022

McDougall, T. J., P. Barker, R. Holmes, R. Pawlowicz, S. Griffies, and P. Durack, The interpretation of temperature and salinity variables in numerical ocean model output, and the calculation of heat fluxes and heat content, *Geoscientific Model Development*, *14*, 6445–6466, doi:10.5194/gmd-14-6445-2021, 2021. 592, 705

McIntosh, P. C., and T. J. McDougall, Isopycnal averaging and the residual mean circulation., *Journal of Physical Oceanography*, *26*, 1655–1660, 1996. 1983, 1996

McWilliams, J., *Fundamentals of Geophysical Fluid Dynamics*, Cambridge University Press, Cambridge, Cambridge, UK, 2006. 1050, 1059, 1078, 1522, 1719, 1872

McWilliams, J., and G. Flierl, On the evolution of isolated, nonlinear vorticies, *Journal of Physical Oceanography*, *9*, 1155–1182, doi:10.1175/1520-0485(1979)009⟨1155:OTEOIN⟩2.0.CO;2, 1979. 1072

McWilliams, J. C., Submesoscale, coherent vortices in the ocean, *Reviews of Geophysics*, *23*, 165–182, 1985. 844

McWilliams, J. C., Submesoscale currents in the ocean, *Proceedings of the Royal Society*, *A472*, doi:10.1098/rspa.2016.0117, 2016. 1669

McWilliams, J. C., There is no horizontal gravity force in geopotential coordinates, *Proceedings of the National Academy of Sciences*, *121*, doi:10.1073/pnas.2416636121, 2024. 344

McWilliams, J. C., M. J. Molemaker, and P. Damien, Baroclinic sea-level, *Journal of Advances in Modeling Earth Systems (JAMES)*, *in review*, 2024. 1128

Mellor, G. L., L.-Y. Oey, and T. Ezer, Sigma coordinate pressure gradient errors and the seamount problem, *Journal of Atmospheric and Oceanic Technology*, *15*, 1122–1131, 1998. 1851

Mermin, N. D., What's wrong with these equations?, *Physics Today*, *42*, 9–11, doi:10.1063/1.2811173, 1989. x

Mertz, G., and D. Wright, Interpretations of the JEBAR term, *Journal of Physical Oceanography*, *22*, 301–305, doi:10.1175/1520-0485(1992)022⟨0301:IOTJT⟩2.0.CO;2, 1992. 1281

Meyer, R., *Introduction to mathematical fluid dynamics*, Dover Publications, New York, 1971. 645, 650, 652

Middleton, J. F., and J. W. Loder, Skew fluxes in polarized wave fields, *Journal of Physical Oceanography*, *19*, 68–76, doi:10.1175/1520-0485(1989)019⟨0068:SFIPWF⟩2.0.CO;2, 1989. 1924, 1959, 1970, 1972, 1975, 2003

Milder, D. M., A note regarding 'on hamilton's principle for surface waves', *Journal of Fluid Mechanics*, *83*, 159–161, doi:10.1017/S0022112077001116, 1977. 1457, 1468, 1469

Miles, J. W., On the stability of heterogeneous shear flows, *Journal of Fluid Mechanics*, *10*, 496–508, doi:10.1017/S0022112061000305, 1961. 1723, 1757

Miles, J. W., On hamilton's principle for surface waves, *Journal of Fluid Mechanics*, *83*, 153–158, doi:10.1017/S0022112077001104, 1977. 1457, 1468

Minobe, S., M. Terada, B. Qiu, and N. Schneider, Western boundary sea level: A theory, rule of thumb, and application to climate models, *Journal of Physical Oceanography*, *47*, 957–977, doi:10.1175/JPO-D-16-0144.1, 2017. 1119

Misner, C., K. Thorne, and J. Wheeler, *Gravitation*, W.H. Freeman and Co., 1279 pages, 1973. 13, 71

Mitrovica, J. X., M. E. Tamisiea, J. L. Davis, and G. A. Milne, Recent mass balance of polar ice sheets inferred from patterns of global sea-level change, *Nature*, *409*, 1026–1029, 2001. 925, 926

Moffatt, H., Transport effects associated with turbulence with particular attention to the influence of helicity, *Reports on Progress in Physics*, *46*, 621–664, doi:10.1088/0034-4885/46/5/002, 1983. 1924, 1975

Molemaker, M., J. McWilliams, and W. Dewar, Submesoscale instability and generation of mesoscale anticyclones near a separation of the California Undercurrent, *Journal of Physical Oceanography*, *45*, 613–629, doi:10.1175/JPO-D-13-0225.1, 2015. 747, 1177

Montgomery, R. B., Circulation in upper layers of southern North Atlantic, *Papers in Physical Oceanography*, *6*, 55, 1938. 2003

Morel, Y., J. Gula, and A. Ponte, Potential vorticity diagnostics based on balances between volume integral and boundary conditions, *Ocean Modelling*, *138*, 23–35, doi:10.1016/j.ocemod.2019.04.004, 2019. 1211, 1216

Morse, P. M., and H. Feshbach, *Methods of Theoretical Physics Part I and II*, McGraw-Hill Book Company, New York, 1953. 5, 188, 201, 344, 1311

Mory, M., Inertial oscillations, in *Rotating Fluids in Geophysical and Industrial Applications*, International Centre for Mechanical Sciences (Courses and Lectures), Springer, Vienna, doi:10.1007/978-3-7091-2602-8_8, 1992. 1503

Müller, P., Ertel's potential vorticity theorem in physical oceanography, *Reviews of Geophysics*, *33*, 67–97, doi:10.1029/94RG03215, 1995. 1184, 1204, 1337, 1342, 1352

Müller, P., *The Equations of Oceanic Motions*, 1st ed., Cambridge University Press, Cambridge, 302pp, 2006. 689

Müller, P., and C. Garrett, From stirring to mixing in a stratified ocean, *Oceanography*, *15*, 12–19, 2002. 1989

Munk, W., and E. Palmén, Note on the dynamics of the Antarctic Circumpolar Current, *Tellus*, *3*, 53–55, 1951. 765, 1008, 1010

Munk, W. H., On the wind-driven ocean circulation, *Journal of Meteorology*, *7*, 79–93, 1950. 1111

Nakamura, N., A new look at eddy diffusivity as a mixing diagnostic, *Journal of the Atmospheric Sciences*, *58*(24), 3685–3701, doi:10.1175/1520-0469(2001)058⟨3685:ANLAED⟩2.0.CO;2, 2001. 1989

Naveira Garabato, A., E. Frajka-Williams, C. Spingys, A. Legg, K. Polzin, A. Forryan, E. Abrahamsen, C. Buckingham, S. Griffies, S. McPhail, K. Nicholls, L. Thomas, and M. Meredith, Rapid mixing and exchange of deep-ocean waters in an abyssal boundary current, *Proceedings of the National Academy of Sciences*, doi:10.1073/pnas.1904087116, 2019. 1222

Neumann, G., and W. Pierson, *Principles of Physical Oceanography*, Prentice-Hall, Englewood Cliffs, USA, 545 pp, 1966. 1488

Noether, E., Invariante variationsprobleme, *Nachrichten von der Gesellschaft der Wissenschaften zu Göttingen, Math-phys. Klasse*, pp. 235–257, 1918. 310, 351, 1310, 1325

Noether, E., and M. Tavel, Invariant variational problems, *arXiv:physics/0503066 [physics.hist-ph]*, 2018. 310, 351, 1310, 1325

Nurser, A. G., and S. M. Griffies, Relating diffusive surface salinity fluxes to boundary freshwater and salt fluxes, *Journal of Physical Oceanography*, *49*, 2365–2376, doi:10.1175/JPO-D-19-0037.1, 2019. 1950, 2030, 2060

Nurser, A. G., and M.-M. Lee, Isopycnal averaging at constant height. Part I: The formulation and a case study, *Journal of Physical Oceanography*, *34*, 2721–2739, 2004a. 1983

Nurser, A. G., and M.-M. Lee, Isopycnal averaging at constant height. Part II: Relating to the residual streamfunction in Eulerian space, *Journal of Physical Oceanography*, *34*, 2740–2755, 2004b. 1983

Nurser, A. G., R. Marsh, and R. Williams, Diagnosing water mass formation from air–sea fluxes and surface mixing, *Journal of Physical Oceanography*, *29*, 1468–1487, doi:10.1175/1520-0485(1999)029⟨1468:DWMFFA⟩2.0.CO;2, 1999. 808

Nurser, A. J. G., S. M. Griffies, J. D. Zika, and G. Stanley, Mathematics of circulation in arbitrary fluid property spaces, *Earth and Space Science Open Archive (ESSOar)*, doi:10.1002/essoar.10511370.1, 2022. 15, 69, 2044, 2050

Olbers, D. J., J. Willebrand, and C. Eden, *Ocean Dynamics*, 1st ed., Springer, Berlin, Germany, 704 pages, 2012. xiii, 345, 412, 574, 689, 702, 705, 834, 1012, 1013, 1369, 1405, 1406, 1410, 1423, 1990

Otto, A., F. Otto, O. Boucher, J. Church, G. Hegerl, P. Forster, N. Gillett, J. Gregory, G. Johnson, R. Knutti, N. Lewis, U. Lohmann, J. Maroztke, G. Myhre, D. Shindell, B. Stevens, and M. Allen, Energy budget constraints on climate response, *Nature Geosciences*, *6*, 415–416, doi:10.1038/ngeo1836, 2013. 2036

Padhye, N., and P. J. Morrison, Fluid element particle relabeling, *Physics Letters A*, *219*, 287–292, doi:10.1016/0375-9601(96)00472-0, 1996. 1352

Paparella, F., and W. R. Young, Horizontal convection is non-turbulent, *Journal of Fluid Mechanics*, *466*, 205–214, doi:10.1017/S0022112002001313, 2002. 800

Patmore, R., P. Holland, D. Munday, A. Naveira Garabato, D. Stevens, and M. Meredith, Topographic control of Southern Ocean gyres and the Antarctic Circumpolar Current: a barotropic perspective, *Journal of Physical Oceanography*, *49*, 3221–3244, doi:10.1175/JPO-D-19-0083.1, 2019. 1109, 1167

Pedlosky, J., The stability of currents in the atmosphere and ocean, Part I, *Journal of the Atmospheric Sciences*, *21*, 201–219, doi:10.1175/1520-0469(1964)021⟨0201:TSOCIT⟩2.0.CO;2, 1964. 1787

Pedlosky, J., *Geophysical Fluid Dynamics*, 2nd ed., Springer-Verlag, Berlin Heidelberg New York, 710 + xv pp, 1987. 1795

Pedlosky, J., *Ocean Circulation Theory*, Springer-Verlag, Berlin Heidelberg New York, 403 + xi pp, 1996. 870

Pedlosky, J., *Waves in the Ocean and Atmosphere: Introduction to Wave Dynamics*, Springer-Verlag, Berlin Heidelberg New York, 206 + viii pp, 2003. 1369, 1484, 1532, 1553, 1601, 1602, 1630, 1639, 1659, 1782, 1785, 1795

Pedlosky, J., L. Pratt, M. Spall, and K. Helfrich, Circulation around islands and ridges, *Journal of Marine Research*, *55*, 1199–1251, 1997. 1117

Peterson, H., and J. Callies, Rapid spin up and spin down of flow along slopes, *Journal of Physical Oceanography*, doi:10.1175/JPO-D-21-0173.1, 2022. 922, 1254, 1804

Peterson, K. A., and R. J. Greatbatch, Vorticity fluxes in shallow water ocean models, *Atmosphere-Ocean*, *39*, 1–14, doi:10.1080/07055900.2001.9649662, 2001. 1889

Phillips, N. A., A coordinate system having some special advantages for numerical forecasting, *Journal of Meteorology*, *14*, 184–185, doi:10.1175/1520-0469(1957)014⟨0184:ACSHSS⟩2.0.CO;2, 1957. 1804

Pierce, A. D., Wave equation for sound in fluids with unsteady inhomogeneous flow, *Journal of the Acoustical Society of America*, *87*, 2292–2299, doi:10.1121/1.399073, 1990. 1432, 1446, 1453

Plumb, R. A., Eddy fluxes of conserved quantities by small-amplitude waves, *Journal of Atmospheric Sciences*, *36*, 1699–1704, 1979. 1975

Polton, J., and D. Marshall, Overturning cells in the Southern Ocean and subtropical gyres, *Ocean Science*, *3*, 17–30, 2007. 1196, 1210

Polzin, K., and T. McDougall, Mixing at the ocean's bottom boundary, in *Ocean Mixing : Drivers, Mechanisms and Impacts*, edited by M. Meredith and A. N. Garabato, pp. 145–180, Elsevier, doi:10.1016/B978-0-12-821512-8.00014-1, 2021. 1218

Polzin, K. L., J. M. Toole, J. R. Ledwell, and R. W. Schmitt, Spatial variability of turbulent mixing in the abyssal ocean, *Science*, *276*, 93–96, 1997. 1989

Pope, S. B., *Turbulent Flows*, Cambridge Press, 2000. 149, 412, 422, 435, 475

Pratt, L. J., and J. A. Whitehead, *Rotating Hydraulics: Nonlinear Topographic Effects in the Ocean and Atmosphere*, 589 pp., Springer Science + Business Media, New York, 2008. 696, 981, 1171, 1564, 1598

Pugh, D. T., *Tides, surges, and mean sea-level*, 472 pp., John Wiley and Sons, 1987. 925

Quigg, C., *Gauge Theories of the Strong, Weak, and Electromagnetic Interactions*, Benjamin Cummings: Frontiers in Physics, Menlo Park, California, 1983. 1311, 1336

Ramond, P., *Field Theory: A Modern Primer*, Addison-Wesley Frontiers in Physics, 1990. 1311, 1325, 1336

Rayleigh, L., On the stability, or instability, of certain fluid motions, *Proceedings of the London Mathematical Society*, *9*, 57–70, doi:10.1112/plms/s1-11.1.57, 1880. 1733

Rayleigh, L., *The Theory of Sound*, Macmillan, London, UK, 1894. 1747

Redi, M. H., Oceanic isopycnal mixing by coordinate rotation, *Journal of Physical Oceanography*, *12*, 1154–1158, doi:10.1175/1520-0485(1982)012⟨1154:OIMBCR⟩2.0.CO;2, 1982. 2003, 2004, 2006

Reif, F., *Fundamentals of Statistical and Thermal Physics*, McGraw-Hill, New York, 1965. 404, 412, 555, 558, 559, 1906

Reiner, M., The deborah number, *Physics Today*, *17*, 62, doi:10.1063/1.3051374, 1964. 408

Rhines, P. B., Lectures on geophysical fluid dynamics, in *Fluid Dynamics in Astrophysics and Geophysics*, edited by N. R. Lebovitz, pp. 3–58, American Mathematical Society, 1980. 1076, 1104

Rhines, P. B., Basic dynamics of the large-scale geostrophic circulation, in *WHOI 1982 Summer Study Program*, Woods Hole Oceanographic Institute, 1982. 1980

Rhines, P. B., and W. R. Holland, A theoretical discussion of eddy-driven mean flows, *Dynamics Of Atmospheres And Oceans*, *3*, 289–325, doi:10.1016/0377-0265(79)90015-0, 1979. 1956

Rhines, P. B., and W. R. Young, Homogenization of potential vorticity in planetary gyres, *Journal of Fluid Mechanics*, *122*, 347–367, 1982. 1938, 1940

Ringler, T., J. Saenz, P. Wolfram, and L. Van Roekel, A thickness-weighted average perspective of force balance in an idealized Circumpolar Current, *Journal of Physical Oceanography*, *47*, 285–302, doi:10.1175/JPO-D-16-0096.1, 2017. 808

Rintoul, S. R., The global influence of localized dynamics in the Southern Ocean, *Nature*, *558*, 209–218, doi:10.1038/s41586-018-0182-3, 2018. 766

Rintoul, S. R., and A. C. Naveira Garabato, Dynamics of the Southern Ocean circulation, in *Ocean Circulation and Climate, 2nd Edition: A 21st Century Perspective*, *International Geophysics Series*, vol. 103, edited by G. Siedler, S. M. Griffies, J. Gould, and J. Church, pp. 471–492, Academic Press, 2013. 766

Rintoul, S. R., C. W. Hughes, and D. Olbers, The Antarctic Circumpolar Current system, in *Ocean Circulation and Climate, 1st Edition*, *International Geophysics Series*, vol. 103, edited by G. Siedler, J. Gould, and J. Church, pp. 271–301, Academic Press, 2001. 766

Rooth, C., Hydrology and the ocean circulation, *Progress in Oceanography*, *11*, 131–149, doi:10.1016/0079-6611(82)90006-4, 1982. 2003

Roquet, F., G. Madec, L. Brodeau, and J. Nycander, Defining a simplified yet realistic equation of state for seawater, *Journal of Physical Oceanography*, *45*, 2464–2579, doi:10.1175/JPO-D-15-0080.1, 2015. 2038

Rossby, C.-G., Planetary flow patterns in the atmosphere, *Quarterly Journal of the Royal Meteorological Society (suppl)*, *66*, 68–87, 1940. 1022, 1094

Rossby, C.-G., On displacements and intensity changes of atmospheric vorticity, *Journal of Marine Research*, *7*, 175–187, 1948. 625, 626, 1070

Ruan, X., and R. Ferrari, Diagnosing diapycnal mixing from passive tracers, *Journal of Physical Oceanography*, *51*, 757–767, doi:10.1175/JPO-D-20-0194.1, 2021. 1956

Ruan, X., J. Wenegrat, and J. Gula, Slippery bottom boundary layers: The loss of energy from the general circulation by bottom drag, *Geophysical Research Letters*, *48*, doi:10.1029/2021GL094434, 2021. 922

Ryder, L. H., *Quantum Field Theory*, Cambridge University Press, 443 pp., 1985. 1311, 1320, 1336

Sadourny, R., and C. Basdevant, Parameterization of subgrid scale barotropic and baroclinic eddies in quasi-geostrophic models: anticipated potential vorticity method, *Journal of Atmospheric Sciences*, *42*, 1353–1363, 1985. 1081

Saffman, P. G., *Vortex Dynamics*, Cambridge University Press, Cambridge, England, 1992. 616, 1032, 1033, 1044

Salmon, R., Hamiltonian fluid mechanics, *Annual Review of Fluid Mechanics*, *20*, 225–256, doi:10.1146/annurev.fl.20.010188.001301, 1988. 1310, 1337, 1342, 1346, 1352

Salmon, R., *Lectures on Geophysical Fluid Dynamics*, Oxford University Press, Oxford, England, 378 + xiii pp., 1998. xiii, 384, 404, 412, 448, 644, 939, 1089, 1310, 1337, 1342, 1352

Samelson, R., *The Theory of Large-Scale Ocean Circulation*, Cambridge University Press, Cambridge, UK, 193 pp., 2011. 870, 1271

Santiago, J., and M. Visser, Gravity's universality: The physics underlying Tolman temperature gradients, *International Journal of Modern Physics D*, *27*, doi:10.1142/S021827181846001X, 2018. 586

Schär, C., A generalization of Bernoulli's Theorem, *Journal of the Atmospheric Sciences*, *50*, 1437–1443, doi:10.1029/2003JC001823, 1993. 1196, 1210

Schey, H., *Div, grad, curl and all that: an informal text on vector calculus*, W.W. Norton and Company, Inc., 176 pp, 2004. 35

Schmitt, R. W., Double diffusion in oceanography, *Annual Review of Fluid Mechanics*, *26*, 255–285, 1994. 1989, 2022

Schneider, T., I. M. Held, and S. Garner, Boundary effects in potential vorticity dynamics, *Journal of Atmospheric Sciences*, *60*, 1024–1040, doi:10.1175/1520-0469(2003)60⟨1024:BEIPVD⟩2.0.CO;2, 2003. 808, 1304

Schutz, B. F., *Geometrical Methods of Mathematical Physics*, Cambridge University Press, Cambridge, UK, 250 pp, 1980. 2, 15, 63, 71, 72

Schutz, B. F., *A First Course in General Relativity*, Cambridge University Press, Cambridge, UK, 392 pp, 1985. 66

Segel, L., *Mathematics Applied to Continuum Mechanics*, 590 pp., Dover Publications, 1987. 7, 35, 468, 469, 479, 646, 650

Seliger, R. L., and G. B. Whitham, Variational principles in continuum mechanics, *Proceedings of the Royal Society A*, *305*, 1–25, doi:10.1098/rspa.1968.0103, 1968. 1471

Serrin, J., Mathematical principles of classical fluid mechanics, in *Fluid Mechanics I*, edited by S. Flügge and C. Truesdell, pp. 125–263, Springer-Verlag, Berlin, 1959. 239, 494, 646, 648, 689, 767, 886, 891

Shakespeare, C. J., B. K. Arbic, and A. M. Hogg, Dissipating and reflecting internal waves, *Journal of Physical Oceanography*, *51*, 2517–2531, doi:10.1175/JPO-D-20-0261.1, 2021. 1659

Shao, A., A. Adcroft, R. Hallberg, and S. Griffies, A general-coordinate, nonlocal neutral diffusion operator, *Journal of Advances in Modeling Earth Systems*, *12*, doi:10.1029/2019MS001992, 2020. 2006, 2013

Shchepetkin, A., and J. McWilliams, A method for computing horizontal pressure-gradient force in an ocean model with a non-aligned vertical coordinate, *Journal of Geophysical Research*, *108*, 35.1–35.34, 2002. 1851

Shifrin, T., *Multivariable Mathematics: Linear Algebra, Multivariable Calculus, and Manifolds*, Wiley, 2004. 45

Sieniutycz, S., *Conservation Laws in Variational Thermo-Hydrodynamics*, Kluwer Academic Pulbications, 1994. 1337

Smagorinsky, J., General circulation experiments with the primitive equations: I. The basic experiment, *Monthly Weather Review*, *91*, 99–164, 1963. 720

Smagorinsky, J., Some historical remarks on the use of nonlinear viscosities, in *Large Eddy Simulation of Complex Engineering and Geophysical Flows*, edited by B. Galperin and S. A. Orszag, pp. 3–36, Cambridge University Press, 1993. 654

Smith, K. S., and J. Marshall, Evidence for enhanced eddy mixing at middepth in the southern ocean, *Journal of Physical Oceanography*, *39*, 50–69, 2009. 2001, 2007

Smith, K. S., and G. K. Vallis, The scales and equilibration of midocean eddies: freely evolving flow, *Journal of Physical Oceanography*, *31*, 554–570, doi:10.1175/1520-0485(2001)031⟨0554:TSAEOM⟩2.0.CO;2, 2001. 870, 1061

Smith, K. S., and G. K. Vallis, The scales and equilibration of midocean eddies: forced-dissipative flow, *Journal of Physical Oceanography*, *32*, 1699–1721, 2002. 2001

Smith, R., A hurricane beta drift law, *Journal of Atmospheric Sciences*, *50*, doi:10.1175/1520-0469(1993)050⟨3213:AHBDL⟩2.0.CO;2, 1993. 1072

Smith, R. D., The primitive equations in the stochastic theory of adiabatic stratified turbulence, *Journal of Physical Oceanography*, *29*, 1865–1880, doi:10.1175/1520-0485(1999)029⟨1865:TPEITS⟩2.0.CO;2, 1999. 1986

Smith, R. D., and P. R. Gent, Anisotropic Gent-McWilliams parameterization for ocean models, *Journal of Physical Oceanography*, *34*, 2541–2564, 2004. 2009, 2010, 2012, 2013, 2014

Smyth, W. D., and J. R. Carpenter, *Instability in Geophysical Flows*, Cambridge University Press, Cambridge, UK, 327 pp, 2019. xxxiv, xxxv, 1544, 1667, 1725, 1747, 1748, 1782, 1914

Solomon, H., On the representation of isentropic mixing in ocean models, *Journal of Physical Oceanography*, *1*, 233–234, doi:10.1175/1520-0485(1971)001⟨0233:OTROIM⟩2.0.CO;2, 1971. 2003

Soper, D. E., *Classial Field Theory*, Dover Pulbications, 2008. 1316, 1337

Spence, P., O. A. Saekno, W. Sijp, and M. England, The role of bottom pressure torques on the interior pathways of North Atlantic Deep Water, *Journal of Physical Oceanography*, *42*, 110–125, doi:10.1175/2011JPO4584.1, 2012. 1166

Spence, P., R. M. Holmes, A. McC. Hogg, S. M. Grifies, K. D. Stewart, and M. H. England, Localized rapid warming of West Antarctic subsurface waters by remote winds, *Nature Climate Change*, doi:10.1038/NCLIMATE3335, 2017. 922

Spiegel, M., *Theory and Problems of Vector Analysis*, Schaum's Outline Series, McGraw-Hill International Book Company, New York, 1974a. 35

Spiegel, M., *Fourier Analysis with Applications to Boundary Value Problems*, Schaum's Outline Series, McGraw-Hill International Book Company, New York, 1974b. 163, 168, 173

Squire, H. B., On the stability for three-dimensional disturbances of viscous fluid flow between parallel walls, *Proceedings of the Royal Society of London. Series A*, *142*, 621–628, doi:10.1098/rspa.1933.0193, 1933. 1725

Stakgold, I., *Boundary value problems of mathematical physics, volume I*, SIAM, Philadelphia, 340 pp, 2000a. 125, 142, 153, 156, 188, 199, 207, 239

Stakgold, I., *Boundary value problems of mathematical physics, volume II*, SIAM, Philadelphia, 408 pp, 2000b. 125, 142, 149, 163, 188, 190, 199, 214, 230, 231, 234, 1385, 1390

Staniforth, A. N., *Global Atmospheric and Oceanic Modelling*, Cambridge University Press, 2022. 3, 344

Stanley, G. J., Neutral surface topology, *Ocean Modelling*, doi:10.1016/j.ocemod.2019.01.008, 2019. 840

Stanley, G. J., T. McDougall, and P. Barker, Algorithmic improvements to finding approximately neutral surfaces, *Journal of Advances in Modeling Earth Systems*, *13*, doi:10.1029/2020MS002436, 2021. 840

Starr, V. P., A quasi-Lagrangian system of hydrodynamical equations, *Journal of Meteorology*, *2*, 227–237, doi:10.1175/1520-0469(1945)002⟨0227:AQLSOH⟩2.0.CO;2, 1945. 1798

Stern, M., *Ocean circulation physics*, *International Geophysics Series*, vol. 19, Academic Press, New York, New York, 246 pp, 1975. 1121, 1503, 1517

Stewart, A., and P. Dellar, The role of the complete Coriolis force in cross-equatorial flow of abyssal ocean currents, *Ocean Modelling*, *38*(3-4), 187 – 202, doi:10.1016/j.ocemod.2011.03.001, 2011. 1153

Stewart, A., and J. McWilliams, Gravity is vertical in geophysical fluid dynamics, *Scientific Reports*, *12*, doi:10.1038/s41598-022-10023-3, 2022. 344

Stewart, A., J. McWilliams, and A. Solococh, On the role of bottom pressure torques in wind-driven gyres, *Journal of Physicao Oceanography*, *51*, 1441–1464, doi:10.1175/JPO-D-20-0147.1, 2021. 1110, 1112

Stewart, R., *An Introduction to Physical Oceanography*, 345 pp., Texas A& M, College Station, Texas, USA, 2008. 925

Stommel, H., The westward intensification of wind-driven ocean currents, *Transactions of the American Geophysical Union*, *29*, 202–206, 1948. 1075, 1102, 1111

Straub, D. N., On the transport and angular momentum balance of channel models of the Antarctic Circumpolar Current, *Journal of Physical Oceanography*, *23*, 776–782, doi:10.1175/1520-0485(1993)023⟨0776:OTTAAM⟩2.0.CO;2, 1993. 766

Straub, D. N., On thermobaric production of potential vorticity in the ocean, *Tellus*, *51A*, 314–325, 1999. 1188

Stull, R., *An Introduction to Boundary Layer Meteorology*, 670 pp., Kluwer Academic Publishers, 1988. 901

Sun, S., R. Bleck, C. Rooth, J. Dukowicz, E. Chassignet, and P. D. Killworth, Inclusion of thermobaricity in isopycnic-coordinate ocean models, *Journal of Physical Oceanography*, *29*, 2719–2729, 1999. 1859

Sutherland, B. R., *Internal Gravity Waves*, Cambridge University Press, 2010. 712, 1369, 1531, 1539, 1593, 1601, 1620, 1639, 1640, 1660, 1715

Symon, K., *Mechanics*, Addison-Wesley Publishing Co., Reading, MA, USA, 639 pp, 1971. xi, 263, 264

Talley, L. D., G. L. Pickard, W. J. Emery, and J. H. Swift, *Descriptive Physical Oceanography*, 6th ed., Elsevier, 555pp, 2011. 952, 2043

Tarshish, N., N. Jeevangee, and D. Lecoanet, Buoyant motion of a turbulent thermal, *Journal of the Atmospheric Sciences*, *75*, 3233–3244, doi:10.1175/JAS-D-17-0371.1, 2018. 823, 856, 857

Taylor, G., Diffusion by continuous movements, *Proceedings of the London Mathematical Society*, *20*, 196–212, 1921. 1901, 1989

Taylor, J. R., *Classical Mechanics*, University Science Books, 786 pp., 2005. 264, 285

Tennekes, H., and J. Lumley, *A First Course in Turbulence*, 300 pp., MIT Press, Cambridge, USA, 1972. 660, 901, 1027

Thomas, L., A. Tandon, and A. Mahadevan, Submesoscale processes and dynamics, in *Eddy resolving ocean models*, edited by M. Hecht and H. Hasumi, Geophysical Monograph 177, pp. 17–38, American Geophysical Union, 2008. 1194, 1222, 1698

Thomas, L., J. R. Taylor, R. Ferrari, and T. Joyce, Symmetric instability in the Gulf Stream, *Deep Sea Research II*, *91*, 96–110, doi:10.1016/j.dsr2.2013.02.025, 2013. 1194, 1222, 1669, 1697, 1705

Thorne, K., and R. Blandford, *Modern Classical Physics*, Princeton University Press, Princeton, USA, 1511 + xl pp, 2017. xvi, 2, 75, 163, 339, 689, 692, 1140, 1369, 1410, 1425, 1453

Thorpe, S., The dynamics of the boundary layers of the deep ocean, *Science Progress*, *72*, 189–206, 1988. 901

Thorpe, S., *The Turbulent Ocean*, 439 pp., Cambridge University Press, Cambridge, UK, 2005. 901

Tomczak, M., and J. S. Godfrey, *Regional Oceanography: An Introduction*, Pergamon Press, Oxford, England, 422 + vii pp, 1994. 726, 954, 1117

Towne, D. H., *Wave phenomena*, Dover Publications, New York, 482 pp, 1967. 1430

Tracy, E. R., A. J. Brizard, A. S. Richardson, and A. N. Kaufman, *Ray Tracing and Beyond: Phase Space Methods in Plasma Wave Theory*, Cambridge University Press, 2014. xvi, 249, 1405, 1414, 1415

Treguier, A. M., I. M. Held, and V. D. Larichev, On the parameterization of quasi-geostrophic eddies in primitive equation ocean models, *Journal of Physical Oceanography*, *27*, 567–580, doi:10.1175/1520-0485(1997)027⟨0567:POQEIP⟩2.0.CO;2, 1997. 1785, 1989, 2001, 2007

Tromp, J., *Theoretical and Computational Seismology*, Princeton University Press, Princeton, USA, 2025a. xvi, 2, 13, 33, 63, 71, 75, 416, 448, 449, 450, 459, 461, 464, 488, 627, 1310, 1332, 1336, 1337, 1342

Tromp, J., *A Geometrical Introduction to Tensor Calculus*, Princeton University Press, Princeton, USA, 2025b. 63, 71, 75, 448, 449, 450, 461

Truesdell, C., The mechanical foundations of elasticity and fluid dynamics, *Journal of Rational Mechanics and Analysis*, *1*, 125–300, 1952. 632

Truesdell, C., Notes on the history of the general equations of hydrodynamics, *American Mathematical Monthly*, *60*, 445–458, doi:10.2307/2308407, 1953. 416, 419, 422

Truesdell, C., *The kinematics of vorticity*, Dover Publications, Mineola, New York, 1954. 49, 416, 417, 419, 422, 538

Tyler, R. H., and R. Käse, A string function for describing the propagation of large-scale energy anomalies in a rotating fluid, *Geophysical and Astrophysical Fluid Dynamics*, *92*, 31–64, doi:10.1080/03091920008203710, 2000. 1585

Tyler, R. H., and R. Käse, A string function for describing the propagation of baroclinic anomalies in the ocean, *Journal of Physical Oceanography*, *31*, 765–776, doi:10.1175/1520-0485(2001)031⟨0765:ASFFDT⟩2.0.CO;2, 2001. 1585

Vallis, G., and B.-L. Hua, Eddy viscosity of the anticipated potential vorticity method, *Journal of the Atmospheric Sciences*, *45*, 617–627, doi:10.1175/1520-0469(1988)045⟨0617:EVOTAP⟩2.0.CO;2, 1988. 1081

Vallis, G. K., *Atmospheric and Oceanic Fluid Dynamics: Fundamentals and Large-scale Circulation*, 1st ed., Cambridge University Press, Cambridge, 745 + xxv pp, 2006. 972, 1016

Vallis, G. K., *Atmospheric and Oceanic Fluid Dynamics: Fundamentals and Large-scale Circulation*, 2nd ed., Cambridge University Press, Cambridge, 946 + xxv pp, 2017. xxxiv, xxxv, 110, 344, 345, 347, 412, 574, 591, 614, 656, 689, 712, 726, 766, 768, 777, 800, 806, 814, 826, 829, 834, 870, 882, 891, 901, 920, 939, 951, 954, 958, 1013, 1061, 1070, 1082, 1107, 1111, 1112, 1147, 1188, 1216, 1240, 1300, 1369, 1471, 1484, 1522, 1539, 1544, 1548, 1597, 1598, 1601, 1638, 1639, 1640, 1659, 1747, 1765, 1785, 1795, 1906, 1912, 1924, 1938, 1987, 1991

Vallis, G. K., *Essentials of Atmospheric and Oceanic Dynamics*, 1st ed., Cambridge University Press, Cambridge, 2019. 1599

van Heijst, G., Dynamics of vortices in rotating and stratified flows, in *Fronts, Waves, and Vortices in Geophysical Flows*, Lecture notes in Physics 805, p. 192, Springer, 2010. 890, 900

Van Roekel, L., A. Adcroft, G. Danabasoglu, S. M. Griffies, B. Kauffman, W. Large, M. Levy, B. Reichl, T. Ringler, and M. Schmidt, The KPP boundary layer scheme for the ocean: revisiting its formulation and benchmarking one-dimensional simulations relative to LES, *Journal of Advances in Modeling Earth Systems*, doi:10.1029/2018ms001336, 2018. 2033

van Sebille, E., S. M. Griffies, R. Abernathey, T. Adams, P. Berloff, A. Biastoch, B. Blanke, E. Chassignet, Y. Cheng, C. Cotter, E. Deleersnijder, K. Döös, H. Drake, S. Drijfhout, S. Gary, A. Heemink, J. Kjellsson, I. Koszalka, M. Lange, C. Lique, G. MacGilchrist, R. Marsh, G. M. Adame, R. McAdam, F. Nencioli, C. Paris, M. Piggott, J. Polton, S. Rühs, S. Shah, M. Thomas, J. Wang, P. Wolfram, L. Zanna, and J. Zika, Lagrangian ocean analysis: fundamentals and practices, *Ocean Modelling*, *121*, 49–75, doi:10.1016/j.ocemod.2017.11.008, 2018. 425

Venaille, A., G. K. Vallis, and S. M. Griffies, The catalytic role of beta effect in barotropization processes, *Journal of Fluid Dynamics*, doi:10.1017/jfm.2012.344, 2012. 1061

Veronis, G., Large scale ocean circulation, *Advances in Applied Mechanics*, *13*, 2–92, doi:10.1016/S0065-2156(08)70143-1, 1973. 343, 344, 394

Veronis, G., The role of models in tracer studies, in *Numerical Models of Ocean Circulation*, pp. 133–146, National Academy of Sciences, 1975. 2003

von Arx, W. S., *An Introduction to Physical Oceanography*, Addison-Wesley Publishing Company, Reading, Massachusetts, USA, 422 pp, 1962. 896, 912, 916

Wåhlin, A., R. Muench, L. Arneborg, G. Björk, H. Ha, S. Lee, and A. Alsén, Some implications of Ekman layer dynamics for cross-shelf exchange in the amundsen sea, *Journal of Physical Oceanography*, *42*, 1461–1474, doi:10.1175/JPO-D-11-041.1, 2012. 921, 922

Wald, R. M., *General Relativity*, University of Chicago Press, Chicago, USA, 1984. 1336

Waldman, R., and H. Giordani, Ocean barotropic vorticity balances: theory and application to numerical models, *Journal of Advances in Modeling Earth Systems*, *15*(4), e2022MS003,276, doi:10.1029/2022MS003276, 2023. 1282

Walin, G., A theoretical framework for the description of estuaries, *Tellus*, *29*(2), 128–136, doi:10.1111/j.2153-3490.1977.tb00716.x, 1977. 2054

Walin, G., On the relation between sea-surface heat flow and thermal circulation in the ocean, *Tellus*, *34*, 187–195, doi:10.1111/j.2153-3490.1982.tb01806.x, 1982. 2054

Wallace, J., and P. Hobbs, *Atmospheric Science: An Introductory Survey*, Academic Press, 2006. 1016

Ward, M., and A. Hogg, Establishment of momentum balance by form stress in a wind-driven channel, *Ocean Modelling*, *40*(133–146), doi:10.1016/j.ocemod.2011.08.004, 2011. 993

Waterhouse, A. F., J. A. MacKinnon, J. D. Nash, M. H. Alford, E. Kunze, H. L. Simmons, K. L. Polzin, L. C. St. Laurent, O. M. Sun, R. Pinkel, L. D. Talley, C. B. Whalen, T. N. Huussen, G. S. Carter, I. Fer, S. Waterman, A. C. Naveira Garabato, T. B. Sanford, and C. M. Lee, Global Patterns of Diapycnal Mixing from Measurements of the Turbulent Dissipation Rate., *Journal of Physical Oceanography*, *44*(7), 1854–1872, doi:10.1175/JPO-D-13-0104.1, 2014. 1989

Waterman, S., and B. J. Hoskins, Eddy shape, orientation, propagation, and mean flow feedback in western boundary current jets, *Journal of Physical Oceanography*, *43*, 1666–1690, 2013. 1055

Waterman, S., and J. Lilly, Geometric decomposition of eddy feedbacks in barotropic systems, *Journal of Physical Oceanography*, *45*, 1009–1024, 2015. 1055

Webb, D., R. Holmes, P. Spence, and M. England, Barotropic Kelvin wave-induced bottom boundary layer warming along the West Antarctic Peninsula, *Journal of Geophysical Research: Oceans*, *124*, 1595–1615, doi:10.1029/2018JC014227, 2019. 922

Webb, D. J., and B. A. de Cueves, On the fast response of the Southern Ocean to changes in the zonal wind, *Ocean Science*, *3*, 417–427, doi:10.5194/os-3-417-2007, 2007. 765, 1014

Weiss, J., The dynamics of enstrophy transfer in two-dimensional hydrodynamics, *Physica D*, *273–294*, 1991. 478

Welander, P., Wind-driven ocean circulation in one and two layer oceans of variable depth, *Tellus*, *20*, 1–16, doi:10.1111/j.2153-3490.1968.tb00347.x, 1968. 1076, 1111, 1119

Wenegrat, J., L. Thomas, J. Gula, and J. McWilliams, Effects of the submesoscale on the potential vorticity budget of the ocean mode waters, *Journal of Physical Oceanography*, *48*, 2141–2165, doi:10.1175/JPO-D-17-0219.1, 2018. 1222

Whalen, C. B., L. D. Talley, and J. A. MacKinnon, Spatial and temporal variability of global ocean mixing inferred from argo profiles, *Geophysical Research Letters*, *39*(18), n/a–n/a, doi:10.1029/2012GL053196, 2012. 1989

Whitham, G. B., *Linear and nonlinear waves*, John Whiley and Sons, New York, 636 + xvi pp, 1974. 1373, 1401, 1403, 1405, 1414, 1415, 1456, 1468, 1471

Wise, A., C. W. Hughes, and J. Polton, Bathymetric influence on the coastal sea level response to ocean gyres at western boundaries, *Journal of Physical Oceanography*, *481*, 2949–2964, doi:10.1175/JPO-D-18-0007.1, 2018. 1117, 1119

Wise, A., C. W. Hughes, J. A. Polton, and J. M. Huthnance, Leaky slope waves and sea level: Unusual consequences of the beta effect along western boundaries with bottom topography and dissipation, *Journal of Physical Oceanography*, *50*, 217–237, doi:10.1175/JPO-D-19-0084.1, 2020a. 1119

Wise, A., J. A. Polton, C. W. Hughes, and J. M. Huthnance, Idealised modelling of offshore-forced sea level hot spots and boundary waves along the north american east coast, *Ocean Modelling*, *155*, doi:10.1016/j.ocemod.2020.101706, 2020b. 1119

Wolfe, C., Approximations to the ocean's residual circulation in arbitrary tracer coordinates, *Ocean Modelling*, *75*, 20–35, doi:10.1016/j.ocemod.2013.12.004, 2014. 1983

Woods, L. C., *The Thermodynamics of Fluid Systems*, Oxford University Press, Oxford, UK, 359pp, 1975. 681

Yassin, H., Normal modes with boundary dynamics in geophysical fluids, *Journal of Mathematical Physics*, *62*, doi:10.1063/5.0048273, 2021. 1473

Yassin, H., and S. Griffies, On the discrete normal modes of quasigeostrophic theory, *Journal of Physical Oceanography*, *52*, 243–259, doi:10.1175/JPO-D-21-0199.1, 2022. 1300, 1473, 1767

Yeager, S., Topographic coupling of the Atlantic overturning and gyre circulations, *Journal of Physical Oceanography*, *45*, 1258–1284, doi:10.1175/JPO-D-14-0100.1, 2015. 1277

Young, W. R., Dynamic enthalpy, Conservative Temperature, and the seawater Boussinesq approximation, *Journal of Physical Oceanography*, *40*, 394–400, doi:10.1175/2009JPO4294.1, 2010. 801, 802, 806

Young, W. R., An exact thickness-weighted average formulation of the Boussinesq equations, *Journal of Physical Oceanography*, *42*, 692–707, doi:10.1175/JPO-D-11-0102.1, 2012. 808, 1871, 1878, 1879, 1880, 1881, 1888, 1889, 1959, 1983, 1986, 1999

Yourgrau, W., and S. Mandelstam, *Variational Principles in Dynamics and Quantum Theory*, Dover Publications, 201 pp., 1968. 249, 304

Zanna, L., S. Khatiwala, J. Gregory, J. Ison, and P. Heimbach, Global reconstruction of historical ocean heat storage and transport, *Proceedings of the National Academy of Science*, doi:10.1073/pnas.1808838115, 2019. 239

Zdunkowski, W., and A. Bott, *Dynamics of the Atmosphere: A Course in Theoretical Meteorology*, Cambridge University Press, Cambridge, UK, 719 pp, 2003. 891

Zeitlin, V., *Geophysical Fluid Dynamics: Understanding (almost) everything with rotating shallow water models*, Oxford University Press, 2018. xix

Zhang, X., M. Nikurashin, B. Peña-Molino, S. R. Rintoul, and E. Doddridge, Maintenance of the zonal momentum balance in the Antarctic Circumpolar Current by barotropic dynamics, *Journal of Physical Oceanography*, *in review*, 2024. 1013, 1014

Zhao, R., and G. K. Vallis, Parameterizing mesoscale eddies with residual and Eulerian schemes, and a comparison with eddy-permitting models, *Ocean Modelling*, *23*, 1–12, doi:10.1016/j.ocemod.2008.02.005, 2008. 1999

Zinnser, W., *Writing to Learn*, Harper Perennial, 1993. xv

INDEX